



THE VISUAL NEUROSCIENCES

VOLUME 1

EDITED BY LEO M. CHALUPA AND JOHN S. WERNER

THE VISUAL NEUROSCIENCES

THE VISUAL NEUROSCIENCES

Edited by

Leo M. Chalupa and John S. Werner

Editorial Advisory Board:

Colin Barnstable
Ralph Freeman
Lamberto Maffei
John Maunsell
Robert Shapley
Murray Sherman
Lothar Spillmann
Mriganka Sur
David I. Vaney

A BRADFORD BOOK

THE MIT PRESS

CAMBRIDGE, MASSACHUSETTS

LONDON, ENGLAND

© 2004 Massachusetts Institute of Technology

All rights reserved. No part of this book may be reproduced in any form by any electronic or mechanical means (including photocopying, recording, or information storage and retrieval) without permission in writing from the publisher.

This is a work in two volumes, not sold separately. This ISBN refers to the set and is therefore used to identify both volumes.

This book was set in Baskerville by SNP Best-set Typesetter Ltd., Hong Kong and was printed and bound in the United States of America.

Library of Congress Cataloging-in-Publication Data

The visual neurosciences / edited by Leo M. Chalupa and John S. Werner.

p. ; cm.

“A Bradford book.”

Includes bibliographical references and index.

ISBN 0-262-03308-9

1. Visual pathways. 2. Visual cortex. 3. Visual perception. 4. Neurosciences. I. Chalupa, Leo M. II. Werner, John Simon.

[DNLM: 1. Vision—physiology. 2. Neurosciences—methods. 3. Visual Perception—physiology. WW 103 V83117 2003]

QP475.V274 2003

612.8'4—dc21

2003056137

CONTENTS

Preface xiii

I HISTORICAL FOUNDATIONS 1

1. Vision Structure and Function: The Early History *Mitchell Glickstein* 3
2. The Role of Single-Unit Analysis in the Past and Future of Neurobiology
Horace Barlow 14

II DEVELOPMENTAL PROCESSES 31

3. Molecular Regulation of Vertebrate Retinal Development
Colin J. Barnstable 33
4. Neurotrophins, Electrical Activity, and the Development of Visual Function
Nicoletta Berardi and Lamberto Maffei 46
5. Developmental and Genetic Control of Cell Number in the Retina
Robert W. Williams and Sally A. Moody 63
6. Development of the Vertebrate Retina *Rachel O. L. Wong and
Leanne Godinho* 77
7. The Development of Retinal Decussations *Carol Mason and
Lynda Erskine* 94
8. The Development of Eye-Specific Segregation in the Retino-Geniculo-Striate
Pathway *Barbara Chapman* 108

9. The Role of Neural Activity in the Development of Orientation Selectivity
Chiayu Chiu and Michael Weliky 117
10. Mechanisms of Plasticity in the Visual Cortex *Nigel W. Daw* 126
11. Ontogenesis of Cortical Connectivity *Henry Kennedy and
Andreas Burkhalter* 146
12. Neural Limitations on Visual Development in Primates *Lynne Kiorpes and
J. Anthony Movshon* 159
13. Development of Spatial Selectivity and Response Timing in Humans
Anthony M. Norcia 174
14. The Effects of Selected Forms of Early Visual Deprivation on Perception
Donald E. Mitchell 189
15. Toward a Future for Aging Eyes *R. A. Weale* 205

III RETINAL MECHANISMS AND PROCESSES 213

16. Visual Transduction by Rod and Cone Photoreceptors *Marie E. Burns and
Trevor D. Lamb* 215
17. How Retinal Circuits Optimize the Transfer of Visual Information
Peter Sterling 234
18. ON and OFF Pathways in the Vertebrate Retina and Visual System
Ralph Nelson and Helga Kolb 260
19. Retinal Synapses *Martin Wilson* 279
20. Retinal Neurotransmitters *Robert E. Marc* 304
21. Excitation in the Retina: The Flow, Filtering, and Molecules of Visual Signaling
in the Glutamatergic Pathways from Photoreceptors to Ganglion Cells
David R. Copenhagen 320
22. Peptide and Peptide Receptor Expression and Function in the Vertebrate Retina
Nicholas C. Brecha 334
23. Inhibition in the Retina *Malcolm M. Slaughter* 355
24. Anatomy, Circuitry, and Physiology of Vertebrate Horizontal Cells
Ido Perlman, Helga Kolb and Ralph Nelson 369
25. Retinal Amacrine Cells *David I. Vaney* 395
26. Ganglion Cells in Mammalian Retinae *Paul R. Martin and
Ulrike Grünert* 410
27. Retinal Ganglion Cell Excitability *Andrew T. Ishida* 422

28.	Direction Selectivity in Retinal Ganglion Cells	<i>Richard H. Masland</i>	451
29.	Spatial Regularity among Retinal Neurons	<i>Jeremy E. Cook</i>	463
IV ORGANIZATION OF VISUAL PATHWAYS			479
30.	The M, P, and K Pathways of the Primate Visual System	<i>Ehud Kaplan</i>	481
31.	Parallel Visual Pathways: A Comparative Perspective	<i>Vivien A. Casagrande and Xiangmin Xu</i>	494
32.	Organization of Visual Areas in Macaque and Human Cerebral Cortex	<i>David C. Van Essen</i>	507
33.	Communications between Cortical Areas of the Visual System	<i>Jean Bullier</i>	522
34.	Ventral and Dorsal Cortical Processing Streams	<i>Leslie G. Ungerleider and Tatiana Pasternak</i>	541
V SUBCORTICAL PROCESSING			563
35.	The Visual Relays in the Thalamus	<i>S. Murray Sherman and R. W. Guillery</i>	565
36.	The Visual Functions of the Pulvinar	<i>Christian Casanova</i>	592
37.	Feedback Systems in Visual Processing	<i>Adam M. Sillito and Helen E. Jones</i>	609
38.	Light Responsiveness and Photic Entrainment of the Mammalian Circadian Clock	<i>Johanna H. Meijer and Joseph S. Takahashi</i>	625
39.	Learning from the Pupil: Studies of Basic Mechanisms and Clinical Applications	<i>John L. Barbur</i>	641
40.	Blindsight	<i>Larry Weiskrantz</i>	657
VI PROCESSING IN PRIMARY VISUAL CORTEX			671
41.	Functional Connectivity in the Pathway from Retina to Striate Cortex	<i>R. Clay Reid and W. Martin Usrey</i>	673
42.	Cell Types and Local Circuits in Primary Visual Cortex of the Macaque Monkey	<i>Edward M. Callaway</i>	680

43.	Assembly of Receptive Fields in Primary Visual Cortex	<i>David Ferster</i>	695
44.	A Modern View of the Classical Receptive Field: Linear and Nonlinear Spatiotemporal Processing by V1 Neurons	<i>Gregory C. DeAngelis and Akiyuki Anzai</i>	704
45.	Beyond the Classical Receptive Field: Contextual Modulation of V1 Responses	<i>Victor A. F. Lamme</i>	720
46.	Contributions of Vertical and Horizontal Circuits to the Response Properties of Neurons in Primary Visual Cortex	<i>Thomas R. Tucker and David Fitzpatrick</i>	733
47.	Nonlinear Properties of Visual Cortex Neurons: Temporal Dynamics, Stimulus Selectivity, Neural Performance	<i>Duane G. Albrecht, Wilson S. Geisler and Alison M. Crane</i>	747
48.	Binocular Interaction in the Visual Cortex	<i>Ralph D. Freeman</i>	765
49.	From Binocular Disparity to the Perception of Stereoscopic Depth	<i>Andrew J. Parker</i>	779

VII DETECTION AND SAMPLING 793

50.	Formation and Acquisition of the Retinal Image	<i>David R. Williams and Heidi Hofer</i>	795
51.	Thresholds and Noise	<i>Theodore E. Cohn</i>	811
52.	Ideal Observer Analysis	<i>Wilson S. Geisler</i>	825
53.	Scotopic Vision	<i>Walter Makous</i>	838
54.	Visual Adaptation	<i>Adam Reeves</i>	851
55.	Rod-Cone Interactions in Human Vision	<i>Steven L. Buck</i>	863

VIII BRIGHTNESS AND COLOR 879

56.	Brightness and Lightness	<i>Adriana Fiorentini</i>	881
57.	Color Appearance	<i>Kenneth Knoblauch and Steven K. Shevell</i>	892
58.	Chromatic Discrimination	<i>Joel Pokorny and Vivianne C. Smith</i>	908
59.	The Role of Color in Spatial Vision	<i>Karen K. De Valois</i>	924
60.	Pattern-Selective Adaptation in Color and Form Perception	<i>Michael A. Webster</i>	936

61.	Color Constancy	<i>David H. Brainard</i>	948
62.	Comparative Color Vision	<i>Gerald H. Jacobs</i>	962
63.	Molecular Genetics of Human Color Vision and Color Vision Defects	<i>Maureen Neitz and Jay Neitz</i>	974
64.	Linking Retinal Circuits to Color Opponency	<i>David J. Calkins</i>	989
65.	Neural Coding of Color	<i>Russell L. De Valois</i>	1003
66.	The Processing of Color in Extrastriate Cortex	<i>Karl R. Gegenfurtner and Daniel C. Kiper</i>	1017
67.	Improbable Areas in Color Vision	<i>Semir Zeki</i>	1029
IX FORM, SHAPE, AND OBJECT RECOGNITION			1041
68.	Spatial Scale in Visual Processing	<i>Robert F. Hess</i>	1043
69.	Spatial Channels in Vision and Spatial Pooling	<i>Hugh R. Wilson and Frances Wilkinson</i>	1060
70.	Contour Integration and the Lateral Connections of V1 Neurons	<i>David J. Field and Anthony Hayes</i>	1069
71.	Shape Dimensions and Object Primitives	<i>Charles E. Connor</i>	1080
72.	Shape and Shading	<i>Jan J. Koenderink and Andrea J. van Doorn</i>	1090
73.	Visual Perception of Texture	<i>Michael S. Landy and Norma Graham</i>	1106
74.	Visual Segmentation and Illusory Contours	<i>Robert Shapley, Nava Rubin and Dario Ringach</i>	1119
75.	Global Yet Early Processing of Visual Surfaces	<i>Yukiyasu Kamitani and Shinsuke Shimojo</i>	1129
76.	Image Parsing Mechanisms of the Visual Cortex	<i>Rüdiger von der Heydt</i>	1139
77.	Inferotemporal Response Properties	<i>Keiji Tanaka</i>	1151
78.	Invariant Object and Face Recognition	<i>Edmund T. Rolls</i>	1165
79.	The Ventral Visual Object Pathway in Humans: Evidence from fMRI	<i>Nancy Kanwisher</i>	1179

X MOTION, DEPTH, AND SPATIAL RELATIONS 1191

80. Motion Cues in Insect Vision and Navigation *Mandyam Srinivasan and Shaowu Zhang* 1193
81. The Middle Temporal Area: Motion Processing and the Link to Perception
Kenneth H. Britten 1203
82. Merging Processing Streams: Color Cues for Motion Detection and Interpretation *Karen R. Dobkins and Thomas D. Albright* 1217
83. Functional Mapping of Motion Regions *Guy A. Orban and Wim Vanduffel* 1229
84. Optic Flow *William H. Warren* 1247
85. The Cortical Analysis of Optic Flow *Charles J. Duffy* 1260
86. The Perceptual Organization of Depth *Roland Fleming and Barton L. Anderson* 1284
87. Stereopsis *Clifton M. Schor* 1300
88. Binocular Rivalry *Randolph Blake* 1313
89. Sensorimotor Transformation in the Posterior Parietal Cortex
Hansjörg Scherberger and Richard A. Andersen 1324

XI EYE MOVEMENTS 1337

90. Gaze Control under Natural Conditions *Robert M. Steinman* 1339
91. Eye Movements in Daily Life *Michael F. Land* 1357
92. Selection of Targets for Saccadic Eye Movements *Jeffrey D. Schall* 1369
93. Visual Perception during Saccades *David C. Burr and M. Concetta Morrone* 1391
94. Smooth Pursuit Eye Movements: Recent Advances *Stephen J. Heinen and Edward L. Keller* 1402
95. Neural Control of Vergence Eye Movements *Lawrence E. Mays* 1415
96. The Primate Frontal Eye Field *Charles J. Bruce, Harriet R. Friedman, Michael S. Kraus and Gregory B. Stanton* 1428
97. Changing Views of the Role of Superior Colliculus in the Control of Gaze
Neeraj J. Gandhi and David L. Sparks 1449

98. The Dialogue between Cerebral Cortex and Superior Colliculus: Implications for Saccadic Target Selection and Corollary Discharge *Marc A. Sommer and Robert H. Wurtz* 1466
99. Cerebellar Control of Eye Movements *David S. Zee and Mark F. Walker* 1485

XII ATTENTION AND COGNITION 1499

100. Visual Perception and Cognition in Honeybees *Shaowu Zhang and Mandyam Srinivasan* 1501
101. A Neural Basis for Human Visual Attention *Sabine Kastner* 1514
102. Neural and Behavioral Measures of Change Detection *Daniel J. Simons and Michael Silverman* 1524
103. The Role of Attention in Visual Cerebral Cortex *John H. R. Maunsell* 1538
104. Volition and the Prefrontal Cortex *Earl K. Miller and Jonathan D. Wallis* 1546

XIII THEORETICAL AND COMPUTATIONAL PERSPECTIVES 1561

105. The Evolution of the Visual System in Primates *Jon H. Kaas* 1563
106. Gestalt Factors in the Visual Neurosciences *Lothar Spillmann and Walter H. Ehrenstein* 1573
107. Neural Mechanisms of Natural Scene Perception *Jack L. Gallant* 1590
108. Principles of Image Representation in Visual Cortex *Bruno A. Olshausen* 1603
109. Local Analysis of Visual Motion *Eero P. Simoncelli* 1616
110. Visual Boundaries and Surfaces *Stephen Grossberg* 1624
111. How the Visual Cortex Recognizes Objects: The Tale of the Standard Model *Maximilian Riesenhuber and Tomaso Poggio* 1640

112.	Plasticity of Orientation Processing in Adult Visual Cortex	<i>Valentin Dragoi and Mriganka Sur</i>	1654
113.	Synchrony, Oscillations, and Relational Codes	<i>Wolf Singer</i>	1665
114.	The Neuronal Basis of Visual Consciousness	<i>Christof Koch and Francis Crick</i>	1682
List of Contributors			C1
Index			II

PREFACE

Perhaps the most remarkable thing about vision is the utter simplicity of the act of seeing. We open our eyes and a three-dimensional panorama of colored images—some stationary, others in motion—unfolds before us. In most cases, the brain makes sense of this information seemingly instantaneously, allowing us to function reasonably well under a wide range of lighting conditions. The retinal image is constantly changing as we move about and yet the objects around us are perceived as stable. This seemingly effortless nature of sight beguiles the profound complexity of the processes underlying the perception of even the simplest visual stimulus. Indeed, no machine can currently perform the myriad visual recognition tasks we normally take for granted, and it is still unclear whether such technology will become available in the foreseeable future.

Vision is the dominant sense in humans and other primates, with nearly 30% of our cortical surface representing information that is predominantly visual. Reflecting the importance of vision to the formation of human experience, more effort has gone into studying the visual system than any other sensory modality. As a consequence, we have accumulated an impressive amount of information about vision at many different levels, ranging from genes and molecules to theoretical computations. Our long-term objective is to explain how the brain transforms the spatiotemporal patterns defined by the photons impinging on the retina at any given moment into a coherent visual world. The information derived from understanding these basic processes will ultimately help us prevent and treat the many disorders that impair our ability to see.

Almost 10% of people living today suffer from a visual disorder stemming from a defect of the retina or the visual centers of the brain. Effective treatment of these visual impairments is possible in only a few types of cases because we lack the basic knowledge to understand the dysfunction underlying these disorders. Although we have made significant progress in the visual neurosciences, much remains to be done. The scope of the overall effort has intensified in recent years, reflecting in part, the advent of new technologies, ranging from those of modern molecular biology to the functional imaging of the human brain. Such methodologies have now made it possible to pursue a host of previously unanswerable questions.

There is a plethora of professional journals devoted to vision research, and a number of excellent books dealing with perception as well as the neural bases of vision. No single source, however, has attempted to provide a comprehensive and authoritative account of the visual neurosciences. In an attempt to remedy this situation, we invited 100 of the world's leading researchers in this field to summarize their area of specialization in a manner understandable to the nonspecialist. The response by our colleagues was immensely gratifying. Virtually everyone invited agreed to participate, and some suggested the inclusion of additional chapters, so the final number of contributions was increased to 114.

Each chapter was reviewed by other experts, and authors made revisions based on their feedback. As editors we strove to preserve the individual “voice” of each author, and we also agreed to tolerate a certain degree of redundancy across chapters, provided they

offered valuable insights into the topic under consideration. *The Visual Neurosciences* is a work in progress so some disagreement was expected among authors regarding specific issues. We made little attempt to broker a compromise between dissimilar viewpoints held by different authors, as long as these were supported by empirical evidence. Controversy is what often makes science fun, and we leave it for future generations to decide the relative merits of currently held positions.

The Visual Neurosciences begins with two historical chapters and an appraisal of the prospects for single-unit approaches in neurobiology. They are followed by Chapters 3–15 on Developmental Processes. This section, as in the book as whole, is organized from molecules to pathways to systems. The section on Retinal Mechanisms and Processes (Chapters 16–29) presents the current state of knowledge on phototransduction, retinal synapses, and physiology, with authors explaining how these mechanisms ostensibly optimize the processing of visual information. These chapters set the stage for the next section on the Organization of Visual Pathways (Chapters 30–34) and the subsequent elaboration of projections for Subcortical Processing (Chapters 35–40) and for Processing in Primary Visual Cortex (Chapters 41–49). Most of the chapters in these first six sections provide an anatomical and physiological context for understanding the psychophysical, perceptual, and neurophysiological chapters that follow in the next four sections, beginning with Detection and Sampling (Chapters 50–55) and proceeding to higher-level processing of Brightness and Color (Chapters 56–67), Form, Shape, and Object Recognition (Chapters 68–79), and Motion, Depth, and Spatial Relations (Chapters 80–89). These chapters illustrate how 20th Century neuroscience unraveled many phenomenological conundrums of the 19th Century. Of course, 20th Century psychology raised still other challenges for neuroscience, including the role of nonsensory variables in perception and cognition. Sections on Eye Movements (Chapters 90–99) and Attention and Cognition (Chapters 100–104) address these questions with detailed accounts of the coordination of eye position and information processing by subcortical and cortical circuits underlying cognitive phenomena. The final section, Theoretical and Computational Perspectives (Chapters 105–114), provides an integration of ideas from neuroscience, psychology, and computer science that are likely to guide future discoveries in the visual neurosciences.

For an undertaking of this scope, the entire project went remarkably smoothly. For this we thank all of the authors for adhering good-naturedly (in most cases) to the rather tight schedule. We also thank the countless anonymous reviewers, members of the Editorial Advisory Board for their input at all stages of this undertaking, and Barbara Murphy, our editor at the MIT Press, for her support and keen professional advice. It is our hope that *The Visual Neurosciences* will serve to motivate and inspire the next generation of researchers, whether they are currently beginning students, clinical practitioners, or established researchers in other fields of endeavor.

Leo M. Chalupa and John S. Werner
7 January 2003

I HISTORICAL FOUNDATIONS

1 Vision Structure and Function: The Early History

MITCHELL GLICKSTEIN

Introduction

This chapter deals with the early history of the study of visual processing by the eye and brain. I begin by considering the first recognition of how images are formed in the vertebrate eye and early contributions to understanding the structure and function of the retina. I go on to discuss the connections from the retina to the cortex by way of the lateral geniculate nucleus (LGN), and the evidence that led to the recognition and spatial mapping of the visual fields on the primary visual cortex. Finally, I describe some of the studies that began to reveal the multiplicity of visual cortical areas and their functions. Because of space limitations, many interesting aspects of the history, such as color vision, visual reflexes, subcortical visual structures, and the controversies over the interpretation of macular sparing after visual cortex lesions must be beyond the scope of this chapter. The emphasis is on fundamentals of structure and its relation to visual function.

Image formation

The cornea and lens form an inverted image of the visual scene at the back of the eye. The optics of image formation in the vertebrate eye were unknown until the theoretical and experimental advances of the seventeenth century. Prior to that time, scientists were troubled by the idea of an upside-down image in the eye even though they knew of the *camera obscura*, a dark chamber with a pinhole aperture that admits light and forms an inverted image of an illuminated scene. As early as the eleventh century, Ibn Al-Haithem, an Arab scholar (cited in Polyak, 1941), wrote a treatise in which the principles of image formation by the camera obscura were clearly described. Even though the optics of the camera obscura appeared to be similar in some ways to that of the eye, inversion of the image troubled earlier thinkers. Leonardo da Vinci (sixteenth century; Windsor Collection) tried to construct a scheme whereby an inverted image would first be received somewhere in the lens and then reinverted to form an upright image at the back of the eye. He wrote:

No image, of however small a body, penetrates into the eye without being turned upside-down and, in penetrating the crystalline sphere, it will be turned the right way again.

The true nature of image formation by the eye was first put forward by Kepler (1604) on theoretical grounds and confirmed experimentally by Scheiner (1619 and 1652), who removed some of the opaque tissue at the back of an excised eye and directly demonstrated the inverted image. The principle of image formation by the human eye was beautifully illustrated by Des Cartes (1677; cited in Polyak, 1941).

The retina

Following Kepler's analysis and Scheiner's demonstration, the inverted image became an accepted fact. There was, however, little understanding of how the pattern of light and darkness in the image is converted into a signal by the retina. Thomas Young (1802) speculated that there must be a finite number of receptor types, say three, which would be sufficient to account for human color vision. But the actual structure of the retinal elements remained poorly understood. Invention of the compound microscope in the early nineteenth century led to an explosion of new knowledge about the structure and function of tissues in general and of the retina in particular. Among the most important of the early contributors was Max Schultze (1866), who described clearly the three major cell layers of the retina, with special attention to the distribution and morphology of the rods and cones (Fig. 1.1). He noted that there is a predominance of thin, rod-like receptors in the retina of strongly nocturnal animals and of thicker, cone-like receptors in diurnal animals. On the basis of comparative evidence and the distribution of receptors in the human eye, Schultze suggested that the two distinct classes of receptors might be associated with vision under two different conditions of illumination.

Schultze and his contemporaries were vague about the connections between the successive elements of the receptors and the ganglion cells. The prevailing view of nervous tissue in general, and the retina in particular, was that it has a reticular structure in which successive elements are continuous and fused. The three prominent cell layers of the retina were thought of as swellings on optic nerve fibers. The anatomic research of Santiago Ramon y Cajal changed that view. Cajal first saw an example of the then new Golgi

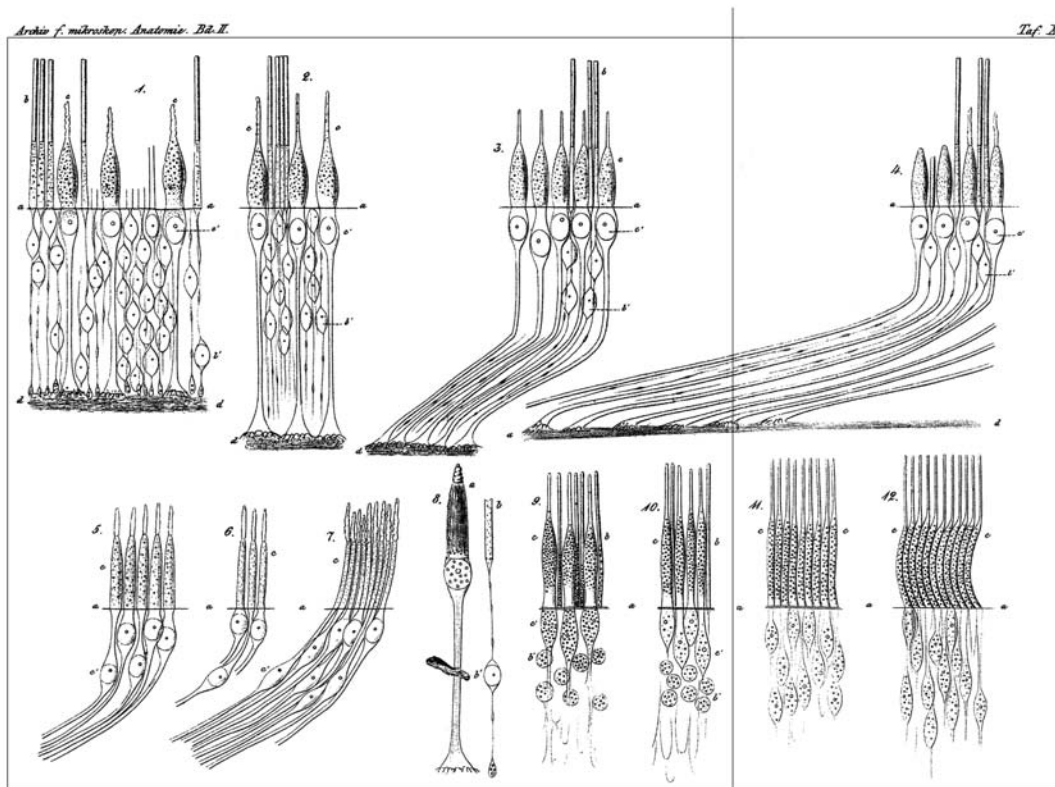


FIGURE 1.1. Schultze's drawings illustrating the structure of the retinal elements, with special reference to the morphological difference between rods and cones. Cones and rods are shown with their fibers up to the inner nuclear layer of the human retina. All of the figures, with the exception of Fig. 8, are drawn at a magnification of 500x. Figs. 1-8 are taken from teased pieces of retina which were placed in osmic acid for 24 hours (1:700). They were from a fresh healthy eye. Figures 9-12 were from an eye with an atrophied optic nerve which was hardened in Müller's solution. *a* always refer to the external limiting membrane, *b* the rods, *c* the cones, *b'* the rod nuclei on the inner part of the external granular layer, *c'* the cone nucleus, and *d* the inner nuclear layer. The outer segments of the cone are incomplete since they were shriveled by the osmic acid. The outer segments of the rods are shown as they would appear in a fresh condition.

Fig. 1. From the peripheral region of the retina. The space between *a* and *d* is completely filled by the rod and cone nuclei (the latter are always adjacent to the external limiting membrane). In the figure, a place has been selected in which the individual rod nuclei are removed in order to make the course of the fibers which remain apparent throughout their entire length. The cone nuclei end in a cone-shaped swelling that breaks up into fine fibers at the upper border of the inner nuclear layer. The rod fibers, which have exquisite fine varicosities, also end in the internal granular layer in an expanded varicosity at the point at which they make connections.

Fig. 2. The same elements from a region outside of the macula lutea. The fibers of the cones and rods have become measurably longer, but their associated nuclei remain in the same relative position, so that now in the external granular layer *d*, there is a region without nuclei that consists only of the radial fibers of the external granular layer, which can reach an even greater length than the figure illustrates. It is this same place which H. Müller says appears to arise as a thickening of the inner nuclear layer and which Henle calls the *external fiber layer* of the retina.

Fig. 3. A region of the retina which is closer to the macula. In the inner part of the external granular layer there is a change

of direction of the fibers away toward the ora serrata. With a reduction in their number, the rods have the same course as the adjacent cone fibers. Otherwise, all courses are as previously described.

Fig. 4. At the border of the macula lutea. The diagonal course of the rod and cone fibers is even more marked.

Figs. 5-7. These figures show the cones in the macula lutea and the fovea centralis. *a* is the outer limiting membrane in all cases next to the cone nuclei. As was partly seen earlier, the cone nuclei appear to follow a radial course. The fibers become so long before they reach the inner nuclear layer that a complete depiction is not possible. The one illustrated is six times longer than the one in Fig. 4. The outer segments of the cones, as stated previously, are shriveled.

Fig. 8. (*a*) A cone from the peripheral region of the retina fixed in osmic acid and enlarged 1000-fold. The outer segment is shriveled. The inner segment and the cone nucleus have a fine fibrous structure, somewhat like that of the substance of the central ganglion cells. This apparently stops at the nuclear swelling of the cone just under the external limiting membrane, only to reappear in the cone fiber, where it is continuous with the end swelling. (*b*) This is an equivalently magnified rod, but without its outer segment: *b'* is the nuclear portion of the rod fiber, the so-called rod nucleus.

Figs. 9-12. These figures show cones and rods of the macula lutea and its surroundings from a thin retina hardened with Müller's fluid and then teased with needles. The preparation is shown to illustrate the fact that even if the rods and cones themselves are not present, the nuclei of the rods and cones (*b'* and *c'*) can be distinguished, and those connected to the thin cones of the fovea centralis are similar to the nuclei of peripheral cones. But the preparation is not suitable to illustrate the cone fibers, which may be attributable to their long immersion in Müller's fluid or else to a pathological condition. The eye had been excised because of intercalary staphyloma, and showed atrophy of the optic nerve and ganglion cells. (From Schultze, 1866.)

staining technique when he visited his colleague in Madrid, Don Luis Simarro, in 1878. Struck by the beauty and promise of the method, he began to apply the Golgi staining technique systematically to the study of the vertebrate retina and brain. Cajal's classic monograph on the retina was published in French (1892) and translated into English (1972) (Fig. 1.2). Cajal was convinced that the reticular theory of organization of the nervous system was wrong. The retina, as well as the brain and spinal cord, he argued, are made up of individual elements, later called *neurons* by Waldeyer. Neurons may touch one another, but they do not fuse. In his monograph, Cajal described in detail the major cell types in all three retinal layers. He emphasized that the direction of conduction is from the receptors, through the horizontal, bipolar, and amacrine cells of the inner nuclear layer, ultimately to the ganglion cells, whose axons constitute the optic nerve. Cajal's descriptions have remained the basis for all subsequent anatomical studies.

On the central course of the optic nerve fibers and the pattern of decussation in the chiasma

Early anatomists saw a prominent nerve exiting the back of each eye directed toward the brain. It was usually assumed that the nerves originated in the brain and extended out to the eye. The fibers arising from each eye appeared first to unite and then to cross the midline in the X-shaped optic chiasm. With earlier techniques of crude dissection, the pattern of crossing was not clear, so the true picture was not accepted until the late nineteenth century. The rearrangement of fibers in the chiasm was briefly described by Isaac Newton in his second book on optics (1704). Newton wrote:

Are not the Species of Objects seen with both Eyes united where the optick Nerves meet before they come into the Brain, the fibres on the right side of both Nerves uniting there, and after union going thence into the Brain in the Nerve which is on the right side of the Head, and the fibres on the left side of both nerves uniting in the same place, and after union going into the Brain in the nerve which is on the left side of the Head, and these two Nerves meeting in the Brain in such manner that their fibres make but one entire Species or Picture, half of which on the right side of the Sensorium comes from the right side of both Eyes through the right side of both optick Nerves to the place where the Nerves meet, and from thence on the right side of the Head into the Brain, and the other half on the left side of the Sensorium comes in like manner from the left side of both Eyes. For the optick Nerves of such Animals as look the same way with both Eyes (as of Men, Dogs, Sheep, Oxen & cet.) meet before they come into the brain, but the optick Nerves of such Animals as do not look the same way with both Eyes (as of Fishes and of the Chameleon) do not meet, if I am rightly informed.

Although he incorrectly assumed that the origin of the optic nerves is within the brain, Newton described correctly

the course of the optic nerves in the optic tracts, and he was also aware of differences in the pattern of decussation in animals with laterally placed eyes. But despite Newton's scientific authority, the true picture failed to penetrate to the medical or biological literature. Over 100 years later, William Wollaston (1824), describing his own temporary hemianopia, wrote:

It is now more than twenty years since I was first affected with the peculiar state of vision, to which I allude, in consequence of violent exercise I had taken for two or three hours before. I suddenly found that I could see but half the face of a man whom I met; and it was the same with respect to every object I looked at. In attempting to read the name JOHNSON over a door, I saw only SON; the commencement of the name being wholly obliterated to my view.

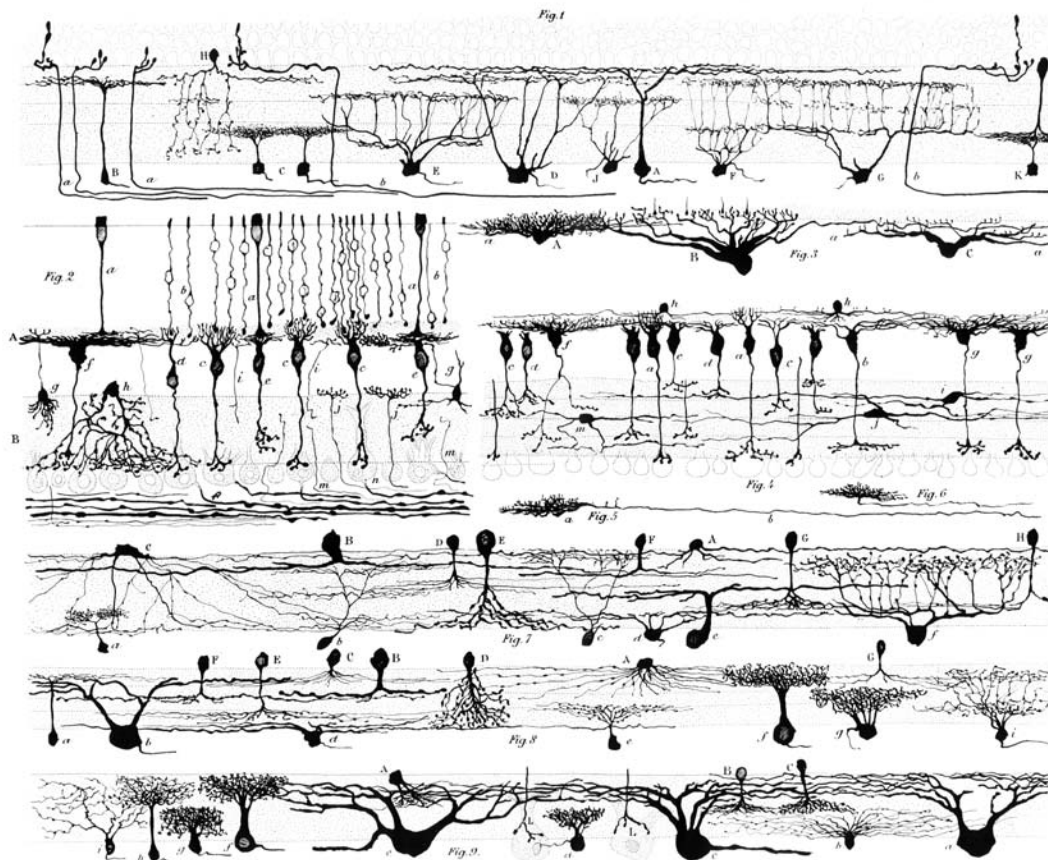
Unaware of Newton's suggested scheme for the course of the optic nerves, Wollaston wrote:

It is plain that the cord, which comes finally to either eye under the name of the optic nerve, must be regarded as consisting of two portions, one half from the right thalamus, and the other from the left thalamus nervorum opticorum. According to this supposition, decussation will take place only between the adjacent halves of the two nerves. That portion of the nerve which proceeds from the right thalamus to the right side of the right eye, passes to its destination without interference: and in a similar manner the left thalamus will supply the left side of the left eye with one part of its fibres, while the remaining half of both nerves in passing over to the eyes of the opposite sides must intersect each other, either with or without intermixture of their fibres.

Wollaston rediscovered hemidecussation by observing his own transient hemianopia. Despite Newton's scientific authority and Wollaston's evidence, the pattern of hemidecussation was still largely unrecognized. Wollaston's report was cited one year later by a news item in the Boston Medical and Surgical Intelligencer as an isolated curiosity in the same paragraph that described a boy in Philadelphia who allegedly saw a candle flame upside down. As late as 1880, H. Charlston Bastian (1880), Professor of Pathological Anatomy and Medicine at University College London (I blush), could still write:

Although the subject is by no means free from doubt and uncertainty, the weight of the evidence seems now most in favour of the view that decussation at the Optic Commissure is as complete in Man as it is known to be in lower Vertebrates.

In spite of Dr. Bastian's opinion, within a few years the true picture was soon clarified. By the time Gowers wrote his Textbook of Neurology (1892), the pattern of decussation and visual loss associated with lesions of the optic tract, the visual radiations, or the striate cortex was widely accepted.



On the termination of the optic tract fibers in the lateral geniculate nucleus

Vision, like all sensory inputs, except for olfaction, is relayed to the cerebral cortex by way of the thalamus. The thalamic relay for vision is the LGN. The LGN in humans and Old World monkeys has an obvious striped appearance, with six layers of neurons separated by interleaved fiber layers. Although, by the end of the nineteenth century, it was clear that the eye projects to the LGN, the pattern of termination of optic tract fibers was not well understood. The true picture was revealed by study of transneuronal atrophy and degeneration. Cells in the LGN that are deprived of their input from the eye shrink or die. Mieczyslaw Minkowski (1920), working in Zurich, studied the LGN of a monkey that had had one eye removed 8 months earlier and that of a 75-year-old woman who had had amblyopia due to a unilateral cataract for 38 years before she died. Minkowski saw that cells in the LGN layers opposite the blind eye, layers 1, 4, and 6, were atrophied. In the ipsilateral LGN, layers 2, 3, and 5 were affected. The technique of studying transneuronal atrophy has revealed the organization of the LGN in a large number of mammals. The six-layered pattern is virtually identical in the apes and the Old World primates.

In some cases, the existence of a hidden laminar pattern can be revealed by transneuronal atrophy. For example, in the squirrel monkey, *Saimiri*, the dorsal parvocellular region of the LGN is not obviously laminated. One year after unilateral enucleation, a clear six-layer pattern emerges which is similar to that of the Old World primates (Doty et al., 1966).

On the representation of the visual fields in the LGN and cortex; orthograde and retrograde degeneration in the visual system

In the 1920s and 1930s, anatomists (e.g., Brouwer and Zeeman, 1926) studied orthograde projections from the retina to the LGN by making restricted retinal lesions and identifying degenerating fiber terminals in the LGN using the Marchi stain. Geniculocortical projections were studied by making lesions of the primary visual cortex and mapping retrograde degeneration of cells in the LGN (e.g., Clark, 1932). These anatomical studies confirmed that there is an orderly projection from the retina to the LGN and from the LGN to the visual cortex. Neighboring points in the visual fields are represented at neighboring points on the cerebral cortex. In later studies (Van Buren, 1963), it

FIGURE 1.2. Cajal's drawings showing the cell types in the mammalian retina. This is Cajal's description (from Thorpe and Glickstein's 1972 translation). All figures show cells from the mammalian retina with the exception of Fig. 1, which shows the nerve cells from the chicken retina.

Fig. 1. *A*, ganglion cell destined for the first sublayer; *B*, ganglion cell destined for the second sublayer; *C*, small ganglion cells with granular clusters which spread in the fourth sublayer; *D*, multipolar cell destined for the second sublayer; *E*, a cell which forms two horizontal plexuses—one below the fourth sublayer and another in the third sublayer; *F*, small cell with two fine plexuses—one in the second sublayer and the other in the fourth sublayer; *G*, giant cell which forms three plexuses—in the second, third, and fourth sublayers; *H*, bistratified amacrine cell; *J*, cell with an extremely fine plexus destined for the third sublayer; *K*, cell which arborizes in the fourth sublayer and whose branches interlace with the end branches of an amacrine cell lying in the same layer; *a*, centrifugal fibers; *b*, another centrifugal fiber whose termination extends horizontally above the inner plexiform layer.

Fig. 2. A section through the retina of an adult dog. *a*, cone fiber; *b*, cell body and fiber of a rod; *c*, bipolar cell with an ascending cluster destined for the rods; *d*, very small bipolar cell for the rods with a sparse upper cluster; *e*, bipolar cell with a flat cluster destined for the cones; *f*, giant bipolar cell with a flat cluster; *h*, diffuse amacrine cell whose varicose branches lie, for the most part, just above the ganglion cells; *i*, ascending nerve fibrils; *j*, centrifugal fibers; *g*, special cells which are very rarely impregnated; they have an ascending axis cylinder; *n*, ganglion cell which receives the terminal cluster of a bipolar cell destined for the rods; *m*, nerve fiber which disappears in the inner plexiform layer; *p*, nerve fiber of the optic fiber layer. *A*, outer plexiform layer; *B*, inner plexiform layer.

Fig. 3. Horizontal cells from the adult dog retina. *A*, outer horizontal cell; *B*, middle-sized inner horizontal cell with no descending protoplasmic processes; *C*, another, smaller inner horizontal cell; *a*, horizontal cell axis cylinder.

Fig. 4. Nerve cells from the ox retina. *a*, bipolar cell with an ascending cluster; *b*, bipolar cell with a flat upper terminal cluster destined for the cones; *c*, *d*, *e*, bipolar cells of the same type whose lower cluster, however, arborizes in the more external sublayers of the inner plexiform layer; *g*, bipolar cell with a flat cluster of enormous extent; *f*, another bipolar cell with a giant upper cluster characterized by the rich, irregular arborization formed by the ascending processes; *h*, oval cells lying outside the outer plexiform layer; *i*, amacrine cell located within the second sublayer of the inner plexiform layer; *j*, amacrine cell occupying the third sublayer; *m*, another amacrine cell whose branches apparently disappear in the third and fourth sublayers.

Fig. 5. Horizontal axis cylinder from the outer plexiform layer. *a*, terminal arborization as seen from the side; *b*, nerve fiber.

Fig. 6. Another terminal arborization of the same type.

Fig. 7. Nerve elements from the ox retina stained with chromium-silver according to the double impregnation method. *A*, semilunar amacrine cell whose enormously long branches arborize in the first sublayer; *B*, large amacrine cell with thick branches in the second sublayer; *F*, another amacrine cell, which is rather small and arborizes in the second sublayer; *D*, amacrine cell with a stellate cluster destined for the third sublayer; *G*, *H*, amacrine cells destined for the fourth sublayer; *E*, large amacrine cell destined for the fifth sublayer; *C*, special type of amacrine cell with very thin branches which spread preferentially in the first and fifth sublayers. *a*, small ganglion cell destined for the fourth sublayer; *b*, ganglion cell whose branches form three superimposed plexes; *c*, small ganglion cell with branches arborizing in the first sublayer; *d*, middle-sized ganglion cell with branches in the fourth sublayer; *f*, ganglion cell which is similar to the multilayered cells (branching in three sublayers) in the reptile and bird; their branches form two plexes—one in the fourth sublayer and another in the second sublayer; *e*, giant ganglion cell destined for the third sublayer.

Fig. 8. Amacrine cells and ganglion cells from the dog retina. *A*, stellate amacrine cell destined for the first sublayer and a portion of the second sublayer; *B*, giant amacrine cell of the third sublayer; *C*, *G*, stellate amacrine cells destined for the second sublayer; *F*, small amacrine cell destined for the third sublayer; *E*, amacrine cell destined for the fourth sublayer; *D*, unstratified amacrine cell; *a*, ganglion cell whose upper cluster spreads in the second sublayer; *b*, giant ganglion cell destined for the second sublayer; *e*, small ganglion cell whose cluster spreads in the fourth sublayer; *f*, middle-sized ganglion cell which arborizes in the first and in a portion of the second sublayers; *g*, ganglion cell which arborizes in the third and a portion of the fourth sublayers; *i*, two-layered cell (*cellule bistratifiée*).

Fig. 9. Ganglion cells from the dog retina. *a*, giant ganglion cell whose cluster spreads in the first and a portion of the second sublayers; *b*, small ganglion cell whose multiple processes disappear in the fifth sublayer; *c*, giant cell whose cluster seems to spread mainly in the second sublayer; *e*, giant ganglion cell of the second sublayer; *d*, *g*, small ganglion cells with clusters in the fourth sublayer; *f*, middle-sized ganglion cells destined for the first sublayer; *h*, another ganglion cell destined for the second and partially for the first sublayer; *i*, unstratified ganglion cell; *A*, *B*, *C*, spongioblasts (amacrine cells); *L*, lower terminal arborization of a bipolar cell. (From Cajal, 1892.)

was discovered that in addition to retrograde degeneration in the LGN that is caused by cortical lesions, there is also transneuronal degeneration in the retinal ganglion cell layer after lesion of the cerebral cortex.

On the primary visual cortex

By the end of the eighteenth century, the gross structure of the cerebral cortex was beautifully illustrated in anatomical texts, but the cortex was portrayed as structurally homoge-

neous. One part of the cortex was depicted as looking like any other. The first recognition that the cerebral cortex is not uniform in structure was made by an Italian medical student, Francesco Gennari, working in the newly re-founded University of Parma (Gennari, 1782; Glickstein and Rizzolatti, 1984). Gennari packed brains in ice, which allowed him to make clean, flat cuts through them. He noted a thin white line, and sometimes two lines within the cortex, running parallel to and about halfway between the pial surface above and the white matter below. The line coalesces

into a prominent single stripe in the caudal part of brain, “in that region near the tentorium.” Gennari first saw the stripe in 1776 and described it in his monograph *De Peculiari* (1782) some 6 years later (Fig. 1.3).

Gennari’s monograph was published in a limited edition and he came from what was then an obscure university, so although it was cited by some authors, it was often ignored. The same cortical stripe was discovered independently a few years later by the more eminent anatomist Vicq D’Azyr. The stripe was described in his *Traité D’Anatomie* (1786) 3 years later. It was the Austrian anatomist Obersteiner (1888) who found Gennari’s earlier description of the white line and named it the *stripe of Gennari*.

Although regional variability in cortical structure was soon accepted, there was no agreement about possible differences in the functions of different cortical areas. Two of the major authorities at the beginning of the nineteenth century, Gall (Gall and Spurzheim, 1810–1819) and Flourens (1824), held opposing views. Gall and his followers, the cranioscopists/phrenologists, asserted that the cerebral cortex is made up of a number of individual areas, each associated with a specific personality characteristic. If a person has a good memory, for example, the memory area of the cortex is relatively enlarged. Enlargement of a cortical area is associated with corresponding change in the shape of the skull, hence a bump on the head. Person-

ality, ability, and character could be read by palpating the head.

The earliest experimentalists failed to confirm Gall’s views. In a typical experiment, Flourens (1824) made lesions in the brains of birds and mammals and observed the resulting effects on the animals’ behavior. Although Flourens was convinced that the cerebral cortex is responsible for sensation, movement, and thought, he could find no evidence that any of these functions is localized to a particular site on the cerebral cortex.

In later years, evidence began to accumulate in favor of functional localization in the cerebral cortex. A series of postmortem observations of focal injuries in the brains of patients who had lost the power of speech culminated in Broca’s (1861) description of the lesion in the left frontal lobe of the patient “Tan,” a man who had been unable to say any word other than *tan* for the past several years. The evidence for brain localization of speech was soon accepted, and within a few years experiments began to provide additional evidence that different areas of the cerebral cortex are specialized for different functions. The single most important experiment that led to modern understanding of the localization of motor and sensory functions in the cortex was done by Gustav Fritsch and Eduard Hitzig (1870). They electrically stimulated restricted regions of the frontal lobe of a dog and elicited movement of the face or limb on the opposite side of the body. Fritsch and Hitzig’s discovery of a specifically motor area of the cortex was instrumental in prompting a search for other functions, including vision. There had been indications (Panizza, cited by Mazzarello and Della Sala, 1993) that lesions in the caudal part of the brain are associated with visual deficits, but the clearest and most influential evidence for the visual function of the occipital lobe was provided by Hermann Munk, professor of physiology in the Veterinary Institute in Berlin. Munk (1881) made lesions in the occipital lobe of dogs and monkeys. He reported that if he destroyed one occipital lobe, the monkeys became hemianopic. Bilateral lesions caused blindness (Fig. 1.4).

Munk’s discovery focused the attention of clinicians and scientists on the role of the occipital lobe in vision. Salomon Henschen (1890) summarized the postmortem findings in a group of patients who had suffered from hemianopia as a result of a stroke. He compared these patients with a similar number who had sustained a comparable loss of brain tissue that had not become hemianopic. Henschen confirmed the location of the primary visual area, and he suggested a scheme for the way in which the visual fields are mapped on the primary visual cortex. Henschen recognized that the left hemisphere receives its input from the right visual field and the upper bank of the calcarine fissure from the upper retina, hence the lower visual field. But Henschen also suggested that the periphery of the visual field is projected

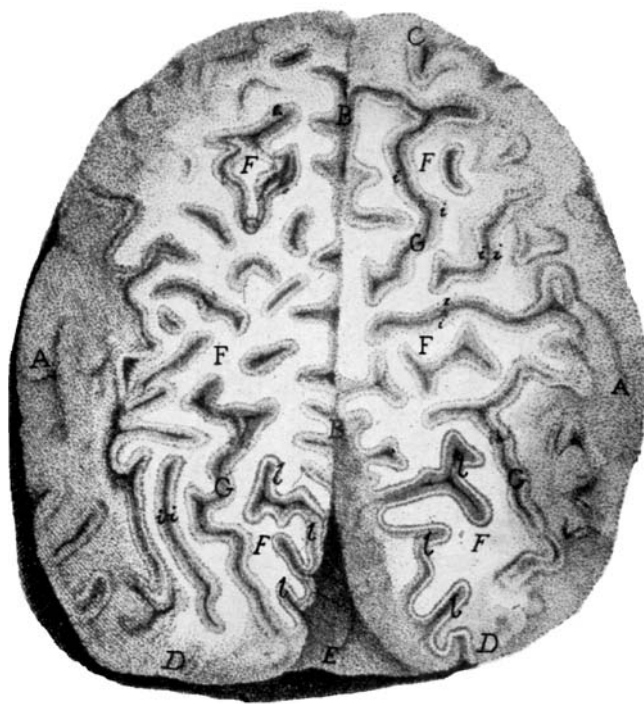


FIGURE 1.3. The first recognition of the presence of a fiber layer within the cerebral cortex (labeled *l* in the picture) which Gennari described as being “particularly prominent in that region near to the tentorium.” (From Gennari, 1782.)

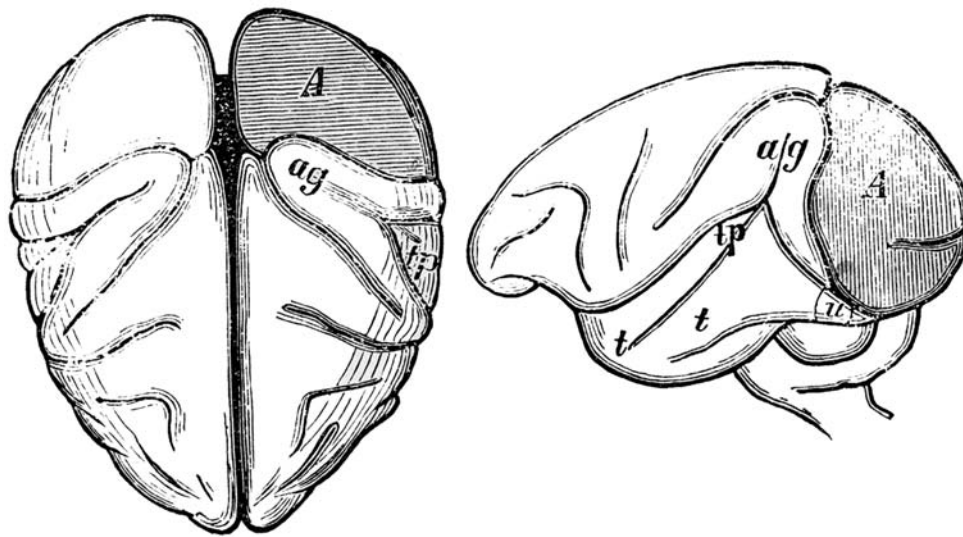


FIGURE 1.4. Munk clearly illustrates the locus of the visual area of the monkey cortex. Unilateral occipital lobe lesions cause hemianopia. (From Munk, 1881.)

onto the caudal end of the striate cortex, with the fovea represented anteriorly. In this, he was in error.

Henschen's error is understandable, since the lesions in the brains that he studied were diffuse. What was needed to establish a more accurate spatial mapping was evidence of partial field defects, scotomas, caused by smaller, subtotal lesions of the striate cortex. Such lesions, regrettably, arise in wartime. One of the earliest clear pictures of the representation of the peripheral-central visual field representation was made by a young Japanese ophthalmologist, Tatsuji Inouye (Glickstein and Whitteridge, 1987; Inouye, 1909). Inouye was in the medical service of the Japanese Army during the Russo-Japanese war of 1904–1905. His responsibility was to evaluate the extent of visual loss in casualties of the war. Inouye used the opportunity to study the visual field defects caused by penetrating brain injuries. In that war the Russians used a newly developed rifle which fired small-caliber bullets at high velocity. Unlike most bullets used in previous wars, these bullets often penetrated the skull at one point and then exited at another, making a straight path through the brain. Inouye devised a three-dimensional coordinate system for recording the entry and exit wounds. He then calibrated the course of the bullet through the brain and estimated the extent of the damage it would have caused to the primary visual cortex or the optic radiations. Based on his study of visual field defects in 29 patients, Inouye produced a map of the representation of the visual fields on the cortex. The central fields were now placed correctly in the most caudal part of the striate cortex, with the peripheral visual fields represented anteriorly, and there was an over-representation of the central visual fields in the primary visual cortex.

Based on his studies of the visual field defects sustained by soldiers of the First World War, Gordon Holmes (1918a) produced a more accurate and detailed map of the representation of the visual fields on the striate cortex, which still forms the basis for interpreting partial visual loss in humans.

Confirmation of the map by electrical stimulation and recording of evoked potentials

In the period between the First and Second World Wars, the basic arrangement of the visual fields was confirmed in studies using electrical stimulation of the brain in neurosurgical patients. Ottfried Foerster (1929) operated under local anesthetic on patients who suffered from seizures caused by focal scarring of the brain. Electric current was applied at a specific site on the cerebral cortex, and the resultant sensation was reported by the patient. Electrical stimulation of the cortex at the occipital pole caused phosphenes that were centered in front of the patient. Stimulation of the upper lip of the calcarine fissure 5 cm anterior to the occipital pole produced a phosphene that was centered in the lower visual field opposite the side of the brain that had been stimulated. Foerster's studies, and later those of Wilder Penfield (Penfield and Rasmussen, 1952), confirmed the representation of the visual fields on the human striate cortex that had been revealed by the analysis of the scotomas caused by focal lesions.

Electrical recording of neural activity in the primary visual cortex

In the 1930s Philip Bard (1938) and his collaborators, one of whom was Wade Marshall, began to record the electrical

activity that is evoked on the surface of the cerebral cortex of experimental animals by stimulation of the body surface. The electrodes at the time were too large to record the activity of individual neurons but small enough to detect focal activity in a restricted group of cells. There is an orderly representation of the body surface on the primary somatosensory cortex, with neighboring points on the body represented at neighboring points on the brain. Marshall later collaborated with William Talbot in studying the activity evoked on the striate cortex of cats and Old World monkeys. They focused small spots of light on the retina of a monkey and marked the locus of maximal evoked activity on the cerebral cortex. Figure 1.5 is from their report.

Talbot and Marshall's recordings were limited to the dorsolateral surface of the macaque cortex, comprising only roughly the central 10 degrees of the visual field. The work was extended by Peter Daniel and David Whitteridge (1961), who recorded more anterior cortical areas within the calcarine fissure of baboons, extending the mapping into the peripheral visual field.

The evidence from visual loss in humans and monkeys caused by cortical lesions, electrical stimulation of the cortex in humans, and recording in monkeys was all consistent. The visual fields are represented in an orderly way on the primary visual cortex.

Early electrical recording from visual areas outside of the primary visual cortex

Early workers had suggested that the regions outside of the primary visual cortex might have a related visual function. Hermann Munk (1881), for example, labeled a region outside of the primary visual cortex in dogs as an area con-

cerned with the storage of visual memories. William Talbot (1942) made a brief report to the Federated Society for Experimental Biology and Medicine which initiated modern study of the way in which the visual fields are represented beyond the primary visual cortex. Talbot recorded potentials evoked by vision from the surface of a cat brain. As expected, he found that the visual field is mapped in an orderly way on the primary visual cortex, with neighboring points in the visual field represented at neighboring points on the cortex. As Talbot continued to record lateral to the representation of the vertical meridian, he found that the cortex was still activated by focused spots of light, but from increasingly peripheral regions of the visual field. Talbot had discovered a second visual area, later called *Visual Area 2*, which is mapped on the cortex like a mirror image of the primary representation. Talbot had started a growth industry. Some years after Talbot's report, Margaret Clare and George Bishop (1954) described another visual area that is located on the lateral suprasylvian gyrus of cats, in which flash stimuli evoke a gross potential. Although the pioneering work of electrical mapping was done in cats, the visual cortex in these animals is not "primary" in the sense that it is in monkeys and humans. In monkeys and humans, the overwhelming majority of geniculocortical fibers terminate in the striate cortex. In cats, Visual Area 2 receives a direct and equally powerful input from the LGN (Glickstein et al., 1967).

In the 1950s, techniques were developed for isolating the activity of individual neurons, and single-unit recording has since become a standard method of studying visual processing by the brain. The contribution to our understanding of vision from single-unit recording is described in this book by Horace Barlow (Chapter 2). Here we note

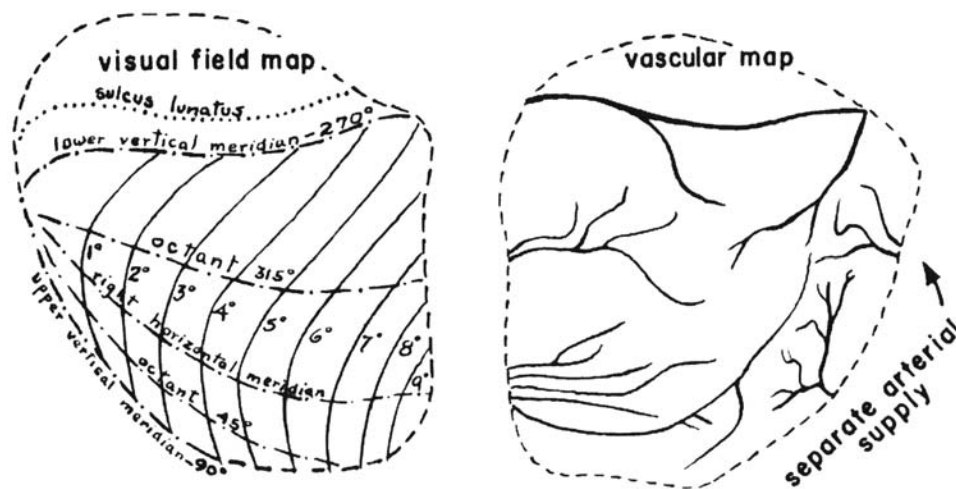


FIGURE 1.5. Mapping of the visual fields onto the monkey striate cortex revealed by evoked responses to small, focused spots of light. (From Talbot and Marshall, 1941.)

briefly the way in which these studies increased the number of recognized visual areas in the cerebral cortex. After Talbot's discovery of Visual Area 2 and Clare and Bishop's description of the lateral suprasylvian visual area, David Hubel and Torsten Wiesel (1965) identified another area by recording from cells on the medial bank of the lateral fissure of cats, an area they called *Visual Area 3*. A few years later, John Allman and Jon Kaas (1971), studying the owl monkey *Aotus*, and Semir Zeki (1978), studying Old World macaques, identified more extrastriate visual areas, each of which appeared to be specialized for analyzing color, motion, or form. By a count made in 1992, there are no less than 32 visual areas in the monkey brain (Van Essen et al., 1992). There are doubtless at least as many in the human cortex.

Early behavioral evidence for the functions of extrastriate visual areas

In humans and monkeys the striate area is virtually the sole cortical target of cells in the LGN, but the cortex adjacent to the primary visual cortex is also dominated by vision. An estimated one-third or more of the monkey cerebral cortex is devoted to visual processing. There are two large groupings of visual areas outside the primary visual cortex (Glickstein and May, 1982; Ungerleider and Mishkin, 1982), a medial group centered in the parietal lobe and a lateral group centered in the temporal lobe.

The visual areas of the parietal lobe

In monkeys, all of the parietal lobe cortex from the primary visual area as far rostrally as the intraparietal fissure has direct or indirect input from the primary visual cortex. The angular gyrus is a major part of this area. When David Ferrier stimulated the angular gyrus of the monkey brain electrically, he observed that the stimulation caused eye movements. When he ablated the region, the monkey appeared to be blind. Ferrier concluded that this region must be the primary visual cortex (Ferrier, 1876; Glickstein, 1985) (Fig. 1.6).

Ferrier's first experiments were done in the 1870s, prior to the widespread use of antiseptic techniques in experimental surgery. His animals were killed 3 days after he operated on them, since longer survival times inevitably led to infections. In later experiments, Ferrier adopted the sterile surgical techniques of his colleague at King's College London, Joseph Lister. His animals could now live for weeks, months, or years after the operation. With Gerald Yeo he replicated his studies of the behavioral effect of angular gyrus lesions. They now reported that his animals were not blinded by the angular gyrus lesion but suffered a *temporary* loss of vision (Ferrier and Yeo, 1884). Ferrier's protocols

demonstrate that rather than blindness, his monkeys suffered a severe impairment in guiding their movements under visual control. Virtually identical symptoms were described by Rudolf Balint (1909) in a patient who had suffered bilateral lesions of the parietal lobes and by Gordon Holmes (1918b), who studied casualties among British soldiers in the First World War. Ferrier's monkeys, Balint's patient, and Holmes's soldiers were all unable to guide their movements accurately under visual control. The visual areas of the parietal lobe are principally concerned with spatial localization in the visual field (Ungerleider and Mishkin, 1982) and the visual guidance of movement (Glickstein and May, 1982).

On visual deficits following lesioning of the temporal lobe

Temporal lobe lesions cause an impairment in recognizing and remembering forms. In early studies of the effects of large temporal lobe lesions in monkeys (Brown and Schäfer,

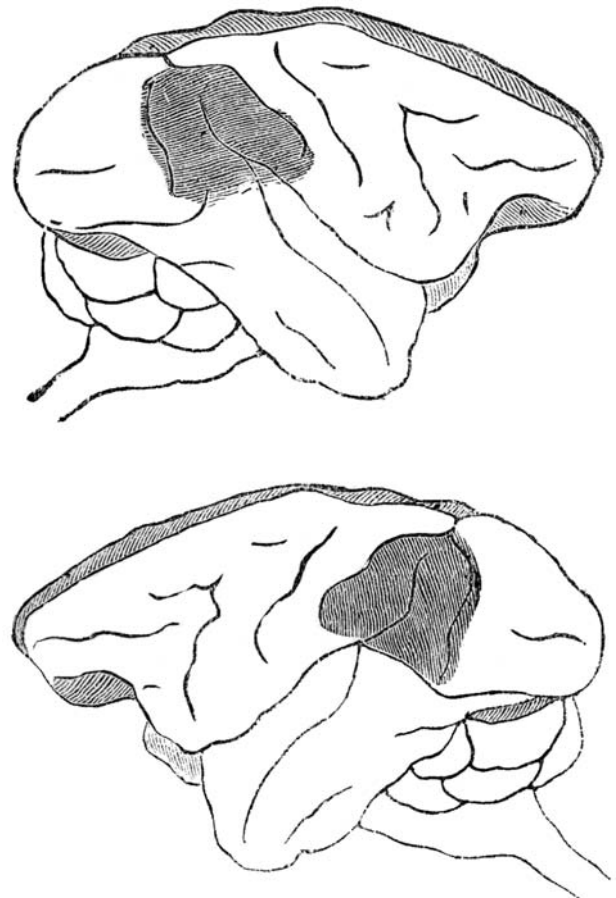


FIGURE 1.6. Lesions of the angular gyrus of the parietal lobe. Ferrier initially interpreted the resultant deficit as blindness. His later study (Ferrier and Yeo, 1884) shows that the monkey was not blind but had a profound deficit in visual guidance of movement following bilateral angular gyrus lesioning. (From Ferrier, 1876.)

1888; Klüver and Bucy, 1938) in addition to other symptoms, there were visual deficits. The specifically visual function of the inferotemporal cortex was further clarified when animals were tested after smaller, more restricted lesions of the temporal lobes were produced. K. L. Chow (1951) showed that lesions of the inferotemporal cortex cause a specific impairment in the acquisition and retention of visual discrimination learning. Mishkin (1966) demonstrated that the essential input to the inferotemporal cortex is by a series of corticocortical connections originating in the striate cortex.

A note on the aims of this chapter and its sources

This chapter has attempted to outline some of the major questions and discoveries that led from the first understanding of image formation by the eye, the recognition of the nature of the photoreceptors, and the connections from the eye to the primary visual cortex. The single most useful volumes for exploring the topics presented here are the two masterful scholarly works of Stephan Polyak, *The Retina* (1941) and *The Vertebrate Visual System* (1957). Both have extensive bibliographies and references which are invaluable for finding the early literature. An excellent source for the history of neuroscience in general is Clarke and O'Malley (1968). Useful also are Von Bonin's (1950) translations of several of the papers cited here. I recognize that there are many other aspects of the history of the study of vision that are of equal interest and relevance. For example, the fascinating story of color vision has only briefly been touched on in the reference to Thomas Young (1802). There is also a tradition based on the subjective study of visual phenomena that began with Goethe, was powerfully advanced by Purkinje and Hering, and contributed to the later understanding of color coding by the brain. While apologizing for these omissions, I hope I have given an outline of some of the early contributions that formed the basis for much of the material to be covered in this volume.

REFERENCES

- Allman, J., and J. Kaas, 1971. Representation of the visual field in striate and adjoining cortex of the owl monkey (*Aotus trivirgatus*), *Brain Res.*, 35:89–106.
- Balint, R., 1909. Seelenlähmung des "Schauens", optische Ataxie, räumliche Störung der Aufmerksamkeit, *Monatsschr. Psychiatr. Neurol.*, 25:51–81.
- Bard, P., 1938. Studies on the cortical representation of somatic sensibility, *Harvey Lectures*, 143–169.
- Bastian, H., 1880. *The Brain as an Organ of Mind*, London: Kegan.
- Broca, P., 1861. Remarque sur la siège de la faculté du langage articulé suivie d'une observation d'aphémie (perte de la parole), *Bull. Soc. Anat. Paris*, 36:330–357.
- Brouwer, B., and W. Zeeman, 1926. The projection of the retina in the primary optic neuron in monkeys, *Brain*, 49:1–35.
- Brown, S., and E. Schäfer, 1888. An investigation into the functions of the occipital and temporal lobes in the monkey's brain, *Phil. Trans. R. Soc. Lond (Biol)*, 179:303–327.
- Cajal, S. Ramon y, 1892. *La rétine des vertébrés (La Cellule*, English trans.; S. Thorpe and M. Glickstein, trans., 1972), Springfield: Thomas.
- Chow, K. L., 1951. Effects of partial extirpation of posterior association cortex on visually mediated behavior in monkeys, *Comp. Psychol. Monogr.*, 20:187–218.
- Clare, M., and G. Bishop, 1954. Responses from an association area secondarily activated from optic cortex, *J. Neurophysiol.*, 17:271–277.
- Clark, W. E. Le Gros, 1932. The structure and connections of the thalamus, *Brain*, 55:406–470.
- Clarke, E., and E. O'Malley, 1968. *The Human Brain and Spinal Cord*, Berkeley and Los Angeles: University of California Press.
- Daniel, P., and D. Whitteridge, 1961. The representation of the visual field on the cerebral cortex in monkeys, *J. Physiol.*, 159:203–221.
- Des Cartes, R., 1677. *L'Homme et la Formation de la Foetus*, 2nd ed. Cited in Polyak, 1941.
- Doty, R., M. Glickstein, and W. Calvin, 1966. Lamination of the lateral geniculate nucleus in the squirrel monkey, *Saimiri sciureus*, *J. Comp. Neurol.*, 127:335–340.
- Ferrier, D., 1876. *The Functions of the Brain*, London: Smith-Elder.
- Ferrier, D., and G. Yeo, 1884. On the effects of brain lesions in monkeys, *Phil. Trans. R. Soc. Lond.*, 2:494.
- Flourens, P., 1824. *Recherches Expérimentales sur les Propriétés et les Fonctions du Système Nerveux dans les Animaux Vertébrés*, Paris: Chevot, pp. 85–122.
- Foerster, O., 1929. Beiträge zur Pathophysiologie der Sehbahn und der Sehphäre, *J. Psychol. Neurol. Leipzig*, 39:463–485.
- Fritsch, G., and E. Hitzig, 1870. Über die elektrische Erregbarkeit des Grosshirns, *Arch. Anat. Physiol. Wissensch. Med. Leipzig*, 300–332.
- Gall, F., and J. Spurzheim, 1810–1819. *Anatomie et physiologie du système nerveux et du cerveau en particulier avec des observations sur la possibilité de reconnaître plusieurs dispositions intellectuelles et morales de l'homme et des animaux par la configuration de leurs têtes*. Paris: N. Maze.
- Gennari, F., 1782. *De peculiari structura cerebri nonnulisque ejus morbis*, Parma: Regio Typographico.
- Glickstein, M., 1985. Ferrier's mistake, *Trends Neurosci.*, 8:341–344.
- Glickstein, M., R. King, J. Miller, and M. Berkley, 1967. Cortical projections from the dorsal lateral geniculate nucleus of cats, *J. Comp. Neurol.*, 130:55–76.
- Glickstein, M., and J. May, 1982. Visual control of movement: the circuits which link visual to motor areas of the brain with special reference to the visual input to the pons and cerebellum, in *Contributions to Sensory Physiology* (W. D. Neff ed.), New York: Academic Press.
- Glickstein, M., and G. Rizzolatti, 1984. Francesco Gennari and the structure of the cerebral cortex, *Trends Neurosci.*, 7:464–467.
- Glickstein, M., and D. Whitteridge, 1987. Tatsuji Inouye and the mapping of the visual fields in the human cerebral cortex, *Trends Neurosci.*, 9:350–353.
- Gowers, W., 1892. *Diseases of the Nervous System*, 2nd ed. vol. 2, *Brain and General Functional Diseases*, London: Churchill.
- Henschen, S., 1890. *Klinische und anatomische Beiträge zur Pathologie des Gehirns Part I*, Uppsala: Almqvist and Wiksell.
- Holmes, G., 1918a. Disturbances of vision by cerebral lesions, *Br. J. Ophthalmol.*, 2:353–384.
- Holmes, G., 1918b. Disturbances of visual orientation, *Br. J. Ophthalmol.*, 2:449–468; 506–516.

- Hubel, D., and T. Wiesel, 1965. Receptive fields and functional architecture in two non-striate visual areas (18 and 19) of the cat, *J. Neurophysiol.*, 28:229–289.
- Inouye, T., 1909. *Die Sehstörungen bei Schussverletzungen der kortikalen Sehsphäre nach Beobachtungen an Verwundeten der letzten japanische Kriege*, Leipzig: Engelmann.
- Kepler, J., 1604. *Ad Vitellionem*, Frankfurt: Marnium and Haez.
- Klüver, H., and P. Bucy, 1938. An analysis of certain effects of bilateral temporal lobectomy in the rhesus monkey with special reference to psychic blindness, *J. Psychol.*, 5:33–54.
- Leonardo da Vinci 16th Century Diagram from the Windsor Collection reproduced in Leonardo da Vinci (1989) Plate 97 in the catalog of an exhibition at the Hayward Gallery, London. London and New Haven; South Bank Centre and Yale University Press.
- Mazzarello, P., and S. Della Sala, 1993. The demonstration of the visual area by means of atrophic degeneration methods in the work of Bartolomeo Panizza (1855), *J. Hist. Neurosci.*, 2:315–322.
- Minkowski, M., 1920. Über den Verlauf, die Endigung und die zentrale Repräsentation von gekreuzten und ungekreuzten Sehnervfasern bei einigen Säugetieren und beim Menschen, *Schweiz. Arch. Neurol. Psychiatr.*, 6:201–252; 7:268–303.
- Mishkin, M., 1966. Visual mechanisms beyond the striate cortex, in *Frontiers in Physiological Psychology* (R. Russell, ed.), New York: Academic Press.
- Munk, H., 1881. *Über die Funktionen der Grosshirnrinde*, Berlin: Hirschwald.
- Newton, I., 1704. *Second Book of Opticks: Treatise of Light*, London: Smith and Walford.
- Obersteiner, H., 1888. *Anleitung beim Studium des baues der Nervösen Centralorgane im gesunden und kranken Zustande*, Leipzig and Vienna: Toeplitz und Deuticke.
- Penfield, W., and T. Rasmussen, 1952. *The Cerebral Cortex of Man*, New York: Macmillan.
- Polyak, S., 1941. *The Retina*, Chicago: University of Chicago Press.
- Polyak, S., 1957. *The Vertebrate Visual System*, Chicago: University of Chicago Press.
- Scheiner, C. 1619, 1652. *Oculus*. Innsbruck: Oenoponti.
- Schultze, M., 1866. Zur Anatomie und Physiologie der Retina, *Arch. Mikroskopische Anat.*, 2:175–286.
- Talbot, S., 1942. A lateral localization in cat's visual cortex, *Fed. Proc.*, 1:84.
- Talbot, S., and W. Marshall, 1941. Physiologic studies on neural mechanisms of visual localization and discrimination, *Am. J. Ophthalmol.*, 2:1255–1261.
- Ungerleider, L., and M. Mishkin, 1982. Two cortical visual systems, in *Analysis of Visual Behavior* (D. Ingle and M. Goodale, eds.), Cambridge, MA, MIT Press, pp. 459–486.
- Van Buren, J., 1963. Trans-synaptic retrograde degeneration in the visual system, *Neurol. Neurosurg. Psychiatr.*, 26:402–409.
- Van Essen, D., C. Anderson, and D. Felleman, 1992. Information processing in the primate visual system: an integrated systems perspective, *Science*, 225:419–423.
- Vicq d'Azyr, F., 1786. *Traité d'anatomie et de physiologie*, Paris: Didot.
- Von Bonin, G., 1950. *Essays on the Cerebral Cortex*, Springfield: Thomas.
- Wollaston, W., 1824. On semi-decussation of optic nerves, *Phil. Trans. R. Soc.*, 114:222–231.
- Young, T., 1802. On the theory of light and colours, *Phil. Trans.*, 92:12–18.
- Zeki, S., 1978. Uniformity and diversity of structure and function in rhesus monkey prestriate visual cortex, *J. Physiol.*, 277:273–290.

2 The Role of Single-Unit Analysis in the Past and Future of Neurobiology

HORACE BARLOW

Introduction

This chapter starts with a brief history of single-unit recording, biased, I am afraid, toward recounting the parts I know best, namely, those that interested me or those I took part in. It stops well short of the present, except for a brief account of some studies on MT neurons in awake behaving monkeys that I believe point the way ahead. The quantitative statistical approach of signal detection theory should enable one to follow a single quantity, the signal-to-noise ratio, through all stages from the sensory stimulus itself, through single-neuron responses at all levels, to reports of perceptual experiences or other behavioral responses. But statistical arguments have pitfalls. First, the source or sources of limiting noise must be correctly identified; second, they are good for establishing limits to what is possible but not very good as a basis for direct models because we know so little about how the brain computes statistics. I think the implications of statistical measures are most easily understood in terms of rules stating when signal-to-noise ratios are conserved, how they can be increased, and when they decrease. Using the rules, statistical arguments can give much insight into the role of single units in sensory systems, for neurons are the only elements capable of collecting together the information relevant to a particular task, which in turn is the only way to obtain high signal-to-noise ratios.

I believe we need to open our eyes to the much more complex types of computation that, as cell biology is beginning to show, might be accomplished by single neurons, so I could not refrain from speculating about this at the end of the chapter. Finally, at the editor's instigation, I have recounted in an Appendix some of my personal experiences in the remarkable department, created by Lord Adrian, in which I had the extraordinary good fortune to grow up scientifically.

This, then, is a personal view. Please do not read this chapter in the hope of finding a complete historical account that leads to a balanced view of the role of single units in vision; desirable though that would be, it is not what the title proclaims and it is not what you will find.

History

By the beginning of the twentieth century, the basic layout of the sensory systems of the brain, including vision, was surprisingly well understood. If, for example, one reads Schäfer's account of the cerebral cortex in his two-volume *Textbook of Physiology* (1900), at first one cannot fail to be amazed by how much was known. There is a good deal about cortical localization, the neuron doctrine was in place, and there were Cajal's beautiful pictures of neurons with all sorts of shapes and sizes, sometimes with putative circuits showing how messages flowed into the dendrites through synapses and out along axons to distant destinations. But on reflection one becomes aware of what was then missing, for the nature of the activity that was localized, and the nature of the messages that passed from place to place in the brain, were quite unknown. Müller's doctrine of specific nerve energies was based on the similar sensation produced whenever a given type of sensory nerve fiber was excited, regardless of the means employed to excite it. It was sometimes taken to imply that the messages were different in different fibers, rather than that the same message had different meanings when carried by different fibers, but with no knowledge of the nature of the messages, this misunderstanding is perhaps not surprising. The all-or-none law had been formulated for heart muscle, but it was not known to apply to nerve impulses; indeed, it was not clear that nerve messages were composed of impulses. In other words, it was well understood that nerve fibers were communication channels, but it was not understood at all how or what they communicated.

The reason for this ignorance is simple: there were no methods available either for isolating the activity of an individual nerve fiber or for detecting and recording the activity if it had been isolated. Intracellular recording was unheard of, and as we now know, the potential from an impulse that can be recorded through an external electrode placed close to a nerve fiber is a brief (<1 msec) triphasic pulse, often no more than a few microvolts in amplitude. Until these pulses could be amplified electronically, there was no way they could be detected. Action potentials from the synchronized syncytium of muscle fibers in the heart could

be recorded, as could the synchronized action potentials from an electrically stimulated peripheral nerve, but in spite of interesting and ingenious technological devices such as the capillary electrometer, string galvanometer, and rheotome, no method combined the speed and sensitivity required to detect single nerve impulses. The nature of the nerve impulse as a locally generated, self-propagating, all-or-nothing electrical disturbance traveling down individual nerve fibers was soon to be established, perhaps chiefly by Keith Lucas (1909) in a series of closely argued and compelling experiments, but the arguments were indirect: he never recorded all-or-none impulses from single fibers.

PERIPHERAL SENSORY NERVE FIBERS The vacuum tube amplifier, or thermionic valve, was invented in the early 1900s by Fleming and De Lee Forest, and this provided the answer. Among the earliest users in physiology were Gasser and Newcomer (1921), and a year or two later, E. D. Adrian (Keith Lucas's student and colleague) wrote to Gasser asking for details of his amplifier; he then constructed one, and in 1925 for the first time recorded action potentials traveling in sensory nerve fibers. By 1928, after collaborations with Sybil Creed (*née* Cooper), Rachel Matthews (*née* Eckhardt), and Yngve Zotterman, he had recorded from nerves carrying sensory messages from many different types of sensory endings and was able to write *The Basis of Sensation* (Adrian, 1928), a book of only 120 pages telling us that all sensory messages are composed of trains of all-or-none nerve impulses. They vary in frequency according to the intensity of the stimulus; they often (but not always) adapt, that is, the frequency of the train declines over time when the stimulus intensity is sustained; and sometimes they are highly regular (for instance, from the stretch organs of muscle) and sometimes highly irregular (for instance, from taste endings in the tongue). These were exciting years; see Hodgkin (1979) for a fuller and more detailed account of Adrian's early work.

Adrian's main method of isolating the activity of a single nerve fiber was to place a complete peripheral nerve on a pair of recording electrodes and then cut away at the nerve between the electrodes and sensory endings until there was only a single sensory fiber remaining to conduct impulses from sensory ending to recording site. He judged when this had been accomplished by observing that all the action potentials reaching the electrodes became uniform in height and shape, and those from some endings were also regularly spaced in time. This method did not always work. In the experiments that are most relevant for this chapter, on the optic nerve of the eel (Adrian and Matthews, 1927a, 1927b, 1928), they were not successful in recording from single active fibers. Their three papers illustrate their resourcefulness when they could not achieve what they wanted, and they had many indirect results foreshadowing later work, but

discussion of recordings from retinal ganglion cells will be deferred.

I said above that the vacuum tube amplifier provided the answer that overcame the problem of recording from single neurons, but it only provided the tool to obtain the answer. The choice of biological tissue, of the arrangements for recording from the nerve, of the means of stimulating sensory endings, and, above all, of the controls needed to show that the weak potentials recorded really were from sensory fibers—all these depended on the experimenter. Adrian's papers describe with transparent simplicity and directness what he and his colleagues did, why they did it, what they observed, and what this means. It all seems so simple that one asks oneself, "Why are not all papers this easy to follow and understand?" I think the answer is that Adrian was skilful enough to make critical observations whose message was clear without elaborate interpretation. He did not waste time describing results whose meaning was not clear, and when there was any doubt about what they meant, he refused to speculate further. For more than 20 years, important results from him and a galaxy of internationally famous collaborators tumbled out of his laboratory, and he remained at the forefront of neurophysiology, but little of this work involved single units and it will not be described here. He gave up experimental work only when his laboratory was flooded in 1958, and for many years afterward he continued to fill influential and important administrative positions. At the editor's suggestion, I provide a few reminiscences about him and his lab in the Appendix.

RETINAL GANGLION CELLS By 1930, then, the neural code used by peripheral nerve fibers had been broken, but there were 10^{10} neurons in the central nervous system busy communicating with each other, and it was far from certain that they used the same code. The next major step toward resolving this question came in the late 1930s, when Keffer Hartline in Philadelphia and Ragnar Granit in Stockholm recorded from retinal ganglion cells, which are separated by at least two synapses from the sensory cells themselves. Granit and Svaetichin (1939) used platinum-tipped glass electrodes about $15\mu\text{m}$ in diameter to record extracellular potentials, and sometimes the action potentials from a single retinal ganglion cell could be isolated (see Rushton, 1949). The development of this method of recording from neurons, in which Gunnar Svaetichin also had a hand, was an important advance, and with minor modifications provided the main means of recording from single neurons in sensory systems until brain slices and patch electrodes were developed many years later.

The physiological aspect of Granit's work on the retina (Granit, 1947) was not so successful. He chose to attack the color problem, using large-area, spectrally pure stimuli, and

he described units with broadband *dominator* and narrower-band *modulator* spectral sensitivity curves. The dominators were relatively stable in position and had scotopic spectral sensitivity curves in dark-adapted conditions and photopic curves in light-adapted conditions. The modulators were not stable and seemed to come in many different varieties. They probably correspond to the spectrally opponent units recorded many years later from fish retina (Svaetichin and MacNichol 1958; Wagner et al., 1960) and from monkey lateral geniculate nucleus (LGN) (DeValois et al., 1967), but it was not really until this later work accrued that progress was made on the color problem.

Hartline developed a technique for raising optic nerve fibers onto recording electrodes as they ran on the surface of the retina from the ganglion cells in the periphery toward the optic disc. His beautiful papers (Hartline, 1938, 1940a, 1940b) give a first insight into how a couple of layers of synaptic connections and lateral interactions create a pattern of activity in the retinal ganglion cells that constitutes a spatiotemporally transformed version of the optical image. He observed that different ganglion cells respond to different temporal phases of the stimulus, some at “on,” some at “off,” and some at both phases. He defined *receptive fields*, noting that they are so large that there must be extensive overlap between the receptive fields of neighboring retinal ganglion cells, and he emphasized the exceptional sensitivity of many cells to movement of the light stimulus. Curiously, he did not discover lateral inhibition in the vertebrate retina, though he certainly would have done so if he had extended his studies of spatial summation to larger diameters of stimulating spots. Instead he switched to the *Limulus* preparation and described it there (Hartline, 1949), so lateral inhibition in the vertebrate eye was left to Kuffler (1952, 1953) and I (Barlow, 1950, 1953) to discover in the cat and the frog, respectively.

SINGLE NEURONS IN THE CENTRAL NERVOUS SYSTEM The task ahead, breaking the code of the 10^{10} neurons of the brain, was a daunting one, not only because of the technical difficulties of recording from them one at a time, but also because of the sheer numbers: How could one possibly hope to sample the activity of a sufficient number of these cells to form an impression of their overall state of activity? And anyway, what guarantee was there that the output of a single cell was at all meaningful by itself? To break the code, it might be necessary to take into account the simultaneous activities of other cells, the details of which would, of course, remain unknown if the cells were recorded one at a time. But the results sketched above convinced some people that single-unit recording was a viable and illuminating technique, and more results followed during the next two decades.

Lettvin and his colleagues (1959) argued that the frog’s retina and superior colliculus extracted behaviorally impor-

tant features from the retinal image. Hubel and Wiesel (1959, 1962, 1968) showed that neurons in the cat’s (and later the monkey’s) visual cortex were sensitive to the orientation of stimuli, and color opponency of neurons in fish retina and monkey lateral geniculate were sorted out (DeValois et al., 1967; Svaetichin and MacNichol, 1958; Wagner et al., 1960). Enroth-Cugell and Robson (1966) applied systems theory to retinal ganglion cell responses and unexpectedly revealed a strong distinction between *X cells*, which behaved linearly, and *I cells*, which behaved nonlinearly, in the way they responded to sinusoidal spatial gratings. Other varieties of selectivity in single units were described and analyzed, such as selectivity for direction and velocity of motion in the rabbit retinal ganglion cells (Barlow et al., 1964) and for disparity in the cat visual cortex (Barlow et al., 1967; Pettigrew et al., 1967). In addition, it was found that the sensitivity of single neurons often approached that of the whole animal quite closely (Barlow et al., 1957, 1971). There were also reports of pattern selectivity in the responses of optic nerve fibers in crustaceans (Wiersma and Yanigasawa, 1971; Wiersma et al., 1961).

In 1972 (Barlow, 1972) I reviewed much evidence showing that single neurons had sensitivity, selectivity, and reliability of an order that would have been considered out of the question 20 years earlier. The results suggested that sensory representations are sparsely coded, that is, only a small proportion of all available sensory neurons are active at any one time in the representations that are responsible for perception. With such sparse coding, single neurons carry a much greater burden in classifying and representing our sensations and perceptions than had previously been supposed, and their ability to respond in a highly selective manner to their inputs becomes crucial. It is sometimes suggested, however, that the early promise of single-unit analysis has not been fulfilled, because units at higher levels responding to more and more specialized features of the environment have not been found. This deserves a comment.

UNITS CAN BE VERY SELECTIVE, BUT THEY ALSO GENERALIZE Perhaps the most striking feature of the early results from single-unit recording was their selectivity: a retinal ganglion cell responds better to a spot of light in exactly the right place on the retina than it does to flooding the whole retina with light, a cortical neuron responds poorly even to a well-placed spot but instead requires a line of the right orientation, and some neurons require a line in the right position in each eye. Some of the *local edge detectors* described by Levick (1967) in the rabbit retina are extraordinarily difficult to excite and characterize. They do not fire spontaneously, nor to whole field illumination, nor even to a line if it is too long, and they ignore their favorite stimulus, a small spot of light, if it is moving too fast. I recall, with some qualms,

leaving Bill Levick just after he had isolated a unit, and coming back an hour and a half later after a good lunch to find that he had made only limited progress toward characterizing it. “I know the receptive field is somewhere near here,” he said, pointing to a mark on the plotting screen, “but there’s something special about its trigger feature.” Then, after perhaps another hour’s further work, he demonstrated that a short black edge at the right orientation, moved very slowly, would invariably elicit a vigorous response, but very little else that could be done on the plotting screen had any detectable effect on that particular unit.

The existence of this degree of selectivity, even in the retina, makes one appreciate how difficult it must have been for Gross and his colleagues (1972) to characterize trigger features as complex as their *hand detectors* or *face detectors* in the inferotemporal cortex of monkeys, or for Rolls and colleagues (Mora et al., 1976; Rolls et al., 1979) to demonstrate *food object* detectors in lateral hypothalamus. These reports were in fact treated with very great skepticism in the early days, though the repeatability of the findings has now established their validity beyond reasonable doubt; one wonders how many more examples of comparable selectivity are waiting to be discovered. But the main point I want to make is that although single-unit results sometimes do show amazing selectivity, they also show evidence of another process—generalization.

One of the surprises in Hartline’s results was the large size of the receptive fields: a retinal ganglion cell collects the activity not just from its fair share of photoreceptors, but from a vastly greater number. Complex cells described by Hubel and Wiesel (1962) in V_1 were orientationally selective but did not have receptive fields that could explain this property, as those of the simple cells could. They proposed that complex cells collect the outputs of many simple cells, thereby retaining the pattern-selective property but generalizing it for position over a small region of visual space. Levick and I found the same in the direction-selective ganglion cells of the rabbit retina (Barlow & Levick, 1965): they apparently collect the outputs of subunits that are selective for the same sequence of activation occurring in their inputs at different positions. This work also showed that selectivity is not necessarily achieved by AND-type logic, but can result from inhibition “vetoing” responses to a subset of stimuli. Another recent example of the way neurons achieve selectivity and generalization is to be found in the work of Thomas and colleagues (2002) showing that some cells in V_2 of monkey are selective for the relative disparity of stereoscopic stimuli; this is thought to be achieved by the appropriate pattern of connections to V_1 cells having absolute disparity selectivities.

The answer to the question raised in this subsection is therefore that cells do become more selective at higher levels, but they also relax their response requirements and gener-

alize in appropriate ways. Selectivity and generalization seem to be the basic operations needed to generate the mythical grandmother cell; the final cell must be selective enough for details so that it responds to a particular elderly lady, not just any elderly lady, but it must also generalize for the dispositions of these details so that it can recognize grandmother in all her possible poses, positions, gestures, and clothing. One can grasp in outline how a hierarchy of neurons, each capable of both selectivity and generalization, might trace a path through the jungle of possibilities resulting from the combinatorial explosion, culminating in a neuron with the properties of a reasonable object detector. I don’t, however, think this has yet been demonstrated in detail in any specific instance as complex and arbitrary as a grandmother cell—if indeed neurons with this degree of selectivity and arbitrariness exist.

The discovery of these unexpected attributes of brain cells obviously took one a step forward, and a sizable fraction of the rest of this book includes later results of single-unit recording in the visual system. I regard this work as the “present” of single-unit analysis and shall not attempt to review it in this chapter, but there is a group of experiments that I shall return to since they are, in my opinion, showing the way ahead. These use statistical measures that can be applied to the sensory signals used to drive the neural responses, to the responses they evoke from single units, and to the behavioral responses of an animal or human observer. First, the approach itself must be described.

The power and pitfalls of the statistical approach

Developments in electronic engineering not only brought us the tools for recording the activities of single neurons, they also brought into prominence the problem of *noise*, the random stochastic voltages that interfere with the *signal* one is interested in and ultimately set a limit to its detectability. But the problem the electrical engineers introduced us to attracted the attention of statisticians, who have provided us with the concepts needed for measuring and understanding signals and noise.

These are the concepts of statistical decision theory (Neyman and Pearson, 1933), which also formed the basis of signal detection theory and which were, in turn, imported into psychology for measuring psychophysical performance within an absolute framework (Swets, 1964). The key advance here was to emphasize signal-to-noise ratios (SNRs) rather than thresholds. Whenever a signal is being detected against a background of noise, there comes a point, as you reduce the signal intensity, when its presence or absence cannot be decided reliably. Before the days of signal detection theory, this was regarded as the threshold of perception, but there is a range in which it can be shown that the value of this threshold is dependent on the number of

false-positive responses the subject makes. From both a theoretical and a practical viewpoint, it is preferable to use a measure that is not dependent on the false-positive rate, and this is provided by the measure that an engineer would naturally use when specifying the magnitude of a signal in a noisy background, the SNR. This is the ratio of the response to the signal divided by the standard deviation of the responses with no signal present. The measure d -prime in signal detection theory estimates from the psychometric responses the SNR of the representation of the stimuli on the decision variable.

The reason this measure is so valuable depends first on the fact that it can be applied equally well to the signals being used as sensory stimuli, to data obtained from the neural firing rates of individual neurons, and to data derived from perceptual responses of human observers or from behavioral responses of animals. It can thus provide the common currency for establishing quantitative relations all along the way from the initial stimulus itself, through single-unit responses, to final behavioral output.

A second reason for attaching great importance to these measures is that the statistical aspects of perceptual performance are in many ways the ones of greatest interest. This cannot be argued here in detail, but my reading of the lesson to be derived from nearly 50 years of work in computer vision is that natural visual systems effortlessly and efficiently extract signals from noisy backgrounds, while computer systems initially struggle to do so. However, once a visual task has been defined in sufficient detail, it can usually be performed as well or better by a computer system. The visual system's superiority seems to lie in the selection of tasks it performs well, for these tasks are just those required to enable an animal to survive and flourish in a competitive, inherently variable, barely predictable environment that has the statistical characteristics of the one we experience. Perhaps one should not be surprised at this, considering that the animals do survive, but one cannot help being impressed.

THE IMPORTANCE OF EXTRINSIC NOISE The ability to detect specific signals buried in extrinsic noise, with an efficiency not far below the theoretical limit, is central to such tasks. The first pitfall is to ignore this, but there is an excuse for doing so because it was none other than J. von Neuman (1956) who suggested that the main problem was to understand how the brain achieves reliable performance using noisy components. Noise is certainly generated inside the brain by neurons themselves, so there is no doubt that intrinsic noise is a problem, but it makes no sense to regard it as the most important one simply because picking out the signal from the extrinsic noise has to be done whether the components are noisy or noiseless. Intrinsic noise is not the essential problem, it is an additional one.

It is extremely difficult to find and isolate the signals from the environment that are necessary for performing a task such as driving a car down a busy street, because of the clutter of other very similar signals that is continuously bombarding the sensory system. Solving the similar problems that arise for prey and predator in the jungle would bring great competitive advantages, and sensory systems must surely have evolved mainly under this pressure. Intrinsic noise is interesting and is probably the limiting factor at the absolute threshold of vision, but quantum fluctuations and extrinsic noise are surely the limiting factors in a much wider range of conditions. One should see how this is handled before worrying too much about intrinsic noise, for this becomes important only when it produces effects comparable in magnitude to those of extrinsic noise, and this tends to occur only when extrinsic noise is artificially reduced to a very low level. For instance, the thermal stability of rhodopsin is probably important at the absolute threshold of vision; but otherwise, the ability to catch the largest possible fraction of quanta is much more important (Barlow, 1956).

THREE RULES ABOUT SNRS Attaining the high SNRs that are needed for reliable behavior in a noisy environment is not an easy task, and the following three rules may help to understand the process better, and thereby illuminate how sensory mechanisms achieve the high standard of performance required for survival in a competitive world.

Rule 1. Noise cannot be removed from a message once it has been added to it. Since signal can easily be lost and more noise can easily be added, this sets a one-sided limit. SNRs decline for any of a large number of possible reasons, but it is hard to sustain them at the same value and still harder to raise them. Note that one immediate and obvious implication of this rule is that you can never obtain a message with a higher SNR than that present in the stimulus delivered, provided that all the available information from the stimulus has already been utilized. Following the SNR through the system can therefore tell the inquisitive neurophysiologist how much irretrievable information loss occurs and where it occurs. We shall see later that there is suggestive evidence that the losses, up to the level of single-unit responses in MT, can be low (Mogi and Barlow, 1999) and that for the most favored types of stimulus, not much more is lost even up to the level where behavioral decisions are made (Barlow and Tripathy, 1997).

Rule 2. The only way to raise an SNR is by adding further relevant information. Relevant information usually means other messages with new signal from the same source, but with noise that is independent (at least partially) of that contained in the original message. The optimal way of incorporating new information is considered below, but

note here that the signal parts of the original and new messages add directly, while it is the variances of the noise parts that add, not their standard deviations, so the combined standard deviation rises more slowly than the signal—hence the possibility of improving the SNR.

Rule 3. The optimal SNR for a given target with graded parameters is obtained by matching all the parameters of the detector to those of the stimulus. This matching assigns weights to the messages from different parts of the target, each weight being proportional to the SNR contributed by that particular part of the target. It can be shown that this maximizes the signal collected and minimizes the noise that accompanies it. Obviously this is an important rule for understanding how a sensory system should design detectors for the features in the environment that are important for its survival, and it adds much significance to the receptive field of a neuron, for its shape, considered as a weighting function, tells one the target for which it is an optimally matched detector.

Recall that the parameters of receptive fields, even those in the same column, differ from each other considerably, so each is a matched detector for a different target; in general, any two neurons in MT are likely to have only moderate overlap of response regions in the multidimensional space defined by the selectivities of the neurons (see Lennie, 1998). Note also that neurons are the only components we know of in the brain that might combine messages in the appropriate way to obtain optimal improvements in SNRs. There are other methods of combining signals, such as picking the maximum, or so-called probability summation, but in general, these are suboptimal.

Experimental statistical studies

With this theoretical background, the history of experimental studies of single neurons can be resumed. Among the earliest uses of signal detection theory in visual neurophysiology were FitzHugh's studies (1957, 1958) of the threshold responses of cat retinal ganglion cells. These and other studies showed how the maintained discharge of neurons constitutes noise limiting what can be detected (Barlow and Levick, 1969; Kuffler et al., 1957; Werner and Mountcastle, 1963). Good neurophysiological SNRs can be obtained for stimuli that are of the same order of magnitude as behavioral or psychophysical absolute thresholds (Barlow et al., 1971). The power of using the approach at several successive levels in the same visual pathway was shown by Laughlin (1973, 1974a, 1974b), who demonstrated the improvement that occurs as information from several insect photoreceptors is brought together on a single higher level neuron.

Note that noise may be represented in other than ways as a variable neural discharge rate. Intracellular biophysical variables often depend on rather small numbers of molecules, implying a high level of random variability which is certainly liable to interfere with the processing of sensory information. On the other hand, a high level of variability does not necessarily limit performance: this will occur only when the intrinsic variability is comparable to or greater than the variability arising from the extrinsic noise which enters with the sensory stimulus.

I learned this lesson in Kuffler's lab. Before going there, I had been struggling to establish that noise was important in human vision (Barlow, 1956, 1957), and I was expecting it to be similarly inconspicuous neurophysiologically. I could not believe my ears when I heard the dreadful irregular cacophony produced by a cat's retinal ganglion cell, and it took some time for Steve and Dick to convince me that this noisiness was not an artifact (Kuffler et al., 1957). The apparent paradox became clear when we measured the ganglion cell's sensitivity to light (Barlow et al., 1957), for like a good radar operator or ham radio enthusiast, the retina turns up the gain far enough to make the noise easily detectable but not so far that it swamps the signal. I strongly suspect that MT does a similar job with correspondence noise.

USING BOTH NEURAL AND BEHAVIORAL RESPONSES Mountcastle (1984) defined three stages of analysis of sensation, in the last of which single units were recorded in alert animals while doing sensory discriminations. The studies of this sort that I think show most promise for sorting out the roles of single units in vision are those on the detection of coherent motion by neurons in MT of the monkey, and I shall concentrate on the following five papers: those of Britten et al., (1992, 1993, 1996), Celebrini and Newsome (1994), and Shadlen et al. (1996). These are referred to collectively as "work from Newsome's lab."

Using alert, trained macaques, these authors recorded the responses of single neurons in MT while the monkey was performing a behavioral discrimination task and signaling its apparent result. The task chosen was to discriminate between two opposite directions of motion of a random dot kinematogram in which the proportion of dots moving coherently in one direction could be varied. The recordings from the isolated neurons gave the distributions in numbers of impulses for different coherence levels for movements in both preferred and null directions, while the behavioral responses gave the proportions with which the monkey correctly identified the direction of motion in their forced-choice task.

The authors plotted the behavioral results as the percentage correct at the varying coherence levels and found that, like humans, the monkeys could perform this task very well, achieving 82% correct responses at coherences

of 10% or less. The criterion of 82% they chose for threshold corresponds to a d -prime value of 1.13 and can be obtained directly from the percentage correct in a two-alternative forced-choice task (e.g., from Elliott's tables in Swets, 1964).

To obtain comparable curves for the neural responses, they used the following method: they assumed that there was another neuron, which they called the *anti-neuron*, with exactly the same properties as the one they were recording from but having a reversed directional preference; they then took the number of impulses in each trial, and said that it signaled the preferred direction if it was a number more likely to have been generated by preferred direction trials at that particular coherence level and null if it was more likely to have been generated by null direction trials.

There are two slight problems with this way of making unit responses comparable with psychometric responses. First, there is little if any evidence that the monkey brain actually uses an anti-neuron in making its decisions, and it is a pity for such an uncertain feature to be so deeply embedded in the comparisons and models made. Second, the authors' neurometric curve shows the performance expected of two neurons, the hypothetical anti-neuron as well as the one they actually recorded from, and this is, of course, better than that expected from a single neuron, provided that, as they assume, the neurons give independent information about the signal.

There seems no good reason to avoid expressing a single neuron's performance directly as an SNR in the way an engineer would naturally express measurements of a signal variable, that is, as the difference between the mean responses at a given coherence and at zero coherence, divided by the standard deviation of the response at zero coherence. This is merely a step in thinking clearly about what can and cannot be done with signals such as those that have been recorded, and it does not necessarily entail the assumption that the brain actually uses the expected response to zero coherence in making its decisions. The unit's SNR at the coherence required for an 82% correct behavioral threshold can be compared directly with 1.13, the value of d -prime for their psychometric measure at 82% correct.

It is worth pointing out that the two-alternative forced-choice task the monkeys performed is a method devised by psychophysicists to determine the ratio of signal response on the decision variable to the noisiness of that representation—that is, its standard deviation. The neuron/anti-neuron artifice seems to be a way of doing this in reverse, going from recorded signal responses back to expected psychophysical-like performance, but why do this? The neurophysiologist has, or hopes he is going to have, access to the signals from which decision variables are constructed, so why go backward? Why use psychophysical performance as the currency for comparisons?

The main result of their study was to show an astonishing agreement between the psychometric curves obtained behaviorally and those obtained from single units using the anti-neuron method. It is true that there was a large range in sensitivities, the ratio of neurometric to psychometric threshold varying over a 10-fold range, with many neurometric sensitivities exceeding the psychometric sensitivity, but the mean ratio was close to 1. Furthermore, the agreement extended to the slopes of the curves as well as to their means. Note, however, that these exact agreements depend in part on the assumption that the decision is based on the use of all of the 2000-msec responses collected from the neuron; this is implausible, for the monkey's life must often depend on much more rapid responses to moving stimuli. Departing from this assumption is likely to spoil the exactness of the agreement, but the change would probably not be large enough to alter the main conclusion—that MT neurons can signal the direction of coherent motion in a random dot kinematogram with a sensitivity comparable to that attainable by the whole animal. This is in agreement with a good body of other work showing that single neurons are very sensitive, and I personally think it is about as far as their results take us at present. But there is hope of further progress from measurements of *choice probabilities* (called the *sender operating characteristics* in Celebrini and Newsome, 1994, and the *predictive index* in Shadlen and Newsome, 2001).

Choice probability is a measure of the way the monkey's behavioral responses covary with the neural responses of a recorded neuron, and it is related to the area under the receiver operating characteristic (ROC) curve in signal detection theory. It represents the probability of determining the behavioral response correctly from an optimal analysis of a particular single unit's responses. If the neural response fully determined the behavioral response, choice probability would have a value of 1, whereas if there was only a chance relationship, it would have a value of 0.5. In fact, the authors found that the average value for all neurons analyzed was significantly above 0.5, though not by very much. A few neurons seem to have had considerably higher values, but they imply that these were untrustworthy chance results. Higher average values have been reported from other experiments on MT (Dodd et al., 2001), in which many neurons seemed to have values above 0.8, and Shadlen and Newsome (2001) and Horwitz and Newsome (2001a, 2001b) have also obtained much higher values in parietal cortex and superior colliculus, where they actually used a much shorter analysis period.

From the point of view of SNR analysis, the choice probability is a measure of the amount of noise added between unit response and behavioral choice: high choice probabilities near 1 are evidence of little added noise, whereas low probabilities near 0.5 are evidence of much added noise.

The trouble is that a high choice probability does not prove that a neuron did actually determine the behavioral response; it only proves that it could have done so, and the possibility that other neurons actually did so is not excluded. Similarly, a low choice probability near 0.5 does not prove that the neuron played no role at all in the behavioral response, for it may have stepped in and caused a correct response on rare occasions when no other neuron was able to do so. What a low choice probability does prove is that that particular neuron, by itself, could not have been responsible for all the correct decisions made behaviorally, and this remains true even if the neuron's SNR was as high as or higher than that given by the psychometric results. It is an important additional measure that has to be taken into account in figuring out how single units control behavior.

In the final paper of the series, Newsome's group tried to model how the brain derives the decision variable underlying the behavioral responses from a set of neural responses and choice probabilities such as those they recorded, but although I admire the attempt, I feel it is not the final solution for the following five reasons:

1. It fails to take into account the fact that, if the conclusion reached by Barlow and Tripathy (1997) is accepted, *correspondence noise*, which is extrinsic, is a major factor limiting the performance of the MT system. Correspondence noise arises from the correspondence problem—that is, from the lack of information about which dots are to be considered as pairs in successive frames of a random dot kinematogram. If we know how such stimuli have been generated, its magnitude can be calculated (Barlow and Tripathy, 1997). Human coherence thresholds behave as if they were limited by it over wide ranges of variation of the principal parameters of the target stimulus, and under optimum conditions, statistical efficiencies for detecting coherent motion are quite high. Newsome's group does recognize the problem of correlations between responses of MT neurons, but this measure does not seem to differentiate between correlations due to the signal being shared and correlations due to the noise being shared, yet these have very different implications.

If correspondence noise is the major natural problem in detecting and analyzing motion signals, one is unlikely to understand how the visual analysis of motion is organized without taking it into account. It is also a pity not to exploit the possibility of estimating SNRs on the stimulus as well as on the responses, for this enables one to follow the losses of efficiency directly. It is these losses of efficiency that are of most practical importance to the monkey, since they have the greatest effect on the utility and survival value of the system for detecting coherent visual motion.

2. One can expect to be able to derive the behavioral decision variable from the neural responses only if the

measure of these responses that is used for the analysis actually corresponds to the measure that the brain uses. The only measure of the neural responses Newsome's group used was the total number of impulses over 2000 msec, but it seems unlikely that an animal that spends its life jumping around in the treetops uses only 2000-msec totals for controlling its responses to motion signals that might save its life if reacted to quickly. Bair and Koch (1996) have shown that the temporal frequency response of the motion detection system peaks at around 3 Hz, so perhaps the monkey makes a decision every 300 msec, and, if forced to wait before responding, bases its delayed response on some kind of probability summation among the stored results of these previous decisions, or perhaps simply uses the most recent, up-to-date one. The decrease in efficiency of psychophysical performance for durations above about 400 msec (Barlow and Tripathy, 1997), together with the margin by which the performance of many neurons exceed their behavioral performance, suggests that it would be hard to exclude such a possibility.

3. The neuronal data the authors used to model the formation of the final decision were collected for stimuli that were only approximately optimal for each of the individual neurons. No signal can be optimal for all the different neurons, even those in a single column, but the extent of the loss of performance from mismatching is obviously hard to estimate. Note particularly that the importance of disparity selectivity was not fully recognized when the data were collected, so this parameter was not optimized.

4. I think that at this stage of our understanding of the problem, we should use statistical arguments to derive limits on what is possible, and it is premature to attempt a direct model. The three rules stated earlier make it fairly easy to derive such limits. Note that if the statistical efficiency of the early stages is as high as some estimates indicate (Mogi and Barlow, 1999), the limits become more stringent and are more informative about which models are viable and which can be excluded.

5. At present, we have very little understanding of the way the brain does its statistical computations, important though these are for all decisions. Advancing knowledge of the cell biology of cortical neurons suggests that they may be able to do computations we have not hitherto suspected, as described in the final section of this chapter. It is not clear how this will affect the problem, but it seems unwise to pin one's faith (or one's model) on the assumption that they can do little more than compute weighted sums of impulse numbers, even though this is a crucial step in collecting the evidence needed for good decision making.

It's evident that the last two objections are swayed by prejudice and stylistic preference. Further analysis (Gold and Shadlen, 2000, 2001) shows interesting convergence with independent psychophysical measurements (Carpenter

and Williams, 1995; Reddi and Carpenter, 2000), and may well prove these and my other doubts to be unfounded. Whatever happens in the future, Newsome's group has already shown that statistical analysis of single-unit responses greatly improves our understanding of behavioral decisions; including the role of extrinsic noise in this analysis will surely bring further insight into this crucial aspect of perceptual decision making.

Why study single neurons?

Different people would answer this question in different ways. For instance, Adrian (1932) clearly regarded himself as an empiricist, saying:

In all branches of natural science there are two methods of approach, that of the strategist who can devise a series of crucial experiments that will reveal the truth by a sort of Hegelian dialectic, and that of the empiricist who merely looks about to see what he can find.

In his hands, "merely looking about to see what one can find" was astonishingly fruitful, but I confess that I have often aspired to the more theoretical approach that Adrian described first in the above passage. As a research student I was intrigued by information theory and cybernetics, which were then coming to the fore (Shannon and Weaver, 1949; Wiener, 1961), by early work on computer pattern recognition (Grimsdale et al., 1959; Selfridge and Neisser, 1960), and by the ideas of ethologists about *fixed action patterns* and *innate releasing factors* that were being popularized by Niko Tinbergen (1953) and Konrad Lorenz (1961) at about that time. But theories can close your eyes as well as open them.

One of the first experimentally satisfactory experiments I did on the frog's retina gave a result that made nonsense of the theory I was testing, but I was so fixated by the theory that I nearly missed an important new fact that was staring me in the face. Having previously mapped the receptive field of a retinal ganglion cell, I measured its sensitivity to circular spots of increasing size. My theory predicted that while it was within the receptive field, sensitivity would rise either in proportion to the area of the stimulus spot or in proportion to its square root, depending on the type of unit. My theory attached great importance to which of these rules it followed, but the results showed that the sensitivity rose at a rate almost exactly halfway between the alternatives expected. I went home late at night in great gloom, thinking the experiment had failed and was not worth repeating. It was only as I was falling asleep that I remembered that the sensitivity had plunged to a nonsensical-seeming near-zero value for the largest spot size when it spread outside the excitatory receptive field. I then realized that this unpredicted near-zero result actually provided direct evidence for

something more interesting than my previous theorizing: it strongly suggested that the retinal ganglion cell had an inhibitory surround, a new fact that was only later described by Hartline (1949) and Kuffler (1952).

This event might justify ignoring theoretical and philosophical issues altogether, but, of course, the real lesson is to stay awake and be ready with a new theory whenever the facts demand it.

For Steve Kuffler, linking single-unit function to known (or discoverable) anatomical structure was probably the main inspiration, as it was for his most famous followers, David Hubel and Torsten Wiesel. Their school of thought was extraordinarily influential, for it diverted the main efforts of neurophysiologists in the United States away from the study of evoked potentials and massed responses to single units. Single-unit recordings are never going to make much sense unless they are related to the anatomy, but this needs no further emphasis.

Obviously, one important aim of neuroscientists is to explain subjective experience, and the role of single neurons in mediating this process adds much zest to their investigation. However, I think this appeal has been seductive rather than productive. We know so little about the nature of conscious experience that it would not help very much even if we were able to establish tight relations with single-unit activities. Instead, the qualitative parallels are weak and tend to fall apart when closely examined, so I shall not discuss them further, feeling that the quantitative parallels that signal detection theory has established are far more significant. There has, however, been one very simple and direct demonstration of the relation between subjective experience and single impulses in a single unit.

Vallbo and colleagues (see Valbo, 1989) demonstrated that human subjects (actually, the experimenters themselves) can detect the occurrence of a single impulse in a single sensory fiber. They inserted a fine metal microelectrode, insulated up to its tip, into the nerve that runs from the hand to the spinal cord and then connects to the brain. With fortunate placement of the electrode it is possible to record the activity of just one fiber, and in such a case a certain region on the hand or finger may be found that, when touched, causes a succession of brief, equal-sized pulses to appear on the oscilloscope screen and to be heard through the loudspeaker as a volley of brief clicks. These action potentials come from a single sensory fiber, and one can reduce the intensity of the mechanical stimulus until it only causes, on average, a single action potential. Will this minimal response ever be felt? For some types of touch receptors at the fingertip, it can: it is felt as a brief and very light touch. For other types of receptors, and at other positions on the skin, this is not the case, and even where it is, one is not forced to conclude that conscious awareness accompanies a single impulse, for it is quite possible that a single one in the peripheral fiber causes several

impulses at later stages. All the same, these facts do seem to show that sensory experience does not necessarily depend on hundreds of impulses in hundreds of fibers: a single impulse in a single fiber sometimes makes a perceptible difference.

For myself, the reason for retaining a keen interest in single neurons is simply that they are the main computing elements of the brain, and I cannot believe that we shall get our models right until we understand them better; the properties of neurons define the work that a network can do, whereas the network connections only permit (or prevent) that work being done.¹ So at this point I shall indulge in some guesswork about how our notions of pyramidal cells may evolve over the next decade or so.

A glimpse of the future

This section is obviously speculative, but there is one feature of the brain that may make speculations more reliable than you would expect. Pyramidal neurons occupy a specific place in a highly organized system, so we know quite a lot about the nature of their inputs. Advances in understanding of their cell biology can only reinforce what existing results already suggest—that neurons are capable of more complex computations than we previously thought. Now, assuming constant requirements for speed and accuracy, an increase in computational capacity is not much use unless there are more data to be handled, but we already know that most data arrive along the inputs to the neuron in question. If nodes can handle more data than we used to think they could, what are these extra data? Where do they come from?

The first possible answer that ought to be considered is that neurons use information that is not often mentioned, namely, knowledge of the time of day. Many cells in the body that have no part in generating the overall circadian rhythm nevertheless have most of the biochemical machinery of the circadian clock (Hastings and Maywood, 2000), and cortical neurons are among them. The timing of the clock in a group of cells is indicated by the phase at which the *mPer1* and *mPer2* genes are expressed, and this can be determined by in situ hybridization. If one compares a diurnally active animal (ground squirrel) with a nocturnally active one (hamster), the clocks in their suprachiasmatic nuclei are both found to be synchronized with the overall light/dark cycle, *mPer1* and *mPer2* expression peaking about 5 hours after the beginning of the light cycle. Now their motor cortices also show a diurnal rhythm, but this is not

synchronized with the suprachiasmatic nucleus (Mrosovsky et al., 2001). In the hamster it peaks at the time when its normal period of *nocturnal* motor activity is starting at the start of the dark period, 5 hours after the *mPer1* peak in the suprachiasmatic nucleus; and in the ground squirrel it peaks at the start of its normal period of *diurnal* motor activity, some 4 hours before the *mPer1* peak in its suprachiasmatic nucleus.

It is not yet known how the phase of the local clock is determined, but it is tempting to suppose that the local activity of the cells provides a synchronizing signal to the cell's cycle, so that *mPer1* expression comes to coincide with the expectation of activity—an increase in the prior probability that a particular cortical neuron will be activated, based on the proportion of activations at that time 24, 48, 72, and so on hours earlier. This machinery in our dog's cortical neurons could presumably become synchronized with the important daily events of her life, thus preparing her to bark at the arrival of the postman or to roll on her back when one of us comes home. Time is only a single variable, but the daily cycle of expectations, signaled intraneurally, might form a nontrivial addition to each cortical neuron's data input.

The second possible answer is that neurons use more thoroughly the data we already know that they receive through ordinary input channels: perhaps they store their inputs temporarily and operate on the temporal patterns and sequences they contain, not just on the present input and that of the very recent past. I shall try to show in the next few paragraphs that the idea that the main job of cortical neurons is to exploit, for the benefit of the brain's owner, the absolute time and the relative timing of sensory signals is a very reasonable extension of our current concepts of what they do, though I think it may take a while to get used to it.

HOW BIOPHYSICAL KNOWLEDGE OF PYRAMIDAL CELLS HAS EVOLVED Our knowledge of the biophysical processes that occur in pyramidal cells has increased enormously since Cajal drew those beautiful pictures of them, but our concept of what they do to help their owner survive in a hostile world has not kept pace. I don't think anyone now accepts the challenging notion of Pitts and McCulloch that they are elementary AND, OR, and NOT logic elements whose task is perform more complex logical functions. We have also progressed from the Sherringtonian model of a neuron that "integrates" central excitatory and central inhibitory states, through Eccles' simple integrate-and-fire model controlled by excitatory and inhibitory synaptic potentials, then through Rall's compartmental treatment of proximal and distal dendrites, and have reached the elaborated compartmental model (Koch and Segev, 1998) by including many different forms of ion channels, including voltage-sensitive

¹There is, however, an intriguing possibility that network studies will tell us what neurons *should* do to make the whole brain able to compute what cognitive studies show that it *does* compute.

ones. These provide a formidable battery of possible biophysical mechanisms, but what do they all add up to? What functions do these cells perform that aid the survival of their owner?

By far the most significant functional addition has been the modifiable synapse postulated by Hebb. This not only adds the function of memory to the nodes, but also increases their computational capacity by an enormous factor. Without memory, a neuron can exist in only two states, on or off, and it cannot change between them in less than about 1 msec. That's not much of a unit, and a cell with, say, 10,000 synapses, each of which can be in several different states, certainly commands much more respect. But there are more additions.

Nerve cells have second messenger systems, working on slower time scales than transmitters that operate on ionic membrane channels. In addition, they have calcium-induced calcium release (CICR) which can not only produce powerful effects at the locality in the dendrite where it occurs, but can also propagate down the endoplasmic reticulum of a dendrite at a speed of about 40 $\mu\text{m}/\text{sec}$ (Jaffé and Brown, 1994). It is remarkable that this striking mechanism has not yet been shown to be responsible for a correspondingly striking functional process in neurons, though there are hopes (Barlow, 1996; Euler et al., 2002) that it may turn out to be responsible for directional selectivity. When considering the time scale on which pyramidal neurons operate, one should realize that metabotropic glutamate receptors activated at the tip of a 2 mm long apical dendrite might initiate a wave of CICR that would produce powerful effects in the soma nearly a minute later!

We do not know what these intracellular processes achieve any more than we know what the various channels in the elaborated compartmental model neuron achieve; they are potential mechanisms, and we still have to find tasks whose performance we can pin on them. It is certainly worthwhile to look at what such mechanisms are known to achieve in *Escherichia coli* and other simple systems. Bray (1990, 1995) has pointed out several instances of biochemical pathways interacting to form control systems that would require many interacting nodes in a network model. But instead of occurring in a whole network of different nodes, in *E. coli* these occur inside a single small cell that is about the size of a synaptic bouton of a pyramidal cell. It would take about a quarter million *E. coli* to fill the whole cytoplasm of a pyramidal cell.

The potential computational capacity of these intracellular mechanisms is hard to assess; they are slower to switch than the ionic channels of membranes, but there are potentially so many of them, all reasonably well isolated from each other, that the complexity of the computations the whole cell might achieve must be increased by a huge factor (Barlow, 1996).

PHASE SEQUENCES AND PYRAMIDAL CELLS Now let us consider what has to be explained by the actions of pyramidal cells. Donald Hebb (1949) was the first person to discuss seriously how the properties of neurons might explain psychological function, and his landmark book made the influential proposal that memory, or information storage, occurs at modifiable synapses. But another influential concept he introduced, that of *cell assemblies*, has not fared so well. As Hebb explained, the reason he advanced this idea was that times of the order of hundreds of milliseconds seemed to be involved in the *phase sequences* that were being discussed by psychologists at that time (see Lashley, 1951), whereas a nerve impulse was very brief and could not produce a sustained effect. He therefore postulated that a group of neurons sustains an excitatory input for the required duration by reverberatory, self-reexcitatory action. There can be little doubt that sequences of activity in the brain follow each other not as independently excited events, but rather as chains in which one event prepares the brain for the next: the sensory stimuli and motor actions at one choice point in a maze prepare the rat for the next choice point, hearing one syllable of a word or one note of a tune prepares the brain for the next, and so forth. But, Hebb argued, nerves work on a very rapid time scale; a mechanism is needed to make excitation persist long enough to carry over to the next element in a phase sequence, and that is what his self-reexciting cell assemblies were supposed to do.

This argument does not really stand up. Even in a peripheral nerve, the passage of an impulse allows sodium ions to enter, and the time constant for pumping them out is much longer than the times Hebb was concerned about. At synapses, as we have seen, there are second messenger systems and CICR that occur slowly. The principal reason Hebb gave for postulating the existence of cell assemblies, the evanescent nature of nerve activity, is no longer convincing, nor is there good experimental evidence for self-reexciting chains performing the function he postulated. All the same, we should not disregard the need he saw for slow processes. Instead, we should ask: is it possible that pyramidal cells on their own can work on the slow time scale appropriate for phase sequences?

Given that pyramidal cells have Hebbian synapses modifiable by experience, this question resolves into two different ones. First, might pyramidal cells be capable of responding selectively to much more complex spatiotemporal patterns than our present concepts would allow? Might they detect a whole tune rather than the separate notes of a tune? The second question follows naturally: if they can detect and discriminate such spatiotemporal patterns, could they acquire these abilities through experience? I think it is plausible to suggest that the answer is "Yes" in both cases, and shall briefly discuss these possibilities.

RADICAL INSEPARABILITY The first proposal moves almost as far away as possible from the integrate-and-fire model. This dealt primarily with the integration of inputs to the neuron through different synapses, which I shall call *spatial integration*; temporal integration could occur through the persistence in time of postsynaptic potentials, but differences in times of persistence were assumed to be unimportant, and so far as this assumption was valid, one could regard spatial and temporal integration as separable processes.

It has actually been clear for a long time that this simplification is not valid. Temporal and spatial summation in vision are not independent of each other (Barlow, 1958), and even in comparatively simple neurons such as retinal ganglion cells, direct measurements of responses to sinusoids of different temporal and spatial frequencies have shown nonseparability (Enroth-Cugell et al., 1983). Furthermore, inseparability in time and space have been shown to be characteristic properties of the neurons in V_1 that are directionally selective (DeAngelis et al., 1995).

Let us suppose that separability is completely wrong, and that the synapses of each neuron have time courses and/or delays that differ from each other, influence each other, and fall into perhaps a dozen or more different categories. It's clear that this neuron is far more complicated than a simple integrate-and-fire neuron, but it can also achieve much more. Directional selectivity would be easy to obtain with only two different categories of synapses having two different positions and delays; so would velocity selectivity. Acceleration, deceleration, and change of direction would require at least three. Oscillatory motions, which are often characteristics of innate releasers, could be detected with rather more, as could the sequences of syllables in a word or of the notes and rhythm of a tune. These and many more are surely possibilities to which we should be opening our eyes.

SUPER-HEBBIAN SYNAPSES Could a pyramidal cell learn to combine information from its many synapses in this radically inseparable way? Recent evidence (Bi and Poo, 1998; Feldman, 2000; Markram et al., 1997) shows that the timing of pre- and postsynaptic activity determine the polarity of the change in synaptic effectiveness that results from joint activity: this is increased when presynaptic firing occurs first and is decreased when it occurs after the postsynaptic firing. But is the time at which the switch occurs always the same at all synapses? Could it be different for synapses located on different parts of the dendritic tree? Is it even possible that there are different mechanisms at the same synapse that are reinforced at different pre-post intervals (Barlow, 1996)? Either of these mechanisms could enable a neuron to learn the spatiotemporal pattern of a movement sequence, a speech sound, or a tune.

Other possibilities will surely appear as we learn more about the cell biology of the large neurons of the brains of higher animals, but at the moment, the difficult problem seems to be that of determining their functional significance. Maybe we need to turn to simpler animals, with simpler behavioral repertoires, to bridge this gap between cell biology and cognition, for I think it is clear that a cell with the kinds of capacities I have sketched above would be a useful component at many levels of behavioral complexity. Such capacities are, however, unlikely to be discovered by experimenters who confine their attention to a brain slice in a dish.

If even a few of these possibilities turn out to be true, the neurophysiology of the cortex is going to be an exciting field over the next few decades. Single neurons are not just the elements whose activity represents what is happening in the outside world; they are also the elements that do the computation in the brain. So their analysis should tell us not only how experience is represented, it should also tell us how it is computed.

Appendix: recollections of Lord Adrian

I was one of Lord Adrian's very small number of graduate students. The Ph.D. was not a popular degree in Cambridge until well after the Second World War, and especially in physiology, even those going into academic research more often took a medical degree, as I had done myself. But when I qualified in 1947, I was faced with the choice of many years of internships and residencies to climb the medical ladder or having a go at physiological research, and I chose the latter. I needed a research studentship, so I came to Cambridge to explore the possibility of getting one.

The first problem was to find Adrian, as he was universally known, both before and after his elevation to the peerage. I knew he was in Cambridge, and often in the Physiological Laboratory, but whenever I called he was not in his office. After several visits his secretary rather reluctantly admitted that he was probably downstairs in his lab, but when I asked if I could find him there, her jaw dropped and she said, "Well, er . . ." I got the message but went down to look for him all the same. The entrance was guarded by his assistant, Leslie, who said, "He's in there with a pony² and does not want any visitors." This time I took the hint, but as I was leaving the lab I met one of my former lecturers (Tunncliffe) and explained my problem. He at once told me I was not alone in finding it difficult to catch Adrian, but, he

²There is some artistic license here—it may have been a hedgehog. But he certainly did do an experiment, singlehanded during the anesthetization, on a Shetland pony at around this time (Adrian, 1946).

said, "He usually goes to Trinity on his bicycle around lunch time, and if you stand in front of him he won't run you down." So I lurked around the lab entrance for a few lunchtimes, and the tactic worked: as I stood triumphantly over the front wheel of his bike he said, "Come to my office at 2 o'clock."

There he asked if I had any ideas I wanted to work on, quickly demolished the ones I proposed, but then said I might be interested in looking at the paper by Marshall and Talbot (1942) on small eye movements to see if there was anything in their idea, and, by the way, he thought he could get me a research studentship from the Medical Research Council. The total duration of the interview was certainly no more than 5 minutes; Adrian believed in getting a lot done in his time outside the lab as well as inside it.

I read the paper, and although it was not the beginning of my interest in vision, it probably was the beginning of my realization that visual motion is an important topic. When I reported for work a few days later, Adrian seemed surprised to see me, and even more surprised when I asked him what I should do, but he said something like "We've discussed that—Marshall and Talbot, don't you know." I was beginning to get the hang of things and quickly got out some words like "I need apparatus—a recording camera, don't you know," whereupon he said "Leslie will see to that." I still had absolutely no idea of what I was expected to do, but ended up the next day in possession of a beautiful mahogany-cased 35mm cinecamera of 1920s vintage with a manual crank for driving it and no lenses, and, of course, no film. It was fun converting it to record eye movements, and I eventually got some film, but I was very glad I was never asked to return the camera in full working order.

ADRIAN AS A RESEARCH SUPERVISOR He mainly left me to find my own way and did not give me very much direction or advice, but the advice he did give was always direct, to the point, valuable, and correct, even if it was often a bit discouraging. I remember him suggesting relevant references and pointing me to various people who might help with problems I was encountering. When I was massacring the movie camera he pointed me to Bryan Matthews, and it was he who explained to me what the unexpected cylindrical lens near the image plane in a recording camera does. Another was Andrew Huxley on a statistical problem, and I remember him explaining patiently that the variances of independent samples add, so my problem became instantly soluble.

After about a year, I knew a good deal more about how much the human eye moves: it moves a lot, but not in ways that make sense for Marshall and Talbot's hypothesis. I realized I was not going to discover much more and wanted to move on, so when Adrian popped his head round my

door a week or so later, I explained where I had got to with eye movements and told him that I wanted to repeat some of Hartline's experiments on the frog's retina because I was puzzled by the very large receptive fields he had described. Adrian's immediate response was, "Oh, I wouldn't do that—Hartline's a very clever chap, you know." But I persisted, driven largely by the theoretical drive that told me the frog's eye would not work very well if there was no more to it than Hartline had described, so I wrote him a note a few days after his visit about the equipment I needed.

At that time, one could buy war surplus electronic equipment at absurdly low prices. It was sold by weight, and one could buy a photon multiplier complete with all circuitry for about 25 cents. I reckoned that with the help of others who had followed the same path, I could build a suitable amplifier for less than 20 dollars. I wrote Adrian a letter asking if I could go ahead and pick it all up from London the following week, but got the letter back the next day with a note scribbled on the back: "Is this a request for leave of absence or something?" I think he was actually more worried about my spending all my time on the equipment (a real danger) than about my wasting the lab's money, and I got the stuff anyway.

A month or two later, I had got it all assembled and in sometimes-working condition when Adrian came unannounced into my lab with a visitor smoking a large cigar and speaking completely incomprehensible English.

A few minutes before their arrival I had dropped the electrode on the floor. I had just remounted it and was lowering it onto a frog retina, without much hope of success, when they came in, so I turned on the light and started explaining what I was trying to do and how. At this point, the visitor was standing under the room light and took a deep puff from his cigar. As he exhaled the smoke, its shadow fell on the preparation and it gave a long, vigorous "off" discharge. Ragnar Granit, for that was who it turned out to be, was astonished. So was I, and his English became at least partly intelligible as we discussed the technicalities of what makes a good electrode and so forth.

ADRIAN'S LABORATORY Adrian definitely did not like visitors in his laboratory, and I only entered it once or twice. I think the first time was when Leslie took me round to see what recording cameras were available. It was a large room, 600sq ft I would guess, completely full of tables with apparatus on them, with more bits and pieces stacked around the walls. The room was in the basement, and in my memory it has a mud floor with no tiles, boards, carpet, or anything luxurious. That is probably wrong, but superficially it was indistinguishable from a mud floor. I remember the frame of a motor bike without its engine resting under one window, and then noticing the engine under an operating table being used as a respiration pump.

I was fascinated, trying to guess what all the old equipment had been used for, but had to attend to the job in hand. Leslie wanted me to take a *falling plate camera*, a device with dashpots and levers and a wooden frame that fell at a controlled speed when one pushed the trigger, but I asked what recording material it used. "It takes a glass plate," said Leslie. "Are they available?" I asked. "Well," said Leslie, "we have many of the glass plates, and you can coat them yourself." That explained why Leslie wanted to get rid of the camera, but it did not make it into a good choice for me, so after a few more false starts I got the beautiful camera I described above, delivered the next day by Leslie after he had checked that it was okay for me to have it.

I recall only one other very brief visit, for a purpose that I cannot recall, when Adrian was actually doing an experiment. Now whenever he was in the physiology lab, Adrian was always moving, never at rest, always reacting. His body movements were like saccadic eye movements, jerking incessantly from one object of attention to another. Ordinarily these movements, while much more frequent than most people's, were quite well spaced out and synchronized with other events occurring around him, so that he surprised one with an unexpected shift of attention only, say, once every 30 seconds or so. But in his own laboratory they seemed to occur every second, and each of one's own movements elicited a response. On the occasion of my visit, he was doing an experiment on a monkey that was infected with amebic dysentery—the reason, he explained, why he was able to get hold of it. If I turned toward the table to ask a question, he seemed to jump to intervene between me and the monkey, and my attention was so riveted by his heightened state of reactivity that I could take in nothing about his laboratory or the experiment he was conducting.

He was an amazing person, and I have never met anyone who had more than a very superficial knowledge of him who was not similarly amazed. I'm sure he broke all records for the number of sound decisions per minute that he could make. I shall tell one more story about him that reveals an aspect of his character of which he was certainly himself aware, and which may have contributed a lot to his success both as a scientist and as an administrator.

After his wife died he came to live in Trinity College, and as the senior fellow he often presided after dinner, when fellows and their guests meet to converse over more wine and cheese. On these occasions those who serve the wine and cheese leave quite early, and it is left to the last departing fellow to extinguish the candles and lock up the room. On one occasion when Adrian was presiding I had consumed a fair amount of port, but considered that I was still well able to perform these functions and indicated to Adrian that I would do so. In spite of this he followed me around, checking every candle and testing the door I had just locked as we left. I suppose I was a little marked by this and turned to him,

saying, "Good heavens, I wish I had ever had a colleague in the lab who was as meticulous and careful as you are!" I don't think I used the word *obsessional*, but it was certainly in my mind and, equally certainly, he knew it. But he turned to me and said with a smile, "Yes, there are not many like us, are there?" Of course, that made my day—and makes it again whenever I recall it.

The Physiological Laboratory at Cambridge in the 1950s was a truly remarkable place, but it's only years later, when I think about the scientific achievements of Adrian, Rushton, Hodgkin, and Huxley, that I realize just how extraordinarily fortunate I was to be there.

REFERENCES

- Adrian, E. D., 1928. *The Basis of Sensation*, London: Christophers.
- Adrian, E. D., 1932. *The Mechanism of Nervous Action*, Philadelphia: University of Pennsylvania Press.
- Adrian, E. D., 1946. The somatic receiving area in the brain of the Shetland pony, *Brain*, 69:1–8.
- Adrian, E. D., and R. Matthews, 1927a. The action of light on the eye. I. The discharge of impulses in the optic nerve and its relation to the electric changes in the retina, *J. Physiol. (Lond.)*, 63:378–414.
- Adrian, E. D., and R. Matthews, 1927b. The action of light on the eye. II. The processes involved in retinal excitation, *J. Physiol. (Lond.)*, 64:279–301.
- Adrian, E. D., and R. Matthews, 1928. The action of light on the eye. III. The interaction of retinal neurons, *J. Physiol. (Lond.)*, 65:273–298.
- Bair, W., and C. Koch, 1996. Temporal precision of spike trains in extrastriate cortex of the behaving macaque monkey, *Neural Comp.*, 8:1185–1202.
- Barlow, H. B., 1950. The receptive fields of ganglion cells in the frog retina, in *Proceedings of the XVIII International Physiological Congress*, Copenhagen: Bianco Lunos Bogtrykkeri, pp. 88–89.
- Barlow, H. B., 1953. Summation and inhibition in the frog's retina, *J. Physiol. (Lond.)*, 119:69–88.
- Barlow, H. B., 1956. Retinal noise and absolute threshold, *J. Opt. Soc. Am.*, 46:634–639.
- Barlow, H. B., 1957. Increment thresholds at low intensities considered as signal/noise discriminations, *J. Physiol. (Lond.)*, 136:469–488.
- Barlow, H. B., 1958. Temporal and spatial summation in human vision at different background intensities, *J. Physiol. (Lond.)*, 141:337–350.
- Barlow, H. B., 1972. Single units and sensation: a neuron doctrine for perceptual psychology? *Perception*, 1:371–394.
- Barlow, H. B., 1996. Intraneuronal information processing, directional selectivity and memory for spatio-temporal sequences, *Network: Comput. Neural Systems*, 7:251–259.
- Barlow, H. B., C. Blakemore, and J. D. Pettigrew, 1967. The neural mechanism of binocular depth discrimination, *J. Physiol.*, 193:327–342.
- Barlow, H. B., R. FitzHugh, and S. W. Kuffler, 1957. Dark adaptation, absolute threshold and Purkinje shift in single units of the cat's retina, *J. Physiol.*, 137:327–337.
- Barlow, H. B., R. M. Hill, and W. R. Levick, 1964. Retinal ganglion cells responding selectively to direction and speed of motion in the rabbit, *J. Physiol.*, 173:377–407.

- Barlow, H. B., and W. R. Levick, 1965. The mechanism of directionally selective units in the rabbit's retina, *J. Physiol.*, 178:477–504.
- Barlow, H. B., and W. R. Levick, 1969. Three factors limiting the reliable detection of light by retinal ganglion cells of the cat, *J. Physiol.*, 200:1–24.
- Barlow, H. B., W. R. Levick, and M. Yoon, 1971. Responses to single quanta of light in retinal ganglion cells of the cat, *Vis. Res.*, 11(Suppl 3):87–101.
- Barlow, H. B., and S. P. Tripathy, 1997. Correspondence noise and signal pooling in the detection of coherent visual motion, *J. Neurosci.*, 17:7954–7966.
- Bi, G., and M.-M. Poo, 1998. Synaptic modification in cultured hippocampal neurons: dependence on spike timing, synaptic strength, and post-synaptic cell type, *J. Neurosci.*, 2:32–48.
- Bray, D., 1990. Intracellular signalling as a parallel distributed process, *J. Theoret. Biol.*, 143:215–231.
- Bray, D., 1995. Protein molecules as computational elements in living cells, *Nature (Lond.)*, 376:307–312.
- Britten, K. H., W. T. Newsome, M. N. Shadlen, S. Celebrini, and J. A. Movshon, 1996. A relationship between behavioural choice and the visual responses of neurons in macaque MT, *Visual Neurosci.*, 13:87–100.
- Britten, K. H., M. N. Shadlen, W. T. Newsome, and J. A. Movshon, 1992. The analysis of visual motion: a comparison of neuronal and psychophysical performance, *J. Neurosci.*, 12:4745–4765.
- Britten, K. H., M. N. Shadlen, W. T. Newsome, and J. A. Movshon, 1993. Responses of neurons in macaque MT to stochastic motion signals, *Visual Neurosci.*, 10:1157–1169.
- Carpenter, R. H. S., and M. L. L. Williams, 1995. Neural computation of log likelihood in the control of saccadic eye movements, *Nature (Lond.)*, 377:59–62.
- Celebrini, S., and W. T. Newsome, 1994. Neuronal and psychophysical sensitivity to motion signals in extrastriate area MST of the macaque monkey, *J. Neurosci.*, 14:4109–4124.
- DeAngelis, G. C., I. Ohzawa, and R. D. Freeman, 1995. Receptive field dynamics in the central visual pathways, *TINS*, 18:451–458.
- DeValois, R. L., I. Abramov, and W. R. Mead, 1967. Single cell analysis of wavelength discrimination at the lateral geniculate nucleus in the macaque, *J. Neurophysiol.*, 30:415–433.
- Dodd, J. V., K. Krug, B. G. Cumming, and A. J. Parker, 2001. Perceptually bistable three-dimensional figures evoke high choice probabilities in cortical area MT, *J. Neurosci.*, 21:4809–4821.
- Enroth-Cugell, C., and J. G. Robson, 1966. The contrast sensitivity of retinal ganglion cells of the cat, *J. Physiol. (Lond.)*, 187:517–552.
- Enroth-Cugell, C., J. G. Robson, D. E. Schweitzer-Tong, and A. B. Watson, 1983. Spatio-temporal interactions in cat retinal ganglion cells showing linear spatial summation, *J. Physiol. (Lond.)*, 341:279–307.
- Euler, T., P. B. Detwiler, and W. Denk, 2002. Directionally selective calcium signals in dendrites of starburst amacrine cells, *Nature (Lond.)*, 418:845–852.
- Feldman, D., 2000. Timing-based LTP and LTD at vertical inputs to layer II/III pyramidal cells in rat barrel cortex, *Neuron*, 27:45–56.
- FitzHugh, R., 1957. The statistical detection of threshold signals in the retina, *J. Gen. Physiol.*, 40:925–948.
- FitzHugh, R., 1958. A statistical analyser for optic nerve impulses, *J. Gen. Physiol.*, 41:675–692.
- Gasser, H. C., and C. Newcomer, 1921. Physiological action currents in the phrenic nerve: an application of the thermionic vacuum tube to neurophysiology, *Am. J. Physiol.*, 57:1–27.
- Gold, J. L., and M. H. Shadlen, 2000. Representation of a perceptual decision in developing oculomotor commands, *Nature (Lond.)*, 404:390–394.
- Gold, J. I., and M. N. Shadlen, 2001. Neural computations that underlie decisions about sensory stimuli, *Trends Cogn. Sci.*, 5:10–16.
- Granit, R., 1947. *Sensory Mechanisms of the Retina*, London: Oxford University Press.
- Granit, R., and G. Svaetichin, 1939. Principles and technique of the electrophysiological analysis of colour reception with the aid of microelectrodes, *Uppsala Läkaref Förh.*, 65:161–177.
- Grimsdale, R. L., F. H. Sumner, C. J. Tunis, and T. Kilburn, 1959. A system for the automatic recognition of patterns, *Proc. Inst. Electr. Eng., B*, 106:210–221.
- Gross, C. G., C. E. Rocha-Miranda, and D. B. Bender, 1972. Visual properties of neurons in infero-temporal cortex of macaque, *J. Neurophysiol.*, 35:96–111.
- Hartline, H. K., 1938. The response of single optic nerve fibres of the vertebrate eye to illumination of the retina, *Am. J. Physiol.*, 121:400–415.
- Hartline, H. K., 1940a. The receptive fields of optic nerve fibres, *Am. J. Physiol.*, 130:690–699.
- Hartline, H. K., 1940b. The effects of spatial summation in the retina on the excitation of the fibers of the optic nerve, *Am. J. Physiol.*, 130:700–711.
- Hartline, H. K., 1949. Inhibition of activity of visual receptors by illuminating nearby retinal areas in *Limulus*, *Fed. Proc.*, 8:69.
- Hastings, M., and E. S. Maywood, 2000. Circadian clocks in the mammalian brain, *BioEssays*, 22:23–31.
- Hebb, D. O., 1949. *The Organisation of Behaviour*, New York: Wiley.
- Hodgkin, A. L., 1979. Edgar Douglas Adrian, Baron Adrian of Cambridge; 1889–1977, *Biographical Memoirs R. Soc.*, 25:1–73.
- Horwitz, G. D., and W. T. Newsome, 2001a. Target selection for eye movements: direction selective visual responses in the superior colliculus, *J. Neurophysiol.*, 86:2527–2542.
- Horwitz, G. D., and W. T. Newsome, 2001b. Target selection for saccadic eye movements: prelude activity in the superior colliculus during a direction discrimination task colliculus, *J. Neurophysiol.*, 86:2543–2558.
- Hubel, D. H., and T. N. Wiesel, 1959. Receptive fields of single neurones in the cat's striate cortex, *J. Physiol.*, 148:574–591.
- Hubel, D. H., and T. N. Wiesel, 1962. Receptive fields, binocular interaction, and functional architecture in the cat's visual cortex, *J. Physiol.*, 195:215–243.
- Hubel, D. H., and T. N. Wiesel, 1968. Receptive fields and functional architecture of monkey striate cortex, *J. Physiol.*, 195:215–243.
- Jaffé, D. B., and T. H. Brown, 1994. Metabotropic glutamate receptor activation induces calcium waves within hippocampal dendrites, *J. Neurophysiol.*, 72:471–474.
- Koch, C., and I. Segev (eds.), 1998. *Methods in Neuronal Modelling: From Ions to Networks*, 2nd ed., Cambridge, Mass: MIT Press.
- Kuffler, S. W., 1952. Neurons in the retina: organisation, inhibition and excitation problems, *Cold Spring Harbor Symp. Quant. Biol.*, 17:281–292.
- Kuffler, S. W., 1953. Discharge patterns and functional organisation of mammalian retina, *J. Neurophysiol.*, 16:37–68.
- Kuffler, S. W., R. FitzHugh, and H. B. Barlow, 1957. Maintained activity in the cat's retina in light and darkness, *J. Gen. Physiol.*, 40:683–702.
- Lashley, K. S., 1951. The problem of serial order in behaviour, in *Cerebral Mechanisms in Behaviour*, New York: Wiley, pp. 112–146.

- Laughlin, S. B., 1973. Neural integration in the first optic neuropile of dragonflies. I. Signal amplification in dark-adapted second-order neurons, *J. Comp. Physiol.*, 84:335–355.
- Laughlin, S. B., 1974a. Neural integration in the first optic neuropile of dragonflies. II. Receptor signal interactions in the lamina, *J. Comp. Physiol.*, 92:357–375.
- Laughlin, S. B., 1974b. Neural integration in the first optic neuropile of dragonflies. III. The transfer of angular information, *J. Comp. Physiol.*, 92:377–396.
- Lennie, P., 1998. Single units and visual cortical organization, *Perception*, 27:889–935.
- Lettvin, J. Y., H. R. Maturana, W. S. McCulloch, and W. H. Pitts, 1959. What the frog's eye tells the frog's brain, *Proc. Inst. Radio Eng.*, 47:1940–1951.
- Levick, W. R., 1967. Receptive fields and trigger features of ganglion cells in the visual streak of the rabbit's retina, *J. Physiol. (Lond.)*, 188:285–307.
- Lorenz, K., 1961. *King Solomon's Ring* (M. K. Wilson, trans.), Cambridge: Cambridge University Press. (Translated from German; first published 1952.)
- Lucas, K., 1909. The "all or none" contraction of amphibian skeletal muscle fibre, *J. Physiol. (Lond.)*, 38:113–133.
- Markram, H., J. Lübke, M. Frotscher, and B. Sakmann, 1997. Regulation of synaptic efficacy by coincidence of post-synaptic APs and EPSPs, *Science*, 275:213–215.
- Marshall, W. H., and S. A. Talbot, 1942. Recent evidence for neural mechanisms in vision leading to a general theory of sensory acuity, *Biol. Symp.* (J. Cattell, ed.), 7:117–164.
- Mogi, K., and H. B. Barlow, 1999. The source of variability in neural responses from MT, *J. Physiol. (Lond.)*, 515:101P–102P.
- Mora, F., E. T. Rolls, and M. J. Burton, 1976. Modulation during learning of the responses of neurons to the sight of food, *Exp. Neurol.*, 53:508–519.
- Mountcastle, V. B., 1984. Central nervous mechanisms in mechanoreceptive sensibility, in *Handbook of Physiology, Section 1, The Nervous System*, vol. III, part 2 (J. M. Brookhart and V. B. Mountcastle, eds.), Bethesda: American Physiological Society, pp. 789–878.
- Mrosovsky, M., K. Edelstein, M. H. Hastings, and E. S. Maywood, 2001. Cycle of *period* gene expression in a diurnal mammal (*Spermophilus tridecemlineatus*): implications for non-photic phase shifting, *J. Biol. Rhythms*, 16:471–478.
- Neumann, J. von, 1956. Probabilistic logics and the synthesis of reliable organisms from unreliable components, in *Automatic Studies*, Princeton: Princeton University Press.
- Neyman, J., and E. S. Pearson, 1933. On the problems of the most efficient tests of statistical hypotheses, *Phil. Trans. R. Soc., Series A*, 231:289–337.
- Pettigrew, J. D., T. Nikara, and P. O. Bishop, 1967. Binocular interaction on single units in cat striate cortex: simultaneous stimulation by single moving slit with receptive fields in correspondence, *Exp. Brain Res.*, 6:391–410.
- Reddi, B. A. J., and R. H. S. Carpenter, 2000. The influence of urgency on decision time, *Nature Neurosci.*, 3:827–830.
- Rolls, E. T., M. K. Sanghera, and A. Roper-Hall, 1979. The latency of activation of neurons in the lateral hypothalamus and substantia innominata during feeding in the monkey, *Brain Res.*, 164:121–135.
- Rushton, W. A. H., 1949. The structure responsible for action potential spikes in the cat's retina, *Nature (Lond.)*, 164:743–745.
- Schäfer, E. A., 1900. The cerebral cortex, in *Textbook of Physiology* (E. A. Schäfer, ed.), Edinburgh and London: Young & Pentland, pp. 697–782.
- Selfridge, O., and U. Neisser, 1960. Pattern recognition by machine, *Sci. Am.*, 203(2):60–68.
- Shadlen, M. N., K. H. Britten, W. T. Newsome, and J. A. Movshon, 1996. A computational analysis of the relationship between neuronal and behavioural responses to visual motion, *J. Neurosci.*, 16:1486–1510.
- Shadlen, M. N., and W. T. Newsome, 2001. Neural basis for a decision in the parietal cortex (Area LIP) of the rhesus monkey, *J. Neurophysiol.*, 86:1916–1936.
- Shannon, C. E., and W. Weaver (eds.), 1949. *The Mathematical Theory of Communication*, Urbana: University of Illinois Press.
- Svaetichin, G., and E. R. MacNichol, 1958. Retinal mechanisms for chromatic and achromatic vision, *Ann. NY Acad. Sci.*, 74:385–404.
- Swets, J. A. (ed.), 1964. *Signal Detection Theory by Human Observers*, New York: Wiley.
- Thomas, O. M., B. G. Cummings, and A. J. Parker, 2002. A specialisation for relative disparity in V2, *Nature Neurosci.*, 5:472–478.
- Tinbergen, N., 1953. *The Herring Gull's World*, London: Collins.
- Vallbo, Å. B., 1989. Single fibre microneurography and sensation, in *Hierarchies in Neurology: A Reappraisal of a Jacksonian Concept* (C. Kennard and M. Swash, eds.), London: Springer, pp. 93–109.
- Wagner, H. G., E. R. MacNichol, and M. L. Wolbarsht, 1960. The response properties of single ganglion cells in the goldfish retina, *J. Gen. Physiol.*, 43(Suppl):115–128.
- Werner, G., and V. B. Mountcastle, 1963. The variability of central neural activity in a sensory system, and its implications for the central reflection of sensory events, *J. Neurophysiol.*, 26:958–977.
- Wiener, N., 1961. *Cybernetics*, Boston: MIT Press.
- Wiersma, C. A. G., T. H. Waterman, and B. M. H. Bush, 1961. The impulse traffic in the optic nerve of decapod crustacea, *Science*, 134:1453.
- Wiersma, C. A. G., and K. Yanigasawa, 1971. On types of interneurons responding to visual stimulation present in the optic nerve of the rock lobster *Panulirus interruptus*, *J. Neurobiol.*, 2:291–309.

II DEVELOPMENTAL PROCESSES

3 Molecular Regulation of Vertebrate Retinal Development

COLIN J. BARNSTABLE

Introduction

For well over a century, the retina has been a favorite model system for experimental studies of the central nervous system (CNS). Anatomical studies, including the pioneering studies of Ramon y Cajal, have identified the ordered laminar arrangement of the five neuronal and two glial cell types, as well as the numerous subclasses of each cell type (see Chapter 20). The retina has also been used extensively by experimental embryologists, and we now have a detailed description of how many of the cell types of the retina are formed from a sheet of primitive neuroepithelium. Such a rich background of information has made it possible for more recent biochemical studies to explain many of these events in molecular terms.

In the plane of the retina, many cell types form a mosaic whose spacing and connectivity patterns vary with position. Retinal position also dictates the topographical connectivity of ganglion cell terminals. Here too, classical anatomical and physiological studies have defined the timing and specificity of this connectivity, and recent studies in the retina have now begun to suggest molecular pathways by which positional specification might be effected.

This chapter will discuss the major steps of retinal development in molecular terms. In particular, it will try to show that several general principles govern many steps of development. First, many developmental steps consist of transcriptional changes in response to one or more morphogenetic gradients in the concentration of diffusible factors (usually peptides). Second, transcription factors that delineate tissue compartments often reciprocally inhibit transcription factors in adjacent compartments. As described later, a combination of these two principles leads to the formation of sharp boundaries. Third, the same families of molecules, even the same molecules, are used at multiple stages of development. This has the experimental advantage that understanding how one retinal cell type is formed can provide many clues about the mechanisms involved in the formation of other retinal cell types.

While our understanding of the molecular mechanism of retinal development has advanced dramatically in recent years, we probably have only the crudest outline of the

whole process. Nevertheless, this outline seems to be robust, and new information is likely to expand, not replace, our current view.

Initial demarcation of eye fields

The developing neural plate acquires an anterior-posterior axis using the same cues as the rest of the early embryo. This axis provides positional information to cells of the developing neuroepithelium. At the anterior edge of the neural plate, a patch of cells becomes specified to develop into the neural components of the eye—the eye field. These cells of the eye field are morphologically identical to surrounding cells but can be characterized by the expression of a variety of transcription factors. The two earliest genes expressed in the eye field are both paired-like homeodomain genes, *Rax/Rx* and *Pax-6* (Furukawa et al., 1997; Hill and Hanson, 1992; Mathers et al., 1997). Both can be detected in mouse by embryonic day 8.5 (E8.5) and in *Xenopus* by stage 12.5 (Furukawa et al., 1997; Hirsch and Harris, 1997). *Pax-6* first appears as two lateral stripes that pass through presumptive forebrain, midbrain, and hindbrain. *Rx* or *Rax* also first appears in areas that will give forebrain and midbrain structures. *Pax-6* expression is maintained in many regions throughout development whereas *Rax/Rx* expression rapidly becomes restricted to the developing eye field. Whether one of these two genes regulates the other or whether they represent parallel developmental pathways with separate functions is not entirely clear. Experimentally it has been found that in *Pax-6* mutants *Rax/Rx* shows normal activation in the anterior neural plate. In *Rax/Rx* mutants, on the other hand, *Pax-6* is not upregulated in the presumptive eye fields (Zhang et al., 2000). This suggests that *Rax/Rx* is an earlier determinant of retina or eye formation.

In recent years there has been a lot of discussion on whether a single gene can trigger complete eye development and thus be thought of as a *master gene*. In a series of elegant experiments, Gehring and his colleagues showed that expression of *Pax-6* in *Drosophila* imaginal discs changed the fate of cells such that ectopic eyes were formed on legs and antennae (Halder et al., 1995). In vertebrates the situation is clearly more complex. First, other cells in the neural plate

express *Pax-6* and do not form eyes. Second, ectopic expression of *Xenopus Pax-6* can induce ectopic eyes but only in certain regions of the head (Chow et al., 1999; Hirsch and Harris, 1997). One convenient synthesis of these findings is that *Pax-6* can specify eye formation in the unique environment of a *Drosophila* imaginal disc but that in the more complex developing neural tissue of the vertebrate, it is one of a series of molecules that are all essential for eye formation.

After expression of *Rax/Rx* and *Pax-6*, three other genes are switched on in the early eye field region. These are *ET*, *Six-3*, and *Optx*, all of which are also transcription factors (Li et al., 1997; Toy et al., 1998). *Pax-6* can induce all three of these genes, suggesting a hierarchical relationship among this set. It is likely that each of these transcription factors regulates the activity of a number of other genes, but these have not been identified.

The next stage in retinal development is the separation of the single eye field into two distinct eye primordia. This is controlled by the underlying prechordal mesoderm. The separation itself is caused by the migration and growth of neuroepithelial cells into the midline region rather than any change of fate in eye field cells. This process is part of the maturation of a dorsoventral axis in the developing brain and is controlled by a number of soluble factors. One of the best characterized of these, sonic hedgehog (Shh), is released from the prechordal mesoderm. Defects in Shh signaling lead to the *cyclops* mutant in zebrafish in which the separation into two eye fields does not occur (MacDonald et al., 1995). Other secreted factors that regulate the dorsoventral patterning, most notably bone morphogenetic proteins 4 and 5, can also disrupt eye field separation and lead to a cyclopean phenotype (Golden et al., 1999).

By this stage of retinal development, cells have undergone substantial molecular changes in response to two sets of external stimuli, but they remain morphologically identical to the surrounding neuroepithelial cells. At the next step, however, a morphologically distinct structure begins to form.

The optic cup and regionalization

The first morphological specialization detectable in the formation of a retina is the outgrowth of a neuroepithelial sheet from the ventrolateral wall of the forebrain vesicle. This occurs before the neural tube has closed at its anterior end and can be detected in rats at E9.5. This outpocketing grows out and up between the forebrain and the surface ectoderm, forming the optic vesicle. Although both layers of the optic vesicle are a single cell thick, the presumptive retina facing the surface ectoderm already looks thicker.

The next major morphological event is the invagination of the optic vesicle to form the optic cup. This is a complex series of events involving both the neuroepithelium and the

surface ectoderm. The surface ectoderm expands and forms a lens vesicle. The neuroepithelial sheet invaginates, and the two layers become even more distinct. The presumptive retina becomes a pseudostratified epithelium with many layers of nuclei, whereas the presumptive retinal pigment epithelium remains as a monolayered epithelium. The optic cup remains connected to the forebrain by the cells of the optic stalk. As indicated in Figure 3.1A, the optic vesicle is all dorsal to the optic stalk. As the optic cup develops, growth and movement of the neuroepithelial sheet extend down below the stalk to form a disc with the stalk approximately in the center. The optic fissure formed when the two edges of the optic cup meet then fuses to form continuous retinal and *retinal pigment epithelium* (RPE) layers.

At the molecular level, the optic vesicle begins to express new transcription factors and to show a patterned expression of others. Among the new gene products expressed in the optic vesicle is that of the homeodomain transcription factor gene *Vax-1*, a close relative of the *emx* and *Not* genes that play important roles in the patterning of many forebrain regions (Hallonet et al., 1999). *Vax-1* is expressed in the basal forebrain and the optic stalk. Other genes that are expressed at this time include *Pax-2*, which is expressed in the ventral optic vesicle and then becomes restricted to the optic stalk, and *MITF*, a basic helix-loop-helix (bHLH) transcription factor gene that regulates many other genes including the enzymes involved in pigment formation in the RPE. *Otx-2*, a transcription factor important in early forebrain vesicle development, becomes restricted to the presumptive RPE region of the optic vesicle at this stage. If we were able to look at the expression of *Vax-1*, *Pax-2*, *MITF*, and *Pax-6* in a single section of the early optic cup we would see some differences, with *Vax-1* and *Pax-2* in the stalk and ventral regions and *Pax-6* in the dorsal surface layer, but there would be extensive overlap. With maturation of the optic cup this changes such that *Pax-6* is restricted to the front (retinal) layer of the optic cup, *MITF* is restricted to the back (RPE) layer, and *Pax-2* and *Vax-1* are found only in the optic stalk (Fig. 3.1B). Such a change from an overlapping distribution to separate domains of expression is a relatively common feature in the developing nervous system. There is increasing evidence that this refinement of territories of transcription factor expression occurs by reciprocal inhibition (Fig. 3.2). For example, *Pax-2* and *Pax-6* show reciprocal transcriptional repression (Schwarz et al., 2000). *Vax-1* also inhibits expression of *Pax-6* (Hallonet et al., 1999). Similarly, *Pax-6* and *MITF* have a positive feedback effect on their own transcription but can inhibit the activity of the other (Planque et al., 2001). The midline secreted factor Shh can increase expression of *Vax-1* and thus might be responsible for a cascade that helps form distinct regions within the optic cup. Of course, a single factor initiating such a cascade

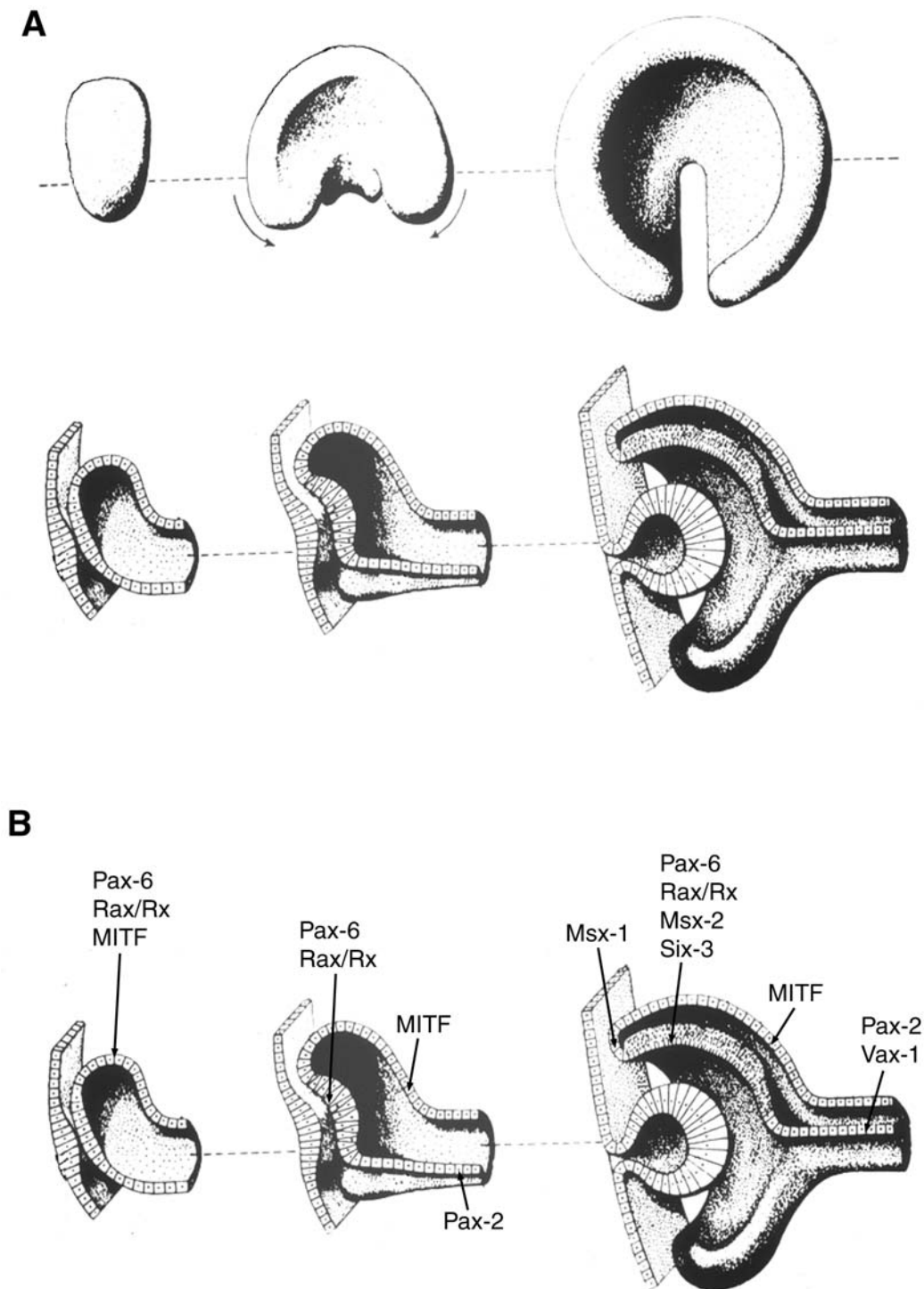


FIGURE 3.1. *A*, Diagrammatic representation of optic cup development showing the outgrowth of the optic vesicle (*left*), the invagination (*middle*), and the downward movement to form the ventral portion of the cup (*right*). This process takes place at the same time that the surface ectoderm is bulging in to form a lens vesicle and mesenchymal cells are beginning to form vascular and other structural components of the eye. *B*, Expression patterns of

transcription factors in the optic vesicle and optic cup. Many of the factors are initially expressed over much of the optic vesicle neuroepithelium but gradually become restricted to specific compartments. In the mature optic cup, the optic stalk, retinal pigment epithelium, ciliary margin, and retina can all be recognized both morphologically and biochemically.

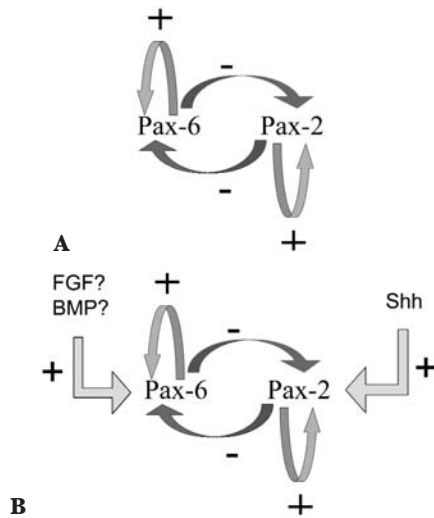


FIGURE 3.2. *A*, Diagrammatic representation of transcription factor interactions in the developing optic cup. *B*, Extrinsic factors can influence transcription factor expression.

might result in the whole optic cup taking on properties of the optic stalk, that is, elevated Pax-2 and Vax-1 expression and suppressed Pax-6 expression. It is likely that a second gradient exists in the opposite direction. One candidate for this is the fibroblast growth factor (FGF) family, possibly FGF8. FGFs can increase expression of retinal transcription factors and thus might work to counterbalance the effect of Shh.

Similar pathways of repressive interactions probably refine the expression patterns of other regulatory molecules. For example, two members of the Msh-like family of transcription factors, *Msx-1* and *Msx-2*, are important markers of optic cup regionalization. *Msx-2* is initially expressed in both layers of the optic vesicle but only in the retinal layer of the optic cup (Monaghan et al., 1991). *Msx-1* is expressed only in the margins of the optic cup that will go on to form the ciliary epithelium. Many of the transcription factors also stimulate expression of other transcription factors. *Pax-6*, for example, regulates expression of other transcription factors including *Six-3* and *optx*, the functions of which are unknown.

The regionalization that began in the optic vesicle is now complete, with gene products including Pax-6, Rax/Rx, Six-3, and *Msx-2* demarcating the retina, Otx-2 and MITF the RPE, *Msx-1* the ciliary margin, and Vax-1 and Pax-2 the optic stalk. The relationships between the multiple markers of each compartment are not entirely clear. While they might be part of a single linear developmental pathway, some evidence favors the idea that they are carrying out separate functions in parallel pathways. In the RPE layer of the optic cup, mutations in MITF lead to lack of further development such that the cells remain as an

immature epithelial monolayer. Loss of Otx-2 in addition to MITF, however, leads to a change in cell phenotype such that the cells turn into retina (Bumsted and Barnstable, 2000).

In all of the dramatic changes of morphology and transcription factor profiles leading up to the optic cup, there is no evidence yet for expression of what can be thought of as retina-specific genes. If no retina-specific genes are expressed, could we define an isolated cell as belonging to retina as opposed to any other part of the nervous system? The answer is a qualified yes. Although each gene we know to be expressed in the retinal epithelium is also expressed at other places and times in development, there are few if any other cells in the embryo that contain the same spectrum of expressed genes. Thus, definition of a cell or tissue type can be achieved through the use of a spectrum of markers rather than a single molecule. Individual markers are more characteristic of the more specialized cells of the terminally differentiated derivatives of the optic cup. The first such signs of terminal differentiation can be detected in the RPE layer with the formation of pigment granules following the expression of tyrosinase and in the retinal layer with the formation of the first postmitotic neurons.

Retinal neurogenesis

The order in which postmitotic cells are formed in the retina, and the relationships between them, have been studied using a variety of tracers. The formation of retinal neurons has been studied using thymidine or BrdU to label cells during their terminal mitosis. All vertebrate retinas studied to date generate retinal cell types in the same order and at approximately the same time when expressed as a proportion of total gestation. All mitoses occur at the ventricular edge of the retinal epithelium, the edge facing the RPE. The space between the two layers is continuous with the forebrain ventricle at the optic vesicle stage, so the retina is like other parts of the CNS in having a proliferative ventricular layer. The other surface of the retina, the vitreal surface, is topologically equivalent to the pial surface of other brain regions.

The major classes of retinal neurons and their laminar arrangement are indicated in Figure 3.3. Ganglion cells become postmitotic in the mouse over the period E12–E15. Beginning just after this, but showing considerable overlap, cone photoreceptors and horizontal cells are generated. In the middle period of development, another major class of retinal interneurons, the amacrine cells, are generated. During the early postnatal period, the last three retinal cell types are formed. These are rod photoreceptors, their post-synaptic targets bipolar cells, and the intrinsic glial cell of the retina, the Müller cell. In addition to the temporal overlap in the generation of retinal cells, there is substantial

spatial overlap such that different cell types are being formed in close proximity to each other. There is a time delay between development of central and peripheral retinas, with central retina several days more advanced in mice and rats. Thus, at any one point on the retina, a spectrum of cell types is being formed, and in adjacent regions a slightly different spectrum is being formed. Such complexity suggests that development is not tightly controlled by an extrinsic factor but rather that much of the timing of cell formation is under intrinsic control.

To determine whether retinal cell types are generated from specific progenitor lines or from common progenitors, lineage tracing has been performed using markers that label dividing cells. Studies using retroviruses in mice or labeled dextrans in *Xenopus* have indicated that multiple cell types can be formed from a single proliferating progenitor cell (Holt et al., 1988; Turner and Cepko, 1987; Turner et al., 1990; Wetts and Fraser, 1988). This means that the fate of cells is not determined in the early epithelium but at a later stage, probably as cells enter their final mitosis. Most current evidence supports the idea that the pool of proliferating progenitor cells is not the same throughout retinal develop-

ment. This means that the vast majority of mouse retinal progenitors at E13 cannot make rod photoreceptors and the progenitors at postnatal day 1 (PN1) cannot make ganglion cells.

Thus, the model we have of early retina is a sheet of neuroepithelium that is distinct from neighboring areas in which each cell initially has the ability to form any retinal cell type but, with time, its potential for development becomes more restricted. Much of the ongoing control of retinal neurogenesis must be intrinsic to the tissue because isolated embryonic retinas can continue to generate all the cell types on an almost normal schedule (Sparrow et al., 1990).

Differentiation of inner retinal cells

In *Drosophila*, neurogenesis in the eye imaginal disc occurs as a wave across the tissue. At the active site of this wave, the morphogenetic furrow, precursor cells differentiate into a regular mosaic of photoreceptors in ommatidia. The secreted protein hedgehog regulates this morphogenetic furrow. There is no morphogenetic furrow in vertebrate retinas, but some studies suggest that the process of retinal

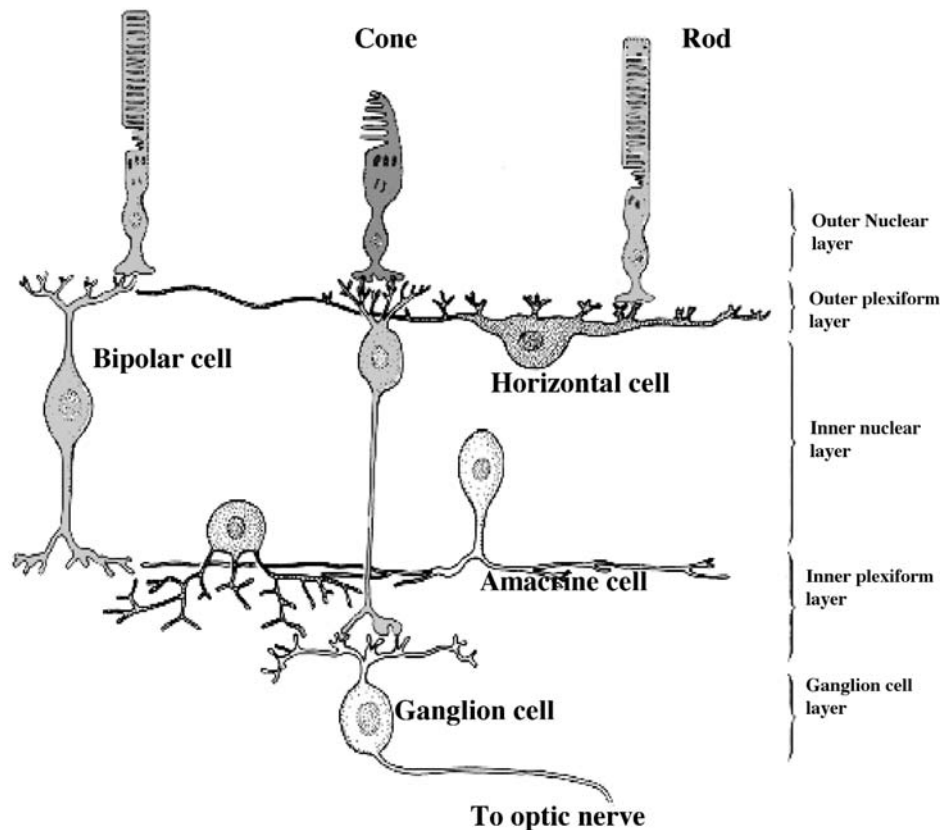


FIGURE 3.3. The five major classes of neurons in the retina form a laminated structure that contains the radial pathway from rod or cone photoreceptor, through bipolar cell, to output ganglion cell and the lateral modulatory pathway consisting of horizontal cells in the outer retina and amacrine cells in the inner retina.

neurogenesis may have some similarities. It appears that one or more of the vertebrate hedgehog isoforms is produced by the RPE and influences the spread of neurogenesis from a small central area outward to the periphery (Neumann and Nusslein-Volhard, 2000; Stenkamp et al., 2000).

We do not yet know how hedgehog proteins influence retinal neurogenesis. There are, however, clues to two important parts of the process. Both of these were first characterized in the development of the *Drosophila* nervous system. The membrane receptor protein Notch and its ligand Delta play an important role at the time a dividing precursor chooses to divide again or to spin off a differentiated daughter cell. Activation of Notch by Delta decreases the production of retinal ganglion cells, and decreasing Notch activity increases the production of ganglion cells (Austin et al., 1995). The Notch system is active throughout retinal development, and changing the activation of Notch can affect production of late-generated cells such as rod photoreceptors and Müller glial cells. Most of the available evidence suggests that the Notch system dictates a differentiation/no differentiation switch, with Notch activation maintaining a cell in an undifferentiated state, but does not control what cell types are formed. At present, we also do not know what controls the selective activation of Notch. One way in which Notch can act is by altering expression of a set of transcription factors essential for triggering the movement of a progenitor into a differentiation pathway. In *Drosophila*, a set of proneural genes of the *aschaete-scute* complex and *atonal* are essential for the development of neural competence by proneural cells. These genes encode proteins of the bHLH class, named for the structural characteristics of their DNA-binding domains, and a number of vertebrate orthologs are known to be important in retinal development. The mouse ortholog of *atonal*, *Math5*, is transiently expressed in developing mouse retinas beginning at E11, a time coincident with the onset of ganglion cell differentiation. Mice in which *Math5* had been deleted showed >80% loss of ganglion cells and an increase in amacrine cells (Wang et al., 2001). In *Drosophila*, *Notch* acts as a negative regulator of *atonal* and it is tempting to speculate that a similar relationship holds for *Notch* and *Math5* in the mouse. Other genes may cooperate with *Math5* in triggering ganglion cell differentiation. For example, *Otx-2* also shows transient expression in ganglion cells just after they become postmitotic (Baas et al., 2000). Whether *Math5* and *Otx-2* are acting in concert or in independent pathways is not known.

Among the earliest markers of ganglion cell differentiation are the POU-domain transcription factors of the *Brn-3* family. These can be detected soon after the ganglion cells have become postmitotic and before they have migrated to

the ganglion cell layer. *Math5* can transactivate a gene coupled to a *Brn-3* promoter (Liu et al., 2001).

Taking all the above results together, we can suggest a pathway in which the process of differentiation from competent precursors is initiated by the action of Shh. This factor influences the pattern of Notch activation, and in cells in which Notch is not activated *Math5* is expressed. This, perhaps in conjunction with other factors like *Otx-2*, irreversibly triggers cells into a ganglion cell fate and promotes expression of characteristic genes such as *Brn-3*. This is clearly an oversimplification and ignores interactions with other cells undergoing other fate choices. A related bHLH protein, NeuroD, is vital for amacrine cell formation. *Math5* can inhibit expression of NeuroD. Thus, in addition to promoting ganglion cell formation, *Math5* is inhibiting amacrine cell formation. By analogy with the mechanisms of optic cup regionalization discussed earlier, we should perhaps be looking for more examples of reciprocal inhibition of bHLH genes involved in specifying retinal cell types and for other extrinsic factors that can initiate a cascade of these reciprocal interactions.

Just as important as the mechanisms initiating cell differentiation in retina are those that regulate the number of each cell type produced. There is abundant evidence for a negative feedback in the production of ganglion and amacrine cells. In many species of fish and amphibians, the retina continues to grow throughout life by adding new cells at the tissue margin. Thus, the radial dimension from center to periphery recapitulates the developmental history of the retina. Dopaminergic amacrine cells are normally formed at the retinal margin at a constant density. Destruction of these cells with 6-OH-dopamine, followed by a sufficient recovery period, led to production of a higher than normal density of new dopaminergic cells (Negishi et al., 1982). Similar experiments in larval frogs gave essentially identical results (Reh and Tully, 1986). In an extension of these experiments, other retinal cell types were destroyed by treatment with kainic acid, and the number of new cells formed was increased in proportion to the damage to the differentiated neurons (Reh, 1987). The conclusion from these studies was that an inhibitory feedback signal was produced by differentiated cells that limited the number of that cell type produced. This possibility has been explored in more detail using retinal cultures. In reaggregate cultures using retinal cells of different ages, differentiated amacrine cells were found to inhibit the production of amacrine cells by embryonic cells (Belliveau and Cepko, 1999). Similarly, ganglion cell production was reduced in cultures of chick embryonic retinal cells when cultured adjacent to older retinal cells (Waid and McLoon, 1998). This type of experiment suggests that the inhibitory signal is diffusible, although its identity has yet to be established.

Differentiation of outer retinal cells

We know more about the differentiation of rod photoreceptors than about any other CNS neuron. The extensive background of molecular information derived from numerous studies of phototransduction has provided an excellent set of markers, and the medical importance of photoreceptor degenerative diseases has spurred extensive studies of this cell type. As indicated earlier, most rods become postmitotic near the end of retinal development, in the first few postnatal days in mice and rats. A few rods can be labeled by thymidine injection as early as E14, although they show further signs of differentiation at the same time as the vast majority of rods born later (Morrow et al., 1998). This suggests that the events occurring during the final mitosis can be separated from those of overt differentiation. Rods are formed from late progenitors, some of which can also form bipolar cells and Müller glial cells.

The visual pigment protein opsin is one of the earliest markers of rod differentiation and, because its early appearance is under transcriptional regulation, it has frequently been used to designate rod formation (Treisman et al., 1988). If retinal cells from postnatal rats or mice are plated in dilute monolayer culture, they form many opsin-expressing rods. If cells from early or midembryonic stages are plated, no opsin-positive rods are detected. On the other hand, if the embryonic tissue is maintained as an explant culture or dissociated and allowed to reaggregate, opsin-positive rods are detected at a time equivalent to the normal time of expression. This suggests that the information required to generate rods is intrinsic to the retina but that it needs cell-cell interactions for expression. Embryonic cells mixed with neonatal retinal cells (that are at their peak of rod differentiation) form more rods but only after the appropriate number of days in culture (Watanabe and Raff, 1992). These and related experiments suggest that there are factors present within retina that can promote formation of rod photoreceptors, but only when the progenitor cells are competent to respond to them. At present, the relative roles of factors located on the cell surface and secreted factors are unknown. Numerous factors including FGFs, retinoids, and even compounds like taurine can increase opsin expression in culture. There is, however, little direct evidence that any of them act directly on cell determination or opsin transcription pathways. It is more likely that they have relatively nonspecific effects that make the cells more healthy and better able to express differentiated functions.

In contrast to the positive effects of the growth factors mentioned above, treatment of retinal explants with cytokines of the interleukin-6 (IL-6) family, such as ciliary neurotrophic factor (CNTF) or leukemia inhibitory factor (LIF), completely inhibits the production of rod photore-

ceptors, as judged by opsin expression (Ezzeddine et al., 1997; Neophytou et al., 1997). These cytokines are known to bind to multisubunit membrane receptors and activate a tyrosine kinase. The intracellular transduction pathways activated by cytokine binding include those characterized by MAPK and STAT proteins. Activation of either of these can lead to changes in transcription. By using pharmacological blockers of MAPK and viruses expressing either constitutively active or dominant negative STAT proteins, we have shown that the MAPK pathway is likely to be involved in Müller glial cell formation and the STAT pathway (specifically STAT3) in rod formation. Activation of STAT3 leads to a change in expression of several key transcription factors. Most relevant are increases in the levels of Otx-2 and HES-1. Otx-2 is thought to play a role in the decision of progenitors to become either bipolar cells or rods. Since reduced levels of Otx-2 lead to production of more rods, it is reasonable to assume that elevated levels will help prevent rod formation. *Hes-1* is an important regulator of development in a number of tissues, is a bHLH protein homologous to the *hairy* and *enhancer of split* genes of *Drosophila*, and generally acts as a repressor of transcription. Its expression can be increased by activation of the Notch pathway. We do not yet know whether the cytokine-induced increase in Hes-1 expression is mediated through a Notch signaling pathway or whether this is another example of regulation through two independent pathways.

Positive regulators of rod formation include a number of bHLH transcription factors. The best studied of these is *Neuro D*, the same gene that influences amacrine cell production. Transfection of *Neuro D* into retinal cultures can increase the number of rods formed, and blocking of *Neuro D* can diminish rod production. *Hes-1* inhibits *Neuro D* expression; thus, this pathway may be responsible for the cytokine-induced inhibition of rod formation.

At present, we do not know how *Neuro D* facilitates rod formation. It does not appear to have a direct effect on the *opsin* gene, suggesting that there must be several steps between *Neuro D* expression and *opsin* expression. It has also been found that inhibition of *Neuro D* function increases the production of Müller glial cells. This suggests that *Neuro D* functions at the time a retinal progenitor is making a choice of cell differentiation pathway.

Molecular regulation of opsin expression

Promoter mapping studies using transgenic mice have suggested that all the information for correct temporal and spatial regulation of *opsin* expression is contained in about 1.5 kb of DNA 5' to the *opsin* gene. Most of the information is in the first few hundred bases 5' to the transcription start site. *Opsin* is a classical gene with a full TATA box for

assembly of the transcription complex. In a region just upstream of this is a region of DNA that appears to become completely covered with transcription factors, several of which have now been identified (Fig. 3.4). RET-4 has been defined as a nuclear protein binding site at -39 to -52, although the identity of the binding protein is unknown. Nrl is a zinc-finger protein that binds at -55 to -70 in the rat rod opsin promoter. Crx is a homeodomain protein that probably binds to the BAT-1 site at -82 to -98 on the opsin promoter. A key promoter site for regulation of opsin expression lies at -110 to -37. This site, labeled RET-1 or PCE, is found in a number of other rod photoreceptor genes, suggesting that a common transcriptional regulatory pathway may exist (Morabito et al., 1991). Its importance is also suggested by the finding that *opsin* genes from species as diverse as humans and *Drosophila* have RET-1/PCE sites in their promoters. Although high levels of Crx can activate transcription from this site, other transcription factors act with higher efficiency. Among these are other homeodomain proteins including *Rax* and another member of the *emx* family *Vax-2* (Kimura et al., 2000; Martinez and Barnstable,

1998). Since neither of these show peak expression in the mature photoreceptor layer, it is likely that either a still undescribed protein is important in *opsin* gene transcription or the affinity of another protein such as Crx can be altered by complex formation with another protein. The transcription factors necessary for *opsin* expression all seem to have different developmental profiles, suggesting that different pathways regulate their expression. What we do not have at present is evidence for a single trigger for rod photoreceptor differentiation, though *Neuro D* may serve this function in some way.

Maturation of retinal cells

The complex set of interactions that trigger the appearance of characteristic molecules is only the first step in the formation of a fully differentiated retinal cell type. Rod photoreceptors undergo a major developmental step of outer segment formation about a week after opsin expression can first be detected. Rod outer segments represent a complex morphological specialization and contain the light-sensing

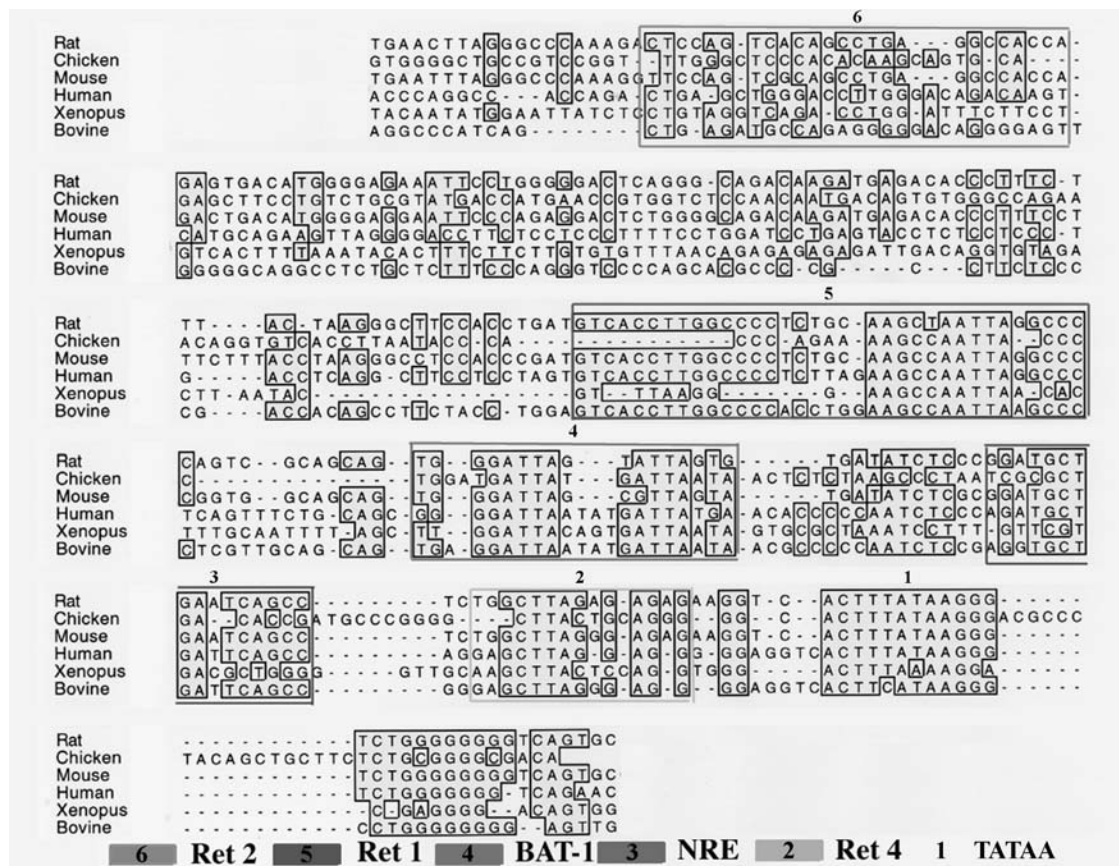


FIGURE 3.4. Comparison of the sequences upstream of the *opsin* gene of various vertebrates. Homologous regions are boxed, and known transcription factor or nuclear protein binding sites are labeled in order from the transcription start site. 1, TATAA box; 2, Ret-4; 3, NRE; 4, BAT-1; 5, Ret-1; 6, Ret-2.

and transduction machinery. It is not surprising, therefore, that outer segment formation is accompanied by the de novo expression of a large number of rod-specific genes. Among these are the structural proteins involved in maintaining rod disc shape, such as peripherin and Rom-1, and components of the transduction cascade, such as transducin, phosphodiesterase (PDE), and the cGMP-gated cation channel. Although most of these appear to be regulated at the transcriptional level, we have little idea of the transcription factors regulating their expression. Both in vitro and in vivo studies have shown that the presence of an RPE cell layer is vital for the full development of outer segments but not for their initiation. Explants of retinas from many species will develop normally up to the stage of forming outer segments but then stop. In the *mi/mi* mutant mouse, an RPE layer is present but the cells remain in an immature state. The retina adjacent to this does not develop normally. Electron microscopy has shown that the rod photoreceptors begin to make membrane expansions that are the beginning of outer segments, and molecular studies have shown that several transduction genes are turned on. Thus, it appears that the RPE does not provide a triggering signal for outer segment formation but is vital for continued growth. Whether it provides important nutritional factors or mechanical support is not yet known.

The role of glia in retinal development and function

Most vertebrate retinas contain three types of glial cells. Müller glia are intrinsic glia that span the whole width of the tissue and are derived from the same set of progenitors as the retinal neurons. Astrocytes that reside in the optic nerve fiber layer migrate in through the optic stalk. Microglia also migrate into the retina, and many move from the ganglion cell layer to a position just below the outer plexiform layer. The timing of this migration coincides with the wave of developmental cell death that occurs during postnatal maturation, and these cells are thought to be intimately involved in removing dead cells from the tissue.

Müller glia serve a variety of roles. They form the inner and outer limiting membranes at either side of the retina and thus serve an important barrier function for substances moving into and out of the retina. Through their glycogen stores and their ability to process transmitters such as glutamate and GABA, they play a vital role in retinal metabolism. They also clearly serve a structural role, and defects in Müller cells can lead to severe disruptions and rosette formation in the photoreceptor layer. Müller cells are also capable of producing a variety of important peptide mediators. In response to lack of oxygen, Müller cells can produce vascular endothelial growth factor (VEGF) that can act on adjacent blood vessels and stimulate their growth. Müller cells can also produce trophic factors such as CNTF

and FGF. Experimentally, this production is usually seen after an insult such as bright light exposure or excitotoxin treatment. It is thought that the Müller cell response may be part of a homeostatic mechanism to lessen the deleterious effects of these insults. Since a number of aspects of retinal development involve similar trophic factors, it is tempting to think that Müller cells, or their precursors, also release these factors as key developmental regulators.

Positional information across the retina

The developmental mechanisms discussed so far in this chapter can begin to explain how distinct cell types arise from an initially uniform epithelium. They cannot, however, account for differences within the same cell class seen in central versus peripheral retina. Some differences, such as the size of the dendritic field or changes in the spacing of an orderly mosaic of cone photoreceptors, are intraretinal, but others, such as the position of synaptic targets in other visual areas, require translation of retinal position into complex patterns of growth and connectivity. It is important to try to distinguish those events in which position is reflected in expression of unique or unique amounts of particular molecules from those that arise as epiphenomena of other processes. One of the most dramatic differences seen in dendritic field morphology is in bipolar cells and retinal ganglion cells where in the human fovea a cone photoreceptor interacts with one or two bipolar cells but in the periphery hundreds of photoreceptors converge onto a single bipolar cell. We do not know whether this difference is inherent in molecular differences between the cells, a consequence of developmental processes that affect relative cell numbers, or a late event that changes from an initially more uniform pattern. Although these intrinsic retinal properties reflect positional information, the axes are more commonly defined by readout, as defined by the retinotopic mapping of ganglion cell axon terminals in target areas such as the superior colliculus.

Many studies have attempted to define the molecular correlates of retinal position. A number of molecules can be found in gradients. Some surface proteins and carbohydrate groups can be found in a dorsoventral gradient (Constantine-Paton et al., 1986; Trisler et al., 1981). Some transcription factors seem to divide the retina into nasal and temporal halves (Hatini et al., 1994). To date, however, only two classes of retinal gradient are known to convey positional information. The first is retinoic acid, which is present in a gradient along the dorsoventral axis created by corresponding gradients in synthetic enzymes with different substrate affinities (Drager et al., 1998). Retinoic acid is critical for the formation of ventral retina in zebrafish (Hyatt et al., 1996). In addition, the gradient of retinoic acid may be used in mouse retina for patterning different cone types.

The other classes of molecules found in a graded distribution are the Eph receptor tyrosine kinases and their ephrin ligands (Flanagan and Vanderhaeghen, 1998). This ligand receptor family was originally identified using a culture assay to measure topographic modulation of the growth of retinal ganglion cell axons (e.g., see Ciossek et al., 1998). Ephrins were isolated as molecules that could inhibit growth by inducing growth cone collapse. The receptor EphA3 is expressed in retinal ganglion cells as a temporal-nasal gradient, and its ligand ephrin A2 is expressed in a posterior-anterior gradient in the tectum. A second tectal ligand for EphA3, ephrin A5, is also expressed in a graded fashion in the tectum. A variety of *in vitro* assays, knockouts, and ectopic expression studies have provided strong evidence for the role of this receptor-ligand system in retino-tectal connectivity. For example, in ephrin A5 and ephrin A2 knockouts, retinal ganglion cell axons terminate in more posterior locations exactly as predicted if a repulsive influence was removed (Feldheim et al., 2000).

There is still debate whether ephrins and Eph receptors are important in both retinal axes. EphB2 and EphB3 receptors show a dorsoventral gradient of expression in the retina, and ephrin B ligands show a medial-lateral gradient in the superior colliculus. The importance of this group of ephrins and their receptors in retinotopic mapping is currently unknown.

As well as interpreting molecular gradients, tissues such as the retina need a molecular mechanism for their establishment. As discussed earlier, the transcription factor Vax-2 is preferentially expressed in ventral retina. In Vax-2 mutant animals, ephrins and their receptors show altered gradients in both nasal-temporal and dorsoventral axes, suggesting that this transcription factor is one specifier of axial polarity in the retina (Mui et al., 2002). Exactly how Vax-2 can produce different levels of expression in different cells is not known.

The gradients described to date cannot fully explain the formation of topographic maps. Unless there is some mechanism for producing and sensing absolute levels of a receptor or ligand, a single gradient is unlikely to be able to give a clear topographic organization. It has often been suggested that a pair of gradients in opposite directions is a more efficient mechanism because it allows the sensing of relative levels to determine position. It seems likely that this other gradient is attractive rather than repulsive, although its nature has yet to be characterized.

Retinal cell survival and cell death

Understanding the ways in which retinal cells develop is very important for providing therapies for diseases that lead to retinal cell death. Use of growth factors to promote cell survival, use of transplanted retinal cells as replacement

therapy, and even use of retinal stem cells all require a knowledge of pathways that regulate retinal cell phenotypes.

The most common forms of blindness occur through the death of retinal ganglion cells or photoreceptors. Loss of ganglion cells is the defining characteristic of glaucoma, which remains one of the leading causes of blindness in adults (Quigley et al., 1995). Loss of photoreceptors can involve rods, as in retinitis pigmentosa; or cones, as in macular degeneration; or both, as in rod-cone dystrophies and various syndromes.

A major risk factor for glaucoma is elevated intraocular pressure, which is thought to cause mechanical deformation as the ganglion cells axons leave the eye. This deformation may prevent the retrograde transport of neurotrophic factors. Based on developmental studies showing that brain derived neurotrophic factor (BDNF) is a vital neurotrophic factor for ganglion cells, it has been suggested that BDNF, or agents that mimic BDNF at later points in its pathway of action, might have therapeutic benefit. A second major cause of ganglion cell death in glaucoma is thought to be excitotoxic injury caused by excess glutamate. This might occur as a result of ischemic damage from elevated intraocular pressure or from other retinal defects in cases where pressure seems normal. Excess glutamate has been measured in glaucomatous eyes, and experimental application of glutamate can certainly induce ganglion cell death (Dreyer et al., 1996; Otori et al., 1998). One mechanism that might account for abnormal glutamate metabolism is abnormal uptake or handling by Müller glial cells (Kawasaki et al., 2000). Although glaucomatous eyes do appear to have lower levels of the Müller cell glutamate transporter, it has yet to be shown that this is a primary cause of the disease. Defects at other steps in the glutamate pathway, including glutamine synthetase and glutamine transporters, are also candidates for causing glaucoma. Since several of these molecules show regulation by extrinsic molecules such as corticosteroids, changes in their function could arise from a number of causes. The differences between normal and diseased retinas may initially be very slight. In addition to defects in specific molecules, overall developmental differences that, for example, alter the relative numbers or spacing of ganglion cells and Müller glial cells could influence the tissue's ability to metabolize glutamate.

Retinitis pigmentosa (RP) is an inherited condition in which loss of rod photoreceptors leads to loss of night vision and, later, deleterious secondary changes in cone photoreceptors (Berson, 1993). A wide array of genes have been identified as causing RP including most of those specific to the phototransduction cascade. Some are loss of function, such as mutations in the cGMP phosphodiesterase; some are structural, such as mutations in the rod outer segment protein peripherin; and still others are "metabolic," such as mutations in the visual pigment protein *opsin* that seem to

clog up the Golgi apparatus of the cell. Mutations in the *CRX* transcription factor gene can cause loss of rods, and later of cones as well (Freund et al., 1997). Thus, many of the molecules that are thought of as developmental regulators may also play a role in later disease. Trophic factors are thought to play an ongoing role in rod photoreceptor survival. In mouse and rat models of RP, it has been shown that some of the same trophic factors important in rod development and survival can prevent cell death for extended periods (LaVail et al., 1998). Interestingly, one of the factors that helps is CNTF, a factor that can completely block rod formation during development. Such a difference emphasizes that the same molecule can have very different functions at different stages of development.

Only a few clearly inherited forms of macular degeneration (MD) have been described. MD is generally much later in onset and can probably result from many different initial causes (Stone et al., 2001). Most vision loss in MD is caused by rapid proliferation of blood vessels between the RPE and the photoreceptor layer of the retina. This is thought to occur as a secondary consequence of changes in the RPE layer, the photoreceptor layer, or both. It may turn out that the majority of cases of MD are due to defects in the RPE layer. As expected for such a late-onset disease, most forms of MD do not show clear patterns of inheritance. This is probably due to the influence of multiple genes. The best-studied examples of gene mutations that cause MD suggest that abnormal handling of retinoid metabolism in the visual cycle can lead to deposits that cause cone photoreceptor death. It remains to be seen whether mutations in transcription factor genes, such as the homologs of *CRX*, can also cause specific cone diseases.

One of the therapies under investigation for photoreceptor degenerative disease is transplantation or cell replacement. For this to be effective, it is essential to know how to treat tissue so that photoreceptors survive and remain functional. We still need to know much more about the factors regulating formation of photoreceptors, particularly those regulating outer segment development. With the increased interest in and potential of stem cell therapies, it is essential that we understand the nature and sequence of factors necessary to turn a cell from a multipotential stem cell or progenitor into the desired phenotype of photoreceptor.

Conclusions

This chapter has presented a very narrow view of retinal development in terms of a series of biochemical pathways. Prior to the completion of the sequencing of the human genome, it was often argued that the complexity of the nervous system arose because of the existence of a vast number of "brain-specific" genes. This does not appear to be the case. Many of the genes used in neural development

are also used in other organs. Many of the genes are also used in multiple regions and at multiple times. Thus, using different combinations of molecules, or the same combinations in temporally and spatially distinct compartments, can generate complexity in the organization of regions of the nervous system. A number of examples of this in retinal development have been discussed. Gene products such as Pax-6 are important in the development of multiple brain regions. Nevertheless, this molecule is critical for eye formation and, in the correct environment, can initiate the whole process of optic vesicle formation. The protein Otx-2 is used in both RPE and retinal compartments, but these are made distinct by expression of other molecules. Otx-2 is also expressed during the development of several retinal cell types but, since these develop at different times from different sets of progenitors, its functions at each stage are unique.

Retinal development does not stop with the events of neurogenesis and maturation described in this chapter. There is obviously much more that could be written about the mechanisms of process growth within, and outside of, the retina and the molecular mechanisms governing synaptogenesis. These phenomena can be studied at the same level of molecular detail as earlier developmental stages. In the foreseeable future, we should have a reasonably complete description of retinal development. If the past is any guide, insights that arise from these studies will be of great value in understanding not only other parts of the visual system, but also other parts of the brain.

Acknowledgments

Work from my own laboratory has been supported by NIH Grants EY 11356 and EY 13 865, as well as by the Allene Reuss Memorial Trust, the Kemper Foundation, and Research to Prevent Blindness, Inc.

REFERENCES

- Austin, C. P., D. E. Feldman, J. A. Ida, and C. L. Cepko, 1995. Vertebrate retinal ganglion cells are selected from competent progenitors by the action of Notch, *Development*, 121:3637–3650.
- Baas, D., K. M. Bumsted, J. A. Martinez, F. M. Vaccarino, K. C. Wikler, and C. J. Barnstable, 2000. The subcellular localization of *Otx2* is cell-type specific and developmentally regulated in the mouse retina, *Mol. Brain Res.*, 78:26–37.
- Belliveau, M. J., and C. L. Cepko, 1999. Extrinsic and intrinsic factors control the genesis of amacrine and cone cells in the rat retina. *Development—Suppl.*, 126:555–566.
- Berson, E. L., 1993. Retinitis pigmentosa. The Friedenwald Lecture, *Invest. Ophthalmol. Vis. Sci.*, 34:1659–1676.
- Bumsted, K. M., and C. J. Barnstable, 2000. Dorsal retinal pigment epithelium differentiates as neural retina in the microphthalmia (mi/mi) mouse, *Invest. Ophthalmol. Vis. Sci.*, 41:903–908.
- Chow, R. L., C. R. Altmann, R. A. Lang, and A. Hemmati-Brivanlou, 1999. Pax6 induces ectopic eyes in a vertebrate, *Development—Suppl.*, 126:4213–4222.

- Ciossek, T., B. Monschau, C. Kremoser, J. Loschinger, S. Lang, B. K. Müller, F. Bonhoeffer, and U. Drescher, 1998. *Eph* receptor-ligand interactions are necessary for guidance of retinal ganglion cell axons in vitro, *Eur. J. Neurosci.*, 10:1574–1580.
- Constantine-Paton, M., A. S. Blum, R. Mendez-Otero, and C. J. Barnstable, 1986. A cell surface molecule distributed in a dorsoventral gradient in the perinatal rat retina, *Nature*, 324:459–462.
- Drager, U. C., E. Wagner, and P. McCaffery, 1998. Aldehyde dehydrogenases in the generation of retinoic acid in the developing vertebrate: a central role of the eye, *J. Nutr.*, 128:463S–466S.
- Dreyer, E. B., D. Zurakowski, R. A. Schumer, S. M. Podos, and S. A. Lipton, 1996. Elevated glutamate levels in the vitreous body of humans and monkeys with glaucoma, *Arch. Ophthalmol.*, 114:299–305.
- Ezzeddine, Z. D., X. Yang, T. DeChiara, G. Yancopoulos, and C. L. Cepko, 1997. Postmitotic cells fated to become rod photoreceptors can be respecified by CNTF treatment of the retina, *Development*, 124:1055–1067.
- Feldheim, D., Y. Kim, A. Bergemann, J. Frisen, M. Barbacid, and J. Flanagan, 2000. Genetic analysis of ephrin-A2 and ephrin-A5 shows their requirement in multiple aspects of retinocollicular mapping, *Neuron*, 25:563–574.
- Flanagan, J. G., and P. Vanderhaeghen, 1998. The ephrins and Eph receptors in neural development, *Annu. Rev. Neurosci.*, 21:309–345.
- Freund, C. L., C. Y. Gregory-Evans, T. Furukawa, M. Papaioannou, J. Looser, L. Ploder, J. Bellingham, D. Ng, J. A. Herbrick, A. Duncan, S. W. Scherer, L. C. Tsui, A. Loutradis-Anagnostou, S. G. Jacobson, C. L. Cepko, S. S. Bhattacharya, and R. R. McInnes, 1997. Cone-rod dystrophy due to mutations in a novel photoreceptor-specific homeobox gene (*CRX*) essential for maintenance of the photoreceptor, *Cell*, 91:543–553.
- Furukawa, T., C. A. Kozak, and C. L. Cepko, 1997. *Rax*, a novel paired-type homeobox gene, shows expression in the anterior neural fold and developing retina, *Proc. Natl. Acad. Sci. USA*, 94:3088–3093.
- Golden, J. A., A. Bracilovic, K. A. McFadden, J. S. Beesley, J. L. RR, and J. B. Grinspan, 1999. Ectopic bone morphogenetic proteins 5 and 4 in the chicken forebrain lead to cyclopia and holoprosencephaly, *Proc. Natl. Acad. Sci. USA*, 96:2439–2444.
- Halder, G., P. Callaerts, and W. J. Gehring, 1995. Induction of ectopic eyes by targeted expression of the *eyeless* gene in *Drosophila*, *Science*, 267:1788–1792.
- Hallonet, M., T. Hollemann, T. Pieler, and P. Gruss, 1999. *Vax1*, a novel homeobox-containing gene, directs development of the basal forebrain and visual system, *Genes Dev.*, 13:3106–3114.
- Hatini, V., W. Tao, and E. Lai, 1994. Expression of winged helix genes, *BF-1* and *BF-2*, define adjacent domains within the developing forebrain and retina, *J. Neurobiol.*, 25:1293–1309.
- Hill, R. E., and I. M. Hanson, 1992. Molecular genetics of the *Pax* gene family, *Curr. Opin. Cell Biol.*, 4:967–972.
- Hirsch, N., and W. A. Harris, 1997. *Xenopus Pax-6* and retinal development, *J. Neurobiol.*, 32:45–61.
- Holt, C. E., T. W. Bertsch, H. M. Ellis, and W. A. Harris, 1988. Cellular determination in the *Xenopus* retina is independent of lineage and birth date, *Neuron*, 1:15–26.
- Hyatt, G. A., E. A. Schmitt, N. Marsh-Armstrong, P. McCaffery, U. C. Drager, and J. E. Dowling, 1996. Retinoic acid establishes ventral retinal characteristics, *Development*, 122:195–204.
- Kawasaki, A., Y. Otori, and C. J. Barnstable, 2000. Müller cell protection of rat retinal ganglion cells from glutamate and nitric oxide neurotoxicity, *Invest. Ophthalmol. Vis. Sci.*, 41:3444–3450.
- Kimura, A., D. Singh, E. F. Wawrousek, M. Kikuchi, M. Nakamura, and T. Shinohara, 2000. Both *PCE-1/RX* and *OTX/CRX* interactions are necessary for photoreceptor-specific gene expression, *J. Biol. Chem.*, 275:1152–1160.
- LaVail, M. M., D. Yasumura, M. T. Matthes, C. Lau-Villacorta, K. Unoki, C. H. Sung, and R. H. Steinberg, 1998. Protection of mouse photoreceptors by survival factors in retinal degenerations, *Invest. Ophthalmol. Vis. Sci.*, 39:592–602.
- Li, H., C. Tierney, L. Wen, J. Y. Wu, and Y. Rao, 1997. A single morphogenetic field gives rise to two retina primordia under the influence of the prechordal plate, *Development*, 124:603–615.
- Liu, W., Z. Mo, and M. Xiang, 2001. The *Ath5* proneural genes function upstream of *Brn3* POU domain transcription factor genes to promote retinal ganglion cell development, *Proc. Natl. Acad. Sci. USA*, 98:1649–1654.
- MacDonald, R., K. A. Barth, Q. Xu, N. Holder, I. Mikkola, and S. W. Wilson, 1995. Midline signalling is required for *Pax* gene regulation and patterning of the eyes, *Development*, 121:3267–3278.
- Martinez, J. A., and C. J. Barnstable, 1998. *Erx*, a novel retina-specific homeodomain transcription factor, can interact with Ret 1/PCEI sites, *Biochem. Biophys. Res. Commun.*, 250:175–180.
- Mathers, P. H., A. Grinberg, K. A. Mahon, and M. Jamrich, 1997. The *Rx* homeobox gene is essential for vertebrate eye development, *Nature*, 387:603–607.
- Monaghan, A. P., D. R. Davidson, C. Sime, E. Graham, R. Baldock, S. S. Bhattacharya, and R. E. Hill, 1991. The *Msh*-like homeobox genes define domains in the developing vertebrate eye, *Development*, 112:1053–1061.
- Morabito, M. A., X. Yu, and C. J. Barnstable, 1991. Characterization of developmentally regulated and retina-specific nuclear protein binding to a site in the upstream region of the rat *opsin* gene, *J. Biol. Chem.*, 266:9667–9672.
- Morrow, E. M., M. J. Belliveau, and C. L. Cepko, 1998. Two phases of rod photoreceptor differentiation during rat retinal development, *J. Neurosci.*, 18:3738–3748.
- Mui, S. H., R. Hindges, D. M. D. O'Leary, G. Lemkel, and S. Bertuzzi, 2002. The homeodomain protein *Vax2* patterns the dorsoventral and nasotemporal axes of the eye, *Development*, 129:797–804.
- Negishi, K., T. Teranishi, and S. Kato, 1982. New dopaminergic and indoleamine-accumulating cells in the growth zone of goldfish retinas after neurotoxic destruction, *Science*, 216:747–749.
- Neophytou, C., A. B. Vernallis, A. Smith, and M. C. Raff, 1997. Müller-cell-derived leukaemia inhibitory factor arrests rod photoreceptor differentiation at a postmitotic pre-rod stage of development, *Development*, 124:2345–2354.
- Neumann, C. J., and C. Nüsslein-Volhard, 2000. Patterning of the zebrafish retina by a wave of *sonic hedgehog* activity, *Science*, 289:2137–2139.
- Otori, Y., J. Y. Wei, and C. J. Barnstable, 1998. Neurotoxic effects of low doses of glutamate on purified rat retinal ganglion cells, *Invest. Ophthalmol. Vis. Sci.*, 39:972–981.
- Planque, N., C. Leconte, F. M. Coquelle, P. Martin, and S. Saule, 2001. Specific *Pax-6*/microphthalmia transcription factor interactions involve their DNA-binding domains and inhibit transcriptional properties of both proteins, *J. Biol. Chem.*, 276:29330–29337.
- Quigley, H. A., R. W. Nickells, L. A. Kerrigan, M. E. Pease, D. J. Thibault, and D. J. Zack, 1995. Retinal ganglion cell death in experimental glaucoma and after axotomy occurs by apoptosis, *Invest. Ophthalmol. Vis. Sci.*, 36:774–786.

- Reh, T. A., 1987. Cell-specific regulation of neuronal production in the larval frog retina, *J. Neurosci.*, 7:3317–3324.
- Reh, T. A., and T. Tully, 1986. Regulation of tyrosine hydroxylase-containing amacrine cell number in larval frog retina, *Dev. Biol.*, 114:463–469.
- Schwarz, M., F. Cecconi, G. Bernier, N. Andrejewski, B. Kammandel, M. Wagner, and P. Gruss, 2000. Spatial specification of mammalian eye territories by reciprocal transcriptional repression of *Pax2* and *Pax6*, *Development—Suppl.*, 127:4325–4334.
- Sparrow, J. R., D. Hicks, and C. J. Barnstable, 1990. Cell commitment and differentiation in explants of embryonic rat neural retina. Comparison with the developmental potential of dissociated retina, *Dev. Brain Res.*, 51:69–84.
- Stenkamp, D. L., R. A. Frey, S. N. Prabhudesai, and P. A. Raymond, 2000. Function for Hedgehog genes in zebrafish retinal development, *Dev. Biol.*, 220:238–252.
- Stone, E. M., V. C. Sheffield, and G. S. Hageman, 2001. Molecular genetics of age-related macular degeneration, *Hum. Mol. Genet.*, 10:2285–2292.
- Toy, J., J. M. Yang, G. S. Leppert, and O. H. Sundin, 1998. The *optx2* homeobox gene is expressed in early precursors of the eye and activates retina-specific genes, *Proc. Natl. Acad. Sci. USA*, 95:10643–10648.
- Treisman, J. E., M. A. Morabito, and C. J. Barnstable, 1988. Opsin expression in the rat retina is developmentally regulated by transcriptional activation, *Mol. Cell. Biol.*, 8:1570–1579.
- Trisler, G. D., M. D. Schneider, and M. Nirenberg, 1981. A topographic gradient of molecules in retina can be used to identify neuron position, *Proc. Natl. Acad. Sci. USA*, 78:2145–2149.
- Turner, D. L., and C. L. Cepko, 1987. A common progenitor for neurons and glia persists in rat retina late in development, *Nature*, 328:131–136.
- Turner, D. L., E. Y. Snyder, and C. L. Cepko, 1990. Lineage-independent determination of cell type in the embryonic mouse retina, *Neuron*, 4:833–845.
- Waid, D. K., and S. C. McLoon, 1998. Ganglion cells influence the fate of dividing retinal cells in culture, *Development*, 125:1059–1066.
- Wang, S. W., B. S. Kim, K. Ding, H. Wang, D. Sun, R. L. Johnson, W. H. Klein, and L. Gan, 2001. Requirement for *math5* in the development of retinal ganglion cells, *Genes Dev.*, 15:24–29.
- Watanabe, T., and M. C. Raff, 1992. Diffusible rod-promoting signals in the developing rat retina, *Development*, 114:899–906.
- Wetts, R., and S. E. Fraser, 1988. Multipotent precursors can give rise to all major cell types of the frog retina, *Science*, 239:1142–1145.
- Zhang, L., P. H. Mathers, and M. Jamrich, 2000. Function of Rx, but not *Pax6*, is essential for the formation of retinal progenitor cells in mice, *Genesis: J. Geneti. Dev.*, 28:135–142.

4 Neurotrophins, Electrical Activity, and the Development of Visual Function

NICOLETTA BERARDI AND LAMBERTO MAFFEI

Introduction

Vision in mammals is very poor at birth and develops over a relatively long period (weeks, months, or years, according to the species; Fig. 4.1A) in parallel with the anatomical and functional maturation of the visual system, particularly the visual cortex. If visual experience is altered during this period, called the *critical period*, dramatic consequences follow both in visual cortical development and in the development of vision. For instance, if during the critical period one eye is deprived of patterned vision, as with unilateral congenital cataract, the great majority of visual cortical neurons stop responding to the deprived eye, being driven only by the normal eye, and vision for the deprived eye develops poorly (amblyopia). There seems to be a close link between visual cortical development, critical period duration, and maturation of some visual functions, as shown in Figure 4.1A: the closure of the critical period for monocular deprivation roughly coincides with completion of visual acuity development in a number of species, from rat to monkey to human.

Manipulations of sensory experience also have been shown to affect the development of auditory and somatosensory systems, leading to the widely accepted assumption that the final stage of development of neural connections in sensory systems is under the irreplaceable control of sensory experience. The studies then converged into what may be the various stages for the fulfillment of the task initiated by sensory experience.

The first link in the chain is likely to be electrical activity, the language into which sensory experience is translated, which is already known to guide nervous circuit rearrangements and synapse formation. Here we reexamine the role of electrical activity, both spontaneous and visually driven, in the “construction” of the visual system by analyzing the interactions between electrical activity and neurotrophins in the completion of visual function development. Neurotrophins are an essential link in the chain of events leading to maturation of visual connections, a link so necessary that electrical activity in the absence of neurotrophins fails to drive developing visual cortical circuits into their final functional state. For instance, even if visual experience is normal,

development of visual function is abnormal if specific neurotrophins are missing. Surprisingly, neurotrophins also seem sufficient to drive the development of some aspects of vision in the absence of visual experience.

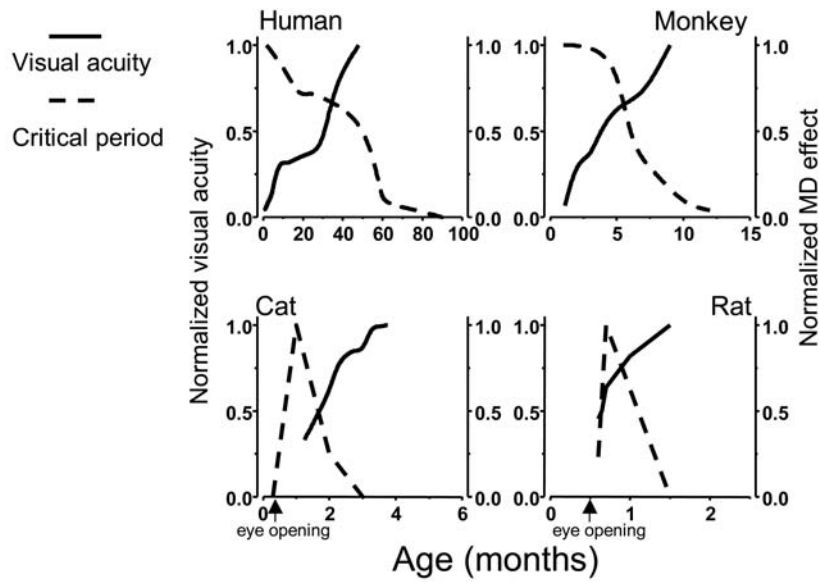
In presenting the fascinating story of the role of electrical activity and neurotrophins in the development of the visual system, studies which blossomed in the past 10–15 years, we shall follow an historical criterion, which allows us to introduce the various experimental paradigms and the experimental models used. (For recent reviews, see Berardi and Maffei, 1999; Cellerino and Maffei, 1996; McAllister et al., 1999; Pizzorusso and Maffei, 1996).

The neurotrophins

Neurotrophins have usually been considered for their involvement in the development of the nervous system and for the differentiation and maintenance of specific functions of certain classes of neurons (see Box 1). The neurotrophins so far identified in addition to NGF, which is the progenitor of the entire family, are BDNF, NT4-5, NT3, and finally NT6, which has been described only in fish (Lewin and Barde, 1996). The action of neurotrophins requires their binding to particular receptors. Each neurotrophin binds to a specific tyrosine kinase receptor (trk) through which it exerts its biological functions. These specific receptors are trkA for NGF, trkB for BDNF and NT4-5, and trkC for NT3 (Bothwell, 1995). Neurotrophic factors also bind to the low-affinity receptor p75, the role of which has been studied particularly in relation to the ligand NGF. Where NGF is concerned, one of the roles of p75 is to augment trkA function, lowering the concentration of NGF necessary for signal transduction. In addition to this role, p75 can act as an inducer of apoptosis.

The classical neurotrophic hypothesis was that developing neurons compete for target-derived neurotrophic factors which are produced in limited amounts by nonneuronal targets (the skin for sensory neurons, the muscle for proprioceptive neurons); neurotrophins bind to their receptors, are internalized, and are transported retrogradely to the neuronal soma, where they promote neuronal survival. If one neurotrophin or its receptor is antagonized or missing,

A



B

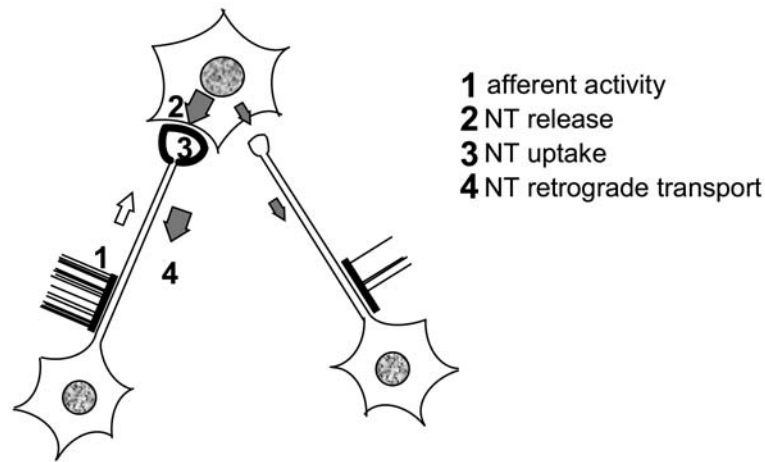


FIGURE 4.1. *A*, The development of visual acuity for man, monkey, cat, and rat is reported as a function of age and compared with the critical period for monocular deprivation. By the end of the critical period visual acuity reaches its final value, indicating that maturation of sensory functions and decline of experience-dependent plasticity are two closely interconnected processes based on the maturation and activity-dependent stabilization of neural connections in the visual cortex. A variation of the critical period duration implies a variation of the rate of visual function development (see Fig. 4.8). *B*, Activity-dependent synapse stabilization. The crucial elements for the new neurotrophic hypothesis are depicted

here: production, release, and uptake of neurotrophins (NT) are activity dependent. The connections with electrical activity (depicted as a sequence of action potentials above the fiber) which is higher, more patterned, and richer in transients receive a greater NT supply (*thick, gray arrow*) and stabilize or enlarge their synaptic contacts (*big, thick knob* at the end of the fiber) with the target neuron, while the connections with poor electrical activity get weak neurotrophic support (*thin, gray arrow*) and lose their synaptic contacts (*small, thin knob*). Anterograde action of NT is also possible (*white arrow*). (Adapted from Berardi et al., 2000.)

Box 1. *Classical Neurotrophic Hypothesis*

During development of the nervous system, neuronal populations undergo a process of naturally occurring cell death at the time their axons innervate target areas. It is believed that this process ensures a match between the size of the innervating population and the size of its target territory. The classical neurotrophic hypothesis states that production of trophic factors by target organs regulates this matching process. Limited amounts of neurotrophic factors are produced by target cells: neurotrophic factors bind specific receptors, are internalized by projecting neurons, and are transported retrogradely to the soma, where they promote survival.

This hypothesis was first formulated for PNS neurons by Hamburger, Levi-Montalcini, and coworkers (reviews in Levi-Montalcini, 1987; Purves, 1988) on the basis of their landmark experiments with nerve growth factor (NGF), the first neurotrophic factor discovered: they demonstrated *in vivo* that this factor is essential for survival of sympathetic and nociceptive sensory neurons. Subsequently, each of the major predictions of the classical neurotrophic hypothesis for NGF was confirmed:

NGF is produced by the nonneuronal targets of sympathetic and sensory neurons but not by the neurons themselves; target ablation or blockage of axonal transport results in the death of neonatal sympathetic and sensory neurons; administration of NGF prevents naturally occurring cell death; NGF binds to specific receptors (trkA) and is retrogradely transported. Now this hypothesis has been extended to the other neurotrophins: brain-derived neurotrophic factor (BDNF), neurotrophin 3 (NT3), and neurotrophin 4 (NT4). The specific receptor for BDNF and NT4 is trkB and for NT3 it is trkC; all neurotrophins, NGF included, also bind to p75. It is now clear from examination of mutant mice carrying deletions for the genes encoding neurotrophins and their receptors that specific neuronal populations require trophic support of specific neurotrophins from their final targets. A table of neuronal losses in neurotrophin and receptor deficient mice is presented below. For a review on neurotrophic factors and their receptors see Bothwell (1995), Lewin and Barde (1996), and Reichardt and Farinas (1997).

Neuronal Population	trkA Deletion	NGF Deletion	trkB Deletion	BDNF Deletion	NT4 Deletion	trkC Deletion	NT3 Deletion
<i>Sensory</i>							
Trigeminal	75%	75%	60%	30%	n.s.	ND	60%
Dorsal root ganglia	70%	70%	30%	35%	n.s.	20%	60%
	Nociceptive and thermoreceptive neurons missing			Proprioceptive fibers (1a) present		Proprioceptive neurons missing	Proprioceptive and cutaneous mechanoreceptors missing
<i>Sympathetic</i>							
Superior cervical ganglion	>95%	>95%	ND	n.s.	n.s.	n.s.	50%

Neuronal losses are expressed as the percentage of neurons lost in mutant compared to wild-type controls. n.s. = not significantly different. ND = not determined. Only some of the populations examined in the original papers are reported for the sake of brevity.

specific neuronal populations in the peripheral and autonomic nervous systems fail to develop or do not survive (see Box 1). For instance, in mice deficient in trkA or NGF, virtually all sympathetic neurons in the superior cervical ganglion die, while in mice deficient in trkC or NT3, proprioceptive neurons die.

At variance with what is found in the peripheral or autonomic nervous system, no central nervous system (CNS) population is solely dependent on one neurotrophin for its survival. Indeed, in neurotrophin knockout mice, there is no loss of any specific population of neurons in the CNS (Thoenen, 1995).¹

With hindsight, this observation already hinted at the possibility that the role of neurotrophins in the CNS was not neuronal survival. However, it took a completely dif-

ferent series of experiments to show clearly that neurotrophins have an important role in the plasticity of the CNS, leading to the formulation of a new neurotrophic hypothesis. These experiments were performed in the developing visual system.

¹Note: Several authors have employed neurotrophins to save neurons from lesion-induced death. Paradigmatic is the effect of NGF on the survival of cholinergic basal forebrain neurons after axotomy. Retinal ganglion cell survival is also increased by exogenous neurotrophins. This, however, does not mean that the exogenous neurotrophin can substitute for the loss of the target-derived endogenous one. Indeed, blockage of axonal transport does not cause appreciable death of retinal ganglion cells.

A new neurotrophic hypothesis

Functional properties of mammalian visual cortical neurons are immature at eye opening and develop gradually during the first months of postnatal life (Fagiolini et al., 1994). Development of the visual system is strongly influenced by depriving one eye of patterned vision during a short period of postnatal development called the *critical period for the effects of monocular deprivation* (which, from now on, will be referred to as simply the *critical period*). Modifications of cortical circuitry in response to an imbalance between the inputs from the two eyes are extremely rapid; for instance, a few hours of monocular deprivation during the critical period are sufficient to shift the ocular dominance distribution of visual cortical cells toward the nondeprived eye, and a few days are enough to produce a shift which is equal to that induced by a deprivation lasting for the entire critical period. What are the mechanisms leading to such dramatic modifications of cortical connections?

Wiesel and Hubel introduced in visual physiology the important concept of *binocular competition* (Wiesel and Hubel, 1963). The two eyes compete for functional possession of the binocular cortical neurons, and the competition takes the form of electrical activity. If electrical activity in the two sets of thalamic fibers, those driven by the contralateral eye and those driven by the ipsilateral eye, is temporally correlated, then both sets of fibers will be allowed to maintain connections with the same cortical neuron. If, however, the activity in the two sets of fibers is not temporally correlated, only one set of fibers will be allowed to keep its hold on the postsynaptic neuron, the one whose activity is more able to drive it. In normal development, where the activity in the two sets of fibers driven by either eye is equally strong and temporally patterned, this process of activity-dependent competition leads to the existence of binocular neurons and to a balanced ocular dominance distribution: neurons in the visual cortex have very similar probabilities of being dominated by either eye. During monocular deprivation the competition between the two eyes becomes uneven, because electrical activity in the afferent fibers driven by the deprived eye is both uncorrelated with that of the fibers driven by the undeprived eye and weaker; as a result, the closed eye loses the fight at cortical level, leaving the dominance of cortical neurons to the undeprived eye.

It is not clear what the two eyes compete for at a molecular level. A reasonable hypothesis is that they compete for a reward important for their function. A reward can be thought of as chemical messages that strengthen nervous connections; therefore, it can be said that the two eyes, during development, compete for eating. Our initial hypothesis (see Fig. 4.1*B*) was that the fibers driven by either eye compete for a neurotrophic factor available in only a limited amount at cortical level (Maffei et al., 1992).

This introduced the neurotrophic hypothesis in the CNS, transforming neurotrophins from survival factors for neurons, derived from nonneuronal targets, to survival factors for neural connections, exchanged from neuron to neuron as they establish functional connections. This new neurotrophic hypothesis envisaged two broad fields of action for neurotrophins in the CNS. The first stage could influence the probability of formation of synaptic contacts between incoming fibers and target neurons. The second stage could be the regulation of synaptic efficacy, maintenance of connections, and development of a function, as in binocular vision development. This hypothesis implies that the production and uptake of the neurotrophic factor are functions of the quantity and pattern of electrical activity at both presynaptic and postsynaptic levels, and that neurotrophic factors, in turn, can enhance synaptic transmission at both the functional and morphological levels, thus firmly linking together neurotrophins and electrical activity in the control of visual development. It should be noted that at the time this new hypothesis concerning the role of neurotrophins in activity-dependent synaptic plasticity was put forth, the reciprocal control between neurotrophins and electrical activity, now well characterized, was totally unknown. The first demonstrations that neurotrophin production was under the control of electrical activity occurred around 1990 (Ernfors et al., 1991; Zafra et al., 1990), showing that artificially increasing the electrical activity in the hippocampus or neocortex increased both the mRNA and protein of neurotrophins; later on, it was shown that this also promoted their release (Blochl and Thoenen, 1995). Also, protocols inducing long-term potentiation (LTP) in the hippocampus were then shown to increase neurotrophin mRNA (Castren et al., 1993). Complementary to this, a decrease of activity by tetrodotoxin (TTX) decreased neurotrophin mRNA (Castren et al., 1992).

In addition to the two main differences already pointed out between the classical neurotrophic hypothesis for the PNS and the new one for the CNS (formation and survival of connections and not of neurons, produced by neurons and not by nonneuronal targets), another difference is emerging from the literature, namely, the possibility of an anterograde action of neurotrophins as opposed to the classical target-derived action. This significantly changes the frame of thought: in addition to thinking that cortex-derived factors guide, in concert with electrical activity, stabilization of thalamic afferents on cortical neurons, we may have to consider that thalamic fibers themselves release factors which promote and guide the formation and maintenance of their synapses on cortical neurons and that corticothalamic afferents may contribute to the development of the pattern of thalamocortical connectivity. The evidence for anterograde actions is illustrated in Box 2.

Box 2. Anterograde and Retrograde Actions of Neurotrophins

Following the experiments in the PNS, the concept had been accepted that neurotrophins are transported retrogradely and that this is the basis of their action.

This idea has been passively extended to the interpretation of CNS data.

In some instances, particularly for NGF and the cholinergic projection from the basal forebrain to the hippocampus, this assumption seems to hold. In other cases, it is supported only by the observation that exogenous neurotrophins injected into specific brain regions are retrogradely transported. However, recent experiments studying the transport of BDNF/NGF in the optic nerve of the rat have shown that the situation is somewhat more complicated. If one ligates the optic nerve and observes the accumulation of neurotrophins at both sides of the ligature, only accumulation of BDNF on the retinal side is seen; by contrast, if NGF and BDNF are injected in the superior colliculus and lateral geniculate nucleus, both promptly accumulate at the distal side of the ligature. This suggests that transport of exogenous neurotrophins is not proof of the transport of endogenous ones and that anterograde actions are more important than was previously thought (Caleo et al., 2000). Evidence for anterograde actions has also been obtained in the visual cortex (Kohara et al., 2001) and in the chick visual system (von Bartheld et al., 1996).

NGF and monocular deprivation

The rationale for most of the experiments performed to assess the role of neurotrophins in the changes induced at

the visual cortical level in monocularly deprived and strabismic animals is the following: if one provides exogenously the neurotrophic factor to the neural competitors, they should not have any reason to fight and even the geniculocortical axons driven by the eye unstimulated or not properly stimulated by vision might achieve enough neurotrophic factor at the level of its cortical projections to ensure its physiological development.

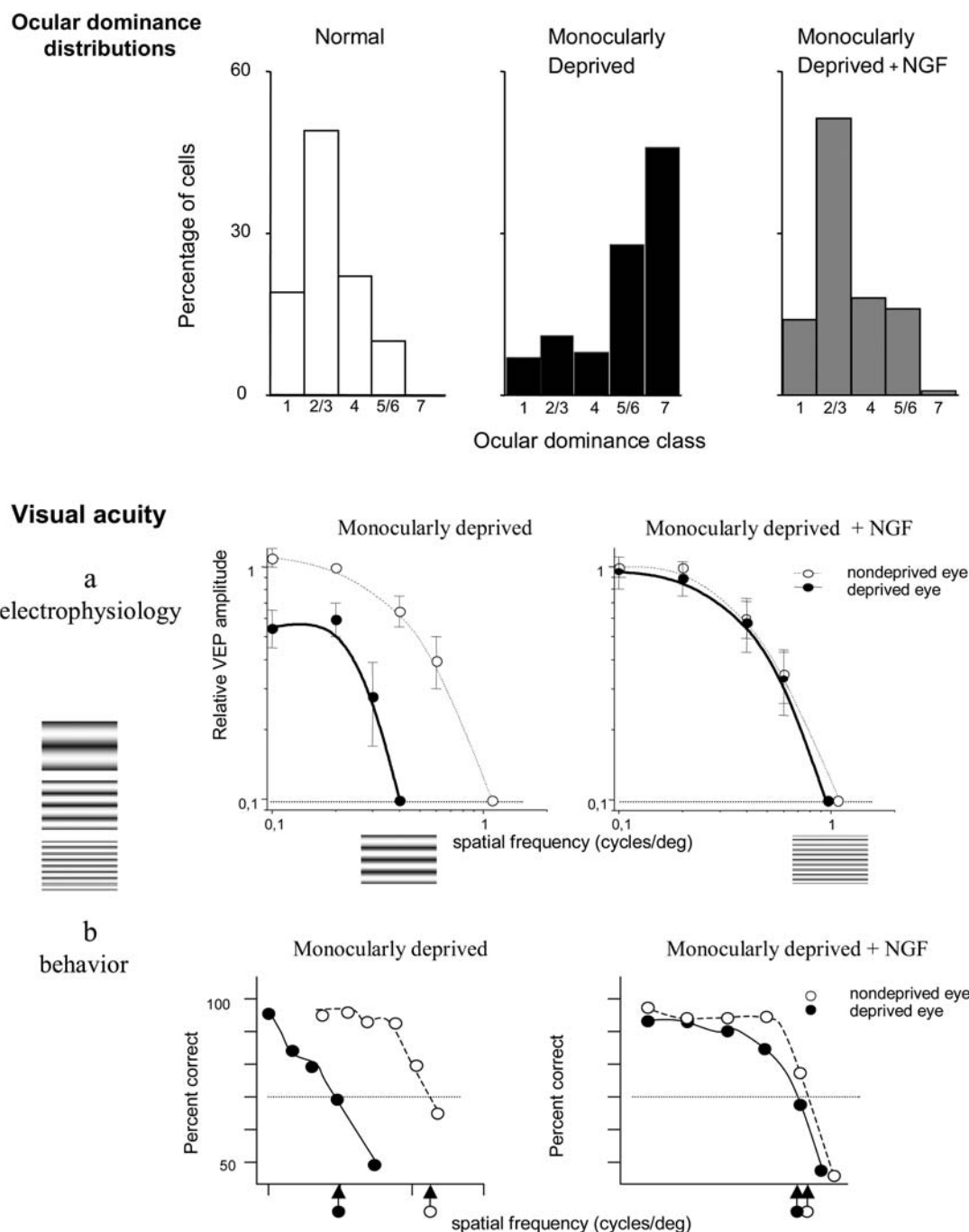
In short, the working hypothesis is that the effects of monocular deprivation or strabismus should be prevented by an exogenous supply of NGF.

This hypothesis may now appear somewhat simple-minded, but it turned out to be very appropriate operationally. Indeed, an intraventricular exogenous supply of NGF in the rat prevents all the tested effects of monocular deprivation and (convergent) strabismus (Domenici et al., 1991, 1992; Maffei et al., 1992). Interestingly, these results have been recently confirmed in another rodent, the mouse, by Fagiolini and Stryker (1996). In cats, an intraventricular supply of NGF was effective in attenuating monocular deprivation effects up to the behavioral level; visual acuity of the deprived eye developed normally in kittens treated with NGF (Fiorentini et al., 1995). A synopsis of the main results concerning NGF and monocular deprivation is presented in Figure 4.2.

More recently, NGF was directly provided to cortical neurons by intracortical infusion; this also prevented monocular deprivation effects on ocular dominance (Lodovichi et al., 2000), suggesting that the receptors for NGF should be

FIGURE 4.2. Intraventricular NGF administration counteracts the effects of monocular deprivation on ocular dominance and visual acuity. *Top*: Ocular dominance distributions for normal rats, rats monocularly deprived during the critical period and rats monocularly deprived and treated with NGF throughout the deprivation period (postnatal days 15–45, P15–P45). Cells were classified according to the Hubel and Wiesel criteria, with cells in classes 1 and 7 being monocular and driven exclusively by the contralateral and ipsilateral eye, respectively; cells in ocular dominance classes 2/3 and 5/6 being binocular and driven preferentially by the contralateral and ipsilateral eye, respectively; and cells in class 4 being binocular and driven equally by the two eyes. It is evident that the shift in ocular dominance distribution in monocularly deprived rats is absent in NGF-treated rats. (Data replotted from Maffei et al., 1992.) *Middle: A*, Visual evoked potentials (VEP) recorded in the visual cortex contralateral to the deprived eye in response to sinusoidal gratings of increasing spatial frequencies (examples of sinusoidal gratings with spatial frequency in the ratio 1:2:4 are reported on the left of the graphs). Mean relative VEP amplitude (normalized to the amplitude of the signal recorded for 0.2 cycle/deg) is reported as a function of stimulus spatial frequency for monocularly deprived control animals and monocularly deprived NGF-treated animals. Vertical bars represent standard deviations. The noise level is indicated by the dotted line. As the spatial frequency of the stimulus increases, the signal amplitude decreases until it falls

to the noise level. The highest spatial frequency still evoking a reliable signal with a maximal stimulus contrast is taken as the visual acuity. The symbols just above the noise level correspond to estimated mean visual acuity for the deprived and nondeprived eyes, which is 0.4 ± 0.7 vs. 1 ± 0.04 cycles/deg in monocularly deprived control animals and 0.97 ± 0.1 vs. 1 ± 0.08 cycles/deg in monocularly deprived NGF-treated animals. The difference between visual acuity in the deprived and undeprived eyes is significant for monocularly deprived animals but not for monocularly deprived animals treated with NGF (replotted from Domenici et al., 1991). To visualize the difference in acuity brought about by NGF in deprived animals, the ratio between the spatial frequency of the gratings below the abscissa is 1:2.5, which is the ratio between visual acuity for the deprived eye in control animals and for the deprived eye in NGF-treated animals. *Bottom: B*, Percentage of correct responses in a behavioral forced choice discrimination of a grating versus a uniform gray ($N = 85$ trials per point) plotted as a function of the spatial frequency of the grating for a kitten monocularly deprived from P30 to P45 and for a littermate deprived for the same period but treated with NGF. The estimated visual acuities (corresponding to 70% correct) for the deprived and nondeprived eyes are indicated by the arrows on the abscissa (adapted from Fiorentini et al., 1995). It is clear that the beneficial effects of NGF in preventing deprivation amblyopia (loss of visual acuity in the deprived eye) are present at the level of visual behavior.



present at the cortical level. Indeed, *trkA* and *p75* are present in the visual cortex during the critical period, and activation of cortical *trkA* receptors is sufficient to allow normal development of ocular dominance in monocularly deprived rats, mimicking the effects of NGF (Pizzorusso et al., 1999).

Thus, even in the presence of an abnormal visual experience, an increase in NGF availability to cortical neurons or activation of NGF cortical receptors allows normal development of visual cortical connectivity and, ultimately, of vision.

Administration of neurotrophins during dark rearing can replace the lack of visual experience

Without visual experience the visual cortex does not develop normally, and it remains largely immature even after the end of the critical period (Fagiolini et al., 1994; Timney et al., 1978). The classical signs of dark-rearing effects on cortical development are reported in Figure 4.3 and include abnormal habituation of cortical responses and decreased visual acuity.

Following the experiments on the effects of NGF in monocularly deprived animals, the hypothesis was advanced that visual experience during development promotes normal maturation of the visual cortex by regulating the availability of neurotrophins to visual cortical circuits or to structures projecting to them (Fagiolini et al., 1997; Pizzorusso et al., 1997). The physiological alterations induced by lack of visual experience in dark-reared animals could be due simply to an alteration in the level of expression of neurotrophins in the visual cortex. If so, increasing the availability of neurotrophins could replace, at least partly, the lack of visual experience during dark rearing. This hypothesis has been tested for NGF and BDNF.

Supplying animals with suitable doses of neurotrophins during the whole period of dark rearing poses technically difficult problems. It is known that neurotrophins do not cross the blood-brain barrier and therefore must be administered directly to the brain. Daily administration of neurotrophins, for instance, into the ventricles, is practically impossible or troublesome during dark rearing. To overcome this problem, three different methods have been used. All of them have been successful and could have a bearing on clinical applications of neurotrophins in humans. Conceptually the first two methods are very similar, in that they aim at implanting in the lateral ventricles biological minipumps delivering sufficient doses of neurotrophins (in this case NGF) throughout the whole period of dark rearing. As biological minipumps, either Schwann cells or polymer-encapsulated cells genetically engineered to release NGF have been employed (for details of the methods and results, see Fagiolini et al., 1997; Pizzorusso et al., 1997).

The results, summarized in Figure 4.3, show that NGF allows a normal or nearly normal development in dark-reared animals with respect to the tested parameters. In particular, Figure 4.3 shows that development of visual acuity is normal in dark-reared rats treated with NGF.

More recently, the problem of supplying neurotrophins to the CNS has been solved by taking advantage of BDNF overexpression in the postnatal forebrain of mice (Huang et al., 1999; see Fig. 4.7). Also in these animals, all tested parameters were normal despite dark rearing (Fig. 4.3).

In addition, in dark-reared BDNF-overexpressing mice we have observed that the critical period, which is normally prolonged by dark rearing, ends at the same time as in normally reared wild-type mice (P45). Thus, development of visual function can proceed almost normally even in the absence of visual experience, provided that neurotrophins are supplied.

A possible interpretation of these results is that visual experience controls development of visual function by controlling the expression of neurotrophins. Indeed, expression and function of neurotrophins are altered in dark-reared animals (Castren et al., 1992; Pollock et al., 2001; Vieg-

et al., 2002), suggesting that the effects of dark rearing could, at least in part, be attributed to the lack of appropriate neurotrophin action.

This allows us to speculate that neurotrophins engage in an innate program of visual development which is normally triggered by visual experience. This program is dependent on activity in the visual pathways, in particular on spontaneous activity. Blockage of spontaneous activity of retinal ganglion cells, at least in the case of monocular deprivation, caused a failure of NGF action (Caleo et al., 1999).

Blockage of endogenous NGF affects development of the visual system

If neurotrophic factors are a crucial link between activity and development of appropriate connectivity in the visual system, either by acting as retrograde messages from neurons or dendrites to nerve terminations, to selectively reinforce active inputs, as Donald Hebb envisaged, or by acting anterogradely, then the blockage of endogenous neurotrophins during the critical period should interfere with development of the visual system: connections should remain immature and the system plastic—for instance, sensitive to monocular deprivation—beyond the critical period. These predictions were tested by the intraventricular transplant of cells secreting antibodies against NGF during development (Berardi et al., 1994; Domenici et al., 1994), and it was shown that they were fulfilled (Fig. 4.4). Visual acuity was reduced, receptive fields remained large, and the critical period for monocular deprivation was abnormally prolonged, effects very similar to those produced by dark rearing.

Very similar results have been obtained in cats blocking endogenous trkB ligands; infusion of BDNF and NT4 scavengers (trkB-IgG fusion proteins) into the visual cortex (Cabelli et al., 1997) disrupts ocular dominance column formation (Fig. 4.5), an effect reminiscent of that produced by binocular deprivation (Crair et al., 1998).

Thus, not only can the deleterious effects of an abnormal or absent visual experience on development be counteracted by increasing neurotrophin availability to visual neurons, but a normal visual experience is unable to normally drive development and closure of the critical period if the action of endogenous neurotrophins is blocked. This last result strongly suggests that neurotrophins may be the crucial link in the chain of events linking visual experience with development of vision.

Do BDNF, NGF, NT4, and NT3 play similar or different roles in cortical plasticity and development?

The question now arose, what were the roles played by the different neurotrophins in developmental visual cortical plasticity? This question occurred because, over the years,

Effects of neurotrophins in dark rearing

DR	DR+NGF	DR+BDNF
•Decreased visual acuity	Normal visual acuity	Normal visual acuity
•Increased receptive field size	Normal receptive fields	Normal receptive fields
•Decreased orientation selectivity	Slightly decreased orientation selectivity	Slightly decreased orientation selectivity
•Increased binocularity	Normal binocularity	Normal binocularity
•Habituating responses to visual stimulation	Normal responses	Normal responses

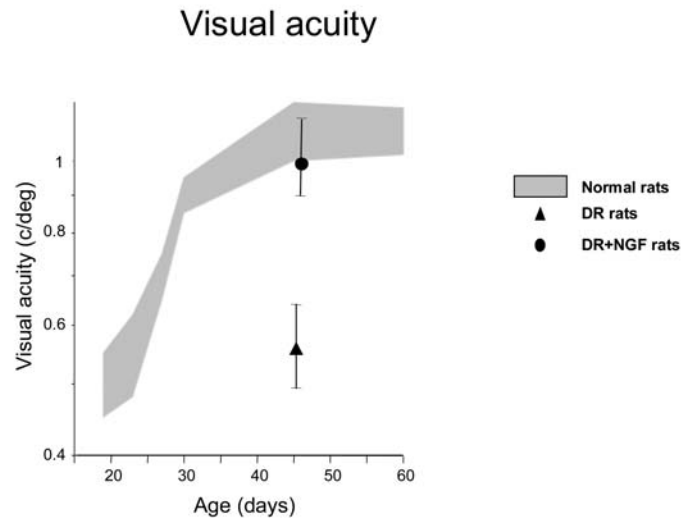


FIGURE 4.3. *Top left:* summary of the functional properties affected by dark rearing (DR). Habituation is the progressive attenuation of cell responses to repetitive visual stimulation: typically, cell responses disappears after three or four passages of a drifting bar over the receptive field in DR animals (DR from birth to P60). Habituation is absent in normally reared animals. *Middle and right:* the deficits induced by DR are absent (no significant differences with respect to normal) or strongly attenuated (orientation selectivity, small difference with respect to normal) in rats subjected to intraventricular implant of NGF-producing cells (DR + NGF) or

in mice overexpressing BDNF in the telencephalon (DR + BDNF). *Bottom:* Summary of the results obtained for visual acuity in DR rats. The shaded area represents the range (mean \pm one standard deviation) of visual acuities for normal rats during development from P20 to adulthood. At each age and for each animal visual acuity was estimated by VEP, as in Figure 4.2. DR up to P45 strongly decreases visual acuity (*filled triangle*); visual acuity of DR rats with intraventricular implant of NGF-producing cells is, however, normal (*filled circle*).

some differences in the actions of the neurotrophins became apparent and a debate developed about the nature of the active neurotrophin(s). As for the effects on cortical development, only BDNF and NT4 disrupt ocular dominance columns in kittens (Cabelli et al., 1995); however, all neurotrophins influence dendritic growth in developing ferret visual cortex (McAllister et al., 1995, 1997). As for the

effects on plasticity, injection into the visual cortex of microbeads conjugated with neurotrophins has shown that NT4, and only NT4, is effective in preventing the shrinkage of lateral geniculate nucleus (LGN) neurons induced by monocular deprivation in ferrets (Riddle et al., 1995). On the other hand, BDNF was found to be able to prevent the shift of the ocular dominance distribution of cortical

Effects of Blocking Endogenous NGF During Development of Rat Visual System

- Shrinkage of LGN neurons
- Reduction of visual acuity
- Decrease in binocularity
- Larger receptive fields

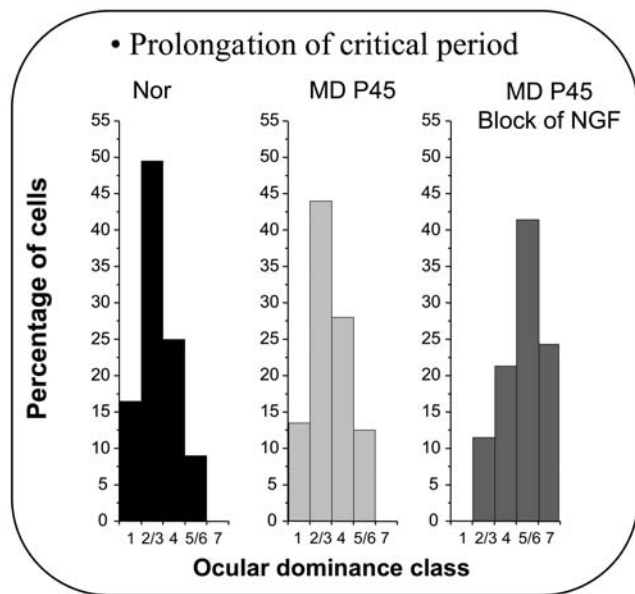


FIGURE 4.4. *Top*: Summary of the main effects of the blockage of endogenous NGF action by implantation in the lateral ventricle of hybridoma cells secreting antibodies to NGF. The implant was done at the beginning of the critical period (P15). Rats implanted with parental myeloma cells were used as controls. Animals were left to develop normally, with both eyes open. LGN soma size, visual acuity, cell ocular dominance, and receptive field size were measured at P45. *Bottom*: The effects of NGF blockage on the critical period. Animals were left to develop normally, with both eyes open, up to P45, which is past the end of the rat critical period, and then were monocularly deprived; the effects of monocular deprivation were assessed electrophysiologically 1 month later. It is evident that monocular deprivation is still able to shift the ocular dominance distribution toward the nondeprived eye in rats with blockage of NGF (MD P45, blockage of NGF) but not in control rats (MD P45). (Adapted from Domenici et al., 1994).

neurons induced by monocular deprivation in cats (Galuske et al., 1996). It became necessary, therefore, to assess whether the differences observed were simply due to different experimental conditions, like the use of different animals, different methods of drug administration, and different ages of the animal, or whether different neurotrophins played different roles.

Another important question concerned the effects of neurotrophins on visual cortical cell electrical activity. Many studies had shown that neurotrophins, in particular BDNF, strongly modulate synaptic transmission and electrical activity of cortical neurons in vitro (see McAllister et al., 1999,

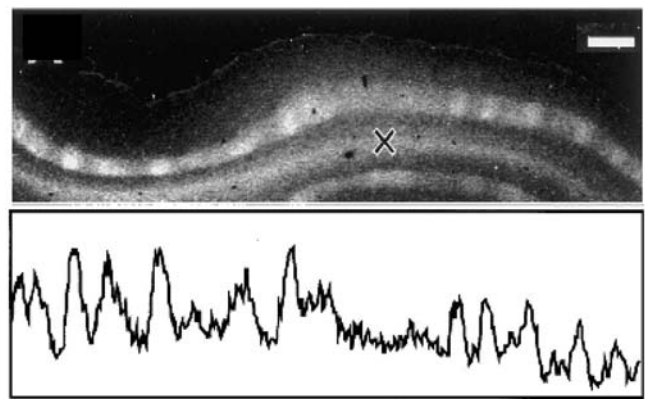


FIGURE 4.5. An example of the effects of trkB-IgG infusion on ocular dominance columns. trkB-IgG was infused into cat visual cortex from P21 to P42 at a rate of 2.5 mg/ml. To label ocular dominance patches in layer IV, geniculocortical afferents were labeled with the transneuronal tracer $[^3\text{H}]$ -proline injected into the vitreous chamber of one eye. *Top*: darkfield image from an infused brain; *bottom*: corresponding profile of silver grain density in layer 4. The position of the tip of the infusion cannula is marked with an X. Scale bar, 1 mm. It is evident that the regular alternation of labeled patches (axons of LGN neurons driven by the injected eye) and of gaps (axons of LGN neurons driven by the noninjected eye) is disrupted in the portion of visual cortex infused with trkB-IgG (zone above the cannula tip). (Adapted from Cabelli et al., 1997.)

for review). The most striking effect of BDNF was documented by Kafitz et al. (1999) in cultured hippocampal neurons: BDNF was as fast and potent as glutamate, a classical excitatory neurotransmitter, in exciting the neurons onto which it was puffed (Kafitz et al., 1999). Knowledge of neurotrophin effects on cortical cell activity in vivo is essential to understand more thoroughly their mechanisms of action in regulating visual cortical plasticity. Any strong direct effect on visual cortical cell electrical activity is bound to influence developmental cortical plasticity (Ramoia et al., 1988; Reiter and Stryker, 1988; Shaw and Cynader, 1984).

A recent study has compared in vivo the actions of all four neurotrophins—NGF, BDNF, NT3, and NT4—on cortical plasticity and on electrical activity in the same species, in animals of the same age, and in the same experimental conditions. This has been done in the rat, employing monocular deprivation as a plasticity test (Lodovichi et al., 2000). NGF and NT4 were found to be very effective in counteracting the shift in the ocular dominance distribution of rat visual cortical neurons induced by monocular deprivation. This protective effect was not accompanied by any detectable changes in cell responsiveness or in orientation selectivity. BDNF, even at much higher doses than NGF and NT4, was less effective in counteracting monocular deprivation effects and, in addition, was the only neurotrophin which altered visual cortical cell electrical activity, both spontaneous and evoked. These results suggest that the partial effect of BDNF on monocular deprivation could stem from its ability to dramatically alter the electrical activity of cor-

tical neurons. NT3 is ineffective in preventing ocular dominance shift, both at a dose comparable to that of NGF and NT4 and at a much higher dose. Thus, the differences found in the literature for neurotrophin action in visual cortical plasticity cannot be attributed solely to species differences: different neurotrophins play their roles in visual cortical plasticity through different mechanisms and, in particular, through a different interplay with electrical activity. This could be due to a difference in the cellular targets of neurotrophins (see below for the peculiar link between BDNF and intracortical inhibitory circuitry) and/or to differences in the intracellular signaling cascades activated. Diversity in the postreceptor transduction pathways is likely to be a necessary explanation for the differences between NT4 and BDNF actions, since they both bind trkB.

Neurotrophins and the modulation of synaptic transmission in the visual cortex

A possible mechanism of action of neurotrophins on neural plasticity is the modulation of synaptic efficacy (see McAllister et al., 1999, for review). To investigate whether neurotrophins can modulate synaptic transmission in the visual cortex, a very convenient *in vitro* preparation, visual cortex synaptosomes, has recently been used. Synaptosomes contain mainly the presynaptic component of synapses, with all the machinery for neurotransmitter release. The advantage of this preparation is that the effectiveness of one neurotrophin in modulating each neurotransmitter system can be investigated in isolation (Fig. 4.6). For instance, an effect of BDNF on acetylcholine release can be attributed to a direct action of BDNF on cholinergic terminals, and not secondary to release of another neurotransmitter acting on cholinergic terminals.

Both NGF and BDNF potentiate glutamate (Glu) and acetylcholine (ACh) release, while only BDNF does so for GABA release (Sala et al., 1998) (Fig. 4.6). trkA plays the major role in mediating NGF effects, with p75 playing a small facilitatory role. This suggests a direct trkA-mediated effect of NGF on synaptic terminals of glutamatergic neurons in the visual cortex. More recently, the effects of NT4 on synaptic release were investigated in the same preparation. Like BDNF, NT4 potentiated GABA and Glu release but was much less effective than BDNF in potentiating acetylcholine release.

Two conclusions can be drawn at this point. First, modulation of synaptic transmission is an important mechanism of action for neurotrophins in the developing visual cortex. Second, different neurotrophins have different targets: NGF modulates synaptic release of cholinergic and glutamatergic terminals but not of GABAergic interneurons; BDNF is active on all three neurotransmitter systems and NT4 on glutamatergic and GABAergic terminals. Putting this informa-

tion together with data on the expression of trk receptors in the visual cortex and with data on retrograde transport of cortically injected NGF (Domenici et al., 1994), it can be concluded that NGF is likely to act directly on cholinergic afferents from the basal forebrain and on a population of glutamatergic cortical neurons and, indirectly, by modulation of the cholinergic function, on cortical inhibitory interneurons (Xiang et al., 1998); BDNF targets are cortical pyramidal cells (glutamatergic), inhibitory interneurons, cholinergic afferents, and serotonergic afferents; NT4 acts on thalamic afferents (glutamatergic), probably pyramidal neurons, and certainly inhibitory interneurons. The likely action of NT4 on thalamic afferents could explain its effectiveness in preventing monocular deprivation effects without disturbing visual cortical neuron electrical activity. The same ability could be conferred on NGF by its combined action on a neuromodulatory system such as the cholinergic system (which also provides indirect control of some interneuronal populations) and on a selected population of glutamatergic cortical neurons. BDNF emerges as the neurotrophin with the largest spectrum of targets and the strongest effectiveness on cortical neurons, both pyramidal and interneurons.

BDNF overexpression accelerates the functional development of the visual cortex

The experiments on the role of neurotrophins in modulating synaptic release show that BDNF has a strong effect in potentiating GABA release which is not shared by NGF. These results show that neurotrophins (in particular BDNF and NT4) also act on the inhibitory circuitry. trkB is present on cortical interneurons, and BDNF regulates the development of at least one class of inhibitory interneurons.

The relationship between neurotrophins and the development of inhibitory processes has been investigated, using an elegant transgenic mouse with postnatal overexpression of BDNF in the forebrain (Huang et al., 1999), as shown in Figure 4.7*A,B*. In these animals, the levels of BDNF expression typical of adult age is reached in the second postnatal week (Fig. 4.7*B*). This precocious expression of BDNF is accompanied by a precocious development of inhibitory synapses (Fig. 4.7*C*, GAD staining) and of inhibitory currents (Fig. 4.7*C*, insert).

This accelerated development of inhibition is paralleled by changes in the functional development of the visual system: there is precocious development of visual acuity with respect to the wild type and precocious closure of the critical period, possibly accompanied by precocious opening. Figure 4.8 clearly illustrates that in BDNF mice there is a shift toward younger ages of the curve describing the developmental time course of visual acuity and of the curve describing the decline of monocular deprivation effective-

Neurotrophins potentiate neurotransmitter release in the visual cortex

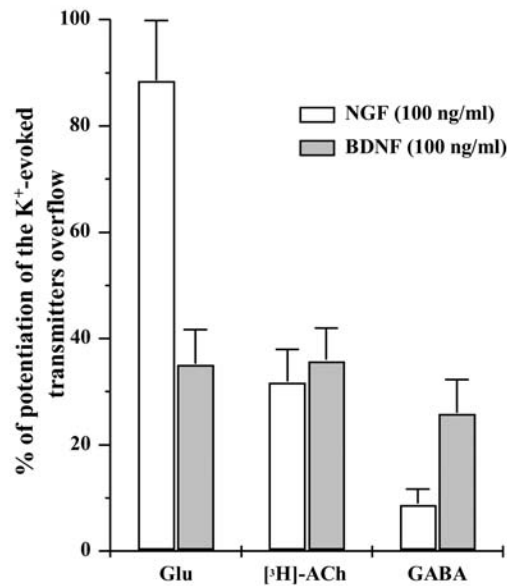
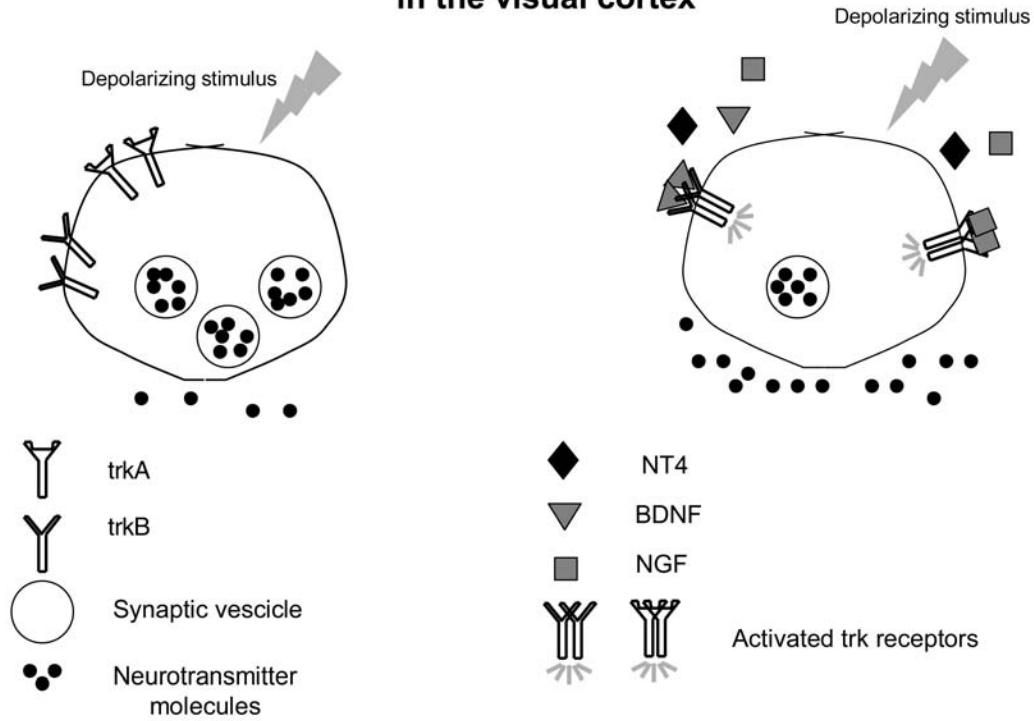


FIGURE 4.6. *Top:* Sketch of the experiment. *Left:* A synaptosome containing synaptic vesicles filled with neurotransmitter and presenting receptors for neurotrophins is subjected to depolarizing stimuli (high K⁺ concentrations); this causes release of transmitter (molecules outside the synaptosome). *Right:* A synaptosome subjected to depolarization is also exposed to neurotrophins. Neurotrophins activate their receptors, and the ensuing transduction

signals cause an increased release of neurotransmitter. *Bottom:* NGF and BDNF effects on K⁺-induced release of neurotransmitter from synaptosomes isolated from P23 rat visual cortices. Each point represents the mean \pm SEM of five to seven experiments run in triplicate. The small increase in GABA release is not statistically significant. (Adapted from Sala et al., 1998.)

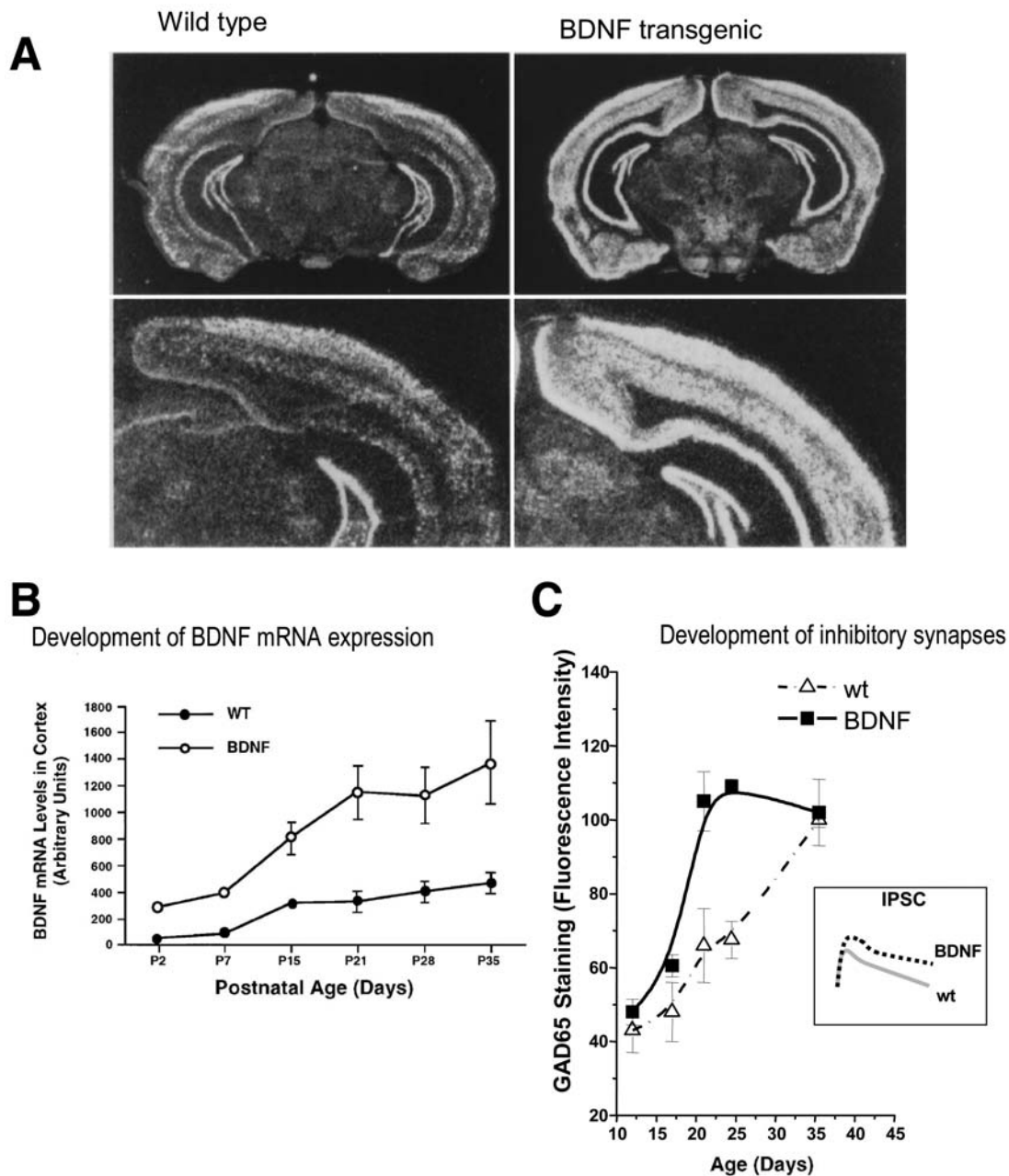


FIGURE 4.7. Precocious expression of BDNF in the telencephalon causes accelerated development of inhibition in the visual cortex. *A*, Spatial expression of the BDNF transgene revealed by in situ hybridization. Coronal brain sections from 4-week-old transgenic (*right*) and wild-type mice (*left*) hybridized with a BDNF oligonucleotide probe that detects both the endogenous and transgenic BDNF mRNA. Expression is restricted to the telencephalon. *B*, Quantification of total BDNF mRNA levels in the cerebral cortex at different developmental ages (data from Northern blotting experiments) for wild-type and transgenic mice. It is evident that the levels of expression normally reached after the third postnatal week

in wild-type mice are reached at P7 in BDNF mice. *C*, Development of GAD65, the synthetic enzyme for the inhibitory neurotransmitter GABA, in the visual cortex of wild-type and transgenic mice. Quantification of GAD65 expression in the presynaptic boutons of GABAergic interneurons was done around the soma of the target neurons. In BDNF mice there is accelerated maturation of GABAergic synapses. In the insert, examples of maximal inhibitory postsynaptic currents (IPSCs) recorded at P23–P26 from visual cortical slices of wild-type and transgenic mice. IPSCs are larger in transgenic mice. (Adapted from Huang et al., 1999.)

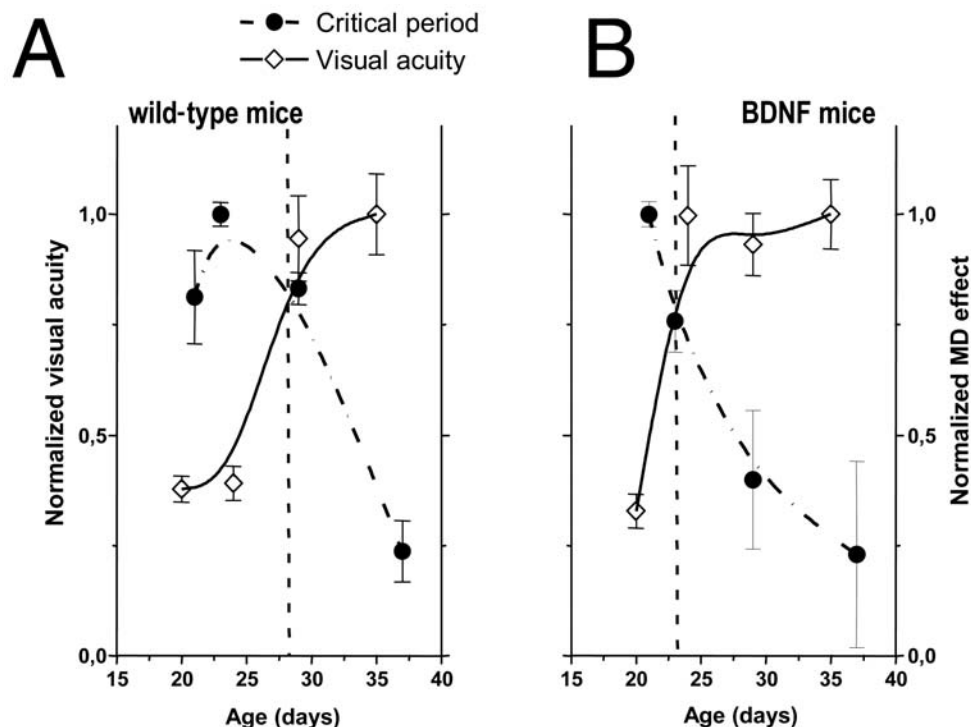


FIGURE 4.8. Critical periods for monocular deprivation and development of visual acuity are reported for wild-type mice, *A* and transgenic mice with precocious expression of BDNF, *B*. For BDNF mice, both the critical period (*dotted line*) and the visual acuity (*solid*

line) curves are shifted to the left (see crossing points, *dashed lines*). This indicates that precocious expression of BDNF induces both accelerated development of visual function and an early closure of critical period.

ness during the critical period. This reinforces the close link between the time course for visual acuity development and the time course of the critical period discussed in the Introduction.

The data presented in Figures 4.7 and 4.8 suggest the following considerations, which are relevant for the studies on development of neocortex:

1. Transgenic animals can be extremely useful in studies on development of visual function.
2. Modulation of a single molecule, in this case BDNF, can have dramatic consequences for the development of visual processes and the duration of the critical period. The observation that in the presence of normal visual experience overexpression of BDNF causes precocious development of vision can be considered the mirror finding to that obtained with blockage of endogenous neurotrophins: in that case, normal visual experience was unable to drive development, suggesting that neurotrophins are crucial effectors through which visual experience drives development of visual function. In BDNF-overexpressing mice, as in dark-reared animals with an increased supply of neurotrophins, neurotrophins seem to “substitute” for experience in driving development.

3. There is a new player on the stage of visual development, namely, inhibition. That inhibition is important for plasticity was previously suggested by experiments showing

that monocular deprivation is less effective in mice with reduced inhibitory transmission (GAD65 knockout mice) (Hensch et al., 1998). The data on the BDNF mouse, with precocious closure of the critical period and normal monocular deprivation effectiveness, clearly indicate that development of inhibition is important for the time course of the critical period. This point is further strengthened by the elegant experiment of Fagiolini and Hensch (2000) showing that precocious enhancement of inhibitory tone accelerates the opening of the critical period.

4. It seems that both NGF and BDNF are important in determining the timing of the critical period and of visual cortical development, pointing toward a more complex role for neurotrophins: they do not seem to be only retrograde, activity-dependent rewards for active thalamic afferents, but also important determinants of development for populations of cortical neurons.

Experience and neurotrophins: intracellular mechanisms

Several intracellular mechanisms are likely to be important in mediating the action of electrical activity and neurotrophins on structural and functional plasticity. Amongst these we have chosen to illustrate the involvement of a particular cascade, the ERK 1,2, also called p42/p44 MAPK.

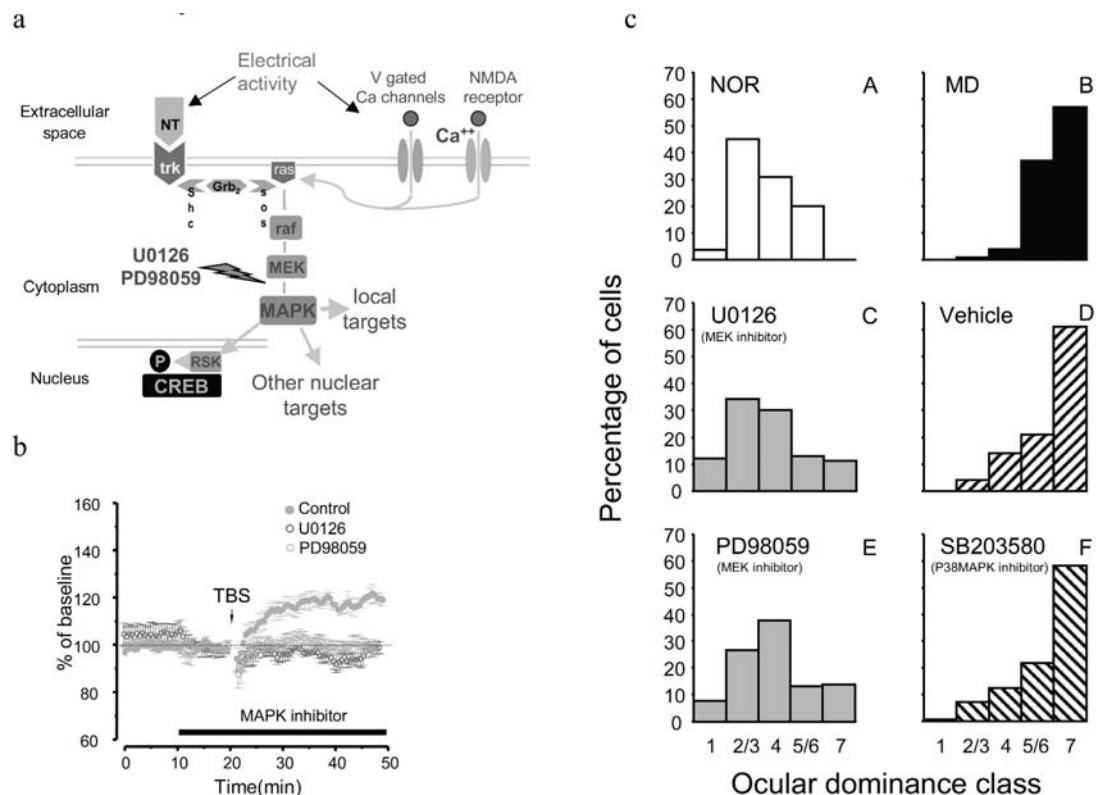


FIGURE 4.9. MAPK activation is required for visual cortical plasticity. *A*, Pathways of MAPK activation. MAPK is activated both by neurotrophins (NT) binding to their trk receptors via the transduction cascade of *ras* and by the influx of calcium through voltage-gated (V-gated) calcium channels and through glutamate NMDA receptors, also acting on *ras*. Electrical activity can therefore activate MAPK via two different converging pathways, and MAPK is a crucial converging point for the integrated action of electrical activity and neurotrophins. Activated MAPK can both act on local targets (synaptic proteins, adhesion molecules) and translocate to the nucleus, where, via kinases such as RSK, it can activate CREB, a transcription factor crucial for many plasticity phenomena. Other pathways impinging on MAPK are omitted for simplicity. The site of action of the two MAPK blockers employed in the experiment is indicated by the arrow. *B*, MAPK inhibitors

U0126 and PD98059 block LTP induction visual cortical slices. Average time course of layer III field potential amplitude before and after TBS of the white matter in the presence of U0126, PD98059, or vehicle. Field potentials recorded in layer III can be potentiated by TBS in control slices but not in U0126- and PD98059-treated slices. *C*, Blockage of MAPK activation prevents experience-dependent plasticity in the visual cortex. Ocular dominance distributions for normal P28 animals (NOR) and for animals monocularly deprived from P21 to P28, either untreated (MD) or treated with U0126, vehicle, PD98059, or SB203580 (an inhibitor of a kinases of the same family as MAPK). It is evident that blockage of MAPK activation by U0126 or PD98059 prevents the ocular dominance shift produced by monocular deprivation; the effect is specific for MAPK blockage, since inhibition of the related p38 kinase is ineffective. (Adapted from Di Cristo et al., 2001.)

The MAPK cascade has been involved in phenomena of synaptic plasticity and learning and memory from *Aplysia* to mammals (see Grewal et al., 1999, for review), but the characteristic which attracted our attention is that this biochemical cascade is sensitive to both electrical activity and neurotrophins, thus being a crucial converging point for the integrated action of the two. In the visual cortex, evidence that neurotrophins activate MAPK has been obtained only recently (Pizzorusso et al., 2000). The authors also show that MAPK activation is crucial for BDNF-induced cAMP response element binding protein (CREB) phosphorylation, which is likely to be an important step in BDNF action on synaptic plasticity.

In Figure 4.9*A* the principal pathways of MAPK activation are shown. It is clear from the figure that MAPK is a

hub linking neurotrophins and electrical activity with both cytoplasmatic and nuclear targets, an ideal position for a candidate player in visual cortical plasticity.

Recently, it has been shown that MAPK is important for experience-dependent plasticity in the visual cortex (Di Cristo et al., 2001). MAPK activation has been blocked with two specific inhibitors. The arrow in Figure 4.9*A* indicates the exact point of the transduction cascade where the block is performed (the molecule immediately upstream of MAPK, MEK).

Two approaches have been used, one in vivo, employing the paradigm of monocular deprivation, to investigate experience-dependent plasticity and one in vitro, using the paradigm of long-term potentiation (LTP) to investigate synaptic plasticity.

Patterned electrical stimulation (theta burst stimulation, TBS) of the white matter, which readily triggers LTP of field potentials recorded in layers II–III, rapidly triggers MAPK activation. Blockage of MAPK activation abolishes induction of LTP in the visual cortex (Fig. 4.9B). The link between MAPK activation and synaptic plasticity in the visual cortex is further confirmed by the observation that abolishing the ability of TBS to trigger LTP with an N-methyl-D-aspartate (NMDA) receptor antagonist also inhibits the ability of TBS to activate MAPK (Di Cristo et al., 2001).

In vivo, it has been found that visual experience rapidly triggers MAPK activation. In turn, MAPK activation is crucial for experience-dependent plasticity: the ocular dominance shift induced by monocular deprivation is prevented by both MAPK blockers employed U0126 and PD98050 (Fig. 4.9C). It is important to note that blockage of MAPK activation prevents experience-dependent plasticity without affecting the development of the visual cortex. Visual acuity, receptive fields, and orientation selectivity were normal in PD98050- and U0126-treated animals (Di Cristo et al., 2001).

The conclusion is that MAPK, acting on both local and nuclear targets, promotes strengthening of synaptic transmission under the control of electrical activity and neurotrophins. Thus, the effects of neurotrophins in preventing the ocular dominance shift induced by monocular deprivation could be attributed to activation of MAPK, which promotes stabilization of synaptic contacts even for the fibers driven by the deprived eye possessing only spontaneous electrical activity.

Conclusions

The results reported in this chapter show that visual experience and neurotrophins cooperate in guiding the development of vision. The actions of neurotrophins and electrical activity are linked in a functional chain which is often reciprocal: activity affects neurotrophin production and uptake, neurotrophins regulate synaptic transmission and may affect electrical activity in visual cortical neurons; visual experience is not sufficient to drive visual cortical development if endogenous neurotrophin action is antagonized, and exogenous neurotrophins become ineffective if electrical activity is blocked. At the other end, neurotrophins seem to be able to promote visual development even in the absence of visual experience, as suggested by the experiments with dark-reared animals.

The neurotrophins active in visual cortical development and plasticity—BDNF, NT4, and NGF—seem to play their roles by acting on different targets: each neurotrophin has its particular subset of targets among the intracortical neurons and the cortical afferents. Some targets are direct, as with the inhibitory circuitry and the neurotrophins BDNF and NT4; some are indirect, in that the action of the neurotrophin is mediated by a neuromodulatory system, such as the cholinergic system. The possible sites of action of neurotrophins in visual cortical plasticity are sketched in Figure 4.10. It is evident that neurotrophin action is not limited to thalamic afferents but involves both cortical circuitry and subcortical afferents.

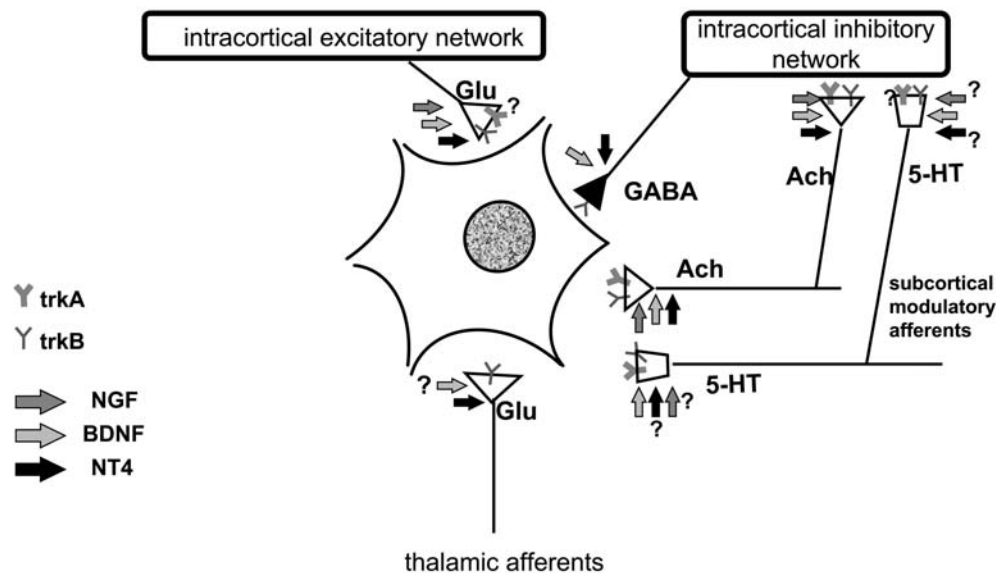


FIGURE 4.10. Possible sites of action of neurotrophins on visual cortical plasticity. Synergistic and antagonistic effects of neurotrophins, however clearly possible, are not included in the model. Even so, it is clear that several neural circuits are involved. Some targets of neurotrophin action could be common, such as the basal

forebrain cholinergic neurons or the intracortical excitatory circuitry. Some could be specific targets for specific neurotrophins; for instance, NT4 seems to be most effective on thalamic afferents, and BDNF/NT4 seem to be specifically active on inhibitory intracortical circuitry.

Up to 10 years ago, neurotrophins were known for their involvement in survival, differentiation, and maintenance of specific classes of neurons in the PNS. Now the scenario has completely changed, and their involvement is at least equally prominent in the CNS. In the CNS, however, neurotrophins are not survival factors for neurons, but rather survival factors for neural connections. In the developing CNS, neurotrophins are essential for the formation, maintenance, and plasticity of synaptic contacts and are crucial for the development of sensory functions. In adult life, they are likely to be still at work in the control of cortical plasticity, and modifications of their activity could be responsible for the slow decline of cognitive functions with age.

REFERENCES

- Berardi, N., A. Cellerino, L. Domenici, M. Fagiolini, T. Pizzorusso, A. Cattaneo, and L. Maffei, 1994. Monoclonal antibodies to nerve growth factor affect the postnatal development of the visual system, *Proc. Natl. Acad. Sci. USA*, 91:684–688.
- Berardi, N., and L. Maffei, 1999. From visual experience to visual function, *J. Neurobiol.*, 41(1):119–126.
- Berardi, N., T. Pizzorusso, and L. Maffei, 2000. Critical periods during sensory development, *Curr. Opin. Neurobiol.*, 10(1):138–145.
- Bloch, A., and H. Thoenen, 1995. Characterization of nerve growth factor (NGF) release from hippocampal neurons: evidence for a constitutive and an unconventional sodium-dependent regulated pathway, *Eur. J. Neurosci.*, 7(6):1220–1228.
- Bothwell, M., 1995. Functional interactions of neurotrophins and neurotrophin receptor, *Annu. Rev. Neurosci.*, 18:223–253.
- Cabelli, J., A. Hohn, and C. J. Shatz, 1995. Inhibition of ocular dominance column formation by infusion of NT-4/5 or BDNF, *Science*, 267:1662–1666.
- Cabelli, R. J., D. L. Shelton, R. A. Segal, and C. J. Shatz, 1997. Blockade of endogenous ligands of TrkB inhibits formation of ocular dominance columns, *Neuron*, 19:63–76.
- Caleo, M., C. Lodovichi, and L. Maffei, 1999. Effects of nerve growth factor on visual cortical plasticity require afferent electrical activity, *Eur. J. Neurosci.*, 11(8):2979–2984.
- Caleo, M., E. Menna, S. Chierzi, M. C. Cenni, and L. Maffei, 2000. Brain-derived neurotrophic factor is an anterograde survival factor in the rat visual system, *Curr. Biol.*, 10(19):1155–1161.
- Castren, E., M. Pitkanen, J. Sirvio, A. Parsadanian, D. Lindholm, H. Thoenen, and P. J. Riekkinen, 1993. The induction of LTP increases BDNF and NGF mRNA but decreases NT-3 mRNA in the dentate gyrus, *Neuroreport*, 4(7):895–898.
- Castren, E., F. Zafra, H. Thoenen, and D. Lindholm, 1992. Light regulates expression of brain-derived neurotrophic factor mRNA in the rat visual cortex, *Proc. Natl. Acad. Sci. USA*, 89:9444–9448.
- Cellerino, A., and L. Maffei, 1996. The action of neurotrophins in the development and plasticity of the visual cortex, *Prog. Neurobiol.*, 49:53–71.
- Crair, M. C., D. C. Gillespie, and M. P. Stryker, 1998. The role of visual experience in the development of columns in cat visual cortex, *Science*, 279(5350):566–570.
- Di Cristo, G., N. Berardi, L. Cancedda, T. Pizzorusso, E. Putignano, G. M. Ratto, and L. Maffei, 2001. Requirement of ERK activation for visual cortical plasticity, *Science*, 292(5525):2337–2340.
- Domenici, L., G. Fontanesi, A. Cottaneo, P. Bagroli and L. Maffei, 1996. Nerve growth factor (NGF) uptake and transport following injection in the developing rat visual cortex, *Vis. Neurosci.*, 11:1083–1102.
- Domenici, L., A. Cellerino, N. Berardi, A. Cattaneo, and L. Maffei, 1994. Antibodies to nerve growth factor (NGF) prolong the sensitive period for monocular deprivation in the rat, *Neuroreport*, 5:2041–2044.
- Domenici, L., N. Borardi, G. Comignolo, G. Vantini, and L. Maffei, 1991. Nerve growth factor promotes the amblyopic effects of monocular deprivation, *Proc. Natl. Acad. Sci. USA*, 88(19):8811–8815.
- Domenici, L., V. Parisi, and L. Maffei, 1992. Exogenous supply of NGF prevents the effects of strabismus in the rat, *Neuroscience*, 51:19–24.
- Ernfors, P., J. Bengzon, Z. Kokaia, H. Persson, and O. Lindvall, 1991. Increased levels of messenger RNAs for neurotrophic factors in the brain during kindling epileptogenesis, *Neuron*, 7(1):165–176.
- Fagiolini, M., and T. K. Hensch, 2000. Inhibitory threshold for critical-period activation in primary visual cortex, *Nature*, 404(6774):183–186.
- Fagiolini, M., T. Pizzorusso, N. Berardi, L. Domenici, and L. Maffei, 1994. Functional postnatal development of the rat primary visual cortex and the role of visual experience: dark-rearing and monocular deprivation, *Vis. Res.*, 34:709–720.
- Fagiolini, M., T. Pizzorusso, V. Porciatti, M. C. Cenni, and L. Maffei, 1997. Transplant of Schwann cells allows normal development of the visual cortex of dark-reared rats, *Eur. J. Neurosci.*, 9:102–112.
- Fagiolini, M., and M. P. Stryker, 1996. Delayed onset of NGF effects on ocular dominance plasticity in mice, *Soc. Neurosci. Abs.*, 22:682.11.
- Fiorentini, A., N. Berardi, and L. Maffei, 1995. Nerve growth factor preserves behavioral visual acuity in monocularly deprived kittens, *Vis. Neurosci.*, 12(1):51–55.
- Galuske, R. A. W., D.-S. Kim, E. Castren, H. Thoenen, and W. Singer, 1996. Brain-derived neurotrophic factor reverses experience-dependent synaptic modifications in kitten visual cortex, *Eur. J. Neurosci.*, 8:1554–1559.
- Grewal, S. S., R. D. York, and P. J. Stork, 1999. Extracellular-signal-regulated kinase signalling in neurons, *Curr. Opin. Neurobiol.*, 9(5):544–553.
- Hensch, T. K., M. Fagiolini, N. Mataga, M. P. Stryker, S. Baekkeskov, and S. F. Kash, 1998. Local GABA circuit control of experience-dependent plasticity in developing visual cortex, *Science*, 282(5393):1504–1508.
- Huang, Z. J., A. Kirkwood, T. Pizzorusso, V. Porciatti, B. Morales, M. F. Bear, L. Maffei, and S. Tonegawa, 1999. BDNF regulates the maturation of inhibition and the critical period of plasticity in mouse visual cortex, *Cell*, 98(6):739–755.
- Kafitz, K. W., C. R. Rose, H. Thoenen, and A. Konnerth, 1999. Neurotrophin-evoked rapid excitation through TrkB receptors, *Nature*, 401(6756):918–921.
- Kohara, K., A. Kitamura, M. Morishima, and T. Tsumoto, 2001. Activity-dependent transfer of brain-derived neurotrophic factor to postsynaptic neurons, *Science*, 291(5512):2419–2423.
- Levi-Montalcini, R., 1987. The nerve growth factor 35 years later, *Science*, 237:1154–1162.
- Lewin, G. R., and Y.-A. Barde, 1996. Physiology of the neurotrophins, *Annu. Rev. Neurosci.*, 19:289–317.

- Lodovichi, C., N. Berardi, T. Pizzorusso, and L. Maffei, 2000. Effects of neurotrophins on cortical plasticity: same or different? *J. Neurosci.*, 20(6):2155–2165.
- Maffei, L., L. Berardi, L. Domenici, V. Parisi, and T. Pizzorusso, 1992. Nerve growth factor (NGF) prevents the shift in ocular dominance distribution of visual cortical neurons in monocularly deprived rats, *J. Neurosci.*, 12:4651–4662.
- McAllister, A. K., D. C. Lo, and L. C. Katz, 1995. Neurotrophins regulate dendritic growth in developing visual cortex, *Neuron*, 15:791–803.
- McAllister, A. K., L. C. Katz, and D. C. Lo, 1997. Opposing roles for endogenous BDNF and NT-3 in regulating cortical dendritic growth, *Neuron*, 18:767–778.
- *McAllister, A. K., L. C. Katz, and D. C. Lo, 1999. Neurotrophins and synaptic plasticity, *Annu. Rev. Neurosci.*, 22:295–318.
- Pizzorusso, T., N. Berardi, F. M. Rossi, A. Viegi, K. Venstrom, L. F. Reichardt, and L. Maffei, 1999. TrkA activation in the rat visual cortex by antirat trkA IgG prevents the effect of monocular deprivation, *Eur. J. Neurosci.*, 11(1):204–212.
- Pizzorusso, T., and L. Maffei, 1996. Plasticity in the developing visual system, *Curr. Opin. Neurol.*, 9:122–125.
- Pizzorusso, T., V. Porciatti, J. L. Tseng, P. Aebischer, and L. Maffei, 1997. Transplant of polymer-encapsulated cells genetically engineered to release nerve growth factor allows a normal functional development of the visual cortex in dark-reared rats, *Neuroscience*, 80:307–311.
- Pizzorusso, T., G. M. Ratto, E. Putignano, and L. Maffei, 2000. Brain-derived neurotrophic factor causes cAMP response element-binding protein phosphorylation in absence of calcium increases in slices and cultured neurons from rat visual cortex, *J. Neurosci.*, 20(8):2809–2816.
- Pollock, G. S., E. Vernon, M. E. Forbes, Q. Yan, Y. T. Ma, T. Hsieh, R. Robichon, D. O. Frost, and J. E. Johnson, 2001. Effects of early visual experience and diurnal rhythms on BDNF mRNA and protein levels in the visual system, hippocampus, and cerebellum, *J. Neurosci.*, 21(11):3923–3931.
- Purves, D., 1988. *Body and Brain. A Trophic Theory of Neural Connections*. Cambridge: Harvard University Press.
- Ramoa, A. S., M. A. Paradiso, and R. D. Freeman, 1988. Blockade of intracortical inhibition in kitten striate cortex: effects on receptive field properties and associated loss of ocular dominance plasticity, *Exp. Brain. Res.*, 73(2):285–296.
- Reichardt, L. F., and I. Farinas, 1997. Neurotrophic factors and their receptors, in *Molecular and Cellular Approaches to Neural Development* (W. Maxwell Cowan, T. M. Jessel, and S. L. Zipursky, eds.), New York: Oxford University Press.
- Reiter, H. O., and M. P. Stryker, 1988. Neural plasticity without postsynaptic action potentials: less-active inputs become dominant when kitten visual cortical cells are pharmacologically inhibited, *Proc. Natl. Acad. Sci. USA*, 85(10):3623–3627.
- Riddle, D. R., D. C. Lo, and L. C. Katz, 1995. NT-4 mediated rescue of lateral geniculate neurons from effects of monocular deprivation, *Nature*, 378:189–191.
- Sala, R., A. Viegi, F. M. Rossi, T. Pizzorusso, G. Bonanno, M. Raiteri, and L. Maffei, 1998. NGF and BDNF increase transmitter release in the rat visual cortex, *Eur. J. Neurosci.*, 10:2185–2191.
- Shaw, C., and M. Cynader, 1984. Disruption of cortical activity prevents ocular dominance changes in monocularly deprived kittens, *Nature*, 308(5961):731–734.
- Thoenen, H., 1995. Neurotrophins and neuronal plasticity, *Science*, 270:593–598.
- Timney, B., D. E. Mitchell, and F. Giffin, 1978. The development of vision in cats after extended periods of dark-rearing, *Exp. Brain. Res.*, 31:547–560.
- Viegi, A., T. Cotrufo, N. Berardi, L. Mascia, and L. Maffei, 2002. Effects of dark rearing on phosphorylation of neurotrophin Trk receptors, *J. Neurosci.*, 16:1925–1930.
- von Bartheld, C. S., M. R. Byers, R. Williams, and M. Bothwell, 1996. Anterograde transport of neurotrophins and axodendritic transfer in the developing visual system, *Nature*, 379(6568):830–833.
- Wiesel, T. N., and D. H. Hubel, 1963. Single cell responses of striate cortex of kittens deprived of vision in one eye, *J. Neurophysiol.*, 26:1003–1017.
- Xiang, Z., J. R. Huguenard, and D. A. Prince, 1998. Cholinergic switching within neocortical inhibitory networks, *Science*, 281(5379):985–988.
- Zafra, F., B. Hengerer, J. Leibrock, H. Thoenen, and D. Lindholm, 1990. Activity dependent regulation of BDNF and NGF mRNAs in the rat hippocampus is mediated by non-NMDA glutamate receptors, *EMBO J.*, 9(11):3545–3550.

5 Developmental and Genetic Control of Cell Number in the Retina

ROBERT W. WILLIAMS AND SALLY A. MOODY

Now, nearly a century after Weismann, it is self-evident that the missing chapters of the Modern Synthesis—the merging of genetics with development and the merging of development with evolution—remain the major tasks before us. Buss (1987)

Introduction

The retina is one of the most highly conserved parts of the central nervous system (CNS), with unambiguous homology of major cell types among most chordates. These cells and their progenitors therefore share common patterns of gene activity. This widespread commonality is illustrated most dramatically by the *Pax6* genes—a small family of transcription factors that trigger the formation of retinas, ommatidia, and photoreceptors in animals as diverse as fruit flies, squid, ascidians, fish, frogs, mice, and humans (Gehring and Ikeo, 1999; Onuma et al., 2002).

Retinas differ strikingly, however, in terms of the number and distribution of cells. Structural diversity of the vertebrate retina is generated using a relatively constant palette of cell types (Walls, 1942). Downstream effects mediated by transcription factors such as *Pax6*, and a rapidly expanding list of trophins, hormones, cytokines, and other signaling molecules, can produce significant changes in the number and ratio of cells and their interconnections. Evolution of the retina has therefore involved the episodic modulation of developmental processes that often adjust quantities, not quality.

The contrast between universal mechanisms and structural diversity highlights the need to study development using complementary approaches. The first approach focuses on fundamental qualitative features that are common denominators; the second approach focuses on quantitative adaptations of genetic networks that underlie functional and evolutionary transformations, as well as individual differences. This review is divided into sections that consider developmental, genetic, and functional factors that modulate the types and numbers of cells in the vertebrate retina from these two complementary viewpoints.

There are approximately 65 to 70 distinct cell types in the retina (Marc and Jones, 2002; Chapter 20, Retinal Neurotransmitters), each with its own idiosyncratic developmental history, and we only consider key themes and a few exem-

plar cell types. In Part 1, we cover the initial stages of visual system development, in which cell proliferation and differentiation produce the cellular substrates common to all vertebrate retinas. Most of our examples are drawn from studies of the South African clawed frog, *Xenopus laevis*, a long-favored experimental subject for developmental analyses. In Part 2, we consider the relation between cell number and visual system performance, addressing the question of how much variation is tolerated within species and why. Finally, we describe a novel approach called *complex trait analysis* that is being used to uncover the genetic basis of individual differences in retinal development. Combined developmental and genetic approaches should eventually provide a much better understanding of how evolutionary modifications have produced such amazing arrays of almost perfectly adapted eyes and retinas, a subject that gave Darwin serious pause (and a cold chill) a century and a half ago (Darwin, 1899; Dawkins, 1996).

PART 1: THE GENERATION OF A MENAGERIE OF RETINAL CELLS

A wide variety of retinal cell types are generated in appropriate numbers by sequential and cooperative changes in patterns of gene expression that are coupled with cell division, cell differentiation, and cell death. These changes start at very early stages, even before gastrulation and the establishment of the neural plate, and changes continue through to late stages of fetal development. Differentiation and cell division are directed by factors that act at different spatial scales and stages, but both ultimately affect the activity of enhancer and promoter response elements in single cells. Broadly speaking, these factors include (1) inherited maternal determinants, (2) regional molecular gradients, (3) cell autonomous lineage factors, and (4) local intercellular signals. In this section we consider some of the key mechanisms involved in selecting the embryonic progenitors of the retina, partitioning part of the forebrain neuroectoderm into a field of specified retinal stem cells, and the progressive differentiation of the many cell types common to all vertebrate retinas that are eventually derived from these stem cells.

Molecular complexity of the retina

The adult retina expresses at least 25,000 transcripts from over 20,000 genes (Sharon et al., 2002). Even more genes are likely to be expressed throughout development. The majority of these genes undoubtedly have common roles in cellular differentiation and metabolism, but a significant fraction—including many so-called housekeeping genes—are likely to contribute to unique features of retinal development and function. This is demonstrated clearly by the fact that over 10% of 12,422 transcripts quantified in triplicate using microarrays (Affymetrics U74Av2) differ more than twofold in abundance between retina and other brain regions such as cerebellum, brainstem, and forebrain (see the databases at www.nervenet.org/array). Even with modest numbers of samples, the expression levels of well over 20% of retinal transcripts differ significantly from forebrain transcripts using standard statistical criteria at the $p < 0.05$ level.

Given the imposing molecular complexity of development of the eye and retina, the reliability of the process is astonishing. The robust molecular systems that ensure the production of a functional retina clearly are built on a principle of genetic redundancy and feedback interactions. While a few genes are essential for eye development (e.g., *Pax6*), most genetic processes are sensitive to context and can adapt to significant perturbations. The inactivation of important genes is often associated with only mild ocular and retinal effects. For example, the loss of the retinoic acid alpha receptor early in retinal development has essentially no effect on the inner retina despite early and intense expression among the pool of progenitors (Mori et al., 2001; Zhou et al., 2001). A process that is controlled by a complex developmental network involving genetic and epigenetic interactions is likely to produce greater variance and flexibility, and is also likely to be more resistant to environmental perturbations (Waddington and Robertson, 1966). As presented below, flexibility is built into the retinal developmental program from beginning (progenitor competence) to end (cell type specification).

The first step: selecting competent retinal progenitors

Retinal development can be divided into several steps, some of which occur even before overt morphogenesis of the eye cup (Fig. 5.1). First, a subset of the pluripotent embryonic cells acquires the competence to contribute to the retina. From this competent pool, a smaller subset is biased to become the retina-forming cells. Later, a specified retinal stem cell population emerges from the descendants of the biased embryonic cells to form the eye field in the anterior neural plate. Further interactions during neural tube morphogenesis segregate this population into three major com-

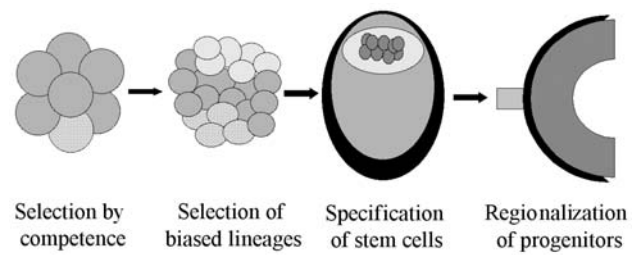


FIGURE 5.1. Early steps of retinogenesis. Retinal development begins with several steps that set aside embryonic precursors. First, a subset of embryonic cells (green) becomes competent to contribute to the retina. The blue-hatched cell is inhibited from forming retina. Next, a smaller subset (yellow) is biased to become the retina-forming cells. Then a specified retinal stem cell population (red) emerges from the descendants of the biased embryonic cells (yellow) to form the eye field in the anterior neural plate (green). Finally, during neural tube morphogenesis, this specified population is segregated into three major compartments: neural retina (red), pigmented retina (black), and optic stalk (blue). (See color plate 1.)

partments: neural retina, pigmented retina, and optic stalk. Each of these compartments goes on to produce different subsets of specialized cells with distinct functions in the mature eye.

An initial question is, how and when during development do pluripotent embryonic cells acquire the differential competence to contribute to the retina? Is this a partly stochastic process, or do early factors bias or restrict the selection of retina-forming embryonic progenitors? *Xenopus* embryos have been crucial for studying the roles of maternal determinants, lineage effects, and cell-cell inductions at this early stage (even before gastrulation) because eggs and blastomeres are large and easily manipulated (Moody, 1999). Each retina in *Xenopus* descends from a stereotypic subset of 9 animal blastomeres at the 32-cell stage (Fig. 5.2), and each of these blastomeres produces characteristic proportions of the cells that make up the mature retina (Huang and Moody, 1993). Are these nine cells the only cells that are competent to form the retina, and just how fixed is their commitment to a retinal fate?

These questions have been largely answered by transplanting single cells to novel positions at a very early stage when only maternally inherited transcripts are expressed. The first key finding is that even at this stage, not all blastomeres are equally competent to contribute to the retina. For example, vegetal blastomeres transplanted to the most retinogenic coordinates never contribute progeny to the retina (Huang and Moody, 1993). This developmental restriction could not be overcome by providing components of the known maternal signaling pathways involved in neural and dorsal fate specification (see below), even in situations in which ectopic heads and eyes were induced successfully (Moore and Moody, 1999).

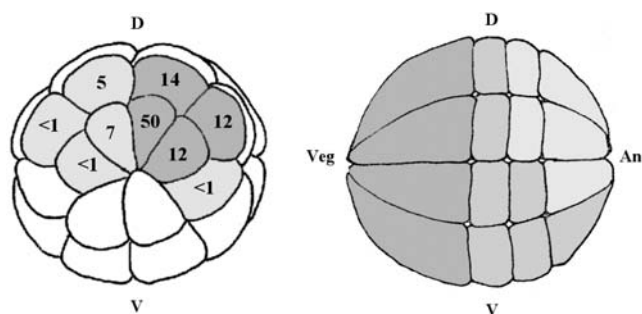


FIGURE 5.2. Retina competent and biased blastomeres in *Xenopus laevis* embryos. *Left*: animal pole view of a 32-cell embryo showing the major (orange) and minor (yellow) blastomeres that contribute to the retina. The numbers within each cell indicate the percentage of retinal cells that derive on average from each blastomere. *Right*: side view of a 32-cell embryo showing the retina-forming blastomeres (yellow), the blastomeres that do not make retina but are competent to do so (green), and the vegetal blastomeres that are inhibited by maternal factors from making retina (blue). Data are from Huang and Moody (1993). An, animal pole; D, dorsal; V, ventral; Veg, vegetal pole. (See color plate 2.)

These results indicate that vegetal blastomeres contain one or more maternal molecules that repress the transcription of genes that are critical in the initial steps of retinal differentiation.

Other blastomeres are not so refractive. Both ventral animal blastomeres and equatorial blastomeres that normally do not contribute progeny to the retina can reprogram when transplanted to the center of the retinogenic zone (Huang and Moody, 1993). Furthermore, if the most retinogenic blastomere is deleted, a ventral implant will be respecified in response to interactions with neighboring cells to help produce a normal-sized retina (Huang and Moody, 1993).

Complementing these findings, the retina-forming blastomeres are biased but not completely committed. When transplanted to a ventral vegetal site that normally produces gut and tail, they retain their neural fate but fail to make retina (Gallagher et al., 1991). Collectively, these embryonic manipulations demonstrate that the correct cellular coordinates within the animal hemisphere are necessary from the earliest stage for a blastomere to produce its normal cohort of mature retinal cells.

The position-specific selection of retina-forming blastomeres from the competent pool appears to be mediated by the local signaling environment within the blastula. The ectopic expression of components of several growth factor pathways involved in embryo patterning, such as activin, fibroblast growth factor (FGF), and bone morphogenetic protein (BMP), demonstrates that competent blastomeres acquire the ability to express a retinal fate by being located in an environment in which BMP signaling is repressed (Moore and Moody, 1999). Expression of BMP4 in a

blastomere that normally is a major contributor to the retina inhibits its retinal fate, whereas repressing BMP signaling in a blastomere that normally gives rise to epidermis induces retinal cells within that lineage. Consistent with this model in frog, *Bmp7* null mice are anophthalmic (Dudley et al., 1995) and rat embryos cultured in anti-BMP7 antibodies have reduced or absent eyes (Solorsh et al., 1996). The inhibition of BMP signaling in the dorsal part of the embryo defines the domain of presumptive retina, just as it defines the domain of presumptive neural plate (Harland, 2000).

Although fate maps show that there are nine retina-forming blastomeres in *Xenopus* (Fig. 5.2), not every one of these cells contributes to retina in every embryo. In the initial map (Moody, 1987), the major progenitors contributed to retina 85–100% of the time, whereas the minor progenitors contributed only 20–50% of the time. Thus, there is surprising individual variation in the number of embryonic cells that produce the retinal lineage. There also is individual variation in the number of retinal cells descended from each retina-forming blastomere (Huang and Moody, 1993). For the major progenitor, there is a 2-fold range in descendants between embryos, but for the others there is as much as a 10-fold range. These data have been verified in many subsequent studies using similar techniques. They demonstrate that the ultimate numbers of progeny produced by each lineage are not predetermined and that individual variation is well tolerated within consistent limits. This is apparently just as true in mammals as in *Xenopus* (Goldowitz et al., 1996; Williams and Goldowitz, 1992a).

The second step: specifying stem cells

The next step in retinogenesis is to select from the competent pool those cells that will become specified as retinal stem cells (Fig. 5.1). After the neural plate is established, it is subdivided into fields that give rise to different CNS domains. Both retinas arise from a common anterior midline group of cells called the *eye field*, which is specified as the sole source of retinal cells when the neural plate is established (Perron and Harris, 1999; Saha and Grainger, 1992).

A number of transcription factors regulate pattern formation in the anterior neural plate and eye field, and they are crucial in determining whether neuroepithelial cells express a retinal fate as opposed to another anterior neural fate. *Otx2*, a vertebrate homolog of the *Drosophila orthodenticle* gene, has at least two potential functions in the formation of the eye field. Early *Otx2* expression in the anterior endoderm appears necessary for the induction of the anterior neural plate (Acampora et al., 1995; Ang et al., 1996; Rhinn et al., 1998), and its continued expression is required to initiate or maintain the expression of several other key neurogenic factors (Rhinn et al., 1998), leading to the

regionalization of the neural plate that allows the eye field to form. *Bf1*, a fork head/winged helix transcription factor, is expressed in the forebrain and in the future nasal retina (Hatini et al., 1994; Tao and Lai, 1992). The *Xenopus* homolog *Fkh4* is expressed in the anterior margin of the neural plate and then in the eye field (Dirksen and Jamrich, 1995). *Pax6*, the potent paired box and homeodomain transcription factor mentioned in the Introduction, is highly expressed in the eye field, and its ectopic expression causes the formation of ectopic eye structures in fly and frog (Altmann et al., 1997; Chow et al., 1999; Halder et al., 1995; Kenyon et al., 2001). *Rx1*, a novel homeobox gene, is expressed exclusively in the eye field, retina, and pineal gland (Casarosa et al., 1997; Furukawa et al., 1997; Mathers et al., 1997). Its overexpression in *Xenopus* causes enlargement of native eye tissue and ectopic patches of pigmented retina (Kenyon et al., 2001; Mathers et al., 1997). *Six3*, related to the *Drosophila sine oculis* gene, is expressed in the eye field and optic vesicle (Oliver et al., 1995). Overexpression of mouse *Six3* in fish or mouse causes ectopic retinal tissues to form (Lagutin et al., 2001; Loosli et al., 1999). Another *six* family gene, *Otx2*, is also expressed in the eye field and optic vesicle (Toy et al., 1998), and when *Otx2* is overexpressed, it transforms more caudal neural plate into eye field (Bernier et al., 2000). Loss-of-function mutations of *Bf1*, *Otx2*, *Pax6*, and *Rx1* each lead to loss of retinal tissue, indicating that all are likely to have important roles during establishment of the eye field.

The segregation of the anterior neural plate into eye field versus non-eye field domains is likely to result from the localized expression of several transcription factors, including those described above, which then initiate eye-specific transcriptional programs. In addition, some of these genes are involved in even earlier retinal fate decisions. *Otx2*, *Pax6*, and *Rx1* are expressed more widely and diffusely at stages just before the formation of the eye field, and they can cause ventral epidermal-forming blastomeres to contribute to retina by altering gastrulation movements that allow their descendants access to the eye field (Kenyon et al., 2001). Thus, these genes appear to regulate the selection of retinal stem cells at multiple levels: transcriptional modulation, signaling, and cell movements.

This complex program of selecting retina-specific stem cells provides several opportunities for adjustments in cell number. From the pregastrula competent pool of cells, only a subset forms the eye field. Expressing the correct genetic program increases the probability of competent cells being selected to become retinal stem cells. For example, in the experiments of Kenyon et al. (2001), not every cell that ectopically expressed the exogenously supplied retinal gene expressed a retinal fate. Some cells migrated into the eye field and others did not. Some of the ventrally derived retinal clones were composed of hundreds of cells, and some were composed of fewer than ten cells. These data indicate that

there are local cues that also influence these fate decisions. Subtle epigenetic variations in these cues have significant effects on final retinal cell numbers by altering the size of the initial stem cell pool.

The third step: specification of different cell types

After the compartmental domains of the future eye are defined during neural plate and neural tube stages, cells within the optic cup begin to differentiate into the many different cell types that characterize the functional vertebrate retina. They exit the cell cycle in a defined spatiotemporal pattern, migrate to appropriate layers, turn on the correct neurotransmitters or visual pigments, and develop the correct pre- and postsynaptic connections. The ganglion cells project long axons to very distinct targets, whereas intrinsic cells make highly specialized connections locally. Intricate choreography! A large number of factors and interactions affect the diversity and number of distinct retinal cell types that are generated during this period of retinogenesis (reviewed in Cepko, 1999; Harris, 1997; Livesey and Cepko, 2001; Vetter and Brown, 2001; Vetter and Moore, 2001).

ROLES OF ENVIRONMENTAL AND LINEAGE IN CELL FATE The optic cup was one of the first vertebrate tissues in which the issue of lineage regulation of cell phenotype specification was addressed. Vertebrate embryos, with their enormous numbers of cells, are difficult subjects for complete lineage studies because it is not technically feasible to map every mitotic division. Nonetheless, parts of retinal lineages have been defined by intracellular injection of tracers into proliferating cells of the optic vesicle/cup (Holt et al., 1988; Wetts and Fraser, 1988) or by injecting a recombinant retrovirus that infects proliferating cells and marks their clones (Turner and Cepko, 1987; Turner et al., 1990). Both techniques showed that dividing cells of the optic vesicle/cup are multipotent; labeled clones spanned the entire thickness of the retina and were composed of various combinations of cells. They also retain striking pluripotency right up to their last division, often producing daughters consisting of two very different cell types—for example, Müller glial cells and bipolar cells (Turner and Cepko, 1987). The great majority of retinal stem cells are not committed to produce only a single phenotype, nor do they appear to be restricted to an identifiable invariant combination of cell types.

With the exception of retinal astrocytes, which originate from separate progenitors in the optic stalk (Chang-Ling and Stone, 1991), it was initially thought that lineage restriction plays little if any role in determining types or numbers of retinal cells. However, the amazing diversity in the cellular composition and size of clones labeled at very early stages (Williams and Goldowitz, 1992a) suggested the presence of

matched heterogeneity among retinal progenitors, which implies some form of differential commitment of the progenitors (Goldowitz et al., 1996; Williams and Goldowitz, 1992b). The original lineage tracing techniques could not label single identified progenitors across different animals—a criterion by which lineage mechanisms are usually identified—and this left the original data open to alternative interpretations.

MULTIPLE RETINAL STEM CELL TYPES We now know that the eye field stem cells are a heterogeneous population (Dyer and Cepko, 2001; Moody et al., 2000). There are at least two kinds of cells, those that produce radial clones and those that produce layer-restricted clones. In *Xenopus* these two progenitors differ in the layer distribution of their constituents, their cellular complexity, and the number of cell divisions remaining in their respective lineages. These two different eye field stem cell types may represent either two different determinative states or separate lineages for the early-formed primary (layered) versus later-formed secondary (radial) retina, similar to what has been described for neural plate progenitors of primary and secondary spinal neurons (Hartenstein, 1989). Two kinds of clones (single cells and radial columns) also have been described in the early chick and mouse retina (Fekete et al., 1994; Reese et al., 1999). Cellular diversity in type and number could easily be generated by changes in the processes that separate the original stem cell pool into different subsets of progenitors that have different ultimate fates. This could result in correlated shifts in populations that participate in common visual function—a primary example being scotopic and photopic subsystems.

Although lineage studies show that progenitor cells in the optic vesicle and cup are multipotent, recent *in vitro* studies also suggest that this pool contains differentially biased precursors (Alexiades and Cepko, 1997; Bellevue and Cepko, 1999; Jensen and Raff, 1997; Marrow et al., 1998). In fact, the concept that retinal lineages are not homogeneously multipotent but are differentially biased was elegantly demonstrated by a statistical analysis (Williams and Goldowitz, 1992b) of published data (Turner et al., 1990); the frequency of clones containing only two cell types was much higher than expected, and the frequency of clones extending across all layers was much lower than expected. Furthermore, *in vitro* studies showed that some rat optic cup progenitors are biased to produce amacrine and horizontal cells (Alexiades and Cepko, 1997). Other progenitors appear biased to produce either rod or bipolar cells (Marrow et al., 1999).

One model put forward to reconcile the strong evidence of extrinsic control of retinal cell differentiation and the strong evidence of fate-biased determination acting via committed progenitors is simply that retinal progenitors pass

through a series of determinative states, each of which is intrinsically specified to respond to particular environmental cues that influence the cell types produced (Cepko, 1999). For example, embryonic retinal progenitor cells differ in many characteristics from neonatal ones (Alexiades and Cepko, 1997; Lillien and Cepko, 1992; Marrow et al., 1998; Waid and McLoon, 1995; Watanabe and Raff, 1990), and these states can be influenced by the presence of other cell populations (Austin et al., 1995; Bellevue and Cepko, 1999; Reh, 1992; Reh and Tully, 1986; Waid and McLoon, 1998) and cytokines (Harris, 1997). An important aspect of this process is a cell-autonomous “clock” that regulates the competence of progenitors (Rapaport et al., 2001). Subtle changes in the timing of the determinative states and/or progenitor competence could be significant contributors to individual variation in cell numbers and types.

LINEAGE BIAS OF SOME AMACRINE SUBTYPES One approach used to eliminate the problem of labeling progenitors at random was to map the origins of specific cell types from the “identified” retina-forming blastomeres of the 32-cell frog embryo (Fig. 5.2). When specific progeny within retinal clones were identified by neurotransmitter expression, certain subtypes of amacrine cells—dopamine (DA), neuropeptide Y (NPY), and serotonin (5-hydroxytryptamine, 5-HT) were observed to arise from different subsets of blastomeres, whereas others (GABA, glycine) did not (Huang and Moody, 1995, 1997). This novel information likely was revealed because blastomeres can be consistently identified, unlike single progenitors in the optic cup, and each subtype of cell may follow its own subprogram of developmental instructions that would not be obvious from studying the broad population. This proposed lineage bias of DA, NPY, and 5-HT amacrine cell specification could result from the asymmetric distribution of intrinsic (i.e., maternal) factors that autonomously influence the different amacrine fates, or from inductive signaling related to the position in which the blastomere descendants differentiate. To test whether amacrine fate is intrinsically biased, blastomeres with distinct amacrine fates were transplanted to a position that normally expresses a different amacrine fate (Moody et al., 2000). A lateral animal blastomere expressed its normal, large number of DA amacrine cells after it was transplanted into a position that normally produces few of these cells, suggesting an intrinsic bias in amacrine fate within this lineage. However, another blastomere changed amacrine fate in accord with its new position. These experiments illustrate that the retina-producing blastomeres are already a mosaic of intrinsically biased and positionally specified progenitors.

At later stages of development, there also is evidence for lineage bias in the specification of amacrine cell subtypes.

When DA, NPY, and 5-HT amacrine cell subtypes first differentiate, they are arranged as single cells scattered across the inner nuclear layer (Huang and Moody, 1995, 1997). As more cells differentiate, the first cells are joined by like-expressing cells to form small clusters (Huang and Moody, 1995, 1997). If amacrine cell clusters are induced to express the same neurotransmitter by local interactions with their peers, then clusters should form even in the absence of cell division and after the emergence of the first amacrine cell. This is true of 5-HT clusters (Moody et al., 2000). In sharp contrast, DA and NPY clusters are virtually eliminated by blocking mitosis, indicating that cells in these clusters are generated by continued asymmetrical divisions of a strongly biased lineage. An important point is that even within a single cell class, specification of subtypes can be modulated by surprisingly different processes and at different stages of development.

LOCAL INTERCELLULAR SIGNALS Local signaling in the developing retina is critical in the progressive changes in retinal progenitors and in the subsequent differentiation of many cell types (Adler and Hatlee, 1989; Gan et al., 1996, 1999; Harris, 1997; Reh, 1992; Repka and Adler, 1992). A growing number of secreted factors have effects on cellular differentiation, usually as assayed in tissue culture and explants. Ciliary neurotrophic factor (CNTF) (Ezzeddine et al., 1997; Fuhrmann et al., 1995; Kirsch et al., 1996), brain-derived neurotrophic factor (BDNF) (Rickman and Rickman, 1996), (GDNF) (Politi et al., 2001), (TGF α) (Lillien, 1995), retinoic acid and thyroid hormone (Kelley et al., 1994, 1995), *sonic hedgehog* (Shh) (Levine et al., 1997), FGFs (Hyer et al., 1998; McFarlane et al., 1998; Opas and Dziak, 1994; Pittack et al., 1991, 1997), and BMPs (Belecky-Adams and Adler, 2001) all appear to have important roles in discriminating among different retinal class fates, in some cases also shifting relative numbers of early- and late-generated cell types. Activin signaling, for example, decreases the number of photoreceptors and increases the number of nonphotoreceptor cells present in low-density retinal cultures in a dose-dependent manner (Davis et al., 2000). Retinoic acid can do the opposite (Kelley et al., 1994). Chick ganglion cells express BMP receptors, and retinal explants exposed to BMPs contain enhanced numbers of ganglion cells (Carri et al., 1998). FGF2 has been reported to either stimulate (Hicks and Courtois, 1992) or suppress (Perron and Harris, 1999) photoreceptor numbers. There is convincing evidence that in the intact embryo, FGF2 may not alter photoreceptor number per se but may affect the ratio of rods to cones (Patel and McFarlane, 2000). Increased FGF2 signaling also reduces the number of Müller glial cells and increases the number of retinal ganglion cells (Patel and McFarlane, 2000). These examples highlight the fact that signaling factors have diverse effects on cell fate specifica-

tion. Local signaling can profoundly influence the cell types generated in culture.

RETINAL TRANSCRIPTIONAL CASCADES A large number of transcriptional regulators are involved in retinal cell fate decisions. Several of the same genes that establish the eye field also are expressed in distinct patterns in the developing retina (Perron and Harris, 1999). *Otx2*, *Pax6*, *Rx1*, and *Six3* are expressed by the stem cells at the margins of the retina, and it has been proposed that their collective expression maintains a retinal identity in these cells (Perron et al., 1998). *Otx2* has been implicated in transforming pigmented retina into neural retina (Toy et al., 1998). Many of these genes also are implicated in regulating the proliferation of the optic vesicle and cup progenitor cells (Loosli et al., 2001; Martinez-Morales et al., 2001). For example, retinoblasts transfected with *Otx2* produce clones that are twofold larger than control clones, and its overexpression early in embryogenesis results in giant eyes (Zuber et al., 1999).

Furthermore, eye field genes are expressed differentially as retinal cells differentiate (Perron and Harris, 1999). Ganglion and amacrine cells express *Pax6* and *Six3*; cells in the outer zone of the inner nuclear layer express *Six3*, *Rx1*, and *Otx2*; and photoreceptor cells express *Rx1*. Added to this complexity is the differential expression of a large number of basic helix-loop-helix (bHLH) differentiation factors (Perron and Harris, 1999; Vetter and Brown, 2001). Different combinations of these latter genes are expressed as cells transit from the purely stem cell zone at the margin, through more restricted progenitor zones, and finally into their retinal layers. Photoreceptors require *NeuroD* and *Ngn2*; bipolar cells require *Ash1*, *Ash3*, and *Ngn2*; amacrine cells require *NeuroD* and *Ath3*; and ganglion cells require *Ath5*. There is compelling evidence that *Pax6* directly regulates several of the bHLH genes (Marquardt et al., 2001) and that *Pax6*, *Six3*, and *Rx1* modulate a cell's responsiveness to the bHLH genes (Inoue et al., 2002).

Many of these genes also cross-regulate each other: when a gene manipulation eliminates one cell class, other classes are significantly enlarged. This indicates that the transcriptional program that specifies one cell type is interrelated with programs that specify other cell types, forming transcriptional webs. This suggests that individual and evolutionary changes in the expression of single genes, the main topic of the next section, will frequently have pleiotropic effects that lead to coordinate changes in several cell types.

PART 2: FUNCTIONAL AND GENETIC ANALYSIS OF INDIVIDUAL DIFFERENCES

The types and numbers of cells that are generated and distributed across the retina represent an explicit, although still incompletely deciphered, summary of a species' relationship

with its visual world (Hayes and Brooke, 1990; Østerberg, 1935; Walls, 1942). These cellular parameters can be modified relatively rapidly in response to changes in selective pressure (Jeffery and Martasian, 1998; Jeffery et al., 2000; Williams et al., 1993). Variation is by no means limited to retina, and there are even more striking quantitative differences in the size and structure of the complex quilt of visual areas that extend from occipital pole into temporal and parietal neocortex of mammals (Chapter 32, Organization of Visual Areas in Macaque and Human Cerebral Cortex; Chapter 105, the Evolution of the Visual System in Primates).

In this part, we first consider the functional relevance of variation in numbers of neurons and photoreceptors and review what we are beginning to learn about the genetic basis of individual differences within species. As illustrated by a few specific examples as the end of this part, variation in retinal structure traces back to specific allelic differences that affect developmental processes.

Functional perspective on cell population size

NEED FOR LARGE NUMBERS An enormous number of cells and synapses are needed to generate and interpret multiple neural representations of the visual world. The advantage of having large numbers of cells is most obvious in the vertebrate fovea (e.g., Collin and Collin, 1999; Wikler et al., 1990). Cones are often packed together in a tight triangular mosaic with peak densities that reach up to 300,000/mm² in humans (Curcio et al., 1987, 1990). Trios of photoreceptors, midretinal bipolar cells, and retinal ganglion cells are organized with nearly pixel-like precision to recapture and transmit the high spatial frequencies into the central visual system. Several remarkable developmental events help to generate large numbers of these cells in central retina (Hendrickson, 1994; LaVail et al., 1991; Lia et al., 1987; Provis et al., 1998; Springer, 1999), the most surprising being a shift of cones toward fovea from surrounding retina late in retinal development (Packer et al., 1990).

The need for large numbers cascades through the dorsal lateral geniculate nucleus (LGN) to the primary visual cortex. Ratios of retinal ganglion cells and projection neurons in the LGN are close to 1:1 in both rhesus monkeys and humans (Spear et al., 1996; Williams and Rakic, 1988). Cell densities are about 25% higher in the posterior region that represents fovea (Ahmad and Spear, 1993). The numbers increase 300- to 400-fold in visual cortex. An average of 350 million neurons are packed into area 17 of both macaques and humans (Suner and Rakic, 1996; Tolhurst and Ling, 1988). Cell densities may be twice as high as those in other neocortical areas (Powell and Hendrickson, 1981; Rockel et al., 1980). A staggering 2–3 trillion synapses are involved in the first stage cortical analysis of the visual world (Colonnier and O’Kusky, 1981; O’Kusky and Colonnier,

1982). Further amplifying these numbers, area 17 devotes disproportionate computational resources to the foveal representation. The central 1 mm² of both retinas contains a total of about 150,000 cones that view the central 12 square degrees of visual space. These receptors feed signals bilaterally to 400–500 mm² of visual cortex that contains approximately 50 million neurons and 150 billion synapses (estimate computed for both hemispheres by combining data in O’Kusky and Colonnier, 1982; Tolhurst and Ling, 1988; and van Essen et al., 1984).

FUNCTIONAL CORRELATE A behavioral corollary of high numbers in fovea and the visual cortex is extremely high acuity, that is, an ability to resolve spatial frequencies of 60–100 cycles per degree (Banks et al., 1991). Even more remarkable, humans can detect misalignments of short line segments finer than the grain of the photoreceptor mosaic. Detection thresholds can be as low as 10 arc-seconds. This computational feat, referred to as *vernier hyperacuity* (Kumar and Glaser, 1993; Westheimer, 1981), depends in part on maintaining high spatiotemporal precision across large numbers of coactivated neurons (Kandil and Fahle, 2001).

NUMBERS AND NEURAL NOISE Impressive visual capabilities of this type depend on minimizing noise at all levels of the retinogeniculocortical system. Noise is suppressed roughly as a function of the square root of n , where n is numbers of active neurons, synapses, and synaptic vesicle fusion events (Sterling, 1998). Small gains in signal-to-noise ratios may appreciably improve fitness due to increased acuity, and this in turn may have fueled steep evolutionary increases in numbers of cells in several vertebrate lineages. For example, the prominent expansion of the peristriate visual cortex in hominids may have been driven both by the complexity of simultaneously processing multiple streams of visual information (Dacey, 2000) and by selective pressure to improve the signal-to-noise ratios of cortical circuits.

EVEN LOW-LIGHT VISION REQUIRES LARGE NUMBERS OF CELLS Vision in low light also demands high numbers of cells, but for reasons other than visual acuity. A wide belt of the retina that usually surrounds the fovea at 10–15 degrees of eccentricity has rod densities that can rise to 500,000–850,000 cells/mm² in primates (Dkhissi-Benyahya et al., 2001; Wikler and Rakic, 1990), cats (Williams et al., 1993), and mice (Jeon et al., 1998). Even in the far periphery of humans, rod density is still typically above 40,000 cells/mm² (Williams, 1991).

An explanation for the high density and small size of rods is that they must be able to convert the absorption of a single photon into a distinct reduction in the transmitter release (Rodieck, 1998). This requires an exceedingly slender rod

outer segment in which a single photon will generate a sufficient reduction in cGMP concentration to shut cation channels. The high impedance of rods converts small fluctuations in outer segment currents into corresponding voltage fluctuations at the synaptic terminal. The great majority of the outer surface of the retina is tiled by rod outer segments to ensure efficient capture of the few photons available under low light. Their signals are averaged and integrated by AII amacrine cells, and these cells appear to define the acuity limit under low-light conditions (Mills and Massey, 1999), much as ganglion cell densities define the acuity limit in daylight.

Because of the inherent noise of the sporadic arrival of photons and receptor noise generated by spontaneous isomerization of rhodopsin and Poisson variance in vesicle release, detecting and interpreting objects in the dark is a challenging computational task. The consequence of these particular environmental and photochemical characteristics is that the population of rods in the human retina is incredibly high—typically ranging from 100 to 150 million (Curcio et al., 1990). Even a mouse retina has approximately 6 million rods. Having very large photoreceptor populations ensures high acuity (cones) in daylight or higher sensitivity and lowered noise levels (rods) in the dark.

CELL FUNCTION AND CELL NUMBERS The functional relationship between cell number and visual system performance is not always as clear-cut as suggested by these examples. There are approximately 60 cell types in the retina and certainly just as many or more in the central part of the visual system, each of which, by definition, makes somewhat different contributions to vision. Some cells, such as horizontal cells and the population of photosensitive retinal ganglion cells that project to hypothalamic circadian pacemaker cells, have computational roles that can best be summarized as averaging mean illuminance (Hattar et al., 2002). In the case of horizontal cells, this averaged signal provides a negative feedback to photoreceptors. Losing all horizontal cells has severe consequences, reducing retinal transduction efficiency and increasing the latency of visual evoked potentials in the cortex (Peachey et al., 1997). However, the crucial biometric parameter in this case is not numbers of channels but uniform field coverage. Small numbers of cells with extensive dendritic and axonal arbors may provide equivalent or even superior feedback compared to larger numbers of cells with smaller fields. Cells with this sort of role will have a number:performance function that is relatively flat or even negative when their numbers exceed the optimum.

EVOLUTIONARY FLEXIBILITY OF NUMBERS Given these considerations, populations of neurons in evolving species will ratchet up or down in numbers at somewhat idiosyncratic

rates that depend on their functional contributions to visual performance. For example, populations of rods are higher in domestic cats than in ancestral wildcats (Williams et al., 1993), and populations of retinal ganglion cells are lower in domestic cats and dogs than in wildcats and wolves (Peichl, 1992; Williams et al., 1993); in addition, both domestic species are likely to have lower acuity than their wild peers. Numbers of neurons will reach asymptotes at which further changes are blunted by countervailing selective pressure, such as the metabolic load associated with increased population size (Franco et al., 2000).

The final cell number is a compromise between the marginal utility of adding yet more cells and the metabolic costs that these extra neurons inevitably incur. An interesting consequence of reaching a functional asymptote is that cell populations within a species will typically be maintained at levels around which significant numerical deviation is surprisingly well tolerated by individual animals (see the list below). Near the asymptote, the relation between number and function is nearly flat, and visual system performance will be robust even in the face of surprisingly large deviations in numbers and ratios of cells that may be introduced by rare alleles and mutations, population admixture, developmental noise, environmental perturbation, or disease.

VARIATION WITHIN SPECIES AND GENOTYPE Ranges of normal variation in absolute numbers of cells and in ratios of cells within a species are often large. There is usually no obvious functional effect. The estimates of variation that are listed below come from small samples, and these examples therefore are likely to underestimate the actual range of variation. In most cases, the examples illustrate variation among individuals.

1. Foveal cone densities vary at least threefold among humans without retinal disease (Curcio et al., 1990; $n = 8$).
2. Ratios of L and M cones (red and green) in human central retina can range from 1:1 to 3.8:1 without evident (or with only subtle) differences in the categorization of colors (Roorda and Williams, 1999; $n = 2$).
3. Even within a single retina, the ratio of rods and cones can vary twofold. In one case, adjacent large fields in the periphery of a normal human retina had rod:cone ratios of 1:2 and 2:1 (Williams, 1991).
4. Twofold differences in horizontal cell number and density are common among normal inbred strains of mice (Williams et al., 1998a). A single strain of inbred mouse does not provide a good index of a typical ratio of cell types (see Williams et al., 1998b). For example, the ratio of ganglion cells to horizontal cells in mice varies from 3.2:1 to 6.7:1.
5. The population of retinal ganglion cells—the information bottleneck of the entire visual system—varies from 1,000,000 to 1,600,000 in humans and macaques (Provis et

al., 1985; Rakic and Riley, 1983; Spear et al., 1996). This population varies from 45,000 to 75,000 among strains of mice (Williams et al., 1996).

6. The population of projection neurons in the dorso-lateral geniculate varies as much as twofold within cat, mouse, and macaque (Ahmad and Spear, 1993; Williams and Rakic, 1988; $n < 10$ in cat and macaque; $n = 100$ in mouse). For example, in mouse, the population of projection neurons varies from 12,000 in CE/J to 22,000 in AKR/J (Kulkarni et al., 2000).

7. The surface area and cell population of primary visual cortex in both humans and macaques vary two- or even threefold (Gillisen and Zilles, 1996; Leuba and Kraftsik, 1994; Suner and Rakic, 1996; van Essen et al., 1984; $n \leq 20$).

8. Ocular dominance column numbers along the vertical meridian range from 101 to 154 in macaques. The width of columns ranges from 400 to nearly 700 μm (Horton and Hocking, 1996; $n = 12$ hemispheres).

THE PARADOX OF HIGH VARIATION The magnitude of this variation may be puzzling, particularly in species that are highly dependent on vision. Stabilizing selection, a process that normally trims away the tails of a distribution of phenotypes, would normally limit the range of variation that is tolerated in an interbreeding population. But the examples above provide ample demonstration that wide variation is well tolerated even in species, such as macaques and humans, that are utterly dependent on vision. The apparent paradox is resolved if we come back to the point that the visual system is overengineered and that there is much functional and developmental redundancy built into the retinas of most individuals. This also means that directional selection has plenty of variation with which to work on an evolutionary scale. Selection is highly effective in changing the cellular demographics of the retina and other parts of the visual system. Rapid changes in cell number have occurred in at least two carnivore lineages—wolves and wildcats—over an interval of less than 20,000 years (Peichl, 1992; Williams et al., 1993). In cats, the population of retinal ganglion cells has eroded from about 240,000 in wildcats to 160,000 in domestic cats. Even more extreme changes have been uncovered in response to rapid changes in habitat—for example, isolation in lightless cave systems in which the eyes regress due to the accumulation of deleterious mutations in genes critical at several stages of eye development (Jeffery and Martasian, 1998).

Genetic basis of individual difference in retinal structure

GENETIC POLYMORPHISM WITHIN SPECIES The striking differences in the retinal architecture of the mouse and the

human arose from natural genetic variation generated and selected within single species. Roughly one-fifth of the genes in most species have functional polymorphisms that produce changes in the electrophoretic mobility of the corresponding proteins. This reservoir of genetic variation often translates into correspondingly high heritability estimates for quantitative retinal traits (Williams, 2000; Zhou and Williams, 1999). For example, variation in retinal ganglion cell number in mice has a heritability above 80% (Williams et al., 1996), demonstrating strong genetic modulation of this population under typical laboratory conditions. The goal of a new field of genetics called *complex trait analysis* is to convert these bland estimates of heritability into the much more interesting and informative gene variants. These gene variants or polymorphisms can, in turn, be used to explore the genetic control of retinal development.

MENDELIAN AND QUANTITATIVE GENETICS Mendelian methods of gene analysis, with which most readers will be familiar, assume that single gene variants—usually rare alleles or mutations—generate essentially all interesting differences. For example, mutation of the tyrosinase gene (albinism) causes a 35% reduction in the fraction of retinal ganglion cells with ipsilateral projections in mice, regardless of genetic background (Rice et al., 1995).

In contrast to Mendelian genetics, complex trait analysis begins with the assumption that differences in cell populations are generated by the combined effects of a large number of polymorphic genes scattered across the genome. The goal is to map this set of genes to precisely delimited chromosomal locations and then proceed to identify these genes and the molecular pathways of which they are part. The types of genes that are part of these multigenic systems are known as *quantitative trait loci* (QTLs). Overwhelming technical difficulties prevented QTLs from being mapped in vertebrates even a decade ago. However, with the introduction of efficient polymerase chain reaction (PCR)-based methods to genotype animals and sophisticated statistical programs to discover associations between gene variants and phenotypes, the prospects for QTL mapping are now greatly improved. It is possible to target virtually any heritable quantitative trait for what is called *genetic dissection*. This is particularly the case if one can exploit strains of inbred mice.

USE OF ISOGENIC LINES An inbred strain is essentially an isogenic clone of fully homozygous animals that are able to reproduce sexually. They are a remarkable tool with which it is possible to resample the same genetic individual at different stages and after different treatments. They can also be used to obtain reliable quantitative estimates of traits that have high noise caused either by technical error or by stochastic developmental variation. If two or more inbred lines

differ substantially in a set of retinal traits under a common environment, then the difference traces back to genetic differences between those lines. These characteristics have been exploited to map and characterize novel gene loci that modulate cell populations in the retina.

The population of retinal ganglion cells has been counted in over 1000 mice belonging to 60 isogenic lines. Numbers range from 45,000 in strain CAST/Ei to 75,000 in BXD32 (Williams et al., 1996). While individual values have a normal distribution, when cases are pooled by strain the histogram has a characteristic multimodal structure in which the different modes represent different combinations of genotypes at several QTLs. The most prominent pair of modes is present in neonatal mice before ganglion cells have been eliminated by apoptosis (Strom and Williams, 1998). This indicates that the QTL responsible for these modes, the *Nnc1* locus, has a modulatory effect on the proliferation or differentiation of retinal ganglion cells.

MAPPING NEUROGENIC GENES Crosses between strains with high and low ganglion cell numbers have been used to map *Nnc1* and three other QTLs responsible for much of the variation in ganglion cell number (Strom, 1999; Williams et al., 1998b). The gene mapping method can be distilled to statistical tests of association between differences in cell number and differences in genotype (genotypes are often scored in a numerical format: AA = 1, Aa = 0, aa = -1). For example, the correlation between ganglion cell number and genotypes at *Nnc1* reaches a peak of 0.72 on chromosome (Chr) 11. The other three QTLs that modulate ganglion cell number map to Chr 7 at 65 cM (*Nnc2*, likelihood adds ratio [LOD] score of 5.9), Chr 1 at 82 cM (*Nnc3*, LOD of 9.3), and Chr 16 at 42 cM (*Nnc4*, LOD of 6.0).

Nnc1 has the largest effect, and this QTL maps to a 6 million base pair stretch of DNA on Chr 11 between *Hoxb* and *Krt1*. This region contains two obvious candidate genes—the retinoic acid alpha receptor and the thyroid hormone alpha receptor. The addition of exogenous retinoic acid to tissue cultures increases rod production at the expense of amacrine cells (Kelley et al., 1994). However, knockouts of the retinoic acid receptor have no detectible effect on retinal ganglion number, a surprising result given the high expression of this gene in ganglion cells from very early stages (Zhou et al., 2001). In contrast, inactivation of the thyroid hormone alpha receptor neatly reproduces a 15% predicted difference in cell number. This result suggests that the QTL on Chr 11 corresponds to a polymorphism of the thyroid hormone receptor gene (Strom, 1999), but this idea has not yet been confirmed by sequence comparison. However, the hypothesis is attractive because thyroid hormone has long been known to control retinal ganglion cell proliferation during *Xenopus* metamorphosis—the stage in this species' development when a population of ipsilater-

ally projecting ganglion cells is first generated (Hoskins, 1985). The thyroid receptor is a transcription factor that often pairs with a retinoid X receptor to control gene expression. It may not be coincidental that the QTL on Chr 1 that modulates ganglion cell number overlaps the position of the *Rxrg* gene (Strom, 1999).

Conclusion

It is already apparent that many developmental processes are intertwined in such a way as to maintain general conformity in retinal structure and cellular content while still permitting substantial latitude for individual variation. A growing number of molecules and processes are now known to affect the diversity and number of retinal cell types generated in multiple steps during retinogenesis (Cepko, 1999; Harris, 1997; Livesey and Cepko, 2001; Vetter and Brown, 2001; Vetter and Moore, 2001). Experimental tests to sort out their relative contributions also demonstrate that there are numerous stages at which the final numbers and relative proportions of the different retinal phenotypes can be changed. Understanding this process of differentiation at a quantitative level will require an analysis of the transcriptome and proteome of the lineages of the major cell types, and an understanding of the processes that occur during the very early embryonic stages to bias and then select the retinal stem cells. Although we are still far from being able to navigate through the molecular labyrinths that generate different retinal cell types in appropriate numbers, the pace of research is now so rapid that it is hard not to be optimistic.

REFERENCES

- Acampora, D. S., S. Mazan, Y. Lallemand, V. Avantaggiato, M. Maury, A. Simeone, and P. Brulet, 1995. Forebrain and midbrain regions are deleted in *Otx2*^{-/-} mutants due to a defective anterior neuroectoderm specification during gastrulation, *Development*, 121:3279–3290.
- Adler, R., and M. Hatlee, 1989. Plasticity and differentiation of embryonic retinal cells after terminal mitosis, *Science*, 243:391–393.
- Ahmad, A., and P. D. Spear, 1993. Effects of aging on the size, density, and number of rhesus monkey lateral geniculate neurons, *J. Comp. Neurol.*, 334:631–643.
- Alexiades, M. R., and C. L. Cepko, 1997. Subsets of retinal progenitors display temporally regulated and distinct biases in the fates of their progeny, *Development*, 124:1119–1131.
- Altmann, C. R., R. L. Chow, R. A. Lang, and A. Hemmati-Brivanlou, 1997. Lens induction by *Pax-6* in *Xenopus laevis*, *Dev. Biol.*, 185:119–123.
- Ang, S. L., O. Jin, M. Rhinn, N. Daigle, L. Stevenson, and J. Rossant, 1996. A targeted mouse *Otx2* mutation leads to severe defects in gastrulation and formation of axial mesoderm and to deletion of rostral brain, *Development*, 122:243–252.
- Austin, C. P., D. E. Feldman, J. A. Ida, and C. L. Cepko, 1995. Vertebrate retinal ganglion cells are selected from competent

- progenitors by the action of Notch, *Development*, 121:3637–3650.
- Banks, M. S., A. B. Sekuler, and S. J. Anderson, 1991. Peripheral spatial vision: limits imposed by optics, photoreceptors, and receptor pooling, *J. Opt. Soc. Am. A*, 8:1775–1787.
- Belecky-Adams, T., and R. Adler, 2001. Developmental expression patterns of bone morphogenetic proteins, receptors, and binding proteins in the chick retina, *J. Comp. Neurol.*, 430:562–572.
- Belleveau, M. J., and C. L. Cepko, 1999. Extrinsic and intrinsic factors control the genesis of amacrine and cone cells in the rat retina, *Development*, 26:555–566.
- Bernier, G., F. Panitz, X. Zhou, T. Hollemann, P. Gruss, and T. Pieler, 2000. Expanded retina territory by midbrain transformation upon overexpression of *Six6* (*optx2*) in *Xenopus* embryos, *Mech. Dev.*, 93:59–69.
- Buss, L. W., 1987. *The Evolution of Individuality*, Princeton: Princeton University Press.
- Carri, N. G., H. Bengtsson, M. F. Charette, and T. Ebendal, 1998. BMPR-II expression and OP-1 effects in developing chicken retinal explants, *Neuroreport*, 9:1097–1101.
- Casarsa, S., M. Andreazzoli, A. Simeone, and G. Barsacchi, 1997. *Xrx1*, a novel *Xenopus* homeobox gene expressed during eye and pineal gland development, *Mech. Dev.*, 61:187–198.
- Cepko, C. L., 1999. The roles of intrinsic and extrinsic cues and bHLH genes in the determination of retinal cell fates, *Curr. Opin. Neurobiol.*, 9:37–46.
- Chang-Ling, T., and J. Stone, 1991. Factors determining the migration of astrocytes into the developing retina: migration does not depend on intact axons or patent vessels, *J. Comp. Neurol.*, 303:375–386.
- Chow, R. L., C. R. Altmann, R. A. Lang, and A. Hemmati-Brivanlou, 1999. *Pax6* induces ectopic eyes in a vertebrate, *Development*, 126:4213–4222.
- Collin, S. P., and H. B. Collin, 1999. The foveal photoreceptor mosaic in the pipefish, *Corythoichthys paxtoni* (Syngnathidae, Teleostei), *Histol. Histopathol.*, 14:369–382.
- Colonnier, M., and J. O'Kusky, 1981. Number of neurons and synapses in the visual cortex of different species, *Rev. Can. Biol.*, 40:91–99.
- Curcio, C. A., K. R. Sloan, R. E. Kalina, and A. E. Hendrickson, 1990. Human photoreceptor topography, *J. Comp. Neurol.*, 292:497–523.
- Curcio, C. A., K. R. Sloan, O. Packer, A. E. Hendrickson, and R. E. Kalina, 1987. Distribution of cones in human and monkey retina: individual variability and radial asymmetry, *Science*, 236:579–582.
- Dacey, D. M., 2000. Parallel pathways for spectral coding in primate retina, *Annu. Rev. Neurosci.*, 23:743–775.
- Darwin, C., 1899. *The Life and Letters of Charles Darwin*, vol. 2 (Francis Darwin, ed.), New York: D. Appleton and Co., pp. 66–67.
- Davis, A. A., M. M. Matzuk, and T. A. Reh, 2000. Activin A promotes progenitor differentiation into photoreceptors in rodent retina, *Mol. Cell. Neurosci.*, 15:11–21.
- Dawkins, R., 1996. *Climbing Mount Improbable*, New York: W. W. Norton.
- Dirksen, M. L., and M. Jamrich, 1995. Differential expression of fork head genes during early *Xenopus* and zebrafish development, *Dev. Genet.*, 17:107–116.
- Dkhissi-Benyahya, O., A. Szel, W. J. Degrip, and H. M. Cooper, 2001. Short and mid-wavelength cone distribution in a nocturnal Strepsirrhine primate (*Microcebus murinus*), *J. Comp. Neurol.*, 438:490–504.
- Dudley, A. T., K. M. Lyons, and E. J. Robertson, 1995. A requirement for BMP7 during development of the mammalian kidney and eye, *Genes Dev.*, 9:2795–2805.
- Dyer, M. A., and C. L. Cepko, 2001. p27Kip1 and p57Kip2 regulate proliferation in distinct retinal progenitor cell populations, *J. Neurosci.*, 21:4259–4271.
- Ezzeddine, Z. D., X. Yang, T. DeChira, G. Yancopoulos, and C. T. Cepko, 1997. Postmitotic cells fated to become rod photoreceptors can be respecified by CNTF treatment of the retina, *Development*, 124:1055–1067.
- Fekete, D. M., J. Perez-Miguelsanz, E. F. Ryder, and C. L. Cepko, 1994. Clonal analysis in the chicken retina reveals tangential dispersion of clonally related cells, *Dev. Biol.*, 166:666–682.
- Franco, E. C., B. L. Finlay, L. C. Silveira, E. S. Yamada, and J. C. Crowley, 2000. Conservation of absolute foveal area in New World monkeys. A constraint on eye size and conformation, *Brain Behav. Evol.*, 56:276–286.
- Fuhrmann, S., M. Kirsch, and H. D. Hofmann, 1995. Ciliary neurotrophic factor promotes chick photoreceptor development in vitro, *Development*, 121:2695–2706.
- Furukawa, T., C. A. Kozak, and C. L. Cepko, 1997. *rax*, a novel paired-type homeobox gene, shows expression in the anterior neural fold and developing retina, *Proc. Natl. Acad. Sci. USA*, 94:3088–3093.
- Gallagher, B. C., A. M. Hainski, and S. A. Moody, 1991. Autonomous differentiation of dorsal axial structures from and animal cap cleavage stage blastomeres in *Xenopus*, *Development*, 112:1103–1114.
- Gan, L., S. W. Wang, Z. Huang, and W. H. Klein, 1999. POU domain factor Brn-3b is essential for retinal ganglion cell differentiation and survival but not for initial cell fate specification, *Dev. Biol.*, 210:469–480.
- Gan, L., M. Xiang, L. Zhou, D. S. Wagner, W. H. Klein, and J. Nathans, 1996. POU domain factor Brn-3b is required for the development of a large set of retinal ganglion cells, *Proc. Natl. Acad. Sci. USA*, 93:3920–3925.
- Gehring, W. J., and K. Ikeo, 1999. *Pax 6*: mastering eye morphogenesis and eye evolution, *Trends Genet.*, 15:371–377.
- Gilissen, E., and K. Zilles, 1996. The calcarine sulcus as an estimate of the total volume of human striate cortex: a morphometric study of reliability and intersubject variability, *J. Hirnforsch.*, 37:57–66.
- Goldowitz, D., D. S. Rice, and R. W. Williams, 1996. Clonal architecture of the mouse retina, *Prog. Brain Res.*, 108:3–15.
- Halder, G., P. Callaerts, and W. J. Gehring, 1995. Induction of ectopic eyes by targeted expression of the eyeless gene in *Drosophila*, *Science*, 267:1788–1792.
- Harland, R., 2000. Neural induction, *Curr. Opin. Genet. Dev.*, 10:357–362.
- Harris, W. A., 1997. Cellular diversification in the vertebrate retina, *Curr. Opin. Genet. Dev.*, 7:651–658.
- Hartenstein, V., 1989. Early neurogenesis in *Xenopus*: the spatio-temporal pattern of proliferation and cell lineages in the embryonic spinal cord, *Neuron*, 3:399–411.
- Hatini, V., W. Tuo, and E. Lai, 1994. Expression of winged helix genes, *BF-1* and *BF-2*, define adjacent domains within the developing forebrain and retina, *J. Neurobiol.*, 25:1293–1309.
- Hattar, S., H. W. Liao, M. Takao, D. M. Berson, and K. W. Yan, 2002. Melanopsin-containing retinal ganglion cells: architecture, projections, and intrinsic photosensitivity, *Science*, 295:1065–1070.

- Hayes, B. P., and M. D. Brooke, 1990. Retinal ganglion cell distribution and behaviour in procellariiform seabirds, *Vision Res.*, 30:1277–1289.
- Hendrickson, A. E., 1994. Primate foveal development: a microcosm of current questions in neurobiology, *Invest. Ophthalmol. Vis. Sci.*, 35:3129–3133.
- Hicks, D., and Y. Courtois, 1992. Fibroblast growth factor stimulates photoreceptor differentiation in vitro, *J. Neurosci.*, 12:2022–2033.
- Holt, C. E., T. W. Bertsch, H. M. Ellis, and W. A. Harris, 1988. Cellular determination in the *Xenopus* retina is independent of lineage and birthdate, *Neuron*, 1:15–26.
- Horton, J. C., and D. R. Hocking, 1996. Intrinsic variability of ocular dominance column periodicity in normal macaque monkeys, *J. Neurosci.*, 16:7228–7239.
- Hoskins, S. G., 1985. Control of the development of the ipsilateral retinorecipient projection in *Xenopus laevis* by thyroxine: results and speculation, *J. Neurobiol.*, 17:203–229.
- Huang, S., and S. A. Moody, 1993. Retinal fate of *Xenopus* cleavage stage progenitors is dependent upon blastomere position and competence: studies of normal and regulated clones, *J. Neurosci.*, 13:3193–3210.
- Huang, S., and S. A. Moody, 1995. Asymmetrical blastomere origin and spatial domains of dopamine and neuropeptide Y amacrine subtypes in *Xenopus* tadpole retina, *J. Comp. Neurol.*, 360:442–453.
- Huang, S., and S. A. Moody, 1997. Three types of serotonin-containing amacrine cells in tadpole retina have distinct clonal origins, *J. Comp. Neurol.*, 387:42–52.
- Hyer, J., T. Mima, and T. Mikawa, 1998. FGF1 patterns the optic vesicle by directing the placement of the neural retina domain, *Development*, 125:869–877.
- Inoue, T., M. Hojo, Y. Bessho, Y. Tano, J. E. Lee, and R. Kageyama, 2002. *Math3* and *NeuroD* regulate amacrine cell fate specification in the retina, *Development*, 129:831–842.
- Jeffery, W. R., and D. P. Martasian, 1998. Evolution of eye regression in the cavefish *Astyanax*: apoptosis and the *pax6* gene, *Am. Zool.*, 38:685–696.
- Jeffery, W. R., A. G. Strickler, S. Guiney, D. Heyser, and S. I. Tomarev, 2000. *Prox1* in eye degeneration and sensory compensation during development and evolution of the cavefish *Astyanax*, *Dev. Genes Evol.*, 210:223–230.
- Jensen, A. M., and M. C. Raff, 1997. Continuous observation of multipotential retinal progenitor cells in clonal density culture, *Dev. Biol.*, 188:267–279.
- Jeon, C.-J., E. Strettoi, and R. H. Masland, 1998. The major cell populations of the mouse retina, *J. Neurosci.*, 18:8936–8946.
- Kandil, F. I., and M. Fahle, 2001. Purely temporal figure-ground segregation, *Eur. J. Neurosci.*, 13:2004–2008.
- Kelley, M. W., J. K. Turner, and T. A. Reh, 1994. Retinoic acid promotes differentiation of photoreceptors in vitro, *Development*, 120:2091–2102.
- Kelley, M. W., J. K. Turner, and T. A. Reh, 1995. Ligands of steroid/thyroid receptors induce cone photoreceptors in vertebrate retina, *Development*, 121:3777–3785.
- Kenyon, K. L., N. Zaghoul, and S. A. Moody, 2001. Transcription factors of the anterior neural plate alter cell movements of epidermal progenitors to specify a retinal fate, *Dev. Biol.*, 240:77–91.
- Kirsch, M., M. Y. Lee, V. Meyer, A. Wiese, and H. D. Hofmann, 1996. Evidence for multiple, local functions of ciliary neurotrophic factor (CNTF) in retinal development: expression of CNTF and its receptors and in vitro effects on target cells, *J. Neurochem.*, 68:979–990.
- Kulkarni, A. L., D. C. Airey, and R. W. Williams, 2000. Genetic architecture of the mouse retinogeniculate system: a QTL analysis of numerical matching, *Neurosci. Abstr.*, 26:1087.
- Kumar, T., and D. A. Glaser, 1993. Initial performance, learning and observer variability for hyperacuity tasks, *Vision Res.*, 33:2287–2300.
- Lagutin, O., C. C. Zhu, Y. Furuta, D. H. Rowitch, A. P. McMahon, and G. Oliver, 2001. *Six3* promotes the formation of ectopic optic vesicle-like structures in mouse embryos, *Dev. Dyn.*, 221:342–349.
- LaVail, M. M., D. H. Rapaport, and P. Rakic, 1991. Cytogenesis in the monkey retina, *J. Comp. Neurol.*, 309:86–114.
- Leuba, G., and R. Kraftsik, 1994. Changes in volume, surface estimate, three-dimensional shape and total number of neurons of the human primary visual cortex from midgestation until old age, *Anat. Embryol.*, 190:351–366.
- Levine, E. M., H. Roelink, J. Turner, and T. A. Reh, 1997. Sonic hedgehog promotes rod photoreceptor differentiation in mammalian retinal cells in vitro, *J. Neurosci.*, 17:6277–6288.
- Lia, B., R. W. Williams, and L. M. Chalupa, 1987. Formation of retinal ganglion cell topography during prenatal development, *Science*, 236:848–851.
- Lillien, L., 1995. Changes in retinal cell fate induced by overexpression of EGF receptor, *Nature*, 377:158–162.
- Lillien, L., and C. L. Cepko, 1992. Control of proliferation in the retina: temporal changes in responsiveness to FGF and TGF alpha, *Development*, 115:253–266.
- Livesay, F. J., and C. L. Cepko, 2001. Vertebrate neural cell-fate determination: lessons from the retina, *Nature Neurosci.*, 2:109–118.
- Loosli, F., S. Winkler, C. Burgdorf, E. Wurmbach, W. Ansorge, T. Henrich, C. Grabher, D. Arendt, M. Carl, A. Krine, E. Grzebisz, and J. Wittbrodt, 2001. *Medaka* eyeless is the key factor linking retinal determination and eye growth, *Development*, 128:4035–4044.
- Loosli, F., S. Winkler, and J. Wittbrodt, 1999. *Six3* overexpression initiates the formation of ectopic retina, *Genes Dev.*, 13:649–654.
- Marc, R. E., and B. W. Jones, 2002. Molecular phenotyping of retinal ganglion cells, *J. Neurosci.*, 22:413–427.
- Marquardt, T., R. Ashery-Padan, N. Andrejewski, R. Scardigli, F. Guillemot, and P. Gruss, 2001. *Pax6* is required for multipotent state of retinal progenitor cells, *Cell*, 105:43–55.
- Marrow, E. M., M. J. Belliveau, and C. L. Cepko, 1998. Two phases of rod photoreceptor differentiation during rat retinal development, *J. Neurosci.*, 18:3738–3748.
- Marrow, E. M., T. Furukawa, J. E. Lee, and C. L. Cepko, 1999. *NeuroD* regulates cell fate determination in the developing neural retina, *Development*, 126:23–26.
- Martinez-Morales, J. R., M. Signore, D. Acampora, A. Simeone, and P. Bovolenta, 2001. *Otx* genes are required for tissue specification in the developing eye, *Development*, 128:2019–2030.
- Mathers, P. H., A. Grinberg, K. A. Mahon, and M. Jamrich, 1997. The *Rx* homeobox gene is essential for vertebrate eye development, *Nature*, 387:603–607.
- McFarlane, S., M. E. Zuber, and C. E. Holt, 1998. A role for the fibroblast growth factor receptor in cell fate decisions in the developing vertebrate retina, *Development*, 125:3967–3975.
- Mills, S. L., and S. C. Massey, 1999. AII amacrine cells limit scotopic acuity in central macaque retina: an analysis with calretinin labeling, confocal microscopy and intracellular dye injection, *J. Comp. Neurol.*, 411:19–34.
- Moody, S. A., 1987. Fates of the blastomeres of 32-cell stage *Xenopus* embryo, *Dev. Biol.*, 122:300–319.

- Moody, S. A., 1999. Testing the cell fate commitment of single blastomeres in *Xenopus laevis*, in *Advances in Molecular Biology: A Comparative Methods Approach to the Study of Oocytes and Embryos* (J. Richter, ed.), New York: Oxford University Press.
- Moody, S. A., I. Chow, and S. Huang, 2000. Intrinsic bias and lineage restriction in the phenotype determination of dopamine and neuropeptide Y amacrine cells, *J. Neurosci.*, 20:3244–3253.
- Moore, K. B., and S. A. Moody, 1999. Animal-vegetal asymmetries influence the earliest steps in retina fate commitment in *Xenopus*, *Dev. Biol.*, 212:25–41.
- Mori, M., N. B. Ghyselinck, P. Chambon, and M. Mark, 2001. Systematic immunolocalization of retinoid receptors in developing and adult mouse eyes, *Invest. Ophthalmol. Vis. Sci.*, 42:1312–1318.
- O'Kusky, J., and M. Colonnier, 1982. A laminar analysis of the number of neurons, glia, and synapses in the adult cortex (area 17) of adult macaque monkeys, *J. Comp. Neurol.*, 210:278–290.
- Oliver, G., A. Mailhos, R. Wehr, N. G. Copeland, N. A. Jenkins, and P. Gruss, 1995. *Six3*, a murine homologue of the sine oculis gene, demarcates the most anterior border of the developing neural plate and is expressed during eye development, *Development*, 121:4045–4055.
- Onuma, Y., S. Takahashi, M. Asashima, S. Kurata, and W. J. Gehring, 2002. Conservation of *Pax 6* function and upstream activation by Notch signaling in eye development of frogs and flies, *Proc. Natl. Acad. Sci. USA*, 99:2020–2025.
- Opas, M., and E. Dziak, 1994. bFGF-induced transdifferentiation of RPE to neuronal progenitors is regulated by the mechanical properties of the substratum, *Dev. Biol.*, 161:440–454.
- Østerberg, G., 1935. Topography of the layer of rods and cones in the human retina, *Acta Ophthalmol.*, 13(Suppl)6:1–103.
- Packer, O., A. E. Hendrickson, and C. A. Curcio, 1990. Developmental redistribution of photoreceptors across the *Macaca nemestrina* (pigtail macaque) retina, *J. Comp. Neurol.*, 298:472–493.
- Patel, A., and S. McFarlane, 2000. Overexpression of FGF-2 alters cell fate specification in the developing retina of *Xenopus laevis*, *Dev. Biol.* 222:170–180.
- Peachey, N. S., L. Roveri, A. Messing, and M. A. McCall, 1997. Functional consequences of oncogene-induced horizontal cell degeneration in the retinas of transgenic mice, *Vis. Neurosci.*, 14:627–632.
- Peichl, L., 1992. Topography of ganglion cells in the dog and wolf retina, *J. Comp. Neurol.*, 324:303–320.
- Perron, M., and W. A. Harris, 1999. Cellular determination in amphibian retina, in *Cell Lineage and Fate Determination* (S. A. Moody, ed.), San Diego: Academic Press, pp. 353–368.
- Perron, M., S. Kanekar, M. L. Vetter, and W. A. Harris, 1998. The genetic sequence of retinal development in the ciliary margin of the *Xenopus* eye, *Dev. Biol.*, 199:185–200.
- Pittack, C., G. B. Grunwald, and T. A. Reh, 1997. Fibroblast growth factors are necessary for neural retina but not pigmented epithelial differentiation in chick embryos, *Development*, 124:805–816.
- Pittack, C., M. Jones, and T. A. Reh, 1991. Basic fibroblast growth factor induces retinal pigment epithelium to generate neural retina in vitro, *Development*, 113:577–588.
- Politi, L. E., N. P. Rotstein, and N. G. Carri, 2001. Effect of GDNF on neuroblast proliferation and photoreceptor survival: additive protection with docosahexaenoic acid, *Invest. Ophthalmol. Vis. Sci.*, 42:3008–3015.
- Powell, T. P., and A. E. Hendrickson, 1981. Similarity in number of neurons through the depth of the cortex in the binocular and monocular parts of area 17 of the monkey, *Brain Res.*, 216:409–413.
- Provis, J. M., C. M. Diaz, and B. Dreher, 1998. Ontogeny of the primate fovea: a central issue in retinal development, *Prog. Neurobiol.*, 54:549–580.
- Provis, J. M., D. van Driel, F. A. Billson, and P. Russell, 1985. Human fetal optic nerve: overproduction and elimination of retinal axons during development, *J. Comp. Neurol.*, 238:92–100.
- Rakic, P., and K. P. Riley, 1983. Overproduction and elimination of retinal axons in the fetal rhesus monkey, *Science*, 219:1441–1444.
- Rapaport, D. H., S. L. Patheal, and W. A. Harris, 2001. Cellular competence plays a role in photoreceptor differentiation in the developing *Xenopus* retina, *J. Neurobiol.*, 49:129–141.
- Reese, B. E., B. D. Necessary, P. P. Tam, B. Faulkner-Jones, and S. S. Tan, 1999. Clonal expansion and cell dispersion in the developing mouse retina, *Eur. J. Neurosci.*, 11:2965–2978.
- Reh, T. A., 1992. Cellular interactions determine neuronal phenotypes in rodent retinal cultures, *J. Neurobiol.*, 23:1067–1083.
- Reh, T. A., and T. Tully, 1986. Regulation of tyrosine hydroxylase-containing amacrine cell number in larval frog retina, *Dev. Biol.*, 114:463–469.
- Repka, A., and R. Adler, 1992. Differentiation of retinal precursor cells born in vitro, *Dev. Biol.*, 153:242–249.
- Rhinn, M., A. Dierich, W. Shawlot, R. R. Behringer, M. Le Meur, and S. L. Ang, 1998. Sequential roles for *Otx2* in visceral endoderm and neuroectoderm for forebrain and midbrain induction and specification, *Development*, 125:845–856.
- Rice, D. S., R. W. Williams, and D. Goldowitz, 1995. Genetic control of retinal projections in inbred strains of albino mice, *J. Comp. Neurol.*, 354:459–469.
- Rickman, D. W., and C. B. Rickman, 1996. Suppression of *trkB* expression by antisense oligonucleotides alters a neuronal phenotype in the rod pathway of the developing rat retina, *Proc. Natl. Acad. Sci. USA*, 93:12564–12569.
- Rockel, A. J., R. W. Hiorns, and T. P. Powell, 1980. The basic uniformity in structure of the neocortex, *Brain*, 103:221–244.
- Rodieck, R. W., 1998. *The First Steps in Seeing*. Sunderland, MA: Sinauer.
- Roorda, A., and D. R. Williams, 1999. The arrangement of the three cone classes in the living human eye, *Nature*, 397:520–522.
- Saha, M. S., and R. M. Grainger, 1992. A labile period in the determination of the anterior-posterior axis during early neural development in *Xenopus*, *Neuron*, 8:1003–1014.
- Sharon, D., S. Blackshaw, C. L. Cepko, and T. P. Dryja, 2002. Profile of the genes expressed in the human peripheral retina, macula, and retinal pigment epithelium determined through serial analysis of gene expression (SAGE), *Proc. Natl. Acad. Sci. USA*, 99:315–320.
- Solursh, M., R. M. Langill, J. Wood, and T. K. Sampath, 1996. Osteogenic protein-1 is required for mammalian eye development, *Biochem. Biophys. Res. Commun.*, 214:438–443.
- Spear, P. D., C. B. Kim, A. Ahmad, and B. W. Tom, 1996. Relationship between numbers of retinal ganglion cells and lateral geniculate neurons in the rhesus monkey, *Vis. Neurosci.*, 13:199–203.
- Springer, A. D., 1999. New role for the primate fovea: a retinal excavation determines photoreceptor deployment and shape, *Vis. Neurosci.*, 16:629–636.
- Sterling, P., 1998. Retina, in *Synaptic Organization of the Brain*, 4th ed., New York: Oxford University Press, pp. 205–253.
- Strom, R. C., 1999. *Genetic analysis of variation in neuron number*. Ph.D. dissertation, University of Tennessee. <http://www.nervenet.org/papers/Strom99/Chapter5.html>

- Strom, R. C., and R. W. Williams, 1998. Cell production and cell death in the generation of variation in neuron number, *J. Neurosci.*, 18:9948–9953.
- Suner, I., and P. Rakic, 1996. Numerical relationship between neurons in the lateral geniculate nucleus and primary visual cortex in macaque monkeys, *Vis. Neurosci.*, 13:585–590.
- Tao, W., and E. Lai, 1992. Telencephalon-restricted expression of BF-1, a new member of the HNF-3/fork head gene family, in the developing rat brain, *Neuron*, 8:957–966.
- Tolhurst, D. J., and L. Ling, 1988. Magnification factors and the organization of the human striate cortex, *Hum. Neurobiol.*, 6:247–254.
- Toy, J., J. M. Yang, G. S. Leppert, and O. H. Sundin, 1998. The *optx2* homeobox gene is expressed in early precursors of the eye and activates retina-specific genes, *Proc. Natl. Acad. Sci. USA*, 95:10643–10648.
- Turner, D. L., and C. L. Cepko, 1987. A common progenitor of neurons and glia persists in rat retina late in development, *Nature*, 328:131–136.
- Turner, D. L., E. Y. Snyder, and C. L. Cepko, 1990. Lineage independent determination of cell type in the embryonic mouse retina, *Neuron*, 4:833–845.
- van Essen, D. C., W. T. Newsome, and J. H. Maunsell, 1984. The visual field representation in striate cortex of the macaque monkey: asymmetries, anisotropies, and individual variability, *Vision Res.*, 24:429–448.
- Vetter, M. L., and N. L. Brown, 2001. The role of basic helix-loop-helix genes in vertebrate retinogenesis, *Semin. Cell Dev. Biol.*, 12:491–498.
- Vetter, M. L., and K. B. Moore, 2001. Becoming glial in the neural retina, *Dev. Dyn.*, 221:146–153.
- Waddington, C. H., and E. Robertson, 1966. Selection for developmental canalization, *Genet. Res.*, 7:303–312.
- Waid, D. K., and S. C. McLoon, 1995. Immediate differentiation of ganglion cells following mitosis in the developing retina, *Neuron*, 14:117–124.
- Waid, D. K., and S. C. McLoon, 1998. Ganglion cells influence the fate of dividing retinal cells in culture, *Development*, 125:1059–1066.
- Walls, G. L., 1942. *The Vertebrate Eye and Its Adaptive Radiation*, Bloomfield Hills MI: Cranbrook Institute of Science.
- Watanabe, T., and M. C. Raff, 1990. Rod photoreceptor development in vitro: intrinsic properties of proliferating neuroepithelial cells change as development proceeds in the rat retina, *Neuron*, 2:461–467.
- Westheimer, G., 1981. Visual hyperacuity, *Prog. Sensory Physiol.*, 1:1–37.
- Wetts, R., and S. E. Fraser, 1988. Multipotent precursors can give rise to all major cell types of the frog retina, *Science*, 239:1142–1145.
- Wikler, K. C., and P. Rakic, 1990. Distribution of photoreceptor subtypes in the retina of diurnal and nocturnal primates, *J. Neurosci.*, 10:3390–3401.
- Wikler, K. C., R. W. Williams, and P. Rakic, 1990. Photoreceptor mosaic: number and distribution of rods and cones in the rhesus monkey retina, *J. Comp. Neurol.*, 297:499–508.
- Williams, R. W., 1991. The human retina has a cone-enriched rim, *Vis. Neurosci.*, 6:403–406.
- Williams, R. W., 2000. Mapping genes that modulate brain development: a quantitative genetic approach, in *Mouse Brain Development* (A. F. Goffinet and P. Rakic, eds.), New York: Springer Verlag, pp. 21–49.
- Williams, R. W., C. Cavada, and F. Reinoso-Suarez, 1993. Rapid evolution of the visual system: a cellular assay of the retina and dorsal lateral geniculate nucleus of the Spanish wildcat and the domestic cat, *J. Neurosci.*, 13:208–228.
- Williams, R. W., and D. Goldowitz, 1992a. Structure of clonal and polyclonal cell arrays in chimeric mouse retina, *Proc. Natl. Acad. Sci. USA*, 89:1184–1188.
- Williams, R. W., and D. Goldowitz, 1992b. Lineage versus environment in embryonic retina: a revisionist perspective, *Trends Neurosci.*, 15:368–373.
- Williams, R. W., and P. Rakic, 1988. Elimination of neurons from the rhesus monkey's lateral geniculate nucleus during development, *J. Comp. Neurol.*, 272:424–436.
- Williams, R. W., R. C. Strom, and D. Goldowitz, 1998b. Natural variation in neuron number in mice is linked to a major quantitative trait locus on Chr 11, *J. Neurosci.*, 18:138–146.
- Williams, R. W., R. C. Strom, D. S. Rice, and D. Goldowitz, 1996. Genetic and environmental control of variation in retinal ganglion cell number in mice, *J. Neurosci.*, 16:7193–7205.
- Williams, R. W., R. C. Strom, G. Zhou, and Z. Yan, 1998a. Genetic dissection of retinal development, *Semin. Cell Dev. Biol.*, 9:249–255.
- Zhou, G., R. C. Strom, V. Giguere, and R. W. Williams, 2001. Modulation of retinal cell populations and eye size in retinoic acid receptor knockout mice, *Mol. Vis.*, 7:253–260.
- Zhou, G., and R. W. Williams, 1999. *Eye1* and *Eye2*: gene loci that modulate eye size, lens weight, and retinal area in mouse, *Invest. Ophthalmol. Vis. Sci.*, 40:817–825.
- Zuber, M. E., M. Perron, A. Philpott, A. Bang, and W. A. Harris, 1999. Giant eyes in *Xenopus laevis* by overexpression of XOptx2, *Cell*, 98:341–352.

6 Development of the Vertebrate Retina

RACHEL O. L. WONG AND LEANNE GODINHO

Introduction

The neural retina, the light-sensitive part of the eye, converts light into electrical signals that are relayed to visual centers in the brain. The retina is part of the central nervous system (CNS), originating from the neural ectoderm during development. In vertebrates, the retina begins as an apparently homogeneous collection of cells in a single-layered neuroepithelium. With maturation, however, it develops into a laminated tissue with seven major cell classes, each of which occupies characteristic positions within the retina. The structural and functional development of the retina has long been studied because of its importance in vision, and because its highly organized structure is ideally suited for studying cell fate, differentiation, and patterning of synaptic networks in the nervous system.

Generation of cellular components

CELL GENESIS Like other regions of the CNS, the retina is derived from the neural tube (Pei and Rhodin, 1970). Each eye begins as an outgrowth on either side of the neural tube. These outgrowths, called *optic vesicles*, invaginate to form a double-layered, cup-shaped structure. The thin outer wall becomes the pigment epithelium, while the inner wall develops into the neural retina. At this stage, the neural retina is a single-layered, pseudostratified epithelium. An extended period of cell proliferation begins to furnish the structure that will become multilayered.

Cell proliferation in the retinal neuroepithelium occurs in a manner peculiar to the CNS. With their cytoplasmic processes extending from the pigment epithelial end to the internal limiting membrane, the nuclei of individual progenitor cells engage in a back-and-forth movement, undergoing different phases of the cell cycle at specific depths within the retinal neuroepithelium (Sidman, 1961; Young, 1985a). This nuclear movement, termed *interkinetic migration*, was first observed in the developing chick neural tube (Sauer, 1935). In the retina, mitosis (M-phase) occurs at the outermost surface, near the pigment epithelium. Each daughter cell resulting from a mitotic division extends a process toward the opposing vitreal surface while maintaining contact with the ventricular side. The daughter nuclei then enter G₁, a resting phase, while migrating within their cytoplasmic pro-

jections toward the vitreal surface. At their destination, nuclei replicate their DNA (S-phase) and subsequently enter the G₂ resting phase on their inward journey to the ventricular surface. Upon arriving, cells retract their cytoplasmic processes from the opposing end and remain poised for the next mitotic division (Robinson, 1991; Sidman, 1961; Young, 1985a). The resulting daughter cells then either reenter the cell cycle or leave it to become postmitotic neuroblasts.

Cohorts of progenitors leave the cell cycle throughout the period of retinal development to differentiate into one of seven cell classes (Carter-Dawson and LaVail, 1979; Sidman, 1961; Young, 1985a, 1985b). The developmental time point at which this occurs for a particular cell type can be referred to as its *birth date*. The “birth dates” of each of the seven retinal cell classes have been deduced by exposing retinal cells to ³H-thymidine at known time points during development and examining the identity of the most heavily labeled nuclei in the mature retina (Carter-Dawson and LaVail, 1979; Sidman, 1961; Young, 1985a, 1985b). Each retinal cell type has a characteristic period during which its entire population is generated. However, there is considerable temporal overlap between the generation periods of most cell classes. Across species, retinal neuroblasts destined to become ganglion cells are the first to become postmitotic. Amacrine, horizontal, and cone photoreceptor cells are generated next; bipolar and Müller glial cells then follow. There is still some debate as to whether an early and transient population of Müller glial cells is generated during the period when ganglion and amacrine cells are born (Robinson, 1991). Rod photoreceptors are generated almost throughout the entire period of cytogenesis in the retina (Carter-Dawson and LaVail, 1979; Sidman, 1961; Young, 1985a, 1985b). Figure 6.1 summarizes the temporal order of appearance and placement of the cell types in the retina.

In addition to the sequential addition of cells across the depth of the retina, cytogenesis also proceeds in a strict centropерipheral sequence. The first postmitotic retinal cells are found in a region (see the section “Cell Distribution”) close to the optic nerve head. Cell genesis occurs last, near the ora serrata (Carter-Dawson and LaVail, 1979; Sidman, 1961; Young, 1985a, 1985b). In many species, the centropерipheral sequence of cell genesis holds true for every retinal cell type.

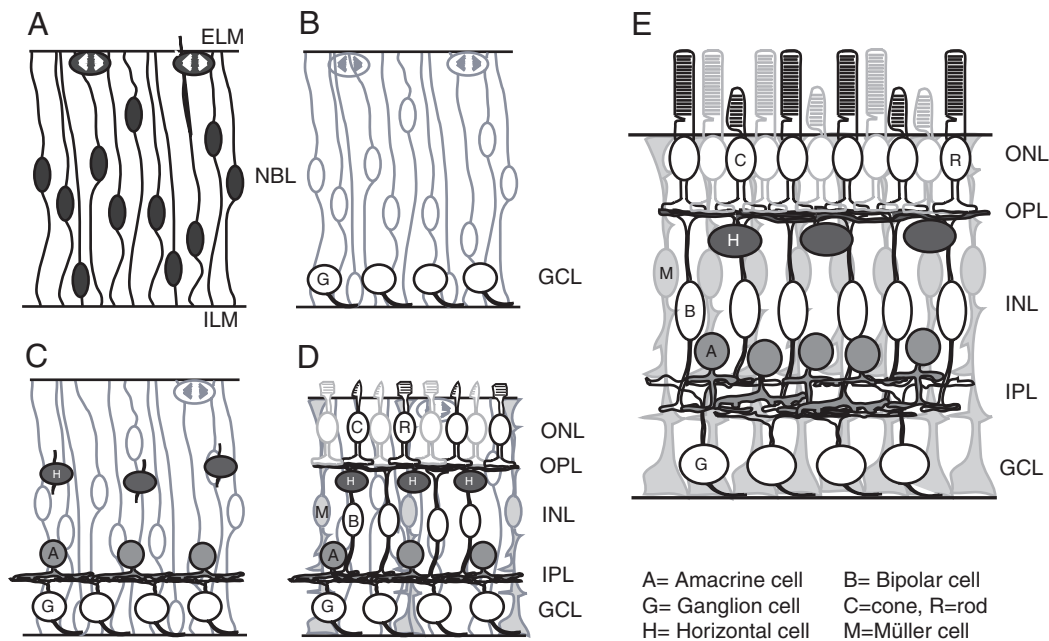


FIGURE 6.1. Basic structure and temporal order of cell differentiation of the vertebrate retina. *A*, The neural retina begins as a sheet of neuroepithelial cells (NBL, neuroblastic layer) with processes that contact the internal (ILM) and external (ELM) limiting membranes. *B*, Ganglion cells are the first cell type to differentiate and migrate toward the ILM to form the ganglion cell layer (GCL). *C*, Amacrine cells and horizontal cells differentiate next. Cone photoreceptors are born at this stage but do not differentiate until later. The first network of connections, between amacrine cells and ganglion cells, is established as a continuous inner plexiform layer (IPL).

forms across the retina. *D*, In the inner nuclear layer (INL), bipolar cells and Müller glial cells are generated and differentiate. At this stage, both cone and rod photoreceptors comprising the outer nuclear layer (ONL) begin to mature, bearing few outer segments or discs. The outer plexiform layer (OPL) emerges, and connections between photoreceptors, horizontal cells, and bipolar cells are formed. Cell genesis (mainly rods) continues at this stage but to a greatly reduced degree. *E*, At maturity, all cell types are present, connections in both plexiform layers are established, and photoreceptor outer segments are well developed.

CELL FATE Cell fate determination in the vertebrate retina is complex. Separate progenitors, each exclusively dedicated to the production of a single retinal cell type, do not exist. Instead, progenitor cells in the retina are regarded as multipotent (Holt et al., 1988; Turner and Cepko, 1987; Turner et al., 1990; Wetts and Fraser, 1988), that is, they are capable of producing more than one retinal cell class. How they adopt distinct fates during development has therefore been an area of intense research. The findings of numerous studies have resulted in a proposed model of retinal development in which cues both intrinsic and extrinsic to progenitors contribute to the determination of the cell fate (Cepko et al., 1996; Livesey and Cepko, 2001; Marquardt and Gruss, 2002).

In this model, progenitor cells are believed to move sequentially through a series of stages, during which they are capable of producing only a limited repertoire of cell types (Cepko et al., 1996). For example, progenitor cells taken from chick retina at an early age when ganglion cells are exclusively produced continue to produce this cell type alone even when transplanted into a later retinal environment when signals conducive to a rod cell fate are present (Austin

et al., 1995). This limited competence of progenitor cells to produce only a small number of cell types at any given stage is thought to result from their genetic makeup. Progenitor cells destined for ganglion cell fates have been shown to express transcription factors such as Brain-3 (Brn-3) and retina-derived POU-domain factor-1 (RPF-1) (reviewed in Harris, 1997). Subsets of progenitors in the rat retina that express markers of mature amacrine and horizontal cells (syntaxin 1a and VC1.1) are biased toward producing these cell types (Alexiades and Cepko, 1997). Thus, the progenitor cell population is a heterogeneous one that is biased toward producing different cell fates. It is on this heterogeneous population of progenitors that extrinsic signals exert their influence.

Extrinsic signals that have been implied in cell fate determination include neurotrophic factors such as nerve growth factor (NGF) and ciliary neurotrophic factor (CNTF), as well as other factors such as transforming growth factor α and β (TGF- α and - β), insulin-like growth factor (IGF), retinoic acid, thyroid hormone, and the amino acid taurine (reviewed in Harris, 1997). A direct role in cell fate determination is more evident for some factors such as CNTF (promotes

bipolar cell fates) and retinoic acid and taurine [rod photoreceptor cell fate (Altshuler et al., 1993)], while for others it remains unclear whether they are also involved in neurogenesis, differentiation, and cell survival. Of course, extrinsic signals that promote a particular cell fate are only positively received by cells competent to respond to them.

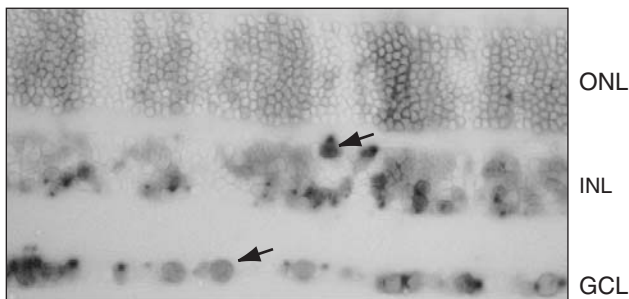
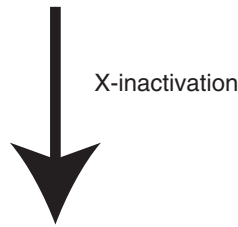
Environmental signals could also act to suppress cell fates. Postmitotic neurons might be the source of such factors providing feedback to progenitors to cease the production of a particular cell type. This has been shown for ganglion cells; a still unidentified diffusible factor produced by ganglion cells limits the further production of this cell type (Waid and McLoon, 1998). While diffusible factors are a means of signaling between retinal cells during cell fate determination, communication also occurs by contact-mediated lateral inhibition. The receptor Notch and its ligand Delta have been shown to play a role in controlling cell fate. All cells start off with equal amounts of Notch and Delta. Activation of Notch blocks differentiation of the cell, at the same time leading to a reduction in its Delta levels. Expression of an activated form of Notch in progenitor cells from *Xenopus* and rat essentially inhibited cell differentiation and caused cells to remain in a progenitor-like state (Bao and Cepko, 1997; Dorsky et al., 1995). Conversely, when antisense oligonucleotides were used to reduce Notch activity in the retina, the number of ganglion cells produced was greatly increased (Austin et al., 1995). By misexpressing Delta in the *Xenopus* retina, Dorsky et al. (1997) demonstrated how the Notch-Delta pathway regulates cellular differentiation in the retina. At early stages of development, cells with high levels of Delta adopt a ganglion cell or cone photoreceptor fate when surrounded by wild-type cells because their neighbors failed to suppress their differentiation. Misexpression at older stages leads to a high proportion of photoreceptor fate. Delta overexpressors, however, failed to differentiate when they were surrounded by cells with similarly high Delta levels. In contrast, reduction of Delta levels by expression of a dominant negative form of Delta resulted in an increase in the percentage of cells with an earlier fate. Thus the Notch-Delta pathway is important for regulating the competence of progenitors to differentiate and respond to signals biasing their choice of fate at each stage of development.

CELL MIGRATION All cells are effectively “born” at the outer surface of the retina, apposed to the pigment epithelium (Sidman, 1961). Postmitotic cells must therefore migrate some distance to occupy positions characteristic of their phenotype within the retina. Unlike the cerebral cortex, another highly laminated structure, cell positioning in the vertical dimension of the retina is not strictly related to cell genesis. Cells born at similar times, for example, horizontal cells and amacrine cells, can end up in different layers.

In the cerebral cortex, postmitotic neuroblasts migrate radially along radial glial fibers from the ventricular zone toward the pia to take up their final positions (Rakic, 1971, 1990). Retinal neuroblasts are also believed to disperse radially from their point of origin. However, whether such radially migrating neuroblasts use glial guides, like their counterparts in the cortex, remains contentious. The presence of a radial glial scaffold in the immature retina was suggested by studies based on electron microscopy and immunohistochemistry with glial-specific antibodies (Meller and Tetzlaff, 1976; Wolburg et al., 1991). However, the positive identification of such glial structures by electron microscopy remains unclear, and glial markers such as vimentin may not be specific to such cells during development (Bennett and DiLullo, 1985; Lemmon and Rieser, 1983).

Perikaryal translocation has been proposed as an alternative mechanism to account for radial migration within the retina (Book and Morest, 1990; Morest, 1970; Snow and Robson, 1994, 1995). This theory suggests that a newly postmitotic cell, located at the scleral surface of the neuroepithelium, extends a process toward the vitreal surface, its nucleus moving to its final destination within this process. The cell maintains an attachment with the scleral side of the neuroepithelium as its nucleus translocates, losing this attachment and that from the vitreal surface only when migration is complete. Evidence in support of perikaryal translocation in the retina originally came from studies of the morphology of retinal neuroblasts by Golgi impregnations (Morest, 1970; Prada et al., 1981). Observations from the retrograde labeling of ganglion cells (Dunlop, 1990; Snow and Robson, 1994, 1995) and immunohistochemical studies using ganglion cell-specific antibodies (McLoon and Barnes, 1989) support this hypothesis. All these studies reported postmitotic cells with a bipolar morphology, attached by processes to both surfaces of the retinal epithelium, and somata located at various depths within the neuroepithelium.

Whatever mechanism is employed, it is now well accepted that newborn retinal cells migrate to their final positions in a radial fashion. When single or small numbers of progenitor cells were marked early in development by the injection of retroviral constructs or fluorescent dyes (Fekete et al., 1994; Turner and Cepko, 1987; Turner et al., 1990), and the distribution of their progeny was examined in the mature retina, they were seen to be distributed radially across the entire depth of the retina in tightly organized columns. Such a cell dispersion pattern was suggestive of the way in which retinal neuroblasts move from their point of origin in the germinal zone. Not all cells move strictly in the radial axis, however. When larger numbers of progenitors were labeled using transgenic (Fig. 6.2; Reese et al., 1995, 1999) or chimeric mice (Williams and Goldowitz, 1992), a small



X-Gal stained section of adult retina

FIGURE 6.2. Schematic depicting the creation of X-inactivation transgenic mosaic retinas. A transgenic mouse line was created in which the *lacZ* transgene was inserted into one of the X-chromosomes (depicted as a blue-colored X). Early in development, all progenitor cells express β -galactosidase, the protein product of the *lacZ* transgene, as both chromosomes are active. In female transgenic mice, through the natural phenomenon of X-inactivation, one of the two X-chromosomes is randomly inactivated. This results in roughly equal numbers of transgene-expressing and -nonexpressing cells. In the adult, only the progeny of transgene-active cells express β -galactosidase. When histochemically detected, these cells appear blue. Alternating radial columns of blue and white can be seen in a section of retina from such a transgenic mouse, indicative of their mode of dispersion. Occasionally however, individual blue cells can be seen tangentially removed from blue radial columns (arrow). ONL, outer plexiform layer; INL, inner nuclear layer; GCL, ganglion cell layer. (L. Godinho and S. S. Tan, unpublished.) (See color plate 3.)

percentage of clonally related cells were found to stray outside the boundaries of the radial columns. Such cells are regarded to have dispersed tangentially from their point of origin in the germinal zone. Importantly, whether a cell dispersed radially or tangentially from its birthplace appears to be linked to its ultimate phenotype. Cells destined for rod photoreceptor, bipolar, and Müller glial cell fates were always found to disperse radially; radial columns are always composed of these cell types. Cells that disperse tangentially include cone photoreceptors and horizontal, amacrine, and ganglion cells (Reese et al., 1995).

CELL DISTRIBUTION At maturity, retinal neurons are often densely packed in a small region, typically referred to as *central retina*, which is actually located temporal to the optic nerve head. In primates this corresponds to the fovea, the center of which is a deep pit-like structure where cone photoreceptor density is at its highest (Chapter 26). Not all animals have a fovea, however; in some species, cell densities peak at a small patch called the *area centralis*. Spatial resolution of the retina is limited by the densities of cone photoreceptors and ganglion cells at the fovea and the area centralis (Rodieck, 1998). As the retina grows, cell density in the peripheral retina declines steeply, but it is reduced by a relatively smaller amount in the central retina (reviewed by Robinson, 1991). In primates, a further step takes place in fovea development, in which ganglion cell bodies become displaced from the center of the fovea with maturation, giving rise to the foveal pit. This lateral movement occurs after synapses have formed on the ganglion cells and may involve active migration of the cell bodies while their connections are “anchored” in place (reviewed by Kirby and Steineke, 1996).

How do retinal cells become differentially distributed? Selective neurogenesis and naturally occurring cell death could contribute to the sharpening of the centropertipheral gradients in cell density. While there is little evidence for selective cell addition across the retina, cell death, particularly in the ganglion cell layer, is common and widespread (Robinson, 1991). In fact, about half the population of ganglion cells dies by maturity. But there is no well-defined spatiotemporal pattern of cell death across the retina, although this process, like other maturation events, follows a centropertipheral gradient. Differential expansion of the retina in which the peripheral region becomes stretched, like the surface of a balloon, has been suggested to be an important mechanism which shapes the density gradients of retinal neurons (Lia et al., 1987; Mastronarde et al., 1984; Robinson, 1991). This is because cell gradients continue to sharpen even after the period of neurogenesis and cell death. No one mechanism, however, appears to account for the final centropertipheral density gradients of each cell type (Robinson, 1991; Wikler and Rakic, 1996). Understanding how each gradient of cell density is determined,

and whether there is coordination in setting up these neuronal gradients, will reflect on how the convergence or divergence of information is established in the retina during development.

Cell differentiation and formation of the plexiform layers

Cell differentiation in the developing retina is clearly reflected by the emergence of the inner and outer plexiform layers. These laminar synaptic regions appear before functional synaptic inputs are formed, as retinal neurons extend neurites toward each other in an apparently coordinated fashion. Here we will discuss what is known about process outgrowth in retinal neurons and what mechanisms might direct and coordinate their morphological differentiation, as well as produce laminar organizations of their connections.

CELL POLARITY AND PROCESS OUTGROWTH The patterns of early neurite outgrowth in the retina have largely been investigated for retinal ganglion cells, mainly because of interest in the organization of their axonal projections to visual targets in the brain. Upon becoming postmitotic, retinal ganglion cells become polarized, generating an axon which is directed toward the vitreal surface and dendrites which project toward the neuroblastic layer (Fig. 6.3). Comparing the morphology of dye-labeled cells at different stages in development suggests that the axon may arise *de novo* from the cell body or is derived from the vitreally directed ventricular process (Hinds and Hinds, 1974; Maslim et al., 1986; Thanos and Mey, 2001). Axon outgrowth begins even prior to the arrival of the cell body to take a position in the forming ganglion cell layer. From static images of cells at different ages, it appears that dendritic outgrowth begins only when the cell body reaches the vitreal surface and when the

process attached to the ventricular surface retracts (Fig. 6.3). Axonal growth cones reach the optic fissure to form the optic nerve, and in some species they arrive at their central targets even before dendrites elaborate within the retina (Thanos and Mey, 2001).

Coculture studies demonstrate that ganglion cell axonal and dendritic growth is directed or promoted by the microenvironment of the inner and outer retina, respectively (Bauch et al., 1998; Stier and Schlosshauer, 1998). Radial glial cells, thought to be Müller glia, influence the outgrowth of axons or dendrites in a highly selective way; their vitreal endfeet provide cues that encourage axon outgrowth, whereas cues from the region of the glial cell body direct dendritic, rather than axonal, outgrowth. The molecular interactions that polarize retinal ganglion cells are not yet fully understood, but some key players have been identified. For example, in the absence of Brn-3b, a POU-domain transcription factor, most retinal ganglion cells fail to extend axons, and instead prefer to generate dendrites (Wang et al., 2000).

Compared to retinal ganglion cells, there is relatively little information concerning differentiation and process outgrowth of other inner retinal neurons. The majority of amacrine interneurons do not have polarized axons and dendrites; this makes these cells interesting candidates for studying how a single neurite can achieve this dual function. Neurite outgrowth from amacrine cells has been studied by serially reconstructing these cells by electron microscopy (Hinds and Hinds, 1983). These studies suggest that amacrine cells may be derived from retinal ganglion cells that have lost their axons, or that they may originate directly from ventricular neuroblasts. However, direct evidence demonstrating how amacrine cells differentiate and extend neurites to form the inner plexiform layer is still lacking. The observations of Hinds and Hinds do suggest that neurite outgrowth from amacrine cells is unlikely to be directed exclusively toward the ganglion cell–amacrine

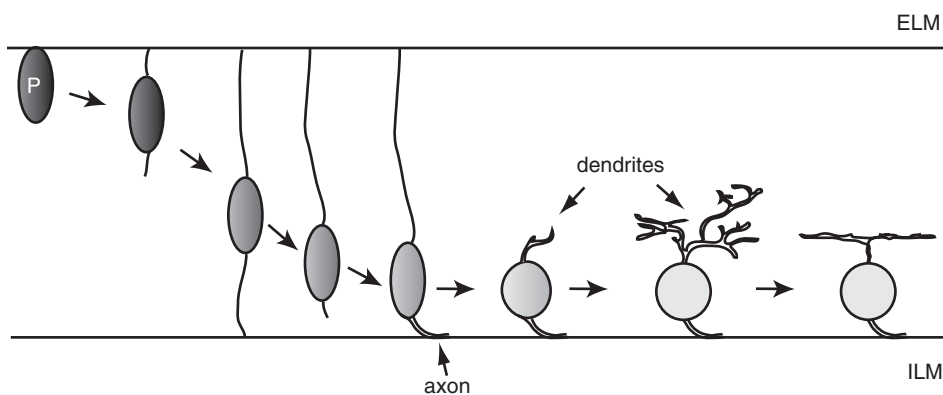


FIGURE 6.3. Presumed sequence of retinal ganglion cell differentiation. *P*, postmitotic ganglion cell; *ELM* and *ILM*, external and internal limiting membranes, respectively. Ganglion cells are first recognized when their axons appear.

cell border. Instead, it is possible that neurite outgrowth in amacrine cells is initially random or multidirectional, but that in time only processes growing laterally are maintained and elaborate to form the inner plexiform layer (Hinds and Hinds, 1983).

How bipolar cells become polarized has not been investigated, but it is possible that the cues that direct ganglion cell polarization may be involved. The difficulty in following bipolar cell development has been the lack of bipolar cell-specific markers that are needed to identify these cells early in development. The earliest available marker is recoverin, which labels a subset of bipolar cells (Milam et al., 1993). However, recoverin also labels photoreceptors before they differentiate. Markers that distinguish different bipolar cell classes in the mature retina, such as protein kinase C or calbindin, appear relatively late, that is, when bipolar axonal terminals are already stratified in the inner plexiform layer (Miller et al., 1999). In the future, the use of molecular approaches to drive fluorescent protein expression in subsets of bipolar cells will be invaluable once suitable promoters are identified.

In the outer retina, process outgrowth begins even before an outer plexiform layer is apparent (Robinson, 1991). Interestingly, photoreceptor terminals which in the mature retina stratify only within this outer lamina may do so only after retracting processes from the inner plexiform layer. In the ferret, recoverin-immunoreactive rods and cones transiently project an axon to the inner plexiform layer before bipolar cells differentiate and the outer plexiform layer forms (Johnson et al., 1999). The function of this early projection is not known, but if connections are made with inner retinal neurons, these early projections would suggest the presence of a novel circuit in the developing retina. The first indica-

tion of a forming outer plexiform layer is when horizontal cells elaborate processes laterally, demarcating a border between the inner and outer retina. Initially, these cells put out processes in multiple directions, some even reaching the inner plexiform layer (Schnitzer and Rusoff, 1984). Eventually, horizontal cells maintain only processes that elaborate laterally. What signals direct the lateral growth of horizontal cell processes at the relevant position and time remain a mystery.

CELL TYPE-SPECIFIC ARBORIZATIONS Shortly after retinal neurons extend neurites, they undergo a period of extensive process outgrowth. In some cells, a great deal of structural remodeling takes place before the final morphologies are attained. Factors, intrinsic and extrinsic to the cells, that may influence the final patterning of neurites in retinal neurons have largely been studied for the inner retinal neurons, particularly for ganglion cells.

Dendritic development of retinal ganglion cells is complex, requiring each cell to achieve a specific pattern of branching, arbor size, and stratification within the inner plexiform layer. As dendrites emanate from the cell body, a rudimentary tree is formed, which elaborates by branching and process extension (Dunlop, 1990; Maslim et al., 1986). However, dendrites also retract, suggesting that the final spatial arrangement results from selective elaboration and elimination of processes (Fig. 6.4).

A combination of genetic factors, environmental cues, and cell-cell interactions is likely to govern dendritic elaboration and retraction in retinal ganglion cells. Evidence for intrinsic control of dendritic patterning in ganglion cells comes from studies in which neonatal cat ganglion cells, dissociated and cultured without contacting neighboring cells,

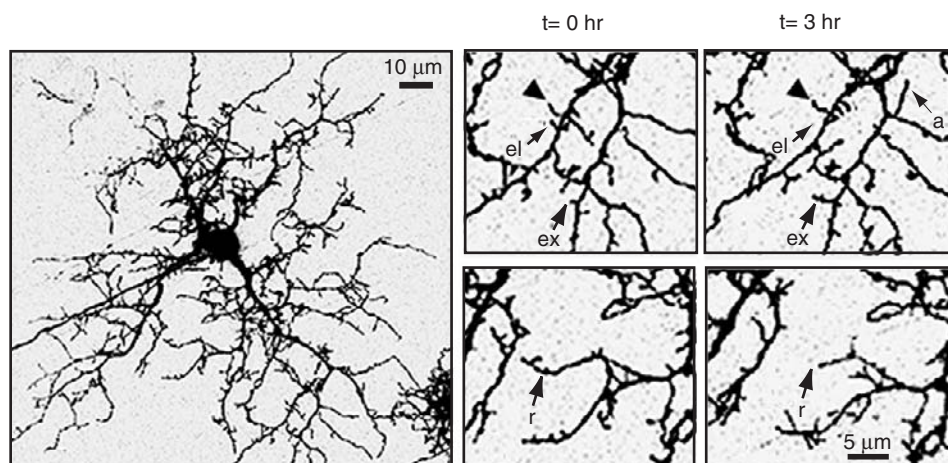


FIGURE 6.4. The dendritic arbor of retinal ganglion cells is sculpted by the addition and elimination of processes over time. Shown here is a ganglion cell from an embryonic chick retina labeled after transfection with plasmid encoding green fluorescent

protein. Images obtained 3 hours apart indicate that whereas some processes are stable (*arrowhead*), others are eliminated (*el*), have extended (*ex*), or have retracted (*r*). New processes are also added (*a*). (W. T. Wong and R. O. L. Wong, unpublished.)

regrow dendritic arbors that are diverse in morphology but resemble that of mature cells (Montague and Friedlander, 1989). Whether the neonatal cells reexecute an earlier plan to elaborate specific patterns of dendritic arborizations is unknown, but the observations suggest that patterning of the arbor can emerge in the absence of direct cell-cell contact. Also, cells with distinctive patterns such as large-field alpha-like cells can be found across several species (Peichl, 1991), implying that the basic “dendritic plan” of ganglion cell classes may be specified intrinsically. Of course, whether there is a complement of genes issuing branching instructions to generate “alpha-like” patterns remains unknown, but it is tempting to speculate about such a possibility. Finally, the dendritic terminals of alpha-like cells in the ferret form dendro-dendritic contacts or fascicles early in development only if they are destined to be of the same ON or OFF subtype (Lohmann and Wong, 2001). Together, these observations encourage investigation into the genetic makeup of retinal ganglion cell classes.

There is also substantial support for a role for cell-cell interactions or environmental cues that regulate the final dendritic patterning of retinal ganglion cells. Neurotrophins such as BDNF and NT-4 affect the patterning of retinal ganglion cell dendrites (Lom and Cohen-Cory, 1999); the source of these neurotrophins may be outside or inside the retina. In addition, neighbor relationships influence the size and symmetry of the ganglion cell dendritic arbor. In all species examined, dendritic field size varies inversely with cell density across the retina. This relationship is present before the retina matures (Sernagor et al., 2001). Experimental manipulations to increase or decrease eye size, and thus affect cell density distributions, result in adjustments in dendritic field area (Troilo et al., 1996). A direct relationship between cell density and the patterning of the dendritic arbor is evident from studies in which ganglion cells have been ablated in some regions of the retina (Deplano et al., 1994; Perry and Linden, 1982). Ganglion cells reorient their dendrites toward the lesion zone apparently in an attempt to cover the cell-depleted area. It is still unclear whether such rearrangements are due to a loss of neighboring ganglion cells of the same class or subclass (Ault et al., 1993; Weber et al., 1998). This knowledge will provide more insight into whether cell-cell interactions between specific cell types are needed to maintain, for example, coverage of the retina by a single cell class (see Chapter 29) or whether it is the overall availability of presynaptic terminals that is key to regulating dendritic patterns. What is apparent, however, is that neurotransmission is involved in regulating the dendritic patterning of retinal ganglion cells (Sernagor and Grzywacz, 1996; Wong et al., 2000a, 2000b).

Much less is known about how the many classes of amacrine and bipolar cells achieve their characteristic arborizations. Cholinergic amacrine cells which differentiate

early in development (Galli-Resta et al., 1997) have radially arranged arbors that undergo some structural remodeling with maturation (Wong and Collin, 1989; Fig. 6.5). In contrast, process outgrowth in another amacrine cell with a radiating arbor, the so-called fireworks cell, may be more “deterministic.” The characteristic nonbranching, radiating processes of this type of amacrine cell are evident even during embryonic development (Fig. 6.5). However, studies in the rodent retina suggest that cell-cell interactions are also important for defining the arborization patterns of amacrine cells. Signaling involving neurotrophins (Rickman, 2000) and reelin (Rice et al., 2001) shape the projection patterns of AII amacrine cells.

LAMINATION From a developmental point of view, it is intriguing to find that the retinal layers are generated sequentially, and normally, without error in their order of appearance. For instance, in all species studied, the inner plexiform layer appears before the outer plexiform layer. As noted in the section on “Cell Genesis,” apart from ganglion cells, when a retinal cell type is generated does not necessarily predict where it will ultimately reside. Thus, environmental factors must come into play to organize the layering of the retina in terms of cell body location and where their processes eventually elaborate.

Another intriguing aspect of lamination concerns how the layers become contiguous across the retina. Not only do the major lamination patterns extend across the retina, but for each type of inner retinal neuron, such as amacrine cells, processes of the same kind ramify in one or a few distinct sublaminae, forming a contiguous plexus (or plexuses) across the retinal surface. How does this happen? Zebrafish mutants have provided some insights into how this might occur for both the inner and outer plexiform layers. In *lakritz* mutants, a continuous inner plexiform layer still develops, suggesting that the formation of this synaptic lamina does not require the presence of ganglion cells, which fail to differentiate in this mutant (Kay et al., 2001). In other zebrafish mutants, however, such as *young*, there are no obvious plexiform layers; this may be because of the perturbed final stages of morphological differentiation of retinal neurons (Link et al., 2000). The outer plexiform layer forms in the absence of transmission from photoreceptors, implying that elaboration of processes within this layer does not require this form of cell-cell communication (Allwardt et al., 2001). Although our knowledge of the mechanisms that regulate layering in the retina is still sketchy, it is likely that this situation will change when more lamination mutants and the genes responsible for these mutations are identified.

The actions of multiple well-coordinated mechanisms come to mind when we also realize that within the inner plexiform layer, up to 10 or more functionally distinct sublaminae are established by maturity (see Chapter 18). Of

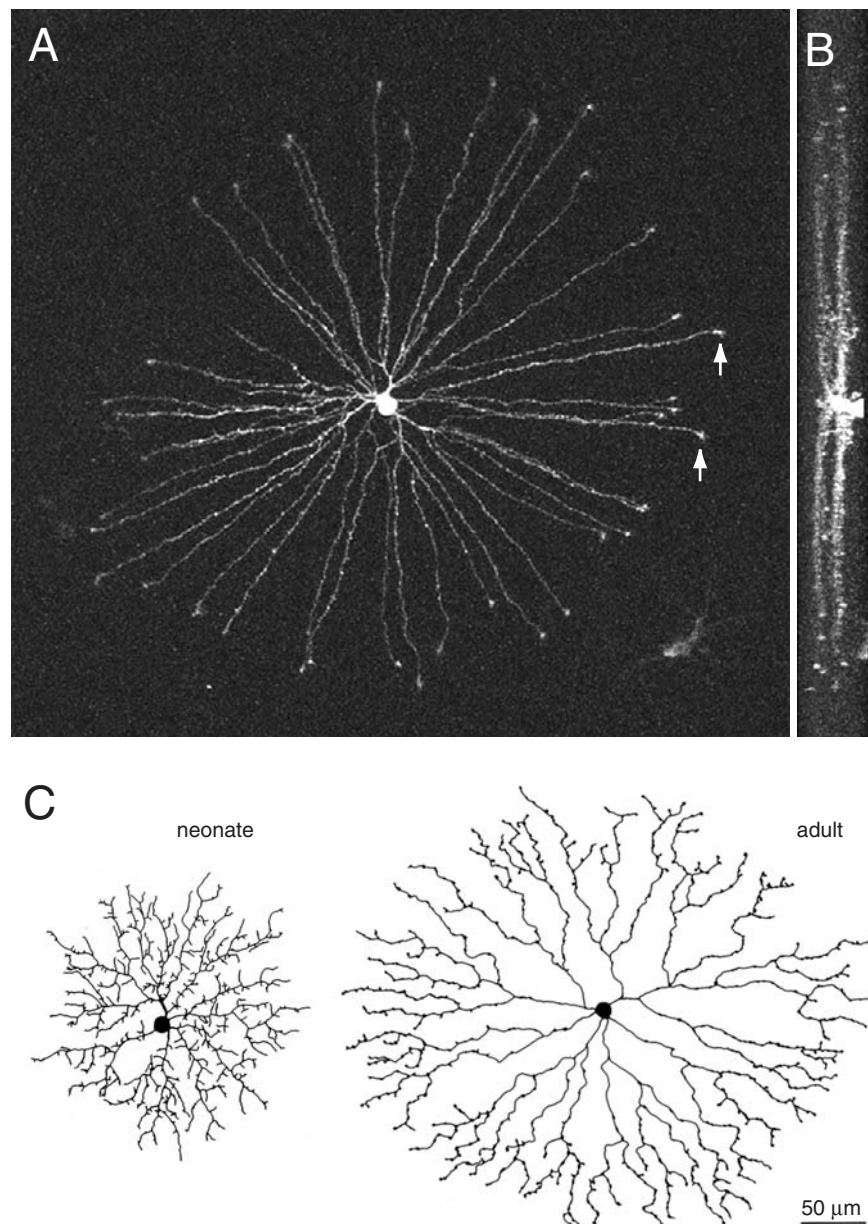


FIGURE 6.5. Development of amacrine cell processes. *A*, A “fireworks” type of amacrine cell in the embryonic chick retina sends out processes radially without much branching. Each process is tipped with a growth cone (examples, *arrows*). Even at this immature stage, the arbor morphology of this cell type is already patterned. Moreover, the processes are already confined to two distinct

strata in the inner plexiform layer (*B*, side view of the cell). The cell was labeled after transfection with plasmid encoding green fluorescent protein. *C*, In contrast, the processes of cholinergic amacrine cells (from the rabbit retina) undergo remodeling with maturation. Many small branches are eliminated with age (Wong and Collin, 1989). Cells labeled by intracellular dye filling.

most interest is how ON and OFF sublamination takes place, an event that commences well before eye opening and requires the sorting out of three sets of neuronal processes—the dendrites of ganglion cells, processes of amacrine cells, and axons of bipolar cells. Morphological studies show that much structural reorganization takes place before the dendrites of ganglion cells become confined to the ON or OFF sublamina (Fig. 6.6; Bodnarenko and Chalupa, 1993;

Bodnarenko et al., 1999; Kirby and Steineke, 1996; Lohmann and Wong, 2001; Maslim and Stone, 1988). Retinal ganglion cells which at maturity have either ON- or OFF-center responses receive converging inputs from ON and OFF bipolar cells when their arbors have not yet stratified (Wang et al., 2001). Thus, importantly, developmental rearrangements in the dendritic structure of the ganglion cells underlie their functional maturation.

How ganglion cell dendritic stratification is achieved is not yet known, but it is a subject of intense investigation. The first indication that transmission from presynaptic interneurons is involved in dendritic stratification of retinal ganglion cells came from studies in which 2-amino-4-phosphonobutyric acid (APB), an agonist of mGluR6 receptors, was injected intraocularly during the period in which dendritic arbors of ganglion cells became stratified (Bodnarenko et al., 1995, 1999). Retinal ganglion cells failed to stratify in the APB-treated eyes. Although APB treatment disrupts the stratification of ganglion cell dendrites, it is unlikely that glutamatergic transmission initiates this process. This is because the process of stratification begins before bipolar cells have differentiated. Amacrine cells, which differentiate earlier than bipolar cells and around the same time as ganglion cells, may mediate the early stratification process. Knockout mice in which populations of amacrine cells are ablated or their function perturbed will be useful for assessing the role of these interneurons. Examination of mice lacking the beta2 subunit of the cholinergic receptor indicated that ganglion cell stratification still occurs, although there may be some abnormalities (Bansal et al., 2000). However, it may be that not all ganglion cell dendritic arbors are affected in beta2 knockout mice because not all ganglion cells may be major postsynaptic targets of cholinergic amacrine cells. Because there are many other popula-

tions of amacrine cells, determining whether ganglion cell dendritic stratification is affected by amacrine transmission will require detailed consideration of subcircuits within the inner retina. This will involve determining which amacrine cells form the major input onto each type of ganglion cell, a task that is extremely challenging. Finally, bipolar cell interactions are likely to be important for the maintenance of stratification in the ganglion cells. Selective perturbation of transmission from ON or OFF bipolar cells should help determine whether bipolar cell inputs affect structural reorganization of the ganglion cell dendritic arbor. Ganglion cell dendritic stratification in mGluR6 knockout mice appears normal, but this may be because activity is enhanced in the ON bipolar cells rather than suppressed (Tagawa et al., 1999).

How could neurotransmission help determine the stratification of ganglion cell arbors? One possibility is that initially, synaptic inputs are not equally distributed across the dendritic arbor. Through competitive interactions that favor the retention of more “active” or collectively “stronger” inputs, dendrites in one sublamina may be selectively maintained or eliminated. To date, however, the initial distributions and synaptic strengths of inputs onto the dendritic arbor of retinal ganglion cells are unknown, but their measurement would be very helpful in understanding how the inner retinal circuitry is established.

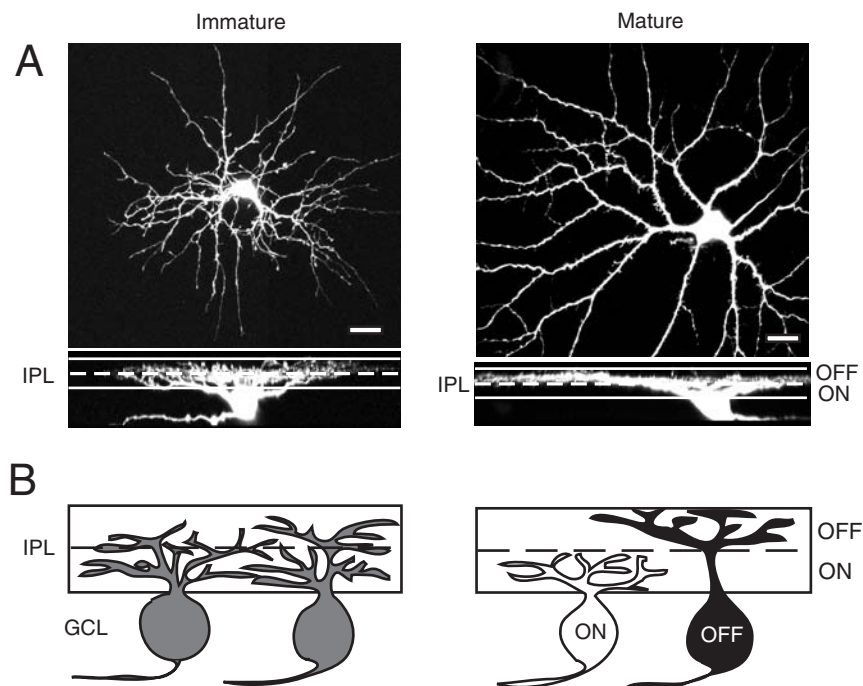


FIGURE 6.6. The dendritic arbors of retinal ganglion cells undergo structural reorganization during the period of synapse formation and maturation. *A*, Reconstructions from confocal images of alpha-like ganglion cells in the newborn (*left*) and 3-week-old (*right*) ferret retina. Below, orthogonal view of the cells. Scale bars,

20 μ m. The distribution of dendrites within the inner plexiform layer (IPL) becomes gradually restricted to either the ON or OFF sublamina with age. *B*, Schematic representation of the stratification process. *GCL*, ganglion cell layer. (*A* adapted from Lohmann and Wong, 2001.)

Even though interactions between amacrine cells and bipolar cells may influence the segregation of ON and OFF pathways within the retina, other nonactivity-dependent mechanisms must be considered. This is because there are other aspects of dendritic development in ganglion cells that may not depend on neurotransmission alone. Notably, mechanisms which regulate the arbor size of retinal ganglion cells during mosaic formation are likely to include molecular cues (Sernagor et al., 2001). Thus, the remodeling of dendritic arbors during development of retinal ganglion cells possibly requires several mechanisms that act together to shape their lateral and vertical distributions in a coordinated way. While contact between retinal interneurons and ganglion cells might direct their stratification according to depth within the inner plexiform layer, contact between retinal ganglion cells themselves may organize the lateral extent of their dendritic territory (see also Chapter 9).

If amacrine and bipolar cell interactions effect the dendritic stratification of ganglion cells, what controls the stratification of these interneurons? Although an answer is still far off, deletion of one of the three major inner retinal cell classes during development should provide important insights. What is known so far is that in rodents, ganglion cells are not needed for amacrine or bipolar cell processes to stratify in the inner plexiform layer (Gunhan-Agar et al., 2000).

Wiring up the retina

NEUROTRANSMITTERS AND RECEPTORS The functional maturation of retinal circuits depends on the expression of neu-

rotransmitters and their receptors, as well as the formation of synaptic contacts. We will discuss briefly the timing and patterns of expression of the major excitatory and inhibitory transmitters in the retina and summarize when receptors for these transmitters appear (see Fig. 6.7).

Glutamate is the major excitatory transmitter in the adult retina, present in photoreceptors, bipolar cells, and retinal ganglion cells. Immunolabeling for glutamate in the developing retina demonstrates that expression of this amino acid is first detected in undifferentiated cells in the ventricular zone of the retina before the plexiform layers appear. Surprisingly, cell bodies in the ganglion cell layer are immunonegative for glutamate until bipolar cells and Müller glial cells have differentiated. This may be because ganglion cells synthesize glutamate from glutamine that is normally provided by the Müller glia. In the outer retina, photoreceptors express glutamate long before they differentiate and form connections. Functional receptors for glutamate are expressed by retinal ganglion cells and amacrine cells before they receive synaptic inputs (Liets and Chalupa, 2001; Wong, 1999). The distribution of the various ionotropic glutamate receptor subunits has been assessed by immunocytochemistry: both Alpha-amino-3-hydroxy-5-methylisoxazole-4-propionic acid (AMPA) and N-methyl-D-aspartate (NMDA) receptor subunit staining becomes restricted to distinct bands within the inner plexiform layer by the time of eye opening (Grunder et al., 2000a, 2000b). These banding patterns appear in retinas immunolabeled for AMPA receptor subunits before those of NMDA receptor subunits.

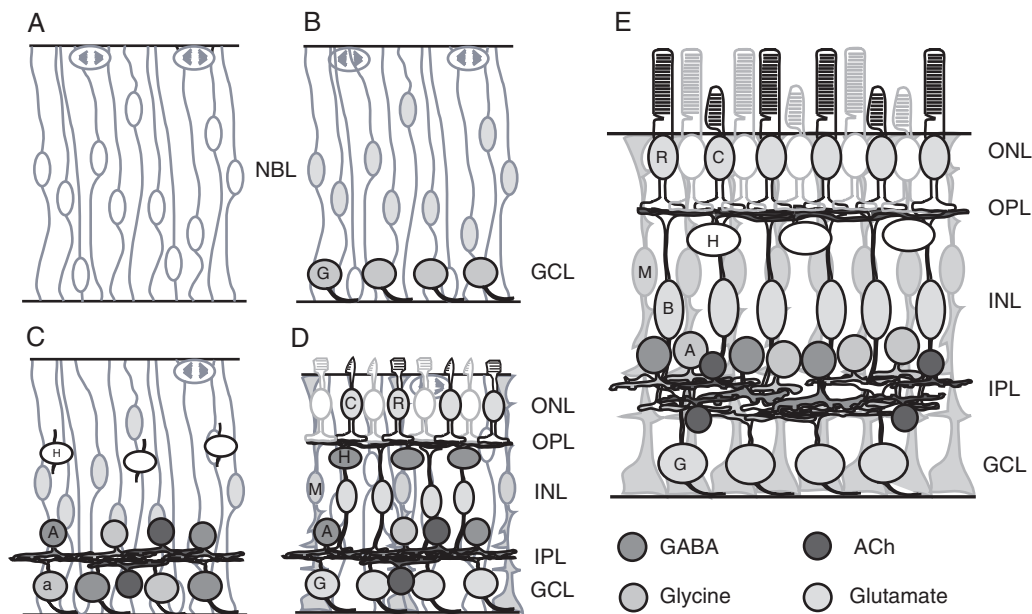


FIGURE 6.7. Expression patterns of major excitatory and inhibitory neurotransmitters in the developing and adult retina. Labeling of cell types and retinal layers are provided in Figure 6.1. *GABA*, gamma-aminobutyric acid; *ACh*, acetylcholine. (See color plate 4.)

The other major excitatory fast neurotransmitter in the retina is acetylcholine. Immunolabeling for choline acetyltransferase (ChAT) has been carried out in a large range of species. ChAT expression is present early in development, often prenatally, and cholinergic transmission takes place before glutamatergic transmission is apparent (see the section "Spontaneous Activity"). In mammal and chick, retinal neuroblasts in the ventricular cell layer demonstrate an increase in intracellular calcium upon stimulation with muscarinic receptor agonists (Sakaki et al., 1996; Wong, 1995a). Whether the expression of these receptors has a major functional role in the differentiation of these cells remains to be determined. Amacrine and ganglion cells, prior to the formation of synapses, are also able to respond to applied nicotine (Wong, 1995b). Thus, like ionotropic glutamate receptors, retinal neurons express functional cholinergic receptors prior to the emergence of synaptic networks.

There has been much interest in the development of the inhibitory systems of the retina, primarily because GABA and glycine have been linked to cell survival and differentiation in many neuronal systems (Cherubini et al., 1991). GABA immunoreactivity is first detected in amacrine cells and in some ganglion cells just before birth in the rabbit and in rodents. Ganglion cell expression disappears at maturity. In mammals, horizontal cells are transiently immunoreactive for GABA at the time when cone photoreceptors can respond to this amino acid (Huang and Redburn, 1996). Glycine immunoreactivity is dominant in the ganglion cell layer and the fiber layer in the immature retina. With maturation, glycine immunoreactivity disappears from the ganglion cells and becomes restricted to amacrine cells and a few bipolar cells (Pow et al., 1994). In contrast to cells at maturity, retinal neurons, including ganglion cells, are depolarized by GABA and glycine early in development (Wong et al., 2000b; Yamashita and Fukuda, 1993). This is because, like other neurons in the developing CNS, immature retinal ganglion cells have a relatively high intracellular chloride concentration. This is probably because the K-Cl cotransporter (KCC2) that extrudes chloride from cells increases in expression only after birth (Vu et al., 2000). Interestingly, KCC2 expression in the inner retina precedes that in the outer retina, suggesting that prior to eye opening, GABA action in the outer plexiform layer may differ from that in the inner retina.

A common feature, then, of the developing neurotransmitter system in the retina is that expression of the transmitters and their receptors occurs before visual processing, and even before electrical activity can be detected. It is possible that communication between retinal neurons still occurs, perhaps through release of transmitter from growth cones (Gordon-Weeks et al., 1984). Such communication could be important for maturation events in the retina,

although direct evidence for a developmental role for transmitter-mediated interactions in cell differentiation is still lacking. During the period of synaptogenesis, however, neurotransmission appears to be important for the maintenance of dendritic structure, as discussed earlier (Wong et al., 2000a). Furthermore, early transmission, before vision, is also necessary for establishing the correct patterns of connections between the retina and visual centers in the brain (see the section "Spontaneous Activity"). The availability of knockout mice lacking synthetic enzymes for various neurotransmitters and the ability to generate conditional knockouts of these mice will no doubt be useful in the future for assessing the importance of the early expression of neurotransmitter systems in the retina and in other parts of the nervous system.

SYNAPSE FORMATION Synapse formation in the retina has largely been assessed by electron microscopy (see Robinson, 1991, for a review). In many species, synaptogenesis in both plexiform layers begins before eye opening, occurring first in the inner plexiform layer about two-thirds of the way through gestation. In particular, amacrine cells form synapses with ganglion cells, and between themselves, shortly after these populations of neurons extend neurites into the inner plexiform layer (Maslim and Stone, 1986; Nishimura and Rakic, 1985, 1987).

Membrane thickenings are observed in the inner plexiform layer before synaptic vesicles can be recognized. Studies of primate retina suggest that these thickenings or specializations occur first in postsynaptic processes, the dendrites of ganglion cells, before they are apposed by amacrine cell processes (Nishimura and Rakic, 1985, 1987). Maturation of conventional synapses involves the acquisition of an increasing number of synaptic vesicles. Bipolar synapses, which are characterized by the presence of a ribbon-like structure, appear after conventional synapses are formed in the retinal periphery of primates. Initially, serial electron microscopy indicates that putative bipolar terminals are observed without ribbons. Then ribbon-containing terminals form dyads, making contact with a single postsynaptic process. With maturation, the typical triad arrangement is seen when each bipolar terminal contacts two processes, which could belong to amacrine or ganglion cells. In contrast to the retinal periphery, in the fovea bipolar synapses appear before conventional synapses are observed (Crooks et al., 1995). It may be that in cone-dominated regions of the retina, bipolar synapses develop before amacrine synapses (see Hendrickson, 1996).

Synapses in the outer plexiform layer are first formed between photoreceptors and horizontal cells (McArdle et al., 1977). The last cellular element to enter into the circuitry is the bipolar cell that appears to be contacted first by cones. Rod bipolar cell differentiation may occur later, and

synapses from rods are therefore established after those of cones, although there is substantial overlap in timing. Synaptogenesis in the outer plexiform layer continues after eye opening, raising the possibility that the properties of this outer synaptic layer may be more susceptible to sculpting by visual stimulation compared to synapses in the inner plexiform layer (Robinson, 1991).

The ultrastructural observations provide a broad view of the order of appearance of synapses within the retina, as well as provide clues as to how various connections may arise. To gain an understanding of the nature of the initial interactions that result in the contact and maturation of synapses between retinal neurons, it will be necessary to watch how pre- and postsynaptic processes behave in living tissue. Although this has not yet been achieved, recent imaging experiments of dendritic motility in the isolated developing retina suggest that contact between inner retinal neurons may involve transient filopodia-like structures that are highly dynamic in nature (Wässle, 1988; Wong and Wong, 2000; Wong et al., 2000b). These filopodia-like structures, which extend and retract over the course of seconds to minutes, are most abundant during the period of synaptogenesis in the inner retina. Because of their high density and motility, dendritic filopodia effectively increase the volume of dendrite that can be contacted by incoming amacrine or bipolar afferents. Although this potential role for dendritic filopodia has yet to be demonstrated, their regulation by neurotransmission supports the notion that afferent signaling encourages contact with dendrites by promoting their motility (Wong and Wong, 2001).

Many questions, of course, remain. How do the many classes and subclasses of retinal neurons find their appropriate synaptic partners? How much remodeling of the initial connectivity occurs in retinal circuits? What determines the lamination and sublamination of the plexiform layers? How is synapse formation coordinated across the plexiform layers and within each lateral and vertical network? Is the mature mammalian retina capable of regenerating connections?

Physiology of the developing retina

SPONTANEOUS ACTIVITY Neurotransmission occurs in the developing retina even before photoreceptors mature, and begins around the time that amacrine inputs to ganglion cells are formed. This early transmission between amacrine and ganglion cells sustains a unique pattern of retinal activity that has important developmental roles. Retinal ganglion cells fire action potentials during the period when their connections with central targets undergo reorganization. Recordings from rat fetuses in vivo demonstrated that immature ganglion cells fire spikes in bursts that occur periodically, about once every minute (Galli and Maffei, 1988;

Maffei and Galli-Resta, 1990). Simultaneous recordings from neighboring ganglion cells using multielectrode arrays (Fig. 6.8) later showed that bursts of spikes from the ganglion cells are temporally synchronized (Meister et al., 1991). This is because activity propagates across the retinal surface as waves, which are clearly seen using optical imaging techniques (Fig. 6.8).

All major classes of retinal ganglion cells and subpopulations of amacrine cells participate in the wave activity. The waves are generated by mechanisms requiring synaptic input from amacrine cells, and later with maturation, transmission from bipolar cells (reviewed in Wong, 1999). Exactly how this inner retinal circuitry generates the wave pattern of activity is not fully known, but transmission from cholinergic amacrine cells is important early on (Feller et al., 1996; Sernagor et al., 2001). Waves are abolished in the presence of neuronal nicotinic receptor antagonists and are absent in mice which lack specific subunits of these receptors (Bansal et al., 2000).

The spontaneous activity patterns of the immature ganglion cells contain several spatiotemporal cues that could be important for the refinement of their connectivity with their central targets. First, spiking in bursts appears necessary for long-term potentiation of synapses between retinal ganglion cells and the lateral geniculate nucleus (Mooney et al., 1996). Second, the propagating waves ensure that activity of neighboring cells is better correlated compared to cells that are more distant. This feature provides a means for geniculate neurons to gauge intercellular distance within the retina based on the timing of their spikes. Such information could be important in helping refine the retinotopic map, which becomes sharpened in many species with maturation. Third, because waves occur randomly and are relatively infrequent, waves from the two eyes are unlikely to be synchronized. Such asynchronous activity from the two eyes is thought to drive the segregation of connections from the two eyes which initially converge onto single geniculate neurons. Indeed, the projections from the left and right eyes are abnormal in nicotinic receptor knockout mice and in ferrets that have been injected intraocularly with epibatidine, a nicotinic receptor antagonist, during the period of axonal segregation (Penn et al., 1998; Bansal et al., 2000). Although activity from the retinas prior to visual stimulation is important for establishing the projection patterns of the ganglion cells during development, direct evidence for patterned activity underlying these events has yet to be obtained. This would require maintaining spontaneous activity but altering the spatiotemporal relationship between spiking of neighboring ganglion cells.

Prior to eye opening in the ferret, the spontaneous spiking patterns of retinal ganglion cells are altered in their temporal characteristics in a cell-type-specific manner. Although waves are still present and each wave synchronizes the spiking of neighboring ON and OFF cells, OFF cells spike

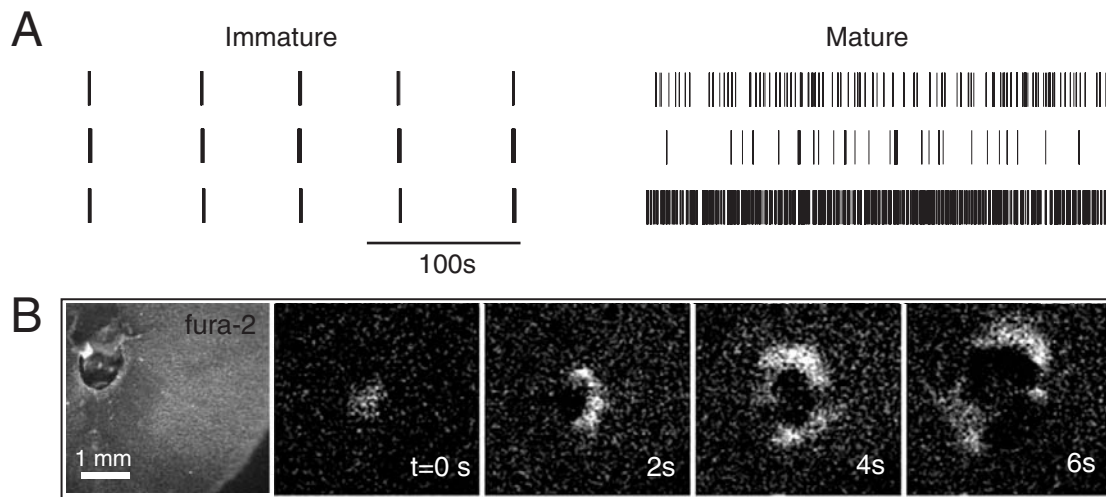


FIGURE 6.8. Patterns of spontaneous activity in the developing retina. *A*, Spike recordings from the mouse retinal ganglion cell layer using a multielectrode array before (immature) and after (mature) eye opening. *B*, Calcium imaging of the immature mouse

retina showing labeling of the retina with the calcium indicator, fura-2, and the spread of activity, indicated by the white pixels, across the retinal surface over time. (*A*, J. Demas and R. O. L. Wong, unpublished; *B*, R. O. L. Wong, unpublished.)

more frequently between waves than ON cells (Wong and Oakley, 1996). This change in the activity patterns of the ON and OFF ganglion cells occurs during the period when the axonal projections of these ganglion cells to the geniculate nucleus becomes refined. Theoretical studies suggest that the decrease in correlated activity between ON and OFF ganglion cells is sufficient to cause their inputs onto geniculate neurons to segregate over time (Lee et al., 2002). By the time of eye opening, waves disappear and the spontaneous spike activity of retinal ganglion cells is no longer patterned, instead appearing randomly (Fig. 6.8). However, different rates of spontaneous firing occur even in the adult retina, although their correlation with retinal ganglion cell type has yet to be established.

The mechanisms that underlie the progressive change in spontaneous activity patterns of the ganglion cells are not yet fully uncovered. It is likely that the developmental maturation of the spike patterns is shaped by both intrinsic properties of the ON and OFF ganglion cells and by their circuitry (Myhr et al., 2001). It is also possible that maturation of the outer retina, particularly the emergence of light sensitivity in photoreceptors, affects the patterns of spontaneous spiking of ganglion cells.

LIGHT RESPONSES Light responses emerge as the photoreceptor-bipolar pathway begins to mature shortly before eye opening (Dacheux and Miller, 1981a, 1981b; Masland, 1977; Tootle, 1993). Electrophysiological recordings from retinal ganglion cells show several major trends in the maturation of their responses to light. The early response of retinal ganglion cells to light stimulation is weak and the cells adapt rapidly (Masland, 1977; Tootle, 1993). But when robust responses to light become detectable a few

days later, the concentric center-surround organization of the receptive fields, as well as ON and OFF center responses, are already present (Bowe-Anders et al., 1975; Masland, 1977; Tootle, 1993). Whether the connectivity that underlies these physiological properties is established before photoreceptors are present is unknown. Determining how surround inhibition appears in the retinal ganglion cells has not been straightforward. Some immature rabbit retinal ganglion cells have silent surrounds that, when stimulated, can suppress the response to center stimulation, but direct stimulation of the surround does not evoke a response (Masland, 1977). In the cat, however, the strength of the antagonistic surround relative to that of the center does not seem to change with postnatal maturation (Tootle, 1993).

Recordings from ferrets, however, clearly demonstrate that connectivity in the inner retina is remodeled with maturation. In the postnatal ferret, alpha- and beta-like retinal ganglion cells have convergent ON and OFF inputs prior to maturity (Wang et al., 2001). In these cells, maturation of the receptive field center responses thus involves the loss of one type of input. Specialized receptive field properties such as direction selectivity also develop before eye opening (Masland, 1977; Sernagor and Grzywacz, 1995), although the synaptic basis for this property remains to be determined.

How then is the ganglion cell receptive field established during development? Visual experience after eye opening does not appear to alter the receptive field properties of mammals that were raised in an environment with unidirectionally moving stimuli (Daw and Wyatt, 1974). But this may be because, in rabbits, ganglion cell receptive fields are fairly mature by the time of eye opening (Masland, 1977). In contrast, the peak firing rate of retinal ganglion cells

in response to light stimulation is decreased in dark-reared mice (Tian and Copenhagen, 2001). Cells also respond more sluggishly in dark-reared animals. The spatial organizations of the receptive fields have not yet been assessed after dark rearing of mice. In turtles, which become light responsive prior to hatching, dark rearing causes an increase in receptive field size (Sernagor and Grzywacz, 1996). However, this study also suggested that it is spontaneous activity rather than visual stimulation that regulates the receptive field size.

Clearly, much remains to be done to fill our knowledge gaps concerning how the light responses of retinal neurons are established in ways that are characteristic of each cell type. While in the past such properties were largely studied using electrophysiological methods, it is likely that the combination of physiology with molecular and live-imaging techniques will now aid investigations in this important area of retinal development.

REFERENCES

- Alexiades, M. R., and C. L. Cepko, 1997. Subsets of retinal progenitors display temporally regulated and distinct biases in the fates of their progeny, *Development*, 124:1119–1131.
- Allwardt, B. A., A. B. Lall, S. E. Brockerhoff, and J. E. Dowling, 2001. Synapse formation is arrested in retinal photoreceptors of the zebrafish *nrc* mutant, *J. Neurosci.*, 21:2330–2342.
- Altshuler, D., J. J. Lo Turco, J. Rush, and C. Cepko, 1993. Taurine promotes the differentiation of a vertebrate retinal cell type in vitro, *Development*, 119:1317–1328.
- Ault, S. J., K. G. Thompson, Y. Zhou, and A. G. Leventhal, 1993. Selective depletion of beta cells affects the development of alpha cells in cat retina, *Vis. Neurosci.*, 10:237–245.
- Austin, C. P., D. E. Feldman, J. A. Ida, Jr., and C. L. Cepko, 1995. Vertebrate retinal ganglion cells are selected from competent progenitors by the action of *Notch*, *Development*, 121:3637–3650.
- Bansal, A., J. H. Singer, B. J. Hwang, W. Xu, A. Beaudet, and M. B. Feller, 2000. Mice lacking specific nicotinic acetylcholine receptor subunits exhibit dramatically altered spontaneous activity patterns and reveal a limited role for retinal waves in forming ON and OFF circuits in the inner retina, *J. Neurosci.*, 20:7672–7681.
- Bao, Z. Z., and C. L. Cepko, 1997. The expression and function of *Notch* pathway genes in the developing rat eye, *J. Neurosci.*, 17:1425–1434.
- Bauch, H., H. Stier, and B. Schlosshauer, 1998. Axonal versus dendritic outgrowth is differentially affected by radial glia in discrete layers of the retina, *J. Neurosci.*, 18:1774–1785.
- Bennett, G. S., and C. DiLullo, 1985. Transient expression of a neurofilament protein by replicating neuroepithelial cells of the embryonic chick brain, *Dev. Biol.*, 107:107–127.
- Bodnarenko, S. R., and L. M. Chalupa, 1993. Stratification of ON and OFF ganglion cell dendrites depends on glutamate-mediated afferent activity in the developing retina, *Nature*, 364:144–146.
- Bodnarenko, S. R., G. Jeyarasasingam, and L. M. Chalupa, 1995. Development and regulation of dendritic stratification in retinal ganglion cells by glutamate-mediated afferent activity, *J. Neurosci.*, 15:7037–7045.
- Bodnarenko, S. R., G. Yeung, L. Thomas, and M. McCarthy, 1999. The development of retinal ganglion cell dendritic stratification in ferrets, *Neuroreport*, 10:2955–2959.
- Book, K. J., and D. K. Morest, 1990. Migration of neuroblasts by perikaryal translocation: role of cellular elongation and axonal outgrowth in the acoustic nuclei of the chick embryo medulla, *J. Comp. Neurol.*, 297:55–76.
- Bowe-Anders, C., R. F. Miller, and R. Dacheux, 1975. Developmental characteristics of receptive organization in the isolated retina-eyecup of the rabbit, *Brain Res.*, 87:61–65.
- Carter-Dawson, L. D., and M. M. LaVail, 1979. Rods and cones in the mouse retina. II. Autoradiographic analysis of cell generation using tritiated thymidine, *J. Comp. Neurol.*, 188:263–272.
- Cepko, C. L., C. P. Austin, X. Yang, M. Alexiades, and D. Ezzeddine, 1996. Cell fate determination in the vertebrate retina, *Proc. Natl. Acad. Sci. USA*, 93:589–595.
- Cherubini, E., J. L. Gaiarsa, and Y. Ben-Ari, 1991. GABA: an excitatory transmitter in early postnatal life, *Trends Neurosci.*, 14:515–519.
- Crooks, J., M. Okada, and A. E. Hendrickson, 1995. Quantitative analysis of synaptogenesis in the inner plexiform layer of macaque monkey fovea, *J. Comp. Neurol.*, 360:349–362.
- Dacheux, R. F., and R. F. Miller, 1981a. An intracellular electrophysiological study of the ontogeny of functional synapses in the rabbit retina. I. Receptors, horizontal, and bipolar cells, *J. Comp. Neurol.*, 198:307–326.
- Dacheux, R. F., and R. F. Miller, 1981b. An intracellular electrophysiological study of the ontogeny of functional synapses in the rabbit retina. II. Amacrine cells, *J. Comp. Neurol.*, 198:327–334.
- Daw, N. W., and H. J. Wyatt, 1974. Raising rabbits in a moving visual environment: an attempt to modify directional sensitivity in the retina, *J. Physiol.*, 240:309–330.
- Deplano, S., G. M. Ratto, and S. Bisti, 1994. Interplay between the dendritic trees of alpha and beta ganglion cells during the development of the cat retina, *J. Comp. Neurol.*, 342:152–160.
- Dorsky, R. I., D. H. Rapaport, and W. A. Harris, 1995. *Notch* inhibits cell differentiation in the *Xenopus* retina, *Neuron*, 14:487–496.
- Dorsky, R. I., W. S. Chang, D. H. Rapaport, W. A. Harris, 1997. Regulation of neuronal diversity in the *Xenopus* retina by Delta signalling, *Nature*, 385:67–70.
- Dunlop, S. A., 1990. Early development of retinal ganglion cell dendrites in the marsupial *Setonix brachyurus*, *quokka*, *J. Comp. Neurol.*, 293:425–447.
- Fekete, D. M., J. Perez-Miguelsanz, E. F. Ryder, and C. L. Cepko, 1994. Clonal analysis in the chicken retina reveals tangential dispersion of clonally related cells, *Dev. Biol.*, 166:666–682.
- Feller, M. B., D. P. Wellis, D. Stellwagen, F. S. Werblin, and C. J. Shatz, 1996. Requirement for cholinergic synaptic transmission in the propagation of spontaneous retinal waves, *Science*, 272:1182–1187.
- Galli, L., and L. Maffei, 1988. Spontaneous impulse activity of rat retinal ganglion cells in prenatal life, *Science*, 242:90–91.
- Galli-Resta, L., G. Resta, S. S. Tan, and B. E. Reese, 1997. Mosaics of islet-1-expressing amacrine cells assembled by short-range cellular interactions, *J. Neurosci.*, 17:7831–7838.
- Gordon-Weeks, P. R., R. O. Lockerbie, and B. R. Pearce, 1984. Uptake and release of [3H]GABA by growth cones isolated from neonatal rat brain, *Neurosci. Lett.*, 52:205–210.

- Grunder, T., K. Kohler, and E. Guenther, 2000a. Distribution and developmental regulation of AMPA receptor subunit proteins in rat retina, *Invest. Ophthalmol. Vis. Sci.*, 41:3600–3606.
- Grunder, T., K. Kohler, A. Kaletta, and E. Guenther, 2000b. The distribution and developmental regulation of NMDA receptor subunit proteins in the outer and inner retina of the rat, *J. Neurobiol.*, 44:333–342.
- Gunhan-Agar, E., D. Kahn, and L. M. Chalupa, 2000. Segregation of on and off bipolar cell axonal arbors in the absence of retinal ganglion cells, *J. Neurosci.*, 20:306–314.
- Harris, W. A., 1997. Cellular diversification in the vertebrate retina, *Curr. Opin. Genet. Dev.*, 7:651–658.
- Hendrickson, A. E., 1996. Synaptic development in macaque monkey retina and its implications for other developmental sequences, *Perspect. Dev. Neurobiol.*, 3:195–201.
- Hinds, J. W., and P. L. Hinds, 1974. Early ganglion cell differentiation in the mouse retina: an electron microscopic analysis utilizing serial sections, *Dev. Biol.*, 37:381–416.
- Hinds, J. W., and P. L. Hinds, 1983. Development of retinal amacrine cells in the mouse embryo: evidence for two modes of formation, *J. Comp. Neurol.*, 213:1–23.
- Holt, C. E., T. W. Bertsch, H. M. Ellis, and W. A. Harris, 1988. Cellular determination in the *Xenopus* retina is independent of lineage and birth date, *Neuron*, 1:15–26.
- Huang, B. O., and D. A. Redburn, 1996. GABA-induced increases in $[Ca^{2+}]_i$ in retinal neurons of postnatal rabbits, *Vis. Neurosci.*, 13:441–447.
- Johnson, P. T., R. R. Williams, K. Cusato, and B. E. Reese, 1999. Rods and cones project to the inner plexiform layer during development, *J. Comp. Neurol.*, 414:1–12.
- Kay, J. N., K. C. Finger-Baier, T. Roeser, W. Staub, and H. Baier, 2001. Retinal ganglion cell genesis requires *lakritz*, a zebrafish atonal homolog, *Neuron*, 30:725–736.
- Kirby, M. A., and T. C. Steineke, 1996. Morphogenesis of retinal ganglion cells: a model of dendritic, mosaic, and foveal development, *Perspect. Dev. Neurobiol.*, 3:177–194.
- Lee, C. W., S. J. Eglén, and R. O. L. Wong, 2002. Segregation of On and Off retinogeniculate connectivity directed by patterned spontaneous activity, *J. Neurophysiol.*, 88:2311–2321.
- Lemmon, V., and G. Rieser, 1983. The development distribution of vimentin in the chick retina, *Brain Res.*, 313:191–197.
- Lia, B., R. W. Williams, and L. M. Chalupa, 1987. Formation of retinal ganglion cell topography during prenatal development, *Science*, 236:848–851.
- Liets, L. C., and L. M. Chalupa, 2001. Glutamate-mediated responses in developing retinal ganglion cells, *Prog. Brain Res.*, 134:1–16.
- Link, B. A., J. M. Fadool, J. Malicki, and J. E. Dowling, 2000. The zebrafish young mutation acts non-cell-autonomously to uncouple differentiation from specification for all retinal cells, *Development*, 127:2177–2188.
- Livesey, F. J., and C. L. Cepko, 2001. Vertebrate neural cell-fate determination: lessons from the retina, *Nat. Rev. Neurosci.*, 2:109–118.
- Lohmann, C., and R. O. L. Wong, 2001. Cell-type specific dendritic contacts between retinal ganglion cells during development, *J. Neurobiol.*, 48:150–162.
- Lom, B., and S. Cohen-Cory, 1999. Brain-derived neurotrophic factor differentially regulates retinal ganglion cell dendritic and axonal arborization in vivo, *J. Neurosci.*, 19:9928–9938.
- Maffei, L., and L. Galli-Resta, 1990. Correlation in the discharges of neighboring rat retinal ganglion cells during prenatal life, *Proc. Natl. Acad. Sci. USA*, 87:2861–2864.
- Marquardt, T., and P. Gruss, 2002. Generating neuronal diversity in the retina: one for nearly all, *Trends Neurosci.*, 25:32–38.
- Masland, R. H., 1977. Maturation of function in the developing rabbit retina, *J. Comp. Neurol.*, 175:275–286.
- Maslim, J., and J. Stone, 1986. Synaptogenesis in the retina of the cat, *Brain Res.*, 373:35–48.
- Maslim, J., and J. Stone, 1988. Time course of stratification of the dendritic fields of ganglion cells in the retina of the cat, *Brain Res. Dev. Brain Res.*, 44:87–93.
- Maslim, J., M. Webster, and J. Stone, 1986. Stages in the structural differentiation of retinal ganglion cells, *J. Comp. Neurol.*, 254:382–402.
- Mastronarde, D. N., M. A. Thibeault, and M. W. Dubin, 1984. Non-uniform postnatal growth of the cat retina, *J. Comp. Neurol.*, 228:598–608.
- McArdle, C. B., J. E. Dowling, and R. H. Masland, 1977. Development of outer segments and synapses in the rabbit retina, *J. Comp. Neurol.*, 175:253–274.
- McLoon, S. C., and R. B. Barnes, 1989. Early differentiation of retinal ganglion cells: an axonal protein expressed by pre-migratory and migrating retinal ganglion cells, *J. Neurosci.*, 9:1424–1432.
- Meister, M., R. O. L. Wong, D. A. Baylor, and C. J. Shatz, 1991. Synchronous bursts of action potentials in ganglion cells of the developing mammalian retina, *Science*, 252:939–943.
- Meller, K., and W. Tetzlaff, 1976. Scanning electron microscopic studies on the development of the chick retina, *Cell. Tissue Res.*, 170:145–159.
- Milam, A. H., D. M. Dacey, and A. M. Dizhoor, 1993. Recoverin immunoreactivity in mammalian cone bipolar cells, *Vis. Neurosci.*, 10:1–12.
- Miller, E. D., M. N. Tran, G. K. Wong, D. M. Oakley, and R. O. L. Wong, 1999. Morphological differentiation of bipolar cells in the ferret retina, *Vis. Neurosci.*, 16:1133–1144.
- Montague, P. R., and M. J. Friedlander, 1989. Expression of an intrinsic growth strategy by mammalian retinal neurons, *Proc. Natl. Acad. Sci. USA*, 86:7223–7227.
- Mooney, R., A. A. Penn, R. Gallego, and C. J. Shatz, 1996. Thalamic relay of spontaneous retinal activity prior to vision, *Neuron*, 17:863–874.
- Morest, D. K., 1970. The pattern of neurogenesis in the retina of the rat, *Z. Anat. Entwicklungsgesch.*, 131:45–67.
- Myhr, K. L., P. D. Lukasiewicz, and R. O. L. Wong, 2001. Mechanisms underlying developmental changes in the firing patterns of ON and OFF retinal ganglion cells during refinement of their central projections, *J. Neurosci.*, 21:8664–8671.
- Nishimura, Y., and P. Rakic, 1985. Development of the rhesus monkey retina. I. Emergence of the inner plexiform layer and its synapses, *J. Comp. Neurol.*, 241:420–434.
- Nishimura, Y., and P. Rakic, 1987. Development of the rhesus monkey retina: II. A three-dimensional analysis of the sequences of synaptic combinations in the inner plexiform layer, *J. Comp. Neurol.*, 262:290–313.
- Pei, Y. F., and J. A. Rhodin, 1970. The prenatal development of the mouse eye, *Anat. Rec.*, 168:105–125.
- Peichl, L., 1991. Alpha ganglion cells in mammalian retinae: common properties, species differences, and some comments on other ganglion cells, *Vis. Neurosci.*, 7:155–169.
- Penn, A. A., P. A. Riquelme, M. B. Feller, and C. J. Shatz, 1998. Competition in retinogeniculate patterning driven by spontaneous activity, *Science*, 279:2108–2112.

- Perry, V. H., and R. Linden, 1982. Evidence for dendritic competition in the developing retina, *Nature*, 297:683–685.
- Pow, D. V., D. K. Crook, and R. O. L. Wong, 1994. Early appearance and transient expression of putative amino acid neurotransmitters and related molecules in the developing rabbit retina: an immunocytochemical study, *Vis. Neurosci.*, 11:1115–1134.
- Prada, C., L. Puelles, and J. M. Genis-Galvez, 1981. A Golgi study on the early sequence of differentiation of ganglion cells in the chick embryo retina, *Anat. Embryol.*, 161:305–317.
- Rakic, P., 1971. Guidance of neurons migrating to the fetal monkey neocortex, *Brain Res.*, 33:471–476.
- Rakic, P., 1990. Principles of neural cell migration, *Experientia*, 46:882–891.
- Reese, B. E., A. R. Harvey, and S. S. Tan, 1995. Radial and tangential dispersion patterns in the mouse retina are cell-class specific, *Proc. Natl. Acad. Sci. USA*, 92:2494–2498.
- Reese, B. E., B. D. Necessary, P. P. Tam, B. Faulkner-Jones, and S. S. Tan, 1999. Clonal expansion and cell dispersion in the developing mouse retina, *Eur. J. Neurosci.*, 11:2965–2978.
- Rice, D. S., S. Nusinowitz, A. M. Azimi, A. Martinez, E. Soriano, and T. Curran, 2001. The reelin pathway modulates the structure and function of retinal synaptic circuitry, *Neuron*, 31:929–941.
- Rickman, D. W., 2000. Neurotrophins and development of the rod pathway: an elementary deduction, *Microsc. Res. Tech.*, 50:124–129.
- Robinson, S. R., 1991. Developmental of the mammalian retina, in *Neuroanatomy of the Visual Pathways and Their Development* (B. Dreher and S. R. Robinson, eds.), London: U.K. Macmillan.
- Rodieck, R. W., 1998. *The First Steps in Seeing*, Sunderland, MA: Sinauer.
- Sakaki, Y., Y. Fukuda, and M. Yamashita, 1996. Muscarinic and purinergic Ca^{2+} mobilizations in the neural retina of early embryonic chick, *Int. J. Dev. Neurosci.*, 14:691–699.
- Sauer, F. C., 1935. Mitosis in the neural tube, *J. Comp. Neurol.*, 62:377–405.
- Schnitzer, J., and A. C. Rusoff, 1984. Horizontal cells of the mouse retina contain glutamic acid decarboxylase-like immunoreactivity during early developmental stages, *J. Neurosci.*, 4:2948–2955.
- Sernagor, E., S. J. Eglén, and R. O. L. Wong, 2001. Development of retinal ganglion cell structure and function, *Prog. Retin. Eye Res.*, 20:139–174.
- Sernagor, E., and N. M. Grzywacz, 1995. Emergence of complex receptive field properties of ganglion cells in the developing turtle retina, *J. Neurophysiol.*, 73:1355–1364.
- Sernagor, E., and N. M. Grzywacz, 1996. Influence of spontaneous activity and visual experience on developing retinal receptive fields, *Curr. Biol.*, 6:1503–1508.
- Sidman, R. L., 1961. Histogenesis of mouse retina studies with thymidine- H^3 , in *Structure of the Eye* (G. K. Smelser, ed.), New York: Academic Press, pp. 487–506.
- Snow, R. L., and J. A. Robson, 1994. Ganglion cell neurogenesis, migration and early differentiation in the chick retina, *Neuroscience*, 58:399–409.
- Snow, R. L., and J. A. Robson, 1995. Migration and differentiation of neurons in the retina and optic tectum of the chick, *Exp. Neurol.*, 134:13–24.
- Stier, H., and B. Schlosshauer, 1998. Different cell surface areas of polarized radial glia having opposite effects on axonal outgrowth, *Eur. J. Neurosci.*, 10:1000–1010.
- Tagawa, Y., H. Sawai, Y. Ueda, M. Tauchi, and S. Nakanishi, 1999. Immunohistological studies of metabotropic glutamate receptor subtype 6-deficient mice show no abnormality of retinal cell organization and ganglion cell maturation, *J. Neurosci.*, 19:2568–2579.
- Thanos, S., and J. Mey, 2001. Development of the visual system of the chick. II. Mechanisms of axonal guidance, *Brain Res. Brain Res. Rev.*, 35:205–245.
- Tian, N., and D. R. Copenhagen, 2001. Visual deprivation alters development of synaptic function in inner retina after eye opening, *Neuron*, 32:439–449.
- Tootle, J. S., 1993. Early postnatal development of visual function in ganglion cells of the cat retina, *J. Neurophysiol.*, 69:1645–1660.
- Troilo, D., M. Xiong, J. C. Crowley, and B. L. Finlay, 1996. Factors controlling the dendritic arborization of retinal ganglion cells, *Vis. Neurosci.*, 13:721–733.
- Turner, D. L., and C. L. Cepko, 1987. A common progenitor for neurons and glia persists in rat retina late in development, *Nature*, 328:131–136.
- Turner, D. L., E. Y. Snyder, and C. L. Cepko, 1990. Lineage-independent determination of cell type in the embryonic mouse retina, *Neuron*, 4:833–845.
- Vu, T. Q., J. A. Payne, and D. R. Copenhagen, 2000. Localization and developmental expression patterns of the neuronal K-Cl cotransporter (KCC2) in the rat retina, *J. Neurosci.*, 20:1414–1423.
- Waid, D. K., and S. C. McLoon, 1998. Ganglion cells influence the fate of dividing retinal cells in culture, *Development*, 125:1059–1066.
- Wang, G. Y., L. C. Liets, and L. M. Chalupa, 2001. Unique functional properties of on and off pathways in the developing mammalian retina, *J. Neurosci.*, 21:4310–4317.
- Wang, S. W., L. Gan, S. E. Martin, and W. H. Klein, 2000. Abnormal polarization and axon outgrowth in retinal ganglion cells lacking the POU-domain transcription factor Brn-3b, *Mol. Cell. Neurosci.*, 16:141–156.
- Wässle, H., 1988. Dendritic maturation of retinal ganglion cells, *Trends Neurosci.*, 11:87–89.
- Weber, A. J., R. E. Kalil, and L. R. Stanford, 1998. Dendritic field development of retinal ganglion cells in the cat following neonatal damage to visual cortex: evidence for cell class specific interactions, *J. Comp. Neurol.*, 390:470–480.
- Wetts, R., and S. E. Fraser, 1988. Multipotent precursors can give rise to all major cell types of the frog retina, *Science*, 239:1142–1145.
- Wikler, K. C., and P. Rakic, 1996. Development of photoreceptor mosaics in the primate retina, *Perspect. Dev. Neurobiol.*, 3:161–175.
- Williams, R. W., and D. Goldowitz, 1992. Structure of clonal and polyclonal cell arrays in chimeric mouse retina, *Proc. Natl. Acad. Sci. USA*, 89:1184–1188.
- Wolburg, H., E. Willbold, and P. G. Layer, 1991. Müller glia endfeet, a basal lamina and the polarity of retinal layers form properly in vitro only in the presence of marginal pigmented epithelium, *Cell. Tissue Res.*, 264:437–451.
- Wong, R. O. L., 1995a. Cholinergic regulation of $[\text{Ca}^{2+}]_i$ during cell division and differentiation in the mammalian retina, *J. Neurosci.*, 15:2696–2706.
- Wong, R. O. L., 1995b. Effects of glutamate and its analogs on intracellular calcium levels in the developing retina, *Vis. Neurosci.*, 12:907–917.
- Wong, R. O. L., 1999. Retinal waves and visual system development, *Annu. Rev. Neurosci.*, 22:29–47.

- Wong, R. O. L., and D. M. Oakley, 1996. Changing patterns of spontaneous bursting activity of on and off retinal ganglion cells during development, *Neuron*, 16:1087–1095.
- Wong, R. O. L., and S. P. Collin, 1989. Dendritic maturation of displaced putative cholinergic amacrine cells in the rabbit retina, *J. Comp. Neurol.*, 287:164–178.
- Wong, W. T., B. E. Faulkner-Jones, J. R. Sanes, and R. O. L. Wong, 2000a. Rapid dendritic remodeling in the developing retina: dependence on neurotransmission and reciprocal regulation by Rac and Rho, *J. Neurosci.*, 20:5024–5036.
- Wong, W. T., K. L. Myhr, E. D. Miller, and R. O. L. Wong, 2000b. Developmental changes in the neurotransmitter regulation of correlated spontaneous retinal activity, *J. Neurosci.*, 20:351–360.
- Wong, W. T., and R. O. L. Wong, 2000. Rapid dendritic movements during synapse formation and rearrangement, *Curr. Opin. Neurobiol.*, 10:118–124.
- Wong, W. T., and R. O. L. Wong, 2001. Changing specificity of neurotransmitter regulation of rapid dendritic remodeling during synaptogenesis, *Nat. Neurosci.*, 4:351–352.
- Yamashita, M., and Y. Fukuda, 1993. Calcium channels and GABA receptors in the early embryonic chick retina, *J. Neurobiol.*, 24:1600–1614.
- Young, R. W., 1985a. Cell proliferation during postnatal development of the retina in the mouse, *Brain Res.*, 353:229–239.
- Young, R. W., 1985b. Cell differentiation in the retina of the mouse, *Anat. Rec.*, 212:199–205.

7 The Development of Retinal Decussations

CAROL MASON AND LYNDA ERSKINE

Introduction

In the vertebrate visual system, retinal ganglion cell (RGC) axons from each eye grow toward the brain and meet at the midline of the ventral diencephalon. Here they establish an X-shaped pathway, the optic chiasm. This major brain decussation, or crossing, carries fibers from the retina to targets in the thalamus (the lateral geniculate nuclei, LGN) and the midbrain (superior colliculus, or optic tectum in lower vertebrates). The projection through the chiasm establishes connections in central targets for an orderly topographic map of the retina. During development of the optic chiasm, RGC axons from each eye diverge from one another to grow to the optic tract on the same and opposite sides of the brain, a projection pattern that subserves binocular vision in higher animals.

Here we will review optic chiasm development, including the axon paths and behaviors of RGCs during their growth as they form the chiasm, and the relationships of RGC growth cones to specialized cells positioned in and around the optic chiasm. Where relevant, we will highlight differences across species in terms of degree of binocularity and the developmental principles underlying the plan of retinal projection. We will then discuss the recent progress on uncovering the cellular and molecular mechanisms directing chiasm formation. Finally, we will discuss aberrations in chiasm development, such as in albinos, in which reduced ocular pigment is linked to a decrease in uncrossed projections, and in a rarer condition in which complete failure of optic chiasm development occurs.

Principles of optic chiasm organization

THE BINOCULAR PLAN The patterns of RGC axon projection at the optic chiasm in different species range from complete crossing and segregation of fibers from each eye to partial decussation and formation of an ipsilateral projection with complex intermingling of the fibers from the two eyes. The presence and relative size of the ipsilateral projection depend on the degree of binocular overlap in the visual field. In lower vertebrates, such as fish, that lack binocular vision, the fibers from each eye are segregated and the mature visual system contains an entirely crossed projection (Fig. 7.1). Amphibian tadpoles also have an entirely crossed projection. However, in some species, for example, *Xenopus*

laevis, an ipsilateral projection develops at metamorphosis when the eyes change position and binocularity develops to subserve their now predatory lifestyle (Grant and Keating, 1986). In chickens, as in fish, there is nearly complete crossing but the fibers intercalate as they cross and, early in development, there is a transient ipsilateral projection (Drenhaus and Rager, 1992; O'Leary et al., 1983; Thanos et al., 1984). In mammals, partial decussation occurs, the extent of which varies widely among species. In humans and primates, all RGC axons originating from the nasal retina cross the midline to project into the contralateral optic tract and all RGC axons from the temporal retina project into the ipsilateral optic tract (Chalupa and Lia, 1991; Polyak, 1957; Stone et al., 1973). By contrast, in mouse, only a small proportion of RGCs (<5%) located in the peripheral temporal retina project ipsilaterally, and these cells are intermingled with RGCs whose axons project contralaterally (Godement et al., 1990) (Fig. 7.1).

CHANGES IN RGC AXON ORGANIZATION IN THE OPTIC NERVE, CHIASM, AND TRACT In all species, as RGC axons grow from the eye to their targets in the thalamus and midbrain, several changes in axon organization occur. In the optic nerve immediately behind the eye, RGC axons are organized by retinal quadrant of origin and display a faithful point-to-point retinotopic order. In nonprimates, the retinotopic but not the quadrant organization is lost rapidly. In the chiasm, axons become ordered in an age-related manner, traversing along radial glial endfeet at the pial surface, but cross the midline in eye-specific bundles deep to the pia. In fish, the fibers from each optic nerve remain bundled and each bundle overlaps to form the chiasm, whereas in higher vertebrates, there are increasingly finer degrees of eye-specific bundle interleaving at the chiasmatic crossing. Chronotopic order is reestablished in the later chiasm and optic tracts and, subsequently, axons regroup according to retinal quadrant but in a different spatial arrangement distinct from that found in the optic nerve (see Chan and Chung, 1999; Colello and Guillery, 1992, 1998; Drenhaus and Rager, 1994; Guillery, 1995; Guillery et al., 1995; Horton et al., 1979; Jeffery, 2001; Mitrofanis et al., 1997; Reese, 1996; and Silver and Rutishauser, 1984, for more detailed descriptions). The functional significance and mechanisms underlying these patterns of rearrangement are not known.

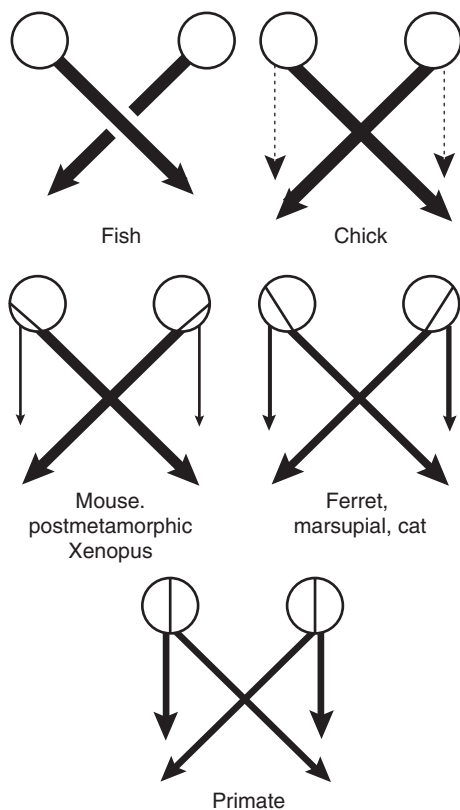


FIGURE 7.1. Basic plan for binocular vision: wiring to the optic chiasm and targets. Line thickness reflects approximate proportions of fibers projecting to ipsilateral or contralateral targets.

Perhaps the most complex change in RGC axon arrangement that occurs along the optic pathway, and the focus of this review, is the divergence of crossed and uncrossed axons at the optic chiasm. An early view of RGC axon behavior during divergent growth was made by Ramón y Cajal. His drawing of the chiasm of the kitten revealed that some uncrossed axons grow directly into the ipsilateral optic tract, while others project toward the midline and then curve back to project ipsilaterally (Ramon y Cajal, 1911). Similarly, in mouse, the best-studied mammalian species, the axons that give rise to the permanent ipsilateral projection arise specifically in the ventrotemporal part of the retina and separate from axons destined to project contralaterally close to the midline (Colello and Guillery, 1992; Godement et al., 1990, 1994). There is no obvious segregation of fibers that will grow ipsilaterally from those projecting across the midline. By contrast, in the marsupial, the ipsilaterally projecting axons diverge laterally and never approach the midline (Jeffery and Harman, 1992; Taylor and Guillery, 1995). Direct growth of RGC axons into the ipsilateral optic tract also occurs during early stages of mouse chiasm development (Colello and Guillery, 1990; Marcus et al., 1995; Silver and Rutishauser, 1984), the formation of the transient ipsilateral projection in

the chick (Hoyt and Luis, 1963; Thanos et al., 1984), and possibly also at the primate chiasm (Hoyt and Luis, 1963; Meissirel and Chalupa, 1994). Although the routes taken by RGC axons through the chiasm may be fundamentally different, in all species the mechanisms that regulate RGC axon divergence at the chiasm must include distinct properties encoded by the ipsilaterally and contralaterally projecting RGCs such that their axons respond differentially to guidance cues arrayed at the midline (see below).

OTHER PROJECTION PATTERNS FOUND AT THE OPTIC CHIASM

In addition to the normal projection into the optic tract, a subset of RGC axons originating in the nasal part of the retina extend through the chiasm into the contralateral optic nerve. This retinoretinal projection has been described in developing rodents (Bunt and Lund, 1981; Plump et al., 2002), chicks (McLoon and Lund, 1982; Thanos, 1999), and the regenerating frog visual system (Bohn and Stelzner, 1981). The growth cones of these axons terminate superficially in the temporal part of the contralateral retina and fail to penetrate into deeper layers of the retina. In all species, this retinoretinal projection is eliminated later in development. Thus, it is not clear if the growth of fibers from one eye to the other has a developmental significance or simply represents an erroneous projection.

Axons also extend from the brain into the optic nerve (Reese and Geller, 1995; Thanos, 1999). These fibers originate early in development in the ventrolateral diencephalon prior to outgrowth of axons from the retina. In the ferret, these axons enter the optic nerve and grow toward but never invade the retina. By contrast, in the chick, they terminate on amacrine and displaced ganglion cells of the contralateral retina. Again, the function of this projection is not known, but it could potentially serve a guidance function for the later developing RGC axons.

Development of the optic chiasm: growth cone behaviors at the midline and the cellular environment

In the past 20 years, much has been learned, particularly in the mouse, about the birth dates and properties of ipsilateral and contralateral RGCs and the timing of axon growth through the optic chiasm (Colello and Guillery, 1990; Dräger, 1985; Sretavan, 1990). Static and dynamic analyses have revealed the behavior of crossed and uncrossed axons and have uncovered cell and molecular cues in the pathway that direct RGC axon outgrowth (see Dingwell et al., 2000; Mason and Erskine, 2000).

STATIC AND DYNAMIC CHRONICLES OF RGC AXON BEHAVIOR AT THE CHIASM Dye tracing of small groups of axons in fixed tissue has provided a picture of the sequential steps in chiasm development and demonstrated that, in the mouse,

formation of the chiasm occurs in two separate phases (Colello and Guillery, 1992; Godement et al., 1990; Marcus et al., 1995; Marcus and Mason, 1995) (Fig. 7.2). In the first phase, axons of early-generated RGCs located in dorsocentral retina enter the ventral diencephalon at E12–E12.5 (E, embryonic day) and grow across the midline to establish the position of the chiasm along the anterior-posterior axis of the brain. Subsequently, at E13–E14, axons from more peripheral parts of the retina enter the nascent chiasm and make specific pathfinding choices into either the ipsilateral or contralateral optic tract (Fig. 7.2*B*).

Analysis of dye-labeled axons and growth cones in fixed preparations has demonstrated that growth cones on axons from ventrotemporal retina are highly complex and spread when positioned near the midline, some appearing as though they are making a U turn (Godement et al., 1990). Dynamic chronicles using time-lapse video microscopy confirmed that at the midline growth cones pause frequently and become highly complex prior to making a turn (Fig. 7.2*A*). This is in contrast to the optic nerves and tracts, in which pausing is less common and the growth cones tend to adopt more streamlined shapes, or in targets during arbor formation when branches have smaller tips (Chan et al., 1998; Godement et al., 1994; Harris et al., 1987; Mason and Wang, 1997; Sretavan and Reichardt, 1993).

The static analyses initially led to the hypothesis that growth cone morphology is related to position along the pathway: complex and spread at the chiasm and streamlined in the optic nerve and tract (Bovolenta and Mason, 1987; Fig. 7.2*A*). The dynamic chronicles revealed that growth cone form is in fact behavior specific. In all regions of the pathway, pausing growth cones have complex forms and advancing growth cones have streamlined shapes (Fig. 7.2*A*). Moreover, while the rate of advance and the duration of each pause period during advance are similar throughout the pathway (about 60 $\mu\text{m/hr}$ and 30–40 minutes, respectively), the duration of the advance periods and the total number of pauses per unit distance vary widely along the trajectory from the retina. At the midline, growth cones pause frequently, interspersed with short periods of advance, but in the optic nerve and tracts, they can spend up to an hour or more in straight advance without pausing. Thus, complex growth cones are more common in the chiasm midline, and streamlined growth cones predominate in the optic nerve and tracts (Fig. 7.2*A*). Consequently, since distinct behaviors occur in different regions of the pathway, growth cone form appears to be position specific (Mason and Wang, 1997). The changes in growth cone dynamics that occur at the midline have been interpreted as reflecting interactions of the growth cones with guidance cues localized to this region. Similar conclusions have been drawn from other studies of growth cone behavior in both vertebrates and invertebrates (e.g., Caudy and Bentley,

1986; Holt, 1989; Mason and Erskine, 2000; Tosney and Landmesser, 1985).

CELLULAR SPECIALIZATIONS AT THE VENTRAL MIDLINE The region of the ventral diencephalon in which the optic chiasm develops contains a number of cellular specializations that have been implicated in regulating RGC axon guidance. Rostral to the developing chiasm in both the chick and mouse is the glial knot, a dense interwoven cluster of non-neuronal cells (Silver and Rutishauser, 1984; Silver et al., 1987). This cellular formation is located at the boundary between the diencephalon and telencephalon and has been postulated to serve as a barrier that prevents the RGC axons from extending anteriorly into the telencephalon.

At the site where the optic chiasm forms in the mouse, two additional groups of cells are located: a specialized group of midline radial glia that have molecular expression patterns distinct from those of surrounding radial glia cells and an early-born population of diencephalic neurons (Marcus and Mason, 1995; Marcus et al., 1995; Mason and Sretavan, 1997; Sretavan et al., 1994) (Fig. 7.2*B*). These cells mark the site where the RGC axons diverge and the posterior boundary of the chiasm. The cell bodies of the midline glia are positioned close to the floor of the third ventricle, and during the establishment of the permanent ipsilateral projection, their radial processes extend to about one-third of the width of the mediolateral extent of the chiasm (Marcus and Mason, 1995). All growth cones enter the glial palisade before either crossing or turning back from the midline. Ultrastructural analysis of neuronal-glial interactions in this region has demonstrated that the lamellae of the growth cones interdigitate with and wrap around the radial glial processes, suggesting that the interactions between these cells may play a critical role in directing RGC axon pathfinding (Marcus et al., 1995).

The early-born diencephalic neurons comprise a V-shaped template of cells with the tip of the V pointing anteriorly along the midline (Fig. 7.2*B*). These cells form the posterior boundary of the chiasm and express a panel of specific markers including carbohydrate epitopes (e.g., stage-specific embryonic antigen-1, SSEA-1) and the hyaluronan binding protein CD44 (Kaprielian et al., 2001; Marcus et al., 1995; Sretavan et al., 1994). It appears likely that these diencephalic neurons (CD44/SSEA neurons) are the mammalian homolog of the cells that generate the tract of the postoptic commissure (TPOC) in lower vertebrates such as fish and amphibians (Easter et al., 1993; Mason and Sretavan, 1997). In the first stage of RGC axon outgrowth in the mouse, crossed and uncrossed axons follow the contour of the early-born diencephalic neurons, thereby establishing the position of the chiasm within the ventral diencephalon. Later, when the permanent pattern is established, the axons diverge at the rostral tip of the neuronal array (Fig. 7.2*B*).

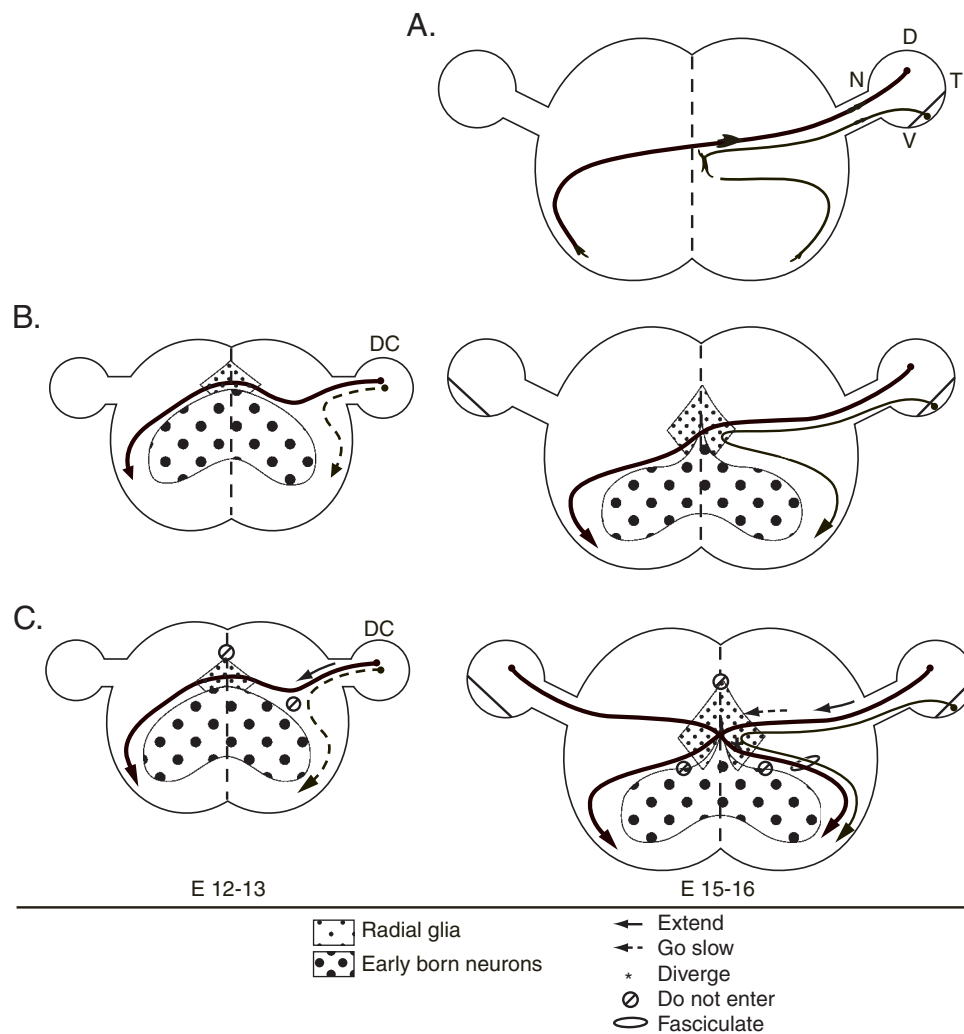


FIGURE 7.2. Trajectory of retinal ganglion cell axons during early and late phase of chiasm formation. Horizontal view of axon growth and cells of the ventral diencephalon during the early (E12–E13) and later (E15–E16) phases of axon growth. Specialized radial glia (*small dots*) form palisades on either side of the midline, and express RC2, as well as *slit2* (rostrally), EphA and EphB receptors, and NrCAM. The early-born neurons (*large dots*) express CD44 and SSEA-1, as well as ephrinA's, Slit1, Robo1, and Robo2, and sulfated proteoglycans. *Slit1* is expressed dorsal to and around the optic nerve as it enters the brain and, more weakly, by the CD44/SSEA neurons. *Slit2* is strongly expressed in the preoptic region directly dorsal and anterior to the chiasm. *A*, At E15–E16, during the major phase of retinal axon divergence, growth cones have different forms, depending on their locale and behavior. Crossing (*thick line*) and uncrossed (*thin line*) fibers have slender streamlined growth cones in the optic nerve and

optic tract. Near the midline, all axons pause and have more spread forms. Uncrossed growth cones extend along the midline in highly complex shapes before turning back to the ipsilateral optic tract. *B*, In the early phase of retinal axon growth, the first-born uncrossed retinal axons from the dorsocentral retina (DC) enter the ipsilateral optic tract directly, quite far from the midline, similar to marsupial RGCs. In contrast, in the later period, uncrossed axons travel toward the midline and diverge from crossing axons within the radial glial palisade. Crossed axons at both ages traverse the midline close to the rostral tip of the early-born neurons. All retinal axons at both ages grow around the contours of the early-born neurons. *C*, Maneuvers of retinal axons with respect to the resident cells of the optic chiasm. See key and text for details. DC, dorsocentral; D, dorsal; V, ventral; N, nasal; T, temporal.

Cell and molecular mechanisms underlying the patterning and formation of the optic chiasm

CELLULAR SPECIALIZATIONS AT THE MIDLINE REGULATE RGC AXON GROWTH AND DIVERGENCE A number of different approaches have provided direct evidence that the cellular

specializations of the ventral diencephalon (radial glia, CD44/SSEA neurons; see above and Fig. 7.2*B*) express cues that regulate RGC axon growth and guidance. In mouse embryos, ablation of the CD44/SSEA neurons early in development results in failure of the optic chiasm to develop and stalling of the RGC axons prior to crossing the midline

(Sretavan et al., 1995). This agenesis of the chiasm is not due to general damage of the neuroepithelium but is specific to the loss of the CD44/SSEA neurons. Puncturing the neuroepithelium at the junction of the optic stalks and ventral diencephalon prior to ingrowth of RGC axons does not prevent optic chiasm formation. By contrast, in amphibians, the presence of axon pathways within the ventral diencephalon is not essential for RGC axon pathfinding. When eyes are transplanted from older tadpoles into younger *Xenopus* embryos at a stage when the first axon tracts have not yet developed, the ectopic RGC axons pathfind normally (Cornel and Holt, 1992).

Additional support for a critical role of the resident cells of the ventral diencephalon in rodent chiasm development has come from tissue culture studies. Culturing retinal explants on membranes or cells derived from the ventral midline of the diencephalon inhibits RGC axon outgrowth (Wang et al., 1995; Wizenmann et al., 1993). Furthermore, axons from ventrotemporal retina, the main source of ipsilaterally projecting axons in the rodent retina, are more inhibited by these cells or membranes than are axons from the remainder of the retina. This strongly suggests that the cellular specializations of the ventral diencephalon express cues that direct RGC axon divergence at the optic chiasm. The ventral diencephalon also secretes a diffusible signal that dampens the growth of all retinal axons to a similar extent (Wang et al., 1996). Coculturing in collagen gels retinal explants from all four quadrants of the retina at a short distance from ventral diencephalon tissue results in a decrease in the number and length of the RGC axons extending from the explants into the collagen. The retinal axons are not repelled by the diencephalic tissue but instead continue to grow toward it, but at a greatly reduced rate. This inhibitory activity has therefore been termed *chemosuppression* and may underlie the slowed growth of RGC axons extending in situ as they approach the midline (Godement et al., 1994; Mason and Wang, 1997; see above).

INTERACTIONS BETWEEN FIBERS FROM EACH EYE When uncrossed axons turn back from the midline, they come into close association with axons from the opposite eye that have crossed the midline. In rodents and ferrets, removing one eye early in development results in failure of many ipsilaterally projecting axons to exit the chiasm and enter the optic tract (Chan and Guillery, 1993; Godement et al., 1987; Guillery, 1989; but see Sretavan and Reichardt, 1993). Because the cellular specializations at the midline are arrayed normally after eye removal (Chan et al., 1999), it has been proposed that binocular fiber interactions are essential for the formation of the ipsilateral projection in rodents. However, this is not true in all species. In marsupials, removal of one eye at any time during development does not affect development

of the uncrossed pathway (for a review see Guillery et al., 1995).

The in vitro demonstration that cues emanate from chiasm cells, coupled with static and dynamic views of dye-labeled axons, suggests the maneuvers of RGCs as they establish the optic chiasm. These maneuvers include maintenance of fasciculation as the axons enter the ventral diencephalon, crossing the midline at the proper anteroposterior point and avoiding the glial knot or preoptic area rostrally; uncrossed fiber divergence from crossed fibers; fasciculation of uncrossed fibers subsequent to turning with crossed fibers from the other eye; avoidance of growth into the zone of early-born CD44/SSEA neurons; and formation of the optic tract (Fig. 7.2C). The molecular factors mediating some of these aspects of RGC pathfinding are discussed below.

MOLECULAR FACTORS CRITICAL FOR OPTIC CHIASM DEVELOPMENT In recent years, a number of different molecular factors have been identified that play a critical role in regulating RGC axon guidance at the optic chiasm and in the path from eye to targets (for reviews see Dingwell et al., 2000; Jeffery, 2001; Thanos and Mey, 2001). Due to the current rapid rate of advance in this field of study, it is not our intention to provide an exhaustive list of all the factors implicated in regulating the development of the optic chiasm. Instead, we focus on the function of a few key molecules, many of them relevant to guidance in other midline structures (Kaprielian et al., 2001; Shu and Richards, 2001; Stoeckli and Landmesser, 1998).

NETRIN/DELETED IN COLORECTAL CANCER Netrins are a family of secreted guidance molecules that can both promote and inhibit outgrowth of different types of neurons. Deleted in Colorectal Cancer (DCC) is an immunoglobulin superfamily member that appears to act as a netrin receptor (Culotti and Merz, 1998). In the developing eye, DCC is expressed by RGCs and netrin-1 is strongly expressed around the optic disc and at the junction of the optic nerve and brain. However, in contrast to the spinal cord, no netrin-1 expression is found at the diencephalic midline (Deiner and Sretavan, 1999; Deiner et al., 1997; Höpker et al., 1999). In vitro, netrin-1, acting through DCC, can promote RGC axon outgrowth (de la Torre et al., 1997; Wang et al., 1996). In netrin-1- or DCC-deficient mice many RGC axons fail to exit the optic disc, resulting in optic nerve hypoplasia. Those axons that do exit the eye approach the chiasm at an abnormal angle but then decussate normally (Deiner and Sretavan, 1999; Deiner et al., 1997). This abnormal angular growth of the RGC axons as they approach the chiasm is not simply a consequence of the decreased number of axons found in the optic nerves; in *Pax6* heterozygous mice that also have optic nerve hypoplasia, the optic chiasm develops

normally (Deiner and Sretavan, 1999). The netrin-1- and DCC-deficient mice also exhibit defects in the formations of other hypothalamic axon pathways and in the location of specific subpopulations of neurons, raising the possibility that the abnormal trajectory of the RGC axons may occur secondarily to these patterning defects. Nevertheless, these results clearly show that unlike spinal commissural axons, guidance of RGC axons to the ventral midline of the diencephalon does not require midline expression of netrin-1.

EPHS/EPHRINS The Eph receptors constitute the largest subfamily of receptor tyrosine kinases and can be subdivided into two groups: the EphA receptors that bind preferentially to the glycosylphosphatidylinositol (GPI)-linked ephrinA ligands and the EphB receptors that bind preferentially to the transmembrane ephrinB ligands (Flanagan and Vanderhaeghen, 1998). Specific Ephs and ephrins are expressed in distinct regions of the developing retina and brain and are key regulators of many different aspects of nervous system development, including the establishment of the topographic map of visual projections within the tectum/superior colliculus (Holder and Klein, 1999). More recently, these molecules have been implicated as playing a pivotal role in regulating axon growth and divergence at the optic chiasm. Both the receptors and ligands are expressed in complex patterns in the developing retina and ventral diencephalon at the time when RGC axons are actively navigating through this region (Marcus et al., 1996a, 2000; Nakagawa et al., 2000). Eph/ephrins are expressed by the midline radial glia and in a region caudal to the site where the chiasm develops. Clusters of Eph/ephrin-expressing cells derived from the ventral diencephalon inhibit RGC axon outgrowth; this inhibition is reduced in the presence of soluble EphA5-Fc that blocks Eph/ephrinA subclass interactions (Marcus et al., 2000). Thus, Ephs/ephrins may play a role in generally dampening the growth of retinal axons within the chiasm region.

The divergence of RGC axons at the chiasm midline may also be critically regulated by Eph/ephrin interactions. In *Xenopus*, during the period when the permanent ipsilateral projection is actively being generated, but not at earlier stages, there is discrete expression of an ephrinB at the site where the RGC axons diverge. Ectopic expression ephrinB2 at the midline in early tadpoles induces a precocious ipsilateral projection that arises specifically from EphB-expressing RGCs in the ventral retina. Furthermore, comparative studies between species that have (postmetamorphic frogs, mice) and do not have (premetamorphic frogs, fish, chicks) a permanent ipsilateral projection at the optic chiasm have shown that there is a correlation between midline ephrinB expression and divergent RGC axon growth at the chiasm (Mann and Holt, 2001; Nakagawa et al., 2000). In mice, the ephrinB expressed at the chiasm

midline has been identified as ephrinB2. Similar to the situation in frogs, its expression in this region is under tight temporal regulation and can only be detected during the period when the ipsilateral projection is produced (Marcus et al., 2000; L. Erskine, S. E. Williams, and C. A. Mason, unpublished results). A critical challenge for the future will be to establish if this midline expression of ephrinB is both necessary and sufficient for the establishment of the ipsilateral pathway.

The expression of ephrins by the RGCs themselves may also play a critical role in regulating chiasm development. In the developing retina, both ephrinA and ephrinB ligands are expressed in complementary gradients to their respective receptors (Marcus et al., 1996a). Overexpressing ephrinA2 or ephrinA5 in the chick retina results in the establishment of a stable ipsilateral projection at the optic chiasm as well as topographic projection errors in the tectum (Dütting et al., 1999; Hornberger et al., 1999). The ipsilaterally projecting axons diverge from their normal path proximal to the midline and are maintained long after the transient ipsilateral projection in chick is eliminated normally. The mechanisms by which ephrin overexpression in the retina perturbs axon guidance at the chiasm remain unclear.

ROUNABOUT (ROBOS)/SLITS The Roundabout (Robos) and Slits are highly evolutionarily conserved families of axon guidance receptors and ligands, respectively. They were initially identified in *Drosophila*, where they play a critical role in regulating axon divergence at the midline of the developing nervous system (Kidd et al., 1999; Seeger et al., 1993). To date, three Robo (Robo1, 2, 3) and three Slit (Slit1, 2, 3) homologs have been identified in vertebrates and implicated as possible mediators of a number of axon guidance events within the developing spinal cord and brain (for reviews see Brose and Tessier-Lavigne, 2000; Nguyen-Ba-Charvet and Chedotal, 2002).

In the developing visual system of both mouse and fish, one of the three *robos* (*robo2*) is expressed by RGCs from the time that the first RGC axons begin to extend into the brain and, within the diencephalon, the Slits are expressed around the path of the RGC axons as they extend through the optic chiasm and toward their targets (Erskine et al., 2000; Fricke et al., 2001; Hutson and Chien, 2002; Niclou et al., 2000; Ringstedt et al., 2000). *Slit1* is expressed dorsal to and around the optic nerve as it enters the brain and, more weakly, by the CD44/SSEA neurons. *Slit2* is strongly expressed in the preoptic region directly dorsal and anterior to the chiasm. Interestingly, in all species examined to date, none of the *slits* are expressed in the region where the RGC axons actually cross the midline. Using in vitro assays, both Slit1 and Slit2 have been found to induce collapse and inhibit outgrowth of RGC axons (Erskine et al.,

2000; Niclou et al., 2000; Plump et al., 2002; Ringstedt et al., 2000).

Direct evidence that the Robos and Slits play an essential role in regulating optic chiasm development has come from analysis of mutants with disrupted expression of these genes. In *astray* zebrafish mutants the gene encoding *robo2* is defective, and RGC axons make severe axon pathfinding errors (Fricke et al., 2001; Karlstrom et al., 1996; Fig. 7.3). These include straying along the anterior and posterior midline, excessive midline crossing, and defasciculation of the retinal projection. Similarly, in mice with disrupted expression of two of the three *slit* genes (*slit1* and *slit2*), RGC axon pathfinding at the chiasm is grossly perturbed. An ectopic chiasm forms anterior to the normal optic chiasm, and RGC axons stray dorsally and posteriorly along the midline and within the lateral diencephalon (Plump et al., 2002; Fig. 7.3). There also is a significant increase in the number of fibers that extend ectopically into the contralateral optic nerve. These pathfinding defects are not due to alterations in the structure of the brain or in the arrangement of the resident cells of the ventral diencephalon which are positioned similar to those in wild-type mice. Moreover, although it appears that fewer axons may project ipsilaterally in the *slit*-deficient mice, it is likely that this is due to the large number of axons that fail to reach the chiasm midline as opposed to a disruption of the crossing/noncrossing decision per se. These data indicate that Robos and Slits play an essential role in restraining the RGC axons to their normal pathway, and that this function is conserved from fish to mammals.

PROTEOGLYCANS Proteoglycans are composed of a protein core to which various types of carbohydrate side chains (glycosaminoglycans) are attached. They are a structurally diverse group of molecules that can promote or inhibit and consequently direct nerve growth (reviewed by Letourneau et al., 1994). Chondroitin sulfate proteoglycans (CSPGs) are expressed in the developing visual system of several species (Chung et al., 2000a; McAdams and McLoon, 1995) and, in vitro, are potent inhibitors of RGC axon outgrowth (Snow et al., 1991). In mouse, CSPGs are highly expressed at the ventral midline of the diencephalon and posterior to the chiasm in a domain that corresponds to the position of the CD44/SSEA neurons (Chung et al., 2000a). Enzymatic removal of the CS chains from an in vitro semi-intact preparation of the retina, optic nerves, and brain results in severe RGC axon pathfinding defects. RGC axons stray anteriorly away from their normal decussation point, project aberrantly into the contralateral optic nerve, and fail to turn into the ipsilateral optic tract (Chung et al., 2000b). These experiments suggest that CSPGs are an important component of the guidance machinery regulating chiasm development. However, an important caveat to this conclusion is that it is

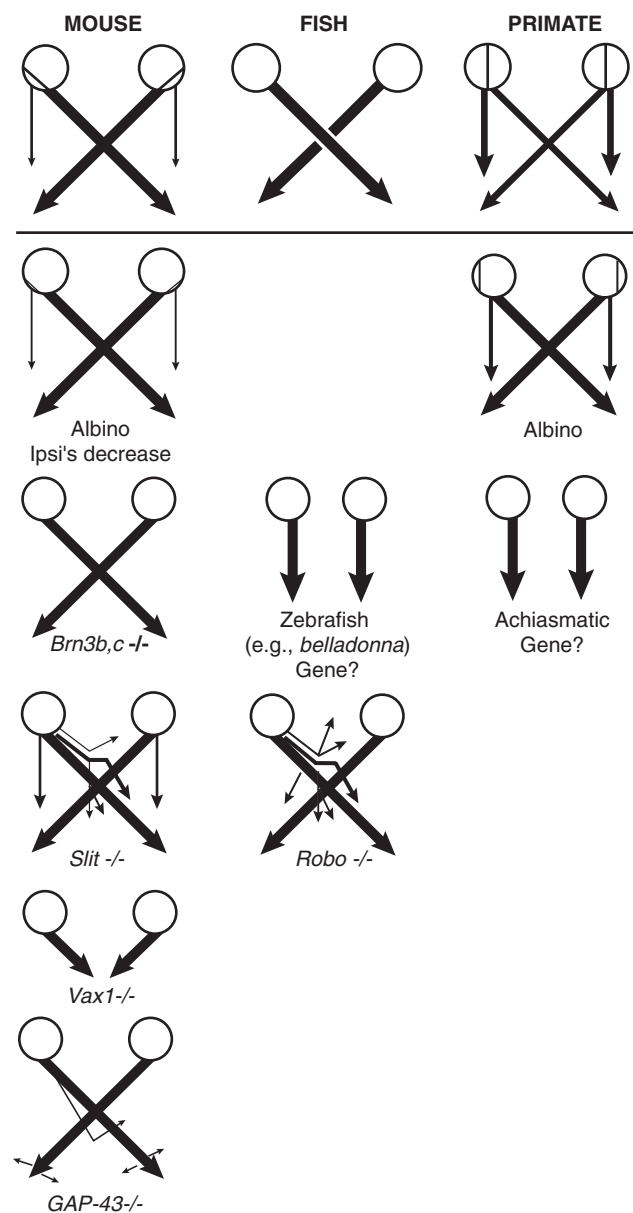


FIGURE 7.3. Mutations of genes expressed in the ventral diencephalon lead to perturbations of chiasm formation. Disruption of known regulatory genes encoding for transcription factors (*Brn3b*, *Brn3c*, *Vax1*), guidance and signaling molecules (*Robo*, *Slit*, *GAP-43*), or pigment (albino—*tyrosinase*) leads to a change in the proportion of ipsilateral to contralateral fibers, as well as aberrant axon projection in and around the chiasm.

not known if the expression patterns of other guidance molecules are disrupted following the enzymatic treatment.

GAP-43 GAP-43 is a major growth cone protein that is highly expressed in developing and regenerating axons and may form part of the signaling machinery linking extracellular signals to changes in growth cone behavior (Benowitz and Routtenberg, 1997). In mice lacking GAP-43 the optic chiasm fails to develop. RGC cross the midline but then stall

and fail to progress normally into the optic tracts (Strittmatter et al., 1995; Fig. 7.3). Later in development, some axons do manage to extend into the optic tracts. However, the routing of these axons is randomized, with axons of cells distributed throughout the retina projecting into either optic tract (Sretavan and Kruger, 1998). These pathfinding errors are due to cell autonomous loss of GAP-43 in the RGC axon growth cones (Kruger et al., 1998) and appear to occur because, in the absence of GAP-43 function, both ipsilaterally and contralaterally projecting RGC axons are inhibited from extending into the lateral diencephalon. In the absence of GAP-43, RGC axons exhibit reduced growth in the presence of lateral diencephalic cell membranes. Furthermore, culturing a semi-intact preparation of the retina, optic nerve, and chiasm such that, from the chiasm, RGC axons extend out of the brain onto a laminin or collagen substratum or into transplanted mid-brain tissue results in robust RGC axon outgrowth from the chiasm (Zhang et al., 2000).

Regulation of chiasm development by control of gene transcription in the retina and brain

During development, a number of different regulatory genes are expressed in specific domains in the region of the brain where the optic chiasm develops. In general, the expression patterns of these genes reflect the longitudinal subdivisions of the forebrain, and RGC axons tend to grow parallel to these subdivisions (Marcus et al., 1999). Analysis of animals with disrupted expression of regulatory genes has revealed a critical role of specific factors in directing the normal development of the optic chiasm.

PAX2 *Pax2*, a paired box transcription factor, is initially expressed in the ventral half of the optic vesicle but later becomes confined to regions destined to contribute to the optic nerve and chiasm. In *Pax2*-deficient mice, the morphology and patterning of the ventral diencephalon are abnormal and the optic chiasm fails to develop. Instead, all RGC axons project into the ipsilateral optic tracts and never approach the midline (Torres et al., 1996). Ectopic ipsilaterally projecting RGC axons are also found in zebrafish *Pax2* (*noi*) mutants in addition to other RGC pathfinding errors (Macdonald et al., 1997). In both species, there is ectopic expression of the patterning gene *sonic hedgehog* (*Shh*) at the ventral midline. In addition to its well-described role in regulating cell fate, recent work has demonstrated that *Shh* can act as an inhibitory guidance cue for RGC axons (Trousse et al., 2001). Thus, the failure of RGC axons to extend across the midline in *Pax2*-deficient animals may result from the inhibitory influence of the ectopic *Shh* expressed in this region.

VAX1 AND VAX2 The homeobox gene *Vax1* is normally expressed at the ventral midline of the developing forebrain and by the optic nerve. In mice lacking *Vax1*, the RGC axons fail to enter the brain in significant numbers and, consequently, do not form an optic chiasm (Fig. 7.3). Disruption of *Vax1* expression does not grossly affect the expression patterns of other regulatory genes in the ventral diencephalon. However, the expression of distinct axon guidance molecules is altered. The attractive guidance cue, netrin-1, is no longer expressed along the optic pathway whereas expression of the inhibitory signal Slit1, is maintained. Thus, it appears that *Vax1* regulates chiasm development by controlling the disposition of specific guidance cues within the ventral diencephalon (Bertuzzi et al., 1999; Hallonet et al., 1999).

The expression of the related factor, *Vax2*, is normally restricted to the ventral part of the retina. In two independently generated mouse lines with disrupted expression of *Vax2*, the patterning of the retina was found to be abnormal and RGC axons make targeting errors in the superior colliculus (Barbieri et al., 2002; Mui et al., 2002). However, these studies reported differential effects on RGC axon guidance at the optic chiasm. In the first study, no effect was found on the development of the ipsilateral pathway despite the fact that the projection from the ventral temporal retina was the most perturbed in the contralateral superior colliculus (Mui et al., 2002). By contrast, Barbieri et al. (2002) reported almost the complete absence of the ipsilateral projections. The reason for this discrepancy is not known. Thus, further study will be required to clarify the role of *Vax2* in optic chiasm development.

BRN3B/C The *Brn3* POU domain transcription factors are expressed early in retinal development and play an essential role in regulating the differentiation and survival of RGCs. They also have been implicated in forming part of the hierarchical program that regulates the response properties of RGC axons to guidance cues along their pathway. In mice with disrupted expression of *Brn3b*, fewer than normal RGCs are generated and the axons of those cells that are produced make pathfinding errors at numerous points along their pathway (Fig. 7.3). At the optic chiasm, some axons stall and fail to exit the chiasm, while others project aberrantly into the ipsilateral optic tract or contralateral optic nerve, or ventrally along the midline. The establishment of the topographic map in the superior colliculus is also perturbed (Erkman et al., 2000). Interestingly, in mice lacking both *Brn3b* and *Brn3c*, similar RGC axon guidance defects are observed, except that no axons project ipsilaterally (Wang et al., 2002). This raises the possibility that *Brn3c* may be a critical component of the signaling machinery specifying ipsilaterally projecting RGCs.

In summary, mutations of genes expressed in the ventral diencephalon lead to perturbations of chiasm formation and disruption of guidance molecule expression in this region. Mutation of these and other genes expressed in the retina also cause aberrant chiasm formation. Understanding of the role of regulatory genes in directing chiasm development will depend on discerning the contribution of these genes to patterning of the ventral diencephalon and to the specification of RGC response properties during growth toward targets.

Defects in chiasm development are associated with lack of ocular pigment

In albino animals, a point mutation in tyrosinase, the key enzyme in melanin synthesis, results in the absence of pigment in the retinal pigment epithelium (RPE) and severe visual deficits. These include underdevelopment of the central retina, a reduction in the number of rod-photoreceptor cells, and an abnormally small, uncrossed RGC projection at the optic chiasm (Dräger and Olsen, 1980; Guillery et al., 1995; Jeffery, 1997; Rice et al., 1995; Fig. 7.3). Insertion of a functional tyrosinase gene into albino mice restores normal pigmentation and normal RGC projections at the optic chiasm (Jeffery, 1997; Jeffery et al., 1994), demonstrating that the tyrosinase gene is involved in determining the projection phenotype of RGCs. However, it is unlikely that tyrosinase itself is the critical factor. A decrease in the number of ipsilaterally projecting RGC axons is found in other pigment-deficient mutants with normal tyrosinase activity (Balkema and Dräger, 1990). Mutations in genes responsible for melanin synthesis, packaging, and transport all cause albino-like visual defects (McGarry et al., 1999; Oetting and King, 1999; Orlow and Brilliant, 1999), as does a loss of function of the OA1 (ocular albinism 1) gene product, a G-protein couple receptor implicated in regulating melanosome biogenesis (Samaraweera et al., 2001; Schiaffino et al., 1999). It is not known which component of the pigment pathway—factors leading to melanin formation or melanin itself—affects the ratio of crossed to uncrossed RGC axons.

There are two possible sites of gene action that could lead to an imbalance in the number of cells that cross or do not cross the midline in hypopigmented mammals. The first is the retina, leading to a decrease in the induction of ipsilaterally projecting RGCs. The second is the optic chiasm, the site of retinal axon divergence. Pigment cells in the optic stalk are avoided by RGC axons and have been implicated in directing RGC axon guidance at the midline (Silver and Sapiro, 1981). Using anatomical techniques and a retinal-chiasm chimeric coculture approach, Marcus et al. (1996b) provided direct evidence that the albino mutation acts on

specification of RGC growth properties at the retinal level. They found that the morphology and cellular composition of the ventral diencephalon of albino animals are indistinguishable from those of normally pigmented animals. Furthermore, in vitro, axons from pigmented retinal explants behaved similarly when cultured on diencephalic cells derived from either pigmented or albino animals, whereas the percentage of axons from albino retinas strongly inhibited by these cells was markedly reduced. This strongly suggests that the albino mutation acts by respecifying the properties of the RGCs rather than by altering the signals for divergence associated with the diencephalic midline (Marcus et al., 1996b). In support of this, no correlation has been found between the size of the adult ipsilateral projection and the existence of optic stalk melanin during development (Colello and Jeffery, 1991).

The mechanism by which lack of pigment affects the size of the uncrossed pathway is enigmatic. Evidence that the effect is extracellular/non-cell autonomous comes from mosaic animals in which the size of the uncrossed projection correlates with the amount of pigment in the RPE and not with the genotype of the RGCs. During development, proliferating retinal progenitor cells are located in a ventricular zone adjacent to the RPE and are in contact with the RPE layer at the time of mitosis. Furthermore, the timing of pigment production and the onset of neurogenesis in the retina are tightly correlated. In retinæ of normally pigmented mice, tyrosinase expression is first detected at E10.5, and the first melanin and RGCs are produced approximately half a day later (Colello and Guillery, 1990; Dräger, 1985). Birthdating studies of pigmented mice (Dräger, 1985) have shown that RGCs that project either ipsilaterally or contralaterally are born concurrently but that the production of ipsilateral cells terminates at E16, while the birth of contralaterally projecting cells continues until birth. This, combined with comparisons of patterns of cell generation in albino and normally pigmented retinæ, has led to the suggestion that perturbations in the temporal features of neurogenesis (Ilia and Jeffery, 1996) and/or retinal maturation (Webster and Rowe, 1991) underlie the abnormal development of the albino retina. More recently, using cell type-specific markers and refined birthdating methods, it has been demonstrated that, relative to normally pigmented mice, more RGCs are born in early stages of neurogenesis in the albino retina and that the spatial organization of these cells is perturbed (Rachel et al., 2002). Thus, the evidence to date suggests that spatiotemporal defects in RGC production in the albino retina act to alter the proportion of cells with axons that project ipsilaterally and contralaterally at the optic chiasm.

How might a factor in the pigment pathway affect the cell cycle kinetics and projection phenotype of cells located on

the opposite side of the retina? It is possible that the RPE normally emits a diffusible signal that acts to regulate retinal neurogenesis. Alternatively, melanin may act as a sink for a factor or ion produced in the neural retina (Dräger, 1985) that, in excess, perturbs normal development. Further studies will be needed to distinguish between these possibilities and identify the factor in the pigment pathway essential for normal retinal development.

Failure of optic chiasm development in the absence of other brain abnormalities

In a breed of Belgian sheepdogs with an autosomal recessive mutation in an unknown gene, the optic chiasm fails to develop (Williams et al., 1994). Instead, all RGCs, irrespective of their site of origin within the retina, extend into the ipsilateral optic tract. Despite the fact that approximately 80% of RGCs in these animals project to targets on the wrong side of the brain, the RGCs terminate appropriately in their targets. Consequently, in the LGN, noncongruent mirror-image maps of visual space are formed in adjacent layers. Other than elimination of the optic chiasm, no other gross brain malformations have been identified in these dogs. The retinae and optic nerves are also relatively normal in size (Hogan and Williams, 1995).

Similar defects in optic chiasm development have been described in a small number of humans (Fig. 7.3). This condition, termed *nondecussating retinofugal fiber syndrome*, results in complete absence of the optic chiasm and projection of all RGC axons to ipsilateral visual targets (Apkarian et al., 1994). With the exception of abnormal eye movements, the affected individuals are otherwise mentally and physically normal and have no other gross brain abnormalities. Their vision is also remarkably normal, possibly as a result of transfer of visual information between the visual hemispheres via the corpus callosum (Victor et al., 2000).

The achiasmatic phenotype is opposite to that found in albinism, in which the size of the ipsilateral projection is increased (see above and Fig. 7.3). However, it is unlikely that this represents a true anti-albino. In a few of the Belgian sheepdogs a small, abnormal chiasm develops. However, in these animals there is no peripheral shift in the retinal line that separates the crossed and uncrossed RGCs, as found in albinism. Instead, the cells that give rise to the residual crossing axons are distributed throughout the retina (Hogan and Williams, 1995).

Summary and perspectives

The optic chiasm represents one of the simpler choice points for growing axons in the developing nervous system. At this

site, axons from each eye either cross or turn back from the ventral midline, thereby projecting to targets on both sides of the brain. In recent years, considerable progress has been made in deciphering the cellular and molecular mechanisms underlying the positioning of the X-shaped chiasm within the ventral diencephalon and the divergence of crossed and uncrossed axons. Dynamic imaging studies have brought the behavior of the RGC axons to life, highlighting the tempo of growth and the various forms of growth cone morphology during the different maneuvers along the pathway. Cellular specializations at the ventral midline have been uncovered, and the molecular mechanisms that orchestrate the formation of the optic chiasm are being revealed. Furthermore, a zebrafish genetic screen has produced mutants that affect RGC axon pathfinding (Baier et al., 1996; Karlstrom et al., 1996; Fig. 7.3). As the genes underlying these defects (Karlstrom et al., 1999) and others seen in mice (Rachel et al., 2000) are identified, additional insights into the mechanisms underlying chiasm development should follow.

The molecular factors critical for chiasm development fall into three broad categories: (1) molecules involved in patterning the retina and ventral diencephalon such that the response properties of the RGCs are encoded properly and the guidance cues in the ventral diencephalon are arrayed correctly (e.g., regulatory genes such as *Vax1*, *Pax2*, and *Brn3b*); (2) inhibitory guidance cues that restrain the RGC axons to their appropriate path and ensure that the chiasm forms at the appropriate position along the anteroposterior axis of the diencephalon (e.g., Slits, ephrins, CSPG); and (3) guidance cues that have a differential effect on ipsilateral and contralateral projecting RGC axons, thereby directing axon divergence at the optic chiasm (ephrinB2). It is clear, though, that many more molecular factors essential for chiasm development remain to be uncovered. It is also important to remember that, in vivo, RGC axons will encounter multiple coexpressed guidance cues simultaneously as they navigate through the chiasm. Thus, in the future, it will be important not only to identify the individual molecules important for chiasm development but also to determine the relative hierarchy of these cues and their interactive effects on RGC axon guidance. In addition, we need to unravel how perturbations in aspects of neurogenesis, as found in albinism, relate to the specification of crossed and uncrossed RGCs.

REFERENCES

- Apkarian, P., L. Bour, and P. G. Barth, 1994. A unique achiasmatic anomaly detected in non-albinos with misrouted retinal-fugal projections, *Eur. J. Neurosci.*, 6:501–507.
- Baier, H., S. Klostermann, T. Trowe, R. O. Karlstrom, C. Nusslein-Volhard, and F. Bonhoeffer, 1996. Genetic dissection of the retinotectal projection, *Development*, 123:415–425.

- Balkema, G. W., and U. C. Dräger, 1990. Origins of uncrossed retinofugal projections in normal and hypopigmented mice, *Vis. Neurosci.*, 4:595–604.
- Barbieri, A. M., V. Broccoli, P. Bovolenta, G. Alfano, A. Marchitello, C. Mocchetti, L. Crippa, A. Bulfone, V. Marigo, A. Ballabio, and S. Banfi, 2002. *Vax2* inactivation in mouse determines alteration of the eye dorsal-ventral axis, misrouting of the optic fibres and eye coloboma, *Development*, 129:805–813.
- Benowitz, L. I., and A. Routtenberg, 1997. GAP-43: An intrinsic determinant of neuronal development and plasticity, *Trends Neurosci.*, 20:84–91.
- Bertuzzi, S., R. Hindges, S. H. Mui, D. D. O'Leary, and G. Lemke, 1999. The homeodomain protein *Vax1* is required for axon guidance and major tract formation in the developing forebrain, *Genes Dev.*, 13:3092–3105.
- Bohn, R. C., and D. J. Stelzner, 1981. The aberrant retino-retinal projection during optic nerve regeneration in the frog. I. Time course of formation and cells of origin, *J. Comp. Neurol.*, 196:605–620.
- Bovolenta, P., and C. A. Mason, 1987. Growth cone morphology varies with position in the developing mouse visual pathway from retina to first targets, *J. Neurosci.*, 7:1447–1460.
- Brose, K., and M. Tessier-Lavigne, 2000. Slit proteins: key regulators of axon guidance, axonal branching, and cell migration, *Curr. Opin. Neurobiol.*, 10:95–102.
- Bunt, S. M., and R. D. Lund, 1981. Development of a transient retino-retinal pathway in hooded and albino rats, *Brain Res.*, 211:399–404.
- Caudy, M., and D. Bentley, 1986. Pioneer growth cone morphologies reveal proximal increases in substrate affinity within leg segments of grasshopper embryos, *J. Neurosci.*, 6:364–379.
- Chalupa, L. M., and B. Lia, 1991. The nasotemporal division of retinal ganglion cells with crossed and uncrossed projections in the fetal rhesus monkey, *J. Neurosci.*, 11:191–202.
- Chan, S. O., and K. Y. Chung, 1999. Changes in axon arrangement in the retinofugal [correction of “retinofungal”] pathway of mouse embryos: confocal microscopy study using single- and double-dye label, *J. Comp. Neurol.*, 406:251–262.
- Chan, S. O., K. Y. Chung, and J. S. Taylor, 1999. The effects of early prenatal monocular enucleation on the routing of uncrossed retinofugal axons and the cellular environment at the chiasm of mouse embryos, *Eur. J. Neurosci.*, 11:3225–3235.
- Chan, S. O., and R. W. Guillery, 1993. Developmental changes produced in the retinofugal pathways of rats and ferrets by early monocular enucleations: the effects of age and the differences between normal and albino animals, *J. Neurosci.*, 13:5277–5293.
- Chan, S. O., K. F. Wong, K. Y. Chung, and W. H. Yung, 1998. Changes in morphology and behaviour of retinal growth cones before and after crossing the midline of the mouse chiasm—a confocal microscopy study, *Eur. J. Neurosci.*, 10:2511–2522.
- Chung, K. Y., K. M. Leung, L. Lin, and S. O. Chan, 2001. Heparan sulfate proteoglycan expression in the optic chiasm of mouse embryos, *J. Comp. Neurol.*, 436:236–247.
- Chung, K. Y., D. K. Shum, and S. O. Chan, 2000a. Expression of chondroitin sulfate proteoglycans in the chiasm of mouse embryos, *J. Comp. Neurol.*, 417:153–163.
- Chung, K. Y., J. S. Taylor, D. K. Shum, and S. O. Chan, 2000b. Axon routing at the optic chiasm after enzymatic removal of chondroitin sulfate in mouse embryos, *Development*, 127:2673–2683.
- Colello, R. J., and R. W. Guillery, 1990. The early development of retinal ganglion cells with uncrossed axons in the mouse: retinal position and axonal course, *Development*, 108:515–523.
- Colello, R. J., and R. W. Guillery, 1992. Observations on the early development of the optic nerve and tract of the mouse, *J. Comp. Neurol.*, 317:357–378.
- Colello, S. J., and R. W. Guillery, 1998. The changing pattern of fibre bundles that pass through the optic chiasm of mice, *Eur. J. Neurosci.*, 10:3653–3663.
- Colello, R. J., and G. Jeffery, 1991. Evaluation of the influence of optic stalk melanin on the chiasmatic pathways in the developing rodent visual system, *J. Comp. Neurol.*, 305:304–312.
- Cornel, E., and C. Holt, 1992. Precocious pathfinding: retinal axons can navigate in an axonless brain, *Neuron*, 9:1001–1011.
- Culotti, J. G., and D. C. Merz, 1998. DCC and netrins, *Curr. Opin. Cell Biol.*, 10:609–613.
- de la Torre, J. R., V. H. Hopker, G. L. Ming, M. M. Poo, M. Tessier-Lavigne, A. Hemmati-Brivanlou, and C. E. Holt, 1997. Turning of retinal growth cones in a netrin-1 gradient mediated by the netrin receptor DCC, *Neuron*, 19:1211–1224.
- Deiner, M. S., T. E. Kennedy, A. Fazeli, T. Serafini, M. Tessier-Lavigne, and D. W. Sretavan, 1997. Netrin-1 and DCC mediate axon guidance locally at the optic disc: loss of function leads to optic nerve hypoplasia, *Neuron*, 19:575–589.
- Deiner, M. S., and D. W. Sretavan, 1999. Altered midline axon pathways and ectopic neurons in the developing hypothalamus of netrin-1- and DCC-deficient mice, *J. Neurosci.*, 19:9900–9912.
- Dingwell, K. S., C. E. Holt, and W. A. Harris, 2000. The multiple decisions made by growth cones of RGCs as they navigate from the retina to the tectum in *Xenopus* embryos, *J. Neurobiol.*, 44:246–259.
- Dräger, U. C., 1985. Birth dates of retinal ganglion cells giving rise to the crossed and uncrossed optic projections in the mouse, *Proc. R. Soc. Lond. B Biol. Sci.*, 224:57–77.
- Dräger, U. C., and J. F. Olsen, 1980. Origins of crossed and uncrossed retinal projections in pigmented and albino mice, *J. Comp. Neurol.*, 191:383–412.
- Drenhaus, U., and G. Rager, 1992. Organization of the optic chiasm in the hatched chick, *Anat. Rec.*, 234:605–617.
- Drenhaus, U., and G. Rager, 1994. Formation of alternating tiers in the optic chiasm of the chick embryo, *Anat. Rec.*, 240:555–571.
- Dütting, D., C. Handwerker, and U. Drescher, 1999. Topographic targeting and pathfinding errors of retinal axons following overexpression of ephrinA ligands on retinal ganglion cell axons, *Dev. Biol.*, 216:297–311.
- Easter, S. S. J., L. S. Ross, and A. Frankfurter, 1993. Initial tract formation in the mouse brain, *J. Neurosci.*, 13:285–299.
- Erkman, L., P. A. Yates, T. McLaughlin, R. J. McEvilly, T. Whisenhunt, S. O'Connell, A. I. Krones, M. A. Kirby, D. H. Rapaport, J. R. Bermingham, D. D. M. O'Leary, and M. G. Rosenfeld, 2000. A POU domain transcription factor-dependent program regulates axon pathfinding in the visual system, *Neuron*, 28:779–792.
- Erskine, L., S. E. Williams, K. Brose, T. Kidd, R. A. Rachel, C. S. Goodman, M. Tessier-Lavigne, and C. A. Mason, 2000. Retinal ganglion cell axon guidance in the mouse optic chiasm: expression and function of robos and slits, *J. Neurosci.*, 20:4975–4982.
- Flanagan, J. G., and P. Vanderhaeghen, 1998. The ephrins and Eph receptors in neural development, *Annu. Rev. Neurosci.*, 21:309–345.
- Fricke, C., J. S. Lee, S. Geiger-Rudolph, F. Bonhoeffer, and C. B. Chien, 2001. *astray*, a zebrafish roundabout homolog required for retinal axon guidance, *Science*, 292:507–510.
- Godement, P., J. Salaün, and C. A. Mason, 1990. Retinal axon pathfinding in the optic chiasm: divergence of crossed and uncrossed fibers, *Neuron*, 5:173–196.

- Godement, P., J. Salaün, and C. Métin, 1987. Fate of uncrossed retinal projections following early or late prenatal monocular enucleation in the mouse, *J. Comp. Neurol.*, 255:97–109.
- Godement, P., L.-C. Wang, and C. A. Mason, 1994. Retinal axon divergence in the optic chiasm: dynamics of growth cone behavior at the midline, *J. Neurosci.*, 14:7024–7039.
- Grant, S., and M. J. Keating, 1986. Ocular migration and the metamorphic and postmetamorphic maturation of the retinotectal system in *Xenopus laevis*: an autoradiographic and morphometric study, *J. Embryol. Exp. Morphol.*, 92:43–69.
- Guillery, R. W., 1989. Early monocular enucleations in fetal ferrets produce a decrease of uncrossed and an increase of crossed retinofugal components: a possible model for the albino abnormality, *J. Anat.*, 164:73–84.
- Guillery, R. W., 1995. A comparison of eutherian and marsupial optic chiasms: a brief review, *Rev. Brasil. Biol.*, 55(Suppl 1):1–10.
- Guillery, R. W., C. A. Mason, and J. S. H. Taylor, 1995. Developmental determinants at the mammalian optic chiasm, *J. Neurosci.*, 15:4727–4737.
- Hallonet, M., T. Hollermann, T. Pieler, and P. Gruss, 1999. *Vax1*, a novel homeobox-containing gene, directs development of the basal forebrain and visual system, *Genes Dev.*, 13:3106–3114.
- Harris, W. A., C. E. Holt, and F. Bonhoeffer, 1987. Retinal axons with and without their somata, growing to and arborizing in the tectum of frog embryos: a time-lapse video study of single fibers *in vivo*, *Development*, 101:23–133.
- Hogan, H., and R. W. Williams, 1995. Analysis of the retinas and optic nerves of achiasmatic Belgian sheepdogs, *J. Comp. Neurol.*, 352:367–380.
- Holder, N., and R. Klein, 1999. Eph receptors and ephrins: effectors of morphogenesis, *Development*, 126:2033–2044.
- Holt, C. E., 1989. A single-cell analysis of early retinal ganglion cell differentiation in *Xenopus*: from soma to axon tip, *J. Neurosci.*, 9:2402–2411.
- Höpker, V. H., D. Shewan, M. Tessier-Lavigne, M. Poo, and C. Holt, 1999. Growth-cone attraction to netrin-1 is converted to repulsion by laminin-1, *Nature*, 401:69–73.
- Hornberger, M. R., D. Dutting, T. Ciossek, T. Yamada, C. Handwerker, S. Lang, F. Weth, J. Huf, R. Wessel, C. Logan, H. Tanaka, and U. Drescher, 1999. Modulation of EphA receptor function by coexpressed ephrinA ligands on retinal ganglion cell axons, *Neuron*, 22:731–742.
- Horton, J. C., M. M. Greenwood, and D. H. Hubel, 1979. Non-retinotopic arrangement of fibres in cat optic nerve, *Nature*, 282:720–722.
- Hoyt, W. F., and O. Luis, 1963. The primate optic chiasm. Details of visual fibre organization studied by silver impregnation techniques, *Arch Ophthalmol.*, 70:69–85.
- Hutson, L. D., and C. B. Chien, 2002. Pathfinding and error correction by retinal axons: the role of *astray/robo2*, *Neuron*, 33:205–217.
- Ilia, M., and G. Jeffery, 1996. Delayed neurogenesis in the albino retina: evidence of a role for melanin in regulating the pace of cell generation, *Dev. Brain. Res.*, 95:176–183.
- Jeffery, G., 1997. The albino retina: an abnormality that provides insight into normal retinal development, *Trends Neurosci.*, 20:165–169.
- Jeffery, G., 2001. Architecture of the optic chiasm and the mechanisms that sculpt its development, *Physiol. Rev.*, 81:1393–1414.
- Jeffery, G., and A. Harman, 1992. Distinctive pattern of organisation in the retinofugal pathway of a marsupial: II. Optic chiasm, *J. Comp. Neurol.*, 325:57–67.
- Jeffery, G., G. Schutz, and L. Montoliu, 1994. Correction of abnormal retinal pathways found with albinism by introduction of a functional tyrosinase gene in transgenic mice, *Dev. Biol.*, 166:460–464.
- Kaprielian, Z., E. Runko, and R. Imondi, 2001. Axon guidance at the midline choice point, *Dev. Dyn.*, 221:154–181.
- Karlstrom, R. O., W. S. Talbot, and A. F. Schier, 1999. Comparative synteny cloning of zebrafish you-too: mutations in the Hedgehog target *gli2* affect ventral forebrain patterning, *Genes Dev.*, 13:388–393.
- Karlstrom, R. O., T. Trowe, S. Klostermann, H. Baier, M. Brand, A. D. Crawford, B. Grunewald, P. Haffter, H. Hoffmann, S. U. Meyer, B. K. Muller, S. Richter, F. J. van Eeden, C. Nusslein-Volhard, and F. Bonhoeffer, 1996. Zebrafish mutations affecting retinotectal axon pathfinding, *Development*, 123:427–438.
- Kidd, T., K. S. Bland, and C. S. Goodman, 1999. Slit is the midline repellent for the robo receptor in *Drosophila*, *Cell*, 96:785–794.
- Kruger, K., A. S. Tam, C. Lu, and D. W. Sretavan, 1998. Retinal ganglion cell axon progression from the optic chiasm to initiate optic tract development requires cell autonomous function of GAP-43, *J. Neurosci.*, 18:5692–5697.
- Letourneau, P. C., M. L. Condic, and D. M. Snow, 1994. Interactions of developing neurons with the extracellular matrix, *J. Neurosci.*, 14:915–928.
- Lustig, M., L. Erskine, C. A. Mason, M. Grumet, and T. Sakurai, 2001. Nr-CAM expression in the developing mouse nervous system: ventral midline structures, specific fiber tracts, and neuropilar regions, *J. Comp. Neurol.*, 434:13–28.
- Macdonald, R., J. Scholes, U. Strähle, C. Brennan, N. Holder, M. Brand, and S. W. Wilson, 1997. The Pax protein Noi is required for commissural axon pathway formation in the rostral forebrain, *Development*, 124:2397–2408.
- Mann, F., and C. E. Holt, 2001. Control of retinal growth and axon divergence at the chiasm: lessons from *Xenopus*, *Bioessays*, 23:319–326.
- Marcus, R. C., R. Blazeski, P. Godement, and C. A. Mason, 1995. Retinal axon divergence in the optic chiasm: uncrossed axons diverge from crossed axons within a midline glial specialization, *J. Neurosci.*, 15:3716–3729.
- Marcus, R. C., N. W. Gale, M. E. Morrison, C. A. Mason, and G. D. Yancopoulos, 1996a. Eph family receptors and their ligands distribute in opposing gradients in the developing mouse retina, *Dev. Biol.*, 180:786–789.
- Marcus, R. C., and C. A. Mason, 1995. The first retinal axon growth in the mouse optic chiasm: axon patterning and the cellular environment, *J. Neurosci.*, 15:6389–6402.
- Marcus, R. C., G. A. Matthews, N. W. Gale, G. D. Yancopoulos, and C. A. Mason, 2000. Axon guidance in the mouse optic chiasm: retinal neurite inhibition by ephrin “A”-expressing hypothalamic cells *in vitro*, *Dev. Biol.*, 221:132–147.
- Marcus, R. C., K. Shimamura, D. Sretavan, E. Lai, J. L. Rubenstein, and C. A. Mason, 1999. Domains of regulatory gene expression and the developing optic chiasm: correspondence with retinal axon paths and candidate signaling cells, *J. Comp. Neurol.*, 403:346–358.
- Marcus, R. C., L.-C. Wang, and C. A. Mason, 1996b. Retinal axon divergence in the optic chiasm: midline cells are unaffected by the albino mutation, *Development*, 122:859–868.
- Mason, C., and L. Erskine, 2000. Growth cone form, behavior, and interactions *in vivo*: retinal axon pathfinding as a model, *J. Neurobiol.*, 44:260–270; erratum 45:134.

- Mason, C. A., and D. W. Sretavan, 1997. Glia, neurons, and axon pathfinding during optic chiasm development, *Curr. Opin. Neurobiol.*, 7:647–653.
- Mason, C. A., and L.-C. Wang, 1997. Growth cone form is behavior-specific and, consequently, position-specific along the retinal axon pathway, *J. Neurosci.*, 17:1086–1100.
- McAdams, B. D., and S. C. McLoon, 1995. Expression of chondroitin sulfate and keratan sulfate proteoglycans in the path of growing retinal axons in the developing chick, *J. Comp. Neurol.*, 353:594–606.
- McGarry, M., M. Reddington, E. Novak, and R. Swank, 1999. Survival and lung pathology of mouse models of Hermansky-Pudlak syndrome and Chediak-Higashi syndrome, *Proc. Soc. Exp. Biol. Med.*, 220:162–168.
- McLoon, S. C., and R. D. Lund, 1982. Transient retinofugal pathways in the developing chick, *Exp. Brain Res.*, 45:277–284.
- Meissirel, C., and L. M. Chalupa, 1994. Organization of pioneer retinal axons within the optic tract of the rhesus monkey, *Proc. Natl. Acad. Sci. USA*, 26:3906–3910.
- Mitrofanis, J., K. L. Earle, and B. E. Reese, 1997. Glial organization and chondroitin sulfate proteoglycan expression in the developing thalamus, *J. Neurocytol.*, 26:83–100.
- Mui, S. H., R. Hinges, D. D. O'Leary, G. Lemke, and S. Bertuzzi, 2002. The homeodomain protein Vax2 patterns the dorsoventral and nasotemporal axes of the eye, *Development*, 129:797–804.
- Nakagawa, S., C. Brennan, K. G. Johnson, D. Shewan, W. A. Harris, and C. E. Holt, 2000. Ephrin-B regulates the ipsilateral routing of retinal axons at the optic chiasm, *Neuron*, 25:599–610.
- Nguyen-Ba-Charvet, K. T., and A. Chedotal, 2002. Role of Slit proteins in the vertebrate brain, *J. Physiol. (Paris)*, 96:91–98.
- Niclou, S. P., L. Jia, and J. A. Raper, 2000. Slit2 is a repellent for retinal ganglion cell axons, *J. Neurosci.*, 20:4962–4974.
- Oetting, W., and R. King, 1999. Molecular basis of albinism: mutations and polymorphisms of pigmentation genes associated with albinism, *Hum. Mutat.*, 3:99–115.
- O'Leary, D. D., C. R. Gerfen, and W. M. Cowan, 1983. The development and restriction of the ipsilateral retinofugal projection in the chick, *Brain Res.*, 312:93–109.
- Orlow, S., and M. Brilliant, 1999. The pink-eyed dilution locus controls the biogenesis of melanosomes and levels of melanosomal proteins in the eye, *Exp. Eye Res.*, 68:147–154.
- Plump, A. S., L. Erskine, C. Sabatier, K. Brose, C. J. Epstein, C. S. Goodman, C. A. Mason, and M. Tessier-Lavigne, 2002. Slit1 and Slit2 cooperate to prevent premature midline crossing of retinal axons in the mouse visual system, *Neuron*, 33:219–232.
- Polyak, S. L., 1957. *The Vertebrate Visual System*, Chicago: University of Chicago Press.
- Rachel, R., J. Murdoch, F. Beermann, A. Copp, and C. Mason, 2000. Retinal axon misrouting at the optic chiasm in mice with neural tube closure defects, *Genesis*, 27:32–47.
- Rachel, R. A., G. Dölen, N. L. Hayes, A. Lu, L. Erskine, R. Nowakowski, and C. A. Mason, 2002. Spatiotemporal features of early neurogenesis differ in wildtype and albino retina, *J. Neurosci.*, 22:4249–4263.
- Ramon y Cajal, S., 1911. *Histologie du système nerveux de l'homme et des vertèbres*, Paris, Maloine.
- Reese, B. E., 1996. The chronotopic reordering of optic axons, *Perspect. Dev. Neurobiol.*, 3:233–242.
- Reese, B. E., and S. F. Geller, 1995. Precocious invasion of the optic stalk by transient retinopetal axons, *J. Comp. Neurol.*, 353:572–584.
- Rice, D. S., R. W. Williams, and D. Goldowitz, 1995. Genetic control of retinal projections in inbred strains of albino mice, *J. Comp. Neurol.*, 354:459–469.
- Ringstedt, T., J. E. Braisted, K. Brose, T. Kidd, C. Goodman, M. Tessier-Lavigne, and D. D. O'Leary, 2000. Slit inhibition of retinal axon growth and its role in retinal axon pathfinding and innervation patterns in the diencephalon, *J. Neurosci.*, 20:4983–4991.
- Samaraweera, P., B. Shen, J. M. Newton, G. S. Barsh, and S. J. Orlow, 2001. The mouse ocular albinism 1 gene product is an endolysosomal protein, *Exp. Eye Res.*, 72:319–329.
- Schiaffino, M., M. d'Addio, A. Alloni, C. Baschiroto, C. Valetti, K. Cortese, C. Puri, M. Bassi, C. Colla, M. deLuca, C. Racchetti, and A. Ballabio, 1999. Ocular albinism: evidence for a defect in an intracellular signal transduction system, *Nat. Genet.*, 23:108–112.
- Seeger, M. A., G. Tear, D. Ferres-Marco, and C. S. Goodman, 1993. Mutations affecting growth cone guidance in *Drosophila*. Genes necessary for guidance toward or away from the midline, *Neuron*, 10:409–426.
- Shu, T., and L. J. Richards, 2001. Cortical axon guidance by the glial wedge during the development of the corpus callosum, *J. Neurosci.*, 21:2749–2758.
- Silver, J., M. Poston, and U. Rutishauser, 1987. Axon pathway boundaries in the developing brain. I. Cellular and molecular determinants that separate the optic and olfactory projections, *J. Neurosci.*, 7:2264–2272.
- Silver, J., and U. Rutishauser, 1984. Guidance of optic axons in vivo by a preformed adhesive pathway on neuroepithelial endfeet, *Dev. Biol.*, 106:485–499.
- Silver, J., and J. Sapiro, 1981. A mechanism for the guidance and topographic patterning of retinal ganglion cell axons, *J. Comp. Neurol.*, 189:101–111.
- Snow, D. M., M. Watanabe, P. C. Letourneau, and J. Silver, 1991. Chondroitin sulfate proteoglycan may influence the direction of retinal ganglion cell outgrowth, *Development*, 113:1473–1485.
- Sretavan, D. W., 1990. Specific routing of retinal ganglion cell axons at the mammalian optic chiasm during embryonic development, *J. Neurosci.*, 10:1995–2007.
- Sretavan, D. W., L. Feng, E. Pure, and L. F. Reichardt, 1994. Embryonic neurons of the developing optic chiasm express L1 and CD44, cell surface molecules with opposing effects on retinal axon growth, *Neuron*, 12:957–975.
- Sretavan, D. W., and K. Kruger, 1998. Randomized retinal ganglion cell axon routing at the optic chiasm of GAP-43 deficient mice: association with midline recrossing and lack of normal ipsilateral axon turning, *J. Neurosci.*, 18:10502–10513.
- Sretavan, D. W., E. Pure, M. W. Siegel, and L. F. Reichardt, 1995. Disruption of retinal axon ingrowth by ablation of embryonic mouse optic chiasm neurons, *Science*, 269:98–101.
- Sretavan, D. W., and L. F. Reichardt, 1993. Time-lapse video analysis of retinal ganglion cell axon pathfinding at the mammalian optic chiasm: growth cone guidance using intrinsic chiasm cues, *Neuron*, 10:761–777.
- Stoeckli, E. T., and L. T. Landmesser, 1998. Axon guidance at choice points, *Curr. Opin. Neurobiol.*, 8:73–79.
- Stone, J., J. Leicester, and M. S. Sherman, 1973. The nasotemporal division of the monkey's retina, *J. Comp. Neurol.*, 150:333–348.
- Strittmatter, S. M., C. Fankhauser, P. L. Huang, H. Mashimo, and M. C. Fishman, 1995. Neuronal pathfinding is abnormal in mice lacking the neuronal growth cone protein GAP-43, *Cell*, 80:445–452.

- Taylor, J. S., and R. W. Guillery, 1995. Effect of a very early monocular enucleation upon the development of the uncrossed retinofugal pathway in ferrets, *J. Comp. Neurol.*, 357:331–340.
- Thanos, S., 1999. Genesis, neurotrophin responsiveness, and apoptosis of a pronounced direct connection between the two eyes of the chick embryo: a natural error or a meaningful developmental event? *J. Neurosci.*, 19:3900–3917.
- Thanos, S., F. Bonhoeffer, and U. Rutishauser, 1984. Fiber-fiber interaction and tectal cues influence the development of the chicken retinotectal projection, *Proc. Natl. Acad. Sci. USA*, 81:1906–1910.
- Thanos, S., and J. Mey, 2001. Development of the visual system of the chick. II. Mechanisms of axonal guidance, *Brain Res. Brain Res. Rev.*, 35:205–245.
- Torres, M., E. Gomez-Pardo, and P. Gruss, 1996. *Pax2* contributes to inner ear patterning and optic nerve trajectory, *Development*, 122:3381–3391.
- Tosney, K. W., and L. T. Landmesser, 1985. Growth cone morphology and trajectory in the lumbosacral region of the chick embryo, *J. Neurosci.*, 5:2345–2358.
- Trousse, F., E. Marti, P. Gruss, M. Torres, and P. Bovolenta, 2001. Control of retinal ganglion cell axon growth: a new role for Sonic hedgehog, *Development*, 128:3927–3936.
- Victor, J. D., P. Apkarian, J. Hirsch, M. M. Conte, M. Packard, N. R. Relkin, K. H. Kim, and R. M. Shapley, 2000. Visual function and brain organization in nondecussating retinal-fugal fibre syndrome, *Cereb. Cortex*, 10:2–22.
- Wang, L.-C., R. A. Rachel, R. C. Marcus, and C. A. Mason, 1996. Chemosuppression of retinal axon growth by the mouse optic chiasm, *Neuron*, 17:849–862.
- Wang, L.-C., J. Dani, P. Godement, R. C. Marcus, and C. A. Mason, 1995. Crossed and uncrossed retinal axons respond differently to cells of the optic chiasm midline *in vitro*, *Neuron*, 15:1349–1364.
- Wang, S. W., X. Mu, W. J. Bowers, D.-S. Kim, D. J. Plas, M. C. Crair, H. J. Federoff, L. Gan, and W. H. Klein, 2002. *Brn3b/Brn3c* double knockout mice reveal an unsuspected role for Brn3c in retinal ganglion cell axon outgrowth, *Development*, 129:467–477.
- Webster, M. J., and M. H. Rowe, 1991. Disruption of developmental timing in the albino rat retina, *J. Comp. Neurol.*, 307:460–474.
- Williams, R. W., D. Hogan, and P. E. Garrahy, 1994. Target recognition and visual maps in the thalamus of achiasmatic dogs, *Nature*, 367:637–639.
- Wizenmann, A., S. Thanos, Y. von Boxberg, and F. Bonhoeffer, 1993. Differential reaction of crossing and non-crossing rat retinal axons on cell membrane preparations from the chiasm midline: an *in vitro* study, *Development*, 117:725–735.
- Zhang, Q., C. Lu, C. Severin, and D. W. Sretavan, 2000. GAP-43 mediates retinal axon interactions with lateral diencephalic cells during optic tract formation, *Development*, 127:969–980.

8 The Development of Eye-Specific Segregation in the Retino-Geniculostriate Pathway

BARBARA CHAPMAN

Introduction

In the adult visual system of higher mammals, information from the two eyes is kept separate through the early stages of visual processing. In the lateral geniculate nucleus (LGN), retinal ganglion cell axons from the two eyes project to separate eye-specific layers, and all LGN cells respond only to visual stimulation through one or the other eye. In primary visual cortex, LGN afferents serving the two eyes are segregated into eye-specific patches or stripes in cortical layer IV, forming the anatomical basis for ocular dominance columns (radial columns of cells throughout the depth of the cortex that tend to respond better to visual stimuli presented to one or the other eye). The development of this eye-specific segregation has been widely studied and is used extensively as a model system for the development of specific neuronal connections throughout the nervous system.

Historically, the development of eye-specific segregation was first studied using electrophysiological recordings in primary visual cortex. The pioneering work of Hubel and Wiesel showed that ocular dominance columns can be drastically modified by visual experience during a *critical period* early in development. Raising an animal with one eye closed (monocular deprivation) results in a primary visual cortex where cells can no longer respond to visual stimuli through the eye that was closed and are driven almost exclusively by the eye that had remained open (Hubel and Wiesel, 1970; Wiesel and Hubel, 1965). Transneuronal labeling with radioactive amino acids injected into one eye confirmed that this physiological response to monocular deprivation is associated with a profound reduction in the size of the geniculocortical projection from the closed eye (Hubel et al., 1977; Fig. 8.1). The first hints of the mechanisms underlying the development of eye-specific segregation came from comparing the results of monocular deprivation experiments with those of binocular deprivation experiments in which animals were raised with both eyes closed. In binocularly deprived animals, ocular dominance columns develop normally, with equal inputs to cortex from the two eyes (Wiesel

and Hubel, 1965). This result, together with the fact that ocular dominance columns are present in some species at birth (Horton and Hocking, 1996; Rakic, 1976) clearly indicates that visual experience is not needed for the normal development of ocular dominance columns. Comparison of the results of monocular and binocular deprivation also suggests that development of ocular dominance columns might occur through a competitive process: when neuronal activity in the two eyes is equal, either because both eyes are open (as in normal animals) or both eyes are closed (as in binocularly deprived animals), normal ocular dominance columns form, whereas when the activity in the two eyes is not equal (in monocularly deprived animals), the more active eye has a competitive advantage in maintaining or expanding its LGN afferent connections to the cortex.

This chapter will discuss some of the large number of experiments that have been performed since the groundbreaking work described above. Many of these experiments have been designed to answer the following questions: (1) does the development of eye-specific layers in the LGN follow the same rules as the development of ocular dominance columns? (2) Are there two separate stages of development, an initial phase in which ocular dominance columns are established and a second phase in which they are maintained or undergo plasticity? (3) Is the role of activity in the development and plasticity of eye-specific segregation instructive (patterns of activity actually guide the development of specific neuronal connections) or merely permissive (activity is necessary only to enable other developmental cues that guide connections)?

Development of eye-specific lamination in the lateral geniculate nucleus

The adult pattern of segregated inputs from the two eyes to distinct layers in the LGN is not present early in development. Instead, axons from the two eyes are initially completely overlapping throughout a large portion of the LGN in both carnivores and primates (Linden et al., 1981; Rakic,

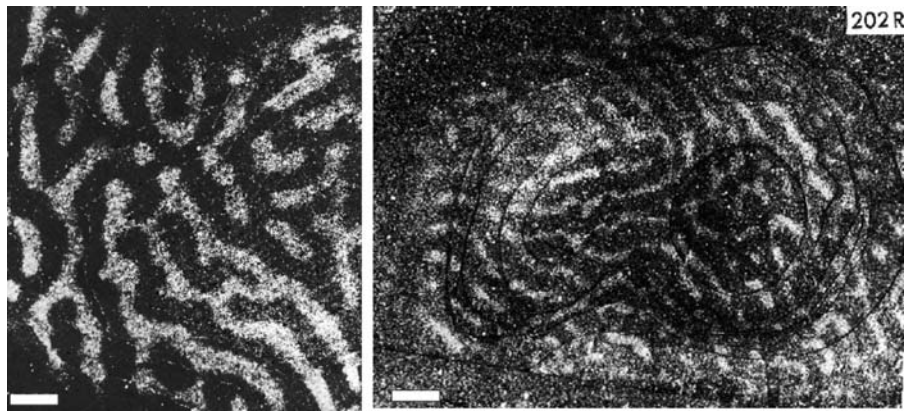


FIGURE 8.1. Ocular dominance columns from a normal monkey (*left*) and a monkey subjected to monocular deprivation during the critical period (*right*). In the normal monkey the ipsilateral eye was injected with [^3H]proline, which was transported transneuronally through the LGN and can be seen as the white stripes in the figure. In the normal monkey, the ocular dominance columns from the injected eye (white stripes) and the uninjected eye (dark

stripes) are equal in width. In the monocularly deprived monkey, [^3H]proline was injected into the deprived eye. The white stripes, representing the ocular dominance columns from this deprived eye, are much narrower than those seen in the normal animal or than those from the nondeprived eye (dark stripes) in this animal. (From LeVay et al., 1980.)

1976; Shatz, 1983). During normal development in the carnivore, adult-like eye-specific segregation of afferents gradually appears as axonal branches in inappropriate locations are pruned and branches in appropriate locations grow and elaborate (Sretavan and Shatz, 1986). In the primate, few inappropriate axonal branches are seen during development, and eye-specific segregation of axons appears to occur through the loss of entire retinal fibers innervating inappropriate regions of the LGN (Lachia and Casagrande, 1988; Snider et al., 1998). Evidence that the segregation of retinal axons into eye-specific layers might be occurring through a competitive process in both carnivores and primates came originally from experiments in which one eye was removed from an animal early in development. When the axonal projection from the remaining eye was labeled later in development or in adulthood, axons were found to occupy nearly the entire LGN (Chalupa and Williams, 1984; Rakic, 1981). This indicates that interactions between the afferents from the two eyes, not just interactions between afferents and LGN cells, are necessary for normal eye-specific segregation in the LGN. The normal segregation of retinal afferents into layers in the LGN occurs in utero in most species and before eye opening in others; therefore, this process clearly does not depend on visual experience. However, the process of segregation has been found to depend on spontaneous activity of retinal ganglion cells. Retinal ganglion cells have been shown to be spontaneously active in utero (Galli and Maffei, 1988). Pharmacological blockade of this spontaneous activity prevents the segregation of retino-geniculate afferents (Penn et al., 1998; Shatz and Stryker, 1988), resulting in an LGN where afferents from the two eyes remain overlapping throughout most of the nucleus. The activity blockade,

however, does not prevent axonal growth: axons in treated animals grow extensively (Sretavan et al., 1988). Nor does the activity blockade completely abolish the axons' ability to interact with postsynaptic targets: the axons in treated animals are not confined to the normal layers of the LGN, but they are confined to the LGN itself and do not grow into adjacent nuclei (Sretavan et al., 1988). These results suggest that during normal development a competitive, activity-dependent process is responsible for driving eye-specific segregation in the LGN.

Further evidence for competition between axons from the two eyes during development of eye-specific layers in the LGN comes from experiments in which the amount of neuronal activity in one eye is pharmacologically altered. If spontaneous activity in one eye is completely blocked, then the LGN territory occupied by that silenced eye's ganglion cell axons is reduced, while the territory occupied by axons from the normal eye is expanded (Penn et al., 1998). Conversely, if the amount of spontaneous activity in one eye is pharmacologically increased, that eye's axons gain territory in the LGN (Stellwagen and Shatz, 2002). These experiments show that the more active eye always "wins," regardless of whether it has normal or enhanced levels of activity, while the less active eye always "loses," regardless of whether it has normal or reduced levels of activity. The LGN layers, however, develop normally when both eyes are pharmacologically induced to have more spontaneous activity than normal (Stellwagen and Shatz, 2002), again indicating the importance of relative levels of activity between the two retinæ.

The activity-dependent, competitive processes involved in the development of eye-specific segregation in the LGN

also appear to be important (at least for some period of time) in maintaining segregation. If spontaneous activity is blocked during a developmental time immediately after the retinogeniculate afferents have segregated, the axons actually desegregate and the projections from the two retinas become completely overlapping in the LGN (Chapman, 2000).

Normal development and plasticity of ocular dominance columns

Until recently, it has been generally accepted that the initial development of ocular dominance columns, like the development of eye-specific segregation in the LGN, involves an activity-dependent, competitive process. Transneuronal labeling with radioactive amino acids showed that early in development the geniculate afferents serving one eye spread uniformly along layer IV, suggesting that at this age the projections serving the two eyes are completely overlapping. Gradually, over a period of weeks, fluctuations in the label-

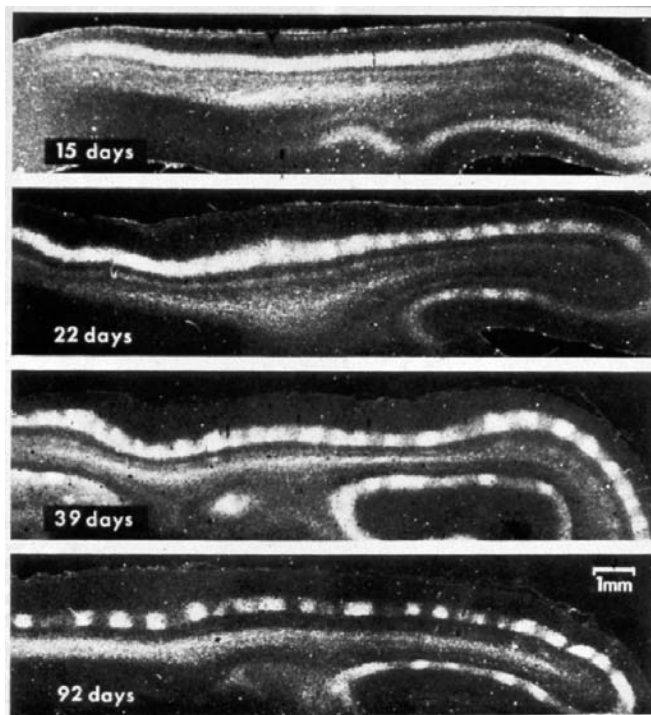


FIGURE 8.2. The development of ocular dominance columns in the cat. In each panel, the ipsilateral eye was injected with [^3H]proline. Different transneuronal labeling patterns are seen at the different developmental stages illustrated in the four panels. At the earliest age, labeling is continuous throughout cortical layer IV; increasingly strong fluctuations in label are seen at later ages. These results were originally interpreted to mean that LGN axons serving the two eyes are initially overlapping in the cortex and gradually segregate out into ocular dominance columns over time. (From LeVay et al., 1978.)

ing density appear and grow stronger, presumably representing segregation of the two eyes' afferents into adult-like ocular dominance columns (Crair et al., 2001; Finney and Shatz, 1998; LeVay et al., 1978; Ruthazer et al., 1999; Fig. 8.2). If activity is blocked in both eyes during development, the segregation into ocular dominance columns is never seen. Instead, the immature pattern of uniform labeling in layer IV is maintained, suggesting that activity is necessary for geniculocortical afferents to segregate into ocular dominance columns (Stryker and Harris, 1986).

However, recent experiments have raised doubts about this view of the development of ocular dominance columns. Injections of neuronal tracers into an individual eye-specific LGN layer in ferrets at different ages show that initially axonal arborizations are very sparse, and it is impossible to tell whether or not axons from the two eyes are segregated. Quite soon after the axons grow into the cortex, however, such LGN injections produce a patchy pattern of labeling in the cortex, reminiscent of ocular dominance columns (Crowley and Katz, 2000; Fig. 8.3). This labeling pattern is seen at postnatal day 16–18 in the ferret, equivalent to E 58–60 in the cat, 2 to 3 weeks earlier than columns were seen in transneuronal labeling studies in cats and ferrets (Crair et al., 2001; Finney and Shatz, 1998; LeVay et al., 1978; Ruthazer et al., 1999).

What could explain the differences between the LGN labeling results, which suggest that columns appear extremely early in development, possibly without a period of initial overlap of axons serving the two eyes, and that the transneuronal results show much later segregation of axons from an initially overlapping projection pattern into columns? The authors of the new study suggest that the transneuronal results might be artifactual (Katz and

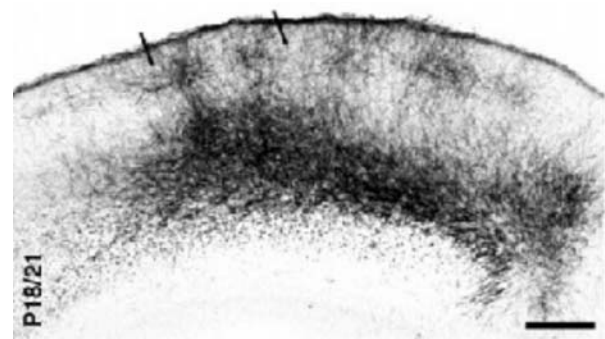


FIGURE 8.3. Early ocular dominance columns revealed by injection of label into a single LGN layer in the ferret. Patchy labeling of geniculocortical afferents thought to represent ocular dominance columns can be seen in very young animals 2 to 3 weeks earlier in development than ocular dominance columns are seen with transneuronal labeling techniques. (From Crowley and Katz, 2000.)

Crowley, 2002). The initial uniform labeling pattern seen in the transneuronal study could be due to the fact that “spillover” of the transneuronal label from one LGN layer to another occurs in very young animals. This means that in the youngest animals, LGN axons serving both eyes could have taken up the label, such that the cortical pattern of continuous labeling reflects the result which would be expected if both eyes’ ocular dominance columns were labeled (Crowley and Katz, 2000). However, this explanation cannot account for the fact that other methods of assessing the development of ocular dominance columns, including metabolic labeling with 2-deoxyglucose (Rathjen and Löwel, 2000), electrophysiological recordings (Crair et al., 2001), and optical imaging of intrinsic signals (Crair et al., 2001), are all in agreement with the transneuronal labeling studies, showing no eye-specific segregation before 2 weeks of age in the cat, and gradually developing columns appearing first between 2 and 3 weeks.

Alternatively, it is possible that the differences between the transneuronal labeling pattern and that seen from LGN injections could be explained if the patches seen following LGN injections do not really represent ocular dominance columns. This explanation seems unlikely, given that these patches closely resemble adult ocular dominance columns in their spacing and degree of segregation (Crowley and Katz, 2000). However, such an explanation remains possible given that it has not been feasible to label axons from the two eyes’ LGN layers with different labels to show that the gaps in the patches seen in labeling from one layer are in fact filled in by axons from the other layer. It seems that resolving the differences in results seen with transneuronal labeling versus those seen with LGN injections will have to await further experimentation.

If, in fact, the results from the LGN injection experiments do represent the true story of how ocular dominance columns form, what are the broader implications of these results? The LGN injections show very early appearance of ocular dominance columns without an obvious initial period of overlap of axons serving the two eyes, which can be interpreted to mean that ocular dominance columns form by an activity-independent process, possibly guided by molecular cues in visual cortex (Crowley and Katz, 2000). How could such a view be reconciled with earlier experiments showing that retinal activity blockade prevents the segregation of axons serving the two eyes into ocular dominance columns (Stryker and Harris, 1986)? If ocular dominance columns do in fact form very early in development, the lack of segregation seen with retinal activity blockade might not represent the blocking of the normal development of ocular dominance columns, but might rather represent the desegregation of previously existing columns (Crowley and Katz, 2000) similar to the desegregation of eye-specific layers in the LGN seen with retinal activity blockade (Chapman,

2000). Additional evidence that the initial formation of ocular dominance columns might be activity independent comes from experiments in which both eyes were removed early in development. In such animals, apparent ocular dominance columns could still be seen via injections of tracer into individual LGN layers, showing that at least retinal activity is not needed to form the patchy geniculocortical projections (Crowley and Katz, 1999).

None of these results, however, rule out a role for activity in the development of ocular dominance columns. Even if these results are taken at face value, it is still possible that activity is necessary for column formation. The early appearance of columns visualized by LGN injections still occurs about a week after axons grow into the cortex, so it is possible that spontaneous retinal activity during this time period is needed for the normal formation of columns (Katz and Crowley, 2002). In fact, there is direct evidence that neuronal activity may be important this early in development; the blockade of neuronal activity during the time period when geniculocortical axons are first growing into layer IV has been shown to radically alter their arborizations, prevent normal branching, and interfere with target selection (Catalano and Shatz, 1998; Herrmann and Shatz, 1995). The apparent existence of ocular dominance columns in animals in which both eyes were removed early in development also cannot rule out a role for neuronal activity in the development of columns. Highly correlated activity within LGN layers and less correlated activity between layers may be present in the absence of retinal input and could be sufficient to drive ocular dominance segregation by an activity-dependent process (Katz and Crowley, 2002; Weliky and Katz, 1999). This explanation is supported by the fact that in animals without eyes, ocular dominance columns are apparently maintained, whereas in animals with pharmacologically silenced retinas, ocular dominance columns apparently desegregate; this suggests that LGNs without retinal input must retain the patterns of activity necessary to maintain ocular dominance columns.

Convincing evidence that ocular dominance column formation occurs through activity-independent mechanisms would require the identification of molecular cues involved in the process; so far, no such molecules have been found. On the other hand, there is also little direct evidence that the initial development of ocular dominance columns does require activity. It is clear that a competitive activity-dependent process *can* produce segregated columns from the two eyes resembling cortical ocular dominance columns. One example of such ocular dominance-like segregation is seen in the tectum of the three-eyed frog. In normal frogs, each tectum receives retinal ganglion cell input only from the contralateral eye. However, if a third eye is surgically transplanted into the developing frog, axons from this eye project to an optic tectum, which also receives input from

one of the normal eyes. The axons from the transplanted and normal eyes segregate into a regular pattern of alternating columns in the tectum (Constantine-Paton and Law, 1978; Fig. 8.4). The development of these columns is prevented by retinal activity blockade (Reh and Constantine-Paton, 1985). The tectal ocular dominance columns develop from an initially completely overlapping state by an activity-dependent process, similar to the traditional model of how cortical ocular dominance columns develop. In this system, where normally each tectum is enervated by only one eye, there is no reason to suspect the presence of any molecular cues in the tectum that could guide the development of ocular dominance columns. Realistic-looking ocular dominance columns can also be produced by computational models using purely activity-dependent competitive mechanisms and starting with an initial state of overlapping axons serving the two eyes (Erwin and Miller, 1998; Jones et al., 1991; Miller et al., 1989; Swindale, 1980; Von Der Marlsburg and Willshaw, 1976). Thus ocular dominance columns *could* develop using activity instead of molecules. However, convincing proof that the development of cortical ocular dominance columns *does* involve activity would require, first, that the controversy over the timing of the development of ocular dominance columns be resolved and, second, that experiments blocking activity be redone at the correct developmental time.

Despite the controversy over the timing and mechanisms of the initial establishment of cortical ocular dominance columns, there is good agreement that ocular dominance columns do undergo activity-dependent plasticity during a critical period of development. The first manipulations demonstrating critical period plasticity involved altering visual experience. As discussed in the Introduction, monocular deprivation results in profound changes in the ocular dominance columns, with the closed eye losing much of its cortical territory and most of its ability to drive cortical cells (Hubel and Wiesel, 1970; Hubel et al., 1977; Wiesel and Hubel, 1965). Other manipulations of visual experience during the critical period, such as experimentally induced strabismus, also affect the ocular dominance columns. In strabismic animals, in which the misalignment of the eyes causes the animal to see double, neurons in primary visual cortex become almost exclusively monocular, driven by one or the other eye but not by both (Hubel and Wiesel, 1965; Van Sluyters and Levitt, 1980). This physiological change is accompanied by an anatomical change; the ocular dominance columns seen by transneuronal labeling are sharper in strabismic animals than in normals (Shatz et al., 1977). Visual experience is not necessary, however, to induce ocular dominance plasticity during the critical period. An imbalance in the levels of spontaneous retinal activity between the two eyes in the absence of vision can be produced by pharmacologically blocking all action potentials from one retina



FIGURE 8.4. Tectal “ocular dominance columns” can be seen in three-eyed frogs. *Top*: [^3H]proline was injected into one eye of a normal frog, resulting in labeling of the entire superficial neuropil of the contralateral tectum. *Bottom*: [^3H]proline was injected into one normal eye of a three-eyed frog. Labeling in the contralateral tectum shows a striped pattern of alternating inputs from the labeled eye and the unlabeled supernumerary eye reminiscent of cortical ocular dominance columns. (From Constantine-Paton, 1981.)

while lid suturing the other eye (to prevent form vision) or raising the animals in the dark (to prevent all vision). In such animals, tested after the pharmacological blockade wears off, many more cortical cells respond to vision through the spontaneously active eye than through the eye which had all activity blocked (Chapman et al., 1986). In this regard, plasticity of ocular dominance columns is very similar to the plasticity seen in the segregation of retinal axons in the LGN; the process does not require vision, and the more active eye “wins.”

Even disregarding the controversy over the mechanisms involved in the initial establishment of ocular dominance columns, there is some evidence that ocular dominance plasticity may be distinct from initial ocular dominance development. First, there is a clearly *defined precritical period* during which an imbalance in the activity of the two eyes does not effect ocular dominance, as assessed either physiologically (Crair et al., 1998; Hubel and Wiesel, 1970; Issa et al., 1999; Olson and Freeman, 1980) or anatomically (Crowley and Katz, 2000). Second, during this time period, the cortex is strongly dominated both anatomically and physiologically by input from the contralateral eye (Crair et al., 2001). These

two facts indicate that the simplest version of a competitive, activity-dependent process cannot be operating during this early time period in the development of ocular dominance columns. If competition were acting in the precritical period as it does during the critical period, then decreasing the activity of one retina during this period would result in ocular dominance plasticity. Additionally, if the same rules were followed during the precritical period, then the contralateral eye would maintain or increase its dominance of the cortex, and the ipsilateral eye would have no way of winning back territory such that the two eyes would have almost equal inputs to the cortex, as they do during the critical period. The existence of the precritical period can be interpreted to indicate that the establishment of ocular dominance columns and the plasticity of those columns occur by completely different mechanisms, with the former involving molecular cues and the latter relying on activity-dependent competition (Crowley and Katz, 2000). However, it is also possible that both periods of development show the same activity-dependent competition; early retinal inputs do not drive LGN cells as strongly as descending corticogeniculate inputs (Weliky and Katz, 1999), so the early development of ocular dominance columns could be driven by activity in the geniculocortical loop following the same rules as later activity-dependent plasticity driven by imbalances in retinal inputs once the retinal inputs become stronger (Crair et al., 2001).

Does activity play an instructive or permissive role in the development of the visual system?

It is clear that activity plays an important role in the development and plasticity of eye-specific segregation in the LGN and in at least the plasticity of ocular dominance columns. A long-standing question in the field of visual system development is whether the role of activity is instructive (the development of connections is specifically guided by patterns of activity) or permissive (some threshold level of activity is necessary for connections to be guided by activity-independent cues) (for reviews, see Crair, 1999; Katz and Shatz, 1996; Sur et al., 1999). At its most basic level, this question was answered by the earliest experiments on ocular dominance plasticity. The rearrangements of connections caused by monocular deprivation cannot be explained by a permissive role for activity. If the deprived eye were losing cortical territory merely because it did not maintain a necessary level of activity, then binocular deprivation would result in the loss of inputs to the cortex from both eyes. Similarly, the plasticity of ocular dominance in response to experimentally induced strabismus rules out a purely permissive role for activity. In strabismic animals, the levels of activity in both eyes are normal; it is only the patterns of activity that have been changed by misaligning the two eyes.

It has been proposed that the instructive role of activity could work through “Hebbian” synapses, that is, synapses that are strengthened when pre- and postsynaptic cells fire together and (by extension) weakened when they fire asynchronously (Hebb, 1949). Such synapses between LGN afferents and cortical cells could explain the monocular deprivation effect. Retinotopy in the geniculocortical projection is well established during the critical period, so neighboring LGN afferents giving input to a single cortical cell would tend to be driven together by visual stimuli in the open eye and would therefore tend to activate the postsynaptic cell, strengthening the synapse. Firing in the deprived eye in the absence of vision, on the other hand, would tend to be random, so neighboring LGN afferents giving input to a single cell would be unlikely to fire together. Therefore, the cortical cell would be less likely to reach threshold, weakening the synapse between an active axon and a silent cortical cell. Hebbian synapses could also explain the effects of strabismus, in which neighboring LGN axons from each eye are driven by visual stimuli to fire in synchrony, but the visual stimulation of the two eyes is different, so (unlike in normal vision) there is no synchrony of neighboring axons from the two eyes. In this situation, each eye’s LGN axons will strengthen synapses with any cell where they had an initial advantage and weaken other synapses, resulting in a loss of binocularity in the cortex. Correlated activity in the two eyes driven by vision is important not only for maintaining binocularity during normal development, but also for the physiological and behavioral recovery from monocular deprivation. In kittens subjected to monocular deprivation and then allowed to recover normally with both eyes open, substantial recovery of vision through the deprived eye is seen. If, however, strabismus is induced following the monocular deprivation, recovery of vision in the deprived eye is much less complete (Kind et al., 2002).

One approach to testing whether this sort of patterning of activity might be involved in the development of ocular dominance columns is to produce artificial manipulations of the patterns of activity during development. Such manipulations are obviously difficult to perform, but one such experiment has been successfully completed. In this experiment, kittens were raised with all natural retinal activity pharmacologically blocked, but with artificial activity produced by stimulating electrodes placed in the optic nerves or optic chiasm (Stryker, 1986; Stryker and Strickland, 1984). If stimulation alternated between the two nerves such that the two eyes’ inputs were never firing at the same time, then sharper than normal ocular dominance columns developed, similar to those seen in strabismic animals. If, on the other hand, the same amount of stimulation was performed at the chiasm, so that both eyes’ inputs were always firing at the same time, then no ocular dominance columns were seen and LGN axons from the two eyes remained overlapping (or

desegregated) in visual cortex. These results support a role for Hebbian synapses. When both eyes are equally but asynchronously active (as is also the case in strabismus), both eyes will maintain equal input to the cortex by strengthening synapses to any cells where they had an initial advantage, but binocularity will be lost. When the two eyes are equally and synchronously activated, however, synapses from both eyes onto all cortical cells, are strengthened, resulting in no segregation of the inputs from the two eyes.

Other experiments have provided more direct evidence for the existence of Hebbian synapses involved in the plasticity of ocular dominance columns. If an animal is monocularly deprived, and its cortical cells are pharmacologically silenced without affecting the geniculocortical afferents, then the open eye actually become *less* effective than the deprived eye at driving cortical cells (Reiter and Stryker, 1988), and the open eye *loses* territory in the cortex (Hata and Stryker, 1994). Thus, the effects of monocular deprivation do not depend on the levels of activity in the two eyes, but rather on correlations between pre- and postsynaptic activity. If cortical cells are responsive, they will be better driven by the open eye, so their activity will be correlated with that of the open eye, and the open eye will “win.” If, on the other hand, the cortical cells are silenced, their activity will be not be correlated with the open eye and so the open eye will “lose.” Such Hebbian synapses have been directly demonstrated in another series of experiments in which the activity of LGN afferents was controlled by visual stimulation, and the activity of postsynaptic cortical cells was artificially controlled by current injections (Fregnac et al., 1988). In these experiments the ocular dominance of a cortical cell was determined, and then visual stimulation through one eye was paired with artificial firing of the cell while visual stimulation through the other eye was paired with artificial silencing of the cell. After a period of such pairings, the cell increased its response to visual stimulation through the eye whose stimulation had been paired with postsynaptic firing and decreased its response to stimulation through the other eye. This result shows that when pre- and postsynaptic activity of the cell was correlated, the synapse was strengthened, while when activity was uncorrelated, the synapse was weakened.

The results of such experiments, in which manipulating the patterns of activity by changing the correlations either between two sets of inputs (in alternating or synchronous stimulation experiments) or between inputs and target cells (in experiments manipulating postsynaptic activity) causes altered patterns of connectivity, clearly demonstrate that activity plays an instructive role in the plasticity of ocular dominance columns. It has been more difficult to rule out a purely permissive role for activity in the development and plasticity of eye-specific segregation in the LGN. Since the development of eye-specific segregation in the LGN occurs prior to the development of functional photoreceptors, it has

not been possible to determine the effects of manipulations of visual experience like monocular deprivation or strabismus. Instead, until recently, manipulations of activity in experiments studying LGN development involved reducing levels of activity in one or both eyes (Penn et al., 1998; Shatz and Stryker, 1988; Sretavan et al., 1988). Therefore, the results of these manipulations could merely reflect a permissive role for activity; retinal ganglion cell axons in manipulated animals could have changed their behavior due to lack of a threshold level of activity necessary for them to interact with some molecular cue that would normally guide their connections. The recent experiment pharmacologically increasing levels of activity in one eye rules out such a purely permissive role for activity in LGN development (Stellwagen and Shatz, 2002). It remains to be determined, however, whether patterns of activity are truly instructing the development of eye-specific segregation in the LGN; so far, no experiments have directly addressed this question. It is interesting to note that while activity does not play a purely permissive role in the development of eye-specific segregation, it may play such a role in the development of normal lamination of retinal inputs to the LGN. Activity is clearly involved in the development of layers of retinal input to the LGN; blocking activity blocks the formation of layers (Penn et al., 1998; Shatz and Stryker, 1988; Sretavan et al., 1988). However, a number of experiments show that although normal retinal activity leads to normal *segregation* of retinal afferents to the LGN, it may not in all cases lead to normal *lamination* of those afferents. Such a pattern is seen in animals with coat color mutations which affect the number of retinal axons crossing at the chiasm; in such animals, retinal activity is normal and retinal axons from the two eyes to the LGN segregate, but they segregate into patches instead of into layers (Cucchiario and Guillery, 1971; Guillery, 1969). A similar situation is seen in “rewired” ferrets in which retinal input is surgically rerouted to terminate in auditory thalamus; in these animals retinal activity is normal, and inputs from the two eyes are again segregated into patches instead of layers (Angelucci et al., 1997). Finally, segregation of retinal axons into patches instead of layers is also seen in animals in which the segregation of retinal axons in the LGN has been temporarily blocked during the time when retinal axons normally segregate by either a genetic (Muir-Robinson et al., 2002) or a pharmacological (Huberman et al., 2002) manipulation of activity, and then retinal activity is allowed to return to normal. These results suggest that although lamination of retinal axons in the LGN is activity-dependent, patterns of activity are not driving the layout of the layers. Instead there may be molecular cues in the LGN which are involved in layer formation, and whose proper function requires activity during a specific time period of development. Additional evidence for molecular cues involved in layer formation comes from the study of mutant

dogs lacking an optic chiasm. In normal animals, ipsilaterally projecting fibers come from the temporal (lateral) portion of the retina, while contralateral projections come from the nasal (medial) portion of the retina. In the achiasmatic dogs, all retinal fibers from each eye remain ipsilateral. However, the LGN in these animals is relatively normal, anatomically, with well-developed laminae where temporal retinal fibers project to what would normally be the ipsilateral layer and nasal retinal fibers project to what would normally be the contralateral layer (Williams et al., 1994). This result is consistent with the possibility that molecular affinities between retinal axons from the two sides of the retina and LGN cells from the two laminae guide the development of LGN layers in both normal and achiasmatic animals.

Conclusion

In the past four decades since the initial experiments showing plasticity of ocular dominance columns in response to monocular deprivation, a great deal has been learned about the processes involved in the development of eye-specific segregation in the retino-geniculo-striate pathway. It is clear that activity is important for the development and plasticity of segregation in the LGN and for plasticity of ocular dominance columns. It remains unclear whether activity also plays a role in the initial establishment of the columns. Activity has been shown to play a truly instructive role in the plasticity of ocular dominance columns, and to play more than a purely permissive role in the plasticity of retinal afferent segregation in the LGN. The exact patterning of activity needed to cause plasticity in the cortex and the LGN, as well as the role of activity in the initial development of both ocular dominance columns and LGN layers, remains to be discovered. The possible involvement of activity-independent molecular cues in the initial establishment of ocular dominance columns and in the formation of layers in the LGN also remains an active area of research.

REFERENCES

- Angelucci, A., F. Clascá, E. Bricolo, K. S. Cramer, and M. Sur, 1997. Experimentally induced retinal projections to the ferret auditory thalamus: development of clustered eye-specific patterns in a novel target, *J. Neurosci.*, 17:2040–2055.
- Catalano, S. M., and C. J. Shatz, 1998. Activity-dependent cortical target selection by thalamic axons, *Science*, 281:559–562.
- Chalupa, L. M., and R. W. Williams, 1984. Organization of the cat's lateral geniculate nucleus following interruption of prenatal binocular competition, *Hum. Neurobiol.*, 3:103–107.
- Chapman, B., 2000. Necessity for afferent activity to maintain eye-specific segregation in ferret lateral geniculate nucleus, *Science*, 287:2479–2482.
- Chapman, B., M. D. Jacobson, H. O. Reiter, and M. P. Stryker, 1986. Ocular dominance shift in kitten visual cortex caused by imbalance in retinal electrical activity, *Nature*, 324:154–156.
- Constantine-Paton, M., 1981. Induced ocular dominance zones in tectal cortex, in *The Organization of the Cerebral Cortex: Proceedings of a Neuroscience Research Program Colloquium* (F. O. Schmitt, F. G. Worden, G. Adelman, and S. G. Dennis, eds.), Cambridge, MA: MIT Press, pp. 47–67.
- Constantine-Paton, M., and M. I. Law, 1978. Eye-specific termination bands in tecta of three-eyed frogs, *Science*, 202:639–641.
- Crair, M. C., 1999. Neuronal activity during development: permissive or instructive? *Curr. Opin. Neurobiol.*, 9:88–93.
- Crair, M. C., D. C. Gillespie, and M. P. Stryker, 1998. The role of visual experience in the development of columns in cat visual cortex, *Science*, 279:566–570.
- Crair, M. C., J. C. Horton, A. Antonelli, and M. P. Stryker, 2001. Emergence of ocular dominance columns in cat visual cortex by 2 weeks of age, *J. Comp. Neurol.*, 430:235–249.
- Crowley, J. C., and L. C. Katz, 1999. Development of ocular dominance columns in the absence of retinal input, *Nat. Neurosci.*, 2:1125–1130.
- Crowley, J. C., and L. C. Katz, 2000. Early development of ocular dominance columns, *Science*, 290:1321–1324.
- Cucchiari, J., and R. W. Guillery, 1971. An abnormal retinogeniculate projection in the albino ferret (*Mustela furo*), *Brain Res.*, 33:482–485.
- Erwin, E., and K. D. Miller, 1998. Correlation-based development of ocularly matched orientation and ocular dominance maps: determination of required input activities, *J. Neurosci.*, 18:9870–9895.
- Finney, E. M., and C. J. Shatz, 1998. Establishment of patterned thalamocortical connections does not require nitric oxide synthase, *J. Neurosci.*, 18:8826–8838.
- Fregnac, Y., D. Shulz, S. Thorpe, and E. Bienenstock, 1988. A cellular analogue of visual cortical plasticity, *Nature*, 333:367–370.
- Galli, L., and L. Maffei, 1988. Spontaneous impulse activity of rat retinal ganglion cells in prenatal life, *Science*, 242:90–91.
- Guillery, R. W., 1969. An abnormal retinogeniculate projection in Siamese cats, *Brain Res.*, 14:739–741.
- Hata, Y., and M. P. Stryker, 1994. Control of thalamocortical afferent rearrangement by postsynaptic activity in developing visual cortex, *Science*, 265:1732–1735.
- Hebb, D. O., 1949. *The Organization of Behavior*, New York: Wiley.
- Herrmann, K., and C. J. Shatz, 1995. Blockade of action potential activity alters initial arborization of thalamic axons within cortical layer 4, *Proc. Natl. Acad. Sci. USA*, 92:11244–11248.
- Horton, J. C., and D. R. Hocking, 1996. An adult-like pattern of ocular dominance columns in striate cortex of newborn monkeys prior to visual experience, *J. Neurosci.*, 16:1791–1807.
- Hubel, D. H., and T. N. Wiesel, 1965. Binocular interaction in striate cortex of kittens raised with artificial squint, *J. Neurophysiol.*, 28:1041–1059.
- Hubel, D. H., and T. N. Wiesel, 1970. The period of susceptibility to the physiological effects of unilateral eye closure in kittens, *J. Physiol.*, 206:419–436.
- Hubel, D. H., T. N. Wiesel, and S. LeVay, 1977. Plasticity of ocular dominance columns in monkey striate cortex, *Phil. Trans. R. Soc. Lond. B*, 278:377–409.
- Huberman, A. D., D. Stellwagen, and B. Chapman, 2002. Decoupling eye-specific segregation from lamination in the lateral geniculate nucleus, *J. Neurosci.*, 22(21):9419–9429.
- Issa, N. P., J. T. Trachtenberg, B. Chapman, K. R. Zahs, and M. P. Stryker, 1999. The critical period for ocular dominance

- plasticity in the ferret's visual cortex, *J. Neurosci.*, 19:6965–6978.
- Jones, D. G., R. C. Van Sluyters, and K. M. Murphy, 1991. A computational model for the overall pattern of ocular dominance, *J. Neurosci.*, 11:3794–3808.
- Katz, L. C., and J. C. Crowley, 2002. Development of cortical circuits: lessons from ocular dominance columns, *Nat. Rev. Neurosci.*, 3:34–42.
- Katz, L. C., and C. J. Shatz, 1996. Synaptic activity and the construction of cortical circuits, *Science*, 274:1133–1138.
- Kind, P. C., D. E. Mitchell, B. Ahmed, C. Blakemore, T. Bonhoeffer, and F. Sengpiel, 2002. Correlated binocular activity guides recovery from monocular deprivation, *Nature*, 416:430–433.
- Lachia, E. A., and V. A. Casagrande, 1988. Development of primate retinogeniculate axon arbors, *Vis. Neurosci.*, 1:103–123.
- LeVay, S., M. P. Stryker, and C. J. Shatz, 1978. Ocular dominance columns and their development in layer IV of the cat's visual cortex: a quantitative study, *J. Comp. Neurol.*, 179:223–244.
- LeVay, S., T. N. Wiesel, and D. H. Hubel, 1980. The development of ocular dominance columns in normal and visually deprived monkeys, *J. Comp. Neurol.*, 191:1–51.
- Linden, D. C., R. W. Guilery, and J. Cucchiari, 1981. The dorsal lateral geniculate nucleus of the normal ferret and its postnatal development, *J. Comp. Neurol.*, 203:189–211.
- Miller, K. D., J. B. Keller, and M. P. Stryker, 1989. Ocular dominance column development: analysis and simulation, *Science*, 245:605–615.
- Muir-Robinson, G., B. J. Hwang, and M. B. Feller, 2002. Retinogeniculate axons undergo eye-specific segregation in the absence of eye-specific layers, *J. Neurosci.*, 22(13):5259–5264.
- Olson, C. R., and R. D. Freeman, 1980. Profile of the sensitive period for monocular deprivation in kittens, *Exp. Brain Res.*, 39:17–21.
- Penn, A. A., P. A. Riquelme, M. B. Feller, and C. J. Shatz, 1998. Competition in retinogeniculate patterning driven by spontaneous activity, *Science*, 279:2108–2112.
- Rakic, P., 1976. Prenatal genesis of connections subserving ocular dominance in the rhesus monkey, *Nature*, 261(5560):467–471.
- Rakic, P., 1981. Development of visual centers in the primate brain depends on binocular competition before birth, *Science*, 214:928–931.
- Rathjen, S., and S. Löwel, 2000. Early postnatal development of functional ocular dominance columns in cat primary visual cortex, *Neuroreport*, 11:2363–2367.
- Reh, T. A., and M. Constantine-Paton, 1985. Eye-specific segregation requires neural activity in three-eyed *Rana pipiens*, *J. Neurosci.*, 5:1132–1143.
- Reiter, H. O., and M. P. Stryker, 1988. Neural plasticity without postsynaptic action potentials: less-active inputs become dominant when kitten visual cortical cells are pharmacologically inhibited, *Proc. Natl. Acad. Sci. USA*, 85:3623–3627.
- Ruthazer, E. S., G. E. Baker, and M. P. Stryker, 1999. Development and organization of ocular dominance bands in primary visual cortex of the sable ferret, *J. Comp. Neurol.*, 407:151–165.
- Shatz, C. J., 1983. The prenatal development of the cat's retinogeniculate pathway, *J. Neurosci.*, 3:482–499.
- Shatz, C. J., S. H. Lindstrom, and T. N. Wiesel, 1977. The distribution of afferents representing the right and left eyes in the cat's visual cortex, *Brain Res.*, 131:103–116.
- Shatz, C. J., and M. P. Stryker, 1988. Prenatal tetrodotoxin infusion blocks segregation of retinogeniculate afferents, *Science*, 242:87–89.
- Snider, C. J., C. Dehay, M. Berland, H. Kennedy, and L. M. Chalupa, 1998. Prenatal development of retinogeniculate axons in the macaque monkey during segregation of binocular inputs, *J. Neurosci.*, 19:220–228.
- Sretavan, D. W., and C. J. Shatz, 1986. Prenatal development of cat retinogeniculate axon arbors in the absence of binocular interactions, *J. Neurosci.*, 6:990–1003.
- Sretavan, D. W., C. J. Shatz, and M. P. Stryker, 1988. Modification of retinal ganglion cell axon morphology by prenatal infusion of tetrodotoxin, *Nature*, 336:468–471.
- Stellwagen, D., and C. J. Shatz, 2002. An instructive role for retinal waves in the development of retinogeniculate connectivity, *Neuron*, 33:357–367.
- Stryker, M. P., 1986. Evidence for a possible role of spontaneous electrical activity in the development of the mammalian visual cortex, in *Developmental Neurophysiology* (P. Kellaway and D. Purpura, eds.), Baltimore: Johns Hopkins University Press.
- Stryker, M. P., and W. A. Harris, 1986. Binocular impulse blockade prevents the formation of ocular dominance columns in cat visual cortex, *J. Neurosci.*, 6:2117–2133.
- Stryker, M. P., and S. L. Strickland, 1984. Physiological segregation of ocular dominance columns depends on the pattern of afferent electrical activity, *Invest. Ophthalmol. Vis. Sci.*, 25:278.
- Sur, M., A. Angelucci, and J. Sharma, 1999. Rewiring cortex: the role of patterned activity in development and plasticity of neocortical circuits, *J. Neurobiol.*, 41:33–43.
- Swindale, N. V., 1980. A model for the formation of ocular dominance stripes, *Proc. R. Soc. Lond. B*, 208:243–264.
- Van Sluyters, R. C., and F. B. Levitt, 1980. Experimental strabismus in the kitten, *J. Neurophysiol.*, 43(3):686–699.
- Von der Malsburg, C., and D. J. Willshaw, 1976. A mechanism for producing continuous neural mappings: ocularity dominance stripes and ordered retino-tectal projections, *Exp. Brain Res.*, 35(Suppl. 1):463–469.
- Weliky, M., and L. C. Katz, 1999. Correlational structure of spontaneous neuronal activity in the developing lateral geniculate nucleus in vivo, *Science*, 285:599–604.
- Wiesel, T. N., and D. H. Hubel, 1965. Comparison of the effects of unilateral and bilateral eye closure on cortical unit responses in kittens, *J. Neurophysiol.*, 28:1029–1040.
- Williams, R. W., D. Hogan, and P. E. Garraghty, 1994. Target recognition and visual maps in the thalamus of achiasmatic dogs, *Nature*, 367:637–639.

9 The Role of Neural Activity in the Development of Orientation Selectivity

CHIAYU CHIU AND MICHAEL WELIKY

Introduction

In the adult visual cortex, neurons are selectively responsive to particular stimulus features in the visual world. One of the most well-known functional properties of cortical neurons is orientation selectivity, in which cortical cells fire most intensely to lines and edges of specific orientations. Since the discovery of orientation-tuned cells in the primary visual cortex (Hubel and Wiesel, 1962), much attention has been devoted to elucidating the mechanisms underlying its development. Current evidence suggests that orientation selectivity develops in two stages: initial establishment followed by subsequent maturation and stabilization. The earliest emergence of orientation selectivity does not require visual experience, as indicated by the observation of well-tuned cells before or at the time of eye opening (Blakemore and Van Sluyters, 1975; Chapman and Stryker, 1993; Wiesel and Hubel, 1963). However, patterned vision after eye opening is essential to the maturation and maintenance of orientation specificity. Disrupting normal visual experience by binocular lid suture or dark rearing causes orientation tuning to deteriorate (Crair et al., 1998; White et al., 2001). Because visual deprivation significantly reduces the level of neural activity within the visual system, it has remained unclear whether natural physiological levels of activity simply permit the development of orientation selectivity to occur or whether patterns of activity have a deeper instructive role. If activity plays an instructive role in the development of orientation tuning, then spatiotemporally organized patterns of spontaneous or visually driven activity would be expected to drive this process. Correlations in firing between different neurons, when combined with Hebbian synaptic developmental processes, would lead to the strengthening or weakening of distinct synapses. Indeed, recent work reveals that manipulations in the precise correlational structure of neural activity block the maturation of orientation tuning (Chapman and Gödecke, 2000; Ramoa et al., 2001; Weliky and Katz, 1999). These results are consistent with correlation-based models of visual cortical development in which patterned spontaneous activity within the immature visual pathway serves to guide the development of orientation preference (Miller, 1992, 1994).

Historically, the cat has served as the model system for studying the role of visual experience on the development of orientation selectivity (Blakemore and Van Sluyters, 1975; Frégnac, 1979; Pettigrew, 1974; Wiesel and Hubel, 1963). However, research has been limited in the cat due to technical difficulties in performing experimental manipulations in young animals during the time when orientation tuning first develops. The recent shift toward the use of the ferret as an animal model in the study of the development of orientation specificity has enabled researchers to investigate activity-dependent processes at the earliest stages of development. This is because while the ferret visual system is quite similar to that of the cat (Law et al., 1988), the ferret is born approximately 3 weeks earlier in development (Linden et al., 1981). In this chapter, we review the literature on the development of orientation specificity in the cat and ferret in order to better understand the multifaceted role that neural activity plays in this process.

Anatomical and functional organization of the early stages of visual processing

Visual input in the cat and ferret is first processed by the retina and the lateral geniculate nucleus (LGN) before being passed on to the visual cortex (Fig. 9.1). Light hitting the retina of each eye is converted into nerve impulses, which are conveyed to the LGN by retinal ganglion cells. There are two main classes of retinal ganglion cells: ON-center and OFF-center. ON-center cells respond best to a spot of light shone onto the center of their receptive field, whereas OFF-center cells fire most strongly when the central area of the receptive field is not illuminated. Cells within the LGN are segregated into two functionally distinct layers. Layers A and A1 receive input from the contra- and ipsilateral retinas, respectively. LGN cells have circular receptive fields like those of retinal ganglion cells. ON- and OFF-center LGN cells exhibit receptive field properties functionally similar to

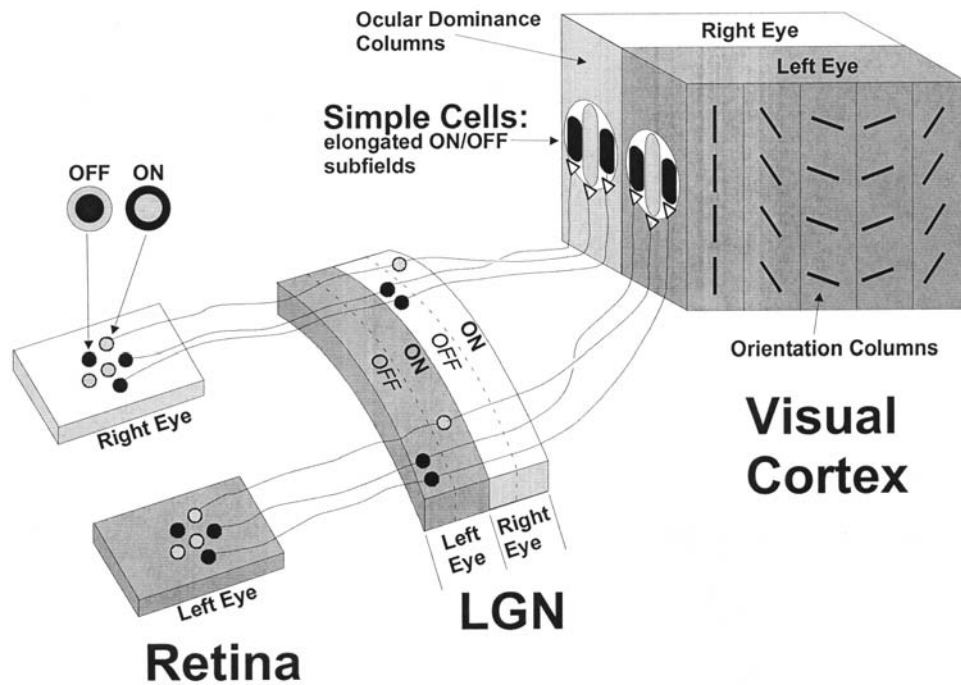


FIGURE 9.1. Anatomical and functional organization of the early stages of the visual pathway. In the retina, ganglion cells have ON-center and OFF-center circular receptive fields. Ganglion cell axons project to eye- and center-type specific functional layers within the LGN. In the ferret, each eye projects to a separate functional LGN layer, and these layers are divided into ON and OFF sublaminae which receive input from ON-center and OFF-center retinal ganglion cells, respectively. Receptive fields of LGN cells are similar to those of retinal ganglion cells. Cells within the LGN form

synaptic contacts with layer 4 simple cells in visual cortex. Simple cell receptive fields consist of alternating ON and OFF subregions which are formed by the spatial segregation of LGN ON and OFF cell inputs. This receptive field organization endows simple cells with the property of orientation tuning. Cells within the visual cortex are functionally organized into orientation and ocular dominance columns which are jointly mapped across the cortex. (From Weliky, 2000).

those of their ON and OFF retinal ganglion cell counterparts and are intermixed within each layer in the cat. In the ferret, each A and A1 layer is further divided into ON and OFF sublaminae.

LGN neurons make synaptic connections with layer 4 simple cells in primary visual cortex. The receptive fields of simple cells contain elongated ON and OFF subregions, which are formed by the spatial alignment of LGN ON- and OFF-center cell inputs. The parallel arrangement of these subregions endows simple cells with the property of orientation tuning, in which cells preferentially respond to bars or edges oriented at a particular angle. In addition to simple cells, there are two other types of orientation-selective cells: complex and hypercomplex (Hubel and Wiesel, 1962; Pettigrew et al., 1968). Whereas the receptive field of simple cells has elongated ON/OFF antagonistic parallel zones, complex cells tend to have a somewhat larger receptive field that does not exhibit any antagonistic arrangements. Hypercomplex cells can be discriminated from simple and complex cells by their particularly strong inhibitory zones at one or both ends of the receptive field.

Most of the cells in the visual cortex are orientation selective. In the cat, more than 90% of visual cortical neurons are well tuned to stimulus orientation (Bishop and Henry, 1972; Chapman and Stryker, 1993). The adult ferret cortex, however, contains fewer cells, about 75%, that show orientation-specific responses (Chapman and Stryker, 1993). The orientation-selective cells are not randomly arranged within the cortex but exhibit a highly ordered organization. Neurons with similar orientation preferences cluster together to form iso-orientation domains, which extend vertically through all cortical layers to form orientation columns (Hubel and Wiesel, 1962; Thompson et al., 1983). Single-unit electrophysiological mapping of receptive field properties in the visual cortex has demonstrated that cells within a vertical column exhibit similar orientation preferences, irrespective of laminar position. With the advent of optical imaging technology, the high-resolution visualization of orientation-specific responses over a wide area of cortex has become possible (Blasdel and Salama, 1986; Chapman et al., 1996; Grinvald et al., 1986). Optical imaging of intrinsic signals has revealed a number of unique features of the map in the cat and ferret (Bonhoeffer and Grinvald, 1991; Weliky

et al., 1996). In addition to the continuous progression of orientation selectivity across the cortical surface, orientation maps contain singularities such as pinwheel centers, in which neurons exhibiting the entire range of orientation preferences are found (Maldonado et al., 1997), and fractures, in which orientation selectivity abruptly changes between neighboring cells.

The role of visual experience in the development of orientation selectivity

The role of visual experience in the development of cortical orientation selectivity has been extensively studied. Patterned vision in the cat occurs when the eyes open about a week after birth. However, electrophysiological experiments reveal that orientation-selective cells are already present at around that time (Blakemore and Van Sluysers, 1975; Wiesel and Hubel, 1963). The actual number of orientation-tuned cells in visually naive kittens is controversial. Reported values range from 0% (Pettigrew, 1974) to 20% (Blakemore and Van Sluysers, 1975) to 100% (Wiesel and Hubel, 1963). This disparity has been attributed to the low level of responsiveness of the immature cat cortex to visual stimuli. This problem is bypassed in studies using ferrets because the cortex of young ferrets is very responsive to visual stimulation. Orientation selectivity in the ferret is first detected at postnatal day (P) 23, 9–12 days before eye opening (Chapman and Stryker, 1993). Although only 25% of neurons in these very young animals are orientation specific, many of them exhibit orientation tuning as sharp as that found in the adult. The presence of well-tuned cells before eye opening suggests that visual experience is not necessary for the initial development of orientation selectivity. There is recent evidence that orientation-specific responses can be elicited through closed eyelids (Krug et al., 2001), suggesting that visual experience may occur before natural eye opening. This raises the possibility that visually evoked activity may be involved in the formation of orientation-specific cells prior to eye opening. However, rearing young animals in complete darkness such that they never have normal visual experience does not prevent the emergence of orientation-selective cells (Frégnac, 1979; White et al., 2001). Thus, the earliest emergence of orientation selectivity does not require patterned vision.

There is also considerable evidence to suggest that normal visual experience is unimportant for the formation of orientation maps. Cortical maps of orientation preference are present very early in development in both cats and ferrets. Clear orientation maps can be optically imaged by 2 weeks of age in the cat, regardless of whether the eyes are open or not (Crair et al., 1998). Similarly, organized orientation maps have been observed in P31–P36 ferrets at the time of natural eye opening as shown in Figure 9.2 (Chapman et al., 1996). Because these maps are present even in young ferrets reared

in the dark (White et al., 2001), visual experience prior to eye opening cannot account for their formation. The optically imaged orientation maps in the cat and ferret are initially low in signal amplitude, reflecting the immature state of orientation selectivity at the time. Over the course of about a week, as orientation-specific cells increase in number and in their sharpness of tuning, the orientation map matures appreciably, as reflected by the increase in image signal contrast. Despite these significant changes following natural eye opening, the general layout of the orientation map remains remarkably constant (Chapman et al., 1996; Gödecke et al., 1997). Longitudinal analysis of orientation map development within the same animal reveals that the size, shape, and location of iso-orientation domains do not vary from the time maps are first detected. Such stability in map structure demonstrates that the orientation map is initially established independent of visual experience.

Although the initial emergence of orientation selectivity occurs without normal visual experience, subsequent maturation and maintenance of orientation specificity critically depends on exposure to patterned visual stimuli. Studies in the cat and ferret demonstrate that maturation of orientation tuning proceeds only to a limited extent in the absence of normal vision (Crair et al., 1998; White et al., 2001). Immediately following the time of natural eye opening, there is a period of increasing orientation selectivity, even in animals reared in complete darkness. However, continued blockade of normal visual experience past this period of time leads to a progressive degradation of orientation tuning until most cells have become unselective. In the ferret, differential effects of dark rearing versus binocular lid suture upon the development of orientation tuning have been demonstrated (White et al., 2001). Animals are reared either in the dark or under binocular lid suture for varying periods of time ranging from 1 to 5 weeks after eye opening. Binocular lid suture alters visual experience by allowing only very low spatial and temporal frequencies to be passed through the closed eyelids to the retina, while dark rearing abolishes all light-driven retinal activity. Interestingly, as shown in Figure 9.3, lid suture has a more severe effect upon the maturation of orientation tuning than dark rearing. Like normally reared animals, dark-reared animals show an increase in orientation selectivity up to the age of about 6 weeks, approximately 7 to 12 days after eye opening. Following this initial maturational period, orientation tuning in dark-reared animals declines at a constant rate. In contrast, the level of orientation selectivity in the lid-sutured animals is similar to that in normal animals only up to the time of eye opening. With continued deprivation, lid-sutured animals show an immediate decrease in orientation selectivity that is maintained at a steady level after this time. Reduced levels of orientation tuning were observed at all time points after eye

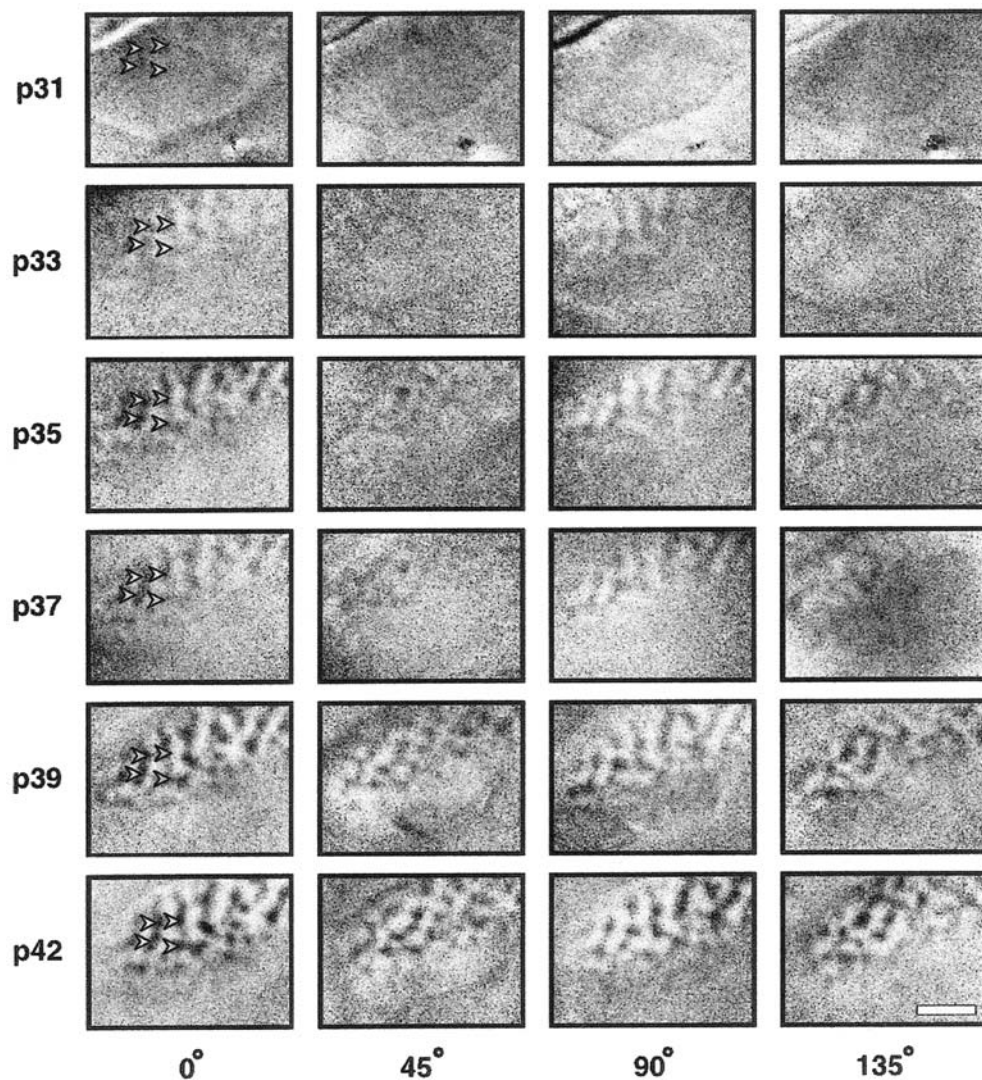


FIGURE 9.2. Development of orientation maps revealed by chronic optical imaging. Single-condition orientation maps recorded at six different ages in one animal. Each row of the figure shows orientation maps recorded in the left primary visual cortex of one ferret at the age indicated at the *left* of the row. Each column of single-condition maps shows orientation maps recorded in response to a particular orientation of a moving square-wave grating (0° = horizontal). For each map, caudal is *up* and medial is to the *left*. The curve in the *upper left corner* of each map indicates the location of the caudal pole of the cortex, behind which the skull

remained intact over the cerebellum. The approximate location of the area 17/18 border can be seen in each image as a *line* rostral to which no orientation activity is seen. In this example, the first clear orientation maps can be seen at P33. Early maps are stronger for horizontal and vertical orientations than for the two obliques. Individual iso-orientation domains remain stable over time and do not change their position, shape, or size. The four *red arrows* shown in each horizontal single-condition map highlight this stability by pointing to particular features in the map. Scale bar, 2 mm. (From Chapman et al., 1996.)

opening in lid-sutured animals compared to dark-reared animals. While these results confirm previous findings that orientation selectivity and orientation maps can develop in the absence of visual experience, they extend these previous findings by demonstrating that visual experience needs to consist of appropriate spatial and temporal frequencies to be effective in driving the subsequent maturation of orientation selectivity.

In the ferret, the development of orientation selectivity occurs in a layer-specific manner (Chapman and Stryker,

1993). At postnatal weeks 4–5, the majority of cells within all cortical layers are unselective for stimulus orientation. Significant differences in the degree of orientation specificity between cortical layers are observed during week 6, when the proportion of cells that are orientation selective has increased only within layers 2/3. Further maturation of orientation selectivity within layer 6 lags behind by about a week or two such that by week 8, the distribution of orientation specificity within layer 6 is equivalent to that within layers 2/3. In contrast, there is very little development of ori-

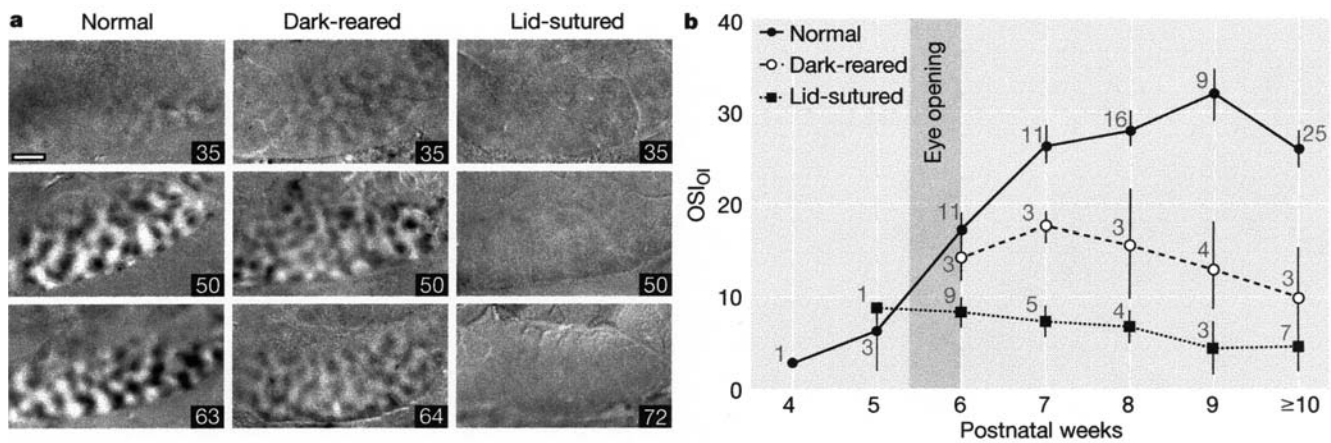


FIGURE 9.3. Quantitative assessment of orientation preference in normal and visually deprived ferrets. *A*, Cardinal difference images show the increase in selectivity seen in normal ferrets after eye opening, the substantial development of the map in dark-reared ferrets, and the devastating effects of lid suture (numbers indicate postnatal age; scale bar: 1 mm). *B*, Plot of OSI_{oi} (mean \pm standard

error) versus postnatal age for each treatment group (numbers next to symbols indicate sample size). After week six, rearing condition was significant ($F_{2,99} = 3.3$, $P < 0.05$), as was the condition/age interaction ($F_{8,99} = 3.6$, $P < 0.001$) with significant differences among all conditions ($P < 0.01$, *post hoc* Tukey-Kramer Honestly Significant Difference). (From White et al., 2001).

entation selectivity in layer 4. Cells within this layer remain relatively unselective for orientation even in adult ferrets. Preventing patterned vision by binocular lid suture for more than 7 weeks results in a reduction in the level of orientation selectivity within layers 2/3 and 6 when compared to normally reared animals at equivalent ages. However, the degree of orientation selectivity in layer 4 is unaffected by visual deprivation.

In the case of the orientation map, visual experience has been demonstrated to play little or no role even late in development. Following 3 weeks of visual deprivation, at a time when selectivity rapidly degrades, clear orientation maps can still be obtained in kittens (Crair et al., 1998; Gödecke et al., 1997). These maps exhibit the same orderly arrangement of cells, with an orientation preference similar to that of normally reared animals. Likewise, in the ferret, even after 64 days of dark rearing, orientation maps are well expressed (White et al., 2001). Experiments rearing kittens in visual environments with a limited set of orientations further reinforce the idea that orientation maps develop independently of visual experience (Sengpiel et al., 1999). These “stripe-rearing” studies demonstrate that although visual experience has been restricted to a narrow range of stimulus orientations, neurons in these animals still exhibit preferences for orientations to which they had never been exposed. This initially experience-independent establishment of orientation specificity results in the formation of a normal orientation map.

Moreover, it has been demonstrated in reverse monocular occlusion experiments that exposure to different visual experiences in the two eyes cannot cause different orientation maps to form (Gödecke and Bonhoeffer, 1996). In

kittens raised with exclusively monocular visual experience for several weeks, the orientation map for the open eye develops. However, the map for the deprived eye cannot be detected, indicating either that the circuitry underlying map formation for the occluded eye is not present or that the connections are intact but cannot be seen by traditional optical imaging techniques. Monocular deprivation has been shown to dramatically decrease the effectiveness of the sutured eye in driving cortical cells, such that most of the cortex is dominated by the open eye (Hubel and Wiesel, 1963). Following reverse occlusion, the orientation map for the originally deprived eye is detectable. This may reflect recovery in the strength and efficacy of the synaptic connections from that eye to the cortex rather than reestablishment of the circuitry underlying map formation. In support of this possibility, there is evidence of a weak residual orientation map for the deprived eye in the cat (Crair et al., 1997). Detailed analysis of the orientation maps for the two eyes optically imaged at separate times during development reveals that they are identical despite never having common visual experience. Thus, the organization of orientation maps is determined and maintained by mechanisms independent of visual experience.

Mechanisms of activity-dependent development

It has been shown that neural activity is necessary for the development of orientation selectivity. Chronically silencing the cortex by infusion of tetrodotoxin (TTX), a sodium channel blocker, completely prevents the maturation of orientation specificity in ferrets (Chapman and Stryker, 1993). At postnatal week 7 and beyond, when orientation

selectivity should have reached adult levels, the number of orientation-selective cells in the TTX-treated animals remains low. The distribution of orientation specificity in these experimental animals is equivalent to that seen in normal animals at postnatal week 4, corresponding to the time when TTX treatment is initiated. Thus, orientation specificity fails to develop in the absence of neural activity. While this experiment demonstrates that neural activity is crucial in the development of orientation selectivity, the precise role of activity cannot be determined.

Current concepts of how activity contributes to the development of neural circuits in general, and of orientation selectivity specifically, revolve around activity playing either a permissive or an instructive role. In a permissive capacity, natural physiological levels of activity simply allow developmental processes to occur, whereas other molecular or genetic mechanisms specify and guide these processes. When activity levels are substantially reduced, these other mechanisms fail to function. For example, manipulations in which neural activity within the visual pathway is pharmacologically blocked (Chapman and Stryker, 1993) or visual experience is abolished, such as in dark rearing (Frégnac, 1979; White et al., 2001), remove a significant portion of neural activity from the visual pathway. For this reason, results from these experiments can only be used to support a permissive role of activity in the development of orientation tuning; such approaches cannot determine whether it is the specific pattern of activity that is important or just the presence of this activity. In order to address directly the instructive role of activity in the development of orientation selectivity, it must be demonstrated that specific manipulation of the spatiotemporal patterns of neural activity disrupts this process.

Recent experiments have tested whether patterns of neural activity carried within the separate ON- and OFF-center pathways are necessary for the development of orientation selectivity in visual cortex (Chapman and Gödecke, 2000). Daily intravitreal injections of DL-2-amino-4-phosphonobutyric acid (APB), an mGluR6 receptor agonist which selectively blocks visually driven activity within the developing ON-center pathway, are made into both eyes starting at P21 in the ferret and continued throughout the period of orientation selectivity maturation until P45–P54. These APB injections completely block the maturation of orientation selectivity, suggesting that neural activity within both ON- and OFF-center visual pathways is required for normal development of orientation specificity. Furthermore, there is a critical period to this activity-dependent process. Orientation selectivity cannot be rescued when APB treatment is continued past P50, and no effects on orientation tuning have been observed when APB injections begin late in development. However, because APB suppresses ON responses, the overall level of activity is reduced in the visual

system. It is also unclear to what extent APB affects spontaneous activity. Therefore, it cannot be determined directly whether orientation selectivity fails to develop following repeated injections of APB due to a reduced level of activity (spontaneous or visually driven) or due to the disruption of specific patterns of correlated activity between ON- and OFF-center cells. A more recent result that is crucial for the proper interpretation of this experiment is that at P21 when the injections were begun, the ON and OFF pathways are not fully segregated. This is demonstrated by the finding that 70% of retinal ganglion cells are multistratified and exhibit both ON and OFF responses (Wang et al., 2001). Segregation of the ON and OFF pathways occurs gradually such that the proportion of ON to OFF ganglion cells decreases to about 12% at P45–P55. Importantly, APB blocked both ON and OFF responses in these multistratified ganglion cells, demonstrating that APB eye injections were likely more disruptive than was previously believed.

Chronic electrical stimulation of the optic nerve has been used to introduce abnormal levels of correlated activity between ON- and OFF-center retinal ganglion cells within the visual pathway in the ferret without reducing the overall level of activity (Weliky and Katz, 1997). In this study, the optic nerve is artificially stimulated only 10% of the time. Despite having normal activity 90% of the time, the orientation tuning of stimulated animals is significantly disrupted, although not completely abolished. Laminar analysis of orientation tuning in control and stimulated animals shows that the disruption is confined to the upper and lower cortical layers. In control animals, cells within the upper and lower cortical layers have significantly sharper orientation tuning than cells located within intermediate layers, which exhibit weak selectivity. Cells within intermediate layers in both stimulated and control animals exhibit similarly weak orientation selectivity; however, in stimulated animals, cells within the upper and lower layers are also weakly tuned. This suggests that chronic stimulation preferentially disrupts intrinsic cortical circuits underlying the sharpening of orientation tuning within superficial and deep cortical layers, similar to the effect seen in binocularly deprived animals (Chapman and Stryker, 1993). While orientation tuning is disrupted, the spatial organization of the orientation map remains unaffected. Optical imaging of orientation preference maps reveals a normal size, spacing, and pattern of orientation domains; however, the magnitude of the signal in these maps is on average 1.6 times weaker than that in control animals. This reduction in signal amplitude would be expected from the extracellular recordings that demonstrate reduced orientation selectivity of individual cells. Since the period of stimulation spanned both pre- and post-eye opening, these results cannot be used to discriminate between the role of spontaneous activity and visually driven activity in the development of orientation selectivity.

Nevertheless, it validates the importance of normal patterns of neural activity in this process.

A recent finding provides a mechanism at the molecular and cellular levels by which the disruption of normal patterns of correlated neural activity may perturb the development of orientation selectivity. With the use of antisense oligonucleotides, Ramoa et al. (2001) demonstrate that the development of orientation selectivity is prevented when cortical *N*-methyl-D-aspartate (NMDA) receptor function is suppressed. NMDA receptors have been postulated to act as a correlation detector for pre- and postsynaptic activity (Bourne and Nicoll, 1993). Under normal conditions, the NMDA receptor is nonfunctional due to a voltage-dependent Mg^{2+} blockade. Mg^{2+} is released when the postsynaptic membrane is sufficiently depolarized by the synchronous firing of a large number of presynaptic cells. In this way, NMDA receptor function may serve to preferentially strengthen the connections between pre- and postsynaptic cells that fire together, thereby causing these cells to wire together. When NMDA receptor function is reduced, the correlational structure of activity in the ON and OFF visual pathways cannot be as reliably conveyed to the postsynaptic cell, thereby disrupting the development of neural connections that underlie orientation selectivity.

These experimental results fit well with a correlation-based model in which activity-dependent interactions within the developing ON- and OFF-center pathways drive the ON/OFF subfield segregation of oriented simple cell receptive fields (Miller, 1994). There are three primary components to this model. First, it presumes that coactive neurons tend to strengthen their inputs to the same postsynaptic cells according to a Hebbian-style rule. Second, the model incorporates an element of competition such that only the synapses of one group of coactive neurons will remain on a given postsynaptic cell, while other groups are eliminated. Finally, computer simulations show that the process of simple cell ON/OFF subfield segregation requires specific patterns of correlated activity among the LGN ON and OFF inputs (Fig. 9.4). In this model, the like center-type inputs (both ON-center or both OFF-center) should be more correlated than the opposite center-type inputs at small retinotopic distances, but at larger retinotopic distances the opposite center-type inputs should be more coactive than the like center-type inputs. In this way, ON and OFF inputs would segregate according to the Hebbian rule so as to form the characteristic elongated parallel zones of ON/OFF subregions, thus conferring orientation selectivity on the simple cells. Such a model can explain the differential effects of binocular lid suture and dark rearing on the development of orientation selectivity in the ferret (White et al., 2001). Abnormal visual experience through light-scattering eyelids may coactivate converging ON- and OFF-center LGN inputs to target layer 4 cells over a broader spatial scale than

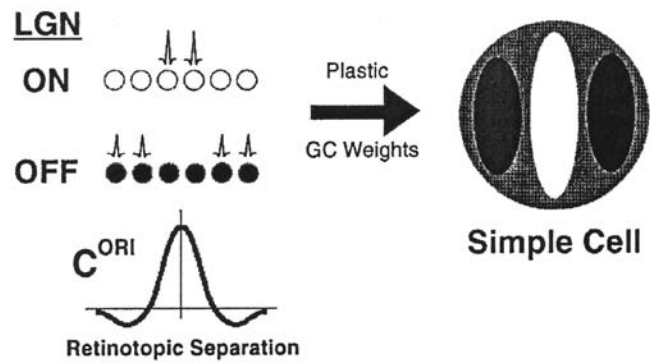


FIGURE 9.4. Model requirements for development of simple cell receptive fields. Correlation-based mechanisms of synaptic development lead a cell to acquire a “most-correlated” set of inputs. For such a set to consist of ON-center and OFF-center inputs from spatially segregated adjacent regions, as in the simple-cell receptive field at the right (*white*: ON inputs; *black*: OFF inputs), these inputs must tend to fire together. This is illustrated at the *top left*: a local group of ON-center cells should tend to fire together and to be coactive with OFF-center cells in adjacent regions. This statistical tendency can be summarized by a correlation function, C^{ORI} (*bottom left*). C^{ORI} describes, for a given retinotopic separation between two inputs, the degree to which two inputs of the same center type (both ON-center or both OFF-center) tend to be more coactive than two inputs of opposite center types (one ON-center and one OFF-center). If, as illustrated, C^{ORI} is positive at smaller retinotopic separations (meaning that same center-type pairs are more coactive than opposite center-type pairs at those separations) but negative at larger retinotopic separations (opposite center types more coactive than same center types), then simple cells will form under correlation-based development of geniculocortical (GC) weights. (From Miller et al., 1999.)

in normal animals. This has the effect of increasing the correlation of these inputs, thus inhibiting their further segregation into ON- and OFF-center bands within layer IV simple cell receptive fields (Miller et al., 1999). It is possible that orientation tuning is less severely disrupted in dark-reared animals because patterns of spontaneous activity, which have components appropriate for the continued maturation of orientation tuning, are preserved under this condition, while in lid-sutured animals these endogenous patterns of spontaneous activity are overwhelmed by visually evoked activity having an improper correlational structure.

If neural activity plays an instructive role in the establishment of orientation selectivity, dark-rearing studies demonstrate that this must occur early in development using spontaneously generated activity. As early as birth, periodic waves of action potentials propagate across the ferret retina (Meister et al., 1991). Thus, these retinal waves generate a pattern of correlated activity in which neighboring retinal ganglion cells are more coactive than those that are separated by larger retinotopic distances. Furthermore, spontaneous activity among like and opposite center-type cells

within the developing LGN has a highly specific correlational structure (Weliky and Katz, 1999). Correlated activity is higher between like center-type cells and weaker between opposite center-type cells within the same eye-specific layer. At the level of the cortex, synchronous bursts of activity occur over large visual cortical regions (Chiu and Weliky, 2001). Multielectrode recordings reveal long-range spatial patterns of coincident activity between discrete cortical patches, which may link iso-orientation columns. However, this relationship between patterns of correlated activity and the organization of orientation selectivity is yet to be established.

While the exact mechanisms guiding the development of orientation selectivity are not well understood, it has become increasingly clear that neural activity is intimately involved in the process. Before eye opening, patterns of spontaneous activity may drive the initial establishment of orientation selectivity and orientation preference maps. After eye opening, it has been suggested that the maturation of orientation selectivity requires appropriate patterns of neural activity evoked during visual experience. In this way, both endogenous and visually driven activity appears to play important roles in the development of orientation selectivity at different times.

Conclusions

By using new methods to manipulate and record spatiotemporal patterns of neuronal activity directly within the developing visual pathway, the mechanisms by which activity shapes and refines the orientation tuning of visual cortical cells is becoming better understood. These studies reveal highly organized patterns of correlated neuronal activity within different levels of the developing visual system, and demonstrate that manipulation of these patterns can dramatically disrupt the normal development of orientation selectivity. However, it remains unclear whether these activity patterns drive the initial establishment of orientation selectivity or determine the layout of orientation preference maps. For example, the finding that orientation maps are initially established without visual experience suggests either that spontaneous activity may drive this process or that their layout is determined by molecular or genetic factors. While recent results provide evidence that neuronal activity can play an instructive role in shaping cortical circuits during development, it is likely that neuronal activity plays a more complex role that may be either instructive or permissive during different developmental periods. Experiments will need to be designed to distinguish between the potential roles that genetic factors, molecular targeting cues, and neuronal activity play in the development of orientation tuning.

REFERENCES

- Bishop, P. O., and G. H. Henry, 1972. Striate neurons: receptive field concepts, *Invest. Ophthalmol.*, 11:346–354.
- Blakemore, C., and R. C. Van Sluyters, 1975. Innate and environmental factors in the development of the kitten's visual cortex, *J. Physiol.*, 248:663–716.
- Blasdel, G. G., and G. Salama, 1986. Voltage-sensitive dyes reveal a modular organization in monkey striate cortex, *Nature*, 321:579–585.
- Bonhoeffer, T., and A. Grinvald, 1991. Iso-orientation domains in cat visual cortex are arranged in pinwheel-like patterns, *Nature*, 353:429–431.
- Bourne, H. R., and R. Nicoll, 1993. Molecular machines integrate coincident synaptic signals, *Cell*, 72(Suppl):65–75.
- Chapman, B., and I. Gödecke, 2000. Cortical cell orientation selectivity fails to develop in the absence of ON-center retinal ganglion cell activity, *J. Neurosci.*, 20:1922–1930.
- Chapman, B., and M. P. Stryker, 1993. Development of orientation selectivity in ferret visual cortex and effects of deprivation, *J. Neurosci.*, 13:5251–5262.
- Chapman, B., M. P. Stryker, and T. Bonhoeffer, 1996. Development of orientation preference maps in ferret primary visual cortex, *J. Neurosci.*, 16:6443–6453.
- Chiu, C., and M. Weliky, 2001. Spontaneous activity in developing ferret visual cortex in vivo, *J. Neurosci.*, 21:8906–8914.
- Crair, M. C., D. C. Gillespie, and M. P. Stryker, 1998. The role of visual experience in the development of columns in cat visual cortex, *Science*, 279:566–570.
- Crair, M. C., E. S. Ruthazer, D. C. Gillespie, and M. P. Stryker, 1997. Relationship between the ocular dominance and orientation maps in visual cortex of monocularly deprived cats, *Neuron*, 19:307–318.
- Frégnac, Y., 1979. Development of orientation selectivity in the primary visual cortex of normally and dark reared kittens. I. Kinetics, *Biol. Cybernetics*, 34:187–193.
- Gödecke, I., and T. Bonhoeffer, 1996. Development of identical orientation maps for two eyes without common visual experience, *Nature*, 379:251–254.
- Gödecke, I., D. Kim, T. Bonhoeffer, and W. Singer, 1997. Development of orientation preference maps in area 18 of kitten visual cortex, *Eur. J. Neurosci.*, 9:1754–1762.
- Grinvald, A., E. E. Lieke, R. D. Frostig, C. D. Gilbert, and T. N. Wiesel, 1986. Functional architecture of cortex revealed by optical imaging of intrinsic signals, *Nature*, 324:361–364.
- Hubel, D. H., and T. N. Wiesel, 1962. Receptive fields, binocular interaction and functional architecture in the cat's visual cortex, *J. Physiol.*, 160:106–154.
- Hubel, D. H., and T. N. Wiesel, 1963. Receptive fields of cells in striate cortex of very young, visually inexperienced kittens, *J. Neurophysiol.*, 26:994–1002.
- Krug, K., C. J. Akerman, and I. D. Thompson, 2001. Responses of neurons in neonatal cortex and thalamus to patterned visual stimulation through the naturally closed lids, *J. Neurophysiol.*, 85:1436–1443.
- Law, M. I., K. R. Zahs, and M. P. Stryker, 1988. Organization of primary visual cortex (area 17) in the ferret, *J. Comp. Neurol.*, 278:157–180.
- Linden, D. C., R. W. Guillery, and J. Cucchiari, 1981. The dorsal lateral geniculate nucleus of the normal ferret and its postnatal development, *J. Comp. Neurol.*, 203:189–211.

- Maldonado, P. E., I. Godecke, C. M. Gray, and T. Bonhoeffer, 1997. Orientation selectivity in pinwheel centers in cat striate cortex, *Science*, 276:1551–1555.
- Meister, M., R. O. L. Wong, D. A. Baylor, and C. J. Shatz, 1991. Synchronous bursts of action potentials in ganglion cells of the developing mammalian retina, *Science*, 252:939–943.
- Miller, K. D., 1992. Development of orientation columns via competition between ON- and OFF-center inputs, *Neuroreport*, 3:73–76.
- Miller, K. D., 1994. A model for the development of simple cell receptive fields and the ordered arrangement of orientation columns through activity-dependent competition between ON- and OFF-center inputs, *J. Neurosci.*, 14:409–441.
- Miller, K., E. Erwin, and A. Kayser, 1999. Is the development of orientation selectivity instructed by activity? *J. Neurobiol.*, 41:44–57.
- Pettigrew, J. D., 1974. The effect of visual experience on the development of stimulus specificity by kitten cortical neurons, *J. Physiol.*, 237:49–74.
- Pettigrew, J. D., T. N. Nikara, and P. O. Bishop, 1968. Responses to moving slits by single units in cat striate cortex, *Exp. Brain Res.*, 6:373–390.
- Ramo, A. S., A. F. Mower, D. Liao, and S. I. A. Jafri, 2001. Suppression of cortical NMDA receptor function prevents development of orientation selectivity in the primary visual cortex, *J. Neurosci.*, 21:4299–4309.
- Sengpiel, F., P. Stawinski, and T. Bonhoeffer, 1999. Influence of experience on orientation maps in cat visual cortex, *Nat. Neurosci.*, 2:727–732.
- Thompson, I. D., M. Kossut, and C. Blakemore, 1983. Development of orientation columns in cat striate cortex revealed by 2-deoxyglucose autoradiography, *Nature*, 301:712–715.
- Wang, G.-Y., L. C. Liets, and L. M. Chalupa, 2001. Unique functional properties of On and Off pathways in the developing mammalian retina, *J. Neurosci.*, 21:4310–4317.
- Weliky, M., 2000. Correlated neuronal activity and visual cortical development, *Neuron*, 27:427–430.
- Weliky, M., W. H. Bosking, and D. Fitzpatrick, 1996. A systematic map of direction preference in primary visual cortex, *Nature*, 379:725–728.
- Weliky, M., and L. C. Katz, 1997. Disruption of orientation tuning in visual cortex by artificially correlated neuronal activity, *Nature*, 386:680–685.
- Weliky, M., and L. C. Katz, 1999. Correlational structure of spontaneous neuronal activity in the developing lateral geniculate nucleus in vivo, *Science*, 285:599–604.
- White, L. E., D. M. Coppola, and D. Fitzpatrick, 2001. The contribution of sensory experience to the maturation of orientation selectivity in ferret visual cortex, *Nature*, 411:1049–1052.
- Wiesel, T. N., and D. H. Hubel, 1963. Single-cell responses in striate cortex of kittens deprived of vision in one eye, *J. Neurophysiol.*, 26:1003–1017.

10 Mechanisms of Plasticity in the Visual Cortex

NIGEL W. DAW

Introduction

The visual cortex has been a model for plasticity in the nervous system ever since the pioneering work of Wiesel and Hubel (1963). It is a model for neural plasticity at the synaptic level, the best illustration of the nature-nurture controversy about the development of the nervous system, and the best example of the mechanisms that underlie clinical deficits in development. In particular, monocular deprivation, produced by closing the eyelids of one eye, which corresponds to unilateral cataract in the human, has significant physiological and anatomical results. These underlie the resulting amblyopia (poor vision which has no obvious cause in the retina) that can amount to total unilateral blindness in severe cases. Thus, the anatomy and physiology can be correlated with behavioral consequences by studying the visual system.

Many forms of plasticity have been studied in the visual cortex. While the physiology has been studied in most forms and the anatomy in many, most experiments concerned with biochemical mechanisms have been done on three: ocular dominance plasticity, orientation and direction plasticity, and long-term potentiation and long-term depression. These are the three forms that will be discussed in this chapter.

Ocular dominance plasticity

Ocular dominance plasticity is a shift in the ocular dominance of cells in the visual cortex, that is, a shift in whether the cells are dominated by the left eye, the right eye, or both. Changes in ocular dominance are found with monocular deprivation, strabismus, anisometropia, and other conditions. Most experiments on mechanisms have been done with monocular deprivation, which leads to total dominance by the nondeprived eye after a few days in young animals (see Chapters 8 and 14). There is a critical period for these effects lasting from eye opening to close to puberty. Animals are most susceptible early in the critical period around 4–5 weeks in the cat (Olson and Freeman, 1980), 4 weeks in the rat (Fagiolini et al., 1994; Guire et al., 1999) and mouse (Gordon and Stryker, 1996),

and 6 weeks in the ferret (Issa et al., 1999), these four species being the ones usually used for experiments on mechanisms.

At the present time, almost everybody thinks of ocular dominance shifts in terms of changes at glutamate synapses: for example, the effect of the GABA agonist muscimol on ocular dominance shifts is interpreted in terms of the hyperpolarization that it produces in glutamate cells (Reiter and Stryker, 1988). There may also be long-term changes in the inhibitory postsynaptic potentials produced at GABA synapses. Suppression of input from the amblyopic eye by the normal eye in strabismus suggests some increase in inhibitory interactions (Harrad et al., 1996). An early paper pointed out that administration of the GABA antagonist bicuculline brings back binocular input after monocular deprivation (Duffy et al., 1976). However, it is also true that bicuculline can make cells more binocular in normal animals, to a similar extent as it does in monocularly deprived animals (Sillito et al., 1981), so the possibility of an effect at GABA synapses has been discounted. Unfortunately, the techniques required to test long-term changes at GABA synapses in monocularly deprived animals are difficult and time consuming, so it seems unlikely that the question will be investigated much more in the near future.

Orientation and direction plasticity

Orientation and direction selectivity is an important feature of cells in the visual cortex, distinguishing them clearly from the cells found in the lateral geniculate nucleus. Orientation selectivity can be tested with stationary or moving bars or gratings. In practice, moving stimuli are almost always used because results can be obtained more quickly. A cell is said to be selective for orientation of the stimulus if the response along one axis is significantly larger than the response along the perpendicular axis. If the response in one direction along the preferred axis is significantly better than the response in the opposite direction, the cell is also said to be direction selective.

Several mechanisms contribute to orientation selectivity. The original suggestion by Hubel and Wiesel (1962) that

cortical cells receive input from a set of lateral geniculate cells with receptive fields lined up along the preferred orientation axis is supported by a variety of experiments (Chapman et al., 1991; Ferster et al., 1996; Reid and Alonso, 1995). There are also lateral inhibitory connections within visual cortex that contribute to orientation selectivity (Crook et al., 1997; Hata et al., 1988; Sillito, 1979; Tsumoto et al., 1979). Orientation selectivity is a dynamic property which increases and then decreases with time after the presentation of a stimulus, suggesting that recurrent excitatory connections within cortex also contribute (Pei et al., 1994; Ringach et al., 1997). Direction selectivity, on the other hand, is believed to be primarily due to lateral inhibitory connections (Crook et al., 1997; Sillito, 1977); according to the model worked out for rabbit retina (Barlow and Levick, 1965; Wyatt and Daw, 1975), although some excitatory influences may play a role (see Rivadulla et al., 2001).

The critical period for changes in direction selectivity ends earlier than the critical period for ocular dominance. Direction selectivity cannot be changed significantly after 7 weeks of age, when ocular dominance is still mutable (Berman and Daw, 1977; Daw and Wyatt, 1976). Indeed, animals reared to 5 weeks of age with the left eye open looking at a drum continually moving to the left, then reared from 5 to 12 weeks of age with the right eye open looking at a drum continually moving to the right, have a majority of cells dominated by the right eye and preferring movement to the left (Daw et al., 1978). Whether the same is true for orientation selectivity is not known. Orientation selectivity is fully developed, while ocular dominance is still mutable in the ferret, in which the characteristic has been most carefully studied (Chapman and Stryker, 1993; Chapman et al., 1996). However, the end of the critical period for orientation selectivity has not been tested by starting a regime that should disrupt or alter orientation selectivity at different ages.

Long-term potentiation and long-term depression

Long-term potentiation (LTP) and long-term depression (LTD) test plasticity at the synaptic level. LTP is an increase in the size of the excitatory postsynaptic potential (EPSP), and LTD is a decrease in the size of the EPSP lasting for more than 30 minutes. LTP is commonly produced by high-frequency stimulation and LTD by low-frequency stimulation (Kirkwood and Bear, 1994a, 1994b). Most recordings are made in layer 3/2, with stimulation of layer 4 or white matter, measuring field potentials in slices of visual cortex. LTP can also be seen in the visual cortex of the intact animal from stimulation of the optic nerves (Tamura et al., 1992) and from intracellular or whole cell recordings of single cells in slices (Artola and Singer, 1987; Dudek and Friedlander,

1996). The result also depends on the state of the GABA system and the polarization of the cell: for example, 50 Hz applied to white matter produces LTP with 0.3 (μ M) bicuculline, LTD with 0.1–0.2 μ M bicuculline, and neither without bicuculline (Artola et al., 1990). LTP of inhibitory postsynaptic potentials (IPSPs) also occurs (Komatsu and Iwakiri, 1993).

A more direct way to measure LTP and LTD is to impale a cell, stimulate its input to produce an EPSP, and also elicit an action potential (AP) by depolarizing the cell. LTP occurs when the EPSP precedes the AP by 0–20 msec and is maximal with an interval of 10 msec (Feldman, 2000). LTD occurs when the AP precedes the EPSP by 0 to 100 msec or more and is maximal with an interval of 15–25 msec. The maximal amplitude of the LTP is larger than that of the LTD. Clearly, high frequency produces LTP because the magnitude of the LTP is larger for short intervals, and low frequency produces LTD because the magnitude of the LTD is larger for long intervals.

Of course, cells in vivo do not fire in a regular fashion, either with a constant high frequency or with a constant low frequency. However, the results from pairs of connected cells can be used to predict what happens with simulated random firing comparable to firing in vivo. The model that best fits the data is one which includes interactions between an AP and its nearest neighbors, but not neighbors farther away, and ignores the contribution from LTD if there is also a contribution from LTP (Sjöström et al., 2001). Recordings from pairs of layer 5 cells in visual cortex show that random firing produces LTP with an average frequency greater than 35 Hz and LTD with an average frequency less than 35 Hz (Sjöström et al., 2001), in agreement with results from constant frequency stimulation.

The magnitude of LTP and LTD changes with age in a complicated fashion. Several forms of LTP decrease with age: LTP in layers 2–3 in the rat from stimulation of white matter between 2 and 4 weeks of age (Kato et al., 1991; Kirkwood et al., 1995) and LTP of IPSPs in layer 5 cells of rat visual cortex between 2 and 10 weeks of age (Komatsu, 1994). LTP in layers 2/3 from stimulation of layer 4 is constant with age (Kirkwood et al., 1995). Only one set of measurements (Komatsu et al., 1988) shows either LTP or LTD increasing as plasticity for ocular dominance plasticity increases and decreasing as ocular dominance plasticity decreases. Recordings from rat show LTP increasing early in development but maximal at 11–20 days of age (Perkins and Teyler, 1988), before the critical period for ocular dominance starts (Fagiolini et al., 1994; Guire et al., 1999). Thus, the majority of results show LTP and LTD declining as the cortex becomes more plastic for ocular dominance changes, as well as over the period during which the cortex becomes less plastic for ocular dominance shifts. This point, of course, raises the question: does one associate a

decline in LTP with an increase or a decrease in plasticity? Until this question is answered, there will be doubt about the claim that LTP and LTD are closely related to ocular dominance plasticity.

Rearing in the dark

Rearing in the dark extends the critical period for ocular dominance plasticity. That is, animals reared in the dark to several months of age, then monocularly deprived, have a larger ocular dominance shift than animals reared in the light and monocularly deprived for the same period of time (Cynader and Mitchell, 1980). Rearing in the dark also delays the start of plasticity (Mower, 1991), so that early in the critical period the ocular dominance shift occurs more slowly (Beaver et al., 2001a). This produces the interesting result that dark-reared animals are *less* plastic than normal at 5–6 weeks of age, equally plastic at 8–9 weeks of age, and *more* plastic than normal at 12–20 weeks of age. This provides a very powerful criterion to distinguish factors related to plasticity from factors related to activity. Factors related to plasticity should be less active than normal in dark-reared animals at 5–6 weeks and more active than normal in dark-reared animals at 12–20 weeks, or vice versa (antiplasticity factors), whereas factors related to activity should steadily increase or decrease with age.

Rearing in the dark reduces LTD and increases LTP (Kirkwood et al., 1996; Sermasi et al., 2000). This tallies with the observation that cats reared in the dark to 12–20 weeks of age are more plastic than normal. Unfortunately, this experiment has not been done with cats reared in the dark to 5 weeks of age compared to cats reared in the dark to 12–20 weeks of age. If there is a true parallel between LTP, LTD, and ocular dominance plasticity, one would expect LTP to be reduced and LTD to be increased in cats reared in the dark to 5 weeks of age.

The importance of activity

The effects of visual deprivation are specific to the deprivation. For example, monocular deprivation affects ocular dominance but not direction selectivity; rearing in an environment continually moving in one direction affects direction selectivity but not ocular dominance; rearing in a pattern of vertical stripes reduces the percentage of cells responding to horizontal bars; rearing in a pattern of horizontal stripes reduces the percentage of cells responding to vertical bars; and so on. Clearly, these results depend on the pattern of electrical activity reaching the visual cortex from the retina. Thus, it is not surprising that abolition of this activity by infusion of TTX abolishes the ocular dominance shifts from monocular deprivation (Stryker and Strickland, 1984).

The initial establishment of ocular dominance and orientation columns proceeds in the absence of patterned activity by some molecular process that is not yet understood (Crowley and Katz, 2000, 2002; see Chapter 8). The columnar arrangement may then be degraded if patterned activity is disrupted by TTX (Stryker and Harris, 1986). However, this chapter is concerned with postnatal changes that occur as a result of visual deprivation, so mechanisms involved in the initial development will not be considered further.

Evaluation of factors involved in plasticity

As factors that may be involved in plasticity are considered, we will evaluate six questions: (1) Do antagonists to the factor disrupt ocular dominance plasticity? (2) Is orientation plasticity disrupted? (3) Is LTP disrupted? (4) Is LTD disrupted? (5) Does the activity or concentration of the factor increase as cortex becomes more plastic and decrease as the cortex becomes less plastic, or vice versa? (6) Is the concentration or activity of the factor smaller in dark-reared animals at 5–6 weeks of age and larger at 12–20 weeks of age, or vice versa? Not many factors have been tested for all these criteria, but the evidence is rapidly accumulating, and a handful of factors clearly fulfill all criteria.

Instructive factors and modulatory factors

We will distinguish between factors that affect the instructive pathway for plasticity, factors that may modulate this instructive pathway, and factors that are involved with both. Given that plasticity is driven by the pattern of activity reaching the visual cortex from the retina, glutamate receptors are clearly on the instructive pathway, and so are calcium and second messengers activated by glutamate receptors. Modulatory factors include state of attention, state of sleep, nonspecific signals from the thalamus, eye movements, and the transmitters that carry signals about these states, such as noradrenaline, acetylcholine, and serotonin. Amongst the neurotrophins, trkB ligands [brain-derived neurotrophic factor (BDNF) and neurotrophic factor 4/5 (NT4/5)] are located on the instructive pathway (Silver and Stryker, 2001), while the trkA ligand, nerve growth factor (NGF), is located on the modulatory pathway coming from the basal forebrain (Domenici et al., 1994b; Silver et al., 2001). Kinases and phosphatases activated by calcium and second messengers, immediate early genes activated by the kinases and phosphatases, and eventually the genes responsible for the formation and degradation of synapses are affected by both instructive and modulatory influences. We will discuss the instructive factors first and the modulatory factors second.

N-methyl-D-aspartate receptors

N-methyl-D-aspartate (NMDA) receptors have long been postulated to be important in plasticity because the NMDA channels are both ligand gated and voltage sensitive (Mayer and Westbrook, 1984; Nowak et al., 1984). Thus, activation of NMDA receptors produces a nonlinear response, which can be measured in visual cortex (Fox et al., 1990), with a nonlinearity that is predicted by the properties of the channels (Fox and Daw, 1992). The nonlinearity makes it more likely that the postsynaptic cell will fire when the presynaptic cell fires, and consequently more likely to fulfill Hebb's postulate that synapses are strengthened when pre- and postsynaptic cells fire together (Hebb, 1940).

Antagonists at the NMDA receptor reduce ocular dominance plasticity (Bear et al., 1990). The specificity of this result was questioned on the grounds that the NMDA receptor antagonist might reduce activity and therefore act like TTX (Miller et al., 1989). However, ocular dominance plasticity is reduced by treatments that affect NMDA receptors but have little effect on activity (Daw et al., 1999a; Roberts et al., 1998). NMDA receptor antagonists abolish some forms of LTP (Artola and Singer, 1987; Kimura et al., 1989) and LTD (Kirkwood and Bear, 1994b) but not others (Kato, 1993; Komatsu et al., 1991). In addition, antisense oligonucleotides for NMDA receptors reduce orientation selectivity but not direction selectivity, emphasizing the difference in mechanism between these two properties (Ramoa et al., 2001).

Overall levels of NMDA receptors increase with age to the peak of the critical period for ocular dominance plasticity and then decline (Bode-Greuel and Singer, 1989; Gordon et al., 1991; Reynolds and Bear, 1991). The NMDA receptor consists of the NMDA receptor 1 (NR1) subunit, found in all receptors, in combination with NR2 subunits in various combinations. The NR1, NR2B, and NR2A subunits all increase with the rise of plasticity and then decline with the fall in plasticity (Chen et al., 2000). The NR2B subunit is reduced in 5-week dark-reared cats compared to normal and increased in 20-week dark-reared cats (Chen et al., 2000). There is downregulation of the NMDA contribution to the visual response which can be seen by recording from single cells in these layers (Fox et al., 1989; Tsumoto et al., 1987). This downregulation is also delayed by rearing in the dark (Fox et al., 1991, 1992). Thus, NMDA receptors are clearly involved in plasticity in the visual cortex, by all the criteria listed above, with the NR2B subunit being most closely related to plasticity. However, overexpression of the NR2B subunit does not affect ocular dominance plasticity (Philpot et al., 2001).

There is a switch during development from the NR2B subunit to the NR2A subunit, which is delayed by rearing in the dark (Carmignoto and Vicini, 1992) and can be altered

quite rapidly (Quinlan et al., 1999). Receptors with the NR2A subunit have a shorter open time. This reduces the probability of overlap of firing between pre- and postsynaptic cells and the chance that the Hebb postulate will be fulfilled, and also affects the amount of calcium that will enter the cell through NMDA receptor channels. The switch to NR2A is correlated with a decrease in LTP between P0 and P7 (P, postnatal day) in the rat (Carmignoto and Vicini, 1992), and the presence of NR2B is correlated with increased plasticity in the cat (Chen et al., 2000). Thus, greater NMDA function is related to plasticity by a variety of experiments.

Metabotropic glutamate receptors

Metabotropic glutamate receptors may also be a mediator for plasticity, because they release calcium from internal stores in the cell and affect various second messengers such as cAMP. Moreover, glutamate stimulation of phosphoinositide turnover follows the critical period for ocular dominance plasticity in cat visual cortex (Dudek and Bear, 1989). There are three groups of metabotropic glutamate receptors. Group I (mGluR's 1 and 5) has facilitatory postsynaptic actions in the visual cortex (Jin et al., 2001), as it does in other parts of the nervous system, affects phosphoinositide metabolism, and increases cAMP. Groups II (mGluR's 2 and 3) and III (mGluR's 4, 6, 7, and 8) have depressive presynaptic actions (Beaver et al., 1999, 2002a; Jin and Daw, 1998), also similar to their actions in other parts of the nervous system, and decrease cAMP. Group II mGluR's and mGluR5 are developmentally regulated and affected by rearing in the dark, but mGluR1 is not (Beaver et al., 1999; Reid and Romano, 2001; Reid et al., 1997). Most of the changes during development and with dark rearing do not correlate with plasticity, except for the point that Group II mGluR's disappear from layer 4 between 3 and 6 weeks of age, when ocular dominance columns are segregating, and this disappearance is delayed by rearing in the dark (Beaver et al., 1999; Reid and Romano, 2001). Thus, the variation in glutamate-stimulated phosphoinositide turnover must be due to a variation in phosphoinositide metabolism rather than a variation in mGluR receptors (Daw et al., 1999b).

The general mGluR antagonist, α -methyl-4-carboxyphenylglycine (MCPG), does not affect ocular dominance plasticity (Hensch and Stryker, 1996). However, MCPG is not very potent. It acts as an antagonist against the mGluR agonist aminocyclopentane-trans-1, 3-dicarboxylic acid (ACPD), but is not effective against glutamate-stimulated phosphoinositide (PI) turnover or glutamate-stimulated spike adaptation (Huber et al., 1998a). Recent work shows that the Group I antagonist *N*-phenyl-7-(hydroxylamino)cyclopropa[b]chromen-1a-carboxamide

(PHCCC) does reduce ocular dominance plasticity slightly, while the mGluR5 antagonist 2-methyl-6-(phenylethynyl) pyridine hydrochloride (MPEP) does not (Fischer et al., 2001), implying that the effect is due to mGluR1. Since it is mGluR5 that is developmentally regulated, rather than mGluR1, the significance of this result is unknown. There is agreement that LTP is not affected by MCPG (Haruta et al., 1994; Hensch and Stryker, 1996; Huber et al., 1998a), but some forms of LTD and reversal of LTP do depend on mGluRs (Haruta et al., 1994; Hensch and Stryker, 1996; Kato, 1993). In summary, metabotropic glutamate receptors may play a role in ocular dominance plasticity in the visual cortex, but the role is weak compared to that of NMDA receptors.

Calcium and calcium-stimulated kinases and phosphatases

Activation of NMDA receptors lets calcium into the cell (Takahashi et al., 1993). Calcium has been implicated in synaptic plasticity in the hippocampus by several experiments (Lynch et al., 1983; Mulkey and Malenka, 1992; see also Malenka and Nicoll, 1999). The current hypothesis is that small increases in calcium that persist over a long period of time lead to depression, and large increases produced over a short period of time lead to potentiation (Lisman, 1989; Yang et al., 1999). It is therefore almost a tautology that calcium must be involved in ocular dominance plasticity in the visual cortex. Unfortunately, nobody has been able to think of an experiment to test the involvement of calcium in ocular dominance plasticity directly, because calcium is involved in so many other cell processes that any disruption of the calcium system would have numerous effects besides its effect on ocular dominance plasticity, and it would be hard to control for the other effects. Indirect evidence involves mainly experiments with LTP and LTD and changes during development.

Both LTP and LTD are blocked by injection of calcium chelators into the cell (Brocher et al., 1992a; Komatsu and Iwakiri, 1992; Yoshimura et al., 1991). In some situations, LTP is blocked but not LTD (Kimura et al., 1990). Presumably this occurs because the block is partial, in accordance with the hypothesis that low rises in calcium lead to LTD, while large transient rises lead to LTP (Hansel et al., 1997). The hypothesis is also supported by simultaneous measurements of calcium and LTP or LTD (Yasuda and Tsumoto, 1996). LTP at inhibitory synapses also depends on calcium (Komatsu and Yoshimura, 2000).

Some developmental changes in calcium correlate with ocular dominance plasticity, and some do not. Binding sites for voltage-dependent calcium channels in the cat decrease steadily with age, during the period when plasticity is increasing (14–28 days), as well as during the period that

plasticity is decreasing (28–70 days), suggesting that they are related to activity rather than plasticity (Bode-Greuel and Singer, 1988). Rearing in the dark has no effect on these binding sites (Bode-Greuel and Singer, 1988). Calcium currents decline in layer 4 and increase in layer 3 between 5 weeks and adulthood in the cat (Bode-Greuel and Singer, 1991). Unfortunately, animals at ages earlier than 28 days were not tested. Calcium uptake through NMDA receptors in the cat declines steadily between 26 and 90 days of age, with few measurements before 28 days of age, again unfortunately for the interpretation of the relationship to plasticity (Feldman et al., 1990).

Calcium stimulates a number of kinases and phosphatases. The hypothesis is that high levels of calcium stimulate kinases to produce potentiation, and low levels stimulate phosphatases to produce depression (Lisman, 1989, 2001). Experiments that have been done in the visual cortex have used primarily α -calcium/calmodulin kinase II (α CaMKII) and calcineurin. In mice mutant for α CaMKII, ocular dominance plasticity was greatly diminished in half of the cases, and in the other half it was normal (Gordon et al., 1996). A more specific mutant that cannot autophosphorylate shows ocular dominance plasticity for long periods of monocular deprivation but not for short periods (Tara et al., 2002). LTP is reduced by about 50% and LTD by about 30% in 4- to 5-week α CaMKII mutant mice, and LTP is almost abolished in adult mutants, in which LTD is minimal (Kirkwood et al., 1997). Thus, α CaMKII has a larger effect in the less plastic cortex. The calcineurin inhibitor FK506 blocks induction of LTD in slices of rat visual cortex (Torii et al., 1995) and makes the induction of LTP more likely (Funauchi et al., 1994). Much of this is consistent with the hypothesis, but the exact role of α CaMKII is not clear.

In summary, calcium is almost certainly an important link in plasticity in the visual cortex, between activation of glutamate receptors and activation of various kinases and phosphatases. However, more NMDA receptors is what makes the cortex more plastic at the peak of the critical period, not more of some property of calcium or calcium channels. There is no evidence that any property of calcium or calcium channels corresponds to both the rising and falling phases of the critical period or is affected by dark rearing in the same manner as plasticity. In other words, calcium is a link but is not the factor that makes the cortex plastic.

GABA

The role of the GABA system in ocular dominance plasticity is complicated and interesting. Monocular deprivation combined with infusion of the GABA_A receptor agonist muscimol leads to an ocular dominance shift toward the deprived eye, known as a *reverse ocular dominance shift* (Reiter

and Stryker, 1988). Infusion of bicuculline has a less pronounced but similar effect, with no effect on orientation selectivity (Ramoia et al., 1988). The hypothesis is that the postsynaptic cell is hyperpolarized and not firing, while the presynaptic terminals are not affected, and the connections between the more strongly activated eye are weakened relative to the less activated eye. Anatomical experiments show that terminals from the deprived eye occupy a larger space in the area affected by muscimol relative to the space occupied by the terminals of the nondeprived eye (Hata and Stryker, 1994). The primary effect is retraction of terminals from the nondeprived eye: terminals from the deprived eye do not change much over the 2 weeks of monocular deprivation tested (Hata et al., 1999). This demonstrates a mechanism for weakening at specific terminals in ocular dominance plasticity, rather than a specific mechanism for strengthening accompanied by a general mechanism for weakening. Since the weakening takes place in the absence of activity in the postsynaptic cell, it seems likely that there is a trophic factor released by the postsynaptic cell independent of activity, and that the less active presynaptic afferents serving the deprived eye have a lower requirement for trophic support.

There are two forms of the enzyme that synthesizes GABA, which is glutamic acid decarboxylase: GAD65 and GAD67. GAD67 is found primarily in soma and dendrites. GAD65 is found primarily in presynaptic terminals and is responsible for the rapid production of GABA in response to stimuli. Ocular dominance plasticity is abolished in mice that are mutant for GAD65 and can be brought back again by infusion of the benzodiazepene agonist diazepam, which increases the open probability and channel conductance of the GABA_A receptor in a use-dependent manner (Hensch et al., 1998). Diazepam brings forward both the start and the end of the critical period (Iwai et al., 2001). LTD is reduced in these mice (Choi et al., 2001) but LTP is not affected, nor is orientation selectivity or receptive field size (Hensch et al., 1998).

Mice that overexpress the *trkB* ligand BDNF produce an excess of GABA (Huang et al., 1999). LTP produced in layer 3 by stimulation of white matter in these mice declines with age by 22 rather than 30 days and can be brought back by infusion of picrotoxin (Huang et al., 1999). GAD65 develops early, and so does visual acuity (Huang et al., 1999). These mice also have a precocious critical period for ocular dominance plasticity (Hanover et al., 1999).

A confusing array of hypotheses has been put forward regarding these results. The suggestion from the result that LTP in BDNF-overexpressing mice ends early was that increased production of GABA brings plasticity to an end (Huang et al., 1999). This is also the suggestion for the result that LTP in layer 3 declines with age with stimulation of

white matter but not with stimulation of layer 4: there is a layer 4 plasticity *gate* which closes as GABA develops with age and brings plasticity to an end (Kirkwood and Bear, 1994a). The suggestion from the precocious critical period in both BDNF-overexpressing mice and GAD65 knockout mice treated with diazepam is that an increase in GABA starts the critical period rather than brings it to an end, and that this sets in train a series of reactions involving other factors, which eventually brings the critical period to an end (Iwai et al., 2001). However, GABA antagonists may also produce plasticity in adult animals (Harauzov et al., 2001). How could this happen if the critical period had already been brought to an end by other processes? Moreover, it obviously does not make sense to say that GABA leads to increased plasticity at early ages, decreased plasticity at intermediate ages, and increased plasticity again in the adult. Thus, we are left in a quandary.

In spite of this quandary, we can still say that the GABA system can be modulated to affect plasticity in a variety of ways. However, the GABA system itself is not correlated with the critical period or affected by monocular deprivation or by dark rearing in the same way that plasticity is affected by dark rearing. GAD65 immunoreactivity in deprived and nondeprived eye columns is not affected by either 2 or 7 days of monocular deprivation (Silver and Stryker, 2000). There are no differences in the density or laminar distribution of GABA-positive neurons between normal and dark-reared cats (Mower et al., 1988). The expression and laminar distribution of GAD67 and GAD65 are similar in normal and dark-reared cats (Mower and Guo, 2001). The GABA_A subunits α_1 and α_3 increase to 10 weeks of age with a small decline after that, and the subunit α_2 decreases steadily with age (Chen et al., 2001). There are increases in these subunits in dark-reared animals compared to normal at both 5 and 20 weeks of age (Chen et al., 2001). Other changes are found in dark-reared animals, such as a reduction in GABAergic neurons in the deprived eye columns of adult macaque monkeys (Hendry and Jones, 1986) and an increase in the mRNA for GAD in dark-reared animals compared to normal (Neve and Bear, 1989), but these results can all be related to activity rather than plasticity. Thus, the GABA system is likely to be a link in the chain of processes involved in plasticity, controlled by BDNF and possibly other factors, just as calcium is a link controlled by NMDA and metabotropic glutamate receptors.

Cyclic AMP and protein kinase A

Protein kinase A (PKA) is clearly an important factor in plasticity in the visual cortex. PKA inhibitors abolish ocular dominance plasticity (Beaver et al., 2001b) and induction of LTP and LTD (Liu and Daw, 2001). Mutants missing the

R1 β subunit of PKA have normal ocular dominance plasticity, but this is almost certainly due to upregulation of the R1 α subunit to compensate (Hensch et al., 1996). Cyclic AMP activates PKA, and cAMP produced by the metabotropic glutamate agonist, ACPD, follows the critical period for ocular dominance plasticity closely (Reid et al., 1996). In dark-reared animals, the amount of cAMP is reduced at 5 weeks of age and increased at 15 weeks of age compared to normal in agreement with the effects of monocular deprivation. Thus, there is a close correlation between cAMP and plasticity. This is not due to variations with age and dark rearing in the number of metabotropic glutamate receptors (Reid et al., 1997; Reid and Romano, 2001). What controls the variations is the amount of cAMP between birth and 15 weeks of age, with a decline after that which is due to a decline in metabotropic glutamate receptors (Daw et al., 1999b; Reid et al., 1996).

The effect of protein kinase inhibitors on orientation selectivity is complicated. PKA inhibitors do not affect orientation selectivity in normal animals. Orientation selectivity is also normal in monocularly deprived animals, assayed by stimulating the nondeprived eye. However, orientation selectivity is degraded in animals with monocular deprivation plus PKA inhibitors in both deprived and nondeprived eyes (Beaver et al., 2002b). The hypothesis is that monocular deprivation degrades orientation selectivity as seen through the deprived eye, that PKA inhibitors maintain binocularity, and that the deprived eye instructs the nondeprived eye to reduce orientation selectivity in both eyes.

Other protein kinases and phosphatases

Nitric oxide affects LTP in the hippocampus, and so does its target, protein kinase G (PKG) (Izumi and Zorumski, 1993; O'Dell et al., 1991; Schuman and Madison, 1991; Zhuo et al., 1994). However, neither affect ocular dominance plasticity in the visual cortex (Beaver et al., 2001b; Reid et al., 1996; Ruthazer et al., 1996). In the visual cortex, LTP is abolished by PKG antagonists, but LTD is not (Liu and Daw, 2001). This suggests that ocular dominance plasticity can get underway with depressive processes in place but potentiating processes absent, which is reminiscent of the anatomical finding that ocular dominance shifts are seen after retraction of terminals from the deprived eye, with no changes in the terminals from the nondeprived eye (Antonini and Stryker, 1993, 1996).

Preliminary studies suggest that protein kinase C (PKC) inhibitors also do not affect ocular dominance plasticity (Daw and Beaver, 2001). However, the membrane form of PKC follows the critical period for ocular dominance plasticity (Sheu et al., 1990). The effect of protein kinase C in

LTP and LTD, and the effect of dark rearing to a variety of ages on PKC, have not been studied.

Mitogen activated protein (MAP) kinase is affected by activity and is downstream of neurotrophins and other kinases, so it could therefore be a point of convergence for several signals involved in plasticity (Grewal et al., 1999). MAP kinase inhibitors abolish ocular dominance plasticity and LTP (Di Cristo et al., 2001) without affecting orientation selectivity. Exactly where MAP kinase fits into the pathways involved in plasticity, which signals feed into it, and where it acts downstream remain to be worked out.

An intriguing recent paper shows that there are two phosphorylation sites on GluR1 receptors (Lee et al., 2000). One is phosphorylated by CaMKII, associated with LTP, and dephosphorylated by protein phosphatase 1 and protein phosphatase 2A, associated with depotentiation. The other is dephosphorylated by protein phosphatase 1 and protein phosphatase 2A, associated with LTD, and phosphorylated with protein kinase A, associated with dedepression. Unfortunately, nobody has yet tested the role of PP1 and PP2A in ocular dominance plasticity.

CREB

Cyclic AMP activates the calcium/cAMP response element binding protein known as CREB, which in turn affects protein synthesis. CREB is therefore an obvious candidate for involvement in plasticity. Monocular deprivation for at least 12 hours during the critical period leads to a delayed and persistent expression of CREB (Pham et al., 1999). Injection of a dominant negative form of CREB using herpes simplex virus abolishes ocular dominance plasticity in the affected region but does not affect the recovery from monocular deprivation (Liao et al., 2001). The activation of CREB depends on BDNF and MAP kinase but not on calcium (Pizzorusso et al., 2000). CREB can, in turn, activate the genes for BDNF and c-Fos, demonstrating a feedback loop in the pathway (Pham et al., 1999). However, the metabotropic glutamate agonist, ACPD, intensifies immunostaining for CREB in neurons in all layers before the critical period, in layer 4 at the peak of the critical period, and in glial cells after the critical period, and rearing in the dark delays these changes (Reid, 2001). Moreover, CREB DNA binding activity is not appreciably modulated during development (Kaminska et al., 1995). Thus, CREB may just be another link in the chain, although the observation that it affects ocular dominance shifts from monocular deprivation but not recovery after this, suggesting that it may be a link only in the chain leading to degradation, is most intriguing (Liao et al., 2002). The role of CREB in LTP and LTD in the visual cortex has not been studied. In summary, the

role of CREB in ocular dominance plasticity needs to be evaluated further.

BDNF

BDNF has numerous effects on plasticity in the visual cortex. One of the first observations was that infusion of BDNF into the visual cortex inhibits the formation of ocular dominance columns in layer 4 of the cortex (Cabelli et al., 1995). This appears to be due to a proliferative action of BDNF, which occurs in kittens but not in cats (Hata et al., 2000). Interestingly, the same result is obtained with infusion of trkB-IgG, which binds BDNF (Cabelli et al., 1997). Presumably, BDNF acts by leading to nonspecific sprouting, and its antagonist acts by halting retraction when the trophic factor does not bind to its receptor. When monocular deprivation is combined with infusion of BDNF, the result is a shift toward the deprived eye and a loss of orientation selectivity, which is seen in kittens during the critical period but not in adult animals (Galuske et al., 1996, 2000). Results seen with the other trkB ligand, NT4/5, are fairly similar, but the reverse ocular dominance shift is not noticeable (Gillespie et al., 2000; Lodovichi et al., 2000).

This last result, the reverse ocular dominance shift, is reminiscent of the reverse ocular dominance shift seen with the GABA receptor agonist, muscimol. The two are related, because activity regulates cortical inhibition through BDNF (Rutherford et al., 1997). As mentioned above, mice that overexpress BDNF have a precocious rise in GABA (Huang et al., 1999), and so should behave like mice given a GABA receptor agonist. There are also similarities in the precocious critical period for ocular dominance plasticity produced by BDNF-overexpressing mice and mice treated with the GABA potentiator diazepam (Hanover et al., 1999).

BDNF blocks LTD and enhances LTP, while trkB antagonists block LTP and enhance LTD (Akaneya et al., 1996, 1997; Huber et al., 1998b), although the result may depend on the location of the stimulation electrode (Sermasi et al., 2000). The LTP produced by BDNF is found in young rats at 13–17 and 19–24 days but not in adult rats, lasts for 4–8 hours, then decreases over 15–16 hours (Jiang et al., 2001). Experiments with cells in culture show that the LTD blocked by BDNF is an LTD at glutamate synapses onto glutamate cells due to a presynaptic action of BDNF (Kumura et al., 2000). Whole cell recordings show that BDNF increases the size of EPSCs through an increase in the probability of release, suggesting a presynaptic mechanism for that phenomenon as well (Carmignoto et al., 1997). NMDA and AMPA currents are equally potentiated, supporting this conclusion.

The mechanism of action of BDNF needs to be clarified. Several authors have suggested that BDNF may be transported retrogradely to activate presynaptic neurons, but

direct evidence shows that it is transferred from presynaptic to postsynaptic neurons more than the reverse (Kohara et al., 2001). BDNF is expressed in pyramidal neurons, which are glutamate neurons, but not in interneurons, which are GABA neurons (Aoki et al., 2000; Gorba and Wahle, 1999). Its receptor, trkB, is expressed on both glutamate and GABA neurons, mainly parvalbumin neurons, and at geniculocortical synapses (Aoki et al., 2000; Gorba and Wahle, 1999; Silver and Stryker, 2001). Putting all of this together, BDNF should be released by glutamate neurons to activate both glutamate and GABA neurons. In fact, BDNF increases the release of glutamate but not GABA (Sala et al., 1998) and increases EPSCs (Rutherford et al., 1998). On the other hand, chronic overexpression of BDNF increases GABA function (Huang et al., 1999).

There is some relationship between BDNF and the critical period. mRNA for BDNF follows the critical period for ocular dominance plasticity in the rat quite well, whereas mRNA for NGF does not (Schoups et al., 1995).

Activity affects BDNF, and so does light. Dark rearing decreases BDNF, but this occurs at all ages including adulthood and so may be an activity effect (Castrén et al., 1992; Lein and Shatz, 2000; Schoups et al., 1995). The decrease produced by monocular deprivation in the contralateral cortex in the rat may be a similar effect (Bozzi et al., 1995; Rossi et al., 1999). It seems likely that the effects on BDNF are activity effects, whereas the effects of BDNF on the system are plasticity effects.

Gene expression and protein synthesis

Protein synthesis must be involved in ocular dominance plasticity if some synapses are to be created and others destroyed. The protein synthesis that is required occurs in the visual cortex rather than the lateral geniculate nucleus (Taha and Stryker, 2002). With modern techniques of molecular biology, it has now become possible to identify genes that are particularly related to plasticity (Nedivi et al., 1996; Prasad and Cynader, 1994; Prasad et al., 2001). They include the obvious candidates, such as proteins for neurotransmitter release, receptors, postsynaptic density, neurofilament assembly, cell-cell interaction, cell remodeling, and general house-keeping. As in the hippocampus, protein synthesis is not required for rapid LTP, depending on NMDA receptors, but is required for a more slowly developing form of LTP, depending on L-type calcium channels (Kurotani et al., 1996).

The most stringent criterion for a candidate plasticity gene is to test whether it is downregulated in dark-reared animals at 5 weeks of age compared to normal and upregulated in dark-reared animals at 20 weeks of age (Mower, 1991), or vice versa, as well as whether it is upregulated at the peak of the critical period compared to before and afterward. Genes that are simply upregulated in dark-reared animals com-

pared to normal at one particular age may be related to activity rather than plasticity. This most stringent criterion has turned up some interesting candidate plasticity genes (cpgs) and some candidate antiplasticity genes (capgs). One is a gene that is probably involved in dendritic and axonal arbor restructuring and synaptic maturation, known as *cpg-15* (Lee and Nedivi, 2002). Another is the mouse homolog of one of the *Drosophila* uncoordinated genes, *Munc13-3*, which codes for a presynaptic protein at glutamate receptors (Yang et al., 2002). Some mitochondrial genes also fulfill the stringent criteria (Yang et al., 2001). So does the immediate early gene *Fos* (Mower and Kaplan, 1999).

Few immediate early genes have been tested for their relationship to plasticity using knockout mice. One of the few is *egr1* (Mataga et al., 2001). In these mice, ocular dominance plasticity is normal after both brief and long-term occlusion of one eye. However, *egr1* is modulated by light and dark. Thus, it is an activity factor rather than a plasticity factor.

Of course, the real question in relation to gene expression and protein synthesis is: what controls the array of genes involved in the formation of axon terminals, dendritic spines, and synapses, as opposed to the array of genes involved in their degradation, and how are levels of calcium, PKA, and other factors involved in plasticity related to turning on one set of genes and turning off the other? Could *Fos* turn on the genes used for synapse formation, and could some other immediate early gene turn on the genes used for synapse degradation? So far, the only clue is the observation that CREB is involved in monocular deprivation but not in recovery from monocular deprivation (Liao et al., 2002).

Effect of modulatory states on ocular dominance plasticity

The state of the nervous system affects plasticity. The clearest example of this is the effect of sleep. Six hours of sleep after 6 hours of monocular deprivation enhances the effect of the monocular deprivation, but 6 hours of wakefulness in the dark does not (Frank et al., 2001). There are nonspecific afferents to the cortex coming from the intermedullary laminae of the thalamus, and stimulation of these also accentuates plasticity (Singer and Rauschecker, 1982). As mentioned above, ocular dominance plasticity is not seen in animals paralyzed and anesthetized with halothane in nitrous oxide plus oxygen, but ocular dominance changes can be seen if the eyes are moved mechanically in these animals (Freeman and Bonds, 1979). Presumably the state of attention also affects plasticity, although the point has not been specifically tested in relation to ocular dominance. While it is the afferents from the retina that instruct plasticity, there are clearly also modulatory influences.

Role of modulatory transmitters

Signals about the state of the nervous system come from the basal forebrain, carried by acetylcholine; from the locus coeruleus, carried by noradrenaline; from the raphe nuclei, carried by serotonin; from the midbrain, carried by dopamine; and from the intermedullary nuclei of the thalamus, carried by glutamate. In the first four cases, it is quite easy to distinguish the role of the modulatory pathways from the role of the instructive pathways by interrupting these pathways or applying antagonists to these transmitters. An early experiment suggested that abolition of the noradrenaline pathway by lesions of the dorsal noradrenergic bundle with injections of 6-hydroxydopamine (6-OHDA) abolishes ocular dominance plasticity (Kasamatsu and Pettigrew, 1979). Later experiments showed that this result was due to nonspecific effects induced by the high concentrations of 6-OHDA used: lower doses of 6-OHDA, and other treatments more specific to the noradrenaline pathway, do not have the same result (Daw et al., 1985; Gordon et al., 1988). However, antagonists to α -adrenergic receptors do have a very small effect on the ocular dominance shift (Kasamatsu and Shirokawa, 1985).

Antagonists to muscarinic acetylcholine receptors reduce ocular dominance plasticity somewhat and also affect orientation selectivity, probably through their action on M₁ receptors (Gu and Singer, 1993). Excitotoxic lesions of the cholinergic cells in the basal forebrain also reduce ocular dominance plasticity, and a combination of this treatment with lesioning of the dorsal noradrenergic bundle by 6-OHDA essentially abolishes ocular dominance plasticity (Bear and Singer, 1986). Bear and Singer also showed that high doses of 6-OHDA antagonize the action of acetylcholine, but it was not certain whether the combined action of the basal forebrain and dorsal noradrenergic bundle lesions could be attributed to acetylcholine alone. Serotonin neurotoxins and a combination of antagonists to 5-HT₁ and 5-HT₂ receptors (5-HT, 5-hydroxytryptamine) also reduce ocular dominance plasticity (Gu and Singer, 1995). The role of dopamine in visual cortex plasticity has not been studied. Thus, acetylcholine and serotonin afferents definitely have an effect, but evidence about other modulators is uncertain. The modulatory pathways also facilitate (Brocher et al., 1992b; Kirkwood et al., 1999; Kojic et al., 1997) or depress (Edagawa et al., 2001) LTP and LTD.

Several aspects of the modulatory pathways are developmentally regulated. Some rise to a peak with the critical period for plasticity and then decline. Included are 5-HT levels, 5-HT receptor binding, α -adrenergic receptor binding (Jonsson and Kasamatsu, 1983), acetylcholinesterase-positive fibers in layers 4–6 (Bear et al., 1985), and a transient clustering of 5-HT_{1C} receptors in layer 4 and lower layer 3 during the critical period (Dyck and Cynader,

1993). Several experiments have observed the effect of dark rearing on modulators, but none has been tested with the stringent criterion mentioned above.

How modulators might act

How the modulatory pathways might act on ocular dominance plasticity is not definitely known. Acetylcholine agonists increase the response of cells in the visual cortex to visual stimuli (Sato et al., 1987; Sillito and Murphy, 1987). Noradrenaline has been said to change the signal-to-noise ratio in these cells, but later experiments have questioned this point (Eco-Stengel et al., 2002; Videen et al., 1984). Serotonin enhances responses to excitatory amino acids (Nedergaard et al., 1987), particularly NMDA responses (Reynolds et al., 1988). Acetylcholine, noradrenaline, and serotonin all affect multiple receptors, with different results. This is particularly clear in the case of noradrenaline, where stimulation of the locus coeruleus can have both facilitatory and depressive effects on visual responses in the visual cortex, depending on whether α_1 , α_2 , β_1 , or β_2 receptors are activated (Sato et al., 1989). Thus, all the modulators can affect the activity of cells in the visual cortex, and thereby affect the probability that the postsynaptic cell will fire when the presynaptic cell fires.

There are also effects on various second messengers. Phospholipase C and phosphoinositides, with release of calcium from intracellular stores, are activated by acetylcholine M_1 and M_3 receptors, noradrenaline α_1 receptors, and serotonin 5-HT₂ receptors. Adenylate cyclase is inhibited by acetylcholine M_2 receptors, noradrenaline α_2 receptors, and serotonin 5-HT₁ and 5-HT₅ receptors. Adenylate cyclase is activated by noradrenaline β receptors and serotonin 5-HT₄ and 5-HT₆ receptors (Hardman et al., 2001). The increase in calcium elicited by glutamate can be enhanced by noradrenaline (Yang et al., 1996). All of these are second messengers involved in the instructive pathways, onto which the modulatory pathways may also converge.

NGF

NGF has little effect on plasticity in the visual cortex of the cat. NGF does not affect the development of geniculocortical endings into ocular dominance columns (Cabelli et al., 1995; Silver et al., 2001), nor does the antagonist at its receptor, trkA-IgG (Cabelli et al., 1997). Infusion of NGF into the visual cortex does not affect ocular dominance changes from monocular deprivation in kittens during the critical period (Galuske et al., 2000; Gillespie et al., 2000; Silver et al., 2001). An orientation selectivity map is not seen in the deprived eye, presumably because the deprived eye no longer drives cortical cells (Galuske et al., 2000; Silver et al., 2001). Interestingly, the same treatment in adult animals leads to a paradoxical

shift toward the deprived eye (Galuske et al., 2000; Gu et al., 1994). Infusion of NGF into the ventricle can lead to a small reduction in the ocular dominance shift, which could be due to activation of trkB receptors, due to the high concentrations used (Carmignoto et al., 1993). In any case, the results do not add up to a role for NGF in ocular dominance plasticity, particularly since the effects are noticeable in adult cats more than in kittens during the critical period.

Results in the rat are somewhat different. Most of the earlier experiments were done by infusion of NGF into the ventricle, and consistently showed that this treatment prevents the shift in ocular dominance from monocular deprivation (Maffei et al., 1992). Moreover, injection of antibodies to NGF into the ventricle late in the critical period (P45) produces an ocular dominance shift (Domenici et al., 1994a). A more recent experiment, with activation of trkA by infusion directly into the visual cortex, leads to a similar effect (Pizzorusso et al., 1999). Indeed, the effect is greater with NGF than with BDNF (Lodovichi et al., 2000). Thus, the results in the rat are clearly different from those in the cat. This does not seem to be a methodological difference in infusion sites, since both intracortical and intraventricular infusions have been used in both species. There could be more cross-reactivity between the various growth factors and their receptors in the rat, in which distances are smaller, so that effective concentrations can be higher at the site of action. The cholinergic projections from the basal forebrain may be wider and more powerful in the rat. Perhaps such differences over a wider area of brain could even lead to different attention or behavioral states sufficient to affect plasticity. There is also a well-known species difference in the acetylcholine systems: there are no intracortical acetylcholine cells in the cat, whereas some bipolar cells in the rat cerebral cortex are cholinergic (Eckstein and Baughman, 1984). However, it is not known whether the intracortical acetylcholine cells in the rat have trkA receptors on them (Domenici et al., 1994b) or how these cells might affect ocular dominance plasticity. Thus, the species differences remain unresolved.

Similar confusion reigns concerning LTP and LTD, where all the experiments have been done on the rat, so that no species differences occur. Some investigators have found that NGF does not affect LTP (Akaneya et al., 1997) or LTD (Akaneya et al., 1996), while others have found that it does (Carmignoto et al., 1997). Other experiments show that delivery of NGF through the recording pipette can block the maintenance phase of LTP, acting in the same manner as blockade of muscarinic receptors, and that LTP may be reintroduced by muscarine later in the critical period (Pesavento et al., 2000). Whatever the final resolution of these conflicting results, the lack of agreement suggests that NGF is not an important component of the generation of either LTP or LTD.

Growth factors and acuity

A small number of studies have investigated the effect of growth factors on acuity, with intriguing and unexplained results. Acuity is reduced in the deprived eye of monocularly deprived animals, and this reduction is prevented by infusion of NGF into the ventricle in both rats (Domenici et al., 1991) and cats (Fiorentini et al., 1994). In addition, antibodies to NGF reduce acuity in normal animals (Berardi et al., 1994). Proliferation of axons and dendrites by NGF would not be expected to improve acuity, and nobody knows whether the acetylcholine system affects acuity, so the mechanism of action here is not understood. With BDNF the results are more understandable. Mice that overexpress BDNF show premature development of acuity (Huang et al., 1999). Since BDNF leads to an accelerated development of inhibition, and since inhibition is known to reduce the size of the receptive fields of cells, which can be related to an improvement in acuity, there is a logical explanation for this result.

Relationship of ocular dominance plasticity, LTP, and LTD

The results are all summarized in Table 10.1, and looking at it is a good way to think about the relationship between

ocular dominance plasticity, LTP, and LTD. If both LTP and LTD are abolished or substantially reduced by antagonists to a factor, then so is ocular dominance plasticity in most cases (see NMDA receptors, PKA, and BDNF). If a factor facilitates LTP and LTD, then its antagonist generally has some effect on ocular dominance plasticity (see acetylcholine, noradrenaline, and serotonin). Where either LTP or LTD is reduced, but not the other, ocular dominance plasticity remains. Ocular dominance plasticity may be found with LTD present and LTP absent (see PKG: Liu and Daw, 2001; and GAD65: Choi et al., 2001) or with LTP present and LTD absent (see the mGluR receptor antagonist MCPG, references above), or with LTP and LTD and depotentiation absent but a form of pairing potentiation present (see PKA ($\text{RI}\beta$) mutants: Hensch et al., 1998). Thus, it seems that both LTP and LTD must be totally abolished for ocular dominance plasticity to be abolished. In other words, neither LTP by itself nor LTD by itself is necessary for ocular dominance plasticity to occur.

Bringing back plasticity in older animals

The holy grail for most people working on plasticity is to find some factor that will bring back plasticity in older animals. Most intriguing here are recent observations that inhibition

TABLE 10.1
Summary of the effects of various factors on plasticity in the visual cortex

Factor	Ocular Dominance	Orientation Selectivity	LTP	LTD	Critical Period	Dark Rearing
NMDA receptors	Yes	Yes	Some forms	Some forms	Yes	Yes
mGluR's	mGluR1	Not tested	No	Partial	No	Maybe
Calcium	Not tested	Not tested	Yes	Yes	No	No
αCaMKII	Yes	No	Reduced	Reduced	No	Not tested
GAD65	Yes	No	No	Yes	No	No
PKA	Yes	No	Yes	Yes	Yes	Yes
PKC	No	Not tested	Not tested	Not tested	Yes	Not tested
PKG	No	Not tested	Yes	No	Not tested	Not tested
Nitrous oxide	No	No	Not tested	Not tested	Not tested	Not tested
MAP kinase	Yes	No	Yes	Not tested	Not tested	Not tested
BDNF	Yes	Yes	Yes	Yes	Yes	Partly
CREB	Yes	Not tested	Not tested	Not tested	Maybe	Yes
IEGs	Not tested	Not tested	Not tested	Not tested	Yes	Yes
Acetylcholine	Reduced	Reduced	Yes	Yes	Yes	Not tested
Noradrenaline	Small	Reduced	Yes	Yes	Yes	Not tested
Serotonin	Reduced	Reduced	Yes	Yes	Yes	Not tested
NGF	No	No	Conflicting	Conflicting	No	No

Note: The second column states whether ocular dominance plasticity is affected by an antagonist to the factor; third column, whether orientation selectivity is affected; the fourth and fifth columns, whether LTP and LTD are affected; the sixth column, whether the factor or its receptor peak with the critical period for plasticity; and the seventh column, whether dark rearing affects the factor and plasticity similarly, according to the strict criterion that distinguishes candidate plasticity factors from candidate activity factors.

of the GABA system can do this in rats, with inhibition of GAD by mercaptopropionic acid, or inhibition of GABA_A receptors by their antagonist picrotoxin (Harauzov et al., 2001). This, of course, is reminiscent of the plasticity gate hypothesis, in which development of the GABA system in layer 4 is suggested to bring plasticity to an end (Kirkwood and Bear, 1994a; Komatsu, 1983). Given the differences that have been found between the rat and cat in the action of NGF, and the diversity of findings on the role of GABA in plasticity, these experiments will need to be repeated in the cat and/or ferret to demonstrate the generality of the finding.

Several treatments that increase the activation of PKA (cholera toxin, forskolin, and dibutylyl cAMP) lead to changes in ocular dominance in adult animals with monocular deprivation (Imamura et al., 1999). So does infusion of noradrenaline into the cortex of adult cats (Kasamatsu and Pettigrew, 1979) and stimulation of the locus coeruleus (Kasamatsu et al., 1985). However, all of these changes amount to a loss of binocular cells rather than a shift toward the nondeprived eye. The PKA activator Sp-8-Cl-cAMPS, given late in the critical period, leads to a slightly larger shift toward the nondeprived eye than is seen in untreated animals, but the effect is not statistically significant (Beaver et al., 2001b). NGF given to the adult animal with monocular deprivation leads to a shift toward the deprived eye (Galuske et al., 2000; Gu et al., 1994). Thus, none of these treatments leads to what could be considered a restoration of plasticity as seen in the critical period, that is, a significant shift toward the nondeprived eye after monocular deprivation. Two treatments do. One is infusion of the noradrenaline precursor L-threo-3,4-dihydroxyphenylserine, done in a limited series of three 7- to 8-month-old cats (Mataga et al., 1992). The other is degradation of chondroitin sulphate proteoglycans in the extracellular matrix by chondroitinase-ABC (Pizzorusso et al., 2002). Hopefully, these observations will be followed up. The general conclusion is that many more explorations will be necessary before the holy grail is found.

Synthesis of results

It is tempting to suggest that there are two parallel series of reactions involved in ocular dominance plasticity (Fig. 10.1). One leads from afferent activity to NMDA and metabotropic glutamate receptors to entry of calcium into the cell, to activation of adenylate cyclase, production of cAMP, and activation of PKA and CaMKII. The other leads from afferent activity to activation of BDNF and the GABA system. They may converge at the level of MAP kinase or CREB. They must diverge to produce decreases in physiological efficacy as well as increases in physiological efficacy, and expansion of anatomical connections as well as retraction of anatomical connections.

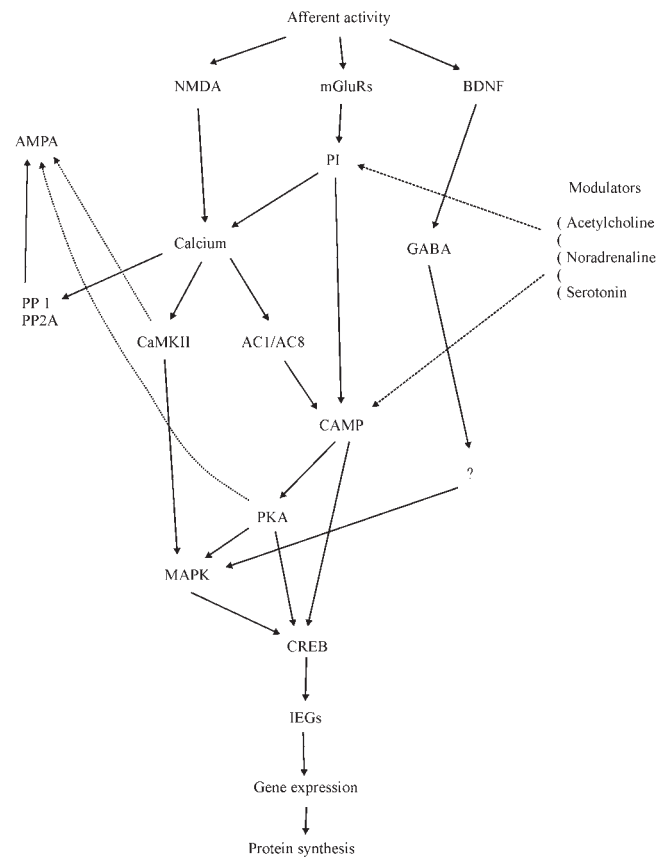


FIGURE 10.1. Factors involved in plasticity in the visual cortex.

Unfortunately, the situation is more complicated than this. There are feedback pathways. For example, PKA and CaMKII can phosphorylate the AMPA receptor GluR1, and protein phosphatases 1 and 2A can dephosphorylate it (Lee et al., 2000). There are points of divergence. For example, high levels of calcium have been proposed to activate kinases and low levels to activate phosphatases (Lisman, 1989, 2001). There are also examples of convergence. For example, CaMKII, PKA, MAPK, and neurotrophins all activate CREB (see Mower et al., 2002). New interactions and intermediaries are continually being discovered.

Few biologists reveal their basic assumptions. In the case of visual cortex plasticity, most people assume that LTP and LTD are related to ocular dominance plasticity, but almost nobody explains how. One possible hypothesis is that there is a pair of pathways, one leading from high levels of activity in the nondeprived eye to expansion of axons and dendrites, the other leading from low levels of activity in the deprived eye to retraction of axons and dendrites (Fig. 10.2A). This can accommodate the Hebb hypothesis, and also the concept of competition if the postsynaptic cell fires only when several nondeprived eye inputs fire together, or when both eyes are nondeprived and their firing is coordinated. However, it is simplistic. Inter alia, neither LTP nor

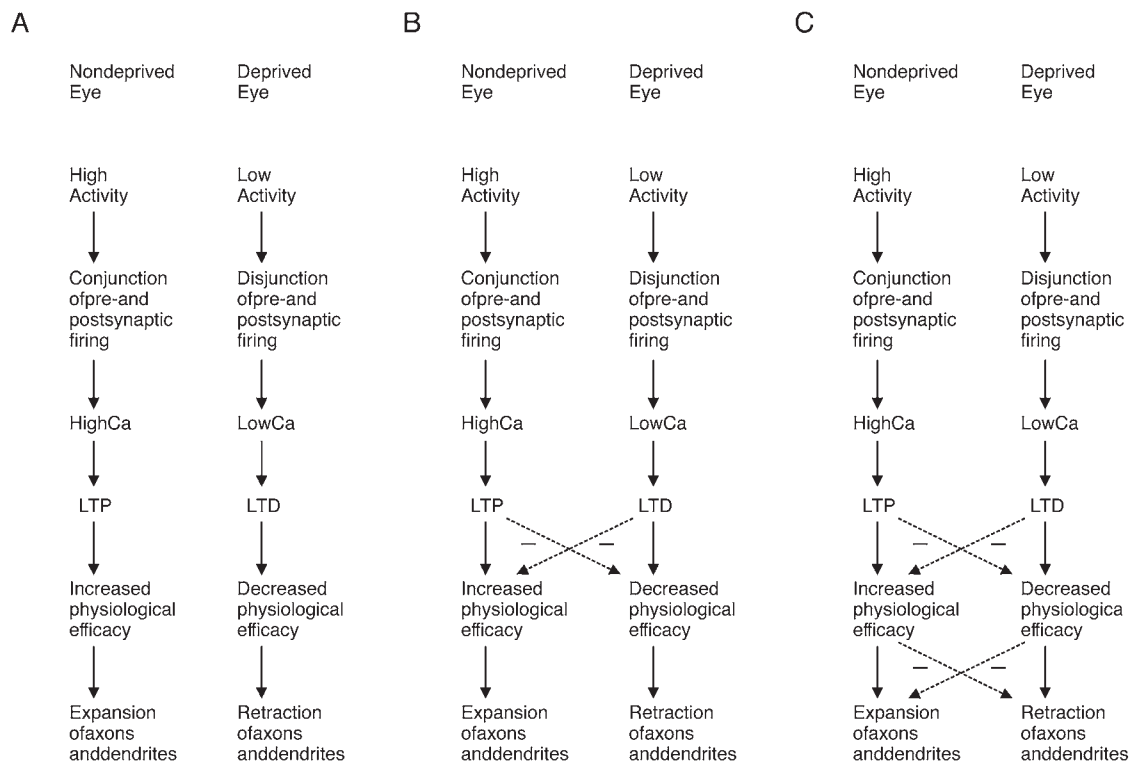


FIGURE 10.2. Three possible assumptions about plasticity. *A*, Increased physiological efficacy is assumed to result from LTP and decreased efficacy from LTD. *B*, Increased physiological efficacy can result from either LTP or LTD, and so can decreased physio-

logical efficacy. *C*, Expansion of axons and dendrites can result from either increased or decreased physiological efficacy, and so can retraction of axons and dendrites.

LTD is necessary for ocular dominance plasticity. In other words, ocular dominance plasticity can occur with either LTP or LTD present and the other absent. This suggests that an interaction must occur, as illustrated in Figure 10.2*B* and shown by Tsumoto and Suda (1979). This could be one place where GABA influences and the balance between excitation and inhibition come in. Other interactions might also occur between changes in physiological efficacy and anatomical alterations (Fig. 10.2*C*).

Another fundamental question is: where in the pre- and postsynaptic cells does all of this take place? Broadly speaking, there are four possibilities—local postsynaptic reactions in the dendritic spine; local presynaptic reactions in the presynaptic terminal; conveyance of signals to the nucleus in the postsynaptic cell for gene expression; and conveyance of signals to the nucleus in the presynaptic cell, also for protein synthesis (Fig. 10.3). Ocular dominance changes after 4 days of monocular deprivation in the mouse are abolished by the protein synthesis inhibitor cycloheximide when infused into the visual cortex but not when infused into the lateral geniculate nucleus (Taha and Stryker, 2002). This must mean that no new axon terminals are created in this period, since it is hard to believe that a new axon terminal could be created without protein synthesis. Can the changes in physiological efficacy that take place over the first 2 days

be accounted for entirely in terms of local reactions? This question remains unanswered. From work in the hippocampus we know that CaMKII and PKA are both located in the postsynaptic density (PSD), and both can phosphorylate AMPA receptors (Colledge et al., 2000; Lee et al., 2000; Lisman and Zhabotinsky, 2001). AMPA receptors can also be inserted into the PSD to make the postsynaptic response larger and removed from it to make the postsynaptic response smaller (Feldman et al., 1999). On the other hand, protein synthesis is required for late LTP in the hippocampus (Huang et al., 1994; Krug et al., 1984), which occurs in an hour or so, so perhaps it is also required for the physiological changes in ocular dominance plasticity which can be seen after a few hours.

The question of which of the changes are presynaptic and which postsynaptic is also unanswered. To address this question, one really needs a slice preparation with whole cell or intracellular recording where one would, of course, be looking at LTP and LTD rather than ocular dominance plasticity. Most investigations of LTP and LTD in the visual cortex have involved field potentials rather than intracellular recordings, so very few investigations on the point have been carried out. However, one does have some information from indirect evidence. For example, nitric oxide, which has been shown to be a feedback factor in the hip-

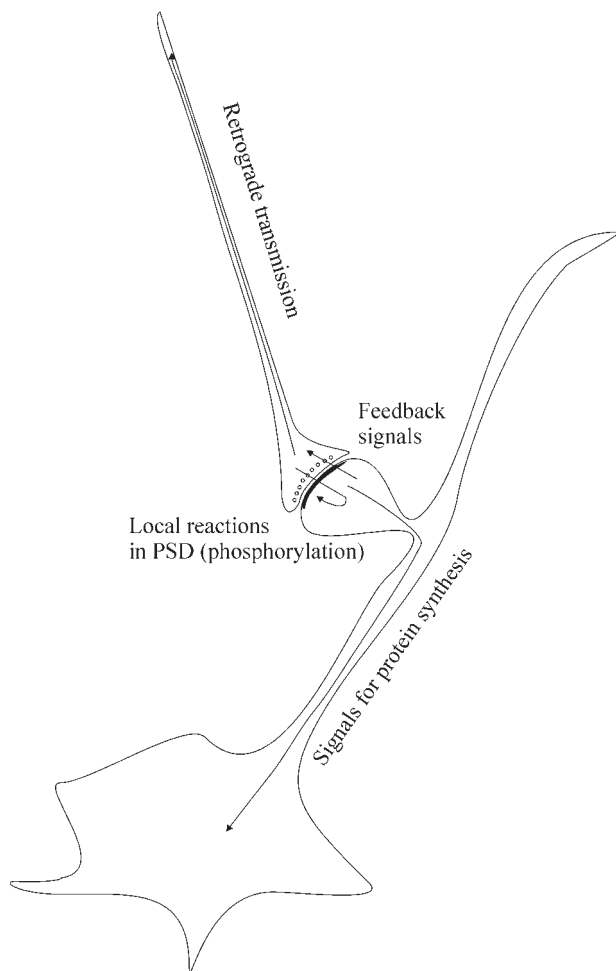


FIGURE 10.3. Four places where plasticity changes can occur: pre- or postsynaptic local reactions and pre- or postsynaptic gene expression.

pocampus, released by the postsynaptic cell to activate cGMP and PKG in the presynaptic cell, is not involved in ocular dominance plasticity, because neither nitric oxide synthase inhibitors nor PKG inhibitors affect ocular dominance plasticity (Beaver et al., 2001b; Reid et al., 1996; Ruthazer et al., 1996).

Thus, it is clear that there is a long way to go. It is unfortunate that LTP and LTD are not necessary precursors to ocular dominance plasticity, because this means that experiments done on LTP and LTD, which can be done rapidly, have to be repeated with ocular dominance plasticity, where results come more slowly. It is also unfortunate that results obtained with LTP and LTD in the hippocampus do not always apply to the visual cortex, as evidenced by the role of PKG. However, it is clear that several factors are necessary for ocular dominance plasticity, have greater activity at the peak of the critical period, and are affected by dark rearing, just as ocular dominance plasticity is affected. These include NMDA receptors, PKA, and BDNF. These are the factors

that contribute to plasticity during the critical period, and probably their lack is responsible for the absence of plasticity at other times. The modulatory factors acetylcholine, noradrenaline, and serotonin may also be more active during the critical period. Other factors, such as calcium and GABA, are important links in the chain of processes without which plasticity would not occur, but these are not the factors that make the cortex more plastic at the peak of the critical period. Thus, an enormous amount has been learned in the past 10 years, and progress continues to be rapid. The problem will finally be resolved when one can construct a composite figure in which the elements of Figures 10.1 and 10.2 can both be mapped onto Figure 10.3.

Acknowledgments

The author's work described in this review is supported by PHS Grants EY00053 and EY11353. The author is a Senior Scientific Investigator for Research to Prevent Blindness. I thank the members of my laboratory, Quentin Fischer, Shaolin Liu, Yan Rao, Xue-Feng Wang, and Yupeng Yang, and also Hiromichi Sato and Satoshi Shimegi, all of whom have made comments on the manuscript.

REFERENCES

- Akaneya, Y., T. Tsumoto, and Y. Hatanaka, 1996. Brain-derived neurotrophic factor blocks long-term depression in rat visual cortex, *J. Neurophysiol.*, 76:4198–4201.
- Akaneya, Y., T. Tsumoto, S. Kinoshita, and Y. Hatanaka, 1997. Brain-derived neurotrophic factor enhances long-term potentiation in rat visual cortex, *J. Neurosci.*, 17:6707–6716.
- Antonini, A., and M. P. Stryker, 1993. Rapid remodelling of axonal arbors in the visual cortex, *Science*, 260:1819–1821.
- Antonini, A., and M. P. Stryker, 1996. Plasticity of geniculocortical afferents following brief or prolonged monocular occlusion in the cat, *J. Comp. Neurol.*, 369:64–82.
- Aoki, C., K. Wu, A. Elste, G. Len, S. Lin, G. McAuliffe, and I. B. Black, 2000. Localization of brain-derived neurotrophic factor and trkB receptors to postsynaptic densities of adult rat cerebral cortex, *J. Neurosci. Res.*, 59:454–463.
- Artola, A., S. Brocher, and W. Singer, 1990. Different voltage-dependent thresholds for inducing long-term depression and long-term potentiation in slices of rat visual cortex, *Nature*, 347:69–72.
- Artola, A., and W. Singer, 1987. Long-term potentiation and NMDA receptors in rat visual cortex, *Nature*, 330:649–652.
- Barlow, H. B., and W. R. Levick, 1965. The mechanism of directionally selective units in rabbit's retina, *J. Physiol. (Lond.)*, 178:477–504.
- Bear, M. F., K. M. Carnes, and F. F. Ebner, 1985. Postnatal changes in the distribution of acetylcholinesterase in kitten striate cortex, *J. Comp. Neurol.*, 237:519–532.
- Bear, M. F., A. Kleinschmidt, Q. Gu, and W. Singer, 1990. Disruption of experience dependent synaptic modifications in striate cortex by infusion of an NMDA receptor antagonist, *J. Neurosci.*, 10:909–925.

- Bear, M. F., and W. Singer, 1986. Modulation of visual cortical plasticity by acetylcholine and noradrenaline, *Nature*, 320:172–176.
- Beaver, C. J., Q. Fischer, Q.-H. Ji, and N. W. Daw, 2002b. Orientation selectivity is reduced by monocular deprivation in combination with PKA inhibitors, *J. Neurophysiol.*, 88:1933–1940.
- Beaver, C. J., Q.-H. Ji, and N. W. Daw, 1999. Effect of the Group II metabotropic glutamate agonist, 2R,4R-APDC, varies with age, layer and visual experience in the visual cortex, *J. Neurophysiol.*, 82:86–93.
- Beaver, C. J., Q.-H. Ji, and N. W. Daw, 2001a. Layer differences in the effect of monocular vision in light- and dark-reared kittens, *Vis. Neurosci.*, 811–820.
- Beaver, C. J., Q.-H. Ji, Q. Fischer, and N. W. Daw, 2001b. cAMP-dependent protein kinase mediates ocular dominance shifts in cat visual cortex, *Nat. Neurosci.*, 4:159–163.
- Beaver, C. J., Q.-H. Ji, X.-T. Jin, and N. W. Daw, 2002a. Activation of Group III mGluRs increases the activity of neurons in area 17 of the cat, *Vis. Neurosci.*, 19:355–364.
- Berardi, N., A. Cellerino, L. Domenici, M. Fagiolini, T. Pizzorusso, A. Cattaneo, and L. Maffei, 1994. Monoclonal antibodies to nerve growth factor affect the postnatal development of the visual system, *Proc. Natl. Acad. Sci. USA*, 91:684–688.
- Berman, N. J., and N. W. Daw, 1977. Comparison of the critical period for monocular and direction deprivation in cats, *J. Physiol. (Lond.)*, 265:249–259.
- Bode-Greuel, K. M., and W. Singer, 1988. Developmental changes of the distribution of binding sites for organic Ca^{++} channel blockers in cat visual cortex, *Brain Res.*, 70:266–275.
- Bode-Greuel, K. M., and W. Singer, 1989. The development of *N*-methyl-D-aspartate receptors in cat visual cortex, *Dev. Brain Res.*, 46:197–204.
- Bode-Greuel, K. M., and W. Singer, 1991. Developmental changes of calcium currents in the visual cortex of the cat, *Exp. Brain Res.*, 84:311–318.
- Bozzi, Y., T. Pizzorusso, F. Cremisi, F. M. Rossi, G. Barsacchi, and L. Maffei, 1995. Monocular deprivation decreases the expression of messenger RNA for brain-derived neurotrophic factor in the rat visual cortex, *Neuroscience*, 69:1133–1144.
- Brocher, S., A. Artola, and W. Singer, 1992a. Intracellular injection of Ca^{2+} chelators blocks induction of long-term depression in rat visual cortex, *Proc. Natl. Acad. Sci. USA*, 89:123–127.
- Brocher, S., A. Artola, and W. Singer, 1992b. Agonists of cholinergic and noradrenergic receptors facilitate synergistically the induction of long-term potentiation in slices of rat visual cortex, *Brain Res.*, 573:27–36.
- Cabelli, R. J., A. Hohn, and C. J. Shatz, 1995. Inhibition of ocular dominance column formation by infusion of NT-4/5 or BDNF, *Science*, 267:1662–1666.
- Cabelli, R. J., D. L. Shelton, R. A. Segal, and C. J. Shatz, 1997. Blockade of endogenous ligands of trkB inhibits formation of ocular dominance columns, *Neuron*, 19:63–76.
- Carmignoto, G., R. Canella, P. Candeo, M. C. Comelli, and L. Maffei, 1993. Effects of nerve growth factor on neuronal plasticity of the kitten visual cortex, *J. Physiol. (Lond.)*, 464:343–360.
- Carmignoto, G., T. Pizzorusso, S. Tia, and S. Vicini, 1997. Brain-derived neurotrophic factor and nerve growth factor potentiate excitatory synaptic transmission in the rat visual cortex, *J. Physiol. (Lond.)*, 498:153–1674.
- Carmignoto, G., and S. Vicini, 1992. Activity-dependent decrease in NMDA receptor responses during development of the visual cortex, *Science*, 258:1007–1011.
- Castrén, E., F. Zafra, H. Thoenen, and D. Lindholm, 1992. Light regulates expression of brain-derived neurotrophic factor mRNA in rat visual cortex, *Proc. Natl. Acad. Sci. USA*, 89:9444–9448.
- Chapman, B., and M. P. Stryker, 1993. Development of orientation selectivity in ferret visual cortex and effects of deprivation, *J. Neurosci.*, 13:5251–5262.
- Chapman, B., M. P. Stryker, and T. Bonhoeffer, 1996. Development of orientation preference maps in ferret primary visual cortex, *J. Neurosci.*, 16:6443–6453.
- Chapman, B., K. R. Zahs, and M. P. Stryker, 1991. Relation of cortical cell orientation selectivity to alignment of receptive fields of the geniculocortical afferents that arborize within a single orientation column in ferret visual cortex, *J. Neurosci.*, 11:1347–1358.
- Chen, L., N. G. F. Cooper, and G. D. Mower, 2000. Developmental changes in the expression of NMDA receptor subunits (NR1, NR2A, NR2B) in the cat visual cortex and the effects of dark rearing, *Mol. Brain Res.*, 78:196–200.
- Chen, L., C. Yang, and G. D. Mower, 2001. Developmental changes in the expression of GABA_A receptor subunits (α_1 , α_2 , α_3) in the cat visual cortex and the effects of dark rearing, *Mol. Brain Res.*, 88:135–143.
- Choi, S. Y., B. Morales, H.-K. Lee, and A. Kirkwood, 2001. Absence of long-term depression in the visual cortex-GAD65 knockout mice, *J. Neurosci.*, 22:5271–5276.
- Colledge, M., R. A. Dean, G. K. Scott, L. K. Langenberg, R. L. Huganir, and J. D. Scott, 2000. Targeting of PKA to glutamate receptors through a MAGUK-AKAP complex, *Neuron*, 27:107–119.
- Crook, J. M., Z. F. Kisvárdy, and U. T. Eysel, 1997. GABA-induced inactivation of functionally characterized sites in cat striate cortex: effects on orientation tuning and direction selectivity, *Vis. Res.*, 14:141–158.
- Crowley, J. C., and L. C. Katz, 2000. Development of ocular dominance columns in the absence of retinal input, *Nat. Neurosci.*, 2:1125–1130.
- Crowley, J. C., and L. C. Katz, 2002. Ocular dominance development revisited, *Curr. Opin. Neurobiol.*, 12:104–109.
- Cynader, M. S., and D. E. Mitchell, 1980. Prolonged sensitivity to monocular deprivation in dark-reared cats, *J. Neurophysiol.*, 43:1026–1040.
- Daw, N. W., and C. J. Beaver, 2001. Developmental changes and ocular dominance plasticity in the visual cortex, *Keio J. Med.*, 50:192–197.
- Daw, N. W., N. J. Berman, and M. Ariel, 1978. Interaction of critical periods in the visual cortex of kittens, *Science*, 199:565–567.
- Daw, N. W., B. Gordon, K. D. Fox, H. J. Flavin, J. D. Kirsch, C. J. Beaver, Q.-H. Ji, S. M. Reid, and D. Czepita, 1999a. Injection of MK-801 affects ocular dominance shifts more than visual activity, *J. Neurophysiol.*, 81:204–215.
- Daw, N. W., S. M. Reid, and C. J. Beaver, 1999b. Development and function of metabotropic glutamate receptors in cat visual cortex, *J. Neurobiol.*, 41:102–107.
- Daw, N. W., T. O. Videen, D. Parkinson, and R. K. Rader, 1985. DSP-4 (*N*-(2-chloroethyl)-*N*-ethyl-2-bromobenzylamine) depletes noradrenaline in kitten visual cortex without altering the effects of visual deprivation, *J. Neurosci.*, 5:1925–1933.
- Daw, N. W., and H. J. Wyatt, 1976. Kittens reared in a unidirectional environment: evidence for a critical period, *J. Physiol. (Lond.)*, 257:155–170.
- Di Cristo, G., N. Berardi, L. Cancedda, T. Pizzorusso, E. Putignano, G. M. Ratto, and L. Maffei, 2001. Requirement of ERK activation for visual cortical plasticity, *Science*, 292:2337–2340.

- Domenici, L., N. Berardi, G. Carmignoto, G. Vantini, and L. Maffei, 1991. Nerve growth factor prevents the amblyopic effects of monocular deprivation, *Proc. Natl. Acad. Sci. USA*, 88:8811–8815.
- Domenici, L., A. Cellerino, N. Berardi, A. Cattaneo, and L. Maffei, 1994a. Antibodies to nerve growth factor (NGF) prolong the sensitive period for monocular deprivation in the rat, *Neuro-Report*, 5:2041–2044.
- Domenici, L., G. Fontanesi, A. Cattaneo, P. Bagnoli, and L. Maffei, 1994b. Nerve growth factor (NGF) uptake and transport following injection in the developing rat visual cortex, *Vis. Neurosci.*, 11:1093–1102.
- Dudek, S. M., and M. F. Bear, 1989. A biochemical correlate of the critical period for synaptic modification in the visual cortex, *Science*, 246:673–675.
- Dudek, S. M., and M. J. Friedlander, 1996. Developmental down-regulation of LTD in cortical layer IV and its independence of modulation by inhibition, *Neuron*, 16:1097–1106.
- Duffy, F. H., S. R. Snodgrass, J. L. Burchfield, and J. L. Conway, 1976. Bicuculline reversal of deprivation amblyopia in the cat, *Nature*, 260:256–257.
- Dyck, R. H., and M. S. Cynader, 1993. Autoradiographic localization of serotonin receptor subtypes in cat visual cortex: transient regional, laminar and columnar distributions during postnatal development, *J. Neurosci.*, 13:4316–4338.
- Eckenstein, F., and R. W. Baughman, 1984. Two types of cholinergic innervation in cortex—one colocalized with vasoactive intestinal peptide, *Nature*, 309:153–155.
- Eco-Stengel, V., V. Bringuier, and D. E. Shulz, 2002. Noradrenergic modulation of functional selectivity in the cat visual cortex: an *in vivo* extracellular and intracellular study, *J. Neurosci.*, 22:111:275–289.
- Edagawa, Y., H. Saito, and K. Abe, 2001. Endogenous serotonin contributes to a developmental decrease in long-term potentiation in the rat visual cortex, *J. Neurosci.*, 21:1532–1537.
- Fagiolini, M., T. Pizzorusso, N. Berardi, L. Domenici, and L. Maffei, 1994. Functional postnatal development of the rat primary visual cortex and the role of visual experience: dark rearing and monocular deprivation, *Vis. Res.*, 34:709–720.
- Feldman, D. E., R. A. Nicoll, and R. C. Malenka, 1999. Synaptic plasticity at thalamocortical synapses in developing rat somatosensory cortex: LTP, LTD and silent synapses, *J. Neurobiol.*, 41:92–101.
- Feldman, D. E., J. E. Sherin, W. A. Press, and M. F. Bear, 1990. *N*-methyl-D-aspartate-evoked calcium uptake by kitten visual cortex maintained in vitro, *Exp. Brain Res.*, 80:252–259.
- Feldman, D. E., 2000. Timing-based LTP and LTD at vertical inputs to layer II/III pyramidal cells in rat barrel cortex, *Neuron*, 27:45–56.
- Ferster, D., S. Chung, and H. S. Wheat, 1996. Orientation selectivity of thalamic input to simple cells of cat visual cortex, *Nature*, 380:249–252.
- Fiorentini, A., N. Berardi, and L. Maffei, 1994. Nerve growth factor preserves behavioral visual acuity in monocularly deprived kittens, *Vis. Neurosci.*, 12:51–56.
- Fischer, Q. S., C. J. Beaver, and N. W. Daw, 2001. Evidence for convergent glutamate receptor mediated pathways in ocular dominance plasticity, *Soc. Neurosci. Abs.*, 27:27.7.
- Fox, K. D., and N. W. Daw, 1992. A model for the action of NMDA conductances in the visual cortex, *Neural Comp.*, 4:59–83.
- Fox, K. D., N. W. Daw, H. Sato, and D. Czepita, 1991. Dark-rearing delays the loss of NMDA-receptor function in kitten visual cortex, *Nature*, 350:342–344.
- Fox, K. D., N. W. Daw, H. Sato, and D. Czepita, 1992. The effect of visual experience on development of NMDA receptor synaptic transmission in kitten visual cortex, *J. Neurosci.*, 12:2672–2684.
- Fox, K. D., H. Sato, and N. W. Daw, 1989. The location and function of NMDA receptors in cat and kitten visual cortex, *J. Neurosci.*, 9:2443–2454.
- Fox, K. D., H. Sato, and N. W. Daw, 1990. The effect of varying stimulus intensity on NMDA-receptor activity in cat visual cortex, *J. Neurophysiol.*, 64:1413–1428.
- Frank, M. G., N. P. Issa, and M. P. Stryker, 2001. Sleep enhances plasticity in the developing visual cortex, *Neuron*, 30:275–287.
- Freeman, R. D., and A. B. Bonds, 1979. Cortical plasticity in monocularly deprived immobilized kittens depends on eye movement, *Science*, 206:1093–1095.
- Funauchi, M., H. Haruta, and T. Tsumoto, 1994. Effects of an inhibitor for calcium/calmodulin-dependent protein phosphatase, calcineurin, on induction of long-term potentiation in rat visual cortex, *Neurosci. Res.*, 19:269–278.
- Galuske, R. W., D.-S. Kim, E. Castrén, and W. Singer, 2000. Differential effects of neurotrophins on ocular dominance plasticity in developing and adult visual cortex, *Eur. J. Neurosci.*, 12:3315–3330.
- Galuske, R. W., D. S. Kim, E. Castrén, H. Thoenen, and W. Singer, 1996. Brain-derived neurotrophic factor reverses experience-dependent synaptic modifications in kitten visual cortex, *Eur. J. Neurosci.*, 8:1554–1559.
- Gillespie, D. C., M. C. Crair, and M. P. Stryker, 2000. Neurotrophin 4/5 alters responses and blocks the effect of monocular deprivation in cat visual cortex during the critical period, *J. Neurosci.*, 20:9174–9186.
- Gorba, T., and P. Wahle, 1999. Expression of TrkB and TrkC but not BDNF mRNA in neurochemically identified interneurons in rat visual cortex *in vivo* and in organotypic cultures, *Eur. J. Neurosci.*, 11:1179–1190.
- Gordon, B., E. E. Allen, and P. Q. Trombley, 1988. The role of norepinephrine in plasticity of visual cortex, *Prog. Neurobiol.*, 30:171–191.
- Gordon, B., N. W. Daw, and D. Parkinson, 1991. The effect of age on binding of MK-801 in the cat visual cortex, *Dev. Brain Res.*, 62:61–67.
- Gordon, J. A., D. Cioffi, A. J. Silva, and M. P. Stryker, 1996. Deficient plasticity in the primary visual cortex of alpha-calcium/calmodulin-dependent protein kinase II mutant mice, *Neuron*, 17:491–499.
- Gordon, J. A., and M. P. Stryker, 1996. Experience-dependent plasticity of binocular responses in the primary visual cortex of the mouse, *J. Neurosci.*, 16:3274–3286.
- Grewal, S. S., R. D. York, and P. J. Stork, 1999. Extracellular-signal-related kinase signalling in neurons, *Curr. Opin. Neurobiol.*, 9:544–553.
- Gu, Q., Y. Liu, and M. S. Cynader, 1994. Nerve growth factor-induced ocular dominance plasticity in adult cat visual cortex, *Proc. Natl. Acad. Sci. USA*, 91:8408–8412.
- Gu, Q., and W. Singer, 1993. Effects of intracortical infusion of anticholinergic drugs on neuronal plasticity in kitten striate cortex, *Eur. J. Neurosci.*, 5:475–485.
- Gu, Q., and W. Singer, 1995. Involvement of serotonin in developmental plasticity of kitten visual cortex, *Eur. J. Neurosci.*, 7:1146–1153.
- Guire, E. S., M. E. Lickey, and B. Gordon, 1999. Critical period for the monocular deprivation effect in rats: assessment with sweep visually evoked potentials, *J. Neurophysiol.*, 81:121–128.

- Hanover, J. L., Z. J. Huang, S. Tonegawa, and M. P. Stryker, 1999. Brain-derived neurotrophic factor overexpression induces precocious critical period in mouse visual cortex, *J. Neurosci.*, 19:RC40.
- Hansel, C., A. Artola, and W. Singer, 1997. Relation between dendritic Ca^{2+} levels and the polarity of synaptic long-term modifications in rat visual cortex neurons, *Eur. J. Neurosci.*, 9:2309–2322.
- Harauzov, A., G. Di Cristo, N. Berardi, and L. Maffei, 2001. Modification of the ratio between intracortical inhibition and excitation restores ocular dominance plasticity in adult rats, *Soc. Neurosci. Abs.*, 27:27.10.
- Hardman, J. G., L. E. Limberd, and A. G. Gilman, 2001. *The Pharmacological Basis of Therapeutics*, 10th ed., New York: McGraw-Hill.
- Harrad, R., F. Sengpiel, and C. Blakemore, 1996. Physiology of suppression in strabismic amblyopia, *Br. J. Ophthalmol.*, 80:373–377.
- Haruta, H., T. Kamashita, T. P. Hicks, M. P. Takahashi, and T. Tsumoto, 1994. Induction of LTD but not LTP through metabotropic glutamate receptors in visual cortex, *NeuroReport*, 5:1829–1832.
- Hata, Y., M. Ohshima, S. Ichisaka, M. Wakita, M. Fukada, and T. Tsumoto, 2000. Brain-derived neurotrophic factor expands ocular dominance columns in visual cortex in monocularly deprived and nondeprived kittens but does not in adult cats, *J. Neurosci.*, 20:RC57.
- Hata, Y., and M. P. Stryker, 1994. Control of thalamocortical afferent rearrangement by postsynaptic activity in developing visual cortex, *Science*, 265:1732–1735.
- Hata, Y., T. Tsumoto, H. Sato, K. Hagihara, and H. Tamura, 1988. Inhibition contributes to orientation selectivity in visual cortex of cat, *Nature*, 335:815–817.
- Hata, Y., T. Tsumoto, and M. P. Stryker, 1999. Selective pruning of more active afferents when cat visual cortex is pharmacologically inhibited, *Neuron*, 22:375–381.
- Hebb, D. O., 1940. *The Organization of Behaviour*, New York: Wiley.
- Hendry, S. C., and E. G. Jones, 1986. Reduction in number of immunostained GABAergic neurones in deprived-eye dominance columns of monkey area 17, *Nature*, 320:750–753.
- Hensch, T. K., M. Fagiolini, N. Mataga, M. P. Stryker, S. Baekkeskov, and S. F. Kash, 1998. Local GABA circuit control of experience-dependent plasticity in developing visual cortex, *Science*, 282:1504–1508.
- Hensch, T. K., J. A. Gordon, E. P. Brandon, G. S. McKnight, R. L. Iderzda, and M. P. Stryker, 1998. Comparison of plasticity *in vivo* and *in vitro* in the developing visual cortex of normal and protein kinase A $\text{R1}\beta$ -deficient mice, *J. Neurosci.*, 18:2108–2117.
- Hensch, T. K., and M. P. Stryker, 1996. Ocular dominance plasticity under metabotropic glutamate receptor blockade, *Science*, 272:554–557.
- Huang, Y.-Y., X. C. Li, and E. R. Kandel, 1994. cAMP contributes to mossy fiber LTP by initiating both a covalently mediated early phase and a macromolecular synthesis-dependent late phase, *Cell*, 79:69–79.
- Huang, Z. J., A. Kirkwood, T. Pizzorusso, V. Porciatti, B. Morales, M. F. Bear, L. Maffei, and S. Tonegawa, 1999. BDNF regulates the maturation of inhibition and the critical period of plasticity in mouse visual cortex, *Cell*, 98:739–755.
- Hubel, D. H., and T. N. Wiesel, 1962. Receptive fields, binocular interaction and functional architecture in the cat's visual cortex, *J. Physiol. (Lond.)*, 160:106–154.
- Huber, K. M., N. B. Sawtell, and M. F. Bear, 1998a. Effects of the metabotropic glutamate receptor antagonist MCPG on phosphoinositide turnover and synaptic plasticity in visual cortex, *J. Neurosci.*, 18:1–9.
- Huber, K. M., N. B. Sawtell, and M. F. Bear, 1998b. Brain-derived neurotrophic factor alters the synaptic modification threshold in visual cortex, *Neuropharmacology*, 37:571–579.
- Imamura, K., T. Kasamatsu, T. Shirokawa, and T. Ohashi, 1999. Restoration of ocular dominance plasticity mediated by adenosine 3',5'-monophosphate in adult visual cortex, *Proc. R. Soc. Ser. B*, 266:1507–1516.
- Issa, N. P., J. L. Trachtenberg, B. Chapman, K. R. Zahs, and M. P. Stryker, 1999. The critical period for ocular dominance plasticity in the ferret's visual cortex, *J. Neurosci.*, 19:6965–6978.
- Iwai, Y., H. Katagiri, and T. K. Hensch, 2001. Ocular dominance plasticity: time course of induction by inhibition, *Soc. Neurosci. Abs.*, 27:27.8.
- Izumi, Y., and C. F. Zorumski, 1993. Nitric oxide and long-term synaptic depression in the rat hippocampus, *NeuroReport*, 4:1131–1134.
- Jiang, B., Y. Akenaya, M. Ohshima, S. Ichisaka, Y. Hata, and T. Tsumoto, 2001. Brain-derived neurotrophic factor induces long-lasting potentiation of synaptic transmission *in vivo* in young rats, but not in the adult, *Eur. J. Neurosci.*, 14:1–12.
- Jin, X.-T., C. J. Beaver, Q.-H. Ji, and N. W. Daw, 2001. Effect of the group I metabotropic glutamate agonist DHPG on the visual cortex, *J. Neurophysiol.*, 86:1622–1631.
- Jin, X.-T., and N. W. Daw, 1998. The group III metabotropic glutamate receptor agonist, L-AP4, reduces EPSPs in some layers of rat visual cortex, *Brain Res.*, 797:218–224.
- Jonsson, G., and T. Kasamatsu, 1983. Maturation of monoamine neurotransmitters and receptors in cat occipital cortex during postnatal critical period, *Exp. Brain Res.*, 50:449–458.
- Kaminska, B., G. Mosieniak, M. Gierdalski, M. Kossut, and L. Kaczmarek, 1995. Elevated AP-1 transcription factor DNA binding activity at the onset of functional plasticity during development of rat sensory cortical areas, *Mol. Brain Res.*, 33:295–304.
- Kasamatsu, T., and J. D. Pettigrew, 1979. Preservation of binocularity after monocular deprivation in the striate cortex of kittens treated with 6-hydroxydopamine, *J. Comp. Neurol.*, 185:139–162.
- Kasamatsu, T., and T. Shirokawa, 1985. Involvement of β -adrenoceptors in the shift of ocular dominance and monocular deprivation, *Exp. Brain Res.*, 59:507–514.
- Kasamatsu, T., K. Watabe, P. Heggelund, and E. Scholler, 1985. Plasticity in cat visual cortex restored by electrical stimulation of the locus coeruleus, *Neurosci. Res.*, 2:365–386.
- Kato, N., 1993. Dependence of long-term depression on postsynaptic metabotropic glutamate receptors in visual cortex, *Proc. Natl. Acad. Sci. USA*, 90:3650–3654.
- Kato, N., A. Artola, and W. Singer, 1991. Developmental changes in the susceptibility to long-term potentiation of neurones in rat visual cortex slices, *Dev. Brain Res.*, 60:43–50.
- Kimura, F., A. Nishigori, T. Shirokawa, and T. Tsumoto, 1989. Long-term potentiation and *N*-methyl-D-aspartate receptors in the visual cortex of young rats, *J. Physiol. (Lond.)*, 414:125–144.
- Kimura, F., T. Tsumoto, A. Nishigori, and Y. Yoshimura, 1990. Long-term depression but not potentiation is induced in Ca^{2+} -chelated visual cortex neurons, *NeuroReport*, 1:65–68.
- Kirkwood, A., and M. F. Bear, 1994a. Hebbian synapses in visual cortex, *J. Neurosci.*, 14:1634–1645.
- Kirkwood, A., and M. F. Bear, 1994b. Homosynaptic long-term depression in the visual cortex, *J. Neurosci.*, 14:3404–3412.
- Kirkwood, A., H. K. Lee, and M. F. Bear, 1995. Co-regulation of long-term potentiation and experience-dependent synaptic

- plasticity in visual cortex by age and experience, *Nature*, 375: 328–331.
- Kirkwood, A., M. G. Rioult, and M. F. Bear, 1996. Experience-dependent modification of synaptic plasticity in visual cortex, *Nature*, 381:526–528.
- Kirkwood, A., C. Rozas, J. Kirkwood, F. Perez, and M. F. Bear, 1999. Modulation of long-term synaptic depression in visual cortex by acetylcholine and norepinephrine, *J. Neurosci.*, 19:1599–1609.
- Kirkwood, A., A. J. Silva, and M. F. Bear, 1997. Age-dependent decrease of synaptic plasticity in the neocortex of alpha-CamKII mutant mice, *Proc. Natl. Acad. Sci. USA*, 94:3380–3383.
- Kohara, K., A. Kitamura, M. Morishima, and T. Tsumoto, 2001. Activity-dependent transfer of brain-derived neurotrophic factor to postsynaptic neurons, *Science*, 291:2419–2423.
- Kojic, L., Q. Gu, R. M. Douglas, and M. S. Cynader, 1997. Serotonin facilitates synaptic plasticity in kitten visual cortex—an in vitro study, *Dev. Brain Res.*, 101:299–304.
- Komatsu, Y., 1983. Development of cortical inhibition in kitten striate cortex investigated by a slice preparation, *Dev. Brain Res.*, 8:136–139.
- Komatsu, Y., 1994. Age-dependent long-term potentiation of inhibitory synaptic transmission in rat visual cortex, *J. Neurosci.*, 14:6488–6499.
- Komatsu, Y., K. Fujii, J. Maeda, H. Sakaguchi, and K. Toyama, 1988. Long-term potentiation of synaptic transmission in kitten visual cortex, *J. Neurophysiol.*, 59:124–141.
- Komatsu, Y., and M. Iwakiri, 1992. Low-threshold Ca^{2+} channels mediate induction of long-term potentiation in kitten visual cortex, *J. Neurophysiol.*, 67:401–410.
- Komatsu, Y., and M. Iwakiri, 1993. Long-term modification of inhibitory synaptic transmission in developing visual cortex, *NeuroReport*, 4:907–910.
- Komatsu, Y., S. Nakajima, and K. Toyama, 1991. Induction of long-term potentiation without participation of *N*-methyl-D-aspartate receptors in kitten visual cortex, *J. Neurophysiol.*, 65:20–32.
- Komatsu, Y., and Y. Yoshimura, 2000. Activity-dependent maintenance of long-term potentiation at visual cortical inhibitory synapses, *J. Neurosci.*, 20:7539–7546.
- Krug, M., B. Lossner, and T. Ott, 1984. Anisomycin blocks the late phase of long-term potentiation in the dentate gyrus of freely moving rats, *Brain Res. Bull.*, 13:39–42.
- Kumura, E., F. Kimura, N. Taniguchi, and T. Tsumoto, 2000. Brain-derived neurotrophic factor blocks long-term depression in solitary neurones cultured from rat visual cortex, *J. Physiol. (Lond.)*, 524:195–204.
- Kurotani, T., S. Higashi, H. Inokawa, and K. Toyama, 1996. Protein and RNA synthesis-dependent and -independent LTPs in developing rat visual cortex, *NeuroReport*, 8:35–39.
- Lee, H.-K., M. Barbarosie, K. Kameyama, M. F. Bear, and R. L. Huganir, 2000. Regulation of distinct AMPA receptor phosphorylation sites during bidirectional synaptic plasticity, *Nature*, 405:955–959.
- Lee, W. C. A., and E. Nedivi, 2002. Extended plasticity of visual cortex in dark-reared animals may result from prolonged expression of *cpg15*-like genes, *J. Neurosci.*, 22:1807–1815.
- Lein, E. S., and C. J. Shatz, 2000. Rapid regulation of brain-derived neurotrophic factor mRNA within eye-specific circuits during ocular dominance column formation, *J. Neurosci.*, 20:1470–1482.
- Liao, D. S., A. E. Medina, R. L. Neve, C. Sato-Biglee, and A. S. Ramoa, 2002. Different mechanisms for loss and recovery of binocularity in the visual cortex, *J. Neurosci.*, 22:9015–9023.
- Lisman, J. E., 1989. A mechanism for the Hebb and the anti-Hebb processes underlying learning and memory, *Proc. Natl. Acad. Sci. USA*, 86:9574–9578.
- Lisman, J. E., 2001. Three Ca^{2+} levels affect plasticity differently: the LTP zone, the LTD zone and no man's land, *J. Physiol. (Lond.)*, 532:285.
- Lisman, J. E., and A. M. Zhabotinsky, 2001. A model of synaptic memory: a CaMKII/PP1 switch that potentiates transmission by organizing an AMPA receptor anchoring assembly, *Neuron*, 31:191–201.
- Liu, S., and N. W. Daw, 2001. Role of PKA and PKG in synaptic plasticity in the visual cortex, *Soc. Neurosci. Abs.*, 31:275.15.
- Lodovichi, C., N. Berardi, T. Pizzorusso, and L. Maffei, 2000. Effects of neurotrophins on cortical plasticity: same or different? *J. Neurosci.*, 20:2165.
- Lynch, G., J. Larson, S. Kelso, G. Barrionuevo, and F. Schottler, 1983. Intracellular injections of EGTA block induction of hippocampal long-term potentiation, *Nature*, 305:719–721.
- Maffei, L., N. Berardi, L. Domenici, V. Parisi, and T. Pizzorusso, 1992. Nerve growth factor (NGF) prevents the shift in ocular dominance distribution of visual cortical neurons in monocularly deprived rats, *J. Neurosci.*, 12:4651–4662.
- Malenka, R. C., and R. A. Nicoll, 1999. Long-term potentiation—a decade of progress? *Science*, 285:1870–1874.
- Mataga, N., S. Fujishima, B. G. Condie, and T. K. Hensch, 2001. Experience-dependent plasticity of mouse visual cortex in the absence of the neuronal activity-dependent marker *egr1/zif268*, *J. Neurosci.*, 21:9724–9732.
- Mataga, N., K. Imamura, and Y. Watanabe, 1992. *L*-threo-3,4-dihydroxyphenylserine enhanced ocular dominance plasticity in adult cats, *Neurosci. Lett.*, 142:115–118.
- Mayer, M. L., and G. L. Westbrook, 1984. Mixed-agonist action of excitatory amino acids on mouse spinal cord neurones under voltage clamp, *J. Physiol. (Lond.)*, 354:29–53.
- Miller, K. D., B. Chapman, and M. P. Stryker, 1989. Visual responses in adult visual cortex depend on *N*-methyl-D-aspartate receptors, *Proc. Natl. Acad. Sci. USA*, 86:5183–5187.
- Mower, A. F., D. S. Liao, E. J. Nestler, R. L. Neve, and A. S. Ramoa, 2002. CAMP/ Ca^{++} response-binding element protein function is essential for ocular dominance plasticity, *J. Neurosci.*, 22:2237–2245.
- Mower, G. D., 1991. The effect of dark rearing on the time course of the critical period in cat visual cortex, *Dev. Brain Res.*, 58:151–158.
- Mower, G. D., and Y. H. Guo, 2001. Comparison of the expression of two forms of glutamic acid decarboxylase (GAD67 and GAD65) in the visual cortex of normal and dark-reared cats, *Dev. Brain Res.*, 126:65–74.
- Mower, G. D., and I. V. Kaplan, 1999. Fos expression during the critical period in visual cortex: differences between normal and dark reared cats, *Mol. Brain Res.*, 64:264–269.
- Mower, G. D., R. Rustad, and W. F. White, 1988. Quantitative comparisons of gamma-aminobutyric acid neurons and receptors in the visual cortex of normal and dark-reared cats, *J. Comp. Neurol.*, 272:293–302.
- Mulkey, R. M., and R. C. Malenka, 1992. Mechanisms underlying induction of homosynaptic long-term depression in area CA1 of the hippocampus, *Neuron*, 9:967–975.

- Nedergaard, S., I. Engberg, and J. A. Flatman, 1987. The modulation of excitatory amino acid responses by serotonin in the cat visual cortex, *Cell Mol. Neurobiol.*, 7:367–379.
- Nedivi, E., S. Fieldust, L. E. Thiell, and D. Hevroni, 1996. A set of genes expressed in response to light in the adult cerebral cortex and regulated during development, *Proc. Natl. Acad. Sci. USA*, 93:2048–2053.
- Neve, R. L., and M. F. Bear, 1989. Visual experience regulates gene expression in the developing striate cortex, *Proc. Natl. Acad. Sci. USA*, 86:4781–4784.
- Nowak, L., P. Bregetowski, A. Ascher, A. Herbet, and A. Prochiantz, 1984. Magnesium gates glutamate-activated channels in mouse central neurones, *Nature*, 307:462–465.
- O'Dell, T. J., R. D. Hawkins, E. R. Kandel, and O. Arancio, 1991. Tests of the roles of two diffusible substances in long-term potentiation: evidence for nitric oxide as a possible early retrograde messenger, *Proc. Natl. Acad. Sci. USA*, 88:11285–11289.
- Olson, C. R., and R. D. Freeman, 1980. Profile of the sensitive period for monocular deprivation in kittens, *Exp. Brain Res.*, 39:17–21.
- Pei, X., T. R. Vidyasagar, M. Volgushev, and O. D. Creutzfeldt, 1994. Receptive field analysis and orientation selectivity of postsynaptic potentials of simple cells in cat visual cortex, *J. Neurosci.*, 14:7130–7140.
- Perkins, A. T., and T. J. Teyler, 1988. A critical period for long-term potentiation in the developing rat visual cortex, *Brain Res.*, 439:222–229.
- Pesavento, E., E. Margotti, M. Righi, A. Cattaneo, and L. Domenici, 2000. Blocking the NGF-TrkA interaction rescues the developmental loss of LTP in the rat visual cortex: role of the cholinergic system, *Neuron*, 25:165–175.
- Pham, T. A., S. Impey, D. R. Storm, and M. P. Stryker, 1999. CRE-mediated gene transcription in neocortical neuronal plasticity during the developmental critical period, *Neuron*, 22:63–72.
- Philpot, B. D., M. P. Weisberg, M. S. Ramos, N. B. Sawtell, Y. P. Tang, J. Z. Tsien, and M. F. Bear, 2001. Effect of transgenic overexpression of NR2B on NMDA receptor function and synaptic plasticity in visual cortex, *Neuropharmacology*, 41:762–770.
- Pizzorusso, T., N. Berardi, F. M. Rossi, A. Viegl, K. Venstrom, L. F. Reichardt, and L. Maffei, 1999. TrkA activation in the rat visual cortex by antirat trkA IgG prevents the effect of monocular deprivation, *Eur. J. Neurosci.*, 11:204–212.
- Pizzorusso, T., P. Medini, N. Berardi, S. Chievzi, J. W. Fawcett, and L. Maffei, 2002. Reactivation of ocular dominance plasticity in the adult visual cortex, *Science*, 298:1248–1251.
- Pizzorusso, T., G. M. Ratto, E. Putignano, and L. Maffei, 2000. Brain-derived neurotrophic factor causes cAMP response element-binding protein phosphorylation in the absence of calcium increases in slices and cultured neurons from rat visual cortex, *J. Neurosci.*, 20:2809–2816.
- Prasad, S. S., and M. S. Cynader, 1994. Identification of cDNA clones expressed selectively during the critical period for visual cortex development by subtractive hybridization, *Brain Res.*, 639:73–84.
- Prasad, S. S., L. Z. Kojic, P. Li, D. E. Mitchell, A. Hachisuka, J. Sawada, Q. Gu, and M. S. Cynader, 2001. Gene expression patterns during enhanced periods of visual cortex plasticity, *Neurosci.*, 111:36–42.
- Quinlan, E. M., B. D. Philpot, R. L. Huganir, and M. F. Bear, 1999. Rapid, experience-dependent expression of synaptic NMDA receptors in visual cortex *in vivo*, *Nat. Neurosci.*, 2:352–357.
- Ramoa, A. S., A. F. Mower, D. Liao, and S. I. A. Jafri, 2001. Suppression of cortical NMDA receptor function prevents development of orientation selectivity in the primary visual cortex, *J. Neurosci.*, 21:4299–4309.
- Ramoa, A. S., M. A. Paradiso, and R. D. Freeman, 1988. Blockade of intracortical inhibition in kitten striate cortex: effects on receptive field properties and associated loss of ocular dominance plasticity, *Exp. Brain Res.*, 73:285–296.
- Reid, S. M., 2001. The response of phosphorylated CREB and MAP2 to ACPD in visual cortical cells, *Soc. Neurosci. Abs.*, 27:27.12.
- Reid, R. C., and J.-M. Alonso, 1995. Specificity of monosynaptic connections from thalamus to visual cortex, *Nature*, 378:281–284.
- Reid, S. M., N. W. Daw, D. Czepita, H. J. Flavin, and W. C. Sessa, 1996. Inhibition of nitric oxide synthase does not alter ocular dominance shifts in kitten visual cortex, *J. Physiol. (Lond.)*, 494:511–517.
- Reid, S. M., and C. Romano, 2001. Developmental and sensory-dependent changes of Group II metabotropic glutamate receptors, *J. Comp. Neurol.*, 429:270–276.
- Reid, S. M., C. Romano, T. Hughes, and N. W. Daw, 1997. Developmental and sensory-dependent changes of phosphoinositide-linked metabotropic glutamate receptors, *J. Comp. Neurol.*, 388:1–7.
- Reiter, H. O., and M. P. Stryker, 1988. Neural plasticity without postsynaptic action potentials: less-active inputs become dominant when kitten visual cortical cells are pharmacologically inhibited, *Proc. Natl. Acad. Sci. USA*, 85:3623–3627.
- Reynolds, I. J., and M. F. Bear, 1991. Effects of age and visual experience on 3H MK801 binding to NMDA receptors in the kitten visual cortex, *Exp. Brain Res.*, 85:611–615.
- Reynolds, J. N., A. Baskys, and P. L. Carlen, 1988. The effects of serotonin on *N*-methyl-D-aspartate and synaptically evoked depolarizations in rat neocortex, *Brain Res.*, 456:286–292.
- Ringach, D. L., M. J. Hawken, and R. Shapley, 1997. Dynamics of orientation tuning in macaque primary visual cortex, *Nature*, 387:281–284.
- Rivadulla, C., J. Sharma, and M. Sur, 2001. Specific roles of NMDA and AMPA receptors in direction-selective and spatial phase-selective responses in visual cortex, *J. Neurosci.*, 21:1710–1719.
- Roberts, E. B., M. A. Meredith, and A. S. Ramoa, 1998. Suppression of NMDA receptor function using antisense DNA blocks ocular dominance plasticity while preserving visual responses, *J. Neurophysiol.*, 80:1021–1032.
- Rossi, F. M., Y. Bozzi, T. Pizzorusso, and L. Maffei, 1999. Monocular deprivation decreases brain-derived neurotrophic factor immunoreactivity in the rat visual cortex, *Neuroscience*, 90:363–368.
- Ruthazer, E. S., D. C. Gillespie, T. M. Dawson, S. H. Snyder, and M. P. Stryker, 1996. Inhibition of nitric oxide synthase does not prevent ocular dominance plasticity in kitten visual cortex, *J. Physiol. (Lond.)*, 494:519–528.
- Rutherford, L. C., A. DeWan, H. M. Lauer, and G. G. Turrigiano, 1997. Brain-derived neurotrophic factor mediates the activity-dependent regulation of inhibition in neocortical cultures, *J. Neurosci.*, 17:4527–4535.
- Rutherford, L. C., S. B. Nelson, and G. G. Turrigiano, 1998. BDNF has opposite effects on the quantal amplitude of pyramidal neuron and interneuron excitatory synapses, *Neuron*, 21:521–530.
- Sala, R., A. Viegl, F. M. Rossi, T. Pizzorusso, G. Bonanno, M. Raiteri, and L. Maffei, 1998. Nerve growth factor and brain-derived neurotrophic factor increase neurotransmitter release in the rat visual cortex, *Eur. J. Neurosci.*, 10:2185–2191.

- Sato, H., K. D. Fox, and N. W. Daw, 1989. Effect of electrical stimulation of locus coeruleus on the activity of neurons in the visual cortex, *J. Neurophysiol.*, 62:946–958.
- Sato, H., Y. Hata, H. Masui, and T. Tsumoto, 1987. A functional role of cholinergic innervation to neurons in the cat visual cortex, *J. Neurophysiol.*, 58:765–780.
- Schoups, A. A., R. C. Elliott, W. J. Friedman, and I. B. Black, 1995. NGF and BDNF are differentially modulated by visual experience in the developing geniculocortical pathway, *Dev. Brain Res.*, 86:326–334.
- Schuman, E. M., and D. V. Madison, 1991. A requirement for the intracellular messenger nitric oxide in long-term potentiation, *Science*, 254:1503–1506.
- Sermasi, E., E. Margotti, A. Cattaneo, and L. Domenici, 2000. TrkB signalling controls LTP but not LTD expression in the developing rat visual cortex, *Eur. J. Neurosci.*, 12:1411–1419.
- Shatz, C. J., and M. P. Stryker, 1978. Ocular dominance in layer IV of the cat's visual cortex and the effects of monocular deprivation, *J. Physiol. (Lond.)*, 281:267–283.
- Sheu, F. S., T. Kasamatsu, and A. Routtenberg, 1990. Protein kinase C activity and substrate (F1/GAP-43) phosphorylation in developing cat visual cortex, *Brain Res.*, 524:144–148.
- Sillito, A. M., 1977. Inhibitory processes underlying the directional specificity of simple, complex and hypercomplex cells in the cat's visual cortex, *J. Physiol. (Lond.)*, 271:699–720.
- Sillito, A. M., 1979. Inhibitory mechanisms influencing complex cell orientation selectivity and their modification at high resting discharge levels, *J. Physiol. (Lond.)*, 289:33–53.
- Sillito, A. M., J. A. Kemp, and C. Blakemore, 1981. The role of GABAergic inhibition in the cortical effects of monocular deprivation, *Nature*, 291:318–320.
- Sillito, A. M., and P. C. Murphy, 1987. The cholinergic modulation of cortical function, in *Cerebral Cortex* (E. G. Jones and A. Peters, eds.), New York: Plenum, pp. 161–185.
- Silver, M. A., M. Fagioli, D. C. Gillespie, C. L. Howe, M. G. Frank, N. P. Issa, A. Antonini, and M. P. Stryker, 2001. Infusion of nerve growth factor (NGF) into kitten visual cortex increases immunoreactivity for NGF, NGF receptors, and choline acetyltransferase in basal forebrain without affecting ocular dominance plasticity or column development, *Neuroscience*, 108:569–585.
- Silver, M. A., and M. P. Stryker, 2000. Distributions of synaptic vesicle proteins and GAD65 in deprived and nondeprived ocular dominance columns in layer IV of kitten primary visual cortex are unaffected by monocular deprivation, *J. Comp. Neurol.*, 422:652–664.
- Silver, M. A., and M. P. Stryker, 2001. TrkB-like immunoreactivity is present on geniculocortical afferents in layer IV of kitten primary visual cortex, *J. Comp. Neurol.*, 436:391–398.
- Singer, W., and J. P. Rauschecker, 1982. Central core control of developmental plasticity in the kitten visual cortex: II. Electrical activation of mesencephalic and diencephalic projections, *Exp. Brain Res.*, 47:223–233.
- Sjöström, P. J., G. G. Turrigiano, and S. B. Nelson, 2001. Rate, timing and cooperativity jointly determine cortical synaptic plasticity, *Neuron*, 32:1149–1164.
- Stryker, M. P., and W. A. Harris, 1986. Binocular impulse blockade prevents the formation of ocular dominance columns in cat visual cortex, *J. Neurosci.*, 6:2117–2133.
- Stryker, M. P., and S. L. Strickland, 1984. Physiological segregation of ocular dominance columns depends on the pattern of afferent electrical activity, *Inv. Ophthalmol.*, 25(Suppl):278.
- Taha, S. A., and M. P. Stryker, 2002. Rapid ocular dominance plasticity requires cortical but not geniculate protein synthesis, *Neuron*, 34:425–436.
- Takahashi, M., M. Sugiyama, and T. Tsumoto, 1993. Contribution of NMDA receptors to tetanus-induced increase in postsynaptic Ca^{2+} in visual cortex of young rats, *Neurosci. Res.*, 17:229–230.
- Tamura, H., T. Tsumoto, and Y. Hata, 1992. Activity-dependent potentiation and depression of visual cortical responses to optic nerve stimulation in kittens, *J. Neurophysiol.*, 68:1603–1612.
- Tara, S., J. L. Hanover, A. J. Silva, and M. P. Stryker, 2002. Autophosphorylation of α CaMKII is required for ocular dominance plasticity, *Neuron*, 36:483–491.
- Torii, N., T. Kasmashita, Y. Otsu, and T. Tsumoto, 1995. An inhibitor for calcineurin, FK506, blocks induction of long-term depression in rat visual cortex, *Neurosci. Lett.*, 185:1–4.
- Tsumoto, T., W. Eckart, and O. D. Creutzfeldt, 1979. Modification of orientation selectivity of cat visual cortex neurons by removal of GABA-mediated inhibition, *Exp. Brain Res.*, 34:351–363.
- Tsumoto, T., K. Hagihara, H. Sato, and Y. Hata, 1987. NMDA receptors in the visual cortex of young kittens are more effective than those of adult cats, *Nature*, 327:513–514.
- Tsumoto, T., and K. Suda, 1979. Cross-depression: an electrophysiological manifestation of binocular competition in the developing visual cortex, *Brain Res.*, 168:190–194.
- Videen, T. O., N. W. Daw, and R. K. Rader, 1984. The effect of norepinephrine on visual cortical neurons in kittens and adult cats, *J. Neurosci.*, 4:1607–1617.
- Wiesel, T. N., and D. H. Hubel, 1963. Single cell responses in striate cortex of kittens deprived of vision in one eye, *J. Neurophysiol.*, 26:1003–1017.
- Wyatt, H. J., and N. W. Daw, 1975. Directionally sensitive ganglion cells in the rabbit retina: specificity for stimulus direction, size and speed, *J. Neurophysiol.*, 38:613–626.
- Yang, B. D., Y. Wang, and M. S. Cynader, 1996. Synergistic interactions between noradrenaline and glutamate in cytosolic calcium influx in cultured visual cortical neurons, *Brain Res.*, 721:181–190.
- Yang, C. B., Y. T. Zhang, G. Y. Li, and G. D. Mower, 2002. Identification of MVNC 13-3 as a candidate gene for critical period neuroplasticity in visual cortex, *J. Neurosci.*, 22:8614–8618.
- Yang, C., B. Silver, S. R. Ellis, and G. D. Mower, 2001. Bidirectional regulation of mitochondrial gene expression during developmental neuroplasticity of visual cortex, *Biochem. Biophys. Res. Commun.*, 287:1070–1074.
- Yang, S. N., Y.-G. Tang, and R. S. Zucker, 1999. Selective induction of LTP and LTD by postsynaptic $[\text{Ca}^{2+}]_i$ elevation, *J. Neurophysiol.*, 81:781–787.
- Yasuda, H., and T. Tsumoto, 1996. Long-term depression in rat visual cortex is associated with a lower rise of postsynaptic calcium than long-term potentiation, *Neurosci. Res.*, 24:265–274.
- Yoshimura, Y., T. Tsumoto, and A. Nishigori, 1991. Input-specific induction of long-term depression in Ca^{2+} -chelated visual cortex neurons, *Neurosci. Res.*, 2:393–396.
- Zhuo, M., Y. Hu, C. Schultz, E. R. Kandel, and R. D. Hawkins, 1994. Role of guanylyl cyclase and cGMP-dependent protein kinase in long-term potentiation, *Nature*, 368:635–639.

11 Ontogenesis of Cortical Connectivity

HENRY KENNEDY AND ANDREAS BURKHALTER

AN UNDERSTANDING of the neuronal mechanisms underlying visual perception has played a major role in shaping our understanding of how the brain extracts information concerning the world. In turn, insight into the development of this process is enormously conditioned by existing theories of brain function.

Over the last century, anatomical and physiological studies have provided a description of the point-to-point connectivity of the visual system where neighboring relations in the retina are conserved in their central projections. Hence, the primary visual cortex has been shown to contain a retinotopic map of the visual world in which each point is represented by neurons with specialized receptive fields that encode basic visual features. Initially, the primary visual cortex was thought to function as the cortical retina before relaying its activity to additional areas in the surrounding association cortex. It was in the association cortex that the important but highly mysterious business of seeing was thought to take place. Increasingly, the system came to be construed as being hierarchically organized, and successive levels were thought to subserve progressively higher functions. Essentially, the visual system was seen to be a highly passive system, whereby information in the retinal image was extracted in central structures, as reflected in the changing receptive field organization at successive levels (Hubel, 1995). The understanding of corticogenesis, which evolved in parallel, was that the early development of the cortex was dictated by the peripheral sense organ (Van der Loos and Woolsey, 1973), whereas later stages were dictated by the sensory experience of the animal (Blakemore and Cooper, 1970).

Recently, our understanding of the neuronal mechanisms underlying vision has shifted from a passive role of analysis of the retinal image to one of inference and the construction of constancy. Increasingly, the visual system is seen as a dynamic one where the individual stations are involved together in a computational process aimed at determining the probabilities of feature constellations in the visual environment (Scannell and Young, 2002; Young, 2000; Young, 2001; Zeki, 1993). In some ways, this modern synthesis has much to do with the Platonic understanding of the brain, in which the sensory impressions were compared to ideas of the world. In parallel to the release of central states from the dictatorship of the sensory periphery, developmental biologists are increasingly detecting the intrinsic constraints,

largely of a molecular nature, which determine early neuronal development of higher levels of the visual system (Rakic, 1988).

One can argue, therefore, that our understanding of the development of the brain being environmentally driven or, alternatively, determined by internal constraints has largely been influenced by theories of brain function. The intrinsic and extrinsic control of cortical development has been epitomized in protomap and protocortex theories (O'Leary, 1989; Rakic, 1988). Although these theories have been considered by some to be antagonistic, it is becoming increasingly clear that normal development of the cortex involves a synthesis of both intrinsic and extrinsic control (Yuste and Sur, 1999).

Early studies of cortical connectivity tended to be dominated by a view that immature connections were imprecise and that mature patterns of connections were largely the consequence of pruning of exuberant, early-formed connections (Innocenti et al., 1977). More recently, it has become clear that, although some early-formed connections undergo pruning, others exhibit precise connectional features from the onset of their formation (Dehay et al., 1988a). Distinguishing between these two possibilities is important because different contributions of each might be expected to underlie the development of very different functions. In this chapter, the authors shall attempt to give an up-to-date account of where development of the connectivity of the visual cortex is thought to be driven by activity in the periphery and where connectivity is prespecified, presumably by molecular cues that lay down the basic structure of the system.

It is becoming increasingly evident that the physiology of the visual cortex can be interpreted usefully in terms of feed-forward and feedback mechanisms underlying the hierarchical organization of the cortex (Felleman and Van Essen, 1991; Lamme and Roelfsema, 2000; Shao and Burkhalter, 1996). This approach provides a conceptual framework for interpreting the feedforward input from the thalamus to the cortex in terms of the recurrent excitation provided by the intracortical and intercortical processing (Douglas et al., 1995; Shao and Burkhalter, 1996). This approach turns out to be highly innovative because instead of viewing the role and development of geniculostriate and corticocortical connectivity as separate entities, it shows that these two sets of connections, in fact, share key features. Hence, the

development of feedforward projections from the thalamus to the cortex exhibits common features with the development of feedforward corticocortical connections; moreover, there are fundamentally different developmental mechanisms operant in the feedback and feedforward pathway.

Development of thalamocortical pathways

When Torston Wiesel presented his Nobel address, he pointed out that his and David Hubel's pioneering work on the effects of sensory deprivation on the development of the functional architecture of the visual cortex had been inspired by early eighteenth century speculation that congenital blindness resulted in defective visual perception, presumably as a result of malformation of the brain (Von Senden, 1960). Earlier, Hubel and Wiesel had demonstrated that adjacent territories of area 17 receive input alternatively from the right and left eye. These so-called ocular dominance columns had been explored both by single-unit recording in the cortex, as well as by injections of anterograde tracers in the eye, followed by transsynaptic transport of the tracer to area 17 (Hubel and Wiesel, 1962, 1977). To investigate the role of the sensory periphery, they carried out similar experiments in normal kittens as well as kittens having one eye, closed throughout development. These experiments suggested that, during normal development, the ocular dominance columns emerge from an immature stage in which input from the two eyes overlaps. If one eye is closed during development, then only the experienced eye drives most neurons in the adult (Wiesel and Hubel, 1963). Transsynaptic labeling has shown that, following monocular deprivation, there is an expansion of the columns receiving input from the open eye and a reduction of the columns receiving input from the deprived eye (LeVay et al., 1980). These experiments gave rise to the concept that, during normal development, the geniculate afferents conveying responses to the right and left eye initially are extensive and, therefore, overlap. Because binocular deprivation allowed segregation of the two sets of inputs while segregation was prevented by blockade of activity (Stryker and Harris, 1986), it was thought that the formation of ocular dominance columns depended on competitive interactions between inputs from both eyes during a so-called critical period. These experiments emphasized the role of sensory experience in shaping neuronal connections and defined a time window during which sensory experience has a profound effect on the development of the brain.

Although experiments involving monocular deprivation clearly show that the brain is susceptible to deprivation, they fail to elucidate the role of experience during normal development. Further, they have failed to provide insight into the normal process of development at the cellular level. It was assumed for many years that the segregation of ocular dominance columns was attributable to pruning of the thalamic

axonal arbor in layer 4 of the primary visual cortex. However, few experiments have actually attempted to examine this issue. When single geniculostriate axonal arbors have been examined at different developmental stages, the main event that is documented is the progressive increase in total axon length and complexity of axonal arbors (Antonini and Stryker, 1993; Friedlander and Martin, 1989). Pruning of extended branches either does not happen, or happens very rarely.

The role of visual experience in constructing ocular dominance columns was challenged by a study involving newborn monkeys. After prolonged in utero development and, therefore, in the absence of stimulation of the retina, the left and right eye inputs to the cortex were found to be well segregated into ocular dominance columns (Horton and Hocking, 1996; Rakic, 1976). This led to the suggestion that spontaneous activity, possibly originating in the periodic waves of excitation in the immature retina, drove segregation (Galli and Maffei, 1988; Meister et al., 1991; Mooney et al., 1993; Wong et al., 1993). However, a number of studies have suggested that the development of ocular dominance columns can actually proceed relatively normally in the total absence of the retina. Cytochrome oxidase-rich blobs in layers 2/3 in the monkey relate to the ocular dominance columns (Hendrickson, 1985; Hendry and Yoshioka, 1994) and have been shown to develop in the absence of the retina (Dehay et al., 1989; Kennedy et al., 1990; Kuljis and Rakic, 1990) and to show a normal periodicity (Kennedy et al., 1990). More direct evidence for the formation of ocular dominance columns in the absence of the retina has recently been obtained from studies of neonatal enucleated ferrets in which tracer injection in the lateral geniculate nucleus (LGN) revealed alternating stripes of label in the striate cortex (Crowley and Katz, 1999). Not only did ocular dominance columns appear to develop independently of the retina, but they were shown to appear well before the critical period and the period in which geniculostriate axons had been thought to undergo refinement and retraction (Crowley and Katz, 2000). Further, geniculate axons formed ocular dominance columns shortly after innervation of layer 4, and at this early stage, imbalance caused by removal of one eye fails to change the periodicity of the input to the cortex (Crowley and Katz, 2000). Although these results do not exclude a role for the sensory periphery in central development, they suggest that molecular cues play a major role in the formation of ocular dominance columns.

The influence of visual experience on the development of orientation columns has a long and controversial history. Unlike ocular dominance columns, where experimental manipulations quickly establish developmental plasticity, the effects of deprivation on the development of orientation columns has been a highly disputed issue (Blakemore and Cooper, 1970; Hirsch and Spinelli, 1970; Stryker and Sherk,

1975). The issue has recently been reexamined using optical imaging of orientation columns during development in normal and deprived animals. This work shows that, in agreement with earlier observations, orientation selectivity develops independently of visual experience, but neuronal activity is required to fine-tune and maintain the orientation map into adulthood (Crair et al., 1998; Sengpiel et al., 1999; White et al., 2001; Wiesel and Hubel, 1974). Although activity may not be necessary for the development of orientation columns, cross-modal rewiring experiments strongly suggest that visual afferents can create orientation columns in the auditory cortex (Sharma et al., 2000).

The emerging consensus on the development of the functional architecture of the cortex is that the construction of both orientation and ocular dominance columns is largely activity independent, but that the fine-tuning and maintenance of columns during the critical period depends on activity. These findings imply that early development of the columnar organization relies on molecular markers that may tag columns in the early phase of thalamic innervation of the cortex and that may share certain features with molecules known to be expressed in the embryonic cortex (Donoghue and Rakic, 1999; Flanagan and Vanderhaeghen, 1998).

Development of corticocortical pathways

During phylogeny, there is a progressive shifting of visual processing to more central structures of the brain. One consequence is that, in the mammal, more than 90% of the synapses in the brain occur in the cerebral cortex. Quantitative investigation of the cortex shows that 95% or more of synapses in the cortex are of cortical origin (Kennedy and Falchier, unpublished). One consequence of these figures is that developmental processes of the corticocortical pathways could have a major impact on the development of visual function.

It is now firmly established that the connectivity of infragranular-layer neurons is determined during the last round of mitosis in the ventricular zone prior to migration to the cortical plate (Polleux et al., 1998a; Polleux et al., 2001). Hence, commitment to a corticothalamic, corticocortical, and corticospinal fate is made independently of environmental influences in the cortical plate (Arimatsu et al., 1999; Koester and O'Leary, 1993; Polleux et al., 1997). There is evidence that specification of neuronal phenotype in the supragranular layers occurs at a later stage, so one might expect the determination of corticocortical neurons to be influenced more by epigenetic factors than is the case with other cortical connections. (McConnell, 1988). For many years, the callosal pathway linking the two hemispheres was the major model for the study of the develop-

ment of cortical connectivity. Because the callosal connections in the adult are largely concentrated at the areal boundaries of area 17, the demonstration that these connections are initially more widespread suggested that elimination of so-called exuberant connections is largely responsible for forming the adult connectivity pattern (Innocenti et al., 1977). Although the elimination of exuberant callosal connections has been demonstrated in a wide range of species, its generality is nevertheless questioned by the fact that this developmental phenomenon does not occur in area 17 of primates and rats (Dehay et al., 1988b; Chalupa et al., 1989; Hernit et al., 1996). This further raises the question of how important axon retraction is in the development of other types of cortical connections.

The connections of the cortex can be subdivided into two broad categories in which developmental control seems to differ. Intrinsic cortical connections (also known as intra-areal, horizontal, lateral, or tangential connections) link neurons within a cortical area, whereas extrinsic (or inter-areal) cortical connections link neurons in different cortical areas. In numerical terms, intrinsic connections constitute the vast majority of cortical connections, whereas extrinsic connections have been demonstrated to have much sparser connectivity (Kennedy et al., 2000).

HORIZONTAL INTRINSIC CONNECTIONS Horizontal intrinsic connections have been implicated in the elaboration of receptive field properties of individual neurons, including mediating inhibitory and excitatory effects from outside the classical receptive field (Das and Gilbert, 1999). Long-distance horizontal connections in superficial layers originate from pyramidal and spiny stellate neurons and form periodic clusters (Gilbert and Wiesel, 1979; Martin and Whitteridge, 1984; McGuire et al., 1991; Rockland and Lund, 1982). These connections have been shown to preferentially link columns with similar orientation preferences (Gilbert and Wiesel, 1989; Ts'o et al., 1986; Weliky and Katz, 1994), and similar or dissimilar ocular dominance columns (Livingstone and Hubel, 1984; Malach et al., 1993; Yoshioka et al., 1996).

Although developmental studies agree that the clustered connectivity that is characteristic of the adult emerges from a nonclustered juvenile situation, there is some uncertainty as to what extent this involves the elimination of inappropriate connections or the addition of appropriate connections. Studies that have focused on the maximum extent of connectivity have claimed tangential extensions of 10 mm in the kitten, compared to the adult configuration of 2 to 4 mm (Luhmann et al., 1986). This contrasts with later studies showing that the maximum extent of connections does not change significantly during development (Callaway and Katz, 1990, 1991; Lubke and Albus, 1992a, 1992b). These

later studies agree that, in kittens, clusters are formed by the end of the second postnatal week, shortly after eye opening. The studies by Callaway and Katz (1990) claim that crude clusters are present at the end of the second postnatal week and are later refined. However, the idea of a prolonged period of cluster refinement has been challenged by Lubke and Albus (1992a, 1992b), who showed that adult-like clusters are already present at the end of the second week. Lubke and Albus argue that the apparent late refinement of clusters seen by Callaway and Katz could be the consequence of using relative large tracer injections. Studies of the formation of clustered horizontal connections further differ on the reported effects of visual deprivation. Whereas dark rearing appeared to delay cluster refinement in some studies (Callaway and Katz, 1991; White et al., 2001), the rapid formation of clustered tangential connections was not influenced by dark rearing in the study of Lubke and Albus (1992a, 1992b).

The consensus remains that it is the emergence of clusters, rather than the restriction of tangential extent, that characterizes the formation of horizontal connections. However, the size of the tracer injection may govern whether one observes late refinement of cluster formation and an effect of dark rearing (Lubke and Albus, 1992b). Although one cannot exclude the possibility that increasing injection size introduces an experimental artifact, there is another possibility. Using paired injections of two distinguishable tracers with known interinjection separation, it is possible to examine the topographic organization of connections of large populations of neurons in the visual cortex. Such experiments show that, during development, the divergence and convergence values of intrinsic connections in area 17 remain constant for most area-17 neurons. However, a small contingent of neurons, less than 2%, do show much higher divergence values in the immature cortex than in the adult cortex (Kennedy et al., 1994). Thus, small injections or injections of single cells tend to emphasize the connectivity of the majority of neurons and may fail to detect the refinement of a subpopulation of neurons with widespread connections. The developmental significance of this subpopulation of immature corticocortical neurons with large divergence values remains to be explored.

VERTICAL INTRINSIC CONNECTIONS How information flows through the cortex is determined by the specific set of connections linking the cortical layers (Gilbert, 1983; Martin and Whitteridge, 1984). Throughout development, interlaminar connections show high target specificity, and the linking of cortical layers appears not to involve elimination of inappropriate connections (Callaway and Katz, 1992; Callaway and Lieber, 1996; Dantzker and Callaway, 1998; Katz and Callaway, 1992). These results suggest that layer-specific cues enable developing axons to form appropriate

connections at early stages of axonal outgrowth. The role of intrinsic influences has been examined in *in vitro* experiments. Immature cortical slices maintained in culture show that layer-specific connections of layers 5/6, but not 2/3, develop in the absence of extrinsic influences (Bolz et al., 1992; Butler et al., 2001; Dantzker and Callaway, 1998; Yamamoto et al., 1992).

The intrinsic cortical cues, which are used by growing axons interconnecting the cortical layers, are thought to be both molecular and activity dependent in origin. Axons from presumptive layer 6 precursors preferentially grow on membranes prepared from layer 4, the laminar targets of layer 6. This finding supports the notion that molecular surface bound cues promote axonal growth of layer 6 neurons on layer 4 (Castellani and Bolz, 1997). However, layer 6 neurons apparently require activity to contact their targets in layer 4 correctly. This has been demonstrated experimentally by maintaining cortical slices in the presence of the sodium channel blocker tetrodotoxine (TTX), which blocks spontaneous activity. In normal development, layer 6 axons grow through layer 5 and form axonal branches in layer 4. However, in the presence of TTX, layer 6 neurons form extensive branches in layer 5 (Callaway and Lieber, 1996; Dantzker and Callaway, 1998). In contrast, layer 5 neurons show normal targeting and specifically contact layers 2/3 in the absence of spontaneous activity (Butler et al., 2001).

The ability of infragranular layers to form layer-specific connections is independent of extrinsic cortical factors, and these connections, therefore, develop normally *in vitro*. This contrasts with the supragranular layers, which apparently fail to form layer-specific connections *in vitro*, suggesting that neurons in layers 2/3 depend on extrinsic factors for their appropriate development (Butler et al., 2001). Layers 2/3 are the major source of feedforward projections to higher cortical areas, and feedforward neurons in these layers receive monosynaptic input from feedback projections from these same areas (Johnson and Burkhalter, 1997). One possibility is that the feedback projections from higher areas are required for the normal development of the layer 2/3 interlaminar connectivity.

INTERAREAL CONNECTIVITY In all mammals, the visual cortex is divided into multiple distinct areas that are organized into a hierarchical network (Coogan and Burkhalter, 1993; Felleman and Van Essen, 1991; Krubitzer and Huffman, 2000). Individual areas often show different cytoarchitectures, have distinct inputs and outputs, and emphasize the representation of specific attributes of the retinal image (Van Essen and Gallant, 1994). These functional specializations are reflected in receptive field properties that, in the primary visual cortex, encode simple features, such as the orientation of light bars or edges, and

that in higher areas represent increasingly more complex aspects of the visual scene (Felleman and Van Essen, 1991). The neuronal activity at different levels of the cortical hierarchy critically depends on ascending connections linking lower with higher visual cortical areas (Vanduffel et al., 1997). These all-important inputs are provided by a surprisingly small number of feedforward connections that account for only 1% to 3% of asymmetric synapses in the target region (Anderson et al., 1998; Johnson and Burkhalter, 1996). Feedforward inputs terminate principally in layer 4 in a topographically organized fashion (Maunsell and Van Essen, 1983; Price et al., 1994; Rockland and Pandya, 1979; Rockland and Virga, 1990). It is thought that these inputs contribute to the construction of progressively larger and more complex receptive fields at successive levels of the hierarchy (Felleman and Van Essen, 1991). In addition to these functions, feedforward connections channel inputs into the ventral and dorsal processing streams that are specialized for the representation of visual objects and spatial relationships (Maunsell and Newsome, 1987).

Pathways leading from higher to lower areas are provided by feedback connections. There is every indication that these connections are at least as numerous as the feedforward connections (Johnson and Burkhalter, 1996; Kennedy et al., 2000). Unlike feedforward pathways, feedback connections terminate outside of layer 4 and distribute their outputs over more extensive parts of the visuotopic map than do feedforward projecting neurons (Perkel et al., 1986). Widespread feedback connections not only provide input from noncorresponding regions of the map, but also are thought to combine signals from distinct processing streams (Rockland et al., 1994; Rockland and Virga, 1989; Zeki and Shipp, 1988).

The physiological role of feedback connections has been most effectively studied by reversible cooling of higher cortical areas and recording of the effects on neuronal responses in lower areas. Experiments in monkeys have shown that feedback inputs from both V3 and V2 to V1 facilitate responses to stimuli moving within the classical receptive field (Sandell and Schiller, 1982) and enhance suppression from outside the receptive field (Hupé et al., 1998). These effects suggest that feedback connections are involved in the discrimination of objects relative to the background. However, indirect evidence strongly suggests that feedback connections mediate top-down influence that result from attention, memory retrieval, and imagery (Chelazzi et al., 2001; Ishai and Sagi, 1995; McAdams and Maunsell, 2000; Motter, 1994; Naya et al., 2001).

In a widely held view, perceptual abilities are, to a large extent, determined by the organization and processing capabilities of feedforward and feedback circuits interconnecting areas at different hierarchical levels. Networks of such enormous complexity must vary in their detailed synaptic

organization. These differences may account for the wide range of cognitive abilities among individuals. Variability in hierarchical networks may arise from both the implementation of genetic programs and the patterns of activation during development. To determine the role of each of the factors in the development of feedforward and feedback connections, a number of studies have investigated when and how inter-areal pathways acquire a lamina specific and topographic organization, segregate into functionally distinct channels, form specific hierarchical relationships, and acquire distinct balances of excitation and inhibition.

INTER-AREAL CONNECTIONS OF PREPLATE NEURONS The earliest inter-areal connections are formed before the cortical plate by neurons of the marginal zone. A major population of cells in the primordial layer 1 are Cajal-Retzius (CR) neurons that constitute a diverse group of neurons composed of derivatives of the subpial granular layer of the preplate and the neuroepithelium behind the olfactory bulb (Meyer and Wahle, 1999). Some CR neurons send out axons that are completely confined to layer 1, extend for millimeters, and are long enough to interconnect different cortical areas (Derer and Derer, 1990; Marin-Padilla, 1984). Unlike inter-areal projections of cortical plate neurons that branch mainly at the end of the pathway, axons of CR neurons branch near the cell body, mainly issuing boutons of passage and distributing outputs over large parts of the cerebral cortex (Derer and Derer, 1990). This projection pattern indicates that connections of CR neurons are not point-to-point and are not designed to preserve the spatial relationship of sensory maps. Instead, they may provide a network for synchronizing activity of pyramidal neurons in different areas (Schwartz et al., 1998). The most fascinating feature of these connections is that they are not permanent. In fact, in the rat and monkey, they are eliminated in the first 1 to 3 weeks after birth owing to the death of CR neurons (Derer and Derer, 1990; Huntley and Jones, 1990). The reason for their demise remains unknown, but some of the consequences have been documented. One of these is that ablation of CR neurons in newborn mice arrests the migration of neurons to superficial layers of cerebral cortex (Super et al., 2000). Similar experiments in the developing hippocampus have further shown that CR neurons are necessary for the development of the lamina-specific innervation by afferents from the entorhinal cortex (Del Rio et al., 1997). In the mature cerebral cortex, layer 1 is thought to be strongly innervated by inter-areal feedback connections (Coogan and Burkhalter, 1993; Rockland and Virga, 1989). By contrast, feedforward inputs to layer 1 are sparse (Coogan and Burkhalter, 1993; Felleman and Van Essen, 1991). These distinct laminar innervation patterns emerge during development. Interestingly, feedforward connections acquire

their lamina specificity during a period in which layer 1 is occupied by CR neurons (Knutsen et al., 1997; Patel et al., 1999). However, as soon as CR neurons begin to vacate the marginal zone, feedback connections start to innervate layer 1. Whether these events are causally related is not known. However, the synchrony in which they occur suggests that CR neurons may play a gatekeeper role for the innervation of layer 1.

Support for this idea derives from experiments in cortical slices that show that high levels of a chemorepellant near the marginal zone keep pyramidal cell axons away from layer 1 (Polleux et al., 1998b). The postulated repulsion of feedforward axons may be caused by a factor that is secreted by CR neurons. At first glance, this scenario seems to contradict the growth-promoting activity attributed to hippocampal CR neurons (Del Rio et al., 1997). However, the recent demonstration that attraction and repulsion depends on the intracellular amount of cyclic nucleotides (Song et al., 1998) suggests that the different responses may be attributable to diverse concentrations of second messengers in neocortical and paleocortical projection neurons.

During late fetal or early postnatal development, subplate neurons, a different, perhaps better known, population of short-lived preplate neurons (Luskin and Shatz, 1985), form connections with subcortical structures (De Carlos and O'Leary, 1992; McConnell et al., 1989). Intracortical connections of subplate neurons also have been observed within the subplate, as well as to the cortical plate, and have been reported, in one study, to extend to the homotypic areas of the opposite hemisphere (Antonini and Shatz, 1990; Friauf et al., 1990). There is currently no evidence that subplate neurons form inter-areal connections. Thus, the postulated role of subplate neurons as pioneer neurons that provide a scaffold for the development of cortical pathways might only apply to descending pathways (De Carlos and O'Leary, 1992; McConnell et al., 1989), but some researchers dispute that such a scaffold role ever applies in descending pathways (Clasca et al., 1995).

FEEDFORWARD CONNECTIONS In vivo retrograde tracing experiments in the visual cortex of fetal monkeys and DiI tracing studies in the fixed brains of monkeys and humans have demonstrated that feedforward connections from lower to higher cortical areas emerge prenatally during the third trimester of gestation (Barone et al., 1996; Burkhalter et al., 1993; Coogan and Burkhalter, 1988). In the cat, feedforward connections from area 17 to area 18 are well established at birth (Kennedy et al., 1994; Price and Blakemore, 1985a; Price et al., 1994), suggesting that they emerge at late fetal stages. In rodents, the earliest connections between V1 and V2 were observed at postnatal day 1 (Coogan and Burkhalter, 1988; Knutsen et al., 1997; Patel, 1994; Patel et al., 1999). Relative to the time point when neuronal

migration ends (Ignacio et al., 1995; Rakic and Nowakowski, 1981; Shatz and Luskin, 1986), the onset of the formation of inter-areal connections in cats is 2 to 3 weeks earlier than in rodents and primates.

In newborn kittens, feedforward connections from area 17 to area 18 originate from superficial and deep layers (Price and Blakemore, 1985a; Price et al., 1994). As development proceeds, the number of projection neurons in upper layers increases to a peak, after which it declines to the adult level (Price et al., 1994). Quantitatively similar developmental processes have been observed in forward pathways of the monkey visual cortex. Here, feedforward projections from V1 to V4, V2 to V4, and V3A to V4 in both the adult and the fetus principally originate from supragranular layers (Barone et al., 1996; Batardière et al., 2002; Coogan and Van Essen, 1996).

In the adult cat, feedforward projecting neurons from area 17 to area 18 form distinct clusters (Gilbert and Kelly, 1975) that contain cells with similar receptive field properties (Gilbert and Wiesel, 1989). Retrograde tracing studies have shown that, at birth, projection neurons in superficial and deep layers are distributed uniformly and that the clusters emerge during the first 3 postnatal weeks (Bullier et al., 1984; Price and Blakemore, 1985b). Although these findings suggest that inappropriate connections are eliminated, the demonstration in newborn kittens that anterogradely labeled feedforward connections from area 17 form distinct clusters in deep layers of area 18 (Price and Zumbroich, 1989) clearly indicates that feedforward connections develop with a high degree of spatial precision. A complementary retrograde study has shown that this is true for the bulk of feedforward connections, and has further demonstrated that inappropriate feedforward connections in newborn kittens are the result of a small population of neurons with widespread axonal connections (Kennedy et al., 1994). Most of these connections are formed by supragranular neurons (Caric and Price, 1996). This mode of development is not a peculiarity of cat area 17 to area 18 connections. In the monkey, the earliest (embryonic day 112) feedforward projecting neurons from V2 to V4 are clustered and are in register with regions of high acetylcholinesterase activity (Barone et al., 1996). Similar clusters, albeit weaker, have been observed after white matter injections of E129 fetuses. Clusters in older animals were more distinct than in animals at an early stage of development. Together, these findings indicate that feedforward axons grow to roughly the correct location and then enter gray matter, after which axon arbors undergo minor remodeling. In the monkey, this process is largely complete at birth. Although these results strongly argue for precise target selection by feedforward axons, it remains unknown whether similar mechanisms guide the development in the vertical dimension to form connections with the correct layers.

FEEDBACK CONNECTIONS Retrograde and anterograde tracing studies have shown that cortical feedback connections emerge at about the same time as feedforward connections. In the monkey, feedback connections to V1 begin to form at E108 (Fig. 11.1; Barone et al., 1995; Coogan and Van Essen, 1996). In humans, they are present at 37 weeks

of gestation (Burkhalter et al., 1993). In the cat, feedback connections to areas 17 and 18 are present at birth, indicating that they emerge at late fetal stages (Batardière et al., 1998; Dehay et al., 1984; Kato et al., 1991). In mice and rats, sparse feedback connections are present at postnatal day 1 (Knutsen et al., 1997; Patel et al., 1999).

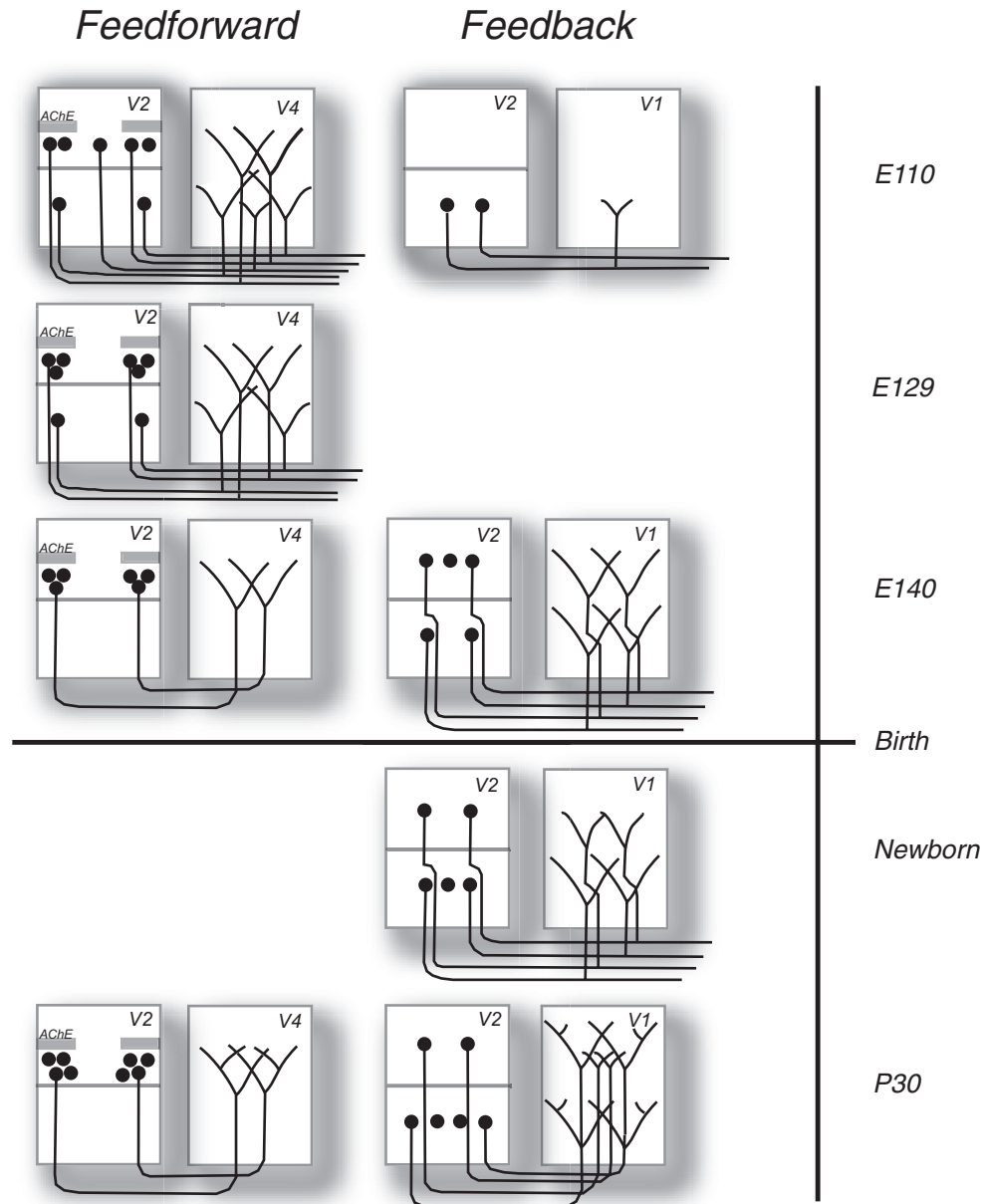


FIGURE 11.1. Schematic representation of the development of inter-areal feedforward and feedback connections in monkey visual cortex (Barone et al., 1995; Barone et al., 1996; Batardière et al., 2002). The development of the laminar and tangential distribution of axon arbors is inferred from the distribution of retrogradely labeled neurons; it has not yet been shown directly by anterograde tracing of axonal connections. The diagram illustrates a highly dichotomous strategy of the development of feedforward and feed-

back connections. Feedforward connections are complete early in prenatal life, and their development largely depends on directed growth and target recognition mechanisms that do not involve large-scale elimination of inappropriate axons. In contrast, the development of feedback connections requires prolonged remodeling, massive postnatal pruning of early-formed axon connections, and elaboration of branches. *AChE*, acetylcholinesterase-rich bands in area V2 (Barone et al., 1995).

In vivo retrograde tracing studies in the cat and monkey have shown that, early in development, feedback connections are formed by both supragranular and infragranular neurons (Barone et al., 1995; Batardière et al., 1998; Kato et al., 1991; Kennedy et al., 1989; Meissirel et al., 1991). For unknown reasons, DiI tracing in fixed tissue of monkey and human visual cortex has failed to reveal early feedback connections from upper layers (Burkhalter et al., 1993; Coogan and Van Essen, 1996), and similar results have been reported in the developing rat visual cortex (Coogan and Burkhalter, 1988). Recent experiments in mouse visual cortex with biotinylated dextran amine, however, have revealed feedback projecting neurons originating from upper layers (Q. Wang and A. Burkhalter, unpublished observations), suggesting that technical reasons may account for the failure to label upper-layer neurons in some earlier studies. Regardless, it is clear from experiments in the cat and monkey that many feedback connections from upper layers are transient and gradually eliminated over a prolonged period that begins at fetal stages and ends about 1 to 2 months after birth (Barone et al., 1995; Batardière et al., 1998; Batardière et al., 2002). The elimination of upper layer neurons leads to both a reduction in the overall strength of the connection and a small increase in the topographic precision (Barone et al., 1995; Batardière et al., 1998; Batardière et al., 2002). In contrast, during maturation, deep-layer connections become stronger and more widespread, presumably by delayed ingrowth of axons into the target (Barone et al., 1995). All of these insights have been obtained by retrograde tracing experiments; it will be critical to see with anterograde labeling techniques whether, and in what way, the present concepts need to be revised.

Studies in rodents show that feedback axons reach their final laminar targets several days after feedforward connection (Knutsen et al., 1997; Patel et al., 1999). This is consistent with the notion that feedback connections mature over a longer period than do feedforward connections. At this point, the most important fact is that shaping of the feedback pathway takes longer than that of the feedforward pathway and involves more extensive remodeling of early connections, which, to a significant degree, occurs after birth. Comparison of rodent and primate development shows that essentially similar processes are involved, with the first formed connections stemming from the infragranular layers (Batardière et al., 2002; Coogan and Burkhalter, 1988). This suggests that the major role of pathfinding resides in the axonal outgrowth of infragranular-layer neurons when distances to be covered between cortical areas are relatively short compared to those in later stages, particularly in the monkey. This is followed by a later overshoot of the numbers of supragranular-layer neurons projecting in feedback pathways and the subsequent massive reduction of projections from supragranular layers.

Quantitative studies of the visual cortex in adult monkeys have shown that feedforward connections have a higher percentage of supragranular projection neurons than do feedback connections, and that, in each type of pathway, the percentage of supragranular neurons is correlated with the relative hierarchical rank of a given area (Barone et al., 2000). Recently, this framework has been used to interpret results from retrograde tracing of connections of V4 in the developing monkey visual cortex (Batardière et al., 2002). These studies have revealed that the hierarchical relations of extrastriate areas are invariant during development.

Clearly, feedforward and feedback pathways develop according to different strategies. Feedforward pathways are created largely through directed growth and target recognition and do not involve large-scale axon elimination. Feedback pathways, in contrast, require substantial and prolonged refinement of early-formed connections. Most interestingly, the relative rank of areas in the cortical hierarchy is established prenatally, weeks before the inter-areal connections have acquired their mature laminar, compartmental, and topographic organization. This implies that the identity, in terms of connectivity, of individual areas in monkey visual cortex is already specified at the time when feedforward and feedback connections first emerge. Therefore, it seems unlikely that inter-areal connections play a major role in the specification of cortical areas.

EFFECTS OF VISUAL DEPRIVATION The role of visual experience in the development of inter-areal connections has been studied mainly in the feedforward pathway. Studies of kittens raised with both eyes sutured closed—from before natural eye opening to up to 80 days postnatally—have revealed no apparent effects on clustering of neurons projecting from area 17 to 18 (Price and Blakemore, 1985a) or on the size and shape of axonal projections in area 18 (Zufferey et al., 1999). Furthermore, the retraction of early-formed connections from deep layers is independent of visual stimulation. However, in monocularly deprived kittens, the clusters of feedforward projecting neurons in area 17 are ~10% larger, suggesting a minor role of binocular competition in the refinement of topographic mapping (Price et al., 1994). These findings are consistent with the notion that, at the present level of resolution, feedforward connections are largely specified prenatally and that the development and maintenance are largely independent of patterned visual stimulation. Whether similar rules apply to the development of feedback connections is an interesting question. The protracted development that in monkey continues for weeks after birth certainly offers the opportunity for epigenetic influences on these connections.

SYNAPTIC ORGANIZATION So far, the issue of connectivity at the global level has been addressed. However, the actual

response of neurons to visual stimuli is the consequence of the activation by excitatory projection neurons of local excitatory and inhibitory neurons in the projection target. Based on the cortical processing of thalamocortical inputs, it was proposed that the local excitatory and inhibitory interactions are performed by a canonical circuit that is similar throughout cortex (Douglas and Martin, 1991). The key features of the model are that cortical activation is produced by a small number of afferent synapses whose excitatory effects are opposed by weak intracortical inhibition that, in turn, controls access to large numbers of excitatory, recurrent, intracortical connections that amplify the primary response. It has been shown recently that the basic structure of the canonical circuit applies to inter-areal feedforward and connections (Johnson and Burkhalter, 1996). In rodent, cat, and monkey visual cortex, mature inter-areal feedforward and feedback connections form asymmetrical synapses on pyramidal and nonpyramidal neurons (Anderson et al., 1998; Johnson and Burkhalter, 1996; Lowenstein and Somogyi, 1991). In adult rats, about 10% of both feedforward and feedback inputs between areas V1 and V2 are sent to nonpyramidal cells that all belong to the same family of parvalbumin expressing GABAergic neurons (Gonchar and Burkhalter, 1999). The remaining 90% of connections are formed on pyramidal neurons.

Stimulation of feedforward or feedback inputs to pyramidal cells elicits monosynaptic excitatory responses followed by disynaptic inhibition (Dong et al., 1999; Shao and Burkhalter, 1996; Shao et al., 1996). Although postsynaptic excitation is similar in both pathways, inhibitory responses in the feedback pathway are smaller and less frequent than in the feedforward pathway (Dong et al., 1999; Shao and Burkhalter, 1996). One factor that might contribute to this difference is that feedback inputs terminate on thinner GABAergic dendrites than do feedforward inputs (Gonchar and Burkhalter, 1999). During development, this pathway difference emerges, after animals open their eyes 14 days postnatally, by selective elimination of feedback synapses from thick GABAergic dendrites (Yamashita et al., 2000). In parallel with these structural changes, during the third and fourth postnatal week, inhibition generated by feedback inputs becomes weaker, whereas inhibition in the feedforward circuit increases (Dong et al., 1999; Shao and Burkhalter, 1998). In mice raised with one eye closed for 36 days, this transformation of the feedback circuit is arrested, and inhibition of pyramidal neurons remains as strong as in the feedforward circuit (Dong et al., 2001). The effect is specific to the binocular region of area 17, suggesting that the development of intracortical inhibition is influenced by competitive mechanisms. The transformation of inhibition in the feedback pathway from a level that is similar to the feedforward circuit to a significantly lower amount fails to occur in BDNF-overexpressing mice (Dong et al., 2000).

This suggests that the pathway-specific balance of excitation and inhibition in inter-areal circuits is determined by the activity-dependent competition for a neurotrophic factor. Further studies are needed to determine whether, in BDNF-overexpressing mice, feedback synapses fail to retract from thick GABAergic dendrites (Yamashita et al., 2000).

Conclusion

Distinguishing between feedforward and feedback projections in the cortex suggest that they follow different sorts of developmental control. The feedback connections appear to undergo prolonged maturation in which inappropriate connections are eliminated so that activity-mediated processes can be implemented. Feedforward projections show directed growth and target selection and are precociously formed, suggesting that molecular guidance mechanisms may be more predominantly used in these pathways. Studies suggest that similar differences in the development of feedforward and feedback pathways are to be found in the ascending pathways. The terminal arbors of retinal feedforward projection to the LGN show progressive increases in size and target appropriate territories (Kennedy et al., 2001; Snider et al., 1999). As discussed earlier, similar findings characterize the feedforward projections from the LGN to the visual cortex. Not much is known about the development of feedback projections from the cortex to the thalamus, but interestingly, in the adult, corticogeniculate arbors span several layers of the LGN (Murphy and Sillito, 1996). This is in sharp contrast to the feedforward input from the retina to the LGN. These results suggest similar developmental mechanisms in feedback and feedforward projections at different levels and hint that they may share common physiological functions. In this respect, the role of feedback projections to the LGN in controlling mode of firing (Sherman, 2001) may prove to be significant for understanding the role of corticocortical feedback projections onto feedforward neurons (Johnson and Burkhalter, 1997). At the level of the cortex, the development and maintenance of feedback projections that perform the processing of retinal inputs necessary for the segmentation and interpretation of the visual scene (Lamme and Roelfsema, 2000) may depend on visual experience.

REFERENCES

- Anderson, J. C., T. Binzegger, K. A. Martin, and K. S. Rockland, 1998. The connection from cortical area V1 to V5: a light and electron microscopic study, *J. Neurosci.*, 18:10525–10540.
- Antonini, A., and C. J. Shatz, 1990. Relation between putative transmitter phenotypes and connectivity of subplate neurons during cerebral cortical development, *Eur. J. Neurosci.*, 2:744–761.
- Antonini, A., and P. M. Stryker, 1993. Rapid remodeling of axonal arbors in the visual cortex, *Science*, 260:1819–1821.

- Arimatsu, Y., M. Ishida, M. Sato, and M. Kojima, 1999. Cortico-cortical associative neurons expressing latexin: specific cortical connectivity formed in vivo and in vitro, *Cereb. Cortex*, 9:569–576.
- Barone, P., A. Batardière, K. Knoblauch, and H. Kennedy, 2000. Laminar distribution of neurons in extrastriate areas projecting to V1 and V4 correlates with the hierarchical rank and indicates the operation of a distance rule, *J. Neurosci.*, 20:3263–3281.
- Barone, P., C. Dehay, M. Berland, J. Bullier, and H. Kennedy, 1995. Developmental remodeling of primate visual cortical pathways, *Cereb. Cortex*, 5:22–38.
- Barone, P., C. Dehay, M. Berland, and H. Kennedy, 1996. Role of directed growth and target selection in the formation of cortical pathways: prenatal development of the projection of area V2 to area V4 in the monkey, *J. Comp. Neurol.*, 374:1–20.
- Batardière, A., P. Barone, K. Knoblauch, P. Giroud, M. Berland, A. M. Dumas, and H. Kennedy, 2002. Early specification of the hierarchical organization of visual cortical areas in the macaque monkey, *Cereb. Cortex*, 12:453–465.
- Batardière, A., P. Barone, C. Dehay, and H. Kennedy, 1998. Area-specific laminar distribution of cortical feedback neurons projecting to cat area 17: quantitative analysis in the adult and during ontogeny, *J. Comp. Neurol.*, 396:493–510.
- Blakemore, C., and G. F. Cooper, 1970. Development of the brain depends on the visual environment, *Nature*, 228:477–478.
- Bolz, J., N. Novak, and V. Staiger, 1992. Formation of specific afferent connections in organotypic slice cultures from rat visual cortex cocultured with lateral geniculate nucleus, *J. Neurosci.*, 12:3054–3070.
- Bullier, J., C. DeHay, and H. Kennedy 1984. Axonal bifurcation and cortico-cortical connectivity in the kitten visual cortex, *J. Physiol.*, 353:22.
- Burkhalter, A., K. L. Bernardo, and V. Charles, 1993. Development of local circuits in human visual-cortex, *J. Neurosci.*, 13:1916–1931.
- Butler, A. K., J. L. Dantzker, R. B. Shah, and E. M. Callaway, 2001. Development of visual cortical axons: layer-specific effects of extrinsic influences and activity blockade, *J. Comp. Neurol.*, 430:321–331.
- Callaway, E. M., and L. C. Katz, 1990. Emergence and refinement of clustered horizontal connections in cat striate cortex, *J. Neurosci.*, 10:1134–1153.
- Callaway, E. M., and L. C. Katz, 1991. Effects of binocular deprivation on the development of clustered horizontal connections in cat striate cortex, *Proc. Natl. Acad. Sci. USA*, 88:745–749.
- Callaway, E. M., and L. C. Katz, 1992. Development of axonal arbors of layer 4 spiny neurons in cat striate cortex, *J. Neurosci.*, 12:570–582.
- Callaway, E. M., and J. L. Lieber, 1996. Development of axonal arbors of layer 6 pyramidal neurons in ferret primary visual cortex, *J. Comp. Neurol.*, 376:295–305.
- Caric, D., and D. J. Price, 1996. The organization of visual cortico-cortical connections in early postnatal kittens, *Neuroscience*, 73:817–829.
- Castellani, V., and J. Bolz, 1997. Membrane-associated molecules regulate the formation of layer-specific cortical circuits, *Proc. Natl. Acad. Sci. USA*, 94:7030–7035.
- Chalupa, L., H. P. Killackey, C. J. Snider, and B. Lia, 1989. Callosal projection neurons in area 17 of the fetal rhesus monkey, *Dev. Brain Res.*, 46:303–308.
- Chelazzi, L., E. K. Miller, J. Duncan, and R. Desimone, 2001. Responses of neurons in macaque area V4 during memory-guided visual search, *Cereb. Cortex*, 11:761–772.
- Clasca, F., A. Angelucci, and M. Sur, 1995. Layer-specific programs of development in neocortical projection neurons, *Proc. Natl. Acad. Sci. USA*, 92:11145–11149.
- Coogan, T. A., and A. Burkhalter, 1988. Sequential development of connections between striate and extrastriate visual cortical areas in the rat, *J. Comp. Neurol.*, 278:242–252.
- Coogan, T. A., and A. Burkhalter, 1993. Hierarchical organization of areas in rat visual cortex, *J. Neurosci.*, 13:3749–3772.
- Coogan, T. A., and D. C. Van Essen, 1996. Development of connections within and between areas V1 and V2 of macaque monkeys, *J. Comp. Neurol.*, 372:327–342.
- Crair, M. C., D. C. Gillespie, and M. P. Stryker, 1998. The role of visual experience in the development of columns in cat visual cortex, *Science*, 279:566–570.
- Crowley, J. C., and L. C. Katz, 1999. Development of ocular dominance columns in the absence of retinal input, *Nat. Neurosci.*, 2:1125–1130.
- Crowley, J. C., and L. C. Katz, 2000. Early development of ocular dominance columns, *Science*, 290:1321–1324.
- Dantzker, J. L., and E. M. Callaway, 1998. The development of local, layer-specific visual cortical axons in the absence of extrinsic influences and intrinsic activity, *J. Neurosci.*, 18:4145–4154.
- Das, A., and C. D. Gilbert, 1999. Topography of contextual modulations mediated by short-range interactions in primary visual cortex, *Nature*, 399:655–661.
- De Carlos, J. A., and D. D. M. O’Leary, 1992. Growth and targeting of subplate axons and establishment of major cortical pathways, *J. Neurosci.*, 12:1194–1211.
- Dehay, C., J. Bullier, and H. Kennedy, 1984. Transient projections from the frontoparietal and temporal cortex to areas 17, 18 and 19 in the kitten, *Exp. Brain Res.*, 57:208–212.
- Dehay, C., G. Horsburgh, M. Berland, H. Killackey, and H. Kennedy, 1989. Maturation and connectivity of the visual cortex in monkey is altered by prenatal removal of retinal input, *Nature*, 337:265–267.
- Dehay, C., H. Kennedy, and J. Bullier, 1988a. Characterisation of transient cortical projections from auditory, somatosensory and motor cortices to visual areas 17, 18 and 19 in the kitten, *J. Comp. Neurol.*, 272:68–89.
- Dehay, C., H. Kennedy, J. Bullier, and M. Berland, 1988b. Absence of interhemispheric connections of area 17 during development in monkey, *Nature*, 331:348–350.
- Del Rio, J. A., B. Heimrich, V. Borrell, E. Forster, A. Drakew, S. Alcantara, K. Nakajima, T. Miyata, M. Ogawa, K. Mikoshiba, P. Derer, M. Frotscher, and E. Soriano, 1997. A role for Cajal-Retzius cells and reelin in the development of hippocampal connections, *Nature*, 385:70–74.
- Derer, P., and M. Derer, 1990. Cajal-Retzius cell ontogenesis and death in mouse brain visualized with horseradish peroxidase and electron microscopy, *Neuroscience*, 36:839–856.
- Dong, H., Z. J. Huang, S. Tonegawa, and A. Burkhalter, 2000. Regulation of inhibition in developing interareal forward and feedback circuit in developing mouse visual cortex, *Soc. Neurosci. Abstr.*, 26:855.
- Dong, H., M. Lee, and A. Burkhalter, 2001. Experience-dependent modification of the balance of synaptic excitation and inhibition in interareal feedback circuit in developing mouse visual cortex, *Soc. Neurosci. Abstr.*, 27:1584.
- Dong, H., Z. Shao, and A. Burkhalter, 1999. Different balance of excitation and inhibition in interareal forward and feedback pathways of mouse visual cortex, *Soc. Neurosci. Abstr.*, 25:2191.

- Donoghue, M. J., and P. Rakic, 1999. Molecular evidence for the early specification of presumptive functional domains in the embryonic primate cerebral cortex, *J. Neurosci.*, 19:5967–5979.
- Douglas, R. J., C. Koch, M. Mahowald, K. A. Martin, and H. H. Suarez, 1995. Recurrent excitation in neocortical circuits, *Science*, 269:981–985.
- Douglas, R. J., and K. A. Martin, 1991. A functional microcircuit for cat visual cortex, *J. Physiol.*, 440:735–769.
- Felleman, D. J., and D. C. Van Essen, 1991. Distributed hierarchical processing in the primate cerebral cortex, *Cereb. Cortex*, 1:1–47.
- Flanagan, J. G., and P. Vanderhaeghen, 1998. The ephrins and Eph receptors in neural development, *Annu. Rev. Neurosci.*, 21:309–345.
- Friauf, E., S. K. McConnell, and C. J. Shatz, 1990. Functional synaptic circuits in the subplate during fetal and early postnatal development of cat visual cortex, *J. Neurosci.*, 10:2601–2613.
- Friedlander, M. J., and K. A. C. Martin, 1989. Development of y-axon innervation of cortical area 18 in the cat, *J. Physiol.*, 416:183–213.
- Galli, L., and L. Maffei, 1988. Spontaneous impulse activity of rat retinal ganglion cells in prenatal life, *Science*, 242:90–91.
- Gilbert, C. D., 1983. Microcircuitry of the visual cortex, *Annu. Rev. Neurosci.*, 6:217–247.
- Gilbert, C. D., and J. P. Kelly, 1975. The projections of cells in different layers of the cat's visual cortex, *J. Comp. Neurol.*, 163:81–105.
- Gilbert, C. D., and T. N. Wiesel, 1979. Morphology and intracortical projections of functionally characterised neurones in the cat visual cortex, *Nature*, 280:120–125.
- Gilbert, C. D., and T. N. Wiesel, 1989. Columnar specificity of intrinsic horizontal and corticocortical connections in cat visual cortex, *J. Neurosci.*, 9:2432–2442.
- Gonchar, Y., and A. Burkhalter, 1999. Differential subcellular localization of forward and feedback interareal inputs to parvalbumin expressing GABAergic neurons in rat visual cortex, *J. Comp. Neurol.*, 406:346–360.
- Hendrickson, A. E., 1985. Dots, stripes and columns in monkey visual cortex, *Trends Neurosci.*, 8:406–410.
- Hendry, S. H. C., and T. Yoshioka, 1994. A neurochemically distinct third channel in the macaque dorsal lateral geniculate nucleus, *Science*, 264:575–577.
- Hernit, C. S., K. M. Murphy, and R. C. Van Sluyters, 1996. Development of the visual callosal cell distribution in the rat: mature features are present at birth, *Visual Neurosci.*, 13:923–943.
- Hirsch, H. V., and D. N. Spinelli, 1970. Visual experience modifies distribution of horizontally and vertically oriented receptive fields in cats, *Science*, 168:869–871.
- Horton, J. C., and D. R. Hocking, 1996. Anatomical demonstration of ocular dominance columns in striate cortex of the squirrel monkey, *J. Neurosci.*, 16:5510–5522.
- Hubel, D., 1995. *Eye, Brain and Vision*, New York: Freeman and Co.
- Hubel, D. H., and T. N. Wiesel, 1962. Receptive fields binocular interaction and functional architecture in the cat visual cortex, *J. Physiol.*, 160:106–154.
- Hubel, D. H., and T. N. Wiesel, 1977. Functional architecture of macaque monkey visual cortex, *Proc. R. Soc. Lond. [Biol.]*, 198:1–59.
- Huntley, G. W., and E. G. Jones, 1990. Cajal-Retzius neurons in developing monkey neocortex show immunoreactivity for calcium binding proteins, *J. Neurocytol.*, 19:200–212.
- Hupé, J. M., A. C. James, B. R. Payne, S. G. Lomber, P. Girard, and J. Bullier, 1998. Cortical feedback improves discrimination between figure and background by V1, V2 and V3 neurons, *Nature*, 394:784–787.
- Ignacio, M. P. D., E. J. Kimm, G. H. Kageyama, J. Yu, and R. T. Robertson, 1995. Postnatal migration of neurons and formation of laminae in the rat cerebral cortex, *Anat. Embryol.*, 191:89–100.
- Innocenti, G. M., L. Fiore, and R. Caminiti, 1977. Exuberant projection into the corpus callosum from the visual cortex of newborn cats, *Neurosci. Lett.*, 4:237–242.
- Ishai, A., and D. Sagi, 1995. Common mechanisms of visual imagery and perception [see comments], *Science*, 268:1772–1774.
- Johnson, R. R., and A. Burkhalter, 1996. Microcircuitry of forward and feedback connections within rat visual cortex, *J. Comp. Neurol.*, 368:383–398.
- Johnson, R. R., and A. Burkhalter, 1997. A polysynaptic feedback circuit in rat visual cortex, *J. Neurosci.*, 17:7129–7140.
- Kato, N., J. M. R. Ferrer, and D. J. Price, 1991. Regressive changes among corticocortical neurons projecting from the lateral suprasylvian cortex to area-18 of the kittens visual cortex, *Neuroscience*, 43:291–306.
- Katz, L. C., and E. M. Callaway, 1992. Development of local circuits in mammalian visual cortex, *Annu. Rev. Neurosci.*, 15:31–56.
- Kennedy, H., P. Barone, and A. Falchier, 2000. Relative contributions of feedforward and feedback inputs to individual area, *Eur. J. Neurosci.*, 12:489.
- Kennedy, H., J. Bullier, and C. Dehay, 1989. Transient projections from the superior temporal sulcus to area 17 in the newborn macaque monkey, *Proc. Natl. Acad. Sci. USA*, 86:8093–8097.
- Kennedy, H., C. Dehay, L. M. Chalupa, P. Giroud, V. Cortay, L. Renaud, and M. Berland, 2001. Directed ingrowth of retinogeniculate axons into eye-specific domains in the fetal monkey, *Soc. Neurosci. Abstr.*, 27:475–472.
- Kennedy, H., C. Dehay, and G. Horsburgh, 1990. Striate cortex periodicity, *Nature*, 348:494.
- Kennedy, H., P. Salin, J. Bullier, and G. Horsburgh, 1994. Topography of developing thalamic and cortical pathways in the visual system of the cat, *J. Comp. Neurol.*, 348:298–319.
- Knutsen, R., D. L. Stanton, and A. Burkhalter, 1997. Emergence of topographic specificity in forward and feedback pathways of rat visual cortex, *Soc. Neurosci. Abstr.*, 23:1665.
- Koester, S. E., and D. D. M. O'Leary, 1993. Connectional distinction between callosal and subcortically projecting cortical neurons is determined prior to axon extension, *Dev. Biol.*, 160:1–14.
- Krubitzer, L., and K. J. Huffman, 2000. Arealization of the neocortex in mammals: genetic and epigenetic contributions to the phenotype, *Brain Behav. Evol.*, 55:322–335.
- Kuljis, R., and P. Rakic, 1990. Hypercolumns in primate visual cortex can develop in the absence of the cues from the photoreceptors, *Proc. Natl. Acad. Sci. USA*, 87:5303–5306.
- Lamme, V. A., and P. R. Roelfsema, 2000. The distinct modes of vision offered by feedforward and recurrent processing, *Trends Neurosci.*, 23:571–579.
- LeVay, S., T. N. Wiesel, and D. H. Hubel, 1980. The development of ocular dominance columns in normal and visually deprived monkeys, *J. Comp. Neurol.*, 191:1–51.
- Livingstone, M. S., and D. H. Hubel, 1984. Specificity of intrinsic connections in primate primary visual cortex, *J. Neurosci.*, 4:2830–2835.
- Lowenstein, P. R., and P. Somogyi, 1991. Synaptic organization of cortico-cortical connections from the primary visual cortex to the posteromedial lateral suprasylvian visual area in the cat, *J. Comp. Neurol.*, 310:253–266.

- Lubke, J., and K. Albus, 1992a. Lack of exuberance in clustered intrinsic connections in the striate cortex of one-month-old kitten, *Eur. J. Neurosci.*, 4:189–192.
- Lubke, J., and K. Albus, 1992b. Rapid rearrangement of intrinsic tangential connections in the striate cortex of normal and dark-reared kittens: lack of exuberance beyond the second postnatal week, *J. Comp. Neurol.*, 323:42–58.
- Luhmann, H. J., L. Martinez Millan, and W. Singer, 1986. Development of horizontal intrinsic connections in cat striate cortex, *Exp. Brain Res.*, 63:443–448.
- Luskin, M. B., and C. J. Shatz, 1985. Neurogenesis of the cat's primary visual cortex, *J. Comp. Neurol.*, 242:611–631.
- Malach, R., Y. Amir, M. Harel, and A. Grinvald, 1993. Relationship between intrinsic connections and functional architecture revealed by optical imaging and *in vivo* targeted biocytin injections in primate striate cortex, *Proc. Natl. Acad. Sci. USA*, 90:10469–10473.
- Marin-Padilla, M., 1984. Neurons of layer 1: a developmental analysis, in *Cerebral Cortex*, New York: Plenum, pp. 447–475.
- Martin, K. A., and D. Whitteridge, 1984. Form, function and intracortical projections of spiny neurones in the striate visual cortex of the cat, *J. Physiol.*, 353:463–504.
- Maunsell, J. H., and W. T. Newsome, 1987. Visual processing in monkey extrastriate cortex, *Annu. Rev. Neurosci.*, 10:363–401.
- Maunsell, J. H. R., and D. C. Van Essen, 1983. The connections of the middle temporal visual area (MT) and their relationship to a cortical hierarchy in the macaque monkey, *J. Neurosci.*, 3:2563–2586.
- McAdams, C. J., and J. H. Maunsell, 2000. Attention to both space and feature modulates neuronal responses in macaque area V4, *J. Neurophysiol.*, 83:1751–1755.
- McConnell, S. K., 1988. Fates of visual cortical neurons in the ferret after isochronic and heterochronic transplantation, *J. Neurosci.*, 8:945–974.
- McConnell, S. K., A. Ghosh, and C. J. Shatz, 1989. Subplate neurons pioneer the first axon pathway from the cerebral cortex, *Science*, 245:978–982.
- McGuire, B. A., C. D. Gilbert, P. K. Rivlin, and T. N. Wiesel, 1991. Targets of horizontal connections in macaque primary visual cortex, *J. Comp. Neurol.*, 305:370–392.
- Meissirel, C., C. Dehay, M. Berland, and H. Kennedy, 1991. Segregation of callosal and association pathways during development in the visual cortex of the primate, *J. Neurosci.*, 11:3297–3316.
- Meister M., R. O. L. Wong, D. A. Baylor, and C. J. Shatz, 1991. Synchronous bursts of action potentials in ganglion cells of the developing mammalian retina, *Science*, 252:939–943.
- Meyer, G., and P. Wahle, 1999. The paleocortical ventricle is the origin of reelin-expressing neurons in the marginal zone of the foetal human neocortex, *Eur. J. Neurosci.*, 11:3937–3944.
- Mooney, R., D. V. Madison, and C. J. Shatz, 1993. Enhancement of transmission at the developing retinogeniculate synapse, *Neuron*, 10:815–825.
- Motter, B. C., 1994. Neural correlates of feature selective memory and pop-out in extrastriate area V4, *J. Neurosci.*, 14:2190–2199.
- Murphy, P. C., and A. M. Sillito, 1996. Functional morphology of the feedback pathway from area 17 of the cat visual cortex to the lateral geniculate nucleus, *J. Neurosci.*, 16:1180–1192.
- Naya, Y., M. Yoshida, and Y. Miyashita, 2001. Backward spreading of memory-retrieval signal in the primate temporal cortex, *Science*, 291:661–664.
- O'Leary, D. D. M., 1989. Do cortical areas emerge from a proto-cortex? *Trends Neurosci.*, 12:400–406.
- Patel, G., G. W. Harding, and A. Burkhalter, 1999. Emergence of topography and laminar specificity of interareal forward and feedback connections in mouse visual cortex, *Soc. Neurosci. Abstr.*, 23:1665.
- Patel, N. H., 1994. Developmental evolution: insights from studies of insect segmentation, *Science*, 266:581–589.
- Perkel, D. J., J. Bullier, and H. Kennedy, 1986. Topography of the afferent connectivity of area 17 in the macaque monkey: a double labelling study, *J. Comp. Neurol.*, 253:374–402.
- Polleux, F., C. Dehay, A. Goffinet, and H. Kennedy, 2001. Pre- and post-mitotic events contribute to the progressive acquisition of area-specific connectional fate in the neocortex, *Cereb. Cortex*, 11:1027–1039.
- Polleux, F., C. Dehay, and H. Kennedy, 1997. The timetable of laminar neurogenesis contributes to the specification of cortical areas in mouse isocortex, *J. Comp. Neurol.*, 385:95–116.
- Polleux, F., C. Dehay, and H. Kennedy, 1998a. Neurogenesis and commitment of corticospinal neurons in reeler, *J. Neurosci.*, 18:9910–9923.
- Polleux, F., R. J. Giger, D. D. Ginty, A. L. Kolodkin, and A. Ghosh, 1998b. Patterning of cortical efferent projections by semaphorin-neuropilin interactions, *Science*, 282:1904–1906.
- Price, D. J., and C. Blakemore, 1985a. The postnatal development of the association projection from visual cortical area 17 to area 18 in the cat, *J. Neurosci.*, 5:2443–2452.
- Price, D. J., and C. Blakemore, 1985b. Regressive events in the postnatal development of association projections in the visual cortex, *Nature*, 316:721–724.
- Price, D. J., J. M. R. Ferrer, C. Blakemore, and N. Kato, 1994. Postnatal development and plasticity of corticocortical projections from area 17 to area 18 in the cats visual cortex, *J. Neurosci.*, 14:2747–2762.
- Price, D. J., and T. J. Zumbroich, 1989. Postnatal development of corticocortical efferents from area 17 in the cat's visual cortex, *J. Neurosci.*, 9:600–613.
- Rakic, P., 1976. Prenatal genesis of connections subserving ocular dominance in the rhesus monkey, *Nature*, 261:467–471.
- Rakic, P., 1988. Specification of cerebral cortical areas, *Science*, 241:170–176.
- Rakic, P., and R. S. Nowakowski, 1981. The time of origin of neurons in the hippocampal region of the rhesus monkey, *J. Comp. Neurol.*, 196:99–128.
- Rockland, K. S., and J. S. Lund, 1982. Widespread periodic intrinsic connections in the tree shrew visual cortex, *Science*, 215:1532–1534.
- Rockland, K. S., and D. N. Pandya, 1979. Laminar origins and terminations of cortical connections to the occipital lobe in the rhesus monkey, *Brain Res.*, 179:3–20.
- Rockland, K. S., K. S. Saleem, and K. Tanaka, 1994. Divergent feedback connections from areas V4 and TEO in the macaque, *Visual Neurosci.*, 11:579–600.
- Rockland, K. S., and A. Virga, 1989. Terminal arbors of individual "feedback" axons projecting from area V2 to V1 in the macaque monkey: A study using immunohistochemistry of anterogradely transported Phaseolus vulgaris-leucoagglutinin, *J. Comp. Neurol.*, 285:54–72.
- Rockland, K. S., and A. Virga, 1990. Organization of individual cortical axons projecting from area V1 (area 17) to V2 (area 18) in the macaque monkey, *Visual Neurosci.*, 4:11–28.

- Sandell, J. H., and P. H. Schiller, 1982. Effect of cooling area 18 on striate cortex cells in the squirrel monkey, *J. Neurophysiol.*, 48:38–48.
- Scannell, J. W., and M. P. Young, eds., 2002. Primary visual cortex within the cortico-cortico-thalamic network, in *Cerebral cortex* (A. Peters, E. G. Jones, and B. R. Payne, eds.), vol. 15, *Cat primary visual cortex*, New York: Plenum.
- Schwartz, T. H., D. Rabinowitz, V. Unni, V. S. Kumar, D. K. Smetters, A. Tsiola, and R. Yuste, 1998. Networks of coactive neurons in developing layer 1, *Neuron*, 20:541–552.
- Sengpiel, F., P. Stawinski, and T. Bonhoeffer, 1999. Influence of experience on orientation maps in cat visual cortex, *Nat. Neurosci.*, 2:727–732.
- Shao, Z., and A. Burkhalter, 1998. Development of synaptic inhibition in intracortical pathways of rat visual cortex, *Soc. Neurosci. Abstr.*, USA, 24:1518.
- Shao, Z. W., and A. Burkhalter, 1996. Different balance of excitation and inhibition in forward and feedback circuits of rat visual cortex, *J. Neurosci.*, 16:7353–7365.
- Sharma, J., A. Angelucci, and M. Sur, 2000. Induction of visual orientation modules in auditory cortex, *Nature*, 404:841–847.
- Shatz, C. J., and M. B. Luskin, 1986. The relationship between the geniculocortical afferents and their cortical target cells during development of the cat's primary visual cortex, *J. Neurosci.*, 6:3655–3668.
- Sherman, S. M., 2001. A wake-up call from the thalamus, *Nat. Neurosci.*, 4:344–346.
- Snider, C. J., C. Dehay, M. Berland, H. Kennedy, and L. M. Chalupa, 1999. Prenatal development of retinogeniculate axons in the macaque monkey during segregation of binocular inputs, *J. Neurosci.*, 19:220–228.
- Song, H., G. Ming, Z. He, M. Lehmann, L. McKerracher, M. Tessier-Lavigne, and M. Poo, 1998. Conversion of neuronal growth cone responses from repulsion to attraction by cyclic nucleotides, *Science*, 281:1515–1518.
- Stryker, M. P., and W. A. Harris, 1986. Binocular impulse blockade prevents the formation of ocular dominance columns in cat visual cortex, *J. Neurosci.*, 6:2117–2133.
- Stryker, M. P., and H. Sherk, 1975. Modification of cortical orientation selectivity in the cat by restricted visual experience: a reexamination, *Science*, 190:904–906.
- Super, H., J. A. Del Rio, A. Martinez, P. Perez-Sust, and E. Soriano, 2000. Disruption of neuronal migration and radial glia in the developing cerebral cortex following ablation of Cajal-Retzius cells, *Cereb. Cortex*, 10:602–613.
- Ts'o, D. Y., C. D. Gilbert, and T. N. Wiesel, 1986. Relationships between horizontal interactions and functional architecture in cat striate cortex as revealed by cross-correlation analysis, *J. Neurosci.*, 6:1160–1170.
- Van der Loos, H., and T. A. Woolsey, 1973. Somatosensory cortex: structural alteration following early injury to sense organs, *Science*, 179:395–398.
- Vanduffel, W., B. R. Payne, S. G. Lomber, and G. A. Orban, 1997. Functional impact of cerebral connections, *Proc. Natl. Acad. Sci. USA*, 94:7617–7620.
- Van Essen, D. C., and J. L. Gallant, 1994. Neural mechanism of form and motion processing in the primate visual system, *Neuron*, 13:1–10.
- Von Senden, M., 1960. *Space and Sight*, Glencoe: The Free Press.
- Weliky, M., and L. C. Katz, 1994. Functional mapping of horizontal connections in developing ferret visual cortex: experiments and modeling, *J. Neurosci.*, 14:7291–7305.
- White, L. E., D. M. Coppola, and D. Fitzpatrick, 2001. The contribution of sensory experience to the maturation of orientation selectivity in ferret visual cortex, *Nature*, 411:1049–1052.
- Wiesel, N., and D. H. Hubel, 1963. Single-cell responses in striate cortex of kittens deprived of in one eye, *J. Neurophysiol.*, 26:1003–1017.
- Wiesel, T. N., and D. H. Hubel, 1974. Ordered arrangement of orientation columns in monkeys lacking visual experience, *J. Comp. Neurol.*, 158:307–318.
- Wong, R. O. L., M. Meister, and C. J. Shatz, 1993. Transient period of correlated bursting activity during development of the mammalian retina, *Neuron*, 11:923–938.
- Yamamoto, N., K. Yamada, T. Kurotani, and K. Toyama, 1992. Laminar specificity of extrinsic cortical connections studied in coculture preparations, *Neuron*, 9:217–228.
- Yamashita, A., Y. Gonchar, and A. Burkhalter, 2000. Rearrangement of synaptic connections with inhibitory neurons in interareal forward and feedback circuits in developing mouse and rat visual cortex, *Soc. Neurosci. Abstr.*, 26:854.
- Yoshioka T., C. G. Blasdel, J. B. Levitt, and J. S. Lund, 1996. Relation between patterns of intrinsic lateral connectivity, ocular dominance, and cytochrome oxidase-reactive regions in macaque monkey striate cortex, *Cereb. Cortex*, 6:297–310.
- Young, M. P., 2000. The architecture of visual cortex and inferential processes in vision, *Spat. Vision*, 13:137–146.
- Young, M. P., ed., 2001. Connectional organization and function in the macaque cerebral cortex, in A. Schüz and R. Miller, *Cortical areas: unity and diversity*, In the series *Conceptual Advances in Brain Research*. London and New York: Taylor and Francis, pp. 351–377, 2002.
- Yuste, R., and M. Sur, 1999. Development and plasticity of the cerebral cortex: from molecules to maps, *J. Neurobiol.*, 41:1–6.
- Zeki, S., 1993. *A Vision of the Brain*, Oxford: Blackwell Scientific.
- Zeki, S., and S. Shipp, 1988. The functional logic of cortical connections, *Nature*, 335:311–317.
- Zufferey, P. D., F. Jin, H. Nakamura, L. Tettoni, and G. M. Innocenti, 1999. The role of pattern vision in the development of cortico-cortical connections, *Eur. J. Neurosci.*, 11:2669–2688.

12 Neural Limitations on Visual Development in Primates

LYNNE KIORPES AND J. ANTHONY MOVSHON

NEWBORN PRIMATES see poorly. Their visual capacities improve over time, with a course that varies somewhat depending on the measure used to define visual function and the species studied. Many common measures of vision reach adult levels by the age of about 1 year in macaque monkeys and about 5 years in humans; during the period of maturation, performance typically improves roughly 10- to 30-fold. Figure 12.1 caricatures the effect on vision of two of these measures, spatial resolution and sensitivity to spatial contrast. The panel on the left shows a cityscape as seen by an adult, whereas the panel on the right shows the same scene transformed to represent the view of a newborn infant. The “infant view” has been spatially lowpass-filtered (blurred) and reduced in contrast.

Figure 12.2 shows developmental measurements of spatial resolution (Kiorpes, 1992a; Movshon and Kiorpes, 1988) and contrast sensitivity (Boothe et al., 1988) taken from macaque monkey infants. Figure 12.2A shows grating activity data from a group of young monkeys tested cross-sectionally; Figure 12.2B shows a series of contrast sensitivity functions measured longitudinally in two representative individual animals. Figure 12.2B emphasizes that different animals develop at different rates, so in Figure 12.2C we show the range of sensitivity and resolution values measured across a population of six monkeys. Both resolution and sensitivity develop smoothly over the first 6 to 12 months of life. These functions mature somewhat more rapidly when measured electrophysiologically using a visual evoked potential (VEP) technique in monkeys (Skoczenski et al., 1995) and humans (Kelly et al., 1997; Norcia et al., 1990; Chapter 13; see also Peterzell et al., 1995). This discrepancy between techniques is not surprising given that the VEP signal arises from the summed activity of visual cortical neurons. As we discuss later, neurons in infant visual cortex are considerably more mature than behavior would suggest.

We want to understand the processes that limit visual development. In the first part of this chapter we will consider what aspects of visual system organization and function limit performance in newborn infants, and what factors develop to permit attainment of adult level of visual performance. We are also interested in the modifiable mecha-

nisms that are responsible for the altered visual development that occurs when normal vision is disrupted, and in the second part of the chapter we will explore the neural factors responsible for this behavioral plasticity.

Visual input

Many aspects of the eye and the optical and retinal elements involved in the initial encoding of the visual stimulus improve postnatally. The macaque eye grows by about 40% from infancy to adulthood, increasing the magnification of the retinal image (Blakemore and Vital-Durand, 1986a; Williams and Boothe, 1981). The quality of the eye’s optics improves over the same span (Williams and Boothe, 1981), increasing the resolution and contrast of the retinal image. Even in the absence of neural changes, the increased retinal magnification would cause a proportionate improvement in visual resolution as long as retinal sampling was held constant. The optical changes are less likely to be important for infant vision, as they primarily affect spatial frequencies well beyond the behavioral resolution limit at any age. So optical factors seem unlikely to account for more than about a 40% change in visual resolution. Retinal changes, however, may be more significant.

Hendrickson and her colleagues have shown that the morphology and distribution of cone photoreceptors undergo marked changes after birth in both humans and monkeys (Hendrickson and Kupfer, 1976; Hendrickson and Yuodelis, 1984; Packer et al., 1990; Yuodelis and Hendrickson, 1986). The foveal concentration of cones that is characteristic of adult retinae is much less marked in neonates; during development, cones migrate toward the center of the fovea. Figure 12.3A shows this effect in data from five macaque monkeys aged 1 week to adult. The data in Figure 12.3A are plotted in terms of units of visual angle, so they incorporate both the effects of retinal changes and the effects of eye growth (which act in the opposite direction to the increase in retinal cone density created by migration). The combination of these factors changes the linear sampling density of the foveal cone mosaic by about a factor of 3 from 1 week to adulthood. This change is captured in Figure 12.3A by plotting the Nyquist frequency of the retinal



FIGURE 12.1. Simulation of the visual worlds of an adult and young infant primate. To create the simulated image on the right, the image on the left was convolved with a Gaussian, the σ of which was 1° ; the image contrast was reduced by a factor of 5. The angular width of the view shown is approximately 10° .

mosaic, the highest spatial frequency that can be accurately reconstructed from samples spaced like foveal cones; this value grows from about 18 cycles/degree at 1 week to about 55 cycles/degree in adulthood. Comparing these values with the behavioral measurements of resolution in Figure 12.2A shows that in no case does the spacing of foveal cones seem to impose an important limit on visual resolution. Figure 12.3A shows that much of the change in foveal cone density takes place by 4 weeks of age in macaques, but the period over which the photoreceptor array matures to its final adult levels is still somewhat unclear. Peak cone density is approximately 75% of adult density by 6 months of age in monkeys, and only about 50% of adult density by 4 years of age in humans (Hendrickson, 1992, 1993).

While photoreceptor migration is taking place, the structure of individual cones is also changing. Initially, their outer segments are short and stubby; but they develop over time to achieve the elongated, slender morphology of adult photoreceptors. This maturation permits the outer segment to capture light efficiently; in the immature retina, a far higher fraction of incident quanta fails to be absorbed by photopigment than in the adult retina (Banks and Bennett, 1988; Brown et al., 1987). Foveal cone outer segments appear generally adult-like by 12 weeks of age in monkeys and 15 months in humans; however, elongation of outer segments continues over the first year in monkeys and beyond 4 years in humans (Hendrickson, 1992, 1993).

The effects of such diverse factors as changes in the size and optical quality of the eye and changes in the morphology and distribution of receptors are critical for the performance of central visual mechanisms, but can be difficult to work out intuitively. They can conveniently be analyzed with

the theory of the “ideal observer” (Geisler, 1984, and Chapter 52, Ideal Observer Analysis). An ideal observer model uses the properties of optics and early visual elements to calculate ideal performance given just the early limitations; the cascade of factors is schematically shown in Fig. 12.3B. The ideal observer simulates each of the early steps in seeing from the incidence of light at the cornea to its absorption and representation by the photoreceptor array. The ideal observer is internally noise-free; its performance is limited only by the Poisson fluctuations in the number of photons absorbed by photoreceptors. As such, it is not a model of the nervous system; rather, it simulates the performance of a perfect nervous system limited only by the optical and photoreceptor apparatus available. It therefore provides an objective benchmark against which the performance of real, imperfect observers can be measured.

Following the work of Geisler (1984) and Banks and Bennett (1988), we created an ideal observer model for the infant macaque monkey and used it to compare real and ideal performance (Kiorpes et al., 2000b). We modeled ideal performance at three ages: 1 week, 4 weeks, and 24 weeks. To make as accurate a model as possible, we made as many measurements as possible from the same macaque species from which the behavioral data were drawn. The key parameters for the model at the different age points are listed in Table 12.1. The photoreceptor and cone density data and pupil diameters were measured directly from *Macaca nemestrina* monkeys; the other values were taken or estimated from the literature. The structure of the ideal observer model is shown in Figure 12.3B. To determine contrast threshold for each of a set of stimulus conditions chosen to be

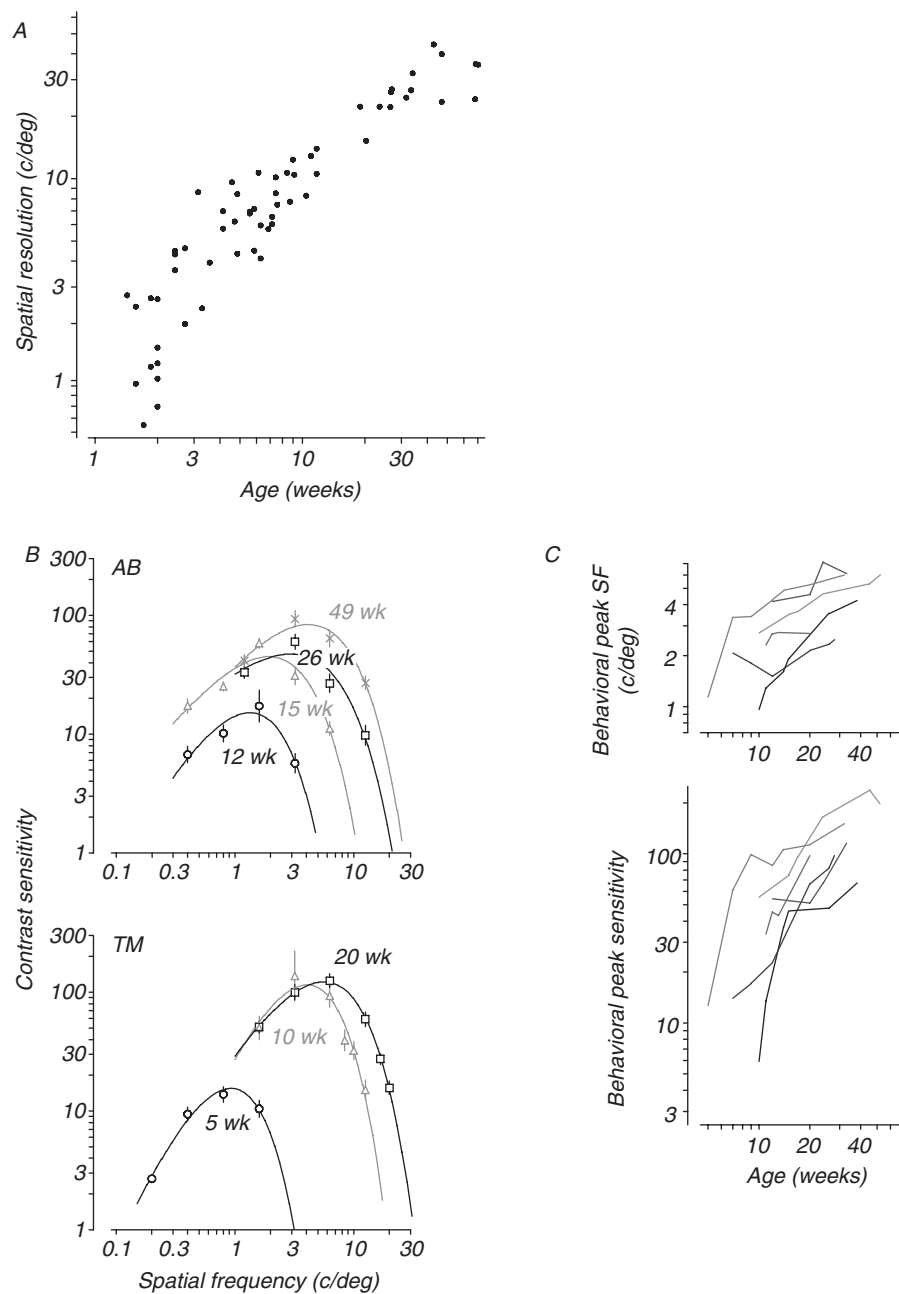


FIGURE 12.2. The development of spatial vision in infant macaque monkeys. *A*, Spatial resolution data from a set of 17 normal infant macaques (taken from Kiorpes, 1992a; Movshon and Kiorpes, 1988). The measure of spatial resolution was grating acuity, the highest spatial frequency at which a grating could reliably be distinguished from a uniform field of the same luminance. Animals younger than 16 weeks were tested using a forced-choice, preferential looking technique. Older animals were tested in a standard two-choice operant discrimination task. *B*, Spatial contrast

sensitivity functions, measured using operant techniques, in two infant macaques at a range of ages (as indicated) (data from Boothe et al., 1988). Error bars indicate the standard error of the mean threshold determined by Probit analysis. *C*, The range of rates of development of spatial contrast sensitivity in six infant macaques. Each line represents the course of contrast sensitivity development in an individual monkey. The two plots indicate the horizontal and vertical positions of the peaks of the measured contrast sensitivity functions. (Redrawn from Movshon and Kiorpes, 1988.)

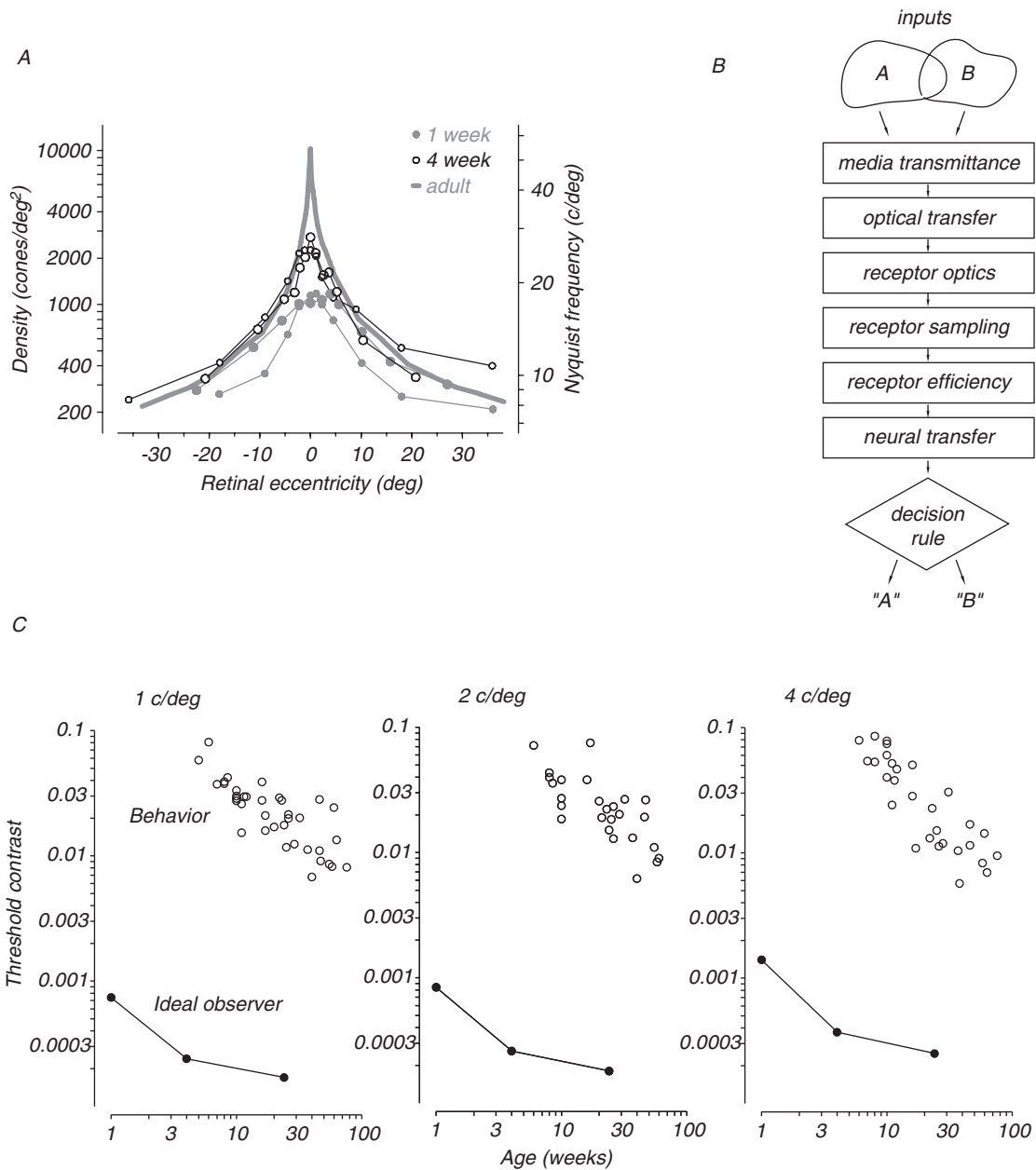


FIGURE 12.3. Assessing the influence of retinal development on spatial vision. *A*, Cone density along the horizontal meridian of the visual field in five macaque monkeys, aged 1 week to adult. Density is expressed on the left ordinate in units of areal density in visual space, and on the right ordinate as the Nyquist frequency of a perfect hexagonal array. The Nyquist frequency is the highest spatial frequency that can be accurately reconstructed from a given set of sample points. (Unpublished measurements by C. Henry,

M. J. Hawken, J. A. Movshon, and L. Kiorpes). *B*, A schematic illustration of the stages of analysis in an ideal observer model (after Geisler, 1984). See text for details. *C*, Comparison of contrast thresholds for macaques and for the macaque ideal observer model (Kiorpes et al., 2000b). Simulated thresholds for the ideal observer are shown as solid symbols connected by lines. Real thresholds, measured behaviorally in 13 macaques, are shown as open symbols (data from Kiorpes and Movshon, 1998).

TABLE 12.1

Key parameters for macaque ideal observer simulations

	1 Week	4 Weeks	24 Weeks
Line spread function width at half height (min arc)	2.25	1.69	1.33
Pupil diameter (mm)	4.8	5.3	6
Posterior nodal distance (mm)	10.91	11.84	13.52
Cone density (cone/mm ²)	37268	110374	202905
Outer segment diameter (μm)	1.94	2.09	1.79
Outer segment length (μm)	13.6	31.8	40.0

comparable to conditions used to gather data from monkeys, we simulated responses to a stimulus and a blank (inputs A and B). We filtered the inputs by the transfer function for the eye, sampled the stimulus using the measured photoreceptor mosaic, incorporated Poisson photon noise, computed the likelihood of a stimulus or blank, and chose the more likely (“A” or “B”). We repeated this process 1000 times for each condition, compiled the resulting data into psychometric functions, and analyzed them exactly as we analyze behavioral data. The results of these simulations for gratings of three spatial frequencies at the three chosen ages are shown in Figure 12.3C as filled points connected by lines. Comparable behavioral measurements are shown as isolated open symbols.

The first point to note is that the absolute sensitivity of the ideal observer is at least 100 times higher than the monkeys’; in other words, the animals’ quantum efficiency was no better than 1%. This value is comparable to that determined in humans (Banks and Bennett, 1988; Geisler, 1984; Pelli, 1990) and reflects the fact that observers do not seem to be capable of using all the information available in the pattern of photoreceptor quantum absorptions. However, ideal observer simulations are nonetheless useful for comparing *relative* performance, here given by the relative shapes of the trends for real and ideal observers. Developmental changes in sensitivity shown by the ideal observer are largely confined to the first 4 postnatal weeks, whereas the bulk of the change measured behaviorally takes place after 4 weeks. Therefore, very little of the change in contrast threshold beyond 4 weeks can be accounted for by changes in the visual periphery in macaque monkeys. Banks and Bennett (1988) performed a similar analysis in human infants, arguing that peripheral factors play a somewhat more prominent role in the development of contrast sensitivity. Our conclusions differ from theirs for two reasons: first, photoreceptors in infant monkeys are somewhat more mature than in human infants; second, we used a more realistic calculation to estimate the way that photopigment absorptions depend on outer segment morphology. In any case, our conclusions and Banks and Bennett’s differ only in detail, and suggest that the great bulk of postnatal develop-

ment in contrast sensitivity depends on neural factors and not on optical and retinal maturation.

Subcortical visual structures

Largely for technical reasons, little is known about the development of the physiological organization of retinal ganglion cell receptive fields. In cats, Rusoff and Dubin (1977) reported the presence of adult-like center responses within a week of eye opening in kittens; however, receptive field surrounds were weak compared to adult surrounds. Because the optical quality of the kitten eye is poor (Bonds and Freeman, 1978), the maturity of retinal neural circuits is not easy to assess from these data. There have been no studies of ganglion cell receptive fields in infant monkeys.

The primary recipients of information from the retina, the lateral geniculate nucleus (LGN) and superior colliculus (SC), have been studied in infant primate, as has the nucleus of the optic tract (NOT), which receives a small but direct input from the retina (Kourouyan and Horton, 1997; Telkes et al., 2000).

The organization of the optokinetic system, whose visual inputs come through the NOT and the dorsal terminal nucleus of the accessory optic system, is qualitatively adult-like between 5 and 12 weeks after birth (Distler et al., 1999), but there is little quantitative information available on neuronal sensitivity or receptive field organization in these structures. The functional organization and receptive field properties of neurons in newborn monkey SC are remarkably mature (Wallace et al., 1997). Topographic organization is adult-like in the neonate, as are many receptive field properties. However, receptive field sizes—particularly for neurons with receptive fields near the fovea—are larger in the newborn than in the adult. Visual responses are also more sluggish throughout the SC, and visual latencies are significantly longer than in adults. Wallace et al. (1997) have argued that the retinotectal input is the primary determinant of SC response properties in infants, with little contribution from corticotectal projections. They have suggested that the immaturities of SC response properties may be explained by postnatal maturation of retinotectal myelination and changes in the retina itself. This conclusion is based on the assumption that the properties of cortical receptive fields in infants are quite immature; however, as documented later in this chapter, neurons in the primary visual cortex are surprisingly mature in infants. Thus it is equally plausible that the visual responses of SC neurons in infants primarily reflect the properties of afferent input from cortex, as they do in adults (Schiller et al., 1974).

The development of receptive field properties of LGN cells in Old-World primates has been studied more extensively than SC and NOT (Blakemore and Vital-Durand,

1986a; Hawken et al., 1997; Movshon et al., 1997). Like SC neurons, LGN cells in newborn monkeys often respond sluggishly to visual stimuli, and they have longer latencies than are found in adults. Blakemore and Vital-Durand (1986a) have found visual latencies to be mature by about 10 weeks of age. There is an overall improvement in visual responsiveness and spatial resolution in both parvocellular and magnocellular layers of the LGN over the first postnatal year in macaque monkeys, and Blakemore and Vital-Durand reported a sevenfold improvement in the visual resolution of LGN cells over this period. Moreover, Hawken and colleagues (1997) have demonstrated that the overall envelope of neuronal contrast sensitivity shows a profile much like that of behavioral development, with contrast sensitivity and spatial resolution developing concurrently. They found an early rapid development of contrast sensitivity over the first 2 months, followed by a more gradual progression to adult levels by about 8 months of age. Taken together, these studies suggest that the development of LGN spatial properties matches behavioral development, and that the properties of LGN cells or their afferents set an important limit on vision during development (Movshon and Kiorpes, 1993). Our own results (Movshon et al., 1997), however, present a somewhat different picture.

To compare behavioral development to physiological changes in LGN responses, we recorded from LGN cells in 1-week-, 4-week-, and 24-week-old macaque monkeys, and made quantitative measurements of their responses to spatial targets. For comparison with behavioral measurements, we concentrated on two aspects of LGN responses: sensitivity to contrast and sensitivity to spatial frequency. The results are shown in Figure 12.4, which places the data from the LGN in direct comparison with the behavioral data from Figure 12.2C. The shaded range and left-hand ordinates on each plot represent the changes in the position of the peak of the contrast sensitivity function (CSF) measured behaviorally. The symbols and right-hand ordinates represent the results of our LGN recordings. Each symbol represents the geometric mean (\pm the standard deviation of the distribution) of measurements from our whole population of LGN cells. The filled symbols show data from magnocellular neurons, whereas the open symbols represent data from parvocellular neurons. The upper plot shows values of the characteristic spatial frequency—this is the spatial frequency at which the response of the receptive field (RF) center mechanism, inferred from a fitted difference-of-Gaussians model, falls to $1/e$ of its peak (Enroth-Cugell and Robson, 1966; Linsenmeier et al., 1982). The lower plot shows values of responsivity, the slope of the initial linear segment of the contrast-response function, measured with optimal drifting grating targets (Linsenmeier et al., 1982). There is an improvement in both the sensitivity and spatial resolution of LGN cells between birth and 6 months, but a comparison

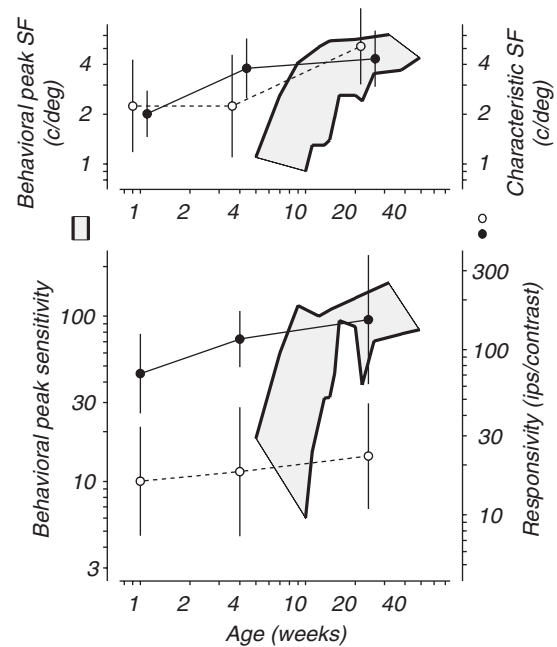


FIGURE 12.4. Comparison of behavioral contrast sensitivity development with the development of spatial contrast sensitivity in LGN neurons. The gray zone in each part of the figure represents (using the left-hand ordinates) the range between the slowest and fastest development in a population of six monkeys tested longitudinally (Boothe et al., 1988). The upper plot shows the development of the spatial frequency at which peak contrast sensitivity was observed; the lower plot shows the development of the peak contrast sensitivity value. The symbols and lines represent (using the right-hand ordinates) population data obtained from 355 LGN neurons recorded from 10 monkeys aged 1 to 24 weeks. Each symbol represents the geometric mean of the measured values of characteristic spatial frequency and responsivity in impulses per second (IPS) for parvocellular (*open circles*) and magnocellular (*filled circles*) neurons (see text for details). The error bars indicate ± 1 SD to convey a sense of the span of the underlying distribution. Note that the right- and left-hand ordinates are arbitrarily shifted so that the data sets meet at adult levels; no absolute relationship is implied.

of the physiological and behavioral data shows that the magnitude of the change is far too small to account for the observed behavioral changes. Moreover, although the physiological changes are, by most measures, largely complete by the age of 4 weeks, most behavioral changes occur later. We conclude that developmental changes in LGN response properties—and, by inference then, in the retinal afferents to LGN—are modest and do not account for behavioral change. In fact, the changes in LGN cell properties are similar to those expected of an ideal macaque observer (Fig. 12.3C), which as we have discussed is also an inadequate account of behavioral development. Our results differ from those presented in earlier reports (Blakemore and Vital-Durand, 1986a; Hawken et al., 1997) primarily in that we found far more adult-like spatial receptive fields in our youngest animals than they did. The difference may be

attributable to the different anesthetic techniques used. (Our studies used opiate anesthesia, whereas those of Blakemore and his colleagues used a combination of N_2O and barbiturates.)

Visual cortex

The primary visual cortex (V1) has long been known to show considerable postnatal modifiability by visual experience; moreover, the development of visual cortical response properties is seriously disrupted by visual deprivation. There is compelling evidence that normal vision is required for normal cortical development, and that abnormal vision can distort cortical development. This has led to the widespread view that the visual cortex is very immature at birth and that its development is actively “instructed” by visual input. An alternative view is that visual experience is not required to instruct development, but is merely “permissive,” allowing the normal sequence of developmental events to take place (for reviews, see Movshon and Kiorpes, 1990; Movshon and Van Sluyters, 1981). A crucial piece of evidence that distinguishes these views is the status of the visual cortex in very young animals. If, as initially claimed, the visual cortex of neonates is responsive to visual stimuli and contains at least some neurons with adult-like selectivity (Hubel and Wiesel, 1963), it would seem unlikely that visual experience served as a strong instructor for development. If, however, the neonatal visual cortex contains few neurons with adult-like responses, the argument for a strong active role for visual experience in visual development is much more plausible (Blakemore and Van Sluyters, 1975; Pettigrew, 1974). This debate initially centered on development in kittens, but the same differences of view have been recapitulated in the literature on development in monkeys (Blakemore, 1990; Blasdel et al., 1995; Chino et al., 1997; Movshon and Kiorpes, 1993; Wiesel and Hubel, 1974).

To revisit these questions and to explore the relationship between the development of physiological response properties of V1 cells and behavioral visual development, the authors recorded from cells in macaque monkeys, aged 1 week, 4 weeks, 16 weeks, and adult (Movshon et al., 1999, 2000), and made quantitative measurements of the animals’ responses to spatial stimuli. We studied a variety of response properties at each age point, including receptive field size and spatial frequency tuning, selectivity for orientation and direction of motion, and selectivity for stimulus area as an indication of the strength of receptive field surrounds. Figure 12.5 shows the development of six derived measures that summarize these developmental data. In each case, the algebraic or geometric mean value for the measure is given (\pm the standard deviation of the distribution; details of the analyses are given in the figure legend).

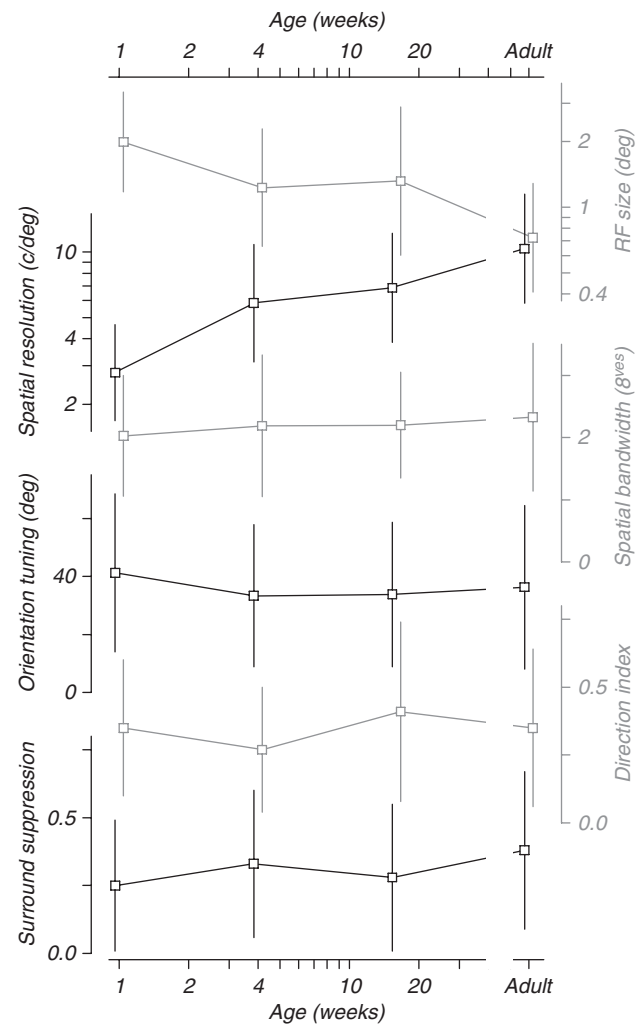


FIGURE 12.5. Development of the receptive field (RF) properties of V1 neurons in macaques (from Movshon et al., 1999, 2000). Each panel of the plot represents the development of a particular receptive field property in a study of 453 V1 neurons representing the central 5° of the visual field, recorded from 11 animals at the indicated ages. Each point represents the mean or the geometric mean, as appropriate, of the values measured for all neurons recorded at a particular age; the error bars indicate ± 1 SD to convey a sense of the span of the underlying distribution. In sequence from the top, the parameters displayed are *receptive field size*, defined as the size of an otherwise optimal patch of grating that elicited at least 95% of the maximum response (Cavanaugh et al., 2002); *spatial resolution*, defined as the highest spatial frequency at which the cell gave a response of at least 10% of its maximum; *spatial bandwidth*, defined as the ratio between the highest and lowest spatial frequencies giving at least half-maximal response, expressed in octaves; *orientation tuning*, defined as the change in orientation from the peak that causes the response to fall by one half; *direction index*, defined as $1 - np/p$, where p is the response to an optimal grating moving in the preferred direction and np is the response to the same grating moving 180° from the preferred; *surround suppression*, defined as the fractional reduction in response resulting from the enlargement of an optimal-size patch of grating to cover the full screen (Cavanaugh et al., 2002).

The two upper graphs in Figure 12.5 show the development of the spatial scale of V1 receptive fields by plotting receptive field size and spatial resolution for grating stimuli as a function of age. Both measures suggest that, from the age of 1 week to adulthood, receptive fields shrink on average by about a factor of 3, a value comparable to that seen for similar measures in LGN cells (see Fig. 12.4). The four lower graphs in Figure 12.5 show the development of four indices of receptive field selectivity. These show that, with remarkable consistency, the spatial structure of V1 receptive fields remains constant during development. None of the parameters that measure receptive field structure—selectivity for spatial frequency and orientation, selectivity for direction of movement, or strength of neuronal surround suppression—varies at all with age. In some other respects, V1 neuronal properties are immature in infants. For example, peak response magnitudes and sensitivity to rapid stimulus change are substantially less in 1-week-old animals than in adults; however, the visual effects of these changes are, to some degree, ameliorated by the curious fact that responses in 1-week-old animals are substantially more reliable than in adults (Rust et al., 2002).

The simplest picture that emerges from these data is that the receptive fields of visual cortex neurons gradually reduce in size during development, without changing any of their

other spatial properties. The degree to which they do this seems to be identical to the rate at which the receptive fields of LGN cells change size and the spacing between foveal cones decreases, but this is substantially slower than the rate at which behavioral changes take place. Figure 12.6A compares the evolution of several spatial properties during development. The graph plots visual acuity (from Fig. 12.2A), along with the development of spatial resolution of LGN and V1 cells and with the development of the cone mosaic as indicated by the Nyquist frequency. Changes in behavioral acuity are more extensive than changes in any of the neural properties plotted, and all these neural properties seem to develop in step, as evidenced by their parallel progressions across the plot.

The comparison shown in Figure 12.6A suggests that the changes in V1 spatial properties simply follow changes at the periphery. One explanation, articulated by Wilson (1988), is illustrated in Figure 12.6B (see also Brown et al., 1987; Peterzell et al., 1993; and Peterzell and Teller, 1996). Cortical receptive fields can be considered to be a map of connections directly back to the mosaic of cones whose signals drive them. As noted earlier, cones in infant retina are spaced widely (*top left*), and the receptive fields of cortical neurons (given in cross-section, *middle*) are correspondingly broad. This corresponds to a selectivity for relatively low spatial

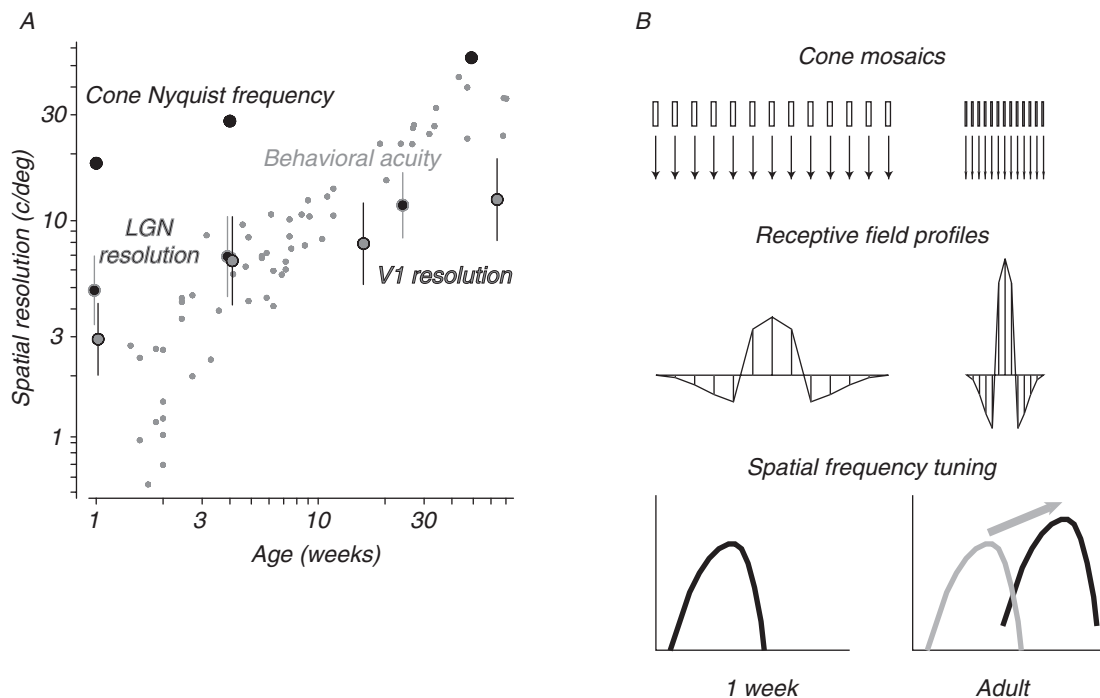


FIGURE 12.6. Relative development of different elements of spatial vision. *A*, The development of grating acuity (from Fig. 12.2A) is compared to three measures of neural development: Nyquist frequency (taken from the peak values of the cone density distributions in Fig. 12.3A); the spatial resolution of neurons in the

LGN (average of P and M cells, from Fig. 12.4); and the spatial resolution of neurons in V1 (from Fig. 12.5). *B*, A conceptual account of how cortical receptive field development would result from migration of cones; see text for details.

frequencies (*bottom*). Let us suppose that cortical receptive fields—as defined by their connections to cones—are unchanged during development. Now as the cones migrate toward the center of the fovea and become more tightly packed (*top right*), cortical receptive fields shrink in proportion (*middle right*), and neurons consequently develop a preference for higher spatial frequencies without changing the shape of their tuning curves (*bottom right*). Because of the changes in cone outer segment morphology (discussed earlier), the sensitivity of individual cones increases slightly during development, leading to a slight increase in contrast sensitivity, which, in turn, leads to the slight upward shift in the tuning curve (*bottom right*). Our finding that the resolution of V1 and LGN cells change at a rate similar to the change in peak density of cone photoreceptors, combined with the complete stability of neuronal selectivity for orientation and spatial frequency during development (see Fig. 12.5), suggests that cortical receptive field properties passively follow the retina as it develops. We earlier developed the argument that retinal changes are too small and happen too early in development to explain behavioral development; it follows, then, that postnatal changes at the level of the visual cortex also fail to account for the normal course of behavioral development.

The results of direct investigation of neonatal monkey cortex argue against the notion that visual experience is strongly instructive and instead support the idea that normal visual experience is simply permissive to normal visual development. The other important piece of the puzzle is to identify what specific changes take place in the face of abnormal visual experience.

Abnormal visual experience and amblyopia

It seems paradoxical that V1 receptive field development passively follows peripheral organization, which is not influenced by visual experience in primates (Blakemore and Vital-Durand, 1986b; Hendrickson et al., 1987; Levitt et al., 2001; Movshon et al., 1987), whereas decades of evidence has accumulated for experience-dependent plasticity in V1. Most studies of the effect of visual experience on development in primates have used monocular or binocular deprivation to manipulate visual experience (Baker et al., 1974; Blakemore, 1990; Blakemore and Vital-Durand, 1986b; Horton, 1984; LeVay et al., 1980; von Noorden and Crawford, 1978; Wiesel, 1982; Wiesel and Hubel, 1974). This kind of deprivation typically devastates spatial vision, reducing contrast sensitivity and resolution so severely that in some cases blindness results (Harwerth et al., 1983; von Noorden, 1973; von Noorden et al., 1970). The most obvious consequence of monocular deprivation is a dramatic loss of influence of the deprived eye over cells in the visual cortex, evident physiologically and anatomically, even

when the deprivation lasts for as short a period as 1 week. Physiologically, cortical binocularity is lost, and most neurons can be influenced only through the nondeprived eye. Anatomically, there is a nearly complete takeover of deprived eye territory by the nondeprived eye.

The obvious correlation between the loss of cortical influence by the deprived eye and the loss of vision has been interpreted to mean that visual function is determined by the number of cortical neurons influenced by a given eye; changes in this balance during development lead to changes in vision. None of these studies has quantified the spatial, temporal, or contrast response properties of deprived cortex, as there are few responsive cells to study. It may be that experience-dependent plasticity in primate V1 is restricted to the balance of inputs from the two eyes, and does not affect the spatial properties of individual neurons. But data on the effects of binocular deprivation suggest that cortical receptive field properties can be altered by experience (Blakemore, 1990). We wanted to establish whether cortical receptive field properties could be influenced by abnormal visual experience that was less radical than complete form deprivation, and we have therefore studied visual behavior and cortical organization in animals raised in a way that creates more modest and experimentally tractable visual deficits.

Visual disorders that occur in early childhood, such as strabismus (crossed eyes) and anisometropia (monocular defocus), are associated with *amblyopia*, literally meaning “blunted” vision. Visual acuity and contrast sensitivity in the amblyopic eyes of monkeys and humans are reduced, but not nearly so severely as they are following visual deprivation (Blakemore and Vital-Durand, 1981; Harwerth et al., 1983; Kiorpes, 1992b, 1996, 2001; Kiorpes et al., 1987; Kiorpes et al., 1993; Kiorpes and Movshon, 1996; Levi and Carkeet, 1993; Smith et al., 1985). Figure 12.7*A* shows the development of spatial resolution in each eye of a population of strabismic monkeys (Kiorpes, 1992b) and compares it to the development of resolution in normal monkeys tested monocularly. Resolution in the fellow (nondeviating) eyes develops normally, but resolution development in the strabismic eyes lags. Figure 12.7*B* illustrates losses in contrast sensitivity for three monkeys, each made experimentally amblyopic by a different technique. Normally, contrast sensitivity is similar for both eyes of an individual (*upper left panel, T7*). The other three panels show contrast sensitivity for each eye in monkeys in which the development of amblyopia followed experimentally produced strabismus, blur created by extended wear of a defocusing contact lens (anisometropia), or blur created by chronic instillation of atropine. Contrast sensitivity functions for the amblyopic eyes, regardless of the origin of amblyopia, are shifted to lower sensitivity and lower spatial frequencies. If we compare the functions obtained from amblyopic eyes with functions from young normal animals (Fig. 12.2*B*). There is

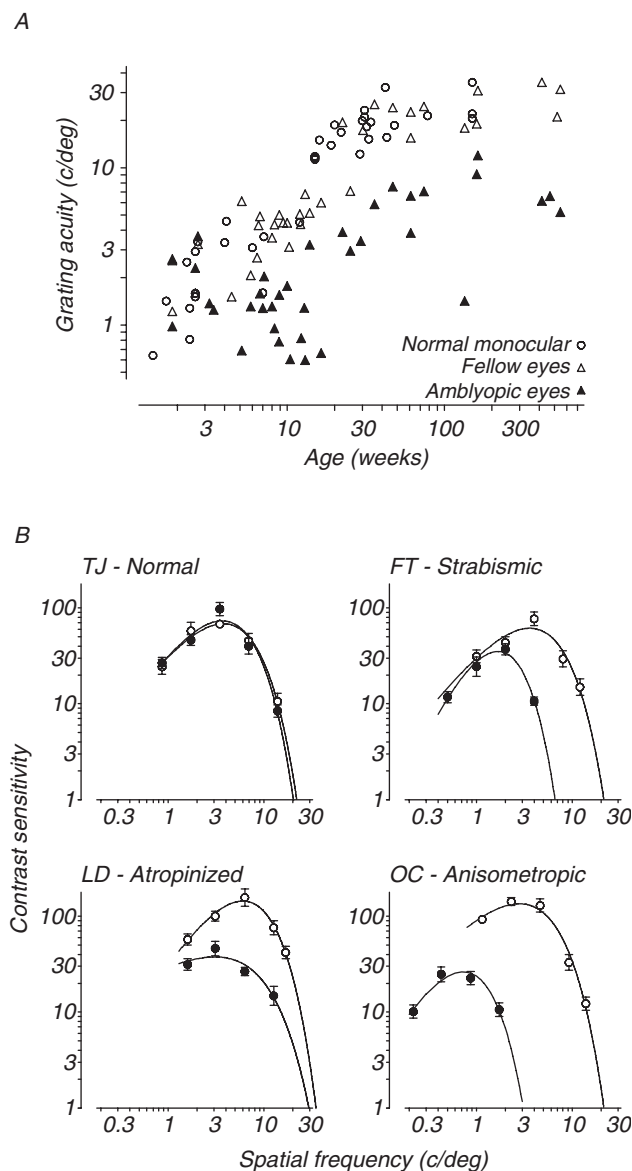


FIGURE 12.7. Spatial vision in amblyopic monkeys. *A*, Spatial resolution data obtained longitudinally from a set of six strabismic infant macaques (data from Kiorpes, 1992b). Data taken monocularly from each eye of the strabismic animals (triangles) are compared with monocular data taken from normal animals (circles; compare to Fig. 12.2*A*). The measure of spatial resolution was grating acuity, the highest spatial frequency at which a grating could be distinguished reliably from a uniform field of the same luminance. Animals younger than 16 weeks were tested using a forced-choice, preferential looking technique. Older animals were tested using a standard two-choice operant discrimination task. *B*, Monocular spatial contrast sensitivity functions for each eye of four macaque monkeys (one normal and three amblyopic), measured using operant techniques (data from Kiorpes et al., 1987, 1998).

a distinct similarity; this similarity is also evident when other visual functions are measured (Kiorpes, 1992b; Levi and Carkeet, 1993).

To explore the neuronal correlates of amblyopia, we analyzed the responses of V1 neurons in amblyopic monkeys (Kiorpes et al., 1998; Movshon et al., 1987). We studied selectivity for orientation, spatial frequency, drift rate, and contrast response properties of neurons driven by each eye, as well as binocular organization. In all types of amblyopic monkeys, there was a disruption of the binocular organization of V1 neurons. Figure 12.8*A* presents V1 eye dominance distributions from normal monkeys and from four groups of monkeys with amblyopia. Monocularly deprived monkeys were found to show the most marked loss of input from the amblyopic eye. The other three groups of amblyopic monkeys each showed substantial losses in binocular neurons, but in none of these groups was there a complete loss of cortical input from the amblyopic eye. Because all the animals in these groups had behaviorally documented amblyopia, this finding indicates that a loss of neurons influenced by the amblyopic eye is not sufficient to account for amblyopia. Thus it is important to evaluate the quality of the visual signals carried by the neurons driven by each eye.

In strabismic and anisometropic amblyopia, the spatial organization of receptive fields driven by the amblyopic eye is degraded. The distributions of preferred spatial frequency and spatial resolution are shifted to lower spatial frequencies relative to those for cells driven by the fellow eye. However, there is no consistent elevation in contrast threshold for neurons driven by the amblyopic eye. The combined results of two studies (Kiorpes et al., 1998; Movshon et al., 1987) are shown in Figure 12.8*B*, which summarizes and compares the behavioral and physiological findings for contrast sensitivity and peak spatial frequency in amblyopia. In each panel, the measures plotted are the interocular ratios of spatial frequency and contrast sensitivity. For behavior, these values are taken from the peaks of the contrast sensitivity functions (e.g., Fig. 12.7*B*). For physiology, the values are the geometric means of the values measured for populations of neurons driven by each eye. A comparison of the upper two panels shows that the range of behavioral deficits is large, whereas the range of physiological deficits is relatively smaller. Nonetheless, both measures show correlated losses in peak contrast sensitivity and peak spatial frequency. The same data are reorganized in the two lower panels to make a direct comparison of behavioral and physiological losses in peak spatial frequency and peak contrast sensitivity. There is a strong correlation between behavioral and physiological loss for peak spatial frequency ($r = 0.60$), although the physiological deficit is consistently smaller than the behavioral one. The relationship for contrast sensitivity is weaker ($r = 0.37$), and does not achieve statistical

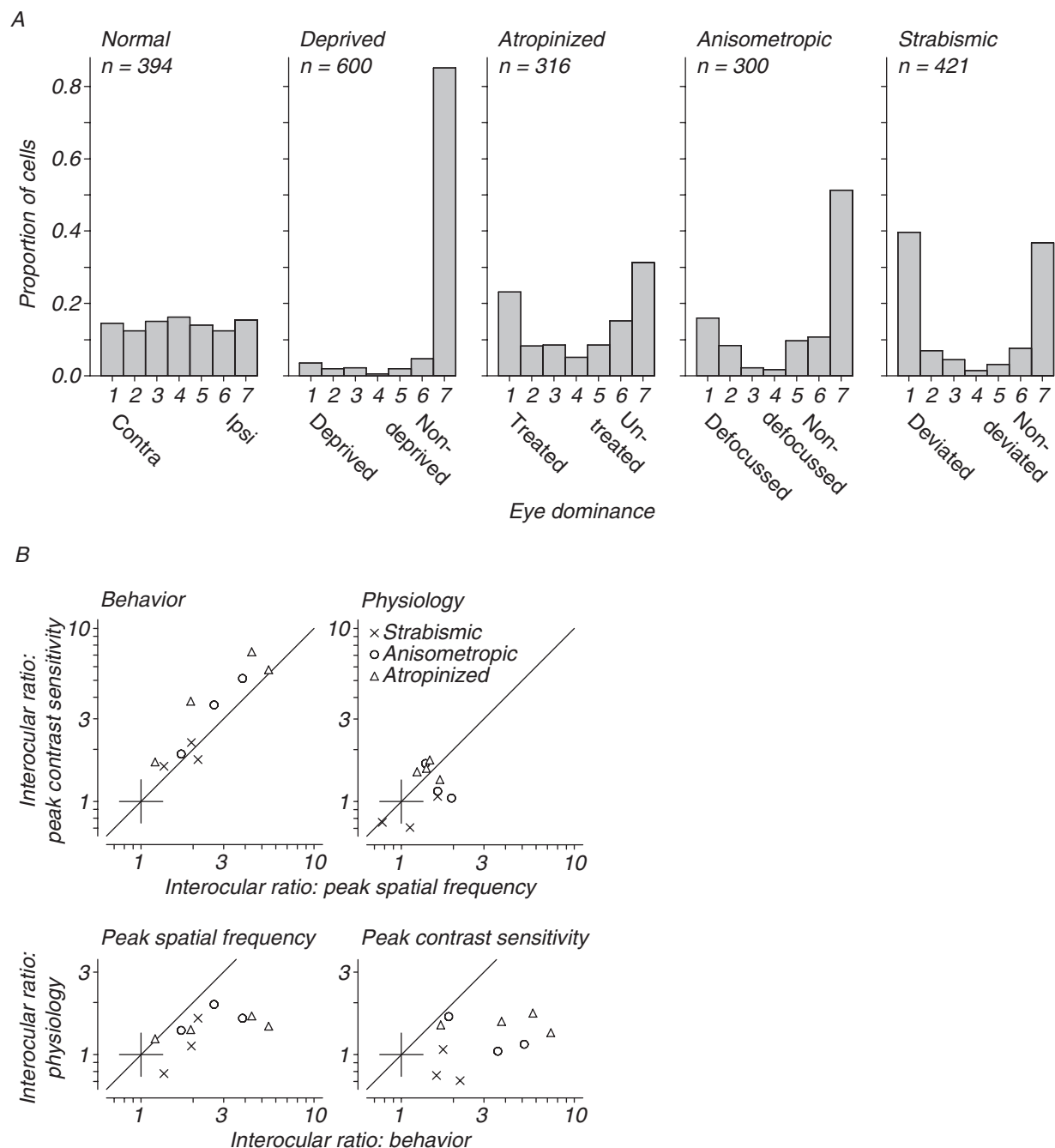


FIGURE 12.8. Physiological measurements of spatial vision in amblyopes. *A*, Distributions of cortical eye dominance obtained from five populations of macaque monkeys. The eye dominance scale is that of Hubel and Wiesel (1962), but only for the normal animals is the eye assignment based on group 1 being contralateral and group 7 being ipsilateral. The distributions for the other four groups are keyed so that the amblyopic eye corresponds to group 1 in all cases. The data for normal subjects and for the three right-hand groups of amblyopes are from Kiorpes et al. (1998) and Movshon et al. (1987). The data for the monocularly deprived

animals are from LeVay et al. (1980). *B*, Comparisons of physiological and behavioral data for 10 amblyopic monkeys studied by Kiorpes et al. (1998) and Movshon et al. (1987). Each axis represents the ratio of the indicated performance value between the amblyopic and fellow eye. For behavioral measures, the values compared are the peak spatial frequency and the peak contrast sensitivity from data like those shown in Fig. 12.7*B*. For physiological measures, the values compared are the geometric means of measured values for populations of cells tested monocularly through the amblyopic and fellow eyes.

significance. There was also no consistent effect of amblyopia on overall visual responsiveness, orientation tuning, or temporal tuning.

Thus, neuronal correlates of amblyopia are evident in the spatial properties of cells in V1, but the observed deficits do not fully explain the spatial losses in amblyopia—that is, the physiological losses are relatively small compared to the behavioral ones. A qualitative account of the visual loss in amblyopia might be constructed by combining the losses in spatial sensitivity with the alterations in eye dominance and binocularity (Fig. 12.8A), but we are aware of no quantitative model that supports this conjecture.

It is notable that, just as vision in an amblyopic eye resembles the vision of a younger normal eye, so, too, do the properties of cortical neurons driven by the amblyopic eye resemble the properties of neurons driven by a younger normal eye. However, this similarity is unlikely to reflect similar mechanisms in the two cases. We have already argued that the properties of developing cortical neurons are largely determined by the development of the foveal cone mosaic, but there is no reason to believe that retinal development is abnormal in amblyopic animals. LGN cell responses are quantitatively very similar in normal and amblyopic eyes (Blakemore and Vital-Durand, 1986b; Levitt et al., 2001). The disruption of cortical receptive fields in amblyopia must, therefore, result from changes in intracortical or intercortical circuits and not from degraded peripheral inputs. The changes observed are consistent with a broadening and blurring of the structure of cortical receptive fields, reminiscent of the far more extensive changes reported to result from complete binocular form deprivation (Blakemore, 1990). Like our data on V1 development, these results seem to favor a permissive view of the role of the environment in development, but with the added feature that not only visual experience, but *the right kind* of visual experience is required for normal development. In the animals raised with blurred vision in one eye, our experiments can be seen as a selective case of visual deprivation in which cells preferring the highest spatial frequencies are the most penalized by the experience of continuously blurred vision. Perhaps it is only natural that these cells would be the ones most affected, or even lost, resulting in distributions of preferred frequency that are shifted in the way that we have observed (Kiorpes et al., 1998; Movshon et al., 1987). But this account is incomplete—it does not suggest an explanation for the effects of strabismus, which does not cause image blur or the consequent loss of high spatial frequency stimulation.

It seems significant that the relationship between cortical signals and behavioral responses is consistent across development and amblyopia, even if the relationship is quantita-

tively imperfect. It is therefore natural to wonder about the course of development and the effects of visual experience in cortical areas outside V1.

Extrastriate cortex

We have until now considered the development of and effects of abnormal visual experience on the structure and function of the visual pathway, up to and including the primary visual cortex, V1. But in primates, there is a very extensive collection of cortical areas outside V1, which in aggregate involve about three times as much cortical tissue as V1 (Felleman and Van Essen, 1991). The functional properties of neurons in these areas and their relationship to behavior are a very active focus of study (see, for example, Chapter 34, Ventral and Dorsal Cortical Processing Streams; Chapter 78; Chapter 81; and Chapter 103), yet little attention has been paid to the way that they change during development or after abnormal visual experience. The visual responsiveness of extrastriate areas has been documented using 2-deoxyglucose autoradiography (Bachevalier et al., 1991; Distler et al., 1996). These measurements show that higher cortical areas are relatively delayed in their development compared to V1, and moreover that the development of the ventral “form” areas occurs over a longer time course than the development of dorsal “motion” areas. This general distinction is confirmed by the observation that neurons in inferotemporal visual areas do not appear to be visually responsive until about 6 months of age in macaques, whereas neurons in the dorsal area MT are responsive in much younger monkeys (Rodman et al., 1993). Anatomical experiments suggest that the normal connections of extrastriate cortical areas are probably present around the time of birth, and are organized approximately as in adults (e.g., Barone et al., 1996; Coogan and Van Essen, 1996), although some refinement certainly continues postnatally (e.g., Barone et al., 1995). Indeed, there is some evidence that higher-order areas have exuberant corticocortical connections that are later lost (Rodman and Consuelos, 1994; Webster et al., 1995). Although normal connections are present in infancy, synaptogenesis continues throughout the cortex for many weeks after birth (Rakic et al., 1986), and immunocytochemical studies reveal substantial changes in the distribution of various chemical markers during the first months of life (e.g., Conde et al., 1996; Hendrickson et al., 1991).

Behavioral data on the development of complex visual functions and the influence of amblyopia suggest that functions dependent on the action of extrastriate areas may develop more slowly than simpler acuity and contrast detection tasks in both monkeys and humans. For example, contour integration ability develops over a protracted

time course in comparison to simple grating acuity (Kiorpes et al., 2000a, 2001; Kovacs et al., 1999). Contour integration ability is also susceptible to disruption in amblyopia (Chandna et al., 2001; Hess et al., 1997; Kovacs et al., 2000; Kozma et al., 2000).

These findings lead to our concluding conjecture that a complete picture of the factors that limit visual development and vision after abnormal experience will not be obtained until we have an account of extrastriate cortical development. There is modest evidence that the binocularity and response properties of neurons in V4 are affected in amblyopia (Movshon et al., 1987), and we have argued that changes in binocular organization in area MT following strabismus show that an independent mechanism of cortical binocular plasticity operates during development in this area (Kiorpes et al., 1996). Also, disruption of binocular organization has recently been reported in several extrastriate cortical areas in amblyopic cats (Schroder et al., 2002).

Our analysis of the relationship between visual neuronal function and visual behavior in normal and abnormal development suggests that neuronal properties up to V1 offer only an incomplete account. Neither the changes in V1 neuronal properties during development nor the effects of amblyopia on those properties are quantitatively concordant with the behavioral changes we observe. If the answer does not lie at or before the level of the primary visual cortex, it seems clear that it must lie beyond.

Acknowledgments

The research from our laboratories described in this chapter was supported by grants from the National Institutes of Health (EY 2017 to JAM, EY 5864 to LK, and RR00166 to the Washington Regional Primate Research Center). We are grateful to Michael Gorman, Jasmine Allen Siegel, Laura Albanese, Jeanine Dimitri, and Suzanne Fenstermaker for their assistance, and to our many students and colleagues for their invaluable contributions to this work.

REFERENCES

- Bachevalier, J., C. Hagger, and M. Mishkin, 1991. Functional maturation of the occipitotemporal pathway in infant rhesus monkeys, in *Alfred Benzon Symposium 31, Brain Work and Mental Activity* (N. A. Lassen, D. H. Ingvar, M. E. Raichle, and L. Friberg L., eds.), Copenhagen: Munksgaard, pp. 231–240.
- Baker, H. F., P. Grigg, and G. K. von Noorden, 1974. Effects of visual deprivation and strabismus on the response of neurons in the visual cortex of monkey, including studies on the striate and prestriate cortex in the normal animal, *Brain Res.*, 66:185–208.
- Banks, M. S., and P. J. Bennett, 1988. Optical and photoreceptor immaturities limit the spatial and chromatic vision of human neonates, *J. Opt. Soc. Am. A*, 5(12):2059–2079.
- Barone, P., C. Dehay, M. Berland, J. Bullier, and H. Kennedy, 1995. Developmental remodeling of primate visual cortical pathways, *Cerebr. Cortex*, 5:22–38.
- Barone, P., C. Dehay, M. Berland, and H. Kennedy, 1996. Role of directed growth and target selection in the formation of cortical pathways: prenatal development of the projection of area V2 to area V4 in the monkey, *J. Comp. Neurol.*, 374:1–20.
- Blakemore, C., 1990. Maturation of mechanisms for efficient spatial vision, in *Vision: Coding and Efficiency* (C. Blakemore, ed.), Cambridge: Cambridge University Press, pp. 254–256.
- Blakemore, C., and R. C. Van Sluyters, 1975. Innate and environmental factors in the development of the kitten's visual cortex, *J. Physiol.*, 248:663–716.
- Blakemore, C., and F. Vital-Durand, 1986a. Organization and post-natal development of the monkey's lateral geniculate nucleus, *J. Physiol.*, 380:453–491.
- Blakemore, C., and F. Vital-Durand, 1986b. Effects of visual deprivation on the development of the monkey's lateral geniculate nucleus, *J. Physiol.*, 380:493–511.
- Blakemore, C., and F. Vital-Durand, 1981. Postnatal development of the monkey's visual system, in *The Fetus and Independent Life* (Ciba Foundation Symposium 86), pp. 152–171.
- Blasdel, G., K. Obermayer, and L. Kiorpes, 1995. Organization of ocular dominance and orientation columns in the striate cortex neonatal macaque monkeys, *Vis. Neurosci.*, 12(3):589–603.
- Bonds, A. B., and R. D. Freeman, 1978. Development of optical quality in the kitten eye, *Vis. Res.*, 18(4):391–398.
- Boothe, R. G., L. Kiorpes, R. A. Williams, and D. Y. Teller, 1988. Operant measurements of contrast sensitivity in infant macaque monkeys during normal development, *Vis. Res.*, 28(3):387–396.
- Brown, A. M., V. Dobson, and J. Maier, 1987. Visual acuity of human infants at scotopic, mesopic and photopic luminances, *Vis. Res.*, 27(10):1845–1858.
- Cavanaugh, J. R., W. Bair, and J. A. Movshon, 2002. Selectivity and spatial distribution of signals from the receptive field surround in macaque V1 neurons, *J. Neurophysiol.*, 88:2547–2556.
- Chandna, A., P. M. Pennefeather, I. Kovacs, and A. M. Norcia, 2001. Contour integration deficits in anisometropic amblyopia, *Invest. Ophthalmol. Vis. Sci.*, 42(3):875–878.
- Chino, Y. M., E. L. Smith III, S. Hatta, and H. Cheng, 1997. Post-natal development of binocular disparity sensitivity in neurons of the primate visual cortex, *J. Neurosci.*, 17(1):296–307.
- Conde, F., J. S. Lund, and D. A. Lewis, 1996. The hierarchical development of monkey visual cortical regions as revealed by the maturation of parvalbumin-immunoreactive neurons, *Dev. Brain Res.*, 96:261–276.
- Coogan, T. A., and D. C. Van Essen, 1996. Development of connections within and between areas V1 and V2 of macaque monkeys, *J. Comp. Neurol.*, 372:327–342.
- Distler, C., J. Bachevalier, C. Kennedy, M. Mishkin, and L. G. Ungerleider, 1996. Functional development of the corticocortical pathway for motion analysis in the macaque monkey: a 14C-2-deoxyglucose study, *Cerebr. Cortex*, 6:184–195.
- Distler, C., F. Vital-Durand, R. Korte, H. Kornhuber, and K. P. Hoffmann, 1999. Development of the optokinetic system in macaque, *Vis. Res.*, 39(23):3909–3919.
- Enroth-Cugell, C., and J. G. Robson, 1966. The contrast sensitivity of retinal ganglion cells of the cat, *J. Physiol.*, 187:517–552.
- Felleman, D. J., and D. C. Van Essen, 1991. Distributed hierarchical processing in the primate cerebral cortex, *Cerebr. Cortex*, 1:1–47.
- Geisler, W. S., 1984. Physical limits of acuity and hyperacuity, *J. Opt. Soc. Am. A*, 1(7):775–782.

- Harwerth, R. S., E. L. Smith III, R. L. Boltz, M. L. Crawford, and G. K. von Noorden, 1983. Behavioral studies on the effect of abnormal early visual experience in monkeys: spatial modulation sensitivity, *Vis. Res.*, 23(12):1501–1510.
- Hawken, M. J., C. Blakemore, and J. W. Morley, 1997. Development of contrast sensitivity and temporal-frequency selectivity in primate lateral geniculate, *Exp. Brain Res.*, 114(1):86–98.
- Hendrickson, A. E., 1992. A morphological comparison of foveal development in man and monkey, *Eye*, 6:136–144.
- Hendrickson, A. E., 1993. Morphological development of the primate retina, in *Early Visual Development, Normal and Abnormal* (K. Simons, ed.), New York: Oxford University Press, pp. 287–295.
- Hendrickson, A. E., and C. Kupfer, 1976. The histogenesis of the fovea in the macaque monkey, *Invest. Ophthalmol.*, 15:746–756.
- Hendrickson, A. E., J. A. Movshon, H. M. Eggers, M. S. Gizzi, R. G. Boothe, and L. Kiorpes, 1987. Effects of early unilateral blur on the macaque's visual system. II. Anatomical observations, *J. Neurosci.*, 7(5):1327–1339.
- Hendrickson, A. E., J. F. Van Brederode, K. A. Mulligan, and M. R. Celio, 1991. Development of the calcium-binding protein parvalbumin and calbindin in monkey striate cortex, *J. Comp. Neurol.*, 307:626–646.
- Hendrickson, A. E., and C. Yuodelis, 1984. The morphological development of the human fovea, *Ophthalmology*, 91(6):603–612.
- Hess, R. F., W. McIlhagga, and D. J. Field, 1997. Contour integration in strabismic amblyopia: the sufficiency of an explanation based on positional uncertainty, *Vis. Res.*, 37:3145–3161.
- Horton, J. C., 1984. Cytochrome oxidase patches: a new cytoarchitectonic feature of monkey visual cortex, *Philos. Trans. R. Soc. Lond. [Biol.]*, 304(1119):199–253.
- Hubel, D. H., and T. N. Wiesel, 1962. Receptive fields, binocular interaction, and functional architecture in the cat's visual cortex, *J. Physiol. (Lond.)*, 160:106–154.
- Hubel, D. H., and T. N. Wiesel, 1963. Receptive fields of cells in striate cortex of very young, visually inexperienced kittens, *J. Neurophysiol.*, 26:994–1002.
- Kelly, J. P., K. Borchert, and D. Y. Teller, 1997. The development of chromatic and achromatic contrast sensitivity in infancy as tested with the sweep VEP, *Vis. Res.*, 37(15):2057–2072.
- Kiorpes, L., 1992a. Development of vernier acuity and grating acuity in normally reared monkeys, *Vis. Neurosci.*, 9:243–251.
- Kiorpes, L., 1992b. Effect of strabismus on the development of vernier acuity and grating acuity in monkeys, *Vis. Neurosci.*, 9:253–259.
- Kiorpes, L., 1996. Development of contrast sensitivity in normal and amblyopic monkeys, in *Infant Vision* (F. Vital-Durand, J. Atkinson, and O. Braddick, eds.), Oxford: Oxford University Press.
- Kiorpes, L., 2001. Sensory processing: animal models of amblyopia, in *Amblyopia: A Multidisciplinary Approach* (M. Moseley and A. Fielder, eds.), Oxford: Butterworth-Heinemann Press.
- Kiorpes, L., S. A. Bassin, and J. A. Movshon, 2000a. Development of contour integration, *Neuroscience Abstr.*, 26:1080.
- Kiorpes, L., S. A. Bassin, and J. A. Movshon, 2001. Development of contour integration, *Invest. Ophthalmol. Vis. Sci.*, 42:122.
- Kiorpes, L., R. G. Boothe, A. E. Hendrickson, J. A. Movshon, H. M. Eggers, and M. S. Gizzi, 1987. Effects of early unilateral blur on the macaque's visual system. I. Behavioral observations, *J. Neurosci.*, 7(5):1318–1326.
- Kiorpes, L., D. C. Kiper, and J. A. Movshon, 1993. Contrast sensitivity and vernier acuity in amblyopic monkeys, *Vis. Res.*, 33(9):2301–2311.
- Kiorpes, L., D. C. Kiper, L. P. O'Keefe, J. R. Cavanaugh, and J. A. Movshon, 1998. Neuronal correlates of amblyopia in the visual cortex of macaque monkeys with experimental strabismus and anisometropia, *J. Neurosci.*, 18(16):6411–6424.
- Kiorpes, L., and J. A. Movshon, 1996. Amblyopia: a developmental disorder of the central visual pathways, *Cold Spring Harb. Symp. Quant. Biol.*, 61:39–48.
- Kiorpes, L., and J. A. Movshon, 1998. Peripheral and central factors limiting the development of contrast sensitivity in macaque monkeys, *Vis. Res.*, 38(1):61–70.
- Kiorpes, L., C. Tang, and J. A. Movshon, 2000b. Ideal observer analysis of spatial contrast sensitivity development in infant macaque monkeys, *Invest. Ophthalmol. Vis. Sci.*, 41(4):729.
- Kiorpes, L., P. J. Walton, L. P. O'Keefe, J. A. Movshon, and S. G. Lisberger, 1996. Effects of early onset strabismus on pursuit eye movements and on neuronal responses in area MT of macaque monkeys, *J. Neurosci.*, 16(20):6537–6553.
- Kourouyan, H. D., and J. C. Horton, 1997. Transneuronal retinal input to the primate Edinger-Westphal nucleus, *J. Comp. Neurol.*, 381(1):68–80.
- Kovacs, I., U. Polat, P. M. Pennefather, A. Chandna, and A. M. Norcia, 2000. A new test of contour integration deficits in patients with a history of disrupted binocular experience during visual development, *Vis. Res.*, 40:1775–1783.
- Kovacs, I., P. Kozma, A. Feher, and G. Benedek, 1999. Late maturation of visual spatial integration in humans, *Proc. Natl. Acad. Sci. USA*, 96(21):12204–12209.
- Kozma, P., L. Kiorpes, and J. A. Movshon, 2000. Contour integration in amblyopic monkeys, *Invest. Ophthalmol. Vis. Sci.*, 41(4):703.
- LeVay, S., T. N. Wiesel, and D. H. Hubel, 1980. The development of ocular dominance columns in normal and visually deprived monkeys, *J. Comp. Neurol.*, 191(1):1–51.
- Levi, D. M., and A. Carkeet, 1993. Amblyopia: A consequence of abnormal visual development, in *Early Visual Development: Normal and Abnormal* (K. Simons, ed.), New York: Oxford University Press, pp. 391–408.
- Levitt, J. B., R. A. Schumer, S. M. Sherman, P. D. Spear, and J. A. Movshon, 2001. Visual response properties of neurons in the LGN of normally reared and visually deprived macaque monkeys, *J. Neurophysiol.*, 85(5):2111–2129.
- Linsenmeier, R. A., L. J. Frishman, H. G. Jakiela, and C. Enroth-Cugell, 1982. Receptive field properties of x and y cells in the cat retina derived from contrast sensitivity measurements, *Vis. Res.*, 22(9):1173–1183.
- Movshon, J. A., H. M. Eggers, M. S. Gizzi, A. E. Hendrickson, L. Kiorpes, and R. G. Boothe, 1987. Effects of early unilateral blur on the macaque's visual system. III. Physiological observations, *J. Neurosci.*, 7(5):1340–1351.
- Movshon, J. A., and L. Kiorpes, 1993. Biological limits on visual development in primates, in *Early Visual Development, Normal and Abnormal* (K. Simons, ed.), New York: Oxford University Press, pp. 296–305.
- Movshon, J. A., and L. Kiorpes, 1990. The role of experience in visual development, in *The Development of Sensory Systems in Mammals* (J. R. Coleman, ed.), John Wiley and Sons, New York, 1990.
- Movshon, J. A., and L. Kiorpes, 1988. Analysis of the development of spatial contrast sensitivity in monkey and human infants, *J. Opt. Soc. Am. A.*, 5(12):2166–2172.
- Movshon, J. A., L. Kiorpes, J. R. Cavanaugh, and M. J. Hawken, 1999. Receptive field properties and surround interactions in

- V1 neurons in infant macaque monkeys, *Neuroscience Abstr.*, 25:1048.
- Movshon, J. A., L. Kiorpes, J. R. Cavanaugh, and M. J. Hawken, 2000. Developmental reorganization of receptive field surrounds in V1 neurons in macaque monkeys, *Invest. Ophthalmol. Vis. Sci.*, 41(4):333.
- Movshon, J. A., L. Kiorpes, M. J. Hawken, A. M. Skoczenski, J. R. Cavanaugh, and N. V. Graham, 1997. Sensitivity of LGN neurons in infant macaque monkeys, *Perception*, 26S:2.
- Movshon, J. A., and R. C. Van Sluyters, 1981. Visual neural development, *Ann. Rev. Psychol.*, 32:477–522.
- Norcia, A. M., C. W. Tyler, and R. D. Hamer, 1990. Development of contrast sensitivity in the human infant, *Vis. Res.*, 30(10):1475–1486.
- Packer, O., A. E. Hendrickson, and C. A. Curcio, 1990. Development redistribution of photoreceptors across the *Macaca nemestrina* (pigtail macaque) retina, *J. Comp. Neurol.*, 298(4):472–493.
- Pelli, D. G., 1990. The quantum efficiency of vision, in *Vision: Coding and Efficiency* (C. Blakemore, ed.), Cambridge: Cambridge University Press.
- Peterzell, D. H., and D. Y. Teller, 1996. Individual differences in contrast sensitivity functions: the lowest spatial frequency channels, *Vis. Res.*, 36(19):3077–3085.
- Peterzell, D. H., J. S. Werner, and P. S. Kaplan, 1993. Individual differences in contrast sensitivity functions: the first four months of life in humans, *Vis. Res.*, 33(3):381–396.
- Peterzell, D. H., J. S. Werner, and P. S. Kaplan, 1995. Individual differences in contrast sensitivity functions: longitudinal study of 4-, 6-, and 8-month-old infants, *Vis. Res.*, 35(7):961–979.
- Pettigrew, J. D., 1974. The effect of visual experience on the development of stimulus specificity by kitten cortical neurones, *J. Physiol.*, 237(1):49–74.
- Rakic, P., J. P. Bourgeois, M. F. Eckenhoff, N. Zecevic, and P. S. Goldman-Rakic, 1986. Concurrent overproduction of synapses in diverse regions of the primate cerebral cortex, *Science*, 232:232–235.
- Rodman, H. R., and M. J. Consuelos, 1994. Cortical projections to anterior inferior temporal cortex in infant macaque monkeys, *Vis. Neurosci.*, 11:119–133.
- Rodman, H. R., S. P. Scialidhe, and C. G. Gross, 1993. Response properties of neurons in temporal cortical visual areas of infant monkeys, *J. Neurophysiol.*, 70:1115–1136.
- Rusoff, A. C., and M. W. Dubin, 1977. Development of receptive-field properties of retinal ganglion cells in kittens, *J. Neurophysiol.*, 40(5):1188–1198.
- Rust, N. C., S. R. Schultz, and J. A. Movshon, 2002. A reciprocal relationship between reliability and responsiveness in developing visual cortical neurons, *J. Neurosci.*, 22(24):10519–10523.
- Schiller, P. H., M. Stryker, M. Cynader, and N. Berman, 1974. Response characteristics of single cells in the monkey superior colliculus following ablation or cooling of visual cortex, *J. Neurophysiol.*, 37(1):181–194.
- Schroder, J. H., P. Fries, P. R. Roelfsema, W. Singer, and A. K. Engel, 2002. Ocular dominance in extrastriate cortex of strabismic amblyopic cats, *Vis. Res.*, 42(1):29–39.
- Skoczenski, A. M., C. D. Brown, L. Kiorpes, and J. A. Movshon, 1995. Development of contrast sensitivity and visual efficiency in macaque monkeys measured with sweep VEPs, *Invest. Ophthalmol. Vis. Sci.*, 36:S442.
- Smith, E. L. III, R. S. Harwerth, and M. L. Crawford, 1985. Spatial contrast sensitivity deficits in monkeys produced by optically induced anisometropia, *Invest. Ophthalmol. Vis. Sci.*, 26(3):330–342.
- Telkes, I., C. Distler, and K. P. Hoffmann, 2000. Retinal ganglion cells projecting to the nucleus of the optic tract and the dorsal terminal nucleus of the accessory optic system in macaque monkeys, *Eur. J. Neurosci.*, 12(7):2367–2375.
- von Noorden, G. K., 1973. Experimental amblyopia in monkeys. Further behavioral observations and clinical correlations, *Invest. Ophthalmol.*, 12(10):721–726.
- von Noorden, G. K., and M. L. Crawford, 1978. Morphological and physiological changes in the monkey visual system after short-term lid suture, *Invest. Ophthalmol. Vis. Sci.*, 17(8):762–768.
- von Noorden, G. K., J. E. Dowling, and D. C. Ferguson, 1970. Experimental amblyopia in monkeys. I. Behavioral studies of stimulus deprivation amblyopia, *Arch. Ophthalmol.*, 84(2):206–214.
- Wallace, M. T., J. G. McHaffie, and B. E. Stein, 1997. Visual response properties and visuotopic representation in the newborn monkey superior colliculus, *J. Neurophysiol.*, 78(5):2732–2741.
- Webster, M. J., J. Bachevalier, and L. G. Ungerleider, 1995. Transient subcortical connections of inferior temporal areas TE and TEO in infant macaque monkeys, *J. Comp. Neurol.*, 352:213–226.
- Wiesel, T. N., 1982. Postnatal development of the visual cortex and the influence of environment, *Nature*, 299(5884):583–591.
- Wiesel, T. N., and D. H. Hubel, 1974. Ordered arrangement of orientation columns in monkeys lacking visual experience, *J. Comp. Neurol.*, 158(3):307–318.
- Williams, R. A., and R. G. Boothe, 1981. Development of optical quality in the infant monkey (*Macaca nemestrina*) eye, *Invest. Ophthalmol. Vis. Sci.*, 21:728–736.
- Wilson, H. R., 1988. Development of spatiotemporal mechanisms in infant vision, *Vis. Res.*, 28(5):611–628.
- Yuodelis, C., and A. Hendrickson, 1986. A qualitative and quantitative analysis of the human fovea during development, *Vis. Res.*, 26(6):847–855.

13 Development of Spatial Selectivity and Response Timing in Humans

ANTHONY M. NORCIA

THE VISUAL SYSTEM of the human, like other altricial species, undergoes an extensive period of postnatal development. Development is both quantitative (e.g., visual performance improves substantially with age) and qualitative (e.g., the visual system of the neonate displays a number of attributes that are absent in the adult). This chapter selectively reviews major aspects of quantitative and qualitative change. The emphasis is on functions that are thought to be the province of the early stages of the visual pathway, where the neural image is formed and primitive features of visual objects are first extracted. Large areas of activity in the field of infant visual development, such as object permanence, attention, and the recognition of objects and faces, are not covered. As with most reviews of human visual development, this review starts with a consideration of methodological issues unique to the field.

Research methods

Methodological considerations are of paramount importance in studies of human visual development. Because the behavioral repertoire is so limited (and constantly changing with development) and because infant observers cannot be instructed, specialized behavioral techniques have been developed (Dobson, 1990; Hainline, 1993; Hamer and Mayer, 1994). Electrophysiological measures, such as the visual evoked potential (VEP) require no overt behavioral responses other than fixation and accommodation. Because the VEP is generated in visual cortex, it is ideally suited for studying the early elements of the visual pathway, the development of which is the focus of this review.

The VEP is a far-field potential that is time- or phase-locked to the visual stimulus. It is this synchronization of the response to the stimulus that allows the investigator to design filters that can select out the visually driven activity from the background electroencephalographic (EEG) and other sources of biological and industrial noise. VEPs were first detected in the early 1950s by averaging the EEG record over fixed time intervals that were precisely aligned with the stimulus onset. The logic of averaging is that all activity that is not synchronized with the stimulus onset is random; thus, the average of these random signals will tend to zero in the

limit of an infinitely large number of averaged records. The time-locked activity, by contrast, is not diminished by the averaging process. As the number of records in the average increases, the time-locked activity represents an ever-increasing proportion of the variance in the record.

THE STEADY-STATE VEP When the stimulus is presented at periodic time intervals, the VEP can also be isolated using spectral analysis procedures. Periodic inputs (stimuli) lead to periodic outputs (responses), and the location of these responses in the spectrum is under the control of the investigator. This prior knowledge of what frequencies in the EEG are relevant (phase-locked at a frequency related to the input frequency) and which are irrelevant (non-phase-locked or of the wrong frequency) makes it possible to design frequency-specific filters that are highly effective in separating the signal from the noise.

Figure 13.1A shows an example of a typical steady-state VEP (SSVEP) spectrum obtained in response to a low spatial frequency grating that was reversed in contrast at 7.25 Hz (14.5 pattern reversals per second). This spectrum is compared to that obtained with the subject viewing a blank screen (lower spectrum in Fig. 13.1A). The SSVEP is composed of several response peaks that occur at exact integer multiples of the stimulus frequency. In the case of the pattern reversal stimulus, the response is symmetrical for each reversal of the pattern, and the spectrum comprises even harmonics (2F, 4F, 6F . . . where F is the stimulus frequency). Because the stimulus is periodic, the response waveform is also periodic, as illustrated in Figure 13.1B. The waveform is not sinusoidal and has two large positive and negative peaks corresponding to the frequency doubling of the response that is apparent in the spectrum.

The SSVEP differs critically from the EEG in that the phase of the SSVEP is constant over repeated presentations, whereas that of the EEG is random. This is illustrated in Figure 13.1C, which plots the SSVEP in polar coordinates. The components of the SSVEP response are complex numbers; that is, the response has both an amplitude and a phase value. The phase of the response is nonzero owing to the presence of neural delays and integration processes. The fact that the response phases from individual trials

cluster around a value of 180° in the figure (*filled symbols*) indicates that the response is synchronized with the stimulus. A phase angle of 180° is consistent with relative delays with respect to the stimulus of 34.5, 103.5, 148.0 . . . , ms for the 14.5-Hz response frequency. This ambiguity is due to phase being a modulo 2π variable. The phase of the EEG is random (see Figure 13.1C, *open symbols*). If one averages the x values (real part) and the y values (imaginary part) and computes the magnitude of the resulting vector, the SSVEP has an amplitude that is not consistent with zero, given the error, but the EEG is consistent with zero (see

larger and smaller filled and open symbols in Figure 13.1C, respectively).

THE SWEEP-PARAMETER VEP Spectral analysis of the SSVEP often results in signal-to-noise ratios that are sufficiently high to detect the response and to measure its amplitude and phase using relatively short data records; as the stimulus value is systematically varied (Regan, 1977). This technique, known as the swept-parameter or sweep VEP, is useful for measuring sensory thresholds—based extrapolation of VEP response functions (Campbell and Maffei, 1970).

It is a general property of sensory systems that evoked response amplitude increases as a function of stimulus intensity over a range of stimulus values. Figure 13.2 shows examples of response functions obtained in experiments where either the spatial frequency (*left panel*) or contrast (*right panel*) of a grating pattern was systematically varied over presentations lasting 10 seconds. In each case, the spectrum analysis was carried out at a series of 1-second intervals in order to map out the shape of the spatial frequency tuning or contrast response functions. Repeated measurements of the response functions were averaged as in Figure 13.1 (*bottom*), with all repetitions from the first second of the sweep being averaged together, all repetitions from the second being averaged together, and so on.

The SSVEP response is a roughly linear function of log-contrast (see Figure 13.2, *right panel*), suggesting that a contrast threshold can be estimated by extrapolation of this function to zero amplitude. This threshold extrapolation technique yields estimates of contrast threshold that are generally within a factor of 2 or 3 of adult psychophysical contrast thresholds (Campbell and Kulikowski, 1971; Cannon,

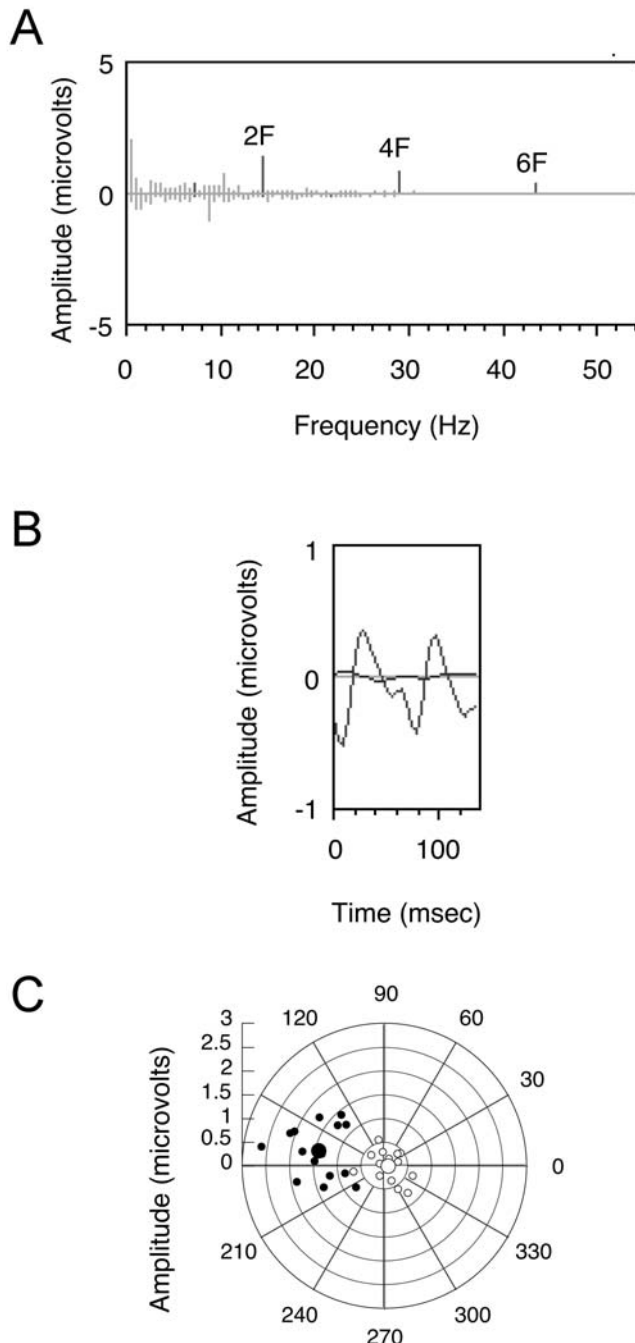


FIGURE 13.1. *A*, Spectra for steady-state VEP (data plotted above the x axis) and background EEG (data plotted below the x axis). The spectrum of the 7.25-Hz pattern reversal response comprises narrow peaks at frequencies that are even multiples of the stimulus frequency (e.g., $2F = 14.5$, $4F = 29$, $6F = 43.5$ Hz). The response (signal) is larger than the EEG (noise) at each of these frequencies in the spontaneous EEG and at nearby frequencies in the record obtained during visual stimulation. *B*, Time averages for the steady-state VEP shown in *A* and for the spontaneous EEG. The time average is periodic, with a base period equal to twice the stimulus period of 138 msec. The averaged response to a blank screen is also shown, indicating the experimental noise level (line near zero). *C*, Amplitude and phase of the steady-state VEP for each of 16 10-second trials composing the averages for stimulus-present (*filled symbols*) and EEG (*open symbols*) conditions previously shown in figure parts *A* and *B*. The VEP responses from individual trials cluster around a phase of 175° , indicating that they are synchronized with the visual stimulus. The spontaneous EEG shows a random phase relationship, with the resulting vector average (*open large dot*) being only a fraction of a microvolt.

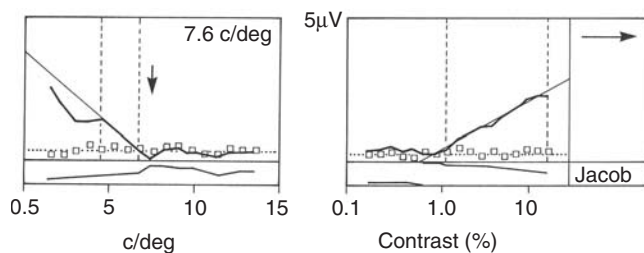


FIGURE 13.2. Spatial frequency (*left panel*) and contrast (*right panel*) sweep records. VEP amplitude (*upper solid curves*) is plotted as a function of linear spatial frequency (*left*) or log stimulus contrast (*right*). Threshold was estimated by an extrapolation to zero amplitude based on a linear regression that used the amplitude values between the dotted cursors. In this example, the estimated grating resolution was 7.6 c/deg (*left panel*), and the contrast threshold was 0.8% (*right panel*). The open squares plot the amplitude recorded simultaneously at a slightly different frequency in the EEG where there was no visual activity. The lower panels plot the response phase, which shows an upward trend as spatial frequency increases (phase lag or increasing delay) and a downward trend on the contrast function as contrast increases (phase lead or decreasing delay). In each case, the phase behavior is indicative of an increase in speed of the response as the stimulus becomes more visible.

1983; Norcia et al., 1990b). The observation that voltage is a linear function of log contrast near threshold suggests that voltage will be a linear function of spatial frequency, given that the contrast sensitivity function is linear on semi-log coordinates (Campbell and Green, 1965). Thus, the same regression procedures can be applied to acuity estimation from the spatial frequency tuning function (see Figure 13.2, *left panel*).

Development of photoreceptor responses

Visual sensitivity is mediated by three cone types (short-wavelength-sensitive [SWS], mid-wavelength-sensitive [MWS], and long-wavelength-sensitive [LWS] cones) and by rods. The outputs of the cones are combined in subsequent stages of processing to support both chromatic and achromatic detection and discrimination.

Photoreceptor components are first present in the human fetal retina by 14 to 15 weeks' gestation, when the precursors of cone inner segments are visible (Narayanan and Wadhwa, 1998). By 18 to 19 weeks' gestation, the photoreceptor inner segments are arranged in a mosaic pattern with large cone inner segments (presumed to be SWS cones) being surrounded by several small cone inner segments (prospective red/green cones; Narayanan and Wadhwa, 1998). Rod inner segments are also identifiable at this age. The cone inner segments then elongate considerably between 19 and 25 weeks. At 24 to 25 weeks' gestation, the rod outer segments begin to emerge, ahead of the outer segments of the cones (Narayanan and Wadhwa, 1998).

Consistent with the emergence of photopigment in the outer segments, visual responses are first recordable at around 24 weeks in the VEP (Kos-Pietro et al., 1997; Taylor et al., 1987).

Each photoreceptor class has a characteristic spectral sensitivity; thus, measurements of spectral sensitivity and receptor isolation conditions have been used to determine when each class of photoreceptor becomes functional. Spectral sensitivity measurements with the scotopic VEP indicate that rods are functioning at 4 weeks of age (Werner, 1982). Similarly, the SWS cones show an adult spectral sensitivity by 4 weeks of age (Volbrecht and Werner, 1987). Photopic spectral sensitivity, measured with the VEP, is similar to that of the adult in 8-week-olds, suggesting that LWS cones are functional by this age (Bieber et al., 1995; Dobson, 1976). Knoblauch et al. (1998) found VEP responses to MWS- and LWS-cone isolating stimuli as early as 4 weeks of age, and Bieber et al. (1998) found adult-like action spectra for both MWS- and LWS-cone classes in 8- to 12-week-olds. Thus, all major photoreceptor classes are known to be functional by no later than 4 weeks of age.

Although all major photoreceptor classes are functional early in infancy, foveal cones are dramatically immature relative to more peripheral cones (Hendrickson and Drucker, 1992; Hendrickson and Yuodelis, 1984). At birth, foveal cones lack outer segments, whereas those in the parafovea are 30% to 50% of adult length. In the midperiphery cone, outer segments are 50% longer than they are in the parafovea, making them relatively adult-like. Despite the relative immaturity of the central retina, throughout development, visual acuity appears to be highest in the central visual field, compared to the peripheral field (Allen et al., 1996; Spinelli et al., 1983).

Spatiotemporal contrast sensitivity development

Perception of the visual world requires that the visual system must transduce light incident on the retina into neural signals. At the earliest stages, neural responses are dependent on the number of absorbed quanta. At the level of the inner plexiform layer, responses are recoded in terms of contrast, that is, spatial and temporal variations in light intensity. Spatiotemporal contrast forms the basis of all subsequent form processing, and contrast sensitivity forms a fundamental limit on what information is made available to visual cognition.

There is a long tradition, based on the theory of linear systems, of using sinusoidal gratings to measure contrast sensitivity (Campbell and Robson, 1968). In this framework, thresholds are measured as a function of spatial frequency (e.g., the number of grating cycles per degree of visual angle). Figure 13.3 shows the development of contrast sensitivity in human infants during the first 8 months of

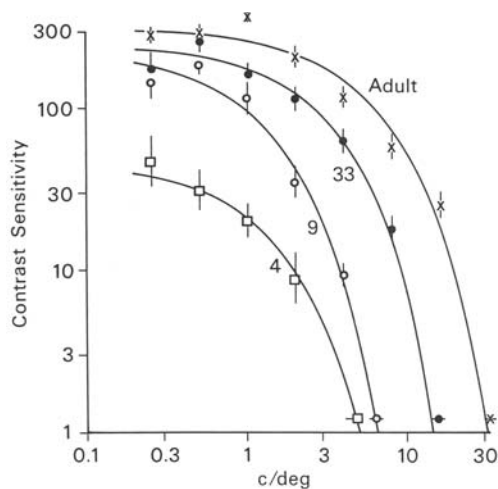


FIGURE 13.3. Development of contrast sensitivity for 6-Hz reversing gratings. Between 4 weeks (*open squares*) and 9 weeks (*open circles*), the contrast sensitivity function shifts upward by a factor of approximately 5 to 6. Between 9 and 33 weeks (*filled circles*), the function shifts rightward, with little increase in maximum sensitivity at low spatial frequencies. Between 33 weeks and adulthood (*x's*), further increases in resolution occur (rightward shift), along with a small increase in overall sensitivity (upward shift).

life (data from Norcia et al., 1990b). In the figure, sensitivity was measured using the swept-parameter technique for gratings that were contrast-reversed at 6 Hz. Thresholds were measured at several spatial frequencies in each infant, with the result being a series of *contrast sensitivity functions*.

The contrast sensitivity function for this temporal frequency has a simple form at all ages: an exponential decline in sensitivity (Norcia et al., 1990b). At 4 weeks of age, peak contrast sensitivity is about a factor of 5 to 6 lower than that of adults. Between 6 and 9 weeks of age, sensitivity at all spatial frequencies increases by a factor of about 3. Between 10 weeks and 33 weeks, sensitivity at low spatial frequencies is constant, but there is a progressive increase in sensitivity at high spatial frequencies.

Contrast sensitivity depends on both spatial and temporal frequency. Relatively little is known about the full range of spatiotemporal contrast sensitivity, as it is difficult in infant studies to obtain the large number of thresholds needed to map the complete spatiotemporal surface. Sensitivity at low spatial frequency and high temporal frequency has been assessed by Apkarian (1993), who measured the critical flicker frequency for the VEP in infants aged birth to 1 year of age and in adults. She found that temporal sensitivity increased to near adult levels by 20 to 30 weeks of age. Gordon and McCulloch (1999) have found that the temporal tuning of responses to low *spatial* frequency targets flickering at 12 Hz is adult-like in 5-, 8-, and 11-year-old children, but that the spatial tuning of responses to high

spatial frequency gratings flickering at 6 Hz is still immature at 5 and 8 years of age. Similarly, psychophysical temporal contrast sensitivity has been found to be mature by the age of 4 years, but grating acuity continues to improve until about the age of 6 years (Ellemberg et al., 1999; see also the section that follows, Development of Resolution Acuity).

Chromatic contrast sensitivity (sensitivity for stimuli that vary in color but not in mean luminance) develops roughly in parallel to achromatic contrast sensitivity during the first 6 months of life (Allen et al., 1993; Kelly et al., 1997; Morrone et al., 1993). However, the waveform of the chromatic VEP continues to develop well after that of the achromatic VEP (see the section "Development of Response Timing" that follows).

NOISE AS A LIMITING FACTOR IN CONTRAST SENSITIVITY DEVELOPMENT The data shown in Figure 13.3 suggest that there are two processes underlying the development of contrast sensitivity. One operates early in development, controlling sensitivity at all spatial frequencies, and a second process operates after 10 weeks of age, primarily affecting higher spatial frequencies.

Contrast sensitivity is limited by several physical processes, including scatter in the optical media of the eye, the efficiency by which photons are captured by the photoreceptors, the size of the eye, and photoreceptor density (Banks and Bennett, 1988; Wilson, 1993). Sensitivity is also limited by noise in the visual pathway.

An estimate of the amount of neural noise can be obtained by measuring contrast thresholds in the presence of varying amounts of spatiotemporal white noise (Pelli, 1990). Using this approach, one determines the maximum amount of noise that can be added to the stimulus without affecting the observer's contrast sensitivity. The idea here is that if neural noise is limiting performance, the visual system will be insensitive to noisy variations in the stimulus that produce responses that are, on average, smaller than the so-called *intrinsic noise* of the visual system. Thus, the goal is to determine the amount of stimulus noise that is *equivalent* to the intrinsic noise by observing the tolerance of contrast threshold to imposed noise. The technique assumes that the imposed stimulus noise (which is spatiotemporally random) approximates the internal noise of the visual system.

Figure 13.4A shows an example of a grating presented either with or without noise. Figure 13.4B shows contrast response functions measured either in the presence of noise (*open circles*) or without noise (*filled circles*). Thresholds were estimated by extrapolating the contrast response function to zero amplitude. Thresholds are higher in the presence of noise, and the contrast response function is shifted rightward. Figure 13.4C plots contrast threshold as a function

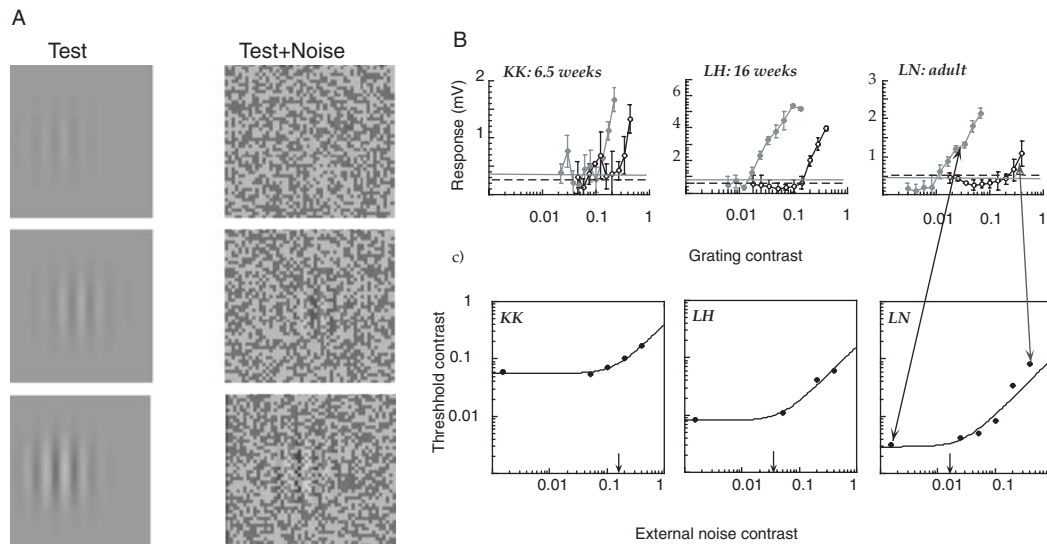


FIGURE 13.4. Equivalent noise paradigm. *A*, Schematic illustration of stimuli used to measure equivalent noise. Contrast response functions were measured from gratings of increasing contrast without noise (*Test*) and then again in the presence of spatiotemporal noise of a fixed level (*Test + Noise*). *B*, Contrast response functions measured without noise (*filled circles*) and in the presence of noise (*open circles*). Added noise raises contrast threshold and shifts the response function rightward. *C*, Contrast thresholds

(vertical axis) as a function of added noise contrast (*x* axis). The solid curve is the fit to an additive model of internal and external noise summation. Equivalent noise, estimated as the point where contrast threshold is elevated by a factor of 1.4, is higher in infants than adults. Note, however, that infant and adult thresholds are similar at high noise levels. (Adapted from Skoczenski and Norcia, 1998.)

of the contrast of the imposed masking noise. As masking noise contrast increases, there is eventually a point at which contrast threshold increases. A consistent estimate of the point at which contrast threshold is elevated by 1.4 (equivalent noise, N_{eq}) was obtained by fitting a two-parameter model (*solid curve*). The equivalent noise contrast is that amount of stimulus contrast that elevates threshold by the same amount as the internal noise.

As noted in the discussion of Figure 13.3, contrast sensitivity increases rapidly before 10 weeks of age, reaching an asymptote that is about a factor of 2 to 3 lower than adults at between 10 and 30 weeks. Equivalent noise declines with a similar profile (Skoczenski and Norcia, 1998). Figure 13.5 shows that, throughout development, the relationship between contrast sensitivity and equivalent noise has a slope very near 1, suggesting that intrinsic noise is a critical limitation on contrast sensitivity at all ages (Skoczenski and Norcia, 1998).

As soon as the noise masker elevates threshold, the entire contrast response function is shifted rightward (see contrast response functions in Fig. 13.4). This rightward shift is the signature of a nonlinear process known as *contrast gain control*. Gain control mechanisms shift the dynamic range of the visual response in a way that depends on the prevailing contrast values in the image. Gain control allows the response of neurons with limited dynamic range to avoid saturation at high contrast, provided the stimulus context is also high contrast. The topic of contrast gain control is discussed

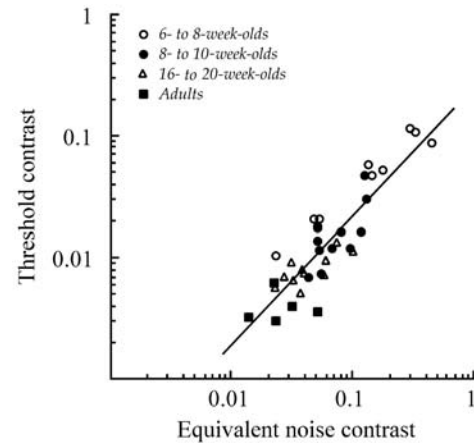


FIGURE 13.5. Relationship between contrast sensitivity and equivalent noise over development. Contrast sensitivity and equivalent noise covary in a 1:1 relationship throughout development. Age is not explicitly plotted, but the high sensitivity points are contributed by progressively older observers. (From Skoczenski and Norcia, 1998.)

further in the section on Orientation-specific Pattern Masking.

Development of resolution acuity

The second major change in the spatial contrast sensitivity function is the marked improvement in sensitivity at high spatial frequencies. The rightward limit of the contrast

sensitivity function indicates the highest resolvable spatial frequency (grating acuity). Several laboratories have measured grating acuity with the swept-parameter technique. In these studies, the spatial frequency of a high contrast grating was systematically varied, and acuity was measured by extrapolating the VEP amplitude versus spatial frequency function to zero amplitude.

Figure 13.6 plots measurements of grating acuity from six studies (Allen et al., 1996; Auestad et al., 1997; Birch et al., 1998; Norcia and Tyler, 1985; Norcia et al., 1990b; Sokol et al., 1992). In each study, grating acuity was found to develop from around 5 c/deg at 1 month to around 15 to 20 c/deg by 8 months. Adult grating acuity is higher, by about a factor of 2, than that attained by 8 months.

Between 4 and 9 weeks of age, the increase in grating acuity visible in Figure 13.3 can be accounted for by an overall increase in contrast sensitivity, presumably brought about by a decrease in intrinsic noise in early processing stages, such as the retina. After that point, resolution increases, without a correlated increase in peak contrast sensitivity. Increases in resolution could be attributable to a number of factors that change over development, including decreasing intercone spacing, increasing photon capture secondary to maturation of the outer segments, and decreasing receptive field size in the lateral geniculate nucleus (LGN) and visual cortex (Hawken et al., 1997; Jacobs and Blakemore, 1988). Optical quality of the eye and eye size contribute little to this improvement (Banks and Bennett, 1988).

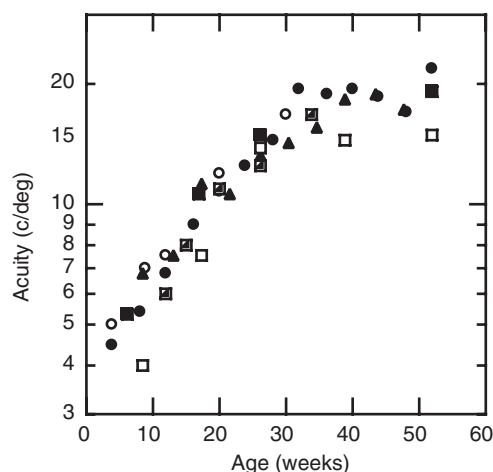


FIGURE 13.6. Development of sweep VEP grating acuity for 5- to 10-Hz pattern reversal stimuli. Acuity growth functions are similar across studies, with acuity increasing from 4 to 6 cycles per degree in 1-month-olds to around 15 to 20 cycles per degree around 8 months of age. (Data replotted from Norcia and Tyler, 1985 [filled circles]; Norcia et al., 1990b [open circles]; Allen et al., 1996 [half-filled squares]; Sokol et al., 1992 [triangles]; Auestad et al., 1997 [open squares]; Birch et al., 1998 [filled squares]). (Redrawn from Norcia and Manny, 2003.)

Development of orientation selectivity

The perception of objects requires more than just the registration of spatiotemporal variations in contrast. The first step along the path to object recognition is taken in primary visual cortex where neurons first begin to display selectivity for the orientation and direction of motion of image elements. Orientation selectivity, of at least a primitive form, appears to develop without the need for visual experience in both cats and monkeys (Albus and Wolf, 1984; Blakemore and Van Sluyters, 1975; Blasdel et al., 1995; Braastad and Heggelund, 1985; Chino et al., 1997; LeVay et al., 1980; Sherk and Stryker, 1976; Wiesel and Hubel, 1974). Human infants can discriminate the orientation of static lines within the first week after birth (Atkinson et al., 1988; Slater and Kirby, 1998). The detection of changing orientation in dynamic patterns has not been measurable at birth, but can be measured both behaviorally (Atkinson et al., 1988) and by VEP (Braddick et al., 1986) by 6 to 7 weeks of age. Hood et al. (1992) found that 1-month-old infants could discriminate orientation changes at 3 Hz, but not at 8 Hz, suggesting the presence of a postnatal maturation period of unknown extent for orientation-selective mechanisms. Manny (1992) used the VEP method of Braddick et al. (1986) to measure orientation tuning in 3-month-old infants. She found that orientation-tuning bandwidths were within a factor of 2 of those of adults. Chino et al. (1997) have found that orientation tuning of V1 cells in the macaque is present in newborn animals and becomes adult-like by 4 weeks of age (see also Chapter 12, Neural Limitations on Visual Development in Primates). It is generally considered that 1 week of monkey life is equivalent to 1 month of life in humans (Boothe et al., 1985); thus, these two measurements of basic orientation selectivity are in substantial agreement.

DEVELOPMENT OF ORIENTATION-SPECIFIC PATTERN MASKING

The visual system is rarely confronted with isolated lines or edges. Rather, objects appear in the midst of cluttered backgrounds and behind occluding surfaces and contours. The detectability of an oriented pattern is degraded by the presence of similar patterns presented to the same location, a phenomenon known as pattern masking. In adults, patterns of the same orientation are much more effective as maskers than are patterns of different orientation.

In Figure 13.4, examples were shown of the masking effect of two-dimensional white noise on the contrast response function. The masker had the effect of raising the threshold, with a concomitant rightward shift of the contrast response function. The author and coworkers repeated these experiments using one-dimensional, rather than two-dimensional, noise maskers in order to study the development of orientation-selective pattern masking (Skoczenski

et al., 1999). Schematic examples of the stimuli are shown in Figure 13.7A. Note that the grating is more visible in the presence of the cross-oriented masker than in the presence of a masker of the same orientation (*cf* Campbell and Kulikowski, 1966).

In 11-month-olds and adults, a noise masker of the same orientation as the test grating was found to elevate threshold by a factor of about 6, whereas an orthogonally oriented masker elevated threshold by much less (a factor of about 3) (see Fig. 13.7B, *right panel*). Remarkably, in 3-month-old infants, both maskers were equally effective; that is, threshold was elevated by a factor of 3 by same- and cross-oriented maskers (see Fig. 13.7B). Orientation-selective pattern masking was first seen by 8 months of age and was adult-like at 11 months.

The lack of orientation-specific masking could be attributable to a lack of orientation-selective mechanisms capable of responding to the 5-Hz contrast-reversing grating. In order to test this hypothesis, the author and colleagues used a technique developed by Regan and Regan (1987) for measuring orientation bandwidths in the VEP. With this technique, the test and mask gratings are modulated at slightly different temporal frequencies. The responses to the test and mask grating thus appear in different bins in the spectrum, and the influence of one stimulus on the other can be measured even though the patterns are presented simultaneously. Regan and Regan (1987) showed that the spectrum of the response to two gratings of the same orientation but of different temporal frequency contained several response components, in addition to the harmonics of the two input gratings. These responses occurred at frequencies that were combinations of the two input frequencies, that is, the sum and difference of the two input frequencies. Figure 13.8 shows an example from Candy et al. (2001). In the top left panel, the response to a single grating counterphase modulated at 3.3 Hz is shown. The response is composed of a series of spectral lines at even harmonics of the input frequency (6.6, 13.2, 19.8 Hz, etc.). When a second grating, modulated at 8.3 Hz, is superimposed, two things happen: the amplitude of the response to the first stimulus is reduced, and strong responses are seen at 5 Hz and 11.8 Hz (Fig. 13.8, *top right*). The 5-Hz response occurs at the difference between the two input frequencies, and the 11.8-Hz response occurs at the “sum frequency.” These additional components at the sum and difference frequency are due to the two inputs having both passed through a nonlinear processing stage. In the present context, this presumably arises from a combination of threshold and network nonlinearities (for a discussion of possible mechanisms, see Candy et al., 2001). Regan and Regan (1987) showed that these combination frequencies could be used to measure VEP orientation-tuning functions.

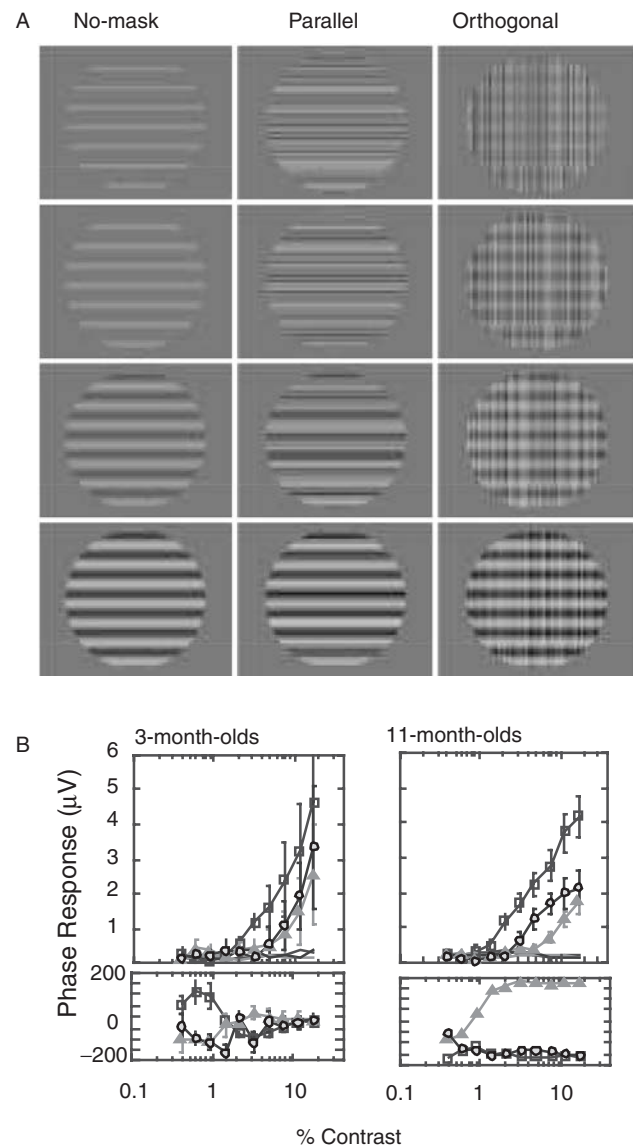


FIGURE 13.7. Orientation-specific masking paradigm utilizing one-dimensional spatiotemporal noise maskers. *A*, VEP contrast response functions were measured without noise (*No mask*) and in the presence of one-dimensional spatiotemporal noise that was at the same orientation as that of the test grating (*Parallel*) or at an orthogonal orientation (*Orthogonal*). Note that the grating is more visible when the masking is oriented orthogonally. *B*, Masked and unmasked contrast response functions for 3- and 11-month-olds. Parallel and orthogonal maskers shift the contrast response rightward by the same amount at 3 months; however, at 11 months, the parallel masker shifts the response function further to the right (rightmost curve plotted as triangles) than does the orthogonal masker (middle curve plotted as circles).

Theoretically, if infants lacked oriented cortical cells, they should generate just as much activity at the combination frequencies for cross-oriented targets as they did for similarly oriented targets. This is not the case, as can be seen in the bottom panel of Figure 13.8, which plots the amplitude of the sum term for two infants (14 and 20 weeks of age) and an adult. In this experiment, the contrast of a masking grating was fixed throughout the trial at a highly suprathreshold value. The contrast of the test grating was swept from below threshold to well above it. The results from three conditions are shown: the swept test, presented alone (*open squares*); the test presented with an orthogonal masker (*triangles*); and the test presented with a masker of the same orientation as the test (*circles*). There is no response at the combination frequency when only one of the inputs is presented or when an orthogonally oriented masker is presented, but there is a robust response when the target and mask share the same orientation. This signature of orientation selectivity was present even in younger infants in whom the pattern-masking effect was nonselective.

Young infants clearly have orientation selectivity, but contrast-gain control, although present, does not show the adult pattern of orientation selectivity. Young infants appear to

possess a gain control mechanism that is activated equally by all orientations, whereas adults show additional masking if the patterns share the same orientation. Gain control in the immature state could rely on equal pooling of inhibition across orientation columns in visual cortex (see, for example, Heeger, 1992). Alternatively, gain control comprise both intracortical and presynaptic mechanisms (Freeman et al., 2002). Intracortical inhibition may be shared preferentially among like orientations, whereas synaptic depression acting on the geniculocortical input would be nonspecific owing to the lack of orientation tuning in the LGN. According to this view, the neonatal visual system may lack intracortical masking processes that are orientation specific, but possess the presynaptic depression mechanism that is nonspecific with respect to orientation.

Development of position sensitivity

Pattern discrimination requires that the visual system not only be able to encode the orientation of features in an image, but also their relative positions. The adult visual system is extremely sensitive to positional offsets between nearby features, such as pairs of lines. Positional acuity, also

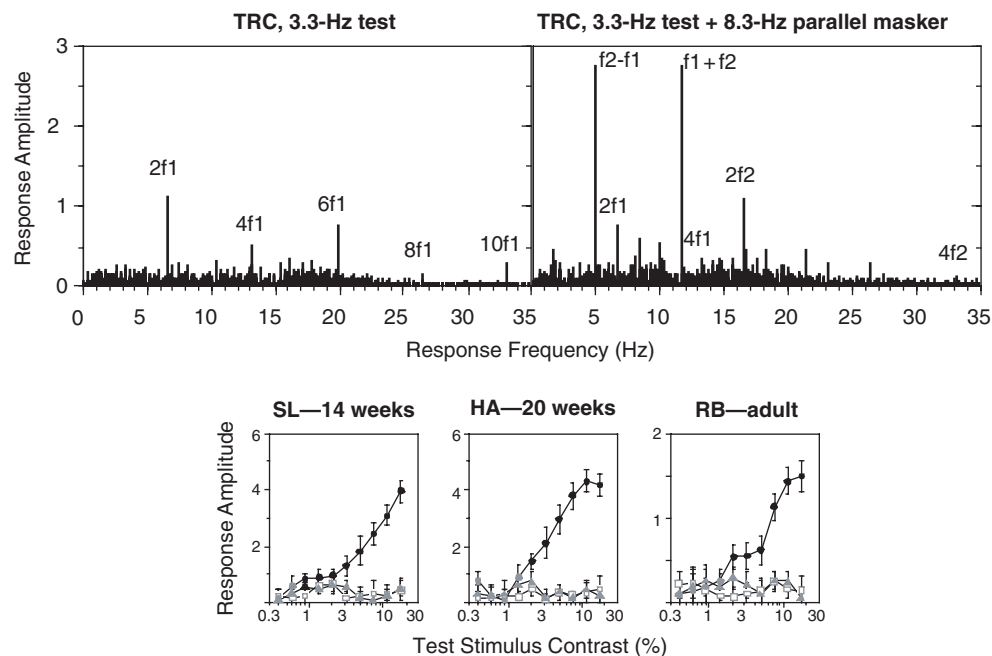


FIGURE 13.8. Demonstration of orientation selectivity in infants using nonlinear response components in a grating-on-grating masking paradigm. *Top panel*, The left panel shows the response of an adult to a single grating contrast reversing at 3.3 Hz (f_1). The response consists of several even harmonic components (e.g., $2f_1$; 6.6 Hz, $4f_1$; 13.2 Hz, etc.). The right panel shows the response spectrum obtained when a second grating of the same orientation (reversing at 8.3 Hz; f_2) is added to the 3.3-Hz grating. The response spectrum now contains prominent activity at the sum (f_2

+ f_1 ; 11.6 Hz) and difference ($f_2 - f_1$; 5.0 Hz) frequencies. Response amplitude at the harmonics of the 3.3-Hz grating are reduced and components related to the 8.3-Hz masker are also visible at frequencies equal to $2f_2$ and $4f_2$. *Bottom panel*, Contrast response functions for the nonlinear sum term. This term is large for parallel test and mask orientations (*open squares*), but is absent with orthogonal maskers or for the test presented alone (*gray curves*). The sum term thus indicates the presence of orientation selectivity in both infants and adults. (Redrawn from Candy et al., 2001.)

known as Vernier acuity, is finer than the spacing of the cone lattice that forms the limiting factor for grating acuity in the adult (Westheimer and McKee, 1977).

Positional sensitivity can be inferred from the VEP by showing that the response is dependent on the relative position or configuration of the stimulus. A demonstration of position sensitivity in infants is illustrated in Figure 13.9, which plots data from Skoczenski and Norcia (1999). Responses were measured using stimuli composed of a series of oscillating grating panels that were sandwiched between static grating panels. The motion of the oscillating panels was constant and equal to one-fourth of a period of the grating making up the oscillating pattern. The author compared the responses to the oscillating pattern when the static pattern was positioned symmetrically with respect to the two extremes of the motion (symmetric misalignment/misalignment), and when the static pattern was shifted by 90° of spatial phase, which yielded a stimulus that alternated between a simple grating and a grating with offsets (alignment/misalignment). If all that is being detected is the motion of the moving panels, the two stimulus configurations should produce the same response because the amount of motion is the same. However, the response to the alignment/misalignment condition has a large first harmonic component that is not present in the symmetric misalignment/misalignment condition. Zemon and Ratliff (1984) performed the original experiments in adults, upon which the author's experiment is based. Their study revealed that the first harmonic was actually a non-linear term owing to an interaction between the moving elements (frequency of 3 Hz, in this case) and the static elements (frequency of 0 Hz), yielding a sum/difference frequency component of 3 Hz. Grose-Fifer et al. (1994) showed that this nonlinear interaction was present in infants,

but that it had a very different temporal tuning than in adults.

The response at the first harmonic in the offset grating task is a marker of position sensitivity that persists down to very small offsets equal to the psychophysical threshold for discriminated left/right shifts of the moving elements relative to the static elements (Norcia et al., 1999). In their experiment, vernier offset size was swept over a range of values spanning the psychophysical discrimination threshold, and VEP thresholds were estimated by extrapolating the VEP amplitude versus displacement function to zero amplitude.

Vernier acuity, measured with the swept-parameter VEP, shows a long developmental sequence in humans, with adult values first being reached between 10 and 14 years of age (Skoczenski and Norcia, 2002; see also Fig. 13.10). Vernier thresholds were 20 to 40 times lower than adult levels in the youngest infant tested. By the second semester, thresholds were between 1 and 2 arc min, or a factor of 4 to 8 below those of the adults (0.25 minutes or 15 arc sec). It is only after the age of 6 years that VEP Vernier acuity exceeds grating acuity.

Development of direction selectivity and sensitivity

The detection of motion involves the determination of speed and direction. Directionally appropriate eye movements can be seen at term or even before term (Dubowitz et al., 1980; Hainline, 1993). However, it is unclear whether these early ocular following responses are controlled by cortical or subcortical pathways. Direction selectivity has been demonstrated behaviorally using forced-choice preferential looking (FPL) and looking-time habituation methods by 6 to 8 weeks of age (Wattam-Bell, 1996a; Wattam-Bell, 1996b). In these studies, 6- to 8-week-old infants demonstrated a

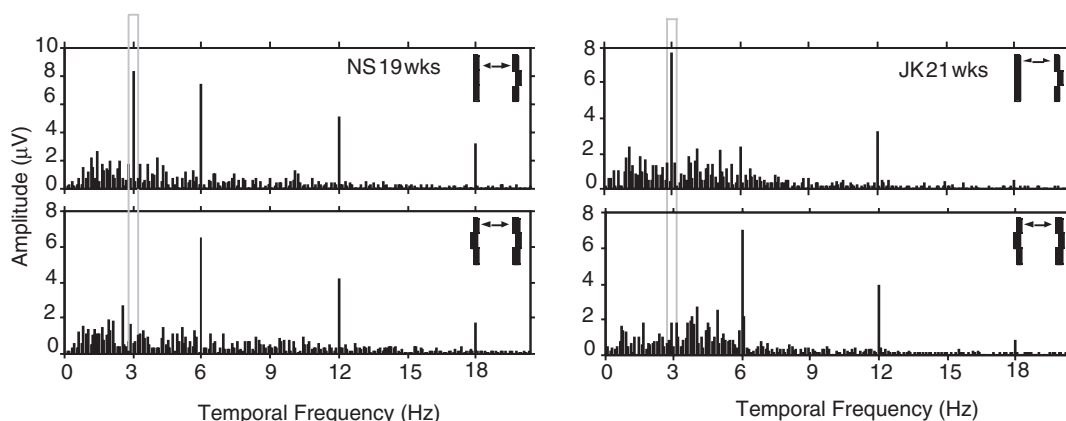


FIGURE 13.9. Demonstration of position sensitivity in infants. Response spectra are plotted from two infants for two stimulus conditions: alignment/misalignment (*top*) and misalignment/misalignment (*bottom*). The two conditions are identical in the amount of motion present, but differ in the relative positioning of the static

reference bars and the moving bars. The alignment/misalignment response contains a prominent response component at the stimulus frequency (3 Hz; *gray box*) that is absent from the misalignment/misalignment response. (Replotted from Skoczenski and Norcia, 1999, Fig.2.)

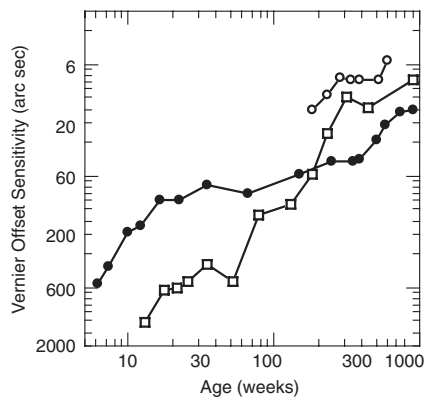


FIGURE 13.10. Development of Vernier acuity. Filled symbols plot VEP measurements (Skoczenski and Norcia, 2002). Behavioral data from Carkeet et al., 1997 (*open circles*) and Zanker et al., 1992 (*open squares*) are plotted for comparison. Vernier acuity reaches adult levels only in later childhood. (Reprinted from Norcia and Manny, 2003.)

behavioral discrimination between random-dot displays containing uniform motion versus displays in which alternate panels moved in opposite directions. Younger infants did not demonstrate this discrimination. VEP responses specifically associated with changes of direction have been recorded by 10 weeks of age (Wattam-Bell, 1991). Sensitivity to change of direction first emerged for lower stimulus velocities (5 versus 20°/second).

The sensitivity of directionally selective mechanisms can be measured with oscillating patterns similar to those used to measure Vernier acuity (Hamer and Norcia, 1994). Thresholds for oscillatory motion in the adult VEP are around 20 to 30 arc sec, similar in magnitude to vernier offset thresholds. Figure 13.11 shows oscillatory motion thresholds measured using the swept parameter VEP (Hamer and Norcia, 1994), compared to vernier offset thresholds taken from the study by Skoczenski and Norcia, 1999. Both functions show similar improvement over the first 6 months of life. Vernier thresholds in older infants are slightly lower than those for motion, but relative to the adult values of 15 versus 26 arc sec, the two functions show a similar degree of immaturity.

DEVELOPMENTAL MOTION ASYMMETRY One of the most striking immaturities in normally developing infants is an asymmetry of responsiveness to visual motion that can only be detected under monocular viewing conditions. This response asymmetry is manifested both in ocular following responses (optokinetic nystagmus [OKN]) and in the VEP. In the case of OKN, smooth ocular following is robust for motions that are nasally directed in the visual field (left to right motion in the left eye, right to left in the right eye), but is weak or primarily saccadic for motions that are temporal in direction (Naegele and Held, 1982). A similarly organized

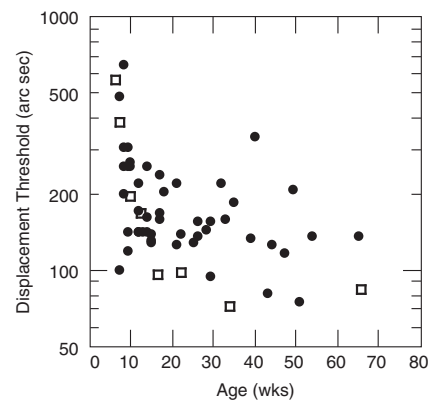


FIGURE 13.11. Full-field motion thresholds (*filled circles*; Hamer and Norcia, 1994) compared to vernier offset thresholds (*open circles*; Skoczenski and Norcia, 1999) in infants. Both thresholds are around 500 arcsec in the youngest infants. Thresholds mature to between 70 and 150 arcsec by the end of the first year. At this age, each threshold is worse, by about a factor of 5, than that in adults.

bias in responsiveness is also apparent in the monocular VEP to oscillatory motion (Birch et al., 2000; Hamer and Norcia, 1994; Jampolsky et al., 1994; Mason et al., 2001; Norcia et al., 1991). In normal adults, the monocular response to oscillatory motion is equal for the two directions of motion, and the VEP response is composed of even harmonics of the input temporal frequency. In normally developing infants, one finds a large first harmonic component that is 180° temporally out of phase between the two eyes (Fig. 13.12, *left*). The presence of a first harmonic component is consistent with the response being larger in one direction of motion than the other. The 180° phase shift between the eyes is consistent with a response bias organized in a nasalward/temporalward direction, although whether the stronger direction is nasalward versus temporalward cannot be determined directly from the steady-state response. Mason et al. (2001) found that 90 displacements of bar gratings elicited a larger monocular response when the motion was temporally directed (e.g., left-to-right motion in the right eye), opposite the dominant direction of the molecular OKN asymmetry.

The monocular VEP direction asymmetry persists down to the oscillatory motion threshold (Hamer and Norcia, 1994), indicating that the thresholds presented in Figure 13.11 are those of direction-selective mechanisms. The VEP motion asymmetry is thus an additional marker for the presence of cortical directional selectivity (Norcia et al., 1991). Birch et al. (2000) have found that this marker is absent in infants younger than 1 month of age, but it can be recorded in those as young as 6 weeks of age at 6 Hz 1 c/deg.

The degree of motion asymmetry, and thus, the degree of immaturity, can be quantified by calculating the proportion of the response at the first harmonic relative to the sum of

the response at the first and second harmonics (Jampolsky et al., 1994; Norcia et al., 1995). At moderate temporal frequencies (6 Hz) and low spatial frequencies (1 c/deg), a symmetric response is achieved by 5 to 6 months of age (Birch et al., 2000; Jampolsky et al., 1994; Mason et al., 2001; Norcia et al., 1995; see Fig. 13.12, *left*). The age at which a symmetric motion response is achieved depends on both spatial and temporal frequency (Norcia et al., 1990a). Figure 13.13 shows data obtained at four different spatiotemporal frequencies (the combinations of 1 and 3 c/deg and 6- and 10-Hz oscillation frequency). At each spatiotemporal combination, the first harmonic shows a decline with age and the second harmonic shows an increase with age. If one considers the age at which the two curves cross (the point where first and second harmonics are of equal amplitude), one observes that this criterion value is reached first for the 6-Hz and 1 c/deg condition (14 weeks), next at 6 Hz and 3 c/deg (27 weeks), then at 10 Hz and 1 c/deg (57 weeks), and finally, at 78 weeks for the 10-Hz and 3 c/deg condition. Brown et al. (1998) found that infant monkeys achieved adult levels of symmetry at 6 Hz and 0.25 c/deg by 6 weeks of age, which is similar to the case in humans, given the 4:1 correction for equivalent developmental ages that has been applied in other contexts (Boothe et al., 1985).

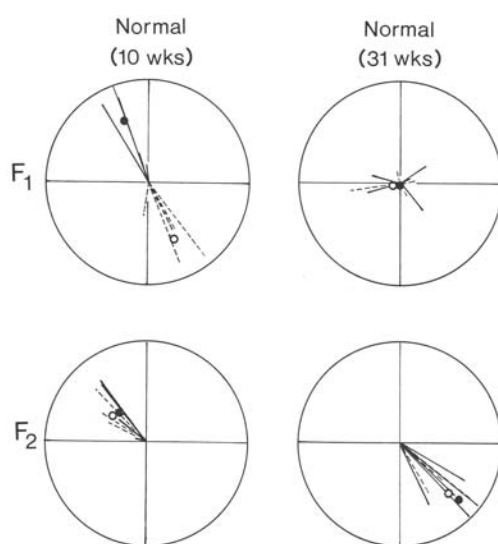


FIGURE 13.12. Developmental immaturity of the response to monocular oscillatory motion. VEP responses to a 6-Hz, 1 c/degree grating are shown in polar form for 6 Hz (first harmonic, *top panels*) and 12 Hz (second harmonic, *bottom panels*). Each vector represents the response amplitude and phase for a single 10-second trial. Filled and open symbols plot the vector average response. In the younger infant (*left panels*), the first harmonic response (F_1) is large relative to the second harmonic (F_2) and is 180° out of phase in the two eyes. The first harmonic response is absent in the older infant. (Reprinted from Norcia and Manny, 2003.)

The maturation of the oscillatory motion response depends on normal binocular interaction during a period of time that is similar to that over which the normal response matures (Birch et al., 2000; Norcia et al., 1995; Norcia et al., 1991). Individuals with constant strabismus present during the first 6 months of life have motion responses that retain the infantile motion asymmetry, a condition that persists well after the age that normal infant responses become symmetrical (Birch et al., 2000; Fawcett and Birch, 2000; Jampolsky et al., 1994). A similar response asymmetry is present in monkeys that develop strabismus during the first months of life (Tychsen and Boothe, 1996). Surgical correction of the strabismus results in a reduction of the magnitude of the motion asymmetry if the eyes are aligned prior to the age of about 2 years (Norcia et al., 1995). The amount of recovery is greatest at spatiotemporal frequencies that mature first.

Development of binocularity

The fact that humans have two laterally placed eyes, each with a slightly different view of the world, allows the brain to calculate object distances from the disparities in the retinal images, a process known as *stereopsis*. The different views afforded by the two eyes also poses a challenge, that is, the brain must select a unique visual direction for each object in the visual field, a process known as *fusion*. There has been considerable interest in determining the developmental sequences for fusion and stereopsis, especially since these functions are disrupted in strabismus (eye misalignment), a condition that occurs commonly in infancy and early childhood.

The most direct approach for determining the onset of sensory fusion in human infants has been to record a “cyclopean” VEP using one of two different stimuli. The first approach presents a uniform field or pattern to each eye that are modulated at different temporal frequencies in the two eyes (e.g., 8 Hz—for the right eye, 6 Hz—for the left eye). A cortical response, recorded at either the sum (14 Hz) or the difference frequency (2 Hz, also termed the beat frequency), indicates the presence of binocular neurons that integrate and respond to input from both eyes. Using this approach, France and Ver Hoeve (1994) reported that a binocular response was present in most normal infants by 2 months of age. The two-frequency approach has also been used by Brown et al. (1999) to study the development of fusion and rivalry. In that study, beat frequency response was recordable only for stimuli that had the same orientation in the two eyes.

The second approach for exploring the integration of information from the two eyes employs dynamic random-dot correlograms. Correlograms consist of a field of random dots presented dichoptically to the two eyes. Correlograms alternate between two different phases, a correlated and anticorrelated phase. In the correlated phase, the dot patterns are identical

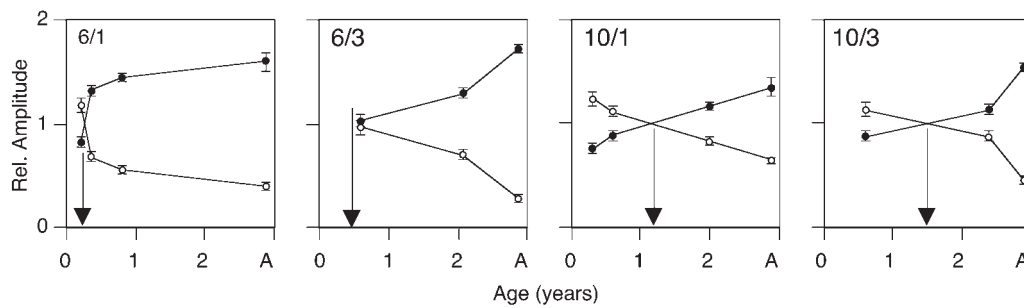


FIGURE 13.13. Development of symmetrical monocular motion VEP response as a function of spatial and temporal frequency. Infants were presented with high-contrast (80%) oscillating gratings (90° phase shifts) at four spatiotemporal frequencies (6 Hz, 1 c/deg; 6 Hz, 3 c/deg; 10 Hz, 1 c/deg; and 10 Hz, 3 c/deg). Response amplitudes for each harmonic were normalized by dividing by the mean response amplitude measured across all responses for each combination of eye (left and right), harmonic (first and second), and

recording channels (Oz vs. O1 and Oz vs. O2). The age at which the first and second harmonics are equal (crossing point) was used as an estimate of age to maturity for each spatiotemporal condition. Maturity on this measure is first reached for 6 Hz, 1 c/deg (18 weeks), and development extends to almost 78 weeks at 10 Hz, 3 c/degree. Development continues beyond these midpoint estimates and extends at least into the third year at 10 Hz, 3 c/deg. Rel., relative

in the two eyes. In the anticorrelated phase, a dark dot in the pattern presented to one eye corresponds to a bright dot in the pattern presented to the fellow eye and vice versa. The cortical response to the alternation between the two phases is recorded. The “cyclopean VEP” response to these correlated/anticorrelated stimuli has been interpreted as being indicative of fusion without stereopsis as horizontal disparities are not induced by the stimuli. Using this approach, the onset of sensory fusion has been reported to occur typically at between 3 and 5 months of age (Braddick et al., 1980; Petrig et al., 1981), but possibly as early as 5 weeks of age (Skarf et al., 1993). Responses to random-dot patterns with disparity also emerge at about the same age (Birch and Petrig, 1996; Braddick et al., 1980; Petrig et al., 1981; Skarf et al., 1993). Stereo-acuity development through adulthood has been reviewed in Norcia and Manny (2003).

Development of response timing

Visual response latency is very much delayed in infants relative to adults. The most well-studied example of this general process is the maturation of the latency of the first positive peak (P100) of the pattern reversal response (Kos-Pietro et al., 1997; McCulloch and Skarf, 1991; Sokol and Jones, 1979). Figure 13.14 plots the latency of the first positive peak as a function of age and spatial frequency. The latency of the first positive peak rapidly declines to near adult levels by approximately 5 months of age for low spatial frequency targets. Longer maturational sequences are seen when finer scale patterns are used (Kos-Pietro et al., 1997; McCulloch and Skarf, 1991), and small latency decreases continue during childhood and adolescence (Allison et al., 1983; Zemon et al., 1997).

The latency of the evoked response is controlled by the neural integration time required in the retina, the conduction

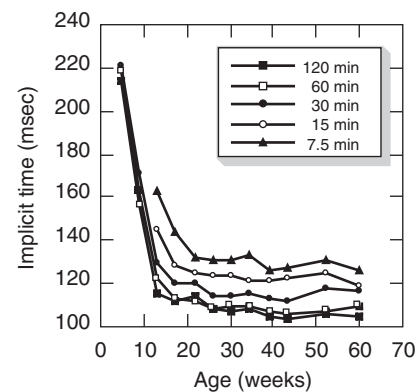


FIGURE 13.14. Latency of the P100 component of the transient pattern reversal response as a function of age. Response latency declines rapidly between birth and 6 months of age for a range of check-sizes between 120 and 7.5 arcmin. The decline in latency is more rapid for the larger check-sizes. (Data from McCulloch and Skarf, 1991, as replotted in Norcia and Manny, 2003.)

velocity through the retinogeniculate pathway, and finally, cortical integration time. Fiorentini and Trimarchi (1992) compared latencies of simultaneously recorded pattern electroretinogram (ERG) and VEP responses. In adults, there was a 50-msec difference in latency between retinal and cortical responses. This difference was 125 msec at 5 weeks of age, indicating that much of the change in delay of VEP latency that occurs during the first 5 months is attributable to changes in postretinal mechanisms, most likely in the cortex itself.

Visual responses are faster for stimuli that are well above threshold than for stimuli that are near threshold (Kubova et al., 1995; Parker et al., 1982). Contrast sensitivity develops rapidly over the same time frame that latency is decreasing; thus, some of the apparent speeding of the cortical response could be due to increasing contrast sensitivity. If one compares response phase at a constant factor above threshold,

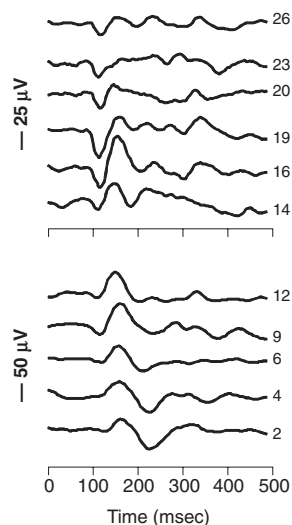


FIGURE 13.15. Development of chromatic VEP waveforms for 2- to 26-year-old observers recorded in response to purely chromatic stimuli modulated about white along the LWS/MWS cone excitation axis. In young observers, the response consists of a positive/negative complex. The negativity at 250 msec, seen in the youngest observers, is absent in adults. Starting at around 5 years of age, an earlier negativity, at approximately 150 msec, emerges and is retained into adulthood. (Reprinted from Madrid and Crognale, 2000, Fig. 2.)

this sensitivity difference can be factored out. In Figure 13.7, response phase for 3-month-old infants at 10% physical contrast is about 0° . At 8 to 11 months, contrast threshold is improved by a factor of 2, and the phase of the response at 5% contrast (a comparable multiple of threshold) has advanced by 100° . This speed-up is independent of stimulus visibility and is equivalent to 25 msec of delay at the response frequency of 11 Hz.

In contrast to the relatively precocious development of low-spatial-frequency achromatic mechanisms, low-spatial-frequency chromatic mechanisms show continued development through late adolescence (Madrid and Crognale, 2000). Figure 13.15 shows response waveforms for 2- to 26-year-old observers recorded in response to purely chromatic stimuli modulated about white along the LWS/MWS cone excitation axis. In young observers, the response consists of a positive/negative complex. The negativity at 250 msec, seen in the youngest observers, is absent in adults. Starting around the age of 5 years, an earlier negativity at approximately 150 msec emerges, and this persists into adulthood. A similarly protracted developmental sequence has been observed for stimuli that preferentially excite the SWS cone pathway.

Summary

Depending on what visual function is measured, adult-like performance can be seen at as early as 8 to 10 weeks of age (low-spatial-frequency contrast sensitivity) or as late as 10 to

14 years (Vernier acuity, chromatic VEP waveforms; for a more complete listing of late-maturing functions, see also Norcia and Manny, 2003). These different developmental sequences presumably reflect fundamental limitations at different levels of the visual system. Studies of nonhuman primates (see Chapter 12, Neural Limitations on Visual Development in Primates) have provided suggestions about limiting factors in the retina and primary visual cortex that may affect the processing of simple stimuli, such as gratings. Our understanding of the developing retina and visual cortex, particularly the extrastriate cortex, is far from complete. It is hoped that future advances in electrophysiological, behavioral, and imaging techniques will help fill in these large gaps in knowledge.

Acknowledgments

AMN is supported by EY06579, EY01248, and the Smith-Kettlewell Eye Research Foundation

REFERENCES

- Albus, K., and W. Wolf, 1984. Early post-natal development of neuronal function in the kitten's visual cortex: a laminar analysis, *J. Physiol.*, 348:153–185.
- Allen, D., M. S. Banks, and A. M. Norcia, 1993. Does chromatic sensitivity develop more slowly than luminance sensitivity? *Vis. Res.*, 33:2553–2562.
- Allen, D., C. W. Tyler, and A. M. Norcia, 1996. Development of grating acuity and contrast sensitivity in the central and peripheral visual field of the human infant, *Vis. Res.*, 36:1945–1953.
- Allison, T., C. C. Wood, and W. R. Goff, 1983. Brain stem auditory, pattern-reversal visual, and short-latency somatosensory evoked potentials: latencies in relation to age, sex, and brain and body size, *Electroencephalogr. Clin. Neurophysiol.*, 55:619–636.
- Apkarian, P., 1993. Temporal frequency responsivity shows multiple maturational phases: state-dependent visual evoked potential luminance flicker fusion from birth to 9 months, *Vis. Neurosci.*, 10:1007–1018.
- Atkinson, J., B. Hood, J. Wattam-Bell, S. Anker, and J. Tricklebank, 1988. Development of orientation discrimination in infancy, *Perception*, 17:587–595.
- Auestad, N., M. B. Montalto, R. T. Hall, K. M. Fitzgerald, R. E. Wheeler, W. E. Connor, M. Neuringer, S. L. Connor, J. A. Taylor, and E. E. Hartmann, 1997. Visual acuity, erythrocyte fatty acid composition, and growth in term infants fed formulas with long chain polyunsaturated fatty acids for one year. Ross Pediatric Lipid Study, *Pediatr. Res.*, 41:1–10.
- Banks, M. S., and P. J. Bennett, 1988. Optical and photoreceptor immaturities limit the spatial and chromatic vision of human neonates, *J. Opt. Soc. Am. [A]*, 5:2059–2079.
- Bieber, M. L., K. Knoblauch, and J. S. Werner, 1998. M- and L-cones in early infancy: II. Action spectra at 8 weeks of age, *Vis. Res.*, 38:1765–1773.
- Bieber, M. L., V. J. Volbrecht, and J. S. Werner, 1995. Spectral efficiency measured by heterochromatic flicker photometry is similar in human infants and adults, *Vis. Res.*, 35:1385–1392.
- Birch, E., and B. Petrig, 1996. FPL and VEP measures of fusion, stereopsis and stereoacuity in normal infants, *Vis. Res.*, 36:1321–1327.

- Birch, E. E., S. Fawcett, and D. Stager, 2000. Co-development of VEP motion response and binocular vision in normal infants and infantile esotropes, *Invest. Ophthalmol. Vis. Sci.*, 41:1719–1723.
- Birch, E. E., D. R. Hoffman, R. Uauy, D. G. Birch, and C. Prestidge, 1998. Visual acuity and the essentiality of docosahexaenoic acid and arachidonic acid in the diet of term infants, *Pediatr. Res.*, 44:201–209.
- Blakemore, C., and R. C. Van Sluyters, 1975. Innate and environmental factors in the development of the kitten's visual cortex, *J. Physiol.*, 248:663–716.
- Blasdel, G., K. Obermayer, and L. Kiorpes, 1995. Organization of ocular dominance and orientation columns in the striate cortex of neonatal macaque monkeys, *Vis. Neurosci.*, 12:589–603.
- Boothe, R. G., V. Dobson, and D. Y. Teller, 1985. Postnatal development of vision in human and nonhuman primates, *Annu. Rev. Neurosci.*, 8:495–545.
- Braastad, B. O., and P. Heggelund, 1985. Development of spatial receptive-field organization and orientation selectivity in kitten striate cortex, *J. Neurophysiol.*, 53:1158–1178.
- Braddick, O., J. Atkinson, B. Julesz, W. Kropfl, I. Bodis-Wollner, and E. Raab, 1980. Cortical binocularity in infants, *Nature*, 288:363–365.
- Braddick, O. J., J. Wattam-Bell, and J. Atkinson, 1986. Orientation-specific cortical responses develop in early infancy, *Nature*, 320:617–619.
- Brown, R. J., T. R. Candy, and A. M. Norcia, 1999. Development of rivalry and dichoptic masking in human infants, *Invest. Ophthalmol. Vis. Sci.*, 40:3324–3333.
- Brown, R. J., J. R. Wilson, A. M. Norcia, and R. G. Boothe, 1998. Development of directional motion symmetry in the monocular visually evoked potential of infant monkeys, *Vis. Res.*, 38:1253–1263.
- Campbell, F. W., and D. G. Green, 1965. Optical and retinal factors affecting visual resolution, *J. Physiol.*, 181:576–593.
- Campbell, F. W., and J. J. Kulikowski, 1966. Orientational selectivity of the human visual system, *J. Physiol.*, 187:437–445.
- Campbell, F. W., and J. J. Kulikowski, 1971. An electrophysiological measure of the psychophysical contrast threshold, *J. Physiol.*, 217:54P–55P.
- Campbell, F. W., and L. Maffei, 1970. Electrophysiological evidence for the existence of orientation and size detectors in the human visual system, *J. Physiol.*, 207:635–652.
- Campbell, F. W., and J. G. Robson, 1968. Application of Fourier analysis to the visibility of gratings, *J. Physiol.*, 197:551–566.
- Candy, T. R., A. M. Skoczinski, and A. M. Norcia, 2001. Normalization models applied to orientation masking in the human infant, *J. Neurosci.*, 21:4530–4541.
- Cannon, M. W., Jr., 1983. Contrast sensitivity: Psychophysical and evoked potential methods compared, *Vis. Res.*, 23:87–95.
- Carkeet, A., D. M. Levi, and R. E. Manny, 1997. Development of Vernier acuity in childhood, *Optom. Vis. Sci.*, 74:741–750.
- Chino, Y. M., E. L. Smith III, S. Hatta, and H. Cheng, 1997. Postnatal development of binocular disparity sensitivity in neurons of the primate visual cortex, *J. Neurosci.*, 17:296–307.
- Dobson, V., 1976. Spectral sensitivity of the 2-month infant as measured by the visually evoked cortical potential, *Vis. Res.*, 16:367–374.
- Dobson, V., 1990. The behavioral assessment of visual acuity in human infants, in *Comparative Perception* (M. A. Berkeley and W. C. Stebbins, eds.), Pittsburgh: Wiley & Sons, pp. 487–521.
- Dubowitz, L. M., V. Dubowitz, A. Morante, and M. Verghote, 1980. Visual function in the preterm and fullterm newborn infant, *Dev. Med. Child. Neurol.*, 22:465–75.
- Ellemberg, D., T. L. Lewis, C. H. Liu, and D. Maurer, 1999. Development of spatial and temporal vision during childhood, *Vis. Res.*, 39:2325–2333.
- Fawcett, S. L., and E. E. Birch, 2000. Motion VEPs, stereopsis, and bifoveal fusion in children with strabismus, *Invest. Ophthalmol. Vis. Sci.*, 41:411–416.
- Fiorentini, A., and C. Trimarchi, 1992. Development of temporal properties of pattern electroretinogram and visual evoked potentials in infants, *Vis. Res.*, 32:1609–1621.
- France, T. D., and J. N. Ver Hoeve, 1994. VECF evidence for binocular function in infantile esotropia, *J. Pediatr. Ophthalmol. Strabismus*, 31:225–231.
- Freeman, T. C., S. Durand, D. C. Kiper, and M. Carandini, 2002. Suppression without inhibition in visual cortex, *Neuron*, 35:754–771.
- Gordon, G. E., and D. L. McCulloch, 1999. A VEP investigation of parallel visual pathway development in primary school age children, *Doc. Ophthalmol.*, 99:1–10.
- Große-Fifer, J., V. Zemon, and J. Gordon, 1994. Temporal tuning and the development of lateral interactions in the human visual system, *Invest. Ophthalmol. Vis. Sci.*, 35:2999–3010.
- Hainline, L., 1993. Conjugate eye movements of infants. in *Early Visual Development, Normal and Abnormal* (K. Simons, ed.), New York: Oxford University Press, pp. 47–79.
- Hamer, R., and L. Mayer, 1994. The development of spatial vision, in *Principles and Practice of Ophthalmology: Basic Sciences* (D. M. Albert and F. A. Jakobiec, eds.), Philadelphia: W. B. Saunders, pp. 578–608.
- Hamer, R. D., and A. M. Norcia, 1994. The development of motion sensitivity during the first year of life, *Vis. Res.*, 34:2387–2402.
- Hawken, M. J., C. Blakemore, and J. W. Morley, 1997. Development of contrast sensitivity and temporal-frequency selectivity in primate lateral geniculate nucleus, *Exp. Brain Res.*, 114:86–98.
- Heeger, D. J., 1992. Normalization of cell responses in cat striate cortex, *Vis. Neurosci.*, 9:181–197.
- Hendrickson, A., and D. Drucker, 1992. The development of parafoveal and mid-peripheral human retina, *Behav. Brain Res.*, 49:21–31.
- Hendrickson, A. E., and C. Yuodelis, 1984. The morphological development of the human fovea, *Ophthalmology*, 91:603–612.
- Hood, B., J. Atkinson, O. Braddick, and J. Wattam-Bell, 1992. Orientation selectivity in infancy: behavioural evidence for temporal sensitivity, *Perception*, 21:351–354.
- Jacobs, D. S., and C. Blakemore, 1988. Factors limiting the postnatal development of visual acuity in the monkey, *Vis. Res.*, 28:947–958.
- Jampolsky, A., A. M. Norcia, and R. D. Hamer, 1994. Preoperative alternate occlusion decreases motion processing abnormalities in infantile esotropia, *J. Pediatr. Ophthalmol. Strabismus*, 31:6–17.
- Kelly, J. P., K. Borchert, and D. Y. Teller, 1997. The development of chromatic and achromatic contrast sensitivity in infancy as tested with the sweep VEP, *Vis. Res.*, 37:2057–2072.
- Knoblauch, K., M. L. Bieber, and J. S. Werner, 1998. M- and L-cones in early infancy: I. VEP responses to receptor-isolating stimuli at 4- and 8-weeks of age, *Vis. Res.*, 38:1753–1764.
- Kos-Pietro, S., V. L. Towle, R. Cakmur, and J. P. Spire, 1997. Maturation of human visual evoked potentials: 27 weeks conceptional age to 2 years, *Neuropediatrics*, 28:318–323.
- Kubova, Z., M. Kuba, H. Spekreijse, and C. Blakemore, 1995. Contrast dependence of motion-onset and pattern-reversal evoked potentials, *Vis. Res.*, 35:197–205.

- LeVay, S., T. N. Wiesel, and D. H. Hubel, 1980. The development of ocular dominance columns in normal and visually deprived monkeys, *J. Comp. Neurol.*, 191:1–51.
- Madrid, M., and M. A. Crognale, 2000. Long-term maturation of visual pathways, *Vis. Neurosci.*, 17:831–837.
- Manny, R. E., 1992. Orientation selectivity of 3-month-old infants, *Vis. Res.*, 32:1817–1828.
- Mason, A. J., O. J. Braddick, J. Wattam-Bell, and J. Atkinson, 2001. Directional motion asymmetry in infant VEPs—Which direction? *Vis. Res.*, 41:201–211.
- McCulloch, D. L., and B. Skarf, 1991. Development of the human visual system: monocular and binocular pattern VEP latency, *Invest. Ophthalmol. Vis. Sci.*, 32:2372–2381.
- Morrone, M. C., D. C. Burr, and A. Fiorentini, 1993. Development of infant contrast sensitivity to chromatic stimuli, *Vis. Res.*, 33:2535–2552.
- Naegele, J. R., and R. Held, 1982. The postnatal development of monocular optokinetic nystagmus in infants, *Vis. Res.*, 22:341–346.
- Narayanan, K., and S. Wadhwa, 1998. Photoreceptor morphogenesis in the human retina: a scanning electron microscopic study, *Anat. Rec.*, 252:133–139.
- Norcia, A. M., H. Garcia, R. Humphry, A. Holmes, R. D. Hamer, and D. Orel-Bixler, 1991. Anomalous motion VEPs in infants and in infantile esotropia, *Invest. Ophthalmol. Vis. Sci.*, 32:436–439.
- Norcia, A. M., R. D. Hamer, A. Jampolsky, and D. Orel-Bixler, 1995. Plasticity of human motion processing mechanisms following surgery for infantile esotropia, *Vis. Res.*, 35:3279–3296.
- Norcia, A. M., R. D. Hamer, and D. Orel-Bixler, 1990a. Temporal tuning of the motion VEP in infants, *Invest. Ophthalmol. (Suppl.)*, 31:10.
- Norcia, A. M., and R. E. Manny, 2003. Development of vision in infancy, in *Adler's Physiology of the Eye*, 10th ed. (P. Kaufman and A. Alm, eds.), St. Louis: Mosby, pp. 531–551.
- Norcia, A. M., and C. W. Tyler, 1985. Spatial frequency sweep VEP: Visual acuity during the first year of life, *Vis. Res.*, 25:1399–1408.
- Norcia, A. M., C. W. Tyler, and R. D. Hamer, 1990b. Development of contrast sensitivity in the human infant, *Vis. Res.*, 30:1475–1486.
- Norcia, A. M., W. Wesemann, and R. E. Manny, 1999. Electrophysiological correlates of vernier and relative motion mechanisms in human visual cortex, *Vis. Neurosci.*, 16:1123–1131.
- Parker, D. M., E. A. Salzen, and J. R. Lishman, 1982. Visual-evoked responses elicited by the onset and offset of sinusoidal gratings: latency, waveform, and topographic characteristics, *Invest. Ophthalmol. Vis. Sci.*, 22:675–680.
- Pelli, D. G. 1990. The quantum efficiency of vision, in *Coding and Efficiency* (C. Blakemore, ed.), Cambridge: Cambridge University Press, pp. 3–24.
- Petrig, B., B. Julesz, W. Kropfl, G. Baumgartner, and M. Anliker, 1981. Development of stereopsis and cortical binocularity in human infants: electrophysiological evidence, *Science*, 213:1402–1405.
- Regan, D., 1977. Speedy assessment of visual acuity in amblyopia by the evoked potential method, *Ophthalmologica*, 175:159–164.
- Regan, D., and M. P. Regan, 1987. Nonlinearity in human visual responses to two-dimensional patterns, and a limitation of Fourier methods, *Vis. Res.*, 27:2181–2183.
- Sherk, H., and M. P. Stryker, 1976. Quantitative study of cortical orientation selectivity in visually inexperienced kitten, *J. Neurophysiol.*, 39:63–70.
- Skarf, B., M. Eizenman, L. M. Katz, B. Bachynski, and R. Klein, 1993. A new VEP system for studying binocular single vision in human infants, *J. Pediatr. Ophthalmol. Strabismus*, 30:237–242.
- Skoczenski, A. M., T. R. Candy, and A. M. Norcia, 1999. Orientation masking identifies a late immaturity in infant pattern vision, *Invest. Ophthalmol. Vis. Sci.*, (Suppl.), 39:S1089.
- Skoczenski, A. M., and A. M. Norcia, 1998. Neural noise limitations on infant visual sensitivity, *Nature*, 391:697–700.
- Skoczenski, A. M., and A. M. Norcia, 1999. Development of VEP Vernier acuity and grating acuity in human infants, *Invest. Ophthalmol. Vis. Sci.*, 40:2411–2417.
- Skoczenski, A. M., and A. M. Norcia, 2002. Late maturation of vernier hyperacuity, *Psychol. Sci.*, 13:537–541.
- Sokol, S., and K. Jones, 1979. Implicit time of pattern evoked potentials in infants: Aan index of maturation of spatial vision, *Vis. Res.*, 19:747–755.
- Sokol, S., A. Moskowitz, and G. McCormack, 1992. Infant VEP and preferential looking acuity measured with phase alternating gratings, *Invest. Ophthalmol. Vis. Sci.*, 33:3156–3161.
- Spinelli, D., M. Pirchio, and G. Sandini, 1983. Visual acuity in the young infant is highest in a small retinal area, *Vis. Res.*, 23:1133–1136.
- Taylor, M. J., R. Menzies, L. J. MacMillan, and H. E. Whyte, 1987. VEPs in normal full-term and premature neonates: longitudinal versus cross-sectional data, *Electroencephalogr. Clin. Neurophysiol.*, 68:20–27.
- Tychsen, L., and R. G. Boothe, 1996. Latent fixation nystagmus and nasotemporal asymmetries of motion visually evoked potentials in naturally strabismic primate, *J. Pediatr. Ophthalmol. Strabismus*, 33:148–152.
- Volbrecht, V. J., and J. S. Werner, 1987. Isolation of short-wavelength-sensitive cone photoreceptors in 4–6-week-old human infants, *Vis. Res.*, 27:469–478.
- Wattam-Bell, J., 1991. Development of motion-specific cortical responses in infancy, *Vis. Res.*, 31:287–297.
- Wattam-Bell, J., 1996a. Visual motion processing in one-month-old infants: Habituation experiments, *Vis. Res.*, 36:1679–1685.
- Wattam-Bell, J., 1996b. Visual motion processing in one-month-old infants: preferential looking experiments, *Vis. Res.*, 36:1671–1677.
- Werner, J. S., 1982. Development of scotopic sensitivity and the absorption spectrum of the human ocular media, *J. Opt. Soc. Am.*, 72:247–258.
- Westheimer, G., and S. P. McKee, 1977. Spatial configurations for visual hyperacuity, *Vis. Res.*, 17:941–947.
- Wiesel, T. N., and D. H. Hubel, 1974. Ordered arrangement of orientation columns in monkeys lacking visual experience, *J. Comp. Neurol.*, 158:307–318.
- Wilson, H. R., 1993. Theories of infant visual development, in *Early Visual Development: Normal and Abnormal* (K. Simons, ed.), New York: Oxford University Press, pp. 560–572.
- Zanker, J., G. Mohn, U. Weber, K. Zeitler-Driess, and M. Fahle, 1992. The development of vernier acuity in human infants, *Vis. Res.*, 32:1557–1564.
- Zemon, V., E. E. Hartmann, J. Gordon, and A. Prunte-Glowazki, 1997. An electrophysiological technique for assessment of the development of spatial vision, *Optom. Vis. Sci.*, 74:708–716.
- Zemon, V., and F. Ratliff, 1984. Intermodulation components of the visual evoked potential: responses to lateral and superimposed stimuli, *Biol. Cybern.*, 50:401–408.

14 The Effects of Selected Forms of Early Visual Deprivation on Perception

DONALD E. MITCHELL

STUDIES OF THE PERCEPTUAL effects of early selected visual deprivation have had at least three motives. Arguably, the primary motive has been to identify the functional consequences of the cortical changes induced by early, selected, visual deprivation imposed within defined critical periods in an animal's early life, and *en passant*, to help shed light on the relationship between the physiological properties of neurons within area 17 and perception. A related motive has been to provide data pertinent to the debate over the complex and, indeed, sometimes paradoxical issue (e.g., Pettigrew, 1978) of how and why periods of abnormal visual experience exert such dramatic effects on certain aspects of cortical physiology for a long time after adult characteristics are present. Finally, the third motive behind a subset of studies has been to arrive at an understanding of the origins of certain common developmental disorders affecting human vision. Of particular interest have been the three major forms of amblyopia, one associated with the presence of strabismus (strabismic amblyopia), one with anisometropia (anisometropic amblyopia), and the last with a severe peripheral impediment to form vision in one eye (stimulus-deprivation amblyopia).

Over time, the inquiry into experiential influences on visual cortical neurons and perception has focused on a limited number of forms of visual deprivation. As a starting point, there were studies of the consequences of binocular visual deprivation. In these studies, animals were either deprived of all visual input as a result of being reared in total darkness, or else they were deprived of patterned visual input in the two eyes by means of bilateral eyelid suture. As a group, the remaining forms of deprivation involved selected visual input biased to one extreme of the range within which each of the major visual response characteristics of cortical neurons (ocular dominance, orientation selectivity, and directional selectivity) are distributed in the normal adult striate cortex. With respect to ocular dominance, two forms of selected visual deprivation have been used widely in an attempt to alter the distribution of cortical ocular dominance in area 17. These are monocular deprivation, whereby one eye is deprived of either patterned or all visual input, and manipulations, such as strabismus or alternating monocular deprivation, which involve an

attempt to reduce or eliminate simultaneous or concordant visual input to the two eyes. Attempts to manipulate the distribution of preferences of orientation or directionally selective neurons in area 17 have employed various procedures designed to reduce early visual input to a narrow range of the spectrum of contour orientations or directions of motion that would be encountered in the environment and represented in the visual cortex of normally reared animals. Studies of experiential influences on the development of the physiological representation of directional selectivity have employed an additional form of selected visual exposure—namely, stroboscopic rearing—that virtually eliminates direction-selective neurons in area 17.

The effects of these various forms of early selected visual exposure on perception are described for various species that have been studied extensively, namely, monkeys, cats, and, to a limited extent, rodents. Where possible, results are included for humans in whom the early visual input was either known to be, or could be inferred to have been, biased in a manner similar to that imposed experimentally on animals. However, to begin, it is first necessary to discuss the behavioral methods that have been employed in the context of the existence of critical periods for the various physiological effects of early visual deprivation.

THE BENEFITS AND SHORTCOMINGS OF COMMON BEHAVIORAL TESTING METHODS With respect to data collected on visually deprived animals, the behavioral testing procedures can be classified according to two main categories. Belonging to the first category are methods that require extensive training and that can be employed only for assessment of the perceptual capacities of mature animals, albeit with great precision. As such, they are useful for documenting the long-standing deficits that follow extended periods of deprivation. When employed in animals subjected to periods of selected visual deprivation that do not extend to the end of the critical period, the final perceptual deficit revealed by such methods may be reduced from that present immediately after the deprivation owing to partial recovery afterward.

The second category includes methods that require little or no training and can be employed on young animals.

Unlike the first category of methods that require animals to be trained to make unfamiliar motor responses, such as a nose or key press, these methods exploit the natural motor behaviors of young animals and require only that the behaviors be linked to particular visual stimuli. A prime example is forced-choice preferential looking (FPL), which exploits the natural tendency of infant primates and, to a lesser extent, kittens (Sireteanu, 1985) to prefer to look at certain visual stimuli over others. For instance, these animals often prefer contoured stimuli over homogeneous fields, and moving over stationary stimuli (Teller et al., 1974). For kittens, a technique based on a Lashley jumping stand that exploits the natural tendency for kittens to jump has been used to measure perceptual abilities in animals as young as 30 days of age (Mitchell et al., 1977; Mitchell et al., 1976; Murphy and Mitchell, 1987). In general, such methods permit longitudinal studies of the normal development of various perceptual abilities, as well as documentation of the immediate effects of periods of selected visual deprivation and the speed of the subsequent recovery. A disadvantage of some of these methods is that their use may be restricted to animals before a certain age.

THE MAGNITUDE OF THE VISUAL DEFICITS INDUCED BY DEPRIVATION IN DIFFERENT SPECIES Because visual thresholds can differ substantially across species, specification of the absolute magnitude of the postdeprivation thresholds may not allow for ease of comparison of the deficits. Consequently, in the case of spatial resolution, deficits are specified, according to common practice, in terms of octaves. An octave represents a factor of 2 difference from normal values; it is defined formally as the logarithm to the base 2 of the ratio of the measured resolution to normal values.

The effects of binocular visual deprivation

Study of the consequences of binocular visual deprivation has a long history, beginning with consideration of the documented findings from cases of “recovery from blindness” reported in the last 500 years. These cases represent individuals in whom visual input was restored by surgery after a long period of blindness, supposedly beginning near birth and caused by a peripheral obstruction to vision, such as bilateral cataracts. The findings fueled debate, beginning in the seventeenth century, over the issue of whether experience was necessary to see. The reader is referred to Morgan (1977) for summaries of the early reports and to Ackroyd et al. (1974), Fine et al. (2002), Valvo (1968), and Gregory and Wallace (1963), for descriptions of more recent cases. A particularly readable account of a case, which later formed the basis for the movie *At First Sight*, was published by the neurologist, Oliver Sacks (1993). In the fall of 2002, the

British Broadcasting Corporation devoted a television program (“the Man who Learnt to See”) to a case of a man, M.M., who had patterned visual input restored 43 years following severe binocular corneal scarring from a chemical explosion that he experienced when he was 3 years old. The rehabilitation of M.M. following surgery can be followed on his website: <http://www.senderogroup.com/perception.htm>. As summarized earlier (Mitchell and Timney, 1984), the findings from these cases can be difficult to interpret because of the frequent lack of quantitative measures of basic visual functions and the lack of precise information concerning the time of onset and course of progression of the visual deprivation. However, in situations in which the deprivation was known to be severe, to have begun early, and to have been prolonged, the visual rehabilitation was very slow (lasting more than a year), incomplete, and accompanied by periods of regression and/or emotional depression. Many of the obstacles to interpretation of binocular deprivation that characterized the early studies of humans are not present in animal studies because of the control over the timing and nature of the visual deprivation. In turn, the results from animal studies have informed the design of recent studies of humans with congenital binocular cataract, described later in this chapter (see also Fine et al., 2002).

With respect to controlled experiments conducted on animals, a distinction may need to be drawn between the consequences of rearing animals in complete darkness and of performing binocular eyelid suture. The latter permits both light and some patterned images on the retina, particularly in young kittens, monkeys, or ferrets (see Crawford and Marc, 1976; Krug et al., 2001; Loop and Sherman, 1977; Spear et al., 1978). Evidence that the two forms of binocular deprivation may not be equivalent can be found in the vast differences between the potential for recovery afterward. Considerable physiological recovery, including experientially dependent, selective development, is observed after dark rearing, but not after binocular eyelid suture (Cynader and Mitchell, 1980; Mower et al., 1981). Although there is no generally accepted explanation for the differences in recovery in these two conditions, it is possible that the different results may reflect differences in the degree of deprivation. Dark rearing eliminates all visually driven activity in the visual pathways, thereby allowing observation of the extent of development of a particular function that is made possible solely through the operation of intrinsic mechanisms of development alone. On the other hand, the limited form information that passes the eyelids of binocularly lid-sutured animals, which is presumably confined to low spatial frequencies, has the potential to allow some experientially guided patterning of cortical activity. In turn, the patterned cortical activity may lead to specification of cortical neurons, which may make them more resistant to

change in response to biased visual input imposed later. This explanation finds partial support in the observation that binocular lid-suturing fails to disturb development of orientation maps in area 17 of kittens during the first 3 weeks of life (Crair et al., 1998).

Although experimental studies have been conducted on animals, including chimpanzees (Riesen et al., 1951), for more than 50 years, the modern era of such studies, spurred by the results of electrophysiological investigations of visually deprived animals, can be traced from the mid-1960s. The results from these modern animal studies are summarized by species; this discussion is then followed by a description of the findings in humans after surgery for congenital binocular cataract.

CATS As might have been anticipated from prior electrophysiological investigations, the severity and permanence of the behavioral effects vary with the length of the deprivation. The deficits observed immediately after termination of deprivation and extending to 3 months or more are extremely profound. These animals appear blind, based on both omnibus qualitative tests of visuomotor function and on tests utilizing the jumping stand, being unable to distinguish between an open and a closed door except by use of tactile cues (Kaye et al., 1982; Timney et al., 1978). Although the deficits evident on gross tests of visuomotor behavior disappear quickly, precise quantitative tests of reaching behavior with the forepaw in kittens dark-reared until 6 months of age reveal small residual deficits in both reaction time and accuracy after 5 to 6 years of recovery (Fabre-Thorpe et al., 1990). In contrast to the fast recovery of gross visuomotor behavior, the recovery of visual acuity measured on the jumping stand is slow and becomes increasingly so as the deprivation lengthens (Mitchell, 1988a). This latter point is demonstrated in Figure 14.1, which shows the time required for 17 dark-reared animals to exhibit the first sign of vision on the jumping stand as a function of the period of deprivation. Although recovery is slow, the vision that is eventually attained can approach normal levels in animals subjected to periods of deprivation that terminate at or before 4 months of age. Animals that are visually deprived to 4 months of age appear blind on the jumping stand for 9 to 30 days, but achieve normal or near-normal levels of grating acuity after 4 months of visual exposure (Kaye et al., 1982; Mitchell, 1988a; Timney et al., 1978). However, as illustrated in Figure 14.2, animals reared in darkness for longer periods of time attain progressively lower final acuities, albeit considerably better than those achieved in the deprived eye of animals monocularly deprived for equivalent periods (see Fig. 14.6). The degree of visual acuity recovery observed following even longer periods of binocular deprivation is consistent with the substantial functional recovery of stimulus response properties of neurons in area

17 of animals that have been either dark-reared or binocularly deprived by bilateral eyelid suture until 11 to 15 months of age and then allowed 6 to 12 months of normal visual exposure (Cynade et al., 1976).

In addition to results obtained from dark-reared animals, Figure 14.2 displays data obtained using the same testing procedure from two laboratories (Mitchell, 1988a; Smith et al., 1980) on kittens reared from normal eyelid opening with bilateral lid suture. One animal (C79, Mitchell, 1988a) that acquired a pendular nystagmus never developed evidence of form vision. Moreover, both animals for which longitudinal measurements were recorded took approximately twice as long as kittens that had been dark-reared for the same time to show any signs of vision on the jumping stand. An additional comparison study of the extent of recovery of visual acuity following these two forms of binocular deprivation was conducted by Mower et al. (1982) on two binocularly lid-sutured kittens and three others that were dark-reared to 4 months of age. Only the mean data for the two groups of animals were provided, and these are depicted in Figure 14.2 by the triangle symbols. Of particular note was the lower mean acuity (2.67 versus 5.05 cycles/degree, or 0.92 octaves) attained by the animals that had been deprived by binocular lid suturing (open triangle symbols). Thus, like the differing physiological effects of these two forms of deprivation on the visual cortex (e.g., Mower et al., 1981), the long-standing deficits in visual acuity from the

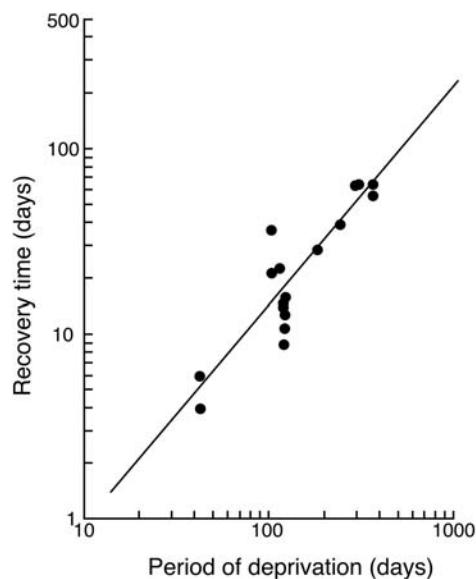


FIGURE 14.1. The time (T) to recovery of the first signs of vision on the jumping stand (operationally defined as the ability to jump to a closed door, as opposed to an adjacent open door, by use of visual cues alone) in 17 kittens dark-reared from birth for the period (t) shown. The increase of T with t has been fitted by the following function: $T = 0.067t^{1.2}$. (Redrawn from Mitchell, 1988a.)

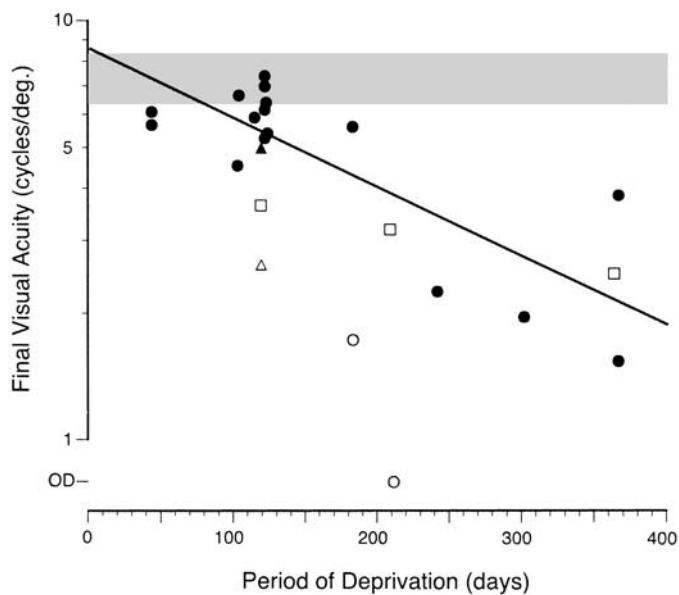


FIGURE 14.2. The grating acuity eventually attained by kittens binocularly deprived from birth is seen to decline with length of deprivation. The line shows the best exponential fit to the data from dark-reared animals (*filled symbols*). The open symbols represent data from three groups of animals that were binocularly deprived by eyelid suture (Mitchell, 1988a [*open circles*]; Mower et al., 1982 [*triangle*]; Smith et al., 1980 [*squares*]). The shaded region indicates the range of grating acuities for normal animals tested using the same procedure. Vision that is so poor as to enable only the ability to distinguish a closed from an open door on the jumping stand is depicted as OD.

latter form of binocular deprivation may be more substantial than those following equivalent periods of dark rearing.

Measurements of visual acuity probe the ability of binocularly deprived animals to see fine spatial detail (high spatial frequencies), but does not provide information on the visibility of coarse patterns (low or medium spatial frequencies). This missing information is supplied by measurements of contrast sensitivity functions, which have been obtained by only two groups using the behavioral technique of conditioned suppression (Blake and Di Gianfilippo, 1980; Lehmkuhle et al., 1982) on three dark-reared and two binocularly lid-sutured animals. The mean spatial contrast sensitivity functions reported by Lehmkuhle et al. (1982) for two animals dark-reared to 5 months and two other cats that were binocularly deprived by eyelid suture up until either 5 or 12 months of age are displayed in Figure 14.3A, together with the mean data for two normal cats. In addition, Figure 14.3B displays the results obtained by Blake and Di Gianfilippo (1980) on one animal that had been dark-reared until 6 months of age. The contrast sensitivity functions for the two forms of binocular deprivation are similar in shape, although there is a tendency for the sensitivities to be lower for the animals deprived by binocular lid suture. Overall, the data indicate a uniform reduction of sensitivity

for all spatial frequencies with respect to normal values. A point of special note that emerged from the investigation of Lehmkuhle et al. (1982), as well as from other data (Mitchell, 2002), is that the deficits that follow binocular deprivation are worse than those that follow ablation of area 17 in normal animals. This finding implies that the effects of deprivation extend to other visual areas besides area 17. Moreover, the greater losses, at both low and high spatial frequencies, than those observed after cortical lesions point to the fact that binocular deprivation affects both the X and the Y pathway (Stone, 1983), with possibly a larger influence on the latter pathway.

There is substantial evidence that dark rearing may have more pronounced effects on other perceptual capabilities than it does on spatial resolution. A substantial proportion of dark-reared cats, even when deprivation extends to 1 year of age, subsequently develops a convergent misalignment of the visual axes (Cynader et al., 1976; Cynader, 1979). It could be argued that the presence of an acquired strabismus may prevent the development of stereoscopic vision. Interestingly, tests of depth perception suggest that all dark-reared cats lack stereopsis, whether they acquire a strabismus or not (Kaye et al., 1982). Tests of depth perception in normal cats on a jumping stand, where the animal has to jump toward the closer of two stimuli viewed through the glass plate onto which the cat jumps, reveal that the threshold perceivable difference in depth between the two stimuli is smaller by a factor of about 8 when both eyes are open than when one eye is covered. This superiority has been attributed to the contribution of the binocular depth cue of stereopsis in the former situation (Mitchell et al., 1979). Animals that are dark-reared to 4 months of age, despite recovering normal or near-normal visual acuity, perform no better on the depth task binocularly than monocularly (Kaye et al., 1982), a result that suggests that they may not possess stereoscopic vision.

MONKEYS The early studies of dark-reared chimpanzees revealed severe degeneration of retinal ganglion cells after periods of deprivation lasting up to at least 16 months of age, thereby making it impossible to attribute the behavioral results to changes at the cortical level. By contrast, no abnormalities have been reported in the retinas of dark-reared monkeys (Chow, 1955, 1973), including the retinas of those employed (Hendrickson and Boothe, 1976) in one modern behavioral study (Regal et al., 1976). The animals of the latter study were not deprived from birth, but from 2 weeks of age, in order that they could be trained to self-feed. Three animals, dark-reared until 3 months and tested by preferential looking on one or two occasions after having spent 22 to 137 days in the light, exhibited grating acuities that were lower by between 1 and 2 octaves than those of age-matched control animals. The grating acuity deficits exhibited by two

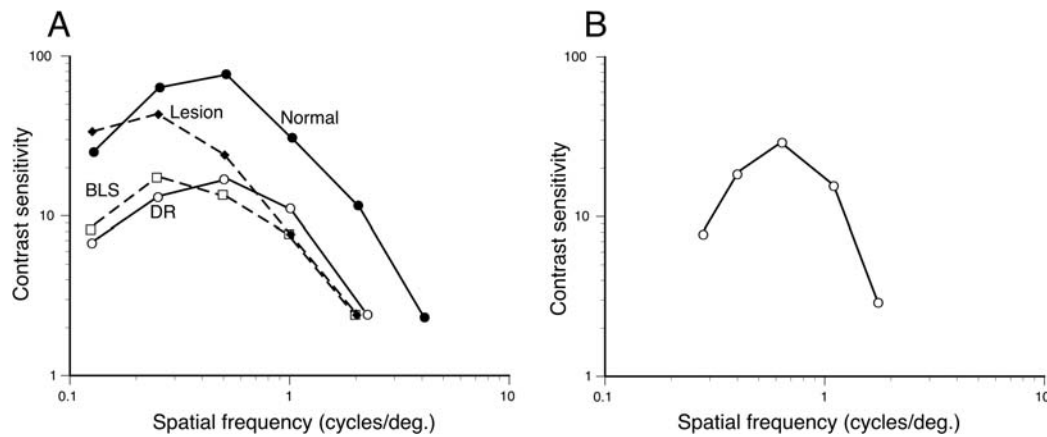


FIGURE 14.3. *A*, The mean spatial contrast sensitivity functions for two normal cats (*filled circles*), two cats following ablation (*Lesion*) of area 17 (*filled diamonds*), two dark-reared (*DR*) cats (*open circles*), and two cats binocularly deprived by lid suture (*BLS*) (*open squares*).

B, Spatial contrast sensitivity function measured with counter-phased gratings (1.5 Hz) for a cat dark-reared to 6 months of age. (*A*, Data redrawn from Lehmkuhle et al., 1982. *B*, Redrawn from Blake and Di Gianfilippo, 1980.)

animals that were deprived until 6 months were no worse (0.6 to 1.5 octaves). By contrast, the latter animals appeared more impaired on several qualitative tests of visuomotor functions, such as visual placing and visual avoidance.

A more extensive study that included measurements of both spatial and temporal contrast sensitivity functions, as well as tests of stereopsis, was conducted later on five monkeys that were deprived for 2 to 16 weeks by bilateral eyelid suture beginning at 2 weeks of age (Harwerth et al., 1991). Only animals deprived for 7 weeks or more exhibited deficits in contrast sensitivity, and even these were restricted to spatial frequencies greater than 0.75 cycles/degree for two animals and 4 cycles/degree for another. By comparison, deficits in temporal contrast sensitivity for uniform field flicker were either nonexistent or else were very small, and did not vary in a systematic manner with temporal frequency. Whereas measurements of increment threshold spectral sensitivities revealed only minor variations from normal values, none of the binocularly deprived animals possessed stereopsis, including those with no contrast sensitivity loss. Although it could be argued that the small and variable losses in contrast sensitivity may be related to either the short period of deprivation or the prior 2-week period of normal vision, it is noteworthy that, like dark-reared cats, binocularly deprived monkeys appear to be stereoblind. Subsequent electrophysiological recordings from area 17 of these animals revealed a physiological explanation for this finding, namely a dramatic reduction in the proportion of cells that could be excited through either eye from a value of 76% (observed in normal animals) to 20% (observed in binocularly deprived cats) (Crawford et al., 1991). Nevertheless, confirmation that this population of cells lacks the ability to extract disparity and/or interocular phase information that relies on inhibitory inputs from the two eyes has yet to be made.

HUMANS Systematic explorations have been made of the visual abilities of humans following surgical intervention for congenital bilateral cataracts and restoration of a clear optical image to both eyes (Birch et al., 1998; Ellemberg et al., 1999; Mioche and Perenin, 1986; Tytla et al., 1988). Despite variation between studies in the length of deprivation prior to surgery and of the period of aphakia prior to full optical correction, there is considerable agreement on the major findings. As with binocularly eyelid-sutured monkeys, the spatial contrast sensitivities at low spatial frequencies (<2 cycles/degree) are within normal limits; however, beyond this range, the contrast sensitivities decline progressively from normal values with increasing spatial frequency. The grating acuity was reduced on average by 1.5 octaves (Ellemberg et al., 1999). As with binocularly deprived monkeys, temporal vision appears to be affected far less severely, with small deficits in uniform field flicker evident only at low temporal frequencies (5 to 10 Hz). Moreover, the deficits in spatial contrast sensitivity do not vary with the rate of temporal modulation of the grating pattern (Tytla et al., 1988).

The effects of monocular visual deprivation

Selected (monocular) visual deprivation is by far the most studied condition at all different levels of analysis, from its anatomical and physiological sequelae to its behavioral effects. Not only are the consequences of monocular deprivation profound and robust, but arguably, the key concept that has emerged from studies of experiential effects on development—namely, the idea that these effects occur only during certain critical periods—has been derived and subsequently refined by studies of this form of deprivation. A second important finding that has emerged from studies of the physiological effects of monocular deprivation is that

the effects in area 17 are far more profound than those that follow equivalent periods of binocular deprivation. This finding is the cornerstone of the hypothesis that the effects of monocular deprivation are a result of competitive interactions for synaptic space between the afferents from the two eyes. As with the physiological effects of monocular deprivation, the behavioral effects are far more profound than those that follow binocular deprivation in any form.

CATS The use of the jumping stand permits both an assessment of the immediate effects of various periods of deprivation on the vision of the deprived eye, as well as the time course and extent of any subsequent recovery following either restoration of normal visual input (referred to as binocular recovery) or imposition of a period of reverse deprivation (reverse occlusion) whereby the formerly non-deprived eye is closed during the recovery period. As might be anticipated from the physiological effects, the immediate effects of even short periods (6 days) of monocular deprivation, when imposed in the first 2 months of life (Mitchell et al., 2001), are profound. Animals subjected to monocular deprivation appear blind when first forced to use their deprived eye. However, after such short periods of deprivation, the vision of the deprived eye begins to recover within just a few hours. Studies of the rate and extent of the recovery of the vision of the deprived eye following periods of monocular deprivation imposed from the time of natural eye opening and terminated at different ages reveal two main trends (Mitchell, 1988a). First, as the length of deprivation increases, the period before signs of vision are exhibited by the deprived eye becomes progressively longer. Second, the vision that is recovered by this eye declines from levels close to normal, in terms of visual acuity, with very short periods of deprivation, to more severe deficits with only rudimentary light perception when deprivation extends to a year or more. These points are evident in the results shown in Figure 14.4, which plots the recovery of the vision of the deprived eye in three animals that were monocularly deprived from near birth until 42, 94, or 302 days of age and thereafter allowed binocular visual input (binocular recovery). Whereas the animal that was monocularly deprived for 6 weeks recovered sufficient form vision in the deprived eye within 5 days to permit measurements of visual acuity, the animals that were deprived for 94 and 302 days displayed no signs of pattern vision for 17 and 145 days, respectively. Moreover, in the animal that was monocularly deprived the longest, the deprived eye appeared completely blind for 2 months, and for an additional 2 months was capable of discriminating only between an open and a closed door on the jumping stand. In parallel with the progressive increase in the time for the first signs of form vision to emerge with increasing length of deprivation, there was a substantial decline in the level of visual acuity that was

eventually recovered by the deprived eye. For the animal deprived for 302 days, the deprived eye recovered an acuity of only 1.35 cycles/degree, a value 2.45 octaves below normal average values.

The generality of these two trends for both conditions of recovery are evident in the combined data from many animals, displayed in Figures 14.5 and 14.6. These figures show, respectively, a plot of the time interval for animals to exhibit the first sign of vision with the deprived eye and the final acuity achieved by the deprived eye as a function of the length of deprivation. The initial speed of recovery appears to be similar for both recovery conditions. For short periods of deprivation that extend to only 4 to 6 weeks of age, signs of vision emerge in the deprived eye within only 2 or 3 days. However, for deprivation lasting 12 to 18 months, a period of at least 4 months, and in some, as long as 12 months, elapses before animals begin to see. Although the initial speed of recovery of vision is similar for the two recovery conditions, for periods of deprivation of 4 months or less, animals that are reverse occluded (*filled symbols*) recover slightly better acuity than do those that have both eyes open during recovery (*open symbols*). With increasing length of deprivation, the vision that is eventually recovered declines regardless of the recovery condition. A proportion of animals that are deprived for a year or more never recover sufficient form vision to permit measurement of visual acuity; the remainder acquire only rudimentary form vision (visual acuity <1 cycle/degree).

Before passing to other matters, there are two caveats to consider with respect to the points made concerning the data displayed in Figures 14.5 and 14.6. First, close examination of the *initial* speed of improvement of vision in the deprived

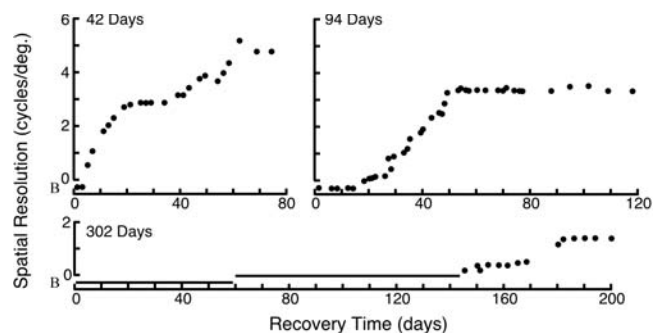


FIGURE 14.4. The time course of vision recovery in the deprived eye of three kittens monocularly deprived to 42, 94, or 302 days of age, after which both eyes were open. The letter “B” denotes the situation in which the animal appears blind on the jumping stand. Throughout the period indicated by the horizontal line corresponding to zero on the ordinate for the animal deprived to 302 days, the animal was capable of discriminating a closed door from an open door on the jumping stand but could not pass a formal test of form vision. (Redrawn from Mitchell, 1988a.)

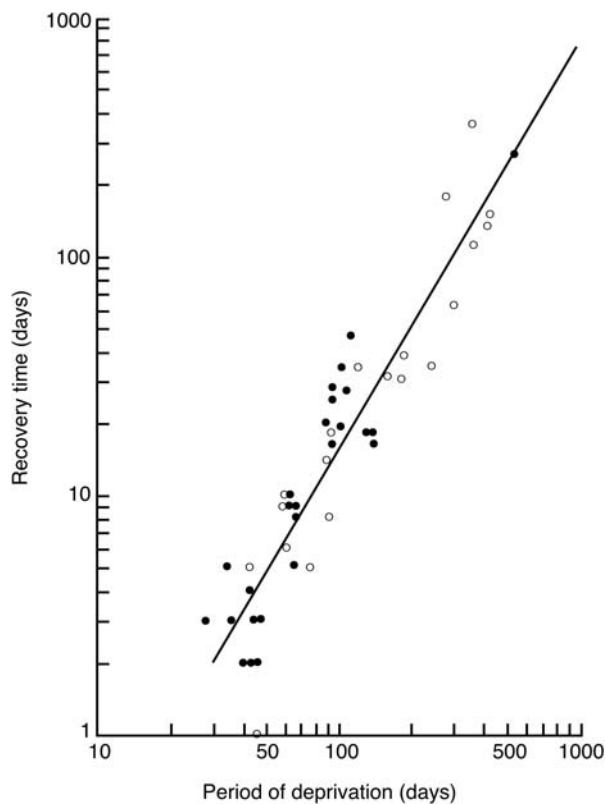


FIGURE 14.5. Recovery time increases with length of visual deprivation. The graph shows the time interval for the deprived eye to exhibit the first sign of vision as a function of the length of the period of monocular deprivation. Open and closed symbols depict data from animals in the situation of binocular recovery or reverse occlusion, respectively, throughout the recovery period. A single regression line has been drawn for the data from both conditions of recovery. (Redrawn from Mitchell, 1988a.)

eye of animals following very short periods (6 days) of monocular deprivation reveals that it is faster in animals that have both eyes open following deprivation than it is in those that are reverse occluded (Mitchell et al., 2001). This finding provides further evidence for the operation of cooperative associative mechanisms of recovery in the underlying neural substrate whereby the nondeprived eye serves as a guide or “teacher” for recovery of the deprived eye (Kind et al., 2002). Such mechanisms may mediate recovery in circumstances in which mechanisms based on binocular competition are ineffective. Second, the recovery that occurs during reverse occlusion and that is plotted in Figure 14.6 may not be maintained afterward when normal visual input is restored to the formerly nondeprived eye. The example of this phenomenon, shown in Figure 14.7, involves a kitten that had been monocularly deprived to 4 weeks of age. The kitten then underwent a 3-week period of reverse occlusion during which the vision of the initially deprived eye recovered from blindness to 3.4 cycles/degree (Mitchell et al., 1984b). However, shortly after opening the initially

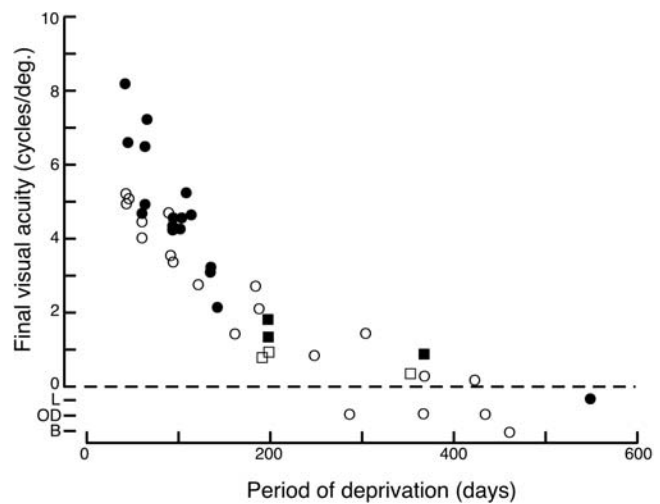


FIGURE 14.6. Less vision is recovered as the period of deprivation lengthens. The visual acuity eventually attained by the deprived eye in 37 monocularly deprived kittens is presented as a function of the length of the prior period of monocular deprivation. Open and closed symbols depict data from animals in the situation of binocular recovery or reverse occlusion, respectively, throughout the recovery period. Visual function is denoted by letters, as follows: B, complete blindness; OD, the ability to discriminate an open from a closed door on the jumping stand; L, the ability to pass a formal luminance discrimination test on the jumping stand. The square symbols show equivalent data from six animals studied by Smith and Holdefer (1985). (Redrawn from Mitchell, 1988a.)

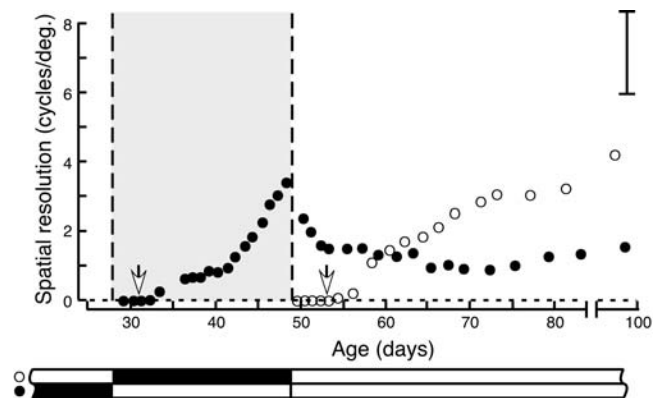


FIGURE 14.7. An example of a situation in which the vision recovered in the deprived eye during reverse occlusion was not retained afterward. The graph shows the changes in the grating acuity of the deprived eye (filled symbols) and nondeprived eye (open symbol) of monocularly deprived kittens during reverse occlusion (shaded area) and after a 3-week period of reverse occlusion imposed at 4 weeks of age. The animal’s visual history is depicted in schematic fashion beneath the graph. The open arrows indicate the first day on which the animal could discriminate an open from a closed door on the jumping stand, whereas the bracket to the right indicates the range of acuity values recorded for normal animals. (Redrawn from Mitchell et al., 1984b.)

nondeprived eye, the vision of the initially deprived eye began to drop to low levels from which it never recovered. Meanwhile, the vision of the initially nondeprived eye improved gradually but never to normal levels. This finding has been explored thoroughly in a number of research articles, some of which address the obvious relevance to patching therapy for amblyopia (Mitchell, 1991; Mitchell et al., 1984a; Murphy and Mitchell, 1987).

Measurements of contrast sensitivity functions (CSFs) reveal that the losses of contrast sensitivity in the deprived eye are far more severe than the final deficits in grating acuity. The four examples from two studies (Lehmkuhle et al., 1982; Mitchell, 1988a), displayed in Figure 14.8, show results following either a short (6 to 8 weeks) or extended (8 to 16 months) period of deprivation. Even the animals subjected to a brief period of deprivation exhibited 10- to 20-fold differences in contrast sensitivities between the two eyes, compared to a difference of less than an octave in visual acuity. The cats deprived for the longest periods showed increased losses of contrast sensitivity (30-fold) at all spatial frequencies; moreover, the losses were approximately the same at all temporal frequencies (Lehmkuhle et al., 1982). As was also evident in the visual acuity data (compare Figs. 14.2 and 14.6), the long-standing deficits in contrast sensitivity following monocular deprivation were far greater than those that followed an equivalent period of binocular deprivation (Fig. 14.3).

MONKEYS In monkeys, monocular deprivation results in a more extensive range of visual deficits, as well as larger losses, than those reported in cats. Most significantly, monkeys that are monocularly deprived at 1 or 2 months of age for a period of 18 months exhibit reduced scotopic sensitivities (by as much as 3 to 4 log units), and also demonstrate changes involving both the shape and absolute sensitivity of their photopic spectral sensitivity functions (Harwerth et al., 1986). In contrast to the losses in contrast sensitivity and resolution, for which the critical period extended to 25 months, the deficits in scotopic and photopic sensitivity have quite short critical periods extending to only 3 and 6 months of age, respectively.

The earliest studies of the effects on spatial vision of monocular lid-suturing, imposed for a year or more in the first month of life, revealed that the animals were unable to demonstrate any pattern vision with their deprived eye, even after extended periods of reverse occlusion. Later research, which incorporated shorter periods of deprivation (2 to 4 weeks), revealed similar loss of pattern vision when imposed in the first month and severe, irreversible effects on visual acuity followed occlusion beginning in the first 9 weeks of postnatal life (von Noorden, 1973).

Extensive studies of spatial contrast sensitivity have explored not just the effects of the timing of the deprivation,

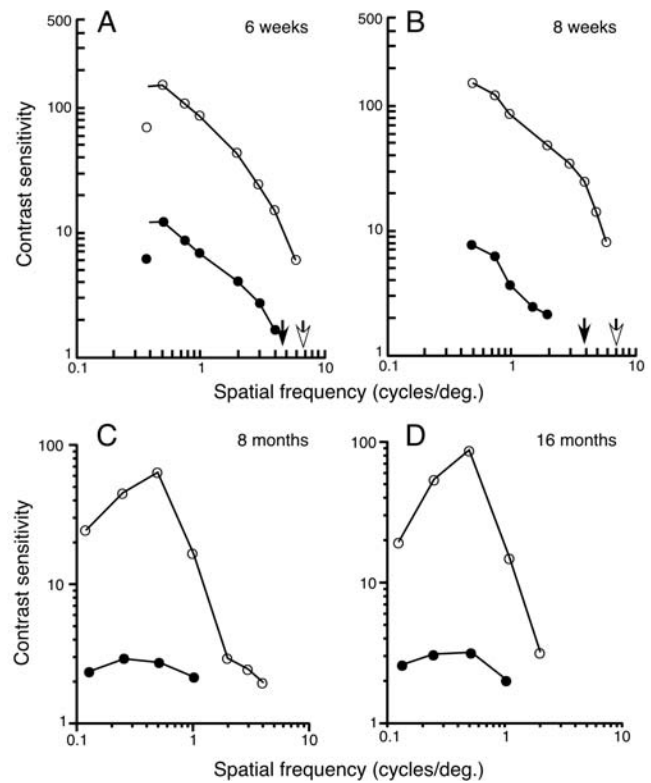


FIGURE 14.8. The graph shows contrast sensitivity functions for the nondeprived (*open symbols*) and deprived (*filled symbols*) eyes of four cats that were monocularly deprived from near birth to 6 weeks (A), 8 weeks (B), 8 months (C), or 16 months (D) of age. The open and closed arrows indicate the measured grating acuity of the nondeprived and deprived eye, respectively. (A and B, Data redrawn from Mitchell, 1988a. C and D, Data redrawn from Lehmkuhle et al., 1982.)

but also the outcomes from different variants of the deprivation itself, including eyelid suture, anisometropia produced by lenses, and chronic monocular cycloplegia (Boothe et al., 1982; Harwerth et al., 1983a; Kiopres et al., 1987; Smith et al., 1985). The profound magnitude of the effects of eyelid suture on CSFs is shown in Figure 14.9 for three animals from the study of Harwerth et al. (1983a). Whereas the CSFs for the nondeprived eyes of all three animals were similar to those of normal animals, the CSFs for the deprived eyes revealed a profound loss of contrast sensitivity at all spatial frequencies. The extrapolated cut-off frequencies for the deprived eyes (approximately 0.3 cycles/degree) were worse than those for the fellow eye by a factor of 100 or more. Moreover, the CSFs for the deprived eyes were essentially the same for either long-term or short-term deprivation, and they remained unchanged despite 2 to 3 years of binocular experience. The similarity of the deficits observed in animals subjected to vastly different lengths of deprivation may result from an effective continuation of the deprivation beyond the time the eyelids are opened due to the development of form deprivation myopia (Daw, 1995) even after short periods of

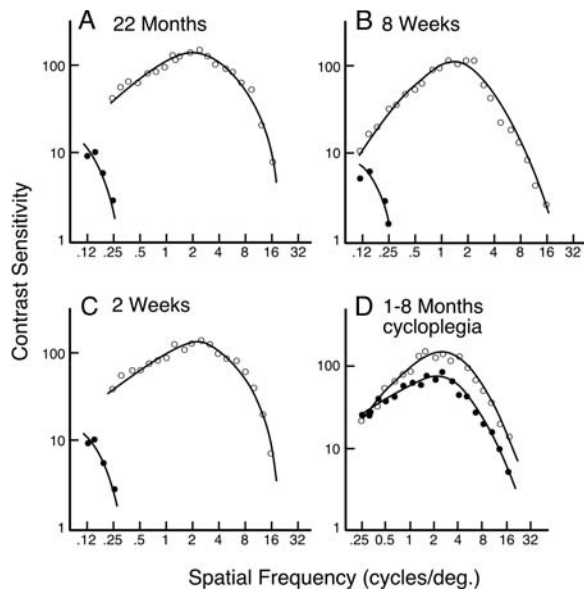


FIGURE 14.9. The graph shows contrast sensitivity functions (CSFs) for the nondeprived (*open symbols*) and deprived (*filled symbols*) eyes of four monkeys that were monocularly deprived by eyelid suture from about 30 days of age to 22 months (A), 8 weeks (B), or 2 weeks (C). D, The CSFs are shown for a monkey reared from 1 to 8 months of age with chronic monocular cycloplegia. (Data redrawn from Harwerth et al., 1983a.)

eyelid suture. Temporal modulation functions for uniform field flicker reveal deficits in the deprived eye at all temporal frequencies, but these increase with frequency beyond the peak of the temporal CSF. Nevertheless, the deficits in temporal modulation sensitivity at all temporal frequencies are less severe than the spatial contrast sensitivity deficits (Harwerth et al., 1983b).

In contrast to the effects of monocular eyelid suture, the consequences of image blur resulting from chronic monocular cycloplegia are far less severe and show greater inter-animal variability (Harwerth et al., 1983a; Kiorpes et al., 1987). As illustrated by the representative animal shown in Figure 14.9D, no loss of contrast sensitivity may be observed at all at low spatial frequencies. A similar outcome was reported in animals reared with anisometropia induced by a $-10D$ lens worn in front of one eye for at least 60 days beginning at 30 days of age (Smith et al., 1985). Contrast sensitivities were reduced in the treated eye for spatial frequencies exceeding 1 cycle/degree. The cut-off frequencies for this eye were about 1 octave lower than those for the fellow eye. The deficits in contrast sensitivity lay in the midrange of values reported for humans with anisometropic amblyopia (Sen, 1980). In addition to the clinical relevance based on the magnitude of the deficit, the ratio of the contrast sensitivities between the two eyes did not vary with luminance, a finding common to human anisometropic, but not strabismic, amblyopes.

HUMANS There are a number of naturally occurring conditions arising at or near birth in humans that result in monocular degradation of form vision similar in nature and severity to that imposed experimentally in animals. The two most common of these conditions are congenital unilateral cataract and ptosis in which the upper eyelid partially or completely covers the pupil. Following restoration of sharp retinal images in later life by surgical interventions combined with appropriate optical correction of any refractive error, affected individuals manifest irreversible deficits in spatial vision that collectively define the clinical entity referred to as stimulus deprivation amblyopia (von Noorden and Maumenee, 1968). The severity of the deprivation and its similarity to that imposed experimentally in animals distinguishes it from amblyopia associated with strabismus and anisometropia. Despite lack of complete documentation of the extent of the deprivation in the perinatal months, as well as variability with respect to both the presence of any co-existing conditions, such as strabismus, and the type and duration of any subsequent treatment, there is general agreement on a number of points. In patients who receive aggressive treatment early, deficits in contrast sensitivity for static gratings may not be present at all for low spatial frequencies (<1 cycle/degree), but may increase with spatial frequency beyond this point. As the length of deprivation increases, the deficits extend to progressively lower spatial frequencies (Ellemberg et al., 2000; Tytla et al., 1988). For temporally modulated gratings, the deficits in contrast sensitivity are either greater for low temporal frequencies (Birch et al., 1998; Ellemberg et al., 2000; Tytla et al., 1988) or else show no dependence on temporal frequency at all (Hess et al., 1981).

When deprivation is long standing (lasting a year or more), a variety of very severe outcomes may result. Two groups have described patients with a complete loss of spatial (pattern) vision for either all spatial frequencies, or else spatial frequencies above 0.5 cycle/degree for certain temporal conditions. One group (Hess et al., 1981) described patients with no form vision for either static or temporally modulated gratings, leaving only the perception of flicker in the latter case. A patient described by the other group (Levi and Harwerth, 1980) had no pattern vision at all above 0.5 cycle/degree for gratings temporally modulated at 10 Hz but could resolve gratings over a wide range of spatial frequencies when they were not temporally modulated. One patient with a severe loss of contrast sensitivity was unable to discern flicker of temporally modulated gratings at any temporal frequency (Manny and Levi, 1982b). This patient, as well as one reported by Hess et al. (1981), exhibited deficits in temporal contrast sensitivity to uniform field flicker similar to those reported in monocularly deprived monkeys; that is, the deficits increased in magnitude with temporal frequency (Manny and Levi, 1982a). Because a pattern of increasing

losses at progressively higher temporal frequencies appear to be associated with the longest periods of deprivation, it has been suggested by Ellemberg et al. (2000) that these deficits may reflect retrograde changes at the level of the retina.

RODENTS Studies of the postnatal development of the visual cortex of rats (e.g., Fagiolini et al., 1994), mice (Drager, 1978; Gordon and Stryker, 1996), and hamsters (Emerson et al., 1982) have revealed experience-dependent changes that are qualitatively similar to those observed in cats and monkeys. However, as with the shifts of ocular dominance (Fagiolini et al., 1994; Gordon and Stryker, 1996), the behavioral effects of monocular deprivation are far less severe than those produced in higher mammals in which pattern vision in the deprived eye can be completely lost. In terms of the visual acuity of the deprived eye, the long-term consequences of periods of monocular deprivation imposed from near birth and extending through the presumed duration of the critical period are similar, but minimal, for all rodent species. For rats, behavioral measurements (Prusky et al., 2000) reveal a deficit of 0.58 octaves in the acuity of the deprived eye (0.65 versus 0.97 cycles/degree), a deficit smaller than that estimated (1.39 octaves) from evoked cortical potentials (Fagiolini et al., 1994). In hamsters and mice, behavioral measurements reveal deficits of 0.6 (Emerson et al., 1982) and 0.74 (Prusky and Douglas, 1998) octaves, respectively.

The effects of decorrelated binocular input

In addition to depriving one eye of patterned visual input, monocular deprivation also results in the two eyes receiving discordant visual input. However, there are forms of deprivation that dissociate the visual input to the two eyes without placing one eye at a chronic disadvantage. One such type of deprivation is artificial strabismus, a misalignment of the visual axes created either by surgical manipulation of one or more extraocular muscles or optically, by use of prisms. Another means to the same end is to rear the animal with alternating monocular occlusion so that the animal is never permitted to see with both eyes at the same time. Such deprivation can produce a near-complete breakdown of binocularity among neurons in area 17 in kittens to the extent that only a very small proportion of cells can be excited by either eye, with each eye retaining an equal representation overall (Daw, 1995; Mitchell, 1988b; Movshon and Kiorpes, 1990). In monkeys and, to some extent, in kittens, strabismus produced by surgical intervention results in a shift of ocular dominance among cortical neurons away from the deviating eye, as well as reduced vision in that eye (reviewed by Mitchell, 1988b; Movshon and Kiorpes, 1990). However, the ubiquitous finding of a reduction in the proportion of binocularly excitable cells associated with rearing conditions

that reduce the concordance of the visual input to the two eyes might have important implications for binocular vision in general and stereopsis in particular. Humans with stimulus deprivation amblyopia are stereoblind, and even when surgical interventions occur very early, it is rare for anything but rudimentary stereopsis to develop (Mitchell and MacKinnon, 2002). Moreover, humans with strabismus or other associated conditions that result in discordant visual input show impaired interocular transfer of visual aftereffects, a phenomenon dependent on the functional integrity of binocular neurons (Daw, 1995; Mitchell and Timney, 1984; Movshon and Kiorpes, 1990). The implications of the early rearing of animals with decorrelated early visual input have been explored in a number of animal studies, the results of which are presented in a later section without regard to species.

Two studies have documented the consequences for binocular depth perception of early alternating monocular occlusion in kittens. In both, the visual input to the two eyes was alternated on a daily basis up to either 6 months of age (Blake and Hirsch, 1975; unrestricted duration each day) or 3 months of age (Packwood and Gordon, 1975; 1 hour/day). The results for each study were consistent with a complete absence of stereopsis in adulthood. The study of Blake and Hirsch (1975) employed indirect tests for stereopsis based on comparison of binocular and monocular depth thresholds; the absence of superior performance of the former over the latter was interpreted as evidence of a lack of the uniquely binocular depth cue of stereopsis. The kittens had to detect whether the middle of three vertical rods was closer to them than the ones on either side. With both eyes open, a normal kitten could discriminate between differences in depth between the rods; these differences were one-tenth the size of those detectable when allowed to use only one eye. For cats reared with alternating monocular occlusion, the binocular and monocular thresholds were identical; moreover, they were no different than the monocular thresholds of normal cats. By contrast, Packwood and Gordon (1975) employed a shadow caster and red and green filters to provide anaglyphic presentation of three rods, of which the center one could be made to appear at a different depth on the basis of retinal disparity cues. Whereas normal cats, when subjected to relative retinal disparities of either 3 or 10 minutes of arc, could detect the middle rod as lying in a different depth plane than the flanking rods, the cats reared with alternating monocular occlusion responded at chance to all tested disparities. A study using similar methods, conducted by Kaye et al. (1982), indicated that stereopsis failed to develop in kittens in which strabismus was introduced by sectioning of an extraocular muscle.

Tests for the presence of global stereoscopic vision have been conducted in monkeys reared with discordant early

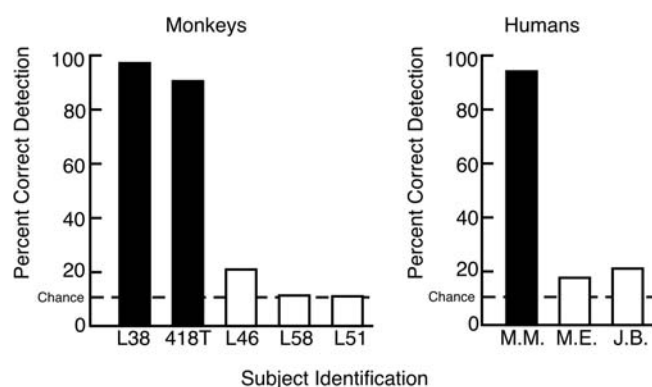


FIGURE 14.10. Performance data are shown for two normal monkeys (L38 and 418T, *filled bars*) and three monkeys reared with an optically induced strabismus (L46, L58, and L51, *open bars*). The animals were tested for global stereopsis with dynamic, random dot stereograms. Shown, for comparison, are the results obtained in a normal human (M.M.) and two humans (M.E. and J.B.; *open bars*) with a history of strabismus in early life. (Redrawn from Crawford et al., 1983.)

visual input using dynamic, random dot, stereographic displays. These displays revealed a cyclopean grating pattern in the presence of stereopsis (Crawford et al., 1983). In this study, three monkeys were reared from postnatal days 30 to 60 wearing helmets that contained two prisms (10 and 17 prism diopters) that dissociated the visual input to the two eyes in all positions of gaze (Crawford and von Noorden, 1980). As illustrated in Figure 14.10, all three of these monkeys (*open bars*) performed at chance on cyclopean detection of dynamic, random dot stereograms, whereas normal monkeys (*filled bars*) were 90% correct or better. The apparent stereoblindness of the helmet-wearing monkeys could not be attributed to amblyopia associated with optically induced strabismus, as measurements of CSF revealed either no deficit (L51) or extremely mild amblyopic deficits. (Also shown, for comparison, are comparable results from three humans performing the same task. One [M.M.] was normal, whereas the other two [M.E. and J.B.] had histories of disrupted early binocular input by strabismus.) Three years later, electrophysiological recordings from area 17 of these animals revealed that only 22% of the cells could be excited through either eye, as compared to 81% of the cells in normal control monkeys (Crawford et al., 1984).

Although tests of stereoscopic vision with more recent probes, such as those for linear and nonlinear stereopsis (Hess and Wilcox, 1994), may reveal some residual stereopsis in animals reared with discordant visual input, there is no doubt that such animals are stereoblind by most conventional assays. Moreover, such animals demonstrate other loss of binocular function, such as binocular summation of thresholds, whereby, for example, spatial contrast sensitivity measurements made binocularly are no better than those

made monocularly (Crawford et al., 1983). By contrast, binocular thresholds are superior by a factor of about 2 in normal animals.

The effect of selective exposure to particular contour orientations

Although both the robustness and interpretation of the physiological consequences of early exposure of animals to a restricted range of contour orientations are controversial (e.g., Mitchell and Timney, 1984; Movshon and Kiorpes, 1990; Movshon and Van Sluyters, 1981; but see also Sengpiel et al., 1999), the behavioral effects appear clear-cut. The earliest behavioral measurements were made in kittens reared in cylinders, like the animals of one of the pioneering physiological studies, so as to restrict the visual input to stripes of a single orientation (horizontal or vertical). Among these animals, measurements of grating acuity in adulthood revealed differences in the acuity for horizontal and vertical gratings of 0.26 to 0.87 octaves; the best acuity was always achieved for the orientation experienced as kittens in the cylinder (Muir and Mitchell, 1973, 1975). Later measurements (Blasdel et al., 1977), made in kittens that were restrained in order to lessen inappropriate visual stimulation through changes of head and body orientation with respect to the stripes, revealed deficits of similar direction and magnitude (0.49 to 0.73 octave).

In the context of the prevailing controversy that centered on the robustness of the physiological findings from selected exposure to restricted orientations, the small magnitude of the concurrent behavioral deficit did little to resolve matters. However, the rediscovery of “astigmatic” or meridional amblyopia in humans known to have received their initial optical correction of high astigmatism in late childhood reinforced the findings from the animal experiments. People with uncorrected astigmatism typically see contours of only one orientation clearly; other contours appear progressively more blurred with increasing departure from the favored orientation. Figure 14.11A illustrates the appearance of the target on the left to individuals with the two most common types of astigmatism who see only horizontal (*middle*) or vertical (*right*) contours sharply. Spurred by the initial “stripe-rearing” animal experiments, other researchers examined a large group of such astigmatic individuals. Their studies revealed that, even after full optical correction of refractive error, substantial differences (as much as an octave) existed in the acuity for gratings parallel to the principal meridians of the astigmatism, which are most commonly close to vertical and horizontal (Cobb and MacDonald, 1978; Freeman et al., 1972; Mitchell et al., 1973). Moreover, as illustrated in Figure 14.11B, for all subjects in whom the ratio of acuities for vertical and horizontal gratings lay outside the range observed among normal subjects, the best acuity always

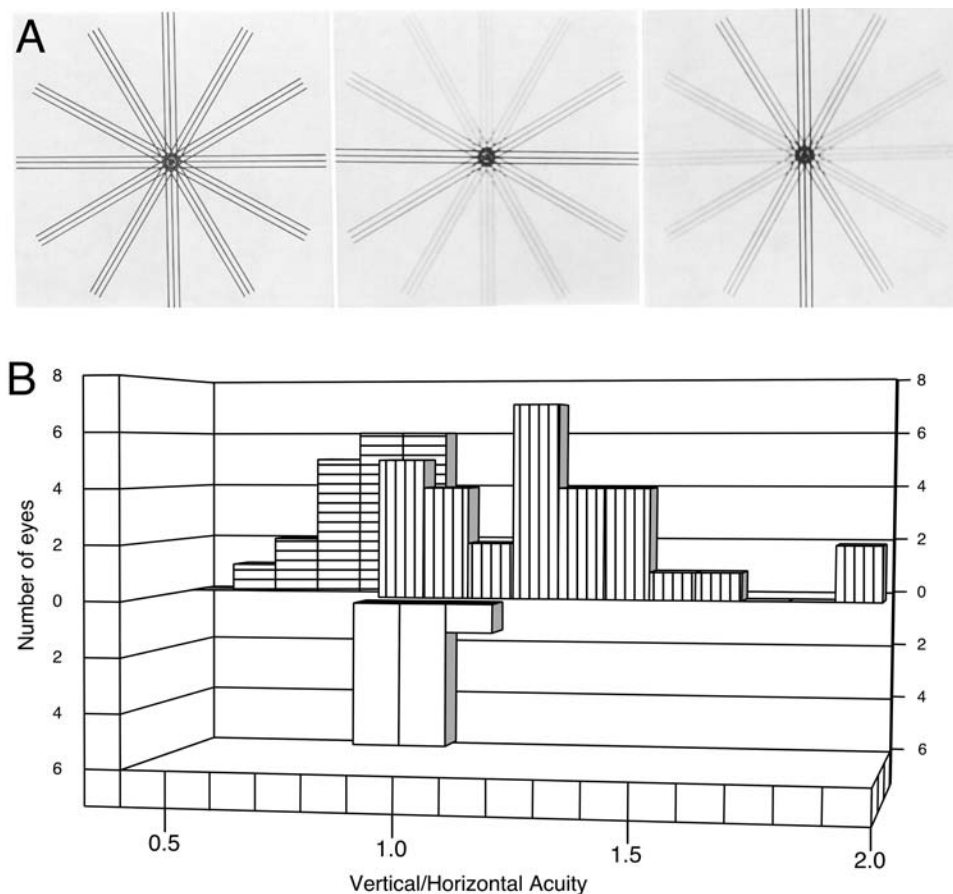


FIGURE 14.11. *A*, Simulation of how the pattern on the left appears to astigmatic observers having the two most common forms of astigmatism in which either only horizontal (*middle*) or vertical (*right*) contours are sharply visualized. *B*, Histograms show the relationship between the meridional variations in acuity of 50 adult astigmatic eyes and 11 normal eyes (*open bars*) after complete optical correction of their refractive error and the visual experience of the uncorrected eye. Plotted on the abscissa is the vertical-to-horizontal grating acuity ratio, which has values of

>1.0 when vertical acuity is superior and <1.0 when the acuity for horizontal gratings is superior. Vertical and horizontal hatching depicts eyes for which vertical and horizontal contours, respectively, are seen most sharply by the uncorrected eye. For all astigmatic eyes for which the ratio of vertical to horizontal acuities exceeded the range of values observed in normal eyes, the grating orientation for which acuity was best was found to coincide with the contour orientation focused best by the uncorrected eye. (Redrawn from Mitchell et al., 1973.)

coincided with the orientation of contours least defocused by the *uncorrected* eye. This result is consistent with the idea that experience influences either the number or the tuning of orientation-specific cells in the human visual cortex, or both.

Measurements of CSFs for gratings parallel to the principal meridians of the astigmatism have revealed small deficits at even very low spatial frequencies, but which become larger with increasing spatial frequency (Freeman and Thibos, 1975; Mitchell and Wilkinson, 1974). The existence of deficits at very low spatial frequencies, as well as other considerations (Charman and Voisin, 1993; Gwiazda et al., 1986), point to a complex relationship between the presumed early optical error and the characteristics of meridional amblyopia.

Evidence that meridional amblyopia is a consequence of early astigmatism, and not promoted by another unknown factor that causes *both* astigmatism and the meridional variations in acuity, was provided by the demonstration of the development of meridional amblyopia in monkeys reared as infants with externally applied astigmatism (Boothe and Teller, 1982). Additional evidence of a link between astigmatism and the emergence of meridional amblyopia was provided by demonstrations of meridional amblyopia in four monkeys that developed astigmatism in one or both eyes. One of the animals was a normal control; for the other three animals, the astigmatism emerged in the nondeprived eye of animals that had been monocularly deprived from near birth (Harwerth et al., 1980; Harwerth et al., 1983c).

Two experiential manipulations have been shown to influence the development of directionally selective neurons in area 17. Of these, strobe rearing of kittens (rearing kittens in environments illuminated intermittently by very brief stroboscopic light flashes at 8 Hz) has been found to have particularly profound effects. Such intermittent illumination is known to destroy the appearance of smooth movement to humans. In kittens, strobe rearing virtually eliminates direction-selective neurons in areas 17 and 18 (Cynader and Chernenko, 1976; Kennedy and Orban, 1983; Pasternak et al., 1985), as well as in the lateral suprasylvian cortical visual area (Spear et al., 1985), with minimal or no effects on other stimulus response properties (Fig. 14.12A). Although the second manipulation—selective exposure to contours moving in only a single direction—can produce a substantial bias in the distribution of directionally selective neurons in area 17 (Daw, 1995), the consequences of this rearing procedure for motion perception have not yet been examined.

Accompanying the loss of directionally selective neurons associated with strobe rearing are substantial deficits in the perception of motion, as documented by Pasternak and colleagues (Pasternak et al., 1990; Pasternak and Leinen, 1986; Pasternak et al., 1985). These researchers have demonstrated that many aspects of pattern and temporal vision are normal in such animals, and that the small deficits that do exist may be attributable to the low luminance and limited total visual exposure associated with the brief duration (3 μ sec) of the strobe flashes during rearing. Thus, strobe-reared cats exhibit normal orientation discrimination thresholds, normal temporal frequency resolution (critical fusion frequency), and normal contrast sensitivities at low spatial frequencies (but slightly lower contrast sensitivities at higher spatial frequencies) (Pasternak and Leinen, 1986). Moreover, when exposed to stimuli of high contrast, the strobe-reared animals are able to discriminate, at performance levels comparable to those of normal cats, between stimuli moving in opposite directions over a wide range of stimulus speeds. However, severe abnormalities were noted in these animals in relation to tasks requiring comparison of contrast thresholds for detecting moving gratings versus discrimination of direction of motion. As illustrated in Figure 14.12B, normal cats could discriminate the direction of motion for drifting gratings of low spatial frequency at contrasts that were very close to detection threshold at all drift rates. However, strobe-reared cats, despite having only slightly lower detection thresholds than normal animals, required contrasts about 10 times higher in order to discriminate the direction of motion (Pasternak et al., 1985). These differences were even more pronounced for gratings of higher spatial frequency (Pasternak and Leinen, 1986).

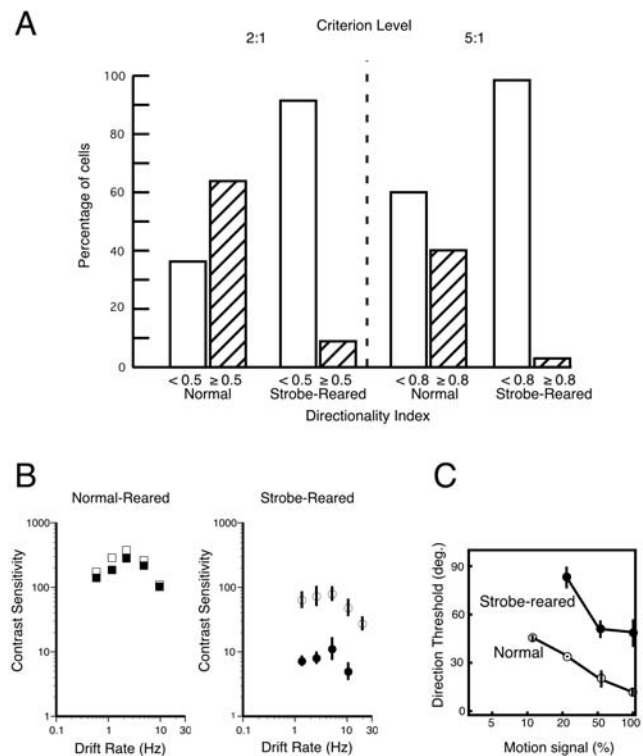


FIGURE 14.12. *A*, The directional selectivity of cells in area 17 is reduced in strobe-reared cats as compared to normal cats. The histograms show the percentage of cells classified as directional (hatched bars) or nondirectional (open bars) in normal ($N = 245$ cells) and strobe-reared ($N = 129$ cells) cats with respect to a directionality index. The index is defined as $1 - np/p$, where np is the response in the nonpreferred direction and p is the response in the preferred direction. The results are shown for two criterion levels with respect to p and np (2:1 or 5:1). *B*, Mean contrast sensitivity for two normal and three strobe-reared cats for the detection (open symbols) and discrimination (filled symbols) of the direction of motion of a 0.28-cycle/degree grating drifting at the rates shown on the abscissa. Normal animals could discriminate the direction of motion at or close to detection threshold. By contrast, in strobe-reared animals, direction discrimination required that the contrast be 10 times greater. *C*, Mean direction difference thresholds for dynamic, random dot displays were measured in two normal and three strobe-reared cats and presented as a function of the proportion of dots with the biased direction signal (% motion signal). The two extreme values for the motion signal represent displays in which dots move in random directions (0%) versus displays in which all the dots move in the same direction (100%). (*A* and *B*, Data redrawn from Pasternak et al., 1985. *C*, Data from Pasternak et al., 1990.)

Recent research has shown that strobe-reared cats also exhibit severe deficits in the ability to perceive global motion in dynamic, random dot displays consisting of multiple, localized, motion vectors (Pasternak et al., 1990). The most severe deficits (see Fig. 14.12C) are in the discrimination thresholds for differences in direction; these deficits are even large when all the dots in the display are directionally biased (see legend for Fig. 14.12).

Conclusions

The functional consequences of selected early visual deprivation can be extremely profound, as evidenced by the immediate effects of monocular deprivation. However, even the subtle deficits associated with other forms of deprivation, such as selected exposure to particular contour orientations, are robust, and as such, provide important data pertaining to the controversy surrounding the physiological effects of visual deprivation (Movshon and van Sluyters, 1981). The documented perceptual abnormalities associated with certain forms of selective deprivation have provided some insight into the relationship between properties of neurons and perception. However, to the extent that the effects of selected deprivation extend beyond area 17, definitive statements as to the relationship between the properties of neurons in area 17 and perception must be made with caution.

REFERENCES

- Ackroyd, C., N. K. Humphrey, and E. K. Warrington, 1974. Lasting effects of early blindness: a case study, *Q. J. Exp. Psychol.*, 26:114–124.
- Birch, E. E., D. Stager, J. Leffler, and D. Weakley, 1998. Early treatment of congenital unilateral cataract minimizes unequal competition, *Invest. Ophthalmol. Vis. Sci.*, 39:1560–1566.
- Blake, R., and A. Di Gianfilippo, 1980. Spatial vision in cats with selective neural deficits, *J. Neurophysiol.*, 43:1197–1205.
- Blake, R., and H. V. B. Hirsch, 1975. Deficits in binocular depth perception in cats after alternating monocular deprivation, *Science*, 190:1114–1116.
- Blasdel, G. G., D. E. Mitchell, D. W. Muir, and J. D. Pettigrew, 1977. A physiological and behavioural study in cats of the effects of early visual experience with contours of a single orientation, *J. Physiol. (Lond.)*, 265:615–636.
- Boothe, R. G., L. Kiorpes, and A. Hendrickson, 1982. Anisometropic amblyopia in *Macaca nemestrina* monkeys produced by atropinization of one eye during development, *Invest. Ophthalmol. Vis. Sci.*, 22:228–233.
- Boothe, R. G., and D. Y. Teller, 1982. Meridional variations in acuity and CSF's in monkeys (*macaca nemestrina*) reared with externally applied astigmatism, *Vis. Res.*, 22:801–810.
- Charman, W. N., and L. Voisin, 1993. Astigmatism, accommodation, the oblique effect and meridional amblyopia, *Ophthalmic Physiol. Opt.*, 13:73–81.
- Chow, K. L., 1955. Failure to demonstrate changes in the visual system of monkeys kept in darkness or in colored light, *J. Comp. Neurol.*, 102:597–606.
- Chow, K. L., 1973. Neuronal changes in the visual system following visual deprivation, in *Handbook of Sensory Physiology*, vol. VII/3A (R. Jung, ed.), New York: Springer, pp. 599–630.
- Cobb, S. R., and C. F. MacDonald, 1978. Resolution acuity in astigmats: Evidence for a critical period in the human visual system, *Br. J. Physiol. Opt.*, 32:38–49.
- Crair, M. C., D. C. Gillespie, and M. P. Stryker, 1998. The role of visual experience in the development of columns in cat visual cortex, *Science*, 279:566–570.
- Crawford, M. L. J., and R. E. Marc, 1976. Light transmission of cat and monkey eyelids, *Vis. Res.*, 16:323–324.
- Crawford, M. L. J., T. W. Pesch, G. K. von Noorden, R. S. Harwerth, and E. L. Smith, 1991. Bilateral form deprivation in monkeys. Electrophysiologic and anatomical consequences, *Invest. Ophthalmol. Vis. Sci.*, 32:2328–2336.
- Crawford, M. L. J., E. L. Smith, R. S. Harwerth, and G. K. von Noorden, 1984. Stereoblind monkeys have few binocular neurons, *Invest. Ophthalmol. Vis. Sci.*, 25:779–781.
- Crawford, M. L. J., and G. K. von Noorden, 1980. Optically induced concomitant strabismus in monkeys, *Invest. Ophthalmol. Vis. Sci.*, 19:1105–1109.
- Crawford, M. L. J., G. K. von Noorden, L. S. Meharg, J. W. Rhodes, R. S. Harwerth, E. L. Smith, and D. D. Miller, 1983. Binocular neurons and binocular function in monkeys and children, *Invest. Ophthalmol. Vis. Sci.*, 24:491–495.
- Cynader, M., 1979. Interocular alignment following visual deprivation in the cat, *Invest. Ophthalmol. Vis. Sci.*, 18:726–741.
- Cynader, M., N. Berman, and A. Hein, 1976. Recovery of function in cat visual cortex following prolonged deprivation, *Exp. Brain Res.*, 25:139–156.
- Cynader, M., and D. E. Mitchell, 1980. Prolonged sensitivity to monocular deprivation in dark-reared cats, *J. Neurophysiol.*, 43:1026–1040.
- Cynader, M. S., and G. Chernenko, 1976. Abolition of directional selectivity in the visual cortex of the cat, *Science*, 193:504–505.
- Daw, N. W., 1995, *Visual Development*, New York: Plenum Press.
- Drager, U. C., 1978. Observations on monocular deprivation in mice, *J. Neurophysiol.*, 41:28–42.
- Ellemberg, D., T. L. Lewis, D. Maurer, and H. P. Brent, 2000. Influence of monocular deprivation during infancy on the later development of spatial and temporal vision, *Vis. Res.*, 40:3283–3295.
- Ellemberg, D., T. L. Lewis, D. Maurer, C. H. Lui, and H. P. Brent, 1999. Spatial and temporal vision in patients treated for bilateral congenital cataracts, *Vis. Res.*, 39:4380–4389.
- Emerson, V. F., L. M. Chalupa, I. D. Thompson, and R. J. Talbot, 1982. Behavioural, physiological, and anatomical consequences of monocular deprivation in the golden hamster (*Mesocricetus auratus*), *Exp. Brain Res.*, 45:168–178.
- Fabre-Thorpe, M., F. Levesque, and E. Gary-Bobo, 1990. Long-term effects of dark-rearing on a visually guided reaching movement in cats, *Neurosci. Lett.*, 118:201–204.
- Fagioli, M., T. Pizzorusso, N. Beradi, L. Domenici, and L. Maffei, 1994. Functional postnatal development of the rat primary visual cortex and the role of visual experience: Dark rearing and monocular deprivation, *Vis. Res.*, 34:709–720.
- Fine, I., H. S. Smallman, P. Doyle, and D. I. A. MacLeod, 2002. Visual function before and after the removal of bilateral congenital cataracts in adulthood, *Vis. Res.*, 42:191–210.
- Freeman, R. D., D. E. Mitchell, and M. Millodot, 1972. A neural effect of partial visual deprivation in humans, *Science*, 175:1384–1386.
- Freeman, R. D., and L. N. Thibos, 1975. Contrast sensitivity in humans with abnormal early visual experience, *J. Physiol. (Lond.)*, 247:687–710.
- Gordon, J. A., and M. P. Stryker, 1996. Experience-dependent plasticity of binocular responses in the primary visual cortex of the mouse, *J. Neurosci.*, 15:3274–3286.
- Gregory, R. L., and J. G. Wallace, 1963. Recovery from early blindness: A case study, *Exp. Psychol. Soc. Monogr.*, Cambridge: Heffer, No. 2.

- Gwiazda, J., J. Bauer, F. Thorn, and R. Held, 1986. Meridional amblyopia *does* result from astigmatism in early childhood, *Clin. Vis. Sci.*, 1:145–152.
- Harwerth, R. S., E. L. Smith, and R. L. Boltz, 1980. Meridional amblyopia in monkeys, *Exp. Brain Res.*, 39:351–356.
- Harwerth, R. S., E. L. Smith, R. L. Boltz, M. L. J. Crawford, and G. K. von Noorden, 1983a. Behavioral studies on the effect of abnormal early visual experience in monkeys: spatial modulation sensitivity, *Vis. Res.*, 23:1501–1510.
- Harwerth, R. S., E. L. Smith, R. L. Boltz, M. L. J. Crawford, and G. K. von Noorden, 1983b. Behavioral studies on the effect of abnormal early visual experience in monkeys: temporal modulation sensitivity, *Vis. Res.*, 23:1511–1517.
- Harwerth, R. S., E. L. Smith III, G. C. Duncan, M. L. J. Crawford, and G. K. von Noorden, 1986. Multiple sensitive periods in the development of the primate visual system, *Science*, 232:235–238.
- Harwerth, R. S., E. L. Smith, and O. J. Okundaye, 1983c. Oblique effects, vertical effects and meridional amblyopia in monkeys, *Exp. Brain Res.*, 53:142–150.
- Harwerth, R. S., E. L. Smith, A. D. Paul, M. L. J. Crawford, and G. K. von Noorden, 1991. Functional effects of bilateral form deprivation in monkeys, *Invest. Ophthalmol. Vis. Sci.*, 32:2311–2327.
- Hendrickson, A., and R. Boothe, 1976. Morphology of the retina and dorsal lateral nucleus in dark-reared monkeys (*Macaca nemestina*), *Vis. Res.*, 16:517–521.
- Hess, R. F., T. D. France, and U. Tulanay-Keesey, 1981. Residual vision in humans who have been monocularly deprived of pattern stimulation in early life, *Exp. Brain Res.*, 44:295–311.
- Hess, R. F., and L. M. Wilcox, 1994. Linear and non-linear contributions to stereopsis, *Vis. Res.*, 34:2431–2438.
- Kaye, M., D. E. Mitchell, and M. Cynader, 1982. Depth perception, eye alignment and cortical ocular dominance of dark-reared cats, *Dev. Brain Res.*, 2:37–53.
- Kennedy, H., and G. A. Orban, 1983. Response properties of visual cortical neurons in cats reared in stroboscopic illumination, *J. Neurophysiol.*, 49:686–704.
- Kind, P. C., D. E. Mitchell, B. Ahmed, C. Blakemore, T. Bonhoeffer, and F. Sengpiel, 2002. Correlated binocular activity guides recovery from monocular deprivation, *Nature*, 416:430–433.
- Kiorpes, L., R. G. Boothe, A. E. Hendrickson, J. A. Movshon, H. M. Eggers, and M. S. Gizzi, 1987. Effects of early unilateral blur on the macaque's visual system. I. Behavioral observations, *J. Neurosci.*, 7:1318–1326.
- Krug, K., C. J. Akerman, and I. F. Thompson, 2001. Responses of neurons in neonatal cortex and thalamus to patterned visual stimulation through the naturally closed lids, *J. Neurophysiol.*, 85:1436–1443.
- Lehmkuhle, S., Kratz, K. E., and Sherman, S. M., 1982. Spatial and temporal sensitivity of normal and amblyopic cats, *J. Neurophysiol.*, 48:372–387.
- Levi, D. M., and R. S. Harwerth, 1980. Contrast sensitivity in amblyopia due to stimulus deprivation, *Br. J. Ophthalmol.*, 64:15–20.
- Loop, M. S., and S. M. Sherman, 1977. Visual discrimination during eyelid closure in the cat, *Brain Res.*, 128:329–339.
- Manny, R. E., and D. M. Levi, 1982a. Psychophysical investigations of the temporal modulation sensitivity function in amblyopia: uniform field flicker, *Invest. Ophthalmol. Vis. Sci.*, 22:515–524.
- Manny, R. E., and D. M. Levi, 1982b. Psychophysical investigations of the temporal modulation sensitivity function in amblyopia: spatiotemporal interactions, *Invest. Ophthalmol. Vis. Sci.*, 22:525–534.
- Mioche, L., and M. Perenin, 1986. Central and peripheral residual vision in humans with bilateral deprivation amblyopia, *Exp. Brain Res.*, 62:259–272.
- Mitchell, D. E., 1988a. The extent of visual recovery from early monocular or binocular visual deprivation in kittens, *J. Physiol. (Lond.)*, 395:639–660.
- Mitchell, D. E., 1988b. Animal models of human strabismic amblyopia: some observations concerning the interpretation of surgically induced strabismus in cats and monkeys, in *Advances in Neural and Behavioral Development* (P. G. Shinkman, ed.), Norwood, NJ: Ablex Publishing Corp., pp. 209–269.
- Mitchell, D. E., 1991. The long-term effectiveness of different regimens of occlusion on recovery from early monocular deprivation in kittens, *Philos. Trans. R. Soc. [Biol.]*, 333:51–79.
- Mitchell, D. E., 2002. Behavioral analyses of the contributions of cat primary visual cortex to vision, in *The Cat primary Visual Cortex* (B. R. Payne and A. Peters, eds.), San Diego: Academic Press, pp. 655–694.
- Mitchell, D. E., R. D. Freeman, M. Millodot, and G. Haegerstrom, 1973. Meridional amblyopia: evidence for modification of the human visual system by early visual experience, *Vis. Res.*, 13:535–558.
- Mitchell, D. E., F. Giffin, and B. Timney, 1977. A behavioral technique for the rapid assessment of the visual capabilities of kittens, *Perception*, 6:181–193.
- Mitchell, D. E., F. Giffin, F. Wilkinson, P. Anderson, and M. L. Smith, 1976. Visual resolution in young kittens, *Vis. Res.*, 16:363–366.
- Mitchell, D. E., G. Gingras, and P. C. Kind, 2001. Initial recovery of vision after early monocular deprivation in kittens is faster when both eyes are open, *Proc. Natl. Acad. Sci. USA*, 98:11662–11667.
- Mitchell, D. E., M. Kaye, and B. Timney, 1979. Assessment of depth perception in cats, *Perception*, 8:389–396.
- Mitchell, D. E., and S. MacKinnon, 2002. The present and potential impact of research on animal models for clinical treatment of stimulus deprivation amblyopia, *Clin. Exp. Optom.*, 85:5–18.
- Mitchell, D. E., K. M. Murphy, and M. G. Kaye, 1984a. Labile nature of the visual recovery promoted by reverse occlusion in monocularly deprived kittens, *Proc. Natl. Acad. Sci. USA*, 81:286–288.
- Mitchell, D. E., K. M. Murphy, and M. G. Kaye, 1984b. The permanence of the visual recovery that follows reverse occlusion of monocularly deprived kittens, *Invest. Ophthalmol. Vis. Sci.*, 25:908–917.
- Mitchell, D. E., and B. Timney, 1984. Postnatal development of function in the mammalian visual system, in *Handbook of Physiology*, section I: *The Nervous System*, vol. 3, pt. 1, *Sensory processes* (I. Darian-Smith, ed.), Bethesda: American Physiological Society, pp. 507–555.
- Mitchell, D. E., and F. E. Wilkinson, 1974. The effect of early astigmatism on the visual resolution of gratings, *J. Physiol. (Lond.)*, 243:739–756.
- Morgan, M. J., 1977. *Molyneux's Question. Vision, Touch and the Philosophy of Perception*, Cambridge: Cambridge University Press.
- Movshon, J. A., and L. Kiorpes, 1990. The role of experience in visual development, in *Development of Sensory Systems in Mammals* (J. R. Coleman, ed.), New York: Wiley & Sons, pp. 155–202.
- Movshon, J. A., and R. C. Van Sluyters, 1981. Visual neural development, *Ann. Rev. Psychol.*, 32:477–522.

- Mower, G. D., D. Berry, J. L. Burchfiel, and F. H. Duffy, 1981. Comparison of the effects of dark-rearing and binocular suture on development and plasticity of cat visual cortex, *Brain Res.*, 220:255–267.
- Mower, G., C. J. Caplan, and G. Letsou, 1982. Behavioral recovery from binocular deprivation in the cat, *Brain Res.*, 4:209–215.
- Muir, D. W., and D. E. Mitchell, 1973. Visual resolution and experience: acuity deficits in cats following early selective visual deprivation, *Science*, 180:420–422.
- Muir, D. W., and D. E. Mitchell, 1975. Behavioral deficit in cats following early selected visual exposure to contours of a single orientation, *Brain Res.*, 85:459–477.
- Murphy, K. M., and D. E. Mitchell, 1987. Reduced visual acuity in both eyes of monocularly deprived kittens following a short or a long period of reverse occlusion, *J. Neurosci.*, 7:1526–1536.
- Packwood, J., and B. Gordon, 1975. Stereopsis in normal domestic cat, Siamese cat, and cat raised with alternating monocular occlusion, *J. Neurophysiol.*, 38:1485–1499.
- Pasternak, T., J. E. Albano, and D. M. Harvitt, 1990. The role of directionally selective neurons in the perception of global motion, *J. Neurosci.*, 10:3079–3086.
- Pasternak, T., and L. J. Leinen, 1986. Pattern and motion vision in cats with selective loss of cortical directional selectivity, *J. Neurosci.*, 6:938–945.
- Pasternak, T., R. A. Schurmer, M. S. Gizzi, and J. A. Movshon, 1985. Abolition of visual cortical direction selectivity affects visual behavior in cats, *Exp. Brain Res.*, 61:214–217.
- Pettigrew, J. D., 1978. The paradox of the critical period for striate cortex, in *Neuronal Plasticity* (C. W. Cotman, ed.), New York: Raven Press, pp. 311–330.
- Prusky, G. T., and R. M. Douglas, 1998. Developmental plasticity of visual acuity in mice (pt. 2), *Soc. Neurosci. Abstr.*, 24:1876.
- Prusky, G. T., P. W. R. West, and R. M. Douglas, 2000. Experience-dependent plasticity of visual acuity in rats, *Eur. J. Neurosci.*, 12:3781–3786.
- Regal, D. M., R. Boothe, D. Y. Teller, and G. P. Sackett, 1976. Visual acuity and visual responsiveness in dark-reared monkeys (*Macaca nemestrina*), *Vis. Res.*, 16:523–530.
- Riesen, A. H., K. L. Chow, J. Semmes, and H. Nissen, 1951. Chimpanzee vision after four conditions of light deprivation, *Am. Psychol.*, 6:282.
- Sacks, O., 1993, May 10. To see and not see. *The New Yorker*, pp. 59–73.
- Sen, D. K., 1980. Anisometropic amblyopia, *J. Ped. Ophthalmol. Strab.*, 17:180–184.
- Sengpiel, F., P. Stawinski, and T. Bonhoeffer, 1999. Influence of experience on orientation maps in cat visual cortex, *Nat. Neurosci.*, 2:727–732.
- Sireteanu, R., 1985. The development of visual acuity in very young kittens. A study with forced-choice preferential looking, *Vis. Res.*, 25:781–788.
- Smith, D. C., and R. N. Holdefer, 1985. Binocular competitive interaction and recovery of visual acuity in long-term monocularly deprived cats, *Vis. Res.*, 25:1783–1794.
- Smith, D. C., R. Lorber, L. R. Stanford, and M. S. Loop, 1980. Visual acuity following binocular deprivation in the cat, *Brain Res.*, 183:1–11.
- Smith, E. L., R. S. Harwerth, and M. L. J. Crawford, 1985. Spatial contrast sensitivity deficits in monkeys produced by optically induced anisometropia, *Invest. Ophthalmol. Vis. Sci.*, 26:330–342.
- Spear, P., L. Tong, and A. Langsetmo, 1978. Striate cortex neurons of binocularly deprived kittens respond to visual stimuli through the closed eyelids, *Brain Res.*, 155:141–146.
- Spear, P., L. Tong, M. A. McCall, and T. Pasternak, 1985. Developmentally induced loss of directionally selective neurons in cat lateral suprasylvian visual cortex, *Dev. Brain Res.*, 20:281–285.
- Stone, J., 1983. *Parallel Processing in the Visual System*, New York: Plenum Press.
- Teller, D., R. Morse, R. Borton, and D. Regal, 1974. Visual acuity for vertical and diagonal gratings in human infants, *Vis. Res.*, 14:1433–1439.
- Timney, B., D. E. Mitchell, and F. Giffin, 1978. The development of vision in cats after extended periods of dark-rearing, *Exp. Brain Res.*, 31:547–560.
- Tytla, M. E., D. Maurer, T. L. Lewis, and H. P. Brent, 1988. Contrast sensitivity in children treated for congenital cataract, *Clin. Vis. Sci.*, 2:251–264.
- Valvo, A. 1968. Behavior patterns and visual rehabilitation after early and long-lasting blindness, *Am. J. Ophthalmol.*, 65:19–24.
- von Noorden, G. K., 1973. Experimental amblyopia in monkeys. Further behavioral observations and clinical correlations, *Invest. Ophthalmol.*, 12:721–726.
- von Noorden, G. K., and Maumenee, A. E., 1968. Clinical observations on stimulus deprivation amblyopia (amblyopia ex anopsia), *Am. J. Ophthalmol.*, 65:220–224.

15 Toward a Future for Aging Eyes

R. A. WEALE

INTEREST IN THEORIES of aging has undergone a revival during the last three decades or so. This is due partly to the relevant experiments being conducted on a molecular level and partly to studies of nematodes that suggest that life spans of species, that is, a putative maximal number of years alive, need not be fixed. Uncomprehending journalists love to seize on such nuggets of undigested information and to speculate on human longevity, suggesting that life may be extended to 150 years or more. However, most researchers have been taught not to argue from one species to another, so when considering the eyes, the author considers it prudent to confine discussion to the human species, however great the temptation to do otherwise.

A question that keeps cropping up concerns the existence of one or more genes for longevity. It would appear to be universally true that evolution responds to biological pressures, and it is hard to see what pressure could be brought to bear on living organisms to prolong their lives well beyond their reproductive capacity. There is little doubt that there exist genes for promoting cellular repairs, and it is easy to understand that they could develop in efficiency if the survival of a species would demand this. However, this is a concept very different from one postulating the ad hoc existence of genes for longevity. Hence, where applicable, the hypotheses underlying the considerations in this chapter rest on cellular repair, not vital prolongation.

Bits and pieces of aging

One of the quantitative aspects of aging that has received relatively little attention concerns its epidemiology in general, and ocular problems in particular. A large number of human biological attributes show a linear decline. This is equally true for glycosides in the pigment epithelium (Cingle et al., 1996), for the depletion of cells in the trabecular meshwork (Grierson and Howes, 1987), and for the retinal microcirculation (Grunwald et al., 1993), as well as for a host of other properties relating to other parts of the body (Weale, 1993). It is to be expected that such declines ultimately lead to systemic failure and, consequently, to death, even in the absence of any obvious pathology. It is highly significant that, broadly speaking, properties depending on dividing cells exhibit a decline that appears to terminate in the neighborhood of a putative age of ~120 years (Weale, 1993). Currently, the age of +120 years seems to be the approximate

maximal human longevity attainable. The coincidence of these figures alone should suffice to put a damper on hopes for an early increase in human life expectancy.

Possible consequences of a linear decline in human biological functions are illustrated in Figure 15.1. The upper part shows the age-related decline in the lenticular concentration of glutathione (Harding, 1970), a scavenger of free radicals that helps to maintain the transparency of the lens and is, incidentally, of some oncological significance. The lower part contains a digest of studies of the prevalence of cataract (Weale, 1998b). It should be noted that the lower part is plotted on a log scale, correctly apposed to the zero level of the upper section, with the two age scales being in tandem. It is clear that the slopes of the lines aim toward the zero level of the declining glutathione data. This suggests a link between the two; that is, when glutathione is exhausted, lens transparency becomes unsustainable.

This concept has been generalized. The figure of ~120 years, cited earlier as the age for ultimate functional failure, is clearly statistical in nature, with many tens of properties distributed around it with a standard difference of more than two decades (Weale, 1993). On the assumption that system failure results from an accumulation of component failures, it has been shown that the cumulant of the distribution agrees well with mortality data for the longest lived member countries of the United Nations (Weale, 1997).

What is interesting is that the end points of the linear decline of properties of the eye, such as biochemical, vascular, and physiological attributes (e.g., lacrimation), are randomly distributed throughout the more general systemic data (Weale, 1998a). On the face of it, the eye has developed to serve a body lasting, under optimal conditions, 12 decades or so.

What are the exceptions to this sweeping statement, if any?

Presbyopia—a problem partially solved

It is generally understood that the failure to accommodate does not terminate at the age of 120 years, but at less than half this time span, which is why presbyopia has been referred to as a maverick of senescence (Pierscionek and Weale, 1995). It is likely that presbyopia raises a point that should never be overlooked in considerations of senescence:

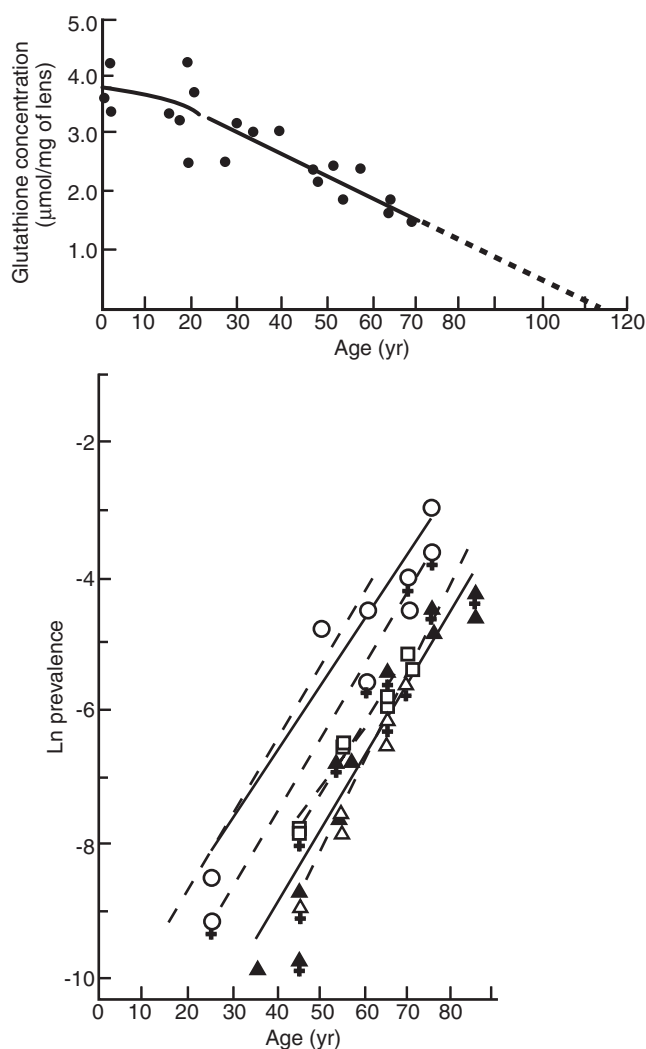


FIGURE 15.1. A suggestive relationship between the age-related decline in the concentration of lenticular glutathione (*top*) and the increase in the (log) prevalence of cataract (Weale, 1998b). The dotted part of the upper curve is a tentative extrapolation. The symbols denote Pima Indians (○ males; ♀ females), European Israelis (△ males; ▲ females), Oriental Israelis (□ males; ■ females), and Oxford UK individuals (●).

that is, any possible influence the environment may exert on aging rates. In other words, although a significant fraction of the aging rate is determined by one's genetic constitution, lifestyle, and external influences—which may include diet—have also been shown to play a role. In the case of presbyopia, climate appears to be a dominant determinant.

Table 15.1 shows how the age of onset of presbyopia (AP) varies with average annual ambient temperature (Rambo and Sangal, 1960). The cooler the climate, the later presbyopia is manifested. It may appear puzzling that humans, a homothermic species that preserves its body temperature, should exhibit such a phenomenon. However, the truth is that it is only the human core temperature that is kept constant. A shell, 1 cm in thickness and extending inward from

TABLE 15.1

*The variation of the age of onset of presbyopia (AP) with the average ambient annual temperature (T)**

Age at Onset of Presbyopia (Yr)	Average Ambient Temperature (F°)	Average Ambient Temperature (C°)
40	84	29
40.5	83	28
40.8	80	27
39.8	79	26
44.8	63	17
45.5	51	11
46	42	6

the surface of the dermis, averages body and environmental temperatures. The eye lens is obviously within that ambit; in addition, it is ill-equipped to benefit from the thermostatic provisions of the body because it has no blood supply: it is therefore exposed to the whims of climatic elements. More recent data suggest that, even at higher temperatures (e.g., in Eritrea or the Philippines), AP may occur at as early an age as the late 20s. Although the lens has been shown to contain heat-resisting protein, the mechanism whereby temperature acts on the rate of loss of accommodation has not been established.

Table 15.1 shows the onset, not the completion, of the symptomatic loss of accommodation, but it has been suggested that the early onset of an unnoticed, very early decline in accommodative amplitude is independent of temperature (Rambo and Sangal, 1960). In other words, the lines of decline for different climates may fan out from a fixed age so as to lead to onsets and terminal ages varying inversely with temperature.

The figures show that this effect does not explain the apparently maverick nature of presbyopia. To achieve success in this respect, it is necessary to try and account for presbyopia in biophysical terms, based on measurements of the properties of the lens.

The lens

A recent bibliography on relevant measurements is to be found in the analysis that attempts to resolve the difference between general systemic aging and the fast rush seen in presbyopia (Weale, 2000). There appear to be two keys to the problem. The first is the age-related variation of the mechanical and geometric properties of the lens. The mechanism of accommodation rests on the capsule molding the lens matrix that it contains; the moduli of elasticity and dimensions of both vary systematically with age. That of the capsule decreases with age (Fisher, 1969), whereas that of the matrix shows an increase. This is the physical counterpart of

why the lens is said to become harder with age (Glasser and Campbell, 1999).

It will be recalled that when a nearby object is fixated, the ciliary muscle is relaxed reflexively, as a result of which the suspensory ligaments of the lens that are attached to it have their tension reduced. Their remote ends being attached to the capsule, the tension therein is also reduced so that its overall surface contracts. This allows the matrix to bulge; that is, its two radii of curvature become smaller, and its optical power increases. The reverse process occurs when a distant object is fixated.

With regard to lenticular dimensions, which represent the second of the two keys to predicting the rate of loss of accommodative amplitude, the lens mass is known to increase with age, and as its specific density remains approximately constant, its volume rises. Although the increase in its sagittal diameter is well documented, there is some uncertainty about the transverse diameter (Strenk et al., 1999; Weale, 2001).

The problem to be solved consists in linking the changes just mentioned to the age-related loss in accommodative power. It may be noted that the decrease in Young's modulus of the capsule (Fisher, 1969) is accompanied by a decrease in the lenticular radii of curvature (Brown, 1974; Dubbelman and Van der Heijde, 2001). This is permanent and independent of whether or not there is any accommodation. Evidently, if the shape of the lens approaches its accommodated form owing to a senescent change in curvature, relaxation of zonular tension will have a smaller effect than is true in the younger, flatter lens. This, then, provides a qualitative explanation of why the accommodative decrement is affected by the reduction in capsular elasticity twice. Reflex changes in ciliary geometry are transmitted less efficiently because the capsule is losing its mechanical power and also because the shape of the lens matrix has moved in that direction owing to age.

The biophysical and optical changes attributable to age are encapsulated in equation 1, where the left represents the achievable change in power at a given age, and the right is made up of the following factors: ϵ , which is the ratio of the capsular elastic modulus to that of the lens matrix; σ , which is the stress applied to the zonule; and \mathcal{R} , which is the anterior radius of curvature. Figure 15.2 shows a comparison between $d\mathcal{F}$ (experimental data) (Brückner et al., 1987) and biophysical attributes of the eye lens, expressed as follows:

$$d\mathcal{F} = k \cdot \epsilon \cdot (1/\mathcal{R}) \cdot \sigma \quad (1)$$

In this equation, k is a calibrating constant. It may be noted that the rate of decline in capsular elasticity is within the compass of the rates of decline mentioned earlier as applying to the human system in general. The agreement between the optical and biophysical data provides tentative support

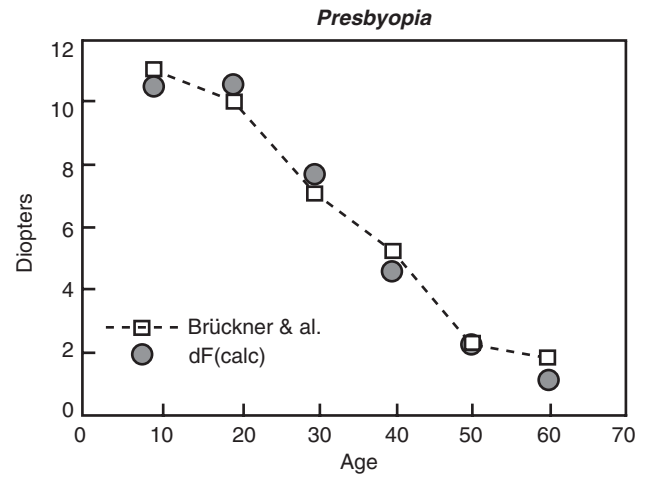


FIGURE 15.2. A comparison between observed data for the decline in accommodative amplitude and values predicted on the basis of underlying biophysical changes (Weale, 2000).

for the view that the maverick nature of presbyopia is due to at least two causal factors, namely, a geometric one and one involving mechanical properties of the lens.

A monkey of a ciliary muscle

In relation to the lens, a word or two may be addressed to a problem relating to the aging ciliary muscle itself. The variation in its cross-section as a function of age has been studied several times (Stieve, 1949). In essence, it was found that the muscle section tends to grow from childhood up to the fourth decade of life, presumably owing to work hypertrophy. As symptomatic presbyopia approaches, this muscle tends to change its shape, to shrink, and to become suffused with hyaloid material. In old age, it assumes a characteristically angular shape (i.e., its inner flank, which, in younger years is rounded and facing the lens, becomes almost angular, if not pointed).

The rate of presbyopia in rhesus monkeys is similar to that in humans when allowance is made for the differences in life expectancies among these species (Bito et al., 1982). However, there exists a significant difference between the age-related changes of the ciliary muscles in these two species (Lütjen-Drecoll, 2001). That is, the rhesus muscle fails to exhibit the above-mentioned angularity. It is tempting to suggest that its shape is typical, and that its human shape is anomalous. It will be appreciated that the angular shape approximates to a situation involving the muscle setting, as it were, in its accommodated form. If true, how could this come about?

Humans were not created to read, yet one of the important differences between the lifestyles of children and rhesus offspring, respectively, is that the former are made to read to such an extent as to promote myopia. Accommodation is

held to deform the eye, increasing the vitreous space, thus distancing the retina from the lens; if close work is carried out for at least 2 hours every day, permanent ocular changes result.

The comparison between the two types of ciliary muscle provides a suggestive, if tentative, example of the fact that senescence can also result from wear and tear. In this instance, it is self-inflicted as a result of the norms of civilization. If this explanation is valid, it does not augur well for the use of malleable lens implants in older patients who have undergone surgery for cataracts in the hope that they may be able to resume accommodating.

Errors and variations

The lens offers an insight into another interesting aspect of senescence, and this relates to the variability of some of its attributes. When population samples for some attribute are obtained, the data hardly ever coincide for a given age group. This can be due to a variety of reasons, even if one excludes faulty experimentation and systematic errors. Plotting the standard errors as a function of age is rarely done, but can be instructive. There are instances in which they are relatively constant, but in other cases, they increase systematically.

In the case of the lens, the age-related variation of standard deviations (std) appears to follow the same rule, no matter whether the elasticity of the lens is considered or some of the optical properties discussed later in this section; the slope of log std against log age is approximately unity or higher (Table 15.2). It can be shown that, if these attributes changed as a direct result of an accumulation of errors, the slope would be expected to be ~ 0.5 . The reason is that the underlying statistic would rest on the “random path” or “drunkard’s walk,” wherein the distance covered is proportional to the square root of the time taken to cover it.

It is clear from Table 15.2 that, overall, standard errors rise with age. If, for example, fluorescence is considered, the ratio of the error to the pertaining average value, the coefficient of variation, can be shown to remain remarkably constant. Lens absorbance does not rise linearly with age, as postulated by some authors (cf. Pokorny et al., 1987), but exponentially (Weale, 1988). This may go some way toward

explaining the high rate of increase in the standard deviation. The reason is that there is good evidence to suggest that more than one cause contributes to the senescence of the light transmission of the lens.

Broadly speaking, the lens becomes yellower and darker with age, even if there is no cataract in the making. This implies that less light of short wavelengths reaches the retina than of longer wavelengths. This affects the interpretation of aging processes in the spectral performance of the retina, which have been studied in considerable detail (Werner et al., 1990; Werner and Steele, 1988). As noted earlier, one of the peculiarities of the lens resides in the fact that it has no blood supply because its transparency needs to be maximized for an efficient functioning of the retina, yet it has to maintain some sort of metabolism to keep going. This leads to the nucleus—which is actually the lens babies are born with, the surrounding cortex accreting after birth—being effectively isolated. Its contents become degraded and yellow.

This, then, is a direct result of aging, although it cannot be viewed as part of a genetic program in the same sense as hair turning gray. This metabolic decay of the lens, however, is not the only factor to determine its appearance and function. The lens also acts as a photic calendar. The extent to which the tissue has been exposed to light is recorded in it, apparently indelibly, partly as additional yellowing, but revealed more systematically in studies of lenticular fluorescence.

The fluorescence of the lens is one of several unpleasant characteristics of this interesting organ. As yet, it remains undecided as to whether lenses of newborn infants, i.e., photically unexposed babies, exhibit any fluorescence. Such a determination would require irradiation of the pupil with violet or ultraviolet radiation and spectral analysis of any radiation emerging from the pupil. If there were any fluorescence, the emerging radiation would be expected to be of a long wavelength; in older eyes, it is typically green, with a peak wavelength of around 480 to ~ 530 nm. Such an experiment would be subject to an ethical barrier, but it would appear that no evidence on this point has been obtained from nonhuman lenses either. Backward extrapolations from accurate age-related measurements (Bleeker et al., 1986) suggest that the onset of fluorescence occurs a year or two after birth.

Of greater importance is the fact that measurements of lenticular fluorescence in widely differing geographical locations yield significantly different results. A comparison of data obtained in Atlanta and Oregon (Lerman, 1988) showed that the lenses of the inhabitants of sunny Atlanta fluoresced more than those of residents of rain-swept Oregon, Atlanta’s average annual solar illumination being some 30% higher. It can be shown that the extent of the southern lenticular fluorescence is correspondingly

TABLE 15.2

Slopes of log magnitude vs. log age for three properties of the lens starting at 10 years of age

Lens Properties	Slope
Fluorescence of the lens (Bleeker et al., 1986)	0.95
Lens absorbance at $\lambda = 460$ nm (Weale, 1982)	1.57
Lens matrix elasticity (Fisher, 1971)	1.28

~30% greater. The agreement may not be entirely coincidental.

There is a very close connection between the age-related absorbance and fluorescence of the lens. This is not surprising as both phenomena depend on the absorption of radiation. However, fluorescence involves the conversion of absorbed radiation of one wave-band into another, typically one with a lower wavelength. The mechanism effecting the conversion is assessed by the photoefficiency of the phenomenon, which is measured in terms of γ , the ratio of quanta emitted per quanta absorbed. At most, γ is a few percent, in stark contrast to the much higher photosensitivity of visual pigments. It is noteworthy that γ rises systematically with age, which is another way of saying that the aging lens becomes more sensitive to short wavelength light as age progresses. The tentative explanation for this phenomenon is that an unraveling of the spatial arrangement of lenticular crystallins occurs, which makes the chromophores increasingly accessible to the incident radiation. On this view, light does not directly harm the lens, but renders it more susceptible to injury from hazards—a better characterization of senescence than the ubiquitous one based on the calendar.

The preceding discussion has offered a sketch of the aging of the eye lens. It is important to keep in mind the various age-related changes as separate entities. Superficial arguments sometimes lead to the suggestion that a temporal sequence needs to be a causal one. Thus, it is said, the completion of presbyopia is accompanied by a noticeable yellowing of the lens. This, in turn, leads to light being scattered, which is ultimately followed by cataract development. However, we have seen that exposure to sunlight can enhance yellowing in younger age groups, that presbyopia differs in its progression in different climates, and that cataract can take different forms, only one of which has so far been linked reliably with solar radiation as a risk factor.

What a nerve!

At one time, it was thought that the rapid course of the loss of accommodative potency might be an exception to the suggestion that human biological functions decline at a rate of a little under 1% per year. However, it has now been established that, as rapidly as presbyopia develops—namely, twice as fast as other functional decrements on average—an additional phenomenon provides a possible explanation, and the condition is consistent with the theory.

There are certain attributes, however, that are not disposed of so easily, and that actually follow a law of their own. They relate to neural structures and the relevant nervous components and responses. All this was suggested explicitly relatively recently (Weale, 1993), but it had already been

surmised from a 30-year-old graph (Danon et al., 1981). The graph showed that the rate of the age-related decline of nerve conduction is one-third or one-quarter slower than that of the properties globally referred to earlier. Thus, whereas these other functional declines terminate hypothetically around the age of ~120 years, the speed of decline of nerve conduction would drop to zero only after nearly 400 years.

The difference between nervous and nonnervous senescence is neatly illustrated with reference to hearing loss. It is well known that there is a progressive, age-related loss of the perception of audible high frequencies, an observation that antedates the self-inflicted losses caused by industrial, disco, and other high-level noise stimuli. In contrast, low (bass) notes continue to be perceived in a relatively undiminished manner. Broadly speaking, the reason for this difference is that, with regard to high frequencies, senescence results from changes in peripheral organs, such as the continuous loss of hair cells, whereas low frequencies are conducted by bone and nerves, the attrition rate of which is incomparably lower.

The aforementioned comparison (Weale, 1993) of a large number of various biological functions has led to the tentative conclusion that tissues consisting of nondividing cells have a potentially longer life than those based on dividing cells. There is an *a priori* reason as to why nervous tissue might have to last for a comparatively longer time than tissues enjoying a rapid metabolic turnover. The prolonged existence of reflexes, innate and acquired, would be parlous if tissue renewal were taking place with the probability that the appropriate responses would have to be reacquired. What is true of such responses applies *a fortiori* to cerebral involvement: it is hard to imagine how memory could be maintained in the presence of a continuous turnover of the necessary component molecules.

The cellular dichotomy makes things rather difficult for the eye, as it is made up of, and functions with, an interesting combination of the two types of cells. We have already noted that the ocular data are distributed randomly among those for other human biological functions, but there is a preponderance of them among those functions with putative end points in excess of ~180 years (Table 15.3).

Clearly, there are standard deviations associated with these values, but overall, the end-point distribution for nondividing-cell tissue differs from that for dividing-cell tissue. Moreover, the former fails as a predictor of mortality, whereas the latter succeeds remarkably well (Weale, 1993). This difference suggests that attempts to tinker with the life span of a species—even when it comes to our own—may have to approach the problem step-by-step, rather than with a blunderbuss attack on genes presumed to control senescence. Such a view is reinforced by a consideration of some age-related disease processes.

TABLE 15.3
Notional ages (*Yr*) of failure (end points) of ocular
neural components*

Ocular Component	Age at Failure
Retinal ganglion cells	194
Rods	242
Optic nerve fibers	303
Cones	326
Retinal pigment epithelium	395

* Gao and Hollyfield, 1992.

Disease

Figure 15.1 showed that the log prevalence ($\log P$, there expressed as $\text{Ln}P$) of cataract is an approximately linear function of age (t), that is,

$$\text{Log}P - \log P_0 = \alpha \cdot t \quad (2)$$

where P_0 is the notional prevalence of the condition at birth, and α is a constant. This implies that the arithmetic function is an exponential:

$$P = P_0 \cdot \exp(\alpha \cdot t) \quad (3)$$

Those readers who are mathematically inclined will realize that this is the integral of

$$dP/dt = \alpha \cdot P \quad (4)$$

which, in turn, implies that the rate of increase of the dependent variable at any time is proportional to the magnitude of the variable. It suggests, for example, that every seed that is produced gives rise to more than one seed in turn, or that this is how epidemics are propagated at their start.

Quite a few other conditions are described similarly; age-related maculopathy, a disease of the fovea and macula involving the loss of cones, is one of them. The most widely quoted example is mortality, even though this simple description is confined to a limited age span, rarely extending over the last 40 years or so of a sample population. Because Gompertz (1825) was the first to have used a version of equation 3, it is sometimes referred to as a Gompertz plot, and P_0 and α as Gompertz constants.

There have been several attempts to increase the range of validity of equation 3, and these have been well summarized (Comfort, 1979). One involves the addition of an arbitrary constant, named after Makeham. Another, more interesting one, is attributable to Teissier (Comfort, 1979); it changes equations 2 and 3 by substituting for the time (t) the expression $t - t_0$ (where t_0 is a constant). Because, in survival data, this formulation implies a delay of the decline associated with aging, Teissier dubbed t_0 the "plateau of adult vigour." It so happens that he overlooked some important attributes of this formulation, which will now be addressed.

To begin, a reconsideration of equation 2 is in order. It contains two constants, namely P_0 and α , which determine the intercept and slope of the straight line. Suppose now that

a given condition, such as the prevalence of age-related maculopathy, has been studied in different countries. Simplicity would lead one to expect that all the studies would produce values of P_0 and α closely clustering around well-defined averages, characterizing the age variation of the prevalence of the disease.

The above-mentioned clustering would have to be not assumed, but demonstrated. A closer look at equation 2 leads to another possibility. One can assume that, although the constants are constant for any one population, they may in fact vary from one population to another. This is not as far-fetched as it might appear; there may be differences in the local genetic set-up, different prevailing risk factors, and so on. Thus, differentiating equation 2, one obtains

$$-d\log P_0 = t \cdot d\alpha \quad (5)$$

which informs on how the slope α varies with the intercept P_0 . Subsequent integration yields

$$-\log P_0 = t \cdot \alpha + \text{const} \quad (6)$$

The value of the constant is determined by setting $\alpha = 0$, whence $-\log P_s = \text{const}$. This is the value of the intercept $\log P_0$ for the (hypothetical) situation in which a condition is unaffected by age. For example, it could represent a constant external hazard. Substitution in equation 6 yields

$$-\log P_0 = t_s \cdot \alpha - \log P_s \quad (7)$$

where the constant t assumes the value t_s , that is, the age at which $\log P_0$ reaches the value $\log P_s$. Thus, substitution in equation 2 leads to a revised form of the Gompertz function, namely

$$\log P - \log P_s = \alpha \cdot (t - t_s) \quad (8)$$

This is akin to Teissier's expression, but with an important difference: P is not expressed as a multiple of P_0 , but of P_s . Equation 8 predicts that, if the prevalence of a condition is measured in different circumstances, yielding different values of P_0 and α , their plot should be rectilinear with an intercept at $\log P_s$. Moreover, it follows from equation 7 that the slope of this line is equal to t_s , that is, the number of years it takes from birth to reach a prevalence of P_s , defined as one for which the associated risk is independent of age.

Figure 15.3 provides remarkable support for the hypothesis here advanced. The data upon which it rests were obtained from various reliable studies (Bressler et al., 1989; Gibson et al., 1985; Klein and Klein, 1982; Martinez et al., 1982; Schachat et al., 1995; Vingerling et al., 1995).

The predicted rectilinearity is plainly confirmed. The value of $\log P_s$ (-0.09 , marked with an X) is lower than in any other corresponding condition, with a correspondingly large figure (102 years) for t_s .

Considering Teissier's concept of the "adult plateau of vigour," one can view this period as one that provides a measure of immunity. It can be shown that similar constants

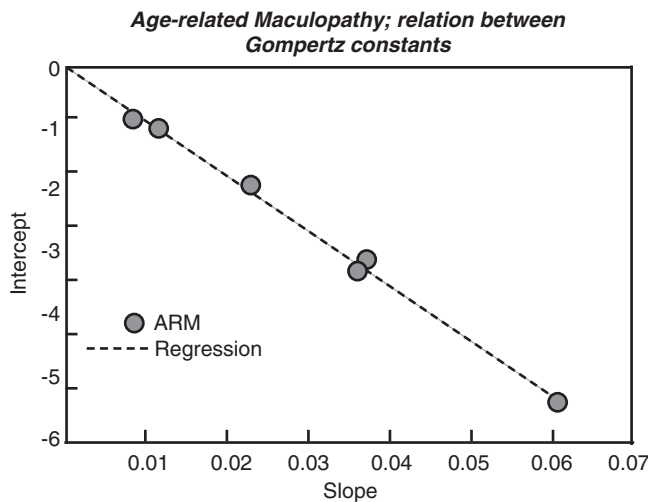


FIGURE 15.3. Gompertz constants for six studies of the prevalence of age-related maculopathy.

can be determined for mortality data, for some types of mental conditions, for Parkinson's disease, and for cataract and glaucoma. What is so remarkable about the figure of 102 years is not its precise value, but that it is higher by far than any other determined up to this time. Analyses of mortality data, to quote one example, give the value for t_x as 60 to 70+ years in women and men.

What follows?

The earlier part of this chapter suggested that tissues consisting of dividing cells help researchers understand why, at present, the longest lived individuals may reach an age of ~120 years. It also set out the reasons why the eyes age in a manner consistent with general systemic aging (Weale, 1995). It was also stressed that nervous tissues do not fit this criterion, as their rate of decline is significantly slower than that of the dividing cells. So, in considering the age-related course of a disease that is apparently tied to neural components of the retina, one finds that, according to one system of measurement, the neural part of the eye shows remarkable resilience, greatly distressing though the condition is.

Hence, on the face of it, the arguments presented in this chapter appear to be consistent. What they highlight—if, indeed, they are valid—is the difficulties faced by those wishing to prolong our health span. Only fools prophesy, but it is important to remember that the 120-year organization is laid down early in life. Benefits for our health span are more likely to be obtained in the first instance by addressing risk factors: lifestyle seems to be the buzz word that has so far been linked principally to the 120-year system. What lifestyle control seems to be achieving—although regress is also observed—is an increase in people's life expectancy. It is likely that the senescence of neural components of the

visual system offer altogether a different problem, hardly though they appear to be.

Acknowledgment

This work has not been funded.

REFERENCES

- Bito, L. Z., C. J. DeRousseau, P. L. Kaufman, and J. W. Bito, 1982. Age dependent loss of accommodative amplitude in rhesus monkeys: an animal model for presbyopia, *Invest. Ophthalmol. Vis. Sci.*, 23:23–31.
- Bleeker, J. C., J. A. van Best, L. Vrij, E. A. van der Velde, and J. A. Oosterhuis, 1986. Autofluorescence of the lens in diabetic and healthy subjects by fluorophotometry, *Invest. Ophthalmol. Vis. Sci.*, 27:791–794.
- Bressler, N. M., S. B. Bressler, S. K. West, S. L. Fine, and H. R. Taylor, 1989. The grading and prevalence of macular degeneration in Chesapeake Bay watermen, *Arch. Ophthalmol.*, 107: 847–852.
- Brown, N., 1974. The change in lens curvature with age, *Exp. Eye Res.*, 19:175–183.
- Brückner, R., E. Batschelet, and F. Huguenschmidt, 1987. The Basel longitudinal study on aging (1955–1978), *Doc. Ophthalmol.*, 64:235–310.
- Cingle, K. A., R. S. Kalski, W. E. Bruner, C. M. O'Brien, P. Erhard, and R. E. Wyszynski, 1996. Age-related changes of glycosidases in human retinal pigment epithelium, *Curr. Eye Res.*, 15:433–438.
- Comfort, A., 1979. *The Biology of Senescence*, 3rd ed. London: Churchill Livingstone, pp. 23–24.
- Danon, D., N. W. Shock, and M. Marois, 1981. *Aging: A Challenge to Science and Society*, Oxford: Oxford University Press, p. 280.
- Dubbelman, M., and G. L. Van der Heijde, 2001. The shape of the aging human lens: curvature, equivalent refractive index and the lens paradox, *Vis. Res.*, 41:1867–1877.
- Fisher, R. F., 1969. Elastic constants of the human lens capsule, *J. Physiol.*, 201:1–19.
- Fisher, R. F., 1971. The elastic constants of the human crystalline lens, *J. Physiol.*, 212:147–180.
- Gao, H., and J. G. Hollyfield, 1992. Aging of the human retina, *Invest. Ophthalmol. Vis. Sci.*, 33:1–17.
- Gibson, J. M., A. R. Rosenthal, and J. A. Lavery, 1985. A study of the prevalence of eye disease in the elderly in an English community, *Trans. Ophthalmol. Soc. UK*, 104:196–203.
- Glasser, A., and M. C. W. Campbell, 1999. Biometric, optical and physical changes in the isolated crystalline lens with age in relation to presbyopia, *Vis. Res.*, 39:1991–2015.
- Gompertz, B., 1825. On the nature of the function expressive of the law of human mortality and on a new mode of determining the value of life contingencies, *Philos. Trans. R. Soc. London [A]*, 115:513–585.
- Grierson, I., and R. C. Howes, 1987. Age-related depletion of the cell population in the human trabecular meshwork, *Eye*, 1:204–210.
- Grunwald, J. E., J. Piltz, N. Patel, S. Bose, and C. E. Riva, 1993. Effect of aging on retinal macular microcirculation: a blue field simulation study, *Invest. Ophthalmol. Vis. Sci.*, 34:3609–3613.
- Harding, J. J., 1970. Free and protein-bound glutathione in normal and cataractous lenses, *Biochem. J.*, 117:957–960.

- Jain, I. S., J. Ram, and A. Gupta, 1982. Early onset of presbyopia, *Am. J. Optom. Physiol. Opt.*, 59:1002–1004.
- Klein, B. E., and R. Klein, 1982. Cataracts and macular degeneration in older Americans, *Arch. Ophthalmol.*, 100:571–573.
- Lerman, S., 1988. Human lens fluorescence aging index, *Lens Res.*, 5:23–31.
- Lütjen-Drecoll, E., 2001. Die Beweglichkeit des Ziliarmuskels ist entscheidend. 99. *Kongress der DOG. Kongressausgabe*, September 9, 2001, p. 7.
- Martinez, G. S., A. J. Campbell, J. Reinken, and B. C. Allan, 1982. Prevalence of ocular disease in a population study of subjects 65 years old and older, *Am. J. Ophthalmol.*, 94:181–189.
- Pierscionek, B. K., and R. A. Weale, 1995. Presbyopia—a maverick of human aging, *Arch. Gerontol. Geriatr.*, 20:229–240.
- Pokorny, J., V. C. Smith, and M. Lütze, 1987. Aging of the human lens, *Appl. Opt.*, 26:1437–1440.
- Rambo, V. C., and S. P. Sangal, 1960. A study of the accommodation of the people of India, *Am. J. Ophthalmol.*, 49:993–1004.
- Schachar, A. P., L. Hyman, M. C. Leske, A. M. Connell, and S. Y. Wu, 1995. Features of age-related macular degeneration in a black population. The Barbados Eye study group, *Arch. Ophthalmol.*, 113:728–735.
- Stieve, R., 1949. Über den Bau des menschlichen Ciliarmuskels, seine Veränderungen während des Lebens und seine Bedeutung für die Akkommodation, *Anat. Anz.*, 97:69–79.
- Strenk, S. A., J. L. Semmlow, L. M. Strenk, P. Munoz, J. Gronlund-Jacob, and J. K. DeMarco, 1999. Age-related changes in human ciliary muscle and lens: A magnetic resonance imaging study, *Invest. Ophthalmol. Vis. Sci.*, 40:1162–1169.
- Vingerling, J. H., I. Dielemans, A. Hofman, D. E. Grobbee, M. Hijmering, C. F. L. Kramer, P. T. V. M. de Jong, 1995. The prevalence of age-related maculopathy in the Rotterdam study, *Ophthalmology*, 102:205–210.
- Weale, R. A., 1982. *A Biography of the Eye—Development, Growth, Age*, London: H. K. Lewis, p. 221.
- Weale, R. A., 1988. Age and the transmittance of the human crystalline lens, *J. Physiol.*, 395:577–587.
- Weale, R. A., 1993. Have human biological functions evolved in support of a lifespan? *Mech. Ageing Devel.*, 69:65–77.
- Weale, R. A., 1995. Why does the human visual system age in the way it does? *Exp. Eye Res.*, 60:49–55.
- Weale, R. A., 1997. Human biological decline and mortality rates, *Mech. Ageing Devel.*, 97:55–72.
- Weale, R. A., 1998a. The eye within the framework of human senescence: biological decline and mortality, *Ophthalmol. Res.*, 30:59–73.
- Weale, R. A., 1998b. Introduction, in *The Epidemiology of Eye Disease* (G. J. Johnson and D. C. Minassian, eds.), London: Chapman & Hall, pp. 1–6.
- Weale, R. A., 2000. Why we need reading glasses before a zimmer-frame, *Vis. Res.*, 40:2233–2240.
- Weale, R. A., 2001. The aging lens, *Vis. Res.*, 41:3089–3091.
- Werner, J. S., D. H. Peterzell, and A. J. Schectz, 1990. Light, vision, and aging, *Optom. Vis. Sci.*, 63:214–229.
- Werner, J. S., and V. G. Steele, 1988. Sensitivity of human foveal color mechanisms throughout the life span, *J. Opt. Soc. Am. [A]*, 5:2123–2130.

III RETINAL MECHANISMS AND PROCESSES

16 Visual Transduction by Rod and Cone Photoreceptors

MARIE E. BURNS AND TREVOR D. LAMB

VISUAL PROCESSING begins with the conversion of light to an electrical signal in retinal photoreceptors. In this review we describe the current state of knowledge of this conversion process. First we summarize the remarkable performance of rod and cone photoreceptors and briefly describe their salient anatomical features. Then we present a brief overview of the transduction process before delving into the details. We divide transduction into activation and inactivation phases because there is a clear distinction between the molecular processes underlying the onset and recovery phases of the light response. Finally, we consider how the balance between activation and inactivation is achieved, and how these processes contribute to photoreceptor adaptation.

PERFORMANCE OF RODS VERSUS CONES Under most conditions, our vision is mediated by cones. Cones operate over an enormous range of intensities; indeed, at any level of illumination where we can make out color, our cones are providing useful signals. Cones also operate very rapidly, a factor that is likely to be of great importance to survival. In addition, our photopic (cone) visual system is extremely sensitive to small changes, being able to detect a contrast (Weber fraction, $\Delta I/I$) of $\sim 0.5\%$. Finally, cones give us color vision, which, among other benefits, helps to break camouflage, again providing a survival advantage.

In evolutionary terms, rods have arisen more recently than cones, and in the retina the specialized rod circuitry gives the appearance of having been superimposed on pre-existing cone circuitry. Despite their more recent origin, rods are numerically the dominant class of photoreceptor in the human eye by far, outnumbering the cones by about 20-fold over most of the retina. Yet, rods do not function over most of the intensity range that we normally experience (they are saturated); instead, they only function at exceedingly low intensities, corresponding to starlight or moonlight conditions. What is their role then, and why are they so numerous?

The answer seems to be that rods are specialized for the detection of individual photons of light (Hecht et al., 1942), and the subsequent circuitry of the scotopic visual system is designed to be able to detect just a few photon hits scattered over large areas (Barlow et al., 1971). This enables the visual system to operate in a “photon-counting” mode (Rose,

1948). The enormous number of rods is employed primarily to catch just about every photon that reaches the retina. Rods do not need to continue operating at intensities much above the level at which their responses to different photons begin overlapping appreciably because the primordial system (of cones) is sufficiently sensitive to operate at those levels.

As long ago as the 1930s, it was proposed that the physical limit to stimulus detection in the scotopic and photopic visual systems was set by the existence of an “equivalent background light” within the photoreceptors (Stiles and Crawford, 1932). Perhaps the greatest difference between rods and cones lies in the magnitude of this so-called dark light. In cones, the dark light corresponds to some hundreds of photon hits per cone per second, whereas for rods, the level is around four orders of magnitude lower, corresponding to just one photon hit per rod every 100 to 200 seconds (see Barlow, 1964). One of the great challenges in phototransduction is to understand how rhodopsin molecules in the rod outer segment are able to achieve such a great advantage over their counterparts in the cones.

It seems that this major advantage of rods over cones brings with it a great cost (Lamb, 1981): namely, the inability of the scotopic system to recover speedily after exposure to extremely intense “bleaching” illumination. This, it seems, may be an inevitable consequence of some sacrifice that has been made in order to achieve the incredibly low dark light that is needed to give the organism a survival advantage in conditions of near-darkness.

PHOTORECEPTOR STRUCTURE IN RELATION TO FUNCTION The ultrastructure of photoreceptors is remarkably similar across the animal kingdom. Photoreceptors consist of three primary functional domains: outer segment, inner segment, and synaptic ending. For the purposes of this chapter, we will focus our brief discussion on the general ultrastructural properties and functions of the outer and inner segments.

By far the most abundant protein in the outer segment is the light-capturing protein, rhodopsin. Historically, the term *rhodopsin* has been applied to the pigment found in those rods that use vitamin A₁ (such as mammalian rods), whereas the term porphyropsin has been applied to vitamin A₂-based rod pigments, and iodopsin to cone pigments. Here, however, we

will adopt the recent loose convention whereby the term rhodopsin will be generalized to refer to all visual pigments; the more explicit terms for rod or cone pigments will be applied only when necessary. Rhodopsin and many of the other components of the transduction cascade reside in (or at the surface of) the lipid material comprising the hundreds to thousands of membrane pairs that are stacked along the outer segment (Fig. 16.1). In cones, these sac-like structures are simply foldings of the plasma membrane, but in rods, the corresponding structures become completely pinched off from the plasma membrane, forming intracellular organelles called discs.

This topological difference between rods and cones represents a major anatomical disparity between the two types of cell, yet we do not at present understand its functional significance. One interesting possibility is that the enormous increase in stability of the rhodopsin molecule is aided in some way by the sealing-off of the discs; thus, perhaps it is advantageous to expose the amino-terminal region, not to the extracellular solution, but instead to the intradiscal medium. For cones, the greatly increased surface-to-volume ratio that is possible with patent sacs may be important, as this speeds the rate of change of intracellular ion concentrations mediated by plasma membrane fluxes; this is likely to be especially important for calcium ions, because calcium levels control negative feedback to the cascade (see “Calcium Feedback Regulation of Phototransduction”).

The lipids and proteins that comprise the discs and sacs eventually deteriorate, so that the photoreceptor needs to perform continual maintenance during its life span. Rods periodically shed old discs from the distal tip of the outer segment, and continually generate new foldings at the base of the outer segment, that in due course pinch off to form discs (reviewed in Young, 1976; see also Steinberg et al., 1980). Thus, rod outer segments are not of uniform age, but rather the newer components “move up” as they achieve seniority. A similar process of renewal and shedding occurs in cones; however, because the entire membrane is continuous, protein components of different age are distributed along the length of the outer segment.

Connecting the outer segment to the inner segment is the ciliary stalk, with a $9 + 2$ arrangement of microtubules and abundant actin filaments. All proteins destined for the outer segment (whether soluble or membrane bound) must pass through this narrow constriction. The mechanisms by which the proteins are transported and the discs are formed are not well understood.

The outermost portion of the inner segment contains a high density of mitochondria called the *ellipsoid*, which supplies adenosine triphosphate (ATP) via diffusion to the metabolically demanding outer segment. The high concentration of mitochondria in the ellipsoid also serves an optical purpose; this region has a high refractive index and helps to funnel photons into the outer segment, thereby increasing the probability that they will be absorbed. This phenomenon is

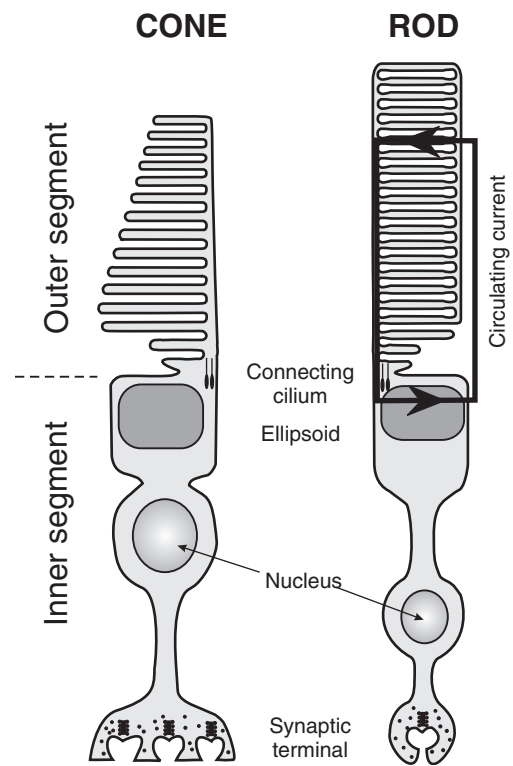


FIGURE 16.1. Anatomical features of rod and cone photoreceptors. The light-sensitive outer segment comprises a very large area of lipid membrane in which the photopigment molecules are densely packed. In cones, the pigment-containing membrane comprises the highly folded plasma membrane, which forms sacs. In rods, the rhodopsin-containing membrane becomes pinched off into discrete discs that are separated from the plasma membrane and from each other. In both cases, new membrane is synthesized at the base of the outer segment, just above the ciliary stalk, where new foldings are continually being formed. The inner segment contains the conventional cellular metabolic machinery. Organelles include the ellipsoid, which is packed with mitochondria, the myoid, endoplasmic reticulum, and the nucleus. At the base of the cell is the synaptic terminal that mediates communication with postsynaptic neurons. The path of the circulating electrical current is shown for the rod.

especially marked in cones, and gives rise to the Stiles–Crawford directional sensitivity effect. The inner segment also contains the endoplasmic reticulum, Golgi apparatus, and nucleus; thus, it performs a cell’s usual housekeeping chores, albeit with higher than average rates of protein synthesis and unusual membrane-trafficking demands. The plasma membrane of the inner segment contains potassium channels, which, in darkness, permit the efflux of potassium ions that balances the influx of cations into the outer segment, completing the loop that gives rise to the “dark current.”

OVERVIEW OF PHOTOTRANSDUCTION Phototransduction in rods and cones is mediated by closely related cascades, which are broadly similar in many respects to the transduction processes utilized in a variety of other G protein-coupled

signaling systems. A receptor protein is activated, causing activation of a G protein, which, in turn, activates a third protein, a so-called effector protein. This brings about a change in the cytoplasmic concentration of a second messenger substance, and thereby leads to modulation of ion channel opening in the plasma membrane. Thereafter, each of the active species must be turned off in order to permit recovery. Phototransduction is the essential first step in vision; thus, it is not surprising that defects in the phototransduction machinery are associated with a variety of blinding diseases in humans (reviewed in Dryja, 2000).

Phototransduction differs from chemoreceptive systems in that the receptor protein does not need to bind a chemical substance before activation can occur; instead, that chemical (a retinoid in the photoreceptor) is already prebound to the receptor. The absorption of light converts the retinoid from a powerful antagonist into a powerful agonist. Another difference from some other systems is that the response to stimulation is upside-down—that is, illumination leads to a reduction of a standing current and, hence, to hyperpolarization of the cell. Why vertebrate photoreceptors should have chosen this inverted response polarity is not entirely clear.

Activation of phototransduction

In this section, we will consider those steps that lead to activation of the light response, and we will postpone until the next section (“Inactivation of the Phototransduction Cascade”) those steps that contribute to inactivation (or recovery) of the light response. First we will outline each of

the molecular mechanisms known to underlie activation. Then we will examine the onset phase of the electrical response that is predicted from theoretical analysis of the activation steps, and we will compare that prediction with experimental results.

MOLECULAR MECHANISMS OF ACTIVATION The molecular reactions underlying the activation stages of vertebrate phototransduction are shown schematically in Figure 16.2 (modified from Lamb and Pugh, 1992, Fig. 1). Upon absorption of a photon of light, the rhodopsin molecule is transformed into an enzymatically active state (R^*) that catalyzes the activation of the G protein transducin (to G^*). Transducin, in turn, activates the effector protein phosphodiesterase (PDE) to PDE^* . The activated PDE hydrolyzes the diffusible messenger cyclic guanosine monophosphate (cGMP) so that the cytoplasmic concentration of cGMP decreases, leading to closure of cGMP-gated ion channels in the plasma membrane. Closure of these channels has the dual effect of generating the photoreceptor’s electrical response (by reducing the circulating current and hyperpolarizing the membrane voltage), and of causing a reduction in cytoplasmic calcium concentration. Each of these molecular steps will now be described.

ACTIVATION OF RHODOPSIN BY A PHOTON Absorption of a photon by the bent 11-*cis* retinal isomer within rhodopsin has a high probability (~ 0.67) of triggering the *cis* to *trans* isomerization of the retinoid. Apparently, the straighter all-trans isomer no longer fits neatly into the hydrophobic pocket so the rhodopsin molecule is strained internally,

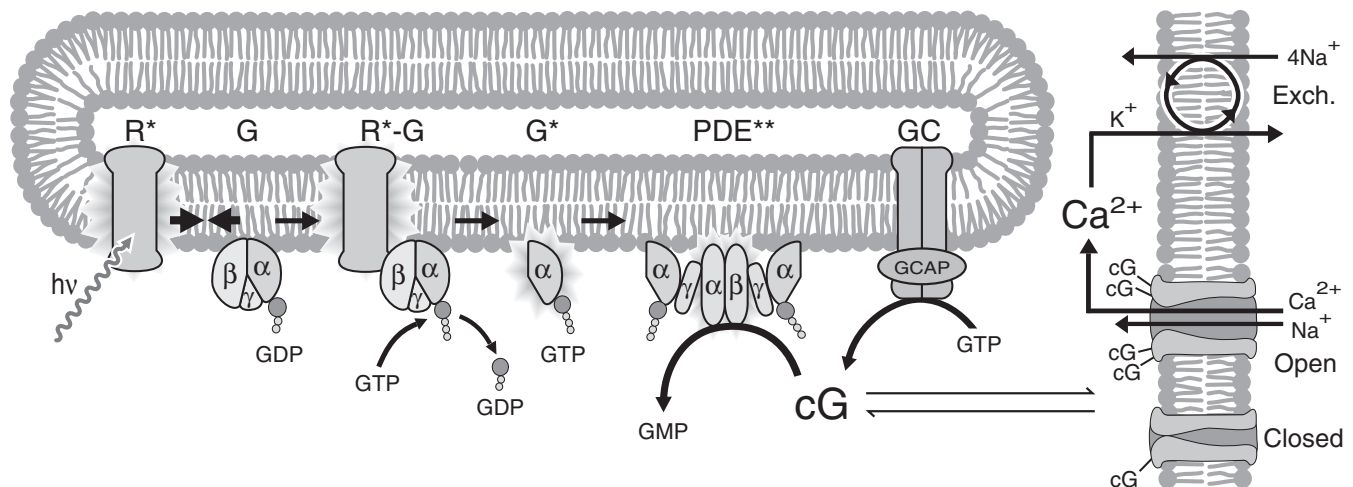


FIGURE 16.2. Schematic representation of molecular reactions underlying activation. Following absorption of a photon ($h\nu$), the activated rhodopsin (R^*) repeatedly contacts molecules of the heterotrimeric G protein (G), catalyzing the exchange of GDP for GTP, producing the active form G^* ($= G\alpha - GTP$). Two G^* s bind to the two inhibitory γ subunits of the phosphodiesterase (PDE), thereby activating the corresponding α and β catalytic subunits,

forming PDE^{**} , which then catalyzes the hydrolysis of cGMP (cG). The consequent reduction in the cytoplasmic concentration of cGMP leads to closure of the cyclic nucleotide gated channels and blockage of the inward flux of Na^+ and Ca^{2+} , thereby reducing the circulating electrical current. The $Na^+/Ca^{2+}, K^+$ exchanger continues to pump Ca^{2+} out, so that the cytoplasmic Ca^{2+} concentration declines during illumination. (See color plate 5.)

undergoing a series of molecular rearrangements that lead to its activation (as R^*). The crystal structure of the ground state of rhodopsin was determined by Palczewski et al. (2000); what is now awaited is a determination of the crystal structure of R^* so that we can better understand the molecular nature of photoactivation. Although the precise structure of R^* is not yet known, many studies have contributed clues to the kinds of changes that must occur.

Historically, the molecular rearrangements underlying photoactivation have been studied spectrophotometrically because each intermediate has a different absorption spectrum, or color. Several transitions occur extremely rapidly, leading within $\sim 100\mu\text{s}$ to the formation of an intermediate named metarhodopsin I (or M_I). The next transition, to the form named metarhodopsin II (or M_{II}), is crucial to the photoresponse, as M_{II} is the form of the protein that is enzymatically active. The transition from M_I to M_{II} takes 1 to 10 ms (depending on temperature) and is thought to involve a substantial structural rearrangement of the protein (recently reviewed by Okada et al., 2001), thereby exposing the site for R^* interaction with the G protein. The conversion to M_{II} involves both a proton translocation and a proton uptake. The H^+ that had, until this stage, been protonating the Schiff base (linking the retinoid to Lys296) jumps across to the Glu113 residue that had been forming the negatively charged counterion that stabilized this configuration; in addition, another proton binds to Glu134 (Arnis and Hofmann, 1993).

CATALYTIC ACTIVATION OF THE G PROTEIN TRANSDUCIN As indicated in Figure 16.2, the molecular basis for activation of transducin is fundamentally the same as for any other G-protein cascade. Upon binding of the quiescent G protein to R^* , the $G\alpha$ subunit releases its bound molecule of guanosine diphosphate (GDP) and takes up a molecule of guanosine triphosphate (GTP) from the cytoplasm. The GTP-bound form of $G\alpha$ represents the active entity, denoted as G^* , which carries forward the activation signal. The activated rhodopsin, R^* , separates from the activated transducin and, unaltered by the interaction, is free to interact with additional molecules of the G protein, thereby catalyzing the activation of many G^* during its active lifetime. We denote the “gain” of this step by the parameter v_G , representing the rate of G^* activation by a single R^* .

Over the last few decades, estimates of the magnitude of v_G have varied widely. At room temperature, a number of biochemical experiments have reported values of $100 G^*s^{-1}$ or lower, whereas light-scattering approaches have yielded values exceeding $1000 G^*s^{-1}$ (e.g., Vuong et al., 1984), and theoretical analysis has suggested that the encounter rate between R^* and G is around $v_{enc} \approx 5000 s^{-1}$ (Lamb and Pugh, 1992). It is only recently that the different approaches have been reconciled, and it now seems clear that a rate of $v_G \approx 150 G^*s^{-1}$ at room temperature is consistent with biochemical, light-scattering, and electrophysiological measure-

ments (Leskov et al., 2000). We shall return to these rates after we have developed the theoretical framework in the section entitled “Predicted Form of the Onset Phase of the Light Response.”

R^* can only activate the G protein when the two molecules come into physical contact. This occurs via lateral diffusion of the molecules (within the membrane for the integral protein rhodopsin, and at the membrane’s cytoplasmic surface for transducin). On this basis, rapid lateral diffusion at the membrane has long been thought to be crucially important to activation. By studying rhodopsin hemizygote mice, Calvert et al. (2001) have provided evidence that the overall amplification of transduction, and hence the rate of G^* activation, depends strongly on membrane fluidity. Their results are consistent with the idea that numerous encounters between R^* and G are required (on average) before the two molecules are in the precise configuration required for binding. Hence, the activation rate (v_G) is indeed proportional to, although far lower than, the rate (v_{enc}) of molecular encounters. Thus, lateral diffusion is crucial to activation. Furthermore, as we discuss later, the results of Calvert et al. (2001) show that lateral diffusion is important not only to activation, but also to inactivation.

COUPLING OF G^* TO THE PDE Although the activated $G\alpha$ -GTP ($= G^*$) is weakly water-soluble, it probably only dissociates from the disc membrane on a relatively slow time scale, or at very high intensities. The usual means by which it encounters molecules of the effector protein PDE is again via lateral diffusion at the surface of the disc membrane.

The PDE is dimeric in structure, comprising a pair of closely homologous hydrolytic subunits (denoted α and β ; see Fig. 16.2). Each of the catalytic subunits binds a small γ subunit which, under resting conditions, inhibits the PDE, preventing hydrolysis of cGMP. When G^* encounters PDE γ , the two bind, thereby relieving the γ subunit’s inhibitory effect and permitting the hydrolysis of cGMP to proceed. Although there have been claims that G^* -PDE γ dissociates from the remainder of the PDE molecule, it is now generally thought more likely that the γ subunits remain closely associated with the $\alpha\beta$ hydrolytic units, ensuring that inhibition can rapidly be restored once G^* is inactivated. One detail that has not yet been clarified is whether or not there is cooperativity in the activation of PDE by G^* , that is, whether the singly activated form G^* -PDE (which we denote PDE*) has exactly half the activity of the doubly activated form G^* -PDE- G^* (denoted as PDE**), or whether the singly activated form might, for example, have much lower activity. However, this detail may be relatively unimportant, as the high density of G^* s in the neighborhood of an R^* is likely to favor the formation of the doubly activated form, PDE**.

How efficient is the coupling of G^* to PDE? Or, in other words, at some arbitrary time during activation, what pro-

portion of the G*s that have been produced will have been able to bind to PDEs? Put another way, what is the ratio of PDE* activation rate to G* activation rate ($c_{GE} = v_G/v_E$; see Fig. 16.3)? Stochastic simulations have shown that, even if G* were activated at the very high rate of several thousand per second set by encounters with R*, then a PDE subunit density of $250\mu\text{m}^{-2}$ (i.e., just 1 PDE subunit per 100 Rh) would be sufficient to achieve a coupling efficiency of 67% ($c_{GE} \approx 0.67$). At the much lower rate (v_G) that is now known to apply to G* activation, the coupling efficiency c_{GE} should be very close to unity. This is just what has been reported by Leskov et al. (2000), who found the mean rates of activation of G* and PDE* (v_G and v_E) both to be around 150s^{-1} in frog rods at room temperature.

Hence it appears that the coupling from activated transducin to activation of the PDE has an efficiency approaching unity (in terms of PDE* subunit activation, equivalent to 0.5 in terms of PDE** holomer activation). For our subsequent calculation of the overall gain of phototransduction, we will need a value for the rate of PDE* activation per R*; as noted earlier, this appears to be around $v_E \approx 150\text{ PDE}^*\text{s}^{-1}$ in amphibian rods.

HYDROLYSIS OF cGMP BY THE PDE The activated PDE** is a highly effective enzyme, and recent measurements indicate that it hydrolyzes cGMP at a rate close to the limit set by aqueous diffusion (Leskov et al., 2000). Its maximal catalytic rate has, for some years, been known to be around $k_{\text{cat}} \approx 4000\text{ cGMPs}^{-1}$, but what has only recently become clear is that its Michaelis constant is far lower than previously thought, at $K_m \approx 10\mu\text{M cGMP}$ (Leskov et al., 2000). Because the cytoplasmic concentration of cGMP is always lower than this value, the rate constant of cGMP hydrolysis is directly proportional to the ratio k_{cat}/K_m , a value that is far higher than previously realized.

This reaction, the hydrolysis by activated PDE of cGMP in the cytoplasm, represents the second amplifying step in phototransduction. In the theoretical analysis presented in the section on “Predicted Form of the Onset Phase of the Light Response,” the gain of the PDE step will be shown to be directly proportional to the parameter k_{cat}/K_m . As the gain achieved by rapid cGMP hydrolysis is cascaded with the first amplifying step—the R*-catalyzed formation of G* (and hence of PDE*)—the overall amplification during the activation phase of phototransduction can be extremely high.

CHANNEL OPENING/CLOSING BY cGMP In darkness, there is a resting concentration of cGMP of several micromolar, and this has the action of directly gating open cyclic nucleotide-gated ion channels in the plasma membrane. For reviews of the channel structure and gating, see Flynn et al. (2001). The decline in cGMP concentration leads to closure of the channels, and this has been shown to occur with a sub-millisecond delay (Karpen et al., 1988) as a combined

result of very rapid radial diffusion in the aqueous medium and extremely fast gating of channels by cGMP. The concentration dependence of channel opening is cooperative, with a Hill coefficient of $n_{\text{chan}} \approx 3$ and a dissociation constant around $K_{\text{chan}} \approx 20\mu\text{M cGMP}$ (although this value depends on calcium concentration; see the section entitled “Calcium Regulation of cGMP-gated Ion Channels: Calmodulin”). At the low cytoplasmic concentrations of cGMP that pertain both in darkness and in the light, the number of open channels can accurately be described as proportional to the cGMP concentration raised to the power n_{chan} , that is, as the cube of the cGMP concentration. This parameter n_{chan} can also be viewed as a gain factor (see the section that follows).

PREDICTED FORM OF THE ONSET PHASE OF THE LIGHT RESPONSE From analysis of the molecular scheme set out in Figure 16.2, and with knowledge of much of the information just presented, a mathematical formulation for the onset phase of the light response was developed by Lamb and Pugh (1992). In order to keep the analysis tractable, all inactivation reactions were ignored, restricting the window of validity to relatively short times after illumination. Several other simplifying assumptions were also made, but were shown not to compromise the validity of the solution under most circumstances. The predictions of the simplified analysis are presented graphically in Figure 16.3.

In response to a single photoisomerization, a single R* is created (after a short delay corresponding mainly to the M_I to M_{II} transition); because inactivation reactions are being ignored, it simply remains present (Fig. 16.3A). The presence of R* catalyzes the activation of G* at a constant rate, so that the quantity $G^*(t)$ ramps as a function of time, t , with a slope of $v_G \approx 150\text{ G}^*\text{s}^{-1}$. Because of the very efficient coupling to PDE, the quantity of activated PDE* subunits, $E^*(t)$, also ramps with time, with a similar slope of $v_E \approx 150\text{ E}^*\text{s}^{-1}$ (Fig. 16.3B).

Figure 16.3C illustrates the predicted time course for the decline of cGMP concentration, $c\text{GMP}(t)$, and for the decline of the fractional inward current, $F(t)$. As the rod photocurrent is relatively insensitive to changes in membrane voltage (Baylor and Nunn, 1986), $F(t)$ also represents the fractional circulating electrical current. Both $c\text{GMP}(t)$ and $F(t)$ decline with an accelerating time course owing to the continually increasing quantity of PDE*. If $E^*(t)$ indeed ramps with time, then it can be shown (Lamb and Pugh, 1992; Pugh and Lamb, 1993) that the electrical response should, to a good approximation, follow a delayed Gaussian time course:

$$F(t) = \exp \left\{ -\frac{1}{2} \Phi A (t - t_{\text{eff}})^2 \right\} \quad (1)$$

where Φ is the number of photoisomerizations (the flash intensity), A is a fixed parameter termed the amplification constant of transduction, and t_{eff} is an effective delay time

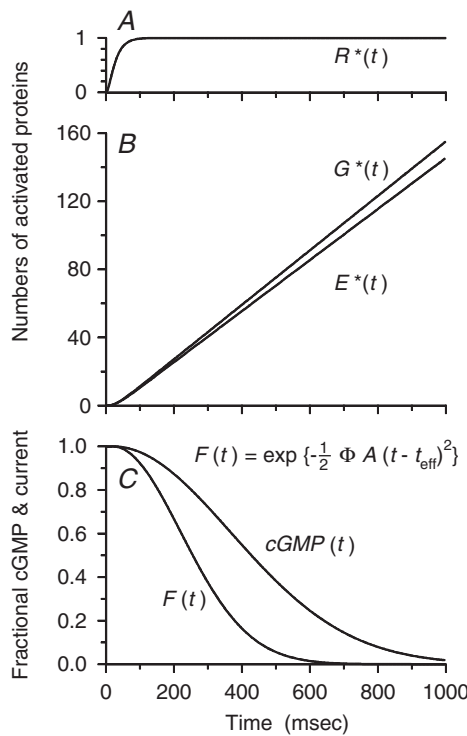


FIGURE 16.3. Predicted time course of activation when inactivation reactions are ignored. *A*, Following photoisomerization, a single R^* is activated. *B*, The quantities $G^*(t)$ and $E^*(t)$ of activated G protein and PDE increase linearly with time after R^* activation; in both cases, the slope is estimated to be around 150 s^{-1} per R^* (see section entitled “Estimated Rate of Activation of the PDE”). *C*, Activation of E^* causes the cGMP concentration to decline. Consequently, cGMP-gated channels close, and the fractional circulating current $F(t)$ declines according to equation 1 (in text). Responses in *C* are shown for a flash delivering $\Phi = 250$ photoisomerizations, with $A = 0.1\text{ s}^{-2}$.

that lumps together a number of very short delays in transduction.

Equation 1 is important because it provides what is essentially a single-parameter description of the onset phase of the light response; thus, apart from the short delay term (t_{eff}), there is only one parameter involved in describing the onset of the electrical response to any arbitrary flash intensity (Φ). All of the physical and biochemical parameters inherent in the scheme of Figure 16.2 have collapsed down into this single parameter, A . Furthermore, this overall amplification constant is specified by the theory as the product of the gains of the underlying stages:

$$A = v_E \beta_{\text{sub}} n_{\text{chan}} \quad (2)$$

where v_E is the rate of PDE* activation in response to a single photoisomerization, β_{sub} is a single PDE* subunit's rate constant for cGMP hydrolysis, and n_{chan} is the Hill coefficient of channel opening by cGMP. Finally, β_{sub} is given by

$$\beta_{\text{sub}} = \frac{\frac{1}{2} k_{\text{cat}} / K_m}{N_{\text{AV}} V_{\text{cyto}} B_{\text{cG}}} \quad (3)$$

where k_{cat}/K_m is the ratio of enzyme parameters for the PDE (described earlier), N_{AV} is Avagadro's number, V_{cyto} is the cytoplasmic volume of the outer segment, and B_{cG} is the cytoplasmic buffering power for cGMP. The factor of $1/2$ provides the conversion from a k_{cat} value for the holoenzyme PDE** to a β_{sub} value for a PDE* subunit.

In Figure 16.3C, the traces are drawn for a flash intensity of $\Phi = 250$ photoisomerizations, in conjunction with an amplification constant of $A = 0.1\text{ s}^{-2}$, typical of an amphibian rod. The theory predicts that, for any other flash intensity, the expected curve would have the same Gaussian shape as drawn, simply with a different time scaling. How does this prediction compare with experiment?

COMPARISON OF THEORY WITH EXPERIMENT In Figure 16.4, we compare the predictions of equation 1 with suction pipette responses from an amphibian rod (*A*) (data from Torre et al., 1986) and from a human rod (*B*) (data from Kraft et al., 1993). In each panel, a single value for the amplification constant A has been chosen, and curves are calculated for the set of measured flash intensities. Clearly, the onset phase of the response is reasonably well described over a wide range of flash intensities. The values of A were 0.065 s^{-2} for the salamander rod and 2 s^{-2} for the human rod. The smaller value of A for the amphibian rod arises primarily because of the much greater cytoplasmic volume of its outer segment (V_{cyto}), which, in the theory, appears in the denominator of equation 3.

For the salamander rod (Fig. 16.4A), the theory traces provide a good fit that extends to later times than one might reasonably expect for a model that ignores inactivation. The reason for the extended period of “good fit” in this cell is that it had been loaded with the calcium buffer BAPTA for the express purpose of slowing down the onset of inactivation reactions. In the same cell, prior to BAPTA incorporation, the experimental traces began deviating from theory by about 300 ms after the flashes (see Fig. 7 of Lamb and Pugh, 1992). As far as we are aware, equation 1 has always been capable of providing a good description of the onset phase of rod responses at suitably early times.

ESTIMATED RATE OF ACTIVATION OF THE PDE In an earlier section, entitled “Catalytic Activation of the G Protein Transducin,” we referred to disparities between different methods for estimating the rates v_G and v_E at which G^* and PDE* are activated in response to a single R^* . Recently, these discrepancies appear to have been reconciled by Leskov et al. (2000). Their biochemical measurements of v_G and v_E were broadly consistent with earlier measurements using comparable methods; both were found to be around 150 s^{-1} . However, in addition, they made new measurements of the PDE hydrolytic parameters and found the value of the Michaelis constant K_m to be far lower than previously

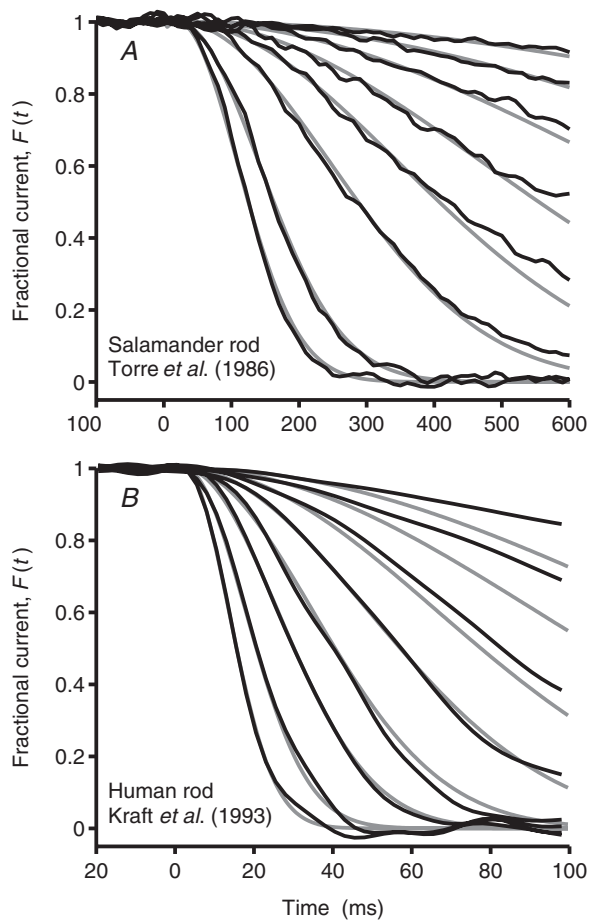


FIGURE 16.4. Comparison of experiment with predicted onset, for families of flash responses from a salamander rod (*A*) and a human rod (*B*), recorded using the suction pipette method. In both panels, the black traces show experiments, whereas the gray traces plot equation 1 (in text) using the calculated number of photoisomerizations, Φ , and a fixed value of the amplification constant A and effective delay time t_{eff} . *A*, Recordings from a salamander rod, following incorporation of the calcium buffer BAPTA, for flashes delivering from 9 to 2000 isomerizations. (Data from Fig. 2*B* of Torre et al., 1986.) Dark current, -29 pA ; amplification constant, $A = 0.065\text{ s}^{-2}$; delay time, $t_{\text{eff}} = 20\text{ ms}$. *B*, Recordings from a human rod for flashes delivering from 34 to 3800 isomerizations. (Data from Fig. 4 of Kraft et al., 1993.) Dark current, -13.5 pA ; amplification constant, $A = 2\text{ s}^{-2}$; delay time, $t_{\text{eff}} = 2.2\text{ ms}$. In both panels, the origin of time has been set to the middle of the flash stimulus, after allowance for the delay introduced by electronic filtering.

reported. Substitution of this value into equations 2 and 3 yielded estimates for v_E from electrophysiological measurements that were consistent with the biochemical values. Thus, with $k_{\text{cat}} = 4400\text{ s}^{-1}$, $K_m = 10\text{ }\mu\text{M}$, and $V_{\text{cyto}} = 0.85\text{ pl}$ for a toad rod outer segment, and assuming $B_{\text{CG}} = 1$ (no cGMP buffering), the parameter β_{sub} in equation 3 was calculated to be $\beta_{\text{sub}} = 4.3 \times 10^{-4}\text{ s}^{-1}$. Then, substituting an amplification constant of $A \approx 0.1\text{ s}^{-2}$ for a toad rod, and a Hill coefficient of $n_{\text{chan}} = 2$ in equation 2, the rate of PDE* subunit

activation was found to be $v_E \approx 120\text{ E}^*\text{ s}^{-1}$, which is in reasonable agreement with the biochemical estimate.

Finally, Leskov et al. (2000) suggested that the estimates from light scattering could also be brought into line if it were assumed that the signal measured by Vuong et al. (1984) originated from the binding of G^* to PDE, rather than from the release of G^* . Such a proposal for the origin of the light-scattering signal had, in fact, already been made by Kamps et al. (1985). If their explanation is correct, then the estimates of protein activation rates from biochemistry, light scattering, and electrophysiology all fall neatly into line with each other.

Inactivation of the phototransduction cascade

Rapid time resolution in the visual system is crucial for survival. However, the overall visual system cannot respond appreciably faster than its photoreceptors, and it is therefore important that the photoreceptor response be as brief as possible, consistent with the achievement of a sufficiently high amplification. Speed of response is most important at increased light intensities at which amplification can be sacrificed. At the very lowest intensities, when the visual system operates in a photon-counting mode and photon hits are few and far between, the speed of response is less critical.

What, then, determines how long the photoreceptor's response to a brief flash of light lingers? Is it determined passively, by the inherent rates of thermal degradation of activated cascade components? Recent results have shown the answer to this question to be a resounding no, with shut-off being an active process in both rods and cones. In this section, we will focus on what is currently known about rhodopsin inactivation in rods, mentioning relevant cone data when it is available.

MOLECULAR MECHANISMS OF RHODOPSIN INACTIVATION

Inactivation of the photopigment molecule is arguably the most important aspect of recovery owing to the high amplification achieved by R^* (see previous section). As long as rhodopsin maintains some level of catalytic activity, an amplified response persists, resembling the presence of steady light and contributing to desensitization and/or saturation of the cell.

At exceedingly low scotopic intensities, at which the visual system operates in its photon-counting mode, it can be argued that reproducibility of both the amplitude and the time course of the single-photon response is important, in order that the system should be better able to count the photons. However, this argument does not apply at higher scotopic intensities, or in the photopic range, where the shape of responses to individual photon hits is irrelevant; at these intensities, all that matters is the shape of the average response. The mechanisms that limit the duration of

rhodopsin's active lifetime, that contribute to its reproducibility under dark-adapted conditions, and that shorten the lifetime even further under light adaptation, are the subject of intense study.

Fast and slow mechanisms contribute to the shut-off of activated rhodopsin. First, R^* is phosphorylated; second, it is capped by the protein arrestin (e.g., Kühn and Wilden, 1987). These two steps rapidly lead to an enormous reduction in rhodopsin's catalytic activity, as described in the next subsections. Subsequent to these fast inactivation steps, the photoisomerized all-*trans* retinal is hydrolyzed from the opsin protein and, in due course, is replaced by 11-*cis* retinal, leading eventually to the total shut-off of catalytic activity. These slower steps, which contribute to dark adaptation and pigment regeneration, are beyond the scope of this review.

PHOSPHORYLATION AS A RAPID FIRST STEP IN SHUT-OFF The first step in shut-off—phosphorylation of rhodopsin's COOH-terminal residues—is performed by rhodopsin kinase (RK) (Kühn and Wilden, 1987), although other protein kinases, such as protein kinase C (e.g., Udovichenko et al., 1997), may play a role under some conditions. Phosphorylation of rhodopsin reduces its catalytic activity substantially (e.g., Wilden et al., 1986) and is essential for recovery of the photoresponse (Nakatani and Yau, 1988b; Sagoo and Lagnado, 1997; see also the section on “Comparison of Effects of Mutations of Inactivation Proteins”).

There are multiple potential sites for phosphorylation by RK in rhodopsin's COOH-terminal domain, six such sites in mice and seven in humans. However, mass spectroscopy of COOH-terminal peptides of rhodopsin following light exposure has suggested that rhodopsin is predominantly monophosphorylated after a flash (Ohguro et al., 1995), raising the interesting possibility that the large number of sites merely serve to increase the rate at which phosphorylation occurs. However, experiments on individual transgenic mouse rods have suggested that multiple phosphorylation is essential for rapid recovery of the single-photon response (Mendez et al., 2000; see also the section on “Comparison of Effects of Mutations of Inactivation Proteins”). Furthermore, mutant mouse rhodopsins containing fewer than three of the six potential phosphorylation sites were found to display first-order inactivation kinetics, suggesting that, under these conditions, a single, stochastic process is responsible for turning off unphosphorylated rhodopsin, and that it is rate-limiting for recovery. Similar behavior is also observed when phosphorylation of R^* is completely prevented (see section cited above). Stochastic shut-off of this kind is quite abnormal, as rhodopsin inactivation in WT rods is fairly reproducible (see the section entitled “Rhodopsin Shut-off: Reproducibility of the Single-

Photon Response”). This suggests that reproducible rhodopsin inactivation requires multiple phosphorylation of R^* (Mendez et al., 2000, Figs. 5 and 6).

ARRESTIN BINDING IS REQUIRED FOR COMPLETION OF THE RAPID PHASE OF R^* INACTIVATION Following phosphorylation, the protein arrestin binds with high affinity to phosphorhodopsin (Wilden et al., 1986). In mouse rods that do not express arrestin (*Arr*^{-/-}; Xu et al., 1997), the dim flash response rises to a peak amplitude comparable to that of normal rods, and begins to recover roughly halfway back to baseline levels (see Figs. 16.5 and 16.6). However, it then enters a period of extremely slow recovery, declining with a final time constant that is on the order of 40 seconds. The time course of the final decline of the response in the *Arr*^{-/-} rods is comparable to that for the disappearance of metarhodopsin II (Cone and Cobbs, 1969).

The failure of normal recovery in *Arr*^{-/-} rods suggests that the binding of arrestin is essential for the rapid quench of rhodopsin's activity, and that in the absence of arrestin, phosphorylated R^* must await hydrolysis of the retinoid. The fact that the failure of normal recovery occurs fairly late in the response suggests that significant rhodopsin activity normally persists throughout the duration of the single-photon response. Slowing the rate of guanosine triphosphate (GTP) hydrolysis by transducin (see the section entitled “Inactivation of the G Protein and the Effector (Transducin and PDE)”) also selectively slows the final recovery of the dim flash response (Sagoo and Lagnado, 1997; Chen et al., 2000). This raises the interesting and yet unanswered question of whether deactivation of rhodopsin or of transducin/PDE is rate-limiting for the recovery of the single-photon response.

Inactivation of cone pigments is also likely to involve phosphorylation and arrestin binding. Because recovery of the photoresponse occurs roughly 10 times faster in cones than in rods, one might expect these biochemical shut-off steps likewise to occur more quickly in cones. Consistent with this possibility was the discovery of a cone-specific isoform of opsin kinase (GRK7), which was first cloned from ground squirrel (Weiss et al., 1998), and has since been identified in other mammals as well. Whether or not this cone-specific isoform is specialized for more rapid inactivation of R^* is unclear, though, partially because of the apparent differences in expression of RK and cone opsin kinases in different species. For example, cones of dogs and pigs exclusively express cone opsin kinase (Weiss et al., 2001), whereas mouse and rat cones express only RK (Lyubarsky et al., 2000; Weiss et al., 2001), and primate cones appear to express both (Chen et al., 2001; Weiss et al., 2001).

A second cone-specific isoform of the regulatory machinery for transduction is cone arrestin (Craft et al., 1994). It

exhibits no detectable binding to light-activated or phosphorylated rod rhodopsin (Maeda et al., 2000), suggesting that it has fundamentally different biochemical properties from rod arrestin. Its role in recovery of the cone photoreceptor has yet to be determined.

RHODOPSIN SHUT-OFF: REPRODUCIBILITY OF THE SINGLE-PHOTON RESPONSE One electrophysiological approach that has been used to estimate the number of stages involved in R^* shut-off is an examination of the degree of reproducibility, or variability, in the shape of a rod's response to different single-photon hits. Rieke and Baylor (1998) and Whitlock and Lamb (1999) conducted experiments of this kind on toad rods and, despite recording apparently similar events, came to quite different conclusions. Rieke and Baylor reported that the single-photon events were highly reproducible in shape, concluding that 10 to 20 stages in R^* 's shut-off needed to be invoked in order to explain such a high degree of reproducibility.

In the same species, Whitlock and Lamb reported that the apparent variability in shut-off timing was twice as large as that found by Rieke and Baylor. They concluded that six or seven stages in R^* shut-off could explain the observed degree of kinetic variability. They went on to speculate that, if a powerful mechanism of calcium feedback were to modulate the R^* lifetime within the single-photon response, then the variability might even be explained by a single stage of shut-off. However, that possibility has now been excluded by the GCAPs (guanylate cyclase-activating proteins)-/- experiments of Burns et al. (2002), which have ruled out calcium feedback onto R^* lifetime within the single-photon response. Accordingly, the electrophysiology of single-photon response is consistent with an apparent number of stages involved in R^* shut-off of around six. Although this number corresponds neatly with the number of sites available for phosphorylation, the agreement may be no more than fortuitous.

INACTIVATION OF THE G PROTEIN AND THE EFFECTOR (TRANSDUCIN AND PDE) Despite the importance of R^* inactivation, that alone is not sufficient for rapid recovery of the electrical response to a flash. It is also important that G^* and PDE^* (the activated transducin and cGMP PDE) be turned off rapidly. As in most heterotrimeric G protein cascades, the rate-limiting step for turning off both the G protein and its effector is the hydrolysis of GTP, that is, the rate at which the GTP's terminal phosphate is cleaved by the $G\alpha$ subunit. For many years, it has been noted that the basal GTPase activity of purified transducin is exceedingly low, with a turnover time of minutes rather than seconds. Thus, it has long been anticipated that mechanisms for speeding the rate of GTP hydrolysis must exist in order to explain the rapid physiological shut-off.

In the last few years, an entirely new family of proteins, called RGS proteins (regulators of G protein signaling; reviewed in Ross and Wilkie, 2000), has been discovered. One member of this family, RGS9-1 (He et al., 1998), is expressed in rods and even more abundantly in cones (Cowan et al., 1998). In photoreceptors, RGS9-1 is obligatorily associated with an orphan G protein β subunit, $G\beta 5L$ (Makino et al., 1999). The resulting RGS9/ $G\beta 5L$ complex is essential for achieving normal rapid shut-off of the light response, both in rods (Chen et al., 2000; see Fig. 16.5) and in cones (Lyubarsky et al., 2001).

Under physiological conditions, it appears that RGS9/ $G\beta 5L$ only affects GTPase activity when G^* is bound to the PDE γ subunit, that is, while the PDE is in its active form, PDE^* (see the earlier section on "Coupling of G^* to the PDE"). It has been known for some time that the acceleration of GTPase activity is aided by $PDE\gamma$ (Arshavsky and Bownds, 1992; Antonny et al., 1993), but the mechanism by which both $PDE\gamma$ and RGS9/ $G\beta 5L$ might work together has been unclear. Recently, it has been found that $PDE\gamma$ increases the affinity of RGS9/ $G\beta 5L$ for $G\alpha$ (Skiba et al., 2000), thereby speeding the rate of GTP hydrolysis and the rate of recovery of the flash response in vivo. Thus, the inactivation of G^*/PDE^* utilizes an elegant method of self-regulation, whereby transducin is prevented from turning off before it has bound to and activated PDE.

The crystal structure of the complex between $G\alpha$ -GTP, $PDE\gamma$, and RGS9 has recently been presented by Slep et al. (2001). Details of the molecular mechanisms involved in the regulation of transducin's GTPase activity are reviewed by Cowan et al. (2001) and Arshavsky et al. (2002).

COMPARISON OF EFFECTS OF MUTATIONS OF INACTIVATION PROTEINS Collaborations between researchers in molecular biology, biochemistry, and physiology are revealing the many levels of regulation that actively turn off the phototransduction machinery, thus speeding recovery of the response to an increment in illumination. Although a great deal has been learned about mechanisms of response shut-off from conventional approaches over several decades, there has been a recent explosion in the application of transgenic approaches to photoreceptors, some of which we will illustrate here. One striking observation to have emerged from gene manipulations in mouse photoreceptors is that rods and cones appear to lack sophisticated compensatory mechanisms to oppose alterations in gene expression of many of the molecules of transduction. Thus, there have been few problems associated with significant changes in expression levels of proteins other than the one under examination. Instead, the most serious and consistent difficulty in creating these transgenic and knockout mice has been the degeneration of photoreceptors, especially in cells with prolonged responses that make them sensitive to steady backgrounds

(Makino et al., 1998). In addition, overexpression or underexpression of rhodopsin can cause degeneration (Li et al., 1996; Lem et al., 1999). These issues can usually be resolved either by careful titration of transgene expression levels (e.g., Mendez et al., 2000) or by rearing the animals in darkness (e.g., Xu et al., 1997).

As examples of the mutations that have been studied in mouse photoreceptors, we present in Figures 16.5 and 16.6 a composite set of responses from cells of different transgenic and knockout mice. In addition to wild-type responses, we illustrate five mutants: three involving disruption of rhodopsin inactivation and two involving the slowing of subsequent stages of recovery. Both figures plot responses to repeated presentations of a very dim flash. In Figure 16.5, the raw responses are shown on a slow time scale, whereas in Figure 16.6, the averaged responses are compared on a faster time scale. In the following descriptions, many of the features we discuss can be seen in these two figures.

R* inactivation Genetic perturbations of rhodopsin inactivation have yielded a wide range of phenotypes that reveal much about the inherent time course of rhodopsin inactivation in intact cells. Phosphorylation of rhodopsin can be prevented by several transgenic techniques: by deleting the entire COOH-terminal domain of rhodopsin (S334ter; Chen et al., 1995), by abolishing the expression of RK (Chen et al., 1999), or by mutating all of the carboxy-terminal serine and threonine residues to alanines (CSM [completely substituted mutant]; Mendez et al., 2000). Under each of these conditions, rhodopsin's activity, measured electrophysiologically, persists for several seconds, with the single-photon response reaching a plateau level of around double the normal amplitude, and then decaying abruptly back to baseline after a long stochastic interval of around 3 to 5 seconds (see Fig. 16.5). Because this interval is considerably shorter than the time course of hydrolysis of

all-*trans* retinal, it can be surmised that mammalian rods possess a backup mechanism that is capable of turning off unphosphorylated R*. Ironically, these large and long-lasting responses are occasionally observed in normal mammalian rods (e.g., Baylor et al., 1984). This suggests that, in normal rods, as many as 1% of all rhodopsin molecules are not capable of being phosphorylated.

The similarity of responses from RK-/-, S334ter, and CSM rods suggests that the sole defect in each case is a lack of rhodopsin phosphorylation, and that the binding of RK has little effect on R*'s catalytic activity. Furthermore,

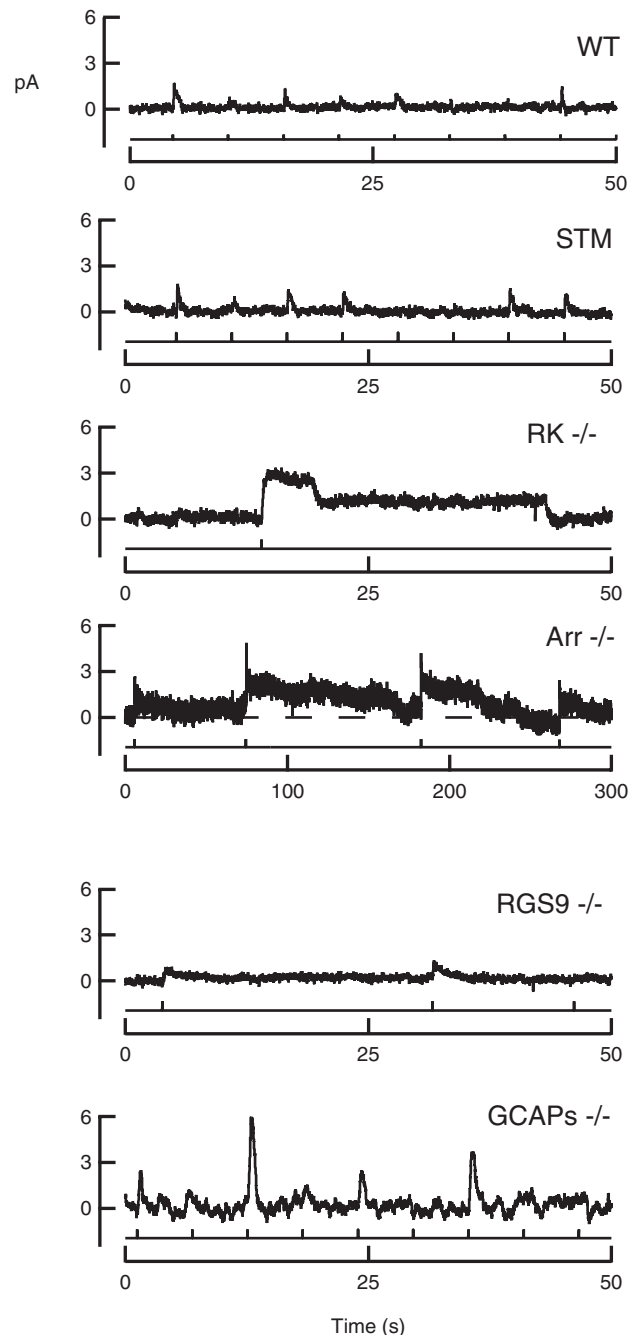


FIGURE 16.5. Dim flash responses recorded from mouse rods of different genotypes. Flashes were delivered at the times indicated by the flash monitor below each recording. Mouse rods expressing mutant rhodopsin with three of the six potential phosphorylation sites (Serine Triple Mutant, STM; Mendez et al., 2000) show responses that are qualitatively similar to wild-type (WT) responses, whereas responses from rods lacking RK (RK-/-; Chen et al., 1999) are prolonged steps of variable duration. Mouse rods lacking arrestin (Arr-/-; recording by AF Almuete in the Burns lab) initially recover, but require much longer times for final inactivation (Xu et al., 1997). Note the sixfold longer time base for the Arr-/- recording. Deficiencies in the rate of GTP hydrolysis (RGS9-/-; Chen et al., 1999) and calcium feedback to guanylate cyclase (GCAPs-/-; Burns et al., 2002) likewise yielded prolonged responses. Note the increased cellular dark noise and very large elementary response amplitude in the GCAPs-/- recording.

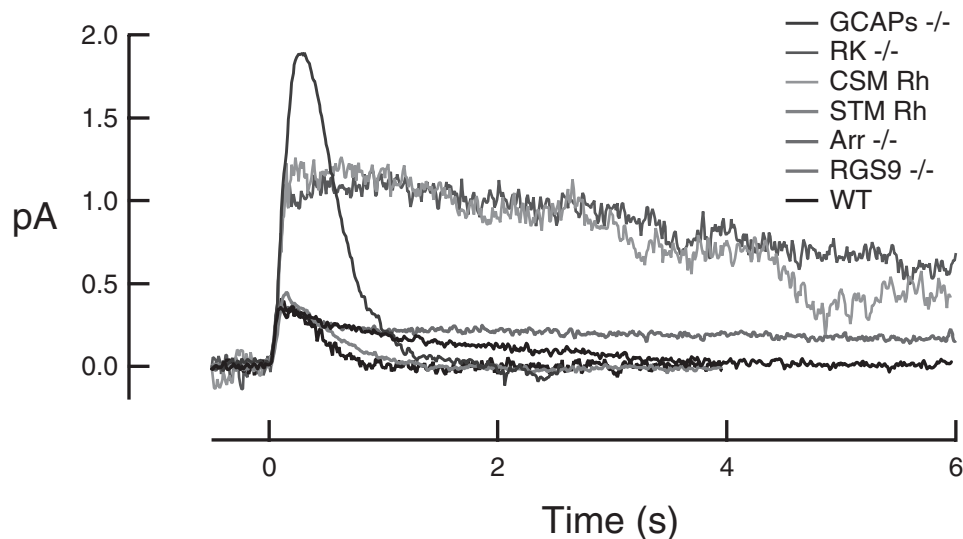


FIGURE 16.6. Form of the average single-photon response from transgenic and knockout mouse rods with perturbed inactivation. Abbreviations are the same as for Figure 16.5. Flashes occurred at $t = 0$.

in each of these examples, the mutant (or knockout) responses deviate from the control responses at roughly 100 msec after the flash, during the rising phase of the flash response. This suggests that, normally, phosphorylation begins to reduce rhodopsin's activity very soon after the R^* is formed.

Experiments on mouse rods that do not express arrestin ($Arr^{-/-}$) have likewise provided important clues regarding the *in vivo* time course of rhodopsin inactivation. First, $Arr^{-/-}$ responses do not differ greatly from wild-type responses until fairly late in the falling phase of the dim flash response (Xu et al., 1997; see also Fig. 16.6). The partial recovery (approximately halfway back to baseline) of the $Arr^{-/-}$ response suggests that phosphorylation alone is sufficient to reduce rhodopsin's catalytic activity by at least 75% (keeping in mind that R^* activity in the absence of all rapid inactivation, such as in the $RK^{-/-}$ rods, generates a response with a peak amplitude roughly twofold larger than normal). On this basis, one might view arrestin as contributing relatively little to inactivation. However, in the absence of arrestin, the final time constant of recovery is nearly 200-fold longer than normal, and roughly 10-fold longer on average than responses of rods that lack rhodopsin phosphorylation. Thus, although the magnitude of the effect of arrestin during the single-photon response is rather small, the implications for the overall function of the rod during prolonged light exposure are astounding.

Inactivation of G^*/PDE^* . Knockout and transgenic approaches have also proven useful for elucidating the mechanisms of G^*/PDE^* inactivation. Experiments on mouse rods expressing a mutant form of $PDE\gamma$ that binds poorly to G^* (W70A; Slepak et al., 1995) have shown that G^*/PDE

interactions are required for normal rates of GTP hydrolysis measured in *in vitro* assays, as well as for the normal amplification and recovery of the flash response (Tsang et al., 1998). An even greater effect on the rate of GTP hydrolysis has been observed in mouse rods expressing neither RGS9-1 nor $G\beta 5$ L ($RGS9^{-/-}$). Retinal homogenates of these mice have shown an impaired rate of GTP hydrolysis that could not be accelerated by the addition of exogenous $PDE\gamma$ (Chen et al., 2000), thereby confirming the notion that RGS9/ $G\beta 5$ L acts on the G^*/PDE^* complex.

CALCIUM-DEPENDENT FEEDBACK Finally, knockout mice have proven to be very effective at isolating the calcium-dependent negative feedback mechanisms. Although such mechanisms have been studied by more conventional physiological and biochemical approaches for decades, the abolition of one such mechanism (e.g., calcium regulation of guanylate cyclase by knocking out GCAPs) in intact cells allows the other calcium-dependent mechanisms to be studied unperturbed. The results and interpretations of these experiments will be described in the section that follows.

Calcium feedback regulation of phototransduction

It has been clear from many investigations conducted since the mid-1980s that the photoreceptor's response to light is accompanied by a decline in cytoplasmic calcium concentration (e.g., as reviewed by Koutalos and Yau, 1996). Here we begin by summarizing those findings.

In darkness, the flow of current into the photoreceptor outer segment is carried primarily by Na^+ ions, but a substantial proportion (~15% in rods) is carried by Ca^{2+} ions.

This steady influx of Ca^{2+} in darkness is balanced by an equal and opposite efflux, driven by the $\text{Na}^+/\text{Ca}^{2+}$, K^+ exchanger that resides in the plasma membrane along with the cyclic nucleotide gated channels. Different estimates have placed the dark resting concentration of free cytoplasmic Ca^{2+} in the range of 200 to 700 nM. During illumination, the outer segment ion channels close (see the section entitled “Channel Opening/Closing by cGMP”), reducing the influx of Ca^{2+} ions. As a result, the exchanger drives down the cytoplasmic Ca^{2+} concentration to a level that has been estimated to be in the range of 10 to 50 nM in saturating light. In amphibian rods, the decline is not especially fast, with an effective time constant of around 1 s. In cones, where the surface-to-volume ratio of the outer segment is much greater, the time course of decline is substantially faster.

It has been known for several decades that a lowered calcium concentration increases the rod's circulating dark current (Hagins and Yoshikami, 1974) and activates guanylate cyclase (Lolley and Racz, 1982), and that elevated calcium concentration enhances light-activated PDE activity (Torre et al., 1986). Furthermore, minimizing the light-induced decline in intracellular calcium by incorporation of calcium buffers or by “calcium clamp” protocols dramatically increases the flash sensitivity of dark-adapted photoreceptors and prevents the onset of normal light adaptation (Torre et al., 1986; Fain et al., 1989; Matthews et al., 1990). However, it has taken some years to unravel the relative importance of the individual molecular mechanisms that participate.

We now know that the decline in calcium concentration orchestrates at least three separate changes in the outer segment. These are often referred to as *negative feedback mechanisms* because any perturbation of the state of the system tends to be opposed. It is now clear that the most important of these feedback mechanisms is the calcium-dependent regulation of guanylate cyclase activity, mediated by GCAPs. In addition, there are also effects of calcium on the disc membrane cascade of reactions leading to PDE activation, probably mediated by the calcium-sensitive protein recoverin, and on the sensitivity of the plasma membrane ion channels to cGMP, mediated in rods by calmodulin. We will discuss each of these three processes in turn.

CALCIUM REGULATION OF GUANYLATE CYCLASE Evidence for calcium regulation of guanylate cyclase originated in the 1980s. Biochemical experiments showed that cyclase activity was regulated in a cooperative manner by a decline in calcium concentration (Pepe et al., 1986; Koch and Stryer, 1988), whereas electrophysiological experiments suggested that cyclase activity was elevated during recovery from saturating flashes (Hodgkin and Nunn, 1988). Today we know that the rapid restoration of circulating current after

a flash is, to a major extent, attributable to activation of guanylate cyclase by the lowered intracellular free calcium concentration.

Ca^{2+} regulation of guanylate cyclase activity is mediated by GCAPs, of which there are three retinal isoforms: GCAP1, GCAP2, and GCAP3. GCAPs belong to the calmodulin superfamily of EF-hand proteins, but contain only three functional Ca^{2+} binding sites (reviewed in Dizhoor and Hurley, 1999). Biochemical studies have shown that at low calcium concentrations, GCAPs activate guanylate cyclases, whereas at high calcium concentrations, the calcium-bound form of GCAPs inhibits guanylate cyclase activity (Dizhoor and Hurley, 1996; Rudnicka-Nawrot et al., 1998). The calcium concentration that has been reported to activate guanylate cyclases half-maximally ($K_{1/2}$) has varied widely depending on experimental conditions, with most reports clustering near ~200 nM (Dizhoor and Hurley, 1996). The activation by calcium is cooperative, and although an early in vitro experiment gave an estimate for the Hill coefficient of about 4 (Koch and Stryer, 1988), subsequent experiments have given values of about 2 (reviewed in Pugh et al., 1997).

Photoreceptors express not only multiple GCAPs, but also multiple isoforms of guanylate cyclase (GC1 and GC2; reviewed in Pugh et al., 1997). The reason for having multiple guanylate cyclases and GCAPs is not known, but presumably they serve distinct functions. GCAP1 activates primarily GC1, whereas GCAP2 and GCAP3 activate both GC1 and GC2 with similar potencies (Haeseleer et al., 1999). It has generally been thought that the calcium dependence of cyclase activation by the GCAPs is similar. However, expression of a GCAP2 transgene in mouse rods lacking endogenous GCAPs (only GCAP1 and GCAP2 occur in mouse rods) has been found to restore maximal calcium-dependent cyclase activity but not to restore normal flash response kinetics (Mendez et al., 2001). In contrast, expression of a GCAP1 transgene in GCAPs $^{-/-}$ rods did restore normal kinetics (Howes et al., 2002). This suggests that GCAP1 and GCAP2 may serve different temporal roles in rods.

Comparison of the steady-state responses of GCAPs $^{-/-}$ rods and wild-type rods suggests that, in a wild-type rod, a given relative change in the cGMP concentration produces an 11-fold larger relative change in the guanylate cyclase activity (Burns et al., 2002). Assuming that the Hill coefficient for channel activation is about 3, this suggests that the Hill coefficient for guanylate cyclase activation by calcium is about 4 in normal rods. However, most biochemical measurements of calcium dependence of guanylate cyclase activity have given a Hill coefficient of about 2 (reviewed in Dizhoor and Hurley, 1999). A satisfactory explanation for this large discrepancy remains to be elucidated.

The power with which calcium regulates guanylate cyclase activity perhaps helps to achieve the surprising speed with which feedback can occur. Experiments on intact GCAPs $^{-/-}$ rods have shown that feedback to guanylate cyclases normally begins very quickly, within roughly 40 ms of the flash (Burns et al., 2002). The rapid feedback to guanylate cyclases causes the rising phase, as well as the amplitude, of the response to be severely attenuated, such that calcium feedback to guanylate cyclases decreases the dark-adapted flash sensitivity (Mendez et al., 2001). In addition, feedback speeds the restoration of the dark current, causing a more rapid recovery of the dim flash response.

Calcium feedback to guanylate cyclase not only reduces the amplitude of the signal (single-photon response) of rods, but also of the noise. In darkness, rods are noisy; spontaneous fluctuations in dark current arise primarily from spontaneous fluctuations in cGMP concentration stemming from thermal activation of rhodopsin and PDE (Baylor et al., 1980; Rieke and Baylor, 1996). Calcium feedback via GCAPs reduces these spontaneous fluctuations, reducing the standard deviation of the dark noise by roughly a factor of 6.3, while at the same time reducing the amplitude of the response by a factor of 4.5. Thus, calcium feedback in the dark-adapted rod serves at least two distinct purposes: (1) it speeds the recovery of the flash response, improving temporal responsiveness at the cost of sensitivity; and (2) it improves the signal-to-noise ratio of the cell by roughly 40%.

Perhaps not surprisingly, GCAPs $^{-/-}$ rods do not adapt normally to steady lights (Mendez et al., 2001). The incremental flash sensitivity is markedly reduced at the brightest backgrounds, reflecting the importance of the steady-state feedback regulation of guanylate cyclase for range extension (see the section entitled "Calcium-dependent Mechanisms of Adaptation"). Thus, both the dynamic and steady-state changes in intracellular calcium have profound effects on guanylate cyclase activity and significant implications for rod function.

CALCIUM REGULATION OF THE DISC MEMBRANE CASCADE OF REACTIONS

Electrophysiology. Electrophysiological evidence for the calcium dependence of the disc membrane reactions that lead to activation of PDE came from experiments in which cGMP was infused into rods. The duration of the bright flash response was shown to be greatly extended under conditions in which Ca^{2+} was expected to have been elevated, even though guanylate cyclase activity had been overridden by the supply of exogenous cGMP (Torre et al., 1986). Prolongation of the flash response has also been seen in experiments in which recombinant recoverin was dialyzed into rods (Gray-Keller et al., 1993; Erickson et al., 1998).

Experiments lowering the Ca^{2+} concentration around the time of flash delivery (Hodgkin et al., 1986; Matthews, 1997) have revealed a shortened response duration and have suggested that the extent of light-dependent PDE activation is determined by the intracellular calcium concentration only near the time that the flash is delivered, presumably while R^* remains in existence. Finally, experiments on truncated salamander rods have suggested that lowered intracellular calcium can speed the quenching of rhodopsin's activity by phosphorylation, as the rate of rise of the flash response is sensitive to both calcium and ATP, but not GTP γ S (Sagoo and Lagnado, 1997).

Biochemical experiments. Biochemical evidence supporting the calcium-dependent regulation of light-dependent PDE activity was first derived from experiments on frog rods (Kawamura, 1992). These experiments demonstrated that rhodopsin phosphorylation was dependent on free calcium concentration and was mediated by the calcium-binding protein recoverin (S-modulin; Kawamura, 1993). The molecular target of recoverin was identified by cross-linking as RK (Sato and Kawamura, 1997). These observations have been extended by several research groups, leading to the hypothesis that recoverin calcium binds to RK in the dark, thereby inhibiting rhodopsin phosphorylation. During light exposure, when the calcium concentration decreases, recoverin unbinds its calcium and its affinity for RK is reduced, so that it no longer inhibits rhodopsin phosphorylation. One as yet unresolved caveat to this hypothesis is that some in vitro measurements have claimed that the extent of rhodopsin phosphorylation is unaffected by light adaptation and changes in intracellular calcium (Ohguro et al., 1995; Otto-Bruc et al., 1998).

CALCIUM REGULATION OF cGMP-GATED ION CHANNELS: CALMODULIN Light-evoked changes in intracellular calcium concentration cause a shift in the $K_{1/2}$ for activation of the cGMP-gated channels by cGMP (Hsu and Molday, 1993). In rod channels, this shift is thought to be mediated by the binding of calmodulin (Weitz et al., 1998) or a calmodulin-like protein (Gordon et al., 1995) to the β subunit of the rod channel (Chen et al., 1994) at high calcium concentrations. The decline in calcium that accompanies the steady-state response to light causes the modulator to dissociate from the channel, increasing the affinity of the channel for cGMP. The contribution of this mechanism to range extension in rods is thought to be rather modest (2- to 10-fold; Koutalos et al., 1995b; Sagoo and Lagnado, 1996; Nikonov et al., 2000;). A similar but more powerful mechanism also appears to operate for cone channels (Rebrik and Korenbrot, 1998; Rebrik et al., 2000; Muller et al., 2001).

In the next section, we will try to evaluate the relative roles of the molecular mechanisms that we have described above in the context of adaptation.

Mechanisms of photoreceptor light adaptation

Photoreceptors have the daunting task of reporting the time course of illumination across an intensity range of at least 10 orders of magnitude. The rod (scotopic) system operates primarily over the dimmest four orders of magnitude, whereas the cone (photopic) system covers the brightest seven, with mesopic vision (both rods and cones functioning) covering a couple of orders of magnitude in the midrange. In human vision, the lowest useful intensity corresponds to $\sim 10^{-2}$ photoisomerizations s^{-1} , whereas the rods have saturated at an intensity of $\sim 10^3$ photoisomerizations s^{-1} , and yet the cones never saturate under steady illumination (see discussion that follows, and Burkhardt, 1994).

Light adaptation causes two characteristic changes in the incremental light response of photoreceptors: it reduces the cell's sensitivity (measured as the peak amplitude per unit of flash intensity) and it speeds the kinetics of response recovery. The cellular events known to contribute to light adaptation encompass at least five categories: (1) response compression; (2) calcium-dependent mechanisms that act on a relatively short time scale; (3) elevated steady-state activity of the PDE, which acts by reducing cGMP's turnover time; (4) recently discovered large-scale movements of protein out of the outer segment; and (5) pigment bleaching. In the following sections we briefly describe the contributions of these phenomena to the overall light adaptation of photoreceptors; for more extensive coverage we refer the reader to several recent reviews (Pugh et al., 1999; Govardovskii et al., 2000; Fain et al., 2001).

An important clue to possible molecular mechanisms of light adaptation comes from the observation that, over a wide range of background intensities, the gain of the transduction process is unaltered by light adaptation (Nikonov et al., 2000). Accordingly, over this range of intensities, any modulation of the cascade of reactions leading up to PDE activation must operate only via effects on the *lifetimes* of active substances, rather than on the *gain* of any activation step, a concept that will be discussed in more detail later in this chapter.

RESPONSE COMPRESSION During steady illumination, the steady level of photoreceptor circulating current decreases, leaving less current available for suppression by additional photon absorptions. Hence, if sensitivity is measured (as it usually is) in terms of absolute, rather than relative, changes in circulating current, then during illumination the sensitivity is bound to decrease because of this effect. Although this effect clearly contributes to measurements of light adapta-

tion, it is difficult to view the phenomenon as an adaptation to background light; rather, it represents an unavoidable consequence of the way that phototransduction operates. In this context, it is worth noting that, in cones, such a drawback is not apparent in measurements of intracellular voltage in the eyecup preparation, where the steady-state hyperpolarization does not exceed half the maximum available range, even at exceedingly high steady intensities (Normann and Perlman, 1979; Burkhardt, 1994). Thus, for the intact cone system, the compressive effect never exceeds a factor of 2, and the cone is able to undergo voltage excursions of roughly equal magnitude for intensity increments and decrements on a background.

CALCIUM-DEPENDENT MECHANISMS OF ADAPTATION Calcium was clearly established as a messenger of light adaptation by the experiments of Nakatani and Yau (1988a) and Matthews et al. (1988). These and subsequent experiments showed that, in the absence of the normal light-induced change in cytoplasmic calcium concentration, the photoreceptor did not display the normal characteristic features of light adaptation. Instead, the photoreceptor simply exhibited response saturation with a much more abrupt decline of sensitivity as a function of increasing background intensity (reviewed in Fain et al., 2001).

These results have sometimes been misinterpreted to indicate that the decline in calcium concentration actually *causes* the decline in flash sensitivity during light adaptation, but nothing could be further from the truth. Instead, the decline in calcium concentration must be viewed as *rescuing* the photoreceptor from the far greater desensitization that would occur in the absence of its intervention, so that it thereby provides an extension of the range of operating intensities (Pugh et al., 1999). In considering the role of calcium, a distinction needs to be made between dynamic and steady-state effects (Pugh et al., 1999; Torre et al., 1986). The rapid transient drop in calcium concentration has been proposed to underlie the rapid recovery of the flash response to its baseline level (Torre et al., 1986), whereas the steady-state change is thought to account for light-adaptation behavior (Koutalos and Yau, 1996).

The role of calcium-dependent modulation of the disc-based reactions in photoreceptor light adaptation is not fully understood, despite our knowledge of the molecular mechanisms listed in a previous section ("Calcium Regulation of the Disc Membrane Cascade of Reactions"). It is clear that the calcium concentration at the time of flash delivery has an effect on the duration of the flash response (see section just cited). In addition, the so-called step-flash effect (whereby the recovery of a bright test flash is accelerated by the prior application of a background) is abolished when changes in calcium concentration are prevented (Fain et al., 1989). Furthermore, this effect also exists in mammalian

rods and is eliminated in rods that do not express recoverin (Dodd, 1998). Hence, the electrophysiological results are consistent with the notion that recoverin-mediated steady-state effects of calcium modulate the disc-based reactions and contribute significantly to overall light-adaptation behavior. Moreover, because of the invariance of the amplification constant of transduction with background intensity (Nikonov et al., 2000; see also the section entitled "Gain Reduction: A Matter of Intensities"), the steady-state effect of calcium must be on the lifetime of intermediate(s), rather than on gain. Finally, a small part of the rescue of sensitivity comes from calcium regulation of the ion channels, through the reduction in $K_{1/2}$ for channel opening by cGMP.

CONTRIBUTION OF ELEVATED STEADY-STATE PDE ACTIVITY Continuous illumination directly causes a steady-state increase in PDE activity, thus increasing the rate constant of cGMP hydrolysis (Hodgkin and Nunn, 1988; Kawamura and Murakami, 1986); this serves to reduce the effective lifetime of the cGMP molecule. Somewhat paradoxically, though, it was not realized until quite recently that this mechanism makes a major contribution to photoreceptor light-adaptation behavior (Nikonov et al., 2000; Pugh et al., 1999). Indeed, this phenomenon appears to represent the rod's most powerful mechanism for steady-state adjustment of sensitivity, and furthermore, it is calcium independent.

A useful way of thinking about this mechanism is to apply the so-called "bath tub" analogy (Pugh et al., 1999), whereby water flows into a bath from a tap and out via a plug hole. The size of the plug hole represents steady PDE activity, whereas the steady inflow through the tap represents steady cyclase activity; the depth of the water represents the cGMP level. In darkness, with a small plug hole and a slow trickle of water from the tap, any perturbation in the water level dies away only slowly. However, in moderate illumination, with a gigantic plug hole and the tap running rapidly, any perturbation comes to equilibrium much more rapidly. From such an analysis it can be shown that, for a given driving function (opening-up of a given additional plug hole), the response measured by the change in water level is both faster and smaller in the adapted state. For a further discussion of this concept, see Govardovskii et al. (2000) and Pugh and Lamb (2000).

GAIN REDUCTION: A MATTER OF INTENSITIES A simple mechanism that one could imagine for reducing flash sensitivity during light adaptation would be a reduction in amplification of the cascade, for example, by reducing the amplifying step between rhodopsin and transducin. Although some studies have suggested that there can be a reduction in rhodopsin-transducin gain during light adapta-

tion (Lagnado and Baylor, 1994; Jones, 1995; Gray-Keller and Detwiler, 1996), other studies have found no evidence for a change in amplification (Torre et al., 1986; Hood and Birch, 1993; Thomas and Lamb, 1999; Nikonov et al., 2000). In attempting to resolve this issue, it is important to restrict consideration to the very earliest times in the light response, before inactivation reactions come into play. Because both the reduction of rhodopsin's catalytic activity by phosphorylation (Chen et al., 1995; Chen et al., 1999; Sagoo and Lagnado, 1997) and calcium activation of guanylate cyclase (Burns et al., 2002) begin during the rising phase of the flash response, the window of relevant times is very short. Bearing in mind this temporal restriction, the most recent analyses have indicated that, for intensities eliciting up to 70% suppression of the circulating current in rods, the amplification of transduction is invariant with intensity (Nikonov et al., 2000, suction pipette; Sokolov et al., 2002, electroretinogram).

By contrast, brighter illumination, sufficient to hold the rods in saturation for a prolonged time, has been found to reduce the amplification (Kennedy et al., 2001; Sokolov et al., 2002). Furthermore, this reduction in gain is associated quantitatively with a large-scale redistribution of transducin within the rod, with a substantial fraction of both the α and $\beta\gamma$ subunits of transducin translocating from the outer segment to the inner segment (Sokolov et al., 2002). The gain reduction that results from the massive movement of transducin from the outer segment is a novel form of light adaptation. However, it is not yet clear whether the purpose of this mechanism is to rescue rods from saturation at higher light intensities than would otherwise be possible, or whether it might perhaps act as a means for minimizing unnecessary metabolism while the rod's photocurrent is saturated.

CONTRIBUTION OF PIGMENT BLEACHING TO LIGHT ADAPTATION The bleaching of photopigment makes a negligible contribution to light adaptation, except at the very highest intensities experienced by cones. In human rods, complete saturation occurs at around 10^3 photoisomerizations s^{-1} , which, with a pigment regeneration time constant on the order of 400 s, corresponds to a steady-state bleach level of 4×10^5 out of $\sim 10^8$ rhodopsin molecules, or less than 0.5%. Hence, rods are completely inoperative at light intensities that cause any appreciable level of bleaching.

Cones, on the other hand, are capable of functioning even when almost all of their pigment has been bleached (Burkhardt, 1994), and it has long been known psychophysically that the cone system does not show saturation under steady illumination of any intensity (Barlow, 1972). This seems to indicate that cones are much less susceptible than rods to the presence of bleaching products, although an additional contributory factor no doubt stems from the fact

that cone pigments exhibit much faster removal of all-trans retinoid and faster return to the native 11-cis form (Shichida et al., 1994). The physiological relevance of the cones' ability to function at very large bleaches is not clear, because large steady-state bleaches are so unpleasant to the observer that they are actively avoided wherever possible. In practice, it seems likely that the steady-state cone pigment bleaching level experienced by human observers seldom exceeds about 90%, contributing a factor of, at most, ~10-fold to reduced quantal catch, even though the cones are fully capable of functioning at much higher bleach levels.

COMPOSITE EFFECT OF ALL THE ADAPTATIONAL MECHANISMS Koutalos et al. (1995a, 1995b) undertook experiments to separate the steady-state effects of calcium feedback on guanylate cyclase, on the cascade leading to PDE activation, and on ion channel activation. They provided a compelling theoretical model of the contributions to light adaptation of these different calcium mechanisms. They reported that the cyclase-mediated effect was most important at relatively low intensities, whereas the effect on the PDE cascade became more important at higher intensities; the effect on the channels was modest at all intensities.

That description would appear to remain valid, with one modification. In view of the analysis of Nikonov et al. (2000) showing the role of steady PDE activation in desensitization, it seems likely that much of the effect that Koutalos et al. (1995b) attributed to calcium-dependent modulation of the cascade might instead arise from light-dependent activation of the cascade. Indeed, Nikonov et al. (2000) presented calculations of the extent to which light adaptation would be perturbed by "knocking out" different components of the calcium feedback system (their Fig. 14). That analysis confirmed the important role of the GCAP/cyclase effect at relatively low intensities, but also attributed a substantial component of desensitization to the light-induced cascade activation of PDE, over a range of intermediate intensities. Their analysis suggested relatively small effects for both the recoverin-mediated effect on the cascade and the modulation of channel sensitivity.

Summary and conclusions

Photoreceptors have a seemingly simple job description: to accurately relay to the rest of the visual system information regarding the timing and number of photon absorptions, and to do this across more than 10 log units of light intensity. Although nature has evolved two separate neural receptors and pathways to mediate vision across this enormous range of intensities, this has clearly not been enough. Rods and cones possess a multitude of specialized mechanisms: (1) mechanisms that serve both to amplify and to deactivate the response in a timely manner; (2) mechanisms that serve to

adapt the cell to light in both the short- and long-term; and finally, (3) mechanisms that serve to maintain these functional abilities, via pigment regeneration and other homeostatic mechanisms that lie beyond the scope of this chapter (e.g., disc shedding and renewal). Our current level of understanding is beginning to reveal our true ignorance regarding the engineering principles with which nature has achieved the generation of signals essential for the visual perceptions of the world around us.

REFERENCES

- Antonny, B., A. Otto-Bruc, M. Chabre, and T. M. Vuong, 1993. GTP hydrolysis by purified alpha-subunit of transducin and its complex with the cyclic GMP phosphodiesterase inhibitor, *Biochemistry*, 32:8646–8653.
- Arnis, S., and K. P. Hofmann, 1993. Two different forms of metarhodopsin II: schiff base deprotonation precedes proton uptake and signaling state, *Proc. Natl. Acad. Sci. USA*, 90:7849–7853.
- Arshavsky, V., and M. D. Bownds, 1992. Regulation of deactivation of photoreceptor G protein by its target enzyme and cGMP, *Nature*, 357:416–417.
- Arshavsky, V. Y., T. D. Lamb, and E. N. Pugh, Jr. 2002. G proteins and phototransduction, *Annu. Rev. Physiol.*, 64:153–187.
- Barlow, H. B., 1964. Dark adaptation: a new hypothesis, *Vis. Res.*, 4:47–58.
- Barlow, H. B., 1972. Dark and light adaptation: psychophysics, in *Handbook of Sensory Physiology*, vol. VII/4 (D. Jameson and L. M. Hurvich, eds.), Berlin: Springer-Verlag, pp. 1–28.
- Barlow, H. B., W. R. Levick, and M. Yoon, 1971. Responses to single quanta of light in retinal ganglion cells of the cat, *Vis. Res.*, 11(Suppl. 3):87–101.
- Baylor, D. A., G. Matthews, and K.-W. Yau, 1980. Two components of electrical dark noise in toad retinal rod outer segments, *J. Physiol.*, 309:591–621.
- Baylor, D. A., and B. J. Nunn, 1986. Electrical properties of the light-sensitive conductance of rods of the salamander *Ambystoma tigrinum*, *J. Physiol.*, 371:115–145.
- Baylor, D. A., B. J. Nunn, and J. L. Schnapf, 1984. The photocurrent, noise and spectral sensitivity of rods of the monkey *Macaca fascicularis*, *J. Physiol.*, 357:575–607.
- Burkhardt, D. A., 1994. Light adaptation and photopigment bleaching in cone photoreceptors *in situ* in the retina of the turtle, *J. Neurosci.*, 14:1091–1105.
- Burns, M. E., A. Mendez, J. Chen, and D. A. Baylor, 2002. Dynamics of cyclic GMP synthesis in retinal rods, *Neuron*, 36:81–91.
- Calvert, P. D., V. I. Govardovskii, N. Krasnoperova, R. E. Anderson, J. Lem, and C. L. Makino, 2001. Membrane protein diffusion sets the speed of rod phototransduction, *Nature*, 411:90–94.
- Chen, C. K., M. E. Burns, W. He, T. G. Wensel, D. A. Baylor, and M. I. Simon, 2000. Slowed recovery of rod photoreponse in mice lacking the GTPase accelerating protein RGS9-1, *Nature*, 403:557–560.
- Chen, C. K., M. E. Burns, M. Spencer, G. A. Niemi, J. Chen, J. B. Hurley, D. A. Baylor, and M. I. Simon, 1999. Abnormal photoresponses and light-induced apoptosis in rods lacking rhodopsin kinase, *Proc. Natl. Acad. Sci. USA*, 96:3718–3722.
- Chen, C. K., K. Zhang, J. Church-Kopish, W. Huang, H. Zhang, Y. J. Chen, J. M. Frederick, and W. Baehr, 2001. Characteriza-

- tion of human GRK7 as a potential cone opsin kinase, *Mol. Vis.*, 7:305–313.
- Chen, J., C. L. Makino, N. S. Peachey, D. A. Baylor, and M. I. Simon, 1995. Mechanisms of rhodopsin inactivation *in vivo* as revealed by a COOH-terminal truncation mutant, *Science*, 267:374–377.
- Chen, T. Y., M. Illing, L. L. Molday, Y. T. Hsu, K.-W. Yau, and R. S. Molday, 1994. Subunit 2 (or beta) of retinal rod cGMP-gated cation channel is a component of the 240-kDa channel-associated protein and mediates Ca^{2+} -calmodulin modulation, *Proc. Natl. Acad. Sci. USA*, 91:11757–11761.
- Cone, R. A., and W. H. Cobbs III, 1969. Rhodopsin cycle in the living eye of the rat, *Nature*, 221:820–822.
- Cowan, C. W., R. N. Fariss, I. Sokal, K. Palczewski, and T. G. Wensel, 1998. High expression levels in cones of RGS9, the predominant GTPase accelerating protein of rods, *Proc. Natl. Acad. Sci. USA*, 95:5351–5356.
- Cowan, C. W., W. He, and T. G. Wensel, 2001. RGS proteins: lessons from the RGS9 subfamily, *Prog. Nucleic Acid Res. Mol. Biol.*, 65:341–359.
- Craft, C. M., D. H. Whitmore, and A. F. Wiechmann, 1994. Cone arrestin identified by targeting expression of a functional family, *J. Biol. Chem.*, 269:4613–4619.
- Dizhoor, A. M., and J. B. Hurley, 1996. Inactivation of EF-hands makes GCAP-2 (p24) a constitutive activator of photoreceptor guanylyl cyclase by preventing a Ca^{2+} -induced “activator-to-inhibitor” transition, *J. Biol. Chem.*, 271:19346–19350.
- Dizhoor, A. M., and J. B. Hurley, 1999. Regulation of photoreceptor membrane guanylyl cyclases by guanylyl cyclase activator proteins, *Methods*, 19:521–531.
- Dodd, R. L., 1998. *The role of arrestin and recoverin in signal transduction by retinal rod photoreceptors*, Doctoral dissertation, Stanford University, Stanford, CA.
- Dryja, T. P., 2000. Molecular genetics of Oguchi disease, fundus albipunctatus, and other forms of stationary night blindness: LVII Edward Jackson Memorial Lecture, *Am. J. Ophthalmol.*, 130:547–563.
- Erickson, M. A., L. Lagnado, S. Zozulya, T. A. Neubert, L. Stryer, and D. A. Baylor, 1998. The effect of recombinant recoverin on the photoresponse of truncated rod photoreceptors, *Proc. Natl. Acad. Sci. USA*, 95:6474–6479.
- Fain, G. L., T. D. Lamb, H. R. Matthews, and R. L. Murphy, 1989. Cytoplasmic calcium as the messenger for light adaptation in salamander rods, *J. Physiol.*, 416:215–243.
- Fain, G. L., H. R. Matthews, M. C. Cornwall, and Y. Koutalos, 2001. Adaptation in vertebrate photoreceptors, *Physiol. Rev.*, 81:117–151.
- Flynn, G. E., J. P. Johnson, Jr., and W. N. Zagotta, 2001. Cyclic nucleotide-gated channels: Shedding light on the opening of a channel pore, *Nat. Rev. Neurosci.*, 2:643–651.
- Gordon, S. E., J. Downing-Park, and A. L. Zimmerman, 1995. Modulation of the cGMP-gated ion channel in frog rods by calmodulin and an endogenous inhibitory factor, *J. Physiol.*, 486:533–546.
- Govardovskii, V. I., P. D. Calvert, and V. Y. Arshavsky, 2000. Photoreceptor light adaptation. Untangling desensitization and sensitization, *J. Gen. Physiol.*, 116:791–794.
- Gray-Keller, M. P., and P. B. Detwiler, 1996. Ca^{2+} dependence of dark- and light-adapted flash responses in rod photoreceptors, *Neuron*, 17:323–331.
- Gray-Keller, M. P., A. S. Polans, K. Palczewski, and P. B. Detwiler, 1993. The effect of recoverin-like calcium-binding proteins on the photoresponse of retinal rods, *Neuron*, 10:523–531.
- Haeseleer, F., I. Sokal, N. Li, M. Pettenati, N. Rao, D. Bronson, R. Wechter, W. Baehr, and K. Palczewski, 1999. Molecular characterization of a third member of the guanylyl cyclase-activating protein subfamily, *J. Biol. Chem.*, 274:6526–6535.
- Hagins, W. A., and S. Yoshikami, 1974. Proceedings: a role for Ca^{2+} in excitation of retinal rods and cones, *Exp. Eye Res.*, 18:299–305.
- He, W., C. W. Cowan, and T. G. Wensel, 1998. RGS9, a GTPase accelerator for phototransduction, *Neuron*, 20:95–102.
- Hecht, S., S. Shlaer, and M. H. Pirenne, 1942. Energy, quanta, and vision, *J. Gen. Physiol.*, 25:819–840.
- Hodgkin, A. L., P. A. McNaughton, and B. J. Nunn, 1986. Effects of changing Ca before and after light flashes in salamander rods, *J. Physiol.*, 372:54P.
- Hodgkin, A. L., and B. J. Nunn, 1988. Control of light-sensitive current in salamander rods, *J. Physiol.*, 403:439–471.
- Hood, D. C., and D. G. Birch, 1993. Light adaptation of human rod receptors: the leading edge of the human a-wave and models of rod receptor activity, *Vis. Res.*, 33:1605–1618.
- Howes, K. A., M. E. Pennesi, I. Sokal, J. Church-Kopish, B. Schmidt, D. Margolis, J. M. Frederick, F. Rieke, K. Palczewski, S. M. Wu, P. B. Detwiler, and W. Baehr, 2002. GCAP1 rescues rod photoreceptor response in GCAP1/GCAP2 knockout mice, *Embo. J.*, 21:1545–1554.
- Hsu, Y. T., and R. S. Molday, 1993. Modulation of the cGMP-gated channel of rod photoreceptor cells by calmodulin, *Nature*, 361:76–79.
- Jones, G. J., 1995. Light adaptation and the rising phase of the flash photocurrent of salamander retinal rods, *J. Physiol.*, 487:441–451.
- Kamps, K. M., J. Reichert, and K. P. Hofmann, 1985. Light-induced activation of the rod phosphodiesterase leads to a rapid transient increase of near-infrared light scattering, *FEBS Lett.*, 188:15–20.
- Karpen, J. W., A. L. Zimmerman, L. Stryer, and D. A. Baylor, 1988. Gating kinetics of the cyclic-GMP-activated channel of retinal rods: flash photolysis and voltage-jump studies, *Proc. Natl. Acad. Sci. USA*, 85:1287–1291.
- Kawamura, S., 1992. Light-sensitivity modulating protein in frog rods, *Photochem. Photobiol.*, 56:1173–1180.
- Kawamura, S., 1993. Rhodopsin phosphorylation as a mechanism of cyclic GMP phosphodiesterase regulation by S-modulin, *Nature*, 362:855–857.
- Kawamura, S., and M. Murakami, 1986. *In situ* cGMP phosphodiesterase and photoreceptor potential in gecko retina, *J. Gen. Physiol.*, 87:737–759.
- Kennedy, M. J., K. A. Lee, G. A. Niemi, K. B. Craven, G. G. Garwin, J. C. Saari, and J. B. Hurley, 2001. Multiple phosphorylation of rhodopsin and the *in vivo* chemistry underlying rod photoreceptor dark adaptation, *Neuron*, 31:87–101.
- Koch, K.-W., and L. Stryer, 1988. Highly cooperative feedback control of retinal rod guanylate cyclase by calcium ions, *Nature*, 334:64–66.
- Koutalos, Y., K. Nakatani, T. Tamura, and K.-W. Yau, 1995a. Characterization of guanylate cyclase activity in single retinal rod outer segments, *J. Gen. Physiol.*, 106:863–890.
- Koutalos, Y., K. Nakatani, and K.-W. Yau, 1995b. The cGMP-phosphodiesterase and its contribution to sensitivity regulation in retinal rods, *J. Gen. Physiol.*, 106:891–921.
- Koutalos, Y., and K. W. Yau, 1996. Regulation of sensitivity in vertebrate rod photoreceptors by calcium, *Trends Neurosci.*, 19:73–81.
- Kraft, T. W., D. M. Schneeweis, and J. L. Schnapf, 1993. Visual transduction in human rod photoreceptors, *J. Physiol.*, 464:747–765.

- Kühn, H., and U. Wilden, 1987. Deactivation of photoactivated rhodopsin by rhodopsin-kinase and arrestin, *J. Recept. Res.*, 7:283–298.
- Lagnado, L., and D. A. Baylor, 1994. Calcium controls light-triggered formation of catalytically active rhodopsin, *Nature*, 367:273–277.
- Lamb, T. D., 1981. The involvement of rod photoreceptors in dark adaptation, *Vis. Res.*, 21:1773–1782.
- Lamb, T. D., and E. N. Pugh, Jr. 1992. A quantitative account of the activation steps involved in phototransduction in amphibian photoreceptors, *J. Physiol.*, 449:719–758.
- Lem, J., N. V. Krasnoperova, P. D. Calvert, B. Kosaras, D. A. Cameron, M. Nicolo, C. L. Makino, and R. L. Sidman, 1999. Morphological, physiological, and biochemical changes in rhodopsin knockout mice, *Proc. Natl. Acad. Sci. USA*, 96:736–741.
- Leskov, I. B., V. A. Klenchin, J. W. Handy, G. G. Whitlock, V. I. Govardovskii, M. D. Bownds, T. D. Lamb, E. N. Pugh, Jr., and V. Y. Arshavsky, 2000. The gain of rod phototransduction: Reconciliation of biochemical and electrophysiological measurements, *Neuron*, 27:525–537.
- Li, T., W. K. Snyder, J. E. Olsson, and T. P. Dryja, 1996. Transgenic mice carrying the dominant rhodopsin mutation P347S: evidence for defective vectorial transport of rhodopsin to the outer segments, *Proc. Natl. Acad. Sci. USA*, 93:14176–14181.
- Lolley, R. N., and E. Racz, 1982. Calcium modulation of cyclic GMP synthesis in rat visual cells, *Vis. Res.*, 22:1481–1486.
- Lyubarsky, A. L., C. Chen, M. I. Simon, and E. N. Pugh, Jr., 2000. Mice lacking G-protein receptor kinase 1 have profoundly slowed recovery of cone-driven retinal responses, *J. Neurosci.*, 20:2209–2217.
- Lyubarsky, A. L., F. Naarendorp, X. Zhang, T. Wensel, M. I. Simon, and E. N. Pugh, Jr., 2001. RGS9-1 is required for normal inactivation of mouse cone phototransduction, *Mol. Vis.*, 7: 71–78.
- Maeda, T., H. Ohguro, H. Sohma, Y. Kuroki, H. Wada, S. Okisaka, and A. Murakami, 2000. Purification and characterization of bovine cone arrestin (cArr), *FEBS Lett.*, 470:336–340.
- Makino, C. L., J. G. Flannery, J. Chen, and R. L. Dodd, 1998. Effects of photoreponse prolongation on retinal rods of transgenic mice, in *Photostasis and Related Phenomena* (T. P. Williams and A. B. Thistle, eds.), New York: Plenum Press, pp. 129–151.
- Makino, E. R., J. W. Handy, T. Li, and V. Y. Arshavsky, 1999. The GTPase activating factor for transducin in rod photoreceptors is the complex between RGS9 and type 5 G protein beta subunit, *Proc. Natl. Acad. Sci. USA*, 96:1947–1952.
- Matthews, H. R., 1997. Actions of Ca^{2+} on an early stage in phototransduction revealed by the dynamic fall in Ca^{2+} concentration during the bright flash response, *J. Gen. Physiol.*, 109: 141–146.
- Matthews, H. R., G. L. Fain, R. L. Murphy, and T. D. Lamb, 1990. Light adaptation in cone photoreceptors of the salamander: a role for cytoplasmic calcium, *J. Physiol.*, 420:447–469.
- Matthews, H. R., R. L. Murphy, G. L. Fain, and T. D. Lamb, 1988. Photoreceptor light adaptation is mediated by cytoplasmic calcium concentration, *Nature*, 334:67–69.
- Mendez, A., M. E. Burns, A. Roca, J. Lem, L. W. Wu, M. I. Simon, D. A. Baylor, and J. Chen, 2000. Rapid and reproducible deactivation of rhodopsin requires multiple phosphorylation sites, *Neuron*, 28:153–164.
- Mendez, A., M. E. Burns, I. Sokal, A. M. Dizhoor, W. Baehr, K. Palczewski, D. A. Baylor, and J. Chen, 2001. Role of guanylate cyclase-activating proteins (GCAPs) in setting the flash sensitivity of rod photoreceptors, *Proc. Natl. Acad. Sci. USA*, 98:9948–9953.
- Muller, F., M. Vantler, D. Weitz, E. Eismann, M. Zoche, K.-W. Koch, and U. B. Kaupp, 2001. Ligand sensitivity of the 2 subunit from the bovine cone cGMP-gated channel is modulated by protein kinase C but not by calmodulin, *J. Physiol.*, 532:399–409.
- Nakatani, K., and K.-W. Yau, 1988a. Calcium and light adaptation in retinal rods and cones, *Nature*, 334:69–71.
- Nakatani, K., and K.-W. Yau, 1988b. Guanosine 3',5'-cyclic monophosphate-activated conductance studied in a truncated rod outer segment of the toad, *J. Physiol.*, 395:731–753.
- Nikonov, S., T. D. Lamb, and E. N. Pugh, Jr., 2000. The role of steady phosphodiesterase activity in the kinetics and sensitivity of the light-adapted salamander rod photoresponse, *J. Gen. Physiol.*, 116:795–824.
- Normann, R. A., and I. Perlman, 1979. Evaluating sensitivity changing mechanisms in light-adapted photoreceptors, *Vis. Res.*, 19:391–394.
- Ohguro, H., J. P. Van Hooser, A. H. Milam, and K. Palczewski, 1995. Rhodopsin phosphorylation and dephosphorylation *in vivo*, *J. Biol. Chem.*, 270:14259–14262.
- Okada, T., O. P. Ernst, K. Palczewski, and K. P. Hofmann, 2001. Activation of rhodopsin: new insights from structural and biochemical studies, *Trends Biochem. Sci.*, 26:318–324.
- Otto-Bruc, A. E., R. N. Fariss, J. P. Van Hooser, and K. Palczewski, 1998. Phosphorylation of photolyzed rhodopsin is calcium-insensitive in retina permeabilized by alpha-toxin, *Proc. Natl. Acad. Sci. USA*, 95:15014–15019.
- Palczewski, K., T. Kumasaka, T. Hori, C. A. Behnke, H. Motoshima, B. A. Fox, I. Le Trong, D. C. Teller, T. Okada, R. E. Stenkamp, M. Yamamoto, and M. Miyano, 2000. Crystal structure of rhodopsin: a G protein-coupled receptor, *Science*, 289:739–745.
- Pepe, I. M., I. Panfoli, and C. Cugnoli, 1986. Guanylate cyclase in rod outer segments of the toad retina. Effect of light and Ca^{2+} , *FEBS Lett.*, 203:73–76.
- Pugh, E. N., Jr., T. Duda, A. Sitaramayya, and R. K. Sharma, 1997. Photoreceptor guanylate cyclases: a review, *Biosci. Rep.*, 17:429–473.
- Pugh, E. N., Jr., and T. D. Lamb, 1993. Amplification and kinetics of the activation steps in phototransduction, *Biochim. Biophys. Acta*, 1141:111–149.
- Pugh, E. N., Jr., and T. D. Lamb, 2000. Phototransduction in vertebrate rods and cones: molecular mechanisms of amplification, recovery and light adaptation, in *Handbook of Biological Physics*, vol. 3, *Molecular Mechanisms of Visual Transduction* (D. G. Stavenga, W. J. de Grip, and E. N. Pugh, Jr., eds.), Amsterdam: Elsevier, pp. 183–255.
- Pugh, E. N., Jr., S. Nikonov, and T. D. Lamb, 1999. Molecular mechanisms of vertebrate photoreceptor light adaptation, *Curr. Opin. Neurobiol.*, 9:410–418.
- Rebrik, T. I., and J. I. Korenbrot, 1998. In intact cone photoreceptors, a Ca^{2+} -dependent, diffusible factor modulates the cGMP-gated ion channels differently than in rods, *J. Gen. Physiol.*, 112:537–548.
- Rebrik, T. I., E. A. Kotelnikova, and J. I. Korenbrot, 2000. Time course and Ca^{2+} dependence of sensitivity modulation in cyclic GMP-gated currents of intact cone photoreceptors, *J. Gen. Physiol.*, 116:521–534.
- Rieke, F., and D. A. Baylor, 1996. Molecular origin of continuous dark noise in rod photoreceptors, *Biophys. J.*, 71:2553–2572.
- Rieke, F., and D. A. Baylor, 1998. Origin of reproducibility in the responses of retinal rods to single photons, *Biophys. J.*, 75: 1836–1857.

- Rose, A., 1948. The sensitivity performance of the human eye on an absolute scale, *J. Opt. Soc. Am.*, 38:196–208.
- Ross, E. M., and T. M. Wilkie, 2000. GTPase-activating proteins for heterotrimeric G proteins: regulators of G protein signaling (RGS) and RGS-like proteins, *Annu. Rev. Biochem.*, 69:795–827.
- Rudnicka-Nawrot, M., I. Surgucheva, J. D. Hulmes, F. Haeseleer, I. Sokal, J. W. Crabb, W. Baehr, and K. Palczewski, 1998. Changes in biological activity and folding of guanylate cyclase-activating protein 1 as a function of calcium, *Biochemistry*, 37: 248–257.
- Sagoo, M. S., and L. Lagnado, 1996. The action of cytoplasmic calcium on the cGMP-activated channel in salamander rod photoreceptors, *J. Physiol.*, 497:309–319.
- Sagoo, M. S., and L. Lagnado, 1997. G-protein deactivation is rate-limiting for shut-off of the phototransduction cascade, *Nature*, 389:392–395.
- Sato, N., and S. Kawamura, 1997. Molecular mechanism of S-modulin action: binding target and effect of ATP, *J. Biochem. (Tokyo)*, 122:1139–1145.
- Shichida, Y., H. Imai, Y. Imamoto, Y. Fukada, and T. Yoshizawa, 1994. Is chicken green-sensitive cone visual pigment a rhodopsin-like pigment? A comparative study of the molecular properties between chicken green and rhodopsin, *Biochemistry*, 33:9040–9044.
- Skiba, N. P., J. A. Hopp, and V. Y. Arshavsky, 2000. The effector enzyme regulates the duration of G protein signaling in vertebrate photoreceptors by increasing the affinity between transducin and RGS protein, *J. Biol. Chem.*, 275:32716–32720.
- Slep, K. C., M. A. Kercher, W. He, C. W. Cowan, T. G. Wensel, and P. B. Sigler, 2001. Structural determinants for regulation of phosphodiesterase by a G protein at 2.0 Å, *Nature*, 409:1071–1077.
- Slepak, V. Z., N. O. Artemyev, Y. Zhu, C. L. Dumke, L. Sabacan, J. Sondek, H. E. Hamm, M. D. Bownds, and V. Y. Arshavsky, 1995. An effector site that stimulates G-protein GTPase in photoreceptors, *J. Biol. Chem.*, 270:14319–14324.
- Sokolov, M., A. L. Lyubarsky, K. J. Strissel, A. B. Savchenko, V. I. Govardovskii, E. N. Pugh, Jr., and V. Y. Arshavsky, 2002. Massive, light-driven translocation of transducin between the two major compartments of rod cells: a novel mechanism of light adaptation, *Neuron*, 34:95–106.
- Steinberg, R. H., S. K. Fisher, and D. H. Anderson, 1980. Disc morphogenesis in vertebrate photoreceptors, *J. Comp. Neurol.*, 190:501–518.
- Stiles, W. S., and B. H. Crawford, 1932. Equivalent adaptational levels in localized retinal areas, in *Report of a Joint Discussion on Vision*, *Physical Society of London*, Cambridge: Cambridge University Press, pp. 194–211. (Reprinted from Stiles, W. S., 1978. *Mechanisms of Colour Vision*, London: Academic Press.)
- Thomas, M. M., and T. D. Lamb, 1999. Light adaptation and dark adaptation of human rod photoreceptors measured from the a-wave of the electroretinogram, *J. Physiol.*, 518:479–496.
- Torre, V., H. R. Matthews, and T. D. Lamb, 1986. Role of calcium in regulating the cyclic GMP cascade of phototransduction in retinal rods, *Proc. Natl. Acad. Sci. USA*, 83:7109–7113.
- Tsang, S. H., M. E. Burns, P. D. Calvert, P. Gouras, D. A. Baylor, S. P. Goff, and V. Y. Arshavsky, 1998. Role for the target enzyme in deactivation of photoreceptor G protein in vivo, *Science*, 282: 117–121.
- Udovichenko, I. P., A. C. Newton, and D. S. Williams, 1997. Contribution of protein kinase C to the phosphorylation of rhodopsin in intact retinas, *J. Biol. Chem.*, 272:7952–7959.
- Vuong, T. M., M. Chabre, and L. Stryer, 1984. Millisecond activation of transducin in the cyclic nucleotide cascade of vision, *Nature*, 311:659–661.
- Weiss, E. R., M. H. Ducceschi, T. J. Horner, A. Li, C. M. Craft, and S. Osawa, 2001. Species-specific differences in expression of G-protein-coupled receptor kinase (GRK) 7 and GRK1 in mammalian cone photoreceptor cells: Implications for cone cell phototransduction, *J. Neurosci.*, 21:9175–9184.
- Weiss, E. R., D. Raman, S. Shirakawa, M. H. Ducceschi, P. T. Bertram, F. Wong, T. W. Kraft, and S. Osawa, 1998. The cloning of GRK7, a candidate cone opsin kinase, from cone- and rod-dominant mammalian retinas, *Mol. Vis.*, 4:27.
- Weitz, D., M. Zoche, F. Muller, M. Beyermann, H. G. Korschen, U. B. Kaupp, and K.-W. Koch, 1998. Calmodulin controls the rod photoreceptor CNG channel through an unconventional binding site in the N-terminus of the beta-subunit, *EMBO J.*, 17:2273–2284.
- Whitlock, G. G., and T. D. Lamb, 1999. Variability in the time course of single photon responses from toad rods: termination of rhodopsin's activity, *Neuron*, 23:337–351.
- Wilden, U., S. W. Hall, and H. Kühn, 1986. Phosphodiesterase activation by photoexcited rhodopsin is quenched when rhodopsin is phosphorylated and binds the intrinsic 48-kDa protein of rod outer segments, *Proc. Natl. Acad. Sci. USA*, 83: 1174–1178.
- Xu, J., R. L. Dodd, C. L. Makino, M. I. Simon, D. A. Baylor, and J. Chen, 1997. Prolonged photoresponses in transgenic mouse rods lacking arrestin, *Nature*, 389:505–509.
- Young, R. W., 1976. Friedenwald Lecture. Visual cells and the concept of renewal, *Invest. Ophthalmol. Vis. Sci.*, 15:700–725.

17 How Retinal Circuits Optimize the Transfer of Visual Information

PETER STERLING

What it means to “understand” the retina

The retina is a thin sheet of *brain* tissue (100 to 250 μm thick) that grows out into the eye to provide neural processing for photoreceptor signals (Fig. 17.1). In cats and macaque monkeys, it weighs about 0.1 g and covers 800 mm^2 , about twice the area of a U.S. quarter (Packer et al., 1989). The retina includes both photoreceptors and the first two to four stages of neural processing. Its output projects centrally over many axons (1.6×10^5 in cats [Williams et al., 1993]; 1.3×10^6 in humans; and 1.8×10^6 in macaques [Potts et al., 1972]), and analysis of these information channels occupies about half of the cerebral cortex (van Essen et al., 1992; Baseler et al., 2002). Because the retina constitutes a significant fraction of the brain (roughly 0.3%), to “solve” it completely would be a significant achievement for neuroscience. This overview considers what a “solution” would entail and summarizes progress toward that goal.

First, we need the basic patterns of connection. The retina’s two synaptic layers span only 60 μm , and most lateral processes span only tens to hundreds of micrometers (versus millimeters to centimeters in cortex). Therefore it has proved technically straightforward to identify, trace, and quantify the neurons and many of their synaptic connections. This reveals the retina to comprise about 75 discrete neuron types connected in specific, highly stereotyped patterns. Second, we need the “neurochemical architecture”. Although information is far from complete, the main neurotransmitters and their receptor types have been identified with the key cell types and synapses. Third, we need the basic response of each cell type. Because the intact retina can be maintained *in vitro*, a cell’s light response can be recorded and the cell filled with dye to determine its morphology. This has permitted the neuroanatomical/neurochemical connections to be interpreted as functional “circuits” (Fig. 17.2).

Such circuits explain both intrinsic retinal mechanisms and also visual performance. For example, known circuits can explain reasonably well how a ganglion cell achieves its “center-surround” receptive field, and how one type of ganglion cell produces a linear, sustained response while a different type yields a nonlinear, transient response. Still other

circuits explain how at night a ganglion cell manages to fire 2 to 3 spikes to a single photon, while by day it fires a similar number of spikes to an increment of 10^5 photons. Finally, we know how different retinal circuits specialize for spatial acuity, motion, and opponent perception of hue (Calkins and Sterling, 1999; Wässle and Boycott, 1991).

CROSSING FROM “HOW” TO “WHY” Deep understanding of any brain region requires that we go beyond mechanism (*how*) to consider the computational purpose (*why*). For instance, why do we need a neural processor within the eye—since all other sense organs transmit spikes directly to the brain (Fig. 17.3)? And what explains the particularities of retinal design? For example, why are mammalian photoreceptors small, whereas in many cold-blooded species they are large? And why do photoreceptor and bipolar cells use presynaptic “ribbons,” since these are absent from the brain itself?

Many biologists dislike asking “why?” because it can be hard to prove that a given feature is truly adaptive, rather than merely decorative or a historical leftover of some evolutionary/developmental program (Gould and Lewontin, 1979). For an engineer, however, “why” is no problem. Every aspect of his design implies some specification of performance, constraints in cost (energy, materials, labor), and many compromises. If an engineer understands his design, he can explain *exactly why* his bridge was built a particular way (Glegg, 1969; Petroski, 1996). If he cannot explain this, stay off! So, the ability to answer “why” measures the depth of our comprehension.

Another test of comprehension is to ask whether circuit components *match optimally*, a condition termed “symmorphosis” (Diamond, 1992, 1993; Diamond and Hammond, 1992; Taylor and Weibel, 1981; Weibel, 2000). Where a neural system can be shown to satisfy the principle of symmorphosis across many levels (behavior \leftrightarrow circuit \leftrightarrow cells \leftrightarrow molecules), it can be chalked up as virtually understood. Many biologists do not care for this question either, reasoning that because evolution is ceaseless, how can we know whether a given feature has reached optimality?

But when a mechanism is shown to meet some physical limit, such as diffraction or diffusion, then natural selection

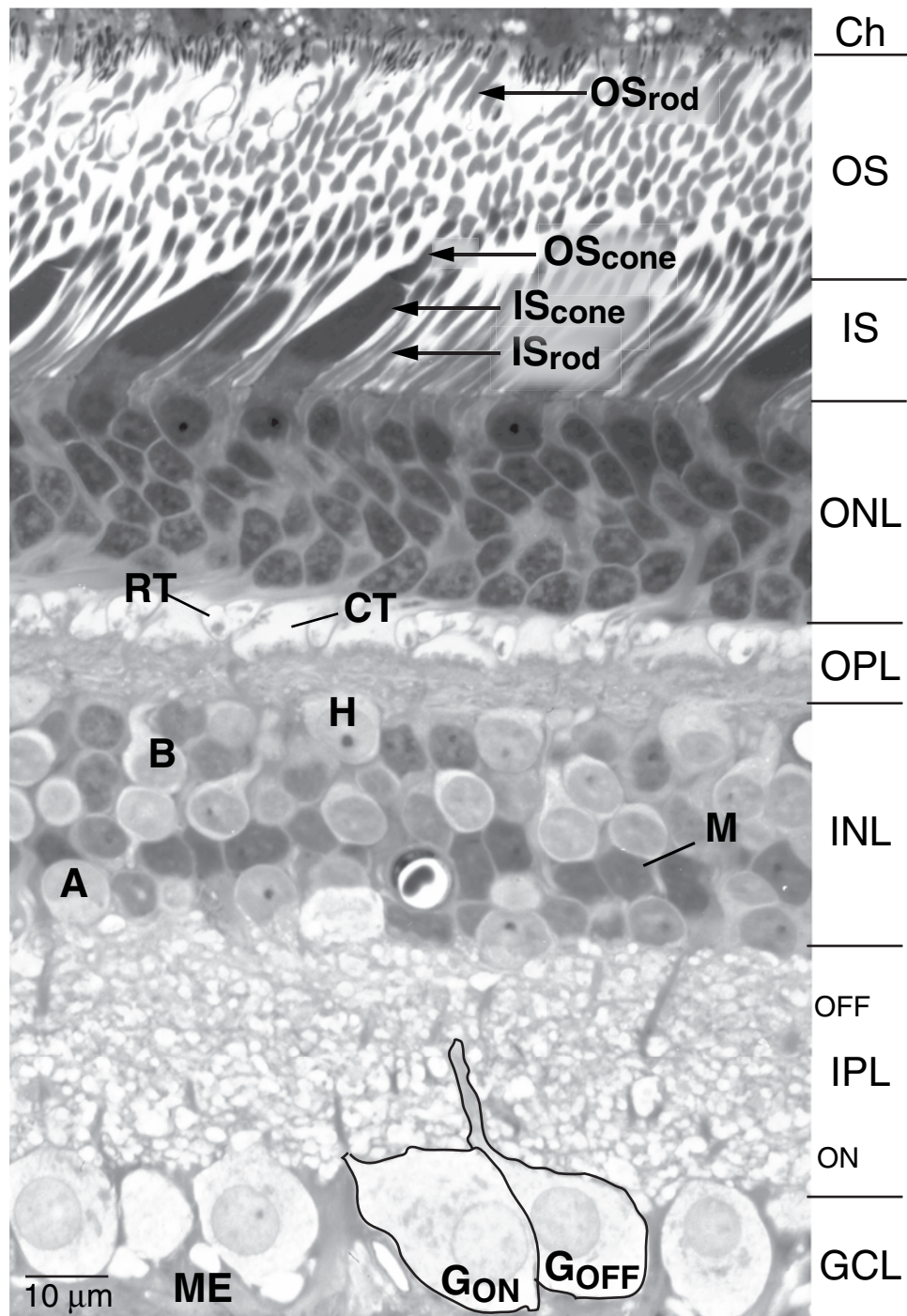


FIGURE 17.1. Radial section through monkey retina about 5 mm ($\sim 25^\circ$) from the fovea. The synaptic layers span only $60\mu\text{m}$. Cone and rod inner segments are easily distinguished from each other, as are their terminals in the outer plexiform layer. Pigmented cells of the choroid layer (Ch) convert vitamin A to its photoactive form and return it to the outer segments. Pigmented cells also phagocytose membrane discs that are shed daily from the outer segment

tips. OS, outer segment; IS, inner segment; ONL, outer nuclear layer; CT, cone terminal; RT, rod terminal; OPL, outer plexiform layer; INL, inner nuclear layer; IPL, inner plexiform layer; GCL, ganglion cell layer; B, bipolar cell; M, Müller cell; H, horizontal cell; A, amacrine cell; ME, Müller end feet; G_{ON} and G_{OFF}, ganglion cells. (Light micrograph by N. Vardi; modified from Sterling, 1998.)

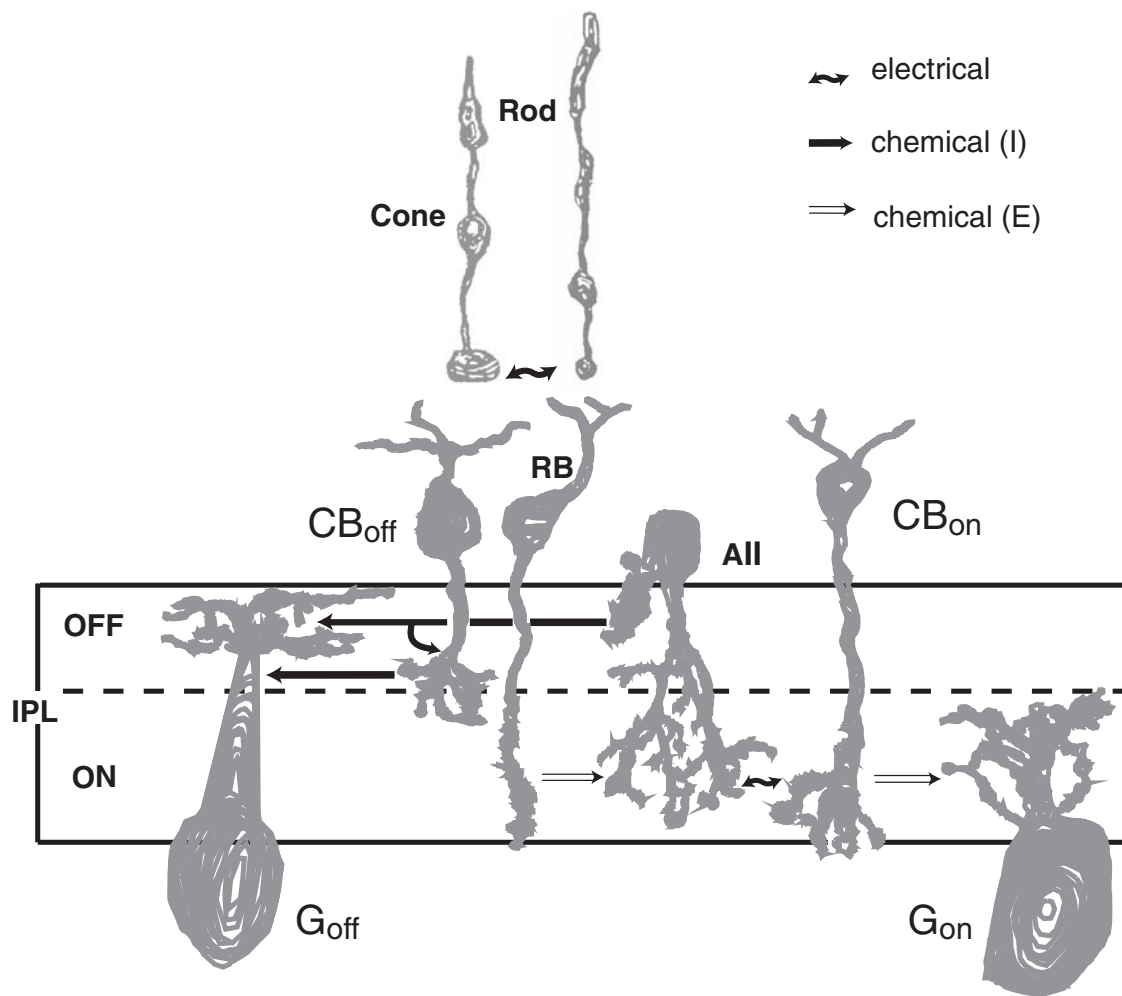


FIGURE 17.2. The basic circuits that relay rod and cone signals through the retina to ganglion cells are known. Cone signals modulate ON and OFF cone bipolar cells (CB) that excite ON and OFF ganglion cells (GC). Rod signals modulate cone terminals via electrical synapse and relay single-photon signals via a private rod

bipolar cell (RB) that excites the AII amacrine cell. The AII is bifunctional, inhibiting the OFF ganglion cell with glycine and exciting the ON ganglion cell via electrical synapse to the ON bipolar terminal. IPL, inner plexiform layer. (Modified from Sterling, 1998.)

has clearly hit the wall. And where several physical constraints conflict, neural design must reflect their compromise. In short, where actual performance approaches “ideal” performance calculated from physical limits, there is a genuine opportunity to address the “why” of a design. Although for most brain regions this is a distant goal, for mammalian retina such questions can now be addressed, and they provide the framework for this overview.

Consider that in nature the visual system operates near threshold. This is easily forgotten living under artificially bright light and viewing mostly high-contrast images, such as newsprint or the computer screen. But go bird watching or hunting (heaven forbid!), and you are quickly reminded that our ancestors strained to see the finest detail at the lowest contrast in the poorest light. To maximize sensitivity their eyes were selected to make each stage—from the optical image to the ganglion cell spike train—as efficient

as possible. Thus each stage should approach the limits set by physical laws and by compromises required by the organism’s “niche.” Thus *every stage* is a potential “bottleneck,” and the purpose at each stage must be to staunch the loss of information up to the physical limit. This hypothesis sets a framework for interpreting the functional architecture.

The central idea of this chapter is that the retina evolved to maximally extract information from the natural spatiotemporal distribution of photons and to convey this information centrally, with minimal loss. Upon this broad goal there are functional constraints: cover a wide range of intensities (10^{10}); respond to very low contrasts ($\sim 1\%$); integrate for short times (~ 0.1 second); keep tissue thin (~ 0.2 mm); and maintain the metabolic rate no higher. There are also basic constraints on biological computation: signal amplitude and velocities are set by properties of biological membranes and

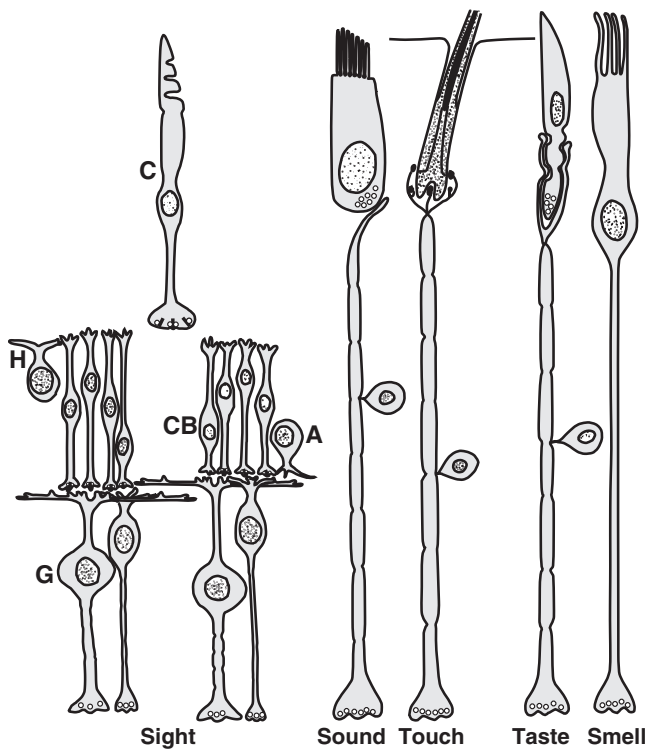


FIGURE 17.3. Only the visual sense requires neural processing at the site of transduction. The mammalian cone (*upper left*) requires lateral integration at its output (horizontal cells [H]), followed by 8 to 10 parallel circuits for a second stage (cone bipolar cells [CB]). Then, it requires more lateral integration (amacrine cells [A]) and finally, 10 to 20 parallel lines (four are shown; ganglion cells [G]) to carry action potentials to the brain. This chapter considers why photoreceptors require such extensive integration and so many parallel circuits before projecting centrally.

the speed of aqueous diffusion; accuracy and reliability of synaptic transmission are constrained by its quantal and Poisson nature. The retina's functional architecture reflects numerous compromises shaped by the interplay of these major factors as they contribute to the organism's overall success in its environment.

WHY NATURAL IMAGES NEED LOTS OF LIGHT Both prey and predators try to merge with the background, so in nature contrast for significant objects tends to be low. Consider the bighorn sheep among the cottonwoods (Fig. 17.4A). The retinal image is represented as peaks and troughs of intensity that differ from the local mean by only ~20%, and much fine structure exhibits far lower contrast, only a few percent (Fig. 17.4B). This range is common in nature (Laughlin, 1994; Srinivasan et al., 1982), and thus our visual threshold for a small stimulus, such as one spanning a single ganglion cell dendritic field, is ~3% contrast (Watson et al., 1983; Dhingra et al., 2003).

To create an optical image at low contrast requires many photons (Rose, 1973; Snyder et al., 1977). Because light is quantized, a small difference from the mean, say 1%, implies that the mean itself must contain at least 100 photons. But photons at each image point arrive randomly in time (Poisson distribution). So even when an image is perfectly still on the retina, the intensity at every point *varies* temporally, with a standard deviation equal to the square root of the mean. Because the minimum detectable contrast (Δn) must differ from the mean by at least one standard deviation, the ability to detect a contrast of 1% implies a mean of at least 10,000 photons:

$$\Delta n/n > \sqrt{n}/n = 100/10,000 = 1\%$$

This root-mean-square fluctuation (\sqrt{n}) is termed "photon noise."

One might think that daylight would provide plenty of photons to represent any scene. But this depends on the extent of photon integration: fine spatial detail implies limited spatial pooling and thus relatively large fluctuations from photon noise (Fig. 17.5A). This might be avoided by increasing temporal integration, but because mammals move swiftly, prolonged integration would blur the spatial image. Thus temporal integration is constrained to ~100 msec (Schneeweis and Schnapf, 1995). Although daylight contains enough photons/100 msec to cast a fine image on the cornea, the excess is not large, nor does it extend to even slightly dimmer situations, for example, when a cloud obscures the sun. The need for intense light to register fine detail at low contrast partly explains why athletes, bird watchers, and the like do not wear sunglasses (Sterling et al., 1992).

Mammalian photoreceptor mosaic

THE NEED FOR TWO TYPES OF DETECTOR The photoreceptor mosaic is optimized to cover the full range of environmental light intensities (10^{10}). This design specification requires two types of detector with different sensitivities, the rod and the cone (see Figs. 17.1, 17.5, and 17.6).¹ The rod serves under starlight where photons are so sparse that over 0.2 second (the rod integration time), they cause only ~1 photoisomerization (R^*)/10,000 rods. Consequently, under starlight and for 3 log units brighter, a rod must give a *binary* response, reporting over each integration time the

¹Of course, insects cover the same intensity range with a single type of photoreceptor, but they differ in many respects, including basic optical design, regeneration of rhodopsin, and use of an entirely different transduction cascade. When insect phototransduction is finally worked out, we may understand better how it manages to compress the full intensity range into a single cell type.

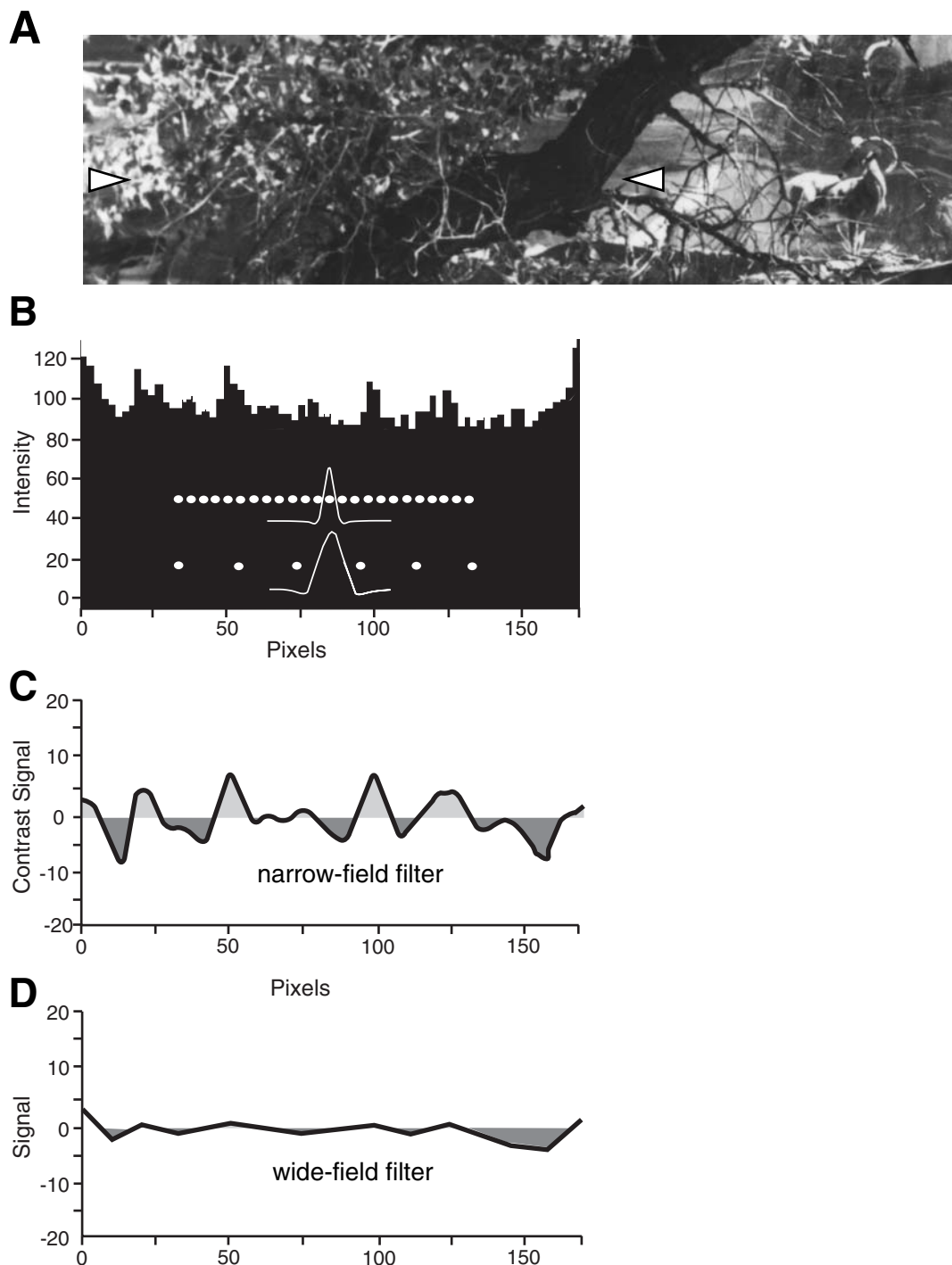


FIGURE 17.4. How narrow-field and wide-field ganglion cell arrays “filter” the transduced image of a natural scene. *A*, Photograph of a bighorn sheep among the cottonwoods. Spatial detail is represented as peaks and troughs of intensity around some mean level (arrowheads mark the area scanned in *B*). *B*, Photometer scan across the middle of the image. Much discernible structure, for example, fine branches, differs from the mean by only a few percent. Were this scene viewed by a cat at 10 meters, 1 pixel would correspond roughly to one cone, and the intensity axis would correspond roughly to the signal amplitude across the cone array. Dimensions and spacings of the narrow and wide receptive fields

are also indicated. *C*, Signal amplitude after filtering by narrow-field array. Subtraction by the surrounds of the shared signal component has reset the mean to zero: pooling by the centers has removed the noisy fluctuations. *D*, Signal amplitude after filtering by the wide-field cell array. Again, a zero mean, but the broad pooling and sparse sampling has removed all but the coarsest spatial detail—thereby clearing the wide-field cell dynamic range to efficiently encode motion. (Photograph by A. Pearlman; computations for *B* to *D* by R. Rao-Mirotznik and M. Eckert; modified from Sterling, 1998.)

occurrence of either 0 or 1 R^* . The rod continues to serve at dawn (or twilight) as photons arrive more densely, providing more than one R^* /integration time. The rod sums these linearly up to 20 R^* /integration time and then gradually saturates, with 100 R^* evoking a maximal photocurrent of ~ 20 pA. Under steady light, the rod adapts (reduces gain), and this allows it to continue signaling up to $\sim 1000 R^*$ /rod/integration time (Nakatani et al., 1991).

The cone serves under full daylight, beginning when photon density reaches ~ 100 photons/receptor/integration time. The cone actually absorbs and transduces single photons, but because its gain is 50-fold lower than the rod's, it requires 100 R^* for the signal to rise above the continuous dark noise. By 1000 R^* /integration time, when rods are nearly saturated, the cone responds strongly. The cone photocurrent saturates at ~ 30 pA (similar to the rod), but this occurs at much higher intensity (Burns and Lamb, 2003). Whether the mammalian cone in situ adapts by reducing gain or simply by saturating remains uncertain, but in any case, this detector serves intensities up to $10^6 R^*$ /cone/integration time (Pugh and Lamb, 1993; Schnapf et al., 1990). Consequently, whereas the rod signal is at first binary and then graded, but always corrupted by photon noise, the cone signal is always graded and far less noisy.

SUBDIVIDING THE RECEPTOR MOSAIC How should space in the receptor mosaic be apportioned? To maximize photon capture, receptors should completely fill the plane, and they *do*, occupying 90% and leaving an irreducible 10% to narrow intercellular channels required for exchange of ions and metabolites (Fig. 17.5). To maximize night vision, rods should fill the plane, but that would reduce daylight vision. Obviously there can be no single "optimal" solution, but only compromises that promote survival in a given niche. For example, the ground squirrel forages only in daylight and expresses only cones. However, most mammals cover the full intensity range and express both types of receptor. Their rods always far outnumber cones, and across species (from mouse to human), the ratio is surprisingly constant, about 20 rods per cone.

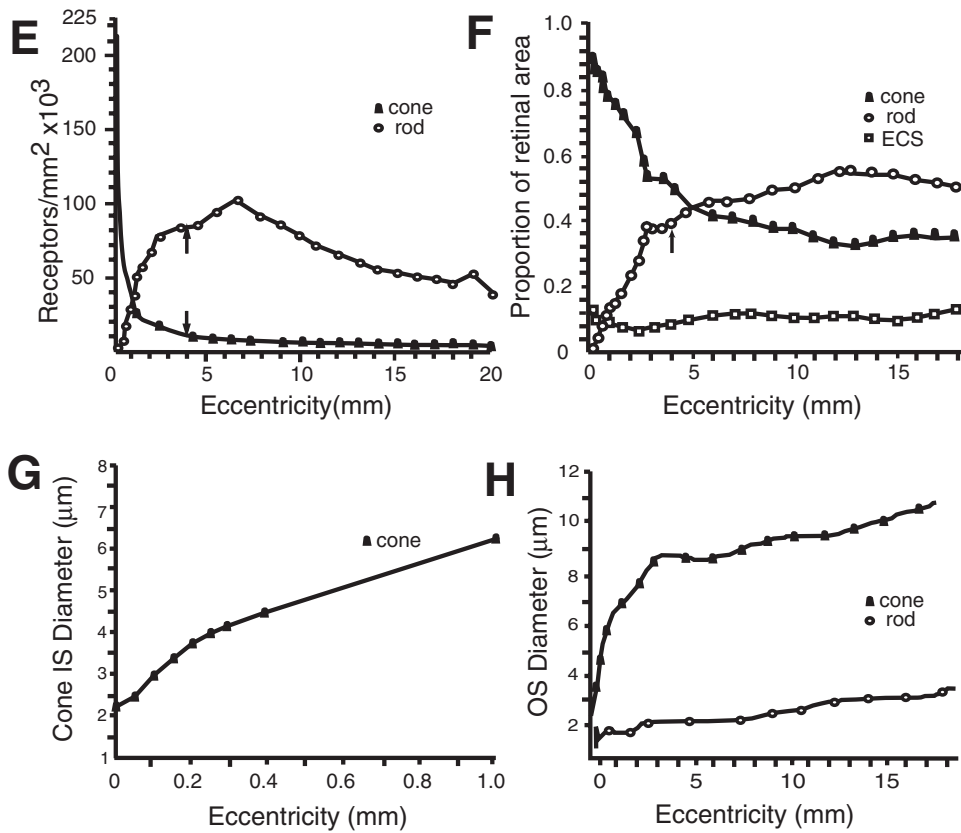
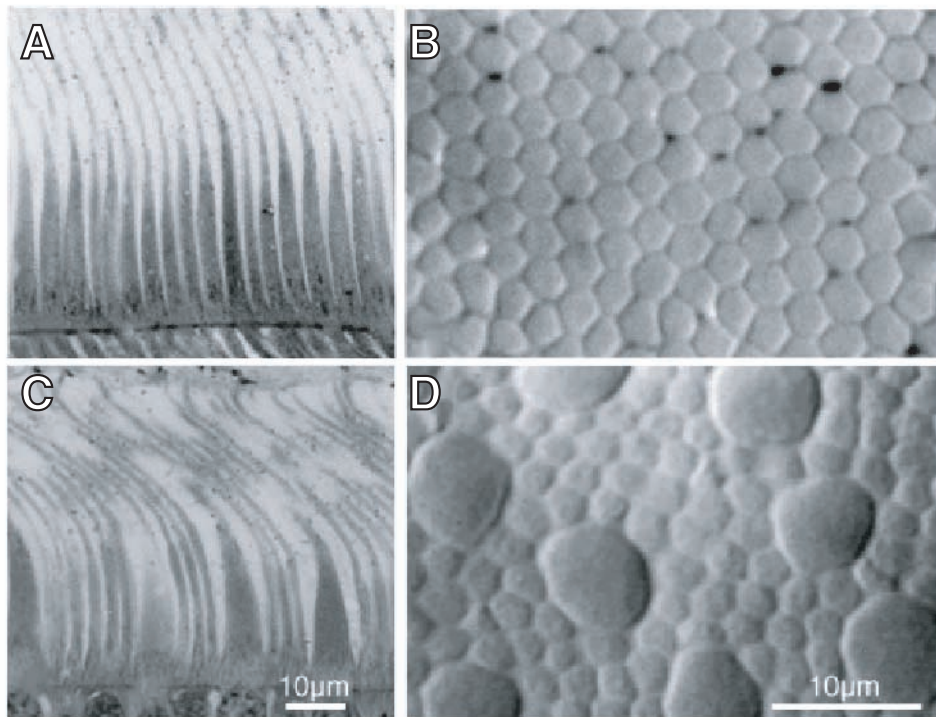
That this ratio genuinely represents a compromise can be appreciated from the many interesting exceptions that have been observed (Hughes, 1977). For one example, cones in the primate fovea completely fill the plane and exclude all rods (see Fig. 17.5). This enhances spatial resolution in daylight, but once light intensity falls below 100 photons/cone/integration time, the cost is utter blindness in this retinal region. To convince yourself, wait for color to disappear at dusk, indicating loss of cone function, then extend your arm and fix steadily on your thumb: it will disappear. This specialization for high spatial acuity requires various auxiliary modifications to the retina, mentioned in a later section.

What sets the basic ratio at 20 rods:1 cone? For the rod system, photons are so sparse that a ganglion cell may sum signals from more than 10,000 rods, yet still be dominated by photon noise. Therefore, the rod system madly competes for territory to catch every photon. But if rods managed to capture the last 5% of the mosaic, their signal-to-noise (S:N) ratio would improve only by $\sqrt{100/95}$, or 2.6%. Of course, there would be no daylight vision. So that is the trade: sacrifice 2.6% in sensitivity at night for the advantage of excellent photodetection by day.

For the cone system, photons are relatively plentiful, so the same ganglion summing signals from only 500 cones (each transducing, say, 1000 photons) will be responding to 500,000 photons. The S:N ratio calculated for photons ($500,000/\sqrt{500,000}$) is ~ 700 . Thus the cone-driven ganglion cell will hardly be affected by photon noise; instead its threshold is set by synaptic gain and neural noise (Dhingra et al., 2003; Freed, 2000a). Consequently for regions of the receptor mosaic where ganglion cells sum broadly, cones cannot improve vision by expanding territory, and thus they are well "satisfied" with 5%.

Where a particular species or retinal region requires higher spatial acuity, the cone territory *does* expand. Here, too, the physical constraints are known: (1) spatial acuity is set by ganglion cell sampling density because Nyquist's limit requires at least two samples for each spatial cycle (reviewed by Wässle and Boycott, 1991; Williams, 2003); (2) ganglion cell dendritic fields shrink and collect from fewer cones. Eventually, photon noise reduces the ganglion cell S:N ratio, and to preserve it cones must capture more territory. For example, in peripheral cat retina, where the dendritic field of a brisk-sustained ganglion cell sums 1000 cones, the rod:cone ratio is 100. However, in the central retina, where the brisk-sustained cell dendritic field shrinks to encompass only 30 cones, the rod:cone ratio is ~ 10 (Cohen and Sterling, 1992; Steinberg et al., 1973; Williams et al., 1993).

WHY THE OUTER SEGMENTS OF MAMMALIAN PHOTORECEPTORS ARE UNIFORM AND SMALL Dimensions of the rod outer segment are surprisingly uniform across mammals. Length is about 20 μm : 18 to 20 μm for cow and rabbit; and 25 μm for cat, Galago (nocturnal prosimian), macaque, and human (Nakatani et al., 1991; Tamura et al., 1991). Diameter is about 1.5 μm : 1 to 1.2 μm for cat (Steinberg et al., 1973; Williams et al., 1993), Galago, and owl monkey (all nocturnal); and 1.8 to 2 μm for rabbit, macaque, and human (Curcio et al., 1987, 1990; Packer et al., 1989). Diameter is somewhat smaller in central retina: cat, 1 μm central versus 1.6 μm peripheral; diurnal primate, 2 μm central versus 4 μm peripheral (Curcio et al., 1987; Packer et al., 1989). It is curious that rods should be smaller in nocturnal species. Possibly, adaptations that enhance photon



gathering in the nocturnal eye (such as a large pupil, reflective tapetum) tend to move the rod circuit away from its high gain, nonlinear regime (Field and Rieke, 2002; van Rossum and Smith, 1998). This switchover can be postponed to a higher environmental light intensity by reducing the rod collecting area.

The cone outer segment is also relatively small and invariant in volume. The shape can vary; for example, it narrows in primate fovea to enhance spatial sampling, and also lengthens (Fig. 17.6). But calculations based on Greeff's drawings suggest that across the human retina, cone outer segment volume is constant to within a factor of 2 (Fig. 17.6). In agreement, the outer segment volumes of isolated macaque cones, judged by their different inner segment diameters to represent all eccentricities, are small and constant: $30 \pm 10 \mu\text{m}$ (Schnapf et al., 1990).

In nonmammals the outer segments can be *much* larger (Fig. 17.7A). Thus, length can increase by orders of magnitude, reaching $60 \mu\text{m}$ in toad and $525 \mu\text{m}$ (!) in deepsea fish (Pugh and Lamb, 1993; Rodieck, 1973). Outer segments can also be much thicker. For example, the salamander outer segment, although only $25 \mu\text{m}$ long, is $11 \mu\text{m}$ in diameter. Thus, mammalian outer segments are reduced in volume by 30- to 80-fold.

This evolutionary "miniaturization" of the mammalian outer segment certainly reduces its efficiency of photon capture. For example, a photon penetrating a primate rod is 2.4-fold less likely to be captured than a photon in a toad rod. The reason is that the membrane discs bearing rhodopsin always stack as densely as possible, 36 discs/ μm (Fig. 17.7B). And the number of rhodopsin molecules per μm^2 of disc membrane is always 25,000 (Liebman et al., 1987). Therefore, as a photon traverses the outer segment, its probability of striking a rhodopsin depends on the number of discs. In this respect the mammalian outer segment is clearly suboptimal, which suggests a competing design constraint.

Recall that to match the mammalian motor system, photoreceptors must be *fast*. Whereas photocurrent in the large amphibian rod rises slowly, peaking at 1 to 2 seconds and with an overall integration time of 2 to 3 seconds, photocurrent in the small mammalian rod rises 10-fold

faster, peaking at 200 msec, with an overall integration time of ~ 300 msec (Baylor et al., 1979; Baylor et al., 1984; Kraft et al., 1993; Nakatani et al., 1991; Tamura et al., 1991). These times are essentially identical across mammals (Nakatani et al., 1991; Tamura et al., 1991), a striking contrast to insects whose different niches require large differences in speed and numerous adaptations to achieve them (Laughlin, 1994). Photocurrent in the mammalian cone rises equally rapidly, about 2 to 3 times faster (60 to 100 msec), but the integration time is shorter (50 msec) because the recovery of the photocurrent is faster and biphasic (Schnapf et al., 1990).

Why does speed require a small outer segment? The photocurrent generated by closing a cGMP-gated cation channel depends on reducing the intracellular concentration of cGMP (Burns and Lamb, 2003). Phosphodiesterase (PDE), the enzyme that hydrolyzes cGMP, is among the fastest enzymes; its catalytic rate approaches the physical limit set by how fast cGMP can reach it by aqueous diffusion (Liebman et al., 1987; Leskov et al., 2000). Thus, evolution cannot produce a faster enzyme. But, each hydrolyzed molecule in the reduced intracellular volume more effectively reduces the *concentration* of cGMP, and this raises transduction speed by 25-fold. Another factor of 4 is explained by increased body temperature: twofold from faster diffusion of the transduction proteins on the disc, which causes R^* to increase its encounter rate with transducin (Gt), and activated transducin (Gt^*) to increase its encounter rate with PDE; another twofold comes from PDE's accelerated catalytic rate, due to faster diffusion.

TRANSDUCTION PROTEINS AND ION CHANNELS ARE OPTIMIZED FOR SENSITIVITY, SPEED, GAIN, AND NOISE Only 20% of the disc membrane is occupied by rhodopsin, implying that denser packing could improve photon capture (sensitivity) by fivefold. In fact, insect rhabdomeres and bacteria do achieve crystalline packing of rhodopsin, so why hasn't evolution achieved this for vertebrate photoreceptors? Furthermore, why hasn't evolution accelerated transduction by increasing PDE density? The answers are not that "evolution is still in progress," but rather that additional factors must be optimized. For example, although rhodopsin density is too low

FIGURE 17.5. The foveal receptor mosaic is optimized for spatial resolution and contrast sensitivity; the peripheral mosaic is optimized for temporal resolution by day and absolute sensitivity by night. A, Human fovea, radial view. Cone inner segments are narrow and gently tapered; outer segments are long and fine. B, Human fovea, tangential view through the base of the inner segments. Hexagonal cone packing provides the finest possible spatial sampling in daylight, but the absence of rods renders the fovea blind from dusk to dawn. C, Human, near periphery, radial view.

Cone inner segments taper sharply and are surrounded by rod inner segments, which are much finer and untapered. D, Human, 20° nasal, tangential view. Large cone inner segments enhance sensitivity to high temporal frequencies, yet "spill" photons at night to surrounding rods. E to H, See text for explanation. IS, inner segment; OS, outer segment; ECS, extracellular space. (A–D, Video-DIC images from Curcio et al., 1990; E and F, Replotted from Packer et al., 1989. Used with permission.)

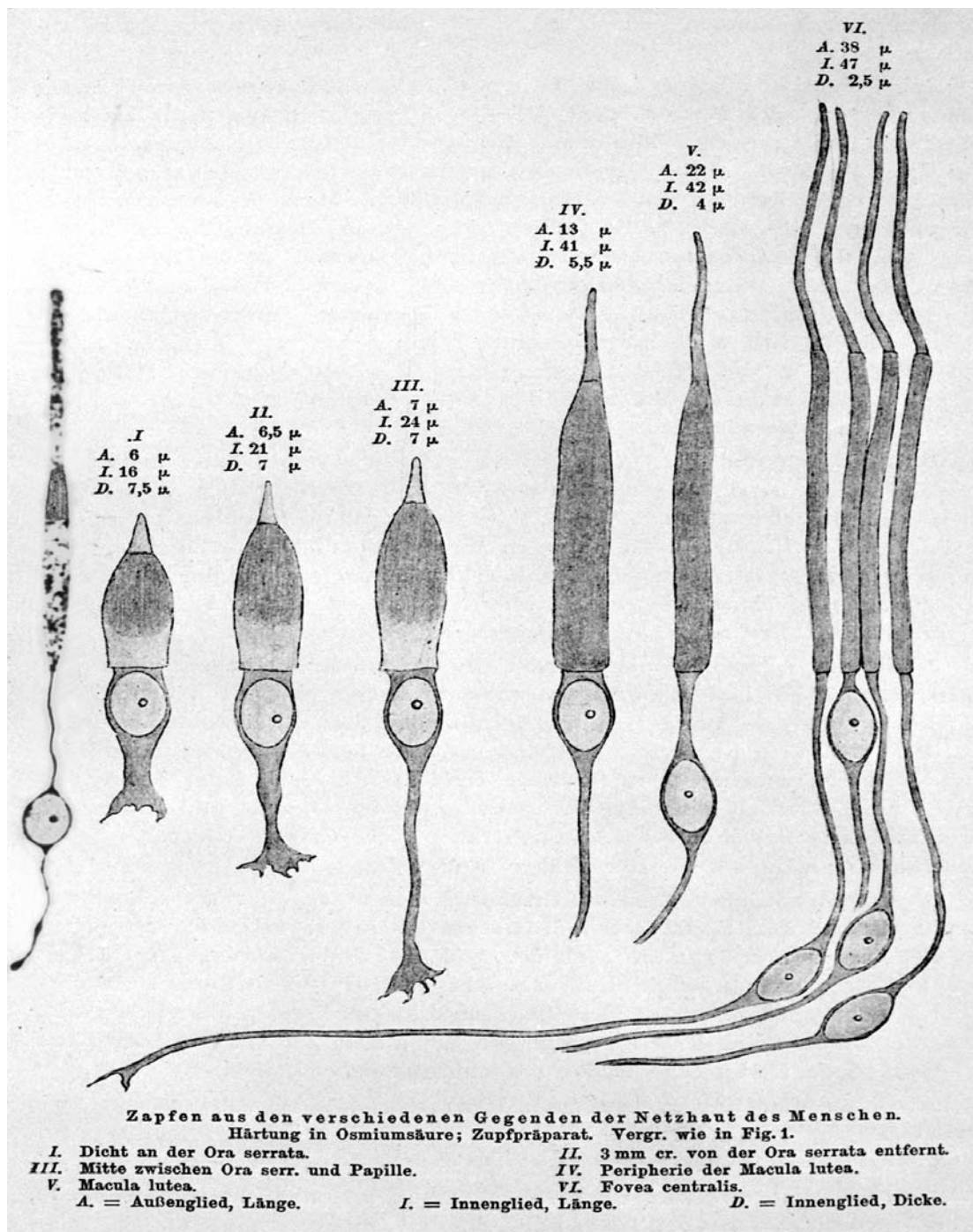


FIGURE 17.6. Cone structure varies across the retina, but rod structure is constant. Human photoreceptors dissociated and fixed with osmium. *Right-to-left*: Cones from the fovea to the periphery, plus one rod. The outer segment for the rod and foveal cone is long and columnar to maximize photon absorption; for the peripheral cone, it is short and tapered, possibly to radiate unabsorbed photons to surrounding rods (Miller and Snyder, 1973). The inner segment for the rod and foveal cone is long and columnar to allow dense packing. Photons that penetrate the cone obliquely escape, but then are captured by the densely packed, neighboring rods (see

Fig. 17.5). The peripheral cone inner segment is greatly enlarged, apparently to enhance photon catch and thus sensitivity to motion. The axon is thick for a cone and thin for a rod (see Fig. 17.8). The cone synaptic terminal is enlarged toward the periphery; the rod terminal is small. Basal processes on the cone terminal reach out to electrically contact other cones and also rods. All of these features appear to reflect the vastly different quantities of information collected by the cone and rod and more modest differences between cones at different eccentricities. (Reprinted from Greff, 1899.)

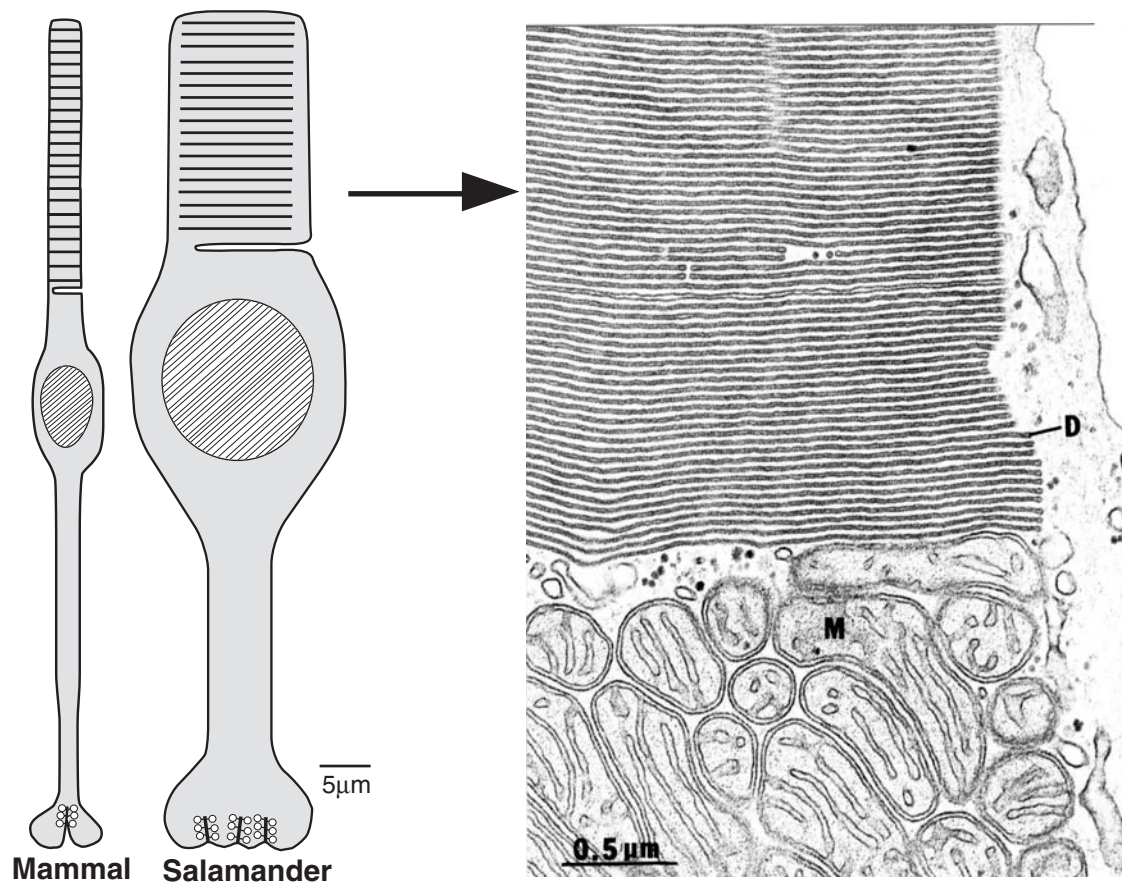


FIGURE 17.7. Mammalian rod outer segments are small in order to be fast. The mammalian outer segment must ensure a high probability of encounter between a photon and a rhodopsin molecule. This is achieved by densely packing rhodopsin on both faces of a membrane disc and then stacking 900 discs at maximal density ($36/\mu\text{m}$), for a total length of $\sim 25\mu\text{m}$. Although slightly longer than a salamander outer segment, the mammal's is much thinner ($\sim 1\mu\text{m}$ vs. $11\mu\text{m}$ in diameter). This greatly reduces its cytoplasmic volume (4% of the salamander rod's). This in turn accelerates its light-evoked fall of cGMP by 25-fold. The mammal's higher temperature further accelerates this process by doubling the rate at which R^* activates transducin (Gt) and the rate at which Gt activates phosphodiesterase (PDE). Consequently, the mammalian rod's amplification constant is about 100-fold faster, and its integration time ($\sim 200\text{msec}$) is about 10-fold shorter than the salamander rod's. The salamander rod's broader cross section and longer integration time provide it with 250-fold more $R^*/\text{integration time}$ than the mammalian rod. Consequently, its later stages are more cone-like: thicker axon, larger synaptic terminal with multiple ribbons (~ 8 ; Townes-Anderson et al., 1985), electrical coupling (Attwell, 1986); and convergence with cones onto the same bipolar cell. D, disc of outer segment; M, mitochondria of inner segment. (Electron micrograph reprinted from Townes-Anderson, 1995.)

for best photon catch, it is already *too high* for greatest speed because crowding slows activated rhodopsin's diffusive search for transducin. Halving rhodopsin's concentration (to 10%) in a transgenic mouse accelerates transduction speed by 1.7-fold (Calvert et al., 2001). Thus, rhodopsin's space on the disc represents an evolutionary compromise that doubles photon catch but nearly halves transduction speed.²

²Given the early evolutionary "decision" to base transduction on multiple stages of protein-protein encounter, the hit rate is increased by restricting the diffusive search to two dimensions (on the disc), rather than three dimensions (Adam and Delbrück, 1968).

One photoisomerization (R^*) in a rod triggers hydrolysis of 10^4 molecules of cGMP, leading to a photocurrent equivalent to $\sim 10^6$ monovalent ions, a gain of 1 million-fold (Burns and Baylor, 2001; Liebman et al., 1987). Gain could be increased if each step in the transduction cascade were activated for longer. But the cost would be slowing of the visual response. As it stands, one R^* in a primate rod evokes a current whose average size is $\sim 0.7\text{pA}$ (Baylor et al., 1984). The event exceeds the continuous dark noise by about five-fold, so noise as large as the photon event will occur rarely ($\sim 1\%$ false alarms). But the S:N ratio in the mouse rod is slightly less, \sim threefold, so many photon events that are smaller than average are indistinguishable from the

One photoisomerization (R^*) in a rod triggers hydrolysis of 10^4 molecules of cGMP, leading to a photocurrent equivalent to $\sim 10^6$ monovalent ions, a gain of 1 million-fold (Burns and Baylor, 2001; Liebman et al., 1987). Gain could be increased if each step in the transduction cascade were activated for longer. But the cost would be slowing of the visual response. As it stands, one R^* in a primate rod evokes a current whose average size is $\sim 0.7\text{pA}$ (Baylor et al., 1984). The event exceeds the continuous dark noise by about five-fold, so noise as large as the photon event will occur rarely ($\sim 1\%$ false alarms). But the S:N ratio in the mouse rod is slightly less, \sim threefold, so many photon events that are smaller than average are indistinguishable from the

continuous noise (see Fig. 17.11; Field and Rieke, 2002; Sterling, 2002). Thus, transduction, while maximizing gain, must also minimize noise due to dark fluctuations of cGMP.

These additional specifications, plus the need for speed, define the optimal molecular ratios of the cascade's effector proteins. Each square micrometer of disc membrane bears 25,000 R:2,500 G_t:330 PDE (Lamb and Pugh, 1992). At these densities, the mean time for an R* to find a G_t by diffusive search just equals the time for which R* binds to G_t. If G_t were sparser, R*'s search would be longer. Then, depending on R*'s lifetime, either transduction would slow, or the gain would fall. On the other hand, if G_t were denser, thermal activation would rise (yielding more false alarms). Similarly, PDE is just dense enough to be efficiently activated by G_t* and sparse enough to minimize basal hydrolysis of cGMP (continuous dark noise).

The rod outer segment bears about 10⁶ cGMP-gated channels, of which 10⁴ are held open by the standing concentration of a few micromolar cGMP. One R* hydrolyzes about 5% of the total cGMP and thus closes about 5% of the open channels. Why should a rod express 50,000 times more channels than needed to span its dynamic range? That is, why does it express 1 million channels instead of 20? Furthermore, why express 1 million channels since, at maximal dark current, only 100,000 channels open (Yau, 1994)?

Because channels behave stochastically (like photons), the ratio of photocurrent to continuous noise (S:N) is determined by n/\sqrt{n} , where n = mean number of channels. Thus, 20 channels could provide an S:N ratio of ~4.5, whereas 10,000 channels could provide an S:N ratio of ~100. By requiring at most 10% of the available channels to be modulated by a given change in cGMP, the channel's affinity for cGMP can be low, which allows a fast OFF rate, and thus rapid closure when cGMP falls. The channel's requirement for three cGMP molecules to open (Hill coefficient = 3) ensures a steep response to small changes in cGMP, that is, high gain (Koshland et al., 1982). Because the intrinsic channel conductance is about 20 pS, 5000 channels open in darkness might saturate the driving force. But this problem is avoided by designing the channel to be partially blocked at depolarized voltages by a magnesium ion, causing it to flicker rapidly and provide a mean functional current of 0.1 pS (Sesti et al., 1994; Yau, 1994).

The cone outer segment resembles the rod outer segment in many respects: opsin photoefficiency; speed of turn on (amplification constant); peak photocurrent; dark concentration of cGMP; number of CNG channels (Pugh and Lamb, 1993; Schnapf et al., 1990; Yau, 1994). In the cone, just like the rod, a single photon effectively triggers the transduction cascade. But, whereas one R* in a rod closes 5% of the open channels, in a cone it closes only

0.1% to 0.01% (Kraft et al., 1993; Schnapf et al., 1990). This sets the cone's gain ~50-fold lower than the rod's, rendering the cone most effective when there are more than 10³ photons/integration time, a regime where photon S:N is high. Cone sensitivity is lower because it depends multiplicatively on the time constant of each transduction step, and all are abbreviated compared to the rod. The advantage is greater temporal resolution and thus greater bandwidth. Because information capacity in any channel rises with the log of S:N ratio and *linearly* with bandwidth (Shannon and Weaver, 1949), the cone's information capacity greatly exceeds the rod's.

WHY THE CONE INNER SEGMENT VARIES The inner segment shifts markedly across the human retina (Figs. 17.5 and 17.6). At the fovea's center, it is tall and columnar, but across the fovea the inner segment gradually thickens. At greater eccentricities the inner segment becomes still broader, shorter, and tapered (quasi-ellipsoid), its aperture ultimately increasing in area by 20-fold. This shift produces concentric rings of cones with progressively greater inner segment diameter. Since the outer segments (both rod and cone) are rather constant, as is the rod inner segment, why should the cone inner segment vary?

The inner segment is crammed with mitochondria that generate ATP for the sodium/potassium transporters that maintain the circulating dark current (Fig. 17.7). But the mitochondria also enhance refractive index, and this converts the inner segment to an optical wave guide. Photons entering roughly parallel to the long axis are trapped and efficiently funneled to the outer segment (Enoch, 1981). The cone inner segments pack triangularly in fovea, so the inner segment diameter sets the number of cones per degree of visual angle and, since private lines are maintained from cone to striate cortex, this determines spatial resolution (Smallman et al., 1996). Of course, narrowing the inner segment to enhance resolution reduces photon catch and thus limits the cone's S:N ratio. Calculations prove that for each light level there exists an optimal balance of spatial resolution versus S:N ratio that maximizes total information (Snyder et al., 1977). Consequently, the fovea's array of concentric rings with progressively larger inner segments should maximize information uptake over a range of daylight intensities.

The inner segment's marked expansion beyond the fovea further enhances photon capture (Figs. 17.5 and 17.6). There is no cost to spatial resolution, which is set outside the fovea by the finest ganglion cell array. But the plump cone inner segments ultimately occupy 40% of the photoreceptor sheet, and appear to impinge on the collecting area needed by rods (Figs. 17.5 and 17.6). This problem seems solved when in dim light the pupil enlarges, allowing much of the light to enter peripheral cones at high angles to their optical

axes. Off-axis photons escape the light guide and spill into neighboring rods. Thus, although receptor ratios and dimensions are fixed, the proportion of light captured by cones and rods shifts adaptively with the optics of the eye. Peripheral cones *need* more light because the eye movements that steady an image on the foveal cones move the image across the peripheral cones, allowing less temporal integration (Eckert and Buchsbaum, 1993).

In summary, vertebrate photoreceptors exemplify the principle of symmorphosis: the mutual optimization of components across many levels. Here, we have considered the apportioning of: (1) space in the receptor mosaic; (2) outer segment volume; (3) numbers of key transduction proteins on a disc and their ratios; (4) reason for the disc; (5) number of cGMP-gated channels; (6) channel binding affinity, cooperativity, and partial blockage; and (7) inner segment size. These features all cooperate to set transduction efficiency, speed, gain, S:N, and bandwidth. They all match for a particular environmental state (e.g., starlight or daylight), and they compromise to promote overall performance (survival). These biophysical factors, by jointly setting the spatiotemporal integration of photons in a receptor, determine the size of its “information packet” to be relayed forward. This, in turn, determines many features of the downstream neural circuitry.

Transmitting the photoreceptor signal

ROD AXON IS THIN AND CONE AXON IS THICK Rod and cone axons are just long enough to traverse their nuclear layer and reach their synaptic targets. Typically, the distance is about 20 μm , but where their axons must course laterally to connect with second order neurons (near the fovea in primates), they are much longer, up to 500 μm (Polyak, 1941). Irrespective of length, the two axon types differ markedly in thickness. The rod axon is thin, about 0.45 μm in diameter, and invariant with species and retinal location; whereas the cone axon is thick, up to 1.6 μm , and varies across the retina, being thinner in the fovea and thicker toward the periphery (Figs. 17.6 and 17.8). The 4-fold difference in diameter implies a 16-fold difference in cross-sectional area.

This sets the number of microtubules in the axon cross-section, because microtubules are evenly spaced at a specific density that is the same for both axons (Fig. 17.8; Hsu et al., 1998). So, a cone axon has ~440 microtubules in its cross-section, whereas a rod axon has only ~35. The rod axon's smaller cross-sectional area also implies a 16-fold smaller volume. Volume of the rod axon terminal is also less than that of the cone axon terminal, so that the combined volume of the rod axon + terminal is less than the combined volume of the cone axon + terminal by 10-fold (Hsu et al., 1998). Were the rod signaling apparatus not

appropriately diminished but equal to that of the cone, the vast number of rods (20 rods/cone) would double the retina's postreceptoral thickness. So there must be pressure to minimize “wire volume” and match it to information capacity (Hsu et al., 1998).

ROD TERMINAL CONTAINS ONE ACTIVE ZONE AND CONE TERMINAL CONTAINS MANY We expect axon diameter to correlate with some *electrical* feature, such as space constant, conduction velocity, and temporal bandwidth. However, models suggest that outside the fovea a thin axon could adequately serve the cone's known electrical properties (Hsu et al., 1998). Instead, axon diameter correlates with the number of active zones.³ The thin rod axon supplies a small terminal with one active zone (Rao-Mirotznik et al., 1995); whereas the thick cone axon supplies a large terminal with many active zones (e.g., 17 in cat central retina, 20 in primate fovea, and 50 in primate periphery) (Fig. 17.9; Haverkamp et al., 2000). As the primate cone terminal enlarges from fovea to periphery, so does the axon (see Fig. 17.6). This rule (axon thickness proportional to number of active zones) also holds for bipolar axons in cat and mouse (Fig. 17.13C; Cohen and Sterling, 1990; Tsukamoto et al., 2001).

Because photoreceptors are tonically depolarized, each active zone releases vesicles tonically, at rates that seem astonishingly high. For example, the cat rod terminal with one active zone is calculated to release ~80 vesicles/second (Fig. 17.9C; Rao et al., 1994; Rao-Mirotznik et al., 1998; van Rossum and Smith, 1998), consistent with capacitance measurements of the salamander rod (Rieke and Schwartz, 1996). The cat cone terminal with 18 active zones (see Fig. 17.9B) is estimated to release ~1500 vesicles/second, consistent with noise measurements in turtle (Ashmore and Copenhagen, 1983). In these examples, transmitter release seems to match information capacity; that is, it is smaller in the rod terminal that transfers an irreducible binary signal (0 or 1 photon/integration time) and greater in the cone terminal that transfers a richer, graded signal (de Ruyter van Steveninck and Laughlin, 1996).

The cone's estimated 15-fold higher release rate apparently requires nearly 15-fold more microtubules. Because microtubules serve as “tracks” for molecular motors to shuttle supplies between cell body and synapse, it makes sense that a terminal whose vesicle release rate matches its information rate should also require a corresponding match of mechanisms for resupply. This observation implies another key constraint in retina, that *information capacity should match wire volume*.

³An active zone is the presynaptic site where synaptic vesicles dock near clusters of voltage-sensitive calcium channels.

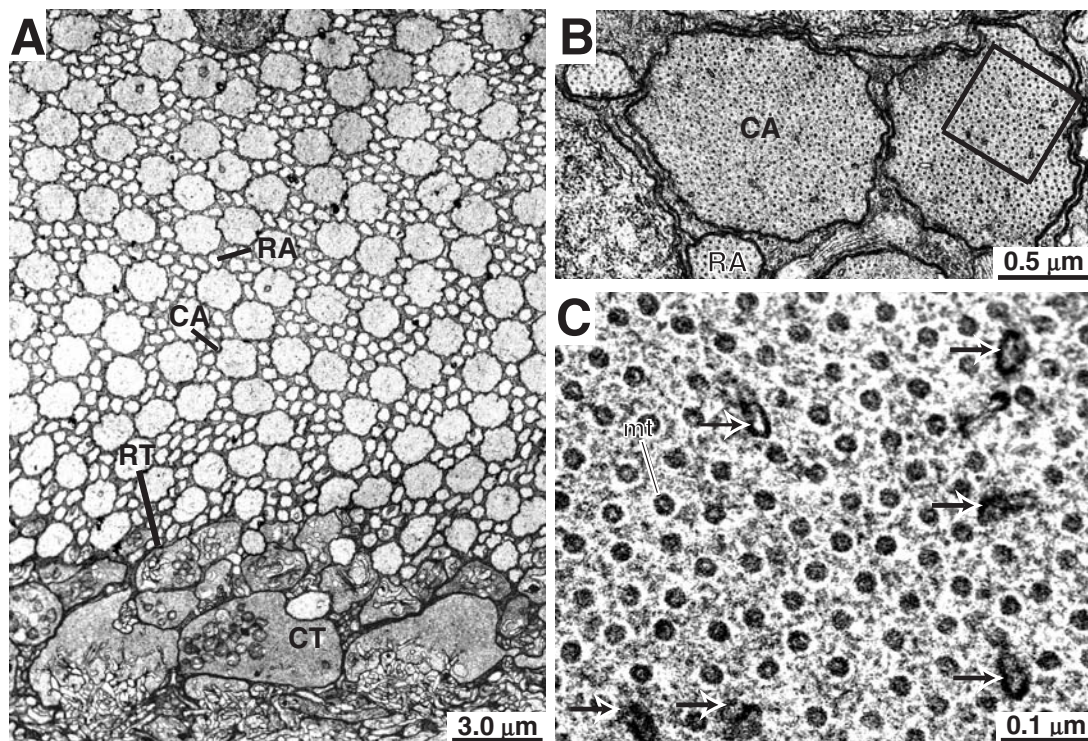


FIGURE 17.8. *A*, Electron micrograph of cross-section through photoreceptor axons in macaque perfovea. Cone axons (CA) are fourfold thicker than rod axons (RA). Cone terminals (CT) are also much larger than rod terminals (RT). *B*, Cone and rod axons are

filled with microtubules at equal densities. The square indicates the region enlarged in *C*. *C*, Microtubules (mt) in the cone axon are evenly spaced and associated with patches of smooth membrane (arrows).

PHOTORECEPTOR SYNAPSES ARE STRUCTURALLY AND FUNCTIONALLY THREE-DIMENSIONAL A signal rich in information coupled to a channel of intrinsically limited capacity, would lose information (Laughlin, 1994). To prevent this, the photoreceptor synapse evolved several coding strategies: (1) compress the signal by bandpass filtering; (2) divide the filtered signal into multiple components and route them over parallel circuits with appropriately matched properties. For example, the weakest rod signals use a private, nonlinear circuit, whereas stronger rod and cone signals share a linear circuit. Strong signals sort further into circuits for different temporal bandwidth. To initiate these key steps in signal processing, the first synapse requires several types of lateral interneuron (horizontal cells) and also *many* types of relay neuron (bipolar cells). To connect with all these neurons while minimizing tissue volume, noise, and metabolic cost, photoreceptors employ a three-dimensional synapse (Haverkamp et al., 2000; Rao-Mirotznik et al., 1995; Vardi et al., 1998).

The synaptic ribbon tethers hundreds of vesicles and anchors to the plasma membrane. There, tens of vesicles along the base of the ribbon are apposed to the presynaptic membrane to form a linear active zone at the apex of an invagination that is 500 nm deep. The invagination houses multiple processes: two horizontal cell spines flank

one or more bipolar dendrites (Fig. 17.9). At the mouth of the invagination and tiling the base of the presynaptic terminal, other bipolar dendrites form specialized contacts: a few for the rod (Hack et al., 1999; Tsukamoto et al., 2001) and *hundreds* for the cone (Fig. 17.9; Haverkamp et al., 2000).

When a vesicle containing $\sim 10^3$ glutamate molecules fuses at the apex of the invagination, some of the molecules diffuse rapidly across the 20-nm cleft to AMPA receptors on the horizontal cell spines. Other glutamate molecules diffuse more slowly down the 500-nm invagination to encounter mGluR6 glutamate receptors on the invaginating or “semi-invaginating” bipolar dendrites (Fig. 17.9). Additional glutamate molecules diffuse still more slowly for 1000 nm or more to reach AMPA and kainate receptors on the “basal” bipolar dendrites that tile the terminal’s base. Consequently, each vesicle delivers glutamate as a brief “pulse” or a slower “puff” to more than 10 (probably closer to 50) postsynaptic processes (DeVries, 2000; Haverkamp et al., 2000; Rao-Mirotznik et al., 1995, 1998).

This three-dimensional synaptic architecture confers two important advantages. First, by allowing every vesicle to affect many postsynaptic processes, the apparent cost of the photoreceptor’s high basal rate of vesicle release is effectively reduced. Second, by allowing each active zone to affect

many postsynaptic processes, considerable synaptic divergence is achieved with minimum wire volume. Although many brain regions disallow “spillover” between synapses, the photoreceptors present a clear case where spillover is both extensive and deliberate; that is, it represents not a failure, but an intrinsic part of the design.

“Engineered spillover” requires that glial processes avoid the synaptic regions. For if the glia invaded, their transporters that rapidly bind and remove extracellular glutamate, would sharply restrict its spatiotemporal distribution (Lehre and Danbolt, 1998). Consequently, Müller glia avoid the invaginations and territory beneath the terminal

(Sarantis and Mobbs, 1992; Burris et al., 2002). Glial membranes do wrap the photoreceptor axon and the upper surface of the terminal (Fig. 17.9). They separate adjacent synaptic terminals except where the membranes are pierced by fine processes that form cone-cone and cone-rod gap junctions.

Three pathways divide the rod system’s intensity range

In starlight the rod system employs many detectors but catches only a few photons, so the signal in each detector is binary: usually 0 and rarely 1. In moonlight the detectors still operate in binary mode, but with fewer 0s and more 1s. In twilight (or dawn) each detector catches more than one photon and thus has a coarsely graded signal. Each condition presents a different challenge for signal processing, each solved with a different circuit (Fig. 17.10).

STARLIGHT CIRCUIT: TWO STAGES OF CONVERGENCE EMPLOY NONLINEAR AMPLIFICATION The challenge in starlight is to separate the small signal in one rod from the continuous dark noise in many rods. The voltage evoked by one photon rises above the dark noise only modestly, by a factor of ~ 4 (Baylor

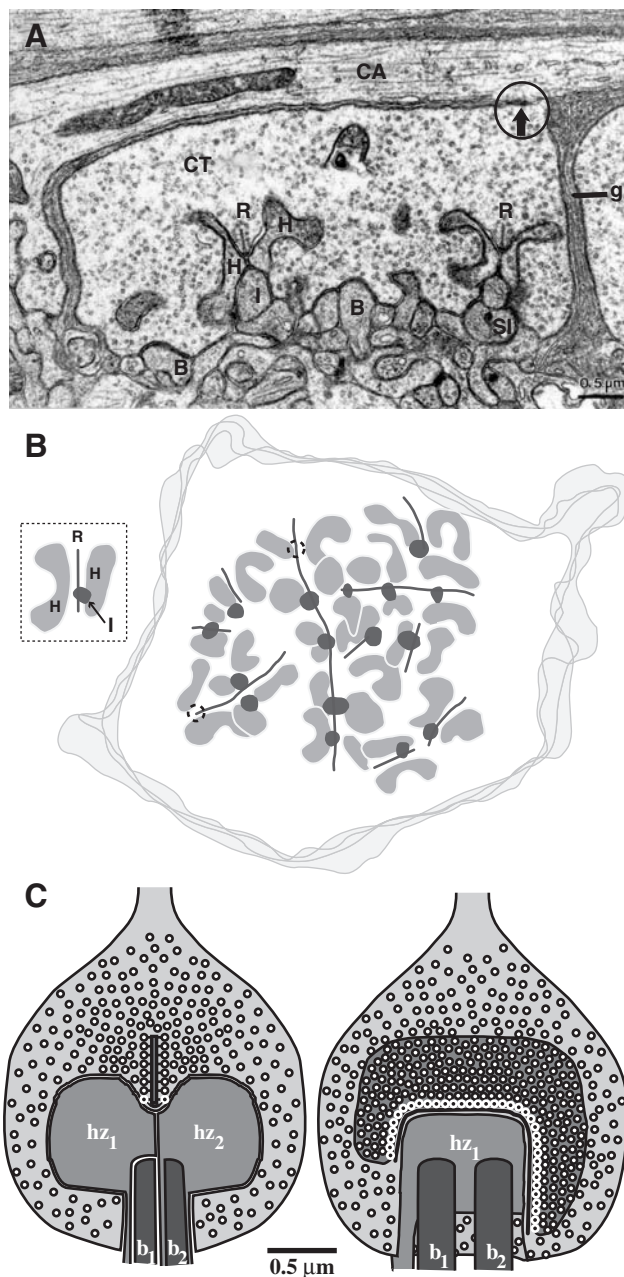


FIGURE 17.9. The cone uses many ribbon synapses to transmit a graded signal; the rod uses one ribbon to transmit a binary signal. *A*, Ultrathin section (~ 90 nm) through a macaque fovea cone terminal. Two ribbons (*R*) and their postsynaptic triads (*H*, *H*, *I*) are present, but full reconstruction shows 20 triads. At the base, semi-invaginating (*SI*) and basal (*B*) dendrites are also shown; full reconstruction shows several hundred such dendrites. The circled arrow indicates the gap junction with the adjacent terminal. Full reconstruction shows that every terminal connects to all its neighbors. Glial wrappings (*g*) separate the terminals, but avoid the terminal’s secretory region, consistent with “engineered spillover” of each vesicle to many postsynaptic processes. *B*, Cone terminal in tangential view, reconstructed from electron micrographs of serial sections (cat central area). Inset shows a triad:ribbon (*R*) with an ON bipolar dendritic tip (dark spot) flanked by two horizontal cell spines (*H*). The terminals contain 11.6 ± 0.9 ribbons. These vary in length from 0.2 to $3.5 \mu\text{m}$, but the total length per terminal is remarkably constant ($9.9 \pm 0.9 \mu\text{m}$; $N = 8$). This provides a constant number of docking sites for synaptic vesicles (~ 600) and a still larger “depot” of vesicles tethered to the faces of the ribbon (~ 3000). The cone terminal has 17 triads. Short ribbons serve a single triad; long ribbons serve up to 5 triads. *C*, Rod terminal in orthogonal views (from three-dimensional reconstruction, cat central area). A single tetrad is present, with one ribbon pointing between two horizontal cell processes (*hz*) toward two rod bipolar dendrites (*b*). Note that the bipolar dendrites are hundreds of nanometers distant from docked vesicles. (*A*, Electron micrograph from Tsukamoto et al., 1992, with permission. *B*, From Harkins & Sterling, unpublished work. *C*, From Rao-Mirotznik et al., 1995, with permission.)

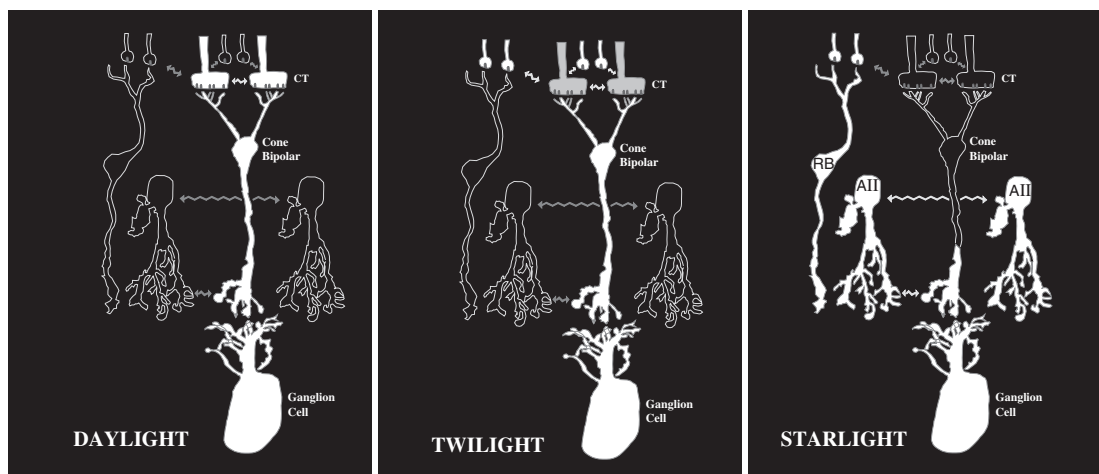


FIGURE 17.10. The final common pathway to the ganglion cell is served by three circuits. In daylight, cone signals are graded and thus require many ribbon synapses for transfer (both at the outer plexiform layer [OPL] and the inner plexiform layer [IPL]). In twilight, rod signals are graded and also require many ribbon synapses. Rods access these synapses by turning on their gap junctions to cone terminals, in effect “parasitizing” the multiple ribbon synapses available at both stages of the cone bipolar circuit. In starlight, rod signals are binary and thus require only one ribbon synapse (see Fig. 17.9C). The single-photon response cannot transfer via coupling to the cone terminal because the many rods lacking a photon add too much noise. Therefore, the rod-cone junction may turn off to transfer the binary signal via the rod’s ribbon synapse to the rod bipolar cell. The latter’s response will be coarsely graded

over some part of the intensity range (owing to rod convergence) and will thus require multiple ribbon synapses, which are present in the rod bipolar terminal. The AII cell’s response will be more finely graded (owing to rod bipolar convergence) and will thus require yet more ribbon synapses. The AII cell gains access to these by turning on its gap junctions with cone bipolar terminals. Coupling of the AII cells—indirectly via the cone bipolar terminals and also directly via AII-AII junctions—spreads current widely enough to enlarge the ganglion cell’s summation area well beyond its dendritic tree. This improves the S:N ratio in very dim light, but would degrade acuity in brighter light. Therefore, both sets of junction are regulated and presumably uncouple in twilight and daylight. See text for further explanation. (Modified from Sterling, 1998.)

et al., 1984). But the next neuron in the circuit, the rod bipolar cell, pools input from many rods ($n = 20$ to 120). If the rod synapse were linear, noise in the bipolar cell would rise as \sqrt{n} and swamp the single-photon event (Baylor et al., 1984). The problem could be solved by a nonlinear synapse that selectively amplified larger signals. This would effectively remove the dark noise by “thresholding,” but at the cost of also removing single-photon events on the small end of the amplitude distribution (van Rossum and Smith, 1998). This mechanism has now been confirmed experimentally and shown to improve overall sensitivity compared to linear transfer (Fig. 17.11; Field and Rieke, 2002).

Of course, signals in each rod bipolar cell are also sparse and each has noise. So the circuit must converge tens of rod bipolar cells onto a second-stage interneuron, the AII amacrine cell, without swamping the signal (Fig. 17.10). Again the solution involves a nonlinearity: larger rod bipolar inputs are selectively amplified by voltage-sensitive sodium channels in the AII cell (Boos et al., 1993; Smith and Vardi, 1995). Then AII cells send current via gap junctions to depolarize ON cone bipolar terminals. Simultaneously the AII also releases inhibitory transmitter (glycine) to hyperpolarize the OFF cone bipolar terminals and OFF ganglion cells. The overall circuit allows a single-photon event to

evoke a discrete “firing event” (1 to 3 spikes) in several ON ganglion cells and to suppress an equal number of spikes in several OFF ganglion cells (Barlow et al., 1971; Mastrorarde 1983).

MOONLIGHT CIRCUIT: LINEAR CHEMICAL SYNAPSE ONTO OFF CONE BIPOLAR As photon density rises slightly, a second rod pathway comes into play. Some rods synapse on dendrites of an OFF cone bipolar cell (Hack et al., 1999; Soucy et al., 1998; Tsukamoto et al., 2001). This synapse amplifies linearly and thus transfers all photon events, which when summed, exceed the noise (Fig. 17.11C; Field and Rieke, 2002; Sterling, 2002). Although only a few rods manage to contact a cone bipolar dendrite, the small gap junctions between rod terminals might couple them at this intensity to pool the signals (Fig. 17.11; Tsukamoto et al., 2001). This pathway has been found so far only in rodents.

TWILIGHT CIRCUIT: ROD ELECTRICAL SYNAPSE ONTO CONE When photon density reaches one photon/rod/ integration time (twilight, dawn), rod signals are processed by cone circuits (Fig. 17.10). Each rod terminal forms gap junctions with two cone terminals, and every cone terminal is

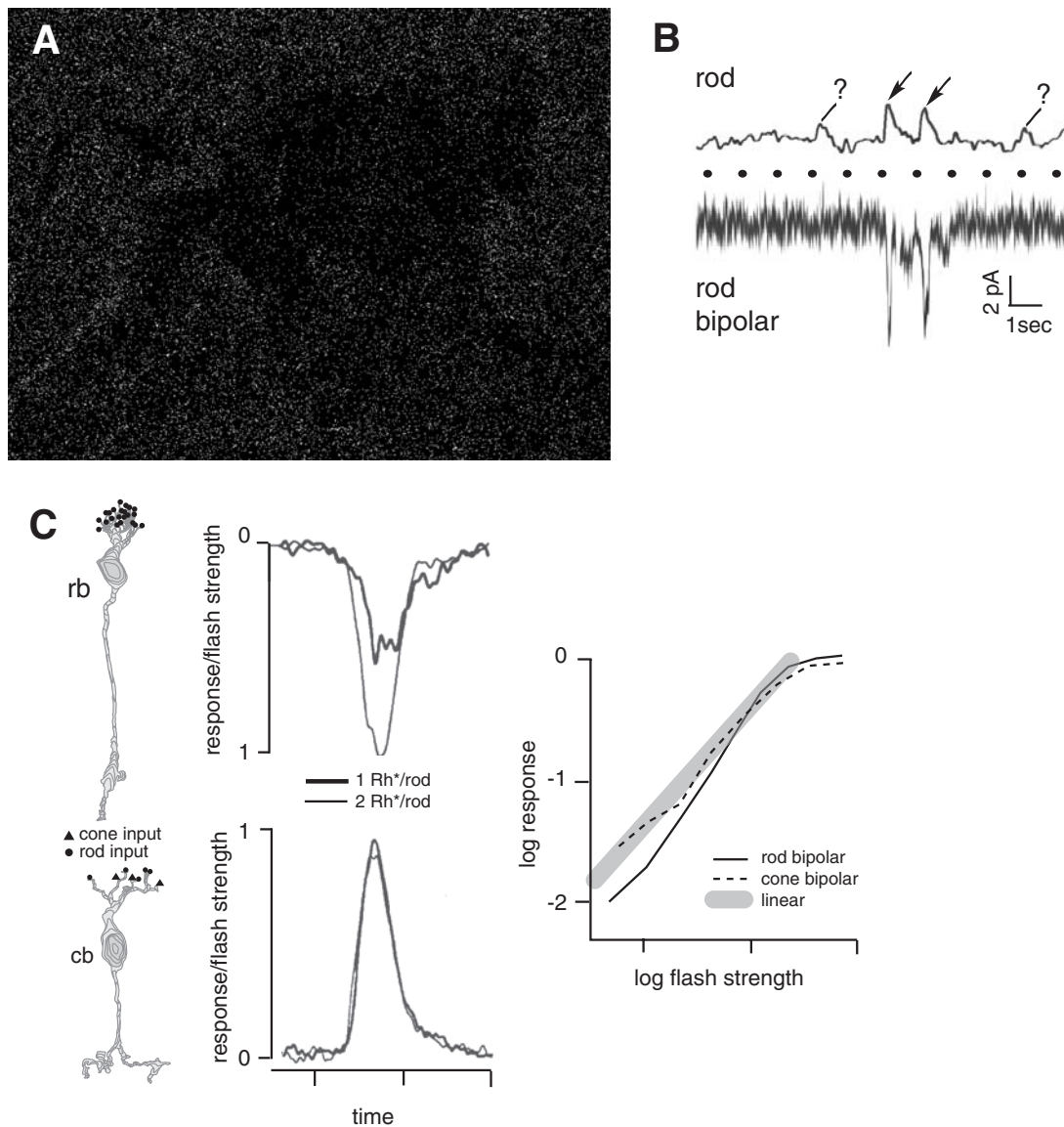


FIGURE 17.11. *A*, Faint image of a baboon in starlight painted by photons in “pointillist” fashion. The probability of each pixel receiving a photon is governed by a Poisson distribution, whose mean corresponds roughly to the intensities used by Field and Rieke (2002). *B*, Single-photon event in a rod rises clearly above the continuous noise (arrows) only when it is considerably larger than average. The same event in the rod bipolar cell is faster, with a much improved signal-to-noise ratio. The dotted trace represents flash timing. *C*, *Left*, A rod bipolar (rb) cell collects chemical synapses from 20 rods, whereas the cone bipolar (cb) cell collects

from only a few rods. However, each rod probably pools signals from neighboring rods via gap junctions. *Middle*, Response amplitudes normalized for flash intensity. The cone bipolar response doubles for twice the intensity, but the rod bipolar response more than doubles. *Right*, Input/output curve for the cone bipolar cell is essentially linear, in contrast to that for the rod bipolar cell, which is clearly nonlinear. (*A*, Image courtesy of A. Hsu and R. Smith. *C*, Neurons, reprinted from Tsukamoto et al., 2001; responses replotted from Field and Rieke, 2002.)

contacted by ~40 rods (Smith et al., 1986; Sterling et al., 1988). The rod signal (recognized by its spectral peak and time course) is observed in recordings from the cone (Nelson, 1977; Schneeweis and Schnapf, 1995, 1999). Rod signals are also present in horizontal cells whose dendrites do not contact rods (Nelson, 1977). Thus, electrical coupling from many rods to each cone allows the graded rod signal to be filtered and relayed by the same circuits used by the graded

cone signals. This design reduces wire volume and metabolic cost.

Daylight circuit requires “bandpass filter” at the cone synapse

Recall that most sensory systems convert a receptor cell’s graded potential into action potentials, either directly or

after interpolating a single synapse (Fig. 17.3). But this requires special mechanisms that precede or accompany transduction to filter out noise and redundant signals. For example, the auditory, vestibular, and somatosensory systems employ complex mechanical filters before transduction to select particular temporal frequencies. And the olfactory and taste senses use more than 1000 different heptahelical receptors to select particular chemical stimuli (Zhang and Firestein, 2002). The eye employs only mild optical filtering,⁴ and cones employ relatively minor molecular filtering (2 to 3 heptahelical receptors) to divide spectral bandwidth. Lacking vigorous preneural filtering or extensive molecular filtering by the transducer, the retina requires neural circuits to perform spatial and temporal bandpass filtering at the first synapse (Fig. 17.12).

The photovoltage arriving at the cone synaptic terminal spreads to neighboring cone terminals. This coupling filters noise intrinsic to the cones. In “steady” light, the cone voltage fluctuates owing to photon noise and biochemical noise arising from the transduction cascade. These noise sources are independent between cones, whereas the signals are locally correlated between cones owing to correlations in the visual scene plus optical blur. Therefore, coupling reduces noise more than the signal. For a coupling strength of about 1 nS, neural blur in human fovea is narrower than the optical blur. Yet, because it gives the cone a slightly broader receptive field than the cone’s optical aperture, it is detectable psychophysically. This lowpass filtering is calculated to improve the S:N ratio by about 60% at the cone terminal for spatial frequencies below 20 cycles/degree (DeVries et al., 2002).

The other essential step is to attenuate signals that are broadly correlated across cones. Correlations arise from the coarse structure in an image (low spatial and temporal frequencies) which delivers similar intensities to neighboring cones. (Think of a blackboard or a uniformly bright wall, or any spatial pattern that is temporally invariant.) These broadly correlated signal components carry little information about image structure and are therefore redundant. Removing them allows the cone synapse to use its dynamic range for what is essential, the *differences* between adjacent regions. In the jargon of signal processing, such filtering is

termed “background subtraction,” “contrast enhancement,” or “highpass filtering.” The theory for optimally matching the spatiotemporal bandpass filter to ambient light intensity is well developed (Srinivasan et al., 1982; van Hateren, 1992).

This essential integrative step is accomplished by the horizontal cell, which collects synaptic input from many cones (Fig. 17.12). The horizontal cell’s spines invaginate the cone terminal, forming the paired, lateral elements of the triad where they express AMPA receptors (Fig. 17.9A; Haverkamp et al., 2001). The horizontal cell pools its signal electrically with neighboring cells. These connections produce a broad receptive field that represents a slightly delayed, center-weighted average of the cone membrane potential. Many diurnal mammals (e.g., cat, rabbit, and guinea pig) express two types of horizontal cell that connect to the same cones. One type is narrow-field with weaker coupling, the other is broad-field with stronger coupling (reviewed by Mills and Massey, 1994; Vaney, 1993). The two patterns of connection cause correspondingly different weighting functions, but they both project feed back negatively onto the cone terminal and bipolar dendrites, creating a receptive field surround with the proper overall weight (see Fig. 17.12; Smith, 1995).

The negative sign of this feedback arises from gamma-aminobutyric acid (GABA), which the horizontal cells synthesize and release via an unconventional mechanism (Schwartz, 1987). These cells lack synaptic vesicles but release the transmitter by reverse action of a GABA transporter, apparently the vesicular GABA transporter (VGAT), which at conventional synapses loads GABA into vesicles (Haverkamp et al., 2000). GABA acts at the bipolar cell dendritic tips which express GABA_A and GABA_C receptors (Haverkamp et al., 2000; Vardi et al., 1992). These ligand-gated chloride channels pose an important puzzle: although GABA’s function is to antagonize the stimulus, light depolarizes some bipolar cells (ON cells) and hyperpolarizes others (OFF cells). So how can the same receptor molecule mediate opposite effects? The current idea is that ON bipolar dendrites express a cotransporter that *accumulates* chloride (NKCC), and OFF bipolar dendrites express a cotransporter that *extrudes* chloride (KCC2). This would set E_{Cl} for the two bipolar classes on opposite sides of the membrane potential, so that GABA would drive their voltages in opposite directions (Vardi et al., 2000). Experimental support for this idea is so far underwhelming (Sato et al., 2001; Billups and Attwell, 2002).

The cone terminal itself may express a GABA_A receptor, but this remains controversial (Pattnaik et al., 2000; Picaud et al., 1998). A different mechanism, perhaps equally controversial, has been proposed for horizontal cell feedback

⁴ Optical blur attenuates spatial frequencies greater than can be resolved by the cone array. For example, optics in the human fovea cut off frequencies above 60 cycles/degree. This precisely matches the foveal sampling rate (120 cones/degree), given Nyquist’s rule that there must be one detector for each half cycle. Although it might seem counterintuitive that optical blur could *improve* vision, frequencies higher than the sampling rate would be seen as lower frequencies, and thus cause a kind of noise termed “aliasing” (Williams, 2003). The matching of optics to cone sampling rate further exemplifies the principle of symmorphosis.

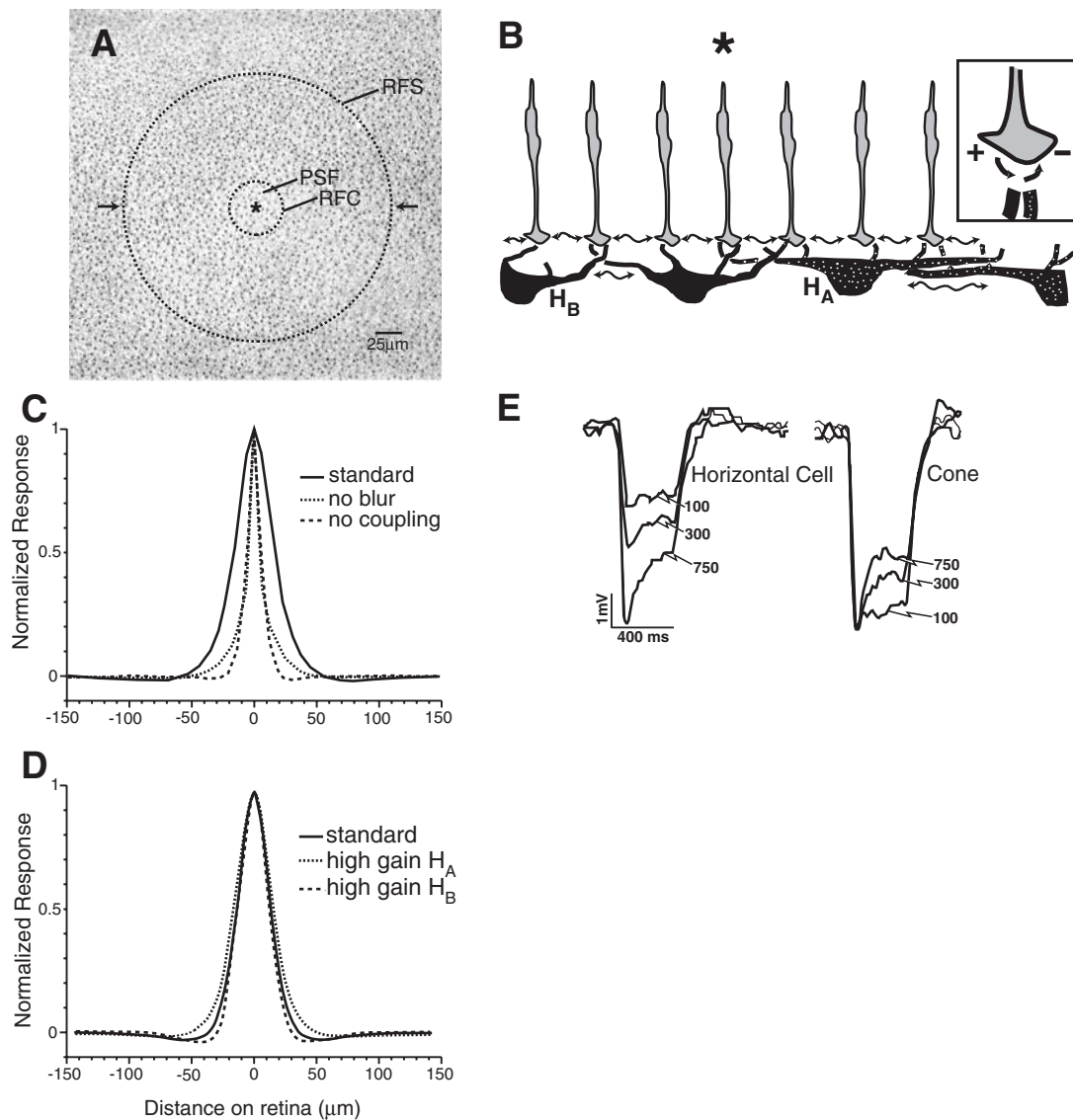


FIGURE 17.12. A center-surround receptive field (“bandpass filter”) arises at the cone terminal. *A*, Cone array, cat central area (24,000/mm²). A point of light striking the cornea spreads, owing to optical blur (PSF, point spread function), to stimulate about 10 cones. The signal spreads further, via coupling at cone terminals, creating a receptive field center (RFC) for one cone (*) that encompasses about 50 cones. Inhibitory feedback via horizontal cells creates a receptive field surround (RFS) encompassing about 1200 cones. *B*, Neural circuit that shapes the cone receptive field. The arrow between the terminals denotes coupling; the surround is shaped by inhibitory feedback (*inset*). *C*, Calculated sensitivity across

the cone receptive field (area between arrows in *A*). To achieve the proper spatial weight requires both optical blur and cone-cone coupling. For surround; narrow, deep region set by the narrow-field H_B cell; broad, shallow region set by the wide-field H_A cell. *D*, Calculated sensitivity as presented in *C*. *E*, Intracellular recordings from squirrel retina. Enlarging a bright spot over a horizontal cell, from 100 μm to 750 μm in diameter, gives progressively larger responses. The same sequence, when applied to a cone, gives the greatest response to a small spot (100 μm) and rising attenuation (somewhat delayed) to larger spots. (*A* to *D*, Adapted from Smith, 1995. *E*, Adapted from Leeper and Charlton, 1985.)

onto the cone terminal (Kamermans et al., 2001). The horizontal cell spine expresses a gap junction channel protein (connexin), but does not form a gap junction with the opposing cone membrane. This dab of connexin is thought to be a hemichannel, observed previously in isolated horizontal cells (DeVries and Schwartz, 1992). The idea is that when the horizontal cell depolarizes, releasing GABA onto bipolar

dendrites, it also injects negative current into the extracellular space near the cone terminal’s voltage-sensitive calcium channels. This reduces the calcium current and thus the cone terminal’s synaptic gain (Kamermans et al., 2002). How these apparently disparate mechanisms cooperate to remove redundant information from the cone terminal remains to be determined.

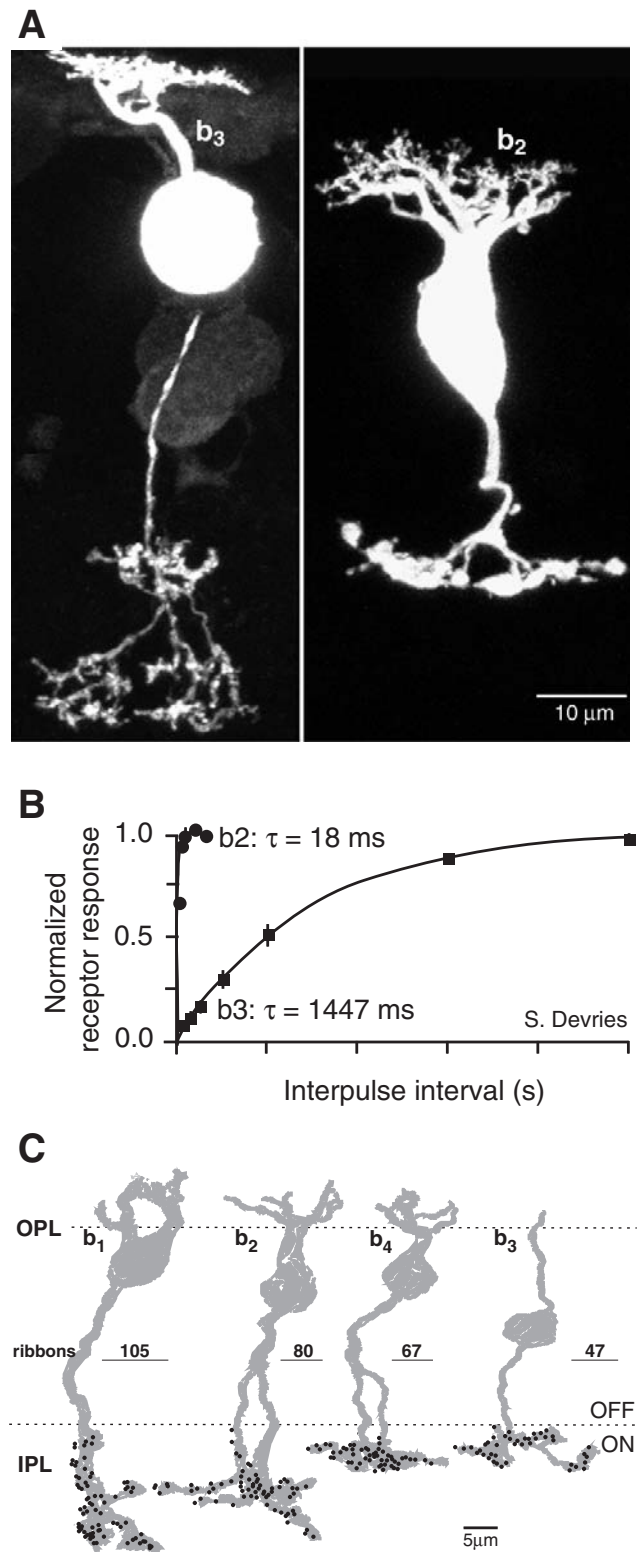
FIGURE 17.13. Two types of OFF cone bipolar cell (b3, b2) from a ground squirrel. *A*, Differences in axon caliber predict few ribbon outputs for b3 and more for b2. *B*, The difference also predicts higher temporal bandwidth for b2. Consistent with this, b2 shows much faster recovery from receptor desensitization, measured by removing the bipolar cells from a slice and measuring paired-pulse responses using a rapid perfusion system. *C*, ON cone bipolar cells (b1 to b4) from cat. Axons decrease in diameter from left to right, expressing fewer ribbons. OPL, outer plexiform layer; IPL, inner plexiform layer, expressing fewer ribbons. (*A* and *B*, From S. DeVries, unpublished. *C*, Modified from Cohen and Sterling, 1990.)

Ten bipolar pathways (!) divide the cone signal

In daylight, the cone system uses relatively few detectors but catches many photons, so the signal in each detector (derived from 10^3 to 10^6 photons) is finely graded. This challenges neural circuitry in a manner opposite to the rod system, not with sparse information, but with a plethora. Even after bandpass filtering, the information in a cone signal exceeds the coding capacity of a single second-order neuron. The solution is to divide the signal into different components and transmit them to the inner retina over multiple circuits (Boycott and Wässle, 1991; Cohen and Sterling, 1990; Euler et al., 1996; Kolb et al., 1981; McGillem and Dacheux, 2001; McGuire et al., 1984).

The contrast signal created by horizontal cell filtering is halved at the cone output⁵ (see Figs. 17.2, 17.4, and 17.12). Signals dimmer than the mean depolarize one class of bipolar cell (OFF cells), and signals brighter than the mean depolarize another class (ON cells). To achieve this, the cone releases glutamate simultaneously onto both bipolar classes, while their dendrites sense it with different receptors. The OFF bipolar dendrites express ionotropic receptors that *open* a cation channel; whereas the ON bipolar dendrites express a metabotropic receptor that *closes* a cation channel. The metabotropic receptor is mGluR6 (Masu et al., 1995; Nomura et al., 1994), which couples to $G_{\alpha o1}$ (Dhingra et al., 2000, 2002), but the rest of the cascade and the channel itself remain elusive.

OFF signals are routed to 3 to 5 types of bipolar cell (Fig. 17.13). The purpose is to divide the signal into different temporal components. In one bipolar type the excitatory postsynaptic current (EPSC) is slow and sustained; in another type it is intermediate; and in a third type it is fast and transient. These kinetic differences arise because the cone's tonic release of glutamate strongly desensitizes iGluR receptors, and the particular iGluRs expressed on each cell type recover



⁵Such circuits must have evolved quite early as they are present even in sharks, the most primitive fish.

at different rates (Fig. 17.13B; DeVries and Schwartz, 1999; DeVries, 2000). The OFF dendrites all contact the base of the cone terminal, but apparently at different distances from the sites of vesicle release: dendrites with large, fast currents are nearest, and dendrites with small, slow currents are farthest (DeVries, personal communication).

ON signals are also routed to five bipolar types, and for the same reason: to divide the signal into slow and fast components (Fig. 13B; Cohen and Sterling, 1990; Freed, 2000a). However, since ON dendrites express only one isoform of mGluR6, the temporal differences must arise differently than in the OFF system. One idea is that the calcium influx through the ON bipolar cation channel, which antagonizes the response (Nawy, 2000), might have different kinetics in each cell type (Awatramani and Slaughter, 2000). This is known to be true for photoreceptors. Further kinetic shaping of the bipolar responses certainly occurs at their axon terminals, owing to autofeedback onto group III metabotropic glutamate receptors and to extrinsic feedback from amacrine processes that release GABA onto GABA_C receptors (Awatramani and Slaughter, 2001; Euler and Masland, 2000; Freed et al., 2003).

BIPOLAR AXONS END IN DIFFERENT STRATA: STRUCTURE MATCHES INFORMATION CONTENT The two major classes of bipolar axon segregate at different levels of the inner plexiform layer, thus dividing it into OFF and ON laminae. Furthermore, within a lamina, each type of bipolar axon occupies a defined stratum, which can be quite thin (~2 μm) (Fig. 17.13). This implies that the inner plexiform layer finely stratifies temporal information, which can be further sharpened by amacrine circuits that extend laterally in fine strata (Roska and Werblin, 2001). Some of these signals are transmitted rapidly and regeneratively over long distances (millimeters) by spiking amacrine cells (Cook et al., 1998; Demb et al., 1999; Stafford and Dacey, 1997).

Because a channel's information content rises directly with bandwidth (Shannon and Weaver, 1949), the bipolar types that signal higher temporal frequencies convey more information. The structural correlates are the same as for the rod and cone. Low frequency ("sustained") bipolar cells have thinner axons with fewer ribbon synapses (~50 to 80); whereas high frequency ("transient") bipolar cells have thicker axons with more synapses (~100 to 120) (Calkins et al., 1994; Cohen and Sterling, 1990; Tsukamoto et al., 2001). The slowest, poorest signal of all belongs to the rod bipolar cell, which has the thinnest axon and fewest ribbon synapses (20 to 40) (Ghosh et al., 2001; McGuire et al., 1984; Tsukamoto et al., 2001).

Design of ganglion cell circuits

CERTAIN GANGLION CELLS SELECT ON OR OFF INPUTS, BUT OTHER TYPES COMBINE THEM Bipolar axons at the inner

plexiform layer deliver packets of information pooled from 5 to 10 cones. These graded signals are further pooled at the ganglion cell and re-encoded as spikes for transmission down the optic nerve. The specific pooling decisions are crucial because they irrevocably set the spatial and temporal resolution of all later stages. These decisions partly reflect the constraints already mentioned (dynamic range, noise, wire volume, and metabolic cost). But ganglion cells project to diverse brain regions that use different regions of the spatiotemporal frequency spectrum. Because further efficiencies can be achieved by matching the message to the "end user," ganglion cells are diverse, comprising some 10 to 20 types (Masland, 2001; O'Brien et al., 2002).

The separate ON and OFF channels established at the cone terminal are retained by ganglion cells. This is straightforward because bipolar cells employ ribbon synapses to release glutamate onto ganglion cell dendrites, and the latter always express iGluR receptors. Therefore, to collect either ON or OFF signals, a ganglion cell simply restricts its dendrites to either the upper or lower stratum of the inner plexiform layer. Indeed, many ganglion cell types continue to encode only the brighter or dimmer half of the contrast range. This is useful because the dynamic range of a neuron's spike-coding mechanism is limited, and this doubles the dynamic range available to encode contrast. Furthermore, to double the contrast range with one neuron, its spike number would need to rise fourfold, a metabolically costly strategy (Attwell and Laughlin, 2001; von der Twer and MacLeod, 2001).

Certain ganglion cells break this rule by sending one set of dendrites to the OFF layer and another to the ON layer. For example, one ganglion cell collects synapses from an ON bipolar cell with exclusively S-cone input (sensitive to **s**hort wavelengths) and additional synapses from OFF bipolar cells with M- and L-cone input (sensitive to **m**iddle and **l**ong wavelengths). This wiring renders the cell most sensitive to light rich in short wavelengths and least sensitive to light rich in middle and long wavelengths (Calkins et al., 1998; Chichilnisky and Baylor, 1999; Dacey and Lee, 1994; Martin et al., 1997). By encoding a spectrally opponent signal (colloquially, "blue minus yellow"), this cell discards spectrally redundant information that in a "generalist" ganglion cell occupies considerable dynamic range and metabolic energy. The spectrally filtered signal is clearly optimized for its particular end user, the koniocellular layer of the lateral geniculate nucleus, which projects to "color circuits" in striate cortex (reviewed in Calkins and Sterling, 1999).

"BRISK" GANGLION CELLS COMPRISE NARROW-FIELD AND WIDE-FIELD TYPES More than half of all ganglion cells fire "briskly" (Fig. 17.14). The spike autocorrelograms rise steeply, and the peak rates are high, more than 100

spikes/second (Cleland and Levick, 1974a; DeVries and Baylor, 1997). The axons of brisk cells are relatively thick and rapidly conducting (e.g., Kirk et al., 1975; Rowe and Stone, 1976a), so their wire volume occupies more than 95% of the optic nerve's cross section (Sterling, unpublished).

About 90% of brisk cells have narrow dendritic fields that collect from relatively few bipolar cells. Transient and sustained bipolar types both contribute, and accordingly, the narrow-field ganglion cell responds to both stimulus components (Cohen and Sterling, 1992; Freed, 2000b). Narrow-field ganglion cells tile the retina (independently for both ON and OFF types), and because they sample space most densely and project 1:1 to parvocellular geniculate neurons, these two cell types set spatial acuity for their main end users, namely, simple cells in striate cortex (Wässle and Boycott, 1991; Smallman et al., 1996).

About 10% of the brisk cells have wide dendritic fields that collect from many bipolar cells. The wide-field ganglion cell is 3-fold broader than the narrow-field cell at the same retinal locus and thus collects from nearly 10-fold more bipolar cells—all of the transient type—and nearly 10-fold more bipolar synapses (Kier et al., 1995; Freed and Sterling, 1988; Freed, 2000a). This design has several important consequences for the end users (superior colliculus and magnocellular pathways of the geniculostriate system). First, summing from many cones via many bipolar cells and bipolar synapses, the wide-field cell, compared to the narrow-field cell, has better S:N ratio and thus greater contrast sensitivity (Kaplan and Shapley, 1986). Threshold for the wide-field, brisk-transient ganglion cell to a spot over its dendritic field can be as low as 0.8% contrast (Dhingra et al., 2003). Second, wide spatial summation reduces sensitivity to high spatial frequencies (which are more effectively carried by narrow-field cells). This frees the cell's limited dynamic range to encode higher *temporal* frequencies and thus to match the input provided by transient bipolar cells (Figs. 17.4 and 17.14).

A third consequence of wide-field summation is that the ganglion cell responds vigorously to a fine stimulus that reverses contrast or moves within the dendritic field (Fig. 17.14; Hochstein and Shapley, 1976). Although the *array* of wide-field cells cannot detect fine detail when it is stationary (Fig. 17.4), the individual wide-field ganglion cell responds sensitively when the grating flickers or drifts (Fig. 17.14). This serves end users, such as neurons in cortical area MT that detect motion based on changes in luminance and contrast (Demb et al., 2001a, 2001b). This response property is termed “nonlinear” because brightening one region while dimming another evokes a vigorous response, whereas in a linear system (such as the narrow-field ganglion cell) the two changes simply cancel.

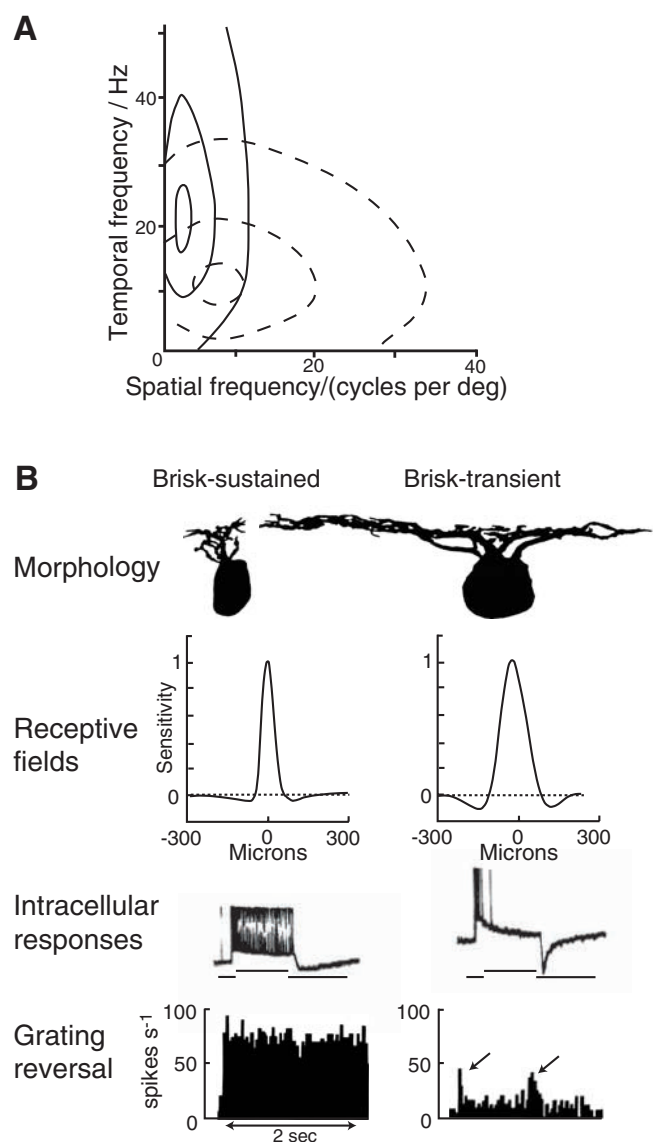


FIGURE 17.14. *A*, The spatiotemporal transfer function of the brisk-transient and brisk-sustained pathways. Contours are at 0.1, 0.5, and 0.9 of the maximum values. The brisk-sustained pathway is tuned to higher spatial frequencies and lower temporal frequencies. *B*, Radial views of ON brisk-sustained (narrow-field) and ON brisk-transient (wide-field) ganglion cells. The narrow-field cell collects 150 synapses (total) from several bipolar cells of each type (b1 to b4 in Fig. 17.13C). Because the bipolar cells have receptive fields broader than their spacing, their rectified responses cancel in the narrow-field ganglion cell and give no response to reversal of a fine grating. The wide-field cell collects about 600 synapses from about 150 bipolar cells, mostly from the transient bipolar cell (b1 in Fig. 17.13). Because the bipolar receptive fields are narrower than the large convergent array, the wide-field cells respond at each grating reversal (arrows). This “frequency doubling” arises because the rectified responses of individual bipolar cells are collected across such a wide field that they cannot cancel (Demb et al., 2001a). (*A*, Reprinted from Eckert and Buchsbaum, 1993. *B*, Modified from Sterling, 1998. Intracellular records from Saito, 1983. Spike histograms from Hochstein and Shapley, 1976.)

The nonlinear mechanism was initially attributed to amacrine circuits because bipolar circuits were thought to be linear. But we now know that the bipolar cell synapse expresses an important nonlinear property, “rectification.” The bipolar synapse releases vesicles at a low basal rate; consequently, depolarization can increase release, but hyperpolarization cannot decrease it. Therefore, dimming an OFF bipolar cell increases release but brightening does not decrease it (and vice versa for an ON bipolar cell). This nonlinearity hardly affects a narrow-field ganglion cell because the bipolar receptive fields overlap due to cone coupling (Cohen and Sterling, 1992; Smith and Sterling, 1990). However, it strongly affects a wide-field cell because bipolar receptive fields are smaller than the extent of the convergent array (Demb et al., 2001a; Freed and Sterling, 1988). This important property of wide-field cells, which arises simply from their extent of spatial convergence, may be the clearest example at the circuit level of an “emergent property.”

SLUGGISH GANGLION CELLS: SMALLER, SLOWER, CHEAPER Nearly half of the ganglion cells fire “sluggishly.” Their spike autocorrelograms show a gradual rise and plateau, and their peak rates are ~10-fold lower than for brisk cells (Cleland and Levick, 1974a; DeVries and Baylor, 1997). The axons of sluggish cells are thin and slowly conducting (Stone and Fukuda, 1974). Consequently, their wire volume is minimal, occupying less than 5% of the optic nerve’s cross-section (Sterling, unpublished). Sluggish cells (also termed “W”) comprise many types with complex response properties, such as directional selectivity and local-edge detection (e.g., Caldwell and Daw, 1978; Cleland and Levick, 1974b; Rowe and Stone, 1976a, 1976b).

Sluggish types have been relatively little studied, partly because, compared to types that fire briskly, these cells seem somehow disadvantaged. Yet, this might actually imply a different coding strategy (Meister and Berry, 1999; Victor, 1999). A cell that responds only to motion of a local edge at low velocity carries fewer possible messages than a cell that responds to a wider range of stimuli. The simpler message might be encoded efficiently by fewer spikes that cost less in energy and in wire volume (Ames and Li, 1992; Ames et al., 1992; Attwell and Laughlin, 2001; Balasubramanian and Berry, 2002). For these benefits, slower conduction velocity seems to be an acceptable cost.

IS INFORMATION CONTENT THE SOLE DETERMINANT OF WIRE VOLUME? The hypothesis that wire volume matches information content arouses a healthy skepticism and thus needs some elaboration. The hypothesis tries to unify three facts: (1) axon thickness rises with number of output synapses; (2) the neurons with thicker axons and more outputs are the ones that transmit higher temporal frequen-

cies; (3) higher temporal frequencies transmit more information. Points 1 and 2 are illustrated in Figure 17.8, 17.13, and 17.14; point 3 comes from Shannon’s equation. The hypothesis claims that more synapses are required at the output because the information capacity of the synapse is limited (de Ruyter van Steveninck and Laughlin, 1996; Laughlin, 1994).

Of course, there may be other reasons why a neuron might need additional synapses and thus a larger axon. For example, the brisk-transient ganglion cell (but not the brisk-sustained cell) typically sends one branch to innervate the lateral geniculate nucleus and another branch to the superior colliculus. Thus, its greater axon thickness may be partly attributable to its greater number of boutons in the geniculate and partly to its need to support an additional arbor. In short, the hypothesis does not exclude additional determinants of wire volume.

Conclusion

Many features of retinal design seem interpretable as evolutionary adaptations to a surprisingly small number of lifestyle decisions and physical constraints:

1. Because mammals move fast, their photoreceptors must be small. Because mammals forage night and day, they need both rods and cones. So rods must be numerous and information poor, whereas cones can be sparse and information rich.
2. The two receptor arrays require different circuits. Rods must converge in large numbers—yet not accumulate noise that would swamp their information-poor signals. This requires several stages, each equipped to remove noise by nonlinear amplification. Cones must converge in smaller numbers—yet not allow their information-rich signals to saturate postsynaptic neurons. This requires bandpass filtering to reduce redundancy and noise.
3. The retina must remain thin and cannot increase its metabolic rate. Therefore, rod and cone circuits must jointly minimize total cellular volume and metabolic cost. Indeed, each circuit seems constrained to expend these quantities in proportion to its information content.

Some additional circuits (mainly amacrine) are known but not described here, and many additional amacrine circuits remain to be discovered. But quite likely their purposes will prove generally similar: to optimize signal transfer using various forms of neural adaptation or gain control. Many of the matches suggested here under the rubric of symmorphosis lack quantitative rigor. This suggests the next large task: to quantify for each retinal circuit, its information rate, metabolic cost, and wire volume, and to test quantitatively the relationships between these three variables. When this is accomplished, the retina will finally be “understood.”

Acknowledgments

I thank Drs. Robert Smith, Martin Wilson, and David Vaney for comments on the manuscript, and Sharron Fina for preparing it. My research has been supported by NEI grants EY00828 and EY08124. I thank Drs. Steven DeVries and Amy Harkins for providing unpublished data for Figures 17.9 and 17.13.

REFERENCES

- Adam, G., and M. Delbrück, 1968. Reduction of dimensionality in biological diffusion processes, in *Structural Chemistry and Molecular Biology* (A. Rich and N. Davidson, eds.), San Francisco, CA: W. H. Freeman & Company.
- Ames, A. I., and Y. -Y. Li, 1992. Energy requirements of glutamatergic pathways in rabbit retina, *J. Neurosci.*, 12:4234–4242.
- Ames, A. I., Y. -Y. Li, E. C. Heher, and C. R. Kimble, 1992. Energy metabolism of rabbit retina as related to function: high cost of Na⁺ transport, *J. Neurosci.*, 12:840–853.
- Ashmore, J. F., and D. Copenhagen, 1983. An analysis of transmission from cones to hyperpolarizing bipolar cells in the retina of the turtle, *J. Physiol.*, 340:569–597.
- Attwell, D., 1986. The Sharpey-Schafer Lecture: ion channels and signal processing in the outer retina, *Q. J. Exp. Physiol.*, 71:497–536.
- Attwell, D., and S. Laughlin, 2001. An energy budget for signaling in the grey matter of the brain, *J. Cerebr. Blood F. Met.*, 21:1133–1145.
- Awatramani, G. B., and M. M. Slaughter, 2000. Origin of transient and sustained responses in ganglion cells of the retina, *J. Neurosci.*, 20:7087–7095.
- Awatramani, G. B., and M. M. Slaughter, 2001. Intensity-dependent, rapid activation of presynaptic metabotropic glutamate receptors at a central synapse, *J. Neurosci.*, 21:741–749.
- Baseler, H. A., A. A. Brewer, L. T. Sharpe, A. B. Moreland, H. Jagle, and B. A. Wandell, 2002. Reorganization of human cortical maps caused by inherited photoreceptor abnormalities, *Nat. Neurosci.*, 5:364–370.
- Balasubramanian, V., and M. J. Berry II, 2002. A test of metabolically efficient coding in the retina, *Network*, 13:531–552.
- Barlow, H. B., W. R. Levick, and M. Yoon, 1971. Responses to single quanta of light in retinal ganglion cells of the cat. *Vis. Res.*, S3:87–101.
- Baylor, D. A., T. D. Lamb, and K.-W. Yau, 1979. Responses of retinal rods to single photons, *J. Physiol.*, 288:613–634.
- Baylor, D. A., B. J. Nunn, and J. L. Schnapf, 1984. The photocurrent, noise and spectral sensitivity of rods of the monkey *Macaca fascicularis*, *J. Physiol.*, 357:575–607.
- Billups, D., and D. Attwell, 2002. Control of intracellular chloride concentration and GABA response polarity in rat retinal ON bipolar cells, *J. Physiol.*, 545:183–198.
- Boos, R., H. Schneider, and H. Wässle, 1993. Voltage- and transmitter-gated currents of AII-amacrine cells in a slice preparation of the rat retina, *J. Neurosci.*, 13:2874–2888.
- Boycott, B. B., and H. Wässle, 1991. Morphological classification of bipolar cells of the primate retina, *Eur. J. Neurosci.*, 3:1069–1088.
- Burns, M. E., and D. A. Baylor, 2001. Activation, deactivation, and adaptation in vertebrate photoreceptor cells, *Annu. Rev. Neurosci.*, 24:779–805.
- Burns, M. E., and T. D. Lamb, 2003. Visual transduction by rod and cone photoreceptors, in *Visual Neurosciences* (L. Chalupa and J. S. Werner eds.), Cambridge MA: MIT Press.
- Burris, C., K. Klug, I.-T. Ngo, P. Sterling, and S. Schein, 2002. How Müller glial cells in macaque fovea coat and isolate the synaptic terminals of cone photoreceptors, *J. Comp. Neurol.*, 453:100–111.
- Caldwell, J. H., and N. W. Daw, 1978. New properties of rabbit retinal ganglion cells, *J. Physiol.*, 276:257–276.
- Calkins, D. J., S. Schein, Y. Tsukamoto, and P. Sterling, 1994. M and L cones in Macaque fovea connect to midget ganglion cells via different numbers of excitatory synapses, *Nature*, 371:70–72.
- Calkins, D. J., and P. Sterling, 1999. Evidence that circuits for spatial and color vision segregate at the first retinal synapse, *Neuron*, 24:313–321.
- Calkins, D. J., Y. Tsukamoto, and P. Sterling, 1998. Microcircuitry and mosaic of a blue/yellow ganglion cell in the primate retina, *J. Neurosci.*, 18:3373–3385.
- Calvert, P. D., V. I. Govardovskii, N. Krasnoperova, R. E. Anderson, J. Lem, and C. L. Makino, 2001. Membrane protein diffusion sets the speed of rod phototransduction, *Nature*, 411:90–94.
- Chichilnisky, E. J., and D. A. Baylor, 1999. Receptive-field microstructure of blue-yellow ganglion cells in primate retina, *Nat. Neurosci.*, 2:889–893.
- Cleland, B. G., and W. R. Levick, 1974a. Brisk and sluggish concentrically organized ganglion cells in the cat's retina, *J. Physiol. (Lond.)*, 240:421–456.
- Cleland, B. G., and W. R. Levick, 1974b. Properties of rarely encountered types of ganglion cells in the cat's retina and an overall classification, *J. Physiol.*, 240:457–492.
- Cohen, E., and P. Sterling, 1990. Demonstration of cell types among cone bipolar neurons of cat retina, *Philos. Trans. R. Soc. Lond. B*, 330:305–321.
- Cohen, E., and P. Sterling, 1992. Parallel circuits from cones to the on-beta ganglion cell, *Eur. J. Neurosci.*, 4:506–520.
- Cook, P. B., P. D. Lukasiewicz, and J. S. McReynolds, 1998. Action potentials are required for the lateral transmission of glycinergic transient inhibition in the amphibian retina, *J. Neurosci.*, 18:2301–2308.
- Curcio, C. A., K. R. Sloan, R. E. Kalina, and A. E. Hendrickson, 1990. Human photoreceptor topography, *J. Comp. Neurol.*, 292:497–523.
- Curcio, C. A., K. R. Sloan, Jr. O. Packer, A. E. Hendrickson, and R. E. Kalina, 1987. Distribution of cones in human and monkey retina: individual variability and radial asymmetry, *Science*, 236:579–582.
- Dacey, D. M., and B. B. Lee, 1994. The “blue-on” opponent pathway in primate retina originates from a distinct bistratified ganglion cell type, *Nature*, 367:731–735.
- de Ruyter van Steveninck, R., and S. B. Laughlin, 1996. The rate of information transfer at graded-potential synapses, *Nature*, 379:642–645.
- Demb, J. B., K. Zaghloul, L. Haarsma, and P. Sterling, 2001a. Bipolar cells contribute to nonlinear spatial summation in the brisk transient (Y) ganglion cell in mammalian retina, *J. Neurosci.*, 21:7447–7454.
- Demb, J. B., L. Haarsma, M. A. Freed, and P. Sterling, 1999. Functional circuitry of the retinal ganglion cell's nonlinear receptive field, *J. Neurosci.*, 19:9756–9767.

- Demb, J. B., K. Zaghoul, and P. Sterling, 2001b. Cellular basis for the response to second-order motion cues in Y retinal ganglion cells, *Neuron*, 32:711–721.
- DeVries, S. H., and E. A. Schwartz, 1992. Hemi-gap-junction channels in solitary horizontal cells of the catfish retina, *J. Physiol.*, 445:201–230.
- DeVries, S. H., 2000. Bipolar cells use kainate and AMPA receptors to filter visual information into separate channels, *Neuron*, 28:847–856.
- DeVries, S. H., and D. A. Baylor, 1997. Mosaic arrangement of ganglion cell receptive fields in rabbit retina, *J. Neurophysiol.*, 78:2048–2060.
- DeVries, S. H., X. Qi, R. G. Smith, W. Makous, and P. Sterling, 2002. Electrical coupling between mammalian cones, *Curr. Biol.*, 12:1900–1907.
- DeVries, S. H., and E. A. Schwartz, 1999. Kainate receptors mediate synaptic transmission between cones and “Off” bipolar cells in a mammalian retina, *Nature*, 397:157–160.
- Dhingra, A., M. Jiang, T.-L. Wang, A. Lyubarsky, A. Savchenko, T. Bar-Yehuda, P. Sterling, L. Birnbaumer, and N. Vardi, 2002. Light response of retinal ON bipolar cells requires a specific splice variant of $G_{\alpha o}$, *J. Neurosci.*, 22:4878–4884.
- Dhingra, A., A. Lyubarsky, M. Jiang, E. N. Pugh, Jr., L. Birnbaumer, P. Sterling, and N. Vardi, 2000. The light response of ON bipolar neurons requires $G_{\alpha o}$, *J. Neurosci.*, 20:9053–9058.
- Dhingra, N. K., Y.-H. Kao, P. Sterling, and R. G. Smith, 2003. Contrast threshold of a brisk-transient ganglion cell, *J. Neurophysiol.* (in press).
- Diamond, J., 1993. Evolutionary physiology, in *The Logic of Life* (C. A. R. Boyd and D. Noble, eds.), New York: Oxford University Press, pp. 89–111.
- Diamond, J., and K. Hammond, 1992. The matches, achieved by natural selection, between biological capacities and their natural loads, *Experientia*, 48:551–557.
- Diamond, J. M., 1992. The red flag of optimality, *Nature*, 355:204–206.
- Eckert, M. P., and G. Buchsbaum, 1993. Efficient coding of natural time varying images in the early visual system, *Philos. Trans. R. Soc. Lond. B*, 339:385–395.
- Enoch, J. M., 1981. Retinal receptor orientation and photoreceptor optics, in *Vertebrate Photoreceptor Optics* (J. M. Enoch and F. L. Tobey Jr., eds.), Berlin: Springer-Verlag.
- Euler, T., and R. H. Masland, 2000. Light-evoked responses of bipolar cells in a mammalian retina, *J. Neurophysiol.*, 83:1817–1829.
- Euler, T., H. Schneider, and H. Wässle, 1996. Glutamate responses of bipolar cells in a slice preparation of the rat retina, *J. Neurosci.*, 16:2934–2944.
- Field, G. D., and F. Rieke, 2002. Nonlinear signal transfer from mouse rods to bipolar cells and implications for visual sensitivity, *Neuron*, 34:773–785.
- Freed, M. A., 2000a. Parallel cone bipolar pathways to ganglion cell use different rates and amplitudes of quantal excitation, *J. Neurosci.*, 20:3956–3963.
- Freed, M. A., 2000b. Rate of quantal excitation to a retinal ganglion cell evoked by sensory input, *J. Neurophysiol.*, 83:2956–2966.
- Freed, M. A., R. G. Smith, and P. Sterling, 2003. Timing of quantal release from the retinal bipolar terminal is regulated by a feedback circuit, *Neuron*, 38:89–101.
- Freed, M. A., and P. Sterling, 1988. The ON-alpha ganglion cell of the cat retina and its presynaptic cell types, *J. Neurosci.*, 8:2303–2320.
- Ghosh, K. K., S. Haverkamp, and H. Wässle, 2001. Glutamate receptors in the rod pathway of the mammalian retina, *J. Neurosci.*, 21:8636–8647.
- Glegg, G. L., 1969. *The Design of Design*, Cambridge: University of Cambridge.
- Gould, S. J., and R. C. Lewontin, 1979. The spandrels of San Marcos and the Panglossian paradigm: a critique of the adaptationist program, *Proc. R. Soc. Lond. B*, 205:581–598.
- Greiff, R., 1899. *Die Mikroskopische Anatomie Des Sehnerven Und Der Netzhaut*, Leipzig: W. Engelmann.
- Hack, I., L. Peichl, and J. H. Brandstätter, 1999. An alternative pathway for rod signals in the rodent retina: rod photoreceptors, cone bipolar cells, and the localization of glutamate receptors, *Proc. Natl. Acad. Sci. USA*, 96:14130–14135.
- Haverkamp, S., U. Grünert, and H. Wässle, 2000. The cone pedicle, a complex synapse in the retina, *Neuron*, 27:85–95.
- Haverkamp, S., U. Grünert, and H. Wässle, 2001. The synaptic architecture of AMPA receptors at the cone pedicle of the primate retina, *J. Neurosci.*, 21:2488–2500.
- Hochstein, S., and R. M. Shapley, 1976. Linear and nonlinear spatial subunits in Y cat retinal ganglion cells, *J. Physiol. (Lond.)*, 262:265–284.
- Hsu, A., Y. Tsukamoto, R. G. Smith, and P. Sterling, 1998. Functional architecture of primate rod and cone axons, *Vis. Res.*, 38:2539–2549.
- Hughes, A., 1977. The topography of vision in mammals of contrasting life style: comparative optics and retinal organisation, in *Handbook of Sensory Physiology* (F. Crescitelli, ed.), Berlin: Springer-Verlag, pp. 615–756.
- Kamermans, M., I. Fahrenfort, K. Schultz, U. Janssen-Bienhold, T. Sjoerdsma, and R. Weiler, 2001. Hemichannel-mediated inhibition in the outer retina, *Science*, 292:1178–1180.
- Kamermans, M., I. Fahrenfort, and T. Sjoerdsma, 2002. GABAergic modulation of ephaptic feedback in the outer retina, *IOVS*, Abstract #2920.
- Kaplan, E., and R. M. Shapley, 1986. The primate retina contains two types of ganglion cells, with high and low contrast sensitivity, *Proc. Natl. Acad. Sci. USA*, 83:2755–2757.
- Kier, C. K., G. Buchsbaum, and P. Sterling, 1995. How retinal microcircuits scale for ganglion cells of different size, *J. Neurosci.*, 15:7673–7683.
- Kirk, D. L., B. G. Cleland, and W. R. Levick, 1975. Axonal conduction latencies of cat retinal ganglion cells, *J. Neurophysiol.*, 38:1395–1402.
- Kolb, H., R. Nelson, and A. Mariani, 1981. Amacrine cells, bipolar cells and ganglion cells of the cat retina: a Golgi study, *Vis. Res.*, 21:1081–1114.
- Koshland, D. E., Jr., A. Goldbeter, and J. B. Stock, 1982. Amplification and adaptation in regulatory and sensory systems, *Science*, 217:220–225.
- Kraft, T. W., D. M. Schneeweis, and J. L. Schnapf, 1993. Visual transduction in human rod photoreceptors, *J. Physiol.*, 464:747–765.
- Lamb, T. D., E. N. Pugh Jr., and V. Y. Arshavsky, 2000. The gain of rod phototransduction: reconciliation of biochemical and electrophysiological measurements, *Neuron*, 27:525–537.
- Lamb, T. D., and E. N. Pugh, Jr., 1992. G-protein cascades: gain and kinetics, *Trends Neurosci.*, 15:291–298.
- Laughlin, S. B., 1994. Matching coding, circuits, cells, and molecules to signals: general principles of retinal design in the fly’s eye, *Prog. Ret. & Eye Res.*, 13:165–196.
- Leeper, H. F., and J. S. Charlton, 1985. Response properties of horizontal cells and photoreceptor cells in the retina of the

- tree squirrel, *Sciurus carolinensis*, *J. Neurophysiol.*, 54:1157–1166.
- Lehre, K. P., and N. C. Danbolt, 1998. The number of glutamate transporter subtype molecules at glutamatergic synapses: chemical and stereological quantification in young adult rat brain, *J. Neurosci.*, 18:8751–8757.
- Leskov, I. B., V. A. Klenchin, J. W. Handy, G. G. Whitlock, V. I. Govardovskii, M. D. Bownds, T. D. Lamb, E. N. Pugh, V. Y. Arshavsky, 2000. The gain of rod phototransduction: reconciliation of biochemical and electrophysiological measurements, *Neuron*, 27:525–537.
- Lieberman, P. A., K. R. Parker, and E. A. Dratz, 1987. The molecular mechanism of visual excitation and its relation to the structure and composition of the rod outer segment, *Annu. Rev. Physiol.*, 49:765–791.
- Martin, P. R., A. J. White, A. K. Goodchild, H. D. Wilder, and A. E. Sefton, 1997. Evidence that blue-on cells are part of the third geniculocortical pathway in primates, *Eur. J. Neurosci.*, 9:1536–1541.
- Masland, R. H., 2001. The fundamental plan of the retina, *Nat. Neurosci.*, 4:877–886.
- Mastrorade, D. N., 1983. Correlated firing of cat retinal ganglion cells. I. Spontaneously active inputs to X- and Y-cells, *J. Neurophysiol.*, 49:303–324.
- Masu, M., H. Iwakabe, Y. Tagawa, T. Miyoshi, M. Yamashita, Y. Fukuda, H. Sasaki, K. Hiroi, Y. Nakamura, and R. Shigemoto, 1995. Specific deficit on the ON response in visual transmission by targeted disruption of the mGluR6 gene, *Cell*, 80:757–765.
- McGille, G. S., and R. F. Dacheux, 2001. Rabbit cone bipolar cells: correlation of their morphologies with whole-cell recordings, *Vis. Neurosci.*, 18:675–685.
- McGuire, B. A., J. K. Stevens, and P. Sterling, 1984. Microcircuitry of bipolar cells in cat retina, *J. Neurosci.*, 4:2920–2938.
- Meister, M., and M. J. I. Berry, 1999. The neural code of the retina, *Neuron*, 22:435–450.
- Miller, W. H., and A. W. Snyder, 1973. Optical function of human peripheral cones, *Vis. Res.*, 13:2185–2194.
- Mills, S. L., and S. C. Massey, 1994. Distribution and coverage of A- and B-type horizontal cells stained with Neurobiotin in the rabbit retina, *Vis. Neurosci.*, 11:549–560.
- Nakatani, K., T. Tamura, and K.-W. Yau, 1991. Light adaptation in retinal rods of the rabbit and two other nonprimate mammals, *J. Gen. Physiol.*, 97:413–435.
- Nawy, S., 2000. Regulation of the On bipolar cell mGluR6 pathway by Ca^{2+} , *J. Neurosci.*, 20:4471–4479.
- Nelson, R., 1977. Cat cones have rod input: a comparison of the response properties of cones and horizontal cell bodies in the retina of the cat, *J. Comp. Neurol.*, 172:109–136.
- Nomura, A., R. Shigemoto, Y. Nakamura, N. Okamoto, N. Mizuno, and S. Nakanishi, 1994. Developmentally-regulated postsynaptic localization of a metabotropic glutamate-receptor in rat rod bipolar cells, *Cell*, 77:361–369.
- O'Brien, B. J., T. Isayama, R. Richardson, and D. M. Berson, 2002. Intrinsic physiological properties of cat retinal ganglion cells, *J. Physiol.* 538:787–802.
- Packer, O., A. Hendrickson, and C. Curcio, 1989. Photoreceptor topography of the retina in the adult pigtail Macaque (*Macaca nemestrina*), *J. Comp. Neurol.*, 288:165–183.
- Pattnaik, B., A. Jellali, J. Sahel, H. Dreyfus, and S. Picaud, 2000. GABA_C receptors are localized with microtubule-associated protein 1B in mammalian cone photoreceptors, *J. Neurosci.*, 20:6789–6796.
- Petroski, H., 1996. *Invention by Design: How Engineers Get From Thought to Thing*, Cambridge, MA: Harvard University Press.
- Picaud, S., B. Pattnaik, D. Hicks, V. Forster, V. Fontaine, J. Sahel, and H. Dreyfus, 1998. GABA_A and GABA_C receptors in adult porcine cones: evidence from a photoreceptor-glia co-culture model, *J. Physiol.*, 513:33–42.
- Polyak, S. L., 1941. *The Retina*, University of Chicago Press.
- Potts, A. M., D. Hodges, C. B. Shelman, K. J. Fritz, N. S. Levy, and Y. Mangnall, 1972. Morphology of the primate optic nerve. I. Method and total fiber count, *Invest. Ophthalmol. Vis. Sci.*, 11:980–988.
- Pugh, E. N. Jr., and T. D. Lamb, 1993. Amplification and kinetics of the activation steps in phototransduction, *Biochim. Biophys. Acta*, 1141:111–149.
- Rao-Mirotnik, R., G. Buchsbaum, and P. Sterling, 1998. Transmitter concentration at a three-dimensional synapse, *J. Neurophysiol.*, 80:3163–3172.
- Rao-Mirotnik, R., A. Harkins, G. Buchsbaum, and P. Sterling, 1995. Mammalian rod terminal: architecture of a binary synapse, *Neuron*, 14:561–569.
- Rao, R., G. Buchsbaum, and P. Sterling, 1994. Rate of quantal transmitter release at the mammalian rod synapse, *Biophys. J.*, 67:57–63.
- Rieke, E., and E. A. Schwartz, 1996. Asynchronous transmitter release: control of exocytosis and endocytosis at the salamander rod synapse, *J. Physiol.*, 493:1–8.
- Rodieck, R. W., 1973. *The Vertebrate Retina: Principles of Structure and Function*, San Francisco CA: W. H. Freeman & Co.
- Rose, A., 1973. *Vision: Human and Electronic*, New York NY: Plenum Press.
- Roska, B., and F. Werblin, 2001. Vertical interactions across ten parallel, stacked representations in the mammalian retina, *Nature*, 410:583–587.
- Rowe, M. H., and J. Stone, 1976a. Conduction velocity groupings among axons of cat retinal ganglion cells, and their relationship to retinal topography, *Exp. Brain Res.*, 25:339–357.
- Rowe, M. H., and J. Stone, 1976b. Properties of ganglion cells in the visual streak of the cat's retina, *J. Comp. Neurol.*, 169:99–126.
- Saito, H.-A., 1983. Morphology of physiologically identified X-, Y-, and W-type retinal ganglion cells of the cat, *J. Comp. Neurol.*, 221:279–288.
- Sarantis, M., and P. Mobbs, 1992. The spatial relationship between Müller cell processes and the photoreceptor output synapse, *Brain Res.*, 584:299–304.
- Satoh, H., M. Kaneda, and A. Kaneko, 2001. Intracellular chloride concentration is higher in rod bipolar cells than in cone bipolar cells of the mouse retina, *Neurosci. Lett.*, 310:161–164.
- Schnapf, J. L., B. J. Nunn, M. Meister, and D. A. Baylor, 1990. Visual transduction in cones of the monkey *Macaca fascicularis*, *J. Physiol.*, 427:681–713.
- Schneeweis, D. M., and J. L. Schnapf, 1995. Photovoltage of rods and cones in the macaque retina, *Science*, 268:1053–1056.
- Schneeweis, D. M., and J. L. Schnapf, 1999. The photovoltage of Macaque cone photoreceptors: adaptation, noise, and kinetics, *J. Neurosci.*, 19:1203–1216.
- Schwartz, E., 1987. Depolarization without calcium can release gamma-aminobutyric acid from a retinal neuron, *Science*, 238:350–355.
- Sesti, F., M. Straforini, T. D. Lamb, and V. Torre, 1994. Gating, selectivity and blockage of single channels activated by cyclic GMP in retinal rods of the tiger salamander, *J. Physiol.*, 474:203–222.
- Shannon, C. E., and W. Weaver, 1949. *The Mathematical Theory of Communication*, Urbana: University of Illinois Press.

- Smallman, H. S., D. I. A. MacLeod, S. He, and R. W. Kentridge, 1996. Fine grain of the neural representation of human spatial vision, *J. Neurosci.*, 16:1852–1859.
- Smith, R. G., 1995. Simulation of an anatomically-defined local circuit: The cone-horizontal cell network in cat retina, *Vis. Neurosci.*, 12:545–561.
- Smith, R. G., M. A. Freed, and P. Sterling, 1986. Microcircuitry of the dark-adapted cat retina: functional architecture of the rod-cone network, *J. Neurosci.*, 6:3505–3517.
- Smith, R. G., and P. Sterling, 1990. Cone receptive field in cat retina computed from microcircuitry, *Vis. Neurosci.*, 5:453–461.
- Smith, R. G., and N. Vardi, 1995. Simulation of the AII amacrine cell of mammalian retina: functional consequences of electrical coupling and regenerative membrane properties, *Vis. Neurosci.*, 12:851–860.
- Snyder, A. W., S. B. Laughlin, and D. G. Stavenga, 1977. Information capacity of eyes, *Vis. Res.*, 17:1163–1175.
- Soucy, E., S. Nirenberg, J. Nathans, and M. Meister, 1998. A novel signaling pathway from rod photoreceptors to ganglion cells in mammalian retina, *Neuron*, 21:481–493.
- Srinivasan, M. V., S. B. Laughlin, and A. Dubs, 1982. Predictive coding: a fresh view of inhibition in the retina, *Proc. R. Soc. Lond. B*, 216:427–459.
- Stafford, D. K., and D. Dacey, 1997. Physiology of the A1 amacrine: a spiking, axon-bearing interneuron of the macaque monkey retina, *Vis. Neurosci.*, 14:507–522.
- Steinberg, R. H., M. Reid, and P. L. Lacy, 1973. The distribution of rods and cones in the retina of the cat (*Felis domesticus*), *J. Comp. Neurol.*, 148:229–248.
- Sterling, P., 1998. Retina, in *The Synaptic Organization of the Brain*, (G. M. Shepherd, ed.), New York: Oxford University Press: pp. 205–253.
- Sterling, P., 2002. Needle from a haystack: optimal signaling by a nonlinear synapse, *Neuron*, 34:670–672.
- Sterling, P., E. Cohen, R. G. Smith, and Y. Tsukamoto, 1992. Retinal circuits for daylight: why ballplayers don't wear shades, in *Analysis and Modeling of Neural Systems* (F. H. Eeckman ed.), Kluwer Academic Publishers: Boston, pp. 143–162.
- Sterling, P., M. A. Freed, and R. G. Smith, 1988. Architecture of the rod and cone circuits to the On-beta ganglion cell, *J. Neurosci.*, 8:623–642.
- Stone, J., and Y. Fukuda, 1974. Properties of cat retinal ganglion cells: a comparison of W-cells with X- and Y-cells, *J. Neurophysiol.*, 37:722–748.
- Tamura, T., K. Nakatani, and K.-W. Yau, 1991. Calcium feedback and sensitivity regulation in primate rods, *J. Gen. Physiol.*, 98: 91–130.
- Taylor, C. R., and E. R. Weibel, 1981. Design of the mammalian respiratory system. I. Problem and strategy, *Respir. Physiol.*, 44:1–10.
- Townes-Anderson, E., 1995. Intersegmental fusion in vertebrate rod photoreceptors. Rod cells structure revisited, *Invest. Ophthalmol. Vis. Sci.*, 36:1918–1933.
- Townes-Anderson, E., P. R. MacLeish, and E. Raviola, 1985. Rod cells dissociated from mature salamander retina: ultrastructure and uptake of horseradish peroxidase, *J. Cell Biol.*, 100:175–188.
- Tsukamoto, Y., P. Masarachia, S. J. Schein, and P. Sterling, 1992. Gap junctions between the pedicles of macaque foveal cones, *Vis. Res.*, 32:1809–1815.
- Tsukamoto, Y., K. Morigiwa, M. Ueda, and P. Sterling, 2001. Microcircuits for night vision in mouse retina, *J. Neurosci.*, 21:8616–8623.
- van Essen, D. C., C. H. Anderson, and D. J. Felleman, 1992. Information processing in the primate visual system: an integrated systems perspective, *Science*, 255:419–423.
- van Hateren, J. H., 1992. Real and optimal neural images in early vision, *Nature*, 360:68–70.
- van Hateren, J. H., 1993. Spatiotemporal contrast sensitivity of early vision, *Vis. Res.*, 33:257–267.
- van Rossum, M. C. W., and R. G. Smith, 1998. Noise removal at the rod synapse of mammalian retina, *Vis. Neurosci.*, 15:809–821.
- Vaney, D. I., 1993. Patterns of neuronal coupling in the retina, *Prog. Ret. & Eye Res.*, 13:301–355.
- Vardi, N., P. Masarachia, and P. Sterling, 1992. Immunoreactivity to GABA_A receptor in the outer plexiform layer of the cat retina, *J. Comp. Neurol.*, 320:394–397.
- Vardi, N., K. Morigiwa, T.-L. Wang, Y.-J. Shi, and P. Sterling, 1998. Neurochemistry of the mammalian cone 'synaptic complex', *Vis. Res.*, 38:1359–1369.
- Vardi, N., L.-L. Zhang, J. A. Payne, and P. Sterling, 2000. Evidence that different cation chloride cotransporters in retinal neurons allow opposite responses to GABA, *J. Neurosci.*, 20:7657–7663.
- Victor, J. D., 1999. Temporal aspects of neural coding in the retina and lateral geniculate, *Network*, 10:R1–R66.
- von der Twer, T., and D. I. A. MacLeod, 2001. Optimal nonlinear codes for the perception of natural colors, *Network*, 12:395–407.
- Wässle, H., and B. B. Boycott, 1991. Functional architecture of the mammalian retina, *Physiol. Rev.*, 71:447–480.
- Watson, A. B., H. B. Barlow, and J. G. Robson, 1983. What does the eye see best? *Nature*, 302:419–422.
- Weibel, E. R., 2000. *Symmorphosis: On Form and Function in Shaping Life*. Cambridge: Harvard University Press.
- Williams, D. R., 2003. Image formation and sampling, in *Visual Neurosciences* (L. Chalupa and J. S. Werner, eds.), Cambridge, MA: MIT Press.
- Williams, R. W., C. Cavada, and F. Reinoso-Suárez, 1993. Rapid evolution of the visual system: a cellular assay of the retina and dorsal lateral geniculate nucleus of the Spanish wildcat and the domestic cat, *J. Neurosci.*, 13:208–228.
- Yau, K.-W., 1994. Phototransduction mechanism in retinal rods and cones, *Invest. Ophthalmol. Vis. Sci.*, 35:9–32.
- Zhang, D. J., and S. Firestein, 2002. The olfactory receptor gene superfamily of the mouse, *Nat. Neurosci.*, 5:124–133.

18 ON and OFF Pathways in the Vertebrate Retina and Visual System

RALPH NELSON AND HELGA KOLB

ON and OFF pathways are feature detectors

A key concept in visual system physiology is the notion of “feature detectors.” The idea of feature detection is that the visual system separates the visual image into components, much the way a publisher creates a color print by separating the picture into separate masks for different colored inks. The idea of feature detection was most forcefully presented by Lettvin et al. (1959) in the classic paper, “What the Frog’s Eye Tells the Frog’s Brain.” In this article, the authors described four different physiological classes of retinal output neurons, that is, four classes of retinal ganglion cells. Ganglion cell axons collectively bundle to form the optic nerve, transmitting visual information to brain visual centers. In this study, each of these classes of ganglion cells was found to be excited by a separate aspect of the visual image. Collectively, the cells sent the visual image to the brain decomposed as four separate channels. Among these four were ON-center and OFF-center cells, ganglion cells selectively specialized for the detection of *highlights* and *shadows*.

Clearly, highlights and shadows are two of the most fundamental features of images. In all vertebrate visual systems studied thus far, highlights and shadows are universally represented, not only by separate sets of ganglion cells, but by separate systems of cells throughout the retina and central nervous system. These are the ON and the OFF pathways. Researchers have come to understand the neural circuitry of these pathways, the cell types that are involved, their morphology and synaptic interconnections, the specialized neurotransmitter systems and receptors used, and the way in which these pathways project to, and are integrated by, the brain.

The lens of the eye projects an optical image of visual space onto the retina. The retina separates this optical image into multiple components. At the outset, this occurs at the photoreceptor level, where rods and cones report different image properties in parallel. Rods deal exclusively with dim signals of slowly varying brightness. Cones deal with bright signals and can detect rapid light fluctuations. Separate cone types sense wavelength with different efficiency, allowing the visual system to detect color. Thus, photoreceptors are the

first neurons in the visual chain to decompose the image into separate parts. The image is differentiated further into component elements at the first synapses of the visual pathway: the synapses between photoreceptors and bipolar cells. Here, typically a dozen different bipolar cell types selectively express different types of receptors for glutamate, the neurotransmitter released in light-modulated fashion by photoreceptors. These different glutamate receptors cause each bipolar type to respond to photoreceptor input in a different manner. As with rods and cones, some bipolar cells are tuned to faster fluctuations and some are tuned to slower fluctuations in the visual signal. There are some bipolar cells expressing rapidly desensitizing, rapidly resensitizing AMPA¹ receptors. AMPA¹ is an acronym for $\pm\alpha$ -Amino-hydroxy-5-methylisoxazole-4-propionic acid. There are others expressing the slowly resensitizing kainate receptors. These kinetic differences allow bipolar cells to respond selectively to different temporal components of visual signals (DeVries, 2000). However, the most extraordinary difference occurs between bipolar cells that express excitatory glutamate receptors versus those that express inhibitory glutamate receptors. Inhibitory glutamate receptors are an uncommon class, but are uniquely emphasized in vertebrate retinas. Excitatory and inhibitory glutamate receptors lead to OFF-center and ON-center bipolar cell responses, respectively. Together, these bipolar cells initiate a set of parallel visual pathways, for shadow and for highlight detection. These are the beginnings of the ON- and the OFF-center pathways.

ON and OFF signals are prominent in retinal field potentials

When the retina is exposed to light, a time-varying transretinal field potential develops. This is referred to as the electroretinogram (ERG). The waveform of the ERG proceeds through a sequence of peaks and troughs. The sequence at light onset and at light offset is roughly similar (Fig. 18.1). Although not a proof, this pattern is certainly suggestive of separate and parallel processes involved in detection of light onset and offset, corresponding to highlights and shadows, respectively. The description of these similar ON and OFF waves of the ERG in a variety

of vertebrate species is generally attributed to Ragnar Granit (1935), winner of a Nobel prize for retinal physiology in 1967. Although all species tested have prominent ON response components, those with high cone density exhibit the greatest OFF component. This difference is attributed to two factors. The first is the relatively sluggish responses of the rods themselves to light offset. The second is a separate and different neural organization within the retina for the processing of rod and cone signals. Figure 18.1 demonstrates the ERG response of a zebrafish eye, typical of cone-dominated retinal responses. The electrical responses at light onset and light offset both exhibit positive-going waves, as if arising from parallel, yet similar, processes. The corneal positive response at light onset is called the b wave. The comparable response at light offset is called the d wave.

Discovery of ON and OFF ganglion cells

Although ERG responses are suggestive, in themselves they are not uniquely interpretable. To help resolve the way the retina actually works, one needs to identify the light responses of individual neurons. This was first achieved by recording the impulse activity of individual nerve fibers in the frog retina (Hartline, 1938). Using the technology available at the time, Hartline lifted bundles of optic nerve fibers onto a cotton wick electrode, similar to the sort used to record ERGs, but much finer. Amplification sometimes consisted of just a single vacuum tube. There were no oscilloscopes. A string galvanometer was used to project a vibrating beam of light onto a moving motion picture film at some distance across a dark room. One would be fortunate to find

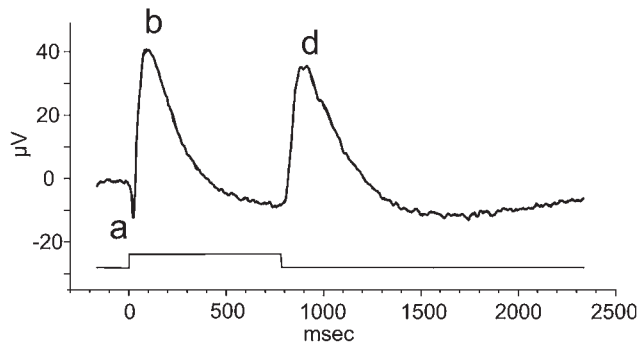


FIGURE 18.1. Light-evoked electrical response of in vitro zebrafish eye. Distinct and nearly symmetrical responses to light onset and light offset are evident. This suggests parallel systems for handling these stimulus events. The a wave (A) is generally attributed to a combination of photoreceptor onset response and inner retinal processing. The b wave (B) response arises, directly or indirectly, from the activity of ON-type bipolar cells. The d wave (D) response arises from the activity of OFF-type bipolar cells. Stimuli are white (xenon arc) and photopic, in the cone range of action. (From Wesolowska et al., 2002.)

such a device in a technological museum today. Nonetheless, recordings of impulse activity from single, isolated, ganglion cell axons were, for the first time, documented by this technique. These impulses were the visual signals sent from retina to brain.

What Hartline found was not a single, monolithic pattern of responses to light, but three different patterns. His classic results appear in Figure 18.2. Although modern recordings are of higher technical quality, in many cases, they represent only a refinement of Hartline's original design. The upper tracing in Figure 18.2 illustrates an ON cell. In addition to a heightened discharge at stimulus onset, it maintains a steady stream of impulses throughout the light stimulus. This stimulus is a small spot positioned in the center of the cell's receptive field. The idea of receptive field is also a concept developed by Hartline (1940). Receptive field defines the restricted regions of space over which ganglion cells respond to photic stimulation. In this region, there is a center of peak sensitivity. The middle tracing in Figure 18.2 illustrates a fiber that exhibits bursts of discharges at stimulus onset and offset, but that is otherwise quiet. This is an ON-OFF retinal ganglion cell. The lower tracing (see Fig. 18.2) shows a ganglion cell fiber with a burst of impulse activity only at stimulus offset. This is the response of an OFF-type retinal ganglion cell.

The multiplicity of light responses in frog ganglion cells surprised Hartline because in parallel studies of invertebrate vision, only a single response pattern had been

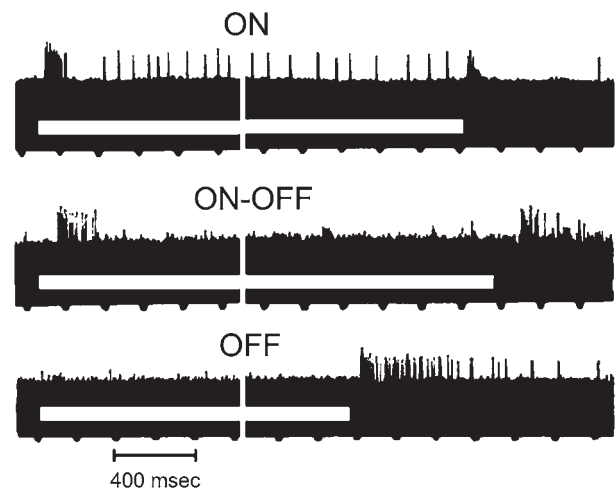


FIGURE 18.2. Hartline's early recordings from retinal ganglion cell axons revealed three different impulse discharge patterns in response to spots of light centered in the receptive field. The ON cell gives a burst of activity at stimulus onset, followed by a maintained discharge during the stimulus. The OFF cell has no discharge during light stimulation, but gives a burst of activity followed by prolonged spiking when the stimulus is turned off. The ON-OFF cell responds with transient bursts of activity at both light onset and offset. (From Hartline, 1938.)

observed: excitation to light (Hartline and Graham, 1932). The results suggested that a good deal of information processing took place within the retina, and this discovery sowed the seed for the development of the notion of parallel visual channels and feature detection. Keffer Hartline won the Nobel Prize in 1967 for his work on the frog's visual system.

Sustained and transient ON and OFF pathways

As mentioned earlier, Lettvin and colleagues (1959) extended the number of physiological ganglion cell types from the three described by Hartline to four. The current theory is that there are about a dozen different physiological types of ganglion cell (Cleland and Levick, 1974b; DeVries and Baylor, 1995). Different types typically project to distinct brain centers. The most sophisticated types are directionally selective ganglion cells. These are excited by movements in one direction, but inhibited by movements in the opposite direction (Barlow and Hill, 1963). Although such cells can be classified, on the basis of stationary spot stimulation, as either ON, ON-OFF, or OFF types, clearly, highlights and shadows are not their specialty. These cells respond equally well to bright or dark objects, so long as the direction of motion is the preferred one.

Among different physiological types of ganglion cell are several distinct classes of ON and OFF center types. The most prominent of these are X (brisk-sustained) and Y (brisk-transient) types (Cleland and Levick, 1974a; Enroth-Cugell and Robson, 1966). X and Y types each come as ON-center and OFF-center varieties, comprising a net of four separate channels from retina to brain: X_{ON} and X_{OFF} , Y_{ON} and Y_{OFF} . X and Y types are distinguished by a battery of properties. Y cells are large in dendritic and receptive field and fast in axonal conduction velocity. Typically, Y-cell processes cover a circular region that is 500 μm in diameter at the surface of the cat retina. These cells are relatively low in density ($\sim 20/\text{mm}^2$). They are excited vigorously by image changes within their receptive field, but appear relatively less interested in standing contrast. These cells are thought to provide a high-speed alerting function for changes in the visual environment. X cells, by contrast, are relatively smaller cells, with dendritic processes covering a diameter of just a few tens of micrometers at the cat retinal surface. They have a high density ($\sim 2000/\text{mm}^2$). They have slower conduction velocities to the brain than Y cells, and respond patiently and in a sustained fashion to steady image patterns. These are thought to be high-acuity cells for fine visual discrimination (Wässle and Boycott, 1991). Comparable sets of cells exist in the primate retina, termed parasol (P) and midget (MP) cells, respectively.

Impulse discharge patterns of an X_{OFF} and a Y_{OFF} cell are shown in Figure 18.3. The stimulus is a one-dimensional

spatial-sine-wave grating, covering a large area of retina. This stimulus is designed to arise suddenly from a homogeneous background of equal mean luminance. When the position of the sine wave is adjusted so that stimulus presentation brightens the receptive field center, the X_{OFF} cell responds with a sustained increase in firing to stimulus withdrawal (see Fig. 18.3, X-type). When the position is adjusted so that the center darkens, the X_{OFF} cell responds with a maintained decrease in firing to stimulus withdrawal. Sustained responses to standing stimuli are characteristic of X cells. For stimulus phases positioned in between, there is a null in the X-cell response. The null suggests net spatiotemporal linearity for X cells; that is, the time course and amplitude of signals arising from regions of the field that are inhibited by increases in brightness are exactly canceled by excitatory signals arising from receptive field regions where brightness is reduced.

No such null positions appear in the Y-cell response (see Fig. 18.3, Y-type). For intermediately positioned stimuli that might be expected to evoke a null response, excitations at both insertion and removal of the stimulus are seen instead. This seems reasonable, as responses to introduction and withdrawal of the stimulus for centered stimuli are far from

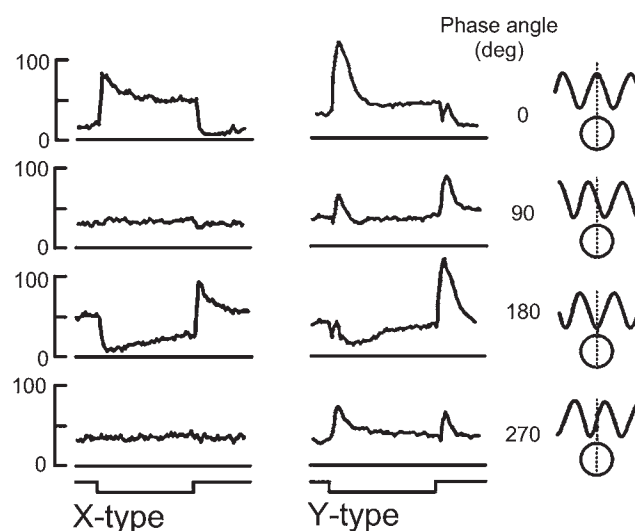


FIGURE 18.3. Spatial properties of X- and Y-type cat retinal ganglion cells. X- and Y-type cells occur in both ON- and OFF-center varieties. OFF types are illustrated here. The stimulus, a one-dimensional spatial-sine-wave grating, is designed to test linearity of spatial summation. This patterned stimulus is turned on from a homogeneous background of equal mean luminance (upward deflections of lowermost traces). As the spatial phase of the stimulus is shifted in respect to the ganglion cell's receptive field, nulls can be found in the X-cell response, indicating spatiotemporal linearity. No such spatial null is recorded for the Y cell. The records are spike-frequency histograms with units of impulses per second. Each record is 2 seconds in length. Downward deflections of the lower traces indicate withdrawal of the pattern. (From Enroth-Cugell and Robson, 1966.)

mirror-symmetric in Y cells. Onset and offset responses are not treated equivalently at any stimulus position: the cell is said to be temporally nonlinear. The mechanisms generating such different waveforms in X cells and Y cells appear not to be intrinsic to the ganglion cells themselves, but rather to selective innervations by physiologically different sets of bipolar cells (Demb et al., 2001). Using the electron microscope, only a single bipolar type can be seen to innervate individual Y cells (Freed and Sterling, 1988; Kolb and Nelson, 1993), whereas two to three types innervate individual X cells (Cohen and Sterling, 1991; Kolb and Nelson, 1993; McGuire et al., 1984). Golgi, flat-mount images of tiny X_{ON} and X_{OFF} beta cells can be seen embedded amongst the dendrites of a much larger Y_{ON} alpha cell in Figure 18.4, together with characteristic stratification patterns, as discussed in a later section.

Discovery of ON and OFF bipolar cells

Retinal ganglion cells are typically only two synapses distant from retinal photoreceptors, yet ganglion cell responses are far more diverse than those of photoreceptors. The most direct pathway from photoreceptors to ganglion cells is through retinal bipolar cells. Thus, it is of great interest to understand how bipolar cells function and, indeed, how all retinal interneurons respond to photic stimuli and interact through synapses and retinal circuitry to produce the diverse types of ganglion cell responses through which visual information is reported to the brain. Extracellular electrodes of the glass or metal type, typically used for ganglion cell recordings, are of little use for recording interneurons within the retinal depths, as impulse activity is rarely produced. Rather, sharp electrode recording holds the greatest promise. With these electrodes, one can penetrate cell membranes and record not only impulse activity, but maintained changes in membrane potential in response to stimuli. Werblin and Dowling (1969) advanced the art of sharp electrode recording in the retina using ultra-high impedance microelectrodes ($10^9\Omega$), and they were among the first to use biological amplifiers based on high-input impedance ($10^{13}\Omega$) field effect transistors. They also introduced intracellular marking of retinal neurons through electrophoretic stain injection. They developed the mudpuppy retina as an animal model of vision processing. This was largely for technical reasons; retinal interneurons in this species are uniformly large and good microelectrode targets. This species, and the closely related tiger salamander, have remained favorites for studies of retinal circuitry. Werblin and Dowling (1969) proposed a physiological, organizational scheme, not just for bipolar cell responses, but for all retinal interneurons. Present research on retinal information processing is, in many cases, based on refinement or modification of the Werblin and Dowling scheme.

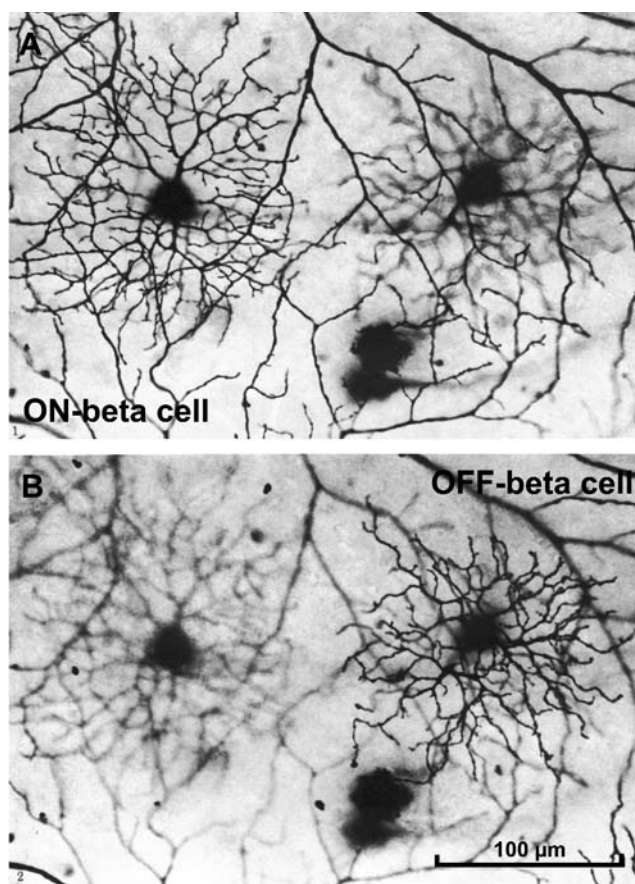


FIGURE 18.4. Flat-mount images of Golgi-stained ON and OFF beta (X-type) ganglion cells in cat retina. Beta dendritic fields are embedded among the dendrites of a much larger ON alpha (Y-type) ganglion cell. *A*, Dendrites of an ON-center beta ganglion cell in the cat retina occupy a plane of focus (*left*) near ganglion cell bodies. The dendrites of an overlying ON alpha (Y-type) ganglion cell cross the field from top to bottom in the same focal plane. This plane is in sublamina *b* of the IPL. *B*, Another, similar-appearing beta ganglion cell lies with its dendritic tree in sharp focus (*right*) deeper in the IPL. This is an OFF-center beta (X-type) ganglion cell. The dendritic plane of focus is in sublamina *a*. ON-type dendrites do not occupy this plane. (From Wässle et al., 1981a.)

Werblin and Dowling (1969) posited that retinal bipolar cells lack impulse activity, and that they process visual signals through integration of synaptic and voltage-gated currents alone. This theory persists. Sodium channels, required for the generation of impulse activity, have not been observed in retinal bipolar cells (Connaughton and Maguire, 1998; Karschin and Wässle, 1990; Lasater, 1988), although under conditions of dark adaptation, 50-msec-long Ca^{2+} spikes have been found in some rod bipolar cell presynaptic terminals (Protti and Llano, 1998). Recent studies have reported voltage-gated Na^+ currents in some cone bipolar cells (Pan and Hu, 2000; Zenisek et al., 2001), though these do not produce spikes.

Werblin and Dowling (1969) proposed also that retinal bipolar cells come in two fundamental varieties: ON-center and OFF-center types (Fig. 18.5). ON-center types were found to be depolarized by small spot stimuli positioned in the receptive field center. OFF-center types were hyperpolarized by the same stimuli. Both types were repolarized by light stimulation of the peripheral receptive field outside the center (see Fig. 18.5). This is the classic, antagonistic, center-surround organization also described for ganglion cell receptive fields (Kuffler, 1953). ON-OFF bipolar cells were not encountered. ON-OFF responses, as described by Hartline (1938), occurred only among neurons at least two synapses removed from photoreceptors. This was the major response type among mudpuppy retinal amacrine cells (Werblin and Dowling, 1969). Thus, although true ON-OFF pathways to brain visual centers exist (Isayama et al., 2000), they originate in the proximal, not the distal retina.

Anatomical investigations of bipolar cells reveal typically a dozen different types in each species (Connaughton and Nelson, 2000; Euler et al., 1996; Kolb et al., 1981; Wu et al., 2000), more than just the two that early physiology implied. Nonetheless, all of these are either ON or OFF types. Their diversity results from other factors, such as differing connectivity with photoreceptors. There are bipolar cells devoted to rods, and others devoted to cones. There are wide-field and narrow-field types, and there are cells expressing various subvarieties of glutamate receptors so as to extract different aspects of the photoreceptor glutamate signal.

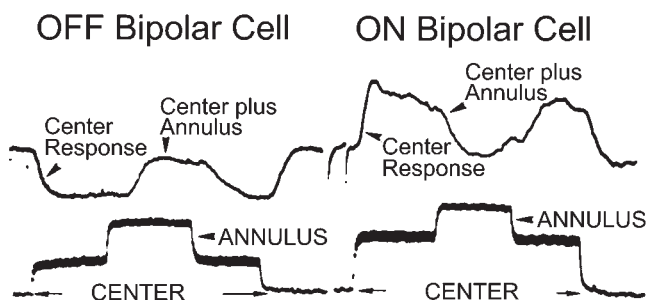


FIGURE 18.5. ON and OFF pathways begin with retinal bipolar cells. Intracellular recordings from mudpuppy retina reveal two sorts of retinal bipolar-cell light responses: those that are hyperpolarized by central illumination (OFF bipolar cell) and those that are depolarized by central illumination (ON bipolar cell). In each case, membrane potential is restored by concomitant illumination of annular regions surrounding the center. Such responses are typically 10 mV in amplitude. They always lack impulse activity. No ON-OFF responses are found. The absolute response latency to the light step is about 100 msec for these suprathreshold stimuli. (From Werblin and Dowling, 1969.)

Different glutamate receptor populations in ON and OFF bipolar cells

ON BIPOLAR CELLS Photoreceptors release only one neurotransmitter—glutamate (Ayoub and Copenhagen, 1991)—yet bipolar cells react to this stimulus with two different responses: ON and OFF. The first investigations into the underlying receptor mechanisms revealed different conductance changes associated with the two responses. The conductance of ON bipolar cells increased in the light, whereas OFF bipolar cell conductance decreased (Nelson, 1973; Toyoda, 1973). The conductance decrease of OFF bipolar cells was easily explained as a loss of excitation by glutamate released from photoreceptors in the dark. The conductance increase in the light, with a positive reversal potential (Nelson, 1973), implied that glutamate was blocking a cation-permeable channel. This was the first evidence of what is now known as *metabotropic* glutamate receptors. These receptors do not form ion channels themselves, but act as isolated antennae on the cell surface, sensing glutamate and activating intracellular pathways and mechanisms that can indirectly affect membrane potential. Whereas elsewhere in the brain, these receptors are involved in regulating synaptic transmission and modifying the activity of voltage-gated channels, thus altering the tuning of neural circuits (Conn and Patel, 1994), in the retina, they are used uniquely in a direct signal transmission pathway: from photoreceptors to ON bipolar cells.

Slaughter and Miller (1981) were the first to observe that the metabotropic glutamate agonist 2-amino-4-phosphonobutyric acid (APB or DL-AP4; it is the L enantiomer that is effective) completely blocks the light responses of ON bipolar cells. In ON bipolar cells, APB acts as a substitute for photoreceptor-released glutamate (Fig. 18.6). These neurons, in the mudpuppy retina at least, use only a metabotropic pathway to sense light-induced variations in photoreceptor glutamate. It is the metabotropic glutamate receptor mGluR6 that is expressed in ON bipolar cells (Nakajima et al., 1993; Nomura et al., 1994). Transgenic knockout mice lacking the mGluR6 gene lack ERG b-wave responses (Fig. 18.7), reflecting a loss of ON bipolar activity (Masu et al., 1995). In addition to mGluR6, the G protein G_o is cytoplasmically localized in the dendritic tips of ON bipolar cells (Vardi et al., 1993). Removal of G_{α_o} by knockout results in loss of ON responses in such mutant mouse retinas (Dhingra et al., 2000), similar to the mGluR6 knockout. This suggests that G_o is directly in the pathway between mGluR6 activation by photoreceptor glutamate and the closing of nonselective cation channels, which leads to the ON response. The exact cascade by which this happens is still unclear; however, it appears that intracellular cyclic guanosine monophosphate (cGMP) is not a

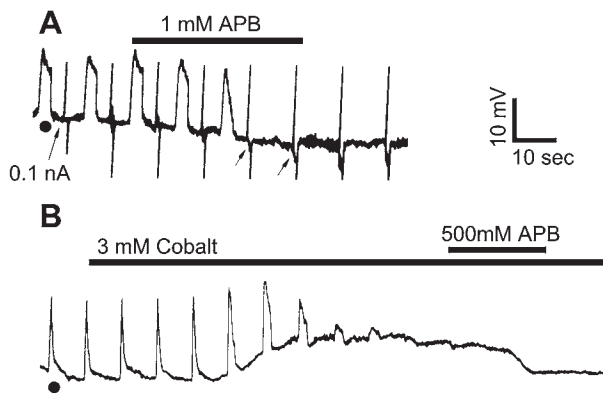


FIGURE 18.6. Metabotropic glutamate receptors in the ON pathway. The glutamate agonist 2-amino-4-phosphonobutyric acid (APB, later terminology DL-AP4) interferes with light responses and membrane physiology of ON-center bipolar cells in mud-puppy retina. *A*, APB abolishes light responses (the rectangular depolarizing events), hyperpolarizes the membrane potential, and increases the membrane resistance. The latter is measured by the size of voltage responses to an injected current pulse (arrows). *B*, Here, 3 mM of cobalt, a blocker for synaptic release of glutamate from photoreceptors, abolishes light responses in an ON bipolar cell and depolarizes the membrane potential. The membrane potential can later be restored by application of APB, which acts as a substitute for the cobalt-blocked photoreceptor glutamate. As APB is selective for a subset of metabotropic glutamate receptors, synaptic transmission of light responses to ON bipolar cells must rely on a metabotropic mechanism. (From Slaughter and Miller, 1981.)

carrier of the light signal as previously suspected (Nawy, 1999).

Metabotropic receptors for ON-center bipolar cells have both sustained and transient subtypes (Awatramani and Slaughter, 2000). The molecular basis is not yet known; however, it appears increasingly likely that sustained and transient responses of ON-center ganglion cells, such as the classic X- and Y-types, may have their origin, at least in part, in the types of glutamate receptors expressed by selectively innervating bipolar cells (Demb et al., 2001).

Ionotropic receptors also exist for ON-center bipolar cells. When these receptors are activated by glutamate released from photoreceptors, a chloride conductance is activated, thus hyperpolarizing the cells in the dark (Fig. 18.8). Release from this inhibition occurs in the light, and bipolar cells depolarize (see Fig. 18.8). The receptor is related to glutamate transporters and requires $[Na^+]_o$. Thus far, this mechanism has been found only in bipolar cells of teleosts (Connaughton and Nelson, 2000; Grant and Dowling, 1995; Grant and Dowling, 1996), although it has been reported in both turtle and salamander photoreceptors (Grant and Werblin, 1996; Picaud et al., 1995; Tachibana and Kaneko, 1988) and in mammalian central nervous system (Otis and Jahr, 1998). The ionotropic mechanism is used for maintained transmission between cones and bipolar cells in

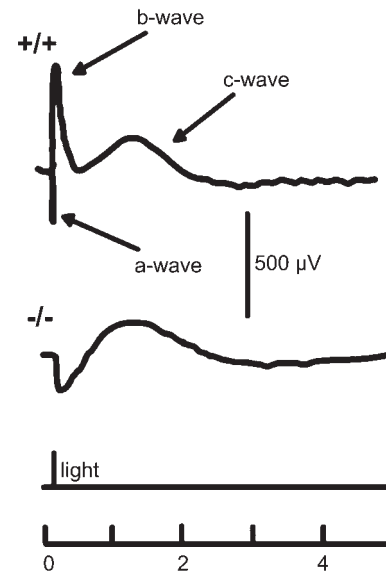


FIGURE 18.7. Light-evoked responses from the eye of a wild-type mouse (+/+) and a mutant mouse (-/-) deficient in the gene encoding mGluR6, the metabotropic glutamate receptor used in ON bipolar cells. The b wave, which originates in the light responses of ON bipolar cells, is absent in the mutant mouse. (From Masu et al., 1995.)

teleost retinas (Saito et al., 1981), and is likely to be a fast mechanism as compared to metabotropic pathways which are often relatively slow (Nelson, 1973).

OFF BIPOLAR CELLS Like ON bipolar cells, OFF bipolar cells express a diversity of glutamate receptor types. In the case of OFF bipolar cells, all the receptors are ionotropic; none are metabotropic. There are three principal types of ionotropic glutamate receptor: AMPA, kainate, and *N*-methyl-D-aspartate (NMDA). OFF bipolar cells have never been observed to utilize NMDA receptors, but in the retina of the ground squirrel, there are types that selectively express either AMPA or kainate receptors (DeVries, 2000; DeVries and Schwartz, 1999). These receptors resensitize at different rates after exposure to glutamate (Fig. 18.9), and as a result, emphasize different temporal characteristics of the light signal.

Kainate-type glutamate signals are able to transfer the sustained characteristics of the visual stimulus. AMPA receptors are more selective for the transient components of the signal (DeVries, 2000). The situation is interesting in that neurons that use kainate receptors exclusively are rare in the central nervous system. Nonetheless, AMPA and kainate receptors on retinal bipolar cells are pharmacologically well behaved. Bipolar-cell, AMPA-type responses can be suppressed by the lipophilic AMPA receptor antagonist, GYKI 52466. This ligand does not affect glutamate responses originating from OFF bipolar cells expressing kainate-type receptors. Conversely, bipolar-cell kainate-type

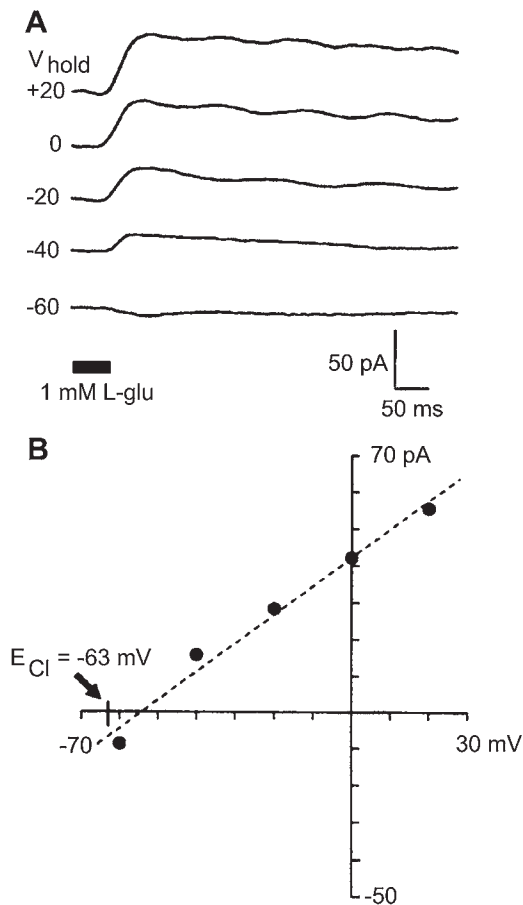


FIGURE 18.8. Ionotropic chloride mechanism for the ON pathway. Puffs of glutamate mimic photoreceptor release in patch recordings from bipolar cells in a zebrafish retinal slice. *A*, Glutamate-evoked currents are outward for physiological ranges of membrane potential, which is consistent with an ON-center mechanism. *B*, The -63 mV reversal potential is consistent with a model in which photoreceptor glutamate opens chloride channels. (From Connaughton and Nelson, 2000.)

responses are blocked by the desensitizing kainate receptor agonist, SYM 2081. This ligand does not interact with bipolar cells that express AMPA receptors (DeVries, 2000).

Although all retinas contain ON and OFF pathways, it is easy to imagine that, among these pathways, natural selection would cause divergence, depending on the visual requirements of the species. The need to flee quickly at the sign of a shadow would be an example. Species diversity appears to be the case. As mentioned earlier, functional ionotropic glutamate channels in ON-type bipolar cells appear to be expressed exclusively in fish retinas. Conversely, in salamander retina, OFF bipolar cells appear to utilize only AMPA receptors (Maple et al., 1999). This may also be the case in zebrafish retina. In this species, dissociated cells fail to respond to the kainate agonist, SYM 2081 (Nelson et al., 2001), and ERG-recorded OFF responses (d waves) are

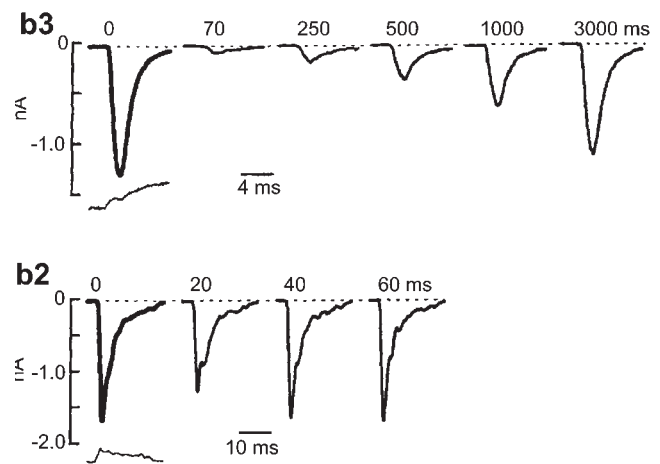


FIGURE 18.9. Different OFF bipolar cells respond to photoreceptor glutamate release with different resensitization rates. In whole-cell patch recordings from ground squirrel retina, bipolar cells are desensitized to an initial glutamate pulse (0). The time course of recovery is followed by the response to a second pulse after different delays. Type b3 bipolar cells use kainate-type glutamate receptors and require several seconds for complete recovery. Type b2 bipolar cells use AMPA-type glutamate receptors and recover 100 times faster. (From DeVries, 2000.)

blocked by the AMPA antagonist, GYKI 52466, but not the kainate-desensitizing agent, SYM 2081 (Wesolowska et al., 2002). One might expect also that, even within the broad classes of AMPA and kainate receptors, subforms may have evolved to fit particular visual niches. This appears to be the case. In the salamander retina, there appear to be separate classes of AMPA receptors that are postsynaptic to rods and to cones (Kim and Miller, 1993; Maple et al., 1999). Thus, the process of splitting the visual signal into multiple pathways tuned to selective visual features begins with differentiation of different photoreceptor types and is greatly elaborated at the synapses between photoreceptors and bipolar cells.

ON and OFF stratification in the inner plexiform layer

GANGLION CELLS In work performed at the National Institutes of Health in the mid-1970s, a collaborative study by Ralph Nelson, Helga Kolb, and Ted Famiglietti revealed that the ON or OFF property of cat retinal ganglion cells was related to the level of stratification of dendrites within the retinal inner plexiform layer (IPL). In Golgi studies, pairs of cells were often found that were otherwise identical, except for stratification level. An example of this appears in Figure 18.4, where two adjacent beta cells are stained. The dendrites of these cells occupy entirely different planes of focus. Beta ganglion cells, with their characteristic compact, bushy, dendritic arbors, are associated with X-type physiological responses (Boycott and Wässle, 1974). Similar

stratification pairing was also found in cat alpha ganglion cells. These are cells with very wide dendritic arbors, particularly narrowly stratified in either of just two IPL bands. Alpha cells are the morphological types associated with Y-type physiological responses (Boycott and Wässle, 1974).

Famiglietti and Kolb (1976) proposed that anatomically paired cell types were, in fact, the physiological ON and OFF types. At roughly the same time, intracellular marking experiments were progressing in an adjacent laboratory (Nelson et al., 1978). These marking experiments generated direct evidence that the theory was not only true, but also held for all morphological types of ganglion cell, regardless of whether they were paired types. This led to the schema illustrated in Figure 18.10. The dendrites of OFF-center ganglion cells always arborize distal to the dendrites of ON-center ganglion cells. The zone of OFF-center dendritic arborization is called sublamina *a*, whereas the zone of ON-center dendritic arborization is called sublamina *b* (see Fig. 18.10). Within each sublamina, ganglion cells make selective contacts with ON- or OFF-type bipolar cells. The pattern of ON and OFF layering of ganglion cells in the IPL, originally discovered in cat retina, has proved to be general and applicable to other vertebrate retinas, including rabbit (Amthor et al., 1989b; Bloomfield and Miller, 1986).

ON and OFF stratification is particularly pronounced in retinas in which ganglion cell types are predominantly monostратified. In more anatomically complex retinas, such as in the turtle, which has many multistratified or diffusely stratified ganglion cell types, the branching rule still applies to monostратified types, but is more difficult to apply

with the others. Nonetheless, even among multistratified ganglion cell types, it appears that morphological and physiological patterns are closely linked (Ammermüller and Kolb, 1995).

The discovery of ON and OFF layering in the IPL has generated further conjecture, namely, the theory that true ON-OFF ganglion cell types would be bistratified, receiving OFF inputs from sublamina *a*, and ON inputs from sublamina *b*. In fact, there is such a population of ON-OFF cells in the cat retina (Isayama et al., 2000). Moreover, there is a major class of ON-OFF, directionally selective cells in the rabbit retina, also bistratified (Amthor et al., 1989a). On a further variation of the theme, a blue-ON, yellow-OFF color opponent cell in the primate retina has been found to be bistratified. Blue excitation arises from the dendrites stratified in sublamina *b*, whereas yellow inhibition arises from dendrites stratified in sublamina *a* (Dacey and Lee, 1994).

The discovery of ON-OFF stratification also prompted a reevaluation of the spatial distributions of alpha and beta cat ganglion cells, as spatial mosaics are thought to govern spatial acuity (DeVries and Baylor, 1997; Wässle and Boycott, 1991). When this was done, it was discovered that Y_{ON} types and Y_{OFF} types were individually much more regularly arranged than the combined ON-OFF grouping (Peichl and Wässle, 1981; Wässle et al., 1981b). The same was found for X_{ON} and X_{OFF} types (Wässle et al., 1981a). Nonetheless, the ON and OFF mosaics themselves appear to be linked spatially (Zhan and Troy, 2000). In situations in which ganglion cell mosaics limit visual acuity, such as with the beta ganglion cells of cat retina, it is an open question whether the

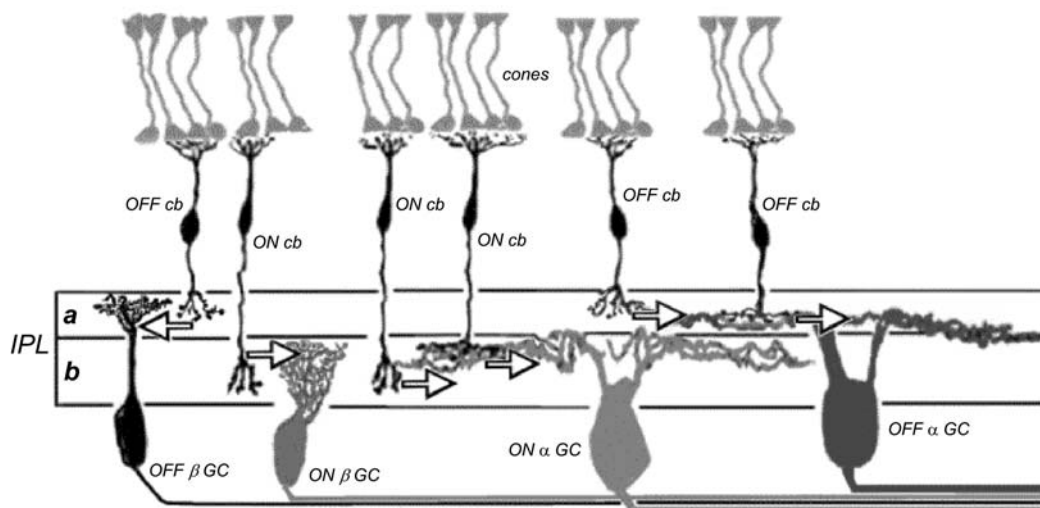


FIGURE 18.10. ON and OFF stratification patterns in the retinal inner plexiform layer (IPL). OFF ganglion cell dendrites (OFF α GC and OFF β GC) and OFF cone bipolar (OFFcb) cell axons co-stratify in sublamina *a* of the IPL. ON bipolar axons (ONcb) and ON ganglion cell (ON α GC and ON β GC) dendrites co-stratify in

sublamina *b* of the IPL. Thus, the sign of the cone bipolar response generated at the cone pedicle through different glutamate receptor mechanisms is faithfully passed to ganglion cells through separate systems of connections within the neuropil of the IPL. These are the parallel ON and OFF cone-system pathways. (See color plate 6.)

limit is achieved jointly or separately among ON and OFF systems.

CONE BIPOLAR CELLS The work of DeVries (2000) and Awatramani and Slaughter (2000) suggests the hypothesis that each bipolar cell type expresses a unique glutamate receptor, and that this receptor expression is somehow linked to a corresponding, discrete, axonal layering pattern within the IPL. That is an exciting scheme to contemplate. At present, though, what appears to be generally true is that axon terminal arborizations of OFF-type bipolar cells lie in sublamina *a*, together with the dendrites of OFF-type ganglion cells, whereas the axon terminal arborizations of ON type bipolar cells lie in sublamina *b* of the IPL, together with the dendrites of ON-center ganglion cells. This is the classic circuitry model (see Fig. 18.10) put forward by Nelson et al. (1978) and Famiglietti and Kolb (1976). Indeed, direct, selective, synaptic contacts between OFF bipolar cells and OFF ganglion cells within sublamina *a*, or ON bipolar cells and ON ganglion cells within sublamina *b*, have been observed with the electron microscope (Cohen and Sterling, 1991; Kolb, 1979; Kolb and Dekorver, 1991; Kolb and Nelson, 1993; McGuire et al., 1984; Nelson and Kolb, 1983). Synapses between unmatched pairs of bipolar and ganglion cells are never observed, even where processes come in close proximity (Kolb, 1979).

After studying salamander retina, Awatramani and Slaughter (2000) proposed a further refinement of the stratification scheme for bipolar cell axons. They suggested that bipolar cells with a glutamate receptor physiology that emphasized transients in the visual pattern were layered more toward the center of the IPL, whereas those with receptor patterns emphasizing sustained contrast were layered more toward the inner and outer edges of the IPL. Such a pattern would be in agreement with the layering of the sustained X- and transient Y-type ganglion cells of the cat retina, as well as the P and M cells of the primate retina. Wu et al. (2000) discovered a similar pattern, but attributed it to the expression of fast signals from cone bipolar terminals in the middle of the IPL, and the expression of slow signals from rod bipolar terminals at both edges of the IPL. Although this further overlay of functional organization within the IPL is exciting to contemplate, most of the evidence is as yet limited to one species.

Relatively exhaustive correlations of ON or OFF bipolar cell physiology with axonal stratification patterns are now available for several species. These involve measurements of light responses or, as a surrogate for light responses, dendritic glutamate responses, coupled with observations of axonal morphology through microelectrode staining. In rat retina, bipolar-cell, axon-terminal arborization appears to obey perfectly the rule of ON and OFF layering. Five cone bipolar-cell morphological types with axons branching in the

outer half of rat IPL were identified. These responded with inward currents when stimulated with kainate. This is the response appropriate to OFF bipolar cells. Of a combined total of 15 recordings, only 1 of these *a*-layered cells responded to APB (DL AP-4), a glutamate agonist selective for ON-center bipolar cells. Three cone bipolar cell types with axons branching in the inner half of rat IPL were identified. In net, 12 of 14 of these *b*-layered cells responded with outward currents to APB, whereas only 1 responded to kainate (Euler et al., 1996). This suggests better than 90% compliance with the ON and OFF stratification rule for bipolar cell axon terminals in rat retina. A limited number of recordings in cat and monkey retinas also suggest that there may be good adherence to this pattern (Dacey and Lee, 1994; Nelson and Kolb, 1983). The salamander retina too appears to be in excellent compliance with ON and OFF stratification of bipolar cell axon terminals (Wu et al., 2000), as does carp retina (Famiglietti et al., 1977; Saito et al., 1985).

This orderliness breaks down to some extent in species in which multistratified, bipolar cell axons are common. Although monkeys and cats have some multistratified cells (Kolb et al., 1981; Mariani, 1983), these types are very much more common in lower vertebrates, such as birds, reptiles, and fishes, or cone-dominant mammals, such as squirrels. Such types are typically cone-contacting bipolar cells (Scholes, 1975), and so may be characteristic of cone-dominated species. Where broad or multistratified patterns are restricted to either the ON or the OFF sublaminae, the ON and OFF stratification rules apply, but not where the axonal stratification pattern crosses the ON-OFF boundary. In this case, cells may be either ON-type or OFF-type (Ammermuller and Kolb, 1995; Connaughton and Nelson, 2000; Wu et al., 2000). In some cases, such multistratified bipolar cells may even express both physiologies (Wu et al., 2000). Stratification patterns of bipolar axon terminals of the zebrafish retina represent this more general vertebrate pattern (Fig. 18.11). Bipolar cells with one or two terminal boutons restricted either to sublamina *a* or sublamina *b* obey the ON and OFF stratification rule. OFF cells branching in sublamina *a* express AMPA/Kainate-type receptors. ON cells branching in sublamina *b* express either or both of two inhibitory glutamate mechanisms: ionotropic or metabotropic. Multistratified bipolar cells with boutons in both sublaminae may be either ON or OFF types. Multistratified ON types use only the inhibitory ionotropic glutamate mechanism (Connaughton and Nelson, 2000).

ROD BIPOLAR CELLS Rod bipolar cells represent a unique case. Judged by the axonal stratification pattern and contacts with photoreceptors, there is only a single class of rod bipolar cell in mammals (Cajal, 1972; Kolb, 1970). The

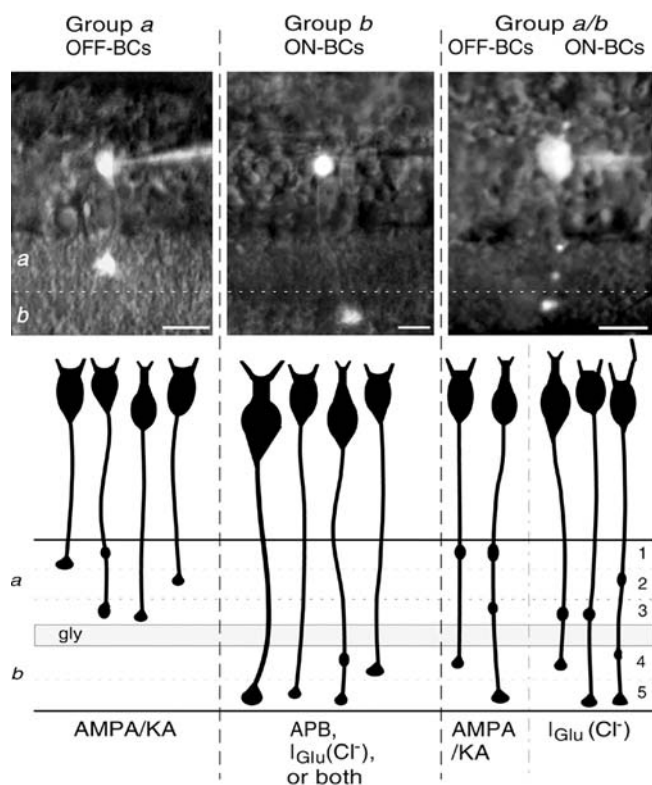


FIGURE 18.11. ON and OFF stratification patterns of bipolar-cell axon terminals in zebrafish retina. Monostratified or bistratified cells with terminal boutons only in sublamina *a* express AMPA/Kainate receptors (AMPA/KA) appropriate to OFF-type bipolar cells (OFF BCs). Those with either one or two boutons only in sublamina *b* express metabotropic (APB-sensitive) glutamate receptors, glutamate-gated chloride channels (I_{glu}), or both. These receptors are both appropriate for ON center cells. Bistratified or tristratified cells with terminal boutons in both sublaminae *a* and *b* express either AMPA/KA, an OFF-type receptor, or I_{glu} , an ON-type receptor. Curiously, metabotropic ON receptors are not seen in *a/b* branching cells, perhaps because these are cone-selective types. (From Connaughton and Nelson, 2000.)

bulbous axon arborizes deep in the ON sublamina of the IPL, just adjacent to ganglion cells. The rod bipolar cell is an ON type (Dacheux and Raviola, 1986), using metabotropic APB-sensitive, glutamate receptors (de la Villa et al., 1995; Yamashita and Wässle, 1991).

For the rod signals transferred by rod bipolar cells, ON and OFF pathways begin in the IPL. This bipolar cell does not contact ganglion cells directly, but instead contacts amacrine cells. It is the AII rod amacrine cell (Kolb and Famiglietti, 1974; Nelson, 1982) that is the intermediary in transferring rod bipolar signals to ON and OFF cone bipolar pathways. It achieves this through direct innervation of cone bipolar processes within the IPL. Cone bipolar cells also participate, even without amacrine intermediation, in transferring ON and OFF rod signals from the distal to the proximal retina. This occurs because of direct rod-cone interphotoreceptor contacts, a pathway emphasized in higher

mammals (Kolb, 1977; Nelson, 1977; Raviola and Gilula, 1973; Smith et al., 1986; Tsukamoto et al., 2001). It may also occur through direct dendritic contact of cone bipolar cells with rods (Dacheux, 1982; Hack et al., 1999; Ishida et al., 1980; Jacobs et al., 1976; Lasansky, 1973; Stell, 1977; Tsukamoto et al., 2001), a pathway particularly prominent in lower vertebrates.

AMACRINE CELLS Amacrine cells are interneurons of the retinal IPL. Most of them are inhibitory and release either gamma-aminobutyric acid (GABA) or glycine. Although this class of cells contains both ON, OFF, and ON-OFF light responses (Ammermüller and Kolb, 1995; Bloomfield and Miller, 1986; Kolb and Nelson, 1996; Naka et al., 1975; Nelson, 1982; Nelson and Kolb, 1985; Werblin and Dowling, 1969), it is among the least obedient to ON and OFF layering within the IPL. Only the widely studied cholinergic “starburst” amacrine cells consistently follow this rule (Bloomfield and Miller, 1986; Famiglietti, 1991; Tauchi and Masland, 1984; Taylor and Wässle, 1995). Starburst amacrine cells are prominent, monostratified types found in morphological pairs, one monostratified in sublamina *a*, the OFF type, and the other monostratified in sublamina *b*, the ON type. These cells provide additional center excitation selective for moving stimuli to ON- and OFF-type retinal ganglion cells (He and Masland, 1997).

Even in retinas with predominantly monostratified bipolar and ganglion cells, such as those in the cat (Kolb et al., 1981) or human (Kolb et al., 1992), about half of amacrine types arborize in both ON and OFF IPL sublaminae. Broadly stratified amacrine cells may be either ON or OFF types (Ammermüller and Kolb, 1995; Kolb and Nelson, 1996). Furthermore, monostratified ON-OFF amacrine types are commonly encountered (Ammermüller and Kolb, 1995; Freed et al., 1996; Jensen and DeVoe, 1982), although other ON-OFF types are clearly bistratified (Ammermüller and Kolb, 1995).

Cross-correlation in the firing patterns of retinal ganglion cells suggests that amacrine cells, and particularly broadly stratified types, provide for cross talk between ON and OFF pathways (Mastrorade, 1983a, 1983b). The AII amacrine cell of mammalian retinas may be thought of as the archetypical example of the broadly stratified amacrine pattern. The AII cell is a narrow-field, concentric, ON-center cell (Bloomfield, 1992; Dacheux and Raviola, 1986; Nelson, 1982). Its principal roles appear to be receiving signals from rod bipolar cells, spatially integrating them, transforming the rod pathway signals to emphasize ON transients, and distributing these signals to ON and OFF pathways (Kolb and Famiglietti, 1974; Nelson, 1982; Vardi and Smith, 1996). The AII amacrine dendrites branch within all strata of the IPL, yet the ultrastructural organization within IPL layers differs (Fig. 18.12). Deep in the prox-

imal IPL, near ganglion cell bodies, the AII dendritic terminals receive ON-center ribbon synaptic input from rod bipolar axon terminals. In the middle of the IPL, they transfer this signal to ON-center cone bipolar cells through heterologous gap junctions. High in the distal IPL, near amacrine cell bodies, AII amacrine processes synapse directly onto OFF-center ganglion cells (Kolb, 1979; Kolb and Nelson, 1993) and OFF-center bipolar cells (Chun et al., 1993; McGuire et al., 1984) using a glycinergic inhibitory mechanism. Glycinergic ON inhibition, perhaps originating with the AII cells, has been confirmed in dark-adapted, OFF-center ganglion cells (Wässle et al., 1986).

Examination of other narrow-field, diffuse amacrine cells in cat retina suggests that, despite lack of clear evidence for ON-OFF layering at the light microscopic level, such cells exhibit stratified synaptic input and output at the ultrastructural level (Kolb and Nelson, 1996). In the rod system, broadly stratified amacrine cells perform a function similar to cone bipolar cells, generating dual ON and OFF path-

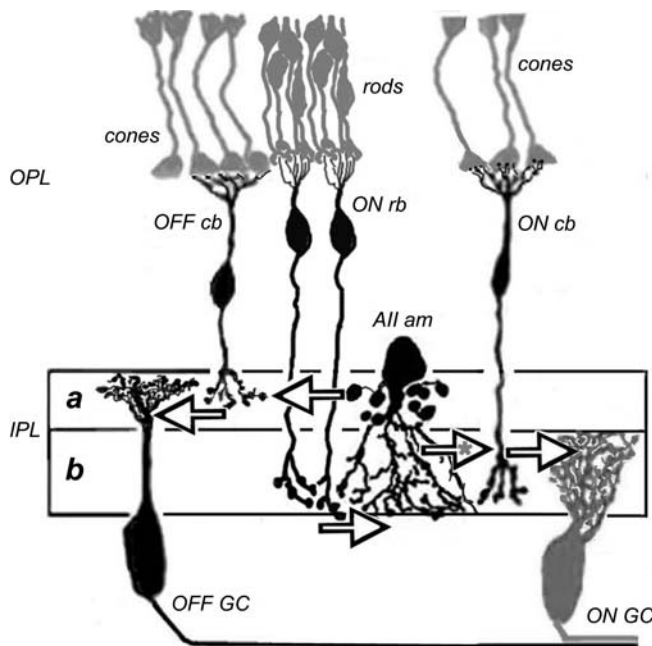


FIGURE 18.12. The rod pathway through the mammalian retina splits into parallel ON and OFF channels within the inner plexiform layer (IPL), where amacrine cells contact bipolar and ganglion cells, rather than at the outer plexiform layer (OPL), where photoreceptors contact bipolar cells. ON rod bipolar signals are established at metabotropic glutamate receptors on dendritic spines within OPL rod spherules. This rod ON signal is split into ON and OFF components by the AII amacrine (*AII am*) cell. Rod ON signals flow from rod bipolar (*ONrb*) to *AII* to ON cone bipolar (*ONcb*) at gap junctions (*asterisk*) in sublamina *b*. Rod OFF signals are generated at the inhibitory glycinergic synapses between AII amacrine cells and both OFF cone bipolar cells (*OFFcb*) and OFF ganglion cells (*OFF GC*) within sublamina *a*.

ways from a single signal substrate, in this case, the rod bipolar cell. In the cone system, broadly stratified amacrine cells may act to reinforce ON and OFF signals through inhibitory cross talk (Mastronarde, 1983a; Mastronarde, 1983b).

Central projections of ON and OFF ganglion cells

Ganglion cells send axons across the retinal surface to form the optic nerve. Optic nerve axons terminate in brain visual centers. In higher mammals, the principal target is the dorsal lateral geniculate nucleus (LGNd), the visual part of the thalamus. In lower mammals and cold-blooded vertebrates, the principal target is the superior colliculus. Neurons of LGNd project through optic radiations to the visual cortex. Neurons of LGNd are all ON-center or OFF-center types. In the visual cortex, "simple cells" are found in layer 4, the layer where axons of LGNd output neurons terminate after traveling through the optic radiations. These cortical "simple cells" are clearly either ON-center or OFF-center types, although unlike ganglion cells, they are very elongate in terms of receptive field structure. Other visual cortical cells are "complex" and often difficult to classify as either ON or OFF types (Hubel, 1988; Hubel and Wiesel, 1959). These complex types finally appear to combine signals from both pathways. Thus, ON and OFF emphasis remains distinct, even to the early stages of visual cortical processing in the occipital lobe.

Some ganglion cells project to brainstem visual centers, either solely or by axon collaterals arising from within the LGNd. Y-type ganglion cells represent a major bifurcating pathway. The principal target in the brainstem is the superior colliculus or optic tectum. This is the main termination of the optic nerve fibers in fishes, reptiles, birds, amphibians, and lower mammals, such as rabbits, rodents, and ground squirrels. Many ganglion cells projecting to the superior colliculus have receptive fields more complex than simple ON or OFF types.

By simultaneous recording of light responses from individual ganglion cells and LGNd neurons in the cat, it can be shown that each geniculate neuron is innervated by one to three retinal ganglion cells. ON-type ganglion cells synapse only with ON-type LGNd neurons; likewise, OFF-type ganglion cells synapse only with OFF-type LGNd neurons (Cleland et al., 1971a). Furthermore, X and Y (sustained and transient) pathways are not mixed on LGNd neurons. These pathways, too, are maintained as separate through to the visual cortex (Cleland et al., 1971b).

LATERAL GENICULATE LAYERS KEEP THE INPUTS FROM EACH EYE SEPARATE The LGNd is a layered structure. The exact number of layers varies from species to species. Common

household pets, like the cat and ferret, have three layers (Fig. 18.13). Primates typically have six layers. Each layer reflects the input of only one of the two eyes. The layers are organized, however, so that equivalent parts of the visual image, as seen by each eye, are in registry. Despite this very organized anatomical overlaying of image inputs from the two eyes, there are no binocularly driven geniculate cells. In the cat, layer A₁ receives input from the ipsilateral eye (see Fig. 18.13), whereas layers A and C receive input from the contralateral eye. Although not illustrated in Figure 18.13, it should be noted that layer C can be subdivided into four sublayers: C, C1, C2, and C3, with C3 lying closest to the optic radiations. Sublayer C contains larger cell bodies than sublayers C1 to C3. Although sublayers C1 to C3 are not histologically distinguishable in themselves, retrograde tracers indicate alternating projection of contralateral and ipsilateral eyes; C1, like A₁, receives ipsilateral input, whereas C2, like C, receives contralateral input. C3 does not receive ocular input (Hickey and Guillery, 1974).

The size and patterns of X-type and Y-type ganglion cell axonal arborizations within the geniculate differ (Bowling and Michael, 1980; Bowling and Michael, 1984; Sur and Sherman, 1982; Sur et al., 1987; Tamamaki et al.,

1995). Y-cell arbors are broader than X-cell arbors within the A layers and have many more boutons (see Fig. 18.13). Furthermore, Y cells always send branches to layer C, as well as the superior colliculus. X cells rarely arborize in layer C, and they never send branches to the superior colliculus (Tamamaki et al., 1995). Projections to the pretectum by axon collaterals of both X-type and Y-type ganglion cells have also been identified (Tamamaki et al., 1995).

ON AND OFF LEAFLETS IN THE LATERAL GENICULATE LAYERS

The synaptic fidelity of ON and OFF pathways within the LGNd argues for an underlying morphological segregation of processes. In the cat, there is a suggestion of ON and OFF layering within LGNd. Y_{ON} axonal arborizations may be more hour-glass in shape, whereas Y_{OFF} axon terminals may be more pyramidal (see Fig. 18.13). Y_{ON} terminals ascend into the upper half of layer A₁, whereas Y_{OFF} terminals are densely clustered in the lower half. Although this subtle morphological distinction between Y_{ON} terminals and Y_{OFF} terminals has not been noted by all investigators (Sur et al., 1987), a corresponding and distinct predominance of ON-type units is found in the upper half of layers A and A₁, whereas OFF-type units are more common toward the bottoms of these layers, that is, the edge closer to the optic tract. Layer C contains mainly OFF units (Berman and Payne, 1989; Bowling and Wieniawa-Narkiewicz, 1986). There is also a strong suggestion of columnar or modular clustering of ON and OFF units within all geniculate layers of the cat (Berman and Payne, 1989).

The tendency toward sublaminal distribution of ON and OFF geniculate pathways in LGNd is much more pronounced in ferret and mink retinas, where layers A and A₁ each are composed of two bisublaminal leaflets, one for OFF-center cells, and one for ON-center cells (LeVay and McConnell, 1982; Stryker and Zahs, 1983). There is also evidence for anatomical segregation of ON and OFF geniculate pathways in the monkey and tree shrew LGNd (Conway and Schiller, 1983; Schiller and Malpeli, 1978). In the macaque, geniculate layers 5 and 6 contain mainly ON types, whereas layers 3 and 4 contain mainly OFF types. Layers 1 and 2 are mixed in type (Michael, 1988; Schiller and Malpeli, 1978). No anatomical separation of ON or OFF pathways has been seen in cat or monkey visual cortex; however, there is evidence for ON and OFF patchiness in ferret visual cortex (Zahs and Stryker, 1988). The continued physiological and anatomical separation of ON and OFF pathways in the central nervous system strengthens the notion that vertebrates contain paired visual systems that, from retina to brain, are functionally separate.

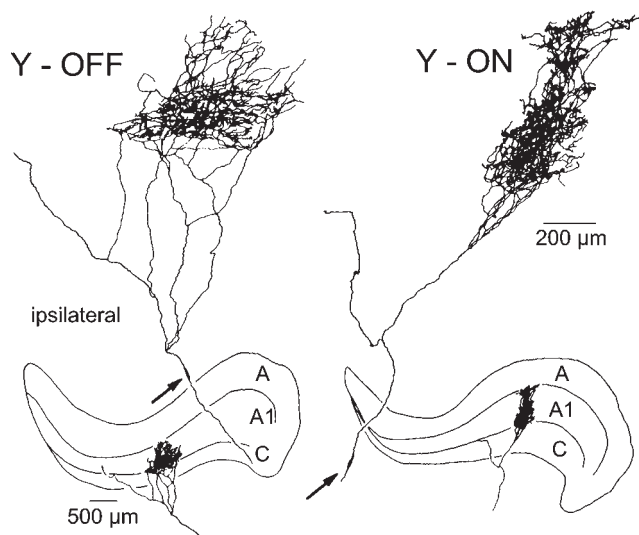


FIGURE 18.13. Axons of ON and OFF Y-type ganglion cells have terminal arborizations in the dorsal lateral geniculate body (LGNd). Axons from the ipsilateral eye project to layer A₁, whereas axons from the contralateral eye project to layers A and C. Projections are organized so that features of the visual images from each eye overlay one another. The Y-OFF axon branches densely in the lower leaflet of lamina A₁ while the Y-ON axon projects, in addition, to the upper leaflet. Although the difference in ON and OFF stratification is subtle in the cat, ON and OFF geniculate sublamination is quite pronounced in other species. Y cells also project to layer C, to the pretectum, and to the superior colliculus. Some X-cells project to the pretectum also. (From Bowling and Michael, 1984.)

Behavioral and clinical implications of ON and OFF pathways

The evidence presented thus far suggests that ON and OFF pathways are deeply embedded in the visual processing of vertebrates. These two processing systems remain separate through at least the first four synapses in vision, until being combined in visual cortex. The reasons for a two-system approach are less clear. Photographic film does not utilize ON and OFF substrates, nor do video cameras. Nonetheless, these media readily transcribe detailed and recognizable images. Hartline, the discoverer of ON and OFF systems in vertebrates, spent much of his career studying the limulus visual system. The optic nerve of the limulus contains only ON-center responses (Hartline and Graham, 1932). One might also argue that either ON or OFF X-type vertebrate retinal ganglion cells, with linear summation of dimming and brightening areas of the stimulus (see Fig. 18.3), are quite capable individually of transmitting information about both shadows and highlights within the image.

The uniqueness of the metabotropic glutamate receptor mGluR6 utilized in the ON pathway of vertebrate vision makes it vulnerable to selective elimination without affecting other neural pathways. Thus, the behavioral implications of eliminating the ON pathway can be studied. This can be accomplished either by the use of selective pharmacological blocking agents, such as APB, or by site-directed mutagenesis designed to eliminate the mGluR6 receptors themselves from the genome. Further, there are naturally occurring mutations and disease processes that selectively affect the ON system. Surprisingly, humans and animal models with ON-system deficit perform visual tasks relatively normally. The major deficit is loss of nocturnal vision, which appears to be dependent on the ON pathway.

MICE WITH ON-PATHWAY KNOCKOUT PERFORM VISUAL TASKS The electrophysiological consequences of site-directed mutagenesis directed at the ON pathway are seen in Figure 18.7 for mGluR6-deficient mice. The electroretinographic b-wave component, which arises from the activity of ON bipolar cells, is abolished (Masu et al., 1995). Furthermore, this study demonstrates that light-evoked field potentials from the superior colliculus, which in the mouse is the main termination site for ganglion cell axons, lack ON responses. In wild-type mice, transient collicular waves are seen at both onset and cessation of light stimuli, but in the mutant, only OFF-type waves appear.

Nonetheless, no deficit in visual behavior was readily observed. In a shuttle box avoidance learning analysis, both mutant and wild-type mice performed equally well. Although the mutant mice were capable of performing visual tasks, some visual system alterations were noted. Mutant mice had normal circadian clocks, but the daily

activity pattern was altered. The normal light-induced reduction in activity was greatly delayed (Takao et al., 2000). Pupillary responses were observed only at high light levels, and optokinetic responses were noted only at high contrasts in mutant mice (Iwakabe et al., 1997), suggesting a general loss of sensitivity. Nonetheless, these studies indicate that the OFF pathway alone can mediate vision, even if in a somewhat impaired way. Interestingly, the morphological layering of ON and OFF ganglion cell types persists in the mutants (Tagawa et al., 1999).

DISEASES OF THE ON PATHWAY

Melanoma-associated retinopathy. Some patients with malignant melanomas lose night vision. They may further report hallucinations consisting of shimmering blobs of white light (Berson and Lessell, 1988; Ripps, 1982). Visual processing in daylight appears otherwise normal. Color vision is not affected, nor is visual acuity dramatically worsened. ERG studies reveal ON pathway deficits for these patients. As with mGluR6-deficient mice, the b wave is selectively absent in both rod- and cone-driven responses (Alexander et al., 1992). The ON pathway loss is more serious for the rod system, as it is the only rod pathway, or at least the only one involved in processing of nocturnal vision. The syndrome is termed “melanoma-associated retinopathy” (MAR). Although originally thought to be a side effect of chemotherapy (Ripps, 1982), it became clear that the syndrome might arise in patients prior to chemotherapy (Alexander et al., 1992; Berson and Lessell, 1988). The immunoglobulin G (IgG) serum fraction of patients with MAR induces reversible electroretinographic disturbances similar to those associated with MAR when injected into the eyes of monkeys (Lei et al., 2000). The ERG documented a waves and d waves remain, but the b wave is lost from both rod and cone responses (Fig. 18.14). MAR appears to be caused by an autoimmune attack on retinal ON pathways for rod and cone vision. Antibodies induced against the melanoma cause the visual deficit.

Congenital stationary night blindness. Congenital stationary night blindness (CSNB) is an inherited retinal disease producing very similar symptoms to MAR. In the Schubert-Bornschein or complete type of the dysfunction (Schubert and Bornschein, 1952), there is loss of nocturnal or rod vision, but in daylight, cone-mediated color vision and visual acuity are relatively normal (Goodman and Bornschein, 1957; Miyake et al., 1986). The sensitivity of cone vision is somewhat reduced (Miyake et al., 1986). The disease appears to be X-linked, affecting primarily males (Miyake et al., 1986). ERGs reveal a loss of b waves for both the rod and cone systems. ON pathways for both rod and cone signals appear greatly depressed or absent, OFF cone

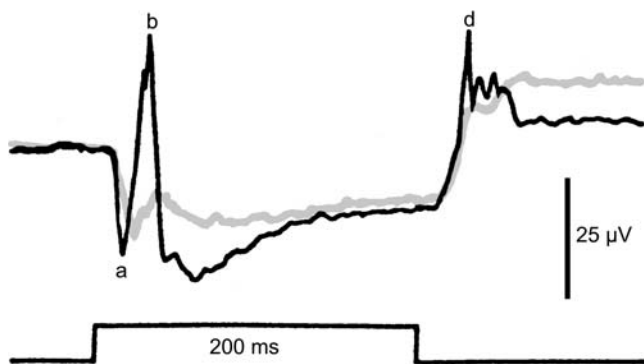


FIGURE 18.14. In melanoma-associated retinopathy (MAR), autoantibodies are generated that attack the retina, selectively targeting the ON pathway. The ERG recordings shown here are from a nonhuman primate model of the disease. The thin black trace represents a normal ERG with a, b, and d waves. The heavier gray trace was recorded from an eye treated with an intravitreal injection of IgG from a patient experiencing MAR. The immune serum causes a marked reduction in the b wave, an index of ON pathway activity in the retina. (From Lei et al., 2000.)

pathways, as represented by the ERG d wave, are spared (Alexander et al., 1992), as is the rod a wave (Goodman and Bornschein, 1957). The presence of a rod a wave but not a b wave provided the first suggestion of a genetic, postreceptor, neural processing disease in the retina (Goodman and Bornschein, 1957).

CSNB can be separated into two types: *complete* and *incomplete*. Genetic analysis reveals that the *complete* form involves defects in the glycoprotein nyctalopin (Bech-Hansen et al., 2000). Mutant nyctalopin may disrupt ON bipolar-cell development. The genetic defect in *incomplete* CSNB occurs in a gene similar to the L-type calcium channel alpha subunit, but uniquely expressed in retina (Bech-Hansen et al., 1998). The gene is CACNA1F—an example of a human retinal channelopathy.

VISUAL PROCESSING WITH PHARMACOLOGICAL BLOCKADE OF THE ON PATHWAY The responses of visual neurons in the central nervous system of primates have been investigated under conditions of ON-channel blockade using the metabotropic glutamate receptor agonist APB (DL AP-4). Recordings from LGNd indicate that light responses of ON-center geniculate neurons are completely blocked by APB applied to the retina. This includes both center and surround components. At the level of this thalamic relay, there appears to be no cross-innervations of ON by OFF channels (Schiller, 1982; Schiller, 1984). ON-center geniculate cells are also blocked selectively in rabbit LGNd (Knapp and Mistler, 1983). The performance of geniculate neurons with pharmacological blockade of the ON pathway confirms conclusions reached earlier by simultaneous recording of ganglion and geniculate cells, namely, that ON and OFF

pathways do not interconnect in LGNd (Cleland et al., 1971a).

Recordings of light responses of individual neurons in visual cortex suggest final integration of ON and OFF pathways. Complex cells, which under control conditions respond to both the leading and trailing boundaries of a bright square passing through the receptive field, only respond to the trailing light-dark transition after perfusion of the eye with APB (Fig. 18.15). In other words, the ON responses of complex cells are selectively eliminated, whereas the OFF responses remain. Even simple cells, normally classifiable as either ON or OFF types, reveal underlying input from both pathways (Schiller, 1982). Consistent with behavioral results, other properties of neurons in the visual cortex remain unperturbed by APB blockade of the ON system. These include preferred orientation and selectivity for direction of motion. These properties appear to be built up separately in each channel and then combined (Schiller, 1982). In a parallel study, monkeys undergoing APB blockade were found to have much poorer perception of light increments than light decrements, but relatively unimpaired perception of simultaneous spatial contrast (Dolan and Schiller, 1994).

DIM LIGHT RESPONSES ARE CONVEYED BY ON PATHWAYS

One common feature of rod-dominated mammalian retinas is the emergence of a single, ON-type rod bipolar cell (Dacheux and Raviola, 1986; de la Villa et al., 1995; Yamashita and Wässle, 1991) dominated by the metabotropic, mGluR6 glutamate receptor. Pharmacological blockade of this pathway leads to severe behavioral, as well as physiological, deficits in night vision. This is true behaviorally for both light increments and decrements (Dolan and Schiller, 1989), as well as for dim light responses in ON or OFF ganglion cells (Müller et al., 1988). Blockade of the ON pathway in mGluR6-deficient mice also leads to loss of light sensitivity, as is evident on ERG studies (Masu et al., 1995). As noted earlier, ON pathway diseases in humans are always accompanied by a loss of nocturnal vision. The secondary rod pathways that utilize cone-system OFF bipolar cells appear not to be involved in rod-mediated nocturnal vision.

Perspectives

In the parallel ON and OFF pathways to the brain, one sees a nearly coequal pair of image detection systems. The systems are based on feature detectors for highlights and shadows, each with separately evolved neurotransmitter systems expressed at photoreceptor to bipolar cell synapses. Each of these images, both the ON and the OFF, appear to be separately competent. Each is a separate visual system capable of color discrimination and sophisticated spatial

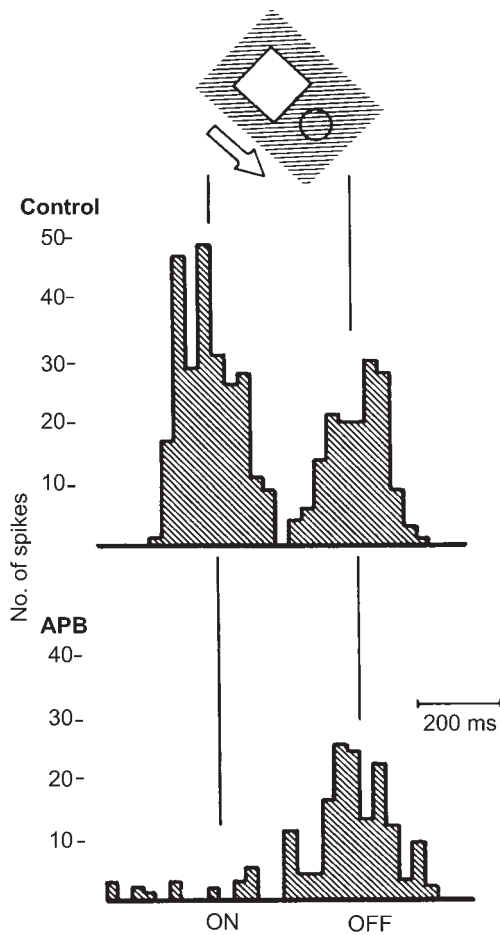


FIGURE 18.15. Effects of ON pathway blockade on a complex cortical cell. At the top, a bright square moves through the receptive field of a complex cell in the visual cortex. Vigorous discharges occur as the leading edge (an ON transition) and the trailing edge (an OFF transition) pass through the field. The neuron is selectively excited only by movements in one direction (arrow). With the ON pathway responses blocked by APB (below), the leading edge (ON) excitation disappears. Only the trailing edge (OFF) excitation remains. This complex cell integrates information from both ON and OFF pathways for edge responses of each contrast. (From Schiller, 1982.)

analysis of features, such as contrast and motion. In mammals, one system—the ON-pathway—dominates nocturnal vision. When the ON pathway is lost, loss of nocturnal vision is the most obvious deficit. That aside, both ON and OFF pathways are competent visual subsystems whose separate analyses are only combined late in the visual process. Although feature detectors may be a universal strategy of visual systems (exquisite, directionally selective cells are found in the medulla of the insect visual system [DeVoe and Ockelford, 1976; Riehle and Franceschini, 1984]), ON and OFF pathways are not invariably found. These may instead be a particular strategy, developed early in the vertebrate lineage, as a solution to unique environmental issues, but there is little to suggest a universal necessity.

REFERENCES

- Alexander, K. R., G. A. Fishman, N. S. Peachey, A. L. Marchese, and M. O. Tso, 1992. 'On' response defect in paraneoplastic night blindness with cutaneous malignant melanoma, *Invest. Ophthalmol. Vis. Sci.*, 33:477–483.
- Ammermüller, J., and H. Kolb, 1995. The organization of the turtle inner retina. I. ON- and OFF-center pathways, *J. Comp. Neurol.*, 358:1–34.
- Amthor, F. R., E. S. Takahashi, and C. W. Oyster, 1989a. Morphologies of rabbit retinal ganglion cells with complex receptive fields, *J. Comp. Neurol.*, 280:97–121.
- Amthor, F. R., E. S. Takahashi, and C. W. Oyster, 1989b. Morphologies of rabbit retinal ganglion cells with concentric receptive fields, *J. Comp. Neurol.*, 280:72–96.
- Awatramani, G. B., and M. M. Slaughter, 2000. Origin of transient and sustained responses in ganglion cells of the retina, *J. Neurosci.*, 20:7087–95.
- Ayoub, G. S., and D. R. Copenhagen, 1991. Application of a fluorometric method to measure glutamate release from single retinal photoreceptors, *J. Neurosci. Methods*, 37:7–14.
- Barlow, H. B., and R. M. Hill, 1963. Selective sensitivity to direction of movement in ganglion cells of the rabbit retina, *Science*, 139:412–414.
- Bech-Hansen, N. T., M. J. Naylor, T. A. Maybaum, W. G. Pearce, B. Koop, G. A. Fishman, M. Mets, M. A. Musarella, and K. M. Boycott, 1998. Loss-of-function mutations in a calcium-channel $\alpha 1$ -subunit gene in Xp 11.23 cause incomplete X-linked congenital stationary night blindness, *Nat. Genet.*, 19:264–267.
- Bech-Hansen, N. T., M. J. Naylor, T. A. Maybaum, R. L. Sparks, B. Koop, D. G. Birch, A. A. Bergen, C. F. Prinsen, R. C. Polomeno, A. Gal, A. V. Drack, M. A. Musarella, S. G. Jacobson, R. S. Young, and R. G. Weleber, 2000. Mutations in NYX, encoding the leucine-rich proteoglycan nyctalopin, cause X-linked complete congenital stationary night blindness, *Nat. Genet.*, 26:319–323.
- Berman, N. E., and B. R. Payne, 1989. Modular organization of ON and OFF responses in the cat lateral geniculate nucleus, *Neuroscience*, 32:721–737.
- Berson, E. L., and S. Lessell, 1988. Paraneoplastic night blindness with malignant melanoma, *Am. J. Ophthalmol.*, 106:307–311.
- Bloomfield, S. A., 1992. Relationship between receptive and dendritic field size of amacrine cells in the rabbit retina, *J. Neurophysiol.*, 68:711–725.
- Bloomfield, S. A., and R. F. Miller, 1986. A functional organization of ON and OFF pathways in the rabbit retina, *J. Neurosci.*, 6:1–13.
- Bowling, D. B., and C. R. Michael, 1980. Projection patterns of single physiologically characterized optic tract fibres in cat, *Nature*, 286:899–902.
- Bowling, D. B., and C. R. Michael, 1984. Terminal patterns of single, physiologically characterized optic tract fibers in the cat's lateral geniculate nucleus, *J. Neurosci.*, 4:198–216.
- Bowling, D. B., and E. Wieniawa-Narkiewicz, 1986. The distribution of on- and off-centre X- and Y-like cells in the A layers of the cat's lateral geniculate nucleus, *J. Physiol.*, 375:561–572.
- Boycott, B. B., and H. Wässle, 1974. The morphological types of ganglion cells of the domestic cat's retina, *J. Physiol.*, 240:397–419.
- Cajal, S. R., 1972. *The Structure of the Retina* (S. A. Thorpe and M. Glickstein, translator), Springfield, IL: Charles C Thomas.

- Chun, M. H., S. H. Han, J. W. Chung, and H. Wässle, 1993. Electron microscopic analysis of the rod pathway of the rat retina, *J. Comp. Neurol.*, 332:421–432.
- Cleland, B. G., M. W. Dubin, and W. R. Levick, 1971a. Simultaneous recording of input and output of lateral geniculate neurones, *Nat. New Biology.*, 231:191–192.
- Cleland, B. G., M. W. Dubin, and W. R. Levick, 1971b. Sustained and transient neurones in the cat's retina and lateral geniculate nucleus, *J. Physiol.*, 217:473–496.
- Cleland, B. G., and W. R. Levick, 1974a. Brisk and sluggish concentrically organized ganglion cells in the cat's retina, *J. Physiol.*, 240:421–456.
- Cleland, B. G., and W. R. Levick, 1974b. Properties of rarely encountered types of ganglion cells in the cat's retina and an overall classification, *J. Physiol.*, 240:457–492.
- Cohen, E., and P. Sterling, 1991. Microcircuitry related to the receptive field center of the on-beta ganglion cell, *J. Neurophysiol.*, 65:352–359.
- Conn, P. J., and J. Patel, 1994. *The Metabotropic Glutamate Receptors*, Totawa, NJ: Humana Press.
- Connaughton, V. P., and G. Maguire, 1998. Differential expression of voltage-gated K^+ and Ca^{2+} currents in bipolar cells in the zebrafish retinal slice, *Eur. J. Neurosci.*, 10:1350–1362.
- Connaughton, V. P., and R. Nelson, 2000. Axonal stratification patterns and glutamate-gated conductance mechanisms in zebrafish retinal bipolar cells, *J. Physiol. (Lond)*, 524:135–146.
- Conway, J. L., and P. H. Schiller, 1983. Laminar organization of tree shrew dorsal lateral geniculate nucleus, *J. Neurophysiol.*, 50:1330–1342.
- Dacey, D. M., and B. B. Lee, 1994. The 'blue-on' opponent pathway in primate retina originates from a distinct bistratified ganglion cell type, *Nature*, 367:731–735.
- Dacheux, R. F., 1982. Connections of the small bipolar cells with the photoreceptors in the turtle. An electron microscope study of Golgi-impregnated, gold-toned retinas, *J. Comp. Neurol.*, 205:55–62.
- Dacheux, R. F., and E. Raviola, 1986. The rod pathway in the rabbit retina: a depolarizing bipolar and amacrine cell, *J. Neurosci.*, 6:331–345.
- de la Villa, P., T. Kurahashi, and A. Kaneko, 1995. L-glutamate-induced responses and cGMP-activated channels in three subtypes of retinal bipolar cells dissociated from the cat, *J. Neurosci.*, 15:3571–3582.
- Demb, J. B., K. Zaghloul, L. Haarsma, and P. Sterling, 2001. Bipolar cells contribute to nonlinear spatial summation in the brisk-transient (Y) ganglion cell in mammalian retina, *J. Neurosci.*, 21:7447–7454.
- DeVoe, R. D., and E. M. Ockelford, 1976. Intracellular responses from cells of the medulla of the fly, *Calliphora erythrocephala*, *Biol. Cybern.*, 23:13–24.
- DeVries, S. H., 2000. Bipolar cells use kainate and AMPA receptors to filter visual information into separate channels, *Neuron*, 28:847–856.
- DeVries, S. H., and D. A. Baylor, 1995. An alternative pathway for signal flow from rod photoreceptors to ganglion cells in mammalian retina, *Proc. Natl. Acad. Sci. USA*, 92:10658–10662.
- DeVries, S. H., and D. A. Baylor, 1997. Mosaic arrangement of ganglion cell receptive fields in rabbit retina, *J. Neurophysiol.*, 78:2048–2060.
- DeVries, S. H., and E. A. Schwartz, 1999. Kainate receptors mediate synaptic transmission between cones and "Off" bipolar cells in a mammalian retina, *Nature*, 397:157–160.
- Dhingra, A., A. Lyubarsky, M. Jiang, E. N. Pugh, L. Birnbaumer, P. Sterling, and N. Vardi, 2000. The light response of ON bipolar neurons requires $G\alpha_o$, *J. Neurosci.*, 20:9053–9058.
- Dolan, R. P., and P. H. Schiller, 1989. Evidence for only depolarizing rod bipolar cells in the primate retina, *Vis. Neurosci.*, 2:421–424.
- Dolan, R. P., and P. H. Schiller, 1994. Effects of ON channel blockade with 2-amino-4-phosphonobutyrate (APB) on brightness and contrast perception in monkeys, *Vis. Neurosci.*, 11:23–32.
- Enroth-Cugell, C., and J. G. Robson, 1966. The contrast sensitivity of retinal ganglion cells of the cat, *J. Physiol. (Lond)*, 187:517–552.
- Euler, T., H. Schneider, and H. Wässle, 1996. Glutamate responses of bipolar cells in a slice preparation of the rat retina, *J. Neurosci.*, 16:2934–2944.
- Famiglietti, E. V., Jr., 1991. Synaptic organization of starburst amacrine cells in rabbit retina: analysis of serial thin sections by electron microscopy and graphic reconstruction, *J. Comp. Neurol.*, 309:40–70.
- Famiglietti, E. V., Jr., A. Kaneko, and M. Tachibana, 1977. Neuronal architecture of on and off pathways to ganglion cells in carp retina, *Science*, 198:1267–1269.
- Famiglietti, E. V., Jr., and H. Kolb, 1976. Structural basis for ON- and OFF-center responses in retinal ganglion cells, *Science*, 194:193–195.
- Freed, M. A., R. Pflug, H. Kolb, and R. Nelson, 1996. ON-OFF amacrine cells in cat retina, *J. Comp. Neurol.*, 364:556–566.
- Freed, M. A., and P. Sterling, 1988. The ON-alpha ganglion cell of the cat retina and its presynaptic cell types, *J. Neurosci.*, 8:2303–2320.
- Goodman, G., and H. Bornschein, 1957. Comparative electoretinographic studies in congenital night blindness and total color blindness, *Arch. Ophthalmol.*, 58:174–182.
- Granit, R., 1935. Two types of retinæ and their electrical responses to intermittent stimuli in light and dark adaptation, *J. Physiol. (Lond)*, 85:421–438.
- Grant, G. B., and J. E. Dowling, 1995. A glutamate-activated chloride current in cone-driven ON bipolar cells of the white perch retina, *J. Neurosci.*, 15:3852–3862.
- Grant, G. B., and J. E. Dowling, 1996. On bipolar cell responses in the teleost retina are generated by two distinct mechanisms, *J. Neurophysiol.*, 76:3842–3849.
- Grant, G. B., and F. S. Werblin, 1996. A glutamate-elicited chloride current with transporter-like properties in rod photoreceptors of the tiger salamander, *Vis. Neurosci.*, 13:135–144.
- Hack, I., L. Peichl, and J. H. Brandstatter, 1999. An alternative pathway for rod signals in the rodent retina: rod photoreceptors, cone bipolar cells, and the localization of glutamate receptors, *Proc. Natl. Acad. Sci. USA*, 96:14130–14135.
- Hartline, H. K., 1938. The response of single optic nerve fibers of the vertebrate eye to illumination of the retina, *Am. J. Physiol.*, 121:400–415.
- Hartline, H. K., 1940. The receptive fields of optic nerve fibers, *Am. J. Physiol.*, 130:690–699.
- Hartline, H. K., and C. R. Graham, 1932. Nerve impulses from single receptors in the eye, *J. Cellular Comp. Physiol.*, 1:227–295.
- He, S., and R. H. Masland, 1997. Retinal direction selectivity after targeted laser ablation of starburst amacrine cells, *Nature*, 389:378–382.
- Hickey, T. L., and R. W. Guillery, 1974. An autoradiographic study of retinogeniculate pathways in the cat and the fox, *J. Comp. Neurol.*, 156:239–253.

- Hubel, D. H., 1988. *Eye, Brain, and Vision*, New York: Scientific American Library (Distributed by W. H. Freeman).
- Hubel, D. H., and T. N. Wiesel, 1959. Receptive fields of single neurons in the cat's striate cortex, *J. Physiol. (Lond)*, 148:574–591.
- Isayama, T., D. M. Berson, and M. Pu, 2000. Theta ganglion cell type of cat retina, *J. Comp. Neurol.*, 417:32–48.
- Ishida, A. T., W. K. Stell, and D. O. Lightfoot, 1980. Rod and cone inputs to bipolar cells in goldfish retina, *J. Comp. Neurol.*, 191:315–335.
- Iwakabe, H., G. Katsuura, C. Ishibashi, and S. Nakanishi, 1997. Impairment of pupillary responses and optokinetic nystagmus in the mGluR6-deficient mouse, *Neuropharmacology*, 36:135–143.
- Jacobs, G. H., S. K. Fisher, D. H. Anderson, and M. S. Silverman, 1976. Scotopic and photopic vision in the California ground squirrel: Physiological and anatomical evidence, *J. Comp. Neurol.*, 165:209–227.
- Jensen, R. J., and R. D. DeVoe, 1982. Ganglion cells and (dye-coupled) amacrine cells in the turtle retina that have possible synaptic connection, *Brain Res.*, 240:146–150.
- Karschin, A., and H. Wässle, 1990. Voltage- and transmitter-gated currents in isolated rod bipolar cells of rat retina, *J. Neurophysiol.*, 63:860–876.
- Kim, H. G., and R. F. Miller, 1993. Properties of synaptic transmission from photoreceptors to bipolar cells in the mudpuppy retina, *J. Neurophysiol.*, 69:352–360.
- Knapp, A. G., and L. A. Mistler, 1983. Response properties of cells in rabbit's lateral geniculate nucleus during reversible blockade of retinal on-center channel, *J. Neurophysiol.*, 50:1236–1245.
- Kolb, H., 1970. Organization of the outer plexiform layer of the primate retina: electron microscopy of Golgi-impregnated cells, *Philos. Trans. R. Soc. Lond. [Biol.]*, 258:261–283.
- Kolb, H., 1977. The organization of the outer plexiform layer in the retina of the cat: electron microscopic observations, *J. Neurocytol.*, 6:131–153.
- Kolb, H., 1979. The inner plexiform layer in the retina of the cat: electron microscopic observations, *J. Neurocytol.*, 8:295–329.
- Kolb, H., and L. Dekorver, 1991. Midget ganglion cells of the parafovea of the human retina: a study by electron microscopy and serial section reconstructions, *J. Comp. Neurol.*, 303:617–636.
- Kolb, H., and E. V. Famiglietti, 1974. Rod and cone pathways in the inner plexiform layer of cat retina, *Science*, 186:47–49.
- Kolb, H., K. A. Linberg, and S. K. Fisher, 1992. Neurons of the human retina: a Golgi study, *J. Comp. Neurol.*, 318:147–187.
- Kolb, H., and R. Nelson, 1993. OFF-alpha and OFF-beta ganglion cells in cat retina: II. Neural circuitry as revealed by electron microscopy of HRP stains, *J. Comp. Neurol.*, 329:85–110.
- Kolb, H., and R. Nelson, 1996. Hyperpolarizing, small-field, amacrine cells in cone pathways of cat retina, *J. Comp. Neurol.*, 371:415–436.
- Kolb, H., R. Nelson, and A. Marianti, 1981. Amacrine cells, bipolar cells and ganglion cells of the cat retina: a Golgi study, *Vis. Res.*, 21:1081–1114.
- Kuffler, S. W., 1953. Discharge patterns and functional organization of mammalian retina, *J. Neurophysiol.*, 16:47–68.
- Lasansky, A., 1973. Organization of the outer synaptic layer in the retina of the larval tiger salamander, *Philos. Trans. R. Soc. (Lond) B: Biol. Sci.*, 265:471–489.
- Lasater, E. M., 1988. Membrane currents of retinal bipolar cells in culture, *J. Neurophysiol.*, 60:1460–1480.
- Lei, B., R. A. Bush, A. H. Milam, and P. A. Sieving, 2000. Human melanoma-associated retinopathy (MAR) antibodies alter the retinal ON-response of the monkey ERG in vivo, *Invest. Ophthalmol. Vis. Sci.*, 41:262–266.
- Lettvin, J. Y., H. R. Maturana, W. S. McCulloch, and W. H. Pitts, 1959. What the frog's eye tells the frog's brain, *Proceedings of the Institute of Radio Engineers*, 47:1940–1951.
- LeVay, S., and S. K. McConnell, 1982. ON and OFF layers in the lateral geniculate nucleus of the mink, *Nature*, 300:350–351.
- Maple, B. R., F. Gao, and S. M. Wu, 1999. Glutamate receptors differ in rod- and cone-dominated off-center bipolar cells, *Neuroreport*, 10:3605–3610.
- Marianti, A. P., 1983. Giant bistratified bipolar cells in monkey retina, *Anat. Rec.*, 206:215–220.
- Mastrorade, D. N., 1983a. Correlated firing of cat retinal ganglion cells. I. Spontaneously active inputs to X- and Y-cells, *J. Neurophysiol.*, 49:303–324.
- Mastrorade, D. N., 1983b. Correlated firing of cat retinal ganglion cells. II. Responses of X- and Y-cells to single quantal events, *J. Neurophysiol.*, 49:325–349.
- Masu, M., H. Iwakabe, Y. Tagawa, T. Miyoshi, M. Yamashita, Y. Fukuda, H. Sasaki, K. Hiroi, Y. Nakamura, R. Shigemoto, M. Takada, K. Nakamura, K. Nakao, M. Katsuki, and S. Nakanishi, 1995. Specific deficit of the ON response in visual transmission by targeted disruption of the mGluR6 gene, *Cell*, 80:757–765.
- McGuire, B. A., J. K. Stevens, and P. Sterling, 1984. Microcircuitry of bipolar cells in cat retina, *J. Neurosci.*, 4:2920–2938.
- Michael, C. R., 1988. Retinal afferent arborization patterns, dendritic field orientations, and the segregation of function in the lateral geniculate nucleus of the monkey, *Proc. Natl. Acad. Sci. USA*, 85:4914–4918.
- Miyake, Y., K. Yagasaki, M. Horiguchi, Y. Kawase, and T. Kanda, 1986. Congenital stationary night blindness with negative electroretinogram. A new classification, *Arch. Ophthalmol.*, 104:1013–1020.
- Müller, F., H. Wässle, and T. Voigt, 1988. Pharmacological modulation of the rod pathway in the cat retina, *J. Neurophysiol.*, 59:1657–1672.
- Naka, K., P. Z. Marmarelis, and R. Y. Chan., 1975. Morphological and functional identifications of catfish retinal neurons. III. Functional identification, *J. Neurophysiol.*, 38:92–131.
- Nakajima, Y., H. Iwakabe, C. Akazawa, H. Nawa, R. Shigemoto, N. Mizuno, and S. Nakanishi, 1993. Molecular characterization of a novel retinal metabotropic glutamate receptor mGluR6 with a high agonist selectivity for L-2-amino-4-phosphonobutyrate, *J. Biol. Chem.*, 268:11868–11873.
- Nawy, S., 1999. The metabotropic receptor mGluR6 may signal through G_o, but not phosphodiesterase, in retinal bipolar cells, *J. Neurosci.*, 19:2938–2944.
- Nelson, R., 1973. A comparison of electrical properties of neurons in *Necturus* retina, *J. Neurophysiol.*, 36:519–535.
- Nelson, R., 1977. Cat cones have rod input: a comparison of the response properties of cones and horizontal cell bodies in the retina of the cat, *J. Comp. Neurol.*, 172:109–135.
- Nelson, R., 1982. All amacrine cells quicken time course of rod signals in the cat retina, *J. Neurophysiol.*, 47:928–947.
- Nelson, R., E. V. Famiglietti, Jr., and H. Kolb, 1978. Intracellular staining reveals different levels of stratification for on- and off-center ganglion cells in the cat retina, *J. Neurophysiol.*, 41:472–483.
- Nelson, R., A. T. Janis, T. N. Behar, and V. P. Connaughton, 2001. Physiological responses associated with kainate receptor immunoreactivity in dissociated zebrafish retinal neurons: a voltage probe study, *Prog. Brain Res.*, 131:255–265.

- Nelson, R., and H. Kolb, 1983. Synaptic patterns and response properties of bipolar and ganglion cells in the cat retina, *Vis. Res.*, 23:1183–1195.
- Nelson, R., and H. Kolb, 1985. A17: A broad-field amacrine cell in the rod system of the cat retina, *J. Neurophysiol.*, 54:592–614.
- Nomura, A., R. Shigemoto, Y. Nakamura, N. Okamoto, N. Mizuno, and S. Nakanishi, 1994. Developmentally regulated postsynaptic localization of a metabotropic glutamate receptor in rat rod bipolar cells, *Cell*, 77:361–369.
- Otis, T. S., and C. E. Jahr, 1998. Anion currents and predicted glutamate flux through a neuronal glutamate transporter, *J. Neurosci.*, 18:7099–7110.
- Pan, Z. H., and H. J. Hu, 2000. Voltage-dependent Na⁺ currents in mammalian retinal cone bipolar cells, *J. Neurophysiol.*, 84:2564–2571.
- Peichl, L., and H. Wässle, 1981. Morphological identification of on- and off-centre brisk transient (Y) cells in the cat retina, *Proc. R. Soc. Lond. B: Biol. Sci.*, 212:139–153.
- Picaud, S. A., H. P. Larsson, G. B. Grant, H. Lecar, and F. S. Werblin, 1995. Glutamate-gated chloride channel with glutamate-transporter-like properties in cone photoreceptors of the tiger salamander, *J. Neurophysiol.*, 74:1760–1771.
- Protti, D. A., and I. Llano, 1998. Calcium currents and calcium signaling in rod bipolar cells of rat retinal slices, *J. Neurosci.*, 18:3715–3724.
- Raviola, E., and N. B. Gilula, 1973. Gap junctions between photoreceptor cells in the vertebrate retina, *Proc. Natl. Acad. Sci. USA*, 70:1677–1681.
- Riehle, A., and N. Franceschini, 1984. Motion detection in flies: parametric control over ON-OFF pathways, *Exp. Brain Res.*, 54:390–394.
- Ripps, H., 1982. Night blindness revisited: from man to molecules. Proctor lecture, *Invest. Ophthalmol. Vis. Sci.*, 23:588–609.
- Saito, T., H. Kondo, and J. Toyoda, 1981. Ionic mechanisms of two types of on-center bipolar cells in the carp retina. II. The responses to annular illumination, *J. Gen. Physiol.*, 78:569–589.
- Saito, T., T. Kujiraoka, T. Yonaha, and Y. Chino, 1985. Reexamination of photoreceptor-bipolar connectivity patterns in carp retina: HRP-EM and Golgi-EM studies, *J. Comp. Neurol.*, 236:141–160.
- Schiller, P. H., 1982. Central connections of the retinal ON and OFF pathways, *Nature*, 297:580–583.
- Schiller, P. H., 1984. The connections of the retinal on and off pathways to the lateral geniculate nucleus of the monkey, *Vis. Res.*, 24:923–932.
- Schiller, P. H., and J. G. Malpeli, 1978. Functional specificity of lateral geniculate nucleus laminae of the rhesus monkey, *J. Neurophysiol.*, 41:788–797.
- Scholes, J. H., 1975. Colour receptors, and their synaptic connections, in the retina of a cyprinid fish, *Philos. Trans. R. Soc. Lond. B: Biol. Sci.*, 270:61–118.
- Schubert, G., and H. Bornschein, 1952. Bertrag zur analyse der menschlichen, *Ophthalmologica*, 123:396–413.
- Slaughter, M. M., and R. F. Miller, 1981. 2-amino-4-phosphonobutyric acid: a new pharmacological tool for retina research, *Science*, 211:182–185.
- Smith, R. G., M. A. Freed, and P. Sterling, 1986. Microcircuitry of the dark-adapted cat retina: functional architecture of the rod-cone network, *J. Neurosci.*, 6:3505–3517.
- Stell, W. K., 1977. Structural basis for On- and Off-center responses in retinal bipolar cells, *Science*, 198:1269–1271.
- Stryker, M. P., and K. R. Zahs, 1983. On and off sublaminae in the lateral geniculate nucleus of the ferret, *J. Neurosci.*, 3:1943–1951.
- Sur, M., M. Esguerra, P. E. Garraghty, M. F. Kritzer, and S. M. Sherman, 1987. Morphology of physiologically identified retinogeniculate X- and Y- axons in the cat, *J. Neurophysiol.*, 58:1–32.
- Sur, M., and S. M. Sherman, 1982. Retinogeniculate terminations in cats: morphological differences between X and Y cell axons, *Science*, 218:389.
- Tachibana, M., and A. Kaneko, 1988. L-glutamate-induced depolarization in solitary photoreceptors: a process that may contribute to the interaction between photoreceptors in situ, *Proc. Natl. Acad. Sci. USA*, 85:5315–5319.
- Tagawa, Y., H. Sawai, Y. Ueda, M. Tauchi, and S. Nakanishi, 1999. Immunohistological studies of metabotropic glutamate receptor subtype 6-deficient mice show no abnormality of retinal cell organization and ganglion cell maturation, *J. Neurosci.*, 19:2568–2579.
- Takao, M., K. Morigiwa, H. Sasaki, T. Miyoshi, T. Shima, S. Nakanishi, K. Nagai, and Y. Fukuda, 2000. Impaired behavioral suppression by light in metabotropic glutamate receptor subtype 6-deficient mice, *Neuroscience*, 97:779–787.
- Tamamaki, N., D. J. Uhlrich, and S. M. Sherman, 1995. Morphology of physiologically identified retinal X and Y axons in the cat's thalamus and midbrain as revealed by intraaxonal injection of biocytin, *J. Comp. Neurol.*, 354:583–607.
- Tauchi, M., and R. H. Masland, 1984. The shape and arrangement of the cholinergic neurons in the rabbit retina, *Proc. R. Soc. Lond. B: Biol. Sci.*, 223:101–119.
- Taylor, W. R., and H. Wässle, 1995. Receptive field properties of starburst cholinergic amacrine cells in the rabbit retina, *Eur. J. Neurosci.*, 7:2308–2321.
- Toyoda, J., 1973. Membrane resistance changes underlying the bipolar cell response in the carp retina, *Vis. Res.*, 13:283–294.
- Tsukamoto, Y., K. Morigiwa, M. Ueda, and P. Sterling, 2001. Microcircuits for night vision in mouse retina, *J. Neurosci.*, 21:8616–8623.
- Vardi, N., D. F. Matesic, D. R. Manning, P. A. Liebman, and P. Sterling, 1993. Identification of a G-protein in depolarizing rod bipolar cells, *Vis. Neurosci.*, 10:473–478.
- Vardi, N., and R. G. Smith, 1996. The AII amacrine network: Coupling can increase correlated activity, *Vis. Res.*, 36:3743–3757.
- Wässle, H., and B. B. Boycott, 1991. Functional architecture of the mammalian retina, *Physiol. Rev.*, 71:447–480.
- Wässle, H., B. B. Boycott, and R. B. Illing, 1981a. Morphology and mosaic of on- and off-beta cells in the cat retina and some functional considerations, *Proc. R. Soc. Lond. B: Biol. Sci.*, 212:177–195.
- Wässle, H., L. Peichl, and B. B. Boycott, 1981b. Morphology and topography of on- and off-alpha cells in the cat retina, *Proc. R. Soc. Lond. B: Biol. Sci.*, 212:157–175.
- Wässle, H., I. Schafer-Trenkler, and T. Voigt, 1986. Analysis of a glycinergic inhibitory pathway in the cat retina, *J. Neurosci.*, 6:594–604.
- Werblin, F. S., and J. E. Dowling, 1969. Organization of the retina of the mudpuppy, *Necturus maculosus*. II. Intracellular recording, *J. Neurophysiol.*, 32:339–355.
- Wesolowska, A., R. Nelson, and V. P. Connaughton, 2002. Glutamate mechanisms involved in the OFF pathway of zebrafish retina, Association for Research in Vision and Ophthalmology Annual Meeting, Program No. 1826.
- Wu, S. M., F. Gao, and B. R. Maple, 2000. Functional architecture of synapses in the inner retina: segregation of visual signals by

- stratification of bipolar cell axon terminals, *J. Neurosci.*, 20:4462–4470.
- Yamashita, M., and H. Wässle, 1991. Responses of rod bipolar cells isolated from the rat retina to the glutamate agonist 2-amino-4-phosphonobutyric acid (APB), *J. Neurosci.*, 11:2372–2382.
- Zahs, K. R., and M. P. Stryker, 1988. Segregation of ON and OFF afferents to ferret visual cortex, *J. Neurophysiol.*, 59:1410–1429.
- Zenisek, D., D. Henry, K. Studholme, S. Yazulla, and G. Matthews, 2001. Voltage-dependent sodium channels are expressed in non-spiking retinal bipolar neurons, *J. Neurosci.*, 21:4543–4550.
- Zhan, X. J., and J. B. Troy, 2000. Modeling cat retinal beta-cell arrays, *Vis. Neurosci.*, 17:23–39.

19 Retinal Synapses

MARTIN WILSON

SYNAPSES ARE THE CORE of the retina as a computational machine, so much so that a proper review of retinal synapses would, in effect, be a description of how the retina works. We are still a long way from a complete description of how the retina works, but the last few years have seen great advances in our understanding of retinal synapses, and it seems likely that the retina will be the first neural machine of any complexity that we will truly understand at a cellular level.

An understanding of retinal synapses requires answers to two related but distinct questions. The first is the question of connectivity: which types of retinal neuron synapse with which other types of neuron? The second question relates to how these synapses behave. As has become increasingly clear over the last decades, this is not simply a question of whether a synapse is excitatory or inhibitory, but requires knowledge of the kinetics of transmitter release and clearance, details of postsynaptic channel gating and modulation, and more. The two issues—connectivity and function—have very different histories, and it is worth reflecting that, whereas the outline of connectivity was appreciated by Cajal in the early 1890s, the mechanisms of synaptic function were a complete mystery as recently as the middle of the twentieth century. To gauge how far the field has developed in the last 50 years, we might consider the state of contemporary understanding of retinal synaptic function, as summarized by Steven Polyak writing in 1955: “Speaking figuratively, it seems that there is not so much an actual passage of a material substratum or a direct transmission of nervous excitation as rather an emanation of a certain imponderable ‘influence’ as yet to be precisely defined in terms of microdynamics” (Polyak, 1957).

What has happened with retinal synapses since Polyak wrote this unenlightening synopsis? Several advances spring to mind. First, the work begun by Cajal in providing anatomical descriptions of synapses between the cell types in the retina has been enormously extended, largely through the electron microscope, to the point that there are now quantitative descriptions of the synapses between some retinal neurons. Second, the identity of transmitter substances in the retina has been almost completely uncovered. This has not been a straight path, and even in the case of the photoreceptor transmitter, there have been numerous wrong turns. The simple story, now firmly established, is that glutamate is the transmitter in the direct pathway, photorecep-

tors to bipolar cells, bipolar cells to ganglion cells; and that gamma-aminobutyric acid (GABA) is the main transmitter in the lateral and feedback pathways mediated by horizontal cells in the outer retina and amacrine cells in the inner retina. Third, something is now known about the molecular identity of the transmitter receptors found on many of the cells in the retina. This molecular characterization is still at an early stage, but has already indicated a level of complexity in retinal organization that goes well beyond our present understanding of how the retina works, leaving the unsettling impression that the retina is a much more subtle machine than we presently acknowledge. Lastly, the way in which transmitters are released from presynaptic terminals in the retina is beginning to be understood, although clearly there are major advances still to be made in this area.

Fifty years have produced a vast increase in the understanding of retinal synapses, but even so, it would be quite wrong to imagine that, but for a few details, retinal synapses are understood. Certainly, the outer retina is much better understood than the inner retina, largely because it has fewer types of neurons and has a simpler organization. Even in the outer retina though, there are important, unanswered questions, and the patterns of connectivity, although closely investigated for several decades, continue to reveal unexpected novelty. Two recent examples of this are provided by two studies describing an uncommon, unsuspected but nevertheless important synapse between mammalian rods and OFF cone bipolar cells (Hack et al., 1999; Tsukamoto et al., 2001), as well as the finding that there may be a layer of anatomically strange and unexplored synapses lying beneath the terminals of mammalian cones (Haverkamp et al., 2000).

The connections within the inner retina, with the exception of a few special pathways, are not known in detail, and our understanding of the physiology of defined synapses is scant. A major task in the inner retina will be the elucidation of the many modulation pathways that are suspected to exist there. This is a particularly challenging area because not only are the mechanisms of modulation largely unknown, but it is also not really clear what modulation contributes to retinal processing.

My intentions in this review are to set out the basic pattern of synaptic organization in the retina, to draw attention to recent advances, and to point out the unsolved problems

of retinal synapses. The direct pathway of photoreceptors to bipolar cells to ganglion cells is presented first; then, lateral pathways and feedback loops involving horizontal cells and amacrine cells are described. Lastly, a brief description of spinules highlights an example of plasticity in the retina. Synaptic function, rather than connectivity, is the focus of this chapter, but even with this restriction, a great amount of important work has to be left out including, among other things, any discussion of efferent input, interplexiform cells, and glycine or dopamine as transmitters.

The basic plan

The synaptic plan of the vertebrate retina is shown in Figure 19.1 in a way that emphasizes the symmetry of its organization. In both the outer and the inner retina, there is a direct transmission pathway, from photoreceptors to bipolar cells, and from bipolar cells to ganglion cells, as well as transmission to lateral interneurons that provide both feedback and negative feedforward. Although this is the basic plan, it must be emphasized that each element in this diagram represents not a single cell, but a class of cells comprising more than one type, each of which makes a characteristic pattern of connections with a subset of types from the other classes. There are species variations in the number of types in a class, but an “average” retina might have 4 types of pho-

toreceptors, 2 types of horizontal cell, 10 types of bipolar cell, several dozen types of amacrine cell, and about 20 types of ganglion cell. The rules of connection for most of these neuronal types are those set out in Figure 19.1, but there are numerous deviations from this plan too tedious to enumerate. One well-known and important exception, though, is the major pathway from rod photoreceptors in the mammalian retina. These photoreceptors have their own exclusive bipolar cell that synapses, not with a ganglion cell, but with an amacrine cell, the AII amacrine, which forms a glycinergic synapse onto a cone bipolar cell and is electrically coupled to yet another type of bipolar cell (Muller et al., 1988).

The direct pathway

PHOTORECEPTORS

Photoreceptor to bipolar cell; presynaptic mechanisms. The first synapses in the retina sort information into categories that are kept separate for several more processing steps. Signals representing local increments or decrements in luminance are separated into two streams, carried by the ON and OFF bipolar cells. Within these two general classes, there is a further splitting of signals into channels in which luminance changes are represented with different temporal filtering. How do synapses achieve this sorting and respond reliably

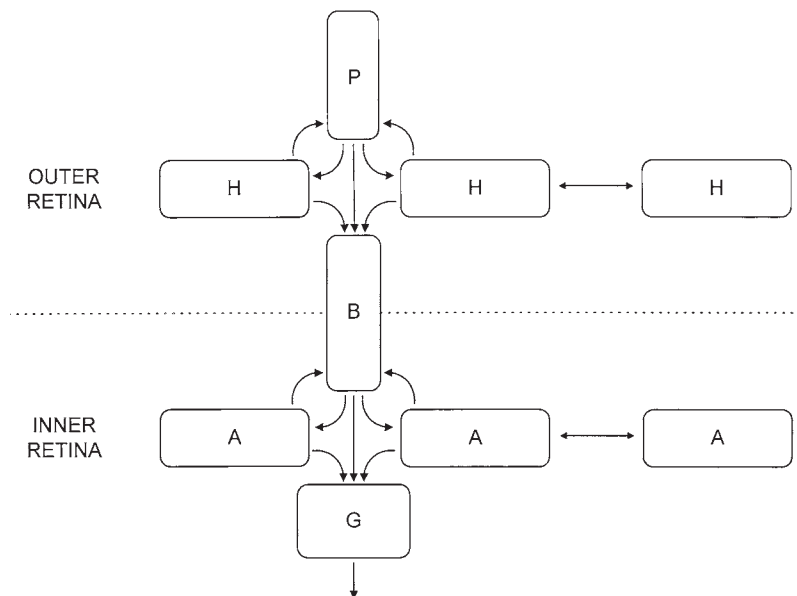


FIGURE 19.1. Schematic layout of the retina showing the basic plan of its synaptic organization. Photoreceptors (P) synapse with the two classes of second-order neurons, bipolar cells (B) and horizontal cells (H). Horizontal cells are lateral interneurons and provide both feedback to photoreceptors and feedforward to bipolar cells. The same general pattern is repeated in the inner retina, where bipolar cells synapse directly with ganglion cells (G),

but also provide input to amacrine cells, the lateral interneurons of the inner retina. Amacrine cells (A) provide feedback to bipolar cells and feedforward to ganglion cells, in addition to having extensive synaptic connections amongst themselves. Electrical synapses mediated by gap junctions couple many of the neuron types within and, in some cases, between classes, but for simplicity, these connections have been omitted.

to signals in photoreceptors that are as small as 1 mV (Schneeweis and Schnapf, 1995)?

Photoreceptors make two anatomically distinguishable kinds of synapses with second-order cells. These have several names, but they are referred to here as superficial and invaginating synapses. Superficial synapses are relatively simple structures with postsynaptic densities and intramembranous particles presynaptically, not unlike many synapses elsewhere

in the brain. Invaginating synapses, in contrast, are remarkably complex. Typically, there are three postsynaptic elements at an invaginating synapse, all of which are pushed into the synaptic terminal of a photoreceptor (Fig. 19.2) and constitute a "triad." Usually, the central element of these three is a bipolar cell dendrite; the two lateral elements are the dendrites of horizontal cells. On the presynaptic side of this synapse, a flat plate, the synaptic ribbon, is held

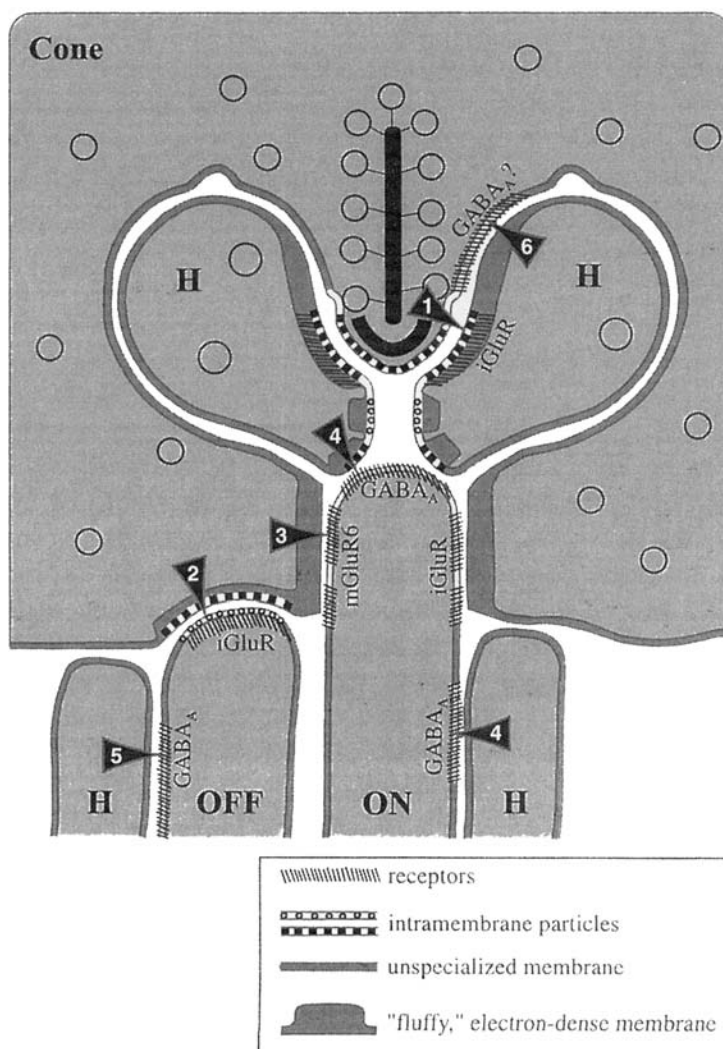


FIGURE 19.2. Schematic layout of a cone terminal synapse in a mammalian retina. Shown here are the distributions of receptors, identified immunocytochemically, and other membrane-associated features from which synaptic interactions (numbered arrowheads) can be inferred. The presynaptic ribbon, in reality a plate upon which synaptic vesicles are aligned, is shown cut transversely. The dendrite of an ON bipolar cell forms the central element of a triad in which the lateral positions are taken by horizontal cell dendrites, seen here also in transverse section. The dendritic tips of OFF bipolar cells do not invaginate the cone terminal, but instead make superficial synapses. Ionotropic glutamate receptors are found on horizontal cell membranes apposed to the likely site of presynaptic vesicle fusion (7). Glutamate released at this fusion site diffuses

some distance to reach the mGluR6 receptors and the ionotropic GluRs on the dendrite of the ON bipolar cell (3). Tips of the OFF bipolar cells express iGluRs, but it is not entirely clear where transmitter for this synapse originates (2). GABA_A receptors are found on both ON and OFF bipolar cells adjacent to superficial horizontal cells (4, 5), from which GABA is thought to be released. GABA_A receptors are also found on the tips of ON bipolar dendrites (4), where they probably receive input from the lateral elements of the triad (4). The presence of GABA_A receptors on the synaptic ridge of the cone is speculative, but may be the location of the feedback to cones (6). (Reprinted from Vardi et al. [1998], copyright 1998 with permission from Elsevier Science.)

perpendicular to the presynaptic membrane, and about 60 nm from it, by filamentous connections to an electron-dense material, the arciform density adjacent to the plasma membrane. Ribbons, or similar structures, are found also in retinal bipolar cells, auditory hair cells, and the electroreceptors of fish. All of these cells carry small, graded, voltage signals and are thought to have the capacity to release transmitter continuously.

Ribbons are very complex structures built from many proteins, most of which have not yet been identified. However, they include forms of the motor protein, kinesin (Muresan et al., 1999), and probably myosin (el-Amraoui et al., 1996; Schlamp and Williams, 1996). Ribbon synapses, despite their unique presynaptic anatomy, have many of the synaptic proteins found at more commonplace synapses (Von Kriegstein et al., 1999), with the notable exception of synapsin (Mandell et al., 1990), which, in other synapses, anchors synaptic vesicles to the cytoskeleton but releases them when phosphorylated. Ribbons themselves are able to bind synaptic vesicles in an orderly array on both faces of the ribbon by holding them on thin filaments approximately 20 to 30 nm long. One protein of unknown function, RIBEYE, is a major component of ribbons and thus far is the only protein unique to these structures (Schmitz et al., 2000). Very likely, ribbons serve in some capacity to collect vesicles from the surrounding cytoplasm and facilitate release, although exactly how this is accomplished is not yet certain.

Patterns of connections between photoreceptors and their postsynaptic partners vary with species and the particular class of photoreceptor. In mammals, a cone makes 25 to 40 invaginating synapses, but a rod makes only a single invaginating synapse that, in darkness, has been estimated to release transmitter at a minimum rate of 40 vesicles per second (Rao et al., 1994). The anatomy of this synapse has been carefully examined (Rao-Mirotznik et al., 1995) with the aim of finding out how it is suited to its unique task of transmitting one bit of information: the presence or absence of a single photon. At the presynaptic membrane, on either side of a ribbon, is a row of about 65 docking sites, making a total of 130 sites at this single active zone, many more than found at conventional bouton synapses. The double row of docking sites is, at least superficially, similar to the structure found at the neuromuscular junction (Harlow et al., 2001), but the presence of the ribbon has no obvious counterpart. The ribbon, in addition to holding 130 vesicles at docking sites, holds a reserve of some 640 vesicles. Both the large number of docking sites and the reserve of available vesicles on the ribbon would appear to be adaptations to permit continuous, high rates of release.

Although invaginating synapses in the outer retina characteristically have three postsynaptic elements, the mammalian rod synapse actually has four, two dendritic processes

from rod bipolar cells flanked by two horizontal cell processes. The three-dimensional synaptic cleft created by this complicated geometry is about 20 times the volume of a typical bouton synapse; moreover, the receptors on the bipolar cell dendrites are at some distance (400 to 800 nm) from the active zone (Vardi et al., 2000). Why? A possible advantage of this arrangement might be that the shot noise of quantal release is smoothed out by the relatively long diffusion pathway, whereas the penalty of slowness imposed by long diffusion is unimportant, as a single-photon signal in a rod has a time course measured in hundreds of milliseconds (Burns and Baylor, 2001).

Glutamate is the transmitter used by both rods and cones. A great deal of work has contributed to this conclusion, but several clever experiments have helped to clinch this. The release of an excitatory amino acid from turtle rods and cones was demonstrated by showing that depolarization of these cells released a substance that could open *N*-methyl-D-aspartate (NMDA) receptors in an isolated patch of membrane on the tip of a recording pipette held near the photoreceptor terminal (Copenhagen and Jahr, 1989). The fact that this amino acid was L-glutamate was demonstrated in an experiment in which a single photoreceptor terminal was drawn into the lumen of a pipette containing NAD^+ and the enzyme glutamate dehydrogenase, which can use only L-glutamate as a substrate. The production of NADH, detected by an increase in fluorescence when the photoreceptor was depolarized, indicated that L-glutamate was released (Ayoub and Copenhagen, 1991).

Release of transmitter from photoreceptors is continuous in darkness while photoreceptors experience a relatively depolarized membrane potential of about -40 mV. Light hyperpolarizes photoreceptors, thereby closing voltage-gated Ca^{2+} channels in the synaptic terminal and diminishing transmitter release. Unlike fast synapses, such as the squid giant synapse at which hundreds of μM Ca^{2+} are required to activate transmitter release (Adler et al., 1991), rods release glutamate in the dark at an estimated Ca^{2+} concentration of between 2 and $4 \mu\text{M}$. As would be expected of a continuously releasing synapse, the rate of endocytosis of vesicles is closely matched to the rate of exocytosis (Rieke and Schwartz, 1996), although exactly how this is achieved is not clear.

A problem posed by the release of photoreceptor transmitter as a consequence of Ca^{2+} influx through voltage-gated Ca^{2+} channels is that these channels activate only positive to about -45 mV, implying that only small-voltage signals close to the photoreceptor dark potential can be transmitted to second-order cells. This actually seems to be the case for dark-adapted salamander rods, but for reasons related to the electrical coupling of rods in this retina, the limited transmission window may not be a problem (Attwell et al., 1987). For cones, though, this problem may be solved by having a

separate mechanism of Ca^{2+} entry, independent of voltage-gated Ca^{2+} channels, that permits transmitter release over the entire voltage range of the cone from -40 mV down to -70 mV . This entry pathway is thought to be a cyclic guanosine monophosphate (cGMP)-gated channel (Rieke and Schwartz, 1994), but it is not at all clear how cGMP concentration at the terminal is coupled to the cone membrane voltage, as it would have to be if this mechanism is used for transmitting cone signals. Cones express soluble G cyclase, and this is probably the source of cGMP in the synaptic terminal. Because nitric oxide, which upregulates this cyclase, is known to be synthesized in the outer retina (Blute et al., 2000), it may well serve to modulate Ca^{2+} entry, and it could perhaps be involved in light adaptation, but it is too slow to transmit cone signals.

All information passing from photoreceptors to second-order cells is first coded as glutamate concentration in the synaptic cleft. In principle, this could be done in two different ways. Each vesicle of transmitter could produce a brief pulse of postsynaptic current integrated by the relative slow electrical time constant of the postsynaptic dendrite. Alternatively, the large volume of the synaptic cleft and the relatively long distances to postsynaptic receptors might imply that transmitter concentration is effectively smoothed out. This issue is not completely settled yet, but on balance, quantitative analysis of this problem favors the idea that smoothing of the concentration seen by the postsynaptic receptors is a minor effect (Rao-Mirotznik et al., 1998). In either case, the rate of glutamate removal from the cleft is an important consideration. High-affinity glutamate transporters, found on the plasma membranes of photoreceptor terminals and glial cells (Eliasof et al., 1998), clearly play a critical role in this, as inhibiting them leads to glutamate concentrations that saturate postsynaptic receptors (Eliasof and Werblin, 1993). The exact disposition of these transporters, though presently unknown in any retina, is likely to be a crucial factor in determining how far glutamate can diffuse from its release site, which, as discussed later, is key to understanding cone synapses. A salient aspect of glutamate transport by photoreceptors is that it is coupled to a Cl^- conductance, as first described by Sarantis and colleagues (1988). Because the glutamate transporter acts as an autoreceptor and opens a Cl^- channel, this arrangement works as a negative feedback on transmitter release by photoreceptors (Picaud et al., 1995).

Multiple forms of negative feedback apparently act at the photoreceptor synapse, quite apart from the feedback mediated by horizontal cells. In rat retina, photoreceptor terminals express the group III metabotropic receptor mGluR8, which functions as an autoreceptor, decreasing Ca^{2+} concentration in the terminal, and thereby decreasing glutamate release (Koulen et al., 1999). Very likely, this works via G-protein control of L-type Ca^{2+} channels. In the cat retina,

mGluR1 is found presynaptically in rod terminals (Cai and Pourcho, 1999), but it is presently unknown how this works. Even more mysterious than this is the expression of NMDA NR1 subunits in the terminals of both rods and cones of the rat (Fletcher et al., 2000). A particularly interesting form of negative feedback has recently been suggested at mammalian cone terminals (DeVries, 2001). At this synapse, and perhaps others, too, the release of transmitter is accompanied by the release of protons that are highly concentrated within synaptic vesicles. This has the effect of acidifying the synaptic cleft and immediately suppressing the Ca^{2+} current by acting directly on the nearby Ca^{2+} channels. This, in turn, is thought to diminish glutamate release.

BIPOLAR CELLS In all retinas, the subclasses of bipolar and horizontal cells are restricted in the types of synapse they make with photoreceptors, some types being postsynaptic only at invaginating synapses and others only at superficial synapses. In the mammalian retina, ON bipolars are postsynaptic only at invaginating synapses, whereas OFF bipolars synapse only at superficial synapses. In other retinas, such as the amphibian retina, the rules are different (Lasansky, 1978). Unlike invaginating synapses, where synaptic vesicles coat both sides of the ribbon and are found in an abundant cloud around the ribbon, the presynaptic locations of superficial synapses are generally almost devoid of vesicles. Whether this implies an unusual, avascular form of transmitter release at superficial synapses is not yet clear. An alternative possibility is that the transmitter released at ribbon synapses is able to diffuse to the receptors at superficial synapses, a pathway that is approximately 500 to 950 μm long (Morigiwa and Vardi, 1999). The suggestion that the ribbon provides glutamate even to superficial synapses casts the cone “synapse” as an extraordinarily complex, layered structure with numerous, carefully positioned, postsynaptic elements (Fig. 19.3) (Haverkamp et al., 2000; Vardi et al., 1998).

Photoreceptor to bipolar cell; postsynaptic mechanisms. At photoreceptor synapses, signals are channeled to ON bipolar cells that depolarize to increments of light and to OFF bipolar cells that hyperpolarize to increments of light. Because photoreceptors hyperpolarize to increments of light, this means that the photoreceptor to OFF bipolar cell synapse is sign preserving, whereas the synapse to ON bipolar cells is sign inverting.

The postsynaptic mechanism of ON bipolar cells is unusual. Here, the transmitter glutamate decreases a postsynaptic conductance to cations. In this way, then, hyperpolarization of photoreceptors by light, because it reduces glutamate release, results in the depolarization of the bipolar cell. The glutamate receptor through which this mechanism operates is mGluR6, a member of the type III mGluR

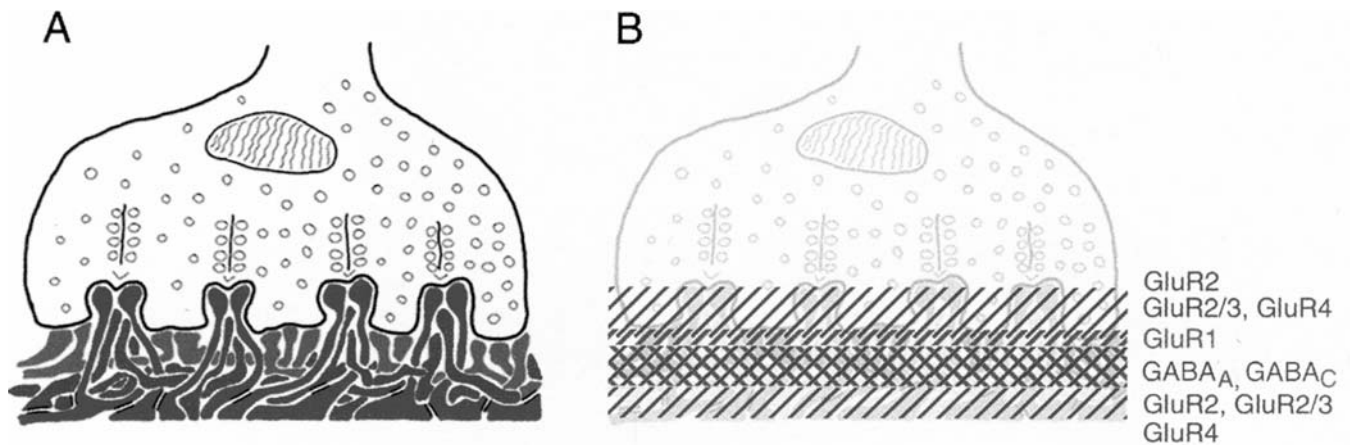


FIGURE 19.3. Schematic drawing of the synaptic complex (A) of a cone terminal showing the layering of transmitter receptors (B). ON bipolar cells are shown in green, OFF bipolar cells are depicted in blue, and the dendrites of horizontal cells are colored red. The whole structure shows a precise lamination in the expression of glutamate and GABA receptor subunits. In addition to receptors at

invaginating and superficial synapses, there appears to be yet another layer of receptors lying 1 to 2 μm below the cone terminal associated with desmosome-like junctions (indicated by double black bars). (Reprinted from Haverkamp et al. [2000], copyright 2000 with permission from Elsevier Science.) (See color plate 7.)

receptors for which APB (L-2-amino-4-phosphonobutyric acid, also known as L-AP4) is a selective and potent agonist (Slaughter and Miller, 1981). The binding of glutamate to mGluR6 results in the closure of cation channels through which Ca^{2+} enters the cell and plays a role in postsynaptic light adaptation (Nawy, 2000; Shiells and Falk, 1999). Until recently, the mechanism of channel closure was thought to resemble phototransduction in that the cation channels were thought to be gated by cGMP, which was destroyed by a phosphodiesterase (PDE) whose activity, in this case, was increased when glutamate was bound by the receptor. The similarities to phototransduction turn out to be more superficial than was at first thought. The G protein, G_o , rather than transducin, the G protein of phototransduction, is involved here, as suggested by the anatomical finding that G_o alpha colocalizes with mGluR6 in bipolar dendrites on the tips of ON bipolar cells (Vardi, 1998). This was confirmed by the absence of ON bipolar responses in the G_o alpha null mouse (Dhingra et al., 2000). The notion that the cation channels are gated by cGMP was supported by results showing that PDE inhibitors could increase the cation current; however, in a recent study glutamate responses were found to be unaffected by PDE inhibitor, as well as by non-hydrolyzable cGMP (Fig. 19.4) (Nawy, 1999). From these experiments, one might reasonably conclude that cGMP is a modulator of the cation channel, but is not in the direct-signaling pathway. A crucial gap in our understanding of this system concerns the identity of the cation channel; until the channel is identified, progress on this problem is likely to be slow.

We might wonder why such an unusual postsynaptic mechanism is employed in ON bipolar cells. Some insight into this issue is provided by a recent study examining rod

to rod (ON) bipolar cell transmission in the mouse retina (Field and Rieke, 2002; discussed in Wilson, 2002). Counterintuitively, this study showed that at very dim light levels a majority of the scarce photon signals generated in rods are not transmitted to rod bipolar cells. In fact, only the biggest amplitude single-photon signals are passed through this synapse. Although the synapse wastes precious photon signals in doing this, it actually confers a net benefit by also filtering out the inevitable and irreducible noise generated in the rods that would otherwise be indistinguishable from genuine photon hits. Very likely, the essential mechanism for this thresholding operation at the synapse lies in the postsynaptic transduction machinery, so that as suggested by van Rossum and Smith (1998), the fluctuating levels of glutamate in the dark are saturating, and only when glutamate falls below some threshold concentration is this able to cause an opening of cation channels.

The APB-sensitive cation channel system, although incompletely understood, is widely acknowledged to be the chief postsynaptic mechanism at photoreceptor to ON bipolar synapses. There are, nevertheless, several other mechanisms that, with different degrees of certainty, are thought to play a role. The best documented of these is the conductance associated with cone input to ON bipolar cells found in teleost fish (Saito et al., 1979). Although rod synapses on these neurons use the APB-sensitive mechanism, glutamate from cones causes a conductance increase to anions. The properties of this glutamate current are unusual, in that it is not blocked by any ionotropic or metabotropic glutamate receptor antagonists, nor by strychnine or picrotoxin. The reversal potential for this current follows E_{Cl} but it has a requirement for extracellular Na^+ (Grant and Dowling, 1995, 1996). Almost certainly, this

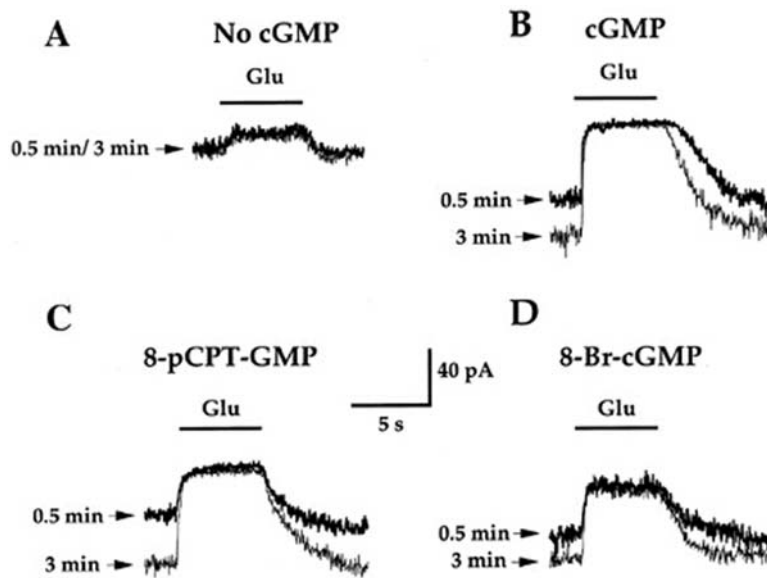


FIGURE 19.4. cGMP potentiates the glutamate response of ON bipolar cells, even when cGMP hydrolysis is inhibited. *A*, Glutamate suppresses an inward current seen in the ON bipolar cells of the tiger salamander retina. *B*, Inward current is increased when cGMP is included in the patch pipette. The times noted (0.5 and 3 minutes), refer to the time after internal perfusion of the cell begins. *C* and *D*, Two nonhydrolyzable analogs of cGMP also

potentiate the inward current, but do not interfere with the ability of glutamate to close these cation channels. The implication of these experiments is that cGMP, though it modulates the cation channel, is not the messenger whose destruction is responsible for channel closure. (From Nawy [1999], copyright 1999, the Society for Neuroscience.)

cone-driven mechanism is mediated by a glutamate transporter that gates a Cl^- channel the same as, or similar to, that seen in the terminals of photoreceptors.

In mammalian retinas, immunocytochemistry shows that rod bipolar cell dendrites express α -amino-3-hydroxy-5-methyl-4-isoxa-2-oleopropionate receptor (AMPA) subunits (Hack et al., 2001; Hughes, 1997; Morigiwa and Vardi, 1999). This finding is shocking, as it implies that rod bipolar cells have a sign-preserving synapse from photoreceptors working against the APB-sensitive, sign-inverting synapse. The most careful physiological study to date finds no evidence for an ionotropic GluR in these bipolar cells (Hartveit, 1996), but the issue is not yet resolved. It is possible that these channels contribute little to the postsynaptic current of the cell, but nevertheless might admit some Ca^{2+} that plays a modulatory role (Hack et al., 2001). A more radical alternative is that these AMPAR subunits, instead of forming channels, associate with G-protein subunits and have a metabotropic role, as they do in some cortical neurons (Wang et al., 1997). Even less well understood than the presence of AMPAR subunits is the possible presence of NR1 subunits (Hughes, 1997), which are capable of forming homomeric channels. In addition to mGluR6, the group I receptors mGluR1 and mGluR5 (Koulen et al., 1997) are found in ON bipolar dendrites. Presumably, these have a modulatory role, but what that might be remains unknown.

In comparison to the unusual postsynaptic mechanisms of ON bipolar cells, those found at OFF bipolar cells are orthodox, involving AMPA- or kainate (KA)-preferring receptors. In the mammalian retina, there are approximately three to five anatomically defined classes of OFF bipolar cells. Although all of these connect to every cone cell, they each carry a different signal by virtue of their different glutamate receptors. Of the three types examined in the ground squirrel retina (DeVries, 2000), two are kainate-preferring and one is an AMPA-preferring receptor. The important difference between these receptors seems to be the rate at which they recover from desensitization. The AMPA receptor on the B2 bipolar cell recovers quickest, and the kainate receptor on the B3 the slowest, with the kainate receptor on B7 having an intermediate recovery rate. The consequence of these kinetic differences is that, while they probably all experience similar glutamate kinetics, the glutamate receptors filter the signal differently, determining that the B2 cell will carry a transient signal and that the B3 cell will carry a sustained signal. Similar kinetic differences are thought to exist among ON bipolar cell classes, but in that case, it is not known how these kinetic differences are achieved.

Bipolar cell to ganglion cell; presynaptic mechanisms. Bipolar cells pass signals to ganglion cells. ON bipolar cells synapse chiefly with ON ganglion cells; similarly, OFF bipolar cells synapse with OFF ganglion cells. The synapses of OFF cells

lie in sublamina *a* of the inner plexiform layer, and ON cells synapse in the lower sublamina *b*. Bipolar cell terminals make dyad ribbon synapses at which there are typically two postsynaptic elements, one usually a ganglion cell dendrite and the other belonging to an amacrine cell. Glutamate is thought to be the transmitter used by bipolar cells. Tachibana and Okada (1991) demonstrated directly, by using a catfish horizontal cell as a detector, that an isolated bipolar cell releases an excitatory amino acid when depolarized in the presence of extracellular Ca^{2+} . Glutamate is certainly the transmitter used by most bipolar cells, but is it the exclusive transmitter for all bipolar cells? Suggestive evidence exists that, at least in the amphibian retina, some bipolar cells may use GABA as a transmitter, perhaps in addition to glutamate (Yang and Wang, 1999).

Much of what is known about transmitter release from bipolar cells comes from work on the Mb1 bipolar cell from goldfish (reviewed in Lagnado, 2000; Tachibana, 1999; von Gersdorff and Matthews, 1999). These bipolar cells are driven chiefly by rods and, in response to a step of light, show a transient depolarization of about 200 msec followed by a smaller tonic depolarization (Saito et al., 1979). The chief recommendation of these cells is that they possess a single, giant, synaptic terminal having a diameter of about 10 μm . Two indirect methods have been applied to these terminals to examine transmitter release. The first method uses a high-frequency voltage sinusoid to determine the membrane capacitance of a voltage-clamped cell. The fusion of vesicles with the plasma membrane increases membrane capacitance linearly with the number of vesicles fused, and though vesicles are too small to be resolved individually, the concerted fusion of thousands of vesicles generates a signal that allows insight into the rapid kinetics of vesicle cycling. A limitation of this technique is that it reports the difference between exocytosis and endocytosis, giving rise to an ambiguity if neither of these rates is known. The second method is complementary to the capacitance method, as it has a lower time resolution but is able to report exocytosis and endocytosis independently. In this method, the fluorescence of a styryl dye, usually FM1-43, is monitored as it partitions into newly exposed vesicle membranes, or is lost from vesicle membranes in exocytosis.

A combination of these two methods has provided a picture of release more complete than at any other synapse, and it is one that integrates very well with the anatomy of these terminals (Fig. 19.5) (von Gersdorff et al., 1996). A typical terminal has 60 ribbons holding on either face, an array of about 66 vesicles. The bottommost row on either face of a ribbon is thought to be aligned with 11 fusion sites on the plasma membrane. L-type Ca^{2+} channels, very likely situated just beneath the ribbon, open with membrane depolarization (Heidelberger and Matthews, 1992), thereby increasing the Ca^{2+} concentration in the immediate vicinity

of the docked vesicles. This first row of vesicles held at docking sites can be exocytosed very quickly (Neves and Lagnado, 1999), with a time constant of 0.5 msec when the activation of the Ca^{2+} current is not the rate-limiting step (Mennerick and Matthews, 1996). Maintained high Ca^{2+} levels lead to a second phase of release, lasting about 200 msec, associated with the release of the rest of the 4500 or so vesicles attached to the ribbons (von Gersdorff et al., 1996). Interestingly, the release of this pool of vesicles seems to occur at a fixed rate until it suddenly runs out of vesicles, suggesting perhaps that vesicles are moved in a coordinated fashion down the ribbon to the release site (Neves and Lagnado, 1999). ATP is a necessary factor for exocytosis, but is apparently not required for the release of vesicles once they are docked (Heidelberger, 1998). Because ribbons contain a kinesin motor protein, it might be thought that the ATP is required to allow movement of vesicles on the ribbon. However, this seems unlikely since, without ATP, the number of vesicles that can be released is more than just those initially held at the docking sites (Heidelberger, 1998). The ATP-dependent step seems to be a required readying step that happens to vesicles while they are aligned on the ribbon.

A third kinetic component of release is indefinitely sustainable at a rate of about 1000 vesicles per second and involves recruitment of vesicles to ribbons from the reservoir of about 750,000 vesicles found throughout the terminal (Neves and Lagnado, 1999; Rouze and Schwartz, 1998). This tonic form of release is not universally accepted (Matthews, 1998) and is invisible as a capacitance change, arguably because exocytosis and endocytosis are balanced. Nevertheless, a technically sophisticated study combining capacitance measurements with the use of AMPARs as transmitter detectors failed to document any continuous release; instead, it showed that the vesicle pool could readily be exhausted (von Gersdorff et al., 1998). How this important discrepancy can be resolved remains to be seen.

Retrieval of vesicle membranes by endocytosis occurs in two kinetic forms, one with a time constant of about 1 second and a slow form with a time constant about 10-fold longer (Neves and Lagnado, 1999; von Gersdorff and Matthews, 1994). The molecular processes controlling these different retrieval mechanisms are presently unknown, but might correspond to a "classical" endocytosis needing clathrin and a rapid form of endocytosis without clathrin that recovers incompletely collapsed vesicles (Pyle et al., 2000). Once endocytosed, recovered vesicles are refilled with transmitter and returned to the releasable pool within 1 minute (Lagnado et al., 1996), thereby allowing continuous turnover of the entire pool of 750,000 vesicles in a terminal within a few minutes.

Calcium has several described effects on vesicle cycling in Mb1 bipolar cells. It can, for example, increase the recruit-

ment of vesicles to the ribbon and the rate of movement along the ribbon (Gomis et al., 1999), but there are contradictions in the quantitative account of the most central of these processes, exocytosis. Studies using FM1-43 show that no exocytosis takes place at resting levels of Ca^{2+} , but that only a moderate increase—to around 500 nM (Lagnado et al., 1996) or 800 nM (Rouze and Schwartz, 1998)—is necessary to promote continuous vesicle fusion. An important technical point is that these studies raised the level of Ca^{2+} uniformly within the terminal by uncaging it photolytically, rather than admitting it through Ca^{2+} channels, where it would have created very local domains of high concentration. Set against these results are those based on capacitance measurements, showing that phasic exocytosis requires at least 50 μM Ca^{2+} (von Gersdorff and Matthews, 1994) and is only half-saturated at 194 μM Ca^{2+} (Heidelberger et al.,

1994), similar to the high Ca^{2+} requirement found in the squid giant synapse (Adler et al., 1991). One potential resolution of these discrepancies is that both a high Ca^{2+} - and a low Ca^{2+} - affinity mechanism of exocytosis exist at this synapse, and they separately mediate continuous and phasic release of transmitter. This possibility may not seem to fit well with a structure as homogeneous as the presynaptic ribbon, but as described later, release at the bipolar cell ribbon may not be completely uniform. An alternative possibility is that the Ca^{2+} dependence of exocytosis might be modifiable, perhaps in a Ca^{2+} -dependent way. Some evidence consistent with this general idea comes from experiments examining use-dependent synaptic depression. In addition to depression resulting from depletion of vesicle pools (von Gersdorff and Matthews, 1997), there is evidence that, after an episode of exocytosis, further exocytosis is less sensitive to Ca^{2+} (Burrone and Lagnado, 2000).

A clever variation on the FM1-43 method employs evanescent wave microscopy to look exclusively at the behavior of single vesicles very close to the plasma membrane as they dock and fuse (Zenisek et al., 2000). From this work, several new findings have emerged. Vesicles are held about 20 nm from the plasma membrane, presumably at the bottom of a ribbon, before undergoing docking to the plasma membrane. Once docked, about 250 msec is required for “priming” before fusion can take place.

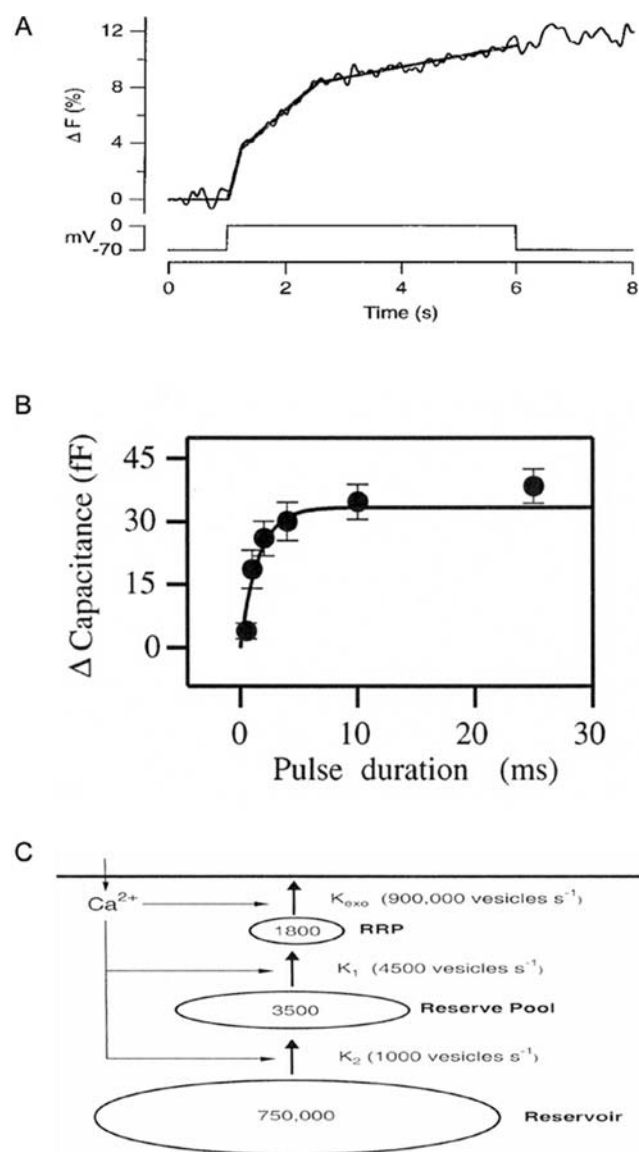


FIGURE 19.5. Transmitter release from Mb1 cells of the goldfish has three kinetic components. *A*, Vesicle fusion with the synaptic terminal membrane, measured as an increase in fluorescence of the dye FM1-43 entering newly exposed vesicle membrane. Immediately after the membrane voltage is stepped from -70 to 0 mV, a very rapid increase in fluorescence corresponds to the fusion of all the docked vesicles. Following this, there is a linear increase at a lower rate corresponding to the exocytosis of all the vesicles on all the ribbons of the terminal. An even slower subsequent rate corresponds to the continuous exocytosis of vesicles as they are recruited from the reservoir pool to the ribbon and then docked and released. *B*, The fastest phase of exocytosis is better resolved from measurements of membrane capacitance. By varying the length of a depolarizing pulse, the kinetics of this form of exocytosis can be investigated. The time constant of this phase, shown by the exponential fit, is 1.5 msec. *C*, The relative numbers of vesicles in the three pools and their rates of movement are indicated in this diagram. The rapidly releasable pool (RRP) of 1800 vesicles corresponds to all the vesicles docked below all of the ribbons in the terminal. The reserve pool corresponds to vesicles held by ribbons, and the much larger reservoir of 750,000 vesicles represents those vesicles that form a cloud around the ribbons and can be recruited to them. Calcium is thought to affect the movement of vesicles in each of these three steps. (*A*, From Lagnado [2000], copyright 2000, Experimental Physiology and the Physiological Society. *B*, From Mennerick and Matthews [1996], copyright 1996, with permission from Elsevier Science. *C*, From Gomis et al. [1999], copyright 1999, the Society for Neuroscience.)

However, fusion is not inevitable, and some docked vesicles escape, implying that docking is reversible. Although most vesicles dock and fuse at a few sites believed to correspond to ribbons, some fusions occur elsewhere, suggesting, as is thought to be the case for hair cells in the auditory system (Lenzi et al., 1999), that ribbons are not absolutely required for vesicle fusion.

Just as the photoreceptor synapse has autoreceptors that extend the dynamic range of the synapse by applying negative feedback, so, too, at the output synapses of bipolar cells. mGluRs, which by their pharmacological profile belong to group III, exercise rapid feedback for moderate and strong stimulation of salamander bipolar cells (Awatramani and Slaughter, 2001). The identity of the mGluR in the experiments of Awatramani and Slaughter is not certain, but it is probably not mGluR7; it may, however, be mGluR8. Because mGluR7 is also known to be located at the presynaptic terminal of bipolar cells (Brandstätter et al., 1996), it presumably is exercising a different kind of feedback. There is some evidence that mammalian rod bipolar cells express NMDA receptor subunits in their terminals (Wenzel et al., 1997), but as is often the case, whether these are functional and what function they might serve is unknown.

Bipolar cell to ganglion cell; postsynaptic mechanisms. The organization of glutamate receptors in the inner retina is much less well described than is the case for the outer retina. Numerous studies have examined the distribution of the different glutamate receptor subunits within the inner plexiform layer, and though it is clear that almost the whole inventory of receptors can be found in ganglion cells, the resolution of this picture allows only a few isolated examples where the identity of both presynaptic and postsynaptic partners are known. Of the AMPA receptor subunits, GluR2, at least in the cat (Qin and Pourcho, 1999), is relatively scarce among ganglion cells. Because this is the subunit that can render an AMPAR impermeable to Ca^{2+} , it might be expected that, in general, AMPARs in ganglion cells will admit Ca^{2+} . NMDARs are commonly found in ganglion cells and are usually seen at one of the two postsynaptic elements of a dyad (Fletcher et al., 2000; Pourcho et al., 2001). Metabotropic glutamate receptors are also common, with almost all ganglion cells of the rat having mGluR1 and mGluR4, and some having others besides (Hartveit et al., 1995).

Consistent with this immunocytochemical picture, numerous physiological studies indicate that both NMDA and AMPA/KA receptors mediate excitatory input from bipolar cells to ganglion cells (e.g., Mittman et al., 1990). In the salamander retina, studies with selective antagonists have shown that AMPA receptors, rather than KA receptors, provide the non-NMDA input (Lukasiewicz et al., 1997), although in

other retinas, KA subunits are found in ganglion cells (Qin and Pourcho, 2001).

Much of the interest in glutamatergic input to ganglion cells has centered on the question of how ganglion cells acquire their kinetic and receptive field properties. As already described, it is now clear that some bipolar cell types have transient responses, whereas others are sustained. Because transient bipolar cells generally connect to transient ganglion cells, and sustained bipolar cells generally connect to sustained ganglion cells (Awatramani and Slaughter, 2000), part of the kinetic difference between ganglion cell types is already accounted for. Along with amacrine cell input to ganglion cells, the behavior of postsynaptic glutamate receptors in ganglion cells also contributes to the kinetic properties of ganglion cells responses. Inferences from fluctuation analysis, a method for estimating the responses to single vesicles of transmitter from an examination of voltage noise, suggest that different bipolar cells converging to the same ganglion cell release transmitter at very different rates and have very unequal quantal responses. The response of a cat ON-beta ganglion cell to a vesicle of transmitter from a b1 bipolar cell is estimated to be $240\mu\text{V}$, whereas $30\mu\text{V}$ is all that the b2 and b3 cells produce (Freed, 2000). Most likely, this is due to differences in the type or number of postsynaptic channels at the different synapses, but conceivably, it could be due to differences in a presynaptic property, such as the number of glutamate molecules per vesicle.

Desensitization of AMPA receptors abbreviates the bipolar input to ON-OFF ganglion cells in salamander, as revealed in experiments in which AMPA receptor desensitization was abolished by thiazide compounds (Lukasiewicz et al., 1995). A second contributor to this abbreviation of glutamate inputs is made by glutamate transporters, probably on Müller cells, which play an important role in reducing glutamate responses tens of milliseconds after the stimulus (Higgs and Lukasiewicz, 1999). Although single quanta of transmitter are cleared effectively by diffusion, multiple quanta are not cleared well by diffusion and rely on uptake, suggesting that some degree of spillover of glutamate from one synapse to another might occur during strong stimulation.

Surprisingly, perhaps, physiological and pharmacological studies of ganglion cells reveal no differences between types. For example, alpha and beta cells of the cat (Cohen et al., 1994) and both ON and OFF midget and parasol ganglion cells from the primate retina are indistinguishable in terms of their ionotropic GluRs (Zhou et al., 1994). Does this mean that all ganglion cells are physiologically identical? Probably not. Very likely, differences between ganglion cells exist at a finer scale than is at present experimentally approachable and different bipolar cells are presynaptic to different combinations of glutamate receptors, as suggested

by the fluctuation analysis of Freed (2000). What is needed is a map of which receptors are postsynaptic to which bipolar cells.

NMDA receptors clearly contribute a significant fraction of excitatory input to ganglion cells, and this helps shape ganglion cell responses (Diamond and Copenhagen, 1993), but what function, if any, is served by the Ca^{2+} admitted through these channels? One possible role for this Ca^{2+} is the stimulation of nitric oxide synthase and the production of nitric oxide. Ganglion cell bodies, as well as dendrites, are known to produce nitric oxide when stimulated through NMDAR-mediated Ca^{2+} influx (Blute et al., 2000) and, unexpectedly, nitric oxide does not appear to spread extensively once generated. The functional significance of nitric oxide production for ganglion cell behavior is presently unknown, but very likely, its effects are via stimulation of soluble G cyclase.

NMDA receptors are themselves modulated by Ca^{2+} . The NMDA component of excitatory postsynaptic potentials (EPSPs) is reduced when Ca^{2+} is raised, either by influx through voltage-gated Ca^{2+} channels or else by release from the ER (Akopian and Witkovsky, 2001). Ca^{2+} seems to play an important and complex role in regulating the behavior of ganglion cells. Moreover, Ca^{2+} , admitted through different mechanisms, exercises different kinds of control. In salamander ganglion cells, glutamate acts at a group III mGluR to inhibit L-type Ca^{2+} channels via the release of Ca^{2+} from internal stores; however, glutamate also acts to inhibit N-type Ca^{2+} channels via Ca^{2+} admitted through ionotropic GluRs (Shen and Slaughter, 1998).

The Lateral Pathways

HORIZONTAL CELLS

Photoreceptor to horizontal cell; postsynaptic mechanisms. Horizontal cells constitute the pathway for lateral information flow in the outer retina. They mediate lateral inhibition that subserves gain control and, in some retinas, color opponency. Horizontal cells are the lateral elements in invaginating synapses, where they receive glutamatergic input from both rods and cones. Glutamate receptor subunits have been localized on the horizontal cell membranes at triads, and there is abundant physiological evidence for glutamatergic input. In the mammalian retina, immunocytochemistry shows the presence of AMPA-preferring subunits (e.g., Qin and Pourcho, 1996), for which there is also physiological evidence (Blanco and de la Villa, 1999), as well the KA-preferring subunits GluR6/7 (Morigiwa and Vardi, 1999), all located on the invaginating tips of horizontal cell dendrites. Good physiological evidence shows the presence of NMDA receptors on the horizontal cells of stingray and catfish retinas (Linn and Christensen, 1992; O'Dell and

Christensen, 1989), but this is not usual, even in other fish. The AMPA receptors of fish horizontal cells admit Ca^{2+} (Linn and Christensen, 1992; Okada et al., 1999), which, at least in some retinas, is part of the pathway that controls the rapid changes in synaptic morphology that accompany light and dark adaptation (Okada et al., 1999), described later.

Transmission from horizontal cells. Horizontal cells are widely thought to use GABA as a transmitter and to generate the surrounds of bipolar cells by being presynaptic to both photoreceptor terminals and bipolar cells; however, every one of these points has been challenged. A curious feature of horizontal cells is that their cytoplasm at presumed synapses is generally without the typical aggregation of presynaptic vesicles. It is generally accepted now that GABA release from horizontal cells is unconventional and uses a transporter whose rate and direction depend on membrane voltage and the Na^+ gradient, but not strongly on Ca^{2+} concentration (Schwartz, 1987). Calculations of the concentrations for external GABA suggest that, even assuming a constant Na^+ gradient, this mode of transmission generates equilibrium values for external GABA of between $4\mu\text{M}$ at -70mV membrane potential and $28\mu\text{M}$ at a horizontal cell membrane potential of -20mV . Very likely, this is within the useful range for postsynaptic GABA receptors (Attwell et al., 1993).

It was thought that the GABA transporter in horizontal cells was probably GAT-1, as this is commonly found in neuronal plasma membranes and has similar biophysical properties to those of the horizontal cell transporter (Cammack et al., 1994). No GAT-1 immunoreactivity, however, has been found on horizontal cells (Yang et al., 1997); instead, VGAT, the GABA transporter thought to be unique to synaptic vesicles, is located at or close to the plasma membrane of horizontal cells at triads (Haverkamp et al., 2000). This might, therefore, be the transporter responsible for GABA release. If so, it raises a number of questions, not the least of which is how a transporter that normally operates at the very low pH of synaptic vesicles could work efficiently at extracellular pH. The most recent work on rat and mouse retina (Cueva et al., 2002) suggests that VGAT is actually found in the cytoplasm of the tips of horizontal cell processes where, presumably, it is associated with the small number of vesicles found there. This finding might resolve the problem of what VGAT is doing in horizontal cells, but at the same time, it reopens the question of how GABA is released from horizontal cells.

Horizontal cell to horizontal cell. Horizontal cells have GABA receptors. The immunocytochemical evidence for this is not overwhelming, but physiological evidence supports this statement. Isolated rabbit horizontal cells show pharmacological

evidence of GABA_A receptors (Blanco et al., 1996), and fish and amphibian horizontal cells show both GABA_A and GABA_C ionotropic receptors (Dong et al., 1994; Qian and Dowling, 1993). These GABA receptors probably mediate chemical transmission between adjacent horizontal cells, but they also act as autoreceptors. A striking feature of horizontal cell light responses is that they can be remarkably slow in the dark-adapted retina, even though their glutamate receptors comprise unremarkable subunits closer to the synaptic release site of photoreceptors than those of ON bipolar cells, whose responses are much faster.

The slowness of horizontal cell light responses is the consequence of positive feedback, in that depolarization of horizontal cells increases extracellular GABA concentration, via the GABA transporter, which, in turn, further depolarizes the horizontal cell through ionotropic GABA receptors (Kamermans and Werblin, 1992). In horizontal cells, E_{Cl} is between -10 mV and -20 mV , so Cl^- conductances are generally depolarizing. When light hyperpolarizes photoreceptors, the glutamatergic input to horizontal cells is reduced quickly. However, the positive feedback loop considerably slows the horizontal cell hyperpolarization, not because the loop has any long delays, but rather because the loop gain is very low when the horizontal cell is depolarized but increases as the membrane potential gets further away from E_{Cl} .

Horizontal cell to photoreceptor. The properties of the synapses from horizontal cells to cone terminals and bipolar cells are not well described and have been obtusely resistant to simple characterization. With the exception of Greferath et al. (1995), who showed GABAR subunits in rod and cone terminals, antibodies have failed to locate GABARs in photoreceptors, although Vardi et al. (1998) reported that PCR finds alpha subunit mRNA in rat rods. A simple, robust result that compels belief in a GABAergic feedback pathway is that isolated cones show strong GABA_A responses when GABA is applied to their terminals (Tachibana and Kaneko, 1984). Nevertheless, careful physiological examinations of this synapse have turned up results that do not easily fit with this idea. In the salamander, a careful study (Hare and Owen, 1996) showed that surround responses in bipolar cells were not abolished with the combined presence of antagonists to GABA_A, GABA_B, and GABA_C receptors. Conceivably, the pharmacology of the receptor is novel, or perhaps the drugs used were unable to reach their targets, but the simplest explanation, as the authors conclude, is that GABA input from horizontal cells does not generate the receptive field surround of bipolar cells.

Parallel difficulties exist in the fish retina, where feedback to cones from horizontal cells establishes spectral opponency (Kamermans and Spekreijse, 1999). As a way of accommodating a number of awkward experimental results, it

has been proposed that the feedback mechanism is not GABAergic, but rather works by an electrical mechanism (Kamermans et al., 2001). The idea, similar to one suggested originally by Byzov and Shura-Bura (1986), is that horizontal cell terminals act as current sinks within the restricted space of the invaginating synapse. An unexpected finding supporting this idea is that the terminals of horizontal cells express connexin 26, a gap junction protein for which no partner exists on the apposed cone terminal membrane (Kamermans et al., 2001). The resulting hemijunctions, in effect, couple horizontal cells to the extracellular space of the synaptic triad. Because the Ca^{2+} channels responsible for photoreceptor transmitter release experience their voltage as the voltage difference between this extracellular space and the cone cytoplasm, this might allow horizontal cells to exercise an ephaptic feedback on the release of photoreceptor transmitter.

Horizontal cell to bipolar cell. Bipolar cell dendrites receive GABAergic input from horizontal cells. GABA_A subunits are found on the dendrites of both ON and OFF bipolar cells adjacent to horizontal cell processes (Haverkamp et al., 2000; Vardi et al., 1998). GABA_C subunits are also seen in dendrites, but they are not obviously located at synapses (Haverkamp et al., 2000; Wässle et al., 1998) and their function is unknown. Physiological recordings from bipolar cells confirm that bipolar dendrites have both GABA_A and GABA_C receptors (e.g., Du and Yang, 2000).

Because both ON and OFF bipolar cells have apparently similar GABA receptors, a problem is posed as surround illumination hyperpolarizes ON bipolars but depolarizes OFF bipolars, even though both effects are mediated by the same horizontal cells. A solution to this problem is suggested by the finding that the Cl^- transporters in the two types of bipolar cell are different (Fig. 19.6; Vardi et al., 2000). The dendrites of OFF bipolars heavily express KCC2, a Cl^- transporter that normally extrudes Cl^- , thus making E_{Cl} more negative. ON bipolar cells, on the other hand, express NKCC, a transporter that imports Cl^- and normally makes E_{Cl} more positive. This suggests that E_{Cl} is different in the two classes of bipolar cell in just the way that could explain how GABA depolarizes one while hyperpolarizing the other. Perhaps surprisingly, rod ON bipolar cells also express KCC2, but at the other end of the cell, in the axon terminals, implying that E_{Cl} is different in those two regions of a cell that are only $100\text{ }\mu\text{m}$ apart. On its face, this would imply a continuous and energetically wasteful Cl^- flux from the dendrites to the axon terminal unless these neurons have some way to compartmentalize Cl^- .

AMACRINE CELLS In the inner plexiform layer, synaptic patterns become very complex and the pharmacology of

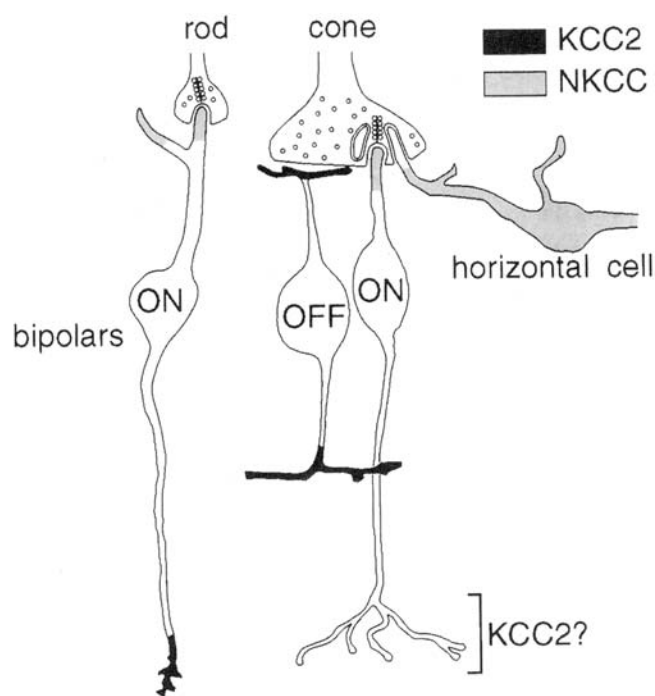


FIGURE 19.6. Diagram summarizing the distribution of the two Cl^- transporters, KCC2 and NKCC, at bipolar cell membranes. KCC2 is found in the dendrites of OFF bipolar cells and is thought to produce a negative E_{Cl} . ON bipolar cells, by contrast, express NKCC in their dendrites, implying a more positive E_{Cl} . These presumed differences in E_{Cl} are consistent with bipolar cell inhibitory surrounds, depolarizing in OFF bipolar cells and hyperpolarizing in ON bipolar cells, produced by GABA from horizontal cells. Both rod (ON) bipolar cells and OFF bipolar cells express KCC2 in their terminals, where GABAergic input from amacrine cells is hyperpolarizing. (From Vardi et al. [2000], copyright 2000, the Society for Neuroscience.)

synaptic responses is only vaguely understood. The basic plan, though, is that most amacrine cells are inhibitory, and of these, most are GABAergic, with a minority being glycinergic and an even smaller minority using other transmitters. In goldfish, a recent study (Marc and Liu, 2000) estimated that 92% of synapses in the inner plexiform layer, excluding those made by bipolar cells, were made by GABAergic amacrine cells. Amacrine cells receive glutamatergic input from bipolar cells and, in turn, provide negative feedback to bipolar cell terminals and inhibitory feedforward to ganglion cells, as well as input to other amacrine cells. As described later, the individual feedback and feedforward pathways are complex, both in their pharmacology and especially in their modulation, about which little is understood. The task of working out the patterns of synaptic connections is truly daunting, especially since we do not yet have a complete classification of the dozens of amacrine cells likely to be found in any retina. Beyond these difficult questions, though, are higher-order questions of how and why inhibitory amacrine

cells are connected in networks, and why so many inhibitory cells are needed.

Bipolar cell to amacrine cell. Only a few studies have examined the bipolar input to amacrine cells, and of these, most are concerned with input from the mammalian rod bipolar cell to the two postsynaptic partners at the dyad, the AII amacrine cells and the A17 amacrine cells (also known as AI amacrine cells). The AII amacrine cells lie on the direct signal pathway to ganglion cells, and the A17 cells are lateral elements providing feedback. These two different roles are subserved by different teams of postsynaptic receptors whose identity is now becoming clearer. Physiological work shows that AMPA/KA receptors dominate input to A17 amacrine cells in the rat (Menger and Wässle, 2000), and in these cells, there seems to be no NMDA input. Immunohistochemical studies have shown that A17s are likely to have kainate-type receptors incorporating the orphan δ receptor subunit (Ghosh et al., 2001). AII amacrine cells, on the other hand, express standard AMPAR subunits, but in addition to responding to non-NMDAR agonists, they also respond to NMDA (Hartveit and Veruki, 1997). This does not necessarily imply that normal bipolar input is mediated through these receptors, though. A cautionary result is reported by Matsui et al. (2001) for transient ON amacrine cells of the mouse retina. In these cells, bipolar input is normally mediated by AMPA receptors; only when the inhibitory feedback from amacrine cells is disabled is the enhanced release of glutamate from bipolar terminals able to activate NMDA receptors.

Metabotropic glutamate receptors are found in amacrine cells and very likely play important modulatory roles. A member of the group II mGluRs, mGluR2 has been found in cholinergic amacrine cells in both ON and OFF sublaminae (Hartveit et al., 1995) and also in A17 cells, where it has been proposed as a mechanism that decreases GABA release at the reciprocal synapse back to rod bipolar cells (Brandstätter et al., 1998). Group I mGluRs are also found on amacrine dendrites postsynaptic to bipolar cells (Koulen et al., 1997). Group I mGluRs are characterized by their coupling to phospholipase C (PLC) and the release of Ca^{2+} from internal stores. Ca^{2+} imaging experiments on amacrine cells from the chick show that two distinct mGluRs are functional in these cells (Kreimborg et al., 2001).

The typical pattern of connection in the inner plexiform layer is that bipolar cells make synapses with two postsynaptic elements, of which one is generally an amacrine cell. However, in addition to this usual arrangement, there are also monads, triads, and tetrads (Marc and Liu, 2000). It is not presently clear what the significance of these patterns is, nor the extent to which these arrangements are specific to particular neuronal types, rather than inconsequential

variations on a theme. Some electron microscopic sections show an amacrine cell process postsynaptic to a bipolar cell that is itself receiving a synaptic feedback from the same amacrine cell. This common anatomical arrangement is termed a “reciprocal synapse.”

Amacrine cell to bipolar cell. Tachibana and Kaneko (1987), using isolated Mb1 bipolar cells from the goldfish retina, showed that GABA sensitivity was high at the axon terminal where GABAergic amacrine cells could provide negative feedback (Fig. 19.7). Like the glutamatergic input to bipolar cells in the outer plexiform layer, the GABAergic input in the inner plexiform layer is turning out to be different in different classes of bipolar cell (Euler and Wässle, 1998; Lukasiewicz and Wong, 1997; Shields et al., 2000), reinforcing the idea that every bipolar cell type carries a unique representation of the pattern of photoreceptor signals. All three kinds of GABA receptor—the ionotropic A and C and the metabotropic $GABA_B$ receptors—are thought to be expressed in bipolar cell terminals. $GABA_C$ receptors activate and deactivate relatively slowly, show little desensitization, and, compared to $GABA_A$ receptors, require a low concentration of GABA for their activation. There is general agreement from both immunocytochemical and physiological studies that $GABA_C$ receptors provide a large fraction of the feedback to the terminals of most bipolar cells (Lukasiewicz et al., 1994; Lukasiewicz and Werblin, 1994; Wässle et al., 1998), but $GABA_A$ receptors also play a role (e.g., Pan, 2001).

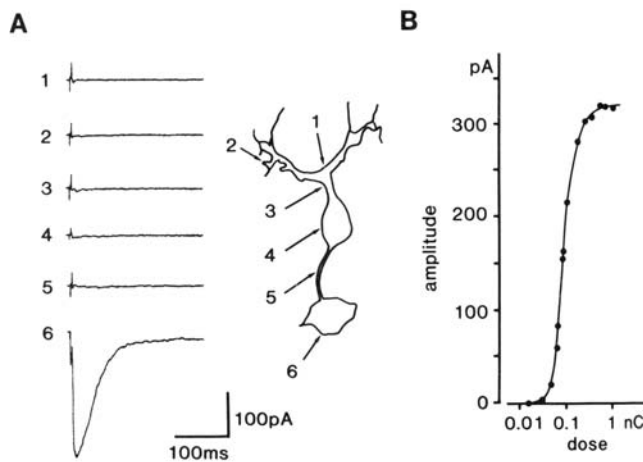


FIGURE 19.7. Currents recorded from a voltage-clamped, isolated Mb1 cell from the goldfish retina. A fine-tipped pipette containing GABA was moved around the cell to the positions indicated by numbers. At each position, an identical dose of GABA was applied iontophoretically. Only when the pipette was placed next to the synaptic terminal (6) was a large, inward Cl^- current seen. (From Tachibana and Kaneko [1987], with permission of the authors.)

The mammalian rod bipolar cell is the best-examined mammalian bipolar cell. Fast-acting GABAergic reciprocal feedback to this bipolar cell is provided by the A17 amacrine cell. This amacrine cell has a powerful ability to extend the dynamic range of the bipolar cell with respect to light intensity, as demonstrated by depressing $GABA_A$ and $GABA_C$ input pharmacologically, or alternatively, cutting off the axon terminal (Fig. 19.8) (Euler and Masland, 2000). $GABA_A$ and $GABA_C$ receptors, though both present on the terminals of rod bipolar cells, do not colocalize (Koulen et al., 1998), raising the question of which amacrine cell provides $GABA_A$ and which $GABA_C$ feedback. An alternative possibility is that A17 cells themselves form both $GABA_A$ -only and $GABA_C$ -only synapses. Is depolarization of a single rod bipolar cell sufficient to drive its own reciprocal inhibition? Direct voltage-clamp experiments on rat rod bipolar cells show that it is (Hartveit, 1999). This result is remarkable, as a single A17 cell, at least in the cat, contacts on the order of 1000 rod bipolar cell terminals (Nelson and Kolb, 1985), leading to the expectation that input from a single rod bipolar cell would generate a negligible signal in the amacrine cell. The fact that this expectation is not fulfilled might suggest that reciprocal synapses act locally. A version of this idea was proposed earlier (Ellias and Stevens, 1980), whereby amacrine cells were thought to act locally by virtue of a restricted spread of their electrical signal. Unfortunately, this idea is not easily consistent with the receptive field properties of amacrine cells (Bloomfield, 1992) and is not widely believed. It might be time to revisit the idea of local

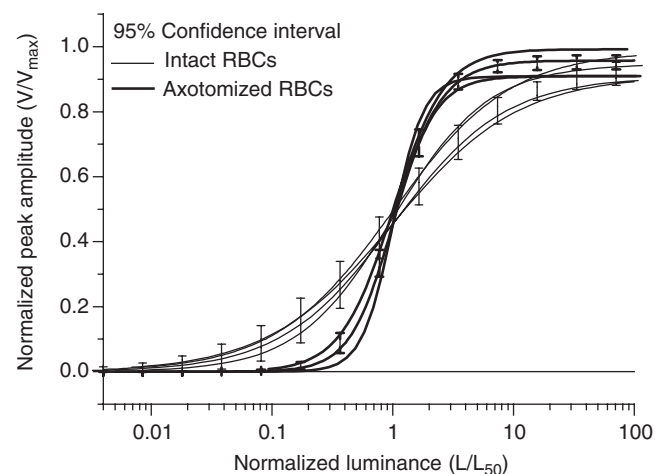


FIGURE 19.8. Normalized peak responses of rod bipolar cells to flashes of different luminance, recorded in retinal slices of a rat. Intact rod bipolar cells have a significantly shallower response curve than those in which the axon terminal has been removed. The implication of this difference is that the feedback at the axon terminal of bipolar cells can extend the sensitivity of these cells. (From Euler and Masland [2000], copyright 2000, The American Physiological Society.)

interactions, this time with the idea that they might be based on local cytoplasmic Ca^{2+} concentration, as it is now well established that this ubiquitous messenger can be locally controlled. In this context an important recent finding has been revealed by 2-photon Ca^{2+} imaging applied to starburst amacrine cells while moving patterns of light were applied to the retina (Euler et al., 2002). Voltage recordings from the somata of these neurons showed no directional preference but the Ca^{2+} signals in individual dendrites were strongly selective for patterns moving centrifugally relative to the soma.

The relative importance of different GABA receptors in generating feedback to bipolar cells other than mammalian rod bipolar cells is somewhat controversial. A confusing factor in untangling this problem is that the pharmacology of GABA_C receptors has not been completely described and differs between preparations. The hallmark insensitivity to bicuculline is consistent, but picrotoxin, which inhibits these channels in ferrets (Lukasiewicz and Wong, 1997) and amphibians (Lukasiewicz et al., 1994), fails to block the channel in the rat (Feigenspan et al., 1993). As described by Shen and Slaughter (2001), there are two pharmacologically distinct GABA_C receptors, one blocked by picrotoxin and the other blocked by I4AA (imidazole-4-acetic acid).

In the salamander retina, Shen and Slaughter (2001) claim that GABA_A input to bipolar cells is small and that the metabotropic GABA_B receptors and the ionotropic GABA_C receptors contribute approximately equally to inhibitory feedback. Lukasiewicz and Werblin (1994), however, failed to confirm an earlier report (Maguire et al., 1989) that GABA_B receptors in bipolar terminals controlled Ca^{2+} current and hence, transmitter release. In addition to uncertainties in the pharmacology of the various GABA receptors, another possible reason for differences in interpretation is that the GABA_B pathway may not be driven strongly by brief step of light, the conventional stimulus (Shen and Slaughter, 2001).

Amacrine cell to ganglion cell. Inhibitory feedforward from amacrine cells to ganglion cells, like feedback to bipolar cells, is an area of pharmacological controversy. There is general agreement that inhibitory feedforward is a powerful mechanism, but disagreement concerns the receptors that mediate this. GABA_A receptor subunits are found expressed on ganglion cells with different subunits at different synapses on the same cell (Wässle et al., 1998), where they mediate transient inhibition (Lukasiewicz and Shields, 1998). Lukasiewicz and Shields (1998) report that GABA_A receptors alone mediate inhibition to ganglion cells of the amphibian retina, but other work suggests there is also GABA_C (Zhang and Slaughter, 1995) and GABA_B input to ganglion cells (Shen and Slaughter, 2001).

As described by Zhang et al. (1997b), there are two separate GABA_B receptors on salamander ganglion cells. For one of these, baclofen is an agonist; for the other, *cis*-aminocrotonic acid (CACA) is an agonist. Both GABA_B receptors reduce Ca^{2+} currents, but the baclofen-sensitive receptor seems to work through a G protein that directly interacts with an N-type Ca^{2+} channel, whereas the CACA-sensitive pathway affects Ca^{2+} entry through L-type Ca^{2+} channels. The regulation of the CACA-sensitive pathway involves cGMP that can be stimulated through the effect of nitric oxide on G cyclase, whereas regulation of the baclofen-sensitive pathway involves calmodulin, which, in turn, can apparently produce both upregulation and downregulation at the receptor.

Already, this is a very complicated picture implying several levels of inhibition under different control mechanisms. Calcium entry clearly plays a significant role in the control of this inhibition, and it is apparent that Ca^{2+} can enter not only through the N- and L-type Ca^{2+} channels of ganglion cells, but possibly, also through NMDA receptors and Ca^{2+} -permeable AMPA receptors. As already described, glutamate seems to regulate L- and N-type Ca^{2+} channels (Shen and Slaughter, 1998), thus allowing an interaction of the two transmitters—GABA and glutamate—at the level of the ganglion cell second-messenger pathways and dendritic Ca^{2+} concentration. Working out how this level of control is regulated normally will be a difficult task since we presently have no good picture of which amacrine cells provide input to which ganglion cells. Conceivably, the complex situation described here for the amphibian retina will turn out to be less complicated in the mammalian retina, as the evidence for GABA_B receptors in the latter is presently not strong.

Amacrine cell to amacrine cell. Electron microscopic anatomy has shown that amacrine cells are extensively interconnected by conventional synapses. In some retinas, such as those of the frog and pigeon, synapses in the inner plexiform layer at which amacrine cells are presynaptic outnumber those at which bipolar cells are presynaptic, by a factor of almost 11 to 1 (Dubin, 1970). As already pointed out, the patterns of amacrine to amacrine connections are clearly complex, involving loops of synapses in addition to presumed electrical connections mediated by gap junctions (Vaney, 1999).

Like reciprocal synapses, “serial synapses” are defined anatomically and describe the common situation in which one amacrine cell process is seen to be presynaptic to another, which is presynaptic to another, and so on. Identifying these chains depends on lucky electron microscopic sections, so it can be assumed that chains of amacrine cell synapses are even more common than they appear. A simple

physiological experiment involving the application of a glycinergic antagonist to the retina (Zhang et al., 1997a) shows that serial synapses are important. With this treatment, inhibition was decreased in most ganglion cells, but was increased in one-third of the ganglion cells examined. The explanation for this is that blockade of glycinergic amacrine cell synapses is disinhibitory for some GABAergic amacrine cells, and for about one-third of ganglion cells, these disinhibited GABAergic amacrine cells provide the bulk of the inhibitory input. A similar result was obtained when GABAergic input was blocked, and in an analogous way, this implies that, for some ganglion cells, disinhibited glycinergic amacrine cells provide the chief inhibitory input. Clearly, if the pattern of connectivity is complex and contains nested loops (Marc and Liu, 2000), the outcome of blocking a whole class of transmission will be hard to predict without knowing the relative synaptic strengths and dynamics of the synapses. Needless to say, this knowledge is not imminent.

Although most amacrine cells are GABAergic, some of these cells may release other fast transmitters in addition to GABA. The best-known example of this is the starburst amacrine cell, which is thought to release both GABA and acetylcholine (ACh). Studies examining the release of radioactively labeled GABA and ACh (O'Malley et al., 1992) provide convincing evidence that ACh is released by depolarization and light stimuli in a Ca^{2+} -dependent way, consistent with conventional vesicular transmitter release. The results concerning the release of ^3H -GABA are less easy to interpret, but point to a Ca^{2+} -independent exchange mechanism like that described in horizontal cells (Schwartz, 1987). Because these studies were carried out in intact retinas, ^3H -GABA efflux is the sum of efflux from all GABAergic cells in the retina, including horizontal cells, of course. Since GABAergic amacrine cells have conventional synapses with clear vesicles, it seems dubious that GABA transport would be the only mode of release in these cells. More recent studies using cultures of amacrine cells that accumulate both GABA and ACh suggest that, in addition to some GABA release via a transporter, both transmitters are released in a Ca^{2+} -dependent manner. Release of the two transmitters is, nevertheless, slightly different in that GABA release prefers Ca^{2+} entry through L-type Ca^{2+} channels, whereas ACh release seems to prefer entry of Ca^{2+} through N-type channels (Santos et al., 1998). If true, many intriguing questions follow from the implication that a single amacrine cell can release two transmitters. Are the two transmitters released by different patterns of input? Are the two transmitters located at different synapses, and if so, what are the postsynaptic cells at those synapses? These questions have rich implications, as the starburst amacrine cell is a key element in the establishment of directional cell activity in ganglion cells (Yoshida et al., 2001), and the differential

release of the two transmitters might well play a central role in this.

Much has been learned about the release of GABA from amacrine cells by the application of electrophysiological techniques to transmission between synaptically connected pairs of cultured chick amacrine cells. Consistent with the anatomy, which shows vesicles in presynaptic locations (Gleason and Wilson, 1989), transmission is quantal when examined with brief depolarizations (Fig. 19.9). Depolarization to about -45 mV is required to evoke transmission, and Ca^{2+} entry is chiefly through L-type Ca^{2+} channels, though another unidentified high voltage activated (HVA) Ca^{2+} channel plays a minor role in promoting release (Gleason et al., 1993). An important feature of these synapses is that, although buffering cytoplasmic Ca^{2+} to zero abolishes all release, these synapses release transmitter, albeit at a low rate, even at resting cytoplasmic levels of Ca^{2+} (around 100 nM) (Frerking et al., 1997). This is a little surprising, as these are conventional synapses for which the expectation is that about $100\text{ }\mu\text{M}$ of Ca^{2+} is required to activate release; in this regard, these synapses are similar to the ribbon synapses in photoreceptor and bipolar cells. Recordings from goldfish amacrine cells in slices show a continuous barrage of quantal input from other GABAergic amacrine cells, even in the absence of all glutamatergic input (Watanabe et al., 2000). It is not clear how this input is maintained, but it seems plausible that it represents the collective input from several amacrine cells releasing quanta at a basal rate.

Strong depolarizations of chick amacrine cells elicit an initial burst of transmitter release, followed by sustained release at a much lower rate (Fig. 19.10) (Borges et al., 1995). This result supports a "fire and reload" model in which vesicles already docked and primed at release sites are discharged soon after Ca^{2+} entry, but once these have fused with the plasma membrane, the release rate slows down considerably as the docking or priming of fresh vesicles becomes the rate-limiting step. Once again, this is qualitatively similar to the situation with the bipolar cell ribbon, except that only a single vesicle is capable of immediate release at the amacrine cell active zone, as opposed to the 22 at the bipolar cell ribbon. Like bipolar cell synapses, cessation of Ca^{2+} influx does not result in immediate termination of transmitter release because the low residual concentrations of Ca^{2+} are sufficient to promote transmitter release. This observation in cultured cells has a counterpart in retinal slices, where depolarization of a rat rod bipolar cell results in a long-lasting inhibitory input presumed to be from an A-17 amacrine cell (Hartveit, 1999).

Because low concentrations of cytoplasmic Ca^{2+} are sufficient to promote transmitter release, the removal of Ca^{2+} plays a role in the kinetics of transmitter release. At synapses that require a high concentration of Ca^{2+} , diffusion alone is

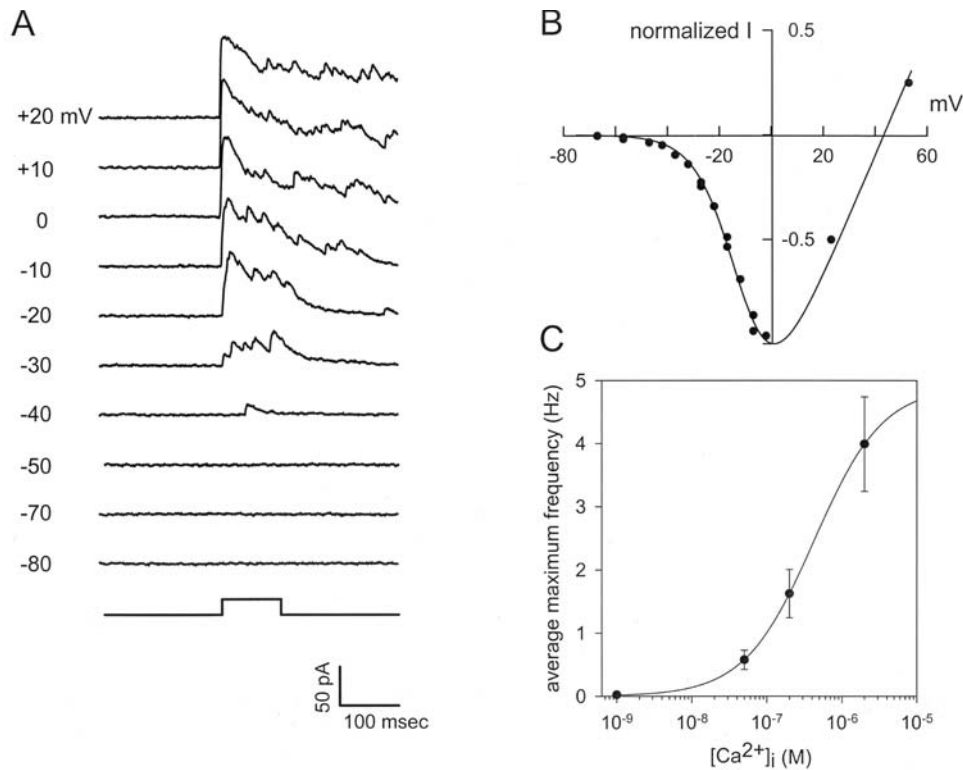


FIGURE 19.9. The Ca^{2+} requirement for transmitter release from amacrine cells. *A*, Postsynaptic currents recorded from a cultured chick amacrine cell held in voltage clamp while the presynaptic cell is depolarized from -70 mV to the voltages indicated to the left of each record. The presynaptic voltage step to -40 mV elicits a single, discrete, outward current corresponding to the release of a single vesicle of transmitter. As the voltage is made increasingly positive, the numbers of vesicles released increases, and transmitter release clearly continues after the presynaptic cell has been repolarized. *B*, The normalized peak Ca^{2+} currents, elicited from a voltage-clamped, isolated amacrine cell. Current begins to activate at about -40 mV, the voltage at which transmission begins in *A*. Pharmacological data show that this inward current is chiefly, but not exclusively, an L-type Ca^{2+} current. *C*, Dependence of the rate of transmitter release on cytoplasmic Ca^{2+} concentration. Buffered Ca^{2+} was internally perfused in 49 amacrine cells while the maximum rate of their transmitter release was recorded. The most important feature of this plot is that, while the release rate is zero at 1 nM Ca^{2+} , 50 and 200 nM Ca^{2+} clearly produces continuous release of transmitter at a low rate. (*A*, From Gleason et al. [1993], copyright 1993, the Society for Neuroscience. *B* and *C*, From Wilson, M. Synaptic transmission between retinal neurons, in Chalupa and Finlay [1998], Copyright 1998, Plenum Press, New York.)

sufficient to clear Ca^{2+} very quickly once Ca^{2+} channels close. The ribbon synapses of photoreceptors and bipolar cells apparently rely on the plasma membrane Ca^{2+} ATPase, the Ca^{2+} pump, for Ca^{2+} clearance (Krizaj and Copenhagen, 1998; Zenisek and Matthews, 2000), but at chick amacrine cell synapses, the Na^+ - Ca^{2+} exchanger is important (Fig. 19.11) (Gleason et al., 1994). Disabling exchange by removing external Na^+ can enormously extend synaptic transmission in these cells, but the mechanism by which this works is indirect. The seemingly obvious interpretation, that Ca^{2+} entering through Ca^{2+} channels remains longer when the Na^+ - Ca^{2+} exchanger is unable to function, is wrong. Instead, even when the exchanger is working normally, a large fraction of the Ca^{2+} responsible for synaptic transmission comes, not from Ca^{2+} entry from the outside, but rather from internal Ca^{2+} stores triggered to release by the Ca^{2+} entering

through Ca^{2+} channels (Hurtado et al., 2002). Calcium increases in amacrine cell dendrites can be very local and “spontaneous.” Using two-photon microscopy, Denk and Detwiler (1999) have observed local Ca^{2+} variations in dendrites and spontaneous Ca^{2+} increases, even in the absence of light stimulation.

Synaptic plasticity

Because the retina has to operate efficiently over a huge range of light intensities, it has the ability to tune its configuration to suit the prevailing lighting. The processes of dark and light adaptation are the transitions from one state to another and represent changes in many aspects of retinal organization, including functional changes to synapses. One of the most striking forms of plasticity is the change in

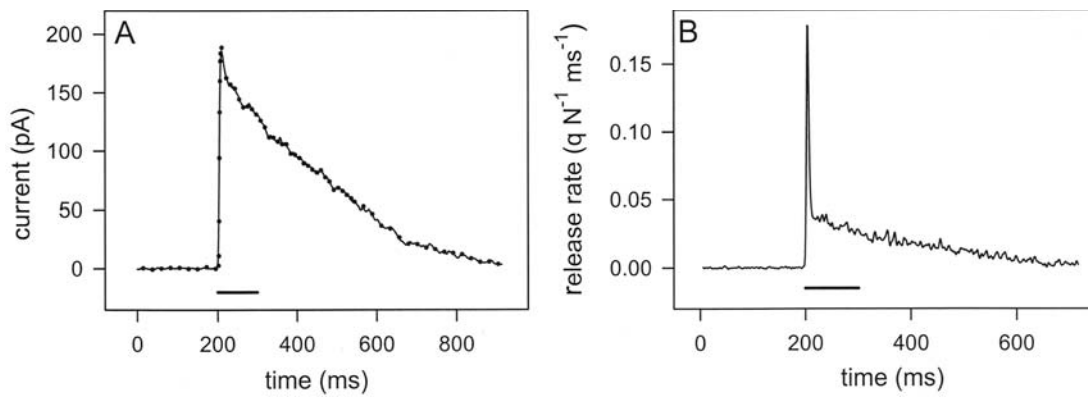


FIGURE 19.10. The kinetics of transmitter release from cultured chick amacrine cells. *A*, The average postsynaptic current elicited by repeatedly stepping the presynaptic voltage from -70 to 0 mV during the period indicated by the bar. The postsynaptic current shown here is the sum of responses to many individual quanta of transmitter. *B*, Using the measured average response to a single quantum of transmitter, a mathematical deconvolution has been used to generate the instantaneous release rate, given in number of quanta released per release site per millisecond. What is revealed

here is that depolarization brings about a sharp, transient increase in release rate, followed by a much slower rate that continues even after presynaptic Ca^{2+} channels close. The initial spike of release probably corresponds to the fusion of vesicles already docked at the release site, whereas the slower, continuous rate is limited by some other process, such as the docking of fresh vesicles. (From Borges et al. [1995], Copyright 1987, National Academy of Sciences, USA.)

synaptic anatomy that takes place in teleost fish retinas (reviewed in Wagner and Djamgoz, 1993).

SPINULES Exposure of a dark-adapted teleost retina to light brings about dramatic physiological (Mangel et al., 1994) as well as morphological changes at cone terminals, on a time scale of minutes. As already described, horizontal cells typically form the two lateral elements of invaginating synapses in which the postsynaptic elements push deeply into the presynaptic terminal, assuming a position opposite the synaptic ribbon. The major morphological change produced by light is that horizontal cell dendrites push out new finger-like processes called spinules, the tips of which are lined with electron-dense material, which further invade the synaptic terminal of cones (Fig. 19.12). The prevailing view has been that spinules are the site of feedback to cones from horizontal cells; in support of this idea is the finding that some changes in horizontal cell physiological properties exactly parallel spinule formation. For example, one sort of horizontal cell, the C-type H2 cell, changes its spectral responses in parallel with spinule formation. When light adapted, it shows depolarization to red light but hyperpolarization to all other wavelengths, whereas when dark adapted, it hyperpolarizes regardless of wavelength (Weiler and Wagner, 1984). A popular theory of the way in which color opponency is generated in light-adapted cones and horizontal cells implicates feedback to cones from horizontal cells as a critical component (Stell et al., 1975), consistent with the “spinules as feedback sites” idea. Further support for this comes from the finding that cytochalasin, which inhibits spinule formation, also prevents the development of spectral opponency in H2 cells (Ter-Margarian and Djamgoz, 1992).

The notion that spinules serve to mediate feedback is an attractive idea, but one based chiefly on correlation, rather than demonstrated causation, and this interpretation has recently been questioned (Weiler et al., 1996). One objection to the concept of spinules as feedback sites is that no GABA_A receptors have been identified immunocytochemically on the cone terminal membranes surrounding the spinule (Yazulla et al., 1989). However, as discussed earlier, it is possible that feedback might be ephaptic (Kamermans et al., 2001), with no need of GABA receptors. The fact that spinules are generally without vesicles is not a strong objection since horizontal cells are thought to release GABA in a non-vesicular fashion (Schwartz, 1987). However, under some circumstances, vesicles in the cone align themselves with the tips of spinules, suggesting that horizontal cell spinules might actually be postsynaptic, rather than presynaptic, structures (Weiler et al., 1996).

The mechanisms involved in the formation and retraction of spinules have been widely investigated. Separate mechanisms seem to be involved in the formation, retraction, and, perhaps, maintenance of spinules, and though none of these pathways have been fully worked out, progress has been made in identifying the likely initial steps. Retinoic acid, a by-product of phototransduction, may well be the main signal for spinule formation, as it is potentially effective at this task (Weiler et al., 1998). Activation of protein kinase C is also very effective and is a likely early step (Kohler et al., 1990). Dopamine, which has multiple actions in mediating light adaptation, is also, to a lesser extent, capable of spinule induction (Kirsch et al., 1991), but may be working through a parallel pathway.

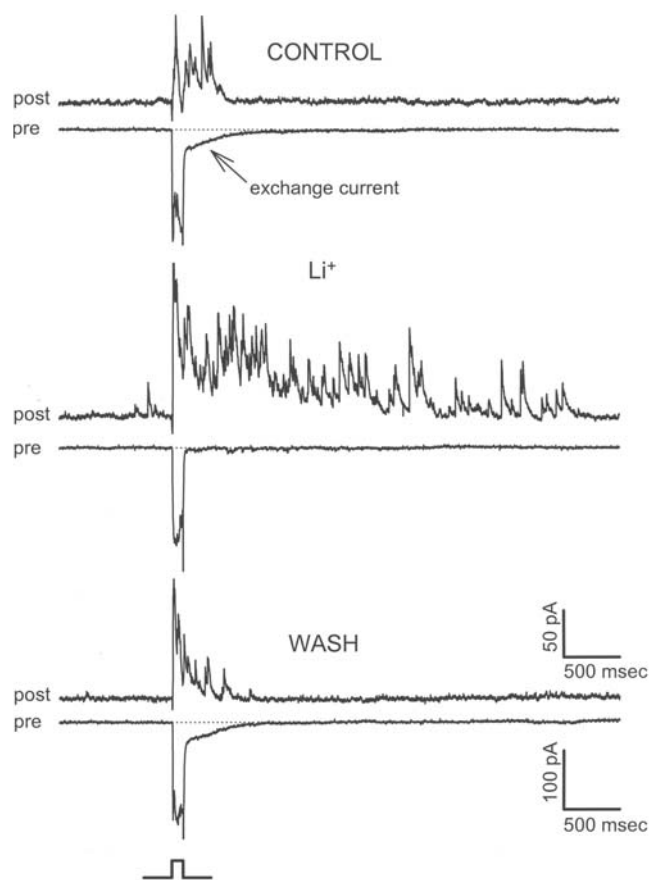


FIGURE 19.11. Simultaneous presynaptic and postsynaptic recordings from a synaptically connected pair of cultured chick amacrine cells. These records show the importance of the $\text{Na}^+\text{-Ca}^{2+}$ exchanger in controlling the release of transmitter. When the presynaptic cell is depolarized for 100 msec, an inward Ca^{2+} current is elicited, followed by a slowly decaying, inward current that is the signature current of the $\text{Na}^+\text{-Ca}^{2+}$ exchanger. During presynaptic depolarization, and for some time afterward, the postsynaptic cell shows a noisy, outward current generated by the release of GABA quanta. When Li^+ replaces external Na^+ , the $\text{Na}^+\text{-Ca}^{2+}$ exchanger is disabled, and the exchanger's signature current is abolished. Under these conditions, the release of GABA quanta is greatly prolonged. Restoring normal external Na^+ restores the normal kinetics of transmitter release. (Modified from Gleason et al. [1994], copyright 1994, with permission from Elsevier Science.)

The dark-adaptation signal for spinule retraction probably operates via AMPA receptors in the horizontal cell membrane. This seems reasonable because darkness would be expected to increase glutamate release from photoreceptors and could, therefore, open AMPA channels. The spinule retraction signal requires external Ca^{2+} to be admitted to horizontal cells, but not through NMDA receptors or voltage-gated Ca^{2+} channels. Only AMPA receptors, presumably without the GluR2 subunit and probably homomeric GluR3 (Schultz et al., 2001), seem to be involved (Okada et al., 1999). Several pieces of evidence contribute to this conclusion, including the finding that a selective

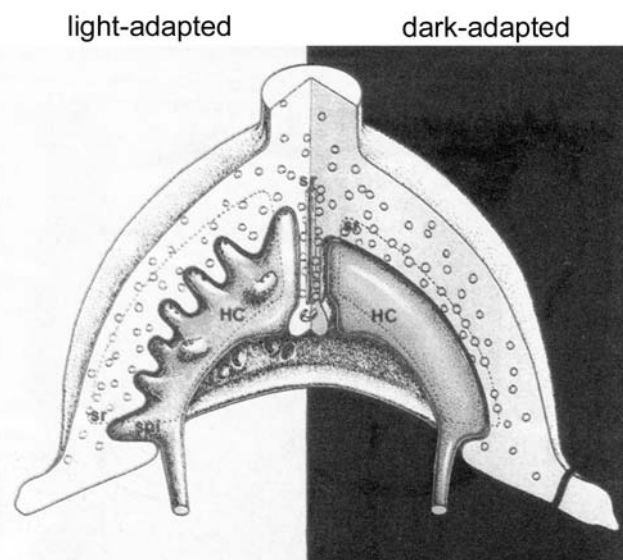


FIGURE 19.12. A cut-away schematic view of a cone terminal shown in its light-adapted state (*left*) and dark-adapted state (*right*). In the light-adapted state, the horizontal cell dendrites that form the lateral elements of triads push out finger-like spinules that are retracted during dark adaptation. (From Wagner and Djamgoz [1993], copyright 1993, with permission from Elsevier Science.)

antagonist for AMPA receptors inhibits spinule retraction. The Ca^{2+} that is admitted through these channels probably activates CaM KII, as inhibition of this kinase or calmodulin also prevents spinule retraction.

The terminals of bipolar cells also show spinule formation, though less is known about this process. The transition between light and dark adaptation produces substantial changes in membrane area in bipolar cell terminals, and spinule formation is one part of this more general rearrangement. ON bipolar cells show spinule formation during dark adaptation (Yazulla and Studholme, 1992), whereas OFF bipolar cells form spinules in light adaptation (Behrens and Wagner, 1996), like horizontal cells. In both cases, the spinules of the inner retina are finger- or mushroom-shaped projections of the bipolar terminal that invaginate an amacrine cell process. The cytoplasm in the tip of the spinule contains vesicles and is lined with membrane densities, as is the apposing amacrine cell membrane.

The isolated Mb1 cell from the goldfish that has proved so useful in the examination of vesicle cycling, has recently become the subject of studies on spinule formation. Depolarization of isolated Mb1 cells from the goldfish, mimicking the effect of light, has been shown to increase the amount of F actin in the terminal in a way that requires Ca^{2+} influx through L-type channels, as well as the stimulation of protein kinase C (PKC) (Job and Lagnado, 1998). Disappointingly, though, this study finds that the cytoskeletal change does not affect the continuous cycling of vesicles.

Using slightly different methods, however, Minami et al. (1998) found that activation of PKC could augment transmitter release. This seems to be accomplished by increasing the size of the available vesicle pool (Tachibana, 1999).

As is true for horizontal cell spinules, the function of spinules in bipolar cells has not been elucidated convincingly. However, Yazulla and Studholme (1992) have proposed that, in the case of the Mb cells, spinules are the sites of GABAergic input to bipolar cells from amacrine cells since the amacrine cell processes that host spinules stain positive for glutamic acid decarboxylase (GAD), the GABA-synthesizing enzyme (Yazulla and Studholme, 1991). This simple proposal is complicated, though, by the finding that, instead of GABA receptors, glycine receptors are found on the bipolar cell spinule membrane.

Summary and future directions

It will, I hope, be clear from this brief review that the field of retinal synapses offers the neuroscientist a rare opportunity to understand the mechanism of a neural machine in a way that can be related to the function and overall design of the machine. There is an abundance of first-rate questions, and because the field is in its early growth phase, the answers to these questions tend to generate still more questions.

In the outer retina, the working of the synaptic complex of cones remains a puzzle, but one that might be addressable in the near future. There are very particular questions associated with this issue. For example, does all the glutamate come from the release sites adjacent to the ribbon, or is glutamate also released at the base of the cone terminal? The overarching question, though, is what engineering problem is solved by this baroque structure?

In the inner retina, there are many pressing questions. The presence of multiple metabotropic receptors in the inner retina has brought the modulation of synapses high up the agenda. Quite apart from modulation of synapses by the metabotropic receptors already discussed is the action of the many peptides found in amacrine cells. Extremely little is known about what these peptides do, and almost nothing is known about how they are released and where their target receptors lie. Because the retina contains dozens of neuropeptides, it seems implausible that they are all involved in light/dark adaptation, the only form of modulation about which we have some understanding.

Release of transmitter from amacrine cells probably has some novel mechanisms. The release of more than one transmitter from a single cell is clearly an important problem, as is the possibility of local control of release. In approaching these issues, a confounding factor is that much of the connectivity of amacrine cells is unexplored territory. A practical approach would be to concentrate on the best-known amacrine cells and to examine closely their synaptic

physiology. The obvious choice would be the AII and the A17 cells postsynaptic to rod bipolar cells in the mammalian retina.

Acknowledgments

This work was supported by a grant from the NEI, EY04112.

REFERENCES

- Adler, E. M., G. J. Augustine, S. N. Duffy, and M. P. Charlton, 1991. Alien intracellular calcium chelators attenuate neurotransmitter release at the squid giant synapse, *J. Neurosci.*, 11:1496–1507.
- Akopian, A., and P. Witkovsky, 2001. Intracellular calcium reduces light-induced excitatory post-synaptic responses in salamander retinal ganglion cells, *J. Physiol.*, 532:43–53.
- Attwell, D., B. Barbour, and M. Szatkowski, 1993. Nonvesicular release of neurotransmitter, *Neuron*, 11:401–407.
- Attwell, D., S. Borges, S. M. Wu, and M. Wilson, 1987. Signal clipping by the rod output synapse, *Nature*, 328:522–524.
- Awatramani, G. B., and M. M. Slaughter, 2000. Origin of transient and sustained responses in ganglion cells of the retina, *J. Neurosci.*, 20:7087–7095.
- Awatramani, G. B., and M. M. Slaughter, 2001. Intensity-dependent, rapid activation of presynaptic metabotropic glutamate receptors at a central synapse, *J. Neurosci.*, 21:741–749.
- Ayoub, G. S., and D. R. Copenhagen, 1991. Application of a fluorometric method to measure glutamate release from single retinal photoreceptors, *J. Neurosci. Methods*, 37:7–14.
- Behrens, U. D., and H. J. Wagner, 1996. Adaptation-dependent changes of bipolar cell terminals in fish retina: effects on overall morphology and spinule formation in Ma and Mb cells. *Vis. Res.*, 36:3901–3911.
- Blanco, R., and P. de la Villa, 1999. Ionotropic glutamate receptors in isolated horizontal cells of the rabbit retina, *Eur. J. Neurosci.*, 11:867–873.
- Blanco, R., C. F. Vaquero, and P. de la Villa, 1996. The effects of GABA and glycine on horizontal cells of the rabbit retina, *Vis. Res.*, 36:3987–3995.
- Bloomfield, S. A., 1992. Relationship between receptive and dendritic field size of amacrine cells in the rabbit retina, *J. Neurophysiol.*, 68:711–725.
- Blute, T. A., M. R. Lee, and W. D. Eldred, 2000. Direct imaging of NMDA-stimulated nitric oxide production in the retina, *Vis. Neurosci.*, 17:557–566.
- Borges, S., E. Gleason, M. Turelli, and M. Wilson, 1995. The kinetics of quantal transmitter release from retinal amacrine cells, *Proc. Natl. Acad. Sci. USA*, 92:6896–6900.
- Brandstätter, J. H., P. Koulen, R. Kuhn, H. van der Putten, and H. Wässle, 1996. Compartmental localization of a metabotropic glutamate receptor (mGluR7): two different active sites at a retinal synapse, *J. Neurosci.*, 16:4749–4756.
- Brandstätter, J. H., P. Koulen, and H. Wässle, 1998. Diversity of glutamate receptors in the mammalian retina, *Vis. Res.*, 38:1385–1397.
- Burns, M. E., and D. A. Baylor, 2001. Activation, deactivation, and adaptation in vertebrate photoreceptor cells, *Annu. Rev. Neurosci.*, 24:779–805.

- Burrone, J., and L. Lagnado, 2000. Synaptic depression and the kinetics of exocytosis in retinal bipolar cells, *J. Neurosci.*, 20:568–578.
- Byzov, A. L., and T. M. Shura-Bura, 1986. Electrical feedback mechanism in the processing of signals in the outer plexiform layer of the retina, *Vis. Res.*, 26:33–44.
- Cai, W., and R. G. Pourcho, 1999. Localization of metabotropic glutamate receptors mGluR1alpha and mGluR2/3 in the cat retina, *J. Comp. Neurol.*, 407:427–437.
- Cammack, J. N., S. V. Rakhilin, and E. A. Schwartz, 1994. A GABA transporter operates asymmetrically and with variable stoichiometry, *Neuron*, 13:949–960.
- Chalupa, L. M., B. L. Finlay, and North Atlantic Treaty Organization, Scientific Affairs Division, 1998. *Development and Organization of the Retina: From Molecules to Function*, New York: Plenum Press.
- Chen, W. R., W. Xiong, and G. M. Shepherd, 2000. Analysis of relations between NMDA receptors and GABA release at olfactory bulb reciprocal synapses, *Neuron*, 25:625–633.
- Cohen, E. D., Z. J. Zhou, and G. L. Fain, 1994. Ligand-gated currents of alpha and beta ganglion cells in the cat retinal slice, *J. Neurophysiol.*, 72:1260–1269.
- Copenhagen, D. R., and C. E. Jahr, 1989. Release of endogenous excitatory amino acids from turtle photoreceptors, *Nature*, 341:536–539.
- Cueva, J. G., S. Haverkamp, R. J. Reimer, R. Edwards, H. Wässle, and N. C. Brecha, 2002. Vesicular gamma-aminobutyric acid transporter expression in amacrine and horizontal cells, *J. Comp. Neurol.*, 445:227–237.
- Denk, W., and P. B. Detwiler, 1999. Optical recording of light-evoked calcium signals in the functionally intact retina, *Proc. Natl. Acad. Sci. USA*, 96:7035–7040.
- DeVries, S. H., 2000. Bipolar cells use kainate and AMPA receptors to filter visual information into separate channels, *Neuron*, 28:847–856. [Comment in: *Neuron*, 2000;28(3):628–629 UI: 21094470].
- DeVries, S. H., 2001. Exocytosed protons feedback to suppress the Ca^{2+} current in mammalian cone photoreceptors, *Neuron*, 32:1107–1117.
- Dhingra, A., A. Lyubarsky, M. Jiang, E. N. Pugh, Jr., L. Birnbaumer, P. Sterling, and N. Vardi, 2000. The light response of ON bipolar neurons requires $\text{G}[\alpha]_o$, *J. Neurosci.*, 20:9053–9058.
- Diamond, J. S., and D. R. Copenhagen, 1993. The contribution of NMDA and non-NMDA receptors to the light-evoked input-output characteristics of retinal ganglion cells, *Neuron*, 11:725–738.
- Dong, C. J., S. A. Picaud, and F. S. Werblin, 1994. GABA transporters and GABAC-like receptors on catfish cone- but not rod-driven horizontal cells, *J. Neurosci.*, 14:2648–2658.
- Du, J. L., and X. L. Yang, 2000. Subcellular localization and complements of GABA(A) and GABA(C) receptors on bullfrog retinal bipolar cells, *J. Neurophysiol.*, 84:666–676.
- Dubin, M. W., 1970. The inner plexiform layer of the vertebrate retina: a quantitative and comparative electron microscopic analysis, *J. Compar. Neurol.*, 140:479–505.
- el-Amraoui, A., I. Sahly, S. Picaud, J. Sahel, M. Abitbol, and C. Petit, 1996. Human Usher 1B/mouse shaker-1: the retinal phenotype discrepancy explained by the presence/absence of myosin VIIA in the photoreceptor cells, *Hum. Mol. Genet.*, 5:1171–1178.
- Eliasof, S., J. L. Arriza, B. H. Leighton, M. P. Kavanaugh, and S. G. Amara, 1998. Excitatory amino acid transporters of the salamander retina: identification, localization, and function, *J. Neurosci.*, 18:698–712.
- Eliasof, S., and F. Werblin, 1993. Characterization of the glutamate transporter in retinal cones of the tiger salamander, *J. Neurosci.*, 13:402–411.
- Ellias, S. A., and J. K. Stevens, 1980. The dendritic varicosity: a mechanism for electrically isolating the dendrites of cat retinal amacrine cells? *Brain Res.*, 196:365–372.
- Euler, T., P. B. Detwiler, and W. Denk, 2002. Directionally selective calcium signals in dendrites of starburst amacrine cells, *Nature*, 418:845–852.
- Euler, T., and R. H. Masland, 2000. Light-evoked responses of bipolar cells in a mammalian retina, *J. Neurophysiol.*, 83:1817–1829.
- Euler, T., and H. Wässle, 1998. Different contributions of GABAA and GABAC receptors to rod and cone bipolar cells in a rat retinal slice preparation, *J. Neurophysiol.*, 79:1384–1395.
- Feigenspan, A., H. Wässle, and J. Bormann, 1993. Pharmacology of GABA receptor Cl^- channels in rat retinal bipolar cells, *Nature*, 361:159–162.
- Field, G. D., and F. Rieke, 2002. Nonlinear signal transfer from mouse rods to bipolar cells and implications for visual sensitivity, *Neuron*, 34:773–785.
- Fletcher, E. L., I. Hack, J. H. Brandstätter, and H. Wässle, 2000. Synaptic localization of NMDA receptor subunits in the rat retina, *J. Comp. Neurol.*, 420:98–112.
- Freed, M. A., 2000. Parallel cone bipolar pathways to a ganglion cell use different rates and amplitudes of quantal excitation, *J. Neurosci.*, 20:3956–3963.
- Ferking, M., S. Borges, and M. Wilson, 1997. Are some minis multiquantal? *J. Neurophysiol.*, 78:1293–1304.
- Ghosh, K. K., S. Haverkamp, and H. Wässle, 2001. Glutamate receptors in the rod pathway of the mammalian retina, *J. Neurosci.*, 21:8636–8647.
- Gleason, E., S. Borges, and M. Wilson, 1993. Synaptic transmission between pairs of retinal amacrine cells in culture, *J. Neurosci.*, 13:2359–2370.
- Gleason, E., S. Borges, and M. Wilson, 1994. Control of transmitter release from retinal amacrine cells by Ca^{2+} influx and efflux, *Neuron*, 13:1109–1117.
- Gleason, E., and M. Wilson, 1989. Development of synapses between chick retinal neurons in dispersed culture, *J. Comp. Neurol.*, 287:213–224.
- Gomis, A., J. Burrone, and L. Lagnado, 1999. Two actions of calcium regulate the supply of releasable vesicles at the ribbon synapse of retinal bipolar cells, *J. Neurosci.*, 19:6309–6317.
- Grant, G. B., and J. E. Dowling, 1995. A glutamate-activated chloride current in cone-driven ON bipolar cells of the white perch retina, *J. Neurosci.*, 15:3852–3862.
- Grant, G. B., and J. E. Dowling, 1996. On bipolar cell responses in the teleost retina are generated by two distinct mechanisms, *J. Neurophysiol.*, 76:3842–3849.
- Greferath, U., U. Grünert, J. M. Fritschy, A. Stephenson, H. Möhler, and H. Wässle, 1995. GABAA receptor subunits have differential distributions in the rat retina: in situ hybridization and immunohistochemistry, *J. Comp. Neurol.*, 353:553–571.
- Hack, I., M. Frech, O. Dick, L. Peichl, and J. H. Brandstätter, 2001. Heterogeneous distribution of AMPA glutamate receptor subunits at the photoreceptor synapses of rodent retina, *Eur. J. Neurosci.*, 13:15–24.
- Hack, I., L. Peichl, and J. H. Brandstätter, 1999. An alternative pathway for rod signals in the rodent retina: rod photoreceptors,

- cone bipolar cells, and the localization of glutamate receptors, *Proc. Natl. Acad. Sci. USA*, 96:14130–14135.
- Hare, W. A., and W. G. Owen, 1996. Receptive field of the retinal bipolar cell: a pharmacological study in the tiger salamander, *J. Neurophysiol.*, 76:2005–2019.
- Harlow, M. L., D. Röss, A. Stoschek, R. M. Marshall, and U. J. McMahan, 2001. The architecture of active zone material at the frog's neuromuscular junction, *Nature*, 409:479–484.
- Hartveit, E., 1996. Membrane currents evoked by ionotropic glutamate receptor agonists in rod bipolar cells in the rat retinal slice preparation, *J. Neurophysiol.*, 76:401–422.
- Hartveit, E., 1999. Reciprocal synaptic interactions between rod bipolar cells and amacrine cells in the rat retina, *J. Neurophysiol.*, 81:2923–2936.
- Hartveit, E., J. H. Brandstätter, R. Enz, and H. Wässle, 1995. Expression of the mRNA of seven metabotropic glutamate receptors (mGluR1 to 7) in the rat retina: An in situ hybridization study on tissue sections and isolated cells, *Eur. J. Neurosci.*, 7:1472–1483.
- Hartveit, E., and M. L. Veruki, 1997. AII amacrine cells express functional NMDA receptors, *Neuroreport*, 8:1219–1223.
- Haverkamp, S., U. Grünert, and H. Wässle, 2000. The cone pedicle, a complex synapse in the retina, *Neuron*, 27:85–95.
- Heidelberger, R., 1998. Adenosine triphosphate and the late steps in calcium-dependent exocytosis at a ribbon synapse, *J. Gen. Physiol.*, 111:225–241.
- Heidelberger, R., C. Heinemann, E. Neher, and G. Matthews, 1994. Calcium dependence of the rate of exocytosis in a synaptic terminal, *Nature*, 371:513–515.
- Heidelberger, R., and G. Matthews, 1992. Calcium influx and calcium current in single synaptic terminals of goldfish retinal bipolar neurons, *J. Physiol.*, 447:235–256.
- Higgs, M. H., and P. D. Lukasiewicz, 1999. Glutamate uptake limits synaptic excitation of retinal ganglion cells, *J. Neurosci.*, 19:3691–3700.
- Hughes, T. E., 1997. Are there ionotropic glutamate receptors on the rod bipolar cell of the mouse retina? *Vis. Neurosci.*, 14:103–109.
- Hurtado, J., S. Borges, and M. Wilson, 2002. Na⁺-Ca²⁺ exchanger controls the gain of the Ca²⁺ amplifier in the dendrites of amacrine cells, *J. Neurophysiol.*, 88:2765–2777.
- Job, C., and L. Lagnado, 1998. Calcium and protein kinase C regulate the actin cytoskeleton in the synaptic terminal of retinal bipolar cells, *J. Cell Biol.*, 143:1661–1672.
- Kamermans, M., I. Fahrenfort, K. Schultz, U. Janssen-Bienhold, T. Sjoerdsma, and R. Weiler, 2001. Hemichannel-mediated inhibition in the outer retina, *Science*, 292:1178–1180.
- Kamermans, M., and H. Spekreijse, 1999. The feedback pathway from horizontal cells to cones: A mini review with a look ahead, *Vis. Res.*, 39:2449–2468.
- Kamermans, M., and F. Werblin, 1992. GABA-mediated positive autofeedback loop controls horizontal cell kinetics in tiger salamander retina, *J. Neurosci.*, 12:2451–2463.
- Kirsch, M., H. J. Wagner, and M. B. Djamgoz, 1991. Dopamine and plasticity of horizontal cell function in the teleost retina: regulation of a spectral mechanism through D1-receptors, *Vis. Res.*, 31:401–412.
- Kohler, K., W. Kolbinger, G. Kurz-Isler, and R. Weiler, 1990. Endogenous dopamine and cyclic events in the fish retina. II: Correlation of retinomotor movement, spinule formation, and connexon density of gap junctions with dopamine activity during light/dark cycles, *Vis. Neurosci.*, 5:417–428.
- Koulen, P., J. H. Brandstätter, R. Enz, J. Bormann, and H. Wässle, 1998. Synaptic clustering of GABA(C) receptor rho-subunits in the rat retina, *Eur. J. Neurosci.*, 10:115–127.
- Koulen, P., R. Kuhn, H. Wässle, and J. H. Brandstätter, 1997. Group I metabotropic glutamate receptors mGluR1alpha and mGluR5a: localization in both synaptic layers of the rat retina, *J. Neurosci.*, 17:2200–2211.
- Koulen, P., R. Kuhn, H. Wässle, and J. H. Brandstätter, 1999. Modulation of the intracellular calcium concentration in photoreceptor terminals by a presynaptic metabotropic glutamate receptor, *Proc. Natl. Acad. Sci. USA*, 96:9909–9914.
- Kreimborg, K. M., M. L. Lester, K. F. Medler, and E. L. Gleason, 2001. Group I metabotropic glutamate receptors are expressed in the chicken retina and by cultured retinal amacrine cells, *J. Neurochem.*, 77:452–465.
- Krizaj, D., and D. R. Copenhagen, 1998. Compartmentalization of calcium extrusion mechanisms in the outer and inner segments of photoreceptors, *Neuron*, 21:249–256.
- Lagnado, L., 2000. The Wellcome Prize Lecture. Visual signals in the retina: from photons to synapses, *Exp. Physiol.*, 85:1–16.
- Lagnado, L., A. Gomis, and C. Job, 1996. Continuous vesicle cycling in the synaptic terminal of retinal bipolar cells, *Neuron*, 17:957–967.
- Lasansky, A., 1978. Contacts between receptors and electrophysiologically identified neurones in the retina of the larval tiger salamander, *J. Physiol.*, 285:531–542.
- Lenzi, D., J. W. Runyeon, J. Crum, M. H. Ellisman, and W. M. Roberts, 1999. Synaptic vesicle populations in saccular hair cells reconstructed by electron tomography, *J. Neurosci.*, 19:119–132.
- Linn, C. P., and B. N. Christensen, 1992. Excitatory amino acid regulation of intracellular Ca²⁺ in isolated catfish cone horizontal cells measured under voltage- and concentration-clamp conditions, *J. Neurosci.*, 12:2156–2164.
- Lukasiewicz, P. D., J. E. Lawrence, and T. L. Valentino, 1995. Desensitizing glutamate receptors shape excitatory synaptic inputs to tiger salamander retinal ganglion cells, *J. Neurosci.*, 15:6189–6199.
- Lukasiewicz, P. D., B. R. Maple, and F. S. Werblin, 1994. A novel GABA receptor on bipolar cell terminals in the tiger salamander retina, *J. Neurosci.*, 14:1202–1212.
- Lukasiewicz, P. D., and C. R. Shields, 1998. Different combinations of GABAA and GABAC receptors confer distinct temporal properties to retinal synaptic responses, *J. Neurophysiol.*, 79:3157–3167.
- Lukasiewicz, P. D., and F. S. Werblin, 1994. A novel GABA receptor modulates synaptic transmission from bipolar to ganglion and amacrine cells in the tiger salamander retina, *J. Neurosci.*, 14:1213–1223.
- Lukasiewicz, P. D., J. A. Wilson, and J. E. Lawrence, 1997. AMPA-preferring receptors mediate excitatory synaptic inputs to retinal ganglion cells, *J. Neurophysiol.*, 77:57–64.
- Lukasiewicz, P. D., and R. O. Wong, 1997. GABAC receptors on ferret retinal bipolar cells: a diversity of subtypes in mammals? *Vis. Neurosci.*, 14:989–994.
- Maguire, G., B. Maple, P. Lukasiewicz, and F. Werblin, 1989. Gamma-aminobutyrate type B receptor modulation of L-type calcium channel current at bipolar cell terminals in the retina of the tiger salamander, *Proc. Natl. Acad. Sci. USA*, 86:10144–10147.
- Mandell, J. W., E. Townes-Anderson, A. J. Czernik, R. Cameron, P. Greengard, and P. De Camilli, 1990. Synapsins in the vertebrate retina: Absence from ribbon synapses and heterogeneous distribution among conventional synapses, *Neuron*, 5:19–33.

- Mangel, S. C., W. H. Baldrige, R. Weiler, and J. E. Dowling, 1994. Threshold and chromatic sensitivity changes in fish cone horizontal cells following prolonged darkness, *Brain Res.*, 659:55–61.
- Marc, R. E., and W. Liu, 2000. Fundamental GABAergic amacrine cell circuitries in the retina: nested feedback, concatenated inhibition, and axosomatic synapses, *J. Comp. Neurol.*, 425:560–582.
- Matsui, K., J. Hasegawa, and M. Tachibana, 2001. Modulation of excitatory synaptic transmission by GABAC receptor-mediated feedback in the mouse inner retina, *J. Neurophysiol.*, 86:2285–2298.
- Matthews, G., 1998. A lie detector test for presynaptic capacitance measurements [comment], *Neuron*, 21:940–941.
- Menger, N., and H. Wässle, 2000. Morphological and physiological properties of the A17 amacrine cell of the rat retina, *Vis. Neurosci.*, 17:769–780.
- Mennerick, S., and G. Matthews, 1996. Ultrafast exocytosis elicited by calcium current in synaptic terminals of retinal bipolar neurons, *Neuron*, 17:1241–1249.
- Minami, N., K. Berglund, T. Sakaba, H. Kohmoto, and M. Tachibana, 1998. Potentiation of transmitter release by protein kinase C in goldfish retinal bipolar cells, *J. Physiol.*, 512:219–225.
- Mittman, S., W. R. Taylor, and D. R. Copenhagen, 1990. Concomitant activation of two types of glutamate receptor mediates excitation of salamander retinal ganglion cells, *J. Physiol.*, 428:175–197.
- Morigiwa, K., and N. Vardi, 1999. Differential expression of ionotropic glutamate receptor subunits in the outer retina, *J. Comp. Neurol.*, 405:173–184.
- Muller, F., H. Wässle, and T. Voigt, 1988. Pharmacological modulation of the rod pathway in the cat retina, *J. Neurophysiol.*, 59:1657–1672.
- Muresan, V., A. Lyass, and B. J. Schnapp, 1999. The kinesin motor KIF3A is a component of the presynaptic ribbon in vertebrate photoreceptors, *J. Neurosci.*, 19:1027–1037.
- Nawy, S., 1999. The metabotropic receptor mGluR6 may signal through G(o), but not phosphodiesterase, in retinal bipolar cells, *J. Neurosci.*, 19:2938–2944.
- Nawy, S., 2000. Regulation of the on bipolar cell mGluR6 pathway by Ca^{2+} , *J. Neurosci.*, 20:4471–4479.
- Nelson, R., and H. Kolb, 1985. A17: a broad-field amacrine cell in the rod system of the cat retina, *J. Neurophysiol.*, 54:592–614.
- Neves, G., and L. Lagnado, 1999. The kinetics of exocytosis and endocytosis in the synaptic terminal of goldfish retinal bipolar cells, *J. Physiol.*, 515:181–202.
- O'Dell, T. J., and B. N. Christensen, 1989. A voltage-clamp study of isolated stingray horizontal cell non-NMDA excitatory amino acid receptors, *J. Neurophysiol.*, 61:162–172.
- Okada, T., K. Schultz, W. Geurtz, H. Hatt, and R. Weiler, 1999. AMPA-preferring receptors with high Ca^{2+} permeability mediate dendritic plasticity of retinal horizontal cells, *Eur. J. Neurosci.*, 11:1085–1095.
- O'Malley, D. M., J. H. Sandell, and R. H. Masland, 1992. Co-release of acetylcholine and GABA by the starburst amacrine cells, *J. Neurosci.*, 12:1394–1408.
- Pan, Z. H., 2001. Voltage-activated Ca^{2+} channels and ionotropic GABA receptors localized at axon terminals of mammalian retinal bipolar cells, *Vis. Neurosci.*, 18:279–288.
- Picaud, S., H. P. Larsson, D. P. Wellis, H. Lecar, and F. Werblin, 1995. Cone photoreceptors respond to their own glutamate release in the tiger salamander, *Proc. Natl. Acad. Sci. USA*, 92:9417–9421.
- Polyak, S. L., 1957. *The Vertebrate Visual System: Its origin, Structure, and Function and Its Manifestations in Disease with an Analysis of Its Role in the Life of Animals and in the Origin of Man*, preceded by a historical review of investigations of the eye, and of the visual pathways and centers of the brain. Chicago: University of Chicago Press.
- Pourcho, R. G., P. Qin, and D. J. Goebel, 2001. Cellular and sub-cellular distribution of NMDA receptor subunit NR2B in the retina, *J. Comp. Neurol.*, 433:75–85.
- Pyle, J. L., E. T. Kavalali, E. S. Piedras-Renteria, and R. W. Tsien, 2000. Rapid reuse of readily releasable pool vesicles at hippocampal synapses, *Neuron*, 28:221–231.
- Qian, H., and J. E. Dowling, 1993. Novel GABA responses from rod-driven retinal horizontal cells, *Nature*, 361:162–164.
- Qin, P., and R. G. Pourcho, 1996. Distribution of AMPA-selective glutamate receptor subunits in the cat retina, *Brain Res.*, 710:303–307.
- Qin, P., and R. G. Pourcho, 1999. AMPA-selective glutamate receptor subunits GluR2 and GluR4 in the cat retina: an immunocytochemical study, *Vis. Neurosci.*, 16:1105–1114.
- Qin, P., and R. G. Pourcho, 2001. Immunocytochemical localization of kainate-selective glutamate receptor subunits GluR5, GluR6, and GluR7 in the cat retina, *Brain Res.*, 890:211–221.
- Rao, R., G. Buchsbaum, and P. Sterling, 1994. Rate of quantal transmitter release at the mammalian rod synapse, *Biophys. J.*, 67:57–63.
- Rao-Mirotnik, R., G. Buchsbaum, and P. Sterling, 1998. Transmitter concentration at a three-dimensional synapse, *J. Neurophysiol.*, 80:3163–3172.
- Rao-Mirotnik, R., A. B. Harkins, G. Buchsbaum, and P. Sterling, 1995. Mammalian rod terminal: architecture of a binary synapse, *Neuron*, 14:561–569.
- Rieke, F., and E. A. Schwartz, 1994. A cGMP-gated current can control exocytosis at cone synapses, *Neuron*, 13:863–873.
- Rieke, F., and E. A. Schwartz, 1996. Asynchronous transmitter release: control of exocytosis and endocytosis at the salamander rod synapse, *J. Physiol.*, 493:1–8.
- Rouze, N. C., and E. A. Schwartz, 1998. Continuous and transient vesicle cycling at a ribbon synapse, *J. Neurosci.*, 18:8614–8624.
- Saito, T., H. Kondo, and J. I. Toyoda, 1979. Ionic mechanisms of two types of on-center bipolar cells in the carp retina. I. The responses to central illumination, *J. Gen. Physiol.*, 73:73–90.
- Santos, P. F., A. L. Carvalho, A. P. Carvalho, and C. B. Duarte, 1998. Differential acetylcholine and GABA release from cultured chick retina cells, *Eur. J. Neurosci.*, 10:2723–2730.
- Sarantis, M., K. Everett, and D. Attwell, 1988. A presynaptic action of glutamate at the cone output synapse, *Nature*, 332:451–453.
- Schlamp, C. L., and D. S. Williams, 1996. Myosin V in the retina: localization in the rod photoreceptor synapse, *Exp. Eye Res.*, 63:613–619.
- Schmitz, F., A. Konigstorfer, and T. C. Sudhof, 2000. RIBEYE, a component of synaptic ribbons: a protein's journey through evolution provides insight into synaptic ribbon function, *Neuron*, 28:857–872.
- Schneeweis, D. M., and J. L. Schnapf, 1995. Photovoltage of rods and cones in the macaque retina, *Science*, 268:1053–1056.
- Schultz, K., U. Janssen-Bienhold, and R. Weiler, 2001. Selective synaptic distribution of AMPA and kainate receptor subunits in the outer plexiform layer of the carp retina, *J. Comp. Neurol.*, 435:433–449.
- Schwartz, E. A., 1987. Depolarization without calcium can release gamma-aminobutyric acid from a retinal neuron, *Science*, 238:350–355.

- Shen, W., and M. M. Slaughter, 1998. Metabotropic and ionotropic glutamate receptors regulate calcium channel currents in salamander retinal ganglion cells, *J. Physiol.*, 510:815–828.
- Shen, W., and M. M. Slaughter, 2001. Multireceptor GABAergic regulation of synaptic communication in amphibian retina, *J. Physiol.*, 530:55–67.
- Shields, C. R., M. N. Tran, R. O. Wong, and P. D. Lukasiewicz, 2000. Distinct ionotropic GABA receptors mediate presynaptic and postsynaptic inhibition in retinal bipolar cells, *J. Neurosci.*, 20:2673–2682.
- Shiells, R. A., and G. Falk, 1999. A rise in intracellular Ca^{2+} underlies light adaptation in dogfish retinal 'on' bipolar cells, *J. Physiol.*, 514:343–350.
- Slaughter, M. M., and R. F. Miller, 1981. 2-amino-4-phosphonobutyric acid: a new pharmacological tool for retina research, *Science*, 211:182–185.
- Stell, W. K., D. O. Lightfoot, T. G. Wheeler, and H. F. Leeper, 1975. Goldfish retina: functional polarization of cone horizontal cell dendrites and synapses, *Science*, 190:989–990.
- Tachibana, M., 1999. Regulation of transmitter release from retinal bipolar cells, *Prog. Biophys. Mol. Biol.*, 72:109–133.
- Tachibana, M., and A. Kaneko, 1984. gamma-Aminobutyric acid acts at axon terminals of turtle photoreceptors: difference in sensitivity among cell types, *Proc. Natl. Acad. Sci. USA*, 81:7961–7964.
- Tachibana, M., and A. Kaneko, 1987. gamma-Aminobutyric acid exerts a local inhibitory action on the axon terminal of bipolar cells: evidence for negative feedback from amacrine cells, *Proc. Natl. Acad. Sci. USA*, 84:3501–3505.
- Tachibana, M., and T. Okada, 1991. Release of endogenous excitatory amino acids from ON-type bipolar cells isolated from the goldfish retina, *J. Neurosci.*, 11:2199–2208.
- Ter-Margarian, A., and M. B. Djamgoz, 1992. Cytochalasin inhibits light-dependent synaptic plasticity of horizontal cells in teleost retina, *Neurosci. Lett.*, 147:131–135.
- Tsukamoto, Y., K. Morigiwa, M. Ueda, and P. Sterling, 2001. Microcircuits for night vision in mouse retina, *J. Neurosci.*, 21:8616–8623.
- van Rossum, M. C., and R. G. Smith, 1998. Noise removal of the rod synapse of mammalian retina, *Vis. Neurosci.*, 15:809–821.
- Vancey, D. I., 1999. Neuronal coupling in the central nervous system: lessons from the retina, *Novartis Foundation Symp.*, 219:113–125; discussion, 125–133.
- Vardi, N., 1998. Alpha subunit of Go localizes in the dendritic tips of ON bipolar cells, *J. Comp. Neurol.*, 395:43–52.
- Vardi, N., R. Duvoisin, G. Wu, and P. Sterling, 2000. Localization of mGluR6 to dendrites of ON bipolar cells in primate retina, *J. Comp. Neurol.*, 423:402–412.
- Vardi, N., K. Morigiwa, T. L. Wang, Y. J. Shi, and P. Sterling, 1998. Neurochemistry of the mammalian cone 'synaptic complex,' *Vis. Res.*, 38:1359–1369.
- von Gersdorff, H., and G. Matthews, 1994. Dynamics of synaptic vesicle fusion and membrane retrieval in synaptic terminals [see comments], *Nature*, 367:735–739.
- von Gersdorff, H., and G. Matthews, 1997. Depletion and replenishment of vesicle pools at a ribbon-type synaptic terminal, *J. Neurosci.*, 17:1919–1927.
- von Gersdorff, H., and G. Matthews, 1999. Electrophysiology of synaptic vesicle cycling, *Annu. Rev. Physiol.*, 61:725–752.
- von Gersdorff, H., T. Sakaba, K. Berglund, and M. Tachibana, 1998. Submillisecond kinetics of glutamate release from a sensory synapse [see comments], *Neuron*, 21:1177–1188.
- von Gersdorff, H., E. Vardi, G. Matthews, and P. Sterling, 1996. Evidence that vesicles on the synaptic ribbon of retinal bipolar neurons can be rapidly released, *Neuron*, 16:1221–1227.
- Von Kriegstein, K., F. Schmitz, E. Link, and T. C. Südhof, 1999. Distribution of synaptic vesicle proteins in the mammalian retina identifies obligatory and facultative components of ribbon synapses, *Eur. J. Neurosci.*, 11:1335–1348.
- Wagner, H. J., and M. B. Djamgoz, 1993. Spinules: A case for retinal synaptic plasticity [see comments], *Trends Neurosci.*, 16:201–206.
- Wang, Y., D. L. Small, D. B. Stanimirovic, P. Morley, and J. P. Durkin, 1997. AMPA receptor-mediated regulation of a Gi-protein in cortical neurons, *Nature*, 389:502–504.
- Wässle, H., P. Koulen, J. H. Brandstätter, E. L. Fletcher, and C. M. Becker, 1998. Glycine and GABA receptors in the mammalian retina, *Vis. Res.*, 38:1411–1430.
- Watanabe, S., A. Koizumi, S. Matsunaga, J. W. Stocker, and A. Kaneko, 2000. GABA-mediated inhibition between amacrine cells in the goldfish retina, *J. Neurophysiol.*, 84:1826–1834.
- Weiler, R., K. Schultz, and U. Janssen-Bienhold, 1996. Ca^{2+} -dependency of spinule plasticity at dendrites of retinal horizontal cells and its possible implication for the functional role of spinules, *Vis. Res.*, 36:3891–3900.
- Weiler, R., K. Schultz, M. Potte, S. Tieding, and U. Janssen-Bienhold, 1998. Retinoic acid has light-adaptive effects on horizontal cells in the retina, *Proc. Natl. Acad. Sci. USA*, 95:7139–7144.
- Weiler, R., and H. J. Wagner, 1984. Light-dependent change of cone-horizontal cell interactions in carp retina, *Brain Res.*, 298:1–9.
- Wenzel, A., D. Benke, H. Mohler, and J. M. Fritschy, 1997. N-methyl-D-aspartate receptors containing the NR2D subunit in the retina are selectively expressed in rod bipolar cells, *Neuroscience*, 78:1105–1112.
- Wilson, M., 2002. Retinal processing: smaller babres thrown out with the bathwater. *Curr. Biol.*, R625–627.
- Yang, C. Y., N. C. Brecha, and E. Tsao, 1997. Immunocytochemical localization of gamma-aminobutyric acid plasma membrane transporters in the tiger salamander retina, *J. Comp. Neurol.*, 389:117–126.
- Yang, C. Y., and H. H. Wang, 1999. Anatomical and electrophysiological evidence for GABAergic bipolar cells in tiger salamander retina, *Vis. Res.*, 39:3653–3661.
- Yazulla, S., and K. M. Studholme, 1991. Glycine-receptor immunoreactivity in retinal bipolar cells is postsynaptic to glycinergic and GABAergic amacrine cell synapses, *J. Comp. Neurol.*, 310:11–20.
- Yazulla, S., and K. M. Studholme, 1992. Light-dependent plasticity of the synaptic terminals of Mb bipolar cells in goldfish retina, *J. Comp. Neurol.*, 320:521–530.
- Yazulla, S., K. M. Studholme, J. Vitorica, and A. L. de Blas, 1989. Immunocytochemical localization of GABAA receptors in goldfish and chicken retinas, *J. Comp. Neurol.*, 280:15–26.
- Yoshida, K., D. Watanabe, H. Ishikane, M. Tachibana, I. Pastan, and S. Nakanishi, 2001. A key role of starburst amacrine cells in originating retinal directional selectivity and optokinetic eye movement, *Neuron*, 30:771–780. [Comment in: *Neuron*, 2001 Jun; 30(3):644–646 UI: 21324759].
- Zenisek, D., and G. Matthews, 2000. The role of mitochondria in presynaptic calcium handling at a ribbon synapse, *Neuron*, 25:229–237.

- Zenisek, D., J. A. Steyer, and W. Almers, 2000. Transport, capture and exocytosis of single synaptic vesicles at active zones [see comments], *Nature*, 406:849–854.
- Zhang, J., C. S. Jung, and M. M. Slaughter, 1997a. Serial inhibitory synapses in retina, *Vis. Neurosci.*, 14:553–563.
- Zhang, J., W. Shen, and M. M. Slaughter, 1997b. Two metabotropic gamma-aminobutyric acid receptors differentially modulate calcium currents in retinal ganglion cells, *J. Gen. Physiol.*, 110:45–58.
- Zhang, J., and M. M. Slaughter, 1995. Preferential suppression of the ON pathway by GABAC receptors in the amphibian retina, *J. Neurophysiol.*, 74:1583–1592.
- Zhou, Z. J., D. W. Marshak, and G. L. Fain, 1994. Amino acid receptors of midget and parasol ganglion cells in primate retina, *Proc. Natl. Acad. Sci. USA*, 91:4907–4911.

20 Retinal Neurotransmitters

ROBERT E. MARC

FAST SYNAPTIC SIGNALING in the vertebrate retina encodes presynaptic voltages as time-varying modulations in extracellular neurotransmitter concentrations and decodes neurotransmitter signals with postsynaptic transmembrane ionotropic or heptahelical receptor arrays. Additional heptahelical receptor pathways conditionally modulate synaptic signaling, often on lower temporal and spatial frequency scales. The six major retinal neurotransmitters—glutamate, gamma-aminobutyric acid (GABA), glycine, acetylcholine, dopamine, and serotonin—are synthesized in group-transfer reactions associated with distinctive cells. The sources and targets of less circumscribed, small-molecule modulators are mentioned only briefly, and peptides are treated elsewhere. Vertical channels deploy fast, high-gain glutamatergic synapses between photoreceptors (PRs) and their bipolar cell (BC) and horizontal cell (HC) targets, and between bipolar cells and their amacrine cell (AC) and ganglion cell (GC) targets. Lateral channels composed of horizontal cells and amacrine cells primarily use fast, low-gain, sign-inverting GABAergic and glycinergic synapses, with specialized circuits employing high-gain, sign-conserving cholinergic signaling. Four modes of fast synaptic transfer dominate neuronal receptive field circuits: high-gain, sign-conserving (\Rightarrow) or sign-inverting ($i\Rightarrow$) transfers, and low-gain, sign-conserving (\rightarrow) or sign-inverting ($i\rightarrow$) transfers. The following sections summarize metabolic networks, transporters, receptors, and circuitries for each neurotransmitter species, concluding with a summary of future directions. Figures 20.1 to 20.6 encapsulate metabolic network diagrams, Enzyme Commission (EC) and Transport Commission (TC) codes, localizations of macromolecules associated with a neurotransmitter phenotype, and other data. References are restricted to reviews or recent exemplars of concepts from which original literature may be traced.

The vertical channel neurotransmitter: L-glutamate

GLUTAMATE METABOLIC NETWORKS L-glutamate is a net anion at physiological pH and the central amino acid in a vast network of group transfers in all cells. No enzyme exclusively controls intracellular glutamate levels and no enzyme cluster yet defines a glutamatergic phenotype. Cellular contents of glutamate and other small molecules reflect group transfer, energetic, redox, osmoregulatory, and signaling demands that require supramillimolar concentrations

≈ 10 to 100 times greater than those required to charge transfer RNAs (tRNAs) for protein synthesis. Many transport epithelia and other somatic cells maintain 1 to 10 mM of glutamate, levels as high as photoreceptors, bipolar cells, and ganglion cells; neurons are not unique in this regard. Neuronal glutamate is predominantly derived from glutamine produced in Müller cells (MCs), but the retinal pigmented epithelium (RPE) maintains 2 to 10 mM glutamine and could be a source for photoreceptors. Normal Müller cells display avid glutamate transport but contain less glutamate than neurons (50 to 500 μ M) owing to robust conversion by glutamine synthetase (glutamate-ammonia ligase, Fig. 20.1). Glial glutamine export appears driven by transactivated System N (SN1) transporters (Chaudhry et al., 1999) and neuronal glutamine import by the Na^+ -dependent Glt1 transporter (Varoqui et al., 2000). Glutaminase on the inner mitochondrial membrane exterior deamidates glutamine to glutamate within the intermembrane space, from whence glutamate may either be transported to the mitochondrial matrix to drive 2-oxoglutarate synthesis or escape to the cytosol via porin channels.

GLUTAMATE TRANSPORTERS Vesicular glutamate import is mediated by VGluT1 and VGluT2 transporters, members of the Na^+ -dependent plasma membrane PO_4^- symporter family (e.g., Takamori et al., 2000). VGluT1 is strongly expressed in both the outer and inner plexiform layers (Stobrawa et al., 2001), and VGluT2 has yet to be mapped, although it is differentially distributed in brain (Varoqui et al., 2002). Anionic glutamate import ($K_m \approx 1$ to 3 mM) is strongly coupled to $\Delta\psi$ generated by vacuolar ATPase (vATPase)-mediated proton accumulation. The number of VGluTs per vesicle, their transfer numbers, and resultant vesicular glutamate concentrations are all undetermined. Electron microscopic immunocytochemical data in lamprey spinal cord have yielded estimates of vesicular glutamate levels of ≈ 60 mM, but true levels could be up to 10-fold lower.

Plasma membrane high-affinity glutamate transporters ($K_m \approx 5$ to 50 μ M) are single, 10-transmembrane domain (TMD), 1-reentrant loop polypeptides and members of the widely distributed Na^+ -dependent acidic and neutral amino acid transporter superfamily (Seal and Amara, 1999). Import is coupled to the sodium gradient ($\Delta p\text{Na}$) and $\Delta\psi$ (increased transport at negative potentials), and

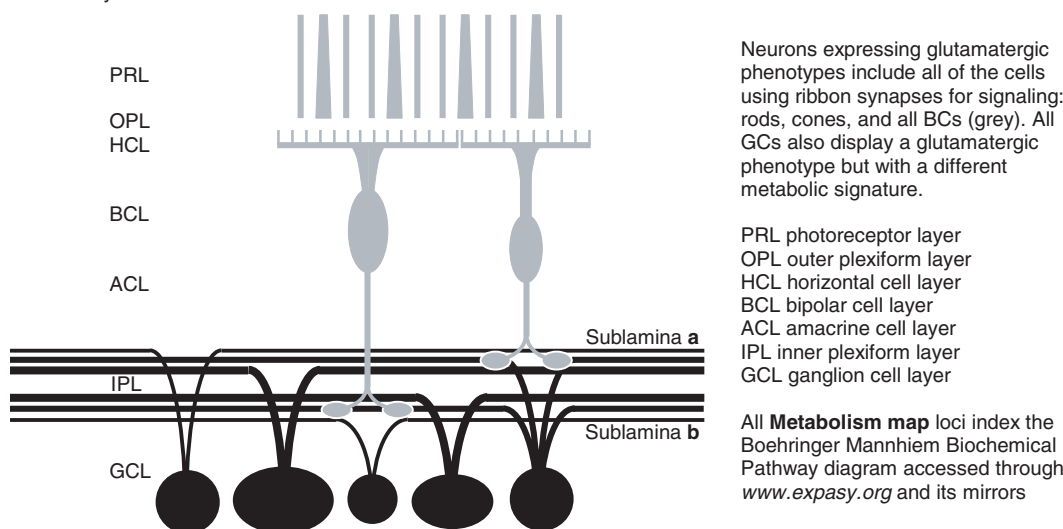
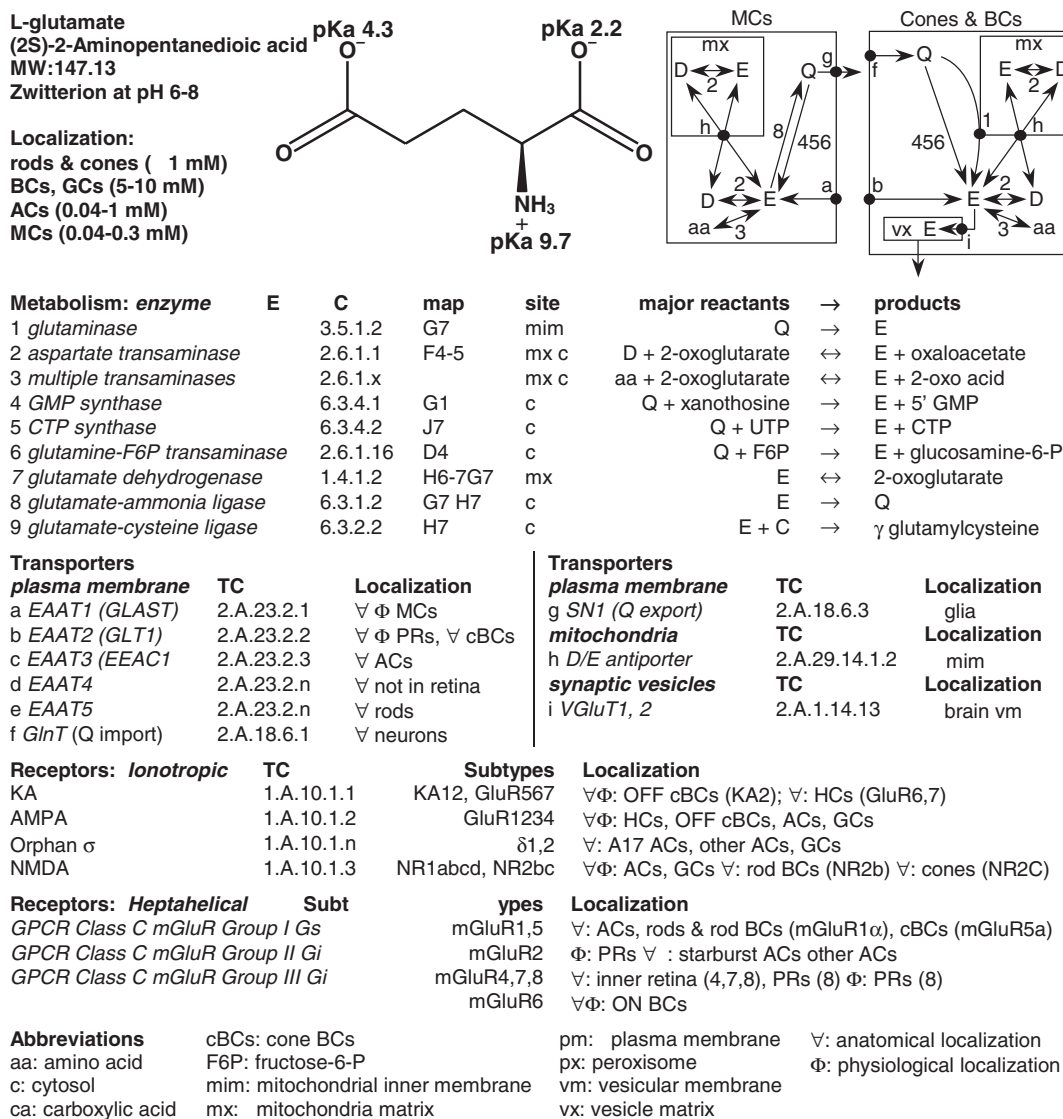


FIGURE 20.1.

experimental collapse of these gradients activates transporter export sufficient to empty a neuron of glutamate in minutes. Physiologically, export is gradually activated by increasingly positive potentials, although the net import/export balance is not known. Import is weakly electrogenic owing to Na^+/H^+ symport, but it can be strongly electrogenic by activating nonstoichiometric Cl^- channel conductance increases ($\uparrow\text{gCl}$). Four glutamate transporters are expressed in the mammalian retina: predominantly EAAT1 in Müller cells; EAAT2 in cones and bipolar cells; EAAT3 in horizontal cells, amacrine cells, and ganglion cells; EAAT5 in nonmammalian Müller cells and mammalian rods (Pow et al., 2000).

Plasma membrane glutamate transporters likely shape synaptic kinetics, control glutamate overflow, and recycle carbon skeletons. Horizontal cell response kinetics are shaped by cone glutamate transporters (Gaal et al., 1998; Vandenbranden et al., 1996), and EAAT2 should act similarly at $\text{BC} \Rightarrow \text{AC}$ and $\text{BC} \Rightarrow \text{GC}$ synapses. The relative roles of intrasynaptic neuronal and extrasynaptic glial transport are unresolved. Neuronal transport may couple intrasynaptic glutamate levels to cone voltage via transporter $\Delta\psi$ dependence (Gaal et al., 1998) when Ca^{2+} flux through voltage-independent cone inner segment cation channels drives vesicle fusion at potentials below Ca^{2+} channel activation (Rieke and Schwartz, 1994).

EAATs on bipolar cell dendrites could have novel, receptor-like activity by activating $\uparrow\text{gCl}$, but ON-center bipolar cell responses are abolished in mGluR6 knockout mice (Masu et al., 1995), and all bipolar cell responses can be blocked with glutamate receptor-specific agents. EAAT-like involvement in $\text{PR} \Rightarrow \text{ON-center BC}$ signaling is more compelling in fishes where hyperpolarizations arise from glutamate-activated $\uparrow\text{gCl}$ (Grant and Dowling, 1996).

IONOTROPIC GLUTAMATE RECEPTORS (iGluRs) Vertebrate iGluRs are a diverse group (Dingledine et al., 1999), decoding glutamate signals as cation currents via ionotropic KA and AMPA receptors: apparently nonordered tetramers of 3-transmembrane domain/1-reentrant loop subunits with mid-to-high micromolar glutamate thresholds, separable pharmacologies, and transient channel-opening properties. AMPA receptor GluR1–4 subunits are produced by a single gene family, with a large number of alternatively spliced and RNA edited forms, whereas KA receptor GluR5–7 and KA1, two subunits arise from two gene families, also with posttranslational modifications. The *orphan* receptor subunits $\delta 1,2$ are yet another family of likely iGluR subunits. This diversity potentially yields iGluR assemblies with varied unitary conductances, ionic selectivities, kinetics, and affinities, as well as protein kinase A and C (PKA, PKC) modulation, and postsynaptic aggregation control through specialized “PDZ”-like domains. Receptor diversity is

further enhanced by mixed iGluR expression (e.g., Ghosh et al., 2001) and the coexistence of different functional AMPA assemblies in one cell (Zhang et al., 1995). AMPA and KA receptors tend to activate brief conductances in the 1 pS to 20 pS range, although some KA receptors can activate larger conductances, whereas AMPA receptors containing GluR2(R) subunits have substantially smaller unitary conductances.

Functional NMDA receptors are obligate heteromeric 3-transmembrane domain/1-reentrant loop tetramers or pentamers of NR1 and NR2 subunits. They require concurrent glutamate and glycine binding and depolarization relief of uncompetitive Mg^{2+} channel block, and gate unitary conductances two to three times larger than those of AMPA/KA receptors. NMDA receptor currents activate/deactivate more slowly, with less desensitization than AMPA/KA receptor currents, and they are more glutamate sensitive. Coactivated with AMPA receptors in retina (Diamond and Copenhagen, 1995), functional NMDA-activated pathways appear restricted to amacrine cell and ganglion cell subsets (Fletcher et al., 2000; Marc, 1999).

Heptahelical glutamate receptors. Heptahelical glutamate receptors are G-protein coupled receptor (GPCR) group C members requiring homodimer formation for signaling. The only heptahelical receptor that completely regulates a synaptic pathway is the mGluR group III mGluR6 localized to ON-center bipolar cell dendrites (Vardi, et al., 2000a). How mGluR6 activation effects closure of ON-center bipolar cell cation channels is unknown, and, because all ON-center bipolar cells in mammals express a single isoform of mGluR6, any filtering differences must arise within or after the G-protein signaling path, where $\text{G}\alpha_o$ appears to be the coupler (Dhingra et al., 2000). ON-center bipolar cells in tetrapods, but perhaps not fishes, appear to be under the complete control of mGluR6 signaling.

Other mGluRs have been localized to the retina, but specific pathway functions have not been delineated. Group I-like systems generally mediate intracellular Ca^{2+} modulations, and isoforms of both mGluR1 and mGluR5 have been localized to the inner retina (Koulen, et al., 1997b). Group II mGluR2 isoforms may inhibit synaptic release, and the most distinctive, but likely not exclusive, localization is the expression of mGluR2 by starburst amacrine cells (Koulen et al., 1996). Group III mGluRs (4,7,8) are widely expressed in the inner retina, but their functional roles await analysis. However, there is a striking localization of mGluR8 in rod and cone synaptic terminals and evidence that mGluR8 activation decreases presynaptic calcium levels, acting as a negative feedback process (Koulen et al., 1999). The kinetics, sensitivity, and desensitization of this process are uncertain, and it is not known how steady-state release rates are maintained. In cones, at least,

constitutive Ca^{2+} leaks could override the mGluR8 feedback signal. mGluR1 α receptors have also been localized in rod terminals and could play a similar role (Cai and Pourcho, 1999).

GLUTAMATERGIC SIGNAL PROCESSING AMPA receptors dominate physiological PR \Rightarrow HC signaling (Blanco and de la Villa, 1999), although horizontal cells may coexpress AMPA GluR2,3,4 (Haverkamp et al., 2001; Morigiwa and Vardi, 1999) and KA GluR6,7 receptors (Brändstatter et al., 1997). Cone \rightarrow OFF BC signaling in mammals is decoded by KA receptors in two classes of OFF-center bipolar cells and AMPA receptors in a third (DeVries, 2000), generating fast AMPA-driven and slower KA-driven bipolar cell classes, perhaps initiating transient and sustained OFF channels, analogous to the ON-center bipolar cell shaping of transient and sustained ON channels described by Awatramani and Slaughter (2000). OFF-center bipolar cells of nonmammals may be dominated by AMPA receptors. Signaling via mGluR6 appears to be the sole process controlling ON-center bipolar cells in mammals. Rod bipolar cells have been shown to express GluR2 AMPA subunits, but their role is yet unknown.

BC \Rightarrow AC and GC signaling in all vertebrates is dominated by AMPA receptors (Marc, 1999), although KA receptors may shape some responses. Amacrine cells and ganglion cells display cell-specific responses to glutamate agonists, and responsivity fractionation suggests that physiological attributes, such as “sluggish” or “brisk” responses, may be determined, in part, by different AMPA receptor assemblies (Marc and Jones, 2002). NMDA receptor expression varies across amacrine cells and ganglion cells, and both immunocytochemical and physiological mappings reveal that specific inner plexiform layer strata driven by cone bipolar cells are enriched with amacrine cell and ganglion cell dendrites bearing NMDA receptors (Fletcher et al., 2000; Marc, 1999). Conversely, rod bipolar cell sublayer amacrine cell targets lack NMDA receptors (Ghosh et al., 2001; Marc, 1999).

GLUTAMATE: FUTURE DIRECTIONS Is there a macromolecular signature for a glutamatergic neuron phenotype? VGluT is currently the sole identifier of a glutamatergic phenotype (Eiden, 2000), but other gene products, such as EAAT2, may be coordinately regulated with VGluT, and transcription factor clusters may ultimately define the glutamatergic phenotype. Detailed spatial mapping and biophysics will be required to resolve the contributions of glial and neuronal EAAT transporters to synaptic kinetics. The mGluR6 transduction pathway and its target channel remain major puzzles. Do adapter proteins modify their properties, and does receptor oligomerization influence signaling? What are the consequences of expressing mixed AMPA, KA, and δ

receptors? Do mGluRs shape specific networks, or are they diffuse, subtle, adaptive elements? Why are NMDA receptors relegated to subsets of amacrine cells and ganglion cells and absent from rod bipolar cell targets?

The dominant lateral channel fast inhibitory neurotransmitter: GABA

GABA METABOLIC NETWORKS GABA, an achiral, zwitterionic, nonprotein amino acid, evolved into a signaling molecule from its ancestral metabolic role. Vertebrate GABA synthesis from glutamate is driven by two glutamic acid decarboxylases (GAD1/GAD67 and GAD2/GAD65; Fig. 20.2) that differ in targeting and regulation. GABA catabolism is aerobic, largely driven by mitochondrial matrix GABA transaminase serial oxidation of GABA to succinate semialdehyde and succinate, driving the citrate cycle (Kalloniatis and Tomisich, 1999). Most GAD-containing retinal neurons are likely GABAergic, although some somatic tissues synthesize GAD and GABA, and developing glutamatergic motor neurons in *Drosophila* require GAD expression (Featherstone et al., 2000). Supramillimolar GABA content remains a strong marker of GABAergic function, and neuronal GABA signals span the inner plexiform layer in all species.

Subsets of horizontal cells and amacrine cells have been shown to express GABA signals, GABA transport, and GAD content (reviewed by Marc, 1992). Most amacrine cells are GABA-positive and GAD-positive, although a total match has yet to be achieved. GABA signal strengths vary widely across amacrine cell classes (≈ 1 to 10+ mM), forming characteristic, quantitative, GABAergic signatures. All cholinergic, serotonergic, and many peptidergic amacrine cells express GABAergic signatures and are, thus, multi-neurotransmitter neurons. Interplexiform cells (IPCs) are amacrine cell variants whose processes target the outer retina, and several IPC classes may contain GABA (Marc, 1995).

Vertebrate horizontal cells remain neurochemically recalcitrant despite a long history of physiological analysis. GABA content, GABA transport, and GAD are expressed by subsets of horizontal cells in many species, but many horizontal cells express no known neurotransmitter signature. A neurotransmitter-free model of feedback signaling via connexin currents has been proposed by Kamermans et al. (2001), although not all problems are thereby solved. Why do any horizontal cells contain GABA if they use connexins for feedback? Some nonmammalian horizontal cells form conventional synapses onto glycinergic IPCs and other targets in fishes (reviewed in Marc, 1992; Marc, 1995), but may use connexin signaling for cone feedback. Horizontal cells in mammals are equally challenging. Rodent horizontal cells are GABA-negative but express GABA in develop-

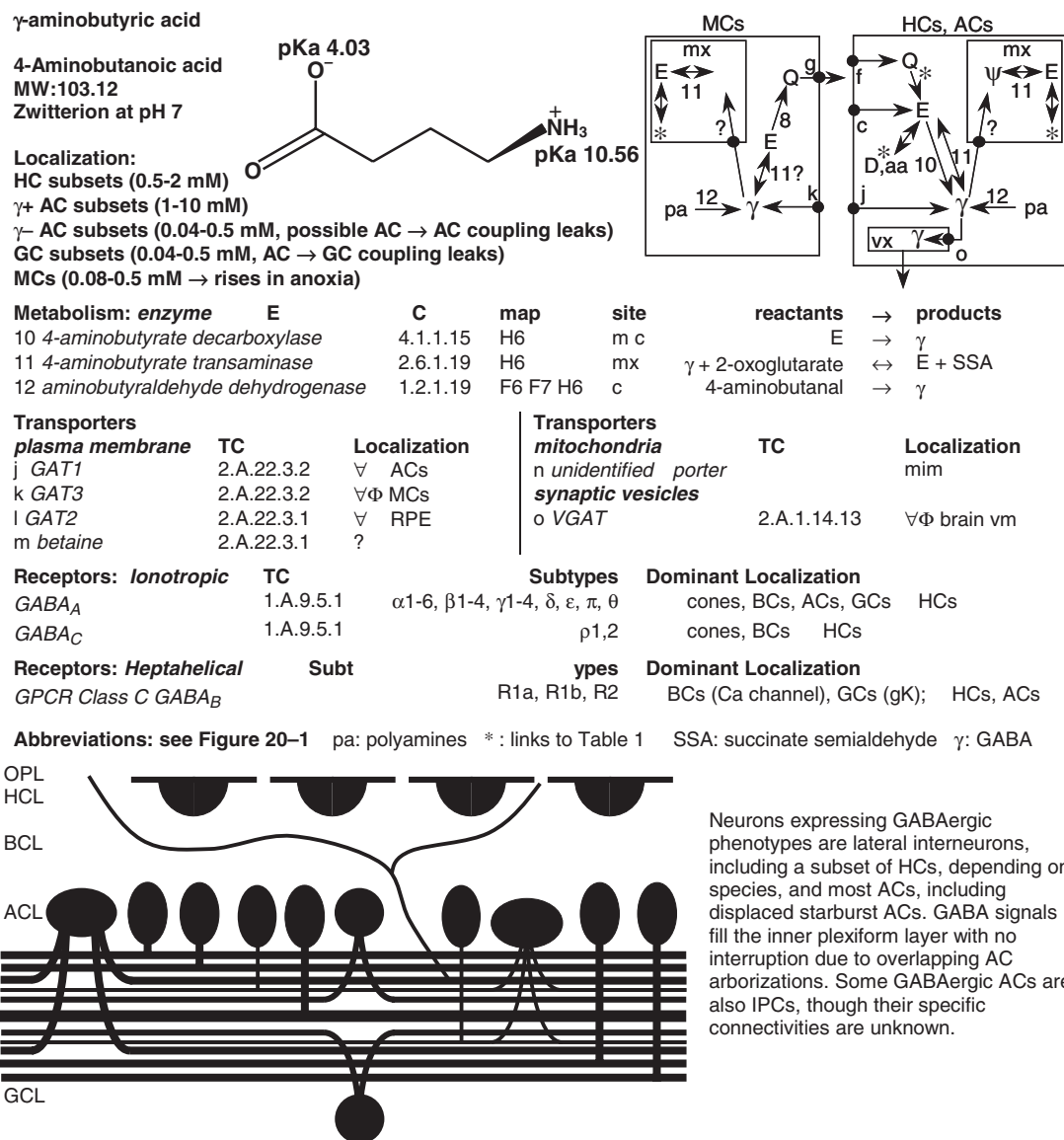


FIGURE 20.2.

ment; macular primate horizontal cells are GABA-positive but become GABA-negative in the periphery; rabbit type B horizontal cells are all GABA-negative, whereas type A horizontal cells are GABA-positive in the streak and GABA-negative in the periphery. Even so, all rabbit horizontal cells are GAD67-immunoreactive at their dendritic tips, suggesting fine regulation of signaling (Johnson and Vardi, 1998). All feline, canine, and porcine horizontal cells express GABA (Kalloniatis and Tomisich, 1999; Marc, 1992).

Many species display weak GABA signals in small subsets of the bipolar cell cohort, and some have been shown to contain GAD. Some may acquire GABA through heterocellular coupling, whereas others may be true sign-inverting elements. The ganglion cell layer in many species contains many GABA-positive cells, mostly displaced starburst

amacrine cells, whereas the remainder are ganglion cells coupled to GABAergic amacrine cells (Marc and Jones, 2002).

GABA TRANSPORTERS The vesicular transporter VGAT is a 10-transmembrane domain polypeptide related to the plant amino acid permease family. It is two- to threefold selective for GABA ($K_m \approx 5$ mM) over glycine (McIntire et al., 1997), and it is widely distributed in the inner plexiform layer and in mammalian horizontal cells (Haverkamp et al., 2000).

Most nonmammals express only neuronal amacrine cell and horizontal cell GABA transport, whereas mammals express neuronal amacrine cell and glial Müller cell transport. Three single-polypeptide, 12-transmembrane domain,

Na⁺-coupled GABA transporters (GAT1,2,3) are present in mammals (Johnson et al., 1996), although GAT2 is more closely related to the epithelial osmoregulatory GABA/betaine transporter and is expressed in the retinal pigmented epithelium, which contains no detectable GABA. GAT1 is widely expressed in some, but not all, GABAergic amacrine cells, whereas Müller cells preferentially display GAT3. No horizontal cell has been found to express these proteins, even those horizontal cells with robust GABA transport.

GATs may regulate synaptic kinetics as they are localized on presynaptic GABAergic neurons and neuronal transporter blockade can dramatically slow inhibitory postsynaptic potential (IPSP) kinetics (Cherubini and Conti, 2001). GAT3-mediated GABA transport by Müller cells is avid in mammals, buffering any additional synaptic overflow, although nonmammals do not require glial support.

Is GABA export a surrogate for or an adjunct to vesicular GABAergic synaptic transmission (O'Malley et al., 1992; Schwartz, 1999; Yazulla, 1995)? GABA import is ΔpNa - and $\Delta\psi$ -coupled, with greater import at negative potentials. Collapse of ΔpNa or decreasing $\Delta\psi$ activates ligand export, but is it physiologically significant? Isolated fish horizontal cells can export physiologically detectable GABA in vitro upon depolarization (Schwartz, 1999), suggesting that transport can mediate feedback or feedforward. However, neither GABA transport nor GATs have been detected in mammalian horizontal cells, and reconciliation of these observations awaits new research.

IONOTROPIC GABA RECEPTORS GABA_A and GABA_C receptors, members of the ligand-gated channel superfamily, are partially ordered pentameric assemblies of four-transmembrane domain α (1–6), 2β (1–3), γ (1–4), δ , ϵ , θ , and π subunits, some with splice variants. Coassembly of 2α and 2β subunits, at least, is required to form functional surface-expressed GABA_A receptors (Connor et al., 1998). GABA_A receptors gate large, rapidly desensitizing $\uparrow gCl$ with GABA thresholds in the 10- μ M range. GABA_C receptors are homomeric assemblies of ρ (1–3) subunits, are more GABA-sensitive than GABA_A receptors, and activate weaker but relatively nondesensitizing $\uparrow gCl$. Cones, bipolar cells, and ganglion cells are known to express functional GABA_A and GABA_C receptors concurrently (Feigenspan and Bormann, 1994; Picaud et al., 1998; Zhang, et al., 1997b).

HEPTAHELICAL GABA RECEPTORS Functional GABA_B receptors (group C GPCRs) are R1–R2 isoform heterodimers (Jones et al., 1998; Sullivan et al., 2000). R1a and R1b versions have been mapped to horizontal cells, amacrine cells, and ganglion cells (Koulen et al., 1998; Zhang, et al., 1998a), and physiological data have shown ganglion cells and bipolar cells to bear functional, pharma-

cologically defined GABA_B receptors, in some cases exhibiting complex switching behavior (Zhang, et al., 1997b; Zhang, et al., 1998b). GPCR coupling of GABA_B receptors can activate $\uparrow gK$, hyperpolarizing target neurons, whereas others gate increases in $[Ca^{2+}]_i$ (Zhang, et al., 1997b) or inhibit presynaptic Ca^{2+} currents (Matthews et al., 1994).

GABAERGIC SIGNAL PROCESSING GABAergic signaling is primarily inhibitory, effected through ionotropic hyperpolarizations/shunts or GPCR pathways. The HC $i \rightarrow$ cone GABAergic pathway has been difficult to validate owing to its varied expression. HC $i \rightarrow$ cone feedback in amphibians clearly involves ionotropic GABA receptors (Wu, 1994), and most of the components of the pathway are expressed in most vertebrates. Unconventional feedback mechanisms, such as connexin-based feedback currents and $\Delta\psi$ -coupled GABA transporter export, enrich signaling possibilities but do not reduce uncertainty. Mammalian horizontal cells lack GABA transport, whereas the presence of VGAT provokes the idea that vesicular transmission can occur from horizontal cell dendrites. Horizontal cells do display presynaptic vesicle clusters within photoreceptor synaptic terminals, but these have been documented infrequently (e.g., Linberg and Fisher, 1988).

The existence of a functional horizontal cell to bipolar cell path has been posited from anatomical data, but the relative horizontal cell- and amacrine cell-driven surround strengths remain unclear. Bipolar cells express dendritic GABA_A and GABA_C receptors (Greferath et al., 1994; Haverkamp et al., 2000; Koulen, et al., 1997a) consistent with GABAergic HC $i \rightarrow$ OFF bipolar cell signaling through $\uparrow gCl$, forming a proper surround polarity. GABAergic HC \rightarrow ON BC signaling through $\uparrow gCl$ must be *sign-conserving* for proper surround polarity, and specialized chloride importers likely shift ON-center bipolar cell dendritic E_{Cl} to positive levels to achieve polarity reversal, while preserving a proper negative E_{Cl} at the axon terminal (Vardi, et al., 2000b).

The AC $i \rightarrow$ BC signaling is supported by abundant evidence in all vertebrates. How GABA_A and GABA_C receptors differentially shape bipolar cell responses is just now emerging. GABA-sensitive, comparatively slower GABA_C receptors may initiate feedback control at low contrasts, with less sensitive, faster GABA_A receptors dominating at high contrast. The involvements of GABA_B receptors appear complex and may vary over bipolar cell types. GABAergic AC $i \rightarrow$ AC signaling numerically dominates retinal circuitry and is largely GABA_A mediated (Lukasiewicz and Shields, 1998), with concatenated inhibitory chains enriching the network assembly (Marc and Liu, 2000). All ganglion cells show significant GABAergic inputs, much of it driven by receptors with GABA_A-like pharmacologies (Akopian et al.,

1998), although some clearly use concurrent GABA_A/GABA_B/GABA_C signaling (Zhang, et al., 1997).

GABA: FUTURE DIRECTIONS Diverse data support GABAergic signaling by some horizontal cells, but inconsistencies persist, and many horizontal cells lack detectable GABA. How do these cells function? Where are the synapses and GABA transporters in mammalian horizontal cells? The mysteries involving AC $i \rightarrow$ BC, AC, GC signaling events are more straightforward. The functional consequences of GABA receptor types and subtype mixtures must be understood. What are the contributions of glial and neuronal GATs to synaptic kinetics, and do amacrine cells use GABA export to supplant or augment vesicular release?

The minor lateral channel fast inhibitory neurotransmitter: glycine

GLYCINE METABOLIC NETWORKS Glycine is an achiral zwitterion at physiological pH with limited conformers (Fig. 20.3). Glycine content is elevated in specific amacrine cells with sparse, varicose dendrites (e.g., AII and DAPI-3 amacrine cells of mammals). Lower glycine levels are found in ON-center bipolar cells that acquire glycine by coupling leakage from AII amacrine cells. Amacrine cells with high glycine levels may also contain low GABA levels in many species, perhaps as a result of heterocellular coupling. Retinal glycine synthesis is still an unresolved process. Although glycine hydroxymethyltransferase is reportedly

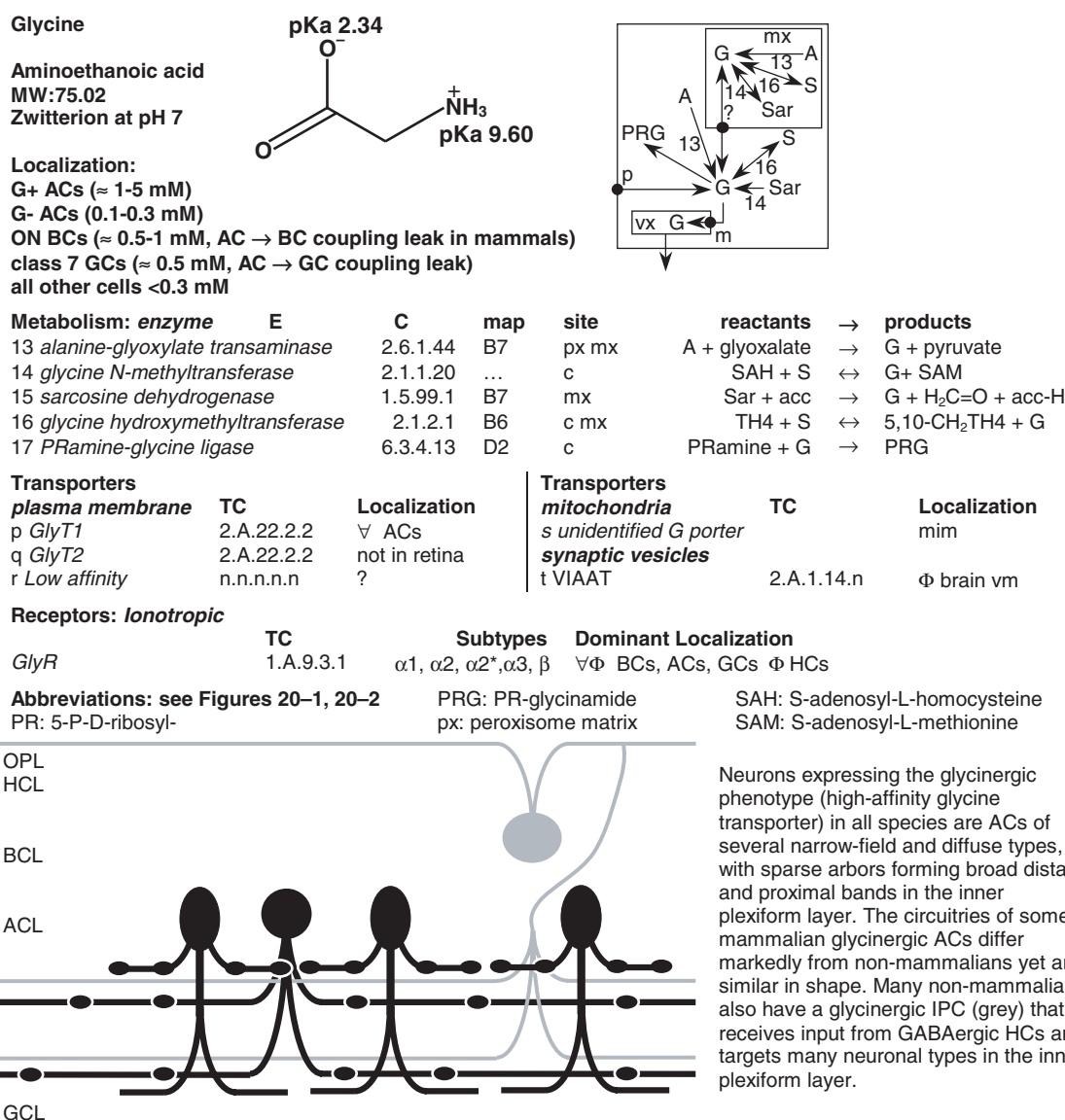


FIGURE 20.3.

elevated in retina and spinal cord, and converts precursor serine to glycine, glycinergic amacrine cells contain no significant precursor serine (Kalloniatis and Tomisich, 1999). Of course, many GABAergic amacrine cells contain little glutamate, so precursors are not proven indices of phenotype. Conversely, somatic cells also use alanine-glyoxylate transferase to produce glycine, and precursor L-alanine is elevated in retina and perhaps in glycinergic amacrine cells. Glycine transport has been proposed as a novel mechanism for elevating amacrine cell glycine levels based on the depletion of amacrine cell glycine by sarcosine (methylglycine), a glycine transport agonist (Pow, 1998), although this effect may have been complicated by transactivated glycine export.

GLYCINE TRANSPORTERS No glycine-selective vesicular transporter has been identified, and the nominal inhibitory amino acid vesicle transporter, VIAAT, transports GABA and glycine with similar efficacy, whereas VGAT is only two- to threefold selective for GABA over glycine. Either might serve a neuron with elevated levels of glycine and no GABA.

Plasma membrane amacrine cell glycine transport is mediated by GlyT1, a member of the sodium-coupled solute symporter family and the signature macromolecule of the retinal glycinergic phenotype. As with EAATs and GATs, collapse of $\Delta\psi$ or ΔpNa can evoke complete glycine export in minutes, but under normal conditions, GlyT1 likely regulates synaptic kinetics.

IONOTROPIC GLYCINE RECEPTORS Glycinergic signaling is exclusively mediated by ionotropic glycine receptors (GlyRs), apparently nonordered multimers of $\alpha 1$ –4 and β subunits. Subunit $\alpha 1$ is abundant in the mammalian inner plexiform layer and is expressed on bipolar cells and ganglion cells (Wässle et al., 1998), although amacrine cells with well-documented anatomical glycinergic inputs must certainly express GlyRs as well. Glycine activates a large, rapidly desensitizing $\uparrow gCl$, especially in ganglion cells. Because glycine activates gCl in parallel with GABA_A and GABA_C receptors, often on adjacent synapses (Marc and Liu, 2000), glycinergic signaling may avoid inhibitory *occlusion*, that is, subadditivity due to GABA spillover at adjacent synapses.

GLYCINERGIC SIGNAL PROCESSING The best-known glycinergic circuit is the rod $i \Rightarrow$ rod BC \Rightarrow AII AC $i \Rightarrow$ cone OFF BC pathway, where OFF bipolar cell glycine receptors render the pathway net sign-conserving, as is appropriate for OFF-center channels. This arcane evolutionary capture of cone pathways to serve scotopic signaling is absent in advanced nonmammalian retinas expressing complete, separable rod and cone ON and OFF pathways to ganglion cells. Most ganglion cells receive glycinergic input, and the

distributions of glycine receptors on identified ganglion cells match relative GABAergic and glycinergic presynaptic process densities in specific inner plexiform layer strata. Although their processes are sparse, glycinergic amacrine cells are potent and mediate complex behavior via local and wide-field systems, intercalating in sign-inverting chains with GABAergic amacrine cells (Cook et al., 2000; Marc and Liu, 2000; Zhang, et al., 1997a).

The glycinergic IPC of nonmammals is best characterized in teleosts (Marc, 1995). It is presynaptic and postsynaptic in both plexiform layers, and part of its role may be to transfer H1 horizontal cell signals to the inner plexiform layer, bypassing the bipolar cell spatial filter.

GLYCINE: FUTURE DIRECTIONS The vesicle transporter of glycinergic amacrine cells and the mechanism that elevates glycine content remain unknown. Does glycine transport shape synaptic kinetics in the retina? Does glycinergic transmission prevent synaptic occlusion? Why are glycinergic amacrine cells of mammals and ectotherms structurally similar but involved in such different networks?

The lateral channel fast excitatory neurotransmitter: acetylcholine

ACETYLCHOLINE METABOLIC NETWORKS Acetylcholine (ACh) is a small quaternary cation synthesized by cholineacetyl transferase (ChAT), a cholinergic phenotype signature macromolecule (Fig. 20.4). Attempts to localize retinal acetylcholine by immunocytochemistry have not succeeded. Conversely, 3H choline uptake autoradiography and ChAT immunocytochemistry label the same amacrine cells. Extracellular retinal acetylcholinesterase (AChE) terminates synaptic acetylcholine signaling.

ACETYLCHOLINE AND CHOLINE TRANSPORTERS Acetylcholine is transported into amacrine cell vesicles by vesicular acetylcholine transporter (VACHT) (Koulen, 1997), a member of the toxin-extruding, proton-translocating, antiporter family, under coordinate regulation with ChAT expression. The ligands for these transporters are cations, so proton antiport and ΔpH dominate vesicle loading.

Synaptic or overflow acetylcholine is cleared by AChE with a transfer rate of $\approx 10^4$, effecting rapid hydrolysis of acetylcholine into choline and acetate. Choline is a significant agonist at some acetylcholine receptors, and Na^+ -coupled choline transport via ChT1 may be essential to prevent adventitious receptor desensitization, as well as to allow for choline recovery.

IONOTROPIC ACETYLCHOLINE RECEPTORS Ionotropic cholinergic transmission is mediated by nicotinic acetylcholine receptors (nAChRs), ordered pentameric assemblies

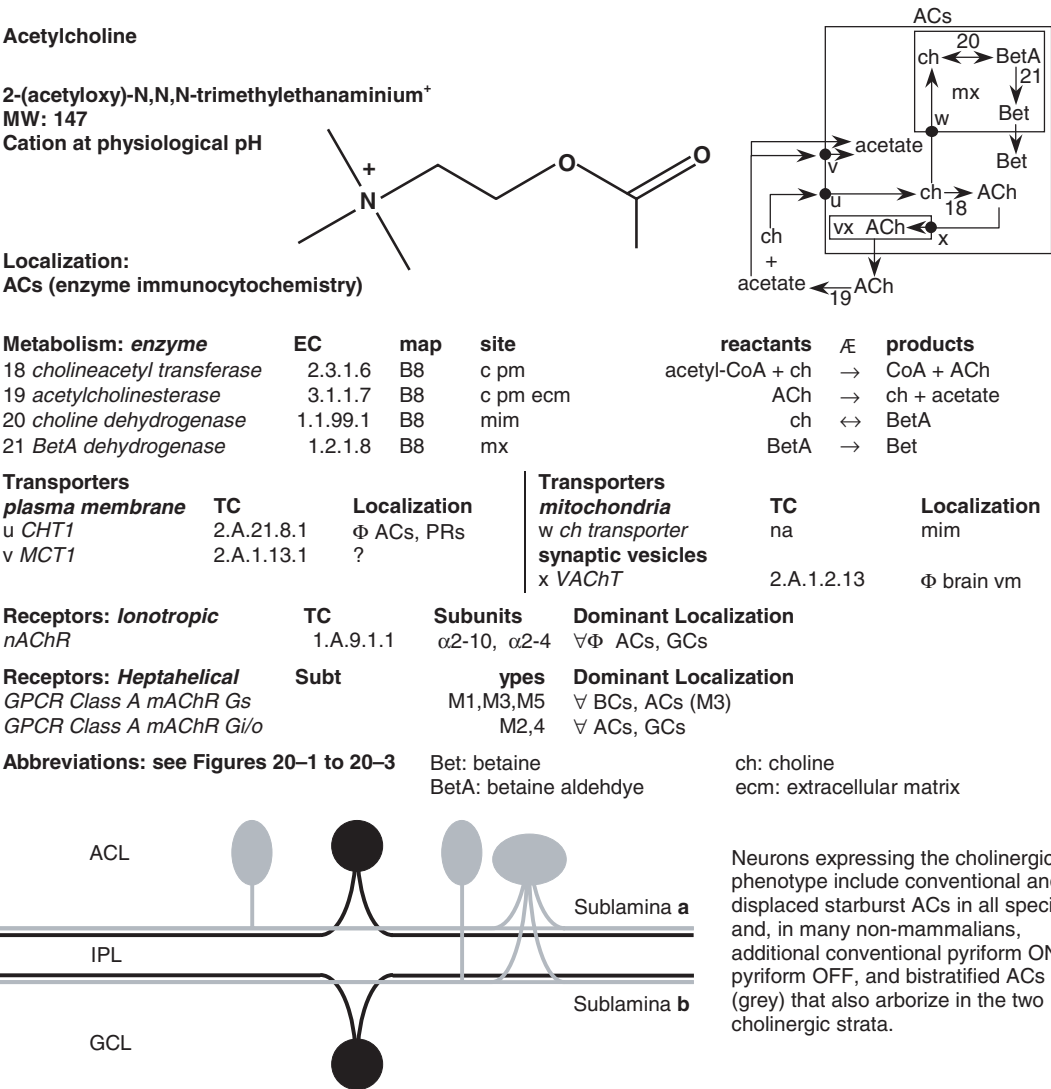


FIGURE 20.4.

of four-transmembrane domain α , β , and γ subunits. Nine neuronal α subunits are known, imparting distinctive properties to channels; for example, $\alpha 7$ subunits are thought to form homomers with high Ca^{2+} permeability and are expressed widely in the inner plexiform layer. The $\beta 2$ subunit is also abundant in amacrine cells and ganglion cells (Keyser et al., 2000), and $\alpha 3\beta 2$ assemblies are apparently involved in developmental excitatory periodicity linked to retinothalamic patterning (Bansal et al., 2000).

HEPTAHELICAL ACETYLCHOLINE RECEPTORS The muscarinic acetylcholine receptors (mAChRs) are group A GPCRs. Subtypes M_2 , M_3 , and M_4 have been immunolocalized in avian retinas and are expressed by ganglion cells, amacrine cells, and bipolar cells (Fischer et al., 1998). Cholinergic starburst amacrine cells express type M_2 receptors consistent with autoreceptor regulation of acetylcholine release.

CHOLINERGIC SIGNAL PROCESSING Every vertebrate displays displaced ON and conventional OFF cholinergic starburst amacrine cell homologues and bistratification of cholinergic signatures in the inner plexiform layer. Non-mammals express two or three additional cholinergic amacrine cells, although the functions of the additional cells are unknown. All cholinergic amacrine cells are also GABAergic, confounding simple circuitry analysis. Only starburst amacrine cell circuits have been properly analyzed (Famiglietti, 1991), and they are driven by cone bipolar cells through a high-sensitivity AMPA receptor (Marc, 1999), primarily targeting ganglion cells. Unclassified GABAergic amacrine cells may be excited by starburst amacrine cells through nAChRs (Dmitrieva et al., 2001), perhaps amplifying surround inhibition of ganglion cells in dim photopic conditions. Any direct signaling between starburst amacrine cells is likely GABAergic and sign-inverting, as starburst

amacrine cell receptive fields are small. Starburst amacrine cells drive directionally selective ganglion cells in the rabbit retina through nAChRs, but are not needed for directional selectivity per se (He and Masland, 1997; Kittila and Massey, 1997).

ACETYLCHOLINE: FUTURE DIRECTIONS Understanding cholinergic function requires more physiological data in light-driven preparations, discrimination of cholinergic and GABAergic synapses, and pharmacological dissection of nAChRs and mAChRs. Although starburst amacrine cells can be driven to release GABA by export (O'Malley et al., 1992), they lack the neuronal GABA transporter GAT1 (Dmitrieva et al., 2001): which do they use? Does ChT1 play any role in signal termination?

The global modulator: dopamine

DOPAMINE METABOLIC NETWORKS Dopaminergic retinal neurons are amacrine cells or IPCs (reviewed by Witkovsky and Dearry, 1991) that express tyrosine 3-mono-oxygenase (tyrosine hydroxylase, TH) and lack conversion of dopamine (Fig. 20.5) to norepinephrine and epinephrine. Their sparse processes facilitate global signaling, and dopamine is not spatially buffered, effectively reaching sites tens of microns from the inner plexiform layer (Witkovsky et al., 1993). Tyrosine is an essential amino acid acquired exogenously and accumulated through TAT1 aromatic amino acid transport. In dopaminergic neurons, it is converted to dihydroxyphenylalanine (DOPA) by tyrosine hydroxylase and DOPA to dopamine by aromatic L-amino acid decarboxylase.

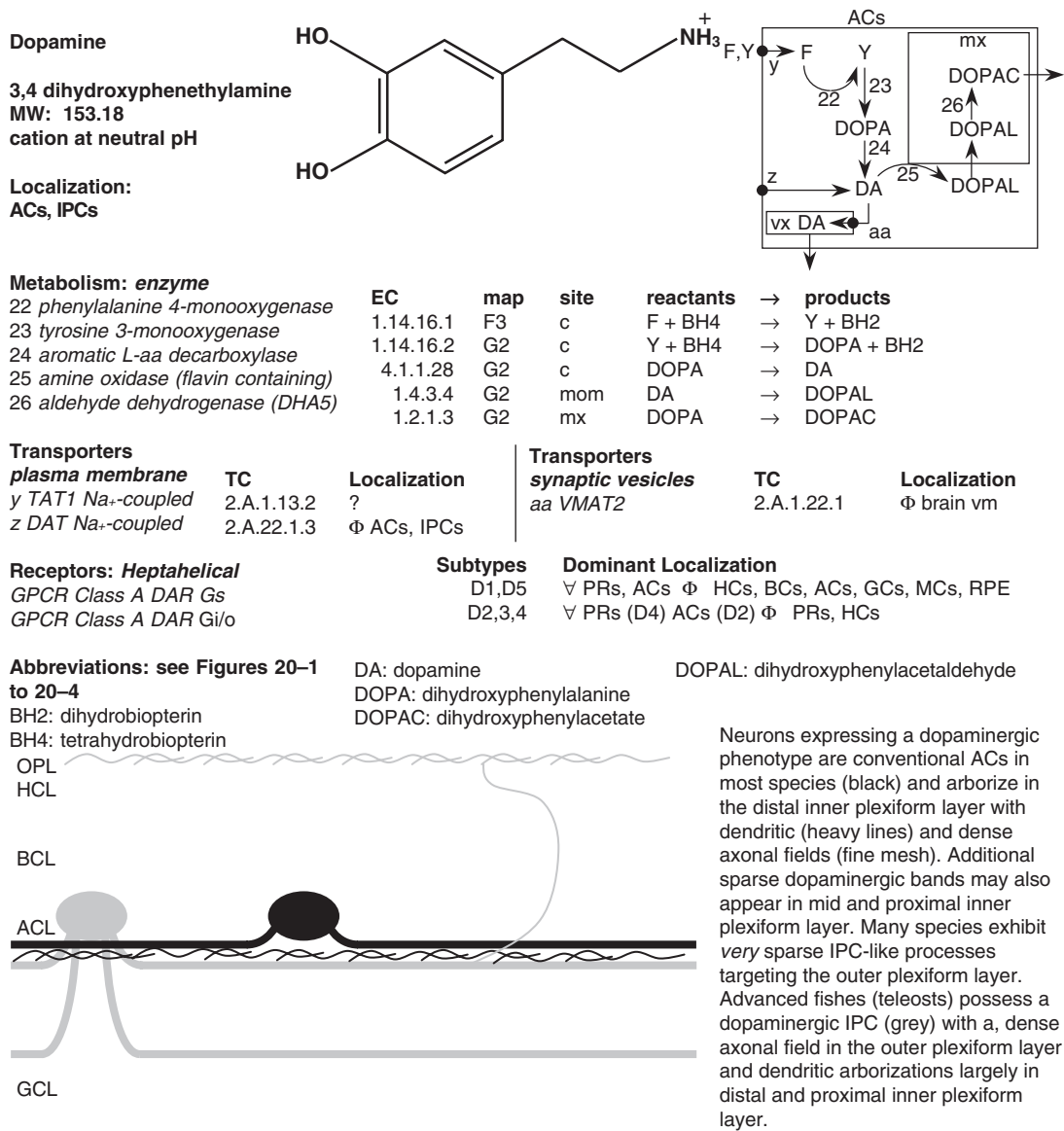


FIGURE 20.5.

Aromatic amines are highly oxidizable, and rapid turnover is common in aminergic neurons. Mitochondrial monoamine oxidase converts dopamine to dihydroxyphenylacetaldehyde (DOPAL), a highly toxic intermediate, then converted to the acetate form for export, apparently by diffusion. As tyrosine hydroxylase is the first stage in tyrosine conversion to neuroactive monoamines, it is present in rare additional neurons that may synthesize norepinephrine or epinephrine, although little is known of their dispositions and roles.

DOPAMINE TRANSPORTERS Dopamine is loaded into synaptic vesicles by VMAT2, the neuronal form of the vesicle amine transporter family (Erickson and Varoqui, 2000). As with other cationic amines, loading is strongly coupled to ΔpH .

The 12-transmembrane domain dopamine transporter DAT is similar to most other Na^+ -coupled transporters, and is susceptible to transactivation of dopamine export via transporter agonists, such as amphetamines. Its involvement in spatial buffering is somewhat unclear, as diffusing dopamine is a potent signal. However, dopaminergic neurons form many synapse-like contacts and highly targeted axonal fields, suggesting that specific connective zones are more highly regulated than others.

HEPTAHELICAL DOPAMINE RECEPTORS All known dopamine receptors are heptahelical group A (rhodopsin-like) GPCRs, coupled through G_s (subtypes D1, D5) or $G_{i/o}$ (D2, D3, D4), and grouped as pharmacological D1/D2 adenylyl cyclase-activating/-suppressing cohorts, respectively. No retinal cell, including Müller cells and the retinal pigmented epithelium, lacks some form of dopamine receptor, and many express both.

DOPAMINERGIC SIGNAL PROCESSING Dopaminergic neurons apparently signal the onset of photopic epochs through vesicular release and dopaminergic effects emerge in seconds to minutes, rather than milliseconds. In teleosts, dopamine activates cone contraction, uncouples horizontal cells, and renders ganglion cells more transient through D1 mechanisms, mimicking light adaptation (Vaquero et al., 2001; Witkovsky and Dearry, 1991). Coupling control between horizontal cells in teleosts is effected by the axonal fields of dopaminergic IPCs, whereas that between A_{II} amacrine cells in mammals is effected by axonal fields of dopaminergic amacrine cells in the distal inner plexiform layer (Hampson et al., 1992). In amphibians, dopamine shifts the balance of $PR \Rightarrow HC$ signaling in favor of cones, in part by reducing rod I_h currents via D2 receptors (Akopian and Witkovsky, 1996). The actual patterning and control of dopamine release remains uncertain, but dopaminergic amacrine cells/IPCs appear to be under massive GABA_A receptor-

gated suppression, and relief from inhibition uncovers spontaneous dopamine release, perhaps generated by constitutive repetitive spiking (Feigenspan et al., 1998). Nevertheless, many dopaminergic neurons also receive explicit bipolar cell inputs and express iGluRs, so the situation is far from clear. Mammalian, reptilian, and avian dopaminergic amacrine cells have also been reported to contain GABA, complicating interpretations further.

DOPAMINE: FUTURE DIRECTIONS A tremendous amount of analysis of dopamine receptor pharmacology has already been done, but how those signaling pathways are themselves regulated and how adaptation state controls, and is controlled by, dopaminergic neurons demands further exploration.

The mystery neurotransmitter: serotonin

SEROTONIN METABOLIC NETWORKS Serotonin is present at high levels in specific nonmammalian amacrine cell subsets (Fig. 20.6). The retinas of mammals contain, at most, 10-fold less serotonin than dopamine, much of that attributable to platelets and photoreceptor synthesis of melatonin. In the central nervous system, the phenotype-defining enzyme tryptophan hydroxylase (TrpH) converts TAT1-imported tryptophan to 5-hydroxytryptophan, but thereafter, the same enzymes expressed in all other aminergic neurons control serotonin production. There is yet no evidence that any mammalian amacrine cell expresses TrpH.

SEROTONIN TRANSPORTERS As for dopaminergic neurons in brain, VMAT2 is the obligatory vesicular serotonin transporter, although its intraretinal distribution is yet unknown. The content of VMAT2-expressing vesicles thus tracks the substrate amine content of cytosol, and VMAT2 expression is not a phenotype signature. All known and suspected serotonergic amacrine cells are also GABAergic neurons, perhaps expressing both VMAT2 and VGAT.

High-affinity serotonin transport is mediated by SERT, a classic Na^+ -coupled single polypeptide, 12-transmembrane domain transporter susceptible to inhibition by numerous agents, such as fluoxetine. In many vertebrates, more neurons express serotonin transport (photoreceptors, bipolar cell subsets, amacrine cell subsets) than are immunoreactive for serotonin, including the GABAergic mammalian A17/S1/S2 amacrine cells. No satisfactory explanation for this has emerged; some of these cells may truly express SERT, whereas others (e.g., some bipolar cells) may have a coupling leak with a bona fide serotonergic amacrine cell.

IONOTROPIC SEROTONIN RECEPTORS The 5HT3 serotonin receptor is an assembly of unknown stoichiometry of

cological complexities of serotonin receptors, the fact that many GPCRs have constitutive activity, and that many agents act as inverse agonists, capable of generating effects in the absence of signaling. Serotonergic amacrine cells may be a central switch in controlling retinal function, although these amacrine cells must also serve GABAergic roles. Nonmammalian serotonergic amacrine cells are directly driven by mixed rod-cone OFF-center bipolar cells, form feedback synapses to bipolar cells, and target ganglion cells and amacrine cells with feedforward synapses (Marc et al., 1988). However, no data exist to discriminate GABAergic versus serotonergic signaling at these sites, and serotonin may act globally through diffusion. Serotonin reciprocally modulates ON and OFF channels: 5HT₃R activation suppresses scotopic mammalian OFF-center ganglion cell responses, whereas 5HT₃R antagonism inhibits ON-center ganglion cell responses, sparing cone-driven responses (Jin and Brunken, 1998). These complex reciprocal effects could act at photoreceptors or bipolar cells, and much remains to be resolved.

SEROTONIN: FUTURE DIRECTIONS The serotonin-transporting amacrine cell of mammals lacks histochemically and immunochemically detectable serotonin. Is an undiscovered monoamine involved, or are serotonergic synapses and vesicles rare, and serotonin synthesis restricted to small dendritic volumes? Is TrpH or VMAT2 expressed in mammalian amacrine cells? Does serotonergic signaling involve photoreceptor-derived serotonin, and are TRP receptors involved?

Other neuroactive molecules

Many nonpeptide species can target ionotropic receptors, GPCRs, tyrosine kinase receptors, and intracellular response elements, and more will likely be found. These additional signals emanate from multifarious sources and modulate signaling within diverse neuronal, glial, and epithelial targets, although none is known to be a primary fast signal.

Nitric oxide that is derived from Ca²⁺-coupled nitric oxide synthase arginine-citrulline cycling potentially arises from numerous vertical and lateral channel sources and can target an array of cells through guanyl cyclase activation (Eldred, 2001). The effects are potent and include cGMP modulation of cone synaptic Ca²⁺ channels and horizontal cell coupling. The involvement of *carbon monoxide signaling* in the retina is only now being explored.

Melatonin signaling, somewhat the inverse of dopamine signaling, initiates with melatonin production in scotophase photoreceptors. Melatonin diffuses to target melatonin receptors (Wiechmann and Smith, 2001), and activates dark-adapted states and suppresses light-adapted states. Melatonin signaling is coupled to intrinsic circadian oscilla-

tor pathways in photoreceptors, but such pathways are complex, and so simple assignment of photic states to melatonin-versus-dopamine signaling is certainly inaccurate.

The retina expresses a variety of adenosine triphosphate (ATP)-activated, ionotropic P2X receptors on neurons and Müller cells (Pannicke et al., 2000; Taschenberger et al., 1999). P2Y GPCRs are also expressed in retina (Deng et al., 1998), although the ATP sources and magnitudes of receptor-gated signaling have yet to be resolved.

One of the newest signal candidates in retina is *anandamide* (N-arachidonylethanolamine) or a related molecule that activates cannabinoid CB1 and CB2 GPCRs expressed on retinal neurons (Straiker et al., 1999; Yazulla et al., 1999). Retinal distributions of central nervous system anandamide transporters and potential interactions with vanilloid receptors are terra incognita.

REFERENCES*

- Akopian, A., R. Gabriel, and P. Witkovsky, 1998. Calcium released from intracellular stores inhibits GABAA-mediated currents in ganglion cells of the turtle retina, *J. Neurophysiol.*, 80:1105–1115.
- Akopian, A., and P. Witkovsky, 1996. D2 dopamine receptor-mediated inhibition of a hyperpolarization-activated current in rod photoreceptors, *J. Neurophysiol.*, 76:1828–1835.
- Awatramani, G. B., and M. M. Slaughter, 2000. Origin of transient and sustained responses in ganglion cells of the retina, *J. Neurosci.*, 20:7087–7095.
- Bansal, A., J. H. Singer, B. J. Hwang, W. Xu, A. Beaudet, and M. B. Feller, 2000. Mice lacking specific nicotinic acetylcholine receptor subunits exhibit dramatically altered spontaneous activity patterns and reveal a limited role for retinal waves in forming ON and OFF circuits in the inner retina, *J. Neurosci.*, 20:7672–7681.
- Blanco, R., and P. de la Villa, 1999. Ionotropic glutamate receptors in isolated horizontal cells of the rabbit retina, *Eur. J. Neurosci.*, 11:867–873.
- Brändstatter, J. H., P. Koulen, and H. Wässle, 1997. Selective synaptic distribution of kainate receptor subunits in the two plexiform layers of the rat retina, *J. Neurosci.*, 17:9298–9307.
- Cai, W., and R. G. Pourcho, 1999. Localization of metabotropic glutamate receptors mGluR1alpha and mGluR2/3 in the cat retina, *J. Comp. Neurol.*, 407:427–437.
- Chaudhry, F. A., R. J. Reimer, D. Krizaj, D. Barber, J. Storm-Mathisen, D. Copenhagen, and R. H. Edwards, 1999. Molecular analysis of System N suggests novel physiological roles in nitrogen metabolism and synaptic transmission, *Cell Tissue Kinetics*, 99:769–780.
- Cherubini, E., and F. Conti, 2001. Generating diversity at GABAergic synapses, *Trends Neurosci.*, 24:155–162.
- Connor, J. X., A. J. Boileau, and C. Czajkowski, 1998. A GABA_A receptor α 1 subunit tagged with Green Fluorescent Protein requires a β subunit for functional surface expression, *J. Biol. Chem.*, 273:28906–28911.

*Expository references.

- Cook, P. B., P. D. Lukasiewicz, and J. S. McReynolds, 2000. GABA_C receptors control adaptive changes in a glycinergic inhibitory pathway in salamander retina, *J. Neurosci.*, 20: 806–812.
- Davies, P. A., M. Pistis, M. C. Hanna, J. A. Peters, J. J. Lambert, T. G. Hales, and E. F. Kirkness, 1999. The 5-HT_{3B} subunit is a major determinant of serotonin-receptor function, *Nature*, 397: 359–363.
- Deng, G., C. Matute, C. K. Kumar, D. J. Fogarty, and R. Miledi, 1998. Cloning and expression of a P2Y purinoceptor from the adult bovine corpus callosum, *Neurobiol. Dis.*, 5:259–270.
- DeVries, S., 2000. Bipolar cells use kainate and AMPA receptors to filter visual information into separate channels, *Neuron*, 28: 847–856.
- Dhingra, A., A. Lyubarsky, M. Jiang, E. N. J. Pugh, L. Birnbaumer, P. Sterling, and N. Vardi, 2000. The light response of ON bipolar neurons requires G α_o , *J. Neurosci.*, 20:9053–9058.
- Diamond, J. S., and D. R. Copenhagen, 1995. The relationship between light-evoked synaptic excitation and spiking behaviour of salamander retinal ganglion cells, *J. Physiol.*, 487:711–725.
- Dingledine, R., K. Borges, D. Bowie, and S. F. Traynelis, 1999. The glutamate receptor ion channels, *Pharmacol. Rev.*, 51:8–61.
- Dmitrieva, N. A., J. M. Lindstrom, and K. T. Keyser, 2001. The relationship between GABA-containing cells and the cholinergic circuitry in the rabbit retina, *Vis. Neurosci.*, 18:93–100.
- Eiden, L. E., 2000. The vesicular neurotransmitter transporters: Current perspectives and future prospects, *FASEB J.*, 14: 2396–2400.
- Eldred, W. D., 2001. Real time imaging of the production and movement of nitric oxide in the retina, *Progr. Brain Res.*, 131:109–122.
- Erickson, J. D., and H. Varoqui, 2000. Molecular analysis of vesicular amine transporter function and targeting to secretory organelles, *FASEB J.*, 14:2450–2458.
- Famiglietti, E. V., 1991. Synaptic organization of starburst amacrine cells in rabbit retina: analysis of serial thin sections by electron microscopy and graphic reconstruction, *J. Comp. Neurol.*, 309:40–70.
- Featherstone, D. E., E. M. Rushton, M. Hilderbrand-Chae, A. M. Phillips, F. R. Jackson, and K. Broadie, 2000. Presynaptic glutamic acid decarboxylase is required for induction of the postsynaptic receptor field at a glutamatergic synapse, *Neuron*, 27:71–84.
- Feigenspan, A., and J. Bormann, 1994. Differential contributions of GABA_A and GABA_C receptors on rat retinal bipolar cells, *Proc. Natl. Acad. Sci. USA*, 91:10893–10897.
- Feigenspan, A., S. Gustincich, B. P. Bean, and E. Raviola, 1998. Spontaneous activity of solitary dopaminergic cells of the retina, *J. Neurosci.*, 18:6776–6789.
- Fischer, A. J., L. A. McKinnon, N. M. Nathanson, and W. K. Stell, 1998. Identification and localization of muscarinic acetylcholine receptors in the ocular tissues of the chick, *J. Comp. Neurol.*, 392:273–284.
- Fletcher, E. L., I. Hack, J. H. Brandstatter, and H. Wässle, 2000. Synaptic localization of NMDA receptor subunits in the rat retina, *J. Comp. Neurol.*, 420:98–112.
- Gaal, L., B. Roska, S. A. Picaud, S. M. Wu, R. E. Marc, and F. S. Werblin, 1998. Postsynaptic response kinetics are controlled by a glutamate transporter at cone photoreceptors, *J. Neurophysiol.*, 79:190–196.
- Ghosh, K. K., S. Haverkamp, and H. Wässle, 2001. Glutamate receptors in the rod pathway of the mammalian retina, *J. Neurosci.*, 21:8636–8647.
- Grant, G. B., and J. E. Dowling, 1996. On bipolar cell responses in the teleost retina are generated by two distinct mechanisms, *J. Neurophysiol.*, 76:3842–3949.
- Greferath, U., U. Grünert, F. Müller, and H. Wässle, 1994. Localization of GABA_A receptors in the rabbit retina, *Cell Tissue Res.*, 276:295–307.
- Hampson, E. C., D. I. Vaney, and R. Weiler, 1992. Dopaminergic modulation of gap junction permeability between amacrine cells in mammalian retina, *J. Neurosci.*, 12:4911–4922.
- Haverkamp, S., U. Grünert, and H. Wässle, 2001. The synaptic architecture of AMPA receptors at the cone pedicle of the primate retina, *J. Neurosci.*, 21:2488–2500.
- Haverkamp, S., U. Grünert, and H. Wässle, 2000. The cone pedicle, a complex synapse in the retina, *Neuron*, 27:85–95.
- He, S., and R. H. Masland, 1997. Retinal direction selectivity after targeted laser ablation of starburst amacrine cells, *Nature*, 389:378–382.
- Jin, X. T., and W. J. Brunken, 1998. Serotonin receptors modulate rod signals: a neuropharmacological comparison of light- and dark-adapted retinas, *Vis. Neurosci.*, 15:891–902.
- Johnson, J., T. K. Chen, D. W. Rickman, C. Evans, and N. C. Brecha, 1996. Multiple γ -aminobutyric acid plasma membrane transporters (GAT-1, GAT-2, GAT-3) in the rat retina, *J. Comp. Neurol.*, 375:212–224.
- Johnson, M. A., and N. Vardi, 1998. Regional differences in GABA and GAD immunoreactivity in rabbit horizontal cells, *Vis. Neurosci.*, 15:743–753.
- Jones, K. A., B. Borowsky, J. A. Tamm, D. A. Craig, M. M. Durkin, M. Dai, W. J. Yao, M. Johnson, C. Gunwaldsen, L. Y. Huang, C. Tang, Q. Shen, J. A. Salon, K. Morse, T. Laz, K. E. Smith, D. Nagarathnam, S. A. Noble, T. A. Branchek, and C. Gerald, 1998. GABA_B receptors function as a heteromeric assembly of the subunits GABA_BR1 and GABA_BR2, *Nature*, 396:674–679.
- Kalloniatis, M., and G. Tomisich, 1999. Amino acid neurochemistry of the vertebrate retina, *Progr. Retinal Eye Res.*, 18:811–866.
- Kamermans, M., I. Fahrenfort, K. Schultz, U. Janssen-Bienhold, T. Sjoerdsma, and R. Weiler, 2001. Hemichannel-mediated inhibition in the outer retina, *Science*, 292:1178–1180.
- Keyser, K. T., M. A. MacNeil, N. Dmitrieva, F. Wang, R. H. Masland, and J. M. Lindstrom, 2000. Amacrine, ganglion, and displaced amacrine cells in the rabbit retina express nicotinic acetylcholine receptors, *Vis. Neurosci.*, 17:743–752.
- Kittila, C. A., and S. C. Massey, 1997. Pharmacology of directionally selective ganglion cells in the rabbit retina, *J. Neurophysiol.*, 77:675–689.
- Koulen, P., 1997. Vesicular acetylcholine transporter (VACHT): A cellular marker in rat retinal development, *Neuroreport*, 8:2845–2848.
- Koulen, P., J. H. Brandstatter, S. Kroger, R. Enz, J. Bormann, and H. Wässle, 1997a. Immunocytochemical localization of the GABA_C receptor rho subunits in the cat, goldfish, and chicken retina, *J. Comp. Neurol.*, 380:520–532.
- Koulen, P., R. Kuhn, H. Wässle, and J. H. Brandstatter, 1997b. Group I metabotropic glutamate receptors mGluR1 α and mGluR5a: localization in both synaptic layers of the rat retina, *J. Neurosci.*, 17:2200–2211.
- Koulen, P., R. Kuhn, H. Wässle, and J. H. Brandstatter, 1999. Modulation of the intracellular calcium concentration in

- photoreceptor terminals by a presynaptic metabotropic glutamate receptor, *Proc. Natl. Acad. Sci. USA*, 96:9909–9914.
- Koulen, P., B. Malitschek, R. Kuhn, B. Bettler, H. Wässle, and J. H. Brandstätter, 1998. Presynaptic and postsynaptic localization of GABA_B receptors in neurons of the rat retina, *Eur. J. Neurosci.*, 10:1446–1456.
- Koulen, P., B. Malitschek, R. Kuhn, H. Wässle, and J. H. Brandstätter, 1996. Group II and group III metabotropic glutamate receptors in the rat retina: distributions and developmental expression patterns, *Eur. J. Neurosci.*, 8:2177–2187.
- Linberg, K. A., and S. K. Fisher, 1988. Ultrastructural evidence that horizontal cell axon terminals are presynaptic in the human retina, *J. Comp. Neurol.*, 268:281–297.
- Lukasiewicz, P. D., and C. R. Shields, 1998. Different combinations of GABA_A and GABA_C receptors confer distinct temporal properties to retinal synaptic responses, *J. Neurophysiol.*, 79:3157–3167.
- Marc, R. E., 1992. Structural organization of GABAergic circuitry in ectotherm retinas, *Progr. Brain Res.*, 90:61–92.
- Marc, R. E., 1995. Interplexiform cell connectivity in the outer retina, in *Neurobiology of the Vertebrate Outer Retina* (S. Archer, M. B. Djamgoz, and S. Vallerga, eds.), London: Chapman and Hall, pp. 369–393.
- Marc, R. E., 1999. Mapping glutamatergic drive in the vertebrate retina with a channel-permeant organic cation, *J. Comp. Neurol.*, 407:47–64.
- Marc, R. E., and B. W. Jones, 2002. Molecular phenotyping of retinal ganglion cells, *J. Neurosci.*, 22:413–427.
- Marc, R. E., and W. Liu, 2000. Fundamental GABAergic amacrine cell circuitries in the retina: nested feedback, concatenated inhibition, and axosomatic synapses, *J. Comp. Neurol.*, 425:560–582.
- Marc, R. E., W. L. Liu, K. Scholz, and J. F. Müller, 1988. Serotonergic and serotonin-accumulating neurons in the goldfish retina, *J. Neurosci.*, 8:3427–3450.
- Masu, M., H. Iwakabe, Y. Tagawa, T. Miyoshi, M. Yamashita, Y. Fukuda, H. Sasaki, K. Hiroi, Y. Nakamura, and R. Shigemoto, 1995. Specific deficit on the ON response in visual transmission by targeted disruption of the mGluR6 gene, *Cell*, 80:757–765.
- Matthews, G., G. S. Ayoub, and R. Heidelberger, 1994. Presynaptic inhibition by GABA is mediated via two distinct GABA receptors with novel pharmacology, *J. Neurosci.*, 14:1079–1090.
- McIntire, S. L., R. J. Reimer, K. Schuske, R. H. Edwards, and E. M. Jørgensen, 1997. Identification and characterization of the vesicular GABA transporter, *Nature*, 389:870–876.
- Morigiwa, K., and N. Vardi, 1999. Differential expression of ionotropic glutamate receptor subunits in the outer retina, *J. Comp. Neurol.*, 405:173–184.
- O'Malley, D. M., J. H. Sandell, and R. H. Masland, 1992. Corelease of acetylcholine and GABA by the starburst amacrine cells, *J. Neurosci.*, 12:1394–1408.
- Pannicke, T., W. Fischer, B. Biedermann, H. Schädlich, J. Grosche, F. Faude, P. Wiedemann, C. Allgaier, P. Illes, G. Burnstock, and A. Reichenbach, 2000. P2X7 receptors in Müller glial cells from the human retina, *J. Neurosci.*, 20:5965–5972.
- Picaud, S., B. Pattnaik, D. Hicks, V. Forster, V. Fontaine, S. Sahel, and H. Dreyfus, 1998. GABA_A and GABA_C receptors in adult porcine cones: evidence from a photoreceptor—glia co-culture model, *J. Physiol.*, 513:33–42.
- Pootanakit, K., and W. J. Brunken, 2001. Identification of 5-HT(3A) and 5-HT(3B) receptor subunits in mammalian retinas: potential pre-synaptic modulators of photoreceptors, *Brain Res.*, 896:77–85.
- Pootanakit, K., K. J. Prior, D. D. Hunter, and W. J. Brunken, 1999. 5-HT_{2a} receptors in the rabbit retina: Potential presynaptic modulators, *Vis. Neurosci.*, 16:221–230.
- Pow, D. V., 1998. Transport is the primary determinant of glycine content in retinal neurons, *J. Neurochem.*, 70:2628–2636.
- Pow, D. V., N. L. Barnett, and P. Penfold, 2000. Are neuronal transporters relevant in retinal glutamate homeostasis? *Neurochem. Int.*, 37:191–198.
- Rieke, F., and E. A. Schwartz, 1994. A cGMP-gated current can control exocytosis at cone synapses, *Neuron*, 13:863–873.
- Schwartz, E. A., 1999. A transporter mediates the release of GABA from horizontal cells, in *The Retinal Basis of Vision* (J.-I. Toyoda, M. Murkani, A. Kaneko, and T. Saito, eds.), Amsterdam: Elsevier, pp. 93–101.
- Seal, R. P., and S. G. Amara, 1999. Excitatory amino acid transporters: a family in flux, *Annu. Rev. Pharmacol. Toxicol.*, 39:431–456.
- Stobrawa, S. M., T. Breiderhoff, S. Takamori, D. Engel, M. Schweizer, A. A. Zdebik, M. R. Bösl, K. Ruether, H. Jahn, A. Draguhn, R. Jahn, and T. J. Jentsch, 2001. Disruption of ClC-3, a chloride channel expressed on synaptic vesicles, leads to a loss of the hippocampus, *Neuron*, 29:185–196.
- Straiker, A., N. Stella, D. Piomelli, K. Mackie, H. J. Karten, and G. Maguire, 1999. Cannabinoid CB1 receptors and ligands in vertebrate retina: localization and function of an endogenous signaling system, *Proc. Natl. Acad. Sci. USA*, 96:14565–14570.
- Sullivan, R., A. Chateaufneuf, N. Coulombe, L. F. Kolakowski, Jr., M. P. Johnson, T. E. Hebert, N. Ethier, M. Belley, K. Metters, M. Abramovitz, G. P. O'Neill, and G. Y. Ng, 2000. Coexpression of full-length GABA_B receptors with truncated receptors and metabotropic glutamate receptor 4 supports the GABA_B heterodimer as the functional receptor, *J. Pharmacol. Exp. Ther.*, 293:460–467.
- Takamori, S., J. Rhee, C. Rosenmund, and R. Jahn, 2000. Identification of a vesicular glutamate transporter that defines a glutamatergic phenotype in neurons, *Nature*, 407:189–194.
- Taschenberger, H., R. Jüttner, and R. Grantyn, 1999. Ca²⁺-permeable P2X receptor channels in cultured rat retinal ganglion cells, *J. Neurosci.*, 19:3353–3366.
- Vandenbranden, C. A., J. Verweij, M. Kamermans, L. J. Müller, J. M. Ruijter, G. F. Vrensen, and H. Spekrijse, 1996. Clearance of neurotransmitter from the cone synaptic cleft in goldfish retina, *Vis. Res.*, 36:3859–3874.
- Vaquero, C. F., A. Pignatelli, G. J. Partida, and A. T. Ishida, 2001. A dopamine- and protein kinase A-dependent mechanism for network adaptation in retinal ganglion cells, *J. Neurosci.*, 21:8624–8635.
- Vardi, N., R. Duvoisin, G. Wu, and P. Sterling, 2000a. Localization of mGluR6 to dendrites of ON bipolar cells in primate retina, *J. Comp. Neurol.*, 423:402–412.
- Vardi, N., L.-L. Zhang, J. A. Payne, and P. Sterling, 2000b. Evidence that different cation chloride cotransporters in retinal neurons allow opposite responses to GABA, *J. Neurosci.*, 20:7657–7663.
- Varoqui, H., M. K.-H. Schafer, H. Zhu, E. Weihe, and J. D. Erickson, 2002. Identification of the differentiation-associated Na⁺/PI Transporter as a novel vesicular glutamate transporter expressed in a distinct set of glutamatergic synapses, *J. Neurosci.*, 22:142–155.
- Varoqui, H., H. Zhu, D. Yao, H. Ming, and J. D. Erickson, 2000. Cloning and functional identification of a neuronal glutamine transporter, *J. Biol. Chem.*, 275:4049–4054.

- Wässle, H., P. Koulen, J. H. Brändstatter, E. L. Fletcher, and C. M. Becker, 1998. Glycine and GABA receptors in the mammalian retina, *Vis. Res.*, 38:1411–1430.
- Wiechmann, A. F., and A. R. Smith, 2001. Melatonin receptor RNA is expressed in photoreceptors and displays a diurnal rhythm in *Xenopus* retina, *Mol. Brain Res.*, 91:104–111.
- Witkovsky, P., and A. Dearth, 1991. Functional roles of dopamine in the vertebrate retina, *Progr. Retinal Res.*, 11:247–292.
- Witkovsky, P., C. Nicholson, M. E. Rice, K. Bohmaker, and E. Meller, 1993. Extracellular dopamine concentration in the retina of the clawed frog, *Xenopus laevis*, *Proc. Natl. Acad. Sci. USA*, 90:5667–56671.
- Wu, S. M., 1994. Synaptic transmission in the outer retina, *Ann. Rev. Physiol.*, 56:141–168.
- Yazulla, S., 1995. Neurotransmitter release from horizontal cells, in *Neurobiology and Clinical Aspects of the Outer Retina* (S. Archer, M. B. Djamgoz, and S. Vallerger, eds.), London: Chapman and Hall, pp. 249–271.
- Yazulla, S., K. M. Studholme, H. H. McIntosh, and D. G. Deutsch, 1999. Immunocytochemical localization of cannabinoid CB1 receptor and fatty acid amide hydrolase in rat retina, *J. Comp. Neurol.*, 415:80–90.
- Zhang, C., B. Bettler, and R. Duvoisin, 1998a. Differential localization of GABA_B receptors in the mouse retina, *Neuroreport*, 9:3493–3497.
- Zhang, D., N. J. Sucher, and S. A. Lipton, 1995. Co-expression of AMPA/kainate receptor-operated channels with high and low Ca²⁺ permeability in single rat retinal ganglion cells, *Neuroscience*, 67:177–188.
- Zhang, J., C. S. Jung, and M. M. Slaughter, 1997a. Serial inhibitory synapses in retina, *Vis. Neurosci.*, 14:553–563.
- Zhang, J., W. Shen, and M. M. Slaughter, 1997b. Two metabotropic γ -aminobutyric acid receptors differentially modulate calcium currents in retinal ganglion cells, *J. Gen. Physiol.*, 110:45–58.
- Zhang, J., N. Tian, and M. M. Slaughter, 1998b. Neuronal discriminator formed by metabotropic γ -aminobutyric acid receptors, *J. Neurophysiol.*, 80:3365–3378.

21

Excitation in Retina: The Flow, Filtering, and Molecules of Visual Signaling in the Glutamatergic Pathways from Photoreceptors to Ganglion Cells

DAVID R. COPENHAGEN

Introduction

The neural retina serves both to transduce the visual scene into biologically relevant electrical signals and to “pre-process” the visual scene before transmission to the brain. The demands of the visual system require rapid and reliable signal transmission through the retinal synapses. Extraction and enhancement of salient features in the visual scene by the retina are motivated, in part, by the limited carrying capacity of the optic nerve exiting from the eye. In humans, only 1 million fibers are available to carry visual information to the brain. This section of the book discusses the anatomical and physiological processes underlying visual processing in the retina. This chapter focuses on the pathways, properties, and underlying mechanisms by which excitatory signals are conducted from rods and cones to bipolar cells to RGCs (retinal ganglion cells). This circuit is commonly referred to as the “vertical” or “radial” pathway. This chapter begins with the anatomical wiring of this vertical pathway, then discusses functional attributes of signal transfer, and finally ends with the cellular and molecular mechanisms that mediate signal transmission. Many of the topics discussed herein are covered in other previously published reviews (Dowling, 1987; Matthews, 1996; Thoreson and Witkovsky, 1999; Toyoda et al., 1999; Wilson, 1994; Wu, 1994).

Pathways

THE VERTICAL PATHWAY LINKS PHOTORECEPTORS TO BIPOLAR CELLS TO GANGLION CELLS A general template for the conduction of light-evoked excitatory signals encompasses photoreceptor to bipolar cell to ganglion cell synaptic transmission. This pathway utilizes the fast-acting neurotransmitter glutamate at both the photoreceptor–bipolar cell synapses and bipolar cell–ganglion cell synapses. Cone pathways in mammalian retina observe this basic template

pattern. Within the pattern there is some diversity. In primate retinas, midget bipolar cells in the high acuity foveal region of the retina usually contact a single cone. In the perifoveal and in the peripheral regions of the retina the midget bipolar cells contact a greater number of cones. Another class of bipolar cell has much more diffuse dendrites and contacts many more cones than the midget bipolar cells (Kolb et al., 1992). A third class, the blue-cone bipolar cells, contacts one or two blue cones exclusively (Kouyama and Marshak, 1992).

A rod pathway is “layered” onto the cone pathways in mammalian retinas. Rod ON bipolar cells are thought to be driven exclusively by synaptic inputs from rods. These rod ON bipolar cells do not activate RGCs but instead provide glutamatergic inputs to a class of amacrine cells classified as AII type. The processes of AII cells make chemical synaptic connections with the terminals of cone OFF bipolar cells. Other AII processes make gap junctions with cone ON bipolar cells. Thus, light-driven rod signals can reach both ON and OFF RGCs via the AII to cone bipolar cell connections. Light-induced depolarization of rod ON bipolar cells depolarizes AII cells via excitatory, sign preserving glutamate synapses. This depolarization evokes a depolarization in the cone ON bipolar cells via sign-converting transfer through the gap junctions. The depolarization in the AII cells evokes a hyperpolarization in the OFF cone bipolar cells via the inhibitory glycinergic synapse made at the AII–OFF cone bipolar synapses. Figure 21.1 illustrates these cone and rod pathways. Nonmammalian retinas are not thought to exhibit the same degree of pathway specializations observed in primate retina. It is generally observed that rod and cone signals are mixed in both bipolar and ganglion cells.

OTHER SYNAPTIC AND ELECTRICAL SYNAPSES ALLOW FOR SIGNAL CONDUCTION VIA ALTERNATIVE PATHWAYS Morphological, immunohistochemical, and electrophysiological

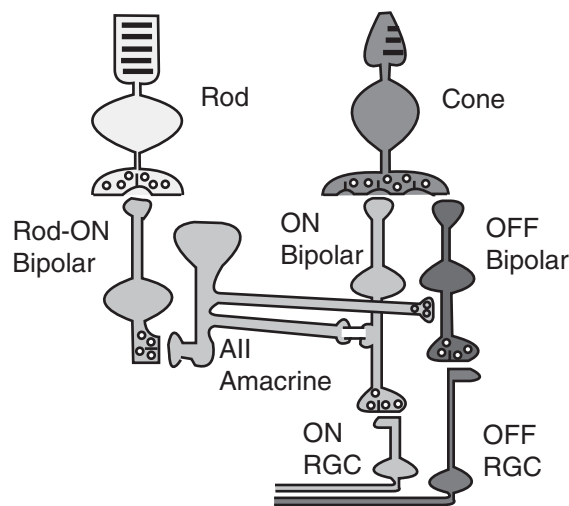


FIGURE 21.1. Vertical pathways from photoreceptors to ganglion cells. Cones connect to both ON and OFF bipolar cells. ON bipolar cells synaptically drive, via glutamatergic synapses, ON ganglion cells. OFF bipolar cells drive OFF ganglion cells, also via glutamatergic synapses localized in the distal half of the IPL (inner plexiform layer). ON-OFF ganglion cells (not shown) receive inputs from both ON and OFF bipolar cells and have dendritic processes in both halves of the IPL. Rods synaptically activate rod ON bipolar cells. These cells, in turn, synaptically drive the AII amacrine cells, whose output is onto cone ON and OFF bipolar cells. AII cells are coupled to ON bipolar cells via gap junctions and to OFF bipolar cells by glycinergic chemical synapses. Drawing is adapted from DeVries and Baylor (1995).

studies have revealed several alternative pathways by which photoresponses can be conducted to ganglion cells. Accumulating evidence demonstrates that light-evoked rod responses are not exclusively transmitted from rod ON bipolar cells through AII-type amacrine cells to couple into the cone ON and OFF pathways. Rod signals can be conducted directly by gap junctions to cones, and then transmitted through the vertical cone bipolar pathways. Evidence in support of this pathway includes the finding that light-evoked rod responses are observed in macaque monkey cones (Schneeweis and Schnapf, 1995). Also, rod-driven light responses in cat retina are seen in cones and in horizontal cells that are exclusively connected to cones (Nelson, 1977). Moreover, rod-driven light responses are observed in rabbit ganglion cells under conditions when the rod to rod ON bipolar cell synapses are blocked pharmacologically (DeVries and Baylor, 1995).

A second alternative pathway for rod signals is via rod synapses onto cone bipolar cells. Immunolocalization studies of the AMPA receptor subunits in rat retina showed GluR1 and GluR2 isoforms on OFF bipolar cell dendrites that contact rod photoreceptor synaptic terminals (Hack et al., 1999). Similarly in mouse retina, OFF bipolar cells make contacts with rod synaptic terminals (Tsukamoto et al., 2001). Electrophysiological recordings from the *coneless*

mouse strain reveal that rod signals can be observed in RGCs (Soucy et al., 1998). Because cones are nonfunctional in this mouse strain, these findings provided strong evidence for the functional transmission of rod signals through the OFF cone bipolar cells.

Human psychophysical and electroretinogram (ERG) measurements provide evidence that there are two alternative pathways for rod signals in retina (Stockman et al., 1995). The slower, higher gain rod pathway is thought to be mediated via the conventional rod bipolar to AII amacrine cells. The faster responding rod pathway is postulated to be mediated by rod signals coupled into the cone pathway at the outer retina.

IN YOUNGER ANIMALS EXCITATORY SYNAPTIC CIRCUITS REMAIN MODIFIABLE Although it is believed that the physical “wiring” of retinal pathways is fixed, it is now being appreciated that glutamatergic retinal synaptic pathways retain some degree of morphological and functional plasticity after eye opening. As discussed above, in mammalian retina, ON bipolar cells make exclusive synaptic contacts with rod photoreceptors. In retinas from transgenic pigs and *rd* mice with severe rod photoreceptor degeneration, ON rod bipolar cells develop ectopic synaptic contacts with cones. Analysis of light-evoked ERG from transgenic porcine retinas provides evidence that the newly formed cone to ON rod bipolar cell synapses are functional (Peng et al., 2000).

Pharmacological blockade of glutamatergic inputs to ON bipolar cells can modify the pattern of synaptic inputs to RGCs. At early postnatal ages a significant percentage of ganglion cell dendrites are bistratified. In cat retina, approximately 40% of the RGCs have dendrites in both the ON and OFF sublaminae of the inner plexiform layer (IPL). By eye opening less than 20% of the RGCs exhibit bistratified dendrites (Bodnarenko et al., 1999). Intravitreal injections of APB, a glutamate agonist for the mGluR6 receptor that drives ON bipolar cells, suppresses the loss of bistratified RGCs (Bodnarenko and Chalupa, 1993). The consequences of APB injections were reflected in the light responses from optic nerve and dorsal lateral geniculate. In normal adult cats, virtually all cells respond as either ON or OFF cells. In animals treated with the intravitreal injections of APB for their first postnatal month, 37% of the cells responded as ON-OFF cells (Bisti et al., 1998). This result suggests that the increased number of bistratified RGCs that remained in APB-treated retinas retained functional synaptic inputs from ON and OFF bipolar cells.

In a visual deprivation paradigm it was demonstrated that dark rearing can regulate the excitatory spontaneous synaptic inputs to mouse RGCs. In animals reared in cyclic light, there is a prolonged burst in the frequency of spontaneous EPSCs in RGCs that occurs approximately 2 weeks after eye

opening (Tian and Copenhagen, 2001). This burst is thought to reflect an increased probability of release from bipolar cell terminals. Interestingly, dark rearing reduces the magnitude of the increase in spontaneous EPSCs seen after eye opening (Tian and Copenhagen, 2001). Taken together, these findings show a degree of plasticity in the formation of the excitatory retinal pathways.

Gap junction coupling between photoreceptors can improve reliability of the transmission of light-evoked signals to bipolar cells David Vaney (Chapter 25) discusses gap junction coupling between many different classes of retinal neuron. Here, it is instructive to consider the functional advantages of coupling between photoreceptors in terms of how the light-evoked excitatory signals are transmitted to the second-order neurons. Gap junctions between photoreceptors exist in virtually every vertebrate species (Cook and Becker, 1995). These gap junctions are formed by pairs of connexons, which are made of connexin subunits arranged to form a pore that passes small molecules (<1 kD), including small ions that carry electrical current. Functional electrical coupling was first identified by studying the spread of light-evoked and injected electrical current between neighboring cones (Baylor et al., 1971) and rods (Copenhagen and Owen, 1976). Electrical coupling is found between rods and cones of mammals (including primates) and reptiles (Schneeweis and Schnapf, 1995; Schwartz, 1975). The gap junction-mediated mixing of rod and cone signals may at first appear disadvantageous since it blurs the spectral selectivity afforded by having separate classes of rod and cones. One functional advantage of the rod to cone coupling may be that it extends the rods' dynamic range by providing a pathway from rods to ganglion cells independent of the high-gain rod to ON bipolar cell pathway. This second pathway could increase the sensitivity of photon detection in the mesopic range of vision (DeVries and Baylor, 1995). Coupling signals between photoreceptors can serve to increase the signal-to-noise ratio for detection of dim lights. At low luminances where photon noise is significant relative to its signal power, coupling reduces the noisiness associated with fluctuations from the random absorption of photons by a factor of 10 or more (Lamb and Simon, 1976). Electrotonic coupling can also facilitate neurotransmission of light-evoked signals by limiting voltage excursions that would take the presynaptic potential into lower gain regions of the input/output relationship. Basically, by spreading light signals across many rod terminals, neurotransmission is accomplished in the linear region of the synapse (Tessier-Lavigne and Attwell, 1988). In summary, coupling is useful because it spreads the signal which might saturate a single synapse over many rods. The random noise intrinsic to individual rods and cones will be reduced by averaging through the coupled network. The coupling between rods and cones

can provide alternative pathways for signals from each of these types of photoreceptors to second- and third-order neurons in the retina.

Gain, filtering, and delay in the transmission of light-evoked signals

LIGHT-EVOKED VOLTAGES IN THE EXCITATORY PATHWAY TO RGCs ARE SLOW, NONSPIKING RESPONSES Luminance changes in the environment vary around a mean level. Rods, cones, and bipolar cells signal these luminance changes not as changes in the rate of action potentials, commonly used for signaling in the nervous system and in amacrine and RGCs, but as graded variations in membrane potential. These changes in membrane potential regulate the mean rate of glutamate release. The advantages of graded signaling are that small increments and decrements can be transmitted with comparable sensitivity and the synapses have a larger bandwidth, making it possible to transmit more information than spike-driven synapses (Juusola et al., 1996).

THE EXCITATORY PATHWAYS ARE CAPABLE OF RELIABLY TRANSMITTING VERY SMALL MEMBRANE POTENTIAL PERTURBATIONS That small-amplitude signals can be transmitted from photoreceptors to ganglion cells is made clear by considering rod-mediated vision at very low levels of light. The light levels present in starlight correspond to one or fewer photon absorptions within an integration time for each mammalian rod outer segment (Rao et al., 1994). At illumination levels that produce only 1 to 2 photons/s/100 rods, toads are capable of reliable visually guided prey-catching (Aho et al., 1993). Humans are capable of detecting the simultaneous absorption of 5 to 7 photons over an area covering several hundred rods. Thus light detection is accomplished with very minimal stimulation of the rods. In considering the relative reliability of transduction in rods versus signal transmission in the retina, it appears that signal conduction is quite noise-free. Behavioral studies of prey catch by toads shows that the limit on absolute visual sensitivity originates principally from thermally activated isomerizations of rhodopsin, which itself is very stable, having a half-life for thermal isomerization of greater than 500 years (Aho et al., 1988). Thus, the excitatory pathways are capable of transmitting very low amplitude signals.

The size of light-evoked hyperpolarizations in rods and cones that evoke action potentials in RGCs is on the order of 10 μ V (Copenhagen et al., 1990; Fain et al., 1977). Although these voltage estimates were derived from experiments with very defined and arbitrary background lights, it is becoming evident that such small signals may be used primarily for signaling the visual image at all ambient background intensities. Analysis of natural scenes shows that

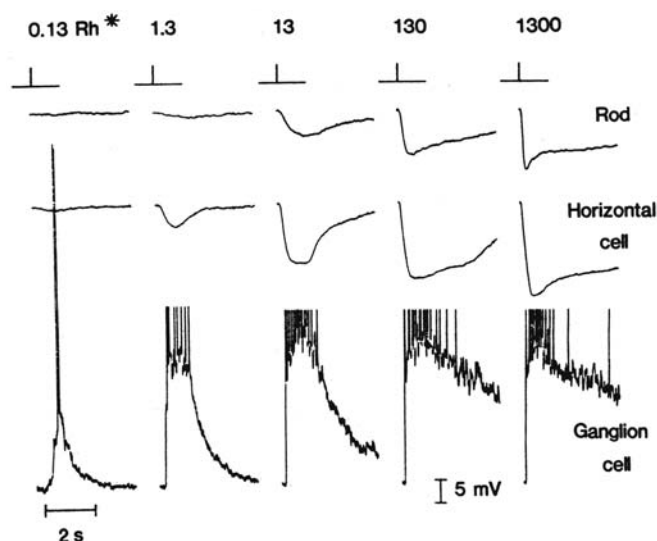


FIGURE 21.2. Comparison of rod, horizontal cell, and ganglion cell responses to the same 5 flash intensities. All responses are shown at the same amplification. For clarity, the action potentials were truncated in the responses to higher flash intensities. All these responses were recorded by microelectrodes in dark-adapted toad retina. (Taken from Copenhagen et al., 1990.)

most of the reflected light from a scene has a contrast $<50\%$. Given that photoreceptors exhibit a maximum response range of $\sim 30\text{ mV}$ over intensity ranges of several orders of magnitude, this implies that most “seeing” originates from photoreceptor responses that are only a few millivolts in amplitude (Vu et al., 1997).

SYNAPTIC TRANSMISSION OF LIGHT-EVOKED SIGNALS IS ASSOCIATED WITH VOLTAGE GAIN Comparison of the light-evoked voltages in photoreceptor, bipolar, and ganglion cells reveals that each stage of synaptic transfer boosts the signal. Figure 21.2 demonstrates the gain in the light-evoked signals of the toad retina. Here, intracellular voltage responses of a rod, horizontal, and ganglion cell to light flashes are plotted in adjacent rows. The dimmest light, which produced 0.13 photoisomerizations per rod, depolarized the ganglion cell by 12 to 15 mV and consequently generated an action potential. The rod terminals were hyperpolarized by approximately $20\mu\text{V}$ by this same stimulus (Copenhagen et al., 1990). Defining gain as the ratio of the peak presynaptic voltage in rods to the peak depolarization in the RGC, one can estimate that the overall gain was ~ 60 in this example. Paired recordings from rods and bipolar cells in toads showed that voltage gain for dim flashes at this first synapse was ~ 10 (Belgium and Copenhagen, 1988). Using similar approaches, the gain from cones to bipolar cells in turtle retina was estimated to be around 10 (Copenhagen et al., 1983). In skate retina, voltage gains from rods to ON bipolar

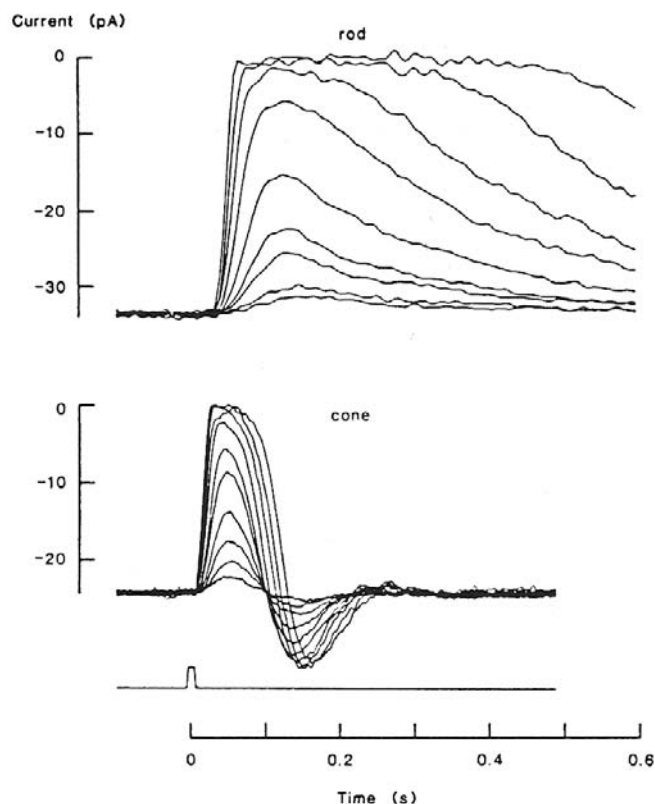


FIGURE 21.3. Photocurrents recorded from a rod and red cone of the monkey retina. Each series of tracings shows light-evoked responses to a sequence of flashes of increasing intensity. Rod responses are slower and more sensitive to light than cones. (Taken from Baylor, 1987.)

cells were seen to be as high as 200 (Ashmore and Falk, 1980).

DELAYS AND TEMPORAL FILTERING SHAPE THE SIGNALS AS THEY ARE TRANSMITTED THROUGH THE EXCITATORY PATHWAYS OF THE RETINA It is well known that responses of rods are much slower than those of cones. Figure 21.3 illustrates the kinetic differences between these two types of photoreceptors. One important question has been whether signal transmission in the retina is matched in any way to the kinetics of the rod and cone light responses. An elegant study in turtle retina demonstrated the differences in signal delay through the ON and OFF pathways and the slower conduction of rod signals versus cone signals. Single rods or cones, impaled with a microelectrode, were depolarized and hyperpolarized with current. RGC responses were simultaneously recorded (Baylor and Fettiplace, 1977a). The latency for the signal in the cone to OFF RGC pathway was on the order of 100 msec. Latencies for cone to ON RGCs and rod to RGCs were approximately 1.5-fold longer for comparable stimulus conditions. An analysis of the kinetics of

synaptic transfer in the OFF pathway showed that rod signals were slower by approximately fivefold, comparable to the differences in the kinetics of the rod and cone single-photon responses (Baylor and Fettiplace, 1977b). These findings reveal that signal transfer is faster in OFF pathways and that the conduction of rod signals is slower than that of cone signals.

Many studies have investigated the temporal properties of synaptic transmission at the photoreceptor and bipolar cell synapses. One important result is that the delays observed by electrical stimulation, discussed above, are not reflected in the speed of glutamate release from the synaptic terminals. Exocytosis of glutamate from photoreceptor and bipolar terminals can be very fast. In fish retina, pulses of transretinal currents were used to depolarize photoreceptors. Glutamate release was monitored by recording membrane potentials in horizontal cells. Evoked postsynaptic potentials were recorded within 2 msec of the stimulus (Kaneko and Shimazaki, 1976). In ground squirrel, single cones were depolarized with a patch pipette while recording the response of bipolar cells (DeVries and Schwartz, 1999). The synaptic currents were similarly evoked with delays of ~ 1 msec. Depolarization-evoked exocytosis in goldfish bipolar terminals occurred within 1 msec (Mennerick and Matthews, 1996). Electrical stimulation of single bipolar cells in newt retina evoked glutamatergic currents in simultaneously recorded ganglion cells with a delay on the order of just a few milliseconds (Matsui et al., 1998). In other experiments in which isolated catfish horizontal cells were used to detect stimulated release from goldfish bipolar cells, AMPA receptor-mediated currents in the horizontal cells were detected within 1 msec (von Gersdorff et al., 1998). These studies indicate that the glutamatergic synapses are inherently capable of releasing vesicles with a very short delay. Delays in the transmission of visual-evoked signals must be accounted for by other mechanisms.

No comprehensive kinetic model of signal transfer in the excitatory pathways has been formulated to date. However, experimental studies in the outer retina do show that some of the differences between ON and OFF pathways and between rod and cone signaling can be accounted for by temporal filtering in the transfer of signals from the photoreceptors. Dim light flashes were recorded simultaneously in rod–horizontal cell and cone–horizontal cell pairs. Analysis of synaptic transfer characteristics showed that signal transfer from the rods was slowed approximately 8- to 10-fold compared to transfer from cones (Schnapf and Copenhagen, 1982). A similar analysis estimated that cone to ON bipolar cell transfer was approximately 10-fold slower than the transfer from cones to OFF bipolar cells (Copenhagen et al., 1983). Figure 21.4 shows the impulse response function of synaptic transfer from rods and cones to the H1 type of horizontal cell in turtle retina. Also shown

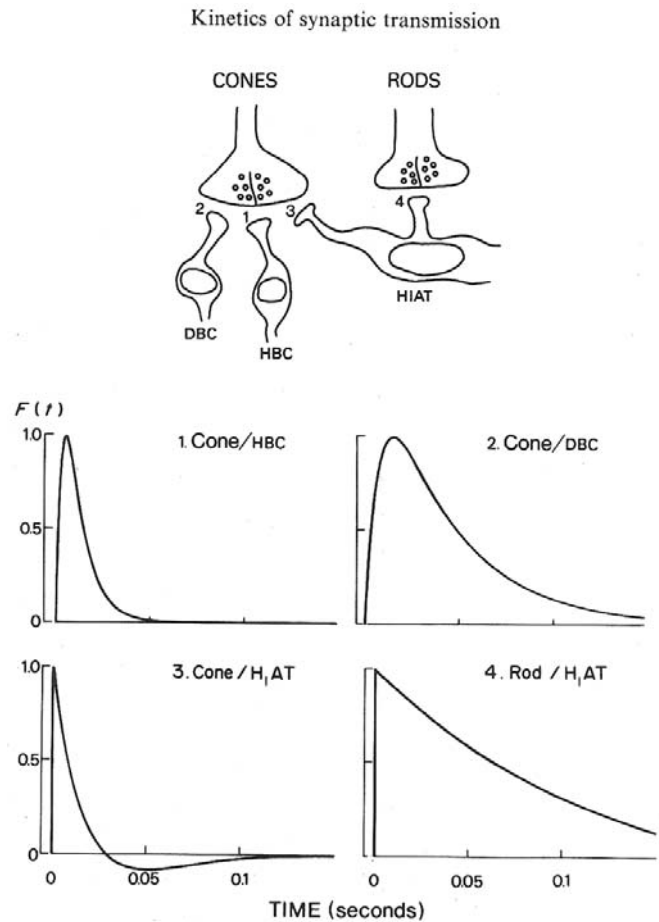


FIGURE 21.4. Synaptic impulse responses of bipolar and horizontal cells. These functions represent the waveform produced in postsynaptic cells in response to a brief depolarization of the synaptic terminals of the rods or cones. The kinetics of the cone to horizontal cell transfer is approximately 10 times faster than the transfer to the same cell from rods. The transfer from cones to OFF bipolar cells (HBCs) is several-fold faster than the transfer to the ON bipolar cells (DBCs). (Taken from Copenhagen et al., 1983.)

is the impulse response function for cone to ON and OFF bipolar cells in turtle retina.

A recent study in ground squirrels shows that synaptic transfer from cones to one type of cone-bipolar cell (b2-type) is mediated by kainate glutamate receptors. In contrast, synaptic transmission from cones to b3- and b7-type bipolar cells is mediated by AMPA-type receptors. The AMPA receptors remained desensitized longer than the kainate receptors in this retina. Temporally, this confers a much lower frequency response on signal transfer from the cone to b3 and b7 bipolar cells (DeVries, 2000). As cone to bipolar cell and bipolar cell to RGC synapses are studied in more detail, many variations in the kinetics of synapses between specific cell types will undoubtedly be revealed.

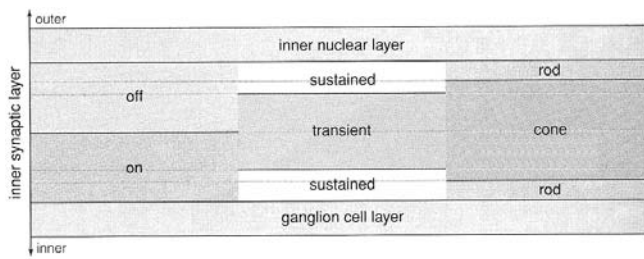


FIGURE 21.5. Stratification of transient and sustained responses in the IPL. ON and OFF responses are transmitted to postsynaptic cells in the proximal and distal halves, respectively, of the IPL. Sustained responses and rod signals are transferred closer to the inner and outer border of the IPL. Cone signals and transient responses are transmitted preferentially at the middle of the IPL. (Taken from Rodieck, 1998.)

TRANSIENT COMPONENTS OF LIGHT RESPONSES ARE ACCENTUATED IN SOME OF THE EXCITATORY RETINAL PATHWAYS In the outer retina, photoreceptors have sustained responses to light. In the inner retina, many amacrine and ganglion cells respond only to the onset and termination of stimuli. The responses of these transient cells encode light-dark transitions. In ganglion cells the form of light-evoked responses to steps of light ranges from brief transient burst of action potentials at the onset or termination of the light to a more sustained discharge either during or after light onset.

Several mechanisms work in coordination to generate the transient responses observed in the inner retinal neurons. Before discussing these alternatives, it is interesting to note that there is a morphological correlate of the sustained and transient response patterns. Several studies have revealed a functional lamination of response patterns across the IPL. As shown in Figure 21.5 (Rodieck, 1998), retinal neurons with synaptic processes at the distal and proximal margins of the IPL tend to have a greater sustained component in their light responses. Neurons with processes closer to the middle of the IPL tend to be more transient. A recent study in rabbit retina utilized a combination of electrophysiological recording and intracellular staining of RGCs to elegantly document this anatomical/physiological separation of transient and sustained responses across the IPL (Roska and Werblin, 2001).

Given that in response to a sustained depolarization, the spike discharge patterns of many neurons in the CNS decline, one must consider the possibility that a similar spike train adaptation accounts for the transience in the retina. By this mechanism, time-varying conductances intrinsic to these inner retinal neurons would truncate the more sustained light responses. This idea has received no experimental verification, as no difference has been observed in the membrane properties of transient versus sustained retinal cells. Currents injected into these different classes of cell gener-

ally produce sustained spiking. The transience must then be attributed to temporal modulation of synaptic inputs. This could result from either transient release of excitatory synaptic neurotransmitter from the bipolar terminals due to inherent ionic processes within these neurons, or from synaptic interactions between bipolar, amacrine, and RGCs that actively truncate the responses. Evidence exists for both mechanisms.

A recent study in salamander retina suggests that at least part of the mechanisms creating transient responses may reflect temporal differentiation at the inputs to bipolar cells in the outer plexiform layer (OPL). It was reported that ON bipolar cells can be classified into transient and sustained groups based on the waveform of their light responses. Pharmacological manipulations led to the suggestion that synaptic transduction in the dendrites of these two classes of cell conferred different degrees of transience (Awatramani and Slaughter, 2000). This hypothesis, while appealing, awaits confirmation. Surprisingly, no other studies examining bipolar cell responses have identified two groups of kinetically separable ON bipolar cell classes.

Amacrine cells are known to make synaptic contacts directly onto RGC dendrites and, via reciprocal synapses, onto the axon terminals of bipolar cells. Amacrine cells serve as inhibitory interneurons, releasing either GABA or glycine from their synapses. Synaptic inhibitory inputs could therefore modulate excitation, and hence the transience of responses, through feedforward or feedback pathways. Some experimental results support a feedforward component. Many ganglion cells are inhibited by GABA (Belgium et al., 1984), so it is plausible that amacrine cell inputs could shorten the excitatory response by offsetting the depolarization induced by the glutamatergic inputs. Evidence for this temporal truncation in RGCs was shown in salamanders (Bieda and Copenhagen, 2000). A large group of studies support a feedback mechanism for amacrine cell-mediated truncation of the responses. Functional GABA receptors are found on synaptic terminals of isolated bipolar cells (Tachibana and Kaneko, 1987) and GABA currents resulting from amacrine cell stimulation are recorded from bipolar cells in slice preparations (Lukasiewicz and Shields, 1998). Analysis of GABA receptor subtypes supports the idea that a majority of the feedback to bipolar cells is mediated by the slower decaying GABA_C-type receptors and feedforward is mediated by the GABA_A subunit (Lukasiewicz and Shields, 1998; Shields et al., 2000).

It is very likely that cellular processes in the bipolar cell terminals might contribute to transience. Support for the idea that amacrine cell synaptic interactions cannot account for all the transience is derived from experiments in which light responses are recorded from RGCs in the presence of GABA and glycine receptor antagonists. The light responses to a step of light are prolonged under these conditions;

however, they remain transient (Bieda and Copenhagen, 2000). Some of the inherent mechanisms within bipolar cell synaptic terminals that could truncate glutamate release include (1) depletion of vesicles in the bipolar cell synaptic terminals upon stimulation (von Gersdorff and Matthews, 1997) and (2) transient calcium currents that regulate exocytosis. In rodent bipolar cells, a rapidly inactivating calcium current has been identified (Kaneko et al., 1989; Pan, 2000). Calcium entry through this calcium channel has been shown to modulate exocytosis (Pan et al., 2001).

In summary it is evident that a number of processes and neuronal interactions in the excitatory pathways serve to transform light responses such that temporal changes are amplified.

Cellular mechanisms of excitatory transmission

SIGNAL TRANSFER RELIES ON VESICLE-MEDIATED SYNAPTIC TRANSMISSION Vesicle-mediated synaptic neurotransmission is the dominant mode at the glutamatergic synapses in retina. Immunocytochemical, electrophysiological, and morphological studies demonstrate the existence of the molecular machinery that underlies vesicle-mediated exocytosis and the existence of spontaneous quantal events in the postsynaptic retinal neurons.

Virtually every electronmicrograph ever published shows small clear vesicles filling the synaptic terminals of photoreceptor and bipolar cells. The size of these vesicles is comparable to synaptic vesicles in CNS neurons, but the quantity of vesicles is many orders of magnitude greater. Terminals of rod bipolar cells of goldfish retina contain 500,000 to 700,000 vesicles (von Gersdorff et al., 1996). Electron microscopy also reveals a dense ribbon-like structure in the terminals of both bipolar and photoreceptor cells. Often, vesicles are aligned along the edge of this ribbon, suggesting a mechanism to sequester vesicles for more efficient release near the “active site,” presumed to be at the juncture between the ribbon and the basal surface of the photoreceptors. Rod photoreceptors have fewer ribbons than cones. In macaque monkey retina, cones have 20 to 40 synaptic ribbons (Chun et al., 1996). MbI-type bipolar cell terminals of goldfish have upwards of 50 ribbons (von Gersdorff et al., 1996).

Photoreceptor and bipolar terminals generally express the full complement of synaptic proteins thought to be involved in vesicle-mediated synaptic transmission at glutamatergic synapses in the CNS (von Kriegstein et al., 1999; Morgans, 2000). However, there are some notable differences in which Synapsin I and rabphilin are absent in retina. Synapsin III is expressed and may substitute for Synapsin I. Vesicular glutamate transporters, proteins that catalyze the concentration of glutamate in vesicles, are richly expressed in both photoreceptor and bipolar terminals (Johnson et al., 2003).

Membrane capacitance changes provide evidence for vesicle-mediated quantal release of neurotransmitter from bipolar and photoreceptor cells. In these experiments, depolarization of presynaptic terminals using whole-cell patch pipettes produces a calcium-dependent increase in membrane capacitance that reflects the exocytosis-associated incorporation of vesicle membrane into the plasma membrane of the neurons (Lagnado et al., 1996; Rieke and Schwartz, 1996; von Gersdorff and Matthews, 1994). Simultaneous measurement of capacitance and glutamate release from MbI goldfish bipolar cells demonstrated that a calcium-dependent capacitance increase on depolarization was linked to glutamate release (Sakaba et al., 1997).

Postsynaptically recorded synaptic currents show glutamatergic “events” that result from exocytosis of single vesicles in the presynaptic terminals. AMPA receptor-mediated synaptic events typical of those observed in CNS neurons have been recorded in ganglion cells and bipolar cells (Maple et al., 1994; Taylor et al., 1995). Estimates of the rates of release in darkness range from 22 quanta/sec/synapse (cat bipolar cells; Freed, 2000) to ~30 quanta/sec/synapse (turtle cones; Ashmore and Copenhagen, 1983) to ~40 quanta/sec/synapse (cat rods; Rao et al., 1994).

The modest rate of tonic release is considerably below the rate that can be evoked by depolarization of individual bipolar cells. Analysis of the magnitude and kinetics of capacitance changes in MbI bipolar cells reveals rate on the order of 50,000 vesicles per second for voltage steps from -60 to 0 mV (von Gersdorff and Matthews, 1994; von Gersdorff et al., 1996). However, the rates estimated for in vivo tonic release are much lower, suggesting that the glutamatergic retinal neurons operate in the range in which vesicle turnover is much lower than can be evoked with artificial stimulation.

BOTH CALCIUM ENTRY AND EXTRUSION REGULATE TRANSMISSION OF EXCITATORY SIGNALS In common with all glutamatergic synapses, glutamate release from photoreceptors and bipolar cells is regulated by the depolarization-stimulated influx of calcium through voltage-activated calcium channels. These channels are so-called high voltage activated L-type channels. The relationship between presynaptic voltage, calcium channel activation, and glutamate release from photoreceptor terminals was derived from some elegant experiments measuring endogenous glutamate release from toad photoreceptors (Schmitz and Witkovsky, 1997). This relation is plotted in Figure 21.6. Interestingly, a novel subtype of the pore-forming α subunit of an L-type channel was isolated from human rods ($\alpha 1F$; Strom et al., 1998), suggesting that photoreceptor calcium channels are structurally distinct from other voltage-gated L-type calcium channels. It should be noted that in cones, an additional

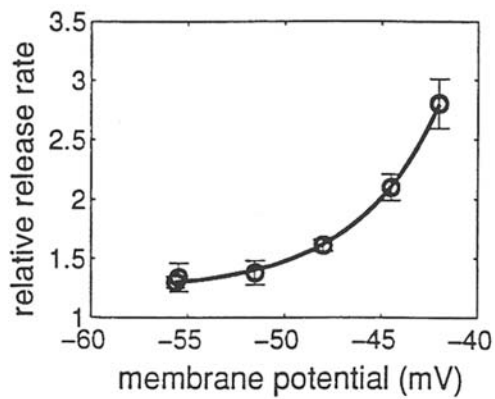


FIGURE 21.6. Relationship between rod voltage and calcium current-mediated glutamate release. The separate relations between light and glutamate release and between light and membrane potential are combined in this figure. By parameterizing the data with respect to light, the dependence of glutamate release on membrane potential is derived. The solid curve shows the activation of the L-type calcium current of rods. This Boltzmann curve is well-fitted to the data points, supporting the hypothesis that L-type calcium channels play a major role in regulating glutamate release. (Taken from Witkovsky et al., 1997.)

component of Ca^{2+} flux may be contributed by a cGMP-gated Ca^{2+} -permeable channel (Rieke and Schwartz, 1994; Savchenko et al., 1997). In bipolar cells, glutamate release is modulated by L-type currents (Tachibana et al., 1993) and T-type calcium currents (Pan et al., 2001).

The direction of light-evoked membrane polarization in photoreceptors and OFF bipolar cells makes it important to consider the role of calcium extrusion in controlling the kinetics of these responses. Light hyperpolarizes these neurons with the resultant closing of calcium channels. Therefore, light-evoked signals transmitted to the postsynaptic neurons are carried by a net decrease in the rate of glutamate released from the terminals. Thus, the kinetics of these signals will depend on the rate at which calcium is extruded from the terminals. In photoreceptors, calcium extrusion is performed exclusively by PMCA (plasma membrane calcium ATPase) transporters (Krizaj and Copenhagen, 1998; Morgans et al., 1998). PMCA transporters are also expressed in bipolar cell terminals (Krizaj et al., 2002).

GLUTAMATE/GLUTAMINE RECYCLING REPLENISHES EXCITATORY GLUTAMATERGIC TERMINALS Glutamate/glutamine recycling plays an important role in maintaining a source of synaptic glutamate for transmission in the nervous system and in the retina, as well. In the basic recycling pathway, synaptically released glutamate is taken up by Na-dependent transporters located in the plasma membrane of nearby glial cells. The glutamate is amidated by glutamine synthetase (GS) to generate glutamine. Glutamine is then transported out of the glial cells to the extracellular space, where it is

transported back into presynaptic neuronal terminals to be converted into glutamate by mitochondrial-bound phosphate-activated glutaminase (PAG). A full description of the evidence supporting recycling is reviewed by Broer and Brookes (2001). Figure 21.7 illustrates glutamate/glutamine recycling.

Strong evidence supports the hypothesis that glutamate/glutamine recycling plays an important role in maintaining glutamatergic synaptic transmission in retina. Here, glutamate is taken up by Müller cells, the radial glia of retina. After conversion from glutamate, glutamine is “released” from these Müller cells to be taken up by photoreceptors and bipolar cells. Briefly, supportive evidence includes the findings that: (1) photoreceptor and bipolar cell synapses are enveloped by Müller cell processes (Sarantis and Mobbs, 1992); (2) Müller cells express GLAST or GLAST-like high-affinity plasmalemmal-bound glutamate transporters, which have been very well characterized electrophysiologically (Rauen and Weissner, 2000); (3) Müller cells express glutamine synthetase (Rieke and Norenberg, 1977); (4) inhibition of GS with MSO depletes photoreceptors and bipolar cells of glutamate and causes a buildup of glutamate in the Müller cells (Barnett et al., 2000; Pow and Robinson, 1994); (5) retinal incubation in MSO, an inhibitor of GS, reduces the b-wave of the ERG, an indicator of

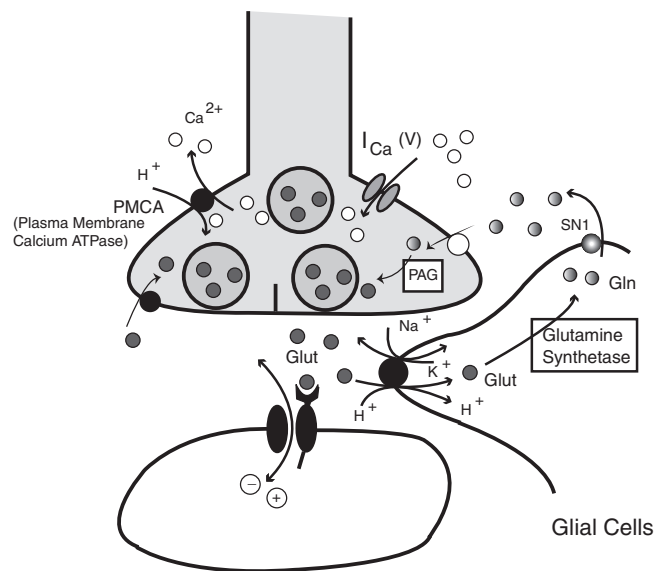


FIGURE 21.7. Schematic diagram of glutamate/glutamine recycling at glutamatergic synapses in retina. Glutamate released from presynaptic neurons activates receptors on the postsynaptic cells and then is sequestered into Müller glial cells, where it is converted to glutamine. Glutamine is then shuttled back to the presynaptic neurons, where it is converted back to glutamate by a phosphate-activated glutaminase (PAG). Also shown in this diagram are glutamate transporters that sequester glutamate directly back into the presynaptic terminals. In addition, the PMCA extrusion pump and calcium channels are illustrated. (See color plate 8.)

photoreceptor to bipolar synaptic transmission (more importantly, the b-wave can be “rescued” in MSO by exogenous glutamine, consistent with the hypothesis that glutamine provides a substrate to restore glutamate [Barnett et al., 2000]); and (6) PAG, which converts glutamine to glutamate, has been immunolocalized to photoreceptors (Gebhard, 1992).

Other pathways exist by which glutamate used for synaptic transmission could be replenished without going through the glutamate/glutamine cycle. Because most of the glutamate taken into astrocytes is oxidized rather than being converted to glutamine, substrates such as lactate, malate, and alpha-ketoglutarate are proposed as precursors for glutamate in neurons (Schousboe et al., 1997). These suggestions are not consistent with in vivo nuclear magnetic resonance studies, which show that a large percentage of glutamine is incorporated into neuronal glutamate (Sibson et al., 2001). In retina inhibition of GS with MSO depleted neuronal glutamate pools, as shown with immunohistochemistry and electrophysiology. This occurred in spite of the availability of other potential substrates for glutamate synthesis (Barnett et al., 2000). Therefore, glutamate/glutamine recycling very likely plays a major role in replenishing synaptic glutamate in retinal neurons.

SYNAPTICALLY RELEASED GLUTAMATE CAN CONTROL THE TRANSMISSION OF LIGHT-EVOKED SIGNALS THROUGH FEEDBACK MECHANISMS There are examples at both excitatory and inhibitory synapses in the CNS that exocytosed neurotransmitter autoregulates further release by feeding back signals to the presynaptic terminals (e.g., Trombley and Westbrook, 1992). In the excitatory pathways of retina several such feedback mechanisms have been proposed. The metabotropic glutamate receptor mGlu-R8 has been immunolocalized to photoreceptors in rat retina (Koulen et al., 1999). Intracellular calcium levels in isolated photoreceptors are decreased by exogenous glutamate and by the class III metabotropic agonist APB (L-2-amino-4-phosphonobutyrate). This decrease in calcium is thought to reduce glutamate release.

Additionally, activation of a plasmalemmal glutamate transporter in synaptic terminals of salamander cones (see Fig. 21.7) is proposed to activate an anionic current that hyperpolarizes cones. Here synaptically released glutamate is proposed to inhibit further release as it is being taken back up into the terminals (Picaud et al., 1995).

A third separate feedback mechanism has also been proposed. It has recently been shown that protons released from synaptic vesicles inhibit the calcium current of ground squirrel cones (DeVries, 2001). Sequestration of glutamate into synaptic vesicles is known to require a proton gradient that acidifies the inside of the vesicles. When glutamate is released, the sequestered protons are also released. Inhibi-

tion of adjacent calcium channels serves to inhibit subsequent calcium-triggered release of glutamate (DeVries, 2001).

In the inner retina, it is proposed that activation of an APB-sensitive metabotropic glutamate receptor on bipolar synaptic terminals can attenuate release of glutamate from these terminals (Awatramani and Slaughter, 2001). The magnitudes of light- and potassium-evoked EPSCs and the rates of spontaneous EPSCs in salamander ganglion cells were reduced in APB, which is thought to be acting presynaptically on the axon terminals of bipolar cells. Functionally, all of the above autofeedback mechanisms would help to extend the dynamic range of the each synapse. Part of this action would be to prevent the synapse from saturating.

EXCITATION IS SIGNED BY BOTH IONOTROPIC AND METABOTROPIC GLUTAMATE RECEPTORS AND GLUTAMATE TRANSPORTERS Most of the currently cloned glutamate neurotransmitter receptors are expressed in retina. Little is known about what specific functional attributes are conferred upon signal transmission by the differential expression patterns of the receptor subunits. Clear evidence, however, shows that the dichotomy between the response properties of ON and OFF bipolar cells derives directly from the expression of the metabotropic (G-protein linked) mGlu-R6 receptor in ON bipolar cells versus the ionotropic (AMPA and kainate-type) receptors, which mediate the responses of OFF bipolar cells. It is also becoming a truism that RGC light responses are mediated by the simultaneous activation of NMDA- and AMPA-type ionotropic glutamate receptors.

ON bipolar cells are hyperpolarized by exogenous glutamate and the class III metabotropic receptor agonist L-AP4. Light, by decreasing glutamate release from photoreceptors, depolarizes the ON bipolar cells. Much evidence verifies that the action of glutamate at the photoreceptor–ON bipolar synapses is mediated by the mGlu-R6 receptor. Antibodies to mGlu-R6 localize to the dendrites of ON bipolar cells. The product of the reporter gene (*LacZ*) attached to mGluR6 is localized similarly to the dendrites of these cells (Nomura et al., 1994; Vardi et al., 2000). A mouse strain in which the *mGluR6* gene has been deleted has a very much reduced light-evoked b-wave in the ERG and ON responses recorded in the superior colliculus (Masu et al., 1995; Sugihara et al., 1997).

The slowness of the light response in ON bipolar cells, compared to OFF bipolar cells, can be attributed in part to the fact that mGlu-R6 modulation of the ionic conductances in the cell requires activation of a G-protein and subsequent regulation of one or more enzymatic steps. In contrast, activation of OFF bipolar cells is mediated by the rapid opening of an ionic channel that is part of the ionotropic glutamate receptors on these cells. Figure 21.8 illustrates glutamate activation of ON and OFF bipolar cells.

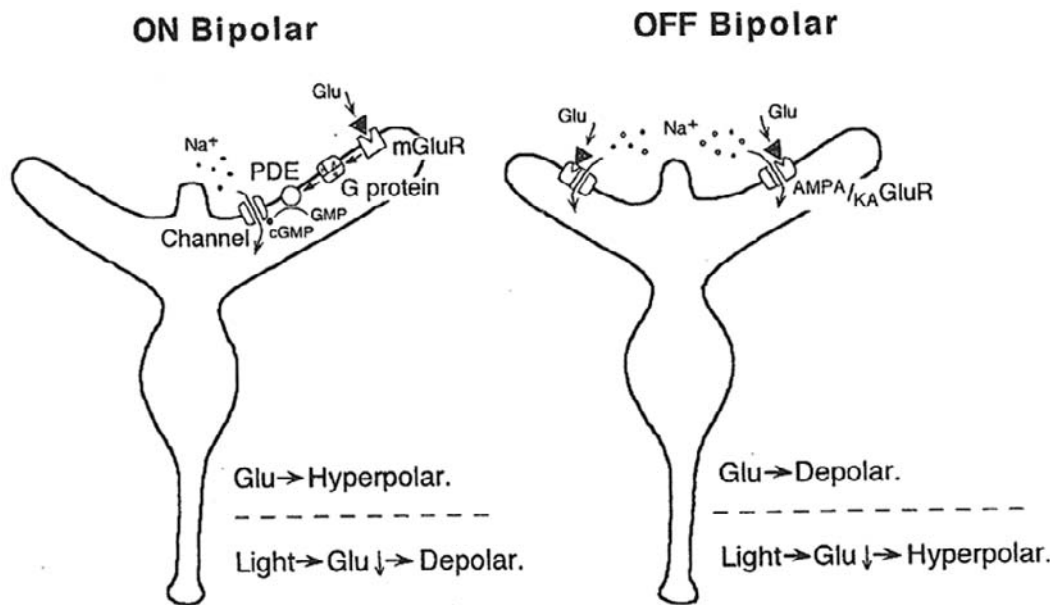


FIGURE 21.8. Schematic diagram of proposed glutamate-mediated transduction mechanisms in ON and OFF bipolar cells. In ON cells, glutamate activates an mGluR6 metabotropic receptor, which triggers an enzymatic cascade consisting of GTP-binding protein and phosphodiesterase (PDE). PDE activity controls the level of cyclic GMP in the cells. cGMP-gated channels regulate current flow through cationic channels in the plasma membrane of

these cells. In OFF cells, glutamate activates an ionotropic receptor that directly opens a nonselective cationic channel. In darkness glutamate release is maximal. Light, by reducing activation of post-synaptic glutamate receptors, produces a depolarization in the ON cells and a hyperpolarization in the OFF bipolar cells. (Taken from Kaneko, 1999.)

One unresolved functional question regarding glutamatergic activation of ON bipolar cells is the role of ionotropic glutamate receptor subunits found on the ON bipolar cell dendrites. In different species various NMDA receptor (NRI, NR2D) and AMPA receptor subunits (GluR2, GluR2/3, and GluR4) are immunolocalized to ON bipolar cells (Hughes, 1997; Hughes et al., 1992; Peng et al., 1995). The role of these ionotropic receptors remains unknown.

OFF bipolar cells can be potentially driven by one or more ionotropic glutamate receptors. In situ hybridization studies reveal mRNA expression of GluR1-7 and KA1-2 subunits in mammalian OFF bipolar cells (reviewed in Thoreson and Witkovsky, 1999; Hamassaki-Britto et al., 1993). Antibody staining suggests the expression of GluR4, GluR6/7, and KA2 in presumed OFF bipolar cells (reviewed in Thoreson and Witkovsky, 1999; Hack et al., 2001). Electrophysiological recordings of OFF bipolar cells reveal that light responses and glutamate currents are abolished almost entirely by CNQX, an AMPA/kainate receptor antagonist (cat: Sasaki and Kaneko, 1996; rat: Euler et al., 1996; zebra fish: Connaughton and Nelson, 2000). Moreover, spontaneous EPSCs recorded in OFF bipolar cells of newt and salamander are blocked by CNQX (Kawai, 1999; Maple et al., 1994). In newt these spontaneous EPSCs were prolonged by cyclothiazide, an AMPA receptor-specific drug that reduces desensitization (Kawai, 1999). In ground squirrel, one type

of OFF bipolar cell is driven by kainate receptors and two other classes are driven by AMPA receptors (DeVries, 2000). These findings strongly support a functional role for AMPA and kainate receptors in the transmission of signals from photoreceptors to OFF bipolar cells.

In fish retina, cone and rod inputs to ON bipolar cells activate two different synaptic mechanisms (Saito et al., 1978; Nawy and Copenhagen, 1987). Rod inputs are mediated by the mGluR6 receptor. The cone inputs may be mediated by an anionic current that is produced when glutamate is transported into the bipolar cell. In zebra fish ON bipolar cells, glutamate activates a chloride conductance that is reduced by lithium substitution for sodium (Connaughton and Nelson, 2000). In white perch, glutamate evokes a chloride current that is insensitive to ionotropic glutamate receptor antagonists, CNQX and DNQX, and is not activated by APB or quisqualate, metabotropic glutamate receptor agonists (Grant and Dowling, 1995). Taken together, these results suggest a glutamate transporter-activated current mediates cone inputs. In contrast, other findings suggest that the cone inputs are mediated by modulation of a potassium conductance. Goldfish ON bipolar cells exhibit a glutamate-activated current that is cesium sensitive and has a negative reversal potential (Nawy and Copenhagen, 1990). Because cesium blocks potassium conductances, these findings are taken as evidence that glutamate regulates a potassium conductance in these ON bipolar cells.

In the inner retina, bipolar-RGC synapses appear to be somewhat more straightforward than the photoreceptor-bipolar synapses of the OPL. Light-evoked glutamatergic excitation of RGCs by bipolar cells relies solely on the concomitant activation of both NMDA and non-NMDA ionotropic receptors. Light-evoked synaptic currents and spiking is blocked when both NMDA and NMDA glutamate receptors are antagonized pharmacologically. However, separate activation of either NMDA or non-NMDA receptors will support light responses in the RGCs (Diamond and Copenhagen, 1993; Mittman et al., 1990). The non-NMDA receptors are most likely AMPA-type, as cyclothiazide enhances the light responses and AMPA-receptor antagonists, including NBQX, GYKI52466, and GYKI53655, suppress light responses (Cohen and Miller, 1994; Lukasiewicz et al., 1995, 1997).

An interesting paradox concerns the localization of NMDA and non-NMDA receptors on the RGCs. Light-evoked responses have dual NMDA and non-NMDA components at all light intensities (Diamond and Copenhagen, 1993). It would be presumed that, similar to other glutamatergic synapses in the CNS, the receptors would therefore be colocalized adjacent to the site of glutamate release from bipolar cells. Interestingly, spontaneous quantal release activates an AMPA-mediated response only. Even though the NMDA receptors have a higher sensitivity to glutamate, no NMDA component has been detected in the quantal events (Matsui et al., 1998; Taschenberger and Grantyn, 1995; Taylor et al., 1995). One possible explanation for the paradox is that NMDA receptors are localized in perisynaptic regions of the synapse and are only stimulated by evoked release of several vesicles (Taylor et al., 1995). Recent findings in rat retina demonstrated that blockade of glutamate uptake caused spontaneous EPSCs to acquire an NMDA component. This argues that glutamate uptake limits the activation of NMDA receptors during release of single quanta (Chen and Diamond, 2002).

Summary

Extensive work by scores of investigators has given us a reasonably good idea of the major features of glutamatergic synaptic transmission in retina. Many of the properties of synaptic transmission, such as the type of glutamate receptors, calcium control of exocytosis, and glutamate uptake, are closely analogous to those utilized by glutamatergic neurons in the CNS. Other features, such as the slower signal transfer and tonic release of neurotransmitter, are unique to the retina. Future studies will reveal much more about how the cellular signaling of visual information is modulated by light and dark and paracrine/hormonal influences.

Acknowledgements

The author gratefully acknowledges research support from NIH, Research to Prevent Blindness (DRC is the recipient of a Senior Investigator's Award), and That Man May See, UCSF.

REFERENCES

- Aho, A. C., K. Donner, S. Helenius, L. O. Larsen, and T. Reuter, 1993. Visual performance of the toad (*Bufo bufo*) at low light levels: retinal ganglion cell responses and prey-catching accuracy, *J. Comp. Physiol. Abstr.*, 172:671–682.
- Aho, A. C., K. Donner, C. Hyden, L. O. Larsen LO, et al., 1988. Low retinal noise in animals with low body temperature allows high visual sensitivity, *Nature*, 334:348–350.
- Ashmore, J. F., and D. R. Copenhagen, 1983. An analysis of transmission from cones to hyperpolarizing bipolar cells in the retina of the turtle, *J. Physiol.*, 340:569–597.
- Ashmore, J. F., and G. Falk, 1980. Responses of rod bipolar cells in the dark-adapted retina of the dogfish, *Scyliorhinus canicula*, *J. Physiol.*, 300:115–150.
- Awatramani, G. B., and M. M. Slaughter, 2001. Intensity-dependent, rapid activation of presynaptic metabotropic glutamate receptors at a central synapse, *J. Neurosci.*, 21:741–749.
- Awatramani, G. B., and M. M. Slaughter, 2000. Origin of transient and sustained responses in ganglion cells of the retina, *J. Neurosci.*, 20:7087–7095.
- Barnett, N. L., D. V. Pow, and S. R. Robinson, 2000. Inhibition of Müller cell glutamine synthetase rapidly impairs the retinal response to light, *Glia*, 30:64–73.
- Baylor, D. A., 1987. Photoreceptor signals and vision. Proctor lecture, *Invest Ophthalmol Vis. Sci.*, 28(1):34–49.
- Baylor, D. A., M. G. Fuortes, and P. M. O'Bryan, 1971. Receptive fields of cones in the retina of the turtle, *J. Physiol.*, 214:265–294.
- Baylor, D. A., and R. Fettiplace, 1977a. Transmission from photoreceptors to ganglion cells in turtle retina, *J. Physiol.*, 271:391–424.
- Baylor, D. A., and R. Fettiplace, 1977b. Kinetics of synaptic transfer from receptors to ganglion cells in turtle retina, *J. Physiol.*, 271:425–448.
- Belgum, J. H., D. R. Dvorak, and J. S. McReynolds, 1984. Strychnine blocks transient but not sustained inhibition in mudpuppy retinal ganglion cells, *J. Physiol.*, 354:273–286.
- Belgum, J. H., and D. R. Copenhagen, 1988. Synaptic transfer of rod signals to horizontal and bipolar cells in the retina of the toad (*Bufo marinus*), *J. Physiol.*, 396:225–245.
- Bieda, M. C., and D. R. Copenhagen, 2000. Inhibition is not required for the production of transient spiking responses from retinal ganglion cells, *Vis. Neurosci.*, 17:243–254.
- Bisti, S., C. Gargini, and L. M. Chalupa, 1998. Blockade of glutamate-mediated activity in the developing retina perturbs the functional segregation of ON and OFF pathways, *J. Neurosci.*, 18:5019–5025.
- Bodnarenko, S. R., and L. M. Chalupa, 1993. Stratification of ON and OFF ganglion cell dendrites depends on glutamate-mediated afferent activity in the developing retina, *Nature*, 364:144–146.
- Bodnarenko, S. R., G. Yeung, L. Thomas, and M. McCarthy, 1999. The development of retinal ganglion cell dendritic stratification in ferrets, *Neuroreport*, 10:2955–2959.

- Broer, S., and N. Brookes, 2001. Transfer of glutamine between astrocytes and neurons, *J. Neurochem.*, 77:705–719.
- Chen, S., and J. S. Diamond, 2002. Synaptically released glutamate activates extrasynaptic NMDA receptors on cells in the ganglion cell layer of rat retina, *J. Neurosci.*, 22:2165–2173.
- Chun, M. H., U. Grunert, P. R. Martin, and H. Wässle, 1996. The synaptic complex of cones in the fovea and in the periphery of the macaque monkey retina, *Vis. Res.*, 36:3383–3395.
- Cohen, E. D., and R. F. Miller, 1994. The role of NMDA and non-NMDA excitatory amino acid receptors in the functional organization of primate retinal ganglion cells, *Vis. Neurosci.*, 11:317–332.
- Connaughton, V. P., and R. Nelson, 2000. Axonal stratification patterns and glutamate-gated conductance mechanisms in zebrafish retinal bipolar cells, *J. Physiol.*, 524 Pt 1:135–146.
- Cook, J. E., and D. L. Becker, 1995. Gap junctions in the vertebrate retina, *Microsc. Res. Tech.*, 31:408–419.
- Copenhagen, D. R., and W. G. Owen, 1976. Coupling between rod photoreceptors in a vertebrate retina, *Nature*, 260:57–59.
- Copenhagen, D. R., J. F. Ashmore, and J. K. Schnapf, 1983. Kinetics of synaptic transmission from photoreceptors to horizontal and bipolar cells in turtle retina, *Vis. Res.*, 23:363–369.
- Copenhagen, D. R., S. Hemila, and T. Reuter, 1990. Signal transmission through the dark-adapted retina of the toad (*Bufo marinus*). Gain, convergence, and signal/noise, *J. Gen. Physiol.*, 95:717–732.
- DeVries, S. H., and D. A. Baylor, 1995. An alternative pathway for signal flow from rod photoreceptors to ganglion cells in mammalian retina, *Proc. Natl. Acad. Sci. USA*, 92:10658–10662.
- DeVries, S. H., and E. A. Schwartz, 1999. Kainate receptors mediate synaptic transmission between cones and OFF bipolar cells in a mammalian retina, *Nature*, 397:157–160.
- DeVries, S. H., 2000. Bipolar cells use kainate and AMPA receptors to filter visual information into separate channels, *Neuron*, 28:847–856.
- DeVries, S. H., 2001. Exocytosed protons feedback to suppress the Ca^{2+} current in mammalian cone photoreceptors, *Neuron*, 32:1107–1117.
- Diamond, J. S., and D. R. Copenhagen, 1993. The contribution of NMDA and non-NMDA receptors to the light-evoked input-output characteristics of retinal ganglion cells, *Neuron*, 11:725–738.
- Dowling, J., 1987. *The Retina*. Cambridge, MA: Harvard University Press.
- Euler, T., H. Schneider, and H. Wässle, 1996. Glutamate responses of bipolar cells in a slice preparation of the rat retina, *J. Neurosci.*, 16:2934–2944.
- Fain, G. L., A. M. Granda, and J. M. Maxwell, 1977. Voltage signal of photoreceptors at visual threshold, *Nature*, 265:181–183.
- Gebhard, R., 1992. Histochemical demonstration of glutamate dehydrogenase and phosphate-activated glutaminase activities in semi-thin sections of the rat retina, *Histochem.*, 97:101–103.
- Grant, G. B., and J. E. Dowling, 1995. A glutamate-activated chloride current in cone-driven ON bipolar cells of the white perch retina, *J. Neurosci.*, 15(5 Pt 2):3852–3862.
- Hack, I., M. Frech, O. Dick, L. Peichl, and J. H. Brandstätter, 2001. Heterogeneous distribution of AMPA glutamate receptor subunits at the photoreceptor synapses of rodent retina, *Eur. J. Neurosci.*, 13:15–24.
- Hack, I., L. Peichl, and J. H. Brandstätter, 1999. An alternative pathway for rod signals in the rodent retina: rod photoreceptors, cone bipolar cells, and the localization of glutamate receptors. *Proc. Natl. Acad. Sci. USA*, 96:14130–14135.
- Hamassaki-Britto, D. E., I. Hermans-Borgmeyer, S. Heinemann, and T. E. Hughes, 1993. Expression of glutamate receptor genes in the mammalian retina: the localization of GluR1 through GluR7 mRNAs, *J. Neurosci.*, 13:1888–1898.
- Hughes, T. E., 1997. Are there ionotropic glutamate receptors on the rod bipolar cell of the mouse retina? *Vis. Neurosci.*, 14:103–109.
- Hughes, T. E., I. Hermans-Borgmeyer, and S. Heinemann, 1992. Differential expression of glutamate receptor genes (GluR1–5) in the rat retina, *Vis. Neurosci.*, 8:49–55.
- Johnson, J., N. Tian, M. S. Caywood, R. J. Reimer, R. H. Edwards, and D. R. Copenhagen, 2001. Vesicular neurotransmitter transport expression in developing postnatal rodent retina: GABA and glycine precede glutamate, *J. Neurosci.*, 23:518–529.
- Juusola, M., A. S. French, R. O. Uusitalo, and M. Weckström, 1996. Information processing by graded-potential transmission through tonically active synapses, *Trends Neurosci.*, 19:292–297.
- Kaneko, A., 1999. Responses of bipolar cells: on and off pathways, in *The Retinal Basis of Vision* (J.-I. Toyoda, M. Mrkani, A. Kaneko, and T. Saito, eds.), Amsterdam: Elsevier Science B. V.
- Kaneko, A., and H. Shimazaki, 1976. Synaptic transmission from photoreceptors to bipolar and horizontal cells in the carp retina, *Cold Spring Harb. Symp. Quant. Biol.*, 40:537–546.
- Kaneko, A., L. H. Pinto, and M. Tachibana, 1989. Transient calcium current of retinal bipolar cells of the mouse, *J. Physiol.*, 410:613–629.
- Kawai, F., 1999. Characterization of spontaneous excitatory synaptic currents in newt retinal bipolar cells, *Neurosci. Lett.*, 271:49–52.
- Kolb, H., K. A. Linberg, and S. K. Fisher, 1992. Neurons of the human retina: a Golgi study, *J. Comp. Neurol.*, 318:147–187.
- Koulen, P., R. Kuhn, H. Wässle, and J. H. Brandstätter, 1999. Modulation of the intracellular calcium concentration in photoreceptor terminals by a presynaptic metabotropic glutamate receptor, *Proc. Natl. Acad. Sci. USA*, 96:9909–9914.
- Kouyama, N., and D. W. Marshak, 1992. Bipolar cells specific for blue cones in the macaque retina, *J. Neurosci.*, 12:1233–1252.
- Krizaj, D., and D. R. Copenhagen, 1998. Compartmentalization of calcium extrusion mechanisms in the outer and inner segments of photoreceptors, *Neuron*, 21:249–256.
- Krizaj, D., S. J. Demarco, J. Johnson, E. E. Strehler, and D. R. Copenhagen, 2002. Cell-specific expression of plasma membrane calcium ATPase isoforms in retinal neurons, *J. Comp. Neurol.*, 451(1):1–21.
- Lagnado, L., A. Gomis, and C. Job, 1996. Continuous vesicle cycling in the synaptic terminal of retinal bipolar cells, *Neuron*, 17:957–967.
- Lamb, T. D., and E. J. Simon, 1976. The relation between intercellular coupling and electrical noise in turtle photoreceptors, *J. Physiol.*, 263:257–286.
- Lukasiewicz, P. D., J. E. Lawrence, and T. L. Valentino, 1995. Desensitizing glutamate receptors shape excitatory synaptic inputs to tiger salamander retinal ganglion cells, *J. Neurosci.*, 15:6189–6199.
- Lukasiewicz, P. D., J. A. Wilson, and J. E. Lawrence, 1997. AMPA-preferring receptors mediate excitatory synaptic inputs to retinal ganglion cells, *J. Neurophysiol.*, 77:57–64.
- Lukasiewicz, P. D., and C. R. Shields, 1998. Different combinations of GABA_A and GABA_C receptors confer distinct temporal properties to retinal synaptic responses, *J. Neurophysiol.*, 79:3157–3167.
- Maple, B. R., F. S. Werblin, and S. M. Wu, 1994. Miniature excitatory postsynaptic currents in bipolar cells of the tiger salamander retina, *Vis. Res.*, 34:2357–2362.

- Masu, M., H. Iwakabe, Y. Tagawa, T. Miyoshi, et al., 1995. Specific deficit of the ON response in visual transmission by targeted disruption of the mGluR6 gene, *Cell*, 80:757–765.
- Matsui, K., N. Hosoi, and M. Tachibana, 1998. Excitatory synaptic transmission in the inner retina: paired recordings of bipolar cells and neurons of the ganglion cell layer, *J. Neurosci.*, 18:4500–4510.
- Matthews, G., 1996. Neurotransmitter release, *Annu. Rev. Neurosci.*, 19:219–223.
- Mennerick, S., and G. Matthews, 1996. Ultrafast exocytosis elicited by calcium current in synaptic terminals of retinal bipolar neurons, *Neuron*, 17:1241–1249.
- Mittman, S., W. R. Taylor, and D. R. Copenhagen, 1990. Concomitant activation of two types of glutamate receptor mediates excitation of salamander retinal ganglion cells, *J. Physiol.*, 428:175–197.
- Morgans, C. W., O. El Far, A. Berntson, H. Wässle, and W. R. Taylor, 1998. Calcium extrusion from mammalian photoreceptor terminals, *J. Neurosci.*, 18:2467–2474.
- Morgans, C. W., 2000. Presynaptic proteins of ribbon synapses in the retina, *Microsc. Res. Tech.*, 50:141–150.
- Nawy S., and D. R. Copenhagen, 1987. Multiple classes of glutamate receptor on depolarizing bipolar cells in retina, *Nature*, 325:56–58.
- Nawy S., and D. R. Copenhagen, 1990. Intracellular cesium separates two glutamate conductances in retinal bipolar cells of goldfish, *Vis. Res.*, 30:967–972.
- Nelson, R., 1977. Cat cones have rod input: a comparison of the response properties of cones and horizontal cell bodies in the retina of the cat, *J. Comp. Neurol.*, 172:109–135.
- Nomura, A., R. Shigemoto, Y. Nakamura, N. Okamoto, N. Mizuno, and S. Nakanishi, 1994. Developmentally regulated postsynaptic localization of a metabotropic glutamate receptor in rat rod bipolar cells, *Cell*, 77:361–369.
- Pan, Z. H., 2000. Differential expression of high- and two types of low-voltage-activated calcium currents in rod and cone bipolar cells of the rat retina, *J. Neurophysiol.*, 83:513–527.
- Pan, Z. H., H. J. Hu, P. Perring, and R. Andrade, 2001. T-type Ca^{2+} channels mediate neurotransmitter release in retinal bipolar cells, *Neuron*, 32:89–98.
- Peng, Y. W., C. D. Blackstone, R. L. Huganir, and K. W. Yau, 1995. Distribution of glutamate receptor subtypes in the vertebrate retina, *Neurosci.*, 66:483–497.
- Peng, Y. W., Y. Hao, R. M. Petters, and F. Wong, 2000. Ectopic synaptogenesis in the mammalian retina caused by rod photoreceptor-specific mutations, *Nat. Neurosci.*, 3:1121–1127.
- Picaud, S., H. P. Larsson, D. P. Wellis, H. Lecar, and F. S. Werblin, 1995. Cone photoreceptors respond to their own glutamate release in the tiger salamander, *Proc. Natl. Acad. Sci. USA*, 92:9417–9421.
- Pow, D. V., and S. R. Robinson, 1994. Glutamate in some retinal neurons is derived solely from glia, *Neurosci.*, 60:355–366.
- Rao, R., G. Buchsbaum, and P. Sterling, 1994. Rate of quantal transmitter release at the mammalian rod synapse, *Biophys. J.*, 67:57–63.
- Rauen, T., and M. Wiessner, 2000. Fine tuning of glutamate uptake and degradation in glial cells: common transcriptional regulation of GLAST1 and GS, *Neurochem. Int.*, 37:179–189.
- Rieke, F., and E. A. Schwartz, 1994. A cGMP-gated current can control exocytosis at cone synapses, *Neuron*, 13:863–873.
- Rieke, F., and E. A. Schwartz, 1996. Asynchronous transmitter release: control of exocytosis and endocytosis at the salamander rod synapse, *J. Physiol.*, 493:1–8.
- Rieke, R. E., and M. D. Norenberg, 1977. Müller cell localisation of glutamine synthetase in rat retina, *Nature*, 268:654–655.
- Rodieck, R. W., 1998. *The First Steps of Seeing*, Sunderland, MA: Sinauer Associates.
- Roska, B., and F. Werblin, 2001. Vertical interactions across ten parallel, stacked representations in the mammalian retina, *Nature*, 410:583–587.
- Saito, T., H. Kondo, and J. Toyoda, 1978. Rod and cone signals in the ON-center bipolar cell: their different ionic mechanisms, *Vis. Res.*, 18:591–595.
- Sakaba, T., M. Tachibana, K. Matsui, and N. Minami, 1997. Two components of transmitter release in retinal bipolar cells: exocytosis and mobilization of synaptic vesicles, *Neurosci. Res.*, 27:357–370.
- Sarantis, M., and P. Mobbs, 1992. The spatial relationship between Müller cell processes and the photoreceptor output synapse, *Brain Res.*, 584:299–304.
- Sasaki, T., and A. Kaneko, 1996. L-Glutamate-induced responses in OFF-type bipolar cells of the cat retina, *Vis. Res.*, 36:787–795.
- Savchenko, A., S. Barnes, and R. H. Kramer, 1997. Cyclic-nucleotide-gated channels mediate synaptic feedback by nitric oxide, *Nature*, 390:694–698.
- Schmitz, Y., and P. Witkovsky, 1997. Dependence of photoreceptor glutamate release on a dihydropyridine-sensitive calcium channel, *Neurosci.*, 78:1209–1216.
- Schnapf, J. L., and D. R. Copenhagen, 1982. Differences in the kinetics of rod and cone synaptic transmission, *Nature*, 296:862–864.
- Schneeweis, D. M., and J. L. Schnapf, 1995. Photovoltage of rods and cones in the macaque retina, *Science*, 268:1053–1056.
- Schousboe, A., N. Westergaard, H. S. Waagepetersen, O. M. Larsson, I. J. Bakken, and U. Sonnewald, 1997. Trafficking between glia and neurons of TCA cycle intermediates and related metabolites, *Glia*, 21:99–105.
- Schwartz, E. A., 1975. Cones excite rods in the retina of the turtle, *J. Physiol.*, 246:639–651.
- Shields, C. R., M. N. Tran, R. O. Wong, and P. D. Lukasiewicz, 2000. Distinct ionotropic GABA receptors mediate presynaptic and postsynaptic inhibition in retinal bipolar cells, *J. Neurosci.*, 20:2673–2682.
- Sibson, N. R., G. F. Mason, J. Shen, G. W. Cline, A. Z. Herskovits, J. E. Wall, K. L. Behar, D. L. Rothman, and R. G. Shulman, 2001. In vivo (^{13}C) NMR measurement of neurotransmitter glutamate cycling, anaplerosis and TCA cycle flux in rat brain during, *J. Neurochem.*, 76(4):975–989.
- Soucy, E., Y. Wang, S. Nirenberg, J. Nathans, and M. Meister, 1998. A novel signaling pathway from rod photoreceptors to ganglion cells in mammalian retina, *Neuron*, 21:481–493.
- Stockman, A., L. T. Sharpe, K. Ruther, and K. Nordby, 1995. Two signals in the human rod visual system: a model based on electrophysiological data, *Vis.*, 12:951–970.
- Strom, T. M., G. Nyakatura, E. Apfelstedt-Sylla, H. Hellebrand, B. Lorenz, B. H. Weber, K. Wutz, N. Gutwillinger, K. Ruther, B. Drescher, C. Sauer, E. Zrenner, T. Meitinger, A. Rosenthal, and A. Meindl, 1998. An L-type calcium-channel gene mutated in incomplete X-linked congenital stationary night blindness, *Nat. Genet.*, 19:260–263.
- Sugihara, H., T. Inoue, S. Nakanishi, and Y. Fukuda, 1997. A late ON response remains in visual response of the mGluR6-deficient mouse, *Neurosci. Lett.*, 233:137–140.
- Tachibana, M., and A. Kaneko, 1987. λ -Aminobutyric acid exerts a local inhibitory action on the axon terminal of bipolar cells: evidence for negative feedback from amacrine cells, *Proc. Natl. Acad. Sci. USA*, 84:3501–3505.

- Tachibana, M., T. Okada, T. Arimura, K. Kobayashi, and M. Piccolino, 1993. Dihydropyridine-sensitive calcium current mediates neurotransmitter release from bipolar cells of the goldfish retina, *J. Neurosci.*, 13:2898–2909.
- Taschenberger, H., and R. Grantyn, 1995. Several types of Ca^{2+} channels mediate glutamatergic synaptic responses to activation of single Thy-1-immunolabeled rat retinal ganglion neurons, *J. Neurosci.*, 15:2240–2254.
- Taylor, W. R., E. Chen, and D. R. Copenhagen, 1995. Characterization of spontaneous excitatory synaptic currents in salamander retinal ganglion cells, *J. Physiol.*, 486 (Pt 1):207–221.
- Tessier-Lavigne, M., and D. Attwell, 1988. The effect of photoreceptor coupling and synapse nonlinearity on signal:noise ratio in early visual processing, *Proc. R. Soc. Lond. Biol. Sci.*, 234:171–197.
- Thoreson, W. B., and P. Witkovsky, 1999. Glutamate receptors and circuits in the vertebrate retina, *Prog. Retin. Eye Res.*, 18:765–810.
- Tian, N., and D. R. Copenhagen, 2001. Visual deprivation alters development of synaptic function in inner retina after eye opening, *Neuron*, 32:439–449.
- Toyoda, J.-I., M. Murakami, A. Kaneko, and T. Saito (eds.), 1999, *The Retinal Basis of Vision*. Amsterdam: Elsevier.
- Trombley, P. Q., and G. L. Westbrook, 1992. L-AP4 inhibits calcium currents and synaptic transmission via a G- protein-coupled glutamate receptor, *J. Neurosci.*, 12:2043–2050.
- Tsukamoto, Y., K. Morigiwa, M. Ueda, and P. Sterling, 2001. Microcircuits for night vision in mouse retina, *J. Neurosci.*, 21:8616–8623.
- Vardi, N., R. Duvoisin, G. Wu, and P. Sterling, 2000. Localization of mGluR6 to dendrites of ON bipolar cells in primate retina, *J. Comp. Neurol.*, 423:402–412.
- von Gersdorff, H., and G. Matthews, 1994. Dynamics of synaptic vesicle fusion and membrane retrieval in synaptic terminals, *Nature*, 367:735–739.
- von Gersdorff, H., E. Vardi, G. Matthews, and P. Sterling, 1996. Evidence that vesicles on the synaptic ribbon of retinal bipolar neurons can be rapidly released, *Neuron*, 16:1221–1227.
- von Gersdorff, H., and G. Matthews, 1997. Depletion and replenishment of vesicle pools at a ribbon-type synaptic terminal, *J. Neurosci.*, 17:1919–1927.
- von Gersdorff, H., T. Sakaba, K. Berglund, and M. Tachibana, 1998. Submillisecond kinetics of glutamate release from a sensory synapse, *Neuron*, 21:1177–1188.
- von Kriegstein, K., F. Schmitz, E. Link, and T. C. Sudhof, 1999. Distribution of synaptic vesicle proteins in the mammalian retina identifies obligatory and facultative components of ribbon synapses, *Eur. J. Neurosci.*, 11:1335–1348.
- Vu, T. Q., S. T. McCarthy, and W. G. Owen, 1997. Linear transduction of natural stimuli by dark-adapted and light-adapted rods of the salamander, *Ambystoma tigrinum*, *J. Physiol.*, 505 (Pt 1):193–204.
- Wilson, M., 1994. Glutamate-gated channels in the outer retina, in *Handbook of Membrane Channels* (C. Peracchia ed.), New York: Academic Press, pp. 287–302.
- Witkovsky, P., Y. Schmitz, A. Akopian, D. Krizaj, and D. Tranchina, 1997. Gain of rod to horizontal cell synaptic transfer: relation to glutamate release and a dihydropyridine-sensitive calcium current, *J. Neurosci.*, 17(19):7297–7306.
- Wu, S. M., 1994. Synaptic transmission in the outer retina, *Annu. Rev. Physiol.*, 56:141–146.

22 Peptide and Peptide Receptor Expression and Function in the Vertebrate Retina

NICHOLAS C. BRECHA

Introduction

The retina contains a rich variety of transmitters and related signaling molecules, including neuroactive peptides and growth factors. Peptides and growth factors have multiple roles in the retina, including participation in cellular signaling and slow synaptic transmission that contribute to visual function (Akopian et al., 2000; Savchenko et al., 2001; Veruki and Yeh, 1992; Zalutsky and Miller, 1990b). Evidence for abundant peptide expression in the vertebrate retina began with descriptions in the late 1970s of peptide activity and peptide receptor binding sites in retinal extracts and peptide immunoreactivity in amacrine cells (Brecha, 1983). Peptides are generally localized to wide-field amacrine cells, which form low-density cell populations that likely have a wide influence on other retinal neurons. A few peptides (e.g., pituitary adenylate cyclase activating polypeptide [PACAP] and substance P [SP]) are also localized to ganglion cells in some species (Brecha et al., 1987; Cuenca et al., 1995; Hannibal et al., 1997). More recently, peptide receptor mRNAs and immunoreactivity have been identified in retinal extracts and localized to multiple retinal cell types (Casini et al., 1997; Johnson et al., 2000; Tsuchida et al., 1990). Interestingly, there is often a difference between the localization of peptide-containing cells and processes, and the cellular distribution of their receptors, suggesting that peptides act in a paracrine manner and therefore have a broad influence on retinal circuits in both the outer and inner retina. Peptides can influence transmitter release from the retina (Bruun and Ehinger, 1993), and they modulate the cellular activity of multiple retinal neurons (Akopian et al., 2000; Feigenspan and Bormann, 1994; Zalutsky and Miller, 1990a). In general, peptide actions are characterized as being slow in onset, long lasting, and potent at low concentrations. Recent cellular studies have shown that peptides influence multiple intracellular effectors, including cAMP and Ca^{2+} , and that they modulate K^+ and Ca^{2+} currents and GABA_A receptor currents in retinal neurons (Akopian et al., 2000; Bruun et al., 1994; Feigenspan and Bormann, 1994; Johnson et al., 2001). Peptides, therefore, influence the efficacy of synaptic transmission in the retina by regulating cellular excitability as well as by modulating the release of GABA and glutamate from

presynaptic axonal terminals. Peptide actions are too slow to participate in light-activated responses, and since their actions are long lasting, peptides are likely to have an important role in adaptive mechanisms, such as light and dark adaptation. Together, these findings provide strong support for a functional role of peptides in the retina.

This chapter is mainly focused on neuropeptide Y (NPY), PACAP, SP, somatostatin (SRIF), and vasoactive intestinal polypeptide (VIP) as examples of peptides that are expressed in and affect the mammalian retina via the activation of selective receptors (Table 22.1). These peptides are characterized by a widespread distribution and abundant expression in the peripheral and central nervous system, where they provoke a broad spectrum of biological actions (Arimura, 1998; Gozes and Brenneman, 1989; McDonald, 1988; Otsuka and Yoshioka, 1993; Patel, 1999).

Peptide and Peptide Receptor Expression and Function

Peptide content. Early evidence for the presence of neuroactive peptides in the retina comes from experiments in the 1950s by Euler and his colleagues showing SP bioactivity in dog and bovine retinal extracts (Dunér et al., 1954). However, it was not until the late 1970s with the development of additional bioassay systems and radioimmunoassays (RIAs) that the rich variety of peptides, including cholecystokinin (CCK), the enkephalins, glucagon, SRIF, SP, thyrotropin-releasing hormone (TRH), and VIP, was shown to be present in the vertebrate retina (Brecha, 1983). At the present time over 20 peptides have been shown to be expressed in the vertebrate retina (Table 22.2).

In general, bioassay and RIA studies reported low to moderate levels of peptides in retinal extracts (Brecha, 1983; Ekman and Tornqvist, 1985; Rorstad et al., 1979). In most cases, findings from these investigations are congruent with those of immunohistochemical studies, which demonstrate that these peptides are found in subsets of amacrine and ganglion cells. For instance, SRIF immunoreactive content in the rat retina is relatively low, and this peptide is mainly localized to sparsely occurring amacrine and displaced amacrine cells (Eskay et al., 1980; Larsen et al., 1990; Sagar

TABLE 22.1
Peptides and peptide receptors in the retina.

Peptides	Preferred Receptors
Neuropeptide Y	Y _{1,2,4,5}
Pituitary adenylate cyclase activating polypeptide	PAC1, VAC1, VAC2
Somatostatin	sst ₁₋₅
Tachykinin peptides	
• Substance P	NK-1
• Neurokinin A	NK-2
• Neurokinin B	NK-3
Vasoactive intestinal polypeptide	VAC1, VAC2

TABLE 22.2
Peptide expression in the vertebrate retina.

Angiotensin II
Cholecystokinin
Corticotropin-releasing hormone
Enkephalins
• Leu ₅ -enkephalin
• Met ₅ -enkephalin
β-endorphin
FMRFamide
Glucagon
Luteinizing hormone releasing hormone
Natriuretic peptides
Atrial natriuretic peptide (α-ANP and γ-ANP)
Brain natriuretic peptide
C-type natriuretic peptide
Neurotensin
Neuropeptide Y
Nociceptin
Pituitary adenylate cyclase activating polypeptide
Peptide histidine isoleucine
Somatostatin
Tachykinin peptides
• Substance P
• Neurokinin A
• Neurokinin B
Thyrotropin-releasing hormone
Vasoactive intestinal polypeptide

et al., 1985). Many earlier studies also showed that peptides detected in the vertebrate retina corresponded in molecular structure to the same peptide in other tissues or the authentic peptide. For instance, glucagon, NPY, SRIF, and VIP immunoreactivity in retinal extracts were shown to correspond in molecular size to authentic peptides using gel or high-pressure liquid chromatography (Bruun et al., 1991; Ekman and Tornqvist, 1985; Sagar et al., 1985).

Peptide mRNAs. Peptide mRNAs have been detected in rat and human retinal extracts using Northern blots and RT-PCR, and in tissue sections using *in situ* hybridization histochemistry. For instance, preprotachykinin (PPT) I and PPT II mRNAs are in rat retinal extracts, indicating that all three TK peptides are expressed in the rat retina (Brecha et al., 1989). PACAP, SRIF, and VIP mRNAs have also been reported in rat retina (Casini et al., 1994; Larsen et al., 1990; Olianias et al., 1997). These findings indicate that the mammalian retina synthesizes various peptides, and it is reasonable to assume, based on these findings, that other peptides located in the retina by RIA or immunohistochemistry are also synthesized by retinal neurons.

Peptide localization. Immunohistochemical studies beginning in the late 1970s and early 1980s reported numerous peptides in the vertebrate retina (Brecha, 1983; Tornqvist et al., 1982). Peptides are most commonly localized to amacrine and ganglion cells, and usually to a single-cell population as defined by their morphology and neurochemistry (Brecha, 1983; Casini and Brecha, 1991; Hannibal et al., 2002; Vaney et al., 1989). Peptide immunoreactivity is commonly reported in very low to medium density wide-field amacrine cell populations. These cells are characterized by processes that are localized to distinct laminae of the inner plexiform layer (IPL) (Cajal, 1893). In addition, these processes ramify widely and overlap to form a network across the retinal surface. Some wide-field amacrine cell types that contain peptide immunoreactivity also have axon-like processes (Cuenca et al., 1995; Rickman et al., 1996; Sagar and Marshall, 1988). These amacrine cell types are likely to be polyaxonal amacrine cells, which are characterized by a distinct dendritic field and multiple axons that extend beyond their major field of dendrites (Volgyi et al., 2001). Finally, interplexiform cells, which are characterized by processes that ramify in both the IPL and outer plexiform layer (OPL) may also be considered an amacrine cell variant (Wässle and Boycott, 1991). There are several examples of a few peptide immunoreactive processes crossing the inner nuclear layer (INL) and ramifying in the OPL (Brecha, 1983; Spira et al., 1984). Wide-field amacrine cell populations, because of their low density and the widespread distribution of their processes, are thought to have broad influence on multiple retinal neurons and to participate in regulatory events such as dark adaptation rather than in more rapid events involving through-conducting pathways mediated by narrow-field and high-density cell populations (Masland, 1988; Wässle and Boycott, 1991). Peptide-containing ganglion cells are characterized by multistratified dendrites and wide dendritic fields. Peptide-containing ganglion cells usually innervate multiple retinorecipient targets, including those in the hypothalamus and midbrain (Brecha et al., 1987; Hannibal et al., 1997). There are only a few reports of peptide immunore-

activity in bipolar or horizontal cells (Marshak et al., 1990; Thier and Bolz, 1985).

There have been a modest number of ultrastructural investigations concerning the connectivity of peptide immunoreactive cells in rat, guinea pig, and primate retina (Cuenca and Kolb, 1998; Kang et al., 2001; Lee et al., 1995; Marshak, 1989; Oh et al., 2002). Several peptide-containing amacrine cell types have been studied in the macaque monkey retina (Marshak, 1989). In general, the main input to peptide immunoreactive processes is from amacrine cells, whereas the major output formed by conventional synapses is onto amacrine and ganglion cells. There is a smaller percentage of input and output connections with bipolar cell axonal terminals. The large degree of synaptic connections with amacrine cells indicates that peptide-containing cells are influenced principally by other amacrine cells and to a lesser degree by bipolar cells. There is more limited information about the connectivity of peptide-containing cells in other species, although overall the pattern of connectivity of these cells appears to be quite similar to that observed in monkey retina.

A feature of many wide-field amacrine cells is the coexpression of GABA and a peptide (Casini and Brecha, 1992; Vaney and Young, 1988). For example, in rat, cat, and monkey retina, GABA is colocalized with NPY, SP, and VIP in different amacrine cell types (Casini and Brecha, 1992; Cuenca and Kolb, 1998; Oh et al., 2002; Pourcho and Goebel, 1988a; Vaney et al., 1989). In addition, glutamate, the predominant ganglion cell transmitter, is coexpressed with PACAP in ganglion cells that innervate the suprachiasmatic nucleus (SCN) of the hypothalamus (Hannibal et al., 2000). These observations are consistent with findings elsewhere in the nervous system reporting the coexpression and corelease of classical transmitters and peptides from the same cell (Hökfelt et al., 2000). Interestingly, a differential release of classic transmitters and peptides depending on the frequency and pattern of cell firing has been shown in several systems (Lundberg, 1996). GABA or glutamate and peptides can act together at the same site, or the peptides can diffuse through the tissue and act at more distant cellular sites. There is evidence for both modes of action in the retina. GABA and peptides released from wide-field amacrine cells may act locally at GABA_A receptors; for instance, both VIP and GABA act on GABA_A receptors expressed by bipolar cell axons and ganglion cells (Veruki and Yeh, 1992). Peptides can also diffuse from their release site and act in a paracrine manner as suggested, for example, by the different distributions of SRIF immunoreactive processes and SRIF receptors, which are expressed by multiple retinal cell types (Johnson et al., 2000).

Peptide binding sites and localization. High-affinity peptide binding sites have been reported in many mammalian species using binding assay protocols and radiolabeled pep-

tides (Kossut et al., 1989; Nilsson et al., 1994; Orianas and Onali, 1995; Osborne, 1984). Autoradiographic techniques have also been used to define the regional distribution of peptide binding sites. For example, SRIF binding sites, identified with SRIF and the SRIF analog octreotide, are on photoreceptors and over both plexiform layers of the mouse and rat retina (Ferriero, 1992; Kossut et al., 1989). SP and VIP binding sites are homogeneously distributed across the inner retina (Denis et al., 1991a; Denis et al., 1991b; Mantyh et al., 1989). However, there are major difficulties in defining the cell types associated with these binding sites because of the low resolution of the autoradiographic technique. Furthermore, there are very few selective peptide agonists or antagonists available to distinguish between the different receptor isoforms. For example, octreotide binds to several somatostatin receptor types (Hoyer et al., 1995), and therefore there is a high likelihood that multiple receptors were detected in the autoradiographic studies of mouse and rat retina (Ferriero, 1992; Kossut et al., 1989).

Functional peptide receptors. Peptide receptors act through G-protein-coupled receptors to regulate intracellular signaling pathways. NPY and SRIF potently inhibit forskolin-induced cAMP accumulation (Bruun et al., 1994; Colas et al., 1992). The potent stimulation of adenylate cyclase activity by VIP is well established (Brecha, 1983; D'Agata and Cavallaro, 1998; Osborne, 1991). In addition, PACAP-27 and PACAP-38 are positively coupled to adenylate cyclase activity (D'Agata and Cavallaro, 1998; Nilsson et al., 1994; Orianas et al., 1997). Finally, the TK peptides stimulate inositol phosphate accumulation and Ca²⁺ mobilization (Osborne and Ghazi, 1989). These investigations, along with peptide binding and autoradiographic studies, have been valuable in establishing the presence of functional peptide receptors in the retina.

Peptide receptor mRNAs. Multiple peptide receptor mRNAs, including SRIF subtype (sst), TK or neurokinin (NK), and VIP/PACAP, are in rat retinal extracts. Multiple isoforms of these peptide receptor mRNAs are found in the retina; for instance, all five sst receptor mRNAs with different relative levels of abundance are expressed in rat and rabbit retinal extracts (Cristiani et al., 2000; Johnson et al., 1999; Mori et al., 1997). In addition, all of the known NK receptor mRNAs are present in rat eye extracts (Tsuchida et al., 1990). Finally, mRNAs of both the selective PACAP receptor, PAC1, and the VIP/PACAP-preferring receptors, VPAC1 and VPAC2, are found in retinal extracts (D'Agata and Cavallaro, 1998; Orianas et al., 1997). These findings indicate that multiple peptide receptors are synthesized by the mammalian retina, in agreement with binding, autoradiographic, and immunohistochemical studies, which corroborate the expression of multiple peptide receptors in the retina.

Peptide receptor localization. Numerous peptide receptors, including Y receptors, three different sst receptors, and the NK receptors have been localized to the retina (Casini et al., 1997; Cristiani et al., 2000; D'Angelo et al., 2000; Helboe and Moller, 1999; Johnson et al., 2000; Oyamada et al., 1999). These receptors are expressed by one or more retinal cell types. The cellular distributions of peptides and their receptors usually differ; peptides are often localized to a single or at most a few cell types, and their receptors are typically expressed by multiple cell types. For example, in rat retina, TK immunoreactive cells are sparsely distributed and ramify primarily in laminae 1, 3, and 5 of the IPL (Brecha et al., 1989; Zhang and Yeh, 1992). In contrast, NK-1 and NK-3 receptor immunoreactivity is predominantly expressed by numerous GABA-containing amacrine cells with processes over the entire IPL and OFF-type bipolar cells with dendritic processes in the OPL and axonal processes in laminae 1 and 2 of the IPL (Blumauer and Brecha, 1998; Casini et al., 1997; Oyamada et al., 1999). These studies are beginning to define the peptide expression pattern in the retina, which in turn is providing important insights into the mode of action of peptides in the retina.

Cellular physiology studies—ion channels and Ca^{2+} imaging. Experimental approaches using patch clamp and Ca^{2+} imaging techniques have been used to investigate peptide modulation of ion channels expressed by retinal neurons. In goldfish retina, several peptides, including SP, SRIF, and met-enkephalin, inhibit a voltage-dependent Ca^{2+} current in rod bipolar cell axon terminals (Ayoub and Matthews, 1992). In the mammalian retina, SRIF and VIP modulate ion channels in several cell types. For instance, a low concentration of SRIF reduces a K^{+} -stimulated increase of intracellular Ca^{2+} ($[Ca^{2+}]_i$) via voltage-activated L-type Ca^{2+} channels in rod bipolar cell terminals (Akopian et al., 2000; Johnson et al., 2000; Petrucci et al., 2001). SRIF also modulates both K^{+} and Ca^{2+} currents in salamander photoreceptors and rabbit rod bipolar cells (Akopian et al., 2000; Petrucci et al., 2001). In addition, VIP is reported to modulate Cl^{-} currents evoked by GABA at $GABA_A$ receptors in bipolar, amacrine, and ganglion cells of the rat retina (Feigenspan and Bormann, 1994; Veruki and Yeh, 1992). These findings show that peptides modulate ion channels, which in turn would influence cellular activity and transmitter release. For example, the modulation of voltage-activated Ca^{2+} currents in photoreceptor and bipolar cell terminals would influence transmitter release from these terminals.

Peptide modulation of transmitter release. Several investigations have been concerned with the influence of peptides on transmitter release from the retina. The general experimental paradigm is to preload the retina with a radiolabeled

transmitter, such as GABA, glycine, or dopamine, and, following a washout period, to add the peptide and measure changes of radiolabeled transmitter levels induced by the peptide. Low concentrations of exogenously applied NPY stimulate the release of glycine, dopamine, acetylcholine, and 5-hydroxytryptamine from the rabbit retina (Bruun and Ehinger, 1993). A variant of this approach involves the use of flashing light to stimulate transmitter release to determine if peptides influence this light-evoked transmitter release. For example, SRIF and SP do not change the level of light-evoked release of acetylcholine from rabbit retina (Cunningham and Neal, 1983). By contrast, the mu opioid receptor agonist, [D-Ala2, MePhe4, Gly-ol5]-enkephalin (DAMGO), increases light-evoked release of acetylcholine from rabbit retina (Neal et al., 1994).

Functional studies—electroretinogram (ERG), intracellular and extracellular recordings. The action of peptides on the retina has also been evaluated using ERG, as well as extracellular and intracellular recordings. The experimental approach that has been used most often is an in vitro retinal eyecup preparation and the bath application of a given peptide. In rabbit retina eyecups, application of low concentrations of SRIF increases the amplitude of the ERG a-, b- and c-waves, but several other peptides, including CCK and SP (Cunningham and Neal, 1983; Zalutsky and Miller, 1990b), do not affect the ERG. Studies using extracellular recordings of retinal neurons report that peptides increase the general excitability of cells (Downing and Djamgoz, 1993; Jensen, 1993; Zalutsky and Miller, 1990a, 1990b). Peptide actions are characterized as slow in onset, long lasting, and potent at low concentrations. Intracellular recordings indicate direct peptide actions on amacrine and ganglion cells. There is also some specificity in peptide action. For example, in rabbit retina, where the actions of SRIF, TK peptides, and VIP on ganglion cells have been studied, SRIF acts on all ganglion cell types; by contrast, SP acts on most brisk ganglion cells and VIP acts on ON- and OFF-center brisk ganglion cell types, respectively (Jensen, 1993; Zalutsky and Miller, 1990a, 1990b). Overall, peptide actions are characterized as being modulatory and too slow to participate in fast, light-evoked responses.

NPY, SRIF, SP, and VIP / PACAP expression and function

NPY, SRIF, SP, and VIP / PACAP expression in the mammalian retina. NPY, SRIF, SP, and VIP have been extensively studied in numerous mammalian species, including mouse, rat, guinea pig, rabbit, cat, monkey, and human retina.

NPY in amacrine and ganglion cells. NPY immunoreactivity is reported in the retina of numerous mammalian species

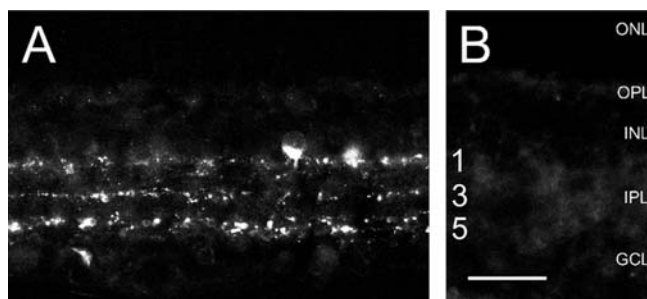


FIGURE 22.1. NPY immunoreactive cells in the rat retina. *A*, NPY immunostaining was localized to cell bodies in the proximal INL and varicose fibers distributed in laminae 1, 3, and 5 of the IPL. *B*, NPY immunoreactivity was absent from a retinal section incubated with the NPY antibody that was preincubated with 10^{-6} M NPY. Scale bar = 30 μ m. (From Oh et al., 2002.)

(Bruun et al., 1991; Ferriero and Sagar, 1989). Chromatographic studies show that NPY immunoreactivity isolated from mammalian retinal extracts corresponds to authentic NPY (Bruun et al., 1991). In addition, the NPY gene is expressed by cells located in the INL and GCL of the mouse retina (Ammar et al., 1998; Sinclair and Nirenberg, 2001).

NPY immunoreactivity is mainly localized to wide-field amacrine and displaced amacrine cells. Overall, these cells are similar in their appearance and distribution across species (Bruun et al., 1984; Bruun et al., 1986; Hutsler and Chalupa, 1994; Kang et al., 2001; Marshak, 1989; Oh et al., 2002; Sinclair and Nirenberg, 2001; Tornqvist and Ehinger, 1988) (Fig. 22.1). Immunoreactive amacrine cells have thin, varicose processes that ramify narrowly in lamina 1 of the IPL and, in some species, processes in laminae 3 and 5 of the IPL. In addition, in other species there are a few NPY immunoreactive displaced amacrine cells. In cat retina, immunoreactive cells only ramify in lamina 1 of the IPL (Hutsler and Chalupa, 1994). Furthermore, the mouse and rat retina have a well-defined displaced amacrine cell population (Oh et al., 2002; Sinclair and Nirenberg, 2001) with cells ramifying in lamina 5 of the IPL. NPY immunoreactivity is also reported in ganglion cells of the cat and human retina (Hutsler et al., 1993; Jen et al., 1994; Straznicky and Hiscock, 1989). In rat, guinea pig, and macaque monkey retina, the synaptic inputs to immunoreactive processes are predominantly from amacrine cell processes and from a small percentage of bipolar cell axon terminals (Kang et al., 2001; Marshak, 1989; Oh et al., 2002). Immunoreactive processes form conventional synaptic output mainly with amacrine cell processes and ganglion cell dendrites.

NPY immunoreactive cells are distributed to all retinal regions. These cells form different density cell populations in the mouse, rat, and cat retina. Cell density in rat retina is about 260 cells/mm² in the INL and 86 cells/mm² in the GCL (Oh et al., 2002), in the mouse retina is about 1452

cells/mm² in the INL and 644 cells/mm² in the GCL (Sinclair and Nirenberg, 2001), and in the cat retina, is about 1000 cells/mm² in central retinal regions and 390 cells/mm² in peripheral retina (Hutsler and Chalupa, 1994).

NPY immunoreactivity occurs also in ganglion cells of the cat retina and perhaps in the human retina (Hutsler et al., 1993; Jen et al., 1994; Straznicky and Hiscock, 1989). In cat retina, NPY immunoreactivity is in a subpopulation of gamma-type ganglion cells that have a small to medium cell body and sparsely branching dendrites that ramify in the ON sublamina of the IPL (Hutsler et al., 1993). These ganglion cells are sparsely distributed across the retina, are highest in density in area centralis, and number about 2000 per retina. NPY immunoreactive ganglion cells terminate in the C layers of the lateral geniculate nucleus and the superior colliculus. In adult human retina, NPY immunoreactivity is mainly in large ganglion cells that are distributed to all retinal regions (Straznicky and Hiscock, 1989) and that make up about 6% of the total ganglion cell population. Only a few, possibly wide-field NPY immunoreactive amacrine cells are reported in this study. In contrast, in the fetal human retina, NPY immunoreactive ganglion cell bodies are small and are identified solely on the basis of their localization to the GCL (Jen et al., 1994). These putative NPY immunoreactive ganglion cells appear to be the same size as the immunoreactive amacrine cells, suggesting that they may be displaced amacrine cells. The reports of NPY-containing ganglion cells are in contrast to the findings from other studies that describe NPY immunoreactive amacrine and displaced amacrine cells in adult and fetal human retina (Jotwani et al., 1994; Tornqvist and Ehinger, 1988).

Y receptor expression. The cellular actions of NPY are mediated via multiple Y receptors. The presence of NPY receptors is indicated by the potent inhibition of forskolin-induced cAMP accumulation by NPY (Bruun et al., 1994). Pharmacological studies have indicated the presence of several functionally coupled Y receptors, including the Y₂ receptor in the pigmented epithelium (Ammar et al., 1998). Therefore, NPY released by amacrine cells in the inner retina must have a paracrine mode of action to affect Y receptors expressed by the pigmented epithelium. Y₁ receptor immunoreactivity is in horizontal cell bodies in the distal INL and their processes in the OPL (D'Angelo et al., 2002). Immunoreactive amacrine cell processes ramify in lamina 2/3 and 4, and immunoreactive puncta are distributed to laminae 4 and 5 of the IPL. Immunoreactivity in lamina 2/3 and 4 of the IPL is localized to cholinergic amacrine cell processes (Voigt, 1986). The presence of NPY-containing amacrine and displaced amacrine cells and Y₁ receptor immunoreactive amacrine and horizontal cells (D'Angelo et al., 2002; Oh et al., 2002) suggests that this peptide acts on multiple cells in the inner and outer retina.

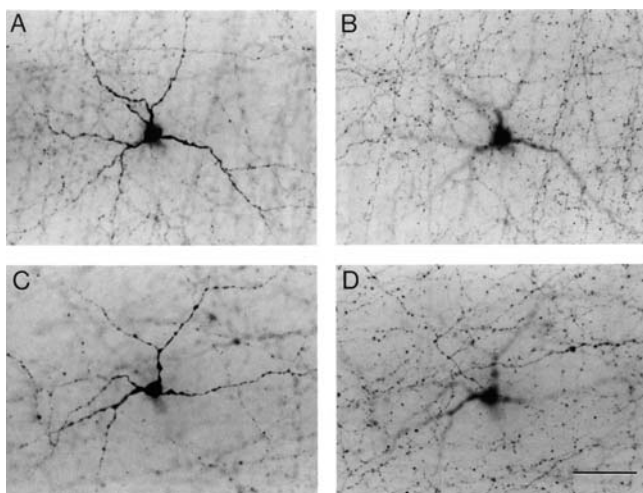


FIGURE 22.2. SRIF immunoreactive cells in a whole mount preparation of the rabbit retina. *A, C*, SRIF immunoreactive cell body located in the GCL. Primary processes ramify in lamina 5 of the IPL. *B, D*, Same fields as in *A* and *C*, respectively, with the plane of focus at lamina 1 of the IPL. A network of fine varicose processes is present in this lamina. Scale bar = 50 μ m. (From Rickman et al., 1996.)

SRIF in amacrine and ganglion cells. SRIF immunoreactivity and bioactivity are described in many mammalian species (Brecha, 1983; Eskay et al., 1980; Marshak and Yamada, 1984). Bioassay and chromatographic studies indicate that SRIF-14 is the predominant form in the rat and human retina and the larger SRIF-28, in addition to SRIF-14, is in guinea pig and rabbit retina (Larsen et al., 1990; Rorstad et al., 1980; Sagar et al., 1985; Sagar et al., 1982; Spira et al., 1984). In rat retina, SRIF mRNA-containing cells are in the INL and GCL (Larsen et al., 1990; Xiang et al., 2001). The coexpression of SRIF mRNA and SRIF immunoreactivity (Gaur et al., 1990) further confirms that amacrine and displaced amacrine cells in the rat retina synthesize this peptide.

SRIF immunoreactivity is localized to sparsely distributed, wide-field amacrine and displaced amacrine cells in the mouse (unpublished observations), rat (Larsen et al., 1990; Sagar et al., 1985), guinea pig (Spira et al., 1984; Tornqvist et al., 1982), and human retina (Tornqvist and Ehinger, 1988). In the rabbit, cat, macaque monkey, the New World monkey *Tupaia belangeri*, and human retina, most SRIF immunoreactive cells are displaced amacrine cells (Engelmann and Peichl, 1996; Marshak, 1989; Mitrofanis et al., 1989; Rickman et al., 1996; Sagar, 1987a; Sagar and Marshall, 1988; White et al., 1990) (Fig. 22.2). SRIF immunoreactive cells in rabbit and human retina have also been classified as “associational ganglion cells” on the basis of an intraretinal axon (Sagar, 1987a; Sagar and Marshall, 1988). These cells are also considered to be an amacrine cell variant, called a polyaxonal amacrine cell (Volgyi et al., 2001). Immunoreactive somata have thin varicose fibers that

form a narrow and continuous plexus in lamina 1 of the IPL. In many species, there is also a narrow plexus of varicose fibers in laminae 3 and 5 of the IPL. Frequently, a smooth, thin-caliber, axon-like process is observed to arise from a cell body or a primary process cross the retinal surface (Marshak, 1989; Rickman et al., 1996; Sagar and Marshall, 1988). A few immunoreactive fibers also cross the INL to ramify in the OPL in both ventral and dorsal retina. These fibers can be traced to the plexus in lamina 1 of the IPL. Finally, in rabbit retina, there is a dense accumulation of SRIF immunoreactive fibers along the retinal margin, which form a circumferential band in all retinal regions (Rickman et al., 1996). In macaque monkey retina, the predominant synaptic input is from amacrine cell processes and bipolar cell axon terminals. Synaptic output, formed by conventional synapses, is onto amacrine cell processes and ganglion cell dendrites (Marshak, 1989). In cat retina, synaptic connections differ from those in macaque retina, with input from amacrine cell processes, and output of immunostained profiles having both ribbon and conventional synaptic specializations to amacrine and ganglion cell processes (see Chun et al., 1992, for a discussion of the immunolabeled ribbon-containing profiles).

The larger proportion of displaced amacrine cells and their predominant distribution to the ventral retina are major features of the SRIF expression in the rabbit, cat, and human retina (Rickman et al., 1996; Sagar, 1987a; Sagar and Marshall, 1988; White et al., 1990). Furthermore, in rabbit and cat retina, there is a band of immunoreactive cells along the retinal margin. SRIF immunoreactive displaced amacrine cells form a low-density cell population in rabbit, cat, and human retina (Mitrofanis et al., 1989; Rickman et al., 1996; Sagar, 1987a; White et al., 1990). Immunoreactive cells are distributed predominantly in the ventral retina with few cells in the dorsal retina. Many immunoreactive cells are located along the retinal margin adjacent to the ora serrata. Cell density is very low; for example, in rabbit retina, cell density ranges from 6 cells/mm² in ventral retina to 11 cells/mm² at the retinal margins (Rickman et al., 1996). The total number of SRIF immunoreactive cells is correspondingly very low and in rabbit number about 1100 cells per retina (Rickman et al., 1996; Sagar et al., 1986). A very low-density SRIF-containing cell population is also present in cat and human retina (Mitrofanis et al., 1989; White et al., 1990). The distribution of SRIF immunoreactive cells in the guinea pig retina also differs from the general patterns of SRIF expression (Spira et al., 1984). SRIF immunoreactive cells are sparsely distributed along the margin of the retina in all retinal regions, and cells are located in the INL, IPL, and GCL. In the guinea pig, there is a density of about 35 cells/mm² in the area along the retinal margin (Spira et al., 1984). In contrast, SRIF immunoreactive cells in *Tupaia belangeri* are distributed in all retinal regions (Engelmann and

Peichl, 1996). The SRIF immunoreactive cell density is many times higher than in other vertebrate retinas (Engelmann and Peichl, 1996) with about 5000 cells/mm² in central retinal regions and 100 cells/mm² in peripheral retina.

SRIF immunoreactivity is also in a small percentage of ganglion cells (Engelmann and Peichl, 1996; White and Chalupa, 1991). In *Tupaia belangeri* retina, about 5% of the total number of SRIF immunoreactive cells are ganglion cells (Engelmann and Peichl, 1996). In cat retina, SRIF immunoreactivity is predominantly localized to a very small number of OFF-center alpha ganglion cells that are predominantly distributed to the inferior retina (White and Chalupa, 1991).

SRIF binding sites, localization, and coupling to adenylate cyclase. High-affinity binding sites for SRIF have been found in the retina of several species (Colas et al., 1992; Ferriero, 1992; Kossut et al., 1989; Liapakis and Thermos, 1992). Furthermore, SRIF binding sites, identified with SRIF and the SRIF analog SMS 204-090, have been localized to photoreceptors and both plexiform layers (Ferriero, 1992; Kossut et al., 1989). Functionally coupled SRIF receptors are indicated by the potent inhibition of VIP-induced cAMP accumulation by SRIF (Colas et al., 1992).

SRIF subtype (sst) receptor expression. SRIF actions are mediated through five sst receptors, sst₁–sst₅, and two sst₂ receptor isoforms, sst_{2A} and sst_{2B}, derived from alternative mRNA splicing (Hoyer et al., 1995). All five sst receptor mRNAs are in rat and rabbit retinal extracts (Cristiani et al., 2000; Johnson et al., 1999; Mori et al., 1997). In rat retina, sst₂ and sst₄ receptor mRNAs are the most abundant, whereas sst₁, sst₃, and sst₅ receptor mRNAs are at low abundance (Mori et al., 1997). In contrast, in rabbit retina, sst₁ receptor mRNA is the most abundant, sst₂ receptor mRNA is moderate, and sst₃, sst₄, and sst₅ receptor mRNAs are low in abundance (Cristiani et al., 2000).

Sst₁ receptor immunoreactivity is reported in amacrine and very sparsely occurring ganglion cells in the rat and rabbit retina (Cristiani et al., 2000; Helboe and Moller, 1999). In rat retina, sst₁ receptor immunoreactivity is in SRIF-containing amacrine and displaced amacrine cells (Helboe and Moller, 1999). A few ganglion cells, identified on the basis of their position, are also reported to contain sst₁ receptor immunoreactivity. In addition, Müller cell endfeet are strongly immunoreactive. The sst₁ receptor immunoreactivity pattern in the rabbit retina is different and more complex (Cristiani et al., 2000). Numerous amacrine cell types, including all tyrosine hydroxylase-containing and SRIF-containing cells, are sst₁ receptor immunoreactive. In addition, there are numerous amacrine cells that only have strong somatic immunostaining. These cells have a moder-

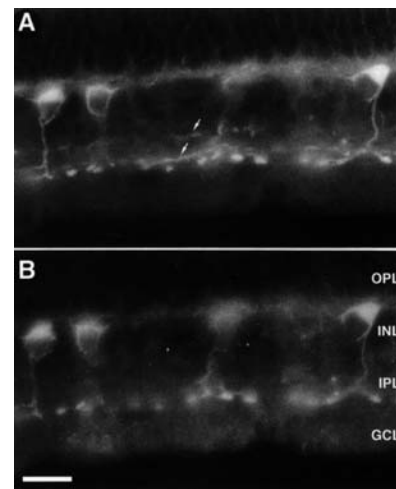


FIGURE 22.3. Sst_{2A} receptor immunoreactive rod bipolar cells in the rabbit retina. Coexpression of sst_{2A} receptor immunoreactivity (A) and protein kinase C (PKC) immunoreactivity (B) in rod bipolar cells. PKC is a cell-specific marker for rod bipolar cells in the rabbit retina. Sst_{2A} receptor immunoreactive amacrine cell processes (arrows) are also found in the rabbit retina. Scale bar = 15 μ m. (From Johnson et al., 1998.)

ate overall density of 112 cells/mm². In addition, there are a very small number of sst₁ receptor-containing ganglion cells, identified on the basis of cell body size, morphology, and disappearance following optic nerve transection.

Sst_{2A} receptor immunoreactivity is localized to multiple cell types in all regions of the mouse, rat, and rabbit retina (Fontanesi et al., 2000; Helboe and Moller, 1999; Johnson et al., 1998; Johnson et al., 1999; Petrucci et al., 2001; Vasilaki et al., 2001). In mouse, rat, and rabbit retina, three different sst_{2A} receptor immunoreactive patterns have been reported. In the mouse and rat retina, sst_{2A} receptor immunoreactivity is in cone photoreceptor terminals, many bipolar cells including rod bipolar cells, horizontal cells, and TH-containing amacrine cells (Johnson et al., 1999). A second study (Helboe and Moller, 1999) reports a less extensive distribution of this receptor with immunoreactivity localized to the inner segments of cone photoreceptors, many amacrine cells including the TH-containing amacrine cells, and Müller cell processes in the inner retina. In contrast to these studies, a third report (Vasilaki et al., 2001) describes sst_{2A} receptor immunoreactivity solely localized to rod bipolar cells. In rabbit retina, sst_{2A} receptor immunoreactivity is localized to all rod bipolar cells and to sparsely occurring amacrine cells (Johnson et al., 1998) (Fig. 22.3). Immunoreactive amacrine cells give rise to widely ramifying and overlapping processes in laminae 2 and 4 of the IPL. Two other studies report a similar pattern of expression in the rabbit retina, with sst_{2A} receptor immunoreactivity in many rod bipolar cells, amacrine cells including some TH-containing amacrine cells, and rare putative horizontal cells

(Fontanesi et al., 2000; Petrucci et al., 2001). Not all rod bipolar (68%) and TH-containing (34%) cells express sst_{2A} receptor immunoreactivity. Finally, an investigation (Vasilaki et al., 2001) describes sst_{2A} receptor immunoreactivity in rabbit rod bipolar cells. There is no obvious explanation for these discrepant observations, which might be due to differences in antibody specificity and sensitivity. One antibody is made to a fusion protein of the C-terminal part of the human sst_{2A} receptor (Helboe and Moller, 1999), and the other three antibodies are made to different synthetic peptides corresponding to the C-terminus of the sst_{2A} receptor (Fontanesi et al., 2000; Johnson et al., 1998; Vasilaki et al., 2001).

Sst_{2B} receptor immunoreactivity has been reported on photoreceptor outer segments of the rat retina (Vasilaki et al., 2001).

In situ hybridization experiments describe sst_4 receptor mRNA expressing cells in the GCL and INL (Mori et al., 1997). Sst_4 receptor immunoreactivity is in medium and large cell bodies in the GCL and numerous multistratified processes in the IPL (Brecha et al., 2002). Immunoreactivity is also in the optic nerve fiber layer and the optic nerve. Together, these findings indicate the presence of SRIF receptors on ganglion cells.

Additional investigations are needed to establish the exact cell types expressing the sst_{2A} receptor; in view of the very different immunostaining patterns reported to date. There is better agreement regarding sst_1 receptor expression on SRIF immunoreactive amacrine and displaced amacrine cells. The presence of sst_1 receptor would provide a mechanism for inhibitory feedback to modulate SRIF release. Finally, the sst_4 receptor appears to be only localized to ganglion cells (Brecha et al., 2002). The presence of sparsely distributed SRIF mRNA-containing and immunoreactive amacrine and displaced amacrine cells (Gaur et al., 1990; Larsen et al., 1990; Rickman et al., 1996; Sagar, 1987a; Sagar et al., 1985) and the widespread cellular expression of sst receptors suggest that SRIF acts on multiple cells in the retina via a paracrine mode of action and has a broad modulatory influence in the retina.

Cellular physiology—ion channels and Ca^{2+} imaging. SRIF modulates both voltage-activated K^+ and L-type Ca^{2+} currents in photoreceptor terminals in a salamander retina slice preparation (Akopian et al., 2000) (Fig. 22.4). SRIF enhances a delayed outwardly rectifying K^+ current in both rod and cone photoreceptors. SRIF differentially modulates L-type Ca^{2+} channel currents; SRIF reduces the Ca^{2+} current in rods and increases the Ca^{2+} current in cones. Ca^{2+} imaging experiments are consistent with these findings. These findings suggest that SRIF has a role in the regulation of transmitter release from photoreceptors through modulation of voltage-gated K^+ and Ca^{2+} currents.

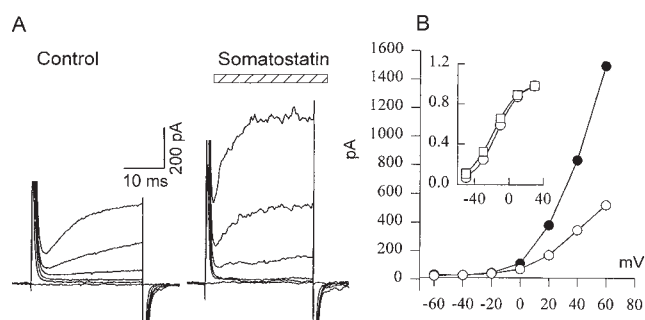


FIGURE 22.4. SRIF enhances a delayed outward K^+ current in rods. *A*, SRIF increased voltage-activated K^+ current. *B*, I-V relationship of the K^+ current obtained by holding cells at -70 mV and stepping from -60 to $+40$ mV in 20 mV increments. (From Akopian et al., 2000.)

In rat rod bipolar cells, there is no detectable change in $[\text{Ca}^{2+}]_i$ levels following direct application of SRIF (Johnson et al., 2001). However, SRIF strongly inhibits a K^+ -stimulated increase of $[\text{Ca}^{2+}]_i$ via L-type Ca^{2+} channels in a dose-dependent manner in rod bipolar axon cell terminals (Fig. 22.5). SRIF also enhances GABA-evoked whole-cell currents in amacrine cells likely due to GABA_A receptor phosphorylation following activation of adenylate cyclase (Feigenspan and Bormann, 1994). In rabbit retina, SRIF and octreotide, an SRIF agonist, reduce a K^+ -stimulated increase in $[\text{Ca}^{2+}]_i$ (Petrucci et al., 2001). In addition, SRIF inhibits Ca^{2+} -activated K^+ channels in these cells. The octreotide effect is prevented by L-Tyr8-Cyanamid 154806, an sst_2 receptor antagonist, indicating that SRIF effects are likely to be mediated by sst_2 receptor activation (Petrucci et al., 2001). Together, these investigations indicate that SRIF modulates both voltage-gated channels and ligand-gated receptors in mammalian retinal neurons.

Functional studies. In rabbit retina, low concentrations of SRIF excite all ganglion cell types, change their “signal-to-

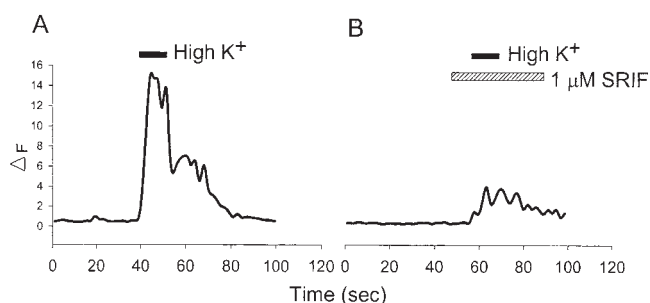


FIGURE 22.5. SRIF strongly inhibits a K^+ -stimulated increase of $[\text{Ca}^{2+}]_i$ via L-type Ca^{2+} channels in a rod bipolar axon cell terminal. *A*, K^+ -stimulated increase of $[\text{Ca}^{2+}]_i$ in an axonal terminal. *B*, Inhibition of K^+ -stimulated increase of $[\text{Ca}^{2+}]_i$ in an axonal terminal by SRIF treatment (striped bar). (From Johnson et al., 2001.)

noise ratio” discharge activity, and shift their center-surround balance toward a more dominant center (Zalutsky and Miller, 1990a) (Fig. 22.6). SRIF actions are characterized as being slow in onset and having a long latency. SRIF is also reported to act on multiple cells in the inner and outer retina; it directly affects bipolar, amacrine, and ganglion cells and influences the horizontal cell network. SRIF is also reported to increase input resistance of amacrine and bipolar cells, suggesting an action on ion channels. This would be consistent with other studies showing that SRIF affects K^+ and Ca^{2+} currents in retinal neurons (Akopian et al., 2000; Johnson et al., 2001; Petrucci et al., 2001). Together these observations indicate that SRIF acts on multiple retinal circuits to produce long-lasting changes in ganglion cell activity and receptive field organization, which is consistent with the hypothesis that this peptide acts as a modulator to affect adaptation in the retina.

TK peptides in amacrine and ganglion cells. SP and the related peptides, neurokinin A and neurokinin B, have a common C-terminus and are collectively referred to as the tachykinins (TKs), or TK peptides (Otsuka and Yoshioka, 1993). The TK peptides are products of two genes; SP and neurokinin A are derived from preprotachykinin (PPT) I by alternative processing, and neurokinin B is derived from a second gene, PPT II.

SP immunoreactivity is reported in the retina of numerous mammalian species, and chromatographic studies indicate the presence of authentic SP in retinal extracts (Brecha, 1983; Eskay et al., 1981; Osborne, 1984). PPT I and PPT II mRNAs are in rat retinal extracts, and *in situ* hybridization histochemistry studies show a differential expression of PPT mRNAs, with PPT I mRNA in cells distributed to the INL, IPL, and GCL and PPT II mRNA in cells distributed to the GCL (Brecha et al., 1989).

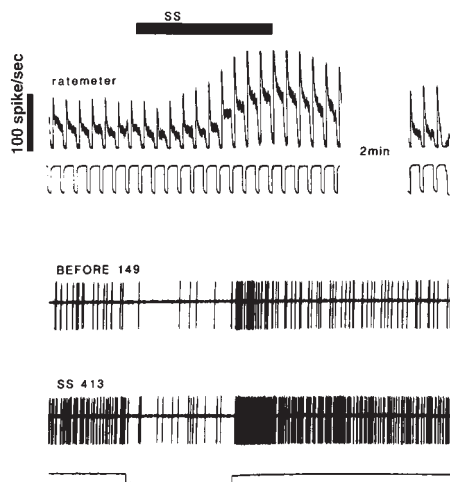


FIGURE 22.6. SRIF excitation of ganglion cells. A, Rate meter record. B, C, An OFF ganglion cell response before and after SRIF application. (From Zalutsky and Miller, 1990a.)

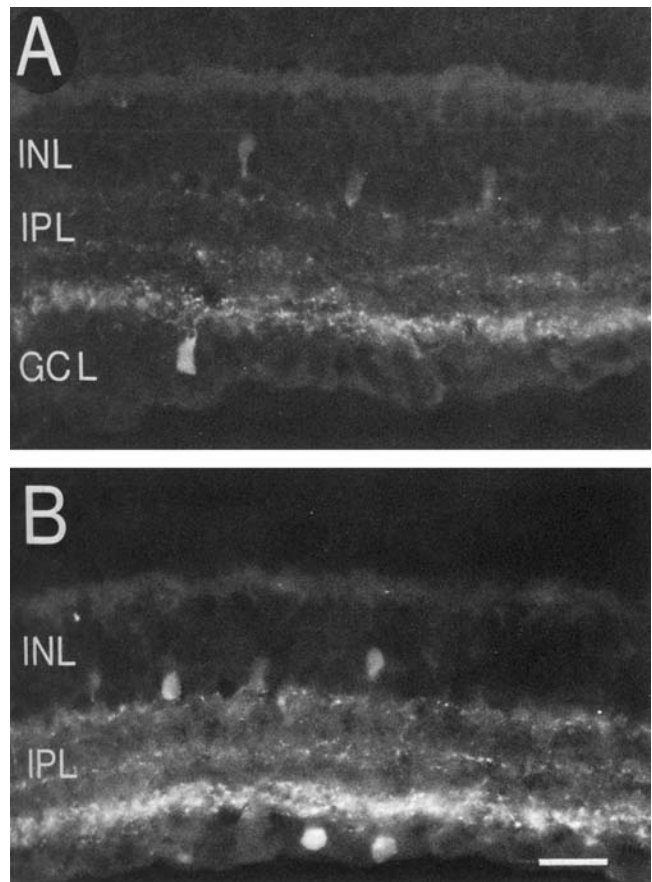


FIGURE 22.7. SP immunoreactivity in the rat retina. Immunoreactive cell bodies are localized to the INL and GCL, and processes are mainly distributed to laminae 1, 3, and 5 of the IPL. Scale bar = 25 μ m. (From Brecha et al., 1989.)

SP immunoreactivity is mainly localized to sparsely distributed wide-field amacrine and displaced amacrine cells in all retinal regions (Brecha, 1983; Kolb et al., 1995). Similar to other peptide-containing cells, SP immunoreactive somata have varicose processes that ramify extensively in the retina. In mouse, rat, rabbit, and primate (monkey and human) retina, immunoreactive processes are distributed to laminae 1, 3, and 5 of the IPL (Brecha, 1983; Brecha et al., 1989; Cuenca et al., 1995; Fukuda et al., 1981; Haverkamp and Wässle, 2000; JenLi and Lam, 1990; Li et al., 1999; Marshak, 1989; Oyamada et al., 1999; Tornqvist and Ehinger, 1988; Zhang and Yeh, 1992) (Fig. 22.7). There are differences in the laminar distribution of processes in the IPL; for example, in rat, hamster, and rabbit retina, processes are mainly in lamina 5, and in primate retina they are mainly in lamina 3 of the IPL. Primate retina is also characterized by numerous immunoreactive cell bodies in lamina 3 of the IPL, and most of the immunoreactive processes are in this lamina. In contrast, SP immunoreactive processes in the guinea pig retina ramify in laminae 4 and 5 of the IPL (Lee et al., 1995). Furthermore, in cat retina, processes mainly ramify in lamina 3/4 and more sparsely in

lamina 1 of the IPL (Pourcho and Goebel, 1988b; Vaney et al., 1989). In several species a few SP immunoreactive processes cross the INL and ramify in the OPL. Axon-like processes are also described in the human retina (Cuenca et al., 1995). They are present in several IPL laminae and they cross the INL and run in the OPL. In some cases, these axon-like processes are associated with retinal vessels. SP immunoreactivity is also in ganglion cells of the rat, hamster, rabbit, and monkey (Brecha et al., 1987; Kolb et al., 1995; Miguel-Hidalgo et al., 1994). Immunoreactive ganglion cells terminate in several CNS structures located in the hypothalamus, thalamus, and midbrain. In primate and guinea pig retina, the synaptic inputs to immunoreactive processes are mainly from amacrine cell processes and about 30% of the input is from bipolar cells (Cuenca and Kolb, 1998; Lee et al., 1995; Li et al., 1999; Marshak, 1989). There are differences in the output of the immunoreactive processes: most of the output in guinea pig is to ganglion cells; in monkey it is to amacrine and ganglion cells; in human retina it is to bipolar, amacrine, and ganglion cells. Interestingly, SP immunoreactive fibers also terminate on blood vessels, suggesting an influence of TK peptides on retinal blood flow (Cuenca and Kolb, 1998).

SP immunoreactive cells are distributed to all retinal regions and form low- to medium-density cell populations. For example, in rat retina, SP-containing cells in the INL are reported in all retinal regions, whereas immunoreactive cells in the GCL are restricted to the superior temporal retina (Zhang and Yeh, 1992). Cell density is 300 to 900 cells/mm² in the INL and 100 to 400 cells/mm² in the GCL. In rabbit retina, there are 1000 to 1400 cells/mm² in the visual streak and 125 to 200 cells/mm² in peripheral retina (Brecha et al., 1987). Finally, in human retina, cell density of SP immunoreactive cells is lower: 35 cells/mm² in temporal superior retina (5 to 9 mm from the fovea) and 5 to 9 cells/mm² in a more peripheral area of the inferior temporal retina (12 to 15 mm from the fovea) (Cuenca et al., 1995).

SP-containing ganglion cells are present in the rat, hamster, rabbit, monkey, and human retina. These cells have been identified by either retrograde transport of fluorescent tracers injected into retinorecipient nuclei or by the loss of immunostaining following optic nerve section. SP-containing ganglion cells terminate in several CNS structures. For instance, in the rat, SP immunoreactive ganglion cells project to the suprachiasmatic nucleus (SCN) and olivary pretectal nucleus (OPN) and perhaps the superior colliculus (Caruso et al., 1990; Klooster et al., 2000; Miguel-Hidalgo et al., 1994; Takatsuji et al., 1991). In hamster, about 3% of all retinal ganglion cells contain SP immunoreactivity, and immunoreactivity is eliminated in the lateral geniculate nucleus (LGN) following optic nerve section (Li et al., 1999). Similarly, in rabbit, 25% to 35% of all retinal ganglion cells contain SP immunoreactivity (Brecha et al., 1987). These cells have

medium to large somata and dendrites that ramify extensively in lamina 5 of the IPL. Their axons terminate in several retinorecipient nuclei, including the LGN, superior colliculus, and accessory optic nuclei. In human retina, weakly staining SP-containing ganglion cells have also been identified on the basis of their morphology (Cuenca et al., 1995). These cells have a large cell body and ramify in lamina 3 of the IPL. Furthermore, in the monkey (*Macaca fuscata yakui*), the presence of SP immunoreactive ganglion cells is suggested by the partial loss of SP immunoreactive processes in the pregeniculate nucleus and the OPN following bilateral eye enucleation (Nakagawa et al., 1988).

TK binding sites, localization, and coupling to phospholipase C. The cellular actions of the TK peptides are mediated through three receptors, known as NK-1, NK-2, and NK-3 (Otsuka and Yoshioka, 1993). The preferred ligands for the NK-1, NK-2, and NK-3 receptors are SP, neurokinin A (also called substance K), and neurokinin B (also called neuromedin K), respectively (Otsuka and Yoshioka, 1993).

High-affinity SP binding sites have been reported in retinal extracts and are homogeneously distributed over the IPL and GCL in tissue sections (Denis et al., 1991b; Mantyh et al., 1989; Osborne, 1984). In addition, substance K and neuromedin K binding sites are evenly distributed over the IPL of the guinea pig retina (Mantyh et al., 1989). Finally, the presence of functional NK receptors in the rabbit retina has been shown by the dose-dependent stimulation of inositol phosphate accumulation and [Ca²⁺]_i mobilization by SP, neurokinin A, and neurokinin B (Osborne and Ghazi, 1989).

NK receptor expression. All NK receptor mRNAs are detected in rat eye extracts (Tsushima et al., 1990). *In situ* hybridization experiments in the rat retina report the localization of NK-1 and NK-3 receptor mRNAs to cells in the inner retina (Kondoh et al., 1996; Shughrue et al., 1996). NK-3 mRNA is mainly distributed to the middle and outer regions of the INL, corresponding to the location of bipolar cell bodies.

NK-1 receptor immunoreactivity is in numerous amacrine cell bodies in the INL and in some small and large cell bodies in the GCL in the rat (Casini et al., 2000; Casini et al., 1997; Oyamada et al., 1999) (Fig. 22.8). Immunoreactivity is prominent in all IPL laminae, and there are fine caliber and varicose processes in the OPL and a few processes in the ganglion cell axon layer. Most NK-1 receptor immunoreactive amacrine cells contain GABA immunoreactivity, suggesting that they comprise multiple amacrine cell subpopulations. NK-1 receptor immunoreactivity is also in tyrosine hydroxylase-containing cell bodies and their processes in the OPL. Some ganglion cells, based on cell body size, appearance, and position, are also likely to express NK-1 receptor immunoreactivity.

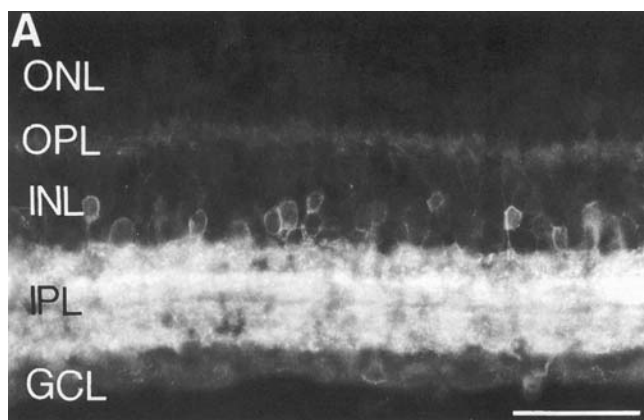


FIGURE 22.8. NK-1 receptor immunoreactivity in the rat retina. Immunoreactive amacrine cell bodies are localized to the INL and GCL and processes are dense in all IPL laminae. Scale bar = 50 μ m. (From Casini et al., 1997.)

There are differences in the NK-1 immunoreactivity and mRNA hybridization patterns in the INL and GCL (Casini et al., 2000; Casini et al., 1997; Kondoh et al., 1996; Oyamada et al., 1999). NK-1 receptor immunoreactivity is in numerous amacrine cell bodies and some putative ganglion cells. In contrast, there are few NK-1 mRNA-containing amacrine cells in the INL, and many ganglion cells are reported to contain NK-1 mRNAs (Kondoh et al., 1996). There is no simple explanation for these differences, which may be due to the NK-1 antibodies cross-reacting with other proteins, NK-1 mRNA not being translated to protein, or nonspecific hybridization to cells in the GCL.

NK-3 receptor immunoreactivity is in OFF-type cone bipolar cells and tyrosine hydroxylase-containing amacrine cells (Blumauer and Brecha, 1998; Casini et al., 2000; Chen et al., 2000; Oyamada et al., 1999). NK-3 immunoreactivity is primarily in cell bodies in the middle of the INL, and processes in the OPL and IPL. NK-3 immunoreactive bipolar cells ramify in laminae 1 and 2 of the IPL, suggesting they are cone bipolar (Cb)1 or Cb2 cells that were previously classified using intracellular labeling (Euler and Wässle, 1995; Hartveit, 1997). Many NK-3 receptor immunoreactive bipolar cells also contain recoverin immunoreactivity, a marker for Cb2 bipolar cells (Euler and Wässle, 1995). Together, these findings show that NK-3 receptor immunoreactivity is localized to at least two types of cone bipolar cells, Cb1 and Cb2 (Blumauer and Brecha, 1998). In addition, NK-3 immunoreactivity is also in tyrosine hydroxylase-containing amacrine cells (Chen et al., 2000).

The presence of amacrine and displaced amacrine cells containing both TK immunoreactivity and PPT mRNAs indicates that all three TK peptides are present in the retina.

These findings, regarding the presence of high-affinity TK binding sites and the distribution of NK-1 and NK-3 receptor mRNAs and immunoreactivity in the inner retina, suggest that a major site of action for SP is GABA-containing amacrine cells and the site of action for neurokinin B is OFF-type cone bipolar cells. In addition, these two peptides likely act on dopaminergic amacrine cells, since they express both NK-1 and NK-3 receptor immunoreactivity.

Cellular physiology studies—ion channels. In goldfish retina, SP reduces a voltage-dependent inhibition of Ca^{2+} currents in rod bipolar cell axonal terminals (Ayoub and Matthews, 1992) with a maximum reduction of the Ca^{2+} current of about 27%.

Functional studies. SP at low to moderate concentrations excites most brisk ganglion cells, including ON- and OFF-center and ON-OFF directionally selective ganglion cells in the rabbit retina (Zalutsky and Miller, 1990b). SP exerts these excitatory effects without affecting ganglion cell receptive field properties. The latency of the SP response was faster than that of SRIF (Zalutsky and Miller, 1990a). Intracellular recordings show that SP depolarized amacrine cells, including GABA-containing amacrine cells. These experiments are consistent with the expression of NK-1 receptor immunoreactivity by GABA-containing amacrine cells in the rat retina (Casini et al., 1997). SP did not affect horizontal cell activity, consistent with the lack of TK binding sites and of NK-1 or NK-3 immunostaining in the outer retina. Investigations in mudpuppy and fish retina also report that SP excites most ganglion cells (Dick and Miller, 1981; Downing and Djamgoz, 1993; Glickman and Adolph, 1982). Together, these findings indicate that TK peptides act in the inner retina and affect the general excitability of ganglion cells and their level of spontaneous activity, rather than altering the characteristics of ganglion cell receptive field properties, like SRIF and VIP.

VIP in amacrine cells. VIP immunoreactivity is present in mammalian retinas, and chromatographic studies show that it corresponds to authentic VIP (Brecha, 1983; Ekman and Tornqvist, 1985; Stone et al., 1990). In rat retina, VIP mRNA is in sparsely distributed cells in the inner retina (Casini et al., 1994; Okamoto et al., 1992). Double label studies show that VIP mRNA and VIP immunoreactivity occur in the same amacrine cells (Casini et al., 1994), confirming that this peptide is synthesized by these cells.

VIP immunoreactivity is localized to sparsely distributed wide-field amacrine cells in the mammalian retina (Tornqvist et al., 1982) (Fig. 22.9). VIP immunoreactive cells in the rabbit retina also coexpress peptide histidine isoleucine (PHI) immunoreactivity (Pachter et al., 1989), and

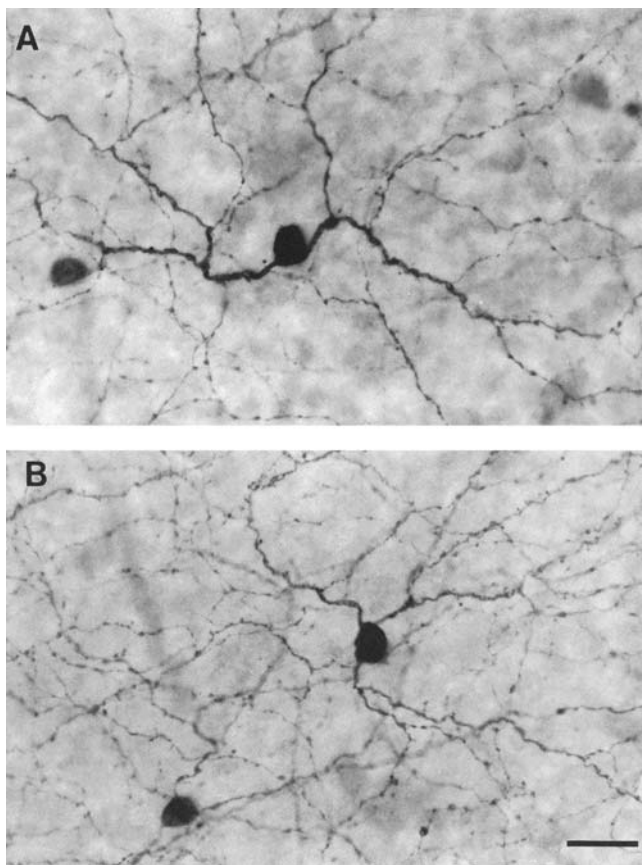


FIGURE 22.9. VIP immunoreactivity in the rabbit retina. Immunoreactive amacrine cell bodies are localized to the INL and processes ramify in laminae 1, 3, and 5 of the IPL. Whole-mount preparation. Scale bar = 50 μ m. (From Casini and Brecha, 1991.)

in rat and monkey retina, the PHI immunoreactivity matches the pattern of VIP immunoreactivity (Marshak, 1989; Mikkelsen et al., 1987; Tornqvist and Ehinger, 1988) consistent with VIP and PHI translation from the same VIP/PHI gene (Itoh et al., 1983). Overall, VIP immunoreactive amacrine cells are similar in their appearance and distribution in different mammalian retina (Casini and Brecha, 1991; Casini et al., 1994; JenLi and Lam, 1990; Lammerding-Koppel et al., 1991; Marshak, 1989; Sagar, 1987b; Tornqvist and Ehinger, 1988; Tornqvist et al., 1982). Immunoreactive cells are most often located in the proximal INL. They are characterized by multiple varicose processes and collaterals that ramify in laminae 1, 3, and 5 of the IPL. The immunostaining pattern in the baboon and cynomolgus monkey retinas are exceptions, with their cell bodies and processes in laminae 3 of the IPL (Tornqvist et al., 1982). In macaque monkey and rabbit retina, the synaptic inputs to immunoreactive processes are predominantly from amacrine cell processes (Marshak, 1989; Pachter et al., 1989). VIP immunoreactive processes form conventional

synaptic outputs mainly to unlabeled amacrine cell processes and to ganglion cell dendrites.

VIP mRNA-containing and immunoreactive cells are in all retinal regions and they form low-density cell populations (Casini and Brecha, 1991; Casini et al., 1994; Lammerding-Koppel et al., 1991; Sagar, 1987b). For example, in rat retina, neurons expressing VIP/PHI mRNA have an overall density of about 190 cells/mm² (Casini et al., 1994). There is a lower density of VIP immunoreactive cells in rabbit and monkey retina: in rabbit, immunoreactive cells have an overall cell density of 25 cells/mm² in the retina; in monkey, there is an overall cell density of 50 cells/mm² in the INL and 12 cells/mm² in the GCL (Casini and Brecha, 1991; Lammerding-Koppel et al., 1991; Sagar, 1987b).

PACAP in ganglion cells. PACAP is structurally homologous to VIP. There are two molecular forms of PACAP, PACAP-27 and -38 (Arimura, 1998). PACAP mRNA has been reported in human retinal extracts (Olianas et al., 1997). PACAP-27 and -38 immunoreactivities are in the retina of many mammalian species (Onali and Olianas, 1994), and PACAP immunoreactivity is reported in many cell types, processes in the IPL, and ganglion cell axon layer of the rat retina (Seki et al., 2000). However, no detailed information is given about the individual cell types and the distribution of processes of the immunoreactive cells. In contrast, another group reports a sparse population of PACAP immunoreactive ganglion cells in the rat retina; these cells are characterized by 2 to 4 thin dendrites that ramify in multiple laminae of the IPL and axons that innervate the SCN of the hypothalamus and the intergeniculate leaflet of the thalamus (Hannibal et al., 1997). PACAP mRNA-containing and immunoreactive ganglion cells form a low-density cell population; there is a differential distribution of cells with a density of 31 to 37 cells/mm² in the superior retina and 5 to 8 cells/mm² in the inferior retina (Hannibal et al., 2002). PACAP immunoreactive ganglion cells also contain glutamate immunoreactivity (Hannibal et al., 2000) and melanopsin immunoreactivity (Hannibal et al., 2002). The presence of the photopigment melanopsin in PACAP immunoreactive ganglion cells, the activation of these cells by light during subjective day (Hannibal et al., 2001), and the demonstration that both glutamate and PACAP have a role in light entrainment generated in the SCN (Mintz et al., 1999; Nielsen et al., 2001) provide compelling evidence that this ganglion cell population participates in the circadian light response.

VIP and PACAP binding sites, localization, and coupling to adenylate cyclase. Several different experimental approaches have indicated the presence of PACAP and VIP receptors in the mammalian retina. High-affinity VIP binding sites are in rat

and rabbit retinal extracts, and VIP binding sites are homogeneously distributed over all layers of the retina (Denis et al., 1991a). The potent stimulation of adenylate cyclase activity by VIP is well established in several retinas (Brecha, 1983; D'Agata and Cavallaro, 1998; Schorderet et al., 1984). PHI also can stimulate adenylate cyclase activity (Pachter et al., 1989). PACAP-27 and -38 positively couple to adenylate cyclase in retinal homogenates, and their actions are more potent than VIP, indicating the presence of the PACAP-preferring receptors known as PAC1 receptors (D'Agata and Cavallaro, 1998; Nilsson et al., 1994; Orianas et al., 1997; Onali and Orianas, 1994). Furthermore, in rat retinal homogenates, PACAP-27 and -38, but not VIP, show a dose-dependent stimulation of inositol phosphate levels, suggesting multiple signal transduction pathways for the PACAP peptides (D'Agata and Cavallaro, 1998).

PACAP/VIP receptor expression. The cellular actions of VIP and PACAP are mediated through three PACAP/VIP receptors: PACAP-preferring type 1 (PAC1) and the VIP/PACAP-preferring types (VPAC1 and VPAC2) receptor (Harmar et al., 1998). PAC1 receptors have a higher affinity for PACAP than VIP; VPAC1 and VPAC2 have a similar affinity for both PACAP and VIP.

PAC1, VPAC1, and VPAC2 receptor mRNAs are in rat and human fetal retinal extracts (D'Agata and Cavallaro, 1998; Orianas et al., 1997). A brief report describes a high level of PACAP receptor mRNA hybridization signal, distributed homogeneously over the entire INL and GCL with lower levels of hybridization signal distributed over the IPL, ONL, and OPL (Seki et al., 1997). Furthermore, using an antibody that cross-reacts with different PACAP receptor splice variants, immunoreactivity is reported in scattered and faintly stained cell bodies in the INL and GCL (Seki et al., 1997). No immunostained processes are observed in the IPL or OPL. The presence of VPAC1 and VPAC2 receptor mRNA and immunoreactivity have not yet been reported.

Cellular physiology studies—ion channels. There is no detectable change in membrane currents following direct application of VIP to isolated rod bipolar and ganglion cells (Gillette and Dacheux, 1995; Veruki and Yeh, 1992). However, VIP influences GABA's action at GABA_A receptors. VIP potentiates GABA-evoked whole-cell currents in bipolar cells by 65% and ganglion cells by 54% (Fig. 22.10). The onset of VIP action was slow and there was a long recovery period. VIP-induced potentiation of whole-cell GABA currents is mediated via phosphorylation of GABA_A receptors following adenylate cyclase activation (Feigenspan and Bormann, 1994; Veruki and Yeh, 1994). The activation of a cAMP-dependent pathway is consistent with numerous other

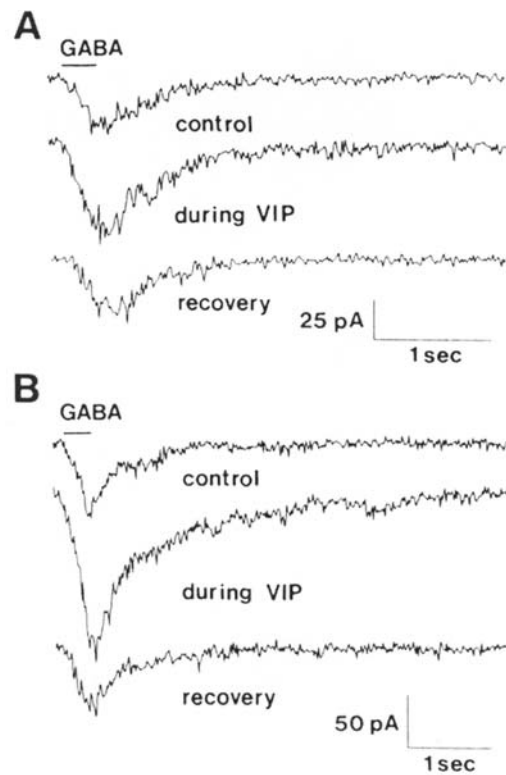


FIGURE 22.10. VIP potentiation of GABA-evoked Cl^- current in a bipolar cell (A) and a ganglion cell (B). A, The whole cell GABA-evoked current in both the bipolar and ganglion cells were potentiated after a 11 second application of VIP.

studies showing that VIP increases cAMP levels in the mammalian retina (Brecha, 1983; Longshore and Makman, 1981; Osborne, 1991). In contrast to these observations in rat, VIP reduces GABA-evoked whole-cell currents of rabbit bipolar cells by 37% (Gillette and Dacheux, 1995). Finally, in rat amacrine cells, VIP also enhances GABA-evoked whole-cell currents, likely due to GABA_A receptor phosphorylation by the activation of adenylate cyclase (Feigenspan and Bormann, 1994).

Functional studies. VIP excites ON- and OFF-center brisk ganglion cells in the rabbit retina (Jensen, 1993). Similar to observations using SRIF and SP, VIP is potent at low concentrations and there is a delay in the onset of its action on ganglion cells. The maintained activity of ON- and OFF-center ganglion cells is increased by VIP and their excitatory responses to flashes of light are unaffected or slightly reduced in the presence of VIP. In contrast, VIP has little effect on the maintained activity of ON/OFF directionally selective ganglion cells and the response of these cells to a moving stimulus. Finally, the action of VIP on ganglion cells in rabbit retina is consistent with other reports of the action of VIP on GABA currents on isolated ganglion cells in the rat retina (Veruki and Yeh, 1992).

Expression and function of other peptides in retinal neurons

Expression of other peptides in the mammalian retina. Several other peptides are also found in the mammalian retina. These include atrial natriuretic peptide (ANP), angiotensin II of the renin-angiotensin system, CCK, corticotropin releasing hormone (CRH), and opioids.

ANP expression. ANP mRNA could not be detected in rat retina using RT-PCR, but ANP immunoreactivity was shown to be in the retina based on RIA and chromatography studies (Gaspar et al., 1991; Stone and Glembotski, 1986). Another study reports the presence of brain natriuretic peptide (BNP) and C-type natriuretic peptide (CNP) mRNAs in the mammalian retina (Fernandez-Durango et al., 1995). Alpha-ANP₁₋₂₈ immunoreactivity has been described in both the OPL and IPL (Palm et al., 1989), and the immunoreactivity of the related peptide, gamma-ANP₁₋₂₅, has been found in rat rod bipolar cells (Haverkamp et al., 1999). High-affinity ANP binding sites are reported in retinal extracts (Fernandez-Durango et al., 1989), although they have not been detected by autoradiography (Mantyh et al., 1986). Finally, ANP, BNP, and CNP receptor mRNAs are reported in the retina (Fernandez-Durango et al., 1995). Consistent with these latter findings is the presence of particulate guanylate cyclase, which is coupled to natriuretic peptide receptors (Ahmad and Barnstable, 1993; Kutty et al., 1992).

Renin and angiotensin expression. The renin-angiotensin system (Phillips, 1987) has been found in mammalian retina. The angiotensin II precursors, angiotensinogen and renin, and angiotensin converting enzyme (ACE) are present in the mammalian retina (Deinum et al., 1990; Kohler et al., 1997; Wagner et al., 1996). Renin immunoreactivity is localized to Müller cells (Berka et al., 1995). Angiotensin II immunoreactivity is reported in rabbit, cat, and bovine retina with weak immunoreactivity in amacrine cells of the rabbit retina. However, pretreatment of the rabbit and cat retina with protease inhibitors and incubation in angiotensin II before immunostaining result in enhanced immunoreactivity, revealing processes in the INL and ONL and possibly ganglion cells (Kohler et al., 1997). This treatment also results in immunoreactivity in Müller cells.

Angiotensin II binding sites are present in the rabbit retina (Mallorga et al., 1989). Furthermore, angiotensin II (AT_{1A} and AT₂) receptor mRNAs are in rat retinal extracts (Murata et al., 1997; Wheeler-Schilling et al., 1999). A role for angiotensin II in regulating vascular tone is indicated by the presence of angiotensin II binding sites on arterioles, but not veins or capillaries, in the cat retina (Ferrari-Dileo et al., 1991). Consistent with this suggestion is a decrease of sys-

temic blood pressure following the intravenous injection of an ACE inhibitor, which depletes angiotensin II levels in the retina (Jacobi et al., 1994).

Weak AT₂ receptor mRNA hybridization signal is localized to neurons sparsely distributed in the INL and GCL (Murata et al., 1997; Wheeler-Schilling et al., 1999). In addition, weak AT₁ immunoreactivity is localized to cell bodies in the INL and most cell bodies in the GCL. Very few weakly staining processes are observed in the IPL or OPL. These latter findings indicate an action by angiotensin II on retinal neurons. Consistent with this suggestion are findings that angiotensin II influences both N- and L-type Ca²⁺ currents in rat ganglion cells (Guenther et al., 1997). Finally, application of angiotensin does not change the level of light-evoked release of acetylcholine from rabbit retina (Cunningham and Neal, 1983), although inhibition of ACE in the cat retina, which depletes angiotensin II levels, results in increased sensitivity and gain of the rod b-wave amplitude of the ERG (Jacobi et al., 1994).

CCK expression. CCK prepropeptide precursor immunoreactivity is in two types of amacrine cells and cone bipolar cells of the monkey retina (Marshak et al., 1990), and CCK immunoreactivity is in amacrine and horizontal cells of the cat retina (Thier and Bolz, 1985). In macaque monkey retina, CCK immunoreactivity is in all blue cone bipolar cells, which terminate in lamina 5 of the IPL (Marshak et al., 1990). These cells form synaptic contacts with amacrine and ganglion cell dendrites. Immunoreactivity is also in two types of wide-field amacrine cells: bistratified amacrine cells with their somata in the INL and GCL and processes that ramify extensively in laminae 2 and 4 of the IPL, and unistratified amacrine cells with processes in the same laminae. The majority of synaptic contacts are with other amacrine cells. Functionally, iontophoresis of CCK onto ganglion cells in the intact retina suppresses maintained and light evoked ganglion cell activity (Thier and Bolz, 1985).

CRH expression. CRH immunoreactivity is in wide-field amacrine and displaced amacrine cells of the rat and monkey retina (Marshak, 1989; Yeh and Olschowka, 1989). In rat retina, CRH-containing amacrine and displaced amacrine cells are distributed in all retinal regions with a slightly higher density in superior temporal retina (Yeh and Olschowka, 1989). There appear to be two cell types, based on the distribution of their processes in the IPL. Cell bodies in both the INL and GCL give rise to two cell types: an unistratified cell type that ramifies in lamina 5 of the IPL, and a second bistratified type that primarily ramifies in lamina 5 and with a fine process in lamina 1. There is a greater density of displaced amacrine cell bodies; in the GCL, cell density is about 120 cells/mm² and in the INL, cell density is about 35 cells/mm². In macaque monkey retina, immunoreactivity

is in sparsely occurring displaced amacrine cells with processes in laminae 1, 3, and 5 of the IPL (Marshak, 1989). These cells receive most of their synaptic input from amacrine cells and form conventional synapses onto amacrine and ganglion cells. These cells have a similar appearance and morphology to SRIF immunoreactive displaced amacrine cells. High-affinity CRH binding sites are present in several mammalian retinas, and CRH stimulates adenylate cyclase activity in these retinas, suggesting functional CRH receptors (Olianas and Onali, 1995; Olianas et al., 1993).

Opioid expression. The endogenous opioid enkephalin is expressed by amacrine cells in nonmammalian retinas (Brecha, 1983). However, there is little evidence for the expression of opioid peptides in the adult mammalian retina, except for reports of enkephalin immunoreactive amacrine cells in the guinea pig retina (Altschuler et al., 1982). Consistent with these observations are chromatographic studies indicating the presence of enkephalins in guinea pig retina (Hoffman, 1983). Interestingly, enkephalin immunoreactivity was not detected in the rat retina using the same antibody to detect enkephalin in the guinea pig retina (Altschuler et al., 1982).

There are three endogenous opioid receptors, known as mu, delta, and kappa. Opiate binding sites were first reported in rat retinal homogenates in the mid-1970s (Brecha, 1983), and mu opioid binding sites are distributed homogeneously over the IPL and GCL of the rat and monkey retina (Wamsley et al., 1981). The presence of functional mu opioid receptor (MOR) in rabbit retina is suggested by the increased levels of acetylcholine release evoked by flickering light in the presence of the MOR agonist, DAMGO (Neal et al., 1994). Consistent with autoradiographic localization studies, MOR immunoreactivity is localized to bistratified ganglion cells of the rat retina (Brecha et al., 1995). These ganglion cells are distributed to all retinal regions and ramify extensively in laminae 2/3 and 4 of the IPL. Furthermore, MOR immunoreactive axons and axonal terminals are detected in retinorecipient nuclei, with the highest levels of immunostaining in the accessory optic nuclei and the OPN, and with moderate levels in the LGN and superior colliculus. Immunoreactivity in these nuclei is reduced or eliminated in the case of the accessory optic nuclei following retinal enucleation (Brecha et al., 1995). Furthermore, ultrastructural studies report MOR immunoreactivity on retinal terminals in the accessory optic nuclei (Ding et al., 1995). Together, these findings show that in the rat, bistratified ganglion cells give rise to MOR immunoreactivity in several retinorecipient structures. The failure to detect enkephalin immunoreactivity in the adult rat retina and the prominent MOR immunostaining in the terminals of ganglion cells suggests that endoge-

nous opioids have a presynaptic action on ganglion cell axonal terminals.

Orphan receptor-like 1 is related to opioid receptors and its endogenous ligand orphanin FQ or nociceptin (Mollereau et al., 1994; Nothacker et al., 1996) may also be expressed in the retina (Neal et al., 1997). High-affinity nociceptin binding sites are in the rabbit retina, and nociceptin inhibits acetylcholine release evoked by flickering light.

Peptide function in the retina

Peptides act as slow transmitters whose actions are mediated by multiple intracellular effectors, including cAMP, Ca^{2+} , protein kinases, and phosphatases, to modulate ion channels, ligand-gated channels, transporters, and receptors, as well as to affect nuclear transcription factors (Greengard, 2001). These peptide actions are characterized by long-lasting changes in cellular properties that modulate both transmitter release from axon terminals and neuronal activity. Peptide actions are often characterized as being modulatory, compared to the rapid action of excitatory and inhibitory transmitters at ligand-gated ion channels.

There are experimental findings consistent with peptides acting as slow transmitters in the retina. Several peptides, including NPY, PACAP, SRIF, SP, and VIP, acting via G-protein-coupled receptors, influence adenylate cyclase or phospholipase C activity in retinal homogenates and whole retina. Peptides also have potent modulatory effects on both Ca^{2+} and K^{+} currents in retinal neurons. For example, (1) low concentrations of SRIF partially inhibit Ca^{2+} currents of isolated ON-type bipolar cells from rat and rabbit rod bipolar cells, (2) SRIF enhances a delayed outwardly rectifying K^{+} current in salamander rod and cone photoreceptors, (3) SRIF inhibits the large conductance and Ca^{2+} - and voltage-dependent K^{+} current in rabbit rod bipolar cells, and (4) SRIF partially inhibits a K^{+} -stimulated $[\text{Ca}^{2+}]_i$ increase via an L-type Ca^{2+} channel in axon terminals of rat rod bipolar cells and salamander photoreceptors (Akopian et al., 2000; Johnson et al., 2001; Petrucci et al., 2001). In addition, the action of GABA at GABA_A receptors is modulated by VIP via phosphorylation of GABA_A receptors by protein kinase A in rat rod bipolar, amacrine, and ganglion cells (Feigenspan and Bormann, 1994; Veruki and Yeh, 1992, 1994). Presumably these peptide actions result in the regulation of transmitter release and the excitability of retinal neurons, leading to the modulation of the efficacy of synaptic transmission in the retina.

The concept that peptides act as modulators of retinal circuitry or networks is based on both anatomical and physiological studies. Peptide-containing cells in most cases are wide-field amacrine cells that are characterized by a very low to medium cell density. These cells ramify widely and have overlapping processes that cover the entire retinal surface.

Therefore, they would have a broad influence on a large number of cells and are unlikely to mediate discrete point-to-point information processing. Connectivity studies show that most synaptic input onto peptide-containing amacrine cell processes is from amacrine cells, and these cells in turn terminate mainly on amacrine and ganglion cells. Peptides released from these cells could therefore influence synaptically multiple cells in a local fashion. In addition, a consistent finding for several peptides is a differential distribution of peptide-containing and peptide receptor-bearing processes and cells. These findings suggest that peptides are likely to diffuse from their release sites and act at a distance in a paracrine fashion. Together, these findings suggest that peptides can have a widespread effect on multiple types of retinal neurons.

Functional studies also support the concept that peptides act as modulators of retinal circuitry. In general, the cellular effects of peptides have a slow onset, are long lasting, and occur at multiple locations in the retina. For instance, both SRIF and VIP produce excitatory changes in the range of seconds to minutes in the spontaneous activity and neuronal discharge patterns of ganglion cells (Jensen, 1993; Zalutsky and Miller, 1990a). Moreover, SRIF affects the center-surround balance of all types of ganglion cells. Thus SRIF appears to play a role in light/dark adaptation (Zalutsky and Miller, 1990a). The role of other peptides in visual function is less well understood. However, as their wide-ranging actions are also likely to be too slow to mediate fast, throughput signaling, these peptides will probably act in modulatory processes that occur on longer timescales (Dowling and Ripps, 1977) and participate in adaptive mechanisms that globally affect the state of retinal circuits and networks.

Acknowledgments

I thank Drs. Arlene Hirano and Catia Sternini for their comments and invaluable assistance in preparing this chapter. I also thank Alex Vila for his assistance, including preparing the figures.

Support has been provided by NEI EY 04067 and a VA Career Scientist Award.

REFERENCES

- Ahmad, I., and C. J. Barnstable, 1993. Differential laminar expression of particulate and soluble guanylate cyclase genes in rat retina, *Exp. Eye Res.*, 56:51–62.
- Akopian, A., J. Johnson, R. Gabriel, N. Brecha, and P. Witkovsky, 2000. Somatostatin modulates voltage-gated K^+ and Ca^{2+} currents in rod and cone photoreceptors of the salamander retina, *J. Neurosci.*, 20:929–936.
- Altschuler, R. A., J. L. Mosinger, D. W. Hoffman, and M. H. Parakkal, 1982. Immunocytochemical localization of enkephalin-like immunoreactivity in the retina of the guinea pig, *Proc. Natl. Acad. Sci. USA*, 79:2398–2400.
- Ammar, D. A., B. A. Hughes, and D. A. Thompson, 1998. Neuropeptide Y and the retinal pigment epithelium: receptor subtypes, signaling, and bioelectrical responses, *Invest. Ophthalmol. Vis. Sci.*, 39:1870–1878.
- Arimura, A., 1998. Perspectives on pituitary adenylate cyclase activating polypeptide (PACAP) in the neuroendocrine, endocrine, and nervous systems, *Jpn. J. Physiol.*, 48:301–331.
- Ayoub, G. S., and G. Matthews, 1992. Substance P modulates calcium current in retinal bipolar neurons, *Vis. Neurosci.*, 8:539–544.
- Berka, J. L., A. J. Stubbs, D. Z. Wang, R. DiNicolantonio, D. Alcorn, D. J. Campbell, and S. L. Skinner, 1995. Renin-containing Müller cells of the retina display endocrine features, *Invest. Ophthalmol. Vis. Sci.*, 36:1450–1458.
- Blumauer, N., and N. C. Brecha, 1998. Off-type cone bipolar cells express neurokinin-3 (NK-3) receptors in the rat retina, *Soc. Neurosci.*, 24:2091.
- Brecha, N. C., 1983. Retinal neurotransmitters: histochemical and biochemical studies, in *Chemical Neuroanatomy* (I. P. C. Emson ed.), New York: Raven Press, pp. 85–129.
- Brecha, N. C., D. Johnson, J. Bolz, S. Sharma, J. G. Parnavelas, and A. R. Lieberman, 1987. Substance P-immunoreactive retinal ganglion cells and their central axon terminals in the rabbit, *Nature*, 327:155–158.
- Brecha, N. C., J. Johnson, R. Kui, B. Anton, D. Keith, Jr., C. Evans, and C. Sternini, 1995. Mu opioid receptor immunoreactivity is expressed in the retina and retinal recipient nuclei, *Analgesia*, 1:331–334.
- Brecha, N. C., C. Sternini, K. Anderson, and J. E. Krause, 1989. Expression and cellular localization of substance P/neurokinin A and neurokinin B mRNAs in the rat retina, *Vis. Neurosci.*, 3:527–535.
- Brecha, N. C., A. Vila, and J. M. Allen, 2002. Somatostatin subtype receptor 4 expression in mouse and rat retina, *Invest. Ophthalmol. Vis. Sci.*, 43:e-abstract 268.
- Bruun, A., L. Edvinsson, and B. Ehinger, 1994. Neuropeptide Y inhibits adenyl cyclase activity in rabbit retina, *Acta Ophthalmol. (Copenh.)*, 72:326–331.
- Bruun, A., and B. Ehinger, 1993. NPY-induced neurotransmitter release from the rabbit and chicken retina, *Acta Ophthalmol. (Copenh.)*, 71:590–596.
- Bruun, A., B. Ehinger, and R. Ekman, 1991. Characterization of neuropeptide Y-like immunoreactivity in vertebrate retina, *Exp. Eye Res.*, 53:539–543.
- Bruun, A., B. Ehinger, F. Sundler, K. Tornqvist, and R. Uddman, 1984. Neuropeptide Y immunoreactive neurons in the guinea-pig uvea and retina, *Invest. Ophthalmol. Vis. Sci.*, 25:1113–1123.
- Bruun, A., K. Tornqvist, and B. Ehinger, 1986. Neuropeptide Y (NPY) immunoreactive neurons in the retina of different species, *Histochem.*, 86:135–140.
- Cajal, S. R., 1893. La retine des vertebres, *La Cellule*, 9:119–257.
- Caruso, D. M., M. T. Owczarzak, and R. G. Pourcho, 1990. Colocalization of substance P and GABA in retinal ganglion cells: a computer-assisted visualization, *Vis. Neurosci.*, 5:389–394.
- Casini, G., and N. C. Brecha, 1991. Vasoactive intestinal polypeptide-containing cells in the rabbit retina: Immunohistochemical localization and quantitative analysis, *J. Comp. Neurol.*, 305:313–327.
- Casini, G., and N. C. Brecha, 1992. Colocalization of vasoactive intestinal polypeptide and GABA immunoreactivities in a population of wide-field amacrine cells in the rabbit retina, *Vis. Neurosci.*, 8:373–378.

- Casini, G., N. C. Brecha, L. Bosco, and D. W. Rickman, 2000. Developmental expression of neurokinin-1 and neurokinin-3 receptors in the rat retina, *J. Comp. Neurol.*, 421:275–287.
- Casini, G., M. Molnar, and N. C. Brecha, 1994. Vasoactive intestinal polypeptide/peptide histidine isoleucine messenger RNA in the rat retina: adult distribution and developmental expression, *Neurosci.*, 58:657–667.
- Casini, G., D. W. Rickman, C. Sternini, and N. C. Brecha, 1997. Neurokinin 1 receptor expression in the rat retina, *J. Comp. Neurol.*, 389:496–507.
- Chen, L. W., L. C. Wei, H. L. Liu, L. Duan, G. Ju, and Y. S. Chan, 2000. Retinal dopaminergic neurons (A17) expressing neuromedin K receptor (NK(3)): a double immunocytochemical study in the rat, *Brain Res.*, 885:122–127.
- Chun, M. H., N. Brecha, and H. Wässle, 1992. Light- and electron-microscopic studies of the somatostatin-immunoreactive plexus in the cat retina, *Cell Tissue Res.*, 267:57–66.
- Colas, B., A. M. Valencia, J. C. Prieto, and E. Arilla, 1992. Somatostatin binding and modulation of adenylate cyclase in ovine retina membranes, *Molec. Cell. Endocrinol.*, 88:111–117.
- Cristiani, R., G. Fontanesi, G. Casini, C. Petrucci, C. Viollet, and P. Bagnoli, 2000. Expression of somatostatin subtype 1 receptor in the rabbit retina, *Invest. Ophthalmol. Vis. Sci.*, 41:3191–3199.
- Cuenca, N., J. De Juan, and H. Kolb, 1995. Substance P-immunoreactive neurons in the human retina, *J. Comp. Neurol.*, 356:491–504.
- Cuenca, N., and H. Kolb, 1998. Circuitry and role of substance P-immunoreactive neurons in the primate retina, *J. Comp. Neurol.*, 393:439–456.
- Cunningham, J. R., and M. J. Neal, 1983. Effect of gamma-aminobutyric acid agonists, glycine, taurine and neuropeptides on acetylcholine release from the rabbit retina, *J. Physiol. (Lond.)*, 336:563–577.
- D'Agata, V., and S. Cavallaro, 1998. Functional and molecular expression of PACAP/VIP receptors in the rat retina, *Brain Res. Mol. Brain Res.*, 54:161–164.
- D'Angelo, I., S.-J. Oh, M.-H. Chun, and N. B. Brecha, 2002. Localization of neuropeptide Y1 receptor immunoreactivity in the rat retina and the synaptic connectivity of Y1 immunoreactive cells, *J. Comp. Neurol.*, 454:373–382.
- Deinum, J., F. H. Derkx, A. H. Danser, and M. A. Schalekamp, 1990. Identification and quantification of renin and prorenin in the bovine eye, *Endocrinol.*, 126:1673–1682.
- Denis, P., M. Dussaillant, J. P. Nordmann, P. P. Elena, H. Saraux, and W. Rostene, 1991a. Autoradiographic characterization and localization of vasoactive intestinal peptide binding sites in albino rat and rabbit eyes, *Exp. Eye Res.*, 52:357–366.
- Denis, P., V. Fardin, J. P. Nordmann, P. P. Elena, L. Laroche, H. Saraux, and W. Rostene, 1991b. Localization and characterization of substance P binding sites in rat and rabbit eyes, *Invest. Ophthalmol. Vis. Sci.*, 32:1894–1902.
- Dick, E., and R. F. Miller, 1981. Peptides influence retinal ganglion cells, *Neurosci. Lett.*, 26:131–135.
- Ding, Y. Q., S. Nomura, T. Kaneko, and N. Mizuno, 1995. Presynaptic localization of mu-opioid receptor-like immunoreactivity in retinal axon terminals within the terminal nuclei of the accessory optic tract: a light and electron microscope study in the rat, *Neurosci. Lett.*, 199:139–142.
- Dowling, J. E., and H. Ripps, 1977. The proximal negative response and visual adaptation in the skate retina, *J. Gen. Physiol.*, 69:57–74.
- Downing, J. E., and M. B. Djamgoz, 1993. Electrophysiological effects of tachykinin analogues on ganglion cell activity in cyprinid fish retina, *Neuropeptides*, 24:109–116.
- Dunér, H., U. S. von Euler, and B. Permow, 1954. Catecholamines and substance P in the mammalian eye, *Acta Physiol. Scand.*, 31:113–118.
- Ekman, R., and K. Tornqvist, 1985. Glucagon and VIP in the retina, *Invest. Ophthalmol. Vis. Sci.*, 26:1405–1409.
- Engelmann, R., and L. Peichl, 1996. Unique distribution of somatostatin-immunoreactive cells in the retina of the tree shrew (*Tupaia belangeri*), *Eur. J. Neurosci.*, 8:220–228.
- Eskay, R. L., J. F. Furness, and R. T. Long, 1981. Substance P activity in the bullfrog retina: localization and identification in several vertebrate species, *Science*, 212:1049–1050.
- Eskay, R. L., R. T. Long, and P. M. Iuvone, 1980. Evidence that TRH, somatostatin and substance P are present in neurosecretory elements of the vertebrate retina, *Brain Res.*, 196:554–559.
- Euler, T., and H. Wässle, 1995. Immunocytochemical identification of cone bipolar cells in the rat retina, *J. Comp. Neurol.*, 361:461–478.
- Feigenspan, A., and J. Bormann, 1994. Facilitation of GABAergic signaling in the retina by receptors stimulating adenylate cyclase, *Proc. Natl. Acad. Sci. USA*, 91:10893–10897.
- Fernandez-Durango, R., D. J. Nunez, and M. J. Brown, 1995. Messenger RNAs encoding the natriuretic peptides and their receptors are expressed in the eye, *Exp. Eye Res.*, 61:723–729.
- Fernandez-Durango, R., D. Sanchez, J. Gutkowska, F. Carrier, and A. Fernandez-Cruz, 1989. Identification and characterization of atrial natriuretic factor receptors in the rat retina, *Life Sci.*, 44:1837–1846.
- Ferrari-Dileo, G., E. B. Davis, and D. R. Anderson, 1991. Angiotensin II binding receptors in retinal and optic nerve head blood vessels. An autoradiographic approach, *Invest. Ophthalmol. Vis. Sci.*, 32:21–26.
- Ferriero, D. M., 1992. Developmental expression of somatostatin receptors in the rat retina, *Brain Res. Devel. Brain Res.*, 67:309–315.
- Ferriero, D. M., and S. M. Sagar, 1989. Development of neuropeptide Y-immunoreactive neurons in the rat retina, *Brain Res. Devel. Brain Res.*, 48:19–26.
- Fontanesi, G., C. Gargini, and P. Bagnoli, 2000. Postnatal development of somatostatin 2A (sst2A) receptors expression in the rabbit retina, *Brain Res. Devel. Brain Res.*, 123:67–80.
- Fukuda, M., Y. Kuwayama, S. Shiosaka, I. Ishimoto, Y. Shimizu, H. Takagi, S. Inagaki, M. Sakanaka, E. Semba, K. Takatsuki, and M. Tohyama, 1981. Demonstration of a substance P-like immunoreactivity in retinal cells of the rat, *Neurosci. Lett.*, 23:239–242.
- Gaspar, L., R. Fernandez-Durango, N. G. Seidah, M. Chretien, and J. Gutkowska, 1991. ANF mRNA is detected by the polymerase chain reaction technique in the chorioid and bodies but not in the retina of the rat eye, *Endocrinol.*, 129:559–561.
- Gaur, V. P., K. Yamaguchi, and J. E. Turner, 1990. Somatostatin in rat retina: localization by in situ hybridization histochemistry and immunocytochemistry, *Tohoku J. Exp. Med.*, 162:121–126.
- Gillette, M. A., and R. F. Dacheux, 1995. GABA- and glycine-activated currents in the rod bipolar cell of the rabbit retina, *J. Neurophysiol.*, 74:856–875.
- Glickman, R. D., and A. R. Adolph, 1982. Acetylcholine and substance P: action via distinct receptors on carp retinal ganglion cells, *Invest. Ophthalmol. Vis. Sci.*, 22:804–808.
- Gozes, I., and D. E. Brenneman, 1989. VIP: Molecular biology and neurobiological function, *Mol. Neurobiol.*, 3:201–236.
- Greengard, P., 2001. The neurobiology of slow synaptic transmission, *Science*, 294:1024–1030.

- Guenther, E., B. Hewig, E. Zrenner, and K. Kohler, 1997. Angiotensin II-induced inhibition and facilitation of calcium current subtypes in rat retinal ganglion cells, *Neurosci. Lett.*, 231:71–74.
- Hannibal, J., J. M. Ding, D. Chen, J. Fahrenkrug, P. J. Larsen, M. U. Gillette, and J. D. Mikkelsen, 1997. Pituitary adenylate cyclase-activating peptide (PACAP) in the retinohypothalamic tract: a potential daytime regulator of the biological clock, *J. Neurosci.*, 17:2637–2644.
- Hannibal, J., P. Hindersson, S. M. Knudsen, B. Georg, and J. Fahrenkrug, 2002. The photopigment melanopsin is exclusively present in pituitary adenylate cyclase-activating polypeptide-containing retinal ganglion cells of the retinohypothalamic tract, *J. Neurosci.*, 22:RC191.
- Hannibal, J., M. Møller, O. P. Ottersen, and J. Fahrenkrug, 2000. PACAP and glutamate are co-stored in the retinohypothalamic tract, *J. Comp. Neurol.*, 418:147–155.
- Hannibal, J., N. Vrang, J. P. Card, and J. Fahrenkrug, 2001. Light-dependent induction of cFos during subjective day and night in PACAP-containing ganglion cells of the retinohypothalamic tract, *J. Biol. Rhythms*, 16:457–470.
- Harmar, A. J., A. Arimura, I. Gozes, L. Journot, M. Laburthe, J. R. Pisegna, S. R. Rawlings, P. Robberecht, S. I. Said, S. P. Sreedharan, S. A. Wank, and J. A. Waschek, 1998. International Union of Pharmacology. XVIII. Nomenclature of receptors for vasoactive intestinal peptide and pituitary adenylate cyclase-activating polypeptide, *Pharmacol. Rev.*, 50:265–270.
- Hartveit, E., 1997. Functional organization of cone bipolar cells in the rat retina, *J. Neurophysiol.*, 77:1716–1730.
- Haverkamp, S., H. Kolb, T. A. Blute, L. Cao, and W. D. Eldred, 1999. Gamma-atrial natriuretic peptide 1–25 is found in bipolar cells in turtle and rat retinas, *Vis. Neurosci.*, 16:771–779.
- Haverkamp, S., and H. Wässle, 2000. Immunocytochemical analysis of the mouse retina, *J. Comp. Neurol.*, 424:1–23.
- Helboe, L., and M. Møller, 1999. Immunohistochemical localization of somatostatin receptor subtypes sst1 and sst2 in the rat retina, *Invest. Ophthalmol. Vis. Sci.*, 40:2376–2382.
- Hoffman, D. W., 1983. Chromatographic identification of enkephalins in the guinea pig retina, *Neurosci. Lett.*, 40:67–73.
- Hökfelt, T., C. Broberger, Z. Q. Xu, V. Sergeev, R. Ubink, and M. Diez, 2000. Neuropeptides—an overview, *Neuropharmacol.*, 39:1337–1356.
- Hoyer, D., G. I. Bell, M. Berelowitz, J. Epelbaum, W. Feniuk, P. P. Humphrey, A. M. O’Carroll, Y. C. Patel, A. Schonbrunn, J. E. Taylor, and T. Reisne, 1995. Classification and nomenclature of somatostatin receptors, *Trends Pharmacol. Sciences*, 16:86–88.
- Hutsler, J. J., and L. M. Chalupa, 1994. Neuropeptide Y immunoreactivity identifies a regularly arrayed group of amacrine cells within the cat retina, *J. Comp. Neurol.*, 346:481–489.
- Hutsler, J. J., C. A. White, and L. M. Chalupa, 1993. Neuropeptide Y immunoreactivity identifies a group of gamma-type retinal ganglion cells in the cat, *J. Comp. Neurol.*, 336:468–480.
- Itoh, N., K. Obata, N. Yanaihara, and H. Okamoto, 1983. Human preprovasoactive intestinal polypeptide contains a novel PHI-27-like peptide, PHM-27, *Nature*, 304:547–549.
- Jacobi, P. C., H. Osswald, B. Jurkies, and E. Zrenner, 1994. Neuromodulatory effects of the renin-angiotensin system on the cat electroretinogram, *Invest. Ophthalmol. Vis. Sci.*, 35:973–980.
- Jen, P. Y., W. W. Li, and D. T. Yew, 1994. Immunohistochemical localization of neuropeptide Y and somatostatin in human fetal retina, *Neurosci.*, 60:727–735.
- JenLi, H. B., and D. M. Lam, 1990. Localization of neuropeptide-immunoreactive neurons in the human retina, *Brain Res.*, 522:30–36.
- Jensen, R. J., 1993. Effects of vasoactive intestinal peptide on ganglion cells in the rabbit retina, *Vis. Neurosci.*, 10:181–189.
- Johnson, J., M. L. Caravelli, and N. C. Brecha, 2001. Somatostatin inhibits calcium influx into rat rod bipolar cell axonal terminals, *Vis. Neurosci.*, 18:101–108.
- Johnson, J., D. W. Rickman, and N. C. Brecha, 2000. Somatostatin and somatostatin subtype 2A expression in the mammalian retina, *Microsc. Res. Tech.*, 50:103–111.
- Johnson, J., H. Wong, J. H. Walsh, and N. C. Brecha, 1998. Expression of the somatostatin subtype 2A receptor in the rabbit retina, *J. Comp. Neurol.*, 393:93–101.
- Johnson, J., V. Wu, H. Wong, J. H. Walsh, and N. C. Brecha, 1999. Somatostatin receptor subtype 2A expression in the rat retina, *Neurosci.*, 94:675–683.
- Jotwani, G., K. Itoh, and S. Wadhwa, 1994. Immunohistochemical localization of tyrosine hydroxylase, substance P, neuropeptide-Y and leucine-enkephalin in developing human retinal amacrine cells, *Brain Res. Dev. Brain Res.*, 77:285–289.
- Kang, W. S., M. Y. Lim, E. J. Lee, I. B. Kim, S. J. Oh, N. C. Brecha, C. B. Park, and M. H. Chun, 2001. Light- and electron-microscopic analysis of neuropeptide Y-immunoreactive amacrine cells in the guinea pig retina, *Cell Tissue Res.*, 306:363–371.
- Klooster, J., W. Kamphuis, G. F. Vrensen, 2000. Immunohistochemical localization of substance P and substance P receptor (NK1) in the olivary pretectal nucleus of the rat, *Exp. Brain Res.*, 131:57–63.
- Kohler, K., T. Wheeler-Schilling, B. Jurkies, E. Guenther, and E. Zrenner, 1997. Angiotensin II in the rabbit retina, *Vis. Neurosci.*, 14:63–71.
- Kolb, H., E. Fernandez, J. Ammermuller, and N. Cuenca, 1995. Substance P: a neurotransmitter of amacrine and ganglion cells in the vertebrate retina, *Histol. Histopathol.*, 10:947–968.
- Kondoh, A., T. Houtani, T. Ueyama, K. Baba, M. Ikeda, K. Yamagishi, H. Miki, M. Uyama, S. Nakanishi, and T. Sugimoto, 1996. In situ hybridization analysis of substance P receptor in the rat retina, *Exp. Brain Res.*, 112:181–186.
- Kossut, M., T. Yamada, L. B. Aldrich, and L. H. Pinto, 1989. Localization and characterization of somatostatin binding sites in the mouse retina, *Brain Res.*, 476:78–84.
- Kutty, R. K., R. T. Fletcher, G. J. Chader, and G. Krishna, 1992. Expression of guanylate cyclase-A mRNA in the rat retina: detection using polymerase chain reaction, *Biochem. Biophys. Res. Commun.*, 182:851–857.
- Lammerding-Koppel, M., P. Thier, and W. Koehler, 1991. Morphology and mosaics of VIP-like immunoreactive neurons in the retina of the rhesus monkey, *J. Comp. Neurol.*, 312:251–263.
- Larsen, J. N., M. Bersani, J. Olcese, J. J. Holst, and M. Møller, 1990. Somatostatin and prosomatostatin in the retina of the rat: an immunohistochemical, in-situ hybridization, and chromatographic study, *Vis. Neurosci.*, 5:441–452.
- Lee, M. Y., M. H. Chun, S. H. Han, S. J. Oh, and J. W. Chung, 1995. Light- and electron-microscopic study of substance P-immunoreactive neurons in the guinea pig retina, *Cell Tissue Res.*, 281:261–271.
- Li, H. B., K. F. So, and W. Cheuk, 1999. Substance P-immunoreactive neurons in hamster retinas, *Vis. Neurosci.*, 16:475–481.
- Liapakis, G., and K. Thermos, 1992. Characterization of [125I]Tyr11-somatostatin binding sites in the rabbit retina, *Neuropeptides*, 21:13–19.

- Longshore, M. A., and M. H. Makman, 1981. Stimulation of retinal adenylate cyclase by vasoactive intestinal peptide (VIP), *Eur. J. Pharmacol.*, 70:237–240.
- Lundberg, J. M., 1996. Pharmacology of cotransmission in the autonomic nervous system: integrative aspects on amines, neuropeptides, adenosine triphosphate, amino acids and nitric oxide, *Pharmacol. Rev.*, 48:113–178.
- Mallorga, P., R. W. Babilon, and M. F. Sugrue, 1989. Angiotensin II receptors labelled with ^{125}I -[Sar¹, Ile⁸]-Ang in albino rabbit ocular tissues, *Curr. Eye Res.*, 8:841–849.
- Mantyh, C. R., L. Kruger, N. C. Brecha, and P. W. Mantyh, 1986. Localization of specific binding sites for atrial natriuretic factor in peripheral tissues of the guinea pig, rat, and human, *Hypertens.*, 8:712–721.
- Mantyh, P. W., T. Gates, C. R. Mantyh, and J. E. Maggio, 1989. Autoradiographic localization and characterization of tachykinin receptor binding sites in the rat brain and peripheral tissues, *J. Neurosci.*, 9:258–279.
- Marshak, D. W., 1989. Peptidergic neurons of the macaque monkey retina, *Neurosci. Res.*, 10(Suppl.):S117–S130.
- Marshak, D. W., L. B. Aldrich, J. Del Valle, and T. Yamada, 1990. Localization of immunoreactive cholecystokinin precursor to amacrine cells and bipolar cells of the macaque monkey retina, *J. Neurosci.*, 10:3045–3055.
- Marshak, D. W., and T. Yamada, 1984. Characterization of somatostatin-like immunoreactivity in vertebrate retinas, *Invest. Ophthalmol. Vis. Sci.*, 25:112–115.
- Masland, R. H., 1988. Amacrine cells, *Trends Neurosci.*, 11:405–410.
- McDonald, J. K., 1988. NPY and related substances, *Crit. Rev. Neurobiol.*, 4:97–135.
- Miguel-Hidalgo, J. J., E. Senba, K. Takatsuji, and M. Tohyama, 1994. Projections of tachykinin- and glutaminase-containing rat retinal ganglion cells, *Brain Res. Bull.*, 35:73–84.
- Mikkelsen, J. D., J. N. Larsen, J. Fahrenkrug, and M. Møller, 1987. Peptide histidine-isoleucine (PHI)-immunoreactive amacrine cells in the retina of the rat, *Neurosci. Lett.*, 79:281–285.
- Mintz, E. M., C. L. Marvel, C. F. Gillespie, K. M. Price, and H. E. Albers, 1999. Activation of NMDA receptors in the suprachiasmatic nucleus produces light-like phase shifts of the circadian clock in vivo, *J. Neurosci.*, 19:5124–5130.
- Mitrofanis, J., S. R. Robinson, and J. M. Provis, 1989. Somatostatinergic neurones of the developing human and cat retinae, *Neurosci. Lett.*, 104:209–216.
- Mollereau, C., M. Parmentier, P. Mailleux, J. L. Butour, C. Moisand, P. Chalon, D. Caput, G. Vassart, and J. C. Meunier, 1994. ORL1, a novel member of the opioid receptor family: Cloning, functional expression and localization, *FEBS Lett.*, 341:33–38.
- Mori, M., M. Aihara, and T. Shimizu, 1997. Differential expression of somatostatin receptors in the rat eye: SSTR4 is intensely expressed in the iris/ciliary body, *Neurosci. Lett.*, 223:185–188.
- Murata, M., M. Nakagawa, and S. Takahashi, 1997. Expression and localization of angiotensin II type 1 receptor mRNA in rat ocular tissues, *Ophthalmologica*, 211:384–386.
- Nakagawa, S., Y. Hasegawa, T. Kubozono, and K. Takumi, 1988. Substance P-like immunoreactive retinal terminals found in two retinorecipient areas of the Japanese monkey, *Neurosci. Lett.*, 93:32–37.
- Neal, M. J., J. R. Cunningham, S. J. Paterson, and A. T. McKnight, 1997. Inhibition by nociceptin of the light-evoked release of ACh from retinal cholinergic neurones, *Br. J. Pharmacol.*, 120:1399–1400.
- Neal, M. J., S. J. Paterson, and J. R. Cunningham, 1994. Enhancement of retinal acetylcholine release by DAMGO: possibly a direct opioid receptor-mediated excitatory effect, *Br. J. Pharmacol.*, 113:789–794.
- Nielsen, H. S., J. Hannibal, S. M. Knudsen, and J. Fahrenkrug, 2001. Pituitary adenylate cyclase-activating polypeptide induces period1 and period2 gene expression in the rat suprachiasmatic nucleus during late night, *Neurosci.*, 103:433–441.
- Nilsson, S. F., P. De Neef, P. Robberecht, and J. Christophe, 1994. Characterization of ocular receptors for pituitary adenylate cyclase activating polypeptide (PACAP) and their coupling to adenylate cyclase, *Exp. Eye Res.*, 58:459–467.
- Nothacker, H. P., R. K. Reinscheid, A. Mansour, R. A. Henningsen, A. Ardati, F. J. Monsma, Jr., S. J. Watson, and O. Civelli, 1996. Primary structure and tissue distribution of the orphanin FQ precursor, *Proc. Natl. Acad. Sci. USA*, 93:8677–8682.
- Oh, S.-J., I. D'Angelo, E.-J. Lee, M.-H. Chun, and N. B. Brecha, 2002. Distribution and synaptic connectivity of neuropeptide Y (NPY) immunoreactive amacrine cells in the rat retina, *J. Comp. Neurol.*, 446:219–234.
- Okamoto, S., H. Okamura, H. Terubayashi, Y. Akagi, H. Okamoto, and Y. Ibata, 1992. Localization of vasoactive intestinal peptide (VIP) messenger RNA (mRNA) in amacrine cells of rat retina, *Curr. Eye Res.*, 11:711–715.
- Olianas, M. C., A. Inganni, V. Sogos, and P. Onali, 1997. Expression of pituitary adenylate cyclase-activating polypeptide (PACAP) receptors and PACAP in human fetal retina, *J. Neurochem.*, 69:1213–1218.
- Olianas, M. C., V. Loi, M. Lai, E. Mosca, and P. Onali, 1993. Corticotropin-releasing hormone stimulates adenylyl cyclase activity in the retinas of different animal species, *Regul. Pept.*, 47:127–132.
- Olianas, M. C., and P. Onali, 1995. G protein-coupled corticotropin-releasing hormone receptors in rat retina, *Regul. Pept.*, 56:61–70.
- Onali, P., and M. C. Olianas, 1994. PACAP is a potent and highly effective stimulator of adenylyl cyclase activity in the retinas of different mammalian species, *Brain Res.*, 641:132–134.
- Osborne, N. N., 1984. Substance P in the bovine retina: localization, identification, release, uptake and receptor analysis, *J. Physiol.*, 349:83–93.
- Osborne, N. N., 1991. Inhibition of cAMP production by alpha 2-adrenoceptor stimulation in rabbit retina, *Brain Res.*, 553:84–88.
- Osborne, N. N., and H. Ghazi, 1989. The effect of substance P and other tachykinins on inositol phospholipid hydrolysis in rabbit retina, superior colliculus and retinal cultures, *Vis. Res.*, 29:757–764.
- Otsuka, M., and K. Yoshioka, 1993. Neurotransmitter functions of mammalian tachykinins, *Physiol. Rev.*, 73:229–308.
- Oyamada, H., K. Takatsuji, E. Senba, P. W. Mantyh, and M. Tohyama, 1999. Postnatal development of NK1, NK2, and NK3 neurokinin receptors expression in the rat retina, *Brain Res. Devel. Brain Res.*, 117:59–70.
- Pachter, J. A., D. W. Marshak, D. M. Lam, and K. R. Fry, 1989. A peptide histidine isoleucine/peptide histidine methionine-like peptide in the rabbit retina: colocalization with vasoactive intestinal peptide, synaptic relationships and activation of adenylate cyclase activity, *Neurosci.*, 31:507–519.
- Palm, D. E., L. C. Keil, J. W. Sassani, and W. B. Severs, 1989. Immunoreactive atrial natriuretic peptide in the retina of rats and rabbits, *Brain Res.*, 504:142–144.
- Patel, Y. C., 1999. Somatostatin and its receptor family, *Front. Neuroendocrinol.*, 20:157–198.
- Petrucchi, C., V. Resta, F. Fieni, A. Bigiani, and P. Bagnoli, 2001. Modulation of potassium current and calcium influx by

- somatostatin in rod bipolar cells isolated from the rabbit retina via sst2 receptors, *Naunyn-Schmiedeberg's Arch. Pharmacol.*, 363:680–694.
- Phillips, M. I., 1987. Functions of angiotensin in the central nervous system, *Annu. Rev. Physiol.*, 49:413–435.
- Pourcho, R. G., and D. J. Goebel, 1988a. Colocalization of substance P and gamma-aminobutyric acid in amacrine cells of the cat retina, *Brain Res.*, 447:164–168.
- Pourcho, R. G., and D. J. Goebel, 1988b. Substance P-like immunoreactive amacrine cells in the cat retina, *J. Comp. Neurol.*, 275:542–552.
- Rickman, D. W., J. C. Blanks, and N. C. Brecha, 1996. Somatostatin-immunoreactive neurons in the adult rabbit retina, *J. Comp. Neurol.*, 365:491–503.
- Rorstad, O. P., M. J. Brownstein, and J. B. Martin, 1979. Immunoreactive and biologically active somatostatin-like material in rat retina, *Proc. Natl. Acad. Sci. USA*, 76:3019–3023.
- Rorstad, O. P., M. K. Senterman, K. M. Hoyte, and J. B. Martin, 1980. Immunoreactive and biologically active somatostatin-like material in the human retina, *Brain Res.*, 199:488–492.
- Sagar, S. M., 1987a. Somatostatin-like immunoreactive material in the rabbit retina: immunohistochemical staining using monoclonal antibodies, *J. Comp. Neurol.*, 266:291–299.
- Sagar, S. M., 1987b. Vasoactive intestinal polypeptide (VIP) immunohistochemistry in the rabbit retina, *Brain Res.*, 426:157–163.
- Sagar, S. M., and P. E. Marshall, 1988. Somatostatin-like immunoreactive material in associational ganglion cells of human retina, *Neurosci.*, 27:507–516.
- Sagar, S. M., P. E. Marshall, and D. M. Landis, 1985. Immunoreactive somatostatin in the rat retina: light microscopic immunocytochemistry and chromatographic characterization, *Brain Res.*, 336:235–242.
- Sagar, S. M., P. E. Marshall, S. T. Onesti, and D. M. Landis, 1986. Somatostatin immunocytochemistry in the rabbit retina, *Invest. Ophthalmol. Vis. Sci.*, 27:316–322.
- Sagar, S. M., O. P. Rorstad, D. M. Landis, M. A. Arnold, and J. B. Martin, 1982. Somatostatin-like immunoreactive material in the rabbit retina, *Brain Res.*, 244:91–99.
- Savchenko, A., T. W. Kraft, E. Molokanova, and R. H. Kramer, 2001. Growth factors regulate phototransduction in retinal rods by modulating cyclic nucleotide-gated channels through dephosphorylation of a specific tyrosine residue, *Proc. Natl. Acad. Sci. USA*, 98:5880–5885.
- Schorderet, M., P. Hof, and P. J. Magistretti, 1984. The effects of VIP on cyclic AMP and glycogen levels in vertebrate retina, *Peptides*, 5:295–298.
- Seki, T., S. Shioda, S. Izumi, A. Arimura, and R. Koide, 2000. Electron microscopic observation of pituitary adenylate cyclase-activating polypeptide (PACAP)-containing neurons in the rat retina, *Peptides*, 21:109–113.
- Seki, T., S. Shioda, D. Ogino, Y. Nakai, A. Arimura, and R. Koide, 1997. Distribution and ultrastructural localization of a receptor for pituitary adenylate cyclase activating polypeptide and its mRNA in the rat retina, *Neurosci. Lett.*, 238:127–130.
- Shughrue, P. J., M. V. Lane, and I. Merchenthaler, 1996. In situ hybridization analysis of the distribution of neurokinin-3 mRNA in the rat central nervous system, *J. Comp. Neurol.*, 372:395–414.
- Sinclair, J. R., and S. Nirenberg, 2001. Characterization of neuropeptide Y-expressing cells in the mouse retina using immunohistochemical and transgenic techniques, *J. Comp. Neurol.*, 432:296–306.
- Spira, A. W., Y. Shimizu, and O. P. Rorstad, 1984. Localization, chromatographic characterization, and development of somatostatin-like immunoreactivity in the guinea pig retina, *J. Neurosci.*, 4:3069–3079.
- Stone, R. A., and C. C. Glembofski, 1986. Immunoactive atrial natriuretic peptide in the rat eye: molecular forms in anterior uvea and retina, *Biochem. Biophys. Res. Commun.*, 134:1022–1028.
- Stone, R. A., C. M. Wilson, and C. C. Glembofski, 1990. Chromatographic characterization of vasoactive intestinal polypeptide in guinea pig and rhesus monkey eyes, *Curr. Eye Res.*, 9:287–291.
- Straznick, C., and J. Hiscock, 1989. Neuropeptide Y-like immunoreactivity in neurons of the human retina, *Vis. Res.*, 29:1041–1048.
- Takatsuki, K., J. J. Miguel-Hidalgo, and M. Tohyama, 1991. Substance P-immunoreactive innervation from the retina to the suprachiasmatic nucleus in the rat, *Brain Res.*, 568:223–229.
- Thier, P., and J. Bolz, 1985. Cholecystokinin in the cat retina. Action of exogenous CCK8 and localization of cholecystokinin-like immunoreactivity, *Invest. Ophthalmol. Vis. Sci.*, 26:266–272.
- Tornqvist, K., and B. Ehinger, 1988. Peptide immunoreactive neurons in the human retina, *Invest. Ophthalmol. Vis. Sci.*, 29:680–686.
- Tornqvist, K., R. Uddman, F. Sundler, and B. Ehinger, 1982. Somatostatin and VIP neurons in the retina of different species, *Histochem.*, 76:137–152.
- Tsuchida, K., R. Shigemoto, Y. Yokota, and S. Nakanishi, 1990. Tissue distribution and quantitation of the mRNAs for three rat tachykinin receptors, *Eur. J. Biochem.*, 193:751–757.
- Vaney, D. I., G. E. Whittington, and H. M. Young, 1989. The morphology and topographic distribution of substance-P-like immunoreactive amacrine cells in the cat retina, *Proc. R. Soc. Lond. B Biol. Sci.*, 237:471–488.
- Vaney, D. I., and H. M. Young, 1988. GABA-like immunoreactivity in NADPH-diaphorase amacrine cells of the rabbit retina, *Brain Res.*, 474:380–385.
- Vasilaki, A., R. Gardette, J. Epelbaum, and K. Thermos, 2001. NADPH-diaphorase colocalization with somatostatin receptor subtypes sst2A and sst2B in the retina, *Invest. Ophthalmol. Vis. Sci.*, 42:1600–1609.
- Veruki, M. L., and H. H. Yeh, 1992. Vasoactive intestinal polypeptide modulates GABA_A receptor function in bipolar cells and ganglion cells of the rat retina, *J. Neurophysiol.*, 67:791–797.
- Veruki, M. L., and H. H. Yeh, 1994. Vasoactive intestinal polypeptide modulates GABA_A receptor function through activation of cyclic AMP, *Vis. Neurosci.*, 11:899–908.
- Voigt, T., 1986. Cholinergic amacrine cells in the rat retina, *J. Comp. Neurol.*, 248:19–35.
- Volgyi, B., D. Xin, Y. Amarillo, and S. A. Bloomfield, 2001. Morphology and physiology of the polyaxonal amacrine cells in the rabbit retina, *J. Comp. Neurol.*, 440:109–125.
- Wagner, J., A. H. Jan Danser, F. H. Derkx, T. V. de Jong, M. Paul, J. J. Mullins, M. A. Schalekamp, and D. Ganten, 1996. Demonstration of renin mRNA, angiotensinogen mRNA, and angiotensin converting enzyme mRNA expression in the human eye: Evidence for an intraocular renin-angiotensin system, *Br. J. Ophthalmol.*, 80:159–163.
- Wamsley, J. K., J. M. Palacios, and M. J. Kuhar, 1981. Autoradiographic localization of opioid receptors in the mammalian retina, *Neurosci. Lett.*, 27:19–24.
- Wässle, H., and B. B. Boycott, 1991. Functional architecture of the mammalian retina, *Physiol. Rev.*, 71:447–480.
- Wheeler-Schilling, T. H., K. Kohler, M. Sautter, and E. Guenther, 1999. Angiotensin II receptor subtype gene expression and

- cellular localization in the retina and non-neuronal ocular tissues of the rat, *Eur. J. Neurosci.*, 11:3387–3394.
- White, C. A., and L. M. Chalupa, 1991. Subgroup of alpha ganglion cells in the adult cat retina is immunoreactive for somatostatin, *J. Comp. Neurol.*, 304:1–13.
- White, C. A., L. M. Chalupa, D. Johnson, and B. C. Brecha, 1990. Somatostatin-immunoreactive cells in the adult cat retina, *J. Comp. Neurol.*, 293:134–150.
- Xiang, Z., L. Jiang, and Z. Kang, 2001. Transient expression of somatostatin mRNA in developing ganglion cell layers of rat retina, *Brain Res. Devel. Brain Res.*, 128:25–33.
- Yeh, H. H., and J. A. Olschowka, 1989. A system of corticotropin releasing factor-containing amacrine cells in the rat retina, *Neurosci.*, 33:229–240.
- Zalutsky, R. A., and R. F. Miller, 1990a. The physiology of somatostatin in the rabbit retina, *J. Neurosci.*, 10:383–393.
- Zalutsky, R. A., and R. F. Miller, 1990b. The physiology of substance P in the rabbit retina, *J. Neurosci.*, 10:394–402.
- Zhang, D., and H. H. Yeh, 1992. Substance-P-like immunoreactive amacrine cells in the adult and the developing rat retina, *Brain Res. Devel. Brain Res.*, 68:55–65.

23 Inhibition in the Retina

MALCOLM M. SLAUGHTER

AMACRINE CELLS PRODUCE a complex array of inhibition to bipolar cells, ganglion cells, and other amacrine cells. Gamma-aminobutyric acid (GABA) and glycine are the primary inhibitory neurotransmitters, each contained in about 35% of all amacrine cells, with little coexpression. Both provide feedback inhibition to bipolar cells, although GABAergic feedback is more prominent. It is most evident in ON bipolar cells, where the GABA_C receptor is particularly important. This feedback improves spatial and temporal contrast and increases the dynamic range at the synapse. There is lateral inhibition between amacrine cells, notably long-range glycinergic inhibition. Both GABAergic and glycinergic amacrine cells feed forward to inhibit ganglion cells. They produce sustained and transient surround inhibition that shortens the response time and improves the resolution of ganglion cells. Glycinergic synapses are often responsible for transient inhibition. There are also inhibitory GABAergic bipolar cells and both glycinergic and GABAergic interplexiform cells. This chapter reviews the history of inhibitory amino acid neurotransmitters in retina, the properties of the receptors, the synaptic mechanisms, and the retinal circuits.

Background history

Kishida and Naka (1967) were the first to show that GABA and glycine inhibit spike activity of retinal ganglion cells. This was at a time when neuroscientists were just discovering inhibitory amino acid transmitters. Retinal experiments were a spearhead of this research, satisfying the criteria for neurotransmitters, including autoradiographic localization of GABA and glycine within the retina (Ehinger and Falck, 1971), measurements of endogenous amino acid levels, and demonstrating that light caused transmitter release (Ehinger and Lindberg, 1974; Voaden and Starr, 1972).

EFFECTS OF GABA AND GLYCINE INHIBITION It rapidly became apparent that the retina was unusual in the juxtaposition of GABA and glycine inhibition. A central question arose that is still not fully answered: why are two very similar transmitters in the same circuit? Clearly there must be a division of labor. The earliest study suggested that some ganglion cells received GABAergic IPSPs exclusively, and others, glycinergic IPSPs (Miller et al., 1977). The two transmitters regulate different visual processes. GABAergic inhibition is

essential for the formation of directional selectivity in ganglion cells; glycine has key effects on other receptive field properties (Caldwell et al., 1978). Glycine is linked to inhibitory surrounds in X cells, GABA in Y cells (Kirby, 1979). Both control the activity of the only known excitatory amacrine cell, the cholinergic starburst amacrine cell (Massey and Neal, 1979b; Neal and Cunningham, 1995). In an intriguing forerunner of recent research, early field potential studies suggested that GABAergic inhibition produced the sustained to transient transition that is a hallmark of retinal ganglion cells (Mooney, 1978). Hence, there was a phenomenological separation of function, but there was no evidence of principle that guided this division.

Thus, within the first decade of discovery the key elements and enduring puzzles were in place. After that stunning progress, there was a change in focus over the next two decades. This led to discovery of new receptors and inhibitory mechanisms. It also helped resolve some of the apparently contradictory observations that had emerged.

DISTINCT INHIBITORY FUNCTIONS The earliest studies in vertebrate retinal physiology revealed that ganglion cell signals are divided into ON and OFF pathways, or alternatively divided into sustained and transient pathways. The physiological characterization was reinforced by anatomical differences, and the distinctions existed not only in the retina, but also in the lateral geniculate and cortex. Naturally, attention turned to the roles that GABA and glycine play in formation or modulation of these essential pathways.

At one end of the spectrum arose the concept that there is a direct correlation between these pathways and the two transmitters. For example, Ikeda and Sheardown (1983) examined inhibition that occurs in ganglion cells at the offset of an excitatory synaptic stimulus. They found that GABA was responsible for this inhibition in ON-center ganglion cells, and glycine in OFF-center ganglion cells. This was true for both transient and sustained cells. While no other laboratory has reported such a stark delineation, many have found that GABAergic inhibition is more prominent in the ON pathway. Belgium and colleagues (1984) found a different correlation; transient inhibition derived exclusively from glycinergic synapses. Transient glycinergic IPSPs were found in ON, OFF, and ON-OFF ganglion cells. Again, other experimenters found that glycine is preferentially, though perhaps not exclusively, involved in transient inhibition.

TABLE 23.1
Properties of retinal inhibitory receptors

	GABA Receptors*				Glycine Receptors	
	Ionotropic: Increase Cl ⁻ Conductance		Metabotropic: Modulate Voltage-dependent K ⁺ and Ca ²⁺ Channels		Ionotropic: Increase Cl ⁻ Conductance	
Receptor Subtype or Variety	GABA _A Fast activation and desensitization	GABA _C Slow activation and little desensitization	GABA _B Baclofen- sensitive	GABA _B CACA- sensitive	Glycine _{fast} Fast activation and desensitization	Glycine _{slow} Slow activation and little desensitization
Antagonists	Bicuculine SR95531, Picrotoxin	Picrotoxin I4AA, TPMPA, APMPA	CGP35348, CGP55845, Saclofen, Phaclofen		Strychnine	DCKA, Strychnine
Agonists	Muscimol, THIP, I4AA		Baclofen, 3AP, APMPA	CACA	Glycine	Glycine
Modulators	Suppressed by Zn and Ca, Enhanced by PKA	Suppressed by Zn and PKC	Suppressed by Ca	Enhanced by NO, cGMP	Enhanced by PKC, Bimodal effect of Zn	Suppressed by PKC

*Abbreviations: APMPA: 3-aminopropyl(methyl)phosphonic acid; TPMPA: (1,2,5,6-tetrahydropyridine-4-yl)-methylphosphonic acid; I4AA: imidazole-4-acetic acid; THIP: 4,5,6,7-tetrahydroisoxazolo(5,4-c)pyridin-3-ol; 3AP: 3-aminopropylphosphonic acid; DCKA: 5,7-dichlorokynurenic acid.

While these two extreme models are clearly contradictory, a moderate interpretation is probably correct: GABA is more involved in inhibition of the ON pathway, and glycine is more involved in transient inhibition. A less restricted model has been presented by Frumkes and colleagues (1981) postulating a complex mixture of GABAergic and glycinergic interactions. One commentator noted that this model was so complex it must be right! While the retina is clearly not striving for simplicity, these models still beg the question why the retina uses two transmitter systems with such apparently similar properties when one might suffice. Part of the answer can be found in the receptors, particularly the GABA receptors.

Receptors

During the first decade of discovery, it was recognized that both GABA and glycine increase chloride conductance. The properties of the two receptors were uncannily similar, including not only ion selectivity, but also conductance. That similarity began to unravel in 1980 with the discovery of the metabotropic GABA_B receptor (Bowery et al., 1980). Retinal pharmacology was even more dramatically altered by the discovery of the rho subunit and its association with the GABA_C receptor (Cutting et al., 1991). Both the molecular subunit and the unusual receptor were first detailed in retina, although the link between the subunit and the receptor took a while to establish. Thus, there are at least three distinct types of ionotropic inhibitory amino acid receptor in retina (Table 23.1). This can be seen, for example, in the kinetics

of spontaneous IPSCs in mouse amacrine cells, where there is one type of glycinergic and two types of GABAergic synaptic responses (Frech et al., 2001).

IONOTROPIC GABA RECEPTORS The GABA_C receptor, like the GABA_A receptor, is an ionotropic receptor that is permeable to chloride. But the GABA_C receptor has several unique properties, including higher affinity for GABA, slower activation kinetics, and less desensitization (Feigenspan et al., 1993; Qian and Dowling, 1993) (Table 23.2). In rat bipolar cells, the GABA_C receptor has a main single channel conductance of 7.9 pS, compared to 29.6 for the GABA_A receptor. GABA_C receptors have an EC₅₀ of 4 μM; for GABA_A receptors the EC₅₀ is 27 μM. The mean open time of the GABA_C receptor is 150 ms, about sixfold greater than the GABA_A receptor (Feigenspan and Bormann, 1994a). These characteristics make GABA_C receptors ideal for the modulation of the slow, prolonged graded potentials found in retina. Thus, it is not surprising that the GABA_C receptor plays a particularly prominent role in the inhibitory feedback to the bipolar cell axon terminal (Lukasiewicz et al., 1994).

METABOTROPIC GABA RECEPTORS The GABA_B receptor is a G-protein-linked receptor that modulates voltage-dependent calcium and potassium channels. In some cases the modulation is through a direct action of the G-protein with the channel, in other cases a more complex second-messenger cascade is involved (Shen and Slaughter, 1998). It is likely to function as an autoreceptor in GABAergic

TABLE 23.2
GABA_A and GABA_C receptors

Relative Response Properties	
Activation Rate	GABA _A > GABA _C
Desensitization Rate	GABA _A > GABA _C
Mean Channel Open Time	GABA _C > GABA _A
Single Channel Conductance	GABA _A > GABA _C
Receptor Affinity	GABA _C > GABA _A
Retinal Distribution	GABA _A > GABA _C

TABLE 23.3
Metabotropic GABA receptors

Actions of Two GABA _B Receptors	
Baclofen-Sensitive	CACA-sensitive
Suppress L-type calcium channels in fish ganglion cells and in ~20% of amphibian bipolar cells	Suppress L-type calcium channels in goldfish Mbl bipolar cells
Enhance inward-rectifying potassium channels and L-type calcium channels in amphibian ganglion cells	Suppress L-type calcium channels in amphibian ganglion cells
Suppress N-type calcium channels in amphibian ganglion cells	

amacrine cells (Koulen et al., 1998). It is also an important postsynaptic receptor, suppressing bipolar cell transmitter release (Maguire et al., 1989) and altering the response properties of ganglion cells (Cook et al., 2000; Shen and Slaught-ter, 1998, 1999a; Zhang et al., 1997b).

The GABA_B receptor system in retina exhibits a variety that has not yet been found in the rest of the brain (Table 23.3). In fish retina, baclofen suppresses an L-type calcium channel in ganglion cells (Bindokas and Ishida, 1991). But in goldfish bipolar cells, GABA suppresses an L-type calcium channel through a baclofen-insensitive receptor. This receptor is a metabotropic GABA_B receptor, but its preferred agonist is cis-aminocrotonic acid (CACA) (Heidelberger and Matthews, 1991). These two GABA_B receptors are coex-pressed in amphibian ganglion cells, but have different actions (Zhang et al., 1997b). The baclofen-sensitive GABA_B receptors suppress N-type calcium channels but facilitate L-type calcium channels, whereas the CACA-sensitive recep-tors suppress the L-type channel. Thus, there is a diversity within the GABA_B receptors, which is compounded by a diversity of second-messenger mechanisms and effector targets.

GLYCINE RECEPTORS GABA release can activate metabotropic receptors and two subtypes of ionotropic receptor. Glycine receptors have not exhibited the same diversity. There are fast- and slow-activating ionotropic

glycine receptors that have some analogy with the GABA_A and GABA_C receptors (Han et al., 1997). In ganglion cells, rapid application of glycine produces a fast-rising chloride current that decays to a plateau. Nanomolar strychnine blocks the peak response but not the plateau, consequently leaving a slowly rising response with little desensitization. In contrast, 5,7 dichlorokynurenic acid (DCKA) inhibits this slow current but not the fast current. Thus, glycine produces two currents: one that activates and desensitizes rapidly, and another that activates and desensitizes slowly. Unlike the action of GABA at the fast GABA_A and slow GABA_C recep-tors, glycine is equally potent in eliciting both responses.

Among the major neurotransmitters in retina, only glycine lacks a metabotropic receptor. A possible explana-tion for this deficit is that glycinergic amacrine cells obtain their glycine from uptake instead of synthesis (Pow, 1998). This implies that there are relatively high ambient levels of extracellular glycine in the inner plexiform layer, making high affinity metabotropic glycine receptors impractical.

RECEPTOR VARIETY The molecular and pharmacological evidence for subdivisions within the GABA_A, GABA_B, and GABA_C receptors requires added terminology. For this chapter, we will use convention in referring to GABA_A, GABA_B, and GABA_C receptors as subtypes of the GABA receptor. Within these subtypes, receptors with different properties will be called *varieties*. We have alluded to varieties of the GABA_B receptor. There are also varieties of the GABA_C receptor, based on molecular composition and the action of various receptor antagonists (Gao et al., 2000; Qian et al, 1998; Shen and Slaught-ter, 2001). The GABA rho subunit can form a functional, homomeric receptor. Five rho subunits have been cloned from white perch retina, each with distinctive biophysical properties (Qian et al., 1998). The implications of this molecular diversity are yet to be explored. Even the original, GABA_A receptor comprises several varieties, based on subunit composition and the diverse effect of a series of GABA_A receptor antagonists (Frumkes and Nelson, 1995; Wang et al., 2000). Overall, there are at least two varieties of each of the three subtypes of GABA receptor.

There is a spatial distribution of receptor varieties that implies functional distinctions. The $\alpha 1$ subunit of the GABA_A receptor is expressed mainly in bipolar and hori-zontal cell layers, the $\alpha 2$ in the amacrine and ganglion cell layers, and the $\alpha 4$ in a subset of amacrine cells (Greferath et al., 1993). The GABA_A receptors in the proximal retina are sensitive to benzodiazepine, but those in the distal retina are not (Lin and Yazulla, 1994). There is a separation in glycine receptors as well, with the $\alpha 1$ found mainly in the distal inner plexiform layer (IPL), the $\alpha 2$ in the proximal IPL, and the $\alpha 3$ throughout the IPL (Greferath et al., 1994).

In light of these findings, the colocalization of glycine and GABA in the IPL no longer seems redundant. But then we come full circle with the finding that the rho-1 subunit, which creates such a distinctive response in the GABA_C receptor, can form heteromeric channels with the gamma-2 subunit of the GABA_A receptor or the α 1 or the α 2 subunit of the glycine receptor (Pan et al., 2000). So the molecular analysis has started to again blur the distinction between GABA and glycine receptors. Similarly, there appears to be a synergy between the actions of glycine and GABA in some retinal neurons, so that in combination the two transmitters produce a much larger response than the sum of their individual responses (Li and Yang, 1998).

Pharmacology of inhibitory receptors

THE GLYCINE RECEPTORS The pharmacology of retinal glycine receptors is thought to be comparatively simple. No metabotropic receptor has been identified, and the ionotropic receptor is blocked by strychnine. This contrasts with the differential distribution of alpha subunits across the retinal layers. The only evidence of pharmacological diversity is the work of Han, Zhang, and Slaughter (1997), which indicates that there are some glycine responses that are less sensitive to strychnine and are selectively blocked by DCKA (a potent blocker of the glycine recognition site on the NMDA receptor).

An issue that has lingered in the literature is whether there are glycine-like receptors activated by glycine but with selectivity for related compounds such as serine, alanine, or taurine. Taurine, in particular, has periodically been proposed as a neurotransmitter. But cross-desensitization experiments have provided no support for this hypothesis (Pan and Slaughter, 1995).

THE METABOTROPIC GABA RECEPTORS The GABA_B receptor is linked to a G-protein second-messenger cascade. The retina possesses the baclofen-sensitive GABA_B receptor that is similar to that described throughout the CNS; one that is sensitive to antagonists such as 2-hydroxysaclofen, CGP35348, and CGP55845. This receptor suppresses L-type calcium channels in amphibian bipolar cells (Maguire et al., 1989) and fish ganglion cells (Bindokas and Ishida, 1991), and N-type calcium channels in amphibian ganglion cells (Zhang et al., 1997b).

As mentioned above, there is another GABA_B receptor that is potently activated by CACA. CACA acts on a baclofen-insensitive GABA receptor through a G-protein cascade that may involve a cGMP pathway. In retina, this receptor has only been linked to suppression of L-type voltage-gated calcium channels (Heidelberger and Matthews, 1991; Zhang et al., 1997b). Unfortunately, an antagonist has not yet been found.

IONOTROPIC GABA RECEPTORS The GABA_A and GABA_C receptors have distinct pharmacological properties that permit their separation. The GABA_A receptor can be blocked by bicuculline and SR95531. The GABA_C receptor can be blocked by TPMPA, APMPA, and I4AA (the former seems selective, the other two are also agonists at the GABA_B and GABA_A receptor, respectively). GABA_{A&C} receptors are blocked by picrotoxin (except in rat retina). But TPMPA may not block all GABA_C responses, so the common experimental method of separation is to apply bicuculline to block GABA_A receptors, and then apply picrotoxin to measure the remaining GABA_C receptor response. This may be problematic, because I4AA blocks some GABA_C receptors that are not blocked by picrotoxin (Gao et al., 2000; Shen and Slaughter, 2001). There is also evidence that not all GABA_A receptors have the same sensitivity to bicuculline and to SR95531 (Frumkes et al., 1995; Lin and Yazulla, 1994).

Despite these ambiguities, pharmacological tools can be used to separate the subtypes of GABA receptor. In addition, subtle differences between antagonists suggest that it may be possible to distinguish receptor varieties, although that is not yet achievable. Nevertheless, it is evident that retinal circuits use inhibitory receptor diversity to process specialized components of the visual scene such as motion, edge enhancement, contrast, and gain.

Receptor modulation

Receptor modulation is an enormous field and can be viewed at several levels, from short-term effects such as phosphorylation to longer-term aspects such as protein expression and sorting. With respect to the former, both the glycine and GABA receptors are controlled by a number of mechanisms that have recently been explored. Modulators often alter the kinetics of the receptors, regulating several varieties in concert to produce a net change in the temporal properties of inhibition.

GLYCINE RECEPTOR MODULATION The glycine receptors are modulated by protein kinase A and protein kinase C (Han and Slaughter, 1998). There are fast and slow glycine responses, probably reflecting the responses of two receptor subtypes. The slow response is suppressed by protein kinase A, and the fast response is enhanced by protein kinase C. Thus, both phosphorylation pathways contribute to shifting the balance of the composite glycine response toward a more phasic signal. Because glycine is involved in transient inhibition, protein kinases can regulate this key aspect of glycine function in retina.

Zinc has a concentration-dependent, biphasic effect on the magnitude of the glycine response, but it only

influences the fast glycine response (Han and Wu, 1999). Low doses of zinc enhance this response; high concentrations suppress the fast glycine response. Zinc is a transmitter candidate, suggesting that it is used in retinal circuits to modulate glycine synaptic kinetics. Low concentrations of zinc may be synergistic with protein kinase C, both acting to increase the synaptic weight of the most phasic glycine signals.

GABA RECEPTOR MODULATION The GABA receptor is also modulated by phosphorylation and by zinc. Unlike the fast glycine response, the GABA_A receptor and the GABA_C receptor are only inhibited by zinc (Dong and Werblin, 1996; Li and Yang, 1999). Zinc's IC₅₀ for the GABA_A receptor is about 67 μ M, compared to about 2 μ M for the GABA_C receptor (Kaneda et al., 2000). Thus, low concentrations of zinc that enhance the fast glycine receptor also suppress the slow GABA_C receptor. Zinc can also increase the net kinetics of the GABA response, slowing the activation of the GABA_C receptor while accelerating that of the GABA_A receptor. Thus, low concentrations of zinc enhance the relative contribution of both fast glycinergic and fast GABAergic inhibition.

Protein kinases modulate GABA receptors, akin to the effect on glycine receptors. The GABA_A receptor response is enhanced by protein kinase A, a pathway that can be stimulated by dopamine (Feigenspan and Bormann, 1994b). Protein kinase C suppresses the GABA_C receptor (Feigenspan and Bormann, 1994c). Thus, protein kinase A enhances the fast GABA_A response and reduces the slow glycine response; protein kinase C enhances the fast glycine response but suppresses the slow GABA_C responses. The net effect is that fast inhibition is relatively greater after stimulation of either kinase system.

Internal calcium modulates ionotropic and metabotropic GABA receptors. The GABA_A receptor is suppressed by internal calcium released through ryanodine and IP₃ receptors (Akopian et al., 1998). Elevated calcium activates a calmodulin-dependent phosphatase that directly or indirectly suppresses the GABA_A receptor. The apparent affinity of the baclofen-sensitive GABA_B receptor is reduced by internal calcium release from ryanodine-sensitive stores that then activates calmodulin (Shen and Slaughter, 1999a). It is well known that one important function of GABA is to suppress transmitter release by inhibition of calcium channels (Pan and Lipton, 1995). But in retina there is a reciprocal pathway, whereby elevated internal calcium may abrogate this inhibition.

Anatomy of inhibition

INTERAMACRINE INHIBITION GABA and glycine are inhibitory in most neurons because of their negative chloride

reversal potential (around -60 mV). An exception is the horizontal cell, where both GABA and glycine produce a depolarization (Stockton and Slaughter, 1991), and the bipolar cell dendrite, at least in fish (Saito, 1981). This correlates with the K-Cl cotransporter found in ganglion cells (which extrudes chloride) and the Na-K-Cl cotransporter found in horizontal cells and ON bipolar cell dendrites (which accumulates chloride) (Vardi et al., 2000). Commonly, amacrine cells passively distribute chloride, resulting in silent inhibition, while the chloride reversal potential is more negative than the resting potential in ganglion cells, resulting in IPSPs.

Inhibitory amacrine cells feedback to bipolar cells, feedforward to ganglion cells, and also feed laterally to other amacrine cells. This lateral inhibition is often ignored although it is considerable. Anatomically, glycinergic amacrine cells frequently synapse on other amacrine cells (Pourcho and Owczarzak, 1991), and the majority of all synaptic input to glycinergic amacrine cells comes from other amacrine cells (Zucker and Ehinger, 1993). When examining inhibitory signals to ganglion cells, it is often observed that blocking either GABA or glycine receptors results in more inhibition rather than less (Zhang et al., 1997a). This paradox is due to serial lateral inhibition among amacrine cells (Marc and Liu, 2000). Blocking one of these receptors produces disinhibition of many other inhibitory amacrine cells.

INHIBITION OF GANGLION CELLS Feedforward inhibition is also considerable. All, or almost all, ganglion cells possess both GABA and glycine receptors. But commonly only one or the other set of inhibitory receptors is used (Miller et al., 1977; Protti et al., 1997). Ganglion cells are excited by glutamate input from bipolar cells and inhibited by both glycinergic and GABAergic amacrine cells. The balance favors inhibition. For instance, ON alpha ganglion cells in cat contain about 4400 synapses, 86% of which come from amacrine cells (Freed and Sterling, 1988). Of that amacrine cell input, about a quarter is from amacrine cells that take up glycine. Thus, the apparent glycinergic synapses alone are 1.5 times as numerous as the glutamatergic synapses. However, this may be an overestimate. Zucker and Ehinger (1992) found that only 56% of the synapses made by glycine-containing amacrine cells are onto postsynaptic elements that are glycine receptor immunoreactive. The implication is that these glycinergic amacrine cells also possess other neurotransmitters, which are released at almost half the synapses. If this statistic applied to the ON alpha ganglion cell, then glycinergic synapses would be nearly equivalent in number to the glutamatergic synapses. Nevertheless, when GABAergic synapses are considered as well, inhibitory synapses far outnumber excitatory synapses.

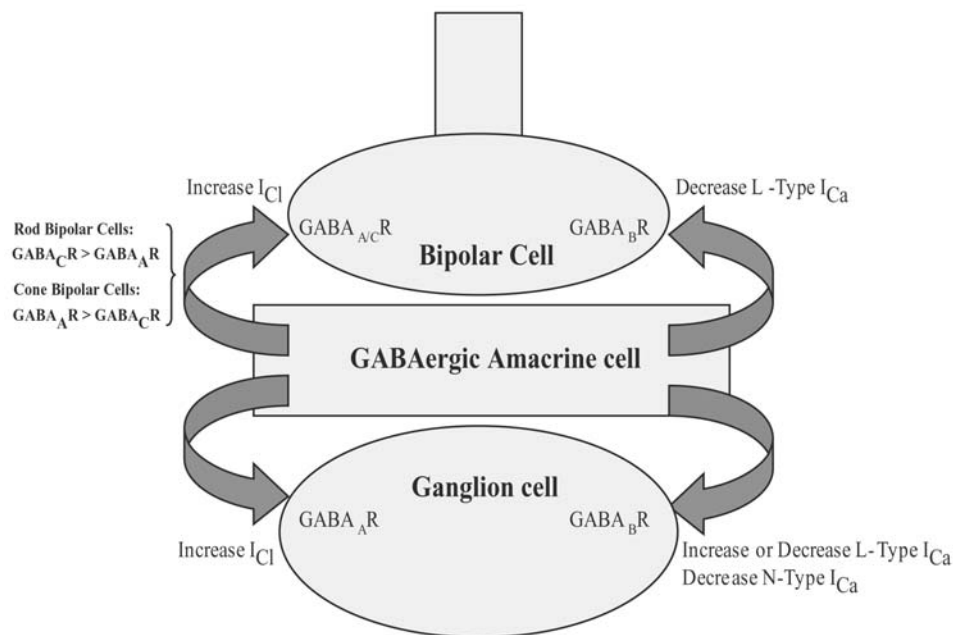


FIGURE 23.1. Actions of feedback and feedforward GABAergic pathways. GABA shunts responses of bipolar cells by activating $GABA_{A/C}$ receptors and also suppresses transmitter release by inhibiting L-type calcium channels. GABA also shunts responses in ganglion cells through $GABA_A$ receptors, while baclofen- and CACA-sensitive $GABA_B$ receptors have complex and sometimes opposing effects on several subtypes of voltage-gated calcium channel.

INHIBITION OF BIPOLAR CELLS GABA receptors are prominently involved in inhibitory feedback to bipolar cells (Fig. 23.1). Glycine seems to have a very limited role in this pathway. All three types of GABA receptors participate in this circuit, although their relative distribution varies markedly. In amphibian retina, Maguire and colleagues (1989) found that only about 20% of bipolar cells were responsive to baclofen and could be distinguished by having axon terminals near the middle of the IPL. The implication is that these are transiently responding bipolar cells and that $GABA_B$ receptors may be involved in motion detection. In the same retina, most bipolar cells express $GABA_C$ receptors (Lukasiewicz et al., 1994). $GABA_C$ receptors in the IPL seem to be localized exclusively at bipolar cell axon terminals. The ratio of $GABA_C$ to $GABA_A$ receptors varies in different types of mammalian bipolar cells, being highest in rod bipolar cells (Euler and Wässle, 1998; McGillem et al., 2000).

Morphology of inhibition

CENTRAL EXCITATION AND PERIPHERAL INHIBITION Whereas bipolar cells have compact dendritic and axonal terminals, the dendritic morphologies of amacrine and ganglion cells are extensive. Both amacrine and ganglion cells receive excitatory input from bipolar cells and inhibitory input from an array of amacrine cells. Consequently, the

excitatory input is compact whereas the inhibitory input sums over a larger receptive field. This disparity can be considerable; the inhibitory field may be 2 to 3 times the diameter of the excitatory field in amphibian ganglion cells (Lukasiewicz and Werblin, 1990). The inhibition is GABAergic and glycinergic; the latter has a slightly larger extent. A similar disparity between excitatory and inhibitory inputs is found in amphibian amacrine cells. Stimulation of the distal retina just above the amacrine cell produced mainly excitation, but stimulation 400 μm to the side produced only an inhibitory glycinergic response (Barnes and Werblin, 1987). Thus, the geometrical disparity between inhibitory and excitatory neurons produces an inhibitory surround response in the inner retina.

EFFECTS OF PERIPHERAL INHIBITION There is sometimes a correspondence between presynaptic input and postsynaptic receptor distribution. In amphibian amacrine cells, excitatory receptors are localized within 200 μm of the soma, and inhibitory receptors extend up to 300 μm (Cook and Werblin, 1994). Interestingly, calcium channels are prominent along the extremities of the dendrites in these wide-field amacrine cells, suggesting that synaptic output occurs near the tips of dendrites. Thus, inhibitory input synapses are located between the site of excitatory input and inhibitory output. This placement almost guarantees that inhibitory input will eliminate synaptic output

from the dendritic tips. This distribution of inhibition would effectively convert the neuron into a narrow receptive field cell.

A similar phenomenon is seen in the marmoset New World monkey, where glycine receptors were quantified based on an antibody to the α -1 subunit. In midget and parasol ganglion cells, the density of glycine receptors was about sixfold greater in distal dendrites as compared to proximal dendrites (Lin et al., 2000). This peripheral inhibition would exaggerate the difference between excitatory and inhibitory receptive fields resulting from the geometries of presynaptic inputs and shrink the ganglion cell's excitatory receptive field.

Inhibitory pathways

GABAergic and Glycinergic Neurons GABA and glycine are both found in amacrine cells, each in approximately 30% to 40% of these neurons (Ball and Brandon, 1986). There is only a small degree of overlap (~5%), probably representing one particular subset of amacrine cell (Yazulla and Yang, 1988). Glycine is found in some interplexiform cells (Marc and Lam, 1981), as is GABA. GABA is also present in some horizontal cells. Comparatively, GABAergic amacrine cells are more involved in feedback to bipolar cells, and glycinergic amacrine cells in interamacrine cell synapses. Overall, GABAergic amacrine cells may be more diverse. In the all-cone lizard retina, 23 different types of amacrine cell were discerned, of which 17 were GABAergic and only 3 were glycinergic. But in macaque amacrine cells, there are four dominant glycinergic types and four GABAergic (Kalloniatis et al., 1996). This section will provide a review of the retinal circuits where functional aspects of inhibitory amino acid receptors have been revealed.

The GABAergic horizontal cell has received much attention over the years, because it is believed to be responsible for the antagonistic surround response: the lateral inhibition of the distal retina (Mangel and Miller, 1987; Vardi and Sterling, 1994). However, this chapter will not discuss this pathway because it is unresolved. Hare and Owen (1996) found no evidence for GABAergic inhibition in formation of the antagonistic surround response in distal retina; Kamermans and colleagues (2001) observed that hemichannels, rather than a chemical synapse, produce this response. Therefore, the discussion of inhibitory circuitry will concentrate on inhibitory neurons of the proximal retina, primarily amacrine cells, with a brief commentary on interplexiform and bipolar cells.

DIRECTIONAL SELECTIVITY The circuit responsible for directional selectivity has received the most attention for the longest duration of any retinal inhibitory pathway. Barlow

and Levick (1965) analyzed the properties of directionally selective (DS) ganglion cells in rabbit retina, concluding that an unidentified asymmetrical inhibitory pathway provided the suppressive null direction response that is the hallmark of this phenomenon. This null inhibition pathway is GABAergic (Ariel and Daw, 1982b; Wyatt and Daw, 1975). The DS ganglion cells receive excitatory input activating nicotinic and NMDA receptors, and the GABAergic cells that mediate null direction inhibition are driven by kainate/AMPA receptors (Kittila and Massey, 1997). Unfortunately, the source of the asymmetrical inhibition is still an enigma.

One of the most perplexing components of the circuit is the cholinergic starburst amacrine cell. These cells form an array of mirror image neurons that contain and release GABA as well as acetylcholine (Brecha et al., 1988; O'Malley and Masland, 1989). They play a key role in encoding directionality, yet acetylcholine receptor blockers do not eliminate directional selectivity (Ariel and Daw, 1982a; Kittila and Massey, 1997). This suggests that their inhibitory action may be important in encoding directionality. Because these are the only neurons in retina that contain acetylcholine, their activity can be reliably monitored by measuring acetylcholine release (Massey and Neal, 1979a). Starburst amacrine cells possess GABA and glycine receptors (Zhou and Fain, 1995), which control acetylcholine release (Massey and Neal, 1979b; Massey and Redburn, 1982). GABA, but not glycine, suppresses basal release. The release of acetylcholine is inhibited by activation of either GABA_A or GABA_C receptors, although GABA_A receptor inhibitors block directional selectivity (Massey et al., 1997). The glycine inhibition involves a feedback loop that is itself suppressed by GABA acting through GABA_B receptors (Neal and Cunningham, 1995). How inhibition of the starburst cells contributes to directional selectivity in ganglion cells is unclear, and there is no evidence for asymmetry of the cholinergic neurons or in their inhibition.

Directional selectivity is reputed to be an intrinsic property of two classes of ganglion cells: the ON-OFF and ON DS cells. But activation of GABA_B receptors by baclofen uncovered directional selectivity in non-DS ganglion cells in amphibian retina (Pan and Slaughter, 1991). The tentative conclusion is that DS is a distributed property in retinal ganglion cells, but DS synaptic inputs have a greater weighting factor in DS ganglion cells. In non-DS ganglion cells, the directional signals are smaller and obscured by other inputs. Presumably, baclofen suppresses these other inputs, thereby unmasking directional signals.

INHIBITORY FEEDBACK TO BIPOLAR CELLS The output of bipolar cells is regulated by reciprocal synapses from amacrine cells. This is true of the rod and cone systems, and much of this feedback is GABAergic. For example, in cat rod

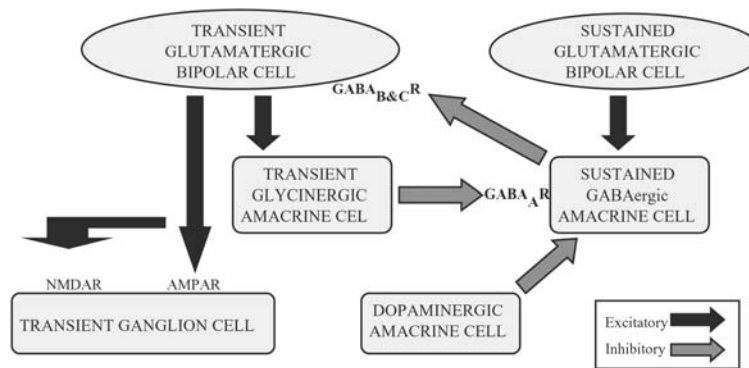


FIGURE 23.2. Pathways involved in GABAergic control of transient ganglion cell signals. Feedback to GABA_{B&C} receptors on bipolar cells contributes to the transient time course of transmitter release in some bipolar cells. This is produced by a sustained but delayed inhibitory feedback to bipolar cells where the delay is controlled by fast, transient input from glycinergic amacrine cells.

bipolar cells, 90% of reciprocal amacrine cell processes take up GABA. In fish retina, GABA uptake is seen in almost all amacrine cell processes going to ON and OFF bipolar cells; glycine is rarely seen in these feedback circuits (Muller and Marc, 1990). This is despite the physiological evidence that bipolar cells are responsive to both GABA and glycine in several species (Attwell et al., 1987; Suzuki et al., 1990), although not in fish retina, where only GABA responses are seen (Kaneko et al., 1991; Kondo and Toyoda, 1983). The balance between GABA_A and GABA_C receptors on bipolar cell axon terminals vary. GABA_C receptors account for 70% of the current in rat rod bipolar cells; that number is closer to 20% in cone bipolar cells, although there is some variance with cone bipolar cell type (Euler and Wassle, 1998). The GABA_A receptor confers speed, and the GABA_C receptor provides an increase in the dynamic range of inhibition (Pan and Lipton, 1995). Thus, when rat rod bipolar cells are axotomized, their light responses have a longer latency and half the dynamic range (Euler and Masland, 2000).

GABA_C receptor feedback to bipolar cells. One of the most intriguing pathways to emerge recently is that of the GABA_C receptor on bipolar cell axon terminals. Shortly after the cloning of the rho subunit of the GABA receptor, it was found that homomers of this protein formed channels that had high affinity for GABA, but were slow to activate, deactivate, and desensitize. GABA receptors with these properties were found in retinal neurons. With the notable exception of subunits from the rat retina, the receptors were blocked by picrotoxin but not bicuculline. Using this pharmacological tool, Lukasiewicz and colleagues (1994) identified a GABA receptor with similar properties in bipolar cell axon terminals. This GABA_C receptor receives delayed feedback from amacrine cells, resulting in a suppression of bipolar cell transmitter release. Blocking this receptor prolongs the excitatory response of ganglion cells. Furthermore, blocking this

receptor alters edge detection in retina (Jacobs and Werblin, 1998).

The GABA_C receptor feedback requires a transient glycinergic amacrine cell to produce the synaptic delay (Fig. 23.2). The circuit begins when the bipolar cell releases glutamate, which excites GABAergic and glycinergic amacrine cells. The glycinergic amacrine cell transiently inhibits the GABAergic amacrine cell. After this fast glycinergic inhibition fades, the GABAergic amacrine cell feedback to bipolar cell GABA_C receptors begins, inhibiting further release of glutamate (Roska et al., 1998).

Overall, there seems to be more GABA_C receptor feedback in the ON, compared with the OFF, bipolar cells. This is certainly evident in rod bipolar cells, but it seems true of other bipolar cells as well (Shields et al., 2000). Stimulation of the GABA_C receptors preferentially suppressed the ON pathway, as judged by the relative responses of ON-OFF ganglion cells (Zhang and Slaughter, 1995). This is an example of preferential GABAergic inhibition of the ON system, alluded to in the Introduction.

The regulation of glutamate release from bipolar cells also influences the type of glutamate receptor activated at the postsynaptic membrane (Minami et al., 1998). In mouse retina, ON bipolar cells release glutamate that activates non-NMDA receptors in ON amacrine cells. If GABA_C receptors are blocked, then more glutamate is released and postsynaptic NMDA receptors are also activated. These NMDA receptors are presumably perisynaptic and only activated when transmitter "spills over" from the synapse (see Fig. 23.2).

There are a number of hypotheses on the function of GABA_C receptor feedback. Pan and Lipton (1995) suggest that it increases the dynamic range of the synapse, Dong and Werblin (1998) propose that it improves temporal contrast, and Jacobs and Werblin (1998) indicate that it is important in edge detection. These conclusions are not contradictory, because a similar mechanism may be involved in all these processes.

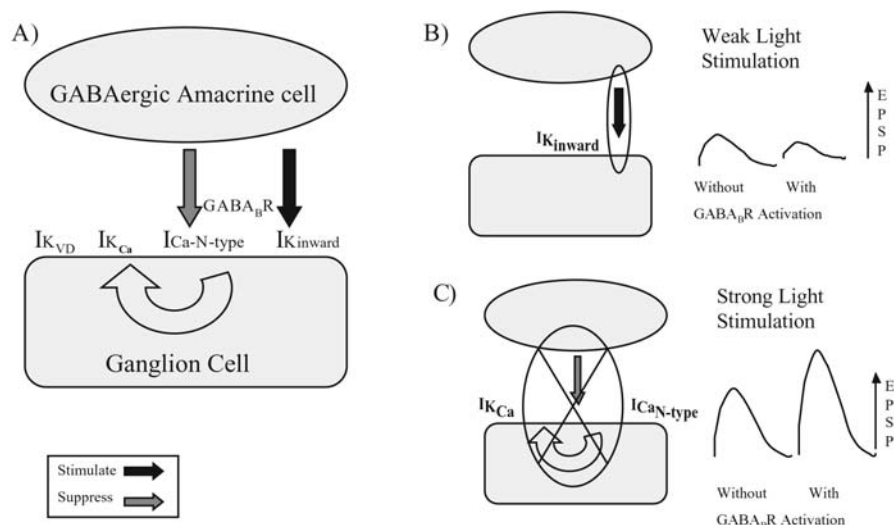


FIGURE 23.3. *A*, The channel mechanisms regulated by baclofen-sensitive $GABA_B$ receptors in the formation of an intensity signal discriminator in ganglion cells. *B*, During weak light stimulation, $GABA_B$ receptors open a small inward-rectifying potassium conductance that shunts small EPSPs, while the calcium-activated

potassium current is not significantly activated. *C*, With stronger light stimulation, $GABA_B$ receptors suppress a larger inward-rectifying calcium-dependent potassium conductance allowing a potentiation of larger EPSPs, while the shunting inward rectifier current is not significant.

GABA_B receptor feedback to bipolar cells. Bipolar cell transmitter release is dependent on voltage-gated L-type calcium channels. In amphibian retina, about 20% of bipolar cells possess baclofen-sensitive $GABA_B$ receptors that suppress these calcium channels and thus reduce transmitter release (Maguire et al., 1989). A proposed function of this selective inhibitory feedback is to create transient signals associated with motion detection (Werblin et al., 1988). The bipolar cells that are sensitive to baclofen are near the midline of the IPL, the presumed site where transient signals are formed. The proposed circuit includes narrow-field, sustained GABAergic amacrine cells that feedback to a subset of bipolar cells. The feedback makes that subset of bipolar cells release transmitter transiently (see Fig. 23.2).

It is curious that bipolar cells (the Mb1 cells) in goldfish retina contain baclofen-insensitive $GABA_B$ receptors (Heidelberger and Matthews, 1991), although there are baclofen-sensitive $GABA_B$ receptors in fish ganglion cells (Bindokas and Ishida, 1991). If there is commonality between these species, it would imply that some bipolar cells possess CACA-sensitive and others baclofen-sensitive $GABA_B$ receptors. But CACA-sensitive bipolar cells have not been reported in any other species of retina.

A GABAERGIC BIPOLAR CELL The general flowchart of the retina includes excitation produced by glutamate-releasing photoreceptors and bipolar cells, modulated by inhibitory horizontal cells and amacrine cells. Yet it appears that a significant subset of bipolar cells may be inhibitory. For a while it was thought that many bipolar cells released glycine, but recent evidence suggests that these cells are

“contaminated” with glycine that diffuses into the bipolar cells from gap junction connections with glycinergic amacrine cells (Vaney et al., 1998). However, there is substantial evidence that about 10% of bipolar cells are truly inhibitory. These neurons have all the hallmarks, including being GAT immunopositive and taking up GABA (Yang, 1997; Yang and Wang, 1999). Furthermore, stimulation of bipolar cells produces an inhibitory response in ganglion cells when the excitatory (glutamatergic) bipolar cells are blocked. GABA-immunopositive bipolar cells are also found in human retina (Van Haesendonck and Missotten, 1993). The function of these inhibitory bipolar cells has yet to be determined.

GABA_B RECEPTOR CREATES A NEURAL DISCRIMINATOR

One of the functions of a sensory system is to discriminate between signals that are relayed to the brain and others that are suppressed. One obvious criterion is signal strength. The $GABA_B$ receptor regulates two conductances in ganglion cells that combine to form an intensity discriminator (Fig. 23.3) (Zhang et al., 1998). The consequence is that small excitatory inputs to ganglion cells are suppressed, and larger EPSPs are enhanced. This phenomenon arises from the confluence of $GABA_B$ receptor activation of a small potassium conductance (probably an inward rectifier) and the suppression of a high-voltage activated calcium-dependent potassium current (an outward rectifier). Thus, small EPSPs are thwarted by activation of the inward rectifying potassium conductance. Larger EPSPs normally activate a calcium-dependent potassium conductance, which is inhibitory. But the $GABA_B$ receptor suppresses that calcium

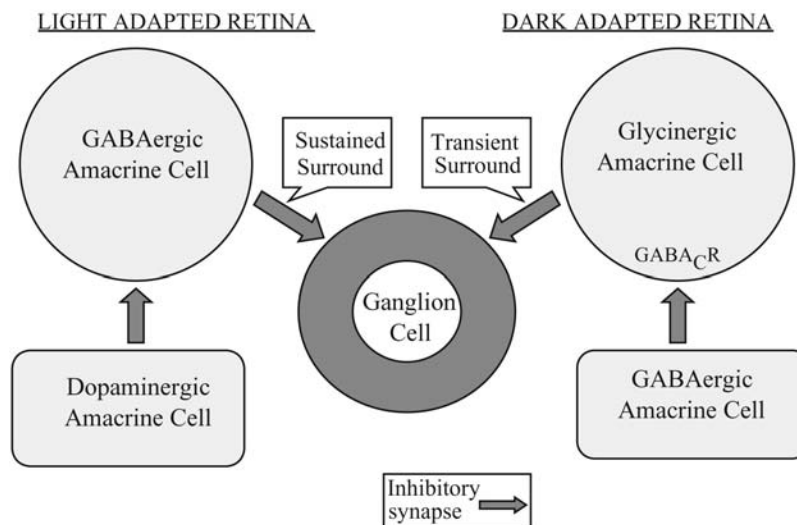


FIGURE 23.4. Regulation of IPL surround inhibition. Transient glycinergic surround inhibition is reduced by GABAergic inhibition in dark adapted retina, becoming disinhibited and more prominent during light adaptation. Similarly, sustained GABAergic inhibition is suppressed during light adaptation.

current and the associated potassium conductance. Thus, the EPSP is enhanced. This system does not require extensive circuitry and the level of GABA_B receptor activation can regulate discrimination.

GLYCINE IN THE ON PATHWAY One of best described and interesting inhibitory circuits is that of the AII glycinergic amacrine cell. The mammalian rod pathway uses the ON bipolar cell, predominantly or exclusively, yet there are both ON and OFF scotopic responses in ganglion cells. The ON responses are explained by the rod ON bipolar cell indirect excitation of ganglion cells, but the OFF excitation is more circuitous. The ON bipolar cell synapses with the AII amacrine cells, which in turn make glycinergic synapses with cone OFF bipolar cells. When the light is ON, the AII cell is depolarized and inhibits the OFF bipolar cell. When the light is OFF, the OFF cone bipolar cell is disinhibited, thereby producing the OFF response in ganglion cells. In sheer numbers, a majority of glycine receptors seem committed to this function. In macaque retina, 70% of the glycine receptors are found in strata 1 and 2 (based on an antibody to receptor $\alpha 1$ subunit), and most are associated with the AII amacrine cell (Grunert and Wassle, 1996).

The AII amacrine cell is inhibited by GABAergic amacrine cells, creating an OFF inhibitory surround (Bloomfield and Xin, 2000). This inhibition is another example of the cross-talk between these two inhibitory systems. In this case, it is generated by an ON amacrine cell, and this surround inhibition is blocked by tetrodotoxin, suggesting that it results from distant lateral circuits.

Besides this rod circuit, there is another glycinergic pathway from the ON to the OFF pathway. When the ON

pathway is blocked, responses in OFF ganglion cells are enhanced. This enhancement is blocked by strychnine, implying that the ON pathway inhibits the OFF pathway (Wassle et al., 1986). But there must be one other member of the circuit, because the ON system is quiescent when glycine is suppressing the OFF system. Presumably, a sign-inverting synapse is interposed, probably another example of serial amacrine cell synapses.

Inhibitory surround

As mentioned, the disparity in the spatial extent of excitatory and inhibitory inputs to ganglion cells contributes to formation of inhibitory surrounds. In amphibian retina, inhibitory IPL surround responses can be parsed into GABAergic sustained surrounds (evoked by a stationary windmill stimulus) and glycinergic transient surrounds (produced by a rotating windmill stimulus). In dark-adapted retina, the sustained surround is dominant, and the transient surround is weak or absent (Fig. 23.4). But with brief light adaptation, the sustained inhibition declines while the transient inhibition increases. The decline in the sustained surround is mediated by dopamine; the increase in the transient surround appears to be due to removal of GABAergic inhibition, mediated by GABA_C receptors (Cook et al., 2000; Cook and McReynolds, 1998). Thus, surround responses are a product of amacrine cell circuits and are modulated by interamacrine synapses.

A comparable process is seen in the surround responses of rabbit OFF ganglion cells. The ON surround response is absent in dark-adapted retina, but can be restored when glycine receptors are blocked (Jensen, 1991). This seems to be the converse of the amphibian circuitry, but once

again exemplifies the importance of cross-talk between inhibitory amacrine cells. The final product of these interamacrine cell circuits may be inhibition of ganglion cells or bipolar cells.

In *Xenopus*, the surround responses are eliminated in both ON and OFF bipolar cells when glycine (but not GABA) is applied to the retina (Stone and Schutte, 1991). But it is not clear whether this is a direct effect on bipolar cells, or is it more likely to be secondary to interamacrine effects?

Roska et al. (2000) examined three inhibitory surround mechanisms that sharpen the ganglion cell response in both time and space. In distal retina, an inhibitory surround is attributed to horizontal cells. Another is mediated by GABAergic amacrine cell feedback to bipolar cells, through GABA_C receptors. This feedback produces a time-delayed, spatial contraction of the image. The third level of surround is produced by feedforward inhibition of ganglion cells, through GABA_A receptors. This sharpens the response, both spatially and temporally. These three surround mechanisms combine to perform the classic role of surround inhibition in a neural network: correcting the signal scattering that occurs in the retinal layers.

GLYCINERGIC AND GABAERGIC INTERPLEXIFORM CELLS

While the best studied of the interplexiform cells contains dopamine, interplexiform cells in various species contain either GABA or glycine (Eldred and Cheung, 1989; Smiley and Basinger, 1988; Yang and Yazulla, 1988). Both of these inhibitory amino acids depolarize horizontal cells because of the unusually high chloride concentrations found in these neurons. The GABA effect may not relate to the function of interplexiform cells because horizontal cells release GABA. But the only source of glycine in the outer retina is the terminals of the interplexiform cell. Glycinergic IPSPs are also observed at bipolar cell dendrites, where they appear to be driven by OFF bipolar cell stimulation of interplexiform cells in salamander retina (Maple and Wu, 1998). Unfortunately, little is known about the function of interplexiform cells that contain inhibitory amino acids. It is not even clear if they are part of a centrifugal or centripetal pathway, because glycinergic interplexiform cells get input from horizontal cells and send output to GABAergic amacrine cells in the goldfish retina (Yazulla and Studholme, 1991).

GABA AND THE DOPAMINERGIC SYSTEM There is a mutual negative interaction between GABAergic and dopaminergic circuits. GABAergic neurons suppress dopamine release; glycinergic neurons do not. This is mediated primarily by GABA_A receptors, with a smaller contribution from GABA_B receptors (Boatright et al., 1994). The distinctions are even more eclectic, for $\alpha 3$ -containing GABA_A receptors are distributed throughout the dopaminergic amacrine cell dendritic tree, but receptors containing $\alpha 1$ GABA subunits are

only in the larger dendrites (Gustincich et al., 1999). Isolated dopaminergic neurons show bursting activity that is inhibited by GABA (Gustincich et al., 1997), suggesting that dopamine release is stimulated by disinhibition. In contrast, dopamine suppresses GABA_C receptors in both bipolar cells and horizontal cells, acting through cAMP (Dong and Werblin, 1994; Wellis and Werblin, 1995). In bipolar cells, where GABA_C receptors play a notable role in regulating transmitter release, dopamine can facilitate bipolar input to the inner retina (Matsui et al., 2001).

Summary

Inhibition in the IPL possesses a richness that is bestowed in part by circuitry, but more by receptor diversity. Recent studies have identified new inhibitory amino acid receptors and linked them to specific aspects of retinal function. Perhaps even more exciting is the inchoate evidence that receptor diversity is more extensive and this portends further specialization in encoding of visual information.

REFERENCES

- Akopian, A., R. Gabriel, and P. Witkovsky, 1998. Calcium released from intracellular stores inhibits GABAA-mediated currents in ganglion cells of the turtle retina, *J. Neurophysiol.*, 80:1105–1115.
- Ariel, M., and N. W. Daw, 1982a. Effects of cholinergic drugs on receptive field properties of rabbit retinal ganglion cells, *J. Physiol.*, 324:135–160.
- Ariel, M., and N. W. Daw, 1982b. Pharmacological analysis of directionally sensitive rabbit retinal ganglion cells, *J. Physiol.*, 324:161–185.
- Attwell, D., P. Mobbs, M. Tessier-Lavigne, and M. Wilson, 1987. Neurotransmitter-induced currents in retinal bipolar cells of the axolotl, *Ambystoma mexicanum*, *J. Physiol.*, 387:125–161.
- Ball, A. K., and C. Brandon, 1986. Localization of 3H-GABA, -muscimol, and -glycine in goldfish retinas stained for glutamate decarboxylase, *J. Neurosci.*, 6:1621–1627.
- Barlow, H. B., and W. R. Levick, 1965. The mechanism of directionally selective units in rabbit's retina, *J. Physiol.*, 178: 477–504.
- Barnes, S., and F. Werblin, 1987. Direct excitatory and lateral inhibitory synaptic inputs to amacrine cells in the tiger salamander retina, *Brain Res.*, 406:233–237.
- Belgum, J. H., D. R. Dvorak, and J. S. McReynolds, 1984. Strychnine blocks transient but not sustained inhibition in mudpuppy retinal ganglion cells, *J. Physiol.*, 354:273–286.
- Bindokas, V. P., and A. T. Ishida, 1991. (–)-baclofen and gamma-aminobutyric acid inhibit calcium currents in isolated retinal ganglion cells, *Proc. Natl. Acad. Sci. USA*, 88:10759–10763.
- Bloomfield, S. A., and D. Xin, 2000. Surround inhibition of mammalian AII amacrine cells is generated in the proximal retina, *J. Physiol.*, 523:771–783.
- Boatright, J. H., N. M. Rubim, and P. M. Iuvone, 1994. Regulation of endogenous dopamine release in amphibian retina by gamma-aminobutyric acid and glycine, *Vis. Neurosci.*, 11:1003–1012.
- Bowery, N. G., D. R. Hill, A. L. Hudson, A. Doble, D. N. Middlemiss, J. Shaw, and M. Turnbull, 1980. (–)Baclofen decreases

- neurotransmitter release in the mammalian CNS by an action at a novel GABA receptor, *Nature*, 283:92–94.
- Brecha, N., D. Johnson, L. Peichl, and H. Wässle, 1988. Cholinergic amacrine cells of the rabbit retina contain glutamate decarboxylase and gamma-aminobutyrate immunoreactivity, *Proc. Natl. Acad. Sci. USA*, 85:6187–6191.
- Caldwell, J. H., N.W. Daw, and H. J. Wyatt, 1978. Effects of picrotoxin and strychnine on rabbit retinal ganglion cells: lateral interactions for cells with more complex receptive fields, *J. Physiol.*, 276:277–298.
- Cook, P. B., P. D. Lukasiewicz, and J. S. McReynolds, 2000. GABA(C) receptors control adaptive changes in a glycinergic inhibitory pathway in salamander retina, *J. Neurosci.*, 20:806–812.
- Cook, P. B., and J. S. McReynolds, 1998. Modulation of sustained and transient lateral inhibitory mechanisms in the mudpuppy retina during light adaptation, *J. Neurophysiol.*, 79:197–204.
- Cook, P. B., and F. S. Werblin, 1994. Spike initiation and propagation in wide field transient amacrine cells of the salamander retina, *J. Neurosci.*, 14:3852–3861.
- Cutting, G. R., L. Lu, B. F. O'Hara, L. M. Kasch, C. Montrose-Rafizadeh, D. M. Donovan, S. Shimada, S. E. Antonarakis, W. B. Guggino, and G. R. Uhl, 1991. Cloning of the gamma-aminobutyric acid (GABA) rho 1 cDNA: A GABA receptor subunit highly expressed in the retina, *Proc. Natl. Acad. Sci. USA*, 88:2673–2677.
- Dong, C. J., and F. S. Werblin, 1994. Dopamine modulation of GABAC receptor function in an isolated retinal neuron, *J. Neurophysiol.*, 71:1258–1260.
- Dong, C. J., and F. S. Werblin, 1996. Use-dependent and use-independent blocking actions of picrotoxin and zinc at the GABAC receptor in retinal horizontal cells, *Vis. Res.*, 36:3997–4005.
- Dong, C. J., and F. S. Werblin, 1998. Temporal contrast enhancement via GABAC feedback at bipolar terminals in the tiger salamander retina, *J. Neurophysiol.*, 79:2171–2180.
- Ehinger, B., and B. Falck, 1971. Autoradiography of some suspected neurotransmitter substances: GABA glycine, glutamic acid, histamine, dopamine, and L-dopa, *Brain Res.*, 33:157–172.
- Ehinger, B., and B. Lindberg, 1974. Light-evoked release of glycine from the retina, *Nature*, 251:727–728.
- Eldred, W. D., and K. Cheung, 1989. Immunocytochemical localization of glycine in the retina of the turtle (*Pseudemys scripta*), *Vis. Neurosci.*, 2:331–338.
- Euler, T., and R. H. Masland, 2000. Light-evoked responses of bipolar cells in a mammalian retina, *J. Neurophysiol.*, 83:1817–1829.
- Euler, T., and H. Wässle, 1998. Different contributions of GABAA and GABAC receptors to rod and cone bipolar cells in a rat retinal slice preparation, *J. Neurophysiol.*, 79:1384–1395.
- Feigenspan, A., and J. Bormann, 1994a. Differential pharmacology of GABAA and GABAC receptors on rat retinal bipolar cells, *Eur. J. Pharmacol.*, 288:97–104.
- Feigenspan, A., and J. Bormann, 1994b. Facilitation of GABAergic signaling in the retina by receptors stimulating adenylate cyclase, *Proc. Natl. Acad. Sci. USA*, 91:10893–10897.
- Feigenspan, A., and J. Bormann, 1994c. Modulation of GABAC receptors in rat retinal bipolar cells by protein kinase, *J. Physiol.*, 481:325–330.
- Feigenspan, A., H. Wässle, and J. Bormann, 1993. Pharmacology of GABA receptor Cl⁻ channels in rat retinal bipolar cells, *Nature*, 361:159–162.
- Frech, M. J., J. Perez-Leon, H. Wässle, and K. H. Backus, 2001. Characterization of the spontaneous synaptic activity of amacrine cells in the mouse retina, *J. Neurophysiol.*, 86:1632–1643.
- Freed, M. A., and P. Sterling, 1988. The ON-alpha ganglion cell of the cat retina and its presynaptic cell types, *J. Neurosci.*, 8:2303–2320.
- Frumkes, T. E., R. F. Miller, M. Slaughter, and R. F. Dacheux, 1981. Physiological and pharmacological basis of GABA and glycine action on neurons of mudpuppy retina. III. Amacrine-mediated inhibitory influence on ganglion cell receptive field organization: a model, *J. Neurophysiol.*, 45:783–804.
- Frumkes, T. E., and R. Nelson, 1995. Functional role of GABA in cat retina: I. Effects of GABAA agonists, *Vis. Neurosci.*, 12:641–650.
- Frumkes, T. E., R. Nelson, and R. Pflug, 1995. Functional role of GABA in cat retina: II. Effects of GABAA antagonists, *Vis. Neurosci.*, 12:651–661.
- Gao, F., B. R. Maple, and S. M. Wu, 2000. 14 AA-Sensitive chloride current contributes to the center light responses of bipolar cells in the tiger salamander retina, *J. Neurophysiol.*, 83:3473–3482.
- Greferath, U., J. H. Brandstätter, H. Wässle, J. Kirsch, J. Kuhse, and U. Grunert, 1994. Differential expression of glycine receptor subunits in the retina of the rat: a study using immunohistochemistry and in situ hybridization, *Vis. Neurosci.*, 11:721–729.
- Greferath, U., F. Müller, H. Wässle, B. Shivers, and P. Seeburg, 1993. Localization of GABAA receptors in the rat retina, *Vis. Neurosci.*, 10:551–561.
- Grunert, U., and H. Wässle, 1996. Glycine receptors in the rod pathway of the macaque monkey retina, *Vis. Neurosci.*, 13:101–115.
- Gustincich, S., A. Feigenspan, W. Sieghart, and E. Raviola, 1999. Composition of the GABA(A) receptors of retinal dopaminergic neurons, *J. Neurosci.*, 19:7812–7822.
- Gustincich, S., A. Feigenspan, D. K. Wu, L. J. Koopman, and E. Raviola, 1997. Control of dopamine release in the retina: a transgenic approach to neural networks, *Neuron*, 18:723–736.
- Han, Y., and M. M. Slaughter, 1998. Protein kinases modulate two glycine currents in salamander retinal ganglion cells, *J. Physiol.*, 508:681–690.
- Han, Y., and S. M. Wu, 1999. Modulation of glycine receptors in retinal ganglion cells by zinc, *Proc. Natl. Acad. Sci. USA*, 96:3234–3238.
- Han, Y., J. Zhang, and M. M. Slaughter, 1997. Partition of transient and sustained inhibitory glycinergic input to retinal ganglion cells, *J. Neurosci.*, 17:3392–3400.
- Hare, W. A., and W. G. Owen, 1996. Receptive field of the retinal bipolar cell: a pharmacological study in the tiger salamander, *J. Neurophysiol.*, 76:2005–2019.
- Heidelberger, R., and G. Matthews, 1991. Inhibition of calcium influx and calcium current by gamma-aminobutyric acid in single synaptic terminals, *Proc. Natl. Acad. Sci. USA*, 88:7135–7139.
- Ikeda, H., and M. J. Sheardown, 1983. Functional transmitters at retinal ganglion cells in the cat, *Vision Res.*, 23:1161–1174.
- Jacobs, A. L., and F. S. Werblin, 1998. Spatiotemporal patterns at the retinal output, *J. Neurophysiol.*, 80:447–451.
- Jensen, R. J., 1991. Involvement of glycinergic neurons in the diminished surround activity of ganglion cells in the dark-adapted rabbit retina, *Vis. Neurosci.*, 6:43–53.
- Kalloniatis, M., R. E. Marc, and R. F. Murry, 1996. Amino acid signatures in the primate retina. [published erratum appears in *J. Neurosci.*, 1997;17:500–503], *J. Neurosci.*, 16:6807–6829.

- Kamermans, M., I. Fahrenfort, K. Schultz, U. Janssen-Bienhold, T. Sjoerdsma, and R. Weiler, 2001. Hemichannel-mediated inhibition in the outer retina, *Science*, 292:1178–1180.
- Kaneda, M., B. Andrasfalvy, and A. Kaneko, 2000. Modulation by Zn²⁺ of GABA responses in bipolar cells of the mouse retina, *Vis. Neurosci.*, 17:273–281.
- Kaneko, A., S. Suzuki, L. H. Pinto, and M. Tachibana, 1991. Membrane currents and pharmacology of retinal bipolar cells: a comparative study on goldfish and mouse, *Comp. Biochem. Physiol. C*, 98:115–127.
- Kirby, A. W., 1979. The effect of strychnine, bicuculline, and picrotoxin on X and Y cells in the cat retina, *J. Gen. Physiol.*, 74:71–84.
- Kishida, K., and K. I. Naka, 1967. Amino acids and the spikes from the retinal ganglion cells, *Science*, 156:648–650.
- Kittila, C. A., and S. C. Massey, 1997. Pharmacology of directionally selective ganglion cells in the rabbit retina, *J. Neurophysiol.*, 77:675–689.
- Kondo, H., and J. Toyoda, 1983. GABA and glycine effects on the bipolar cells of the carp retina, *Vis. Res.*, 23:1259–1264.
- Koulen, P., B. Malitschek, R. Kuhn, B. Bettler, H. Wässle, and J. H. Brandstätter, 1998. Presynaptic and postsynaptic localization of GABA(B) receptors in neurons of the rat retina, *Eur. J. Neurosci.*, 10:1446–1456.
- Li, P., and X. L. Yang, 1998. Strong synergism between GABA(A) and glycine receptors on isolated carp third-order neurons, *Neuroreport*, 9:2875–2879.
- Li, P., and X. L. Yang, 1999. Zn²⁺ differentially modulates glycine receptors versus GABA receptors in isolated carp retinal third-order neurons, *Neurosci. Lett.*, 269:75–78.
- Lin, B., P. R. Martin, S. G. Solomon, and U. Grunert, 2000. Distribution of glycine receptor subunits on primate retinal ganglion cells: a quantitative analysis, *Eur. J. Neurosci.*, 12:4155–4170.
- Lin, Z. S., and S. Yazulla, 1994. Heterogeneity of GABA_A receptor in goldfish retina, *J. Comp. Neurol.*, 345:429–439.
- Lukasiewicz, P. D., B. R. Maple, and F. S. Werblin, 1994. A novel GABA receptor on bipolar cell terminals in the tiger salamander retina, *J. Neurosci.*, 14:1202–1212.
- Lukasiewicz, P. D., and F. S. Werblin, 1990. The spatial distribution of excitatory and inhibitory inputs to ganglion cell dendrites in the tiger salamander retina, *J. Neurosci.*, 10:210–221.
- Maguire, G., B. Maple, P. Lukasiewicz, and F. Werblin, 1989. Gamma-aminobutyrate type B receptor modulation of L-type calcium channel current at bipolar cell terminals in the retina of the tiger salamander, *Proc. Natl. Acad. Sci. USA*, 86:10144–10147.
- Mangel, S. C., and R. F. Miller, 1987. Horizontal cells contribute to the receptive field surround of ganglion cells in the rabbit retina, *Brain Res.*, 414:182–186.
- Maple, B. R., and S. M. Wu, 1998. Glycinergic synaptic inputs to bipolar cells in the salamander retina, *J. Physiol.*, 506:731–744.
- Marc, R. E., and D. M. Lam, 1981. Glycinergic pathways in the goldfish retina, *J. Neurosci.*, 1:152–165.
- Marc, R. E., and W. Liu, 2000. Fundamental GABAergic amacrine cell circuitries in the retina: nested feedback, concatenated inhibition, and axosomatic synapses, *J. Comp. Neurol.*, 425:560–582.
- Massey, S. C., D. M. Linn, C. A. Kittila, and W. Mirza, 1997. Contributions of GABA_A receptors and GABA_C receptors to acetylcholine release and directional selectivity in the rabbit retina, *Vis. Neurosci.*, 14:939–948.
- Massey, S. C., and M. J. Neal, 1979a. Release of [3H]-acetylcholine from the isolated retina of the rat by potassium depolarization: dependence on high affinity choline uptake, *J. Neurochem.*, 32:1327–1329.
- Massey, S. C., and M. J. Neal, 1979b. The light evoked release of acetylcholine from the rabbit retina in vivo and its inhibition by gamma-aminobutyric acid, *J. Neurochem.*, 32:1327–1329.
- Massey, S. C., and D. A. Redburn, 1982. A tonic gamma-aminobutyric acid-mediated inhibition of cholinergic amacrine cells in rabbit retina, *J. Neurosci.*, 2:1633–1643.
- Matsui, K., J. Hasegawa, and M. Tachibana, 2001. Modulation of excitatory synaptic transmission by GABA(C) receptor-mediated feedback in the mouse inner retina, *J. Neurophysiol.*, 86:2285–2298.
- McGille, G. S., T. C. Rotolo, and R. F. Dacheux, 2000. GABA responses of rod bipolar cells in rabbit retinal slices, *Vis. Neurosci.*, 17:381–389.
- Miller, R. F., R. F. Dacheux, and T. E. Frumkes, 1977. Amacrine cells in Necturus retina: evidence for independent gamma-aminobutyric, *Science*, 198:748–750.
- Minami, N., K. Berglund, T. Sakaba, H. Kohmoto, and M. Tachibana, 1998. Potentiation of transmitter release by protein kinase C in goldfish retinal bipolar cells, *J. Physiol.*, 512:219–225.
- Mooney, R. D., 1978. GABA-mediated control of transient signals in the inner retina, *Brain Res.*, 145:97–115.
- Muller, J. F., and R. E. Marc, 1990. GABA-ergic and glycinergic pathways in the inner plexiform layer of the goldfish retina, *J. Comp. Neurol.*, 291:281–304.
- Neal, M. J., and J. R. Cunningham, 1995. Baclofen enhancement of acetylcholine release from amacrine cells in the rabbit retina by reduction of glycinergic inhibition, *J. Physiol.*, 482:363–372.
- O'Malley, D. M., and R. H. Masland, 1989. Co-release of acetylcholine and gamma-aminobutyric acid by a retinal neuron, *Proc. Natl. Acad. Sci. USA*, 86:3414–3418.
- Pan, Z. H., and S. A. Lipton, 1995. Multiple GABA receptor subtypes mediate inhibition of calcium influx at rat retinal bipolar cell terminals, *J. Neurosci.*, 15:2668–2679.
- Pan, Z. H., and M. M. Slaughter, 1991. Control of retinal information coding by GABA_B receptors, *J. Neurosci.*, 11:1810–1821.
- Pan, Z. H., and M. M. Slaughter, 1995. Comparison of the actions of glycine and related amino acids on isolated third order neurons from the tiger salamander retina, *Neurosci.*, 64:153–164.
- Pan, Z. H., D. Zhang, X. Zhang, and S. A. Lipton, 2000. Evidence for coassembly of mutant GABA_C rho1 with GABA_A gamma2S, glycine alpha1 and glycine alpha2 receptor subunits in vitro, *Eur. J. Neurosci.*, 12:3137–3145.
- Pourcho, R. G., and M. T. Owczarzak, 1991. Connectivity of glycine immunoreactive amacrine cells in the cat retina, *J. Comp. Neurol.*, 307:549–561.
- Pow, D. V., 1998. Transport is the primary determinant of glycine content in retinal neurons, *J. Neurochem.*, 70:2628–2636.
- Protti, D. A., H. M. Gerschenfeld, and I. Llano, 1997. GABAergic and glycinergic IPSCs in ganglion cells of rat retinal slices, *J. Neurosci.*, 17:6075–6085.
- Qian, H., and J. E. Dowling, 1993. Novel GABA responses from rod-driven retinal horizontal cells, *Nature*, 361:162–164.
- Qian, H., J. E. Dowling, and H. Ripps, 1998. Molecular and pharmacological properties of GABA-rho subunits from white perch retina, *J. Neurobiol.*, 37:305–320.
- Roska, B., E. Nemeth, L. Orzo, and F. S. Werblin, 2000. Three levels of lateral inhibition: a space-time study of the retina of the tiger salamander, *J. Neurosci.*, 20:1941–1951.
- Roska, B., E. Nemeth, and F. S. Werblin, 1998. Response to change is facilitated by a three-neuron disinhibitory pathway in the tiger salamander retina, *J. Neurosci.*, 18:3451–3459.

- Saito, H., 1981. The effects of strychnine and bicuculline on the responses, *Brain Res.*, 212:243–248.
- Shen, W., and M. M. Slaughter, 1998. Metabotropic and ionotropic glutamate receptors regulate calcium channel currents in salamander retinal ganglion cells, *J. Physiol.*, 510:815–828.
- Shen, W., and M. M. Slaughter, 1999a. Internal calcium modulates apparent affinity of metabotropic GABA receptors, *J. Neurophysiol.*, 82:3298–3306.
- Shen, W., and M. M. Slaughter, 1999b. Metabotropic GABA receptors facilitate L-type and inhibit N-type calcium channels in single salamander retinal neurons, *J. Physiol.*, 516:711–718.
- Shen, W., and M. M. Slaughter, 2001. Multireceptor GABAergic regulation of synaptic communication in amphibian retina, *J. Physiol.*, 530:55–67.
- Shields, C. R., M. N. Tran, R. O. Wong, and P. D. Lukasiewicz, 2000. Distinct ionotropic GABA receptors mediate presynaptic and postsynaptic inhibition in retinal bipolar cells, *J. Neurosci.*, 20:2673–2682.
- Smiley, J. F., and S. F. Basinger, 1988. Somatostatin-like immunoreactivity and glycine high-affinity uptake colocalize to an interplexiform cell of the *Xenopus laevis* retina, *J. Comp. Neurol.*, 274:608–618.
- Stockton, R. A., and M. M. Slaughter, 1991. Depolarizing actions of GABA and glycine on amphibian retinal horizontal cells, *J. Neurophysiol.*, 65:680–692.
- Stone, S., and M. Schutte, 1991. Physiological and morphological properties of off- and on-center bipolar cells in the *Xenopus* retina: effects of glycine and GABA, *Vis. Neurosci.*, 7:363–376.
- Suzuki, S., M. Tachibana, and A. Kaneko, 1990. Effects of glycine and GABA on isolated bipolar cells of the mouse retina, *J. Physiol.*, 421:645–662.
- Van Haesendonck, E., and L. Missotten, 1993. A subgroup of bipolar cells in human retina is GABA-immunoreactive, *Neurosci. Lett.*, 161:187–190.
- Vaney, D. I., J. C. Nelson, and D. V. Pow, 1998. Neurotransmitter coupling through gap junctions in the retina, *J. Neurosci.*, 18:10594–10602.
- Vardi, N., and P. Sterling, 1994. Subcellular localization of GABA_A receptor on bipolar cells in macaque and human retina, *Vis. Res.*, 34:1235–1246.
- Vardi, N., L. L. Zhang, J. A. Payne, and P. Sterling, 2000. Evidence that different cation chloride cotransporters in retinal neurons allow opposite responses to GABA, *J. Neurosci.*, 20:7657–7663.
- Voaden, M. J., and M. S. Starr, 1972. The efflux of radioactive GABA from rat retina in vitro, *Vis. Res.*, 12:559–566.
- Wang, H., K. M. Standifer, and D. M. Sherry, 2000. GABA(A) receptor binding and localization in the tiger salamander retina, *Vis. Neurosci.*, 17:11–21.
- Wassle, H., I. Schafer-Trenkler, and T. Voigt, 1986. Analysis of glycinergic inhibitory pathway in the cat retina, *J. Neurosci.*, 6:594–604.
- Wellis, D. P., and F. S. Werblin, 1995. Dopamine modulates GABA_A receptors mediating inhibition of calcium entry into and transmitter release from bipolar cell terminals in tiger salamander retina, *J. Neurosci.*, 15:4748–4761.
- Werblin, F., G. Maguire, P. Lukasiewicz, S. Eliasof, and S. M. Wu, 1988. Neural interactions mediating the detection of motion in the retina of the tiger salamander, *Vis. Neurosci.*, 1:317–329.
- Wyatt, H. J., and N. W. Daw, 1975. Directionally sensitive ganglion cells in the rabbit retina: specificity for stimulus direction, size, and speed, *J. Neurophysiol.*, 38:613–626.
- Yang, C. Y., 1997. L-glutamic acid decarboxylase- and gamma-aminobutyric acid-immunoreactive bipolar cells in tiger salamander retina are of ON- and OFF-response types as inferred from Lucifer Yellow injection, *J. Comp. Neurol.*, 385:651–660.
- Yang, C. Y., and H. H. Wang, 1999. Anatomical and electrophysiological evidence for GABAergic bipolar cells in tiger salamander retina, *Vis. Res.*, 39:3653–3661.
- Yang, C. Y., and S. Yazulla, 1988. Light microscopic localization of putative glycinergic neurons in the larval tiger salamander retina by immunocytochemical and autoradiographical methods, *J. Comp. Neurol.*, 272:343–357.
- Yazulla, S., and K. M. Studholme, 1991. Glycinergic interplexiform cells make synaptic contact with amacrine cell bodies in goldfish retina, *J. Comp. Neurol.*, 310:1–10.
- Yazulla, S., and C. Y. Yang, 1988. Colocalization of GABA and glycine immunoreactivities in a subset of retinal neurons in tiger salamander, *Neurosci. Lett.*, 95:37–41.
- Zhang, J., C. S. Jung, and M. M. Slaughter, 1997a. Serial inhibitory synapses in retina, *Vis. Neurosci.*, 14:553–563.
- Zhang, J., W. Shen, and M. M. Slaughter, 1997b. Two metabotropic gamma-aminobutyric acid receptors differentially modulate calcium currents in retinal ganglion cells, *J. Gen. Physiol.*, 110:45–58.
- Zhang, J., and M. M. Slaughter, 1995. Preferential suppression of the ON pathway by GABA_A receptors in the amphibian retina, *J. Neurophysiol.*, 74:1583–1592.
- Zhang, J., N. Tian, and M. M. Slaughter, 1998. Neuronal discriminator formed by metabotropic gamma-aminobutyric acid receptors, *J. Neurophysiol.*, 80:3365–3368.
- Zhou, Z. J., and G. L. Fain, 1995. Neurotransmitter receptors of starburst amacrine cells in rabbit retinal slices, *J. Neurosci.*, 15:5334–5345.
- Zucker, C. L., and B. Ehinger, 1992. Heterogeneity of receptor immunoreactivity at synapses of glycine-utilizing neurons, *Proc. Roy. Soc. Lond. B: Biol. Sci.*, 249:89–94.
- Zucker, C. L., and B. Ehinger, 1993. Synaptic connections involving immunoreactive glycine receptors in the turtle retina, *Vis. Neurosci.*, 10:907–914.

24 Anatomy, Circuitry, and Physiology of Vertebrate Horizontal Cells

IDO PERLMAN, HELGA KOLB, AND RALPH NELSON

S-potentials: the first intracellularly recorded photoresponses in the vertebrate retina

S-potentials were the first light-evoked electrical responses recorded with intracellular microelectrodes from nerve cells in the vertebrate retina (Svaetichin, 1953). As shown in Figure 24.1, S-potentials are negative-going changes in membrane potential that last for as long as the light stimulus is present. The graded character of the S-potential is evident in Figure 24.1A. The brighter the stimulus, the larger the amplitude of the S-potential until a saturation level is reached. In Figure 24.1B, the duration of a light stimulus of fixed intensity is altered to examine the effects of this parameter on the S-potential. For long stimuli, the S-potential changes in duration but the amplitude remains constant (the two leftmost responses in Fig. 24.1B). Further reduction in the stimulus duration causes a decrease in amplitude (Fig. 24.1B). This illustrates the temporal summation of the S-potential, following the psychophysical Bloch's law (Roufs, 1972). Up to a certain stimulus duration, the amplitude is directly related to the quantal *content* of the stimulus (quantal flux \times duration); while for stimuli of longer duration, the amplitude is related to the quantal *flux*. It is likely that S-potentials were named in honor of their discoverer, Gunnar Svaetichin, although S-potentials have come to mean slow potentials.

S-potentials evoked puzzlement among neurophysiologists of the late 1950s when they were first described. At that time, neurons were thought only to be depolarized (inside becoming more positive relative to outside) by excitatory synaptic inputs. If the depolarization was of sufficient amplitude, action potentials, or nerve spikes, were generated to transfer signals down the length of the axon. S-potentials, however, had neither light-induced depolarizations nor nerve impulses.

At first, the cell type of origin of S-potentials was not really known other than that they were recorded somewhere in the outer retina. In fact, initially S-potentials were thought to arise from cones, as indicated by the title of the 1953 article by Gunnar Svaetichin ("The cone action potential"). However, later intracellular marking techniques, in which dyes were injected from electrode tips into the cytoplasm of

the recorded neuron, revealed horizontal cells to be the source of the S-potentials (Kaneko, 1970; Werblin and Dowling, 1969). Since first described in fish retinas, S-potentials have been recorded from retinal horizontal cells in all vertebrate classes, including cold-blooded vertebrates (Byzov and Trifonov, 1968; Fuortes and Simon, 1974; Itzhaki and Perlman, 1984; Naka, 1976; Naka and Rushton, 1966, 1967; Normann and Perlman, 1979; Norton et al., 1968; Werblin and Dowling, 1969), mammals (Bloomfield and Miller, 1982; Dacheux and Raviola, 1982; Nelson, 1977; Nelson et al., 1975; Niemeyer and Gouras, 1973; Steinberg, 1969a, 1969b), and primates (Dacey et al., 1996; Dacheux and Raviola, 1990; Verweije et al., 1999). Horizontal cells have now been studied by numerous investigators using anatomical, biochemical, pharmacological, and electrophysiological techniques. In this chapter, we shall try to summarize our current knowledge of horizontal cells in the vertebrate retina.

Morphology and circuitry of horizontal cells

Horizontal cells are second-order neurons interconnecting photoreceptors laterally across the plane of the outer plexiform layer of the retina. These cell types were first described as huge bricklike structures occupying much of the inner nuclear layer in the fish retina (Yamada and Ishikawa, 1965). Early interpretations assumed these cells to be glial cells, mainly because they gave rise to hyperpolarizing slow S-potential responses rather than true depolarizing spikes like "real" neurons. Now we know horizontal cells to be true neurons that have synapses and exhibit most of the ultrastructural characteristics of neurons. Through Golgi staining, intracellular marking, and immunostaining techniques we have learned of the various morphologies horizontal cells can adopt in the retinas of different vertebrate species (Fig. 24.2) (Boycott and Dowling, 1969; Boycott et al., 1978; Cajal, 1892; Gallego, 1986; Kolb, 1970; Leeper, 1978a, 1978b; Peichl et al., 1998; Polyak, 1941; Sandmann et al., 1996a, 1996b; Stell and Lightfoot, 1975; Wässle and Riemann, 1978).

There are two morphological types of horizontal cell in the majority of vertebrate retinas, B-types with axons and

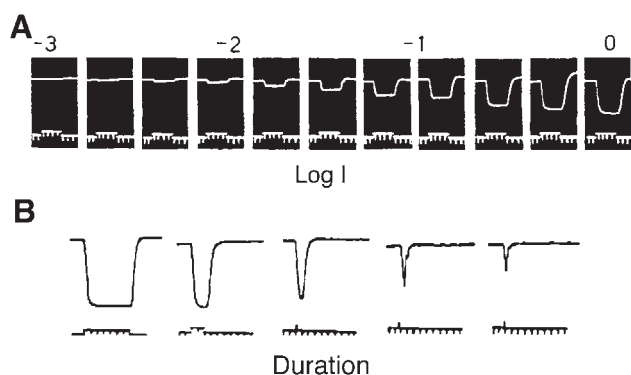


FIGURE 24.1. The S-potential of the fish retina. Light stimuli of fixed intensity but different durations (*A*) and light stimuli of fixed duration but different intensities (*B*) were used to elicit these potentials. Lower traces in *A* and *B* record light-stimulus duration and provide 100-msec tick-marks (from Svaetichin, 1953).

A-types that are axonless (see Fig. 24.2). In nonmammalian species, horizontal cells come in further axonless subtypes with color-specific cone connections (Fig. 24.2, axonless). Figure 24.2 shows the morphologies of these different types of horizontal cells in the various species indicated. Also shown are the spectral types of cone (red, blue, and green dots) that connect with the horizontal cells. Rod-dominated nonmammalian retinas like those of fish also have a horizontal cell type devoted only to the rods (not shown); rod-dominated mammalian retinas have adapted the axonal terminal portion of the B-type cell to connect purely with rods (Fig. 24.2, gray shaded areas over the axon terminal).

B-Type horizontal cells are concerned solely with light intensity changes and shaping adaptational and spatial responses of vertical pathway neurons. They are the luminosity type horizontal cells, which will be discussed later. B-Type cells can often be identified with antibodies against calcium-binding proteins (Cuenca et al., 2000; Wässle and Boycott, 1991; Wässle et al., 1989) and GABA neurotransmitters (Marc, 1999; Marc et al., 1978). In turtle retina, acetylcholine has been localized to H1-type horizontal cell dendrites, where they invaginate the cone pedicles (Cuenca et al., 2000). The dendrites of B-type horizontal cells in mammalian retinas are bushy and contact all cones in their dendritic field; while their axon terminals collect from large numbers of rods at some distance from the cone-connecting dendritic field. The length and thinness of the axon is believed to electrically isolate one portion of the cell from the other, thereby separating a cone photoreceptor-involved compartment of the cell from a rod photoreceptor-involved compartment (Nelson et al., 1975). In species where there are few rods (Fig. 24.2, turtle) the B-type cell's axon terminal has sparse contacts with red cones and the few rods present in this retina (Leeper, 1978a, 1978b).

A-Type horizontal cells in mammals are pure coneconnecting (most species have only green and blue cones). They

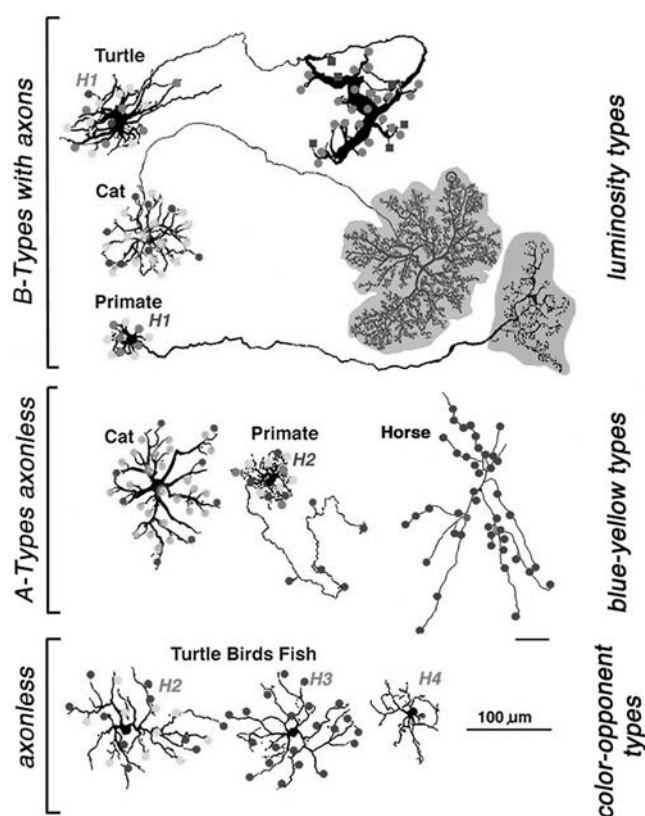


FIGURE 24.2. The morphologies of different types of horizontal cells and their known connectivities with rod and cone photoreceptors. The cells are drawn from Golgi-stained or Neurobiotin-filled retinal staining techniques and viewed in flat whole-mounted preparations. B-type cells with axons and axonless cell types exist in most vertebrate retinas. The physiological type that has been proved associated with the morphological type is indicated to the right of the figure; i.e., luminosity, blue-yellow, and color-opponent types. Red dots, red cones; green dots, green cones; blue dots, blue cones; black squares; or shaded gray areas represent rod inputs. (Horse image from Sandmann et al., 1996a.) (See color plate 9.)

have no connections with rod photoreceptors at all. Even in the case of the H2-type cell of the trichromatic primate retina, where one or more dendrites are elongated and axonlike, their connections are with cones and interestingly enough with blue cones. This may be a general theme for mammalian axonless horizontal cells that is only now being realized. In certain big cats (not yet confirmed in domestic cat), the elongated dendritic tips of A-type cells contact blue cones, and the dendrites closer to the cell body are in contact with both green cones and blue cones (Ahnelt et al., 2000). In horses the A-type cell is apparently only connected to blue cones (see Fig. 24.2) (Peichl et al., 1998; Sandmann et al., 1996a).

In turtles, birds, and fish, species with excellent color vision, type H2 and type H3 horizontal cells are large, stellate cells, lacking axons, and are concerned solely with cone pathways (Fig. 24.2, axonless, color-opponent types). Thus,

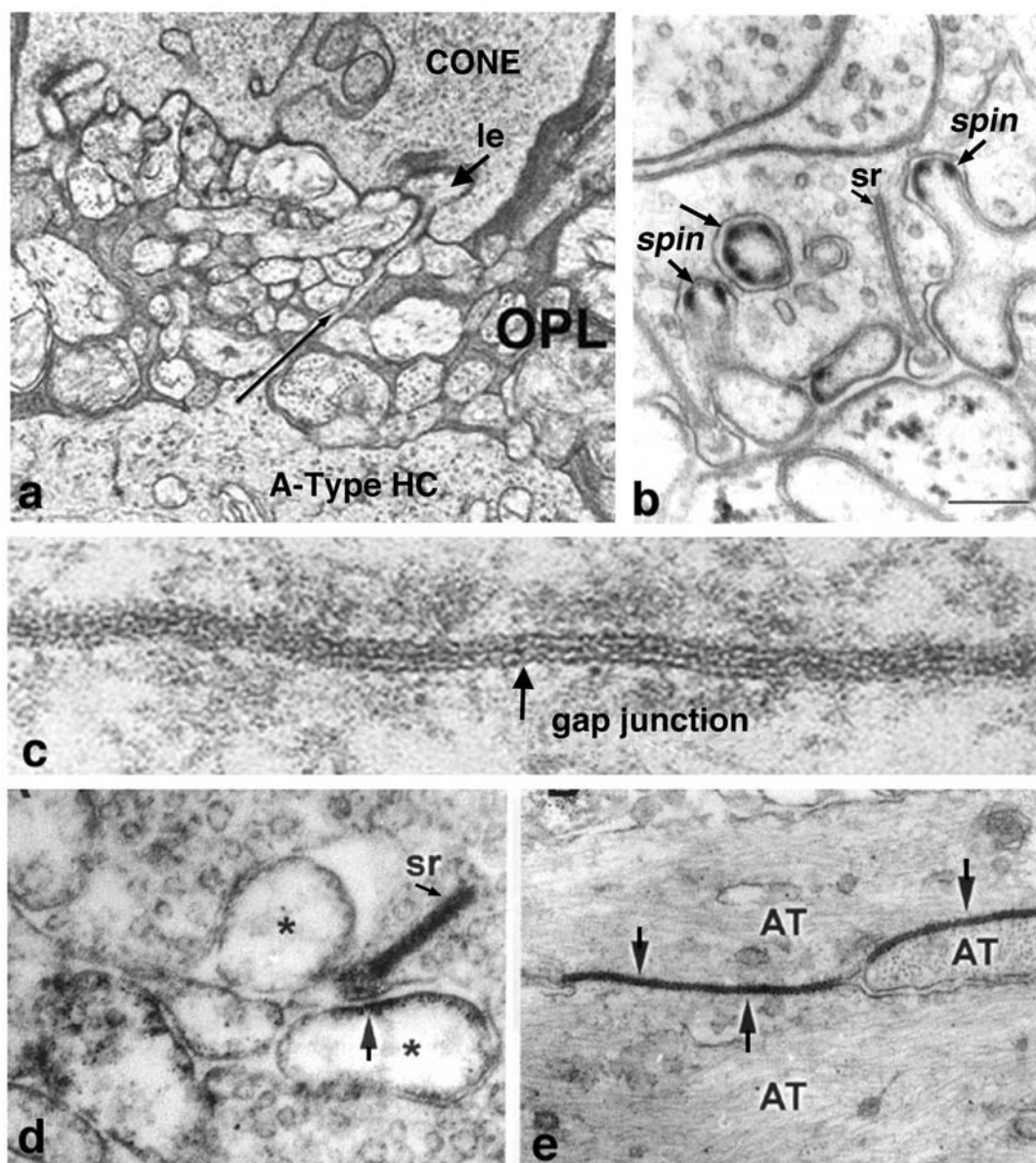


FIGURE 24.3. *A*, Electronmicroscopy of cat outer plexiform layer (OPL) shows an A-type horizontal cell's dendritic terminal entering an overlying cone pedicle to form a lateral element (le) at a ribbon triad. *B*, Light-adapted fish retina exhibits spinules (spin) on horizontal cell lateral elements in cone pedicles at synaptic ribbon (sr) synapses. (From DeJuan and Garcia, 2001.) *C*, High-magnification electronmicrograph of a gap junction between two A-type horizontal cell dendrites in the cat retina. *D*, Electronmi-

crograph shows the location of C \times 26 as revealed by immunocytochemistry (*asterisks*) in the hemi-gap junction (*arrow*) of the horizontal cell lateral element in the turtle retina. *E*, Electronmicrograph shows the location of C \times 26, as revealed by immunocytochemistry, in the full connexon extent of a gap junction between two H1 axon terminals (AT) in the turtle retina. (*D* and *E* from Janssen-Bienhold et al., 2001.)

in turtle (pentachromats) and fish (trichromats or tetrachromats), H2 horizontal cells connect to green and blue cones and H3 to blue cones (Fig. 24.2) (Fuortes and Simon, 1974; Leeper, 1978a, 1978b; Lipetz, 1978; Miller et al., 1973; Stell and Lightfoot, 1975). The C-type horizontal cells of the turtle can be labeled with antibodies to nitric oxide synthase and calcium-binding proteins (Cuenca et al., 2000), suggesting a role for nitric oxide in their functioning.

Horizontal cells always interact with photoreceptor terminals at what are known as lateral elements at presynaptic ribbons (Fig. 24.3*A*, le, *arrow*). In fish retinas, the horizontal cell connections with cones at the lateral elements are characterized by minute projections called *spinules* (Fig. 24.3*B*). Spinules are dynamic and change shape with the level of illumination. During background illumination, the spinules are stimulated to form, while darkness causes contraction

(Raynauld et al., 1979; Weiler and Wagner, 1984). These spinules are also under an endogenous circadian control but need centrifugal control from the brain via FMR-amide-like and gonadotropin-releasing hormone (GnRH)-like hormone-releasing hormones (Munz et al., 1982; Stell et al., 1984) acting on the dopaminergic interplexiform cell system in the retina (DeJuan and Garcia, 2001; Zucker and Dowling, 1987).

Retinal horizontal cells in all species are connected to their homologous neighbors by areas of gap junctions between their dendrites, their axon terminals, and occasionally between their dendrites and cell bodies. These areas of gap junction can be extremely large, appearing as plaques of electrical junction (Fig. 24.3C). First described in fish retinas by Yamada and Ishikawa (1965), gap junctions were considered “fused membrane structures” specialized for electrical transmission of stimuli. Procion yellow dye diffusion between morphologically similar horizontal cells was noted by Kaneko (1971) and indicated that the electrical junctions could pass small molecules freely through the so-called S-space of horizontal cells (Naka and Rushton, 1967).

Gap junctions are formed at closely applied plasma membranes (2 to 4 nm gap) of the two horizontal cell structures (Fig. 24.3C). Each half of the cell supplies connexons or hemichannels to complete the gap junction channel. These channels can consist of homomeric or heteromeric connexons, thus allowing a huge variety of gap junctions with slightly different properties to exist between various neurons of the nervous system. Each connexon channel contains six connexins (Cx) surrounding the channel pore. In fish and turtle retinas Cx43 and Cx26 (Fig. 24.3E) have been demonstrated to comprise the horizontal cell gap junction connexons (Janssen-Bienhold et al., 2001; McMahon et al., 1989). Not only dye molecules, but also ion and cytoplasmic molecules of small size can pass through the connexon pores of the gap junction, so changing horizontal cell activities and ionic properties. These ionic conductances are modulated by various agents, such as dopamine, nitric oxide, and retinoic acid. We shall deal with this aspect of horizontal cells in later sections of this chapter.

Physiological types of horizontal cell: luminosity and chromaticity

The vertebrate retina contains a mosaic of rod and cone photoreceptors that serve for dark- and light-adapted vision, respectively. Multiple cone types with visual pigments tuned to different regions of the visible spectrum provide vertebrates with the opportunity to discriminate colors. Most mammals are dichromats (having two different cone types); however, Old World monkeys, humans, and many cold-blooded species are trichromats (three different cone types) or even tetrachromats (four different cone types). In the

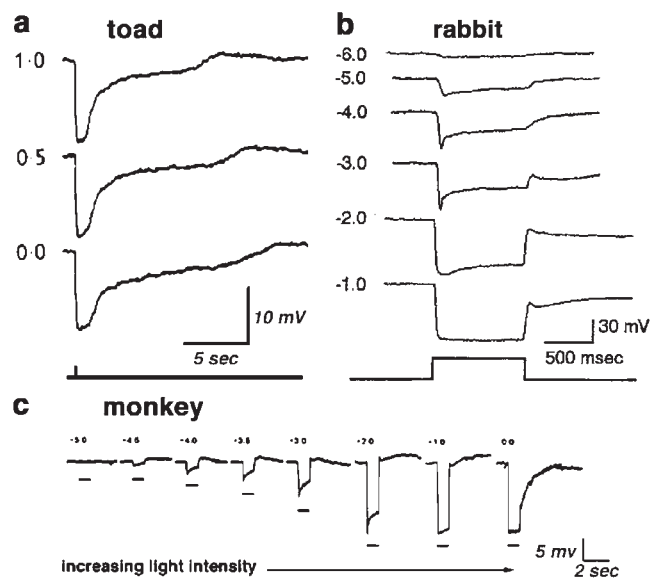


FIGURE 24.4. Photoresponses that were recorded from luminosity-type horizontal cells from the toad (Normann and Pochobradsky, 1976), rabbit (Bloomfield and Miller, 1982), and monkey (Dacheux and Raviola, 1990) retinas. In each case, photoresponses were elicited by light stimuli of different intensities.

retinas of birds, fish, and reptiles, a class of cones that are sensitive to ultraviolet light can also be found (Ammermüller et al., 1998; Goldsmith, 1980; Hughes et al., 1998) in addition to the red-, green-, and blue-sensitive cones. Because rods and cones of different spectral types are directly connected to horizontal cells, it is of interest to explore how horizontal cells integrate and process this richness of spectral information.

Two physiological types of horizontal cell are known to exist: luminosity and chromaticity. These cell types can be identified by their photoresponses to chromatic light stimuli. The luminosity (L-type) horizontal cells always respond with hyperpolarization to light stimuli of any wavelength within the visible range of the spectrum. The chromaticity (C-type) horizontal cells respond with different polarity to light stimuli of different wavelengths (Svaetichin and MacNichol, 1958).

L-type horizontal cells are found in every retina that has been studied, from cold-blooded vertebrates to mammals and primates. Figure 24.4 shows the photoresponses of luminosity-type horizontal cells from the toad (A), rabbit (B), and monkey (C) retinas. These cells respond with graded hyperpolarization to light stimuli of any wavelength. The amplitude and duration of the photoresponse depends on the intensity and duration of the light stimulus. In some species, two classes of L-type horizontal cells can be identified according to their anatomical structure and physiological properties. In the turtle retina, the L1 and L2 types are similar in their spectral sensitivity but differ in receptive field

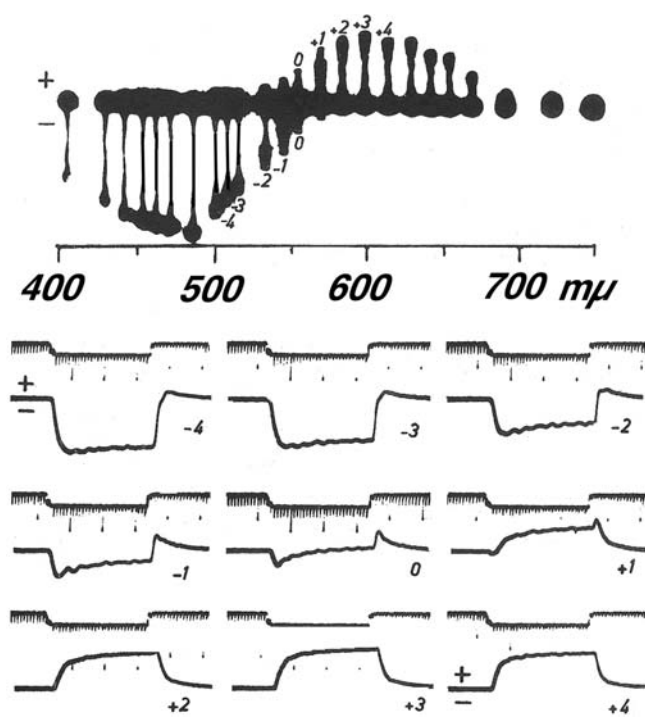


FIGURE 24.5. Color opponency of S-unit in the fish retina. Responses were recorded as a function of wavelength covering the entire visible spectrum using light stimuli of different wavelength but similar quantal content. The responses elicited by light stimuli of wavelength close to the transition from hyperpolarizing to depolarizing pattern (denoted in the upper part of the figure by +4 to -4) are shown in faster time scale (Svaetichin and MacNichol, 1958).

size and in the kinetics of their photoresponses to red and green light (Perlman & Normann, 1979; Simon, 1973). Anatomically, these two L-type horizontal cells are, respectively, the soma and axon terminal of the H1 horizontal cell (see Fig. 24.2). In the rabbit retina, type A and B luminosity horizontal cells differ in morphology and in their major excitatory input but respond only with hyperpolarizations to light stimuli (Bloomfield & Miller, 1982; Dacheux & Raviola, 1982).

In 1958, Svaetichin and MacNichol first reported on wavelength-dependency of the S-potentials (Fig. 24.5). As shown in the figure, the photoresponses of this S-unit reverses in polarity at a wavelength of about 560 nm. The photoresponse to light stimuli of longer wavelength are depolarizing; stimuli of shorter wavelengths elicit hyperpolarizing responses. These color opponent S-units are called chromaticity, or C-type horizontal cells. C-type horizontal cells have been extensively studied in turtle and fish retinas (Ammermüller and Kolb, 1995, 1996; Asi and Perlman, 1998; Fuortes and Simon, 1974; Kamermans and Spekreijse, 1995; Kolb and Lipetz, 1991; Naka and Rushton, 1966; Saito et al., 1974; Spekreijse and Norton, 1970; Twig et al., 2001, 2002; Yazulla, 1976). C-type horizontal cells are

identified by the number of wavelengths at which response polarity reverses:

- no reversal—monophasic cells
- one reversal—biphasic cells
- two reversals—triphasic cells

The wavelength at which response polarity reverses is called the null wavelength. In fish retinas, two types of chromaticity horizontal cells have been described: biphasic and triphasic (Gottesman and Burkhardt, 1987; Kamermans and Spekreijse, 1995). In the bowfin retina, the null wavelength for the biphasic cells is around 640 nm; and for the triphasic cells, the null wavelengths are one in the region of 500 to 530 nm and the other in 650 to 670 nm (Gottesman and Burkhardt, 1987). The biphasic and triphasic C-type horizontal cells of the fish retina are identified morphologically as H2 and H3 types, respectively (see Fig. 24.2).

In the turtle retina, two classes of biphasic C-type horizontal cells have been identified (Asi and Perlman, 1998; Fuortes and Simon, 1974; Twig et al., 2002). Typical photoresponses of L-type and C-type horizontal cells in the turtle *Mauremys caspica* to light stimuli of different wavelength and intensity are shown in Figure 24.6. For each wavelength, a series of photoresponses to different intensities is shown. The L-type horizontal cell (Fig. 24.6, first row) responds to all stimuli with graded hyperpolarizations regardless of wavelength. The red/green C-type horizontal cell (Fig. 24.6, second row) responds with graded depolarizations to red light stimuli and with graded hyperpolarizations to yellow and blue stimuli. The yellow/blue horizontal cell (Fig. 24.6, third row) responds with depolarizations to red and yellow light stimuli and with hyperpolarizations to blue light stimuli.

To define the spectral properties of the horizontal cells, monochromatic light stimuli of dim intensities are used to elicit small amplitude (<1 mV) photoresponses. These photoresponses are within the linear range of the cells and can be used to calculate light sensitivities. The relationship between light sensitivity and wavelength is the action spectrum of the cell and describes its spectral properties. Figure 24.7 shows the action spectra of 8 L-types, 7 red/green types, and 6 yellow/blue types of horizontal cell (A, B, and C, respectively) from the turtle *Mauremys caspica*. These spectra clearly demonstrate that the L-type horizontal cells are most sensitive to long-wavelength stimuli, as expected since their major excitatory input is from red cones (Asi and Perlman, 1998; Fuortes and Simon, 1974). These cells receive additional excitatory input from green cones and to a lesser extent from blue cones (Asi and Perlman, 1998). The red/green C-type horizontal cells are characterized by reversal of response polarity around 600 nm (Fig. 24.7B). These cells receive excitatory input from green and blue cones and inhibitory input from red cones (Asi and Perlman,

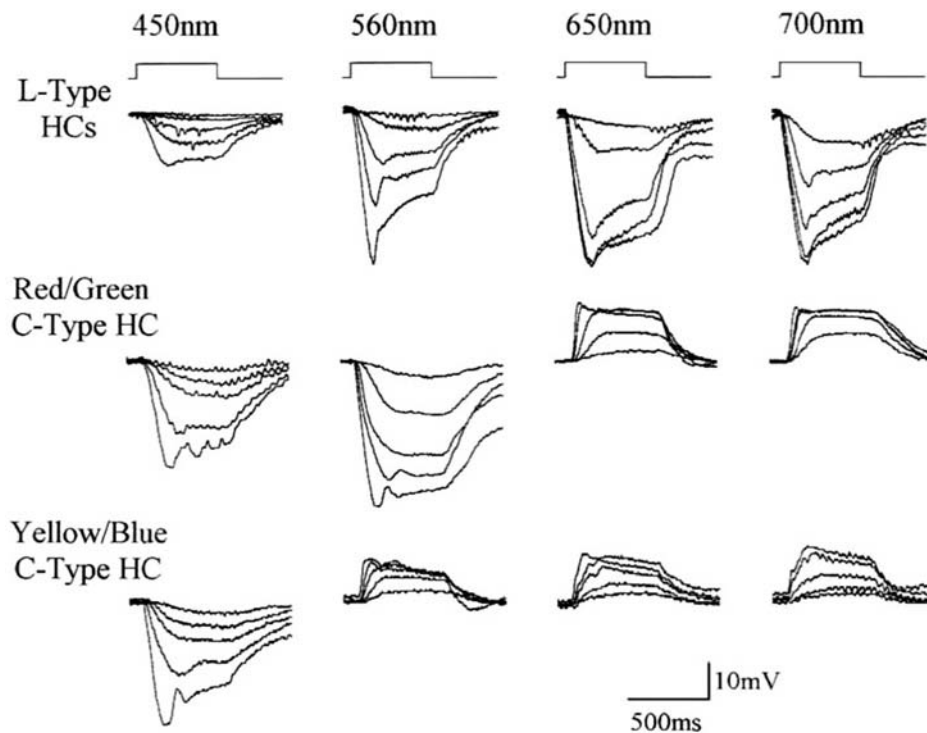


FIGURE 24.6. Wavelength dependency of the photoresponses from an L-type, a red/green C-type, and a yellow/blue C-type horizontal cells in the retina of the turtle *Mauremys caspica*. For each wavelength, several intensities were used.

1998; Fuortes and Simon, 1974). The yellow/blue C-type horizontal cells receive inhibitory inputs from green and red cones and excitatory input from blue cones (Asi and Perlman, 1998; Fuortes and Simon, 1974) and interestingly, also from UV cones (Ammermüller et al., 1998). Consequently, their photoresponses reverse in polarity around 540 nm (Fig. 24.7C).

Given the horizontal cell diversity from lower vertebrates, where the axonless types are chromatically opponent, it is surprising that in mammalian retinas, where the axonless horizontal cell type is also present, only L-type horizontal cell responses can be recorded (Nelson, 1985; Niemeyer and Gouras, 1973; Steinberg, 1969a, 1969b). For example, both cat A- and B-types are luminosity (see Fig. 24.2). Although dominated by red-cone input, low-level synergistic input from blue cones can be seen when tested using specific spectral stimulating and adapting conditions (Nelson, 1985).

In primate retina, horizontal cells also only occur as luminosity types (Dacey et al., 1996; Dacheux and Raviola, 1990). Some of these cells receive synergistic signals from long- and medium-wavelength cones (red and green cones), and others receive synergistic input from all three spectral types of cones; long- medium-, and short-wavelength (red, green, and blue cones) as shown in Figure 24.8. Anatomically H1-type horizontal cells tend to avoid the pedicles of blue cones (Fig. 24.8, *left*) (Ahnelt and Kolb, 1994a, 1994b; Dacey et al., 1996) and are therefore not responsive to blue

light stimuli (E in Fig. 24.8, *left*). On the other hand, large numbers of dendrites of H2-type horizontal cells make synaptic contacts with blue cone pedicles (outlined clusters, Fig. 24.8, *right*) (Ahnelt and Kolb, 1994a, 1994b; Dacey et al., 1996). The H2 cell is indeed very sensitive to the blue end of the spectrum (E in Fig. 24.8, *right*). Yet the responses of both horizontal cell types are only hyperpolarizing to the three wavelengths (Dacey et al., 1996). Thus, it appears that subsets of mammalian and primate L-type horizontal cells are devoted primarily to processing of either blue signals or red and green signals, but spectral opponency is not part of the processing regime (see Figs. 24.5, 24.6, and 24.7).

Rod and cone contributions to horizontal cells

ROD-CONE MIXING Steinberg (1969a, 1969b) was the first to record S-potentials in a mammalian retina. He made intracellular recordings from horizontal cells in the cat retina and saw the typical graded hyperpolarizing responses that depended on the intensity of the light stimulus. However, Steinberg's S-potential recordings revealed separate rod and cone contributions to the response, as might be expected in a rod-dominated retina. A very slow phase of membrane repolarization that was seen after termination of the light stimulus was identified as the rod contribution based on spectral adaptation. He called it the "rod after effect" (Fig. 24.9). The difference in offset kinetics for rod and cone signal

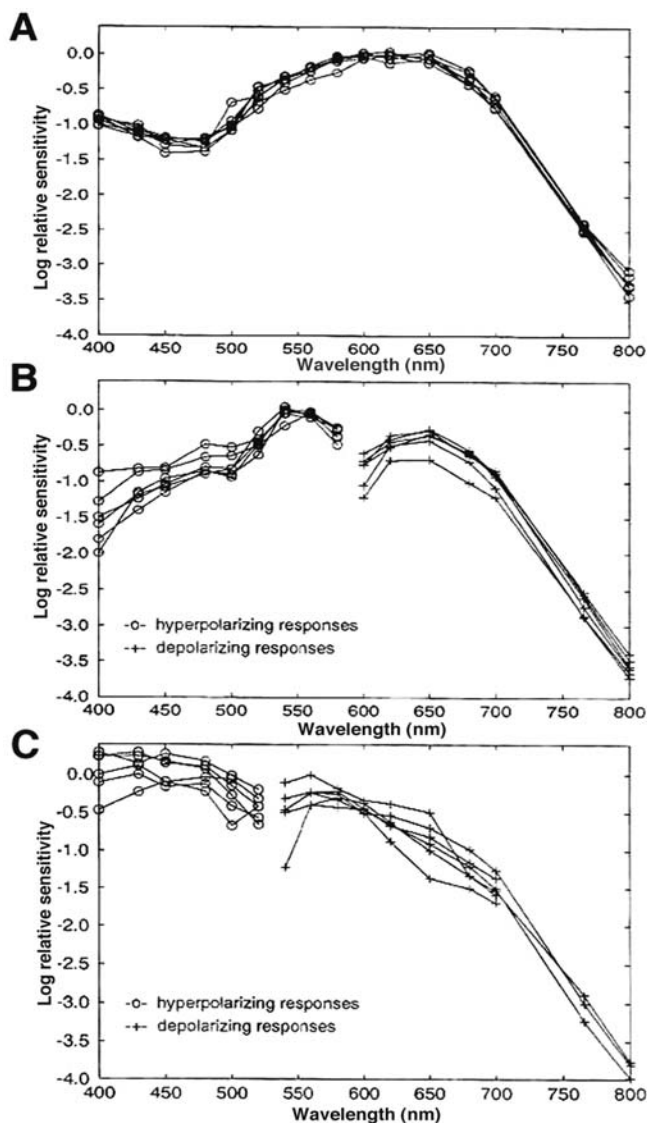


FIGURE 24.7. Action spectra of 8 L-type (A), 7 red/green C-type (B), and 6 yellow/blue C-type (C) horizontal cells in the turtle *Mauremys caspica* retina. Sensitivity data were calculated from photoresponses of small amplitude ($<1\mu\text{V}$). In order to compare the different action spectra, the spectrum of each cell was normalized to the peak sensitivity (Asi and Perlman, 1998).

components provides a convenient assay for rod and cone signal composition of S-potentials in rod-dominated mammalian retinas (Nelson, 1977; Nelson et al., 1976). In Figure 24.9, typical mixed rod and cone signals of all three horizontal cell structures in cats are shown (Nelson et al., 1976). In A- and B-type horizontal cell bodies, rod and cone signals are about equal in amplitude, whereas in the axon terminal of the B-type cell, the response has a slowly recovering waveform, characteristic of rod signals. The “rod after effect” is most evident with bright light stimuli (Fig. 24.9, bottom).

Further evidence for the mixing of rod and cone inputs to horizontal cells is seen during adaptation to background

lights. When retinas are light adapted by steady background lights, rod function saturates even at low levels of illumination and their contributions to the horizontal cell photoresponses decrease significantly. Meanwhile, the cones adapt to the conditions of ambient illumination and their input remains. These properties of rod and cone inputs are easily seen in the photoresponses of mammalian horizontal cells. The photoresponses of B-type horizontal cell axon terminals are virtually abolished by light adaptation, consistent with their rod-dominated physiology. In the horizontal cell bodies (A and B types) that receive mixed rod and cone inputs, light adaptation selectively reduces the rod contribution but large cone signals remain; therefore, these horizontal cell elements continue to respond well in the presence of background lights (Nelson, 1977).

We know that the axon terminals of the axon-bearing horizontal cells in the cat receive an excitatory feedforward input from rods, but the cell bodies of A-type and B-type cells contact only cones. So where does the large rod component of the S-potential in these structures of horizontal cells come from? Electron-microscope observations show that small gap junctions link rod and cone photoreceptors in the outer plexiform layer (Kolb, 1977; Raviola and Gilula, 1975). These electrical synapses introduce rod signals into cones and thence into horizontal cells. This rod-cone mixing in the photoreceptors is now considered a major pathway whereby rod-driven inputs pass to horizontal cells and to all subsequent second- and third-order cells in the retina (Smith et al., 1986; Sterling, 1990).

In other species, similar characteristics of rod-cone mixing can be found in horizontal cells. In the rabbit retina, as in the cat retina, rod-dominated input to the axon terminal is identified by waveform, sensitivity, and after-potentials (Dacheux and Raviola, 1982; Massey and Miller, 1987). Also, in primate retina, the axon terminals of the axon-bearing H1-type horizontal cells are connected to rods while the cell body is connected to cones (Dacheux and Raviola, 1990; Verweije et al., 1999). Similar to other mammalian retinas, the somata of primate H1-type horizontal cells receive rod input indirectly via gap junctions between rods and cones (Verweije et al., 1999).

Horizontal cells in cold-blooded vertebrates are also characterized by mixing of rod and cone signals. In the retina of the turtle *Chelydra serpentina*, the photoresponses of H1 axon terminals contain slow, low-amplitude components that are contributed by rod photoreceptors, despite their major excitatory input being from long-wavelength sensitive cones. The cell bodies of the same H1 horizontal cells receive input only from long- and medium-wavelength sensitive cones (Leeper and Copenhagen, 1979).

PASSIVE ELECTRICAL MODELS All vertebrate retinas contain one horizontal cell type that is an axon-bearing cell (see Fig.

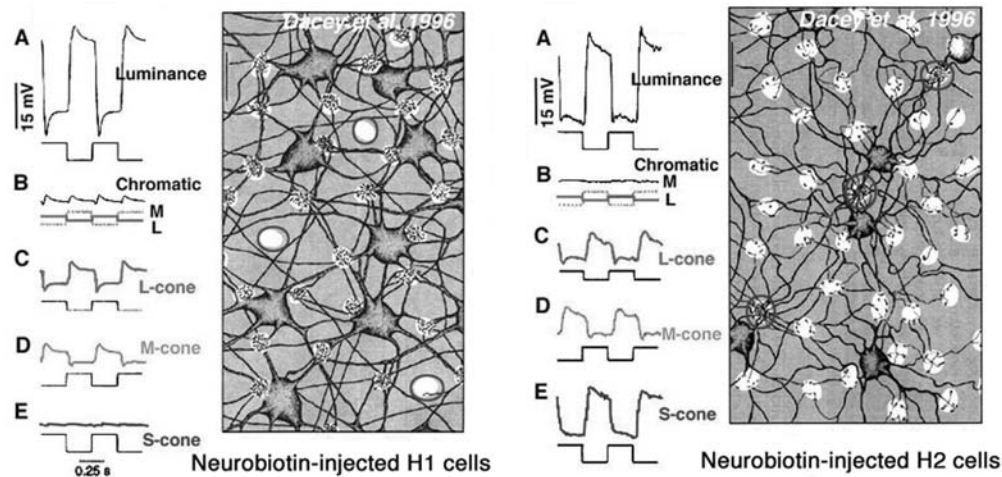


FIGURE 24.8. *Left*, Intracellular staining and chromatic responses of H1 cells in monkey retina. The H1 cells avoid having dendritic contact with blue cones (blue-outlined white circles), and the S-potential shows no response to stimulation with blue light (trace E). *Right*, Intracellular staining and chromatic responses of H2 cells in

monkey retina. The H2 cells send many dendrites to blue cones (blue-outlined cones) as well as to red and green cones. The S-potential is very large to stimulation with blue light (E). (Dacey et al., 1996). (See color plate 10.)

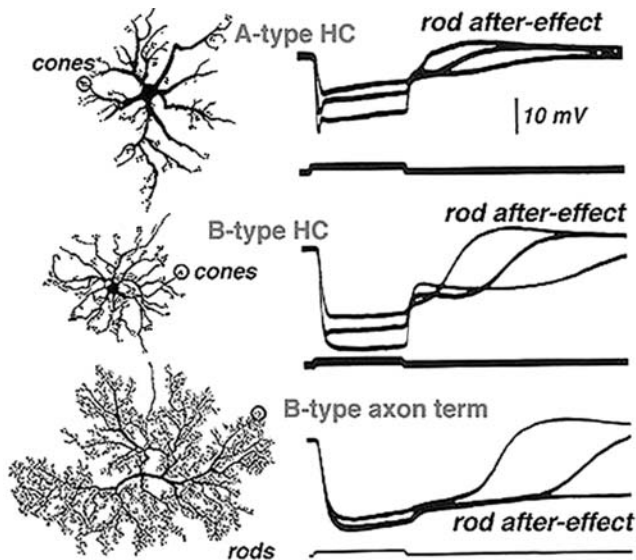


FIGURE 24.9. Rod-cone mixing in horizontal cells of the cat retina. Responses to light stimuli of different intensities were recorded from the cell bodies of A-type and B-type horizontal cells and from the axon terminal of the B-type horizontal cell (Nelson et al., 1976).

24.2, B type). The axon terminal and the somata of this horizontal cell type are connected by a long thin axon, but both parts behave as isolated physiological units. In the turtle *Pseudemys scripta elegans*, both axon terminal and somata receive excitatory input mainly from red cones, but they are characterized by different spatial properties and different kinetics to red and green light stimuli (Perlman and Normann, 1979; Simon, 1973). In the turtle *Chelydra serpentina*, the axon terminal receives excitatory input from red

cones and rods while the cell body dendrites contact red and green cones (Leeper and Copenhagen, 1979). In mammals (cat, rabbit) and in primates (monkey), the dendrites of the cell body receive input from cones while the terminals of the axon contact thousands of rods. No evidence has been found to indicate any synaptic or electrical interaction between the axon terminal and the soma of the same cell in any of these cases.

Where horizontal cell types have the dendritic portion of the cell much distant from the axonal ending (Fig. 24.2, B cells), calculations based on the anatomical dimensions and geometry of the neuron, and ohmic linear properties of cell membrane and cytoplasm, indicate that the axons are too long and thin to allow passive electrotonic conduction of signals from one end of the cell to the other (Leeper, 1978a, 1978b; Leeper and Copenhagen, 1979; Nelson et al., 1975). Such models tell us that signals in cell bodies of horizontal cells reflect the local synaptic inputs from cones and signals in axon terminals reflect the local synaptic inputs from rods. Indeed, the two portions of the same cell act as independent units (Nelson et al., 1975).

Ionic conductances in horizontal cells

LIGAND-GATED CHANNELS Photoreceptors make excitatory (sign-conserving) synapses onto horizontal cells. In darkness, the photoreceptors continuously release an excitatory neurotransmitter that opens cation channels with a depolarized reversal potential. Therefore, the horizontal cells are maintained at a relatively depolarized potential in darkness. When the photoreceptors are hyperpolarized by a light stimulus, transmitter release is reduced, the postsynaptic ligand-

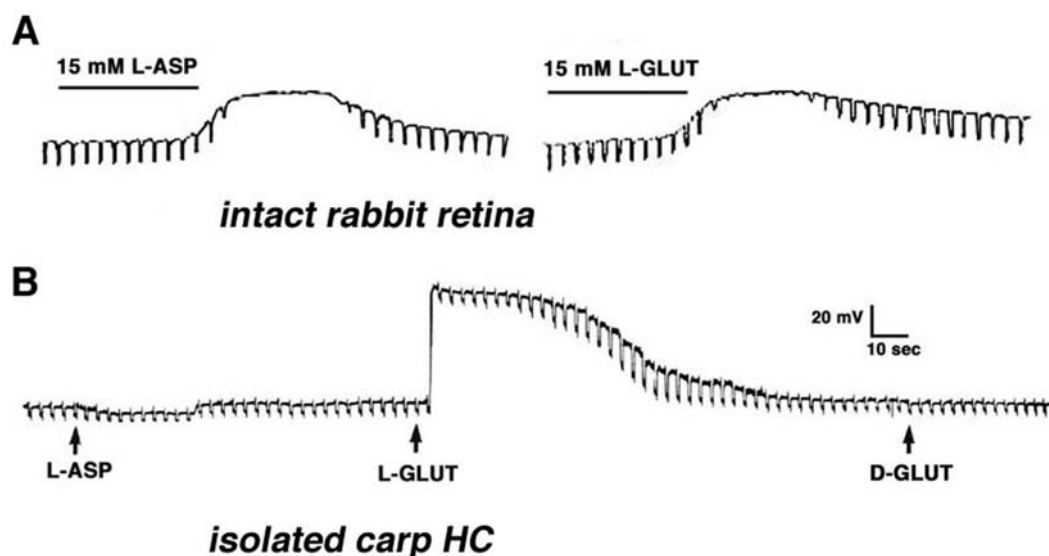


FIGURE 24.10. *A*, The effects of L-aspartate and L-glutamate on the membrane potential and photoresponses of a horizontal cell in the rabbit retina (Bloomfield and Dowling, 1985). The photoresponses were elicited by diffuse light stimuli. *B*, The effects of L-aspartate, L-glutamate, and D-glutamate on the membrane

potential of a horizontal cell isolated from the carp retina (Lasater and Dowling, 1982). Each application pipette was filled with 500 μ M of drug. Current pulses are used to assess changes in membrane resistance.

gated channels close, and horizontal cells hyperpolarize. Transmitter release from photoreceptor terminals is calcium dependent. Thus, exposing the retina to solutions that interfere with calcium influx through voltage-dependent calcium channels causes block of transmitter release and horizontal cell hyperpolarization (Cervetto and Piccolino, 1974; Dowling and Ripps, 1973; Kaneko and Shimazaki, 1975).

Early experiments in intact retinas pointed to the excitatory amino acids L-glutamate and L-aspartate as putative candidates for the photoreceptor neurotransmitter (Bloomfield and Dowling, 1985; Cervetto and MacNichol, 1972; Marshall and Werblin, 1978; Negishi and Drujan, 1979; Normann et al., 1986). Exposing the retina to either L-glutamate or L-aspartate caused depolarization of the horizontal cells and loss of their photoresponses, as shown in Figure 24.10*A* for rabbit horizontal cells in the intact retina (Bloomfield and Dowling, 1985). In the experiment described in Figure 24.10*A*, 15 mM solutions of L-aspartate or L-glutamate were needed to induce depolarization of rabbit horizontal cells and loss of their photoresponses. These observations are consistent with the notion of an excitatory amino acid neurotransmitter being continuously released by the photoreceptors in the dark, and that light-induced electrical activity in the horizontal cells reflects the removal of the neurotransmitter from the synaptic cleft. Accordingly, exogenously applied neurotransmitter saturates the receptor sites in the horizontal cells, causing further depolarization. Because the horizontal cells are saturated with the neurotransmitter, modulation of endogenous trans-

mitter release by light stimuli have no effect on membrane potential and the photoresponses are eliminated. These and other studies raised two major questions: (1) Why were relatively high concentrations (millimolar range) of excitatory amino acids needed to exert the effects shown in Figure 24.10*A*? (2) Which of the two excitatory amino acids was the real neurotransmitter?

The first question was answered by the identification of efficient uptake systems for excitatory amino acids in retinal cells (Eliasof et al., 1998; Rauen et al., 1998). These uptake mechanisms remove the excitatory amino acids from the superfusing solution, thereby preventing the chemicals from reaching the cone–horizontal cell synapses. Thus, when nontransportable agonists of excitatory amino acids are used, considerably lower concentrations are needed to exert effects on horizontal cells (Massey and Miller, 1987; Yang and Wu, 1991a). This is illustrated in Figure 24.11 where the effects of 10 mM L-glutamate (*A*) are compared to those of 0.1 mM kainic acid (*B*). Kainic acid, a nontransportable agonist for glutamate-type receptors in vertebrate horizontal cells, exerts similar effects to those of L-glutamate at a concentration lower by 100-fold. In contrast, kynurenic acid, a nonselective antagonist of excitatory amino acid receptors (Mayer and Westbrook, 1987), induces the opposite effects (Fig. 24.11*C*). The horizontal cell hyperpolarizes and loses its photoresponses.

The identity of the neurotransmitter was a subject of debate for more than a decade. A variety of experiments in intact retinas were designed to decide between L-glutamate and L-aspartate, and conflicting conclusions were achieved.

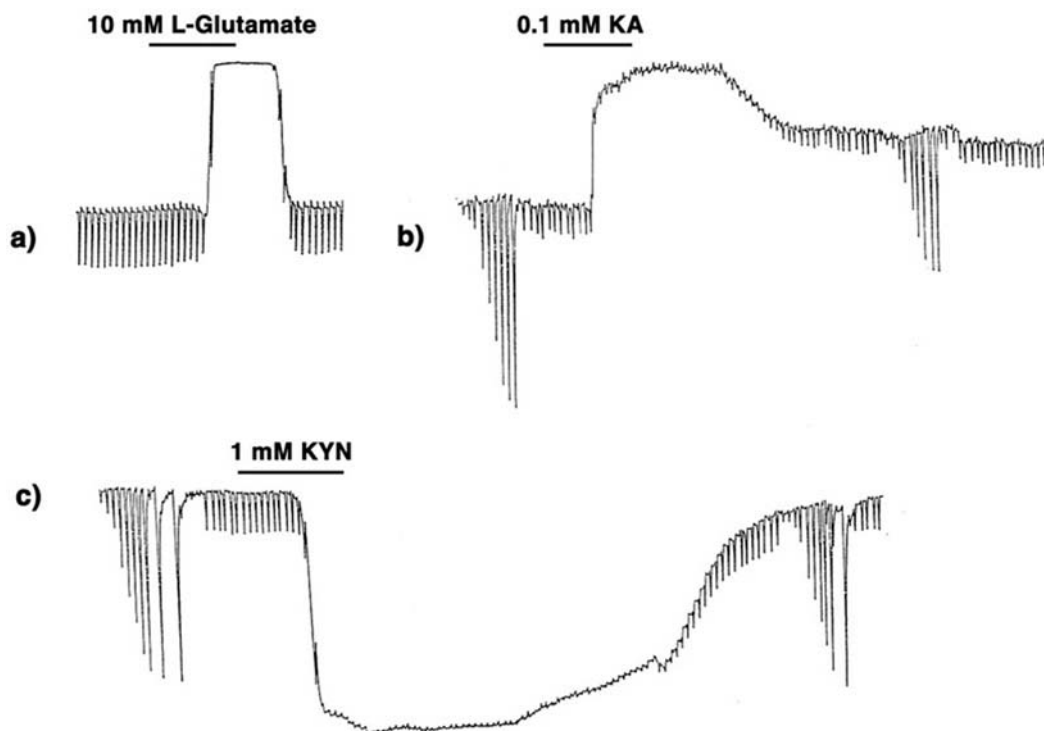


FIGURE 24.11. The effects of L-glutamate (a), kainic acid (b), and kynurenic acid (c) on the membrane potential and photoresponses of L-type horizontal cells in the retina of the turtle *Mauremys caspica*.

It was not until the development of the isolated cell preparation that a clear answer to this question was obtained. Lasater and Dowling (1982), in their pioneering work, isolated horizontal cells from the carp retina and recorded their membrane potentials with sharp microelectrodes. The horizontal cells in culture were characterized by hyperpolarized resting potentials (close to the potassium equilibrium potential) because they were separated from the retina circuitry. Application of L-glutamate, but *not* of L-aspartate or D-glutamate, induced depolarization, indicating that specific receptors for L-glutamate existed in the horizontal cell membrane (Fig. 24.10B). With this experimental approach, a low concentration of L-glutamate was sufficient to induce effects, because in this preparation, removal of extracellular L-glutamate by uptake systems is negligible.

Voltage- and current-clamp techniques have been applied to isolated horizontal cells from a variety of species to reveal the properties of the glutamate-gated channels. These channels have a reversal potential around 0 mV, depending on the composition of the intrapipette and extracellular solutions (Hals et al., 1986; Perlman et al., 1989; Tachibana, 1985; Yang and Wu, 1991a). Pharmacological analysis of the properties of the glutamate-gated channels in horizontal cells, using specific agonists and antagonists, revealed them to be of the AMPA/KA type. They are specifically activated by α -amino-3-hydroxy-5-methyl-4-isoxazole propionic acid (AMPA) or kainic acid (KA) and are antagonized by 6-

cyano-7-nitroquinoxaline (CNQX) or cis-2,3-piperidine-dicarboxylic acid (PDA) (reviews in Peng et al., 1995; Wu, 1994). When these ion channels are activated by the agonist kainic acid, the induced currents are considerably larger than those elicited by L-glutamate, even at higher concentrations (O'Dell and Christensen, 1989; Perlman et al., 1989). This effect has been attributed to fast desensitization of the AMPA/KA type channels by L-glutamate but not by kainic acid (Eliasof and Jahr, 1997; Schmidt et al., 1994). More recently, selective blockers of the glutamate-induced desensitization (e.g., cyclothiazide) have shown that the glutamate-induced currents are increased by severalfold, thereby concluding that horizontal cells express exclusively AMPA-type glutamate receptors (Blanco and de la Villa, 1999; Yang et al., 1998). Catfish horizontal cells, which express NMDA receptors in addition to AMPA/KA receptors, appear to be the lone exception to the above general conclusion (O'Dell and Christensen, 1989).

VOLTAGE- AND TIME-DEPENDENT IONIC CONDUCTANCES The photoresponses of horizontal cells from cold-blooded, as well as warm-blooded mammalian retinas, are shaped by voltage- and time-dependent ionic conductances in their plasma membrane (Lasater, 1986, 1991; Lohrke and Hofmann, 1994; Ueda et al., 1992). Five types of ionic currents—a sodium current, a calcium current, and three types of potassium current—have been identified in isolated horizontal

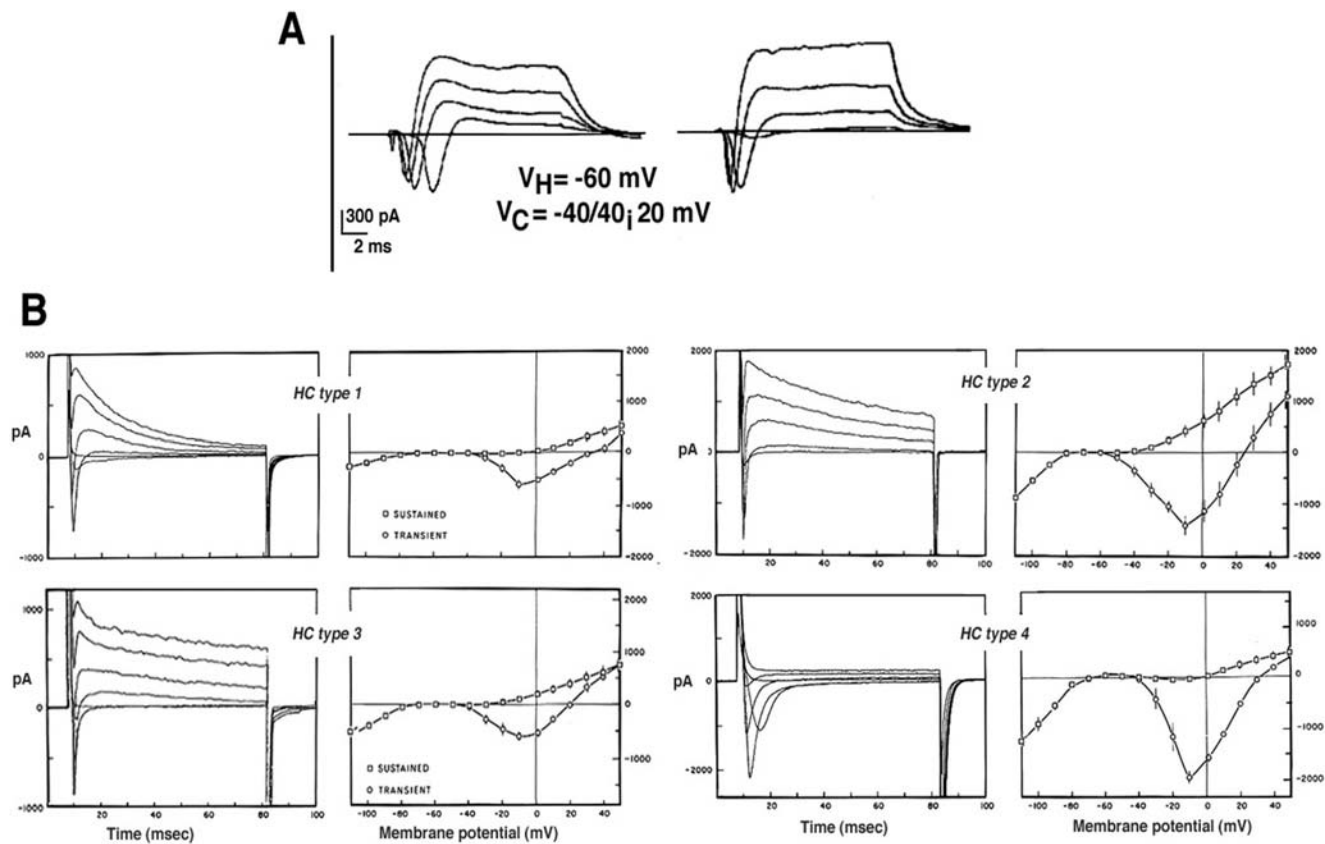


FIGURE 24.12. Voltage- and time-dependent ionic conductances in isolated horizontal cells. *A*, Current pulses to different voltage steps from a holding potential at -60 mV in horizontal cells from the rabbit retina (Lohrke and Hofmann, 1994). *B*, Current responses and I-V curves from four types of horizontal cells that were isolated from the retina of the white perch (Lasater, 1986).

cells of goldfish (Tachibana, 1983), catfish (Shingai and Christensen, 1986), white perch (Lasater, 1986), skate (Malchow et al., 1990), turtle (Golard et al., 1992), rabbit (Lohrke and Hofmann, 1994), and cat (Ueda et al., 1992).

Figure 24.12 shows the current responses to voltage steps of two types of horizontal cells from the rabbit retina (*A*) and four types of horizontal cells isolated from white perch retina (*B*). In rabbit horizontal cells, the inward sodium current is clearly evident during the first 10 ms of the current responses; at the steady state, a sustained outward potassium current is seen (Fig. 24.12*A*). The fish horizontal cells exhibit a more complex array of currents, as evident from the current pulses and transient and sustained I-V curves (Fig. 24.12*B*). All four types of fish horizontal cells exhibit similar ionic currents that differ only in relative magnitude. The sodium current is inward going and is seen during the initial 10 ms of the current pulses recorded when the horizontal cells are depolarized from a negative holding potential (about -70 mV) to around 0 mV. It is very similar to the regenerative sodium current typical of spiking neurons. The physiological role of this current in horizontal cells is not known because these cells do not respond with action potentials. Three types of potassium channel have been identified

by their voltage and time dependency and by their sensitivity to specific blockers. The inwardly rectifying channels conduct an inward current when the cells are hyperpolarized below potassium equilibrium potential. In some species, extracellular sodium ions also determine the reversal potential of these channels, making the currents functional at physiological potentials (Pfeiffer-Linn et al., 1995). The sustained outward potassium current (delayed rectifier) is activated at potentials more depolarized than the resting, dark potential of the horizontal cells. The outward transient potassium current (I_A) is activated by a fast depolarization from negative potentials. In the intact turtle retina, the outward transient potassium current is activated after termination of a bright light stimulus to enhance the recovery of the L-type horizontal cell potential back to the dark level. This effect allows the L-type horizontal cells to follow fast flickering stimuli and thus improves the frequency response curve of the cells (Perlman et al., 1993).

Gap junctions and spatial characteristics

GAP JUNCTIONS In all vertebrate retinas, including mammals, horizontal cells are characterized by large-

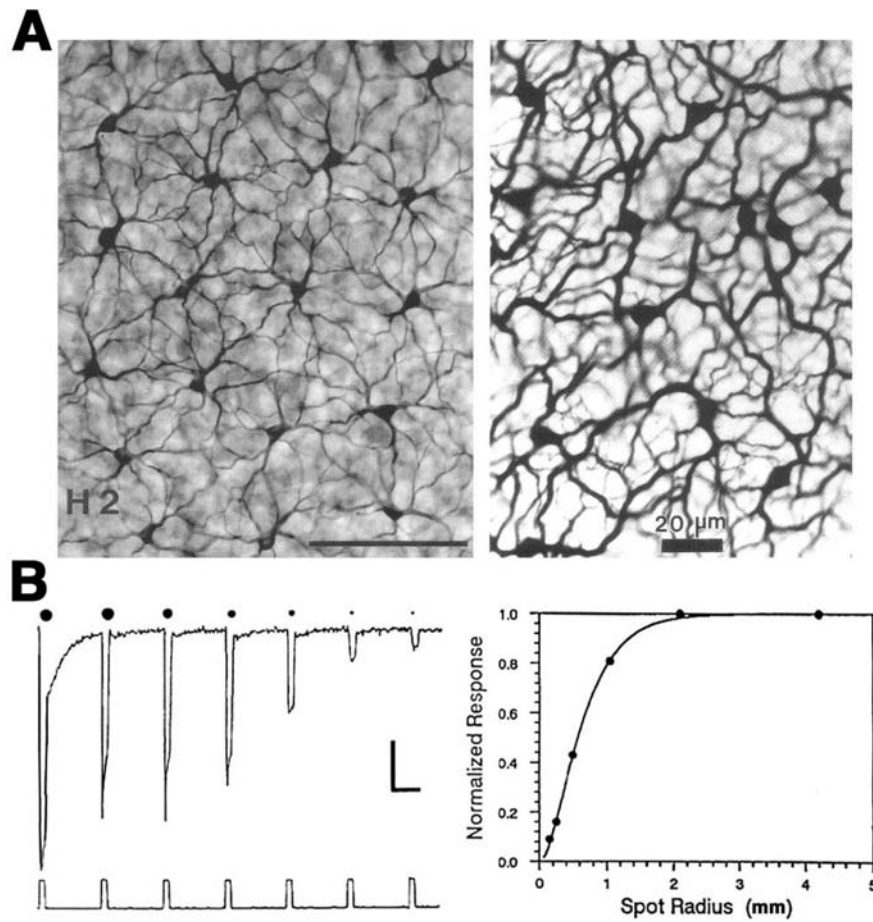


FIGURE 24.13. *A*, The syncytia of H2 cells of the turtle (*left*) and A-type horizontal cells in the rabbit (*right*) as revealed by Neurobiotin injection into one cell in each syncytium (Ammermüller and Kolb, 1996; Mills and Massey, 1994). *B*, The properties of the receptive field of turtle L-type horizontal cell as determined from

the photoresponses elicited by concentric light stimuli of different diameter (*left*). The peak amplitude, normalized to the response to full-field illumination, is plotted as a function of spot radius to derive the length constant (*right*) (Perlman and Ammermüller, 1994).

surface-area gap junctions (Fig. 24.3C and E) between each others' dendrites (Kolb, 1977; Witkovsky and Dowling, 1969). These junctions allow lateral flow of small molecules and ions within the horizontal cell network. Lucifer yellow or Neurobiotin injected into one horizontal cell in the layer spreads to hundreds of neighboring cells, forming striking images of the interconnected horizontal cell network (Fig. 24.13A and B) (Ammermüller and Kolb, 1996; Bloomfield and Miller, 1982; Kaneko, 1971; Mills and Massey, 1994; Teranishi et al., 1983; Vaney, 1994). Gap junctions are formed only between neighboring horizontal cells of the same physiological type, as shown in Figure 24.13. Networks of turtle H2 cells (Fig. 24.13, *left*) and of rabbit A-type cells (Fig. 24.13, *right*) are demonstrated by Neurobiotin injection into one cell of the network. The conductance of the gap junctions between horizontal cells and therefore dye coupling is influenced by the intracellular and extracellular milieu and by chemicals such as dopamine, retinoic acid, and nitric oxide that are released by other retinal cells (see later section).

RECEPTIVE FIELD PROPERTIES The gap junctions between horizontal cells are highly permeable to small ions and therefore serve as low-resistance pathways for electrical signals to spread laterally within the horizontal cell layer. Thus, horizontal cells receive excitatory input via chemical synapses from photoreceptors and via gap junctions from neighboring horizontal cells. The physiological consequences of the gap junctions between horizontal cells are that these cells have very large receptive fields that spread out to retinal regions outside the range of their immediate dendritic fields (Kaneko, 1971; Naka and Rushton, 1967).

Different procedures have been used to characterize the receptive fields of horizontal cells. The most common experimental procedures have been the application of a series of concentric spots of increasing diameter but fixed intensity, or moving a narrow slit of light across the retina. An experiment in which an L-type horizontal cell in the retina of the turtle *Pseudemys scripta elegans* was stimulated with a series of concentric spots of fixed intensity is shown in Figure 24.13B.

The first photoresponse to the left was elicited with a stimulus of supersaturating intensity that illuminated the entire receptive field of the cell. This is the maximal photoresponse of the cell. A series of six photoresponses that were elicited by light stimuli of fixed intensity and wavelength (650 nm) but different diameters are shown. The amplitudes of the photoresponses gradually decrease as the size of the illuminated retinal area is reduced (Fig. 24.13*B*, *left*). This diminution is not due to lesser summation of inputs from photoreceptors but to shunting of the direct input to the horizontal cell by neighboring horizontal cells. With full-field illumination, all the horizontal cells are evenly illuminated and are equipotential, and therefore no current flows between them. With small spot illumination, the membrane potential of nonilluminated horizontal cells is different from that of illuminated cells, causing electrical currents to flow between them and thus to shunt the responses of the illuminated cells.

The dimension of the horizontal cell receptive field can be quantified by the diameter of the spot that elicits a response that does not differ from that elicited by a full-field illumination or by the length constant (λ). The mathematical definition of λ and the ways of measuring it vary (Kamermans et al., 1996; Lamb, 1976; Lankheet et al., 1990; Nelson, 1977; Nelson et al., 1990; Owen and Hare, 1989). However, it is generally agreed that the receptive field size is directly related to λ and that λ is directly related to the membrane resistance of the horizontal cell and inversely related to the coupling resistance between the horizontal cells.

The relationship between peak amplitude of the photoresponse and the radius of the illuminated retinal area used to elicit it, while analytically given by a Bessel function (Lamb, 1976; Nelson et al., 1990), can be approximated by an exponential equation (Owen and Hare, 1989):

$$V_r/V_{ff} = 1 - [1 + (r/\underline{\lambda})]e^{(-r/\lambda)}$$

Where V_r and V_{ff} are the amplitudes of the photoresponses elicited by a light spot of radius r and by full-field illumination, respectively. $\underline{\lambda}$ is 0.81 of the one-dimensional length constant λ for the horizontal cell network (Hare and Owen, 1990). The relationship between peak response amplitude that was normalized to the amplitude obtained with full-field illumination and spot radius was constructed for the photoresponses in Figure 24.13*B*, *left* and is shown in Figure 24.13*B*, *right*. The continuous curve represents the best fit of the above equation to the data points with $\underline{\lambda} = 280 \mu\text{m}$ ($\lambda = 345 \mu\text{m}$).

Another common method for determining the length constant is to measure the photoresponses that are elicited by long narrow slits of light presented at different distances from the recorded horizontal cell (Nelson, 1977). The relationship between response amplitude and distance of the slit from the cell can be described by an exponential function. For slit stimuli much narrower than the length constant, the

length constant is approximately the distance between the slit of light and the recorded cell that elicits a response that is $1/e$ of that elicited when the slit directly illuminates the cell.

Horizontal cells have been classified according to their physiological type and according to the size and properties of their receptive fields. In the turtle retina, two types of luminosity horizontal cells have been described: L1 and L2 (Simon, 1973), or large receptive field (LRF) and small receptive field (SRF) horizontal cells (Perlman and Normann, 1979). The L1 (LRF) cells are characterized by receptive fields of large diameter ($>3 \text{ mm}$); the L2 (SRF) cells have a receptive field diameter of about 2 mm. These two L-type horizontal cells also differ with regard to spectral properties (Perlman et al., 1985) and responsiveness to surround illumination (Piccolino et al., 1981). The spatial properties of C-type horizontal cells in the turtle retina also depend on the color of the light stimuli (Kato, 1979; Twig et al., 2002). The waveform of the photoresponses of C-type horizontal cells may change dramatically when the spatial pattern of the light stimulus is changed, especially when the wavelength of the light is close to the zone where response polarity reverses (Twig et al., 2002).

The horizontal cell syncytium cannot be described by a simple array of resistors interconnected by coupling resistors. The resistances of the horizontal cell layer change with illumination and time; therefore, the size of the receptive field (magnitude of length constant) changes with light intensity and with time (Borenstein, 1999; Bykov and Shura-Bura, 1983; Kamermans et al., 1996). In general, the diameter of the receptive field (length constant) is directly related to the intensity of the light stimulus used to measure it (Lamb, 1976; Perlman and Ammermüller, 1994; Perlman et al., 1985; Pottek et al., 1997). When the irradiance of the ambient illumination is increased, the length constant first increases to a peak value and then decreases to a steady-state value (Borenstein, 1999; Kamermans et al., 1996; Nelson, 1977).

Feedback

Horizontal cells are postsynaptic to the photoreceptors, but in certain cold-blooded species they are also presynaptic to the photoreceptors. Horizontal cells send visual information back to cones through feedback pathways (Baylour et al., 1971; Burkhardt, 1977; Fuortes et al., 1973; Lasansky, 1981; O'Bryan, 1973; Wu, 1991). The effects of these pathways can be revealed by adjusting the properties of the light stimuli. In Figure 24.14, the photoresponses of a cone from the retina of the tiger salamander are shown (Lasansky, 1981). Each pair of responses was elicited by light stimuli of the same intensity but different size. The ON phase of each pair of photoresponses (initial hyperpolarization) is identical

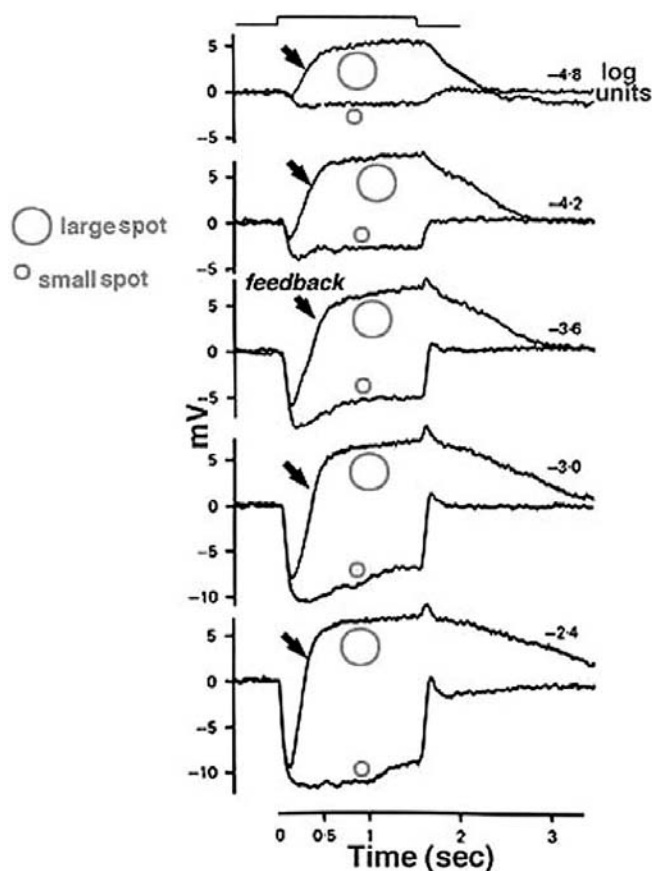


FIGURE 24.14. The contribution of the feedback pathway from L-type horizontal cells to cone responses in the retina of the tiger salamander. Photoresponses were elicited by light stimuli of different intensities covering a small or a large spot (indicated) (Lasansky, 1981).

regardless of the size of the stimulus, but the later phases are considerably affected by the stimulus size. With a small spot stimulus, after the initial hyperpolarization, the cell slightly recovers toward the dark potential but the membrane potential is maintained at a hyperpolarized level for the entire duration of the stimulus. When a large spot stimulus is used, a significant depolarization is seen after the initial hyperpolarizing phase despite continuous illumination (Fig. 24.14, arrows). This late depolarizing potential reflects the activation of the negative feedback pathway from the horizontal cells.

In turtle retina, the feedback pathway from horizontal cells to cones can be revealed by experiments using light stimuli of different sizes and colors (Fig. 24.15). Red and green light stimuli of different diameters were used to excite a red cone (L-cone) and a green cone (M-cone). With small-field stimuli, the photoresponses of the red cone are very similar in shape (Fig. 24.15, upper left pair of responses). However, with large-field stimuli, the large excitatory input from the green cones to the L-type horizontal cells that is activated by the bright green light stimulus activates the feedback pathway and

causes the response of the red cone to the green light stimulus to become narrower (Fig. 24.15, lower left traces). In the green cone, the contribution of the feedback pathway from the L-type horizontal cells is more apparent and a depolarizing photoresponse is elicited with a large-diameter red light stimulus (Fig. 24.15, bottom traces). Blue cones (S-cones) also get feedback pathways from L-type horizontal cells (Itzhaki et al., 1992) as shown in Figure 24.15 (right-hand traces). A large-diameter red light stimulus was used to selectively isolate possible inputs that were mediated by feedback pathways from L-type horizontal cells to blue cones. In the dark-adapted state, a small depolarizing afterpotential was seen after the initial hyperpolarizing phase (Fig. 24.15, trace 1). During a red background light that selectively desensitized the L-cones, a pure hyperpolarizing photoresponse was elicited by the red light stimulus (trace 2), while the blue background augmented the relative contribution of the feedback pathway and, therefore, a depolarizing photoresponse was obtained (trace 3). These and other anatomical and physiological studies formed the basis for the theory that a feedback model between cones and horizontal cells underlied color opponency in nonmammalian retinas (Kamermans and Spekreijse, 1995; Stell and Lightfoot, 1975; Witkovsky et al., 1995; review in Piccolino, 1995).

The negative feedback circuit from horizontal cells to cones is thought to take place through the horizontal cell lateral elements invaginating the photoreceptor terminal at the triad ribbon synapse (see Fig. 24.3). The problem has been that no images of a synapse with vesicle clusters in the lateral elements have ever been seen, except for in human retina (Linberg and Fisher, 1988). Fish retinas have distinctive spinules on the dendritic endings of the horizontal cells' lateral elements in cone pedicles (Fig. 24.3bB). Spinules have been suggested to be the sites of feedback from horizontal cells to cones because they change shape and enlarge during background illumination when the effects of negative feedback are most apparent (Djamgoz et al., 1989; Downing and Djamgoz, 1989; Kirsch et al., 1990; Raynauld et al., 1979; Wagner, 1980; Weiler and Wagner, 1984).

GABA has been suggested as the candidate for the inhibitory feedback neurotransmitter between H1 cells and photoreceptors in some species (Cuenca et al., 2000; Marc et al., 1978). GABA-induced currents can be recorded from the terminals of red-sensitive and green-sensitive cones isolated from the turtle retina (Tachibana and Kaneko, 1984). Furthermore, color opponency in fish C-type horizontal cells is eliminated on exposure to GABA or its antagonists (Murakami et al., 1982a, 1982b). However, studies in other species have failed to show effects supportive for a role of GABA as the inhibitory neurotransmitter of the horizontal cell (Perlman and Normann, 1990; Stone et al., 1990). In L-type horizontal cells of turtle, GABA and related drugs induce depolarizations that are consistent only with the

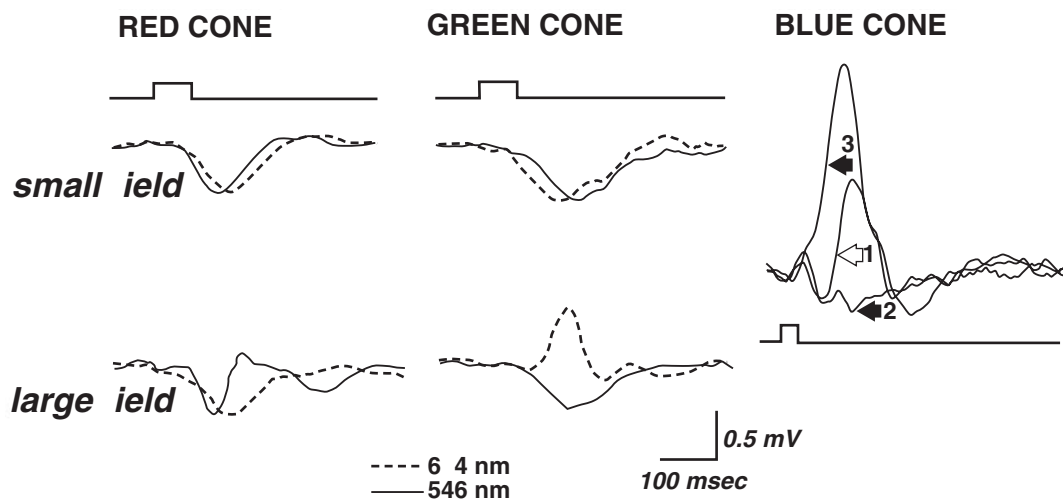


FIGURE 24.15. The contribution of the negative feedback from L-type horizontal cells to the photoresponses of cones in the turtle retina. The red and green cones were stimulated with small-field and large-field stimuli of red and green light (Perlman et al., 1985).

The blue cone from the retina of the turtle *Mauremys caspica* was stimulated with a red (700-nm) light stimulus covering a large retinal area in the dark-adapted state (trace 1) and during red (trace 2) or blue (trace 3) background lights (Itzhaki et al., 1992).

activation of electrogenic GABA transporters in the horizontal cell membrane (Kamermans and Werblin, 1992; Perlman and Normann, 1990). Thus, the idea that GABA mediates the negative feedback of horizontal cells to cone photoreceptors has gone out of favor in recent years, although GABA could still have a feedforward action directly on bipolar cell dendrites.

A different approach to the question of horizontal cell feedback has been taken recently (Verweij et al., 1996). Using voltage-clamp recordings from cones during illumination with spots or annuli of light, these authors have suggested that negative feedback modulates the voltage dependency of the calcium channels in the cone pedicles. The idea takes off from an old electrical model (Byzov and Trifonov, 1968) and proposes that horizontal cells can initiate large extracellular current flow through hemi-gap junction channels at the lateral element synapse into the intercellular space at the triad synapse of the cone (Fig. 24.3D) (Janssen-Bienhold et al., 2001; Kamermans et al., 2001). During light stimulation, the L-type horizontal cells hyperpolarize and the magnitude of the extracellular current is reduced, so affecting the voltage-dependent calcium channels in the cone pedicle and its resultant membrane potential. The idea finds some support because when the hemi-channels are blocked with carbenoxolone (a specific gap junction blocker), the feedback signal in the cone is eliminated (Kamermans et al., 2001).

Modulation of horizontal cell physiology

The properties of horizontal cells can be modulated by a variety of chemicals that are released by retinal cells during

changing conditions of illumination. These chemicals are generally referred to as neuromodulators. They are believed to alter modes of information processing to adjust retinal function to any new state of adaptation. These chemicals can reach the horizontal cells either via direct synaptic interactions or via volume transmission. In the latter mode, intercellular communication is mediated by a chemical that is released into the extracellular space and reaches its targets by simple diffusion. The most extensively studied neuromodulator is dopamine, but in recent years nitric oxide and retinoic acid have also been studied. In this section, some effects of these neuromodulators on vertebrate horizontal cells will be discussed.

DOPAMINE Dopamine-containing neurons reside in the amacrine cell layer of the retina in most species. In some species (e.g., fish, where they were first demonstrated), dopaminergic cells are interplexiform cells (IPCs) that send long processes to the outer plexiform layer to make synaptic contact with horizontal cells at synapses. In other species (e.g., turtle), the dopaminergic cells are amacrine cells; therefore, dopamine has to reach the horizontal cells by volume diffusion through the inner nuclear layer. The action of dopamine on vertebrate horizontal cells has been extensively studied (see reviews in Dowling, 1991; Witkovsky and Dearry, 1991).

In cold-blooded vertebrates, dopamine has several influences on horizontal cells. (1) The size of the receptive field is reduced, as shown by dye coupling and by electrophysiological determination of receptive field size (Dong and McReynolds, 1991; Mangel and Dowling, 1985; Negishi and Drujan, 1979; Perlman and Ammermüller, 1994; Piccolino

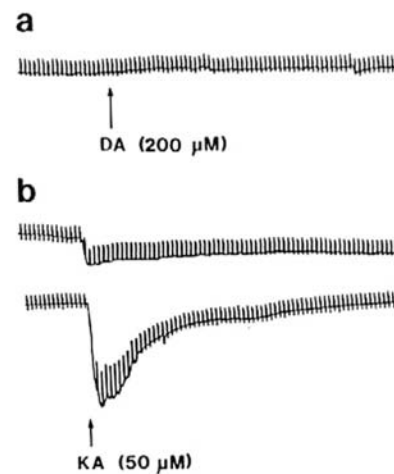
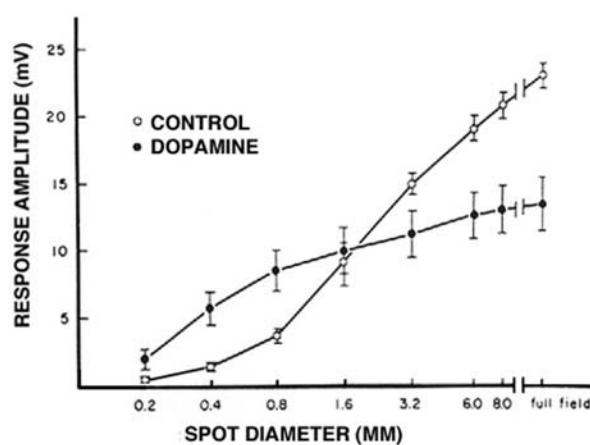


FIGURE 24.16. The effects of dopamine on the physiology of fish horizontal cells. Photoresponses were recorded from a horizontal cell in the intact retina using light stimuli of fixed intensity but different diameter, under control conditions and after exposure to dopamine (*left*) (Mangel and Dowling, 1985). Voltage-clamp

recordings from isolated white perch horizontal cells (*right*) indicate dopamine-induced augmentation of kainate (KA)-induced current (compare lower and upper traces in *B*). Dopamine (DA) by itself (*A*) did not elicit any current (Knapp and Dowling, 1987).

et al., 1984; Teranishi et al., 1983). This effect reflects a reduction of gap junction conductance induced by activation of adenylate cyclase by dopamine at D1-type receptors (see Dowling, 1991 for review). (2) Dopamine induces the formation of spinules in fish horizontal cells in a manner similar to that seen with bright light background illumination (Djamgoz et al., 1989; Weiler et al., 1988). (3) In some species, the interaction between L-glutamate and its receptors on the horizontal cell membrane is modulated by dopamine so that the amplitude of the photoresponse is reduced to any given light stimulus (Mangel and Dowling, 1985; Yang et al., 1988). However, it is not clear that this happens in the turtle retina (Perlman and Ammermüller, 1994; Piccolino et al., 1984). (4) Dopamine changes the balance between rod and cone inputs to horizontal cells in *Xenopus* retina to augment the rod contribution in the dark-adapted state and the cone contribution in the light-adapted state (Witkovsky et al., 1989).

Figure 24.16 demonstrates the effects of dopamine on horizontal cells in the intact fish retina (*left*) in contrast to horizontal cells that were isolated from the fish retina (*right*). Light stimuli of constant intensity but different diameters were used to study the effects of dopamine on the receptive field size in the intact retina (Fig. 24.16, *left*). With small spot stimuli, the photoresponses that were recorded during superfusion with dopamine solutions were larger in amplitude than those recorded with the same stimuli under control conditions. The increase in the response to spot stimuli indicates less shunting by neighboring nonilluminated horizontal cells and is consistent with the notion that dopamine uncouples horizontal cells from the network (Lasater and Dowling, 1985). Another effect of dopamine is a reduction in the maximum amplitude of the photoresponses elicited

by light stimuli that illuminate the entire receptive field of the cell (Fig. 24.16, *left*). This was explained by the observation that dopamine modulated the interaction between L-glutamate and its receptors on the horizontal cell membrane itself (Knapp and Dowling, 1987). In Figure 24.16 (*right*), the effect of dopamine on the inward current elicited by a given dose of kainic acid is shown. Dopamine by itself evoked no current in the horizontal cell (Fig. 24.16*A*, *right*), but it significantly augmented the kainate-induced current (Fig. 24.16*B*, *right*). This was interpreted to mean that dopamine increased the affinity of the glutamate-gated channels on the horizontal cell membrane to its agonist. In the intact retina, the photoresponses of horizontal cells reflect the unbinding of glutamate from its receptors. If dopamine increases the affinity of glutamate for its receptors on the horizontal cell membrane, then unbinding during a light stimulus will be at a slower rate and the photoresponse is expected to be of smaller amplitude.

In the mammalian retina a similar but lesser magnitude of uncoupling of horizontal cells due to dopamine has been reported (Bloomfield et al., 1995; Mills and Massey, 1994). Similar to the findings in cold-blooded vertebrates, horizontal cell uncoupling in the mammalian retina is mediated by activation of cyclic AMP synthesis through the interaction of dopamine with D1-type receptors (Hampson et al., 1994).

NITRIC OXIDE Involvement of nitric oxide in physiological mechanisms is indicated by the presence of cells containing the enzyme nitric oxide synthase (NOS), which synthesizes nitric oxide from L-arginine (Nathan, 1992). Immunoreactivity to NOS isoforms or demonstration of NADPH-diaphorase activity has been seen in some populations of cells in every retina studied (Koistinaho and Sagar, 1995). In

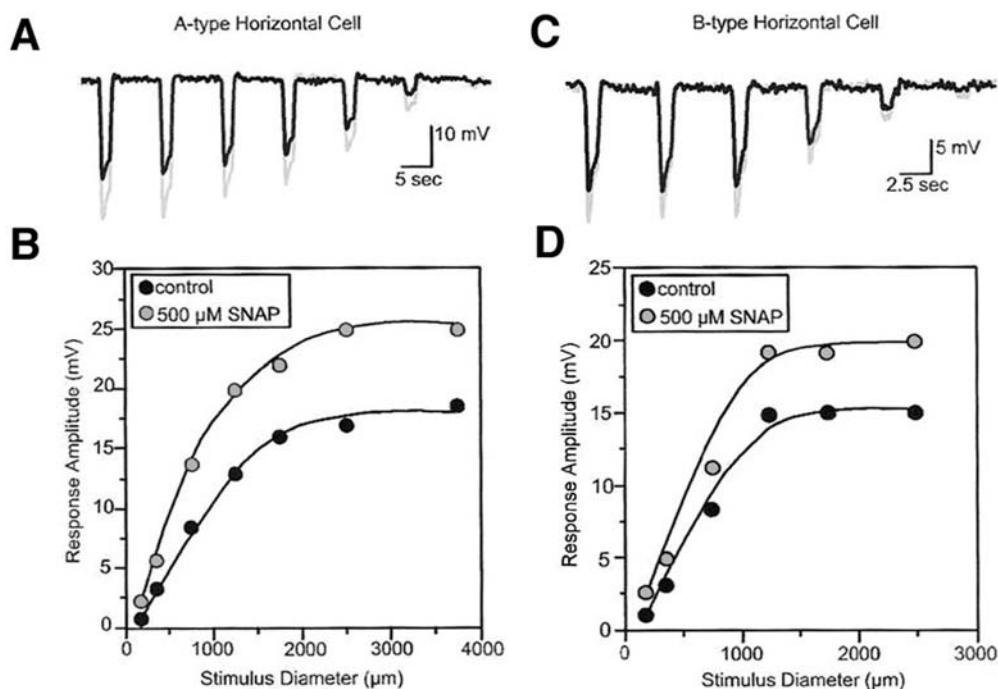


FIGURE 24.17. The effects of nitric oxide (NO) on the physiology of horizontal cells in the rabbit retina. The effects of NO were tested by adding SNAP, an NO donor, and testing its effects on the photoresponses elicited by light stimuli of fixed intensity but different diameters (black traces, control; gray traces, SNAP). The

relationship between response amplitude and stimulus diameter indicates that NO augments the photoresponses of the horizontal cell and reduces its receptive field size (Xin and Bloomfield, 2000).

all species NOS occurs in amacrine cells, but reports of NOS in photoreceptors, horizontal cells, bipolar cells, and Müller cells have also been published. In fish retinas, evidence for NOS in horizontal cells has been demonstrated by immunostaining and NADPH diaphorase histochemistry (Liepe et al., 1994; Ostholm et al., 1994; Weiler and Kewitz, 1993). In the turtle retina, n- and e-isoforms of NOS have been found in horizontal cell processes at the photoreceptor ribbon synapses and in the inner segments of the photoreceptors, in amacrine cells and in Müller cells (Blute et al., 1997; Cuenca et al., 2000; Haverkamp and Eldred, 1998; Haverkamp et al., 1999). In the rabbit retina, NADPH diaphorase activity in horizontal cells has been shown to depend on the state of adaptation and the activity of glutamatergic pathways. It is increased in the dark-adapted state (Zemel et al., 1996) or by activation of AMPA/KA type receptors (Zemel et al., 2001).

Regardless of the exact cellular source of nitric oxide, this molecule exerts profound effects on the physiology of horizontal cells. Raising nitric oxide level by either exogenous application (nitric oxide donors) or by addition of L-arginine reduces the size of the horizontal cell receptive field (Miyachi et al., 1990; Pottek et al., 1997; Xin and Bloomfield, 2000). This effect reflects direct action of nitric oxide on the gap junctions between horizontal cells. It is thought to be mediated through cGMP-dependent protein kinase pathways

(DeVries and Schwartz, 1989; Lu and McMahon, 1997; Xin and Bloomfield, 2000).

Figure 24.17 shows the effects of nitric oxide on A-type (A and B) and B-type (C and D) horizontal cells in the rabbit retina. The photoresponses were elicited by a series of light stimuli of fixed intensity and different radii, in control conditions and during exposure to SNAP (a nitric oxide donor). For every light stimulus, the photoresponse is larger during SNAP application (gray responses). This is better illustrated in Figure 24.17B and D, where the peak amplitudes of the photoresponses are plotted as a function of stimulus diameter. SNAP clearly causes augmentation of the photoresponses to large-diameter stimuli. Thus, nitric oxide acts in the distal rabbit retina to augment the photoresponses of the horizontal cells and to reduce the receptive field size (Xin and Bloomfield, 2000).

A similar augmentation of horizontal cell responses by nitric oxide has been seen in L-type horizontal cells of carp (Pottek et al., 1997) and turtle retinas (Levy, 2001). Nitric oxide's effect can reflect an action directly on the phototransduction process in the outer segments of the photoreceptors (Levy, 2001; Tsuyama et al., 1993) and/or on neurotransmitter release from the photoreceptors (Kurenny et al., 1994). Furthermore, nitric oxide can modulate the interaction between L-glutamate and its receptors on the horizontal cell membrane (McMahon and Ponomareva,

1996) and thus, can alter the responsivity of horizontal cells independently of effects on the photoreceptors (Levy, 2001).

Nitric oxide, like dopamine, also induces cone contraction and horizontal cell spinule formation (Haamedi and Djamgoz, 2002).

RETINOIC ACID Retinoids are of great importance in the eye, having roles in both the photopigment cycle and in development of the eye. Retinoic acid is produced in the pigment epithelium as a side effect of the rhodopsin transduction process in bright illumination. In the form of a retinaldehyde, it is part of the rhodopsin molecule, the visual pigment of the vertebrate photoreceptors (Dowling and Wald, 1960; Wald, 1935); in the form of retinoic acid, it activates transcription factors that are important in the development of the eye (Dräger et al., 2001; Wagner et al., 1992). Most recently a third role for retinoic acid has been proposed, that of a neuromodulator linked to background adaptation affecting horizontal cells in particular (Pottek and Weiler, 2000; Weiler et al., 2001; Weiler et al., 1998).

Retinoic acid induces synaptic plasticity at the terminal dendrites of horizontal cells and promotes the growth of spinules in a pattern similar to that induced by background lights (Pottek and Weiler, 2000; Weiler et al., 1998). It exerts a pronounced effect on the electrical coupling between horizontal cells in mammalian and nonmammalian retinas and reduces the receptive fields of the horizontal cells (Weiler et al., 2001; Weiler and Vaney, 1999), as shown in Figure 24.18. Adding retinoic acid to retinal preparations of carp, rabbit, and mouse reduces the conductance of the gap junctions between neighboring horizontal cells, thus reducing the degree of dye coupling in a manner similar to that seen during background illumination (Fig. 24.18A). Intracellular recordings in horizontal cells also show that retinoic acid produces effects similar to those of light adaptation. The amplitudes of the horizontal cell photoresponses to full-field stimuli are increased by retinoic acid (Fig. 24.18B). The responses to stimulation with light annuli are reduced by retinoic acid, and those to spot illumination are increased (Fig. 24.18C). Thus, retinoic acid, like dopamine and nitric oxide, seems to modulate the physiological properties of vertebrate horizontal cells in order to adjust their function during background illumination.

Functional roles

The major functional roles of horizontal cells in the vertebrate retina are (1) creating spatially opponent receptive field organization for second- and third-order neurons in the retina, and (2) modulating the photoreceptor signal under different lighting conditions, a form of neuronal adaptation at the first synaptic level in the retina.

SPATIAL SURROUND ORGANIZATION Bipolar cells are the first visual neurons exhibiting spatial organization of their receptive fields. These cells respond with opposite polarity to light stimuli illuminating either the center or the surround (Dowling, 1970; Werblin and Dowling, 1969). Figure 24.19A shows a cartoon of the original model of photoreceptor and horizontal cell interactions with the bipolar cells that underlie spatial opponent organization of the latter (Werblin and Dowling, 1969). Specifically, direct input from photoreceptors is believed to contribute to the central response of bipolar cells, and the horizontal cells form the surround component. In experiments where horizontal cell membrane potentials are directly polarized by injections of current through an intracellular microelectrode, ganglion cell discharges characteristic of “surround responses” or “large-spot responses” are evoked (Mangel, 1991; Naka, 1971). This current-evoked response could reflect the negative feedback pathway from horizontal cells to cones and/or direct input from the horizontal cells to bipolar cells. Evidence for both possibilities has been reported. The glutamate agonist 2-amino-4-phosphonobutyrate (APB), selective for transmission between cones and ON-center bipolar cells, blocks the light responses of ON-center ganglion cells and also the current-evoked responses in ganglion cells (Mangel, 1991). Moreover, submillimolar concentrations of cobalt ions selectively block the feedback pathway from horizontal cells to cone photoreceptors, resulting in the absence of surround components in ganglion cells in proximal retina (Vigh and Witkovsky, 1999).

Horizontal cell feedback is not necessarily the only way of influencing bipolar cell receptive field architecture. Horizontal cells can impinge directly on bipolar cells, feeding visual information forward to these second-order retinal neurons. Direct horizontal to bipolar synapses have been described in several mammalian and nonmammalian species’ retinas (Dowling, 1970; Fisher and Boycott, 1974; Kolb and Jones, 1984). In one study using APB to block synaptic transmission from photoreceptors to ON-center bipolar cells, the light stimulus induced a hyperpolarizing response in the bipolar cell, thus supporting the idea of a direct excitatory input from horizontal cells (Yang and Wu, 1991b). The best candidate for the feedforward neurotransmitter is GABA (Wu, 1986).

There are exceptions to every model, though. Not all bipolar cells exhibit spatial antagonism. The ON-bipolar for the rod system and some OFF-center cone bipolar cells in cat retina appear to lack surrounds (Nelson and Kolb, 1983). Regardless of the exact neuronal pathway, whether feedforward or feedback, it is generally accepted that horizontal cells play an important role in spatial information processing in retinal neurons after the photoreceptors (Ammermüller and Kolb, 1995, 1996; Hare and Owen, 1990; Kaneko, 1970; Lasansky, 1978; Marchiafava and

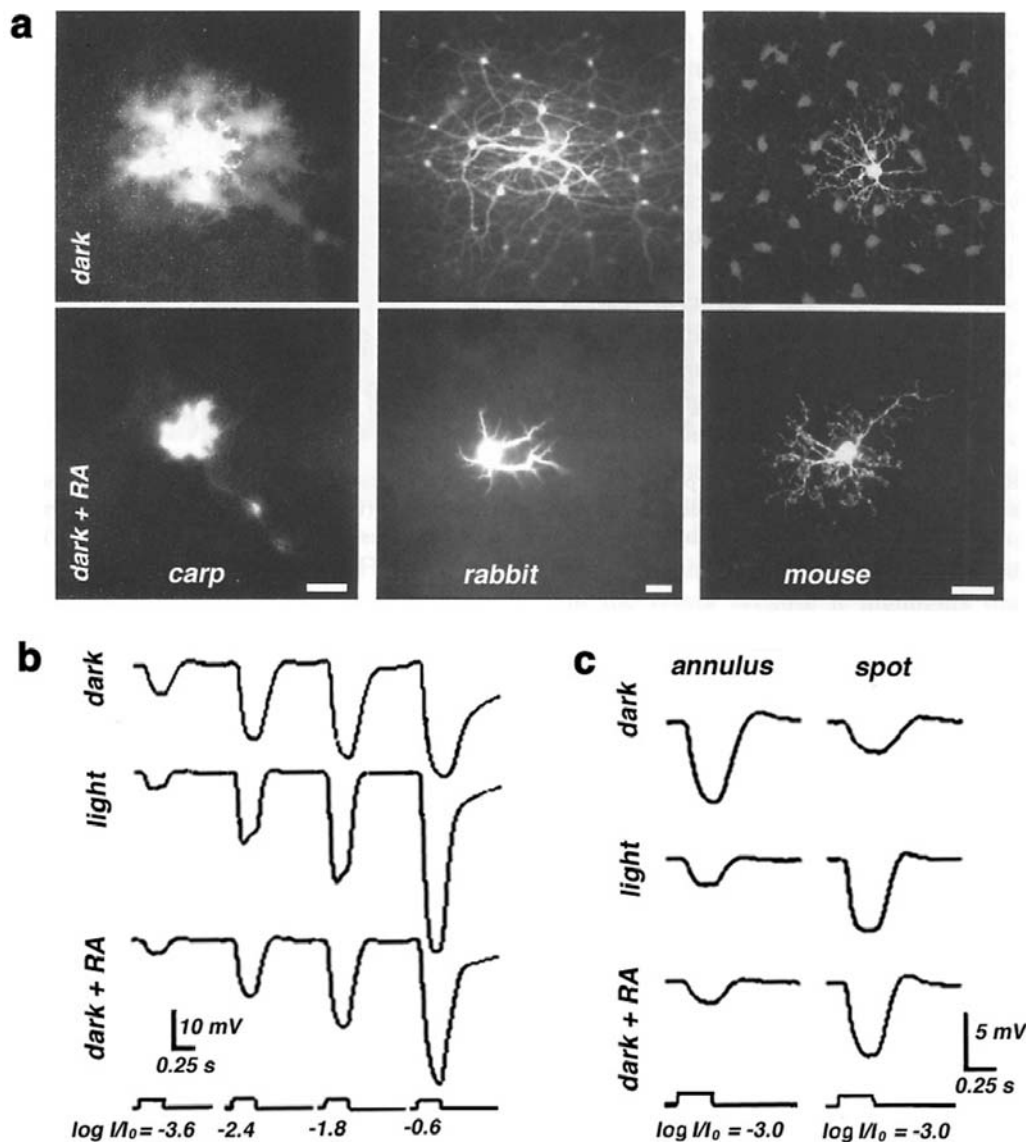


FIGURE 24.18. The effects of retinoic acid on the physiology of horizontal cells in different species. *a*, In carp, rabbit, and mouse retinas, retinoic acid added in the dark-adapted state reduces the extent of dye coupling. *b*, Retinoic acid added in the dark-adapted state exerts effects similar to those of light adaptation by aug-

menting the photoresponses of fish horizontal cells. *c*, Retinoic acid, like background illumination, reduces the response to an annulus stimulus and augments that to a spot stimulus in fish horizontal cells (Weiler et al., 2001).

Weiler, 1980; McReynolds and Lukasiewicz, 1989; Naka, 1971, 1976; Saito et al., 1979, 1981; Werblin and Dowling, 1969).

Horizontal cell feedback to bipolar cells probably also serves to generate color opponency in bipolar cells and therefore in ganglion cells. Figure 24.19*B* summarizes, in cartoon form, the manner in which single and double opponent bipolar cell receptive fields could be formed in the fish retina according to the cascade model of color opponency (Kamermans and Spekrijse, 1995; Stell, 1976; Stell and Lightfoot, 1975). The opponent surround of the single opponent cell is easy to model (Fig. 24.19*B*, *top*). This bipolar

cell receives an excitatory input from red cones only and therefore is defined as a red OFF-center cell. The negative feedback from the monophasic and biphasic horizontal cells oppose each other in the red range of the spectrum and strengthen each other in the green and blue range. If the degree of feedback from both horizontal cells is the same, then the bipolar surround will be of an ON pattern with spectral sensitivity highest in the green range of the spectrum. If the feedback from the monophasic horizontal cell is weaker compared to that of the biphasic horizontal cell, then the spectral response of the bipolar cell to surround illumination will be hyperpolarizing for red light and depolar-

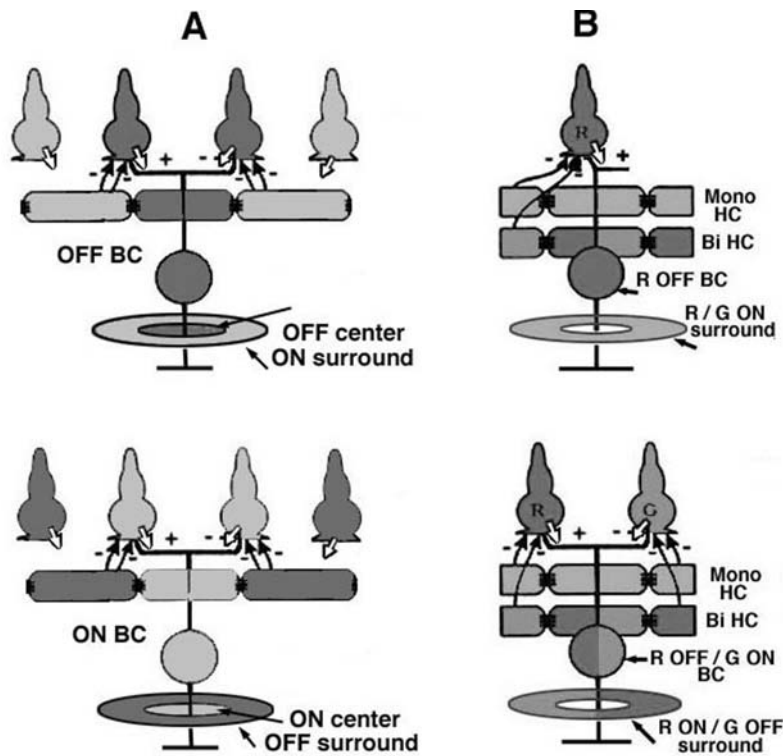


FIGURE 24.19. Cartoon to show how the horizontal cell lateral inhibition on the cones helps to form the concentrically organized receptive fields of bipolar cells. *A*, A simple feedback from monophasic (L-type) horizontal cells onto cones can affect the hyperpolarizing OFF-center or depolarizing ON-center bipolar cells to provide the opponent ON- or OFF-surround, respectively. *B*, Possible models for the generation of color-opponent responses in bipolar cells are shown (Kamermans and Spekreijse, 1995). The

cartoon illustrates the manner in which biphasic (Bi) chromaticity horizontal cells and monophasic (Mono) luminosity horizontal cells can feedback through a single cone type to give the opponent color surround to a red OFF bipolar cell. In the lower cartoon, red cones provide excitatory input and green cone inhibitory input to produce a red OFF, green ON center double opponent bipolar cell. The red ON and green OFF surround is added by the chromatic (Bi) and luminosity (mono) horizontal cells.

izing for green light ($R-G^+$) (Kamermans and Spekreijse, 1995).

The double opponent bipolar cell (Fig. 24.19*B*, bottom) responds in its center with hyperpolarization to red stimuli and with depolarization to green and blue stimuli. This central color opponency is generated by different types of inputs from different types of cones: excitatory input from the red cones and inhibitory input from the green cones. If the monophasic and biphasic horizontal cells feedback onto both spectral types of cones (Kamermans and Spekreijse, 1995), the feedback through the green cones would work against the feedback through the red cones because of the different synaptic interactions. When the feedback pathways from each horizontal cell onto the red and green cones differ, color opponency can be generated by the feedback pathways. However, when the strength of the feedback from each horizontal cell to both types of cones is equal, the surround response can be achromatic. Under these conditions, color opponency in the surround of the bipolar cell can occur only through direct input from one or both horizontal cells to the bipolar cell itself.

PHOTORECEPTOR MODULATION UNDER DIFFERENT LIGHTING CONDITIONS Calcium entry into synaptic structures induces the release of neurotransmitter by promoting fusion of neurotransmitter-laden synaptic vesicles with the presynaptic membrane. Calcium entry occurs through specialized membrane channels regulated by both voltage and second messengers. In a simple model of horizontal cell modulation of gain at cone synapses (Kamermans et al., 2001; Verweij et al., 1996), depolarized, dark-adapted horizontal cells produce an electrical gradient in the extracellular space that reduces the rate of calcium entry into cone terminals. This, in turn, reduces the rate of neurotransmitter release. Background illumination, which hyperpolarizes horizontal cells, alters the extracellular currents, thereby shifting the voltage dependency of the calcium channels in the cone terminals and increasing the rate of transmitter release for a given potential of the cone.

This modulation also serves to complete the negative feedback loop between horizontal cells and cones, which regulates the horizontal cell membrane potential. When horizontal cells become depolarized, calcium influx into the cone

synapse is reduced, as is transmitter efflux from the synapse. The effect sends horizontal cell membrane potential in a hyperpolarized direction. The horizontal cell membrane potential becomes controlled by the network, rather than by factors intrinsic to the cell. Interestingly, bipolar cells perceive this negative feedback effect and synaptic gain modulation as a further spatial opponency effect. This is true for both ON- and OFF-center bipolar cells. The increase in transmitter release caused by horizontal cell hyperpolarization is just the reverse of the decrease in transmitter release that occurs as cones are hyperpolarized by small spots of light.

When horizontal cells are hyperpolarized by wide-field, bright light stimuli, cone signals evoked in second-order neurons both increase in amplitude and become quicker in time course. Such effects are commonly observed when small spots are flashed in the presence of large background fields (Chappell et al., 1985). Similarly, under dark conditions the horizontal cells can increase the sensitivity of both the rod and cone pathways by switching to a large receptive field organization and response characteristics of the scotopic range.

Horizontal cell modulatory effects on the cones can be utilized for interpretation of electrophysiological tests at the clinical level in human patients. A test known as suppressive rod-cone interaction (SRCI) is often recorded in clinical electroretinograms (Goldberg et al., 1983). In the SRCI, large, dim green stimuli, seen only by rods, cause observers to perceive focal, red stimuli, seen only by cones, as being brighter. Analogous physiological effects involving rod and cone signals occur in horizontal cells and bipolar cells themselves (Frumkes and Eysteinnsson, 1987; Nelson et al., 1990; Pflug et al., 1990). Flickering cone signals are evoked in cat horizontal cells by flickering red stimuli of various sizes. When the stimuli are small, flicker amplitudes can be increased by superimposing steady blue backgrounds, which selectively excite rods. Thus the amplitude of the cone flicker signals is modulated by wide-field, rod-driven horizontal cell stimulation, probably through increased gain at horizontal cell to cone synapses.

In the 50 years since Svaetichin first described S-potentials in the vertebrate retina, we have made significant progress in our understanding of the many ways that horizontal cells can influence the kinetics, plasticity, and spatial organization of the photoreceptor response. We have discussed most of these ways in previous sections of this chapter. They include rod-cone balance changes, differences in the horizontal cell's receptive field, often under neuro-modulatory control by dopamine and other neuroactive agents and biochemical second-messenger mechanisms. The horizontal cells are essential elements in visual information processing and play a crucial role in the genesis of the recep-

tive fields of inner retinal cells. Finally, the horizontal cells form an important link between inner and outer retina because this cell type is almost certainly under the influence of centrifugal input from within the retina and even from the brain itself.

Acknowledgements

We dedicate this chapter to the following scientists who have been very influential on us in the field of horizontal cell physiology. They include Elliot Simon, Mike Fuortes, Henry Wagner, Matthew Alpern, and Ken Naka. We thank other colleagues for their valuable advice and the National Institutes of Health (USA), Research to Prevent Blindness Organization (USA), and the Israel Science Foundation for continued support over the years.

REFERENCES

- Ahnelt, P. K., E. Fernández, O. Martínez, J. A. Bolea, and A. Kübber-Heiss, 2000. Irregular S-cone mosaics in felid retinas. Spatial interaction with axonless horizontal cells, revealed by cross correlation, *J. Opt. Soc. Am. A*, 17:580–588.
- Ahnelt, P., and H. Kolb, 1994a. Horizontal cells and cone photoreceptors in primate retina: a Golgi-light microscope study of spectral connectivity, *J. Comp. Neurol.*, 343:387–405.
- Ahnelt, P., and H. Kolb, 1994b. Horizontal cells and cone photoreceptors in human retina: a Golgi-electron microscopic study of spectral connectivity, *J. Comp. Neurol.*, 343:406–427.
- Ammermüller, J., A. Itzhaki, R. Weiler, and I. Perlman, 1998. UV-sensitive input to horizontal cells in the turtle retina, *Eur. J. Neurosci.*, 10:1544–1552.
- Ammermüller, J., and H. Kolb, 1995. The organization of the turtle inner retina. I. The organization of ON- and OFF-center pathways, *J. Comp. Neurol.*, 358:1–34.
- Ammermüller, J., and H. Kolb, 1996. Functional architecture of the turtle inner retina, *Prog. Ret. Eye Res.*, 15:393–433.
- Asi, H., and I. Perlman, 1998. Neural interactions between cone photoreceptors and horizontal cells in the turtle (*Mauremys caspica*) retina, *Vis. Neurosci.*, 15:1–13.
- Baylor, D. A., M. G. F. Fuortes, and P. M. O'Bryan, 1971. Receptive fields of the cones in the retina of the turtle, *J. Physiol. (Lond.)*, 214:265–294.
- Blanco, R., and P. de la Villa, 1999. Ionotropic glutamate receptors in isolated horizontal cells of the rabbit retina, *Eur. J. Neurosci.*, 11:867–873.
- Bloomfield, S. A., and J. E. Dowling, 1985. Roles of aspartate and glutamate in synaptic transmission in rabbit retina. I. Outer plexiform layer, *J. Neurophysiol.*, 53:699–713.
- Bloomfield, S. A., and R. F. Miller, 1982. A physiological and morphological study of the horizontal cell types of the rabbit retina, *J. Comp. Neurol.*, 208:288–303.
- Bloomfield, S. A., D. Xin, and S. E. Persky, 1995. A comparison of receptive field and tracer coupling size of horizontal cells in the rabbit retina, *Vis. Neurosci.*, 12:985–999.
- Blute, T. A., B. Mayer, and W. D. Eldred, 1997. Immunocytochemical and histochemical localization of nitric oxide synthase in the turtle retina, *Vis. Neurosci.*, 14:717–729.

- Borenstein, O., 1999. Lateral spread of electrical signals in the horizontal cells layer of the turtle retina. Ph.D. thesis, Technion-Israel Institute of Technology, Haifa, Israel.
- Boycott, B. B., and J. E. Dowling, 1969. Organization of the primate retina: light microscopy, *Phil. Trans. R. Soc. B*, 255: 109–184.
- Boycott, B. B., L. Peichl, and H. Wässle, 1978. Morphological types of horizontal cell in the retina of the domestic cat, *Proc. R. Soc. (Lond.) B*, 203:229–245.
- Burkhardt, D. A., 1977. Responses and receptive-field organization of cones in perch retina, *J. Neurophysiol.*, 40:53–62.
- Byzov, A. L., and T. M. Shura-Bura, 1983. Spread of potentials along the network of horizontal cells in the retina of the turtle, *Vis. Res.*, 23:389–397.
- Byzov, A. L., and Y. A. Trifonov, 1968. The response to electrical stimulation of horizontal cells in the carp retina, *Vis. Res.*, 8:817–822.
- Cajal, S. R., 1892. *The Structure of the Retina* (S. A. Thorpe and M. Glickstein, transl.), Springfield, IL: Thomas, 1972.
- Cervetto, L., and E. F. MacNichol, 1972. Inactivation of horizontal cells in turtle retina by glutamate and aspartate, *Science*, 178:767–768.
- Cervetto, L., and M. Piccolino, 1974. Synaptic transmission between photoreceptors and horizontal cells in the turtle retina, *Science*, 183:417–419.
- Chappell, R. L., K.-I. Naka, and M. Sakuranaga, 1985. Dynamics of turtle horizontal cell response, *J. Gen. Physiol.*, 86:423–453.
- Cuenca, N., S. Haverkamp, and H. Kolb, 2000. Choline acetyltransferase and nitric oxide synthase are found in horizontal cells of the turtle retina, *Brain Res.*, 878:228–239.
- Dacey, D. M., B. B. Lee, D. K. Stafford, J. Pokorny, and V. C. Smith, 1996. Horizontal cells of the primate retina: cone specificity without spectral opponency, *Science*, 271:656–659.
- Dacheux, R. F., and E. Raviola, 1982. Horizontal cells in the retina of the rabbit, *J. Neurosci.*, 2:1486–1493.
- Dacheux, R. F., and E. Raviola, 1990. Physiology of HI horizontal cells in the primate retina, *Proc. R. Soc. Lond. B*, 239:203–221.
- DeJuan, J., and M. Garcia, 2001. Spinules and nematosomes in retinal horizontal cells: a thorny issue, in *Concepts and Challenges in Retinal Biology: A Tribute to John E. Dowling* (H. Kolb, H. Ripps, and S. Wu, eds.), Amsterdam: Elsevier, pp. 519–537.
- DeVries, S. H., and E. A. Schwartz, 1989. Modulation of an electrical synapse between solitary pairs of catfish horizontal cells by dopamine and second messengers, *J. Physiol. (Lond.)*, 414:351–375.
- Djamgoz, M. B. A., M. Kirsch, and H.-J. Wagner, 1989. Haloperidol suppresses light-induced spinule formation and biphasic responses of horizontal cells in fish (roach) retina, *Neurosci. Lett.*, 107:200–204.
- Dong, C.-J., and J. S. McReynolds, 1991. The relationship between light, dopamine and horizontal cell coupling in the mudpuppy retina, *J. Physiol. (Lond.)*, 440:291–309.
- Dowling, J. E., 1970. Organization of vertebrate retinas, *Invest. Ophthalmol.*, 9:655–680.
- Dowling, J. E., 1991. Retina neuromodulation: the role of dopamine, *Vis. Neurosci.*, 7:87–97.
- Dowling, J. E., and H. Ripps, 1973. Effects of magnesium on horizontal cell activity in the skate retina, *Nature*, 242:101–103.
- Dowling, J. E., and G. Wald, 1960. The biological function of vitamin A acid, *Proc. Natl. Acad. Sci. USA.*, 46:587–608.
- Downing, J. E. G., and M. B. A. Djamgoz, 1989. Quantitative analysis of cone photoreceptor-horizontal cell connectivity patterns in the retina of a cyprinid fish: electron microscopy of functionally identified and HRP-labelled horizontal cells, *J. Comp. Neurol.*, 289:537–553.
- Dräger, U. C., H. Li, E. Wagner, and P. McCaffery, 2001. Retinoic acid synthesis and breakdown in the developing mouse retina, *Prog. Brain Res.*, 131:579–587.
- Eliasof, S., and C. E. Jahr, 1997. Rapid AMPA receptor desensitization in catfish cone horizontal cells, *Vis. Neurosci.*, 14:13–18.
- Eliasof, S., J. L. Arriza, B. H. Leighton, S. G. Amara, and M. P. Kavanaugh, 1998. Localization and function of five glutamate transporters cloned from the salamander retina, *Vis. Res.*, 38: 1443–1454.
- Fisher, S. K., and B. B. Boycott, 1974. Synaptic connexions made by horizontal cells within the outer plexiform layer of the retina of the cat and the rabbit, *Proc. R. Soc. Lond. B*, 186:317–331.
- Frumkes, T. E., and T. Eysteinnsson, 1987. Suppressive rod-cone interaction in distal vertebrate retina: intracellular records from *Xenopus* and *Necturus*, *J. Neurophysiol.*, 57:1361–1382.
- Fuortes, M. G. F., E. A. Schwartz, and E. J. Simon, 1973. Colour dependence of cone responses in the turtle retina, *J. Physiol. (Lond.)*, 234:199–216.
- Fuortes, M. G. F., and E. J. Simon, 1974. Interactions leading to horizontal cell responses in the turtle retina, *J. Physiol. (Lond.)*, 240:177–199.
- Gallego, A., 1986. Comparative studies on horizontal cells and a note on microglial cells, *Prog. Ret. Res.*, 5:165–206.
- Golard, A. G., P. Witkovsky, and D. Tranchina, 1992. Membrane currents of horizontal cells isolated from turtle retina, *J. Neurophysiol.*, 68:351–361.
- Goldberg, S. H., T. E. Frumkes, and R. W. Nygaard, 1983. Inhibitory influence of unstimulated rods in the human retina: evidence provided by examining cone flicker, *Science*, 221: 180–182.
- Goldsmith, T. H., 1980. Hummingbirds see near ultraviolet light, *Science*, 207:786–788.
- Gottesman, J., and D. A. Burkhardt, 1987. Response properties of C-type horizontal cells in the retina of the bowfin, *Vis. Res.*, 27:179–189.
- Haamedi, S. N., and M. B. A. Djamgoz, 2002. Dopamine and nitric oxide control both flickering and steady-light-induced cone contraction and horizontal cell spinule formation in the teleost (carp) retina: serial interaction of dopamine and nitric oxide, *J. Comp. Neurol.*, 449:120–128.
- Hals, G., B. N. Christensen, T. O'Dell, M. Christensen, and R. Shingai, 1986. Voltage-clamp analysis of currents produced by glutamate and some glutamate analogues on horizontal cells isolated from the catfish retina, *J. Neurophysiol.*, 56:19–31.
- Hampson, E. C. G. M., R. Weiler, and D. I. Vaney, 1994. pH-gated dopaminergic modulation of horizontal cell gap junctions in mammalian retina, *Proc. Royal Soc. Lond. B*, 255:67–72.
- Hare, W. A., and W. G. Owen, 1990. Spatial organization of the bipolar cells receptive field in the retina of the tiger salamander, *J. Physiol. (Lond.)*, 421:223–245.
- Haverkamp, S., and W. D. Eldred, 1998. Localization of nNOS in photoreceptor, bipolar and horizontal cells in turtle and rat retinas, *Neuroreport*, 9:2231–2235.
- Haverkamp, S., H. Kolb, and N. Cuenca, 1999. Endothelial nitric oxide synthase (eNOS) is localized to Müller cells in all vertebrate retinas, *Vis. Res.*, 39:2299–2303.
- Hughes, A., S. Saszik, J. Billota, P. J. Demarco, Jr., and W. F. Patterson, II, 1998. Cone contributions to the photopic spectral sensitivity of the zebrafish ERG, *Vis. Neurosci.*, 15:1029–1037.

- Itzhaki, A., S. Malik, and I. Perlman, 1992. The spectral properties of short wavelength (blue) cones in the turtle retina, *Vis. Neurosci.*, 9:235–241.
- Itzhaki, A., and I. Perlman, 1984. Light adaptation in luminosity horizontal cells in the turtle retina: role of cellular coupling, *Vis. Res.*, 24:1119–1126.
- Janssen-Bienhold, U., K. Schultz, W. Hoppenstedt, and R. Weiler, 2001. Molecular diversity of gap junctions between horizontal cells, in *Concepts and Challenges in Retinal Biology: A Tribute to John E. Dowling* (H. Kolb, H. Ripps, and S. Wu, eds.), Amsterdam: Elsevier, pp. 93–107.
- Kamermans, M., I. Fahrenfort, K. Schultz, U. Janssen-Bienhold, T. Sjoerdsma, and R. Weiler, 2001. Hemichannel-mediated inhibition in the outer retina, *Science*, 292:1178–1180.
- Kamermans, M., J. Haak, J. B. A. Habraken, and H. Spekrijse, 1996. The size of the horizontal cell receptive fields adapts to the stimulus in the light adapted goldfish retina, *Vis. Res.*, 36:4105–4119.
- Kamermans, M., and H. Spekrijse, 1995. Spectral behavior of cone-driven horizontal cells in teleost retina, *Prog. Ret. Eye Res.*, 14:313–360.
- Kamermans, M., and F. Werblin, 1992. GABA-mediated positive autofeedback loop controls horizontal cell kinetics in tiger salamander, *J. Neurosci.*, 12:2451–2463.
- Kaneko, A., 1970. Physiological and morphological identification of horizontal, bipolar and amacrine cells in goldfish retina, *J. Physiol. (Lond.)*, 207:623–633.
- Kaneko, A., 1971. Electrical connexions between horizontal cells in the dogfish retina, *J. Physiol. (Lond.)*, 213:95–105.
- Kaneko, A., and H. Shimazaki, 1975. Effects of external ions on the synaptic transmission from photoreceptors to horizontal cells in the carp retina, *J. Physiol. (Lond.)*, 252:509–522.
- Kato, S., 1979. C-type horizontal cell responses to annular stimuli, *Exp. Eye Res.*, 28:627–639.
- Kirsch, M., M. B. A. Djamgoz, and H.-J. Wagner, 1990. Correlation of spinule dynamics and plasticity of the horizontal cell spectral response in cyprinid fish retina: quantitative analysis, *Cell Tiss. Res.*, 260:123–130.
- Knapp, A. G., and J. E. Dowling, 1987. Dopamine enhances excitatory amino acid-gated conductances in cultured retinal horizontal cells, *Nature*, 325:437–439.
- Koistinaho, J., and S. M. Sagar, 1995. NADPH-diaphorase-reactive neurons in the retina, *Prog. Ret. Eye Res.*, 15:69–87.
- Kolb, H., 1970. Organization of the outer plexiform layer of the primate retina: electron microscopy of Golgi-impregnated cells, *Phil. Trans. R. Soc. (Lond.): B*, 258:261–283.
- Kolb, H., 1977. The organization of the outer plexiform layer in the retina of the cat: electron microscopic observations, *J. Neurocytol.*, 6:131–153.
- Kolb, H., and J. Jones, 1984. Synaptic organization of the outer plexiform layer of the turtle retina: an electron microscope study of serial sections, *J. Neurocytol.*, 13:567–591.
- Kolb, H., and L. E. Lipetz, 1991. The anatomical basis for colour vision in the vertebrate retina, in *Vision and Visual Dysfunction*, vol. 6 *The Perception of Colour* (P. Gouras, ed.), London: Macmillan Press Ltd., pp. 128–145.
- Kurenny, D. E., L. L. Moroz, R. W. Turner, K. A. Sharkey, and S. Barnes, 1994. Modulation of ion channels in rod photoreceptors by nitric oxide, *Neuron*, 13:315–324.
- Lamb, T. D., 1976. Spatial properties of horizontal cell responses in the turtle retina, *J. Physiol. (Lond.)*, 263:239–255.
- Lankheet, M. J. M., M. A. Frens, and W. A. Van de Grind, 1990. Spatial properties of horizontal cell responses in the cat retina, *Vis. Res.*, 30:1257–1275.
- Lasansky, A., 1978. Contacts between receptors and electrophysiologically identified neurones in the retina of the larval tiger salamander, *J. Physiol. (Lond.)*, 285:531–542.
- Lasansky, A., 1981. Synaptic action mediating cone responses to annular illumination in the retina of the larval tiger salamander, *J. Physiol. (Lond.)*, 310:205–214.
- Lasater, E. M., 1986. Ionic currents of cultured horizontal cells isolated from white perch retina, *J. Neurophysiol.*, 55:499–513.
- Lasater, E. M., 1991. Membrane properties of distal retinal neurons, *Prog. Ret. Res.*, 11:215–246.
- Lasater, E. M., and J. E. Dowling, 1982. Carp horizontal cells in culture respond selectively to L-glutamate and its agonists, *Proc. Natl. Acad. Sci. USA*, 79:936–940.
- Lasater, E. M., and J. E. Dowling, 1985. Dopamine decreases conductance of the electrical junctions between cultured retinal horizontal cells, *Proc. Natl. Acad. Sci. USA*, 82:3025–3029.
- Leeper, H. F., 1978a. Horizontal cells of the turtle retina. I. Light microscopy of Golgi preparations, *J. Comp. Neurol.*, 182:777–794.
- Leeper, H. F., 1978b. Horizontal cells of the turtle retina II. Analysis of interconnections between photoreceptor cells and horizontal cells by light microscopy, *J. Comp. Neurol.*, 182:795–810.
- Leeper, H. F., and D. R. Copenhagen, 1979. Mixed rod-cone responses in horizontal cells of the snapping turtle retina, *Vis. Res.*, 19:407–412.
- Levy, H., 2001. The role of nitric oxide in information processing in the distal retina of the turtle. Ph.D. dissertation, Faculty of Medicine, Technion-Israel Institute of Technology, Haifa, Israel.
- Liepe, B. A., C. Stone, J. Koistinaho, and D. R. Copenhagen, 1994. Nitric oxide synthase in Müller cells and neurons of salamander and fish retina, *J. Neurosci.*, 14:7641–7654.
- Linberg, K. A., and S. K. Fisher, 1988. Ultrastructural evidence that horizontal cell axon terminals are presynaptic in the human retina, *J. Comp. Neurol.*, 268:281–297.
- Lipetz, L. E., 1978. A model of function at the outer plexiform layer of cyprinid retina, in *Frontiers of Visual Science* (S. J. Cool and E. L. Smith, eds.), Berlin-Heidelberg: Springer-Verlag, pp. 471–482.
- Lohrke, S., and H. D. Hofmann, 1994. Voltage-gated currents of rabbit A- and B-type horizontal cells in retinal monolayer cultures, *Vis. Neurosci.*, 11:369–378.
- Lu, C., and D. G. McMahon, 1997. Modulation of hybrid bass retinal gap junctional channel gating by nitric oxide, *J. Physiol. (Lond.)*, 499:689–699.
- Malchow, R. P., H. Qian, H. Ripps, and J. E. Dowling, 1990. Structural and functional properties of two types of horizontal cell in the skate retina, *J. Gen. Physiol.*, 95:177–198.
- Mangel, S. C., 1991. Analysis of the horizontal cell contribution to the receptive field surround of ganglion cells in the rabbit retina, *J. Physiol. (Lond.)*, 442:211–234.
- Mangel, S. C., and J. E. Dowling, 1985. Responsiveness and receptive field size of carp horizontal cells are reduced by prolonged darkness and dopamine, *Science*, 229:1107–1109.
- Marc, R. E., 1999. The structure of vertebrate retinas, in *The Retinal Basis of Vision* (Toyoda et al., eds.), Amsterdam: Elsevier, pp. 3–19.
- Marc, R. E., W. K. Stell, D. Bok, and D. M. K. Lam, 1978. GABAergic pathways in the goldfish retina, *J. Comp. Neurol.*, 182:221–246.
- Marchiafava, P. L., and R. Weiler, 1980. Intracellular analysis and structural correlates of the organization of inputs to ganglion

- cells in the retina of the turtle, *Proc. R. Soc. (Lond.) B*, 208:103–113.
- Marshall, L. M., and F. S. Werblin, 1978. Synaptic transmission to the horizontal cells in the retina of the larval tiger salamander, *J. Physiol. (Lond.)*, 279:321–346.
- Massey, S. C., and R. F. Miller, 1987. Excitatory amino acid receptors of rod- and cone-driven horizontal cells in the rabbit retina, *J. Neurophysiol.*, 57:645–659.
- Mayer, M. L., and G. L. Westbrook, 1987. The physiology of excitatory amino acids in vertebrate central nervous system, *Prog. Neurobiol.*, 28:197–276.
- McMahon, D. G., A. G. Knapp, and J. E. Dowling, 1989. Horizontal cell gap junctions: single channel conductance and modulation by dopamine, *Proc. Natl. Acad. Sci. USA*, 86:7639–7643.
- McMahon, D. G., and L. V. Ponomareva, 1996. Nitric oxide and cGMP modulate retinal glutamate receptors, *J. Neurophysiol.*, 76:2307–2315.
- McReynolds, J. S., and P. D. Lukasiewicz, 1989. Integration of synaptic input from on and off pathways in mudpuppy retinal ganglion cells, in *Neurobiology of the Inner Retina* (R. Weiler and N. N. Osborne, eds.), Berlin, Heidelberg: Springer-Verlag, pp. 209–220.
- Miller, W. H., Y. Hashimoto, T. Saito, and T. Tomita, 1973. Physiological and morphological identification of L- and C-type S-potentials in the turtle retina, *Vis. Res.*, 13:443–447.
- Mills, S. K., and S. C. Massey, 1994. Distribution and coverage of A-type and B-type horizontal cells stained with Neurobiotin in the rabbit retina, *Vis. Neurosci.*, 11:549–560.
- Miyachi, E., M. Mutakami, and T. Nakaki, 1990. Arginine blocks gap junctions between retinal horizontal cells, *Neuroreport*, 1:107–110.
- Münz, H., B. Class, W. E. Stumpf, and L. Jennes, 1982. Centrifugal innervation of the retina by luteinizing hormone releasing hormone (LHRH)-immunoreactive telencephalic neurons in teleostean fishes, *Cell Tiss. Res.*, 222:313–323.
- Murakami, M., Y. Shimoda, K. Nakatani, E. Miyachi, and S. Watanabe, 1982a. GABA-mediated negative feedback from horizontal cells to cones in carp retina, *Jpn. J. Physiol.*, 32:911–926.
- Murakami, M., Y. Shimoda, K. Nakatani, E. Miyachi, and S. Watanabe, 1982b. GABA-mediated negative feedback and color opponency in carp retina, *Jpn. J. Physiol.*, 32:927–935.
- Naka, K.-I., 1971. Receptive field mechanism in the vertebrate retina, *Science*, 171:691–693.
- Naka, K.-I., 1976. Neuronal circuitry in the catfish retina, *Invest. Ophthalmol.*, 5:926–935.
- Naka, K.-I., and W. A. H. Rushton, 1966. S-potentials from colour units in the retina of fish (*Cyprinidae*), *J. Physiol. (Lond.)*, 185:536–555.
- Naka, K.-I., and W. A. H. Rushton, 1967. The generation and spread of S-potentials in fish (*Cyprinidae*), *J. Physiol. (Lond.)*, 192:437–461.
- Nathan, C., 1992. Nitric oxide as a secretory product of mammalian cells, *FASEB J.*, 6:3051–3064.
- Negishi, K., and B. D. Drujan, 1979. Effects of catecholamines and related compounds on horizontal cells in the fish retina, *J. Neurosci. Res.*, 4:311–334.
- Nelson, R., 1977. Cat cones have rod input: a comparison of the response properties of cones and horizontal cell bodies in the retina of the cat, *J. Comp. Neurol.*, 172:109–136.
- Nelson, R., 1985. Spectral properties of cat horizontal cells, *Neurosci. Res.*, 2(Suppl):S167–S183.
- Nelson, R., and H. Kolb, 1983. Synaptic patterns and response properties of bipolar and ganglion cells in the cat retina, *Vis. Res.*, 23:1183–1195.
- Nelson, R., H. Kolb, E. V. Famiglietti, Jr., and P. Goures, 1976. Neural responses in the rod and cone systems of the cat retina: intracellular records and procion stains, *Invest. Ophthalmol.*, 15:946–953.
- Nelson, R., R. Pflug, and S. M. Baer, 1990. Background induced flicker enhancement in cat retinal horizontal cells. II: Spatial properties, *J. Neurophysiol.*, 64:326–340.
- Nelson, R., A. von Lutzow, H. Kolb, and P. Gouras, 1975. Horizontal cells in cat with independent dendritic systems, *Science*, 189:137–139.
- Niemeyer, G., and P. Gouras, 1973. Rod and cone signals in S-potentials of the isolated perfused cat eye, *Vis. Res.*, 13:1603–1612.
- Normann, R. A., and I. Perlman, 1979. Signal transmission from red cones to horizontal cells in the turtle retina, *J. Physiol. (Lond.)*, 235:207–223.
- Normann, R. A., I. Perlman, and S. J. Daly, 1986. The effects of continuous superfusion of L-aspartate and L-glutamate on horizontal cells of the turtle retina, *Vis. Res.*, 26:259–268.
- Normann, R. A., and J. Pochobradsky, 1976. Oscillations in rod and horizontal cell membrane potentials: evidence for feedback to rods in the vertebrate retina, *J. Physiol. (Lond.)*, 261:15–29.
- Norton, A. L., H. Spekreijse, M. L. Wolbarsht, and H. G. Wagner, 1968. Receptive field organization of the S-potential, *Science*, 160:1021–1022.
- O'Bryan, P. M., 1973. Properties of the depolarizing synaptic potential evoked by peripheral illumination in cones of the turtle retina, *J. Physiol. (Lond.)*, 235:207–223.
- O'Dell, T. J., and B. N. Christensen, 1989. A voltage-clamp study of isolated stingray horizontal cells non-NMDA excitatory amino acid receptors, *J. Neurophysiol.*, 61:175–190.
- Ostholm, T., B. I. Holmqvist, P. Alm, and P. Ekstrom, 1994. Nitric oxide synthase in the CNS of the atlantic salmon, *Neurosci. Lett.*, 168:233–237.
- Owen, W. G., and W. Hare, 1989. Signal transfer from photoreceptors to bipolar cells in the retina of the tiger salamander, *Neurosci. Res.*, 10(Suppl):77–88.
- Peichl, L., D. Sandman, and B. B. Boycott, 1998. Comparative anatomy and function of mammalian horizontal cells, in *Development and Organization of the Retina* (L. M. Chalupa and B. L. Finlay, eds.), New York: Plenum Press, pp. 147–172.
- Peng, Y.-W., C. D. Blackstone, R. L. Haganir, and K.-W. Yau, 1995. Distribution of glutamate receptor subtypes in the vertebrate retina, *Neurosci.*, 66:483–497.
- Perlman, I., and J. Ammermüller, 1994. The receptive field size of L1 horizontal cells in the turtle retina: the effects of dopamine and background light, *J. Neurophysiol.*, 72:2786–2795.
- Perlman, I., A. G. Knapp, and J. E. Dowling, 1989. Responses of isolated white perch horizontal cells to changes in the concentration of photoreceptor transmitter agonists, *Brain Res.*, 487:16–25.
- Perlman, I., and R. A. Normann, 1979. Short-wavelength input to luminosity-type horizontal cells in the turtle retina, *Vis. Res.*, 19:903–906.
- Perlman, I., and R. A. Normann, 1990. The effects of GABA and related drugs on horizontal cells in the isolated turtle retina, *Vis. Neurosci.*, 5:469–477.
- Perlman, I., R. A. Normann, A. Itzhaki, and S. J. Daly, 1985. Chromatic and spatial information processing by red cones and L-type horizontal cells in the turtle retina, *Vis. Res.*, 25:543–549.

- Perlman, I., J. M. Sullivan, and R. A. Normann, 1993. Voltage and time dependent potassium conductances enhance the frequency response of horizontal cells in the turtle retina, *Brain Res.*, 619:89–97.
- Pfeiffer-Linn, C. L., I. Perlman, and E. M. Lasater, 1995. Sodium dependency of the inward potassium rectifier in horizontal cells isolated from the white bass retina, *Brain Res.*, 701:81–88.
- Pflug, R., R. Nelson, and P. K. Ahnelt, 1990. Background induced flicker enhancement in cat retinal horizontal cells. I: Temporal and spectral properties, *J. Neurophysiol.*, 64:313–325.
- Piccolino, M., 1995. The feedback synapse from horizontal cells to cone photoreceptors in the vertebrate retina, *Prog. Ret. Eye Res.*, 14:141–196.
- Piccolino, M., J. Neyton, and H. M. Gerschenfeld, 1981. Center-surround antagonistic organization in small-field luminosity horizontal cells of turtle retina, *J. Neurophysiol.*, 45:363–375.
- Piccolino, M., J. Neyton, and H. M. Gerschenfeld, 1984. Decrease of gap junction permeability induced by dopamine and cyclic adenosine 3-5-mono-phosphate in horizontal cells of the turtle retina, *J. Neurosci.*, 4:2477–2488.
- Polyak, S. L., 1941. *The Retina*. Chicago: University of Chicago.
- Pottek, M., K. Schultz, and R. Weiler, 1997. Effects of nitric oxide on the horizontal cell network and dopamine release in the carp retina, *Vis. Res.*, 37:1091–1102.
- Pottek, M., and R. Weiler, 2000. Light-adaptive effects of retinoic acid on receptive field properties of retinal horizontal cells, *Eur. J. Neurosci.*, 12:437–445.
- Rauen, T., W. R. Taylor, K. Kuhlbrodt, and M. Wiessner, 1998. High-affinity glutamate transporters in the rat retina: a major role of the glial glutamate transporter GLAST-1 in transmitter clearance, *Cell Tiss. Res.*, 291:19–31.
- Raviola, E., and N. B. Gilula, 1975. Intramembrane organization of specialized contacts in the outer plexiform layer of the retina: a freeze-fracture study in monkeys and rabbits, *J. Cell Biol.*, 65:192–222.
- Raynauld, J.-P., J. R. Laviolette, and H.-J. Wagner, 1979. Goldfish retina: a correlate between cone activity and morphology of the horizontal cell in cone pedicles, *Science*, 204:1436–1438.
- Roufs, J. A. J., 1972. Dynamic properties of vision. I. Experimental relationships between flicker and flash thresholds, *Vis. Res.*, 12:261–278.
- Saito, T., H. Kondo, and Toyoda, J.-I., 1979. Ionic mechanisms of two types of ON-center bipolar cells in the carp retina: I. The responses to central illumination, *J. Gen. Physiol.*, 73:73–90.
- Saito, T., H. Kondo, and Toyoda, J.-I., 1981. Ionic mechanisms of two types of ON-center bipolar cells in the carp retina: II. The responses to annular illumination, *J. Gen. Physiol.*, 78:569–589.
- Saito, T., W. H. Miller, and Tomita, T., 1974. C- and L-type horizontal cells in the turtle retina, *Vis. Res.*, 14:119–123.
- Sandmann, D., B. B. Boycott, and L. Peichl, 1996a. Blue cone horizontal cells in the retinae of horses and other Equidae, *J. Neurosci.*, 16:3381–3396.
- Sandmann, D., B. B. Boycott, and L. Peichl, 1996b. The horizontal cells of artiodactyls retinae: a comparison with Cajal's description, *Vis. Neurosci.*, 13:735–746.
- Schmidt, K.-F., M. Kruse, and H. Hatt, 1994. Dopamine alters glutamate receptor desensitization in retinal horizontal cells of the perch (*Perca fluviatilis*), *Proc. Natl. Acad. Sci. USA*, 91:8288–8291.
- Shingai, R., and B. N. Christensen, 1986. Excitable properties and voltage-sensitive ion conductances of horizontal cells isolated from catfish (*Ictalurus punctatus*) retina, *J. Neurophysiol.*, 56:32–49.
- Simon, E. J., 1973. Two types of luminosity horizontal cells in the retina of the turtle, *J. Physiol. (Lond.)*, 230:199–211.
- Smith, R. G., M. A. Freed, and P. Sterling, 1986. Microcircuitry of the dark-adapted cat retina: functional architecture of the rod-cone network, *J. Neurosci.*, 6:3503–3517.
- Spekreijse, H., and A. L. Norton, 1970. The dynamic characteristics of color-coded S-potentials, *J. Gen. Physiol.*, 56, 1–15.
- Steinberg, R. H., 1969a. Rod and cone contributions to S-potentials from the cat retina, *Vis. Res.*, 9:1319–1329.
- Steinberg, R. H., 1969b. Rod-cone interactions in S-potentials from the cat retina, *Vis. Res.*, 9:1331–1344.
- Stell, W. K., 1976. Functional polarization of horizontal cell dendrites in goldfish retina, *Invest. Ophthalmol.*, 15:895–908.
- Stell, W. K., and D. O. Lightfoot, 1975. Color-specific interconnections of cones and horizontal cells in the retina of the goldfish, *J. Comp. Neurol.*, 159:473–501.
- Stell, W. K., S. E. Walker, K. S. Chohan, and A. K. Ball, 1984. The goldfish nervous terminalis: a luteinizing hormone-releasing hormone and molluscan cardioexcitatory peptide immunoreactive olfactoryretinal pathway, *Proc. Natl. Acad. Sci. USA*, 81:940–944.
- Sterling, P., 1990. Retina, in *The Synaptic Organization of the Brain*, 3rd ed. (G. M. Shepard, ed.), New York: Oxford University Press, pp. 170–213.
- Stone, S., P. Witkovsky, and M. Schutte, 1990. A chromatic horizontal cell in the *Xenopus* retina: intracellular staining and synaptic pharmacology, *J. Neurophysiol.*, 64:1683–1694.
- Svaetichin, G., 1953. The cone action potential, *Acta Physiol. Scand.*, 29:565–599.
- Svaetichin, G., and E. F. MacNichol, Jr., 1958. Retinal mechanisms for chromatic and achromatic vision, *Ann. N.Y. Acad. Sci.*, 74:385–404.
- Tachibana, M., 1983. Ionic currents of solitary horizontal cells isolated from goldfish retina, *J. Physiol. (Lond.)*, 345:329–351.
- Tachibana, M., 1985. Permeability changes induced by L-glutamate in solitary horizontal cells isolated from *Carassius auratus*, *J. Physiol. (Lond.)*, 358:153–167.
- Tachibana, M., and A. Kaneko, 1984. γ -Aminobutyric acid acts at axon terminals of turtle photoreceptors: difference in sensitivity among cell types, *Proc. Natl. Acad. Sci. USA*, 81:7961–7964.
- Teranishi, T., K. Negishi, and S. Kato, 1983. Dopamine modulates S-potential amplitude and dye-coupling between external horizontal cells in carp retina, *Nature*, 301:243–246.
- Tsuyama, Y., G. N. Noll, and K.-F. Schmidt, 1993. L-arginine and nicotinamide adenine dinucleotide phosphate alter dark voltage and accelerate light response recovery in isolated retinal rods of the frog (*Rana temporaria*), *Neurosci. Lett.*, 149:95–98.
- Twig, G., H. Levy, and I. Perlman, 2001. Turtle C-type horizontal cells behave as push-pull devices, *Vis. Neurosci.*, 18:893–900.
- Twig, G., H. Levy, and I. Perlman, 2002. Spatial-chromatic interactions in C-type horizontal cells of the turtle (*Mauremys caspica*) retina, *Vis. Neurosci.*, 19:71–84.
- Ueda, Y., A. Kaneko, and M. Kaneda, 1992. Voltage-dependent ionic currents in solitary horizontal cells isolated from cat retina, *J. Neurophysiol.*, 68:1143–1150.
- Vaney, D. I., 1994. Patterns of neuronal coupling in the retina, *Prog. Ret. Eye Res.*, 13:301–355.
- Verweije, J., D. M. Dacey, B. B. Peterson, and S. L. Buck, 1999. Sensitivity and dynamics of rod signals in H1 horizontal cells of the macaque monkey retina, *Vis. Res.*, 39:3662–3672.
- Verweij, J., M. Kamermans, and H. Spekreijse, 1996. Horizontal cells feed back to cones by shifting the cone calcium-current activation range, *Vis. Res.*, 36:3943–3953.

- Vigh, J., and P. Witkovsky, 1999. Sub-millimolar cobalt selectively inhibits the receptive field surround of retinal neurons, *Vis. Neurosci.*, 16:159–168.
- Wagner, H.-J., 1980. Light dependent plasticity of the morphology of horizontal cell terminals in cone pedicles of fish retinas, *J. Neurocytol.*, 9:573–590.
- Wagner, M., B. Han, and T. M. Jessell, 1992. Regional differences in retinoid release from embryonic neural tissue detected by in vitro reporter assay, *Development*, 116:55–66.
- Wald, G., 1935. Carotenoids and the visual cycle, *J. Gen. Physiol.*, 19:351–361.
- Wässle, H., and B. B. Boycott, 1991. Functional architecture of the mammalian retina, *Physiol. Rev.*, 71:447–480.
- Wässle, H., B. B. Boycott, and J. Röhrenbeck, 1989. Horizontal cells in the monkey retina: cone connections and dendritic network, *Eur. J. Neurosci.*, 1:421–435.
- Wässle, H., and H. J. Riemann, 1978. The mosaic of nerve cells in the mammalian retina, *Proc. R. Soc. Lond. B*, 200:441–461.
- Weiler, R., and B. Kewitz, 1993. The marker for nitric oxide synthase, NADPH-diaphorase, co-localizes with GABA in horizontal cells and cells of the inner retina in carp retina, *Neurosci. Lett.*, 158:151–154.
- Weiler, R., K. Kohler, M. Kirsch, and H.-J. Wagner, 1988. Glutamate and dopamine modulate synaptic plasticity in horizontal cell dendrites of fish retina, *Neurosci. Lett.*, 87:205–209.
- Weiler, R., M. Pottek, K. Schultz, and U. Janssen-Bienhold, 2001. Retinoic acid, a neuromodulator in the retina, in *Concepts and Challenges in Retinal Biology: A Tribute to John E. Dowling* (H. Kolb, H. Ripps, and S. Wu, eds.), Amsterdam: Elsevier, pp. 309–318.
- Weiler, R., K. Schultz, M. Pottek, S. Tieding, and U. Janssen-Bienhold, 1998. Retinoic acid has light-adaptive effects on horizontal cells in the retina, *Proc. Natl. Acad. Sci. USA*, 95:7139–7144.
- Weiler, R., and D. I. Vaney, 1999. Retinoic acid modulates gap junctional permeability between horizontal cells of the mammalian retina, *Eur. J. Neurosci.*, 11:3346–3350.
- Weiler, R., and H.-J. Wagner, 1984. Light-dependent change of cone-horizontal cell interactions in carp retina, *Brain Res.*, 298:1–9.
- Werblin, F. S., and J. E. Dowling, 1969. Organization of the retina of the mudpuppy, *Necturus maculosus*. II. Intracellular recording, *J. Neurophysiol.*, 32:339–355.
- Witkovsky, P., and A. Dearry, 1991. Functional role of dopamine in the vertebrate retina, *Prog. Ret. Res.*, 11:247–292.
- Witkovsky, P., and J. E. Dowling, 1969. Synaptic relationships in the plexiform layers of carp retina, *Z. Zellforsch.*, 100:60–82.
- Witkovsky, P., R. Gabriel, D. Krizaj, and A. Akopian, 1995. Feedback from luminosity horizontal cells mediates depolarizing responses of chromaticity horizontal cells in the *Xenopus* retina, *Proc. Natl. Acad. Sci. USA*, 92:3556–3560.
- Witkovsky, P., S. Stone, and D. Tranchina, 1989. Photoreceptor to horizontal cell synaptic transfer in the *Xenopus* retina: modulation by dopamine ligands and circuit model for interactions of rod and cone inputs, *J. Neurophysiol.*, 62:864–881.
- Wu, S. M., 1986. Effects of gamma-aminobutyric acid on cones and bipolar cells of the tiger salamander retina, *Brain Res.*, 365:70–77.
- Wu, S. M., 1991. Input-output relations of the feedback synapse between horizontal cells and cones in the tiger salamander retina, *J. Neurophysiol.*, 65:1197–1206.
- Wu, S. M., 1994. Synaptic transmission in the outer retina, *Annu. Rev. Physiol.*, 56:141–168.
- Xin, D., and S. A. Bloomfield, 2000. Effects of nitric oxide on horizontal cells in the rabbit retina, *Vis. Neurosci.*, 17:799–811.
- Yamada, E., and T. Ishikawa, 1965. The fine structure of the horizontal cells in some vertebrate retinas, *Cold Spring Harbor Symp. Quant. Biol.*, 30:383–392.
- Yang, X.-L., B. Maple, F. Gao, G. Maguire, and S. M. Wu, 1998. Postsynaptic responses of horizontal cells in the tiger salamander retina are mediated by AMPA-preferring receptors, *Brain Res.*, 797:125–134.
- Yang, X.-L., K. Tornqvist, and J. E. Dowling, 1988. Modulation of cone horizontal cell activity in the teleost fish retina. II. Role of interplexiform cells and dopamine in regulating light responsiveness, *J. Neurosci.*, 8:2269–2278.
- Yang, X.-L., and S. M. Wu, 1991a. Coexistence and function of glutamate receptor subtypes in the horizontal cells of the tiger salamander retina, *Vis. Neurosci.*, 7:377–382.
- Yang, X.-L., and S. M. Wu, 1991b. Feedforward lateral inhibition in retinal bipolar cells: input-output relation of the horizontal cell–depolarizing bipolar cell synapse, *Proc. Natl. Acad. Sci. USA*, 88:3310–3313.
- Yazulla, S., 1976. Cone input to horizontal cells in the turtle retina, *Vis. Res.*, 16:727–735.
- Zemel, E., O. Eyal, B. Lei, and I. Perlman, 1996. NADPH diaphorase activity in the mammalian retina is modulated by the state of visual adaptation, *Vis. Neurosci.*, 13:863–871.
- Zemel, E., B. Lei, and I. Perlman, 2001. NADPH diaphorase activity in the rabbit retina is modulated by glutamatergic pathways, *J. Comp. Neurol.*, 431:28–38.
- Zucker, C. L., and J. E. Dowling, 1987. Centrifugal fibres synapse on dopaminergic interplexiform cells in the teleost retina, *Nature*, 300:166–168.

25 Retinal Amacrine Cells

DAVID I. VANEY

Interneurons of the inner retina

Detailed studies of the neuronal interactions that occur at the terminal pedicle of cone photoreceptors have created a cohesive framework for understanding the complexity of visual processing in the outer retina and, in particular, the neuronal mechanisms that give rise to the parallel visual pathways mediated by the different types of bipolar cells (see Chapter 17, How Retinal Circuits Optimize the Transfer of Visual Information). By contrast, our understanding of how the visual signals are further processed in the inner retina has advanced comparatively little in the past decade, notwithstanding the detailed documentation of the neuronal diversity of both the amacrine and ganglion cells (see Chapter 26). In Ramón y Cajal's final paper addressing "the enigma of the amacrine cells," he pointed out that the functions of most types of amacrine cells remained unknown almost 50 years after their discovery (Cajal, 1933). Although our present understanding of amacrine cell function is now informed by the knowledge that these cells are primarily inhibitory neurons and that they make and receive synapses on their dendrites (Dowling and Boycott, 1966), anyone who has looked down a microscope at Golgi-stained or dye-filled amacrine cells can appreciate how Cajal was bewildered by these cells.

Amacrine cells first came to prominence in the late 1880s. Although Müller (1851) had recognized that the cells at the vitread margin of the inner nuclear layer formed a distinct sublayer (*spongöse schicht*), it was not until Tartuferi (1887) first applied the Golgi method to the retina that the detailed morphology of the spongioblasts was revealed. Shortly afterward, Cajal (1893) and Dogiel (1891) independently came to the conclusion that spongioblasts do not give rise to a classical axon, leading Cajal (1893) to name these inner retinal neurons amacrine cells, from the Greek *a-makrós-inos* meaning "without-long-fiber." Cajal also recognized that some spongioblasts in the bird retina do give rise to a short intraretinal axon; these cells he called association spongioblasts or association amacrine cells, to distinguish them from amacrine cells proper. In keeping with Cajal's broad view, this review encompasses all retinal interneurons that receive their primary input in the inner retina, including the amacrine cells of the inner nuclear layer, the "displaced" amacrine cells of the ganglion cell

layer, the association amacrine cells, and the interplexiform cells.

AI and AII cells: prototypical amacrine cells

In the mammalian retina, rod bipolar cells do not contact ganglion cells directly but, instead, their ribbon synapses are presynaptic to a pair of amacrine varicosities, typically arising from different types of amacrine cells, originally termed the AI and AII cells (Kolb, 1979; Kolb and Famiglietti, 1974). More informatively, the AII cell has also been called the rod amacrine cell because it is the third-order neuron in the scotopic pathway, and the AI cell has been called the reciprocal rod amacrine cell because the AI varicosities invariably make a reciprocal synapse back to the rod bipolar terminal. The AI amacrine cell is a wide-field GABAergic neuron, and the AII amacrine cell is a small-field glycinergic neuron, with each cell type being generally representative of the numerous other amacrine types with the same neurotransmitter. Thus, a detailed comparison of these two well-characterized cell types illustrates the diversity of structure and function shown by contrasting types of amacrine cells. The extensive literature on rod-signal circuits in the mammalian retina has been reviewed recently by Sharpe and Stockman (1999) and by Bloomfield and Dacheux (2001).

AMACRINE CELLS: SMALL-FIELD GLYCINERGIC NEURONS

The AII amacrine cells have a characteristic bilaminar morphology, with a stout vertically directed primary dendrite giving rise to a necklace of delicate lobular appendages in sublamina *a* of the inner plexiform layer, before branching to form a conical arborization in sublamina *b* (Famiglietti and Kolb, 1975). The AII amacrine cells receive extensive excitatory input from rod bipolar cells terminating deep in sublamina *b*, and the ON-signal in the AII cells is then fed into cone bipolar cells. In sublamina *a*, the lobular appendages make sign-inverting inhibitory synapses with OFF-center cone bipolar cells, whereas in strata 3 and 4 of sublamina *b*, the arboreal dendrites make sign-conserving electrical synapses with ON-center cone bipolar cells (Kolb, 1979; Sterling et al., 1988; Strettoi et al., 1992). Thus, the cone bipolar cells are both second-order neurons in the photopic pathway and fourth-order neurons in the scotopic pathway. In contrast to the cone signal, where the ON- and

OFF-pathways are established in the outer plexiform layer, the rod signal is not directed to separate ON and OFF pathways until the inner plexiform layer (see Chapter 18). The cone bipolar cells piggyback the rod signal, carrying it both to the ganglion cells and to the interposed circuitry that underlies complex visual processing in the inner retina (Strettoi et al., 1992).

Although the level of endogenous glycine in AII amacrine cells is relatively low compared to most glycinergic amacrine cells (Pourcho and Goebel, 1987; Wright et al., 1997), the AII cells clearly use glycine as their neurotransmitter because the glycine transporter GLYT1 is strongly expressed in the cell membrane (Vaney et al., 1998) and the output synapses on the lobular appendages are presynaptic to the $\alpha 1$ subunit of the glycine receptor (Sassoè-Pognetto et al., 1994). Correspondingly, application of the glycine antagonist strychnine blocks the scotopic light response in OFF-center ganglion cells, as would be expected if the ON response in the AII amacrine cells is sign inverted at a glycinergic synapse (Müller et al., 1988).

Under dark-adapted conditions, the AII amacrine cells show a strong center-surround organization of the receptive field, responding to center illumination with a transient-sustained depolarization and to surround illumination with a steady hyperpolarization (Dacheux and Raviola, 1986; Nelson, 1982). Under light-adapted conditions, the center responds to both the ONset and OFFset of light, apparently reflecting cone bipolar inputs mediated by both the heterologous gap junctions with arboreal dendrites (ON response) and ribbon synapses onto the lobular appendages (OFF response). It is unclear how the responses elicited under light-adapted conditions contribute to the processing of cone signals and whether these would degrade the acuity of the cone bipolar pathways (Dacey, 1999; Xin and Bloomfield, 1999).

There are over 500,000 AII cells in the retina of the cat or rabbit, accounting for ~11% of all amacrine cells (Vaney, 1985; Vaney et al., 1991). The dendritic-field size of the AII amacrine cells decreases with increasing density, which reaches a maximum of 5000 cells/mm² in the cat central area and 3000 cells/mm² in the rabbit visual streak. The lobular appendages of neighboring AII cells tile the retina with minimal overlap and therefore the lobular-appendage field is only ~20 μ m wide in the central retina. The arboreal dendrites spread further, typically showing a two- to four fold coverage of their dendritic fields. In the macaque retina, the AII amacrine cells have a peak density of ~5000 cells/mm² in the perifovea, suggesting that the central scotopic acuity is limited by the sampling density of the AII cells (Mills and Massey, 1999; Wässle et al., 1995).

In keeping with this interpretation, the receptive field of rabbit AII amacrine cells is only slightly larger than the

dendritic field under both dark-adapted and light-adapted conditions (Bloomfield et al., 1997). However, under intermediate conditions in the light-sensitized retina, the receptive-field center increases about sixfold in diameter, and this reflects increased electrical coupling through the homologous gap junctions that connect the arboreal dendrites of neighboring AII cells (Kolb and Famiglietti, 1974; Strettoi et al., 1992). Both the homologous and heterologous gap junctions are permeable to small biotinylated tracers, and this enables changes in the coupling to be assessed microscopically (Vaney, 1991). Bloomfield and colleagues (1997) showed that the changes in receptive-field size under different lighting conditions are closely mirrored by changes in the extent of tracer coupling. The homologous gap junctions between AII cells are uncoupled by exogenous dopamine (Hampson et al., 1992), and it has been proposed that endogenous dopamine underlies the constriction of the AII receptive field in the light-adapted retina, but it has yet to be demonstrated that dopaminergic antagonists affect either the receptive-field size or the extent of tracer coupling.

Two properties of the AII cells appear to be representative of the glycinergic amacrine cells in the mammalian retina. First, it appears that all glycinergic amacrine have small- or medium-sized dendritic trees, which show only limited dendritic-field overlap (Menger et al., 1998; Pourcho and Goebel, 1985; Wright et al., 1997). Second, the dendrites of glycinergic amacrine cells are not confined to a single stratum but typically connect bipolar cells and/or ganglion cells branching in two or more strata of the inner plexiform layer. In particular, most of the glycinergic amacrine cells have the capacity to integrate information between the ON- and OFF-sublaminae.

AI AMACRINE CELLS: WIDE-FIELD GABAERGIC NEURONS
Electronmicroscopy of the cat retina showed that the AI varicosities providing the reciprocal input to the rod bipolar terminals are connected by very fine intervaricose dendrites of ~0.1 μ m diameter (Kolb, 1979; Kolb and Famiglietti, 1974). Parallel Golgi studies identified the wide-field A17 amacrine cell as the probable morphological correlate of the AI amacrine cell (Kolb et al., 1981), and this was confirmed by electron microscopy of A17 cells that had been filled with horseradish peroxidase after their light responses were recorded (Nelson and Kolb, 1985). The A17 amacrine cell gives rise to a spray of fine beaded dendrites, which cover a field of 600 to 2000 μ m diameter (Fig. 25.1). Proximal to the soma, the dendrites spread diffusely throughout the inner plexiform layer but, more distally, they are essentially unistratified deep in sublamina *b*. Small round varicosities are located every 10 to 50 μ m along the dendrites and may number 1000 or more in a single cell.

The AI processes are homologically coupled by small gap junctions (Kolb and Famiglietti, 1974) and, following intra-

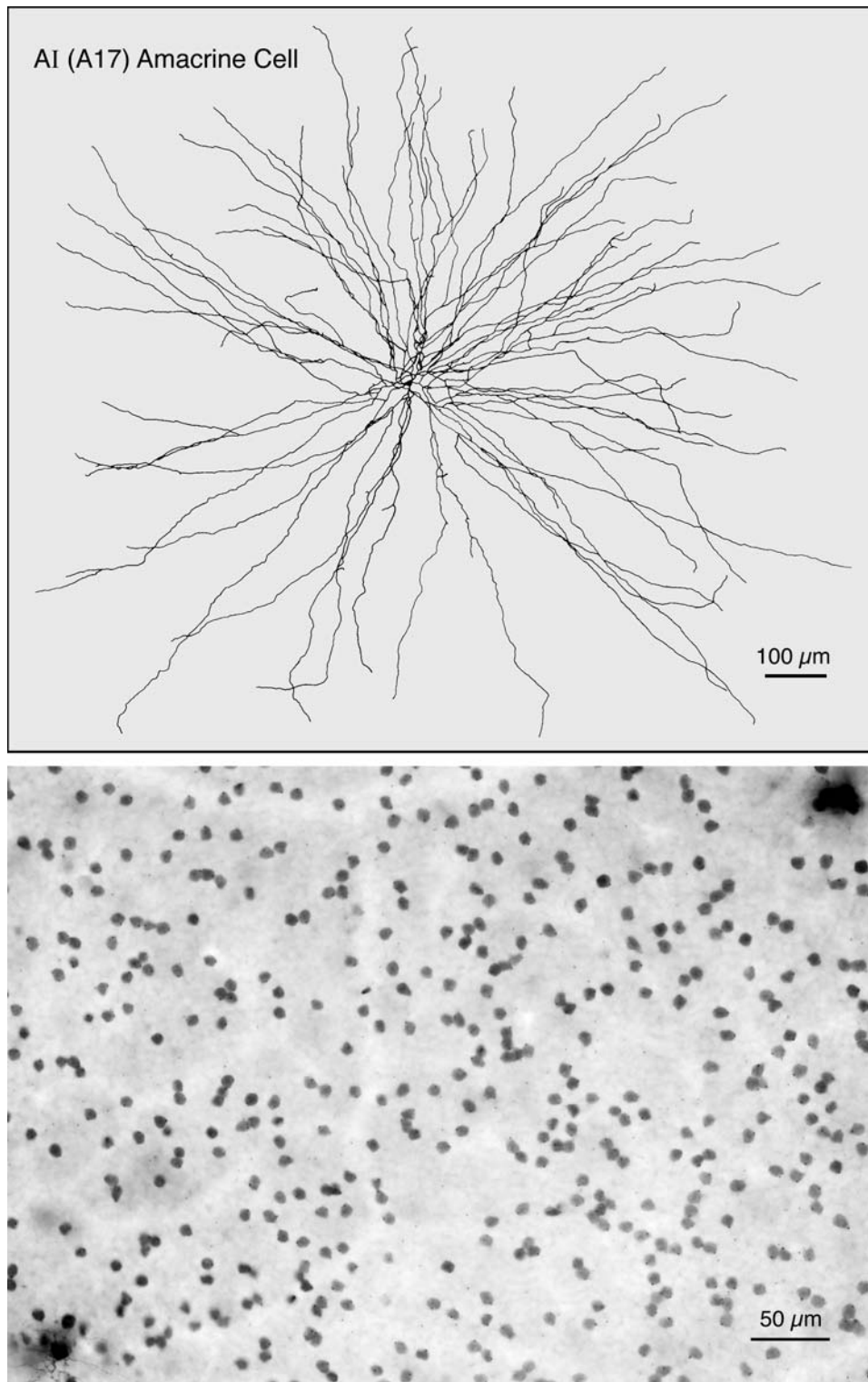


FIGURE 25.1 Reciprocal rod amacrine cells. *Top*, drawing of a Neurobiotin-filled AI (A17) amacrine cell in the cat retina. *Bottom*, somatic array of AI amacrine cells in the central area of the cat retina, labeled by homologous tracer coupling following the injection of Neurobiotin into two AI cells at the bottom-left and top-right of the field (D. I. Vaney, unpublished).

cellular injection with Neurobiotin, tracer coupling reveals the local population of A17 amacrine cells, whose density ranges from 300 cells/mm² in the far periphery of the cat retina to ~2500 cells/mm² in the central area (Vaney, 1996). The high cell density coupled with the large dendritic fields produces an extraordinarily high dendritic-field overlap: each point on the cat retina is covered by ~700 A17 amacrine cells and about 1 million of their varicosities are packed into each square millimeter of retina. This high density of varicosities is readily accounted for when it is considered that there are 40,000 rod bipolar cells/mm² in the central area and each rod bipolar terminal has ~30 ribbon synapses, some 75% of which are presynaptic to indoleamine-accumulating varicosities thought to arise from A17 amacrine cells (Freed et al., 1987; Holmgren-Taylor, 1982; McGuire et al., 1984).

Retinal amacrine cells that appear morphologically similar to the A17 amacrine cell have been described in a variety of mammals. In the rabbit retina, there are two distinct types of reciprocal rod amacrine cells, which have been termed S1 and S2 amacrine cells (Sandell and Masland, 1986; Vaney, 1986). Both types selectively accumulate indoleamines, and together they account for almost all of the varicosities that are reciprocal to the rod bipolar ribbons (Sandell et al., 1989). The S1 and S2 amacrine cells differ in their dendritic-field diameter, the initial course of their dendrites, and the form of their varicosities, but it is not clear which of the two cell types should be considered homologous to the A17 cell. The amacrine cells in the cat retina have not been investigated as systematically as those in the rabbit retina, and it is possible that the A17 amacrine cells may comprise more than one cell type; alternatively, the 25% of reciprocal varicosities that do not accumulate indoleamines in the cat retina may arise from a cell type—such as the A13 amacrine cell—that is homologous to one of the two types in the rabbit retina (Kolb and Nelson, 1996; Vaney, 1990).

The reciprocal rod amacrine cells (A17, S1/S2 cells) respond to light with a transient-sustained depolarization and the receptive field recorded at the soma is coextensive with the dendritic field (Bloomfield, 1992; Nelson and Kolb, 1985). These cells contain elevated levels of GABA (Osborne and Beaton, 1986; Pourcho and Goebel, 1983), and they appear to provide inhibitory feedback at the reciprocal synapse to the rod bipolar terminals, mediated predominantly by GABA_C receptors but probably also by GABA_A receptors (Bloomfield and Xin, 2000; Fletcher and Wässle, 1999; Hartveit, 1999). Although intracellular recordings indicate that the rod bipolar cells do not have a receptive-field surround generated in the outer plexiform layer, the inhibitory feedback from the reciprocal rod amacrine cells creates a surround at the level of the rod bipolar terminals, and pharmacological experiments

indicate that this is the source of the OFF-surround in the dark-adapted AII amacrine cells (Bloomfield and Xin, 2000).

There are interesting parallels between the neuronal circuits underlying the generation of the receptive-field surround in the photopic and scotopic pathways. In the photopic pathway, inhibitory feedback from horizontal cells to the cone photoreceptor terminal creates a surround before the OFF-center cone signal is split into separate OFF and ON pathways through the action of sign-conserving and sign-inverting glutamatergic synapses on the OFF- and ON-center cone bipolar cells, respectively (see Chapter 18). In the scotopic pathway, inhibitory feedback from the reciprocal rod amacrine cells to the rod bipolar terminal creates a surround before the ON-center rod signal is passed onto the AII amacrine cells and then split into the separate OFF and ON pathways through the action of sign-inverting glycinergic synapses and sign-conserving electrical synapses. It is not clear why two types of reciprocal rod amacrine cell are required in the rabbit retina, although the same can also be said for the two types of horizontal cells which, like the S1 and S2 amacrine cells, appear to differ primarily in the size of their receptive fields (Bloomfield and Miller, 1982; Hack and Peichl, 1999).

The AI amacrine cells are typical of other wide-field GABAergic amacrine cells in that they appear to rely on actively propagated sodium spikes to transmit synaptic signals along their dendrites and, consequently, the application of tetrodotoxin reduces both the receptive field of the AI amacrine cells and the surround response of the AII amacrine cells (Bloomfield, 1992; Bloomfield and Xin, 2000; Hartveit, 1999). Other wide-field amacrine cells usually branch in only one stratum of the inner plexiform layer and, therefore, the diffuse form of the AI cells appears atypical at first sight. However, electron microscope and physiological studies indicate that these cells are functionally unistratified, in that they interact directly with only one cell type in the vertical retinal pathways, namely the rod bipolar cells. The AI amacrine cells also receive input throughout the inner plexiform layer from other types of amacrine cells, but it is not known how this modulates the reciprocal interactions with the rod bipolar cells (Nelson and Kolb, 1985; Sandell et al., 1989).

RECIPROCAL CONE AMACRINE CELLS The ribbon synapses of cone bipolar cells are also presynaptic to a pair of processes, one of which is typically a GABAergic amacrine varicosity that makes a reciprocal synapse back to the cone bipolar terminal (Pourcho and Owczarzak, 1989). It might be expected that each type of cone bipolar cell would be served by a reciprocal amacrine cell with morphology comparable to that of the reciprocal rod amacrine cell, thus enabling the output of the bipolar terminal to be modulated

by the activity in surrounding bipolar cells of the same type. Moreover, it might also be expected that the reciprocal cone amacrine cells would come in paramorphic pairs serving the OFF- and ON-center cone bipolar cells in sublamina *a* and *b*, respectively. For example, one pair of amacrine cells could provide reciprocal input to the bipolar cells synapsing on transient alpha ganglion cells, and another pair could provide reciprocal input to the bipolar cells synapsing on sustained beta ganglion cells. However, the only well-characterized pair of GABAergic amacrine cells are the ON- and OFF-center starburst cells, which co-stratify with the ON-OFF direction-selective ganglion cells, but the starburst amacrine cells do not appear to provide reciprocal input to the bipolar cells that drive the neurons (Famiglietti, 1991).

Contrary to these expectations, the few reciprocal cone amacrine cells that have been identified are surprisingly heterogeneous in morphology, including some small-field and/or glycinergic types in addition to the expected wide-field GABAergic types (Kolb, 1997; Sassoè-Pognetto et al., 1994; Strettoi et al., 1992). However, the functions of the reciprocal cone amacrine cells appear to be different from those of the reciprocal rod amacrine cell, given that the surround of cone bipolar cells appears to be generated in the outer retina, and this will be reflected in differences in their morphology. Although it appears that spiking amacrine cells do contribute to the generation of the surround in retinal ganglion cells (Cook and McReynolds, 1998; Roska et al., 2000; Taylor, 1999), this may reflect feedforward inhibition onto the ganglion cells rather than feedback inhibition to the bipolar terminals (see Chapter 23).

Morphological diversity of amacrine cells

Cajal (1893) described three main categories of amacrine cells: the diffuse cells were subdivided into small and large varieties, and the stratified and bistratified cells were first subdivided according to their level of branching, and then by differences in their size and dendritic morphology. The Golgi-stained retinas were usually cut in vertical sections, making it impossible to trace the full extent of medium- and wide-field neurons. Thus, Cajal's original reports of the great neuronal diversity in the inner retina were not substantiated until the 1970s, when several researchers developed methods for staining whole-mounted retinas.

In these studies, the Golgi-impregnated neurons were sorted into separate types based on their dendritic branching pattern, stratification level, and dendritic-field size. Kolb and colleagues (1981) identified 22 different types of amacrine cells in the cat retina, and subsequent studies have identified as many as 26 types in the primate retina (Kolb et al., 1992; Mariani, 1990) and 70 types in the teleost retina (Wagner and Wagner, 1988). Moreover, Golgi staining is rather capricious, and some amacrine types were repre-

sented by only one or a few labeled cells; apart from the problems of characterizing a neuronal type with so few cells, probability alone indicates that some other types of amacrine cells would be missing from the sample. Because of the qualitative nature of these Golgi-impregnation studies, the extraordinary neuronal diversity that they revealed was not accepted widely until other means were found to validate individual types of amacrine cells, usually by methods that specifically stained a whole population of cells.

More recently, Masland and colleagues have developed a noncapricious alternative to Golgi staining in which a fluorescent product is created within an individual cell by focal irradiation of its nucleus (MacNeil and Masland, 1998; MacNeil et al., 1999). This "photofilling" technique had a 94% success rate when 261 amacrine cells in the rabbit retina were targeted systematically, with the only bias imposed by the oversampling of neurons with larger cell bodies. The photofilled neurons were then sorted by criteria similar to those used in Golgi studies, with no account taken of their relative frequencies. A total of 28 amacrine cell types were distinguished by this method, and almost all of these types could be identified in a parallel sample of 208 Golgi-impregnated amacrine cells (Fig. 25.2).

MacNeil and colleagues (1999) used the relative frequencies of the photofilled types to derive their cell densities and then calculated the retinal coverage of each type by multiplying the cell density by the mean dendritic-field area. This indicated that every type of small- and medium-field amacrine cell covered at least 80% of the retina and thus met an important criterion for a neuronal type established from previous studies on other classes of retinal neurons. This provided independent validation that the neuronal diversity of the amacrine cells had not been overestimated in the photofilled catalogue, but does allow for the possibility that some amacrine cell types with multiple coverage of the retina might actually comprise more than one natural type.

The 24% of the photofilled amacrine cells that had wide-field dendritic trees (>200 μm diameter) were sorted into 10 types (MacNeil et al., 1999), but this should be regarded as a minimum estimate for two reasons. First, the photofilling technique poorly labels both the distal dendrites of wide-field cells and the very thin intraretinal axons produced by some cell types, making it difficult to appreciate fully the morphological diversity of the wide-field amacrine cells. Second, some types of wide-field cells account for only one amacrine cell in a thousand (Vaney, 1990) and could easily be missed in a random sample of 261 cells; this appears to be the case for the type 2 catecholaminergic cells found by Tauchi and colleagues (1990). The random injection of rabbit amacrine cells with Neurobiotin has revealed at least five types of wide-field amacrine cells that are not present in

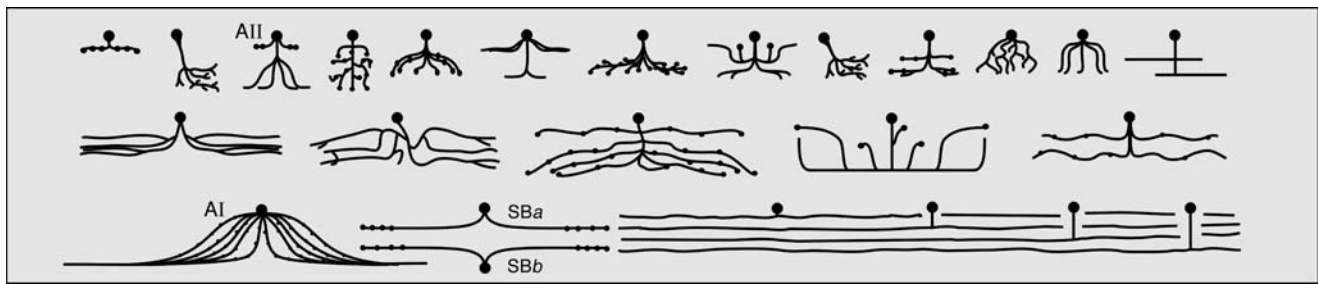


FIGURE 25.2. Amacrine cells of the rabbit retina. Schematic drawing of the different types of amacrine cells identified by MacNeil and colleagues (1999) using the photofilling technique. The cells are drawn as they would be seen in vertical section, with the somata in the inner nuclear layer and the dendrites in the inner plexiform layer. The multiple types of wide-field amacrine

cells branching in each stratum are represented by a generic cell whose dendrites have been significantly truncated. Labels mark the rod amacrine cell (AII), the reciprocal rod amacrine cell (AI), and the OFF- and ON-starburst cells (SBa, SBb). (After Masland, 2001).

the photofilled catalogue (D. I. Vaney, unpublished). It seems possible, therefore, that the number of distinct amacrine cell types in the mammalian retina may yet approach 40 (Vaney, 1990).

All of the quantitative studies lead back to the qualitative conclusion that retinal neurons with distinct dendritic morphologies are likely to comprise different cell types, subject to three important caveats. First, it is necessary to avoid creating artificial cell types based on arbitrary criteria, for example, the presence of two or three primary dendrites (Rodieck and Brening, 1983). Second, it is essential to take into account changes in morphology with retinal eccentricity and cell density, as shown by Boycott and Wässle (1974) in their classic study of ganglion cells in the cat retina. Third, the retina contains imperfections like any natural system and a small minority of retinal neurons display aberrant morphologies or make aberrant connections that are not typical of the population as a whole. For example, there are about 300 serotonin-accumulating amacrine cells in the rabbit retina that send processes into the outer plexiform layer, but they are randomly distributed and their outer retinal processes cover only 6% of the retina (Sandell and Masland, 1989; Vaney, 1990). These neurons cannot be considered a natural type because they do not have a regular spatial distribution and a uniform dendritic coverage.

ASSOCIATION AMACRINE CELLS Although it has long been known that many types of amacrine cells produce depolarizing spikes (Werblin and Dowling, 1969), it has only become apparent in the past decade that amacrine cells giving rise to axonlike processes are a regular feature of the mammalian retina. Such association amacrine cells, which were first described by Cajal (1893) in the bird retina, were the only amacrine cells to which Cajal ascribed a definite function because they showed a clear dynamic polarization, receiving input from centrifugal fibers on their cell bodies and providing output through their short axons to other retinal neurons. In the last decade, Golgi-staining and dye-injection studies have revealed that the mammalian retina contains

~10 types of association amacrine cells (Famiglietti, 1992b; D.I. Vaney, unpublished) (Fig. 25.3). Two of these cell types have been studied in particular detail; one is the classic dopaminergic amacrine cell (Dacey, 1990) and the other is a distinctive type of polyaxonal amacrine cell whose somata commonly occupy an interstitial position in the inner plexiform layer (Dacey, 1989; Famiglietti, 1992a; Stafford and Dacey, 1997).

The dopaminergic amacrine cells were the first retinal neurons to be identified neurochemically, and they have been the focus of numerous studies in the past four decades (Witkovsky and Dearth, 1992). It is thus ironic that these cells are quite atypical amacrine cells in two important respects. First, they are present at very low density; in the rabbit retina, for example, the two morphological types each account for only one amacrine cell in a thousand (Tauchi et al., 1990; Vaney, 1990). Second, they give rise to both a sparsely branched dendritic tree and a much more extensive axonal arborization, which is formed by a single axon arising near the cell body (Dacey, 1990). In both respects, the dopaminergic amacrine cells resemble the type 1 nitroergic amacrine cells (Sagar, 1986; Vaney and Young, 1988b), although the multiple axons of the latter cells arise from more distal dendrites. The axonal arbors of the dopaminergic and nitroergic amacrine cells may extend for almost 10 mm across the retina, and this accounts for the extraordinarily rich plexus revealed by tyrosine-hydroxylase immunocytochemistry and NADPH-diaphorase histochemistry, respectively.

Intracellular recordings from the interstitial polyaxonal cells, termed the A1 amacrine cells in the monkey retina (Stafford and Dacey, 1997), showed that they produce large spikes over a receptive field that matches the relatively restricted dendritic tree, suggesting that the axonal arbor serves to transmit spikes distally from initiation sites near the soma. These cells probably have a global modulatory function like the dopaminergic amacrine cells, which are thought to facilitate the transition from scotopic to photopic vision, perhaps through the diffuse release of

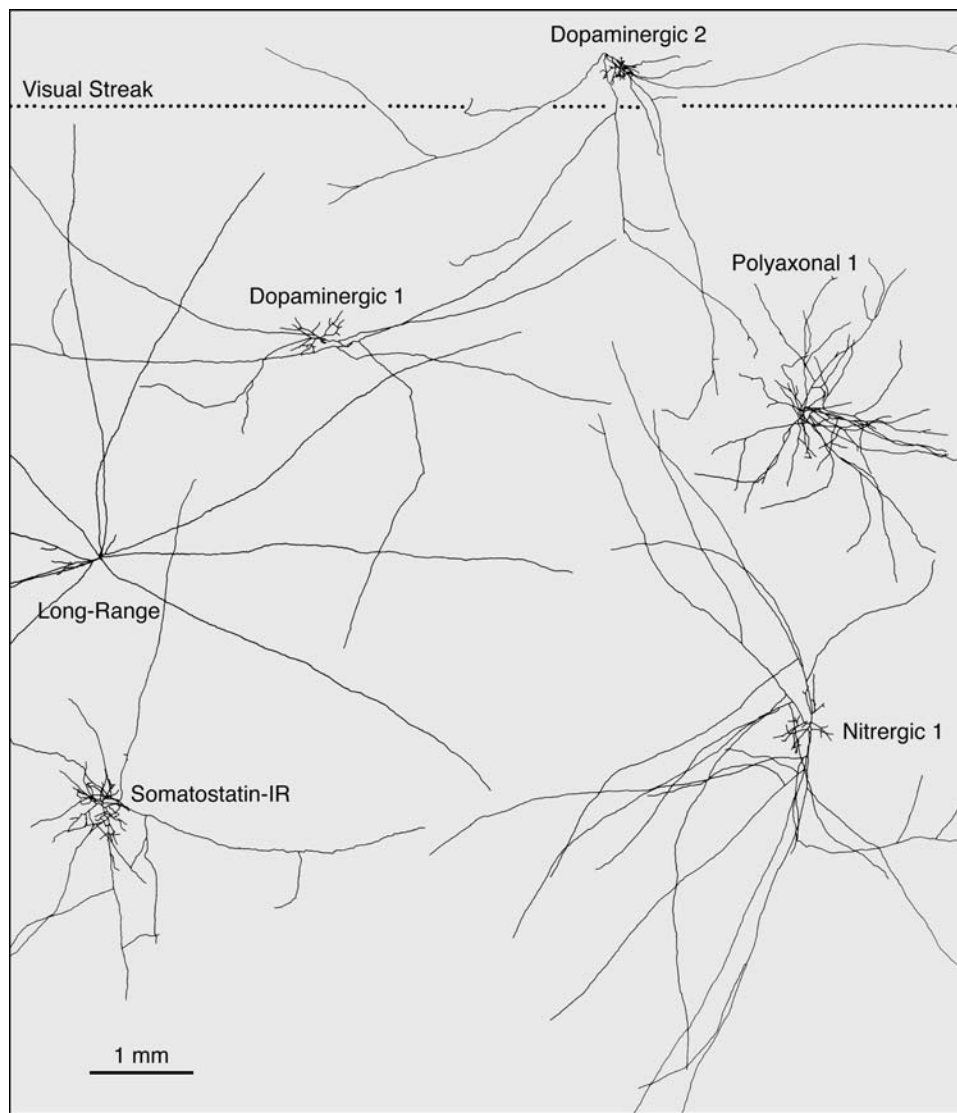


FIGURE 25.3. Association amacrine cells. Drawing of six types of axon-bearing amacrine cells in the rabbit retina, labeled by the intracellular injection of Neurobiotin; each cell is correctly placed with respect to its retinal eccentricity from the horizontal visual

streak. Note that the axonal arbors of these cells may span almost 10 mm of retina, thus covering one-third of the visual field (D. I. Vaney, unpublished).

dopamine from the axonal arbor (Witkovsky and Deary, 1992). In some vertebrates, the dopaminergic axonal arbor extends to the outer plexiform layer (Dowling and Ehinger, 1975) but, in other respects, these dopaminergic interplexiform cells are clearly homologous to the dopaminergic amacrine cells found in other retinas. Thus the interplexiform cells should not be considered as a separate class of retinal neurons but rather as a subgroup of the association amacrine cells.

TRACER-COUPLING STUDIES Cell types that account for only a few amacrine cells in every thousand are encountered so infrequently by random labeling methods that other means must be found to characterize them. For example,

many of the association amacrine cells have comparatively large somata, enabling them to be preferentially targeted for intracellular dye injection. However, it is difficult to establish a cell type based on only a few labeled examples; therefore, any technique that selectively labels a whole population of amacrine cells greatly strengthens the legitimacy of the cell type. Biotinylated tracers readily pass through the gap junctions that connect retinal neurons (Vaney, 1991), and tracer coupling has proved to be a powerful tool for selectively labeling local arrays of many types of amacrine cells, both by homologous coupling following injection of a single cell and by heterologous coupling following injection of a ganglion cell or a different type of amacrine cell (Vaney, 1994a, 1999). In fact, more types of amacrine cells can be

selectively labeled by tracer coupling than by immunolabeling with presently available antisera.

The pattern of tracer coupling shown by each type of amacrine cell appears to be relatively stable in different species. For example, the dopaminergic amacrine cells show only weak homologous coupling in both cat and rabbit retinas, and the interstitial polyaxonal cells show heterologous coupling to ganglion cells in both rabbit and monkey retinas (Stafford and Dacey, 1997). Biotinylated tracers do not mask the antigenicity of intracellular epitopes in the coupled cells; therefore, a single preparation can be used to characterize the dendritic morphology, cellular array, and neurotransmitter content of a cell type (Wright et al., 1999).

Neurochemical diversity of amacrine cells

Retinal amacrine cells express a wide variety of neurotransmitters and neuroactive substances; this was critical to early progress in labeling individual populations of cells. The first retinal neurons to be identified neurochemically were several types of monoaminergic amacrine cells, which were labeled by the classic Falck-Hillarp method of formaldehyde-induced fluorescence (Ehinger, 1966; Häggendal and Malmfors, 1965). The first immunocytochemical studies were undertaken in the 1970s to study the retinal localization of neuropeptides (Brecha et al., 1979) and GABAergic markers (Lam et al., 1979). The scope of these studies was greatly extended with the development of techniques for localizing small amino-acid transmitters, both in glutaraldehyde-fixed sections and formaldehyde-fixed whole mounts (Agardh et al., 1986; Mosinger et al., 1986; Pourcho and Goebel, 1987; Pow and Crook, 1993; Pow et al., 1995). In the past decade, antisera against a range of regulatory proteins, including protein kinase C and various calcium-binding proteins, have proved valuable in selectively labeling diverse types of retinal neurons (Gábel and Straznicky, 1992; Negishi et al., 1988; Pasteels et al., 1990).

Almost all retinal amacrine cells contain elevated levels of GABA or glycine; most of the putative GABAergic cells express the GABA-synthesizing enzyme glutamic acid decarboxylase, and most of the putative glycinergic cells express the plasma-membrane glycine transporter GlyT1 (see Chapter 20). In rabbit retina, for example, a double-immunolabeling study showed that 32% of the cells in the amacrine sublayer express GABA, 62% express glycine, 2% express both GABA and glycine, and 4% express neither inhibitory transmitter (Wright et al., 1996) (Fig. 25.4). Many of the unlabeled cells are probably bipolar cells or displaced ganglion cells. Recent tracer-coupling studies have reinforced earlier evidence that different types of amacrine cells express characteristic levels of inhibitory transmitters (Pourcho and Goebel, 1985, 1987); for example, the DAPI-3 amacrine cells consistently show the

strongest glycine immunoreactivity in the rabbit retina whereas the AII amacrine cells are among the most weakly labeled of the glycine-immunopositive cells (Wright et al., 1997).

Although the glycinergic cells account for the majority of amacrine cells in the mammalian retina (Crooks and Kolb, 1992; Koontz et al., 1993; Pourcho and Owczarzak, 1991), the inner plexiform layer is dominated by the processes of GABAergic amacrine cells, which usually have much more extensive dendritic trees than the glycinergic amacrine cells (Menger et al., 1998). Correspondingly, the GABAergic cells account for 80% to 90% of the synapses made by all amacrine cells in the retina (Koontz and Hendrickson, 1990; Marc and Liu, 2000). Although inhibitory interactions in the retina are often represented as simple feedback or feedforward circuits, serial synapses between amacrine processes have long been recognized (Dowling and Boycott, 1966; Dubin, 1970). In fact, a quantitative study of the synaptic connectivity of GABAergic amacrine cells in the goldfish retina indicated that the majority of amacrine cell circuitries are relatively complex, involving nested feedback, nested feedforward, and chains of inhibition (Marc and Liu, 2000).

In many types of amacrine cells, the GABA or glycine is colocalized with another neurotransmitter, including dopamine, serotonin, acetylcholine, nitric oxide, and a diverse range of neuropeptides (Watt et al., 1984; Weiler and Ball, 1984). Such colocalization raised the exciting possibility that each cell type may be identified by a unique neurochemical signature (Lam et al., 1985), comparable to the chemical coding of enteric neurons (Costa et al., 1986). The signature hypothesis has been tested most rigorously by Marc and colleagues, who used postembedding immunocytochemistry and pattern recognition techniques to analyze quantitatively the amino-acid content of all cells in serial plastic sections of goldfish, monkey, and cat retinas (Kalloniatis et al., 1996; Marc et al., 1995, 1998). This analysis partitioned virtually all of the retinal neurons into as many as 15 "theme" classes that had statistically separable amino-acid signatures.

Although the amacrine cells in monkey retina could be divided into four GABA-dominated classes and another four glycine-dominated classes (Kalloniatis et al., 1996), this falls well short of accommodating the known morphological diversity of the amacrine cells. However, a recent study of the ganglion cells in rabbit retina showed that the seven theme classes identified from intrinsic amino-acid signals could be further divided into 14 classes, which may correspond to natural neuronal types, if both an excitation signal and soma size were also included in the parametric space (Marc and Jones, 2002). If the quantitative immunocytochemical analysis of the amacrine cells could be extended to include other parameters, including neuropeptides and the dozens of enzymes involved in neurotransmission, then it is possible

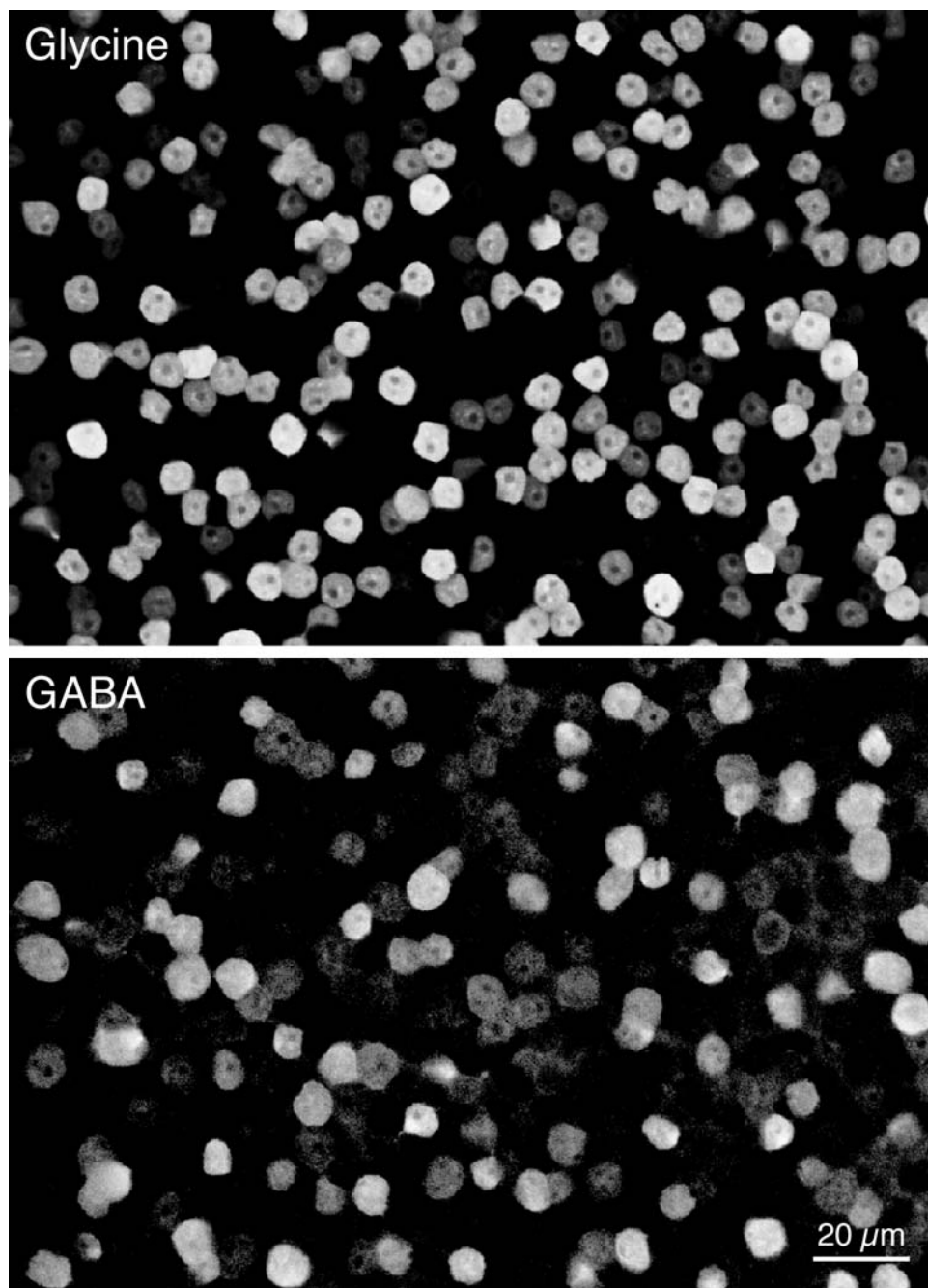


FIGURE 25.4. Almost all amacrine cells express glycine or GABA. Confocal fluorescence micrographs of a rabbit retinal whole mount immunolabeled for glycine and GABA, with the focus on the amacrine sublayer of the inner nuclear layer (L. L. Wright, unpublished).

that the number of theme classes extracted might yet approach the number of morphological types of amacrine cells.

STARBURST AMACRINE CELLS: EXCITATION AND INHIBITION
The principal cholinergic neurons in the retina are amacrine cells that have a distinctive radially symmetrical morphology, with the primary dendrites branching regularly and repeatedly to form numerous terminal dendrites that are studded with varicosities, thus giving the cells the appear-

ance of starburst fireworks (Famiglietti, 1983). The starburst amacrine cells are found throughout the vertebrates and comprise two paramorphic types, with the OFF-starburst cells stratifying in sublamina *a* of the inner plexiform layer and the displaced ON-starburst cells stratifying in sublamina *b* (Perry and Walker, 1980). The starburst amacrine cells contain and release both acetylcholine and GABA (Brecha et al., 1988; O'Malley et al., 1992; Vaney and Young, 1988a), but it is not known whether these fast-

acting excitatory and inhibitory transmitters are used at the same synapses.

In rabbit retina, the ON- and OFF-starburst cells stratify at precisely the same levels as the ON-OFF direction-selective ganglion cells (DSGCs) and, within each stratum, the dendrites of numerous overlapping starburst cells cofasciculate with those of the DSGCs (Vaney and Pow, 2000). The DSGCs receive a powerful cholinergic input (Masland and Ames, 1976), and the role of the starburst amacrine cells in the generation of direction selectivity has been the subject of many studies (Vaney et al., 2001; see also Chapter 28). The ON-OFF DSGCs comprise four subtypes that respond preferentially to image motion in one of the four cardinal ocular directions—upward, downward, forward, and backward (Oyster and Barlow, 1967). Each point on the retina is probably covered by four DSGCs of different subtypes, whereas DSGCs of the same subtype tile the retina in a highly territorial manner with little overlap of their dendritic fields (Amthor and Oyster, 1995; Vaney, 1994b).

The starburst cells receive bipolar and amacrine cell input over the whole dendritic tree, but their output to ganglion cells is confined to the varicose distal zone (Famiglietti, 1991). Vaney and Young (1988a) proposed that this proximodistal segregation of the input and output synapses could provide the spatial asymmetry necessary for the generation of direction selectivity, assuming that the dendrites on different sides of the starburst cells provided selective output to DSGCs with different preferred directions (Vaney et al., 1989).

Classic electrophysiological experiments revealed that the responses of DSGCs are both facilitated by image motion in the preferred direction and strongly inhibited by image motion in the opposite null direction (Barlow and Levick, 1965). The inhibition appears to be mediated by GABAergic amacrine cells because GABA_A-antagonists effectively abolish the direction selectivity of DSGCs (Wyatt and Daw, 1976). Given that the starburst cells contain both acetylcholine and GABA, Vaney and colleagues (1989) proposed that each DSGC could selectively receive either cholinergic input from starburst cells located on the preferred side of the ganglion cell or GABAergic input from starburst cells located on the null side (the preferred and null sides correspond to the flanks first encountered by preferred- and null-direction motion, respectively). If the two mechanisms operated together in a push-pull fashion, then a starburst dendrite pointing in one radial direction would both selectively excite a DSGC with a matching preferred direction and selectively inhibit an overlapping DSGC with the opposite preferred direction. Several related models of direction selectivity have been put forward, in which the spatial asymmetries underlying the different preferred directions are generated by a common radial amacrine cell (Borg-Graham

and Grzywacz, 1992; Grzywacz et al., 1997; Vaney, 1990; Werblin, 1991).

The experimental evidence that the starburst amacrine cells underlie the generation of direction selectivity is contradictory. In the rabbit retina, laser ablation of many ON-starburst cells on the preferred or null side of DSGCs indicated that the starburst cells facilitate the responses of DSGCs in either direction but do not mediate the null-direction inhibition (He and Masland, 1997; see also Vaney et al., 2001). In particular, the DSGCs remained unresponsive to null-direction stimuli following the laser ablation of null-side starburst cells. In the mouse retina, on the other hand, immunoablation of most starburst amacrine cells appeared to abolish direction selectivity, in that all recorded ON-OFF ganglion cells were directional in the control animals but nondirectional in the experimental animals (Yoshida et al., 2001). Moreover, the loss of retinal direction selectivity was reflected in the loss of the optokinetic eye reflex. The immunoablation experiments thus indicate that the starburst amacrine cells are central to the generation of direction selectivity, perhaps by providing the critical null-direction inhibition.

Borg-Graham and Grzywacz (1992) proposed that the terminal dendrites of a starburst amacrine cell would be activated more strongly by centrifugal image motion (away from the soma) than centripetal image motion (toward the soma). For example, a terminal dendrite on the right side of a starburst cell would be activated more strongly by a visual stimulus moving from left to right than in the opposite direction. Consequently, the release of transmitter from a terminal dendrite of a starburst amacrine cell would be directionally selective. Direct evidence for such a differential effect of centrifugal and centripetal image motion on the responses of the distal dendrites has recently been obtained from two-photon imaging of starburst cells filled with a calcium-indicator dye (Euler et al., 2002). If the dendrites on different sides of starburst cells connect selectively to DSGCs with different preferred directions, then the excitatory and/or inhibitory inputs to DSGCs should themselves be direction selective (Grzywacz et al., 1997).

Patch-clamp recordings from turtle DSGCs showed that the excitatory synaptic conductance was larger in the preferred direction than the null direction but, surprisingly, the inhibitory synaptic conductance of many of the DSGCs was also larger in the preferred direction (Borg-Graham, 2001). By contrast, patch-clamp recordings from rabbit DSGCs indicated that the synaptic inputs were almost balanced in the preferred and null directions; this result could be explained most parsimoniously if the component excitatory and inhibitory inputs were nondirectional (Taylor et al., 2000). However, more detailed studies of rabbit DSGCs now indicate that a larger excitatory synaptic conductance in the

preferred direction is coupled with a larger inhibitory synaptic conductance in the null direction (Taylor and Vaney, 2002). In addition to the presynaptic mechanisms that generate directional excitatory and inhibitory inputs, the OFF-responses displayed evidence for postsynaptic interactions between the inputs, by virtue of the fact that the inhibition was coincident with the excitation in the null direction but delayed in the preferred direction.

Fried and colleagues (2002) recently provided direct evidence that asymmetric inputs from starburst amacrine cells underlie the directional inhibitory inputs to DSGCs. They made paired recordings from a DSGC and a starburst cell and then examined how the ganglion cell responded to electrical stimulation of the amacrine cell. Their results indicate that null-side starburst cells inhibit the DSGCs but, surprisingly, that preferred-side starburst cells neither excite nor inhibit the DSGCs. Extracellular recordings had previously established that, although DSGCs cannot be driven by visual stimulation of starburst cells located beyond the dendritic tree of the ganglion cell, such stimuli do facilitate the responses produced by concurrent stimulation of the receptive-field center (Amthor et al., 1996; Yang and Masland, 1992). This led Vaney and colleagues (2001) to suggest that the glutamatergic input from the central bipolar cells somehow gates the cholinergic input from the starburst amacrine cells, either by acting presynaptically on the starburst terminals or postsynaptically on the ganglion cell dendrites. Thus it is possible that electrical stimulation of a preferred-side starburst cell might excite the DSGC if accompanied by concurrent stimulation of the central bipolar cells.

Therefore it is conceivable that the starburst amacrine cells could mediate the larger excitation in the preferred direction as well as the larger inhibition in the null direction. However, the push-pull starburst model of direction selectivity is challenged by several lines of evidence indicating that the starburst cells provide symmetrical cholinergic input to the DSGCs (reviewed by Vaney and Taylor, 2002). It is clear that the spatial and temporal characteristics of the excitatory and inhibitory inputs to DSGCs need to be examined in greater detail, using pharmacological methods to dissect the glutamatergic and cholinergic contributions to the excitation. The developmental mechanisms that would enable each of the four subtypes of DSGCs to receive spatially appropriate inputs from a single starburst cell are certain to be the subject of intensive investigation. When the cotransmission model of direction selectivity was first proposed, Vaney (1990) noted “the concept that pronounced functional asymmetries may be derived from the most symmetrical neurons in the retina is not without irony.” What is now clear is that the radial symmetry of the starburst amacrine cells is probably fundamental to generating the asymmetrical responses of DSGCs.

More structures than functions?

Although it is clear that the functional diversity of retinal amacrine cells is as broad as the morphological diversity, we are still faced with the problem that troubled Cajal (1933): namely, that there appear to be many more types of amacrine cells than required functions. Those amacrine types that have been studied in particular detail—including the AI, AII, dopaminergic, and starburst cells—perform quite distinct tasks, suggesting that the functions of other amacrine types are equally specialized (Masland, 2001). However, it is unclear whether the function of each amacrine type is narrowly restricted, even for cells that have been well characterized. For example, why are there two types of AI cells in the rabbit retina? What is the function of the AII cells in the light-adapted retina? Why do the dopaminergic cells contain GABA? Can the starburst cells excite ganglion cells in a paracrine fashion?

It is not even clear why half the amacrine cells use glycine and the other half use GABA, although it has been proposed that the diversity of inhibitory transmitters and their receptors may reduce cross-talk between adjacent synapses. This hypothesis is not compelling given that there does not appear to be significant cross-talk within the GABAergic circuitry that produces the directional responses of the four subtypes of DSGCs. However, the differences in the dendritic morphology of the glycinergic and GABAergic amacrine cells are clear enough. The glycinergic cells have small- or medium-field dendritic trees that typically occupy two or more strata of the inner plexiform layer; therefore, they can facilitate interactions between the parallel pathways established by the different types of cone bipolar cells. In other words, the glycinergic amacrine cells seem designed to mediate “vertical inhibition” in the retina (Roska and Werblin, 2001). The GABAergic amacrine cells, by comparison, seem designed to mediate the “lateral inhibition” that has normally been attributed to amacrine cells, either via the GABA_C-dominated feedback inhibition of bipolar cells or the GABA_A-dominated feedforward inhibition of ganglion cells and other amacrine cells (Roska et al., 2000).

Whether the inhibition is directed vertically or laterally, the potential connectivity of each type of amacrine cell is limited by its dendritic stratification, which alone imposes substantial functional diversity on the amacrine cells. However, no wiring diagram of the retina could predict the extraordinary morphological diversity of the amacrine cells, suggesting that many subtle aspects of amacrine structure and function have so far eluded us.

Acknowledgements

D. I. Vaney is supported by the National Health & Medical Research Council of Australia.

REFERENCES

- Agardh, E., A. Bruun, B. Ehinger, and J. Storm-Mathisen, 1986. GABA immunoreactivity in the retina, *Invest. Ophthalmol. Vis. Sci.*, 27:674–678.
- Anthor, F. R., and C. W. Oyster, 1995. Spatial organization of retinal information about the direction of image motion, *Proc. Natl. Acad. Sci. USA*, 92:4002–4005.
- Anthor, F. R., N. M. Grzywacz, and D. K. Merwine, 1996. Extra-receptive-field motion facilitation in on-off directionally selective ganglion cells of the rabbit retina, *Vis. Neurosci.* 13:303–309.
- Barlow, H. B., and W. R. Levick, 1965. The mechanism of directionally selective units in rabbit's retina, *J. Physiol.*, 178:477–504.
- Bloomfield, S. A., 1992. Relationship between receptive and dendritic field size of amacrine cells in the rabbit retina, *J. Neurophysiol.*, 68:711–725.
- Bloomfield, S. A., and R. F. Dacheux, 2001. Rod vision: pathways and processing in the mammalian retina, *Prog. Ret. Eye Res.*, 20:351–384.
- Bloomfield, S. A., and R. F. Miller, 1982. A physiological and morphological study of the horizontal cell types of the rabbit retina, *J. Comp. Neurol.*, 208:288–303.
- Bloomfield, S. A., and D. Xin, 2000. Surround inhibition of mammalian AII amacrine cells is generated in the proximal retina, *J. Physiol.*, 523:771–783.
- Bloomfield, S. A., D. Xin, and T. Osborne, 1997. Light-induced modulation of coupling between AII amacrine cells in the rabbit retina, *Vis. Neurosci.*, 14:565–576.
- Borg-Graham, L. J., 2001. The computation of directional selectivity in the retina occurs presynaptic to the ganglion cell, *Nat. Neurosci.*, 4:176–183.
- Borg-Graham, L. J., and N. Grzywacz, 1992. A model of the direction selectivity circuit in retina: transformations by neurons singly and in concert, in *Single Neuron Computation* (T. McKenna, J. Davis, and S. F. Zornetzer, eds.), San Diego: Academic Press, pp. 347–375.
- Boycott, B. B., and H. Wässle, 1974. The morphological types of ganglion cells of the domestic cat's retina, *J. Physiol.*, 240:397–419.
- Brecha, N., D. Johnson, L. Peichl, and H. Wässle, 1988. Cholinergic amacrine cells of the rabbit retina contain glutamate decarboxylase and gamma-aminobutyrate immunoreactivity, *Proc. Natl. Acad. Sci. USA*, 85:6187–6191.
- Brecha, N., H. J. Karten, and C. Laverack, 1979. Enkephalin-containing amacrine cells in the avian retina: immunohistochemical localization, *Proc. Natl. Acad. Sci. USA*, 76:3010–3014.
- Cajal, S. R., 1893. La rétine des vertébrés, *La Cellule*, 9:119–257.
- Cajal, S. R., 1933. Les problèmes histophysiologiques de la rétine, *XIV Conc. Ophthal. Hispan.*, 2:11–19.
- Cook, P. B., and J. S. McReynolds, 1998. Lateral inhibition in the inner retina is important for spatial tuning of ganglion cells, *Nat. Neurosci.*, 1:714–719.
- Costa, M., J. B. Furness, and I. L. Gibbins, 1986. Chemical coding of enteric neurons, *Prog. Brain Res.*, 68:217–239.
- Crooks, J., and H. Kolb, 1992. Localization of GABA, glycine, glutamate and tyrosine hydroxylase in the human retina, *J. Comp. Neurol.*, 315:287–302.
- Dacey, D. M., 1989. Axon-bearing amacrine cells of the macaque monkey retina, *J. Comp. Neurol.*, 284:275–293.
- Dacey, D. M., 1990. The dopaminergic amacrine cell, *J. Comp. Neurol.*, 301:461–489.
- Dacey, D. M., 1999. Primate retina: cell types, circuits and color opponency, *Prog. Ret. Eye Res.*, 18:737–763.
- Dacheux, R. F., and E. Raviola, 1986. The rod pathway in the rabbit retina: a depolarizing bipolar and amacrine cell, *J. Neurosci.*, 6:331–345.
- Dogiel, A. S., 1891. Ueber die nervösen Elemente in der Retina des Menschen, *Arch. Mikrosk. Anat.*, 38:317–344.
- Dowling, J. E., and B. B. Boycott, 1966. Organization of the primate retina: electron microscopy, *Proc. R. Soc. Lond. B*, 166:80–111.
- Dowling, J. E., and B. Ehinger, 1975. Synaptic organization of the amine-containing interplexiform cells of the goldfish and Cebus monkey retinas, *Science*, 188:270–273.
- Dubin, M. W., 1970. The inner plexiform layer of the vertebrate retina: a quantitative and comparative electron microscopic analysis, *J. Comp. Neurol.*, 140:479–505.
- Ehinger, B., 1966. Adrenergic retinal neurons, *Z. Zellforsch.*, 71:146–152.
- Euler, T., P. B. Detwiler, and W. Denk, 2002. Directionally selective calcium signals in dendrites of starburst amacrine cells, *Nature*, 418:845–852.
- Famiglietti, E. V., 1983. "Starburst" amacrine cells and cholinergic neurons: mirror-symmetric ON and OFF amacrine cells of rabbit retina, *Brain Res.*, 261:138–144.
- Famiglietti, E. V., 1991. Synaptic organization of starburst amacrine cells in rabbit retina: analysis of serial thin sections by electron microscopy and graphic reconstruction, *J. Comp. Neurol.*, 309:40–70.
- Famiglietti, E. V., 1992a. Polyaxonal amacrine cells of rabbit retina: morphology and stratification of PA1 cells, *J. Comp. Neurol.*, 316:391–405.
- Famiglietti, E. V., 1992b. Polyaxonal amacrine cells of rabbit retina: PA2, PA3, and PA4 cells. Light and electron microscopic studies with a functional interpretation, *J. Comp. Neurol.*, 316:422–446.
- Famiglietti, E. V., and H. Kolb, 1975. A bistratified amacrine cell and synaptic circuitry in the inner plexiform layer of the retina, *Brain Res.*, 84:293–300.
- Fletcher, E. L., and H. Wässle, 1999. Indoleamine-accumulating amacrine cells are presynaptic to rod bipolar cells through GABA_C receptors, *J. Comp. Neurol.*, 413:155–167.
- Freed, M. A., R. G. Smith, and P. Sterling, 1987. Rod bipolar array in the cat retina: pattern of input from rods and GABA-accumulating amacrine cells, *J. Comp. Neurol.*, 266:445–455.
- Fried, S. I., T. A. Münch, and F. S. Werblin, 2002. Mechanisms and circuitry underlying directional selectivity in the retina, *Nature*, 420:411–414.
- Gábel, R., and C. Straznicky, 1992. Immunocytochemical localization of parvalbumin- and neurofilament triplet protein immunoreactivity in the cat retina: colocalization in a subpopulation of AII amacrine cells, *Brain Res.*, 595:133–136.
- Grzywacz, N. M., J. S. Tootle, and F. R. Anthor, 1997. Is the input to a GABAergic or cholinergic synapse the sole asymmetry in rabbit's retinal directional selectivity? *Vis. Neurosci.*, 14:39–54.
- Hack, I., and L. Peichl, 1999. Horizontal cells of the rabbit retina are non-selectively connected to the cones, *Eur. J. Neurosci.*, 11:2261–2274.
- Häggendal, J., and T. Malmfors, 1965. Identification and cellular localization of the catecholamines in the retina and choroid of the rabbit, *Acta Physiol. Scand.*, 64:58–66.
- Hampson, E. C. G. M., D. I. Vaney, and R. Weiler, 1992. Dopaminergic modulation of gap junction permeability between amacrine cells in mammalian retina, *J. Neurosci.*, 12:4911–4922.
- Hartveit, E., 1999. Reciprocal synaptic interactions between rod bipolar cells and amacrine cells in the rat retina, *J. Neurophysiol.*, 81:2923–2936.

- He, S., and R. H. Masland, 1997. Retinal direction selectivity after targeted laser ablation of starburst amacrine cells, *Nature*, 389:378–382.
- Holmgren-Taylor, I., 1982. Electron microscopical observations on the indoleamine-accumulating neurons and their synaptic connections in the retina of the cat, *J. Comp. Neurol.*, 208:144–156.
- Kalloniatis, M., R. E. Marc, and R. F. Murry, 1996. Amino acid signatures in the primate retina, *J. Neurosci.*, 16:6807–6829.
- Kolb, H., 1979. The inner plexiform layer in the retina of the cat: electron microscopic observations, *J. Neurocytol.*, 8:295–329.
- Kolb, H., 1997. Amacrine cells of the mammalian retina: neurocircuitry and functional roles, *Eye*, 11:904–923.
- Kolb, H., and E. V. Famiglietti, 1974. Rod and cone pathways in the inner plexiform layer of cat retina, *Science*, 186:47–49.
- Kolb, H., K. A. Linberg, and S. K. Fisher, 1992. Neurons of the human retina: a Golgi study, *J. Comp. Neurol.*, 318:147–187.
- Kolb, H., and R. Nelson, 1996. Hyperpolarizing, small-field, amacrine cells in cone pathways of cat retina, *J. Comp. Neurol.*, 371:415–436.
- Kolb, H., R. Nelson, and A. Mariani, 1981. Amacrine cells, bipolar cells and ganglion cells of the cat retina: a Golgi study, *Vis. Res.*, 21:1081–1114.
- Koontz, M. A., and A. E. Hendrickson, 1990. Distribution of GABA-immunoreactive amacrine cell synapses in the inner plexiform layer of macaque monkey retina, *Vis. Neurosci.*, 5:17–28.
- Koontz, M. A., L. E. Hendrickson, S. T. Brace, and A. E. Hendrickson, 1993. Immunocytochemical localization of GABA and glycine in amacrine and displaced amacrine cells of macaque monkey retina, *Vis. Res.*, 33:2617–2628.
- Lam, D. M.-K., H.-B. Li, Y.-Y. T. Su, and C. B. Watt, 1985. The signature hypothesis: colocalizations of neuroactive substances as anatomical probes for circuitry analyses, *Vis. Res.*, 25:1353–1364.
- Lam, D. M.-K., Y.-Y. T. Su, L. Swain, R. E. Marc, C. Brandon, and J.-Y. Wu, 1979. Immunocytochemical localization of L-glutamic acid decarboxylase in the goldfish retina, *Nature*, 278:565–567.
- MacNeil, M. A., J. K. Heussy, R. F. Dacheux, E. Raviola, and R. H. Masland, 1999. The shapes and numbers of amacrine cells: matching of photofilled with Golgi-stained cells in the rabbit retina and comparison with other mammalian species, *J. Comp. Neurol.*, 413:305–326.
- MacNeil, M. A., and R. H. Masland, 1998. Extreme diversity among amacrine cells: implications for function, *Neuron*, 20:971–982.
- Marc, R. E., and B. W. Jones, 2002. Molecular phenotyping of retinal ganglion cells, *J. Neurosci.*, 22:413–427.
- Marc, R. E., and W. Liu, 2000. Fundamental GABAergic amacrine cell circuitries in the retina: nested feedback, concatenated inhibition, and axosomatic synapses, *J. Comp. Neurol.*, 425:560–582.
- Marc, R. E., R. F. Murry, and S. F. Basinger, 1995. Pattern recognition of amino acid signatures in retinal neurons, *J. Neurosci.*, 15:5106–5129.
- Marc, R. E., R. F. Murry, S. K. Fisher, K. A. Linberg, G. P. Lewis, and M. Kalloniatis, 1998. Amino acid signatures in the normal cat retina, *Invest. Ophthalmol. Vis. Sci.*, 39:1685–1693.
- Mariani, A. P., 1990. Amacrine cells of the rhesus monkey retina, *J. Comp. Neurol.*, 301:382–400.
- Masland, R. H., 2001. The fundamental plan of the retina, *Nat. Neurosci.*, 4:877–886.
- Masland, R. H., and A. Ames, 1976. Responses to acetylcholine of ganglion cells in an isolated mammalian retina, *J. Neurophysiol.*, 39:1220–1235.
- McGuire, B. A., J. K. Stevens, and P. Sterling, 1984. Microcircuitry of bipolar cells in cat retina, *J. Neurosci.*, 4:2920–2938.
- Menger, N., D. V. Pow, and H. Wässle, 1998. Glycinergic amacrine cells of the rat retina, *J. Comp. Neurol.*, 401:34–46.
- Mills, S. L., and S. C. Massey, 1999. AII amacrine cells limit scotopic acuity in central macaque retina: a confocal analysis of calretinin labeling, *J. Comp. Neurol.*, 411:19–34.
- Mosinger, J. L., S. Yazulla, and K. M. Studholme, 1986. GABA-like immunoreactivity in the vertebrate retina: a species comparison, *Exp. Eye Res.*, 42:631–644.
- Müller, F., H. Wässle, and T. Voigt, 1988. Pharmacological modulation of the rod pathway in the cat retina, *J. Neurophysiol.*, 59:1657–1672.
- Müller, H., 1851. Zur Histologie der Netzhaut, *Zeits. Wiss. Zool.*, 3:4.
- Negishi, K., S. Kato, and T. Teranishi, 1988. Dopamine cells and rod bipolar cells contain protein kinase C-like immunoreactivity in some vertebrate retinas, *Neurosci. Lett.*, 94:247–252.
- Nelson, R., 1982. AII amacrine cells quicken time course of rod signals in the cat retina, *J. Neurophysiol.*, 47:928–947.
- Nelson, R., and H. Kolb, 1985. A17: a broad-field amacrine cell in the rod system of the cat retina, *J. Neurophysiol.*, 54:592–614.
- O'Malley, D. M., J. H. Sandell, and R. H. Masland, 1992. Corelease of acetylcholine and GABA by the starburst amacrine cells, *J. Neurosci.*, 12:1394–1408.
- Osborne, N. N., and D. W. Beaton, 1986. Direct histochemical localisation of 5,7-dihydroxytryptamine and the uptake of serotonin by a subpopulation of GABA neurones in the rabbit retina, *Brain Res.*, 382:158–162.
- Oyster, C. W., and H. B. Barlow, 1967. Direction-selective units in rabbit retina: distribution of preferred directions, *Science*, 155:841–842.
- Pasteels, B., J. Rogers, F. Blachier, and R. Pochet, 1990. Calbindin and calretinin localization in retina from different species, *Vis. Neurosci.*, 5:1–16.
- Perry, V. H., and M. Walker, 1980. Amacrine cells, displaced amacrine cells and interplexiform cells in the retina of the rat, *Proc. R. Soc. Lond. B*, 208:415–431.
- Pourcho, R. G., and D. J. Goebel, 1983. Neuronal subpopulations in cat retina which accumulate the GABA agonist, (³H)muscimol: a combined Golgi and autoradiographic study, *J. Comp. Neurol.*, 219:25–35.
- Pourcho, R. G., and D. J. Goebel, 1985. A combined Golgi and autoradiographic study of (³H)glycine-accumulating amacrine cells in the cat retina, *J. Comp. Neurol.*, 233:473–480.
- Pourcho, R. G., and D. J. Goebel, 1987. Visualization of endogenous glycine in cat retina: an immunocytochemical study with Fab fragments, *J. Neurosci.*, 7:1189–1197.
- Pourcho, R. G., and M. T. Owczarzak, 1989. Distribution of GABA immunoreactivity in the cat retina: a light- and electron-microscopic study, *Vis. Neurosci.*, 2:425–435.
- Pourcho, R. G., and M. T. Owczarzak, 1991. Connectivity of glycine immunoreactive amacrine cells in the cat retina, *J. Comp. Neurol.*, 307:549–561.
- Pow, D. V., and D. K. Crook, 1993. Extremely high titre polyclonal antisera against small neurotransmitter molecules: rapid production, characterisation and use in light- and electron-microscopic immunocytochemistry, *J. Neurosci. Methods*, 48:51–63.
- Pow, D. V., L. L. Wright, and D. I. Vaney, 1995. The immunocytochemical detection of amino-acid neurotransmitters in paraformaldehyde-fixed tissues, *J. Neurosci. Methods*, 56:115–123.

- Rodieck, R. W., and R. K. Brening, 1983. Retinal ganglion cells: properties, types, genera, pathways and trans-species comparisons, *Brain Behav. Evol.*, 23:121–64.
- Roska, B., E. Nemeth, L. Orzo, and F. S. Werblin, 2000. Three levels of lateral inhibition: a space-time study of the retina of the tiger salamander, *J. Neurosci.*, 20:1941–1951.
- Roska, B., and F. Werblin, 2001. Vertical interactions across ten parallel, stacked representations in the mammalian retina, *Nature*, 410:583–587.
- Sagar, S. M., 1986. NADPH diaphorase histochemistry in the rabbit retina, *Brain Res.*, 373:153–158.
- Sandell, J. H., and R. H. Masland, 1986. A system of indoleamine-accumulating neurons in the rabbit retina, *J. Neurosci.*, 6:3331–3347.
- Sandell, J. H., and R. H. Masland, 1989. Shape and distribution of an unusual retinal neuron, *J. Comp. Neurol.*, 280:489–497.
- Sandell, J. H., R. H. Masland, E. Raviola, and R. F. Dacheux, 1989. Connections of indoleamine-accumulating cells in the rabbit retina, *J. Comp. Neurol.*, 283:303–313.
- Sassoè-Pognetto, M., H. Wässle, and U. Grünert, 1994. Glycinergic synapses in the rod pathway of the rat retina: cone bipolar cells express the $\alpha 1$ subunit of the glycine receptor, *J. Neurosci.*, 14:5131–5146.
- Sharpe, L. T., and A. Stockman, 1999. Rod pathways: the importance of seeing nothing, *Trends Neurosci.*, 22:497–504.
- Stafford, D. K., and D. M. Dacey, 1997. Physiology of the A1 amacrine: a spiking, axon-bearing interneuron of the macaque monkey retina, *Vis. Neurosci.*, 14:507–522.
- Sterling, P., M. A. Freed, and R. G. Smith, 1988. Architecture of rod and cone circuits to the ON-beta ganglion cell, *J. Neurosci.*, 8:623–642.
- Strettoi, E., E. Raviola, and R. F. Dacheux, 1992. Synaptic connections of the narrow-field, bistratified rod amacrine cell (AII) in the rabbit retina, *J. Comp. Neurol.*, 325:152–168.
- Tartuferi, F., 1887. Sull'anatomia della retina, *Arch. Scienze Mediche*, 11:335–358.
- Tauchi, M., N. K. Madigan, and R. H. Masland, 1990. Shapes and distributions of the catecholamine-accumulating neurons in the rabbit retina, *J. Comp. Neurol.*, 293:178–189.
- Taylor, W. R., 1999. TTX attenuates surround inhibition in rabbit retinal ganglion cells, *Vis. Neurosci.*, 16:285–290.
- Taylor, W. R., S. He, W. R. Levick, and D. I. Vaney, 2000. Dendritic computation of direction selectivity by retinal ganglion cells, *Science*, 289:2347–2350.
- Taylor, W. R., and D. I. Vaney, 2002. Diverse synaptic mechanisms generate direction selectivity in the rabbit retina, *J. Neurosci.*, 22:7712–7720.
- Vaney, D. I., 1985. The morphology and topographic distribution of AII amacrine cells in the cat retina, *Proc. R. Soc. Lond. B*, 224:475–488.
- Vaney, D. I., 1986. Morphological identification of serotonin-accumulating neurons in the living retina, *Science*, 233:444–446.
- Vaney, D. I., 1990. The mosaic of amacrine cells in the mammalian retina, *Prog. Retinal Res.*, 9:49–100.
- Vaney, D. I., 1991. Many diverse types of retinal neurons show tracer coupling when injected with biocytin or Neurobiotin, *Neurosci. Lett.*, 125:187–190.
- Vaney, D. I., 1994a. Patterns of neuronal coupling in the retina, *Prog. Retinal Eye Res.*, 13:301–355.
- Vaney, D. I., 1994b. Territorial organization of direction-selective ganglion cells in rabbit retina, *J. Neurosci.*, 14:6301–6316.
- Vaney, D. I., 1996. The A17 (AI) amacrine cells of the cat retina, *Invest. Ophthalmol. Vis. Sci.*, 37:S676.
- Vaney, D. I., 1999. Neuronal coupling in the central nervous system: Lessons from the retina, in *Gap Junction-Mediated Intercellular Signalling in Health and Disease* (Novartis Foundation Symposium 219) Chichester: Wiley, pp. 113–133.
- Vaney, D. I., S. P. Collin, and H. M. Young, 1989. Dendritic relationships between cholinergic amacrine cells and direction-selective retinal ganglion cells, in *Neurobiology of the Inner Retina* (R. Weiler and N. N. Osborne, eds.), Berlin: Springer, pp. 157–168.
- Vaney, D. I., I. C. Gynther, and H. M. Young, 1991. Rod-signal interneurons in the rabbit retina: 2. AII amacrine cells, *J. Comp. Neurol.*, 310:154–169.
- Vaney, D. I., S. He, W. R. Taylor, and W. R. Levick, 2001. Direction-selective ganglion cells in the retina, in *Motion Vision: Computational, Neural, and Ecological Constraints* (J. M. Zanker and J. Zeil, eds.), Berlin: Springer, pp. 13–55.
- Vaney, D. I., J. C. Nelson, and D. V. Pow, 1998. Neurotransmitter coupling through gap junctions in the retina, *J. Neurosci.*, 18:10594–10602.
- Vaney, D. I., and D. V. Pow, 2000. The dendritic architecture of the cholinergic plexus in the rabbit retina: selective labeling by glycine accumulation in the presence of sarcosine, *J. Comp. Neurol.*, 421:1–13.
- Vaney, D. I., and H. M. Young, 1988a. GABA-like immunoreactivity in cholinergic amacrine cells of the rabbit retina, *Brain Res.*, 438:369–373.
- Vaney, D. I., and H. M. Young, 1988b. GABA-like immunoreactivity in NADPH-diaphorase amacrine cells of the rabbit retina, *Brain Res.*, 474:380–385.
- Vaney, D. I., and W. R. Taylor, 2002. Direction selectivity in the retina, *Curr. Opin. Neurobiol.*, 12:405–410.
- Wagner, H. J., and E. Wagner, 1988. Amacrine cells in the retina of a teleost fish, the roach (*Rutilus rutilus*): a Golgi study on differentiation and layering, *Phil. Trans. R. Soc. Lond. B*, 321:263–324.
- Wässle, H., U. Grünert, M. H. Chun, and B. B. Boycott, 1995. The rod pathway of the macaque monkey retina: identification of AII-amacrine cells with antibodies against calretinin, *J. Comp. Neurol.*, 361:537–551.
- Watt, C. B., Y.-Y. T. Su, and D. M.-K. Lam, 1984. Interactions between enkephalin and GABA in avian retina, *Nature*, 311:761–763.
- Weiler, R., and A. K. Ball, 1984. Co-localization of neurotensin-like immunoreactivity and ^3H -glycine uptake system in sustained amacrine cells of turtle retina, *Nature*, 311:759–761.
- Werblin, F., 1991. Synaptic connections, receptive fields, and patterns of activity in the tiger salamander retina. A simulation of patterns of activity formed at each cellular level from photoreceptors to ganglion cells, *Invest. Ophthalmol. Vis. Sci.*, 32:459–483.
- Werblin, F. S., and J. E. Dowling, 1969. Organization of the retina of the mudpuppy, *Necturus maculosus*. II. Intracellular recording, *J. Neurophysiol.*, 32:339–355.
- Witkovsky, P., and A. Dearry, 1992. Functional roles of dopamine in the vertebrate retina, *Prog. Ret. Res.*, 11:247–292.
- Wright, L. L., C. L. Macqueen, G. N. Elston, H. M. Young, D. V. Pow, and D. I. Vaney, 1997. The DAPI-3 amacrine cells of the rabbit retina, *Vis. Neurosci.*, 14:473–492.
- Wright, L. L., D. V. Pow, and D. I. Vaney, 1996. A quantitative immunocytochemical analysis of the distribution of glycinergic and GABAergic amacrine cells in wholemount rabbit retina, *Proc. Aust. Neurosci. Soc.*, 7:190P.

- Wright, L. L., and D. I. Vaney, 1999. The fountain amacrine cells of the rabbit retina, *Vis. Neurosci.*, 16:1145–1156.
- Wyatt, H. J., and N. W. Daw, 1976. Specific effects of neurotransmitter antagonists on ganglion cells in rabbit retina, *Science*, 191:204–205.
- Xin, D., and S. A. Bloomfield, 1999. Comparison of the responses of AII amacrine cells in the dark- and light-adapted rabbit retina, *Vis. Neurosci.*, 16:653–65.
- Yang, G., and R. H. Masland, 1992. Direct visualization of the dendrite and receptive fields of directionally selective retinal ganglion cells, *Science* 258:1949–1952.
- Yoshida, K., D. Watanabe, H. Ishikane, M. Tachibana, I. Pastan, and S. Nakanishi, 2001. A key role of starburst amacrine cells in originating retinal directional selectivity and optokinetic eye movement, *Neuron*, 30:771–780.

26 Ganglion Cells in Mammalian Retinae

PAUL R. MARTIN AND ULRIKE GRÜNERT

IT IS CUSTOMARY to describe the ganglion cells as the output neurons of the retina. By this is meant that trains of action potentials in the axons of ganglion cells carry encoded messages from the eye to the brain. These messages give rise to conscious visual perception and also contribute to diverse, nonconscious aspects of visual function, including eye movements, modulation of attention, and entrainment of the circadian rhythm. This chapter gives an introduction to the basic morphological and functional properties of ganglion cells in the mammalian retina. Special attention is given to the dominant ganglion cell classes in the primate visual system.

Morphological properties

HISTORY Structural analysis of the eye began with the Greek and Arab anatomists, but identification of the cellular elements of the retina was dependent on the development of microscopic technology and histological methods in the eighteenth and nineteenth century. Polyak's historical review (1941) attributes to G. R. Treviranus (1836–1838) the first description of ganglion cells. Treviranus described a subset of “papillae” (presumed to be the photoreceptive terminals of the optic nerve fibers) on the vitreal surface of the retina. The major direction for retinal signal flow—from photoreceptors to the optic nerve—was substantially agreed upon by the end of the nineteenth century by the German and Italian anatomists led by Corti, H. Müller, and Kölliker. In these decades the retina became the object of intense scientific scrutiny, as proponents of the *neuronal* and *reticularist* schools attempted to answer “the basic problem of the intrinsic organisation of the nervous system: reciprocal or mutual relationship of the nervous elements” (Polyak, 1941, p. 169). The evidence and forceful arguments of Cajal prevailed, to give the first clear expression of the modern view: each ganglion cell is an independent functional entity, which forms the final link in a chain of synaptic connectivity beginning with the photoreceptors (Cajal, 1893; for qualifications to this view, see Chapters 17 and 25). Cajal's second major contribution to understanding ganglion cells was the delineation of diverse morphological types, with distinct patterns of dendritic arborization within the inner plexiform layer (Figure 26.1A). In this discovery is the germ of the modern view that the retinal ganglion cells comprise functionally distinct neuronal populations. The different types of ganglion

cells are specialized to encode, in parallel, signals about distinct aspects of the spatial, temporal, and spectral composition of the retinal image.

MORPHOLOGY AS A GUIDE TO FUNCTION Understanding the variety of morphologies presented by ganglion cells has been improved by assuming that there exist multiple natural types¹ of ganglion cell, each of which is present throughout the retina (Rodieck, 1972; Rodieck and Brening, 1983; Stone, 1983; see also Chapters 25 and 30). Members of a given cell type all show consistent features. Some of these features remain constant throughout the retina (e.g., the brain nucleus where the ganglion cell axon terminates); others show systematic variation (e.g., the size of the dendritic tree). Such variation can lead to systematic variation in functional properties and ultimately to variation in the visual functions that rely on the activity of that cell type.

A simplified catalogue of ganglion cell types defined in this way is nevertheless large. More than a dozen natural types of ganglion cell have been distinguished in the retinas of the mammalian species studied in detail (Boycott and Dowling, 1969; Kolb et al., 1992; O'Brien et al., 2002; Rockhill et al., 2002; Watanabe and Rodieck, 1989), and the extent to which homologies can be drawn between functional classes in species of different orders remains controversial (Shapley and Perry, 1986; see Chapter 31). But substantial insight has been gained by addressing two major questions. First, which properties of each ganglion cell type remain constant throughout the retina? Second, which properties are variable? The following discussion will focus on the primate retina as both exemplifying general principles and being most relevant to understanding the visual capacity of humans.

GANGLION CELL TYPES IN THE PRIMATE RETINA

Parasol and midget cells. Polyak (1941) distinguished, in Golgi studies of the primate retina, two types of ganglion cell,

¹The terms “type” and “group” are used according to Rodieck and Brening (1983), where a cell *type* occupies a unique position in a space defined by multiple parameters, whereas a cell *group* has one or more features in common but may contain multiple types. For example, in the following discussion the midget and parasol cells form separate *types*, but both belong to the *group* of ganglion cells with axons which project to the lateral geniculate nucleus.

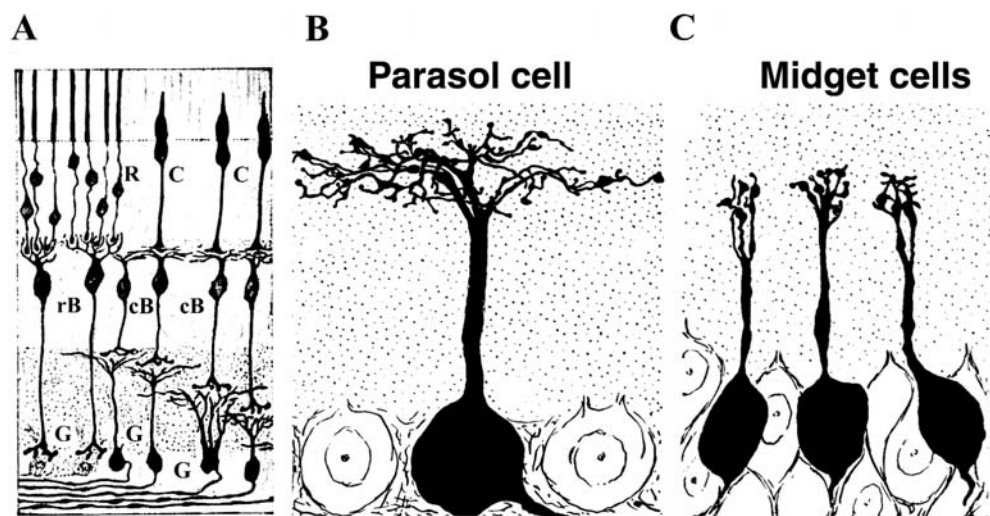


FIGURE 26.1. *A*, signal flow in the retina (Cajal, 1893; modified from Fig. 34 in Polyak, 1941). Summary drawing made from observations of vertical (radial) Golgi-stained sections of bird retina. Rod (*R*) and cone (*C*) photoreceptors make contact with rod bipolar cells (*rB*) and cone bipolar cells (*cB*). Cone bipolar

cells are costratified with distinct types of ganglion cells (*G*) in the inner plexiform layer. *B*, *C*, ganglion cells in Golgi-stained vertical sections of macaque retina (modified from Fig. 70 in Polyak, 1941). *B*, parasol cell from the perifoveal region. *C*, midget cells at the fovea.

which he termed *parasol* and *midget* for the morphology of their dendritic arbour (Figure 26.1*B,C*). Subsequent studies using retrograde transport of injected tracer (Leventhal et al., 1981; Perry et al., 1984; Rodieck and Watanabe, 1993) showed that parasol cells form the dominant projection to the magnocellular layers of the lateral geniculate nucleus of the thalamus, whereas midget cells make up the dominant projection to the parvocellular layers. There can be little doubt that activity of these two cell types is the functional “front end” of most aspects of human conscious visual perception. Parasol and midget cells have been distinguished in the retinas of all primates studied so far (Boycott and Dowling, 1969; Ghosh et al., 1996; Leventhal et al., 1981; Perry et al., 1984; Polyak, 1941; Rodieck, 1988; Rodieck and Watanabe, 1993; Silveira et al., 1994; Yamada et al., 1996). Midget ganglion cells make up approximately 80% of the primate ganglion cell population, and parasol cells make up close to 10%.

Nonmidget, nonparasol cells. The proportion of nonmidget, nonparasol ganglion cells is small in relative terms (about 10%), but in absolute terms (probably about 100,000 cells in primate retina) they approach or outnumber the total complement of ganglion cells in most nonprimate retinas. For example, the retina of the cat probably contains about 120,000 ganglion cells (Williams et al., 1986). A wide range of morphologies is displayed by nonmidget, nonparasol cell populations; these populations are customarily described as wide field or diffuse because their dendrites are less densely branched and cover a larger region of the retina than the dendrites of parasol and midget cells at a given eccentricity

(for a summary of early morphological classification, see Rodieck, 1972, pp. 469–476).

Rapid progress has been made toward the goal of identifying natural types of ganglion cells from these other cell types. Two key technological advances have assisted this progress. First, retrograde labeling techniques allow identification of the central targets of ganglion cell populations. Each central retinorecipient nucleus gets input from only a few types of ganglion cell. The retrograde label thus acts as a “functional sieve” to reveal the morphology and mosaic properties of only a specific fraction of ganglion cells. Second, refinements to *in vitro* recording techniques allow combined functional and morphological measurements of individual neurons (Brown et al., 2000; Dacey and Lee, 1994; Demb et al., 2001; O’Brien et al., 2002). Common functional properties of a population of cells can then be tied to common morphological properties. These principles are well illustrated by the establishment of small bistratified ganglion cells as a natural type in primate retina, as follows.

Small-field bistratified cells. Delineation by Rodieck (1991) and Dacey (1993) of a parvocellular-projecting, bistratified ganglion cell type in macaque and human retina, with a dendritic arbor slightly larger than that of parasol cells, was closely followed by the discovery (Dacey and Lee, 1994) that the small-field bistratified cell corresponds to the “blue-ON” cell known from extracellular *in vivo* recordings in the retina and lateral geniculate nucleus (Derrington et al., 1984; Gouras, 1968). Small bistratified cells and blue-ON type responses have been identified in several primate species,

with the possible exception of the (nocturnal) owl monkey *Aotus*, suggesting that this functional system is common to diurnal primates (Dacey, 1993; Ghosh et al., 1996; Rodieck and Watanabe, 1993; Yamada et al., 1996). Direct correlation of morphology with function has only been made in macaque (Dacey and Lee, 1994). The basis of chromatic selective responses in small bistratified cells is treated elsewhere in this volume (see Chapter 64).

Other wide-field cell types. The central projections and morphological features of several distinct groups of wide-field ganglion cells in primate retina have been delineated (Boycott and Dowling, 1969; Kolb et al., 1992; Peterson and Dacey, 2000; Polyak, 1941; Rodieck and Watanabe, 1993; Telkes et al., 2000; Yamada et al., 1996), but their functional properties remain poorly understood, especially when compared to the analyses recently completed for essentially all ganglion cell types in cat and rabbit retina (O'Brien et al., 2002; Rockhill et al., 2002). One recent and important exception is the delineation of a wide-field class projecting to olivary pretectal nucleus in macaque (Gamlin et al., 2001); this cell shows nonadapting, sustained response to maintained illumination. It remains to be established whether this cell type, like the melanopsin-containing ganglion cell that projects to the suprachiasmatic nucleus (Hattar et al., 2002), attains nonadapting response to ambient light level by intrinsic phototransduction.

SYNAPTIC INPUT TO GANGLION CELLS Multiple types of bipolar and amacrine cells have been distinguished in all mammalian retinas studied so far (Chapter 25). The major excitatory neurotransmitter used by bipolar cells is glutamate, whereas amacrine cells use the inhibitory transmitters GABA and/or glycine. Glutamate, glycine, and GABA_A receptors are present throughout the dendritic tree of both midget and parasol ganglion cell types (Lin et al., 2002; Macri et al., 2000). Figure 26.2 compares the distribution of glutamate and GABA_A receptors on the dendritic tree of two parasol cells. Such light microscopic data are consistent with electronmicroscopic data suggesting parasol cells receive 80% of their synaptic input from amacrine cells and 20% from bipolar cells. By contrast, midget ganglion cells receive closer to 50% of their input from amacrine cells and 50% from bipolar cells (Calkins et al., 1994; Kolb et al., 1992).

Dendritic field stratification. Both Polyak (1941) and Boycott and Dowling (1966), in Golgi studies of primate retina, used the pattern of dendritic stratification in the inner plexiform layer as a defining characteristic for ganglion cell types. The pattern of dendritic stratification remains relatively constant throughout the retina (Watanabe and Rodieck, 1989). Because the absolute width of the inner plexiform layer varies with distance from the fovea, it is customary to express

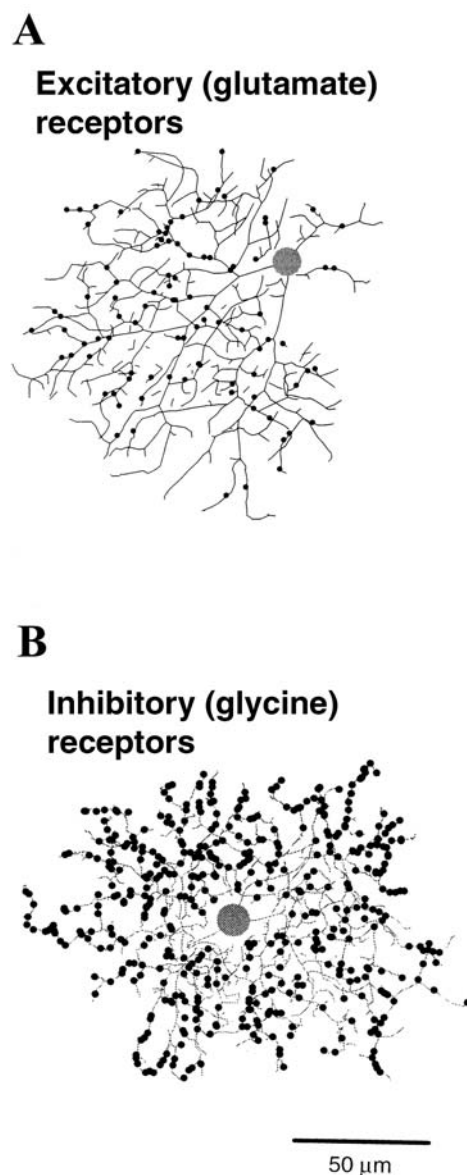


FIGURE 26.2. Neurotransmitter receptors on ganglion cells. Computer reconstruction of the dendritic tree of Neurobiotin-injected parasol cells in marmoset retina. Retinas were processed for immunoreactivity to neurotransmitter receptor subunits: AMPA receptor GluR1 subunit (A); glycine receptor all subunits (B). Solid black circles show colocalized receptor clusters on the ganglion cell dendrites. Large gray circle shows the position of the cell somata. Both receptor types are distributed throughout the dendritic tree; the density of colocalized glutamate receptors is lower than that of colocalized glycine receptors. (Data from Lin, et al., 2000 and Lin et al., 2002.)

the depth of stratification as a percentage of the distance between the inner nuclear layer and the ganglion cell layer. In primate retina, midget cells form two subtypes, which stratify close to 15% and 75% depth; parasol cells form two subtypes, which stratify closer to the center of the inner plexiform layer around 33% and 66% depth (Calkins et al., 1994; Ghosh et al., 1996; Watanabe and Rodieck, 1989).

Wide-field ganglion cell types in primate retina display a variety of stratification patterns: some have dendrites restricted to a small range of depth in the inner plexiform layer, others have multiple layers of dendritic stratification, or dendrites that range in an apparently unconstrained way throughout the inner plexiform layer (Boycott and Dowling, 1969; Dacey, 1993; Kolb et al., 1992; Peterson and Dacey, 2000). Surveys of ganglion cell morphology in nonprimate mammalian retina (O'Brien et al., 2002; Rockhill et al., 2002) likewise show stereotyped patterns of dendritic stratification for each natural cell type. The functional significance of dendritic stratification is thought to lie in selectivity for synaptic input to ganglion cells from distinct classes of bipolar and amacrine cells.

Bipolar cell connectivity. Over 10 different bipolar cell types have been distinguished in primate retina (Boycott and Dowling, 1969; Boycott and Wässle, 1991; Kolb et al., 1992; Rodieck, 1988). The stratification level of bipolar dendrites is a natural constraint on the connectivity with ganglion cells. Polyak (1941) suggested that one-to-one connectivity between midget ganglion cells and midget bipolar cells in the fovea could be the anatomical substrate for high spatial resolution vision. Electron microscopic reconstruction of midget bipolar–ganglion cell pairs has confirmed that the great majority of bipolar synapses to each midget ganglion cell in the fovea derive from a single midget bipolar cell (Calkins et al., 1994; Kolb et al., 1992). Data from other cell types suggests that this “tidy” pattern of connectivity may be unique to the midget system in the foveal retina. Outside the fovea, the dendritic field diameter of midget cells encompasses the dendritic field of many midget bipolar cells. This implies neural convergence from midget bipolar cells to ganglion cells. Data from electronmicroscopic reconstructions of cat ganglion cells (see Chapter 17) also show divergence of bipolar to ganglion cell connections, so a bipolar cell may share its output among several ganglion cells. Electron microscopic analysis of parasol and small-field bistratified cells further shows that there is not unique connectivity between bipolar cells and ganglion cells (Jacoby et al., 2000). For example, the OFF-parasol cell derives synaptic input from two diffuse bipolar cell classes DB3 and DB2 (Jacoby et al., 2000). In summary, “type-to-type” costratification of ganglion cell dendrites with bipolar cell axon terminals gives strong probability of connectivity, but does not mean there is a devoted synaptic circuit.

ECCENTRICITY-DEPENDENCE OF MORPHOLOGY The idea that each natural ganglion cell type shows systematic morphological variation as a function of eccentricity, that is, distance from the retinal locus of highest cone receptor density, was first evaluated quantitatively by Boycott and Wässle (1974) in the cat retina. Figure 26.3 shows eccentricity-

dependent change in ganglion cell morphology for the primate retina. The dendritic field diameter of both midget and parasol cells shows systematic increase with distance from the fovea. This increase is associated with decreasing numbers of each cell type, so the sensorium is completely sampled by constant “coverage” of the retina by each class, albeit with decreasing spatial precision as eccentricity increases (Peichl and Wässle, 1981; Wässle et al., 1981; Yamada et al., 1996; see Chapter 29). Evidence for this principle is given in Figure 26.4 by comparing cells at the same distance from the fovea in nasal or temporal retina. Density is higher in nasal retina, and the dendritic field diameter of both parasol and midget cells is correspondingly smaller (Ghosh et al., 1996; Perry et al., 1984; Watanabe and Rodieck, 1989). This principle is also consistent with the less marked dependence of receptive field diameter on eccentricity for nonmidget, nonparasol cells, where larger dendritic field diameter is associated with a shallower central-peripheral density gradient (Perry et al., 1984; Peterson and Dacey, 2000; Rodieck and Watanabe, 1993).

Special case of the fovea. The special case of the fovea as a specialized region for high-acuity vision was recognized in early morphological studies (Boycott and Dowling, 1969; Cajal, 1893; Polyak, 1941). This specialization gives rise not only to gross changes in the structure of the retinal layers, but also to the characteristic morphology of midget cells as originally defined by Polyak (1941). Midget cells within 9° of the fovea in all diurnal primates described so far have uniform dendritic diameter (between 5 and 15 mm) (Kolb et al., 1992; Perry et al., 1984; Watanabe and Rodieck, 1989; Yamada et al., 1996). The dendritic fields of inner and outer subtypes are tightly packed in two or three sublevels within their respective zones of stratification (Calkins et al., 1994; Perry et al., 1984). These morphological features may reflect some lower limit on the size of a ganglion cell dendritic tree; there may be a requirement to “pack” a minimum number of bipolar and amacrine synapses onto the dendritic arbor. The fovea is also an exception to the general rule that the dendritic field diameter is close to the diameter of the excitatory (center) mechanism of the receptive field: the visual acuity of midget-PC pathway ganglion cells continues to increase toward the foveola but the dendritic field size does not change (Derrington and Lennie, 1984; Perry et al., 1984).

CENTRAL PROJECTIONS There is substantial segregation of central projections of distinct cell types. For most central nuclei studied so far, the functional properties of neurons in the target nucleus are dominated by the properties of the afferent ganglion cells. For example, the properties of most neurons in the magnocellular layers of the lateral geniculate nucleus (small receptive field, high sensitivity

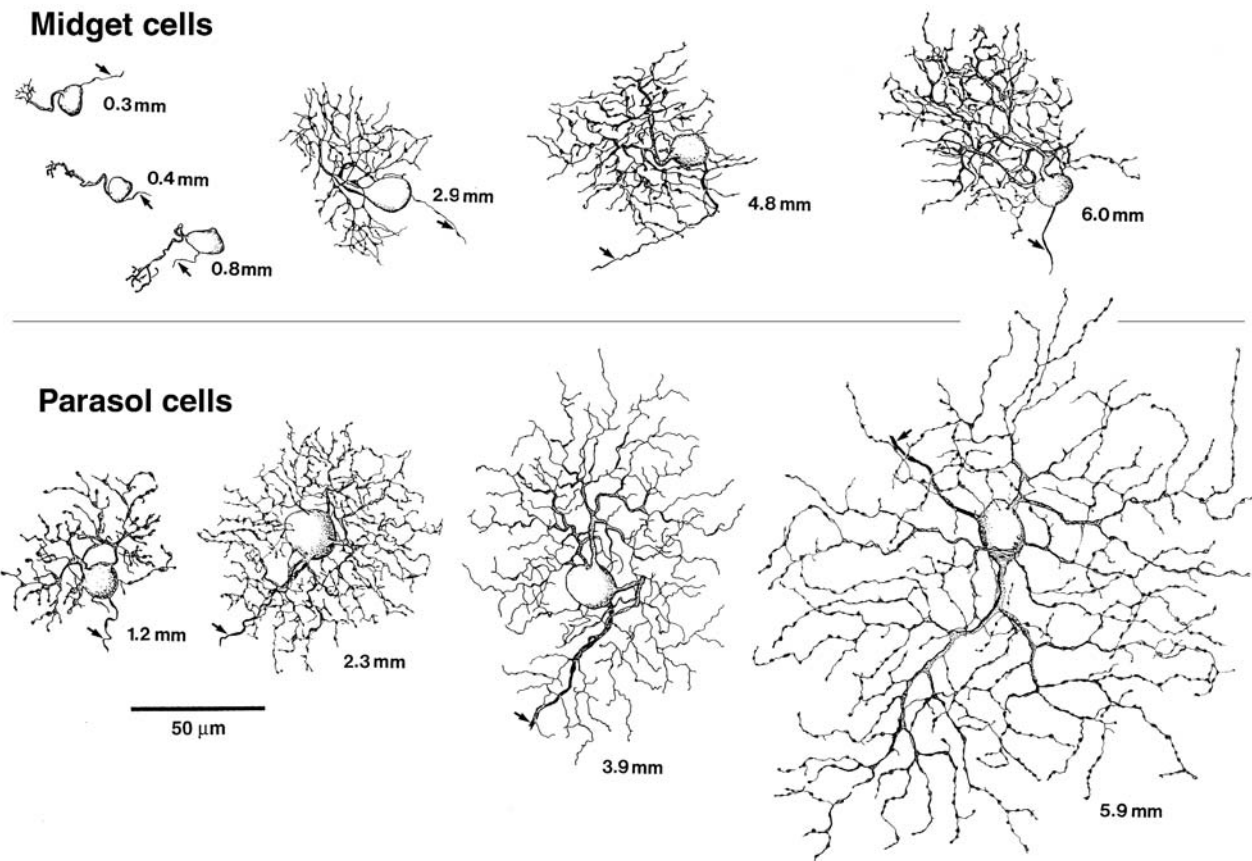


FIGURE 26.3. Eccentricity dependence of ganglion cell morphology. Drawings from Neurobiotin-labeled ganglion cells in marmoset retina. Whole-mount view. Upper row, midget cells; lower

row, parasol cells. Dendritic field diameter of both cell classes increases with distance from the fovea. Arrows point to axons. (Modified from Ghosh et al., 1996, Fig. 5.)

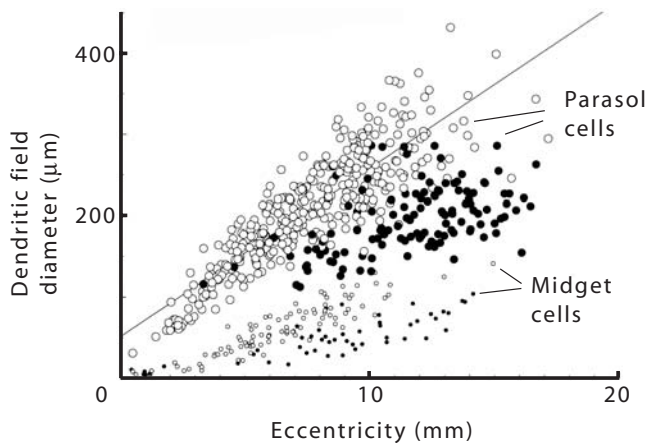


FIGURE 26.4. Dendritic field diameter of parasol and midget cells in macaque retina. Data from horseradish peroxidase-labeled ganglion cells in macaque retina. At any given distance from the fovea the parasol cells have larger dendritic field than midget cells. Cells at a given eccentricity in nasal retina (filled circles) have smaller dendritic field diameter than cells at the same eccentricity in the temporal, upper, and lower quadrants of the retina (open circles). Regression line refers to parasol cells in temporal, upper, and lower quadrants. (Modified from Watanabe and Rodieck, 1989).

to achromatic contrast, high sensitivity to rapid movement) are also properties of the parasol ganglion cells, which project to the magnocellular layers (Croner and Kaplan, 1995; De Monasterio and Gouras, 1975; Derrington and Lennie, 1984; Lee et al., 1990; Wiesel and Hubel, 1966). The central target is thus key for delineating natural types of ganglion cells, but there is also imprecision in this wiring scheme. The axons of some ganglion cell types do branch to innervate more than one central nucleus, and some central nuclei receive afferent projections from more than one ganglion cell type. Two examples follow. First, the axons of the alpha ganglion cell class in cat retina branch to innervate both the lateral geniculate nucleus and the superior colliculus (Illing and Wässle, 1981). Second, the dominant input to the parvocellular division of the primate lateral geniculate is from midget cells, but a proportion of wide-field cells and some small-bistratified ("blue-ON") cells project to the parvocellular layers (Derrington et al., 1984; Leventhal et al., 1981; Perry et al., 1984; Rodieck and Watanabe, 1993; White et al., 1998). Definition of ganglion cell classes by their projection target alone (Shapley and Perry, 1986) should thus be regarded as a convenient simplification,

which applies to most but not all of the projection to any retinorecipient region of a given target nucleus.

Receptive field properties

Very soon after we started we were puzzled and greatly excited to find that uniform illumination of the retina was not the best way to influence the discharges of a ganglion cell; instead, a small spot of light was generally much more effective. Furthermore, the same spot of light could have opposite effects, depending on the exact position of the stimulus on the retina. All one had to do to convert excitation, or “on-response,” into inhibition, or “off-response,” was to shift the spot by a millimeter or less across the retina surface. (Kuffler, 1973, p. 795).

Kuffler’s statement encapsulates most of what today’s student of visual neuroscience must learn about the function of mammalian ganglion cells. First, the action potential discharge rate of each ganglion cell is directly influenced by photon flux in a restricted region of the retina. The *receptive field* of a ganglion cell thus corresponds to a region of visual space where presentation or withdrawal of light causes changes in the rate of action potentials (Barlow, 1953; Kuffler, 1953; Wiesel and Hubel, 1966). Second, the receptive field of most mammalian ganglion cells includes subregions that have opposite effects on the discharge rate of the cell. These subregions usually occupy more or less concentrically organized domains (“center” and “surround”). The rate of action potentials in the ganglion cell is determined by the balance of excitatory and inhibitory influences on the receptive field (Figure 26.5). Responses of such ganglion cells are best thought of as delivering to the brain a simple encoded signal about the local spatial derivative of photon

flux. Parallel studies by Barlow (1953) gave early evidence that there is also a rich variety of receptive field types, particularly in nonmammalian retinas, to which these simple principles do not apply. Such ganglion cells are cryptic, remaining silent until a trigger feature (or “releasing stimulus”) in the visual environment—for example, image movement in a certain direction—produces a burst of action potentials. Responses in such ganglion cells are better thought of as related to specific detection tasks for the visual system, giving rise to the idea of feature detection as a major task of retina ganglion cells (Barlow, 1953; Lettvin et al., 1959).

What have the studies of the intervening decades added to these fundamental observations? The remainder of this chapter summarizes the main advances in understanding receptive field properties of ganglion cells in mammalian retinas, with reference both to the underlying morphological features described above and to those aspects of visual function subserved by the major geniculate-projecting ganglion cell classes in primate retina. Key aspects of the functional properties of preganglion cell circuitry, the generation of ON- and OFF-type responses, and the generation of specialized properties such as direction selectivity are treated in other chapters in this volume (see Chapters 17, 18, 25, and 28). The following discussion treats ganglion cells as independent encoders of the visual scene, in which the encoded message is carried by the spike discharge rate. Evidence that correlated activity between ganglion cells and the fine structure of trains of action potentials may also convey useful additional signals to the brain is reviewed elsewhere (DeVries, 1999; Meister and Berry, 1999; Neuenschwander and Singer, 1996).

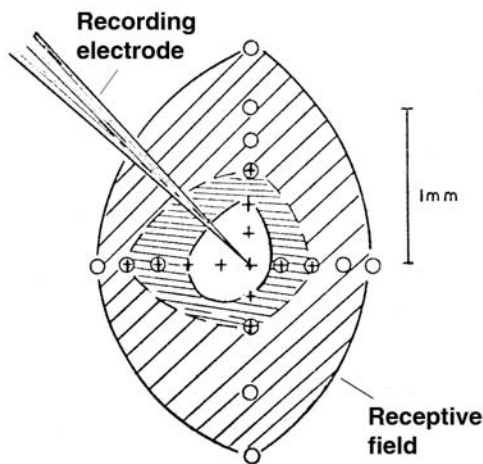


FIGURE 26.5. Receptive field map of a ganglion cell in cat retina made under direct ophthalmoscopic observation during intraocular recording. The area around the tip of the recording electrode defines three zones of the receptive field, where OFF-surround (oblique hatching), ON-center (crosses), and an intermediate zone where both ON- and OFF-responses were elicited. (Modified from Kuffler, 1953, Fig. 6).

CENTER-SURROUND ORGANIZATION Rodieck and Stone (1965) showed that responses of many ganglion cells in cat retina can be accounted for by assuming that the ganglion cell draws antagonistic input from concentrically organized regions with Gaussian distribution of sensitivity to photon flux. Despite well-recognized imperfections, the difference-of-Gaussians (DOG) model (Figure 26.6) remains most widely accepted as a simplified description of the majority of geniculate-projecting ganglion cells in primate retina.

In the midget-parvocellular and parasol-magnocellular cell types, the radius of the surround mechanism is typically 4 to 8 times larger than the radius of the center mechanism (Croner and Kaplan, 1995; Derrington and Lennie, 1984; Irvin et al., 1993; White et al., 2001). The surround mechanism increases in diameter together with the center mechanism, when passing from central to peripheral retina, so gradual uniform changes in illumination give little net response, regardless of the receptive field size or position in the retina (Croner and Kaplan, 1995; Irvin et al., 1993; White et al., 2001).

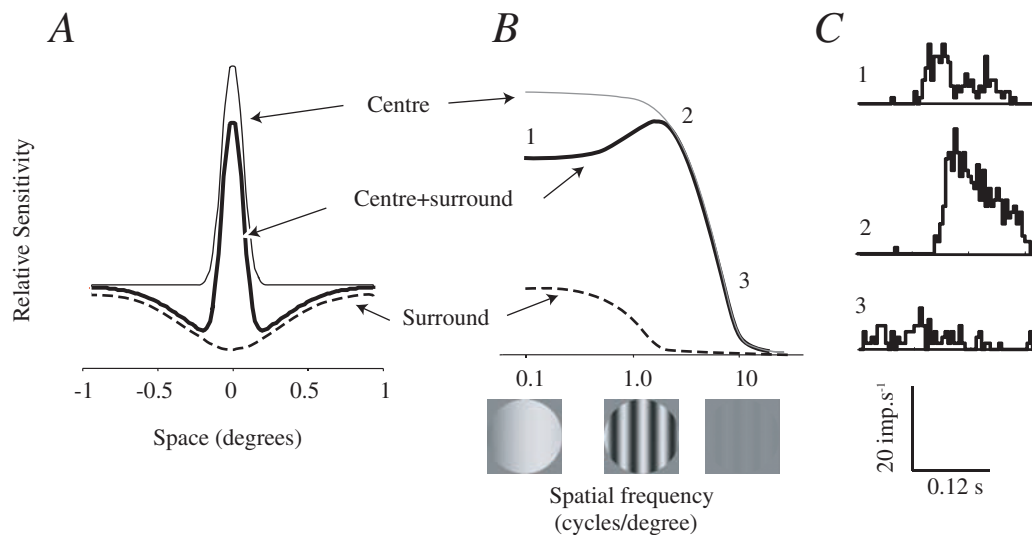


FIGURE 26.6. Difference-of-Gaussians analysis of center-surround receptive fields. *A*, space domain. Center and surround mechanisms are represented by two Gaussians with different contrast sensitivity and space constant. *B*, frequency domain. The center mechanism responds to higher spatial frequencies and is more sensitive than the surround. The frequency response curve

shows bandpass characteristic. *C*, sample peristimulus time histograms recorded from one midget-parvocellular pathway cell in the primate lateral geniculate nucleus. Responses to drifting sinusoidal gratings at the indicated spatial frequencies are shown. The peak response (2) corresponds to the lowest spatial frequency where only the center mechanism is active.

CONTRAST SENSITIVITY Spatial and temporal variations in image intensity cause variations in the discharge rate for the majority of ganglion cells. Sensitivity to such variations (expressed as the variation in discharge rate as a fraction of the variation in intensity, or contrast gain) varies between ganglion cell types. This leads to the idea that different ganglion cell types are tuned to different parts of the spatial and temporal spectrum of the retinal image (see Chapters 17 and 30). In the primate visual system, convergent results from several primate species show that achromatic contrast sensitivity of parasol cells in the retina, and of greater magnocellular cells in the lateral geniculate nucleus, is higher than the sensitivity of midget-parvocellular pathway cells. Responses of cells in the koniocellular division of the lateral geniculate nucleus are assumed to reflect predominantly the properties of nonmidget, nonparasol cells in the retina, and are more heterogeneous than the responses of parvocellular or magnocellular cells (Benardete et al., 1992; Derrington and Lennie, 1984; Irvin et al., 1993; Kaplan and Shapley, 1986; Lee et al., 1990; Norton et al., 1988; Purpura et al., 1988; Sherman et al., 1976; Solomon et al. 1999; Xu et al., 2001). Parasol-magnocellular pathway cells show response compression to high-contrast stimuli (Benardete et al., 1992; Lee et al., 1990; Purpura et al., 1988) indicative of the operation of contrast gain control mechanisms (Shapley et al., 1972). Figure 26.7 shows typical contrast-response relationships and average values for magnocellular, parvocellular, and koniocellular populations.

Two emerging general principles of concentric receptive field organization in mammalian retina are summarized

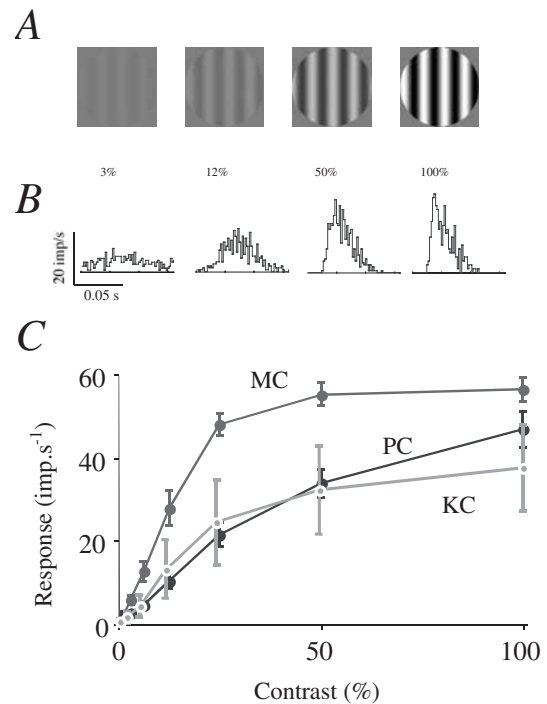


FIGURE 26.7. Contrast sensitivity. *A*, *B*, responses of one midget-parvocellular pathway cell (*B*) to drifting achromatic sinusoidal gratings at optimal spatial frequency at different contrasts (shown in *A*). *C*, average (mean \pm SEM) contrast-response functions of midget-parvocellular (PC), parasol-magnocellular (MC), and koniocellular (KC) pathway cells recorded in marmoset lateral geniculate nucleus. MC and KC cells show high-contrast sensitivity with saturated response to contrast above 50% (data from Solomon et al., 2002, and unpublished).

as follows. First, the contrast sensitivity of the surround mechanism is much lower than that of the center, but the surround integrates over a larger area (16 to 64 times the area of the center mechanism). Second, there is an approximately inverse relationship between area and peak sensitivity of both center and surround mechanisms, so the integrated “volume” of these mechanisms remains relatively constant throughout the retina (Croner and Kaplan, 1995; Irvin et al., 1993; White et al., 2001). The upshot of all this is that the influences of center and surround are rather well balanced (with the center mechanism usually dominating slightly), regardless of cell type or position in the retina. Small deviations from this general relationship confer slightly greater contrast sensitivity, especially for low spatial and high temporal frequencies, on ganglion cells in peripheral retina when compared to their central counterparts.

RELATION TO DENDRITIC FIELD AND SYNAPTIC INPUT The origin of the receptive field center is considered to lie in excitatory, glutamatergic input from bipolar cells (see Chapters 17, 18, and 21). Bipolar cell synapses are distributed

throughout the ganglion cell’s dendritic field (Cohen and Sterling, 1991; Owczarzak and Pourcho, 1999). Accordingly, there is good correspondence between the ganglion cell dendritic field and the size and shape of the receptive field center (Brown et al., 2000; Peichl and Wässle, 1981, 1983; see Fig. 26.8). However, the surround component probably originates at multiple levels of the preganglion cell circuitry. Center-surround interactions are already manifest at the level of the bipolar cell input (see Chapter 17), and direct inhibitory input from amacrine cells makes an additional contribution (Demb et al., 2001; Flores-Herr et al., 2001). Knowledge of the amacrine cells’ contribution to the inhibitory surround is still rudimentary; this is a consequence both of the morphological diversity of amacrine cells and the fact that most amacrine cell types make widespread connections within the retina (see Chapter 25). Recent data suggest that some of the inhibitory input to ganglion cells in rabbit retina depends on activation of voltage-sensitive sodium channels (“spiking” amacrine cells), and the majority of input from amacrine cells depends on GABAergic synaptic activity (Demb et al., 2001; Flores-Herr et al., 2001).

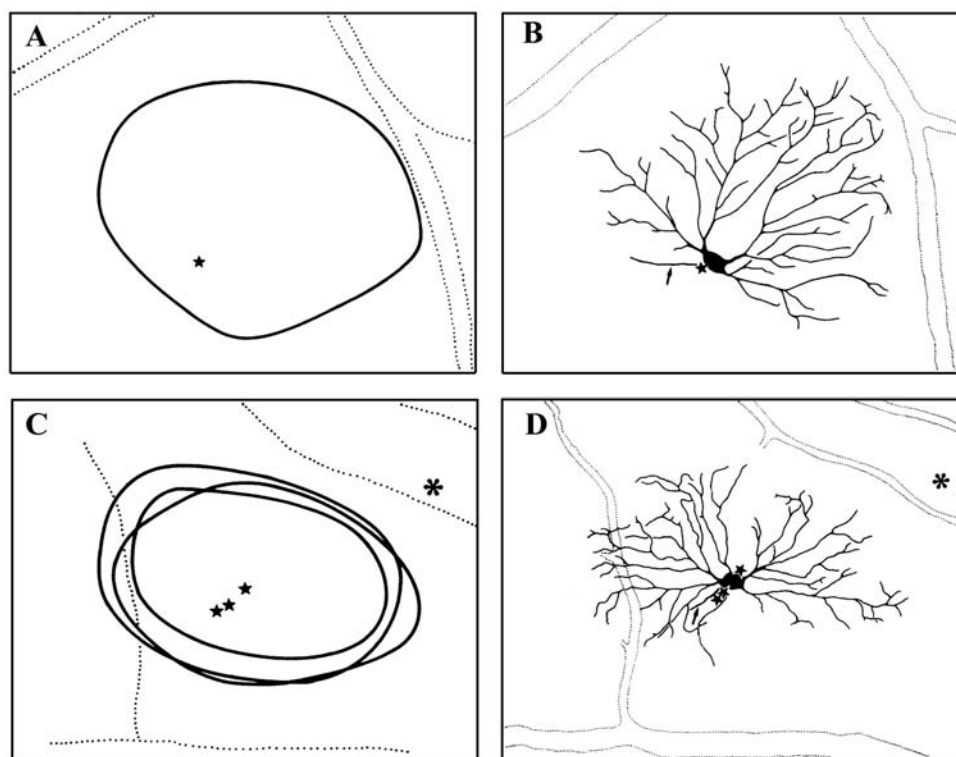


FIGURE 26.8. Correspondence of receptive and dendritic field in alpha cells in cat retina. *A, C*, solid lines show the border of the excitatory receptive field center for two alpha cells encountered in intraocular recordings. Three independent recordings were made from the cell shown in *C*. Stars mark the position of the tip of the recording electrode. *B, D*, drawings of alpha cells (identified postmortem by neurofibrillar stain of the whole-mounted retina) at

the recording sites *A* and *C*, respectively. Note the good correspondence between the size and shape of the dendritic tree and the border of the receptive field center for each cell. *Dotted lines* show borders of local retinal blood vessels. *Flower symbols* in *C* show position of an electrolytic marker lesion. (Modified from Peichl and Wässle, 1981).

LIMITATIONS OF THE DOG MODEL The DOG model may give a reasonable account of the response to spatial contrast for the many ganglion cells, but it is important to understand its limitations. First, there are many receptive fields (e.g., direction-selective cells; see Chapter 28) for which the DOG model simply does not capture the essential functional property of the receptive field. Second, even “ideal”—centrically organized, antagonistic—receptive fields may be more accurately described by *spatially finite* sensitivity functions such as the difference-of-raised-cosines (reviewed by Levick, 1996). Third, spatial sensitivity profiles of a good proportion of ganglion cells in cat, rabbit, and primate retina show deviations from the Gaussian prediction. Fine-grained analysis of the receptive field reveals that the center may contain multiple sensitivity peaks (Brown et al., 2000; Chichilnisky and Baylor, 1999; Cohen and Sterling, 1991; McMahon et al., 2000). Sensitivity within the center is only weakly correlated with the local dendritic branching density. This suggests that bipolar cell inputs, rather than local dendritic computation, create local variation in contrast sensitivity within the receptive field center (Brown et al., 2000; Cohen and Sterling, 1991). Parvocellular cells in the foveal representation in macaque geniculate show nonhomogeneous center sensitivity when assessed using laser interferometry, which bypasses the eye’s optics (McMahon et al., 2000). Because the foveal midget-parvocellular projecting ganglion cells receive input from a single midget bipolar cell, this raises the possibility that bipolar cell inputs may already have irregular receptive field structure.

ORIENTATION SENSITIVITY In the intact visual system, the sensitivity peaks arising from individual cones and bipolar cells are smoothed by combination of optical blur and by dendritic summation in the ganglion cell (Cohen and Sterling, 1991), leaving an overall mild circular asymmetry in most of the concentric receptive fields in ganglion cells and retinorecipient geniculate cells (Fig. 26.8; Leventhal and Schall, 1983; Levick and Thibos, 1982; Passaglia et al., 2002; Smith et al., 1990). In primate retina, the circular anisotropy (expressed as the length ratio of the major to minor axes of the best-fitting ellipse) is larger for midget cells (1.72) than for parasol cells (1.38); for both classes there is a tendency for the receptive fields to be oriented either radially (toward the fovea) or tangentially (Passaglia et al., 2002). These data partially corroborate morphological analyses showing only weak tendency for both midget and parasol cells to be oriented toward the fovea (Watanabe and Rodieck, 1989). The chief functional consequence of the elliptical receptive field is enhanced sensitivity to stimuli oriented along the major axis of the ellipse. Quantitative comparison of orientation bandwidth in subcortical and cortical neurons shows that subcortical orientation bias could account for the orientation

bias in the geniculorecipient layers of primary visual cortex, but that additional mechanisms are required to account for the much greater orientation selectivity of the majority of cortical neurons (Passaglia et al., 2002; Vidyasagar et al., 1996).

SPATIAL SUMMATION In contrast to the situation in many mammalian retinas, the great majority of primate ganglion cells show predominantly linear spatial summation (Kaplan and Shapley, 1982; Sherman et al., 1976; see also Chapter 17). Analyses of responses in nonprimate retina (Demb et al., 2001; Levick, 1996) give a general association of nonlinear summation properties with large receptive field dimensions. This implies that the low proportion of cells showing nonlinear spatial summation in primate vision could be a simple consequence of the dominance of midget cells, which have the smallest receptive fields described among mammalian retinas. A small proportion (<10%) of magnocellular and koniocellular pathway cells show nonlinear summation (Kaplan and Shapley, 1982; White et al., 2001, 2002; Xu et al., 2001), but within these populations there is no clear association of nonlinear response characteristic with larger receptive fields. There is evidence for multiple sites of nonlinear spatial interaction, including bipolar and amacrine cell inputs to ganglion cells (Benardete and Kaplan, 1997; Demb et al., 2001).

CHROMATIC CONTRAST SENSITIVITY Two kinds of interaction between photoreceptors can be identified in responses of ganglion cells. First, at mesopic illuminance levels there is functional interaction between synaptic inputs from rod and cone photoreceptors. These phenomena are described in detail elsewhere (see Chapter 55). There is unequivocal evidence for rod input at mesopic levels to parasol-magnocellular pathway ganglion cells (Lee et al., 1990; Lee et al., 1997; Purpura et al., 1988). Anatomical and physiological studies also suggest a smaller degree of rod input to midget-parvocellular pathway ganglion cells (Grünert, 1997; Lee et al., 1997); the degree of rod input to other ganglion cell types in primate retina may also be small (Dacey and Lee, 1994).

A second kind of chromatic interaction occurs between the different spectral classes (long-, medium-, and short-wavelength sensitive) of cone photoreceptors at photopic illuminance levels. Most of the midget-parvocellular pathway ganglion cells display opponent interactions between long- and medium-wavelength sensitive cones, whereas the small-field bistratified cells receive excitatory ON input from short-wavelength sensitive cones and antagonistic OFF input from the other cone types (Dacey and Lee, 1994; De Monasterio and Gouras, 1975; Derrington et al., 1984; Schiller and Malpeli, 1977; Wiesel and Hubel, 1966). The origin and nature of these interactions is discussed in

Chapter 64. Here it is important to note that for the midget ganglion cells these chromatic interactions are linked to center-surround antagonism, so the excitatory center mechanism derives input primarily from a single cone type, whereas the inhibitory surround mechanism derives input at least partly from the opponent cone type. By contrast, for small bistratified cells the chromatic interactions are generated through ON- and OFF-retinal pathways, so ON-excitation comes from short-wavelength cones and OFF-excitation comes from medium- and long-wavelength sensitive cones.

Receptive fields recorded in the geniculate include cells with inhibitory input from short-wavelength sensitive cones; these presumably reflect inputs from “blue-OFF” ganglion cells. Recent results from combined morphological and physiological recordings show a large, monostратified wide-field ganglion cell type may be the substrate of blue-OFF responses (Dacey et al., 2002).

Parasol-magnocellular pathway cells show some chromatic opponent interactions at low spatial and temporal frequencies (Derrington et al., 1984; Smith et al., 1992; Wiesel and Hubel, 1966), and nonlinear addition of medium- and long-wavelength sensitive cone inputs within the receptive field surround (Lee et al., 1989). Although these effects are small in comparison to the frank cone-opponent responses in midget-parvocellular and small bistratified cells, they render invalid the assumption that chromatic interaction at subsequent levels of visual processing is a definite sign of input from the midget and/or bistratified cell groups.

EXTRAClassical RECEPTIVE FIELD PROPERTIES The extraclassical receptive field is defined as a region of visual space where an appropriate stimulus can modulate the responses evoked from the classical receptive field (see Chapter 45). The effects of extraclassical stimulation are often termed facilitatory (or suppressive) to emphasize this distinction from frank excitatory (or inhibitory) effects on action potential discharge rates. Abrupt rapid movement of large targets outside the classical receptive field was first reported to produce facilitatory or frank excitatory effects in recordings from axons of cat ganglion cells by McIlwain (1964). Subsequent work on cat retina shows that both facilitatory and suppressive effects, originating in an extended region of the visual field, can influence both the evoked and maintained activity of ganglion cells (Barlow et al., 1977; Li et al., 1992; Passaglia et al., 2001). The influence on larger (brisk-transient, Y type spatial summation) receptive fields is generally greater than effects on smaller (brisk-sustained, X type spatial summation) receptive fields (Li et al., 1992). Fewer data are available on primate ganglion cells; recordings from ganglion cell targets in the lateral geniculate nucleus reveal both close-range suppressive and long-range facilitatory extraclassical receptive field regions (Felisberti

and Derrington, 2001; Marrocco and McClurkin, 1985; Solomon et al., 2002), but the extent to which these effects are already present in ganglion cell receptive fields in primates has not yet been established.

Acknowledgements

We are grateful to Ana Lara and Krishna Ghosh for technical assistance, to Leo Peichl and Barry Lee for comments on the manuscript, and to Samuel Solomon and Andrew White for permission to share unpublished data.

REFERENCES

- Barlow, H. B., 1953. Summation and inhibition in the frog's retina, *J. Physiol.*, 119:69–88.
- Barlow, H. B., A. M. Derrington, L. R. Harris, and P. Lennie, 1977. The effects of remote retinal stimulation on the responses of cat retinal ganglion cells, *J. Physiol.*, 269:177–194.
- Benardete, E. A., and E. Kaplan, 1997. The receptive field of the primate P retinal ganglion cell, II: Nonlinear dynamics, *Vis. Neurosci.*, 14:187–205.
- Benardete, E. A., E. Kaplan, and B. W. Knight, 1992. Contrast gain control in the primate retina: P cells are not X-like, some M cells are, *Vis. Neurosci.*, 8:483–486.
- Boycott, B. B., and J. E. Dowling, 1969. Organization of the primate retina: light microscopy, *Phil. Trans. Roy. Soc. Lond. B*, 255:109–176.
- Boycott, B. B., and H. Wässle, 1974. The morphological types of ganglion cells of the domestic cat's retina, *J. Physiol.*, 240:397–419.
- Boycott, B. B., and H. Wässle, 1991. Morphological classification of bipolar cells of the primate retina., *Eur. J. Neurosci.*, 3: 1069–1088.
- Brown, S. P., S. He, and R. H. Masland, 2000. Receptive field microstructure and dendritic geometry of retinal ganglion cells, *Neuron*, 27:371–383.
- Cajal, S. R., 1893. La rétine des vertébrés, *Cellule*, 9:121–255.
- Calkins, D. J., S. J. Schein, Y. Tsukamoto, and P. Sterling, 1994. M and L cones in macaque fovea connect to midget ganglion cells by different numbers of excitatory synapses, *Nature*, 371:70–72.
- Chichilnisky, E. J., and D. A. Baylor, 1999. Receptive-field microstructure of blue-yellow ganglion cells in primate retina, *Nat. Neurosci.*, 2:889–893.
- Cohen, E., and P. Sterling, 1991. Microcircuitry related to the receptive field center of the ON-beta ganglion cell, *J. Neurophysiol.*, 65:352–359.
- Croner, L. J., and E. Kaplan, 1995. Receptive fields of P and M ganglion cells across the primate retina, *Vis. Res.*, 35:7–24.
- Dacey, D. M., 1993. Morphology of a small-field bistratified ganglion cell type in the macaque and human retina, *Vis. Neurosci.*, 10:1081–1098.
- Dacey, D. M., and B. B. Lee, 1994. The blue-ON' opponent pathway in primate retina originates from a distinct bistratified ganglion cell type, *Nature*, 367:731–735.
- Dacey, D. M., B. B. Peterson, and F. R. Robinson, 2002. Identification of an S-cone opponent OFF pathway in the macaque monkey retina: morphology, physiology and possible circuitry, *Invest. Ophthalmol.* (ARVO abstracts), Abstract 2983.

- De Monasterio, F. M., and P. Gouras, 1975. Functional properties of ganglion cells of the rhesus monkey retina, *J. Physiol.*, 251:167–195.
- Demb, J. B., K. Zaghloul, L. Haarsma, and P. Sterling, 2001. Bipolar cells contribute to nonlinear spatial summation in the brisk-transient (Y) ganglion cell in mammalian retina, *J. Neurosci.*, 21:7447–7454.
- Derrington, A. M., J. Krauskopf, and P. Lennie, 1984. Chromatic mechanisms in lateral geniculate nucleus of macaque, *J. Physiol.*, 357:241–265.
- Derrington, A. M., and P. Lennie, 1984. Spatial and temporal contrast sensitivities of neurones in lateral geniculate nucleus of macaque, *J. Physiol.*, 357:219–240.
- DeVries, S. H., 1999. Correlated firing in rabbit retinal ganglion cells, *J. Neurophysiol.*, 81:908–920.
- Felisberti, F., and A. Derrington, 2001. Long-range interactions in the lateral geniculate nucleus of the New World monkey, *Callithrix jacchus*, *Vis. Neurosci.*, 18:209–218.
- Flores-Herr, N., D. A. Protti, and H. Wässle, 2001. Synaptic currents generating the inhibitory surround of ganglion cells in the mammalian retina, *J. Neurosci.*, 21:4852–4863.
- Gamlin, P. D. R., B. B. Peterson, and D. M. Dacey, 2001. Physiology and morphology of retinal ganglion cells projecting to the pretectal olivary nucleus of the rhesus monkey, *Invest. Ophthalmol. Vis. Sci.*, 42:3639.
- Ghosh, K. K., A. K. Goodchild, A. E. Sefton, and P. R. Martin, 1996. Morphology of retinal ganglion cells in a New World monkey, the marmoset *Callithrix jacchus*, *J. Comp. Neurol.*, 366:76–92.
- Gouras, P., 1968. Identification of cone mechanisms in monkey ganglion cells, *J. Physiol.*, 199:533–547.
- Grünert, U., 1997. Anatomical evidence for rod input to the parvocellular pathway in the visual system of the primate, *Eur. J. Neurosci.*, 9:617–621.
- Hattar, S., H. W. Liao, M. Takao, D. M. Berson, and K. W. Yau, 2002. Melanopsin-containing retinal ganglion cells: architecture, projections, and intrinsic photosensitivity, *Science*, 295:1065–1070.
- Illing, R.-B., and H. Wässle, 1981. The retinal projection to the thalamus in the cat: a quantitative investigation and a comparison with the retinotectal pathway, *J. Comp. Neurol.*, 202:265–285.
- Irvin, G. E., V. A. Casagrande, and T. T. Norton, 1993. Center/surround relationships of magnocellular, parvocellular, and koniocellular relay cells in primate lateral geniculate nucleus, *Vis. Neurosci.*, 10:363–373.
- Jacoby, R. A., A. F. Wiechmann, S. G. Amara, B. H. Leighton, and D. W. Marshak, 2000. Diffuse bipolar cells provide input to OFF parasol ganglion cells in the macaque retina, *J. Comp. Neurol.*, 416:6–18.
- Kaplan, E., and R. M. Shapley, 1982. X and Y cells in the lateral geniculate nucleus of macaque monkeys, *J. Physiol.*, 330:125–143.
- Kaplan, E., and R. M. Shapley, 1986. The primate retina contains two types of ganglion cells, with high and low contrast sensitivity, *Proc. Natl. Acad. Sci. USA*, 83:2755–2757.
- Kolb, H., K. A. Linberg, and S. K. Fisher, 1992. Neurons of the human retina: a Golgi study, *J. Comp. Neurol.*, 318:147–187.
- Kuffler, S. W., 1953. Discharge patterns and functional organization of mammalian retina, *J. Neurophysiol.*, 16:37–68.
- Kuffler, S. W., 1973. The single-cell approach in the visual system and the study of receptive fields, *Invest. Ophthalmol.*, 12:794–813.
- Lee, B. B., P. R. Martin, and A. Valberg, 1989. Nonlinear summation of M- and L-cone inputs to phasic retinal ganglion cells of the macaque, *J. Neurosci.*, 9:1433–1442.
- Lee, B. B., J. Pokorny, V. C. Smith, P. R. Martin, and A. Valberg, 1990. Luminance and chromatic modulation sensitivity of macaque ganglion cells and human observers, *J. Opt. Soc. Am. A*, 7:2223–2236.
- Lee, B. B., V. C. Smith, J. Pokorny, and J. Kremers, 1997. Rod inputs to macaque ganglion cells, *Vis. Res.*, 37:2813–2828.
- Lettvin, J. Y., H. R. Maturana, W. S. McCulloch, and W. S. Pitts, 1959. What the frog's eye tells the frog's brain, *Proc. Inst. Radio Engng.*, 47:1940–1951.
- Leventhal, A. G., R. W. Rodieck, and B. Dreher, 1981. Retinal ganglion cell classes in the Old World monkey: morphology and central projections, *Science*, 213:1139–1142.
- Leventhal, A. G., and J. D. Schall, 1983. Structural basis of orientation sensitivity of cat retinal ganglion cells, *J. Comp. Neurol.*, 220:465–475.
- Levick, W. R., 1996. Receptive fields of cat retinal ganglion cells with special reference to the alpha cells, *Prog. Ret. Eye Res.*, 15:457–500.
- Levick, W. R., and L. N. Thibos, 1982. Analysis of orientation bias in cat retina, *J. Physiol.*, 329:243–261.
- Li, C.-Y., Y.-X. Zhou, X. Pei, F.-T. Qiu, C.-Q. Tang, and X.-Z. Xu, 1992. Extensive disinhibitory region beyond the classical receptive field of cat retinal ganglion cells, *Vis. Res.*, 32:219–228.
- Lin, B., P. R. Martin, and U. Grünert, 2002. Expression and distribution of ionotropic glutamate receptor subunits on parasol ganglion cells in the primate retina, *Vis. Neurosci.*, 19:453–465.
- Lin, B., P. R. Martin, S. G. Solomon, and U. Grünert, 2000. Distribution of glycine receptor subunits on primate retinal ganglion cells: a quantitative analysis, *Europ. J. Neurosci.*, 12:4155–4170.
- Macri, J., P. R. Martin, and U. Grünert, 2000. Distribution of the $\alpha 1$ subunit of the GABA_A receptor on midget and parasol ganglion cells in the retina of the common marmoset (*Callithrix jacchus*), *Vis. Neurosci.*, 17:437–448.
- Marrocco, R. T., and J. W. McClurkin, 1985. Evidence for spatial structure in the cortical input to the monkey lateral geniculate nucleus, *Exp. Brain Res.*, 59:50–56.
- McIlwain, J. T., 1964. Receptive fields of optic tract axons and lateral geniculate cells: peripheral extent and barbiturate sensitivity, *J. Neurophysiol.*, 27:1154–1173.
- McMahon, M. J., M. J. M. Lankheet, P. Lennie, and D. R. Williams, 2000. Fine structure of parvocellular receptive fields in the primate fovea revealed by laser interferometry, *J. Neurosci.*, 20:2043–2053.
- Meister, M., and M. J. Berry, 1999. The neural code of the retina, *Neuron*, 22:435–450.
- Neuenschwander, S., and W. Singer, 1996. Long-range synchronization of oscillatory light responses in the cat retina and lateral geniculate nucleus, *Nature*, 379:728–732.
- Norton, T. T., V. A. Casagrande, G. E. Irvin, M. A. Sesma, and H. M. Petry, 1988. Contrast-sensitivity functions of W-, X-, and Y-like relay cells in the lateral geniculate nucleus of bush baby, *Galago crassicaudatus*, *J. Neurophysiol.*, 59:1639–1656.
- O'Brien, B. J., T. Isayama, R. Richardson, and D. M. Berson, 2002. Intrinsic physiological properties of cat retinal ganglion cells, *J. Physiol.*, 538:787–802.
- Owczarzak, M. T., and R. G. Pourcho, 1999. Transmitter-specific input to OFF-alpha ganglion cells in the cat retina, *Anat. Rec.*, 255:363–373.

- Passaglia, C. L., C. Enroth-Cugell, and J. B. Troy, 2001. Effects of remote stimulation on the mean firing rate of cat retinal ganglion cells, *J. Neurosci.*, 21:5794–5803.
- Passaglia, C. L., J. B. Troy, L. Rüttger, and B. B. Lee, 2002. Orientation sensitivity of ganglion cells in primate retina, *Vis. Res.*, 42:683–694.
- Peichl, L., and H. Wässle, 1981. Morphological identification of ON- and OFF-centre brisk transient (Y) cells in the cat retina, *Proc. R. Soc. Lond. Ser. B. Biol. Sci.*, 212:139–156.
- Peichl, L., and H. Wässle, 1983. The structural correlate of the receptive field centre of ganglion cells in the cat retina, *J. Physiol.*, 341:309–324.
- Perry, V. H., R. Oehler, and A. Cowey, 1984. Retinal ganglion cells that project to the dorsal lateral geniculate nucleus in the macaque monkey, *Neurosci.*, 12:1101–1123.
- Peterson, B. B., and D. M. Dacey, 2000. Morphology of wide-field bistratified and diffuse human retinal ganglion cells, *Vis. Neurosci.*, 17:567–578.
- Polyak, S. L., 1941. *The Retina*, Chicago: University of Chicago Press.
- Purpura, K., E. Kaplan, and R. M. Shapley, 1988. Background light and the contrast gain of primate P and M retinal ganglion cells, *Proc. Natl. Acad. Sci. USA*, 85:4534–4537.
- Rockhill, R. L., F. J. Daly, M. A. MacNeil, S. P. Brown, and R. H. Masland, 2002. The diversity of ganglion cells in a mammalian retina, *J. Neurosci.*, 22:3831–3843.
- Rodieck, R. W., 1972. *The Vertebrate Retina*, San Francisco: W.H. Freeman.
- Rodieck, R. W., 1988. The primate retina, in *Comparative Primate Biology*, vol. 4, *Neurosciences* (H. D. Steklis and J. Erwin, eds.), New York: Alan R. Liss, pp. 203–278.
- Rodieck, R. W., 1991. Which cells code for color? in *From Pigments to Perception: Advances in Understanding Visual Processes* (A. Valberg and B. B. Lee, eds.), London: Plenum Press, pp. 83–93.
- Rodieck, R. W., and R. K. Brening, 1983. Retinal ganglion cells: properties, types, genera, pathways and trans-species comparisons, *Brain Behav. Evol.*, 23:121–164.
- Rodieck, R. W., and J. Stone, 1965. Analysis of receptive fields of cat retinal ganglion cells, *J. Neurophysiol.*, 28:833–849.
- Rodieck, R. W., and M. Watanabe, 1993. Survey of the morphology of macaque retinal ganglion cells that project to the pretectum, superior colliculus, and parvocellular laminae of the lateral geniculate nucleus, *J. Comp. Neurol.*, 338:289–303.
- Schiller, P. H., and J. G. Malpeli, 1977. Properties and tectal projections of monkey retinal ganglion cells, *J. Neurophysiol.*, 40:428–445.
- Shapley, R., and V. H. Perry, 1986. Cat and monkey retinal ganglion cells and their visual functional roles, *Trends Neurosci.*, 9:229–235.
- Shapley, R. M., C. Enroth-Cugell, A. B. Bonds, and A. Kirby, 1972. Gain control in the retina and retinal dynamics, *Nature*, 236:352–353.
- Sherman, S. M., J. R. Wilson, J. H. Kaas, and S. V. Webb, 1976. X- and Y-cells in the dorsal lateral geniculate nucleus of the owl monkey (*Aotus trivirgatus*), *Science*, 192:475–477.
- Silveira, L. C. L., E. S. Yamada, V. H. Perry, and C. W. Picano-Diniz, 1994. M and P retinal ganglion cells of diurnal and nocturnal New World monkeys, *Neuroreport*, 5:2077–2081.
- Smith, E. L., Y. M. Chino, W. H. Ridder, III, K. Kitagawa, and A. Langston, 1990. Orientation bias of neurons in the lateral geniculate nucleus of macaque monkeys, *Vis. Neurosci.*, 5:525–545.
- Smith, V. C., B. B. Lee, J. Pokorny, P. R. Martin, and A. Valberg, 1992. Responses of macaque ganglion cells to the relative phase of heterochromatically modulated lights, *J. Physiol.*, 458:191–221.
- Solomon, S. G., A. J. R. White, and P. R. Martin, 1999. Temporal contrast sensitivity in the lateral geniculate nucleus of a New World monkey, the marmoset *Callithrix jacchus*, *J. Physiol.*, 517:907–917.
- Solomon, S. G., A. J. R. White, and P. R. Martin, 2002. Extra-classical receptive field properties of parvocellular, magnocellular and koniocellular cells in the primate lateral geniculate nucleus, *J. Neurosci.*, 22:338–349.
- Stone, J., 1983. *Parallel Processing in the Visual System*, London: Plenum Press.
- Telkes, I., C. Distler, and K.-P. Hoffmann, 2000. Retinal ganglion cells projecting to the nucleus of the optic tract and the dorsal terminal nucleus of the accessory optic system in macaque monkeys, *Eur. J. Neurosci.*, 12:2367–2375.
- Treviranus, G. R., 1836–1838. *Beiträge zur Aufklärung der Erscheinungen und Gesetze des organischen Lebens*, Bremen: Heyse, J.G.
- Vidyasagar, T. R., X. Pei, and M. Volgushev, 1996. Multiple mechanisms underlying the orientation selectivity of visual cortical neurones, *Trends Neurosci.*, 19:272–277.
- Wässle, H., L. Peichl, and B. B. Boycott, 1981. Dendritic territories of cat retinal ganglion cells, *Nature*, 292:344–345.
- Watanabe, M., and R. W. Rodieck, 1989. Parasol and midget ganglion cells of the primate retina, *J. Comp. Neurol.*, 289:434–454.
- White, A. J. R., S. G. Solomon, and P. R. Martin, 2001. Spatial properties of koniocellular cells in the lateral geniculate nucleus of the marmoset *Callithrix jacchus*, *J. Physiol.*, 533:519–535.
- White, A. J. R., A. K. Goodchild, H. D. Wilder, A. E. Sefton, and P. R. Martin, 1998. Segregation of receptive field properties in the lateral geniculate nucleus of a New-World monkey, the marmoset *Callithrix jacchus*, *J. Neurophysiol.*, 80:2063–2076.
- White, A. J. R., H. Sun, W. H. Swanson, and B. B. Lee, 2002. An examination of physiological mechanisms underlying the frequency-doubling illusion, *Invest. Ophthalmol.*, 43:3590–3599.
- Wiesel, T. N., and D. H. Hubel, 1966. Spatial and chromatic interactions in the lateral geniculate body of the rhesus monkey, *J. Neurophysiol.*, 29:1115–1156.
- Williams, R. W., M. J. Bastiani, B. Lia, and L. M. Chalupa, 1986. Growth cones, dying axons, and developmental fluctuations in the fiber population of the cat's optic nerve, *J. Comp. Neurol.*, 246:32–69.
- Xu, X., J. M. Ichida, J. D. Allison, J. D. Boyd, A. B. Bonds, and V. A. Casagrande, 2001. A comparison of koniocellular, magnocellular and parvocellular receptive field properties in the lateral geniculate nucleus of the owl monkey (*Aotus trivirgatus*), *J. Physiol.*, 531:203–218.
- Yamada, E. S., L. C. L. Silveira, F. L. Gomes, and B. B. Lee, 1996. The retinal ganglion cell classes of New World primates, *Rev. Brasil. Biol.*, 56:381–396.

27 Retinal Ganglion Cell Excitability

ANDREW T. ISHIDA

RETINAS ARE GEARED to function as the first cell layers of the visual system by several sorts of signal generation and processing. In addition to transducing light and limiting light sensitivity, photoreceptors help reduce noise, differentially distribute signals to different bipolar cells, and adapt to changes in mean luminance (Sterling, 1998). Before driving retinal ganglion cells to “spike” (i.e., generate action potentials), interneurons help determine the spatial, temporal, and chromatic properties that produce changes in ganglion cell spiking at any moment, and help adjust the sensitivity and response kinetics of cells when the mean, range, and spatial distribution of light intensities change (Meister and Berry, 1999). Finally, the outcome of these processes is enriched by the variety of cellular teams that retinas devote to handling these tasks and, as described in other chapters of this book, this variety arises at least in part from differences in the combinations of bipolar and amacrine cells that converge onto ganglion cells, the synaptic arrangements and transmitter systems that make up the outer and inner plexiform layers, and the transfer and dynamic properties of these synapses.

In the midst of this, ganglion cells may seem to simply be on stand-by, generating a spike anytime some fixed threshold is reached. However, certain responses of the retina also entail changes in signal flow through synapses and single cells. The best known of these include shifts in the balance of rod and cone inputs to shared pathways, modulation of neurotransmitter-gated and voltage-gated ion channels, and changes in coupling at gap junctions (Akopian and Witkovsky, 2002; Barlow, 2001; Dowling, 1991; Vaney, 1999; Wässle and Boycott, 1991; Witkovsky and Dearry, 1991). Because some modulators have recently been found to regulate ion channels in ganglion cells, retinas seem set up to generate their outputs in part because stimuli change the synaptic inputs that drive ganglion cells, and in part because stimuli change the response of ganglion cells to their inputs. This chapter addresses two questions about how ganglion cells fit into an ensemble like this to form the retinal output. First, do all ganglion cells generate spikes in the same way? Second, do individual ganglion cells produce spikes the same way under all lighting conditions?

One reason for considering these possibilities is that they imply that retinas could be organized in different ways to respond to their inputs. A fixed mechanism of ganglion cell

“excitability” (i.e., spike generation) would suffice to send the retina’s output off to remote targets without it degrading along the way, but this would leave information-processing duties in the retina up to the outer and inner nuclear layers. Allowing different ganglion cells to generate spikes at different frequencies, at different moments, or in different temporal patterns could create different outputs for identical inputs, relieve other retinal cells from shaping these spiking patterns, or ensure that critical processing that started in the distal retina was maintained in the retinal output. Equipping individual ganglion cells with spiking mechanisms that change depending on the intensity, distribution, or other attributes of light could enable ganglion cells to modulate the retina’s output, and this could occur independently of or together with changes in the light responses of other retinal neurons.

A second reason for considering ganglion cell excitability is that it could factor into the range of inputs these cells respond to. For example, ganglion cell responses, measured in spike firing rate (i.e., spike “frequency”), saturate within a “dynamic range” of 2.5 log units (Barlow and Levick, 1969; Diamond and Copenhagen, 1995; Enroth-Cugell and Shapley, 1973; Green and Powers, 1982; Sakmann and Creutzfeldt, 1969; Thibos and Werblin, 1978), yet photon fluxes encountered under starlight and sunlight can differ by up to 10 log units (Rodieck, 1998). For ganglion cells to respond over broad ranges of stimulus values, retinas with fixed spike-generation mechanisms in all ganglion cells, or with different mechanisms in different cells, have at least three sorts of options. One is “range fractionation,” the use of different cells to respond to different portions of a parameter’s value range (cf. Albrecht and Hamilton, 1982; Ohzawa et al., 1985). A second way is “receptive field surround inhibition,” the reduction of responses to localized “center” illumination by light that falls within a slightly broader “surround” area (Barlow et al., 1957; Barlow and Levick, 1969; Donner, 1981; Enroth-Cugell and Lennie, 1975). A third would be “adaptation” or “gain control,” which adjust the response that cells produce per unit of input (Shapley, 1997; Shapley and Enroth-Cugell, 1984). Although none of these tactics necessarily entail differences or changes in ganglion cell excitability, differences in the range of inputs that ganglion cells respond to or the range of outputs that ganglion cells generate could contribute to range fractionation, and changes in excitabil-

ity could result from changes in either local or broad-field illumination.

One approach to take here would be to proceed through descriptions of light stimuli, cell types, light responses, mechanisms, and models. Unfortunately, although a number of different models of ganglion cell light responses have been built from comparisons of stimuli and responses, surprisingly few biophysical and intracellular signaling mechanisms that allow these models to work have been established by intracellular recording, imaging, or experimental manipulations. This chapter will therefore start by describing simple light responses of ganglion cells, those of dark-adapted cells to flashes of intermediate intensity. A number of cellular properties that have been found in ganglion cells by patch-clamp and immunocytochemical methods will then be reviewed, and related, where possible, to responses of light-adapted ganglion cells to light flashes and to randomly fluctuating intensities. Two of the main ideas considered here are that ganglion cell spike generation is not an “integrate-and-fire” process that can be described by voltage-gated ion current amplitudes, kinetics, and voltage sensitivities that are identical in all cells and constant under all conditions, and that changes in ganglion cell excitability help adjust the retinal output as the retinal input changes.

Excitability and light responses

DYNAMIC RANGE A number of studies have investigated the contribution of ganglion cell excitability to light responses by comparing light-elicited spikes with spikes elicited by current injections through intracellular electrodes. This was first attempted by measuring spikes with micro-electrodes that penetrated ganglion cell somata (Fig. 27.1; Baylor and Fettiplace, 1979) and thereafter with patch-electrodes that sealed onto ganglion cell somata (e.g., Diamond and Copenhagen, 1995; Fohlmeister and Miller, 1997a; Kim and Rieke, 2001; Mobbs et al., 1992; Sheasby and Fohlmeister, 1999). To begin with, the transformation of current into spikes was studied from the spike frequencies elicited by exogenously injected constant current and by light flashes, and by comparing these with the amplitude of light-evoked whole-cell currents.

At spike frequencies ranging from around 2 Hz (spikes·sec⁻¹) to as high as 80 Hz, spike frequency was found to increase linearly with the amplitude of injected current (Baylor and Fettiplace, 1979; Diamond and Copenhagen, 1995; Mobbs et al., 1992; Robinson and Chalupa, 1997; Vaquero et al., 2001). Likewise, light-evoked spike frequency was found to increase linearly when plotted against the amplitude of light-evoked whole-cell current (Diamond and Copenhagen, 1995). Do these two types of plots coincide? Most studies so far have only measured one of these types of plots; of the plots published so far, some differ considerably in slope

(compare, for example, the data of Baylor and Fettiplace versus those of Mobbs and colleagues). It remains to be seen whether these differences are significant, because the data were collected with different methods and under different recording conditions. Fortunately, one study measured both plots in a single species, under the same recording conditions (Diamond and Copenhagen, 1995). These showed neither a significant difference in slope (both approximately 1 Hz/pA), nor a marked difference in position along the current axis. These similarities are consistent with the possibility that dendritic processing of input currents, if any, does not substantially contribute to light-evoked spike frequencies—a possibility that was recently confirmed by recording the whole-cell current that is activated by light and showing that spikes elicited by this light are similar in frequency and time-course to spikes elicited by injecting that current into somata (Fig. 27.2; Kim and Rieke, 2001).

These results suggest that, under the conditions that these measurements were made, ganglion cells can linearly transform current into spike frequency. Because there is no universal way that this is accomplished, one would like to know how ganglion cells are able to do this, and whether this contributes to ganglion cell function under various conditions. To begin with, these results predict that the dependence of ganglion cell spike frequency on light intensity should be similar to that of the cells that drive them to spike. Consistent with this, rod, cone, bipolar, and ganglion cells have been found to have similar dynamic ranges—around 2.5 log units. A measure of this similarity can be seen in studies that have fitted the Michaelis equation [$R = R_{\max}(I^n)/(I^n + \sigma^n)$] to plots of the amplitude of responses to local illumination against logarithm of light intensity; in this equation, R is response amplitude, R_{\max} is the maximum response amplitude, I is light intensity, and σ is the light intensity that elicits 0.5 R_{\max} (Naka and Rushton, 1966). These studies have found the coefficient “ n ” to be equal to, or not much different from, unity (for examples, see Ashmore and Falk, 1980; Baylor and Fuortes, 1970; Berntson and Taylor, 2000; Diamond and Copenhagen, 1995; Euler and Masland, 2000; Fain and Dowling, 1973; Guenther and Zrenner, 1993; Schneeweis and Schnapf, 1995; Thibos and Werblin, 1978). This does not argue that these fits are necessarily the best for all cells of these classes, but rather that similar dynamic ranges were found in the cells recorded from. At face value, this suggests that the linearity of current-frequency relations in ganglion cells allows their dynamic range to be governed by those of their presynaptic inputs, at least in the steady state.

HIGH VERSUS LOW SPIKE FREQUENCIES Monotonic increases in spike frequency with stimulus current intensity, particularly at low stimulus intensities, are not predicted by the Na⁺, K⁺, and leak currents described by Hodgkin and

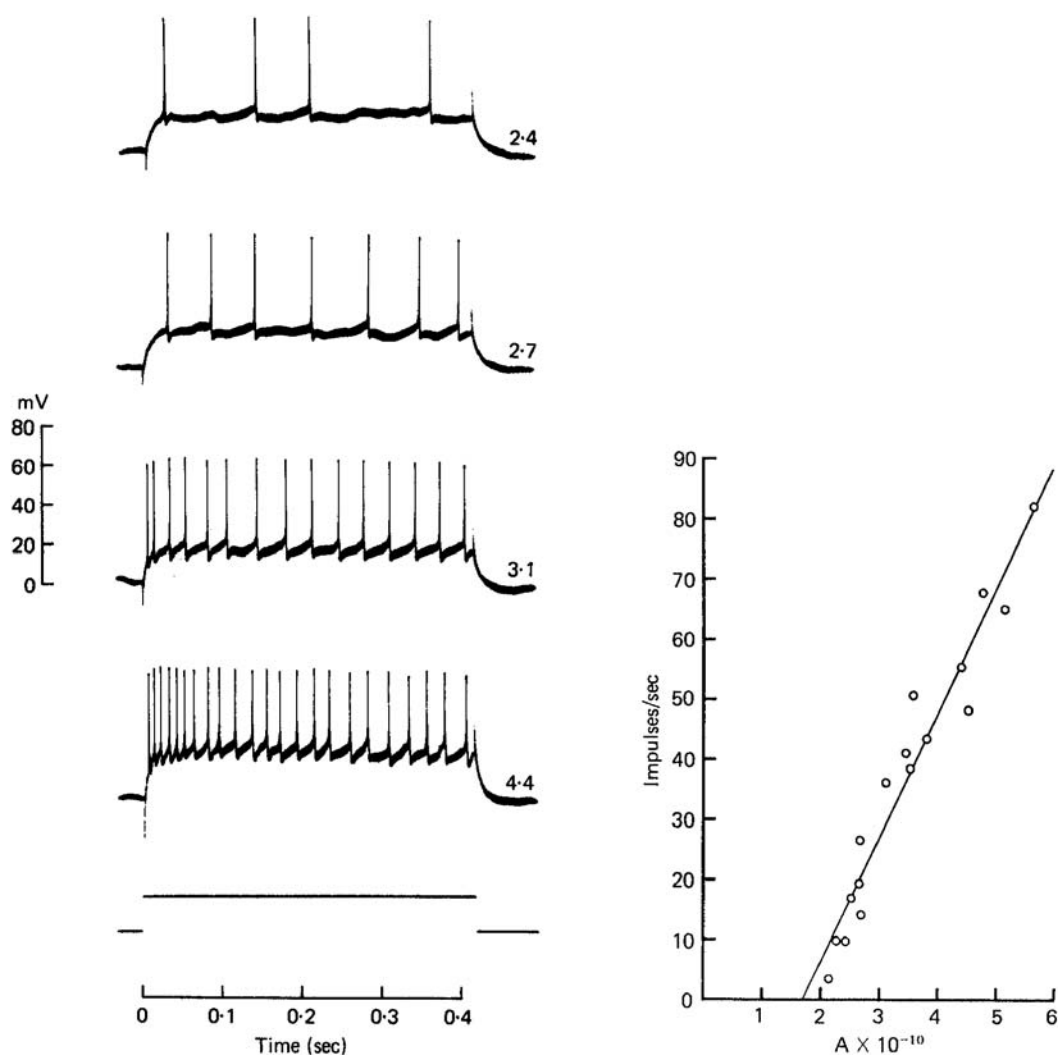


FIGURE 27.1. Responses of a retinal ganglion cell in turtle eyecup to constant current injections are shown at the left. The frequency of spikes elicited by several current injections into this cell are plotted at the right. The numbers next to each trace indicate the

current strength (in 10^{-10} A). The timing and duration of each injection are indicated along the bottom. Resting potential was -70 mV. From Baylor and Fettiplace (1979), with permission of The Physiological Society.

Huxley (1952), and therefore imply the presence of currents that have different properties. Recent studies of currents that facilitate ganglion cell spiking have been propelled by two different interests. One was to learn how, during responses to stimuli of different intensities, ganglion cells avoid large changes in the driving force for the nonselective cation current that bipolar cells activate in them (Diamond and Copenhagen, 1993, 1995; Freed et al., 1992). If, for example, ganglion cells depolarized by amounts that were proportional to light intensity, response amplitudes might increase so much to small inputs that ganglion cells saturate before their presynaptic inputs do.

A key observation was made in turtle ganglion cells that do not spike spontaneously in darkness. Here it was possible to show that dim light flashes elicit subthreshold excitatory postsynaptic depolarizations that sum linearly and that this

linear scaling stops when light flashes are bright enough to elicit spikes (Fig. 27.3; Baylor and Fettiplace, 1979). The recordings of that study, as well as recordings from toad and salamander ganglion cells (Copenhagen et al., 1990; Diamond and Copenhagen, 1995), showed that as light intensity increases, spike frequency increases and spike latency decreases, but the membrane potential that ganglion cells repolarize to between spikes is invariant, or nearly so. The interspike potential was around -50 mV in turtle, and around -40 mV in salamander. To explain this, Diamond and Copenhagen (1995) proposed that voltage-gated conductances “clamp” the membrane potential between spikes to a value that does not vary much with stimulus intensity (or, presumably, duration) and that this helps ganglion cells avoid response saturation due to nonlinear summation of synaptic potentials. The currents and current properties that

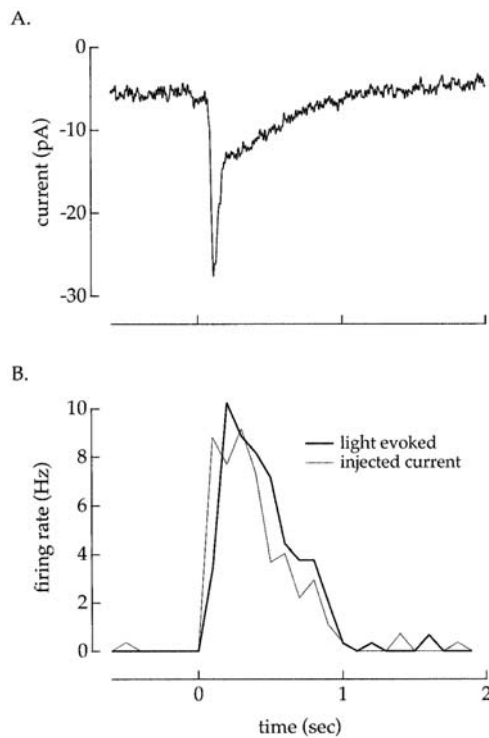


FIGURE 27.2. Responses of a ganglion cell in an isolated larval tiger salamander retina. *A*, whole-cell voltage-clamp current activated by a single flash (10 msec of 1000 photons $\cdot \mu\text{m}^2$ at 575 nm). *B*, poststimulus time histograms of spikes elicited by the same flash as in *A* (thick trace, averaged over 28 presentations) and by injection of the current shown in *A* (thin trace, averaged over 28 injections). From Kim and Rieke (2001), with permission. Copyright 2001 by the Society for Neuroscience.

produce this clamp remain to be identified. Nevertheless, this type of mechanism also seems to help buffer some cat and rabbit ganglion cells against saturation, at least during the first few hundred milliseconds of responses to bright flashes (Freed, 2000a; Fig. 1A of Bloomfield, 1996).

A second set of studies investigated how ganglion cells generate spikes at low frequencies, where the original Hodgkin-Huxley equations predict a discontinuity in response to small input currents. This work proceeded in two steps. First, it showed that Hodgkin-Huxley type equations can be modified to fit single spikes and intensity-frequency plots for salamander ganglion cells using five types of current—a regenerative Na^+ current; a high-threshold Ca^{2+} current; a low-threshold, rapidly inactivating K^+ current; a high-threshold, slowly inactivating K^+ current; and a K^+ current activated by increases in cytoplasmic Ca^{2+} concentration (Benison et al., 2001; Fohlmeister and Miller, 1997a; Sheasby and Fohlmeister, 1999). Next, it showed that incorporation of voltage-gated Na^+ channels into dendrites, and allowing retrograde current flow into these dendrites to dissipate charge, enable ganglion cell models to spike at low

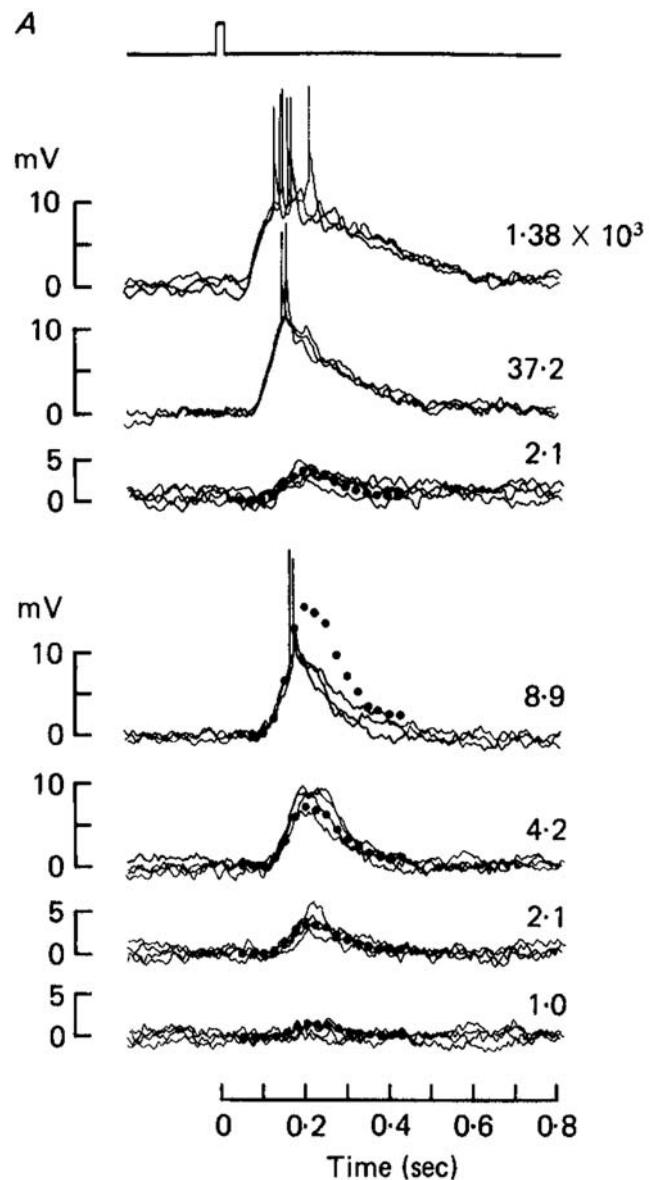


FIGURE 27.3. ON responses of an ON-OFF ganglion cell in turtle eyecup to 6-msec flashes of 640 nm light. Between 3 and 5 traces are superimposed at each intensity. The numbers next to each trace indicate the intensity relative to 74.8 photons per μm^2 . The filled circles plot the response calculated from linear scaling of the response to the dimmest light (i.e., by multiplying the response to dim light, by the ratio of the test intensity to the dim intensity). Resting potential was -59 mV . From Baylor and Fettiplace (1979), with permission of The Physiological Society.

frequencies (Fohlmeister and Miller, 1997b). Although voltage-gated Na^+ channels are found in dendrites of various central neurons (e.g., Stuart and Sakmann, 1994), immunostaining of newt retina with a polyclonal antiserum directed against an amino acid sequence that is widely conserved among Na^+ channels did not reveal Na^+ channels in the inner plexiform layer (Cheon et al., 1998). Also, as mentioned above, a recent test for dendritic processing of input currents

in salamander ganglion cells showed no detectable amount (Kim and Rieke, 2001). On the other hand, patch-clamp recordings have shown that rabbit ganglion cell dendrites are endowed with Na^+ channels (Velte and Masland, 1999) and immunostaining studies have shown Na^+ channel-like immunoreactivity in the inner plexiform layer of cat, monkey, and goldfish retinas (Miguel-Hidalgo et al., 1994; Zenisek et al., 2001). As found recently in cerebellar Purkinje cells and cortical pyramidal cells (Caldwell et al., 2000), an antibody directed against certain Na^+ channel isoforms might help visualize Na^+ channels in salamander ganglion cell dendritic membranes.

TRANSIENT RESPONSES AND BURST FIRING The responses described above differ from those of other ganglion cells to the same stimuli, and from ganglion cell responses to other stimuli, in several respects.

1. Some ganglion cells can be hyperpolarized by light. These hyperpolarizations can be as large as 15 mV below the

membrane potential recorded in darkness (e.g., Ammermüller and Kolb, 1995). In dark-adapted retinas, the response to turning off lights that produce these hyperpolarizations is a step-wise increase in spike frequency (Fig. 27.4; Enroth-Cugell and Lennie, 1975; Jakiela et al., 1976; Müller et al., 1988; Thier and Alder, 1984; Yoon, 1972), leaving these cells to spike continuously in darkness.

2. In light-adapted retinas, depolarizing changes in light intensity elicit transient increases in spike frequency, rather than sustained ones. This can be seen in both the receptive field center and surround responses of ON- and OFF-center ganglion cells—for example, during brightening of ON-cell centers and OFF-cell surrounds, and darkening of ON-cell surrounds and OFF-cell centers (Figs. 27.4, 27.5, and 27.13; Enroth-Cugell and Lennie, 1975; Enroth-Cugell and Shapley, 1973; Jakiela et al., 1976; Lennie, 1981; Müller et al., 1988; Purpura et al., 1990; Thier and Alder, 1984; Yoon, 1972).

3. Maintained presentations of flickering checkerboards (i.e., arrays of squares that fluctuate in intensity and

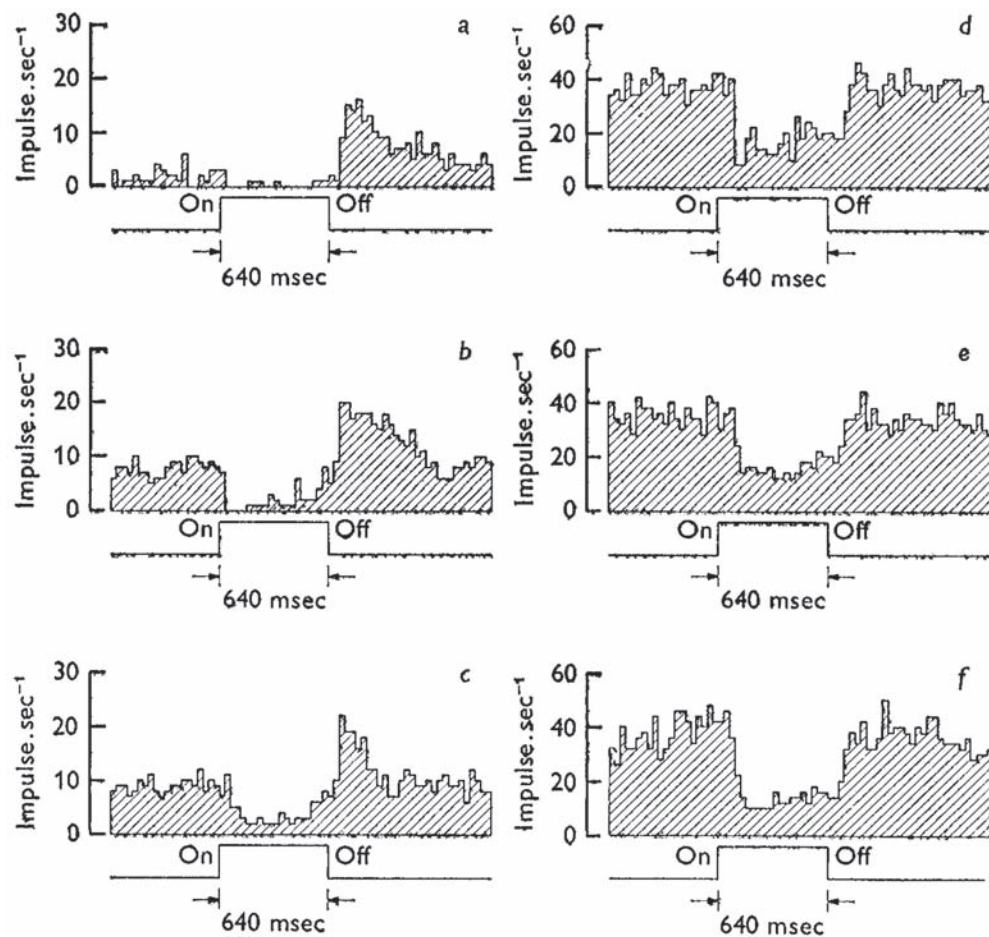


FIGURE 27.4. Poststimulus time histograms of an OFF-center ganglion cell in an in situ cat retina. Background illuminations were: *a*, 2×10^6 ; *b*, 2×10^5 ; *c*, 1.8×10^4 ; *d*, 1.4×10^3 , and *e*, 1.4×10^2

photons·sec⁻¹·deg⁻² (523 nm; 5.7 mm² pupil). No background illumination during the response in *f*. From Yoon (1972), with permission of The Physiological Society.

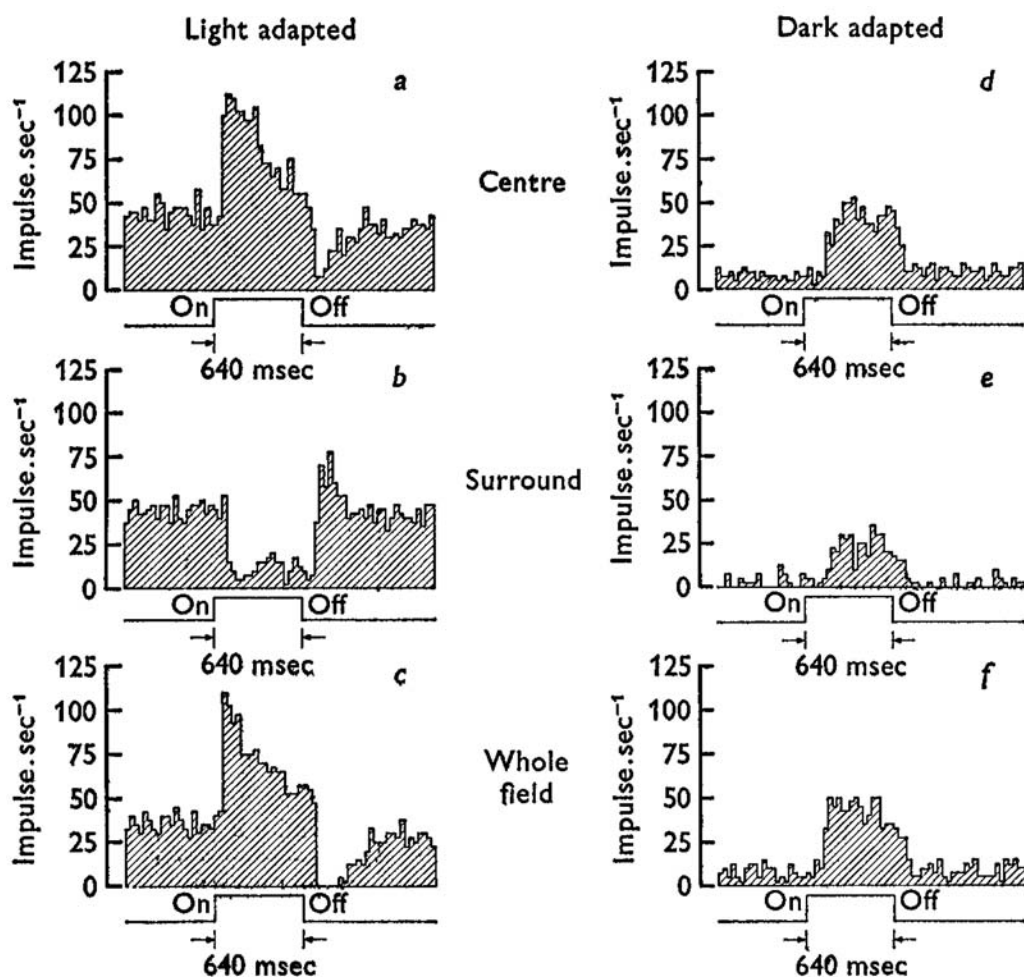


FIGURE 27.5. Poststimulus time histograms of an ON-center ganglion cell in an in situ cat retina. Background illumination at the left was 2×10^6 photons \cdot sec $^{-1}\cdot$ deg $^{-2}$ (5.7 mm 2 pupil). No background illumination during the response at the right. Paired recordings

showing response to receptive field center (*top*), surround (*middle*), and whole-field (*bottom*) illumination. From Yoon (1972), with permission of The Physiological Society.

position) elicit steady rates of spike firing (Brown and Masland, 2001; Chander and Chichilnisky, 2001; Smirnakis et al., 1997). Spatially uniform random flicker, however, elicit spike bursts (Fig. 27.6; Berry and Meister, 1998; Berry et al., 1997; Korenberg et al., 1989; Sakai and Naka, 1987; Sakanaga et al., 1987), meaning that there are both brief periods when cells do not spike (within each burst) and longer periods when cells do not spike (between bursts). These bursts, also called “events,” are preceded in ON-center ganglion cells by brief increases in mean light intensity, and in OFF-center cells by brief decreases in mean light intensity (Fig. 27.7; Meister and Berry, 1999). In response to repeated stimulus presentations over long recording times, the beginning of these events are temporally precise, cells spend relatively small amounts of time firing bursts, and spike-count variability is low (Berry et al., 1997; see also Kara et al., 2000).

4. Ganglion cell light responses can be reduced by increases in the mean light intensity and the amount by which intensity fluctuates relative to the mean (see Barlow and Levick, 1969; Chander and Chichilnisky, 2001; Enroth-Cugell and Shapley, 1973; Green et al., 1975; Kim and Rieke, 2001; Sakai et al., 1995; Sakmann and Creutzfeldt, 1969; Shapley and Enroth-Cugell, 1984; Shapley and Victor 1978; Yeh et al., 1996). These decreases follow various time courses and are commonly referred to as light adaptation and contrast gain control, respectively.

Do the light responses listed here differ from those described in the previous section due to changes in synaptic input alone, or do these responses suggest somehow that ganglion cells differ in excitability and membrane properties, and/or that light stimuli alter these properties? A number of observations are consistent with the latter. To begin with, the transition from sustained to transient spike

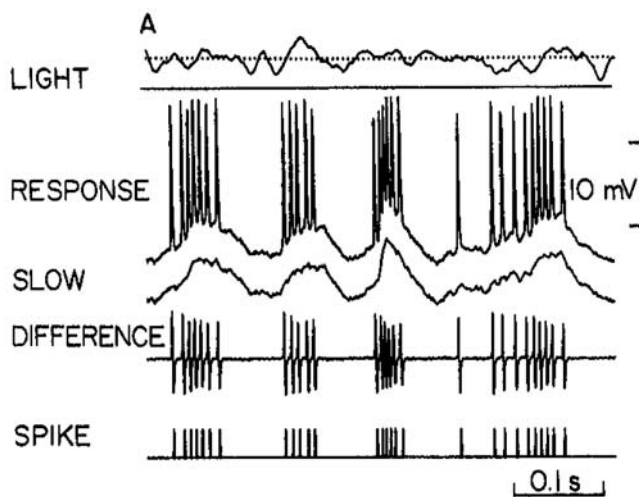


FIGURE 27.6. Intracellular recording of membrane potential (“response”) of a retinal ganglion cell in a catfish eyecup, during presentation of white-noise modulated full-field illumination (“light”). Differentiating the response gave the trace marked “difference.” An algorithm separating the response into analog and discrete signals gave the traces marked “slow” and “spike.” Mean luminance: $5 \mu\text{W}/\text{cm}^2$. Reproduced from Sakuranaga et al. (1987) by copyright permission of The Rockefeller University Press.

firing that occurs during light adaptation of ganglion cells is not accompanied by parallel changes in the light responses of bipolar cells: depolarizing light responses from light-adapted rod bipolar, cone bipolar, and mixed rod-cone bipolar cells are sustained or consist of a transient peak followed by a sustained plateau (Berntson and Taylor, 2000; Dacey et al., 2000; Dacheux and Raviola, 1986; Euler and Masland, 2000; Kaneko et al., 1979; Saito et al., 1978). Furthermore, although transience in ganglion cell responses to input from these bipolar cells might result from a delayed presynaptic or postsynaptic inhibition by amacrine cells, light adaptation can change ganglion cell responses to small spots positioned carefully over the receptive field center from sustained to transient (Yoon, 1972; see also Jakiela et al., 1976).

Secondly, unlike some amacrine cells (Feigenspan et al., 1998), ganglion cells do not spike in the absence of synaptic input. This implies that spikes recorded from ganglion cells in darkness are generated by tonic excitatory synaptic input(s). This input produces as much as a 10-mV difference in the resting potential between ON- and OFF-center ganglion cells (Belgum et al., 1982; Coleman and Miller, 1989;

Saito, 1983), and also gives rise to fluctuations (“noise”) in the membrane potential recorded between spikes (Belgum et al., 1982; Bloomfield and Xin, 1997; see also Freed, 2000b). These inputs might be expected to affect the response of ganglion cells to depolarizing as well as hyperpolarizing inputs, because the voltage-gated and Ca^{2+} -sensitive ion currents that form ganglion cell spikes are subject to inactivation and modulation at these membrane potentials, and because noise would be expected to introduce some jitter in spike timing.

Thirdly, the responses of light-adapted ganglion cells to random fluctuations in the intensity of full-field illumination reflect additional complexities in spike firing mechanisms. In the dark-adapted ganglion cell responses discussed in the previous section, spike threshold appeared to be relatively constant, and there was no sign that the relationship between input current and steady-state spike frequency changed. These properties are consistent with the possibility that ganglion cell spike generation is a simple integrate-and-fire process, in which ganglion cells sum synaptic inputs and then spike whenever their membrane potential reaches a fixed threshold value. A number of modifications of this process have been proposed, for example, to account for the timing of spikes elicited by periodic stimuli in light-adapted ganglion cells (e.g., Reich et al., 1997) and for spike accommodation (e.g., Benison et al., 2001). Recent studies, however, have shown that responses of light-adapted ganglion cells to randomly modulated inputs differ from a simple integrate-and-fire process in at least two ways (Berry and Meister, 1998; Berry et al., 1997). First, these responses consist of spike “events.” Each event is comprised of a relatively fixed number of spikes that fire at a high rate (~ 100 to 200 Hz ; Fig. 27.7). Secondly, each of these events is followed by a relatively long period when cells do not spike. In response to repeated presentations of a randomly fluctuating input, spike events begin at times that vary from trial-to-trial by as little as 1 msec and by not more than 10 msec (Fig. 27.7; see also Berry et al., 1997). The spikes generated under these conditions have therefore been modeled by two signal processing stages (Keat et al., 2001; see also Chichilnisky, 2001; Korenberg et al., 1989), namely a linear filter that transforms light intensity into a generator potential, and a spike generator that starts a spike event when the generator potential exceeds spike threshold.

What cellular mechanisms equip ganglion cells to produce these light responses? Given the variety and complexity of spike-generating mechanisms in other central neurons, it should not be surprising that no complete answer to this question yet exists. However, numerous efforts have been made and are continuing to be made to identify such mechanisms. These efforts have explored how quickly ganglion cells can be depolarized by current injections, what ion channel properties enable ganglion cells to spike, and how

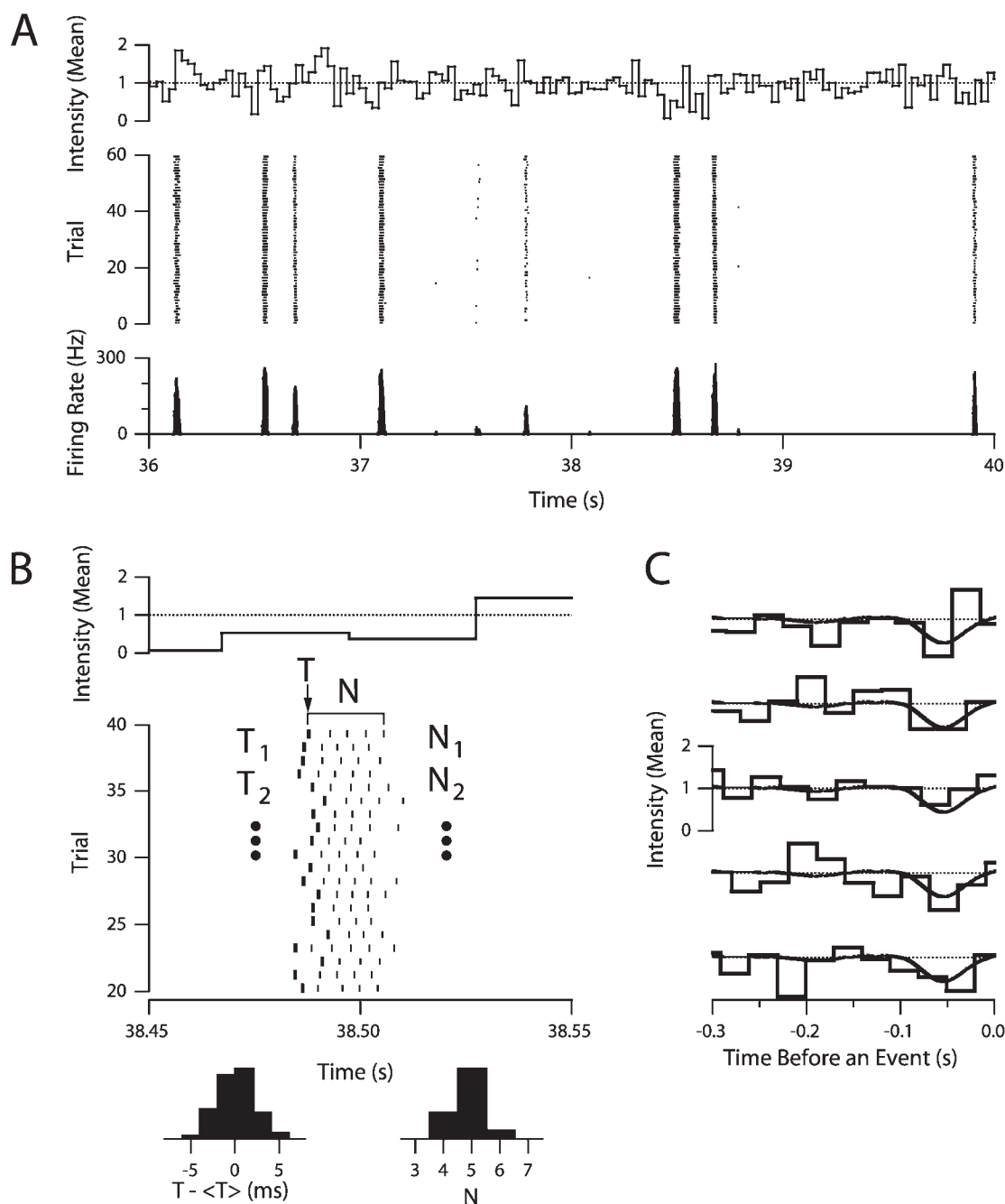


FIGURE 27.7. *A*, spike raster plots (*middle*) and firing rates (*bottom*), recorded from a ganglion cell in salamander retina, in response to 60 presentations of uniform illumination whose intensity was changed to a new value once per 30 msec, from a Gaussian distribution (*top*). Mean light intensity: $4 \times 10^{-3} \text{ W/m}^2$. Standard deviation: 35% of the mean. *B*, spikes comprising the “spike events” recorded during 20 trials, approximately 38.5 msec after the beginning of each trial. Histograms show the time of the first spike in

each event (T), relative to the value averaged across trials ($\langle T \rangle$). N gives the total number of spikes per event. *C*, plot of the intensity (thick line) during the 300-msec period that preceded spike events consisting of, on average, 1.8 to 2.2 spikes. The average intensity that preceded each event is plotted by the thin lines. From Meister and Berry (1999), with permission. Copyright 1999 by Elsevier Science.

these properties change under various conditions. The remainder of this chapter reviews the results of these studies, focusing on four particular areas: membrane time constant, differences in current-clamp and voltage-clamp measurements related to cell-type, modulation of excitability by sub-threshold voltage excursions, and modulation of excitability by dopamine. This will show that a dozen or so types of voltage-gated ion current have been found in ganglion cells so far, that roughly a half dozen conductances could account for ion permeabilities that have been detected around resting potential, and that certain light responses may involve the susceptibility of some of these conductances to modulation. These results begin to suggest that ganglion cells are packed with means to spike differently and to do so to various extents. For reasons given below, however, no attempt to calculate spikes from these data or to compare these data to existing spike models will be made.

Passive properties

MEMBRANE TIME CONSTANT When a pulse of depolarizing current is injected into a cell (either through an electrode or at a synapse), the membrane potential does not instantaneously rise to, or fall from, its steady-state value. The speeds at which these membrane potential changes occur have been measured in many cells, because they are thought to influence the temporal properties of spike firing and the integrative properties of neurons. Within a few mV of resting potential, these changes typically take tens of milliseconds to reach most of their steady-state value (see Spruston and Johnston, 1992).

Several studies have measured this property in ganglion cells. Some of the results are not formally equivalent because different methods were used. However, several values are the time in which membrane potential changed to 63% ($1 - \frac{1}{e}$) of its steady state value during a constant current injection. The values of these “membrane time constants” measured in different cells of the same species, and with similar methods in different species, can therefore be compared. The values reported so far fall into two sets. One was measured near resting potential. These results are summarized here to check for similarities without the complications of synaptic inputs, and in part to compare these values with what has been learned recently about ion permeabilities in resting cells. The second set of measurements give some idea of how time constants differ in cells that receive tonic synaptic inputs.

Using whole-cell patch-electrodes and fits of exponential time functions to membrane potential changes produced

by current injections, Lasater and Witkovsky (1990) found a value of 7 msec in turtle ganglion cells. By fitting single exponentials to similarly produced membrane potential changes, longer time constants have been reported for cat, mudpuppy, and tiger salamander ganglion cells. Robinson and Chalupa (1997) found mean time constants of 23 and 34 msec for beta and alpha ganglion cells, respectively; Lukasiewicz and Werblin (1988) found time constants ranging from 18 to 52 msec (mean: 41 msec), and Coleman and Miller (1989) found time constants ranging from 35 to 126 msec (mean: 68 msec). O’Brien and colleagues (2002) recently reported that the time constants peeled from 8 of 10 morphological types of cat ganglion cells ranged between 20 and 50 msec; that of alpha cells was closer to 5 msec, while zeta cells weighed in at 80 msec. Lastly, by modeling ganglion cells as somata attached to finite cables and fitting equations that describe these structures to the decay of capacitive current transients, Taylor and colleagues (1996) found time constants ranging from 27 to 270 msec (mean: 97 msec).

These data show a couple of trends. First, cells that responded differently to light (ON-center, OFF-center, and ON-OFF; linear vs. nonlinear spatial summation) were found to have similar time constants within individual studies (Coleman and Miller, 1989; Robinson and Chalupa, 1997). Because these types of ganglion cell differ in the level and size of their dendritic arborization, and in some cases the size of their somata (e.g., Wässle and Boycott, 1991), these results indicate that differences in cell shape and size produced no marked difference in time constant. The similarity in time constants reported by O’Brien and colleagues (2002) for the small, tightly branching beta cells and the more sparsely, broadly arborizing delta cells concurs with this; the marked difference between their measurements from alpha cells, beta cells, and zeta cells does not.

Secondly, two groups of cells that differed in sensitivity to current injections—the repetitively spiking “fast” and “slow” cells described by Fohlmeister and Miller (1997a)—had similar time constants. However, Fohlmeister and Miller (1997a) found that “medium” cells had shorter time constants than both slow and fast cells, and that plots of their spike frequency against current intensity were intermediate in slope and position. These data imply that neither of the measured properties depends on time constant. Similar data plots for other cells that have presented different time constants are not available. However, in the recordings of O’Brien and colleagues (2002), one finds (as one would

usually expect) that cells with the shortest time constants (alpha cells) spiked at the lowest rates for a given current intensity, and that cells with the longest time constant (zeta cells) spiked at intermediate rates at much smaller current intensities.

Thirdly, a wide range of time constants has been observed in some ganglion cells. Part of this may be due to species, as the value found in turtle was outside the range of values measured in salamander, mudpuppy, and cat. However, a wide range of values was found in salamanders and mudpuppies alone, even in cells classified for other reasons as single types (Coleman and Miller, 1989; Taylor et al., 1996). This might reflect normal differences in resting membrane resistance, and the ion conductances that determine these resistances. It is also possible that perfusion by the ruptured-patch whole-cell electrodes used to make these measurements altered these conductances in different ways, or to different extents, in different cells. Differences in "passive" membrane properties of the magnitude seen in ganglion cells have been caused in other neurons by this type of recording (Cuevas et al., 1997; Spruston and Johnston, 1992), and as described in the following section, more than one ion permeability in resting ganglion cells may be susceptible to these effects.

RESTING ION PERMEABILITIES A number of studies have shown that, as in other central neurons, the specific membrane resistance of ganglion cells (i.e., the ratio of their time constant to their specific membrane capacitance) is high (e.g., Coleman and Miller, 1989; Fohlmeister and Miller, 1997a; Freed et al., 1992; Taylor et al., 1996). Moreover, the ion permeabilities of resting ganglion cells appear to be "leak-like" because total membrane current amplitude shows no voltage- or time-dependent change when membrane potential is shifted under voltage-clamp around resting potential (i.e., between -65 and -75 mV; see Tabata and Ishida, 1996). One might not be surprised by either of these observations, until the ion permeabilities of resting ganglion cells were examined. To begin with, intracellular recordings suggest that resting ganglion cells are permeable to K^+ , Cl^- , Na^+ , and perhaps Ca^{2+} ions, because (1) increases in extracellular K^+ concentration depolarize dissociated ganglion cells (Bindokas et al., 1994), (2) the reversal potential of current measured just after shifting the voltage in whole-cell patch clamp recordings is K^+ -sensitive (Skaliora et al., 1995), (3) the reversal potential of current in the presence of Na^+ , K^+ , and Ca^{2+} channel blockers is Cl^- -sensitive (Tabata and Ishida, 1999), (4) a small amount of voltage-gated Ca^{2+} conductance resists inactivation at membrane potentials near resting potential (Lee, Hayashida, and Ishida, unpublished observation), and (5) the resting potential typically found in ganglion cells (-65 mV; e.g., Baylor and Fettiplace, 1979; Lukasiewicz and Werblin, 1988) is more positive than

the K^+ equilibrium potential (roughly -100 mV; Stys and Lopachin, 1996).

Recent studies have started to identify ion permeabilities in resting ganglion cells more specifically. Candidates for the resting K^+ and Cl^- permeability include TRAAK, found in ganglion cells by immunostaining and in situ hybridization (Fink et al., 1998; Reyes et al., 2000), and channels like $ClC-1$ (Rosenbohm et al., 1999) or $ClC-3$ (Kawasaki et al., 1994; cf. Stobrawa et al., 2001), because the Cl^- permeability is PKC-regulated (Tabata and Ishida, 1999). At least two non-synaptic routes for Na^+ influx into resting and slightly depolarized ganglion cells have been described: epithelial-type (amiloride-sensitive, voltage-insensitive) Na^+ channels (Matsuo, 1998; Mirshahi et al., 1999) and nonselective cation channels activated by cGMP (Ahmad et al., 1994). In addition to these, the activation and steady-state inactivation curves of Na^+ currents in ganglion cells overlap (Barres et al., 1989; Hidaka and Ishida, 1998; Inceoglu et al., 2002; Kaneda and Kaneko, 1991a; Lasater and Witkovsky, 1990; Lipton and Tauck, 1987; Lukasiewicz and Werblin, 1988; Skaliora et al., 1993), and a small fraction of the voltage-gated Na^+ conductance resists inactivation (Hidaka and Ishida, 1998). This might produce some Na^+ permeability in resting cells, because activation threshold can be as negative as -65 mV (Hidaka and Ishida, 1998). Lastly, "mixed-cation" channels also pass Na^+ ions in addition to K^+ ions, including those that pass the hyperpolarization-activated inward current I_h (Eng et al., 1990; Tabata and Ishida, 1996) and, guessing from the reversal potential measurements published for several preparations (Lasater and Witkovsky, 1990; Lipton and Tauck, 1987; Lukasiewicz and Werblin, 1988), those that carry a substantial fraction of the depolarization-activated outward current. It is not yet possible to state the relative contribution of any of these channel populations to resting membrane resistance (and potential), because the relative permeability of resting ganglion cells to K^+ versus other cations, and K^+ versus anions, has not been measured under physiological conditions. However, resting ganglion cells clearly have several ion permeabilities, and the control of some of these permeabilities by cytoplasmic messengers (e.g., TRAAK, the background Cl^- permeability, and the cyclic nucleotide-gated channels) suggests that membrane resistance (and, in turn, time constant) could be modulated.

MEMBRANE TIME CONSTANTS \pm SYNAPTIC INPUTS Given the high specific membrane resistances that have been found in unstimulated ganglion cells, the membrane time constant of ganglion cells would be expected to decrease when they are barraged by synaptic inputs. The full extent to which this occurs has not yet been worked out, but the three major conductances that might contribute to this effect are those gated by glutamate, inhibitory synaptic inputs, and voltage.

For example, Baylor and Fettiplace (1979) found time constants of 10 to 14 msec by fitting Lapicque's strength-duration equation to the latency of the first spike elicited by different current intensities. Although these measurements were made with sharp microelectrodes, one would also expect them to be shorter than most of those described above because they rely on spike latency, so that these measurements also reflect the effect of conductances that open at subthreshold voltages. A similar conclusion was reached by Coleman and Miller (1989). They reported that ON-center ganglion cells had monoexponential time constants, and that OFF-center and ON-OFF cells did not. By fitting sums of exponentials to the changes in membrane potential produced by stepwise current injections, they found that all cells had a similarly slow membrane time constant (for example, 70 msec for all the mudpuppy ganglion cells recorded from). The faster exponentials (<10 msec) were attributed to voltage-gated conductances activated in OFF-cells by tonically depolarizing synaptic inputs. Consistent with both of the above studies, Diamond and Copenhagen (1993) reported that blocking non-NMDA glutamate receptors in ON-cells, with CNQX, did not significantly alter membrane time constant. The total conductance due to NMDA-type receptors was estimated to be 1.5 times larger than that gated by non-NMDA receptors, suggesting that these conductances might not greatly alter membrane time constant either. These results, and those discussed in the previous section, imply that the ease with which ganglion cells can be driven to spike depends, in part, on the modulation of resting conductances, the voltage-sensitivity and kinetics of currents activating between resting potential and spike threshold, and the deactivation rate of high-threshold K^+ currents.

Voltage-gated ion currents

A number of studies have tried to identify voltage-gated conductances in ganglion cells using patch-clamp methods. Based on the effects of membrane potential changes, ion substitutions, and pharmacological agents, these studies have found that at least some ganglion cells possess a persistent Na^+ current, transient Na^+ current, transient Ca^{2+} current (I_T), conotoxin-sensitive Ca^{2+} current, dihydropyridine-sensitive Ca^{2+} current, toxin-resistant Ca^{2+} current, transient K^+ current (I_A), slowly inactivating K^+ current, one or two Ca^{2+} -activated K^+ currents, I_B (a K^+ current that remains after blocking the other K^+ currents listed here), and an inwardly rectifying cation current (I_h). These results show that in the species examined so far (rat, salamander, turtle, cat, goldfish, rabbit, and ferret), ganglion cells have as many as three "low threshold" ion currents that can be activated by depolarizations at relatively negative membrane potentials, as many as eight "high

threshold" currents that can only activate at more positive membrane potentials, and one current that is activated by hyperpolarization.

A number of questions emerge from these results. Are all of the voltage-gated ion currents listed above found in all ganglion cells? Are the properties of these currents identical among all cells? Have any differences in these currents been shown to account for any functional differences between ganglion cells? These questions have not yet been answered by testing for the presence of all of the currents listed above in any one or more types of cell. However, recordings from numerous cells in the species listed above have shown the following properties:

Na^+ CURRENTS All adult ganglion cells have a Na^+ current that is transient and relatively high-threshold. Some ganglion cells have also been found to have a persistent and low-threshold Na^+ current. The activation threshold of the transient Na^+ current is typically between -50 and -40 mV. Dividing the maximum current amplitude by the total cell capacitance yields a current density of at least 200 pA/pF (Barres et al., 1988; Hidaka and Ishida, 1998; Schmid and Guenther, 1998) consistent with the rise-time of spikes recorded from these cells (roughly 100–200 mV/ms). Complete current blockade is produced by 1 μ M tetrodotoxin (Hidaka and Ishida, 1998; Kaneda and Kaneko, 1991a; Lasater and Witkovsky, 1990; Lukasiewicz and Werblin, 1988; Taschenberger and Grantyn, 1995) consistent with the block of all spike output by tetrodotoxin (Byzov et al., 1970) and the lack of mRNA for tetrodotoxin-resistant Na^+ channels in rat ganglion cells (Fjell et al., 1997). The voltage-sensitivity of this current is complex in several respects. The current does not decline exponentially in amplitude during long (>30-msec) stepwise depolarizations (Hidaka and Ishida, 1998), consistent with the presence of channels that differ in rates of activation or inactivation (cf. Barres et al., 1989). The rate of recovery from inactivation depends on the duration of time spent at conditioning voltages (Kaneda and Kaneko, 1991a), consistent with the presence of multiple kinetic states or different channel subtypes. The voltage sensitivity of steady-state inactivation is susceptible to a left-ward drift in ruptured-patch whole-cell recording (Hidaka and Ishida, 1998), hinting at some sort of on-going regulation. The functional consequences of these complexities are not yet known for sure, but three possibilities are considered below.

"Persistent" Na^+ current—so-named because it resists steady-state inactivation—has been found in rat and goldfish ganglion cells (Hidaka and Ishida, 1998; Stys et al., 1993; Vaquero and Ishida, unpublished observation). The activation threshold of this current is around -65 mV, and at membrane potentials between -40 and -10 mV this current reaches a maximum amplitude that is <1% of the largest transient Na^+ current in the same cells (Hidaka

and Ishida, 1998). Although persistent and transient Na^+ current are both blocked by $1\text{ }\mu\text{M}$ tetrodotoxin, it is not known if they arise from the same channel populations in individual ganglion cells; they are listed here as separate currents because the persistent component has been found in some ganglion cells and not others. The function of this current in ganglion cells is not yet known, but it contributes to spike firing and signal processing in a variety of other cells.

Ca^{2+} CURRENTS All adult ganglion cells have high-threshold Ca^{2+} currents, and most (if not all) ganglion cells also have a low-threshold Ca^{2+} current. The low-threshold current (“T” type Ca^{2+} current or simply “ I_T ”) inactivates almost completely at resting potential (-65 mV ; Lee, Hayashida, and Ishida, unpublished observation) and therefore sizeable amounts of I_T can be activated only by depolarizations from more negative membrane potentials. During these depolarizations, I_T rises and declines in amplitude more slowly than transient Na^+ current, and the maximum current amplitude is typically small ($<10\text{ pA/pF}$). Although previous studies reported that I_T is absent in 25% of the ganglion cells recorded (Bindokas and Ishida, 1996; Guenther et al., 1994; Karschin and Lipton, 1989; Liu and Lasater, 1994a), Miller and colleagues (2002) have recently reported that current density is higher in ganglion cell dendrites than cell bodies. Because dissociations typically shear most or all the dendrites off of cells, this suggests that noticeable amounts of I_T may be present in more ganglion cells than previously reported and, more importantly, serve functions not previously considered.

High-threshold Ca^{2+} current appears to pass through two or three channel populations. One is modulated by dihydropyridine ligands—agonists that augment current at low doses and antagonists that reduce current (Akopian and Witkovsky, 1996; Bindokas and Ishida, 1996; Hirooka et al., 2000; Kaneda and Kaneko, 1991b; Karschin and Lipton, 1989; Liu and Lasater, 1994a; Taschenberger and Grantyn, 1995). Another is blocked by “conotoxins” from *Conus* snails and “agatoxins” from an *Agelenopsis* spider (Bindokas and Ishida, 1996; Hirooka et al., 2000; Karschin and Lipton, 1989; Liu and Lasater, 1994a; Rothe and Grantyn, 1994; Schmid and Guenther, 1998; Tabata et al., 1996; Taschenberger and Grantyn, 1995; Zhang et al., 1997). The third high-threshold Ca^{2+} current found so far is a toxin-resistant component in *Xenopus*, mouse, and rat ganglion cells (Akopian and Witkovsky, 1996; Rothe and Grantyn, 1994; Taschenberger and Grantyn, 1995). Since these current subtypes have been identified, it has become increasingly clear that they mediate the effect of numerous modulators and they do so in complex patterns. To begin with, high-threshold Ca^{2+} currents fuel increases in cytoplasmic Ca^{2+} levels in various subcellular regions of ganglion cells and these regulate nearby ion channels, transmitter receptors,

and signaling cascades (for examples, see Abdel-Majid et al., 2002; Ahljianian et al., 1990; Akopian et al., 1998; Bindokas et al., 1994; Henderson et al., 2001; Karschin and Lipton, 1989; Lipton and Tauck, 1987; Liu and Lasater, 1994a; Lohmann et al., 2002; Shen and Slaughter, 1998; Wang et al., 1998, 1999). These effects are then subject to modulations themselves. For example, GABA and dopamine can both differentially modulate the amplitude of Ca^{2+} currents (e.g., Liu and Lasater, 1994b; Shen and Slaughter, 1999), and glutamate and acetylcholine can exert opposite effects on Ca^{2+} currents (Akopian and Witkovsky, 1996; Baldrige, 1996; Shen and Slaughter, 1998). Thus, while the functions of Ca^{2+} currents obviously depend on their rates of activation and inactivation, it has become clear that these currents coordinate and regulate effects of pathways that converge onto ganglion cells and that this does not depend only on ganglion cell membrane potential. For further details, readers are referred to other chapters in this book and a recent review (Akopian and Witkovsky, 2002).

K^+ CURRENTS All ganglion cells are thought to possess low-threshold and high-threshold K^+ currents, and these have been attributed to as many as five channel populations. The low-threshold current was found in a single study (Lipton and Tauck, 1987) to start activating near -50 mV , inactivate fully around -40 mV , and be blocked by 4-aminopyridine (4-AP); this current was termed I_A . One other study (Guenther et al., 1999) has shown that the activation threshold of this current is around -40 mV . The second type of current reported by most studies has an activation threshold around -25 mV and is blocked by high concentrations of tetraethylammonium (TEA, 10 to 20 mM). A third current is resistant to block by 4-AP and TEA (Guenther et al., 1999; Lukasiewicz and Werblin, 1988; Sucher and Lipton, 1992; Tabata and Ishida, 1999). Although the activation threshold of this current is difficult to say from the published records, this current can be carried by Cs^+ (Tabata and Ishida, 1999) and be blocked by Ba^{2+} (Guenther et al., 1999; Sucher and Lipton, 1992). The two other K^+ currents are activated by depolarization and a concomitant rise in free intracellular Ca^{2+} concentration (Lipton and Tauck, 1987; Lukasiewicz and Werblin, 1988; Skaliara et al., 1995; Wang et al., 1998; see also Henne et al., 2000). These currents are termed BK_{Ca} and SK_{Ca} to signify that the former has a big single-channel conductance (118 pS in cell-attached mode) while that of the latter is small (22 pS). When the cytoplasmic face of these channels was exposed to solutions containing 1 and 10 nM Ca^{2+} , the opening probability and mean open time of BK_{Ca} increased more than those of SK_{Ca} (Wang et al., 1998). Depending on their voltage sensitivity and kinetics, K^+ currents either reduce or facilitate spiking in various preparations. Unfortunately, ascertaining the role of K^+ currents in ganglion cell excitability has been hampered by a number

of problems. One is that reagents commonly used to separate low- and high-threshold K^+ currents (4-aminopyridine and tetraethylammonium) nonselectively block K^+ currents in most, if not all, ganglion cells (Lasater and Witkovsky, 1990; Lukasiewicz and Werblin, 1988; Olson et al., 2000; Skaliara et al., 1995). This has also been found in a recent attempt to unravel K^+ currents and reveal a specific type of low-threshold K^+ current with other pharmacological strategies (Henne et al., 2000). Here, low TEA doses reduced both transient and sustained current (regardless of holding potential) and an agent denoted α -DTX (presumably dendrotoxin) reduced total K^+ current amplitude at membrane potentials above 0 mV but not to any noticeable extent at more negative voltages.

I_h Lastly, the inwardly rectifying cation current I_h has been found in some ganglion cells. The effect of ion substitutions and pharmacological treatments on voltage rectification provided the first evidence of this current in rat optic nerve (Eng et al., 1990). This current was subsequently separated from other currents and measured in goldfish ganglion cell somata (Tabata and Ishida, 1996). The activation threshold of this current is around -65 mV, and thus slightly more negative than that of I_h in photoreceptors. The function of I_h in ganglion cells is not entirely known yet and will certainly depend on its subcellular distribution and the properties of other currents. However, as in other retinal neurons, I_h tends to depolarize ganglion cells while they are hyperpolarized and for some tens of milliseconds after these hyperpolarizations cease (Tabata and Ishida, 1996). Cat ganglion cells have shown voltage rectification and posthyperpolarization spikes (Skaliara et al., 1993; see also O'Brien et al., 2002) consistent with activation of I_h ; recordings from turtle and salamander ganglion cells have shown no measurable amounts of I_h (Lasater and Witkovsky, 1990; Lukasiewicz and Werblin, 1988).

In summary, most studies have found that ganglion cells typically possess a large transient Na^+ current, two types of high-threshold Ca^{2+} current, transient K^+ current (I_A), tetraethylammonium-sensitive K^+ current, one if not two types of Ca^{2+} -activated K^+ current, and a K^+ current that resists block by TEA and 4-AP. The same studies have shown that persistent Na^+ current, transient Ca^{2+} current (I_T), toxin-resistant Ca^{2+} current, and inwardly rectifying cation current (I_h) are present in some ganglion cells and not in others.

SPIKE CALCULATIONS It would be natural to ask why few attempts to use current recordings to calculate ganglion cell spikes have been published so far (for an exception, see Benison et al., 2001). A major reason is undoubtedly that, of the currents alluded to above, the types actually recruited during light responses in specific types of ganglion cell are

unknown. A second reason is that the properties of ion channels in ganglion cell dendrites and axons have not been measured, except for the dendritic Na^+ current recordings of Velte and Masland (1999) and beyond a handful of whole optic nerve recordings and immunostainings (e.g., Boiko et al., 2001; Eng et al., 1990; Stys et al., 1993; Tang et al., 1979).

A third reason is that for most species the amplitudes, kinetics, and voltage sensitivities of the currents listed above have not been described in terms that can readily be incorporated into models. This is both a question of deriving kinetic schemes that describe these currents, and assessing whether data of sufficient quality are at hand. Unfortunately, the method that made it possible to identify and begin to characterize the currents listed above—whole-cell patch clamping in ruptured-patch mode with a continuous single-electrode voltage-clamp amplifier (Hamill et al., 1981)—can also be a source of two types of uncertainties. One is that this method does not provide membrane potential measurements while currents are measured and uncompensated series resistance can significantly distort the measurements of large-amplitude currents (see Armstrong and Gilly, 1992). The other is that rupturing the membrane between the cell cytoplasm and recording pipette solution has been found to confound measurements by changing cytoplasmic divalent cation levels, ion channel phosphorylation and redox states, and activities of signaling cascade components (see Marty and Neher, 1995; Ruppersberg et al., 1991; Tabata and Ishida, 1999; Vaquero et al., 2001; Vargas et al., 1999). Fortunately, perforated-patch recording (Horn and Marty, 1988) and discontinuous single-electrode voltage-clamp amplifiers (Finkel and Redman, 1984) have been developed to circumvent most of these problems. While it is too early to say how differently ganglion cell currents as a whole will look with these methods, a recent study measured voltage-gated Na^+ current in ganglion cells this way and found that the current kinetics and the voltage producing half-maximal steady-state inactivation differ significantly from values reported in previous studies (Inceoglu et al., 2002).

Heterogeneity

Can a case be made for differences in excitability among ganglion cells? If all ganglion cells received the same synaptic inputs, would they be expected to produce similar spike outputs? Can equations incorporating terms for the same currents describe spike generation in all morphological types of ganglion cells?

Baylor and Fettiplace (1979) originally showed that current injections elicit sustained spike firing in turtle ganglion cells even if their light responses were transient. They concluded that this transience could arise presynaptically, and subsequent current injections have also been

found to elicit sustained spike firing in most if not all salamander (Diamond and Copenhagen, 1995; Fohlmeister and Miller, 1997a; Sheasby and Fohlmeister, 1999), ferret (Wang et al., 1997), and goldfish (Vaquero et al., 2001) ganglion cells.

These results are contrasted by reports of transient spiking elicited by current injections into some postnatal rat ganglion cells (Barres et al., 1988) and some larval tiger salamander ganglion cells (Lukasiewicz and Werblin, 1988; Mobbs et al., 1992). While the basis for this transience has not been confirmed by a comparison of recorded spikes versus spikes calculated from recorded currents, a number of possibilities have been proposed. One is that after one or more spikes, the amount of Na^+ current available to produce additional spikes declines faster in transient cells than in sustained cells. This could be due either to steady-state inactivation at relatively negative membrane potentials, current activation at only relatively positive membrane potentials, slow recovery from inactivation, or a combination of these (Barres et al., 1988; Kaneda and Kaneko, 1991a; Skaliara et al., 1993; Wang et al., 1997). A second idea is that transience arises because the gradual inactivation of I_B promotes Na^+ current inactivation (Lukasiewicz and Werblin, 1988). A third idea is that the delayed activation of an outwardly rectifying K^+ current inhibits repetitive spiking (Henne et al., 2000).

A number of immunostaining and in situ hybridization studies have also found that different ganglion cells express different kinds and combinations of Shaker-, Shab-, and Shaw-type K^+ channels (Henne et al., 2000; Klumpp et al., 1995; Yazulla and Studholme, 1998) and different types of voltage-gated Na^+ channels (Fjell et al., 1997; see also Boiko et al., 2001). These results raise even further the possibility that ganglion cells spike in subtly different ways, not just transient versus sustained. However, the actual significance of these results will depend on the outcome of experiments that show the properties of currents carried by these channels and the properties of other currents in these cells.

One problem in understanding the differences summarized here is that all of the voltage-clamp measurements to date have been made either in ganglion cells of unknown subtype or at best, in only a few of the 10 to 20 types of ganglion cells that have been classified anatomically. For this reason, the study of O'Brien and colleagues (2002) is of keen interest, because it sampled excitability in 10 morphologically identified types of adult cat ganglion cell. Depolarizing current injections elicited different maximum spike frequencies, degrees of spike accommodation, and spike widths. This corroborates the observation that salamander ganglion cells differ in spike threshold and spike frequencies elicited by different amounts of current (Fohlmeister and Miller, 1997a; Sheasby and Fohlmeister, 1999), and shows that morphologically distinct cells possess more combinations of dis-

tinct spiking patterns, time constants, and amounts of inward rectification than any previous study suggested. Whether these differences allow different cells to generate outputs over different dynamic ranges, and the extent that these differences result from differences in cell morphology as opposed to the distribution and properties of specific ion currents, all remain to be worked out.

Response-dependent modulation

A number of changes in ganglion cells spikes differ from the simple integrate-and-fire behavior referred to above. Some of these are triggered by voltage changes in ganglion cells, and could therefore be called "response-dependent." Others are a consequence of changes in the chemical environment of ganglion cells, and could therefore be called "input dependent." Both are described below. Although these sections will show that some seemingly simple voltage responses are not readily explained by existing current recordings, comparing these currents and voltage behaviors suggest experiments that might be pursued. Response-dependent modulation is described first, starting with those showing effects of hyperpolarization, and following with those showing effects of depolarization.

PRIMING BY HYPERPOLARIZATION Hyperpolarizations can boost excitability, as evidenced by bursts of spikes seen after hyperpolarizing current injections are terminated (Eng et al., 1990; O'Brien et al., 2002; Skaliara et al., 1993; Tabata and Ishida, 1996). These spikes arise because hyperpolarization of ganglion cells below normal resting potential recruits inward current that can depolarize cells toward spike threshold after the hyperpolarization ceases.

One of these currents is I_h . This current is carried by both Na^+ and K^+ ions, reverses in polarity at voltages more positive than resting potential, and deactivates exponentially with a time constant of roughly 100 msec at resting potential (Tabata and Ishida, 1996). I_h can therefore depolarize ganglion cells until it deactivates, after the hyperpolarization that activates it is terminated. Two other currents that are affected by hyperpolarization are voltage-gated Na^+ current and I_T . Hyperpolarization does not activate these currents, but instead, increases the amount of current available for activation by subsequent depolarization. This occurs because resting membrane potential is positive enough to inactivate these currents—by as much as 25% of the maximum Na^+ current (e.g., Barres et al., 1989; Hidaka and Ishida, 1998; Inceoglu et al., 2002) and around 95% of the maximum I_T (Lee, Hayashida, and Ishida, unpublished observations; see also Bindokas and Ishida, 1996; Karschin and Lipton, 1989). After sufficient hyperpolarizations, the amounts of Na^+ and Ca^{2+} current that recover from inactivation and the I_h that activates would be expected to facil-

itate spiking, because the reversal potentials of all three currents are more positive than spike threshold. This might occur not only at the termination of hyperpolarizing steps of light intensity, but also during the hyperpolarizations that precede spike bursts elicited in OFF-center ganglion cells by randomly fluctuating light intensity (Sakai and Naka, 1987; see also Sakuranaga et al., 1987).

Although the sensitivities to hyperpolarization of I_T and I_h in ganglion cells resemble those of currents that contribute to the function and electrical properties of other central neurons and other tissues, there is little evidence at this time that the effects described above contribute to ganglion cell spiking *in situ*. For that matter, effects of this kind are difficult to reconcile with three observations. First, as noted above, the OFF response of dark-adapted ganglion cells consists of a step-like increase in spike frequency, rather than a transient one. Secondly, the amplitudes of I_T and I_h are typically small; in fact, some species have been reported to lack I_h (turtle: Lasater and Witkovsky, 1990; salamander: Lukasiewicz and Werblin, 1988) and I_T has been reported to be absent in some ganglion cells of all species examined to date (rat, turtle, goldfish, cat: Bindokas and Ishida, 1996; Guenther et al., 1994; Huang and Robinson, 1998; Karschin and Lipton, 1989; Liu and Lasater, 1994a). Thirdly, the membrane potentials that ganglion cells have been found to traverse during hyperpolarizing light stimuli are generally less negative than those that activate I_h and/or prime Na^+ and Ca^{2+} currents in the ways described above. The recordings of O'Brien and colleagues (2002) underscore this point, in that they show voltage rectification at -75 mV and more negative membrane potentials in theta and iota ganglion cells, but only during hyperpolarizations past -90 mV in beta, delta, epsilon, zeta, eta, and lambda cells. As clear as these disparities seem, they leave open the question why some ganglion cells possess I_h and I_T , and why others might not. To date, one study has found that the membrane potential changes calculated for cells assumed to have a leak permeability, I_h , and a depolarizing input that is either monosynaptic or push-pull in origin (Tabata and Ishida, 1996) resemble subthreshold membrane potential changes that occur during transient OFF responses (e.g., Saito, 1983). One might also note that all of the cell types that inwardly rectified in the study of O'Brien and colleagues (2002) spiked transiently after termination of hyperpolarizing currents.

One other current is thought to be primed in ganglion cells by hyperpolarization, namely I_A . This current is prototypically low threshold, transient, and inactivated by depolarization—in other words, it consists of a brief K^+ efflux that begins when cells are depolarized from relatively negative membrane potentials (Hagiwara et al., 1961). This current can delay spiking, and thereby reduce excitability (Connor and Stevens, 1971). The only evidence that this

occurs in ganglion cells is that, in rat, 4-aminopyridine accelerates the repolarizations that are recorded after terminating hyperpolarizing current injections (Eng et al., 1990) and reduces the amplitude of an outward current that is transient and low-threshold (Lipton and Tauck, 1987; see also Guenther et al., 1999). Spikes with very long latencies have been recorded in some rat ganglion cells during depolarizing current injections (Barres et al., 1988), and (as noted above) Shaker-type K^+ channel mRNA has been found in ganglion cells (Henne et al., 2000; Klumpp et al., 1995; Yazulla and Studholme, 1998). However, for reasons that are not yet known, the K^+ current that is transient and blocked by 4-aminopyridine in ganglion cells of all species beside rat begins to activate around -40 mV (salamander: Lukasiewicz and Werblin, 1988; turtle: Lasater and Witkovsky, 1990; cat: Skaliora et al., 1995; ferret: Wang et al., 1997; goldfish: Olson et al., 2000). The point here is not that this current is unusual (see Rudy, 1988), but that this current would work differently than low-threshold K^+ current. The function of 4-aminopyridine-sensitive currents in ganglion cells remains to be seen. So far, two studies have found that altering the properties of I_A included in Hodgkin-Huxley type equations does not affect ganglion cell spiking (Benison et al., 2001; Fohlmeister and Miller, 1997a).

ACCOMMODATION When ganglion cells are depolarized by constant current injections, the interspike interval increases during the first few spikes (Baylor and Fettiplace, 1979; Diamond and Copenhagen, 1995; Fohlmeister and Miller, 1997a; Mobbs et al., 1992; O'Brien et al., 2002; Vaquero et al., 2001; Velte and Masland, 1999). This increase—or the decrease in the “instantaneous” frequency calculated from the inverse of these intervals—is termed “accommodation.” Practically speaking, a decline in spike frequency is termed accommodation if the frequency does not decline to the baseline level (or zero), to distinguish it from “transient” spike firing (Cleland et al., 1971; see also Bieda and Copenhagen, 2000). Although accommodation lowers the spike frequency averaged over the duration of long depolarizations below that measured either during brief depolarizations or during the initial portion of long depolarizations, relatively little is known about what causes it. Simulations of dissociated cells have suggest that a gradual build-up of intracellular Ca^{2+} can lead to accommodation (Benison et al., 2001); accommodation observed under conditions that block voltage-gated Ca^{2+} influx (Vaquero et al., 2001) implies that other mechanisms can also produce accommodation.

CALCIUM-MODULATED SPIKING Another effect of depolarization on ganglion cell excitability is due to depolarization-activated Ca^{2+} influx. Nearly all studies have found that pharmacological agents that reduce high-threshold Ca^{2+}

currents reduce spike frequency. These agents include D_1 -type dopamine receptor agonists, $GABA_B$ -type GABA receptor agonists, Co^{2+} , Cd^{2+} , and the *Conus* toxins ω -MVIIC and ω -GVIA (Liu and Lasater, 1994b; Rothe et al., 1999; Zhang et al., 1997). Because all ganglion cells are thought to have Ca^{2+} -activated K^+ currents, it seems likely that the effects of blocking Ca^{2+} current are due, in part, to reducing Ca^{2+} -activated K^+ currents. If so, then one might expect spike frequency to be decreased by toxins that block these currents. However, two toxins of this sort (apamin and charybdotoxin) have been found to increase spike frequency (Fohlmeister and Miller, 1997a; Wang et al., 1998). Attempts to account for the effect of Ca^{2+} by modeling have led to two different conclusions. One model predicts that blocking Ca^{2+} and Ca^{2+} -activated K^+ currents should increase spike frequency (Fohlmeister and Miller, 1997a). A more recent model (Benison et al., 2001) predicts that Ca^{2+} currents by themselves will not affect spike frequency. These models were formulated differently, in a number of ways, particularly in how they model cytoplasmic Ca^{2+} levels. Figuring out which factors are significant will therefore depend on the outcome of further studies of the cells modeled, particularly their cytoplasmic Ca^{2+} levels and the sensitivity of K^+ currents to Ca^{2+} and voltage.

ADAPTATION INDUCED BY TEMPORAL CONTRAST A very different effect of depolarization has been studied by Kim and Rieke (2001). Their results are the first to have shown that the excitability of at least some ganglion cells is modulated by “temporal contrast” (defined in their study as the ratio of the standard deviation of the photoisomerization of long-wavelength-sensitive cones to the mean rate). This was done in two ways. First, spikes and whole-cell current were measured in response to 8% and 21% contrast in full-field illumination. These responses were used to describe how ganglion cells convert light to whole-cell current in terms of one linear filter and a static nonlinearity, and how ganglion cells convert the whole-cell current to spikes in terms of another linear filter and static nonlinearity. Increasing contrast reduced spike generation more than the conversion of light to current, and did so in the linear filter rather than the static nonlinearity. Secondly, current that fluctuated randomly within a 0 to 50 Hz bandwidth (i.e., Gaussian noise) was injected into ganglion cells. When the modulation depth of the injected current was changed from a value induced by 8% contrast to that induced by 21% contrast, spike frequency declined. Because this reduction did not occur in the presence of a Na^+ channel toxin (tetrodotoxin), while it persisted in the presence of agents that block Ca^{2+} current and some K^+ currents (Cd^{2+} , Ba^{2+} , and apamin), temporal contrast adaptation appeared to be mediated by effects of current variance on Na^+ channels (Fig. 27.8).

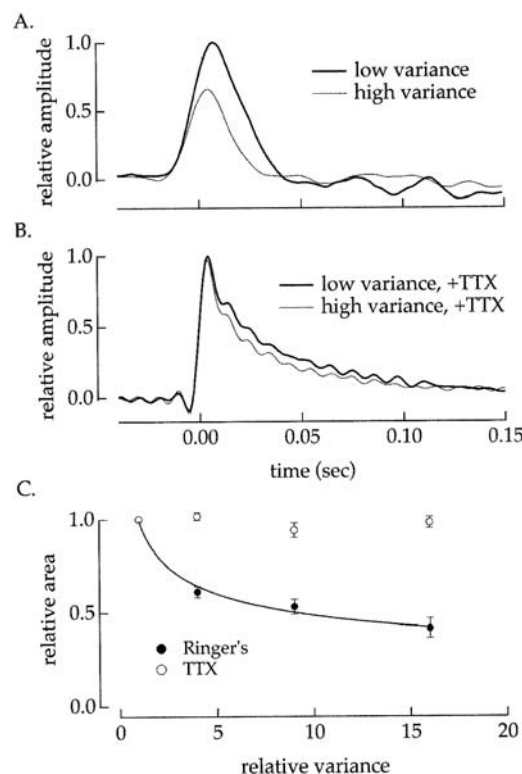


Figure 27.8. Responses of a ganglion cell, in an isolated larval tiger salamander retina, to injections of randomly fluctuating current. Current variance (in the bandwidth 0 to 50 Hz) was set to values recorded in response to low-contrast or high-contrast illumination (16 or 144 pA^2 , respectively). Responses show the change in spike firing rate, calculated as the output of a linear filter in a sandwich model, from cross-correlating the injected current with the spikes recorded, and dividing by power spectrum of the current. Control response (A) decreased on increase in current variance. This decrease was not observed in the presence of 100 nM TTX (B). C, plot of area of response in responses to different current variances, in presence and absence of TTX. From Kim and Rieke (2001), with permission. Copyright 2001 by the Society for Neuroscience.

Kim and Rieke (2001) suggested that increases in current variance increase spike threshold by decreasing the fraction of Na^+ channels that are available for activation. Specifically, Kim and Rieke suggested that this component of adaptation may occur because Na^+ channels recover slowly from inactivation after being activated at subthreshold membrane potentials by increased stimulus contrast. Other effects could also have come into play. For example, because Na^+ current measurements from ganglion cells of the species studied by Kim and Rieke show that activation threshold is -40 mV (Lukasiewicz and Werblin, 1988), contrast might have raised spike threshold because Na^+ channels inactivated without activating. This would be interesting to check in ganglion cells because Na^+ channels in a number of tissues enter, and recover from, this type of inactivation somewhat slowly (e.g., Rudy, 1978), and because a portion of the effect found by

Kim and Rieke is slow in onset and recovery. Also, other studies have shown that, before declining, spike frequency increases sharply just after contrast is increased (Brown and Masland, 2001; Chander and Chichilnisky, 2001; Smirnakis et al., 1997). Therefore, increases in contrast might induce other kinds of slow Na^+ channel inactivation, for example, one that follows fast inactivation during volleys of spikes (e.g., Fleidervish et al., 1996). One further possibility is that increases in contrast reduce excitability because a K^+ conductance is activated by the increased spiking that occurs just after the contrast increment, as found in ferret V1 neurons (Sanchez-Vives et al., 2000). Temporal contrast adapts these cells by activating a Na^+ -dependent K^+ current and, in various preparations, this current is blocked by tetrodotoxin, and not by Cd^{2+} , apamin, or low concentrations of Ba^{2+} (Constanti and Sim, 1987; Koh et al., 1994; Schwindt et al., 1989). It may only be a coincidence, but this pharmacology matches the one found by Kim and Rieke (2001).

Regardless of mechanism, the extent that decreases in ganglion cell excitability account for contrast adaptation remains to be worked out. Earlier studies found contrast adaptation that was relatively broad ranging and attributable to feedback from processes in the inner plexiform layer (Shapley and Victor, 1978). More recent studies have found contrast adaptation that is localized (Brown and Masland, 2001; Donner et al., 1991; Smirnakis et al., 1997) and persists after blocking GABA and glycine receptors (Brown and Masland, 2001; Donner et al., 1991; Rieke, 2001). Moreover, changes in contrast have been found to adapt some bipolar cells more than others (Rieke, 2001). These results imply that adaptation might arise in different ways or to different extents in different ganglion cells (Chander and Chichilnisky, 2001; Donner et al., 1991; Kim and Rieke, 2001).

Input-dependent modulation

Various substances (e.g., dopamine, serotonin, somatostatin, enkephalin, vasoactive intestinal peptide, substance P, and nitric oxide) have been found to affect spontaneous firing rates, light responses, and/or voltage-gated currents of ganglion cells (e.g., Hirooka et al., 2000; Zalutsky and Miller, 1990). These substances are generally termed “neuromodulators” because they exert their effects by altering the amplitude, voltage-sensitivity, and/or kinetics of ion currents, and also because their effects typically take seconds to develop. Of the substances that are thought to act as neuromodulators in the retina, dopamine has been studied the most extensively (Dowling, 1991; Witkovsky and Deary, 1991), and among the many effects that dopamine is known to exert, two recent studies have found that dopamine alters the excitability of dissociated ganglion cells (Liu and Lasater, 1994b; Vaquero et al., 2001). These studies showed that dopamine and SKF-38393 (a D1-type dopamine receptor

agonist) reduce spike frequency, truncate sustained spike firing, and increase spike latency, and that these effects occur without a change in resting potential (i.e., without producing a response opposite in polarity from the response to excitatory transmitters). Two of these effects are observed in ganglion cell responses to light flashes when dark-adapted retinas are light adapted by full-field background illumination. In particular, plots of spike frequency versus stimulus intensity shift rightwardly and spike firing becomes “transient” (as only a few spikes are elicited just after the beginning of constant current injections). The following sections describe what is known about how dopamine might produce these effects.

MECHANISMS OF INHIBITION Three intermediate steps between the release of dopamine by background illumination and modulation of ganglion cell excitability have been identified. First, light elevates cyclic 3',5' adenosine monophosphate (cAMP) levels in ganglion cells (Fig. 27.9; Vaquero et al., 2001). Secondly, dopamine increases cytoplasmic cAMP levels in ganglion cells (Liu and Lasater, 1994b) by activation of D1-type dopamine receptors, and thirdly, the elevated level of cAMP appears to activate a cAMP-dependent protein kinase (PKA; Vaquero et al., 2001). The evidence for these latter two steps is that a D1-type dopamine receptor antagonist (SCH-23390) blocks increases in ganglion cell cAMP levels by exogenous dopamine, that the inhibition of spikes by SKF-38393 is counteracted by a PKA inhibitor (Rp-5,6 DCl-cBIMPS; Fig. 27.10), and that a membrane-permeable cAMP analog that can activate PKA (8-bromo cAMP) also inhibits ganglion cells (Vaquero et al., 2001). As would be expected if light stimulates intraretinal dopamine release and if this dopamine activates D1-type receptors in ganglion cells, SCH-23390 diminishes cAMP levels in light-adapted ganglion cells, whereas sulpiride (a D2-type dopamine receptor antagonist) does not (Vaquero et al., 2001). In concert with these results, cAMP immunoreactivity has been found in the ganglion cell layer somata of light-adapted rat retinas (Vaquero and Ishida, unpublished observations), forskolin increases cAMP immunoreactivity in turtle (Liu and Lasater, 1994b) and rat (Shen et al., 1999; Traverso et al., 2002) ganglion cells, and antisera directed against adenylyl cyclase isoforms immunostain somata throughout the ganglion cell layer of rat and mouse retinas (Abdel-Majid et al., 2002).

The electrophysiological details of how dopamine-activated PKA reduces ganglion cell excitability remain to be worked out. D1-type receptor activation inhibits ganglion cells even after voltage-gated Ca^{2+} influx is blocked by replacing most of the extracellular Ca^{2+} with Mg^{2+} (Fig. 27.11; Vaquero et al., 2001). This suggests that dopamine inhibits ganglion cells by modulating other voltage-gated currents involved in spike generation, for example, voltage-

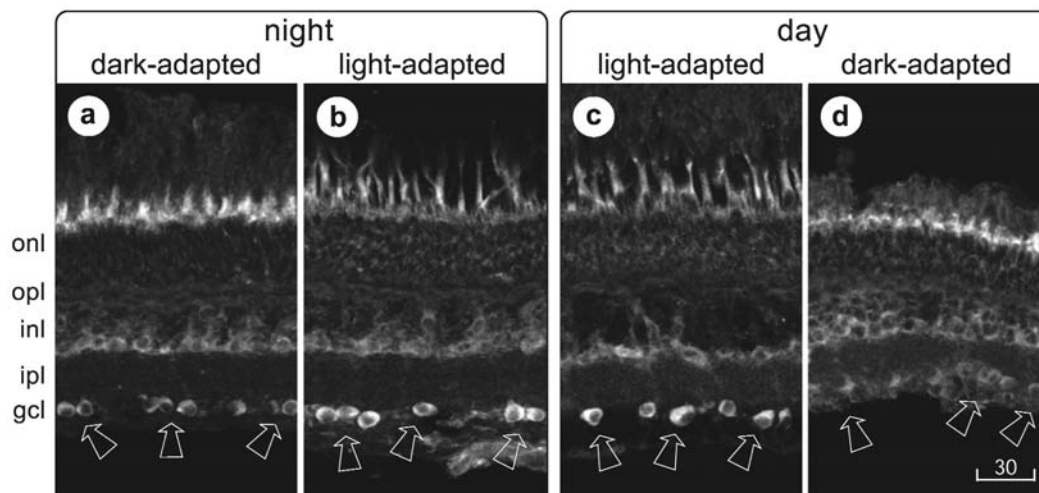


FIGURE 27.9. Transretinal cryosections of goldfish retinas, immunostained with a polyclonal antiserum directed against cyclic 3',5' adenosine monophosphate (cAMP) and imaged on a confocal laser microscope. Dark-adapted retinas were isolated and fixed under infrared illumination, 3 hrs after sunset (*a*), or from fish transferred to complete darkness for a 3-hr period that began 3 hrs after sunrise (*d*). Light-adapted retinas were isolated and fixed under room light 3 hrs after sunrise (*c*), or from fish exposed to roomlight for a 3-hr period that began 3 hrs after sunset (*b*). Level of photoreceptors (onl), outer plexiform layer (opl), inner nuclear layer (inl), inner plexiform layer (ipl), and ganglion cell layer (gcl) indi-

cated along left side of figure. The intensity of fluorescence that passed through a 590-nm long-pass filter is displayed in grayscale, with the brightest fluorescence appearing white. cAMP-like immunoreactivity is most vivid at level of cone photoreceptor inner segments in dark-adapted retinas and in ganglion cell layer in light-adapted retinas. cAMP-like immunoreactivity in photoreceptors is reduced in light-adapted retinas. Arrows point to some of the ganglion cell somata in each section. Magnification is identical in all panels; calibration mark in *d* is 30 μm . From Vaquero et al. (2001). Copyright 2001 by the Society for Neuroscience.

gated Na^+ current and/or voltage-gated K^+ currents. What changes in these currents could explain the inhibition by dopamine? One possibility is that the primary effect of dopamine is like that found in hippocampal pyramidal neurons. Here, dopamine decreases the voltage-gated Na^+ current amplitude and decreases spike frequency (see Fig. 4a in Cantrell and Catterall, 2001). These effects are not thought to involve a change in Na^+ current inactivation (Cantrell et al., 1999).

Dopamine could also reduce ganglion cell excitability and truncate repetitive spiking by modulating outward K^+ current(s). One possibility is that K^+ current deactivates rapidly in the absence of dopamine, so that spike repolarization is short lived and ganglion cells can spike again when they are depolarized; if K^+ current deactivation was then slowed in the presence of dopamine, depolarization back to spike threshold would be postponed, Na^+ current inactivation could accumulate, and spiking would become transient. Although D1 receptor activation is not known to inhibit cells in any tissue this way, this is one way that somatostatin inhibits hippocampal pyramidal neurons (Moore et al., 1988).

Aside from these possibilities, it was originally proposed that dopamine inhibits turtle ganglion cells by decreasing the amplitude of a high-threshold Ca^{2+} current (Liu and Lasater, 1994b). The basis of this suggestion was that spikes are blocked in ganglion cells by other pharmacological agents

that block Ca^{2+} currents. This remains an interesting possibility because it suggests that dopamine might excite some ganglion cells, specifically those whose Ca^{2+} current amplitudes are increased by dopamine (Liu and Lasater, 1994b). One way to resolve this would be to demonstrate that dopamine reduces Ca^{2+} currents in cells that it inhibits, and increases Ca^{2+} currents in cells that it excites.

FEEDFORWARD INHIBITION Regardless of the mechanism(s) underlying the effect of dopamine on ganglion cells, the ability of dopamine to inhibit ganglion cells in the absence of their synaptic inputs implies that this inhibition does not require a decrease in excitatory synaptic inputs to ganglion cells, or a decrease in ganglion cell responses to this input in situ. This constitutes an inhibitory input to ganglion cells that is anatomically feedforward.

What cells and pathways produce this inhibition? A large number of anatomical, immunostaining, release, and electrophysiological studies suggest that dopaminergic input to ganglion cells can be activated by various presynaptic circuits. To begin with, endogenous dopamine and/or tyrosine hydroxylase have been found in processes ramifying in the most distal sublayer ("s1") of the inner plexiform layer in all of around 45 different species examined to date; similar processes also ramify in the middle and most proximal sublayers of most species (Djamgoz and Wagner, 1992; Ehinger, 1983; Frederick et al., 1982; Gustincich et al., 1997;

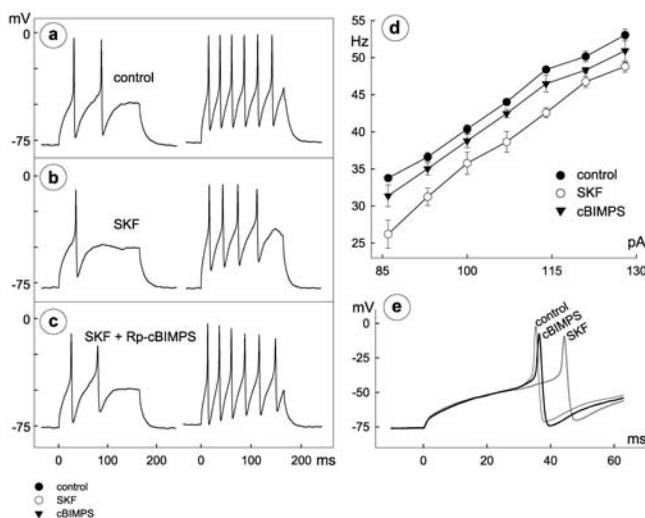


FIGURE 27.10. Intracellular recording of membrane potential of a ganglion cell dissociated from goldfish retina. Spikes are elicited by 165-msec, constant-current injections of 72 and 107 pA in left and right, respectively, of *a–c*. Current injections start at $t = 0$ in each record. Spikes recorded before (*a*) and during (*b*) application of 30 μ M SKF-38393, and during (*c*) subsequent application of a mixture of 30 μ M SKF-38393 plus 100 μ M Rp-5,6-DCI-cBIMPS. The response to the larger current injection in (*b*) shows a lower instantaneous spike frequency than in *a* and *c*; note also that spiking stops around 150 msec after the beginning of the current injection, as in Figure 27.11. *d*, plot of instantaneous spike frequency calculated from the first pair of spikes activated by individual depolarizations. Bars plot ± 1 S.E.M. *e*, plot of lead spike in recording in all three solutions, at fast sweep speed. From Vaquero et al. (2001). Copyright 2001 by the Society for Neuroscience.

Marc, 1995; Nguyen-Legros, 1988; Oyster et al., 1985; Peichl, 1991; Tauchi et al., 1990; Witkovsky and Deary, 1991; Witkovsky and Schütte, 1991). These processes arise from one, two, or possibly three morphological types of cell (namely, different amacrine cells, or amacrine and interplexiform cells; see Hokoç and Mariani, 1988; Kolb et al., 1990; Oyster et al., 1985; Tauchi et al., 1990), and position dopaminergic cells to be controlled by at least two different kinds of synaptic input. One is a direct excitatory input from ON-center bipolar cells (Boelen et al., 1998; Dong and McReynolds, 1992; Pollard and Eldred, 1990; Watt and Glazebrook, 1993; Yazulla and Zucker, 1988); the other allows dopaminergic processes to depolarize by disinhibition, when inhibitory input from GABAergic amacrine cells is reduced by hyperpolarizing input from OFF-center bipolar cells (Critz and Marc, 1992; Gustincich et al., 1997; Kamp and Morgan, 1980; Marshak, 2001; Piccolino et al., 1984).

Consistent with the net effect of these circuits, release studies have shown that dopamine release is augmented by light rather than by darkness (e.g., Kramer, 1971). Unfortunately, the rate at which ganglion cell activity can be

modulated by these circuits has not been measured. Although this should depend to some degree on how quickly extracellular dopamine concentration changes when dopamine release starts and stops, the rates of these changes are not yet known. Some of this could be rapid, given the amacrine and interplexiform cell processes that face synaptic vesicle clusters at ganglion cell dendrites (Pollard and Eldred, 1990; Watt and Glazebrook, 1993; Yazulla and Zucker, 1988), and the dendritic processes that wander down to the ganglion cell layer and even the optic fiber layer (Brunken et al., 1986; Guimarães and Hokoç, 1997; Kallo-niatis and Marc, 1990; Yazulla and Zucker, 1988). On the other hand, dopamine receptors have not yet been localized in ganglion cells at release sites of either dopaminergic amacrine or interplexiform cells. Moreover, a number of studies have reported not finding synapses from dopaminergic processes onto ganglion cells (Gustincich et al., 1997; Hokoç and Mariani, 1987, 1988; Kolb et al., 1990; Pourcho, 1982), even though dopamine receptors have been found in ganglion cells of some of these species (Nguyen-Legros et al., 1997; Tran and Dickman 1992; Verucki and Wässle, 1996). Unless the synapses are scarce enough to have been missed, one might imagine that dopamine reaches these ganglion cells by the paracrine type of transmission that was inferred originally from dopamine sensitivities of horizontal cells, photoreceptors, and pigmented epithelium (Deary and Burnside, 1989; Piccolino et al., 1984, 1987; Pierce and Besharse, 1985).

DOPAMINE “TONE”? It is not known if dopamine modulates ganglion cell light responses in all of the species referred to above, especially by modulating ganglion cell excitability as described above. However, dopamine responses have been studied in fish, reptilian, and mammalian ganglion cells, and at least two effects of dopamine on light responses resemble the effects of dopamine on spiking discussed above and effects of background light on responses to light flashes.

The first of these is to reduce instantaneous and sustained spike frequency. The earliest studies showed that dopamine reduced spike firing in cat ganglion cells, regardless of whether the dopamine was injected intravenously or iontophoretically applied (Straschill and Perwein, 1969; Thier and Alder, 1984). These studies also showed that dopamine inhibited spikes, regardless of whether they were elicited by receptive field centers or surrounds—for example, by illuminating ON-cell centers, darkening ON-cell surrounds, or illuminating OFF-cell surrounds (Straschill and Perwein, 1969; Thier and Alder, 1984); even spontaneous spike firing rates were reduced (Thier and Alder, 1984). When these effects were measured at different light intensities, dopamine was found to produce, in rabbit ON-center and OFF-center ganglion cells, a parallel and rightward shift of semi-

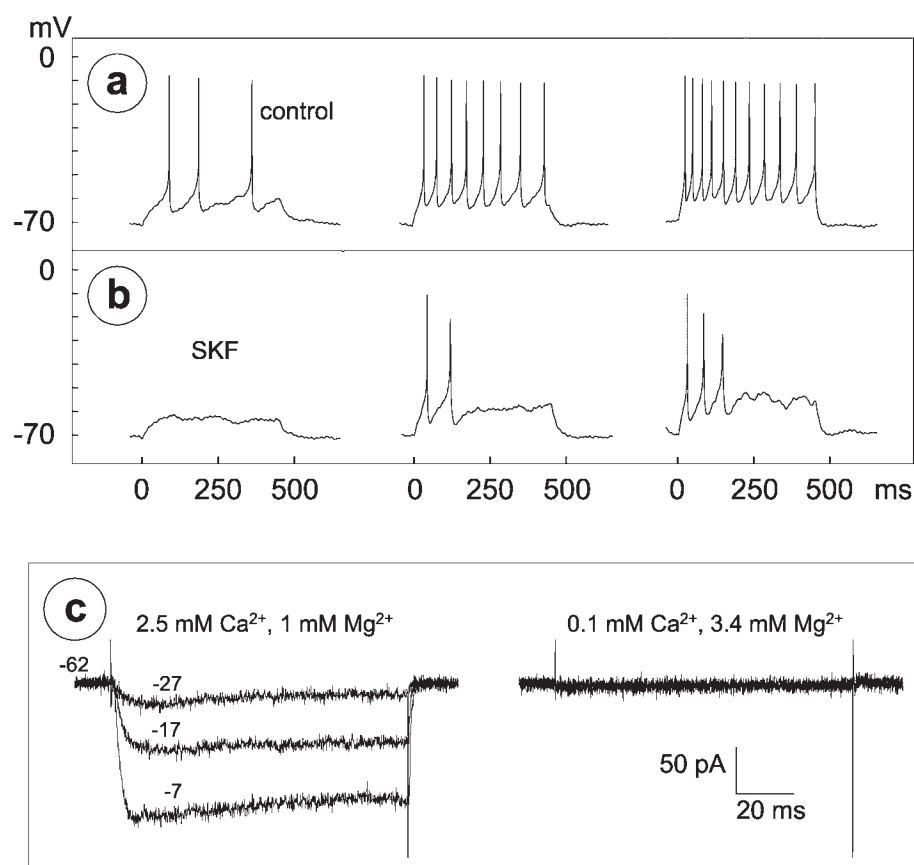


FIGURE 27.11. Intracellular recording of membrane potential of a ganglion cell dissociated from goldfish retina. Spikes are elicited by 450-msec, constant-current injections of 7, 11, and 15 pA in left, middle, and right of *a* and *b*. Current injections start at $t = 0$ in each record. Spikes recorded in a Ringer's solution containing 0.1 mM Ca²⁺ and 2.4 mM Mg²⁺, before (*a*) and during (*b*) application of 30 μM SKF-38393. Note that, in SKF-38393, cell stops spiking around 150 to 200 msec after beginning of the current injections, as in Figure 27.10. *c*, lowering Ca²⁺ (and raising Mg²⁺) blocks whole-cell Ca²⁺ current that normally

activates at voltages traversed during spikes. Traces recorded in voltage-clamp mode, from a single cell (different from that in *a* and *b*) in control Ringer that contained 2.5 mM Ca²⁺ and 1 mM Mg²⁺ (*left*), and in test solution that contained 0.1 mM Ca²⁺ and 3.4 mM Mg²⁺ (*right*). As indicated by numbers next to traces, holding potential was -62 mV, and test potentials were -27, -17, and -7 mV. Compositions of Ringer's and pipette-filling solutions blocked voltage-gated Na⁺ and K⁺ currents. Adapted from Vaquero et al. (2001). Copyright 2001 by the Society for Neuroscience.

logarithmic plots of spike frequency against light intensity (so-called "R-log I curves"; Fig. 27.12; also see p. 846 of Jensen and Daw, 1986). These shifts, being parallel and rightward, resemble those produced by dopamine on spike frequencies elicited by current injections into goldfish ganglion cells (Vaquero et al., 2001), and by uniform background illumination on R-log I curves recorded from ganglion cells in cat (Sakmann and Creutzfeldt, 1969), mudpuppy (Thibos and Werblin, 1978; Werblin and Copenhagen, 1974), and rat (Green and Powers, 1982).

This does not imply that dopamine accounts for the position of R-log I curves measured over a wide range of background intensities. As yet, there is no way to know how much dopaminergic inhibition of ganglion cells contributes to adaptation, because the dependence of intraretinal dopamine concentration on light intensity, and the depen-

dence of both bipolar and ganglion cell light responses on dopamine concentration, remain to be determined. The parallel right-shift of R-log I curves that is produced, however, indicates that dopamine can reduce the light sensitivity of ganglion cells without changing the width of their dynamic range (e.g., Jensen and Daw, 1986)—in other words, dopamine can change σ in the Michaelis equation, without changing n or R_{\max} .

A second effect of dopamine is to truncate repetitive spiking. Dopamine (1) eliminates sustained spiking in dark-adapted OFF-center cells at the offset of central illumination (leaving a transient response only), (2) accelerates the decay of this OFF-response even after it becomes somewhat transient due to light adaptation (see below), and (3) accelerates the decay of spiking elicited in ON-center cells by the onset of central illumination (Fig. 27.13; Thier and Alder,

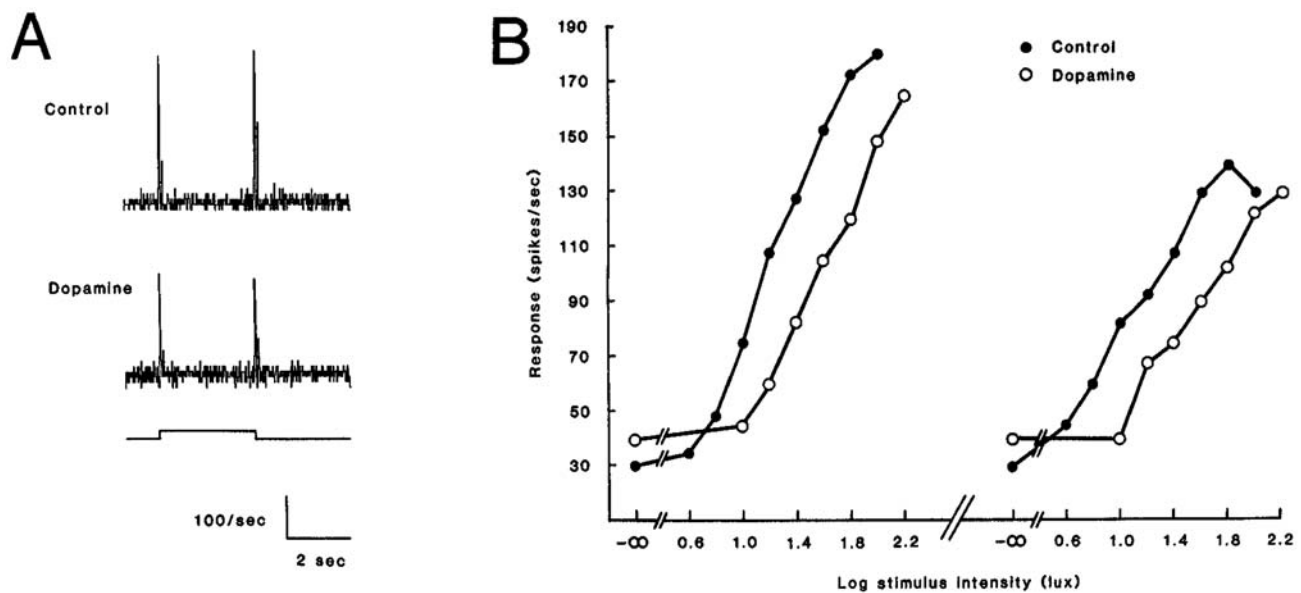


FIGURE 27.12. Poststimulus time histograms of an OFF-center ganglion cell in a rabbit eyecup. Stimulus was a 3-mm square of light at 1.6 log lux. Background illumination was approximately 1.4 log lux. Spike frequencies recorded in this cell at the offset (left) and

onset (right) of various stimulus intensities, in the absence (filled circles) and presence (open circles) of 65 μ M dopamine. (From Jensen and Daw (1986), with permission. Copyright 1986 by Elsevier Science.)

OFF BRISK-TRANSIENT (Y)

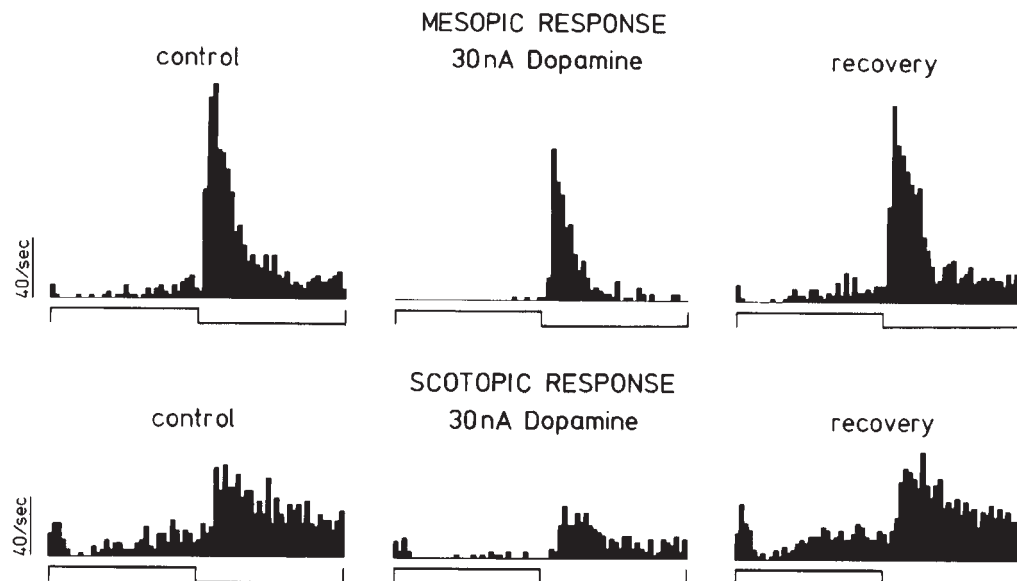


FIGURE 27.13. Peristimulus time histograms of an OFF-center ganglion cell in an in situ cat retina. Top row shows response to 7 cd/m² in presence of 3 cd/m² background illumination. Lower row shows response to 0.02 cd/m² in presence of 0.01 cd/m² background illumination. In each row, light responses were

recorded before (control), during (dopamine), and after (recovery) ionophoretic application of dopamine. Each trace shows 1024 msec of recording, with the stimulus light on (during the upward-step below each recording) for the first 512 msec. (From Thier and Alder (1984), with permission. Copyright 1984 by Elsevier Science.)

1984; see also Ames and Pollen, 1969). This change in spiking pattern emphasizes the transient component of ganglion cell light responses, resembles the effects of light adaptation on ganglion cell responses cited above (e.g., Yoon, 1972), and parallels the decrease in photoreceptor integration time that results from light adaptation (Baylor and Hodgkin, 1974).

The filtering of ganglion cell spiking by dopamine is also of interest because it might explain, to some extent, the shape of light responses that have been recorded after suppressing responses to the fast-acting inhibitory transmitters of the retina, GABA and glycine. The most notable example is that Müller and colleagues (1992) and Frumkes and colleagues (1995) found that GABA and glycine receptor blockers do not transform transient light responses of ganglion cells into sustained responses in well light-adapted cat retinas, whereas Caldwell and Daw (1978) found that this did occur at lower background light intensities. Using an entirely different approach, mouse ganglion cell light responses were found to be prolonged, but still transient, after photoablation of displaced amacrine cells that are likely to be GABAergic (Nirenberg and Meister, 1997). Similarly, in tiger salamander retina, various combinations of bicuculline, CGP35348, picrotoxin, and strychnine do not transform transient ganglion cell light responses into sustained ones, at concentrations that block the GABA_A, GABA_B, GABA_C, and glycine receptors in this species (Bieda and Copenhagen, 2000). And most recently, the recordings of Flores-Herr and colleagues (2001) have shown that rabbit ganglion cells spike more, but still transiently, after direct, hyperpolarizing, GABAergic and glycinergic inputs to these cells were reversed by raising the intracellular Cl⁻ concentration with whole-cell patch electrodes.

To better understand these spiking patterns, light-evoked excitatory postsynaptic current and spikes will have to be recorded under the same conditions, and whether transience arises presynaptically or postsynaptically will have to be checked (e.g., Awatramani and Slaughter, 2000; DeVries, 2000; Freed, 2000b; Hare and Owen, 1995; Heidelberger and Matthews, 1994; Lukasiewicz et al., 1995; Shiells and Falk, 1985). In any event, at least some of the results cited here suggest that dopamine and inhibitory amino acids can both truncate the responses of individual ganglion cells to light flashes. This raises a number of questions. Functionally, the most important would be what purpose this dual inhibition might serve. One clue may be that inhibition by dopamine takes several seconds to develop (Liu and Lasater, 1994b; Straschill and Perwein, 1969; Thier and Alder, 1984; Vaquero et al., 2001), whereas GABA can inhibit ganglion cells more quickly. These differences (and their corresponding recovery rates) suggest that fluctuations in GABA and dopamine release could drive “brisk fluctuating” GABA responses, but only “sluggish sustained” dopamine res-

ponses. Fluctuations in light intensity around a mean value may then produce fluctuating GABA responses superimposed over a relatively constant level of dopamine response. Examining this possibility could be facilitated by the availability of specific dopamine receptor antagonist. However, a number of commonly used agents have been found to produce effects unrelated to dopamine receptors, including changes in ganglion cell membrane potential and voltage-gated currents (Akamine et al., 2002; Guenther et al., 1994; Ito et al., 1997; Jensen, 1992).

Conclusion

During the first few years that patch-clamp methods were used to identify ion conductances in ganglion cells, discoveries of conductances and their voltage sensitivities were welcome news. Now, 15 years later, we want to know even more about ion conductances in ganglion cells, particularly as we find out how these conductances are controlled, which species and cells they reside in, and the conditions under which they might operate. One could argue that major progress along three fronts has been made. First, the number of ion conductances in ganglion cells is unlikely to double any time soon. Second, it appears that the susceptibility of these conductances to regulation by transmitters, extracellular modulators, and cytoplasmic messenger systems will be more the rule than the exception. Third, it now seems more than likely that some morphological types of ganglion cells use different conductances to generate spikes, at least under certain conditions. At the same time, we clearly have no complete “parts list” yet for any ganglion cell, to the extent that its excitability under various conditions can be accounted for in measured biophysical terms. Essentially, no ganglion cell has yet been “disassembled” carefully and thoroughly enough to know how to “assemble” one.

In parallel with this line of study, quantitative comparisons of spikes that ganglion cells generate with the inputs that elicit these spikes, and modeling of the statistical properties of these spikes has progressed to the point that the timing and variability of spike occurrences under certain lighting conditions can be predicted with remarkable accuracy. The model that can make these predictions (Keat et al., 2001) has few variables in it. In fact, the processes this model describes are so few that one would like to think that the properties of the channels underlying the generator and feedback voltages in these models must already have been found. If not, how then are we going to find these? The results reviewed in this chapter give at least some reasons to believe that these properties will be best sought under the conditions that the model applies to, and will be best measured with methods that do not disrupt the intracellular milieu that those conditions create. Fortunately, some of the methods for doing so have been worked out (perforated-

patch recording, different types of amplifiers, and various retinal preparations).

To construct mechanistic descriptions of excitability, maximum whole-cell ion conductances, the dependence of current amplitudes and kinetics on voltage, transmitters, modulators, and second messenger systems, the stationarity and variability of these dependencies, and the dependence of cytoplasmic messenger concentrations on various stimulus conditions, will have to be measured. Without knowing these, it will be difficult to know what component of spike generating models can be experimentally manipulated to test the uniqueness of fits to data and the variety of cells whose behaviors these models might predict. Also, as much as it now seems that spike generation will vary with the conditions it is measured under, one would like to know how much these changes actually amount to, and how well the underlying conductances have been characterized to understand and account for these changes.

Unfortunately, those interested in how ganglion cells spike under various conditions face a mountain of direct and indirect effects to unravel and resolve. For example, a large number of modulatory neurochemicals have been identified in the retina (see Chapters 20 and 22). How do these affect ganglion cell function? Components of several signaling cascades have been localized to ganglion cells, including protein kinase C, calcium/calmodulin-dependent protein kinases, and arachidonic acid. What controls these, and what do they do? More than one ion channel system is affected by some cytoplasmic messengers (Liu and Lasater, 1994b; Vaquero et al., 2001; also see Chapter 23) Are these effects synergistic, and if not, which effects dominate?

How multiple and flexible spike generating mechanisms in ganglion cells contribute to the transfer of information remains to be evaluated. At the level of retinal organization, one could imagine a number of possibilities. For example, modulation of ganglion cell excitability by mechanisms that are purely response dependent could limit the effect of adaptation to local, rather than global, maps. In the horizontal plane of the retina, this could form adaptation pools that are no larger than summation pools. In the vertical axis of the retina, this would enable the retina to adapt ganglion cells without necessarily altering photoreceptor or interneuron light responses. Modulation of ganglion cell excitability by mechanisms that are input dependent could allow ganglion cells to adapt under any conditions that drive the modulatory input (see Vaquero et al., 2001). One difference between this and response-dependent modulation is that tonically released chemical modulators could alter ganglion cell responses with less, if any, dependence on ganglion cell response magnitude and duration. Adaptation could still be spatially discrete if the cell that releases the modulator in question has a relatively small arbor (Brown and Masland, 2001; Kalloniatis and Marc, 1990; Smirnakis et al., 1997) or

if this cell has an inhibitory surround (Ammermüller and Kolb, 1995). By placing receptors for different modulators on single cells, and releasing these modulators with different stimuli, single ganglion cells could change their spike output under a variety of lighting conditions. By placing receptors for a modulator on some cells but not others, different ganglion cells could transform identical synaptic inputs into different spike outputs. Lastly, differences in spike output could obviously result, with or without modulatory inputs, from differences in the types of ion channels that ganglion cells express.

By placing these differences and modulatory mechanisms in the output neurons of the retina, ganglion cells seem not only anatomically positioned, but also electrophysiologically equipped to regulate and condition information flow from the retina to the rest of the visual system. By analogy to the notion that retinal ganglion cell mosaics help to “tile” visual space (Wässle and Boycott, 1991), intrinsic functional differences among ganglion cells, and adaptive mechanisms within ganglion cells, could be parts of strategies that “tile” parameter spaces.

REFERENCES

- Abdel-Majid, R. M., F. Tremblay, and W. H. Baldrige, 2002. Localization of adenylyl cyclase proteins in the rodent retina, *Molec. Brain Res.*, 101:62–70.
- Ahlijanian, M. K., R. E. Westenbroek, and W. A. Catterall, 1990. Subunit structure and localization of dihydropyridine-sensitive calcium channels in mammalian brain, spinal cord, and retina, *Neuron*, 4:819–832.
- Ahmad, I., T. Leinders-Zufall, J. D. Kocsis, G. M. Shepherd, F. Zufall, and C. J. Barnstable, 1994. Retinal ganglion cells express a cGMP-gated cation conductance activatable by nitric oxide donors, *Neuron*, 12:155–165.
- Akamine, T., Y. Nishimura, K. Ito, Y. Uji, and T. Yamamoto, 2002. Effects of haloperidol on K⁺ currents in acutely isolated rat retinal ganglion cells, *Invest. Ophthalmol. Vis. Sci.*, 43:1257–1261.
- Akopian, A., R. Gabriel, and P. Witkovsky, 1998. Calcium released from intracellular stores inhibits GABA_A-mediated currents in ganglion cells from the turtle retina, *J. Neurophysiol.*, 80:1105–1115.
- Akopian, A., and P. Witkovsky, 1996. Activation of metabotropic glutamate receptors decreases a high-threshold calcium current in spiking neurons of the *Xenopus* retina, *Vis. Neurosci.*, 13:549–577.
- Akopian, A., and P. Witkovsky, 2002. Calcium and retinal function, *Molec. Neurobiol.*, 25:113–132.
- Albrecht, D. G., and D. B. Hamilton, 1982. Striate cortex of monkey and cat: contrast response function, *J. Neurophysiol.*, 48:217–237.
- Ames, A. III, and D. A. Pollen, 1969. Neurotransmission in central nervous tissue: a study of isolated rabbit retina, *J. Neurophysiol.*, 32:424–442.
- Ammermüller, J., and H. Kolb, 1995. The organization of the turtle inner retina. I. ON- and OFF-center pathways, *J. Comp. Neurol.*, 358:1–34.

- Armstrong, C. M., and W. F. Gilly, 1992. Access resistance and space clamp problems associated with whole-cell patch clamping, *Meth. Enzymol.*, 207:100–122.
- Ashmore, J. F., and G. Falk, 1980. Responses of rod bipolar cells in the dark-adapted retina of the dogfish, *Scyliorhinus canicula*, *J. Physiol.*, 300:115–150.
- Awatramani, G. B., and M. M. Slaughter, 2000. Origin of transient and sustained responses in ganglion cells of the retina, *J. Neurosci.*, 20:7087–7095.
- Baldrige, W. H., 1996. Optical recordings of the effects of cholinergic ligands on neurons in the ganglion cell layer of mammalian retina, *J. Neurosci.*, 16:5060–5072.
- Barlow, H. B., R. Fitzhugh, and S. W. Kuffler, 1957. Change of organization in the receptive fields of the cat's retina during dark adaptation, *J. Physiol.*, 137:338–354.
- Barlow, H. B., and W. R. Levick, 1969. Changes in the maintained discharge with adaptation level in the cat retina, *J. Physiol.*, 202:699–718.
- Barlow, R., 2001. Circadian and efferent modulation of visual sensitivity, *Progr. Brain Res.*, 131:488–503.
- Barres, B. A., L. L. Chun, and D. P. Corey, 1989. Glial and neuronal forms of the voltage-dependent sodium channel: characteristics and cell-type distribution, *Neuron*, 2:1375–1388.
- Barres, B. A., B. E. Silverstein, D. P. Corey, and L. L. Chun, 1988. Immunological, morphological, and electrophysiological variation among retinal ganglion cells purified by panning, *Neuron*, 1:791–803.
- Baylor, D. A., and R. Fettiplace, 1979. Synaptic drive and impulse generation in ganglion cells of turtle retina, *J. Physiol.*, 288:107–127.
- Baylor, D. A., and M. G. Fuortes, 1970. Electrical responses of single cones in the retina of the turtle, *J. Physiol.*, 207:77–92.
- Baylor, D. A., and A. L. Hodgkin, 1974. Changes in time scale and sensitivity in turtle photoreceptors, *J. Physiol.*, 242:729–758.
- Belgum, J. H., D. R. Dvorak, and J. S. McReynolds, 1982. Sustained synaptic input to ganglion cells of mudpuppy retina, *J. Physiol.*, 326:91–108.
- Benison, G., J. Keizer, L. M. Chalupa, and D. W. Robinson, 2001. Modeling temporal behavior of postnatal cat retinal ganglion cells, *J. Theor. Biol.*, 210:187–199.
- Berntson, A., and W. R. Taylor, 2000. Response characteristics and receptive field widths of on-bipolar cells in the mouse retina, *J. Physiol.*, 524:879–889.
- Berry, M. J., and M. Meister, 1998. Refractoriness and neural precision, *J. Neurosci.*, 18:2200–2211.
- Berry, M. J., D. K. Warland, and M. Meister, 1997. The structure and precision of retinal spike trains, *Proc. Natl. Acad. Sci. USA*, 94:5411–5416.
- Bieda, M. C., and D. R. Copenhagen, 2000. Inhibition is not required for the production of transient spiking responses from retinal ganglion cells, *Vis. Neurosci.*, 17:243–254.
- Bindokas, V. P., and A. T. Ishida, 1996. Conotoxin-sensitive and conotoxin-resistant Ca^{2+} currents in fish retinal ganglion cells, *J. Neurobiol.*, 29:429–444.
- Bindokas, V. P., M. Yoshikawa, and A. T. Ishida, 1994. Na^{+} - Ca^{2+} exchanger-like immunoreactivity and regulation of intracellular Ca^{2+} levels in fish retinal ganglion cells, *J. Neurophysiol.*, 72:47–55.
- Bloomfield, S. A., 1996. Effect of spike blockade on the receptive-field size of amacrine and ganglion cells in the rabbit retina, *J. Neurophysiol.*, 75:1878–1893.
- Bloomfield, S. A., and D. Xin, 1997. A comparison of receptive-field and tracer-coupling size of amacrine and ganglion cells in the rabbit retina, *Vis. Neurosci.*, 14:1153–1165.
- Boelen, M. K., M. G. Boelen, and D. W. Marshak, 1998. Light-stimulated release of dopamine from the primate retina is blocked by 1–2-amino-4-phosphonobutyric acid (APB), *Vis. Neurosci.*, 15:97–103.
- Boiko, T., M. H. Rasband, S. R. Levinson, J. H. Caldwell, G. Mandel, J. S. Trimmer, and G. Matthews, 2001. Compact myelin dictates the differential targeting of two sodium channel isoforms in the same axon, *Neuron*, 30:91–104.
- Brown, S. P., and R. H. Masland, 2001. Spatial scale and cellular substrate of contrast adaptation by retinal ganglion cells, *Nat. Neurosci.*, 4:44–51.
- Brunken, W. J., P. Witkovsky, and H. J. Karten, 1986. Retinal neurochemistry of three elasmobranch species: an immunohistochemical approach, *J. Comp. Neurol.*, 243:1–12.
- Byzov, A. L., N. A. Polishchuk, and G. M. Zenkin, 1970. On the transmission of signals in vertebrate retina in the presence and absence of impulses, *Neirofiziol.*, 2:536–543.
- Caldwell, J. H., and N. W. Daw, 1978. Effects of picrotoxin and strychnine on rabbit retinal ganglion cells: changes in centre surround receptive fields, *J. Physiol.*, 276:299–310.
- Caldwell, J. H., K. L. Schaller, R. S. Lasher, E. Peles, and S. R. Levinson, 2000. Sodium channel $\text{Na}_{v}1.6$ is localized at nodes of Ranvier, dendrites, and synapses, *Proc. Natl. Acad. Sci. USA*, 97:5616–5620.
- Cantrell, A. R., and W. A. Catterall, 2001. Neuromodulation of Na^{+} channels: an unexpected form of cellular plasticity, *Nat. Rev. Neurosci.*, 2:397–407.
- Cantrell, A. R., T. Scheuer, and W. A. Catterall, 1999. Voltage-dependent neuromodulation of Na^{+} channels by D1-like dopamine receptors in rat hippocampal neurons, *J. Neurosci.*, 19:5301–5310.
- Chander, D., and E. J. Chichilnisky, 2001. Adaptation to temporal contrast in primate and salamander retina, *J. Neurosci.*, 21:9904–9916.
- Cheon, E. W., Y. Kaneko, and T. Saito, 1998. Regeneration of the newt retina: order of appearance of photoreceptors and ganglion cells, *J. Comp. Neurol.*, 396:267–274.
- Chichilnisky, E. J., 2001. A simple white noise analysis of neuronal light responses, *Network: Computat. Neural. Syst.*, 12:199–213.
- Cleland, B. G., M. W. Dubin, and W. R. Levick, 1971. Sustained and transient neurones in the cat's retina and lateral geniculate nucleus, *J. Physiol.*, 217:473–496.
- Coleman, P. A., and R. F. Miller, 1989. Measurement of passive membrane parameters with whole-cell recording from neurons in the intact amphibian retina, *J. Neurophysiol.*, 61:218–230.
- Connor, J. A., and C. F. Stevens, 1971. Voltage clamp studies of a transient outward membrane current in gastropod neural somata, *J. Physiol.*, 213:21–30.
- Constanti, A., and J. A. Sim, 1987. Calcium-dependent potassium conductance in guinea-pig olfactory cortex neurones in vitro, *J. Physiol.*, 387:173–194.
- Copenhagen, D. R., S. Hemila, and T. Reuter, 1990. Signal transmission through the dark-adapted retina of the toad (*Bufo marinus*). Gain, convergence, and signal/noise, *J. Gen. Physiol.*, 95:717–732.
- Critz, S. D., and R. E. Marc, 1992. Glutamate antagonists that block hyperpolarizing bipolar cells increase the release of dopamine from turtle retina, *Vis. Neurosci.*, 9:271–278.
- Cuevas, J., A. A. Harper, C. Trequatrini, and D. J. Adams, 1997. Passive and active membrane properties of isolated rat intracardiac neurons: regulation by H- and M-currents, *J. Neurophysiol.*, 78:1890–1902.

- Dacey, D., O. S. Packer, L. Diller, D. Brainard, B. Peterson, and B. Lee, 2000. Center surround receptive field structure of cone bipolar cells in primate retina, *Vis. Res.*, 40:1801–1811.
- Dacheux, R. F., and E. Raviola, 1986. The rod pathway in the rabbit retina: A depolarizing bipolar and amacrine cell. *J. Neurosci.*, 6:331–345.
- Dearry, A., and B. Burnside, 1989. Light-induced dopamine release from teleost retinas acts as a light-adaptive signal to the retinal pigment epithelium, *J. Neurochem.*, 53:870–878.
- DeVries, S. H., 2000. Bipolar cells use kainate and AMPA receptors to filter visual information into separate channels, *Neuron*, 28:847–856.
- Diamond, J. S., and D. R. Copenhagen, 1993. The contribution of NMDA and non-NMDA receptors to the light-evoked input-output characteristics of retinal ganglion cells, *Neuron*, 11:725–738.
- Diamond, J. S., and D. R. Copenhagen, 1995. The relationship between light-evoked synaptic excitation and spiking behaviour of salamander retinal ganglion cells, *J. Physiol.*, 487:711–725.
- Djamgoz, M. B. A., and H. J. Wagner, 1992. Localization and function of dopamine in the adult vertebrate retina, *Neurochem. Int.*, 20:139–191.
- Dong, C. J., and J. S. McReynolds, 1992. Comparison of the effects of flickering and steady light on dopamine release and horizontal cell coupling in the mudpuppy retina, *J. Neurophysiol.*, 67:364–372.
- Donner, K., 1981. Receptive fields of frog retinal ganglion cells: Response formation and light-dark-adaptation, *J. Physiol.*, 391:131–142.
- Donner, K., K. Djupsund, T. Reuter, and I. Vaisanen, 1991. Adaptation to light fluctuations in the frog retina, *Neurosci. Res.*, 15(Suppl):S175–S184.
- Dowling, J. E., 1991. Retinal neuromodulation: the role of dopamine, *Vis. Neurosci.*, 7:87–97.
- Ehinger, B., 1983. Functional role of dopamine in the retina, *Progr. Ret. Res.*, 2:213–232.
- Eng, D. L., T. R. Gordon, J. D. Kocsis, and S. G. Waxman, 1990. Current-clamp analysis of a time-dependent rectification in rat optic nerve, *J. Physiol.*, 421:185–202.
- Enroth-Cugell, C., and P. Lennie, 1975. The control of retinal ganglion cell discharge by receptive field surrounds, *J. Physiol.*, 247:551–578.
- Enroth-Cugell, C., and R. M. Shapley, 1973. Adaptation and dynamics of cat retinal ganglion cells, *J. Physiol.*, 233:271–309.
- Euler, T., and R. H. Masland, 2000. Light-evoked responses of bipolar cells in a mammalian retina, *J. Neurophysiol.*, 83:1817–1829.
- Fain, G. L., and J. E. Dowling, 1973. Intracellular recordings from single rods and cones in the mudpuppy retina, *Science*, 180:1178–1181.
- Feigenspan, A., S. Gustincich, B. P. Bean, and E. Raviola, 1998. Spontaneous activity of solitary dopaminergic cells of the retina, *J. Neurosci.*, 18:6776–6789.
- Fink, M., F. Lesage, F. Duprat, C. Heurteaux, R. Reyes, M. Fosset, and M. Lazdunski, 1998. A neuronal two P domain K⁺ channel stimulated by arachidonic acid and polyunsaturated fatty acids, *EMBO J.*, 17:3297–3308.
- Finkel, A. S., and S. Redman, S., 1984. Theory and operation of a single microelectrode voltage clamp, *J. Neurosci. Methods*, 11:101–127.
- Fjell, J., S. Dib-Hajj, K. Fried, J. A. Black, and S. G. Waxman, 1997. Differential expression of sodium channel genes in retinal ganglion cells, *Molec. Brain Res.*, 50:197–204.
- Fleiderovich, I. A., A. Friedman, and M. J. Gutnick, 1996. Slow inactivation of Na⁺ current and slow cumulative spike adaptation in mouse and guinea-pig neocortical neurones in slices, *J. Physiol.*, 493:83–97.
- Flores-Herr, N., D. A. Protti, and H. Wässle, 2001. Synaptic currents generating the inhibitory surround of ganglion cells in the mammalian retina, *J. Neurosci.*, 21:4852–4863.
- Fohlmeister, J. F., and R. F. Miller, 1997a. Impulse encoding mechanisms of ganglion cells in the tiger salamander retina, *J. Neurophysiol.*, 78:1935–1947.
- Fohlmeister, J. F., and R. F. Miller, 1997b. Mechanisms by which cell geometry controls repetitive impulse firing in retinal ganglion cells, *J. Neurophysiol.*, 78:1948–1964.
- Frederick, J. M., M. E. Rayborn, A. M. Laties, D. M. Lam, and J. G. Hollyfield, 1982. Dopaminergic neurons in the human retina, *J. Comp. Neurol.*, 210:65–79.
- Freed, M. A., 2000a. Parallel cone bipolar pathways to a ganglion cell use different rates and amplitudes of quantal excitation, *J. Neurosci.*, 20:3956–3963.
- Freed, M. A., 2000b. Rate of quantal excitation to a retinal ganglion cell evoked by sensory input, *J. Neurophysiol.*, 83:2956–2966.
- Freed, M. A., R. G. Smith, and P. Sterling, 1992. Computational model of the ON-alpha ganglion cell receptive field based on bipolar cell circuitry, *Proc. Natl. Acad. Sci. USA*, 89:236–240.
- Frumkes, T. E., R. Nelson, and R. Pflug, 1995. Functional role of GABA in cat retina: II. Effects of GABA_A antagonists, *Vis. Neurosci.*, 12:651–661.
- Green, D. G., J. E. Dowling, I. M. Siegel, and H. Ripps, 1975. Retinal mechanisms of visual adaptation in the skate, *J. Gen. Physiol.*, 65:483–502.
- Green, D. G., and M. K. Powers, 1982. Mechanisms of light adaptation in rat retina, *Vis. Res.*, 22:209–216.
- Guenther, E., T. Rothe, H. Taschenberger, and R. Grantyn, 1994. Separation of calcium currents in retinal ganglion cells from postnatal rat, *Brain Res.*, 633:223–235.
- Guenther, E., S. Schmid, D. Reiff, and E. Zrenner, 1999. Maturation of intrinsic membrane properties in rat retinal ganglion cells, *Vis. Res.*, 39:2477–2484.
- Guenther, E., V. Wilsch, and E. Zrenner, 1994. Inhibitory action of haloperidol, spiperone and SCH23390 on calcium currents in rat retinal ganglion cells, *Neuroreport*, 5:1373–1376.
- Guenther, E., and E. Zrenner, 1993. The spectral sensitivity of dark- and light-adapted cat retinal ganglion cells, *J. Neurosci.*, 13:1543–1550.
- Guimarães, M. Z. P., and J. N. Hokoç, 1997. Tyrosine hydroxylase expression in the *Cebus* monkey retina, *Vis. Neurosci.*, 14:705–715.
- Gustincich, S., A. Feigenspan, D. K. Wu, L. J. Koopman, and E. Raviola, 1997. Control of dopamine release in the retina: a transgenic approach to neural networks, *Neuron*, 18:723–736.
- Hagiwara, S., K. Kusano, and N. Saito, 1961. Membrane changes of *Onchidium* nerve cell in potassium-rich media, *J. Physiol.*, 155:470–489.
- Hamill, O. R., A. Marty, E. Neher, B. Sakmann, and F. J. Sigworth, 1981. Improved patch-clamp techniques for high resolution current recording from cells and cell-free membrane patches, *Pflug. Arch.*, 391:85–100.
- Hare, W. A., and W. G. Owen, 1995. Similar effects of carbachol and dopamine on neurons in the distal retina of the tiger salamander, *Vis. Neurosci.*, 12:443–455.
- Heidelberger, R., and G. Matthews, 1994. Dopamine enhances Ca²⁺ responses in synaptic terminals of retinal bipolar neurons, *Neuroreport*, 5:729–732.

- Henderson, D., T. A. Doerr, J. Gottesman, and R. F. Miller, 2001. Calcium channel immunoreactivity in the salamander retina, *NeuroReport*, 12:1493–1499.
- Henne, J., S. Pottering, and G. Jeserich, 2000. Voltage-gated potassium channels in retinal ganglion cells of trout: a combined biophysical, pharmacological, and single-cell RT-PCR approach, *J. Neurosci. Res.*, 62:629–637.
- Hidaka, S., and A. T. Ishida, 1998. Voltage-gated Na⁺ current availability after step- and spike-shaped conditioning depolarizations of retinal ganglion cells, *Pflügers Arch.*, 436:497–508.
- Hirooka, K., D. E. Kourennyi, and S. Barnes, 2000. Calcium channel activation facilitated by nitric oxide in retinal ganglion cells, *J. Neurophysiol.*, 83:198–206.
- Hodgkin, A. L., and A. F. Huxley, 1952. A quantitative description of membrane current and its application to conduction and excitation in nerve, *J. Physiol.*, 117:500–544.
- Hokoç, J. N., and A. P. Mariani, 1987. Tyrosine hydroxylase immunoreactivity in the rhesus monkey retina reveals synapses from bipolar cells to dopaminergic amacrine cells, *J. Neurosci.*, 7:2785–2793.
- Hokoç, J. N., and A. P. Mariani, 1988. Synapses from bipolar cells onto dopaminergic amacrine cells in cat and rabbit retinas, *Brain Res.*, 461:17–26.
- Horn, R., and A. Marty, 1988. Muscarinic activation of ionic currents measured by a new whole cell recording method, *J. Gen. Physiol.*, 92:145–159.
- Huang, S.-J., and D. W. Robinson, 1998. Activation and inactivation properties of voltage-gated calcium currents in developing cat retinal ganglion cells, *Neuroscience*, 85:239–247.
- Inceoglu, A. B., Y. Hayashida, J. Lango, A. T. Ishida, and B. D. Hammock, 2002. A single charged surface residue modifies the activity of iktotoxin, a beta-type Na⁺ channel toxin from *Parabuthus transvaalicus*, *Eur. J. Biochem.*, 269:5369–5376.
- Ito, K., Y. Nishimura, Y. Uji, and T. Yamamoto, 1997. Haloperidol effects on Na current in acutely isolated rat retinal ganglion cells, *Jpn. J. Ophthalmol.*, 41:221–225.
- Jakiela, H. G., C. Enroth-Cugell, and R. Shapley, 1976. Adaptation and dynamics in X-cells and Y-cells of the cat retina, *Exp. Brain Res.*, 24:335–342.
- Jensen, R. J., 1992. Effects of the dopamine antagonist (+)-SCH 23390 on intracellularly recorded responses of ganglion cells in the rabbit retina, *Vis. Neurosci.*, 8:463–467.
- Jensen, R. J., and N. W. Daw, 1986. Effects of dopamine and its agonists and antagonists on the receptive field properties of ganglion cells in the rabbit retina, *Neuroscience*, 17:837–855.
- Kalloniatis, M., and R. E. Marc, 1990. Interplexiform cells of the goldfish retina, *J. Comp. Neurol.*, 297:340–358.
- Kamp, C. W., and W. W. Morgan, 1980. GABA antagonists enhance dopamine turnover in the rat retina in vivo, *Eur. J. Pharmacol.*, 69:273–279.
- Kaneda, M., and A. Kaneko, 1991a. Voltage-gated sodium currents in isolated retinal ganglion cells of the cat: relation between the inactivation kinetics and the cell type, *Neurosci. Res.*, 11:261–275.
- Kaneda, M., and A. Kaneko, 1991b. Voltage-gated calcium currents in isolated retinal ganglion cells of the cat, *Jpn. J. Physiol.*, 41:35–48.
- Kaneko, A., E. V. Famiglietti, Jr., and M. Tachibana, 1979. Physiological and morphological identification of signal pathways in the carp retina, in *Neurobiology of Chemical Transmission* (M. Otsuka and Z. Hall, eds.), New York: Wiley, pp. 235–251.
- Kara, P., P. Reinagel, and R. C. Reid, 2000. Low response variability in simultaneously recorded retinal, thalamic, and cortical neurons, *Neuron*, 27:635–646.
- Karschin, A., and S. A. Lipton, 1989. Calcium channels in solitary retinal ganglion cells from post-natal rat, *J. Physiol.*, 418:379–396.
- Kawasaki, M., S. Uchida, T. Monkawa, A. Miyawaki, K. Mikoshiba, F. Marumo, and S. Sasaki, 1994. Cloning and expression of a protein kinase C-regulated chloride channel abundantly expressed in rat brain neuronal cells, *Neuron*, 12:597–604.
- Keat, J., P. Reinagel, R. C. Reid, and M. Meister, 2001. Predicting every spike: A model for the responses of visual neurons, *Neuron*, 30:803–817.
- Kim, K. J., and F. Rieke, 2001. Temporal contrast adaptation in the input and output signals of salamander retinal ganglion cell, *J. Neurosci.*, 21:287–299.
- Klumpp, D. J., E. J. Song, and L. H. Pinto, 1995. Identification and localization of K⁺ channels in the mouse retina, *Vis. Neurosci.*, 12:1177–1190.
- Koh, D.-S., P. Jonas, and W. Vogel, 1994. Na⁺-activated K⁺ channels localized in the nodal region of myelinated axons of *Xenopus*, *J. Physiol.*, 479:183–197.
- Kolb, H., N. Cuenca, H. H. Wang, and L. Dekorver, 1990. The synaptic organization of the dopaminergic amacrine cell in the cat retina, *J. Neurocytol.*, 19:343–366.
- Korenberg, M. J., H. M. Sakai, and K.-I. Naka, 1989. Dissection of the neuron network in the catfish inner retina. III. Interpretation of spike kernels, *J. Neurophysiol.*, 61:1110–1120.
- Kramer, S. G., 1971. Dopamine: A retinal neurotransmitter. I. Retinal uptake, storage, and light-stimulated release of H³-dopamine in vivo, *Invest. Ophthalmol.*, 10:438–452.
- Lasater, E. M., and P. Witkovsky, 1990. Membrane currents of spiking cells isolated from turtle retina, *J. Comp. Physiol. [A]*, 167:11–21.
- Lennie, P., 1981. The physiological basis of variations in visual latency, *Vis. Res.*, 21:815–824.
- Lipton, S. A., and D. L. Tauck, 1987. Voltage-dependent conductances of solitary ganglion cells dissociated from the rat retina, *J. Physiol.*, 385:361–391.
- Liu, Y., and E. M. Lasater, 1994a. Calcium currents in turtle retinal ganglion cells. I. The properties of T- and L-type currents, *J. Neurophysiol.*, 71:733–742.
- Liu, Y., and E. M. Lasater, 1994b. Calcium currents in turtle retinal ganglion cells. II. Dopamine modulation via a cyclic AMP-dependent mechanism, *J. Neurophysiol.*, 71:743–752.
- Lohmann, C., K. L. Myhr, and R. O. Wong, 2002. Transmitter-evoked local calcium release stabilizes developing dendrites, *Nature*, 418:177–181.
- Lukasiewicz, P. D., J. E. Lawrence, and T. L. Valentino, 1995. Desensitizing glutamate receptors shape excitatory synaptic inputs to tiger salamander retinal ganglion cells, *J. Neurosci.*, 15:6189–6199.
- Lukasiewicz, P. D., and F. Werblin, 1988. A slowly inactivating potassium current truncates spike activity in ganglion cells of the tiger salamander retina, *J. Neurosci.*, 8:4470–4481.
- Marc, R. E., 1995. Interplexiform cell connectivity in the outer retina, in *Neurobiology and Clinical Aspects of the Outer Retina* (M. B. A. Djamgoz, S. N. Archer, and S. Vallergera, eds.), London: Chapman & Hall, pp. 369–393.
- Marshak, D. W., 2001. Synaptic inputs to dopaminergic neurons in mammalian retinas, *Prog. Brain Res.*, 131:83–91.
- Marty, A., and E. Neher, 1995. Tight-seal whole-cell recording, in *Single-Channel Recording*, 2nd ed. (B. Sakmann and E. Neher, eds.), New York: Plenum Press, pp. 31–52.

- Matsuo, T., 1998. Expression of amiloride-sensitive sodium channel in rat eye, *Acta Med. Okayama*, 52:279–283.
- Meister, M., and M. J. Berry, 1999. The neural code of the retina, *Neuron*, 22:435–450.
- Miguel-Hidalgo, J. J., C. J. Snider, K. J. Angelides, and L. M. Chalupa, 1994. Voltage-dependent sodium channel alpha subunit immunoreactivity is expressed by distinct cell types of the cat and monkey retina, *Vis. Neurosci.*, 11:219–228.
- Miller, R. F., K. Stenback, D. Henderson, and M. Sikora, 2002. How voltage-gated ion channels alter the functional properties of ganglion and amacrine cell dendrites, *Arch. Ital. Biol.*, 140:347–359.
- Mirshahi, M., C. Nicolas, S. Mirshahi, N. Golestaneh, F. d'Hermies, and M. K. Agarwal, 1999. Immunohistochemical analysis of the sodium channel in rodent and human eye, *Exp. Eye Res.*, 69:21–32.
- Mobbs, P., K. Everett, and A. Cook, 1992. Signal shaping by voltage-gated currents in retinal ganglion cells, *Brain Res.*, 574:217–223.
- Moore, S. D., S. G. Madamba, M. Joels, and G. R. Siggins, 1988. Somatostatin augments the M-current in hippocampal neurons, *Science*, 239:278–280.
- Müller, F., R. Boos, and H. Wässle, 1992. Actions of GABAergic ligands on brisk ganglion cells in the cat retina, *Vis. Neurosci.*, 9:415–425.
- Müller, F., H. Wässle, and T. Voigt, 1988. Pharmacological modulation of the rod pathway in the cat retina, *J. Neurophysiol.*, 59:1657–1672.
- Naka, K.-I., and W. A. Rushton, 1966. S-potentials from colour units in the retina of fish (*Cyprinidae*), *J. Physiol.*, 185:536–555.
- Nguyen-Legros, J., 1988. Morphology and distribution of catecholamine-neurons in mammalian retina, *Progr. Ret. Res.*, 7:113–147.
- Nguyen-Legros, J., A. Simon, I. Caillé, and B. Bloch, 1997. Immunocytochemical localization of dopamine D1 receptors in the retina of mammals, *Vis. Neurosci.*, 14:545–551.
- Nirenberg, S., and M. Meister, 1997. The light response of retinal ganglion cells is truncated by a displaced amacrine circuit, *Neuron*, 18:637–650.
- O'Brien, B. J., T. Isayama, R. Richardson, and D. M. Berson, 2002. Intrinsic physiological properties of cat retinal ganglion cells, *J. Physiol.*, 538:787–802.
- Ohzawa, I., G. Sclar, and R. D. Freeman, 1985. Contrast gain control in the cat's visual system, *J. Neurophysiol.*, 54:651–667.
- Olson, A. J., A. Picones, and J. I. Korenbrot, 2000. Developmental switch in excitability, Ca^{2+} and K^{+} currents of retinal ganglion cells and their dendritic structure, *J. Neurophysiol.*, 84:2063–2077.
- Oyster, C. W., E. S. Takahashi, M. Cilluffo, and N. C. Brecha, 1985. Morphology and distribution of tyrosine hydroxylase-like immunoreactive neurons in the cat retina, *Proc. Natl. Acad. Sci. USA*, 82:6335–6339.
- Peichl, L., 1991. Catecholaminergic amacrine cells in the dog and wolf retina, *Vis. Neurosci.*, 7:575–587.
- Piccolino, M., J. Neyton, and H. M. Gerschenfeld, 1984. Decrease of gap junction permeability induced by dopamine and cyclic adenosine 3':5'-monophosphate in horizontal cells of turtle retina, *J. Neurosci.*, 4:2477–2488.
- Piccolino, M., P. Witkovsky, and C. Trimarchi, 1987. Dopaminergic mechanisms underlying the reduction of electrical coupling between horizontal cells of the turtle retina induced by d-amphetamine, bicuculline, and veratridine, *J. Neurosci.*, 7:2273–84.
- Pierce, M. E., and J. C. Besharse, 1985. Circadian regulation of retinomotor movements. I. Interaction of melatonin and dopamine in the control of cone length, *J. Gen. Physiol.*, 86:671–689.
- Pollard, J., and W. D. Eldred, 1990. Synaptic analysis of amacrine cells in the turtle retina which contain tyrosine hydroxylase-like immunoreactivity, *J. Neurocytol.*, 19:53–66.
- Pourcho, R., 1982. Dopaminergic amacrine cells in the cat retina, *Brain Res.*, 252:101–109.
- Purpura, K., D. Tranchina, E. Kaplan, and R. M. Shapley, 1990. Light adaptation in the primate retina: analysis of changes in gain and dynamics of monkey retinal ganglion cells, *Vis. Neurosci.*, 4:75–93.
- Reich, D. S., J. D. Victor, B. W. Knight, T. Ozaki, and E. Kaplan, 1997. Response variability and timing precision of neuronal spike trains in vivo, *J. Neurophysiol.*, 77:2836–2841.
- Reyes, R., I. Lauritzen, F. Lesage, M. Ettaiche, M. Fosset, and M. Lazdunski, 2000. Immunolocalization of the arachidonic acid and mechanosensitive baseline K^{+} channel in the nervous system, *Neuroscience*, 95:893–901.
- Rieke, F., 2001. Temporal contrast adaptation in salamander bipolar cells, *J. Neurosci.*, 21:9445–9454.
- Robinson, D. W., and L. M. Chalupa, 1997. The intrinsic temporal properties of alpha and beta retinal ganglion cells are equivalent, *Curr. Biol.*, 7:366–374.
- Rodieck, R. W., 1998. *The First Steps in Seeing*, Sunderland: Sinauer Associates.
- Rosenbohm, A., R. Rudel, and C. Fahlke, 1999. Regulation of the human skeletal muscle chloride channel hClC-1 by protein kinase C, *J. Physiol.*, 514:677–685.
- Rothe, T., and R. Grantyn, 1994. Retinal ganglion neurons express a toxin-resistant developmentally regulated novel type of high-voltage-activated calcium channel, *J. Neurophysiol.*, 72:2542–2546.
- Rothe, T., R. Jüttner, R. Bähring, and R. Grantyn, 1999. Ion conductances related to development of repetitive firing in mouse retinal ganglion neurons *in situ*, *J. Neurobiol.*, 38:191–206.
- Rudy, B., 1978. Slow inactivation of the sodium conductance in squid giant axons. Pronase resistance, *J. Physiol.*, 283:1–21.
- Rudy, B. 1988. Diversity and ubiquity of K^{+} channels, *Neurosci.*, 25:729–749.
- Ruppersberg, J. P., M. Stocker, O. Pongs, S. H. Heinemann, R. Frank, and M. Koenen, 1991. Regulation of fast inactivation of cloned mammalian $\text{I}_{\text{K}}(\text{A})$ channels by cysteine oxidation, *Nature* 352:711–714.
- Saito, H. A., 1983. Morphology of physiologically identified X-, Y-, and W-type retinal ganglion cells of the cat, *J. Comp. Neurol.*, 221:279–288.
- Saito, T., H. Kondo, and J.-I. Toyoda, 1978. Rod and cone signals in the on-center bipolar cell: their different ionic mechanisms, *Vis. Res.*, 18:591–595.
- Sakai, H. M., and K.-I. Naka, 1987. Signal transmission in catfish retina. IV. Transmission to ganglion cells, *J. Neurophysiol.*, 58:1307–1328.
- Sakai, H. M., J. L. Wang, and K.-I. Naka, 1995. Contrast gain control in the lower vertebrate retinas, *J. Gen. Physiol.*, 105:815–835.
- Sakmann, B., and O. D. Creutzfeldt, 1969. Scotopic and mesopic light adaptation in the cat's retina, *Pflügers Arch.*, 313:168–185.
- Sakuranaga, M., Y. Ando, and K.-I. Naka, 1987. Dynamics of the ganglion cell response in the catfish and frog retinas, *J. Gen. Physiol.*, 90:229–259.

- Sanchez-Vives, M. V., L. G. Nowak, and D. A. McCormick, 2000. Cellular mechanisms of long-lasting adaptation in visual cortical neurons in vitro, *J. Neurosci.*, 20:4286–4299.
- Schmid, S., and E. Guenther, 1998. Alterations in channel density and kinetic properties of the sodium current in retinal ganglion cells of the rat during in vivo differentiation, *Neuroscience*, 85:249–258.
- Schneeweis, D. M., and J. L. Schnapf, 1995. Photovoltage of rods and cones in the macaque retina, *Science*, 268:1053–1056.
- Schwindt, P. C., W. J. Spain, and W. E. Crill, 1989. Long-lasting reduction of excitability by a sodium-dependent potassium current in cat neocortical neurons, *J. Neurophysiol.*, 61:233–244.
- Shapley, R., 1997. Retinal physiology: adapting to the changing scene, *Curr. Biol.*, 7:R421–423.
- Shapley, R., and C. Enroth-Cugell, 1984. Visual adaptation and retinal gain controls, *Prog. Ret. Res.*, 3:263–346.
- Shapley, R. M., and J. D. Victor, 1978. The effect of contrast on the transfer properties of cat retinal ganglion cells, *J. Physiol.*, 285:275–298.
- Sheasby, B. W., and J. F. Fohlmeister, 1999. Impulse encoding across the dendritic morphologies of retinal ganglion cells, *J. Neurophysiol.*, 81:1685–1698.
- Shen, S., A. P. Wiemelt, F. A. McMorris, and B. A. Barres, 1999. Retinal ganglion cells lose trophic responsiveness after axotomy, *Neuron*, 23:285–295.
- Shen, W., and M. M. Slaughter, 1998. Metabotropic and ionotropic glutamate receptors regulate calcium channel subtypes in salamander retinal ganglion cells, *J. Physiol.*, 510:815–828.
- Shen, W., and M. M. Slaughter, 1999. Metabotropic GABA receptors facilitate L-type and inhibit N-type calcium channels in single salamander retinal neurons, *J. Physiol.*, 516:711–718.
- Shiells, R. A., and G. Falk, 1985. Dopamine hyperpolarizes and reduces the light responses of rod ON-centre bipolar cells in the retina of the dogfish, *Scyliorhinus canicula*, *Neurosci. Lett.*, 55:331–336.
- Skaliyora, I., D. W. Robinson, L. M. Chalupa, 1995. Properties of K⁺ conductances in cat retinal ganglion cells during the period of activity-mediated refinements in retinofugal pathways, *Eur. J. Neurosci.*, 7:1558–1568.
- Skaliyora, I., R. P. Scobey, and L. M. Chalupa, 1993. Prenatal development of excitability in cat retinal ganglion cells: action potentials and sodium currents, *J. Neurosci.*, 13:313–323.
- Smirnakis, S. M., M. J. Berry, D. K. Warland, W. Bialek, and M. Meister, 1997. Adaptation of retinal processing to image contrast and spatial scale, *Nature*, 386:69–73.
- Spruston, N., and D. Johnston, 1992. Perforated patch-clamp analysis of the passive membrane properties of three classes of hippocampal neurons, *J. Neurophysiol.*, 67:508–529.
- Sterling, P., 1998. Retina, in *The Synaptic Organization of the Brain*, 4th ed. (G. M. Shepherd, ed.), New York: Oxford University Press, pp. 205–253.
- Stobrawa, S. M., T. Breiderhoff, S. Takamori, D. Engel, M. Schweizer, A. A. Zdebik, M. R. Bösl, K. Ruether, H. Jahn, A. Draguhn, R. Jahn, and T. J. Jentsch, 2001. Disruption of ClC-3, a chloride channel expressed on synaptic vesicles, leads to a loss of the hippocampus, *Neuron*, 29:185–196.
- Straschill, M., and J. Perwein, 1969. The inhibition of retinal ganglion cells by catecholamines and gamma-aminobutyric acid, *Pflügers Arch.*, 312:45–54.
- Stuart, G. J., and B. Sakmann, 1994. Active propagation of somatic action potentials into neocortical pyramidal cell dendrites, *Nature*, 367:69–72.
- Stys, P. K., and R. M. Lopachin, Jr., 1996. Elemental composition and water content of rat optic nerve myelinated axons during in vitro post-anoxia reoxygenation, *Neuroscience*, 73:1081–1090.
- Stys, P. K., H. Sontheimer, B. R. Ransom, and S. G. Waxman, 1993. Noninactivating, tetrodotoxin-sensitive Na⁺ conductance in rat optic nerve axons, *Proc. Nat. Acad. Sci. USA*, 90:6976–6980.
- Sucher, N. J., and S. A. Lipton, 1992. A slowly inactivating K⁺ current in retinal ganglion cells from postnatal rat, *Vis. Neurosci.*, 8:171–176.
- Tabata, T., and A. T. Ishida, 1996. Transient and sustained depolarization of retinal ganglion cells by I_h, *J. Neurophysiol.*, 75:1932–1943.
- Tabata, T., and A. T. Ishida, 1999. A zinc-dependent Cl[−] current in neuronal somata, *J. Neurosci.*, 19:5195–5204.
- Tabata, T., B. M. Olivera, and A. T. Ishida, 1996. ω -conotoxin-MVIIID blocks an ω -conotoxin-GVIA-sensitive, high-threshold Ca²⁺ current in fish retinal ganglion cells, *Neuropharmacol.*, 5:633–636.
- Tang, C. M., G. R. Strichartz, and R. K. Orkand, 1979. Sodium channels in axons and glial cells of the optic nerve of *Necturus maculosa*, *J. Gen. Physiol.*, 74:629–642.
- Taschenberger, H., and R. Grantyn, 1995. Several types of Ca²⁺ channels mediate glutamatergic synaptic responses to activation of single Thy-1-immunolabeled rat retinal ganglion neurons, *J. Neurosci.*, 15:2240–2254.
- Tauchi, M., N. K. Madigan, and R. H. Masland, 1990. Shapes and distributions of the catecholamine-accumulating neurons in the rabbit retina, *J. Comp. Neurol.*, 293:178–189.
- Taylor, W. R., S. Mittman, and D. R. Copenhagen, 1996. Passive electrical cable properties and synaptic excitation of tiger salamander retinal ganglion cells, *Vis. Neurosci.*, 13:979–990.
- Thibos, L. N., and F. S. Werblin, 1978. The response properties of the steady antagonistic surround in the mudpuppy retina, *J. Physiol.*, 278:79–99.
- Thier, P., and V. Alder, 1984. Action of iontophoretically applied dopamine on cat retinal ganglion cells, *Brain Res.*, 292:109–121.
- Tran, V. T., and M. Dickman, 1992. Differential localization of dopamine D1 and D2 receptors in rat retina, *Invest. Ophthalmol. Vis. Sci.*, 33:1620–1626.
- Traverso, T., R. A. Bush, P. A. Sieving, and D. Deretic, 2002. Retinal cAMP levels during the progression of retinal degeneration in rhodopsin P23H and S334ter transgenic rats, *Invest. Ophthalmol. Vis. Sci.*, 43:1655–1661.
- Vaney, D. I., 1999. Neuronal coupling in the central nervous system: lessons from the retina, *Novartis Found. Symp.*, 219:113–125.
- Vaquero, C. F., A. Pignatelli, G. J. Partida, and A. T. Ishida, 2001. A dopamine- and protein kinase A-dependent mechanism for network adaptation in retinal ganglion cells, *J. Neurosci.*, 21:8624–8635.
- Vargas, G., T.-Y. J. Yeh, D. K. Blumenthal, and M. T. Lucero, 1999. Common components of patch-clamp internal recording solutions can significantly affect protein kinase A activity, *Brain Res.*, 828:169–173.
- Velte, T. J., and R. H. Masland, 1999. Action potentials in the dendrites of retinal ganglion cells, *J. Neurophysiol.*, 81:1412–1417.
- Veruki, M. L., and H. Wässle, 1996. Immunohistochemistry localization of dopamine D1 receptors in rat retina, *Eur. J. Neurosci.*, 8:2286–2297.
- Wang, G.-Y., G. M. Ratto, S. Bisti, and L. M. Chalupa, 1997. Functional development of intrinsic properties in ganglion cells of the mammalian retina, *J. Neurophysiol.*, 78:2895–2903.

- Wang, G.-Y., D. W. Robinson, and L. M. Chalupa, 1998. Calcium-activated potassium conductances in retinal ganglion cells of the ferret, *J. Neurophysiol.*, 79:151–158.
- Wang, G.-Y., B. A. Olshausen, and L. M. Chalupa, 1999. Differential effects of apamin- and charybdotoxin-sensitive K^+ conductances on spontaneous discharge patterns of developing retinal ganglion cells of the ferret, *J. Neurosci.*, 19:2609–2618.
- Wässle, H., and B. B. Boycott, 1991. Functional architecture of the mammalian retina, *Physiol. Rev.*, 71:447–480.
- Watt, C. B., and P. A. Glazebrook, 1993. Synaptic organization of dopaminergic amacrine cells in the larval tiger salamander retina, *Neuroscience*, 53:527–536.
- Werblin, F. S., and D. R. Copenhagen, 1974. Control of retinal sensitivity. Lateral interactions at the inner plexiform layer, *J. Gen. Physiol.*, 63:88–110.
- Witkovsky, P., and A. Dearry, 1991. Functional roles of dopamine in the vertebrate retina, *Prog. Ret. Res.*, 11:247–292.
- Witkovsky, P., and M. Schütte, 1991. The organization of dopaminergic neurons in vertebrate retinas, *Vis. Neurosci.*, 7:113–124.
- Yazulla, S., and K. M. Studholme, 1998. Differential distribution of Shaker-like and Shab-like K^+ -channel subunits in goldfish retina and retinal bipolar cells, *J. Comp. Neurol.*, 396:131–140.
- Yazulla, S., and C. L. Zucker, 1988. Synaptic organization of dopaminergic interplexiform cells in the goldfish retina, *Vis. Neurosci.*, 1:13–29.
- Yeh, T., B. B. Lee, and J. Kremers, 1996. The time course of adaptation in macaque retinal ganglion cells, *Vis. Res.*, 36:913–931.
- Yoon, M., 1972. Influence of adaptation level on response pattern and sensitivity of ganglion cells in the cat's retina, *J. Physiol.*, 221:93–104.
- Zalutsky, R. A., and R. F. Miller, 1990. The physiology of substance P in the rabbit retina, *J. Neurosci.*, 10:394–402.
- Zenisek, D., D. Henry, K. Studholme, S. Yazulla, and G. Matthews, 2001. Voltage-dependent sodium channels are expressed in nonspiking retinal bipolar neurons, *J. Neurosci.*, 21:4543–4550.
- Zhang, J., W. Shen, and M. M. Slaughter, 1997. Two metabotropic γ -aminobutyric acid receptors differentially modulate calcium currents in retinal ganglion cells, *J. Gen. Physiol.*, 110:45–58.

28 Direction Selectivity in Retinal Ganglion Cells

RICHARD H. MASLAND

DIRECTION SELECTIVITY by retinal ganglion cells—the ability of some cells to report the direction of stimulus movement—was described in classic experiments by Barlow and Levick (Barlow et al., 1964; Barlow and Levick, 1965) more than 35 years ago. Despite much theory and many experiments, the mechanism remains unknown. Indeed, it can be argued, with some embarrassment, that small progress has been made since Barlow and Levick's classic studies. Those studies and subsequent ones have recently been the subject of a careful review by four experienced students of direction selectivity, including its codiscoverer (Vaney et al., 1999). Here I will: (1) outline the cardinal features of direction selectivity—that is, those experimental findings that seem universally accepted; (2) discuss some of the requirements for a mechanistic explanation of it; and (3) comment on certain controversies that have sprung up in the past few years.

Retinal direction selectivity appears deceptively simple. Perhaps for that reason, even sophisticated neurobiologists have sometimes offered theories of its mechanism that could have been seen with a few minutes' careful thought to be unworkable. For that reason, it is important to begin with a statement of the fundamental facts.

Fundamental features of direction selectivity in mammalian retinas

Direction selectivity has been most studied in the retina of the rabbit; work in other species will be noted where appropriate. The behavior of an idealized ON-OFF direction-selective (DS) cell (a separate ON type exists but will not be considered here) is shown in Figure 28.1. The cells can respond to a 50- μ m displacement of a spot of light 50 μ m in diameter. The displacement can happen anywhere within the receptive field, with the preferred direction remaining the same. The cells have the same directional preference for movement of a light spot or a dark spot. Similarly, the cells have the same directional preference for a light edge or a dark edge. If the receptive field is mapped with a flashing spot, ON and OFF responses are encountered at all locations.

These observations eliminate a trivial form of direction selectivity, in which an excitatory zone is flanked by an

inhibitory zone (Fig. 28.1D). In principle, a stimulus moving first across the inhibitory zone and later across the excitatory zone could, with the right timing, generate a null response as inhibition collides with excitation. A stimulus moving in the opposite direction, from the excitatory side to the inhibitory side, would encounter the excitatory zone first and create a positive response. This cannot be the mechanism, first because ON-OFF responses are encountered everywhere, and second because the directional preference is the same for a light or a dark edge (this is a quick diagnostic test for a putatively DS ganglion cell encountered during recordings). Instead, some sort of local subunit is reduplicated throughout the receptive field.

Nothing in the anatomical structure of the ON-OFF DS cell predicts direction selectivity (Amthor et al., 1984; Oyster et al., 1993; Yang and Masland, 1994). A series of ON-OFF DS cells injected after recording are shown in Figure 28.2. There is no correlation between the preferred direction and any feature of the dendritic arbor that has thus far been discerned.

However, one feature of the DS cell's response was explained by the cell's structure: its independence of the sign of contrast. The DS ganglion cell has a bistratified dendritic arbor (Fig. 28.3). One arbor lies within the ON zone in the inner plexiform layer and one arbor in the OFF zone. The ON arbor can mediate direction-selective responses to a light edge; the OFF arbor to a dark edge. The relative independence of these two mechanisms was demonstrated by Kittila and Massey (1995), who eliminated the ON input by blocking the responses of ON bipolar cells pharmacologically. With ON responses blocked, the DS ganglion cell remained direction selective, even though it could respond only to negative contrasts.

A major event in direction selectivity is feedforward inhibition

A series of important experiments on the mechanism of direction selectivity was carried out by Daw and his colleagues (Ariel and Daw, 1982a, 1982b; Caldwell et al., 1978; Wyatt and Daw, 1975). They recorded from ON-OFF DS cells *in vivo*, using electrodes that penetrated the globe, and

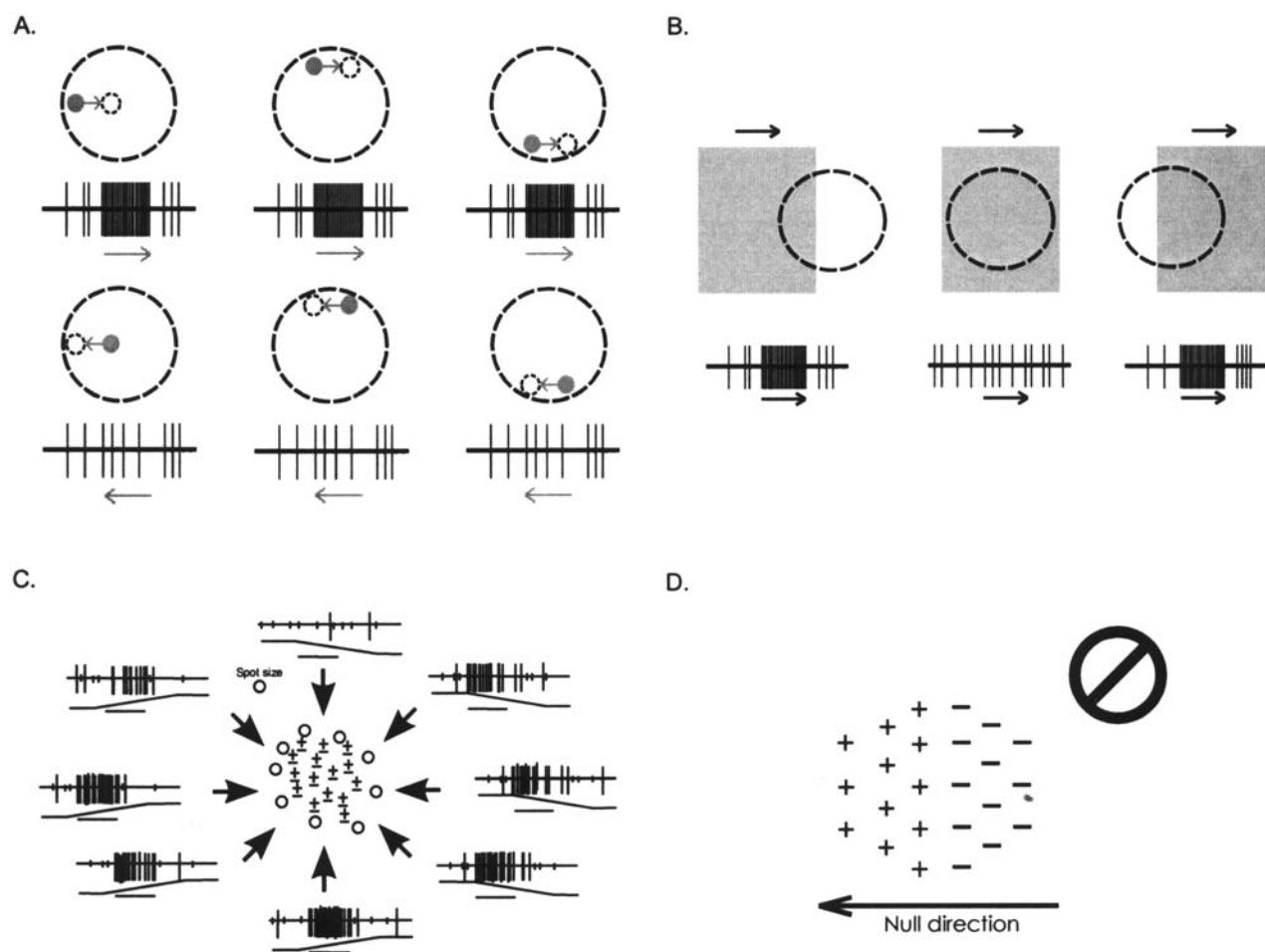


FIGURE 28.1. Response properties of the ON-OFF direction selective neuron in the retina. *A* and *B* are schematic, *C* is the classic illustration of Barlow and Levick (1965). The receptive field is indicated by a dashed line. *A*, The cell responds selectively to movement of a small spot from left to right. The directional preference is maintained for small areas within the receptive field. *B*, Direction-selective cells respond to either sign of contrast.

applied drugs to the retina by infusing them into the ophthalmic artery.

Their first critical observation was that a small moving stimulus that sweeps across the receptive field generates an asymmetrical wave of inhibition. Their result is schematized in Figure 28.4. Note that the cloud of inhibition does not occupy a fixed position, but moves around the receptive field, maintaining a constant position relative to the moving stimulus. When the stimulus moves in the null direction, the cloud of inhibition precedes the arrival of the stimulus in space. When the stimulus moves in the preferred direction, the cloud of inhibition trails the stimulus.

The importance of this inhibition was confirmed by the demonstration that retinal direction selectivity is entirely abolished by the GABA receptor antagonist picrotoxin

C, When the receptive field of an ON-OFF DS cell is mapped with a flashing spot, ON and OFF responses are encountered everywhere within the receptive field. This requires that some sort of local subunit be reduplicated within the field. In other words, the trivial mechanism shown in *D*, in which ON and OFF zones are segregated, cannot explain the behavior of the DS neuron.

(Caldwell et al., 1978). Under control conditions, the excitatory center of the receptive field is only slightly larger than the dendritic arbor of the DS ganglion cell (Yang and Masland, 1994). In the presence of picrotoxin, two things happen: (1) the receptive field almost doubles in size, and (2) all traces of direction selectivity are abolished. From cell to cell there is some biological variation, such that the picrotoxin-influenced receptive field may be slightly asymmetrical, but there is no consistency to this result.

It is also possible to show weak, feedforward excitation (excitation that spreads ahead of the moving stimulus) in the preferred direction (Amthor et al., 1996). However, this is also seen in the null direction as well when the masking inhibition is pharmacologically blocked (Chiao and Masland, 2002).

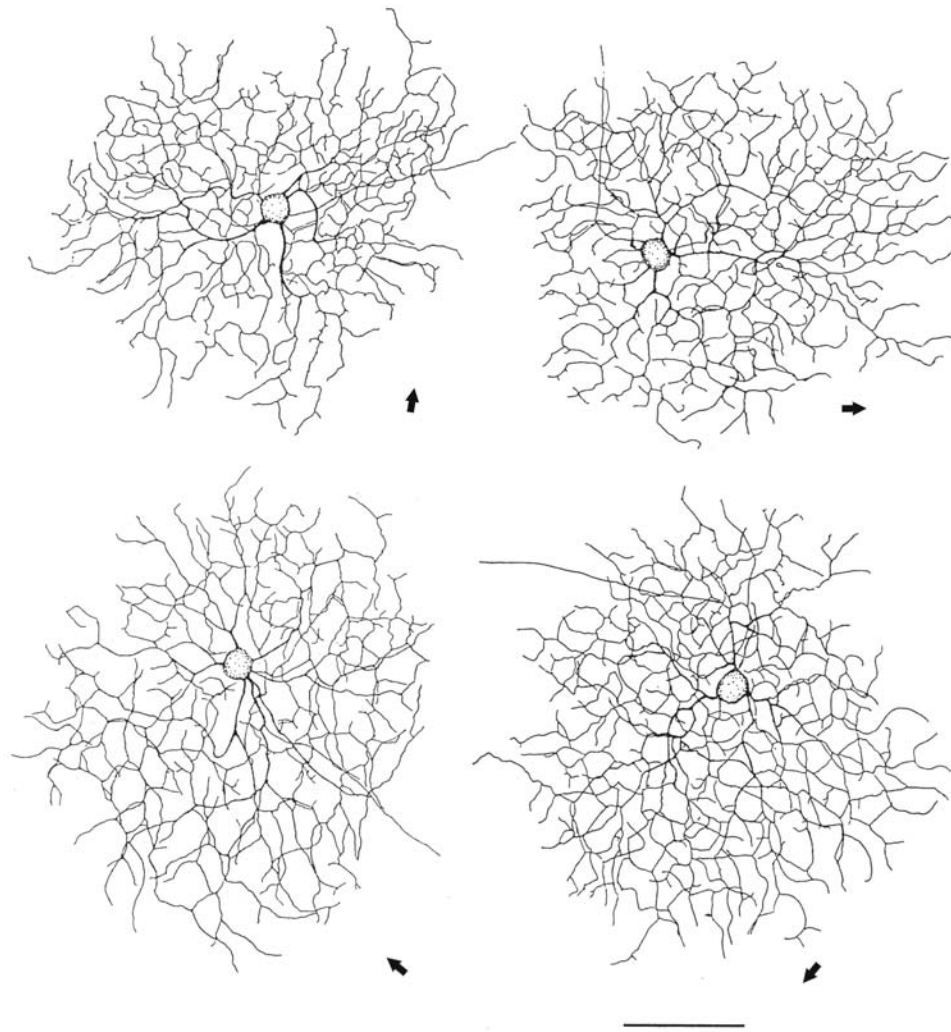


FIGURE 28.2. ON-OFF DS cells injected after recording. An arrow indicates the preferred direction for each cell (Yang and Masland, 1994). Thus far, no one has been able to find any correlation between a morphological feature and the preferred direction. Scale bar, 100 μm .

General requirements for direction selectivity

Barlow and Levick pointed out that two things are required for direction selectivity. There must be, somewhere in the system, a physical asymmetry such that inhibition (or in principle, excitation) is laterally displaced relative to the stimulus. As will be discussed later, this is usually interpreted as the process (axon or dendrite) of a neuron, but that is not necessarily so: one can imagine laterally displaced receptors, laterally displaced waves of intracellular calcium, or other molecular mechanisms that would achieve the same result. Nonetheless, something, somewhere, undergoes a lateral displacement in direction selectivity. The second element that is required is the time delay. The model now commonly termed the Barlow-Levick model invokes the process of a laterally directed inhibition. Some possible arrangements are shown in Figure 28.5.

In its simplest form (Fig. 28.5, *top panel*) such a mechanism, taken at face value, cannot work. A mechanism of direction selectivity must not only prevent responses during movement in the null direction, but *it must also permit responses in the preferred direction*. In the drawing, there is no difference between the total amount of inhibition that the ganglion cell receives in the null direction or the preferred direction. Something else must be postulated.

One such “something else” might be that the inhibition occurs presynaptic to the ganglion cell, rather than directly on it (*middle panel*). Another was imagined very early in the study of visual motion, from studies by Reichardt of insect behavior. From first principles, Reichardt and Hassenstein (Reichardt, 1961) proposed a model that outlined the components necessary for an elementary motion detector. It is in many ways similar to the model proposed by Barlow and Levick, in which a lateral displacement and a time delay are

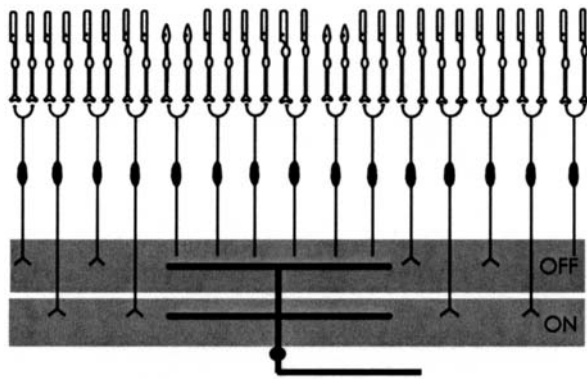


FIGURE 28.3. How the ON-OFF DS cell can respond to both light edges and dark edges. The ON-OFF DS cell is a bistratified neuron. One arbor is stratified within the ON sublayer of the inner plexiform layer and the other within the OFF sublayer. The ON arbor subserves responses to light edges; the OFF arbor to dark edges. Because the retina's ON and OFF pathways are created at the first retinal synapse (between photoreceptors and bipolar cells), this implies that the fundamental mechanism of the directional discrimination is reduplicated for the ON and OFF pathways.

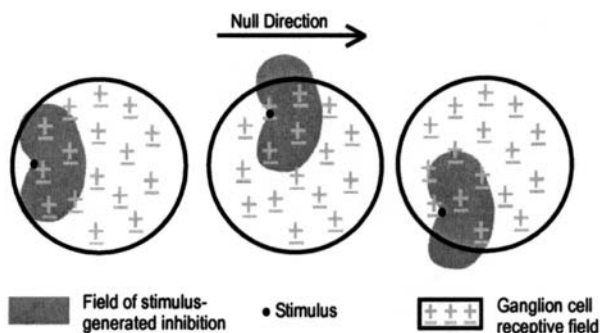


FIGURE 28.4. A moving "cloud" of inhibition precedes a stimulus moving in the null direction. The illustration shows the prediction made from the results of Wyatt and Daw (1975), in which the receptive field was probed with a moving stimulus and a flashed test probe. A heart-shaped contour of inhibition was observed.

required. However, the elementary motion detector was taken to the level of a formal model and had an additional requirement: some nonlinearity in the interaction between the presynaptic and postsynaptic motion-detecting elements (Fig. 28.6). This overcomes the difficulty described in the previous paragraph; namely, that a cell receiving input from many small motion-detecting elements receives the same amount of excitation and inhibition, no matter what the direction of motion, in the absence of another postulated mechanism. The mechanism postulated in the Reichardt model is a multiplicative step between the feedforward information and the straight-through information. There is a time delay, such that the feedforward information from point A arrives at the integrator at the same time as

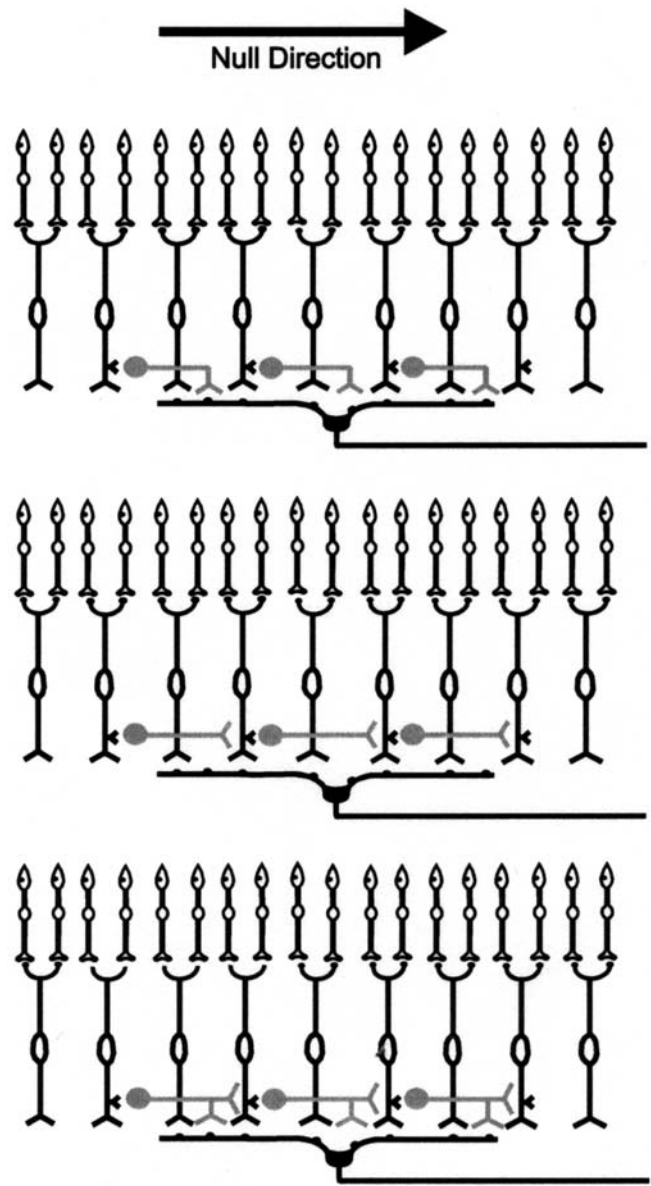


FIGURE 28.5. Several different ways in which a laterally displaced inhibition could be arranged. The top panel shows a "post-synaptic model" in which an inhibitory amacrine cell makes an input onto the ganglion cell that is displaced toward the null direction. As drawn, such a model will probably not work. If the ganglion cell is isopotential (or is any form of simple, linear, integrate-and-fire neuron), the cell will be prevented from responding when the stimulus moves in the null direction, but also will be prevented from responding when the stimulus moves in the preferred direction. Even though the inhibition trails the stimulus, it will be detected by the ganglion cell. As has been pointed out by many, some other nonlinearity is required. The middle panel shows a model in which the inhibition is presynaptic. In this case, the amacrine cell inhibits the output of the bipolar cells (only some of the hypothetical synapses on bipolar cells are shown). This is a "presynaptic model," in which the output of the bipolar cells is direction selective. The two types of model are not mutually exclusive, and the bottom panel shows a case in which both mechanisms operate.

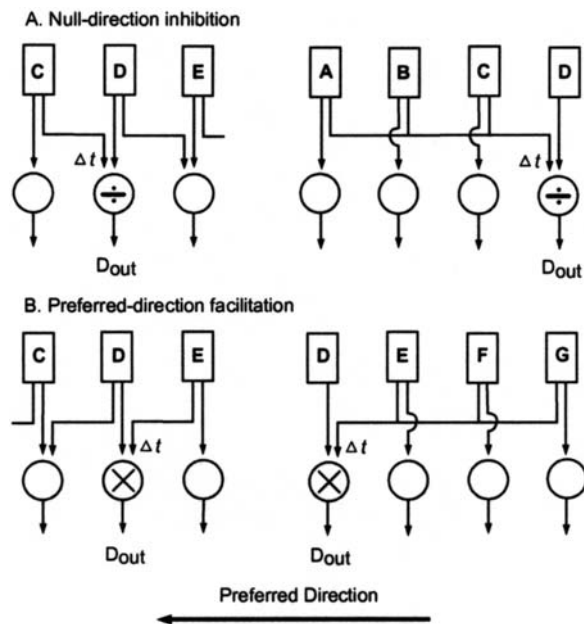


FIGURE 28.6. Schematic illustrations of the spatial asymmetries and nonlinear interactions that could create direction selectivity in retinal ganglion cells. For historical reasons, the inhibitory model is sometimes termed the Barlow-Levick model and the excitatory model the Reichardt model, but they are similar in many regards. The illustration also makes the point that single or multiple cells could participate in the asymmetrical inputs. (From Vancy et al., 1999).

straight-through information from point B. If these merely sum, there will be no difference between the preferred direction and the null direction. However, if they multiply, an asymmetry is created such that the system's output is greater in the preferred direction than the null direction.

The nonlinearity could just as well be divisive. It was later shown that for fly vision a multiplicative step followed by a subtractive step yields the best prediction of fly behavior (Borst and Egelhaaf, 1990). These models offer little in the way of neural mechanism. Instead, they are guideposts and the task, both in flies and in rabbits, is to learn whether and how they are implemented.

Presynaptic versus postsynaptic computation of direction selectivity

A controversy alluded to already (see Fig. 28.5) concerns the locus of the computation of direction selectivity. By this is meant whether the synaptic interactions that create direction selectivity occur on the DS ganglion cell itself or among the neurons afferent to the DS ganglion cell. In the second case, the input to the DS ganglion cell would already be direction selective.

Taylor and colleagues (2000) concluded that the first element to be fully direction selective in the rabbit retina is

the DS ganglion cell (this is what is usually meant by the somewhat imprecise phrase the “site of the DS computation”). They made whole-cell patch recordings from DS ganglion cells and found two kinds of evidence for a postsynaptic locus. First, holding the membrane potential at -30 mV or -70 mV allowed an isolation of excitation and inhibition on the ganglion cell. At -70 mV movement of a stimulus in the preferred direction caused a large depolarization; in the null direction it also caused a depolarization, but a smaller one. When the cell was clamped at -30 mV , the null direction depolarization was converted to a hyperpolarization. This repeats an earlier observation by Marchiafava (1979) in turtle retina. A parsimonious interpretation is that stimulus movement in the null direction causes the ganglion cell to receive a laterally displaced input that opens chloride channels (shunting inhibition, known to result from GABA_A receptors).

In confirmation of this interpretation, Taylor and colleagues carried out a second type of experiment, in which the intracellular concentration of chloride was raised by recording with a patch pipette containing 150 mM of chloride. As chloride diffused from the electrode into the cell, the driving force on chloride was reduced. In that case, shunting inhibition would have become less effective; in fact, the high chloride electrode very much lessened the ganglion cell's direction selectivity. Taylor and colleagues concluded that the asymmetry responsible for direction selectivity is a shunting inhibition of the dendrites of the DS ganglion cell.

In contrast, Borg-Graham argued, from experiments on turtle retinas, that the directional decision is made presynaptically—that the first direction-selective element lies somewhere earlier in the chain of synapses leading to the ganglion cell, so that the excitatory input to the DS ganglion cell is already direction selective (Borg-Graham, 2001). This conclusion was derived from modeling of experiments using patch recording. The presynaptic and postsynaptic models make different predictions for the excitatory and inhibitory synaptic conductance inputs onto the DS ganglion cells during traverse of the receptive field by a stimulus. They were estimated from the modulation of the ganglion cell's input conductance during the visual response and the apparent reversal potential of the evoked inputs. For example, if the computation is postsynaptic, there must be a temporal offset between excitation and inhibition of the ganglion cell. The finding was that the peak and average of the excitatory input was greater for responses generated by stimuli moving in the preferred direction. If correct, this is direct evidence for a presynaptic site of the directional discrimination.

At the moment, this conflict remains unresolved. Given the difficulties of these experiments, one possibility is that both presynaptic and postsynaptic mechanisms operate. The critical biological measurements are difficult ones. Retinal ganglion cells have small (20 to $30\text{ }\mu\text{m}$) somas but large

dendritic arbors. Retinal ganglion cells are not, like billiard balls on a table, a naked target. Instead, they are enveloped in the cytoplasm of the Müller glia and are protected on the surface by the inner limiting membrane, a tough extracellular proteinaceous matrix. The inner limiting membrane must either be penetrated or removed. An advance in this type of recording was the discovery that the inner limiting membrane can be physically peeled away from the ganglion cells, yielding access for patch or sharp electrodes (Peters and Masland, 1996; Taylor and Wässle, 1995). Even so, these cells are much more difficult to access than are, say, Purkinje or hippocampal neurons in a brain slice.

The second major difficulty is that the dendrites of the DS cells are not isopotential. They range up to approximately 800 μm in diameter and the diameters of their dendrites are far from uniform: the thinnest dendrites, approximately 0.3 μm in diameter, can exit directly from major dendrites that have diameters up to 1 μm (He et al., 1999). This creates many electrotonic complexities (indeed, many opportunities for interesting computations) but complicates the analysis of the somatic responses and raises the suggestion of nonlinearities that are invisible to an electrode placed at the soma. Among many other assumptions are that there is a single type of excitatory and a single inhibitory conductance, that the amount of electrotonic isolation is constant under all stimulus conditions; and that the current voltage relations are linear. Both groups of experimenters in this controversy are pushing the limits of current methodologies.

Starburst amacrine cells have features that could contribute to direction selectivity

From the earliest times, likely candidates for the laterally displaced element that creates direction selectivity were horizontal or amacrine cells. Amacrine cells quickly took the ascendancy because of their greater diversity. The original and still the leading candidate was the cholinergic, “starburst” amacrine cell. The first evidence came from electrophysiological experiments, which showed that the DS retinal ganglion cell responds very strongly to acetylcholine, is excited by anticholinesterase, and has its response to light depressed by cholinergic antagonists (Kittalia and Massey, 1997; Masland and Ames, 1976). The cells responded strongly to acetylcholine even when an isolated retina was incubated in medium containing high magnesium and low calcium, conditions that prevent synaptic transmission; this indicated that acetylcholine receptors were located directly on the ganglion cells, a finding subsequently confirmed by using antibodies against those receptors (Keyser et al., 2000). That the acetylcholine-releasing neuron was in fact an amacrine cell was shown directly by autoradiography of the acetylcholine-synthesizing neurons, which formed mirror

symmetrical populations located on either side of the inner plexiform layer and contained acetylcholine within two thin bands within the layer (Masland and Mills, 1979). Famiglietti (1983) then pointed out that a neuron adventitiously stained by the Golgi method stratified at the same level where bands of acetylcholine are present, and nicknamed this neuron the “starburst cell.” Definitive proof of the identity between the acetylcholine-synthesizing cells and the starburst cell (and neurofibrillar-stained cells observed by an independent method; Vaney et al., 1981) came when the starburst cells could be injected using fluorescent staining with DAPI as an intermediate step for targeting (Hayden et al., 1980; Masland et al., 1984a; Tauchi and Masland, 1984; Vaney, 1984).

The first suggestion that starburst cells were involved in direction selectivity was by Masland and colleagues (1984b), on the basis that (1) DS ganglion cells receive a strong cholinergic input, (2) the starburst cell is the only cholinergic neuron known to exist in the retina, and (3) a role in detecting motion would rationalize the apparent redundancy of the overlapping plexuses of starburst dendrites. They proposed that “the dense plexus of cholinergic dendrites and the transient nature of acetylcholine release combine to create the local subunit that enables detection of motion within regions smaller than the ganglion cells’ receptive fields,” but did not suggest a specific mechanism by which the directional discrimination might occur.

Are starburst cells the mechanism of motion discrimination?

Subsequent studies at both the light and electronmicroscopic levels have confirmed an intimate relationship between dendrites of the starburst cells and those of the DS ganglion cells (Famiglietti, 1992; Vaney et al., 1989). An important observation was that the synaptic inputs and outputs of the starburst dendrites are anisotropic (Famiglietti, 1991). The dendrites receive synaptic inputs along their whole length but make outputs primarily along the dendrites’ distal third (Fig. 28.7). This creates a directional polarization, such that, on average, inputs to the cell will be propagated centrifugally, from the center of the cell toward the ends of the dendrites.

This functional polarization of the dendrites represents a potential source for the lateral displacement postulated in all theories of direction selectivity. That it creates a local direction selectivity has recently been elegantly confirmed in experiments using calcium imaging and two-photon microscopy (Euler et al., 2002), show that the starburst cells have large calcium influxes at the distal release sites of their dendrites in response to centrifugal motion but much less to centripetal motion.

From the anatomic evidence, Vaney (1991) had seized upon this asymmetry to suggest a mechanism of direction

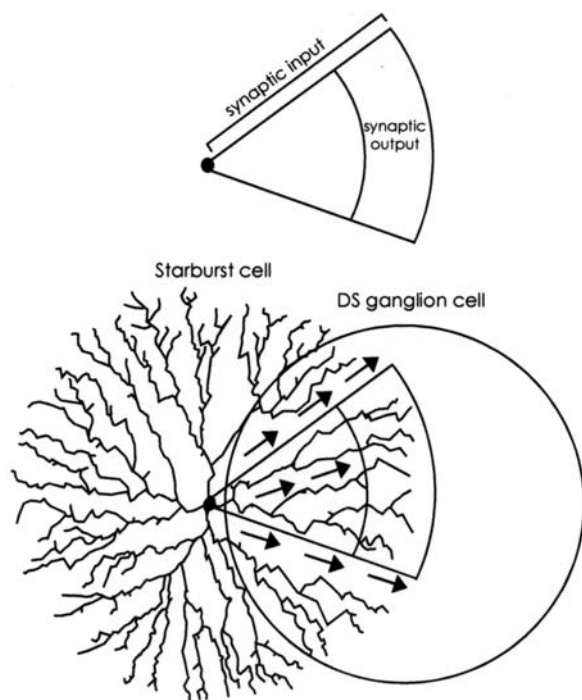


FIGURE 28.7. Synaptic asymmetries in the starburst cell can create an asymmetrical input to DS ganglion cells. At the top is shown the pattern of synaptic input and output on the dendrites of the starburst amacrine cell. Inputs from bipolar cells to the starburst cell occur throughout the length of the dendrites, but synaptic outputs are restricted to the distal third. This results in a net polarization of activity along the dendrites; on average, activity will propagate centrifugally, toward the distal dendrites. If the starburst cell is selectively connected to a DS cell, this asymmetry can create direction selectivity in the ganglion cell. In the illustration shown, the ganglion cell would respond to stimuli moving toward the right. The other, “empty” dendrites of the starburst cell would make outputs to other DS ganglion cells, those with preferred directions upward, downward, or to the left in the diagram. (From He and Masland, 1997).

selectivity. In this model the starburst cells are selectively connected to individual DS ganglion cells. On the upstream (preferred) side, they selectively excite the ganglion cell during movements in the preferred direction. This accords with the polarized nature of their dendritic activity, which tends to transmit signals from central to peripheral areas within the starburst cell’s arbor. This concept has the great appeal that it accounts for the overlap of the starburst cells. In the postulated arrangement (Fig. 28.7), only a fraction of the starburst cell’s dendrites are occupied with one DS cell. What happens to the starburst cell’s other, “empty” dendrites? They contact DS ganglion cells with other preferred directions. In other words, a single population of starburst amacrine cells can provide a directionally biased output to direction selective ganglion cells of several preferred directions. A similar model was formally stated by Borg-Graham and Grzywacz (1992) and was accompanied by modeling

showing many of the premises of the theory to be mathematically plausible.

The simplicity and elegance of this proposed arrangement make it very attractive. However, certain conflicts existed, most notably that under most conditions cholinergic antagonists fail to eliminate direction selectivity (Ariel and Daw, 1982a; He and Masland, 1997; Kittila and Massey, 1997; Masland and Ames, 1976). Those same antagonists (d-tubocurarine, dihydro- β -erythroidine, or mecamlamine) could be shown to prevent acetylcholine’s action on the retina’s acetylcholine receptors; this was done by applying large test doses of acetylcholine, which in the presence of the antagonist could be shown to produce no response from the DS ganglion cell. The antagonists thus are effective at the synapses in question but fail to prevent direction selectivity. This is not conclusive evidence, however, because the starburst cells are unusual in that they contain and release both acetylcholine and GABA (Brecha et al., 1988; O’Malley et al., 1992; Vaney and Young, 1988). The model depicted in Figure 28.7 could be either excitatory or inhibitory (or both, i.e., push-pull).

In an attempt to resolve the issue, He and Masland (1997) used laser microablation of the starburst cells as a further test. They identified starburst cells in isolated retinas by staining with DAPI, recorded the responses of DS ganglion cells, and then laser-microablated a patch of starburst cells on either the preferred side, the null side, or both. The fundamental result was that ablating starburst cells did not eliminate direction selectivity. In the preferred direction, where a vigorous response is normally observed, ablating starburst cells decreased the response to about the level expected from a pharmacological blockade of acetylcholine, but direction selectivity was retained. He and Masland reported a second experiment in which the effect of curare was tested in the presence of picrotoxin. As noted earlier, picrotoxin blocks GABA_A receptors and entirely eliminates direction selectivity. In the presence of picrotoxin, the application of curare caused a *symmetrical* decrease in the magnitude of the response of the cell to movements in any direction. This suggests that the cholinergic input to the DS ganglion cell is isotropic. These two experiments argue that the starburst cells carry out feedforward excitation of the DS cells, but from all sides; they make the ganglion cells motion sensitive but not direction selective (Fig. 28.8). (This amounts to a bidirectional Reichardt correlator.) This would imply that the asymmetrical connectivity postulated by the starburst theory does not exist.

A few years later, this result was contradicted by a different type of experiment, this time carried out in the retina of the mouse. Yoshida colleagues. (2001) immunolesioned the starburst cells in the mouse retinas. This was done by first creating a transgenic mouse in which the promoter for choline acetyltransferase was used to drive the human interleukin-2

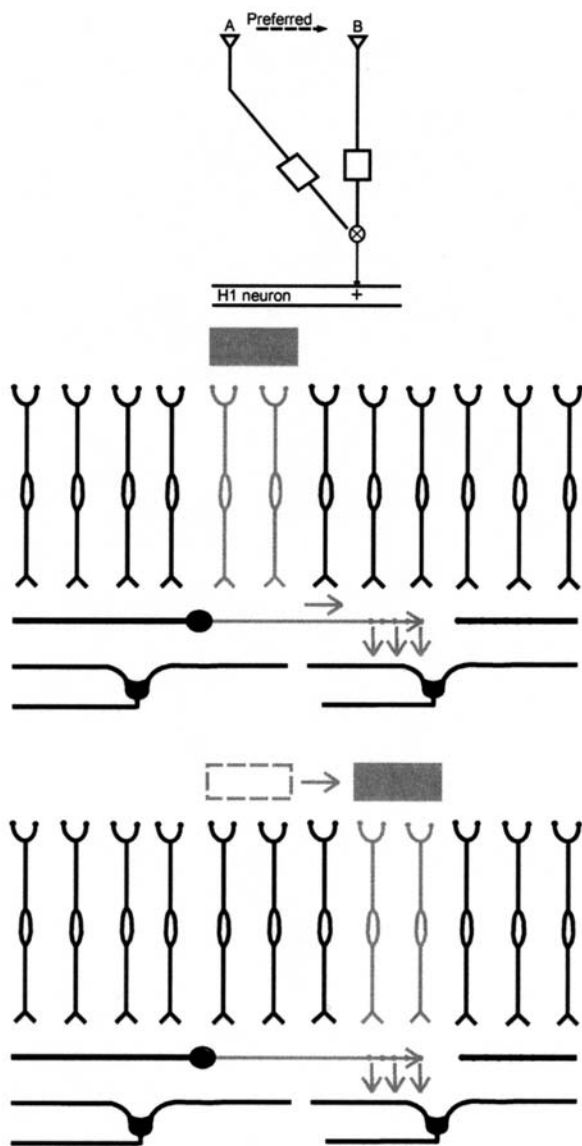


FIGURE 28.8. Another view of the polarized output of the starburst amacrine cell, together with the classic illustration by Reichardt (1961) of a motion detector in insects. The polarization of the starburst cell's inputs and outputs (Fig. 28.7) will cause its synaptic output to be laterally displaced across the retina. When a moving stimulus (*gray rectangle*) traverses the retina, this can create feedforward excitation or inhibition.

receptor α -subunit (hiL-2R α). The foreign receptor was thus expressed in the starburst cells. An immunotoxin conjugated to a monoclonal antibody against hiL-2R α was injected into the vitreous. On binding to the receptor, it was internalized and killed the starburst cells. That the starburst cells were in fact absent could be verified by staining against choline acetyltransferase. After lesioning, these mice contained no DS retinal ganglion cells when studied electrophysiologically. Furthermore, optokinetic responses were depressed. This result would imply that in the mouse the starburst amacrine cells are critical for direction selectivity.

Which of these conclusions is correct? Both experiments have their weak points. It has been suggested that laser ablation of the starburst cells allowed the starburst dendrites to reseal, so that they continued to function in the absence of their cell bodies. This seems extremely unlikely. The laser photocoagulated the cell body and it could be demonstrated that the cell body was permanently (>8 h) accessible to extracellular dyes. Such an explanation would require that not one but all the dendrites reseal, and stay resealed for up to 8 hours. This does not happen in cultured cells and there is no reason to think it would happen in the intact tissue. Furthermore, ablating starburst cells on the preferred side had the expected effect—it depressed the response by about the same amount as did curare. It would be strange for the dendrites to reseal if the starburst cell is located on the preferred side but not when the starburst cell is located on the null side.

If the laser experiment contains an error, the more likely possibility is that it is due to the great redundancy of the starburst plexus. Because hitting a dendrite of a ganglion cell with the laser beam killed that ganglion cell (another reason for not believing in dendritic resealing), only a relatively small patch of starburst cells, outside but overlapping the DS ganglion cell, could be targeted. If a few missed cells were enough to sustain direction selectivity, the experiment would be invalid. Another ambiguity, discovered after the original experiments were carried out, is that there is cross-talk between the ON and OFF arbors of the ON-OFF DS cell. A method was devised that revealed the virtually complete population of amacrine cells (MacNeil et al., 1999; MacNeil and Masland, 1998). Surprisingly, it turned out that roughly half of all amacrine cells violate the ON and OFF borders within the inner plexiform layer. In the case of the ON-OFF DS cell, it can be directly demonstrated that OFF inhibition prevents ON excitation—a crossing of the ON-OFF border (Stasheff and Masland, 2002). Because for practical reasons the laser experiments could only target the ON starburst cells, some kind of cross-talk could have sustained direction selectivity.

The immunolesion experiments run different risks. One is collateral damage, notably the well-established bystander effect, in which a cell that is specifically targeted by a toxin kills its neighbors when it dies (this is presumably due to the release of proteases). Yoshida and colleagues (2001) had little way to know if additional amacrine cells were damaged, because specific stains for most amacrine cells are not available. A second difficulty is that immunolesioning takes a substantial amount of time, and this precludes recording from the same DS cell before and after the lesion. Thus, it was necessary to assume that all ON-OFF ganglion cells encountered in the immunolesioned animals would have been DS cells before the lesion.

Finally, it is not certain that direction selectivity in the mouse and the rabbit are computed in the same way. There

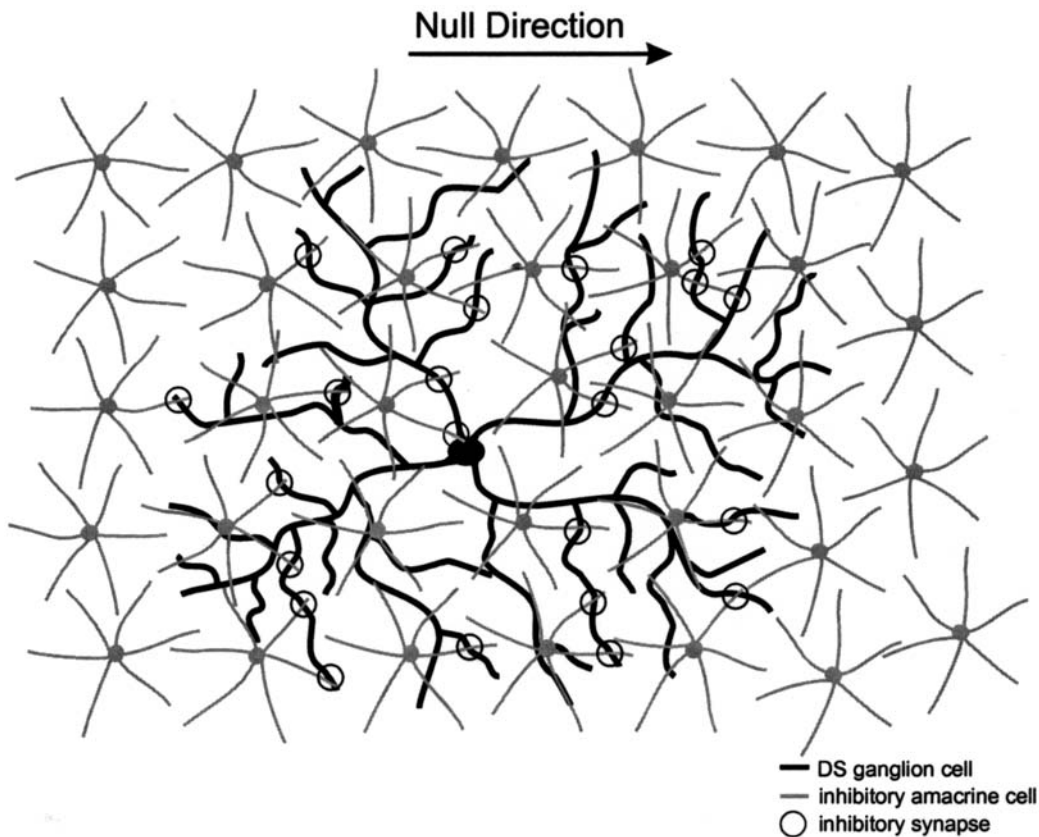


FIGURE 28.9. How a symmetrical amacrine cell could create an asymmetrical output onto a ganglion cell. The postulate is that synapses between the hypothetical amacrine cell and the ganglion cell are polarized, such that they occur only on one side of the dendritic arbor of the amacrine cell. If the amacrine cell is inhibitory and the interaction is divisive, this will create a null direction. The amacrine cell shown is a generic one, not intended to represent any known cell. From Jeon et al. (2002).

is no obvious morphological homolog of the rabbit's ON-OFF DS cell in the mouse (Sun et al., 2002). Direction selectivity has been reinvented many times in different species and different parts of the nervous system, and it is possible (though an inelegant explanation) that there is a species difference.

In conclusion, it seems certain that the starburst cells are involved in a major way in the computation of direction selectivity in the rabbit retina. Whether or not the starburst cells, by themselves, achieve the computation remains unclear. Certainly all of the available information— anatomy, electrophysiology, laser lesion, and immunole- sion—indicates that the starburst cells are important for direction selectivity. Whether they are solely responsible for the directional discrimination or merely contributors remains to be learned.

Alternative anatomies: where does the asymmetry occur?

In the most general case, direction selectivity is understood: A Reichardt-type correlator, with or without bells and whis-

tles, will generate direction selectivity in a neural circuit. The question remains how direction selectivity is biologically implemented. What would constitute proof of a theory of direction selectivity? A commonly held view is that the ultimate understanding will require that we locate the physical basis of the functional asymmetry long recognized as the central requirement of direction selectivity.

The asymmetry is commonly drawn as shown in Figures 28.5 and 28.6, which are suggestive of a neuron with a dendritic or axonal arbor polarized along the preferred-null axis. As noted earlier, other types of asymmetry are possible, including those localized on a molecular scale, but a neuronal asymmetry seems the more likely because of the larger scale (~50 to 100 μm) of the local subunit observed in physiological experiments. What might the asymmetry be? Among the collection of 29 different types of amacrine cells in the rabbit (MacNeil et al., 1999; MacNeil and Masland, 1998), there is no neuron that immediately suggests itself as possessing the kind of physical asymmetry shown in Figures 28.5 and 28.6. In other words, it seems unlikely that we will some day stumble on a neuron that points, arrow-like, up or down the preferred-null axis.

However, it is not necessary that a neuron be spatially biased in gross physical structure to create the preferred-null asymmetry. The specific case of a starburst cell, which is a radially symmetrical neuron that could nonetheless create direction selectivity, has been discussed above. It is important to note, however, that two different elements are confounded in the starburst model. One is the proximal-to-distal asymmetry in the conduction of electrical activity along the starburst cell's dendrites. The second is the postulate that starburst cells are selectively connected to the DS ganglion cell, such that only dendrites aligned along the preferred-null axis are connected to a specific DS cell (the other starburst dendrites are connected to other DS cells, with different preferred directions).

It is not necessary that an amacrine cell have the proximal to distal asymmetry possessed by the starburst cells for that hypothetical amacrine cell to create direction selectivity. Direction selectivity could be created by postulate two alone. How that could happen is illustrated in Figure 28.9. The drawing shows a DS ganglion cell receiving input from a mosaic of hypothetical inhibitory amacrine cells. The key postulate is only that connection between the inhibitory amacrine and the DS cell be asymmetrical, such that only at the “downstream” side of the amacrine cell's arbor does it synapse on the DS ganglion cell. As postulated by Vaney for the starburst cell, the other dendrites of the amacrine cell would be connected to DS cells with different preferred directions. The illustration is drawn as though the inhibition falls directly on the dendrites of the DS ganglion cell. However, it could just as well fall on a neuron afferent to the ganglion cell; for example, it could represent presynaptic inhibition of the release of glutamate by bipolar cells onto the DS cell or a more complicated circuitry involving several neurons.

The point here is to clearly separate the two different assumptions—asymmetrical dendritic conduction and anisotropic connectivity—that are included in the starburst hypothesis. The reason that this seems worthwhile is that postulate two, shown in Figure 28.9, would allow almost any narrow or medium-field amacrine cell to be the amacrine cell that creates the inhibitory asymmetry that finally results in direction selectivity.

Intradendritic microcircuitry within the inner plexiform layer

In their classic studies of the synaptology of the inner plexiform layer, Dowling and Boycott (1966) described a number of local synaptic interrelations. These include the familiar dyad synapse, in which a bipolar cell synapses on adjacent processes of an amacrine cell and a ganglion cell, with the amacrine cell immediately feeding back onto the bipolar cell. But synapses between amacrine cells and synapses of

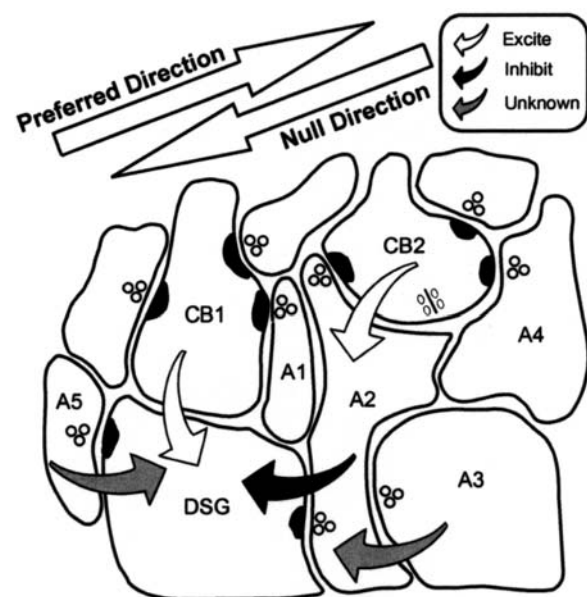


FIGURE 28.10. Local interactions among the dendrites of cone bipolar cells, amacrine cells, and a DS ganglion cell. The ganglion cell was identified by recording; the preferred direction was established, and the cell was injected with HRP for electron microscopic analysis by serial sectioning. Note the complexity of the synaptic interactions, especially the local chains of synapses that can occur over very short distances, here less than 1 μ m for the whole illustration. For example, amacrine cell 4 (A4) synapses on cone bipolar 2 (CB2), which then synapses on A2, which then synapses on a dendrite of the DS ganglion cell. The illustration is taken from Dacheux et al., 2003.

amacrine cells on bipolar cells away from the dyads were also observed, and these arrangements sometimes take complex and baroque forms, an example of which is the observation of chains of synapses among several (3 to 4) amacrine cells (Marc and Liu, 2000).

Recently, Dacheux and colleagues have been carrying out a study of the synapses afferent to an ON-OFF DS ganglion cell using serial section electron microscopy (Dacheux et al., 2003). The cell was recorded; its preferred direction was noted; it was then injected with HRP and processed for electron microscopy. A number of synaptic regularities were observed. Their interpretation will doubtless take some time and may require further serial sectioning to identify the cells of origin of the processes. Even at this stage, though, it is plain that major complexities exist on the synaptic scale of local microcircuitry.

A summary diagram of one such arrangement is shown in Figure 28.10. The preferred and null directions are indicated, as are the dendrite of a DS ganglion cell, two axon terminals of cone bipolars, and several amacrine cells. Note the chain of synapses in which A3 synapses on A2, and A2, which receives an additional input from a cone bipolar axon terminal, then synapses on the dendrite of the DS ganglion cell. Such chain synapses were very common, sometimes

directly involving the dendrite of the DS ganglion cell, and sometimes among the fascicle of processes that surround it. Many of the surrounding processes appear to belong to starburst amacrine cells, which are known to cofasciculate with the dendrites of the DS ganglion cells. However, there are also processes in these fascicles of unknown origin. Figure 28.10 reminds us that another level of neuronal interrelationship exists, on a spatial scale an order of magnitude smaller than the one usually discussed.

Acknowledgments

I thank Steven Stasheff and Chuan-Chin Chiao for comments on the manuscript, Rebecca Rockhill for making the figures, and Lyle Graham for discussions of the symmetry requirement (Fig. 28.9). RHM is a Senior Investigator of Research to Prevent Blindness.

REFERENCES

- Amthor, F. R., N. M. Grzywacz, and D. K. Merwine, 1996. Extra-receptive-field motion facilitation in ON-OFF directionally selective ganglion cells of the rabbit retina, *Vis. Neurosci.*, 13:303–309.
- Amthor, F. R., C. W. Oyster, and E. S. Takahashi, 1984. Morphology of ON-OFF direction-selective ganglion cells in the rabbit retina, *Brain Res.*, 298:187–190.
- Ariel, M., and N. W. Daw, 1982a. Pharmacological analysis of directionally selective rabbit retinal ganglion cells, *J. Physiol. (Lond.)*, 324:161–185.
- Ariel, M., and N. W. Daw, 1982b. Effects of cholinergic drugs on receptive field properties of rabbit retinal ganglion cells, *J. Physiol. (Lond.)*, 324:135–160.
- Barlow, H. B., R. M. Hill, and W. R. Levick, 1964. Retinal ganglion cells responding selectively to direction and speed of image motion in the rabbit, *J. Physiol. (Lond.)*, 173:377–407.
- Barlow, H. B., and W. R. Levick, 1965. The mechanism of directionally selective units in rabbit's retina, *J. Physiol. (Lond.)*, 178:477–504.
- Borg-Graham, L. J., 2001. The computation of directional selectivity in the retina occurs presynaptic to the ganglion cell, *Nat. Neurosci.*, 4:176–183.
- Borg-Graham, L. J., and N. M. Grzywacz, 1992. A model of the directional selectivity circuit in retina: transformations by neurons singly and in concert, in *Single Neuron Computation* (T. McKenna, J. Davis, and S. F. Zornetzer, eds.), New York: Academic Press, pp. 347–376.
- Borst, A., and M. Egelhaaf, 1990. Direction selectivity of blowfly motion-sensitive neurons is computed in a two-stage process, *Proc. Natl. Acad. Sci. USA*, 87:9363–9367.
- Brecha, N., D. Johnson, L. Peichl, and H. Wässle, 1988. Cholinergic amacrine cells of the rabbit retina contain glutamate decarboxylase and gamma-aminobutyrate immunoreactivity, *Proc. Natl. Acad. Sci. USA*, 85:6187–6191.
- Caldwell, J. H., N. W. Daw, and H. J. Wyatt, 1978. Effects of picrotoxin and strychnine on rabbit retinal ganglion cells: lateral interactions for cells with more complex receptive fields, *J. Physiol. (Lond.)*, 276:277–298.
- Chiao, C.-C., and R. H. Masland, 2002. Starburst cells non-directionally facilitate the responses of direction selective ganglion cells, *J. Neurosci.*, 22:10509–10513.
- Dacheux, R., M. F. Chimento, and F. R. Amthor, 2003. Synaptic input to the ON-OFF directionally selective ganglion cell in rabbit retina, *J. Comp. Neurol.*, 456:267–278.
- Dowling, J. E., and B. B. Boycott, 1966. Organization of the primate retina: Electron microscopy, *Proc. R. Soc. Lond. [Biol.]*, 166:80–111.
- Euler, T., P. B. Detwiler, and W. Denk, 2002. Direction-selective calcium signals in dendrites of starburst amacrine cells, *Nature*, 418:845–852.
- Famiglietti, E. V., Jr., 1983. Starburst amacrine cells and cholinergic neurons: mirror-symmetric ON and OFF amacrine cells of rabbit retina, *Brain Res.*, 261:138–144.
- Famiglietti, E. V., Jr., 1991. Synaptic organization of starburst amacrine cells in rabbit retina: analysis of serial thin sections by electron microscopy and graphic reconstruction, *J. Comp. Neurol.*, 309:40–70.
- Famiglietti, E. V., 1992. Dendritic co-stratification of ON and ON-OFF directionally selective ganglion cells with starburst amacrine cells in rabbit retina, *J. Comp. Neurol.*, 324:322–335.
- Hayden, S. A., J. W. Mills, and R. H. Masland, 1980. Acetylcholine synthesis by displaced amacrine cells, *Science*, 210:435–437.
- He, S.-G., Z. F. Jin, and R. H. Masland, 1999. The non-discriminating zone of directionally selective retinal ganglion cells: comparison with dendritic structure and implication for mechanism, *J. Neurosci.*, 19:8049–8056.
- He, S.-G., and R. H. Masland, 1997. Retinal direction selectivity after targeted laser ablation of starburst amacrine cells, *Nature*, 389:378–382.
- Jeon, C.-J., J.-H. Kong, E. Strettoi, R. L. Rockhill, S. F. Stasheff, and R. H. Masland, 2002. The pattern of synaptic excitation and inhibition upon direction selective retinal ganglion cells, *J. Comp. Neurol.*, 449:195–205.
- Keyser, K. T., M. A. MacNeil, N. Dmitrieva, F. Wang, and R. H. Masland, 2000. Amacrine, ganglion, and displaced amacrine cells in the rabbit retina express nicotinic acetylcholine receptors, *Vis. Neurosci.*, 17:743–752.
- Kittila, C. A., and S. C. Massey, 1995. Effect of ON pathway blockade on directional selectivity in the rabbit retina, *J. Neurophysiol.*, 73:703–712.
- Kittila, C. A., and S. C. Massey, 1997. The pharmacology of directionally selective ganglion cells in the rabbit retina, *J. Neurophysiol.*, 77:675–689.
- MacNeil, M. A., J. K. Heussy, R. Dacheux, E. Raviola, and R. H. Masland, 1999. The shapes and numbers of amacrine cells: matching of photofilled with Golgi-stained cells in the rabbit retina and comparison with other mammalian species, *J. Comp. Neurol.*, 413:305–326.
- MacNeil, M. A., and R. H. Masland, 1998. Extreme diversity among amacrine cells: Implications for function, *Neuron*, 20:971–982.
- Marc, R. E., and W.-L. S. Liu, 2000. Fundamental GABAergic amacrine cell circuitries in the retina: nested feedback, concatenated inhibition, and axosomatic synapses, *J. Comp. Neurol.*, 425:560–582.
- Marchiafava, P. L., 1979. The responses of retinal ganglion cells to stationary and moving visual stimuli, *Vis. Res.*, 19:1203–1211.
- Masland, R. H., and A. Ames, III, 1976. Responses to acetylcholine of ganglion cells in an isolated mammalian retina, *J. Neurophysiol.*, 39:1220–1235.

- Masland, R. H., and J. W. Mills, 1979. Autoradiographic identification of acetylcholine in the rabbit retina, *J. Cell Biol.*, 83:159–178.
- Masland, R. H., J. W. Mills, and C. Cassidy, 1984a. The functions of acetylcholine in the rabbit retina, *Proc. R. Soc. Lond. [Biol.]*, 223:121–139.
- Masland, R. H., J. W. Mills, and S. A. Hayden, 1984b. Acetylcholine-synthesizing amacrine cells: identification and selective staining by using autoradiography and fluorescent markers, *Proc. R. Soc. Lond. [Biol.]*, 223:79–100.
- O'Malley, D. M., J. H. Sandell, and R. H. Masland, 1992. Co-release of acetylcholine and GABA by the starburst amacrine cells, *J. Neurosci.*, 12:1394–1408.
- Oyster, C. W., F. R. Amthor, and E. S. Takahashi, 1993. Dendritic architecture of ON-OFF direction-selective ganglion cells in the rabbit retina, *Vis. Res.*, 33:579–608.
- Peters, B. N., and R. H. Masland, 1996. Responses to light of starburst amacrine cells, *J. Neurophysiol.*, 75:469–480.
- Reichardt, W., 1961. Autocorrelation, a principle for the evaluation of sensory information by the central nervous system, in *Sensory Communication* (W. A. Rosenblith, ed.), Cambridge, MA: MIT Press, pp. 303–317.
- Stasheff, S. F., and R. H. Masland, 2002. Functional inhibition in direction-selective retinal ganglion cells: spatiotemporal extent and intralaminar interactions, *J. Neurophysiol.*, 88:1026–1039.
- Sun, W., N. Li, and S. He, 2002. Large-scale morphological survey of mouse retinal ganglion cells, *J. Comp. Neurol.*, 451:115–126.
- Tauchi, M., and R. H. Masland, 1984. The shape and arrangement of the cholinergic neurons in the rabbit retina, *Proc. R. Soc. Lond. [Biol.]*, 223:101–119.
- Taylor, W. R., S. He, W. R. Levick, and D. I. Vaney, 2000. Dendritic computation of direction selectivity by retinal ganglion cells, *Science*, 289:2350.
- Taylor, W. R., and H. Wässle, 1995. Receptive field properties of starburst cholinergic amacrine cells in the rabbit retina, *Eur. J. Neurosci.*, 7:2308–2321.
- Vaney, D. I., 1984. Coronate amacrine cells in the rabbit retina have the starburst dendritic morphology, *Proc. R. Soc. Lond. [Biol.]*, 220:501–508.
- Vaney, D. I., 1991. The mosaic of amacrine cells in the mammalian retina, *Prog. Ret. Res.*, 9:49–100.
- Vaney, D. I., S. P. Collin, and H. M. Young, 1989. Dendritic relationships between cholinergic amacrine cells and directionally-selective retinal ganglion cells, in *Neurobiology of the Inner Retina* (R. Weiler and N. N. Osborne, eds.), Berlin: Springer Verlag, pp. 157–168.
- Vaney, D. I., S.-G. He, R. Taylor, and W. R. Levick, 1999. Direction-selective ganglion cells in the retina, in *Processing Visual Motion in the Real World* (J. Zanker and J. Zeil, eds.), Berlin: Springer Verlag, pp. 1–47.
- Vaney, D. I., L. Peichl, and B. B. Boycott, 1981. Matching populations of amacrine cells in the inner nuclear and ganglion cell layers of the rabbit retina, *J. Comp. Neurol.*, 199:373–391.
- Vaney, D. I., and H. M. Young, 1988. GABA-like immunoreactivity in cholinergic amacrine cells of the rabbit retina, *Brain Res.*, 438:369–373.
- Wyatt, H. J., and N. W. Daw, 1975. Directionally sensitive ganglion cells in the rabbit retina: specificity for stimulus direction, size and speed, *J. Neurophysiol.*, 38:613–626.
- Yang, G., and R. H. Masland, 1994. Receptive fields and dendritic structure of directionally selective retinal ganglion cells, *J. Neurosci.*, 14:5267–5280.
- Yoshida, K., D. Watanabe, H. Ishikane, M. Tachibana, I. Pastan, and S. Nakanishi, 2001. A key role of starburst amacrine cells in originating retinal directional selectivity and optokinetic eye movement, *Neuron*, 30:771–780.

29 Spatial Regularity among Retinal Neurons

JEREMY E. COOK

Patterns and Tiles

In this chapter, we “zoom out” from the study of individual retinal neurons and circuits to a consideration of how these individuals are organized across the retinal surface. In particular, we focus on an almost universal tendency for these neurons to lie in regular patterns. Although regularity can be a consequence of uniform size and tight packing, it also occurs among neurons that are widely spaced. In either case, it fulfills a behavioral requirement that each class of functional circuits should sample the visual scene systematically and completely, so that vital features (such as prey and predators) do not go undetected.

Regular arrays of retinal neurons often extend dendrites in a competitive, territorial manner that minimizes the overlap of their dendritic fields and causes them to tessellate, “tiling” the retina like the individual pieces (Latin: *tesserae*) of a ceramic mosaic. By convention, regular arrays of neuronal somata are often called *neuronal mosaics* even if precise dendritic tiling has not been shown directly, and the term *mosaic* is used in this sense throughout the chapter. It is important to be aware that geneticists and developmental biologists exploit the analogy of the tiled mosaic in another way, using it to describe mixtures or clusters of cells with distinct histories or genotypes and emphasizing the potential for abrupt contrasts at the boundaries of adjacent tesserae; these two senses of *mosaic* may confront each other uneasily in studies of retinal developmental genetics.

Neuronal mosaics are informative in many different ways. The following sections briefly review their implications for the function of the mature retina and the elucidation of its many neuronal types, consider what they can tell us about retinal development and evolution, summarize the methods used for their quantitation, and look ahead to questions that remain.

Retinal mosaics and visual function

The retina is organized in a way that allows each part of the image to be analyzed by many local circuits, working in parallel to assess different aspects of brightness, contrast, color, and movement. These analyses demand different degrees of spatial resolution, so neurons with different functions are repeated across the retina at different intervals. Neurons that

report fine detail are always small and closely spaced, whereas neurons that report movement or the widespread changes in luminosity that may herald a predator are often large and broadly spaced. In general, the spacings of overlapping circuits with distinct functions vary independently, and their mosaics are also spatially independent, so the retina as a whole cannot be accurately described as modular even though there are modular aspects to its function and to its development (Reichenbach and Robinson, 1995; Rockhill et al., 2000). In this respect the retina resembles the visual cortex, where functional maps are also overlaid in a flexible way that is repetitive but not strictly modular (Swindale, 1998).

The significance of the density and geometry of the sampling array is discussed in detail in Chapter 50. Here, we note only that the considerable contrasts of interval and scale between the functional types are made more extreme by regional variations in species that have a visual streak, area centralis, macula, or fovea. Neurons may conserve their branching patterns during retinal growth, but they cannot grow uniformly in all dimensions (allometrically) because growth that maintained a linear scaling relationship between dendritic diameter and length would change their physiological properties (Bloomfield and Hitchcock, 1991). Thus, functionally homologous neurons may look very different in different regions of the same eye and in eyes of differing size even before genuine interspecies variation is taken into account (Fig. 29.1).

Given this complex, multiparametric relationship between neuronal spacing and visual function, there are two distinct ways in which studying the spatial regularities of neurons can help us understand how the retina does its job. One is by helping us to decide how much spatial resolution a particular analytical function demands in a particular retinal region of a particular species at a particular stage in its growth. Simple cell counts can give us partial answers to such questions, but neuronal arrays give higher resolutions when they are regular than when they are not, and some techniques for measuring spatial regularity have the potential to provide more accurate density estimates than simple counting alone. The other, and perhaps more interesting, way is by helping us to draw up a catalogue of the different neuronal types in the retina and their functional roles, which is the subject of the next section.

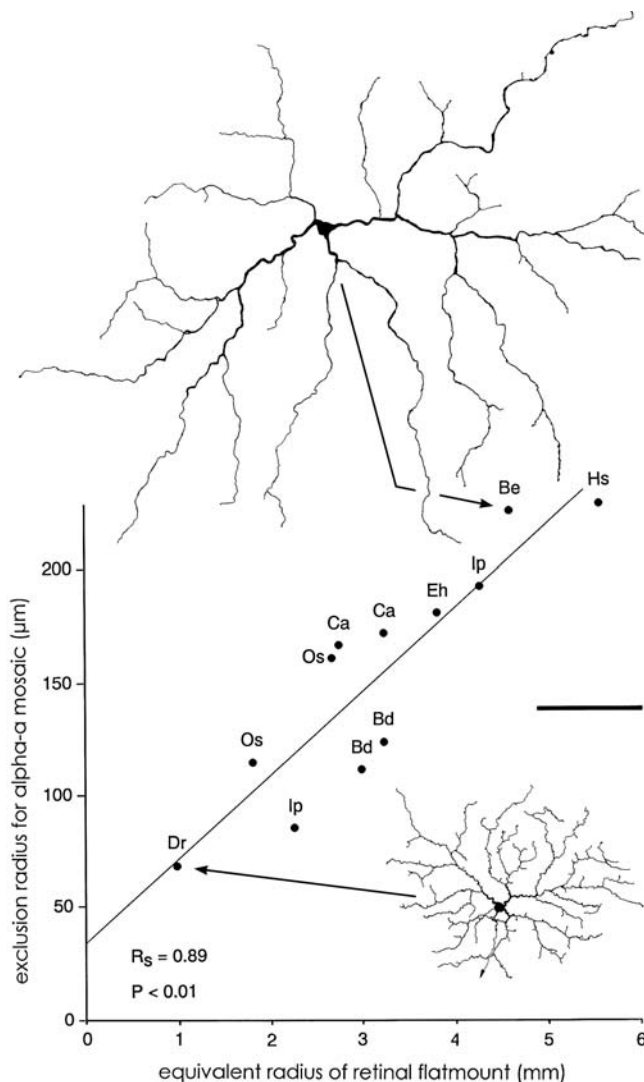


FIGURE 29.1. Variation of mosaic spacing and scale across species. The graph shows how the spacing of the alpha-ganglion cell mosaic varies with eye size (represented as retinal radius) in eight species of teleost fish, four of them at more than one stage of growth. The small alpha-ganglion cell is from an adult zebrafish *Danio rerio* (marked *Dr* on the graph); the large one is from the sculpin *Bero elegans* (*Be*), to the same scale. Bar = 100 μm . For further details, see Cook (1998). © 1998 Plenum Publishing Corporation. Reprinted by permission.

What retinal mosaics tell us about neuronal types

It is hard to discover anything interesting by pooling data from heterogeneous neuronal populations, so a thoughtful neuroscientist must put a high value on understanding the diversity of functionally distinct neuronal types in the system under scrutiny. In the retina, mosaics have contributed greatly to this, not only practically, but also by helping to clarify the very concept of a neuronal type. This is a surprisingly slippery concept to grasp. At one extreme, neurons vary in so many details that (as with snowflakes) one can

argue that no two individuals are ever identical. At the other extreme, the retina is viewed simplistically by some as containing only five basic kinds of neuron (photoreceptors, horizontal cells, bipolar cells, amacrine/interplexiform cells, and ganglion cells). The term *class* can usefully be applied to these most basic divisions; however, within each class, neurons can be further divided into subclasses, types, subtypes, or variants, although there is no consensus yet on the terminology for such a hierarchy (Cook, 1998). Vaney and Hughes (1990) estimated that there could be as many as 70 functionally distinct neuronal types in a given retina, and subsequent studies have already confirmed an inventory of about 55 morphologically distinct neuronal types in mammals (Masland, 2001).

BETWEEN-TYPE AND WITHIN-TYPE VARIATION In attempting to get a grip on neuronal diversity, it is vital to find ways of distinguishing between two radically different forms of variation that neurons—indeed all cells in complex organisms—display. One is the categorical, hierarchical kind that is assumed to underlie cell-fate decisions during development, where transcriptional mechanisms force cells to choose between predefined pathways and positive feedback loops drive those choices to completion. Rowe and Stone (1980) described this, the kind of variation that distinguishes a cone from a ganglion cell or a red-sensitive cone from a blue-sensitive cone, as “between-type” variation. The other kind is the continuous variation of size, shape, and functional properties that we see in the phenotypes of all living things, which Rowe and Stone (1980) termed “within-type” variation. Much of this may be stochastic and inherently unpredictable, but some is correlated with external factors that have predictive power. A classic example is the correlation between the sizes of alpha and beta ganglion cells and their retinal eccentricities in the cat, which first allowed Boycott and Wässle (1974) to distinguish the two populations even though the largest (most peripheral) beta cells overlap in size with the smallest (most central) alpha cells.

In these terms, the task of identifying neuronal types equates to the task of working out which aspects of neuronal diversity are between-type variation and which are within-type variation. At first sight, this redefinition may seem unhelpful, even pedantic, because at the level of individual neurons a distinction may simply not be available. When we measure a character such as cell size across a mixed population, we often find that the overall distribution is unimodal even though the averages for the component types may be distinct. Unless a major source of within-type variation can be factored out (as for the cat ganglion cells just described), it is impossible to assign an individual neuron to a type on this basis, even provisionally. Rodieck and Brening (1983) argued that the problem could be tackled only by examin-

ing many variables at once. In their view, variables of shape, stratification, receptive field, conduction velocity, transmitter content, projection target, and so forth should be viewed as defining a multidimensional virtual space within which every objectively defined neuronal type (natural type) would be represented as a discrete cluster of points, separable in at least one dimension from every other cluster. Their argument was helpful in clarifying the problem, and their approach to solving it remains the ideal approach, but it is so labor intensive that practical applications are rare (for an exception, see Kock et al., 1989).

This is where mosaics show their value. The more we can discover about the within-type variation in a population of neurons, the easier it becomes to isolate between-type differences. The discovery of a regular array of neurons with complete retinal coverage gives us access to a presumptive “natural” type laid out for inspection (Fig. 29.2A). Presented with such an array, we can hypothesize that the variation we see among its members is within-type variation. Then, by noting which features show the most within-type variation over the population, we can avoid relying on these features when attempting to assign individual neurons to specific types.

MOSAICS AS GUIDES TO WITHIN-TYPE VARIATION The first observations of mosaics were made serendipitously, when particular populations drew attention to themselves by having an unusual reaction to staining and/or being in an unusual retinal plane (Stell and Witkovsky, 1973; Wässle and Riemann, 1978). Observers had little difficulty in deciding which neurons belonged to the mosaics they described because the property that drew their attention, often combined with clear evidence of dendritic tessellation, left the issue in no doubt. The concept of a natural type was implicit in the very existence of such a mosaic.

Studies of these self-evident mosaics have led to some valuable and durable conclusions. One, as we have seen, is that absolute soma size is poorly correlated with neuronal type. A second is that patterns of *dendritic* stratification tend to be strongly conserved within a mosaic-forming neuronal type, to the extent that otherwise similar neurons with distinct stratification patterns almost always form spatially independent mosaics (Cook, 1998). A third conclusion, refuting earlier assumptions, is that *somatic* stratification is only weakly correlated with neuronal type. Individual cells sometimes have their somata “misplaced” into the wrong layer even though they meet other criteria for membership of a type and their dendrites tessellate with those of their neighbors (Fig. 29.2B). These “misplaced” cells can even include cells that belong to so-called displaced types but are not actually displaced (amacrine cells: Wässle et al., 1987; ganglion cells: Cook and Noden, 1998). Indeed, in some cases there is no right or wrong layer for the somata of a

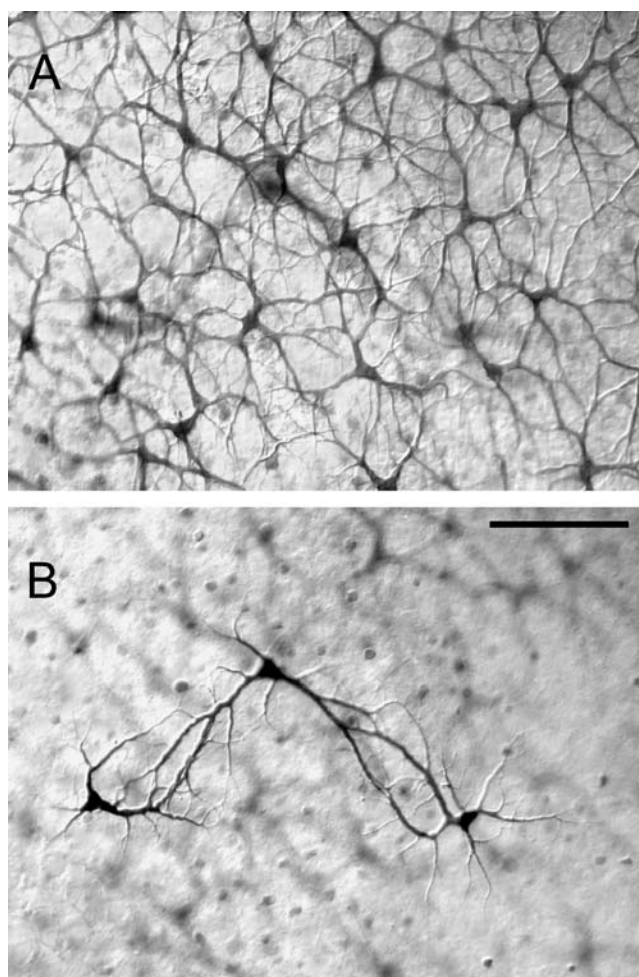


FIGURE 29.2. Sporadic variation within a mosaic-forming neuronal type. These A-type horizontal cells in a cat retina have been immunostained for calbindin. Most of them (A) lie at the border of the outer plexiform and inner nuclear layers, but others (B) are misplaced into the ganglion cell layer, where in different circumstances they could be mistaken for biplexiform ganglion cells. Bar = 100 μ m. For further details, see Wässle et al. (2000). Unpublished photographs reproduced by kind permission of Prof. Heinz Wässle.

mosaic-forming population, and they appear to be arbitrarily distributed in depth (Fig. 29.3). These conclusions exposed serious flaws in traditional morphological classification schemes for retinal neurons.

A further interesting conclusion was reached by blending in some later observations. Chalupa and his colleagues (White and Chalupa, 1991) found that the alpha ganglion cell mosaics of the cat (both outer and inner stratified) contained a subset of cells with somatostatin-like immunoreactivity, confined largely to the inferior (ventral) half of the retina and absent from the region where the density of alpha cells peaks. It has been widely assumed that a neuron's expression of neurotransmitter or neuromodulator genes directly reflects its function, with the result that transmitter

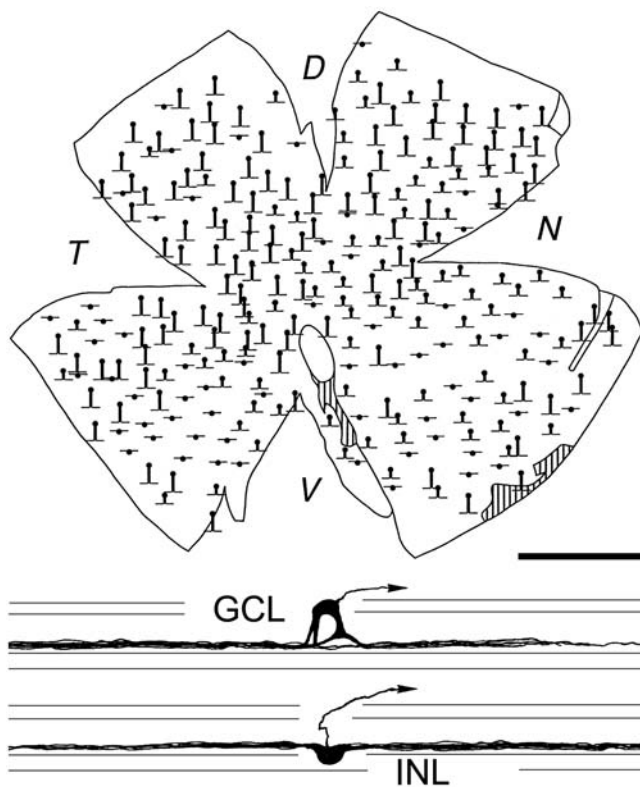


FIGURE 29.3. Continuous variation within a mosaic-forming neuronal type. Two partially overlapping, alpha-a (outer-stratified) ganglion cells from the cichlid fish *Oreochromis spilurus* are seen in profile below; one with its soma in the ganglion cell layer (GCL) and one with its soma in the inner nuclear layer (INL). The complete mosaic is shown above, with iconic symbols representing different degrees of soma displacement. The somatic part of each symbol marks the actual location. The mosaic is highly regular but the distribution of soma depths is arbitrary and sporadic. Bar = 1 mm for retina; 100 μ m for cell profiles. I, D, N, and V show the temporal, dorsal, nasal, and ventral poles of the retina. For further details, see Cook and Becker (1991). © 1991 Wiley-Liss, Inc. Reprinted by permission.

content has often been used as the basis for an arbitrary classification. However, in these studies of a uniform population, the archetypal mosaic of the mammalian inner retina, this neurochemical marker picked out some individuals and not others. Although highly reproducible anomalies are known to occur within some natural types (Masland et al., 1993), and there may be scope for genuine functional differences among mosaic members (Cook, 1998), this example demonstrates that neurochemical phenotypes are no more intrinsically reliable than morphological phenotypes as guides to neuronal taxonomy. It has long been understood in fields outside neuroscience that gene expression can sometimes be nonfunctional; that eukaryotic cells must often tolerate uncontrolled expression because of constraints imposed by combinatorial gene regulation. Bowers (1994) has summarized the evidence for neuroscientists, and all authors (and reviewers) of papers in which neurochemical observations

are taken as evidence of neuronal types should read that summary.

EXPOSING HIDDEN MOSAICS AND TYPES In the outer retina, I have already noted that the high regularity of neuronal mosaics may sometimes allow the identity of a neuron to be confirmed directly by its position. In the less regular world of the inner retina, there is no possibility of this direct approach, but mosaics can help with neuronal identification in less direct ways.

For example, in a preparation where most of the relevant neurons are visible, one can learn much about the type-specific characteristics of an unfamiliar mixed set of neurons merely by attempting to assign them to mosaics. The trick is to start by defining arbitrary cell-type criteria that are based on all the observable differences between neurons that make up clusters or clumps. Clustered neurons with overlapping dendrites are likely to belong to different mosaics, so any features that consistently distinguish between cluster members are prime candidates for between-type variation. These provisional cell-type criteria may need to be adjusted arbitrarily, by trial and error, until a regular, self-consistent set of mosaics emerges. However, their objectivity can then be established by testing the same criteria on new specimens. It was this iterative approach that made it possible to understand an atypical and confusing set of large retinal ganglion cell types in a tree frog (Shamim et al., 1999).

Even by such methods, not all functionally distinct types can be distinguished directly by shape or size. Direction-selective ganglion cells provide good examples of such types and of other ways to expose their hidden order. In the rabbit retina, bistratified ON-OFF direction-selective ganglion cells occur at a much higher spatial density than would seem necessary for uniform retinal coverage; they also appear to be randomly distributed. Their high coverage is explained by the fact that they actually comprise distinct functional types with different preferred directions of motion, overlaid as a polymosaic of overlapping arrays. Even when the distinct types are functionally identified and compared, they remain morphologically indistinguishable. In this case, the key to visualizing them is the intracellular injection of a tracer that passes through gap junctions, selectively coupling cells of the same type. Tracer-coupling shows that they do in fact form regular, independent, beautifully tessellated mosaics (Amthor and Oyster, 1995; Vaney, 1994a). This technique is also useful for revealing the detailed mosaic organization of types that are already morphologically distinguishable (Ammermüller et al., 1993) and for revealing gap-junctional connections between the separate mosaics of different neuronal types (review: Mills, 1999; Vaney, 1994b; Xin and Bloomfield, 1997).

A separate category of direction-selective ganglion cells, again comprising distinct types with different preferred

directions of motion, projects to the accessory optic system. As before, these cells appear almost random in their arrangement when taken together. However, spatial correlogram analysis has been applied to distribution data from a frog, a reptile, a bird, and a mammal to show that these evolutionarily conserved cells possess exactly the kind of cryptic order that is predicted for a polymosaic of overlaid arrays (Cook and Podugolnikova, 2001). Because these apparent exceptions have both turned out to prove the rule, it seems likely that all neurons that integrate signals across their dendritic fields (rather than processing them only locally within the dendrites) may form regular mosaics (DeVries and Baylor, 1997; Rockhill et al., 2000). This being so, the combination of high coverage with low apparent regularity should always trigger a search for hidden mosaics and multiple functional types.

What retinal mosaics tell us about development

Studies of spatial regularity have provided many insights into retinal development. However, our present state of knowledge, accumulated piecemeal from studies of several model systems, fails to point to a unifying mechanism that could underlie all mosaic patterns. On the contrary, there seem to be three separate ways in which mosaics can be established in the retina, with evidence that they may act in combination, in different developmental contexts.

INDUCTIVE INTERACTIONS AND MOLECULAR MARKERS The interlaced and often highly regular mosaics of retinal photoreceptors are obvious targets for developmental studies. In fish in particular, the cone mosaic is often geometrically exact and consists of regularly repeated modules (Engström, 1963), which has led to speculative comparisons with the near-crystalline patterning of the compound eyes of insects. In the eye of a fly, cell fate is known to be determined by a cascade of inductive interactions, mostly between immediate neighbors. The first photoreceptors of the fly (R8 cells) are formed by a multistep process of lateral inhibition within an initially featureless bed of dividing cells and act as reference points for the construction of each ommatidial facet of the eye. This process spreads across the eye in a visible traveling wave, the morphogenetic furrow, which marks a progression of inductive and responsive competence in which the signaling protein Hedgehog plays an important self-regulating role and each cohort of differentiating cells acts as a spatial template for the next (for a summary of the molecular interactions, see Baonza et al., 2001). A traveling wave may be needed to allow a globally coherent pattern to emerge from interactions that involve only immediate neighbors; indeed, when different eye regions in a mutant fly start the process independently, pattern coherence is lost (Heberlein and Moses, 1995).

In the retinas of vertebrates, built to an entirely different structural plan, there is no known equivalent to the morphogenetic furrow. Nevertheless, some of the primary inductive mechanisms are known to have been conserved, and a self-regulating traveling wave of expression of the orthologous gene *Sonic hedgehog* has recently been shown to sweep through the zebrafish retina in the first differentiated neurons, the retinal ganglion cells (Neumann and Nüsslein-Volhard, 2000).

In the fish retina, the earliest regular patterns that can be seen by conventional histology comprise either regular rows of morphologically identical single cones or alternating rows of double and single cones (Fig. 29.4), and in some species these rows are eventually transformed into a modular square mosaic (Engström, 1963; Shand et al., 1999). As morphological distinctions between the photoreceptor types are slow to develop, studies of their earliest relationships require them to be identified in another way, usually by their content of photopigment (opsin) mRNA. Raymond and colleagues have shown that the first opsin to be expressed in the embryonic eyecup of the goldfish is distributed in a predictable pattern, beginning at the nasal margin of the ventral fissure and spreading around the retina in a circular or spiral path. The cells producing this first opsin sometimes form regular rows at the leading edge of the wave (Raymond et al., 1995; Stenkamp et al., 1996). Further, in the zebrafish, an additional wave of *Sonic hedgehog* expression precedes this wave of photoreceptor differentiation and seems to be necessary for it (Stenkamp et al., 2000). The potential parallels with the fly's eye are clear, but it is not yet possible to say whether the fish has a direct equivalent to the fly's prepatterned array of R8 cells, defining modules in the cone mosaic. One reason is that this first opsin is actually found in rod photoreceptors, which are *not* regularly patterned in the adult retina and *not* required for the formation of a normal cone mosaic (Wan and Stenkamp, 2000). Another reason is that we still know very little about the long period of cone differentiation that precedes the expression of cone opsins and next to nothing about the initial spatial relationships of the cells that will develop into the different cone types over this long period (Cook and Chalupa, 2000). However, studies of retinal regeneration after physical wounding or chemical lesioning show that the densest regenerated populations, where opportunities for inductive interaction are greatest, are also typically the most orderly (Stenkamp et al., 2001), so we may speculate that local relationships are important.

Computer-modeling studies (Tohya et al., 1999) confirm that regular mosaics of four different cell types can emerge from cellular-automaton rules of differentiation that involve purely local interactions and are applied to initially random arrangements. Different rules converge on the same simple patterns, precisely matching those observed in real fish, and these rules operate most efficiently when they act at an

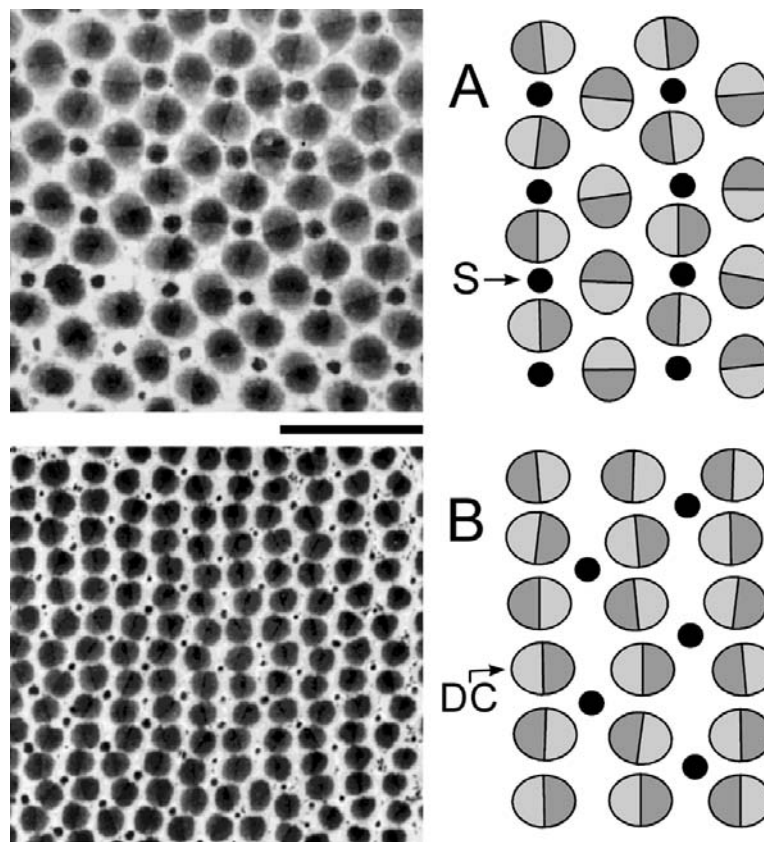


FIGURE 29.4. Quasi-crystalline cone lattice patterns in salmonid fish. Tangential sections through the cone ellipsoids show a typical square mosaic without corner cones (*A*) and a row mosaic (*B*). Where both forms coexist within one retina, the row pattern occupies younger, more peripheral regions. DC = double cone; S = single cone. Bar = 50 μ m for microphotographs. For further details, see Beaudet et al. (1997). © 1997 Wiley-Liss, Inc. Reprinted by permission.

advancing wavefront (such as the fly's furrow or the marginal zone of a growing fish retina) rather than across a large area at once. Whether the biological interactions that underlie the formation of real cone mosaics will turn out to be anything like the assumptions of such models remains to be seen. However, the approach is adaptable: a more recent alternative model is able to create appropriate patterns based on the assumption that the cone mosaics arise by secondary cell rearrangements among predetermined cone types that differ in their adhesion properties (Mochizuki, 2002).

Mammals also have cone mosaics, and those of Old World monkeys such as the macaque have been studied intensively. However, tools for probing opsins are not as precise in mammals as in fish, and the individual cone mosaics are not as precise either (Engström, 1963; Roorda and Williams, 1999). Blue-sensitive cones, which comprise about 10% of the cone population and form regular mosaics in macaques and humans, are present in all mammalian orders (although not all species) but do not always form regular mosaics (see Chapter 50). Red- and green-sensitive cones are derived from an ancestral type that seems not to form a regular mosaic in any placental mammal (Ahnelt and

Kolb, 2000), and recent spectrophotometric studies show that they are intermingled in the human fovea as irregular clumps and clusters (Roorda and Williams, 1999). Other investigations into the origins of mammalian cone patterning were summarized by Cook and Chalupa (2000).

LATERAL MOVEMENTS OF DEVELOPING NEURONS A second way to generate a regular mosaic would be to create a random array of fate-determined neuroblasts and then move them to regularize the spacing of each distinct type. Rockhill and colleagues (2000) noted that such an approach might reduce the aliasing effects that would be expected if successive wavefronts of differentiation laid down overlapping patterns at different scales, and there is now convincing evidence that mosaic-forming neurons do move laterally within the retinal plane during development.

An ingenious method for demonstrating such movements relies on the random and irreversible inactivation of one of the two X-chromosomes in every cell of a female mammalian embryo. This property has been used to generate transgenic mouse embryos whose eyecups contain a pepper-and-salt distribution of multipotential precursor cells, half

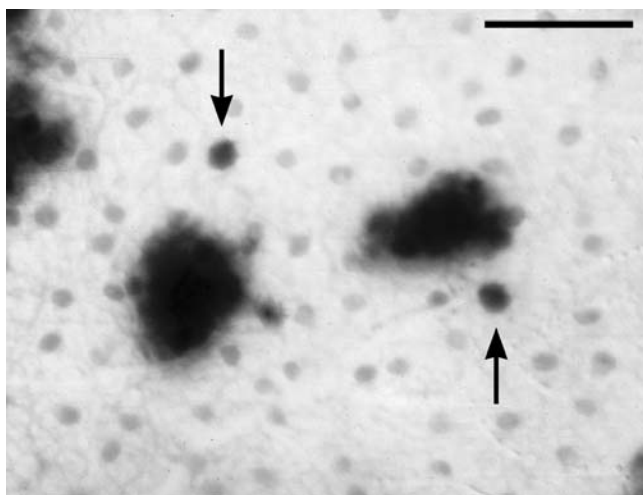


FIGURE 29.5. Evidence for the tangential migration of developing neurons. In this wholemount retina from an adult chimeric mouse, the *dark patches* are columns of lacZ-active cells, derived from a transgenic embryonic stem cell that was injected into the blastocyst. Two individual lacZ-active horizontal cells (*arrows*) have migrated laterally from these columns. They are both immunopositive for calbindin, like the other, lacZ-inactive members of the horizontal cell mosaic. Bar = 50 μ m. For further details, see Reese et al. (1999). © 1999 European Neuroscience Association. Reprinted by permission.

with an active *lacZ* marker gene and half without (Reese et al., 1999). The *lacZ*-active cells go on to generate beta-galactosidase-positive, blue-reacting clones of retinal cells, whereas their neighbors form white, nonreacting clones. Within both white and blue clones, about 85% of all cells maintain strict radial alignment. However, cones, horizontal cells, ganglion cells, and at least one type of amacrine cell, which make up the remaining 15%, are commonly tangentially displaced into clonally unrelated columns (Fig. 29.5)—so commonly, indeed, that it would seem lateral movement is the universal rule. This displacement occurs late, in many cases after birth. Its extent is limited to some 10 or 20 soma diameters, but this could be enough to explain the emergence of mosaics (Reese et al., 1999). Similar evidence of cell dispersal in chick retinas had earlier been interpreted as arising from the migration of precursors, rather than differentiated neurons (Fekete et al., 1994). The same neuronal types were involved, however, and the same explanation now seems likely to apply (review: Reese and Galli-Resta, 2002).

This evidence that the neurons of all the major mosaic-forming classes move laterally during development does not, of course, prove that their movement establishes their mosaics. In many cases this further logical step is hard to take because there is no way to identify a future member of a particular mosaic until that mosaic is complete. However, the cholinergic amacrine cells of rodents bind antibodies to the transcription factor Islet-1 (Galli-Resta et al., 1997) and

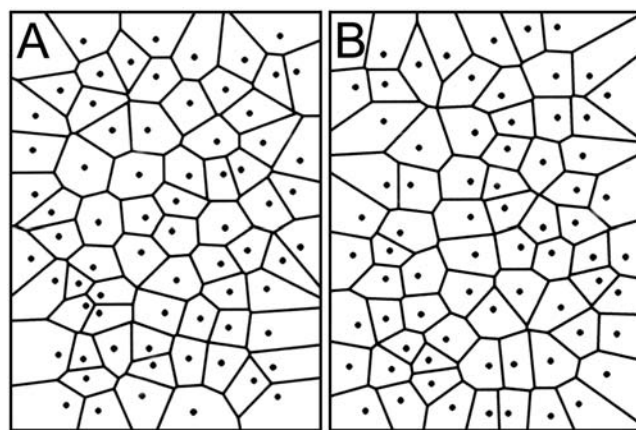


FIGURE 29.6. Minimal-spacing rules as a basis for neuronal mosaic generation. The *dots* in these figures represent young cholinergic amacrine cells in a rat retina during the period of mosaic formation, and the *polygons* represent their Voronoi domains, constructed to include all points that are closer to that dot than to any other. The dots in *A* represent the locations of actual Islet-1-positive amacrine cells in a rectangular sampling region of the inner nuclear layer. The dots in *B* represent the result of a computer simulation in which points were positioned randomly by a probabilistic minimal spacing rule, with the minimal spacing set to $15 \pm 2 \mu\text{m}$ (mean \pm standard deviation). The distributions are indistinguishable, not only to the eye but also to Voronoi and Fast Fourier Transform analysis. For further details see Galli-Resta et al. (1997). © 1997 Society for Neuroscience. Reprinted by permission.

two cholinergic markers (Galli-Resta, 2000) while they are still migrating radially to form two independent mosaics in the inner nuclear layer and the ganglion cell layer. During their migration, they show no spatial order beyond a minimal spacing imposed by their occasional physical contact but by the time they reach the boundary between the inner nuclear layer and the ganglion cell layer, they show a more regular pattern with a minimal spacing several times the soma diameter. Remarkably, their regularity is then maintained throughout a period of 5 days, during which up to 30% more cells of the same type enter each array. To achieve this, existing cells must move sideways to accommodate the newcomers (Galli-Resta et al., 1997).

The mosaics that are seen in this situation can be simulated rather exactly (Fig. 29.6) by a simple computational model in which the only constraint on cell positioning is a probabilistic limit on the minimal spacing between cells (Ammermüller et al., 1993; Galli-Resta, 1998). When neuronal density is relatively high, as it is here (and also in the case of the blue-sensitive cones—but not the rods—of the ground squirrel retina: Galli-Resta et al., 1999), this simple minimal-spacing rule is sufficient to create a fairly regular mosaic. It seems that many, and perhaps all, retinal mosaics may reflect a simple rule of this kind. Whenever spatial autocorrelograms have been computed for inner-retinal neurons,

their dominant feature has always been a central area of low density that represents a zone around each cell from which others of the same type are excluded, and there has been no sign of longer-range order that might suggest a more complex patterning rule. In fact, of all the cell types so far studied in this way, only cones have shown evidence of long-range order (Cook and Noden, 1998; Curcio and Sloan, 1992), and modeling studies show that the particular type of order they possess can be created entirely by short-range interactions (Tohya et al., 1999).

In the case of cones, a minimal spacing is imposed by the requirements of efficient packing, because cone inner segments contact their neighbors directly. It is less clear what might determine the larger minimal spacings of horizontal cells and inner-retinal neurons during development: for example, the minimal spacing of rodent cholinergic amacrine cells is at least three times the soma diameter at this stage (Galli-Resta et al., 1997). A diffusible repulsive or inhibitory signal seems unlikely in this model because the exclusion radius around close pairs of such cells is no greater than that around single cells (Galli-Resta, 2000). An obvious alternative, that such cells might already be in direct contact with their neighbors through transient, fine filopodial processes, is considered below, in the context of dendritic development. Raven and Reese (2003) have shown that a normal complement of cones is not necessary for the formation of the horizontal cell mosaic in mice, so cone afferents do not appear to be required as mediators in the signaling process. Reese and Galli-Resta (2002) provide a more detailed review of many of these issues.

A mechanical, cytoskeleton-mediated basis for mosaic generation is suggested by recent evidence that the precision of some neuronal arrays is reversibly dependent on normal microtubule function (Galli-Resta et al., 2002). One interpretation of this finding is that regularity is directly determined by microtubule-mediated forces between the linked processes of neighboring neurons. However, microtubules have other vital roles, including cytoplasmic transport and the intracellular positioning of the nucleus, so further work is needed to understand this interesting effect.

It is worth noting, in this context, that less is known about the control of nuclear location within dividing or migrating neurons than about practically any other observable aspect of neuronal behavior. Even interkinetic perikaryal translocation in the radial dimension of the retina is poorly understood, despite having been reported more than 30 years ago (see Chapter 6, Development of the Vertebrate Retina). It is actually the position of the nucleus within the complex membranous envelope of a differentiated neuron that determines the regularity of the mosaic as normally measured (see Methods for Measuring Mosaics, below). At present we do not know when, by how much, or by what mechanism a nucleus might move tangentially *within* its neuron in response

to external signals, and we shall not be able to say that we fully understand mosaic development until we do.

EFFECTS OF NEURONAL DEATH ON MOSAIC DEVELOPMENT A third model of mosaic formation involves the selective death of neurons. This is unlikely to be a universal mechanism of mosaic formation because mosaics are a major feature of the retina in all vertebrate groups, whereas in anamniotes the death of differentiated retinal neurons is thought to be rare (Williams and Herrup, 1988). Even so, the massive and widespread increase in programmed cell death within the amniote (and particularly mammalian) radiation must at the very least have disrupted those mosaics that were previously formed by other mechanisms and may have stimulated the emergence of entirely new mosaic-forming mechanisms.

For example, the alpha and beta ganglion cell mosaics of the domestic cat (together forming half of the ganglion cell population) are highly regular in the adult, yet 80% of all ganglion cells die between embryonic day 28 and postnatal week 6 (Williams et al., 1986). How can these observations be reconciled? The most obvious possibility is that programmed cell death, even while it is tending to obliterate any preexisting regularity, might be actively selecting survivors that will form regular arrays. The limited evidence currently available is consistent with such a mechanism (Chalupa et al., 1998). Between postnatal day 12 and adulthood, the overall density of alpha cells in the central region falls by about 20%. Over the same period, the incidence of opposite-sign pairs among nearest-neighbor alpha cells rises from less than 60% (not much higher than when two random populations are overlaid) to about 90% (matching the adult level of regularity). It is not yet known how this rise in opposite-sign pairs is achieved, but postnatal intraocular injection of the sodium-channel blocker tetrodotoxin reduces the regularity of the adult alpha mosaics without increasing their density (Jeyarasasingam et al., 1998). This suggests that electrical activity affects the spatial selectivity of alpha cell death without controlling its extent. Computer simulations confirm that the death of 20% of the original cells could account for the observed increase in regularity, provided that neighbor-pairs of the same sign were selectively targeted and that one from each pair died. However, there are many questions about the role of cell death still to be answered, and it has been shown not to contribute to the regularity of the cholinergic amacrine arrays of the rat (Galli-Resta, 2000).

MOSAICS, COMPETITION, AND THE DEVELOPMENT OF DENDRITIC FIELDS Implicit in the concept of a mosaic is the property of dendritic tessellation, yet we know surprisingly little about how the sizes and shapes of individual dendritic trees are controlled (review: Scott and Luo, 2001). Most studies of dendritic growth have been directed toward ganglion cells. Their patterns of dendritic growth have been

shown to be determined competitively in many experiments involving the elimination of other ganglion cells; their dendritic rearrangement in such circumstances is disrupted by tetrodotoxin and therefore apparently depends on electrical activity (Deplano et al., 1999). However, only a few studies have directly addressed the question of whether dendritic competition is selective between members of a ganglion-cell type, as it must be if it has a role in mosaic formation (Weber et al., 1998). Such a role, while it needs to be confirmed, would be consistent with the observations that ganglion cell types with different receptive-field sizes establish similar levels of functional coverage (DeVries and Baylor, 1997), that coverage is constant across substantial intraretinal gradients of cell density (review: Weber et al., 1998), and that coverage tends to be maintained when cell density is altered by normal or abnormal eye growth (Finlay and Snow, 1998).

Although competitive *dendritic* growth alone cannot account for the regularity of *somatic* mosaics, a recent computational model (Eglen et al., 2000) has shown how cell-type-selective dendritic interactions might provide a controlling mechanism for the lateral migration of somata described above. In this model, differentiated neurons reposition themselves constantly to minimize the overlap between their dendrites. Under some constraints (fixed dendritic field sizes), their distributions have properties that converge with those created by minimal spacing rules, where regularity increases with density up to a packing limit. Under other constraints (adaptive dendritic field sizes), they resemble distributions that have been observed in older retinas, where regularity and density are independent of each other (Eglen et al., 2003).

Models based on dendritic interaction may not seem relevant to the earliest stages of mosaic formation, when neurons lack differentiated dendrites. However, similar interactions may be possible even between immature cells because some immediately postmigratory neurons—for instance, retinal ganglion cells in the chick (Nishimura et al., 1979)—are surrounded by a halo of fine protoplasmic processes that may reach out to more distant neighbors, as do the telodendria of immature S cones (Xiao and Hendrickson, 2000). Such processes also resemble the delicate, hard-to-visualize cytonemes of invertebrates (review: Bryant, 1999), which have been implicated in remote contact-mediated signaling functions. Indeed, they may not differ greatly from the motile filopodia that later cover the dendrites (review: Wong and Wong, 2001). Thus, paradoxically, a model such as that of Eglen and colleagues (2000) might be more relevant to the earliest stages of neuronal differentiation, when most neuronal processes are transient, motile, and unbranched, than to later stages, when a thicket of established dendritic branches must seriously constrain neuronal movement.

In vitro time-lapse imaging techniques have recently revealed much that is new and interesting about the short-term behavior of dendritic filopodia and growth cones and their molecular regulation by extrinsic factors such as neurotransmitters, as well as intrinsic factors such as small GTPases (Wong and Wong, 2001). However, the growth and remodeling of ganglion cell dendrites is a long-term process, not well suited to in vitro study, and the molecular bases of dendritic competition and the cell-type-specific recognition that must underlie it are not yet known, even in outline (Sernagor et al., 2001; see also Chapter 6).

In the fly *Drosophila*, a particular class of segmentally repeated sensory neurons (MD cells) shows type-specific tiling behavior that might more easily be studied directly, in living embryos. The dendritic interactions of MD cells are abnormal in several mutants, disrupting tiling behavior and normal competitive interactions across the midline. The defective gene in at least one of these mutants, *flamingo*, has mammalian homologs and codes for a protocadherin that would appear to be a good candidate for selective cell adhesion (Gao et al., 2000). If MD neurons are as good an experimental model for selective dendritic competition as the initial studies suggest, dendritic tessellation may yet join the large class of vertebrate developmental problems into which significant insights have been gained from invertebrate models.

What retinal mosaics tell us about evolution

We have seen how mosaics help us to develop objective neuronal classifications, which are essential for any useful comparisons between species. In addition, the spatial characteristics of each mosaic (its regularity, density, gradients, coverage) are phenotypic characters in their own right that can be used in identifying cross-species homologies. In these two ways, mosaics help us to understand how neuronal types are interrelated and ultimately how they evolved.

COMPARING NEURONAL TYPES ACROSS SPECIES The notion of a natural type among neurons is closely analogous to the notion of a species among organisms in its implications of self-similarity and isolation, whereas a neuronal class is analogous to a genus. It is disturbing, therefore, that our understanding of most neuronal types remains firmly rooted in an 18th century, Linnaean mode of thought that classifies cells only by morphological and functional similarity, whereas the rest of biology long ago embraced the Darwinian view that it is ancestry, not similarity, that acts as the key to unlock biological meaning. For a full understanding of any part of the brain, we need to see neuronal classifications not only as hypotheses about the boundaries of variation in neuronal structure and function in a single species, but also as hypotheses about the evolutionary relationships between

natural types in different species and the developmental programs that create them (Cook, 1998). Although comparative studies of cone mosaic patterns go back more than half a century (review: Engström, 1963), the scope for a broader evolutionary view can be illustrated by a few of many possible questions to which there are, as yet, no clear answers: Which of the recorded neuronal types in salamander, turtle, cat, and monkey retinas have common ancestors and so are homologous, rather than merely analogous? What developmental mechanisms control the emergence of a new, mosaic-forming, neuronal type and enable it to show self-recognition? Why do mammalian ganglion cell mosaics seem to come in inner- and outer-stratified pairs? The last of these alone is addressed here.

IS THE PAIRED MOSAIC A MAMMALIAN INVENTION? The dominance of mammalian alpha and beta cells in early studies of mosaics, starting with those that first showed the importance of dendritic stratification (review: Wässle and Boycott, 1991), has created a general impression that mosaic-forming neurons are typically organized into pairs of related subtypes that differ only in their stratification and in giving opposite-sign physiological responses to visual stimuli. In fact, such mosaic pairings seem to be unusual among vertebrates as a whole (Cook, 1998), and their predominance in mammals may reflect the emergence of novel, late-acting mechanisms of mosaic formation in response to neuronal death.

However, the paired, monostratified alpha and beta mosaics of the cat are known to be derived from multistratified precursor populations by dendritic remodeling (review: Chalupa et al., 1998). When the definitive adult inner- and outer-stratified mosaics of a pair are overlaid and compared, they show some degree of spatial interdependence (alpha cells: Jeyarasasingam et al., 1998; beta cells: Zhan and Troy, 2000), which is unusual among retinal mosaics in general, even those that are synaptically coupled (Galli-Resta et al., 2000; Rockhill et al., 2000). Thus, it is plausible that some of the order in these paired mosaics is created by a process that encourages neighboring multistratified cells to remodel their dendrites into opposite-sign pairs and that each complementary pair of mosaics may have evolved by the developmental remodeling of a single ancestral mosaic whose neurons remained bistratified or multistratified throughout life. For example, both of the mammalian alpha mosaics might be homologous to a single mosaic of prominently bistratified large ganglion cells (alpha-ab cells: Fig. 29.7) that occurs in fish, frogs, and reptiles (Cook, 1998). To test such hypotheses, we would need either to study the phenotypes of these cells in many more species, especially among reptiles and primitive mammals, or to hack directly into the transcriptional control code that defines each neuronal type and seek homologies at that level. The

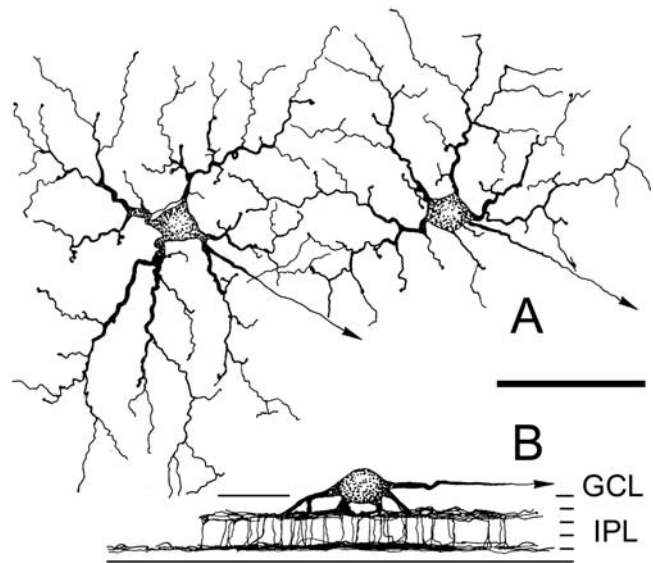


FIGURE 29.7. A bistratified ganglion cell mosaic could be the ancestor of the mammalian alpha mosaics. The two strictly bistratified cells in *A* form part of a highly regular mosaic in a gekkonid lizard. Only their inner trees are shown in plan view here, but the cell on the left is also shown in profile view (*B*). All non-mammalian species studied so far have a single, prominent mosaic of large-bodied ganglion cells that are either bistratified or predominantly inner-stratified. It is likely that these have a mammalian homolog. As mammalian alpha cells are initially multistratified, they are obvious candidates for this role. Bar = 50 μ m. For further details see Cook and Noden (1998). © 1998 S. Karger AG, Basel. Reprinted by permission.

second method should be quicker, once the tools for it become available.

Methods for measuring mosaics

It is the limits of the dendritic field that determine a neuron's excitatory receptive field (see Chapter 26) so, ideally, the quantitation of mosaics would focus on dendrites. However, it is technically challenging to define the individual limits of a large array of partially overlapping dendrites, so mainstream methods of quantitation consider only soma location. The analysis can take several different forms, according to its aims. There is no space here for a detailed discussion of each approach but the references include such discussions.

METHODS BASED ON NEAREST-NEIGHBOR DISTANCE The aim may simply be to establish the objective reality of the mosaic, a step made necessary by the tendency of our own visual systems to perceive pattern in random distributions. The methods first adopted for this task were based on the statistical distribution of the distance from each neuron to its nearest neighbor of the same type (the nearest-neighbor distance, or NND; Wässle and Riemann, 1978). NND-based methods still underlie the most useful general tests of mosaic

significance, but care is needed in interpreting them because some tests overestimate the degree of regularity within a small, irregular or elongated sample (Cook, 1996). The most common, easiest, and most conservative test is based on the *conformity ratio* (mean NND/standard deviation). The sampling distribution of this ratio has now been tabulated for a wide range of sample sizes and shapes so that the significance of an observed value can be found by looking it up on a chart (Cook, 1996).

It is often useful to show that one mosaic is spatially (and so presumably functionally and developmentally) independent of another. Historically, NND methods have been used for this, too, the standard approach being to combine the two mosaics and attempt to show that the NND distribution of the combined set is close to that expected for a random population. This approach is seriously flawed, not only because its sensitivity depends on the orderliness of the individual mosaics and their relative spacings, but also because the sum of two mosaics depends on their spatial relationship within the sampling area (Cook, 1996). Spatial correlograms, discussed in the next section, offer a much more informative approach to issues of this kind.

METHODS BASED ON SPATIAL CORRELATION A powerful technique for the assessment of spatial order is the spatial correlogram, introduced into retinal studies by Rodieck (1991), which reveals coincidences and relationships in two-dimensional space. To create a spatial correlogram, each neuron in an array is placed, in turn, at a central reference point and the locations of all its neighbors are plotted around it. The accumulation of overlaid plots reveals overall trends in neighbor-relationships. *Autocorrelation* of a single array with itself explores its internal spatial relationships and can reveal local order, global order, and some aspects of array geometry, whereas *cross-correlation* of one array with another explores any spatial interactions between the two. Although the correlogram itself is primarily a tool for visualization, it can be used to derive a quantitative measure known as the density recovery profile, or *DRP* (Rodieck, 1991), which is basically a histogram of the mean neuronal density in a series of concentric rings around the correlogram's origin.

The autocorrelation-DRP of a large sample drawn from a random point distribution is completely flat. By contrast, autocorrelation-DRPs from individual neuronal mosaics are never flat, because each neuron is surrounded by a territory from which other neurons of the same type tend to be excluded. This exclusion leads to a central hole in the autocorrelation-DRP and a deep well in the *DRP*. The size of the neighbor-depleted region can be used to derive an objective measure of the minimal spacing within the array (the exclusion radius) and a measure of the regularity of the array (the packing factor; Rodieck, 1991). Autocorrelation-DRPs with

partial-depth wells may be seen when the sample contains a mixture of spatially independent neuronal types (Cook and Podugolnikova, 2001).

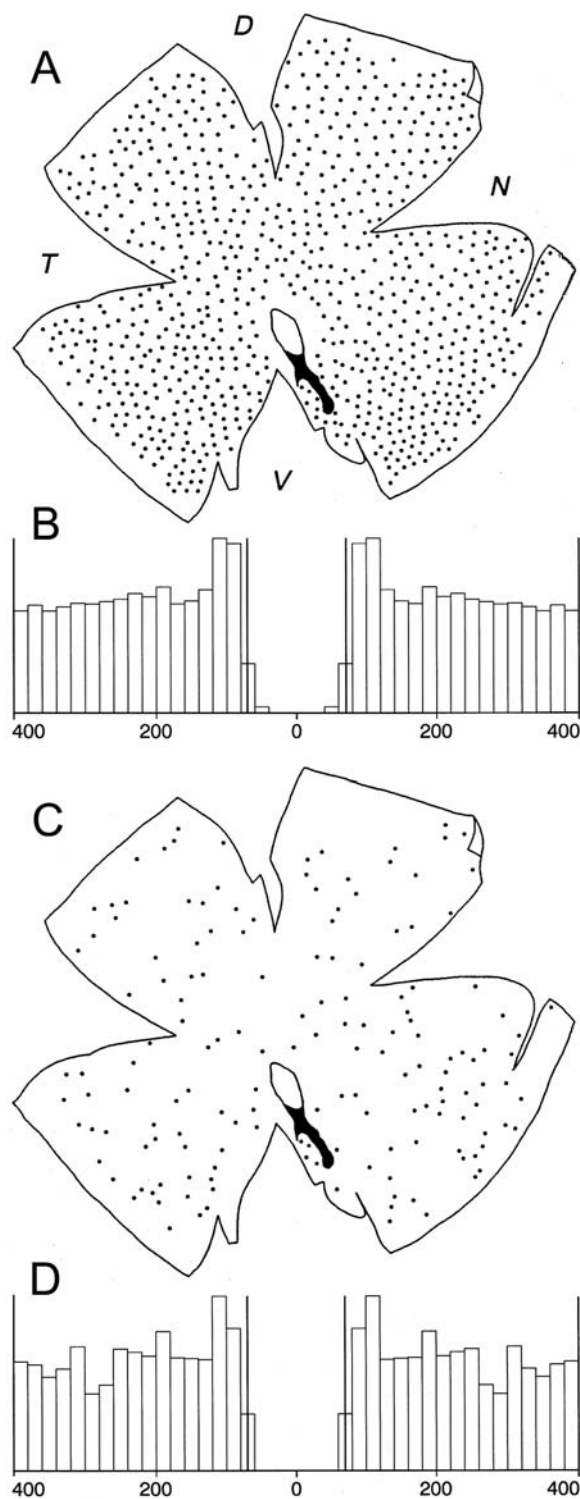
Cross-correlograms derived from two distinct mosaics normally yield essentially flat DRPs, demonstrating spatial independence, although short-range steric hindrance between costratifying neurons can cause minor central deviations. Where the cross-correlation-DRP shows a broad central well like that of an autocorrelation-DRP, the most likely explanation is that the two "mosaics" are actually subsets of a single mosaic.

A major merit of spatial correlograms is their robustness in the face of imperfect sampling procedures. Real neuronal mosaic samples vary in spacing across the sample area and contain gaps where individual neurons or clusters have failed to label or are damaged or obscured. Estimates of the exclusion radius are remarkably resistant to this kind of under-sampling, to the extent that the radius of a regular mosaic may be correctly estimated when as few as 20% of the neurons actually present in the sample area are included in the analysis (Fig. 29.8). In such a case, NND-based methods are virtually useless (Cook, 1996).

METHODS BASED ON VORONOI DOMAIN ANALYSIS A method that is growing in popularity is the analysis of Voronoi polygons, constructed around each cell in a mosaic so as to include all points that are closer to that cell than to any other (Ammermüller et al., 1993; Curcio and Sloan, 1992; see also Fig. 29.6). This approach is potentially more informative than NND analysis in that it allows additional aspects of mosaic geometry to be assessed (e.g., the distribution of the number of neighbors around each neuron) as well as the typical spacing. At present the extra data is of limited use because (as the method itself has been used to confirm) nothing more than the establishment of a certain minimal spacing between neurons may be needed to simulate all their observable properties (Galli-Resta et al., 1999). With a tightly packed, quasi-crystalline mosaic such as the human cone mosaic, however, estimates of domain orientation and neighbor number can be used to identify regional discontinuities within the mosaic (Curcio and Sloan, 1992). The method has been discussed in more detail by Zhan and Troy (2000).

There is a risk with this type of analysis that users will interpret the several different variables that can be computed from a single dataset as though they were statistically independent and thus overestimate their significance. The full utility of this approach will be reached only when there is consensus on a set of tests that can be applied without falling into this trap.

OTHER METHODS Other methods have appeared at various times in the literature, although their advantages have not



always been clear enough to lead to wider uptake. For example, Galli-Resta and colleagues (1997) used a fast Fourier transform method to confirm the close similarity between real mosaics of cholinergic amacrine cells and simulated mosaics created by a minimal-spacing rule, and their paper provides a useful set of direct comparisons between this and standard methods based on NND, spatial correlograms, and Voronoi analysis. Stenkamp and colleagues (2001) have recently used a form of quadrat analysis to assess clustering, as an alternative to the NND-based dispersion index (review: Cook, 1996), which is also capable of measuring the entire spectrum of order from regularity through randomness to clustering.

Looking ahead

The 1980s saw a revival of interest in structural and functional diversity within the retina and the birth (after a long but little-remarked gestation) of the important concept of a natural neuronal type. Concurrently, evidence was accumulating for spatial regularity as a common phenomenon among retinal neurons. In the 1990s, these ideas became more firmly coupled as mosaics were found in a wide range of species and used to address questions of functional diversity and cross-species homology. Recent work suggests that the focus in the next few years will be on exploring the mechanisms through which mosaics develop, whether at the level of cell-fate determination, cell migration, or cell death. What, then, are the big questions that remain?

For the molecular developmental neurobiologist, the key questions must be how neurons acquire their type-diversity and spatial patterning through the interplay of intercellular and intracellular signaling pathways, and how these properties are created and maintained by transcriptional control. These are questions that transcend the visual system and seem likely to be answered first for the spinal cord (review: Lee and Pfaff, 2001), but the diverse and well-defined neuronal mosaics of the retina offer an excellent model in which to test the generality of the answers.

FIGURE 29.8. The exclusion radius is insensitive to undersampling. The alpha-b (inner-stratified) mosaic of *Oreochromis spilurus* is highly regular (A) and has a well-defined minimal spacing, shown clearly by the well in the autocorrelation-DRP (B). This yields an exclusion radius (Rodieck, 1991) of 70 μm . When 80% of these cells are deleted at random, simulating an incompletely sampled mosaic in which only one cell in five is recorded, the mosaic (C) now appears irregular to the untutored eye. However, the autocorrelation-DRP, although “noisier,” is otherwise unchanged (D) and the calculated exclusion radius is still 70 μm . T, D, N, and V show the temporal, dorsal, nasal, and ventral poles of the retina. For further details see Cook (1996). © 1996 Cambridge University Press. Reprinted by permission.

At the cell-biological level, the primary spatial patterning issue must be the molecular mechanisms that are used by members of each mosaic-forming type to recognize each other reliably within a crowd of other types while migrating to appropriate positions, staking out territory, and tiling the retina with their dendritic trees. In this respect, the recent discovery of large families of molecules with the potential to mediate highly selective adhesion, attraction, and repulsion among neuronal processes (Wu and Maniatis, 1999; Yu and Bargmann, 2001) is highly encouraging, as are recent technical advances for studying living, growing neurons in their natural habitat (Lichtman and Fraser, 2001). An interesting secondary issue is the molecular control of type-specific dendritic branching patterns. Factors such as branch density, branch angle, and narrowness of stratification will strongly affect the density of interdendritic contacts at the boundaries of neighboring dendritic fields (Lohmann and Wong, 2001; see also Chapter 6) and so may be related to type-specific variations in coverage factor, precision of tessellation, and the contouring of physiological receptive fields. A third issue needing exploration is the two-edged relationship between spatial regularity and cell death discussed earlier; a fourth is the generality of spatial regularity among neurons elsewhere in the CNS, which has hardly yet been touched upon (Stevens, 1998).

Finally, the key issue for the evolutionary biologist must be to discover what these conspicuous and fascinating patterns can tell us about how retinal neurons have evolved. During which of the evolutionary transitions that shaped the major vertebrate lineages have mosaic-forming neurons (and thus, closing the circle, their transcriptional control systems) undergone duplication or “speciation” to create novel neuronal types with independent functions and tilings? What are the genetic and/or epigenetic mechanisms of adaptation that enable homologous neuronal types to vary their regularity and spacing in response to divergent visual demands in related taxa of a single lineage? Ahnelt and Kolb (2000) have begun to address these difficult questions with respect to mammalian cones, but only when they can be answered for all the major neuronal classes and vertebrate groups shall we be able to say that we understand the relationships between development, structure, and function in the retina.

REFERENCES

- Ahnelt, P. K., and H. Kolb, 2000. The mammalian photoreceptor mosaic—adaptive design, *Prog. Ret. Eye Res.*, 19:711–777.
- Ammermüller, J., W. Möckel, and P. Rujan, 1993. A geometrical description of horizontal cell networks in the turtle retina, *Brain Res.*, 616:351–356.
- Amthor, F. R., and C. W. Oyster, 1995. Spatial organization of retinal information about the direction of image motion, *Proc. Natl. Acad. Sci. USA*, 92:4002–4005.
- Baonza, A., T. Casci, and M. Freeman, 2001. A primary role for the epidermal growth factor receptor in ommatidial spacing in the *Drosophila* eye, *Curr. Biol.*, 11:396–404.
- Beaudet, L., I. Novales Flamarique, and C. W. Hawryshyn, 1997. Cone photoreceptor topography in the retina of sexually mature Pacific salmonid fishes, *J. Comp. Neurol.*, 383:49–59.
- Bloomfield, S. A., and P. F. Hitchcock, 1991. Dendritic arbors of large-field ganglion cells show scaled growth during expansion of the goldfish retina: a study of morphometric and electrotonic properties, *J. Neurosci.*, 11:910–917.
- Boycott, B. B., and H. Wässle, 1974. The morphological types of ganglion cells of the domestic cat’s retina, *J. Physiol. (Lond.)*, 240:397–419.
- Bowers, C. W., 1994. Superfluous neurotransmitters? *Trends Neurosci.*, 17:315–320.
- Bryant, P. J., 1999. Filopodia: fickle fingers of cell fate, *Curr. Biol.*, 9:R655–R657.
- Chalupa, L. M., G. Jeyarasasingam, C. J. Snider, and S. R. Bodnarenko, 1998. Development of ON and OFF retinal ganglion cell mosaics, in *Development and Organization of the Retina: From Molecules to Function* (L. M. Chalupa and B. L. Finlay, eds.), New York: Plenum Press, pp. 77–89.
- Cook, J. E., 1996. Spatial properties of retinal mosaics: an empirical evaluation of some existing measures, *Vis. Neurosci.*, 13:15–30.
- Cook, J. E., 1998. Getting to grips with neuronal diversity: what is a neuronal type? in *Development and Organization of the Retina: From Molecules to Function* (L. M. Chalupa and B. L. Finlay, eds.), New York: Plenum Press, pp. 91–120.
- Cook, J. E., and D. L. Becker, 1991. Regular mosaics of large displaced and non-displaced ganglion cells in the retina of a cichlid fish, *J. Comp. Neurol.*, 306:668–684.
- Cook, J. E., and L. M. Chalupa, 2000. Retinal mosaics: new insights into an old concept, *Trends Neurosci.*, 23:26–34.
- Cook, J. E., and A. J. Noden, 1998. Somatic and dendritic mosaics formed by large ganglion cells in the retina of the common house gecko (*Hemidactylus frenatus*), *Brain Behav. Evol.*, 51:263–283.
- Cook, J. E., and T. A. Podugolnikova, 2001. Evidence for spatial regularity among retinal ganglion cells that project to the accessory optic system in a frog, a reptile, a bird, and a mammal, *Vis. Neurosci.*, 18:289–297.
- Curcio, C. A., and K. R. Sloan, 1992. Packing geometry of human cone photoreceptors: variation with eccentricity and evidence for local anisotropy, *Vis. Neurosci.*, 9:169–180.
- Deplano, S., C. Gargini, and S. Bisti, 1999. Electrical activity regulates dendritic reorganization in ganglion cells after neonatal retinal lesion in the cat, *J. Comp. Neurol.*, 405:262–270.
- DeVries, S. H., and D. A. Baylor, 1997. Mosaic arrangement of ganglion cell receptive fields in rabbit retina, *J. Neurophysiol.*, 78:2048–2060.
- Eglen, S. J., L. Galli-Resta, and B. E. Reese, 2003. Theoretical models of retinal mosaic formation, in *Modelling Neural Development* (A. van Ooyen, ed.), Boston: MIT Press, pp. 133–150.
- Eglen, S. J., A. van Ooyen, and D. J. Willshaw, 2000. Lateral cell movement driven by dendritic interactions is sufficient to form retinal mosaics, *Network: Comput. Neural Syst.*, 11:103–118.
- Engström, K., 1963. Cone types and cone arrangements in teleost retinæ, *Acta Zool. (Stockholm)*, 44:179–243.
- Fekete, D. M., J. Perez-Miguelsanz, E. F. Ryder, and C. L. Cepko, 1994. Clonal analysis in the chicken retina reveals tangential dispersion of clonally related cells, *Devel. Biol.*, 166:666–682.
- Finlay, B. L., and R. L. Snow, 1998. Scaling the retina, micro and macro, in *Development and Organization of the Retina: From Molecules*

- to Function (L. M. Chalupa and B. L. Finlay, eds.), New York: Plenum Press, pp. 245–258.
- Galli-Resta, L., 1998. Patterning the vertebrate retina: the early appearance of retinal mosaics, *Semin. Cell Dev. Biol.*, 9:279–284.
- Galli-Resta, L., 2000. Local, possibly contact-mediated signalling restricted to homotypic neurons controls the regular spacing of cells within the cholinergic arrays in the developing rodent retina, *Development*, 127:1509–1516.
- Galli-Resta, L., E. Novelli, Z. Kryger, G. H. Jacobs, and B. E. Reese, 1999. Modelling the mosaic organization of rod and cone photoreceptors with a minimal-spacing rule, *Eur. J. Neurosci.*, 11:1461–1469.
- Galli-Resta, L., E. Novelli, and A. Vieg, 2002. Dynamic microtubule-dependent interactions position homotypic neurones in regular monolayered arrays during retinal development, *Development*, 129:3803–3814.
- Galli-Resta, L., E. Novelli, M. Volpini, and E. Strettoi, 2000. The spatial organization of cholinergic mosaics in the adult mouse retina, *Eur. J. Neurosci.*, 12:3819–3822.
- Galli-Resta, L., G. Rest, S.-S. Tan, and B. E. Reese, 1997. Mosaics of Islet-1-expressing amacrine cells assembled by short-range cellular interactions, *J. Neurosci.*, 17:7831–7838.
- Gao, F.-B., M. Kohwi, J. E. Brenman, L. Y. Jan, and Y. N. Jan, 2000. Control of dendritic field formation in *Drosophila*: the roles of Flamingo and competition between homologous neurons, *Neuron*, 28:91–101.
- Heberlein, U., and K. Moses, 1995. Mechanisms of *Drosophila* retinal morphogenesis: the virtues of being progressive, *Cell*, 81:987–990.
- Jeyarasasingam, G., C. J. Snider, G.-M. Ratto, and L. M. Chalupa, 1998. Activity-regulated cell death contributes to the formation of ON and OFF alpha ganglion cell mosaics, *J. Comp. Neurol.*, 394:335–343.
- Kock, J., E. Mecke, O. Y. Orlov, T. Reuter, R. A. Väisänen, and J. E. Wallgren, 1989. Ganglion cells in the frog retina: discriminant analysis of histological classes, *Vis. Res.*, 29:1–18.
- Lee, S.-K., and S. L. Pfaff, 2001. Transcriptional networks regulating neuronal identity in the developing spinal cord, *Nature Neurosci.*, 4(Suppl):1183–1191.
- Lichtman, J. W., and S. E. Fraser, S. E., 2001. The neuronal naturalist: watching neurons in their native habitat, *Nat. Neurosci.*, 4(Suppl):1215–1220.
- Lohmann, C., and R. O. L. Wong, 2001. Cell-type specific dendritic contacts between retinal ganglion cells during development, *J. Neurobiol.*, 48:150–162.
- Masland, R. H., 2001. Neuronal diversity in the retina, *Curr. Opin. Neurobiol.*, 11:431–436.
- Masland, R. H., J. F. Rizzo, and J. H. Sandell, 1993. Developmental variation in the structure of the retina, *J. Neurosci.*, 13:5194–5202.
- Mills, S. L., 1999. Unusual coupling patterns of a cone bipolar cell in the rabbit retina, *Vis. Neurosci.*, 16:1029–1035.
- Mochizuki, A., 2002. Pattern formation of the cone mosaic in the zebrafish retina: a cell rearrangement model, *J. Theoret. Biol.*, 215:345–361.
- Neumann, C. J., and C. Nüsslein-Volhard, 2000. Patterning of the zebrafish retina by a wave of Sonic hedgehog activity, *Science*, 289:2137–2139.
- Nishimura, Y., Y. Inoue, and K. Shimai, 1979. Morphological development of retinal ganglion cells in the chick embryo, *Expl. Neurol.*, 64:44–60.
- Raven, M. A., and B. E. Reese, 2003. Mosaic regularity of horizontal cells in the mouse retina is independent of cone photoreceptor innervation, *Invest. Ophthalmol. Vis. Sci.*, in press.
- Raymond, P. A., L. K. Barthel, and G. A. Curran, 1995. Developmental patterning of rod and cone photoreceptors in embryonic zebrafish, *J. Comp. Neurol.*, 359:537–550.
- Reese, B. E., and L. Galli-Resta, 2002. The role of tangential dispersion in retinal mosaic formation, *Prog. Ret. Eye Res.*, 21:153–168.
- Reese, B. E., B. D. Necessary, P. P. L. Tam, B. Faulkner-Jones, and S.-S. Tan, 1999. Clonal expansion and cell dispersion in the developing mouse retina, *Eur. J. Neurosci.*, 11:2965–2978.
- Reichenbach, A., and S. R. Robinson, 1995. Phylogenetic constraints on retinal organisation and development, *Prog. Ret. Eye Res.*, 15:139–171.
- Rockhill, R. L., T. Euler, and R. H. Masland, 2000. Spatial order within but not between types of retinal neurons, *Proc. Natl. Acad. Sci. USA*, 97:2303–2307.
- Rodiek, R. W., 1991. The density recovery profile: a method for the analysis of points in the plane applicable to retinal studies, *Vis. Neurosci.*, 6:95–111.
- Rodiek, R. W., and R. K. Brening, 1983. Retinal ganglion cells: properties, types, genera, pathways and trans-species comparisons, *Brain Behav. Evol.*, 23:121–164.
- Roorda, A., and D. R. Williams, 1999. The arrangement of the three cone classes in the living human eye, *Nature*, 397:520–522.
- Rowe, M. H., and J. Stone, 1980. The interpretation of variation in the classification of nerve cells, *Brain Behav. Evol.*, 17:123–151.
- Scott, E. K., and L. Luo, 2001. How do dendrites take their shape? *Nat. Neurosci.*, 4:359–365.
- Sernagor, E., S. J. Eglon, and R. O. L. Wong, 2001. Development of retinal ganglion cell structure and function, *Prog. Ret. Eye Res.*, 20:139–174.
- Shamim, K. M., P. Tóth, D. L. Becker, and J. E. Cook, 1999. Large retinal ganglion cells that form independent, regular mosaics in the bufonoid frogs *Bufo marinus* and *Litoria moorei*, *Vis. Neurosci.*, 16:861–879.
- Shand, J., M. A. Archer, and S. P. Collin, 1999. Ontogenetic changes in the retinal photoreceptor mosaic in a fish, the black bream, *Acanthopagrus butcheri*, *J. Comp. Neurol.*, 412:203–217.
- Stell, W. K., and P. Witkovsky, 1973. Retinal structure in the smooth dogfish, *Mustelus canis*: general description and light microscopy of giant ganglion cells, *J. Comp. Neurol.*, 148:1–32.
- Stenkamp, D. L., R. A. Frey, S. H. Prabhudesai, and P. A. Raymond, 2000. Function for *Hedgehog* genes in zebrafish retinal development, *Devel. Biol.*, 220:238–252.
- Stenkamp, D. L., O. Hisatomi, L. K. Barthel, F. Tokunaga, and P. A. Raymond, 1996. Temporal expression of rod and cone opsins in embryonic goldfish retina predicts the spatial organization of the cone mosaic, *Invest. Ophthalmol. Vis. Sci.*, 37:363–376.
- Stenkamp, D. L., M. K. Powers, L. H. Carney, and D. A. Cameron, 2001. Evidence for two distinct mechanisms of neurogenesis and cellular pattern formation in regenerated goldfish retinas, *J. Comp. Neurol.*, 431:363–381.
- Stevens, C. F., 1998. Neuronal diversity: too many cell types for comfort? *Curr. Biol.*, 8:R708–R710.
- Swindale, N. V., 1998. Cortical organization: modules, polymaps and mosaics, *Curr. Biol.*, 8:R270–R273.
- Tohya, S., A. Mochizuki, and Y. Iwasa, 1999. Formation of cone mosaic of zebrafish retina, *J. Theor. Biol.*, 200:231–244.
- Vancey, D. I., 1994a. Territorial organization of direction-selective ganglion cells in rabbit retina, *J. Neurosci.*, 14:6301–6316.

- Vaney, D. I., 1994b. Patterns of neuronal coupling in the retina, *Prog. Ret. Eye Res.*, 13:301–355.
- Vaney, D. I., and A. A. Hughes, 1990. Is there more than meets the eye? in *Vision: Coding and Efficiency* (C. Blakemore, ed.), Cambridge, UK: Cambridge University Press, pp. 74–83.
- Wan, J., and D. L. Stenkamp, 2000. Cone mosaic development in the goldfish retina is independent of rod neurogenesis and differentiation, *J. Comp. Neurol.*, 423:227–242.
- Wässle, H., and B. B. Boycott, 1991. Functional architecture of the mammalian retina, *Physiol. Rev.*, 71:447–480.
- Wässle, H., M. H. Chun, and F. Müller, 1987. Amacrine cells in the ganglion cell layer of the cat retina, *J. Comp. Neurol.*, 265:391–408.
- Wässle, H., D. M. Dacey, T. Haun, S. Haverkamp, U. Grünert, and B. B. Boycott, 2000. The mosaic of horizontal cells in the macaque monkey retina: with a comment on bplexiform ganglion cells, *Vis. Neurosci.*, 17:591–608.
- Wässle, H., and H. J. Riemann, 1978. The mosaic of nerve cells in the mammalian retina, *Proc. Roy. Soc. (Lond.) B*, 200:441–461.
- Weber, A. J., R. E. Kalil, and L. R. Stanford, 1998. Dendritic field development of retinal ganglion cells in the cat following neonatal damage to visual cortex: evidence for cell class specific interactions, *J. Comp. Neurol.*, 390:470–480.
- White, C. A., and L. M. Chalupa, 1991. Subgroup of alpha ganglion cells in the adult cat retina is immunoreactive for somatostatin, *J. Comp. Neurol.*, 304:1–13.
- Williams, R. W., M. J. Bastiani, B. Lia, and L. M. Chalupa, 1986. Growth cones, dying axons, and developmental fluctuations in the fiber population of the cat's optic nerve, *J. Comp. Neurol.*, 246:32–69.
- Williams, R. W., and K. Herrup, 1988. The control of neuron number, *Annu. Rev. Neurosci.*, 11:423–453.
- Wong, W. T., and R. O. L. Wong, 2001. Changing specificity of neurotransmitter regulation of rapid dendritic remodeling during synaptogenesis, *Nat. Neurosci.*, 4:351–352.
- Wu, Q., and T. Maniatis, 1999. A striking organization of a large family of human neural cadherin-like cell adhesion genes, *Cell*, 97:779–790.
- Xaio, M., and A. Hendrickson, 2000. Spatial and temporal expression of short, long/medium, or both opsins in human fetal cones, *J. Comp. Neurol.*, 425:545–559.
- Xin, D., and S. A. Bloomfield, 1997. Tracer coupling pattern of amacrine and ganglion cells in the rabbit retina, *J. Comp. Neurol.*, 383:512–528.
- Yu, T. W., and C. I. Bargmann, 2001. Dynamic regulation of axon guidance, *Nat. Neurosci.*, 4(Suppl):1169–1176.
- Zhan, X. J., and J. B. Troy, 2000. Modeling cat retinal beta-cell arrays, *Vis. Neurosci.*, 17:23–39.

IV ORGANIZATION OF VISUAL PATHWAYS

30 The M, P, and K Pathways of the Primate Visual System

EHUD KAPLAN

OVERVIEW

Why are neural streams worth studying?

To our mind's eye, the world appears as a combination of colors, sizes, movements, locations, and other attributes of the visual world. It is tempting to assume that every one of these attributes is handled by a separate neural population, which constitutes an information channel or stream. The observation that the visual system comprises several neuronal populations or streams suggests the possibility that each stream performs a distinct function in vision. We believe that understanding the link between the properties of the neurons in each stream and those visual functions should illuminate the computations that are performed by the visual system as it analyzes the visual world. Here I shall review the current state of our understanding of the three neuronal populations that together make up the output of the primate retina: the so-called M (magnocellular), P (parvocellular), and K (koniocellular) streams. A review is timely for several reasons: (1) Recent intracellular recordings in vitro have generated detailed information about the morphology and physiology of several types of retinal cells, including some cell types that had not been characterized before; (2) a significant new population of cells (the Koniocellular, or K cells) had been identified within the lateral geniculate nucleus (LGN), with distinctive patterns of projection into the visual cortex; (3) detailed microscopic analysis of retinal circuits has revealed new information about synaptic patterns of connections; and (4) more sophisticated stimulation techniques have shed some new light on the details of the organization and dynamics of the various neuronal populations that make up the early visual system of primates.

After a brief review of the relevant anatomical structures of the primate early visual system, I shall consider several aspects of the physiological characteristics of the three main neuronal streams and discuss their functional implications.

Cell types, visual streams, and parallel information processing

When one considers diverse neuronal populations within a neural entity such as the visual system, it is important to have a clear understanding of the taxonomical notion of *cell type*. In the primate visual system, the M, P, and K populations are thought to consist of three different types of neurons. The concept of a neuronal type, and its relationship to visual neuroscience, has been discussed extensively in the past (see, for example, Rodieck and Brening, 1983; Stone, 1983). Usually, one refers to a group of neurons that is distinct from other groups along one or more important dimensions, such as morphology, physiology, or connectivity. Even if along any one dimension the variations among cells form a continuous transition with a unimodal distribution (say, from small to large neurons, or from fast conducting to slow conducting), when the entire cell population is examined along *multiple dimensions*, one typically observes distinct clusters. This point is illustrated for two dimensions in Figure 30.1.

A seductive and widespread hypothesis is that different cell types serve distinct functions. If the various populations also have distinct patterns of connectivity, it is often assumed that we are looking at distinct neuronal streams or functional pathways, each devoted to the representation and analysis of a different aspect of the visual world, for which each stream is specialized. It is thought that the spatiotemporal distribution of light on the two-dimensional retinal surface is transformed by the visual system into a set of higher-order representations, or abstractions, of several aspects of the visual world, such as color, size, edge orientation, or movement. The notion of parallel representation suggests, in turn, that each neuronal type should probably cover the entire visual field, so as to avoid having regions in which one cannot see some important aspect of the world, such as blue or vertical edges or movement.

We do not know currently how many major attributes of the visual world are represented by the visual system, but it is probably safe to assume that the number is larger than 3, though probably less than 20. One might try to estimate the number of possible dimensions by considering how many neuronal types are represented at any point in the retina.

Such information is exceedingly difficult to obtain and is available in only a few cases, such as the elegant work of MacNeil and Masland (1998), who found 29 types of amacrine cells at every point in the rabbit retina. The relatively large number of visual dimensions suggests that each of the three major visual streams we are discussing here (M, P, and K) must deal with more than one attribute of the visual world. We hope to determine at least some of the functions of the various streams by comparisons of the respective properties along some of the dimensions mentioned above, and much of what is to follow will be taken up by that effort.

Anatomical vs. physiological classification

In discussing neuronal streams it is useful to keep in mind the distinction between labeling neurons according to (1) where they are or who they connect with, which is usually

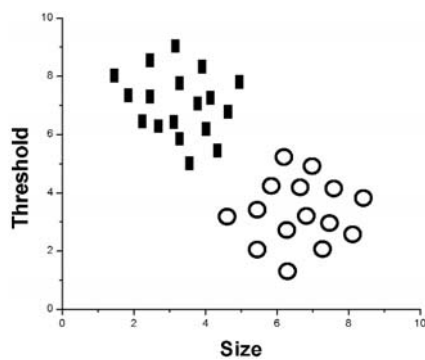


FIGURE 30.1. Two cell populations might have a unimodal distribution along any one dimension, but when analyzed along more than one dimension (two in this example: size and response threshold), they form two distinct clusters.

qualitative and unambiguous; and (2) their physiological (or other) properties, which can vary in quantitative measures (e.g., conduction velocity, response time course, or chromatic opponency). The latter classification is often less certain and more controversial than the former.

Properties of the M, P, and K streams: a summary

Table 30.1 provides a concise overview of our current knowledge of the three major visual streams in the primate visual system: M, P, and K. The subsequent sections will elaborate on some of the entries in the table. We note that much more is known currently about the P and M populations than about the K population, which was discovered more recently, and which is much more difficult to study in isolation. There are several extensive reviews of the M/P pathways at various stages of the visual system (Kaplan et al., 1990; Lee, 1996; Merigan and Maunsell, 1993). Less is known about the K (koniocellular) pathway, but the reader is referred to Irvin et al. (1993), Hendry and Reid (2000), White et al. (2001), and Xu et al. (2001).

THE UNDERLYING ANATOMICAL CIRCUITRY

Retina

GENERAL SCHEME The primate retina follows the general scheme of other vertebrate retinas. After traversing the retina, light is transformed by the photoreceptors into electrical signals that are communicated to the bipolar cells, which relay the message to the ganglion cells, whose axons form the optic nerve. Two additional layers of cells, the horizontal cells and amacrine cells, form lateral connections

TABLE 30.1
Properties of the P, M, and K Pathways

Property	P	M	K
Clear spectral opponency/selectivity	Yes	No	Some (Blue-ON)
Luminance contrast gain	Low	High	High
Receptive field size	Small	Large	Large
Spatial resolution of individual neurons	Similar to M	Similar to P	Variable
Ganglion cells/mm ² (acuity of cell group)	Many (high)	Few (low)	?
Retinal source	Midretinal ganglion cells (RGCs)	Parasol retinal ganglion cells	Unknown (some from blue-ON bistratified RGCs)
LGN projection target	Parvocellular	Magnocellular	Intercalated (K)
V1 projection target	Layer 4C β	Layer 4C α	Layers 2-3, CO blobs
Cell size	Small	Large	Large/varied
Conduction velocity of axons	Low	High	Low/varied
Response to light steps	Tonic	Phasic (transient)	Phasic; some sluggish
Contrast sensitivity at scotopic luminance	Poor	Good	?
Linearity of spatial summation	Linear (X-like)	75% linear, 25% nonlinear (Y-like)	Linear (X-like?)
Fraction of LGN population	~80%	~10%	~10%

with elements of the three major layers, and these are believed to provide the basis for the antagonistic center-surround organization of receptive fields of retinal neurons (Kuffler, 1953; Werblin and Dowling, 1969). All told, the retina of Old World primates comprises approximately 80 cell types: 4 types of photoreceptors, 10 types of bipolar cells, 2 types of horizontal cells, 30 to 40 types of amacrine cells, and 20 types of ganglion cells (for extensive reviews, see Rodieck, 1988; Wässle and Boycott, 1991; Dacey, 2000).

GANGLION CELLS

Parasols and midgets. An early indication that the primate retina contains more than one homogeneous neural stream came from the anatomical studies of Polyak (1941), who described two major types of ganglion cells, distinguished by their morphology: midget and parasol cells. Later work has established that the midget cells of the central few degrees receive their input from bipolar cells that get their input from a single cone, establishing a “private line” from cone to ganglion cell (although each cone connects to one ON and one OFF bipolar cell). The parasol cells, by contrast, receive their inputs from several diffuse bipolar cells, which in turn sample from several cones. This basic anatomical difference results in a dramatic difference in physiological properties and, by inference, in visual function, as we shall discuss below.

Injections of tracers into the LGN have shown that the parasol cells project to the magnocellular layers of the LGN (the bottom 2 layers), whereas the midget ganglion cells innervate the upper 4 layers, the parvocellular layers (Leventhal et al., 1981; Perry et al., 1984). These anatomical destinations have given these two major visual streams their commonly used names, the M (magnocellular projecting) and P (parvocellular projecting). This nomenclature is a source of some unfortunate confusion, since anatomically we speak of *Parasol* (M) and *Midget* (P) retinal ganglion cells. However, the M and P labels have the advantage of being completely unambiguous, because the ganglion cells that project to the LGN synapse either in the parvocellular or in the magnocellular layers, with no overlap.

The segregation of pathways into P and M streams starts right at the very first visual synapse: the midget bipolar cells innervate the midget ganglion cells, the parasol cells are innervated by diffuse bipolar cells (Boycott and Wässle, 1991; Calkins and Sterling, 1999), and each point in the retina is covered by both cell types.

We note that both the M/P and parasol/midget nomenclatures are strictly anatomical and carry no explicit information about the physiological properties of the relevant populations. These properties will be discussed later.

Bistratified and other types. Another distinct morphological type has been added to the parasol and midget cell types with the inclusion of the bistratified ganglion cells, which make synaptic contacts at both the upper and lower sublaminae of the inner plexiform layer (Dacey, 2000; Dacey and Lee, 1994). Because we know that ON and OFF ganglion cells synapse separately in these sublaminae (Famiglietti and Kolb, 1976), the bistratified morphology predicts that the bistratified cells will show ON/OFF responses to light steps; a recent report by Dacey and Lee (1994) confirms that expectation. Backfilling experiments have shown that these ganglion cells project to the intercalated layers (the layers just underneath the major layers of the LGN, which are also called the interlaminar layers, or the koniocellular [K] layers). The cells in these regions had been shown to project to the cytochrome oxidase-rich regions of the upper layers of the primary visual cortex (CO “blobs”) (Diamond et al., 1985; Hendry and Yoshioka, 1994). The properties of other ganglion cells that project to the K layers of the LGN are not yet known. We also note that, although there is evidence that the M and P streams diverge already at the first synapse, between photoreceptor and bipolar cell (Calkins and Sterling, 1999), the situation regarding the K stream is still unknown.

Some typical examples of primate retinal ganglion cells are shown in Figure 30.2, together with their LGN projection targets.

TERMINOLOGY The terms *parasol*, P_α , M (or MC), *phasic*, and *broad-band* have all been used (somewhat loosely) in the literature to refer to the same population of neurons. Similarly, the terms *midget*, P_β , P (or PC), *tonic*, and *color opponent* have been used to refer to the other major type of ganglion cell. The term *midget system*, which is used by some authors, is somewhat more accurate, because it excludes other, quite different, cell types (Rodieck and Watanabe, 1993) that project to the parvocellular layers of the LGN. Koniocellular layers have been called S, interlaminar, intercalated, or K layers. Whatever terminology is used, it is important to keep in mind the distinction between strictly anatomical classification (parasol, P_α , and midget, P_β) and classifications that rely on the physiological properties of the cells (tonic, phasic, color-opponent).

TILING, SAMPLING DENSITY, AND SPATIAL RESOLUTION As mentioned above, each cell type should tile the retina completely, so the visual attribute for which the type is specialized will be represented everywhere in the visual field. In some cases, the tiling might be overlapping, with a coverage factor (the number of cells of a given type at each retinal point) >1 . Dacey (1993) has shown that the midget cells tile the retina with a coverage factor of approximately 1, leaving no holes, but with no overlap of dendritic fields. Similar

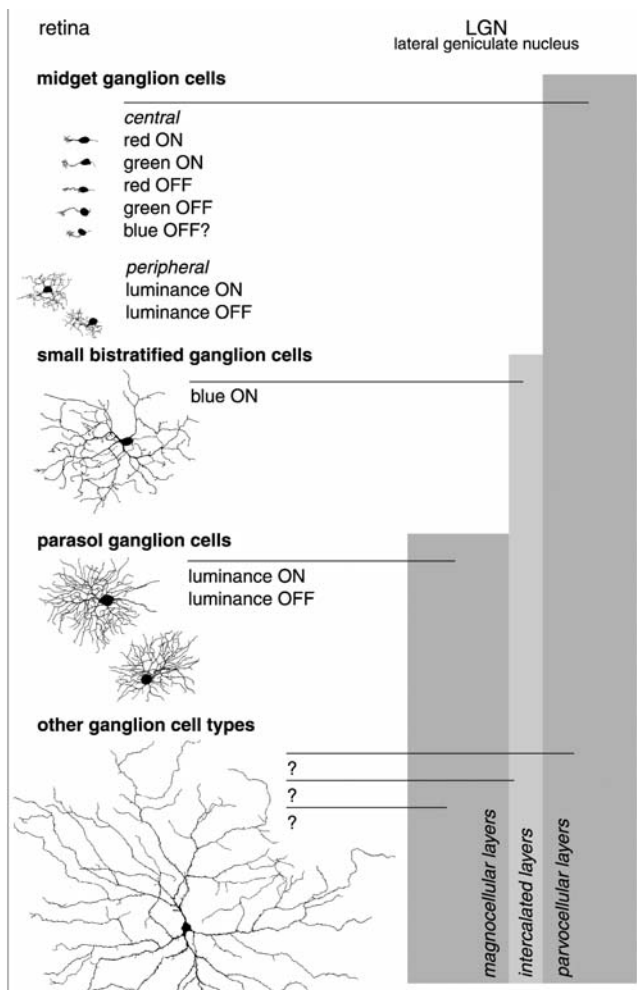


FIGURE 30.2. Examples of the morphology of some of the common ganglion cell types in the primate retina, together with their projection targets in the LGN, and some of their physiological properties (Dacey, 2000).

information for the parasol cells is available from looking at the areal density of the cells, rather from a detailed mapping analysis. This shows that the retinal coverage of the parasol cells is qualitatively similar to that of the midget cells: as their density changes, their dendritic field sizes vary by a similar factor. The lower density of parasol cells explains why the spatial resolution of the parasol (M) system is much lower than that of the P system. Although the spatial resolution of individual M cells is virtually identical to that of individual P cells (Blakemore and Vital-Durand, 1986; Crook et al., 1988) because of their higher sensitivity to luminance contrast (see below, Figure 30.5), their ability to faithfully represent spatial patterns is much poorer than that of the P system, with the difference being determined by the Nyquist limit of spatial sampling (which requires at least two samples along any direction for each cycle of spatial frequency in the stimulus). The similar spatial resolutions of individual M and P cells is clarified in Figure 30.3, which shows that despite

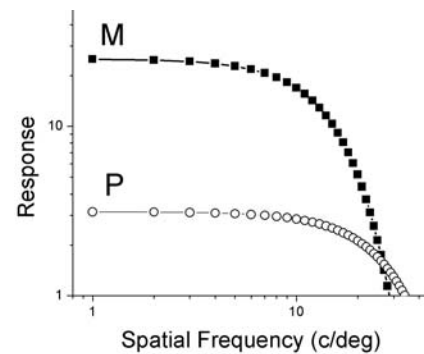


FIGURE 30.3. Large cells (M) can have spatial resolution (ability to respond to fine patterns) that is similar to that of small cells (P) if they are sensitive enough, even though their “cutoff frequencies” (the spatial frequency at which the horizontal and sloping asymptotes intersect) are quite different. The shape (Gaussian), radius and sensitivity of the detectors in this example are similar to those of M and P cells recorded in the laboratory.

the large receptive field center of M cells, their high-contrast gain gives them acuity that is like that of P cells. We note that the high acuity of individual M cells is especially remarkable in view of the fact that parasol cells have been shown to be electrically coupled (Dacey and Brace, 1992), and such coupling is bound to lower their spatial resolution, both individually and as a network.

RETINAL ECCENTRICITY The density of cones and rods varies steeply across the retina, and these gradients are reflected in the subsequent stages of retinal circuitry and function. Several important aspects are mentioned below.

Parasol/midget ratio. Early reports suggested that M cells were less well represented in and around the fovea, but later studies (Perry et al., 1984; Silveira and Perry, 1991) found the ratio of parasol and midget cells in the macaque retina to be uniform across the retina, reinforcing the view that these two streams form true neuronal types in the sense that was discussed above. This uniform coverage casts doubt on attempts to use selective stimulation of the M or P populations by restricting their stimuli to particular retinal eccentricity. However, in humans the situation might be different, because Dacey and Petersen (1992) reported indirect evidence, based on measurements of dendritic field size at two retinal eccentricities, that suggested that the P/M ratio in the central retina might be as high as 30/1.

Receptive field size. The diameter of receptive fields increases for both M and P cells as one moves away from the fovea, but, at any given retinal eccentricity, the diameters of M cells’ receptive fields are larger than those of P cells from the same retinal eccentricity (Croner and Kaplan, 1995). This trend reflects the underlying increase in the dendritic trees of ganglion cells as one moves from fovea to the retinal

periphery and has consequences for the physiological properties of the cells, primarily their contrast sensitivity and chromatic selectivity, but also their state of light adaptation.

Near the fovea the midget bipolar cells receive synaptic input from a single cone and deliver their output to a single midget ganglion cell. This produces a very narrow receptive field center. At retinal eccentricities beyond approximately 7 degrees, the bipolar cells start collecting input from an increasing number of cones, and the midget ganglion cell receives input from an increasing number of bipolar cells. The much larger collecting area of M cells (~6 to 8 times that of P cells; Croner and Kaplan, 1995) accounts for at least some of their relative superiority in luminance contrast gain. Data from the human retina suggests significantly larger areal ratios in the central retina (Dacey and Petersen, 1992).

The effect that receptive field size has on contrast sensitivity is discussed later in this chapter.

LGN

M, P, AND K POPULATIONS We shall now review briefly the LGN anatomy. A recent review can be found in Sherman and Guillery (1996). The primate LGN is comprised of 6 layers, arranged in 2 major divisions, and numbered from the bottom (1) to the top (6). The upper one contains 4 layers of smaller cells, the parvocellular layers; the lower one has 2 layers of larger cells, the magnocellular layers. Layers 6, 4, and 1 receive their input from the *contralateral* eye; layers 5, 3, and 2 are innervated by the *ipsilateral* eye. Intracellular staining of retinal ganglion cells projecting to the cat LGN by Bowling and Michael (1980) shows little violations of layer boundaries. Approximately 80% of the cells in the nucleus are in the parvocellular layers, and 10% are in the magnocellular layers.

More recently, Norton and Casagrande (1982, in the *galago*) and Hendry and Yoshioka (1994, in the macaque monkey), have shown that there is another distinct group of LGN neurons, which are immunoreactive for the alpha subunit of type II calmodulin-dependent protein kinase, and are located under each of the major six layers. These are the intercalated layers, or koniocellular (K) cells, which account for ~10% of the cells in the macaque LGN. They have been shown (Hendry and Yoshioka, 1994) to project directly to the CO-rich regions of the primary visual cortex ("blobs"; Carroll and Wong-Riley, 1984).

In addition to the primary "relay" cells, which receive their input from the retina, there is a small number of inhibitory GABAergic interneurons. The magnocellular layers have four times as many interneurons as the parvocellular layers (Hámori et al., 1983), but the functional significance of that difference is unknown. As is the case in other mammalian species, the primate LGN receives a

massive feedback input from the striate cortex, which has recently been reported to increase the gain of LGN neurons (Przybylski et al., 2000).

Primary visual cortex

CONNECTIONS The information from the LGN is fed primarily into layer 4 of the primary (striate) visual cortex, or V1. Magnocellular cells synapse in layer 4C α , and parvocellular cells synapse in 4C β . Collaterals of both are sent also to layer 6, the layer that, in turn, projects back to the LGN (Gilbert and Kelly, 1975). In addition, the koniocellular cells project into the CO-rich zones of the upper layers, the CO "blobs" (Hendry and Yoshioka, 1994).

From V1 the information is relayed to the rest of the visual system, and the pattern of M/P/K connectivity below and above V1 has given rise to the notion of parallel systems or streams, each handling some portion or aspect of the visual information. Thus the output from the CO blobs is relayed to specialized CO bands in V2, which are embedded among CO-poor pale bands (Livingstone and Hubel, 1984b, 1987). The overall connectivity of the three streams, from the retina through the LGN to the visual cortex, is shown schematically in Figure 30.4.

PHYSIOLOGICAL PROPERTIES

Response dynamics: tonic and phasic cells

The first physiological indication that the primate retina contains more than one functional type of ganglion cell came when Gouras (1968) reported that in response to light steps, some cells responded in a tonic, sustained fashion, whereas others responded phasically. This difference in dynamical properties has remained one of the clearest distinguishing characteristics of these two main cell types. Gouras recorded from the cells inside the eye, so the anatomical characteristics of them were unknown at the time, but subsequent studies have established that the phasic cells correspond to the parasol cells, which project to the magnocellular layers of the LGN, and the tonic cells correspond to midget ganglion cells projecting to the parvocellular layer.

Luminance contrast gain

Another major physiological difference between the M and P populations is the contrast gain (change in response for a unit change in contrast) for luminance patterns, which is high for M cells at low contrasts and low for P cells at all contrasts (Kaplan and Shapley, 1986). Contrast gain depends directly on the photon flux over the receptive field (Enroth-Cugell and Shapley, 1973). At all eccentricities, the flux collected by M cells is greater than that collected by

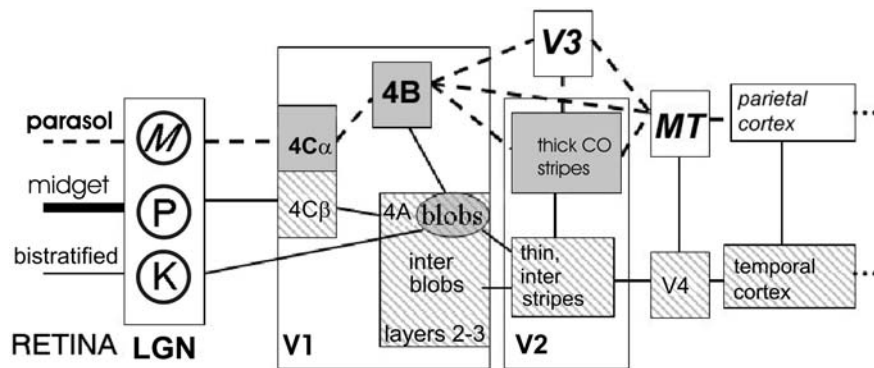


FIGURE 30.4. A simplified connectivity diagram of the M, P, and K pathways in the primate visual system. The magno-dominated dorsal (“where”) stream is marked in *dashed lines and bold italics*; the ventral (“what”) stream is indicated by *solid lines and faint stripes*.

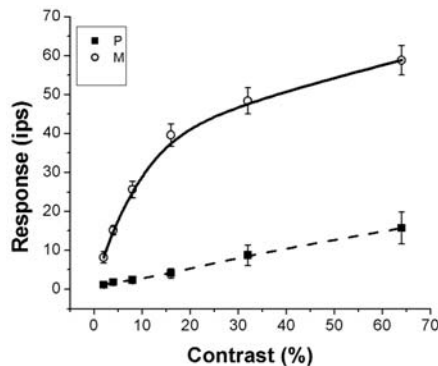


FIGURE 30.5. The luminance contrast gain (slope of the response *vs.* contrast function) of M cells is much higher at low contrasts than that of P cells, but is similar at higher contrasts. The stimulus was a black and white grating, drifting at 4 Hz. All 36 retinal ganglion cells in this data set (28 P and 8 M) were recorded as S potentials in the LGN of the same macaque monkey. Contrast is defined as $C = 100 \cdot \frac{L_{\max} - L_{\min}}{L_{\max} + L_{\min}}$, where L is the luminance level. The response measure was the fundamental Fourier component of the average firing at each contrast (± 1 SEM). (from Kaplan and Shapley, 1986)

P cells, and that accounts for at least some of their superior contrast gain (Croner and Kaplan, 1995; Kaplan and Shapley, 1986; Shapley et al., 1981;). This is shown in Figure 30.5, which shows the average response versus luminance contrast for M and P cells in the retina of one macaque monkey. Kaplan and Shapley (1986) recorded the responses of retinal ganglion cells in the LGN in the form of S potentials, a small extracellular potential that is seen in the LGN each time a spike is fired by a retinal ganglion cell that innervates the LGN neuron near the recording electrode (Bishop, 1953; Kaplan and Shapley, 1984). This approach allows the correct identification of the recorded retinal cells as P or M, as opposed to intraretinal recordings *in vivo*, where one must rely on physiological characterization of the cells to determine their projection targets.

It is not yet certain whether the difference in receptive field size is sufficient to account for the different gains or whether some other process, such as antagonistic cone input, could lower the gain of P cells. It is also possible that some yet unknown process is responsible for the high gain of M cells at low contrast, and that process saturates as contrast exceeds ~15% to 20%, after which the gain of M cells is rather similar to that of P cells. It is possible, then, that the response of M cells is governed by two mechanisms, one for low and the other for high contrasts.

X/Y/W homology and linearity

HOMOLOGY Early studies of primate LGN neurons by Dreher et al. (1976) and Sherman et al. (1976) suggested a correspondence between the cells found in the upper (parvocellular) layers and the X type found in the cat retina (Enroth-Cugell and Robson, 1966). Similarly, cells found in the magnocellular layers were thought to correspond to the Y type of cat retinal ganglion cells. These studies focused on the time course of the responses (X/parvo = sustained, Y/magno = transient), rather than on the linearity of spatial summation, which was the criterion used originally by Enroth-Cugell and Robson to distinguish X from Y ganglion cells in the cat retina. When the original linearity test was applied by Kaplan and Shapley (1982), they reported that all the parvocellular neurons and 75% of the magnocellular cells were X-like, whereas 25% of the magnocellular neurons were Y-like.

Another study that investigated the issue of linearity of spatial summation (Sherman et al., 1984; Levitt et al., 2001) reported that the degree of nonlinearity among the magnocellular neurons was distributed unimodally, rather than bimodally as was found for cat retinal ganglion cells (Hochstein and Shapley, 1976). The cells at the tail of that unimodal distribution were probably the ones that Kaplan and Shapley labeled as “Y-like.” It is worth pointing out that Calkins and Sterling (personal communication) found that

approximately one-third of the parasol cells in their sample received much more amacrine input than the other two-thirds. Because amacrine cells are often nonlinear, this result suggests that these ganglion cells would show stronger nonlinearities, and thus would be classified as “Y-like.” Because of the similarities between the cat X/Y population and the monkey M population, Shapley and Perry (1986) have suggested that these be considered homologous, and that the P cell type was something that primates have developed for higher resolution and perhaps for color vision. Studies of the laminar organization and development of the cat LGN have provided data that support this view as well (Mitzdorf and Singer, 1977; Shatz, 1981, 1983). In addition, a comparative study of several mammalian retinæ by Peichl et al. (1987) showed that in all of them the alpha cells (the ones corresponding to the nonlinear Y-like cells in the cat retina) account for 1% to 4% of all retinal ganglion cells. If we were to accept one-fourth to one-third of the M ganglion cells as Y-like, the monkey will have the same fraction of Y-like ganglion cells as other mammals, namely, 2.5% to 3%.

The K stream has been proposed as the primate homolog of the W population in the cat visual system (Irvin et al., 1986), because many of its cells are sluggish (White et al., 2001). However, because both K and W have a rather heterogeneous morphology and physiology, the value of such a homology in establishing the function of either stream is difficult to establish.

NONLINEAR RESPONSES In addition to the spatial nonlinearity mentioned above, it had been reported (Lee et al., 1989) that the receptive field surround of retinal M cells produces nonlinear responses if a large enough portion of it is stimulated. A thorough investigation of linear and nonlinear responses of the center and surrounds regions of both M and P cells (Benardete et al., 1992; Benardete and Kaplan, 1997a, 1997b, 1999) found evidence for nonlinear components in both populations. One type of nonlinearity, called *contrast gain control*, which was described earlier in cat retinal ganglion cells (Shapley and Victor, 1978), was found in some M cells but not in P cells. This mechanism affects the dynamics of the cell’s response: at higher contrasts, the response to low temporal frequencies is attenuated, and the response phase is advanced (Benardete et al., 1992). It seems reasonable to ascribe the nonlinear components to input from amacrine cells, which are known to produce nonlinear responses. This would suggest that the surround mechanism, and perhaps the center mechanism as well, are made up of at least two components, one originating in the outer and the other in the inner plexiform layers, as suggested by Kaplan and Benardete (2001, their Figure 10).

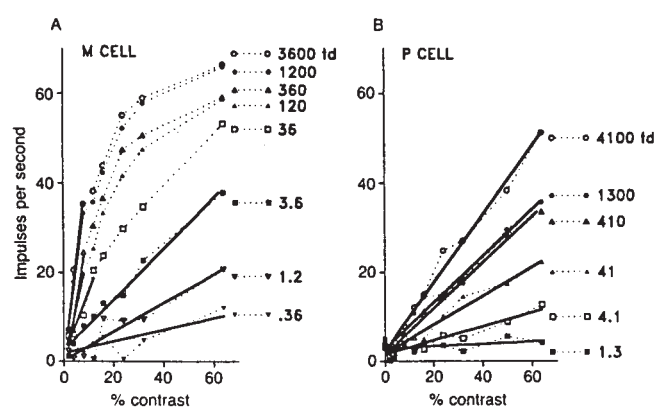


FIGURE 30.6. Contrast gain decreases with decreasing retinal illumination. At scotopic luminance levels the responses of most P cells drown in the noise, whereas M cells still respond to patterns. Shown are the responses of typical M (*left*) and P (*right*) cells to drifting achromatic gratings as a function of contrast (from Purpura et al., 1988).

Light adaptation in M and P cells

Like contrast gain, the adaptation state of a visual neuron is intimately connected to the size of its receptive field, because larger receptive fields collect more photons (Enroth-Cugell and Shapley, 1973). The adaptation state has a profound effect on the dynamics of the response (De Lange, 1958; Dodge et al., 1968; many others). One would expect, then, that M cells would be more light adapted and therefore more transient than P cells at any given luminance level. Purpura et al. (1988, 1990) have shown that, as expected, M cells are always more transient (band pass) than P cells at a given luminance, and that lowering the luminance lowers the steady-state contrast gain of both cell types. These properties are illustrated in Figure 30.5. It is not yet established whether the different dynamical properties of the M and P cells can be attributed entirely to the difference in their size and resulting adaptation level, or whether other factors, such as biophysical properties and/or synaptic input, may contribute as well.

Scotopic (low light) vision

As luminance decreases, the gain of all retinal ganglion cells decreases (Figure 30.6 and Figure 30.7). Because the gain of M cells at all luminance levels is higher than that of P cells, eventually the response of P cells drowns in the noise of their spontaneous activity. Under those conditions, only M cells can still signal the appearance of patterns in the visual field. Note that there are roughly eight times as many P cells as M cells, so if their responses were summed together in the cortex, they could, in principle, compensate for their poorer gain. However, recall that the coverage factor of P cells is

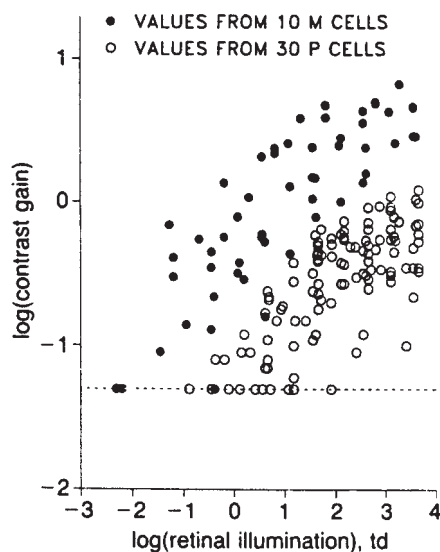


FIGURE 30.7. The contrast gain (slope of functions like the ones in Fig. 30.6) of M cells is higher than that of P cells at all luminance levels (from Purpura et al., 1988).

roughly 1 (Dacey, 1993), so any pooling will have to sacrifice spatial resolution.

Chromatic selectivity

REPRESENTING SPACE AND COLOR It was clear from the very beginning that the M/P populations differ in their chromatic selectivity (Gouras, 1968). Much subsequent work has shown that most P cells are wavelength selective, whereas the selectivity of the M population is more broad-band. Wiesel and Hubel (1966) recognized that cells with antagonistic center-surround receptive fields had to represent two distinct features: space and color. There are only three sensible permutations of center-surround with space/color: cells that care only about *color*, cells that report only about *space*, and cells that represent *both*. Cells that ignore both are useless to a visual system. Wiesel and Hubel (1966) reported that the cells in the macaque LGN indeed fell into these three groups. They called those cells that were chromatically and spatially opponent (77% of parvocellular cells) *type I*, those that were chromatically but not spatially opponent *type II* (7%), and those that were spatially but not chromatically opponent *type III* (16%). The magnocellular cells were mostly of the *type III* variety, although some were reported to have a red-sensitive inhibitory surround, and those were labeled *type IV*.

A subsequent investigation by DeMonasterio and Gouras (1975), who used small spots and annuli of various colors to explore the receptive fields of retinal ganglion cells, has reported a rich variety of chromatic types. However, some of these results might have been contaminated by the use of chromatic adaptation, which attempted to desensitize some

of the cones by bright illumination with light of the color that they are most sensitive to.

Derrington et al. (1984) revisited the subject of chromatic selectivity from the perspective of a theory that transformed an earlier suggestion of MacLeod and Boynton (1979). Derrington et al. postulated three intersecting axes: constant red/green cone excitation, constant blue cone excitation, and a luminance axis that is perpendicular to the two chromatic axes. They have measured the elevation and azimuth of a plane that includes the stimuli that can be silently exchanged for each LGN cell they have studied. The azimuth and elevation values for the various cells clustered around two main groups: red/green and blue/yellow. The measurements were repeated with drifting gratings of various spatial frequencies to assess the cone inputs to the center and surround separately. The authors concluded that *all* cells in the macaque LGN, parvocellular as well as magnocellular, show both chromatic and spatial antagonism.

These results, together with the reports of magnocellular cells (type IV) that show a chromatically selective surround, call into question the widely accepted notion that the M stream does not participate in the analysis of chromatic information, and is blind to isoluminant stimuli.

CONE INPUT TO THE RECEPTIVE FIELD SURROUND The wavelength selectivity of the surrounds of P receptive fields has attracted much attention and is still a rather controversial issue, because anatomical and physiological studies of the primate retina have produced conflicting expectations. Several physiological studies (Benardete and Kaplan, 1999; Reid and Shapley, 1992; Wiesel and Hubel, 1966) have reported that the surrounds appear to receive input from only one cone type. However, several other studies (Boycott et al., 1987; Calkins and Sterling, 1996; Dacheux and Raviola, 1990) have reported that the cellular elements that are believed to generate the surround response of ganglion cells (horizontal and amacrine cells) show remarkable promiscuity, and are innervated by all the cones within the reach of their dendritic trees. This apparent contradiction between the physiological results and the anatomical findings still awaits resolution.

It is worth noting, however, that a chromatically nonselective surround is sufficient for color vision (Lennie et al., 1990; Paulus and Kröger-Paulus, 1983). In addition, the clumpy nature of the random cone mosaic (Roorda and Williams, 1999) will cause many cells with nonselective cone inputs to show strongly biased physiological selectivity.

Multiplexing chromatic and luminance information

The discovery of two (or more) distinct neuronal populations suggested that they subserve distinct visual functions. However, Gouras and Zrenner (1979) reported that ganglion

cells that were color opponent at low temporal frequency lost their chromatic opponency at high temporal frequency, and attributed that change to a progressive increase in the phase lag between the responses of the center and its antagonistic surround. This increase of phase lag with temporal frequency was, indeed, reported by Benardete and Kaplan (1997a). The view that the P channel might multiplex chromatic and luminance information was formalized in the analysis of Ingling and Martinez-Uriegas (1983, 1985), who argued that the spatiotemporal chromatic organization of parvocellular receptive fields allows them to communicate both chromatic and luminance information to the cortex, depending on the spatiotemporal specifics of the stimulus. Note that this analysis requires the cells to be strictly linear; as mentioned above, recent studies have uncovered some nonlinear components in the responses of P cells (Benardete and Kaplan, 1997b).

Homogeneity of the M, P, and K populations

The visual neuroscience literature often treats the M/P streams as if they were monolithic, homogeneous neuronal populations. This is especially true when scientists discuss the roles that the various streams play in the analysis of visual information, or when they attempt to design visual stimuli that will selectively excite or bias one stream at the expense of the other(s). This view is at odds with reality, and much of the controversy in the literature could be attributed to heterogeneity within these major types. The P cells (the parvocellular-projecting), in particular, are probably quite heterogeneous (Rodieck and Watanabe, 1993), and include some of the largest cells in the retina, although the majority of them are probably midget ganglion cells. This heterogeneity is anatomical, and to it one must add functional differences. The M (magnocellular-projecting) cells also seem to comprise at least two populations, based on the amount of amacrine synaptic input they receive (Calkins and Sterling, personal communication), the linearity of their spatial summation (Kaplan and Shapley, 1982), or the pattern of the cortical projection of their LGN targets, which includes a population of larger axons that project to a separate sublamina of 4C α (Blasdel and Lund, 1983).

The physiological properties of K cells have been studied primarily in bushbabies (*galago*) (Irvin et al., 1986; Norton and Casagrande, 1982; Norton et al., 1988), and more recently in owl monkeys (Xu et al., 2001) and marmosets (White et al., 2001). These studies report that the physiological properties of the K stream are quite diverse, although in some respects (size, contrast gain) they appear closer to the M than to the P stream. This diversity makes it especially difficult to study them in isolation or to ascribe a specific visual function to the K stream.

The fact that the K stream has been discovered only recently (Hendry and Yoshioka, 1994; Irvin et al., 1986) is a

reminder of the need for caution when viewing the P and the M cells as homogeneous populations or when considering the visual system as made up of only these three populations. With the advent of new anatomical markers or analysis techniques, it is likely that these populations will be shown to include new subgroups. Another reminder is the intriguing report by Calkins et al. (1994) of two types of midget cells, with distinct patterns of synaptic inputs. The functional significance of these two cell groups is still elusive, although the association of these synaptic types with green-sensitive and red-sensitive cones is suggestive.

Some studies (e.g., Levitt et al., 2001) have argued that, because the distribution of the various parameters they investigated (nonlinearity, conduction velocity, and so on) had unimodal distribution, the neuronal populations should not be subdivided. However, the rather broad distributions of some parameters of receptive field or morphology suggest that the splitters will have more to say before the lumpers' word is final. For example, the analysis of clustering of parameters of the receptive fields in the marmoset LGN by White et al. (2001, Fig. 10) showed considerable overlap among the three major streams.

FUNCTIONAL IMPLICATIONS

What roles might the various pathways play in vision?

The assignment of distinct visual functions to the various neuronal streams has proven to be irresistible to vision scientists, and several similar suggestions have been made. These attempts were based on two very different types of evidence: (1) the clustering of anatomical and physiological properties of the three major streams and (2) lesion studies.

NOTIONS BASED ON CLUSTERING OF FUNCTIONAL PROPERTIES

The small receptive fields and chromatic organization of P cells has suggested, initially, that they participate in the analysis of form and color; while the broad-band, phasic M cells were relegated to detecting motion and conveying information about (achromatic) luminance. In view of the proposed division of the visual system into "what" (dorsal) and "where" (ventral) streams (Ungerleider and Mishkin, 1982), the pattern of cortical projections of the M, P, and K streams suggested that they provide the initial inputs to these two main visual pathways (Livingstone and Hubel, 1984a, 1988; Zeki and Shipp, 1988), with the P stream feeding the *what* pathway and the M stream answering the question *Where?* (see Figure 30.4).

NOTIONS BASED ON LESION STUDIES Several groups (Lynch et al., 1989; Merigan and Maunsell, 1993; Schiller et al.,

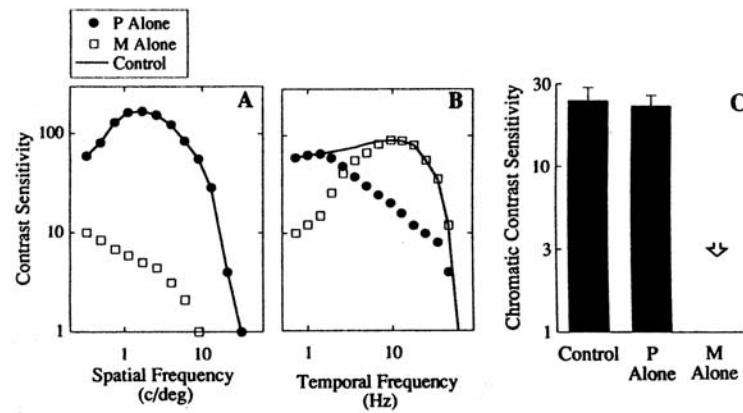


FIGURE 30.8. The effects of selective lesions of the P or M layers of the monkey LGN on spatial (A), temporal (B), or chromatic (C) modulations (from Merigan and Maunsell, 1993). The results support the notion that the P stream is important for spatial and chromatic analysis, and the M stream is involved in temporal analysis.

1990) have used various agents, either systemically or through localized injections, to damage one or the other of the M or P streams. Their results were interpreted as support for the notion that the M and P streams played different roles in vision. The overall impression was that the clusters of anatomical and physiological properties were distinct enough to justify such a view.

In addition, the notion of distinct visual functions implied the independence of the various functions and streams. Thus, movement analysis was said to be independent of color, and so on. An example that illustrates the results of such an approach is shown in Figure 30.8, from the work of Merigan and his colleagues. The data support the notion of specialized function of the P and M pathways along the lines mentioned in the previous section.

However, in evaluating such results today, we should note that the existence of the K channel was unknown at the time of these studies, and the location of its layers makes it virtually impossible to disentangle K lesions from lesions of the overlaying P or M layers.

DYSFUNCTIONS ATTRIBUTED TO SPECIFIC STREAMS The different physiological properties of the various streams have given rise to several hypotheses that related specific neural dysfunctions to one of the three pathways. Two prominent examples are glaucoma and dyslexia, both of which have been attributed to malfunctions or specific damage to the magnocellular pathways (e.g., Livingstone et al., 1991; Quigley, 1999; Yücel et al., 2000; Jenner et al., 1999; Willis and Anderson, 2000). However, despite rigorous research efforts, doubts remain regarding the notion that such damage represents the only (or major) cause of these two serious dysfunctions, and the issue is still quite controversial. The difficulties of validating these hypotheses are similar to those of establishing the functional specificity of any of the streams in vision, as discussed below.

Are the three neural streams functionally distinct and independent?

The seductive simplicity of the association of the visual streams with distinct visual roles has won it broad and rapid acceptance. Many now view the M system as the luminance channel of psychophysics and believe that it is probably involved in motion detection and analysis. The P system seems to be involved in color and form analysis, although which cells within it are responsible for chromatic analysis is still being debated (see, e.g., Rodieck, 1991). The K system is involved in at least some aspects of color vision. The remaining aspects of the visual world are said to be analyzed by both P and M.

However, we should note that the evidence in support of these views is rather weak. The reasons are as follows: (1) The various streams are rather heterogeneous, and it is likely that future research will uncover additional new substreams, perhaps with their own role in vision; (2) much evidence points to interaction among the various visual functions that were said, initially, to be performed in parallel by the various streams (as one of many examples, see Krauskopf and Farell, 1990); (3) the anatomy provides a substrate for numerous pathways to support such interactions among the streams (Figure 30.4). In short, the visual system is a dynamical (and nonlinear) network, and in such a network it is difficult at best to ascribe a specific function to a given element. The evidence from lesion experiments is especially difficult to interpret, because the brain is a plastic, adaptable network, and removing, damaging, or otherwise inactivating any of its parts tells you not what that part is doing, but rather what the brain can (or cannot) do without that part. There are also recent physiological data that suggest that inputs from the P and M streams are combined linearly in the primary visual cortex to detect motion (De Valois and Cottaris, 1998). In short, although the three streams flow

separately from retina to cortex, there is little doubt that their messages are intermingled in the cortex, as they blend to form unified perceptions.

We note that the difficulties in clear-cut assignment of functions to pathways also impact our ability to design stimuli that affect one pathway without affecting others.

CONCLUSIONS

What else do we need to know about visual streams?

Although much has been learned about the various neuronal streams that comprise the early primate visual system, much remains to be learned. Some of the remaining issues are listed below:

1. Are the M, P, and K *all* the streams that exist?
2. How *homogeneous* are they?
3. *Which aspects* of the visual world are handled by each stream?
4. What other ganglion cells, besides the bistratified ganglion cells, project to the LGN K cells?
5. How is the information *integrated* into a uniform percept?
6. Which of the streams' distinct properties are due to biophysical/morphological characteristics, and which emerge from the network in which the cells are embedded?
7. How is the development of the separate streams controlled?

The next few years will undoubtedly provide exciting answers to these questions. However, we should recall that the visual system, like the brain itself, is a highly interconnected, nonlinear dynamical network, and in such a network it might be difficult to allocate a particular function to a specific anatomical entity.

Acknowledgments

This work was supported by NIH grants *EY 12867*, *MH50166*, *EY01867*, and from DARPA. Ehud Kaplan is the Jules and Doris Stein Research-to-Prevent-Blindness Professor in the Depts. of Ophthalmology, Physiology & Biophysics, The Mount Sinai School of Medicine, NY, NY.

REFERENCES

- Benardete, E. A., E. Kaplan, and B. W. Knight, 1992. Contrast gain control in the primate retina: P cells are not X-like, some M cells are, *Vis. Neurosci.*, 8:483–486.
- Benardete, E., and E. Kaplan, 1997a. The receptive field of the primate P retinal ganglion cell, I: Linear dynamics, *Vis. Neurosci.*, 14:169–185.
- Benardete, E., and E. Kaplan, 1997b. The receptive field of the primate P retinal ganglion cell, II: Nonlinear dynamics, *Vis. Neurosci.*, 14:187–205.
- Benardete, E., and E. Kaplan, 1999. The dynamics of primate M retinal ganglion cells, *Vis. Neurosci.*, 16:355–368.
- Bishop, P. O., 1953. Synaptic transmission. An analysis of the electrical activity of the lateral geniculate nucleus in the cat after optic nerve stimulation, *Proc. R. Soc. Lond. B*, 141:362–392.
- Blakemore, C., and F. Vital-Durand, 1986. Organization and postnatal development of the monkey's lateral geniculate nucleus, *J. Physiol. (Lond.)*, 380:453–491.
- Blasdel, G. G., and J. S. Lund, 1983. Termination of afferent axons in macaque striate cortex, *J. Neurosci.*, 3:1389–1413.
- Bowling, D. B., and C. R. Michael, 1980. Projection patterns of single physiologically characterized optic tract fibres in cat, *Nature*, 286:899–902.
- Boycott, B. B., J. M. Hopkins, and H. G. Sperling, 1987. Cone connections of the horizontal cells of the rhesus monkey's retina, *Proc. R. Soc. Lond. B*, 229:345–379.
- Boycott, B. B., and H. Wässle, 1991. Morphological classification of bipolar cells of the primate retina, *Eur. J. Neurosci.*, 3:1069–1088.
- Calkins, D. J., S. J. Schein, Y. Tsukamoto, and P. Sterling, 1994. M and L cones in macaque fovea connect to midget ganglion cells by different numbers of excitatory synapses, *Nature*, 371:70–72.
- Calkins, D. J., and P. Sterling, 1996. Absence of spectrally specific lateral inputs to midget ganglion cells in primate retina, *Nature*, 381:613–615.
- Calkins, D. J., and P. Sterling, 1999. Evidence that circuits for spatial and color vision segregate at the first retinal synapse, *Neuron*, 24(2):313–321.
- Carroll, E. W., and M. T. T. Wong-Riley, 1984. Quantitative light and electron microscopic analysis of cytochrome oxidase-rich zones in the striate cortex of the squirrel monkey, *J. Comp. Neurol.*, 222:1–17.
- Croner, L. J., and E. Kaplan, 1995. Receptive fields of P and M ganglion cells across the primate retina, *Vis. Res.*, 35:7–24.
- Crook, J. M., B. Lange-Malecki, B. B. Lee, and A. Valberg, 1988. Visual resolution of macaque retinal ganglion cells, *J. Physiol. (Lond.)*, 396:205–224.
- Dacey, D. M., 1993. The mosaic of midget ganglion cells in the human retina, *J. Neurosci.*, 13:5334–5355.
- Dacey, D. M., 2000. Parallel pathways for spectral coding in primate retina, *Annu. Rev. Neurosci.*, 23:743–775.
- Dacey, D. M., and S. Brace, 1992. A coupled network for parasol but not midget ganglion cells in the primate retina, *Vis. Neurosci.*, 9:279–290.
- Dacey, D. M., and B. B. Lee, 1994. The blue-ON opponent pathway in primate retina originates from a distinct bistratified ganglion cell type, *Nature*, 367:731–735.
- Dacey, D. M., and M. R. Petersen, 1992. Dendritic field size and morphology of midget and parasol ganglion cells of the human retina, *Proc. Natl. Acad. Sci. USA*, 89:9666–9670.
- Dacheux, R. F., and E. Raviola, 1990. Physiology of HI horizontal cells in the primate retina, *Proc. R. Soc. Lond. B*, 239:213–230.
- De Lange, H., 1958. Research into the dynamic nature of the human fovea—cortex systems with intermittent and modulated light: I. Attenuation characteristics with white and colored light, *J. Opt. Soc. Am.*, 48:777–784.
- DeMonasterio, F. M., and P. Gouras, 1975. Functional properties of ganglion cells of the rhesus monkey retina, *J. Physiol. (Lond.)*, 251:167–195.
- Derrington, A. M., J. Krauskopf, and P. Lennie, 1984. Chromatic mechanisms in lateral geniculate nucleus of macaque, *J. Physiol. (Lond.)*, 357:241–265.

- De Valois, R. L., and N. P. Cottaris, 1998. Inputs to directionally selective simple cells in macaque striate cortex, *Proc. Natl. Acad. Sci. USA*, 95(24):14488–14493.
- Diamond, I. T., M. Conley, K. Itoh, and D. Fitzpatrick, 1985. Laminar organization of geniculocortical projections in *Galago senegalensis* and *Aotus trivirgatus*, *J. Comp. Neurol.*, 242:584–610.
- Dodge, F. A., B. W. Knight, and J. Toyoda, 1968. Voltage noise in *Limulus* visual cells, *Science*, 160:88–90.
- Dreher, B., Y. Fukada, and R. W. Rodieck, 1976. Identification, classification and anatomical segregation of cells with X-like and Y-like properties in the lateral geniculate nucleus of old-world primates, *J. Physiol. (Lond.)*, 258:433–452.
- Enroth-Cugell, C., and J. G. Robson, 1966. The contrast sensitivity of retinal ganglion cells of the cat, *J. Physiol. (Lond.)*, 187: 517–552.
- Enroth-Cugell, C., and R. M. Shapley, 1973. Flux, not retinal illumination, is what cat retinal ganglion cells really care about, *J. Physiol. (Lond.)*, 233:311–326.
- Famiglietti, E. V., and H. Kolb, 1976. Structural basis for ON- and OFF-center responses in retinal ganglion cells, *Science*, 194:193–195.
- Gilbert, C. D., and J. P. Kelly, 1975. The projections of cells in different layers of the cat's visual cortex, *J. Comp. Neurol.*, 163: 81–106.
- Gouras, P., 1968. Identification of cone mechanisms in monkey ganglion cells, *J. Physiol. (Lond.)*, 199:533–547.
- Gouras, P., and E. Zrenner, 1979. Enhancement of luminance flicker by color-opponent mechanisms, *Science*, 205:587–589.
- Hámori, J., P. Pasik, and T. Pasik, 1983. Differential frequency of P-cells and I-cells in magnocellular and parvocellular laminae of monkey lateral geniculate nucleus. An ultrastructural study, *Exp. Brain Res.*, 52:57–66.
- Hendry, S. H. C., and C. R. Reid, 2000. The koniocellular pathway in primate vision, *Annu. Rev. Neurosci.*, 23:127–153.
- Hendry, S. H. C., and T. Yoshioka, 1994. A neurochemically distinct third channel in the macaque dorsal lateral geniculate nucleus, *Science*, 264:575–577.
- Hochstein, S., and R. M. Shapley, 1976. Linear and nonlinear spatial subunits in Y cat retinal ganglion cells, *J. Physiol. (Lond.)*, 262:265–284.
- Ingling, C. R., and E. Martinez-Uriegas, 1983. The relationship between spectral sensitivity and spatial sensitivity for the primate r-g X channel, *Vis. Res.*, 23:1495–1500.
- Ingling, C. R., and Martinez-Uriegas, E. (1985). The spatiotemporal properties of the r-g X-cell channel, *Vis. Res.*, 25:33–38.
- Irvin, G. E., V. A. Casagrande, and T. T. Norton, 1993. Center/surround relationships of magnocellular, parvocellular, and koniocellular relay cells in primate lateral geniculate nucleus, *Vis. Neurosci.*, 10:363–373.
- Irvin, G. E., T. T. Norton, M. A. Sesma, and V. A. Casagrande, 1986. W-like response properties of interlaminar zone cells in the lateral geniculate nucleus of a primate (*Galago crassicaudatus*), *Brain Res.*, 362:254–270.
- Jenner, A. R., G. D. Rosen, and A. M. Galaburda, 1999. Neuronal asymmetries in primary visual cortex of dyslexic and nondyslexic brains, *Ann. Neurol.*, 46(2):189–196.
- Kaplan, E., and E. Benardete, 2001. The dynamics of primate retinal ganglion cells, in *Vision: From Neurons to Cognition* (C. Casanova and M. Ptito, eds.), *Prog. Brain Res.*, 134:1–18.
- Kaplan, E., B. B. Lee, and R. M. Shapley, 1990. New views of primate retinal function, in *Progress in Retinal Research* (N. N. Osborne and G. J. Chader, eds.), vol. 9. New York: Pergamon Press, pp. 273–336.
- Kaplan, E., and R. M. Shapley, 1982. X and Y cells in the lateral geniculate nucleus of macaque monkeys, *J. Physiol. (Lond.)*, 330:125–143.
- Kaplan, E., and R. M. Shapley, 1984. The origin of the S (slow) potential in the mammalian lateral geniculate nucleus, *Exp. Brain Res.*, 55:111–116.
- Kaplan, E., and R. M. Shapley, 1986. The primate retina contains two types of ganglion cells, with high and low contrast sensitivity, *Proc. Natl. Acad. Sci. USA*, 83:2755–2757.
- Krauskopf, J., and B. Farell, 1990. Influence of colour on the perception of coherent motion, *Nature*, 348:328–331.
- Kuffler, S. W., 1953. Discharge patterns and functional organization of mammalian retina, *J. Neurophysiol.*, 16:37–68.
- Lee, B. B., 1996. Receptive field structure in the primate retina, *Vis. Res.*, 36:631–644.
- Lee, B. B., P. R. Martin, and A. Valberg, 1989. Nonlinear summation of M- and L-cone inputs to phasic retinal ganglion cells of the macaque, *J. Neurosci.*, 9:1433–1442.
- Lennie, P., C. Trevarthen, D. Van Essen, and H. Wässle, 1990. Parallel processing of visual information, in *Visual Perception: The Neurophysiological Foundations* (L. Spillmann and J. S. Werner, eds.), San Diego: Academic Press, pp. 103–128.
- Leventhal, A. G., R. W. Rodieck, and B. Dreher, 1981. Retinal ganglion cell classes in the Old World monkey: morphology and central projections, *Science*, 213:1139–1142.
- Levitt, J. B., R. Schumer, S. M. Sherman, P. D. Spear, and J. A. Movshon, 2001. Visual properties of neurons in the LGN of normally reared and visually deprived macaque monkeys, *J. Neurophysiol.*, 85:2111–2129.
- Livingstone, M. S., and D. H. Hubel, 1984a. Specificity of intrinsic connections in primate primary visual cortex, *J. Neurosci.*, 4:2830–2835.
- Livingstone, M. S., and D. H. Hubel, 1984b. Specificity of intrinsic connections in primate primary visual cortex, *J. Neurosci.*, 4:2830–2835.
- Livingstone, M. S., and D. H. Hubel, 1987. Connections between layer 4B of area 17 and the thick cytochrome oxidase stripes of area 18 in the squirrel monkey, *J. Neurosci.*, 7:3371–3377.
- Livingstone, M. S., and D. H. Hubel, 1988. Segregation of form, color, movement, and depth: anatomy, physiology, and perception, *Science*, 240:740–749.
- Livingstone, M. S., G. D. Rosen, F. W. Drislane, and A. M. Galaburda, 1991. Physiological and anatomical evidence for a magnocellular defect in developmental dyslexia, *Proc. Natl. Acad. Sci. USA*, 88:7943–7947.
- Lynch, J. J., W. H. Merigan, and T. A. Eskin, 1989. Subchronic dosing of macaques with 2,5-hexanedione causes long-lasting motor dysfunction but reversible visual loss, *Toxicol. Appl. Pharmacol.*, 98:166–180.
- MacLeod, D. I. A., and R. M. Boynton, 1979. Chromaticity diagram showing cone excitation by stimuli of equal luminance, *J. Opt. Soc. Am.*, 69:1183–1186.
- McNeil, M. A., and R. H. Masland, 1998. Extreme diversity among amacrine cells: implications for function, *Neuron*, 20: 971–982.
- Merigan, W. H., and J. H. R. Maunsell, 1993. How parallel are the primate visual pathways? *Ann. Rev. Neurosci.*, 16:369–402.
- Mitzdorf, U., and W. Singer, 1977. Laminar segregation of afferents to lateral geniculate nucleus of the cat: an analysis of current source density, *J. Neurophysiol.*, 40:1227–1244.
- Norton, T. T., and V. A. Casagrande, 1982. Laminar organization of receptive-field properties in lateral geniculate nucleus of bush baby (*Galago crassicaudatus*), *J. Neurophysiol.*, 47:715–741.

- Norton, T. T., V. A. Casagrande, G. E. Irvin, M. A. Sesma, and H. M. Petry, 1988. Contrast-sensitivity functions of W-, X-, and Y-like relay cells in the lateral geniculate nucleus of bush baby, *Galago crassicaudatus*, *J. Neurophysiol.*, 59:1639–1656.
- Paulus, W., and A. Kröger-Paulus, 1983. A new concept of retinal colour coding, *Vis. Res.*, 23:529–540.
- Peichl, L., H. Ott, and B. B. Boycott, 1987. Alpha ganglion cells in mammalian retinae, *Proc. R. Soc. Lond. B*, 231:169–197.
- Perry, V. H., R. Oehler, and A. Cowey, 1984. Retinal ganglion cells that project to the dorsal lateral geniculate nucleus in the macaque monkey, *Neurosci.*, 12:1101–1123.
- Polyak, S. L., 1941. *The Retina*, Chicago: The University of Chicago Press.
- Przybylski, A. W., J. P. Gaska, W. Foote, and D. A. Pollen, 2000. Striate cortex increases contrast gain of macaque LGN neurons, *Vis. Neurosci.*, 17(4):485–494.
- Purpura, K., E. Kaplan, and R. M. Shapley, 1988. Background light and the contrast gain of primate P and M retinal ganglion cells, *Proc. Natl. Acad. Sci. USA*, 85:4534–4537.
- Purpura, K., D. Tranchina, E. Kaplan, and R. M. Shapley, 1990. Light adaptation in the primate retina: analysis of changes in gain and dynamics of monkey retinal ganglion cells, *Vis. Neurosci.*, 4:75–93.
- Quigley, H. A., 1999. Neuronal death in glaucoma, *Prog. Ret. Eye Res.*, 18(1):39–57.
- Reid, R. C., and R. M. Shapley, 1992. Spatial structure of cone inputs to receptive fields in primate lateral geniculate nucleus, *Nature*, 356:716–718.
- Rodieck, R. W., 1988. The primate retina, in *Comparative Primate Biology*, 4: *Neurosciences*, New York: Alan R. Liss, pp. 203–278.
- Rodieck, R. W., 1991. Which cells code for color? in *From Pigments to Perception* (A. Valberg, and B. B. Lee, eds), New York: Plenum Press, pp. 83–93.
- Rodieck, R. W., and R. K. Brening, 1983. Retinal ganglion cells: Properties, types, genera, pathways and trans-species comparisons, *Brain Behav. Evol.*, 23:121–164.
- Rodieck, R. W., and M. Watanabe, 1993. Survey of the morphology of macaque retinal ganglion cells that project to the pretectum, superior colliculus, and parvocellular laminae of the lateral geniculate nucleus, *J. Comp. Neurol.*, 338:289–303.
- Roorda, A., and D. R. Williams, 1999. The arrangement of the three cone classes in the living human eye, *Nature*, 397:520–522.
- Schiller, P. H., N. K. Logothetis, and E. R. Charles, 1990. Role of the color-opponent and broad-band channels in vision, *Vis. Neurosci.*, 5:321–346.
- Shapley, R., E. Kaplan, and R. Soodak, 1981. Spatial summation and contrast sensitivity of X and Y cells in the lateral geniculate nucleus of the macaque, *Nature*, 292:543–545.
- Shapley, R., and V. H. Perry, 1986. Cat and monkey retinal ganglion cells and their visual functional roles, *Trends Neurosci.*, 9:229–235.
- Shapley, R. M., and J. D. Victor, 1978. The effect of contrast on the transfer properties of cat retinal ganglion cells, *J. Physiol. (Lond.)*, 285:275–298.
- Shatz, C. J., 1981. Inside-out pattern of neurogenesis of the cat's lateral geniculate nucleus, *Soc. Neurosci. Abstr.*, 7:140(#47.4).
- Shatz, C. J., 1983. The prenatal development of the cat's retinogeniculate pathway, *J. Neurosci.*, 3:482–499.
- Sherman, S. M., and R. W. Guillery, 1996. The functional organization of thalamocortical relays, *J. Neurophysiol.*, 76:1367–1395.
- Sherman, S. M., R. A. Schumer, and J. A. Movshon, 1984. Functional cell classes in the macaque's LGN, *Soc. Neurosci. Abstr.*, 10:296.
- Sherman, S. M., J. R. Wilson, J. H. Kaas, and S. V. Webb, 1976. X- and Y- cells in the dorsal lateral geniculate nucleus of the owl monkey (*Aotus trivirgatus*), *Science*, 192:475–477.
- Silveira, L. C. L., and V. H. Perry, 1991. The topography of magnocellular projecting ganglion cells (M-ganglion cells) in the primate retina, *Neurosci.*, 40(1):217–237.
- Stone, J., 1983. *Parallel Processing in the Visual System*, New York and London: Plenum Press.
- Ungerleider, L. G., and M. Mishkin, 1982. Two cortical visual systems, in *Analysis of Visual Behavior* (D. J. Ingle, M. A. Goodale, and R. J. W. Mansfield, eds.), Cambridge, MA: MIT Press, pp. 549–586.
- Wässle, H., and B. B. Boycott, 1991. Functional architecture of the mammalian retina, *Physiol. Rev.*, 71:447–480.
- Werblin, F. S., and J. E. Dowling, 1969. Organization of the retina of the mudpuppy, *Necturus maculosus*. II. Intracellular recording, *J. Neurophysiol.*, 32:339–355.
- White, A. J. R., S. G. Solomon, and P. R. Martin, 2001. Spatial properties of koniocellular cells in the lateral geniculate nucleus of the marmoset *Calithrix jacchus*, *J. Physiol. (Lond.)*, 533:519–535.
- Wiesel, T. N., and D. H. Hubel, 1966. Spatial and chromatic interactions in the lateral geniculate body of the rhesus monkey, *J. Neurophysiol.*, 29:1115–1156.
- Willis, A., and S. J. Anderson, 2000. Effects of glaucoma and aging on photopic and scotopic motion perception, *Invest. Ophthalm. Vis. Sci.*, 41:325–335.
- Xu, X., M. J. Ichida, J. D. Allison, J. D. Boyd, A. B. Bonds, and V. A. Casagrande, 2001. A comparison of koniocellular, magnocellular and parvocellular receptive field properties in the lateral geniculate nucleus of the owl monkey (*Aotus trivirgatus*), *J. Physiol. (Lond.)*, 531:203–218.
- Yücel, Y. H., Q. Zhang, N. Gupta, P. L. Kaufman, and R. L. Weinreb, 2000. Loss of neurons in magnocellular and parvocellular layers of the lateral geniculate nucleus in glaucoma, *Arch. Ophthalmol.*, 118:378–384.
- Zeki, S., and S. Shipp, 1988. The functional logic of cortical connections, *Nature*, 335:311–317.

31 Parallel Visual Pathways: A Comparative Perspective

VIVIEN A. CASAGRANDE AND XIANGMIN XU

IN SPITE OF OBVIOUS differences between species, our knowledge of the structure and function of the human visual system is based almost entirely on extrapolation from studies in a very limited set of animal models. Although a variety of species have been used, the principal models for visual system studies continue to be domestic cats and macaque monkeys. These species, and others used less commonly, differ from humans in a number of respects including millions of years of separate evolutionary history, brain size, and visual behavior. The continued use of just a few species as models for the human visual system is defensible if the organization of the visual system is basically the same among species. Many differences, however, have been documented. For example, in cats the lateral geniculate nucleus (LGN) of the visual thalamus appears to have much more widespread connections with extrastriate cortex than in macaque monkeys or other primates. Differences in visual cortical architecture also have been documented among different primate groups including New and Old World simians and between Old World simians and apes and humans (Preuss, 2000).

Why have so few species been accepted as adequate models? Other than issues of practicality, one reason is that many features of the visual system of mammals appear to be shared across a range of species. Hubel and Wiesel, beginning with their seminal work more than 40 years ago, showed that the basic receptive field organization of cells in the LGN and the primary visual cortex (also called *striate cortex*, *area 17*, or *V1*) of cats and macaque monkeys is quite similar (see Hubel and Wiesel, 1998, for review). They demonstrated that LGN cells respond well to spots of light presented to one eye and, like their retinal ganglion cell inputs, demonstrate center-surround receptive fields of two types: ON or OFF center, with surrounds of opposing sign (Wiesel and Hubel, 1966). In V1 of cats and macaque monkeys, they demonstrated that cells tend to be binocular, are selective for the orientation of a bar of light, and exhibit a systematic organization of orientation preference across cortex. These same features have now been demonstrated in a wide range of mammals, suggesting that they represent general features of the mammalian visual system (LeVay and Nelson, 1991). Nevertheless, as we learn more details about

the visual system, more species differences are being uncovered. The important issue is how we interpret both similarities and differences. In this chapter, we argue that species differences as well as similarities can provide important clues, not only about the organization of the human visual system, but also about how the visual system works. A comparative approach is particularly important in translating findings to humans since the possibilities of direct investigations in humans are so limited.

In this chapter, we focus primarily on primate relatives of humans. The chapter is further limited to an analysis of parallel pathways at the early levels of visual processing from the retina through the LGN to V1. The main purpose of the chapter is not to rehash current views on parallel visual pathways in primates but to point out key issues that remain to be resolved, as highlighted by the comparative perspective. Given that the cat visual system has been studied in the most detail, especially at these early levels of visual processing, comparisons with this species are included. Where relevant, other nonprimate species are also mentioned. Some issues have been omitted, and those concern the segregation of ocular inputs and the segregation of pathways concerned with ON-center and OFF-center responses.

This chapter is divided into six sections in addition to this introduction. The first of these sections highlights key findings from different schools that led to today's views of parallel processing within the visual system. The second section outlines how newer findings have altered the two-pathway view of retinogeniculocortical organization in primates. The third section discusses how the different pathways exiting the LGN are organized within the primary visual cortex (V1). The fourth section considers the functional significance of the parallel LGN pathways within V1. The final two sections are devoted to summaries of key points and an outline of the main questions that remain to be resolved.

Separate visual pathways: a little history

Beginning with the prize-winning work of Gasser and Erlanger (1929) on the somatosensory system, it has been recognized that different qualities within a sensory modality can be transmitted via parallel pathways that are

morphologically distinct. In the somatosensory system, it was suggested that different sensations within a single cutaneous nerve (e.g., pain and temperature versus light touch and pressure) might be carried via axons of different caliber and conduction velocity. By analogy, George Bishop (1933) subsequently argued that the three groups of axons that he identified in the optic nerve of the rabbit, based on axon size and conduction latency, were evidence of parallel processing for visual qualities, although he later changed his mind and argued that axon fiber size reflected evolutionary history (Bishop, 1959). Today the idea that separate retinal ganglion cell classes transmit different sensory messages to the brain is accepted as a basic organizational principle. The issues that remain controversial concern the number of pathways that exist, homologies among pathways across species, the exact content of these pathways, and how these pathways relate to different perceptual attributes.

How we think about parallel processing is a product of several distinct approaches to the problem. Outlined below are four lines of investigation that have strongly impacted our views of parallel processing in the visual system. First, in the mid-1960s, Enroth-Cugell and Robson (1966) sparked a revolutionary shift in thinking about visual processing. Approaching the visual system from an engineering standpoint, they proposed that the visual system works as a series of spatial filters, namely, as spatial-frequency analyzers. The idea was that the visual system represents objects by tuning different cells to different ranges of spatial frequency. Enroth-Cugell and Robson (1966) used this linear systems approach to analyze the responses of ganglion cells in the cat retina. This, in turn, was followed by the application to visual psychophysics of Campbell and Robson (1968). This general approach then led to a flood of studies based on the idea that the visual system's response to any pattern could be predicted from its response to more basic components. In their original work, Enroth-Cugell and Robson (1966) subdivided concentrically organized ON- and OFF-center retinal ganglion cells in cats into two types on the basis of their spatial summation properties. Those that summed luminance changes linearly across their receptive fields were called *X cells*, and those that did not were called *Y cells*. In their report, the authors also described other features that distinguished Y from X ganglion cells including the higher conduction velocities, sensitivity to higher speeds and lower contrasts, lower spatial frequency cutoffs, larger average receptive field center sizes, and more transient responses of Y versus X cells (Enroth-Cugell and Robson, 1966). More than a decade of studies on X and Y cells followed these seminal findings. These studies showed that X and Y cells also could be distinguished based on different distributions in the retina, parallel central projections, and morphology (reviewed by Stone, 1983). From this constellation of traits, it was proposed that X cells were part of a channel

to cortex that subserves high-resolution pattern vision, while Y cells were part of a channel that subserves crude form and motion vision (Stone, 1983). Also during this time, other cell types were discovered in the cat retina that were collectively called *W cells*. From the beginning, it was clear that unlike X and Y cells, which show relatively low within-group variability, the response properties of W cells varied widely, having perhaps little more in common than the attribute of low conduction velocity (see Kaplan, 1991; Stone, 1983, for review). Because many W cells were shown to have heavy projections to the midbrain, it was proposed that they subserved a more primitive form of vision referred to as *ambient vision*. X and Y cells, by contrast, provided *focal vision*, or vision that required cortex. *Ambient vision* was seen as an almost unconscious primitive ability to orient to objects and move through the environment found in all vertebrates, while *focal vision* was seen as the conscious vision used to identify objects typical of primates. The analysis of X, Y, and W cells in cats also led later to a similar set of investigations in primates, where both similarities and differences between cats and primates were uncovered (see Casagrande and Norton, 1991, for review). We will return to the issue of species differences in parallel processing in the next section.

The ambient/focal vision idea was actually linked to a second very influential set of investigations that also began in the 1960s. In 1969 Schneider published an important article in which he proposed that there was an anatomical separation between visual coding of the location of a stimulus and its identification. Based on behavioral/lesion work in hamsters, he argued that there were two pathways: a *where* pathway involving the superior colliculus and a *what* pathway involving the visual cortex (Schneider, 1969). The *where* versus *what* or ambient versus focal pathways were subsequently modified and described as independent pathways, one involving a pathway from colliculus to pulvinar to extrastriate cortex and the other involving the geniculostriate pathway (Casagrande et al., 1972; Diamond and Hall, 1969). The idea that these pathways were capable of independent operation was demonstrated clearly in tree shrews, in which complete removal of striate cortex and complete degeneration of the LGN does not impair discrimination of simple patterns or acuity (Ware et al., 1972, 1974). The dual pathway idea more recently has been suggested as an explanation for the *blind sight* exhibited by humans in the absence of visual cortex (Ungerleider and Mishkin, 1982).

In 1982 the idea of two visual systems *where* versus *what*, took a different form. Ungerleider and Mishkin (1982) proposed that visual object identification (*what*) depended on connections to the temporal cortex, while object location (*where*) required the parietal cortex. They also argued that both areas required primary visual cortex (V1) based on their own data from other lesion studies in monkeys, as well as from human clinical studies. The cortical version of the

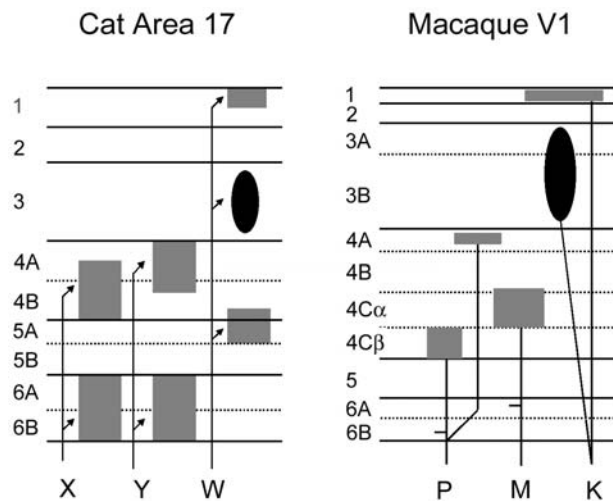


FIGURE 31.1 LGN projection patterns to visual cortex of cats and macaque monkeys. *Left*: projections from the LGN to V1 in the cat. X and Y LGN cells send axons to layers 4 and 6. W cells project CO blobs in layer 3 and to layers 1 and 5a. *Right*: projections from the LGN to V1 in macaque monkey. M and P cells project, respectively, to layers 4C α and 4C β while K cells project to the CO blobs in layer 3 and to layer 1. In addition, P cells have been proposed to send axons to layer 4A. LGN projections to layer 4A are missing in apes, humans, and some other primates. Some M and a few P cells have collateral branches terminating sparsely in layer 6. See text for details. (*Left*: Data from Boyd and Matsubara, 1996; Humphrey et al., 1985; Kawano, 1998; *Right*: modified from Casagrande and Kaas, 1994, with permission of the publisher.)

what versus *where* hypothesis suggested that if the two visual systems originated subcortically, they must both pass through the LGN.

A third avenue of investigations involved efforts to define pathways based on anatomy. The advent of new technologies for tracing degenerating pathways in the 1950s and 1960s, and for anterograde and retrograde transport of tracers in the 1970s and 1980s, provided details of the connections of parallel pathways from retina to the LGN and from the LGN to the cortex in several species. For example, these studies clearly showed that different retinal ganglion cell classes projected to separate cell classes in the cat LGN and to separate layers of the LGN in all primate species examined (Casagrande and Norton, 1991). In addition, studies showed that the parallel arrangement of connections from the retina continued to V1, where X, Y, and W LGN cells in cats, and parvocellular (P) and magnocellular (M) and subsequently koniocellular (K) LGN cells in primates, were shown to project in parallel to separate layers of V1 (Fig. 31.1; see Casagrande and Kaas, 1994; Sherman and Guillery, 2001, for review).

Finally, in the 1980s, a set of studies was published by Livingstone and Hubel (1988) outlining their hypothesis that different attributes such as form, color, and motion were

segregated within the layers and cytochrome oxidase (CO) blob compartments of V1 (Fig. 31.2). They linked various ideas described above together in a very satisfying model. According to this model, the P retinogeniculocortical pathway (form and color) projects ultimately to the what pathway ending in the temporal lobe and the M retinogeniculocortical pathway (motion) to the where pathway in the parietal lobe. Evidence to support the links between the P pathway and form/color and the M pathway and motion came primarily from physiology and connectional anatomy. Physiological studies had shown that P LGN cells exhibit chromatic opponency and have high spatial resolution, and that M cells are not selective for wavelength but exhibit high temporal resolution (reviewed in DeYoe and Van Essen, 1988; Livingstone and Hubel, 1988). Livingstone and Hubel and others provided evidence that linked the P pathway to the CO blob and interblob compartments in cortical layer 3 with appropriate output pathways to the what hierarchy of extrastriate visual areas, as well as evidence that the M pathway connected to the where hierarchy of visual areas via connections within V1 layer 4B (Fig. 31.2). The K pathway was ignored, in part, because it did not fit well with the model and had not been studied in as much detail (Casagrande, 1994; Hendry and Reid, 2000). Nevertheless, it was already known at that time that the K LGN pathway terminated in patches that appeared to coincide with the CO blobs in V1 in macaque monkeys (Livingstone and Hubel, 1982).

The degree of synthesis provided by Livingstone and Hubel's (1988) view of the visual system had a powerful impact on current thinking about the organization of the human visual system. Because of the simplicity of the model, things that did not fit were set aside as ever more streamlined diagrams of the original appeared in textbooks. Recently, however, as more data have been gathered in a variety of primates and in other species, findings have been presented that raise questions about the model. Examples are provided in the next section.

How many parallel retinal pathways project to and through the primate LGN?

In the parallel processing model of Livingstone and Hubel (1988), P and M pathways are the only pathways considered. Since their model was first published, a number of studies have appeared that have added controversy and complexity to the original proposal. Instead of just 2 major retinal pathways (P and M) to the LGN, as many as 10 morphologically distinct classes of ganglion cells have now been identified that project to the macaque monkey LGN, excluding ON-center and OFF-center cells of the same class (see Dacey, 1999, 2000; Dacey et al., 2001; Rodieck and Watanabe, 1993). Of these, at least five types have also been physiologically classified.

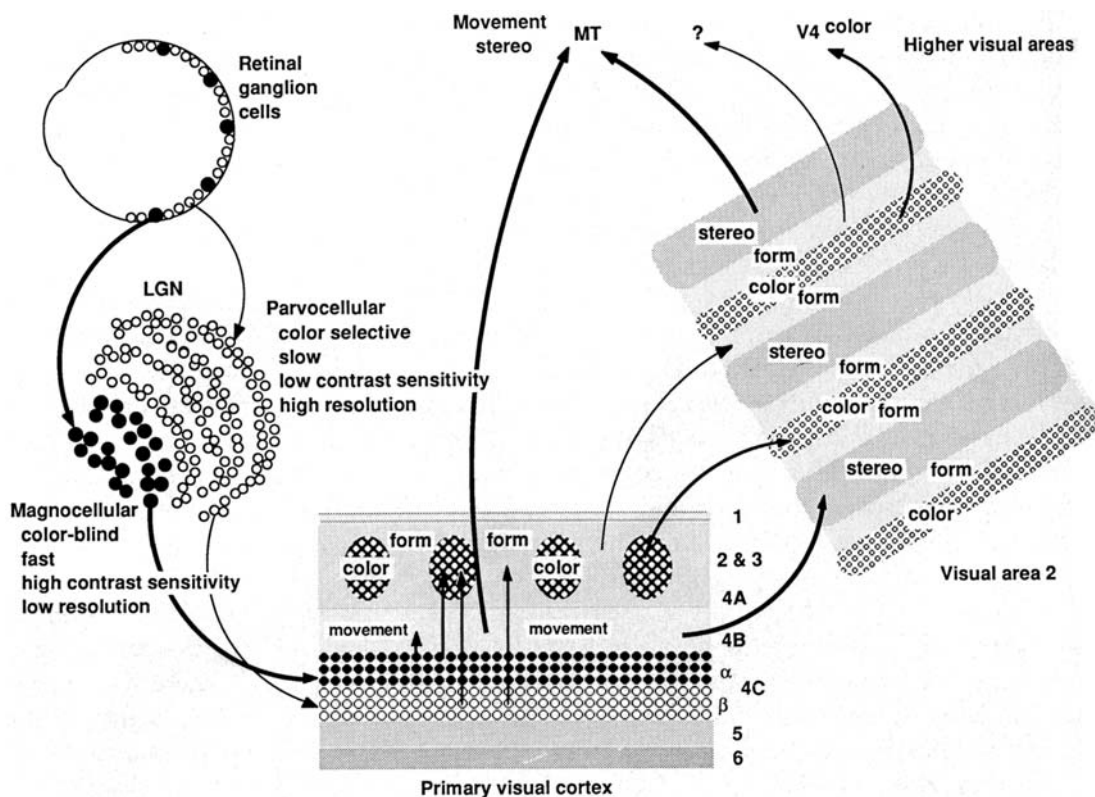


Figure 31.2 Diagram of the functional segregation of the primate visual system. *MT*, middle temporal area; *V4*, visual area 4; *LGN*, lateral geniculate nucleus. (From Livingstone and Hubel, 1988, with permission of the publisher.)

Within the LGN of all primates studied, it is now recognized that P and M LGN cells can be distinguished from K LGN cells based on their neurochemical signatures (Casagrande, 1994; Hendry and Reid, 2000). P and M relay cells contain the calcium binding protein parvalbumin, and K cells contain the calcium binding protein calbindin-D28k. K layers distinguished by the immunomarker calbindin are located primarily (although not exclusively) below all P and M layers. For ease of identification, these small cell layers are numbered from K1 to Kn beginning at the optic tract (Ding and Casagrande, 1997). It is now also established in several simian primates that cells in K3 project principally, although not exclusively, to the CO blobs in cortical layer 3, while those in K1/K2 project mainly to cortical layer 1 (Casagrande et al., 1997; Ding and Casagrande, 1997). It is not entirely clear, however, which LGN cell classes receive input from the 10 ganglion cell classes currently identified as projecting to the LGN from the retina in macaque monkeys. In a number of primate species, midget ganglion cells project to P LGN layers and parasol ganglion cells project to M LGN layers (Dacey, 1999; Rodieck and Watanabe, 1993; Yamada et al., 1998), but the question remains, which LGN cells receive input from the other ganglion cells that project to the LGN?

There is evidence to suggest that the small bistratified ganglion cells, identified as excited by S cone inputs (blue ON),

project to the K3 LGN layer in marmosets (Martin et al., 1997; White et al., 1998) and to layers K3 and K4 in macaque monkeys (Reid et al., 1997). Because K3 axons terminate within the CO blobs, a revision of the Hubel/Livingstone model has been proposed in which the K channel now becomes an S cone color channel (Dobkins, 2000). According to this revised view, S cone signals are sent directly to the CO blobs by means of the K pathway, while L and M cone signals reach the CO blobs indirectly from P channel projections that terminate within 4C β . This still leaves the P pathway performing both as a color and as a high-resolution spatial vision channel. Calkins and Sterling (1999) have gone one step further by proposing that midget ganglion cells that innervate P LGN cells cannot transmit chromatic opponency to the LGN due to the wiring of their surrounds (Dacey, 1996). The surrounds depend on either horizontal or amacrine cell connections; both horizontal and amacrine cells have been found to receive mixed-cone, not single-cone, connections (see Calkins and Sterling, 1999; Dacey, 2000, for review). According to this model, the L and M cone (red and green) channels must project through a nonmidget ganglion cell class: perhaps another type of ganglion cell that sends input to the K pathway. This could mean that all chromatic information reaching V1 travels through the K pathway to the CO blobs (Hendry and Reid, 2000). Other than evidence that the midget to P LGN cell

pathway may not carry pure cone opponent signals, this proposal has appeal if one assumes that true color opponent cells occur in low numbers in the retina and LGN (Calkins and Sterling, 1999). A sparse projection could force cortical terminations to become patchy in order to maintain retinotopic coverage in cortex, thus explaining the presence of CO blobs (Calkins and Sterling, 1999). It is noteworthy in this regard that, even in cats, the only chromatically sensitive retinal ganglion and LGN cells that have been identified are W cells, and these were found to be excited by S cones and inhibited by M cones (Cleland and Levick, 1974). W cells in cats also project to CO blobs (Boyd and Matsubara, 1996).

Appealing as this new proposal is, there are several issues that do not fit. The first concerns the number of K cells required to support both the S and L/M cone channels in macaque monkeys. Counts of K cells immunolabeled with calbindin and α CamII kinase (another marker for K cells in macaque monkeys) have provided evidence that there are too few cells within the foveal and parafoveal representation in macaque LGN to support the acuity of both color channels to cortex (Song et al., 2001). Moreover, in marmosets, only 20% of the total K cell population were found to carry S cone signals; none were found to be L/M cone opponent (White et al., 1998). In the same study, however, two types of P cells were identified: P cells that were L/M opponent and P cells that did not respond selectively to different cone inputs but had good spatial resolution. These same two classes bear a resemblance to the type I and type III P LGN cells identified originally by Wiesel and Hubel (1966). Taken together, these findings suggest that there are two classes of P cells and two classes of K cells but that both P and K channels transmit information related to one color channel, at least in Old World macaque monkeys and New World marmosets. Add to these data new findings indicating that there are two ganglion cell classes in addition to the small bistratified ganglion cells that transmit S cone signals to macaque LGN (Dacey et al., 2001), as well as older data showing that cells responding to S cones as well as to L/M cones have been identified in P layer targets in V1 in macaques and squirrel monkeys (reviewed in LeVay and Nelson, 1991), and the picture becomes even more complex.

Another issue concerns the function of K cells in nocturnal primates that lack S cones such as bush babies and owl monkeys (Jacobs et al., 1996). Both of these primate species have only a single cone type (an M cone), and both have morphologically identified midget and parasol ganglion cells as well as a variety of smaller ganglion cells, although owl monkeys apparently lack small bistratified ganglion cells that carry some of the S cone signals (Yamada et al., 2001). Both bush babies and owl monkeys have well-developed calbindin-positive K layers within the LGN that project to well-defined CO blobs (Casagrande, 1994; Johnson and Casagrande, 1995). Presumably some K cells and some CO

blob cells perform noncolor functions that are defined by inputs from as yet to be classified ganglion cells. Additional evidence for heterogeneity among K cells comes from detailed physiological studies of their spatial and temporal properties in bush babies (Norton et al., 1988), owl monkeys (Xu et al., 2001), and marmosets (White et al., 2001). Given the proposal that diurnal primates arose from a nocturnal common ancestor, it seems likely that the origin of the K pathway and projections to the CO blobs arose originally to support some function or functions other than the processing of chromatic signals, with color processing being added later in evolution (Heesy and Ross, 2001). We consider this issue and the evidence for and against continued functional segregation of LGN parallel pathways within V1 in the next section.

How are parallel LGN pathways organized in V1?

As reviewed above, at least three classes of cells can be distinguished within the LGN based on morphology and physiology in all primates examined, as well as in cats. The basic patterns of geniculate to V1 projections that have been documented in primates and cats suggest that X/P medium-sized LGN cells send axons principally to the lower half of cortical layer 4, Y/M large LGN cells send axons principally to the upper half of cortical layer 4, and K/W small LGN cells send axons mainly to layers above 4 (Fig. 31.1). This pattern of projections appears to represent a basic mammalian plan since it has been identified (with some variation) in several other species (Casagrande and Kaas, 1994). Given the ever-increasing number of classes of retinal ganglion cells that project to the macaque LGN, as well as the many types that have been found previously to project to the LGN of cats (discussed in Isayama et al., 2000), it seems reasonable to suggest that more than three ganglion cell classes is the rule, not the exception. Unfortunately, markers such as the calcium binding proteins parvalbumin and calbindin, even combined with cell size, are not sufficient to distinguish the targets of all of these ganglion cells within the LGN of any species, assuming that the pathways remain separate at this level. Clues about how many pathways are maintained in parallel to and through the LGN to cortex can be gained by examining detailed termination patterns of these axons in primate V1 and connections within V1 itself. Several examples follow.

Within primate V1, there is evidence that projections within and among layers and compartments are more precise and complex than was originally believed. For example, in both macaque monkeys and owl monkeys there is evidence that the main recipient layer, Brodmann's (1909) layer 4C, consists of three, not two, tiers. Morphologically, this tripartite organization was originally noted in Nissl-stained sections in macaque monkeys (Lund, 1988). In owl

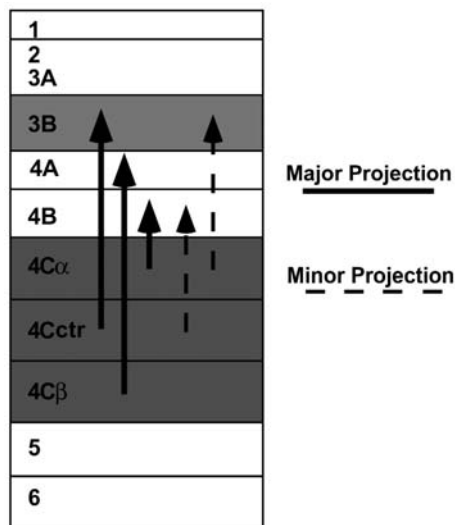


Figure 31.3 Projections from layer 4C to the supragranular layers in V1 of owl monkey. Layer 4C α projects principally to layer 4B, 4C β to 4A, and 4Cctr to 3B. Layer 3A, the major output layer to area V2, receives signals from layer 4 only indirectly via other subdivisions of layer 3 and layer 5. See text for details. (From Boyd et al., 2000, with permission of the publisher.)

monkeys, in vivo studies tracing connections based on small laminar injections revealed that the three tiers of layer 4C projected to different targets within the upper cortical layers (Boyd et al., 2000). As shown in Figure 31.3, cells in 4C β project to 4A, cells in 4Cctr project to 3B, and cells in 4C α project to 4B (Boyd et al., 2000). Intracellular filling of cells in slice preparations within layer 4C in macaque monkeys has identified similar sets of projections (Yabuta and Callaway, 1998). There is also evidence from axon reconstructions in macaque monkeys (Blasdel and Lund, 1983) and in bush babies (Florence and Casagrande, 1987) that axon arbors of some P and some M LGN cells extend through layer 4Cctr, while others are restricted to the top and bottom tiers. Add to these anatomical data the physiological evidence given above that there may be two P LGN cell classes, one color opponent and the other not, as well as evidence suggesting that there are two M LGN cell classes based on linearity of spatial summation in macaque monkeys (Kaplan and Shapley, 1982), and we now have four LGN cell classes projecting to layer 4C of V1.

Examination of LGN projections and connections to cortical layers above layer 4C adds to the complexity. Layer 4A has been proposed to receive input from P cells in macaque and squirrel monkeys (Lund, 1988), yet recent data suggest that cells in this layer in macaque monkeys are excited by S cone stimulation (blue ON), indicating that these cells also could receive input from a class of LGN K cells (Wandell et al., 2002). It is noteworthy that apes (e.g., chimpanzees) lack LGN input to layer 4A (Tigges and Tigges, 1979) and that humans probably also lack such input based on CO stain-

ing (Horton and Hedley-Whyte, 1984; Wong-Riley et al., 1993), even though 4A has been described cytoarchitecturally in humans (Yoshioka and Hendry, 1995). If this is true, it suggests that humans and apes lack this particular blue ON channel since they appear not to have LGN projections to cortical layer 4A, projections that are also lacking in the nocturnal primates owl monkeys and bush babies (Casagrande and Kaas, 1994). Why humans and apes that clearly have S cones would not also have a projection to layer 4A remains a mystery, although the recent discovery of a second class of blue ON ganglion cells in macaques suggests that S cones may not be restricted to a single channel (Dacey et al., 2001). Nevertheless, the fact that layer 4A is morphologically distinct and has unique intracortical projections, even in primates that lack direct LGN input to this layer, would indicate that layer 4A performs a specialized role in most primates.

Cortical layers above 4A receive projections from at least two classes of K axons, those that project primarily to the CO blobs within layer 3B and those that project primarily to cortical layer 1 from the ventral most K layers, LGN layers K1/2 (Ding and Casagrande, 1997). The latter pattern has been demonstrated in both nocturnal (owl monkeys) and diurnal (macaque and squirrel monkeys) Old and New World primates, so it appears to remain independent of lifestyle or phylogenetic history (Casagrande, 1994; Hendry and Reid, 2000). In prosimian bush babies, K layer connections also have been demonstrated to project to the CO blobs and layer 1 (Lachica and Casagrande, 1992). In bush babies, however, no investigations have been done of the more ventral K layers to see if these send axons primarily to layer 1. Given the heterogeneity of the axon projection patterns of K cells even in macaque monkeys (Fig. 31.4A) and the physiologically demonstrated heterogeneity of K cells in the LGN level in several primate species (see above and Fig. 31.4B,C), it seems likely that more than two K axon classes project above cortical layer 4A.

Combining the above data, the following picture of parallel input pathways emerges (Fig. 31.5A). Four classes of LGN axons project to cortical layer 4C, two P and two M classes. Layer 4A receives input from either K or P axons or both, but only in a subset of nonhominid primates. LGN axonal projections above layer 4A come from two or more classes of K axons. Interestingly, in other species such as cats, there also is evidence that X, Y, and especially W cells contain subgroups. Lagged and nonlagged X and Y cells have been described (Saul and Humphrey, 1990). Evidence also suggests that the Y cells within the C lamina and/or the medial interlaminar nucleus (MIN) in cats are not functionally equivalent to those in the A laminae (Boyd et al., 1998). W cells within the parvocellular C laminae of cats have been subdivided into at least two classes, W1/Q and W2, or tonic and phasic cell classes, as well as other types (Rowe and Cox,

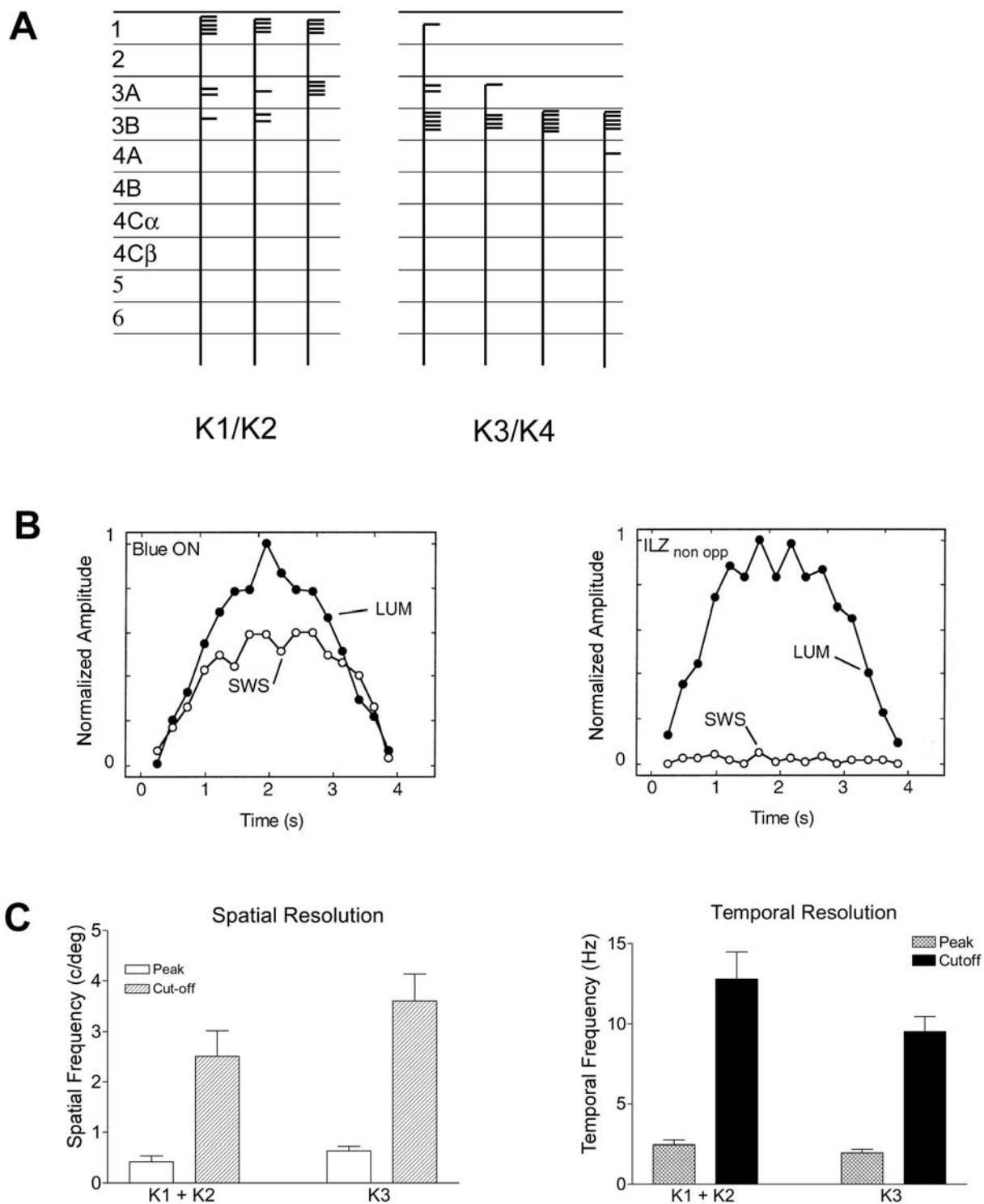


Figure 31.4 Morphological and physiological heterogeneity of K cells. *A*, In macaque monkeys, the geniculocortical projections from different K layers are morphologically distinct; axons from LGN layers K1/K2 mainly project to cortical layer 1, while axons from LGN layers K3/K4 chiefly terminate in cortical layer 3. *B*, Responses of different K cells to a short-wavelength-sensitive (SWS) isolating stimulus and luminance stimulus (LUM). About 20% of K cells in the marmoset LGN are blue ON cells (shown in *B* on the left) and respond to the SWS stimulus; 80% of K cells

[also called *interlaminar zone (ILZ)* cells] show no response to the SWS stimulus (shown in *B* on the right). *C*, Spatial and temporal characteristics of owl monkey K cells in different LGN layers exhibited differences. Cells in K1/K2 tend to be selective for lower spatial frequencies and higher temporal frequencies than cells in layer K3. (*A* from Casagrande et al., 1997; *B* modified from White et al., 1998, with permission of the publisher; *C* modified from Xu et al., 2001, with permission of the publisher.)

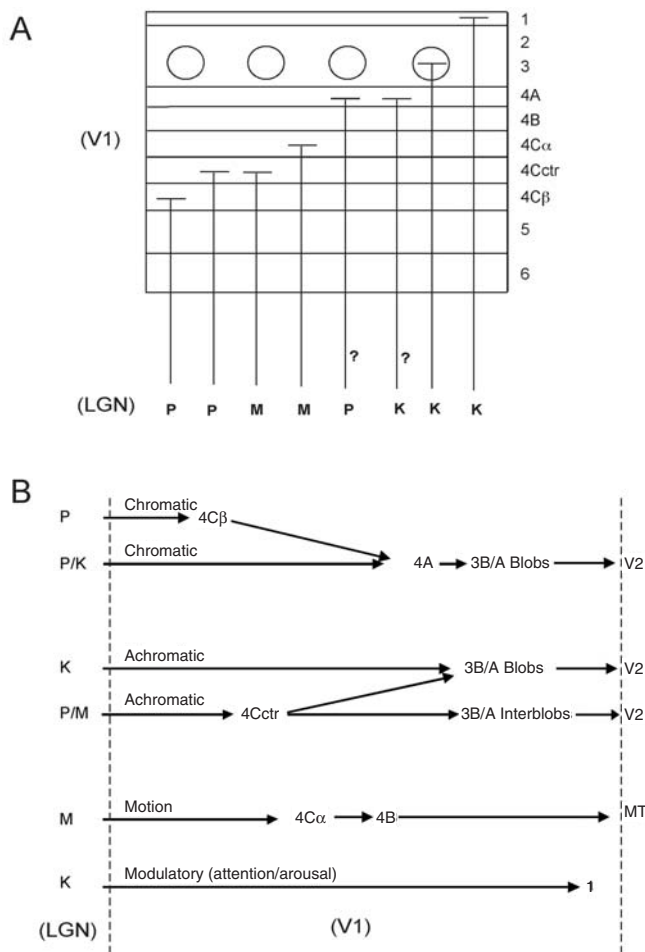


Figure 31.5 Parallel pathways from the LGN to V1 in macaque monkey. *A*, Eight parallel pathways are shown from the LGN to the cortical layers of V1 in macaque monkey: three P channels, three K channels, and two M channels. The circles within layer 3 represent the CO blobs. It is unclear whether K, P, or both pathways project to layer 4A. It is noteworthy that LGN projections to layer 4A represent a specialization of some simians only; chimpanzees, humans, owl monkeys, and bush babies lack this pathway. The layers of cortex are indicated by Arabic numerals. *B*, Connections and possible functions of the eight parallel pathways within V1. In this diagram the ventral to dorsal sequence of layers in V1 is laid out from left to right. V1 projects directly to different compartments within V2 and to area MT. Not shown: V1 also sends axons to DM/V3a which exit from CO blob columns, to area V3, and to area V4. See text for details.

1993; Sur and Sherman, 1982; Troy et al., 1995). All of these data argue against a simple two-channel model for parallel pathways to and through the LGN.

Functional implications of multiple LGN channels to V1

WHY HAVE TWO M CHANNELS? If primates have multiple M, P, and K channels to V1, what are the functional implications of such a model? First, beginning with the M LGN

cells, Blasdel and Lund (1983) found two classes of M axons terminating in layer 4C α in macaque monkeys. The majority of axons arborized throughout layer 4C α , with minor or no collateral input to layer 6, while the arborizations of the others were restricted to the upper half of layer 4C α , with extensive collaterals in layer 6. Later, it was theorized that differences in receptive field sizes and contrast sensitivities in these two populations could account for changes in these properties with depth in layer 4C (Bauer et al., 1999; Lund et al., 1995). Cells at the top of 4C α have larger receptive fields and higher contrast sensitivity than cells deeper within 4C α . In addition, like cells in 4B, many cells at the top of 4C α are orientation and direction selective. This arrangement suggests that the M LGN cells projecting to 4C α are part of a channel allowing for rapid transmission of information important to stimulus motion directly to dorsal stream areas like the middle temporal (MT) visual area via cortical layer 4B or possibly even via synapses on dendrites of large 4B pyramidal cells that dip into 4C α (Fig. 31.5*B*). In cats, the class of Y cells that projects beyond area 17 may play a similar role, providing rapid transmission of motion information to higher areas. One could speculate that in the latter case the transmission is even more direct and unfiltered simply because the lifestyle of cats requires a very rapid reaction to motion.

Why then would one need two M channels? In the most basic sense, P and M populations of LGN cells represent two ends of a continuum in the spatial and temporal frequency domains (Schiller et al., 1990). Either channel alone allows for a much more limited sampling of spatial and temporal frequencies, a limitation imposed at the retina simply because ganglion cells cannot have both small and large dendritic fields simultaneously. The second M channel terminating within layer 4C α could, along with an achromatic P channel, provide the full range of basic spatial and temporal information to cells in the ventral stream concerned with object identification through connections with cortical layer 3 cells.

WHY HAVE TWO P CHANNELS? Dacey (2000) has proposed that the unique midget cell architecture of the fovea evolved first to permit high spatial resolution, which demands cones, and only recently evolved to carry color opponent L/M channels in Old World primates. If one P channel is transmitting information about spatial detail, the other is presumably a color channel. P input in 4C β , with its heavy projections to layer 4A, could represent such a chromatic channel, at least in those primate species that have color vision (Fig. 31.5*B*). Color-selective nonoriented cells have been reported in layers 4C β and 4A, at least in macaque monkeys (see LeVay and Nelson, 1991, for review). As mentioned earlier, it is unclear whether layer 4A also receives input from a subset of K cells, from P cells, or from

both cell classes. Interestingly, physiological studies have noted two populations of cells within layer 4A (Blasdel and Fitzpatrick, 1984). Perhaps both P and K LGN cells project to 4A. Unfortunately, older studies claiming that P LGN cells project to layer 4A were based on tracer injections that included the K layers lying below each P layer (Lund, 1988).

WHY SEGREGATE K AXONS TO THE CO BLOBS? The only documented direct input (based on axon reconstruction) to the cortical layers dorsal to layer 4A are K axons in primates. These K axons are restricted to CO blobs within layer 3B, leaving the interblob columns in layer 3 free of any direct LGN input; K axons also appear to project to all of layer 1 (Casagrande et al., 1997; Ding and Casagrande, 1997; Lachica and Casagrande, 1992). This arrangement certainly suggests that CO blobs and interblobs within layer 3 perform different functions. Also, the fact that CO blobs can be distinguished neurochemically in several other ways from interblobs (Wiencken and Casagrande, 2000) argues that these two compartments do different things. The original proposal from Livingstone and Hubel (1988) was that the CO blobs send signals to extrastriate areas that are relevant to color, while the interblobs are concerned with putting together signals to support form vision. Although this scenario would fit data from diurnal monkeys, it does not fit data from nocturnal primates that appear to have the same direct K LGN projections to CO blobs and the same basic arrangement of intracortical connections in V1 (Casagrande and Kaas, 1994). Interestingly, one difference was found between diurnal and nocturnal simians in the microcircuitry of the CO blobs (Shostak et al., 2002). The subset of K axons that synapse on dendritic shafts in diurnal macaque and squirrel monkeys synapse on significantly larger shafts than in the nocturnal owl monkey. Shostak et al. (2002) have argued that it is possible that the latter shift represents a loss of K axons that carry S cone signals in owl monkeys. Since the majority of K LGN cells probably do not carry color signals anyway (see above) and cannot carry these signals in nocturnal species, we are still left with the question of why the CO blobs exist. Clearly, CO blobs are not necessary for good color vision since many species, such as tree shrews and ground squirrels, have excellent color vision but no CO blobs (Jacobs, 1993; Wong-Riley and Norton, 1988). CO blobs, however, appear to be a universal feature of primate V1. What primates do, more than other species, is to use vision to analyze objects that they manipulate. Cortical layer 3, which sends information into the ventral stream, is particularly well developed in primates. One possibility is that the special demands of high-level object vision require that stimulus attributes be combined in several different ways to support the variety of analyses performed by the ventral stream hierarchy of areas. The compartments within the

CO blobs and interblobs that extend throughout layers 2 and 3 may provide the substrate of the variety of combinations necessary. Further support for this scenario comes from the fact that so many distinct extrastriate visual areas receive input directly from cells located within cortical layer 3, including different compartments within area V2 and areas V3 and V3a and its presumed homolog, the dorsal medial area (DM) (Beck and Kaas, 1999).

An interesting proposal by Allman and Zucker (1990) on the function of CO blobs suggested that cells in CO blobs are designed to analyze scalar variables related to the intensity of the stimulus such as brightness, color contrast, and texture, while interblobs are designed for analysis of geometrical variables such as orientation preference and possibly more complex binocular interactions. From a phylogenetic perspective, this proposal still has considerable appeal since this segregation of function could have evolved first in the absence of color vision, with color contrast added later. CO-blob cells are in a position to integrate the full range of information from different K axons directly and P and M axons indirectly. In this respect it is noteworthy that in cats Cleland and Levick (1974) recorded from an S cone-driven W cell that appeared to substitute rod input for S cone input under scotopic conditions. There have also been other reports in primates that LGN cells carrying S cone signals exhibit rod input under dark-adapted conditions (Virsu et al., 1987). M cells also carry rod signals (Virsu et al., 1987) and tend to have a larger input to CO blobs than to interblobs. Taken together, all of these inputs could provide CO-blob cells with the ability to maintain constancy over a very broad range of stimulus intensities and wavelengths under both scotopic and photopic conditions. From this perspective, it would be interesting to know whether there are any differences in the responses of CO-blob and interblob cells under photopic versus scotopic conditions, as would be predicted by such a model.

WHY SEND LGN SIGNALS TO CORTICAL LAYER 1? As reviewed earlier (Casagrande, 1994), the K axons that project to cortical layer 1 are in a position to modulate activity within many pyramidal cells throughout the depth of V1 since the apical dendrites of some cells in almost all layers extend into cortical layer 1 (Lund, 1988). The K axons that have a branch in cortical layer 1 have been described following injections involving almost all of the K layers (Fig. 31.44; also see Ding and Casagrande, 1997), but the bulk of these projections appear to come from K layers 1 and 2. Jones (1998) has stated that there is a correlation between calcium binding protein content in thalamic relay cells and projection patterns to cortex, with the calbindin-positive cells having projections above layer 4 and being part of a more diffuse system serving a role in recruitment of more widespread areas of cortex, in contrast to the parvalbumin-

containing cells, which are dedicated to sensory transmission. In the K pathway, this scenario would hold only for cells projecting to layer 1 since other K cells clearly project to very limited areas of cortex. Regardless, this hypothesis is of interest given the long history of proposals implicating cortical layer 1 in attention, arousal, and other forms of modulation (Vogt, 1991). Interestingly, both K LGN cells and cells in the adjacent inferior pulvinar are immunoreactive for calbindin, receive input from the superficial colliculus (also implicated in attention), and send axons to cortical layer 1 of V1 (Ogren and Hendrickson, 1977). Evidence for the pulvinar's involvement in attention has a long history (Robinson and Petersen, 1992).

DO DIFFERENCES IN VISUAL LATENCIES OFFER FUNCTIONAL CLUES? One issue that has not been considered is that of differences in visual latencies between pathways and the impact this may have on the responses of cortical neuron targets. Clear differences in the visual onset latencies of K, M, and P cells have been demonstrated at the level of the LGN (e.g., Irvin et al., 1986). As discussed by Maunsell et al. (1999), it is difficult to predict the cortical impact of these differences because stimulus attributes, stimulus intensity, and degree of convergence of inputs on the postsynaptic cell all affect response latency. It is still possible, however, that V1 takes advantage of these timing differences to increase the probability that cells reach threshold. For example, one could imagine that within the CO-blob cells might receive signals from the slower K axons that have direct projections at the same time as signals from the faster M and P pathways that must traverse several synapses. Due to greater convergence from larger numbers (Maunsell et al., 1999), signals from P cells would arrive at about the same time as those from M cells. From this perspective, it would be of interest to know how removal of one of these pathways affects the thresholds of cells within the output layers of V1. The timing differences may also be important in combining signals from the feedforward parallel pathways and the multiple pathways that feed back to V1.

Conclusions

Parallel pathways from the retina via the LGN to V1 presumably act to maintain the integrity of signals that can only be combined at later stages of processing. Since V1 is concerned with local feature analysis, the layer and compartmental geometry of V1 provides a substrate for such independent processing and for the creation of different combinations of output pathways. The evidence reviewed above suggests that there may be as many as 10 pathways that pass through the LGN that could impact V1 processing in different ways; good evidence for at least 8 now exists. The puzzling question is why there are so many. In some cases,

evolutionary history may offer a possible explanation. Cones would be expected to provide input to any system designed for high-resolution vision, like midget ganglion cells. The addition of another cone type would simply provide a potential substrate for transmission of color signals along the same pathway. It is less easy to explain why K cells might carry S cone signals, except that this appears to happen earlier in evolutionary history if one considers that W cells also carry these signals. The coevolution of M and P cells or X and Y cells (and perhaps other subtypes as well) also may be, as mentioned earlier, the result of incompatibility (e.g., sensitivity often is incompatible with spatial resolution). The variety of conventional and unconventional responses of different K cell populations to visual stimulation suggests that LGN channels may do more than perform a simple analysis of spatial and temporal frequencies. The challenge for the future is to understand how V1 cells use the different views of the visual world that each of the parallel pathways provide. This can only be done by taking into account the dynamic aspects of the system by sampling from multiple cells at different levels within the system while the system is exposed to a variety of visual stimuli.

Unanswered questions

- How many pathways project from the retina to and through the LGN? How many of these pathways generalize across primates or across other mammals like the cat?
- If 10 ganglion cell classes project to the LGN in macaque monkeys, are there 10 separate target cell classes in the LGN? If so, what criteria can be used to distinguish them?
- To what extent do different LGN cell classes carry redundant information to V1?
- What is the functional significance of different calcium binding proteins within the different layers of the LGN?
- Why are there so many types of K cells?
- Why do K and W cells get input from the superior colliculus?
- Do LGN K cells and P cells both carry chromatic signals in diurnal primates?
- Why are LGN projections to layer 4A seen in only some primates?
- Why are S cones missing in nocturnal primates?
- Do CO-blob cells function differently in diurnal and nocturnal primates or in cats?
- Why do K cells in primates and W cells in cats send axons to the CO blobs and not to the interblobs?
- V1 projects to three compartments in V2 and also to compartments in V3, V3a/DM, MT, and V4. Do all of these projections arise from separate groups of cells in V1?
- How many extrastriate target areas of V1 are homologous across primates?

Acknowledgments

We are especially grateful to Julia Mavity-Hudson for help with figures and proofing the manuscript, to Shirin Pulous for secretarial help, and to Jennifer Ichida for helpful comments. This research was supported by NIH grant EY01778 (VAC) and core grants EY08126 and HD15052.

REFERENCES

- Allman, J., and S. Zucker, 1990. Cytochrome oxidase and functional coding in primate striate cortex: a hypothesis, *Cold Spring Harbor Symposia on Quantitative Biology*, 55:979–982.
- Bauer, U., M. Scholz, J. B. Levitt, K. Obermayer, and J. S. Lund, 1999. A model for the depth-dependence of receptive field size and contrast sensitivity of cells in layer 4C of macaque striate cortex, *Vis. Res.*, 39:613–629.
- Beck, P. D., and J. H. Kaas, 1999. Cortical connections of the dorsomedial visual area in old world macaque monkeys, *J. Comp. Neurol.*, 406:487–502.
- Bishop, G. H., 1933. Fiber groups in the optic nerves, *Am. J. Physiol.*, 106:460–470.
- Bishop, G. H., 1959. The relation between nerve fiber size and sensory modality: phylogenetic implications of the afferent innervation of cortex, *J. Nerv. Ment. Dis.*, 128:89–114.
- Blasdel, G. G., and D. Fitzpatrick, 1984. Physiological organization of layer 4 in macaque striate cortex, *J. Neurosci.*, 4:880–895.
- Blasdel, G. G., and J. S. Lund, 1983. Termination of afferent axons in macaque striate cortex, *J. Neurosci.*, 3:389–413.
- Boyd, J. D., V. A. Casagrande, and A. B. Bonds, 1998. How distinct are the lateral geniculate nucleus (LGN) inputs to areas 17 and 18 in the cat? *Soc. Neurosci. Abs.*, 24:894.
- Boyd, J. D., and J. A. Matsubara, 1996. Laminar and columnar patterns of geniculocortical projections in the cat: relationship to cytochrome oxidase, *J. Comp. Neurol.*, 365:659–682.
- Boyd, J. D., J. A. Mavity-Hudson, and V. A. Casagrande, 2000. The connections of layer 4 subdivisions in the primary visual cortex (V1) of the owl monkey, *Cereb. Cortex*, 10:644–662.
- Brodman, K., 1909. Localization in the cerebral cortex, translated and edited by L. J. Garey from *Vergleichen lokalisationslehre der grosshirnrinde in ihren prinzipien dargestellt auf grund des zellenbaues*, Leipzig: Johann Ambrosius Barth, London: Smith-Gordon and Co., Ltd.
- Calkins, D. J., and P. Sterling, 1999. Evidence that circuits for spatial and color vision segregated at the first retinal synapse, *Neuron*, 24:313–321.
- Campbell, F. W., and J. G. Robson, 1968. Application of Fourier analysis to the visibility of gratings, *J. Physiol.*, 197:551–566.
- Casagrande, V. A., 1994. A third parallel visual pathway to primate area V1, *Trends in Neuroscience*, 17:305–310.
- Casagrande, V. A., Y. Ding, and J. D. Boyd, 1997. The morphology of LGN axons from different K layers in V1 of macaque monkey, *Soc. Neurosci. Abs.*, 23:2361.
- Casagrande, V. A., J. K. Harting, W. C. Hall, I. T. Diamond, and G. F. Martin, 1972. Superior colliculus of the tree shrew: a structural and functional subdivision into superficial and deep layers, *Science*, 177:444–447.
- Casagrande, V. A., and J. H. Kaas, 1994. The afferent, intrinsic, and efferent connections of primary visual cortex, in *Cerebral Cortex*, vol. 10, *Primary Visual Cortex of Primates* (A. Peters and K. S. Rockland, eds.), New York: Plenum Press, pp. 201–259.
- Casagrande, V. A., and T. T. Norton, 1991. The lateral geniculate nucleus: A review of its physiology and function, in *The Neural Basis of Visual Function* (A. G. Leventhal, ed.), vol. 4, *Vision and Visual Dysfunction* (J. R. Cronley-Dillon, ed.), London: Macmillan, pp. 41–84.
- Cleland, B. G., and W. R. Levick, 1974. Properties of rarely encountered types of ganglion cells in the cat's retina and an overall classification, *J. Physiol.*, 240:457–492.
- Dacey, D. M., 1996. Circuitry for color coding in the primate retina, *PNAS*, 93:582–588.
- Dacey, D. M., 1999. Primate retina: cell types, circuits and color opponency, *Prog. Ret. Eye Res.*, 18:737–763.
- Dacey, D. M., 2000. Parallel pathways for spectral coding in primate retina, *Annu. Rev. Neurosci.*, 23:743–775.
- Dacey, D. M., B. B. Peterson, and F. R. Robinson, 2001. Morphology and physiology of diverse new ganglion cell types that project to the lateral geniculate nucleus in macaque monkey revealed by retrograde “photofilling,” *XXXIVth International Congress of Physiological Sciences*, Sidney, Australia: (abs.), p. 19.
- DeYoe, E. A., and D. C. Van Essen, 1988. Concurrent processing streams in monkey visual cortex, *Trends in Neuroscience*, 11:219–226.
- Diamond, I. T., and W. C. Hall, 1969. Evolution of neocortex, *Science*, 164:251–262.
- Ding, Y., and V. A. Casagrande, 1997. The distribution and morphology of LGN K pathway axons within the layers and CO blobs of owl monkey V1, *Vis. Neurosci.*, 14:691–704.
- Dobkins, K. R., 2000. Moving colors in the lime light, *Neuron*, 25:15–18.
- Enroth-Cugell, C., and J. Robson, 1966. The contrast sensitivity of retinal ganglion cells of the cat, *J. Physiol.*, 187:517–552.
- Florence, S. L., and V. A. Casagrande, 1987. Organization of individual afferent axons in layer IV of striate cortex in a primate, *J. Neurosci.*, 7:3850–3868.
- Gasser, H. S., and J. Erlanger, 1929. The role of fiber size in the establishment of a nerve block by pressure or cocaine, *Am. J. Physiol.*, 88:581–591.
- Heesy, C. P., and C. F. Ross, 2001. Evolution of activity patterns and chromatic vision in primates: morphometrics, genetics and cladistics, *J. Human Evol.*, 40:111–149.
- Hendry, S. H., and C. Reid, 2000. The koniocellular pathway in primate vision, *Annu. Rev. Neurosci.*, 23:127–153.
- Horton, J. C., and E. T. Hedley-Whyte, 1984. Mapping of cytochrome oxidase patches and ocular dominance columns in human visual cortex, *PNAS*, 304:255–272.
- Hubel, D. H., and T. N. Wiesel, 1998. Early exploration of the visual cortex, *Neuron*, 20:401–412.
- Humphrey, A. L., M. Sur, D. J. Uhlich, and S. M. Sherman, 1985. Termination patterns of individual X- and Y-cell axons in the visual cortex of the cat: projections to area 18, to the 17/18 border region, and to both areas 17 and 18, *J. Comp. Neurol.*, 233:190–212.
- Irvin, G. E., T. T. Norton, M. A. Sesma, and V. A. Casagrande, 1986. W-like response properties of interlaminar zone cells in the lateral geniculate nucleus of a primate (*Galago crassicaudatus*), *Brain Res.*, 362:254–270.
- Isayama, T., D. M. Berson, and M. Pu, 2000. Theta ganglion cell type of cat retina, *J. Comp. Neurol.*, 417:32–48.
- Jacobs, G. H., 1993. The distribution and nature of colour vision among the mammals, *Biol. Rev. Cambridge Philos. Soc.*, 68:413–471.
- Jacobs, G. H., M. Neitz, and J. Neitz, 1996. Mutations in S-cone pigment genes and the absence of colour vision in two species of nocturnal primate, *PNAS*, 263:705–710.

- Johnson, J. K., and V. A. Casagrande, 1995. The distribution of calcium-binding proteins within the parallel visual pathways of a primate (*Galago crassicaudatus*), *J. Comp. Neurol.*, 356:238–260.
- Jones, E. G., 1998. Viewpoint: the core and matrix of thalamic organization, *Neuroscience*, 85:331–345.
- Kaplan, E., 1991. The receptive field structure of retinal ganglion cells in cat and monkey, in *The Neural Basis of Visual Function*, vol. 4 (A. G. Leventhal, ed.), *Vision and Visual Dysfunction* series (J. R. Cronley-Dillon, ed.), London: Macmillan, pp. 41–84.
- Kaplan, E., B. B. Lee, and R. M. Shapley, 1990. New views of primate retinal function, *Prog. Ret. Res.*, 9:273–236.
- Kaplan, E., and R. M. Shapley, 1982. X and Y cells in the lateral geniculate nucleus of macaque monkeys, *J. Physiol.*, 330:125–143.
- Kawano, J., 1998. Cortical projections of the parvocellular laminae C of the dorsal lateral geniculate nucleus in the cat: an anterograde wheat germ agglutinin conjugated to horseradish peroxidase study, *J. Comp. Neurol.*, 392:439–457.
- Lachica, E. A., and V. A. Casagrande, 1992. Direct W-like geniculate projections to the cytochrome oxidase (CO) blobs in primate visual cortex: axon morphology, *J. Comp. Neurol.*, 319:141–158.
- LeVay, S., and S. B. Nelson, 1991. Columnar organization of the visual cortex, in *The Neural Basis of Visual Function* (A. G. Leventhal, ed.), Boston: CRC Press, pp. 266–315.
- Livingstone, M. S., and D. H. Hubel, 1982. Thalamic inputs to cytochrome oxidase-rich regions in monkey visual cortex, *PNAS*, 79:6098–6101.
- Livingstone, M. S., and D. H. Hubel, 1988. Segregation of form, color, movement and depth: anatomy, physiology, and perception, *Science*, 240:740–749.
- Lund, J. S., 1988. Anatomical organization of macaque monkey striate visual cortex, *Annu. Rev. Neurosci.*, 11:253–288.
- Lund, J. S., Q. Wu, P. T. Hadingham, and J. B. Levitt, 1995. Cells and circuits contributing to functional properties in area V1 of macaque monkey cerebral cortex: bases for neuroanatomically realistic models, *Anatomy*, 187:563–581.
- Martin, P. R., A. J. R. White, A. K. Goodchild, H. D. Wilder, and A. J. Sefton, 1997. Evidence that Blue-on cells are part of the third geniculocortical pathway in primates, *Eur. J. Neurosci.*, 9:1536–1541.
- Maunsell, J. H. R., M. Ghose, J. A. Assad, C. J. McAdams, C. E. Boudre, and B. D. Noerager, 1999. Visual response latencies of magnocellular and parvocellular LGN neurons in macaque monkeys, *Vis. Neurosci.*, 16:1–14.
- Norton, T. T., V. A. Casagrande, G. E. Irvin, M. A. Sesma, and H. M. Petry, 1988. Contrast-sensitivity functions of W-, X-, and Y-like relay cells in the lateral geniculate nucleus of bush baby, *Galago crassicaudatus*, *J. Neurophysiol.*, 59:1639–1656.
- Ogren, M. P., and A. E. Hendrickson, 1977. The distribution of pulvinar terminals in visual areas 17 and 18 of the monkey, *Brain Res.*, 137:343–350.
- Preuss, T. M., 2000. Preface: from basic uniformity to diversity in cortical organization, *Brain Behav. Evol.*, 55:283–286.
- Preuss, T. M., H. Qi, and J. H. Kaas, 1999. Distinctive compartmental organization of human primary visual cortex, *PNAS*, 96:11601–11606.
- Rafal, R., J. Smith, J. Krantz, A. Cohen, and C. Brennan, 1990. Extrageniculate vision in hemianopic humans: saccade inhibition by signals in the blind field, *Science*, 250:118–121.
- Reid, R. C., J. M. Alonso, and S. H. C. Hendry, 1997. S-cone input is relayed to visual cortex from two koniocellular layers of macaque LGN, *Soc. Neurosci. Abs.*, 23:13.
- Robinson, D. L., and S. E. Petersen, 1992. The pulvinar and visual salience, *Trends in Neuroscience*, 15:127–132.
- Rodiek, R. W., and M. Watanabe, 1993. Survey of the morphology of macaque retinal ganglion cells that project to the pretectum, superior colliculus, and parvocellular laminae of the lateral geniculate nucleus, *J. Comp. Neurol.*, 338:289–303.
- Rowe, M. H., and J. F. Cox, 1993. Spatial receptive-field structure of cat retinal W cells, *Vis. Neurosci.*, 10:765–779.
- Saul, A. B., and A. L. Humphrey, 1990. Spatial and temporal response properties of lagged and nonlagged cells in cat lateral geniculate nucleus, *J. Neurophysiol.*, 64:206–224.
- Schiller, P. H., N. K. Logothetis, and E. R. Charles, 1990. Role of the color-opponent and broad-band channels in vision, *Vis. Neurosci.*, 5:321–346.
- Sherman, S. M., and R. W. Guillery, 2001. *Exploring the Thalamus*, San Diego: Academic Press.
- Schneider, G. E., 1969. Two visual systems, *Science*, 163:895–902.
- Shostak, Y., Y. Ding, J. A. Mavity-Hudson, and V. A. Casagrande, 2002. Cortical synaptic arrangements of the third visual pathway in three primate species: *Macaca mulatta*, *Saimiri sciureus*, and *Aotus trivirgatus*, *J. Neurosci.*, 22:2885–2893.
- Song, Z., J. Broome, J. Mavity-Hudson, A. Wiencken-Barger, J. Malpeli, and V. A. Casagrande, 2001. The distribution of koniocellular lateral geniculate nucleus (LGN) cells in macaque monkey, *Soc. Neurosci. Abs.*, 27:723.5.
- Stone, J., 1983. *Parallel Processing in the Visual System: The Classification of Retinal Ganglion Cells and Its Impact on the Neurobiology of Vision*, New York: Plenum Press, pp. 83–108.
- Sur, M., and S. M. Sherman, 1982. Linear and non-linear W cells in C laminae of the cat's lateral geniculate nucleus, *J. Neurophys.*, 47:869–884.
- Tigges, J., and M. Tigges, 1979. Ocular dominance columns in the striate cortex of chimpanzee (*Pan troglodytes*), *Brain Res.*, 166:386–390.
- Troy, J. B., D. E. Schweitzer-Tong, and C. Enroth-Cugell, 1995. Receptive-field properties of Q retinal ganglion cells of the cat, *Vis. Neurosci.*, 12:285–300.
- Ungerleider, L. G., and M. Mishkin, 1982. Two cortical visual systems, in *Analysis of Visual Behavior* (M. A. Goodale and R. J. W. Mansfield, eds.), Cambridge, MIT Press, pp. 549–586.
- Virsu, V., B. B. Lee, and O. D. Creutzfeldt, 1987. Mesopic spectral responses and the Purkinje shift of macaque lateral geniculate nucleus cells, *Vis. Res.*, 27:191–200.
- Vogt, B. A., 1991. The role of layer I in cortical function, in *Cerebral Cortex*, vol. 9, *Normal and Altered States of Functions* (A. Peters and E. G. Jones, eds.), New York: Plenum Press, pp. 49–80.
- Wandell, B., D. Dacey, B. Peterson, F. Robinson, P. Martin, S. Solomon, B. Lee, E. Callaway, V. Casagrande, D. Ts'o, R. Reid, 2002. Primate color vision, *Soc. Neurosci. Abs.*, Program No. 509.
- Ware, C. B., V. A. Casagrande, and I. T. Diamond, 1972. Does the acuity of the tree shrew suffer from removal of striate cortex? A commentary on the paper by Ward and Masterton, *Brain Behav. Evol.*, 5:18–29.
- Ware, C. B., I. T. Diamond, and V. A. Casagrande, 1974. Effects of ablating the striate cortex on a successive pattern discrimination: further study of the visual system in the tree shrew (*Tupaia glis*), *Brain Behav. Evol.*, 9:264–279.
- White, A. J. R., S. G. Solomon, and P. R. Martin, 2001. Spatial properties of koniocellular cells in the lateral geniculate nucleus of the marmoset *Callithrix jacchus*, *J. Physiol.*, 533:519–535.
- White, A. J., H. D. Wilder, A. K. Goodchild, A. J. Sefton, and P. R. Martin, 1998. Segregation of receptive field properties in

- the lateral geniculate nucleus of a New-World monkey, the marmoset *Callithrix jacchus*, *J. Neurophysiol.*, 80:2063–2076.
- Wiencken, A. E., and V. A. Casagrande, 2000. The distribution of NADPH diaphorase and nitric oxide synthetase (NOS) in relation to the functional compartments of areas V1 and V2 of primate visual cortex, *Cereb. Cortex*, 10:499–511.
- Wiesel, T. N., and D. H. Hubel, 1966. Spatial and chromatic interactions in the lateral geniculate body of the rhesus monkey, *J. Neurophysiol.*, 29:1115–1156.
- Wong-Riley, M. T., R. F. Hevner, R. Cutlan, M. Earnest, R. Egan, J. Frost, and T. Nguyen, 1993. Cytochrome oxidase in the human visual cortex: distribution in the developing and the adult brain, *Vis. Neurosci.*, 10:41–58.
- Wong-Riley, M. T., and T. T. Norton, 1988. Histochemical localization of cytochrome oxidase activity in the visual system of the tree shrew: normal patterns and the effect of retinal impulse blockage, *J. Comp. Neurol.*, 272:562–578.
- Xu, X., J. M. Ichida, J. D. Allison, J. D. Boyd, A. B. Bonds, and V. A. Casagrande, 2001. A comparison of koniocellular, magnocellular and parvocellular receptive field properties in the lateral geniculate nucleus of the owl monkey (*Aotus trivirgatus*), *J. Physiol.*, 531:203–218.
- Yabuta, N. H., and E. M. Callaway, 1998. Functional streams and local connections of layer 4C neurons in primary visual cortex of the macaque monkey, *J. Neurosci.*, 18:9489–9499.
- Yamada, E. S., D. W. Marshak, L. C. Silveira, and V. A. Casagrande, 1998. Morphology of P and M retinal ganglion cells of the bush baby, *Vis. Res.*, 38:3345–3352.
- Yamada, E. S., L. C. Silveira, V. H. Perry, and E. C. Franco, 2001. M and P retinal ganglion cells of the owl monkey: morphology, size and photoreceptor convergence, *Vis. Res.*, 41:119–311.
- Yoshioka, T., and S. H. Hendry, 1995. Compartmental organization of layer IVA in human primary visual cortex, *J. Comp. Neurol.*, 359:213–220.

32 Organization of Visual Areas in Macaque and Human Cerebral Cortex

DAVID C. VAN ESSEN

THE MAMMALIAN visual system contains numerous visual areas that collectively occupy a large fraction of cerebral cortex. For cortical cartographers interested in vision, a fundamental set of objectives is to identify in key species of interest the overall extent of visual cortex, the total number of visual areas, the identities of these areas, and their location in relation to one another and to various gyral and sulcal landmarks. Over the past three decades there has been much progress in this endeavor for a number of primate and nonprimate species. However, the task remains far from complete. Numerous qualitatively different partitioning schemes abound, even for the most intensively studied species. Our fragmentary and rapidly evolving understanding is reminiscent of the situation faced by cartographers of the Earth's surface many centuries ago, when maps were replete with uncertainties and divergent portrayals of most of the planet's surface.

The primary objective of this chapter is to summarize our current understanding of visual cortical organization in two primate species, the macaque monkey and the human. The macaque is the most intensively studied nonhuman primate and has been charted using a wide variety of approaches. Human visual cortex, largely terra incognita until the past decade, is now accessible thanks to modern neuroimaging methods, especially functional magnetic resonance imaging (fMRI; see Chapter 79). A secondary objective, more methodological in nature, is to illustrate the utility of computerized surface-based atlases in elucidating visual cortical organization. In brief, surface-based atlases offer many advantages over conventional atlases (e.g., stereotactic atlases and pictorial representations). These include the ability to (1) visualize the cortical surface in multiple configurations, including smoothed and flattened maps, (2) view any number of partitioning schemes and open-ended amounts of complex data in a convenient and electronically accessible format; (3) represent various types of spatial uncertainty that are associated with real experimental data; (4) compensate for individual variability, and (5) make objective interspecies comparisons of cortical organization.

Visual areas in the macaque monkey

Figure 32.1 shows the estimated extent of visual cortex

in the macaque and its relationship to other sensory modalities and to motor cortex. This is displayed on a surface-based atlas of the right cerebral hemisphere that was generated from a high-resolution structural MRI volume (Van Essen et al., 2002; Van Essen, 2002; see legend to Fig. 32.1 for details). The top panels show lateral and medial views, respectively, of the fiducial (three-dimensional) configuration; the lower left panel (Fig. 32.1C) is a flat map that shows the entire surface in a single view.

The dotted lines on the flat map represent the estimated boundary between regions dominated by different modalities, based on the analysis of Felleman and Van Essen (1991). These boundaries are not sharply defined, as there is considerable intermixing of function in transitional regions between modalities. The blending of colors on the maps in Figure 32.1 qualitatively reflects this functional overlap. Cortex that is predominantly or exclusively visual (blue shading) occupies about half (52%) of the cortical surface area (as measured on the fiducial surface rather than on the flat map, which contains significant distortions). This greatly exceeds the amount devoted to other modalities: somatosensory (green, 10%), auditory (red, 3%), motor (magenta, 8%), and olfactory (brown, 1%). Unassigned cortex (gray, 25%) is mostly cognitive or emotional in function but is not subdivided along these lines in the figure.

Figure 32.1 also shows latitude and longitude isocontours that are determined on a spherical map (*Panel D*) and projected to the flat map (*Panel E*). As with earth maps, spherical coordinates provide a concise and objective way to specify precise locations on the map (Drury et al., 1999; Fischl et al., 1999a, 1999b; Van Essen et al., 2001a).

The identification of distinct visual areas is generally based on finding reliable differences in one or more characteristics related to (1) architecture, (2) connectivity, (3) visual topography, and/or (4) functional characteristics (Felleman and Van Essen, 1991; Kaas, 1997). Using various combinations of these criteria, numerous partitioning schemes for visual cortex in the macaque monkey have been published over the past century. Figure 32.2 shows 10 such schemes

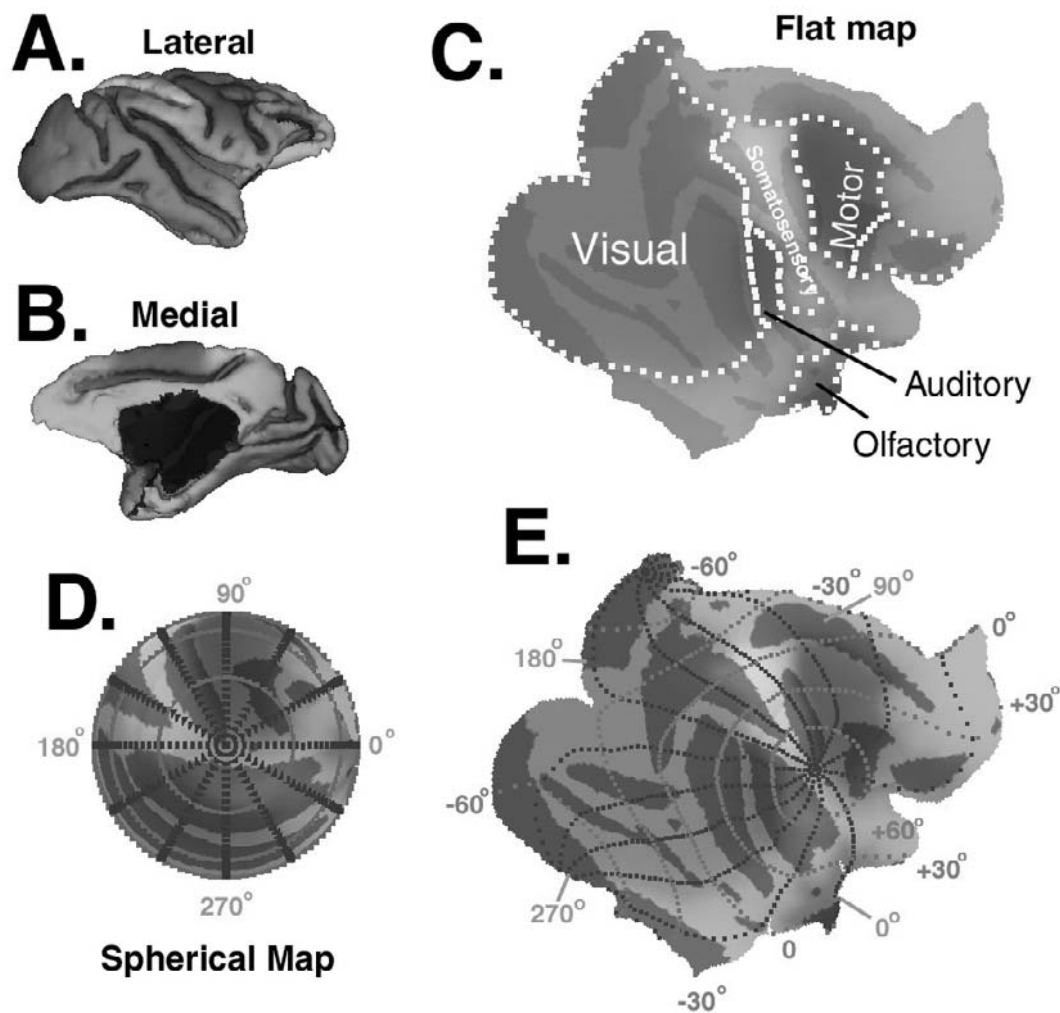


FIGURE 32.1. Visual cortex and other functional modalities mapped onto a surface-based atlas of macaque cerebral cortex. The atlas was generated from a high-resolution (0.5 mm^3 voxels) structural MRI volume generously provided by N. Logothetis (Case F99UA1, *M. mulatta*), using the SureFit segmentation method for surface reconstruction and Caret software for surface manipulation and flattening (Van Essen et al., 2001a). This atlas has many advantages over its predecessors, which include manually generated maps (Felleman and Van Essen, 1991; Van Essen and Maunsell, 1980) and surface-based atlases from a hemisphere that lacked corre-

sponding structural MRI data (Van Essen et al., 2001a). *A*, Lateral view. *B*, Medial view. *C*, Flat map. Surface coloring represents different functional modalities, as identified on the flat map; darker shading represents cortex buried in sulci. *D*, Lateral view of the atlas spherical map, with latitude and longitude isocontours. By convention, the lateral pole is set at the ventral tip of the central sulcus. *E*, Latitude and longitude isocontours displayed on the flat map. Data for Figures 32.1 to 32.3 can be accessed via http://brainmap.wustl.edu:8081/sums/archivelist.do?archive_id=448857 (see color plate 11).

that were mapped to the atlas using a surface-based registration method (Van Essen et al., 1998, 2001b; see legend to Fig. 32.2 for details). *Panels A–C* illustrate three schemes that encompass most or all of the visual cortex. The Felleman and Van Essen (1991) and Ungerleider and Desimone (1986) schemes are based on anatomical and physiological data from many sources. The Lewis and Van Essen (2000a) scheme is based on an architectonic analysis of multiple hemispheres, with the atlas map generated via surface-based registration of a particular individual map. *Panel D* shows several schemes that cover more restricted regions, including a connectivity-based analysis of occipital cortex (Lyon

and Kaas, 2002) and architectonic analyses of temporal and parietal cortex (Seltzer and Pandya, 1978, 1980, 1986). *Panel E* shows two additional architectonic schemes covering temporal (Baylis et al., 1987) and parietal (Preuss and Goldman-Rakic, 1991) regions, plus a visuotopic mapping analysis of dorsal occipital cortex (Galletti et al., 1999). While far from an exhaustive compilation, Figure 32.2 includes most of the partitioning schemes in current use that have been reported in a format suitable for registration to the atlas.

Although there are many similarities, these partitioning schemes differ in many ways for reasons that reflect various

technical impediments faced by cortical cartographers. (1) *Subtle boundaries*. The distinctions between neighboring regions are often subtle, even when evaluated with the most sensitive anatomical and physiological techniques available. (2) *Internal heterogeneity*. Many (perhaps most) visual areas are internally heterogeneous. This heterogeneity may be manifested by *modularity* (repetitive organization at a finer scale than the overall areal dimensions); *asymmetries* (differences between the representations of the upper [superior] and lower [inferior] visual fields); or internal *gradients* (gradual shifts in characteristics rather than discrete modularity). (3) *Individual variability*. The overall size of well-defined visual areas such as V1 and MT can vary twofold or more from one individual to the next (Maunsell and Van Essen, 1987; Van Essen et al., 1984). This is compounded by substantial variability in the exact pattern of convolutions and in the location of areal boundaries relative to gyral and sulcal landmarks.

A compelling case for areal identification entails finding region-specific characteristics that are robust, consistent across multiple approaches, and replicated by multiple laboratories. The diversity among partitioning schemes signifies that a consensus has been achieved for only a minority of the visual areas illustrated in Figure 32.2. Several well-defined areas (V1, V2, V4, and MT) are shown by different colors in Figure 32.2; others are included as part of a regional coloring pattern that includes six clusters discussed below.

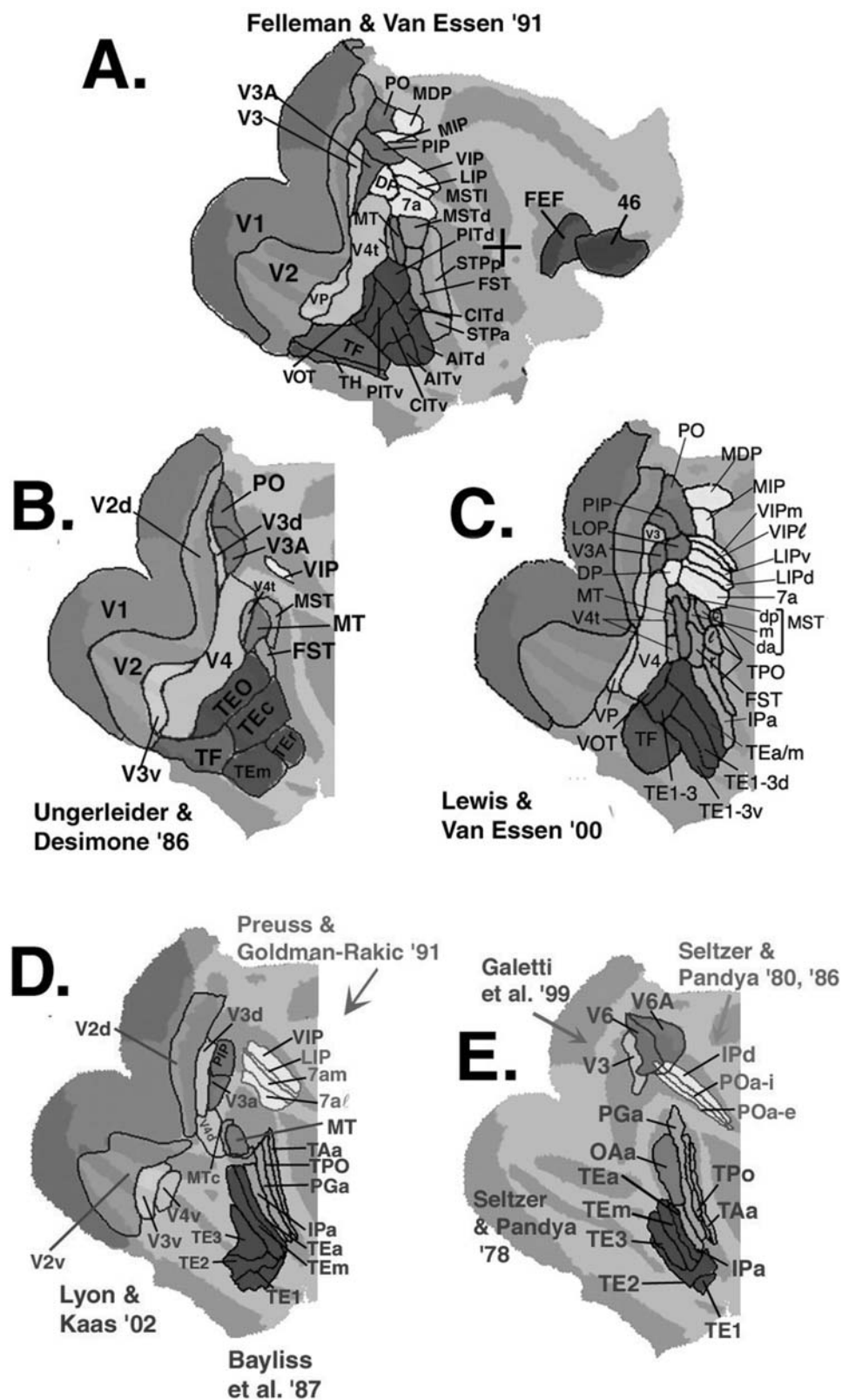
The differences among partitioning schemes can be categorized along four lines. (1) *Terminological equivalence*. Some differences are essentially terminological in that different labels are assigned to what is fundamentally the same visual area. For example, area 17 is equivalent to area V1; MT (Fig. 32.2A–C) is equivalent to V5 (Shipp and Zeki, 1985); and PO (Fig. 32.2A–C) is equivalent to V6 (Fig. 32.2F). (2) *Lumping versus splitting*. Some regions are considered a single area by some investigators (the lumpers) but as two separate areas by other investigators (the splitters). This is an issue, for example, for subdivisions V3d/V3v, V4d/V4v, and LIPd/LIPv. In some cases, it can be helpful to use the term *zone* to describe a consistently identifiable region whose status as a distinct area is uncertain, ambiguous, or contentious (Lewis and Van Essen, 2000a). The term *subdivision* can then encompass both zones and well-defined cortical areas. (3) *Boundary uncertainty*. Even when there is a consensus on the identity of an area and the main criteria for its identification, the location and extent of any particular area on the atlas map vary substantially across schemes (cf. V2 and MT in Fig. 32.2A–D). These differences may reflect (a) the choice of criteria or emphasis among different criteria available for delineating boundaries; (b) variability in the size and location of areas in the individuals studied; (c) inaccuracies in portraying areal boundaries on a

summary diagram in the original publication; and (d) inaccuracies or distortions arising when registering data to the atlas. (4) *Genuine incompatibility*. In some regions, partitioning schemes differ more profoundly than can be explained by the factors just mentioned. For example, in inferotemporal cortex (blue) there is rather little correlation between the areal boundaries in *panel A* versus *panel E*; hence the schemes are largely incompatible.

OCCIPITAL VISUAL AREAS V1 and V2 are both large, well-defined areas, with V1 occupying 13% and V2 occupying 10% of the total cortical surface area (12.6 cm²) in the right hemisphere of the atlas. V1 and V2 have a mirror-symmetric visuotopic organization, with the vertical meridian represented along their common boundary, and with upper fields represented ventrally and lower fields dorsally in each area. In addition, both areas have prominent internal modularity related to the processing streams that course through these areas (Felleman and Van Essen, 1991; Van Essen and Gallant, 1994; Chapter 34). Interestingly, there are significant asymmetries between dorsal V2 (V2d) and ventral V2 (V2v): V2v is notably wider than V2d (Fig. 32.2A–D), and the two subregions differ in the global pattern of thick stripes, thin stripes, and interstripes (Olavarria and Van Essen, 1997).

Area V3 was originally identified as a strip of cortex that adjoins V2 and has mirror-symmetric visuotopic organization (Zeki, 1969). Subsequent studies confirmed this visuotopic organization but revealed that the dorsal and ventral subdivisions are physically separated from one another by the interposition of area V4 (cf. Fig. 32.2A–C). More significantly, evidence for pronounced dorsoventral asymmetries in connectivity (especially with V1), myeloarchitecture, and physiological properties prompted the classification of these dorsal and ventral subdivisions as distinct visual areas: VP (or V3v) and V3 (or V3d), each containing a partial representation of the visual field (cf. Burkhalter et al., 1986). In contrast, Lyon and Kaas (2002) reported relatively symmetric projections of V1 using more sensitive tracers, and they support Zeki's original proposal that V3d and V3v are subdivisions of a single area V3. A sensible interim strategy is to designate these subdivisions as zones V3d and V3v while awaiting additional data on the overall magnitude and nature of V3d/V3v asymmetries, along with insights regarding the asymmetries encountered in other regions and other species (see below). Independent of this terminological debate, it is noteworthy that V3d and V3v vary considerably in location and size among the various maps shown in Figure 32.2.

V4 is a moderately sized area whose lower-field (V4d) and upper-field (V4v) representations are contiguous with one another, in contrast to the physical separation of V3d and V3v. The visuotopic organization of dorsal V4 appears



to be more complex and variable across individuals than that of ventral V4 (Boussaud et al., 1991; Gattass et al., 1988; Maguire and Baizer, 1984; Van Essen et al., 1990). Because analogous but more pronounced dorsoventral asymmetries have been reported for the corresponding region of human cortex (see below), Tootell and Hadjikhani (2001) have suggested that macaque V4d and V4v might themselves constitute distinct visual areas.

Five additional areas adjoin or closely approach V2 along its dorsomedial and ventromedial boundaries. The dorsomedial cluster (magenta in Fig. 32.2) includes areas V3A, PIP, and PO, each of which includes an upper-field as well as a lower-field representation (Colby et al., 1988; Felleman and Van Essen, 1991; Lyon and Kaas, 2002). Area PO, as charted by Colby et al. (1988), corresponds to area V6 of Galletti et al. (1999). The ventromedial cluster (brown in Fig. 32.2) includes areas TF and TH (near the bottom of the flat map), both of which receive visual inputs (see Felleman and Van Essen, 1991). The posterior portion of TF, identified as VTF by Boussaud et al. (1991), is visually responsive but has at best a crude visuotopic organization.

DORSAL TEMPORAL AND POSTERIOR PARIETAL CORTEX The *dorsal stream* of visual areas (Chapter 34) includes cortex in and near the intraparietal sulcus, plus the dorsal part of the superior temporal sulcus. Area MT, the most extensively studied area in the dorsal stream, contains a complete visuotopic map, but with a bias toward lower versus upper visual fields (Maunsell and Van Essen, 1987). Though MT is well defined by several criteria (including a high incidence of direction-selective cells), its precise location and extent on different summary maps vary significantly (cf. Fig. 32.2A–D; see also Desimone and Ungerleider, 1986). Adjoining MT on its lateral side is a narrow strip that has been identified

as V4t (Felleman and Van Essen, 1991; Ungerleider and Desimone, 1986) or MTc (Lyon and Kaas, 2002). Within V4t, architectonically distinct zones V4ta and V4tp have been described (Lewis and Van Essen, 2000a).

A major target of MT is the MST complex (orange in Fig. 32.2), which lies dorsal and medial to MT and is implicated in higher-order motion analysis. MST is heterogeneous both anatomically and physiologically, but it remains unclear whether there are two subdivisions (MSTd and MSTl of Komatsu and Wurtz, 1988a, 1988b, and Felleman and Van Essen, 1991; MSTc and MSTp of Boussaud et al., 1990) or three (MSTdp, MSTm, and MSTl of Lewis and Van Essen, 2000a) and whether these constitute distinct areas or zones within a larger MST complex. Area FST lies ventral to the MST complex and medial to MT, but its position differs markedly in different partitioning schemes (Fig. 32.2A versus 32.2B, C).

Posterior parietal visual cortex (yellow in Fig. 32.2) includes several elongated areas in and near the intraparietal sulcus, plus additional areas in more posterior regions that are represented in some schemes. The most fine-grained scheme (Lewis and Van Essen, 2000a; Fig. 32.2C) is based on immunohistochemical as well as cyto- and myeloarchitecture and includes seven distinct areas (7a, LIPd, LIPv, VIP, MIP, MDP, and DP) plus additional architectonic zones. In the region previously described as area LIP (Blatt et al., 1990), subdivisions LIPd and LIPv differ from one another in architecture, connectivity, and physiological characteristics and are thus likely to constitute separate visual areas (cf. Lewis and Van Essen, 2000a, 2000b). Area VIP, along the fundus of the intraparietal sulcus, contains lateral (VIPl) and medial (VIPm) architectonic zones, but these are not considered distinct areas on the basis of current evidence (Lewis and Van Essen, 2000a, 2000b). Areas LIPd, LIPv, and VIP

FIGURE 32.2. Ten partitioning schemes for macaque visual cortex registered to the atlas and displayed on flat map views. See the abbreviations list for full names of areas. Data were registered to the atlas using a surface-based registration method in which geographic (gyral and sulcal) landmarks were used to constrain the registration (Van Essen et al., 2001b). Depending on the data source, this method was applied to computerized maps (spherical or flat maps) and to scanned images of manually generated flat maps or drawings of the hemispheric surface and of schematically opened sulci. Thus, there are substantial differences in the fidelity of the published representations and in the distortions and uncertainties involved in registering to the atlas, but visualization on a common substrate nonetheless remains advantageous. *A*, Felleman and Van Essen (1991) partitioning scheme for visual areas. Areal boundaries were originally charted on a physical model of an individual hemisphere (case 79O). They were transferred to a computerized surface reconstruction of the same hemisphere and then were registered to the Case F99UA1 atlas using spherical maps of each hemisphere. *B*, Ungerleider and Desimone (1986) scheme (their Figure 1; see

also Figure 2 of Desimone and Ungerleider, 1989). Registration was achieved using geographic landmarks on a manually generated flat map. *C*, Lewis and Van Essen (2000a) scheme from Case 95DR (their Figure 14) registered from the computerized flat maps. *D*, A composite map of partitioning schemes for occipital cortex (Lyon and Kaas, 2002, their Figure 4), parietal cortex (Preuss and Goldman-Rakic, 1991, their Figure 4C) and temporal cortex (Baylis et al., 1987, their Figures 2 and 3). The Lyon and Kaas map was based on a visuotopic analysis of V1 projections as displayed on sections of physically flattened cortex. The Preuss and Goldman-Rakic maps were derived from their illustrations of schematically partially unfolded sulci; the Baylis et al. maps were based on cortex flattened using a *straight-line* unfolding technique. *E*, A composite map of dorsomedial cortex (Galletti et al., 1999, their Figure 17), and parietal and temporal cortex (Seltzer and Pandya, 1978, 1980, 1986), all illustrated on schematically unfolded sulci. Data can be accessed via http://brainmap.wustl.edu:8081/sums/archivelist.do?archive_id=448857 (see color plate 12).

of Lewis and Van Essen (2000a) largely correspond with POa–e, Poa–i, and IPd of Seltzer and Pandya (1980, 1986), except that they are more restricted anteroposteriorly. The relationships with other schemes are somewhat confusing because of “cross-talk” in the terminology: area VIP* of Ungerleider and Desimone corresponds to LIPv of Lewis and Van Essen; areas LIP and VIP of Felleman and Van Essen correspond to LIPd and LIPv/VIPi, respectively, of Lewis and Van Essen.

A second group of areas, near the posterior end of the intraparietal sulcus, includes areas MDP, MIP, and DP, plus zone LOP (Fig. 32.2C). Area MDP corresponds to V6A of Galetti et al. (1999). Zone LOP may correspond to the cIPS subdivision identified physiologically by Taira et al. (2000) based on surface orientation selectivity.

VENTRAL TEMPORAL AREAS Cortex ventral to area MT and anterior to V4 is generally considered part of the ventral processing stream (cf. Chapter 34). This region includes a cluster of inferotemporal areas (blue in Fig. 32.2) that are implicated mainly in pattern recognition and form analysis (Desimone and Ungerleider, 1989; Tanaka, 1997). Another cluster of ventral-STS areas (green in Fig. 32.2) includes polysensory regions and regions involved in both form and motion processing (Cusick, 1997; Oram and Perrett, 1996). The five schemes in Figure 32.2 subdivide ventral temporal cortex along both anteroposterior and dorsoventral axes, but the number of identified subdivisions ranges from 4 to 10 and the location of areal boundaries varies widely as well.

The simplest scheme (Ungerleider and Desimone, 1986; Fig. 32.2B) includes a visuotopically organized area TEO that contains a lower-field and an upper-field representation (see also Boussaoud et al., 1991), plus three areas (TEc, TEr, and TEm) that lack clear visuotopic organization. The Felleman and Van Essen (1991) scheme, based mainly on topographic and connectional data, includes three areas (VOT, PITd, and PITv) in the region corresponding to TEO of Ungerleider and Desimone (1986). VOT contains only an upper-field representation, whereas PITd and PITv are reported to each contain a crude topography with lower-field and upper-field inputs (Van Essen et al., 1990). Areas CITd and CITv of Felleman and Van Essen (1991) together correspond approximately to TEc of Ungerleider and Desimone (1986) but are distinguished from one another by differential connections. More anteriorly on the atlas map, there is reasonable correspondence between AITd and TEr in the two schemes but poor correspondence between AITv and TEm.

The Seltzer and Pandya (1978) architectonic scheme (Fig. 32.2E) includes five inferotemporal areas (TEa, TEm, TE1, TE2, and TE3), plus four additional areas in the superior temporal sulcus (TAa, TPO, PGa, and IPa). The Baylis et al. (1987) scheme (Fig. 32.2D) uses the same criteria and terminology as Seltzer and Pandya (1978), but the areal boundaries

differ significantly on the atlas map. The Lewis and Van Essen (2000a) scheme, like that of Cusick (1997), identifies three subdivisions within TPO (TPOc, TPOi, and TPOr). In inferotemporal cortex, the Lewis and Van Essen (2000a) scheme does not discriminate among TE1, TE2, and TE3 but does identify dorsoventral subdivisions TE1-3d and TE1-3v. The latter correspond approximately to subdivisions TEad and TEav of Yukie et al. (1990) and Saleem and Tanaka (1996).

FRONTAL AREAS Felleman and Van Essen classified areas 8 (FEF) and 46 as part of visual cortex. Areas 8 and 46 have both been partitioned into multiple subdivisions, including eight zones (8A, 8Am, 8Ar, 46d, 46v, 46dr, 46vr, and 46r) by Preuss and Goldman-Rakic (1991) and zones 8Ac, 46p, and 46v by Lewis and Van Essen (2000a).

It remains unclear which of the aforementioned schemes for inferotemporal and parietal cortex best reflect the underlying neurobiological reality. Indeed, alternative possibilities worth bearing in mind are that much of inferotemporal and frontal cortex might contain gradual gradients of properties rather than sharply defined areas, or else irregular clustering whose arrangement varies markedly from one individual to the next.

Figure 32.3 shows a composite map in which all of the 10 schemes represented in the preceding panels are superimposed and displayed in lateral (Fig. 32.3A), medial (Fig. 32.3B), and flat map (Fig. 32.3C) views. Besides the individually colored areas, the composite map includes the six clusters discussed in preceding sections: the dorsomedial occipital complex (DMOcx), posterior parietal complex (PPcx), MST complex (MSTcx), ventral superior temporal complex (VSTcx), inferotemporal complex (ITcx), and TF/TH cluster.

HOW MANY VISUAL SUBDIVISIONS ARE THERE? It is naturally of interest to have a current estimate of the total number of cortical areas and subdivisions associated with visual processing. Given the diversity among partitioning schemes, it is impractical to arrive at a definitive single number. Altogether, there is substantial evidence for more than 40 anatomically and/or functionally distinct subdivisions of visually responsive cortex, but for some the evidence does not warrant identification as separate areas. A conservative lumper can argue that the number of convincing visual areas is only about two dozen. A more generous splitter can make a credible case for at least three dozen distinct areas. The number of areas that show clear visuotopic organization is also difficult to determine precisely but is in the range of 10–12, depending on the designation of zones versus areas.

COPING WITH MULTIPLE SCHEMES, AREAL UNCERTAINTIES, AND INDIVIDUAL VARIABILITY Several general observations emerge from the preceding discussion. First, a multiplicity

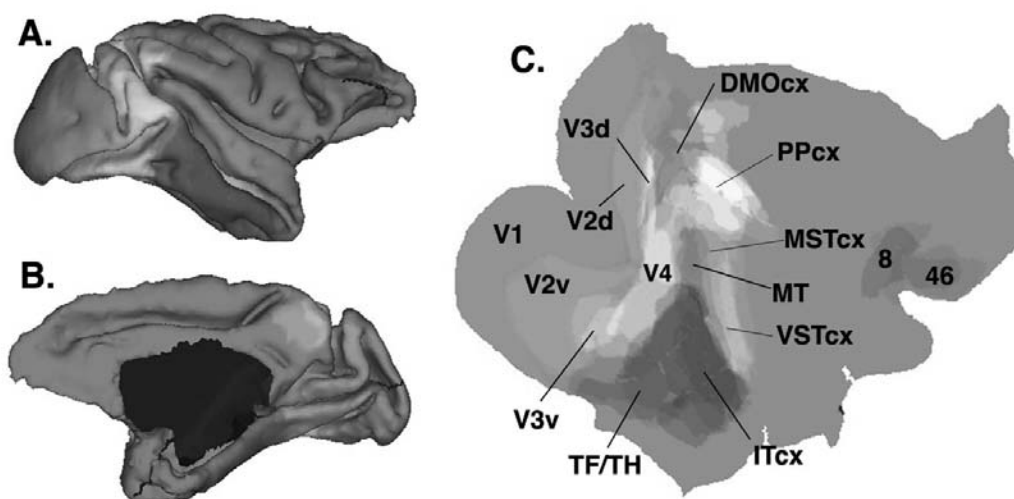


FIGURE 32.3. *A–C*, Lateral, medial, and flat map views of a composite map obtained by superimposing the data from Figure 32.2. Although the specific areal assignments at each location cannot be ascertained by viewing this image, they can be readily obtained using a node-identification option in the Caret visualization software. See the abbreviations list for full names and Figure 32.1 legend for data access information. (See color plate 13.)

of competing partitioning schemes will likely persist for years, because many of the issues remain difficult to resolve with currently available techniques. Second, it is becoming increasingly important to have objective methods for quantifying and visualizing the uncertainties associated with charting areal boundaries and the variability associated with individual differences in cortical organization. This leads to the notion of probabilistic surface-based maps of cortical organization. The composite map in Figure 32.3 constitutes one step in this direction, as it includes many different schemes in a common coordinate system. Another important aspect of a probabilistic approach is to incorporate information about individual variability by registering maps of many individuals on the atlas (Van Essen et al., 2001a).

Another important issue involves the options for accessing and extracting information from surface-based atlases. The fundamental challenge is that existing atlases already contain far more information than can be easily gleaned from static pictorial images such as those shown in this chapter. Moreover, the amount of information represented on such atlases is likely to grow exponentially over the next decade. An attractive alternative is to use computerized visualization software to access atlas data more efficiently and flexibly. For the atlases illustrated here, this can be done by downloading specific data sets (using hyperlinks included in the figure legends) and viewing the maps using the freely available Caret software (Van Essen et al., 2001b; <http://brainmap.wustl.edu/caret>). Existing visualization options in Caret include zooming in on regions of interest; rapid toggling between different partitioning schemes; laying one scheme directly over another; listing areal identities for multiple partitioning schemes when clicking on locations of interest; specifying location by latitude and longitude (cf. Fig. 32.1E); encoding

uncertainty limits for each boundary; and encoding variability by combining maps from different individuals.

HUMAN VISUAL CORTEX The analysis of human visual cortex has benefited greatly from the advent of structural and functional MRI methods that can be routinely carried out on normal subjects. In the top half of Figure 32.4, the extent of visual cortex and other functional modalities is charted on the right hemisphere of a surface-based atlas (the HumanColin atlas) that was generated from high-resolution structural MRI of a particular individual (Holmes et al., 1998; Van Essen, 2002; Van Essen et al., 2002). The surface displays include lateral and medial views of the fiducial surface (Fig. 32.4*A, B*) and the inflated surface (Fig. 32.4*C, D*), plus a flat map (Fig. 32.4*E*). The assignment of different functional modalities was estimated mainly from functional neuroimaging data that were mapped onto the atlas using a combination of methods applied to a number of published data sets (see the legend to Fig. 32.4). Based on these provisional assignments, cortex that is predominantly visual in function occupies about 27% of the total extent of cerebral cortex (950 cm^2) in the right hemisphere of the atlas. By comparison, about 8% of cortex is predominantly auditory, 7% somatosensory, and 7% motor. The remaining half (51%) includes major domains associated with cognition, emotion, and language.

Human area V1 (area 17) has a well-defined architectonic boundary that runs near the margins of the calcarine sulcus but with considerable individual variability (Rademacher et al., 1993). The estimated surface area of V1 on the atlas map (charted using the most likely boundary in the Rademacher et al. study) is 21 cm^2 , or 2.2% of cerebral cortex. This is about one-sixth of its fractional occupancy on the macaque atlas.

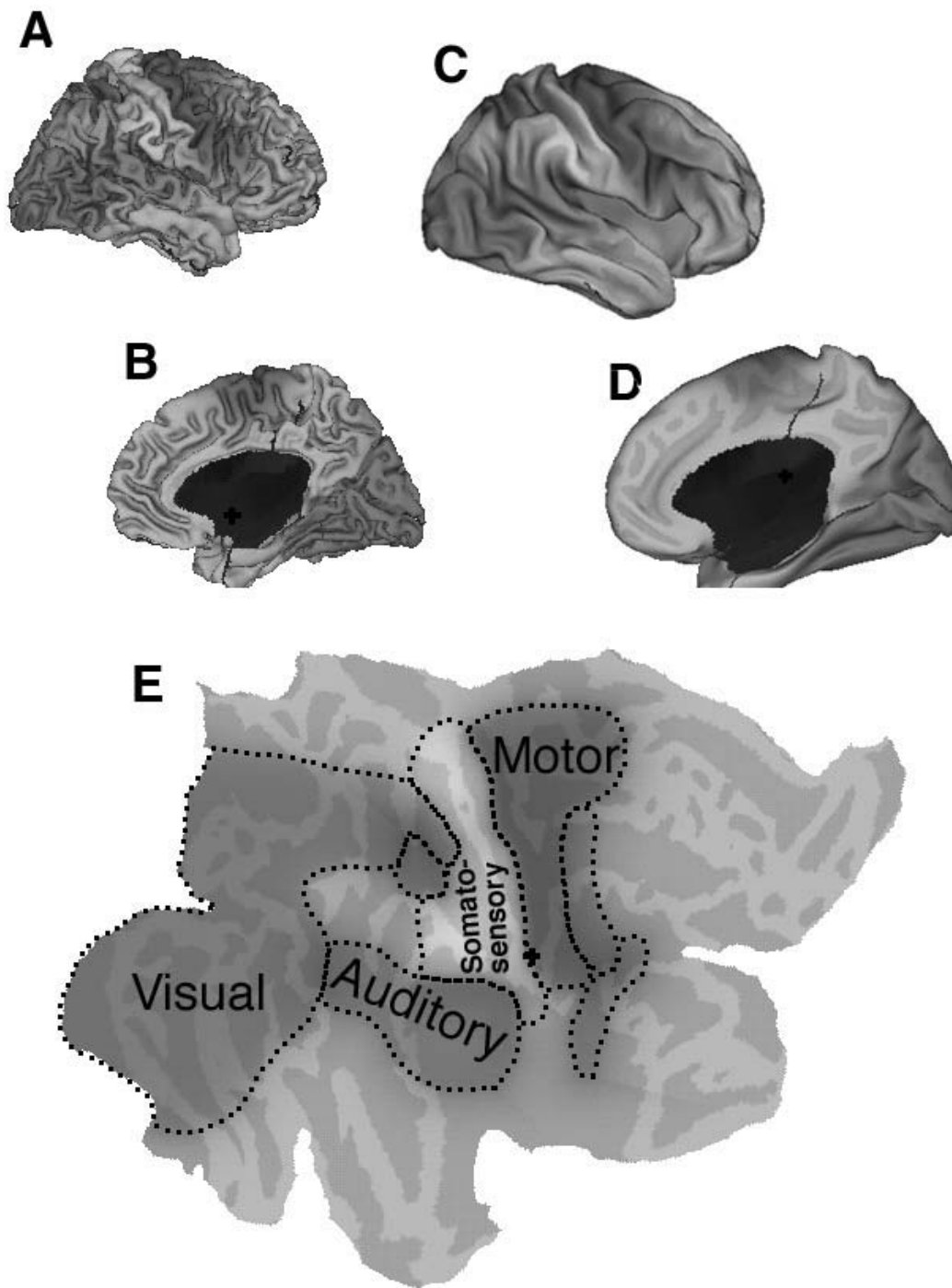


FIGURE 32.4. Visual cortex and other functional modalities mapped onto a surface-based atlas of human cerebral cortex. The atlas was generated from a high-resolution structural MRI volume provided by A. Toga (Case Human.colin) using SureFit and Caret software (cf. Fig. 32.1). This atlas (Van Essen et al., 2002) is higher in quality and supersedes the Visible Man surface-based atlas previously published (Van Essen and Drury, 1997; Van Essen et al., 2001a). Modality assignments were based on (1) stereotactic mapping of fMRI volume data onto the atlas surface from the studies of Corbetta et al. (1998), Lewis and DeYoe (2000), and

Lewis et al. (2001); (2) stereotactic projection of published Talairach coordinates of activation focus centers (Ishai et al., 1999; Kanwisher et al., 1997; Van Essen and Drury, 1997); and (3) manually transposed boundaries related to local geographic and/or functional landmarks from surface maps published by Burton and Sinclair (2000), Press et al. (2001), and Tootell & Hadjikhani (2001). Data for Figures 32.4 and 32.5 can be downloaded via http://brainmap.wustl.edu:8081/sums/archivelist.do?archive_id=449900 (See color plate 14).

Neuroimaging studies have revealed numerous visuotopically organized extrastriate areas in human occipital cortex in an arrangement that shows many similarities to the pattern found in the macaque. Corresponding areas that have fundamentally similar visuotopic organization in the two species include V1, V2, V3 (V3d), VP (V3v), V3A, and V4v (DeYoe et al., 1996; Hadjikhani et al., 1998; Sereno et al., 1995). In addition, tests for motion-related activation have consistently demonstrated a prominent focus in or near the posterior inferotemporal sulcus. This focus is generally presumed to correspond to macaque MT plus part of the MST complex and has therefore been identified as human MT+ (Tootell et al., 1995) or as V5 (Watson et al., 1993).

Figure 32.5 includes many visuotopic areas that were mapped onto the human atlas using surface-based registration of an individual case from Hadjikhani et al. (1998). For technical reasons these maps do not include the representation of the fovea or far periphery, so the extent of the extrastriate areas is likely to be modestly underestimated. Interestingly, the sizes of V3d, V3v, and V3A relative to V1 and V2 are all substantially greater in humans than in the macaque, suggesting a marked evolutionary divergence in the relative sizes of nearby cortical areas. In the region adjoining dorsal V3, Smith et al. (1998) and Press et al. (2001) found evidence for two representations, V3A and V3B, instead of a single V3A, with V3B being located more posterior (lower on the flat map). Area V7 (Press et al., 2001; Tootell and Hadjikhani, 2001) is a visuotopically organized area that lies anterior to V3A; its location and extent are displayed on the atlas using dotted boundaries to signify greater uncertainty.

Human area V4v lies anterolateral to VP/V3v and contains a mirror-symmetric upper-field representation. Interestingly, cortex lateral and dorsal to V4v, identified as LO (Van Oostende et al., 1997) or as the LOC/LOP complex (Tootell and Hadjikhani, 2001), evidently lacks a complementary lower-field representation equivalent to that described for macaque V4d. Instead, the LOC/LOP region represents both upper and lower fields, but with an irregular and inconsistent map of the polar angle and an apparent discontinuity in the transition between central and peripheral eccentricities. LO as described by Grill-Spector et al. (1998a,b; 2001) includes much of LOC/LOP but extends further ventrally and anteriorly (down and to the right on the flat map). Area V8 lies anterior to V4v and contains a complete visuotopic map with a foveal representation near its anterior margin to the right on the flat map (Hadjikhani et al., 1998; but see Wade et al., 2002).

Tests using a variety of stimuli and behavioral paradigms besides those just discussed have revealed several additional regions of functional specialization. Ventral occipitotemporal cortex contains a region preferentially activated by object versus nonobject stimuli. Based on published stereotactic (Talairach) coordinates, foci involved in analysis of faces,

houses, and chairs are concentrated in a region (red dotted outline in Fig. 32.5E) that partially overlaps V8 on the atlas map but extends more anteriorly (Haxby et al., 1999; Ishai et al., 1999; Kanwisher et al., 1997). This region has been proposed to include a fusiform face area (FF) and a parahippocampal place area (PP) (Epstein and Kanwisher, 1998; Kanwisher et al., 1997) and is accordingly identified as FF/PP in Figure 32.5E. Other studies suggest that these may not constitute distinct areas but rather a functional gradient within a larger subdivision (Haxby et al., 2001).

In the parietal lobe, visually related activations have been reported in a large swath of cortex in and near the intraparietal sulcus, dorsal and anterior to the known visuotopic areas. Paradigms effective in activating this region include shifting visual attention, target-directed eye movements, visual motion, and spatial analyses (Corbetta et al., 1998; Haxby et al., 1994; Lewis and DeYoe, 2000; Lewis et al., 2001). This region presumably includes a number of functionally distinct areas or subdivisions that have not been clearly discriminated using existing paradigms and analysis methods.

Macaque-human comparisons

While there are many striking similarities in visual cortical organization between macaque and human, there are numerous differences as well. Some of the differences are in relative size and in the geographic location of areas, but others presumably reflect fundamental differences in the existence of areas or in their topological relationships to one another. A useful general strategy for examining these relationships and candidate homologies is to use surface-based registration between species (Van Essen et al., 1998, 2001a). While neither proving nor disproving any particular homology, interspecies registration of surfaces provides a good testbed for exploring any particular set of proposed homologies implied for the relationships among areas in intervening regions.

In Figure 32.6, the macaque and human maps were registered to one another using explicit landmarks that are likely to reflect genuine homologies. These landmarks (colored contours in Fig. 32.6) include the fundus of the central sulcus (near the boundary between somatosensory and motor cortex); the fundus of the Sylvian fissure (near the boundary between somatosensory and auditory cortex); the boundaries of V1, V2, and MT+; and the boundaries of neocortex along the medial wall (Fig. 32.6A, B). To avoid confounds associated with artificial cuts on the flat maps, the landmarks were first projected to macaque and human spherical maps (not shown); the registration was applied to the spherical maps; and the deformed visual areas were then projected back to the flat maps. This is shown in Figure 32.6D for the human visual areas deformed to the shape of the macaque flat map (and superimposed on the macaque sulcal map). In Figure 32.6D, the corresponding relationships are shown with the macaque visual areas deformed to the shape of

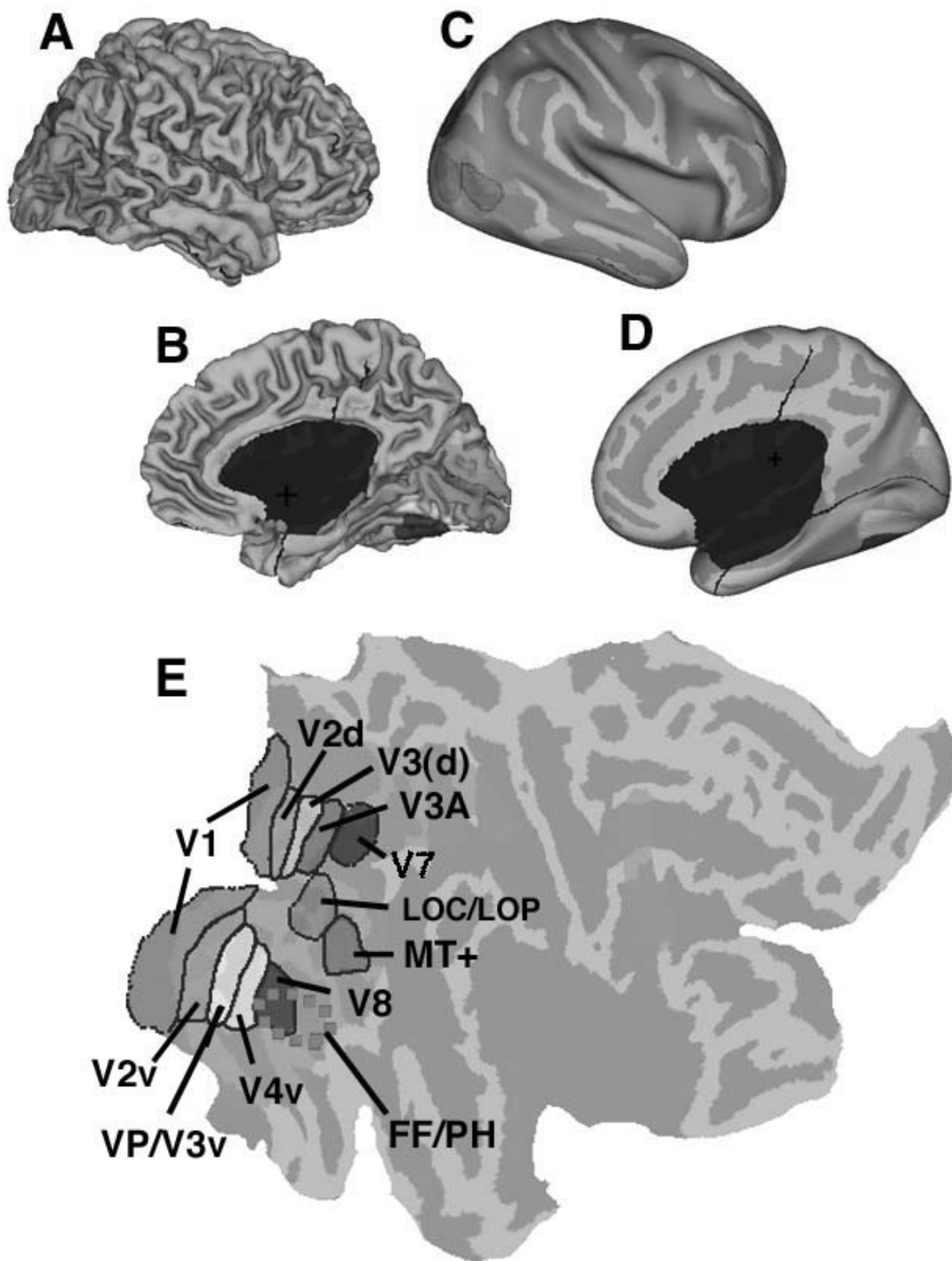


FIGURE 32.5. Identified visual areas on the Human.colin surface-based atlas. See the abbreviations list for full names. The boundary of MT+ on the atlas map was estimated by projecting the motion-related activation foci tabulated by Van Essen and Drury (1997) onto the atlas surface. The visuotopic map from Figure 5A of Tootell and Hadjikhani (2001) was then registered to the atlas using the V1/V2 boundary and the posterior boundary of MT+

as landmarks. Additional areas LO and V7 were drawn manually onto the atlas, based respectively on the studies of Tootell and Hadjikhani (2001) and Press et al. (2001). *A*, Lateral view. *B*, Medial view. *C*, Inflated lateral view. *D*, Inflated medial view. *E*, Flat map view. The red dotted contour represents the main cluster activation focus center involved in face and place analysis (see text). (See color plate 15.)

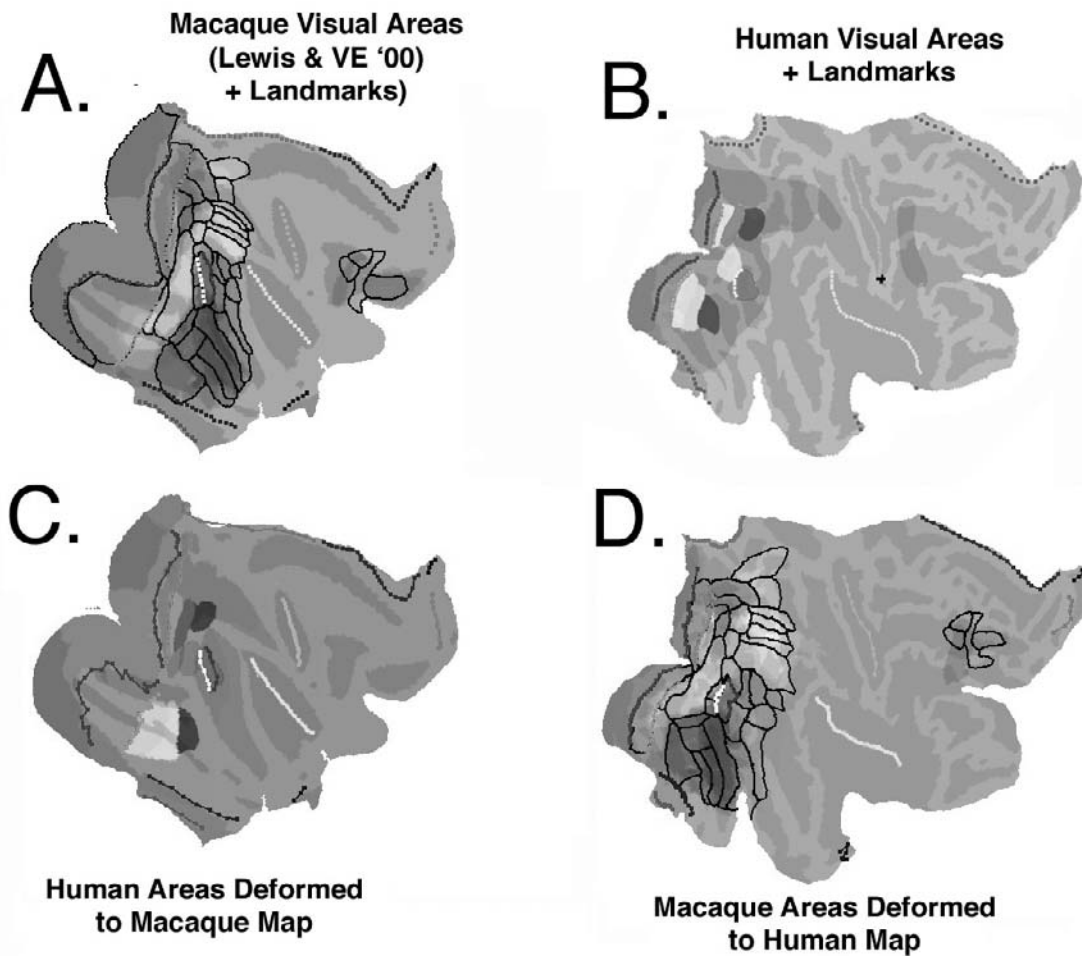


FIGURE 32.6. Comparisons between macaque and human visual cortex using interspecies surface-based registration. *A*, Macaque atlas flat map showing the composite map of visual areas (same as Fig. 32.3*C*) plus the boundaries of the Lewis and Van Essen scheme (same contours as in Fig. 32.2*C*) and the landmarks used to constrain the registration. *B*, Human atlas flat map showing visuotopic and functionally defined areas plus the landmarks used to constrain

the registration. *C*, Deformed human visual areas overlaid on the macaque flat map. *D*, Deformed macaque visual areas overlaid on the human flat map. Data can be accessed via <http://brainmap.wustl.edu/sums/sums-cgi?specfile=Human.colin.Cerebral.R.ATLAS.VanEssen02.Fig6.spec> and http://brainmap.wustl.edu:8081/sums/archivelist.do?archive_id=450135. (See color plate 16.)

the human flat map (and superimposed on the human sulcal map). The macaque map (before and after deformation) includes the composite of all 10 partitioning schemes painted onto the map, plus the Lewis and Van Essen partitioning scheme (black contours). The human map includes the same visuotopic areas delineated in Figure 32.5.

The deformation between species necessarily involves highly nonlinear distortions, mainly because V1 and V2 are much smaller (relative to overall cortical size) in humans versus macaques, and also because the location of MT (relative to foveal V2 and to the Sylvian fissure) is more posterior and ventral in the human versus the macaque map. Consequently, in Figure 32.6*D*, there is considerably more expansion of parietal areas than of inferotemporal areas on the deformed macaque map. The parietal lobe as defined by conventional geographic landmarks is slightly larger in the human atlas compared to the macaque (21% vs. 19% of

total neocortical surface area on the fiducial surface), whereas the size of region bounded by V2, MT, and the fundus of the central sulcus is substantially larger in humans (27% vs. 21% of neocortex). The species difference is even larger in the frontal lobe, which occupies 36% of human neocortex but only 25% in the macaque.

Several potential homologies can be evaluated by comparing individual areas and clusters of areas in the deformed macaque visual areas in Figure 32.6*D* to the human map in Figure 32.6*B* (or, equivalently, comparing the deformed human areas in Fig. 32.6*C* to the macaque map in Fig. 32.6*A*). One particular issue of interest is the relationship between macaque areas V4 and TEO/VOT, on the one hand, and human areas V4v, LOC/LOP, and V8, on the other hand. Deformed macaque V4v overlaps extensively with human V4v, and deformed macaque V4d overlaps with human LOC/LOP, consistent with the proposed homologies

for these areas. In contrast, deformed macaque V4 differs greatly in size and location from human V8. As emphasized by Tootell and Hadjikhani (2001), these and other differences argue strongly against a homology between macaque V4 and human V8, as proposed by Zeki et al. (1998).

Based on its location just anterior to V4v, human V8 is a candidate for homology with area TEO in the Ungerleider and Desimone scheme and with VOT in the Felleman/Lewis/Van Essen schemes. However, the visuotopic organization of human V8 is not in accord with that reported for either TEO or VOT, making a homology implausible on those grounds. For human V7, its location just anterior to V3A makes areas DP and zone LOP the most plausible candidates for homologs in the macaque, but a visuotopic map consistent with that in V7 has not been reported in this region.

Parietal visual cortex in the deformed macaque map overlaps extensively with human parietal visual cortex but is shifted somewhat more lateral (lower on this part of the map). Candidate homologies have been suggested between macaque LIP and human parietal areas involved in attention and eye movements (e.g., Corbetta et al., 1998; Sereno et al., 2001). These and other candidate homologies can be used as additional constraints to test for mappings that bring the overall parietal regions into closer register and may suggest additional homologies.

Deformed macaque inferotemporal and ventral superior temporal areas (blue and green in Fig. 32.4D) lie well anterior (to the right on the flat map) to the known visually responsive regions of human occipitotemporal cortex. One possible explanation for this discrepancy is that human visual cortex extends farther anterior in the temporal lobe than was previously recognized. Alternatively, the homologs of the macaque inferotemporal complex may lie within currently designated human visual cortex, anterior to V8 and/or flanking it. If so, this would signify an even more pronounced overemphasis on parietal visual areas and underemphasis on inferotemporal visual areas in humans compared to macaques.

OTHER SPECIES Although the focus of this chapter has been on the macaque and human, there is an enormous amount to be gained by obtaining a better understanding of visual cortex in other primate and nonprimate species. There has been substantial progress in elucidating visual cortical organization in other nonhuman primates, most notably the owl monkey but also several other species as well (Kaas, 1997; Rosa, 1997). In brief, these reveal similar patterns, especially for occipital visual areas, but also many indications of significant differences.

Rodents, particularly the mouse, are likely to become increasingly important as model systems for studying many aspects of cortical organization. Studies of the rat and

mouse have revealed a primary visual area surrounded by a modest number of extrastriate visual areas (Coogan and Burkhalter, 1990; Wagor et al., 1980). However, the magnitude of differences in the overall number and layout of visual areas from species in different orders remains to be determined. A mouse surface-based atlas, akin to those for the macaque and human illustrated here, has recently been generated (Van Essen et al., 2002) and should aid in charting the detailed organization of mouse visual cortex.

Concluding remarks

Progress in elucidating visual cortical organization is likely to accelerate markedly in the next few years, particularly with the use of fMRI and other imaging methods that can be applied to monkeys (Logothetis et al., 1999; Vanduffel et al., 2001) and to rodents as well as to humans. Because these data are represented digitally from the outset, registering such data to surface-based atlases should be easier and more accurate than for many of the data sets illustrated in this chapter. As the richness and complexity of such atlases and associated databases grow, the ways in which neuroscientists routinely access the data will likely evolve to be progressively more web-based, analogous to how molecular biologists use search engines and large databases to access an increasingly large fraction of the information they use in their research.

Abbreviations

Cortical Areas

DP	dorsal prelunate area
FST	floor of superior temporal area
IPa	area IPa from Cusick et al. (1995)
LIPd	lateral intraparietal (dorsal)
LIPv	lateral intraparietal (ventral)
MDP	medial dorsal parietal area
MIP	medial intraparietal area
MST	medial superior temporal area
MT	middle temporal area
PIP	posterior intraparietal area
PO	parietal-occipital area
TAa	area TAa from Cusick et al. (1995)
TEad	anterodorsal division of TE
TEav	anteroventral division of TE
TF	temporal area F
TH	temporal area H
Tpt	temporoparietal area
TPOc	temporal parietal occipital (caudal)
TPOi	temporal parietal occipital (intermediate)
TPOr	temporal parietal occipital (rostral)
VIP	ventral intraparietal
VIP*	heavily myelinated subdivision of VIP
V1	visual area 1
V2	visual area 2
V3	visual area 3
V3A	visual area V3A

V4	visual area 4
V4t	V4 transitional area
VOT	ventral occipitotemporal area
VP	ventral posterior area
7a	visual area 7a
46	visual area 46
7al	lateral area 7a
DMOcx	dorsomedial occipital complex
IPd	
ITcx	inferotemporal complex
MSTcx	medial superior temporal complex
MTc	caudal to middle temporal
OAA	
PGA	
POa-e	external division of area POa
POa-i	internal division of area POa
PPcx	posterior parietal complex
TE1	subdivision 1 of TE
TE1-3d	dorsal subdivision of TE1-3
TE1-3v	ventral subdivision of TE1-3
TE2	subdivision 2 of TE
TE3	subdivision 3 of TE
TEa/m	subdivisions a and m of TE
TEm	medial division of TE
TPO	temporo-parietal-occipital area
V2d	dorsal division of V2
V2v	ventral division of V2
V3d	dorsal division of V3
V3v	ventral division of V3
V6	visual area 6
V6A	visual area 6A
VSTcx	ventral superior temporal complex
Cortical Zones	
LOP	lateral occipital parietal
MST	medial superior temporal area
MSTd	dorsal subdivision of MST
MSTl	lateral subdivision of MST
MSTda	dorsoanterior subdivision of MST
MSTdp	dorsoposterior subdivision of MST
MSTm	medial subdivision of MST
VIPl	lateral subdivision of VIP
VIPm	medial subdivision of VIP
V4ta	V4 transitional area (anterior)
V4tp	V4 transitional area (posterior)

REFERENCES

- Baylis, G. C., E. T. Rolls, and C. M. Leonard, 1987. Functional subdivisions of the temporal lobe neocortex, *J. Neurosci.*, 7(2): 330–342.
- Blatt, G. J., R. A. Andersen, and G. R. Stoner, 1990. Visual receptive field organization and cortico-cortical connections of the lateral intraparietal area (Area LIP) in the macaque, *J. Comp. Neurol.*, 299:421–445.
- Boussaoud, D., R. Desimone, and L. G. Ungerleider, 1991. Visual topography of area TEO in the macaque, *J. Comp. Neurol.*, 306: 554–575.
- Boussaoud, D. R., L. C. Ungerleider, and R. Desimone, 1990. Pathways for motion analysis: cortical connections of the medial superior temporal and fundus of the superior temporal visual areas in the macaque, *J. Comp. Neurol.*, 296:462–495.
- Burton, H., and R. J. Sinclair, 2000. Attending to and remembering tactile stimuli: a review of brain imaging data and single-neuron responses, *J. Clin. Neurophysiol.*, 17(6):575–591.
- Burkhalter, A., D. J. Felleman, W. T. Newsome, and D. C. Van Essen, 1986. Anatomical and physiological asymmetries related to visual areas V3 and VP in macaque extrastriate cortex, *Vis. Res.*, 26:63–80.
- Colby, C. L., R. Gattass, C. R. Olson, and C. G. Gross, 1988. Topographic organization of cortical afferents to extrastriate visual area PO in the macaque: a dual tracer study, *J. Comp. Neurol.*, 269:392–413.
- Coogan, T. A., and A. Burkhalter, 1990. Conserved patterns of corticocortical connections define areal hierarchy in rat visual cortex, *Exp. Brain Res.*, 80:49–53.
- Corbetta, M., E. Akbudak, T. E. Conturo, A. Z. Snyder, J. M. Ollinger, H. A. Drury, M. R. Linenweber, M. E. Raichle, D. C. Van Essen, S. E. Petersen, and G. L. Shulman, 1998. A common network of functional areas for attention and eye movements, *Neuron*, 21:761–773.
- Cusick, C. G., 1997. The superior temporal polysensory region in monkeys, in *Cerebral Cortex*, vol. 12, *Extrastriate Cortex in Primates* (K. S. Rockland, J. H. Kaas, and A. Peters, eds.), New York: Plenum Press, pp. 435–468.
- Cusick, C. G., B. Seltzer, M. Cola, and E. Griggs, 1995. Chemoarchitectonics and corticocortical terminations with the superior temporal sulcus of the rhesus monkey: evidence for subdivisions of superior temporal polysensory cortex, *J. Comp. Neurol.*, 360: 513–535.
- Desimone, R., and L. B. Ungerleider, 1986. Multiple visual areas in the caudal superior temporal sulcus of the macaque, *J. Comp. Neurol.*, 248:164–189.
- Desimone, R., and L. B. Ungerleider, 1989. Neural mechanisms of visual processing in monkeys, in *Handbook of Neuropsychology*, vol. 2 (F. Boller and J. Grafman, eds.), Elsevier, pp. 267–299.
- DeYoe, E. A., G. Carman, P. Bandettini, S. Glickman, J. Wieser, R. Cox, D. Miller, and J. Neitz, 1996. Mapping striate and extrastriate visual areas in human cerebral cortex, *Proc. Natl. Acad. Sci. USA*, 93:2382–2386.
- Drury, H. A., D. C. Van Essen, M. Corbetta, and A. Z. Snyder, 1999. Surface-based analyses of the human cerebral cortex, in *Brain Warping*, (A. Toga ed.), San Diego: Academic Press, pp. 337–363.
- Epstein, R., and N. Kanwisher, 1998. A cortical representation of the local visual environment, *Nature*, 392:598–601.
- Felleman, D. J., and D. C. Van Essen, 1991. Distributed hierarchical processing in primate cerebral cortex, *Cereb. Cortex*, 1:1–47.
- Fischl, B., M. I. Sereno, and A. M. Dale, 1999a. Cortical surface-based analysis. II: inflation, flattening, and a surface-based coordinate system, *NeuroImage*, 9:195–207.
- Fischl, B., M. I. Sereno, R. B. Tootell, and A. M. Dale, 1999b. High-resolution intersubject averaging and a coordinate system for the cortical surface, *Hum. Brain Mapp.*, 8(4):272–284.
- Galletti, C., P. Fattori, M. Gamberini, and D. F. Kutz, 1999. The cortical visual area V6: brain location and visual topography, *Eur. J. Neurosci.*, 11:3922–3936.
- Gattass, R., A. P. B. Sousa, and C. G. Gross, 1988. Visuotopic organization and extent of V3 and V4 of the macaque, *J. Neurosci.*, 8(6):1831–1845.
- Grill-Spector, K., T. Kushnir, S. Edelman, Y. Itzhak, R. Malach, 1998. Cue-invariant activation in object-related areas of the human occipital lobe, *Neuron*, 21:191–202.
- Grill-Spector, K., T. Kushnir, T. Hendler, S. Edelman, Y. Itzhak, R. Malach, 1998b. A sequence of object-processing stages

- revealed by fMRI in the human occipital lobe, *Human Brain Mapping*, 6:316–328.
- Gill-Spector, K., Z. Kourtzi, and N. Kanwisher, 2001. The lateral occipital complex and its role in object recognition, *Vis. Res.* 41:1409–1422.
- Hadjikhani, N., A. K. Liu, A. M. Dale, P. Cavanagh, and R. B. H. Tootell, 1998. Retinotopy and color sensitivity in human visual cortical area V8, *Nat. Neurosci.*, 1:235–241.
- Haxby, J. V., M. I. Gobbini, M. L. Furey, A. Ishai, J. L. Schouten, and P. Pietrini, 2001. Distributed and overlapping representations of faces and objects in ventral temporal cortex, *Science*, 293(5539):2425–2430.
- Haxby, J. V., B. Horowitz, L. G. Ungerleider, J. M. Maisog, P. Pietrini, and C. L. Grady, 1994. The functional organization of human extrastriate cortex: a PET-rCBF study of selective attention to faces and locations, *J. Neurosci.*, 14:6336–6353.
- Haxby, J. V., L. G. Ungerleider, V. P. Clark, J. L. Schouten, E. A. Hoffman, and A. Martin, 1999. The effect of face inversion on activity in human neural systems for face and object perception, *Neuron*, 22:189–199.
- Holmes, C. J., R. Hoge, L. Collins, R. Woods, A. W. Toga, and A. C. Evans, 1998. Enhancement of MR images using registration for signal averaging, *J. Comp. Assist. Tomogr.*, 22:324–333.
- Ishai, A., L. G. Ungerleider, A. Martin, J. L. Schouten, and J. V. Haxby, 1999. Distributed representation of objects in the human ventral visual pathway, *Proc. Natl. Acad. Sci. USA*, 96:9379–9384.
- Kaas, J. H., 1997. Theories of visual cortex organization in primates, in *Cerebral Cortex*, vol. 12, *Extrastriate Cortex in Primates* (K. S. Rockland, J. H. Kaas, and A. Peters, eds.), New York: Plenum Press, pp. 91–125.
- Kanwisher, N., J. McDermott, and M. M. Chun, 1997. The fusiform face area: a module in human extrastriate cortex specialized for face perception, *J. Neurosci.*, 17:4302–4311.
- Komatsu, H., and R. H. Wurtz, 1988a. Relation of cortical areas MT and MST to pursuit eye movements. I. Localization and visual properties of neurons, *J. Neurophysiol.*, 60(2): 580–603.
- Komatsu, H., and R. H. Wurtz, 1988b. Relation of cortical areas MT and MST to pursuit eye movements. III. Interaction with full-field visual stimulation, *J. Neurophysiol.*, 60:621–644.
- Lewis, J. W., and E. A. DeYoe, 2000. A comparison of visual and auditory motion processing in human cerebral cortex, *Cereb. Cortex*, 10:873–888.
- Lewis, J. W., and D. C. Van Essen, 2000a. Architectonic parcellation of parieto-occipital cortex and interconnected cortical regions in the macaque monkey, *J. Comp. Neurol.*, 428:79–111.
- Lewis, J. W., and D. C. Van Essen, 2000b. Cortico-cortical connections of visual, sensorimotor, and multimodal processing areas in the parietal lobe of the macaque monkey, *J. Comp. Neurol.*, 428: 112–137.
- Lewis, J. W., F. L. Wightman, J. L. Junion Dienger, and E. A. DeYoe, 2001. fMRI activation in response to the identification of natural sounds, *Soc. Neurosci. Abstr.*, 27:512.9.
- Logothetis, N. K., H. Guggenberger, S. Peled, and J. Pauls, 1999. Functional imaging of the monkey brain, *Nat. Neurosci.*, 6: 555–562.
- Lyon, D. C., and J. H. Kaas, 2002. Evidence for a modified V3 with dorsal and ventral halves in macaque monkeys, *Neuron*, 33(3):453–461.
- Maguire, W. M., and J. S. Baizer, 1984. Visuotopic organization of the prelunate gyrus in rhesus monkey, *J. Neurosci.*, 4:1690–1704.
- Maunsell, J. H. R., and D. C. Van Essen, 1987. Topographical organization of the middle temporal visual area in the macaque monkey: representational biases and the relationship to callosal connections and myeloarchitectonic boundaries, *J. Comp. Neurol.*, 266:535–555.
- Olavarria, J. F., and D. C. Van Essen, 1997. The global pattern of cytochrome oxidase stripes in visual area V2 of the macaque monkey, *Cereb. Cortex*, 7:395–404.
- Oram, M. W., and D. I. Perrett, 1996. Integration of form and motion in the anterior superior temporal polysensory area (STPa) of the macaque monkey, *J. Neurophysiol.*, 76:109–129.
- Press, W. A., A. A. Brewer, R. F. Dougherty, A. R. Wade, and B. A. Wandell, 2001. Visual areas and spatial summation in human visual cortex, *Vis. Res.*, 41(10–11):1321–1332.
- Preuss, T. M., and P. S. Goldman-Rakic, 1991. Architectonics of the parietal and temporal association cortex in the strepsirrhine primate galago compared to the anthropoid primate macaca, *J. Comp. Neurol.*, 310:475–506.
- Rademacher, J., V. S. Caviness, Jr., H. Steinmetz, and A. M. Galaburda, 1993. Topographical variation of the human primary cortices: implications for neuroimaging, brain mapping, and neurobiology, *Cereb. Cortex*, 3:313–329.
- Rosa, M. G. P., 1997. Visuotopic organization of primate extrastriate cortex, in *Cerebral Cortex*, vol. 12, *Extrastriate Cortex in Primates* (K. S. Rockland, J. H. Kaas, and A. Peters, eds.), New York: Plenum Press, pp. 127–203.
- Saleem, K. S., and K. Tanaka, 1996. Divergent projections from the anterior inferotemporal area TE to the perirhinal and entorhinal cortices in the macaque monkey, *J. Neurosci.*, 16(15): 4757–4775.
- Seltzer, B., and D. N. Pandya, 1978. Afferent cortical connections and architectonics of the superior temporal sulcus and surrounding cortex in the rhesus monkey, *Brain Res.*, 149:1–24.
- Seltzer, B., and D. N. Pandya, 1980. Converging visual and somatic sensory cortical input to the intraparietal sulcus of the rhesus monkey, *Brain Res.*, 192:339–351.
- Seltzer, B., and D. N. Pandya, 1986. Posterior parietal projections to the intraparietal sulcus of the rhesus monkey, *Exp. Brain Res.*, 62:459–469.
- Sereno, M. I., A. M. Dale, J. B. Reppas, K. K. Kwong, J. W. Belliveau, T. J. Brady, B. R. Rosen, and R. B. H. Tootell, 1995. Borders of multiple visual areas in humans revealed by functional magnetic resonance imaging, *Science*, 268:889–893.
- Sereno, M. I., S. Pitzalis, and A. Martinez, 2001. Mapping of contralateral space in retinotopic coordinates by a parietal cortical area in humans, *Science*, 294(5545):1350–1354.
- Shipp, S., and S. Zeki, 1985. Segregation of pathways leading from V2 to areas V4 and V5 of macaque monkey visual cortex, *Nature*, 315:322–325.
- Smith, A. T., M. W. Grenlee, K. D. Singh, F. M. Kraemer, and J. N. Hennig, 1998. The processing of first- and second-order motion in human visual cortex assessed by functional magnetic resonance imaging (fMRI), *J. Neurosci.*, 18:3816–3830.
- Taira, M., K. I. Tsutsui, M. Jiang, K. Yara, and H. Sakata, 2000. Parietal neurons represent surface orientation from the gradient of binocular disparity, *J. Neurophysiol.*, 83(5):3140–3146.
- Tanaka, K., 1997. Columnar organization in the inferotemporal cortex, in *Cerebral Cortex*, vol. 12, *Extrastriate Cortex in Primates* (K. S. Rockland, J. H. Kaas, and A. Peters, eds.), New York: Plenum Press, pp. 469–495.
- Tootell, R. B. H., and N. Hadjikhani, 2001. Where is “dorsal V4” in human visual cortex? Retinotopic, topographic and functional evidence, *Cereb. Cortex*, 11:298–311.

- Tootell, R. B. H., J. B. Reppas, K. K. Kwong, R. Malach, R. T. Born, T. J. Brady, B. R. Rosen, and J. W. Belliveau, 1995. Functional analysis of human MT and related visual cortical areas using magnetic resonance imaging, *J. Neurosci.*, 15:3215–3230.
- Ungerleider, L. G., and R. Desimone, 1986. Cortical connections of visual area MT in the macaque, *J. Comp. Neurol.*, 248:190–222.
- Vanduffell, W., D. Fize, J. B. Mandeville, K. Nelissen, P. Van Hecke, B. R. Rosen, R. B. Tootell, and G. A. Organ, 2001. Visual motion processing investigated using contrast agent-enhanced fMRI in awake behaving monkeys, *Neuron*, 32:565–577.
- Van Essen, D. C., 2002. Windows on the brain. The emerging role of atlases and databases in neuroscience, *Curr. Op. Neurobiol.*, 12:574–579.
- Van Essen, D. C., J. Dickson, J. Harwell, D. Hanlon, C. H. Anderson, and H. A. Drury, 2001b. An integrated software system for Surface-based analyses of cerebral cortex, *J. Am. Med. Informat. Asso.*, 8:443–459.
- Van Essen, D. C., and H. A. Drury, 1997. Structural and functional analyses of human cerebral cortex using a surface-based atlas, *J. Neurosci.*, 17:7079–7102.
- Van Essen, D. C., and J. L. Gallant, 1994. Neural mechanisms of form and motion processing in the primate visual system, *Neuron.*, 13:1–10.
- Van Essen, D. C., and J. H. R. Maunsell, 1980. Two-dimensional maps of the cerebral cortex, *J. Comp. Neurol.*, 191:255–281.
- Van Essen, D. C., H. A. Drury, S. Joshi, and M. I. Miller, 1998. Functional and structural mapping of human cerebral cortex: solutions are in the surfaces, *Proc. Natl. Acad. Sci. USA*, 95:788–795.
- Van Essen, D. C., D. F. Felleman, E. A. DeYoe, J. F. Olavarria, and J. J. Knierim, 1990. Modular and hierarchical organization of extrastriate visual cortex in the macaque monkey, *Cold Spring Harbor Symp. Quant. Biol.*, 55:679–696.
- Van Essen, D. C., J. Harwell, D. Hanlon, J. Dickson, A. Snyder, and R. W. Cox, 2002. Mapping functional activation patterns onto cerebral and cerebellar surface-based atlases. *NeuroImage* (<http://www.academicpress.com/journals/hbm2002/14798.html>).
- Van Essen, D. C., J. W. Lewis, H. A. Drury, N. Hadjikhani, R. B. H. Tootell, M. Bakircioglu, and M. I. Miller, 2001a. Mapping visual cortex in monkeys and humans using surface-based atlases, *Vis. Res.*, 41:1359–1378.
- Van Essen, D. C., W. T. Newsome, and J. R. H. Maunsell, 1984. The visual field representation in striate cortex of the macaque monkey: asymmetries, anisotropies and individual variability, *Vis. Res.*, 24:429–448.
- Van Oostende, S., S. Sunaert, P. Van Hecke, G. Marchal, and G. A. Orban, 1997. The kinetic occipital (KO) region in man: an fMRI study, *Cereb. Cortex*, 7:690–701.
- Wade, A. R., A. A. Brewer, J. W. Rieger, and B. A. Wandell, 2002. Functional measurements of human ventral occipital cortex: retinotopy and color, *Philos. Trans. R. Soc.*, 357:963–973.
- Wagor, E., N. J. Mangini, and A. L. Pearlman, 1980. Retinotopic organization of striate and extrastriate visual cortex in the mouse, *J. Comp. Neurol.*, 193:187–202.
- Watson, J. G. D., R. Myers, R. S. J. Frackowiak, J. V. Hajnal R. P. Woods, J. C. Mazziotta, S. Shipp, and S. Zeki, 1993. Area V5 of the human brain: evidence from a combined study using positron emission tomography and magnetic resonance imaging, *Cereb. Cortex*, 3:37–94.
- Yukie, M., H. Takeuchi, Y. Hasegawa, and E. Iwai, 1990. Differential connectivity of inferotemporal area TE with the amygdala and the hippocampus in the monkey, in *Vision, Memory, and the Temporal Lobe* (E. Iwai and M. Mishkin, eds.), New York: Elsevier, pp. 129–135.
- Zeki, S. M., 1969. Representations of central visual fields in pres-triate cortex of moneky, *Brain Res.*, 14:271–291.
- Zeki, S., D. J. McKeefry, A. Bartels, and R. S. J. Frackowiak, 1998. Has a new color been discovered? *Nat. Neurosci.*, 1:335–336.

33 Communications between Cortical Areas of the Visual System

JEAN BULLIER

THE MAMMALIAN visual cortex is composed of numerous functional areas that contain a more or less complete representation of the contralateral visual hemifield or, in the case of the inferotemporal cortex, of the entire visual field. Information transmitted by the retinal ganglion cells is relayed by neurons of the dorsal lateral geniculate nucleus (LGN) and, with very few exceptions, is sent to layer 4 neurons of area V1. Thus, the first population of neurons to be activated by the onset of a visual stimulus is found in layer 4 of area V1 (Maunsell and Gibson, 1992; Nowak et al., 1995). After processing in area V1, activity is relayed to a few other cortical areas located close to V1 which themselves transmit activity to additional cortical areas. This pathway that starts in area V1 and spreads information to all visual cortical areas is the feedforward pathway. It will be shown that feedforward connections carry the main excitatory drive to cortical neurons and that they transmit information at different speeds in different regions of the visual cortex.

Cortical neurons do not simply transfer information to other visual areas with feedforward connections; they also process it. This operation is achieved by two sets of connections: the intrinsic, or horizontal, connections that connect together neighboring neurons in a cortical area and the feedback connections that connect cortical areas in the direction opposite to feedforward connections. Little will be said in this chapter about the function of horizontal connections because that is the subject of another chapter (see Chapter 46). On the other hand, the organization and function of feedback corticocortical connections will be examined closely because this has recently been the subject of much discussion and research.

Practically all the connections between areas are made by pyramidal neurons which also send recurrent collaterals to neighboring neurons within a few millimeters (Fig. 33.1). These connections, together with those of inhibitory GABAergic interneurons, constitute the horizontal connections (also called *local* or *intrinsic connections*). Therefore, processing between areas and processing within areas are inevitably related by the simple fact that whatever message is sent by a cortical neuron to neurons of another cortical area is also transmitted by horizontal connections to neighboring neurons within the same area. The local contacted

neurons appear to be almost exclusively pyramidal cells, some of them projecting to the same cortical area as the neurons to which they are connected. Thus, neurons with a common cortical target appear to be interconnected by horizontal connections. They also receive reciprocal connections from the target area (Johnson and Burkhalter, 1997), thus defining a specific network across and within areas.

The first processing stages (areas V1, V2, V3, V4, V5, or MT) contain neurons that have relatively small receptive fields confined to the contralateral visual hemifield. Neurons at higher levels in the inferotemporal and parietal cortex have receptive fields that extend across the vertical meridian. This extension in the ipsilateral hemifield is due to the presence of interhemispheric or callosal connections that link together the visual areas of both cortical hemispheres. Although the anatomical characteristics of these connections are well understood, little is known concerning their function beyond that of linking together the representations of both visual hemifields and producing receptive fields that are not limited to one visual hemifield. The role of callosal connections is also examined in this chapter.

Structure and function of corticocortical connections

GENERAL CHARACTERISTICS Corticocortical connections between functional areas are made almost exclusively by pyramidal neurons. A few exceptions have been noted: in the cat, some spiny stellate cells in area 17 send projections to area 18 (Meyer and Albus, 1981). It has been reported that in the rat, a small contingent of GABAergic smooth stellate cells send connections to neighboring cortical areas (McDonald and Burkhalter, 1993). Interhemispheric connections have also been found to arise from a few presumably inhibitory interneurons in the rat (Hughes and Peters, 1992a, 1992b) and in the cat (Peters et al., 1990). Despite this anatomical evidence, no monosynaptic inhibitory synaptic potential has ever been reported in electrophysiological studies of connections between cortical areas of the same or opposite hemisphere. It can therefore be concluded that interarea and interhemispheric corticocortical connections are massively excitatory. This does not mean that these

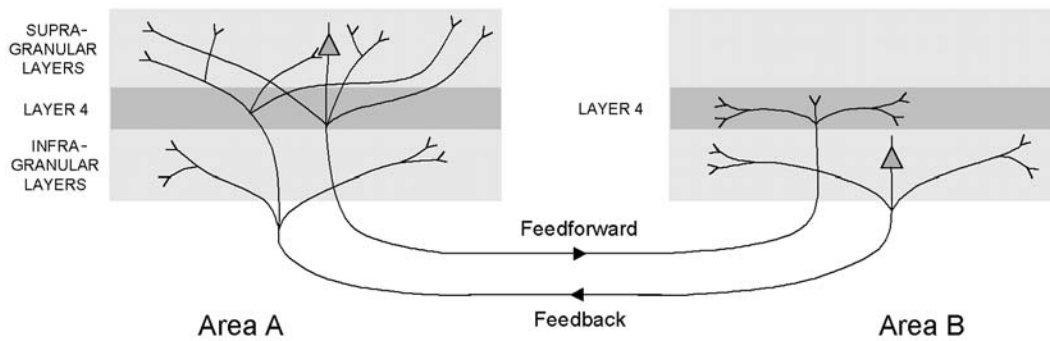


FIGURE 33.1. Schematic representation of the laminar distributions of feedforward and feedback neurons and axonal terminal arborizations. Note the presence of axon collaterals that innervate neighboring neurons and constitute the majority of horizontal connections.

connections have a net excitatory effect on the responses of the target area because they contact pyramidal cells as well as inhibitory interneurons. Therefore, the net effect of corticocortical connections is a mixture of excitatory and inhibitory influences.

It is known that within the local network of horizontal connections, the densest projections are to immediate neighbors. This is demonstrated by placing small injections of anterograde or retrograde tracers in a given site and examining the local distribution of labeled axons and neurons. The higher density of local connections is due to the branching pattern of axons that arborize more profusely near the main axon trunk.¹

In a similar fashion, the densest interarea connections tend to be with neighboring cortical areas. For example, the strongest connections of area V2 are with neighboring areas V1 and V4 in the monkey (Fig. 33.5.4). Similarly, in the cat, the strongest connections of area 17 are with neighboring areas 18 and 19. There are, however, a few examples of adjacent areas that are not interconnected, like the retrosplenial visual area in the monkey that has no connections with area V1, although it is surrounded by it on its caudal and lateral borders. Another exception to the rule of preferential connections with neighboring areas is found in the relationship between visual areas of the occipital, parietal, and temporal lobes with areas of the frontal lobe surrounding the frontal eye field area (FEF in Fig. 33.5.4). These frontal areas, in addition to local connections in the frontal lobe, exchange long-distance connections with parietal, occipital, and inferotemporal cortex. Similarly, areas of the occipital and parietal cortex interconnect with adjacent areas and exchange long-distance connections with the frontal cortex (Jones and Powell, 1970; Schall et al., 1995). This dual set of connec-

tions (to neighboring areas and to frontal cortex) probably corresponds to the different functional roles played by posterior and frontal regions in vision.²

DIFFERENT TYPES OF CORTICOCORTICAL CONNECTIONS
Intrahemispheric corticocortical connections are often divided into two classes: feedforward and feedback. The anatomical differences between feedforward and feedback were first described by Rockland and Pandya (1979), who noted that some connections (forward-going) tend to originate in neurons located in supragranular layers (layers 2 and 3) and terminate around layer 4, whereas reciprocal connections (backward-directed) are predominantly made by neurons in infragranular layers (layers 5 and 6) and project outside layer 4 (Figs. 33.1 and 33.4). This was later formalized by Maunsell and Van Essen (1983) and Felleman and Van Essen (1991), who used the anatomical differences between feedforward and feedback connections³ to construct the hierarchy of cortical areas (see below).

Although feedforward and feedback connections are usually presented in their archetypal form⁴ (Fig. 33.1), there are many variations on the theme: feedforward connections can originate from neurons in infragranular layers (Fig. 33.4.4), and their terminals often extend into the supragranular layers. Terminals of feedback connections

¹The distribution of boutons along axonal branches, on the other hand, appears to be more or less uniform (Braitenberg and Schüz, 1991).

²Frontal cortex is supposed to be more involved in the planning and generation of eye movement than are areas of the posterior cortex, which are thought to analyze visual information transmitted by the retina.

³Felleman and Van Essen also defined a third set of interarea connections called *lateral connections*; their neurons of origin belong to infra- and supragranular layers, and their terminals arborize in all layers. These connections are relatively rare, and their role is not understood.

⁴Feedforward connections originating from supragranular layer neurons and arborizing in layer 4 and feedback connections originating from infragranular layer neurons and arborizing outside layer 4.

usually avoid layer 4, but they often originate from supra- as well as infragranular layers (Fig. 33.4*B*). Quantitative estimates of the proportions of source neurons in infra- versus supragranular layers reveal that there is a continuum in the organization of feedback and feedforward connections instead of two separate homogeneous populations (Barone et al., 2000). Although this has not been quantified, it appears that a similar continuum is found when the laminar distribution of axonal arborization is considered. As argued earlier (Salin and Bullier, 1995), the archetypal organization of feedback connections (neurons located only in infragranular layers and providing exclusive input to layers 1 and 2) is found only for the relatively rare connections between areas that are distant on the cortical surface [such as inferotemporal (IT) cortex and V1; Fig. 33.5*A*]. In contrast, feedback connections between neighboring areas, which are extremely numerous, do not follow the archetypal model. They originate from neurons in supra- as well as infragranular layers and terminate in all layers except the lower portion of layer 4 (Kennedy and Bullier, 1985; Kennedy et al., 1989).

Interhemispheric connections have morphological characteristics that place them in the feedforward group for the laminar position of the source neurons (in layers 2 and 3) and in the feedforward or feedback group for the distributions of the axon terminals. In fact, the laminar organization of axon terminals in interhemispheric connections tends to follow that of intrahemispheric connections. In general, a given area connects to the same areas in both the same and the opposite cortical hemispheres, and the laminar distributions of the terminals are similar for inter- and intrahemispheric connections (Kennedy et al., 1991).

RETINOTOPIC ORGANIZATION As mentioned above, one of the major organizing principles of the visual cortical areas is that each area contains a retinotopic representation of the contralateral visual hemifield. In addition, receptive field sizes vary greatly from one area to another. Receptive field size is smallest in area V1 and increases progressively as one moves from V1 to V2, V4, and TEO to reach receptive fields that cover almost the entire visual field in some neurons of IT cortex. Similarly, receptive fields increase from V1 to V2, MT, MST and areas of the parietal cortex (Fig. 33.2). In addition, all anatomical studies show an important degree of convergence and divergence in corticocortical connections. Typically, a cortical zone a few hundred microns wide projects to and receives from a region that is usually a few millimeters wide but can cover up to 15mm on the cortical surface of a connected area (see the review in Salin and Bullier, 1995).

This large degree of convergence and divergence, and the great variation in receptive field sizes among cortical areas, have important consequences for the retinotopic organiza-

tion of corticocortical connections. It is usually assumed that all connections in the visual system are retinotopically organized, meaning that the receptive field centers of the afferent neurons are included in the receptive field center of the recipient cell. This appears to be the case for thalamocortical connections (Reid and Alonso, 1995; Tanaka, 1983) and feedforward connections, as shown by mapping studies in the cat (Price et al., 1994; Sherk and Ombrellaro, 1988) and inactivation studies in the monkey (Girard and Bullier, 1989; Girard et al., 1991a, 1991b) (Fig. 33.3).

Such is not the case for feedback connections because of the large degree of convergence and the larger receptive field centers of neurons in areas distant from area V1 (Fig. 33.2). Earlier mapping studies showed that the organization of feedback connections is compatible with the rule that neurons tend to interconnect if their receptive field centers overlap at least partially (Salin et al., 1992). As a consequence, the extent of the visual field concerned by the feedback connections to a column of cortex corresponds to the sum of twice the average diameter of the receptive field center in the source area and the average receptive field center in the recipient area (Fig. 33.3). The progressive increase in receptive field center size with distance from V1 (Fig. 33.2) means that feedback connections concern larger and larger regions of visual field as one moves from adjacent to more distant areas. Thus, feedback from area V2 to area V1 comes from neurons coding for a limited region of visual field (a few degrees; Fig. 33.3). On the other hand, feedback projections from IT neurons (Kennedy and Bullier, 1985; Rockland and Hoesen, 1994), which have very large receptive fields, enable neurons in area V1 to be influenced by information concerning very large portions of the visual

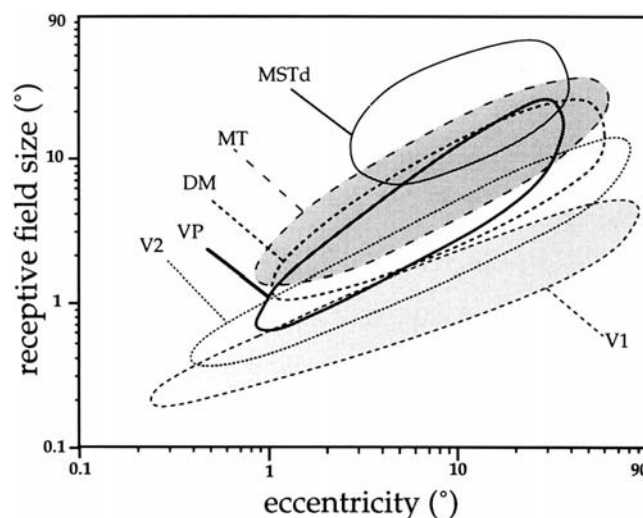


FIGURE 33.2. Receptive field center size as a function of eccentricity in the visual field for areas of the dorsal stream. Note how the receptive field size increases with distance from area V1. (From Rosa, 1997.)

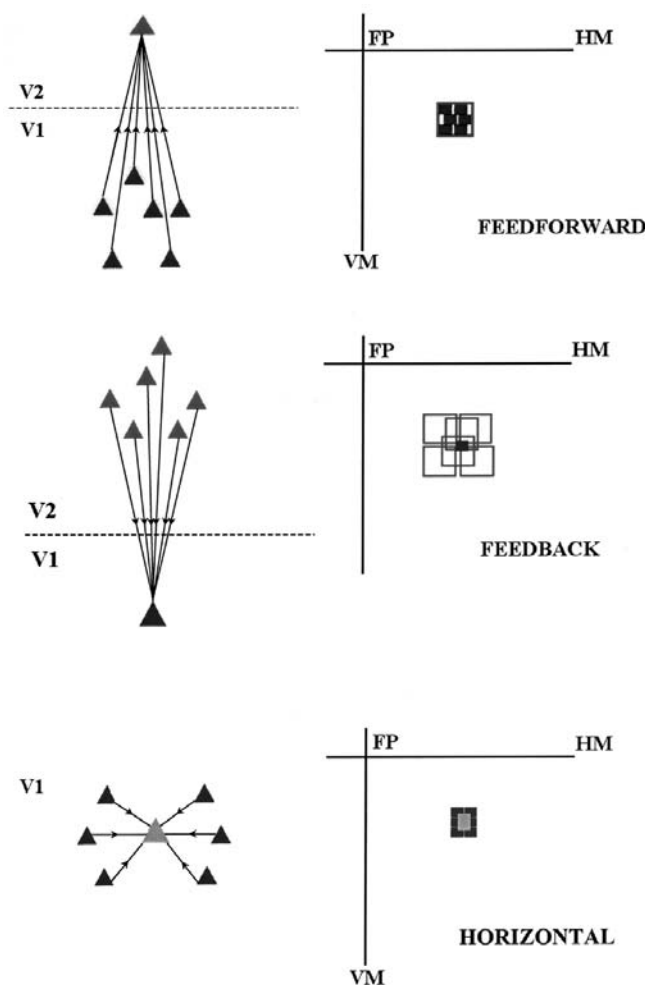


FIGURE 33.3. Retinotopic organization of feedforward, feedback, and horizontal connections. The left part of the figure schematically represents areas V1 and V2 seen from above. Triangles correspond to neuron cell bodies. The direction of the connection is indicated by the arrows on the simplified axons. The right part of the figure represents the right lower visual field of the animal (FP, fixation point; HM, horizontal meridian; VM, vertical meridian). For the *feedforward* connections, the large square represents the receptive field (RF) center of the V2 neuron receiving convergent information from the V1 neurons that have the small black squares as RF centers. The combination of RF centers of the afferent V1 neurons makes up the RF center of the target V2 neuron: feedforward connections are visuotopically organized. For the *feedback* connections, the small black square represents the RF center of the V1 neuron receiving convergent information from V2 neurons with the large open squares as RF centers. The RF centers of V2 neurons cover a larger region of visual field than that covered by the RF center of their target neuron in area V1: the feedback connections are only loosely retinotopic and can be used to mix information from distant regions of the visual field. For the *horizontal* connections, the gray square represents the RF center of the V1 neuron receiving convergent horizontal connections from neighboring neurons with RF centers indicated by the black squares. The combination of the horizontal afferents covers a larger part of the visual field than the RF center of the target neuron: horizontal connections are loosely retinotopic.

field. Feedback connections thus provide a sort of tiling of visual space, with further influences coming from progressively further areas.

In a similar way, but on a much smaller scale, the horizontal connections link together neurons with neighboring and partially overlapping receptive fields. The region of the visual field concerned by the horizontal connections corresponds approximately to the point image, that is, the extent of visual field covered by the receptive fields of neurons that are activated by a light point in the visual field⁵ (Angelucci et al., 2000). Thus, the extent of visual field concerned by the local connections is much smaller than that corresponding to the feedback connections from some of the most distant source areas (Fig. 33.3).

Interhemispheric connections, like horizontal connections, also interconnect neurons with overlapping and partially overlapping receptive fields, particularly around the vertical meridian. In addition, some interhemispheric connections appear to link together neurons with separate receptive fields that sometimes correspond to mirror images in both visual hemifields (Houzel and Milleret, 1999; Innocenti, 1986; Kennedy et al., 1991).

PATCHY ORGANIZATION AND AXONAL BIFURCATION Neuroanatomical tracing studies show that neurons retrogradely filled by a small deposit of retrograde tracer tend to be grouped in small patches a few hundred microns wide and separated by 500 to 1000 μm on the cortical surface, depending on the connection and the species (Fig. 33.4A). Results of anterograde tracer studies also demonstrate that terminal axons labeled by a small amount of tracer placed in a given cortical area are grouped together in small patches (Fig. 33.4C). This was originally discovered for horizontal connections (Rockland and Lund, 1982), and it was found later that extrinsic corticocortical connections also tend to be similarly organized in most species, with the possible exception of the mouse (Braitenberg and Schüz, 1991).

Patchy arborization is usually observed for horizontal (Gilbert and Wiesel, 1983; Rockland and Lund, 1982) and feedforward connections (Bullier et al., 1984; DeYoe and Van Essen, 1985; Shipp and Zeki, 1985; Symonds and Rosenquist, 1984). Coupled injections of different retrograde tracers in different cortical areas produce mostly nonoverlapping patches of labeled cells (Bullier et al., 1984; DeYoe and Van Essen, 1985; Shipp and Zeki, 1985), with very few double-labeled cells in the regions of overlap (Fig. 33.4A). This suggests that a given cortical area sends feedforward connections to several other areas through a system

⁵The point image corresponds to the average scatter of receptive field centers plus the average receptive field center diameter in the area.

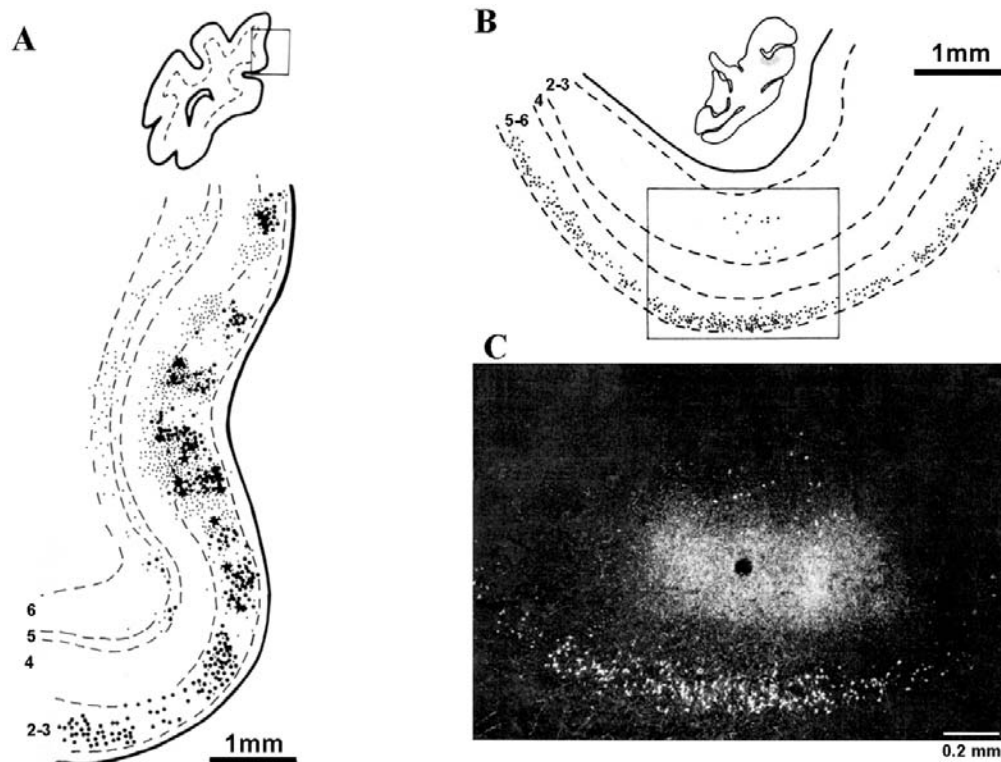


FIGURE 33.4. Patchy organization of corticocortical connections. *A*, distribution of neurons in area 17 sending feedforward connections to areas 18 and 19 of the cat visual cortex (small dots indicate neurons projecting to area 18, large dots neurons projecting to area 19, stars projecting to both areas). Note the predominance of neurons in the supragranular layers (2 and 3), the rare neurons projecting to both areas (stars). *B*, distribution of neurons sending feedback connections from area MT to area V1 in the macaque

monkey. Note the predominance and continuous nonpatchy distribution of feedback neurons in the infragranular layers. *C*, detail of *B*: retrogradely labeled feedback neurons in layers 5 and 6 (white dots) and labeling of feedforward terminal axons in layer 4 (white cloud). Note the contrast between the small patch of feedforward axon terminals and the more extensive and nonpatchy distribution of feedback neurons (*A* modified from Bullier et al., 1984; *C* modified from Kennedy et al., 1989.)

of neuronal populations organized as interdigitating neuron patches. It is likely that these populations share common functional properties and are interconnected by patchy horizontal connections. Although less frequently demonstrated because of the small number of studies using coupled anterograde tracers compared to studies using retrograde tracers, patches of terminal axons also appear to segregate at least partially in the target area for feedforward and interhemispheric connections (Goldman-Rakic and Schwartz, 1982; Morel and Bullier, 1990).

It is likely that the patchy organization and lack of axonal bifurcation in feedforward connections are the marks of the functional specificity of such connections. This is suggested by the observation that the V1 neurons projecting to area MT belong to a specific type with homogeneous properties (Movshon and Newsome, 1996). This result is comparable to that of an earlier work by Henry and his collaborators, which also demonstrated the specific functional properties of neurons projecting from area 17 to the PMLS in the cat (Henry et al., 1978). Similarly, the patchy distribution of feedforward terminals presumably corresponds to the con-

vergence of axon terminals of neurons with some common properties. This is suggested by the elegant experiments of Sherk in the LS area (which is slightly larger than the PMLS) (Sherk, 1990). Using a neurotoxin, she killed the neurons in a small region of that area and recorded from what presumably correspond to the terminals of afferent axons. She found that axon terminals group together according to direction selectivity, thus suggesting that neurons with the same optimal direction tend to terminate in common patches. The neurons innervated by this axon group presumably inherit the property of direction selectivity transmitted by the converging feedforward axons.

The prevalence of patchy organization is more variable in studies of feedback connections. In general, when relatively extensive injections of retrograde tracers are placed in a given area, neurons in extrastriate areas do not group themselves in well-defined patches, as in the case of feedforward connections (Fig. 33.4*B*; Kennedy and Bullier, 1985; Perkel et al., 1986). On the other hand, more localized injections of retrograde tracers in the supragranular layers produce patchy distributions of labeled cells in supragranu-

lar layers (Angelucci et al., 2002; Salin et al., 1995; Shipp and Grant, 1991). Similarly, injections of anterograde tracers produce patchy distributions of terminals, particularly in the supragranular layers (Henry et al., 1991; Salin et al., 1995; Wong-Riley, 1979). A continuous distribution of anterograde labeling has been reported on other occasions, but this may be due to the large size of the injection (Maunsell and Van Essen, 1983; Ungerleider et al., 1983).

There appears to be greater variability in the patchy distribution of feedback than in feedforward. The reason for this difference may be that different categories of feedback connections, concerning different sets of layers, show variable degrees of patchiness. Indeed, direct comparisons of the distributions of labeled cells or axon terminals in different layers for feedback connections show that patchy distributions exist in the connections between supragranular layers, whereas connections from infragranular layers appear to be less segregated (Fig. 33.4*B*), and afferent terminals in lamina 1 always project in a diffuse manner (Henry et al., 1991; Salin et al., 1992; Shipp and Grant, 1991). Similar differences between the topographic organizations of terminals in different laminae are also observed when individual axonal arbors are traced in the target area, as demonstrated by the work of Rockland and her colleagues (Rockland and Drash, 1996; Rockland et al., 1994).

It is interesting that the laminar differences observed for the patchy character of feedback connections are echoed by similar differences in the pattern of axonal bifurcation. Thus, in feedback connections, the proportion of neurons sending bifurcating axons to two cortical areas is higher in infragranular than in supragranular layers (Bullier and Kennedy, 1987). Also, the results of Rockland and her associates demonstrate that some feedback axons have long axonal collaterals in layer 1 that arborize extensively over at least two cortical areas, whereas terminals in layers 2 and 3 are restricted to one cortical area (Rockland et al., 1994).

This difference in organization across layers suggests that for a given set of feedback connections between two areas, different roles are played by different subsets of connections corresponding to different laminar distributions in the source and target areas. Thus, the variability of laminar distribution among feedback connections between areas at different distances on the cortical surface may correspond to different functional roles played by distant feedback connections (e.g., TE to V1) compared to those between adjacent areas (e.g., V2 to V1).

Assuming that the patchy and nonbifurcating nature of feedforward connections reflects the necessity to organize inputs according to specific properties, the more diffuse character of the feedback connections to layer 1 suggests that it plays a more general role, such as controlling the contrast gain or membrane potential of a large population of target neurons. Such a diffuse role cannot be extended to

all feedback connections, however, because feedback connections to layers 2 and 3, with their patchy organization, probably play a very specific role in the processing of visual information.

What differentiates neurons with axonal bifurcation to several cortical areas from neurons that project to only one cortical area? This question is particularly interesting for the feedback connections from the infragranular layers that contain a sizable proportion of axonal bifurcation (Bullier and Kennedy, 1987). It is possible that such bifurcation concerns preferentially axons with fast conduction velocity. As suggested by modeling studies (Murre and Sturdy, 1995), axon size is under strong constraints in the brains of large mammals. Projection of thick axons to several areas by way of bifurcation is one way of limiting their number. Indeed, there are many examples of thick axons that bifurcate: Y cells in the cat LGN that have the largest axons send bifurcations to areas 17 and 18 (Bullier and Kennedy, 1987), and Meynert cells in layer 6 of area V1 send bifurcating axons to at least area MT, and to the superior colliculus (Fries et al., 1985). In functional terms, the bifurcation of thick axons to several cortical areas is an efficient way to coactivate several cortical areas rapidly and simultaneously.

SYNAPTIC TRANSMISSION Given the important anatomical differences between feedforward and feedback connections reviewed above, it is likely that differences also exist in the characteristics of synaptic transmission for these two types of connections. Reports on electron microscopic (EM) studies of all types of corticocortical connections all agree that they make excitatory synapses on their target neurons (Anderson et al., 1998; Gonchar and Burkhalter, 1999; Johnson and Burkhalter, 1996; Lowenstein and Somogyi, 1991). Possible differences between feedforward and feedback connections are therefore likely to be reflected in the excitatory or inhibitory type of neuron that is contacted. The morphology of feedforward connections from V1 to V5 was recently investigated by Anderson and his collaborators (1998). Terminal boutons formed asymmetric (presumably excitatory) synapses and tended to contact preferentially spiny neurons (excitatory, mostly pyramidal), but also terminated on smooth, presumably inhibitory, cells in 20% of the cases. Very similar proportions were reported by Lowenstein and Somogyi (1991) in their study of the feedforward projection from area 17 to PMLS in the cat, an area that has been considered homologous to area MT of primates (Payne, 1993). In a study of feedforward connections between visual cortical areas in the rat, Johnson and Burkhalter (1996) reported a smaller proportion of contacts onto synaptic shafts (10%).

Less is known concerning the synaptic organization of feedback connections. The early results of Johnson and Burkhalter suggested that feedback connections contact

more specifically spines of pyramidal cells (98% of the cases) and rarely terminate on dendritic shafts (Johnson and Burkhalter, 1996). However, a more recent study by the same laboratory found similar proportions of terminals on parvalbumin-rich GABAergic interneurons (10%) in both feedforward and feedback connections in the rat visual system (Gonchar and Burkhalter, 1999). Differences between feedforward and feedback were found at the site of axonal contact to GABAergic parvalbumin-rich interneurons, with feedback connections terminating on distal parts of the dendrites, whereas feedforward contacted dendritic regions closer to the cell body (Gonchar and Burkhalter, 1999). This finding is in keeping with functional data from the same group showing that feedback connections have mostly an excitatory influence, whereas electrical stimulation of intrinsic and feedforward connections tends to recruit inhibitory circuits at relatively low stimulus intensities (Shao and Burkhalter, 1996). The latter results, however, should be treated with caution, because electrical stimulation acts exclusively on axonal branches (Nowak and Bullier, 1998a, 1998b). Therefore, stimulation in one area activates the efferent axons orthodromically, as well as the afferent axons antidromically, and it is impossible to differentiate the synaptic potentials evoked by direct orthodromic activation from those evoked by recurrent collaterals of antidromically activated axons. This confusion probably explains why the laminar pattern of activation elicited in a given cortical area by electrical stimulation in another area does not always fit with that predicted from the laminar distribution of axon terminals (Domenici et al., 1995; Nowak et al., 1997).

The low proportion of terminals on dendritic shafts reported for feedback connections by Burkhalter and his colleagues contrasts with the results of an earlier EM study of the feedback connections between areas 18 and 17 in the cat (Fisken et al., 1975). In that study, the authors concluded that more than 30% of the terminals of feedback connections were located on dendritic shafts. Whether this discrepancy is related to a species difference or whether there is indeed a strong feedback projection to dendritic shafts remains to be determined by further studies.

In conclusion, much remains to be done to understand the differences between the synaptic organizations of feedforward and feedback connections. It appears that both types send excitatory connections, but whether they target different proportions of inhibitory neurons has not been clearly established. Using agonists and antagonists, it will also be interesting to determine the proportions of different receptor channels contacted by these two types of connections. As mentioned above, the task is complicated by the limits of the method of electrical stimulation and by the heterogeneity of feedback connections.

Hierarchical organization of cortical areas

The classification of corticocortical connections in feedforward, feedback, and lateral connections led Maunsell and Van Essen (1983) to define a hierarchy of cortical areas on the basis of a simple rule: the areas are arranged in a series of levels defined by their connections with each other. At the lowest level is area (V1) that receives only feedback connections and sends only feedforward connections to other areas. At the next level is area V2, which receives feedforward connections from V1 but receives only feedback connections from other areas. Above V2 is area V3, which receives feedforward connections from V1 and V2 and feedback connections from other areas. In addition, there is the possibility that two areas belong to the same level if they exchange lateral connections (see also Chapter 32).

It is remarkable that this simple set of rules is in most cases internally consistent: if area A sends feedforward connections to area B, then B sends feedback connections to A; if A sends lateral connections to B, B sends lateral connections to A. A small number of exceptions have been noted (Felleman and Van Essen, 1991). Applying these rules to the areas of the macaque monkey initially generated the pattern shown in Figure 33.5B. More recent versions (Fig. 33.5C) have a similar organization but have become more and more complicated as more connections have been discovered (DeYoe et al., 1994; Felleman and Van Essen, 1991).

This method is useful for organizing the large number of cortical areas of the monkey visual system in a small number of distinct levels, but it has two disadvantages: (1) It is an anatomical classification that says little about the functional interactions between the areas. We will come back to this question in the next section. (2) It is largely underdetermined, as pointed out by Malcolm Young and his associates (Hilgetag et al., 1996). This means that the set of rules used to construct the hierarchy does not produce a unique solution. Optimal solutions lead to smaller numbers of rule violations, but it is usually impossible to identify the optimal configurations because of the lack of knowledge concerning many connections. The consequence of the underdetermined character of the hierarchical scheme is that a given cortical area such as area MT can occupy levels 5 to 10 in the hierarchy. For most pairs of cortical areas beyond V1, V2, and V3,⁶ it is impossible to be certain that one area is at a lower or a higher level than the other, or whether they belong to the same level in the hierarchy.

An attempt has been made recently to specify the character of this hierarchical scheme more precisely by quanti-

⁶For these areas, the numbers of possible levels are small.

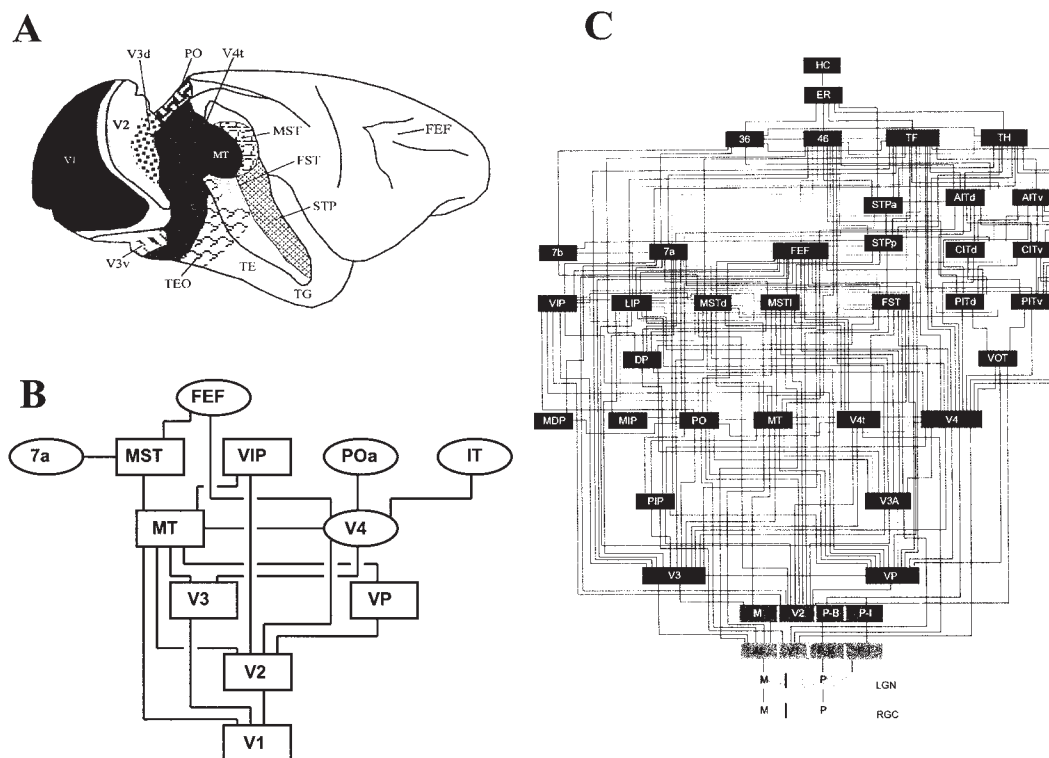


FIGURE 33.5. Hierarchical organization of cortical areas of the macaque monkey visual system. *A*, a schematic representation of the visual areas of the macaque monkey brain. *B*, the early version of the hierarchy. Boxes and ellipses correspond to cortical areas shown in *A*, lines to bidirectional connections. IT corresponds to TE in *A*; 7a, Poa, and VIP are located in the intraparietal sulcus that is located in front of PO in *A*; V3 corresponds to V3d and VP to V3v in *A*. V1 is at the lowest level, and the frontal eye field

(FEF) is at the highest level of the hierarchy. *C*, the 1991 version. Separation is made between magno- and parvocellular layers in the LGN (*M* and *P*) and in the retinal ganglion cells (*RGC*). In V1 the Magno stream (*M*) is separated from the Parvo-Blob (*P-B*) and Parvo-Interblob (*P-I*) streams. At the highest level are found the hippocampal formation (*HC*) and the entorhinal cortex (*ER*). The FEF is seven levels above V1. (*A* modified from Van Essen and Maunsell, 1983; *C* modified from Felleman and Van Essen, 1991.)

fying the proportions of source neurons in supragranular versus infragranular layers (Barone et al., 2000). When this is done, a reasonably good match to the original hierarchy of Maunsell and Van Essen is obtained and, provided that a few adjustments are made, the proportion of labeled neurons in supragranular layers is a good predictor of the level in the hierarchy. However, when the hierarchy obtained by Young and colleagues by modeling (Hilgetag et al., 1996) and that obtained by quantifying the proportion of supragranular layer neurons (Barone et al., 2000) are compared to those published by Van Essen and his colleagues, serious discrepancies are found between the levels at which a given area belongs. For example, the FEF belongs to the highest level in the original map (Fig. 33.5*B*), to the eighth level in the 1991 version (Fig. 33.5*C*), and is brought down to the fourth level when attention is paid to the proportion of supragranular layer neurons (Barone et al., 2000).

The underdetermined character and the variability in the levels occupied by areas in different classification schemes suggest that caution should be applied when attempts are

made to derive functional interpretations from the hierarchical classification. Furthermore, as mentioned below (see the next section), the latencies of neurons in different cortical areas cannot be predicted from the hierarchy of cortical areas, as would be expected if the hierarchical organization corresponded to a functional model with a succession of processing stages along the hierarchy.

An interesting interpretation of the laminar organization of neurons and axon terminals of different corticocortical connections has been proposed by Barbas (1986; Barbas and Rempel-Clower, 1997) for the connections in the monkey frontal cortex. This author claims that the laminar organization of a given connection can be predicted by the laminar organizations of the source and target areas. Most sensory areas have a classic organization with six layers and a well-identified layer 4 (or granular layer). In the frontal cortex, there are also “agranular” areas, lacking the characteristic layer 4, and several areas belonging to the limbic type of cortex with a dense population of neurons in the deep layers. It has been argued that evolutionary steps can be traced by

studying the laminar organization of different cortical regions, and that areas can be classed into different types, from ancient limbic-type cortex to agranular and to more recent granular cortex (Sanides, 1970). Barbas showed that the laminar organizations of corticocortical connections are related to the types of the source and target areas. Thus, areas of the granular type project from the supragranular layers and terminate mostly in the middle and deep layers to less laminated areas, whereas the return projections originate from the deep layers and preferentially target the upper layers (Barbas and Rempel-Clower, 1997). Thus, the differences between feedforward and feedback connections in occipital, parietal, and temporal cortex may simply reflect differences in organization between sensory cortices of the occipital cortex with well-differentiated structures (areas V1 and V2) and areas with less well differentiated structures in the parietal and temporal cortex. One advantage of this model is that it predicts the observed progressive shift toward projections from infragranular layers terminating at higher levels in the target area with increasing distance (in terms of levels of organization which reflect distance on the cortical surface).

Timing of activation in different areas

The hierarchical model of visual cortical areas suggests that information is processed through a succession of stages corresponding to the different levels of the hierarchy. This leads to the prediction that successive levels should contain neurons responding with increasingly long latencies to visual stimulation, the increase in latency reflecting processing occurring at the different levels. Direct tests of this hypothesis, however, have not confirmed such a model of a cascade of processors. Instead, important latency differences are observed between neurons of the dorsal and ventral streams. Although these are treated in detail in another chapter (Chapter 34), a rapid review is presented of the anatomical and functional differences between these two groups of areas.

DORSAL AND VENTRAL STREAMS An important subdivision of the visual system was proposed in the 1970s, that between structures subserving form and space vision. This separation was already present in the early models of the visual system based on the study of nonprimate species, with the superior colliculus involved in space vision and the visual cortex dealing with form vision (Schneider, 1969). A similar distinction was made between structures dealing with focal and ambient vision (Trevarthen, 1968). Since the beginning of the twentieth century, it was known that in humans, lesions in the parietal and temporal cortex lead to deficits in space and form vision, respectively. All these ideas were synthesized in the concept of two functional streams in the primate

visual cortex, with the ventral occipitotemporal stream dealing with form vision and the dorsal occipitoparietal stream involved in space vision. The success of this subdivision was established by the demonstration in the monkey of a double dissociation of the effects of lesions in the parietal and inferotemporal cortex (Pohl, 1973) that mirrored the clinical observations in humans, and by the tracing of anatomical connections between striate cortex and parietal and IT cortex (Ungerleider and Mishkin, 1982). The segregation of cortical connections into dorsal and ventral streams was confirmed by the results of mathematical models grouping together the most densely interconnected areas of the monkey (Jouve et al., 1998; Young, 1992).

Since then, questions have been raised concerning the roles of the two cortical streams. The initial idea was that the dorsal stream is involved in processing *where* an object is located in the visual field, whereas the ventral stream is engaged in the *recognition* of objects (the *where/what* division of Ungerleider and Mishkin, 1982). More recently, the emphasis has shifted to the visuomotor aspects of processing in the dorsal stream. In addition to dealing with where an object is located, the dorsal stream is important for grasping and manipulating an object (Goodale and Milner, 1992; Jeannerod et al., 1995). Despite these evolutions, the basic idea that parietal and IT cortex deal with different aspects of vision has stood the test of time. Anatomical studies partially confirmed this separation by showing that the two streams remain partially separate in the frontal cortex, and that there are regions of convergence in frontal cortex and in the depths of the superior temporal sulcus (Baizer et al., 1991; Bullier et al., 1996; Morel and Bullier, 1990).

THE FAST BRAIN In order to examine the flow of information transfer across the primate visual system, we collected the latencies of neurons to visual stimulation in the different visual areas, as published by research groups working on awake, behaving monkeys (Nowak and Bullier, 1997). As can be seen in Figure 33.6A, these latencies are only loosely correlated with their locations in the hierarchy of cortical areas. For example, neurons in the FEF area have latencies that are longer than those of area 17 by only a few milliseconds (Nowak and Bullier, 1997; Schmolesky et al., 1998), despite the six levels difference between the two areas (Fig. 33.5C). Similarly, latencies of neurons in MT and V2 are comparable (Raiguel et al., 1989; Fig. 33.6A), even though area MT is placed at three levels above V2 in the cortical hierarchy (Fig. 33.5C). On the other hand, areas MST, FEF, and 7a have much shorter latencies than areas of the IT cortex (e.g., TEa, TE1, TE2) that are at the same levels in the hierarchy (Fig. 33.6A).

A much better predictor of the latency to visual stimulation is whether the area is in the dorsal or ventral stream.

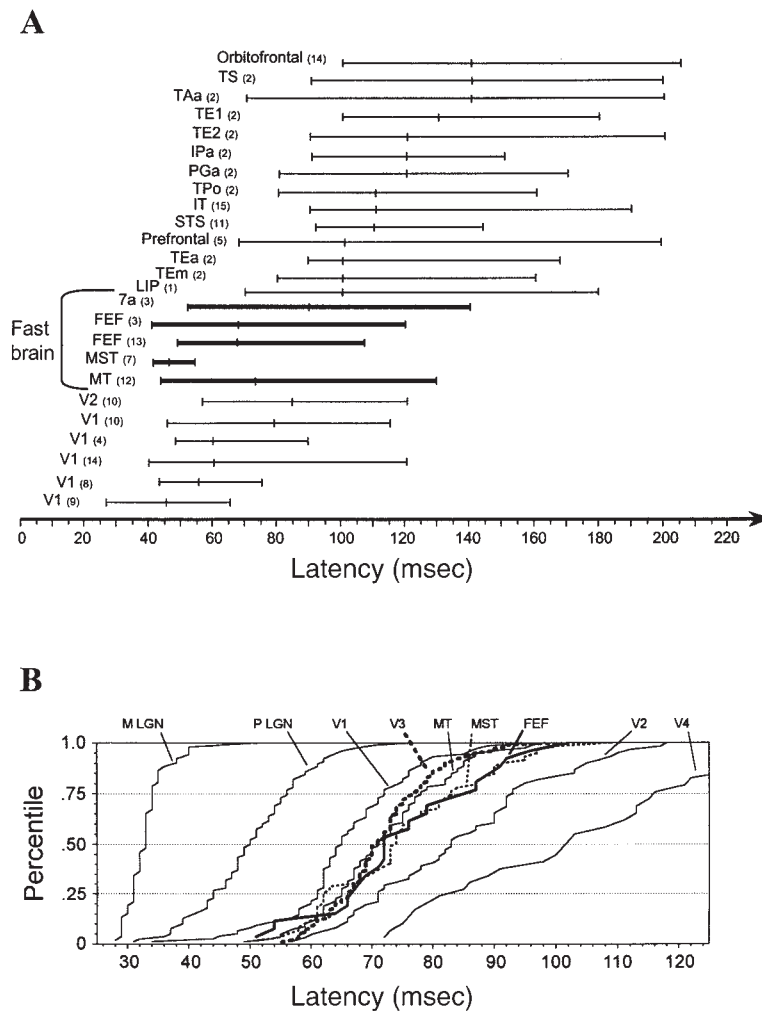


FIGURE 33.6. Temporal aspects of interactions between cortical areas. *A*, latencies of neurons in different cortical areas of the macaque monkey. These were behaving monkeys in all cases except (10). Small flashed stimuli were used in all cases except (7) and (12), for which motion onset was used.⁷ For each published study, the central bar represents the median and the extremities of the line represent the 10% and 90% centiles. Note that the FEF latencies are similar to those in V1 despite the large distance between these two areas in the cortical hierarchy (Fig. 33.5); the same is true of V2 and MT. Thus, the cortical hierarchy is a poor predictor of the

timing of activation of neurons in different cortical areas. *B*, cumulative distributions of visual latencies of neurons recorded in different visual areas in two anesthetized monkeys. [*A*: (1), Barash et al., 1991; (2), Baylis et al., 1987; (3), Bushnell et al., 1981; (4), Celebrini et al., 1993; (5), Funahashi et al., 1990; (6), Goldberg and Bushnell, 1991; (7), Kawano et al., 1994; (8), Knierim and Van Essen, 1992; (9), Maunsell and Gibson, 1992; (10), Nowak et al., 1995; (11), Perrett et al., 1982; (12), Raiguel et al., 1999; (13), Thompson et al., 1996; (14), Thorpe et al., 1983; (15), Vogels and Orban, 1994; *B* modified from Schmolesky et al., 1998.]

Areas of the dorsal stream tend to have short latencies to visual stimulation, whereas areas of the ventral stream have longer latencies. This is apparent in Figure 33.6*A*, with short latencies for areas MT, MST, FEF, and 7a and longer latencies for areas of the IT cortex (TE_m, TE_a, IT, Tpo, PGa, IPa, TE₂, TE₁, TAa, TS). A similar finding was reported by Leventhal and his collaborators (Schmolesky et al., 1998), who recorded neurons of many areas in the same animals

instead of pooling results from different published reports, as we had done. Their results are presented in Figure 33.6*B*: it is clear that neurons of areas V3, MT, MST, and FEF have very short latencies, which differ by only 5 msec from those in area V1, and that these latencies are much shorter than those observed in area V4, which belongs to the ventral stream. Similar results were found by simultaneous recordings in awake monkeys with microelectrodes implanted in numerous cortical areas (Schroeder et al., 1998). This difference between dorsal and ventral streams led us to propose the term *fast brain* (Fig. 33.6*A*) for the parietal cortex and FEF area (Nowak and Bullier, 1997).

⁷No difference was found between latencies to motion onset and to small flashed stimuli (Raiguel et al., 1999).

That neurons of the dorsal pathway respond rapidly to visual stimuli is in keeping with their role in visuomotor interactions: to correct a hand movement in time to catch a ball on a windy day, it is necessary to process visual information rapidly across the different cortical areas involved in the parietal and frontal cortex (Pisella et al., 2000). In contrast, areas of the ventral stream contain neurons with longer latencies to visual stimulation, in keeping with the role of this pathway in object recognition, for which speed is presumably less essential than for visuomotor interactions.

There is an interesting correlation between the short latencies of neurons in the dorsal stream and the rapidity of axons in this pathway. Staining for myelin reveals that the density of myelin is much higher in the gray matter of areas of the dorsal stream than in that of areas of the ventral stream, indicating a higher incidence on axonal ramifications of myelin sheaths that are known to increase conduction velocity (Nowak and Bullier, 1997). Indeed, the hallmark of area MT is the presence of a high density of myelin that has been observed in all primate species so far investigated. Also, it has been found that connections to the dorsal stream involve much higher densities of neurofilament protein than those to the ventral stream (Hof et al., 1996), indicating a much higher proportion of large, myelinated axons that conduct more rapidly than small axons (Nowak and Bullier, 1997). In particular, all V1 neurons projecting to area MT contain neurofilament protein (Hof et al., 1996), in keeping with the very fast conduction velocities of these axons (Movshon and Newsome, 1996).

The elevated level of neurofilament protein in callosal connections afferent to the border between areas V1 and V2 suggests that these connections are very rapid, a necessary condition given the long distance covered by callosal axons (Hof et al., 1997) and the necessity to integrate information rapidly across the two visual hemifields (Kennedy et al., 1991). The high proportion of neurofilament protein in the feedback connections from all cortical areas (Hof et al., 1996) strongly suggests that these connections are fast. Indeed, we found that in the rat as well as in the monkey, feedback connections are matched in conduction speed to feedforward connections (Girard et al., 2001; Nowak et al., 1997). This means that information is transferred as rapidly in the feedforward as in the feedback direction.

Functional roles of feedforward and feedback connections

FEEDFORWARD CONNECTIONS A number of functional studies have attempted to discover the role of feedforward connections by reversibly inactivating the source area of the connection and recording single units in the target area. In the cat, the early work was intended to probe the differences

between the visual systems of cats and primates. In cats, as in other nonprimate mammalian species, inactivating or lesioning area 17 does not lead to a complete cessation of visual responses in other visual cortical areas (see Bullier et al., 1994, and Salin and Bullier, 1995, for review), in contrast to the results reported in monkeys (see below).

The specific role of the feedforward connections from area 17 to area 18 cells in the cat was assessed by methods comparing visual responses before and during reversible inactivation of area 17. Inactivation of a large region of area 17 produced a general decrease of visual responses in numerous area 18 neurons, with a few specific effects (Sherk, 1978). In particular, it was noted that the effects of area 17 inactivation were more pronounced for low-stimulus velocities, in keeping with the finding of Dreher and Cotté (1975) that cells in area 18 are tuned to higher velocities after lesioning of area 17. These results suggest that feedforward inputs from area 17, which contains cells tuned to lower velocities than area 18 (Orban et al., 1981), potentiate the responses of area 18 neurons to low-velocity stimuli.

Similar methods were used to investigate the role of feedforward connections from area 17 to area 21a in the cat (Michalski et al., 1993). Inactivation of large regions of areas 17 and 18 led to a strong decrease in the response of many area 21a neurons and a complete silencing of others. It is quite remarkable that the orientation selectivities of area 21a neurons were retained even when the inactivation of area 17 led to an almost total cessation of the responses. This suggests that area 17 neurons providing feedforward connections to area 21a are very homogeneous in their orientation selectivity, in keeping with the homogeneous character of feedforward connections, as discussed earlier. There is also the possibility that specific mechanisms strengthen orientation selectivity within area 21a.

Some recent studies have used more localized inactivation techniques, and their conclusions point to a specific role for feedforward connections. Molotchnikoff and his colleagues presented evidence for changes in direction selectivity in many simple cells in area 18 during inactivation of a small zone of area 17 a few hundred microns wide. In most cases, this effect was due to a selective decrease in the response to the optimal direction and, in a few cases, to an increase in the nonpreferred direction (Casanova et al., 1992). They also demonstrated that local inactivation of area 17 produced changes in orientation tuning curves in area 18 neurons and that the effects were specific for the cell type (simple or complex cells) (Chabli et al., 1998). Such results confirm that feedforward connections can have a very strong driving input into cortical neurons and that they are organized in a precise column-to-column fashion. It is, however, difficult to deduce from these studies that specific properties such as direction or orientation selectivity are entirely set up by feed-

forward inputs from area 17 to area 18. Indeed, the reported changes with localized inactivation of area 17 could be due to a loss of balance between the excitatory inputs coming from different columns in area 17 converging on the recorded neurons in area 18.

The driving role of feedforward connections in the cat has been confirmed by the work of Vanduffel and collaborators (1997): in awake cats, they used radioactive 2-deoxyglucose to assess the residual neural activity in visual areas during reversible inactivation by cooling cortical areas in the suprasylvian sulcus. The results show strong decreases in activity in areas that receive feedforward connections from areas of the suprasylvian sulcus, in contrast to areas receiving feedback connections, which show a smaller decrease in activity.

In the monkey, our knowledge of the role of feedforward connections is mostly derived from the results of reversible inactivation or lesioning in area V1 and their effects on responses in other cortical areas. In contrast to the results obtained in the cat, inactivation or lesioning of V1 leads to a complete cessation of activity in a number of cortical areas belonging mostly to the ventral or occipitotemporal stream that channel information from V1 to the IT cortex (see the review by Bullier et al., 1994). In contrast, areas of the dorsal occipitoparietal stream remain visually responsive in the absence of input from area 17. At least in the case of area MT, the residual input is channeled through the superior colliculus (see the review in Bullier et al., 1994).

The present consensus is that feedforward connections carry the drive of lower-order areas and that the selectivities of neurons in higher-order areas result at least in part from the converging feedforward inputs of neurons in lower-order areas. This is well illustrated by the study of Movshon and Newsome (1996), who found that the neurons in V1 that project to area MT have receptive fields exactly superimposed on those of the recipient neurons. A similar result had been found earlier in the cat visual system (Bullier et al., 1988; Henry et al., 1978). These studies also produced interesting results concerning the cell type that projects to a given area. Both in the cat (Henry et al., 1978) and in the monkey (Movshon and Newsome, 1996), neurons that send feedforward connections away from area V1 appear to belong to a relatively homogeneous population of neurons in terms of functional properties. The findings of Sherk concerning the patchy organization of area 17 inputs to PMLS described above (Sherk, 1990; Sherk and Ombrellaro, 1988) are also consistent with such a role of convergent feedforward inputs.

This suggests that feedforward connections are important for carrying the visual drive from one neuronal population to the next and that their arrangement is important for shaping the selectivities of neurons in higher-order areas.

Thus, feedforward connections would belong to the “driver” category of the classification of connections⁸ by Sherman and Guillery (1998) and Crick and Koch (1998).

It should be noted, however, that the selective properties of cortical neurons are unlikely to be explained entirely by the properly arranged convergence of feedforward connections. This question has been central to the controversy concerning the mechanisms underlying the orientation and direction selectivity of area 17 neurons: do they result from the arrangement of their thalamic inputs, as predicted by Hubel and Wiesel (1962), or are they shaped mainly by the local network of horizontal connections? Until recently, the presence of inhibitory inputs to cortical neurons proved to be elusive, and it was thought that the orientation selectivity in area 17 neurons results mainly from the convergence of excitatory thalamic inputs (Douglas et al., 1991; Ferster et al., 1996; Hubel, 1996). This conclusion changed with the discovery of strong shunting inhibitory inputs into cortical cells (Borg-Graham et al., 1998) and the demonstration that local cortical inactivation has strong and specific effects on the orientation tuning curves of cortical cells (Crook et al., 1997). The results of Grinvald’s group with optical imaging techniques are also consistent with a major role for local horizontal connections: they showed that an area 17 neuron gives spikes when the network of interconnected cortical patches is activated. Most remarkably, this was observed for visually driven as well as spontaneous activity (Tsodyks et al., 1999). This suggests that local horizontal connections have a major impact on the excitability of cortical neurons and that the response of a neuron in area 17 cannot be explained simply by the simultaneous firing of converging afferent thalamic neurons. Instead, it appears that the cortical network controls the excitability of the cell and that the thalamic input mostly acts as a trigger. It remains to be seen whether interactions similar to those between thalamocortical and horizontal connections are observed between feedforward, horizontal, and feedback corticocortical connections.

FEEDBACK CONNECTIONS

Effects on responses to receptive field center stimulation. Fewer experiments have been devoted to uncovering the role of feedback connections. Several groups have inactivated large portions of a higher-order cortical area to assess the role of feedback connections in anesthetized animals. All concluded that feedback connections mostly tend to facilitate the

⁸In the distinction between drivers and modulators, driver connections are relatively rare and have strong, focused, rapid effects on their target neurons. Modulators have symmetrical properties: they are numerous and have weak, slow, diffuse actions.

responses of neurons in lower-order areas. Sandell and Schiller (1982) inactivated by cooling a region of area V2 in the squirrel monkey and reported effects on a third of the neurons in area V1. Most effects were decreases in responses to visual stimulation and were strongest in the infragranular layers. These results are in keeping with those of Mignard and Malpeli (1991), who concluded that feedback connections from area 18 exert a predominantly facilitatory effect upon neurons in area 17 in the cat. Similar conclusions were recently reached by Dreher and his collaborators concerning the feedback connections from area 21a to area 17 in the cat (Wang et al., 2000) and by our group concerning the feedback connections from area MT to areas V1, V2, and V3 in the monkey (Hupé et al., 1998). In general, effects were observed for a fraction of the population of recorded neurons (10% to 40%). In addition, no clear effects have been reported on orientation tuning curves during inactivation of higher-order areas (Wang et al., 2000).

Overall, inactivating feedback connections produce smaller effects than those for feedforward connections: a smaller proportion of neurons are affected, and the response changes are less dramatic. Only in very rare cases does inactivation of a cortical area lead to a complete cessation of responses in an area receiving feedback connections, as is the case for feedforward connections to the ventral stream in the monkey. As mentioned above, a direct comparison between the effect of inactivating area PMLS on cortical areas receiving feedforward and feedback connections from that area has been done (Vanduffel et al., 1997). The results show that both feedforward and feedback connections have a net excitatory role on their target areas but that the effects are stronger for areas receiving feedforward connections than for those receiving feedback connections.

Not only do feedback connections have a weaker effect on their target neurons than feedforward connections, they also do not appear to be able to drive neurons in the absence of a feedforward drive. Several lines of evidence support this conclusion. In the monkey, numerous neurons in area MT remain visually responsive when V1 is inactivated (Girard et al., 1992; Rodman et al., 1989), and there are strong feedback projections from area MT to V2 (Kennedy and Bullier, 1985). These feedback connections appear unable to drive V2 neurons when they are deprived of their feedforward drive from V1 because all V2 neurons are silenced when V1 is inactivated (Girard and Bullier, 1989; Schiller and Malpeli, 1977). Another line of evidence comes from the observation that, despite the wide spatial convergence of feedback connections (Fig. 33.3), the potentiating effect of feedback connections is present only for the excitatory center of the receptive field (Hupé et al., 2001a), which presumably reflects the converging feedforward inputs.

Such a nonlinear interaction between feedforward and feedback connections is also suggested by the results of

Mignard and Malpeli (1991) in the cat. They compared the effects of inactivating the A layers of the LGN on the responses of neurons in upper layers of area 17 when area 18 is intact or lesioned. When area 18 is intact, most neurons in the upper layers of area 17 retain strong visual responses when the A layers are inactivated (Malpeli, 1983). This contrasts with the strong decrease in the visual responses of these neurons during inactivation of the A layers when area 18 had been lesioned (Mignard and Malpeli, 1991). Without LGN blocking, direct inactivation of area 18 produces a mild response decrease in area 17 cells (Sherk, 1978). Thus, both the feedforward input from the A layers of the LGN and the feedback input from area 18 each has a relatively weak influence on the upper layer neurons of area 17, but their combination has a dramatic effect on the visual responses.

This suggests that feedback connections potentiate the responses of neurons in lower-order areas by nonlinear mechanisms such as gain control. This effect is particularly evident for weak responses, as seen in intracellular recordings (Shao and Burkhalter, 1999, their Figure 7), as well as in extracellular recordings (Bullier et al., 2001). An interesting possibility is that this nonlinear mechanism is used to gate the flow of different circuits in lower-order areas, thus allowing higher-order areas to reorganize processing in lower-order areas.

More specific effects of feedback inactivation were demonstrated by Alonso and his collaborators, who blocked a small region of layer 5 of area 18 while recording in layer 5 of area 17 in the cat (Alonso et al., 1993a, 1993b). The effects were strong and frequent when they inactivated area 18 neurons with overlapping receptive fields and the same properties as those of the recorded neurons in area 17. Effects were observed on the orientation tuning curves and on the speed selectivity of the neurons. Some effects were compatible with a facilitatory action of the feedback, and others suggested an inhibitory effect. The specificity of the demonstrated effect was particularly striking in the case of speed selectivity: Alonso and coworkers demonstrated that 40% of the neurons in layer 5 of area 17 increased their responses to high velocities when the corresponding region of layer 5 of area 18 was blocked (Alonso et al., 1993a, 1993b). This result suggests that the preference for low stimulus velocities of neurons in layer 5 of area 17 is due, at least in part, to an inhibitory input from area 18 neurons that are known to respond to high velocities. Thus, at least in that particular case, feedback connections appear to play a role in sharpening the selectivity of neurons in another cortical area.

The results of Alonso and his colleagues make the important point that feedback connections can have very specific effects and are not limited to the diffuse, unselective role that is often attributed to them. Similar experiments conducted

on the interactions between the upper layers of A18 and the upper layers of area 17 produced more variable results (Martinez-Conde et al., 1999) on orientation tuning curves of area 17 neurons. As argued above for the work of Casanova and collaborators (1992) on feedforward connections, such results could be due to the fact that only a small region of area 18 was inactivated, thus possibly producing a loss of balance of different converging inputs.

Feedback influences on center-surround interactions. So far, we have examined the contribution of feedback connections to the response of the receptive field center. However, the important degree of spatial divergence and convergence of these connections (Fig. 33.3) suggests that they might regulate the strength of center-surround interactions. This is indeed what was found in our study of the role of feedback connections from area MT to areas V1, V2, and V3. Feedback connections appear to potentiate the strength of the inhibitory influence of the receptive field surround on the response generated by stimulating the receptive field center (Bullier et al., 2001; Hupé et al., 1998). However, this effect was found to be specific for stimuli of low salience (a low-contrast bar moving on a noisy background). When the stimulus was of high salience (a high-contrast bar moving on a low-contrast, noisy background), the contribution of the MT feedback to the center-surround inhibitory interactions was small. This is in keeping with the lack of effect of feedback connections from V2 to V1 on center-surround interactions in V1 neurons for high-salience stimuli (Hupé et al., 2001b).

The relative roles of horizontal and feedback connections in shaping the modulatory regions of the receptive field surround of a cortical neuron is a subject of debate (Angelucci and Bullier, 2003; Bullier et al., 2001). It appears that the spatial extent of horizontal connections is too small to carry information from more than a few millimeters away on the cortical surface. Because of the high magnification factor in the central visual field, a few millimeters on the surface of area 17 represent only a few tenths of a degree of visual angle. This is much smaller than the size of the receptive field surround of most V1 neurons (Angelucci et al., 2002; Cavanaugh et al., 2002; Levitt and Lund, 1997). This distance in visual field is also far too small to explain the large extent of the interaction field beyond the receptive field center demonstrated by using colinear lines in a noisy background (Ito and Gilbert, 1999; Kapadia et al., 1995). Thus, it is impossible that monosynaptic horizontal connections can entirely subserve the far-reaching contextual effects demonstrated in area 17. One possibility is offered by multisynaptic information transfer through horizontal connections. However, horizontal connections are much too slow (Girard et al., 2001) to account for the rapid contextual effects seen in responses of neurons in area 17 (Ito and Gilbert, 1999). Because of the high conduction velocity of

feedforward and feedback axons (Girard et al., 2001) and the large spatial convergence and divergence of feedback connections (Fig. 33.3), it is likely that the latter play a major role in shaping the long-range center-surround interactions in the receptive fields of cortical neurons. Experiments are needed to test this prediction directly on behaving animals performing a visual task requiring attention to long-range interactions across the visual field, such as those used by Gilbert and his colleagues (2000).

Feedback influences on the synchrony of neurons in lower-order areas. A number of studies have shown that interconnected cortical neurons tend to synchronize the time of emission of their action potentials (see the review by Nowak and Bullier, 2000). As mentioned above, neurons in a given cortical column exchange reciprocal connections with several columns in other cortical areas. The exact cell-to-cell connectivity within this column-to-column network is not known, but it is likely to be similar to that of intrinsic connections: each axon gives only a few contacts to some neurons in a column, and each neuron in a target column receives convergent input from several neurons. In that case, a powerful way to modulate transfer from one column to another is to synchronize the spike discharges of the neurons belonging to the source column or to change the firing pattern from regular to bursty. In accord with this possibility, it has been proposed that feedback corticogeniculate connections switch the firing mode from bursting to tonic in LGNs through activation of metabotropic receptors (Godwin et al., 1996). The results of Sillito and his group (1994) further indicate that feedback corticothalamic connections synchronize the firing of LGN neurons. However, recent results suggest that there may be an important effect of feedback connections on slow modulation of rate changes instead of a direct effect on spike-to-spike synchronization (Brody, 1998) and specific effects on the receptive-field center mechanism (Rivadulla et al., 2002).

For corticocortical feedback connections, lesion studies showed that when higher-order areas are lesioned in the cat, certain types of synchronization between neurons located in lower-order cortical areas in the opposite hemisphere disappear (Munk et al., 1995). This suggests that feedback connections are involved in the synchronization of activity in neurons of lower-order cortical areas. We tested this hypothesis directly by measuring changes in the synchronization of spike firing induced by inactivating higher-order areas. We found changes in the cross-correlograms and the auto-correlograms of neighboring neurons showing changes in response strength (J. M. Hupé, P. Girard, and J. Bullier, unpublished observations). However, we never observed a change in the strength of the cross-correlogram peaks when there was no change in firing rate in at least one of the neurons. Therefore, despite its attractiveness, the idea that

feedback connections control specifically the synchronization of lower-order neurons independently of their firing rate does not seem tenable at the moment. On the other hand, it would be interesting to determine whether inactivation or activation of a higher-order area leads to a change in the firing pattern of neurons in a lower-order area in a similar way to the conclusions reached by Sherman and his collaborators for the corticogeniculate feedback connections (Godwin et al., 1996).

Figure-ground segregation, attention, top-down activation by internal images. A role for feedback connections in attention has been postulated in many studies but has not been directly tested. Attending to a visual stimulus increases the gain of neuronal responses in most visual cortical areas (Reynolds et al., 2000; Treue and Maunsell, 1999). These effects are strongest for low-contrast stimuli and weak for high-contrast stimuli (Reynolds et al., 2000). This is reminiscent of the effects of inactivating area MT on the responses of neurons in areas V1, V2, and V3 which were strongest for low-salience stimuli, as reviewed above (Bullier et al., 2001; Hupé et al., 1998). It is therefore possible that the mechanisms revealed by inactivation of feedback connections may be at play during modulation of the sensitivity of lower-order areas by spatially directed attention.

It has been claimed that feedback connections play a role in the modulation of responses of neurons in V1 when their receptive field is inside a square object that pops out from the background because of its difference in the orientation of the lines composing the pattern or movement direction of random dots (Lamme, 1995; Lamme et al., 1998; see, however, Rossi et al., 2001). The argument rests on the observation that such modulatory effects are delayed by 40–100 msec with respect to the beginning of the response and that these effects disappear during anesthesia. However, given that higher-order area neurons can have very short latencies (as reviewed above) and that feedback effects appear to be extremely rapid (Hupé et al., 2001a), it is not clear that delayed response modulations are necessarily due to feedback influences. The disappearance of the effect during anesthesia does not speak to the source of the effects, since several studies reviewed above show that clear influences of feedback connections can be revealed during anesthesia. Whether the modulatory effects corresponding to popout are transferred from higher-order areas by feedback connections remains to be tested by directly influencing the responses of neurons in higher-order areas.

A recent study of Myiashita and his group demonstrated a role that has been long suspected for feedback connections: that of activating lower-order area neurons with top-down signals conveying information about categorization of visual images (Tomita et al., 1999). By using a split brain preparation, they were able, in IT cortex neurons, to distinguish

activation by feedforward connections from the drive by feedback connections from the frontal cortex. This is the first direct evidence that feedback connections carry signals corresponding to internal images to lower-order areas of the visual system.

Conclusion

The functions of different types of corticocortical connections are beginning to be more precisely known. The differences at the synaptic level, and the relative functions of feedforward and horizontal connections in shaping the receptive field properties of visual neurons, remain to be determined. The role of feedback connections in modulating the gain control of neurons in low-order areas also needs to be tested directly. To understand the role of feedforward and feedback connections in vision, it will be necessary to develop methods to activate and inactivate cortical neurons while the animal performs various tasks of visual detection and discrimination.

Acknowledgments

I thank Frédéric Sarrato for his expert help with the iconography.

REFERENCES

- Alonso, J. M., J. Cudeiro, R. Perez, F. Gonzalez, and C. Acuna, 1993a. Influence of layer V of area 18 of the cat visual cortex on responses of cells in layer V of area 17 to stimuli of high velocity, *Exp. Brain Res.*, 93(2):363–366.
- Alonso, J. M., J. Cudeiro, R. Perez, F. Gonzalez, and C. Acuna, 1993b. Orientational influences of layer V of visual area 18 upon cells in layer V of area 17 in the cat cortex, *Exp. Brain Res.*, 96(2):212–220.
- Anderson, J. C., T. Binzegger, K. A. Martin, and K. S. Rockland, 1998. The connection from cortical area V1 to V5: a light and electron microscopic study, *J. Neurosci.*, 18(24):10525–10540.
- Angelucci, A., and J. Bullier, 2003. Reaching beyond the classical receptive field of V1 neurons: horizontal or feedback axons? *J. Physiol. (Paris)*, in press.
- Angelucci, A., J. B. Levitt, J. M. Hupé, E. J. S. Walton, J. Bullier, and J. S. Lund, 2000. Anatomical circuits for local and global integration of visual information: intrinsic and feedback connections in macaque visual cortical area V1, *Eur. J. Neurosci.*, 12(Suppl 11):285.
- Angelucci, A., J. B. Levitt, E. J. Walton, J. M. Hupé, J. Bullier, and J. S. Lund, 2002. Circuits for local and global signal integration in primary visual cortex, *J. Neurosci.*, 22(19):8633–8646.
- Baizer, J. S., L. G. Ungerleider, and R. Desimone, 1991. Organization of visual inputs to the inferior temporal and posterior parietal cortex in macaques, *J. Neurosci.*, 11(1):168–190.
- Barash, S., R. M. Bracewell, L. Fogassi, J. W. Gnadt, and R. A. Andersen, 1991. Saccade-related activity in the lateral intraparietal area. I. Temporal properties; comparison with area 7a, *J. Neurophysiol.*, 66(3):1095–1108.

- Barbas, H., 1986. Pattern in the laminar origin of corticocortical connections, *J. Comp. Neurol.*, 252(3):415–422.
- Barbas, H., and N. Rempel-Clower, 1997. Cortical structure predicts the pattern of corticocortical connections, *Cereb. Cortex*, 7(7):635–646.
- Barone, P., A. Batardiere, K. Knoblauch, and H. Kennedy, 2000. Laminar distribution of neurons in extrastriate areas projecting to V1 and V4 correlates with the hierarchical rank and indicates the operation of a distance rule, *J. Neurosci.*, 20(9):3263–3281.
- Baylis, G. C., E. T. Rolls, and C. M. Leonard, 1987. Functional subdivisions of the temporal lobe neocortex, *J. Neurosci.*, 7(2):330–342.
- Borg-Graham, L. J., C. Monier, and Y. Fregnac, 1998. Visual input evokes transient and strong shunting inhibition in visual cortical neurons, *Nature*, 393(6683):369–373.
- Braitenberg, V., and A. Schüz, 1991. *Anatomy of the Cortex. Statistics and Geometry*, Berlin: Springer-Verlag.
- Brody, C. D., 1998. Slow covariations in neuronal resting potentials can lead to artefactually fast cross-correlations in their spike trains, *J. Neurophysiol.*, 80(6):3345–3351.
- Bullier, J., P. Girard, and P. A. Salin, 1994. The role of area 17 in the transfer of information to extrastriate visual cortex, in *Primary Visual Cortex in Primates* (A. Peters and K. S. Rockland, eds.), New York: Plenum Press, pp. 301–330.
- Bullier, J., J. M. Hupé, A. James, and P. Girard, 2001. The role of feedback connections in shaping the responses of visual cortical neurons, *Prog. Brain Res.*, 134:193–204.
- Bullier, J., and H. Kennedy, 1987. Axonal bifurcation in the visual system, *Trends Neurosci.*, 10:205–210.
- Bullier, J., H. Kennedy, and W. Salinger, 1984. Branching and laminar origin of projections between visual cortical areas in the cat, *J. Comp. Neurol.*, 228(3):329–341.
- Bullier, J., M. E. McCourt, and G. H. Henry, 1988. Physiological studies on the feedback connection to the striate cortex from cortical areas 18 and 19 of the cat, *Exp. Brain Res.*, 70(1):90–98.
- Bullier, J., J. D. Schall, and A. Morel, 1996. Functional streams in occipito-frontal connections in the monkey, *Behav. Brain Res.*, 76(1–2):89–97.
- Bushnell, M. C., M. E. Goldberg, and D. L. Robinson, 1981. Behavioral enhancement of visual responses in monkey cerebral cortex: I. Modulation in posterior parietal cortex related to selective visual attention, *J. Neurophysiol.*, 46(4):755–772.
- Casanova, C., Y. Michaud, C. Morin, P. A. McKinley, and S. Molotchnikoff, 1992. Visual responsiveness and direction selectivity of cells in area 18 during local reversible inactivation of area 17 in cats, *Vis. Neurosci.*, 9(6):581–593.
- Cavanaugh, J. R., W. Bair, and J. A. Movshon, 2002. Nature and interaction of signals from the receptive field center and surround in macaque V1 neurons, *J. Neurophysiol.*, 88(5):2530–2546.
- Celebrini, S., S. J. Thorpe, Y. Trotter, and M. Imbert, 1993. Dynamics of orientation coding in area V1 of the awake primate, *Vis. Neurosci.*, 10(5):811–825.
- Chabli, A., D. Y. Ruan, and S. Molotchnikoff, 1998. Influences of area 17 on neuronal activity of simple and complex cells of area 18 in cats, *Neuroscience*, 84(3):685–698.
- Crick, F., and C. Koch, 1998. Constraints on cortical and thalamic projections: the no-strong-loops hypothesis, *Nature*, 391(6664):245–250.
- Crook, J. M., Z. F. Kisvarday, and U. T. Eysel, 1997. GABA-induced inactivation of functionally characterized sites in cat striate cortex: effects on orientation tuning and direction selectivity, *Vis. Neurosci.*, 14(1):141–158.
- DeYoe, E. A., D. J. Felleman, D. C. Van Essen, and E. McClendon, 1994. Multiple processing streams in occipitotemporal visual cortex, *Nature*, 371(6493):151–154.
- DeYoe, E. A., and D. C. Van Essen, 1985. Segregation of efferent connections and receptive field properties in visual area V2 of the macaque, *Nature*, 317(6032):58–61.
- Domenici, L., G. W. Harding, and A. Burkhalter, 1995. Patterns of synaptic activity in forward and feedback pathways within rat visual cortex, *J. Neurophysiol.*, 74(6):2649–2664.
- Douglas, R. J., K. A. C. Martin, and D. Whitteridge, 1991. An intracellular analysis of the visual responses of neurones in cat visual cortex, *J. Physiol.*, 440:659–696.
- Dreher, B., and L. J. Cottet, 1975. Visual receptive-field properties of cells in area 18 of cat's cerebral cortex before and after lesions in area 17, *J. Neurophysiol.*, 38(4):735–750.
- Felleman, D. J., and D. C. Van Essen, 1991. Distributed hierarchical processing in the primate cerebral cortex, *Cereb. Cortex*, 1(1):1–47.
- Ferster, D., S. Chung, and H. Wheat, 1996. Orientation selectivity of thalamic input to simple cells of cat visual cortex, *Nature*, 380(6571):249–252.
- Fisken, R. A., L. J. Garey, and T. P. S. Powell, 1975. The intrinsic, association and commissural connections of area 17 of the visual cortex, *Phil. Trans. Roy. Soc. (Lond.)*, 272(919):487–536.
- Fries, W., K. Keizer, and H. G. Kuypers, 1985. Large layer V1 cells in macaque striate cortex (Meynert cells) project to both superior colliculus and prestriate visual area V5, *Exp. Brain Res.*, 58(3):613–616.
- Funahashi, S., C. J. Bruce, and P. S. Goldman-Rakic, 1990. Visuospatial coding in primate prefrontal neurons revealed by oculomotor paradigms, *J. Neurophysiol.*, 63(4):814–831.
- Gilbert, C., M. Ito, M. Kapadia, and G. Westheimer, 2000. Interactions between attention, context and learning in primary visual cortex, *Vis. Res.*, 40(10–12):1217–1226.
- Gilbert, C. D., and T. N. Wiesel, 1983. Clustered intrinsic connections in cat visual cortex, *J. Neurosci.*, 3(5):1116–1133.
- Girard, P., and J. Bullier, 1989. Visual activity in area V2 during reversible inactivation of area 17 in the macaque monkey, *J. Neurophysiol.*, 62(6):1287–1302.
- Girard, P., J. M. Hupé, and J. Bullier, 2001. Feedforward and feedback connections between areas V1 and V2 of the monkey have similar rapid conduction velocities, *J. Neurophysiol.*, 85(3):1328–1331.
- Girard, P., P. A. Salin, and J. Bullier, 1991a. Visual activity in areas V3A and V3 during reversible inactivation of area V1 in the macaque monkey, *J. Neurophysiol.*, 66(5):1493–1503.
- Girard, P., P. A. Salin, and J. Bullier, 1991b. Visual activity in macaque area V4 depends on area 17 input, *Neuroreport*, 2(2):81–84.
- Girard, P., P. A. Salin, and J. Bullier, 1992. Response selectivity of neurons in area MT of the macaque monkey during reversible inactivation of area V1, *J. Neurophysiol.*, 67(6):1437–1446.
- Godwin, D. W., J. W. Vaughan, and S. M. Sherman, 1996. Metabotropic glutamate receptors switch visual response mode of lateral geniculate nucleus cells from burst to tonic, *J. Neurophysiol.*, 76(3):1800–1816.
- Goldberg, M. E., and M. C. Bushnell, 1991. Behavioral enhancement of visual responses in monkey cerebral cortex. II. Modulation in frontal eye fields related to saccades, *J. Neurophysiol.*, 46(4):773–787.
- Goldman-Rakic, P. S., and M. L. Schwartz, 1982. Interdigitation of contralateral and ipsilateral projections of frontal association cortex in primates, *Science*, 216(4547):755–757.

- Gonchar, Y., and A. Burkhalter, 1999. Differential subcellular localization of forward and feedback interareal inputs to parvalbumin expressing GABAergic neurons in rat visual cortex, *J. Comp. Neurol.*, 406(3):346–360.
- Goodale, M. A., and A. D. Milner, 1992. Separate visual pathways for perception and action, *Trends Neurosci.*, 15(1):20–25.
- Henry, G. H., J. S. Lund, and A. R. Harvey, 1978. Cells of the striate cortex projecting to the Clare-Bishop area of the cat, *Brain Res.*, 151(1):154–158.
- Henry, G. H., P. A. Salin, and J. Bullier, 1991. Projections from area 18 and 19 to cat striate cortex: divergence and laminar specificity, *Eur. J. Neurosci.*, 3:186–200.
- Hilgetag, C. C., M. A. O'Neill, and M. P. Young, 1996. Indeterminate organization of the visual system, *Science*, 271(5250):776–777.
- Hof, P. R., L. G. Ungerleider, M. J. Webster, R. Gattass, M. M. Adams, C. A. Sailstad, and J. H. Morrison, 1996. Neurofilament protein is differentially distributed in subpopulations of cortico-cortical projection neurons in the macaque monkey visual pathways, *J. Comp. Neurol.*, 376(1):112–127.
- Hof, P. R., L. G. Ungerleider, M. M. Adams, M. J. Webster, R. Gattass, D. M. Blumberg, and J. H. Morrison, 1997. Callosally projecting neurons in the macaque monkey V1/V2 border are enriched in nonphosphorylated neurofilament protein, *Vis. Neurosci.*, 14(5):981–987.
- Houzel, J. C., and C. Milleret, 1999. Visual inter-hemispheric processing: constraints and potentialities set by axonal morphology, *J. Physiol. (Paris)*, 93(4):271–284.
- Hubel, D. H., 1996. A big step along the visual pathway, *Nature*, 380(6571):197–198.
- Hubel, D. H., and T. N. Wiesel, 1962. Receptive fields, binocular interaction and functional architecture in the cat visual cortex, *J. Physiol. (Lond.)*, 160:106–154.
- Hughes, C. M., and A. Peters, 1992a. Symmetric synapses formed by callosal afferents in rat visual cortex, *Brain Res.*, 583(1–2):271–278.
- Hughes, C. M., and A. Peters, 1992b. Types of callosally projecting nonpyramidal neurons in rat visual cortex identified by lysosomal HRP retrograde labeling, *Anat. Embryol. (Berl.)*, 186(2):183–193.
- Hupé, J. M., A. C. James, B. R. Payne, S. G. Lomber, P. Girard, and J. Bullier, 1998. Cortical feedback improves discrimination between figure and background by V1, V2 and V3 neurons, *Nature*, 394(6695):784–787.
- Hupé, J. M., A. C. James, P. Girard, S. G. Lomber, B. R. Payne, and J. Bullier, 2001a. Feedback connections act on the early part of the responses in monkey visual cortex, *J. Neurophysiol.*, 85(1):134–145.
- Hupé, J. M., A. C. James, P. Girard, and J. Bullier, 2001b. Response modulation by static texture surround in area V1 of the macaque monkey do not depend on feedback connections from V2, *J. Neurophysiol.*, 85(1):146–163.
- Innocenti, G. M., 1986. General organization of callosal connections in the cerebral cortex, in *Cerebral Cortex*, vol. 5 (E. G. Jones and A. Peters, eds.), New York: Plenum Press, pp. 291–353.
- Ito, M., and C. D. Gilbert, 1999. Attention modulates contextual influences in the primary visual cortex of alert monkeys, *Neuron*, 22(3):593–604.
- Jeannerod, M., M. A. Arbib, G. Rizzolatti, and H. Sakata, 1995. Grasping objects: the cortical mechanisms of visuomotor transformation, *Trends Neurosci.*, 18(7):314–320.
- Johnson, R. R., and A. Burkhalter, 1996. Microcircuitry of forward and feedback connections within rat visual cortex, *J. Comp. Neurol.*, 368(3):383–398.
- Johnson, R. R., and A. Burkhalter, 1997. A polysynaptic feedback circuit in rat visual cortex, *J. Neurosci.*, 17(18):7129–7140.
- Jones, E. G., and T. P. S. Powell, 1970. An anatomical study of converging sensory pathways within the cerebral cortex of the monkey, *Brain*, 93(4):793–820.
- Jouve, B., P. Rosenstiehl, and M. Imbert, 1998. A mathematical approach to the connectivity between the cortical visual areas of the macaque monkey, *Cereb. Cortex*, 8(1):28–39.
- Kapadia, M. K., M. Ito, C. D. Gilbert, and G. Westheimer, 1995. Improvement in visual sensitivity by changes in local context: parallel studies in human observers and in V1 of alert monkeys, *Neuron*, 15(4):843–856.
- Kawano, K., M. Shidara, Y. Watanabe, and S. Yamane, 1994. Neural activity in cortical area MST of alert monkey during ocular following responses, *J. Neurophysiol.*, 71(6):2305–2324.
- Kennedy, H., and J. Bullier, 1985. A double-labelling investigation of the afferent connectivity to cortical areas V1 and V2 of the macaque monkey, *J. Neuroscience*, 5(10):2815–2830.
- Kennedy, H., J. Bullier, and C. Dehay, 1989. Transient projection from the superior temporal sulcus to area 17 in the newborn macaque monkey, *Proc. Natl. Acad. Sci. USA*, 86(20):8093–8097.
- Kennedy, H., C. Meissirel, and C. Dehay, 1991. Callosal pathways in primates and their compliance to general rules governing the organization of cortico-cortical connectivity, in *Vision and Visual Dysfunction*, vol. 3, *Neuroanatomy of the Visual Pathways and their Development* (B. Dreher and S. Robinson, eds.), London: Macmillan, pp. 324–359.
- Knierim, J. J., and D. C. Van Essen, 1992. Neuronal responses to static texture patterns in area V1 of the alert macaque monkey, *J. Neurophysiol.*, 67(4):961–980.
- Lamme, V. A. F., 1995. The neurophysiology of figure-ground segregation in primary visual cortex, *J. Neurosci.*, 15(2):1605–1615.
- Lamme, V. A. F., H. Super, and H. Spekreijse, 1998. Feedforward, horizontal, and feedback processing in the visual cortex, *Curr. Opin. Neurobiol.*, 8(4):529–535.
- Levitt, J. B., and J. S. Lund, 1997. Spatial summation properties of macaque striate neurons, *Soc. Neurosci. Abstr.*, 23:455.
- Lowenstein, P. R., and P. Somogyi, 1991. Synaptic organization of cortico-cortical connections from the primary visual cortex to the posteromedial lateral suprasylvian visual area in the cat, *J. Comp. Neurol.*, 310(2):253–266.
- Malpeli, J. G., 1983. Activity of cells in area 17 of the cat in absence of input from layer A of lateral geniculate nucleus, *J. Neurophysiol.*, 49(3):595–610.
- Martinez-Conde, S., J. Cudeiro, K. L. Grieve, R. Rodriguez, C. Rivadulla, and C. Acuna, 1999. Effects of feedback projections from area 18 layers 2/3 to area 17 layers 2/3 in the cat visual cortex, *J. Neurophysiol.*, 82(5):2667–2675.
- Maunsell, J. H. R., and J. R. Gibson, 1992. Visual response latencies in striate cortex of the macaque monkey, *J. Neurophysiol.*, 68(4):1332–1344.
- Maunsell, J. H. R., and D. C. Van Essen, 1983. The connections of the middle temporal visual area (MT) and their relationship to a cortical hierarchy in the macaque monkey, *J. Neurosci.*, 3(12):2563–2586.
- McDonald, C. T., and A. Burkhalter, 1993. Organization of long-range inhibitory connections with rat visual cortex, *J. Neurosci.*, 13(2):768–781.
- Meyer, G., and K. Albus, 1981. Spiny stellates as cells of origin of association fibres from area 17 to area 18 in the cat's neocortex, *Brain Res.*, 210(1–2):335–341.

- Michalski, A., B. M. Wimborme, and G. H. Henry, 1993. The effect of reversible cooling of cat's primary visual cortex on the responses of area 21a neurons, *J. Physiol.*, 466:133–156.
- Mignard, M., and J. G. Malpeli, 1991. Paths of information flow through visual cortex, *Science*, 251(4998):1249–1251.
- Morel, A., and J. Bullier, 1990. Anatomical segregation of two cortical visual pathways in the macaque monkey, *Vis. Neurosci.*, 4(6):555–578.
- Movshon, J. A., and W. T. Newsome, 1996. Visual response properties of striate cortical neurons projecting to area MT in macaque monkeys, *J. Neurosci.*, 16(23):7733–7741.
- Munk, M. H. J., L. G. Nowak, J. I. Nelson, and J. Bullier, 1995. The structural basis of cortical synchronization. II. Effects of cortical lesions, *J. Neurophysiol.*, 74(6):2401–2414.
- Murre, J. M. J., and D. P. F. Sturdy, 1995. The connectivity of the brain: multi-level quantitative analysis, *Biol. Cybern.*, 73(6):529–545.
- Nowak, L. G., and J. Bullier, 1997. The timing of information transfer in the visual system, in *Extrastriate Visual Cortex in Primates*, vol. 12 (K. S. Rockland, J. H. Kaas, and A. Peters, eds.), New York: Plenum Press, pp. 205–241.
- Nowak, L. G., and J. Bullier, 1998a. Axons, but not cell bodies are activated by electrical stimulation in cortical gray matter. I. Evidence from chronaxie measurements, *Exp. Brain Res.*, 118(4):477–488.
- Nowak, L. G., and J. Bullier, 1998b. Axons, but not cell bodies, are activated by electrical stimulation in cortical grey matter. II. Evidence from selective inactivation of cell bodies and axon initial segments, *Exp. Brain Res.*, 118(4):489–500.
- Nowak, L. G., and J. Bullier, 2000. Cross correlograms for neuronal spike trains. Different types of temporal correlation in neocortex, their origin and significance, in *Time and the Brain, Conceptual Advances in Brain Research* (R. Miller, ed.), Amsterdam: Harwood Academic, pp. 53–96.
- Nowak, L. G., A. C. James, and J. Bullier, 1997. Corticocortical connections between visual areas 17 and 18a of the rat studied in vitro: spatial and temporal organisation of functional synaptic responses, *Exp. Brain Res.*, 117(2):219–241.
- Nowak, L. G., M. H. J. Munk, P. Girard, and J. Bullier, 1995. Visual latencies in areas V1 and V2 of the macaque monkey, *Vis. Neurosci.*, 12(2):371–384.
- Orban, G. A., H. Kennedy, and H. Maes, 1981. Response to movement of neurons in areas 17 and 18 of the cat: velocity sensitivity, *J. Neurophysiol.*, 45(6):1059–1073.
- Payne, B. R., 1993. Evidence for visual cortical area homologs in cat and macaque monkey, *Cereb. Cortex*, 3(1):1–25.
- Perkel, D. J., J. Bullier, and H. Kennedy, 1986. Topography of the afferent connectivity of area 17 of the macaque monkey: a double-labelling study, *J. Comp. Neurol.*, 253(3):374–402.
- Perrett, D. L., E. T. Rolls, and W. Caan, 1982. Visual neurons responsive to faces in the monkey temporal cortex, *Exp. Brain Res.*, 47(3):329–342.
- Peters, A., B. Payne, and K. Josephson, 1990. Transcallosal non-pyramidal cell projections from visual cortex in the cat, *J. Comp. Neurol.*, 302(1):124–142.
- Pisella, L., H. Grea, C. Tilikete, A. Vighetto, M. Desmurget, G. Rode, D. Boisson, and Y. Rossetti, 2000. An “automatic pilot” for the hand in human posterior parietal cortex: toward reinterpreting optic ataxia, *Nat. Neurosci.*, 3(7):729–736.
- Pohl, W., 1973. Dissociation of spatial discrimination deficits following frontal and parietal lesions in monkeys, *J. Comp. Physiol. Psychol.*, 82(2):227–239.
- Price, D. J., J. M. R. Ferrer, C. Blakemore, and N. Kato, 1994. Functional organization of corticocortical projections from area 17 to area 18 in the cat's visual cortex, *J. Neurosci.*, 14(5):2732–2746.
- Raiguel, S. E., L. Lagae, B. Gulyas, and G. A. Orban, 1989. Response latencies of visual cells in macaque areas V1, V2 and V5, *Brain Res.*, 493(1):155–159.
- Raiguel, S. E., D. K. Xiao, V. L. Marcar, and G. A. Orban, 1999. Response latency of macaque area MT/V5 neurons and its relationship to stimulus parameters, *J. Neurophysiol.*, 82(4):1944–1956.
- Reid, C. R., and J. M. Alonso, 1995. Specificity of monosynaptic connections from thalamus to visual cortex, *Nature*, 378(6554):281–284.
- Reynolds, J. H., T. Pasternak, and R. Desimone, 2000. Attention increases sensitivity of V4 neurons, *Neuron*, 26(3):703–714.
- Rivadulla, C., L. M. Martinez, C. Varela, and J. Cudeiro, 2002. Completing the corticofugal loop: a visual role for the corticogeniculate type 1 metabotropic glutamate receptor, *J. Neurosci.*, 22(7):2956–2962.
- Rockland, K. S., and G. W. Drash, 1996. Collateralized divergent feedback connections that target multiple cortical areas, *J. Comp. Neurol.*, 373(4):529–548.
- Rockland, K. S., and G. W. V. Hoesen, 1994. Direct temporal-occipital feedback connection to striate cortex (V1) in the macaque monkey, *Cereb. Cortex*, 4(3):300–313.
- Rockland, K. S., and J. S. Lund, 1982. Widespread periodic intrinsic connections in the tree shrew visual cortex, *Science*, 215(4539):1532–1534.
- Rockland, K. S., and D. N. Pandya, 1979. Laminar origin and terminations of cortical connections of the occipital lobe in the rhesus monkey, *Brain Res.*, 179(1):3–20.
- Rockland, K. S., K. S. Saleem, and K. Tanaka, 1994. Divergent feedback connections from areas V4 and TEO, *Vis. Neurosci.*, 11(3):579–600.
- Rodman, H. R., C. G. Gross, and T. D. Albright, 1989. Afferent basis of visual response properties in area MT of the macaque: I. Effects of striate cortex removal, *J. Neurosci.*, 9(6):2033–2050.
- Rosa, M., 1997. Visuotopic organization of primate extrastriate cortex, in *Cerebral Cortex: Extrastriate Cortex in Primates*, vol. 12 (K. S. Rockland, J. H. Kaas, and A. Peters, eds.), New York: Plenum Press, pp. 127–203.
- Rossi, A. F., R. Desimone, and L. G. Ungerleider, 2001. Contextual modulation in primary visual cortex of macaques, *J. Neurosci.*, 21(5):1698–1709.
- Salin, P. A., and J. Bullier, 1995. Corticocortical connections in the visual system: structure and function, *Physiol. Reviews*, 75(1):107–154.
- Salin, P. A., P. Girard, H. Kennedy, and J. Bullier, 1992. The visuotopic organization of corticocortical connections in the visual system of the cat, *J. Comp. Neurol.*, 320(4):415–434.
- Salin, P. A., H. Kennedy, and J. Bullier, 1995. Spatial reciprocity of connections between areas 17 and 18 in the cat, *Can. J. Physiol. Pharmacol.*, 73(9):1339–1347.
- Sandell, J. H., and P. H. Schiller, 1982. Effect of cooling area 18 on striate cortex cells in the squirrel monkey, *J. Neurophysiol.*, 48(1):38–48.
- Sanides, F., 1970. Functional architecture of motor and sensory cortices in primates in the light of a new concept of neocortex evolution, in *The Primate Brain: Advances in Primatology* (C. R. Noback and W. Montagna, eds.), New York: Appleton-Crofts, pp. 137–208.

- Schall, J. D., A. Morel, D. J. King, and J. Bullier, 1995. Topography of visual cortex connections with frontal eye field in macaque—Convergence and segregation of processing streams, *J. Neurosci.*, 15(6):4464–4487.
- Schiller, P. H., and J. G. Malpeli, 1977. The effect of striate cortex cooling on area 18 cells in the monkey, *Brain Res.*, 126(2):366–369.
- Schmolesky, M. T., Y. Wang, D. P. Hanes, K. G. Thompson, S. Leutgeb, J. D. Schall, and A. G. Leventhal, 1998. Signal timing across the macaque visual system, *J. Neurophysiol.*, 79(6):3272–3278.
- Schneider, G. E., 1969. Two visual systems, *Science*, 163(870):895–902.
- Schroeder, C. E., A. D. Mehta, and S. J. Givre, 1998. A spatiotemporal profile of visual system activation revealed by current source density analysis in the awake macaque, *Cereb. Cortex*, 8(7):575–592.
- Shao, Z. W., and A. Burkhalter, 1996. Different balance of excitation and inhibition in forward and feedback circuits of rat visual cortex, *J. Neurosci.*, 16(22):7353–7365.
- Shao, Z. W., and A. Burkhalter, 1999. Role of GABAB receptor-mediated inhibition in reciprocal interareal pathways of rat visual cortex, *J. Neurophysiol.*, 81(3):1014–1024.
- Sherk, H., 1978. Area 18 cell responses in cat during reversible inactivation of area 17, *J. Neurophysiol.*, 41(1):204–215.
- Sherk, H., 1990. Functional organization of input from areas 17 and 18 to an extrastriate area in the cat, *J. Neurosci.*, 10(8):2780–2790.
- Sherk, H., and M. Ombrellaro, 1988. The retinotopic match between area 17 and its targets in visual suprasylvian cortex, *Exp. Brain Res.*, 72(2):225–236.
- Sherman, S. M., and R. W. Guillery, 1998. On the actions that one nerve cell can have on another: distinguishing “drivers” from “modulators,” *Proc. Natl. Acad. Sci. USA*, 95(12):7121–7126.
- Shipp, S., and S. Grant, 1991. Organization of reciprocal connections between area 17 and the lateral suprasylvian area of cat visual cortex, *Vis. Neurosci.*, 6(4):339–355.
- Shipp, S., and S. M. Zeki, 1985. Segregation of pathways leading from area V2 to areas V4 and V5 of macaque monkey visual cortex, *Nature*, 315(6017):322–325.
- Sillito, A. M., H. Jones, G. L. Gerstein, and D. C. West, 1994. Feature-linked synchronization of thalamic relay cell firing induced by feedback from the visual cortex, *Nature*, 369(6480):479–482.
- Symonds, L. L., and A. C. Rosenquist, 1984. Corticocortical connections among visual areas in the cat, *J. Comp. Neurol.*, 229(1):1–38.
- Tanaka, K., 1983. Cross-correlation analysis of geniculostriate neuronal relationships in cats, *J. Neurophysiol.*, 49(6):1303–1318.
- Thompson, K. G., D. P. Hanes, N. P. Bichot, and J. D. Schall, 1996. Perceptual and motor processing stages identified in the activity of macaque frontal eye field neurons during visual search, *J. Neurophysiol.*, 76(6):4040–4055.
- Thorpe, S. J., E. T. Rolls, and S. Maddison, 1983. The orbitofrontal cortex: Neuronal activity in the behaving monkey, *Exp. Brain Res.*, 49(1):93–115.
- Tomita, H., M. Ohbayashi, K. Nakahara, I. Hasegawa, and Y. Miyashita, 1999. Top-down signal from prefrontal cortex in executive control of memory retrieval, *Nature*, 401(6754):699–703.
- Treue, S., and J. H. Maunsell, 1999. Effects of attention on the processing of motion in macaque middle temporal and medial superior temporal visual cortical areas, *J. Neurosci.*, 19(17):7591–7602.
- Trevarthen, C. B., 1968. Two mechanisms of vision in primates, *Psychol. Forschung*, 31(4):299–337.
- Tsodyks, M., T. Kenet, A. Grinvald, and A. Arieli, 1999. Linking spontaneous activity of single cortical neurons and the underlying functional architecture, *Science*, 286(5446):1943–1946.
- Ungerleider, L. G., T. W. Galkin, and M. Mishkin, 1983. Visuotopic organization of projections from striate cortex to inferior and lateral pulvinar in rhesus monkey, *J. Comp. Neurol.*, 217(2):137–157.
- Ungerleider, L. G., and M. Mishkin, 1982. Two cortical visual systems, in *Analysis of Visual Behavior* (D. J. Ingle, M. A. Goodale, and R. J. W. Mansfield, eds.), Cambridge: MIT Press, pp. 549–586.
- Van Essen, D. C., and J. H. R. Maunsell, 1983. Hierarchical organization and functional streams in the visual cortex, *Trends Neurosci.*, 6:370–375.
- Vanduffel, W., B. R. Payne, S. G. Lomber, and G. A. Orban, 1997. Functional impact of cerebral connections, *Proc. Natl. Acad. Sci. USA*, 94(14):7617–7620.
- Vogels, R., and G. A. Orban, 1994. Activity of inferior temporal neurons during orientation discrimination with successively presented gratings, *J. Neurophysiol.*, 71(4):1428–1451.
- Wang, C., W. J. Waleszczyk, W. Burke, and B. Dreher, 2000. Modulatory influence of feedback projections from area 21a on neuronal activities in striate cortex of the cat, *Cereb. Cortex*, 10(12):1217–1232.
- Wong-Riley, M. T. T., 1979. Columnar cortico-cortical interconnections within the visual system of the squirrel and macaque monkeys, *Brain Res.*, 162(2):201–217.
- Young, M. P., 1992. Objective analysis of the topological organization of the primate cortical visual system, *Nature*, 358(6382):152–155.

34 Ventral and Dorsal Cortical Processing Streams

LESLIE G. UNGERLEIDER AND TATIANA PASTERNAK

MUCH OF OUR DETAILED knowledge of visual cortical organization derives from anatomical and physiological studies of the brains of Old World monkeys, of the genus *Macaca*, in which over 50 separate visual areas have now been described (Felleman and Van Essen, 1991). Similar visual areas and processing stages are now known to exist in both New World species and humans, and thus likely represent a common primate plan. In understanding the contributions of these multiple, functionally distinct visual areas, it is useful to describe two principles of cortical organization. The first principle is that the multiple visual cortical areas are organized into processing streams. According to the model originally proposed by Ungerleider and Mishkin (1982), there are two major processing streams, both of which originate in the primary visual cortex (striate cortex), V1, and both of which consist of multiple extrastriate areas beyond V1: the ventral stream is directed into the temporal lobe and is crucial for the visual recognition of objects, whereas the dorsal stream is directed into the parietal cortex and is crucial for appreciating the spatial relationships among objects and visual guidance toward them (Fig. 34.1A). A simple way to conceptualize the two streams is *what* versus *where*.

The original evidence for separate processing streams for *what* versus *where* was based on the contrasting effects of inferior temporal and posterior parietal cortex lesions in monkeys (for review, see Ungerleider and Mishkin, 1982). Lesions of inferior temporal cortex cause severe deficits on a wide range of visual discrimination tasks (e.g., discriminating objects, colors, patterns, and shapes), but these lesions do not affect animals' performance on visuospatial tasks (e.g., visually guided reaching and judging which of two objects lies closer to a visual landmark). Conversely, posterior parietal lesions do not affect visual discrimination ability but instead cause severe deficits on visuospatial performance (Fig. 34.1B). As will be described in more detail later, physiological studies of cell properties also support the functional distinction between the ventral and dorsal streams. Neurons in areas within the ventral stream respond selectively to visual features relevant for object identification, such as color, shape, and texture, whereas neurons in areas within the dorsal stream instead respond selectively to spatial

aspects of stimuli, such as the direction and speed of stimulus motion, as well as to tracking eye movements (for reviews, see Desimone and Ungerleider, 1989; Maunsell and Newsome, 1987; Merigan and Maunsell, 1993).

The second principle of cortical organization is that within each of the two processing streams, visual areas form processing hierarchies. Anatomical studies have shown that virtually all connections between successive pairs of areas within the ventral stream are reciprocal, that is, projections from one area to the next are reciprocated by projections from the second area back to the first (Felleman and Van Essen, 1991). Yet, in spite of this reciprocity, much of the processing appears to be sequential (e.g., see Desimone and Ungerleider, 1989; Desimone et al., 1985; Maunsell and Newsome, 1987; Van Essen and Maunsell, 1983). For example, neuronal response latencies found in physiological recordings increase steadily as one proceeds from the primary visual cortex (V1) toward the temporal lobe (Nowak and Bullier, 1997). Likewise, the average receptive field (RF) size increases as one moves along the ventral stream (Desimone and Gross, 1979; Gattass et al., 1981, 1988), consistent with the notion that the RFs of cells in later areas are built up from those in earlier areas. Like the ventral stream, the earlier stations of the dorsal stream, including the "motion-sensitive" areas within the superior temporal sulcus (STS), also have a hierarchical organization. Within the parietal lobe portion of the dorsal stream, by contrast, the hierarchy likely gives way to parallel processing among numerous small cortical areas (Fig. 34.2). As we will describe later, some aspects of visual processing are indeed parallel, but much of this parallel processing takes place within each cortical area rather than across areas.

It is thus possible to view much of the neural mechanism for vision, especially object vision, as a bottom-up process in which low-level inputs provided by the retina are transformed into more useful representations through successive stages of processing. In the first part of this chapter, we will describe the anatomical arrangement of components of both the ventral and dorsal streams in monkey cortex. Next, we will consider the physiological properties of neurons in each of the streams, with a focus on emergent neuronal properties as one proceeds from low-level to high-level areas.

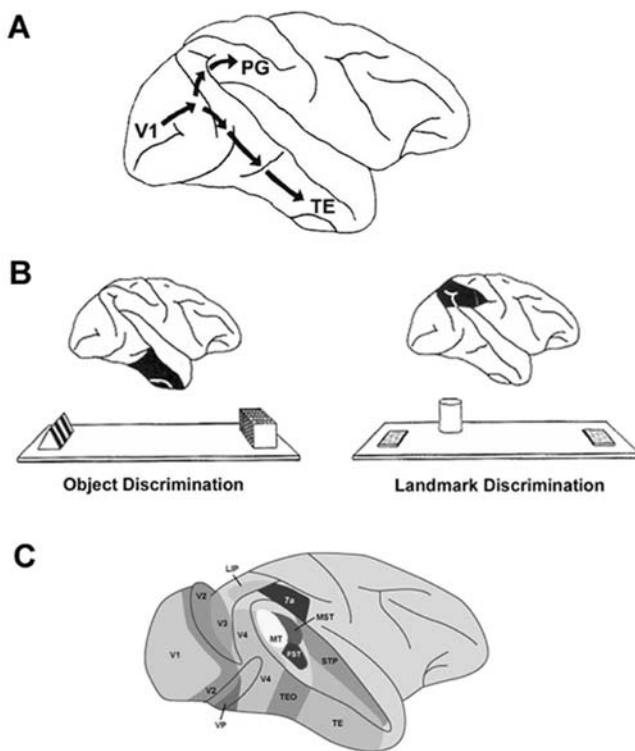


FIGURE 34.1. Two visual processing streams in monkey cortex. *A*, According to the model originally proposed by Ungerleider and Mishkin (1982), both streams originate in primary visual cortex (V1) and both consist of multiple visual areas beyond V1. The ventral stream is directed into the temporal lobe, area TE, and is crucial for the visual recognition of objects, whereas the dorsal stream is directed into the parietal lobe, area PG, and is crucial for appreciating the spatial relationships among objects and for the visual guidance toward them. *B*, The original evidence for separate processing streams was based largely on the contrasting effects of inferior temporal and posterior parietal lesions in monkeys. Lesions of inferior temporal cortex (*left*, in *black*) cause impairments on visual discrimination tasks, such as recognizing an object seen a few seconds previously, whereas posterior parietal lesions (*right*, in *black*) cause impairments on visuospatial tasks, such as judging which of two identical plaques is located closer to a visual landmark—the cylinder. *C*, Lateral view of the monkey brain with the sulci partially opened to illustrate the location of the multiplicity of functionally distinct visual areas that comprise the ventral and dorsal processing streams. For a list of abbreviations, see Table 34.1. (*A* adapted from Mishkin et al., 1983; *B* adapted from Ungerleider and Mishkin, 1982; *C* adapted from Distler et al., 1993.) (See color plate 17.)

We will also describe the behavioral effects of selective lesions of the two streams. Then we will describe interactions between the two processing streams, as well as the differential projections from them to regions within prefrontal cortex, and the role these areas play in vision. Finally, we will conclude with evidence for the existence of homologous visual processing streams in the human cortex.

Anatomical organization of ventral and dorsal processing streams

Much of our knowledge of the areas that comprise the ventral and dorsal streams comes from anatomical tract-tracing studies in nonhuman primates. These studies have demonstrated that regions that make up the ventral stream lie directly anterior to V1 in the occipital lobe and in progressively more anterior and ventral portions of the temporal lobe, whereas regions that make up the dorsal stream also include these early occipital-lobe areas but then occupy sites within the posterior STS and include progressively more anterior sites within this sulcus and more dorsal sites within the parietal lobe. Figure 34.1*C* illustrates the location of these areas within the cortex, and Figure 34.2 diagrams their anatomical connections (see Table 34.1 for a list of abbreviations).

The cortical analysis of objects begins in V1, where information about contour orientation, color composition, brightness, and direction of motion is represented in subsets of neurons responsible for each point in the visual field (Livingstone and Hubel, 1984; Tootell et al., 1988; Ts'o and Gilbert, 1988). Information from V1 is then sent forward to subdivisions or *modules*—interdigitating thin, thick, and interstripe regions—within V2 (Livingstone and Hubel, 1984, 1987). From the thin and interstripe regions in V2, representing mainly color and form information, respectively (De Yoe and Van Essen, 1985; Hubel and Livingstone, 1985, 1987; Livingstone and Hubel, 1984; Shipp and Zeki, 1985), neural signals proceed forward to area V4 on the lateral and ventromedial surfaces of the hemisphere and to a posterior inferior temporal area just in front of V4, area TEO (Gattass et al., 1997; Nakamura et al., 1993). From both V4 and TEO, signals related to object form, color, and texture proceed forward to area TE (Desimone et al., 1980; Distler et al., 1993), the last exclusively visual area within the ventral stream for object recognition (Desimone and Gross, 1979). Together, areas TEO and TE comprise inferior temporal (IT) cortex.

Progressing forward along the ventral stream, there is a gradual shift in the nature of connectivity. Patterns of cortical projections become successively less topographic or *point-to-point*. For example, while connections from V1 to V2 maintain topographic order, they are looser between V2 and V4, and inputs to area TE from V4 and TEO retain no obvious retinotopic organization (Desimone et al., 1980; Distler et al., 1993; Gattass et al., 1997; Livingstone and Hubel, 1983; Rockland and Pandya, 1979). This loss of retinotopy within area TE means that single neurons respond to objects anywhere in the visual field. Thus, explicit information about the spatial location of an object is not retained at the highest levels of the ventral stream.

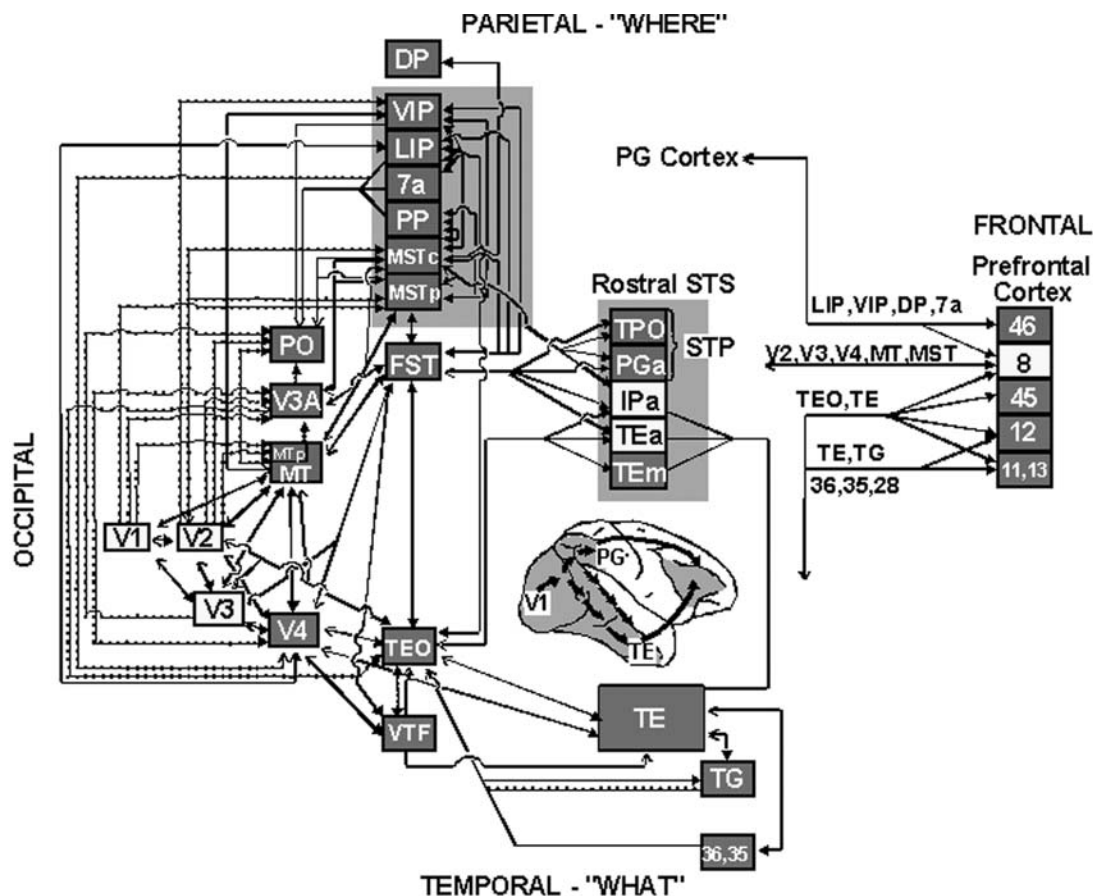


FIGURE 34.2. Anatomical connections of visual areas in the ventral and dorsal streams. Solid lines indicate connections arising from both central and peripheral visual field representations, whereas dotted lines indicate connections restricted to peripheral field representations. Red boxes indicate ventral stream areas associated primarily with object vision; green boxes indicate dorsal

stream areas associated primarily with spatial vision; and yellow boxes indicate areas not clearly allied with either stream. The shaded region on the lateral view of the monkey brain indicates the extent of the cortex included in the diagram. For a list of abbreviations, see Table 34.1. (Adapted from Ungerleider, 1995.) (See color plate 18.)

The cortical analysis of spatial perception also begins in V1, deriving largely from the motion-sensitive cells in layer 4B (Maunsell and Van Essen, 1983a). In turn, cells in layer 4B project primarily to the thick stripes within V2 (Roe and Ts'o, 1995; Zeki and Shipp, 1987) and to V3, where direction of motion information is retained. Together, these three early visual areas provide the input to the middle temporal visual area, MT (Ungerleider and Desimone, 1986), also known as the *motion-sensitive area* of the STS. From MT, information is sent forward within the STS to several additional motion-sensitive areas, including MST (the medial superior temporal area) and FST (the fundus of the superior temporal area; Maunsell and Van Essen, 1983a; Ungerleider and Desimone, 1986), both of which project to area STP (the superior temporal polysensory area) located farther forward on the upper bank of the STS (Boussaoud et al., 1990). Inasmuch as portions of STP also receive ventral stream inputs, these regions may serve as anatomical sites for the integration of visual information about form and motion.

MT is also the source of information for VIP (the ventral intraparietal area; Ungerleider and Desimone, 1986), which in turn projects to several additional parietal areas, including LIP (lateral intraparietal area) and area 7a, located in the inferior parietal lobule (Andersen et al., 1990a; Blatt et al., 1990; Boussaoud et al., 1990). Interestingly, a number of these parietal areas receive direct inputs from the peripheral field representations of V1 and V2, bypassing MT (e.g., Colby et al., 1988), and these inputs may provide rapid activation of regions mediating spatial attention.

Neural processing is not, however, a simple matter of successive elaboration of information from lower-order to higher-order areas. As described earlier, at all stages connections are reciprocal. For example, an area receiving feedforward projections from an area earlier in the ventral stream also provides feedback projections to that area. Whereas feedforward projections provide bottom-up, sensory-driven inputs to subsequent visual areas, and severing these projections disconnects subsequent areas from their

TABLE 34.1
Visual areas in the cortex of monkeys.

Areas with Abbreviations	
DP	dorsal prelunate area
FST	fundus of the STS area
LIP	lateral intraparietal area
MT	middle temporal area
MT _p	MT, peripheral visual field representation
MST	medial superior temporal area
MST _c	MST, central field representation
MST _p	MST, peripheral field representation
PO	posterior occipital area
PP	posterior parietal area
STP	superior temporal polysensory area
VP	ventral posterior area
VIP	ventral intraparietal area
VTF	visually responsive portion of area TF
V1	primary visual (striate) cortex
V2	second visual area
V3	third visual area
V3A	third visual area, part A
V4	fourth visual area
Brodmann (1909) Areas	
7a	inferior parietal
46, 9	dorsolateral prefrontal
45, 12	ventrolateral prefrontal
11, 13	orbital frontal
von Bonin and Bailey (1947) Areas	
PG	inferior parietal
TF	parahippocampal
TEO, TE	inferior temporal
TG	temporal polar

Rostral superior temporal sulcus (STS) areas TPO, PGa, IPa, TEa, and TEm are from Seltzer and Pandya (1978).

visual input (Rocha-Miranda et al., 1975; Schiller and Malpeli, 1977), the precise functions of the reciprocal feedback projections are still unknown. However, they are thought to play a top-down role in vision, such as in selective attention, by modulating activity in earlier areas of the processing stream. In addition to feedforward and feedback projections, there appear to be “intermediate-type” projections that link areas at the same level of the visual hierarchy. These are seen most notably between areas of the ventral and dorsal streams. For example, area V4 is interconnected with areas MT and MST (Maunsell and Van Essen, 1983a; Ungerleider and Desimone, 1986). Thus, there exists an anatomical substrate for interactions between the two processing streams at several levels, which we will discuss when we consider the physiological properties of neurons within the ventral and dorsal streams.

All areas within the ventral and dorsal streams also have heavy interconnections with subcortical structures, including the pulvinar, claustrum, and basal ganglia (Baizer et al., 1993; Benevento and Davis, 1977; Benevento and Rezak, 1976; Boussaoud et al., 1992; Kemp and Powell, 1970; Saint-Cyr et al., 1990; Selemon and Goldman-Rakic, 1985; Ungerleider et al., 1983, 1984; Webster et al., 1993). In addition, each stream receives subcortical modulatory inputs from ascending cholinergic projections from the basal forebrain and ascending noradrenergic projections from the locus coeruleus (Gatter and Powell, 1977; Mesulam and Van Hoesen, 1976; Webster et al., 1993). These projections are thought to play a role in the storage of information in cortex and the influence of arousal on information processing, respectively. Finally, visual information is sent from the last stations of both streams to the most ventral and anterior reaches of the temporal lobe, notably perirhinal cortex and parahippocampal areas TF and TH (Van Hoesen, 1980, 1982). These regions in turn project, via entorhinal cortex, to medial temporal lobe structures, such as the hippocampus, which contribute to forming long-term memories of visual objects and their contexts. Information is also sent from both streams to prefrontal cortex (Barbas and Mesulam, 1985; Cavada and Goldman-Rakic, 1989; Chavis and Pandya, 1976; Ungerleider and Desimone, 1986; Ungerleider et al., 1989; Webster et al., 1994), which plays an important role in working memory (Fuster, 1995; Goldman-Rakic, 1990), that is, holding an object and its location briefly in mind when it is no longer visible. Finally, there are direct projections from the ventral stream to the amygdala (Webster et al., 1993), which is important for attaching emotional valence to a stimulus, and from the dorsal stream to the pons (Boussaoud et al., 1992), which, in conjunction with the cerebellum, likely contributes to the control of eye and head velocity during tracking eye movements.

Neuronal properties within the ventral stream

CELLS ARE SENSITIVE TO INCREASINGLY COMPLEX OBJECT FEATURES Consistent with a role in object recognition, neurons in all areas of the ventral stream share a number of physiological characteristics, including sensitivity to the shape, color, or texture of visual stimuli. Progressing forward along the pathway, there is a general trend toward selectivity for increasingly complex stimulus features or combinations of features. For example, whereas many V1 neurons function as local spatial filters (e.g., signaling the presence of contours at particular positions in the visual field), some V2 cells respond to so-called illusory contours of whole figures (von Der Heydt et al., 1984); a V2 cell selective for the horizontal orientation of an edge placed in its RF may respond similarly to an edge that is perceptually suggested by stimu-

lation of surrounding regions but not physically present. Other cells in V2 are jointly selective for wavelength and small dimensions of stimuli (Baizer et al., 1977; Hubel and Livingstone, 1987); such cells represent an early stage of integration of stimulus features. Moving forward to V4, the trend continues such that a greater proportion of cells are conjointly tuned for multiple dimensions of a stimulus (such as length, width, disparity, and/or wavelength of a bar of light (Cheng et al., 1994; Desimone and Schein, 1987; Desimone et al., 1985; Hinkle and Connor, 2001; Watanabe et al., 2002). In addition, about a third of the neurons in V4 show selectivity to contour features such as curves and angles (Gallant et al., 1996; Pasupathy and Connor, 1999), suggesting an intermediate stage of processing.

Another important property of V4 neurons is the existence of large, silent suppressive zones surrounding the excitatory RFs of cells (Desimone and Schein, 1987; Desimone et al., 1985). These zones are termed *silent* because stimulation of the zones does not normally cause any change from the cell's baseline activity but can have a powerful effect on the response to a stimulus placed in the RF (what is now called by many the *classical* RF). The stimulus-selective properties of the excitatory RF and the suppressive surround are often matched. As a consequence, many V4 cells respond maximally to a stimulus only if it stands out from its background on the basis of a difference in form. This sensitivity to RF/surround differences is thought to be useful for figure/ground segregation—the parcellation of scenes into a collection of objects within them.

Moving forward successively into area TEO and then into posterior and anterior portions of area TE, there is a further increase in the complexity of the critical features needed to activate many neurons and an increase as well in the proportion of cells that are selectively driven by some kind of complex pattern or object (Desimone et al., 1984; Gross et al., 1972). Indeed, many cells in TE require moderately complex features for their activation (Tanaka, 1997). Importantly, the critical features that drive single cells are typically not complex enough to specify a particular object. To represent individual objects instead requires activation of a few to several tens of cells with different critical features.

The work of Tanaka and colleagues has shown that a key property of TE is that it is composed of columns, in many ways similar to those in V1, in which cells with related but slightly different selectivity cluster together (Tanaka, 1993). For example, some cells in a column responsive to faces might respond optimally to different face components, while others might be sensitive to the overall configuration of a face regardless of viewpoint, and still others might respond well to faces specifically in profile. Thus, a given object feature is apparently not represented by the activity of a

single cell, but by the activity of many cells within a column. Representation by multiple cells in a column in which the selectivity varies, but overlaps, from cell to cell satisfies two apparently conflicting requirements in visual recognition: robustness to subtle changes in input and precision of representation. Given this clustering of cells responsive to related features, an object in its entirety would then be represented by a pattern of activity distributed across multiple columns, each of which may participate in representing multiple objects. Whereas the image of an object projected on the retina changes in response to variations in illumination and viewing angle, the pattern of activity in TE should be largely maintained, insofar as the clustering of cells with overlapping but slightly different selectivity should serve as a buffer to absorb such changes.

SOME CELLS IN THE INFERIOR TEMPORAL CORTEX ARE FACE SELECTIVE One of the more striking characteristics of monkey temporal cortex is the presence of neurons with responses selective for face stimuli, first described by Gross and colleagues (Bruce et al., 1981) and by Rolls and colleagues (Perrett et al., 1982). Although the overall numbers of these face-selective cells are small (1% to 5% of all neurons recorded in these regions), their concentration is much higher in the cortex of the lower and upper banks of the STS, where they are found together in clumps and where they may make up as much as 10% to 20% of all cells studied (Baylis et al., 1985). The lower bank of the STS is part of area TE, whereas the upper bank is part of area STP, which responds to auditory and somatic stimuli, as well as to visual stimuli (Bruce et al., 1981).

Face-selective cells vary in the degree and nature of their preference for face stimuli (for review, see Desimone, 1991). Many respond well to both real faces and face pictures but give nearly no response to any other stimuli tested, including other complex objects, texture patterns, and images in which the features making up the face are rearranged or scrambled. Thus, at least some face-selective neurons appear to be sensitive to very general or global aspects of a face, such as the prototypical arrangement of the eyes, nose, and mouth into a face-like configuration (Desimone et al., 1984). Other neurons in TE and STP respond to specific face components, such as the presence of eyes per se, the distance between the eyes, or the extent of the forehead (Baylis et al., 1985; Perrett et al., 1982; Rolls et al., 1985). While such neurons may merely be sensitive to facial features, they are nonetheless likely to participate in circuits responsible for recognizing a particular individual. One subset of face cells that responds to whole faces is particularly sensitive to the direction of gaze of the eyes (looking back directly or turned to the side; Perrett et al., 1985a), which is an important social signal for both monkeys and humans.

THE VENTRAL STREAM EXTRACTS SOME INVARIANT ASPECTS OF OBJECTS The visual information impinging on the retina is a two-dimensional projection of a three-dimensional world, a projection that varies dramatically as a function of changes in an object's position, distance, illumination, and orientation relative to the viewer. Thus, the function of the ventral stream can be defined in large measure as determining and encoding those invariant features of objects that are useful for recognition across myriad circumstances. As described earlier, as one progresses forward from V1 to TE, RFs become larger and the retinotopic maps less precise. By the anterior portions of area TE, RFs can include the entire visual field (Desimone and Gross, 1979; Gross et al., 1972). These large, bilateral RFs signal the presence of a given feature, collection of features, or object, regardless of where in the visual field they fall. In other words, they exhibit invariance of stimulus coding across changes in retinal position (Gross and Mishkin, 1977).

In addition to invariance over position, many neurons in TE show maintained selectivity for their "preferred" stimuli over more complex kinds of transformations, such as size, distance from the subject in depth, or degree of ambient illumination (Hikosaka, 1999; Ito et al., 1995; Sary et al., 1993; Vogels and Orban, 1996), so that they show invariance over a number of the changes that normally take place as a moving object is viewed under naturalistic conditions (or as an observer moves relative to a stationary object). Also, many TE neurons show form-cue invariance: for example, a neuron selective for a particular shape defined by luminance borders (e.g., a white star on a black background) will be selective for the same form defined either by relative texture or by motion cues instead (e.g., a star-shaped region of speckles of the same average luminance as the background moving in a different direction from the background). These various types of response invariance or generalization, taken together, make it possible to understand the types of deficits seen in monkeys when IT cortex is removed (see Plaut and Farah, 1990).

One central question in object recognition has been the degree to which neural representations of objects are object centered (view independent) or viewer centered (view dependent). The question of view dependence has been addressed by a number of single-unit studies of neurons in TE. For example, in one study, monkeys were trained to recognize specific novel three-dimensional objects from any viewpoint after experience with a few prototypical views in a discrimination task (Logothetis et al., 1995). After months of such training, the monkeys were found to have neurons in TE that exhibited strong selectivity for precisely those views on which the animal had been trained. These results support the view-dependent account of object recognition (Bulthoff et al., 1995). Studies of face-selective neurons in

area TE also initially provided strong support for view dependence by finding separate populations of cells tuned for front and profile views in both adult and infant monkeys (Desimone et al., 1984; Rodman et al., 1993). However, other studies showed that at least small subsets of TE neurons respond to faces or objects independent of view, providing evidence for view-independent representations as well. Overall, the issue of view dependence remains an open question, with some evidence for both accounts to be found in the neurophysiological literature as well as in psychophysical studies.

CELLS IN THE VENTRAL STREAM ARE AFFECTED BY ATTENTION With the use of a number of simple but effective behavioral paradigms, such as change blindness (Rensink, 2000), it has become clear that visual attention is necessary for the construction of the visual world we perceive. These behavioral paradigms demonstrate that without the ability to allocate attentional resources, detecting even large changes in the visual world becomes difficult. In the laboratory, directing attention to a specific location of the visual field speeds up detection and increases sensitivity to visual stimuli presented at that location (Bashinski and Bacharach, 1980; Posner et al., 1980; Yantis and Jonides, 1984). Neurophysiological correlates of this enhancement have been found in many visual areas, including V1 (Ito and Gilbert, 1999; Luck et al., 1997; Motter, 1993; Roelfsema et al., 1998), V2 (Luck et al., 1997; Reynolds et al., 1999), V3A (Nakamura and Colby, 2000), V4 (McAdams and Maunsell, 1999; Moran and Desimone, 1985), and areas MT and MST (Seidemann and Newsome, 1999; Treue and Maunsell, 1999).

The enhancement of neural activity associated with the demands of the behavioral task has been studied most extensively in area V4. Neurons in this area show enhanced responses to a visual stimulus when it is placed in the neuron's RF and becomes the target of a saccade or is used by the monkey in a discrimination task (Fischer and Boch, 1981; McAdams and Maunsell, 1999; Moore et al., 1998; Motter, 1994; Reynolds et al., 2000). This attentional enhancement is greatest when the discriminative stimulus is presented at near-threshold contrasts, resulting in an increase in neuronal sensitivity to contrast (Reynolds et al., 2000). Attentional effects on neuronal firing are even more pronounced when two stimuli are placed within the RF of a V4 neuron; in this case, the response is primarily driven by the attended stimulus (Moran and Desimone, 1985; Reynolds et al., 1999). These observations have led to the hypothesis that, within the circuitry of extrastriate cortex, there is a mechanism that gates out unattended stimuli (Desimone, 1998), and that this gating may be due to the interaction between neighboring RFs (Connor et al., 1997). In animals with lesions of V4, attention appears to be

allocated automatically to the most salient stimulus (see below), suggesting that the mechanism that controls the gating may include neurons within V4 (De Weerd et al., 1999; Schiller, 1993).

While earlier studies identified area V4 and the ventral stream as one of the main sites of attentional influences on visual processing, a number of recent studies have demonstrated similar influences in visual cortical areas within the dorsal stream. For example, Treue and Maunsell (1999) showed that directing attention to the RF in areas MT and MST results in an increase in neuronal firing. This effect was more pronounced when two spots moving in the preferred and the nonpreferred directions were placed in the RF and attention was directed from the nonpreferred to the preferred direction. In a subsequent study, Treue and Martinez-Trujillo (1999) demonstrated that attention increases the gain of direction-selective neurons. These effects are similar to those found in area V4, and show that attention enhances the representation of attended stimuli and reduces the influence of unattended stimuli. As discussed by Kastner and Ungerleider (2000), the source of these attentional modulatory influences likely arises from a network of frontal and parietal areas.

CELLS IN THE VENTRAL STREAM ARE AFFECTED BY EXPERIENCE Thus far, we have seen how the ventral stream, especially area TE, represents features that are useful for object recognition. For example, some neurons respond selectively to the salient features in a face, or their relative positions, while ignoring aspects of stimulus appearance that depend on viewing conditions, such as absolute size and luminance. We next consider how the brain represents stimuli over time. In particular, we describe how neurons in TE and the adjacent perirhinal cortex show effects of both recent viewing history and long-term experience with stimuli.

Experiments by Miller and Desimone (1994) have shown how short-term changes in response properties of temporal neurons encode aspects of both stimulus recency and short-term stimulus significance. For example, for many of these cells, responses to an object that is presented repeatedly decrease in a systematic fashion, potentially signaling that the object has been seen recently. Such reduced signals may be useful for redirecting attention to novel objects. This kind of response decrement, termed *repetition suppression*, has been found both under anesthesia and for stimuli which an awake animal is trained to ignore. This habituation-like response is therefore a passive, automatic mechanism by which the visual system edits out recently seen objects. By contrast, if a monkey is trained to do a matching task in which it must hold a particular visual pattern in memory over a short delay, some temporal neurons increase their firing rates, specifically when the to-be-remembered stimulus is recognized. This phenomenon, termed *mnemonic enhancement*, can be thought

of as a mechanism in which bottom-up processing of the stimulus is affected by top-down, cognitive factors, namely, the animal's expectation of the relevant stimulus. Stimuli that are repeated but are not behaviorally relevant in the context of the task do not show this enhancement effect (Desimone, 1996).

Experiments such as these demonstrate that the magnitude of responses of neurons can be affected by the subject's experience with the stimulus and by its significance, at least in the short term. Other studies suggest that the kind of familiarity gained over longer periods of time—akin to the development of expertise—can also be reflected in the responses of TE cells. For example, in monkeys that have been trained for as long as a year to discriminate between objects, more than 30% of the cells show selectivity for those objects, compared to untrained monkeys, in which roughly 10% of the cells show such selectivity (Kobatake et al., 1998).

Perhaps even more fascinating is the finding that some TE cells come to represent the history of association between objects in the activity patterns they exhibit in response to members of a set of stimuli. Using paired associate tasks, in which monkeys are trained to associate arbitrary stimulus patterns with one another for a reward, Sakai and Miyashita (1991) have found that, across the population of cells, TE neurons respond best to stimuli that had been paired together during training. In other words, some cells in temporal cortex developed conjoint selectivity (pair coding) for the members of associated pairs. Further, pair coding by TE cells is decreased by surgically interrupting the feedback projections to them from the perirhinal and entorhinal cortices (Miyashita et al., 1998). Thus, feedback projections appear to play a specific role in associating objects because the pair-coding property depends on them.

Although associative learning effects typically have been seen in studies after weeks or months of training, there is evidence that small but detectable shifts in neuronal population selectivity occur even after only a day or so of experience, suggesting that TE cells tend to develop pair-coding properties more rapidly than was previously thought (Erickson et al., 2000). Thus, the pattern of selectivity shown by TE cells at any given moment in time may partly reflect a record of their exposure to stimuli seen together. Overall, TE circuits appear to represent not only complex visual features, but also the history of their meanings and relationships in a behavioral context.

Behavioral effects of ventral stream lesions

FORM AND COLOR IMPAIRMENTS Lesions of the components of the ventral stream generally result in deficits that are consistent with neuronal RF properties of this processing pathway. Thus, there is evidence that lesions of both V4 and

IT cortex elevate contrast thresholds for relatively simple orientation discriminations (Dean, 1978; Merigan, 1996; Rudolph, 1997; Vogels et al., 1997). Many studies have shown that such lesions also disrupt more complex shape discriminations, with deficits resulting from V4 lesions usually being more pronounced (De Weerd et al., 1996; Heywood and Cowey, 1992; Huxlin et al., 2000; Merigan, 2000; Walsh et al., 1992b; for review, see Merigan and Pasternak, 2003).

The specificity of the effects of IT lesions on form discriminations is well illustrated by a study by Britten et al. (1992). In this study, deficits in discrimination were found when shapes were defined by luminance but not when they were defined by relative motion. This study not only supports the general finding that ventral pathway lesions typically spare motion discriminations but also suggests that form discriminations may be partially spared from the effects of ventral pathway lesions when the form is conveyed by motion.

Although V4 has been identified as one of the areas actively involved in the processing of color information (Zeki, 1973, 1980), V4 lesions result surprisingly in transitory and relatively modest disruption of simple color discriminations (Walsh et al., 1992a, 1993). The effects of V4 lesions on color thresholds and chromatic contrast sensitivity are also relatively mild (Dean, 1979; Heywood et al., 1992; Merigan, 1996; Walsh et al., 1993). This preservation of various forms of color perception is consistent with reports that some portions of the dorsal stream of both macaques and humans have access to chromatic information (Dobkins and Albright, 1994; Gegenfurtner et al., 1994; Seidemann et al., 1999; Wandell et al., 1999). While the function of color processing in the dorsal stream may be primarily to subserve the perception of motion, that in the ventral stream is undoubtedly more related to object recognition and segmentation by color. Color sensitivity found in the dorsal stream may help account for the failure to find large, permanent color vision loss after V4 lesions. It cannot, however, account for the more dramatic, and often permanent, color deficits found after IT lesions (Heywood et al., 1995; Huxlin et al., 2000).

IMPAIRMENTS IN PERCEPTUAL CONSTANCIES Normally, one can recognize an object independent of its size, location in the visual field, viewing distance, and ambient illumination. Several studies have demonstrated that these kinds of perceptual constancies are lost in monkeys with IT lesions (Humphrey and Weiskrantz, 1969; Seacord et al., 1979; Walsh et al., 1993; Weiskrantz and Saunders, 1984). For example, monkeys with IT lesions that have been trained to discriminate between two discs of different absolute size are unable to perform the discrimination when those discs are presented at variable distances (and hence with variable

retinal image sizes). Instead, they respond on the basis of either retinal size or distance (Humphrey and Weiskrantz, 1969). Thus, they have lost size constancy. Similarly, whereas normal monkeys easily generalize a visual discrimination learned in one hemifield to the other, monkeys with IT lesions do not, indicating that they have lost neural representations for objects that are invariant across visual field locations. Finally, whereas normal monkeys are unaffected by changes in the patterns of shadow and light falling on object surfaces, variations in illumination prevent monkeys with IT lesions from seeing the equivalence of objects. These behavioral findings, together with the physiological properties of IT neurons described earlier, indicate that an important role of IT cortex is perceptual constancy, that is, representing the invariant aspects of objects independent of retinal inputs.

MEMORY IMPAIRMENTS In addition to the loss of several visual constancy mechanisms described above, it is well established that monkeys with IT lesions are impaired in learning to discriminate among visual stimuli (including colors, patterns, shapes, and objects) and in recalling previously learned discriminations (Dean, 1976, 1982). Further, these impairments cannot be explained by deficits in basic sensory capacities. Rather, the behavioral impairment seems to result from the loss of a high-level mechanism, although the precise nature of this mechanism is still in dispute.

One proposed model is that monkeys with IT lesions have fewer perceptual categories than normal (Dean, 1976; Gaffan et al., 1986). For example, a brush and a wooden block with the same general shape and color would likely fall within different perceptual categories for a normal monkey but might fall within the same category for a monkey with an IT lesion. Hence, in a visual discrimination task, learning to associate the brush with reward and the wooden block with nonreward might be as difficult for an animal with an IT lesion as learning to discriminate between two slightly different brushes might be for a normal monkey. This concept fits with some models of prosopagnosia, in which it is thought that the underlying impairment may be in discriminating among objects within the same perceptual category rather than in discriminating faces *per se* (Damasio et al., 1982).

Mishkin has argued, by contrast, that a reduction in the number of perceptual categories cannot fully explain the impairments produced by IT lesions. He has proposed that IT lesions also cause a loss of certain perceptual constancies (as described above), a reduction in the visual inputs to a *habit*-learning system involving the basal ganglia, and a profound loss of visual memories (Mishkin, 1982; Mishkin and Appenzeller, 1987). The memory loss is suggested by studies showing that monkeys with IT lesions cannot recognize an object seen as recently as 30–60 seconds

previously (Squire, 1987). Thus, according to this view, IT cortex contains the central representations for visual objects, and the loss of IT cortex leads not only to the loss of old memories but also to an inability to form new ones. Although there are some suggestive physiological data indicating that IT cortex could be the site of memory storage (Brown et al., 1987; Fuster and Jervey, 1981), definitive data on this issue are sorely lacking.

IMPAIRMENT IN VISUAL ATTENTION It is well established that responses of neurons in V4 and IT cortex are modulated by visual attention (e.g., Chelazzi et al., 1998; Connor et al., 1997; Moran and Desimone, 1985; Reynolds et al., 2000). Thus, one would expect to find impairments in visual attention following the loss of these neurons. Indeed, Schiller and Lee (1991) reported that V4 lesions severely disrupted the ability to detect a less salient (smaller, less coarse) odd stimulus in an array of stimuli, but had less effect on the ability to detect a more salient (larger, coarser) odd stimulus. This result is consistent with current views that V4 may be one site where top-down attentional influences modulate bottom-up sensory-driven inputs, such as visual salience (Desimone and Duncan, 1995). Hence, in the absence of V4, relevant but less salient stimuli would be ignored. More recently, De Weerd et al. (1999) showed that monkeys with either V4, TEO, or combined V4 and TEO lesions were minimally impaired on a grating orientation discrimination but were greatly impaired when the grating was surrounded by irrelevant disc distracters. Furthermore, the impairment was proportional to the contrast of the distracters. This result supports the idea that V4 and TEO lesions can alter perception by disrupting the role attention plays in separating visual targets from distracters (Braun, 1994).

Neuronal properties within the dorsal stream

CELLS ARE SENSITIVE TO VISUAL MOTION One of the more prominent features of neurons in the dorsal stream is selectivity for the direction of visual motion. Directionally selective neurons respond vigorously to one direction of motion and respond less or not at all when the same stimulus moves in the opposite direction (Hubel and Wiesel, 1968). This property first appears in V1, where directionally selective neurons are found primarily in layers 4C α and 4B (Hawken et al., 1988), the target layers of the magnocellular neurons of the lateral geniculate nucleus. These V1 neurons are sensitive to low contrasts and have relatively poor spatial resolution (Hawken et al., 1988; Movshon and Newsome, 1996). In area V2, directionally selective neurons are less numerous, show high sensitivity to contrast, and are localized largely in the thick stripes, suggesting magnocellular influences (Burkhalter and Van Essen, 1986; Levitt et al.,

1994a). In area V3, these neurons are much more numerous, exhibit relatively high sensitivity to contrast, and prefer coarse, relatively fast-moving stimuli, indicating a role in processing of motion information. Indeed, neurons in V3 show the ability to integrate local motion signals (Gegenfurtner et al., 1997), a feature indicative of higher-level motion analysis (Movshon et al., 1985). Because of these features, the prominent inputs V3 sends to MT, and its reactivity to CAT-301 antibody, which is characteristic of regions in the dorsal processing stream (De Yoe et al., 1990), V3 often has been associated with the dorsal stream (e.g., Felleman et al., 1997).

Processing of visual motion is even more prevalent in area MT, where selectivity for the direction and speed of motion is found in the majority of neurons (e.g., Albright, 1984; Maunsell and Van Essen, 1983c). MT neurons display directional selectivity to the motion of random dots, bars, and gratings (Britten et al., 1993; Maunsell and Van Essen, 1983c; Mikami et al., 1986), and neurons with similar directional preferences are clustered in columns (Albright et al., 1984). Furthermore, many properties of these neurons are consistent with their role in motion perception. For example, many MT neurons respond to complex motion stimuli consisting of multiple motion vectors in the same part of space, similar to the way such motion is perceived by human observers. Specifically, when presented with a plaid pattern consisting of two component gratings moving in orthogonal directions, MT neurons, unlike V1 neurons, respond to the direction of the plaid rather than to its components (Albright et al., 1984; Rodman and Albright, 1989). The RFs of MT neurons also have strong antagonistic surrounds, which, when stimulated by the same direction and/or speed as the excitatory center, show strong inhibition (Allman et al., 1985a, 1985b; Xiao et al., 1995). This property allows these neurons to code local motion signals according to the context in which this motion appears, suggesting a role in the detection of relative motion and in figure-ground segregation.

Responses of MT neurons to other types of complex motion also support their close connection to perception. In contrast to V1 neurons, which respond equally well to non-transparent and transparent motion, activity of MT neurons to the motion of transparent surfaces moving in different directions is suppressed (Recanzone et al., 1997; Snowden et al., 1991). This suppression is reminiscent of the perception of motion transparency observed in human psychophysical experiments (Qian and Andersen, 1994).

Visual motion is also processed by neurons in the medially adjacent area MST, an important target of MT projections. Its dorsal portion (MSTd) contains neurons with very large RFs, preferring the motion of full-field stimuli (Desimone and Ungerleider, 1986; Saito et al., 1986), a property that suggests a role in integrating visual motion

signals generated during the observer's movement through the environment with eye-movement and vestibular signals (Andersen, 1997). A number of studies have shown that MSTd has the machinery needed to extract and signal the direction of heading from optic flow stimuli (Lappe et al., 1996; Van Den Berg and Beintema, 2000). The evidence that the use of such information may depend on MST has come from Britten and Van Wezel (1998), who showed that electrical microstimulation of MST neurons produced biased decisions about the direction of heading provided by optic flow stimuli.

In contrast to MSTd, neurons in the lateral portion of MST (MSTl) have properties that make them more likely to be involved in the analysis of object motion in the environment (Tanaka et al., 1993) and in the maintenance of pursuit eye movements associated with this motion (Komatsu and Wurtz, 1988). RFs of neurons in this region, similar to neurons in MT, have antagonistic surrounds and respond very strongly to object motion when the motion in the surround is in the opposite direction (Eifuku and Wurtz, 1998), suggesting a role in segmenting moving objects from backgrounds.

A number of areas within parietal cortex also respond to visual motion (e.g., areas VIP and 7a), and these responses are largely reminiscent of responses at earlier stages of processing within the dorsal pathway.

CELLS ARE SENSITIVE TO BINOCULAR DISPARITY Sensitivity to binocular disparity, the property believed to underlie depth perception, is characteristic of many neurons in the dorsal stream. Although the information from the two eyes remains segregated upon their arrival in layer 4 of V1 (Hubel and Wiesel, 1977), there is substantial intermixing of inputs from the two eyes in layers above and below layer 4. This intermixing is reflected in neuronal properties, as there are many V1 neurons that respond best when both eyes are stimulated and many of these neurons are sensitive to absolute retinal disparity (Cumming and Parker, 1999; Poggio et al., 1988), an early stage of processing that leads to stereoscopic depth perception (Cumming and DeAngelis, 2001). Although sensitivity to absolute retinal disparity is still quite common at the level of V2 (Hubel and Livingstone, 1987; Poggio, 1995; Zeki, 1979), some neurons begin to show sensitivity to *relative disparity* between different locations in the visual field, a property absent from V1 neurons (Cumming and Parker, 1999). This property appears to be segregated primarily to neurons in the thick stripes of V2 (Roe and Ts'o, 1995), which project to MT. Disparity sensitivity, also present in some neurons in area V3 (Felleman and Van Essen, 1987), becomes even more prevalent in MT, where the neurons are found clustered according to preferred disparity (DeAngelis and Newsome, 1999). These neurons appear to contribute to stereoscopic depth percep-

tion, as microstimulation of similarly tuned cells can bias the monkey's perceptual judgment of depth toward the preferred disparity (DeAngelis et al., 1998). Apart from depth perception, the disparity tuning of these neurons appears to be relevant to other perceptual phenomena. For example, a difference in disparity of the display consisting of sheets of random dots creates the percept of transparent motion (Bradley et al., 1995), and changing the disparity in the surround of the classical RF modulates not only the response of MT neurons to motion but also the percept of the direction of motion (Bradley et al., 1998). It has also been suggested that MT may be involved in extracting shape from motion (Buracas and Albright, 1996; Dodd et al., 2001), and while there is evidence of the interaction between motion and disparity signals in the same neurons (Bradley et al., 1995), MT neurons do not appear to be tuned to motion in depth (Maunsell and Van Essen, 1983b).

It should be noted that sensitivity to retinal disparity is not unique to the dorsal pathway. Even though disparity in V2 neurons appears to be segregated to the thick stripes, which project to the dorsal stream, neurons in both V4 and IT cortex have been shown to be sensitive to retinal disparity as well (Hinkle and Connor, 2001; Janssen et al., 2000; Watanabe et al., 2002).

CELLS ARE INVOLVED IN PROCESSING OF VISUAL SPACE IN ACTIVE OBSERVERS Many properties of neurons within the dorsal stream point to their role in the processing of location information in active observers. For example, neurons in MSTd are capable of integrating visual information extracted during movement of the observer with signals related to eye and head movements (Andersen et al., 1999; Duffy, 1998). Area LIP, located in parietal cortex that receives inputs from MT and MST as well as from a number of regions within the ventral stream, has also been shown to play a role in sensorimotor transformations in preparation for action (Andersen et al., 1990b; Gnadt and Andersen, 1988). There is evidence that LIP neurons play a role in planning saccades to a remembered location (Mazzoni et al., 1996; Platt and Glimcher, 1997; Snyder et al., 1997) and in storing information in both eye-centered (Duhamel et al., 1992) and body-centered coordinates (Snyder et al., 1998). There is also evidence that responses of LIP neurons are modulated by the salience and behavioral significance of visual stimuli (Colby and Goldberg, 1999). Another intriguing feature of LIP neurons is that the spatial representation of a remembered stimulus is dynamic and shifts to the corresponding retinal location around the time of a saccade (Duhamel et al., 1992). Thus, neurons in parietal cortex update the retinal coordinates of remembered stimuli to anticipate the upcoming eye movement. This *remapping*, important for maintaining a continuous representation of the visual world during eye movements, is not unique to LIP,

as it has also been observed in areas V2, V3, and V3A (Nakamura and Colby, 2002).

Area VIP has also been implicated in the encoding of spatial representations. It has prominent connections with MT, MST, and FST but, unlike LIP, it receives little if any input from ventral stream areas (Boussaoud et al., 1990; Colby et al., 1993). Neuronal responses in VIP show selectivity for optic flow (Colby et al., 1993), are often modulated by eye position, and appear to reflect an encoding in head-centered coordinates (Bremmer et al., 1999; Duhamel et al., 1997). Some VIP neurons seem to prefer stimuli that are close to the animal (Colby et al., 1993), and most also respond to tactile stimuli in locations on the head congruent with their visual RFs (Duhamel et al., 1998). This observation has led to the suggestion that VIP neurons are involved in the construction of a multisensory head-centered representation of near-personal space (Duhamel et al., 1998).

Within the dorsal stream, area 7a represents the final stage in the hierarchy. It is interconnected with a wide range of cortical and subcortical regions, thereby providing visual and visuomotor signals important for the execution of visually guided behavior. Its interconnections include a number of areas in parietal (Cavada and Goldman-Rakic, 1989), prefrontal, and IT cortex, as well as the basal ganglia (Neal et al., 1990; Selemon and Goldman-Rakic, 1988). Neurons in area 7a have large, often bilateral RFs (Blatt et al., 1990) and possess properties similar to those encountered at preceding stages in the dorsal stream. For example, many neurons are sensitive to complex visual motion and optic flow (Sakata et al., 1994; Siegel and Read, 1997). Most notably, responses of 7a neurons are modulated by the behavioral relevance of the visual stimuli (Constantinidis and Steinmetz, 2001; Steinmetz et al., 1994). Since the activity of these neurons is largely unaffected by changes in body or head position during saccades to specific retinal locations, it is likely that these cells encode information in world-referenced spatial coordinates (Snyder et al., 1998).

Behavioral effects of dorsal stream lesions

Most of the lesion studies support the notion of specialization of the dorsal stream for processing of stimulus motion. They also suggest that this pathway is important for the integration of motion information to construct a representation of space that can be used in navigation and other motor behaviors.

MT LESIONS AFFECT SMOOTH PURSUIT EYE MOVEMENTS AND SPEED PROCESSING Area MT has become the area of choice for examining the effects of lesions within the dorsal stream, primarily because of its high incidence of directionally selective neurons, its clearly defined borders within the STS, and its precise retinotopy. The first studies involv-

ing lesions of areas MT and MST used ibotenic acid and examined its effects on eye movement responses. Wurtz and his colleagues reported that MT and MST lesions resulted in retinotopically specific deficits in smooth pursuit eye movements (Dursteler and Wurtz, 1988; Dursteler et al., 1987; Newsome et al., 1985). The monkeys had been trained to pursue moving targets but, after MT and MST lesions, were unable to match the speed of their smooth pursuit eye movements to the speed of the target. The animals also had problems adjusting the amplitude of their saccadic eye movements to compensate for target motion, though they had no problems making saccades to stationary targets. As these effects reflected difficulties in matching the velocity of visual targets, without evidence of motor abnormalities, they were interpreted as impaired perception of stimulus velocity. A similar deficit in smooth pursuit eye movements was later reported (Schiller and Lee, 1994). Subsequently, a number of studies examined the effects of MT/MST lesions on speed discriminations more directly by measuring speed difference thresholds. Substantial and largely permanent loss in the accuracy of speed judgments was found (Orban et al., 1995; Pasternak and Merigan, 1994; Schiller and Lee, 1994).

LESIONS OF MT/MST LEAD TO DEFICITS IN COMPLEX MOTION PERCEPTION A number of studies examined the perception of stimulus motion with displays in which coherence thresholds were measured by adjusting the proportion of coherently and randomly moving dots. For example, Newsome and Pare (1988) used such stimuli to measure motion perception in monkeys with localized lesions placed in MT while the monkeys performed a discrimination task. They found severe deficits in motion coherence thresholds when stimuli were placed in the portion of the visual field affected by the lesion. A similar inability to extract coherent motion in the presence of noise was later reported after MT/MST lesions by Pasternak and Merigan (1994). In a subsequent study, Rudolph and Pasternak (1999) found that MT/MST lesions produced deficits not only in coherence thresholds measured with random dots but also in signal-to-noise thresholds measured with drifting gratings masked by noise. This increased susceptibility to noise was specific to the domain of motion perception, as the same monkeys showed no deficit in discriminating the orientation of gratings masked by two-dimensional noise. Interestingly, monkeys with V4 lesions showed the opposite pattern of impairment (Fig. 34.3).

In addition to producing increased susceptibility to noise, MT/MST lesions result in permanent deficits both in the integration of local motion vectors (Pasternak and Merigan, 1994; Rudolph and Pasternak, 1999) and in the ability to remember such stimuli for brief periods of time (Bisley and Pasternak, 2000). MT lesions have also been shown

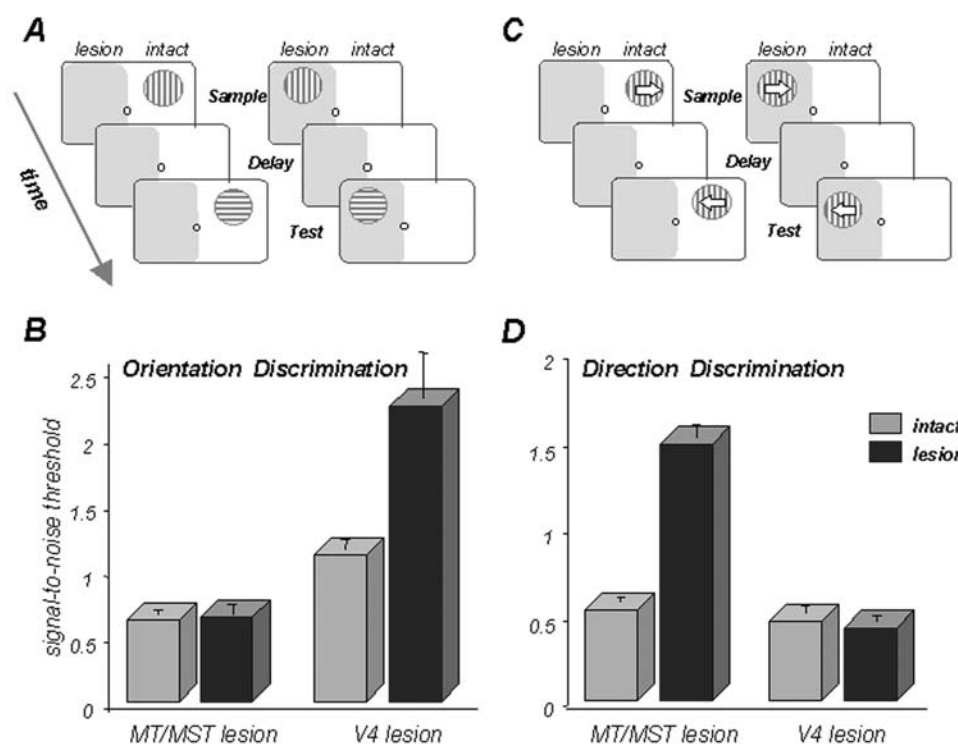


FIGURE 34.3. Effects of V4 and MT/MST lesions on the discrimination of form and motion. *A*, Psychophysical testing procedure for measuring orientation discrimination. The monkeys fixated a small spot for 1 second to initiate the trial. During each trial they viewed sample and test stimuli separated by a 0.2 second delay and indicated whether the orientation of the test was either the same as or different from that of the sample. The orientation of the sample was chosen at random from a set of six and the orientation of the test was the same as or orthogonal to that of the sample. Signal-to-noise thresholds were measured with flickering gratings (1 c/deg, 5 Hz) masked by adding varying amounts of two-dimensional noise in the sample; the test grating was of high contrast and contained no noise. *B*, Effects of a unilateral V4 or MT/MST lesion on orientation discrimination. The performance was measured with stimuli in the intact and affected portions of the visual field. The V4 lesion elevated signal-to-noise thresholds for orientation, while the MT/MST lesion had no significant effect on

performance. *C*, Psychophysical testing procedure for measuring direction discrimination. The task was identical to that described in *A*, except that drifting gratings were used. One of eight possible directions of motion was selected at random as a sample stimulus, and the test stimulus moved either in the same or the opposite direction. Signal-to-noise thresholds were measured by varying the proportion of pixels in the grating that assumed random intensities. *D*, Effect of a unilateral V4 or MT/MST lesion on direction discrimination. The MT/MST lesion elevated signal-to-noise thresholds for discriminating differences in direction. The V4 lesion had no measurable effect on direction discrimination thresholds.

Lesions were made by multiple injections of ibotenic acid. Representative data are shown for a single monkey with a V4 lesion and for another with an MT/MST lesion. (MT/MST lesion data adapted from Rudolph and Pasternak, 1999; V4 lesion data were adapted from Rudolph, 1997.)

to produce modest and largely transient deficits in the detection of motion shear and more severe deficits in the perception of structure from motion (Andersen and Siegel, 1989).

LESIONS OF POSTERIOR PARIETAL CORTEX AFFECT ENCODING OF VISUAL SPACE Neuronal properties in parietal cortex suggest a role in the integration of sensory signals and in constructing a representation of extrapersonal space in preparation for motor action; the few lesion studies performed in nonhuman primates in this region largely confirm this notion. A role of posterior parietal cortex in spatial aspects of task performance was first reported in the mid-1970s (Pohl, 1973; Ratcliff et al., 1977; Ridley and Ettlinger,

1975; for review, see Ungerleider and Mishkin, 1982). Subsequently, Lattin (1986) tested monkeys after bilateral lesions of area 7a and found deficits in the performance of a spatial landmark test. Further evidence for a role of parietal cortex in space coding was reported by Quintana and Fuster (1993), who applied cooling to areas 5 and 7 of the parietal cortex. They found that the monkeys showed decreased speed and accuracy in both reaching and eye movements during the performance of tasks that required the processing and retention of spatial information. More recently, Li et al. (1999) reported deficits in memory-guided saccadic eye movements after reversible inactivation of LIP. They concluded that LIP neurons play a direct role in processing incoming sensory information to program saccadic eye movements.

Inaccuracy in reaching toward visual targets after lesions of areas 7a, 7b, and LIP was observed by Rushworth et al. (1997). Thus, lesions of parietal cortex appear to disrupt the ability of a subject to coordinate movements relative to oneself or relative to other objects located in extrapersonal space (Milner and Goodale, 1996).

Some neurons in both streams integrate information about motion, color, and form

Although processing of the information about color/form and motion/space appears to be segregated and carried largely by segregated pathways, there is evidence of intermixing of properties at various stages of cortical processing.

Evidence of some intermixing and possibly integration of color and motion signals can be found relatively early in the visual cortex. For example, although there is functional segregation of neurons into stripe and interstripe regions in area V2 with respect to color, form, and retinal disparity, this segregation is not complete (Ts'o et al., 2001). It has been reported that the thick stripes, receiving inputs from layer 4B in V1, the magnocellular output layer, also receive inputs from layer 4A, the parvocellular output layer. Furthermore, it is likely that the extensive spread of projections supplied by pyramidal V1 neurons, as well as the horizontal connections between the stripes in V2, may provide an anatomical substrate for interactions between segregated channels in V1 (Levitt et al., 1994b; Malach et al., 1994). Thus, even at the level of V2, there may be intermixing of signals proceeding toward the dorsal and ventral streams, a notion supported by RF properties encountered both within V2 and anterior to it.

While some connections of area V3, the next stage of cortical processing, suggest an association with the dorsal stream, it is also strongly interconnected with V4, a major component of the ventral stream (Beck and Kaas, 1999). Because of this pattern of connectivity, V3 is in a good position to serve as a site where the integration of various visual signals can occur. Indeed, the high incidence of directional selectivity of V3 neurons and their preference for lower spatial and higher temporal frequencies (Gegenfurtner et al., 1997) suggest a role in processing motion information. Yet, the majority of V3 neurons are also orientation selective, and nearly half of all neurons in this area show selectivity for color (Burkhalter et al., 1986). It is interesting that many of the neurons responding to color also show directional selectivity, and a substantial number show directional selectivity to isoluminant gratings. This interaction between color and motion suggests that area V3 may represent a stage in the analysis of the visual scene where interactions between the two streams take place.

Some interactions between the processing of color and motion have also been observed in area MT, an area strongly

influenced by the magnocellular pathway (Maunsell et al., 1990), which itself does not appear to carry color-opponent signals. Thus, many MT neurons maintain significant responses to motion of isoluminant stimuli (Gegenfurtner et al., 1994; Seidemann et al., 1999; Thiele et al., 2001), and the presence of chromatic information has been shown to increase neuronal direction discrimination (Croner and Albright, 1999). While chromatic signals reaching MT are much weaker than the luminance signals, the activity of MT neurons to isoluminant gratings appears to be sufficient to explain the performance of monkeys in a color-based motion discrimination task (Thiele et al., 2001).

An area likely to represent a region of convergence and integration of form and motion information is STP, which receives inputs from both processing streams (Baizer et al., 1991; Boussaoud et al., 1990; Oram and Perrett, 1996). It is a multimodal area, containing neurons that respond to somatosensory and auditory as well as visual stimuli (Bruce et al., 1981). STP neurons have large, gaze-centered RFs and show selectivity to visual motion similar to that observed in areas MT and MST (Anderson and Siegel, 1999; Oram et al., 1993). Some neurons also respond particularly well to biological motion, that is, motion patterns consistent with what one sees when one observes the gait of another animal (Oram and Perrett, 1996; Perrett et al., 1985b). For example, these cells respond when viewing a monkey or human walking, or to equivalent motion patterns generated by so-called Johanssen point-light stimuli (stimuli generated by attaching lights to the joints of a moving animal which is otherwise in the dark). These observations have led to the idea that the primate temporal lobe has evolved specialized mechanisms for the encoding and recognition of biologically significant stimuli (Fig. 34.4).

Finally, it should be noted that properties of neurons within each stream have been shown to respond to the demands of the behavioral task, and features normally not associated with a given area may emerge if they are behaviorally relevant. An interesting example of this phenomenon has been provided by Ferrera et al. (1994), who demonstrated that the activity of neurons in area V4, which rarely show directionally selective responses, was strongly modulated by the direction of a behaviorally significant motion stimulus. This observation illustrates the dynamic nature of processing by the two visual streams; under some circumstances, each stream may contribute to the processing usually associated with the other.

Beyond visual processing streams

In order to execute visually guided behaviors successfully, the information carried by the two streams needs to be integrated. While some aspects of this integration appear to take place within each stream, the integration is only partial at

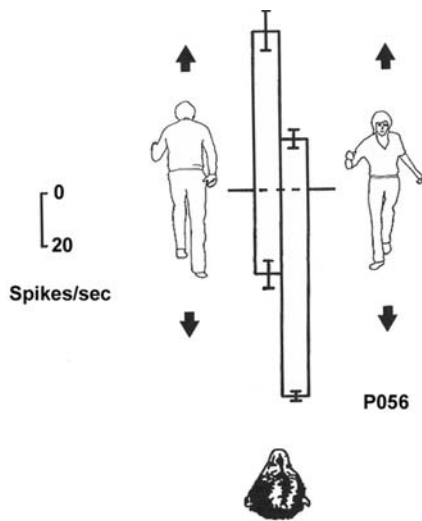


FIGURE 34.4. Sensitivity to walking forward in area STP. The mean and standard error of responses (spikes/sec) to different views of the body when approaching and retreating from the monkey are shown for cell P056. The cell responded most to the body moving in a direction compatible with its orientation (i.e., in the direction it was facing). The cell responded significantly more to the front view than to the back view of the body when it moved toward the monkey ($p < .01$). The response to the back view was greater than that to the front view, however, when it moved away from the monkey ($p < .01$). (From Perrett et al., 1985b.)

best. The question arises: how and where is such integration accomplished? While this question is still the topic of active investigation, there is accumulating evidence that the answer may lie in areas located outside of the visual system, as traditionally defined.

It is well established that both processing streams, dorsal and ventral, have reciprocal connections with regions beyond the modality-specific visual system. One such set of connections includes those with the prefrontal cortex. Anatomical studies have shown that projections from areas in the dorsal stream terminate mainly in and around the principal sulcus, in Brodmann area (BA) 46 of dorsolateral prefrontal cortex (Barbas and Mesulam, 1985; Cavada and Goldman-Rakic, 1989; Ungerleider and Desimone, 1986), whereas projections from areas in the ventral stream terminate mainly on the inferior convexity, in BA 12 and 45 of ventrolateral prefrontal cortex (Chavis and Pandya, 1976; Ungerleider et al., 1989; Webster et al., 1994). Thus, from an anatomical point of view, the domain specificity of spatial versus object vision that is present in the posterior processing areas of the monkey brain appears to extend forward into the prefrontal cortex. These separate prefrontal regions are thought to play an important role in working memory, that is, briefly keeping in mind an object and its location, respectively, after it is no longer visible (Fuster, 1990; Goldman-Rakic, 1990).

Although the inputs to prefrontal cortex from the two streams are anatomically segregated and there is physiological evidence of neuronal specialization for the modality arriving from each stream (Sakagami et al., 2001; Scialdhe et al., 1999; Wilson et al., 1993), regional intermixing of prefrontal neurons active during execution of working memory tasks for objects and spatial locations has been reported (Fuster et al., 1982). Furthermore, recent studies have documented the existence of individual prefrontal neurons that process information about both an object's identity and its location (Rainer et al., 1998; Rao et al., 1997), thus integrating the information arriving from the two streams.

Conclusions: ventral and dorsal processing streams in the human brain

The differential visual impairments produced by focal lesions in clinical cases suggest that human visual cortex, like that of the monkey, contains two anatomically distinct and functionally specialized pathways corresponding to the ventral and dorsal streams (Damasio and Damasio, 1979; Damasio et al., 1982; Newcombe and Russell, 1969; Newcombe et al., 1987; Ratcliff and Davies-Jones, 1972; Ratcliff and Newcombe, 1973; Zihl et al., 1983). The clinical syndromes produced by occipitotemporal lesions include visual object agnosia, as well as prosopagnosia, an inability to recognize familiar faces, and achromatopsia, or cortical color blindness. By contrast, syndromes produced by occipitoparietal lesions include optic ataxia (misreaching), hemispatial neglect, constructional apraxia, gaze apraxia, and akinetopsia (inability to perceive movement).

The advent of functional brain imaging, both positron emission tomography (PET) and functional magnetic resonance imaging (fMRI), has made it possible to map the organization of the human visual cortex with far greater precision than is possible with human lesion studies and without the confounding influence of compensatory responses to brain injury (e.g., see Ungerleider and Haxby, 1994). In experiments by Haxby and colleagues designed to investigate the possible existence of separate object vision and spatial vision pathways in humans, changes in regional cerebral blood flow were measured using PET while subjects performed object identity and spatial location matching-to-sample tasks (Haxby et al., 1994). In the object identity task, the subjects indicated on each trial which of two choice faces matched the sample face, whereas in the spatial location task, the subjects indicated which of two choice stimuli contained a small square in the same location, relative to a double line, as the small square in the sample stimulus (Fig. 34.5). The faces for the object identity task were contained within the small squares, so that identical stimuli were used for face and location matching, with only the task requirements changing. The results identified occip-

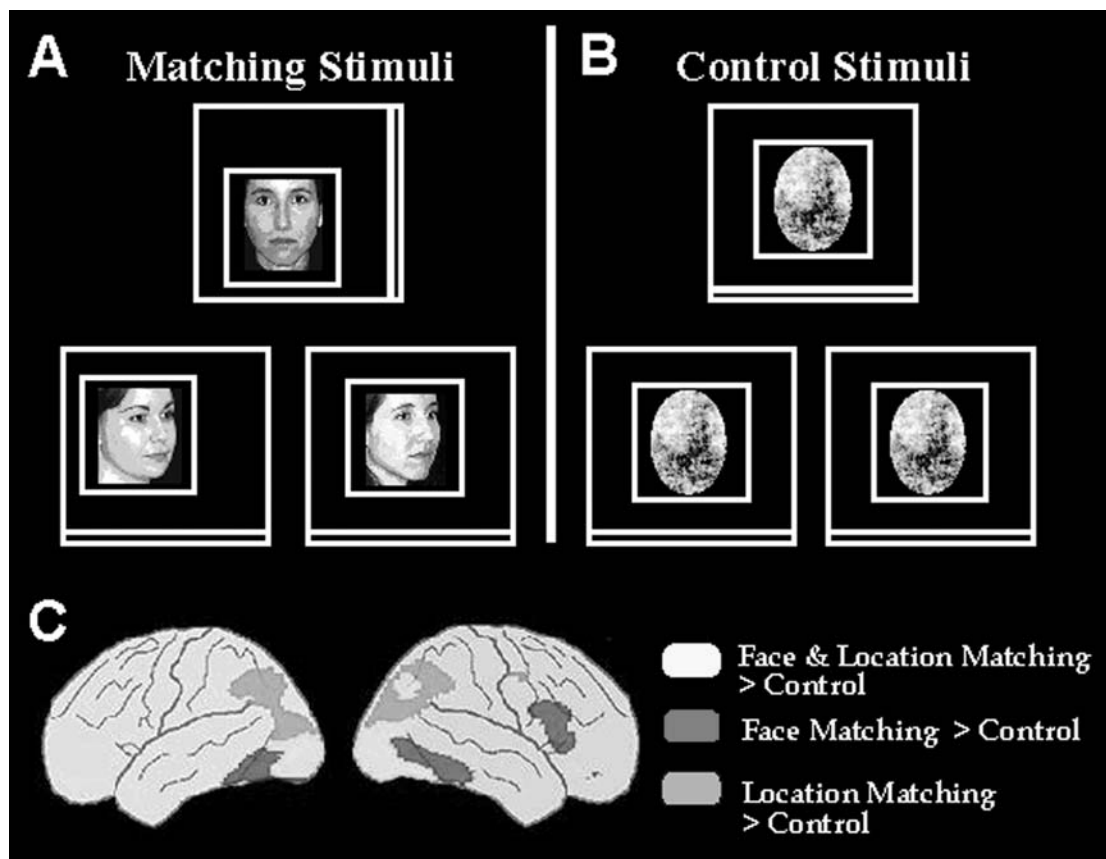


FIGURE 34.5. Two cortical processing streams in human visual cortex, as demonstrated in a PET imaging study of face and location perception. *A*, Sample experimental stimuli used for both face- and location-matching tasks. During face-matching trials, subjects had to indicate with a button press which of the two faces at the bottom was the same person shown at the top. In this example, the correct choice is the stimulus on the right. During location-matching trials, subjects had to indicate with a button press which of the two small squares at the bottom was in the same location relative to the double line as the small square shown at the top. In this example, the correct choice is the stimulus on the left. *B*, Sample control stimuli used during the experiment. During control

trials, subjects saw an array of three stimuli in which the small squares contained a complex visual image. On these trials, which controlled for both visual stimulation and finger movements, they alternated left and right button presses. *C*, Areas shown in red had significantly increased activity during the face-matching but not during the location-matching task compared with activity during the control task. Areas shown in green had significantly increased activity during the location-matching but not during the face-matching task compared with activity during the control task. Areas shown in yellow had significantly increased activity during both face- and location-matching tasks. (Adapted from Haxby et al., 1994.) (See color plate 19.)

itotemporal and occipitoparietal regions associated with face and location matching, respectively, and posterior occipital regions associated with both visual functions. In addition, regions in ventral and dorsal frontal cortex were selectively activated by face and location matching, respectively. These findings thus indicate the existence in humans, as in monkeys, of two functionally specialized and anatomically segregated visual processing streams, both of which receive their inputs from early visual areas. The findings further suggest the extensions of each into the frontal lobe, which plays a role in working memory for objects and their spatial locations.

At a finer level of analysis, functional imaging studies have begun to reveal the individual processing areas within the two streams, and many of these areas appear to be homol-

ogous to monkey visual areas, including V1, V2, V3, V3A, V4, MT, and LIP (De Yoe et al., 1994; Reppas et al., 1995; Sereno et al., 1995, 2001; Shipp et al., 1995; Tootell et al., 1997). On the other hand, it has been discovered that human visual cortex also contains regions specialized for the processing of visual letters and word forms (Nobre et al., 1994; Petersen et al., 1990). These regions could not have evolved for the purpose of reading but instead must have developed in the course of learning to read. These regions thus appear to be similar to those in the temporal cortex of monkeys in which familiarity over long periods of time, leading to expertise, alters the responses of TE neurons (Kobatake et al., 1998). Such findings in humans and monkeys highlight one challenge for future research: to understand how visual experience tunes neuronal selectivities.

REFERENCES

- Albright, T. D., 1984. Direction and orientation selectivity of neurons in visual area MT of the macaque, *J. Neurophysiol.*, 52:1106–1130.
- Albright, T. D., R. Desimone, and C. G. Gross, 1984. Columnar organization of directionally selective cells in visual area MT of the macaque, *J. Neurophysiol.*, 51:16–31.
- Allman, J., F. Miezin, and E. McGuinness, 1985a. Direction- and velocity-specific responses from beyond the classical receptive field in the middle temporal visual area (MT), *Perception*, 14:105–126.
- Allman, J., F. Miezin, and E. McGuinness, 1985b. Stimulus specific responses from beyond the classical receptive field: neurophysiological mechanisms for local-global comparisons in visual neurons, *Annu. Rev. Neurosci.*, 8:407–430.
- Andersen, R. A., 1997. Multimodal integration for the representation of space in the posterior parietal cortex, *Philos. Trans. R. Soc. Lond. B. Biol. Sci.*, 352:1421–1428.
- Andersen, R. A., C. Asanuma, G. Essick, and R. M. Siegel, 1990b. Corticocortical connections of anatomically and physiologically defined subdivisions within the inferior parietal lobule, *J. Comp. Neurol.*, 296:65–113.
- Andersen, R. A., K. V. Shenoy, L. H. Snyder, D. C. Bradley, and J. A. Crowell, 1999. The contributions of vestibular signals to the representations of space in the posterior parietal cortex, *Ann. N. Y. Acad. Sci.*, 871:282–292.
- Andersen, R. A., and R. M. Siegel, 1989. Motion processing in primate cortex, in *Signal and Sense: Local and Global Order in Perceptual Maps* (G. M. Edelman, W. E. Gall, and W. M. Cowan, eds.), New York: Wiley, pp. 163–184.
- Andersen, R. A., R. J. Snowden, S. Treue, and M. Graziano, 1990a. Hierarchical processing of motion in the visual cortex of monkey, *Cold Spring Harb. Symp. Quant. Biol.*, 55:741–748.
- Anderson, K. C., and R. M. Siegel, 1999. Optic flow selectivity in the anterior superior temporal polysensory area, STPa, of the behaving monkey, *J. Neurosci.*, 19:2681–2692.
- Baizer, J. S., R. Desimone, and L. G. Ungerleider, 1993. Comparison of subcortical connections of inferior temporal and posterior parietal cortex in monkeys, *Vis. Neurosci.*, 10:59–72.
- Baizer, J. S., D. L. Robinson, and B. M. Dow, 1977. Visual responses of area 18 neurons in awake, behaving monkey, *J. Neurophysiol.*, 40:1024–1037.
- Baizer, J. S., L. G. Ungerleider, and R. Desimone, 1991. Organization of visual inputs to the inferior temporal and posterior parietal cortex in macaques, *J. Neurosci.*, 11:168–190.
- Barbas, H., and M. M. Mesulam, 1985. Cortical afferent input to the principalis region of the rhesus monkey, *Neuroscience*, 15:619–637.
- Bashinski, H. S., and V. R. Bacharach, 1980. Enhancement of perceptual sensitivity as the result of selectively attending to spatial locations, *Percept. Psychophys.*, 28:241–248.
- Baylis, G. C., E. T. Rolls, and C. M. Leonard, 1985. Selectivity between faces in the responses of a population of neurons in the cortex in the superior temporal sulcus of the monkey, *Brain Res.*, 342:91–102.
- Beck, P. D., and J. H. Kaas, 1999. Cortical connections of the dorsomedial visual area in old world macaque monkeys, *J. Comp. Neurol.*, 406:487–502.
- Benevento, L., and B. Davis, 1977. Topographical projections of the prestriate cortex to the pulvinar nuclei in the macaque monkey: an autoradiographic study, *Exp. Brain Res.*, 30:405–424.
- Benevento, L. A., and M. Rezak, 1976. The cortical projections of the inferior pulvinar and adjacent lateral pulvinar in the rhesus monkey (*Macaca mulatta*): an autoradiographic study, *Brain Res.*, 108:1–24.
- Bisley, J. W., and T. Pasternak, 2000. The multiple roles of visual cortical areas MT/MST in remembering the direction of visual motion, *Cereb. Cortex*, 10:1053–1065.
- Blatt, G. J., R. A. Andersen, and G. R. Stoner, 1990. Visual receptive field organization and cortico-cortical connections of the lateral intraparietal area (area LIP) in the macaque, *J. Comp. Neurol.*, 299:421–445.
- Boussaoud, D., R. Desimone, and L. G. Ungerleider, 1992. Subcortical connections of visual areas MST and FST in macaques, *Vis. Neurosci.*, 9:291–302.
- Boussaoud, D., L. G. Ungerleider, and R. Desimone, 1990. Pathways for motion analysis: cortical connections of the medial superior temporal and fundus of the superior temporal visual areas in the macaque, *J. Comp. Neurol.*, 296:462–495.
- Bradley, D. C., G. C. Chang, and R. A. Andersen, 1998. Encoding of three-dimensional structure-from-motion by primate area MT neurons, *Nature*, 392:714–717.
- Bradley, D. C., N. Qian, and R. A. Andersen, 1995. Integration of motion and stereopsis in middle temporal cortical area of macaques, *Nature*, 373:609–611.
- Braun, J., 1994. Visual search among items of different salience—removal of visual attention mimics a lesion in extrastriate area V4, *J. Neurosci.*, 14:554–567.
- Bremmer, F., W. Graf, S. Ben Hamed, and J. R. Duhamel, 1999. Eye position encoding in the macaque ventral intraparietal area (VIP), *Neuroreport*, 10:873–878.
- Britten, K. H., W. T. Newsome, and R. C. Saunders, 1992. Effects of inferotemporal cortex lesions on form-from-motion discrimination in monkeys, *Exp. Brain Res.*, 88:292–302.
- Britten, K. H., M. N. Shadlen, W. T. Newsome, and J. A. Movshon, 1993. Responses of neurons in macaque MT to stochastic motion signals, *Vis. Neurosci.*, 10:1157–1169.
- Britten, K. H., and R. J. Van Wezel, 1998. Electrical microstimulation of cortical area MST biases heading perception in monkeys, *Nat. Neurosci.*, 1:59–63.
- Brodman, K., 1909. *Vergleichende Lokalisationslehre der Grosshirnrinde*, Leipzig: Barth.
- Brown, M. W., F. A. Wilson, and I. P. Riches, 1987. Neuronal evidence that inferomedial temporal cortex is more important than hippocampus in certain processes underlying recognition memory, *Brain Res.*, 409:158–162.
- Bruce, C., R. Desimone, and C. G. Gross, 1981. Visual properties of neurons in a polysensory area in superior temporal sulcus of the macaque, *J. Neurophysiol.*, 46:369–384.
- Bulthoff, H. H., S. Y. Edelman, and M. J. Tarr, 1995. How are three-dimensional objects represented in the brain? *Cereb. Cortex*, 5:247–260.
- Buracas, G. T., and T. D. Albright, 1996. Contribution of area MT to perception of three-dimensional shape: a computational study, *Vis. Res.*, 36:869–887.
- Burkhalter, A., D. J. Felleman, W. T. Newsome, and D. C. Van Essen, 1986. Anatomical and physiological asymmetries related to visual areas V3 and VP in macaque extrastriate cortex, *Vis. Res.*, 26:63–80.
- Burkhalter, A., and D. C. Van Essen, 1986. Processing of color, form and disparity information in visual areas VP and V2 of ventral extrastriate cortex in the macaque monkey, *J. Neurosci.*, 6:2327–2351.

- Cavada, C., and P. S. Goldman-Rakic, 1989. Posterior parietal cortex in rhesus monkey: II. Evidence for segregated corticocortical networks linking sensory and limbic areas with the frontal lobe, *J. Comp. Neurol.*, 287:422–445.
- Chavis, D. A., and D. N. Pandya, 1976. Further observations on corticofrontal connections in the rhesus monkey, *Brain Res.*, 117:369–386.
- Chelazzi, L., J. Duncan, E. K. Miller, and R. Desimone, 1998. Responses of neurons in inferior temporal cortex during memory-guided visual search, *J. Neurophysiol.*, 80:2918–2940.
- Cheng, K., T. Hasegawa, K. S. Saleem, and K. Tanaka, 1994. Comparison of neuronal selectivity for stimulus speed, length, and contrast in the prestriate visual cortical areas V4 and MT of the macaque monkey, *J. Neurophysiol.*, 71:2269–2280.
- Colby, C. L., J. R. Duhamel, and M. E. Goldberg, 1993. Ventral intraparietal area of the macaque: anatomic location and visual response properties, *J. Neurophysiol.*, 69:902–914.
- Colby, C. L., R. Gattass, C. R. Olson, and C. G. Gross, 1988. Topographical organization of cortical afferents to extrastriate visual area PO in the macaque: a dual tracer study, *J. Comp. Neurol.*, 269:392–413.
- Colby, C. L., and M. E. Goldberg, 1999. Space and attention in parietal cortex, *Annu. Rev. Neurosci.*, 22:319–349.
- Connor, C. E., D. C. Preddie, J. L. Gallant, and D. C. Van Essen, 1997. Spatial attention effects in macaque area V4, *J. Neurosci.*, 17:3201–3214.
- Constantinidis, C., and M. A. Steinmetz, 2001. Neuronal responses in area 7a to multiple stimulus displays: II. Responses are suppressed at the cued location, *Cereb. Cortex*, 11:592–597.
- Croner, L. J., and T. D. Albright, 1999. Segmentation by color influences responses of motion-sensitive neurons in the cortical middle temporal visual area, *J. Neurosci.*, 19:3935–3951.
- Cumming, B. G., and G. C. DeAngelis, 2001. The physiology of stereopsis, *Annu. Rev. Neurosci.*, 24:203–238.
- Cumming, B. G., and A. J. Parker, 1999. Binocular neurons in V1 of awake monkeys are selective for absolute, not relative, disparity, *J. Neurosci.*, 19:5602–5618.
- Damasio, H., and A. R. Damasio, 1979. “Paradoxical” ear extinction in dichotic listening: possible anatomic significance, *Neurology*, 29:644–653.
- Damasio, A. R., H. Damasio, and G. W. Van Hoesen, 1982. Prosopagnosia: anatomic basis and behavioral mechanisms, *Neurology*, 32:331–341.
- De Weerd, P., R. Desimone, and L. G. Ungerleider, 1996. Cue-dependent deficits in grating orientation discrimination after V4 lesions in macaques, *Vis. Neurosci.*, 13:529–538.
- De Weerd, P., M. R. Peralta 3rd, R. Desimone, and L. G. Ungerleider, 1999. Loss of attentional stimulus selection after extrastriate cortical lesions in macaques, *Nat. Neurosci.*, 2:753–758.
- De Yoe, E. A., P. Bandettini, J. Neitz, D. Miller, and P. Winans, 1994. Functional magnetic resonance imaging (fMRI) of the human brain, *J. Neurosci. Methods*, 54:171–187.
- De Yoe, E. A., S. Hockfield, H. Garren, and D. C. Van Essen, 1990. Antibody labeling of functional subdivisions in visual cortex: cat-301 immunoreactivity in striate and extrastriate cortex of the macaque monkey, *Vis. Neurosci.*, 5:67–81.
- De Yoe, E. A., and D. C. Van Essen, 1985. Segregation of efferent connections and receptive field properties in visual area V2 of the macaque, *Nature*, 317:58–61.
- Dean, P., 1976. Effects of inferotemporal lesions on the behavior of monkeys, *Psychol. Bull.*, 83:41–71.
- Dean, P., 1978. Visual cortex ablation and thresholds for successively presented stimuli in rhesus monkeys: I. Orientation, *Exp. Brain Res.*, 32:445–458.
- Dean, P., 1979. Visual cortex ablation and thresholds for successively presented stimuli in rhesus monkeys: II. Hue, *Exp. Brain Res.*, 35:69–83.
- Dean, P., 1982. Analysis of visual behavior in monkeys with inferotemporal lesions, in *Analysis of Visual Behavior* (D. J. Ingle, M. A. Goodale, and R. J. W. Mansfield, eds.), Cambridge: MIT Press, pp. 587–628.
- DeAngelis, G. C., B. G. Cumming, and W. T. Newsome, 1998. Cortical area MT and the perception of stereoscopic depth, *Nature*, 394:677–680.
- DeAngelis, G. C., and W. T. Newsome, 1999. Organization of disparity-selective neurons in macaque area MT, *J. Neurosci.*, 19:1398–1415.
- Desimone, R., 1991. Face selective cells in the temporal cortex of monkey, *J. Cogn. Neurosci.*, 3:1–8.
- Desimone, R., 1996. Neural mechanisms for visual memory and their role in attention, *Proc. Natl. Acad. Sci. USA*, 93:13494–13499.
- Desimone, R., 1998. Visual attention mediated by biased competition in extrastriate visual cortex, *Philos. Trans. R. Soc. Lond. B. Biol. Sci.*, 353:1245–1255.
- Desimone, R., T. D. Albright, C. G. Gross, and C. Bruce, 1984. Stimulus-selective properties of inferior temporal neurons in the macaque, *J. Neurosci.*, 4:2051–2062.
- Desimone, R., and J. Duncan, 1995. Neural mechanisms of selective attention, *Annu. Rev. Neurosci.*, 18:193–222.
- Desimone, R., J. Fleming, and C. G. Gross, 1980. Prestriate afferents to inferior temporal cortex: an HRP study, *Brain Res.*, 184:41–55.
- Desimone, R., and C. G. Gross, 1979. Visual areas in the temporal cortex of the macaque, *Brain Res.*, 178:363–380.
- Desimone, R., and S. J. Schein, 1987. Visual properties of neurons in area V4 of the macaque: sensitivity to stimulus form, *J. Neurophysiol.*, 57:835–868.
- Desimone, R., S. J. Schein, J. Moran, and L. G. Ungerleider, 1985. Contour, color and shape analysis beyond the striate cortex, *Vis. Res.*, 25:441–452.
- Desimone, R., and L. G. Ungerleider, 1986. Multiple visual areas in the caudal superior temporal sulcus of the macaque, *J. Comp. Neurol.*, 248:164–189.
- Desimone, R., and L. G. Ungerleider, 1989. Neural mechanisms of visual perception in monkeys, in *Handbook of Neuropsychology*, vol. 2 (F. B. A. J. Grafman, ed.), Amsterdam: Elsevier, pp. 267–299.
- Distler, C., D. Boussaoud, R. Desimone, and L. G. Ungerleider, 1993. Cortical connections of inferior temporal area TEO in macaque monkeys, *J. Comp. Neurol.*, 334:125–150.
- Dobkins, K. R., and T. D. Albright, 1994. What happens if it changes color when it moves?: the nature of chromatic input to macaque visual area MT, *J. Neurosci.*, 14:4854–4870.
- Dodd, J. V., K. Krug, B. G. Cumming, and A. J. Parker, 2001. Perceptually bistable three-dimensional figures evoke high choice probabilities in cortical area MT, *J. Neurosci.*, 21:4809–4821.
- Duffy, C. J., 1998. MST neurons respond to optic flow and translational movement, *J. Neurophysiol.*, 80:1816–1827.
- Duhamel, J. R., F. Bremmer, S. Benhamed, and W. Graf, 1997. Spatial invariance of visual receptive fields in parietal cortex neurons, *Nature*, 389:845–848.
- Duhamel, J. R., C. L. Colby, and M. E. Goldberg, 1992. The updating of the representation of visual space in parietal cortex by intended eye movements, *Science*, 255:90–92.

- Duhamel, J. R., C. L. Colby, and M. E. Goldberg, 1998. Ventral intraparietal area of the macaque: congruent visual and somatic response properties, *J. Neurophysiol.*, 79:126–136.
- Dursteler, M. R., and R. H. Wurtz, 1988. Pursuit and optokinetic deficits following chemical lesions of cortical areas MT and MST, *J. Neurophysiol.*, 60:940–965.
- Dursteler, M. R., R. H. Wurtz, and W. T. Newsome, 1987. Directional pursuit deficits following lesions of the foveal representation within the superior temporal sulcus of the macaque monkey, *J. Neurophysiol.*, 57:1262–1287.
- Eifuku, S., and R. H. Wurtz, 1998. Response to motion in extrastriate area MSTl: center-surround interactions, *J. Neurophysiol.*, 80:282–296.
- Erickson, C. A., B. Jagadeesh, and R. Desimone, 2000. Clustering of perirhinal neurons with similar properties following visual experience in adult monkeys, *Nat. Neurosci.*, 3:1143–1148.
- Felleman, D. J., A. Burkhalter, and D. C. Van Essen, 1997. Cortical connections of areas V3 and VP of macaque monkey extrastriate visual cortex, *J. Comp. Neurol.*, 379:21–47.
- Felleman, D. J., and D. C. Van Essen, 1987. Receptive field properties of neurons in area V3 of macaque monkey extrastriate cortex, *J. Neurophysiol.*, 57:889–920.
- Felleman, D. J., and D. C. Van Essen, 1991. Distributed hierarchical processing in the primate cerebral cortex, *Cereb. Cortex*, 1:1–47.
- Ferrera, V. P., K. K. Rudolph, and J. H. Maunsell, 1994. Responses of neurons in the parietal and temporal visual pathways during a motion task, *J. Neurosci.*, 14:6171–6186.
- Fischer, B., and R. Boch, 1981. Selection of visual targets activates prelunate cortical cells in trained rhesus monkey, *Exp. Brain Res.*, 41:431–433.
- Fuster, J. M., 1990. Behavioral electrophysiology of the prefrontal cortex of the primate, *Prog. Brain Res.*, 85:313–323.
- Fuster, J. M., 1995. *Memory in the Cerebral Cortex*, Cambridge: MIT Press.
- Fuster, J. M., R. H. Bauer, and J. P. Jervey, 1982. Cellular discharge in the dorsolateral prefrontal cortex of the monkey in cognitive tasks, *Exp. Neurol.*, 77:679–694.
- Fuster, J. M., and J. P. Jervey, 1981. Inferotemporal neurons distinguish and retain behaviorally relevant features of visual stimuli, *Science*, 212:952–955.
- Gaffan, E. A., S. Harrison, and D. Gaffan, 1986. Single and concurrent discrimination learning by monkeys after lesions of inferotemporal cortex, *Q. J. Exp. Psychol. B.*, 38:31–51.
- Gallant, J. L., C. E. Connor, S. Rakshit, J. W. Lewis, and D. C. Van Essen, 1996. Neural responses to polar, hyperbolic, and Cartesian gratings in area V4 of the macaque monkey, *J. Neurophysiol.*, 76:2718–2739.
- Gattass, R., C. G. Gross, and J. H. Sandell, 1981. Visual topography of V2 in the macaque, *J. Comp. Neurol.*, 201:519–539.
- Gattass, R., A. P. B. Sousa, and C. G. Gross, 1988. Visuotopic organization and extent of V3 and V4 of the macaque, *J. Neurosci.*, 8:1831–1845.
- Gattass, R., A. P. B. Sousa, M. Mishkin, and L. G. Ungerleider, 1997. Cortical projections of area V2 in the macaque, *Cereb. Cortex*, 7:110–129.
- Gatter, K. C., and T. P. Powell, 1977. The projection of the locus coeruleus upon the neocortex in the macaque monkey, *Neuroscience*, 2:441–445.
- Gegenfurtner, K. R., D. C. Kiper, J. M. Beusmans, M. Carandini, Q. Zaidi, and J. A. Movshon, 1994. Chromatic properties of neurons in macaque MT, *Vis. Neurosci.*, 11:455–466.
- Gegenfurtner, K. R., D. C. Kiper, and J. B. Levitt, 1997. Functional properties of neurons in macaque area V3, *J. Neurophysiol.*, 77:1906–1923.
- Gnadt, J. W., and R. A. Andersen, 1988. Memory related motor planning activity in posterior parietal cortex of macaque, *Exp. Brain Res.*, 70:216–220.
- Goldman-Rakic, P., 1990. Cellular and circuit basis of working memory in prefrontal cortex of nonhuman primates, in *Progress in Brain Research* (H. B. M. Ylings, C. Eden, J. Bruin, M. Corner, and M. Feenstra, eds.), Amsterdam: Elsevier, pp. 325–336.
- Gross, C. G., and M. Mishkin, 1977. The neural basis of stimulus equivalence across retinal translation, in *Lateralization in the Nervous System* (S. Harnad, R. Doty, J. Jaynes, L. Goldstein, and G. Krauthamer, eds.), New York: Academic Press, pp. 109–122.
- Gross, C. G., C. E. Rocha-Miranda, and D. B. Bender, 1972. Visual properties of neurons in inferotemporal cortex of the macaque, *J. Neurophysiol.*, 35:96–111.
- Hawken, M. J., A. J. Parker, and J. S. Lund, 1988. Laminar organization and contrast sensitivity of direction-selective cells in the striate cortex of the Old World monkey, *J. Neurosci.*, 8:3541–3548.
- Haxby, J. V., B. Horwitz, L. G. Ungerleider, J. M. Maisog, P. Pietrini, and C. L. Grady, 1994. The functional organization of human extrastriate cortex: a PET-rCBF study of selective attention to faces and locations, *J. Neurosci.*, 14:6336–6353.
- Heywood, C. A., and A. Cowey, 1992. The role of the “face-cell” area in the discrimination and recognition of faces by monkeys, *Philos. Trans. R. Soc. Lond. B. Biol. Sci.*, 335:31–37.
- Heywood, C. A., A. Gadotti, and A. Cowey, 1992. Cortical area V4 and its role in the perception of color, *J. Neurosci.*, 12:4056–4065.
- Heywood, C. A., D. Gaffan, and A. Cowey, 1995. Cerebral achromatopsia in monkeys, *Eur. J. Neurosci.*, 7:1064–1073.
- Hikosaka, K., 1999. Tolerances of responses to visual patterns in neurons of the posterior inferotemporal cortex in the macaque against changing stimulus size and orientation, and deleting patterns, *Behav. Brain Res.*, 100:67–76.
- Hinkle, D. A., and C. E. Connor, 2001. Disparity tuning in macaque area V4, *Neuroreport*, 12:365–369.
- Hubel, D. H., and M. S. Livingstone, 1985. Complex-unoriented cells in a subregion of primate area 18, *Nature*, 315:325–327.
- Hubel, D. H., and M. S. Livingstone, 1987. Segregation of form, color, and stereopsis in primate area 18, *J. Neurosci.*, 7:3378–3415.
- Hubel, D. H., and T. N. Wiesel, 1968. Receptive fields and functional architecture of monkey striate cortex, *J. Physiol.*, 195:215–243.
- Hubel, D. H., and T. N. Wiesel, 1977. Ferrier lecture. Functional architecture of macaque monkey visual cortex, *Proc. R. Soc. Lond. B. Biol. Sci.*, 198:1–59.
- Humphrey, N. K., and L. Weiskrantz, 1969. Size constancy in monkeys with inferotemporal lesions, *Q. J. Exp. Psychol.*, 21:225–238.
- Huxlin, K. R., R. C. Saunders, D. Marchionini, H. A. Pham, and W. H. Merigan, 2000. Perceptual deficits after lesions of inferotemporal cortex in macaques, *Cereb. Cortex*, 10:671–683.
- Ito, M., and C. D. Gilbert, 1999. Attention modulates contextual influences in the primary visual cortex of alert monkeys, *Neuron*, 22:593–604.
- Ito, M., H. Tamura, I. Fujita, and K. Tanaka, 1995. Size and position invariance of neuronal responses in monkey inferotemporal cortex, *J. Neurophysiol.*, 73:218–226.

- Janssen, P., R. Vogels, and G. A. Orban, 2000. Three-dimensional shape coding in inferior temporal cortex, *Neuron*, 27:385–397.
- Kastner, S., and L. G. Ungerleider, 2000. Mechanisms of attention in the human cortex, *Annu. Rev. Neurosci.*, 23:315–341.
- Kemp, J. M., and T. P. Powell, 1970. The cortico-striate projection in the monkey, *Brain*, 93:525–546.
- Kobatake, E., G. Wang, and K. Tanaka, 1998. Effects of shape-discrimination training on the selectivity of inferotemporal cells in adult monkeys, *J. Neurophysiol.*, 80:324–330.
- Komatsu, H., and R. H. Wurtz, 1988. Relation of cortical areas MT and MST to pursuit eye movements. I. Localization and visual properties of neurons, *J. Neurophysiol.*, 60:580–603.
- Lappe, M., F. Bremmer, M. Pökel, A. Thiele, and K. P. Hoffmann, 1996. Optic flow processing in monkey STS: a theoretical and experimental approach, *J. Neurosci.*, 16:6265–6285.
- Latto, R., 1986. The role of inferior parietal cortex and the frontal eye-fields in visuospatial discriminations in the macaque monkey, *Behav. Brain Res.*, 22:41–52.
- Levitt, J. B., D. C. Kiper, and J. A. Movshon, 1994a. Receptive fields and functional architecture of macaque V2, *J. Neurophysiol.*, 71:2517–2542.
- Levitt, J. B., T. Yoshioka, and J. S. Lund, 1994b. Intrinsic cortical connections in macaque visual area V2: evidence for interaction between different functional streams, *J. Comp. Neurol.*, 342:551–570.
- Li, C. S., P. Mazzoni, and R. A. Andersen, 1999. Effect of reversible inactivation of macaque lateral intraparietal area on visual and memory saccades, *J. Neurophysiol.*, 81:1827–1838.
- Livingstone, M. S., and D. H. Hubel, 1983. Specificity of cortico-cortical connections in monkey visual system, *Nature*, 304:531–534.
- Livingstone, M. S., and D. H. Hubel, 1984. Anatomy and physiology of a color system in the primate visual cortex, *J. Neurosci.*, 4:309–356.
- Livingstone, M. S., and D. H. Hubel, 1987. Psychophysical evidence for separate channels for the perception of form, color, movement, and depth, *J. Neurosci.*, 7:3416–3468.
- Logothetis, N. K., J. Pauls, and T. Poggio, 1995. Shape representation in the inferior temporal cortex of monkeys, *Curr. Biol.*, 5:552–563.
- Luck, S. J., L. Chelazzi, S. A. Hillyard, and R. Desimone, 1997. Neural mechanisms of spatial selective attention in areas V1, V2, and V4 of macaque visual cortex, *J. Neurophysiol.*, 77:24–42.
- Malach, R., R. B. Tootell, and D. Malonek, 1994. Relationship between orientation domains, cytochrome oxidase stripes, and intrinsic horizontal connections in squirrel monkey area V2, *Cereb. Cortex*, 4:151–165.
- Maunsell, J. H., T. A. Nealey, and D. D. Depriest, 1990. Magnocellular and parvocellular contributions to responses in the middle temporal visual area (MT) of the macaque monkey, *J. Neurosci.*, 10:3323–3334.
- Maunsell, J. H., and W. T. Newsome, 1987. Visual processing in monkey extrastriate cortex, *Annu. Rev. Neurosci.*, 10:363–401.
- Maunsell, J. H., and D. C. Van Essen, 1983a. The connections of the middle temporal visual area (MT) and their relationship to a cortical hierarchy in the macaque monkey, *J. Neurosci.*, 3:2563–2586.
- Maunsell, J. H., and D. C. Van Essen, 1983b. Functional properties of neurons in middle temporal visual area of the macaque monkey. II. Binocular interactions and sensitivity to binocular disparity, *J. Neurophysiol.*, 49:1148–1167.
- Maunsell, J. H., and D. C. Van Essen, 1983c. Functional properties of neurons in middle temporal visual area of the macaque monkey. I. Selectivity for stimulus direction, speed, and orientation, *J. Neurophysiol.*, 49:1127–1147.
- Mazzoni, P., R. M. Bracewell, S. Barash, and R. A. Andersen, 1996. Spatially tuned auditory responses in area LIP of macaques performing delayed memory saccades to acoustic targets, *J. Neurophysiol.*, 75:1233–1241.
- McAdams, C. J., and J. H. R. Maunsell, 1999. Effects of attention on orientation-tuning functions of single neurons in macaque cortical area V4, *J. Neurosci.*, 19:431–441.
- Merigan, W. H., 1996. Basic visual capacities and shape discrimination after lesions of extrastriate area V4 in macaques, *Vis. Neurosci.*, 13:51–60.
- Merigan, W. H., 2000. Cortical area V4 is critical for certain texture discriminations, but this effect is not dependent on attention, *Vis. Neurosci.*, 17:949–958.
- Merigan, W. H., and J. H. Maunsell, 1993. How parallel are the primate visual pathways? *Annu. Rev. Neurosci.*, 16:369–402.
- Merigan, W. H., and T. Pasternak, 2003. Lesions in primate visual cortex leading to deficits of perception, in *Neuropsychology of Vision* (M. Fahle and M. Greenlee, eds.), Oxford: Oxford University Press.
- Mesulam, M. M., and G. W. Van Hoesen, 1976. Acetylcholinesterase-rich projections from the basal forebrain of the rhesus monkey to neocortex, *Brain Res.*, 109:152–157.
- Mikami, A., W. T. Newsome, and R. H. Wurtz, 1986. Motion selectivity in macaque visual cortex. I. Mechanisms of direction and speed selectivity in extrastriate area MT, *J. Neurophysiol.*, 55:1308–1327.
- Miller, E. K., and R. Desimone, 1994. Parallel neuronal mechanisms for short-term memory, *Science*, 263:520–522.
- Milner, A., and M. A. Goodale, 1996. *The Visual Brain in Action*, Oxford: Oxford University Press.
- Mishkin, M., 1982. A memory system in the monkey, *Philos. Trans. R. Soc. Lond. B. Biol. Sci.*, 298:83–95.
- Mishkin, M., and T. Appenzeller, 1987. The anatomy of memory, *Sci. Am.*, 256:80–89.
- Mishkin, M., L. G. Ungerleider, and K. A. Macko, 1983. Object vision and spatial vision: two cortical pathways, *Trends Neurosci.*, 6:414–417.
- Miyashita, Y., M. Kameyama, I. I. Hasegawa, and T. Fukushima, 1998. Consolidation of visual associative long-term memory in the temporal cortex of primates, *Neurobiol. Learn. Mem.*, 70:197–211.
- Moore, T., A. S. Tolias, and P. H. Schiller, 1998. Visual representations during saccadic eye movements, *Proc. Natl. Acad. Sci. USA*, 95:8981–8984.
- Moran, J., and R. Desimone, 1985. Selective attention gates visual processing in the extrastriate cortex, *Science*, 229:782–783.
- Motter, B. C., 1993. Focal attention produces spatially selective processing in visual cortical areas V1, V2, and V4 in the presence of competing stimuli, *J. Neurophysiol.*, 70:909–919.
- Motter, B. C., 1994. Neural correlates of attentive selection for color or luminance in extrastriate area V4, *J. Neurosci.*, 14:2178–2189.
- Movshon, J. A., E. H. Adelson, M. S. Gizzi, and W. T. Newsome, 1985. The analysis of moving visual patterns, in *Pattern Recognition Mechanisms* (C. Chagas, R. Gattas, and C. G. Gross, eds.), Vatican City: Pontifical Academy of Sciences, pp. 117–151.
- Movshon, J. A., and W. T. Newsome, 1996. Visual response properties of striate cortical neurons projecting to area MT in macaque monkeys, *J. Neurosci.*, 16:7733–7741.
- Nakamura, H., R. Gattass, R. Desimone, and L. G. Ungerleider, 1993. The modular organization of projections from areas V1

- and V2 to areas V4 and TEO in macaques, *J. Neurosci.*, 13: 3681–3691.
- Nakamura, K., and C. L. Colby, 2000. Visual, saccade-related, and cognitive activation of single neurons in monkey extrastriate area V3a, *J. Neurophysiol.*, 84:677–692.
- Nakamura, K., and C. L. Colby, 2002. Updating of the visual representation in monkey striate and extrastriate cortex during saccades, *Proc. Natl. Acad. Sci. USA*, 99:4026–4031.
- Neal, J. W., R. C. Pearson, and T. P. Powell, 1990. The ipsilateral corticocortical connections of area 7 with the frontal lobe in the monkey, *Brain Res.*, 509:31–40.
- Newcombe, F., G. Ratcliff, and H. Damasio, 1987. Dissociable visual and spatial impairments following right posterior cerebral lesions: clinical, neuropsychological and anatomical evidence, *Neuropsychologia*, 25:149–161.
- Newcombe, F., and W. R. Russell, 1969. Dissociated visual perceptual and spatial deficits in focal lesions of the right hemisphere, *J. Neurol. Neurosurg. Psychiatry*, 32:73–81.
- Newsome, W. T., and E. B. Pare, 1988. A selective impairment of motion perception following lesions of the middle temporal visual area (MT), *J. Neurosci.*, 8:2201–2211.
- Newsome, W. T., R. H. Wurtz, M. R. Dursteler, and A. Mikami, 1985. Deficits in visual motion processing following ibotenic acid lesions of the middle temporal visual area of the macaque monkey, *J. Neurosci.*, 5:825–840.
- Nobre, A. C., T. Allison, and G. McCarthy, 1994. Word recognition in the human inferior temporal lobe, *Nature*, 372:260–263.
- Nowak, L. G., and J. Bullier, 1997. The timing of information transfer in the visual system, *Cereb. Cortex*, 12:205–241.
- Oram, M. W., and D. I. Perrett, 1996. Integration of form and motion in the anterior superior temporal polysensory area (STPa) of the macaque monkey, *J. Neurophysiol.*, 76:109–129.
- Oram, M. W., D. I. Perrett, and J. K. Hietanen, 1993. Directional tuning of motion-sensitive cells in the anterior superior temporal polysensory area of the macaque, *Exp. Brain Res.*, 97: 274–294.
- Orban, G. A., R. C. Saunders, and E. Vandembussche, 1995. Lesions of the superior temporal cortical motion areas impair speed discrimination in the macaque monkey, *Eur. J. Neurosci.*, 7:2261–2276.
- Pasternak, T., and W. H. Merigan, 1994. Motion perception following lesions of the superior temporal sulcus in the monkey, *Cereb. Cortex*, 4:247–259.
- Pasupathy, A., and C. E. Connor, 1999. Responses to contour features in macaque area V4, *J. Neurophysiol.*, 82:2490–2502.
- Perrett, D. I., E. T. Rolls, and W. Caan, 1982. Visual neurones responsive to faces in the monkey temporal cortex, *Exp. Brain Res.*, 47:329–342.
- Perrett, D. I., P. A. J. Smith, A. J. Mistlin, A. J. Chitty, A. S. Head, D. D. Potter, R. Broennimann, A. D. Milner, and M. A. Jeeves, 1985b. Visual analysis of body movements by neurons in the temporal cortex of the macaque monkey: a preliminary report, *Behav. Brain Res.*, 16:153–170.
- Perrett, D. I., P. A. Smith, D. D. Potter, A. J. Mistlin, A. S. Head, A. D. Milner, and M. A. Jeeves, 1985a. Visual cells in the temporal cortex sensitive to face view and gaze direction, *Proc. R. Soc. Lond. B. Biol. Sci.*, 223:293–317.
- Petersen, S. E., P. T. Fox, A. Z. Snyder, and M. E. Raichle, 1990. Activation of extrastriate and frontal cortical areas by visual words and word-like stimuli, *Science*, 249:1041–1044.
- Platt, M. L., and P. W. Glimcher, 1997. Responses of intraparietal neurons to saccadic targets and visual distractors, *J. Neurophysiol.*, 78:1574–1589.
- Plaut, D. C., and M. J. Farah, 1990. Visual object representation: interpreting neurophysiological data within a computational framework, *J. Cogn. Neurosci.*, 2:320–343.
- Poggio, G. E., 1995. Mechanisms of stereopsis in monkey visual cortex, *Cereb. Cortex*, 5:193–204.
- Poggio, G. F., F. Gonzalez, and F. Krause, 1988. Stereoscopic mechanisms in monkey visual cortex: binocular correlation and disparity selectivity, *J. Neurosci.*, 8:4531–4550.
- Pohl, W., 1973. Dissociation of spatial discrimination deficits following frontal and parietal lesions in monkeys, *J. Comp. Physiol. Psychol.*, 82:227–239.
- Posner, M. I., C. R. Snyder, and B. J. Davidson, 1980. Attention and the detection of signals, *J. Exp. Psychol.*, 109:160–174.
- Qian, N., and R. A. Andersen, 1994. Transparent motion perception as detection of unbalanced motion signals. II. Physiology, *J. Neurosci.*, 14:7367–7380.
- Quintana, J., and J. M. Fuster, 1993. Spatial and temporal factors in the role of prefrontal and parietal cortex in visuomotor integration, *Cereb. Cortex*, 3:122–132.
- Rainer, G., W. F. Asaad, and E. K. Miller, 1998. Memory fields of neurons in the primate prefrontal cortex, *Proc. Natl. Acad. Sci. USA*, 95:15008–15013.
- Rao, S. C., G. Rainer, and E. K. Miller, 1997. Integration of what and where in the primate prefrontal cortex, *Science*, 276:821–824.
- Ratcliff, G., and G. A. Davies-Jones, 1972. Defective visual localization in focal brain wounds, *Brain*, 95:49–60.
- Ratcliff, G., and F. Newcombe, 1973. Spatial orientation in man: effects of left, right, and bilateral posterior cerebral lesions, *J. Neurol. Neurosurg. Psychiatry*, 36:448–454.
- Ratcliff, G., R. M. Ridley, and G. Ettlinger, 1977. Spatial disorientation in the monkey, *Cortex*, 13:62–65.
- Recanzone, G. H., R. H. Wurtz, and U. Schwarz, 1997. Responses of MT and MST neurons to one and two moving objects in the receptive field, *J. Neurophysiol.*, 78:2904–2915.
- Rensink, R. A., 2000. The dynamic representation of scenes, *Vis. Cogn.*, 7:17–42.
- Reppas, J. B., K. K. Kwong, R. Malach, R. T. Born, T. J. Brady, B. R. Rosen, J. W. Belliveau, and R. B. Tootell, 1995. Visual motion aftereffect in human cortical area MT revealed by functional magnetic resonance imaging, *J. Neurosci.*, 15:3215–3230.
- Reynolds, J. H., L. Chelazzi, and R. Desimone, 1999. Competitive mechanisms subserve attention in macaque areas V2 and V4, *J. Neurosci.*, 19:1736–1753.
- Reynolds, J. H., T. Pasternak, and R. Desimone, 2000. Attention increases sensitivity of V4 neurons, *Neuron*, 26:703–714.
- Ridley, R. M., and G. Ettlinger, 1975. Tactile and visuo-spatial discrimination performance in the monkey: the effects of total and partial posterior parietal removals, *Neuropsychologia*, 13:191–206.
- Rocha-Miranda, C. E., D. B. Bender, C. G. Gross, and M. Mishkin, 1975. Visual activation of neurons in inferotemporal cortex depends on striate cortex and forebrain commissures, *J. Neurophysiol.*, 38:475–491.
- Rockland, K. S., and D. N. Pandya, 1979. Laminar origins and terminations of cortical connections of the occipital lobe in the rhesus monkey, *Brain Res.*, 179:3–20.
- Rodman, H. R., and T. D. Albright, 1989. Single-unit analysis of pattern-motion selective properties in the middle temporal visual area (MT), *Exp. Brain Res.*, 75:53–64.
- Rodman, H. R., S. P. O. Scalaidhe, and C. G. Gross, 1993. Response properties of neurons in temporal cortical visual areas of infant monkeys, *J. Neurophysiol.*, 70:1115–1136.

- Roe, A. W., and D. Y. Ts'o, 1995. Visual topography in primate V2: multiple representation across functional stripes, *J. Neurosci.*, 15:3689–3715.
- Roelfsema, P. R., V. A. Lamme, and H. Spekreijse, 1998. Object-based attention in the primary visual cortex of the macaque monkey, *Nature*, 395:376–381.
- Rolls, E. T., G. C. Baylis, and C. M. Leonard, 1985. Role of low and high spatial frequencies in the face-selective responses of neurons in the cortex in the superior temporal sulcus in the monkey, *Vis. Res.*, 25:1021–1035.
- Rudolph, K. K., 1997. Motion and form perception after lesions of cortical areas MT/MST and V4 in the macaque. Doctoral dissertation, Department of Brain and Cognitive Science, Rochester, NY: University of Rochester.
- Rudolph, K. K., and T. Pasternak, 1999. Transient and permanent deficits in motion perception after lesions of cortical areas MT and MST in the macaque monkey, *Cereb. Cortex*, 9:90–100.
- Rushworth, M. F. S., P. D. Nixon, and R. E. Passingham, 1997. Parietal cortex and movement. I. Movement selection and reaching, *Exp. Brain Res.*, 117:292–310.
- Saint-Cyr, J. A., L. G. Ungerleider, and R. Desimone, 1990. Organization of visual cortical inputs to the striatum and subsequent outputs to the pallidum-nigral complex in the monkey, *J. Comp. Neurol.*, 298:129–156.
- Saito, H., M. Yukie, K. Tanaka, K. Hikosaka, Y. Fukada, and E. Iwai, 1986. Integration of direction signals of image motion in the superior temporal sulcus of the macaque monkey, *J. Neurosci.*, 6:145–157.
- Sakagami, M., K. Tsutsui, J. Lauwereyns, M. Koizumi, S. Kobayashi, and O. Hikosaka, 2001. A code for behavioral inhibition on the basis of color, but not motion, in ventrolateral prefrontal cortex of macaque monkey, *J. Neurosci.*, 21:4801–4808.
- Sakai, K., and Y. Miyashita, 1991. Molecule-hippocampus-memory. Part II: hippocampus as a memory control apparatus, *Brain Nerve*, 43:111–128.
- Sakata, H., H. Shibutani, Y. Ito, K. Tsurugai, S. Mine, and M. Kusunoki, 1994. Functional properties of rotation-sensitive neurons in the posterior parietal association cortex of the monkey, *Exp. Brain Res.*, 101:183–202.
- Sary, G., R. Vogels, and G. A. Orban, 1993. Cue-invariant shape selectivity of macaque inferior temporal neurons, *Science*, 260:995–997.
- Scalaidhe, S. P., F. A. Wilson, and P. S. Goldman-Rakic, 1999. Face-selective neurons during passive viewing and working memory performance of rhesus monkeys: evidence for intrinsic specialization of neuronal coding, *Cereb. Cortex*, 9:459–475.
- Schiller, P. H., 1993. The effects of V4 and middle temporal (MT) area lesions on visual performance in the rhesus monkey, *Vis. Neurosci.*, 10:717–746.
- Schiller, P. H., and K. Lee, 1991. The role of the primate extrastriate area V4 in vision, *Science*, 251:1251–1253.
- Schiller, P. H., and K. Lee, 1994. The effects of lateral geniculate nucleus, area V4, and middle temporal (MT) lesions on visually guided eye movements, *Vis. Neurosci.*, 11:229–241.
- Schiller, P. H., and J. G. Malpeli, 1977. Properties and tectal projections of monkey retinal ganglion cells, *J. Neurophysiol.*, 40:428–445.
- Seacord, L., C. G. Gross, and M. Mishkin, 1979. Role of inferior temporal cortex in interhemispheric transfer, *Brain Res.*, 167:259–272.
- Seidemann, E., and W. T. Newsome, 1999. Effect of spatial attention on the responses of area MT neurons, *J. Neurophysiol.*, 81:1783–1794.
- Seidemann, E., A. B. Poirson, B. A. Wandell, and W. T. Newsome, 1999. Color signals in area MT of the macaque monkey, *Neuron*, 24:911–917.
- Selemon, L. D., and P. S. Goldman-Rakic, 1985. Longitudinal topography and interdigitation of corticostriatal projections in the rhesus monkey, *J. Neurosci.*, 5:776–794.
- Selemon, L. D., and P. S. Goldman-Rakic, 1988. Common cortical and subcortical targets of the dorsolateral prefrontal and posterior parietal cortices in the rhesus monkey: evidence for a distributed neural network subserving spatially guided behavior, *J. Neurosci.*, 8:4049–4068.
- Seltzer, B., and D. N. Pandya, 1978. Afferent cortical connections and architectonics of the superior temporal sulcus and surrounding cortex in the rhesus monkey, *Brain Res.*, 149:1–24.
- Sereno, M. I., A. M. Dale, J. B. Reppas, K. K. Kwong, J. W. Belliveau, T. J. Brady, B. R. Rosen, and R. B. H. Tootell, 1995. Borders of multiple visual areas in human revealed by functional magnetic resonance imaging, *Science*, 268:889–893.
- Sereno, M. I., S. Pitzalis, and A. Martinez, 2001. Mapping of contralateral space in retinotopic coordinates by a parietal cortical area in humans, *Science*, 294:1350–1354.
- Shipp, S., J. Watson, R. Frackowiak, and S. Zeki, 1995. Retinotopic maps in human prestriate visual cortex: the demarcation of areas V2 and V3, *NeuroImage*, 2:125–132.
- Shipp, S., and S. Zeki, 1985. Segregation of pathways leading from area V2 to areas V4 and V5 of macaque monkey visual cortex, *Nature*, 315:322–325.
- Siegel, R. M., and H. L. Read, 1997. Analysis of optic flow in the monkey parietal area 7a, *Cereb. Cortex*, 7:327–346.
- Snowden, R. J., S. Treue, R. G. Erickson, and R. A. Andersen, 1991. The response of area MT and V1 neurons to transparent motion, *J. Neurosci.*, 11:2768–2785.
- Snyder, L. H., A. P. Batista, and R. A. Andersen, 1997. Coding of intention in the posterior parietal cortex, *Nature*, 386:167–170.
- Snyder, L. H., K. L. Grieve, P. Brotchie, and R. A. Andersen, 1998. Separate body- and world-referenced representations of visual space in parietal cortex, *Nature*, 394:887–891.
- Squire, L. R., 1987. *Memory and Brain*, New York: Oxford University Press.
- Steinmetz, M. A., C. E. Connor, C. Constantinidis, and J. R. McLaughlin, 1994. Covert attention suppresses neuronal responses in area 7a of the posterior parietal cortex, *J. Neurophysiol.*, 72:1020–1023.
- Tanaka, K., 1993. Neuronal mechanisms of object recognition, *Science*, 262:685–688.
- Tanaka, K., 1997. Columnar organization in inferotemporal cortex, in *Extrastriate Cortex in Primates* (K. S. Rockland, J. H. Kaas, and A. Peters, eds.), New York and London: Plenum Press, pp. 469–498.
- Tanaka, K., Y. Sugita, M. Moriya, and H. Saito, 1993. Analysis of object motion in the ventral part of the medial superior temporal area of the macaque visual cortex, *J. Neurophysiol.*, 69:128–142.
- Thiele, A., K. R. Dobkins, and A. T. D., 2001. Neural correlates of chromatic motion perception, *Neuron*, 32:351–358.
- Tootell, R. B. H., S. L. Hamilton, M. S. Silverman, and E. Switkes, 1988. Functional anatomy of macaque striate cortex. 1. Ocular dominance, binocular interaction, and baseline conditions, *J. Neurosci.*, 8:1500–1530.
- Tootell, R. B., J. D. Mendola, N. K. Hadjikhani, P. J. Ledden, A. K. Liu, J. B. Reppas, M. I. Sereno, and A. M. Dale, 1997. Functional analysis of V3A and related areas in human visual cortex, *J. Neurosci.*, 17:7060–7078.

- Treue, S., and J. C. Martinez-Trujillo, 1999. Feature-based attention influences motion processing gain in macaque visual cortex, *Nature*, 399:575–579.
- Treue, S., and J. H. R. Maunsell, 1999. Effects of attention on the processing of motion in macaque middle temporal and medial superior temporal visual cortical areas, *J. Neurosci.*, 19:7591–7602.
- Ts'o, D. Y., and C. D. Gilbert, 1988. The organization of chromatic and spatial interactions in the primate striate cortex, *J. Neurosci.*, 8:1712–1727.
- Ts'o, D. Y., A. W. Roe, and C. D. Gilbert, 2001. A hierarchy of the functional organization for color, form and disparity in primate visual area V2, *Vis. Res.*, 41:1333–1349.
- Ungerleider, L. G., 1995. Functional brain imaging studies of cortical mechanisms for memory, *Science*, 270:769–775.
- Ungerleider, L. G., and R. Desimone, 1986. Cortical connections of visual area MT in the macaque, *J. Comp. Neurol.*, 248:190–222.
- Ungerleider, L. G., R. Desimone, T. W. Galkin, and M. Mishkin, 1984. Subcortical projections of area MT in the macaque, *J. Comp. Neurol.*, 223:368–386.
- Ungerleider, L. G., D. Gaffan, and V. S. Pelak, 1989. Projections from inferior temporal cortex to prefrontal cortex via the uncinate fascicle in rhesus monkeys, *Exp. Brain Res.*, 76:473–484.
- Ungerleider, L. G., T. W. Galkin, and M. Mishkin, 1983. Visuotopic organization of projections from striate cortex to inferior and lateral pulvinar in rhesus monkey, *J. Comp. Neurol.*, 217:137–157.
- Ungerleider, L. G., and J. V. Haxby, 1994. “What” and “where” in the human brain, *Curr. Opin. Neurobiol.*, 4:157–165.
- Ungerleider, L. G., and M. Mishkin, 1982. Two cortical visual systems, in *The Analysis of Visual Behavior* (D. J. Ingle, R. J. W. Mansfield, and M. S. Goodale, eds.), Cambridge: MIT Press, pp. 549–586.
- Van Den Berg, A. V., and J. A. Beintema, 2000. The mechanism of interaction between visual flow and eye velocity signals for heading perception, *Neuron*, 26:747–752.
- Van Essen, D. C., and J. R. Maunsell, 1983. Hierarchical organization and functional streams in the visual cortex, *Trends Neurosci.*, 6:370–375.
- Van Hoesen, G. W., 1980. The cortico-cortical projections of the posterior parahippocampal area in the rhesus monkey, *Anat. Rec.*, 196:195A.
- Van Hoesen, G. W., 1982. The parahippocampal gyrus: new observations regarding its cortical connections in the rhesus monkey, *Trends Neurosci.*, 5:345–350.
- Vogels, R., and G. A. Orban, 1996. Coding of stimulus invariances by inferior temporal neurons, *Prog. Brain Res.*, 112:195–211.
- Vogels, R., R. C. Saunders, and G. A. Orban, 1997. Effects of inferior temporal lesions on two types of orientation discrimination in the macaque monkey, *Eur. J. Neurosci.*, 9:229–245.
- von Bonin, G., and P. Bailey, 1947. *The Neocortex of Macaca Mulatta*, Urbana: University of Illinois Press.
- von Der Heydt, R., E. Peterhans, G. Baumgartner, and P. Iacovelli, 1984. Illusory contours and cortical neuron responses, *Science*, 224:1260–1262.
- Walsh, V., S. R. Butler, D. Carden, and J. J. Kulikowski, 1992b. The effects of V4 lesions on the visual abilities of macaques: shape discrimination, *Behav. Brain Res.*, 50:115–126.
- Walsh, V., D. Carden, S. R. Butler, and J. J. Kulikowski, 1993. The effects of V4 lesions on the visual abilities of macaques: hue discrimination and colour constancy, *Behav. Brain Res.*, 53:51–62.
- Walsh, V., J. J. Kulikowski, S. R. Butler, and D. Carden, 1992a. The effects of lesions of area V4 on the visual abilities of macaques: colour categorization, *Behav. Brain Res.*, 52:81–89.
- Wandell, B. A., A. B. Poirson, W. T. Newsome, H. A. Baseler, G. M. Boynton, A. Huk, S. Gandhi, and L. T. Sharpe, 1999. Color signals in human motion-selective cortex, *Neuron*, 24:901–909.
- Watanabe, M., H. Tanaka, T. Uka, and I. Fujita, 2002. Disparity-selective neurons in area V4 of macaque monkeys, *J. Neurophysiol.*, 87:1960–1973.
- Webster, M. J., J. Bachevalier, and L. G. Ungerleider, 1993. Subcortical connections of inferior temporal areas TE and TEO in macaque monkeys, *J. Comp. Neurol.*, 335:73–91.
- Webster, M. J., J. Bachevalier, and L. G. Ungerleider, 1994. Connections of inferior temporal areas TEO and TE with parietal and frontal cortex in macaque monkeys, *Cereb. Cortex*, 4:470–483.
- Weiskrantz, L., and R. C. Saunders, 1984. Impairments of visual object transforms in monkeys, *Brain*, 107:1033–1072.
- Wilson, F. A., S. P. O. Scalaidhe, and P. S. Goldman-Rakic, 1993. Dissociation of object and spatial processing domains in primate prefrontal cortex, *Science*, 260:1955–1958.
- Xiao, D. K., S. Raiguel, V. Marcar, J. Koenderink, and G. A. Orban, 1995. Spatial heterogeneity of inhibitory surrounds in the middle temporal visual area, *Proc. Natl. Acad. Sci. USA*, 92:11303–11306.
- Yantis, S., and J. Jonides, 1984. Abrupt visual onsets and selective attention: evidence from visual search, *J. Exp. Psychol. Hum. Percept. Perform.*, 10:601–621.
- Zeki, S. M., 1973. Colour coding in rhesus monkey prestriate cortex, *Brain Res.*, 53:422–427.
- Zeki, S. M., 1979. Functional specialization and binocular interaction in the visual areas of rhesus monkey prestriate cortex, *Proc. R. Soc. Lond. B. Biol. Sci.*, 204:379–397.
- Zeki, S. M., 1980. A direct projection from area V1 to area V3A of rhesus monkey visual cortex, *Proc. R. Soc. Lond. B. Biol. Sci.*, 207:499–506.
- Zeki, S. M., and S. Shipp, 1987. Functional segregation within area V2 of macaque monkey visual cortex, in *Seeing Contour and Color* (J. J. Kulikowski, C. M. Dickinson, and I. J. Murray, eds.), Oxford: Pergamon Press, pp. 120–124.
- Zihl, J., D. von Cramon, and N. Mai, 1983. Selective disturbance of movement vision after bilateral brain damage, *Brain*, 106:313–340.

V SUBCORTICAL PROCESSING

35 The Visual Relays in the Thalamus

S. MURRAY SHERMAN AND R.W. GUILLERY

THE LATERAL GENICULATE nucleus¹ is the thalamic relay of retinal input to the visual cortex. It is the best understood of the thalamic relays and, because there is an overall structure shared by all thalamic nuclei, it can serve as a general model for the thalamus. We first consider the lateral geniculate nucleus and then, using this as a prototype, look at other thalamic relays on the visual pathways, the lateral posterior nucleus and the pulvinar. For convenience, both will be referred to jointly as the *pulvinar region*. We look at features that are shared by the lateral geniculate nucleus and the pulvinar region and explore the extent to which the organizational principles that are well defined for the lateral geniculate nucleus can help us to understand aspects of pulvinar organization. The lateral geniculate nucleus will be treated as a first-order relay (Guillery and Sherman, 2002b; Sherman and Guillery, 2001), sending ascending visual messages from the retina to primary receiving cortex and the pulvinar region as a higher-order relay carrying messages from one cortical area through the thalamic relay to another cortical area and thus playing a potentially crucial role in corticocortical communication. First- and higher-order relays are defined more fully below, but it suffices to note here that the former represent the initial relay of a particular sort of information (e.g., visual or auditory) to cortex, while the latter represent further relay of such information via a cortico-thalamo-cortical loop.

The complex cell and circuit properties of thalamic relays have been defined during the past three or four decades, and these are a clear indication that thalamic circuits must be concerned with significant tasks. In spite of this, thalamic relays are often still treated as they were in the nineteenth century, when it was enough to trace a pathway, such as the auditory, visual, or somatosensory pathway, to the thalamus and then conclude that the function of that part of the thalamus had been defined. Glees and Le Gros Clark (1941) described a one-to-one relationship between incoming retinogeniculate axon terminals and geniculate cells in

macaque monkeys, which suggested a relatively simple transfer of visual information. We now know that this was an error and that, as we show below, the synaptic relationships are, in fact, very complex, with the vast majority of synapses onto relay cells coming from nonretinal sources (Guillery, 1969; Van Horn et al., 2000; Wilson et al., 1984). In spite of this, when, more recently, the distinctive receptive field properties of cells in the retina and the visual cortex were being defined (reviewed in Hubel and Wiesel, 1977), the lateral geniculate nucleus was treated as a simple, machine-like relay. This reflected the great success of the receptive field approach to vision. Initially, in anesthetized animals, this approach showed that receptive fields become increasingly elaborated along the synaptic hierarchies through retina and cortex, with the one glaring exception being the retinogeniculate synapse: the center/surround receptive fields of geniculate relay cells are essentially the same as those of their retinal afferents. From this arose the misleading conclusion that nothing much of interest was happening in the geniculate relay (Hubel and Wiesel, 1977; Zeki, 1993). Indeed, this raises certain questions: Why have a geniculate relay at all? Why not have retinal axons project directly to visual cortex? Or, more generally, why bother with thalamic relays? One of the main purposes of this chapter is to provide a partial answer to these questions. A second purpose is to indicate that currently we are far from having a complete answer. It is highly probable that much of what the thalamus does still remains to be defined.

As we shall see, even on the evidence available today, there is much of interest happening in the geniculate relay, and in retrospect, the lack of receptive field elaboration seen in the geniculate relay is not evidence of nothing happening there but, rather, evidence that something completely different but important occurs. That is, this is a crucial synapse in the visual pathways doing something other than receptive field elaboration: geniculate circuitry is involved in affecting, in a dynamic fashion, the amount and nature of information relayed to cortex. One reason this was missed in earlier studies is that these functions depend largely on the behavioral state of the animal and are suppressed in anesthetized animals. This dynamic control, dependent on the animal's behavioral state and considered below, can be seen to represent the neuronal substrate for many forms of visual attention.

¹By *lateral geniculate nucleus* in this chapter, we mean the *dorsal* lateral geniculate nucleus. Like all thalamic nuclei providing a relay to neocortex, the lateral geniculate nucleus is developmentally a part of the dorsal thalamus. The *ventral* lateral geniculate nucleus, which is part of the ventral thalamus, does not send axons to cortex and will not be considered further.

Functional organization of the lateral geniculate nucleus

For those who still consider the lateral geniculate nucleus as a simple relay, the complexity of its organization will no doubt come as a surprise. The nucleus is organized into a number of layers with a detailed topographic map of visual space that cuts across layers, and its circuitry involves several cell types, many distinctive groups of afferents, and complex synaptic relationships.

MAPS There is a precise map of the contralateral visual hemifield in the lateral geniculate nucleus of all species so far studied, and in this the visual system is like other sensory systems that are mapped in their thalamic relays. The map in the lateral geniculate nucleus is laid out in fairly simple Cartesian coordinates in all species (see Fig. 35.1, where the visual field and its retinal and geniculate representations are shown as tapered arrows). Each layer maps the contralateral hemifield, either through one or the other eye, and all of these maps are aligned across the various layers that characterize the lateral geniculate nucleus of most species (see below and Fig. 35.1). Thus, a point in visual space is represented by a line, called a *line of projection*, that runs perpendicularly through all the layers. The precise alignment of these maps, which matches inputs from the nasal retina of one eye across layers with inputs from the temporal retina of the other eye, is seen in all species and is somewhat surprising when one thinks about the developmental mechanisms needed to produce such a match, which forms before the eyes open and before the two visual images can be matched. We shall see that there are nonretinal afferent axons that innervate the lateral geniculate nucleus and distribute terminals along the lines of projection. In this way, these afferents can have a well-localized action on just one part of the visual input, even though this comes from different eyes and distributes to distinct sets of layers (see the section “Afferents to the A Layers”).

LAYERING The lateral geniculate nuclei of all mammalian species so far studied show some form of layering, although there is considerable difference among species as to what the layers represent functionally. For all mammals, each layer receives input from only one eye, but the distribution of distinct functional types of retinal afferents to the layers differs greatly from one species to another. Chapters 30 and 31 describe the various classes of retinal ganglion cell that give rise to several parallel retinogeniculate pathways, and these frequently relate to specific geniculate layers. Figure 35.2 shows the layering of the lateral geniculate nucleus in the macaque monkey² and the cat, the two best-studied species. The figure illustrates the variation in layering seen across species and introduces the several parallel pathways

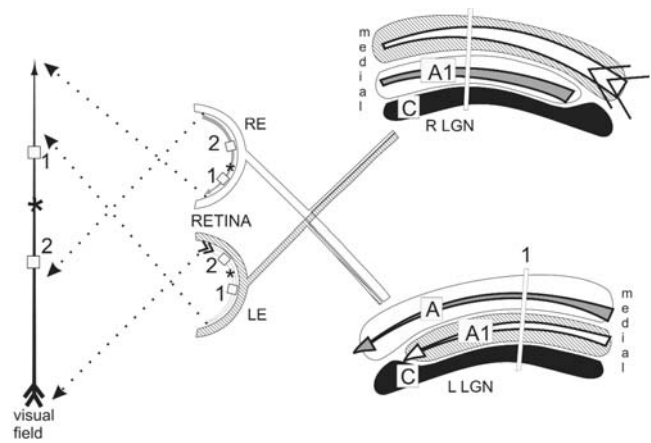


FIGURE 35.1 Schematic view of the representation of the retina and visual field in the layers of the lateral geniculate nucleus of a cat. The visual field is represented by a straight arrow, and the projection of part of this arrow onto each retina is shown. Small white areas of the visual field and corresponding parts of the retina are labeled “1” and “2.” The representation of this part of the visual field in the lateral geniculate nucleus is shown as a corresponding white column going through all of the geniculate layers “like a toothpick through a club sandwich” (Walls, 1953). Each such column is bounded by the lines of projection, which also pass through all of the laminae. A, A1, and C, the major geniculate layers; L LGN and R LGN, left and right lateral geniculate nuclei; LE and RE, left eye and right eye; asterisk, central point of fixation.

that are relayed through the lateral geniculate nucleus to the cortex.

Both species have three main retinal ganglion cell classes that project to the lateral geniculate nucleus. For the macaque monkey (Casagrande, 1994; Casagrande and Kaas, 1994; Hendry and Reid, 2000), these are the P (for parvocellular, meaning small-celled), M (for magnocellular; large-celled), and K (for koniocellular; tiny or dust-like cells) cells, comparable respectively to the X, Y, and W cells in the cat (reviewed in Casagrande and Norton, 1991; Lennie, 1980; Sherman, 1985). The terminology for the macaque monkey relates to the geniculate layers to which the cell classes project. P and M cells project to parvocellular and magnocellular layers, respectively. In the macaque monkey, K cells project to the ventral regions of all layers, where very small cells lie scattered, and the projections overlap with those of M and P cells. However, in *Galago*, a prosimian primate, each of the homologous retinal cell types projects to a separate set of layers (not shown)—koniocellular, par-

²Unless otherwise specified, we shall refer to this as the *monkey* in what follows, noting, however, that the macaque can be regarded as representative of Old World monkeys and that the lateral geniculate nucleus in New World monkeys has a slightly different structure.

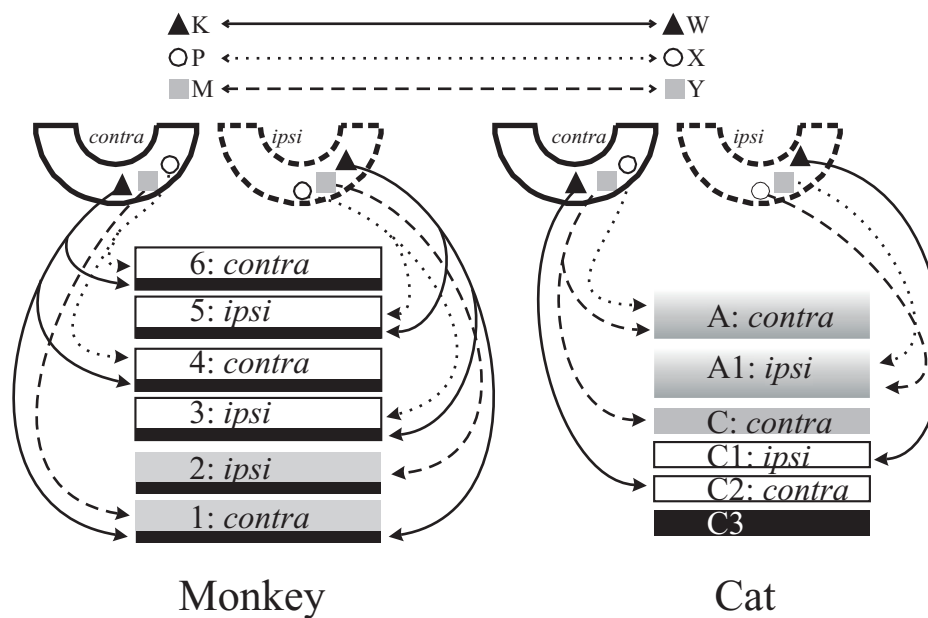


FIGURE 35.2. Comparison of layering in lateral geniculate nucleus of cat and macaque monkey. See text for details. For simplicity, the medial interlaminar nucleus, which is part of the lateral geniculate nucleus medial to the main laminated portion, present in the cat but not in most other species, is not shown.

vocellular, and magnocellular—and it was in this species that the koniocellular pathway was first clearly recognized (Conley et al., 1985; Itoh et al., 1982; Norton et al., 1988). In the cat, X and Y cells have overlapping projections to the A layers, Y cells also project to layer C, and W cells project to layers C1 and C2; there is no retinal input to layer C3, which is therefore shown in black in Figure 35.2 (Hickey and Guillery, 1974). Strictly speaking, layer C3 should perhaps not be included in the lateral geniculate nucleus, which can be defined as the thalamic relay of retinal inputs. What is common to cat and macaque monkey is that each layer is innervated by only one eye. What is different is the partial segregation of parallel pathways through each layer. In the macaque monkey, the P and M pathways use separate layers, the parvocellular for P and the magnocellular for M; the K pathway overlaps with each and is thus represented in all layers. In the cat, the W pathway uses separate layers (C1 and C2), and the Y pathway has exclusive use of layer C, but the X and Y pathways are mingled in the A layers.

Despite the overlap within layers of many of the parallel pathways, there is no functional overlap at the cellular level; within the A layers of the cat, retinal X and Y axons innervate their own classes of relay cell. A similar pattern exists for the macaque monkey, with each of the K, P, and M retinal axons targeting separate classes of geniculate relay cell, whose axons, in turn, have distinct distributions in the visual cortex (see Chapter 31).

New World primates have a slightly different layering arrangement from that shown for the macaque monkey. So

far as we know, the human lateral geniculate nucleus is closely comparable to that of the macaque monkey, although there are commonly more than six layers (Hickey and Guillery, 1979), and we have no direct evidence concerning the distribution of distinct functional types to the different layers.

Thus, layering in the lateral geniculate nucleus separates left eye from right eye afferents and also, to a more limited extent, relates to the separation of functionally distinct parallel pathways. The binocular separation is constant across species, but the functional separation into distinct layers is highly variable, so that the number of layers, their sequence from superficial to deep, and their total number show great variability across species. Most of the information we have for cell and circuit properties of the lateral geniculate nucleus specifically and the thalamus more generally comes from the A layers in the cat, and most details presented below are from these layers. However, this focus on the A layers should not obscure two important facts. One is that in terms of the general arrangements of synaptic circuitry, there is a common thalamic plan that applies to the pulvinar region and to most other parts of the thalamus; the other is that structural details vary significantly among different layers and species. That is, there are details of functional organization that remain unknown but almost certainly will ultimately have to be added to our account of the A layers. For some details of geniculate relays beyond the A layers in the cat and in other species, see Jones (1985), Casagrande and Norton (1991), and Casagrande and Kaas (1994).

CELL TYPES WITHIN THE A LAYERS There are three basic cell types in the A layers of the cat's lateral geniculate nucleus (see Fig. 35.3). These include the two relay cell types, X and Y, and interneurons. The relay cells use glutamate as a neurotransmitter, whereas interneurons use GABA.

Relay cells. X and Y cells represent geniculate relays of two parallel and independent geniculocortical pathways, each innervated by its own retinal X or Y axons, which are excitatory. Retinal Y axons are thicker and conduct more rapidly than do X axons (reviewed in Sherman, 1985). Also, within the A layers, the terminal arbors of retinal Y axons are much larger than those of X axons and give rise to many more synaptic terminals (Bowling and Michael, 1984; Sur et al., 1987). As a result of this and because the postsynaptic relay cell types do not differ much in the number of synapses that they receive from the retina, each retinal Y axon innervates many more relay cells than does an X axon. It has been estimated that the X:Y ratio, which is roughly 10:1 in the retina (Leventhal, 1982; Wässle et al., 1975; Wässle et al., 1981), becomes 1:1 or 2:1 for geniculate relay cells (Sherman, 1985).

These geniculate relay cells differ from one another with respect to their functional and morphological properties. Both cell types have the center/surround organization for their receptive fields typical of retinal and geniculate cells generally. However, Y cells have larger receptive fields and respond better to higher temporal and lower spatial frequencies, whereas X cells have smaller receptive fields and respond better to lower temporal and higher spatial frequencies. Further, Y cells exhibit subtly more nonlinear summation (for further details, see Hochstein and Shapley, 1976a, 1976b; Sherman, 1985). All these receptive field differences are already present in the retinal afferents, and for this reason they will not be considered further.

Morphologically, there are some differences between these relay cell types (Friedlander et al., 1981; Guillery, 1966; LeVay and Ferster, 1977; Wilson et al., 1984). At the light microscopic level (see Fig. 35.3), Y cells have larger cell bodies and smooth dendrites that have cruciate branches in a relatively spherical arbor, with peripheral segments of dendrites often crossing from one layer to another. X cells have arbors that tend to be bipolar and oriented perpendicular to the layers' borders. Their dendrites also have numerous clusters of grape-like appendages located mostly near primary branch points (Fig. 35.3). The functional significance of these morphological differences remains to be defined, although the clustered appendages of the X cells represent the postsynaptic site of retinal inputs, where complex synaptic relationships are formed that are characteristic of X but not of Y cells (the *triadic* arrangements described below).

These and other differences in the microcircuitry of these cells types are described below.

Interneurons. Interneurons have the smallest cell bodies in the A layers and long, sinuous dendrites, and the dendritic arbors are always oriented perpendicular to the layers, often spanning an entire layer (see Fig. 35.3). The dendrites have the appearance of terminal axonal arbors and for that reason have been described as axoniform in appearance (Guillery, 1966). Terminals of these dendritic arbors are presynaptic to local dendrites, containing synaptic vesicles and thus resembling axon terminals, and they are also postsynaptic to other axons, generally those coming from either the retina or the brainstem (see also below and Erişir et al., 1997; Famiglietti and Peters, 1972; Hamos et al., 1985; Ralston, 1971). In addition, most, if not all, interneurons have conventional axons that terminate in the general vicinity of the dendritic arbor. The receptive fields of the few identified interneurons that have been studied are like those of X relay cells and unlike those of Y cells, which suggests that the retinal inputs responsible for their firing are X rather than Y axons (Friedlander et al., 1981; Sherman and Friedlander, 1988).

AFFERENTS TO THE A LAYERS The major sources of inputs to the A layers, besides the retina, include the thalamic reticular nucleus, layer 6 of cortex, and the parabrachial region³ of the midbrain. These are summarized in Figure 35.4. Other afferent sources not shown in Figure 35.4 include the nucleus of the optic tract (midbrain), the dorsal raphe nucleus (midbrain and pons), and the tuberomammillary nucleus (hypothalamus) (reviewed in Sherman and Guillery, 1996, 2001).

Retinal afferents. Retinal afferents to the A layers are glutamatergic (see Fig. 35.4). They are relatively thick axons and have a distinct terminal structure involving richly branched, dense terminal arbors with boutons densely distributed mostly in flowery terminal clusters (not illustrated; see Guillery, 1966). In contrast, most nonretinal inputs described below are thinner, and have an equally distinct structure with smaller terminals *en passant* or on short side branches (see Fig. 35.5, *right*). The retinal axons innervate both relay cells and interneurons in the A layers. Each retinal axon has an arbor strictly limited to one of the A layers, although Y axons and occasional

³ Another term frequently used for this area is *pedunculopontine tegmental nucleus*. We prefer *parabrachial region*, because the scattered cells that innervate the thalamus from this area do not have a clear nuclear boundary, and they are found scattered around the brachium conjunctivum.

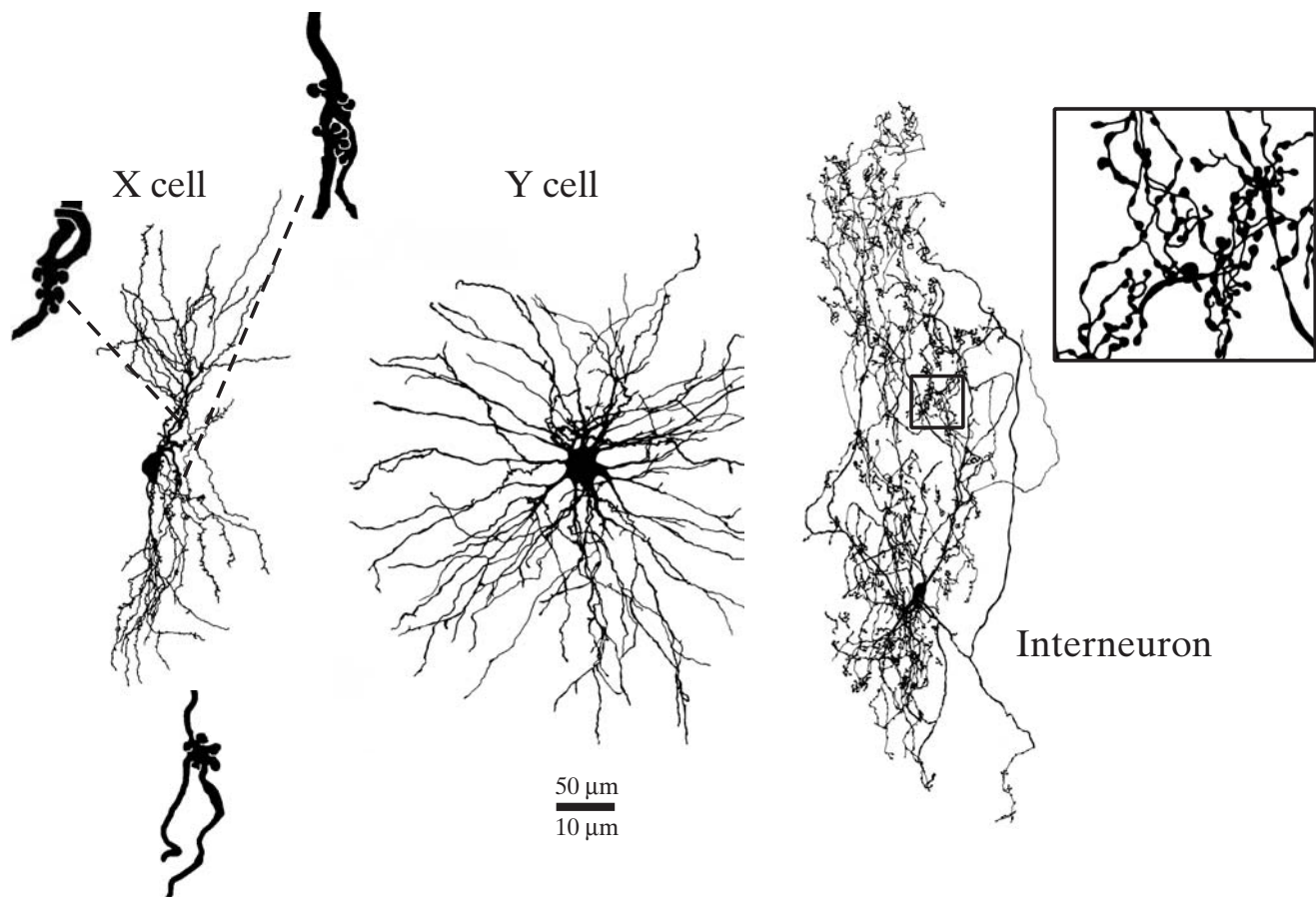


FIGURE 35.3. Reconstruction of an X cell, Y cell, and interneuron from A layers of the cat's lateral geniculate nucleus. The larger scales are for the insets for the X cell and interneuron.

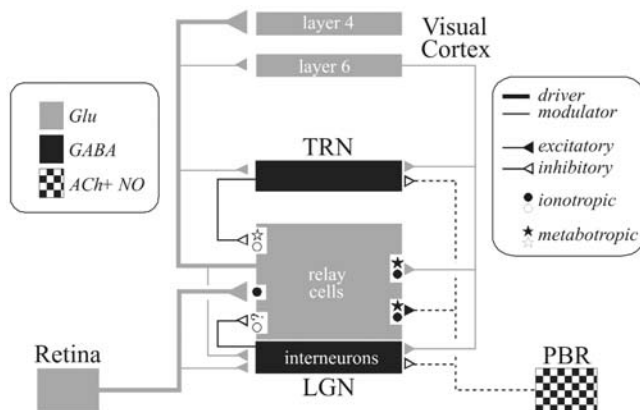


FIGURE 35.4. Neuronal circuitry related to A layers of the cat's lateral geniculate nucleus. Shown are the various inputs, the neurotransmitters associated with them, and the type of receptor, ionotropic or metabotropic, that each activates. Driver versus modulator inputs are also shown (see text for details).

X axons branch to innervate the C layers and/or the medial interlaminar nucleus⁴ as well. As would be expected from the earlier description of the lines of projection, the terminal arbors of the retinogeniculate axons are also organized so that they occupy relatively narrow columns that are bounded by lines of projection, either within a single layer or across more than one layer. Y arbors are larger and contain more boutons than do X arbors. A more subtle difference between them is that the boutons in Y arbors are fairly evenly distributed, while those in X arbors tend to be found in clusters with gaps between them (Bowling and Michael, 1984; Sur et al., 1987). All retinal X and Y axons innervating the lateral geniculate nucleus branch to innervate the midbrain as well (a point that is discussed further below; see also Guillery and Sherman, 2002a,b), but they do not innervate the thalamic reticular nucleus.

⁴The medial interlaminar nucleus is a part of the lateral geniculate nucleus found in carnivores.

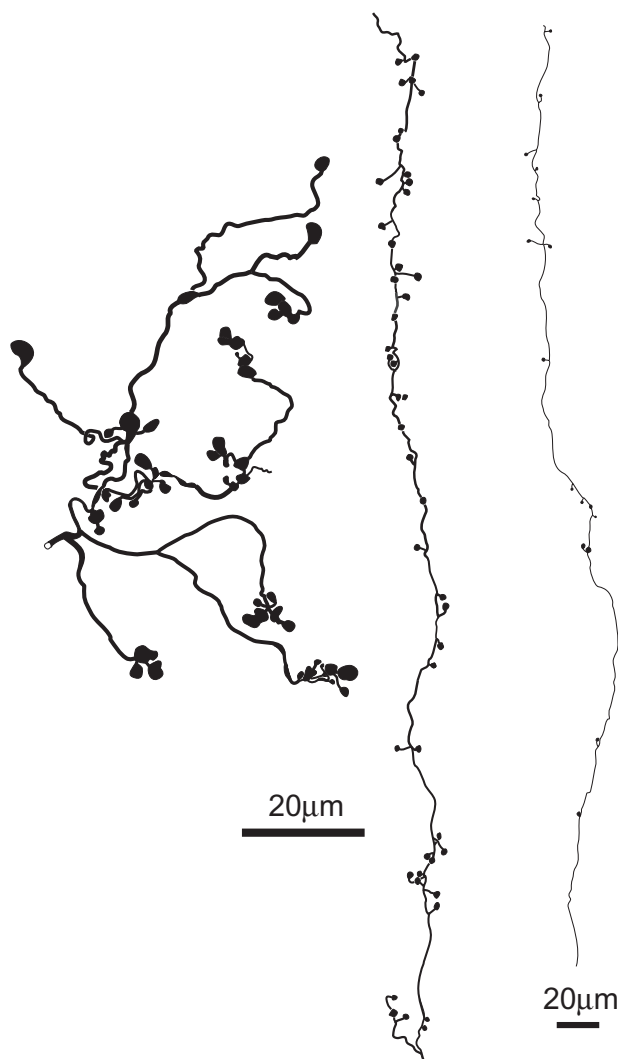


FIGURE 35.5. Tracings of partial terminal arbors of three corticothalamic axons in the pulvinar region labeled by biotinylated dextran amine. The axon on the left exhibits driver morphology from cortical layer 5, and the two axons on the right exhibit modulator morphology from layer 6. (From Sherman and Guillery, 2001.)

Afferents from the thalamic reticular nucleus. The thalamic reticular nucleus is a thin shell of GABAergic neurons that surrounds the entire thalamus laterally, extending somewhat dorsally and ventrally. It derives from the ventral thalamus, together with the ventral lateral geniculate nucleus (see footnote 1), and is divided into sectors, each related to thalamic relay nuclei concerned with a particular modality or function (e.g., auditory, somatosensory, and motor), and as in the main part of the thalamus, sensory surfaces are mapped in the sectors (Crabtree, 1992, 1996, 1998; Crabtree and Killackey, 1989; Montero et al., 1977; reviewed in Guillery et al., 1998). There are strong reciprocal connections between relay cells and reticular cells linking corresponding parts of the reticular and geniculate maps (Pinault and Deschênes,

1998; Pinault et al., 1995a, 1995b; Uhlich et al., 1991), and the cortical afferents from layer 6 (next section) are mapped along the same coordinates (Murphy and Sillito, 1996). That is, the portion of the thalamic reticular nucleus innervating the lateral geniculate nucleus⁵ is mapped in retinotopic coordinates. In addition, the visual sector of the reticular nucleus is linked reciprocally to the pulvinar region (Conley and Diamond, 1990; Pinault et al., 1995a). There is some evidence that the visual sector of the reticular nucleus can be split into two parts, an inner part linked to the lateral geniculate nucleus and an outer part linked to the pulvinar region. The retinotopic mapping in the pulvinar sector of the reticular nucleus is less accurate than that for the geniculate sector, and there may be no map at all in the former.

The cells of the thalamic reticular nucleus, which lie just dorsal to layer A, have moderate to large cell bodies and dendrites oriented mostly parallel to layer A (Uhlich et al., 1991). Their axons descend into the A layers, generally along the lines of projection, with terminal arbors that are moderately branched and contain numerous boutons, mostly *en passant*. These terminals innervate geniculate relay cells, but they provide only a very sparse innervation to interneurons (Cucchiari et al., 1991; Wang et al., 2001). Thus, the thalamic reticular nucleus provides a potent inhibitory GABAergic input to relay cells (Fig. 34.4). Their receptive fields tend to be larger than those of relay cells and are often binocular (So and Shapley, 1981).

Afferents from layer 6 of the cortex. Cortical afferents from layer 6, which are glutamatergic, have thin axons with most boutons located at the end of short side branches (Fig. 34.5; see Murphy and Sillito, 1996). They are topographically organized, with each axon having terminal arbors bounded by lines of projection and passing across more than one layer. These axons enter the A layers after traveling through the thalamic reticular nucleus, where they also give off branches to innervate cells there; this projection, too, is topographic.

Afferents from the parabrachial region. Most of the input from the brainstem to the A layers derives from the parabrachial region (Bickford et al., 1993; de Lima and Singer, 1987). These axons are cholinergic but also appear to colocalize nitric oxide (Bickford et al., 1993; Erişir et al., 1997). Light microscopically, they resemble the cortical afferents more than the retinal afferents, but their terminal arbors are rather diffuse and most appear to terminate in a nontopographic

⁵In the cat, the major portion of the thalamic reticular nucleus innervating the lateral geniculate nucleus is the *perigeniculate nucleus*.

fashion. These axons contact both relay cells and interneurons in the A layers and also branch to innervate cells in the thalamic reticular nucleus.

Other afferents. Some other afferents to the A layers not shown in Figure 35.4 have been described, but they are small in number, not well documented, and will be mentioned only briefly here (for further details, see Sherman and Guillery, 1996, 2001). Lying among the cholinergic cells of the parabrachial region, there are also some noradrenergic cells that innervate the A layers. There is limited serotonergic input from the dorsal raphe nucleus in the midbrain and pons. GABAergic cells of the nucleus of the optic tract in the midbrain also provide limited input. Finally, the tuberomammillary nucleus of the hypothalamus provides a small histaminergic input (Uhlrich et al., 1993).

Postsynaptic receptors. In addition to showing the inputs and their transmitters onto relay cells, Figure 35.4 shows the associated postsynaptic receptors. Note that both ionotropic and metabotropic receptors are postsynaptic in relay cells. There are a number of differences between these two receptor types, but only a few concern us here (for details, see Brown et al., 1997; Conn and Pin, 1997; Mott and Lewis, 1994; Nicoll et al., 1990; Pin and Duvoisin, 1995; Recasens and Vignes, 1995).

Ionotropic receptors include AMPA receptors for glutamate, GABA_A, and nicotinic receptors for acetylcholine. These are complex proteins found in the postsynaptic membrane, and when the transmitter contacts the receptor, it leads to a rapid conformational change that opens an ionic channel, leading to transmembrane flow of ions and a postsynaptic potential. Activation of ionotropic receptors leads to fast responses, typically with a latency for postsynaptic potentials of less than 1 msec and a duration of a few tens of milliseconds. Metabotropic receptors include various glutamate receptors, GABA_B, and various muscarinic receptors for acetylcholine. These are not directly linked to ion channels. Instead, when the transmitter contacts the receptor protein in the membrane, a series of complex biochemical reactions takes place that ultimately leads to the opening or closing of an ion channel, among other postsynaptic events. For thalamic cells, this is primarily a K⁺ channel that, when opened, produces an inhibitory postsynaptic potential (IPSP) as K⁺ flows out of the cell and, when closed, produces an excitatory postsynaptic potential (EPSP) as leakage of K⁺ is reduced. However, these postsynaptic responses are slow: there is usually a latency of 10 msec or longer and a duration of hundreds of milliseconds or more. Also, in general, metabotropic receptors require higher firing rates from inputs to be activated. This is thought to be related to the observation that electron micrographs show these receptors to be located slightly farther from the synaptic site than are

ionotropic receptors, so that more transmitter must be released to reach them.

The more sustained responses associated with metabotropic receptors have a number of important implications. One has to do with the fact that retinal inputs activate only ionotropic receptors in relay cells. This means that retinal EPSPs are relatively fast and brief. This has the virtue that firing in the retinal afferents can reach relatively high levels before temporal summation of the EPSPs occurs, and thus each retinal action potential has a unique postsynaptic response associated with it. If, instead, metabotropic glutamate receptors were activated, the sustained EPSPs would mean that relatively low rates of firing in the afferent would produce temporal summation postsynaptically. This, in turn, means that higher-frequency information would be lost in retinogeniculate transmission or, more formally, that the retinogeniculate synapse would operate like a low-pass temporal device, filtering out higher frequencies. Thus, the fact that retinal inputs activate only ionotropic receptors serves to maximize the transfer of higher temporal frequencies. Note that the population of nonretinal inputs as a whole activates both metabotropic and ionotropic receptors (reviewed in Sherman and Guillery, 1996, 2001). However, it is not clear whether any individual nonretinal axon can activate both ionotropic and metabotropic receptors. Nonetheless, the activation of metabotropic receptors means that these inputs can create sustained changes in baseline membrane potential, which, among other things, means that these inputs can have sustained effects on the overall responsiveness of relay cells. Other consequences of these sustained postsynaptic responses are considered below.

Synaptic structures. Over 95% of all synaptic terminals in the A layers can be placed into one of four categories (reviewed in Sherman and Guillery, 1996, 2001): (1) *RL* (Round vesicle, Large profile) terminals, which are the retinal terminals, are the largest terminals in the A layers. They form asymmetric⁶ contacts consistent with their identity as excitatory inputs. (2) *RS* terminals (Round vesicle, Small profile) are smaller than RL terminals but also form asymmetric contacts. The vast majority of these come from either layer 6 of cortex or the parabrachial region. (3) *FI* terminals (*F*lattened

⁶One ultrastructural characteristic of synaptic contacts is a thickening of the postsynaptic membrane, which includes the postsynaptic receptors (Sheng, 2001). When the thickening is especially prominent, the postsynaptic membranes are much thicker than the presynaptic ones, and this characterizes an *asymmetric* synapse. When the thickening is less prominent, there is a less pronounced difference in thickness between presynaptic and postsynaptic membranes, and this characterizes a *symmetric* synapse. Typically, asymmetric synapses are excitatory, and symmetric ones are inhibitory.

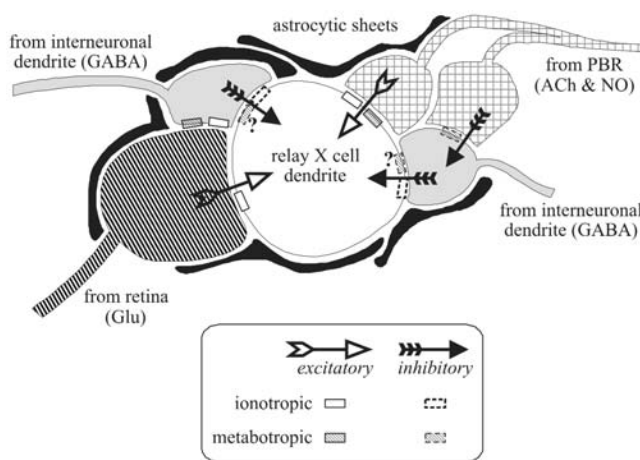


FIGURE 35.6. Schematic view of triadic circuits in a glomerulus of the lateral geniculate nucleus in the cat. The arrows indicate presynaptic to postsynaptic directions. The question marks postsynaptic to the dendritic terminals of interneurons indicate that it is not clear whether or not metabotropic (GABA_B) receptors exist there.

vesicles) form symmetric contacts consistent with their origin from axons of reticular cells or interneurons. (4) F2 terminals represent the dendritic outputs of interneurons; they also have flattened vesicles and form symmetric contacts. Unlike all of the other terminals, which are strictly presynaptic, these are both presynaptic and postsynaptic, with inputs from either retinal or parabrachial terminals.

Triadic synaptic arrangements involving F2 terminals are common in the A layers (Fig. 35.6). In some triads, an RL terminal contacts both an F2 terminal and the dendrite of a relay cell, and the F2 terminal contacts the same relay cell dendrite. A slightly different kind of triad can be formed by a parabrachial terminal contacting an F2 terminal and a different parabrachial terminal from the same axon contacting a relay cell dendrite, again with the F2 terminal contacting the same relay cell dendrite (Fig. 35.6). Nearly all F2 terminals are involved in one or the other form of triad. Curiously, these triads are quite common for relay X cells and rare for Y cells, the latter thus receiving very few inputs from F2 terminals.⁷ Triads are typically found in complex synaptic zones that lack astrocytic processes but are

surrounded by sheets of astrocytic cytoplasm; these are called *glomeruli*. It is not at all clear how the triads function.

Distribution of inputs to relay cells. The dendritic arbors of relay cells can be divided into two distinct sectors with little or no overlap (Erişir et al., 1997; Wilson et al., 1984): a proximal region (up to about $100\mu\text{m}$ from the cell body or generally close to the first branch point) and a distal region (farther than about $100\mu\text{m}$ from the cell body). Retinal terminals contact the former region, whereas cortical terminals contact the latter. F2 and parabrachial terminals also contact relay cells in the proximal zone. Axonal inputs from interneurons mostly contact the proximal zone, whereas those from reticular axons mostly contact the distal zone.

A small minority of synaptic inputs onto geniculate relay cells derive from retina. In the A layers of the cat's lateral geniculate nucleus, for instance, only about 5–10% of the synaptic input to relay cells comes from the retinal axons: roughly 30% comes from local GABAergic cells (interneurons plus reticular cells), 30% from the cortical input, and 30% from the parabrachial region (Van Horn et al., 2000). In the parvocellular C layers, even fewer synapses—2% to 4%—onto relay cells derive from the retina (Raczkowski et al., 1988). If one had only the anatomical data, and for many other thalamic relays that is all we have, one might well conclude that the lateral geniculate nucleus relays parabrachial input to cortex and that the retinal input plays only a minor, undetermined role. For the lateral geniculate nucleus we know that it is the retinal input that is relayed to cortex, so we accept that the small number of retinal afferents serve as the crucial drivers of geniculate function. However, for thalamic nuclei that we do not understand as well as the lateral geniculate nucleus, the point is important, as we will see when we discuss corticocortical communication.

Drivers and modulators. It follows that not all inputs to the thalamus are equal in their action on the relay cells. We have distinguished two different types of input (Sherman and Guillery, 1998, 2001): *drivers* and *modulators*. The drivers are the information-bearing input that is to be relayed to cortex, and this is the retinal input for the lateral geniculate nucleus. All other inputs are modulators. Examples of modulation are provided below, and details of how drivers might generally be distinguished from modulators is provided elsewhere (Sherman and Guillery, 1998, 2001). One difference is seen in Figure 35.4: the driver (retinal) input activates only ionotropic receptors, whereas the modulators activate metabotropic and often ionotropic receptors. Note that, of the main extrinsic inputs to the lateral geniculate nucleus, the retinal input is a driver, but the layer 6 cortical and parabrachial inputs are both modulators. The corticothalamic input must be seen as modulatory because, among other

⁷Recent descriptions of triads that relate to Y cell terminals suggest more similarities between the X and the Y pathways than reported in the earlier studies (e.g., Wilson et al., 1984; Sherman and Friedlander, 1988). Datskovskaia et al. (2001) offer evidence that many retinal Y axons in the A layers terminate on dendritic presynaptic F2 terminals and thus are likely to contribute significantly to triads. Also a recent account of triads related to Y cell axons in the geniculate C layers (Dankowski and Bickford, 2003) adds new information on the subject, and the issue of the extent of triadic circuitry in the Y pathway remains to be resolved.

reasons, its elimination (by cooling, ablation, etc.) has only subtle effects on the receptive fields of geniculate relay cells, not altering their basic center/surround organization (Cudeiro and Sillito, 1996; Geisert et al., 1981; Jones and Sillito, 1991; Kalil and Chase, 1970; McClurkin and Marrocco, 1984; McClurkin et al., 1994). This is in contrast to corticothalamic afferents from layer 5, which go to higher-order thalamic relays but not to the lateral geniculate nucleus, and which must be regarded as drivers because their elimination essentially abolishes the characteristic receptive fields in such target thalamic relays as the posterior medial nucleus or pulvinar region (Bender, 1983; Chalupa, 1991; Diamond et al., 1992; see also the section "The Pulvinar Region as a Visual Relay").

INTRINSIC PROPERTIES OF THALAMIC CELLS IN THE A LAYERS

The relay nature of the lateral geniculate nucleus depends on the mechanisms by which retinal inputs evoke firing in geniculate relay cells, and these mechanisms are also present in thalamic relays more generally. There are three factors that largely control this retinogeniculate transmission, and they are considered below. First are the intrinsic membrane properties of relay cells, including their passive and active membrane properties, because these determine the effect of retinal EPSPs at the cell body or region of action potential generation. Second is the geniculate circuitry that, by affecting many of the intrinsic membrane properties, also controls the effect of retinal EPSPs on relay cell firing. Third, the nature of the postsynaptic receptors largely determines the postsynaptic response of relay (and other) cells to their active inputs; this feature is considered in the section "Control of Response Mode."

Generally, all thalamic cells show a wide range of intrinsic membrane properties that are found generally in neurons of the brain (reviewed in Sherman and Guillery, 1996, 2001). These include passive cable properties, voltage-sensitive and -insensitive conductances, and conductances sensitive to other factors, such as Ca^{2+} concentration. The conductances underlie transmembrane currents, including a leak K^+ current ($I_{\text{K[leak]}}$) that helps control the resting membrane potential, various voltage- and Ca^{2+} -gated K^+ currents (I_{A} , $I_{\text{K[Ca}^{2+}]}$, etc.), and a voltage-gated cation current (I_{h}). Since these are properties found widely in the brain, they will not be considered further here, but additional details of these as they apply to thalamic neurons can be found in Sherman and Guillery (1996, 2001). Two features that are of particular interest in thalamic neurons are considered below. One is the apparent cable properties of interneurons, which suggests that synaptic inputs onto their dendritic terminals affect them locally but have little effect on the cell body and axonal output, permitting these cells to provide numerous input/output routes independently and simultaneously (see below). The other is the presence in all cells of a voltage-

gated Ca^{2+} conductance based on T-type (for transient) Ca^{2+} channels that, when activated, leads to a current (I_{T}) large enough to produce an all-or-none Ca^{2+} spike (reviewed in Sherman and Guillery, 1996, 2001). This spike alters the response properties of the thalamic cells in a functionally highly significant manner.

Passive membrane or cable properties. Determining how current spreads through cells with complex geometries of their dendritic trees poses a formidable computational problem. Modeling the cell and its membranes as a cable provides a useful means of approximating current flow. Details of cable modeling for thalamic neurons can be found in Bloomfield et al. (1987) and Bloomfield and Sherman (1989) and will be briefly summarized here. Relay cells and cells of the thalamic reticular nucleus have relatively thick dendrites that branch in a way that suggests efficient current flow through the dendrites. The result of cable modeling for these cells indicates that they are electrotonically compact, meaning that EPSPs and IPSPs generated even on peripheral dendrites will produce significant voltage changes at the cell body and axon hillock (Bloomfield et al., 1987; Bloomfield and Sherman, 1989). Thus, all synaptic inputs to these cells can be considered influential in affecting the cell's firing. Since the dendrites of relay cells are purely postsynaptic structures, the only synaptic output of these cells is via their axons, so that any synaptic input to the distal dendrites that could not produce a voltage change at the spike-initiating region would be ineffective for spike initiation.

In contrast to relay cells, interneurons are built differently in two ways. First, as noted above, in addition to having a conventional axonal output, these cells have presynaptic terminals on peripheral dendrites, which provide these cells with numerous dendritic outputs. Second, these presynaptic terminals are attached to the stem dendrites by long, thin stalks; overall, the thin dendrites and the nature of the dendritic branching suggest poor current flow through the dendritic trees. Cable modeling suggests that EPSPs and IPSPs generated on the peripheral dendrites, where the retinal and brain stem axons provide significant input to the dendritic presynaptic boutons, will have little influence on the cell body and axon hillock (Bloomfield and Sherman, 1989). Thus, the interneuron appears capable of multiplexing: the axonal output is controlled by synapses located on proximal dendrites, whereas the several separate dendritic outputs are controlled locally and independently of each other by local synaptic inputs. However, this concept of the functioning of the interneuron remains a hypothesis that requires more direct evidence than currently exists (Cox and Sherman, 2000).

Properties of I_{T} in relay cells. The voltage-dependent low-threshold Ca^{2+} spikes that are based on T channels are

The Low Threshold Ca^{2+} Spike

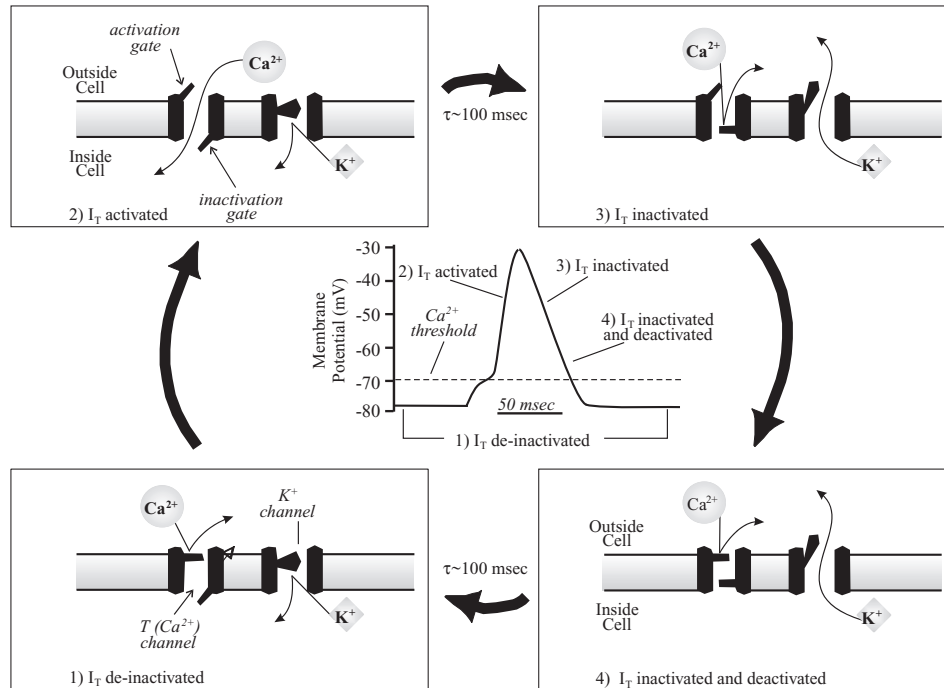


FIGURE 35.7. Highly schematized view of the actions of voltage-dependent T (Ca^{2+}) and K^+ channels underlying a low-threshold Ca^{2+} spike. The four numbered panels show the sequence of channel events, and the central graph shows the effects on membrane potential. The T channel has two voltage-dependent gates: an *activation* gate that closes at hyperpolarized levels and opens with depolarization, and an *inactivation* gate that shows the opposite voltage dependency. The K^+ channel shown is really a conglomeration of several such channels that have only a single gate that opens during depolarization; thus, these channels do not inactivate. 1, At a relatively hyperpolarized resting membrane potential (~ 70 mV), the activation gate of the T channel is closed but the inactivation gate is open, so the T channel is deinactivated. The single gate for the K^+ channel is closed. 2, With sufficient depolarization to reach its threshold, the activation gate of the T channel opens, allowing Ca^{2+} to flow into the cell. This depolarizes the cell, providing the upswing of the low-threshold spike. 3, The inactivation gate of the T channel closes after roughly 100 msec (“roughly,”

because closing of the channel is a complex function of time and voltage), and the K^+ channel also opens. These combined actions lead to the repolarization of the cell. While the inactivation gate of the T channel is closed, the channel is said to be inactivated. There are probably several different kinds of K^+ channels involved with different time constants, but in general, they open more slowly than does the activation gate of the T channel. Also, not shown, K^+ channels dependent on Ca^{2+} entry are probably involved. 4, Even though the initial resting potential is reached, the T channel remains inactivated, because it takes roughly 100 msec (“roughly” having the same meaning as above) of hyperpolarization to deinactivate it; it also takes a bit of time for the various K^+ channels to close. Note that the behavior of the T channel is qualitatively exactly like that of the Na^+ channel involved with the action potential, but with several quantitative differences: the T channel is slower to inactivate and deinactivate, and it operates in a more hyperpolarized regime.

ubiquitous to thalamic relay cells: they have been found in every relay cell of every thalamic nucleus of every mammalian species so far studied (reviewed in Sherman and Guillery, 1996). Figure 35.7 shows the voltage dependence of the T channels and that of K^+ channels also involved in the generation of the low-threshold spikes. The T channels have two voltage-sensitive gates, an activation gate and an inactivation gate, and both must be open for Ca^{2+} to flow into the cell and thus depolarize it. At the normally hyperpolarized resting membrane potentials (Fig. 35.7(1)), the activation gate is closed but the inactivation gate is open, so the channel is deinactivated. The single gate of the K^+ channel is closed at this membrane potential. If the cell is

now sufficiently depolarized (e.g., by an EPSP), the activation gate pops open, and Ca^{2+} flows into the cell, providing the upswing of the low-threshold spike (Fig. 35.7(2)). However, depolarization causes the inactivation gate to close (Fig. 35.7(3)), but this takes time, on the order of 100 msec or so.⁸ The single gate of the K^+ channel, because of its

⁸Actually the opening or closing of the inactivation gate is a complex function of voltage and time (Jahnsen and Llinás, 1984), so that the more depolarized (or hyperpolarized) the more quickly the gate closes (or opens), but the important point is that under normal conditions, roughly 100 msec is required for these actions.

voltage dependency, also opens, and the combined inactivation of the T channel and activation of the K^+ channel serve to repolarize the cell (Fig. 35.7(4)). Although not shown, in addition to voltage-dependent K^+ channels, Ca^{2+} -dependent ones are also activated by the Ca^{2+} entry and assist the repolarization process. While the membrane is repolarized to its initial potential, the T channel remains inactivated, because it takes roughly 100 msec of this hyperpolarization to deinactivate these channels, after which time the initial conditions are reestablished (Fig. 35.7(1)). To reiterate: when the cell is sufficiently hyperpolarized for more than about 100 msec, the T channel is deinactivated; if deinactivated, a suitable depolarization can then activate the channel, but continued depolarization for more than about 100 msec will inactivate it; the inactivation can then be removed by suitable hyperpolarization for more than about 100 msec.

This voltage dependency of the T channels provides the relay cell with two different firing modes: if the cell is relatively depolarized, the T channels are inactivated and do not participate in the cell's responses; here the cell is said to be in *tonic firing mode*. If the cell is relatively hyperpolarized, the T channels are deinactivated and thus primed for action. They can become activated and, on the basis of mechanisms considered below, can affect how the cell fires; here the cell is said to be in *burst firing mode*.

The voltage-dependent properties of the T channels are qualitatively identical to those of the Na^+ channels underlying the action potential, but there are several important quantitative differences: (1) Opening or closing of the inactivation gate is roughly two orders of magnitude faster for the Na^+ channel. (2) The T channels are found in the cell body and membranes, but not in the axon; thus, the low-threshold spike can be propagated through the dendrites and cell body but not along the axon to cortex. That is, the T channels can affect the signal reaching cortex by the effect of the low-threshold spike on the generation of action potentials (see below). (3) The T channels operate in a somewhat more hyperpolarized regime, and their activation at more hyperpolarized levels is the reason the resultant Ca^{2+} spike is called *low threshold*. (4) The T channels operate in a slightly more hyperpolarized regime than the Na^+ channels.

Figure 35.8 shows recordings from relay cells of the cat's lateral geniculate nucleus, illustrating some of the functional consequences of I_T . When the membrane is more depolarized than roughly -60 to -65 mV for more than ~ 100 msec, I_T becomes inactivated (Fig. 35.8A), and activation by a depolarizing pulse evokes a steady stream of action potentials lasting for the duration of the stimulus: this is tonic firing. When the membrane is more hyperpolarized than about -65 to -70 mV for more than ~ 100 msec (Fig. 35.8B), I_T becomes deinactivated. Now the very same depolarizing

pulse activates I_T , leading to a low-threshold spike, which, in turn, leads to a burst of a few action potentials: this is burst firing. Note that the same excitatory stimulus produces two very different signals relayed to cortex, and the difference depends on the initial membrane potential of the relay cell, because this determines the inactivation state of I_T . The stimulus in this example is a current pulse, but the same would apply to a sufficiently large EPSP.

The size of the activated low-threshold spike depends on the extent to which the cell is hyperpolarized before being activated, because the more the cell is hyperpolarized, the more T channels are deinactivated and thus available to contribute to the low-threshold spike (Fig. 35.8C). As would be expected, the larger the low-threshold spike, the larger the number of action potentials evoked in the associated burst (Fig. 35.8C). However, in addition, the low-threshold spike is activated in an all-or-none manner, because at any one initial membrane potential, suprathreshold activating inputs activate low-threshold spikes of essentially the same amplitude, regardless of how far above threshold the activating input is (Fig. 35.8D). One implication of this for the difference in input/output relationships between burst and tonic firing is shown in Figure 35.9. This relationship is fairly linear for tonic firing, because there is a direct link between the input depolarization and activation of action potentials, leading to the monotonic relationship as shown. However, the relationship is indirect for burst firing, since it is the low-threshold spike that controls firing, and, as Figure 35.8D shows, larger activating inputs do not produce larger low-threshold spikes.

Properties of I_T in interneurons and reticular cells. I_T is present in both interneurons and reticular cells, but its action is subtly different in these cells. Its activation in interneurons is a matter of some controversy. Several studies suggest that I_T is rarely activated in these cells, because it is masked by I_A (Pape et al., 1994). I_A is a K^+ conductance with a voltage dependence similar to that of I_T : it is inactivated at depolarized levels and deinactivated at hyperpolarized levels, from which it can be activated (for details, see McCormick, 1991). However, unlike I_T , I_A creates hyperpolarization, since the current is composed of K^+ ions leaving the cell. Some evidence suggests that, in interneurons, the relative voltage dependency of these two currents is such that I_A is typically activated before I_T , thereby preventing activation of I_T (Pape et al., 1994). In relay cells, the relative voltage dependency is different, so that I_T is activated first (Pape et al., 1994). However, other evidence suggests that if the input resistance of the interneuron is high enough, low-threshold spiking is readily produced (Zhu et al., 1999). At present, it is difficult to reconcile these views. Nonetheless, it should be appreciated that tonic firing and burst firing in the interneuron, to the extent that

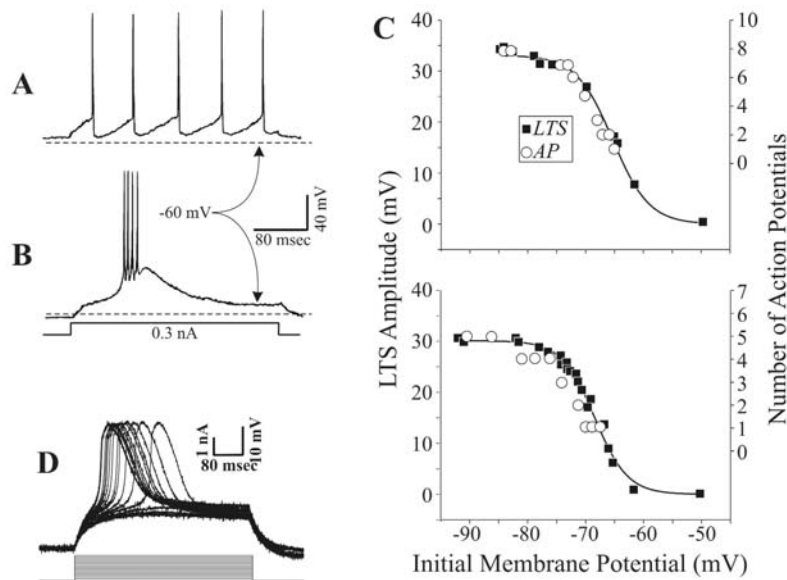


FIGURE 35.8. Properties of I_T and the low-threshold spike; examples from intracellular in vitro recordings of geniculate relay cells of the cat. *A, B*, Voltage dependency of the low-threshold spike. Responses are shown to the same depolarizing current pulse delivered intracellularly but from two different initial holding potentials. With relative depolarization of the cell (*A*), I_T inactivates, and the cell response is a stream of unitary action potentials lasting for the duration of a suprathreshold stimulus. This is the *tonic mode* of firing. With relative hyperpolarization of the cell (*B*), I_T deinactivates, and the current pulse activates a low-threshold spike with four action potentials riding its crest. This is the *burst mode* of firing. *C*, Voltage dependency of low-threshold spike amplitude and associated burst response. Examples for two cells are shown. The number of action potentials were recorded first in the experiment, and then the pro-

cedure was repeated after tetrodotoxin (TTX) application to eliminate action potentials and isolate the low-threshold spike for measurement. The more hyperpolarized the cell before activation (*Initial Membrane Potential*), the more action potentials (*AP*) in the burst (open circles) and the larger the low-threshold spike (filled squares and curve). *D*, All-or-none nature of low-threshold spikes in another geniculate cell, measured in the presence of TTX. After initial hyperpolarization of the cell, current pulses were injected in 10 pA incremental steps. Smaller (subthreshold) pulses produced resistive-capacitive responses, but all larger (suprathreshold) pulses evoked low-threshold spikes that are all of the same amplitude, regardless of how far the depolarizing pulse exceeded activation threshold. (*C* redrawn from Sherman, 2001; Zhan et al., 2000; *D* redrawn from Zhan et al., 1999.)

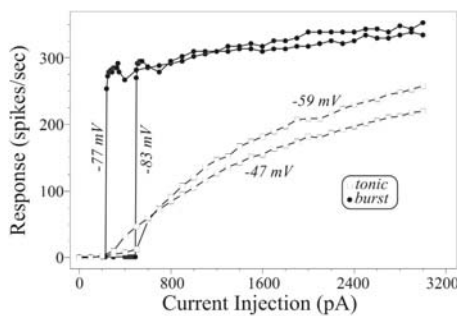


FIGURE 35.9. Input output relationship for a geniculate relay cell recorded intracellularly in vitro. The input variable is the amplitude of the depolarizing current pulse, and the output is the firing frequency of the cell. To compare burst and tonic firing, the firing frequency was determined by the first six action potentials of the response, since this cell usually exhibited six action potentials per burst in this experiment. The initial holding potentials are shown; -47 mV and -59 mV reflect tonic mode (open squares and curves), whereas -77 mV and -83 mV reflect burst mode (filled curves). (Redrawn from Zhan et al., 1999.)

they exist, describe axonal outputs of interneurons, and their dendritic outputs may follow quite different and independent patterns.

Cells of the thalamic reticular nucleus also have burst firing based on voltage-dependent T channels, but the temporal properties are slightly different from those in relay cells, leading to longer low-threshold spikes and more prolonged bursts in reticular cells (for details, see Destexhe et al., 1996).

SIGNIFICANCE OF BURST AND TONIC FIRING The first studies of thalamic bursting in vivo emphasized the presence of rhythmic bursting in thalamic relay cells during slow-wave sleep and certain pathological conditions, such as epilepsy, in which this bursting is synchronized across large cell populations. In these conditions, such bursting also interferes with normal relay functions, and it was thus considered not to be a relay mode of firing (Fanselow et al., 2001; Steriade and Llinás, 1988; Steriade and McCarley, 1990; Steriade et al., 1990, 1993).

Because such rhythmic bursting was not seen during waking behavior, this led to the notion that bursting occurs

only during sleep or pathological state and that tonic firing is the normal relay mode during waking behavior. However, it is now clear that bursting also occurs during normal waking behavior (Edeline et al., 2000; Faselow et al., 2001; Lenz et al., 1998; Magnin et al., 2000; Ramcharan et al., 2000; Swadlow and Gusev, 2001), but because the bursting then is not rhythmic it is harder to detect, and this perhaps explains why it was not emphasized in earlier studies. It may also be that the rhythmic bursting seen during slow-wave sleep provides a positive signal to cortex that nothing is being relayed despite the possible presence of sensory stimuli, and this is less ambiguous than no activity, which could mean either no relay or no stimulus. In contrast, when the bursting is arrhythmic, this arrhythmicity can represent responses evoked by sensory stimuli.

Most relay cells during waking behavior fire more often in tonic mode, and the amount of bursting seems to go down to small values as the animal becomes more alert (Ramcharan et al., 2000; Swadlow and Gusev, 2001). Nonetheless, both modes effectively relay retinal information to cortex (Ramcharan et al., 2000; Reinagel et al., 1999; Sherman, 2001), and thus the presence in an awake animal of both modes, tonic and nonrhythmic bursting, raises the obvious question: what is the significance of these two modes? They represent very different ways in which the relay cell responds to the same input, indicating that the same message is relayed to cortex in one of two different ways. Thus, when messages arrive at the relay cell, the level of its membrane potential, which determines the inactivation state of I_T , can strongly influence the nature of the information that is transmitted to cortex. Receptive field analysis from relay cells of the cat's lateral geniculate nucleus indicates that both response modes convey comparable levels of information in the relay to cortex (Reinagel et al., 1999), although it is also clear that the nature of that information differs between modes (Sherman, 1996, 2001). There may be many differences related to these two modes, but two that have received considerable attention are linearity of the relay process and detectability of the message that is relayed to cortex.

Linearity. From the cellular properties described above (e.g., Fig. 35.9), it is clear that tonic firing represents a more linear relay mode. This is also seen in the responses of geniculate relay cells to visual stimuli. A clear example is shown in Figure 35.10, which shows the responses to a drifting sinusoidal grating of a relay cell recorded in vivo in an anesthetized cat. When the cell is in tonic mode, the response to the grating has a sinusoidal profile (Fig. 35.10*A*, lower). This means that the response level closely matches the changes in contrast, indicating a very linear relay of this input to cortex. However, when the same stimulus is applied to the same cell, but now in burst mode, the response no longer seems sinu-

soidal (Fig. 35.10*B*, lower), indicating considerable nonlinear distortion in the relay. Thus, tonic mode is better at preserving linearity in the relay of information to cortex (Sherman, 1996, 2001).

Detectability. The upper histograms of Figure 35.10 show further that spontaneous activity is lower during tonic than burst firing. Higher spontaneous activity is actually useful for maintaining linearity of response, because it helps prevent rectification of the response to inhibitory phases of visual stimulation, and rectification is a nonlinearity. Perhaps more interesting is the notion that spontaneous activity represents firing without a visual stimulus and can thus be considered a noisy background against which the signal—the response to the visual stimulus—must be detected. In this regard, the signal-to-noise ratio appears to be higher during burst firing, and indeed, the use of a method from signal detection theory involving the calculation of *receiver operating characteristic* curves (Green and Swets, 1966; Macmillan and Creelman, 1991) shows that stimulus detectability is improved during burst firing compared to tonic firing (Sherman, 1996, 2001).

Bursting as a “wake-up call.” The above differences in firing modes as regards linearity and detectability suggest the following hypothesis (Sherman, 1996, 2001). Tonic firing is better for faithful, detailed reconstruction of the stimulus,

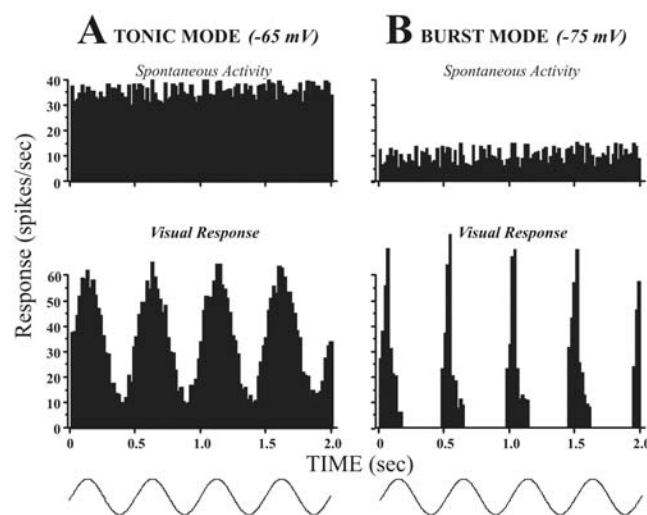


FIGURE 35.10. Tonic and burst responses of relay cells from the cat's lateral geniculate nucleus to visual stimulation. *A*, *B*, Average response histograms of responses of one cell to four cycles of drifting sinusoidal grating (lower) and during spontaneous activity (upper). The contrast changes resulting from the drifting grating are shown below the histograms. The cell was recorded intracellularly in vivo, and current injected through the recording electrode was used to bias membrane potential to more depolarized (-65 mV), producing tonic firing (*A*), or more hyperpolarized (-75 mV), producing burst firing (*B*).

because the nonlinear distortions created during burst firing would limit the extent to which cortex receives an accurate copy of the messages that are being passed through the thalamus. However, burst firing would be better for initial stimulus detectability. For instance, when an animal is drowsy, it might be advantageous to have geniculate relay cells in burst mode to maximize detection of a new visual stimulus; after detection, the relay can be switched to tonic firing for more faithful stimulus analysis (for details of this hypothesis, see Sherman, 1996, 2001). Indeed, there is evidence from the somatosensory system of awake, behaving rabbits that thalamic relay cells in burst mode are much more likely to evoke an action potential in their cortical target cells than when these relay cells are firing in tonic mode (Swadlow and Gusev, 2001). This finding that bursts punch through the thalamocortical synapse much more effectively than tonic firing is consistent with, but of course falls short of proving, the notion that bursts serve as a wake-up call.

Control of response mode. For this hypothesis to be plausible, there must be ways in which thalamic circuitry can be employed to control the firing mode. In fact, the functional circuitry shown schematically in Figure 35.4 provides this requirement. As noted above, to switch the inactivation state of I_T requires a change in membrane voltage that must be sustained for roughly ≥ 100 msec. Sustained depolarization is needed to inactivate I_T and sustained hyperpolarization for deinactivation. Activation of ionotropic receptors with their fast postsynaptic potentials seems poorly suited to this task, because without extensive temporal summation, the changes in membrane polarization would be too transient to affect the inactivation state of I_T significantly. Metabotropic receptors are much better suited for this task, since their activation would produce sufficiently sustained postsynaptic potentials. Thus, activation of metabotropic glutamate receptors from cortex or muscarinic receptors from the parabrachial region produces a sufficiently long EPSP to inactivate I_T and switch the firing mode from burst to tonic. In contrast, activation of $GABA_B$ receptors, mainly from activation of reticular inputs but also possibly from interneuronal inputs, produces a sufficiently long IPSP to deinactivate I_T and switch the firing mode from tonic to burst. Indeed, evidence for such switching from activation of these inputs exists from both in vivo and in vitro studies (reviewed in Sherman and Guillery, 1996, 2001).

Ultimately, it is the cortical and parabrachial inputs that control firing mode via their direct inputs to relay cells, which promote tonic firing, and their indirect inputs, via reticular (and possibly interneuron) inputs, which promote burst firing. At the cellular level, both inputs seem to have the same effect. However, the corticogeniculate pathway is highly topographic and purely visual, so that this pathway would presumably control firing mode for groups of genic-

ulate cells based on specific visual parameters such as different locations within the visual field. The diffuse nature of the parabrachial input suggests that its effects are more widespread in the lateral geniculate nucleus and might relate more globally to overall levels of attention (e.g., more bursting exists during states of drowsiness; see Ramcharan et al., 2000; Swadlow and Gusev, 2001) or to which sensory system is being used.

This is not to say that the only purpose of cortical and brainstem inputs is to control firing mode. For example, the corticogeniculate input seems quite heterogeneous, and several other functions have been proposed for it (e.g., McClurkin and Marrocco, 1984; McClurkin et al., 1994; Schmielau and Singer, 1977; Sillito et al., 1993, 1994). The point here is that these multiple functions are not mutually exclusive.

The functional organization of the pulvinar region

THE PULVINAR REGION AS A VISUAL RELAY Although much less is known about the pulvinar region than about the lateral geniculate nucleus, it provides an important pathway to many, possibly all, higher visual cortical areas. The cells in this complex have visual receptive fields (Bender, 1982; Chalupa, 1991; Hutchins and Updyke, 1989), and their links with extrastriate visual cortical areas have long been recognized (Jones, 1985), but the functional nature of this link has become clear only more recently. In order to appreciate the nature of this link, it is important to recall that the lateral geniculate nucleus receives modulatory afferents from layer 6 of cortex and driving afferents, providing the visual inputs, from the retina. These two types of afferent were described above, and it was shown that they are clearly distinguishable in terms of their light and electron microscopic appearance, in terms of the patterns of synaptic connections that they establish, and in terms of their driving or modulatory functions: silencing the retinal inputs abolishes the receptive field properties of lateral geniculate cells, whereas silencing the cortical inputs changes the receptive field properties of geniculate cells only slightly (Baker and Malpeli, 1977; Geisert et al., 1981; Kalil and Chase, 1970; McClurkin and Marrocco, 1984; McClurkin et al., 1994; Schmielau and Singer, 1977). Further, the receptive field properties of lateral geniculate cells are very similar to those of retinal cells but are not like those of layer 6 cortical cells.

We know from injections of retrograde tracers into the lateral geniculate nucleus that this nucleus receives afferents from cortical layer 6 but not from cortical layer 5 (Gilbert and Kelly, 1975). Further, injections of anterograde tracers into cells in layer 6 of area 17 label the axons having the characteristics of the modulatory afferents described above (Fig. 35.5, *right*), whereas injections of layer 5 cells produce no labeled axons in the lateral geniculate nucleus (Bourassa

and Deschênes, 1995; Rockland, 1996). The pulvinar region is different. Experiments using retrograde and anterograde tracers have shown that it receives afferents from layers 5 and 6 of visual cortex (Abramson and Chalupa, 1985), and apart from a very small region (the geniculate wing, which we regard as part of the lateral geniculate nucleus rather than the pulvinar; see Guillery et al., 1980), it receives no retinal afferents. The afferents from layer 6 seem quite similar to the layer 6 afferents that go to the lateral geniculate nucleus. They have the same characteristic light microscopic appearance (Bourassa and Deschênes, 1995; Ojima et al., 1996), and corticothalamic terminals with the same electron microscopic appearance, and the same distribution of synaptic contacts, have been described in the pulvinar region (Feig and Harting, 1998; Mathers, 1972a; Ogren and Hendrickson, 1979; Rouiller and Welker, 2000). We regard them as modulators, almost certainly functioning very much like the layer 6 modulators to the lateral geniculate nucleus, although currently there is little experimental evidence about their functional roles. The afferents from layer 5 of visual cortex look remarkably like the retinal afferents in the lateral geniculate nucleus in terms of their light microscopic (Bourassa and Deschênes, 1995; Ojima et al., 1996) and electron microscopic appearance (Feig and Harting, 1998; Mathers, 1972a; Ogren and Hendrickson, 1979; Rouiller and Welker, 2000). Further, they establish the same pattern of synaptic contacts. We regard them as the drivers of the pulvinar cells, and it is because these drivers come from areas of cortex classifiable as visual that we see visual receptive fields in the pulvinar region. Evidence that these layer 5 afferents function as drivers is provided by the fact that silencing the cortical areas that send layer 5 afferents to the pulvinar relay abolishes (Bender, 1983) or greatly diminishes (Chalupa, 1991) the visual responses of the pulvinar cells and by the fact that the receptive field properties of pulvinar cells are not unlike those of cells in cortical layer 5 (Chalupa, 1991).

So far, we have not specified which visual areas give rise to which afferents. In the cat, the lateral geniculate nucleus receives layer 6 afferents not just from areas 17, but also from areas 18 and 19 (Gilbert and Kelly, 1975; Murphy et al., 2000; Updyke, 1977) and from other visual cortical areas farther afield (Abramson and Chalupa, 1985; Gilbert and Kelly, 1975; Updyke, 1981). The pulvinar region receives afferents from areas 17, 18, and 19 (in the cat) and from other visual cortical areas such as posteromedial lateral suprasylvian sulcus (PMLS) and posterolateral lateral suprasylvian sulcus (PLLS) (Updyke, 1977, 1981), and many of these are characteristic layer 6 afferents (Guillery et al., 2001). Other inputs to the cat's pulvinar region, however, come from cortical layer 5 and have the characteristics of layer 5 afferents, and these also come from areas 17, 18, and 19 (Fig. 35.5, *left*; see also Abramson and Chalupa, 1985; Guillery et al., 2001).

We look at some of the details of these connections more closely for the cat in the section "The Pulvinar as a Monitor of Motor Outputs." For now, it is sufficient to recognize that the pulvinar region receives two types of cortical afferent and that the layer 6 afferents can be regarded as modulators, whereas all the layer 5 afferents are reasonably regarded as drivers, although currently only some have been tested from this point of view. Closely related to the distinct functional roles of these two cortical afferents to the pulvinar region is the fact that whereas the layer 6 afferents send a rich innervation to the modulatory cells of the thalamic reticular nucleus, the layer 5 afferents do not.

FIRST-ORDER AND HIGHER-ORDER THALAMIC RELAYS The fact that the pulvinar region receives driving afferents from layer 5 of visual cortex shows that the pulvinar serves as a relay in the visual pathways for messages that have already been through cortical processing once. For this reason, the pulvinar region has been called a *higher-order visual relay*, in contrast to the *first-order relay* in the lateral geniculate nucleus, which transfers ascending messages directly to cortex (Guillery, 1995; Guillery and Sherman, 2002b; Sherman and Guillery, 1996, 2001). This distinction between first- and higher-order relays is found not only for the visual pathways but for other relays to cortex as well. However, only the visual relays concern us here. One important point about the higher-order visual relays is that they involve a much greater volume of thalamus, and a much greater area of cortex, than does the first-order visual relay in the thalamus. That is, the pulvinar region is far larger than the lateral geniculate nucleus, and the areas of cortex in receipt of inputs from the pulvinar region are, in total, far greater than area 17.

We have described the pulvinar region as providing higher-order relays to extrastriate cortical areas. However, the possibility that there may also be first-order pulvinar relays of ascending afferents has not been excluded. The small direct input to the pulvinar from the retina was mentioned earlier but, as noted above, we regard this as part of the lateral geniculate nucleus. It clearly represents a first-order relay. The input from the superior colliculus and pretectum to a part of the pulvinar raises another problem. Are these driving or modulatory inputs?

There were strong arguments in the past (Diamond, 1973; Schneider, 1969; Sprague, 1966, 1972; Sprague et al., 1970) for the view that there are two parallel visual pathways going to the cortex. This conclusion was based on behavioral studies primarily in the cat, hamster, and tree shrew and on anterograde tract tracing studies that demonstrated axonal pathways from the region of the tectum to the pulvinar (Altman and Carpenter, 1961). One of these parallel pathways from the retina goes through the lateral geniculate nucleus to striate cortex, and the other relays through the

tectum and then the pulvinar to the extrastriate cortex. However, recordings from cells in the pulvinar region of cats and monkeys have shown that the receptive field properties of cells there are dependent on cortical inputs, not tectal inputs (Bender, 1983; Chalupa, 1991; Chalupa et al., 1972), suggesting that the tectal inputs are not drivers innervating a pulvinar first-order relay (see also Smith and Spear, 1979, on the effects of tectal lesions on responses in higher cortical areas of cats).

The morphological evidence on the structure of the tectopulvinar connections is conflicting (Mathers, 1971; Partlow et al., 1977; Robson and Hall, 1977), with some reports showing terminals like those of the layer 6 modulators and others showing terminals like those of the layer 5 drivers and the retinal terminals. This issue needs to be resolved. Since there are several distinct subdivisions of the pulvinar, which are not easily compared across species, it is possible that there are some tectal drivers innervating some first-order relays in some regions of the pulvinar, with other tectal inputs acting as modulators. It is possible that there are significant species differences in the extent to which such tectopulvinar driver afferents may or may not play a significant role in the transfer of visual information to higher cortical areas (Rodman et al., 1989, 1990). Further, since cells in layer 5 of visual cortex send terminals to the pulvinar region and to the superior colliculus (Guillery et al., 2001), it is possible that lesions or injections in the colliculus will produce changes in the pulvinar region that do not represent a tectopulvinar pathway. The possibility that parts of the pulvinar may be in receipt of drivers from the tectum and also from layer 5 of cortex raises a question addressed in the section "Parallel Pathways through the Pulvinar Region," that arises wherever one finds two driving inputs innervating the same part of the thalamus. Do they interact on single relay cells or do they, like X cells and Y cells in the A layers of the lateral geniculate nucleus, form two essentially independent parallel pathways?

THE PULVINAR REGION AS A KEY RELAY IN CORTICOCORTICAL COMMUNICATION The distinction between first- and higher-order relays outlined above shows the pathways over which the pulvinar region receives its visual inputs from the visual cortex and provides grounds for thinking of these as the drivers of pulvinar cells. Recognizing the pulvinar as a higher-order relay provides a clear functional role for the cells of the pulvinar, at least in the sense that the functional roles of visual, auditory, and somatosensory thalamic relays were assigned in the nineteenth century when the ascending afferent pathways to these relays were defined. That is, the pulvinar serves as a relay from one visual cortical area to other cortical areas. Further, the functional parallel between retinal inputs to the lateral geniculate nucleus and cortical layer 5 inputs to the pulvinar provides a useful key for

comparing these two visual relays, which we explore in subsequent sections. Before looking at these comparisons more closely, however, it is important to stress that the pulvinar as a higher-order relay takes on a vitally important role as a key participant in corticocortical communication.

The pathway that goes from layer 5 in one cortical area, through a pulvinar relay, to another cortical area provides a potentially important, but largely unstudied and often unrecognized, transthalamic route for corticocortical communication. This transthalamic pathway is likely to differ in its functional properties from the more widely studied direct corticocortical route (Van Essen et al., 1992; and see Fig. 35.11). Specifically, the thalamic relay has, as we have seen, properties that can modify transmission in accord with attentional needs, and so far as we know, these properties are not characteristic of the direct corticocortical pathways. Further, the thalamic relay is, as we show below, transmitting information that goes from cortex by a branched axon to thalamus and to lower, motor or premotor centers (Guillery et al., 2001; Guillery and Sherman, 2002a), so that the transthalamic

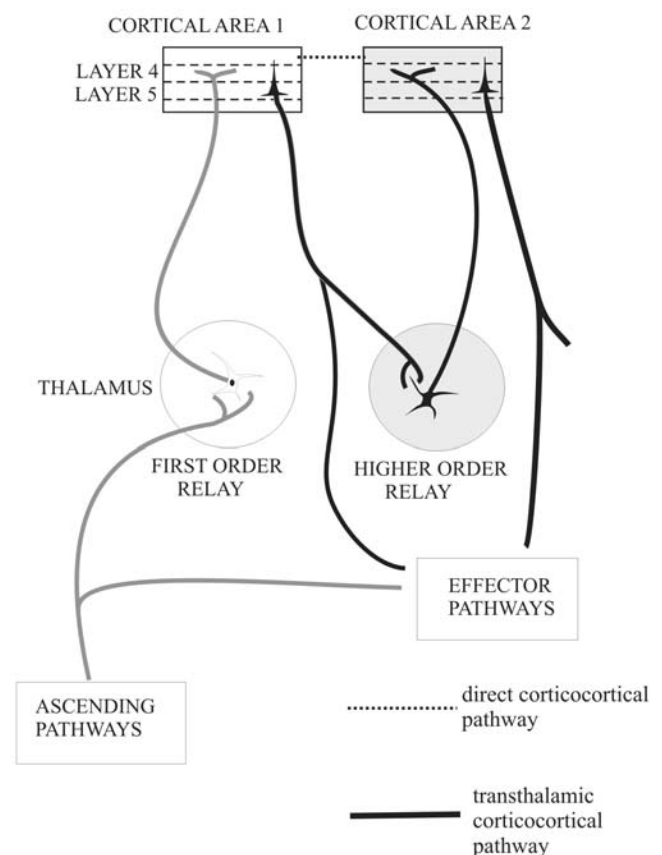


FIGURE 35.11. Schema showing first-order and higher-order thalamic relays and the relationship of each to effector pathways passing through the brainstem. Note the distinction between direct corticocortical pathways and transthalamic corticocortical pathways.

mic pathway can be seen as sending a copy of a motor instruction from one cortical area to another.

There are a number of reasons why the thalamic input to higher cortical areas has received much less attention than has the direct corticocortical input. One is that for many years it was simply not recognized as a possibility, because the layer 5 and layer 6 afferents could not be distinguished from each other, and there was no reason to consider the layer 5 input to thalamus as a driver. A second reason concerns the number of axons involved. The thalamocortical afferents represent a relatively small group of afferents to cortex, and thus attention was directed at the apparently much more massive, direct corticocortical connections. However, this consideration has to be viewed in relation to what we know about the first-order visual relay, where the afferents from retina represent only about 5% to 10% of the synapses in the lateral geniculate nucleus (Van Horn et al., 2000), and the geniculocortical afferents in area 17 also represent only about 5% to 10% of the synapses in cortical layer 4 (Ahmed et al., 1994; Latawiec et al., 2000). The modulators, in fact, far outnumber the drivers in these pathways, and, as noted above, a strategy that considered only the size of an input would not lead one to see the retinal input as a major source of drivers to the lateral geniculate nucleus. The large number of synapses arising from modulators probably reflects the delicate adjustments that the modulators are capable of, and may also indicate that there are modulatory functions that still remain to be explored; the numbers cannot be taken as a good indication of which pathway carries the information that the pathway is processing (the receptive fields in the visual pathways). Insofar as it is reasonable to expect some common organizational pattern to characterize all thalamocortical pathways, one should expect that the main information bearing driver input to higher cortical areas will come from the thalamus, as it does for all first-order cortical areas. That is, the driver visual inputs to area 17 come from the thalamus, not from other cortical areas, which instead are modulators there.

Another important and practical reason why the transthalamic corticocortical pathways have received much less attention than has the direct corticocortical pathway is that it is generally easier to explore the cortical surface than the depths of the thalamus, particularly when it comes to tracing the pathways. We stress in later sections ("Parallel Pathways through the Pulvinar Region" and "Projections from the Pulvinar Region to the Cortex") some of the difficult problems that need to be overcome before we can expect to understand the functional organization of the pathways that are relayed in the pulvinar region. However, looking for evidence about the nature of corticocortical processing by studying the direct corticocortical pathways, which are readily accessible on the surface, and ignoring the deeper

transthalamic pathways, which are likely to prove more difficult, can at best be justified by arguments such as those used by the proverbial drunk, searching for lost keys under the lamppost, where it was light.

So far as we know, all cortical areas receive thalamic afferents, and for almost all higher cortical areas, the functional contribution made by the thalamic afferents remains essentially unexplored. This evidence in itself suggests that schemes tracing connections to primary cortical receiving areas, and from these through corticocortical pathways progressively to higher and higher cortical areas, for perceptual processing and eventually for motor outputs (e.g., Kandel et al., 2000; Van Essen et al., 1992) represent a false view about the connections that underlie the cortical relationships of sensory inputs, perception, and movement control.

Not only do all cortical areas probably receive thalamic inputs, but most, possibly all, have descending outputs from layer 5. The axonal pathways of these layer 5 outputs have been studied for several cortical areas recently by tracing individual axons, and it has been found that where corticofugal axons provide a characteristic driver innervation for a higher-order thalamic relay, they very commonly also send a branch through the thalamus more caudally to the midbrain or pons (reviewed in Guillery and Sherman, 2002a). Although the final destination of these more caudal branches is not always defined, we have to think of the corticothalamic drivers as representing branches of an axon that also has descending, motor connections. This issue is explored in the next section. Here it is important to look at these multiple output pathways from many cortical areas as an important reason for seeing cortical processing as being continually in touch with lower motor centers (Fig. 35.12). Messages may be processed through several stages in many functionally distinct cortical areas on their way to motor cortical areas, but at almost any stage there is direct output to motor or premotor centers. Area 17 sends axons to the superior colliculus, which is concerned with the control of head and eye movements, and there are comparable outputs from many other visual cortical areas that have connections with the pulvinar.

In summary, there is an important difference between conventional views of corticocortical processing for vision and the one that recognizes the importance of transthalamic corticocortical pathways. In the conventional views, information enters striate cortex from the lateral geniculate nucleus and is then processed entirely within cortex. The processing strictly involves direct corticocortical connections among many discrete areas (more than 30 in the monkey and probably fewer in the cat) organized into several (5–6 in the monkey) hierarchical levels, with feedback as well as feedforward connections and, occasionally, with the recognition that there may be some modulatory influences from the thalamus (Olshausen et al., 1993; Van Essen et al., 1992).

there derive from terminals with driver (i.e., RL) morphology. Overall, estimates suggest that driver input in pulvinar and the lateral geniculate nucleus range between roughly 2% and 7%.

We have very little information about the membrane properties of cells in the pulvinar (but see Jahnsen and Llinás, 1984), but on the basis of the structural similarities and on the basis of the ubiquitous distribution throughout thalamus of the critical conductances described in the section “Properties of I_T in Relay Cells,” it is reasonable to conclude that generally the same ground rules for transmission to cortex apply. This is an area where detailed studies may reveal functional differences that are currently undefined. We shall assume that the pulvinar region functions much like the lateral geniculate relay in terms of how modulators act, how the burst and tonic modes are controlled, and how information is transmitted from the drivers to cortex.

LAYERS AND MAPS The pulvinar region can be divided into a number of distinct zones. Some of these zones are defined on the basis of differential staining properties, some are defined on the basis of their connections, and others are defined by mapping the visual field and identifying a new area wherever a new visual field map can be demonstrated (Adams et al., 2000; Graybiel and Berson, 1980a; Gutierrez et al., 2000; Shipp, 2001; Updyke, 1981). This last is basically the same argument that was originally and successfully used for defining cortical areas. Each functionally distinct cortical area was defined as a single map, which may have a particular distortion of the visual field and may even not include the whole visual field, but any one map contains no duplications (Lane et al., 1971; Tusa et al., 1979; Zeki, 1969). At present the differential stains, the connections, and the maps do not produce precisely matching subdivisions, and especially for the monkey, there are some problems still to be resolved before one can clearly identify the separate zones of the pulvinar region.

In the cat, Updyke's studies of receptive fields and of corticothalamic axonal projections have produced a relatively clear picture (Updyke, 1981) that allows one to distinguish a number of major subdivisions, each with its own map and each receiving distinctive patterns of afferents from several visual cortical areas or from the superior colliculus. In each subdivision, it is possible to define lines that correspond roughly to the lines of projection in the lateral geniculate nucleus. That is, the lines correspond roughly to a single point in visual space, although the accuracy of the relation is less than it is in the lateral geniculate nucleus. These lines also correspond, roughly, to single points in the cortical area from which these subdivisions receive their cortical afferents, and thalamic cells grouped around such a line have been called *isocortical columns* (Guillery et al., 2001).

Given that there are maps and lines of projection, the next question is, are there layers? If one is looking for architectonically distinguishable layers such as the A layers of the cat or the parvocellular layers of the monkey, then the answer is “no,” there are no such layers identifiable in the pulvinar region of any species. If, however, one asks whether there are identifiable functional and morphological differences as one moves from one end of an isocortical column to the other, then there is evidence that it may be possible to separate functionally distinct “layers.” In this the pulvinar region may be more like the lateral geniculate nucleus of the rabbit (Holcombe and Guillery, 1984) or the “C” regions of the cat (Hickey and Guillery, 1974), where distinct cell groupings are separated from each other along the lines of projection, but with no overt separation of layers.

The best example of this is the lateral part of the lateral posterior nucleus in the cat, where the isocortical columns run from rostradorsal to caudoventral. Several connectional differences can be recorded along this axis. The layer 5 afferents change their appearance, becoming more compact caudoventrally (Guillery et al., 2001), the cortical afferents come from different sources (cortical areas 5 and 7 most rostrally, areas PMLS and PLLS most caudally) (Heath and Jones, 1971; Kawamura et al., 1974; Robertson and Cunningham, 1981; Updyke, 1981) and whereas areas 17, 18, and 19 all send layer 5 corticothalamic afferents to the middle and ventral parts of the columns, area 19 also sends cortical afferents to the more rostral parts, but these are primarily or entirely from layer 6 (Guillery et al., 2001; Updyke, 1977). The functional implications of these connectional differences have not yet been explored for this part of the pulvinar region, but one should expect to find that, as in the lateral geniculate nucleus, the functional properties of the relay cells change as one moves from one end of an isocortical column to the other.

For other subdivisions of the pulvinar region in cat and in monkey, visual field maps or maps of isocortical columns have also been described (Adams et al., 2000; Graybiel and Berson, 1980b; Gutierrez et al., 2000; Shipp, 2001; Updyke, 1981), but there are no observations about the extent to which connectivity patterns change along the direction of any one column or line of projection. Receptive field properties have been described, and they generally resemble the receptive fields of layer 5 cortical cells. However, the extent to which they may vary from one subdivision of the pulvinar region to another or from one part of a column to another has not been explored.

CORTICAL AFFERENTS TO THE PULVINAR REGION Much of the earlier evidence about the cortical inputs to the pulvinar region comes from experiments using methods such as autoradiographic labeling, horseradish peroxidase labeling,

or axonal degeneration, which label the afferents from layers 5 and 6 together and do not allow the discrimination of one from the other. These have been useful for helping to define the maps in the relay (see above), and have helped to show the several cortical areas that send axons to this region. Only fairly recently have methods become available for labeling just a few cortical cells and their axons, and allowing identification of the cortical layer giving rise to the axons or the morphological characteristics of the axons. As indicated above, cortex sends two types of axon to the pulvinar region: layer 5 cells send axons with large, flowery terminals, and layer 6 sends finer axons with small terminals that are mostly on short, stubby side branches distributed irregularly along the length of the axons. They are readily distinguished from each other (Fig. 35.5).

Cortical areas 17, 18, and 19 in the cat all send layer 5 afferents to the lateral part of the lateral posterior nucleus (Guillery et al., 2001). Small, well-localized injections into any one of these cortical areas label a small number of corticothalamic axons, each having a single small terminal zone 100–200 μm across. These terminal zones from a single small injection site are irregularly scattered around, but not accurately along, the ventral and caudal two-thirds of the isocortical columns (Fig. 35.12). The overall terminal distributions of all layer 5 axons from areas 17, 18, and 19 overlap entirely in this region, and as indicated above, the shapes of the terminal arbors are more compact caudoventrally than rostradorsally (not shown in the figure). This part of the nucleus receives few or no layer 6 afferents from areas 17 and 18 (Abramson and Chalupa, 1985; Guillery et al., 2001), but it does receive a rich layer 6 innervation from area 19. These layer 6 axons have a far more widespread distribution in the nucleus around the areas occupied by the layer 5 terminals and also in the most rostral and dorsal part that receives no layer 5 afferents from area 19 but presumably receives layer 5 drivers from other parts of cortex. Where the cortical injections into area 19 are small, there is a striking local sparsity of layer 6 afferents in the region where layer 5 axons from the same injection site have their termination (Fig. 35.13). Of course, there is no corresponding reciprocity for the axons from areas 17 and 18, since the layer 6 terminals do not go to the same nuclear subdivision as the layer 5 terminals.

These observations on just one subdivision of the pulvinar region show that any one part of a single isocortical column can receive driver afferents from more than one functionally distinct cortical area, and that each cortical area distributes its driver terminals quite broadly along any one isocortical column. Further, the distribution of the modulators from layer 6 suggests that there is no simple rule that relates the distribution of the corticothalamic drivers to the distribution of the modulators for any one cortical region, although the relationships we have described suggest that the

layer 6 input serves to modulate layer 5 inputs that do not come from the same small column of cortex or even from the same cortical area.

PARALLEL PATHWAYS THROUGH THE PULVINAR REGION We have seen that a single small cortical injection site labels axons that have terminals widely distributed along the length of a single isocortical column. If there are functional differences along the length of a column, as the connections and the structural features of the terminals suggest there may be, then there is an interesting parallel to be drawn between the parallel pathways of the retinogeniculate connection and the corticopulvinar connection. That is, for the retinogeniculate pathway, a single small area of retina contains several functionally distinct ganglion cell types. Their axons distribute to different parts of the same line of projection in the lateral geniculate nucleus, and their differential distribution along a line of projection is a signal of their functional differences. To some extent this differential distribution of the terminals in the nucleus relates to the geniculate layers, and to some extent it relates to functional differences that are not expressed by layer separations. It is worthwhile to look at the possibility that closely comparable relationships for parallel processing obtain for the corticopulvinar projection where several functionally distinct cortical layer 5 cells can be expected in any one small cortical area or column. These cortical cells then send axons to the pulvinar region that are segregated along the isocortical columns in accordance with their functional characteristics (Fig. 35.13). This is admittedly speculative, but it provides a guide to studying the distribution of functions that is currently not available for studies of the pulvinar region.

The previous paragraph introduced the idea of parallel processing in the corticopulvinar pathways that is comparable to the parallel processing of the retinogeniculate pathways. However, we have seen that there is another, more obvious type of parallel processing that may also have to be recognized in the pulvinar. This is represented by the fact that any one isocortical column receives driving afferents from several distinct cortical areas. Each of these pathways can be seen as a separate input to the pulvinar region, so that corticopulvinar axons from separate cortical areas may also provide parallel pathways through the pulvinar. The issue of whether these represent parallel pathways like the X and Y pathways going through the A layers of the lateral geniculate nucleus with essentially no interaction, or whether there are integrative interactions between the pathways, remains to be resolved.

Although these observations of the distributions of layer 5 and layer 6 axons from cortical areas 17, 18, and 19 to one small part of the pulvinar region can show how it may be possible to analyze cortical afferents in relation to the isocortical columns, it has to be stressed that even for this one

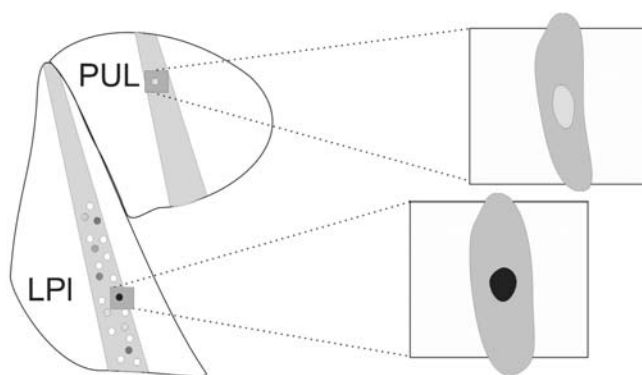


FIGURE 35.13. The lateral part of the lateral posterior nucleus (*LP1*) and the pulvinar (*PUL*) of a cat are shown on the left. The afferents from layer 5 of cortical areas 17, 18, and 19 to *LP1* are shown as for Figure 35.12. In addition, the terminals of two layer 5 afferents from area 19 are shown shaded in the small squares in *LP1* and in *PUL*. The area of these small squares is shown enlarged on the right, where the layer 5 terminals are shown in black for *LP1* and pale gray for *PUL*, and the layer 6 terminals from the same cortical column are shown in intermediate gray. There are virtually no layer 6 terminals in the colored zone occupied by the (colored) layer 5 terminals. The layer 6 terminals extend beyond the layer 5 terminals, especially along the direction of the isocortical columns. Note that we do not know whether the terminals in *LP1* and *PUL* can arise from the same layer 5 cortical cell or always come from different layer 5 cells. They are shown in different shades here, suggesting that they come from different cells. (Based on Guillery et al., 2001.)

part of the complex (the lateral part of the lateral posterior nucleus) our information is incomplete, and for other parts of the complex the information is either entirely unknown or only very sketchy.

PROJECTIONS FROM THE PULVINAR REGION TO THE CORTEX
A vital piece of information needed to understand the function of the pulvinar region is the pattern of projections from the relay cells to the various cortical areas that receive afferents from the pulvinar. This is not merely a question of enumerating the cortical areas that receive afferents from the pulvinar region, although this information is, of course, essential. Studies of retrograde cell degeneration in the thalamus, of retrograde cell labeling, or of anterogradely labeled axonal pathways (Rockland et al., 1999; Walker, 1938; Wong-Riley, 1977) all indicate that there are widespread axonal projections from the pulvinar region to the cortex. To some extent these studies indicate pathways from particular subdivisions of the pulvinar region, but, in general, the information that would allow one to relate each pulvinar subdivision to particular groups of cortical areas is not available.

A more serious consideration arises when one looks at the comparison we have drawn between the pulvinar region and the lateral geniculate nucleus and focuses on differences that can be seen along the lines of projection in the lateral

geniculate nucleus or along the isocortical columns in the pulvinar region. We have focused on the cat's A layers of the lateral geniculate nucleus, which send their axons predominantly to area 17. However, there are also projections to area 18 from the A layers, and these come from the largest cells, which represent the Y cells (Ferster, 1990a, 1990b; Garey and Powell, 1967; Geisert, 1980; Humphrey et al., 1985; Mitzdorf and Singer, 1978; Stone and Dreher, 1973). The C layers in the cat project predominantly to area 19 and to the lateral suprasylvian cortex (Holländer and Vanegas, 1977; Laemle, 1975; Maciewicz, 1975; Raczkowski and Rosenquist, 1980). In the monkey there is also a projection to extrastriate cortical areas, and some of these axons probably arise from the koniocellular elements (Fries, 1981; Yoshida and Benevento, 1981; Yukie and Iwai, 1981). That is, there are two features that make the pattern of cortical projections difficult to analyze. One is that in any one small region along a line of projection there are neighboring cells that are functionally distinct and that also have distinguishable cortical projections. The second is that cells that lie in different sectors of a line of projection are likely to have different cortical projections. Once we have a system of parallel processing passing through a thalamic nucleus, the problem of tracing the separate but intermingled pathways through the thalamic relay becomes particularly difficult, and this applies to both the pulvinar region and the lateral geniculate nucleus. We know almost nothing about the functional significance of thalamic afferents to extrastriate cortex, regardless of whether these are first-order afferents coming through the lateral geniculate nucleus or higher-order afferents coming through the pulvinar. This will, before long, prove to be an important issue for understanding the nature of cortical processing in extrastriate visual cortical areas.

Conclusions

Clearly, the thalamus can no longer be viewed as a passive, machine-like relay of information to cortex. We have outlined a number of important functional properties of a dynamic nature that occur during thalamic relays and that relate to behavioral states such as attention and alertness. This is probably the tip of the iceberg, with many additional functions likely to emerge as our understanding of thalamic properties expands.

It is important to note in this context that the thalamus offers a last "bottleneck" for general behavioral states to have an effect on information processing. Thalamic relays represent a relatively small number of neurons and synapses compared to their target cortical areas. Thus, if the object were to increase or decrease the salience of a particular bit of information, say a visual stimulus at the expense of an auditory one, it would require orders of magnitude less synaptic

processing to modulate at the thalamic level than at the cortical level. For visual processing in mammals, there is no opportunity for the rest of the brain to affect processing in retina. The lateral geniculate nucleus is not only a convenient last bottleneck of information flow, it is the most peripheral site at which such processing can be modulated. In other sensory systems, it is possible to modulate processing more peripherally than at the thalamus, but for all pathways going to cortex, the thalamic level remains the last convenient stage at which modulation can efficiently affect information flow before it is passed to cortex.

When one looks at the visual relays in the thalamus, it is necessary to recognize that there is a quite well-studied *first-order* relay in the lateral geniculate nucleus and a series of more elusive *higher-order* relays in the pulvinar region. The lateral geniculate nucleus relays several functionally distinct, largely independent, topographically organized, parallel visual pathways from the retina to the cortex. It serves, among other possible but currently undefined functions, to modify transmission to visual cortex in accord with attentional needs, acting either in *tonic mode*, where accurate linear transfer of information from the periphery to the cortex is required, or in *burst mode*, where the need is for identification of novel signals that merit attention. Messages from the retina are carried to the lateral geniculate nucleus by the retinogeniculate *drivers*. These represent less than 10% of the afferent synapses to the lateral geniculate nucleus and have characteristic structural features, synaptic connectivity patterns, and functional relationships in terms of transmitters and receptors. The rest of the afferent synapses are formed by *modulators*, which can serve to switch transmission from burst to tonic or from tonic to burst mode. These come from several distinct sources. Some, specifically those from the neocortex and the thalamic reticular nucleus, relate closely to the topographic representation of the retina in the lateral geniculate nucleus and can thus have a local action, whereas others, particularly those from the brainstem, show no topography and appear to have a global action.

The higher-order relays in the pulvinar region serve to transmit information from one cortical area to others. The *drivers* come from pyramidal cells in layer 5 of cortex and represent branches of axons that are going to lower (motor) centers. That is, the pulvinar serves to send copies of motor outputs from one cortical area to another. We stress the likely importance of these transthalamic pathways in corticocortical communication, a role that has not been recognized in the past. Corticopulvinar driver afferents can be analyzed on the basis of comparisons with the lateral geniculate relay. They show a topographical organization between cortex and thalamus. There are multiple parallel corticopulvinar pathways coming from several cortical areas that are relayed through any one small local region of the pulvinar. In addition, it is probable that the afferent drivers coming from any

one of these cortical areas also represent several functionally distinct pathways. An important key to understanding the functional significance of this higher-order thalamic relay will depend on understanding how the several distinct corticopulvinar driver afferents relate to the pathways that go from the pulvinar region to multiple different cortical areas. We know almost nothing about this either in terms of the specific patterns of connectivity that are established or in terms of possible interactions within the thalamic relay. The parallel afferents may prove to show little or no interaction, comparable to the situation in the first-order geniculate relay, or there may be interaction among the several corticopulvinar afferent drivers, and this could strongly influence views of pulvinar functions.

The organization of the modulatory afferents to the pulvinar also merits closer study than it has received to date. We propose that in general terms, the functions of these afferents are comparable to the functions of the modulators in the lateral geniculate nucleus. That is, they serve to switch the relay between the burst and tonic modes. They can do this on a global basis from the brainstem and other sources, or in terms of local parts of the mapped projections from layer 6 of many distinct cortical areas cortex, or from the thalamic reticular nucleus.

REFERENCES

- Abramson, B. P., and L. M. Chalupa, 1985. The laminar distribution of cortical connections with the tecto- and cortico-recipient zones in the cat's lateral posterior nucleus, *Neuroscience*, 15:81–95.
- Adams, M. M., P. R. Hof, R. Gattass, M. J. Webster, and G. L. Ungerleider, 2000. Visual cortical projections and chemoarchitecture of macaque monkey pulvinar, *J. Comp. Neurol.*, 419:377–393.
- Ahmed, B., J. C. Anderson, R. J. Douglas, K. A. C. Martin, and J. C. Nelson, 1994. Polyneuronal innervation of spiny stellate neurons in cat visual cortex, *J. Comp. Neurol.*, 341:39–49.
- Altman, J., and M. B. Carpenter, 1961. Fiber projections of the superior colliculus in the cat, *J. Comp. Neurol.*, 116:157–177.
- Andreas, S. T., M. Stelios, A. Smirnakis, M. Augath, T. Trinath, and M. K. Logothetis, 2001. Motion processing in the macaque: revisited with functional magnetic resonance imaging, *J. Neurosci.*, 21:8594–8601.
- Baker, F. H., and J. G. Malpeli, 1977. Effects of cryogenic blockade of visual cortex on the responses of lateral geniculate neurons in the monkey, *Exp. Brain Res.*, 29:433–444.
- Bender, D. B., 1982. Receptive-field properties of neurons in the macaque inferior pulvinar, *J. Neurophysiol.*, 48:1–17.
- Bender, D. B., 1983. Visual activation of neurons in the primate pulvinar depends on cortex but not colliculus, *Brain Res.*, 279:258–261.
- Bickford, M. E., A. E. Günlük, W. Guido, and S. M. Sherman, 1993. Evidence that cholinergic axons from the parabrachial region of the brainstem are the exclusive source of nitric oxide in the lateral geniculate nucleus of the cat, *J. Comp. Neurol.*, 334:410–430.

- Bloomfield, S. A., J. E. Hamos, and S. M. Sherman, 1987. Passive cable properties and morphological correlates of neurones in the lateral geniculate nucleus of the cat, *J. Physiol. (Lond.)*, 383:653–692.
- Bloomfield, S. A., and S. M. Sherman, 1989. Dendritic current flow in relay cells and interneurons of the cat's lateral geniculate nucleus, *Proc. Natl. Acad. Sci. USA*, 86:3911–3914.
- Bourassa, J., and M. Deschênes, 1995. Corticothalamic projections from the primary visual cortex in rats: a single fiber study using biocytin as an anterograde tracer, *Neuroscience*, 66:253–263.
- Bowling, D. B., and C. R. Michael, 1984. Terminal patterns of single, physiologically characterized optic tract fibers in the cat's lateral geniculate nucleus, *J. Neurosci.*, 4:198–216.
- Brown, D. A., F. C. Abogadie, T. G. Allen, N. J. Buckley, M. P. Caulfield, P. Delmas, J. E. Haley, J. A. Lamas, and A. A. Selyanko, 1997. Muscarinic mechanisms in nerve cells, *Life Sci.*, 60:1137–1144.
- Casagrande, V. A., 1994. A third parallel visual pathway to primate area V1, *Trends Neurosci.*, 17:305–309.
- Casagrande, V. A., and J. H. Kaas, 1994. The afferent, intrinsic, and efferent connections of primary visual cortex in primates, in *Cerebral Cortex* (A. Peters and K. S. Rockland eds.), New York: Plenum Press, pp. 201–259.
- Casagrande, V. A., and T. T. Norton, 1991. Lateral geniculate nucleus: a review of its physiology and function, in *Vision and Visual Dysfunction* (A. G. Leventhal ed.), London: Macmillan, pp. 41–84.
- Chalupa, L. M., 1991. Visual function of the pulvinar, in *The Neural Basis of Visual Function* (A. G. Leventhal ed.), Boca Raton: CRC Press, pp. 140–159.
- Chalupa, L. M., H. Ansel, and D. B. Lindsley, 1972. Visual input to the pulvinar via lateral geniculate, superior colliculus and visual cortex in the cat, *Exp. Neurol.*, 36:449–462.
- Conley, M., E. Birecree, and V. A. Casagrande, 1985. Neuronal classes and their relation to functional and laminar organization to functional and laminar organization of the lateral geniculate nucleus: a Golgi study of the prosimian primate, *Galago crassicaudatus*, *J. Comp. Neurol.*, 242:561–583.
- Conley, M., and I. T. Diamond, 1990. Organization of the visual sector of the thalamic reticular nucleus in *Galago*, *Eur. J. Neurosci.*, 3:211–226.
- Conn, P. J., and J. P. Pin, 1997. Pharmacology and functions of metabotropic glutamate receptors, *Annu. Rev. Pharmacol. Toxicol.*, 37:205–237.
- Cox, C. L., and S. M. Sherman, 2000. Control of dendritic outputs of inhibitory interneurons in the lateral geniculate nucleus, *Neuron*, 27:597–610.
- Crabtree, J. W., 1992. The somatotopic organization within the cat's thalamic reticular nucleus, *Eur. J. Neurosci.*, 4:1352–1361.
- Crabtree, J. W., 1996. Organization in the somatosensory sector of the cat's thalamic reticular nucleus, *J. Comp. Neurol.*, 366:207–222.
- Crabtree, J. W., 1998. Organization in the auditory sector of the cat's thalamic reticular nucleus, *J. Comp. Neurol.*, 390:167–182.
- Crabtree, J. W., and H. P. Killackey, 1989. The topographical organization of the axis of projection within the visual sector of the rabbit's thalamic reticular nucleus, *Eur. J. Neurosci.*, 1:94–109.
- Cucchiari, J. B., D. J. Uhlrich, and S. M. Sherman, 1991. Electron-microscopic analysis of synaptic input from the perigeniculate nucleus to the A-laminae of the lateral geniculate nucleus in cats, *J. Comp. Neurol.*, 310:316–336.
- Cudeiro, J., and A. M. Sillito, 1996. Spatial frequency tuning of orientation-discontinuity-sensitive corticofugal feedback to the cat lateral geniculate nucleus, *J. Physiol.*, 490:481–492.
- Dankowski, A., and M. E. Bickford, 2003. Inhibitory circuitry involving Y cells and Y retinal terminals in the C laminae of the cat dorsal lateral geniculate nucleus, *J. Comp. Neurol.*, 460:368–379.
- Datskovskaia, A., W. B. Carden, and M. E. Bickford, 2001. Y retinal terminals contact interneurons in the cat dorsal lateral geniculate nucleus, *J. Comp. Neurol.*, 430:85–100.
- de Lima, A. D., and W. Singer, 1987. The brainstem projection to the lateral geniculate nucleus in the cat: identification of cholinergic and monoaminergic elements, *J. Comp. Neurol.*, 259:92–121.
- Destexhe, A., D. Contreras, M. Steriade, T. J. Sejnowski, and J. R. Huguenard, 1996. In vivo, in vitro, and computational analysis of dendritic calcium currents in thalamic reticular neurons, *J. Neurosci.*, 16:169–185.
- Diamond, I. T., 1973. The evolution of the tectal-pulvinar system in mammals: structural and behavioral studies of the visual system, *Symp. Zool. Soc. Lond.*, 33:205–233.
- Diamond, M. E., M. Armstrong-James, M. J. Budway, and F. F. Ebner, 1992. Somatic sensory responses in the rostral sector of the posterior group (POM) and in the ventral posterior medial nucleus (VPM) of the rat thalamus: dependence on the barrel field cortex, *J. Comp. Neurol.*, 319:66–84.
- Edeline, J. M., Y. Manunta, and E. Hennevin, 2000. Auditory thalamus neurons during sleep: changes in frequency selectivity, threshold, and receptive field size, *J. Neurophysiol.*, 84:934–952.
- Erişir, A., S. C. Van Horn, M. E. Bickford, and S. M. Sherman, 1997. Immunocytochemistry and distribution of parabrachial terminals in the lateral geniculate nucleus of the cat: a comparison with corticogeniculate terminals, *J. Comp. Neurol.*, 377:535–549.
- Famiglietti, E. V. J., and A. Peters, 1972. The synaptic glomerulus and the intrinsic neuron in the dorsal lateral geniculate nucleus of the cat, *J. Comp. Neurol.*, 144:285–334.
- Fanselow, E. E., K. Sameshima, L. A. Baccala, and M. A. Nicolelis, 2001. Thalamic bursting in rats during different awake behavioral states, *Proc. Natl. Acad. Sci. USA*, 98:15330–15335.
- Feig, S., and J. K. Harting, 1998. Corticocortical communication via the thalamus: ultrastructural studies of corticothalamic projections from area 17 to the lateral posterior nucleus of the cat and inferior pulvinar nucleus of the owl monkey, *J. Comp. Neurol.*, 395:281–295.
- Ferster, D., 1990a. X- and Y-mediated current sources in areas 17 and 18 of cat visual cortex, *Vis. Neurosci.*, 4:135–145.
- Ferster, D., 1990b. X- and Y-mediated synaptic potentials in neurons of areas 17 and 18 of cat visual cortex, *Vis. Neurosci.*, 4:115–113.
- Friedlander, M. J., C.-S. Lin, L. R. Stanford, and S. M. Sherman, 1981. Morphology of functionally identified neurons in lateral geniculate nucleus of the cat, *J. Neurophysiol.*, 46:80–129.
- Fries, W., 1981. The projections from the lateral geniculate nucleus to the prestriate cortex of the macaque monkey, *Proc. R. Soc. Lond. B.*, 213:73–80.
- Galletti, C., M. Gamberini, D. F. Kutz, P. Fattori, G. Luppino, and M. Matelli, 2001. The cortical connections of area V6: an occipito-parietal network processing visual information, *Eur. J. Neurosci.*, 13:1572–1588.
- Garey, L. J., and T. P. S. Powell, 1967. The projection of the lateral geniculate nucleus upon the cortex in the cat, *Proc. R. Soc. Lond. B.*, 169:107–126.
- Geisert, E. E., Jr., 1980. Cortical projections of the lateral geniculate nucleus in the cat, *J. Comp. Neurol.*, 190:793–812.

- Geisert, E. E., Jr., A. Langsetmo, and P. D. Spear, 1981. Influence of the cortico-geniculate pathway on response properties of cat lateral geniculate neurons, *Brain Res.*, 208:409–415.
- Gilbert, C. D., and J. P. Kelly, 1975. The projections of cells in different layers of the cat's visual cortex, *J. Physiol. (Lond.)*, 163:81–106.
- Glees, P., and W. E. Le Gros Clark, 1941. The termination of optic fibres in the lateral geniculate body of the monkey, *J. Anat. (Lond.)*, 75:295–308.
- Graybiel, A. M., and D. M. Berson, 1980a. Autoradiographic evidence for a projection from the pretectal nucleus of the optic tract to the dorsal lateral geniculate complex in the cat, *Brain Res.*, 195:1–12.
- Graybiel, A. M., and D. M. Berson, 1980b. Histochemical identification and afferent connections of subdivisions in the lateralis posterior-pulvinar complex and related thalamic nuclei in the cat, *Neuroscience*, 5:1175–1238.
- Green, D. M., and J. A. Swets, 1966. *Signal Detection Theory and Psychophysics*, New York: Wiley.
- Guillery, R. W., 1966. A study of Golgi preparations from the dorsal lateral geniculate nucleus of the adult cat, *J. Comp. Neurol.*, 128:21–50.
- Guillery, R. W., 1969. A quantitative study of synaptic interconnections in the dorsal lateral geniculate nucleus of the cat, *Z. Zellforsch.*, 96:39–48.
- Guillery, R. W., 1995. Anatomical evidence concerning the role of the thalamus in corticocortical communication: a brief review, *J. Anat.*, 187:583–592.
- Guillery, R. W., S. L. Feig, and D. A. Lozsádi, 1998. Paying attention to the thalamic reticular nucleus, *Trends Neurosci.*, 21:28–32.
- Guillery, R. W., S. L. Feig, and D. P. Van Lieshout, 2001. Connections of higher order visual relays in the thalamus: a study of corticothalamic pathways in cats, *J. Comp. Neurol.*, 438:66–85.
- Guillery, R. W., E. E. Geisert, E. H. Polley, and C. A. Mason, 1980. An analysis of the retinal afferents to the cat's medial interlaminar nucleus and to its rostral thalamic extension, the "geniculate wing," *J. Comp. Neurol.*, 194:117–142.
- Guillery, R. W., and S. M. Sherman, 2002a. Thalamocortical pathways as monitors of ongoing motor instructions. Philosophical Transactions of the Royal Society of London. B: Biological Sciences, 357:1809–1821.
- Guillery, R. W., and S. M. Sherman, 2002b. Thalamic relay functions and their role in corticocortical communication: generalizations from the visual system, *Neuron*, 33:1–20.
- Gutierrez, C., M. G. Cola, B. Seltzer, and C. Cusick, 2000. Neurochemical and connectional organization of the dorsal pulvinar complex in monkeys, *J. Comp. Neurol.*, 419:61–86.
- Hamos, J. E., S. C. Van Horn, D. Raczkowski, D. J. Uhlrich, and S. M. Sherman, 1985. Synaptic connectivity of a local circuit neurone in lateral geniculate nucleus of the cat, *Nature*, 317:618–621.
- Heath, C. J., and E. G. Jones, 1971. The anatomical organization of the of the suprasylvian gyrus of the cat, *Ergeb. Anat. Entwicklungsgeschichte*, 45:1–64.
- Hendry, S. H. C., and R. C. Reid, 2000. The koniocellular pathway in primate vision, *Annu. Rev. Neurosci.*, 23:127–153.
- Hickey, T. L., and R. W. Guillery, 1974. An autoradiographic study of retinogeniculate pathways in the cat and the fox, *J. Comp. Neurol.*, 156:239–254.
- Hickey, T. L., and R. W. Guillery, 1979. Variability of laminar patterns in the human lateral geniculate nucleus, *J. Comp. Neurol.*, 183:221–246.
- Hochstein, S., and R. M. Shapley, 1976a. Linear and non-linear subunits in Y cat retinal ganglion cells, *J. Physiol. (Lond.)*, 262:265–284.
- Hochstein, S., and R. M. Shapley, 1976b. Quantitative analysis of retinal ganglion cell classifications, *J. Physiol. (Lond.)*, 262:237–264.
- Holcombe, V., and R. W. Guillery, 1984. The organization of retinal maps within the dorsal and ventral lateral geniculate nuclei of the rabbit, *J. Comp. Neurol.*, 225:469–491.
- Holländer, H., and H. Vanegas, 1977. The projection from the lateral geniculate nucleus onto the visual cortex in the cat. A quantitative study with horseradish-peroxidase, *J. Comp. Neurol.*, 173:519–536.
- Hubel, D. H., and T. N. Wiesel, 1977. Functional architecture of macaque monkey visual cortex, *Proc. R. Soc. Lond. B.*, 198:1–59.
- Humphrey, A. L., M. Sur, D. J. Uhlrich, and S. M. Sherman, 1985. Termination patterns of individual X- and Y-cell axons in the visual cortex of the cat: projections to area 18, to the 17–18 border region, and to both areas 17 and 18, *J. Comp. Neurol.*, 233:190–212.
- Hutchins, B., and B. V. Updyke, 1989. Retinotopic organization within the lateral posterior complex of the cat, *J. Comp. Neurol.*, 285:350–398.
- Itoh, K., M. Conley, and I. T. Diamond, 1982. Retinal ganglion cell projections to individual layers of the lateral geniculate body in *Galago crassicaudatus*, *J. Comp. Neurol.*, 205:282–290.
- Jahnsen, H., and R. Llinás, 1984. Electrophysiological properties of guinea-pig thalamic neurones: an in vitro study, *J. Physiol. (Lond.)*, 349:205–226.
- Jones, E. G., 1985. *The Thalamus*, New York: Plenum Press.
- Jones, H. E., and A. M. Sillito, 1991. The length-response properties of cells in the feline dorsal lateral geniculate nucleus, *J. Physiol. (Lond.)*, 444:329–348.
- Kalil, R. E., and R. Chase, 1970. Corticofugal influence on activity of lateral geniculate neurons in the cat, *J. Neurophysiol.*, 33:459–474.
- Kandel, E. R., J. H. Schwartz, and T. M. Jessell, 2000. *Principles of Neural Science*, New York: McGraw-Hill.
- Kawamura, S., J. M. Sprague, and K. Nimi, 1974. Corticofugal projections from the visual cortices to the thalamus, pretectum and superior colliculus in the cat, *J. Comp. Neurol.*, 158:339–362.
- Laemle, L. K., 1975. Cell populations of the lateral geniculate nucleus of the cat as determined with horseradish peroxidase, *Brain Res.*, 100:650–656.
- Lane, R. H., J. M. Allman, and J. H. Kaas, 1971. Representation of the visual field in the superior colliculus of the grey squirrel (*Sciurus carolinensis*) and the tree shrew (*Tupaia glis*), *Brain Res.*, 26:277–292.
- Latawiec, D., K. A. C. Martin, and V. Meskenaite, 2000. Termination of the geniculocortical projection in the striate cortex of macaque monkey: a quantitative immunoelectron microscopic study, *J. Comp. Neurol.*, 419:306–319.
- Lennie, P., 1980. Perceptual signs of parallel pathways, *Philos. Trans. R. Soc. Lond. Ser. B Biol. Sci.*, 290:23–37.
- Lenz, F. A., I. M. Garonzik, T. A. Zirh, and P. M. Dougherty, 1998. Neuronal activity in the region of the thalamic principal sensory nucleus (ventralis caudalis) in patients with pain following amputations, *Neuroscience*, 86:1065–1081.
- LeVay, S., and D. Ferster, 1977. Relay cell classes in the lateral geniculate nucleus of the cat and the effects of visual deprivation, *J. Comp. Neurol.*, 172:563–584.
- Leventhal, A. G., 1982. Morphology and distribution of retinal ganglion cells projecting to different layers of the dorsal lateral

- geniculate nucleus in normal and siamese cats, *J. Neurosci.*, 2:1024–1042.
- Maciewicz, R. J., 1975. Thalamic afferents to areas 17, 18 and 19 of cat cortex traced with horseradish peroxidase, *Brain Res.*, 84:308–312.
- Macmillan, N. A., and C. D. Creelman, 1991. *Detection Theory: A User's Guide*, Cambridge: Cambridge University Press.
- Magnin, M., A. Morel, and D. Jeanmonod, 2000. Single-unit analysis of the pallidum, thalamus and subthalamic nucleus in Parkinsonian patients, *Neuroscience*, 96:549–564.
- Mathers, L. H., 1971. Tectal projection to posterior thalamus of the squirrel monkey, *Brain Res.*, 35:357–380.
- Mathers, L. H., 1972a. The synaptic organization of the cortical projection to the pulvinar of the squirrel monkey, *J. Comp. Neurol.*, 146:43–60.
- Mathers, L. H., 1972b. Ultrastructure of the pulvinar of the squirrel monkey, *J. Comp. Neurol.*, 146:15–42.
- McClurkin, J. W., and R. T. Marrocco, 1984. Visual cortical input alters spatial tuning in monkey lateral geniculate nucleus cells, *J. Physiol. (Lond.)*, 348:135–152.
- McClurkin, J. W., L. M. Optican, and B. J. Richmond, 1994. Cortical feedback increases visual information transmitted by monkey parvocellular lateral geniculate nucleus neurons, *Vis. Neurosci.*, 11:601–617.
- McCormick, D. A., 1991. Functional properties of a slowly inactivating potassium current in guinea pig dorsal lateral geniculate relay neurons, *J. Neurophysiol.*, 66:1176–1189.
- Mitzdorf, U., and W. Singer, 1978. Prominent excitatory pathways in the cat visual cortex (A17 and A18): a current source density analysis of electrically evoked potentials, *Exp. Brain Res.*, 33:371–394.
- Montero, V. M., R. W. Guillery, and C. N. Woolsey, 1977. Retinotopic organization within the thalamic reticular nucleus demonstrated by a double label autoradiographic technique, *Brain Res.*, 138:407–421.
- Mott, D. D., and D. V. Lewis, 1994. The pharmacology and function of central GABAB receptors, *Int. Rev. Neurobiol.*, 36:97–223.
- Murphy, P. C., S. G. Duckett, and A. M. Sillito, 2000. Comparison of the laminar distribution of input from areas 17 and 18 of the visual cortex to the lateral geniculate nucleus of the cat, *J. Neurosci.*, 20:845–853.
- Murphy, P. C., and A. M. Sillito, 1996. Functional morphology of the feedback pathway from area 17 of the cat visual cortex to the lateral geniculate nucleus, *J. Neurosci.*, 16:1180–1192.
- Nicoll, R. A., R. C. Malenka, and J. A. Kauer, 1990. Functional comparison of neurotransmitter receptor subtypes in mammalian central nervous system, *Physiol. Rev.*, 70:513–565.
- Norton, T. T., V. A. Casagrande, G. E. Irvin, M. A. Sesma, and H. M. Petry, 1988. Contrast-sensitivity functions of W-, X-, and Y-like relay cells in the lateral geniculate nucleus of bush baby, *Galago crassicaudatus*, *J. Neurophysiol.*, 59:1639–1656.
- Ogren, M. P., and A. E. Hendrickson, 1979. The morphology and distribution of striate cortex terminals in the inferior and lateral subdivisions of the Macaca monkey pulvinar, *J. Comp. Neurol.*, 188:179–199.
- Ojima, H., K. Murakami, and K. Kishi, 1996. Dual termination modes of corticothalamic fibers originating from pyramids of layers 5 and 6 in cat visual cortical area 17, *Neurosci. Lett.*, 208:57–60.
- Olshausen, B. A., C. H. Anderson, and D. C. Van Essen, 1993. A neurobiological model of visual attention and invariant pattern recognition based on dynamic routing of information, *J. Neurosci.*, 13:4700–4719.
- Pape, H.-C., T. Budde, R. Mager, and Z. F. Kisvárdy, 1994. Prevention of Ca^{2+} -mediated action potentials in GABAergic local circuit neurones of rat thalamus by a transient K^{+} current, *J. Physiol. (Lond.)*, 478:403–422.
- Partlow, G. D., M. Colonnier, and J. Szabo, 1977. Thalamic projections of the superior colliculus in the rhesus monkey, *Macaca mulatta*. A light and electron microscopic study, *J. Comp. Neurol.*, 171:285–318.
- Pin, J. P., and R. Duvoisin, 1995. The metabotropic glutamate receptors: structure and functions, *Neuropharmacology*, 34:1–26.
- Pinault, D., J. Bourassa, and M. Deschênes, 1995a. Thalamic reticular input to the rat visual thalamus: a single fiber study using biocytin as an anterograde tracer, *Brain Res.*, 670:147–152.
- Pinault, D., J. Bourassa, and M. Deschênes, 1995b. The axonal arborization of single thalamic reticular neurons in the somatosensory thalamus of the rat, *Eur. J. Neurosci.*, 7:31–40.
- Pinault, D., and M. Deschênes, 1998. Projection and innervation patterns of individual thalamic reticular axons in the thalamus of the adult rat: a three-dimensional, graphic, and morphometric analysis, *J. Comp. Neurol.*, 391:180–203.
- Raczkowski, D., J. E. Hamos, and S. M. Sherman, 1988. Synaptic circuitry of physiologically identified W-cells in the cat's dorsal lateral geniculate nucleus, *J. Neurosci.*, 8:31–48.
- Raczkowski, D., and A. C. Rosenquist, 1980. Connections of the parvocellular C laminae of the dorsal lateral geniculate nucleus with the visual cortex in the cat, *Brain Res.*, 199:447–451.
- Ralston, H. J., III, 1971. Evidence for presynaptic dendrites and a proposal for their mechanism of action, *Nature*, 230:585–587.
- Ramcharan, E. J., J. W. Gnadt, and S. M. Sherman, 2000. Burst and tonic firing in thalamic cells of unanesthetized, behaving monkeys, *Vis. Neurosci.*, 17:55–62.
- Recasens, M., and M. Vignes, 1995. Excitatory amino acid metabotropic receptor subtypes and calcium regulation, *Ann. N.Y. Acad. Sci.*, 757:418–429.
- Reinagel, P., D. W. Godwin, S. M. Sherman, and C. Koch, 1999. Encoding of visual information by LGN bursts, *J. Neurophysiol.*, 81:2558–2569.
- Robertson, R. T., and T. J. Cunningham, 1981. Organization of corticothalamic projections from the parietal cortex in the cat, *J. Comp. Neurol.*, 199:569–585.
- Robson, J. A., and W. C. Hall, 1977. The organization of the pulvinar in the grey squirrel (*Sciurus carolinensis*) II. Synaptic organization and comparisons with the dorsal lateral geniculate nucleus, *J. Comp. Neurol.*, 173:389–416.
- Rockland, K. S., 1996. Two types of corticopulvinar terminations: round (type 2) and elongate (type 1), *J. Comp. Neurol.*, 368:57–87.
- Rockland, K. S., 1998. Convergence and branching patterns of round, type 2 corticopulvinar axons, *J. Comp. Neurol.*, 390:515–536.
- Rockland, K. S., J. Andresen, R. J. Cowie, and D. L. Robinson, 1999. Single axon analysis of pulvinocortical connections to several visual areas in the macaque, *J. Comp. Neurol.*, 406:221–250.
- Rodman, H. R., C. G. Gross, and T. D. Albright, 1989. Afferent basis of visual response properties in area MT of the macaque. I. Effects of striate cortex removal, *J. Neurosci.*, 9:2033–2050.
- Rodman, H. R., C. G. Gross, and T. D. Albright, 1990. Afferent basis of visual response properties in area MT of the macaque.

- II. Effects of superior colliculus removal, *J. Neurosci.*, 10: 1154–1164.
- Rouiller, E. M., and E. Welker, 2000. A comparative analysis of the morphology of corticothalamic projections in mammals, *Brain Res. Bull.*, 53:727–741.
- Schmielau, F., and W. Singer, 1977. The role of visual cortex for binocular interactions in the cat lateral geniculate nucleus, *Brain Res.*, 120:354–361.
- Schneider, G. E., 1969. Two visual systems, *Science*, 163:895–902.
- Sheng, M. H. T., 2001. The postsynaptic specialization, in *Synapses* (W. M. Cowan, T. C. Südhof, and C. F. Stevens, eds.), Baltimore: Johns Hopkins University Press, pp. 315–355.
- Sherman, S. M., 1985. Functional organization of the W-, X-, and Y-cell pathways in the cat: a review and hypothesis, in *Progress in Psychobiology and Physiological Psychology*, vol. 11 (J. M. Sprague and A. N. Epstein, eds.), Orlando: Academic Press, pp. 233–314.
- Sherman, S. M., 1996. Dual response modes in lateral geniculate neurons: mechanisms and functions, *Vis. Neurosci.*, 13:205–213.
- Sherman, S. M., 2001. Tonic and burst firing: dual modes of thalamocortical relay, *Trends Neurosci.*, 24:122–126.
- Sherman, S. M., and M. J. Friedlander, 1988. Identification of X versus Y properties for interneurons in the A-laminae of the cat's lateral geniculate nucleus, *Exp. Brain Res.*, 73:384–392.
- Sherman, S. M., and R. W. Guillery, 1996. The functional organization of thalamocortical relays, *J. Neurophysiol.*, 76:1367–1395.
- Sherman, S. M., and R. W. Guillery, 1998. On the actions that one nerve cell can have on another: distinguishing “drivers” from “modulators,” *Proc. Natl. Acad. Sci. USA*, 95:7121–7126.
- Sherman, S. M., and R. W. Guillery, 2001. *Exploring the Thalamus*, San Diego: Academic Press.
- Shipp, S., 2001. Corticopulvinar connections of areas V5, V4, and V3 in the macaque monkey: a dual model of retinal and cortical topographies, *J. Comp. Neurol.*, 439:469–490.
- Sillito, A. M., J. Cudeiro, and P. C. Murphy, 1993. Orientation sensitive elements in the corticofugal influence on centre-surround interactions in the dorsal lateral geniculate nucleus, *Exp. Brain Res.*, 93:6–16.
- Sillito, A. M., H. E. Jones, G. L. Gerstein, and D. C. West, 1994. Feature-linked synchronization of thalamic relay cell firing induced by feedback from the visual cortex, *Nature*, 369:479–482.
- Smith, D. C., and P. D. Spear, 1979. Effects of superior colliculus removal on receptive-field properties of neurons in lateral suprasylvian visual area of the cat, *J. Neurophysiol.*, 42:57–75.
- So, Y.-T., and R. Shapley, 1981. Spatial tuning of cells in and around lateral geniculate nucleus of the cat: X and Y relay cells and perigeniculate interneurons, *J. Neurophysiol.*, 45:107–120.
- Sprague, J. M., 1966. Interaction of cortex and superior colliculus in mediation of visually guided behavior in the cat, *Science*, 153:1544–1547.
- Sprague, J. M., 1972. The superior colliculus and pretectum in visual behavior, *Invest. Ophthalmol.*, 11:473–482.
- Sprague, J. M., G. Berlucchi, and A. Di Berardino, 1970. The superior colliculus and pretectum in visually guided behavior and visual discrimination in the cat, *Brain Behav. Evol.*, 3:285–294.
- Steriade, M., E. G. Jones, and R. Llinás, 1990. *Thalamic Oscillations and Signalling*, New York: Wiley.
- Steriade, M., and R. Llinás, 1988. The functional states of the thalamus and the associated neuronal interplay, *Physiol. Rev.*, 68:649–742.
- Steriade, M., and R. W. McCarley, 1990. *Brainstem Control of Wakefulness and Sleep*, New York: Plenum Press.
- Steriade, M., D. A. McCormick, and T. J. Sejnowski, 1993. Thalamic oscillations in the sleeping and aroused brain, *Science*, 262:679–685.
- Stone, J., and B. Dreher, 1973. Projection of X- and Y-cells of the cat's lateral geniculate nucleus to areas 17 and 18 of visual cortex, *J. Neurophysiol.*, 36:551–567.
- Sur, M., M. Esguerra, P. E. Garraghty, M. F. Kritzer, and S. M. Sherman, 1987. Morphology of physiologically identified retinogeniculate X- and Y-axons in the cat, *J. Neurophysiol.*, 58:1–32.
- Swadlow, H. A., and A. G. Gusev, 2001. The impact of “bursting” thalamic impulses at a neocortical synapse, *Nat. Neurosci.*, 4:402–408.
- Tusa, R. J., A. C. Rosenquist, and L. A. Palmer, 1979. Retinotopic organization of areas 18 and 19 in the cat, *J. Comp. Neurol.*, 185:657–678.
- Uhlich, D. J., J. B. Cucchiaro, A. L. Humphrey, and S. M. Sherman, 1991. Morphology and axonal projection patterns of individual neurons in the cat perigeniculate nucleus, *J. Neurophysiol.*, 65:1528–1541.
- Uhlich, D. J., K. A. Manning, and T. P. Pienkowski, 1993. The histaminergic innervation of the lateral geniculate complex in the cat, *Vis. Neurosci.*, 10:225–235.
- Updyke, B. V., 1977. Topographic organization of the projections from cortical areas 17, 18, and 19 onto the thalamus, pretectum and superior colliculus in the cat, *J. Comp. Neurol.*, 173:81–122.
- Updyke, B. V., 1981. Projections from visual areas of the middle suprasylvian sulcus onto the lateral posterior complex and adjacent thalamic nuclei in cat, *J. Comp. Neurol.*, 201:477–506.
- Van Essen, D. C., C. H. Anderson, and D. J. Felleman, 1992. Information processing in the primate visual system: an integrated systems perspective, *Science*, 255:419–423.
- Van Horn, S. C., A. Erişir, and S. M. Sherman, 2000. The relative distribution of synapses in the A-laminae of the lateral geniculate nucleus of the cat, *J. Comp. Neurol.*, 416:509–520.
- Walker, A. E., 1938. *The Primate Thalamus*, Chicago: University of Chicago Press.
- Walls, G. L. 1953. The lateral geniculate nucleus and visual histophysiology. Univ. Calif. Berkeley *Publ. Physiol.* No. 1. 1–100.
- Wang, S., M. E. Bickford, S. C. Van Horn, A. Erişir, D. W. Godwin, and S. M. Sherman, 2001. Synaptic targets of thalamic reticular nucleus terminals in the visual thalamus of the cat, *J. Comp. Neurol.*, 440:321–341.
- Wang, S., M. A. Eisenback, and M. E. Bickford, 2002. Relative distribution of synapses in the pulvinar nucleus of the cat: implications regarding the “driver/modulator” theory of thalamic function, *J. Comp. Neurol.*, 454:482–494.
- Wässle, H., B. B. Boycott, and R.-B. Illing, 1981. Morphology and mosaic of on- and off-beta cells in the cat retina and some functional considerations, *Proc. R. Soc. Lond. B.*, 212:177–195.
- Wässle, H., W. R. Levick, and B. G. Cleland, 1975. The distribution of the alpha type of ganglion cells in the cat's retina, *J. Comp. Neurol.*, 159:419–438.
- Wilson, J. R., M. J. Friedlander, and S. M. Sherman, 1984. Fine structural morphology of identified X- and Y-cells in the cat's lateral geniculate nucleus, *Proc. R. Soc. Lond. B.*, 221:411–436.
- Wong-Riley, M. T. T., 1977. Connections between the pulvinar nucleus and the prestriate cortex in the squirrel monkey as revealed by peroxidase histochemistry and autoradiography, *Brain Res.*, 134:225–236.
- Yoshida, K., and L. A. Benevento, 1981. The projection from the dorsal lateral geniculate nucleus of the thalamus to extrastriate

- visual association cortex in the macaque monkey, *Neurosci. Lett.*, 22:103–108.
- Yukie, M., and E. Iwai, 1981. Direct projection from the dorsal lateral geniculate nucleus to the prestriate cortex in macaque monkeys, *J. Comp. Neurol.*, 201:81–97.
- Zeki, S. M., 1993. *A Vision of the Brain*, Oxford: Blackwell Scientific.
- Zeki, S. M., 1969. Representation of central visual fields in prestriate cortex of monkey, *Brain Res.*, 14:271–291.
- Zhan, X. J., C. L. Cox, J. Rinzel, and S. M. Sherman, 1999. Current clamp and modeling studies of low threshold calcium spikes in cells of the cat's lateral geniculate nucleus, *J. Neurophysiol.*, 81:2360–2373.
- Zhan, X. J., C. L. Cox, and S. M. Sherman, 2000. Dendritic depolarization efficiently attenuates low threshold calcium spikes in thalamic relay cells, *J. Neurosci.*, 20:3909–3914.
- Zhu, J. J., D. J. Uhlich, and W. W. Lytton, 1999. Burst firing in identified rat geniculate interneurons, *Neurosci.*, 91:1445–1460.

36 The Visual Functions of the Pulvinar

CHRISTIAN CASANOVA

IN FLIPPING THROUGH a general textbook of neuroscience, very little information on the pulvinar is found. This is regrettable given that the pulvinar of higher mammals is the largest extrageniculate visual thalamic complex and is likely to play a key role in visual and visuomotor processing. This structure lies over the dorsolateral posterior thalamus and runs along the medial edge of the lateral geniculate nucleus (LGN). Through evolution, the primate pulvinar, in parallel with the expansion of the neocortex, has undergone a considerable increase in size and has established extensive reciprocal connections with most visual cortical areas (Fig. 36.1). The almost total omission of the pulvinar from textbooks may come from the fact that its function in normal vision has remained largely elusive. When compared to other subcortical areas such as the LGN or the superior colliculus (SC), few studies have investigated the response properties of neurons in the mammalian pulvinar complex. This may result partly from the difficulty of characterizing these neurons' visual receptive field properties. In addition, research may have been discouraged by a number of behavioral findings that revealed no strong impairment of visual function after destruction of the pulvinar (for a comprehensive review, see Chalupa, 1991). Despite such impediments, several investigators labored on and their work provided contemporary researchers with precious information on the functional organization of the pulvinar complex. This chapter reviews recent findings on the anatomy and physiology of the pulvinar. The information focuses on findings from the cat and monkey, as most of our knowledge of this thalamic region comes from work on these two species. Unraveling the function of the pulvinar is still a formidable challenge to researchers, but new findings have opened promising avenues in deciphering the role of this structure in vision.

Structural and visuotopic organization

The anatomical limits of the pulvinar and the nuclei comprising it are not readily defined. Work on the cat and monkey, using various experimental approaches, has shown this extrageniculate structure to be parceled into several nuclei. As discussed below, these subregions' boundaries vary across studies (especially in primates), and additional work is necessary to establish a clear structural organization that relates to function adequately.

In cats, the pulvinar is referred to as the *lateral posterior-pulvinar* (LP-pulvinar) complex. Internal subdivisions of the LP-pulvinar have been defined by connectivity patterns (Berson and Graybiel, 1978; Updyke, 1977, 1981), cyto- and chemoarchitectonics (Berson and Graybiel, 1980, 1983; Updyke, 1983), and functional properties (Chalupa and Abramson, 1988, 1989; Chalupa et al., 1983). Of note is the histochemical work by Graybiel and Berson (1980) and Berson and Graybiel (1983), who parceled the LP-pulvinar by revealing thalamic acetylcholinesterase (AChE) activity. Several laboratories currently use this method to reveal the three main LP-pulvinar subregions that are generally agreed upon: the lateral and medial parts of the LP nucleus (LPi and LPm) and the pulvinar. Each division contains a representation of the contralateral visual field that encompasses slightly the vertical meridian, and overrepresents the binocular part of the visual field. The overall visuotopic organization of the LP-pulvinar is rather complex because of multiple visual field representations (Raczkowski and Rosenquist, 1981; Updyke, 1983); up to five have been proposed by Hutchins and Updyke (1989). These multiple representations and the large extent of receptive fields contribute to an LP-pulvinar visuotopic organization that is less rigorous than that of the LGN.

The pulvinar of primates is relatively larger than that of cats; the structural boundaries of its subdivisions are more easily differentiated, though firm delimitations using Nissl and myelin stains remain difficult. Four nuclei have been identified on classical cytoarchitectonic grounds (Olszewski, 1952; Walker, 1938): the inferior, lateral, medial, and oral (or anterior) pulvinar. An LP nucleus also exists, but it is not well developed and does not seem to receive any prominent visual input (Jones, 1985). As work progressed, it became evident that there was no clear correspondence between the cytoarchitectonically defined structural organization and the functional and connectional subdivisions of the primate pulvinar (Robinson and Cowie, 1997). In recent years, pulvinar organization has been challenged by studies using a host of chemoarchitectonic techniques. In particular, Cusik and collaborators, with the use of calbindin, AChE, cytochrome oxidase (CO), and parvalbumin stains, have divided the inferior pulvinar into four to five subregions that encompass the entire ventral part of the original lateral pulvinar (Gray et al., 1999; Gutierrez et al., 1995; in humans, Cola et al., 1999). Comparable subdivisions have been described by

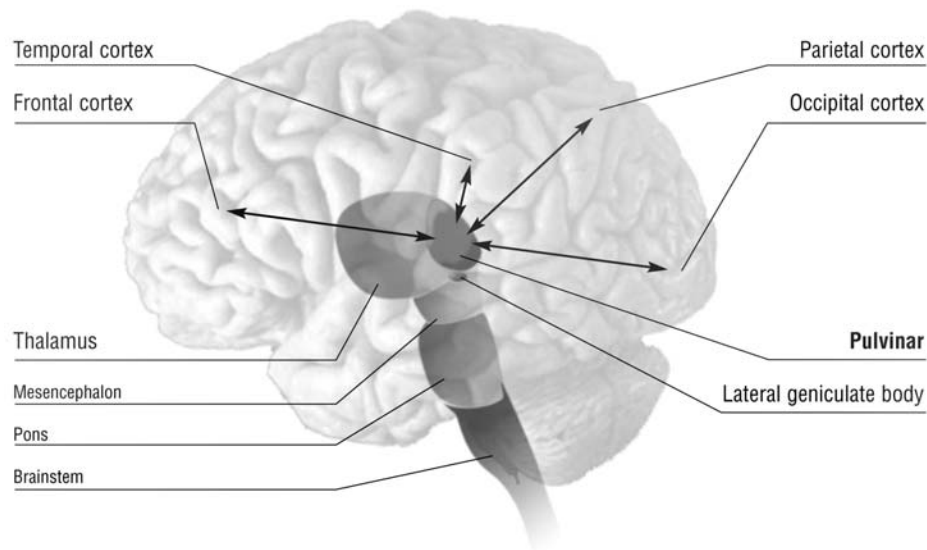


FIGURE 36.1. Schematic representation of the human brain showing the location of the pulvinar. The pulvinar is most fully developed in humans, and based on cat and primate studies, it establishes reciprocal connections with visual areas or visually

related areas of the neocortex. These cortico-thalamo-cortical loops may represent computational modules involved in analyzing specific features of complex visual scenes.

Stepniewska and Kaas (1997) and Adams et al. (2000) using Nissl, calbindin, myelin, CO, AChE, and Cat-301 stains. According to their proposals, however, the inferior pulvinar does not extend strongly over the lateral division. Clearly, the internal organization of the primate pulvinar remains vaguely defined. A solution to this anatomical puzzle is necessary to better understand the pulvinar's anatomic-functional organization and overall function. Nevertheless, the inferior and lateral subdivisions of the pulvinar are generally considered as the main visual nuclei. Both contain a complete topographic representation of the contralateral visual field where receptive field size increases with eccentricity (Bender, 1982; Petersen et al., 1985) and where the central visual field is overrepresented (Bender, 1981). A third area, located in the dorsomedial part of the lateral pulvinar (Pdm), has been described: it does not show a structured visuotopic organization, and the neurons comprising it have large receptive fields (Benevento and Miller, 1981; Petersen et al., 1985).

Afferent and efferent connectivity

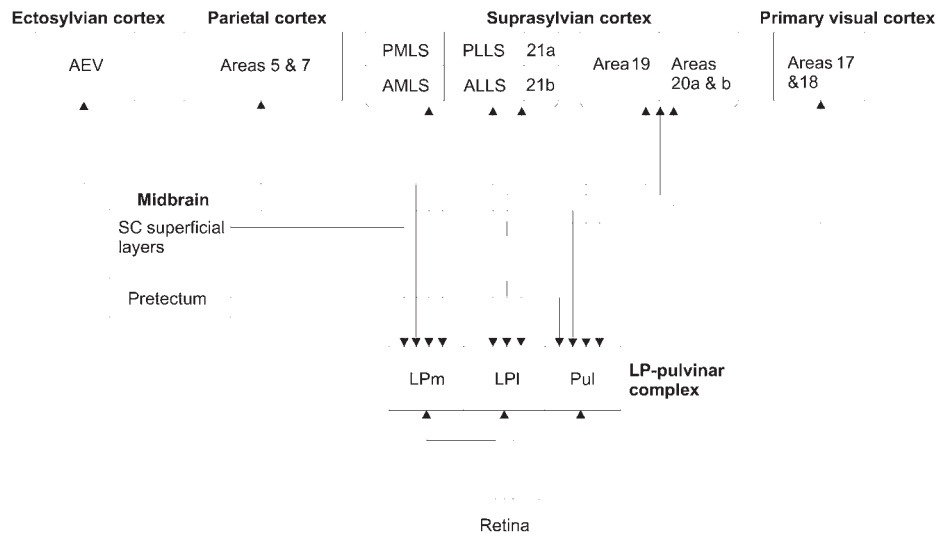
The pulvinar receives visual input from a number of sub-cortical and cortical structures (Fig. 36.2). Only projections that are directly related to establishing the visual responsiveness of pulvinar cells are reviewed here. As discussed later, it is generally accepted that retinal projections are insufficient to account for the overall visual properties of pulvinar neurons in both cats and primates. Unlike its thalamic neighbor, the LGN, the pulvinar seems to receive its primary or driving visual afferents through descending

pathways from the cortex. For this reason, the pulvinar should be considered as a higher-order nucleus, as opposed to a first-order nucleus such as the LGN (Sherman and Guillery, 1998).

RETINAL INPUTS It was long believed that direct retinal projections to the LP-pulvinar complex only reach the lateral edge of the pulvinar in cats (Berman and Jones, 1977; Berson and Graybiel, 1978; Kawamura et al., 1979), and some authors (e.g., Guillery et al., 1980; Mason, 1981) considered this retino-recipient region as part of the geniculate complex (geniculate wing) rather than the pulvinar complex. However, vitreal injection of the B-fragment of the cholera toxin reveals the presence of direct retinal (bilateral, but predominantly contralateral) projections to the medial portion of the pulvinar as well as to the LPI and LPm subdivisions (Boire et al., in prep.). Most terminals exhibit small-caliber axons, and some are similar to the large endings of corticothalamic projections (R-type, see below). The functional properties of these retino-LP fibers are not yet known, though it is now necessary to consider that some receptive field properties in the LP nucleus may be modulated by, or even built from, direct retinal ganglion cell input. It is recognized, however, that ganglion cells reaching the retinorecipient zone of the pulvinar are electrophysiologically defined W cells (Mason, 1981), and subsequent anatomical work indicates that they are e cells (Pu et al., 1994).

In primates, bilateral retinal projections terminate in the inferior pulvinar (Itaya and Van Hoesen, 1983; Mizuno et al., 1982; O'Brien et al., 2001). In the macaque, Cowey

A. Cat



B. Primate

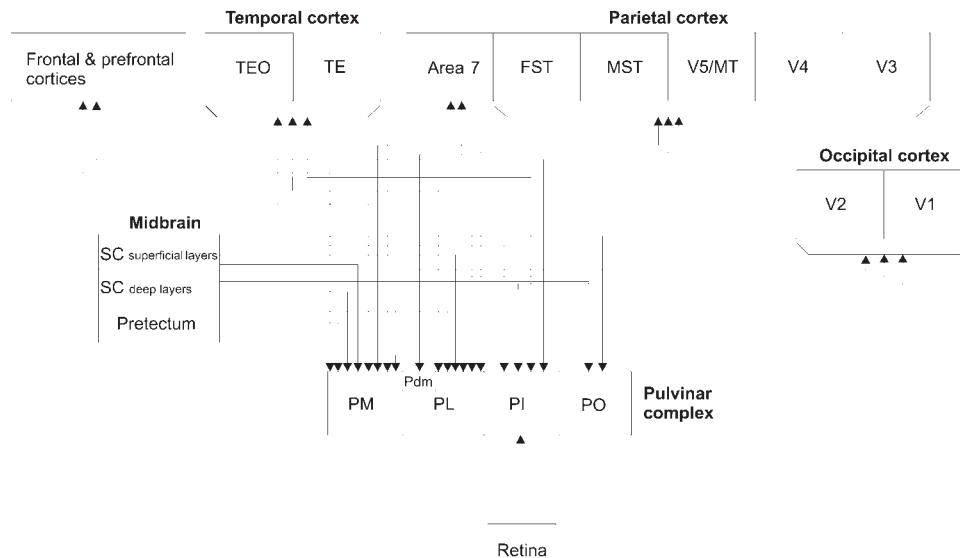


FIGURE 36.2. Schematic diagrams representing the main efferent and afferent connections of the cat's LP-pulvinar complex (*A*) and primate pulvinar (*B*). Abbreviations are defined throughout the text.

et al. (1994) reported that the injection of horseradish peroxidase in the inferior pulvinar labeled all three major ganglion cell classes (note, however, that the authors could not rule out the possible labeling of axons of passage). Some were located near the fovea, but the majority was in eccentric retinal regions. Gamma (γ) cells appeared to form most of the retinal afferents, but α and β cells were also present. Cowey and collaborators have long believed that the pulvinar is likely involved in blindsight (along with the SC and extrastriate areas (for a review, see Stoerig and Cowey, 1997) and that the presence of β retinopulvinar cells may con-

tribute to the postlesion (striate cortex) preservation of visual function.

MIDBRAIN INPUTS There is no doubt that the pathway from the SC to the pulvinar has been the most thoroughly studied, given the SC's key role in the control of fixation and saccadic eye movements. In cats, collicular fibers (also referred to as *tectal fibers*) reaching the LP-pulvinar originate predominantly from the lower part of the stratum griseum superficiale (SGSi) and terminate in the LPm; the latter is considered as the *tectorecipient* zone of the complex (Graybiel

and Berson, 1980; Kawamura et al., 1980). Some of these projection cells are substance P immunoreactive, suggesting that this neuropeptide plays a role in tecto-LP pathway function (Hutsler and Chalupa, 1991). Abramson and Chalupa (1988) have shown that a small contingent of SGS cells, distinct from the above cellular pool, projects to a restricted portion of the LPI adjacent to the pulvinar and identified as the LPI₂. These authors have also reported the existence of another pathway that originates from cells in the stratum opticum and terminates in a region just below the LPM, the ventral division of the LP. There are thus multiple pathways from the SC to the LP-pulvinar, and the exact role of each has yet to be established (the possibility that the pulvinar serves as a relay for collicular signals en route to the visual cortex is discussed later in this chapter). In addition, the tecto-LGN pathway originates from the upper part of the SGS and runs in parallel to the tecto-LP pathway; it would be of interest to determine how these two compare. Since SC cell properties vary according to their laminar position in the SGS, it is likely that these two anatomically defined tectothalamic pathways have distinct functions. Another midbrain region associated with visuomotor reflexes, the pretectum, projects bilaterally to the LP-pulvinar complex. Most terminals appear to use glutamate, to be excitatory, and to end in the pulvinar nucleus (Berson and Graybiel, 1978; Sudkamp and Schmidt, 1995; Weber et al., 1986).

Dense projections from the primate SC to the pulvinar have also been described. Neurons located in the inferior part of the collicular SGS send terminals to the inferior pulvinar and, to a lesser extent, to the lateral subdivision (Benevento and Standage, 1983; Harting et al., 1980; Huerta and Harting, 1983; Marrocco et al., 1981). These projections are mainly ipsilateral and topographically organized. Another pathway arises from the deep collicular layers and reaches the medial and oral pulvinar (Benevento and Fallon, 1975; Benevento and Standage, 1983), and terminals from the pretectum end in the lateral and medial pulvinar (Benevento and Standage, 1983).

CORTICAL INPUTS Cortical afferents appear to represent the main source of visual signals to all subdivisions of the pulvinar. Remarkably, in both species considered here, the pulvinar complex is connected to nearly all visual cortical areas that contain a complete or partial representation of the visual world. Moreover, these connections are reciprocal, allowing for a multitude of cortico-thalamo-cortical loops that may represent distinct computational modules to be established.

In cats, all subdivisions of the LP-pulvinar receive dense cortical projections from extrastriate cortical areas such as areas 19, 20, 21, and the suprasylvian cortex and, in turn, project back to these areas. The density of the projections may vary among subdivisions (Graybiel and Berson, 1980;

Raczkowski and Rosenquist, 1983; Updyke, 1977, 1981). There is one notable observation. The primary visual cortex (areas 17 and 18) projects only to the LPI, which is considered the *striatoprecedent* zone of the cat LP-pulvinar (Abramson and Chalupa, 1985; Graybiel and Berson, 1980). This input is mainly excitatory in nature (Casanova et al., 1997) and may be glutamate- and aspartate-ergic (Fosse et al., 1989). According to Benedek et al. (1983), striate and collicular projections overlap in the caudal part of the LP-pulvinar complex, allowing signals from the two main retinofugal pathways to be combined. It is not known whether there are intrinsic connections between the LPI and LPM, and the aforementioned overlap provides the substrate for a possible collicular modulation of striate input preceding transfer to higher-order areas.

Neuroanatomical studies have shown that most cortical neurons projecting to the LP-pulvinar are pyramidal cells located in layer V and, to a much lesser extent, in layer VI (Abramson and Chalupa, 1985; Norita et al., 1986; Ojima et al., 1996). Cortico-LPI neurons in area 17 are complex cells located in the upper part of layer V (Abramson and Chalupa, 1985; Casanova, 1993). According to Lund et al. (1979), a majority of striate terminals ending in the LPI are collaterals of corticotectal neurons, but this was confirmed only in part by an electrophysiological investigation (Casanova, 1993). This is an important issue, because it may indicate whether striate output signals to the SC and LP-pulvinar are similar or not. If they are similar, the key factor would be a contrast between target-cell processing of this input and that of other afferent signals.

LP-pulvinar cells project to extrastriate neurons in layer IV (and, to a lesser extent, layer I) (Abramson and Chalupa, 1985; Norita et al., 1986), whereas LPI neurons projecting to the primary visual cortex seem to end preferentially in layer I (Abramson and Chalupa, 1985), though projections to layer IV also have been described (Symonds et al., 1981). There is some evidence that individual LP-pulvinar neurons are double-labeled by injection of different tracers in separate cortical areas (Kaufman et al., 1984; Miceli et al., 1991). For instance, a subset of LPI neurons projects to the posteromedial part of the lateral suprasylvian cortex (PMLS) and the primary visual cortex, and some LPM neurons project to both the posterolateral part of the LS (PLLS) and the visual part of the anterior ectosylvian (AEV) cortex (Miceli et al., 1991).

In primates, striate, prestriate, parietal, temporal, and frontal visual or visually related areas project to all subdivisions of the pulvinar (Boussaoud et al., 1991; Ungerleider et al., 1983; Webster et al., 1993; see also Jones, 1985; Robinson and Cowie, 1997). These projections generally present a topographical organization (Campos-Ortega and Hayhow, 1972; Gutierrez and Cusick, 1997; Ungerleider et al., 1983) and are schematically represented in Figure

36.2. Note that a restricted zone of the medial pulvinar, which is not considered a purely visual nucleus, appears to be innervated by cells from areas 17 and 18 (Benevento and Davis, 1977). This region, however, is primarily connected to association cortices, such as the prefrontal cortex and area 7, involved in attentional processing (Baleydier and Mauguière, 1985; Hardy and Lynch, 1992).

The inferior and lateral pulvinar receive their cortical input through layer V neurons of the primary visual cortex and layer VI neurons of extrastriate cortical areas (Lund et al., 1975; Trojanowski and Jacobson, 1977). As shown in cats, these projections are reciprocal: pulvinar fibers end in layers I, II, and III of the striate cortex and in layers I, III, and IV of extrastriate areas (Benevento and Rezak, 1976; Ogren and Hendrickson, 1979; Rezak and Benevento, 1979).

A fundamental question regarding the pulvinar complex and its relationship with cortical areas is the nature of the afferent and efferent terminals. In other words, are the projections likely to drive (i.e., be necessary for establishing response properties in a targeted area) or modulate the activity of recipient cells? V1 and V2 neurons projecting to the cat and primate pulvinar complex exhibit E- and R-type (types 1 and 2, respectively) axon terminals, with a predominance of R-axons (Bickford et al., 1998; Guillery et al., 2001; Rockland, 1996, 1998). This would suggest that projections from the primary visual cortex are mainly driving cellular activity (rather than modulating it; see Sherman and Guillery, 1998, 2001), a concept in agreement with the ultrastructural analysis of terminals (Feig and Harting, 1998) and the electrophysiological findings of Bender (1983, 1988) and Casanova et al. (1997) described below. A different picture seems to emerge for higher-order cortical areas, as projections from primate area MT are predominantly of the E-type, that is, presumably of a modulatory nature (Rockland, 1998).

In primates, neurons projecting from the pulvinar to striate and extrastriate cortices are heterogeneous in their arbor size and terminal fields, suggesting that these projections do not have the same function in all cortical areas. It remains to be determined whether the pulvinocortical terminals are inhibitory or excitatory in nature. More important, perhaps, is to address a question whose answer may establish the relative strength between converging thalamocortical and feedforward corticocortical projections: do pulvinar terminals drive cortical units or is these terminals' action strictly modulatory? Data from Minville and Casanova (1998) have shown that the activity of only a few PMLS neurons is reduced by the deactivation of the LPI, suggesting that these projections are not predominantly of a driving type, despite the fact that they terminate in layer IV.

Another important task is to determine the visual response properties of cells projecting within the cortico- and thalamo-

mofugal systems (e.g., by antidromic activation methods). At this point, very little is known of the stimulus configurations that drive these neurons and trigger output from the cortico- and pulvinofugal systems.

Receptive field properties

Response properties of neurons in the pulvinar complex reflect the presence of prominent descending cortical input and therefore resemble those of cortical rather than subcortical neurons (such as those characterizing the neighboring LGN cells). Whether some of these properties are strictly imposed by the cortex or result from the intrinsic integration of cortical and subcortical inputs remains to be determined.

BASIC ORGANIZATION Most studies investigating the function of the cat's LP-pulvinar neurons were carried out in anesthetized animals. In such preparations, several cells cannot be driven by visual stimuli. Future studies in awake, behaving animals may reveal the function of these seemingly nonresponsive cells. Nevertheless, all studies have shown that receptive fields in the cat LP-pulvinar are generally large, with boundaries that cannot be delimited easily. It has been determined that neurons in the three main LP-pulvinar subdivisions have distinct visual properties.

Most receptive fields in the LPI or striatorecipient zone are orientation- and direction-selective (Casanova et al., 1989; Chalupa and Abramson, 1989; Mason, 1978, 1981; Fig. 36.3). They are binocular and exhibit binocular facilitation, and many are sensitive to relative retinal disparities (Casanova et al., 1989). Receptive fields are composed of superimposed ON and OFF subregions, surrounded by ON or OFF peripheral edges (Chalupa and Abramson, 1989), and are driven by low spatial frequency gratings (generally less than 0.5 c/deg) drifted at a relatively high temporal frequency, between 4 and 8 Hz (Casanova et al., 1989). As expected from their receptive field organization, they do not exhibit a strong response modulation to drifting gratings. The motion sensitivity of LPI neurons is better illustrated by two factors. LPI cells are highly sensitive to textured patterns or visual noise (Casanova and Savard, 1996a), and their responses to sine wave gratings are modulated by the presence of a visual noise background (Casanova and Savard, 1996b). This suggests that the LP-pulvinar complex may be involved in the analysis of the relative motion of an object in its surrounding environment. As a general rule, we have found that gratings and noise patterns are more efficient in driving LP neurons than moving bars or spots. Despite their multiple cortical inputs, LPI cells constitute a relatively homogeneous population with regard to their receptive field properties. This may indicate that striate and extrastriate cortical signals are somewhat integrated at this thalamic level. Overall, receptive field properties resemble those of

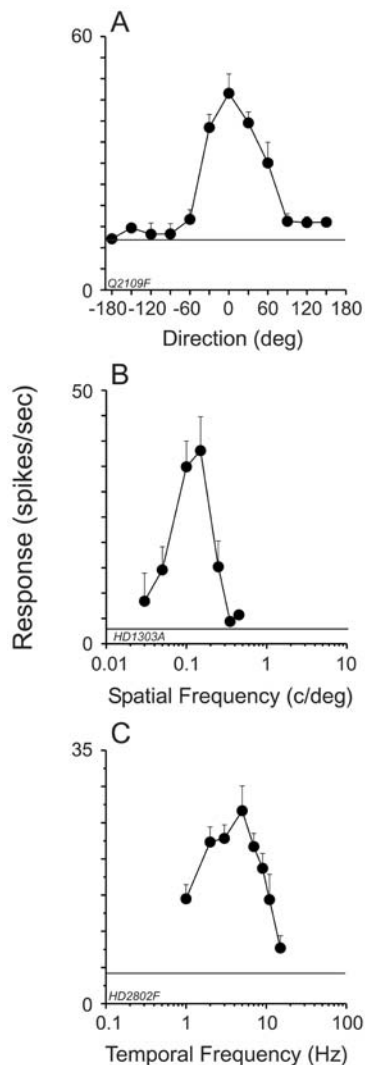


FIGURE 36.3. Examples of representative basic response properties of neurons in the cat's LP-pulvinar. *A*, The neurons respond optimally to an oriented grating drifting in the forward (0 degrees) but not the reverse (180 degrees) direction of motion. *B*, *C*, Spatial and temporal frequency tuning functions in LP-pulvinar. Note that in both cases, the bandpass pattern prevails.

complex cells in the visual cortex. This is in agreement with the fact that striate-LPI cells are complex or special-complex cells (Casanova, 1993) and neurons in extrastriate cortical areas exhibit, for the most part, complex-like properties (for a review, see Spear, 1991).

Three major differences exist between receptive field properties of neurons in the LPm and LPI (Chalupa and Abramson, 1988, 1989; Chalupa et al., 1983). Receptive fields in the LPm are approximately four times larger than those in the LPI, and some may cover the whole contralateral hemifield. They exhibit a more uniform internal organization, that is, they composed of a single ON, OFF, or ON-OFF region. Finally, fewer LPm neurons are orientation selective, and their tuning function is broader.

These differences are likely to reflect the presence of collicular input and the absence of striate projections to the LPm.

The pulvinar remains the least characterized nucleus of the cat LP-pulvinar complex, and additional investigation of its constituent neurons must be carried out. According to Mason (1981), visual properties of pulvinar cells are comparable to those he has described in the LP nucleus [note, however, that very few orientation-selective neurons were found by this author (Mason, 1978, 1981)]. A notable difference has been reported for cells located in the lateral part of the pulvinar (corresponding to Guillery's geniculate wing); neurons in this retinorecipient zone had concentric receptive fields and were mainly of the W type.

Unfortunately, when compared to the cat, there is a dearth of data regarding response properties in the primate pulvinar, and most relevant work was carried out at a time when this region was defined classically on cytoarchitectonic grounds. Most receptive fields in the inferior and medial pulvinar have a small diameter (1 to 5 degrees in the inferior pulvinar; Bender, 1982), but very large ones have been reported (Mathers and Rapisardi, 1973). The majority of cells are binocular and orientation selective, and a subset are direction selective. Color-sensitive cells have also been identified (Bender, 1982; Felsten et al., 1983).

HIGHER-ORDER MOTION SENSITIVITY There is clear evidence that a subset of neurons in the LP-pulvinar complex are capable of signaling the true direction of motion of a plaid pattern [i.e., they can integrate separate motion signals into a single coherently moving percept termed *pattern motion* (PM)]. This implies that these thalamic cells are involved in higher-order motion processing (Merabet et al., 1998; see Casanova et al., 2001; Fig. 36.4). LP-pulvinar neurons selective for PM are distinguished by large receptive fields (suitable for spatial integration) and are located mainly in the LPm. Thus far, this plaid-defined higher-level neuronal operation has been reported solely in higher-order visual areas: PM responses have been described in primate area MT (Movshon et al., 1985) and subsequently in the cat's AEV (Scannell et al., 1996)—two regions reciprocally connected to the pulvinar complex. The involvement of the cat LP-pulvinar complex in higher-order motion processing was further demonstrated by the finding that LP cells signal the direction of complex random dot kinematograms (RDKs), whose elements do not indicate locally the direction of motion (Dumbrava et al., 2001). It is not yet known whether the plaid pattern and complex RDK motion-sensitive neurons described in the cat also exist in the primate pulvinar. The cat model may very well extend to the primate, as reciprocal connections between the pulvinar and area MT exist (Cusick et al., 1993); MT cells are known to respond to similar or comparable higher-order stimuli (Movshon et al., 1985; Newsome and Pare, 1988; Rodman

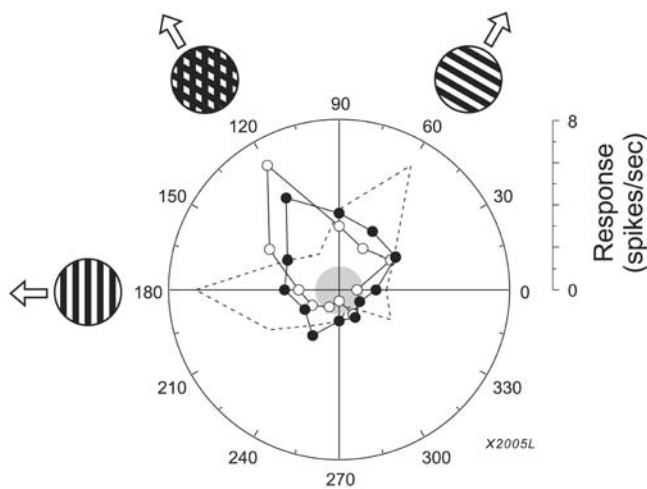


FIGURE 36.4. Higher-order motion characteristics of LP-pulvinar neurons. Polar graph illustrating the responses of a pattern-motion selective LPm neuron to gratings (open symbols) and plaid patterns (filled symbols) drifted in 12 directions of motion. The response to gratings alone is considered the predicted profile for a truly pattern-direction selective unit. The dashed line represents the predicted response to plaids for a component-direction selective unit. The small central circle represents spontaneous activity level.

and Albright, 1989). In addition, there are strong similarities in the organization of cat and primate extrageniculate pathways (Creutzfeldt, 1988).

VISUAL SALIENCE AND ASSOCIATED VISUOMOTOR CHARACTERISTICS There is evidence that the activity of a subset of neurons in the pulvinar complex varies according to the animal's attentional state, to stimulus relevance, and to eye movements associated with scanning a visual scene.

Sudkamp and Schmidt (2000) have demonstrated the existence of three classes of neurons in the pulvinar of awake cats, which, by order of incidence, are purely visual neurons, saccadic visual neurons, and cells that respond solely during a saccade. These authors suggested that saccadic visual neurons could induce arousal in visual cortical areas after self-induced eye movements or external motion lead to changes of the visual scene.

In primates, the Pdm, which is reciprocally connected to the posterior parietal cortex (area 7a), contains neurons with large nonorientation-selective receptive fields whose discharges are enhanced during visual attention tasks. Specifically, Pdm neurons respond more strongly to stimuli relevant to active behavior (targets) than to stimuli not associated as such (Fig. 36.5; Petersen et al., 1985). This enhancement is spatially selective and independent of eye movements. Another subpopulation of Pdm cells characterized by larger receptive fields was found to discharge during and after saccadic eye movements (Petersen et al., 1985; Robinson et al., 1986). These cells may therefore

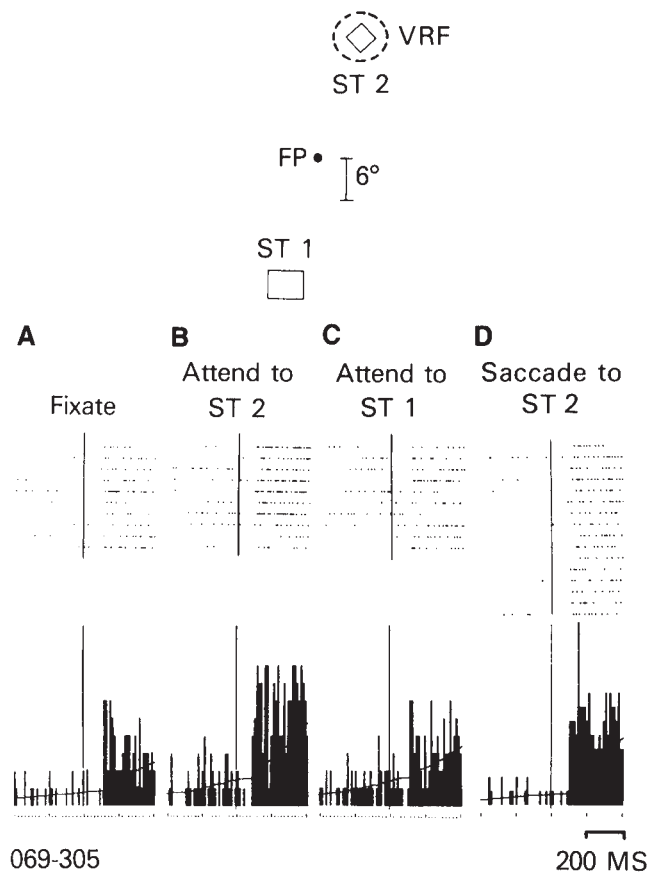


FIGURE 36.5. Responses of cells in the Pdm of primates are modulated by visual spatial attention. *A*, Response of the cell to the stimulation of its receptive field (RF) by the ST 2 stimulus (the animal is fixating FP). *B*, This response is enhanced when ST 2 is used as a target for saccadic eye movements. *C*, There is no increase in the cell's discharge when the animal attends to ST 1, which is located outside the RF. *D*, The response is still enhanced when the monkey attends to ST 2 in the receptive field (no saccade is made). (Modified from Petersen et al., 1985).

signal a change in the axis of gaze and indicate that a fixation period (i.e., an increase of attention) is to occur (Petersen et al., 1987). On the other hand, findings have shown the visual responses of neurons in the inferior and lateral pulvinar to be suppressed during eye movements (Robinson et al., 1991). Robinson's group has also reported that neuronal discharges in the inferior and lateral pulvinar of the behaving macaque vary as a function of orbital position (Robinson et al., 1990). Recent work by Bender and Youakim (2001) has confirmed the involvement of the pulvinar in visual attention: attention during a fixation task increases or reduces excitability (*push-pull* modulation) for about a quarter of inferior and lateral pulvinar cells. They reported, however, that the same attentional fixation task produces only a suppression of neuronal discharges in the Pdm. This last finding is counter to the observations of Petersen et al. (1985). This difference remains somewhat

intriguing and may arise from the nature of the attentional task in the two studies. Nevertheless, Bender and Youakim (2001) suggest that the push-pull form of modulation observed in the pulvinar is similar to that seen in extrastriate cortex associated with early, intermediate, and late stages of cortical processing. This cellular behavior is most likely related to the engagement and disengagement of attention during fixation. Finally, Acuna et al. (1986, 1990) and Cudeiro et al. (1989) have found *reaching cells* in the macaque LP nucleus and in the oral and lateral pulvinar. These neurons respond during intentional movement of the upper limbs that is visually triggered and guided.

What does the pulvinar do?

For many years, most physiologists have regarded thalamic nuclei as stations that passively relay sensory information to the cortex, dependent on the animal's state of arousal, and in which minimal subcortical processing takes place (Sherman and Guillery, 1996; Macchi et al., 1996). This conventional view does not hold when one considers the extensive reciprocal connectivity between the thalamus and the visual cortex and the complex intrinsic response properties described above. Both first- and higher-order thalamic nuclei are closely linked to the cortex through cortico-thalamo-cortical loops, and it has been proposed in recent years that thalamic nuclei may participate actively in the processing of specific information in conjunction with cortical areas (Grieve et al., 2000; Macchi et al., 1996; Miller and Schreiner, 2000; Mumford, 1991; Miller, 1996; Sherman and Guillery, 1996). This may be especially true for the pulvinar, given its remarkable connectivity with the neocortex. In fact, higher-order thalamic nuclei such as the pulvinar may represent a better model for the study of cortico-thalamo-cortical loops. The reason is that unlike first-order nuclei (such as the LGN), higher-order nuclei do not receive powerful retinal inputs that can mask the subtler role of cortical feedback projections and corresponding cortico-thalamic loops. In the next sections, some hypotheses as to the function of the pulvinar in vision are presented.

THE "NOT SO STRONG" RELAY HYPOTHESIS To some extent, the importance of the pulvinar complex was revealed when Diamond and colleagues (Diamond and Hall, 1969; Killackey and Diamond, 1971), Schneider (1967, 1969), and Trevarthen (1968) demonstrated the involvement of a second retinofugal visual system, the retino-collicular pathway, in orienting behavior (the where pathway as opposed to the what or retino-geniculo-cortical pathway). In order to reach the visual cortex, signals from the SC and the pretectum must be relayed via thalamic nuclei, and the pulvinar complex represented the best candidate. Despite the fact that the pulvinar may indeed provide a route along an ascending

tectocortical pathway or between cortical areas, almost all available evidence is against a simple¹ relay function.

In cats, there are major differences between the receptive field organization of collicular (including tecto-LP cells) and LPm neurons (e.g., receptive field size, orientation selectivity, binocular facilitation) that preclude the LPm from acting as a simple relay between the colliculus and visual cortex (Chalupa et al., 1983; Fish and Chalupa, 1979; McIlwain, 1978). It seems that tectal signals undergo substantial transformation within the LP-pulvinar. Subsequent experiments, confirming earlier work using evoked potential recordings by Chalupa et al. (1972), indicate that deactivating the SC by lidocaine injection or cooling fails to influence significantly the visual responsiveness of LPm neurons (Chalupa, 1991). In agreement with the last observation, Smith and Spear (1979) have reported that lesioning the SC has little effect on the response properties of most neurons in LS subregions that are known to receive a prominent input from the LP-pulvinar complex.

Support for the suggestion that the SC does not contribute substantially to establishing response properties in the LP-pulvinar comes from studies carried out in primates. Bender (1983, 1988) has shown that collicular lesions have no effect on receptive field properties in the inferior pulvinar.² The idea that the pulvinar is not simply relaying information to the cortex is further emphasized by the findings that SC and pulvinar lesions do not yield similar behavioral deficits (Bender and Butter, 1987). In addition, SC lesions do not abolish neuronal responses in area MT (Rodman et al., 1990), and the medial nucleus of the inferior pulvinar, the major projection zone to MT, does not receive significant SC input (Stepniewska et al., 1999): such an ascending pathway was often proposed to explain the persistence of activity in area MT after acute or chronic deactivation of the macaque primary visual cortex (Girard et al., 1992; Rodman et al., 1989; but see Kaas and Krubitzer, 1992; Maunsell et al., 1990). This pathway is also considered part

¹The term *simple* may not be adequate, as no such thing as a simple nucleus exists. For example, the LGN, often referred to as a *simple relay nucleus*, receives a number of projections from both the brainstem and primary visual cortex that modulate its visual responsiveness. Nevertheless, the basic structural organization of retinal ganglion cells and LGN neuron receptive fields is virtually the same. Such a close correspondence of properties between a region and its target is not seen at the level of the pulvinar.

²It is interesting to note that the colliculus appears to have a more significant impact on the LP-pulvinar of less telencephalized species (e.g., the rabbit; Casanova and Molotchnikoff, 1990). This may be related to the considerable development of the pulvinar, the neocortex, and of their interconnectivity throughout evolution. As a consequence, the impact of the cortex on LP and pulvinar cells may have increased to the detriment of collicular influence during that period.

of the neural substrate for blindsight (Stoerig and Cowey, 1997), despite a lack of clear evidence for pulvinar involvement in the persistence of visual function in brain-lesioned patients (see, however, Püto et al., 1999, for an interesting case of “spontaneous recovery” that involved a pathway comprising the pulvinar).

Supporting evidence accompanies the possibility that the pulvinar offers another route for primary visual cortex signals to reach extrastriate areas. In cats, cooling the primary visual cortex causes an overall decrease in visual responsiveness for about one-third of LPl neurons tested (Casanova et al., 1997). The persistence of visual responses during cortical deactivation has been confirmed by additional experiments in which area 17 was removed by aspiration (Casanova et al., 1997). In these brain-damaged animals, a few LPl receptive fields within the cortical scotoma remained sensitive to the orientation and/or direction of a moving stimulus. Despite the strong impact of area 17 projections, our data suggest that the extrastriate cortex might also play a role in establishing response properties in the cat's LPl. This is, to some extent, confirmed by the preliminary data of Chalupa (1991), who observed a complete loss of responsiveness in the LP-pulvinar after cryoblockade of a large cortical surface encompassing the striate cortex and most, if not all, extrastriate areas. Nevertheless, it is very likely that the striate cortex may be necessary to fully establish the basic retinotopic map in the LP-pulvinar complex, on which maps of other areas may be superimposed (Fig. 36.6). Primary visual cortex input appears more critical in primates than in cats because its removal yields an almost total loss of visual responses in the pulvinar (Bender, 1983). It would be somewhat erroneous to conclude at this point that the pulvinar is “relaying” information from striate to extrastriate cortex. In primates, the integrity of the primary visual cortex is necessary to maintain activity in most extrastriate areas. For example, the deactivation of area 17 causes complete elimination of cellular responses in areas V3 and V4 (Girard et al., 1991a, 1991b). Should we then consider these two cortical regions as “simple” relay areas? Surely not.

Results from Minville and Casanova (1998) further support the claim that the pulvinar does more than relay signals from the striate cortex. Spatial and temporal contrast properties of PMLS neurons were studied after the pharmacological deactivation of their main thalamic input, that is, the LPl (Grant and Shipp, 1991; Norita et al., 1996). Despite numerous large injections of lidocaine or GABA, deactivation of the LPl had little effect on the spatial and temporal frequency tuning of neurons in the PMLS cortex and on their direction selectivity. Less than 20% of PMLS cells were affected by the deactivation, and the observed effect consisted of a decrease in the cells' overall respon-

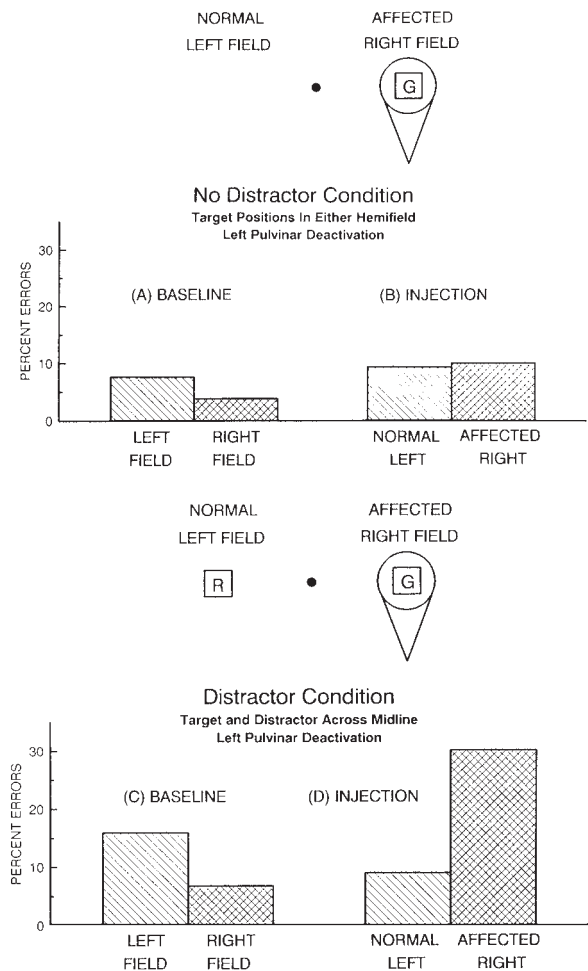


FIGURE 36.6. The pulvinar may participate in visual selection by filtering irrelevant information. After deactivating the inferior pulvinar, the trained monkey could still perform form and color discrimination tasks (*A* and *B*). The animal's performance was slightly reduced when distracting stimuli were added to the right hemifield (*C*) and was dramatically impaired when the pulvinar was deactivated in this condition (*D*). *G*, green; *R*, red. (From Desimone et al., 1990).

siveness. It was concluded that only a small fraction of the projections from LPl to PMLS are necessary to drive cortical neurons and that the signals from the remaining LPl projection cells may be used for more subtle functions (e.g., response modulation to the stimulation context). This last assumption was confirmed by some preliminary data obtained subsequently, which suggest that stimulus-background interactions observed in PMLS cortex (von Grunau and Frost, 1983) may depend on the integrity of the LPl (see Figure 9 in Casanova, 2002). In summary, while the pulvinar complex may be used to bypass corticocortical connections, it should not be regarded as a strict relay nucleus, but rather as an active partner of the visual cortex (see below).

EYE MOVEMENTS The implication of the LP-pulvinar in visuomotor processing was initially precipitated by two findings. LP-pulvinar electrical stimulation evoked conjugated saccades (Crommelinck et al., 1977), and its neurons were reportedly linked polysynaptically to the abducens nucleus (Wilson and Goldberg, 1980). Given its relationship to structures such as the SC, the pretectal and oculomotor nuclei, and cortical areas such as the frontal eye fields (Huerta et al., 1986), the pulvinar complex likely contributes to the visuomotor processing underlying eye movements (particularly saccadic eye movements). As discussed below, this may be closely linked to the identification of salient objects in a visual scene. As previously stated, neural discharges of primate and cat pulvinar cells are correlated with saccades and orbital position (in primates: Petersen et al., 1985, 1987; Robinson et al., 1986, 1990, 1991; in cats: Sudkamp and Schmidt, 2000). It has been proposed that these neurons may be used to enhance the level of attention during fixation and a change in the axis of gaze. Signals from these neurons may also lead to increased visual perception after the occurrence of an eye movement, to initiation or guidance of corrective saccades, and to spatial constancy (Petersen et al., 1987; Robinson and Petersen, 1992; Robinson et al., 1990). Some neurons may also be used to suppress vision during saccadic eye movements (Robinson et al., 1990). In partial support of these hypotheses, bilateral lesions of the macaque pulvinar have been shown to yield abnormally spontaneous and task-related scanning of visual stimuli and prolonged fixation times (Ungerleider and Christensen, 1977, 1979). Similar deficits have been observed in a human patient with a unilateral lesion of the posterior portion of the pulvinar (Ogren et al., 1984).

All primate studies investigating eye movement-related activity were conducted in awake animals that could not move their heads. It is still unknown whether pulvinar cells, like parietal cortex neurons, can encode any changes in head- or body-centered reference frames that accompany head movements (see Grieve et al., 2000).

VISUAL ATTENTION AND SALIENCE Neurophysiological findings that the Pdm, and the inferior and lateral pulvinar of primates, contain neurons exhibiting attention-related discharge modulation (Bender and Youakim, 2001; Petersen et al., 1985; Salzman, 1995) are supported by an elegant series of behavioral experiments. Petersen et al. (1987) showed that injections of muscimol (a potent GABA_A receptor agonist) in the Pdm reduced reaction times during a cued spatial attention task. Conversely, the administration of bicuculline (a GABA antagonist) in the same region had the opposite effect: the monkey's ability to shift its attention from ipsilateral to contralateral visual fields was enhanced. The pulvinar has also been shown to be involved in visual

target selection. Desimone et al. (1990) showed that muscimol deactivation of the lateral pulvinar (more specifically, in the part connected to area V4 and the inferior temporal cortex) impaired the monkey's ability to perform a color discrimination task only when a distractor was present (Fig. 36.6). The pulvinar therefore seems to play a critical role in the filtering of irrelevant visual information, as its deactivation affects the animal's performance only when attention is to be directed to a target presented with a distractor. Overall, the pulvinar may participate in visual selection either by enhancing relevant information (Petersen et al., 1987) or by filtering irrelevant information (Desimone et al., 1990).

Further support for the pulvinar's involvement in mechanisms of attention comes from the work of Acuna's group on the responses associated with intentional, visually guided limb movements (Acuna et al., 1986, 1990; Cudeiro et al., 1989). These authors proposed that the monkey LP-pulvinar would integrate subcortical and cortical signals, allowing for the execution and programming of intentional visually guided movement, and would participate in the maintenance of attention during those movements. Their hypothesis is in agreement with the observation that the destruction of the LP nucleus (but not the pulvinar) leads to a marked impairment in visual guidance in the cat (Fabre-Thorpe et al., 1986).

Human studies have also provided clues to the implication of the pulvinar in visual salience. Rafal and Posner (1987) reported that patients with hemorrhages in the thalamus (clearly, though not exclusively, involving the pulvinar in two out of three patients) exhibited deficiencies in performing the same cued-reaction time task used by Petersen et al. (1987). While these patients exhibited neither visual neglect nor visual field defects, they were slow at engaging attention for a new target location in the visual field contralateral to the lesion. Michael et al. (2001) presented evidence that the efficiency of attentional shifts for the exploration of new relevant stimuli is reduced in patients with thalamic lesions involving the pulvinar. Accordingly, positron emission tomography (PET) work has revealed increases in pulvinar-specific activity when subjects are asked to perform an object-identification task (which requires attentional selection) in the contralateral field (LaBerge and Buchsbaum, 1990). As one of the tests required the selection of a single letter among others (*filtering task*), these data strongly support the concept that the pulvinar is involved in separating relevant from irrelevant visual information. Using the same brain imaging technique, Corbetta et al. (1991) subsequently observed that the pulvinar was activated during a feature discrimination task necessitating selective (as opposed to divided) attention. The contribution of the pulvinar in the selective processing of stimuli was further

demonstrated by Morris et al. (1997). Using a simple visual reaction time task, a recent PET-activation study by Sturm et al. (1999) has shown the pulvinar to be part of a large network, comprising cortical and brainstem areas, involved in intrinsic alertness and defined as an internal control of wakefulness and arousal. Throughout these studies, the importance of corticopulvinar relationships is emphasized, and these relationships may be the key to understanding pulvinar function.

OTHER FUNCTIONAL CLUES REVEALED BY HUMAN STUDIES

Aside from the studies described above associating the pulvinar with visual salience, this structure has been linked to other normal visual functions and to visual deficits observed in neurodegenerative pathologies. Takayama et al. (1994) studied the visual function of a patient with a unilaterally restricted lesion of the pulvinar. Only deficits in the patient's stereoacuity were observed; this is in accord with the finding that binocular LP-pulvinar neurons are sensitive to relative retinal disparity (Casanova et al., 1989). Surprisingly, no impairment of visual spatial attention was seen—a discrepancy that may have resulted from the nature of the task or from the limited extent of the lesion, both of which differed from those mentioned above.

Kuljis (1994) presented evidence that all subdivisions of the pulvinar of Alzheimer's disease (AD) patients exhibit extensive lesions (e.g., amyloid and neuritic plaques). This observation is of interest, as it suggests that some of the visual deficits observed in AD patients [e.g., abnormal eye movements (Fletcher and Sharpe, 1986), reduced global motion sensitivity (Matsumoto et al., 2000), impaired visual attention (Baddeley et al., 2001)] may be due to pulvinar dysfunction and/or to the disruption of associated cortico-thalamo-cortical loops. A recent study using single-photon emission computed tomography (SPECT) also revealed a dysfunction (reduced blood perfusion) of the pulvinar in AD patients displaying psychoses such as visual hallucinations (Mega et al., 2000).

Pulvinar dysfunction has also been reported in schizophrenia. Heckers et al. (2000) have shown that schizophrenic patients (compared to controls) exhibit reduced activation of the right pulvinar (revealed by PET) during tasks that required them to pay attention to or recognize novel visual stimuli. This may be linked to the diminished metabolic rate seen in the thalamus (including the pulvinar) of schizophrenic patients (Buchsbaum et al., 1996; Hazlett et al., 1999) or to an impairment of the connections between thalamic nuclei and prefrontal cortical areas (Portas et al., 1998), which may lead to inefficient filtering of visual information. Again, the disruption of normal activity along the cortico-thalamo-cortical loops may be responsible for the sensory deficits observed in neurodegenerative diseases.

SEEING THE PULVINAR COMPLEX AS AN ACTIVE PARTNER OF CORTICAL AREAS The original statement by Le Gros Clark (1932) on the possible associative or integrative function of the pulvinar is as timely as ever. Given that the pulvinar receives prominent signals from the mesencephalon and the primary visual cortex, it represents a strategic thalamic structure and a unique platform for the integration of neural signals from the two main retinofugal pathways (i.e., retino-tectal and retino-geniculo-striate). In addition, the pulvinar establishes reciprocal connections with most visual cortical areas. It thus finds itself in an exceptional position to influence and/or inform multiple cortical regions of processing in lower- and higher-level areas or to increase the effectiveness (e.g., stimulus salience) of analysis in a given cortical area (Fig. 36.7). Another hypothesis, which does not exclude the others, is to consider the pulvinar complex as the basis for multiple extrageniculate cortico-thalamo-cortical loops that may be implicated in various complex neuronal opera-

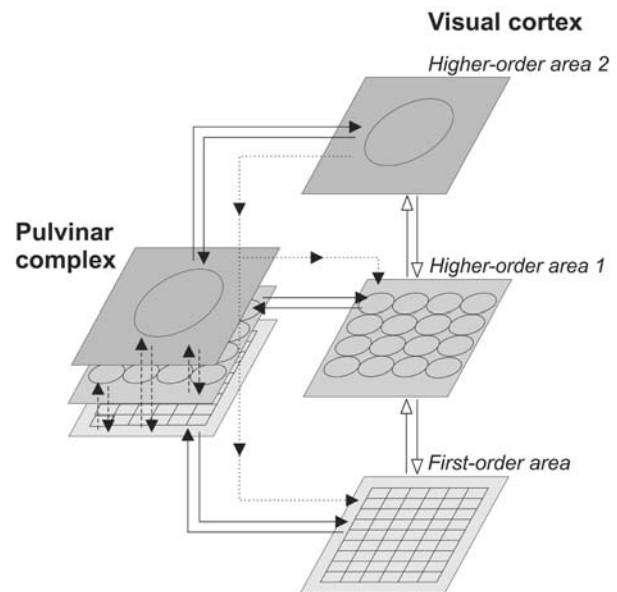


FIGURE 36.7. Hypothetical schematic for visual integration with the pulvinar complex taken into account. Local visual signals are processed in the primary visual cortex and later integrated at second and third cortical levels (increased level of integration is illustrated by an increase in receptive field size). The pulvinar is reciprocally connected to these three cortical levels and contains cell types that were characterized in those areas. One fundamental question is whether pulvinar cells are preferentially connected to neurons with similar properties (yielding specific cortico-thalamic loops; see the *continuous lines* and *filled arrows*) and/or linked to cells with lower- or higher-order motion properties (for an example, see the *dotted line*). In the latter case, activity within a loop could be compared with incoming and outgoing signals and modified accordingly. In addition, such a pathway may be used to short-circuit corticocortical connections (*open arrows*). Besides, it is possible that some integration of cortical signaling levels occurs in the pulvinar through intrinsic connections (*dashed lines*).

tions. In accordance with this hypothesis are the reports of cells in the cat LP-pulvinar responding to moving plaids with pattern-motion responses and of cells coding for the displacement of complex RDKs (Dumbrava et al. 2001; Merabet et al., 1998). It is possible to propose the existence of one loop (e.g., AEV-LPm in the cat) involved in higher-order motion analysis, while another loop (e.g., Pdm and area 7 in monkeys) is implicated in visual attentional processing, and so on. In cats, disrupting the loop by deactivating the cortex has been shown to impair processing in the LPm (Merabet et al., 1998). The effect of pulvinar-complex deactivation on cortical function remains unknown. Mumford (1991) has proposed that the thalamus may act as an active blackboard, through which each cortical area would be informed of the processing taking place in another area and would modify its activity accordingly. The pulvinar may play such a role by maintaining an “up-to-date” copy of the reconstructed visual world, thus allowing cortical areas to be informed of any relevant change in the visual scene that would need new neuronal computations for planning action strategies (see also Jones, 2001; Mumford, 1995). Along the same line, Olshausen et al. (1993) have suggested that the pulvinar may be involved not only in attentional processing but also in pattern recognition, a suggestion supported by the PET activation maps described by Barrett et al. (2001). In addition, some evidence suggests that the cat LP-pulvinar may participate in the synchronization of cortical cell discharges in area 17 (Shumikhina and Molotchnikoff, 1999), a phenomenon that would amplify the effectiveness of synaptic transfer between processing stages and further the resolution of the neuronal assembly engaged by a stimulus (Singer, 1999). Recently, the investigation of the visual function of a patient with unilateral damage of the pulvinar suggest that this nucleus may indeed be involved in feature binding (Ward et al., 2002).

Future research avenues on the pulvinar

Paraphrasing Sillito and Jones (1997), pulvinar and cortical levels of visual processing cannot be separated easily: they form a circuit, not a sequence. As such, the understanding of pulvinar function may depend largely on the researcher's ability to clearly establish the functional significance of the bidirectional connections between this large extrageniculate nucleus and the visual cortex. Uncovering the nature and function of the signals transferred along the cortico-thalamo-cortical loops will prove to be a challenging task, given the number of connections between the neocortex and the thalamus. Throughout the text, some specific questions have been pinpointed. Here are some general issues that need to be addressed.

Is the pulvinar made up of distinct functional modules? Despite the neuroanatomical finding that the pulvinar complex can

be parceled into distinct modules, it is not clear whether these modules have a distinct function in vision. In other words, should the pulvinar be seen as a single entity when it comes to function? While the available electrophysiological data in cat favor functional parcellation (e.g., pattern-motion selectivity was found almost exclusively in the medial part of the LP nucleus), additional studies should be conducted to determine the specificity of each nucleus comprising the pulvinar. This is especially true for primates, in which relatively little is known of pulvinar receptive properties. Once the parcellation of the primate pulvinar is clearly assessed, efforts should be made to reevaluate the characteristics of each module. In particular, higher-order neuronal functions should be assessed, as the pulvinar is likely to be involved in higher-order processing. Specific visual tasks could then be developed to further the study of pulvinar module function through brain imaging or selective pharmacological deactivations.

To what extent are these modules and their cortical counterparts interconnected? Another fundamental issue is to determine whether or not a given pulvinar module is preferentially linked to a specific cortical area; that is, are specific cortico-thalamo-cortical loops involved in particular functions? In order to answer this question, the arbor size, the overall configuration, and the branching of individual axons from projecting neurons must be established. The outcome of these studies is important not only to determine the functional nature of the inputs (e.g., driving vs. modulatory), but also to reveal the level of axonal divergence and convergence onto individual neurons or a pool. Pulvinar neurons projecting to multiple areas via axonal collaterals permit computations along a given loop. These projections also provide a route by which cortical areas are informed of ongoing computations and, by extension, of processes in other cortices connected to the loop. Such a system makes comparisons between different levels of visual analysis possible.

A related research goal is to determine the extent of communications between pulvinar modules that occur via intrinsic connections. As in other thalamic nuclei, pulvinar nuclei comprise projection neurons and intrinsic interneurons (Jones, 1985; Ma et al., 1998). Thalamic nuclei are generally considered to be independent of one another. To my knowledge, however, this issue has not been addressed in the pulvinar, and it may well be that dendritic or axon terminals in one module extend and reach cells located in neighboring subdivisions.

Who's driving whom? Finally, the relative weight of ascending and descending projections must be assessed. At this point, the primary visual cortex seems crucial for establishing an organized visuotopic map in the pulvinar complex. The contribution of extrastriate cortical areas to pulvinar function is not yet known. Another point of interest is that the activity of pulvinar neurons appears to be modulated by

stimulus relevance, but the impact of these “salience” signals (as well as any other signals from the pulvinar) onto cortical receptive fields remains virtually unknown.

Acknowledgments

I am grateful to Karine Minville, research assistant, for her help in the preparation of this chapter and to M. Ptito and D. Boire for constructive comments. I would also like to thank the members of my laboratory who worked on pulvinar-related projects, especially Karine Minville, Lotfi Merabet, Daniela Dumbrava, Alex Desautels, and Tony Savard, as well as the agencies that funded the projects: Canadian Institutes of Health Research, Fonds de la recherche en Santé du Québec, Fonds pour la Formation de chercheurs et l'aide à la recherche.

REFERENCES

- Abramson, B. P., and L. M. Chalupa, 1985. The laminar distribution of cortical connections with the tecto- and cortico-recipient zones in the cat's lateral posterior nucleus, *Neuroscience*, 15:81–95.
- Abramson, B. P., and L. M. Chalupa, 1988. Multiple pathways from the superior colliculus to the extrageniculate visual thalamus of the cat, *J. Comp. Neurol.*, 271:397–404.
- Acuna, C., J. Cudeiro, and F. Gonzalez, 1986. Lateral-posterior (LP) and pulvinar unit activity related to intentional upper limb movements directed to spatially separated targets in behaving *Macaca nemestrina* monkeys, *Rev. Neurol.*, 142:354–361.
- Acuna, C., J. Cudeiro, F. Gonzalez, J. M. Alonso, and R. Perez, 1990. Lateral-posterior and pulvinar reaching cells—comparison with parietal area 5a: a study in behaving *Macaca nemestrina* monkeys, *Exp. Brain Res.*, 82:158–166.
- Adams, M. M., P. R. Hof, R. Gattass, M. J. Webster, and L. G. Ungerleider, 2000. Visual cortical projections and chemoarchitecture of macaque monkey pulvinar, *J. Comp. Neurol.*, 419:377–393.
- Baddeley, A. D., H. A. Baddeley, R. S. Bucks, and G. K. Wilcock, 2001. Attentional control in Alzheimer's disease, *Brain*, 124:1492–1508.
- Baleydier, C., and F. Mauguère, 1985. Anatomical evidence for medial pulvinar connections with the posterior cingulate cortex, the retrosplenial area, and the posterior parahippocampal gyrus in monkeys, *J. Comp. Neurol.*, 232:219–228.
- Barrett, N. A., M. M. Large, G. L. Smith, P. T. Michie, F. Karayanidis, D. J. Kavanagh, R. Fawdry, D. Henderson, and B. T. O'Sullivan, 2001. Human cortical processing of colour and pattern, *Hum. Brain Mapp.*, 13:213–225.
- Bender, D. B., 1981. Retinotopic organization of macaque pulvinar, *J. Neurophysiol.*, 46:672–693.
- Bender, D. B., 1982. Receptive-field properties of neurons in the macaque inferior pulvinar, *J. Neurophysiol.*, 48:1–17.
- Bender, D. B., 1983. Visual activation of neurons in the primate pulvinar depends on cortex but not colliculus, *Brain Res.*, 279:258–261.
- Bender, D. B., 1988. Electrophysiological and behavioral experiments on the primate pulvinar, *Prog. Brain Res.*, 75:55–65.
- Bender, D. B., and C. M. Butter, 1987. Comparison of the effects of superior colliculus and pulvinar lesions on visual search and tachistoscopic pattern discrimination in monkeys, *Exp. Brain Res.*, 69:140–154.
- Bender, D. B., and M. Youakim, 2001. Effect of attentive fixation in macaque thalamus and cortex, *J. Neurophysiol.*, 85:219–234.
- Benedek, G., M. Norita, and O. D. Creutzfeldt, 1983. Electrophysiological and anatomical demonstration of an overlapping striate and tectal projection to the lateral posterior-pulvinar complex of the cat, *Exp. Brain Res.*, 52:157–169.
- Benevento, L. A., and B. Davis, 1977. Topographical projections of the prestriate cortex to the pulvinar nuclei in the macaque monkey: an autoradiographic study, *Exp. Brain Res.*, 30:405–424.
- Benevento, L. A., and J. H. Fallon, 1975. The ascending projections of the superior colliculus in the rhesus monkey (*Macaca mulatta*), *J. Comp. Neurol.*, 160:339–361.
- Benevento, L. A., and J. Miller, 1981. Visual responses of single neurons in the caudal lateral pulvinar of the macaque monkey, *J. Neurosci.*, 1:1268–1278.
- Benevento, L. A., and M. Rezak, 1976. The cortical projections of the inferior pulvinar and adjacent lateral pulvinar in the rhesus monkey (*Macaca mulatta*): an autoradiographic study, *Brain Res.*, 108:1–24.
- Benevento, L. A., and G. P. Standage, 1983. The organization of projections of the retinorecipient and nonretinorecipient nuclei of the pretectal complex and layers of the superior colliculus to the lateral pulvinar and medial pulvinar in the macaque monkey, *J. Comp. Neurol.*, 217:307–336.
- Berman, N., and E. G. Jones, 1977. A retino-pulvinar projection in the cat, *Brain Res.*, 134:237–248.
- Berson, D. M., and A. M. Graybiel, 1978. Parallel thalamic zones in the LP-pulvinar complex of the cat identified by their afferent and efferent connections, *Brain Res.*, 147:139–148.
- Berson, D. M., and A. M. Graybiel, 1980. Some cortical and subcortical fiber projections to the accessory optic nuclei in the cat, *Neuroscience*, 5:2203–2217.
- Berson, D. M., and A. M. Graybiel, 1983. Organization of the striate-recipient zone of the cat's lateralis posterior-pulvinar complex and its relations with the geniculostriate system, *Neuroscience*, 9:337–372.
- Bickford, M. E., W. Guido, and D. W. Godwin, 1998. Neurofilament proteins in Y-cells of the cat lateral geniculate nucleus: normal expression and alteration with visual deprivation, *J. Neurosci.*, 18:6549–6557.
- Boire, D., C. Casanova, and M. Ptito, in preparation. Direct retinal projections to the lateral posterior-pulvinar complex in normal cats.
- Boussaoud, D., R. Desimone, and L. G. Ungerleider, 1991. Visual topography of area TEO in the macaque, *J. Comp. Neurol.*, 306:554–575.
- Buchsbaum, M. S., T. Someya, C. Y. Teng, L. Abel, S. Chin, A. Najafi, R. J. Haier, J. Wu, and W. E. Bunney, Jr, 1996. PET and MRI of the thalamus in never-medicated patients with schizophrenia, *Am. J. Psychiatry*, 153:191–199.
- Campos-Ortega, J. A., and W. R. Hayhow, 1972. On the organization of the visual cortical projection to the pulvinar in *Macaca mulatta*, *Brain Behav. Evol.*, 6:394–423.
- Casanova, C., 1993. Response properties of neurons in area 17 projecting to the striate-recipient zone of the cat's lateralis posterior-pulvinar complex: comparison with cortico-tectal cells, *Exp. Brain Res.*, 96:247–259.
- Casanova, C., 2002. In search of the role of extrageniculate cortico-thalamic loops in visual processing using deactivation techniques, in *Virtual Lesions: Understanding Perception and Cognition*

- with *Reversible Deactivation Techniques* (S. Lomber and R. Galuske, eds.), Oxford: Oxford University Press, pp. 61–81.
- Casanova, C., R. D. Freeman, and J. P. Nordmann, 1989. Monocular and binocular response properties of cells in the striate-recipient zone of the cat's lateral posterior-pulvinar complex, *J. Neurophysiol.*, 62:544–557.
- Casanova, C., L. Merabet, A. Desautels, and K. Minville, 2001. Higher-order motion processing in the pulvinar, *Prog. Brain Res.*, 134:71–82.
- Casanova, C., and S. Molotchnikoff, 1990. Influence of the superior colliculus on visual responses of cells in the rabbit's lateral posterior nucleus, *Exp. Brain Res.*, 80:387–396.
- Casanova, C., and T. Savard, 1996a. Responses to moving texture patterns of cells in the striate-recipient zone of the cat's lateral posterior-pulvinar complex, *Neuroscience*, 70:439–447.
- Casanova, C., and T. Savard, 1996b. Motion sensitivity and stimulus interactions in the striate-recipient zone of the cat's lateral posterior-pulvinar complex, *Prog. Brain Res.*, 112:277–287.
- Casanova, C., T. Savard, and S. Darveau, 1997. Contribution of area 17 to cell responses in the striate-recipient zone of the cat's lateral posterior-pulvinar complex, *Eur. J. Neurosci.*, 9:1026–1036.
- Chalupa, L. M., 1991. Visual function of the pulvinar, in *Vision and Visual Dysfunction. The Neural Basis of Visual Function* (B. Dreher and S. P. Robinson, eds.), Boca Raton: CRC Press, pp. 140–159.
- Chalupa, L. M., and B. P. Abramson, 1988. Receptive-field properties in the tecto- and striate-recipient zones of the cat's lateral posterior nucleus, *Prog. Brain Res.*, 75:85–94.
- Chalupa, L. M., and B. P. Abramson, 1989. Visual receptive fields in the striate-recipient zone of the lateral posterior-pulvinar complex, *J. Neurosci.*, 9:347–357.
- Chalupa, L. M., H. Anchel, and D. B. Lindsley, 1972. Visual input to the pulvinar via lateral geniculate, superior colliculus and visual cortex in the cat, *Exp. Neurol.*, 36:449–462.
- Chalupa, L. M., R. W. Williams, and M. J. Hughes, 1983. Visual response properties in the tectorecipient zone of the cat's lateral posterior-pulvinar complex: a comparison with the superior colliculus, *J. Neurosci.*, 3:2587–2596.
- Cola, M. G., D. N. Gray, B. Seltzer, and C. G. Cusick, 1999. Human thalamus: neurochemical mapping of inferior pulvinar complex, *Neuro Report*, 10:3733–3738.
- Corbetta, M., F. M. Miezin, S. Dobmeyer, G. L. Shulman, and S. E. Petersen, 1991. Selective and divided attention during visual discriminations of shape, color, and speed: functional anatomy by positron emission tomography, *J. Neurosci.*, 11:2383–2402.
- Cowey, A., P. Stoerig, and M. Bannister, 1994. Retinal ganglion cells labelled from the pulvinar nucleus in macaque monkeys, *Neuroscience*, 61:691–705.
- Creutzfeldt, O. D., 1988. Extrageniculate-striate visual mechanisms: compartmentalization of visual functions, *Prog. Brain Res.*, 75:307–320.
- Crommelinck, M., A. Roucoux, and M. Meulders, 1977. Eye movement evoked by stimulation of lateral posterior nucleus and pulvinar in the alert cat, *Brain Res.*, 124:361–366.
- Cudeiro, J., F. Gonzalez, R. Perez, J. M. Alonso, and C. Acuna, 1989. Does the pulvinar-LP complex contribute to motor programming? *Brain Res.*, 484:367–370.
- Cusick, C. G., J. L. Scriptor, J. G. Darensbourg, and J. T. Weber, 1993. Chemoarchitectonic subdivisions of the visual pulvinar in monkeys and their connectional relations with the middle temporal and rostral dorsolateral visual areas, MT and DLR, *J. Comp. Neurol.*, 336:1–30.
- Desimone, R., M. Wessinger, L. Thomas, and W. Schneider, 1990. Attentional control of visual perception: cortical and subcortical mechanisms, *Cold Spring Harb. Symp. Quant. Biol.*, 55:963–971.
- Diamond, I. T., and W. C. Hall, 1969. Evolution of neocortex, *Science*, 164:251–262.
- Dumbrava, D., J. Faubert, and C. Casanova, 2001. Global motion integration in the cat's lateral posterior-pulvinar complex, *Eur. J. Neurosci.*, 13:2218–2226.
- Fabre-Thorpe, M., A. Vievard, and P. Buser, 1986. Role of the extra-geniculate pathway in visual guidance. II. Effects of lesioning the pulvinar-lateral posterior thalamic complex in the cat, *Exp. Brain Res.*, 62:596–606.
- Feig, S., and J. K. Harting, 1998. Corticocortical communication via the thalamus: ultrastructural studies of corticothalamic projections from area 17 to the lateral posterior nucleus of the cat and inferior pulvinar nucleus of the owl monkey, *J. Comp. Neurol.*, 395:281–295.
- Felsten, G., L. A. Benevento, and D. Burman, 1983. Opponent-color responses in macaque extrageniculate visual pathways: the lateral pulvinar, *Brain Res.*, 288:363–367.
- Fish, S. E., and L. M. Chalupa, 1979. Functional properties of pulvinar-lateral posterior neurons which receive input from the superior colliculus, *Exp. Brain Res.*, 36:245–257.
- Fletcher, W. A., and J. A. Sharpe, 1986. Saccadic eye movement dysfunction in Alzheimer's disease, *Ann. Neurol.*, 20:464–471.
- Fosse, V. M., P. Heggelund, and F. Fonnum, 1989. Postnatal development of glutamatergic, GABAergic, and cholinergic neurotransmitter phenotypes in the visual cortex, lateral geniculate nucleus, pulvinar, and superior colliculus in cats, *J. Neurosci.*, 9:426–435.
- Girard, P., P. A. Salin, and J. Bullier, 1991a. Visual activity in macaque area V4 depends on area 17 input, *NeuroReport*, 2:81–84.
- Girard, P., P. A. Salin, and J. Bullier, 1991b. Visual activity in areas V3a and V3 during reversible inactivation of area V1 in the macaque monkey, *J. Neurophysiol.*, 66:1493–1503.
- Girard, P., P. A. Salin, and J. Bullier, 1992. Response selectivity of neurons in area MT of the macaque monkey during reversible inactivation of area V1, *J. Neurophysiol.*, 67:1437–1446.
- Grant, S., and S. Shipp, 1991. Visuotopic organization of the lateral suprasylvian area and of an adjacent area of the ectosylvian gyrus of cat cortex: a physiological and connectional study, *Vis. Neurosci.*, 6:315–338.
- Gray, D., C. Gutierrez, and C. G. Cusick, 1999. Neurochemical organization of inferior pulvinar complex in squirrel monkeys and macaques revealed by acetylcholinesterase histochemistry, calbindin and Cat-301 immunostaining, and *Wisteria floribunda* agglutinin binding, *J. Comp. Neurol.*, 409:452–468.
- Graybiel, A. M., and D. M. Berson, 1980. Histochemical identification and afferent connections of subdivisions in the lateralis posterior-pulvinar complex and related thalamic nuclei in the cat, *Neuroscience*, 5:1175–1238.
- Grieve, K. L., C. Acuna, and J. Cudeiro, 2000. The primate pulvinar nuclei: vision and action, *Trends Neurosci.*, 23:35–39.
- Guillery, R. W., S. L. Feig, and D. P. Van Lieshout, 2001. Connections of higher order visual relays in the thalamus: a study of corticothalamic pathways in cats, *J. Comp. Neurol.*, 438:66–85.
- Guillery, R. W., E. E. Geisert, Jr., E. H. Polley, and C. A. Mason, 1980. An analysis of the retinal afferents to the cat's medial interlaminar nucleus and to its rostral thalamic extension, the "geniculate wing," *J. Comp. Neurol.*, 194:117–142.
- Gutierrez, C., and C. G. Cusick, 1997. Area V1 in macaque monkeys projects to multiple histochemically defined subdivisions of the inferior pulvinar complex, *Brain Res.*, 765:349–356.

- Gutierrez, C., A. Yaun, and C. G. Cusick, 1995. Neurochemical subdivisions of the inferior pulvinar in macaque monkeys, *J. Comp. Neurol.*, 363:545–562.
- Hardy, S. G., and J. C. Lynch, 1992. The spatial distribution of pulvinar neurons that project to two subregions of the inferior parietal lobule in the macaque, *Cereb. Cortex*, 2:217–230.
- Harting, J. K., M. F. Huerta, A. J. Frankfurter, N. L. Strominger, and G. J. Royce, 1980. Ascending pathways from the monkey superior colliculus: an autoradiographic analysis, *J. Comp. Neurol.*, 192:853–882.
- Hazlett, E. A., M. S. Buchsbaum, W. Byne, T. C. Wei, J. Spiegel-Cohen, C. Geneve, R. Kinderlehrer, M. M. Haznedar, L. Shihabuddin, and L. J. Siever, 1999. Three-dimensional analysis with MRI and PET of the size, shape, and function of the thalamus in the schizophrenia spectrum, *Am. J. Psychiatry*, 156:1190–1199.
- Heckers, S., T. Curran, D. Goff, S. L. Rauch, A. J. Fischman, N. M. Alpert, and D. L. Schacter, 2000. Abnormalities in the thalamus and prefrontal cortex during episodic object recognition in schizophrenia, *Biol. Psychiatry*, 48:651–657.
- Huerta, M. F., and J. K. Harting, 1983. Sublamination within the superficial gray layer of the squirrel monkey: an analysis of the tectopulvinar projection using anterograde and retrograde transport methods, *Brain Res.*, 261:119–126.
- Huerta, M. F., L. A. Krubitzer, and J. H. Kaas, 1986. Frontal eye field as defined by intracortical microstimulation in squirrel monkeys, owl monkeys, and macaque monkeys: I. Subcortical connections, *J. Comp. Neurol.*, 253:415–439.
- Hutchins, B., and B. V. Updyke, 1989. Retinotopic organization within the lateral posterior complex of the cat, *J. Comp. Neurol.*, 285:350–398.
- Hutsler, J. J., and L. M. Chalupa, 1991. Substance P immunoreactivity identifies a projection from the cat's superior colliculus to the principal tectorecipient zone of the lateral posterior nucleus, *J. Comp. Neurol.*, 312:379–390.
- Itaya, S. K., and G. W. Van Hoesen, 1983. Retinal projections to the inferior and medial pulvinar nuclei in the Old-World monkey, *Brain Res.*, 269:223–230.
- Jones, E. G., 1985. *The Thalamus*, New York: Plenum Press, pp. 531–572.
- Jones, E. G., 2001. The thalamic matrix and thalamocortical synchrony, *Trends Neurosci.*, 24:595–601.
- Kaas, J. H., and L. A. Krubitzer, 1992. Area 17 lesions deactivate area MT in owl monkeys, *Vis. Neurosci.*, 9:399–407.
- Kaufman, E. F., A. C. Rosenquist, and D. Raczkowski, 1984. The projections of single thalamic neurons onto multiple visual cortical areas in the cat, *Brain Res.*, 298:171–174.
- Kawamura, S., N. Fukushima, and S. Hattori, 1979. Topographical origin and ganglion cell type of the retino-pulvinar projection in the cat, *Brain Res.*, 173:419–429.
- Kawamura, S., N. Fukushima, S. Hattori, and M. Kudo, 1980. Laminar segregation of cells of origin of ascending projections from the superficial layers of the superior colliculus in the cat, *Brain Res.*, 184:486–490.
- Killackey, H., and I. T. Diamond, 1971. Visual attention in the tree shrew: an ablation study of the striate and extrastriate visual cortex, *Science*, 171:696–699.
- Kuljis, R. O., 1994. Lesions in the pulvinar in patients with Alzheimer's disease, *J. Neuropathol. Exp. Neurol.*, 53:202–211.
- LaBerge, D., and M. S. Buchsbaum, 1990. Positron emission tomographic measurements of pulvinar activity during an attention task, *J. Neurosci.*, 10:613–619.
- Le Gros Clark, W. E., 1932. The structure and connections of the thalamus, *Brain*, 55:406–470.
- Lund, J. S., G. H. Henry, C. L. MacQueen, and A. R. Harvey, 1979. Anatomical organization of the primary visual cortex (area 17) of the cat. A comparison with area 17 of the macaque monkey, *J. Comp. Neurol.*, 184:599–618.
- Lund, J. S., R. D. Lund, A. E. Hendrickson, A. H. Bunt, and A. F. Fuchs, 1975. The origin of efferent pathways from the primary visual cortex, area 17, of the macaque monkey as shown by retrograde transport of horseradish peroxidase, *J. Comp. Neurol.*, 164:287–303.
- Ma, T. P., J. C. Lynch, D. K. Donahoe, H. Attallah, and J. A. Rafols, 1998. Organization of the medial pulvinar nucleus in the macaque, *Anat. Rec.*, 250:220–237.
- Macchi, G., M. Bentivoglio, D. Minciacchi, and M. Molinari, 1996. Trends in the anatomical organization and functional significance of the mammalian thalamus, *Ital. J. Neurol. Sci.*, 17:105–129.
- Marrocco, R. T., J. W. McClurkin, and R. A. Young, 1981. Spatial properties of superior colliculus cells projecting to the inferior pulvinar and parabigeminal nucleus of the monkey, *Brain Res.*, 222:150–154.
- Mason, R., 1978. Functional organization in the cat's pulvinar complex, *Exp. Brain Res.*, 31:51–66.
- Mason, R., 1981. Differential responsiveness of cells in the visual zones of the cat's LP-pulvinar complex to visual stimuli, *Exp. Brain Res.*, 43:25–33.
- Mathers, L. H., and S. C. Rapisardi, 1973. Visual and somatosensory receptive fields of neurons in the squirrel monkey pulvinar, *Brain Res.*, 64:65–83.
- Matsumoto, E., Y. Ohigashi, M. Fujimori, and E. Mori, 2000. The processing of global and local visual information in Alzheimer's disease, *Behav. Neurol.*, 12:119–125.
- Maunsell, J. H., T. A. Nealey, and D. D. DePriest, 1990. Magnocellular and parvocellular contributions to responses in the middle temporal visual area (MT) of the macaque monkey, *J. Neurosci.*, 10:3323–3334.
- McIlwain, J. T., 1978. Properties of cells projecting rostrally from the superficial layers of the cat's superior colliculus, *Brain Res.*, 143:445–457.
- Mega, M. S., L. Lee, I. D. Dinov, F. Mishkin, A. W. Toga, and J. L. Cummings, 2000. Cerebral correlates of psychotic symptoms in Alzheimer's disease, *J. Neurol. Neurosurg. Psychiatry*, 69:167–171.
- Merabet, L., A. Desautels, K. Minville, and C. Casanova, 1998. Motion integration in a thalamic visual nucleus, *Nature*, 396:265–268.
- Miceli, D., J. Reperant, L. Marchand, R. Ward, and N. Vesselkin, 1991. Divergence and collateral axon branching in subsystems of visual cortical projections from the cat lateral posterior nucleus, *J. Hirnforsch.*, 32:165–173.
- Michael, G. A., M. Boucart, J. F. Degreef, and O. Godefroy, 2001. The thalamus interrupts top-down attentional control for permitting exploratory shiftings to sensory signals, *NeuroReport*, 12:2041–2048.
- Miller, L. M., and C. E. Schreiner, 2000. Stimulus-based state control in the thalamocortical system, *J. Neurosci.*, 20:7011–7016.
- Miller, R., 1996. Cortico-thalamic interplay and the security of operation of neural assemblies and temporal chains in the cerebral cortex, *Biol. Cybern.*, 75:263–275.
- Minville, K., and C. Casanova, 1998. Spatial frequency processing in posteromedial lateral suprasylvian cortex does not depend on the projections from the striate-recipient zone of the cat's lateral posterior-pulvinar complex, *Neuroscience*, 84:699–711.

- Mizuno, N., K. Itoh, K. Uchida, M. Uemura-Sumi, and R. Matsushima, 1982. A retino-pulvinar projection in the macaque monkey as visualized by the use of anterograde transport of horseradish peroxidase, *Neurosci. Lett.*, 30:199–203.
- Morris, J. S., K. J. Friston, and R. J. Dolan, 1997. Neural responses to salient visual stimuli, *Proc. R. Soc. Lond. B. Biol. Sci.*, 264: 769–775.
- Movshon, J. A., E. H. Adelson, M. S. Gizzi, and W. T. Newsome, 1985. The analysis of moving visual patterns, *Pont. Acad. Sci. Varia.*, 54:117–151.
- Mumford, D., 1991. On the computational architecture of the neocortex. I. The role of the thalamo-cortical loop, *Biol. Cybern.*, 65:135–145.
- Mumford, D., 1995. Neuronal architectures for pattern-theoretic problems, in *Large-Scale Neuronal Theories of the Brain* (C. Koch and J. L. Davis, eds.), Cambridge: MIT Press, pp. 125–152.
- Newsome, W. T., and E. B. Pare, 1988. A selective impairment of motion perception following lesions of the middle temporal visual area (MT), *J. Neurosci.*, 8:2201–2211.
- Norita, M., M. Kase, K. Hoshino, R. Meguro, S. Funaki, S. Hirano, and J. G. McHaffic, 1996. Extrinsic and intrinsic connections of the cat's lateral suprasylvian visual area, *Prog. Brain Res.* 112:231–250.
- Norita, M., L. Mucke, G. Benedek, B. Albowitz, Y. Katoh, and O. D. Creutzfeldt, 1986. Connections of the anterior ectosylvian visual area (AEV), *Exp. Brain Res.*, 62:225–240.
- O'Brien, B. J., P. L. Abel, and J. F. Olavarria, 2001. The retinal input to calbindin-D28K-defined subdivision in macaque inferior pulvinar, *Neurosci. Lett.*, 312:145–148.
- Ogren, M. P., and A. E. Hendrickson, 1979. The morphology and distribution of striate cortex terminals in the inferior and lateral subdivisions of the *Macaca* monkey pulvinar, *J. Comp. Neurol.*, 188:179–199.
- Ogren, M. P., C. A. Mateer, and A. R. Wyler, 1984. Alterations in visually related eye movements following left pulvinar damage in man, *Neuropsychologia*, 22:187–196.
- Ojima, H., K. Murakami, and K. Kishi, 1996. Dual termination modes of corticothalamic fibers originating from pyramids of layers 5 and 6 in cat visual cortical area 17, *Neurosci. Lett.*, 208:57–60.
- Olshausen, B. A., C. H. Anderson, and D. C. Van Essen, 1993. A neurobiological model of visual attention and invariant pattern recognition based on dynamic routing of information, *J. Neurosci.*, 13:4700–4719.
- Olzowski, J., 1952. *The Thalamus of the Macaca mulatta: An Atlas for Use with the Stereotaxic Instrument*, Basel: Karger.
- Petersen, S. E., D. L. Robinson, and W. Keys, 1985. Pulvinar nuclei of the behaving rhesus monkey: visual responses and their modulation, *J. Neurophysiol.*, 54:867–886.
- Petersen, S. E., D. L. Robinson, and J. D. Morris, 1987. Contributions of the pulvinar to visual spatial attention, *Neuropsychologia*, 25:97–105.
- Portas, C. M., J. M. Goldstein, M. E. Shenton, H. H. Hokama, C. G. Wible, I. Fischer, R. Kikinis, R. Donnino, F. A. Jolesz, and R. W. McCarley, 1998. Volumetric evaluation of the thalamus in schizophrenic male patients using magnetic resonance imaging, *Biol. Psychiatry*, 43:649–659.
- Ptito, M., P. Johansson, J. Faubert, and A. Gjedde, 1999. Activation of human extrageniculostriate pathways after damage to area V1, *Neuroimage*, 9:97–107.
- Pu, M., D. M. Berson, and T. Pan, 1994. Structure and function of retinal ganglion cells innervating the cat's geniculate wing: an in vitro study, *J. Neurosci.*, 14:4338–4358.
- Raczkowski, D., and A. C. Rosenquist, 1981. Retinotopic organization in the cat lateral posterior-pulvinar complex, *Brain Res.*, 221:185–191.
- Raczkowski, D., and A. C. Rosenquist, 1983. Connections of the multiple visual cortical areas with the lateral posterior-pulvinar complex and adjacent thalamic nuclei in the cat, *J. Neurosci.*, 3:1912–1942.
- Rafal, R. D., and M. I. Posner, 1987. Deficits in human visual spatial attention following thalamic lesions, *Proc. Natl. Acad. Sci. USA*, 84:7349–7353.
- Rezak, M., and L. A. Benevento, 1979. A comparison of the organization of the projections of the dorsal lateral geniculate nucleus, the inferior pulvinar and adjacent lateral pulvinar to primary visual cortex (area 17) in the macaque monkey, *Brain Res.*, 167:19–40.
- Robinson, D. L., and R. J. Cowie, 1997. The primate pulvinar: structural, functional, and behavioral components of visual salience, in *Thalamus*, vol. 2, *Experimental and Clinical Aspects* (M. Norita, T. Bando, and B. E. Stein, eds.), Oxford: Elsevier Science, pp. 53–92.
- Robinson, D. L., J. W. McClurkin, and C. Kertzman, 1990. Orbital position and eye movement influences on visual responses in the pulvinar nuclei of the behaving macaque, *Exp. Brain Res.*, 82:235–246.
- Robinson, D. L., J. W. McClurkin, C. Kertzman, and S. E. Petersen, 1991. Visual responses of pulvinar and collicular neurons during eye movements of awake, trained macaques, *J. Neurophysiol.*, 66:485–496.
- Robinson, D. L., and S. E. Petersen, 1992. The pulvinar and visual salience, *Trends Neurosci.*, 15:127–132.
- Robinson, D. L., S. E. Petersen, and W. Keys, 1986. Saccade-related and visual activities in the pulvinar nuclei of the behaving rhesus monkey, *Exp. Brain Res.*, 62:625–634.
- Rockland, K. S., 1996. Two types of corticopulvinar terminations: round (type 2) and elongate (type 1), *J. Comp. Neurol.*, 368:57–87.
- Rockland, K. S., 1998. Convergence and branching patterns of round, type 2 corticopulvinar axons, *J. Comp. Neurol.*, 390:515–536.
- Rodman, H. R., and T. D. Albright, 1989. Single-unit analysis of pattern-motion selective properties in the middle temporal visual area (MT), *Exp. Brain Res.*, 75:53–64.
- Rodman, H. R., C. G. Gross, and T. D. Albright, 1989. Afferent basis of visual response properties in area MT of the macaque. I. Effects of striate cortex removal, *J. Neurosci.*, 9:2033–2050.
- Rodman, H. R., C. G. Gross, and T. D. Albright, 1990. Afferent basis of visual response properties in area MT of the macaque. II. Effects of superior colliculus removal, *J. Neurosci.*, 10:1154–1164.
- Salzmann, E., 1995. Attention and memory trials during neuronal recording from the primate pulvinar and posterior parietal cortex (area PG), *Behav. Brain Res.*, 67:241–253.
- Scannell, J. W., F. Sengpiel, M. J. Tovee, P. J. Benson, C. Blakemore, and M. P. Young, 1996. Visual motion processing in the anterior ectosylvian sulcus of the cat, *J. Neurophysiol.*, 76:895–907.
- Schneider, G. E., 1967. Contrasting visuomotor functions of tectum and cortex in the golden hamster, *Psychol. Forsch.*, 31:52–62.
- Schneider, G. E., 1969. Two visual systems, *Science*, 163:895–902.
- Sherman, S. M., and R. W. Guillery, 1996. Functional organization of thalamocortical relays, *J. Neurophysiol.*, 76:1367–1395.
- Sherman, S. M., and R. W. Guillery, 1998. On the actions that one nerve cell can have on another: distinguishing “drivers” from “modulators,” *Proc. Natl. Acad. Sci. USA*, 95:7121–7126.

- Sherman, S. M., and R. W. Guillery, 2001. *Exploring the Thalamus*, San Diego: Academic Press.
- Shumikhina, S., and S. Molotchnikoff, 1999. Pulvinar participates in synchronizing neural assemblies in the visual cortex in cats, *Neurosci. Lett.*, 272:135–139.
- Sillito, A., and H. E. Jones, 1997. Functional organization influencing neurotransmission in the lateral geniculate nucleus, in *Thalamus*, vol. 2, *Experimental and Clinical Aspects* (M. Norita, T. Bando, and B. E. Stein, eds.), Oxford: Elsevier Science, pp. 1–52.
- Singer, W., 1999. Time as coding space? *Curr. Opin. Neurobiol.*, 9:189–194.
- Smith, D. C., and P. D. Spear, 1979. Effects of superior colliculus removal on receptive-field properties of neurons in lateral suprasylvian visual area of the cat, *J. Neurophysiol.*, 42:57–75.
- Spear, P. D., 1991. Functions of extrastriate visual cortex in non-primate species, in *Vision and Visual Dysfunctions. The Neural Basis of Visual Function* (B. Dreher and S. R. Robinson, eds.), Boca Raton: CRC Press, pp. 339–370.
- Stepniewska, I., and J. H. Kaas, 1997. Architectonic subdivisions of the inferior pulvinar in New World and Old World monkeys, *Vis. Neurosci.*, 14:1043–1060.
- Stepniewska, I., H. X. Qj, and J. H. Kaas, 1999. Do superior colliculus projection zones in the inferior pulvinar project to MT in primates? *Eur. J. Neurosci.*, 11:469–480.
- Stoerig, P., and A. Cowey, 1997. Blindsight in man and monkey, *Brain*, 120:535–559.
- Sturm, W., A. de Simone, B. J. Krause, K. Specht, V. Hesselmann, I. Radermacher, H. Herzog, L. Tellmann, H. W. Muller-Gartner, and K. Willmes, 1999. Functional anatomy of intrinsic alertness: evidence for a fronto-parietal-thalamic-brainstem network in the right hemisphere, *Neuropsychologia*, 37:797–805.
- Sudkamp, S., and M. Schmidt, 1995. Physiological characterization of pretectal neurons projecting to the lateral posterior-pulvinar complex in the cat, *Eur. J. Neurosci.*, 7:881–888.
- Sudkamp, S., and M. Schmidt, 2000. Response characteristics of neurons in the pulvinar of awake cats to saccades and to visual stimulation, *Exp. Brain Res.*, 133:209–218.
- Symonds, L. L., A. C. Rosenquist, S. B. Edwards, and L. A. Palmer, 1981. Projections of the pulvinar-lateral posterior complex to visual cortical areas in the cat, *Neuroscience*, 6:1995–2020.
- Takayama, Y., M. Sugishita, T. Kido, M. Ogawa, H. Fukuyama, and I. Akiguchi, 1994. Impaired stereoacuity due to a lesion in the left pulvinar, *J. Neurol. Neurosurg. Psychiatry*, 57:652–654.
- Trevarthen, C. B., 1968. Two mechanisms of vision in primates, *Psychol. Forsch.*, 31:299–348.
- Trojanowski, J. Q., and S. Jacobson, 1977. The morphology and laminar distribution of corticopulvinar neurons in the rhesus monkey, *Exp. Brain Res.*, 28:51–62.
- Ungerleider, L. G., and C. A. Christensen, 1977. Pulvinar lesions in monkeys produce abnormal eye movements during visual discrimination training, *Brain Res.*, 136:189–196.
- Ungerleider, L. G., and C. A. Christensen, 1979. Pulvinar lesions in monkeys produce abnormal scanning of a complex visual array, *Neuropsychologia*, 17:493–501.
- Ungerleider, L. G., T. W. Galkin, and M. Mishkin, 1983. Visuotopic organization of projections from striate cortex to inferior and lateral pulvinar in rhesus monkey, *J. Comp. Neurol.*, 217:137–157.
- Updyke, B. V., 1977. Topographic organization of the projections from cortical areas 17, 18 and 19 onto the thalamus, pretectum and superior colliculus in the cat, *J. Comp. Neurol.*, 173:81–122.
- Updyke, B. V., 1981. Projections from visual areas of the middle suprasylvian sulcus onto the lateral posterior complex and adjacent thalamic nuclei in cat, *J. Comp. Neurol.*, 201:477–506.
- Updyke, B. V., 1983. A reevaluation of the functional organization and cytoarchitecture of the feline lateral posterior complex, with observations on adjoining cell groups, *J. Comp. Neurol.*, 219:143–181.
- von Grunau, M., and B. J. Frost, 1983. Double-opponent-process mechanism underlying RF-structure of directionally specific cells of cat lateral suprasylvian visual area, *Exp. Brain Res.*, 49:84–92.
- Walker, A. E., 1938. *The Primate Thalamus*, Chicago: University of Chicago Press.
- Ward, R., S. Danziger, V. Owen, and R. Rafal, 2002. Deficits in spatial coding and feature binding following damage to spatiotopic map in the human pulvinar, *Nat. Neurosci.*, 5:99–100.
- Weber, J. T., I. L. Chen, and B. Hutchins, 1986. The pretectal complex of the cat: cells of origin of projections to the pulvinar nucleus, *Brain Res.*, 397:389–394.
- Webster, M. J., J. Bachevalier, and L. G. Ungerleider, 1993. Subcortical connections of inferior temporal areas TE and TEO in macaque monkeys, *J. Comp. Neurol.*, 335:73–91.
- Wilson, J. S., and S. J. Goldberg, 1980. Inputs of the pulvinar and lateral posterior nucleus into the abducens nucleus of the cat, *Exp. Neurol.*, 68:72–86.

37 Feedback Systems in Visual Processing

ADAM M. SILLITO AND HELEN E. JONES

ONE OF THE ABIDING challenges in vision is the role of the extensive feedback systems that parallel the ascending feed-forward pathways. In some senses, the way we conceptualize these feedback systems may be misleading because it follows from a view that the process of vision proceeds upward in a series of divergent steps and hence the return connections have to be judged as feedback. Indeed, for a visual world in motion, and taking note of the rapid responses seen in some of the higher visual areas, the feedback connections have the capacity to influence the earliest central processing steps. Thus, they become more a part of a complex and integrated circuit rather than a reflected regulatory influence down a hierarchy.

From some viewpoints, an understanding of the organization of the visual system seems to be best encapsulated by descriptions that invoke a stepwise processing of the retinal input through a hierarchy of areas that build increasingly complex abstractions of the visual world. At higher levels these areas, in turn, could broadly be described as falling into two streams, one concerned with form and the other with motion and location. The earlier levels of the system can also be subdivided into channels subserving the differing “objectives” of the higher-level areas. Aspects of the segregation and the hierarchical nature of the processing in the sequence of cortical steps are, for example, supported by data from imaging studies. On the other hand, an extensive body of anatomical and neurophysiological data suggests a more complex and subtle organization of the central visual mechanism. Firstly, there are substantial interconnections enabling transfer of information between the processing streams at the level of the primary visual cortex (V1) and between higher cortical visual areas. Secondly, feedback connections provide an extensive and potentially very fast influence that can rephrase the local processing mechanisms at earlier levels in the system. Because of the interconnections between many of the higher areas, this also blurs the absolute segregation of the processing streams. Although it has been argued that such influences have a minor effect on visual processing, the evidence now available suggests the potential for a much more significant role. Thus, for example, the feedback from cortex to lateral geniculate nucleus (LGN) has been shown from several lines of evidence to influence both the temporal and spatial characteristics of the way visual information is translated through the LGN. In the cortex, feedback from area MT, associated with

higher-level motion processing, has been shown by a range of techniques to exert a strong influence on many aspects of visual processing in V1. Indeed, the strength and potential speed of MT feedback influences bring into question some of the associations that link to the concept of *feedback systems* and suggest that it might be more appropriate to consider them as components of a circuit. In this chapter, we shall review some of the evidence regarding the function of feedback in the visual system of the cat and primate, with particular, although not exclusive, reference to feedback from the visual cortex to the LGN and area MT to V1.

The geniculo-cortical loop

ANATOMICAL CONSIDERATIONS A common feature of the projections transferring retinal information to higher levels is that numerically the feedforward synapses constitute a relatively small component of the total excitatory synaptic input converging on the cells that relay the input to the next level. Thus, at each level in the system, the transfer of information is potentially subject to influences from both lateral interactions in the local horizontal network and feedback from higher levels in the system. In the LGN of cat and primates the retinal afferents comprise about 10% of the input to relay cells, while the corticofugal feedback connections to the relay cells represent 30% of the input (Sherman, 2001; Wilson, 1993). As well as the relay cells, the cortical feedback connections target intrinsic inhibitory interneurons in the LGN and inhibitory neurons in the thalamic reticular nucleus/perigeniculate nucleus. The main details of the circuitry in the LGN are summarized in Figure 37.1. In the cat the projection to the LGN, which derives primarily from areas 17 and 18, is dense, and individual corticofugal axons’ arborizations have a central core projection of approximately 180–1080 μ with a sparse scattering of long-range axons which spread over 500–2000 μ (Murphy et al., 2000; Murphy and Sillito, 1996; Robson, 1984). This needs to be placed in the perspective of the fact that the average spread of the retinal X axonal arborizations is 150 μ and that of the Y axons is 375 μ (Bowling and Michael, 1984). Thus, even within their central core, individual corticofugal axons innervate an area of the LGN that extends significantly beyond their own location in retinotopic space. These points and the circuitry in the LGN are summarized in Figure 37.1. This, together with their longer-range connections, means they

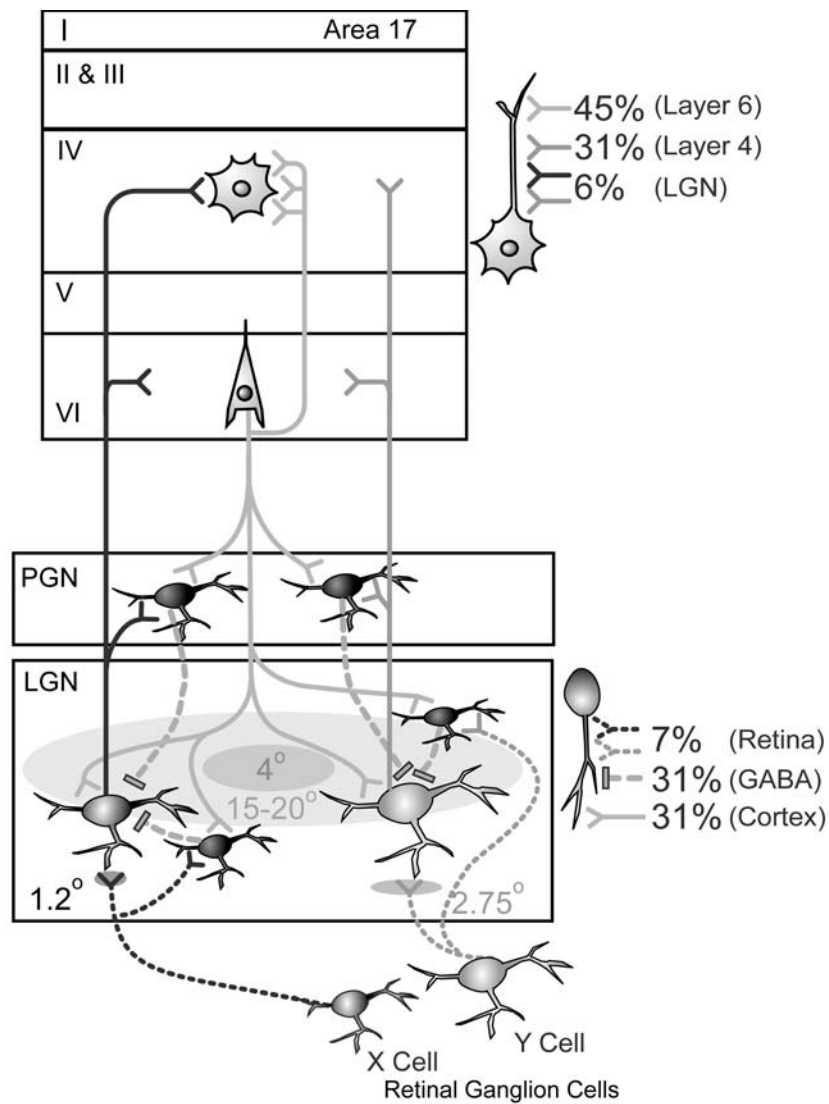


FIGURE 37.1. Schematic summary of the geniculo-cortical loop. Shaded ovals denote the typical retinotopic extent (at 5 degrees of eccentricity from the area centralis) of the axonal arborizations of X and Y retinal ganglion cell axons and corticofugal axons. Two dimensions are given for feedback axons: the smaller dimension depicts the typical spread for the dense central core projection, while the larger dimension depicts the overall coverage of the

axonal arborization. Percentages to the right of the drawing summarize the contribution of synaptic contacts from retinal axons, corticofugal feedback axons, and inhibitory interneurons synapsing on LGN relay cells, as well as the contributions from geniculate axons, layer 6 collaterals, and layer 4 connections synapsing on spiny stellate cells in layer 4 of the cortex.

can influence inputs that may lie outside their own classical receptive field. There is also good evidence favoring the view that the projection comprises axons with several diameters and conduction velocities. Individual axons, both coarse and fine, seem to innervate both perigeniculate nucleus (PGN) and LGN (Murphy and Sillito, 1996; Murphy et al., 2000). Similarly, estimates of the conduction velocity from latency measurements provide support for two groups of corticofugal afferents (Grieve and Sillito, 1995b; Tsumoto et al., 1978) projecting to the LGN and PGN. The fastest pathway allows for a very rapid influence of the corticofugal system on the developing response and would enable the loop from LGN

cell response to cortex and back within approximately 3–5 msec. Even the slower group would enable a loop within 4–10 msec. The organization of layer 6 and its interactions with the LGN in the primate are particularly interesting because there is a clear segregation of cells in relation to the incoming channels. Cells projecting to the parvocellular layers of the LGN lie in the upper part of layer 6, while the lower part contains cells projecting to both magnocellular and parvocellular laminae (Fitzpatrick et al., 1994). Additionally, the intercalated cells in the LGN that send axons to layer 1 and the cytochrome oxidase-rich blobs (Hendry and Yoshioka, 1994) seem to receive feedback from a distinct

group of cells in the deepest part of layer 6 (Fitzpatrick et al., 1994). Cells in the middle of layer 6 do not project to the LGN but may project to the claustrum.

An interesting feature of the organization of feedback connections from the visual cortex to the LGN in the cat is that the most dense component of the terminal arborizations of the corticofugal axons in the LGN exhibits marked asymmetry. These arborizations are extended either parallel or perpendicular to the axis of the orientation preference of the parent cell in layer 6 of the visual cortex (Murphy et al., 1999), as shown in Figure 37.2. This anatomical asymmetry strongly suggests that the feedback might be organized to influence the processing of information relevant to the extraction of the orientation of contours in the visual cortex. We discuss this further in relation to functional data below.

FIRING PATTERNS A key question is whether under normal circumstances layer 6 cells in the visual cortex directly drive LGN relay cells or whether they simply modulate their response to the retinal input. The synaptic input from the corticofugal axons, although extensive, as discussed above, targets the distal portion of the relay cell dendrites via ionotropic and metabotropic receptors (Sherman, 2001; Von Krosigk et al., 1999) while the retinal axons target the proximal dendrites via ionotropic receptors. While it is clear that under certain nonphysiological circumstances (e.g., electrical stimulation of layer 6 cells at 30–50 Hz) the feedback pathway effects are optimized and can drive relay cells directly (Lindstrom and Wróbel, 1990), the balance of the evidence favors a feedback-driven modulation of the probability that relay cells will respond to their retinal input (Sherman and Guillery, 1998). Certainly for visual

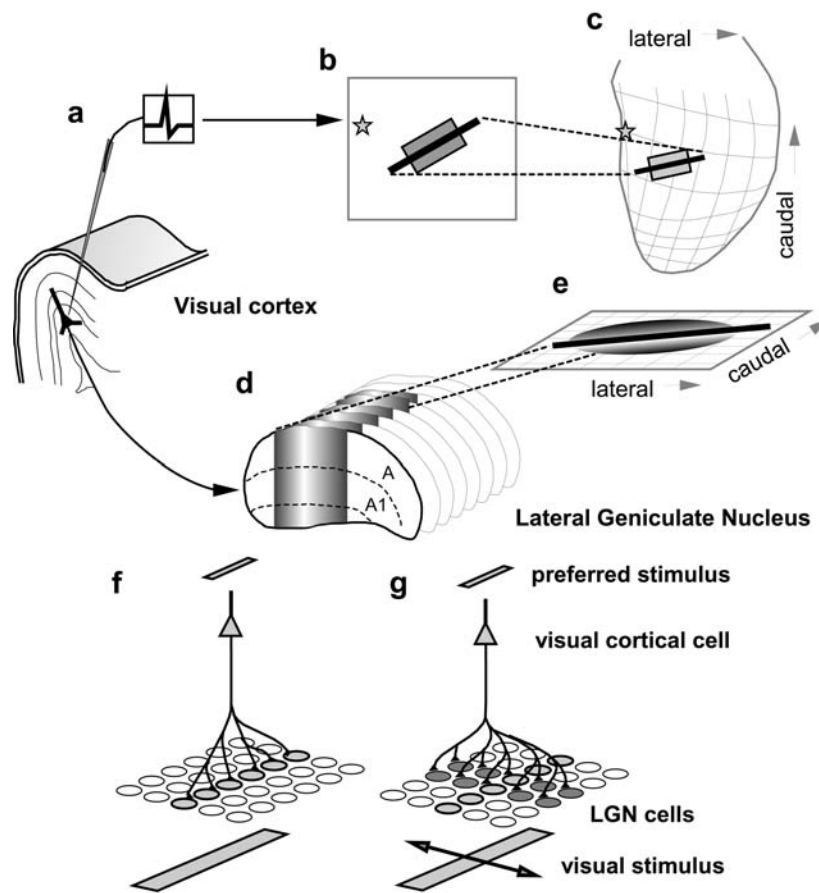


FIGURE 37.2. Asymmetric termination pattern of corticofugal axons links to parent cell response properties. *A–E*, Experimental paradigm. Receptive field properties of layer 6 cortical cells were mapped prior to labeling with biocytin (*A*). The receptive fields (*B*) were superimposed on the geniculate retinotopic map (*C*). Single axons were reconstructed from serial sections and the bouton distribution was quantified in three dimensions, then analyzed with

respect to their relation to the geniculate representation of visual space (*D*, *E*). *F*, *G*, Two main patterns of connectivity were observed. Feedback axons either innervated LGN cells lying along a line corresponding to the preferred orientation of the parent layer 6 cell (*F*) or orthogonal to (hence lying along the preferred axis of stimulus movement) the parent cell orientation preference (*G*). (Data taken from Murphy et al., 1999.)

stimulation, several investigations support the view that virtually all the spikes fired by X- and Y-type relay cells in the cat can be linked to spikes in the retinal ganglion cells providing the input (Cleland and Lee, 1985; Mastronarde, 1987). This point needs further experimental verification with stimuli that will strongly activate layer 6 cells in the visual cortex. Additionally, the suggestion that burst mode firing in relay cells, originally associated with synchronized firing of relay cells and slow-wave sleep, also occurs in the waking state (Guido and Weyand, 1995; Sherman, 2001) adds another dimension of complexity (Rowe and Fischer, 2001). Burst mode firing occurs when relay cells have been hyperpolarized for periods of 100 msec or more and follows the deinactivation of a voltage- and time-dependent calcium current (I_T). Under these conditions, when the cell receives a suprathreshold depolarizing input, there is a calcium influx generating a low-threshold depolarizing spike that then activates a burst of conventional spikes. The size of the low-threshold depolarizing spike and the number of conventional spikes in the burst depend on the degree of hyperpolarization of the membrane, not the magnitude of the suprathreshold activating input. A sustained depolarization of relay cells for 100 msec or more inactivates I_T , and the cell switches to tonic mode firing associated with a linear transmission of sensory information and in this sense associated more conventionally with the waking state.

We suggest that the key to the reported presence of burst firing mode in the waking state is the strength of the hyperpolarization that can follow from the visual input. An example could be a group of OFF-center X cells with receptive fields lying within a bright, featureless, and thus uniform field. This would produce a visually driven hyperpolarization of their membrane potential. The salient components of an image are the loci where a change occurs; thus, in this sense, the hypothetical group of cells would have nothing to signal. On the other hand, the appearance of a moving dark contour over their receptive field would provoke a depolarizing input and a low-threshold calcium spike driving a burst of action potentials.

It has been suggested that burst firing in thalamic cells in the waking state serves as a “wake-up” call to the cortical cells receiving the input (Sherman, 2001). However, in the sense that the cortex is already in the waking state, this may be a slightly misleading description. Rather, the burst of action potentials in the input to the cortex would provide a high-security signal to focus the circuitry on the new feature driving attention in the cortical mechanism. One suggested role for the corticofugal feedback system is that it may contribute to selective attention via its influence on geniculate firing patterns. Because the feedback axons influence LGN relay cells both directly via synapses involving ionotropic and metabotropic receptors (Sherman, 2001; Von Krosigk et al., 1999), and indirectly via an input to inhibitory interneurons,

they have the capacity to exert a complex pattern of control over relay cells that could switch the behavior of LGN cells between tonic and burst modes. Recent work has questioned whether the patterned activity that occurs normally in the visual cortex during visual stimulation might switch the behavior of LGN cells via the feedback system (Wang et al., submitted). While recording simultaneously in cortex and LGN, focal iontophoretic application of a GABA_B receptor antagonist, CGP 55845 (see below), was used to produce local relief of the GABA_B inhibition of layer 6 cells (Fig. 37.3A). This reversibly enhanced the gain of their visually driven responses without affecting their spontaneous firing rate, making it possible to isolate the effects of this change in a controlled fashion. This change in cortical visual responses led to a statistically significant shift in the ratio of burst to tonic firing for 68% of LGN cells tested. Of these, 43% showed a shift from tonic to bursting (e.g., Fig. 37.3B) and 25% from bursting to tonic firing (Fig. 37.3C). These effects did not follow from the drug’s application causing a state-dependent shift in the state of the cortex because simultaneously recorded LGN cells showed opposite direction shifts in firing. Thus, the data indicate that a focal change in the visual response magnitude of layer 6 cells can produce a clear switch in the firing pattern of LGN cells. In some cases, it moves them toward the tonic firing pattern and the faithful relay of their visual input; in others, it moves them to burst firing and a response mode suggested to underlie early signal detection (Sherman, 2001). With the complex input derived from stimuli in the natural visual world, the selective adjustment of the transfer properties of the LGN provides a means of alerting the system to salient change, while at the same time optimizing its capacity to relay accurate information about what has already engaged the system.

SPATIAL INTERACTIONS The corticofugal system also exerts a subtle but clear influence on the spatial properties of the LGN relay cell field. The fundamental effect seems to be an enhancement of the strength of the inhibitory surround in the presence of moving stimuli, so cells are more strongly patch-suppressed (and end-stopped) and the excitatory discharge zone for a moving stimulus is more focused (Cudeiro and Sillito, 1996; Jones et al., 2000; Murphy and Sillito, 1987; Sillito et al., 1993). Thus, the records in Figure 37.4A give an example of the length tuning of simultaneously recorded LGN cells, one with corticofugal feedback and one without. The loss of surround suppression in the absence of feedback is clear. The effect over the group of LGN cells tested is summarized by the block histogram in Figure 37.4B. These effects occurred without changing the degree of suppression associated with a stationary flashing stimulus of varying diameter. The enhancement of the inhibitory surround for moving stimuli also seems to lead to an increased sensitivity to orientation contrast, direction contrast, and

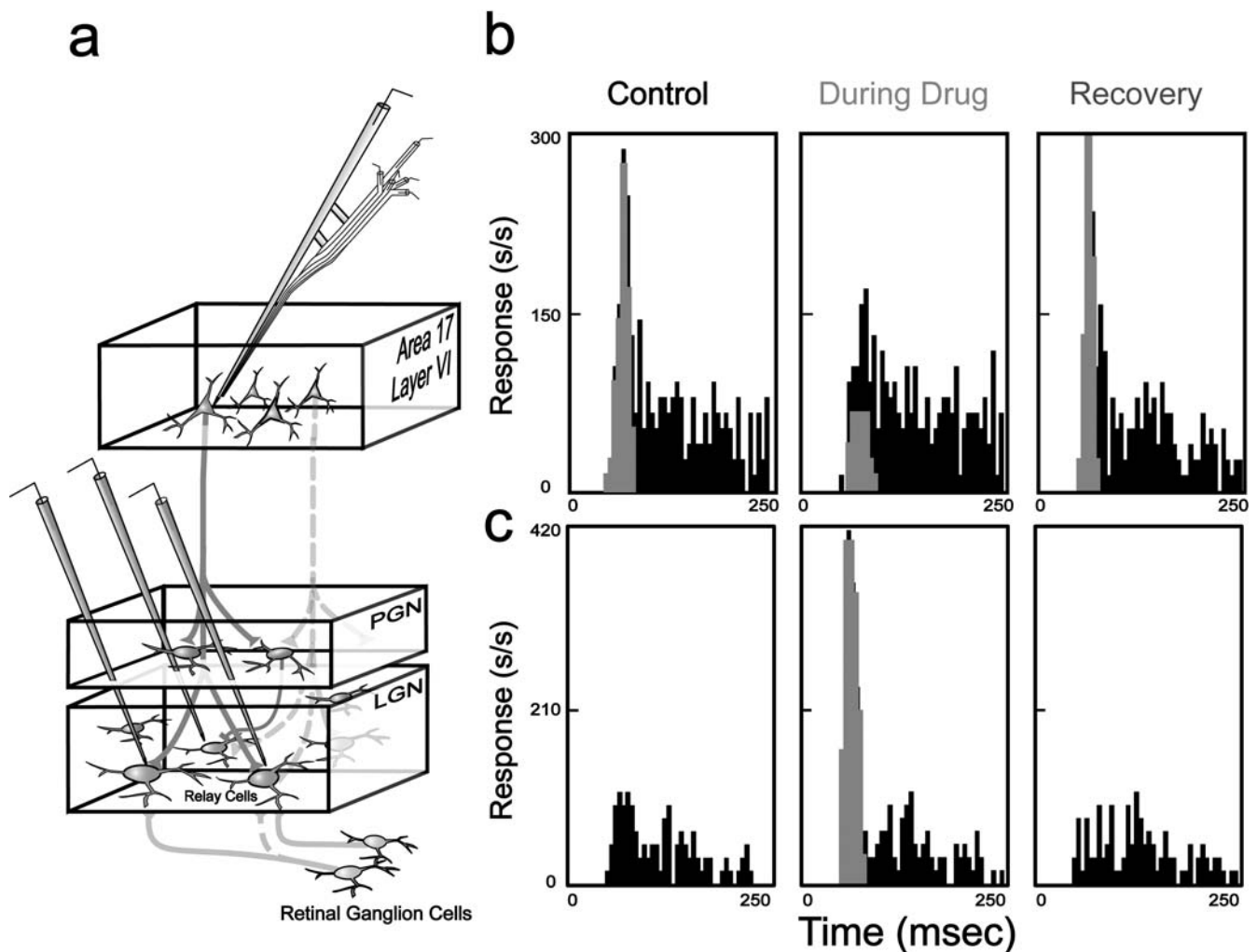


FIGURE 37.3. Effect of corticofugal feedback on LGN cell firing patterns. *A*, Experimental paradigm. Simultaneous recordings were obtained from a layer 6 cell and an LGN cell. Responses to visual stimulation were compared before, during, and after focal iontophoretic application of the GABA_B antagonist CGP in layer 6. Spike trains of LGN cell responses during periods of visual stimulation were divided into periods of burst and tonic activity. The first action potential in a burst showed a preceding silent period of at least 100 msec followed by a second spike with an interspike interval ≤ 4 msec. Any subsequent action potentials with preceding inter-

spike intervals ≤ 4 msec were also considered to be part of a burst. All other spikes were regarded as tonic. *B,C*, The peristimulus time histograms (PSTHs) show the responses of two LGN cells to an optimal diameter flashing spot located over the classical receptive field (CRF) before, during, and after focal enhancement of layer 6. For both cells, there was a clear change in firing pattern during focal enhancement of layer 6. Burst spikes are colored red; tonic spikes are colored black. PSTHs are plotted with 5 msec bins. (Data summarized from Wang et al., submitted.) (See color plate 20.)

temporal/phase contrast between center and surround mechanisms (Cudeiro and Sillito, 1996; Sillito and Jones, 1997; Sillito et al., 1993, 1999). The examples in Figure 37.5*A–D* illustrate the way LGN cells are influenced by direction (*A*), orientation (*B, F*), and temporal frequency (*D*) contrast in the presence of feedback, while the examples in Figure 37.5*C* and 37.5*G* show how the sensitivity to orientation contrast between a central and a surround stimulus is influenced by corticofugal feedback. In the absence of feedback, the sensitivity to the difference in orientation is greatly reduced, as summarized by the population histograms in Figure 37.5*E*. We stress that this reflects a sensitivity to

orientation contrast and is not influenced by the absolute orientation of the stimulus. This point is underlined by the surface plot in Figure 37.5*F*, which shows the response of an LGN cell when the orientations of a central and a surrounding stimulus are varied independently in a random and interleaved fashion. Those instances in which the orientations of the inner and outer stimuli are the same lie along a diagonal from top right to bottom left. This diagonal is marked by a trough of low response levels. Thus, the cell signals orientation contrast. These effects all seem to follow from an increased resolution of the receptive field center-surround mechanism for a discontinuity in moving

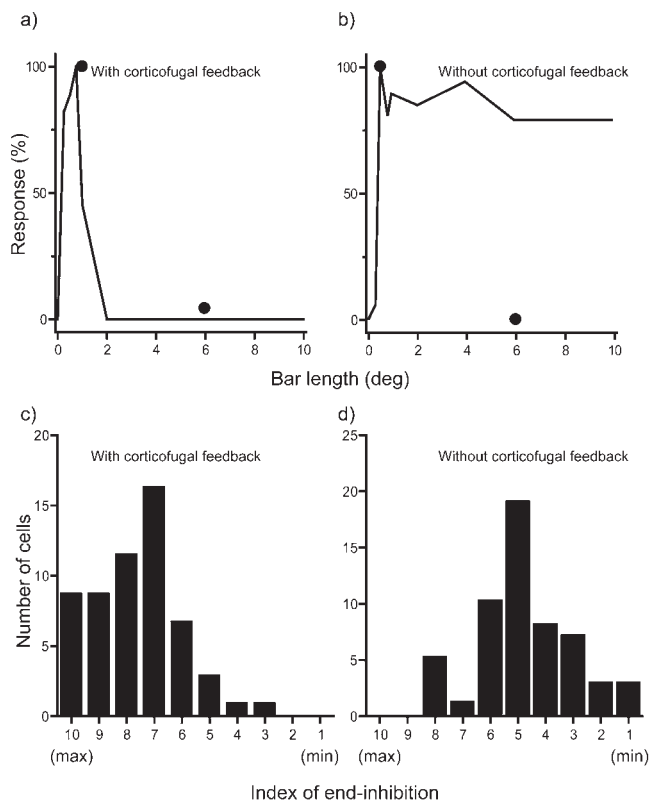


FIGURE 37.4. Effect of corticofugal feedback on LGN cell length tuning. *A,B*, Length tuning curves for two simultaneously recorded LGN cells. One was recorded from an LGN with corticofugal feedback (*A*), the other (*B*) from the other side of the brain from an LGN without feedback. The responses evoked by optimal and larger than optimal stationary spots of light flashed over the receptive field are superimposed on each graph (denoted by the filled spots). *C,D*, Bar histograms summarizing the distribution of end-inhibition with (*C*) and without (*D*) feedback. Cells are grouped into 10 categories for degree of end-inhibition. Category 10 contains cells showing total suppression of response at longer bar lengths, while those in category 1 show no suppression. (Observations summarized from Murphy and Sillito, 1987.)

stimuli and serve to highlight the points of change in the input to the cortex. The influence of the feedback in this sense might broadly be described as enhancing fine-scale segmentation.

The other side of the coin to segmentation is integration. The input from common elements belonging to, say, a moving contour needs to be integrated by a mechanism detecting the presence of the contour. At the most basic level, simple cells in the visual cortex integrate the inputs from LGN cells to detect the presence of contours with a particular orientation (Fig. 37.6). An appropriately oriented bar would coactivate the converging inputs illustrated in Figure 37.6 and synchronize their firing. The degree of synchronization of the inputs has a strong bearing on their ability to influence the simple cell. Indeed, evidence shows supralinear enhancement of transmission from hetero-

synaptic geniculate inputs to layer 4 simple cells in the visual cortex for spikes occurring within ~5 msec of each other (Usrey et al., 2000). It is thus very interesting that the feedback-enhanced center-surround antagonism influences the stimulus-driven synchronization (Andolina et al., submitted) of the discharges of LGN cells when they are precisely coactivated by a moving contour. We suggest in Figure 37.7 that the enhanced surround antagonism “focuses” the effective spatial extent of the receptive field center of LGN cells, leading to greater precision in firing when the two inputs are precisely coactivated. The evidence for this is summarized in Figure 37.6*A–D*. The experiments involved recordings in the cat LGN A laminae, using electrode assemblies configured to sample three cells of varying separation (Fig. 37.6*A*) in the presence and absence of feedback (Andolina et al., submitted). A grating patch was centered over one of the fields and was used to record the responses of the three cells at a range of orientations that included the angles linking each cell pair. Raw cross-correlograms (which show the stimulus-linked information that the second-order neuron sees) were then computed. These reflect the synchronicity of the inputs as “seen” by a theoretical simple cell for each pair at each orientation. Figure 37.6*B* shows representative results for a pair of X cells. A 5 msec window centered at zero lag (red) indicates those spikes that might generate supralinear enhancement of transmission. Note that shifts in orientation as small as 2° to either side of the angle linking the fields changed the count in this integration window. Converting the data to a surface representation of cross-correlogram time against grating orientation (Fig. 37.6*C*) reveals that the peak of the cross-correlogram shifted systematically throughout the time domain as orientation was varied. Interestingly, in the absence of feedback, this shift was less pronounced (Fig. 37.6*D*). As would be expected from this result, orientation tuning curves constructed from the synchronized spikes within the 5 msec window were much broader in the absence of feedback (see Fig. 37.6*E, F*, mean half width at half height 4.4 degrees with feedback and 13.17 degrees without feedback). Essentially this means that feedback greatly enhances the sensitivity to orientation in the stimulus-driven synchronization of the firing of LGN cells and thus the input to simple cells. In this sense, the organization is linked to contour and possibly motion integration.

Transfer of visual information through V1 and feedback from MT

SYNAPTIC ORGANIZATION, AND CIRCUITRY AND LAYER 6 CELL FUNCTION IN V1 In both cat and primate V1, the projections from the LGN provide a surprisingly small component of the excitatory (asymmetric) synaptic input to the main geniculo-recipient cells in layer 4. In the cat, input from the

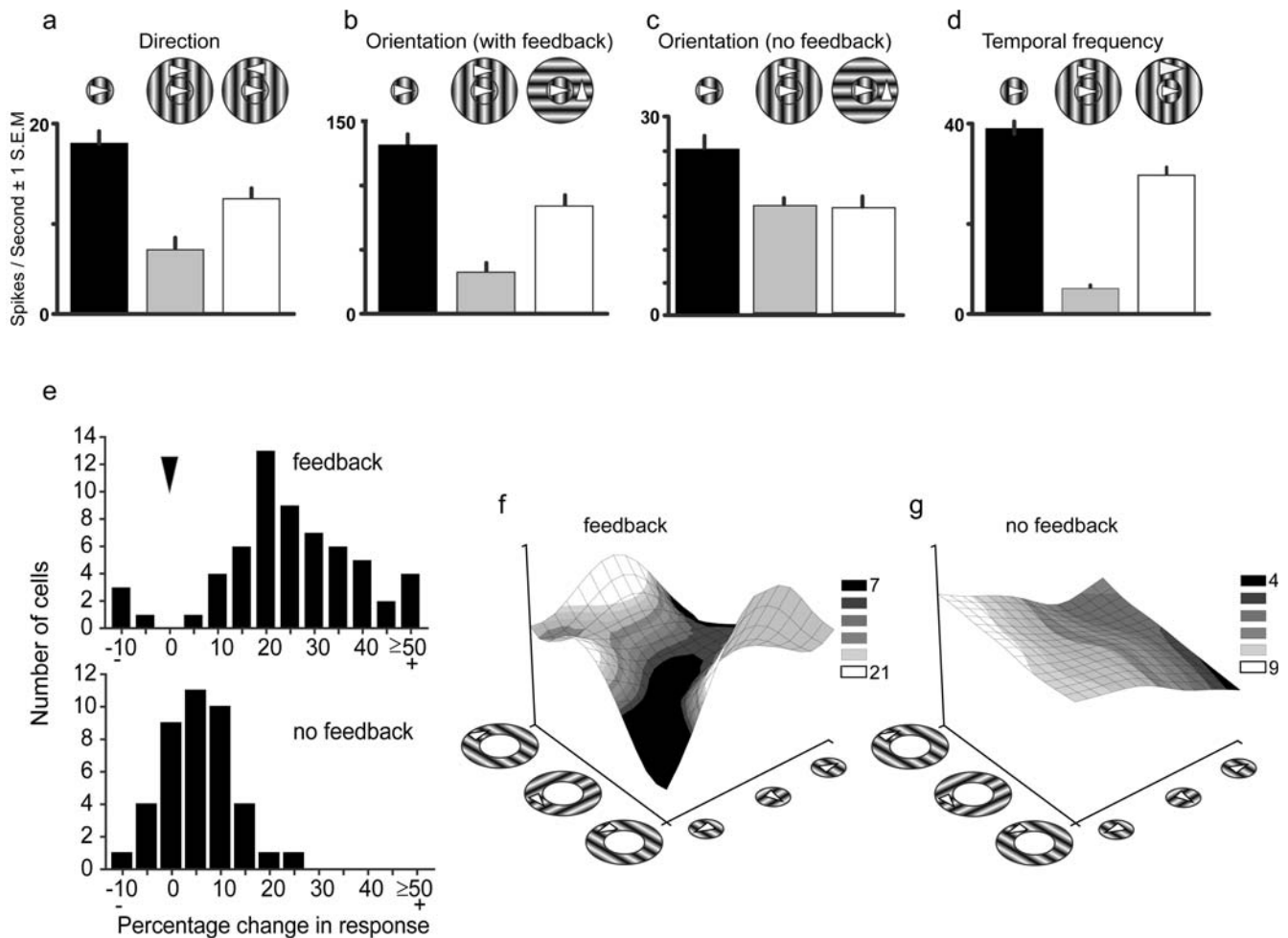


FIGURE 37.5. Corticofugal feedback enhances local segmentation effects in LGN cells. *A*, LGN cell response to direction contrast. The bar histogram shows the cell's response (spikes/second \pm 1 S.E.) to three stimulus conditions (shown diagrammatically by the stimulus icons above). These comprised a circular patch of grating overlying the receptive field (RF) center, the introduction of a surrounding field of identical grating drifting in the same direction of motion, and the presence of a surrounding grating with its direction of drift reversed. Drift direction is denoted by white arrowheads. *B*, LGN cell response to orientation contrast. Stimulus details as for *A*, but the last record shows the effect of changing the orientation of the surround grating. *C*, LGN cell response to orientation contrast in the absence of feedback. Stimulus details as for *B*. *D*, LGN cell response to temporal/phase contrast. Stimulus details as for *A*, but the last record shows the effect of changing the drift rate of the surrounding grating. *E*, Influence of feedback on orientation contrast. The histograms plot the percentage change in response observed between iso-oriented and orthogonally oriented

surround configurations (normalized with respect to the center-only response) in the presence (upper panel) and absence (lower panel) of corticofugal feedback. The mean increase in response magnitude for the switch from iso- to cross-oriented surround was 24.3% in the presence of feedback, which was reduced to 5.6% without feedback. *F*, LGN cells are sensitive to orientation contrast. The surface plot shows the response of an LGN cell (in the presence of feedback) to varying the orientation of an inner patch of grating in the presence of an outer patch of grating also of varying orientation. The diagonal running from bottom left to top right represents all those points where the orientation of the center and surround stimuli were the same over a complete sequence of absolute orientations. Response magnitude is shown by the height and shading of the contour. *G*, Reduction in orientation contrast in the absence of feedback. Stimulus details as for *F*. Note the absence of the pronounced diagonal trough. (Observations summarized from Cudeiro and Sillito, 1996; Sillito and Jones, 1997; Sillito et al., 1993, 1999.)

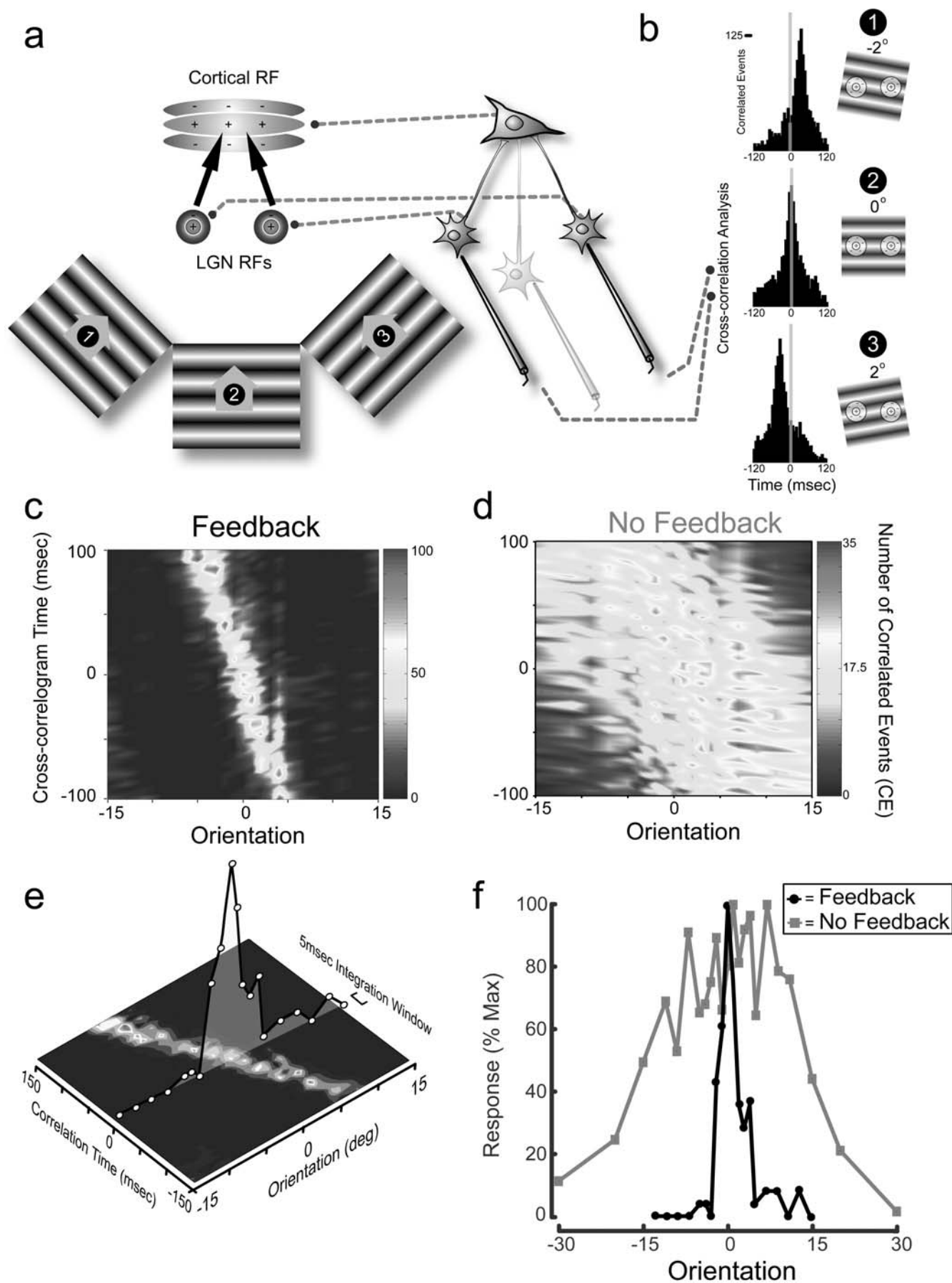


FIGURE 37.6. Corticofugal feedback influences stimulus-linked synchronization between LGN cell pairs. *A*, Experimental paradigm. The responses of pairs of LGN cells to drifting gratings of varying orientation were recorded, and raw cross-correlograms were constructed for each stimulus orientation. *B*, Raw cross-correlograms recorded from a pair of LGN cells for three stimulus orientations. The shaded bar centered at time 0 indicates a 5 msec time span and highlights the correlated events occurring within the supralinear integration window of a cortical layer 4 cell. *C, D*, Surface representation showing the cross-correlation data (y -axis)

versus orientation (x -axis) for LGN cells recorded in the presence (*C*) and absence (*D*) of feedback. The color scale represents the number of correlated events from low (dark blue) to high (dark red). *E*, Schematic example of an orientation tuning curve derived from the number of correlated events occurring in a 5 msec integration window. *F*, Orientation tuning curves for two LGN cells plotting the number of events in a 5 msec integration window recorded in the presence (black line) and absence (red line) of feedback. (Observations summarized from Andolina et al., submitted.) (See color plate 21.)

LGN provides only 6% of excitatory input to layer 4 cells, whereas neighboring spiny stellate cells provide 28% of the input and 45% of the inputs derive from layer 6 cell collaterals (from the same layer 6 cells that project to the LGN) (Ahmed et al., 1994). In the primate, the magnocellular input to layer 4C α comprises 8.7% of the asymmetric synapses and the parvocellular input to 4C β just 6.9% of the asymmetric synapses. The remaining asymmetric synaptic inputs to cells in 4C α and 4C β may be presumed to follow the same overall balance of the pattern reported in the cat, with strong inputs from layer 6 and surrounding spiny stellates (Latawiec et al., 2000). An issue that stands out from this is the role of the layer 6 cells that provide the feedback to the LGN. They sit in a unique position in relation to the transfer of the visual input, contributing numerically the majority of the connections to LGN relay cells and to the spiny stellate cells receiving the input from the relay cells. One cannot truly consider the role of the feedback to the LGN in isolation from that of the collateral projection to layer 4. Indeed, it is interesting to see that Callaway (1998) refers to these collateral connections to layer 4 as *feedback connections* in his analysis of the elements of local circuitry in V1. We have already discussed the functional segregation of the feedback neurons in the primate with respect to three input channels. The connections of these cells in V1 are equally discrete, showing dendritic and axonal configurations that are extremely laminar specific, so that some parvocellular projecting layer 6 cells may have dendritic and axonal arborizations that are, for example, almost exclusively focused on layer 4C β or layers 4C β and 4A. Magnocellular projecting cells, on the other hand, may have axonal and dendritic arborizations that distribute through layer 4C α , while others may distribute through 4C and enter 4A (or above). Cells in the middle of layer 6 do not project to the LGN, although some project to the claustrum, but they have very specific patterns of axonal distribution within 4C and include some that seem to sample both parvocellular and magnocellular sections of 4C (Callaway, 1998). In the cat, there is less apparent specificity amongst corticogeniculate cells in V1 but a very clear difference between LGN and claustrally projecting cells. The LGN projecting cells have extensive dendritic and axonal arborizations in

layer 4 but almost no horizontal arborization in layer 6, and their apical dendrites do not extend beyond layer 3. The claustral projecting cells have axon collaterals arborizing extensively in layer 6 and apical dendrites that reach layer 1 (Katz, 1987).

The detail of the visual response properties of identified corticofugally projecting cells is of considerable interest because it indicates the type of stimuli that might influence the transfer of visual information in the geniculate and layer 4. In the cat, feedback projections originate from both simple and complex cells, with simple cells predominating (Grieve and Sillito, 1995b; Tsumoto et al., 1978). The complex cells are spontaneously active and are strongly binocular, directional, broadly orientation tuned, and capable of responding at high stimulus velocities. The simple cells, on the other hand, have little or no spontaneous activity, are sharply orientation tuned, and include cells strongly or exclusively dominated by one eye. Although it was suggested that the corticofugal projection originates from cells with very long fields (generally 8 degrees or more; Bolz and Gilbert, 1986), the group that projects back to the LGN actually originates from cells with much shorter receptive fields, while the longer field cells project to the claustrum (Grieve and Sillito, 1995b). Indeed, in layer 6 as a whole, short field cells predominate (Grieve and Sillito, 1991b, 1995b). One fact stands out from all the available evidence: both the simple and complex cells projecting to the LGN tend to be strongly directionally sensitive. While there is no direct evidence regarding the properties of corticogeniculate cells in the primate, there is a wide consensus for a preponderance of directionally selective cells in layer 6 (Orban, 1994) along with layer 4 (A, B, and C α). Moreover, directionally selective simple cells have been reported to be the dominant cell type in layer 6, although there is substantive variance among investigators regarding this issue.

All this raises the intriguing question of what the collaterals of the corticogeniculate cells arborizing in layer 4 are doing. Intracellular work in vivo and in vitro (Ferster and Lindstrom, 1985; Tarczy-Hornoch et al., 1999) provides a consistent line of evidence for the layer 6 input to layer 4 cells driving many small excitatory postsynaptic potentials

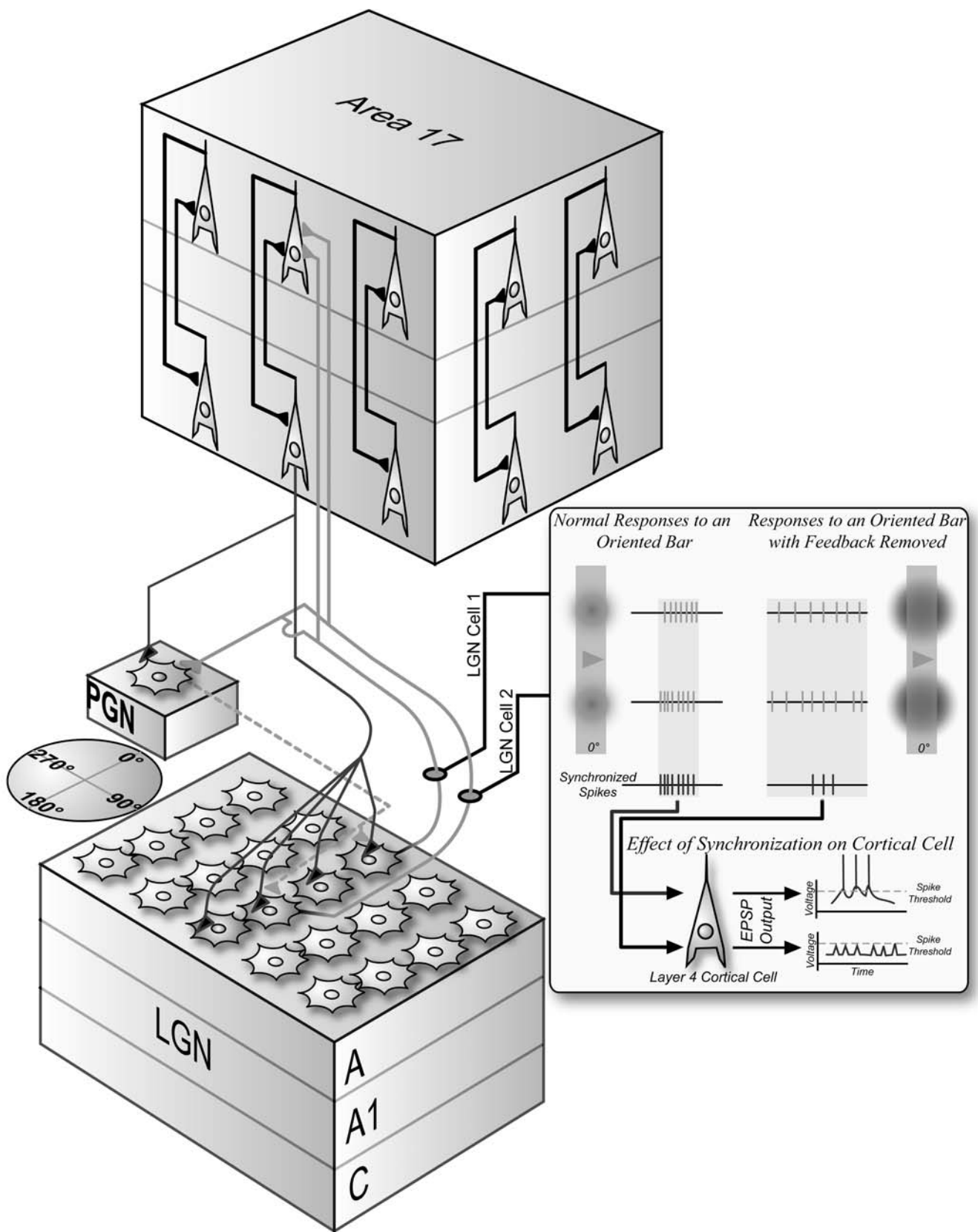


FIGURE 37.7. Diagram summarizing the view that feedback-linked enhanced surround antagonism leads to greater synchronization of LGN cell firing to coherent contours and thus increases the probability of firing in cortical layer 4 cells.

(EPSPs) that show facilitation. This might serve to enhance the responsiveness of layer 4 cells as the visual response evolves. It is interesting to consider the possibility that were the cortex to receive a “burst” from a component of its thalamic input (see the discussion above) highlighting the appearance of a feature in a previously uniform sector of the visual input, the layer 6 input might serve to sustain the excitability of the layer 4 cells to the input as the relay cells switched to tonic mode firing. We know a little about the functional effects of layer 6 cells on layer 4 cell responses. Focal blockade of layer 6 reveals a loss of facilitatory drive to cells in overlying layer 4 (Grieve and Sillito, 1991a, 1995a). For a small proportion of non-end-stopped cells it seems to reduce an inhibitory input. This could follow from the loss of an influence mediated via inhibitory interneurons in layer 4 or a loss of direct inhibitory input from some GABAergic cells that have axon collaterals extending from layer 6 to layer 4 (Grieve and Sillito, 1995a). Overall, though, the predominant influence of layer 6 on layer 4 visual responses seems to be facilitatory (Grieve and Sillito, 1991a, 1995a). This is in accord with the distribution of layer 6 cell synapses to spiny stellate cells (Ahmed et al., 1994) and the electrophysiological data discussed above. The often expressed view that layer 6 cells with long receptive fields provide input to layer 4 inhibitory interneurons and generate end-stopped fields (Bolz and Gilbert, 1986) does not seem to be tenable (for a discussion, see Grieve and Sillito, 1991a, 1995a). Clearly, further work is needed here, but the balance of the evidence seems to favor a predominantly modulatory and facilitatory input. In a global sense, we wonder whether there may not be some mirror-image differentiation in the pattern of influence on visual responses, with the corticofugal connections on balance enhancing inhibitory mechanisms and the layer 4 collaterals enhancing facilitatory mechanisms.

LINKS BETWEEN V1 AND MT A consideration of the interactions between MT and V1 highlights many of the issues that are central to this discussion of the role of feedback. Area MT is associated with motion processing, and most of the cells are highly directionally selective (Orban, 1997). Area MT is particularly interesting in the context of feedback systems because, as discussed below, it uniquely sends feedback connections to V1 that target layer 4B and the depth of layer 6. It thus has the capacity to influence the layer 6 cells sitting at the interface of the input for all three streams of information translating through the thalamus. The output from V1 to MT derives from layers 4B and 6 (Shipp and Zeki, 1989). Layer 4B contains spiny stellates and pyramidal cells and receives input from both layer 4C α and 4C β (Callaway, 1998). The spiny stellate cells project directly to MT and receive input predominantly from layer 4C α together with a component from layer 5 and 6 cells. They

thus provide a strong magnocellular-dominated input to MT. The pyramidal cells in 4B also receive strong input from 4C α but gain a significant component from 4C β as well as a component from layer 5 and 6 cells. Pyramidal cells in layer 4B project directly to MT (Elston and Rosa, 1997), as well as to the thick stripes in V2, and there is a projection from the pyramidal cells in layer 3B of the V2 thick stripes to layer 4 in MT with some terminals in layers 1–3.

The information extracted by MT cells is fed back down the visual system to influence processing at the earlier levels. Feedback connections from layers 3 and 6 of MT target layers 1, 4B, and 6 in V1 (Orban, 1997; Rockland and Knutson, 2000; Shipp and Zeki, 1989); however, this varies with eccentricity. In the central 10 degrees the projection targets layers 4B and 6, while at greater eccentricities the projection focuses on layer 1. There is an interesting blurring in the reciprocal connections between MT and V1. The layer 4B and layer 6 cells projecting to MT from V1 are not uniformly distributed (Shipp and Zeki, 1989), the layer 4B cells are generally clustered together, and the layer 6 cells are restricted to the top of layer 6 (and avoid registration with the centers of blobs). The feedback connections from MT, on the other hand, project to wider patches of layer 4B and the whole of layer 6. Given the divergent connections of the various types of layer 6 cells (Callaway, 1998), including the feedback projections to the LGN, it seems fair to assume that the MT projection has the capacity to exert widespread influence over both magnocellular and parvocellular streams. Indeed, it is pertinent to note that the speed of transmission through the magnocellular pathway to MT is such that feedback from MT can potentially influence the feedforward relay of retinal information through the more slowly conducting parvocellular-dominated pathways of both the LGN and V1 (Orban, 1997).

EFFECTS OF FEEDBACK FROM MT ON RESPONSES IN V1 In considering the functional significance of these connections, one possibility is that the corticocortical feedback projections play a broad and nonspecific role centered on global gain control and that the detail of the connections is largely irrelevant from the viewpoint of processing mechanisms. On the other hand, the very early visual responses seen in MT cells and their pattern of termination in layers 4B and 6 in V1 suggest that MT is in a position to exert substantial influence on the early processing of the input in V1. Indeed, given the feedback from V1 layer 6 to the LGN, MT may additionally influence the responses of LGN cells. Thus, feedback containing information relevant to the high-level processing of motion in the visual world could influence visual processing in V1 for moving stimuli at a very early stage in the development of visual responses. Indeed, the available evidence does suggest a strong influence of MT on processing in V1. Firstly, studies that have either lesioned or reversibly

cooled MT show marked changes in the responses of V1 cells (Hupe et al., 2001; Lamme et al., 1997) including an effect on the earliest component of the responses to both stationary flashing and moving stimuli. However, the effects of cooling can be complex and difficult to control (Volgushev et al., 2000), and the gradient of cooling that logically has to occur will cause cells at a certain distance from the cooling focus to fire at higher levels than normal. Consequently, these procedures may well have influenced more than MT and may not have influenced MT uniformly. Even by removing all the influence of MT, it is not certain that the changes in V1 necessarily reflect the loss of a specific influence from MT on processing in V1. Blockade of MT may have eliminated static biasing influences, resulting in a shift in the balance of the V1 circuitry, which in turn shifted the way the circuitry processed visual stimuli. Thus, although the data from cooling studies provide a strong indication of the potential influence of the feedback from MT, they leave many unanswered questions.

In attempting to unravel the effects of feedback from MT, it is crucial to recognize that MT feedback will provoke the primary change in V1 processing when the stimulus contains features that best activate MT cells. Moreover, these stimuli, by virtue of their spatial focus and specific trigger features such as direction of motion, will provoke differential activation of MT, and the “high spots” of enhanced activity in MT will in turn provide highlights in the pattern of feedback to V1. Although it is clearly possible to generate stimuli that should cause a differential pattern of activation of MT, it is very difficult to dissociate any consequent reflected influence on V1 via feedback from potential direct effects of the stimulus on circuitry in V1. One way of tackling this problem is to use stimuli that will activate MT cells but, in addition, via a drug and recording electrode assembly inserted in area MT, produce very focal and reversible changes in the gain of the response of the recorded MT cells to these stimuli. In many ways, this could be argued to simply increase or decrease the salience of the stimuli to the cell

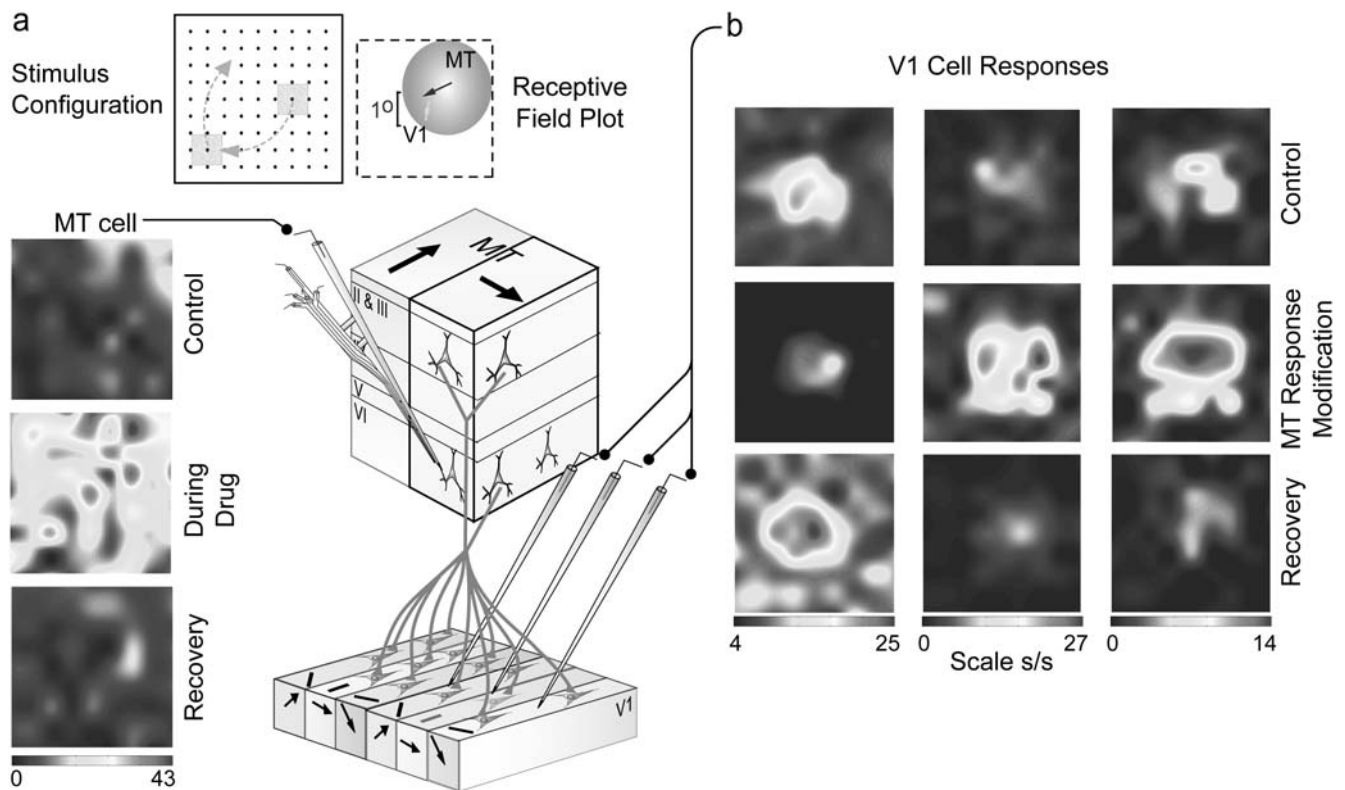


FIGURE 37.8. Effect of MT feedback on V1 cell responses to drifting stimuli. *A*, Experimental protocol. Simultaneous recordings were obtained from one or more V1 cells and an MT cell. Responses to visual stimuli were assessed before, during, and after focal iontophoretic application of the GABA_B antagonist CGP in MT. The stimulus was a patch of drifting texture displaced (in a randomized interleaved sequence) to cover a range of XY locations. The grid was centered over the receptive fields of the V1 cells, as shown by the example diagrammatic icon of the relative

locations of an MT (orange) and a V1 (green) cell receptive field (where the dotted rectangle depicts the total area of visual space covered by the grid). The contour maps show the response of an MT cell before, during, and after CGP iontophoresis. Response magnitude (s/s) is represented by color, from low (dark blue) to high (dark red). *B*, Effects in V1. The contour maps plot the responses of three V1 cells tested in the presence of the type of change in MT shown in *B*. (Observations summarized from Jones et al., submitted.) (See color plate 22.)

recorded by the MT electrode. Because one can reverse this and repeat it, there is a potential for unmasking influence of the MT feedback on V1 cell responses. A diagram summarizing this approach is shown in Figure 37.8A. The experiment involved iontophoretic application of the GABA_B antagonist CGP 55485 to produce a focal change in gain in the visually evoked response of a recorded MT cell without affecting either its background discharge or its response selectivity. The key here is that synaptically released GABA acting via the GABA_B receptor produces a long-lasting hyperpolarization of the cell membrane, moving it away from the depolarization threshold for initiating action potentials. This contrasts with the fast time course of action via GABA_A receptors which is linked to the dynamics of visual processing determining selectivity to the visual stimulus (Borg-Graham et al., 1998; Sillito, 1975). Thus, blockade of the GABA_B receptor, by decreasing the long-lasting hyperpolarization, renders the cells more responsive to their input. An example of the data obtained from the blockade of GABA_B receptors is shown in Figure 37.8. The visual stimulus used was a patch of drifting visual texture (Fig. 37.8A) presented through a series of XY coordinates within the rectangle to encompass the locations of the MT and V1 cell fields. The direction of drift of the stimulus matched the preferred direction of the MT cell, and the stimulus activated it. The responses of the cells are shown in the colored surface plots, and the different locations in the surface plot reflect the effect of the stimulus at each of the points shown in the stimulus icon rectangle. In the surface plots, the color scale denoting response magnitude (in spikes per second) moves from red (highest firing rates) to blue (lowest firing rates). An example of the effect on the responses of an MT cell is shown in Figure 37.8A. The strong increase in response during the GABA_B blockade is clear. The responses of three V1 cells, in the presence of the type of focal change in MT seen in Figure 37.8A, are shown in Figure 37.8B. Two of these examples (middle and right columns) showed enhanced responses when MT responses were enhanced, and one showed a diminished response (left column). These different patterns of effect were seen among simultaneously recorded V1 cells with overlapping fields.

Changes in response magnitude were seen in 76% of the V1 cells tested in this way. At the same time, there were changes in the spatial organization of the area from which the responses to patches of drifting visual texture could be elicited and changes in the response to motion contrast. The types of effects seen could be grouped in several ways. Firstly, most nonoriented cells showed a reciprocal relationship to the response level of the MT cell: when MT cell responses increased, those of the nonoriented cells decreased, while decreasing MT responses (by iontophoresing GABA, for example, with a very low current) led to an increase in the nonoriented cell response. Most simple cell responses, on the

other hand, increased when MT cells responses increased and decreased when they decreased. Complex cells were evenly distributed between the two patterns of linkage to MT cells. Functionally this suggests that MT differentially influences the processes in V1 that are represented by the receptive field characteristics associated with nonoriented and simple cells. A particular issue is that when the gain of the visual response of recorded MT cells was decreased (using GABA), changes in the V1 responses were also seen, with a reciprocal pattern to that for the MT increases in the nonorientation tuned and simple cells. Thus, the normal responses of MT cells seem to provide the basis for the “control” responses of V1 cells, as one might expect. It is also clear that MT influences the way V1 cells process stimulus features extending across visual space that may link together or highlight a focus of change. Thus, applying a second motion field around a central one overlying the V1 fields (Fig. 37.9A, B) and varying the direction of drift of the two reveals different patterns of response in V1 cells and a strong influence from MT on these patterns of response.

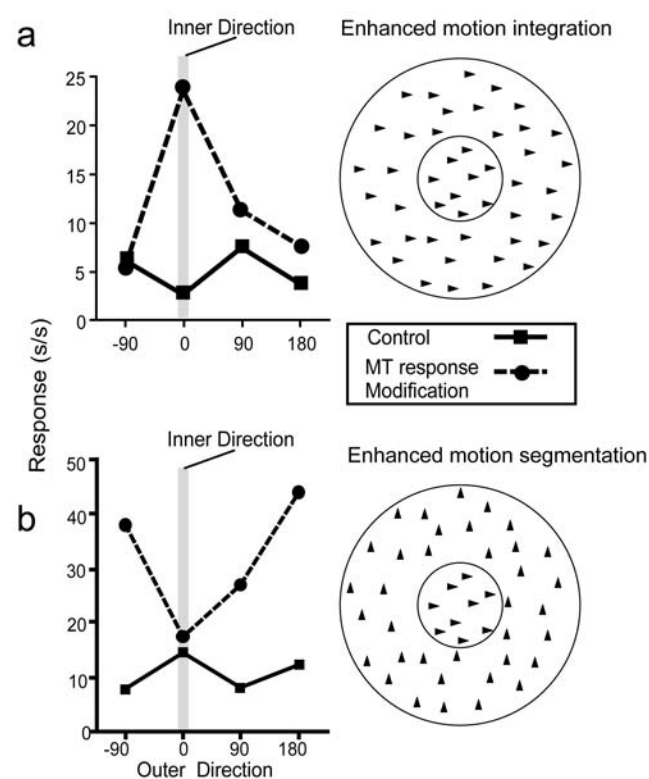


FIGURE 37.9. MT feedback influences responses of V1 cells to direction contrast stimuli. A,B, The tuning curves show the responses (in s/s) of two V1 cells before (solid line) and during (dotted line) MT response enhancement. Each tuning curve plots the effect of varying the outer texture direction (in degrees along the x-axis) while the direction of the inner texture stimulus was held constant (0 degrees—marked on each plot by the gray shading). (Observations summarized from Jones et al., submitted.)

The influence of MT on these cells fell into two categories, either enhancing contour/motion integration (Fig. 37.9A) or enhancing segmentation (Fig. 37.9B) produced by direction contrast. On a larger scale, this has many similarities to the types of effects seen with feedback in the LGN.

Conclusions

On the basis of both the anatomical and functional data, it is clear that the feedback systems highlighted in this account are structured to provide specific patterns of effect that can be linked to the organization of the processing of visual information. In different ways and on varying retinotopic scales, a major role seems to be the enhancement of the respective mechanisms linking to local and global segmentation and integration. The logic underlying this would be that the next stage in the processing stream starts to extract or detect the information that provides the basis for recognizing the common components of a feature or change in components defining different features. This information, reflected back to the earlier stages, seems to be able to enhance the finer resolution of the earlier level to the patterns isolated by the higher level. It would be incorrect to see this as a slow process or a process separate from the sequential processing of the input. For the visual world in motion, the “hand” of MT is present in the responses of V1 cells all the time. We also know that, via its influences in V1, it exerts clear effects in the LGN (H.E. Jones et al., unpublished observations). Feedback influences do not imply long latency. The size of MT cell receptive fields (10 times those of V1 cells; Orban, 1997), and spatial organization of the feedback connections which contact a retinotopic area in V1 that matches or exceeds that driving the input to a particular MT cell, mean that a moving stimulus can exert feedback effects on V1 circuitry that influence the response in V1 to its successive positions with zero latency. Indeed, effects could occur in advance of the arrival of a stimulus at a particular location. Reflected through the feedback projection from V1 to the LGN, this same logic applies to the LGN. The anatomical organization of the feedback to the LGN, which suggests a particular role in direction and orientation processing underlying segmentation and integration, argues for the ability of the feedback, reflected via layer 6 of V1 from higher levels, to exert rapid and structured patterns of effect. Embedded in the influences, and part of the mechanism driving the effects, is a regulation of the patterns of firing of the cells. In the LGN this is clear both in terms of the influence of feedback on the synchronization of the firing of LGN cells commonly activated by a contour and in the switch between burst and tonic firing modes. A key point for the burst versus tonic firing modes is that the cortex via the visually driven feedback can shift the response modes of LGN cells in a way that reflects the optimization best suited

to the visual image. As the image of the visual world contains features differentiated across retinotopic space and time, these in turn selectively activate different foci in the higher visual areas and produce a changing pattern of feedback reflected to the earlier levels. This drives a visually cued mechanism for selective attention to salient features and shifts in the local circuitry to optimize the system's hold on these at all levels. Finally, the question to repeat is whether the term *feedback* for these interconnections in the processing streams is not somewhat misleading. It might be better to consider the organization of the central visual system in terms of local and multilevel circuits.

A crucial step in the next phase of work on the central visual system is the recognition that these multilevel circuits underpin the evolution of the visual response to even simple stimuli, and that we need to unravel the way the feedback adjustments of the lower-level response properties contribute to the abstraction carried out by the higher level. Clearly, the way feedback from MT targets layer 6 in V1 within the central 10 degrees of the visual field suggests that the feedback of information linked to motion cues to layer 6 cells that sit at the “gate” of all the processing streams is important to the translation of the visual input through V1. The reasons for this need to be assessed in models and experiments designed to examine the interactions between different cues in the early visual system with and without manipulation of the feedback. Focusing on the special role of layer 6 cells, another interesting issue is that the majority of the feedback cells are simple cells (Grieve and Sillito, 1995b), and these contact cells in the LGN that are concentric and cells in layer 4 of V1 that are also simple (or concentric, as in primate 4C). The question is, does a particular layer 6 simple cell contact cells in the LGN in a fashion that reflects the spatial phase of the layer 6 cell, that is, does a layer 6 cell with a central ON zone in its receptive field contact ON-center LGN cells that are spatially aligned to the ON zone of the layer 6 cell? Are there direct connections in such an arrangement to OFF-center cells that lie under the OFF surround of the layer 6 cell or do these relay via an inhibitory interneuron? Alternatively, are the connections phase reversed or are phase relationships lost? Similar questions apply to the connections from layer 6 cells to layer 4. A further dimension here is the question of the potential phase relationships between layer 6 and LGN fields and those of the layer 6 collaterals with layer 4 cells. For example, it could be that the connections from layer 6 to the LGN are phased reversed with respect to those to layer 4. The net effect is positive feedback at one location in the circuit translating the retinal input to the cortex and negative feedback at the other. The specificity of such connections would have great significance for the way we interpret what might appear to be putative excitatory connections but would have essentially the opposite action if phase reversed.

These issues need to be resolved experimentally and modeled. Considering other feedback systems to V1, it is relevant to question the significance of the fact that with the exception of the feedback from MT (for the central 10 degrees and that from V3), the bulk of the connections target layer 1. We have no idea how these connections are ordered with respect to function or of the detailed synaptic organization. Possibly the most surprising thing about the organization of feedback systems is how little we know about them. On the other hand, we do know enough from the work over the past decade to know that they have strong effects and that we need to know more if we are to understand the visual system better.

REFERENCES

- Ahmed, B., J. C. Anderson, R. J. Douglas, K. A. C. Martin, and J. C. Nelson, 1994. Polynuclear innervation of spiny stellate neurons in cat visual cortex, *J. Comp. Neurol.*, 341:39–49.
- Andolina, I. M., H. E. Jones, W. Wang, K. L. Kirkland, G. L. Gerstein, and A. M. Sillito, submitted. Stimulus-linked correlation of activity in the lateral geniculate nucleus and the role of feedback.
- Bolz, J., and C. D. Gilbert, 1986. Generation of end-inhibition in the visual cortex via interlaminar connections, *Nature*, 320:362–365.
- Borg-Graham, L. J., C. Monier, and Y. Fregnac, 1998. Visual input evokes transient and strong shunting inhibition in visual cortical neurons, *Nature*, 393:369–373.
- Bowling, D. B., and C. R. Michael, 1984. Terminal patterns of single, physiologically characterized optic tract fibers in the cat's lateral geniculate nucleus, *J. Neurosci.*, 4:198–216.
- Callaway, E. M., 1998. Local circuits in primary visual cortex of the macaque monkey, *Annu. Rev. Neurosci.*, 21:47–74.
- Cleland, B. G., and B. B. Lee, 1985. A comparison of visual responses of cat lateral geniculate neurones with those of ganglion cells afferent to them, *J. Physiol.*, 369:249–268.
- Cudeiro, J., and A. M. Sillito, 1996. Spatial frequency tuning of orientation-discontinuity-sensitive corticofugal feedback to the cat lateral geniculate nucleus, *J. Physiol.*, 490:481–492.
- Elston, G. N., and M. G. Rosa, 1997. The occipitoparietal pathway of the macaque monkey: comparison of pyramidal cell morphology in layer III of functionally related cortical visual areas, *Cereb. Cortex*, 7:432–452.
- Ferster, D., and S. Lindstrom, 1985. Augmenting responses evoked in area 17 of the cat by intracortical axon collaterals of corticogeniculate cells, *J. Physiol.*, 367:217–232.
- Fitzpatrick, D., W. M. Usrey, B. R. Schofield, and G. Einstein, 1994. The sublaminal organization of corticogeniculate neurons in layer 6 of macaque striate cortex, *Vis. Neurosci.*, 11:307–315.
- Grieve, K. L., and A. M. Sillito, 1991a. A re-appraisal of the role of layer VI of the visual cortex in the generation of cortical end inhibition, *Exp. Brain Res.*, 87:521–529.
- Grieve, K. L., and A. M. Sillito, 1991b. The length summation properties of layer VI cells in the visual cortex and hypercomplex cell end zone inhibition, *Exp. Brain Res.*, 84:319–325.
- Grieve, K. L., and A. M. Sillito, 1995a. Non-length-tuned cells in layers II/III and IV of the visual cortex: the effect of blockade of layer VI on responses to stimuli of different lengths, *Exp. Brain Res.*, 104:12–20.
- Grieve, K. L., and A. M. Sillito, 1995b. Differential properties of cells in the feline primary visual cortex providing the corticofugal feedback to the lateral geniculate nucleus and visual claustrum, *J. Neurosci.*, 15:4868–4874.
- Guido, W., and T. Weyand, 1995. Burst responses in thalamic relay cells of the awake behaving cat, *J. Neurophysiol.*, 74:1782–1786.
- Hendry, S. H. C., and T. Yoshioka, 1994. A neurochemically distinct third channel in the macaque dorsal lateral geniculate nucleus, *Science*, 264:575–577.
- Hupe, J. M., A. C. James, P. Girard, S. G. Lomber, B. R. Payne, and J. Bullier, 2001. Feedback connections act on the early part of the responses in monkey visual cortex, *J. Neurophysiol.*, 85:134–145.
- Jones, H. E., I. M. Andolina, N. M. Oakely, P. C. Murphy, and A. M. Sillito, 2000. Spatial summation in Lateral Geniculate Nucleus and visual cortex, *Exp. Brain Res.*, 135:279–284.
- Jones, H. E., W. Wang, I. M. Andolina, T. E. Salt, K. L. Grieve, and A. M. Sillito, submitted. Discrete shift in area MT cell visual response level changes response properties in primary visual cortex.
- Katz, L. C., 1987. Local circuitry of identified projection neurons in cat visual cortex brain slices, *J. Neurosci.*, 7:1223–1249.
- Lamme, V. A., K. Zipser, and H. Spekreijse, 1997. Figure-ground signals in V1 depend on extrastriate feedback, *Invest. Ophthalmol. Vis. Sci.*, 38:S969.
- Latawiec, D., K. A. Martin, and V. Meskenaite, 2000. Termination of the geniculocortical projection in the striate cortex of macaque monkey: a quantitative immunoelectron microscopic study, *J. Comp. Neurol.*, 419:306–319.
- Lindstrom, S., and A. Wróbel, 1990. Frequency dependent corticofugal excitation of principal cells in the cat's dorsal lateral geniculate nucleus, *Exp. Brain Res.*, 79:313–318.
- Mastrorade, D. N., 1987. Two classes of single-input X-cells in cat lateral geniculate nucleus II retinal inputs and the generations of receptive-field properties, *J. Neurophysiol.*, 57(2):381–413.
- Murphy, P. C., S. G. Duckett, and A. M. Sillito, 1999. Feedback connections to the lateral geniculate nucleus and cortical response properties, *Science*, 286:1552–1554.
- Murphy, P. C., S. G. Duckett, and A. M. Sillito, 2000. Comparison of the laminar distribution of input from areas 17 and 18 of the visual cortex to the lateral geniculate nucleus of the cat, *J. Neurosci.*, 20:845–853.
- Murphy, P. C., and A. M. Sillito, 1987. Corticofugal feedback influences the generation of length tuning in the visual pathway, *Nature*, 329:727–729.
- Murphy, P. C., and A. M. Sillito, 1996. Functional morphology of the feedback pathway from area 17 of the cat visual cortex to the lateral geniculate nucleus, *J. Neurosci.*, 16:1180–1192.
- Orban, G. A., 1994. Motion processing in monkey striate cortex, in *Cerebral Cortex*, vol. 10 (A. Peters and K. S. Rockland, eds.), New York: Plenum Press, pp. 431–444.
- Orban, G. A., 1997. Visual processing in macaque area MT/V5 and its satellites (MSTd and MSTv), in *Cerebral Cortex*, vol. 12 (K. S. Rockland, J. H. Kaas, and A. Peters, eds.), New York: Plenum Press, pp. 359–379.
- Robson, J. A., 1984. Reconstruction of corticogeniculate axons in the cat, *J. Comp. Neurol.*, 225:193–200.
- Rockland, K. S., and T. Knutson, 2000. Feedback connections from area MT of the squirrel monkey to areas V1 and V2, *J. Comp. Neurol.*, 425:345–368.
- Rowe, M. H., and Q. Fischer, 2001. Dynamic properties of retinogeniculate synapses in the cat, *Vis. Neurosci.*, 18:219–231.

- Sherman, S. M., 2001. Tonic and burst firing: dual modes of thalamocortical relay, *Trends Neurosci.*, 24:122–126.
- Sherman, S. M., and R. W. Guillery, 1998. On the actions that one nerve cell can have on another: distinguishing “drivers” from “modulators,” *Proc. Natl. Acad. Sci. USA*, 95:7121–7126.
- Shipp, S., and S. Zeki, 1989. The organization of connections between areas V5 and V1 in macaque monkey visual cortex, *Eur. J. Neurosci.*, 1(4):309–332.
- Sillito, A. M., 1975. The contribution of inhibitory mechanisms to the receptive field properties of neurones in the striate cortex of the cat., *J. Physiol.*, 250:305–329.
- Sillito, A. M., I. M. Andolina, and H. E. Jones, 1999. The processing by cells in the cat dLGN of the relative phase between center and surround, *Invest. Ophthalmol. Vis. Sci.*, 40: 3380.
- Sillito, A. M., J. Cudeiro, and P. C. Murphy, 1993. Orientation sensitive elements in the corticofugal influence on center-surround interactions in the dorsal lateral geniculate nucleus, *Exp. Brain Res.*, 93:6–16.
- Sillito, A. M., and H. E. Jones, 1997. Functional organization influencing neurotransmission in the lateral geniculate nucleus, in *Thalamus*, vol. 2, *Experimental and Clinical Aspects* (M. Steriade, E. G. Jones, and D. A. McCormick, eds.), Amsterdam: Elsevier, pp. 1–52.
- Tarczy-Hornoch, K., K. A. Martin, K. J. Stratford, and J. J. Jack, 1999. Intracortical excitation of spiny neurons in layer 4 of cat striate cortex in vitro, *Cereb. Cortex*, 9:833–843.
- Tsumoto, T., O. D. Creutzfeldt, and C. R. Légendy, 1978. Functional organization of the corticofugal system from visual cortex to lateral geniculate nucleus in the cat, *Exp. Brain Res.*, 32:345–364.
- Usrey, W. M., J. M. Alonso, and R. C. Reid, 2000. Synaptic interactions between thalamic inputs to simple cells in cat visual cortex, *J. Neurosci.*, 20:5461–5467.
- Volgushev, M., T. R. Vidyasagar, M. Chistiakova, T. Yousef, and U. T. Eysel, 2000. Membrane properties and spike generation in rat visual cortical cells during reversible cooling, *J. Physiol.*, 522:59–76.
- Von Krosigk, M., J. E. Monckton, P. B. Reiner, and D. A. McCormick, 1999. Dynamic properties of corticothalamic excitatory postsynaptic potentials and thalamic reticular inhibitory postsynaptic potentials in thalamocortical neurons of the guinea-pig dorsal lateral geniculate nucleus, *Neuroscience*, 91:7–20.
- Wang, W., H. E. Jones, I. A. Andolina, T. E. Salt, and A. M. Sillito, submitted. Local gain changes in V1 activate a “feedback searchlight” changing thalamic transmission mode.
- Wilson, J. R., 1993. Circuitry of the dorsal lateral geniculate nucleus in the cat and monkey, *Acta. Anat. (Basel)*, 147:1–13.

38 Light Responsiveness and Photic Entrainment of the Mammalian Circadian Clock

JOHANNA H. MEIJER AND JOSEPH S. TAKAHASHI

THE ROTATION OF the Earth around its axis causes 24-hour rhythms in many aspects of the physical environment, while the Earth's revolution around the sun causes seasonal changes. As an adaptation to daily environmental changes, virtually all living systems have developed endogenous circadian clocks with periods of about 24 hours to anticipate changes in the solar day. Anticipation of, rather than passive responsiveness to, the daily cycle is deeply embedded in biology and perhaps first evolved in cyanobacteria 3–4 billion years ago (Johnson and Golden, 1999). The photic environment was likely the selective agent for optimization of photosynthesis as well as escape from the mutagenic effects of ultraviolet irradiation. In animals, this evolutionary history persists in the circadian rhythms that can be observed at the level of gene expression, cellular metabolism, endocrine function, physiology, and behavior (Takahashi et al., 2001).

For proper functioning, circadian rhythms have to be synchronized, or entrained, to the day-night cycle. The major synchronizing stimulus in the environment is light. Light, rather than temperature variation or other environmental features, is a reliable signal to indicate whether it is day or night, while changes in day length are a reliable signal to indicate the time of the year. Not surprisingly, circadian clocks are responsive to light to subserve entrainment to the daily and annual cycle. In mammals, the circadian clock is located in the suprachiasmatic nuclei (SCN) at the base of the anterior hypothalamus. Light information reaches the SCN via specialized neuronal projections, of which the retinohypothalamic tract appears sufficient for photic entrainment.

Circadian rhythms are generated at the cellular level, and in mammals individual neurons in the SCN are cell autonomous circadian oscillators (Welsh et al., 1995). In the past decade, progress has been made in the identification of “clock” genes that play a role in the generation of circadian rhythms. An autoregulatory transcriptional-translational feedback loop forms the core mechanism of the circadian clock in animals. The positive elements of the oscillator are

Clock and *BMAL1*, whose gene products (CLOCK and BMAL1) form a heterodimeric transcription factor to activate the mammalian *Period* and *Cryptochrome* genes. The negative elements of the oscillator are *Period* and *Cryptochrome*, whose gene products (PERIOD and CRYPTOCHROME) accumulate, associate with each other, and translocate into the nucleus to inhibit the CLOCK/BMAL1 activation of their own transcription. As the negative elements turn over, CLOCK and BMAL1 then become active again to begin a new cycle of transcription of the *Period* and *Cryptochrome* genes (for recent reviews, see King and Takahashi, 2000; Lowrey and Takahashi, 2000; Reppert and Weaver, 2001; Young and Kay, 2001).

This chapter will focus on the light responsiveness of the mammalian circadian pacemaker and will start with an overview of the behavioral responsiveness of circadian rhythms to light as it is measured in the behaving animal. This will be followed by a discussion of light input pathways to the SCN, the neurotransmitters involved, and the light response properties of SCN neurons. The last part of the chapter will deal with intracellular responsiveness of SCN neurons to light, including the effects of light on clock gene expression.

Responsiveness of behavioral circadian rhythms to light

Physiological and molecular experiments eventually intend to offer an explanation for the attributes of the system as they appear in the phenotype. For that reason, a description of the system's behavior can guide the design of experiments at other research levels. Complex attributes of the system that are not directly explainable in terms of their function are not less important in this respect. This section will discuss the several properties of the circadian system in its response to light.

LIGHT-INDUCED PHASE SHIFTS Characteristically, the effects of light on the clock change as a function of time of day. During the night the circadian system responds to light with

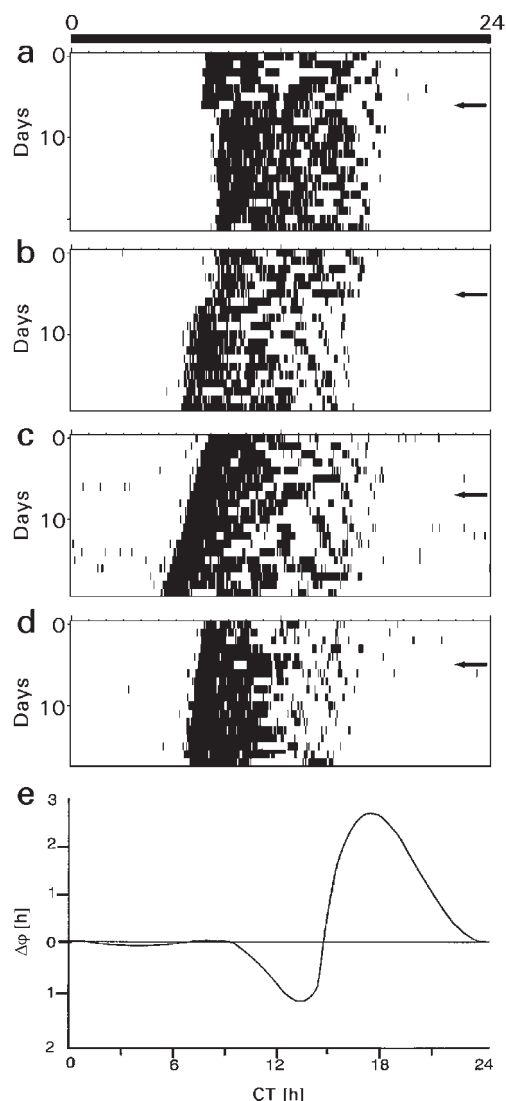
a phase adjustment, while during the day this response is absent. The changing responsivity of the clock to light is essential for photic entrainment and, in fact, is an analytical necessity for the pacemaker to become entrained. When mammals are kept in a constant environment, their activity pattern is still rhythmic but the period of the cycle deviates slightly from 24 hours. The characteristic light response of the circadian pacemaker is best illustrated when animals are kept in constant darkness and exposed to a short pulse of light (e.g., 5–15 minutes) at a particular phase of the circadian cycle. A light pulse that is presented shortly after a nocturnal animal's activity onset (which corresponds to the beginning of the animal's *subjective night*) will induce a phase delay of the circadian cycle. This means that on the next cycle the animal will start its activity later than was expected on the basis of its previous activity rhythm. A light pulse presented toward the end of the animal's activity (which corresponds to the end of the animal's subjective night) will induce a phase advance of the animal's rhythm (Fig. 38.1). During the animal's resting phase (which corresponds to the animal's subjective day), light does not affect the pacemaker's phase.

The behavioral phase shifts that are induced by light pulses are permanent and an indication that the underlying pacemaker has shifted in phase (Fig. 38.1). The effects of light pulses can be summarized in a phase response curve by plotting the light-induced phase shift as a function of the phase of pulse application (Daan and Pittendrigh, 1976;

Takahashi et al., 1984). The phase response curve illustrates how the pacemaker's responsiveness changes during the course of the cycle (Fig. 38.1).

For diurnal species, the phase response curve is nearly identical, and only the time of behavioral activity is shifted from night to day. Light pulses presented at the beginning of the animal's resting phase induce phase delays in diurnal animals, and light pulses at the end of the resting phase produce phase advances. The phase delaying and phase advancing responses at the beginning and end of the subjective night are common features of circadian pacemakers and ensure that animals entrain to a light-dark cycle. For example, when nocturnal animals leave their burrow too early in the evening, the evening light will induce a phase delay, causing them to leave their burrow later on the next cycle. In contrast, the circadian system is advanced when animals return to their burrow too late in the morning and see the morning light. In conclusion, photic entrainment

FIGURE 38.1. Phase-shifting effects of light on running wheel activity in the hamster. Consecutive days are plotted beneath one another. The presence of running wheel activity is recorded with a resolution of 1 minute. Following entrainment to a light-dark cycle (L:D 14:10), hamsters were released in constant darkness, resulting in a free-running rhythm with a period that is slightly deviating from 24 hours. *A*, Presentation of a 15 minute light pulse (100lux) 2 hours after activity onset results in a phase delay of the free-running activity rhythm. *B*, An identical light pulse that is presented 7 hours after activity onset results in a phase advance of the rhythm. Parts *A* and *B* illustrate the phase dependence of the effects of light on the pacemaker. *C*, Ineffectiveness of light presentation 2 hours after activity onset to induce a phase delay in a blinded hamster. *D*, Ineffectiveness of light 7 hours after activity onset in producing a phase advance in a blinded hamster. Parts *C* and *D* illustrate that the effects of light on the pacemaker are dependent on the integrity of retinal input. *E*, Phase-response curve for the phase-shifting effects of light pulses on circadian running wheel activity rhythm in the hamster. Onset of behavioral activity is defined as circadian time 12 (CT 12). The phase-response curve shows that presentation of light in the first few hours after activity onset results in phase delays. Delays are maximal around CT 14. Toward the end of activity, light results in phase advances with maximal advances around CT 19. A dead zone exists in which the animals' circadian clock is not responding to light with a phase shift. (*C* and *D* based on Meijer et al., 1999; *E* based on Takahashi et al., 1984.)



relies on well-directed phase adjustments of the circadian pacemaker that follow from the phase-dependent responsiveness of the pacemaker to light.

Additional response properties of the circadian pacemaker to light further support the animal's ability to entrain. The magnitude of either a phase delay or a phase advance obtained at a particular phase of the cycle depends on (1) light intensity, (2) duration of the light pulse, and (3) wavelength of the light. For light pulses with durations of 5–15 minutes, light intensities up to a threshold level of about 0.1 lux or 10^{11} photons $\text{Rev cm}^2/\text{s}$ for hamsters and 1 lux for rats do not phase shift the circadian clock (Meijer et al., 1986, 1992; Nelson and Takahashi, 1991). This threshold intensity is very high compared to the thresholds for scotopic vision and is similar to the thresholds for photopic vision. Above threshold intensity, the magnitude of the phase shifts increases in a nearly linear way with light intensity. At around 100 lux, saturation occurs and further increments in intensity do not result in a further increase in phase shift. The working range of about 2 log units is very small compared to the range of light intensities that occur in the environment in the course of a day. For example, on a sunny day, intensity levels are about 10^5 lux. If we transform the environmental variations in light intensity using the intensity dependence of the circadian system, the daily cycle of light in the world becomes a rectangular waveform with transitions at dawn and dusk, allowing the system to discriminate between day and night effectively. In view of the function of light in entraining the system to the day-night cycle, this light responsiveness of the pacemaker makes sense.

The duration of light pulses is also an important determinant of light-induced phase shifts (Meijer et al., 1992; Nelson and Takahashi, 1991). In hamsters, durations ranging from milliseconds to hours can reset circadian rhythms, but the optimal duration is about 5 minutes (Nelson and Takahashi, 1991). Short pulses on the order of seconds are not effective stimuli and require very high intensities of light, whereas long pulses on the order of hours saturate the system and so are also less efficient on a quantum basis. Indeed, the intensity-response functions for durations between seconds and hours can all be explained by integration of the total quanta during the pulse. Under these conditions, reciprocity between intensity and duration holds over the range from 1 to 45 minutes, suggesting that the circadian photic entrainment system acts as a *photon counter*.

Wavelength sensitivity is determined largely by the retinal pigments that mediate photic entrainment (to be discussed later in this chapter). The circadian system shows sensitivity to green, blue, and red light (Provencio and Foster, 1995; Takahashi et al., 1984; Yoshimura and Ebihara, 1996). Sensitivity is greatest for blue/green light, with a maximum sensitivity of about 480–500 nm. Phase-shifting responses have also been reported to be induced by pulses of ultraviolet

radiation (Amir and Robinson, 1995; von Schantz et al., 1997).

COMPLEXITY IN LIGHT RESPONSE Several complexities exist in an animal's behavioral responses to light. A phase shift is often not completed on the first circadian cycle after a light pulse but can exhibit transients. Especially for phase advances, several transient cycles occur in which the phase shift gradually grows after a single stimulating light pulse (Fig. 38.1). A two-pulse paradigm has been used to investigate whether the transient cycles reflect the pacemaker's position or whether, alternatively, the pacemaker is fully shifted on the first day after the pulse. In the latter case, transients would be a reflection of secondary mechanisms, that resynchronize to the SCN only slowly (Best et al., 1999; Watanabe et al., 2001). The data indicate that the pacemaker is fully shifted on day 1, at least the light-sensitive part of the pacemaker, while interaction with secondary downstream oscillators either inside or outside the SCN determine the delayed response of the behavioral activity pattern.

The immediate phase-shifting responses of activity onset and activity offset are different. While the activity onset shows transient cycles following a phase-advancing light pulse, the activity offset shows phase shifts that are complete on the first circadian cycle. In other words, the immediate shift in activity offset is larger than the shift in activity onset (Elliot and Tamarkin, 1994; Honma et al., 1985; Meijer and De Vries, 1995). In the course of several cycles, the shift in activity onset grows and the shifts in onset and offset become similar. For phase delays, the shifts in activity onset tend to exceed the shifts in activity offset, and transients are visible in the offset only. Several lines of research indicate that the pacemaker of the SCN consists of different subsets of oscillators (Jagota et al., 2000; Pittendrigh and Daan, 1976). Differences in response properties of these oscillators to light could cause differential phase shifts in onset and offset.

Repeated or prolonged light exposure leads to saturation of the phase shift. The pacemaker shows a reduction in light response in terms of its phase shifting capacity that persists for at least 1 hour after a subsaturating light pulse (Nelson and Takahashi, 1999). Two hours after a light pulse, the pacemaker's responsiveness seems to recover (Best et al., 1999). The decreased responsiveness to light does not correspond with the pacemaker's ability to track day length and suggests that day length is coded for in a different way.

Light pulses cause period changes in addition to phase shifts (DeCoursey, 1989; Hut et al., 1999). The light-induced changes in period depend on the circadian phase of pulse application. The changes in period occur such that they may contribute to photic entrainment (i.e., period lengthening occurs after light pulses during early night, and period shortening occurs following pulses during the late night).

Light is the most important but not the only phase-resetting stimulus since behavioral activity of the animal can also cause phase shifts (Maywood, 1999; Mrosovsky et al., 1989; Reebbs and Mrosovsky, 1989). Behavioral activity of the animal causes phase shifts when the activity is triggered by, for instance, cage cleaning or by presenting a dark pulse against an otherwise illuminated background. Forced activity of the animal is less effective in producing a phase shift. Behavioral activity has phase-shifting effects when it occurs during the day but not when it occurs during the night. Nevertheless, it has the capacity at night to inhibit light-induced phase shifts. Light-induced phase advances but not delays are strongly attenuated and in some cases completely blocked by simultaneous running wheel activity of the animal (Mistlberger and Antle, 1998; Ralph and Mrosovsky, 1992). The effect of behavioral activity on the light-induced phase shift is correlated with the amount of running wheel activity of the animal. The data indicate that physical activity affects the circadian system and its responsiveness to light.

The intensity-response curves for phase shifting and melatonin suppression are different. Melatonin production in the pineal gland is high during the night and low during the day, and still cycles when animals are kept in constant darkness (Illnerova, 1991; Illnerova and Sumova, 1997). The nighttime elevation of melatonin can be suppressed by light. The SCN mediates these light effects on melatonin production. Light suppression of melatonin appears substantially more sensitive to irradiance compared to phase shifting (Nelson and Takahashi, 1991). The difference is 1.4 log units when half-saturation values are compared. As light information reaches the pineal gland via the SCN, the increased sensitivity cannot readily be explained and indicates differences in the organization of input pathways.

Neuronal input pathways

Despite the well-established role for extraretinal photoreception in many vertebrate species, mammals have lost the ability to perceive light extraretinally and photoentrainment is mediated exclusively via the retina (Groos, 1982; Meijer et al., 1999; Yamazaki et al., 1999). Action spectra have indicated a maximal sensitivity of the circadian system in its phase-shifting response to wavelengths of about 500 nm (Boulos, 1995; Provencio and Foster, 1995; Takahashi et al., 1984) and a secondary peak in the near-ultraviolet range of the spectrum (Amir and Robinson, 1995; von Schantz et al., 1997). The maximal sensitivity at about 500 nm may suggest a role for opsin-based photopigments. However, mice that are deficient in both rods and cones show normal phase-shifting responses to 509 nm monochromatic light pulses (Freedman et al., 1999) and normal suppression of pineal melatonin in response to light (Lucas et al., 1999), indicating that classical photoreceptors do not fully account for light

effects on the circadian pacemaker. Recent evidence suggests that a small subset of retinal ganglion cells (about 1% of the total population) contains the photopigment melanopsin (Hattar et al., 2002). Melanopsin is present in the axons, cell bodies, and proximal dendrites of the ganglion cells. Melanopsin-containing ganglion cells innervate the SCN bilaterally and also project to the intergeniculate leaflet (IGL), the pretectum, and, to a lesser extent, the ventral lateral geniculate nucleus. It is suggested, therefore, that melanopsin plays a role in transducing light information to non-image-forming visual brain areas (Hattar et al., 2002).

Melanopsin-containing ganglion cells show direct responsiveness to light (Berson et al., 2002). The ganglion cells also depolarize in response to light, when synaptic input from rods and cones is blocked or when they are surgically detached from the retina. This demonstrates that these ganglion cells are intrinsically photosensitive. The spectral sensitivity function of these ganglion cells shows a peak at 484 nm. Constant illumination of the cells causes a tonic depolarization and an increase in discharge rate, and the change in membrane potential appears to be a function of light intensity. Latencies in response are long, on the order of several seconds. Physiological recordings of retrogradely labeled SCN-projecting ganglion cells have shown similar characteristics. These ganglion cells showed sustained responses to light and receptive field sizes of 2 to 5 degrees (Pu, 2000). It has been suggested that converging W (or type III) cells account for the response characteristics of SCN neurons (Cooper et al., 1993; Groos and Mason, 1980; Hattar et al., 2002). The axons of these cells are fine and unmyelinated and make up the retinohypothalamic tract (RHT), which projects directly via the optic chiasm to the SCN (Moore, 1973). The terminal field is in the ventral and often also in the lateral part of the SCN in most species of rodents (Fig. 38.2). The RHT is probably sufficient for photic entrainment, and we will focus on this pathway in this chapter. Three other photic pathways reach the SCN: via the IGL of the lateral geniculate nucleus, via the raphe, and via the pretectum (see Meijer, 2001, for review). The raphe projects with serotonergic fibers to the SCN, while the IGL projects with GABA, Neuropeptide (NPY), and enkephalins containing neurons (see Harrington, 1997, and Morin, 1994, for reviews). The dominant effect of the raphe and IGL on the SCN is inhibitory.

The RHT contains three different neurotransmitters: (1) excitatory amino acids, (2) pituitary adenylate cyclase activating peptide (PACAP), and (3) substance P. Increased glutamate immunoreactivity has been demonstrated inside the SCN (Castell et al., 1993; De Vries et al., 1993; see Ebling, 1996, for review). In situ hybridization and immunocytochemical studies have indicated the presence of ionotropic and metabotropic (mGluR1) receptor subunits. Ionotropic receptors are usually divided into *N*-methyl-D-

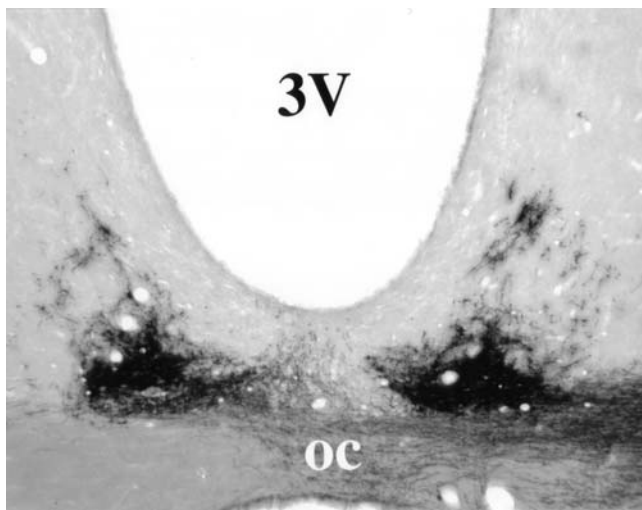


FIGURE 38.2. Retinal innervation of the SCN in the rat as revealed by unilateral injection of cholera toxin-horse radish peroxidase. 3V, third ventricle; OC, optic chiasm. (Photograph provided by Robert Y. Moore, M.D., University of Pittsburgh.)

aspartate (NMDA) and non-NMDA receptors, and both are present in the SCN. Subunits of the NMDA receptor are NMDAR1 and NMDAR2C, and non-NMDA subunits are GluR1, GluR2, and GluR4 (Ebling, 1996). Intraperitoneal administration of a noncompetitive antagonist of the NMDA receptor (MK-801) blocks the phase-shifting effects of light pulses (Colwell et al., 1991) and of electrical stimulation of the RHT (De Vries et al., 1994), whereas application of glutamate or NMDA mimics the effects of light on the pacemaker's phase in vitro (Ding et al., 1994; Shirakawa and Moore, 1994a) as well as in vivo (Mintz et al., 1999; Vindlacheruvu et al., 1992). A role for the NMDA receptor in mediating phase shifts is therefore relatively well established. Several non-NMDA receptor antagonists also block phase shifting by light (see Ebling, 1996).

PACAP is a member of the vasoactive intestinal polypeptide (VIP)/glucagon/secretin/growth-hormone releasing hormone superfamily, and it is present in the terminals of the RHT (Hannibal et al., 1997). PACAP-containing ganglion cells contain the photopigment melanopsin (Hannibal et al., 2001a). PACAP induces phase shifts during the day when it is applied in high dosages (Hannibal et al., 1997) but phase shifts during the night when applied at lower dosages (Harrington, 1999). The latter effect of PACAP is mediated by potentiation of NMDA currents. Both light and PACAP induce phosphorylation of the transcription factor cyclic adenosine monophosphate (cAMP) response element binding protein (CREB) in the SCN (von Gall et al., 1998).

Substance P is contained in retinal ganglion cells projecting to the SCN, and after enucleation, the density of substance P-containing fibers in the SCN is markedly reduced

(Mikkelsen and Larsen, 1993). The acute effect of substance P on SCN neurons is excitatory (see Challet et al., 1998, for review). Substance P potentiates glutamatergic activation (Piggins and Rusak, 1997; Shirakawa and Moore, 1994b), and its phase-shifting effect in vitro is similar to that of glutamate or NMDA (Hamada et al., 1999; Kim et al., 2001). Substance P-induced phase shifts can be blocked not only by the substance P receptor antagonists spantide or L-703,606 but also by NMDA and non-NMDA receptor antagonists (Hamada et al., 1999; Kim et al., 2001). Conversely, however, the substance P antagonist L-703,606 does not block glutamate-induced phase delays, suggesting that glutamate is downstream from substance P (Kim et al., 2001).

Electrophysiological response properties of SCN neurons

SCN neurons are among the smallest in the central nervous system and are difficult to record using intracellular methods without causing damage to the cells. Indeed, it has been shown that membrane potential recordings of SCN neurons interfere with ongoing rhythmicity in membrane potential and membrane resistance (Kim and Dudek, 1993; Schaap et al., 1999). Only a few studies have investigated the membrane properties of retinorecipient SCN neurons with intracellular recording techniques. These studies showed that retinorecipient SCN neurons are characterized by a high input resistance and a membrane potential of about 60 mV (Jiang et al., 1997; Kim and Dudek, 1993). A circadian variation in conductance was demonstrated in SCN neurons with higher conductances observed during subjective day/dawn and lower conductances during subjective dusk, while the membrane potential appeared high during the day and low during the night (de Jeu et al., 1998; Jiang et al., 1997; Schaap et al., 1999). Optic nerve stimulation induced EPSPs in most retinorecipient neurons (Kim and Dudek, 1993; Pennartz et al., 2001; Jiang et al., 1997).

The electrical properties and light responsiveness of SCN neurons have been investigated more extensively by extracellular recordings of neuronal discharge rates. A subpopulation of SCN neurons responds to light stimulation (or stimulation of the RHT) with a change in discharge rate. These light-responsive SCN neurons are located in the terminal field of the RHT (Meijer et al., 1986), indicating that they may be directly driven by it. In the nocturnal rat and hamster, about one-third of the SCN neurons respond to light (Cui and Dyball, 1996; Groos and Mason, 1980; Meijer et al., 1986). In one study, SCN neurons were tested not only under scotopic (dark-adapted) but also under photopic (light-adapted) conditions (Aggelopoulos and Meissl, 2000). Under scotopic but not photopic conditions, light-responsive SCN neurons showed preferred firing intervals of about 18–39 msec. Possibly the higher discharge rate under light

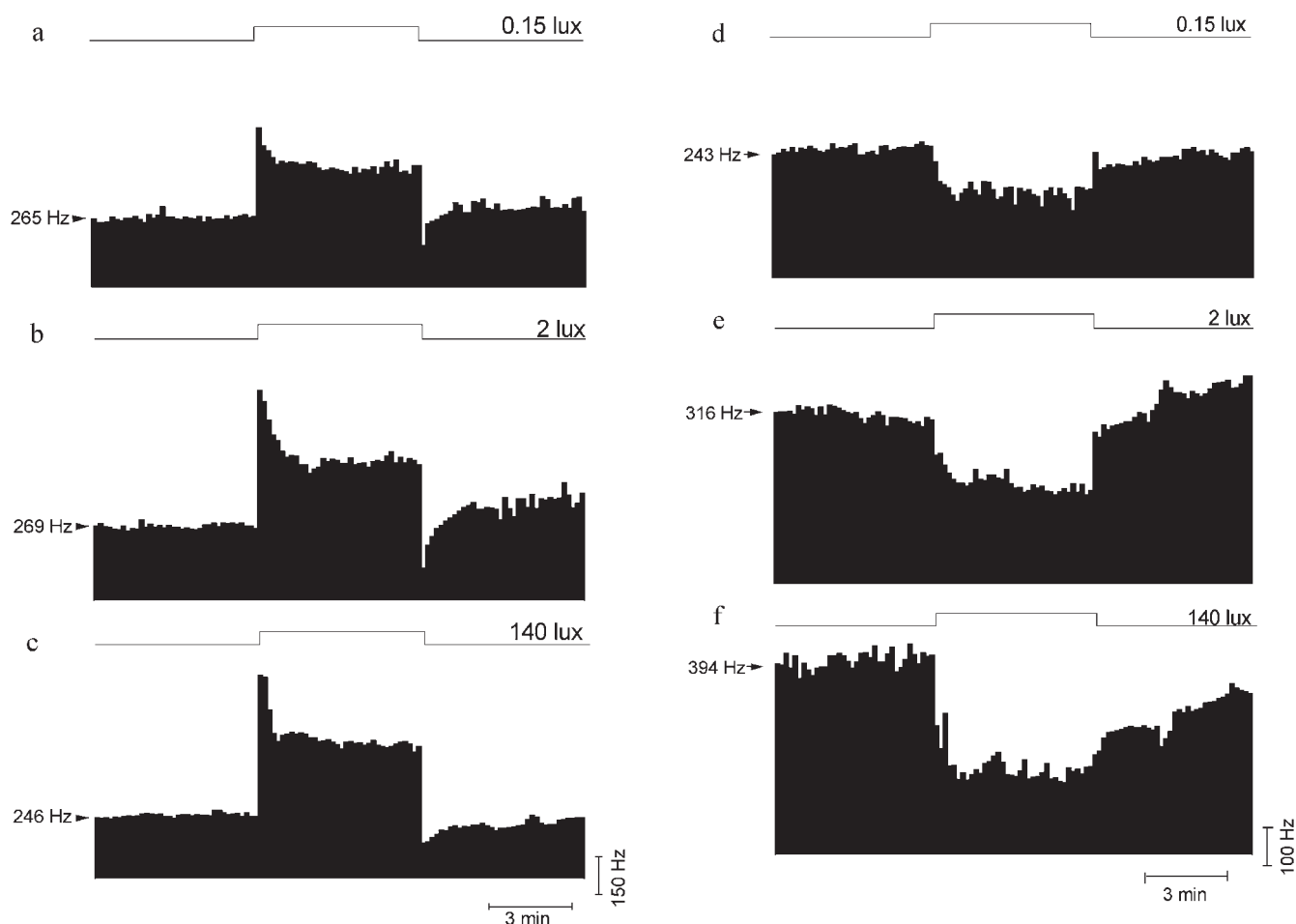


FIGURE 38.3. Light-activated and light-suppressed responses of SCN neurons to different light intensities based on Meijer et al. (1998). *A–C*, Peristimulus time histograms show light-activated responses to a 6 minute light pulse of 0.15, 2, and 140 lux, respectively, against a dark-adapted background. The timing of the light pulse is indicated above the records. The discharge rate of the neuronal population was counted every 10 seconds. The neurons

respond with an initial transient before they reach a sustained steady-state discharge level. The sustained discharge level depends on light intensity. A transient off-response is visible at the offset of the light pulse. *D–F*, Peristimulus time histograms for light-suppressed responses. Suppressed responses lack the characteristic transient response at the onset and offset of a light pulse. The steady-state discharge response is a function of light intensity.

adaptation had unmasked these preferred intervals. The receptive fields of SCN neurons are large, often exceeding 20 degrees in diameter, and are characterized by an absence of antagonistic center-surround organization (Groos and Mason, 1980). This means that SCN neurons respond with either suppression or activation to light spots that are presented throughout large parts of the visual field. Their large receptive fields show that light-responsive SCN neurons integrate light from large areas in the visual field (Groos and Mason, 1980).

Most light-responsive SCN neurons of the rat and hamster show excitation in response to light (light-activated), while a smaller fraction is suppressed by it (light-suppressed; Groos and Mason, 1980). Studies in diurnal 13-lined ground

squirrels (*Spermophilus tridecemlineatus*) and diurnal degus (*Octodon degus*) have demonstrated that in these species, the relative contribution of activated and suppressed neurons is reversed and that the majority of light-responsive SCN neurons are suppressed by light, while the minority are light-activated (Jiao et al., 1999; Meijer et al., 1989). Response latencies are long, ranging from 25 msec to several seconds (Meijer et al., 1986; Sawaki, 1979). Most responses develop fully between 200 msec and 20 seconds after the onset of a light pulse. Very brief light flashes of less than 1 second are not very effective in stimulating these neurons (Meijer et al., 1986; Sawaki, 1979). The time course of the responsiveness is extraordinarily slow compared to responses in visually responsive brain areas and is very similar to the latencies that

have been observed in melanopsin-containing ganglion cells (Berson et al., 2002). The difference in effectiveness of long versus short stimuli reflects a remarkable property of photically responsive SCN cells.

Several features of the response properties of SCN neurons correlate well with the effects of light on behavioral circadian activity rhythms discussed earlier in this chapter. Responses of SCN neurons are typically sustained, despite a short transient “overshoot” at the onset of a light response and a short suppression at light-off. Sustained responses are also found in the pretectum (Trejo and Cicèrone, 1984), the raphe nucleus (Mosko and Jacobs, 1974), and the IGL (Harrington, 1997). Of note, these are the three retinorecipient brain areas that also project to the SCN. The sustained light responsiveness of the SCN, together with its large receptive field properties, allows the SCN to monitor ambient light levels reliably in the natural environment. The light response is also transmitted to the pineal gland to control pineal melatonin synthesis (Illnerova, 1991). During the night pineal melatonin levels are high, whereas during the day they are low. Nighttime melatonin levels can be suppressed by light presentation, and suppression of melatonin corresponds with the duration of light presentation.

The sustained response level of SCN neurons is determined by light intensity (Groos and Mason, 1980; Meijer et al., 1986, 1992, 1998). The steady-state discharge rate that is obtained during a light pulse increases with light intensity for light-activated neurons and decreases for light-suppressed neurons (Fig. 38.3). The intensity response curve for SCN neurons is sigmoid, with a small working range (Meijer et al., 1986, 1998). These response curves are nearly identical with the intensity-response curve for phase shifting (Meijer et al., 1992). The intensity response curve for melatonin suppression is also sigmoid (Nelson and Takahashi, 1991) but shows increased sensitivity. Recordings in the diurnal 13-lined ground squirrels and degus indicated that much higher light intensities were required to stimulate their SCN neurons (Jiao et al., 1999; Meijer et al., 1989). In both studies, light intensities of about 1000 lux were required. The high threshold for light responses corresponds roughly with the high thresholds for melatonin suppression in 13-lined ground squirrels (Reiter, 1985). In humans, light intensities of 180 lux are required to shift the circadian rhythm in temperature (Boivin et al., 1996). Although these intensities are not as high as was expected, they are substantially higher than the threshold intensity in nocturnal animals.

When recording light responses under scotopic conditions (dark-adapted), maximal sensitivity was observed to 505 nm wavelengths (Aggelopoulos and Meissl, 2000). Under photopic conditions, peak sensitivity was observed at 510 nm, with a secondary sensitivity peak in the near-ultraviolet region of the spectrum.

Behavioral activity of the animal attenuates the phase-shifting effects of light. To investigate whether photic and behavioral stimuli interact at the level of the neuronal membrane, electrical recordings were performed in freely moving animals. Behavioral activity by itself appeared to result in suppressions of neuronal activity in the SCN of the rat and hamster (Meijer et al., 1997; Yamazaki et al., 1998). These suppressions are long-lasting, and recovery to baseline levels takes about 20 minutes. To investigate the effect of behavioral activity on light responsiveness in the SCN, light pulses were presented shortly after the animal had been active (Schaap and Meijer, 2001). The data indicate that light and behavioral activity have opposing effects within the same population of neurons (Fig. 38.4). Thus, the discharge level that is reached during a light pulse is strongly reduced by concomitant behavioral activity of the animal and can explain the decreased phase-shifting response of the animals to light when it is active at around the time of the light pulse.

Several studies have shown that the light responsiveness of SCN neurons changes in the course of the circadian cycle (Cui and Dyball, 1996; Meijer et al., 1998). Cui and Dyball (1996) have shown in anesthetized hamsters that the proportion of neurons that responds to optic nerve stimulation during the night exceeds the proportion of responsive neurons during the day (40% vs. 16%, respectively). The increased responsiveness occurred at around the onset of the dark period. With implanted electrodes in freely moving animals, it was shown that the light response during the night is larger than the response during the day (Meijer et al., 1998). In these experiments, the animals were kept in constant darkness throughout the experiment, except for the light stimulations. The baseline discharge rate of SCN neurons in constant darkness is rhythmic and shows high electrical activity during the projected daytime (called *subjective day*) and low electrical activity during the projected night (*subjective night*). The rhythm in light responsiveness is superimposed on the rhythm in baseline activity. During the subjective day, when baseline discharge is high, light presentations elicit only small responses. During the subjective night, when baseline discharge is low, the light responses are large and exceed the response levels that are obtained during daytime (Fig. 38.5). The variation in light response is apparent as a gradual transition in responsiveness and is highest during the middle of the subjective day. These data are also consistent with enhanced NMDA receptor activity during the night (Pennartz et al., 2001). For light-suppressed responses, a similar rhythm is present, and suppressions are minimal during the middle of the subjective day and are maximal during midnight. Long-term single-unit recordings revealed that the change in light sensitivity is also present at the single-neuron level. This indicates that the rhythm is not solely determined by the number of responsive neurons that

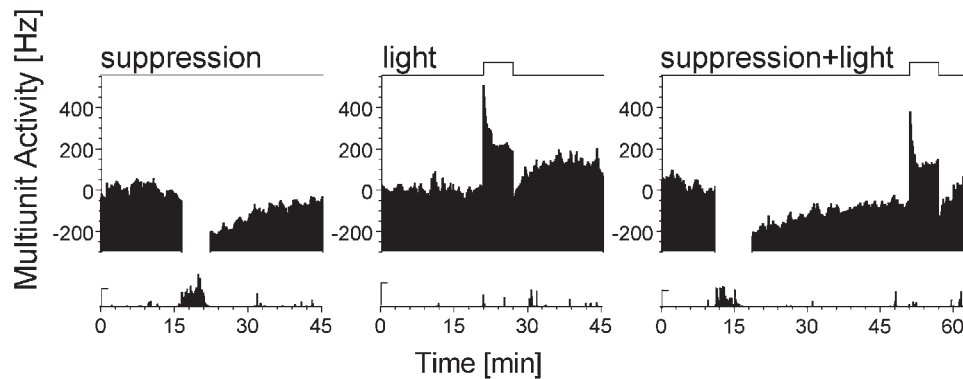


FIGURE 38.4. Behavioral-induced suppression of neuronal activity in the SCN interacts with the effects of light. The discharge rate of SCN neurons is counted per 10 seconds. Above the records, the presentation of a light pulse is indicated. At the bottom of the figures, behavioral activity is indicated. *Left*: Behavioral activity induces a long-lasting suppression of neuronal activity in the SCN. During behavioral activity, reliable recordings of the discharge rate were not possible, which accounts for the missing data in the plot.

Center: A continuation of the same recording shows that the same neuronal population is activated by a light pulse. *Right*: Presentation of a light pulse during the aftereffects of behavioral activity results in a steady-state discharge level that is lower than the discharge rate obtained by light without preceding activity. The data indicate that behavioral activity can reduce the effects of light on SCN neurons. (Based on Schaap and Meijer, 2001.)

contribute to the signal, but this feature is determined at the single-neuron level (Schaap and Meijer, 2001).

The difference in light responsiveness between day and night is especially clear when subsaturating light intensities are applied. When light intensity is increased, response levels are higher. Application of different light intensities at a fixed phase of the cycle shows that at midnight, responses increase rapidly as a function of light intensity, whereas during midday, responses grow slowly and the system saturates at a much higher light intensity. This illustrates that the light sensitivity of the circadian system is higher during the night than it is during daytime. Hence, the light response of an SCN neuron is determined by the combination of light intensity and circadian phase at which light is presented (Fig. 38.6).

Intracellular signaling responses to light

The circadian pacemaker responds to light with a phase delay during the beginning of the night and a phase advance during the end of the night. The direction of the neuronal response to light is either excited or suppressed and does not change in the course of the circadian cycle (Inouye, 1984; Meijer et al., 1998). Thus, the sign of the neuronal light response does not correspond with the bidirectional phase-shifting response of the pacemaker. The absence of phase shifts during the day is also not reflected by the electrophysiological response of the SCN. When light intensity is raised sufficiently, neuronal responses are observed but behavioral phase-shifting effects remain absent.

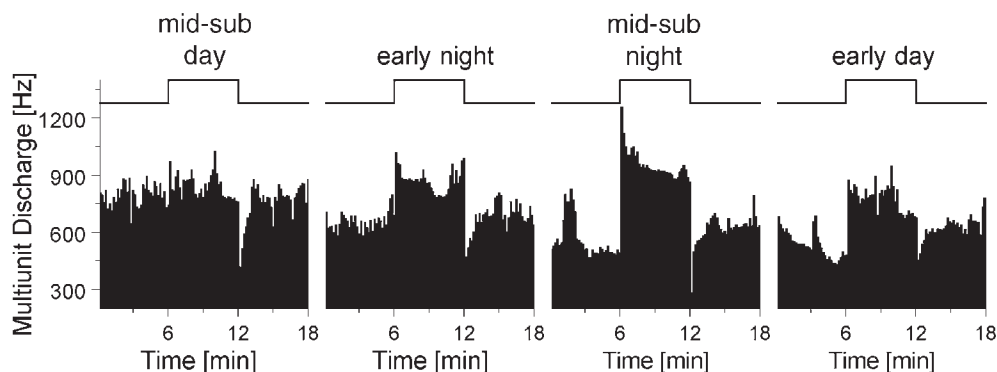


FIGURE 38.5. Light response of SCN neurons as a function of circadian time based on Meijer et al. (1998). The timing of a 6 minute light pulse is indicated above the records. The discharge rate of SCN neurons is given per 10 seconds. Light pulse presentation during midsubjective day (CT 7) to a dark-adapted animal does not induce an increase in electrical activity. At the offset of the pulse,

a transient suppression is visible. During early night (CT 12), light induces a clear, sustained increase in neuronal discharge rate. Maximal light responses are obtained during midsubjective night (CT 19). Toward the end of the night, responses decrease and only small responses are obtained during early subjective day (CT 2).

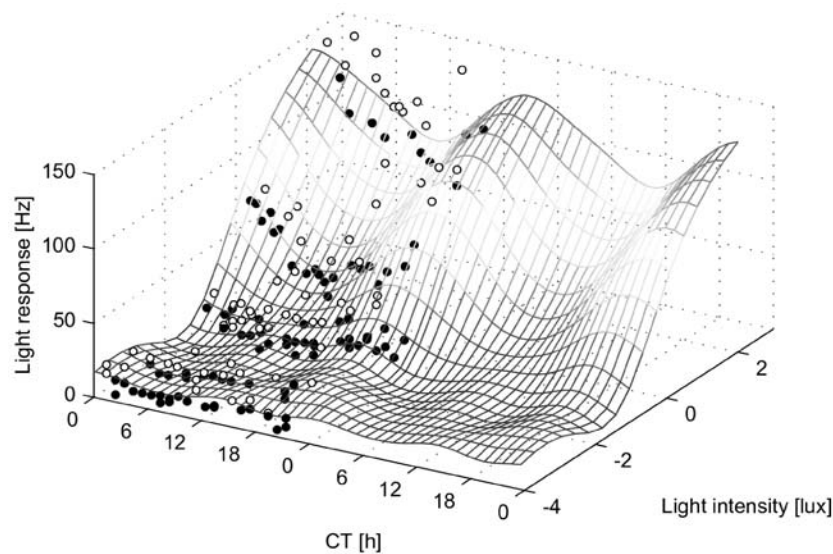


FIGURE 38.6. Two-dimensionally smoothed plot of the light response of SCN neurons as a function of both light intensity and circadian time. Light response is calculated as the difference between the steady-state discharge rate during a light pulse minus the baseline discharge rate immediately preceding the light pulse. The data indicate that for low light intensities a light response is absent throughout the circadian cycle. For increasing light intensi-

ties, light responses exist during the subjective night but not during the subjective day. A further increase in light intensity triggers light responses during both the night and the day. The magnitude of the response, however, is larger during the night than during the day. (J. H. Meijer, P. H. C. Eilers, and J. Schaap, unpublished results.) (See color plate 23.)

Similar data have been obtained in the marine snail *Bulla gouldiana* (for a review, see Block et al., 1993). Pacemaker cells of the snail respond to light throughout the circadian cycle, while their phase response curve is qualitatively identical to that of rodents. For the snail, it has been demonstrated that the neuronal response to light results in an increase of intracellular calcium during the night but not so much during the day, and it was suggested that the intracellular calcium response is of major importance for phase shifting (Block et al., 1993). Recordings in mammalian SCN neurons have now shown that NMDA induces calcium transients that are large during the night and small during the day (Colwell, 2001). Thus, the rhythm in calcium response follows the rhythm in light-induced changes in discharge rate. This is not surprising, as calcium influx is triggered by depolarization of membrane potential. The intracellular calcium response is one of the best-studied intracellular responses to light, and stimulates by itself or in concert with other second messengers a complex cascade of intracellular events. A few elements of the intracellular signal transduction pathway have been identified that lead to transcriptional activation (Gillette, 1997). Light-induced release of glutamate and activation of both NMDA and non-NMDA receptors leads to an increase in intracellular calcium (Tominaga et al., 1994). Intracellular calcium can increase both by calcium influx across the membrane and by calcium release from intracellular stores. Cellular organelles such as the endoplasmic reticulum function in the storage of calcium. Stimulation of calcium channels on intracellular organelles results in phase

delays during early night but not in phase advances during late night. Blocking of the ryanodine receptor by dantrolene and ruthenium red blocks light- and glutamate-induced delays during early night but not the glutamate-induced advances during late night (Ding et al., 1998). These data indicate that the ryanodine receptors play a role that is restricted to the early night.

Intracellular increase in calcium level leads to formation of nitric oxide (NO) (Amir, 1992; Ding et al., 1994) via activation of nitric oxide synthetase (NOS). NO produces phase advances and delays, depending on the circadian time of NO application. The effects of NO are similar to those of light, and blocking of NO transmission disrupts light transmission to the SCN (Amir, 1992; Watanabe et al., 1994).

A third intracellular component of importance is cyclic guanosine monophosphate (cGMP) (Prosser et al., 1989). The SCN is reset by cGMP during the night but not during the day. The effect of cGMP is a phase advance, with a maximum phase shift at midsubjective night. The phase response curve for cGMP shows no delay zone; thus, it does not resemble the phase response curve for light. However, the sensitive part of the phase response curve is similar to the period in which the pacemaker responds to light with a phase shift (Prosser et al., 1989).

Evidence exists that NO can directly activate cGMP (see Ding et al., 1994). However, NO produces phase advances and phase delays, depending on circadian time, whereas cGMP induces advances only. It has been proposed (e.g.,

Ding et al., 1998) that intracellular signaling elements diverge. Late at night, light causes a phase advance by means of a cGMP-dependent pathway, whereas early at night, intracellular release of calcium is involved.

Light has been shown to induce phosphorylation of the CREB in the hamster SCN (Ginty et al., 1993; Kornhauser et al., 1996). CREB becomes phosphorylated on the transcriptional regulatory site, Ser133 (Ginty et al., 1993). Phosphorylation occurs within several minutes after light exposure and only at night (Ginty et al., 1993; Kornhauser et al., 1996). Increased phosphorylation of CREB can be blocked by the NMDA receptor antagonist α -amino-5-phosphonovaleric acid (APV), indicating that it results from activation of the NMDA receptor (Ginty et al., 1993). Depolarization of membrane potential by itself and in the presence of APV is also able to induce CREB, indicating that NMDA receptor activation can be bypassed if membrane depolarization occurs (Ginty et al., 1993).

Intracellular calcium also activates the mitogen activated protein kinase (MAPK) signaling pathway in the SCN. Once phosphorylated, MAPK is translocated from the cytosol into the nucleus, where it can regulate transcriptional activity (Obrietan et al., 1998). MAPK shows an endogenous circadian rhythmicity (Obrietan et al., 1998). Light induces activation of MAPK during the night but not during the day and MAPK activation depends on the duration of light exposure, with 15 minute light pulses being more effective than 5 minute pulses (Obrietan et al., 1998). Glutamate application or membrane depolarization also triggers activation of MAPK. Blocking the MAPK pathway results in a 50% reduction of glutamate-induced CREB phosphoryla-

tion in the SCN. Taken together, these results show that MAPK is an important signaling component for CREB phosphorylation in the SCN (Obrietan et al., 1998).

As discussed earlier in this chapter, low concentrations of PACAP cause phase shifts that resemble the phase-response curve for light pulses. Several studies have indicated that cAMP protein kinase A (PKA) and calcium-dependent pathways are involved in PACAP-induced phase shifts during the night (Kopp et al., 1999; Tischkau et al., 2000; von Gall et al., 1998). Moreover, PACAP can stimulate CREB (Gillette, 1997). There is substantial evidence, therefore, that PACAP is involved in photic entrainment by stimulating intracellular components that also respond to light or NMDA.

Two circadian clock genes, *mPer1* and *mPer2*, are thought to be involved in light-induced resetting of the pacemaker (Albrecht et al., 1997; Field et al., 2000; Hastings et al., 1999; Shearman et al., 1997; Takumi et al., 1998a; Yan et al., 1999; Zylka et al., 1998). These genes are homologs of the *Drosophila* circadian clock gene *period* (Sun et al., 1997; Tei et al., 1997). The expression of *mPer1* and *mPer2* is regulated not only by light but also by the CREB pathway (Gillette, 1997), by NMDA (Moriya et al., 2000), and by PACAP (Nielsen et al., 2001). Increases in *mPer1* occur within 10 minutes after light exposure, which is very rapid (Shigeyoshi et al., 1997) and show peaks in expression about 60 minutes after light exposure (Fig. 38.7) (Albrecht et al., 1997; Shearman et al., 1997; Takumi et al., 1998a). Expression of *mPer1* is initially present in the retinorecipient area of the SCN and spreads through the SCN in the course of 60–120 minutes (Albrecht et al., 1997; Shigeyoshi et al., 1997). In transgenic

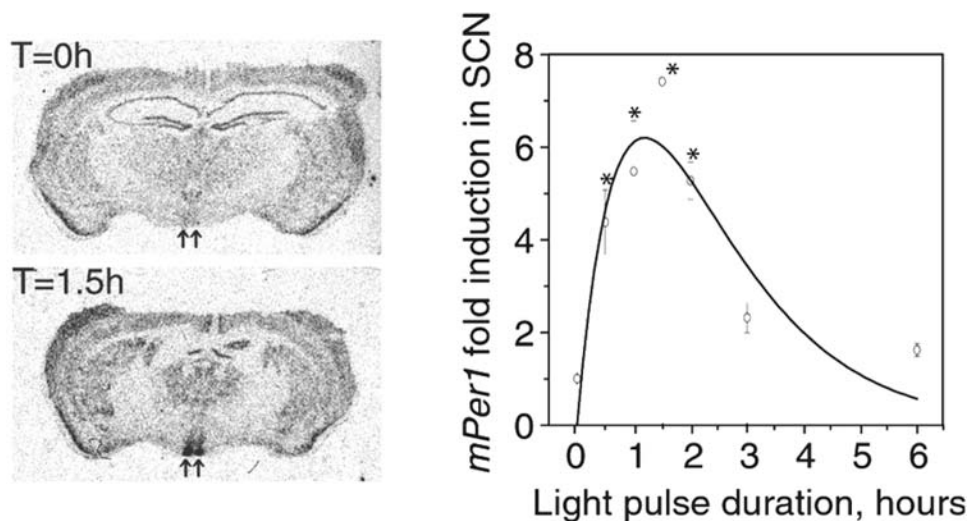


FIGURE 38.7. Light-induced *mPer1* mRNA expression in the SCN. Mice were maintained in constant darkness for at least 7 days prior to the experiment, and the endogenous circadian rhythm of each animal was measured. At CT 17, mice were transferred to a light

box. The graph to the right shows a time course for *mPer1* induction over 6 hours. The y-axis indicates the fold induction from baseline expression at CT 17. (From Wilsbacher et al., 2002.)

rats or mice with a reporter gene under the control of the *mPer1* promoter, light results in increased *mPer1* expression and in rapid shifts of the *mPer1* expression cycle (Kuhlman et al., 2000; Wilsbacher et al., 2002; Yamazaki et al., 2000). In cultured SCN slices with an *mPer1:luc* reporter gene, the cycle in *mPer1* is quickly reset by NMDA (Asai et al., 2001). As with light, *mPer1* induction by NMDA occurs only during the night.

Similar results have been obtained for *mPer2* (Albrecht et al., 1997; Shearman et al., 1997; Takumi et al., 1998a; Zylka et al., 1998). *mPer2* is induced about 90 minutes after light exposure, although different studies show somewhat different results in the time required to show maximal expression. Light-induced *mPer2* expression is dependent on circadian time, and maximal responsiveness exists at the end of the subjective day and during the first part of the night. In contrast to *mPer1* and *mPer2*, *mPer3* appears unresponsive to light (Albrecht et al., 1997; Shearman et al., 1997; Takumi et al., 1998b; Zylka et al., 1998).

Evidence for a role of *mPer1* in light-induced delays is provided by Akiyama et al. (1999), who showed that intracerebroventricular injections of antisense oligonucleotide repress light-induced phase shifts in running wheel activity and that direct application in vitro attenuates glutamate-induced delays of neuronal firing rhythms. A complete block of light-induced phase delays is obtained when both *mPer1* and *mPer2* antisense oligonucleotides are injected, indicating that *mPer1* and *mPer2* have additive effects on photic entrainment (Wakamatsu et al., 2001). In PACAP type 1 receptor-deficient mice, it has been shown that light results in phase delays instead of phase advances late at night and suggests a role for the PACAP type 1 receptor in gating of light information to the clock (Hannibal et al., 2001b). The relative contribution of *mPer1* and PACAP type 1 receptors for phase shifting remains to be shown. To further investigate the role of *mPer1* and *mPer2* in light-induced phase shifting, the responsiveness to light was tested in mice carrying a mutation in the *mPer1* or *mPer2* gene (Albrecht et al., 2001; Zheng et al., 1999). *mPer1* mutant mice appeared unable to advance in response to light stimulation late at night, while *mPer2* mutants cannot delay in response to light presentation early at night (Albrecht et al., 2001; however, see Cermakian et al., 2001). The results indicate that mammalian *Per* genes are not only light-responsive components of the circadian oscillators, but also are involved in resetting of the circadian clock.

Cryptochromes are a possible candidate for the short-wavelength responses, but thus far the mammalian cryptochromes have not been shown to be functional photopigments (Hall, 2000; Sancar, 2000). Rather, in mammals, *mCry1* and *mCry2* are essential components of the molecular clockwork (van der Horst et al., 1999; Vitaterna et al., 1999), where they play a role as negative elements in the autoregulatory feedback loop (King and Takahashi,

2000; Young and Kay, 2001). Indeed, *mCry1/mCry2* double knockouts appear to have intact *mPer1* and *mPer2* light responses in the SCN (Okamura et al., 1999).

Molecular biological lines of research have quickly provided essential contributions to our present insights concerning light-induced phase shifting of the circadian clock. It is expected that in the near future, our knowledge of this issue will be greatly enhanced. As a logical next step to the present lines of research, it will be important to demonstrate that the several clock genes are not only induced by light, but also that their expression is critical for the occurrence of a phase shift. So far, this has been performed for *mPer* but not for the other clock genes. Moreover, it is expected that more genes will become known that play an essential role in either the generation or the shaping of circadian rhythms, and it remains to be determined whether these genes also contribute to phase resetting properties.

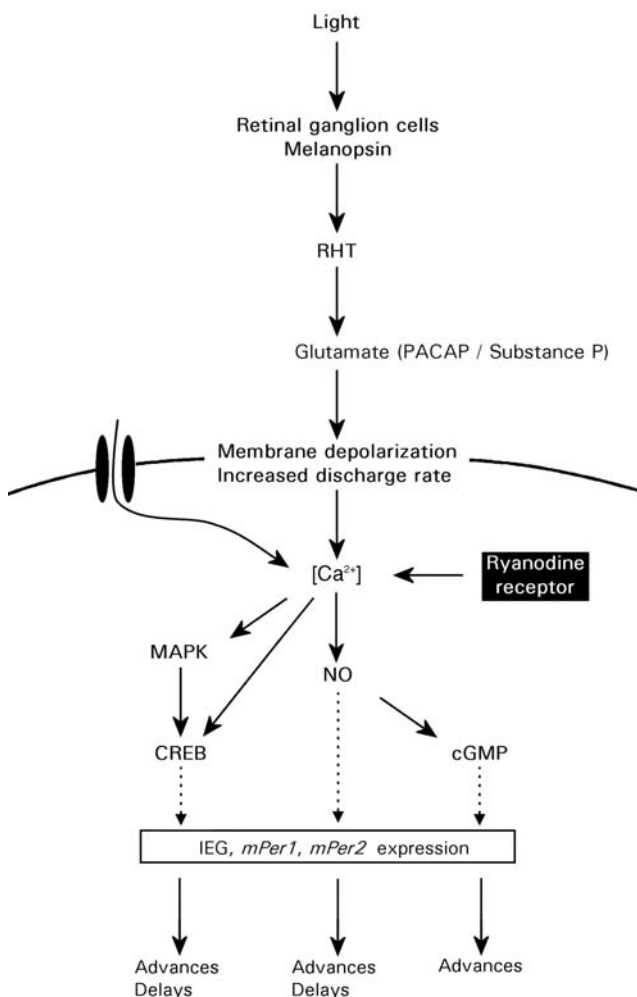


FIGURE 38.8. Schematic overview of light input pathways to the circadian clock. Note that PACAP is thought to support light entrainment in low but not in high concentrations. See text for further details.

At a conceptual level, a major question to be answered is how the phase response curve, with its bidirectional response to light, can be explained. In *Drosophila* and *Neurospora*, there is an indication that light-regulated clock components such as *timeless* and *frq* show a unidirectional response to light throughout the circadian cycle. This response is associated with phase delays and advances solely on the basis of the time by which the response occurs. In mammals, there is substantial evidence for divergence in the intracellular transduction cascade resulting in specific cues that mediate advances and delays. Whether divergence in intracellular signals accounts for phase advances and delays remains to be proven. Alternatively, divergence in input pathways supports the bidirectional phase responsiveness of the mammalian pacemaker but is not required. It will be a major challenge to identify light-responsive elements in the intracellular biochemical and genetic machinery of the cell to construct a general model accounting for the attributes of the circadian pacemaker's light responsiveness.

Summary

It has become evident that the light responsiveness of the SCN differs in many ways from the light responsiveness in brain areas involved in vision (Fig. 38.8). When the light response of the SCN is placed in perspective, it can be concluded that specialized and distinguishable photoreceptors mediate entrainment. A set of novel ganglion cells have now been identified that show direct responsiveness to light and contain the photopigment melanopsin. Via a separate unmyelinated neuronal pathway, light information is transmitted to the SCN to stimulate a subpopulation of SCN neurons. The response of these neurons to prolonged light presentation is sustained, in contrast with that of most image-forming brain areas where responses are mostly transient. SCN neurons code for luminance in a near-linear way for light intensities occurring during dawn and dusk. A time window exists for processing the neuronal response, and while the clock is rendered blind during the day, it responds with bidirectional phase shifts during the night in order to become entrained.

REFERENCES

- Aggelopoulos, N. C., and H. Meissl, 2000. Responses of neurons of the rat suprachiasmatic nucleus to retinal illumination under photopic and scotopic conditions, *J. Physiol.*, 523 (Pt 1):211–222.
- Akiyama, M., Y. Kouzu, S. Takahashi, H. Wakamatsu, T. Morya, M. Maetani, S. Watanabe, H. Tei, Y. Sakai, and S. Shibata, 1999. Inhibition of light- or glutamate-induced *mPer1* expression represses the phase shifts into the mouse circadian locomotor and suprachiasmatic firing rhythms, *J. Neurosci.*, 19:1115–1121.
- Albrecht, U., Z. S. Sun, E. E. Eichele, and C. C. Lee, 1997. A differential response of two putative mammalian circadian regulators, *mPer1* and *mPer2*, to light, *Cell*, 91:1055–1064.
- Albrecht, U., B. Zheng, D. Larkin, Z. S. Sun, and C. C. Lee, 2001. *mper1* and *mper2* are essential for normal resetting of the circadian clock, *J. Biol. Rhythms*, 16(2):100–104.
- Amir, S., 1992. Blocking NMDA receptors or nitric oxide production disrupts light transmission to the suprachiasmatic nucleus, *Brain Res.*, 586:336–339.
- Amir, S., and B. Robinson, 1995. Ultraviolet light entrains rodent suprachiasmatic nucleus pacemaker, *Neuroscience*, 69:1005–1011.
- Asai, M., S. Yamaguchi, H. Isejima, M. Jonouchi, T. Morya, S. Shibata, M. Kobayashi, and H. Okamura, 2001. Visualization of *mPer1* transcription in vitro: NMDA induces a rapid phase shift of *mPer1* gene in cultured SCN, *Curr Biol.*, 11:1524–1527.
- Berson, D. M., F. A. Dunn, and T. Motoharu, 2002. Phototransduction by retinal ganglion cells that set the circadian clock, *Science*, 295:1070–1073.
- Best, J. D., E. S. Maywood, K. L. Smith, and M. H. Hastings, 1999. Rapid resetting of the mammalian circadian clock, *J. Neurosci.*, 19:828–835.
- Block, G. D., S. B. S. Khalsa, D. G. McMahon, S. Michel, and M. Guesz, 1993. Biological clocks in the retina: cellular mechanisms of biological timekeeping, *Int. Rev. Cytol.*, 146:83–144.
- Boivin, D. B., J. F. Duffy, R. E. Kronauer, and C. A. Czeisler, 1996. Dose-response relationships for resetting of human circadian clock by light, *Nature*, 379:540–542.
- Boulos, Z., 1995. Wavelength dependence of light-induced phase shifts and period changes in hamsters, *Physiol. Behav.*, 57:1025–1033.
- Castell, M., M. Belenky, S. Cohen, O. P. Ottersen, and I. Storm-Mathisen, 1993. Glutamate-like immunoreactivity in retinal terminals of the mouse suprachiasmatic nucleus, *Eur. J. Neurosci.*, 5:368–381.
- Cermakian, N., L. Monaco, M. P. Pando, A. Dierich, and P. Sassone-Corsi, 2001. Altered behavioral rhythms and clock gene expression in mice with a targeted mutation in the *Period 1* gene, *EMBO J.*, 20:3967–3974.
- Challet, E., E. Naylor, J. M. Metzger, D. E. MacIntyre, and F. W. Turek, 1998. An NK₁ receptor antagonist affects the circadian regulation of locomotor activity in golden hamsters, *Brain Res.*, 800:32–39.
- Colwell, C. S., 2001. NMDA-evoked calcium transients and currents in the suprachiasmatic nucleus: gating by the circadian system, *Eur. J. Neurosci.*, 13:1420–1428.
- Colwell, C. S., R. G. Foster, and M. Menaker, 1991. NMDA receptor antagonists block the effects of light on circadian behavior in the mouse, *Brain Res.*, 554:105–110.
- Cooper, H. M., M. Herbin, and E. Nevo, 1993. Ocular regression conceals adaptive progression of the visual system in a blind subterranean mammal, *Nature*, 361:156–159.
- Cui, L.-N., and R. E. J. Dyball, 1996. Synaptic input from the retina to the suprachiasmatic nucleus changes with the light-dark cycle in the Syrian hamster, *J. Physiol.*, 492(2):483–493.
- Daan, S., and C. S. Pittendrigh, 1976. A functional analysis of circadian pacemaker in nocturnal rodents, II: the variability of phase response curves, *J. Comp. Physiol.*, 106:253–266.
- DeCoursey, P. J., 1989. Photoentrainment of circadian rhythms: an ecologist's viewpoint, in *Circadian Clocks and Ecology* (T. Hiroshige and K. Honma, eds.), Sapporo: Hokkaido University Press, pp. 187–206.

- De Jeu, M., M. Hermes, and C. M. Pennartz, 1998. Circadian modulation of membrane properties in slices of rat suprachiasmatic nucleus, *Neuroreport*, 9:3725–3729.
- De Vries, M. J., B. Nunes Cardozo, J. Want van der, A. de Wolf, and J. H. Meijer, 1993. Glutamate immunoreactivity in terminals of the retinohypothalamic tract of the brown Norwegian rat, *Brain Res.*, 612:231–237.
- De Vries, M. J., J. A. Treep, E. S. D. de Pauw, and J. H. Meijer, 1994. The effects of electrical stimulation of the optic nerves and anterior optic chiasm on the circadian activity rhythm of the Syrian hamster: involvement of excitatory amino acids, *Brain Res.*, 642:206–212.
- Ding, J. M., G. F. Buchanan, S. A. Tischkau, D. Chen, L. Kuriashkina, L. E. Faiman, J. M. Alster, P. S. McPherson, K. P. Campbell, and M. U. Gillette, 1998. A neuronal ryanodine receptor mediates light-induced phase delays of the circadian clock, *Nature*, 394:381–384.
- Ding, J. M., D. Chen, E. T. Weber, L. E. Faiman, M. A. Rea, and M. U. Gillette, 1994. Resetting the biological clock: mediation of nocturnal circadian shifts by glutamate and NO, *Science*, 266:1713–1717.
- Ebling, F. J. P., 1996. The role of glutamate in the photic regulation of the suprachiasmatic nucleus, *Prog. Neurobiol.*, 50:109–132.
- Elliott, J. A., and L. Tamarkin, 1994. Complex circadian regulation of pineal melatonin and wheel-running in Syrian hamsters, *J. Comp. Physiol. A.*, 174:469–484.
- Field, M. D., E. S. Maywood, J. A. O'Brien, D. R. Weaver, S. M. Reppert, and M. H. Hastings, 2000. Analysis of clock proteins in mouse SCN demonstrates phylogenetic divergence of the circadian clockwork and resetting mechanisms, *Neuron*, 25:437–447.
- Freedman, M. S., R. J. Lucas, B. Soni, M. von Schantz, M. Munoz, Z. David-Gray, and R. Foster, 1999. Regulation of mammalian circadian behavior by non-rod, non-cone, ocular photoreceptors, *Science*, 284:502–504.
- Gillette, M. U., 1997. Cellular and biochemical mechanisms underlying circadian rhythms in vertebrates, *Curr. Opin. Neurobiol.*, 7:797–804.
- Ginty, D. D., J. M. Kornhauser, M. A. Thompson, H. Bading, K. E. Mayo, J. S. Takahashi, and M. E. Greenberg, 1993. Regulation of CREB phosphorylation in the suprachiasmatic nucleus by light and a circadian clock, *Science*, 260:238–241.
- Groos, G. A., 1982. The comparative physiology of extraocular photoreception, *Experientia*, 38:989–1128.
- Groos, G. A., and R. Mason, 1980. The visual properties of rat and cat suprachiasmatic neurons, *J. Comp. Physiol.*, 135:349–356.
- Hall, J. C., 2000. Cryptochromes: sensory reception, transduction, and clock functions subserving circadian systems, *Neurobiology*, 10:456–466.
- Hamada, T., S. Yamanouchi, A. Watanabe, S. Shibata, and S. Watanabe, 1999. Involvement of glutamate release in substance P-induced phase delays of suprachiasmatic neuron activity rhythm in vitro, *Brain Res.*, 836:190–193.
- Hannibal, J., J. M. Ding, D. Chen, J. Fahrenkrug, P. J. Larsen, M. U. Gillette, and J. D. Mikkelsen, 1997. Pituitary adenylate cyclase-activating peptide (PACAP) in the retinohypothalamic tract: a potential daytime regulator of the biological clock, *J. Neurosci.*, 17:2637–2644.
- Hannibal, J., P. Hindersson, S. M. Knudsen, B. Georg, and J. Fahrenkrug, 2001a. The photopigment melanopsin is exclusively present in pituitary adenylate cyclase-activating polypeptide-containing retinal ganglion cells of the retinohypothalamic tract, *J. Neurosci.*, 21(19):1–7.
- Hannibal, J., F. Jamen, H. S. Nielsen, L. Journot, P. Brabet, and J. Fahrenkrug, 2001b. Dissociation between light-induced phase shift of the circadian rhythm and clock gene expression in mice lacking the pituitary adenylate cyclase activating polypeptide type 1 receptor, *J. Neurosci.*, 21(13):4883–4890.
- Harrington, M. E., 1997. The ventral lateral geniculate nucleus and the intergeniculate leaflet: interrelated structures in the visual and circadian systems, *Neurosci. Biobehav. Rev.*, 21:705–727.
- Harrington, M. E., 1999. Pituitary adenylate cyclase activating peptide phase shifts circadian rhythms in a manner similar to light, *J. Neurosci.*, 19:6637–6642.
- Hastings, M. H., M. D. Field, E. S. Maywood, D. R. Weaver, and S. M. Reppert, 1999. Differential regulation of mPER1 and mTIM proteins in the mouse suprachiasmatic nuclei: new insights into a core clock mechanism, *J. Neurosci.*, 19:1–7.
- Hattar, S., H.-W. Liao, M. Takao, D. M. Berson, and K.-W. Yau, 2002. Melanopsin-containing retinal ganglion cells: architecture, projections, and intrinsic photosensitivity, *Science*, 295:1065–1073.
- Honma, K. I., S. Honma, and T. Hiroshige, 1985. Response curve, free-running period, and activity time in circadian locomotor rhythm of rats, *Jpn. J. Physiol.*, 35:643–658.
- Hut, R. A., B. E. H. van Oort, and S. Daan, 1999. Natural entrainment without dawn and dusk: the case of the European ground squirrel, *J. Biol. Rhythms*, 14:290–299.
- Illnerova, H., 1991. The suprachiasmatic nucleus and rhythmic pineal melatonin production, in *Suprachiasmatic Nucleus: The Minds Clock* (D. C. Klein, R. Y. Moore, and S. M. Reppert, eds.), New York: Oxford University Press, pp. 197–216.
- Illnerova, H., and S. Sumova, 1997. Photic entrainment of the mammalian rhythm in melatonin production, *J. Biol. Rhythms*, 12(6):547–555.
- Inouye, S. T., 1984. Light responsiveness of the suprachiasmatic nucleus with the island with the retino-hypothalamic tract spared, *Brain Res.*, 294:263–268.
- Jagota, A., O. Horacio de la Iglesia, and W. J. Schwartz, 2000. Morning and evening circadian oscillations in the suprachiasmatic nucleus *in vitro*, *Nat. Neurosci.*, 3(4):372–376.
- Jiang, Z.-G., Y. Q. Yang, Z.-P. Liu, and C. N. Allen, 1997. Membrane properties and synaptic inputs of suprachiasmatic nucleus neurons in rat brain slices, *J. Physiol.*, 499:141–159.
- Jiao, Y., T. M. Lee, and B. Rusak, 1999. Photic responses of suprachiasmatic area neurons in diurnal degus (*Octodon degus*) and nocturnal rats (*Rattus norvegicus*), *Brain Res.*, 817:93–103.
- Johnson, C. H., and S. S. Golden, 1999. Circadian programs in cyanobacteria: adaptiveness and mechanism, *Annu. Rev. Microbiol.*, 53:389–409.
- Kim, Y. I., and F. E. Dudek, 1993. Membrane properties of rat suprachiasmatic nucleus neurons receiving optic nerve input, *J. Physiol.*, 464:229–243.
- Kim, D. Y., H.-C. Kang, H. C. Shin, K. J. Lee, Y. W. Yoon, H. C. Han, H. S. Na, S. K. Hong, and Y. I. Kim, 2001. Substance P plays a critical role in photic resetting of the circadian pacemaker in the rat hypothalamus, *J. Neurosci.*, 21:4026–4031.
- King, D. P., and J. S. Takahashi, 2000. Molecular genetics of circadian rhythms in mammals, *Annu. Rev. Neurosci.*, 23:713–742.
- Kopp, M. D. A., C. Schomerus, F. Dehghani, H.-W. Kort, and H. Meissl, 1999. Pituitary adenylate cyclase-activating polypeptide and melatonin in the suprachiasmatic nucleus: effects on the calcium signal transduction cascade, *J. Neurosci.*, 19:206–219.

- Kornhauser, J. M., D. D. Ginty, M. E. Greenberg, K. E. Mayo, and J. S. Takahashi, 1996. Light entrainment and activation of signal transduction pathways in the SCN, *Prog. Brain Res.*, 111:133–146.
- Kuhlman, S. J., J. E. Quintero, and D. G. McMahon, 2000. GFP fluorescence reports Period 1 circadian gene regulation in the mammalian biological clock, *NeuroReport*, 11:1479–1482.
- Lowrey, P. H., and J. S. Takahashi, 2000. Genetics of the mammalian circadian system: photic entrainment, circadian pacemaker mechanisms, and posttranslational regulation, *Annu. Rev. Genet.*, 34:533–562.
- Lucas, R. J., M. S. Freedman, M. Munoz, J. M. Garcia-Fernandez, and R. G. Foster, 1999. Regulation of the mammalian pineal by non-rod, non-cone, ocular photoreceptors, *Science*, 284:505–507.
- Maywood, E. S., N. Mrosovsky, M. D. Field, and M. H. Hastings, 1999. Rapid down-regulation of mammalian period genes during behavioral resetting of the circadian clock, *Proc. Natl. Acad. Sci. USA*, 96(26):15211–15216.
- Meijer, J. H., 2001. Photic entrainment in mammals, in: *Handbook of Behavioral Neurobiology*, vol. 12, *Circadian Clocks* (J. S. Takahashi, F. W. Turek, and R. Y. Moore, eds.), New York Kluwer Academic/Plenum, pp. 183–222.
- Meijer, J. H., and M. J. De Vries, 1995. Light induced phase shifts in onset and offset of running-wheel activity in the Syrian hamster, *J. Biol. Rhythms*, 10:4–16.
- Meijer, J. H., G. A. Groos, and B. Rusak, 1986. Luminance coding in a circadian pacemaker: the suprachiasmatic nucleus of the rat and the hamster, *Brain Res.*, 382:109–118.
- Meijer, J. H., B. Rusak, and G. Gänshirt, 1992. The relation between light-induced discharge in the suprachiasmatic nucleus and phase shifts of hamster circadian rhythms, *Brain Res.*, 598:257–288.
- Meijer, J. H., B. Rusak, and M. E. Harrington, 1989. Photically responsive neurons in the hypothalamus of a diurnal ground squirrel, *Brain Res.*, 501:315–323.
- Meijer, J. H., J. Schaap, K. Watanabe, and H. Albus, 1997. Multi-unit activity recordings in the suprachiasmatic nuclei: in vivo versus in vitro models, *Brain Res.*, 753:322–327.
- Meijer, J. H., B. Thio, H. Albus, J. Schaap, and A. C. J. Ruijs, 1999. Functional absence of extraocular photoreception in hamster circadian rhythm entrainment, *Brain Res.*, 831:337–339.
- Meijer, J. H., K. Watanabe, J. Schaap, H. Albus, and L. Détári, 1998. Light responsiveness of the suprachiasmatic nucleus: long-term multiunit and single-unit recordings in freely moving rats, *J. Neurosci.*, 18:9078–9087.
- Mikkelsen, J. D., and P. J. Larsen, 1993. Substance P in the suprachiasmatic nucleus of the rat: an immunohistochemical and in situ hybridization study, *Histochemistry*, 100:3–16.
- Mintz, E. M., C. L. Marvel, C. F. Gillespie, K. M. Price, and H. E. Albers, 1999. Activation of NMDA receptors in the suprachiasmatic nucleus produces light-like phase shifts of the circadian clock in vivo, *J. Neurosci.*, 19(12):5124–5130.
- Mistlberger, R. E., and M. C. Antle, 1998. Behavioral inhibition of light-induced circadian phase resetting is phase and serotonin dependent, *Brain Res.*, 786:31–38.
- Moore, R. Y., 1973. Retinohypothalamic projection in mammals: a comparative study, *Brain Res.*, 49:403–409.
- Morin, L. P., 1994. The circadian visual system, *Brain Res. Rev.*, 67:102–127.
- Moriya, T., K. Horikawa, M. Akiyama, and S. Shibata, 2000. Correlative association between *N*-methyl-D-aspartate receptor-mediated expression of period genes in the suprachiasmatic nucleus and phase shifts in behavior with photic entrainment of clock in hamsters, *Mol. Pharmacol.*, 58(6):1554–1562.
- Mosko, S. S., and B. L. Jacobs, 1974. Midbrain raphe neurons; spontaneous activity and response to light, *Physiol. Behav.*, 13:589–593.
- Mrosovsky, N., S. G. Reebs, G. I. Honrado, and P. A. Salmon, 1989. Behavioral entrainment of circadian rhythms, *Experientia*, 45:696–702.
- Nelson, D. E., and J. S. Takahashi, 1991. Sensitivity and integration in a visual pathway for circadian entrainment in the hamster (*Mesocricetus auratus*), *J. Physiol.*, 439:115–145.
- Nelson, D. E., and J. S. Takahashi, 1999. Integration and saturation within the circadian photic entrainment pathway of hamsters, *Am. J. Physiol.*, 277:R1351–R1361.
- Nielsen, H. S., J. Hannibal, S. M. Knudsen, and J. Fahrenkrug, 2001. Pituitary adenylate cyclase-activating polypeptide induces period 1 and period 2 gene expression in the rat suprachiasmatic nucleus during late night, *Neuroscience*, 103(2):433–441.
- Obrietan, K., S. Impey, and D. R. Storm, 1998. Light and circadian rhythmicity regulate MAP kinase activation in the suprachiasmatic nuclei, *Nat. Neurosci.*, 1:693–700.
- Okamura, H., S. Miyake, Y. Sumi, S. Yamaguchi, A. Yasui, M. Muijtens, J. H. L. Hoeijmakers, and G. T. J. van der Horst, 1999. Photic induction of *mPer1* and *mPer2* in *Cry*-deficient mice lacking a biological clock, *Science*, 286:2531–2534.
- Pennartz, C. M. A., R. Hamstra, and A. M. S. Geurtsen, 2001. Enhanced NMDA receptor activity in retinal inputs to the rat suprachiasmatic nucleus during the subjective night, *J. Physiol.*, 532(1):181–194.
- Piggins, H. D., and B. Rusak, 1997. Effects of microinjections of substance P into the suprachiasmatic nucleus region on hamster wheel-running rhythms, *Brain Res. Bull.*, 42:451–455.
- Pittendrigh, C. S., and S. Daan, 1976. A functional analysis of circadian pacemakers in nocturnal rodents. V. Pacemaker structure: a clock for all seasons, *J. Comp. Physiol.*, 106:333–355.
- Prosser, R. A., A. J. McArthur, and M. U. Gillette, 1989. cGMP induces phase shifts of a mammalian circadian pacemaker at night, in antiphase to cAMP effects, *Proc. Natl. Acad. Sci. USA*, 86:6812–6815.
- Provencio, I., and R. G. Foster, 1995. Circadian rhythms in mice can be regulated by photoreceptors with cone-like characteristics, *Brain Res.*, 694:183–190.
- Pu, M., 2000. Physiological response properties of cat retinal ganglion cells projecting to suprachiasmatic nucleus, *J. Biol. Rhythms*, 15:31–36.
- Ralph, M. R., and N. Mrosovsky, 1992. Behavioral inhibition of circadian responses to light, *J. Biol. Rhythms*, 7:353–359.
- Reebs, S. G., and N. Mrosovsky, 1989. Effects of induced wheel running on the circadian activity rhythms of Syrian hamsters: entrainment and phase response curve, *J. Biol. Rhythms*, 4:39–48.
- Reiter, R. J., 1985. Action spectra, dose-response relationships and temporal aspects of light's effects on the pineal gland, *Ann. N.Y. Acad. Sci.*, 453:215–230.
- Reppert, S. M., and D. R. Weaver, 2001. Molecular analysis of mammalian circadian rhythms, *Annu. Rev. Physiol.*, 63:647–676.
- Sancar, A., 2000. Cryptochrome: the second photoactive pigment in the eye and its role in circadian photoreception, *Annu. Rev. Biochem.*, 69:31–67.

- Sawaki, Y., 1979. Suprachiasmatic nucleus neurones, excitation and inhibition mediated by the direct retinohypothalamic projection in female rats, *Exp. Brain Res.*, 37:127–138.
- Schaap, J., N. P. A. Bos, M. T. G. de Jeu, A. M. S. Geurtsen, J. H. Meijer, and C. M. A. Pennartz, 1999. Neurons of the rat suprachiasmatic nucleus show a circadian rhythm in membrane properties that is lost during prolonged whole-cell recording, *Brain Res.*, 815:154–166.
- Schaap, J., and J. H. Meijer, 2001. Opposing effects of behavioral activity and light on neurons of the suprachiasmatic nucleus, *Eur. J. Neurosci.*, 13:1955–1962.
- Schantz, von M., S. M. Argamaso-Hernan, A. Szél, and R. G. Foster, 1997. Photopigments and photoentrainment in the Syrian golden hamster, *Brain Res.*, 770:131–138.
- Shearman, L. P., M. J. Zylka, D. R. Weaver, L. F. Kolakowski, and S. M. Reppert, 1997. Two period homologs: circadian expression and photic regulation in the suprachiasmatic nuclei, *Neuron*, 19:1261–1269.
- Shigeyoshi, Y., K. Taguchi, S. Yamamoto, S. Tadekida, L. Yan, H. Tei, T. Moriya, S. Shibata, J. J. Loros, J. C. Dunlap, and H. Okamura, 1997. Light-induced resetting of a mammalian circadian clock is associated with rapid induction of the *mper1* transcript, *Cell*, 91:1043–1053.
- Shirakawa, T., and R. Y. Moore, 1994a. Glutamate shifts the phase of the circadian neuronal firing rhythm in the rat suprachiasmatic nucleus in vitro, *Neurosci. Lett.*, 178:47–50.
- Shirakawa, T., and R. Y. Moore, 1994b. Responses of rat suprachiasmatic nucleus neurons to substance P and glutamate in vitro, *Brain Res.*, 642:213–220.
- Sun, Z. S., U. Albrecht, O. Zhuchenko, J. Bailey, G. Eichele, and C. C. Lea, 1997. RIGUI, a putative mammalian ortholog of the *Drosophila* period gene, *Cell*, 90:1003–1011.
- Takahashi, J. S., P. J. Decoursey, L. Bauman, and M. Menaker, 1984. Spectral sensitivity of a novel photoreceptive system mediating entrainment of mammalian circadian rhythms, *Nature*, 308:186–188.
- Takahashi, J. S., F. W. Turek, and R. Y. Moore, eds., 2001. *Handbook of Behavioral Neurobiology*, vol. 12, *Circadian Clocks*, New York: Kluwer Academic/Plenum.
- Takumi, T., C. Matsubara, Y. Shigeyoshi, K. Taguchi, K. Yagita, Y. Maebayashi, Y. Sakakida, K. Okumura, N. Takashima, and H. Okamura, 1998a. A new mammalian period gene predominantly expressed in the suprachiasmatic nucleus, *Genes Cells*, 3(3):167–176.
- Takumi, T., K. Taguchi, S. Miyake, Y. Sakakida, N. Takashima, C. Matsubara, Y. Maebayashi, K. Okumura, S. Takekida, S. Yamamoto, K. Yagita, L. Yan, M. W. Young, and H. Okamura, 1998b. A light-independent oscillatory gene *mPer3* in mouse SCN and OVLT, *EMBO J.*, 16:4753–4759.
- Tei, H., H. Okamura, Y. Shigeyoshi, C. Fukuhara, R. Ozawa, M. Hirose, and Y. Sakaki, 1997. Circadian oscillation of a mammalian homologue of the *Drosophila* period gene, *Nature*, 389:512–516.
- Tischkau, S. A., E. A. Gallman, G. F. Buchanan, and M. U. Gillette, 2000. Differential cAMP gating of glutamatergic signaling regulates long-term state changes in the suprachiasmatic circadian clock, *J. Neurosci.*, 20(20):7830–7837.
- Tominaga, K., M. E. Geusz, S. Michel, and S.-I. T. Inouye, 1994. Calcium imaging in organotypic cultures of the rat suprachiasmatic nucleus, *NeuroReport*, 5:1901–1905.
- Tejro, L. J., and C. M. Ciccone, 1984. Cells in the pretectal olivary nucleus are in the pathway for the direct light reflex of the pupil in the rat, *Brain Res.*, 300:49–62.
- van der Horst, G. T. J., M. Muijtjens, K. Kobayashi, R. Takano, S.-I. Kanno, M. Takao, J. de Wit, A. Verkerk, A. P. M. Eker, D. van Leenen, R. Buys, R. Bootsma, J. H. Hoeijmakers, and A. Yasui, 1999. Mammalian *Cry1* and *Cry2* are essential for maintenance of circadian rhythms, *Nature*, 398:627–663.
- Vindlacheruvu, R. R., F. J. P. Ebling, E. S. Maywood, and M. H. Hastings, 1992. Blockade of glutamatergic neurotransmission in the suprachiasmatic nucleus prevents cellular and behavioral responses of the circadian system to light, *Eur. J. Neurosci.*, 4:673–679.
- Vitaterna, M. H., C. P. Selby, T. Todo, H. Niwa, C. Thompson, E. M. Fruechte, K. Hitomi, R. J. Thresher, T. Ishikawa, J. Miyazaki, J. S. Takahashi, and A. SancaR, 1999. Differential regulation of mammalian *Period* genes and circadian rhythmicity by cryptochromes 1 and 2, *Proc. Natl. Acad. Sci. USA*, 96:12114–12119.
- von Gall, C., G. E. Duffield, M. H. Hastings, M. D. A. Kopp, F. Dehghani, H.-W. Korf, and J. H. Stehle, 1998. CREB in the mouse SCN: a molecular interface coding the phase-adjusting stimuli light, glutamate, PACAP, and melatonin for clockwork access, *J. Neurosci.*, 18(24):10389–10397.
- von Schantz, M., I. Provencio, and R. G. Foster, 1997. Recent developments in circadian photoreception: more than meets the eye, *Invest. Ophthalmol. Vis. Sci.*, 41(7):1605–1607.
- Wakamatsu, H., Y. Yoshinobu, R. Aida, T. Moriya, M. Akiyama, and S. Shibata, 2001. Restricted-feeding-induced anticipatory activity rhythm is associated with a phase-shift of the expression of *mPer1* and *mPer2* mRNA in the cerebral cortex and hippocampus but not in the suprachiasmatic nucleus of mice, *Eur. J. Neurosci.*, 13(6):1190–1196.
- Watanabe, A., T. Hamada, S. Shibata, and S. Watanabe, 1994. Effects of nitric oxide synthase inhibitors on *N*-methyl-D-aspartate-induced phase delay of circadian rhythm of neuronal activity in the rat suprachiasmatic nucleus in vitro, *Brain Res.*, 646(1):161–164.
- Watanabe, K., T. de Boer, and J. H. Meijer, 2001. Light-induced resetting of the circadian pacemaker: quantitative analysis of transient versus steady-state phase shifts, *J. Biol. Rhythms*, 16(6):564–573.
- Welsh, D. K., D. E. Logothetis, M. Meister, and S. M. Reppert, 1995. Individual neurons dissociated from rat suprachiasmatic nucleus express independently phased circadian firing rhythms, *Neuron*, 14:697–706.
- Wilsbacher, L. D., S. Yamazaki, E. D. Herzog, E. J. Song, L. A. Radcliffe, M. Abe, G. Block, E. Spitznagel, M. Menaker, and J. S. Takahashi, 2002. Photic and circadian expression of luciferase in *mPeriod1-luc* transgenic mice in vivo, *Proc. Natl. Acad. Sci. USA*, 99:489–494.
- Yamazaki, S., M. Goto, and M. Menaker, 1999. No evidence for extraocular photoreceptors in the circadian system of the Syrian hamster, *J. Biol. Rhythms*, 14:197–201.
- Yamazaki, S., M. C. Kerbeshian, C. G., Hocker, G. D. Block, and M. Menaker, 1998. Rhythmic properties of the hamster suprachiasmatic nucleus in vivo, *J. Neurosci.*, 18:10709–10723.
- Yamazaki, S., R. Numano, M. Abe, A. Hida, R. Takahashi, M. Ueda, G. D. Bloch, Y. Sakaki, M. Menaker, and H. Tei, 2000. Resetting central and peripheral circadian oscillators in transgenic rats, *Science*, 288:682–685.
- Yan, L., S. Takekida, Y. Shigeyoshi, and H. Okamura, 1999. *Per1* and *Per2* gene expression in the rat suprachiasmatic nucleus: circadian profile and the compartment-specific response to light, *Neuroscience*, 94:141–150.

- Yoshimura, T., and S. Ebihara, 1996. Spectral sensitivity of photoreceptors mediating phase-shifts of circadian rhythms in retinally degenerate CBA/J (rd/rd) and normal CBA/N (+/+) mice, *J. Comp. Physiol. A*, 178:797–802.
- Young, M. W., and S. A. Kay, 2001. Time zones: a comparative genetics of circadian clocks, *Nat. Rev. Genet.*, 2:702–715.
- Zheng, B., D. W. Larkin, U. Albrecht, Z. S. Sun, M. Sage, G. Eichele, C. C. Lee, and A. Bradley, 1999. The *mPer2* gene encodes a functional component of the mammalian circadian clock, *Nature*, 400:169–173.
- Zylka, M. J., L. P. Shearman, D. R. Weaver, and S. M. Reppert, 1998. Three period homologs in mammals: differential light responses in the suprachiasmatic circadian clock and oscillating transcripts outside of brain, *Neuron*, 20:1103–1110.

39 Learning from the Pupil: Studies of Basic Mechanisms and Clinical Applications

JOHN L. BARBUR

THE FUNCTION OF the iris and its response to light in humans have been of great interest to both physiologists and neurologists, who wanted to establish the neural pathways involved in the control of the pupil response, as well as to physicists and biological engineers, who have often described the pupil light reflex (PLR) as a beautiful example of a closed-loop servomechanism. The function of this mechanism was primarily to adjust retinal illuminance with changes in ambient light, although this has often been recognized as a useful simplification. In addition, many clinical, neuro-ophthalmological, and pharmacological studies have attempted to establish the usefulness of the pupil in diagnosing lesions of the visual pathways and the normal functioning of the retina (Loewenfeld, 1999). The often circuitous involvement of a large number of neural pathways in controlling the movements of the iris makes the pupil a rich source of information, but it also ensures that its secrets are hard to unravel. The presence of numerous uncorrelated signals in the pupil makes difficult the extraction of other small signals that can reflect important retinal and cortical processing of visual information. Recent advances in instrumentation and data processing have generated renewed interest in pupil research by overcoming some of the difficulties of extracting small, stimulus-specific signals from much larger “noisy” fluctuations of the pupil that have often been wrongly regarded as random noise.

There is little doubt that the most important and best-studied afferent visual signal that drives the pupil is generated by changing the ambient illumination. The afferent pathways involved in the control of the PLR in humans have been associated entirely with subcortical projections, and this is consistent with some clinical observations which suggest that the pupils continue to respond normally to sudden changes in room illumination, even when the patients are cortically blind (Brindley et al., 1969). The PLR response has therefore been associated with a single subcortical neural pathway. Other studies have examined in greater detail the effect of visual cortical lesions on the pupil response to light, and the results do not always support the classical belief in a single light reflex pathway. We know that the ambient light level determines largely the steady-state size of the pupil and that rapid increments in light flux on

the retina cause a brisk transient constriction of the pupil that is often described as the *dynamic PLR response*. The tacit assumption that a single neural pathway mediates both of these functions has been questioned in previous studies, largely because neural mechanisms with different spatial and temporal properties would ideally be needed to serve these two functions. It is of interest to establish whether the PLR response involves more than one component and to explain why, under some conditions, this response is either absent or significantly reduced in patients with damage to the geniculostriate projection or the visual cortex (Alexandridis et al., 1979; Barbur et al., 1988; Cibis et al., 1975; Harms, 1951; Kardon, 1992).

Pupil responses to other stimulus attributes such as the onset of luminance flicker (Troelstra, 1968), spatially structured patterns (Slooter and van Norren, 1980; Ukai, 1985), coherent motion (Barbur et al., 1991; Sahraie and Barbur, 1997), or colored stimuli (Young and Alpern, 1980; Young et al., 1993) have also been reported, but the mechanisms and neural pathways involved in mediating such responses remain largely unknown. The possible involvement of the PLR and the near-reflex pathways in any of these responses has not always been ruled out. It remains of great interest to establish the extent to which such responses involve the geniculostriate projection and require the processing of specific stimulus attributes in extrastriate visual cortical areas. Finally, if any of these stimulus-specific pupil responses are mediated through central inhibition of the pupillomotor system, as demonstrated in animal studies (Koss et al., 1984; Loewenfeld, 1958; Loewy et al., 1973; Szabadi and Bradshaw, 1996), it is of interest to know how and where these inhibitory signals are integrated into the efferent pupil pathways. This chapter reports the results of recent pupil studies that have addressed some of these questions. These studies involved measurements of the pupil's response to visual stimuli that favor the processing of specific stimulus attributes, both in normal subjects and in patients with selective loss of function as a result of damaged or abnormal visual pathways. The patients studied included dichromats who cannot discriminate certain colors as a result of deficiency in one class of cone receptor, patients with cerebral achromatopsia who cannot see color as a result of lesions to

the ventromedial extrastriate visual cortical areas, patients who are clinically blind in one hemifield as a result of unilateral damage to the primary visual cortex, and patients with selective damage to the pretectal region of the midbrain.

The anatomy of the iris and related disorders, pharmacological aspects of pupil function evaluation, and clinical examination techniques have been discussed in a number of excellent recent reviews (Kardon, 1998; Thompson and Miller, 1998; Wilhelm, 1994), and will not be covered in this chapter.

Pupil pathways

The iris's movement and hence its image, the pupil of the eye, is controlled by the action of two antagonistic muscles, the sphincter and the dilator. Activation of the sphincter of the iris causes the pupil to constrict (i.e., miosis). This constriction is largely under parasympathetic control, while the dilator muscle receives mostly sympathetic innervation and causes the pupil to dilate (i.e., mydriasis). As with any aperture in a lens system, the size of the iris determines the amount of light that is captured by the system and, in the case of the eye, the level of retinal illuminance. In addition, the pupil controls the aberrations and the depth of field of the eye. The parasympathetic pathway is understood better and involves the Edinger-Westphal (EW) nucleus, the ciliary ganglion, and the short ciliary nerves (Kardon, 1998). The firing rate of pupilloconstrictor neurons in the EW nucleus is high, even in the absence of external influences (Sillito and Zbrozyna, 1973). In this respect, the pupilloconstrictor neurons in the EW nucleus act as a signal generator whose output is modulated by a number of inputs, the major one being the afferent projection from the retina via the olivary pretectal nucleus (OPN) of the midbrain (Gamlin et al., 1997; Pierson and Carpenter, 1974). The strength of these modulating inputs can, in turn, be determined by a number of other factors that may involve the cortical processing of specific stimulus attributes.

Strong inhibitory inputs to the EW nucleus from other areas of the brain have also been reported (Smith et al., 1970). The inhibition of the parasympathetic system may involve at least two pathways, a noradrenergic pathway from the nucleus coeruleus to the EW complex (Breen et al., 1983; Koss et al., 1984; Loewy et al., 1973) and a second indirect pathway from A1/A5 nuclei in the brainstem via the hypothalamus (Koss and Wang, 1972; Loewenfeld, 1958; Szabadi and Bradshaw, 1996). Signal changes in these inhibitory pathways can be used to explain a number of other pupil-related observations such as the constriction of the pupil during sleep or anesthesia (Larson et al., 1996), the gradual decrease in pupil size with age (Loewenfeld, 1972), and the slow oscillations of the pupil observed during periods of sleepiness (Lowenstein et al., 1963; Wilhelm et al., 1999).

PLR response

THE STEADY-STATE COMPONENT The accepted clinical view of the pupil's response to light is that the ambient light level largely determines the steady-state size of the pupil and that rapid increments in light flux on the retina cause a brisk constriction of the pupil (Fig. 39.1). The pupil's response to changes in ambient illumination is best served by neural mechanisms that respond to overall light flux changes, cover a large dynamic range, and exhibit large spatial summation.

THE TRANSIENT COMPONENT The transient constriction of the pupil in response to flashes of light requires neurons with different properties, since the steady-state signal is largely discarded and the response reflects only novel changes in luminance contrast (LC), not the absolute light adaptation level. The ideal properties of such neurons include limited spatial summation, bandpass temporal response characteristics, and high contrast gain. A light stimulus presented to the eye is likely to trigger both components, but the relative contribution each component makes to the constriction of the pupil will depend on the size of the stimulus, its luminance contrast, onset temporal characteristics, and location in the visual field. The sustained component also makes a contribution to the transient constriction of the pupil since the neurons involved respond to a range of temporal frequencies in addition to steady light. In other words, these neurons exhibit low-pass temporal response characteristics. The relative contribution of the sustained component is likely to be small, given the range of ambient illumination to which the eye responds. When the stimulus is large and of high LC, the response of the pupil can be dominated entirely by the sustained component because of the limited spatial summation and early contrast response saturation of the transient component. The temporal properties of both transient and sustained neurons are largely determined by the level of light adaptation of the retina. This suggests that under conditions of steady light adaptation, the pupil onset response latency, defined as the time from the onset of the stimulus to the onset of pupil constriction, should not depend on its response amplitude. Visual inspection of the pupil response traces shown in Figure 39.1A would suggest otherwise, but this is largely because the onset constriction is more gradual when the response amplitude is small. When scaled for equal amplitude, as shown in Figure 39.1B, the graphs can be fitted with a single template, and this suggests that the onset time of the response is approximately the same for all traces, independent of initial amplitude.

In spite of such observations and other electrophysiological (Sillito and Zbrozyna, 1973) and psychophysical findings (Young and Kennish, 1993; Young et al., 1993) that demonstrate the involvement of both sustained and transient

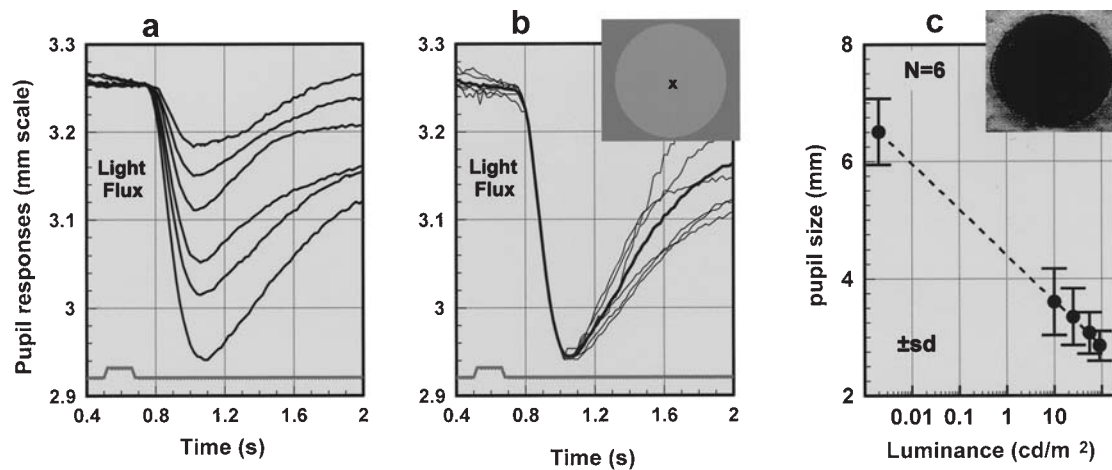


FIGURE 39.1. Examples of dynamic PLR responses (*A*) to flashes of increasing LC, that is, $\delta L/L_b = 0.3, 0.6, 0.9, 1.2, 1.5$, and 2.15 (see stimulus inset in *B*). The dark gray traces show the timing and duration of the flash. The subject was light adapted to a uniform background field (26×21 deg) of luminance 24 cd/m^2 . The test stimulus was a disc of 6 degrees in diameter, and each trace represents the average of 36 to 48 measurements. *B*, The same data scaled for equal pupil constriction amplitude to indicate the

absence of significant differences in pupil response latency. *C*, The steady-state size of the pupil varies as a function of screen luminance. The subjects viewed a uniform screen subtending 33×26 degrees of visual angle. Continuous records of pupil size (of 4 second duration at a sampling rate of 50 Hz) were taken and averaged at each light level to obtain an estimate of mean pupil size. The data points show the mean values for six normal subjects and the corresponding intersubject variation.

neurons in the neural control of pupilloconstrictor activity, the PLR response continues to be associated with a single afferent projection to the midbrain. In this chapter we describe findings from a number of diverse experiments that support the two-component hypothesis of the light reflex response.

EVIDENCE FROM DYNAMIC NOISE EXPERIMENTS Background perturbation techniques have often been used to reduce selectively the sensitivity of some visual mechanisms and hence the contribution these mechanisms can make to the detection of a subsequent test stimulus (Barbur and Ruddock, 1980; Stiles, 1978). We have extended this approach to study pupil response components by presenting a flash of light onto a textured background made up of discrete checks that vary randomly in luminance as a function of time (see inset to Fig. 39. 2). The luminance of each check is allowed to vary with equal probability every 40 to 80 msec in a range specified as a percentage of background luminance. For example, for a background luminance of 24 cd/m^2 and an LC noise amplitude of $\pm 25\%$, the luminance of each check could have any value with equal probability in the range 18 to 30 cd/m^2 . The space-averaged luminance of the textured background remains unchanged throughout the test and equal to that of the uniform background field. The results show that the presence of dynamic LC noise causes the PLR response amplitude to decrease systematically, although this reduction starts to asymptote when the LC noise amplitude exceeds $\sim 30\%$ contrast. Interestingly, a static structured background had no effect on the amplitude

of the PLR response for any of the LC noise amplitudes investigated. Examples of such data are shown in Figure 39.2C. The reduction in pupil response amplitude observed when the spatial distribution of LC noise changes every 50 to 80 msec is likely to reflect the masking of a transient pupil response component.

A further experiment was carried out in a subject with homonymous hemianopia caused by unilateral accidental damage to his left hemisphere (see the magnetic resonance imaging [MRI] scan in Fig. 39.3). Although clinically blind in his right hemifield, the subject can make use of visual information when tested in a number of different ways (Barbur et al., 1980, 1994b). In addition, the subject exhibits *blindsight* (see Chapter 40). The subject's pupil responses measured with the stimulus presented foveally or in the sighted hemifield are normal, but when the stimulus is restricted to his blind hemifield, a number of differences emerge (Barbur et al., 1980, 1993, 1998a; Weiskrantz et al., 1999). In this chapter we report results from a number of experiments that compared pupil responses to blind and sighted hemifield stimulation in this subject. PLR responses in the blind hemifield are in general reduced significantly by comparison to the sighted field. Figure 39.3 shows that the dynamic LC noise has little or no effect when only the blind hemifield is involved (Fig. 39.3B), although a normal response pattern is obtained in the sighted hemifield (Fig. 39.3A). These findings suggest that some aspect of the transient component of the PLR response requires the normal functioning of the geniculostriate projection and primary visual cortex.

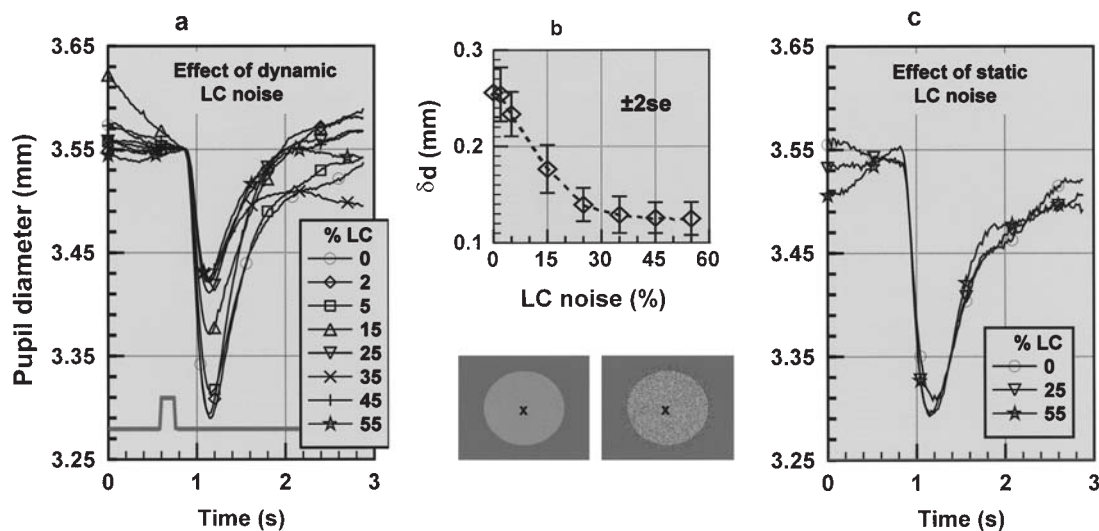


FIGURE 39.2. Effect of dynamic LC noise on pupil response amplitude to a flash of constant LC ($SL/Lb = 0.5$) presented on a uniform background field of luminance 24 cd/m^2 . An array of square checks covered an area slightly larger than the central disc stimulus (see inset). The luminance of each check was selected randomly, with equal probability within a range specified as a percentage of background luminance. This range determined the amplitude of LC noise. The spatial distribution of check luminances varied randomly every 40 to 80 msec so as to generate dynamic LC noise of mean luminance equal to that of the uniform background. Zero amplitude corresponds to a uniform background

field with no modulation (i.e., the luminance of each check remained unchanged and equal to that of the background field). The test flash generated the same light flux increment irrespective of ongoing LC noise amplitude. The peak constriction of the pupil was extracted from each of the traces shown in part *A* and plotted as a function of background noise amplitude in part *B*. The results show that the ongoing dynamic LC noise causes a significant reduction in pupil response amplitude, in spite of the constant LC increment generated by the test flash. Interestingly, static background noise does not in any way affect the pupil response amplitude and is equivalent to a uniform field (*C*).

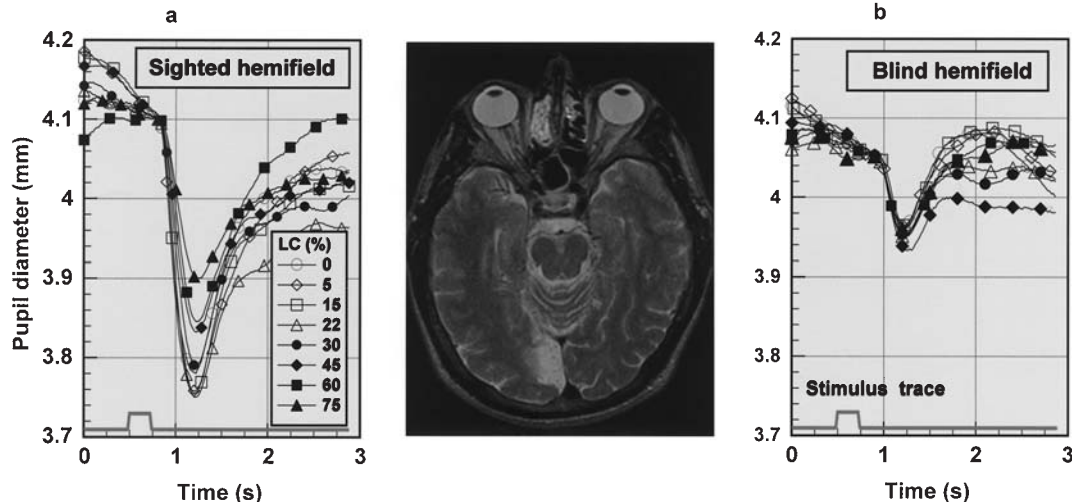


FIGURE 39.3. Comparison of sighted and blind hemifield pupil responses in a subject with homonymous hemianopia caused by damage to the left hemisphere. The MRI scan reveals significant damage to the left primary visual cortex with sparing at the pole (Barbur et al., 1993). The subject is clinically blind in the right hemifield but exhibits small (~ 3.5 degree) macular sparing (Barbur

et al., 1980). The pupil responses measured with the stimulus presented in the blind hemifield (*A*) are either absent or significantly smaller than those elicited in the sighted hemifield. In contrast to the sighted hemifield (*B*), the dynamic LC noise has little or no effect on pupil response amplitude in the blind hemifield.

EVIDENCE FROM SUBJECTS WITH OPTIC NERVE DAMAGE We studied a 12-year-old male diagnosed with optic nerve drusen that affected mostly his left eye. This condition is associated with calcified deposits that protrude over the optic disc and can cause selective damage to optic nerve fibers. Less severe signs of optic disc drusen were also observed in the subject's right eye. Visual acuity was normal in both eyes. The clinical examination revealed signs of a possible left afferent pupil defect. We measured and compared pupil responses with the stimulus presented to each eye (Fig. 39.4).

The results reveal normal consensual responses with a large steady-state afferent pupil defect in the left eye (Fig. 39.4A). In spite of this afferent defect, the PLR response to a brief flash remains normal in the affected eye. This finding is consistent with selective damage of the sustained component fibers of the pupil response, with little or no effect on the transient fibers. Figure 39.4B shows pupil responses in each eye, with and without dynamic LC noise. The results show that the normal transient pupil response in the left eye (i.e., the affected eye) is eliminated almost completely by the presence of dynamic LC noise, but not so in the relatively normal right eye. These findings are consistent with the two-component hypothesis for the control of the PLR response, with the sustained component fibers having been most affected in the subject's left eye.

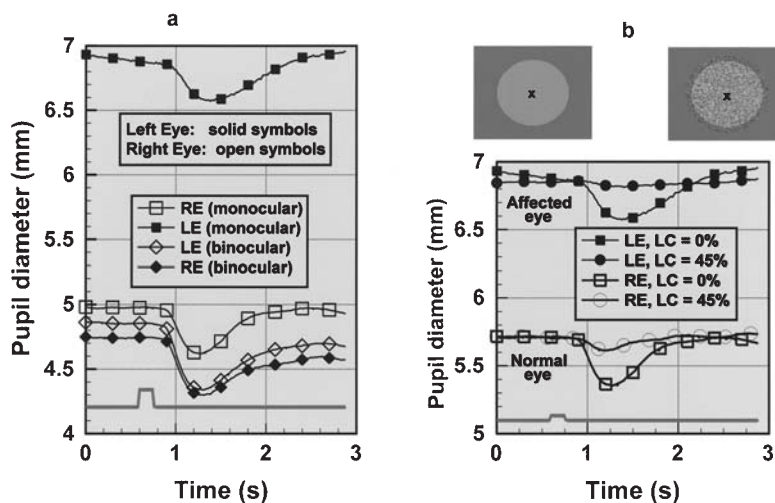


FIGURE 39.4. Example of a relative afferent pupil defect that affects selectively the steady state but not the dynamic PLR response. The subject was 12 years old, with normal visual acuity and chromatic and achromatic sensitivity in the right eye. Optic nerve drusen in the left eye caused loss of visual acuity and achromatic contrast sensitivity, but no loss of chromatic sensitivity. The subject viewed a uniform display subtending 33×26 degrees either binocularly or monocularly. The test stimulus was a central disc, 6 degrees in diameter, as shown in the inset. When the subject views

EVIDENCE FROM PUPIL PERIMETRY STUDIES This series of perimetry experiments involved sinusoidal and square-wave modulation of stimulus contrast (Fig. 39.5), and was driven by the need to minimize the time required for such measurements and to make possible the automatic extraction of pupil response parameters of interest.

Figure 39.6 shows typical response amplitudes and latencies elicited at each of the 24 possible stimulus locations. Discrete Fourier transform analysis of the pupil response trace provides a measure of response amplitude, latency, signal-to-noise ratio, and response nonlinearity (Fig. 39.5). A surprising finding of these studies was the disproportionately large pupil response amplitude that can be elicited with square-wave modulation. An identical stimulus configuration with sinusoidal modulation yields a much smaller pupil response amplitude (Fig. 39.6). We also measured the response of the pupil using sinusoidal modulation of amplitude equal to that of the fundamental frequency at each of the harmonic frequency components present in the square wave. The frequency range was restricted to 5 Hz, given the limited frequency response range of the pupil when tested with sinusoidally modulated stimuli (Bishop and Stark, 1965; Stark and Sherman, 1957). The results show that even under such conditions, the pupil response amplitude to square-wave modulation is significantly larger than the sum of the responses elicited by all of its harmonic components.

the display with his left (affected) eye, the pupils are large in both eyes (~ 7 mm in diameter). The pupils are, however, normal (~ 4.7 mm) when the subject views the display either with the right (normal) eye or with both eyes. The dynamic PLR response is normal in each eye in spite of the large, steady-state, relative afferent pupil defect in the left eye (A). Another interesting observation is that the dynamic PLR response in the left eye is abolished almost completely by the addition of LC noise, but it is only reduced in the normal eye (B).

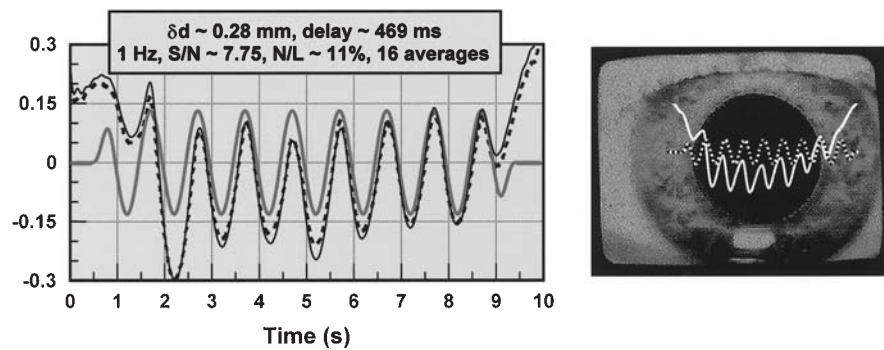


FIGURE 39.5. Example of the mean pupil response to sinusoidal modulation of stimulus luminance, as employed in our pupil perimetry program (see inset in Fig. 39.6). The stimulus trace (shown in gray) was shifted through 469 msec to match the direct (solid black line) and consensual (dotted line) pupil responses. In normal subjects, no significant differences can be measured between the direct and consensual responses. The modulation frequency was 1 Hz, and each stimulus consisted of 10 cycles (with Hanning weighting). Each of the 24 stimulus locations shown in Figure 39.6 was selected randomly and tested eight times to obtain

an averaged response. The signal power and phase shift at the modulation frequency, together with a measure of signal/noise ratio (S/N) and response nonlinearity (N/L), were computed from the discrete Fourier transform of each averaged trace. The N/L parameter was defined as the ratio of the summed signal power in all harmonics and the signal power at the stimulus modulation frequency. A more detailed description of the measurement technique and the analysis of results has been given elsewhere (Barbur et al., 1999).

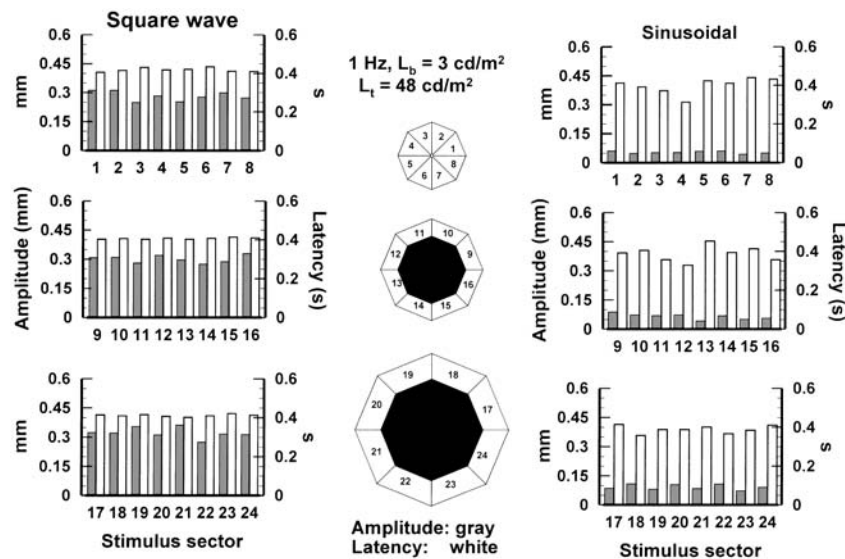


FIGURE 39.6. Example of pupil perimetry data measured with either sinusoidal (*right section*) or square-wave (*left section*) modulation of stimulus luminance. In both cases, the stimulus had a peak luminance of 48 cd/m^2 and was presented against a uniform background of luminance 3 cd/m^2 . The vertical bars indicate the measured pupil response amplitude and latency (as described in Fig. 39.5) for each stimulus location in the visual field (i.e., 1 to 24).

The startling observation is the difference in pupil response amplitude between sinusoidal and square-wave modulation for the same light flux change. The human pupil exhibits low-pass temporal response characteristics with a cutoff upper limit not much above 3 Hz. The much larger pupil response amplitudes elicited with square-wave modulation cannot be accounted for by the additional contribution from higher harmonics in the square wave.

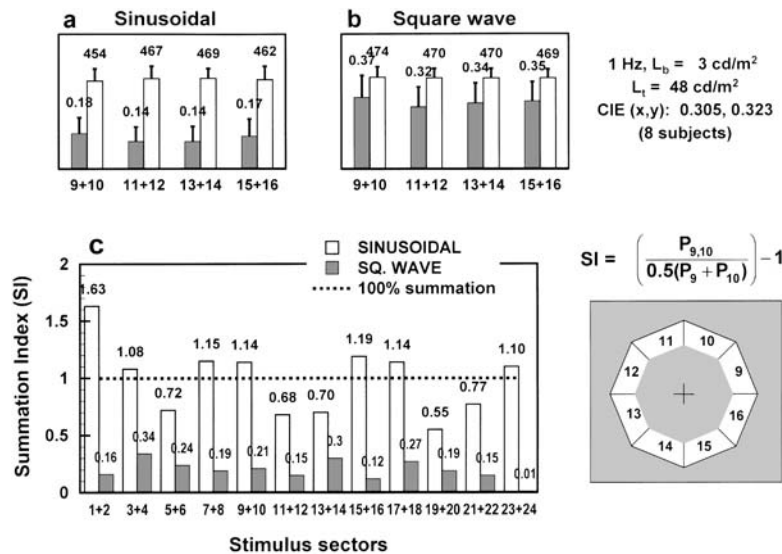


FIGURE 39.7. The spatial summation properties of the pupil response were investigated separately for both sinusoidal and square-wave modulation by comparing the response amplitudes elicited with single and paired stimuli. The top sections show averaged pupil response amplitudes and latencies for eight normal subjects for both sinusoidal and square-wave modulation using paired stimuli. Comparison of results obtained using single and paired stimuli suggests that sinusoidal modulation exhibits large spatial summation, while square-wave modulation does not. These observed differences in spatial summation can be quantified by defining an index of spatial summation that compares the response

amplitudes elicited by single and paired stimuli. Perfect summation of light flux increments over paired stimuli doubles the pupil response amplitude and results in a summation index (*SI*) of 1 (see the inset for definition of *SI*). The absence of spatial summation means no difference in pupil response amplitude between single and paired stimuli and corresponds to an *SI* index of zero. The lower section plots the computed *SI* values over the visual field for both sinusoidal and square-wave modulation. The results show large spatial summation for sinusoidal and little or no spatial summation for square-wave modulation.

In order to reduce the duration of a pupil perimetry test, we grouped together pairs of stimuli (Fig. 39.7). A comparison of pupil response amplitudes with single and double stimuli reveals the much greater spatial summation properties associated with sinusoidal modulation.

The difference in spatial summation index (Fig. 39.7C) for sinusoidal and square-wave modulation suggests that the two modes of presentation favor populations of neurons that have vastly different spatial summation properties. The relationship between stimulus contrast (or modulation depth) and pupil response amplitude was investigated in another study using a single foveal stimulus. The results obtained with sinusoidal and square-wave modulation are shown in Figure 39.8.

The pattern of response is again consistent with the two-component hypothesis. The transient component exhibits high-contrast gain but saturates above 30% to 40% contrast, while the sustained component continues to respond linearly up to the highest LC investigated. This finding is completely consistent with the results shown in Figure 39.2A. The initial rapid reduction in pupil response is amplitude when a test flash is added to a background of dynamic LC noise asymptotes to a constant value as the test flash exceeds 30% to 40% contrast.

PLR RESPONSES IN SUBJECTS WITH CORTICAL DAMAGE A number of pupil studies have demonstrated either reduced or completely absent PLR responses to small stimuli in patients with postgeniculate lesions (Barbur et al., 1988; Harms, 1951; Kardon et al., 1993). These findings are not consistent with a single afferent PLR projection that does not involve, at least indirectly, the geniculostriate pathway. Figure 39.9 shows examples of PLR response deficits in a hemianope. Stimuli of different sizes (Fig. 39.9A) were imaged separately in both the sighted and blind hemifields (see inset to Fig. 39.9). Figure 39.9B shows data for a number of luminance increments but for a fixed stimulus size selected in the middle of the range (i.e., 92 deg²).

The results show that the pupil responses in the blind hemifield are either absent or reduced in amplitude for stimuli of small size and LC. When large light flux increments are involved, the pupil responds well to both blind and sighted hemifield stimulation. The immediate hypothesis that could explain such observations requires more than one afferent pathway to control the pupil's response to light. The results suggest, contrary to classical belief, that the processing of signals along the geniculostriate pathway is normally required to generate a normal PLR response.

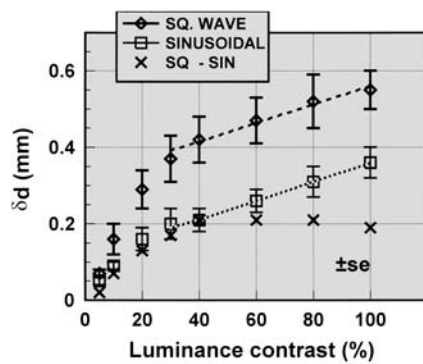


FIGURE 39.8. The data show the effect of LC (i.e., modulation depth) on pupil response amplitudes using sinusoidal and square-wave modulation. For this test the stimulus was a central disc 9 degrees in diameter presented against a uniform background field of luminance 12 cd/m^2 and angular subtense 26×21 degrees. The mean luminance of the test stimulus was 48 cd/m^2 , and this was modulated at 0.8 Hz . The differences in pupil response amplitude between square-wave and sinusoidal modulation suggest that two populations of neurons with different contrast response characteristics drive the PLR response. One population of neurons has high-contrast gain but saturates in response above 40% contrast. The second set of neurons continues to respond to higher LC modulation and may also exhibit larger spatial summation. This finding is completely consistent with the results shown in Figure 39.2A. The results of Figure 39.2 also show that the initial rapid reduction in pupil response amplitude when a test flash is added to a background of dynamic LC noise asymptotes to a constant value as the test flash exceeds 30% to 40% contrast.

Pupil responses to other stimulus attributes

PUPIL MOTION RESPONSE The sudden change from random to coherent motion of randomly distributed checks (see inset to Fig. 39.10) represents an ideal stimulus for studying pupil responses to moving stimuli. This stimulus ensures that there are no additional luminance transients at the onset of coherent motion that could trigger a pupil response. The sudden change from random to coherent motion requires only that the direction of displacement is the same for all checks in the array (Barbur et al., 1992).

The results yield long pupil onset response latencies, little or no dependence on stimulus contrast, and no response to motion offset (i.e., a change from coherent motion to random motion). A sudden angular change in the direction of coherent movement also triggers a transient constriction of the pupil, but only when the change of motion direction exceeds approximately ± 30 degrees (Sahraie and Barbur, 1997). These findings are not unexpected given the extensive motion selectivity and directional tuning of cortical neurons (Dubner and Zeki, 1971; Maunsell and Van Essen, 1983; Orban et al., 1981). Results of experiments that compared pupil responses to coherent motion restricted to the blind and sighted hemifields in a patient with hemianopia are shown in Figure 39.10B. The residual pupil motion response in the blind hemifield is small, but the response amplitude is statistically significant because of the large number of averages employed. These findings complement the results of other studies in this subject that demonstrate

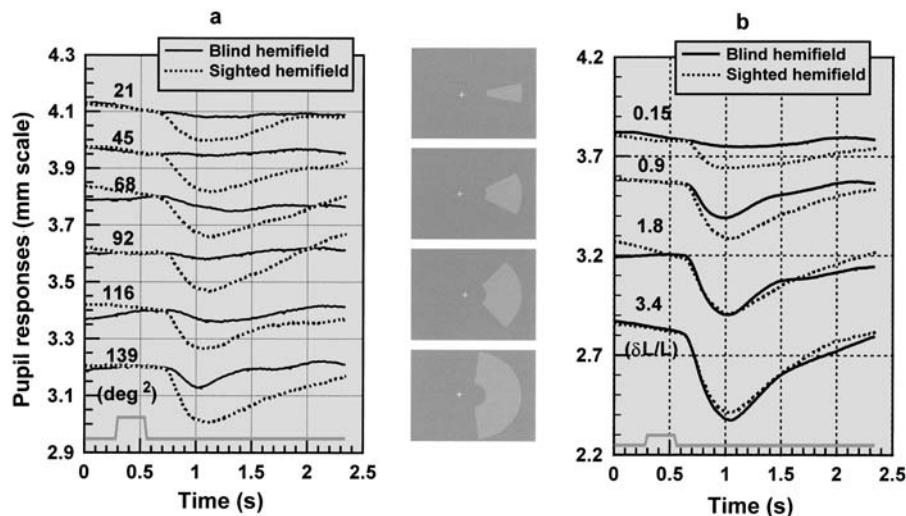


FIGURE 39.9. Comparison of PLR responses elicited by stimulating corresponding regions in the sighted and blind hemifields in a subject with homonymous hemianopia caused by damage to the left hemisphere (see the MRI scan in Fig. 39.3). The subject viewed a uniform background of angular subtense 33×26 degrees and luminance 24 cd/m^2 . The stimulus was a sector of an annulus that

varied systematically in either size (at a fixed contrast of 0.6, part A) or LC (for a fixed size of 92 deg^2 , part B). The results suggest that stimulation of the blind hemifield can, in general, yield highly abnormal PLR responses. When the stimulus causes large increments in light flux, there is little or no difference in PLR response between the blind and sighted hemifields.

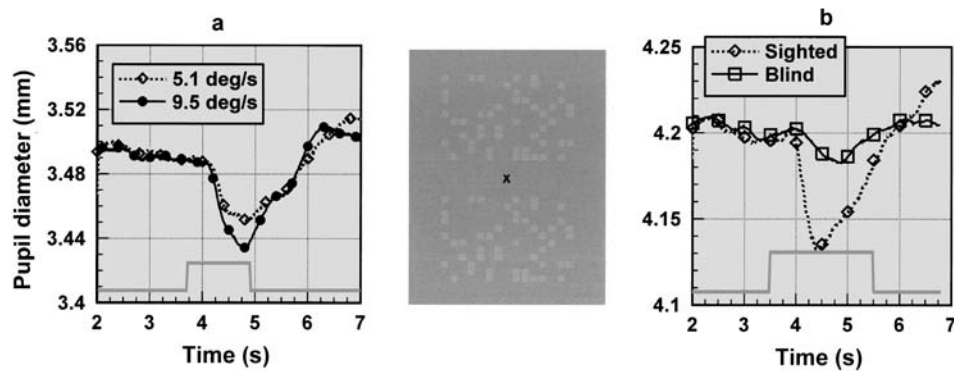


FIGURE 39.10. *A, B*, Examples of pupil responses to the onset of coherent motion. *A*, Data measured in a normal subject for two speeds of movement with the stimulus presented in the foveal region. *B*, Comparison of pupil responses to coherent motion with the stimulus restricted to either the sighted or the blind hemifield of a hemianope. The stimulus (see inset) consists of small, spatially random checks that change position randomly in a number of dif-

ferent directions every 80 msec. This generates dynamic random motion of background checks. During coherent motion, the spatiotemporal characteristics of the stimulus remain unchanged, but all the checks are displaced in the same direction. The pupil motion responses elicited with such stimuli exhibit long latency, some dependence on speed, and little or no dependence on check contrast.

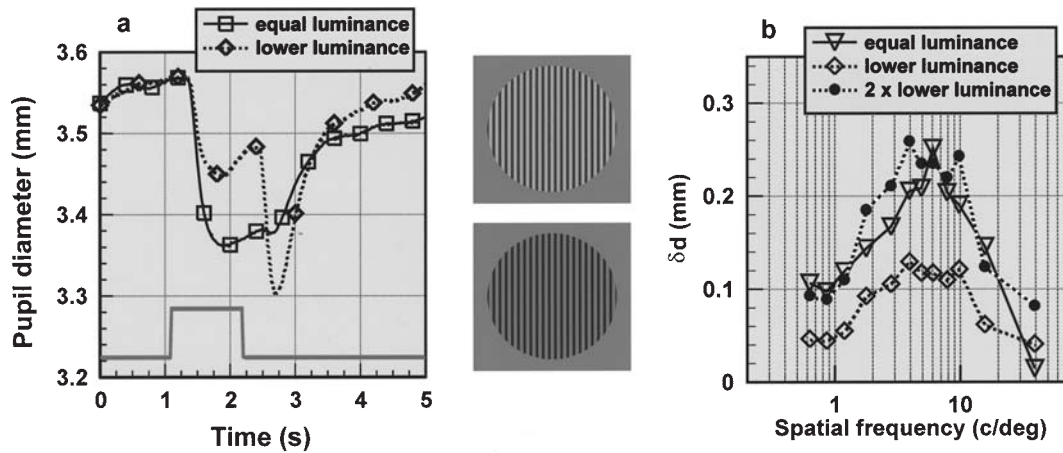


FIGURE 39.11. Pupil responses to grating stimuli as a function of spatial frequency. *A*, Typical pupil traces to equal and lower luminance gratings of 5 c/degree and contrast 0.8. The grating had a diameter of 5 degrees and was generated on a uniform background of luminance 34 cd/m². For the equal-luminance condition, the space-averaged luminance remained the same as that of the uniform background. For the lower-luminance condition, only the peak luminance in the grating remained the same as that of the uniform background field, and hence the space-averaged luminance over the grating was reduced during the stimulus to about 19 cd/m². Each trace represents the average of 64 measurements.

In spite of a net reduction in mean luminance, the pupil constricts to the onset of a lower-luminance grating. This is followed by a second constriction at grating offset. The amplitude of this second constriction is largely independent of spatial frequency and is therefore likely to reflect a PLR response caused by the luminance increment at grating offset. *B*, Spatial frequency dependence of the pupil grating response. Interestingly, the response to an equal-luminance grating that can be described as local increments and decrements in luminance is approximately double the response amplitude elicited with lower-luminance gratings (i.e., a grating defined only by luminance decrements).

residual vision (Barbur et al., 1980) and blindsight (Weiskrantz et al., 1995) for moving stimuli, and the corresponding activation of visual and nonvisual areas of the cortex in functional MRI (fMRI) studies when the moving stimuli were restricted to the subject's blind hemifield (Sahraie et al., 1997a, 1997b).

PUPIL GRATING RESPONSE We have employed two types of grating stimuli, as illustrated in Figure 39.11. *Equal-luminance*

gratings consist of both increments and decrements in local luminance. The mean luminance therefore remains unchanged and equal to that of the uniform background. *Lower-luminance* gratings consist only of dark bars, causing a net reduction in mean luminance over the grating. Both gratings cause an initial constriction of the pupil that varies systematically in amplitude with the spatial frequency of the grating (Fig. 39.11*B*). The pupil onset response latency is the same for both types of grating, but equal-luminance

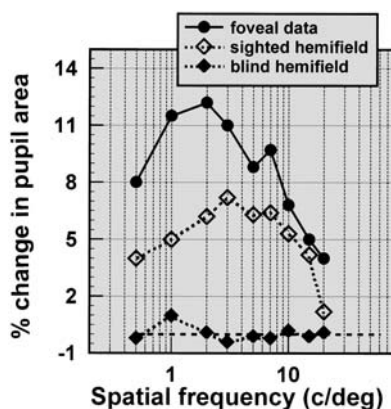


FIGURE 39.12. Comparison of pupil responses to equal-luminance gratings with the stimulus presented either foveally or to the sighted or the blind hemifield of a hemianope. The pupil responses in the blind hemifield are either absent or reduced significantly by comparison with those in the sighted field.

gratings generate a pupil constriction twice as large as lower-luminance gratings (Barbur, 1991). The offset of the grating causes a large constriction of the pupil, for lower-luminance gratings, that increases systematically with grating contrast. The large constriction at stimulus offset for lower-luminance gratings is likely to represent a light reflex response driven by the net increment in luminance when the grating stimulus is returned to the uniform background. Transient responses, but of greatly reduced amplitude, can also be observed at grating offset for equal-luminance gratings, but only in the low spatial frequency range.

Since both sustained and transient neurons are probably activated when a suprathreshold grating is presented to the eye, the small constriction of the pupil at grating offset is not unexpected, particularly in the low spatial frequency range. The doubling of pupil response amplitude when equal-luminance gratings are employed suggests that local increments and decrements in luminance trigger the activity of equal but separate populations of ON and OFF neurons (Fiorentini et al., 1990).

Figure 39.12 shows pupil grating response amplitudes with the stimulus presented foveally and in the sighted and blind hemifields of the hemianopic subject described earlier in this chapter. Although the absence of pupil responses in the blind hemifield is immediately obvious, the small residual response for a grating frequency of 1 c/deg correlates well with other findings from psychophysical studies (Barbur et al., 1994b) and has also been confirmed in a more extensive pupil study that employed larger grating stimuli (Weiskrantz et al., 1998).

PUPIL COLOR RESPONSE Pupil responses can also be elicited with chromatic isoluminant gratings. The gratings employed in these tests were presented in the foveal region and sub-

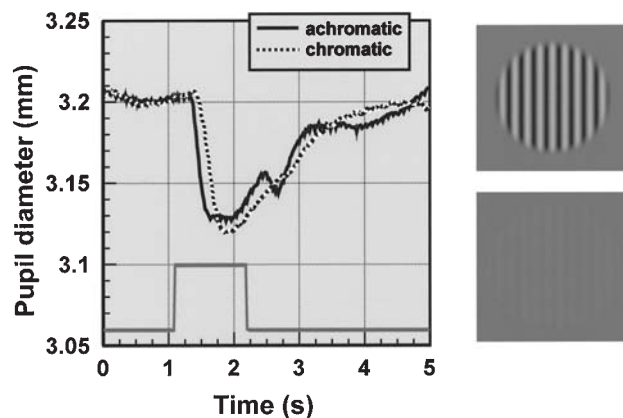


FIGURE 39.13. Comparison of pupil responses to luminance and color-defined gratings (see inset). Pupil responses to isoluminant, chromatic gratings are in general of longer latency, even when of equal response amplitude. (See color plate 24.)

tended a visual angle of some 5 degrees. Figure 39.13 shows two pupil response traces of approximately equal amplitude but significantly different onset latency measured in a normal trichromat. The graph also shows that the pupil responds to the offset of the achromatic, equal-luminance grating, but this response is absent in the case of the isoluminant, colored grating.

In order to avoid the difficulties of setting isoluminance, particularly when transient chromatic stimuli are employed, a new technique based on dynamic random LC masking was developed to isolate the use of chromatic signals (Barbur et al., 1994a). A two-dimensional array of LC-defined checks served as the stimulus template. Vertical bars defined by chromatic contrast (as shown in Fig. 39.14) were then presented to the eye for 0.5 second, buried in the ongoing dynamic LC noise (readers are invited to take a look at our website for a demonstration of such dynamic stimuli and the corresponding color vision tests: <http://www.city.ac.uk/avrc>).

The dynamic LC noise technique is very effective in that dichromats cannot detect the presence of the colored bars even for large chromatic saturations imposed by the phosphors of the display (Barbur et al., 1994a). Figure 39.14A shows the chromatic threshold detection ellipse for a normal trichromat, the color confusion bands for each class of dichromat, and the chromaticities of the test stimuli employed in pupil studies (i.e., crosses on the large dotted circle). We measured pupil color responses using this technique in normal trichromats and in a number of other subjects who do not see the colored pattern for a number of different reasons. The pupil constriction amplitude was computed from each pupil trace and plotted as a function of the direction of chromatic displacement in the (CIE) - (x_2, y) diagram. Each direction of chromatic displacement

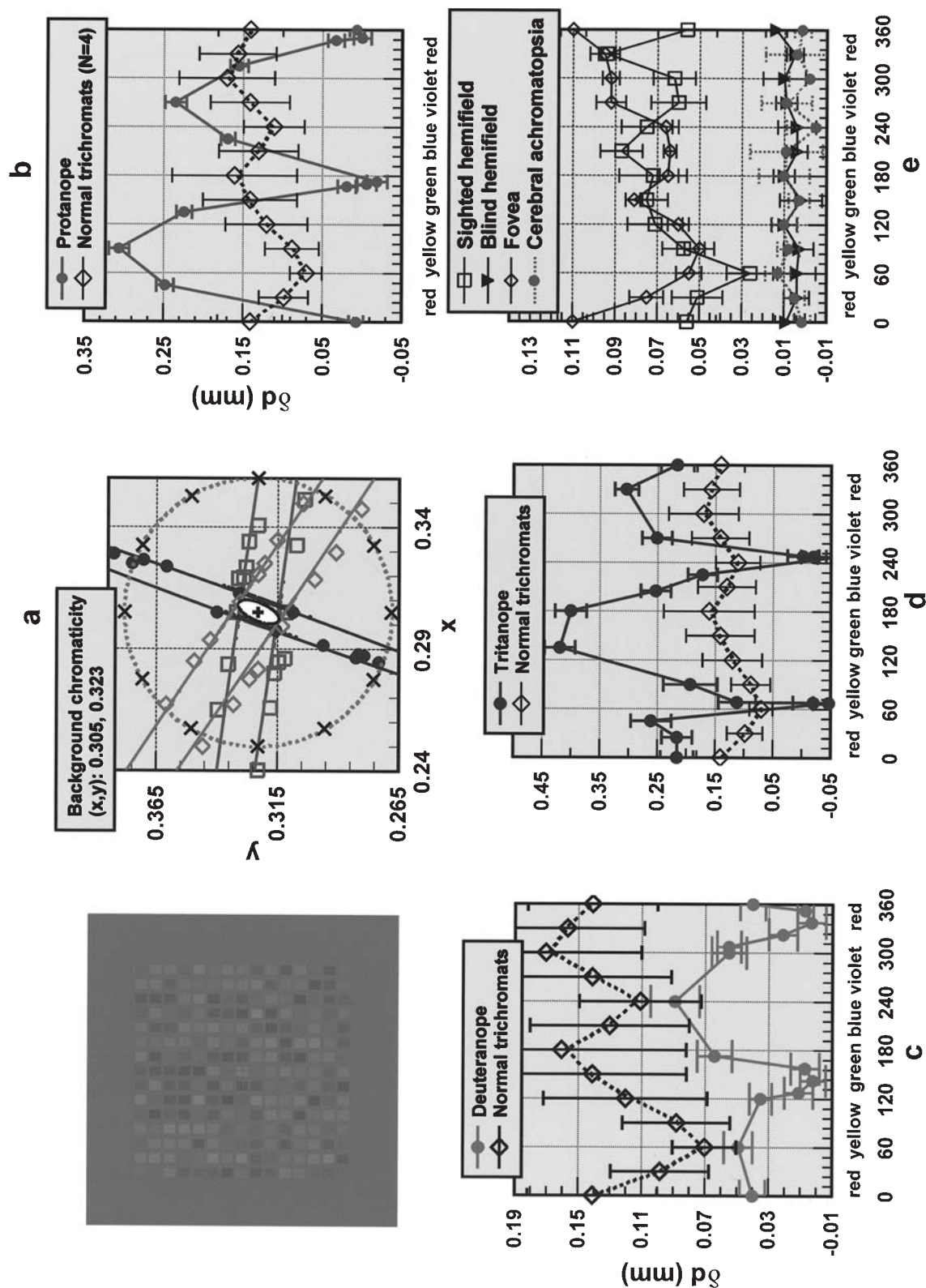


FIGURE 39.14. *A*, Chromatic threshold detection ellipse for a normal trichromat (solid black line) and the color confusion "bands" for each class of dichromat in the CIE $x-y$ chromaticity diagram. The stimulus consisted of vertically aligned colored checks (as shown in the inset) buried in a background of dynamic LC noise (Barbur et al., 1994a). The test stimulus subtended a visual angle of 5×5 degrees, and its mean luminance was 24 cd/m^2 . The stimulus was presented in the center of a uniform background of the same luminance and angular subtense 28×23 degrees. The dynamic LC masking technique isolates the use of chromatic signals even for the most saturated colors, limited only by the phosphors of the display. The dotted circle in *a* shows the suprathreshold chromatic saturation of the colors employed to elicit pupil responses. *B-D*, Pupil color responses in normal trichromats and in each class of dichromat. Pupil color responses in normal trichromats show considerable intersubject variability and exhibit the smallest amplitude for chromatic modulation along the blue-yellow axis. Pupil color responses are completely absent in each class of dichromat, but only for chromatic displacement directions along the corresponding color confusion lines. *E*, Significantly reduced or absent pupil color responses are shown when the stimulus is restricted to the blind hemifield of a hemianope. Similar results are also obtained in a subject with cerebral achromatopsia caused by lesions to the ventromedial prefrontal visual cortical areas. (See color plate 25.)

represents a different color on the spectrum locus. For example, an angle of zero degrees corresponds to a direction parallel to the abscissa and points toward the red region of the spectrum locus, while an angle of 65 degrees points toward the yellow region of the spectrum locus. Results for each class of dichromat are shown in Figure 39.14B–D. These data reveal the complete absence of pupil color responses for directions of chromatic displacement that match the corresponding color confusion lines in each class of dichromat. Figure 39.14E shows similar data measured in a hemianope and in a subject with cerebral achromatopsia. The small colored stimulus employed in this study failed to elicit significant pupil color responses in the hemianope's blind hemifield. Similar results were also obtained in the subject with cerebral achromatopsia with the stimulus presented foveally. The latter finding was surprising given that pupil responses to light flux increments and to luminance modulated gratings were normal in this subject.

Pupil responses in subjects with damage to the dorsal midbrain

PLR RESPONSE Damage to the pretectal region of the brain can cause selective disruption of the normal functioning of midbrain nuclei, and this can affect the various components of the pupil response (Wilhelm et al., 2002). The damage is usually caused by a compressive tumor in the region of the pineal gland and results in a pattern of response deficits, normally described as *Parinaud's syndrome*. These include abnormal PLR responses, vertical gaze palsy, and ocular vergence problems. The near reflex response is usually unaffected, and this observation suggests that the EW nucleus is not damaged in such lesions.

We have investigated how the two components of the PLR response and the observed pupil responses to gratings and colored stimuli are affected when the OPN and other nuclei in the pretectum are damaged. Figure 39.15A shows PLR responses in two subjects with Parinaud's syndrome as a function of the LC of the test flash (see inset). More extensive results, clinical reports, and MRI scans showing the extent of the midbrain damage in each subject have been reported elsewhere (Wilhelm et al., 2002). Comparison data averaged over six normal subjects are shown in Figure 39.15B. Unlike the normal subject group, both Parinaud's syndrome subjects show the almost complete absence of both transient and sustained PLR responses, with little or no dependence on stimulus contrast (Fig. 39.15C). A residual response of small amplitude and longer latency can be demonstrated in each subject by averaging several pupil response traces. These small pupil constrictions passed undetected in the clinical examination.

It is of interest to establish if the sympathetic innervation of the dilator muscle of the iris plays any role in the PLR

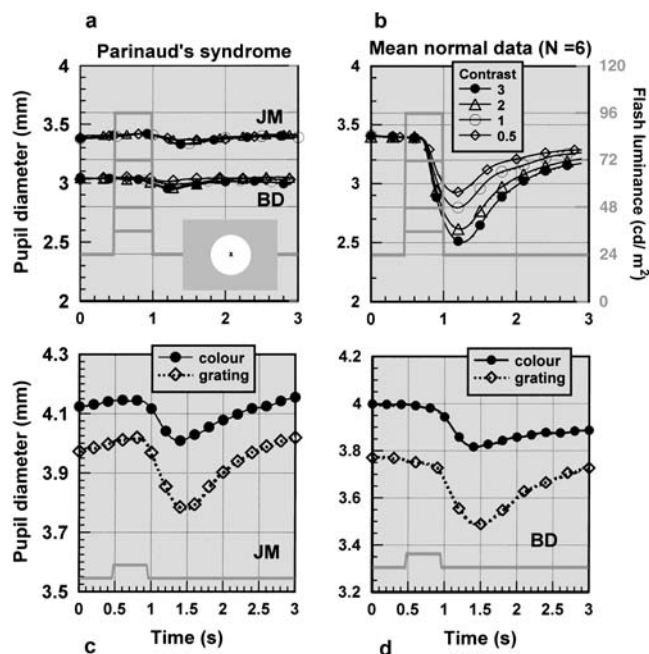


FIGURE 39.15. Pupil responses to light flux increments, isoluminant colors, and achromatic gratings of space-averaged luminance equal to that of the background field in two subjects with Parinaud's syndrome (J.M. and B.D.) caused by damage to the pretectal region of the midbrain. *A*, Examples of PLR responses elicited with a foveal stimulus (see inset) of progressively larger LC. *B*, Data obtained for the same stimuli in a group of six normal subjects. Unlike the normal subject group, the PLR response is largely absent in J.M. and B.D. The stimulus trace (shown in dark gray) shows both the duration and the luminance of the stimulus. Both J.M. and B.D. exhibit normal near-reflex responses when accommodating. The pupil color and pupil grating responses are also within the normal range (*C*, *D*).

response. Although one cannot be certain, this small, residual response to light flux increments may not necessarily involve any subcortical light-reflex projection. The sympathetic pathway involves more stages of neural processing originating in the hypothalamus, and its retinal afferent projections must rely, at least in part, on a direct cortical input (Alexandridis, 1995; Loewenfeld, 1999). A large increment in light flux on the retina could, at least in principle, initiate the weakening of sympathetic innervation to the dilator muscle of the iris in addition to facilitating the parasympathetic control of the sphincter. Such an arrangement could produce a more effective constriction of the pupil. The residual pupil responses observed in the two subjects with damage to pretectal nuclei are of very small amplitude but longer latencies (i.e. ~0.5 second compared to 0.24 second in the normal subject group). We know that pupil response latency shows little or no dependence on response amplitude when the subject is light adapted to a uniform background (Fig. 39.1B). This observation suggests that the small PLR responses that can be demonstrated in the two patients

with Parinaud's syndrome involve the action of mechanisms other than the direct midbrain pathway.

PUPIL COLOR AND PUPIL GRATING RESPONSES Pupil responses to stimulus attributes such as color, spatial structure, or movement must involve the activity of extrastriate visual areas since such responses are either absent or reduced significantly when only subcortical pathways are involved (Figs. 39.10, 39.12, and 39.14). In principle, the cortex can influence the pupil either through direct projections to the EW nucleus or indirectly via other nuclei in the pretectum such as the OPN, which is known to send afferents to the EW nucleus. The two subjects with Parinaud's syndrome have extensive damage to pretectal nuclei, and this causes a pattern of related deficits that includes the absence of a PLR response. It is therefore of great interest to establish whether an intact pretectum region is also needed to generate normal pupil color and grating responses.

The results of this study show that both subjects exhibit pupil grating and pupil color responses, as shown in Figure 39.15C, D. In addition, they exhibit normal slow oscillations of the pupil during sleepiness (Wilhelm et al., 2002). Such fluctuations have been attributed to instability in sympathetic inhibition of the pupillomotor nucleus (Lowenstein et al., 1963; Wilhelm et al., 1999).

Discussion

The diverse experimental findings presented in this chapter illustrate the complexity of the visual pathways involved in the control of the pupil response, and go a long way toward justifying why the pupil has been described by some as a beautiful example of a biological servomechanism for control of retinal illuminance and by others as the "apple of one's eye" or a "window to the soul." In spite of this great diversity of function, a unifying picture is beginning to emerge as the underlying circuitry that drives the PLR is unraveled. Although in the absence of precise anatomical and electrophysiological evidence any model for the control of the pupil response remains speculative, the following scheme accounts well for all the experimental observations reported in this chapter. It also explains the slow pupillary oscillations induced by sleepiness (Lowenstein et al., 1963; Yoss et al., 1978) and the large pupil constriction observed during deep anesthesia (Loewenfeld, 1999).

The principal component of this circuitry is the neural substrate in the pupillomotor nucleus where neurons generate a steady firing rate, even when no external inputs are involved (Sillito, 1968; Sillito and Zbrozyna, 1970, 1973). The amplitude of this signal generator determines the strength of the efferent innervation of the sphincter muscle of the iris and hence the size of the pupil. In the absence of external influences, the efferent signal to the iris is large, and

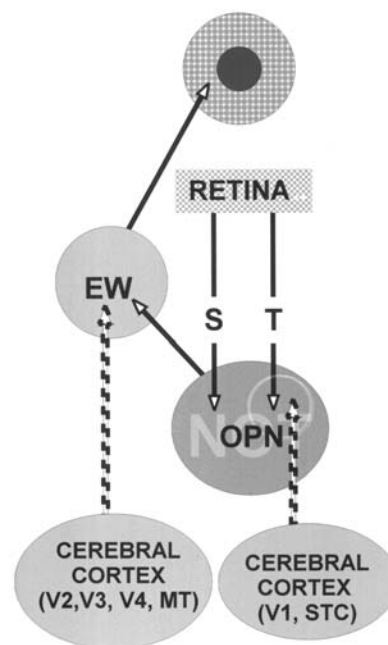


FIGURE 39.16. Schematic diagram of pupil pathways needed to explain the presence of different pupil response components in normal subjects and the absence of some components in patients with damaged primary visual cortex or pretectal nuclei. In this model, the EW nucleus acts as a signal generator whose amplitude is modulated by a number of other inputs. In the absence of such inputs the efferent signal to the retina is high, and this would normally result in miosis. A steady-state inhibitory projection from a number of cortical areas to the EW nucleus ensures that the pupil size remains normal by decreasing the strength of the efferent signal to the sphincter muscle of the iris. Perturbation of neural activity in extrastriate visual areas caused by sudden processing of stimulus attributes such as color, spatial structure, or motion can cause transient weakening of the steady-state inhibitory signal to the sphincter muscle, and this causes the pupil to constrict transiently in response to such stimuli. Changes in inhibition at the level of the EW nucleus may also explain the near-reflex response on accommodation and the irregular oscillations of the pupil caused by sleepiness. The PLR response is likely to involve two projections from the retina to the OPN. Both components respond to transient stimuli but differ in spatial summation, contrast gain, and temporal response characteristics. The sustained component exhibits large spatial summation, a low-pass temporal response, and low contrast gain. For convenience we label this as the steady-state component. The transient pathway exhibits poor spatial summation, a bandpass temporal response, and high contrast gain, properties characteristic of a transient component. The latter projection exhibits response saturation at large contrast (>40%), and its effectiveness is controlled by a direct projection from the cortex. This arrangement explains why patients with damaged primary visual cortex exhibit poor PLR responses to small, low-contrast stimuli but show no difference between the sighted and cortically blind hemifields when large, high-contrast stimuli are employed. This simplified scheme also explains why damage to pretectal nuclei, particularly in the OPN, as observed in patients with Parinaud's syndrome, can affect both the sustained and transient components of the PLR response.

this would normally cause the pupil to constrict. The normal size of the pupil observed under ordinary levels of ambient illumination is due largely to a strong steady-state cortical inhibition of the pupillomotor nucleus. Any transient decrease in this inhibition as a result of sudden perturbation of neural activity in the cortex will cause the pupil to constrict, only to return to its normal size once the steady-state inhibitory signal is restored. This is indicated in Figure 39.16 as a direct projection from extrastriate visual cortical areas to the EW nucleus. We know that the processing of stimulus color, structure, or motion can trigger small constrictions of the pupil, but these responses are either absent or reduced significantly when the normal processing of these signals is disrupted as a result of postgeniculate lesions.

The selective loss of pupil color response in patients with cerebral achromatopsia (Fig. 39.14*E*) provides strong evidence in support of this hypothesis. Central inhibition of the EW may therefore play a major role in the generation of stimulus-specific pupil responses. The exact cortical origin of this projection is not known, but extrastriate visual areas such as those listed in Figure 39.16 may be involved. All pupil responses mediated through cortical inhibition tend to have longer latencies by comparison with the PLR response (Barbur et al., 1992, 1998b; Tsujimura et al., 2001). During deep anesthesia and sleep, the weakening of central inhibition is sufficient to explain the observed miosis, while the slow oscillations of the pupil induced by sleepiness are consistent with intermittent fluctuations in the strength of central inhibition. Both sleepiness waves, the pupil near-reflex response, and pupil grating and color responses are preserved in Parinaud's syndrome, even when damage to the dorsal midbrain region abolishes the PLR response (Wilhelm et al., 2002). These observations suggest that inhibitory cortical signals are integrated into the pupillomotor pathway at the level of the EW nucleus. Some experimental observations suggest that this central inhibitory pathway may also play a part in the PLR response.

The findings presented in this chapter suggest that two distinct pathways, both based on detection of light flux changes, but one with large spatial summation and sustained responses and the other with more transient properties, high-contrast gain, and reduced spatial summation are involved in mediating the PLR response. We know that pupil responses to small, low-contrast stimuli are either absent or reduced significantly in amplitude in patients with postgeniculate lesions (Fig. 39.9*A, B*), but completely normal pupil responses can be elicited in the same patients when large, high-contrast stimuli that favor the sustained component are employed. These observations suggest that the transient PLR component may involve a direct projection to the striate cortex and the integration of this signal into the pupil pathway via the central inhibitory projection to the EW nucleus. This hypothesis does, however, predict that in

addition to the pupil color and pupil grating responses, the transient PLR response component should be spared in patients with dorsal midbrain damage.

Contrary to this prediction, the experimental findings show that both the transient and sustained components of the PLR response are absent in Parinaud patients. The OPN receives projections from the retina, and in principle it can also receive a projection from the cortex. Any cortical component of the transient PLR response could therefore be integrated into the pupil pathway directly as an excitatory signal via the OPN. In the absence of this excitatory cortical component in patients with postgeniculate damage, the afferent retinal projection to the OPN becomes less effective, and this can explain the abnormal pattern of PLR responses observed in hemianopes. The cortex can therefore exercise some influence on the pupil response at the level of the EW nucleus through a sympathetic inhibitory projection and also through an excitatory input to the OPN.

Conclusions

The study of the pupil brings together some of the best aspects of the physiology and the psychology of vision. The normal functioning of geniculostriate and midbrain projections, the detection of light flux changes, the processing of specific stimulus attributes, and the level of anxiety, excitement, and conscious awareness of the subject are among the many parameters that can be reflected in the pupil. Recent advances in visual psychophysics and pupil measurement techniques have rekindled much of the centuries'-old fascination with the pupil. We now know that the pupil's pathways are wired up to respond specifically to different features of a visual stimulus. We can use the pupil to diagnose reliably color deficiency, to measure visual acuity, and to reveal levels of visual processing in the cortex by measuring differences in response latency. We can also reveal the existence of two components in the PLR response. The latter finding can be used to explain unusual PLR response deficits when the damage affects one of these components selectively and also helps us understand better the limitations of pupil perimetry studies. Pupil color responses have been used to unravel the mechanisms for the generation of chromatic afterimages (Barbur et al., 1999), and screening programs based on pupil responses have now been developed to study residual vision and blindsight in patients with postgeniculate damage (Sahraie et al., 2002). The development of dynamic morphing of images in pupil studies makes it possible to manipulate the meaningful content of an image and to investigate the presence of accompanying pupil signals when no light responses are involved. Such techniques will extend the use of the pupil to other studies and, in particular, the measurement of response components that contribute to the sympathetic innervation of the iris that have so far remained

relatively unexplored. In summary, the pupil has become an important tool that can yield useful information in basic neuroscience and clinical research. Although the pupil may not be “the apple of one’s eye” or a true “window to the soul,” the analysis of its response components may provide a “window to the brain.”

Acknowledgments

I would like to thank J. A. Harlow and A. Goodbody for their help with software development and equipment construction and the many subjects who took part in these studies. I am also grateful to D. Edgar, L. Weiskrantz, S. Moro, G. Ruskell, and B. Wilhelm for their critical comments on the manuscript. The studies reported here were carried out with support from the Wellcome Trust and the Medical Research Council of Great Britain.

REFERENCES

- Alexandridis, E., 1995. *The Pupil*, New York: Springer-Verlag.
- Alexandridis, E., H. Krastel, and R. Reuther, 1979. Pupillenreflexstörungen bei Läsionen der oberen Sehbahn, *Albrecht von Graefes Arch. Klin. Ophthalmol.*, 209:199–208.
- Barbur, J. L., 1991. Pupillary responses to grating stimuli, *J. Psychophysiol.*, 5:259–263.
- Barbur, J. L., A. J. Harlow, and G. T. Plant, 1994a. Insights into the different exploits of colour in the visual cortex, *Proc. R. Soc. Lond. B*, 258:327–334.
- Barbur, J. L., A. J. Harlow, and A. Sahraie, 1992. Pupillary responses to stimulus structure, colour and movement, *Ophthalm. Physiol. Opt.*, 12:137–141.
- Barbur, J. L., A. J. Harlow, and L. Weiskrantz, 1994b. Spatial and temporal response properties of residual vision in a case of hemianopia, *Phil. Trans. R. Soc. Lond. B*, 343:157–166.
- Barbur, J. L., M. S. Keenleyside, and W. D. Thomson, 1988. *Investigation of Central Visual Processing by Means of Pupillometry*, Manchester, UK: Northern Eye Institute, pp. 431–451.
- Barbur, J. L., and K. H. Ruddock, 1980. Spatial characteristics of movement detection mechanisms in human vision. I: achromatic vision, *Biol. Cybern.*, 37:77–92.
- Barbur, J. L., K. H. Ruddock, and V. A. Waterfield, 1980. Human visual responses in the absence of the geniculocalcarine projection, *Brain*, 103:905–928.
- Barbur, J. L., A. Sahraie, A. Simmons, L. Weiskrantz, and S. C. Williams, 1998a. Residual processing of chromatic signals in the absence of a geniculostriate projection, *Vis. Res.*, 38:3447–3453.
- Barbur, J. L., A. Sahraie, and L. Weiskrantz, 1991. The processing of movement information is reflected in the pupil response, *Perception*, 20:76.
- Barbur, J. L., J. D. Watson, R. S. Frackowiak, and S. Zeki, 1993. Conscious visual perception without V1, *Brain*, 116:1293–1302.
- Barbur, J. L., L. Weiskrantz, and J. A. Harlow, 1999. The unseen color aftereffect of an unseen stimulus: insight from blindsight into mechanisms of color afterimages, *Proc. Natl. Acad. Sci. USA*, 96:11637–11641.
- Barbur, J. L., J. Wolf, and P. Lennie, 1998b. Visual processing levels revealed by response latencies to changes in different visual attributes, *Proc. R. Soc. Lond. B. Biol. Sci.*, 265:2321–2325.
- Bishop, L. G., and L. Stark, 1965. Pupillary responses in the screech owl, *Otus asio*, *Science*, 148:1750–1752.
- Breen, L. A., R. M. Burde, and A. D. Loewy, 1983. Brainstem connections to the Edinger-Westphal nucleus of the cat: a retrograde tracer study, *Brain Res.*, 261:303–306.
- Brindley, G. S., P. C. Gautier-Smith, and W. Lewin, 1969. Cortical blindness and the functions of the non-geniculate fibres of the optic tracts, *J. Neurol. Neurosurg. Psychiatry*, 32:259–264.
- Cibis, G. W., E. C. Campos, and E. Aulhorn, 1975. Pupillary hemiopia in supragenulate lesions, *Arch. Ophthalmol.*, 93:1322–1327.
- Dubner, R., and S. M. Zeki, 1971. Response properties and receptive fields in an anatomically defined area of the superior temporal sulcus in the monkey, *Brain Res.*, 35:528–532.
- Fiorentini, A., G. Baumgartner, S. Magnussen, P. H. Schiller, and J. P. Thomas, 1990. The perception of brightness and darkness—relations to neuronal receptive fields, in *Visual Perception—The Neurophysiological Foundations* (L. Spillman and J. Werner, eds.), London: Academic Press, pp. 129–161.
- Gamlin, P. D. R., H. Zhang, and R. J. Clarke, 1997. Luminance neurons in the pretectal olivary nucleus mediate the pupillary light reflex in the rhesus monkey, *Exp. Brain Res.*, 106:177–180.
- Harms, H., 1951. Hemianopische Pupillenstarre, *Klin. Mbl. Augenheilk.*, 118:133–147.
- Kardon, R. H., 1992. Pupil perimetry. Editorial review, *Curr. Opin. Ophthalmol.*, 3:565–570.
- Kardon, R. H., 1998. Anatomy and physiology of the pupil, in *Clinical Neuro-ophthalmology* (D. J. Walsh and W. F. Hoyt, eds.), Baltimore: Williams & Wilkins.
- Kardon, R. H., C. L. Hauptert, and H. S. Thompson, 1993. The relationship between static perimetry and the relative afferent pupillary defect, *Am. J. Ophthalmol.*, 115:351–356.
- Koss, M. C., T. Cherezghiler, and A. Nomura, 1984. A CNS adrenergic inhibition of parasympathetic oculomotor tone, *J. Autonomic. Nerv. Syst.*, 10:55–68.
- Koss, M. C., and S. C. Wang, 1972. Brainstem loci for sympathetic activation of the nictitating membrane and pupil in the cat, *Am. J. Physiol.*, 224:900–905.
- Larson, M. D., F. Tayefeh, D. I. Sessler, M. Daniel, and M. Noorani, 1996. Sympathetic nervous system does not mediate reflex pupillary dilation during desflurane anesthesia, *Anesthesiology*, 85:748–754.
- Loewenfeld, I. E., 1958. Mechanism of reflex dilation of the pupil. Historical review and experimental analysis, *Doc. Ophthalmol.*, 12:185–448.
- Loewenfeld, I. E., 1972. Pupillary changes related to age, in *Topics in Neuro-ophthalmology* (H. S. Thompson, R. Daroff, L. Frisén, J. S. Glaser, and M. D. Sanders, eds.), Baltimore: Williams & Wilkins, pp. 124–150.
- Loewenfeld, I. E., 1999. *The Pupil: Anatomy, Physiology, and Clinical Applications*, Boston: Butterworth and Heinemann.
- Loewy, A. D., J. C. Arango, and W. L. Kerr, 1973. Pupillodilator pathways in the brain stem of the cat: anatomical and electrophysiological identification of a central autonomic pathway, *Brain Res.*, 60:65–91.
- Lowenstein, O., R. Feinberg, and I. E. Loewenfeld, 1963. Pupillary movements during acute and chronic fatigue. A new test for the objective evaluation of tiredness, *Invest. Ophthalmol.*, 2:138–157.
- Maunsell, J. H. R., and D. C. Van Essen, 1983. Functional properties of neurons in middle temporal (MT) visual area of the macaque monkey. I. Selectivity for stimulus direction, speed and orientation, *J. Neurophysiol.*, 49:1127–1147.

- Orban, G. A., H. Kennedy, and H. Maes, 1981. Response to movement of neurones in areas 17 and 18 of the cat: velocity sensitivity, *J. Neurophysiol.*, 45:1043–1048.
- Pierson, R. J., and M. B. Carpenter, 1974. Anatomical analysis of pupillary reflex pathways in the rhesus monkey, *J. Comp. Neurol.*, 158:121–144.
- Sahraie, A., and J. L. Barbur, 1997. Pupil response triggered by the onset of coherent motion, *Graefes. Arch. Clin. Exp. Ophthalmol.*, 235:494–500.
- Sahraie, A., L. Weiskrantz, J. L. Barbur, A. Simmons, S. C. Williams, and M. J. Brammer, 1997a. Pattern of neuronal activity associated with conscious and unconscious processing of visual signals, *Proc. Natl. Acad. Sci. USA*, 94:9406–9411.
- Sahraie, A., L. Weiskrantz, J. L. Barbur, A. Simmons, and S. C. R. Williams, 1997b. Motion processing with and without awareness: pattern of increased brain activity using fMRI, *Invest. Ophthalmol. Vis. Sci.*, 37:223.
- Sahraie, A., L. Weiskrantz, C. T. Treveltham, R. Cruce, and A. D. Murray, 2002. Psychophysical and pupillometric studies of spatial channels of visual processing in blindsight, *Exp. Brain Res.*, 143:249–256.
- Sillito, A. M., 1968. The location and activity of pupilloconstrictor neurons in the mid-brain of the cat, *J. Physiol.*, 194:39–40.
- Sillito, A. M., and A. W. Zbrozyna, 1970. The activity characteristics of the preganglionic pupilloconstrictor neurones, *J. Physiol. (Lond.)*, 211:769–779.
- Sillito, A. M., and A. W. Zbrozyna, 1973. The neural control of pupilloconstrictor activity, in *Normal and Disturbed Pupillary Movements* (E. Dodt and K. E. Schrader, eds.), Munich: Verlag J. F. Bergmann, pp. 30–35.
- Slooter, J., and D. van Norren, 1980. Visual acuity measured with pupil responses to checkerboard stimuli, *Invest. Ophthalmol. Vis. Sci.*, 19:105–108.
- Smith, J. D., G. A. Masek, L. Y. Ichinose, T. Watanabe, and L. Stark, 1970. Single neuron activity in the pupillary system, *Brain Res.*, 24:219–234.
- Stark, L., and P. M. Sherman, 1957. A servoanalytic study of consensual pupil reflex to light, *J. Neurophysiol.*, 20:17–26.
- Stiles, W. S., 1978. *Increment Thresholds in the Analysis of Colour-Sensitive Mechanisms of Vision: Historical Retrospect and Comment on Recent Developments. Mechanisms of Colour Vision*, London: Academic Press.
- Szabadi, E., and C. M. Bradshaw, 1996. Autonomic pharmacology of α 2-adrenoceptors, *Psychopharmacology*, 10:6–18.
- Thompson, H., and R. F. Miller, 1998. Disorders of pupillary function, accommodation and lacrimation, in *Walsh & Hoyt's Clinical Neuro-ophthalmology* (N. R. Miller and N. J. Newman, eds.), Baltimore: Williams & Wilkins.
- Troelstra, A., 1968. Detection of time-varying light signals as measured by the pupillary response, *J. Opt. Soc. Am.*, 5:685–690.
- Tsujimura, S., J. S. Wolffsohn, and B. Gilmartin, 2001. A linear chromatic mechanism drives the pupillary response, *Proc. R. Soc. Lond. B*, 268:2203–2209.
- Ukai, K., 1985. Spatial pattern as a stimulus to the pupillary system, *J. Opt. Soc. Am.*, 2:1094–1100.
- Weiskrantz, L., J. L. Barbur, and A. Sahraie, 1995. Parameters affecting conscious versus unconscious visual discrimination with damage to the visual cortex (V1), *Proc. Natl. Acad. Sci. USA*, 92:6122–6126.
- Weiskrantz, L., A. Cowey, and J. L. Barbur, 1999. Differential pupillary constriction and awareness in the absence of striate cortex, *Brain*, 122:1533–1538.
- Weiskrantz, L., A. Cowey, and C. LeMare, 1998. Learning from the pupil: a spatial visual channel in the absence of V1 in monkey and human, *Brain*, 121:1065–1072.
- Wilhelm, B., H. Lüdtke, and H. Wilhelm, 1999. Spontaneous pupillary oscillations—An objective measure for the level of tonic central nervous activation, in *Pupillography Principles, Methods and Applications* (S. Kuhlmann and M. Böttcher, eds.), Zuckschwerdt: Verlag.
- Wilhelm, B., H. Wilhelm, S. Moro, and J. L. Barbur, 2002. Pupil response components—Studies in patients with Parinaud's syndrome, *Brain*, submitted.
- Wilhelm, H., 1994. Pupil examination and evaluation of pupillary disorders, *Neuro-ophthalmology*, 14:283–295.
- Yoss, R. E., N. J. Moyer, and R. W. Hollenhorst, 1978. Pupil size and spontaneous pupillary waves associated with alertness drowsiness and sleep, *Neurology*, 20:545–554.
- Young, R. S. L., and M. Alpern, 1980. Pupil responses to foveal exchange of monochromatic lights, *J. Opt. Soc. Am.*, 70:697–706.
- Young, R. S. L., B. C. Han, and P. Y. Wu, 1993. Transient and sustained components of the pupillary responses evoked by luminance and color, *Vis. Res.*, 33:437–446.
- Young, R. S. L., and J. Kennish, 1993. Transient and sustained components of the pupil response evoked by achromatic spatial patterns, *Vis. Res.*, 33:2239–2252.

40 Blindsight

LARRY WEISKRANTZ

BLINDSIGHT IS A CONDITION associated with damage to human primary visual cortex (V1), which causes blindness in corresponding parts of the affected visual fields, the field defect having a size and shape to be expected from the classical retinocortical maps (Holmes, 1918). The term *blindsight* first arose (Sanders et al., 1974; Weiskrantz et al., 1974; Weiskrantz, 1986) to describe the demonstration of good visual discriminative capacity in patients even though they denied having any visual experience in their blind fields (Pöppel et al., 1973; Weiskrantz, 1986; Weiskrantz et al., 1974; cf. an early report by Bard, 1905). The term enjoys sufficient usage to warrant a dictionary entry: “*Medicine*: a condition in which the sufferer responds to visual stimuli without consciously perceiving them” (*Oxford Concise Dictionary*).

The historical origin of the oxymoron stems from animal work, because it has been known for some decades that monkeys with V1 removal can nevertheless carry out some visual discriminations, which is not surprising because V1 is not the only target in the brain for signals originating in the retina, although it is the major one. There are several extra-striate pathways from the retina to subcortical targets that remain intact after damage to V1, from which information can have a very wide distribution to other cerebral areas, both cortical and subcortical (Benevento and Yoshida, 1981; Cowey and Stoerig, 1991; Fries, 1981; Hernandez-Gonzales and Reinoso-Suarez, 1994; Yukie and Iwai, 1981). In apparent contrast to the animal findings, human subjects with V1 damage are said to be *densely blind* in the corresponding part of the affected visual fields.

There are problems in relating animal to human evidence. In the human brain, it is rare for any lesion of the striate cortex to occur without damage to overlying tissue, including visual association cortex, whereas it is relatively easy for lesions restricted to striate cortex to be studied in experimental animals. Importantly, the effect of enlarging a striate cortex lesion in the monkey so as to include posterior association cortex is reported to lead to a significant reduction in residual visual capacity (Pasik and Pasik, 1971). In addition, evidence regarding these closely adjoining cortical regions suggests that they are functionally segregated and may have partially specialized capacities of a modular type, such as color, movement, spatial features, and form (cf. Cowey, 1985; Zeki, 1978, 1993). Therefore, the pattern of deficits can differ considerably from patient to patient even with relatively slight differences in the disposition of the

lesions, and experimental striate lesions in monkey and clinically occurring lesions in the human are typically not like-with-like.

But there is a deeper methodological difficulty in making monkey-human comparisons. Residual vision in the animal is studied by behavioral methods, typically by making reward contingent on a particular response choice between alternative stimuli, typically entailing a long series of trials. In contrast, human visual assessment is rarely carried out in such a fashion in the clinic. Instead, the negotiation is typically verbal: the patients are given a verbal instruction and are asked to report verbally whether they “see” the preselected stimulus, and to say what it is, as in acuity measurements made with a Snellen chart. Sometimes a response key is substituted for a verbal report, as in automatic devices for plotting fields, but the underlying assumptions are the same.

Blindsight evidence emerged when patients with field defects were tested atypically with animal-type forced-choice methodology—requiring them to make differential responses to the stimuli whether or not they verbally acknowledge seeing them. The history and some of the related background issues are discussed more fully elsewhere (Cowey and Stoerig, 1991, 1992; Stoerig and Cowey, 1997; Weiskrantz and Cowey, 1970; Weiskrantz et al., 1977; Weiskrantz, 1972, 1980, 1986, 1997, 2001b).

Categories of residual visual capacities

As in other areas of neuropsychology, single cases or small-group studies can be especially illuminating because they can reveal what dissociations may be possible. In addition, for reasons alluded to above, work has tended to focus on patients with the appropriately restricted and defined lesions. Much of the intensive research has been carried out with subjects D.B., G.Y., and F.S. [D.B. had surgical removal of tumor from V1 (see Weiskrantz et al., 1974); a magnetic resonance imaging (MRI) scan is not possible because of metal aneurysm clips and CT scans are badly distorted for the same reason, but a high resolution CT scan is possible for upper bank of calcarine cortex, and shows complete loss of V1 in that bank (Weiskrantz, Cowey, and Hodinott-Hill, in preparation), corresponding to the lower visual field where testing has been concentrated. G.Y. suffered a head injury; he has been scanned several times (see Barbur et al., 1993; Baseler et al., 1999) showing complete left V1 removal except for occipital pole, corresponding to 3 degrees of

macular sparing. F.S. suffered a severe craniocerebral trauma, almost completely destroying his left primary visual cortex; the damage is well documented by MRI (see Goebel et al., 2001)]. Taking the evidence collectively, not all necessarily found in all subjects, the findings are as follows:

LOCALIZING AND DETECTION Subjects have been asked to attempt to localize the position of a brief, fixated stimulus by making an eye movement to the supposed locus of the stimulus, typically a briefly flashed spot (Pöppel et al., 1973), or by pointing or touching the locus of a target on a perimeter screen (Weiskrantz et al., 1974), even though they deny seeing the stimulus. In yet another study, G.Y. was trained to give a numerical score on a ruled scale to successfully describe the locus (Barbur et al., 1980). Localizing accuracy is typically not as good as in the intact visual field but nevertheless can be very impressive. Successful detection is obviously a necessary prerequisite for localization or any other discriminative capacity, but detection has also been studied independently of localizing (Azzopardi and Cowey, 1997; Barbur et al., 1980; Stoerig, 1987; Stoerig et al., 1985; Stoerig and Pöppel, 1986; Weiskrantz, 1986).

ACUITY D.B.'s acuity was measured with large Moiré fringe interference gratings (approximating sine-wave gratings) based on forced-choice guessing for the presence of a grating versus a luminance-matched homogeneous patch. The reduction in acuity for the region 16–20 degrees eccentric was about 2 octaves compared to the mirror-symmetric region of the intact field (2.5 c/deg compared with 10 c/deg) (Weiskrantz, 1986). Other acuity measurements have been derived from contrast-sensitivity functions in the scotoma (e.g., with G.Y.), using forced-choice detection of a grating versus a homogeneous patch. Acuity falls to zero at approximately 7 c/deg, which again is approximately a drop of about 2 octaves compared to his intact field (Barbur et al., 1994a; Weiskrantz et al., 1998). The reduction is in agreement with animal evidence (Miller et al., 1980).

ORIENTATION D.B. has repeatedly demonstrated good discriminative capacity for orientation of lines and a grating in the frontal plane in the blind hemifield, although not as sharp as in his good field. He could nevertheless discriminate a difference in orientation of 10 degrees between two gratings presented successively and briefly, even at an eccentricity of 45 degrees in the impaired field, with no acknowledged experience with the gratings or even with the brief flash. Other subjects who have been tested have shown more variable residual capacity for orientation (e.g., Barbur et al., 1980). For example, G.Y. does not show orientation discrimination using gratings, but positive evidence has been obtained using single lines (Morland et al., 1996).

COLOR Spectral sensitivity functions of the blind hemifields of several hemianopes have been measured by Stoerig and Cowey (1989, 1991, 1992; Cowey and Stoerig, 1999) and been found to be qualitatively similar to those of their normal hemifields, although with quantitatively reduced sensitivity. The profiles include the humps and troughs thought to reflect color opponency; they also show the characteristic loss of long-wavelength sensitivity following dark adaptation, the *Purkinje shift*. Strikingly, wavelength *discrimination*, such as red versus green, but even of more closely spaced wavelengths, is possible in some subjects (Stoerig and Cowey, 1992) using forced-choice guessing. Barbur et al. (1994b) demonstrated good discrimination between “colored” patches and achromatic patches matched in luminance using a two-alternative forced-choice (2AFC) paradigm in G.Y. Ruddock and his colleagues (Brent et al., 1994) have also found good discrimination between red and achromatic stimuli in G.Y. It appears, in this connection, that the discriminative sensitivity of the blind field is biased toward the red end of the spectrum. In addition to wavelength discrimination, a strong inference can be drawn from pupilometry that *successive color contrast* is intact in G.Y., another hemianopic blindsight subject (Barbur et al., 1999), and recently also confirmed with D.B.

While residual color mechanisms can be found, it should be stressed that in all of these studies, the subjects *never* reported any experience of color per se. It is worthwhile to note Stoerig and Cowey's comment about the subjects' commentaries:

the patients were often asked whether they could perceive anything when the blind field was tested. Throughout the experiments, which involved from 2 to 4 three-hour sessions per month for approximately six months, they consistently claimed that this was not the case and that they never saw or felt anything that was related to stimulus presentation. (1991, p. 1496)

MOVEMENT AND TRANSIENT STIMULI This subject has long antecedents given the classical evidence of Riddoch (1917) and Poppelreuter (1917/1990), who described wartime gunshot-wound patients who could see moving but not stationary stimuli. Reports of detection and tracking of moving stimuli in their impaired fields are among the earliest observations of human subjects (Barbur et al., 1980; Brindley et al., 1969; Denny-Brown and Chambers, 1955) and of the monkey (Humphrey, 1974). Using threshold determinations, D.B. was shown to have good ability to detect moving bars and spots, although with reduced sensitivity, depending on the location in the blind field (Weiskrantz, 1986). A number of parametric psychophysical studies of *directional* discrimination of moving spots or bars have been carried out by Barbur and his colleagues on G.Y. (Barbur et al., 1993; Sahraie et al., 1997, 1998; Weiskrantz et al., 1995; cf. also Perenin, 1991), who measured the limits of velocity and

contrast for successful directional discrimination in the blind field. Some of these studies led to the experimental exploration of the distinction between *awareness* and *unawareness* modes and also to brain imaging (see below).

While there is no question that blindsight subjects can detect moving bars or spots and discriminate their direction of movement, other modes of movement discrimination, namely, the discrimination of direction of movement of random dot kineograms and plaids, has been found to be lacking (Azzopardi and Cowey, 2001; Cowey and Azzopardi, 2001).

Temporal onset/offset transients also are of particular significance in the blind field. Weiskrantz et al. (1991) carried out a systematic study in G.Y. by varying the temporal slope of the Gaussian envelope of the onset and offset of stimuli in a 2AFC paradigm for gratings versus equiluminant homogeneous patches. Performance improved as the temporal slope increased. In a related study, the manipulation of spatial as well as temporal transients also allowed a specification to be made of both the spatial and temporal parameters required for good detection. From such determinations, it was possible to conclude that G.Y.'s blind field possesses a narrowly tuned spatiotemporal visual *channel*, with a peak of about 1 c/deg and a cutoff (*acuity*) of about 7 c/deg (Barbur et al., 1994a). This can now be linked to a closely similar channel in monkeys revealed by pupillometry (see below). It appears to be characteristic of a number of hemianopic subjects, although with a small variation in the peak spatial frequency.

A somewhat different approach had been used in an early study of D.B. in which the temporal rate of onset was varied systematically over a wide range in a forced-choice discrimination paradigm between a circular, homogeneous luminous disc versus no stimulus. Although the sharper the rate of onset the better the performance, D.B. still performed reliably well above chance, and without acknowledged awareness, even with extremely slow rates of onset (Weiskrantz, 1986, Chapter 9). Therefore, a rapid temporal transient is not a necessary feature for good detection. It also indicates that this mode of blindsight is quite different from that in the early reports by Riddoch (1917) that described vigorous movement in the blind field.

“FORM” Early reports of evidence for shape discrimination were negative or weak (cf. Weiskrantz, 1986). With reaching responses, however, when subjects are asked to grasp solid objects in their blind fields, the situation may be different. Both Marcel (1998) and Perenin and Rossetti (1996) have reported that the subject's hand adopts the appropriate configuration in advance of grasping an object in the blind field. This result is nicely in accord with Milner and Goodale's (1995) thesis that the shape and orientation of objects can be involved in directed visual actions via the dorsoventral

stream toward the objects even when subjects are unable to perceive the objects correctly. Less easy to accommodate on such a basis, on the other hand, is the evidence for color processing and the striking claim by Marcel (1998) that words flashed into the blind field can influence the interpretation of meanings of words subsequently shown in the intact field. This intriguing report is isolated and deserves to be followed up. It would require considerable expansion of the known capacity for residual processing of stationary shapes in the blind field.

EMOTIONAL CONTENT There are reports that conditioned aversive properties of stimuli in normal human subjects can give rise to autonomic responses even when the subjects have no awareness of them (Esteves et al., 1994; Öhman and Soares, 1998). Functional imaging studies have also demonstrated that conditioned fear stimuli rendered invisible by backward masking can nevertheless activate the amygdala via a colliculo-pulvinar pathway (Breiter et al., 1996; Morris et al., 1999). Behavioral evidence from monkeys with V1 removal suggests that the blind field is inert to the emotional content. For example, when a fear-evoking stimulus, such as a strange doll, is presented to the affected hemifield, the animal appears to ignore it completely, although it emits loud shrieks of fear and outrage when it is confronted in the normal visual field. Nor does it react, for example, to a highly prized banana in the blind field (Cowey, 1967; Cowey and Weiskrantz, 1963). On the other hand, no concurrent measures of autonomic activity were made, and it remains possible that emotion-provoking stimuli produce responses in the absence of overt behavioral responses, just as, for example, galvanic skin responses can be recorded to familiar faces in prosopagnosic patients who cannot distinguish familiar from unfamiliar faces perceptually (Tranel and Damasio, 1985).

A recent study of faces with emotional expression projected to G.Y.'s blind field has some direct relevance (de Gelder et al., 1999). G.Y. has been shown to be able to discriminate between different facial expressions in moving (but not stationary) video images projected into his blind field, such as happy versus sad, angry versus fearful. Strikingly, he could also identify which of four different emotional expressions were presented on any single exposure. He failed to “see” the faces as such, and his responses were at chance with inverted faces. Using cross-field interactions between blind and intact hemifields (see below), evidence was found for face processing with stationary exposures. It remains unknown whether his autonomic system would also be sensitive to emotional stimuli that he can discriminate in the absence of seeing. A recent functional MRI (fMRI) study using a conditioned fear paradigm in G.Y. demonstrated that the amygdala is activated by the conditioned stimulus presented to the blind field, and that the amygdala's activity

correlates with activity levels in the superior colliculus and pulvinar. Thus, a route that bypasses V1 evidently remains intact for activation by emotional events (Morris et al., 2001).

ATTENTION IN THE BLIND FIELD It has been demonstrated with G.Y. that attention can confer an advantage in processing stimuli in the blind field either within an attended time interval or at an attended spatial location. Using a Posner cueing paradigm, G.Y.'s discrimination of the location of a stimulus was improved by a visual cue that provides temporal information about the time window within which the targets will appear (Kentridge et al., 1999a). Cues in the blind field that provide information about the likely spatial location of a target also confer an advantage, strikingly in the complete absence of reported awareness of either the cue or the target. Cues in G.Y.'s blind field were effective even in directing his attention to a second location remote from that at which the cue was presented, again under conditions in which there was no reported awareness of the cue or the target (Kentridge et al., 1999b). Such evidence suggests that spatial selection by attention, on the one hand, and conscious awareness of attentional control, on the other, cannot be the same process.

Verbal versus nonverbal approaches

AWARENESS VERSUS UNAWARENESS With the exception of D.B., verbal reports have not been explicitly assembled until recently. But it was noted in D.B. that transient stimuli, for example, of movement, looming and recession, or abrupt onset and offset, gave rise to a report of "awareness," a "feeling," or "knowing" that an event has occurred. These experiences were apt to mislead D.B. as to the identity of the event, so such transients were avoided by varying contrast and other conditions (see Weiskrantz, 1986, Chapter 13), and hence most of the studies with him involved visual discriminations in the absence of any awareness. A similar distinction between performance with and without awareness emerged in studies with G.Y. and other subjects, and has been named as a distinction between *blindsight type 1* (no awareness) and *blindsight type 2* (with awareness but not perceptual seeing) (Weiskrantz, 1998b, 1998c, 2000). The distinction is not necessarily binary, but serves as a convenient label for distinguishing some experience of awareness from complete nonawareness. Comparisons between functions with and without awareness are assessed with a *commentary key* paradigm. In addition to the usual pair of response keys for discriminating the stimulus events, two other commentary keys were introduced with which the subject could signal awareness or no awareness after each trial (Weiskrantz et al., 1995). The application of the paradigm with discrimination of movement direction is shown in Figures 40.1 and 40.2, with variations of velocity or contrast to affect the incidence

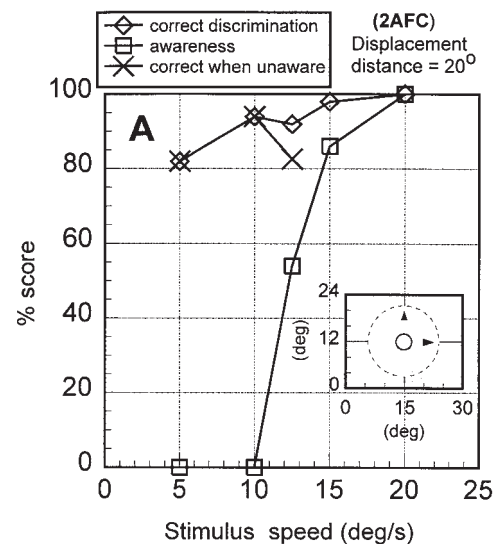


FIGURE 40.1. Directional movement discrimination performance for a moving spot presented to G.Y.'s blind hemifield as a function of stimulus speed. The subject had to discriminate (by guessing, if necessary) whether the stimulus moved horizontally or vertically by pressing the appropriate response key. Commentary keys were provided on which he also had to indicate on each trial whether he had any experience whatever of the stimulus event. *Awareness* refers to the percentage of trials on which he pressed the "yes, had experience" key. *Correct when unaware* refers to performance during those trials when he pressed the "no, I had no experience at all" key. Performance was high even without reported awareness. (From Weiskrantz et al., 1995, with permission. Copyright National Academy of Sciences, USA.)

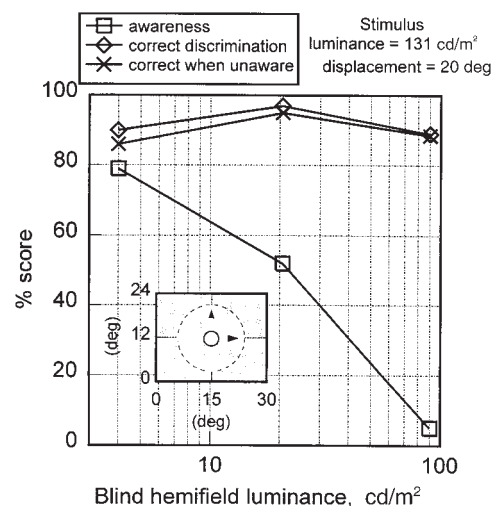


FIGURE 40.2. Conditions as in Figure 40.1, but with stimulus contrast varied instead of speed. The luminance of the test spot was constant, at 131 cd/m², and background luminance changed systematically. Awareness declined steeply as background luminance increased, but performance remained relatively stable. (From Weiskrantz et al., 1995, with permission. Copyright National Academy of Sciences, USA.)

of awareness reports and the corresponding discriminative performance. It can be seen that performance can remain high and relatively independent of awareness levels as such. The relationship between commentaries and confidence reports has also been examined in a further extension, as well as the use of multivalues versus binary scales (Sahraie et al., 1998). The paradigm was applied in an imaging study of the two blindsight modes (Sahraie et al., 1997; see below).

NONVERBAL, INDIRECT METHODS OF REVEALING RESIDUAL VISUAL FUNCTION Particular problems of confidence and credibility arise for many subjects (and some experimenters) about requests to make counterintuitive judgments about stimuli they cannot see. Aside from that, parametric psychophysics carried out by forced-choice guessing or reaching require multiple and lengthy sessions, often totaling thousands of trials. In other areas of cognitive neuropsychology, residual function can be tested quite readily by methods that do not directly assault credibility. For example, the amnesic patient can be asked to try to identify a word when presented with its first three letters, thereby enabling the experimenter to infer that an earlier exposure to the word (the *prime*) has facilitated its identification without requiring the subject to remember as such.

Two general indirect methods have been used in testing for residual visual function without requiring the subject to guess “without seeing”: (1) reflexes to visual stimuli in the blind hemifield and (2) interactions between the intact and impaired hemifields. The field has been reviewed by Weiskrantz (1990) and by Stoerig and Cowey (1997).

Reflexes. Reliable electrodermal responses to lights versus “blanks” in the blind hemifield were found by Zihl et al. (1980). Such responses, however, are difficult to relate in a directly quantitative way to the visual events. The pupil response, in contrast, provides a direct and incisive quantitative measure because it constricts differentially to visual stimuli, depending precisely on the parameters of spatial frequency, wavelength, and movement, even when there is no change in the total luminance of the stimuli (Barbur and Forsyth, 1986; Barbur and Thomson, 1987). As the pupil response is independent of verbal report, it can be used to assess the blind fields of human patients, of animals, and of human infants (cf. Cocker et al., 1994).

In this way, for example, the pupil has been used to measure the profile of sensitivity to gratings in the blind field as a function of spatial frequency, and thereby to obtain an estimate of contrast sensitivity and of visual acuity. Weiskrantz et al. (1998), examined the spatial frequency profiles of the affected hemifields of G.Y. and also of two monkeys with unilateral removal of striate cortex (V1), using *P-scan pupillometry* (Barbur et al., 1987). The results were very clear (Fig. 40.3). In both the human and the monkeys, there

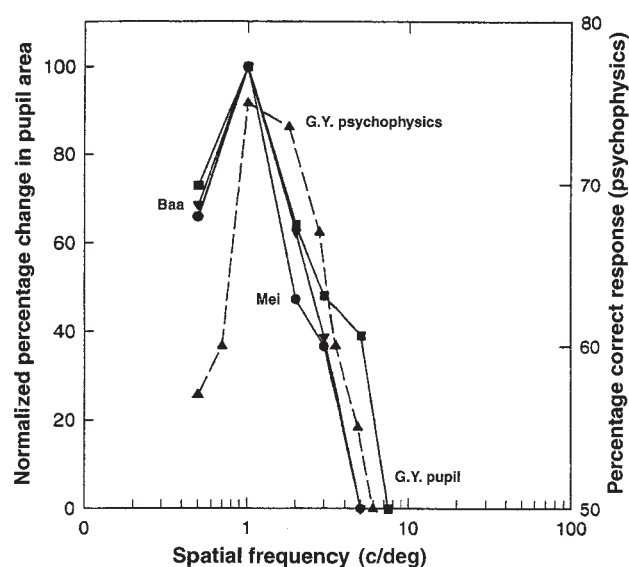


FIGURE 40.3. Relative normalized size (peak at 100) of pupil constriction (*solid lines*) as a function of spatial frequency of an equiluminant grating presented to the blind hemifields of a human subject (G.Y.) and two monkeys (Baa and Mei). The dotted line shows psychophysical performance for G.Y. from an earlier study (Barbur et al., 1994a) for gratings versus an equiluminant featureless stimulus. (From Weiskrantz et al., 1998, with permission. Copyright Oxford University Press.)

is a narrowly tuned response of the pupil to different spatial frequencies of an achromatic grating, with a peak at approximately 1 c/deg. The acuity (the point at which the response falls to zero as spatial frequency increases) is at about 7 c/deg, a reduction of about 2 octaves compared with the intact hemifields under these conditions. G.Y.’s pupillary response could be validated psychophysically with a spatial-temporal tuning curve obtained in an earlier study (Barbur et al., 1994a). The psychophysical function and the pupillary profile map onto each other quite closely (Fig. 40.3), confirming the potential usefulness of pupillometry as a clinical screening device. Recently, it has been possible to make the same comparison between psychophysics and pupillometry for D.B. (L. Weiskrantz and A. Cowey, unpublished), with a similar close agreement (Fig. 40.4). The strikingly close similarity of the monkey and human results is further evidence that similar mechanisms are involved following V1 removal in both species, and is counter to the view that in residual function the human must depend on fragments of intact visual cortex, given that there are demonstrably no such fragments in the monkey. The occurrence of the pupillary response does not depend on the subject’s having blindsight type 2 (see above). It still constricts to a 1 c/deg isoluminant grating even when the onset and offset of the grating are smoothed so as to eliminate G.Y.’s reported awareness of the event (Weiskrantz et al., 1999). Given that pupillometric acuity changes with V1 removal, there must be a direct

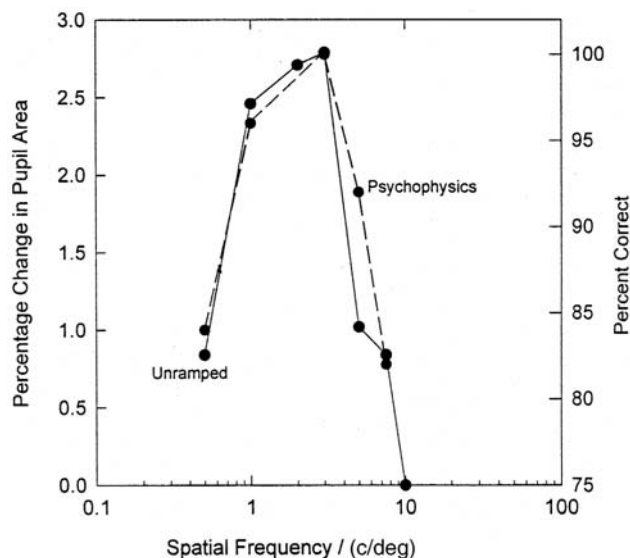


FIGURE 40.4. Change in pupillary area (solid line) for subject D.B. as a function of spatial frequency, and percentage correct discrimination performance for gratings versus equiluminant featureless stimulus, with forced-choice guessing (dotted line). The subject's commentaries for each of the spatial frequencies tested are shown below the figure, together with the relevant percentage of correct performance. (Note that for this subject psychophysical sensitivity is slightly better than for pupillometry; the subjects performance is 75% correct when the pupil fails to respond.) (From L. Weiskrantz and A. Cowey, unpublished.)

downstream influence of cortex reaching the midbrain mechanism that provides the final efferent to the pupillary musculature.

Interactions between intact and blind hemifields. Torjussen's work (1976, 1978) provides the seminal example demonstrating completion of shapes shown to the blind and intact hemifields simultaneously. The subject reports seeing nothing when a stimulus is presented to the blind field but sees a normally completed stimulus which bridges the intact and impaired fields. More recently, this method has been used by Marcel in two hemianopes, one of whom was G.Y. (Marcel, 1998), and also by Perenin et al. (1985).

A related approach was designed by Marzi and colleagues (Corbetta et al., 1990) in which the reaction time of a key-press response to a light in the intact field could be increased by a light presented immediately beforehand in the impaired field of human subjects. A similar finding has been reported for the monkey: an unseen target slows the reaction time to the seen target, especially at delays on the order of 400–500 msec (Stoerig and Cowey, 1997). A contrasting approach, based on facilitation rather than inhibition, was used by Marzi et al. (1986), exploiting the fact that the reaction time to two flashes presented simultaneously is consistently faster than the reaction time to a single flash, whether or not the two flashes appear in the same hemifield or in opposite

fields. The reaction time of hemianopes can be speeded up when the two flashes are presented across the vertical meridian, even though the subject only reports seeing a single stimulus, that is, the one in the intact hemifield. Recently, the same approach has been used by Tamale et al. (1997) to demonstrate visual spatial summation in hemispherectomized subjects. de Gelder et al. (2001) also have used the method to conclude that there was facilitatory interaction of face processing between G.Y.'s blind and intact fields.

Functional brain imaging

G.Y. has been the subject of both positron emission tomography (PET) and MRI investigations. Barbur et al. (1993) studied the difference between moving and stationary bars with PET. The results focused on the activation found in area V5 in association with moving stimuli. In this situation, G.Y. was typically aware of the movement, that is, it was blindsight type 2; blindsight type 1 was not investigated.

The distinction between directional movement discrimination *with and without awareness* (e.g., type 2 vs. type 1) was the explicit focus of a subsequent fMRI study of G.Y. (Sahraie et al., 1997) using parameters that had been previously established (Weiskrantz et al., 1995) to produce good discrimination both with and without awareness. The stimulus contrast and velocity parameters that had previously been used to establish this difference psychophysically (see above) served to design the stimuli in the imaging study. There was an association between the "awareness" mode and activity in dorsolateral prefrontal activity (areas 46 and 47), both when the subject was "aware without seeing" in the blind hemifield and when he was "aware with seeing" in the intact hemifield. In the "unaware" mode but associated with good discrimination, and only in this mode, there was activation in the superior colliculus. Although these associations with awareness and unawareness modes were unique, the main conclusion of the paper stressed the general change in pattern between the two modes—from dorsolateral structures in the former to medial and subcortical structures in the latter.

Another fMRI study focused on colored stimuli, specifically of red and green, presented to G.Y.'s blind hemifield. It had previously been established, both by pupillometry and by psychophysics, that there was a differential sensitivity to red compared with green colors (although it must be stressed again that the subject did not report any experience of color as such). Activation of the superior colliculus was found by a red but not by a green stimulus in the blind hemifield. No such midbrain activation was found in the sighted hemifield (Barbur et al., 1998).

Finally, a recent fMRI study of G.Y. and E.S. reported "surprisingly strong" responses to stimulation of the blind field in ipsilateral extrastriate areas, using stimuli intended

to activate either the dorsal or ventral pathways, but no detectable activity in the early visual areas of the lesioned hemisphere (Goebel et al., 2001).

Animal homologs

As already mentioned, blindsight stemmed from the long-standing evidence that infrahuman primates can make visual discriminations in the absence of striate cortex, while humans with such damage describe themselves as being blind to experience in the relevant parts of the visual fields. With appropriate testing methods, the quantitative effects of visual cortex damage in monkeys and human blindsight subjects are similar in many respects. But an important and much deeper qualitative question remains: does the monkey without striate cortex, which can localize and discriminate visual stimuli so impressively, actually have *visual experience* of those stimuli in its affected hemifield? Seminal experiments addressing this question were carried out by Cowey and Stoerig in 1995. After confirming that monkeys could accurately localize and reach for a briefly presented visual stimulus in their “blind” hemifields, they proceeded to a second experiment with the same animals: they were trained to discriminate between randomly presented “lights” and “no lights” (i.e., blanks) in their intact hemifields and were rewarded for correct responses (reaching for a light or pressing a “blank panel” for a nonlight). The crucial question after this training was completed was, how would the animals respond to a visual stimulus in their blind hemifields? The answer was clear and robust: the monkeys pressed the blank panel. That is, even though the animals had just demonstrated that they could detect the lights with virtually perfect performance, they nevertheless treated them as blanks, as *nonlights*. This is just what a human blindsight subject would do, of course. Some further experimental extensions of this paradigm are discussed by Cowey and Stoerig (1997) in an excellent review of the comparative issues. The matter is also discussed, at a more general level, in Weiskrantz (1997, Chapter 4).

Two important studies carried out by Charles Gross and his colleagues are also relevant to the animal-human parallel. Monkeys were trained to make a saccadic eye movement from the point of fixation to a visual target in their blind hemifields (Moore et al., 1995). Performance was good when they had a warning signal (the turning off of the fixation point). But without such a warning, they failed to initiate the eye movement to the target. The authors draw the parallel with clinical testing of human patients with field defects caused by visual cortex damage: typically in clinical perimetric testing, subjects are not given warning signals and are blind to visual events in their field defects. In blindsight experiments carried out in the laboratory, however, warning signals are routinely used.

But even the need for a warning signal disappears if the unilateral V1 damage is imposed in infancy (Moore et al., 1996). Other animal work (Payne, 1994) also supports the conclusion that greater recovery is possible after early than after late damage to the visual system and is accompanied by anatomical reorganization. It may be relevant that the two most thoroughly studied human patients, D.B. and G.Y., both had visual defects in childhood, G.Y. because of head injury at the age of 8 and D.B. because of an incipient occipital tumor which first gave rise to a clinical problem at the age of 14, although the pathology might well have been present much earlier, perhaps even prenatally (Weiskrantz, 1986).

A related issue concerns the role of practice in recovery of residual function. It was demonstrated some time ago (Cowey, 1967; Mohler and Wurtz, 1977) that if monkeys with visual cortex lesions are given sustained practice with visual discriminations in their blind fields, their sensitivity increases. This increase can be substantial—as much as 3 log units. The size of the field defect also shrinks. But improvement depends directly on whether the animal is actually *required* to practice with stimuli directed within the field defect; in fact, Mohler and Wurtz showed that recovery was specific even to practice *within a subpart* of the field defect. The typical hemianope, whether human or animal, has no particular pressure to exercise the affected hemifield, given the preservation of a normal intact hemifield, which may be why specific practice has to be prescribed. The beneficial effect of practice in human patients, using a procedure based on the method of Mohler and Wurtz, has been demonstrated by Zihl and colleagues (Zihl, 1980, 1981, 2000; Zihl and von Cramon, 1979, 1985). Recently, other investigators (Kasten and Sabel, 1995; Kerkhoff et al., 1994) have also reported encouraging results with human patients, using similar techniques.

Validation issues

Some of the issues of validation and theoretical interpretation are the same throughout all varieties of implicit processing in neuropsychological subjects, and some are unique to blindsight. A fuller treatment of these issues can be found in Weiskrantz (1997, 1998a, 2001a, 2001b). Briefly, however, some of these issues relevant to blindsight are as follows:

STRAY LIGHT, INTRAOCULAR DIFFUSION, EYE MOVEMENTS, AND OTHER POSSIBLE OPTICAL ARTIFACTS Hemianopic subjects have an intact, normal visual hemifield ipsilateral to the lesion, so it is important to rule out the possibility that alleged processing by the blind field is not, in fact, being carried out by stray light or intraocular diffused light reaching the intact hemifield (Campion et al., 1983). Such a factor

could not, of course, apply to stimuli which would be severely degraded by diffusion, such as high spatial frequency gratings for measuring acuity in the impaired field. Stray light has been controlled in a variety of ways—for example, by flooding the intact visual hemifield with high levels of illumination so that if there were any stray light, it could not be detected. The stray light function has also been determined experimentally (Barbur et al., 1994a). The most demanding method to ensure that there can be no effective entrance of stray light into intact parts of the field is to use the *genuinely* blind part of the eye as a control, the optic disc, in which there are no receptors. As the size of this natural absolutely blind area is known (5×7 degrees), maximum diffusion would be no more than half the size of the disc for stimuli that are not detected on the disc. When the subject's performance is at chance for stimuli on the disc, it is above chance on the neighboring region. Weiskrantz and Warrington (cf. Weiskrantz, 1986, Chapter 10), Stoerig et al. (1985), and Tomaiuolo et al. (1997) have used this control effectively. It can be said with assurance that residual visual capacity in the blind field of hemianopes cannot be explained away as a matter of stray light or intraocular diffusion.

Eye movement recordings and monitoring are standard features of many studies, which have ruled out inadvertent fixation shifts, as well as the use of stimuli too brief to survive a saccade. A Purkinje eye-tracking device has also been used with G.Y., which ensured that even if the eye moved, the stimulus would remain fixed on the same retinal location (Kentridge et al., 1997). Residual function cannot be explained away in terms of inadvertent fixation shifts.

INCIDENCE Across a random sample of patients with hemianopias resulting from cortical damage, it is still not known how many would be likely to demonstrate blindsight. Blythe et al. (1987) found 5 patients (one of whom was G.Y.) with evidence of residual function (responses to movement and localization by reaching or eye movements) out of a studied population of 25. Similarly, Weiskrantz (1980) found, in a study of acute hospital patients, that 14 hemianopic patients out of 69 showed some evidence of residual function. In the remainder, either no such evidence was found or it remained inconclusive.

Why should the incidence of residual function apparently be low? Briefly, there are at least four reasons (cf. Weiskrantz, 1998a). One of the most important is likely to be the variable extent of the occipital lesions in human subjects and the unlikelihood of any such lesion being restricted to V1, which itself is buried deep in the medial aspect of the brain. As noted above, animal work has demonstrated that extensions of lesions beyond V1 reduce the degree of residual function, and many lesions seen clinically probably lead to the same diminution, especially as the visual association

areas in the vicinity of V1 are tightly compressed. Secondly, the age at which the lesion occurs could be important, as has already been demonstrated in animal work (Moore et al., 1996; Payne, 1994) (see above). A third reason for possibly variable incidence is the strangeness of the question that the researcher is bound to ask when testing blindsight type 1, when subjects are asked to guess about stimuli of which they have no awareness. Some refuse to do so. The problem is compounded by the need to test subjects extensively over tens of hundreds of trials to obtain parametric families of functions. This no doubt is why research has been carried out on only a relatively small number of long-suffering subjects with the appropriately delimited lesions, who are willing or able to make themselves available, and also why indirect methods have commended themselves (see above).

A final reason is that the stimulus parameters used in testing for residual function can be critical—parameters that may be suitable or even optimal for normal function may not apply to that of the blind field. Even a slight change in the slope of the temporal onset or offset of the stimulus can transform chance performance into virtually perfect performance. For example, Hess and Pointer (1989), using particular fixed parameters of temporal and spatial Gaussian envelopes of unstructured stimuli, concluded that there was no residual function in G.Y. (and other subjects). This negative result was confirmed (Weiskrantz et al., 1991) using the same parameters as Hess and Pointer, but a relatively small change in the parameters led to excellent performance by G.Y. in his blind hemifield. This and another example of an apparently unfortunate choice of parameters is discussed in Weiskrantz (1997, pp. 154–155, 247–248). A more important question lies at the heart of the issue of parameters: whether one chooses fixed parameters of visual stimuli for testing the population or varies the parameters and categories over a wide range for each patient, seeking those that will reveal residual function. The latter approach may be why Teuber et al. (1960) found not a single case of occipital damage in a war-injured population of 46 patients who did not exhibit some measure of residual visual function in the field defect. One may also cite Poppelreuter's conclusion (1917/1990) that he could never find an absolutely blind scotoma in his wartime brain-injured patients. In current research, Sahraie and Weiskrantz (in preparation) have found that in most patients, some residual function can be revealed when spatial frequency and temporal frequency parameters are varied widely until the psychophysically sensitive region is located.

COMPLETENESS OF THE VISUAL CORTIX LESION AND EXTENSIONS TO NONSTRIATE CORTIX It is a complicating fact that damage in human clinical patients is rarely confined to striate cortex. A further possible complication is that the damage to striate cortex itself may not be complete. Some

have argued—along the lines of the late-nineteenth-century view that assigns special higher properties to cerebral cortex (cf. Weiskrantz, 1961, for a critique)—that intact striate cortex is itself necessary for the capacity to make visual discriminations. In particular, Fendrich et al. (1992), Gazzaniga et al. (1994), and Wessinger et al. (1997) have argued that blindsight, when demonstrated, may depend critically not on extrastriate pathways, but on small islands of intact striate cortex. Briefly, they found small islands of intact visual function in an otherwise dead visual hemifield of occipital patients; it was blindsight because the subjects reported no awareness of the stimuli within the island. Brain imaging also revealed a small region of intact striate cortex at the occipital pole (which would be expected, of course, in a subject with macular sparing). Their evidence was found using an eye tracker, which allows the visual image to be fixed on the retina (within limited eccentricities) and which thus eliminates detection due to inadvertent or uncontrolled fixation shifts (although these have been controlled by other methods in earlier blindsight studies; see above).

It may well be that some cases are amenable to an explanation in terms of intact, tiny islands of striate cortex, but it does not follow that this is the only explanation even in such cases, nor can it be a general explanation of all examples of residual visual function with V1 lesions. The question has been reviewed more fully in Weiskrantz (1998a). Briefly, *no* islands were found in G.Y. using the same eye-tracking apparatus and the same parameters as in the Fendrich study (Kentridge et al., 1997).

Secondly, such an account cannot apply to the closely convergent evidence with monkeys, in which the completeness of the lesion and the absence of islands can be confirmed with certainty. Thirdly, “patchiness” of the visual field, when and if it is found, need not imply islands of cortex, because V1 lesions can cause patchy transneuronal degeneration of ganglion cells in the retina (Cowey et al., 1989, 1999; Van Buren, 1963), especially in the p-beta class of cells. The retina itself can be patchy. Finally, high-resolution MRI scans of the most highly studied subject do not reveal intact islands of tissue (aside from those at the pole, corresponding to his region of macular sparing), nor do PET or fMRI scans reveal any functioning visual cortex when he is stimulated in his blind field. (Barbur et al., 1993, 1998; Sahraie et al., 1997; A. Morland, personal communication).

ASSESSMENT OF BLINDSIGHT IN RELATION TO RESPONSE ASSESSMENT AND RESPONSE CRITERIA Stoerig et al. (1985) deliberately varied response criteria without affecting detection thresholds with blindsight subjects, although performance levels were admittedly relatively weak. The demonstration of discriminative performance in blindsight, when it is good, can be assessed in standard statistical terms without any reference to signal detection theory.

In contrast, theoretical concern lies more with the much lower levels of performance, usually chance or near-chance levels. Clinical procedures typically involve a “yes, I see” or “no, I do not see” response to a stimulus in the blind field, which is typically the evidence upon which a claim of blindness is based. In signal detection terms, however, a subject may have high sensitivity (d') even though the measured performance level at 50% because of response criterion bias (e.g., if the subject is very cautious and responds “no” on every trial). Experimental studies of the capacity of the “blind” field, on the other hand, are often carried out with a more rigorous procedure, such as a 2AFC, which tends to be free of response bias. Therefore, the question is whether the dissociation between the reported blindness of the affected field versus its positive residual blindsight function merely reflects different response criteria in the yes/no versus the 2AFC discriminating modes.

Azzopardi and Cowey (1997) addressed this in a signal detection comparison of these two modes of responding, 2AFC versus yes/no, in G.Y. using a grating stimulus versus an equiluminant uniform patch with a range of stimulus contrasts. For both paradigms (“Was the grating in the first or the second temporal interval?” and “Was there a stimulus or not?”), they obtained Receiver Operating Curves, and hence could derive measures of sensitivity (d') that were independent of response criteria. The result was that in normal subjects the two measures of sensitivity were identical—saying “yes” or “no” yielded the same outcome as judging in which of two intervals the stimulus occurred in the 2AFC. But for G.Y. the result was quite different: he was much more sensitive in the 2AFC paradigm than in the yes/no paradigm. This is, of course, exactly the difference implied in the meaning of blindsight itself: there is good performance when the subject is forced to make a response to a stimulus as opposed to making a see/not see judgment, as in clinical perimetry.

However, a deeper question arises regarding the applicability of signal detection theory to evidence for blindsight, which essentially is a disjunction between forced-choice discriminations and the commentaries that relate to them. Signal detection theory is useful and powerful for characterizing the sensitivity and response bias in the performance of discriminations but not for characterizing off-line commentaries made about the discriminations. This raises questions of veracity rather than bias (cf. Weiskrantz, 2001a). An alternative approach is to use scale discriminations and commentaries independently and to plot their correlations or dissociations.

DOES BLINDSIGHT DIFFER QUALITATIVELY OR JUST QUANTITATIVELY FROM NORMAL VISION? Azzopardi and Cowey take their results to imply “that blindsight is not just normal, near-threshold vision and that information about the

stimulus is processed in blindsighted patients in an unusual way” (1997, p. 14190), which is the view originally advanced for blindsight (cf. Weiskrantz, 1986). One important difference between blindsight and normal vision is the serious disjunction between on-line discriminative processes and off-line commentaries or judgments that arise in blindsight. For example, Kentridge et al. (1999a) examined correlations in G.Y. between commentary-key responses (“aware” or “not aware”) and 2AFC spatial localization discriminations in the good and bad fields, selecting approximately similar levels of discrimination for both fields. In fact, a double dissociation emerged: even though G.Y.’s 2AFC performance happened to be poorer in his good field than in his blind field, he had a higher level of awareness commentary responses in the good field than in the blind one. Warrington and Weiskrantz also reported a double dissociation between the intact and impaired fields of D.B., leading to the suggestion of a qualitative dissociation between form and detection between the intact and impaired fields (Weiskrantz, 1986, Chapter 16).

Other considerations speak against the conclusion that the properties of the blind field are simply a weaker version of normal vision. The levels of performance in the blind field can also be very high, approaching or reaching 100%, even when the subject reports complete absence of awareness, unlike the degraded levels characteristic of parathreshold levels in normal vision. Another consideration is that there is a retrograde transneuronal degeneration following V1 lesions both in humans (Van Buren, 1963) and in monkeys, resulting in a shift from a predominance of p-beta ganglion cells of the affected retina toward p-alpha and p-gamma cells. The latter classes of ganglion cells have different structures, different projections in the brain, and different functional properties from p-beta. In other words, the hemiretina corresponding to the field defect is qualitatively different from the normal hemiretina (Covey et al., 1989). Other differences (see above) include the finding that color discrimination and detection, measured psychophysically or by pupillometry in the blind field, appear to favor the red end of the spectrum, unlike a normal field, and the fMRI evidence shows a different pattern of activation in the brain images when G.Y. reports awareness and when he does not, despite comparable levels of performance psychophysically under these contrasting conditions.

Concluding comment

In the absence of V1, parallel extrastriate visual pathways can mediate visual discriminations in humans as well as in other primates, but we are only beginning to characterize the emerging dissociations. The most surprising aspect has been the contrast between subjects’ reported lack of experience of visual stimuli, whether registered verbally or by commentary keys, and their objectively measured capacity or, in

the case of monkeys, their classification of the visual stimuli that they objectively can detect with impressive sensitivity as being blanks. But this same counterintuitive disjunction is found across the entire neuropsychological research spectrum—for example, commissurotomy, amnesia, aphasia, prosopagnosia, and dyslexia (see Schacter et al., 1988; Weiskrantz, 1991, 1997, for reviews.). Indeed, even in normal function, it could be argued that much, perhaps even most, neural processing proceeds without any associated awareness or other off-line measure of competence. An advantage of blindsight research is the greater anatomical and physiological knowledge of the visual system in relation to other syndromes. The hope is that blindsight research, in addition to helping to characterize the function of subcomponents of the visual pathways, may help to elucidate the disjunction between awareness and unawareness more precisely and to open up a route by which its neural underpinnings can be explored.

REFERENCES

- Azzopardi, P., and A. Cowey, 1997. Is blindsight like normal, near-threshold vision? *Proc. of Natl. Acad. Sci. USA*, 94:14190–14194.
- Azzopardi, P., and A. Cowey, 2001. Motion discrimination in cortically blind patients, *Brain*, 124:30–46.
- Barbur, J. L., and P. M. Forsyth, 1986. Can the pupil response be used as a measure of the visual input associated with the geniculo-striate pathway? *Clin. Vis. Sci.*, 1:107–111.
- Barbur, J. L., J. A. Harlow, A. Sahraie, P. Stoerig, and L. Weiskrantz, 1994b. Responses to chromatic stimuli in the absence of V1: pupillometric and psychophysical studies. In: *Vision science and its applications. Opt. Soc. Am. Tech. Dig.*, 2:312–315.
- Barbur, J. L., J. A. Harlow, and L. Weiskrantz, 1994a. Spatial and temporal response properties of residual vision in a case of hemianopia, *Philos. Trans. R. Soc. B*, 343:157–166.
- Barbur, J. L., K. H. Ruddock, and V. A. Waterfield, 1980. Human visual responses in the absence of the geniculo-striate projection, *Brain*, 102:905–927.
- Barbur, J. L., A. Sahraie, A. Simmons, L. Weiskrantz, and S. C. R. Williams, 1998. Processing of chromatic signals in the absence of a geniculostriate projection, *Vis. Res.*, 38:3447–3453.
- Barbur, J. L., and W. D. Thomson, 1987. Pupil response as an objective measure of visual acuity, *Ophthalm. Physiol. Opt.*, 7:425–429.
- Barbur, J. L., W. D. Thomson, and P. M. Forsyth, 1987. A new system for the simultaneous measurement of pupil size and two-dimensional eye movements, *Clin. Vis. Sci.*, 2:131–142.
- Barbur, J. L., J. A. G. Watson, R. A. J. Frackowiak, and S. Zeki, 1993. Conscious visual perception without V1, *Brain*, 116:1293–1302.
- Barbur, J. L., L. Weiskrantz, and J. A. Harlow, 1999. The unseen color after-effect of an unseen stimulus: insight from blindsight into mechanisms of colour afterimages, *Proc. Natl. Acad. Sci. USA*, 96:11637–11641.
- Bard, L., 1905. De la persistance des sensations lumineuses dans le champ aveugle des hemianopsiques, *Sem. Med.*, 22:3–25.
- Baseler, H. A., A. B. Morland, and B. A. Wandell, 1999. Topographic organization of human visual areas in the absence of input from primary cortex, *J. Neurosci.*, 19:2619–2627.

- Benevento, L. A., and K. Yoshida, 1981. The afferent and efferent organization of the lateral geniculo-striate pathways in the macaque monkey, *J. Comp. Neurol.*, 203:455–474.
- Blythe, I. M. C., C. Kennard, and K. J. Ruddock, 1987. Residual vision in patients with retrogeniculate lesions of the visual pathways, *Brain*, 110:887–905.
- Breiter, H. C., N. L. Etcoff, P. J. Whalen, W. A. Kennedy, S. L. Rauch, R. L. Buckner, M. M. Straus, S. E. Hyman, and B. R. Rosen, 1996. Response and habituation of the human amygdala during visual processing of facial expression, *Neuron*, 17:875–887.
- Brent, P. J., C. Kennard, and K. H. Ruddock, 1994. Residual colour vision in a human hemianope: spectral responses and colour discrimination, *Proc. R. Soc. Lond. B*, 256:219–225.
- Brindley, O. S., P. C. Gautier-Smith, and W. Lewin, 1969. Cortical blindness and the functions of the non-geniculate fibres of the optic tracts, *J. Neurol. Neurosurg. Psychiatry*, 32:259–264.
- Campion, J., R. Latto, and Y. M. Smith, 1983. Is blindsight an effect of scattered light, spared cortex, and near-threshold vision? *Behav. Brain Sci.*, 6:423–448.
- Cocker, D., M. J. Moseley, and J. G. Bissenden, 1994. Visual acuity and pupillary responses to spatial structure in infants, *Invest. Ophthalmol. Vis. Sci.*, 35:2620–2625.
- Corbetta, M., C. A. Marzi, G. Tassinari, and S. Aglioti, 1990. Effectiveness of different task paradigms in revealing blindsight, *Brain*, 113:603–616.
- Cowey, A., 1967. Perimetric study of field defects in monkeys after cortical and retinal ablations, *Q. J. Exp. Psychol.*, 19:232–245.
- Cowey, A., 1985. Aspects of cortical organization related to selective attention and selective impairments of visual perception, in *Attention and Performance*, vol. 11 (M. I. Posner and O. S. M. Marin, eds.), Hillsdale, NJ: Erlbaum, pp. 41–62.
- Cowey, A., and P. Azzopardi, 2001. Is blindsight motion blind? in *Out of Mind* (B. deGelder, E. deHaan, and C. A. Heywood, eds.), Oxford: Oxford University Press.
- Cowey, A., and P. Stoerig, 1991. The neurobiology of blindsight, *Trends Neurosci.*, 29:65–80.
- Cowey, A., and P. Stoerig, 1992. Reflections on blindsight, in *The Neuropsychology of Consciousness* (D. Milner and M. D. Rugg, eds.), London: Academic Press, pp. 11–37.
- Cowey, A., and P. Stoerig, 1995. Blindsight in monkeys, *Nature (Lond.)*, 373:247–249.
- Cowey, A., and P. Stoerig, 1997. Visual detection in monkeys with blindsight, *Neuropsychologia*, 35:929–937.
- Cowey, A., and P. Stoerig, 1999. Spectral sensitivity of hemianopic macaque monkeys, *Eur. J. Neurosci.*, 11:2114–2120.
- Cowey, A., P. Stoerig, and V. H. Perry, 1989. Transneuronal retrograde degeneration of retinal ganglion cells after damage to striate cortex in macaque monkeys: selective loss of P-beta cells, *Neuroscience*, 29:65–80.
- Cowey, A., P. Stoerig, and C. Williams, 1999. Variance in transneuronal retrograde ganglion cell degeneration in monkeys after removal of striate cortex: effects of size of the cortical lesion, *Vis. Res.*, 39:3642–3652.
- Cowey, A., and L. Weiskrantz, 1963. A perimetric study of visual field defects in monkeys, *Q. J. Exp. Psychol.*, 15:91–115.
- deGelder, B. G., M. Pourtois, M. van Raamsdonk, J. Vroomen, and L. Weiskrantz, 2001. Unseen stimuli modulate conscious visual experience: evidence from inter-hemispheric summation, *NeuroReport*, 12:385–391.
- de Gelder, B., J. Vrooman, G. Pourtois, and L. Weiskrantz, 1999. Non-conscious recognition of affect in the absence of striate cortex, *NeuroReport*, 10:3759–3763.
- Denny-Brown, D., and R. A. Chambers, 1955. Visuo-motor function in the cerebral cortex, *J. Nerv. Ment. Dis.*, 121:288–289.
- Esteves, F., D. Parra, U. Dimberg, and A. Öhman, 1994. Non-conscious associative learning: pavlovian conditioning of skin conductance responses to masked fear-relevant facial stimuli, *Psychophysiology*, 31:375–385.
- Fendrich, R., C. M. Wessinger, and M. S. Gazzaniga, 1992. Residual vision in a scotoma: implications for blindsight, *Science*, 258:1489–1491.
- Fries, W., 1981. The projection from the lateral geniculate nucleus to the prestriate cortex of the macaque monkey, *Proc. Natl. Acad. Sci. USA*, 213:73–80.
- Gazzaniga, M. S., R. Fendrich, and C. M. Wessinger, 1994. Blindsight reconsidered, *Curr. Dir. Psychol. Sci.*, 3:93–96.
- Goebel, R., L. Muckli, F. E. Zanella, W. Singer, and P. Stoerig, 2001. Sustained extrastriate cortical activation without visual awareness revealed by fMRI studies of hemianopic patients, *Vis. Res.*, 41:1459–1474.
- Hernandez-Gonzalez, C. C., and F. Reinoso-Suarez, 1994. The lateral geniculate nucleus projects to the inferior temporal cortex in the macaque monkey, *NeuroReport*, 5:2692–2696.
- Hess, R. F., and J. S. Pointer, 1989. Spatial and temporal contrast sensitivity in hemianopia. A comparative study of the sighted and blind hemifields, *Brain*, 112:871–894.
- Holmes, G., 1918. Disturbances of vision by cerebral lesions, *Br. J. Ophthalmol.*, 2:353–384.
- Humphrey, N. K., 1974. Vision in a monkey without striate cortex: a case study, *Perception*, 3:241–255.
- Kasten, E., and B. A. Sabel, 1995. Visual field enlargement after computer training in brain-damaged patients with homonymous deficits: an open pilot trial, *Restor. Neurol. Neurosci.*, 8:113–127.
- Kentridge, R. W., C. A. Heywood, and L. Weiskrantz, 1997. Residual vision in multiple retinal locations within a scotoma: implications for blindsight, *J. Cogn. Neurosci.*, 9:191–202.
- Kentridge, R. W., C. A. Heywood, and L. Weiskrantz, 1999a. Effects of temporal cueing on residual discrimination in blindsight, *Neuropsychologia*, 37:479–483.
- Kentridge, R. W., C. A. Heywood, and L. Weiskrantz, 1999b. Attention without awareness in blindsight, *Proc. R. Soc. B*, 266:1805–1811.
- Kerkhoff, G. U., U. Munsinger, and E. Meier, 1994. Neurovisual rehabilitation in cerebral blindness, *Arch. Neurol.*, 51:474–481.
- Marcel, A. J., 1998. Blindsight and shape perception: deficit of visual consciousness or of visual function? *Brain*, 121:1565–1588.
- Marzi, C. A., G. Tassinari, S. Aglioti, and L. Lutzemberger, 1986. Spatial summation across the vertical meridian in hemianopes: a test of blindsight, *Neuropsychologia*, 30:783–795.
- Miller, M., P. Pasik, and T. Pasik, 1980. Extrageniculate vision in the monkey. VII. Contrast sensitivity functions, *J. Neurophysiol.*, 43:1510–1526.
- Milner, A. D., and M. A. Goodale, 1995. *The Visual Brain in Action*, Oxford: Oxford University Press.
- Mohler, C. W., and R. H. Wurtz, 1977. Role of striate cortex and superior colliculus in visual guidance of saccadic eye movements in monkeys, *J. Neurophysiol.*, 40:74–94.
- Moore, T., H. R. Rodman, A. B. Repp, and C. G. Gross, 1995. Localization of visual stimuli after striate cortex damage in monkeys: parallels with human blindsight, *Proc. Natl. Acad. Sci. USA*, 92:8215–8218.
- Moore, T., H. R. Rodman, A. B. Repp, and C. G. Gross, 1996. Greater residual vision in monkeys after striate cortex damage in infancy, *J. Neurophysiol.*, 76:3928–3933.

- Morland, A. J., J. A. Ogilvie, K. H. Ruddock, and J. R. Wright, 1996. Orientation discrimination is impaired in the absence of the striate cortical contribution to human vision, *Proc. R. Soc. B*, 263:633–640.
- Morris, J. S., B. DeGelder, L. Weiskrantz, and R. J. Dolan, 2001. Differential extrageniculate and amygdala responses to presentation of emotional faces in a cortically blind field, *Brain*, 124:1241–1252.
- Morris, J. S., A. Öhman, and R. J. Dolan, 1999. A subcortical pathway to the right amygdala mediating “unseen” fear, *Proc. Natl. Acad. Sci. USA*, 96:1680–1685.
- Öhman, A., and J. J. F. Soares, 1998. Emotional conditioning to masked stimuli: expectancies for aversive outcomes following non-recognized fear-relevant stimuli, *J. Exp. Psychol. Gen.*, 127:69–82.
- Pasik, T., and P. Pasik, 1971. The visual world of monkeys deprived of striate cortex: effective stimulus parameters and the importance of the accessory optic system, in *Visual Processes in Vertebrates* (T. Shipley and J. E. Dowling, eds.), Vision Research Supplement no. 3, Oxford: Pergamon Press, pp. 419–435.
- Payne, B. R., 1994. System-wide repercussions of damage to the immature visual cortex, *Trends Neurosci.*, 17:126–130.
- Perenin, M. T., 1991. Discrimination of motion direction in perimetrically blind fields, *NeuroReport*, 2:397–400.
- Perenin, M. T., P. H. Girard-Madoux, and M. Jeannerod, 1985. From completion to residual vision in hemianopic patients. Paper delivered at the meeting of European Brain and Behaviour Society, Oxford, 1985.
- Perenin, M. T., and Y. Rossetti, 1996. Grasping without form discrimination in a hemianopic field, *NeuroReport*, 7:793–797.
- Perenin, M. T., J. Ruel, and H. Hécaen, 1980. Residual visual capacities in a case of cortical blindness, *Cortex*, 16:605–612.
- Pöppel, E., R. Held, and D. Frost, 1973. Residual visual function after brain wounds involving the central visual pathways in man, *Nature (Lond.)*, 243:295–296.
- Poppelreuter, W., 1990. *Disturbances of Lower and Higher Visual Capacities Caused by Occipital Damage* (trans. by J. Zihl of the 1917 German book). Oxford: Oxford University Press.
- Riddoch, G., 1917. Dissociation of visual perceptions due to occipital injuries, with especial reference to appreciation of movement, *Brain*, 40:15–17.
- Sahraie, A., L. Weiskrantz, and J. L. Barbur, 1998. Awareness and confidence ratings in motion perception without geniculostriate projection, *Behav. Brain Res.*, 96:71–77.
- Sahraie, A., L. Weiskrantz, J. L. Barbur, A. Simmons, S. C. R. Williams, and M. L. Brammer, 1997. Pattern of neuronal activity associated with conscious and unconscious processing of visual signals, *Proc. Natl. Acad. Sci. USA*, 94:9406–9411.
- Sanders, M. D., E. K. Warrington, J. Marshall, and L. Weiskrantz, 1974. “Blindsight”: vision in a field defect, *Lancet*, 707–708.
- Schacter, D. L., M. P. McAndrews, and M. Moscovitch, 1988. Access to consciousness: dissociations between implicit and explicit knowledge in neuropsychological syndromes, in *Thought Without Language* (L. Weiskrantz, ed.), Oxford: Oxford University Press, pp. 242–278.
- Stoerig, P., 1987. Chromaticity and achromaticity: evidence for a functional differentiation in visual field defects, *Brain*, 110:869–886.
- Stoerig, P., and A. Cowey, 1989. Wavelength sensitivity in blindsight, *Nature (Lond.)*, 342:916–918.
- Stoerig, P., and A. Cowey, 1991. Increment threshold spectral sensitivity in blindsight: evidence for colour opponency, *Brain*, 114:1487–1512.
- Stoerig, P., and A. Cowey, 1992. Wavelength sensitivity in blindsight, *Brain*, 115:425–444.
- Stoerig, P., and A. Cowey, 1997. Blindsight in man and monkey, *Brain*, 120:535–559.
- Stoerig, P., M. Hubner, and E. Pöppel, 1985. Signal detection analysis of residual vision in a field defect due to a post-geniculate lesion, *Neuropsychologia*, 23:589–599.
- Stoerig, P., and E. Pöppel, 1986. Eccentricity-dependent residual target detection in visual defects, *Exp. Brain Res.*, 64:469–475.
- Tamale, F., M. Pito, C. A. Marzi, T. Paus, and A. Pito, 1997. Blindsight in hemispherectomized patients as revealed by spatial summation across the vertical meridian, *Brain*, 120:795–803.
- Teuber, H.-L., W. S. Battersby, and M. B. Bender, 1960. *Visual Field Defects After Penetrating Missile Wounds of the Brain*, Cambridge: Harvard University Press.
- Torjussen, T., 1976. Residual function in cortically blind hemifields, *Scand. J. Psychol.*, 17:320–322.
- Tomaiuolo, F., M. Pito, C. A. Marzi, and A. Pito, 1997. Blindsight in hemispherectomized patients as revealed by spatial summation across the vertical meridian, *Brain*, 120:795–803.
- Torjussen, T., 1978. Visual processing in cortically blind hemifields, *Neuropsychologia*, 16:15–21.
- Tranel, D. D., and A. R., Damasio, 1985. Knowledge without awareness: an autonomic index of facial recognition by prosopagnosics, *Science*, 228:1453–1455.
- Van Buren, K. M., 1963. *The Retinal Ganglion Cell Layer*, Charles C Thomas.
- Weiskrantz, L., 1961. Encephalisation and the scotoma, in *Current Problems in Animal Behaviour* (W. H. Thorpe and O. L. Zangwill, eds.), Cambridge: Cambridge University Press, pp. 30–85.
- Weiskrantz, L., 1972. Behavioural analysis of the monkey’s visual nervous system (review lecture), *Proc. R. Soc. B*, 182:427–455.
- Weiskrantz, L., 1980. Varieties of residual experience, *Q. J. Exp. Psychol.*, 32:365–386.
- Weiskrantz, L., 1986. *Blindsight. A Case Study and Implications*. Oxford: Oxford University Press, 1986. (New paperback edition, 1998.)
- Weiskrantz, L., 1987. Residual vision in a scotoma: a follow-up study of “form” discrimination, *Brain*, 110:77–92.
- Weiskrantz, L., 1990. Outlooks for blindsight: explicit methodologies for implicit processes. The Ferrier Lecture, *Proc. R. Soc. B*, 239:247.
- Weiskrantz, L., 1991. Disconnected awareness in detecting, processing, and remembering in neurological patients. The Hughlings Jackson Lecture, *J. R. Soc. Med.*, 84:477–470.
- Weiskrantz, L., 1997. *Consciousness Lost and Found. A Neuropsychological Exploration*, Oxford: Oxford University Press.
- Weiskrantz, L., 1998a. *Blindsight. A Case Study and Implications*, 2nd ed. (1986 ed. with additional material).
- Weiskrantz, L., 1998b. Consciousness and commentaries, in *Towards a Science of Consciousness II—The Second Tucson Discussions and Debates* (S. R. Hameroff, A. W. Kaszniak, and A. C. Scott, eds.), Cambridge: MIT Press, pp. 371–377.
- Weiskrantz, L., 1998c. Pupillary responses with and without awareness in blindsight, *Consciousness Cogn.*, 7:324–326.
- Weiskrantz, L., 2000. Blindsight: implications for the conscious experience of emotion, in *Cognitive Neuroscience of Emotion* (R. Lane, G. Ahern, J. Allen, A. Kaszniak, L. Nadel, S. Rapsak, and G. Schwartz, eds.), New York: Oxford University Press, pp. 277–295.
- Weiskrantz, L., 2001a. Putting beta (β) on the back burner, in *Out of Mind* (B. DeGelder, E. DeHaan, and C. A. Heywood, eds.), Oxford: Oxford University Press.

- Weiskrantz, L., 2001b. Blindsight, in *Handbook of Neuropsychology*, 2nd ed., vol. 4 (M. Behrmann, ed.). Amsterdam: Elsevier.
- Weiskrantz, L., J. L. Barbur, and A. Sahraie, 1995. Parameters affecting conscious versus unconscious visual discrimination without V1, *Proc. Natl. Acad. Sci. USA*, 92:6122–6126.
- Weiskrantz, L., and A. Cowey, 1970. Filling in the scotoma: a study of residual vision after striate cortex lesions in monkeys, in *Progress in Physiological Psychology*, vol. 3 (F. Stellar and J. M. Sprague, eds.), New York: Academic Press, pp. 237–260.
- Weiskrantz, L., A. Cowey, and J. L. Barbur, 1999. Differential pupillary constriction and awareness in the absence of striate cortex, *Brain*, 122:1533–1538.
- Weiskrantz, L., A. Cowey, and C. Le Mare, 1998. Learning from the pupil: a spatial visual channel in the absence of V1 in monkey and human, *Brain*, 121:1065–1072.
- Weiskrantz, L., A. Cowey, and C. Passingham, 1977. Spatial responses to brief stimuli by monkeys with striate cortex ablations, *Brain*, 100:655–670.
- Weiskrantz, L., A. Harlow, and J. L. Barbur, 1991. Factors affecting visual sensitivity in a hemianopic subject, *Brain*, 114:2269–2282.
- Weiskrantz, L., E. K. Warrington, M. D. Sanders, and J. Marshall, 1974. Visual capacity in the hemianopic field following a restricted occipital ablation, *Brain*, 97:709–728.
- Wessinger, C. M., R. Fendrich, and M. S. Gazzaniga, 1997. Islands of residual vision in hemianopic patients, *J. Cogn. Neurosci.*, 9:203–221.
- Yukie, M., and E. Iwai, 1981. Direct projection from dorsal lateral geniculate nucleus to the prestriate cortex in macaque monkeys, *J. Comp. Neurol.*, 201:81–97.
- Zeki, S., 1978. Functional specialization in the visual cortex of the rhesus monkey, *Nature (Lond.)*, 274:423–428.
- Zeki, S., 1993. *A Vision of the Brain*, Oxford: Blackwell Scientific.
- Zihl, J., 1980. “Blindsight”: improvement of visually guided eye movements by systematic practice in patients with cerebral blindness, *Neuropsychologia*, 18:71–77.
- Zihl, J., 1981. Recovery of visual functions in patients with cerebral blindness, *Exp. Brain Res.*, 44:159–169.
- Zihl, J., 2000. *Rehabilitation of Visual Disorders After Brain Injury*. Psychology Press.
- Zihl, J., F. Tretter, and W. Singer, 1980. Phasic electrodermal responses after visual stimulation in the cortically blind hemi-field, *Behav. Brain Res.*, 1:197–203.
- Zihl, J., and D. von Cramon, 1979. Restitution of visual function in patients with cerebral blindness, *J. Neurol. Neurosurg. Psychiatry*, 42:312–322.
- Zihl, J., and D. von Cramon, 1985. Visual field recovery from scotoma in patients with postgeniculate damage: a review of 55 cases, *Brain*, 108:313–340.

VI PROCESSING IN PRIMARY VISUAL CORTEX

41 Functional Connectivity in the Pathway from Retina to Striate Cortex

R. CLAY REID AND W. MARTIN USREY

BECAUSE THE TERM has been used in many different ways, it is important to define *functional connectivity* as it pertains to the early visual pathway: from retina to lateral geniculate nucleus to visual cortex. Although functional connectivity can simply refer to neuronal connections that function, we prefer to use it in much the same way that Hubel and Wiesel (1962, 1977) used the term *functional architecture*. Functional architecture refers to the way anatomical organization relates to neuronal function, such as retinotopy, ocular dominance, or orientation selectivity. Similarly, functional connectivity can be thought of as the presence (or absence) of connections between neurons as they relate to the neurons' visual functions.

Although any use of the term *connectivity* implies that there is a physiological relationship between the neurons (or groups of neurons), it could have many other connotations. Connectivity has been used to describe neurons that are related by a polysynaptic chain and even more loosely for neurons that tend to be coactive. For our purposes, we will use the term *connected* only for pairs of neurons for which the existence of a working synapse has been demonstrated physiologically. The presence of monosynaptic connections between neurons studied in vivo has been revealed almost exclusively with the tool of cross-correlation analysis. While cross-correlations in general cannot demonstrate causal relationships between neurons, in strictly feedforward pathways, monosynaptic connections can be demonstrated with a high degree of certainty (Reid, 2001; Usrey and Reid, 1999).

The distinction between anatomy and functional connectivity must be emphasized. At the finest level of detail, anatomy can show a morphological synapse, but it cannot demonstrate the physiological correlates of the synapse. More importantly for our purposes, anatomy (except in the retina) cannot be used to define the receptive field of a neuron. For instance, in the lateral geniculate nucleus (LGN) of the cat, current anatomical knowledge and techniques allow us to determine whether a projection neuron is an X cell or a Y cell, but not whether it is ON-center or OFF-center or the exact position of its receptive field. Therefore, physiological experiments are necessary to study the function of any given LGN cell.

In this chapter, we will concentrate on the visual system of the cat (particularly the X cell pathway) because of the detailed knowledge of its anatomy, visual physiology, and functional connectivity. For other species, in particular Old World primates, the anatomy and visual physiology of the pathway from retina through layer 4 of visual cortex are perhaps equally well understood. It is only in the cat, however, that functional connectivity as we have defined it has been studied.

In the cat retino-geniculo-cortical pathway, receptive fields of visual neurons are strongly suggestive of the pattern of connections that might be found between each level. In both retina and LGN, neurons have concentric receptive fields with centers, either ON or OFF, and antagonistic surrounds (Hubel and Wiesel, 1962; Kuffler, 1953). Thus, neurons are classified as either ON-center/OFF-surround or OFF-center/ON-surround. In the principal laminae of the LGN, A and A1, these neurons are further classified as either X cells or Y cells on the basis of additional response criteria. X cells sum their visual inputs in a linear fashion and have sustained responses with longer latencies between stimulus and response. Y cells have nonlinear spatial summation and more transient responses with shorter latencies. Because there is very little difference between the receptive fields encountered in the retina and LGN, it has been tempting to speculate that the connections between retinal ganglion cells and geniculate neurons serve the purpose of preserving the center/surround receptive field.

In contrast, in the pathway from LGN to visual cortex there are dramatic transformations in receptive field structure. These transformations are perhaps best documented and most pronounced in the cat (Hubel and Wiesel, 1962), in which a new receptive field type emerges in layer 4: the simple cell. Simple cells have elongated receptive fields with adjacent ON and OFF subregions. They respond best to bars or edges of light of a specific orientation, while their geniculate inputs respond well to stimuli of all orientations. Based on the structure of LGN receptive fields and simple cell receptive fields, Hubel and Wiesel (1962) proposed a straightforward model for the construction of simple cell receptive fields: simple cells receive convergent input from multiple LGN cells whose receptive fields are of the same

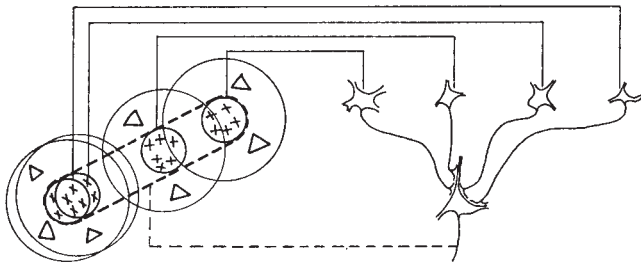


FIGURE 41.1. The Hubel and Wiesel model for the generation of simple cell receptive fields. On the lower right is a simple cell that receives convergent input from multiple LGN cells (only four are shown). The LGN cells have receptive fields that are the same sign (in this example, ON center) and are located along a line of visual space. This organization of LGN input gives the simple cell a receptive field with an elongated ON subregion (indicated by the interrupted lines in the receptive field diagram) and two adjacent OFF subregions. (From Hubel and Wiesel, 1962.)

sign and fall along a line of visual space (Fig. 41.1). Although this model is now generally accepted (Chapman et al., 1991; Ferster et al., 1996; Reid and Alonso, 1995), it was the source of tremendous controversy for over 35 years. As this chapter will show, the study of functional connectivity was key to demonstrating the relationship between geniculate and cortex in terms of how simple cell receptive fields are constructed.

Functional connectivity between retina and LGN: anatomical considerations

Despite the central importance of physiological experiments in the study of functional connectivity, anatomy is of course necessary to put physiological studies in context. The anatomy of a feedforward pathway can be studied at multiple levels of detail. At the broadest level, anatomical techniques can simply demonstrate the existence of a projection pathway, as has been known since classical times for the retinogeniculate pathway (Wade, 1998). Next, slightly finer techniques can be used to trace the projections of smaller groups of neurons, as was done in early studies that demonstrated the retinotopic mapping in the LGN and visual cortex (Le Gros Clark and Penman, 1934; Polyak, 1933). At the next level, single-cell labeling techniques (Golgi, horseradish peroxidase, biocytin) can be used to elucidate the structures of dendritic trees or of axonal arbors. Finally, individual synapses between neurons can be identified either with electron microscopy (Famiglietti and Peters, 1972; Guillery, 1969; Hamos et al., 1987; Mason et al., 1984) or, increasingly, with multiple-label confocal microscopy (e.g., Mills and Massey, 1999).

Although it would be difficult to use anatomy to study functional connectivity, as we have defined it, in the retinogeniculate pathway, our current knowledge of anatomy

allows us to approximate the range of convergent and divergent connections that might be made. Specifically, anatomy allows us to define an upper limit of the number of ganglion cell inputs to an LGN neuron or the number of LGN neurons receiving input from a single ganglion cell. These numbers can be derived in several different ways.

In visual neuroscience, the *coverage factor* has generally been defined as the number of neurons of a certain class whose receptive fields overlap a given point in visual space. A second use of the term is in the context of anatomy: the number of axons or dendrites of a given class that overlap in a given position within a neural structure. For retinal ganglion cells, anatomical and physiological coverage factors are closely related, because receptive-field centers are roughly equal in area to a ganglion cell's dendritic arbor (Wässle et al., 1983; see DeVries and Baylor, 1997).

The anatomical coverage factor is derived by first counting the number of retinal ganglion cells of a given class in 1 mm^2 of retina and then determining the average area occupied by each dendritic arbor. The product of these values yields the total dendritic area of all ganglion cells per square millimeter of retina, which is equivalent to the average number of dendritic arbors that overlap any point. The anatomical coverage factor for β cells in the cat retina (which correspond to X cells) is roughly 3 (Wässle et al., 1981).

Although the retinal coverage factor will in fact prove important for our discussion of the pathway between LGN and cortex, coverage factors in the LGN are more pertinent to our discussion of the retinogeniculate pathway. Although less has been written specifically about geniculate coverage factors (both by ganglion cell arbors and by geniculate dendritic trees), they can be calculated from values in the literature.

The total surface area of the A laminae in the LGN (A plus A1) is roughly 80 mm^2 (10 by $4\text{ mm} \times 2$; Sanderson, 1971), and there are approximately 100,000 X cells in the retina (reviewed in Peters and Payne, 1993); therefore, there are roughly 1250 retinal arbors per square millimeter in each lamina. The axonal arbor of each ganglion cell terminates throughout the thickness of its appropriate layer, but the cross-section is roughly circular, with a diameter of 0.1 mm (area = 0.008 mm^2) (Sur et al., 1984, 1987). The coverage factor of retinal axonal arbors in the LGN is therefore $1250 \times .008 = 10$. The dendritic trees of X-cell relay neurons in the LGN have the same dimensions as the retinal axonal arbors, but because there are roughly 2.5 more relay neurons in the X-cell system than retinal afferents (Peters and Payne, 1993), the coverage factor is 2.5 times greater. In other words, a single dendritic spine of an X cell in the LGN is within the terminal arbors of ~ 10 retinal ganglion X cells, while a single presynaptic bouton is within the dendritic trees of ~ 25 relay neurons. Therefore, simply from the

morphology of single neurons, the total area of the LGN, and the number of neurons, we have bounded the possible values of divergent and convergent inputs in the retinogeniculate system. Each LGN neuron could receive convergent input from more than 10 retinal neurons (because the dendritic arbor is not a single point). Each retinal neuron could diverge to form synapses onto at least 25 relay neurons. Although these morphological features would allow each relay neuron to receive inputs from many different afferents, only a few specific connections are made onto each cell. This specificity is seen physiologically (Cleland et al., 1971a, 1971b; Lee et al., 1977; Usrey et al., 1999; see below), and has also been demonstrated in a heroic ultrastructural study (Hamos et al., 1987) that found that a given retinal afferent makes synapses on fewer than 10% of potential targets in the LGN.

Functional connectivity between retina and LGN: physiological studies

An early indication that LGN neurons receive strong input from one or a few retinal ganglion cells with similar receptive fields came from the early work of Hubel and Wiesel (1961). By recording and comparing action potentials and S-potentials—the synaptic potential evoked by a strong retinal input (Bishop et al., 1958, 1962; Freygang, 1958; Kaplan and Shapley, 1984)—of individual LGN neurons, they demonstrated that connected cell pairs have receptive fields that overlap spatially and have the same response sign (ON or OFF). The major difference between geniculate receptive fields and retinal receptive fields is in the strength of their surrounds. Surround responses from geniculate cells are stronger than surround responses from retinal ganglion cells. By comparing the receptive field of a geniculate neuron's S-potential to the receptive field of the neuron's action potential, a number of more recent studies performed in both cat and monkey have demonstrated that geniculate neurons and their strongest retinal inputs are similar in terms of color selectivity, contrast sensitivity, and X/Y classification (Kaplan et al., 1987; Lee et al., 1983; Reid and Shapley, 1992; So and Shapley, 1981).

One drawback of using S-potentials as a measure of retinal input to a geniculate neuron is the fact that S-potentials can only be measured from retinal inputs that provide very strong input to the geniculate neuron; S-potentials cannot be measured from retinal inputs that provide moderate or weak input. Given this knowledge, it should not be surprising that geniculate neurons and their strongest retinal inputs have very similar receptive fields. By recording directly from the retina and LGN, one can compare the receptive fields of connected neurons, regardless of the strength of their connection. This dual recording technique was pioneered by Levick and colleagues (Cleland

et al., 1971a, 1971b; Levick et al., 1972). By moving the retinal electrode to record from different neurons, they demonstrated that it was possible to compare the receptive fields of multiple presynaptic neurons that converge onto a single geniculate neuron. More recently, the method of dual recording was revisited for the specific purpose of determining the specificity of both strong and weak connections from ganglion cells to geniculate neurons, as determined by cross-correlation analysis (Usrey et al., 1999). As expected, these studies demonstrated that receptive fields of strongly connected cell pairs are very similar in terms of spatial location, response sign, and X/Y classification (Fig. 41.2). In addition, these studies found that even weakly connected pairs are almost always from same-sign retinal cells with partially overlapping receptive fields. In summary, as the similarity between receptive fields decreases, so does the likelihood of connection and the strength of connection.

Functional connectivity between LGN and visual cortex: anatomical considerations

As with the retinogeniculate projection, the convergence and divergence of geniculate inputs onto their cortical targets can be estimated on anatomical grounds. First, the anatomical coverage factor of the thalamic afferents can give an upper bound for the degree of convergence. As reviewed by Peters and Payne (1993), an upper bound for this value can be obtained by multiplying the total number of afferents by the size of their axonal arbors and then dividing by the total cortical area ($240,000 \text{ cells} \times 0.6\text{--}0.9\text{mm}^2$, $399\text{mm}^2 = 360\text{--}540 \text{ cells}$).

The dendrites of stellate cells in layer 4 of cat visual cortex are similar in extent to the axonal arbors of the X-cell afferents, but there are roughly 50 times more stellate cells ($10\text{--}12 \times 10^6$; Beaulieu and Colonnier, 1987; Peters and Yilmaz, 1993) than there are X-cell afferents. The anatomical coverage factor is thus roughly 50 times higher: approximately 18,000–27,000. Therefore, the upper limit of *divergence* would be extremely large, were it not limited by the total number of boutons made by each X-cell arbor: roughly 3300. Even if each X cell never made more than one synapse onto each layer 4 neuron, it would contact only a fraction of potential targets.

An upper bound for the *convergence* onto each potential target in layer 4 can be estimated by similar arguments. Again following Peters and Payne (1993), this number can be estimated by considering the number of synapses from each thalamic afferent. The strategy is first to estimate the total number of geniculate synapses to all of area 17 and then to divide this value by the total number of potential targets. There are roughly 3300 synapses per X-cell arbor (Freund et al., 1985; Humphrey et al., 1985), which gives a total of 8×10^8 synapses for the afferent pool of 240,000 X

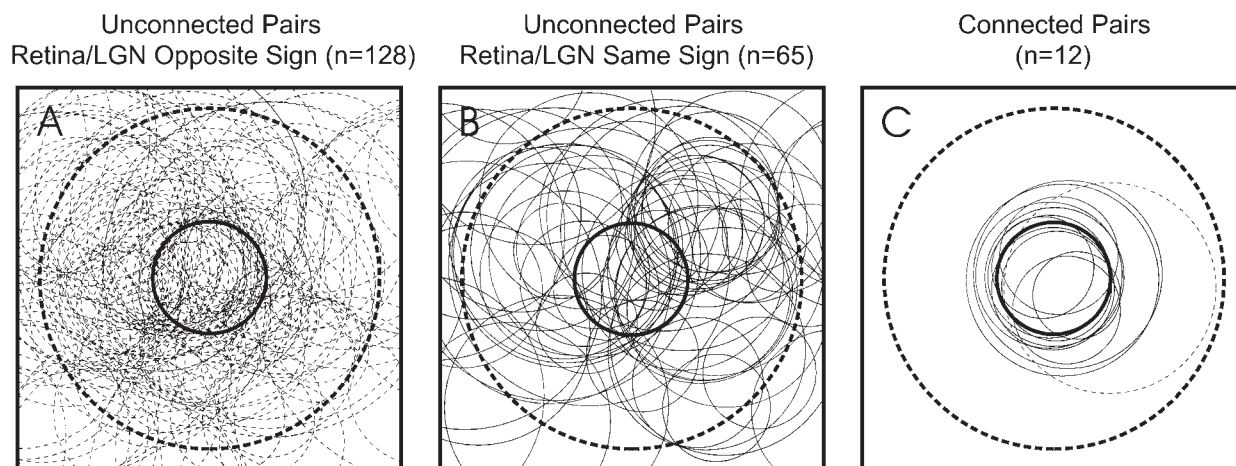


FIGURE 41.2. Summary of the specificity and strength of retinal ganglion cell input LGN neurons. Summary diagrams showing the spatial relationship of receptive fields of (A) unconnected retinal ganglion cells and LGN neurons with opposite (ON versus OFF) response signs, (B) unconnected retinal ganglion cells and LGN

neurons with the same response sign, and (C) connected pairs. In panels A–C, thick circles correspond to the LGN receptive field. Receptive fields were mapped using a white-noise stimulus; connectivity was assessed using cross-correlation analysis. (From Usrey et al., 1999.)

cells. Although we are emphasizing the X-cell pathway, Y cells provide a roughly equal number of synapses onto neurons in layer 4. Therefore, assuming that all cells in layer 4 receive an equal number of thalamic inputs, there are on the order of 150 afferent synapses per layer 4 neuron (16×10^8 synapses, 11×10^6 neurons). This value must be corrected by taking into account synapses onto apical dendrites from other layers that extend into layer 4. As outlined by Peters and Payne (1993), only 62.5% of synapses in layer 4 are onto layer 4 neurons. Therefore, a spiny stellate cell in layer 4 receives approximately 100 synapses from the LGN ($150 \times 62.5\%$).

Given approximately 100 geniculate synapses onto any given neuron in layer 4, one can then ask how many different inputs there might be. Although it is extremely difficult to approach this question anatomically, one ultrastructural study of thalamic input to individual layer 4 neurons provides some insight into the question. Freund et al. (1985) counted the number of synapses made by an individual geniculate axon onto four different cortical neurons in area 17 and found only one synapse per neuron in three cases and eight in the other case. From this very small sampling, the number of different thalamic afferents that converge onto a cortical target could therefore range between the extreme values of more than 10 to somewhat less than 100.

Functional connectivity between LGN and visual cortex: physiological studies

In primary visual cortex of the cat, two major cell types are distinguished on the basis of receptive field structure—simple cells and complex cells (Hubel and Wiesel, 1962). Simple cells, the dominant cell type in layer 4 (Gilbert, 1977),

have elongated receptive fields with separate and adjacent ON and OFF subregions. By contrast, complex cells generally have receptive fields with overlapping ON and OFF subregions. Both cell types respond best to oriented bars or edges of light. Based on the structure of LGN receptive fields (center/surround) and simple cell receptive fields, Hubel and Wiesel (1962) proposed a simple hierarchical model. According to this model, simple cells receive convergent input from multiple LGN cells whose receptive fields have the same sign and are located along a line of visual space (Fig. 41.1). This model could account for the adjacent ON and OFF subregions of the simple cell as well as the orientation selectivity of simple cells. In a similar hierarchical fashion, Hubel and Wiesel (1962) also suggested that complex receptive fields could be constructed via convergence of multiple simple cells.

Early studies examining the connections between the LGN and visual cortex used electrical stimulation to geniculate fibers to determine the functional targets of geniculate projections. As expected from the anatomy, these studies demonstrated that simple cells indeed receive monosynaptic input from the LGN (Bullier and Henry, 1979a, 1979b, 1979c; Creutzfeldt and Ito, 1968; Ferster and Lindstrom, 1983; Martin and Whitteridge, 1984; Singer et al., 1975; Stone and Dreher, 1973).

While electrical stimulation provided strong evidence for monosynaptic input to simple cells, it was unable to demonstrate either the strength of single inputs or their receptive-field properties. These difficulties were overcome by recording simultaneously the responses of cortical cells and their geniculate afferents and performing cross-correlation analysis between spike trains (Alonso et al., 2001; Reid and Alonso, 1995; Tanaka, 1983, 1985). Using this approach,

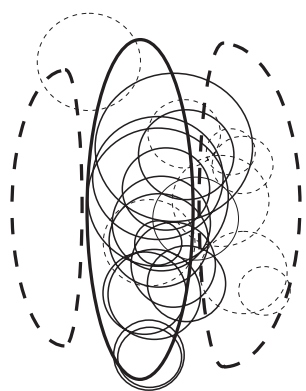


FIGURE 41.3. Summary diagram showing the relationship between the receptive fields of monosynaptically connected pairs of LGN cells and simple cells. To generate this diagram, the receptive field of each simple cell was transformed into a stylized receptive field (shown in the figure with a central subregion, indicated with solid lines, flanked by two adjacent subregions of opposite sign, indicated with dashed lines). The circles indicate the relative size, sign, and locations of the receptive field centers of monosynaptically connected LGN cells. Of the 23 pairs of connected cells (out of a total of 74 pairs recorded), very few mismatches in the sign of overlapping receptive fields were found. Receptive fields were mapped using a white-noise stimulus; connectivity was assessed using cross-correlation analysis. (From Reid and Alonso, 1995, 1996).

Tanaka demonstrated that individual connections were fairly strong—often accounting for up to 10% of the spikes in a simple cell—and that connected cells had appropriately overlapped receptive fields. In addition, Tanaka demonstrated that both X and Y afferents as well as both ON and OFF geniculate cells could project to the same simple cell. While this study demonstrated that LGN neurons with appropriately overlapping receptive fields provide monosynaptic input to a simple cell, the study did not systematically explore the factors determining whether a specific afferent would be connected to any given cortical target.

Implicit in the Hubel and Wiesel model is that certain geniculate afferents should have a high probability of connection to a particular simple cell, while others should not. Reid and colleagues specifically tested this assumption by examining the relationship between receptive field overlap and the probability of connection, again as assessed with cross-correlation analysis (Alonso et al., 2001; Reid and Alonso, 1995; Fig. 41.3). On average, 33% of cells are connected if their receptive fields overlap in any way. More specifically, these studies demonstrated that connections are made between pairs of cells when the signs (ON or OFF) of the overlapping portions of the receptive fields are the same. The probability of connection is greatest, approaching 100%, when the center of an LGN receptive field perfectly overlaps the exact center of a simple subregion. Conversely, inappropriate connections are rarely made between LGN

neurons and simple cells. Restated, if the receptive field of an LGN cell is nonoverlapping or of the opposite sign (ON versus OFF) of an overlapped simple-cell subregion, monosynaptic connections are almost never made.

These studies indicate that roughly 30 LGN afferents synapse onto any given layer 4 neuron. This value is obtained by multiplying the probability of connection (33%) by the total number of thalamic X cells whose receptive field centers overlap the simple cell receptive field in any way ($n = 90$; see Alonso et al., 2001).

Although the spatial outline of a simple receptive field is consistent with the aggregate thalamic input, this does not mean that the responses of simple cells are entirely determined by this thalamic input. Intracortical processing, both excitatory and inhibitory, of course, plays an important role (Douglas et al., 1995; Ferster and Miller, 2000; Sillito et al., 1980; Somers et al., 1995; Sompolinsky and Shapley, 1997). For instance, recent intracellular studies have validated the earlier idea that simple cell subregions are formed by a push/pull mechanism: ON excitation superimposed with OFF inhibition and vice versa (Ferster, 1988; Hirsch et al., 1998; Hubel and Wiesel, 1962; Palmer and Davis, 1981; Tolhurst and Dean, 1987; but see Borg-Graham et al., 1998).

Concluding remarks

In summary, we have examined how neuroanatomy can provide upper and lower bounds for the number of connections between neurons in the retino-geniculo-cortical pathway. These bounds, however, are extremely broad. Further, anatomical results provide only limited information about the physiology of the neurons being studied. Functional connectivity—the relationship between neuronal function (receptive fields) and synaptic connections—is currently a topic that can be addressed only with physiological experiments. In the pathway from retina through LGN to visual cortex, the connections made are strongly determined by the receptive fields of pre- and postsynaptic neurons. This finding is perhaps tautological for the strongest inputs to a cell, which can be seen as determining its receptive field. For weak inputs such as most LGN inputs to a simple cell, however, connections could be made without significantly perturbing the receptive field structure of the target neuron. Nonetheless, virtually no inappropriate synapses are made, although the axons of inappropriate inputs are intertwined with the dendrites of any given target neuron.

The approach we have described works best in the early visual system, before recurrent pathways and divergence make correlations between the spike trains of neurons difficult to interpret in terms of individual synaptic connections. So far, functional connectivity has been studied only from retina to LGN, from LGN to layer 4, and, most recently, from layer 4 to the superficial layers of visual cortex (Alonso

and Martinez, 1998). Pushing this line of research deeper into the cortical processing stream remains a challenge for the future.

REFERENCES

- Alonso, J. M., and L. M. Martinez, 1998. Functional connectivity between simple cells and complex cells in cat striate cortex, *Nat. Neurosci.*, 1:395–403.
- Alonso, J. M., W. M. Usrey, and R. C. Reid, 2001. Rules of connectivity between geniculate cells and simple cells in cat primary visual cortex, *J. Neurosci.*, 21:4002–4015.
- Beaulieu, C., and M. Colonnier, 1987. Effect of the richness of the environment on the cat visual cortex, *J. Comp. Neurol.*, 266:478–494.
- Bishop, P. O., W. Burke, and R. Davis, 1958. Synapse discharge by single fibre in mammalian visual system, *Nature*, 128:728–730.
- Bishop, P. O., W. Burke, and R. Davis, 1962. The interpretation of the extracellular response of single lateral geniculate cells, *J. Physiol.*, 162:451–472.
- Borg-Graham, L. J., C. Monier, and Y. Fregnac, 1998. Visual input evokes transient and strong shunting inhibition in visual cortical neurons, *Nature*, 393:369–373.
- Bullier, J., and G. H. Henry, 1979a. Laminar distribution of first-order neurons and afferent terminals in cat striate cortex, *J. Neurophysiol.*, 42:1271–1281.
- Bullier, J., and G. H. Henry, 1979b. Neural path taken by afferent streams in striate cortex of the cat, *J. Neurophysiol.*, 42:1264–1270.
- Bullier, J., and G. H. Henry, 1979c. Ordinal position of neurons in cat striate cortex, *J. Neurophysiol.*, 42:1251–1263.
- Chapman, B., K. R. Zahs, and M. P. Stryker, 1991. Relation of cortical cell orientation selectivity to alignment of receptive fields of the geniculocortical afferents that arborize within a single orientation column in ferret visual cortex, *J. Neurosci.*, 11:1347–1358.
- Clark, W. E., Le Gros, and G. G. Penman, 1934. The projection of the retina in the lateral geniculate body, *Proc. R. Soc. Lond. B*, 114:291–313.
- Cleland, B. G., M. W. Dubin, and W. R. Levick, 1971a. Simultaneous recording of input and output of lateral geniculate neurones, *Nature New Biol.*, 231:191–192.
- Cleland, B. G., M. W. Dubin, and W. R. Levick, 1971b. Sustained and transient neurones in the cat's retina and lateral geniculate nucleus, *J. Physiol.*, 217:473–496.
- Creutzfeldt, O., and M. Ito, 1968. Functional synaptic organization of primary visual cortex neurones in the cat, *Exp. Brain Res.*, 6:324–352.
- DeVries, S. H., and D. A. Baylor, 1997. Mosaic arrangement of ganglion cell receptive fields in rabbit retina, *J. Neurophysiol.*, 78:2048–2060.
- Douglas, R. J., C. Koch, M. Mahowald, K. A. Martin, and H. H. Suarez, 1995. Recurrent excitation in neocortical circuits, *Science*, 269:981–985.
- Famiglietti, E. V., Jr., and A. Peters, 1972. The synaptic glomerulus and the intrinsic neuron in the dorsal lateral geniculate nucleus of the cat, *J. Comp. Neurol.*, 144:285–334.
- Ferster, D., 1988. Spatially opponent excitation and inhibition in simple cells of the cat visual cortex, *J. Neurosci.*, 8:1172–1180.
- Ferster, D., S. Chung, and H. Wheat, 1996. Orientation selectivity of thalamic input to simple cells of cat visual cortex, *Nature*, 380:249–252.
- Ferster, D., and S. Lindstrom, 1983. An intracellular analysis of geniculo-cortical connectivity in area 17 of the cat, *J. Physiol. (Lond.)*, 342:181–215.
- Ferster, D., and K. D. Miller, 2000. Neural mechanisms of orientation selectivity in the visual cortex, *Annu. Rev. Neurosci.*, 23:441–471.
- Freund, T. F., K. A. Martin, and D. Whitteridge, 1985. Innervation of cat visual areas 17 and 18 by physiologically identified X- and Y-type thalamic afferents. I. Arborization patterns and quantitative distribution of postsynaptic elements, *J. Comp. Neurol.*, 242:263–274.
- Freygang, W. H., Jr., 1958. An analysis of extracellular potentials from single neurons in the lateral geniculate nucleus of the cat, *J. Gen. Physiol.*, 41:543–564.
- Gilbert, C. D., 1977. Laminar differences in receptive field properties of cells in cat primary visual cortex, *J. Physiol.*, 268:391–421.
- Guillery, R. W., 1969. A quantitative study of synaptic interconnections in the dorsal lateral geniculate nucleus of the cat, *Z. Zellforsch.*, 96:39–48.
- Hamos, J. E., S. C. Van Horn, D. Raczkowski, and S. M. Sherman, 1987. Synaptic circuits involving an individual retinogeniculate axon in the cat, *J. Comp. Neurol.*, 259:165–192.
- Hirsch, J. A., J. M. Alonso, R. C. Reid, and L. M. Martinez, 1998. Synaptic integration in striate cortical simple cells, *J. Neurosci.*, 18:9517–9528.
- Hubel, D. H., and T. N. Wiesel, 1961. Integrative action in the cat's lateral geniculate body, *J. Physiol.*, 155:385–398.
- Hubel, D. H., and T. N. Wiesel, 1962. Receptive fields, binocular interaction and functional architecture in the cat's visual cortex, *J. Physiol. (Lond.)*, 160:106–154.
- Hubel, D. H., and T. N. Wiesel, 1977. Functional architecture of macaque monkey visual cortex, *Proc. R. Soc. Lond. B*, 198:1–59.
- Humphrey, A. L., M. Sur, D. J. Uhlrich, and S. M. Sherman, 1985. Projection patterns of individual X- and Y-cell axons from the lateral geniculate nucleus to cortical area 17 in the cat, *J. Comp. Neurol.*, 233:159–189.
- Kaplan, E., K. Purpura, and R. M. Shapley, 1987. Contrast affects the transmission of visual information through the mammalian lateral geniculate nucleus, *J. Physiol.*, 391:267–288.
- Kaplan, E., and R. Shapley, 1984. The origin of the S (slow) potential in the mammalian lateral geniculate nucleus, *Exp. Brain Res.*, 55:111–116.
- Kuffler, S., 1953. Discharge patterns and functional organization of mammalian retina, *J. Neurophysiol.*, 16:37–68.
- Lee, B. B., B. G. Cleland, and O. D. Creutzfeldt, 1977. The retinal input to cells in area 17 of the cat's cortex, *Exp. Brain Res.*, 30:527–538.
- Lee, B. B., V. Virsu, and O. D. Creutzfeldt, 1983. Linear signal transmission from prepotentials to cells in the macaque lateral geniculate nucleus, *Exp. Brain Res.*, 52:50–56.
- Levick, W. R., B. G. Cleland, and M. W. Dubin, 1972. Lateral geniculate neurons of cat: retinal inputs and physiology, *Invest. Ophthalmol.*, 11:302–311.
- Martin, K. A., and D. Whitteridge, 1984. Form, function and intracortical projections of spiny neurones in the striate visual cortex of the cat, *J. Physiol. (Lond.)*, 353:463–504.
- Mason, C. A., R. W. Guillery, and M. C. Rosner, 1984. Patterns of synaptic contact upon individually labeled large cells of the dorsal lateral geniculate nucleus of the cat, *Neuroscience*, 11:319–329.

- Mills, S. L., and S. C. Massey 1999. AII amacrine cells limit scotopic acuity in central macaque retina: a confocal analysis of calretinin labeling, *J. Comp. Neurol.*, 411:19–34.
- Palmer, L. A., and T. L. Davis, 1981. Receptive-field structure in cat striate cortex, *J. Neurophysiol.*, 46:260–276.
- Peters, A., and B. R. Payne, 1993. Numerical relationships between geniculocortical afferents and pyramidal cell modules in cat primary visual cortex, *Cereb. Cortex*, 3:69–78.
- Peters, A., and E. Yilmaz, 1993. Neuronal organization in area 17 of cat visual cortex, *Cereb. Cortex*, 3:49–68.
- Polyak, S. D., 1933. A contribution to the cerebral representation of the retina, *J. Comp. Neurol.*, 57:541–617.
- Reid, R. C., 2001. Divergence and reconvergence: multielectrode analysis of feedforward connections in the visual system, *Prog. Brain. Res.*, 130:141–154.
- Reid, R. C., and J. M. Alonso, 1995. Specificity of monosynaptic connections from thalamus to visual cortex, *Nature*, 378:281–284.
- Reid, R. C., and J. M. Alonso, 1996. The processing and encoding of information in the visual cortex, *Curr. Opin. Neurobiol.* 6:475–480.
- Reid, R. C., and R. M. Shapley, 1992. Spatial structure of cone inputs to receptive fields in primate lateral geniculate nucleus, *Nature*, 356:716–718.
- Sanderson, K. J., 1971. The projection of the visual field to the lateral geniculate and medial interlaminar nuclei in the cat, *J. Comp. Neurol.*, 143:101–108.
- Sillito, A. M., J. A. Kemp, J. A. Milson, and N. Berardi, 1980. A re-evaluation of the mechanisms underlying simple cell orientation selectivity, *Brain Res.*, 194:517–520.
- Singer, W., F. Tretter, and M. Cynader, 1975. Organization of cat striate cortex: a correlation of receptive-field properties with afferent and efferent connections, *J. Neurophysiol.*, 38:1080–1098.
- So, Y. T., and R. M. Shapley, 1981. Spatial tuning of cells in and around lateral geniculate nucleus of the cat: X and Y relay cells and perigeniculate interneurons, *J. Neurophysiol.*, 45:107–120.
- Somers, D. C., S. B. Nelson, and M. Sur, 1995. An emergent model of orientation selectivity in cat visual cortical simple cells, *J. Neurosci.*, 15:5448–5465.
- Sompolinsky, H., and R. M. Shapley, 1997. New perspectives on the mechanisms for orientation selectivity, *Curr. Opin. Neurobiol.*, 7:514–522.
- Stone, J., and B. Dreher, 1973. Projection of X- and Y-cells of the cat's lateral geniculate nucleus to areas 17 and 18 of visual cortex, *J. Neurophysiol.*, 36:551–567.
- Sur, M., M. Esguerra, P. E. Garraghty, M. F. Kritzer, and S. M. Sherman, 1987. Morphology of physiologically identified retinogeniculate X- and Y-axons in the cat, *J. Neurophysiol.*, 58:1–32.
- Sur, M., R. E. Weller, and S. M. Sherman, 1984. Development of X- and Y-cell retinogeniculate terminations in kittens, *Nature*, 310:246–249.
- Tanaka, K., 1983. Cross-correlation analysis of geniculostriate neuronal relationships in cats, *J. Neurophysiol.*, 49:1303–1318.
- Tanaka, K., 1985. Organization of geniculate inputs to visual cortical cells in the cat, *Vis. Res.*, 25:357–364.
- Tollhurst, D. J., and A. F. Dean, 1987. Spatial summation by simple cells in the striate cortex of the cat, *Exp. Brain Res.*, 66:607–620.
- Usrey, W. M., and R. C. Reid, 1999. Synchronous activity in the visual system, *Annu. Rev. Physiol.*, 61:435–456.
- Usrey, W. M., J. B. Reppas, and R. C. Reid, 1999. Specificity and strength of retinogeniculate connections, *J. Neurophysiol.*, 82:3527–3540.
- Wade, N. J., 1998. *A Natural History of Vision*, Cambridge: MIT Press.
- Wässle, H., B. B. Boycott, and R. B. Illing, 1981. Morphology and mosaic of on- and off-beta cells in the cat retina and some functional considerations, *Proc. R. Soc. Lond. B Biol. Sci.*, 212:177–195.
- Wässle, H., L. Peichl, and B. B. Boycott, 1983. A spatial analysis of on- and off-ganglion cells in the cat retina, *Vis. Res.*, 23:1151–1160.

42 Cell Types and Local Circuits in Primary Visual Cortex of the Macaque Monkey

EDWARD M. CALLAWAY

A MAJOR AIM OF VISION research is to understand how neural circuits mediate the computations that underlie visual perception. Since the visual response properties of cortical neurons arise largely as a consequence of the organization and function of their connections with other neurons, it is believed that understanding how neural circuits give rise to the specific visual response properties of individual cortical neurons contributes significantly to this aim.

Local circuits in the primary visual cortex (V1) of primates provide a unique venue for elucidating cortical computations. This is due largely to the highly specialized organization and function of primate V1. Parallel inputs from multiple functionally specialized pathways impinge on V1, and the local circuits here must simultaneously extract the features from each input pathway that are relevant to the computations required for the creation of output neurons with novel receptive field properties and maintain an ordered substrate for interacting efficiently with distant cortical and subcortical neurons. The result is a highly organized structure of multiple circuits that are intertwined at multiple levels of organization. Nevertheless, these circuits remain embedded within a framework that V1 has in common with other cortical areas.

At present, our understanding of the relationships between circuits and function in the visual system is strongest at the levels of areas and modules (layers or columns within an area). There is detailed information about the functional properties and interconnections of dozens of cortical areas (e.g., Felleman and Van Essen, 1991), and for some of these areas (particularly V1) we know that different layers or columns receive input from different sources and that the neurons in these locations have corresponding differences in their responses to visual stimuli (see Callaway, 1998b, and below for review).

But it is apparent that much of the computation that is carried out by visual cortical circuits will not be understood until we understand circuits and function at a finer level of resolution than cortical modules. This is most apparent from the simple observation that any given cortical module contains many functionally and anatomically distinct neuron types. In particular, it appears that the number of anatomically distinct cell types in primate V1 may far exceed that

in other cortical areas. And recent studies of functional connectivity have revealed that anatomically distinct neuron types within the same V1 module are uniquely interconnected (see below). It follows that the diversity of visual response properties within a module is likely to reflect the connectional differences between anatomically distinct neuron types. It is therefore possible to evaluate correlations between circuits and function at a finer level of resolution by taking advantage of the unique anatomical features of each cell type in V1.

The focus of this chapter is on the organization of local circuits in V1 at the level of specific cell types. It is the recognition and exploitation, as well as continuing discovery, of the functional, structural, and connectional diversity of cell types that allows circuits to be linked to function at increasingly fine levels. I will begin with a brief review of the anatomy and function of parallel pathways from the retina and lateral geniculate nucleus (LGN) to V1. I will then turn to the primary focus of the chapter: a detailed description of the cell types which compose V1's local circuits and the specific connectivity of each cell type. The circuitry of excitatory neurons will be considered first, and within this context I will also emphasize how V1 circuits mediate interactions between parallel inputs to V1 and the projection neurons that provide output to various extrastriate cortical areas. Finally, I will describe the circuits suggested by the anatomical and functional diversity of inhibitory interneurons.

The pathways from lateral geniculate nucleus to primary visual cortex

The retino-geniculo-cortical pathways in the macaque monkey are composed of at least three distinct parallel systems, the M, P, and K pathways, which originate in the retina and remain segregated until they reach V1 (see, Chapter 30 in this volume). Each of these systems seems to be specialized for the detection of a unique set of visual cues. At the other end of the visual hierarchy are dozens of extrastriate cortical areas, each of which is also specialized for the detection of particular attributes of visual scenes (cf. Desimone and Ungerleider, 1989; Felleman and Van

Essen, 1991). It is believed that the extrastriate visual areas also compose two more or less parallel systems. One system is specialized for analysis of spatial relationships and involves visual areas in parietal cortex. The other is believed to be responsible for object identification and involves areas in temporal cortex. Since virtually all of the retinal input relayed through the LGN to primate cortical areas converges on area V1 (Benevento and Standage, 1982; Bullier and Kennedy, 1983), V1 provides a unique interface between the M, P, and K pathways and extrastriate cortex. It also provides a unique opportunity for computations requiring early integration of information from more than one stream.

Our understanding of circuits underlying the contributions of the M, P, and K pathways to extrastriate cortical areas is based largely on studies of the flow of information into and out of various functional compartments in V1. These functional compartments include laminar (i.e., layers 4B, 4C α , and 4C β) and columnar (i.e., blob, interblob) divisions. But there are also different cell types within each compartment which are anatomically and/or connectionally distinct. Over the past several decades, considerable progress has been made in relating the functional characteristics of parallel pathways with the functional architecture of V1 and, in turn, the functional differences between neurons providing output to extrastriate areas (see Callaway, 1998b, and below for review). But there is still much to be learned about the functional and anatomical heterogeneities within each pathway and how these are related.

The locations in V1 which receive the combined input from the M, P, and K cells of the LGN correlate closely with the pattern revealed by staining for the mitochondrial enzyme cytochrome oxidase (CO) (Livingstone and Hubel, 1982). The most dense LGN input is to layer 4C, but there is also input to layer 1, blobs in layer 2/3, layer 4A, and layer 6. Each of the M, P, and K pathways has a unique relationship to these afferent termination zones.

THE M PATHWAY Neurons in the most ventral M layers of the LGN project most strongly to the upper division of layer 4C, to layer 4C α , and secondarily to layer 6 (Hendrickson et al., 1978; Hubel and Wiesel, 1972). Anatomical reconstructions of individual afferent axons show that they are heterogeneous. Most innervate the entire depth of layer 4C α , but a subset selectively targets the upper portion of 4C α (Blasdel and Lund, 1983). These termination zones closely mimic the laminar organization of the dendritic arbors of two types of layer 4C α spiny stellate neurons (Yabuta and Callaway, 1998a; see also below). Cells with dendrites in upper 4C α , where they would contact both types of M afferent, project axons to layer 4B and selectively to CO blobs in layer 3. Cells with narrowly stratified dendrites in lower 4C α , where they would contact only one type of M afferent, project axons densely and selectively to CO

interblobs in layer 3. These observations suggest that layer 4B and blobs are influenced by both types of M input, while interblobs are influenced exclusively by the M input that spans the entire depth of layer 4C α (see Fig. 42.1).

M cells could potentially vary from each other with respect to numerous functional attributes, and these variations might be systematically related to the anatomically defined termination zones of M afferents (upper versus lower layer 4C α). We have hypothesized that the functional differences between M afferents that terminate in upper 4C α versus those that terminate throughout 4C α might be related to their linearity (Yabuta and Callaway, 1998a). Some cells in the M layers of the LGN respond to high spatial frequency counterphase gratings with frequency-doubled responses, irrespective of spatial phase (Kaplan and Shapley, 1982; Chapter 30 in this volume). In this respect they are similar to Y cells, which in the cat's visual system arborize preferentially in upper layer 4 of area 17 (Humphrey et al., 1985; Shapley and Perry, 1986). Most M cells in the monkey, however, respond more linearly and in this respect are similar to the cat's X cells, which arborize throughout the depth of layer 4.

Although there may be functional and anatomical similarities between cat X or Y cells and subsets of LGN M cells in the monkey, it is unclear whether these pathways are truly analogous. For example, the parasol cells of the primate retina, which give rise to the M pathway (Leventhal et al., 1981), are most similar to the cat's α -retinal ganglion cells (RGCs) and not the β -RGCs which give rise to the X pathway (Leventhal et al., 1985). Furthermore, it is not clear whether there are discrete classes of linear and nonlinear M cells or whether frequency-doubled cells simply reflect extreme nonlinearity (Levitt et al., 2001). Thus, differences in linearity are just one of many possible functional differences that may distinguish M afferents in upper versus lower 4C α .

P AND K PATHWAYS Neurons in the dorsal LGN layers include not only P cells but also K cells. K cells are located primarily in the intercalated zones between the P layers (and M layers) but are also found scattered within the P layers (Hendry and Yoshioka, 1994). This arrangement has made it difficult to ascertain which layers of V1 receive input from P versus K cells or which of the functionally distinct neuron types recorded in the dorsal LGN correspond to P or K cells. For example, early studies describing anterograde labeling following tracer injections (or lesion-induced degeneration) in the dorsal layers of the LGN reported label in superficial layers (layers 1, 2/3, and 4A) as well as layers 4C β and 6 (Hendrickson et al., 1978; Hubel and Wiesel, 1972). The superficial labeling was originally believed to arise from the P pathway. But we now know that most, if not all, of the label in the superficial layers originated from K cells, not P

cells (see below). Similarly, recordings from LGN neurons in and around the P layers were all attributed to the P pathway before it was appreciated that there is a distinct K pathway. And even with this realization, recordings made in the LGN cannot distinguish P cells from the K cells that are scattered within the P layers.

Despite uncertainty about the precise anatomy and physiology of the K pathway, the available evidence strongly suggests that the great majority of LGN neurons which project axons to layer 4C β are P cells, while only K cells expressing Ca⁺⁺/Calmodulin-dependent Protein Kinase II (α CAMKII) or calbindin (Hendry and Yoshioka, 1994) project to more superficial layers (4A and layer 2/3 blobs). There are three main pieces of evidence which support this configuration: (1) Reconstructions of individual LGN afferents fail to reveal any axons which project densely both to layer 4C β and to superficial layers (Blasdel and Lund, 1983; Freund et al., 1989)—these inputs therefore appear to arise from anatomically distinct populations. (2) The K pathway originates from RGCs with the smallest-diameter axons and these axons innervate the intercalated K layers (Conley and Fitzpatrick, 1989). (3) LGN neurons retrogradely labeled from superficial layers of V1 include cells in the intercalated K layers, along with scattered cells in the P layers, and these cells stain for α CAMKII or calbindin (Hendry and Yoshioka, 1994). Although these findings are strongly suggestive, further studies are required to test more exhaustively the possibility that some afferents might innervate both layer 4C β and superficial layers or that some α CAMKII-expressing cells might connect to layer 4C β . There may also be cells projecting to layer 4A that do not express α CAMKII (Hendry and Yoshioka, 1994).

FUNCTIONAL PROPERTIES OF M, P, AND K CELLS Relative to P or K cells, M cells have excellent contrast sensitivity, prefer lower spatial frequencies and higher temporal frequencies, and lack cone-opponent receptive fields (see Chapter 30 in this volume for review). The most distinctive property of cells recorded in the dorsal layers of the LGN (P and K layers) is that, unlike M cells, they have cone-opponent receptive fields (e.g., Wiesel and Hubel, 1966). These cells are tuned along the cardinal red-green and blue-yellow color axes (Derrington et al., 1984; De Valois et al., 2000). Thus, they either receive input from long-wavelength sensitive (L) cones opposed to middle-wavelength sensitive (M) cones (red-green color opponency) or they have short-wavelength sensitive (S) cone input opposed by the L + M cones (blue-yellow color opponency).

The great majority of cells recorded in and around the P layers have red-green color opponency (Wiesel and Hubel, 1966). Since K cells are only a minority of the cells in this region, it follows that P cells must include cells with red-green opponency. But since there are no direct observations

linking these cell types with receptive-field properties, it is possible that the P pathway might also include cells with blue-yellow color opponency.

There is also compelling evidence that a substantial portion of the K pathway neurons have blue-ON/yellow-OFF receptive fields (see Hendry and Reid, 2000, for review). Blue-ON receptive fields originate with bistratified retinal ganglion cells which connect to intercalated layers K3 and K4 of the LGN. Neurons recorded in the K3 and K4 intercalated layers also have blue-ON receptive fields (see Hendry and Reid, 2000, and personal observation). Neurons with blue-OFF/yellow-ON receptive fields have also been recorded in the dorsal layers of the LGN, but they have not been linked to the P or K pathway (De Valois et al., 2000, and personal observation). It is also not known whether the K pathway includes cells with red-green color opponency.

PROJECTIONS TO EXTRASTRIATE CORTICAL AREAS The next section of this chapter will describe the cell types which receive direct input from the M, P, and K pathways and how they distribute this information to V1's extrastriate cortical projection neurons. In this context, it is therefore also helpful to review briefly the organization of V1 neurons that project to various extrastriate cortical areas and to functionally distinct compartments in area V2.

As a general rule, neurons which project to dorsal visual areas are found in layer 4B, while those that project to ventral visual areas are found in layer 2/3 (see Felleman and Van Essen, 1991, for review). For example, layer 4B neurons provide direct input to areas V3 and MT, while layer 2/3 neurons connect to area V4. But detailed connectivity between areas V1 and V2 has only very recently been studied in the macaque monkey (Sincich and Horton, 2002). Although it was previously appreciated that neurons throughout the cortical depth, from layers 2 to 4B, contain neurons connecting to area V2, their relationships to CO stripe compartments in V2 and to blobs and interblobs in V1 had not been investigated. Because each of the CO stripe compartments in V2 connects to a unique set of cortical areas, this is particularly relevant to the question of how each type of V1 cortical projection neuron distributes information to dorsal and ventral visual areas. In particular, the V2 thick stripes connect to areas V3 and MT, while thin stripes and interstripes connect to V4 (for review see De Yoe and Van Essen, 1988; Zeki and Shipp, 1988).

Input to the CO compartments in V2 is most closely related to the CO organization in V1, not to V1's laminar organization. Layer 2 to 4B neurons in (and under) interblob regions of V1 connect to V2 thick stripes and interstripes, while those in (and under) blob regions connect to V2 thin stripes (Sincich and Horton, 2002). Thus, although it had long been thought that layer 4B provided the only input to V2 thick stripes, it is now clear that layer 2/3 and 4A

interblob neurons also provide input to the thick stripes (Sincich and Horton, 2002). It had also been thought that V2 thin stripes receive input only from layer 2/3 blob neurons, but the new results indicate that the layer 4A and 4B cells under blobs also connect to thin stripes (Sincich and Horton, 2002). It is noteworthy that the input from layer 4B to V2 tends to arise from pyramidal neurons, while the direct input to MT from V1 arises predominantly from layer 4B spiny stellate neurons (Shipp and Zeki, 1989; see further below).

Excitatory cell types in V1, their local connectivity, and relationships to extrastriate cortical areas

Intracellular labeling and anatomical reconstruction of the axonal and dendritic arbors of individual neurons throughout the layers of V1 of macaque monkeys (see Callaway, 1998b, for review) have revealed at least 27 distinct excitatory neuron types (see details below). Photostimulation experiments have revealed the sources of local excitatory input to 14 of these cell types (Briggs and Callaway, 2001; Sawatari and Callaway, 1996, 2000; Yabuta et al., 2001). Systematic differences in the sources of local input to different cell types have revealed that each cell type receives input from unique sources, even when the locations of their cell bodies and/or dendritic arbors are the same (see also Dantzker and Callaway, 2000). Thus, connectivity cannot be predicted based solely on light-level anatomy, because axons that arborize in a particular location selectively connect to the dendrites of certain cell types within that location. In some cases, the sources of functional excitatory input can be highly diverse, even for neurons of the same type (Sawatari and Callaway, 2000). Differences in functional input to each cell type imply that there should be corresponding differences in their visual function in vivo. Future studies will be necessary to reveal any such correlations.

EXCITATORY CELL TYPES AND CONNECTIONS FROM LAYER 4C TO SUPERFICIAL LAYERS As described above, the most dense LGN input to V1 is to layer 4C. Layer 4C neurons, in turn, connect directly to extrastriate projection neurons in more superficial layers (Fig. 42.1). It appears that the most salient features of the classical receptive fields of neurons in superficial cortical layers can be attributed largely to the organization of these connections (cf. Callaway, 1998b). Therefore, understanding the detailed relationships between these circuits and the visual responses of the neurons that form them is expected to be particularly useful for understanding how V1 circuits function.

Within layer 4C α , three distinct types of spiny stellate neuron have been identified (Yabuta and Callaway, 1998a). The first type has dense axonal arbors only within layer 4C α and layer 6; it does not arborize in layer 5 or in superficial layers. The second cell type has dense axonal arbors in layers

4C α and 4B but also makes substantial connections with layers 3B, 5, and 6. The connections in layer 3B are located selectively in the CO blobs. The last type of layer 4C α spiny stellate is the most unusual. It has narrowly stratified dendrites at the bottom of layer 4C α that extend neither into layer 4C β nor to upper layer 4C α . Its M input is therefore limited to those afferents that terminate throughout layer 4C α and not those that target only upper 4C α (Blasdel and Lund, 1983; see also above for possible functional significance). These cells have very dense axonal arbors selectively in the CO interblobs of layer 3B. They have moderate axonal arbors within layer 4C. Together these three cell types receive information from LGN M afferents and distribute it to all three of the major compartments that contain extrastriate projection neurons—blobs, interblobs, and layer 4B (see above). But the narrowly stratified cells that provide input to interblobs are likely to receive only one type of M input, while the cells connecting to layer 4B and blobs receive both types of M input (see also above). Possible functional differences between these sources of LGN input remain unknown.

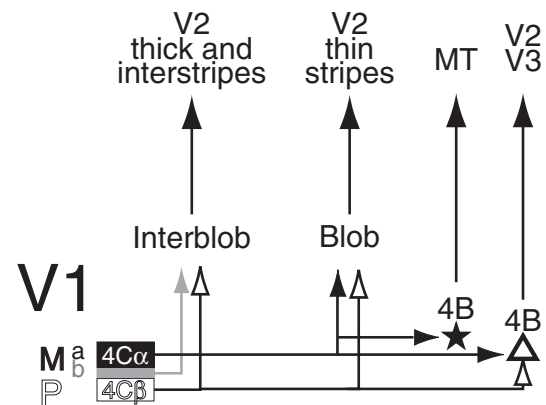


FIGURE 42.1. Schematic of the pathways from magno- (*M*) and parvocellular (*P*) LGN, through V1, to extrastriate cortical areas. Two anatomical types of *M* afferent terminate in either upper layer 4C α of V1 (*Ma* illustrated in *black*) or the entire depth of 4C α . This second type of *M* afferent (*Mb*) thus provides the only input to the middle of layer 4C (illustrated by the *white box*). *P* afferents terminate in layer 4C β . Layer 2/3 CO interblobs receive input from layers 4C β and middle 4C and thus get input from *P* and *Mb* but not *Ma* recipient neurons. Layer 2/3 blobs receive input from neurons throughout the depth of layer 4C and thus get input from *Ma*, *Mb*, and *P* recipient neurons. Layer 4B spiny stellate neurons receive input only from layer 4C α and thus only from *M* recipient neurons, while layer 4B pyramids receive input from both layer 4C α and layer 4C β and thus also receive input from *P* recipient neurons. Interblob neurons, in turn, project to thick stripes and interstripes of V2. Blob neurons project to V2 thin stripes. Layer 4B spiny stellates project to area MT. Layer 4B pyramids project to areas V2 and V3, with the V2 compartment that is targeted being dependent on their position relative to the blobs (see text).

There are two distinct types of layer 4C β spiny stellate cells, although subtle differences in connections to layers 5 and 6 may also be diagnostic of additional types (Callaway and Wiser, 1996; Yabuta and Callaway, 1998a). Cells near the layer 4C α /4C β border have dendritic arbors that span the border and are therefore likely to receive both M and P input. But most layer 4C β spiny stellates confine their dendrites to layer 4C β and therefore can receive LGN input only from P cells. Both of these layer 4C β spiny stellate cell types make extremely dense connections to layer 3B, and these connections lack specificity for blobs or interblobs.

These anatomical observations of layer 4C neurons suggest distinct differences in the sources of input to the extrastriate projection neurons in layers 3B and 4B. But more detailed photostimulation experiments reveal that the connections are even more precise. Neurons in layer 4B provide the output from V1 to areas in the dorsal visual pathway, including areas V2, V3, and MT (see above). Furthermore, there are differences in the cell types projecting to these areas. About one-third of layer 4B excitatory neurons have a spiny stellate morphology, while the remainder are pyramidal (Callaway and Wiser, 1996). But the less common spiny stellates provide the majority of the input to area MT (Shipp and Zeki, 1989), while the pyramids are more likely to connect to V2 and V3. Photostimulation studies (Fig. 42.2; Sawatari and Callaway, 1996; Yabuta et al., 2001) reveal that both cell types receive their strongest local inputs from layer 4C α , as expected from anatomical observations (see above). But pyramidal cells also receive substantial excitatory input from layer 4C β (Figs. 42.1 and 42.2), presumably via their apical dendrites in layer 3. This P-dominated input from layer 4C β is about half the strength of the M-dominated input from layer 4C α . Layer 4B spiny stellates receive no detectable input from layer 4C β . Thus, the direct pathway from layer 4B of V1 to area MT is influenced far less by the P pathway than are indirect pathways from layer 4B pyramids via areas V2 or V3 to MT. These observations imply that there are likely to be differences in the visual receptive field properties of layer 4B spiny stellate versus pyramidal neurons that reflect the differential contributions from the P pathway.

There are also differences in the sources of local excitatory input to different pyramidal cell types in layer 3B. About one-third of the pyramidal neurons in layer 3B of V1 project an axon into the white matter (probably to area V2), while the remaining pyramids have axonal arbors that are completely local to V1 (Callaway and Wiser, 1996; Sawatari and Callaway, 2000). The projecting pyramids have apical dendrites with tufts in layer 1 or layer 2, while the local pyramids rarely have tufted apical dendrites (Sawatari and Callaway, 2000). Photostimulation studies revealed that these anatomical differences were closely correlated with sources of local excitatory input (Sawatari and Callaway, 2000). Most notably, functional excitatory connections from layer

4C β , which provides the most dense anatomical input to layer 3B, could never be detected onto projecting pyramids. In contrast, most local pyramids received strong excitatory input from layer 4C β . There were also systemic differences in the sources of functional excitatory input to layer 3B pyramids in blobs versus interblobs. These differences were consistent with the anatomical differences in local input to blobs and interblobs (see above). It is therefore expected that future in vivo recordings will reveal differences in the visual receptive fields of local versus projecting pyramids and that there will be further correlations with location relative to blobs. Differences between local and projecting pyramids are likely to reflect the functional influence of direct input from layer 4C β . In addition, layer 2/3A also contains both local and projecting pyramids (Callaway and Wiser, 1996) which are also likely to receive different functional inputs and have different receptive fields. And anatomical observations indicate that the sources of input to these cells must differ from those in layer 3B (Callaway and Wiser, 1996; Lachica et al., 1992; Yabuta and Callaway, 1998a). Finally, layer 2/3 pyramids can also be separated into two types based on their patterns of horizontal intralaminar axonal arbors (Yabuta and Callaway, 1998b). While most pyramidal neurons have clustered intralaminar axons projecting for long distances, those located at distances of about 125 μ m from the centers of blobs tend to lack long axons.

EXCITATORY CELL TYPES IN DEEP LAYERS AND THEIR CONNECTIONS The contributions of V1 to visual processing depend on the patterns of activity that are generated in its output neurons. These include not only the extrastriate projection neurons found in superficial cortical layers (see above) but also subcortically projecting neurons found in layers 5 and 6 (Fitzpatrick et al., 1994; Hendrickson et al., 1978; Lund et al., 1975). Interestingly, however, only a minority of layer 5 and layer 6 neurons in macaque V1 have axonal projections outside of V1 (Callaway and Wiser, 1996; Fitzpatrick et al., 1994; Wiser and Callaway, 1996). The majority make connections that are entirely intrinsic to V1. This suggests that the role of these neurons is to influence the patterns of activity that are generated in the output neurons. Other deep layer neurons do project outside of V1, and their local axonal projections and input sources are often distinctly different from those that do not.

These observations, and analyses of local axonal arbors, lead to the hypothesis that there are two distinct classes of deep layer neurons. The first class has local, recurrent axon collaterals that form extensive arbors in superficial cortical layers. The layer 5 pyramidal neurons of this class have axonal arbors that target layers 2–4B, while this class of layer 6 pyramidal neurons targets layer 4C (Fig. 42.3). The second class of deep-layer pyramidal neurons has laterally projecting local axon collaterals that generally avoid superficial

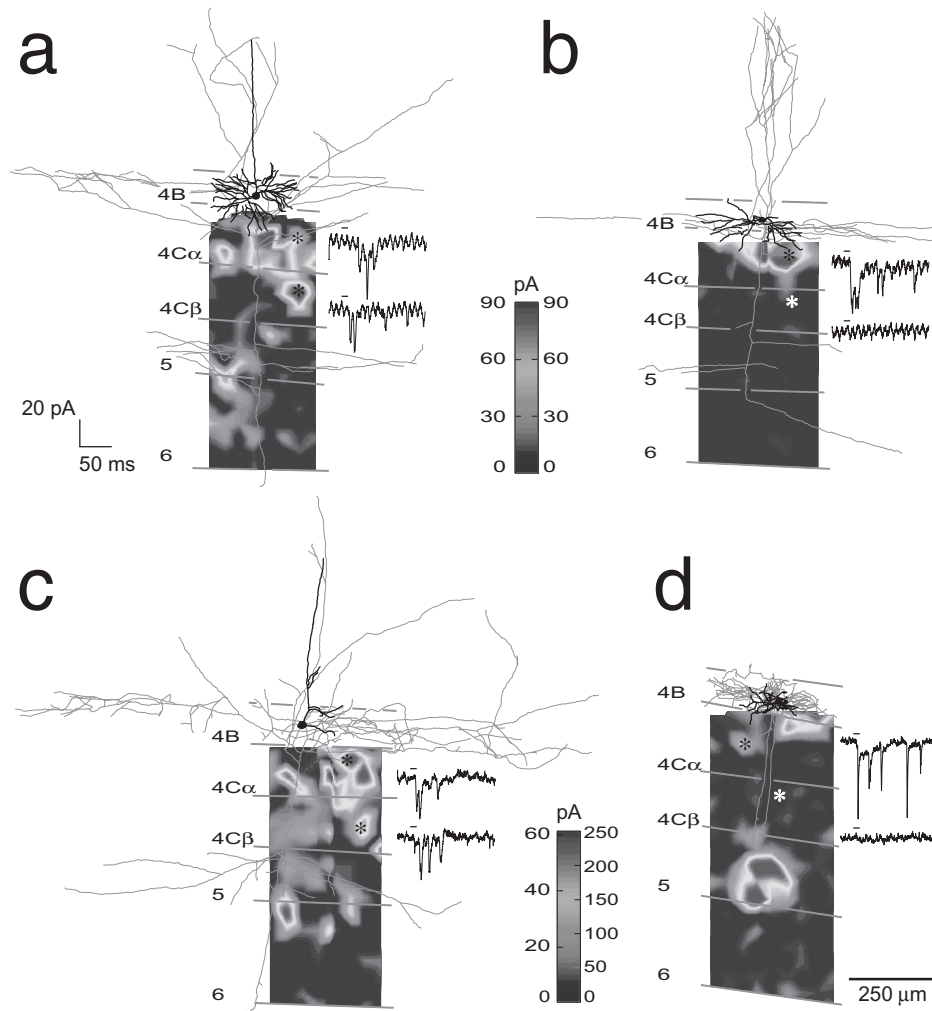


FIGURE 42.2. Laminar excitatory input to layer 4B pyramidal neurons (*a*, *c*), a spiny stellate neuron (*b*), and an inhibitory basket cell (*d*). The pyramidal cells receive strong excitatory input from both layers 4C α and 4C β , while spiny stellate neurons receive input from layer 4C α but not layer 4C β (see text for further details). The excitatory neurons (spiny stellate and pyramidal) get their strongest input from layer 4C, while this inhibitory neuron receives its strongest input from layer 5. These patterns of input to the excitatory neurons versus the inhibitory neurons are reminiscent of input to pyramidal neurons and a subtype of inhibitory basket cell in rat visual cortex (Dantzker and Callaway, 2000). Colored maps indicating patterns of excitatory input to each neuron are linear

interpolations of the estimated evoked input (EEI) (see Yabuta et al., 2001) values measured following photostimulation at discrete sites. Colored vertical scale bars indicate the corresponding EEI values for input maps to the left and right. To the right of each input map are example voltage-clamp recordings made while stimulating presynaptic regions (indicated by asterisks) in layer 4C α (upper traces) or layer 4C β (lower traces). Short dashes above each recording show the onset of photostimulation. Horizontal lines crossing the input maps represent the anatomical laminar borders. Anatomical reconstructions of dendritic (*black*) and axonal arbors (*gray*) are superimposed over the input maps. Scale bars apply to all panels. (From Yabuta et al., 2001.) (See color plate 26.)

cortical layers. These same two cell types have also been distinguished on both anatomical and physiological grounds in other species and cortical areas (cf. Chagnac-Amitai et al., 1990).

Because of our extensive knowledge of the functional organization of macaque V1, it has been possible to make inferences about the functional influences of the different types of deep-layer neurons (Callaway, 1998b). Specifically, deep-layer neurons with local, recurrent axonal arbors appear to have a modulatory rather than a driving influence

on the visual response properties of neurons in superficial layers. Local recurrent pyramidal neurons in layers 5 and 6 have widespread recurrent axon collaterals in layers 2–4B and layer 4C, respectively. Despite these widespread projections, the receptive fields of neurons in layers 2–4C remain relatively small. Furthermore, the projections from deep layers lack specificity for functional compartments (i.e., ocular dominance columns, blobs, interblobs), yet the visual response properties of neurons in the recipient modules appear to be reflective of their inputs from the LGN and

layer 4 (see above and Callaway, 1998b). For example, layer 6 pyramidal neurons have widespread axonal arbors in layer 4C that are not ocular dominance column specific (Wiser and Callaway, 1997). This indicates that under monocular viewing conditions, layer 6 cells connecting to ocular dominance columns corresponding to the closed eye are active, but the recipient layer 4C neurons are not driven above threshold. The layer 6 input cannot by itself activate the layer 4C neurons. The connections are therefore modulatory. A similar argument can be made for the widespread projections from layer 5 to layers 2–4B. The same argument does not hold for the deep-layer neurons that have local, laterally projecting axonal arbors.

Beyond the local, recurrent versus local, lateral distinction that can be made between deep-layer neurons, they can be further classified into at least three types of layer 5 pyramidal neuron and nine types of layer 6 pyramid (Fig. 42.3). The different patterns of axonal and dendritic arborization, as well as differential connectivity of these cell types, suggest that they are likely to be involved uniquely in information processing within V1. Each cell type receives local input from a unique set of sources and provides output to a unique combination of target layers, implying that there are also likely to be corresponding differences in their visual receptive fields.

Neurons in the deep cortical layers, 5 and 6, are even more diverse than those in superficial layers (Briggs and Callaway, 2001; Callaway and Wiser, 1996; Wiser and Callaway, 1996). Three distinct types of layer 5 pyramidal neuron have been identified in macaque V1 (Callaway and Wiser, 1996). One type includes all of the local recurrent neurons found in this layer. They have extensive axonal arbors in superficial layers (2–4B), but not deep layers, and do not project out of V1. A second type has a “back-branching” dendritic morphology, and its local axons project laterally within the bottom of layer 5. The backbranching cells project out of V1, perhaps to the pulvinar nucleus of the thalamus or to the superior colliculus (Callaway and Wiser, 1996; Lund et al., 1975). Finally, there are the Meynert cells, or “tall” pyramids (Lund and Boothe, 1975; Valverde, 1985). They have long (more than 500 μm), lateral basal dendrites and apical dendrites that extend to layer 1. Their large cell bodies suggest that they project to the superior colliculus (Lund et al., 1975). They have not been intracellularly labeled in mature animals, but tall layer 5 pyramids in prenatal animals (Callaway, 1998a) have laterally projecting local axons. Photostimulation-based investigation of the sources of local excitatory input to these cells is in progress.

Nine anatomically distinct types of layer 6 pyramidal neurons have been identified (Fig. 42.3; Briggs and Callaway, 2001; Wiser and Callaway, 1996), and photostimulation reveals systematic differences in the sources of local excitatory input to each type (Briggs and Callaway, 2001).

Layer 6 pyramids are grouped into two classes, I and II. Class I cells have apical dendritic branches and dense axonal arbors in layer 4C. These are divided into five types based on their specific patterns of local axonal arborization within subdivisions of layer 4. They project specifically to either layer 4C α (type I α), 4C β (type I β), the middle of layer 4C/lower 4C α (type Im), 4C β plus 4A (type I β A), or throughout layer 4C plus 3B/4A (type IC). These primary distinguishing features are correlated with the position of the cell body within the depth of layer 6 and with whether the cell projects an axon into the white matter. These features indicate that the class I cells are the source of feedback from V1 to the LGN (see Fitzpatrick et al., 1994; Wiser and Callaway, 1996). The feedback to P layers of the LGN comes from type I β , I β A, and perhaps IC cells. Feedback to M layers of the LGN comes from type IC cells. Type I α and Im cells are found only in the middle of layer 6 and never project axons outside of V1. Thus, each type of class I cell has unique relationships to the M and P pathways, locally in V1, and with respect to input from and feedback to the LGN (see also Briggs and Callaway, 2001). Future studies of the differences in the functional properties of each of these cell types in vivo will provide considerable insight into the functions of these circuits.

Distinct anatomical features and photostimulation studies of local input indicate that class II layer 6 pyramids are likely to have very different functions than class I cells. Only one type of class II cell, type IIA, projects an axon to the white matter. The type IIA cells are found preferentially in the middle of layer 6 and have long, lateral local axons exclusively in deep layers of V1. They are therefore very similar to claustral projecting cells in the cat (Katz, 1987) and are hypothesized to also project to the visual claustrum of the monkey (Wiser and Callaway, 1996). They may therefore have very long receptive fields and play a role in the generation of end-stopped receptive fields (Bolz and Gilbert, 1986; Grieve and Sillito, 1995; Sherk and LeVay, 1983). Type IIB cells provide dense local feedback to superficial layers of V1, while type IIC cells are unusual in receiving diffuse input from all layers of V1 and extending sparse local axons throughout the cortical layers (Briggs and Callaway, 2001). Finally, the layer 6 pyramids also include giant cells of Meynert (Winfield et al., 1981). These project to area MT and are likely to have direction-selective receptive fields (Movshon and Newsome, 1996). The distinct inputs and outputs of each type of class II cell suggest that they are each likely to also have different visual receptive field properties in vivo.

Inhibitory cell types and V1 circuits

Inhibitory neurons are likely to play a crucial role in the processing of visual information in primate V1. Although they

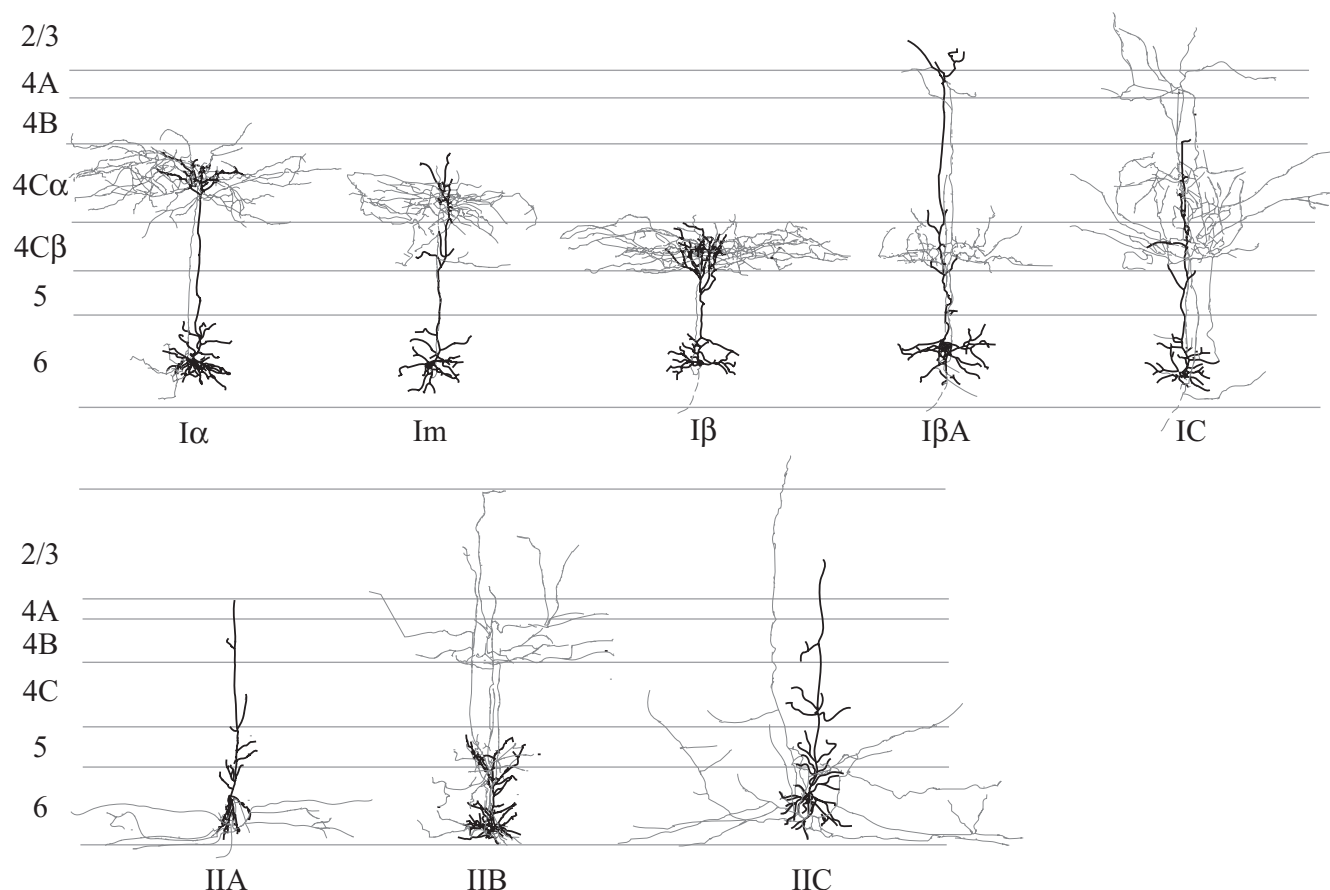


FIGURE 42.3. Eight types of pyramidal neuron identified in layer 6 of macaque V1. Class I neurons (*top row*) have dense axonal and apical dendritic arbors in layer 4C. Each type of class I neuron has a unique distribution of axons and dendrites within layer 4C and therefore a unique relationship to the magno- and parvocellular

streams. Class II neurons (*bottom row*) have more extensive dendritic arbors in layer 5 and project axons primarily to either layers 2–4B (type IIB) or deep layers (types IIA and IIC). See text for further details. (From Briggs and Callaway, 2001.)

rarely send axons outside of the local cortical area and therefore cannot directly relay information about the computations occurring in V1 to other areas, they can profoundly influence local computations and the activity of V1's projection neurons. The diversity of inhibitory interneurons found in the neocortex (see below) is likely to reflect a corresponding diversity of functional roles. Not only are inhibitory neurons believed to perform more straightforward tasks like gain control (Douglas et al., 1995; Heeger et al., 1996), but they can also control the timing of action potential generation (Tamas et al., 2000) and are likely to be able to selectively gate inputs from diverse sources impinging on different parts of the dendritic arbor (cf. Somogyi et al., 1998).

Although there have been extensive anatomical studies of inhibitory cortical neurons in primates, including macaque area V1, nearly all functional studies of inhibitory cortical neurons have been conducted in nonprimate species. Nevertheless, the basic types of inhibitory neurons appear to be conserved across cortical areas and species. We can there-

fore gain some insight into the likely function of macaque V1 inhibitory neurons by considering previous studies of inhibitory neurons in other species. I will therefore begin by reviewing these studies. Detailed Golgi studies of the anatomical features of inhibitory neurons in macaque V1 (Lund, 1987; Lund et al., 1988; Lund and Wu, 1997; Lund and Yoshioka, 1991) indicate, however, that the basic cell types found in other cortical areas/species have become highly specialized in V1. This specialization of inhibitory neurons is reminiscent of the greater diversity of excitatory neurons in V1 compared to other cortical areas or species (see above). And comparisons of the sources of local functional input to pyramidal neurons in layer 2/3 of rat visual cortex (Dantzker and Callaway, 2000), versus excitatory neurons in the equivalent layers of macaque V1 (Sawatari and Callaway, 2000; Yabuta et al., 2001), indicate that the increased anatomical diversity is accompanied by cell type specificity and increased diversity of functional connections. Thus, there is also likely to be a corresponding specificity of input to the multitude of inhibitory neuron types in

macaque V1. I will therefore also review the work of Lund and colleagues, which describes anatomical features characterizing inhibitory cell types in V1.

Cortical circuits are composed of a complex network of many neuron types. The function of the circuits in which these neurons are embedded is largely dependent on three variables: (1) which neurons are functionally interconnected, (2) how their synapses function, and (3) how the information delivered to individual neurons is integrated and transformed within the postsynaptic dendritic arbor. Although a long history of anatomical observations has led to thorough descriptions of the neuronal cell types found in the cortex and their patterns of axonal and dendritic arborization, it is only within the past decade that methodological advances have made possible more detailed functional studies of the cortical network. These studies indicate that for each type of cortical inhibitory neuron, each of the three variables described above is closely regulated (see details below).

Although conventional anatomical studies reveal spatial overlap of axonal and dendritic arbors, and therefore the potential for synaptic connectivity, until recently only tedious electron microscopic (EM) studies had been able to reveal which of the possible connections suggested by the anatomical overlap of axons and dendrites are in fact manifested. These EM studies have, however, pointed toward precisely organized cortical circuits. EM studies correlating synaptic bouton morphologies on individual neurons in layer 4 of cat visual cortex with local and thalamic afferent sources found no difference in the proportion of excitatory and inhibitory inputs received by inhibitory and excitatory neurons (Ahmed et al., 1997; Anderson et al., 1994). These observations are consistent with theories that view cortical connections as largely random, with the purpose of enabling associations among many possible stimuli (e.g., Braitenberg and Schuz, 1991). But other EM studies and increasing evidence from functional studies point to the alternative view, that the cortex is composed of extremely precise circuits mediating specific functions. EM studies suggest that inhibitory interneurons participate in cell-type-specific connections. For example, subcortical brain regions that innervate cortex target specific interneuron types (Freund and Gulyas, 1991; Gibson et al., 1999; Hornung and Celio, 1992; Staiger et al., 1996), and inhibitory neurons form selective connections to other types of interneurons or to particular postsynaptic elements on excitatory neurons (DeFelipe et al., 1999; Gonchar and Burkhalter, 1999; Meskenaite, 1997; Somogyi, 1977; Tamas et al., 1998). Finally, studies of functional cortical connections reveal that excitatory cortical neurons selectively connect to specific subsets of neuron types within the zone of axonal arborization; in particular, axons not only arborize in specific cortical layers, but they connect selectively to certain cell types within those layers (see above; Briggs and Callaway, 2001; Dantzker and Callaway, 2000;

Sawatari and Callaway, 2000; Yabuta et al., 2001). Cell type specificity of cortical connections is therefore likely to be prevalent and perhaps the norm rather than the exception.

Although cortical inhibitory neuron types are numerous, they each express specific and precisely regulated attributes pointing toward the likelihood that each type plays a unique role within the functioning cortical network. For example, each type of inhibitory neuron has diverse but highly correlated morphological, molecular, and physiological properties (Cauli et al., 1997; Gonchar and Burkhalter, 1997, 1999; Gupta et al., 2000; Kawaguchi, 1993; Kawaguchi and Kubota, 1997; Parra et al., 1998; Peters and Regidor, 1981; Thomson and Deuchars, 1997). Further complexity and precision of inhibitory cortical circuits are evident from the striking correlations between functional synaptic dynamics and the cell types that contribute the pre- and postsynaptic elements of each cortical connection (Gupta et al., 2000). And yet another level of complexity is introduced by modern studies of the properties of dendritic arbors. Dendrites are not simply passive filters; they can actively influence the integration of synaptic information (e.g., Johnston et al., 2000; Stuart et al., 1997). Thus, intrinsic membrane properties, which vary systematically among inhibitory neuron types and correlate with morphology and molecular properties, are also likely to have a strong impact on the in vivo function of inhibitory neurons.

Inhibitory neuron types that are common across multiple cortical areas and species can be classified according to numerous parameters, many of which are correlated. The most useful parameters include morphological features (patterns of axonal and dendritic arborization), specific targets innervated (e.g., cell bodies versus distal dendrites or axons), intrinsic firing properties, and expression of chemical markers. For organizational purposes, it is most useful to categorize these cells here primarily according to the targets of their synapses.

BASKET CELLS Basket cells make multiple large synapses on the proximal dendrites and cell bodies of pyramidal neurons (Jones and Hendry, 1984), and therefore even the connections originating from a single neuron may profoundly influence the activity of a recipient pyramid (e.g., Tamas et al., 2000). The typical basket cell expresses parvalbumin (PV) and is fast-spiking (FS) (Cauli et al., 1997; Gonchar and Burkhalter, 1997; Kawaguchi and Kubota, 1997), that is, there is no adaptation of firing frequency upon prolonged intracellular current injection. In contrast, small basket cells express cholecystokinin (CCK), not PV, and fire action potentials with frequency adaptation (referred to as *adapting* or *regular spiking*) or are burst spiking (Gonchar and Burkhalter, 1997; Kawaguchi and Kubota, 1997, 1998; Kubota and Kawaguchi, 1997). Our studies of sources of excitatory

input to FS basket cells in rat visual cortex (Dantzker and Callaway, 2000) indicate that they receive input from the same layers as pyramidal neurons. Since the FS basket cells strongly inhibit pyramidal neurons, this connectional organization is consistent with a role for this cell type in nonlinear cortical operations such as normalization or gain control (Douglas et al., 1995; Heeger et al., 1996). In macaque V1 there are numerous varieties of basket cells in each cortical layer (see below).

AXO-AXONIC “CHANDELIER” CELLS Chandelier cells (Somogyi, 1977; Somogyi et al., 1985) have physiological and molecular features similar to those of FS basket cells—they are FS and express PV (Kawaguchi and Kubota, 1997; Lewis and Lund, 1990). They are unique, however, in their morphology and cellular targets. They have a highly stereotyped appearance due to the formation of large cartridge-like synapses on the axon initial segments of pyramidal neurons (DeFelipe and Farinas, 1992). These cells therefore have the potential to strongly regulate the generation of action potentials by pyramidal neurons.

DENDRITE-TARGETING INTERNEURONS Inhibitory neurons targeting more distal dendrites of excitatory neurons are distinct from basket and chandelier cells but are nevertheless a diverse population. These include neurogliaform, double-bouquet, and Martinotti cells, each of which has distinct morphological and physiological properties (Conde et al., 1994; DeFelipe et al., 1989; DeFelipe and Jones, 1992; Jones, 1984; Kawaguchi and Kubota, 1997). Neurogliaform cells have a dense, local axonal arbor and fire spikes late following ramp depolarization (late-spiking or LS). Double-bouquet cells have dendritic tufts both above and below the cell body and fire spikes in bursts. And Martinotti cells are regular spiking, with axons extending primarily above the cell body. Calbindin (CB) immunoreactivity is associated with all of these cell types, but somatostatin (SOM) is preferentially found in Martinotti cells. Since SOM does not colocalize with CCK or PV (Kawaguchi and Kubota, 1997), this is a particularly helpful marker for distinguishing Martinotti cells from regular spiking basket cells, whose morphology can sometimes appear similar to that of Martinotti cells. Although these intrinsic features point to specific functions for each cell type, more information about the functional interactions of these cells with other cell types is needed.

INTERNEURON-TARGETING INTERNEURONS Superficial cortical layers contain a distinctive population of inhibitory neurons that are immunoreactive for calretinin (CR) and have a bipolar dendritic morphology (DeFelipe et al., 1999; Gonchar and Burkhalter, 1999). Within layer 2/3 these cells synapse predominantly onto other inhibitory neurons

(DeFelipe et al., 1999; Meskenaite, 1997), including CR-positive inhibitory interneurons (Gonchar and Burkhalter, 1999). It is therefore suggested that these cells function to disinhibit cortical pyramidal neurons (Gonchar and Burkhalter, 1999).

MORPHOLOGY OF INHIBITORY CELL TYPES IN MACAQUE V1 Most studies of inhibitory neurons in monkey cortex have relied on antibody staining to reveal the processes of neurons expressing particular neurochemicals. Although these studies can provide information about dendritic morphology or synaptic connectivity of populations at the EM level (see above), they do not reveal the detailed patterns of axonal arbors of the same neurons. The Golgi studies of Lund and colleagues have, however, revealed an extensive array of inhibitory cell varieties in macaque V1 (Lund, 1987; Lund and Wu, 1997; Lund and Yoshioka, 1991; Lund et al., 1988). These studies indicate that morphological features distinguish a highly diverse population of inhibitory cell types, each providing output to particular neuronal populations within V1, as evidenced by their precise patterns of axonal arborization.

Unlike typical inhibitory neurons found in other species or cortical areas, inhibitory neurons in macaque V1 often have not only axonal arbors within the immediate vicinity of their cell body and dendritic arbor (intralaminar axons), but also interlaminar projections that are highly specific, targeting from one to as many as five laminar divisions, depending on the cell type. Lund refers to these different cell types as *varieties* in order to avoid confusion with more general cell type classifications such as basket cells or chandelier cells (see above). She often distinguishes several varieties which have their cell bodies in the same layer and might all be of the same class (e.g., basket cells).

The inhibitory neurons of layer 4C have patterns of axonal arborization that are usually confined to a subset of the layers that receive strong input from the LGN (Lund, 1987). For example, many cells in layers 4C α and 4C β have dense intralaminar axons, along with a projection that arborizes in layer 6. Other layer 4C α or 4C β neurons have interlaminar projections specifically to layer 4A or 3B. And some layer 4C neurons have dense axons throughout layer 4C. A population of inhibitory neurons with very narrowly stratified dendrites at the border between layer 4C and layer 5 (layer 5A) has varieties with axonal arbors similar to those of the layer 4C α and 4C β cells. Because the combinations of layers targeted by the axonal arbors of individual inhibitory neurons are typically not all receiving input from the same functional stream (e.g., M, P, or K; see above), these cells might mediate gating of thalamic inputs from diverse sources or provide gain control across streams. In all, Lund (1987) describes 17 varieties of inhibitory neuron in layers 4C α , 4C β , and 5A.

Inhibitory neurons in the most superficial layers, 2–4B, are likely to have the most direct influence on the output from V1 to extrastriate cortical areas, because this output arises from excitatory neurons in the same layers. Layers 3B, 4A, and 4B differ from more superficial layers (2–3A) in that they receive direct excitatory input from layer 4C (see the discussion of excitatory cell types above). Layers 2–3A are dependent on layers 3B–4B for access to the excitatory output of 4C. Accordingly, Lund provides separate descriptions of the neurons in layers 4B, 4A, and 3B (Lund and Yoshioka, 1991) versus layers 1–3A (Lund and Wu, 1997). This distinction is further justified by striking differences in the overall patterns of axonal arbors of cells in these groups. The neurons in layers 2–3A typically confine their axons to layers 1–3A and rarely have axons extending to deeper layers. In contrast, neurons in layers 3B–4B can, as a group, have axonal arbors in any cortical layer. But, individually, layer 3B–4B inhibitory neurons make extremely precise interlaminar projections, clearly targeting specific combinations of layers while avoiding others (Fig. 42.4). The cells in layers 2–4B include the classic cell types, such as basket cells, chandelier cells, and neurogliaform cells, as well as numerous varieties. While the relative simplicity of layer 2–3A cells yields only six varieties (Lund and Wu, 1997), Lund and Yoshioka (1991) distinguish more than a dozen varieties in layers 3B–4B.

The patterns of axonal arborization of inhibitory neurons in layers 5B and 6 mimic the axonal projection patterns of the local, recurrent pyramidal neurons (see above) found in the same layers. Layer 5B neurons have rising axon projections principally in layer 2/3A, while layer 6 inhibitory

neurons have axonal arbors in layers 4C, 4A, and 3B (Lund et al., 1988). Lund et al. (1988) distinguish five varieties of inhibitory neurons with somata in layer 5B and six varieties in layer 6. These cells appear to be predominantly basket cells, plus some chandelier cells, with the varieties differing in relatively subtle features. But a large group of layer 6 cells which Lund et al. (1988) describe as a single variety (variety 6-6) have precise interlaminar axonal arbors that target either layer 4C α , layer 4C β , midlayer 4C, or layers 4C β plus 4A. These patterns of axonal arborization are again reminiscent of the excitatory cell types found in the same layer (see above). It will be particularly interesting to determine whether these layer 5B and layer 6 inhibitory cell types receive excitatory input from the same layers as their excitatory pyramidal cell counterparts or display some other trends related to the M, P, and K pathways. For example, layer 6 pyramidal neurons with axons in layer 4C receive excitatory input from both layers 4C α and 4C β , regardless of cell type. But only pyramidal cell types with axons in layer 4C α receive excitatory input from M-dominated layer 4B, while neurons with axons layers 4C β (and sometimes 4A) receive excitatory input from P- and K-dominated layer 3 (Briggs and Callaway, 2001). Will the inhibitory cell types of layer 6 show similar trends? Or will they receive specific inputs from layers 4C α , 4C β , and 4A that mimic their patterns of axonal arborization? The answers to these questions have distinctly different implications for the roles of these cells in terms of operations such as feedforward or feedback inhibition and differential shunting of input from diverse sources.

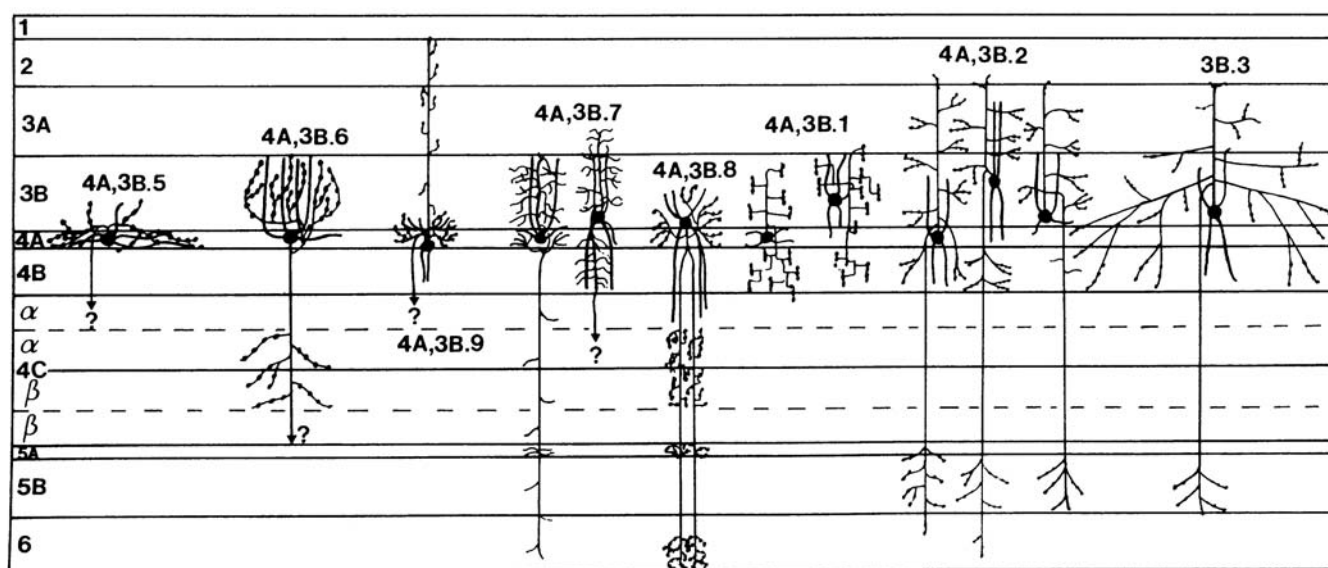


FIGURE 42.4. Schematic diagram illustrating several varieties of inhibitory neurons with cell bodies in layers 3B, 4A, and 4B. Each cell variety has axonal arbors that precisely target particular combinations of layers and sublayers in V1. These cell varieties appear to belong to the basket cell and chandelier cell classes. (From Lund and Yoshioka, 1991.)

Summary and conclusions

Understanding how neural circuits give rise to visual perception requires the understanding of numerous details, most of which are necessary but probably not sufficient for solving the problem. It is clear that we must first understand how the neurons that compose the circuits are connected—what is the circuit? But we must also correlate circuits with function and perturb function in vivo to test hypotheses that emerge from observed correlations. As we come to understand the precision of cortical circuits at increasingly fine levels, it becomes clear that it will also be necessary to develop methods and implement experiments designed to observe correlations between circuitry and function and to perturb function at increasingly fine levels. Studies of the circuitry in V1 have shown that individual cell types are precisely interconnected. Thus, future methods and experiments should be designed to attack function at this same level of resolution.

In this chapter, I have emphasized our understanding of V1 circuits at the level of individual cell types. In particular, it has become increasingly apparent that V1 of the macaque monkey contains dozens of anatomically distinct excitatory and inhibitory cell types. We now know that each of the distinct cell types whose sources of functional input have been investigated have proven to be connected differently from other cell types. This is the case even for neurons with similar cell body positions or similar laminar patterns of dendritic arborization. Our understanding of the connectivity in macaque V1 at this cell-type-specific level of detail is so far confined to excitatory neurons. However, studies of the connectivity of inhibitory neurons in rat visual cortex (Dantzker and Callaway, 2000) and the anatomical diversity of inhibitory neurons in macaque V1 (see above) strongly suggest that functional connectivity will also be strongly correlated with distinct anatomical features of inhibitory cell types in macaque V1. We are therefore likely to gain a great deal of understanding about the functional roles of inhibitory neurons and their interactions with excitatory neurons from future studies revealing the functional connectivity of each inhibitory cell type.

Regardless of the detail with which we understand the connectivity between distinct neuron types, we are unlikely to be able to understand the mechanisms by which these circuits contribute to visual perception without also correlating cell types with function. Future studies should take advantage of the strong correlations between anatomical features and connectivity in V1 in order to correlate visual responses with circuits. For example, in vitro studies show that layer 4B spiny stellate cells and projecting pyramids in layer 3B receive strong functional input from layer 4C α but not 4C β , while layer 4B pyramids and layer 3B local pyramids receive considerable layer 4C β input. Thus, comparing

the visual responses of these four anatomically distinct cell types would provide further insight into the contributions of layers 4C α and 4C β to visual responses in more superficial layers.

It should also be apparent that identifying correlations between circuits and function must be accompanied by perturbations that precisely test any hypotheses that emerge based on correlative studies. The incorporation of modern molecular and genetic methods into the experimental arsenal of primate neurophysiologists is likely to contribute importantly to this process. In particular, distinct cell types can be targeted genetically using cell-type-specific promoters (e.g., Zemelman and Miesenböck, 2001), and replication-incompetent viruses can be used to deliver these genetic constructs to neurons in the primate brain (E.M.C., unpublished observations). This genetic arsenal is in need of fortification from further development of genetic methods for perturbing function, such as methods to allow selective and quickly reversible neuronal inactivation (Lechner et al., 2002) and identification of promoters suitable for driving gene expression specifically in cell types of interest.

REFERENCES

- Ahmed, B., J. C. Anderson, K. A. C. Martin, and J. C. Nelson, 1997. Map of the synapses onto layer 4 basket cells of the primary visual cortex of the cat, *J. Comp. Neurol.*, 380: 230–242.
- Anderson, J. C., R. J. Douglas, K. A. C. Martin, and J. C. Nelson, 1994. Map of the synapses formed with the dendrites of spiny stellate neurons of cat visual cortex, *J. Comp. Neurol.*, 341:25–38.
- Benevento, L. A., and G. P. Standage, 1982. Demonstration of lack of dorsal lateral geniculate nucleus input to extrastriate areas MT and visual 2 in the macaque monkey, *Brain Res.*, 252:161–166.
- Blasdel, G. G., and J. S. Lund, 1983. Termination of afferent axons in macaque striate cortex, *J. Neurosci.*, 3:1389–1413.
- Bolz, J., and C. D. Gilbert, 1986. Generation of end-inhibition in the visual cortex via interlaminar connections, *Nature*, 320:362–365.
- Braitenberg, V., and A. Schuz, 1991. *Anatomy of the Cortex*, Berlin: Springer.
- Briggs, F., and E. M. Callaway, 2001. Layer-specific input to distinct cell types in layer 6 of monkey primary visual cortex, *J. Neurosci.*, 21:3600–3608.
- Bullier, J., and H. Kennedy, 1983. Projection of the lateral geniculate nucleus onto cortical area V2 in the macaque monkey, *Exp. Brain Res.*, 53:168–172.
- Callaway, E. M., 1998a. Prenatal development of layer-specific local circuits in primary visual cortex of the macaque monkey, *J. Neurosci.*, 18:1505–1527.
- Callaway, E. M., 1998b. Local circuits in primary visual cortex of the macaque monkey, *Annu. Rev. Neurosci.*, 21:47–74.
- Callaway, E. M., and A. K. Wiser, 1996. Contributions of individual layer 2–5 spiny neurons to local circuits in macaque primary visual cortex, *Vis. Neurosci.*, 13:907–922.

- Cauli, B., E. Audinat, B. Lambolez, M. C. Angulo, N. Ropert, K. Tsuzuki, S. Hestrin, and J. Rossier, 1997. Molecular and physiological diversity of cortical nonpyramidal cells, *J. Neurosci.*, 17:3894–3906.
- Chagnac-Amitai, Y., H. J. Luhmann, and D. A. Prince, 1990. Burst generating and regular spiking layer 5 pyramidal neurons of rat neocortex have different morphological features, *J. Comp. Neurol.*, 296:598–613.
- Conde, F., J. S. Lund, D. M. Jacobowitz, K. G. Baimbridge, and D. A. Lewis, 1994. Local circuit neurons immunoreactive for calretinin, calbindin D-28k or parvalbumin in monkey prefrontal cortex: distribution and morphology, *J. Comp. Neurol.*, 341:95–116.
- Conley, M., and D. Fitzpatrick, 1989. Morphology of retinogeniculate axons in the macaque, *Vis. Neurosci.*, 2:287–296.
- Dantzker, J. L., and E. M. Callaway, 2000. Laminar sources of synaptic input to cortical inhibitory interneurons and pyramidal neurons, *Nat. Neurosci.*, 3:701–707.
- DeFelipe, J., and I. Farinas, 1992. The pyramidal neuron of the cerebral cortex: morphological and chemical characteristics of the synaptic inputs, *Prog. Neurobiol.*, 39:563–607.
- DeFelipe, J., M. C. Gonzalez-Albo, M. R. Del Rio, and G. N. Elston, 1999. Distribution and patterns of connectivity of interneurons containing calbindin, calretinin, and parvalbumin in visual areas of the occipital and temporal lobes of the macaque monkey, *J. Comp. Neurol.*, 412:515–526.
- DeFelipe, J., S. H. Hendry, and E. G. Jones, 1989. Synapses of double bouquet cells in monkey cerebral cortex visualized by calbindin immunoreactivity, *Brain Res.*, 503:49–54.
- DeFelipe, J., and E. G. Jones, 1992. High-resolution light and electron microscopic immunocytochemistry of colocalized GABA and calbindin D-28k in somata and double bouquet cell axons of monkey somatosensory cortex, *Eur. J. Neurosci.*, 4:46–60.
- Derrington, A. M., J. Krauskopf, and P. Lennie, 1984. Chromatic mechanisms in lateral geniculate nucleus of macaque, *J. Physiol. (Lond.)*, 357:241–265.
- Desimone, R., and L. Ungerleider, 1989. Neural mechanisms of visual processing in monkeys, in *Handbook of Neuropsychology*, vol. 2 (F. Boller and J. Grafman eds.), Amsterdam: Elsevier, pp. 267–299.
- De Valois, R. L., N. P. Cottaris, S. D. Elfar, L. E. Mahon, and J. A. Wilson, 2000. Some transformations of color information from lateral geniculate nucleus to striate cortex, *PNAS*, 97:4997–5002.
- De Yoe, E. A., and D. C. Van Essen, 1988. Concurrent processing streams in monkey visual cortex, *Trends Neurosci.*, 11:219–226.
- Douglas, R. J., C. Koch, M. Mahowald, K. A. Martin, and H. H. Suarez, 1995. Recurrent excitation in neocortical circuits, *Science*, 269:981–985.
- Felleman, D. J., and D. C. Van Essen, 1991. Distributed hierarchical processing in the primate cerebral cortex, *Cereb. Cortex*, 1:1–47.
- Fitzpatrick, D., W. M. Usrey, B. R. Schofield, and G. Einstein, 1994. The sublaminal organization of corticogeniculate neurons in layer 6 of macaque striate cortex, *Vis. Neurosci.*, 11:307–315.
- Freund, T. F., and A. I. Gulyas, 1991. GABAergic interneurons containing calbindin D28K or somatostatin are major targets of GABAergic basal forebrain afferents in the rat neocortex, *J. Comp. Neurol.*, 314:187–199.
- Freund, T. F., K. A. C. Martin, I. Soltesz, P. Somogyi, and D. Whitteridge, 1989. Arborisation pattern and postsynaptic targets of physiologically identified thalamocortical afferents in striate cortex of the macaque monkey, *J. Comp. Neurol.*, 289:315–336.
- Gibson, J. R., M. Beierlein, and B. W. Connors, 1999. Two networks of electrically coupled inhibitory neurons in neocortex, *Nature*, 402:75–79.
- Gonchar, Y., and A. Burkhalter, 1997. Three distinct families of GABAergic neurons in rat visual cortex, *Cereb. Cortex*, 7:347–358.
- Gonchar, Y., and A. Burkhalter, 1999. Connectivity of GABAergic calretinin-immunoreactive neurons in rat primary visual cortex, *Cereb. Cortex*, 9:683–696.
- Grieve, K. L., and A. M. Sillito, 1995. Differential properties of cells in the feline primary visual cortex providing the corticofugal feedback to the lateral geniculate nucleus and visual claustrum, *J. Neurosci.*, 16:1180–1192.
- Gupta, A., Y. Wang, and H. Markram, 2000. Organizing principles for a diversity of GABAergic interneurons and synapses in the neocortex, *Science*, 287:273–278.
- Heeger, D. J., E. P. Simoncelli, and J. A. Movshon, 1996. Computational models of cortical visual processing, *Proc. Natl. Acad. Sci. USA*, 93:623–627.
- Hendrickson, A. E., J. R. Wilson, and M. P. Ogren, 1978. The neuroanatomical organization of pathways between the dorsal lateral geniculate nucleus and visual cortex in Old World and New World primates, *J. Comp. Neurol.*, 182:123–136.
- Hendry, S. H., and R. C. Reid, 2000. The koniocellular pathway in primate vision, *Annu. Rev. Neurosci.*, 23:127–153.
- Hendry, S. H., and T. Yoshioka, 1994. A neurochemically distinct third channel in the macaque dorsal lateral geniculate nucleus, *Science*, 264:575–577.
- Hornung, J. P., and M. R. Celio, 1992. The selective innervation by serotonergic axons of calbindin-containing interneurons in the neocortex and hippocampus of the marmoset, *J. Comp. Neurol.*, 320:457–467.
- Hubel, D. H., and T. N. Wiesel, 1972. Laminar and columnar distribution of geniculocortical fibers in the macaque monkey, *J. Comp. Neurol.*, 146:421–450.
- Humphrey, A. L., M. Sur, D. J. Uhlrich, and S. M. Sherman, 1985. Projection patterns of individual X- and Y-cell axons from the lateral geniculate nucleus to cortical area 17 in the cat, *J. Comp. Neurol.*, 233:159–189.
- Johnston, D., D. A. Hoffman, J. C. Magee, N. P. Poolos, S. Watanabe, C. M. Colbert, and M. Migliore, 2000. Dendritic potassium channels in hippocampal pyramidal neurons, *J. Physiol. (Lond.)*, 525:75–81.
- Jones, E. G., 1984. Neurogliaform or spider web cells, in *Cerebral Cortex*, vol. 1 (A. Peters and E. G. Jones, eds.), New York: Plenum, pp. 409–418.
- Jones, E. G., and S. H. C. Hendry, 1984. Basket cells, in *Cerebral Cortex*, vol. 1 (A. Peters and E. G. Jones, eds.), New York: Plenum, pp. 309–336.
- Kaplan, E., and R. M. Shapley, 1982. X and Y cells in the lateral geniculate nucleus of macaque monkeys, *J. Physiol. (Lond.)*, 330:125–143.
- Katz, L. C., 1987. Local circuitry of identified projection neurons in cat visual cortex brain slices, *J. Neurosci.*, 7:1223–1249.
- Kawaguchi, Y., 1993. Groupings of nonpyramidal and pyramidal cells with specific physiological and morphological characteristics in rat frontal cortex, *J. Neurophysiol.*, 69:416–431.

- Kawaguchi, Y., and Y. Kubota, 1997. GABAergic cell subtypes and their synaptic connections in rat frontal cortex, *Cereb. Cortex*, 7:476–486.
- Kawaguchi, Y., and Y. Kubota, 1998. Neurochemical features and synaptic connections of large physiologically-identified GABAergic cells in the rat frontal cortex, *Neuroscience*, 85:677–701.
- Kubota, Y., and Y. Kawaguchi, 1997. Two distinct subgroups of cholecystokinin-immunoreactive cortical interneurons, *Brain Res.*, 752:175–183.
- Lachica, E. A., P. D. Beck, and V. A. Casagrande, 1992. Parallel pathways in macaque monkey striate cortex: anatomically defined columns in layer III, *Proc. Natl. Acad. Sci. USA*, 89:3566–3570.
- Lechner, H. A. E., E. S. Lein, and E. M. Callaway, 2002. A genetic method for selective and quickly reversible silencing of mammalian neurons, *J. Neurosci.*, 22:5287–5290.
- Leventhal, A. G., R. W. Rodieck, and B. Dreher, 1981. Retinal ganglion cell classes in the Old World monkey: morphology and central projections, *Science*, 213:1139–1142.
- Leventhal, A. G., R. W. Rodieck, and B. Dreher, 1985. Central projections of cat retinal ganglion cells, *J. Comp. Neurol.*, 237:216–226.
- Levitt, J. B., R. A. Schumer, S. M. Sherman, P. D. Spear, and J. A. Movshon, 2001. Visual response properties of neurons in the LGN of normally reared and visually deprived macaque monkeys, *J. Neurophysiol.*, 85:2111–2129.
- Lewis, D. A., and J. S. Lund, 1990. Heterogeneity of chandelier neurons in monkey neocortex: corticotropin-releasing factor- and parvalbumin-immunoreactive populations, *J. Comp. Neurol.*, 293:599–615.
- Livingstone, M. S., and D. H. Hubel, 1982. Thalamic inputs to cytochrome oxidase-rich regions in monkey visual cortex, *Proc. Natl. Acad. Sci. USA*, 79:6098–6101.
- Lund, J. S., 1987. Local circuit neurons of macaque monkey striate cortex: I. Neurons of laminae 4C and 5A, *J. Comp. Neurol.*, 257:60–92.
- Lund, J. S., and R. G. Boothe, 1975. Interlaminar connections and pyramidal neuron organisation in the visual cortex, area 17, of the macaque monkey, *J. Comp. Neurol.*, 159:305–334.
- Lund, J. S., M. J. Hawken, and A. J. Parker, 1988. Local circuit neurons of macaque monkey striate cortex: II. Neurons of laminae 5B and 6, *J. Comp. Neurol.*, 276:1–29.
- Lund, J. S., R. D. Lund, A. E. Hendrickson, A. H. Bunt, and A. F. Fuchs, 1975. The origin of efferent pathways from the primary visual cortex, area 17, of the macaque monkey as shown by retrograde transport of horseradish peroxidase, *J. Comp. Neurol.*, 164:287–303.
- Lund, J. S., and C. Q. Wu, 1997. Local circuit neurons of macaque monkey striate cortex: IV. Neurons of laminae 1–3A, *J. Comp. Neurol.*, 384:109–126.
- Lund, J. S., and T. Yoshioka, 1991. Local circuit neurons of macaque monkey striate cortex: III. Neurons of laminae 4B, 4A, and 3B, *J. Comp. Neurol.*, 311:234–258.
- Meskenaite, V., 1997. Calretinin-immunoreactive local circuit neurons in area 17 of the cynomolgus monkey, *Macaca fascicularis*, *J. Comp. Neurol.*, 379:113–132.
- Movshon, J. A., and W. T. Newsome, 1996. Visual response properties of striate cortical neurons projecting to area MT in macaque monkeys, *J. Neurosci.*, 16:7733–7741.
- Parra, P., A. I. Gulyas, and R. Miles, 1998. How many subtypes of inhibitory cells in the hippocampus? *Neuron*, 20:983–993.
- Peters, A., and J. Regidor, 1981. A reassessment of the forms of nonpyramidal neurons in area 17 of cat visual cortex, *J. Comp. Neurol.*, 203:685–716.
- Sawatari, A., and E. M. Callaway, 1996. Convergence of magno- and parvocellular pathways in layer 4B of macaque primary visual cortex, *Nature*, 380:442–446.
- Sawatari, A., and E. M. Callaway, 2000. Diversity and cell type specificity of local excitatory connections to neurons in layer 3B of monkey primary visual cortex, *Neuron*, 25:459–471.
- Shapley, R., and V. H. Perry, 1986. Cat and monkey retinal ganglion cells and their visual functional roles, *TINS*, 9:229–235.
- Sherk, H., and S. LeVay, 1983. Contribution of the cortico-claustral loop to receptive field properties in area 17 of the cat, *J. Neurosci.*, 11:2121–2127.
- Shipp, S., and S. Zeki, 1989. The organization of connections between areas V5 and V1 in macaque monkey visual cortex, *Eur. J. Neurosci.*, 1:308–331.
- Sincich, L. C., and J. C. Horton, 2002. Divided by cytochrome oxidase: a map of the projections from V1 to V2 in macaques, *Science*, 295:1734–1737.
- Somogyi, P., 1977. A specific “axo-axonal” interneuron in the visual cortex of the rat, *Brain Res.*, 136:345–350.
- Somogyi, P., T. F. Freund, A. J. Hodgson, J. Somogyi, D. Beroukas, and I. W. Chubb, 1985. Identified axo-axonic cells are immunoreactive for GABA in the hippocampus and visual cortex of the cat, *Brain Res.*, 332:143–149.
- Somogyi, P., G. Tamas, R. Lujan, and E. H. Buhl, 1998. Salient features of synaptic organisation in the cerebral cortex, *Brain Res. Brain Res. Rev.*, 26:113–135.
- Staiger, J. F., K. Zilles, and T. F. Freund, 1996. Distribution of GABAergic elements postsynaptic to ventroposteromedial thalamic projections in layer IV of rat barrel cortex, *Eur. J. Neurosci.*, 8:2273–2285.
- Stuart, G., N. Spruston, B. Sakmann, and M. Hausser, 1997. Action potential initiation and backpropagation in neurons of the mammalian CNS, *Trends Neurosci.*, 20:125–131.
- Tamas, G., E. H. Buhl, A. Lorincz, and P. Somogyi, 2000. Proximally targeted GABAergic synapses and gap junctions synchronize cortical interneurons, *Nat. Neurosci.*, 3:366–371.
- Tamas, G., P. Somogyi, and E. H. Buhl, 1998. Differentially interconnected networks of GABAergic interneurons in the visual cortex of the cat, *J. Neurosci.*, 18:4255–4270.
- Thomson, A. M., and J. Deuchars, 1997. Synaptic interactions in neocortical local circuits: dual intracellular recordings in vitro, *Cereb. Cortex*, 7:510–522.
- Valverde, F., 1985. The organizing principles of the primary visual cortex in the monkey, in *Cerebral Cortex*, vol. 3 (A. Peters and E. G. Jones, eds.), New York: Plenum, pp. 207–257.
- Wiesel, T. N., and D. H. Hubel, 1966. Spatial and chromatic interactions in the lateral geniculate body of the rhesus monkey, *J. Neurophysiol.*, 29:1115–1156.
- Winfield, D. A., M. Rivera-Dominguez, and T. P. Powell, 1981. The number and distribution of Meynert cells in area 17 of the macaque monkey, *Proc. R. Soc. Lond. B Biol. Sci.*, 213:27–40.
- Wiser, A. K., and E. M. Callaway, 1996. Contributions of individual layer 6 pyramidal neurons to local circuitry in macaque primary visual cortex, *J. Neurosci.*, 16:2724–2739.
- Wiser, A. K., and E. M. Callaway, 1997. Ocular dominance columns and local projections of layer 6 pyramidal neurons in macaque primary visual cortex, *Vis. Neurosci.*, 14:241–251.

- Yabuta, N. H., and E. M. Callaway, 1998a. Functional streams and local connections of layer 4C neurons in primary visual cortex of the macaque monkey, *J. Neurosci.*, 18:9489–9499.
- Yabuta, N. H., and E. M. Callaway, 1998b. Cytochrome oxidase blobs and intrinsic horizontal connections of layer 2/3 pyramidal neurons in primate V1, *Vis. Neurosci.*, 15:1007–1027.
- Yabuta, N. H., A. Sawatari, and E. M. Callaway, 2001. Two functional channels from primary visual cortex to dorsal visual cortical areas, *Science*, 292:297–300.
- Zeki, S., and S. Shipp, 1988. The functional logic of cortical connections, *Nature*, 335:311–317.
- Zemelman, B. V., and G. Miesenböck, 2001. Genetic schemes and schemata in neurophysiology, *Curr. Opin. Neurobiol.*, 11:409–414.

43 Assembly of Receptive Fields in Primary Visual Cortex

DAVID FERSTER

HUBEL AND WIESEL's characterization of receptive fields in cat visual cortex spawned several completely new lines of research (Hubel and Wiesel, 1962). Almost any description of a sensory receptive field raises similar questions. First, how are the response properties of a cell adapted to help the organism process the signals that arrive through a particular sensory modality? Why, for example, are cells in the visual cortex selective for orientation, and how does that help the brain represent the retinal image or parse it in preparation for object recognition, depth perception, motion detection, and so on? A second, related question is how receptive field properties give rise to the perceptual abilities of the organism. Can we explain an animal's ability to detect motion, for example, in light of the specific motion sensitivities of neurons in the cortex? Third, how do the responses of the neurons develop during early life? In the cortex, for example, specific types of altered experience, such as monocular deprivation or strabismus, profoundly alter some aspects of neuronal responses while leaving others intact. How much of cortical function, then, is genetically predetermined, and how much does it adapt to the environment? Fourth is the question I would like to address here: How are receptive field properties assembled from the neuronal circuitry of the cells and their inputs? In the visual cortex, neuronal receptive fields are completely unlike the receptive fields of the geniculate neurons that provide visual input to the cortex. How are the excitatory and inhibitory synaptic connections organized, both among the cortical cells themselves and between cortical cells and their geniculate inputs, so that the cortical neurons can construct their completely novel representation of the visual image?

For several reasons, this last question as it applies to visual cortex has attracted intense experimental scrutiny, numerous theoretical and computational treatments, and vigorous debate. The cortical transformation of the retinal image is at once sufficiently complex to make it highly interesting and yet extremely well defined so as to be mathematically tractable. Visual stimuli are relatively simple to control experimentally. And visual cortex performs reasonably well under anesthesia, unlike other cortical areas, where the tasks being performed, such as object recognition and high-level reasoning, do not even occur under anesthesia.

Furthermore, the exact nature of the tasks being performed in these other areas is only now being pinned down in any detail. So primary visual cortex holds out the promise of being well understood, of being a part of the brain where we have a chance to learn exactly how cortical circuitry accomplishes a complex bit of neuronal computation. For a long time, then, primary visual cortex has stood in as a proxy for the study of all cortical circuitry and its function.

Feedforward and feedback models of cortical function

Of all the receptive field properties in the visual cortex, orientation selectivity has received the most attention. In the cat, the vast majority of neurons are orientation selective, whereas the neurons of the lateral geniculate nucleus (LGN) show only rudimentary orientation selectivity. Orientation selectivity is also a very striking property and one that is easy to quantify. The first model of orientation selectivity was proposed by Hubel and Wiesel, who first described the receptive fields of cortical neurons (Hubel and Wiesel, 1962). Reasoning from the similarity between the responses of ON centers in ON geniculate neurons and the ON regions of simple cells (and the corresponding similarity between OFF centers and OFF regions), Hubel and Wiesel proposed that simple cell ON regions were constructed from the input of ON center cells whose centers overlapped the ON region. Since the simple cell ON regions are elongated relative to geniculate cell ON centers, they further reasoned that the ON region was constructed from inputs from multiple ON center cells whose receptive fields were distributed in a line down the center of the ON region (Fig. 43.1). A similar arrangement could occur for the OFF region and presynaptic OFF-center geniculate neurons. Some measure of orientation selectivity immediately falls out of the model: when a stimulus such as a bright bar is oriented correctly, it can simultaneously fall onto the centers of all of the presynaptic ON-center geniculate neurons. In the model, the resulting barrage of excitatory synaptic input brings the simple cell to threshold and causes it to fire in response to this optimal stimulus. When the bar is oriented away from the orientation of the subfields, it can only activate a fraction of the presynaptic ON center cells at any one time, so

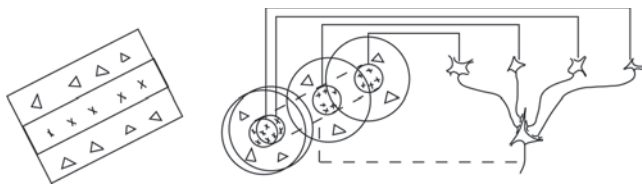


FIGURE 43.1. To the right is the receptive field of a simple cell. Crosses represent ON subfields; triangles represent OFF regions. To the left is Hubel and Wiesel's proposal for how the ON subfield arises from excitatory input from ON-center geniculate relay cells whose receptive fields are aligned in a row. (Adapted from Hubel and Wiesel, 1962.)

that the simple cell never reaches threshold. Note that a bar passing over the simple cell receptive field evokes the same number of spikes from each presynaptic geniculate neuron, so that at every orientation the simple cell receives the same total amount of synaptic excitation. But the excitation from the many inputs is spread out in time for nonpreferred orientations as the bar passes the long way down the receptive field, whereas the excitation is nearly simultaneous for the preferred orientation when the bar hits the receptive field broadside. It is the nonlinearity of the spike threshold that converts the long-lasting, low-amplitude input evoked by the nonpreferred orientation into a lack of spike response and the short, high-amplitude input evoked by the preferred orientation into a significant spike response.

This model and its successors have been referred to as *feedforward models*, since the information flows only in the forward direction, from the LGN to simple cells (and later to complex cells). One could also characterize the cortex in these models as a passive filter: the magnitude of a neuron's response is directly and monotonically related to the strength of the stimulus and to how well the stimulus matches the cell's preferred stimulus.

Hubel and Wiesel's model has an almost irresistible elegance and simplicity that has kept it at the center of the debate for 40 years. But the physiology of simple cells is surprisingly complex, and it has not been easy to account for all the properties of simple cells in detail with quantitative elaborations of Hubel and Wiesel's ideas. The difficulties will be discussed in detail below. But to deal with them, a separate class of models of cortical function has been developed (Ben-Yishai et al., 1995; Douglas et al., 1995; Somers et al., 1995; Sompolinsky and Shapley, 1997). These models are completely different in character from the original. First, they are feedback models as opposed to feedforward models: information reverberates within an excitatory feedback loop formed by the cells in a cortical column, and the responses of the cells are refined on each pass through the loop. Second, these models depend less on the spatially specific organization of the excitatory input from geniculate cells to

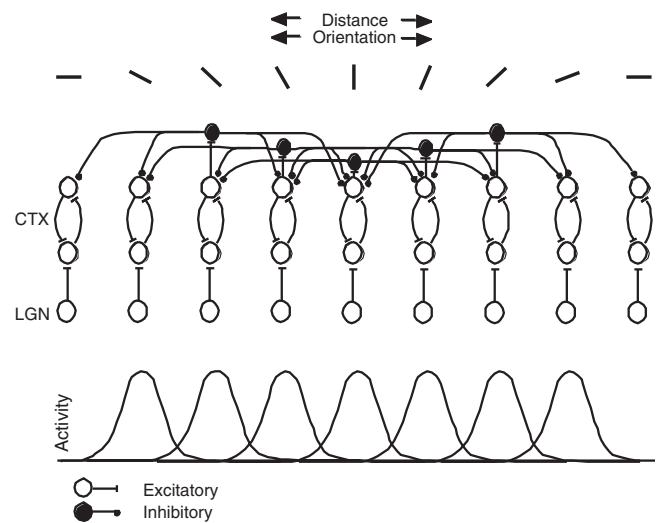


FIGURE 43.2. A diagram of a feedback model of orientation selectivity in visual cortex. Excitatory neurons within a column (*open circles*) excite one another and amplify the input coming from the LGN. Inhibitory neurons are coactivated with the excitatory neurons within their column and inhibit neurons in adjacent columns. As a result, the most stable activity pattern within the cortex is a single bubble of activity (*solid curves below*), but the location of the bubble will depend on which orientation is most prevalent in the image (*dashed curves*).

simple cells and more on the orientation-specific organization of the lateral inhibitory connections within the cortex. Finally, the feedback models do not act merely as passive filters; as will be discussed below, they impose their internal structure, that is, their internal model of the world, on the representation of the retinal image in a way that the feedforward models do not. Thus, the debate over feedforward and feedback models is a debate over the essence of cortical function. In classical fashion, however, the dialectic between the two models and the interplay between experiments and models has increased our understanding of the cortex dramatically.

The structure of the feedback models is illustrated in Figure 43.2. Though details vary from one implementation to another, the models rely on three key features of cortical organization. First, neurons within a column excite one another and, by doing so, amplify any signals coming from the LGN (hence the *feedback*). Second, the amplification from within any one column is prevented from spreading to adjacent columns by lateral inhibitory projections that originate from within the column. (The inhibitory interneurons are coactivated with the excitatory feedback neurons.) Third, the neurons in each column all prefer the same orientation. The circuits operate by implementing a form of winner-take-all behavior. Imagine, for example, that two nearby columns (representing nearby orientations within a small region of the image) are receiving significant input from the LGN, but

one is receiving somewhat stronger input. The column with the stronger input will initially be activated more strongly, and its lateral inhibitory projections will partly suppress the feedback amplification in the column with weaker input. As the feedback develops within each column, the activity and therefore the inhibition originating from the more strongly activated column will grow. At the same time, the more strongly active column will inhibit activity in the more weakly activated column, which will in turn disinhibit the more strongly activated column. Eventually, the column with stronger initial input will become fully active and the column with weaker input will become almost completely silent. The result is a single bubble of activity centered on the location of the strongest input from the LGN, that is, in the column in which the visual stimulus most closely matches the preferred orientation.

The feedback models have a number of important properties. (1) The orientation selectivity of cortical neurons does not depend on strongly orientation-sensitive input from the LGN, as would be generated by the Hubel and Wiesel model. (2) The overwhelming majority of the excitatory input to simple cells comes from other cortical cells and not from the LGN. (3) Only a weak orientation bias in the geniculate input is necessary. (4) Because of the lateral inhibition and local excitatory feedback, the cortex responds to many stimuli that contain more than one orientation with a single bubble of cortical activity centered on one orientation column (Carandini and Ringach, 1997). This relative lack of dependence of the shape of the cortical response on the exact details of the stimulus or of the organization of the geniculate input gives the feedback models their power to account for some properties of cortical neurons. But it also is the way in which the models impose their internal model of the world on the retinal image.

Experimental evidence and the feedforward and feedback models

STRENGTH AND SPATIAL ORGANIZATION OF INPUT TO SIMPLE CELLS FROM THE LATERAL GENICULATE NUCLEUS One basic premise of the feedforward models is that the ON and OFF subregions of simple cells arise from the synaptic input from ON-center and OFF-center geniculate neurons with overlapping receptive field centers. Electrical stimulation of the LGN and intracellular recording in cortex have shown that geniculate relay cells do make strong monosynaptic connections with simple cells (Douglas et al., 1991; Ferster and Lindström, 1983). Convincing evidence for the appropriate spatial arrangement of geniculate input comes from cross-correlation experiments (Reid and Alonso, 1996). In simultaneous recording from neurons in LGN and cortex, these authors found strong short-latency spike correlations which

they identified as monosynaptic connections from geniculate relay cell to simple cell. Such correlations were detected only when the receptive field center of the geniculate relay cell overlapped a subregion in the simple cell of the same polarity (ON or OFF). Thus, the subfields of the simple cell appear to originate from direct geniculate input, exactly as was predicted by Hubel and Wiesel's feedforward model. Furthermore, these monosynaptic connections from the LGN appear to account for much of a simple cell's response. That is, individual inputs from the LGN account for up to 15% of the spikes in the simple cell, and each simple cell likely receives multiple geniculate inputs (Alonso et al., 1996). The geniculate input can therefore account for a large fraction of the visual responses of simple cells.

CORTICAL INACTIVATION EXPERIMENTS The feedback models make an important prediction: that orientation selectivity depends on participation by the full cortical circuit. Unlike the feedforward models, then, the feedback models predict that orientation selectivity should collapse almost completely when the cortex is inactivated. This prediction has been tested in two experiments. In the first, the cortex was inactivated by cooling while simple cells were recorded intracellularly (Ferster et al., 1996). At surface temperatures below 10°C, most cortical cells stopped firing in response to optimal stimuli (except for cells in layer 6, which were reduced in activity by a factor of 5). At the same time, inhibition evoked by electrical stimulation in the LGN disappeared from cortical cells (presumably since the inhibitory interneurons were also silenced by the cooling). And finally, the amplitude of visually evoked modulations in membrane potential was reduced in amplitude by up to 15-fold. All these changes indicate that most of the cortical circuit was inactivated by cooling and that the remaining membrane potential responses recorded intracellularly in simple cells originated from the LGN, which was not affected directly by the cooling. Yet the orientation tuning of these residual responses was almost identical to that seen in the intact cortex. Neither the preferred orientation nor the width of tuning was significantly broadened.

In a second experiment, the cortex was silenced by electrical stimulation rather than by cooling (Chung and Ferster, 1998). A shock to the upper layers of the cortex evoked a large, long-lasting (200 msec) inhibition in nearly every cell within a 1 mm radius throughout the depth of the cortex. During the early part of this inhibition, a briefly flashed, optimally oriented grating evoked no spikes in any of the affected cells, even though it evoked vigorous responses in the absence of the electrical stimulus. In intracellular recordings from simple cells with direct input from the LGN, the electrical stimulus reduced the membrane potential response to the flashed grating by about 50% in amplitude.

Therefore, about half of the visually evoked synaptic input to these simple cells appeared to come from the cortex, whereas the remaining half presumably came from the LGN. Interestingly, the orientation selectivity of this remaining input was not significantly different from the selectivity of the responses recorded while the cortex was fully active.

Both the cooling and electrical stimulation experiments suggest, then, that the geniculate input to simple cells makes up a large fraction of the total input, and that the tuning of the geniculate input is comparable to that of the total input. The amplification of the geniculate input by the cortical circuit appears to be modest in size and appears not to sharpen orientation selectivity significantly.

PREDICTION OF ORIENTATION TUNING FROM THE SPATIAL ORGANIZATION OF THE RECEPTIVE FIELD MAP Despite all this seemingly good news for the feedforward models and bad news for the feedback models, can the feedforward models account quantitatively for all the behavior of simple cells? In the feedforward models, for example, the orientation selectivity of a simple cell arises from the elongation of the receptive field subregions, which in turn is derived from the arrangement of the receptive fields of presynaptic geniculate neurons. As a result, the longer and narrower the receptive field subregions are, the more sensitive the cell should become to small changes in orientation around the preferred orientation, that is, the more sharply tuned for orientation the cell will become. One can test this prediction by making quantitative comparisons between the elongation of the subfields and orientation tuning width in real cells. In several experiments, the tuning width of simple cells was predicted from subfield shape by assuming that the simple cells combine their inputs linearly (Gardner et al., 1999; Jones and Palmer, 1987a, 1987b). Receptive fields were mapped with high precision using small spots of light flashed throughout the receptive field, and orientation selectivity was predicted from those maps using linear summation. In most cases, the predictions failed. Whereas the preferred orientation was always well predicted by the orientation of the receptive field subregions, the width of tuning was not: the cells were most often much more sharply tuned for orientation than the elongation of the subfields would predict.

And yet, in experiments in which receptive fields and orientation tuning were measured extracellularly, this result may not be unexpected. In these experiments, the receptive field maps should predict the orientation tuning of the *synaptic input to the cell*, whereas the orientation tuning was measured from the *spike output*. It has now been shown directly that the orientation tuning measured from spikes is significantly narrower than that measured from synaptic input, that is, the subthreshold changes in membrane poten-

tial. This narrowing originates from the so-called iceberg effect (Carandini and Ferster, 2000; Volgushev et al., 2000): at the fringes of the orientation tuning curve, some orientations evoke small membrane depolarizations that remain subthreshold and therefore do not evoke spikes. Thus, because of the iceberg effect, the mismatch that is observed between predicted and measured orientation tuning is expected.

In two experiments, the orientation tuning of the membrane potential responses were compared to that predicted from the receptive field map. In the first experiment (Volgushev et al., 1996), the mismatch observed in the extracellular experiments remained, whereas in the second experiment (Lampl et al., 2001) the width of the predicted orientation tuning curve matched that of the measured tuning curve in the majority of cells. In this latter experiment, the changes in tuning width that occur with change in stimulus spatial frequency were also accounted for, which is a strong prediction of the feedforward models. It is difficult to know why the two sets of experiments gave different results, but there were differences in experimental design. Volgushev et al. used long-duration flashing spots to map the receptive fields and flashing bars to measure orientation tuning, whereas Lampl et al. used briefly flashed spots and drifting gratings. Lampl et al. also mapped the receptive fields with somewhat higher resolution. Nevertheless, that the orientation tuning of simple cells can be predicted robustly from the receptive field maps under at least one set of experimental conditions lends strong experimental support to the feedforward models, particularly if much of the synaptic input evoked by the flashing stimuli really does originate from geniculate relay cells.

DYNAMICS OF ORIENTATION TUNING For flashing stimuli, the feedforward and feedback models differ in the development of orientation selectivity during the early phase of a response. In the feedforward models, assuming that all the geniculate relay cells presynaptic to a simple cell begin responding to a flashed stimulus at the same time, and that their responses all grow in proportion to one another, the synaptic potentials measured in the simple cell should be well tuned for orientation from the first moment that orientation tuning can be measured. Furthermore, the width of tuning and the preferred orientation should remain stable throughout the early phase of the response. Feedback models, on the other hand, make a different prediction. At the earliest phase of the response, the response is dominated by the geniculate input, which is postulated to be poorly tuned for orientation on its own. Several milliseconds later, the feedback that originates from within the cortex will begin to build, sharpening the orientation tuning relative to what the geniculate can provide. Thus, the orientation tuning width should narrow

during the first several milliseconds of the response. This sharpening has been observed in extracellular recordings from the monkey visual cortex (Ringach et al., 1997). These authors found that orientation tuning at early phases of the response to flashed gratings is, in some cells, relatively broad, narrowing as the response reaches its peak. Such narrowing is not seen, however, when orientation tuning is measured intracellularly from the subthreshold changes in membrane potential (Gillespie et al., 2001). In these experiments, from the earliest moment that the responses emerge far enough out of the noise to allow the orientation tuning to be measured precisely, the width of tuning is identical to that seen at the peak of the response. What is seen in about half of the cells is a downward shift of the membrane potential at all orientations. This shift appears just prior to the peak of the preferred response and could account for any narrowing of the orientation tuning curve seen in extracellular recordings. That is, a lowering of the entire tuning curve relative to threshold could narrow the tuning of the spike output by the iceberg effect. Note that this downward shift is not equivalent to the narrowing of the orientation selectivity of the excitatory input that is predicted by the feedback models. The origin of the downward shift, whether from synaptic inhibition or by depression in the excitatory inputs (see below), remains to be determined.

CONTRAST INVARIANCE OF ORIENTATION TUNING One of the properties of simple cells that seems most difficult for the feedforward models to account for—and most natural for the feedback models—is the contrast invariance of orientation tuning. Orientation tuning curves predicted by the feedforward model for the excitatory geniculate input to a simple cell at different contrasts are shown in Figure 43.3A. Tuning curves recorded intracellularly from a real simple cell are shown in Figure 43.3C. Note that the width of tuning of the real cell is truly invariant with contrast—the curves simply scale in amplitude (Anderson et al., 2000)—whereas the model predicts that the baseline of the curve rises with contrast in addition to the observed rise in amplitude. The spike output of the feedforward model cell is also at odds with what is observed. With a fixed threshold, the rise in both the baseline and the amplitude of the membrane potential tuning curve with contrast means that orientation tuning of the spikes in the feedforward models will gradually broaden and eventually collapse altogether at high contrasts, and the responses of the cell will fail even for the preferred orientation at low contrasts (Fig. 43.3B). And yet, real cells are much better behaved. At all orientations, the spike output of simple cells scales in amplitude with contrast (Fig. 43.3D). As a result, there is no significant change in the width of orientation tuning with contrast (Sclar and Freeman, 1982; Skottun et al., 1987). These apparent failures of the feed-

forward model in explaining the contrast invariance of orientation selectivity for both membrane potential and spike output must be addressed if the model is to lay claim to any validity in describing cortical function.

THE UNTUNED COMPONENT OF THE GENICULATE INPUT Why do the orientation tuning curves in Fig. 43.3C, recorded from real simple cells (Anderson et al., 2000b), not show the rise in baseline with contrast predicted by the simple feedforward models (Fig. 43.3A)? The baseline rise (equivalent to the “untuned” or “DC” component of the responses to sinusoidal grating stimuli) occurs in the model because geniculate neurons themselves are orientation insensitive (Troyer et al., 1998). As discussed at the beginning of this chapter, an orthogonally oriented bar passing across the receptive field of a simple cell evokes the identical responses in each geniculate relay cell as does a properly oriented bar. The only reason the peak response in the simple cell is smaller at the null orientation is that the inputs from all the geniculate neurons are spread out in time as the bar passes down the rows of the geniculate receptive field that make up the ON and OFF subfields. Even though it is small, however, this excitatory input at the null orientation should grow with

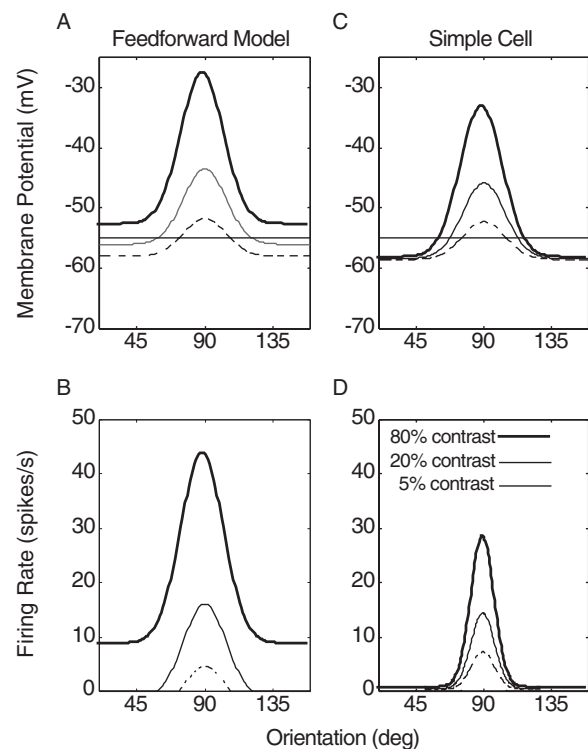


FIGURE 43.3. Orientation tuning curves at different contrasts for (A) membrane potential for the simple feedforward model, (B) spike output of the simple feedforward model, (C) the membrane potential as recorded intracellularly in simple cells, and (D) spike output of simple cells as recorded intra- or extracellularly.

contrast in proportion to the growth of the input at the preferred orientation, and so the baseline of the tuning curves should rise with contrast (Fig. 43.3A).¹

Why, then, does this predicted input at orthogonal orientations not appear in the intracellular records from simple cells (Fig. 43.3C) and why does it not grow with contrast (Anderson et al., 2000b)? The feedback models solve this problem elegantly (Somers et al., 1995). Remember that the feedback models respond with a bubble of activity in the cortex centered on the column with the preferred orientation that most closely matches the orientation present in the stimulus. Most importantly, the shape of the activity bubble depends little on the details of the input from the LGN, as determined either by the anatomical arrangement of the projection from the LGN or by the exact configuration of the stimulus. Instead, the activity pattern is determined largely by the extent of the lateral inhibitory projections within the cortex. The pattern of activity will therefore be relatively independent of the amplitude (contrast) of the stimulus as well. Since the orientation tuning of individual cells is directly related to the spatial pattern of activity in the cortex, the feedback models nicely solve the contrast invariance problem and mimic the contrast invariance observed in real simple cells.

While the simplest form of the feedforward model of Hubel and Wiesel, which relies on geniculate input alone, cannot explain the lack of a rise in baseline, there are two ways in which the model might be amended to account for the missing input at the nonpreferred orientations. The first addition to the feedforward model is a feedforward (not feedback) inhibition via cortical interneurons (Troyer et al., 1998). This inhibition would have exactly the same spatial organization and contrast dependence as the geniculate input to a simple cell. In other words, the interneuron's receptive field would look exactly like that of the simple cell it was inhibiting. As such, it would exactly counteract the predicted rise in baseline of the excitatory geniculate input to the simple cells at nonpreferred orientations. The trick is to prevent the inhibition from counteracting the geniculate input at the preferred orientation. To do so, the subfields of

the interneuron are flipped, OFF for ON and ON for OFF. At the preferred orientation, the interneuron will still respond strongly, but at the opposite spatial phase from the geniculate input. When the bar is maximally stimulating the ON geniculate inputs, it is centered on the interneuron's OFF region, so that the interneuron will not be active and will not affect the simple cell's response. The inhibition and excitation never occur simultaneously in response to stimuli of the preferred orientation, leaving the geniculate input free to fire the simple cell. But at the nonpreferred orientation, the interneuron responds in proportion to its geniculate input, thereby suppressing the effects of the excitatory geniculate input to the simple cells it inhibits (Troyer et al., 1998).

A second mechanism that might account for the lack of a rise in baseline in Figure 43.3C is synaptic depression. Synaptic depression has a disproportionately greater effect on steady-state or slowly varying inputs than it does on rapidly changing inputs (A. E. Krukowski and K. D. Miller, private communication). Thus, it will shorten the duration of the synaptic input from each geniculate neuron evoked by the passage of the stimulus. That is, the synaptic input to the simple cell will tail off faster than the spiking in the geniculate neuron itself. Note that this shortening will have little effect on the peak amplitude of the preferred response of the simple cell when the geniculate inputs are simultaneous. The shortening will, however, reduce the amplitude of the long, slow response to the orthogonal orientation by reducing the degree of temporal overlap between the asynchronous geniculate inputs. Krukowski and Miller estimate that depression at the geniculocortical synapse could reduce the size of the input at the nonpreferred orientation by as much as 60% relative to what is predicted by the simple feedforward models (though depression will have less of an effect in the response to gratings of temporal frequencies above 4 Hz). Whether depression occurs or can play this role in orientation selectivity remains to be determined experimentally.

MODIFYING THE ICEBERG EFFECT Even if the lack of a contrast-dependent baseline shift in the tuning curves of Figure 43.3C can be explained (by feedback, feedforward inhibition, or depression), how can the orientation tuning of the spike output of the neuron remain contrast invariant? Note that a fixed threshold applied to the tuning curves in Figure 43.3C (horizontal line) would appear to generate spike output tuning curves of different widths at different contrasts. In order to answer this question, one must first realize that the graphs of Figure 43.3C and Figure 43.3D are derived from the *averaged* responses of simple cells. That is, each point is derived from the averaged response to many trials of a stimulus with a particular combination of orientation and contrast. The *individual* responses that make up

¹One might think that at the orthogonal orientation, the bar would evoke a decrease in the activity of OFF-center geniculate cells making up the OFF region of the simple cell at the same time that it is evoking an increase in the ON-center cells in the ON region. These effects cannot balance one another at high contrasts, however, since the decrease in OFF-center cell activity saturates at 0 spikes/sec from a starting value of about 15 spikes/sec, which is the spontaneous rate, whereas the increase in ON-center cell activity can increase to well over 200 spikes/sec. Thus, at high contrasts and nonpreferred orientations, the feedforward models predict the presence of a small but nonzero synaptic input, which grows with contrast.

those averages, however, are extremely variable from trial to trial. The response to a low-contrast stimulus at the preferred orientation, for example, can occasionally be as large as the response to a high-contrast stimulus at the preferred orientation. Any orientation that evokes a nonzero response on average can evoke a response that is almost as large as the response to an optimally oriented high-contrast stimulus. What makes the average response to nonoptimal stimuli small (and subthreshold) is that these large individual responses are rare (Anderson et al., 2000b). Unlike optimal responses, on the majority of trials nonoptimal stimuli evoke little or no response at all. Nevertheless, the few suprathreshold responses that do occur contribute enough to the tuning curves at low contrast to broaden them significantly relative to what would be expected from the average membrane potential tuning curves.

Another way to look at the effect of response variability (or noise) is from the perspective of the threshold mechanism. The thick black line in Figure 43.4 shows the typical relationship between membrane potential and spike rate found in neurons: a nonzero threshold followed by a linear relationship. The trial-to-trial variability of the response to a stimulus, however, can be seen as effectively changing the threshold relative to the fixed mean response (Fig. 43.4, green curves). When the noise is high, the threshold is effectively lowered because the noise boosts the chance that the visual response will fire the cell. When the noise is low, the threshold remains effectively high. The average effective threshold can then be calculated by averaging together the numerous curves for individual stimulus trials (Fig. 43.4, red curve). This average can be shown to approximate a power law in which the spike rate is proportional to R^n (Fig. 43.4, blue curve), where R is the mean amplitude of the visually evoked response (relative to rest) and n is approximately 3 (Hansel and van Vreeswijk, 2001; Miller and Troyer, 2002). Thus, the noise has effectively smoothed the discontinuity of the threshold curve intrinsic to the cell's electrical properties. This smoothing is akin to the smoothing-by-noise or dithering phenomenon known in electrical engineering.

It is now possible to understand the relationship between the membrane potential (input) tuning curves of Figure 43.3C and the spike rate (output) tuning curves of Figure 43.3D: the latter should simply be equal to the former raised to the third power. The curves in Figure 43.3C can be well described by Gaussians of different amplitudes but the same of width, σ_1 . And raising a Gaussian to the third power yields a new Gaussian with $\sigma_2 = \sigma_1/\sqrt{3}$.

$$R(\theta, C) = (A_c e^{(\theta - \theta_{\text{pref}})^2 / \sigma_1^2})^3 = A_c e^{(\theta - \theta_{\text{pref}})^2 / (\sigma_1 / \sqrt{3})^2}$$

As a result, if all the widths of the input tuning curves are identical, then all the widths of the output tuning curves will be identical as well, though narrower than the input curves.

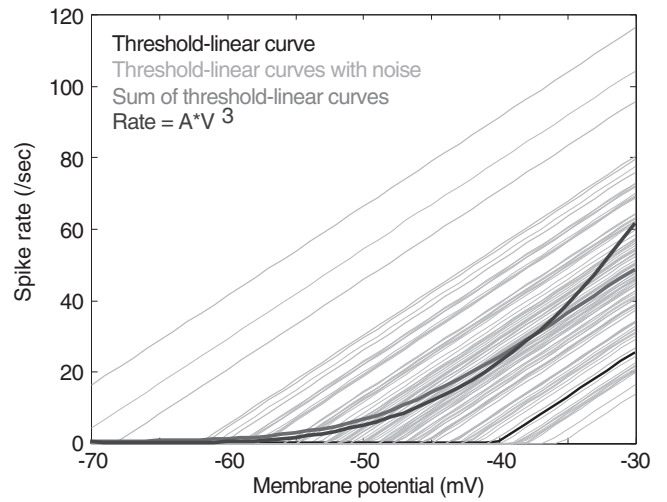


FIGURE 43.4. Smoothing-by-noise of the average relationship between membrane potential and spike rate. *Black curve*: the relationship between membrane potential and spike rate defined by the cell's electrical properties. *Green curves*: the effective threshold is shifted by the presence of trial-to-trial noise in the response to a visual stimulus. Thresholds are distributed normally. *Red curve*: the average of the green curves. *Blue curve*: An approximation to the blue curve by a power function (exponent of 3).

Thus, smoothing by noise predicts contrast invariance of the spike output from the contrast invariance of synaptic input, and yet at the same time allows for a narrowing of tuning relative to that of the synaptic input. This narrowing is similar in magnitude to that observed in real simple cells (Carandini and Ferster, 2000; Volgushev et al., 2000).

CROSS-ORIENTATION INHIBITION Even before the advent of feedback models of cortical function, it was generally thought that intracortical inhibition must sharpen orientation selectivity relative to that provided by the direct geniculate input to simple cells (for all the reasons outlined above). This inhibition would arise from cortical cells with preferred orientations different from the preferred orientation and thus has been called *cross-orientation inhibition*. Evidence for cross-orientation inhibition comes from experiments in which two stimuli are presented to a cortical cell, a test stimulus at the preferred orientation and a conditioning stimulus at the orthogonal orientation (Bonds, 1989; DeAngelis et al., 1992; Morrone et al., 1982). Even though the conditioning stimulus by itself evoked no spikes at all, it still reduces the response to the preferred stimulus alone. The simplest explanation for this behavior is cross-orientation inhibition. Several lines of evidence support this view. Local inactivation of nearby cortical columns with a preferred orientation orthogonal to that of a recorded cell increases the response of the recorded cell to stimuli of the orthogonal orientation, as if that column is providing strong inhibition (Crook et al., 1998; Eysel et al., 1998). Anatomical evidence

has been presented for inhibitory connections between columns of different orientation preference (Matsubara et al., 1985). Similarly, when GABA_A antagonists are applied to the cortex near a recorded cell, orientation selectivity is lessened or abolished, as would be expected were cross-orientation inhibition to play a role in orientation selectivity (Sillito, 1975; Tsumoto et al., 1979).

Effects of GABA_A antagonists can be difficult to interpret, however, since they increase the general excitability of the network and may thereby cause a nonspecific loss of selectivity unrelated to cross-orientation inhibition. Indeed, intracellular blockade of inhibition in one cortical cell seems not to reduce its orientation selectivity (Nelson et al., 1994). Another difficulty with attributing cross-orientation effects to cortical inhibition is that cross-orientation effects tend to be monocular: the suppressive effect of the orthogonal conditioning stimulus is much weaker or absent when present in the opposite eye from the preferred test stimulus, suggesting that cortical cells, which are strongly binocular, may not be the origin of cross-orientation inhibition effects. Finally, intracellular recording shows that synaptic inhibition is much stronger at the preferred orientation than at the orthogonal one, though some inhibition is present at all orientations.

Recent work provides an alternative explanation for cross-orientation effects (Freeman et al., 2002). These authors measured cross-orientation effects under two special circumstances, with the conditioning stimulus drifting at very high temporal frequencies and after prolonged adaptation to the conditioning stimulus. The responses of cortical cells activated by the conditioning stimulus are greatly diminished under both circumstances, and yet cross-orientation effects are almost completely unaffected. This would suggest either that cross-orientation effects are not mediated by cortical neurons at all or that cross-orientation inhibition is mediated by a very special and rare class of cortical neurons that, unlike the vast majority of cortical cells, respond at high temporal frequency *and* are unaffected by adaptation. The authors argue strongly for the first possibility, that cross-orientation effects are mediated not by cortical inhibition but by depression at the synapses between geniculate relay cells and simple cells. They then go on to model the depression and show that it can account for cross-orientation effects. In essence, the extra activity evoked in the relay cells by the conditioning stimulus increases the level of depression at their synapses, thereby reducing the excitatory drive evoked by the test stimulus.

Conclusions

It may seem paradoxical that orientation selectivity, the receptive field property most closely associated with the visual cortex, is largely established at the first synapse in

the cortex, between the axons of the LGN and the simple cells of layer 4. And yet that is what I believe the evidence as summarized here most strongly supports. The original model of Hubel and Wiesel, with minor modifications of smoothing-by-noise, and perhaps synaptic depression and/or feedforward inhibition from other simple cells, can account for many of the properties of simple cells. The strength and spatial organization of the geniculate input are exactly as the model predicts. The spatial organization of the inputs can account quantitatively for the orientation selectivity of the modulatory component of the simple cell membrane potential responses. The threshold nonlinearity can explain the discrepancy between the orientation tuning of the synaptic input and spike output. The orientation selectivity of the synaptic input to simple cells is stable over the course of the response to a flashed stimulus. And nearly complete suppression of the rest of the cortical circuit leaves the major components of orientation tuning of the synaptic input to simple cells intact. This leaves the question of what the vastly complex interconnections among cortical cells are meant to achieve, if not orientation selectivity. But the exact manner in which other receptive field properties—direction selectivity, disparity sensitivity, end stopping, surround suppression and facilitation, spatial frequency selectivity, the effects of attention—act has yet to be determined. Surely these properties, and others yet to be described, will require the fully functional cortical circuit to elaborate them.

REFERENCES

- Alonso, J. M. and W. M. Usrey, 1996. Precisely correlated firing in cells of the lateral geniculate nucleus, *Nature*, 383:815–819.
- Anderson, J. S., M. Carandini, and D. Ferster, 2000a. Orientation tuning of input conductance in cat primary visual cortex, *J. Neurophysiol.*, 84:909–926.
- Anderson, J. S., L. Lampl, and D. Ferster, 2000b. The contribution of noise to contrast invariance of orientation tuning in cat visual cortex, *Science*, 290:1968–1971.
- Ben-Yishai, R., R. L. Bar-Or, and H. Sompolinsky, 1995. Theory of orientation tuning in visual cortex, *Proc. Natl. Acad. Sci. USA*, 92:3844–3848.
- Bonds, A. B., 1989. The role of inhibition in the specification of orientation selectivity of cells in the cat striate cortex, *Vis. Neurosci.*, 2:41–55.
- Carandini, M., and D. Ferster, 2000. Membrane potential and firing rate in cat primary visual cortex, *J. Neurosci.*, 20:470–484.
- Carandini, M., and D. L. Ringach, 1997. Predictions of a recurrent model of orientation selectivity, *Vis. Res.*, 37:3061–3071.
- Chung, S., and D. Ferster, 1998. Strength and orientation tuning of the thalamic input to simple cells revealed by electrically evoked cortical suppression, *Neuron*, 20:1177–1189.
- Crook, J. M., Z. F. Kisvarday, and U. T. Eysel, 1998. Evidence for a contribution of lateral inhibition to orientation tuning and direction selectivity in cat visual cortex: reversible inactivation of functionally characterized sites combined with neuroanatomical tracing techniques, *Eur. J. Neurosci.*, 10:2056–2075.

- DeAngelis, G. C., J. G. Robson, I. Ohzawa, and R. D. Freeman, 1992. Organization of suppression in receptive fields of neurons in cat visual cortex, *J. Neurophysiol.*, 68:144–163.
- Douglas, R. J., C. Koch, M. Mahowald, K. A. Martin, and H. H. Suarez, 1995. Recurrent excitation in neocortical circuits, *Science*, 269:981–985.
- Douglas, R. J., K. A. C. Martin, and D. Whitteridge, 1991. An intracellular analysis of the visual responses of neurones in cat visual cortex, *J. Physiol. (Lond.)*, 440:659–696.
- Eysel, U. T., I. A. Shevelev, N. A. Lazarevo, and G. A. Sharaev, 1998. Orientation tuning and receptive field structure in cat striate neurons during local blockade of intracortical inhibition, *Neuroscience*, 84:25–36.
- Ferster, D., 1986. Orientation selectivity of synaptic potentials in neurons of cat primary visual cortex, *J. Neurosci.*, 6:1284–1301.
- Ferster, D., S. Chung, and H. Wheat, 1996. Orientation selectivity of thalamic input to simple cells of cat visual cortex, *Nature*, 380:249–252.
- Ferster, D., and S. Lindström, 1983. An intracellular analysis of geniculocortical connectivity in area 17 of the cat, *J. Physiol. (Lond.)*, 342:181–215.
- Freeman, T. C. B., S. Durand, D. C. Kiper, and M. Carandini, 2002. Suppression without inhibition in visual cortex, *Neuron*, 35:759–771.
- Gardner, J. L., A. Anzai, J. Ohzawa, and R. D. Freeman, 1999. Linear and nonlinear contributions to orientation tuning of simple cells in the cat's striate cortex, *Vis. Neurosci.*, 16:1115–1121.
- Gillespie, D., L. Lampl, J. S. Anderson, and R. D. Ferster, 2001. Dynamics of the orientation tuned membrane potential response in cat primary visual cortex, *Nat. Neurosci.*, 4:1014–1019.
- Hansel, D., and C. van Vreeswijk, 2002. How noise contributes to contrast invariance of orientation tuning in cat visual cortex, *J. Neurosci.*, 22:5118–5128.
- Hubel, D. H., and T. N. Wiesel, 1962. Receptive fields, binocular interaction and functional architecture in the cat's visual cortex, *J. Physiol. (Lond.)*, 160:106–154.
- Jones, J. P., and L. A. Palmer, 1987a. An evaluation of the two-dimensional Gabor filter model of simple receptive fields in cat striate cortex, *J. Neurophysiol.*, 58:1233–1258.
- Jones, J. P., and L. A. Palmer, 1987b. The two-dimensional spatial structure of simple receptive fields in cat striate cortex, *J. Neurophysiol.*, 58:1187–1211.
- Lampl, L., J. S. Anderson, D. C. Gillespre, and D. Ferster, 2001. Prediction of orientation selectivity from receptive field architecture in simple cells of cat visual cortex, *Neuron*, 30:263–274.
- Matsubara, J., M. Cynader, N. V. Swindale, and M. P. Stryker, 1985. Intrinsic projections within visual cortex: evidence for orientation-specific local connections, *Proc. Natl. Acad. Sci. USA*, 82:935–939.
- Miller, K. D., and T. D. Troyer, 2002. Neural noise can explain expansive, power-law nonlinearities in neural response functions, *J. Neurophysiol.*, 87:653–665.
- Morrone, M. C., D. C. Burr, and L. Maffei, 1982. Functional implications of cross-orientation inhibition of cortical visual cells. I. Neurophysiological evidence, *Proc. R. Soc. (Lond.) Ser. B*, 216:335–354.
- Nelson, S., L. Toth, B. Sheth, and M. Sur, 1994. Orientation selectivity of cortical neurons during intracellular blockade of inhibition, *Science*, 265:774–777.
- Reid, R. C., and J. M. Alonso, 1996. The processing and encoding of information in the visual cortex, *Curr. Opin. Neurobiol.*, 6:475–480.
- Ringach, D. L., M. J. Hawken, and R. Shapley, 1997. Dynamics of orientation tuning in macaque primary visual cortex, *Nature*, 387:281–284.
- Sclar, G., and R. D. Freeman, 1982. Orientation selectivity in the cat's striate cortex is invariant with stimulus contrast, *Exp. Brain Res.*, 46:457–461.
- Sillito, A. M., 1975. The contribution of inhibitory mechanisms to the receptive field properties of neurones in the striate cortex of the cat, *J. Physiol. (Lond.)*, 250:305–329.
- Skottun, B. C., A. Bradley, G. Sclar, I. Ohzawa, and R. D. Freeman, 1987. The effects of contrast on visual orientation and spatial frequency discrimination: a comparison of single cells and behavior, *J. Neurophysiol.*, 57:773–786.
- Somers, D. C., S. B. Nelson, and M. Sur, 1995. An emergent model of orientation selectivity in cat visual cortical simple cells, *J. Neurosci.*, 15:5448–5465.
- Sompolinsky, H., and R. Shapley, 1997. New perspectives on the mechanisms for orientation selectivity, *Curr. Opin. Neurobiol.*, 7:514–522.
- Troyer, T. W., A. E. Krukowski, N. J. Priebe, and K. D. Miller, 1998. Contrast-invariant orientation tuning in cat visual cortex: thalamocortical input tuning and correlation-based intracortical connectivity, *J. Neurosci.*, 18:5908–5927.
- Tsumoto, T., W. Eckart, and O. D. Creutzfeldt, 1979. Modification of orientation sensitivity of cat visual cortex neurons by removal of GABA-mediated inhibition, *Exp. Brain Res.*, 34:351–363.
- Volgushev, M., J. Pernberg, and U. T. Eysel, 2000. Comparison of the selectivity of postsynaptic potentials and spike responses in cat visual cortex, *Eur. J. Neurosci.*, 12:257–263.
- Volgushev, M., T. R. Vidyasagar, and X. Pei, 1996. A linear model fails to predict orientation selectivity of cells in the cat visual cortex, *J. Physiol. (Lond.)*, 496:597–606.

44 A Modern View of the Classical Receptive Field: Linear and Nonlinear Spatiotemporal Processing by V1 Neurons

GREGORY C. DEANGELIS AND AKIYUKI ANZAI

Framework

The receptive field is a central construct in virtually all physiological and computational accounts of the workings of the early visual system. It describes how visual inputs are transformed into neural responses and thus represents the computations performed by a neuron. For this reason, studies of receptive fields are essential for understanding the neural basis of visual perception.

The receptive field of a visual neuron was originally defined as the region of the retina that must be illuminated in order to evoke a response from the neuron (Hartline, 1940). In addition to defining the spatial extent of the receptive field, traditional descriptions specified that particular regions of a receptive field could respond to luminance increments (ON subregions), luminance decrements (OFF subregions), or both (ON-OFF subregions). Using this basic scheme, the spatial organization of receptive fields in the retina, lateral geniculate nucleus (LGN), and striate cortex was elucidated in a series of classic studies (e.g., Barlow, 1953; Hubel and Wiesel, 1961, 1962; Kuffler, 1953), some of which are described below. However, research over the past two decades has revealed a number of response properties that are not easily described within the basic scheme of ON and OFF subregions, suggesting that an expanded view of the receptive field is needed.

There are two major limitations to the traditional characterization of receptive fields. One is that it does not describe the temporal dynamics of neuronal responses. The response of a neuron to a very brief stimulus rises after some delay and then decays over time, and the time course of this response varies among neurons in the early visual pathways (e.g., DeAngelis et al., 1993a; De Valois et al., 2000; Wolfe and Palmer, 1998). In addition, the temporal dynamics may vary dramatically from one spatial location to another within the classically defined receptive field (DeAngelis et al., 1993a; McLean et al., 1994). Thus, it is essential for any

modern description of receptive fields to incorporate both spatial and temporal dimensions.

The second major limitation of the traditional description of receptive fields is that it does not allow for a rigorous characterization of nonlinear response properties. The response of a neuron to multiple stimuli distributed across space and time is often not equal to the linear summation of the responses to the individual stimuli, and in many cases the dominant component of the response is due to nonlinear interactions among stimuli. Thus, a modern description of the receptive field must be able to represent nonlinear response properties in addition to linear characteristics.

In this chapter, we define a receptive field as the spatiotemporal structure that characterizes the transformation between the visual image and a neuron's response, a view that has emerged from research done over the past few decades in numerous laboratories. The main advantage of this modern view is that it describes temporal dynamics of neuronal responses, and it considers the information processing performed by neurons through spatiotemporal interactions (both linear and nonlinear) within the classical receptive field. We show that this view provides new and better explanations for some of the response properties of neurons in primary visual cortex. It should be noted, however, that we do not deal with response modulations originating from outside the classical receptive field, which are described elsewhere in this volume (Chapter 45). Although nonclassical surround effects constitute important receptive field properties, they are not generally elicited by the types of stimuli discussed here and will not be a part of our descriptions.

To characterize the transformation from visual image to neuronal response, it is useful to start by considering the relevant dimensions of the visual input (Adelson and Bergen, 1991). Ignoring color for the sake of simplicity, the image formed on the retina of each eye is a time (T)-varying pattern of luminance across two spatial dimensions (X, Y),

which we denote as $I(X, Y, T)$. The response (instantaneous spike rate) of a neuron, on the other hand, is a function of only time and will be represented here by $R(T)$. In our framework, the receptive field transforms the image, $I(X, Y, T)$, into the neuronal response, $R(T)$, in two possible ways: linearly or nonlinearly (Fig. 44.1A, B). In the linear case, the neuron's response, $R(T)$, is described by a convolution of the image, $I(X, Y, T)$, with the spatiotemporal receptive field, denoted by $RF_L(X, Y, T)$:

$$R(T) = \int \int \int_{X, Y, \tau} RF_L(X, Y, \tau) I(X, Y, T - \tau) d\tau dY dX \quad (1)$$

In other words, the neuron's response is the linear summation of $I(X, Y, T)$ weighted by $RF_L(X, Y, T)$. We shall call $RF_L(X, Y, T)$ a *linear receptive field map* or a *linear map* for short. For a linear neuron, $RF_L(X, Y, T)$ can be obtained by measuring the neuron's response to a small, brief stimulus (i.e., a spatiotemporal impulse) presented at various locations throughout the receptive field. In turn, $RF_L(X, Y, T)$ can be used to predict the response of the linear neuron to any arbitrary stimulus according to equation 1. It follows that the response to a combination of multiple stimuli can be predicted by the sum of responses to the individual stimuli. In reality, neurons' behavior cannot be strictly linear due to the threshold for spike generation. However, if neurons behave otherwise linearly, equation 1 still holds for a limited range of inputs, that is, above threshold. In the third section, we will examine the spatiotemporal structure of linear receptive field maps for neurons in the central visual pathways. We will see that linear maps provide a good account of the response properties, including directional selectivity, of many neurons.

On the other hand, if a neuron combines visual inputs across space and time in a nonlinear fashion, the response will deviate from that predicted by the convolution integral of equation 1. For instance, the response of a nonlinear neuron to a combination of two stimuli would be the sum of responses to the individual stimuli (linear response) combined with the response caused by interactions between the two stimuli (nonlinear response). Thus, to describe the response, $R(T)$, of a nonlinear neuron completely, the nonlinear response due to interactions among combinations of inputs must be specified (Fig. 44.1B). We will call maps that describe this transformation *nonlinear receptive field maps* or *nonlinear maps*. For example, the map that describes nonlinear interactions between two inputs i and j (i.e., second-order interactions) will be a function of the spatial and temporal dimensions associated with the two inputs. We denote this second-order nonlinear map as $RF_{N2}(X_i, Y_i, T_i, X_j, Y_j, T_j)$. Then the response, $R(T)$, of a second-order nonlinear neuron can be described as the sum of two components: a linear response given by equation 1 and a nonlinear

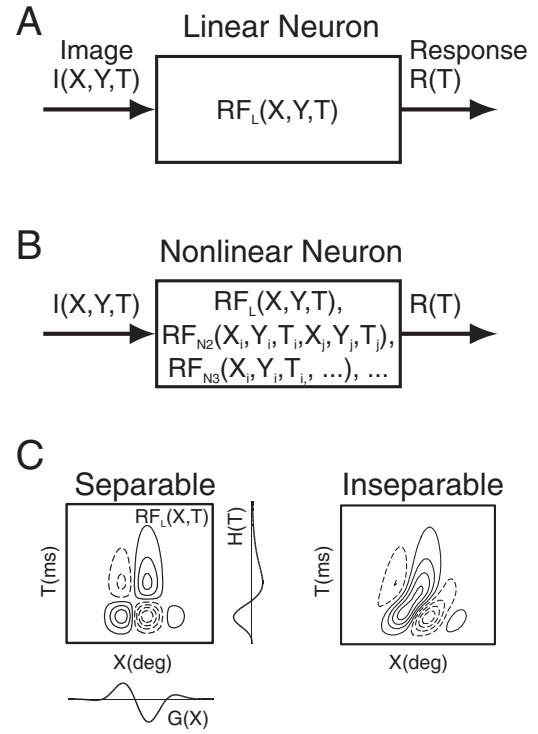


FIGURE 44.1. A visual neuron can be viewed as a system that takes an image, $I(X, Y, T)$, as input and produces a response, $R(T)$, as output. $I(X, Y, T)$ represents a luminance distribution over two dimensions of space (X, Y) and time (T), whereas $R(T)$ denotes the instantaneous spike rate as a function of time. The receptive field of a visual neuron can then be defined as a spatiotemporal structure that characterizes the transformation between the image, $I(X, Y, T)$, and the response, $R(T)$. A, For a linear neuron, this transformation is a linear summation of the image $I(X, Y, T)$ weighted by $RF_L(X, Y, T)$, which we will call a linear receptive field map. B, For a nonlinear neuron, the response is the sum of a linear component due to $RF_L(X, Y, T)$, and a nonlinear component due to interactions among visual inputs over space and time. Transformations between combinations of inputs and nonlinear responses are represented by nonlinear receptive field maps, RF_{Np} , where the subscript p indicates the order of nonlinear interaction. For example, the second-order nonlinear interaction between two inputs, i and j , is denoted by $RF_{N2}(X_i, Y_i, T_i, X_j, Y_j, T_j)$. C, Space-time separable and inseparable receptive fields. Each contour plot shows a spatiotemporal receptive field map, $RF_L(X, Y, T)$, for a hypothetical V1 simple cell (the Y -axis of $RF_L(X, Y, T)$ has been eliminated for simplicity). Solid and dashed contours represent responses to luminance increments (bright stimuli) and decrements (dark stimuli), respectively. The receptive field map on the left is space-time *separable*, meaning that $RF_L(X, Y, T)$ can be described as a product of a spatial function $G(X)$ and a temporal function $H(T)$, that is, $RF_L(X, Y, T) = G(X)H(T)$. The map on the right is *inseparable*; it cannot be decomposed into a spatial function and a temporal function.

response given by a combination of two visual inputs, $I(X_i, Y_i, T_i)$ and $I(X_j, Y_j, T_j)$, weighted by the nonlinear map $RF_{N2}(X_i, Y_i, T_i, X_j, Y_j, T_j)$:

$$R(T) = \iiint_{X_i, Y_i, T_i} \iiint_{X_j, Y_j, T_j} RF_L(X, Y, T) I(X, Y, T - \tau) d\tau dY dX + \iiint_{X_i, Y_i, T_i} \iiint_{X_j, Y_j, T_j} RF_{N2}(X_i, Y_i, T_i, X_j, Y_j, T_j) I(X_i, Y_i, T - \tau_i) I(X_j, Y_j, T - \tau_j) d\tau_i d\tau_j dY_i dY_j dX_i dX_j \quad (2)$$

In theory, nonlinear interactions can be of any order. Therefore, the receptive field of a nonlinear neuron is generally represented by multiple maps. However, responses of many neurons in early visual pathways are well described by just two maps: a linear map and a second-order nonlinear map. As we will see in the fourth section, second-order nonlinear interactions are characteristic of *complex* cells and can be measured with appropriately chosen pairs of stimuli. These interactions serve to extract useful information from the visual image, such as motion and binocular disparity. We will see that the essence of such second-order nonlinear computations can be captured with an *energy* model.

It is worth noting that the temporal dimension, T , of the linear and nonlinear receptive field maps represents the time over which the neuron integrates visual inputs. Thus, it differs from the temporal dimension of the image, $I(X, Y, T)$. One of the central tenets of our framework is that the time dimension needs to be considered as part of receptive field descriptions. If the temporal dynamics of a receptive field map do not depend on spatial location, then the map can be summarized by separate spatial and temporal profiles: $RF_L(X, Y, T) = G(X, Y) H(T)$. This case is referred to as *space-time separable* (Fig. 44.1C). However, as we will see shortly, receptive field maps of neurons in the primary visual cortex often depart from space-time separability in functionally important ways. For these neurons, a joint space-time map is the minimum acceptable descriptor of the receptive field.

Mapping receptive fields in space and time: the white noise approach

The formulation of the receptive fields in terms of equations 1 and 2 is based on linear and nonlinear systems analysis theory, the details of which are beyond the scope of this chapter and will be left for other excellent references (e.g., Marmarelis and Marmarelis, 1978; Pinter and Nabet, 1992; Schetzen, 1980). However, modern methods for mapping receptive fields rest entirely on this theory, and some conceptual understanding of the theory is helpful for interpreting the data described in the following sections. As illustrated in Figures 44.1A and 44.1B, a neuron can be considered a system that takes an input and produces an output. The goal of receptive field mapping is to infer a function that describes the transformation between input and output based solely on measurements of the output to some known

inputs. If one could record from a neuron indefinitely, then one might consider testing the neuron with every conceivable stimulus. Obviously, that approach is not only inefficient but also impractical. Methods are needed that allow one to efficiently collect information that is equivalent to testing a neuron with all possible stimuli. It is also desirable that these methods allow one to measure the linear receptive field map and various orders of nonlinear receptive field maps separately, without one measurement affecting the others.

The approach based on the use of *white noise* stimuli satisfies these requirements (Marmarelis and Marmarelis, 1978). White noise is so named because its frequency spectrum is flat, analogous to the spectral distribution of white light. This means that it contains all possible frequency components and hence can test a neuron exhaustively. When applied to a nonlinear neuron, it allows independent estimation of linear and nonlinear receptive field maps by means of cross-correlation analysis. It also guarantees that when nonlinear maps are truncated at some order of interaction, the maps for interactions up to that order still provide the best approximation to the response of the neuron in a mean-squared error sense. However, these benefits come at the expense of the generality assumed in equations 1 and 2. That is, linear and nonlinear receptive field maps are no longer independent of the stimuli used to obtain them (Marmarelis and Marmarelis, 1978). Nonetheless, as we will see in the next two sections, the maps obtained with various stimuli capture basic linear and nonlinear characteristics of neurons' responses in a qualitatively similar manner.

In recent years, several research groups have implemented receptive field mapping techniques based on white noise analysis (e.g., Anzai et al., 1999b; Chen et al., 1993; De Valois et al., 2000; Eckhorn et al., 1993; Emerson et al., 1987; Jacobson et al., 1993; Jones and Palmer, 1987; Livingstone, 1998; Ohzawa et al., 1990; Reid et al., 1997; Ringach et al., 1997; Victor et al., 1977). In these methods, a sequence of visual stimuli is presented rapidly and randomly to the neuron under study, and the resultant spike train is cross-correlated with the stimulus sequence to obtain linear and/or nonlinear maps of the receptive field. The specifics of the methods vary in a number of ways. Some have presented stimuli one at a time (sparse noise: e.g., DeAngelis et al., 1993a; Jones and Palmer, 1987; Ohzawa et al., 1990), whereas others have presented many stimuli simultaneously (dense noise: e.g., Anzai et al., 1999b; Jacobson et al., 1993; Reid et al., 1997). Some stimuli have contained many levels of luminance (Gaussian noise: e.g., Jacobson et al., 1993), while others have had only a few levels (ternary noise: e.g., Emerson et al., 1987; binary m-sequence: e.g., Anzai et al., 1999b; Reid et al., 1997). Most have operated in the space-time domain, but others have

used sinusoidal stimuli and mapped receptive fields in the spatiotemporal frequency domain (Victor et al., 1977; see also Ringach et al., 1997). Receptive field mapping has generally been performed in anesthetized, paralyzed animals, but has recently been done in alert, fixating animals by compensating for eye movements (Livingstone, 1998; Livingstone and Tsao, 1999). Although each has its strengths and weaknesses, all of these methods share two principal advantages: they allow one to obtain spatial maps of receptive fields efficiently and quantitatively, and they reveal the temporal dynamics of the receptive fields.

Figure 44.2 illustrates one of these receptive field mapping approaches (reverse correlation) developed by Palmer and colleagues (Jones and Palmer, 1987; McLean et al., 1994). The visual stimulus is a sequence of small, briefly flashed bars, and each location on a two-dimensional grid is tested using both bright and dark bars. The result of cross-correlating the stimulus sequence with the spike train is a sensitivity profile as a function of space (X, Y) and time (T , correlation delay). This cube of data corresponds to the linear spatiotemporal receptive field map, $RF_L(X, Y, T)$, that provides the best linear characterization of the neuron's response in a mean-squared-error sense (e.g., Victor, 1992). Strictly speaking, the linear map represents responses to bright bars minus responses to dark bars. However, it is common to call positive values of the map *ON responses* or *bright-excitatory responses* and to call negative values *OFF responses* or *dark-excitatory responses*. We will follow this convention unless otherwise noted.

To obtain a nonlinear receptive field map for the interaction of order p (i.e., RF_{Np}), one needs to use stimuli that contain at least p elements (such as spots and bars) so that interactions among them can be measured. In reality, however, the number of interactions explodes exponentially as the order p increases, and an ordinary recording time is generally not long enough to obtain accurate measures of all interactions. Fortunately, neurons in early stages of visual pathways exhibit relatively modest nonlinearities, mostly second-order. Still, many researchers have focused on specific subsets of second-order interactions (e.g., Fig. 44.8) and tailored their methods for efficiency (e.g., Anzai et al., 1999b; Emerson et al., 1987; Ohzawa et al., 1990).

The procedure for computing nonlinear receptive field maps is the same as that for linear maps: a cross-correlation between the stimulus and the spike train. However, the stimulus in this case is a combination of stimulus elements for which interactions are sought. For second-order interactions, this produces a sensitivity profile as a function of space and time associated with two inputs i and j , $RF_{N2}(X_i, Y_i, T_i, X_j, Y_j, T_j)$. The value at each point on the map represents the difference between responses to a pair of polarity-matched stimuli (bright-bright and dark-dark combinations) and a pair of polarity-mismatched stimuli (bright-dark and dark-bright

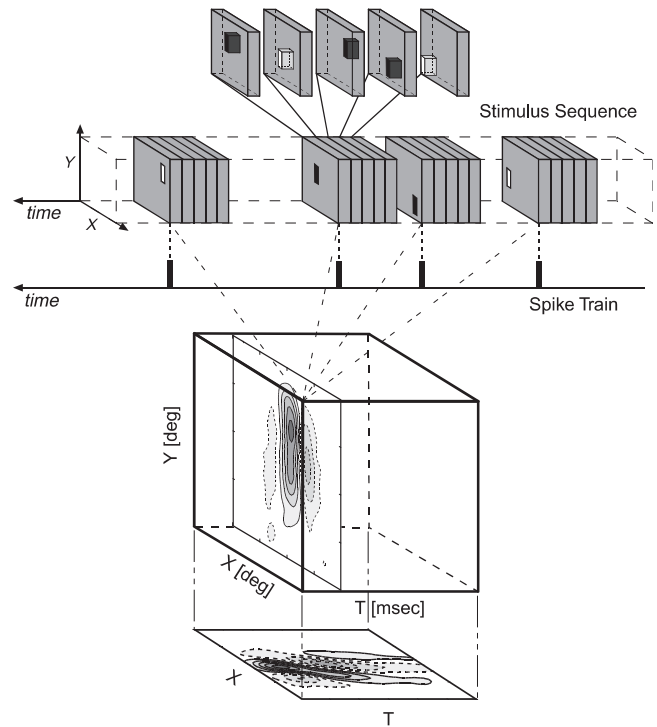


FIGURE 44.2. Illustration of a reverse correlation method for obtaining the linear spatiotemporal receptive field map. *Top*: a portion of the stimulus sequence is shown. Each stimulus is a small bright or dark bar that is presented for 30 to 50 msec on a gray background at one of 20×20 grid locations. The position and polarity of the bars are randomized. Stimuli are presented in rapid succession, with no interstimulus interval. The spike train of the neuron (which is generally much sparser than the stimulus sequence) is shown below the stimulus sequence. *Bottom*: to obtain the linear receptive field map, one averages together the sections of the stimulus sequence (shaded cubes at the top) that precede each spike. Once this procedure is completed for all spikes, the result is equivalent to that obtained by taking a cross-correlation between the spike train and the stimulus sequence. It is a cube of data that represents neuronal sensitivity in two spatial (X, Y) dimensions and one temporal (T , the correlation delay) dimension. A spatial profile of the receptive field map is generally taken at the value of T that yields maximum neuronal sensitivity (shown inside the cube). Alternatively, the cube can be integrated along the Y -axis (which is typically chosen to be parallel to the neuron's orientation preference) to obtain an X - T profile of the receptive field map (shown below the cube). (Adapted from Ohzawa et al., 1996.)

combinations). We will refer to positive and negative values of the map simply as *polarity-matched* and *polarity-mismatched responses*, respectively.

Linear receptive field maps

SPATIAL ORGANIZATION OF RECEPTIVE FIELDS IN THE CENTRAL VISUAL PATHWAY In most mammals, the dominant visual pathway runs from the retina through the LGN of the thalamus to the primary visual cortex (V1). Spiking neurons along the retino-geniculo-cortical pathway exhibit

one of three main receptive field configurations, as illustrated in Figure 44.3. For retinal ganglion cells and LGN neurons, the receptive field has a roughly circular, center-surround organization (Hubel and Wiesel, 1961; Kuffler, 1953). Two primary configurations are observed: one in which the receptive field center is responsive to a luminance increment (ON-center) and the surround is responsive to a luminance decrement (OFF-surround) (Fig. 44.3A), and another in which the respective stimulus polarities are reversed (i.e., OFF-center and ON-surround). As predicted from the circular symmetry of these receptive fields (assuming linear spatial summation), ganglion cells and LGN neurons are generally nonselective for stimulus orientation and broadly tuned for spatial frequency.

A striking transformation of response properties occurs between the LGN and V1, where orientation selectivity and direction selectivity emerge in primates and felines (Hubel and Wiesel, 1962, 1968). Simple cells, which receive most of the geniculate input to V1, have spatially oriented receptive fields (Fig. 44.3B), with alternating elongated subregions that are responsive to bright or dark stimuli. As discussed below, simple cells act roughly as linear filters, and their orientation and direction selectivity can be understood in terms of the spatiotemporal structure of their linear receptive field maps. Hubel and Wiesel (1962) originally proposed that simple cell receptive fields are constructed from arrays of ON- and OFF-center LGN inputs, and a number of elegant recent experiments provide strong support for this view (Chapman et al., 1991; Ferster et al., 1996; Reid and Alonso, 1995; see Ferster and Miller, 2000, for review). Complex cells, the other major physiological cell type in the striate cortex, respond to both bright and dark stimuli placed anywhere within their receptive fields (Fig. 44.3C). Although complex cells are also orientation selective, it is evident from Figure 44.3C that this selectivity cannot be deduced from conventional receptive field maps. As we will see in the fourth section, however, this and other properties of complex cells can be explained by the nonlinear receptive field structure.

SPATIOTEMPORAL RECEPTIVE FIELD MAPS ALONG THE GENICULOSTRIATE PATHWAY The traditional depictions of receptive fields (Fig. 44.3, *left*) are qualitative and strictly spatial in nature. We now describe linear spatiotemporal receptive field maps and examine their temporal dynamics. The spatiotemporal receptive field map can be summarized by an X - T plot. An X - T plot represents how the one-dimensional spatial profile of the receptive field map changes with time (see Fig. 44.2, *bottom*). Figure 44.4 shows X - T plots for seven representative neurons and illustrates how the linear receptive field structure changes along the geniculostriate pathway.

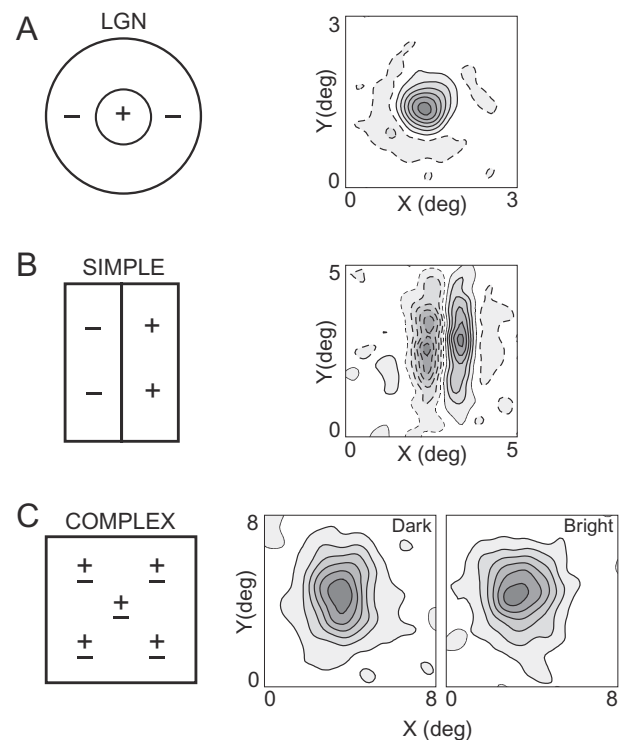


FIGURE 44.3. Spatial receptive field structure of the major classes of neurons in the geniculocortical pathway. *A*, Schematic and empirical receptive field profiles for an LGN neuron from the cat. In the traditional depiction (*left*), the receptive field has a central ON region (+) that is responsive to luminance increments and a surrounding OFF region (−) that is responsive to luminance decrements. On the right is shown a measured two-dimensional spatial (X - Y) receptive field profile. Solid and dashed contours represent regions of visual space in which the cell responds to bright and dark spots, respectively. Gray level saturation is proportional to response strength in each type of subregion. *B*, Depicted schematically on the left, the receptive field of a simple cell consists of alternating elongated subregions that are responsive to either bright (+) or dark (−) stimuli. A measured receptive field profile for a simple cell in cat striate cortex (area 17) is shown on the right (conventions as in *A*). *C*, Spatial receptive field structure of a complex cell. In the traditional illustration shown on the left, pluses and minuses scattered across the receptive field indicate that the cell responds to both bright and dark stimuli anywhere within the receptive field. Panels on the right show the receptive field profiles of an area 17 complex cell in cat. Because regions responsive to bright and dark stimuli overlap extensively, a separate profile is shown for each stimulus. (Adapted from DeAngelis et al., 1995a.)

LGN neurons For LGN cells (Fig. 44.4A, *B*), the X - T plot typically exhibits a center-surround organization in space and a biphasic structure in time (Cai et al., 1997; De Valois et al., 2000; Wolfe and Palmer, 1998). To a first approximation, the X - T profiles of LGN cells are space-time separable; however, many LGN cells (e.g., Fig. 44.4A) show two subtle, yet clear, deviations from separability. The temporal profile of the surround is often delayed slightly with respect to that of the center. In addition, the first temporal phase of the

surround often appears to converge with the second temporal phase of the center, although this may simply be a consequence of the delay in the surround.

Neurons in the magnocellular and parvocellular divisions of the primate LGN appear to have different temporal dynamics. It has long been appreciated that magnocellular neurons prefer higher temporal frequencies and exhibit more transient responses (Merigan and Maunsell, 1993). Recent studies (De Valois and Cottaris, 1998; De Valois et al., 2000) report that the temporal response profiles of magnocellular neurons are typically biphasic (i.e., odd-symmetric), whereas those of parvocellular neurons are roughly monophasic. We shall return to the importance of this temporal diversity shortly.

The feline LGN does not have magno- and parvocellular subdivisions. Nevertheless, cats appear to have two distinct classes of LGN neurons—*lagged* and *nonlagged*—with different temporal properties (Humphrey and Weller, 1988; Mastronarde, 1987; Saul and Humphrey, 1990; but see Wolfe and Palmer, 1998). As in the monkey, both types typically have bi- or triphasic temporal profiles but differ in phase by roughly 90 degrees. For nonlagged cells (e.g., Fig. 44.4A), the first phase of the temporal profile is largest, whereas for lagged cells (e.g., Fig. 44.4B) the second phase typically dominates. This property accounts for the delayed response of lagged cells to a flashed spot stimulus (Cai et al., 1997).

Simple cells Many simple cells, like their LGN inputs, have linear receptive field maps that are space-time separable, as

shown in Figures 44.4C and D. These X - T profiles typically exhibit multiple lobes in both space and time, and are well approximated by the product of a spatial profile and a temporal profile. Thus, the traditional notion that each receptive field has a unique spatial configuration still pertains to these neurons. The spatial profile typically exhibits one to five distinct subregions of alternating polarity and all possible types of spatial symmetry (i.e., spatial phases) (DeAngelis et al., 1993a; Field and Tolhurst, 1986; Hamilton et al., 1989). The temporal profile is typically biphasic

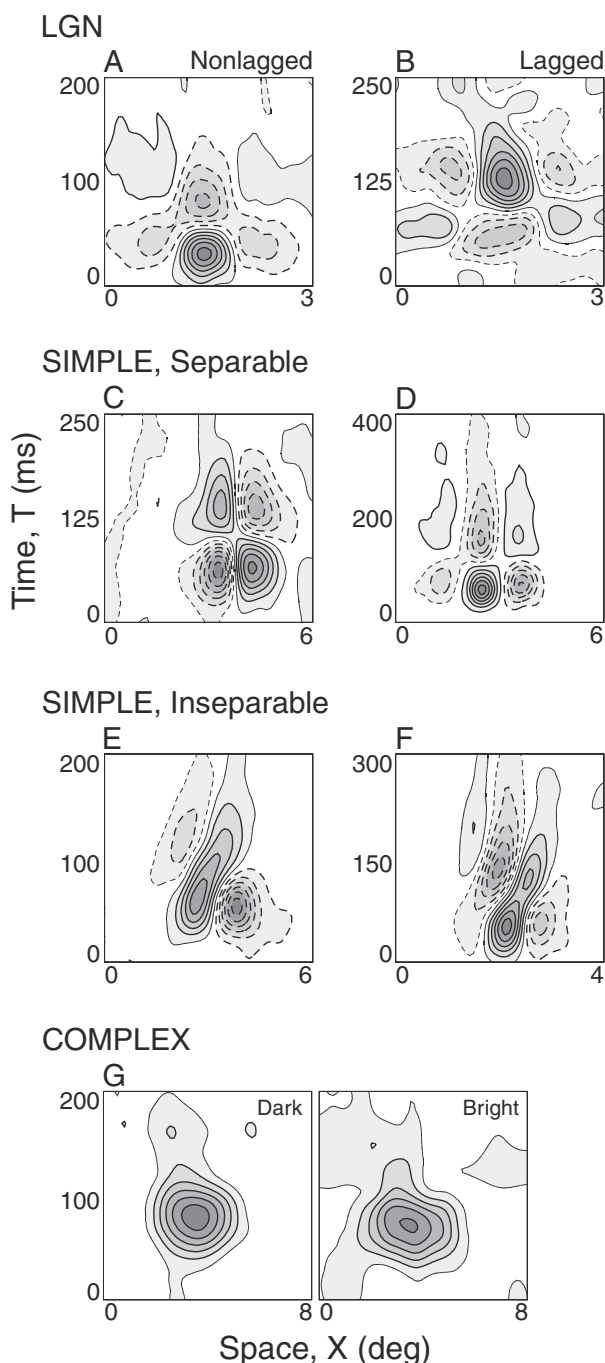


FIGURE 44.4. Linear spatiotemporal receptive field maps (X - T plots) for neurons recorded from LGN and V1 of the cat. For panels A–F, solid contours delimit bright-excitatory (ON) regions, whereas dashed contours indicate dark-excitatory (OFF) regions. A, An X - T profile is shown for a typical ON-center, non-lagged X cell from the LGN. For $T < 50$ msec, the receptive field profile has a bright-excitatory center and a dark-excitatory surround. However, for $T > 50$ msec, the receptive field center becomes dark-excitatory and the surround becomes bright-excitatory. B, An X - T plot for an ON-center, lagged X cell. Note that the second temporal phase of the profile is strongest. C, An X - T profile of a simple cell that is space-time separable. For $T < 100$ msec, the receptive field map exhibits a dark-excitatory subregion to the left of a bright-excitatory subregion. For $T > 100$ msec, each subregion reverses polarity, so that the bright-excitatory region is now on the left. D, Data for another simple cell with an approximately separable X - T profile. E, An inseparable X - T profile of a simple cell. Note how the spatial arrangement of bright- and dark-excitatory subregions (i.e., the spatial phase of the receptive field profile) changes gradually with time. F, Another example of an inseparable X - T profile from a simple cell for which a two-dimensional spatial profile is shown in Figure 44.3B. G, X - T profiles of the complex cell shown in Figure 44.3C. Responses to bright and dark stimuli are shown separately because they overlap extensively. (Adapted from DeAngelis et al., 1995a.)

in cats, although some simple cells exhibit either monophasic or triphasic profiles (DeAngelis et al., 1993a). In monkeys, a much larger fraction of simple cells have monophasic profiles (De Valois et al., 2000).

Hubel and Wiesel (1962) originally suggested that simple-cell receptive fields are created by combining inputs from a group of ON- and OFF-center geniculate neurons with receptive fields that are arranged in rows, a concept that has recently received some strong experimental support (e.g., Alonso et al., 2001; Ferster et al., 1996; Reid and Alonso, 1995). In this light, it is interesting to note that the temporal profile in a single subregion of a separable simple-cell receptive field (e.g., Figs. 44.4C and D) is similar to the temporal structure seen within the receptive field center of either an ON- or OFF-center LGN cell (e.g., Fig. 44.4A). Thus, the temporal organization of separable simple-cell receptive fields seems consistent with the idea that these receptive fields are constructed from arrays of LGN receptive fields (De Valois et al., 2000).

Unlike LGN neurons, however, many simple cells in both cats and monkeys exhibit marked space-time inseparability in their linear maps (e.g., DeAngelis et al., 1993a; McLean and Palmer, 1989; McLean et al., 1994). Two such examples are shown in Figures 44.4E and F. The X - T plots for these cells exhibit ON and OFF subregions that are distinctly tilted in the space-time domain. As a result, there is no unique spatial (or temporal) receptive field profile, because ON and OFF subregions move within the envelope of the receptive field as a function of time. Clearly, for these cells, the very definition of the receptive field must incorporate both space and time.

How are these space-time inseparable receptive fields constructed in V1? Computational studies showed that a pair of separable receptive fields that differ in spatial and temporal phase by 90 degrees could be used to build inseparable receptive fields (Adelson and Bergen, 1985; Watson and Ahumada, 1985). This scheme builds on the previous findings of Pollen and Ronner (1981), who described pairs of adjacent simple cells with receptive field profiles that differed in spatial phase by 90 degrees. Other studies have shown that a population of simple cells with separable receptive fields has the requisite variety of spatial phases to account for the observed diversity of inseparable receptive fields (see also DeAngelis et al., 1993a; De Valois et al., 2000; Field and Tolhurst, 1986; Hamilton et al., 1989). But do simple cells have the necessary diversity of temporal phases? DeValois et al. (1998, 2000) have recently reported that separable simple cells in the monkey form two groups differing in temporal phase by roughly 90 degrees. They suggest that these two groups are driven by magno- and parvocellular neurons of the LGN. In the cat, however, separable simple cells may lack the diversity of temporal phases that would be needed to build inseparable receptive fields (DeAngelis et al.,

1995b). Thus, in the cat, inseparable receptive fields may be constructed directly from a combination of lagged and nonlagged geniculate inputs, as suggested by Saul and Humphrey (1992).

Complex cells Figure 44.4G shows X - T profiles for a complex cell. Responses to bright and dark stimuli are shown separately. Note that the bright and dark responsive regions overlap almost completely in the space-time domain, and no distinct subregions are visible within either domain. Thus, unlike for simple cells, linear receptive field maps give little insight into the stimulus selectivity of complex cells. We shall return to the subject of complex cells in the fourth section.

SPATIOTEMPORAL MECHANISMS UNDERLYING DIRECTION SELECTIVITY In contrast to their geniculate antecedents, many V1 neurons are quite selective for the direction of stimulus motion (e.g., Hubel and Wiesel, 1962; Movshon, 1975; Schiller et al., 1976; Thompson et al., 1994). What accounts for the sudden emergence of directional selectivity in V1 simple cells? Hubel and Wiesel initially suggested that direction selectivity in simple cells could be explained based on the arrangement of ON and OFF subregions within the receptive field. However, subsequent studies revealed that these predictions often failed (Heggelund, 1984; Peterhans et al., 1985). Therefore, it was suggested that direction selectivity is mediated by fundamentally nonlinear mechanisms involving delayed excitation and/or inhibition between different parts of the receptive field (e.g., Barlow and Levick, 1965; Ruff et al., 1987).

In the mid-1980s, theoretical (Adelson and Bergen, 1985; Watson and Ahumada, 1985) and psychophysical (Burr et al., 1986) studies suggested that direction selectivity could be generated from linear filters that are tilted (i.e., inseparable) in the space-time domain. The intuition for this idea comes from the realization that horizontal motion of an object is represented by an oriented stripe in the X - T plane. According to this hypothesis, simple cells with inseparable X - T profiles (e.g., Fig 44.4E, F) should be direction selective, whereas those with separable X - T profiles should not. Several groups have now confirmed this prediction experimentally (e.g., Albrecht and Geisler, 1991; DeAngelis et al., 1993b; McLean et al., 1994; Reid et al., 1991). Figure 44.5 shows data from one of these studies (DeAngelis et al., 1993b), in which direction selectivity of simple cells was measured using drifting sinusoidal gratings and compared with predictions from linear receptive field maps. Note that linear predictions give the correct direction preference for the vast majority of neurons, as evidenced by most of the data points falling in the upper right quadrant of Figure 44.5A (gray shading). However, the linear predictions tend to underestimate the strength of direction selectivity (most points fall

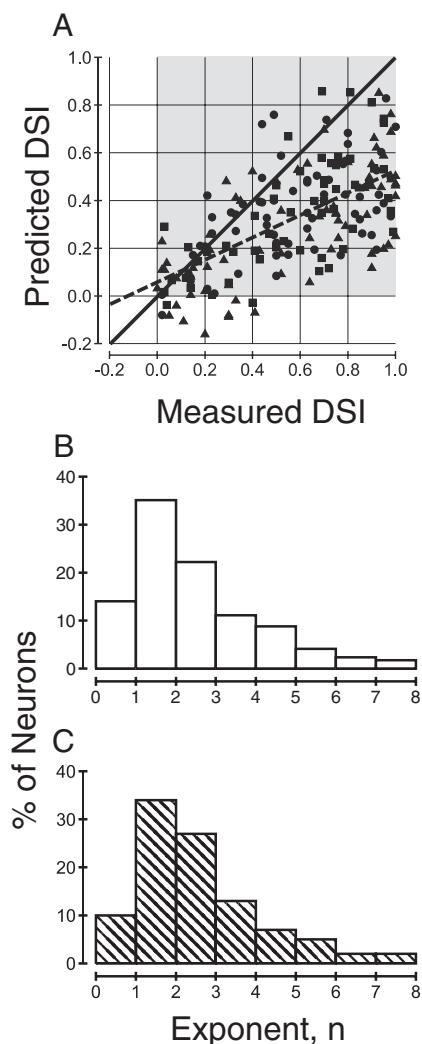


FIGURE 44.5. *A*, Comparison between the direction selectivity index (DSI) measured with drifting grating stimuli (horizontal axis) and the DSI predicted from the linear receptive field map (vertical axis). The DSI is defined as $(R_p - R_n) / (R_p + R_n)$, where R_p is the response to the preferred direction of motion and R_n is the response to the null (opposite) direction. Linear predictions of DSI were obtained from the two-dimensional Fourier transform of the X - T profile (see DeAngelis et al., 1993b). Data are shown for 190 simple cells, 65 from adult cats (*circles*), 55 from 8-week-old kittens (*squares*), and 70 from 4-week-old kittens (*triangles*). A majority of data points fall below the unity slope (*solid line*), indicating that the linear predictions underestimate DSIs measured with gratings. The dashed line shows the result of linear regression ($R = .64$, $P < .0001$); there was no significant main effect of age (ANCOVA, $P > .2$). *B*, The distribution of exponents (n) that would be required to place all of the data points in panel *A* onto the unity-slope diagonal. *C*, The distribution of exponents measured by Albrecht and Hamilton (1982) for a population of 127 cells from cat V1. The exponent value for each neuron was obtained by fitting the contrast-response function with a hyperbolic-ratio curve. (Adapted from DeAngelis et al., 1993b.)

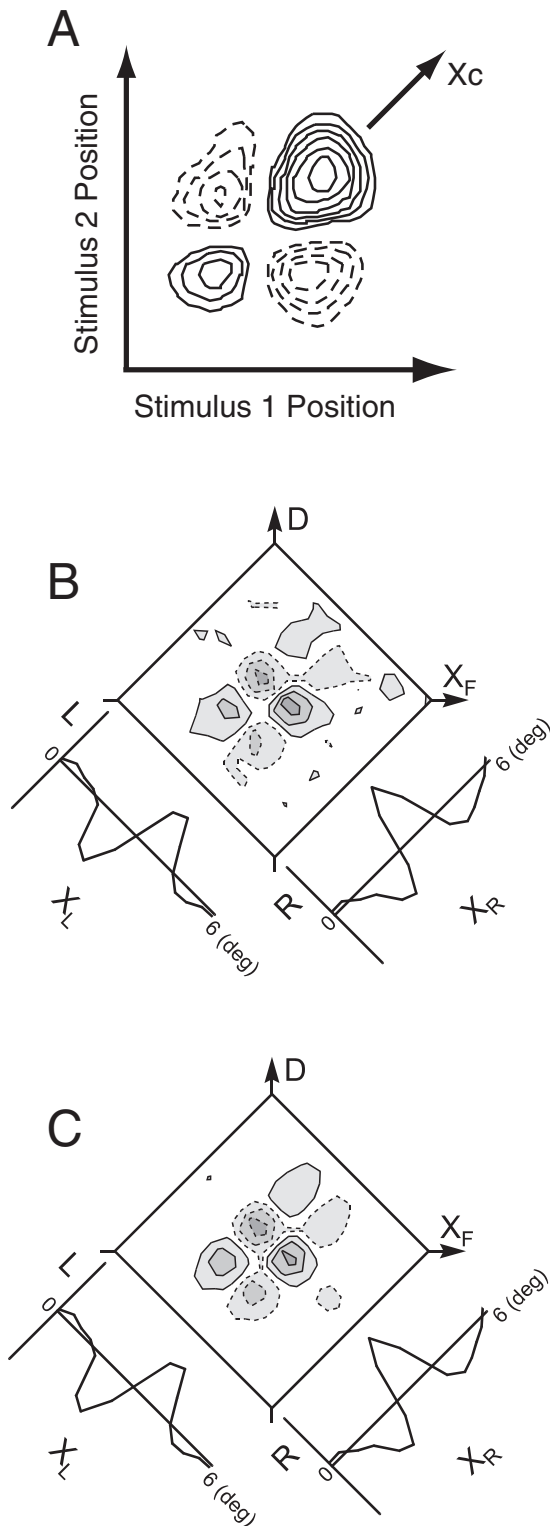
below the diagonal), indicating that simple cells are not strictly linear in their behavior.

Two groups have shown that this discrepancy can largely be accounted for by an expansive nonlinearity at the output of simple cells (Albrecht and Geisler, 1991; DeAngelis et al., 1993b; but see Emerson, 1997). The nonlinearity is generally well described by a power function ($y = x^n$ for $x > 0$). Figure 44.5*B* shows the distribution of exponents (n) that would be needed to equate the predicted and measured indices of direction selectivity for each neuron in Figure 44.5*A* (see also Gardner et al., 1999). For comparison, Figure 44.5*C* shows the exponents measured for a large population of V1 neurons (Albrecht and Hamilton, 1982; see also Anzai et al., 1999b). Although both distributions are rather broad, there is a striking agreement in the shape of the distributions. Therefore, with respect to direction selectivity, responses of simple cells are consistent with those predicted by a linear spatiotemporal filter followed by a static (output) nonlinearity (e.g., Heeger, 1992b). We will discuss this model further in the next section.

Nonlinear receptive field maps

We have thus far examined the spatiotemporal structure of linear receptive field maps for neurons in the LGN and striate cortex. If these neurons indeed sum visual inputs linearly, then their responses to any arbitrary visual pattern can be predicted by convolving the image with the linear receptive field map. On the other hand, if the neurons perform nonlinear summation, then the responses predicted from linear maps will not match the actual responses to stimuli. The deviations of the actual responses from the predicted ones, which can be represented by nonlinear receptive field maps, provide valuable insights into the functions of nonlinear processing.

As described in the first section, these deviations can be attributed to nonlinear interactions among visual inputs. In particular, second-order nonlinear interactions are of fundamental importance in early visual processing. Suppose, for example, that a bar stimulus is presented at one location (x, y) at time t and is subsequently shifted to a new location $(x + \Delta x, y + \Delta y)$ at time $t + \Delta t$. The stimulus will appear to move, provided that Δx , Δy , and Δt are chosen appropriately. Thus, the nonlinear interaction between $I(x, y, t)$ and $I(x + \Delta x, y + \Delta y, t + \Delta t)$ could be a significant factor contributing to detection of the motion. Suppose, instead, that two bars separated by Δx are presented simultaneously (i.e., $\Delta y = 0$, $\Delta t = 0$), one to each eye. They will appear to be a single bar at a certain depth, provided that Δx is within limits. In this case, Δx corresponds to a binocular disparity, and the second-order nonlinear interaction between the two eyes could be an important mechanism for signaling depth. By examining second-order nonlinear receptive field maps, we can learn



how neurons extract information about second-order attributes of the visual scene such as motion and binocular disparity.

We now describe second-order nonlinear spatiotemporal receptive field maps of simple and complex cells. As discussed in the previous section, linear receptive field maps of simple cells account for much of their responses. However, there are some residual responses that can be attributed to static nonlinearities (i.e., nonlinearities that depend on amplitude, not spatial and temporal factors). In contrast, linear maps of complex cells generally explain little of their responses. Responses of most complex cells are dominated by second-order nonlinear interactions and are well described by an energy model.

NONLINEAR INTERACTIONS EXHIBITED BY SIMPLE CELLS

Figure 44.6 shows examples of nonlinear receptive field maps for simple cells. In these maps, solid contours indicate responses to polarity-matched stimuli (e.g., a pair of bright or dark stimuli), whereas dashed contours show responses to polarity-mismatched stimuli (e.g., bright-dark combinations). The map in Figure 44.6A describes the nonlinear spatial interaction between two small squares presented to the same eye (Jacobson et al., 1993). Responses along the main diagonal (X_c) are due to the nonlinear interaction of a stimulus with itself (self-interaction) at various positions in space. Responses along one of the parallel off-diagonals represent the interaction between a pair of stimuli that have a fixed spatial interval between them. The map consists of alternating response regions (solid and dashed contours), which reflect the alternating ON and OFF subregions of the neuron's linear receptive field map (not shown). A pair

FIGURE 44.6. Nonlinear receptive field maps for simple cells and predictions of an $L-N$ model. *A*, A monocular spatial interaction map for a simple cell from monkey V1. The horizontal and vertical axes of the map represent the positions of two stimuli (*small spots*). *Solid contours* indicate responses to polarity-matched stimuli (a pair of bright or dark stimuli), whereas *dashed contours* correspond to responses to polarity-mismatched stimuli (bright-dark combinations). Responses along the X_c diagonal indicate nonlinear interactions when the two stimuli occupied the same location of space (self-interaction). *B*, A binocular spatial interaction map for a simple cell from cat area 17. Nonlinear response is shown as a function of the position of stimuli in the left (X_L) and right (X_R) eyes. Contour conventions are the same as in *A*. Linear receptive field profiles are also shown for each eye along the margins of the plot. The vertical axis, D , represents binocular disparity, whereas the horizontal axis, X_F , indicates position along the frontoparallel plane. *C*, Contours show the binocular interaction map predicted from the product of the monocular receptive field profiles for the same simple cell as in *B*. There is good agreement between the measured (*B*) and predicted (*C*) interaction maps. (*A* adapted from Jacobson et al., 1993; *B* and *C* adapted from Anzai et al., 1999b.)

of bright stimuli presented in ON subregions, or a pair of dark stimuli presented in OFF subregions, produce more response than expected from linear summation (solid contours), and the same is true for a pair of bright and dark stimuli presented in ON and OFF subregions, respectively (dashed contours). The responses vary along the main diagonal (X_c) as well as the opposite diagonal, indicating that the nonlinear interaction depends not only on the spatial interval between two stimuli but also on the individual positions of the stimuli.

Figure 44.6*B* shows that a similar pattern of nonlinear spatial interaction can be observed for a pair of stimuli presented to the two eyes (Anzai et al., 1999b). Solid and dashed contours in the map correspond to regions where linear receptive field profiles for the two eyes (shown in the margins of the nonlinear map) have matching (ON-ON or OFF-OFF) and nonmatching (ON-OFF) subregions, respectively. The responses vary along the diagonal (X_f) as well as the opposite diagonal (D). Thus, the nonlinear interaction depends not only on the interocular position difference, or binocular disparity, but also on the individual monocular positions.

Second-order temporal interactions (between two stimuli presented at the same spatial location but with various time delays) also exhibit similar response patterns (Mancini et al., 1990). In this case, the pattern seems to reflect the bi- or triphasic nature of the temporal profile of the linear receptive field map (e.g., Fig. 44.4). Similar to spatial interactions, nonlinear facilitation occurs when a pair of bright stimuli are presented during ON phases, a pair of dark stimuli are presented during OFF phases, or bright and dark stimuli are presented during ON and OFF phases.

A common feature of the nonlinear receptive field maps of simple cells is the alternating pattern of responses to polarity-matched and polarity-mismatched stimuli, which appears to reflect the arrangement of ON and OFF subregions in the linear receptive field map. These nonlinear maps are generally separable and can be described as a product of two functions. In fact, second-order interaction maps are expected to be proportional to the product of the linear receptive field profiles if the system structure of neurons is consistent with a linear filter followed by a static nonlinearity (L - N structure; Marmarelis and Marmarelis, 1978). However, if the linear map is inseparable in space-time, the second-order space-time interaction map will not be separable even though the system conforms to the L - N structure. It has been shown that some simple cells exhibit inseparable space-time interaction maps (Baker, 2001; Emerson, 1997). Although this second-order space-time inseparability can contribute to direction selectivity of the neuron (Baker, 2001), it does not necessarily require more than a static nonlinearity. A space-time inseparable linear filter followed by a static nonlinearity would exhibit separable maps for

space-space and time-time interactions but would show an inseparable map for space-time interactions.

SYSTEM STRUCTURE OF SIMPLE CELLS If a simple cell can be modeled as a linear filter followed by a static nonlinearity, then the second-order nonlinear map would be proportional to the product of the linear receptive field maps. Anzai et al. (1999b) have examined this prediction by comparing the binocular interaction map (Fig. 44.6*B*) with a product of monocular receptive field profiles (Fig. 44.6*C*). As expected, the nonlinear maps of many simple cells are proportional to the product of their monocular receptive field profiles, consistent with the L - N prediction. Similar analyses have been conducted in the temporal domain (Jacobson et al., 1993; Mancini et al., 1990) and the monocular space-time domain (Baker, 2001; Emerson, 1997; Jacobson et al., 1993). In all of these studies, it was found that many simple cells followed an L - N structure. However, some simple cells deviate from this model in a manner that suggests multiple L - N subsystems arranged in parallel (Anzai et al., 1999b; Baker, 2001; Emerson, 1997; Jacobson et al., 1993). It should be noted that a parallel L - N structure would create some overlap between ON and OFF subregions of different L - N subsystems. Receptive field maps of such neurons would have a profile that is intermediate between the canonical simple and complex types. Although quantitative studies of the simple/complex classification do find a bimodal distribution, there are certainly a fair number of cells that fall between the two modes (Skottun et al., 1991). While it is likely that these neurons may be classified as simple by some criteria, one should realize that they could be classified as complex on other grounds. The existence of such neurons does not diminish the fact that most simple cells are well described by the L - N model.

For simple cells that conform to an L - N structure, it is useful to identify the shapes of the linear filter and the static nonlinearity. Luckily, the shape of the linear filter is already known; it is given by the linear receptive field map (subject to a scaling factor). The shape of the static nonlinearity can then be estimated by plotting the relationship between its input and output. The input to the static nonlinearity is the output of the linear filter, which can be obtained by convolving the visual stimulus with the linear receptive field map. The output of the static nonlinearity is the response of the neuron to the stimulus. Using this method, Anzai et al. (1999b) found that the static nonlinearity of simple cells is an expansive function that can be modeled well by a half-rectified power function (Fig. 44.7*A*; see also Emerson et al., 1989). The exponent of this function across the population of simple cells had a mean of 2.17 (Fig. 44.7*B*), suggesting that the nonlinearity is approximately a half-squaring function (Heeger, 1992b). The distribution in Figure 44.7*B* is completely overlapping with, but narrower than, the

distributions of exponents shown in Figure 44.5*B* and Figure 44.5*C*. This is likely explained by differences in stimulus contrast among the studies, which may have introduced differential effects on contrast gain control (Ohzawa et al., 1985). The data of Figure 44.7*B* were obtained using dense noise stimuli of fixed contrast, whereas the data of Figure 44.5*B* (DeAngelis et al., 1993b; see also Gardner et al., 1999) were derived from responses to two kinds of stimuli, sinusoidal gratings and sparse noise, that had markedly different effective contrasts. The data of Figure 44.5*C* (Albrecht and Hamilton, 1982) were measured with sinusoidal gratings of various contrasts.

NONLINEAR INTERACTIONS EXHIBITED BY COMPLEX CELLS

The first quantitative attempt to characterize the nonlinear

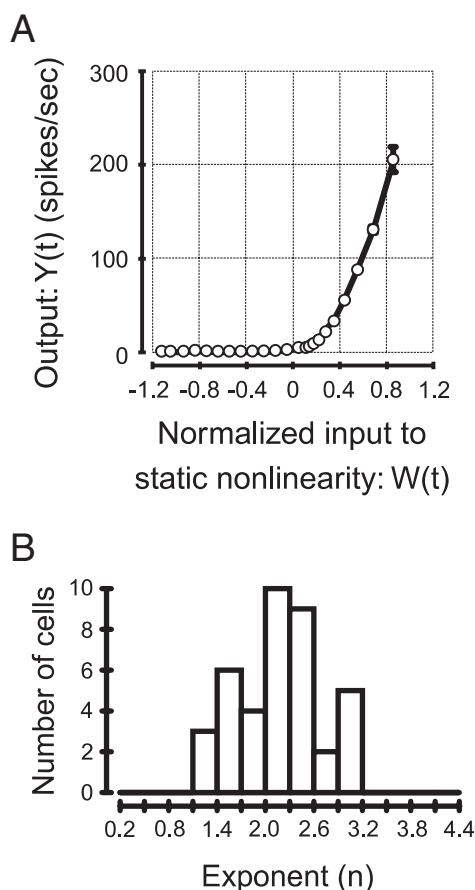


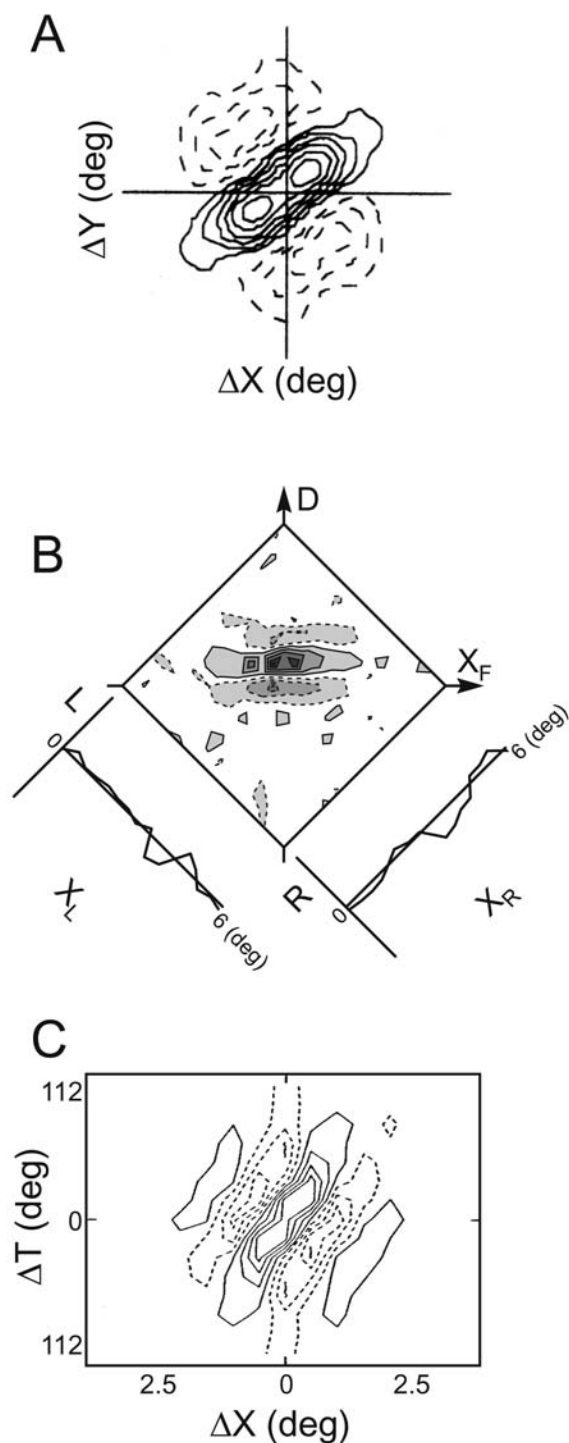
FIGURE 44.7. *A*, Characterization of the static nonlinearity for a simple cell from cat area 17. The input-output relationship of the static nonlinearity is shown. The output, $Y(t)$, is the response of the neuron to receptive field mapping stimuli, and the input, $W(t)$, is obtained by convolving the mapping stimuli with the linear receptive field map. The data are well described by a half-rectified power function ($y = x^n$, for $x > 0$) with an exponent (n) of 2.08. *B*, Distribution of exponents from a population of simple cells. The mean of the distribution is 2.17, indicating that the static nonlinearity is approximately a half-squaring function. (Adapted from Anzai et al., 1999b.)

properties of complex cells was made by Movshon et al. (1978), who measured two-bar interaction profiles by presenting pairs of bars at various positions along the axis perpendicular to the cell's preferred orientation. These interaction profiles exhibited alternating flanks of opposite polarities, similar to ON and OFF subregions of simple cells (see also Baker and Cynader, 1986; Gaska et al., 1994; Rybicki et al., 1972). Importantly, the interaction did not change with bar position as long as the spatial interval between the two bars was kept constant. These two-bar interaction profiles could explain the spatial frequency tuning of complex cells, whereas their linear maps could not (see also Gaska et al., 1994). This supports the idea that complex cells are made up of simple cell-like subunits with overlapping receptive fields (Alonso and Martinez, 1998; Hubel and Wiesel, 1962).

Numerous subsequent studies have examined second-order nonlinear interactions exhibited by complex cells (e.g., Anzai et al., 1999a; Baker, 2001; Emerson et al., 1987; Gaska et al., 1994; Livingstone and Tsao, 1999; Ohzawa et al., 1990; Szulborski and Palmer, 1990). Figure 44.8*A* shows a nonlinear spatial receptive field map measured with two-dimensional white noise presented monocularly (Gaska et al., 1994). Since the spatial interaction is independent of stimulus position, the map is plotted on $\Delta X - \Delta Y$ axes by summing responses over various positions for each spatial interval. This nonlinear map resembles the linear receptive field map of a simple cell, as Movshon et al. (1978) found using pairs of bar stimuli. In addition, the tuning for orientation and spatial frequency predicted by the nonlinear map matches well with that measured using sinusoidal gratings (Heggelund, 1981; see also Gaska et al., 1994; Szulborski and Palmer, 1990).

Figure 44.8*B* shows that a similar result is obtained for complex cells when nonlinear binocular interactions are examined with dichoptic white noise stimuli (see also Anzai et al., 1999a; Livingstone and Tsao, 1999; Ohzawa et al., 1990, 1997). For comparison, these data are shown in the same format as those of the simple cell in Figure 44.6*B*. Unlike simple cells, complex cells show nonlinear maps that are elongated along the constant-disparity diagonal (X_d). Thus, the nonlinear binocular interaction is independent of monocular position, analogous to the findings of Movshon et al. (1978) for monocular spatial interactions. In other words, complex cells respond to stimuli at any position within their receptive field as long as the binocular disparity is appropriate.

Second-order nonlinear interactions have also been examined for complex cells in the space-time domain (Anzai et al., 2001; Baker, 2001; Baker and Cynader, 1986; Emerson et al., 1987, 1992a; Gaska et al., 1994). Figure 44.8*C* shows a nonlinear space-time receptive field map for a complex cell in cat primary visual cortex (from Emerson et al., 1987). The



nonlinear response is plotted as a function of the spatial and temporal intervals between pairs of bar stimuli ($\Delta X - \Delta T$ plot). The map shows a tilt of the response pattern in this domain, reminiscent of the space-time inseparable linear maps for direction-selective simple cells. The space-time structure of these nonlinear maps predicts the direction selectivity of complex cells, whereas their linear maps (Fig. 44.4G) do not.

FIGURE 44.8. Nonlinear receptive field maps for complex cells illustrating second-order interactions. *A*, A monocular spatial interaction map of a V1 complex cell from the monkey. The nonlinear response is plotted as a function of the horizontal (ΔX) and vertical (ΔY) separation between a pair of spots presented over the receptive field. Solid and dashed contours indicate responses to polarity-matched and polarity-mismatched stimuli, respectively. *B*, A binocular spatial interaction map for a complex cell from cat area 17, plotted in the same format as Figure 44.6B for comparison. The linear receptive field profiles shown along the margins are fairly flat, whereas the nonlinear map (contours) exhibits subregions elongated along lines of constant disparity (parallel to the X_F axis). *C*, A monocular space-time interaction map for a complex cell from cat area 17. The nonlinear response is plotted as a function of the spatial (ΔX) and temporal (ΔT) interval between a pair of bars presented across the classical receptive field. (*A* adapted from Gaska et al., 1994; *B* adapted from Anzai et al., 1999a; *C* adapted from Emerson et al., 1987.)

Overall, second-order nonlinear maps account well for the orientation tuning (Gaska et al., 1994; Szulborski and Palmer, 1990), spatial frequency tuning (Gaska et al., 1994; Movshon et al., 1978), temporal frequency tuning (Gaska et al., 1994), direction preference (Emerson et al., 1987; Gaska et al., 1994), speed preference (Baker, 1988), and binocular disparity tuning (Anzai et al., 1999a; Ferster, 1981; Ohzawa et al., 1997) of most complex cells. Thus, second-order nonlinear interactions explain the essential response properties of complex cells, which in turn suggests that higher-order nonlinearities may contribute relatively little. We have noted that the spatiotemporal organization of the subunits of complex cells is strikingly similar to that of simple cells. Although this is consistent with the hierarchical model of Hubel and Wiesel (1962), we must emphasize that these measured subunits do not necessarily represent individual afferent neurons. Because these nonlinear maps are likely to reflect responses of multiple afferent neurons, the subunits should be regarded as functional rather than anatomical.

SYSTEM STRUCTURE OF COMPLEX CELLS AND THE ENERGY MODEL The results described above suggest that complex cells consist of subunits that resemble simple cells. This implies that complex cells may be modeled as a parallel $L-N$ system. If so, how many $L-N$ subunits are necessary to make up a complex cell, and what are the relationships between the subunits?

Recall that nonlinear spatial interaction maps for complex cells are relatively invariant to stimulus position within the receptive field. This suggests that receptive field subunits share common preferences for stimulus parameters such as orientation, spatial frequency, direction of motion, and binocular disparity. However, because complex cells respond to both bright and dark stimuli throughout the receptive field, the ON and OFF regions of subunits' receptive fields must

overlap extensively. In other words, the spatial relationship of subunit receptive fields must be one of the following: (1) subunit receptive fields are located at slightly different positions, as Hubel and Wiesel (1962) originally suggested; (2) they are located at the same position but have different spatial phases; or (3) they vary in both spatial position and phase.

Various models of complex cells have been built upon one of these suppositions (Cavanagh, 1984; Emerson et al., 1992a, 1992b; Glezer et al., 1980, 1982; Jacobson et al., 1993; Ohzawa et al., 1990; Pollen and Ronner, 1983; Pollen et al., 1989; Spitzer and Hochstein, 1985, 1988). Of these models, the *energy* model (Adelson and Bergen, 1985; Watson and Ahumada, 1985) has been the most popular. An energy model generally consists of two parallel L - \mathcal{N} subunits that are in a quadrature phase relationship. Each subunit is a linear bandpass filter followed by a squaring nonlinearity. Figure 44.9 shows a physiologically plausible version of the energy model in that each linear filter is subdivided further into two linear filters that are sign-inverted versions of each other, and their outputs are rectified and then squared. This basic structure has been used to model the monocular spatial characteristics (Pollen and Ronner, 1983), direction selectivity (Emerson et al., 1992a), and binocular disparity selectivity (Fleet et al., 1996; Ohzawa et al., 1990; Qian and Zhu, 1997) of complex cells.

The energy model makes a specific prediction as to the number of subunits and relationships between subunits. That is, two functionally distinct subunits that are in quadrature phase relationship would be sufficient to build a complex cell receptive field (two of the four subunits in Fig. 44.9 are not functionally distinct, differing only in sign from the other two). Anzai et al. (1999a) tried to determine if second-order binocular interaction profiles of complex cells (e.g., Fig. 44.8B) are consistent with this prediction. They performed a singular value decomposition (SVD) analysis to obtain the minimum number of quadrature subunits that are needed to account for the interaction profile. They found that a majority of complex cells required only two subunits (four if sign-inverted versions are assumed), a result consistent with the prediction of an energy model.

Although an energy model provides excellent functional descriptions for many complex cells, some second-order nonlinear maps are not well characterized by an energy model. In the SVD analysis, Anzai et al. (1999a) found that some complex cells required more than two functional subunits. Some of these cells may have had a quadrature pair that consisted of subunits that were not exactly sign-inverted versions of each other. This could explain why linear maps of some complex cells are not completely flat. Another possibility is that spatial pooling of subunits is more extensive than an energy model permits. This could account for some complex cells showing nonlinear receptive field profiles that

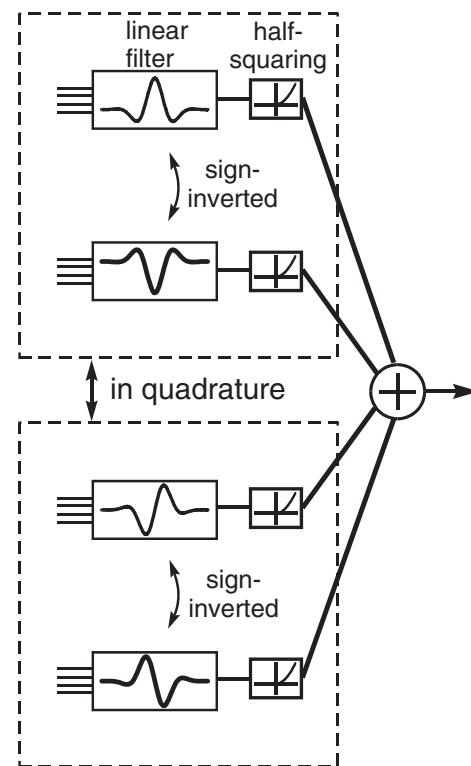


FIGURE 44.9. Schematic illustration of an energy model for a complex cell. The model consists of two major units (enclosed by dashed boxes) that are in quadrature (differing in spatial phase by 90 degrees), which makes the model respond to a stimulus independent of its spatial position/phase. Each quadrature unit consists of a pair of simple cell-like subunits with receptive field profiles of opposite signs so that the model responds equally to both bright and dark stimuli at the same position in space. Each subunit is modeled as a linear filter followed by a static nonlinearity (half-squaring). The linear filters here are depicted by one-dimensional spatial profiles of subunit receptive fields. In reality, each filter is a function of space and time, and can be monocular or binocular. They share similar selectivities for orientation, spatial and temporal frequencies, direction of motion, and binocular disparity.

are larger (i.e., more elongated diagonally in Fig. 44.8B) than expected from an energy model (Anzai et al., 1999a; Ohzawa et al., 1997). This type of spatial pooling could improve the reliability of signals being detected (Fleet et al., 1996; Qian and Zhu, 1997).

Summary and conclusions

Spatiotemporal receptive fields describe how neurons process visual inputs across space and time; hence, they characterize the functionality of neurons. Linear receptive field maps represent the best linear characterization of the transformation between visual input and neuronal response. They provide a good description of the response properties of simple cells, accounting for orientation selectivity, spatial and temporal frequency tuning, direction preference, binoc-

ular disparity tuning, and more. Nonlinear receptive field maps, on the other hand, characterize the responses of neurons that cannot be accounted for by linear summation of visual inputs across space and time. Second-order nonlinear receptive field maps are particularly important at early stages of visual processing since they represent the neural encoding of fundamental visual attributes such as motion and binocular disparity. Second-order nonlinear interactions are relatively modest for simple cells, whereas they account for virtually the entire repertoire of response properties for most complex cells.

Examination of linear and nonlinear maps allows one to formulate quantitative models for visual neurons. The maps of simple cells are consistent with the model of a linear filter followed by a static nonlinearity similar to half-squaring (L - N model). Complex cells are well characterized by an energy model, a parallel combination of simple cell-like L - N subunits that are in a quadrature phase relationship. Although some cells certainly deviate from these two canonical models, the models provide an excellent foundation upon which to build a better understanding of early visual processing. It should be noted, however, that these models exclude some important known nonlinear properties of cortical neurons, such as contrast gain control (e.g., Ohzawa et al., 1985), surround inhibition (e.g., DeAngelis et al., 1994), and contextual modulation (e.g., Zipser et al., 1996). These phenomena are likely to be the result of feedback connections from higher visual areas or lateral connections within V1, and they need to be incorporated eventually into the types of models described here (see Carandini et al., 1997; Heeger, 1992a, 1993).

The receptive fields discussed in this chapter can be thought of as spatiotemporal image filters. The visual system uses them to extract certain spatiotemporal patterns from the stream of visual images striking the retina. A linear filter followed by a squaring nonlinearity acts to extract energy in the input signal that conforms to the spatiotemporal structure of the receptive field. The linear filter creates stimulus selectivity, which in turn is enhanced by the expansive nonlinearity. Simple cells perform this computation for a given position (or phase) in space and time. Complex cells remove this position/phase dependence by combining simple cell-like subunits across space. This makes complex cells behave as spatiotemporal filters for second-order image attributes, which makes them ideally suited for encoding visual cues such as motion and binocular disparity.

Acknowledgments

We thank Andrew Parker, David Van Essen, Daniel Pollen, Lowell Jacobson, Jonathan Victor, Jay Demas, and Stephen Eglén for helpful comments and suggestions.

REFERENCES

- Adelson, E. H., and J. R. Bergen, 1985. Spatiotemporal energy models for the perception of motion, *J. Opt. Soc. Am. A*, 2: 284–299.
- Adelson, E. H., and J. R. Bergen, 1991. The plenoptic function and the elements of early vision., in *Computational Models of Visual Processing* (M. S. Landy and J. A. Movshon, eds), Cambridge, MA: MIT Press.
- Albrecht, D. G., and W. S. Geisler, 1991. Motion selectivity and the contrast-response function of simple cells in the visual cortex, *Vis. Neurosci.*, 7:531–546.
- Albrecht, D. G., and D. B. Hamilton, 1982. Striate cortex of monkey and cat: contrast response function, *J. Neurophysiol.*, 48:217–237.
- Alonso, J. M., and L. M. Martinez, 1998. Functional connectivity between simple cells and complex cells in cat striate cortex, *Nat. Neurosci.*, 1:395–403.
- Alonso, J. M., W. M. Usrey, and R. C. Reid, 2001. Rules of connectivity between geniculate cells and simple cells in cat primary visual cortex, *J. Neurosci.*, 21:4002–4015.
- Anzai, A., I. Ohzawa, and R. D. Freeman, 1999a. Neural mechanisms for processing binocular information II. Complex cells, *J. Neurophysiol.*, 82:909–924.
- Anzai, A., I. Ohzawa, and R. D. Freeman, 1999b. Neural mechanisms for processing binocular information I. Simple cells, *J. Neurophysiol.*, 82:891–908.
- Anzai, A., I. Ohzawa, and R. D. Freeman, 2001. Joint-encoding of motion and depth by visual cortical neurons: neural basis of the Pulfrich effect, *Nat. Neurosci.*, 4:513–518.
- Baker, C. Jr., and M. S. Cynader, 1986. Spatial receptive-field properties of direction-selective neurons in cat striate cortex, *J. Neurophysiol.*, 55:1136–1152.
- Baker, C. L., 1988. Spatial and temporal determinants of directionally selective velocity preference in cat striate cortex neurons, *J. Neurophysiol.*, 59:1557–1574.
- Baker, C. L., 2001. Linear filtering and nonlinear interactions in direction-selective visual cortex neurons: a noise correlation analysis, *Vis. Neurosci.*, 18:465–485.
- Barlow, H. B., 1953. Summation and inhibition in the frog's retina, *J. Physiol.*, 119:69–88.
- Barlow, H. B., and W. R. Levick, 1965. The mechanism of directionally-selective units in the rabbit's retina, *J. Physiol.*, 178:477–504.
- Burr, D. C., J. Ross, and M. C. Morrone, 1986. Seeing objects in motion, *Proc. R. Soc. Lond B*, 227:249–265.
- Cai, D., G. C. DeAngelis, and R. D. Freeman, 1997. Spatiotemporal receptive field organization in the lateral geniculate nucleus of cats and kittens, *J. Neurophysiol.*, 78:1045–1061.
- Carandini, M., D. J. Heeger, and J. A. Movshon, 1997. Linearity and normalization in simple cells of the macaque primary visual cortex, *J. Neurosci.*, 17:8621–8644.
- Cavanagh, P., 1984. Image transforms in the visual system, in *Figural Synthesis* (P. C. Dodwell and T. M. Caelli, eds), Hillsdale, NJ: Erlbaum, pp. 185–218.
- Chapman, B., K. R. Zahs, and M. P. Stryker, 1991. Relation of cortical cell orientation selectivity to alignment of receptive fields of the geniculocortical afferents that arborize within a single orientation column in ferret visual cortex, *J. Neurosci.*, 11:1347–1358.
- Chen, H. W., L. D. Jacobson, J. P. Gaska, and D. A. Pollen, 1993. Cross-correlation analyses of nonlinear systems with spatiotemporal inputs, *IEEE Trans. Biomed. Eng.*, 40:1102–1113.

- DeAngelis, G. C., R. D. Freeman, and I. Ohzawa, 1994. Length and width tuning of neurons in the cat's primary visual cortex, *J. Neurophysiol.*, 71:347–374.
- DeAngelis, G. C., I. Ohzawa, and R. D. Freeman, 1993a. Spatiotemporal organization of simple-cell receptive fields in the cat's striate cortex. I. General characteristics and postnatal development, *J. Neurophysiol.*, 69:1091–1117.
- DeAngelis, G. C., I. Ohzawa, and R. D. Freeman, 1993b. Spatiotemporal organization of simple-cell receptive fields in the cat's striate cortex. II. Linearity of temporal and spatial summation, *J. Neurophysiol.*, 69:1118–1135.
- DeAngelis, G. C., A. Anzai, I. Ohzawa, and R. D. Freeman, 1995b. A spatiotemporal receptive field model for simple cells in the cat's striate cortex, *Invest. Ophthalmol. Vis. Sci. Suppl.*, 36:872.
- DeAngelis, G. C., I. Ohzawa, and R. D. Freeman, 1995a. Receptive-field dynamics in the central visual pathways, *Trends Neurosci.*, 18:451–458.
- De Valois, R. L., and N. P. Cottaris, 1998. Inputs to directionally selective simple cells in macaque striate cortex, *Proc. Natl. Acad. Sci. USA*, 95:14488–14493.
- De Valois, R. L., N. P. Cottaris, L. E. Mahon, S. D. Elfar, and J. A. Wilson, 2000. Spatial and temporal receptive fields of geniculate and cortical cells and directional selectivity, *Vis. Res.*, 40:3685–3702.
- Eckhorn, R., F. Krause, and J. I. Nelson, 1993. The RF-cinematogram. A cross-correlation technique for mapping several visual receptive fields at once, *Biol. Cybern.*, 69:37–55.
- Emerson, R. C., 1997. Quadrature subunits in directionally selective simple cells: spatiotemporal interactions, *Vis. Neurosci.*, 14:357–371.
- Emerson, R. C., J. R. Bergen, and E. H. Adelson, 1992a. Directionally selective complex cells and the computation of motion energy in cat visual cortex, *Vis. Res.*, 32:203–218.
- Emerson, R. C., M. C. Citron, W. J. Vaughn, and S. A. Klein, 1987. Nonlinear directionally selective subunits in complex cells of cat striate cortex, *J. Neurophysiol.*, 58:33–65.
- Emerson, R. C., M. J. Korenberg, and M. C. Citron, 1989. Identification of intensive nonlinearities in cascade models of visual cortex and its relationship to cell classification, in *Advanced Methods of Physiological System Modeling* (V. Z. Marmarelis, ed.), New York: Plenum, pp. 97–111.
- Emerson, R. C., M. J. Korenberg, and M. C. Citron, 1992b. Identification of complex-cell intensive nonlinearities in a cascade model of cat visual cortex, *Biol. Cybern.*, 66:291–300.
- Ferster, D., 1981. A comparison of binocular depth mechanisms in areas 17 and 18 of the cat visual cortex, *J. Physiol.*, 311:623–655.
- Ferster, D., S. Chung, and H. Wheat, 1996. Orientation selectivity of thalamic input to simple cells of cat visual cortex, *Nature*, 380:249–252.
- Ferster, D., and K. D. Miller, 2000. Neural mechanisms of orientation selectivity in the visual cortex, *Ann. Rev. Neurosci.*, 23:441–471.
- Field, D. J., and D. J. Tolhurst, 1986. The structure and symmetry of simple-cell receptive-field profiles in the cat's visual cortex, *Proc. R. Soc. Lond. B*, 228:379–400.
- Fleet, D. J., H. Wagner, and D. J. Heeger, 1996. Neural encoding of binocular disparity: energy models, position shifts and phase shifts, *Vis. Res.*, 36:1839–1857.
- Gardner, J. L., A. Anzai, I. Ohzawa, and R. D. Freeman, 1999. Linear and nonlinear contributions to orientation tuning of simple cells in the cat's striate cortex, *Vis. Neurosci.*, 16:1115–1121.
- Gaska, J. P., L. D. Jacobson, H. W. Chen, and D. A. Pollen, 1994. Space-time spectra of complex cell filters in the macaque monkey: a comparison of results obtained with pseudowhite noise and grating stimuli, *Vis. Neurosci.*, 11:805–821.
- Glezer, V. D., T. A. Tsherbach, V. E. Gauselman, and V. M. Bondarko, 1980. Linear and non-linear properties of simple and complex receptive fields in area 17 of the cat visual cortex. A model of the field, *Biol. Cybern.*, 37:195–208.
- Glezer, V. D., T. A. Tsherbach, V. E. Gauselman, and V. M. Bondarko, 1982. Spatio-temporal organization of receptive fields of the cat striate cortex. The receptive fields as the grating filters, *Biol. Cybern.*, 43:35–49.
- Hamilton, D. B., D. G. Albrecht, and W. S. Geisler, 1989. Visual cortical receptive fields in monkey and cat: spatial and temporal phase transfer function, *Vis. Res.*, 29:1285–1308.
- Hartline, H. K., 1940. The receptive fields of optic nerve fibers, *Am. J. Physiol.*, 130:690–699.
- Heeger, D. J., 1992a. Normalization of cell responses in cat striate cortex, *Vis. Neurosci.*, 9:181–197.
- Heeger, D. J., 1992b. Half-squaring in responses of cat striate cells, *Vis. Neurosci.*, 9:427–443.
- Heeger, D. J., 1993. Modeling simple-cell direction selectivity with normalized, half-squared, linear operators, *J. Neurophysiol.*, 70:1885–1898.
- Heggelund, P., 1981. Receptive field organization of complex cells in cat striate cortex, *Exp. Brain Res.*, 42:90–107.
- Heggelund, P., 1984. Direction asymmetry by moving stimuli and static receptive field plots for simple cells in cat striate cortex, *Vis. Res.*, 24:13–16.
- Hubel, D. H., and T. N. Wiesel, 1961. Integrative action in the cat's lateral geniculate body, *J. Physiol.*, 155:385–398.
- Hubel, D. H., and T. N. Wiesel, 1962. Receptive fields, binocular interaction, and functional architecture in the cat's visual cortex, *J. Physiol.*, 160:106–154.
- Hubel, D. H., and T. N. Wiesel, 1968. Receptive fields and functional architecture of monkey striate cortex, *J. Physiol. (Lond.)*, 195:215–243.
- Humphrey, A. L., and R. E. Weller, 1988. Functionally distinct groups of X-cells in the lateral geniculate nucleus of the cat, *J. Comp. Neurol.*, 268:429–447.
- Jacobson, L. D., J. P. Gaska, H. W. Chen, and D. A. Pollen, 1993. Structural testing of multi-input linear-nonlinear cascade models for cells in macaque striate cortex, *Vis. Res.*, 33:609–626.
- Jones, J. P., and L. A. Palmer, 1987. The two-dimensional spatial structure of simple receptive fields in cat striate cortex, *J. Neurophysiol.*, 58:1187–1211.
- Kuffler, S. W., 1953. Discharge patterns and functional organization of mammalian retina, *J. Neurophysiol.*, 16:37–68.
- Livingstone, M. S., 1998. Mechanisms of direction selectivity in macaque V1, *Neuron*, 20:509–526.
- Livingstone, M. S., and D. Y. Tsao, 1999. Receptive fields of disparity-selective neurons in macaque striate cortex, *Nat. Neurosci.*, 2:825–832.
- Mancini, M., B. C. Madden, and R. C. Emerson 1990. White noise analysis of temporal properties in simple receptive fields of cat cortex, *Biol. Cybern.*, 63:209–219.
- Marmarelis, P. Z., and V. Z. Marmarelis, 1978. *Analysis of Physiological Systems: The White-Noise Approach*, New York: Plenum.
- Mastronarde, D. N., 1987. Two classes of single-input X-cells in cat lateral geniculate nucleus. I. Receptive-field properties and classification of cells, *J. Neurophysiol.*, 57:357–380.

- McLean, J., and L. A. Palmer, 1989. Contribution of linear spatiotemporal receptive field structure to velocity selectivity of simple cells in area 17 of cat, *Vis. Res.*, 29:675–679.
- McLean, J., S. Raab, and L. A. Palmer, 1994. Contribution of linear mechanisms to the specification of local motion by simple cells in areas 17 and 18 of the cat, *Vis. Neurosci.*, 11:271–294.
- Merigan, W. H., and J. H. Maunsell, 1993. How parallel are the primate visual pathways? *Annu. Rev. Neurosci.*, 16:369–402.
- Movshon, J. A., 1975. The velocity tuning of single units in cat striate cortex, *J. Physiol.*, 249:445–468.
- Movshon, J. A., I. D. Thompson, and D. J. Tolhurst, 1978. Receptive field organization of complex cells in the cat's striate cortex, *J. Physiol.*, 283:79–99.
- Ohzawa, I., G. C. DeAngelis, and R. D. Freeman, 1990. Stereoscopic depth discrimination in the visual cortex: neurons ideally suited as disparity detectors, *Science*, 249:1037–1041.
- Ohzawa, I., G. C. DeAngelis, and R. D. Freeman, 1996. Encoding of binocular disparity by simple cells in the cat's visual cortex, *J. Neurophysiol.*, 75:1779–1805.
- Ohzawa, I., G. C. DeAngelis, and R. D. Freeman, 1997. Encoding of binocular disparity by complex cells in the cat's visual cortex, *J. Neurophysiol.*, 77:2879–2909.
- Ohzawa, I., G. Sclar, and R. D. Freeman, 1985. Contrast gain control in the cat's visual system, *J. Neurophysiol.*, 54:651–667.
- Peterhans, E., P. O. Bishop, and R. M. Camarda, 1985. Direction selectivity of simple cells in cat striate cortex to moving light bars. I. Relation to stationary flashing bar and moving edge responses, *Exp. Brain Res.*, 57:512–522.
- Pinter, R. B., and B. Nabet, 1992. *Nonlinear Vision: Determination of Neural Receptive Fields, Function, and Networks*, Boca Raton, FL: CRC Press.
- Pollen, D. A., J. P. Gaska, and L. D. Jacobson, 1989. Physiological constraints on models of visual cortical function, in *Models of Brain Function* (R. M. J. Cotterill, ed.), Cambridge, MA: Cambridge University Press, pp. 115–135.
- Pollen, D. A., and S. F. Ronner, 1981. Phase relationships between adjacent simple cells in the visual cortex, *Science*, 212:1409–1411.
- Pollen, D. A., and S. F. Ronner, 1983. Visual cortical neurons as localized spatial frequency filters, *IEEE Trans. Systems, Man, Cybern.*, 13:907–916.
- Qian, N., and Y. Zhu, 1997. Physiological computation of binocular disparity, *Vis. Res.*, 37:1811–1827.
- Reid, R. C., and J. M. Alonso, 1995. Specificity of monosynaptic connections from thalamus to visual cortex, *Nature*, 378:281–284.
- Reid, R. C., R. E. Soodak, and R. M. Shapley, 1991. Directional selectivity and spatiotemporal structure of receptive fields of simple cells in cat striate cortex, *J. Neurophysiol.*, 66:505–529.
- Reid, R. C., J. D. Victor, and R. M. Shapley, 1997. The use of m-sequences in the analysis of visual neurons: linear receptive field properties, *Vis. Neurosci.*, 14:1015–1027.
- Ringach, D. L., G. Sapiro, and R. Shapley, 1997. A subspace reverse-correlation technique for the study of visual neurons, *Vis. Res.*, 37:2455–2464.
- Ruff, P. I., J. P. Rauschecker, and G. Palm, 1987. A model of direction-selective “simple” cells in the visual cortex based on inhibition asymmetry, *Biol. Cybern.*, 57:147–157.
- Rybacki, G. B., D. M. Tracy, and D. A. Pollen, 1972. Complex cell response depends on interslit spacing, *Nat. New Biol.*, 240:77–78.
- Saul, A. B., and A. L. Humphrey, 1990. Spatial and temporal response properties of lagged and nonlagged cells in cat lateral geniculate nucleus, *J. Neurophysiol.*, 64:206–224.
- Saul, A. B., and A. L. Humphrey, 1992. Evidence of input from lagged cells in the lateral geniculate nucleus to simple cells in cortical area 17 of the cat, *J. Neurophysiol.*, 68:1190–1208.
- Schetzen, M., 1980. *The Volterra and Wiener Theories of Nonlinear Systems*, New York: Wiley.
- Schiller, P. H., B. L. Finlay, and S. F. Volman, 1976. Quantitative studies of single-cell properties in monkey striate cortex. I. Spatiotemporal organization of receptive fields, *J. Neurophysiol.*, 39:1288–1319.
- Skottun, B. C., R. L. DeValois, D. H. Grosof, J. A. Movshon, D. G. Albrecht, and A. B. Bonds, 1991. Classifying simple and complex cells on the basis of response modulation, *Vis. Res.*, 31:1079–1086.
- Spitzer, H., and S. Hochstein, 1985. A complex-cell receptive-field model, *J. Neurophysiol.*, 53:1266–1286.
- Spitzer, H., and S. Hochstein, 1988. Complex-cell receptive field models, *Prog. Neurobiol.*, 31:285–309.
- Szulborski, R. G., and L. A. Palmer, 1990. The two-dimensional spatial structure of nonlinear subunits in the receptive fields of complex cells, *Vis. Res.*, 30:249–254.
- Thompson, K. G., Y. Zhou, and A. G. Leventhal, 1994. Direction-sensitive X and Y cells within the A laminae of the cat's LGNd, *Vis. Neurosci.*, 11:927–938.
- Victor, J. D., 1992. Nonlinear systems analysis in vision: an overview of kernel methods, in *Nonlinear Vision: Determination of Neural Receptive Fields, Function, and Networks* (R. B. Pinter and B. Nabet, eds.), Boca Raton, FL: CRC Press, pp. 1–38.
- Victor, J. D., R. M. Shapley, and B. W. Knight, 1977. Nonlinear analysis of cat retinal ganglion cells in the frequency domain, *Proc. Natl. Acad. Sci. USA*, 74:3068–3072.
- Watson, A. B., and A. Ahumada, Jr., 1985. Model of human visual-motion sensing, *J. Opt. Soc. Am. A*, 2:322–341.
- Wolfe, J., and L. A. Palmer, 1998. Temporal diversity in the lateral geniculate nucleus of cat, *Vis. Neurosci.*, 15:653–675.
- Zipser, K., V. A. Lamme, and P. H. Schiller, 1996. Contextual modulation in primary visual cortex, *J. Neurosci.*, 16:7376–7389.

45 Beyond the Classical Receptive Field: Contextual Modulation of V1 Responses

VICTOR A. F. LAMME

Receptive field tuning properties define the functions of visual areas

The receptive field (RF) of a neuron in visual cortex is the part of the visual field from which action potential responses can be elicited by presenting a stimulus. This stimulus has to meet a number of requirements for the cell to respond; that is, the RF is “tuned” to particular features. For example, cells in primary visual cortex (V1) respond better to some orientations of luminance contrast than to others (Hubel and Wiesel, 1968, 1977). Traditionally, the function of a visual area is derived from the set of features to which the neurons in the area are tuned. MT is called a *motion* area because many of its cells are tuned to direction, speed, or other aspects of motion (Allman et al., 1985a; Maunsell and Newsome, 1987; Maunsell and Van Essen, 1983; Movshon et al., 1986; Newsome et al., 1986); V4 is a *color* or *form* area because cells are tuned to certain wavelengths (Zeki, 1973, 1980) or elementary shapes (Desimone and Schein, 1987; Gallant et al., 1996); and so on. This view is further corroborated by the fact that lesions in these areas typically cause deficits that are related to the processing functions we attribute to these areas by means of their receptive field tuning properties (Dean, 1979; Heywood and Cowey, 1987; Maunsell and Newsome, 1987; Newsome et al., 1985; Schiller, 1993; Schiller and Lee, 1991; Wild et al., 1985). Thus, we arrive at a view whereby visual processing is subdivided into specific modules, each solving a particular subproblem of vision (Livingstone and Hubel, 1988; DeYoe and Van Essen, 1988). Although the strictness of this view is much disputed, it has profoundly pervaded our thinking about the roles of cortical areas in vision.

Combining the distributed information

When the visual field is analyzed by limited RFs within functionally separate modules, extensive and dynamic interactions are required to combine the distributed information. Anatomical connections provide the framework for those interactions (Felleman and Van Essen, 1991). Within each cortical area, horizontal interactions integrate information

from separate parts of the visual field (Gilbert, 1992; Gilbert and Wiesel, 1989). Between areas, information is transferred in a feedforward fashion from low-level areas to higher-level ones. But in addition, feedback connections transfer information in the reverse direction (Salin and Bullier, 1995). When going upstream through the hierarchy of visual areas, RFs obtain increasingly complex tuning properties and rapidly increase in size (Maunsell and Newsome, 1987). These tuning properties can be observed as soon as the neurons start to respond to a visual stimulus. So, RF properties strongly reflect the convergent-divergent feedforward cascade of information processing. But what effect do the horizontal and feedback connections exert on the neural activity? Feedback connections are highly diverging, so their influence on cells in lower areas is not reflected by the small RFs of an area such as V1 (Salin and Bullier, 1995). Also, horizontal connections within V1 spread over much larger distances than the size of RFs would necessitate (Gilbert, 1992, 1993). So, if not “visible” in the tuning properties of cells, when and how do these connections exert their effect on the neuron’s responses?

Once an RF contains some stimulus, the response to this stimulus may be modulated by surrounding stimuli. A key feature of this phenomenon is that the modulating stimuli do not evoke a response when presented alone; they are outside the “classical” RF. The early experiments, in area 17 of anesthetized cats, typically used bars or gratings to stimulate both the RF and its surround. Modulatory effects could be evoked at large distances but were strongest at small distances. Both facilitatory and inhibitory effects were found that could be either nonspecific or any combination of orientation and direction of motion specific (Albus and Fries, 1980; Allman et al., 1985b; Blakemore and Tobin, 1972; Jones, 1970; Maffei and Fiorentini, 1976; Nelson and Frost, 1978). Modulation from outside the RF was also reported in areas beyond V1 (Allman et al., 1985a, 1985b; Desimone et al., 1993). The phenomenon thus seems to be a general property of visual cortical cells.

In this chapter, we will review the phenomenon of contextual modulation and focus on primary visual cortex of the monkey in particular. It will be shown that contextual modulation indeed reflects widespread interactions within

and between cortical areas, interactions that are related to high-level processes such as perceptual organization, object recognition, and visual awareness. V1 is an interesting area in this respect. Its RFs are very small, and their tuning properties are simple. For these reasons, activity reflecting perceptual interpretation of the scene as a whole is least expected here. On the other hand, it can be said that the area is at the top of the hierarchy in terms of feedback connections. If some feedback-related activity is present here that represents the convergence of information from all visual areas, this activity would be expected to clearly reflect a fully evolved perceptual interpretation. In V1, therefore, we can expect RF processing of a sort most detached from scene perception, while contextual modulation might be closely related to it.

Phenomenology of contextual modulation in V1

SINGLE VERSUS MULTIPLE IMAGE ELEMENTS Line segments form ideal stimuli for V1 cells. V1 RFs are typically tuned for their orientation, direction of motion, disparity, size, contrast, or color (DeValois et al., 1982; Hubel and Wiesel 1977; Livingstone and Hubel, 1988; Poggio, 1995; Schiller et al., 1976). V1 neurons are therefore viewed as encoding information about contour segments within their RFs. However, a single line segment on a blank background is a visual scene rarely encountered. In natural scenes, contour segments are combined with many others, forming edges, textures, object boundaries, the one occluded by the other, and so on. In those natural situations, the perceptual interpretation of a single line segment strongly depends on its context. What happens to the V1 responses when the perceptual context of a line segment within the RF is manipulated?

Compare the single line segment of Figure 45.1A with the multiple line segments of Figure 45.1B. The isolated line segment strongly draws attention to itself, while the set of line segments draw attention as a group, where each line segment is of much less importance. In V1, this is expressed in the neuronal responses by means of contextual modulation. If the line segment of Figure 45.1A falls on a V1 RF, and the surrounding line segments that are added in Figure 45.1B fall outside, the response of the neuron is much stronger in the first situation than in the second (Knierim and Van Essen, 1992).

The reduced salience of the center line segment in Figure 45.1B can be increased by having its orientation differ from those of the surrounding elements, as in Figure 45.1C. This results in a perceptual *popout* of the center element (Nothdurft, 1991, 1994). This (partial) restoration of perceptual salience is again expressed by a modulation of V1 responses, which are larger in Figure 45.1C than in Figure 45.1B, although not as large as the response would be for a

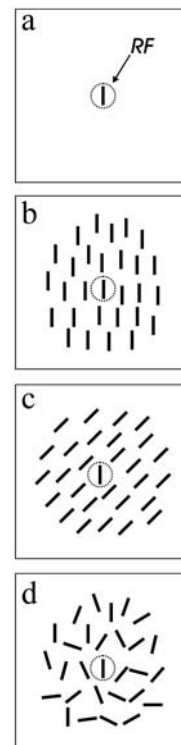


FIGURE 45.1. The context of a line segment changes its perceptual salience. *a*, A lone line segment is perceptually most salient. *b*, The same line segment, now embedded in similar ones, is much less conspicuous. *c*, The line segment may popout when its orientation differs from that of the surrounding line segments, restoring its perceptual salience to some extent. *d*, Global stimulus aspects are taken into consideration, since a similar local orientation difference does not produce popout when surrounding elements all have different orientations. When a V1 neuron is stimulated by presenting these displays, so that its RF only covers the same center line segment in all cases, contextual modulation signals the perceptual salience of the center line segment.

lone element (Fig. 45.1A) (Knierim and Van Essen, 1992). That this is not a purely local phenomenon, that is, governed only by the orientation difference between center and surround stimuli, is illustrated by Figure 45.1D. Here the center line segment is surrounded by line segments of different orientations, as in Figure 45.1C. There is no perceptual popout, however, because the orientation difference between center and surround is not different from the orientation differences among the elements in general (Landy and Bergen, 1991; Nothdurft, 1985, 1994). Likewise, responses of V1 neurons to stimuli like those in Figure 45.1D are not different from the responses to Figure 45.1B stimuli (Kapadia et al., 1995; Knierim and Van Essen, 1992).

A similar phenomenon can be observed in the luminance domain. The perceived brightness of a surface can be modulated by changing the brightness of surrounding surfaces. V1 neurons modulate their activity according to such changes in perceived brightness (Rossi et al., 1996).

GROUPING OF LINE SEGMENTS Another factor that makes line segments segregate from a background of randomly oriented line segments is grouping into elongated chains (Fig. 45.2A). Perceptually, such groupings depend on the relative alignment of the line segments, and important factors are colinearity, relative distance, angle, and axial offset (Field et al., 1993; Kapadia et al., 1995; Kovacs, 1996). For example, the linking is much stronger (and the contour is more visible) in Figure 45.2A than in Figure 45.2B. This is because the relative axial offsets are smaller. By doing experiments like this, using Gabor patches instead of line segments, Hess and coworkers identified an *association field* (Fig. 45.2C), which identifies how distance and relative orientation between Gabor patches determine their grouping strength (Field et al., 1993). Remarkably, these same factors influence contextual modulation in V1 neurons. Line segments that are flanked by colinear ones elicit larger responses (Kapadia et al., 1995; Nelson and Frost, 1985). This depends on relative distance, angle, and axial offset. In fact, neural association fields (Fig. 45.2D,E; Kapadia et al., 2000) have been determined that look very much like the perceptual association fields. These neural association fields map the modulation that is evoked by stimuli surrounding an optimal and RF-centered stimulus. When a surrounding stimulus (with the same orientation) has no effect, the map is flat at that particular position, while excitatory or inhibitory influences are shown by different colors. At 10% to 20% contrast, there is strong facilitation by colinear line segments and weak inhibition by flanking line segments, while at 50% contrast the reverse is the case.

BOUNDARIES, SURFACES, AND FIGURE-GROUND SEGREGATION In Figure 45.3A, the more or less one-dimensional chain of lines of Figure 45.2A has been extended to two dimensions. The line segments, which are now grouped on the basis of orientation similarity, segregate from a background of line segments of another orientation. The stimulus is richer in

some aspect, however, than the one of figure 45.2A. We can distinguish a boundary and a surface of the segregating figure. Where line segments of one orientation juxtapose line segments of the orthogonal orientation, we observe a sharp boundary between the square figure and the background. The line segments within this boundary form a figure surface, which is perceived as if lying in front of the background, which is assumed to continue behind it. The boundary is asymmetrical in that it “belongs” to the figure and not to the background.

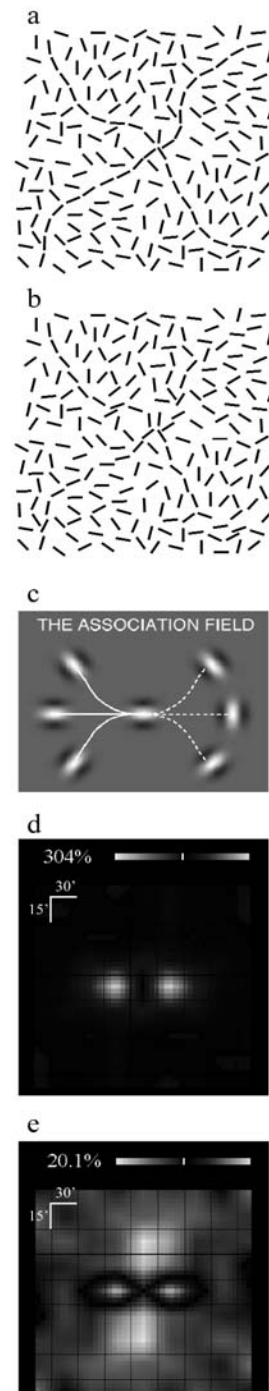


FIGURE 45.2. Colinear grouping and contextual modulation. *a*, An example of the grouping of line segments that lie on a colinear path. *b*, The display is the same as in *a*, except for the relative angles between the line segments that lie on the colinear path. The grouping is less strong. *c*, The relative grouping of neighboring Gabor elements depends on relative orientation, angle, and distance. This constitutes the association field. Strong grouping is depicted by solid lines, weak grouping by dashed lines. *d*, The effect of neighboring line segments on the response of a V1 neuron with a horizontally oriented RF at the center. Blue/white depicts facilitation and red/yellow depicts inhibition for neighboring lines at the given position. At 10% to 20% contrast (shown), the main effect is facilitation by colinear line segments. *e*, The same figure at 50% contrast, where the main effect is inhibition by flanking line segments. (*c* from Field et al., 1993, courtesy of Robert Hess) (*d*, *e* from Kapadia et al., 2000, courtesy of Charles Gilbert.) (See color plate 27.)

Are all these perceptual elements of the scene also reflected in the modulations of V1 responses to the line segments that make up the display? To study this, the responses of V1 neurons to line segments at various positions along the display had to be recorded (Fig. 45.3D). However, during this manipulation, the stimulus within the RF had to be maintained identical. Figure 43.3B shows how this was achieved for the line segments making up the figure surface: the response of a V1 neuron was recorded while it was stimulated either with a display containing a figure or with a display alone (Lamme, 1995; Zipser et al., 1996). The line segments covering the RF were identical in the two displays. Responses to figure and background elements were compared and were subtracted to obtain the modulation signal in isolation (Fig. 45.3C). This result shows that until about 100 msec after stimulus onset, V1 neurons responded identically to the two displays. After that, however, the response to figure elements was larger. The immediate context of the RF line segments was identical, yet still there was strong modulation. Apparently the more global perceptual context, being that of a figure overlying a background, influenced the V1 activity.

That these modulations reflect figure-ground segregation is corroborated by a further analysis in which modulation across the display was studied. In Figure 45.3D the contextual modulation recorded across the figure-ground display of Figure 45.3A is shown. To obtain this plot, responses from a neuron with its RF at different positions relative to the figure and the background were recorded, such that the line segments within the RF were the same for all conditions (Fig. 45.3B; Lamme et al., 1999). Subsequently, the response to a scene with identical line segments, but containing no figure, was subtracted (Fig. 45.3C). As a result, the initial feedforward activity (typically occurring at a latency of 40 to 50 msec) was no longer visible; only the modulation, evoked by recurrent interactions, remained (Lamme et al., 1998a). Positive modulation, that is, a response enhancement from about 80 msec after stimulus onset, is observed at the boundary between figure and ground (see also Nothdurft et al., 2000). After 100 msec, all line segments that belong to the figure uniformly evoke a stronger response than line segments of the background. Note the asymmetry across the figure-ground boundary; while the immediate context is almost identical for a neuron with its RF immediately inside or outside the figure, modulation is present only when the RF is within the figure's boundary. As soon as the RF is outside, modulation is absent. It is as if a neural image of the figure is stamped out of the neural image of the background, closely reflecting our figure-ground percept.

These data illustrate an important point about contextual modulation that is not observed in the results discussed in the previous section. Above (Fig. 45.2), we saw contextual

modulation reflecting local grouping and segregation criteria. But using stimuli such as those in Figure 45.3A, we see that these local criteria can be overridden: at the center of the figure, the line segments are surrounded by similar ones, but nevertheless contextual modulation is the same as it is close to the edge, where elements are flanked by orthogonal ones (although the modulation at the edge occurs at a shorter latency). Immediately outside the boundary between figure and ground, elements are flanked by orthogonal ones, but contextual modulation is absent (i.e., responses are identical to background positions farther away). Apparently, contextual modulation is not limited to reflecting local discontinuities, or differences between RF center and surround stimuli. Contextual modulation in these experiments reflects the figure-ground relationships of the surfaces in the scene.

With respect to this interpretation, it is important to note that the strength of modulation depends on the size of the figure. The results mentioned above were obtained with figures of 4 degrees of visual angle in diameter on a 24×16 degree background. Zipser et al. (1996) found modulation to be much bigger for smaller figures and to decline as figures grew larger. No significant modulation was found for figures larger than 10 degrees. Rossi et al. (2001) found a similar size tuning, but with a much earlier cutoff, with no modulation for figures larger than 3 degrees. The results of Marcus and Van Essen (2002) are in between. It has been argued that this dependence on figure size counters the interpretation of contextual modulation representing figure-ground segregation (Rossi et al., 2001). However, the essential component in the figure-ground interpretation is the finding of asymmetry of modulation across the figure-ground boundary, as explained above. The findings of Rossi et al. do not bear on that issue, as the dependence on figure size was measured only with the RF at the center of the figure. The authors interpreted their sharp size tuning as showing that V1 cells respond only to figure-ground boundaries and that V1 is involved only at a stage prior to figure-ground analysis. To support that claim, however, the authors should have recorded on both sides of the figure-ground boundary and should have found equal modulation in both cases. That was not the case. Of course, that leaves us with the question of why there is a discrepancy in the reported cutoffs in the size tuning curves (Zipser et al., 10 degrees; Rossi et al., 3 degrees; Marcus and Van Essen, 5 degrees). These quantitative differences are probably reconcilable within the domains of intersubject and intersession differences. Factors of importance here include the size of the background, as figure-ground assignment is very much determined by relative size, and stimulus contrast, as salience of the figure probably plays a role. In fact, an alternative interpretation of the figure-ground modulation could be that the neurons representing the perceptually most salient

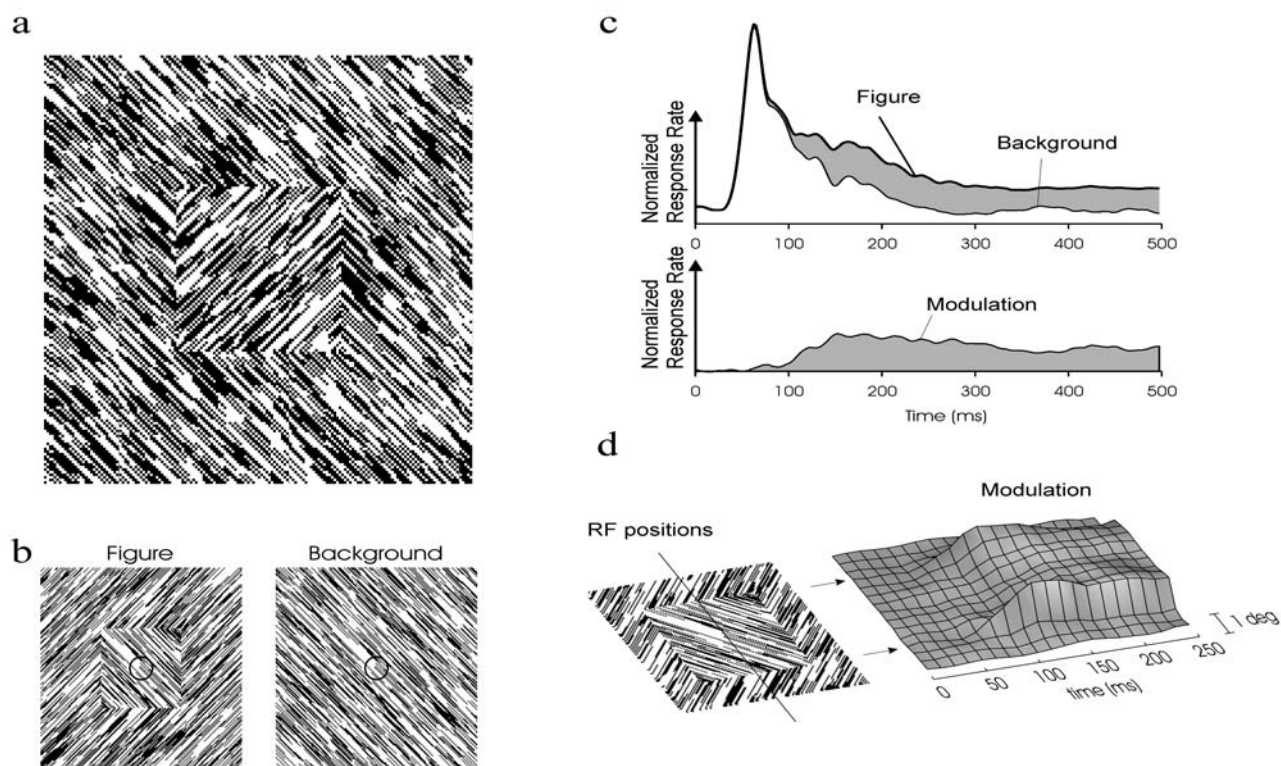


FIGURE 45.3. The neural correlate of figure-ground segregation in V1. *a*, Line segments of similar orientation perceptually group together and segregate from line segments of another orientation. The center square is considered a textured figure on a textured background that perceptually seems to continue behind it. The boundary between figure and ground belongs to the figure surface. *b*, Contextual modulation related to figure-ground segregation can be recorded by stimulation with the two displays shown, while the line segments within the RF are the same for both conditions. *c*, Responses from a population of V1 neurons to the two stimuli shown in *b*. The difference between the superimposed responses, contextual modulation, is shaded in gray and is shown separately

below. *d*, Modulation with the RF at 15 different positions relative to figure and ground, such that the contextual modulation is “scanned” across a line passing over and through the figure. The three-dimensional graph combines the modulation, such that the 15 positions are on the *x*-axis (side), time is on the *y*-axis (in front), and response strength is on the vertical axis. Responses are identical up to about 80 msec after stimulus onset, and no modulation is present. Then responses are “highlighted” at the boundary between figure and ground. This is followed by an equal response enhancement for all positions of the RF within the figure compared to responses for positions of the RF on the background.

elements of the scene, in this case the whole figure, are highlighted relative to the neurons representing less important elements.

Contextual modulation can be elicited by figure-ground displays defined by a variety of cues, such as differences in orientation, direction of motion, disparity, color, or luminance. At the population response level, contextual modulation is of the same magnitude for figures defined by these various cues, while at the single unit level, some cells show complete cue invariance (Lamme, 1995; Zipser et al., 1996). Surprisingly, figure-ground-related contextual modulation bears no relation to the RF properties of the neurons recorded from. For example, modulation for a motion-

defined figure can be recorded in cells without direction selectivity (Lamme, 1995). Also, when cues are combined, modulation is not additive, but instead is identical to the one-cue-alone situation (Zipser et al., 1996). This indicates that the modulation signals figure-ground relationships instead of feature-specific differences; a figure is a figure, no matter how it is defined. It also shows that contextual modulation is mediated by mechanisms far removed from those that shape and tune the local RF.

Also, when more complicated scenes are used, contextual modulation reflects the figure-ground arrangements of the surfaces in that scene. Particularly nice examples can be found in Zipser et al. (1996) and Lee et al. (1998) using sur-

faces containing holes, multiple overlying surfaces, and so on. Under specific conditions, it can sometimes be observed that there is a stronger modulation at the geometrical center of the figures in those scenes (Lee et al., 1998). It has been proposed that this plays a role in representing the medial axes of objects (Kovacs, 1996; Lee et al., 1998).

Mechanisms of contextual modulation

THE EXCITATION-INHIBITION BALANCE From the results discussed thus far, an important problem emerges: the presence of surround stimuli typically results in an inhibition of the response. However, depending on the nature of these surround stimuli, this inhibition can be reduced or sometimes can even revert to facilitation. What mechanisms control this delicate balance between excitation and inhibition? Perceptually, a similar paradox can be formulated: perceptual grouping depends on similar features enhancing each other's representation. Segregation, on the other hand, requires similar features to inhibit each other (Roelfsema et al., 2002). The figure-ground modulation discussed in the previous section is a good example of both processes operating at the same time.

The excitation-inhibition balance seems to depend critically on the contrast of stimuli. Manipulating the contrast of center and surround, such that the cell's RF is stimulated less or more strongly than the surround, may invert the sign of modulation from inhibition to facilitation (Levitt and Lund, 1997). Similarly, in cats, it was found that colinear Gabor patches facilitate the response to a low-contrast Gabor patch on the RF but suppress the response to a high-contrast patch (Mizobe et al., 2001; Polat et al., 1998). The neural association field shown in Figure 45.2D was recorded at 10% to 20% contrast. Figure 45.2E shows the neural association field recorded at 50% contrast (Kapadia et al., 2000). While at high contrast there is strong lateral inhibition and weak colinear facilitation, the opposite is true at low contrast. More generally, it appears that facilitation is stronger the weaker the stimulation of the RF.

The most extreme version of a low-contrast RF stimulus is, of course, no RF stimulus at all. By definition, there should be no response in that case and, consequently, no modulation either. When a cell is excited by such a configuration, the conclusion should simply be that the RF is bigger than it was believed to be. Still, there have been recent reports of cells in V1 being activated by stimuli outside the RF of a neuron, even when the RF itself was not stimulated (Li et al., 2001; Rossi et al., 2001). A possible reason to classify these responses as coming from beyond the RF is that they typically have a very long latency, ~100 msec, clearly in the range of the latency of modulatory effects. Also, they show little specificity for stimulus features such as orienta-

tion. These results might be placed in the context of what we know about the potency of contextual effects when the RF is stimulated at low contrast: What exactly is "no" stimulus on the RF? When a gray area is covering the RF, cells in V1 will still respond to it (after all, we see it; but see also Komatsu et al., 1996; MacEvoy et al., 1998). Perhaps this very faint stimulation is enough to enable modulation from distant sites that are strongly stimulated.

HORIZONTAL CONNECTIONS OR FEEDBACK? The functional properties of contextual modulation we have discussed depend strongly on the anatomical connections between the neuron recorded from (and whose RF is being stimulated) and other neurons. As already pointed out, contextual modulation is mediated by horizontal and feedback connections (Lamme and Roelfsema, 2000). It is difficult to disentangle the relative contributions of these two systems in a particular contextual effect. Some insight might be obtained by studying the latency of contextual effects.

Responses in area V1 have a minimal response onset latency of about 30 msec (Maunsell and Gibson, 1992; Nowak et al., 1995). This can be viewed as the time when processing in V1 begins. In relation to the question of what types of connections (feedforward, horizontal, or feedback) may mediate contextual modulation, it is important to know how long it takes for these modulations to occur once activity has started in V1. The suppressive effect that results from presenting a stimulus in the immediate surround of an RF (Fig. 45.1B) develops quickly. No latency difference (Müller et al., 1997), or a latency difference of only 7 msec, has been reported (Knierim and Van Essen, 1992). Orientation-specific effects, that is, comparing the effect of an identical background with that of an orthogonal background producing perceptual popout (Fig. 45.1B vs. Fig. 45.1C) takes about 20 msec (Knierim and Van Essen, 1992). Modulation related to figure-ground segregation of surfaces (Fig. 45.3) may start 30 to about 70 msec after response onset, depending on the cue that segregates figure from ground (Lamme, 1995; Zipser et al., 1996) and on the distance of the RF from the edge of the surface (Fig. 45.3D).

Once processing has started in V1, contextual modulation apparently occurs within a wide temporal range. The latency of the effects seems to depend on the complexity of the computations underlying the modulation and the spatial extent of the part of the scene that is considered. Short-latency contextual modulation effects are more likely to be generated by feedforward and horizontal connections than by feedback connections, since it is assumed that the latter take some time to exert their effect. However, for some extrastriate visual areas, minimal response latencies as short as those in V1 have been reported (Nowak and Bullier, 1997; Nowak et al., 1995), so even short-latency effects may be caused by feedback.

Insight into the roles of horizontal versus feedback connections also comes from studying the properties of these connections. Of the horizontal connections in V1, we know that (1) at a short range ($\sim 500\mu\text{m}$, i.e., a column's width), connections are excitatory and inhibitory, not very specific, and fall off rapidly with distance (Das and Gilbert, 1999; Kapadia et al., 2000); (2) at a longer range (several millimeters), connections are specific, that is, they preferentially link cells with similar orientation tuning (Malach et al., 1993); and (3) long-range connections between similarly oriented cells are even stronger when these cells have RFs along a colinear axis (Bosking et al., 1997; Schmidt et al., 1997). On the basis of these connections (excluding feedback), many contextual effects can be explained, such as those shown in Figures 45.1 and 45.2, but also the boundary enhancement at figure-ground edges (Fig. 45.3). Particularly striking is the correspondence between the association field (Fig. 45.2C) and what is known about horizontal connections.

There are also effects that cannot be explained by horizontal interactions alone. A good example is the modulation that can be recorded at the center of a figure overlying a background (Fig. 45.3). A model based on horizontal connections predicts enhancement at the figure-ground boundary but also predicts an equal level of activation at the center and at the background (Kapadia et al., 2000; Roelfsema et al., 2002; Fig. 45.4C). Center modulation (Fig. 45.3) can be explained, however, by adding feedback from higher areas. In this model, the higher areas perform the same analysis on their input (coming from lower areas) as the V1 cells, but at coarser spatial scales. Interactions between the horizontal connections at each level, and the feedback signals coming from higher levels, fully explain the asymmetrical figure-ground enhancement observed physiologically (Fig. 45.4A; Roelfsema et al., 2002). That feedback plays a role is further corroborated by lesion experiments. Figure 45.4B shows the results of recording figure-ground-related modulation in an animal that had sustained a large lesion to the extrastriate areas ipsilateral to the recording site. Contextual modulation is still evoked at the boundary between figure and ground, but it is no longer present for the surface elements of the figure (Lamme et al., 1998a). Others have confirmed that figure-ground-related modulation in V1 depends on the integrity of the extrastriate areas (Hupe et al., 1998), while simpler modulatory effects, such as those explained in Figure 45.1, do *not* depend on feedback (Hupe et al., 2000).

ANESTHETIZED VERSUS AWAKE ANIMALS It is crucial to record contextual modulation in awake animals. The effects described above have mostly been recorded in awake and perceiving animals. In anesthetized preparations, RF surround effects are present (Allman et al., 1985b; Kastner et al., 1997; Sillito et al., 1995). To what extent these

effects are similar to contextual modulation in the awake animal is not clear. Thus far, only one investigation has directly compared the awake and anesthetized conditions in the same animals and with the same stimuli. It was found that at the population response level, figure-ground-related contextual modulation is present only in the awake and perceiving animal. In the anesthetized condition, modulation is totally absent. Feedforward RF tuning properties, on the other hand, are not different in the anesthetized and awake conditions (Lamme et al., 1998b). In other studies recording contextual modulation from single units in the anesthetized monkey, effects were either found to be weak compared to those in the awake monkey (Nothdurft et al., 1999) or effects were both positively and negatively correlated with perceptual parameters, so that at the population level the net effect was close to zero (Jones et al., 2001). This could imply that subprocesses underlying normal contextual modulation are operational under anesthesia but fail to produce a coherent effect at the population response level.

Functions of contextual modulation

CONTEXTUAL MODULATION AND PERCEPTUAL GROUPING The computations performed within the separate cortical areas must be combined to produce a coherent output. The role of vision is to segregate objects from each other and to select particular ones for behavioral responses. Image elements and features of the objects that we encounter are processed by cells at different locations, and the results have to be combined so that we can manipulate them (the *binding problem*; Singer and Gray, 1995; Treisman, 1996). To some extent, this might be explained by the feedforward cascade of information processing. The increasingly complex RF tuning properties that one observes when going upstream through the hierarchy of visual areas suggest that low-level features are combined into complex constellations of features in higher areas (Barlow, 1995; Maunsell and Newsome, 1987). Strict feedforward processing, however, has its limitations—for example, in terms of the number of neurons that are needed to map every possible combination of features onto all possible outputs (the *combinatorial explosion*). In this context, many have advocated population coding as opposed to *grandmother* cell hypotheses (Abeles, 1982; Georgopoulos, 1991; Singer and Gray, 1995). In population coding, cells might be engaged in a processing task with one set of neurons (an assembly) at one time but, at another time, might be engaged in a different task with a different set of neurons. For this mechanism to work, cells have to be labeled as belonging to the same assembly, with a label that can rapidly be switched on and off. For example, in processing an image such as Figure 45.3A, the label should tag the neurons that code for the elements of the figure separately from the neurons that code for the background.

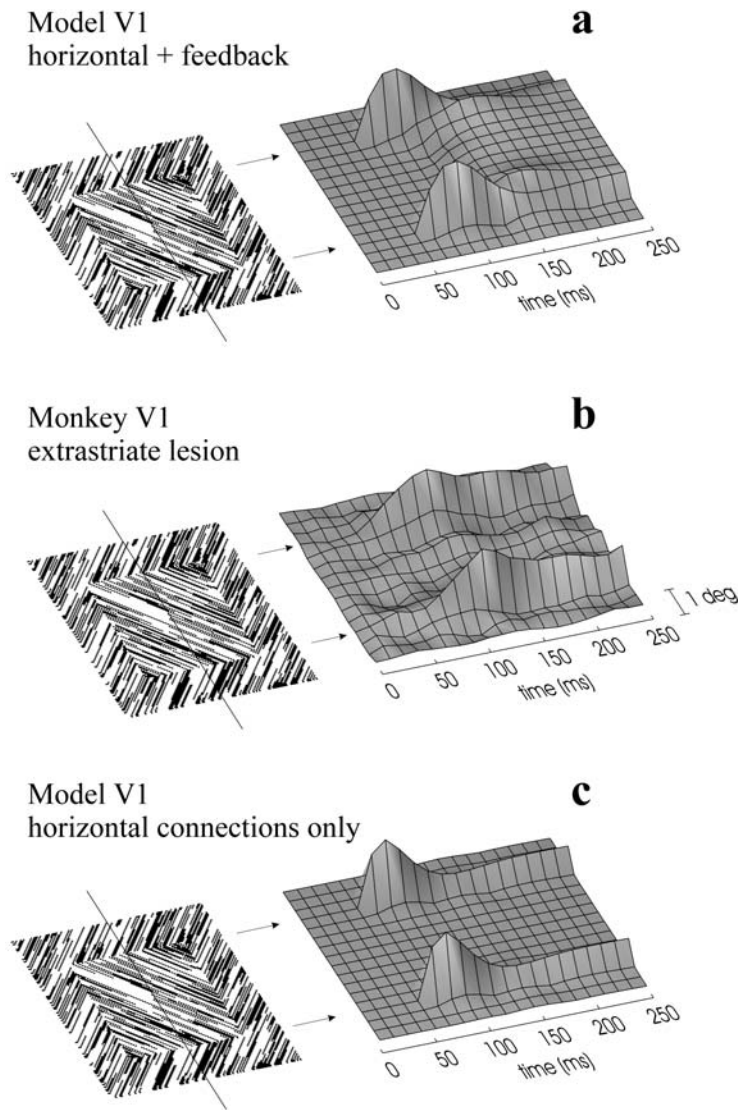


FIGURE 45.4. The relative contribution of horizontal and feedback connections to figure-ground modulation. *a*, Modulation (see Fig. 45.3*d*), “recorded” from V1 neurons of a neural network model. The model uses realistic horizontal interactions in four different “cortical areas” that interact via feedforward and feedback connections. The model mimics the figure-ground boundary enhancement to precede enhancement for the figure surface. *b*,

Modulation recorded from V1 neurons of a monkey that sustained a lesion to the extrastriate areas. Only boundary enhancement remains. *c*, Modulation from V1 model neurons (*a*) without feedback from higher “areas.” The model evokes boundary enhancement with V1 horizontal interactions only. (*a* and *c* from Roelfsema et al., 2002; *b* from Lamme et al., 1998a.)

Synchrony of firing between cells has been proposed to act as such a label (Singer and Gray, 1995). Neurons in V1 fire their action potentials in relative synchrony when their RFs are stimulated with a coherently moving bar, and this synchrony is reduced when the neurons are costimulated with separate bars (Freiwald et al., 1995; Gray et al., 1989). Based on the hypothesis that synchrony labels neurons belonging to the same assembly, one would predict that neurons whose RFs fall within the figure region of an image such as Figure 45.3*A*, fire in synchrony with other neurons whose RFs fall within the figure and do not fire in synchrony with neurons whose RFs fall on the background. We tested

this hypothesis by recording from multiple sites simultaneously in V1 but did not find it to be the case. Synchrony between neurons at considerable distance was found. However, this synchrony could be just as strong between neuron pairs whose RFs were within the figure as between pairs whose RFs were on either side of the boundary between figure and ground (Lamme and Spekreijse, 1998). The results suggested that synchrony reflects the interactions mediated by local and horizontal connections, but does not take into account more global (feedback) interactions that form the basis of the figure-ground percept. Apparently, synchrony in V1 does not operate as a label tagging neurons as

belonging to an assembly coding for the figure-ground percept.

An alternative binding tag could be an enhanced firing rate. In that case, cells engaged in processing features or elements of the same object would have an enhanced firing rate compared to other cells. The results discussed above provide evidence that the neural system might use an enhanced firing rate in this way. All neurons responding to elements of the same figure have an equal amount of response enhancement (Fig. 45.3*D*). Also, colinear line segments that group together share an enhanced firing rate (Kapadia et al., 1995; Sugita, 1999). A drawback of the firing rate as a binding tag is that it is difficult to separate several assemblies from each other, while this can easily be achieved with synchrony as a tag (Singer and Gray, 1995). It is, however, questionable whether the visual system is indeed capable of representing many objects simultaneously. Visual search and change blindness experiments indicate that no more than one to four objects are represented by the visual system at a time (Irwin, 1997; Rensink, 1997; Treisman, 1993; Wolfe and Bennet, 1997).

ATTENTION AND AWARENESS Line segments that group into a coherent object have higher salience than background elements and thus draw attention in bottom-up fashion (Egeth and Yantis, 1997). It is therefore conceivable that the contextual modulations of firing rate we observe are to a large extent attentional modulations or are at least contaminated by attentional effects. This seems all the more possible in light of the recent finding that effects of attention can be recorded in early areas including V1 (Desimone and Duncan, 1995; Ress et al., 2000; Roelfsema et al., 1998; Vidyasagar, 1998). However, in general, contextual modulation appears to be independent of focal spatial attention. For example, two separate and distant figures evoke the same amount of figure-ground-related modulation as one (Lamme et al., 1998b). Instructing the animal to attend to one of several objects does not modify figure-ground modulation very strongly (Landman et al., 2002). The benefits of colinear facilitation in the detection of low-contrast line segments are most pronounced when attention is distributed over the scene (Ito and Gilbert, 1999). The strongest evidence for the independence of contextual effects from attention comes from an Magneto Encephalo Graphy (MEG) study in human subjects. With appropriate paradigms, V1 contextual modulation related to scene segmentation can be recorded in human subjects using electroencephalography (EEG) or MEG (Bach and Meigen, 1992; Caputo and Casco, 1999; Lamme et al., 1992, 1993a, 1993b, 1994; Romani et al., 1999). In one study (Scholte et al., 2002), subjects were not told in advance about the presence of the segmenting stimuli, and their attention was diverted away from

their location. This resulted in the condition of *inattention blindness*, in which subjects reported that they did not see the segmenting objects. Nevertheless, figure-ground MEG modulation was still present, and was in fact just as strong as when subjects did see the objects. Since the condition of inattention blindness ensures that no attention whatsoever was directed to the segmenting stimuli, the finding proves that figure-ground modulation occurs in the absence of attention.

The study makes a second important point: the presence of contextual modulation is not sufficient for a conscious report about the stimulus configuration that evokes the modulation. The same was found in a study where the presence or absence of modulation was related to the behavior of monkeys that were trained to detect textured figures (like those in Fig. 45.3*A*) on a textured background. The figures varied in position and salience, and the animals had to make an eye movement toward that position to obtain a reward. Also, on some trials, no figures were present at all, and on those occasions the animals had to maintain fixation. Surprisingly, on some trials where a figure was presented, the animals still maintained fixation, as if indicating that they did not see the figure. On those trials, contextual modulation was absent or lower than on trials where the figures were correctly detected. Further analysis showed that the occurrence of modulation is *necessary* for the monkey to detect the figures but is not sufficient (Supér et al., 2001). The occurrence of modulation reflects a successful unrolling of perceptual organization, but an independent decision process that follows ultimately determines the animal's answer.

That contextual modulation is necessary for a figure-ground percept is corroborated by a masking study. Presenting a textured screen within 50 msec after presenting a textured figure-ground scene prevents the occurrence of contextual modulation related to the figure-ground segregation. That same manipulation renders the figure invisible (Lamme et al., 2002). A second manipulation that suppresses modulation is to present figure-ground displays of orthogonal orientation to either eye in a binocular setup. Either eye alone still receives (and can "see") a figure-ground display, but in the fused *cyclopean* percept the figure is no longer present (Fig. 45.5). Modulation is absent in this condition (Zipser et al., 1996).

Conclusions

In V1, receptive field properties are relatively simple. As the processing time after stimulus onset grows, however, the V1 responses incorporate information from more and more distant cortical regions. In doing so, they start to reflect perceptual grouping operations of wider and wider spatial

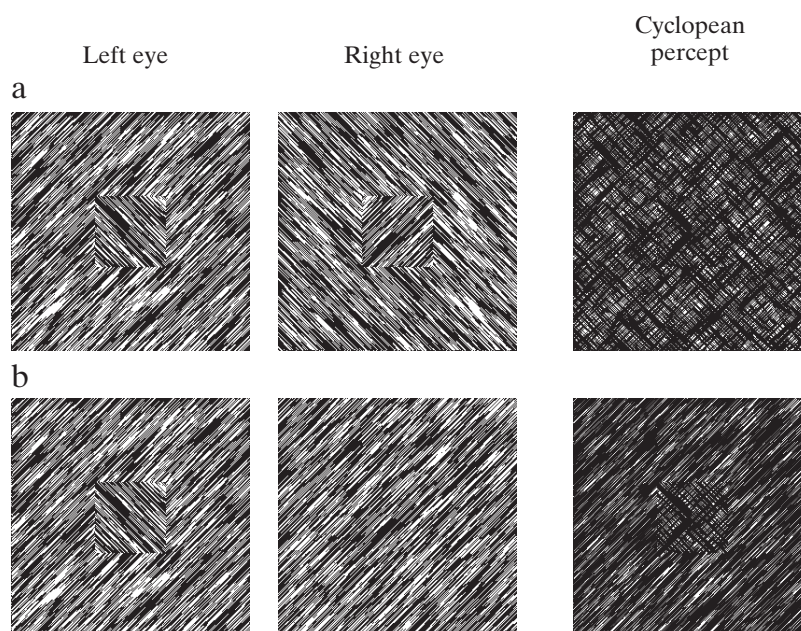


FIGURE 45.5. *a*, Orthogonal textures presented to the two eyes, each containing a figure on a background, yield a cyclopean percept of a homogeneous texture, with no visible figure (at eccentric fixation). *b*, When the figure is present in one eye only, the cyclopean percept is that of a figure on a background. The stimulus in *b* yields figure-ground-related contextual modulation; the stimulus in *a* does not.

range and increasing complexity. This process is mediated by horizontal and feedback corticocortical connections that modulate the feedforward-generated RF tuning properties. Contextual modulation was originally viewed as a relatively unimportant feature of cortical processing, providing the RF with an inhibitory surround, possibly related to gain control or constancy mechanisms. We now know that, instead, contextual modulation reflects potentially widespread corticocortical interactions related to perceptual organization (Lamme and Roelfsema, 2000). Furthermore, contextual modulation plays an important role in generating a coherent phenomenal experience of the visual scene (Lamme et al., 2000a; Lamme et al., 2000b).

REFERENCES

- Abeles, M., 1982. *Local Cortical Circuits*, Berlin: Springer-Verlag.
- Albus, K., and W. Fries, 1980. Inhibitory sidebands of complex receptive fields in the cat's striate cortex, *Vis. Res.*, 20:369–372.
- Allman, J. M., F. Miezin, and E. McGuinness, 1985a. Direction and velocity-specific responses from beyond the classical receptive field in the middle temporal visual area (MT), *Perception*, 14:105–126.
- Allman, J. M., F. Miezin, and E. McGuinness, 1985b. Stimulus specific responses from beyond the classical receptive field: neurophysiological mechanisms for local-global comparisons in visual neurons, *Annu. Rev. Neurosci.*, 8:407–430.
- Bach, M., and T. Meigen, 1992. Electrophysiological correlates of texture segregation in the human visual evoked-potential, *Vis. Res.*, 32:417–424.
- Barlow, H. B., 1995. The neuron doctrine in perception, in *The Cognitive Neurosciences* (M. S. Gazzaniga, ed.), Cambridge, MA: MIT Press, pp. 415–435.
- Blakemore, C., and E. A. Tobin, 1972. Lateral inhibition between orientation detectors in the cat's visual cortex, *Exp. Brain Res.*, 15:439–440.
- Bosking, W. H., Y. Zhang, B. Schofield, and D. Fitzpatrick, 1997. Orientation selectivity and the arrangement of horizontal connections in the tree shrew striate cortex, *J. Neurosci.*, 17:2112–2127.
- Caputo, G., and C. Casco, 1999. A visual evoked potential correlate of global figure-ground segmentation, *Vis. Res.*, 39:1597–1610.
- Das, A., and C. D. Gilbert, 1999. Topography of contextual modulations mediated by short-range interactions in primary visual cortex, *Nature*, 399:655–661.
- Dean, P., 1979. Visual cortex ablation and thresholds for successively presented stimuli in rhesus monkeys: II. Hue, *Exp. Brain Res.*, 35:69–83.
- Desimone, R., and J. Duncan, 1995. Neural correlates of selective visual attention, *Annu. Rev. Neurosci.*, 18:193–222.
- Desimone, R., J. Moran, S. J. Schein, and M. Mishkin, 1993. A role for the corpus callosum in visual area V4 of the macaque, *Vis. Neurosci.*, 10:159–171.
- Desimone, R., and S. J. Schein, 1987. Visual properties of neurons in area V4 of the macaque: sensitivity to stimulus form, *J. Neurophysiol.*, 57:835–868.

- DeValois, R. L., D. G. Albrecht, and L. G. Thorell, 1982. Spatial frequency selectivity of cells in macaque visual cortex, *Vis. Res.*, 22:545–559.
- DeYoe, E. A., and D. C. Van Essen, 1988. Concurrent processing streams in monkey visual cortex, *Trends Neurosci.*, 11:219–226.
- Egeth, H. E., and S. Yantis, 1997. Visual attention: control, representation, and time course, *Annu. Rev. Psychol.*, 48:269–297.
- Felleman, D. J., and D. C. Van Essen, 1991. Distributed hierarchical processing in the primate cerebral cortex, *Cereb. Cortex*, 1:1–47.
- Field, D. J., A. Hayes, and F. Hess, 1993. Contour integration by the human visual system: evidence for a local “association field.” *Vis. Res.*, 33:173–193.
- Freiwald, W. A., A. K. Kreiter, and W. Singer, 1995. Stimulus dependent intercolumnar synchronization of single unit responses in cat area 17, *Neuroreport*, 6:2348–2352.
- Gallant, J. L., C. E. Connor, S. Rakshit, J. W. Lewis, and D. C. Van Essen, 1996. Neural responses to polar, hyperbolic, and cartesian gratings in area V4 of the macaque monkey, *J. Neurophysiol.*, 76:2718–2739.
- Georgopoulos, A. P., 1991. Higher order motor control, *Annu. Rev. Neurosci.*, 14:361–377.
- Gilbert, C. D., 1992. Horizontal integration and cortical dynamics, *Neuron*, 9:1–13.
- Gilbert, C. D., 1993. Circuitry, architecture and functional dynamics of visual cortex, *Cereb. Cortex*, 3:373–386.
- Gilbert, C. D., and T. N. Wiesel, 1989. Columnar specificity of intrinsic horizontal and cortico-cortical connections in cat visual cortex, *J. Neurosci.*, 9:2432–2442.
- Gray, C. M., A. K. Engel, P. König, and W. Singer, 1989. Oscillatory responses in cat visual cortex exhibit intercolumnar synchronization which reflects global stimulus properties, *Nature*, 338:334–337.
- Heywood, C. A., and A. Cowey, 1987. On the role of cortical area V4 in the discrimination of hue and pattern in macaque monkeys, *J. Neurosci.*, 7:2601–2617.
- Hubel, D. H., and T. N. Wiesel, 1968. Receptive fields and functional architecture of monkey striate cortex, *J. Physiol. (Lond.)*, 195:215–243.
- Hubel, D. H., and T. N. Wiesel, 1977. Ferrier Lecture. Functional architecture of macaque monkey visual cortex, *Proc. R. Soc. Lond. B*, 198:1–59.
- Hupe, J. M., A. C. James, B. R. Payne, S. G. Lomber, P. Girard, and J. Bullier, 1998. Cortical feedback improves discrimination between figure and background by V1, V2 and V3 neurons, *Nature*, 394:784–787.
- Hupe, J. M., A. C. James, P. Girard, and J. Bullier, 2000. Response modulations by static texture surround in area V1 of the macaque monkey do not depend on feedback connections from V2, *J. Neurophysiol.*, 85:146–163.
- Irwin, D. E., 1997. Eye movements and scene perception: memory for things observed, *Invest. Ophthalmol. Vis. Sci.*, 38:S707 (ARVO abstract 3274).
- Ito, M., and C. D. Gilbert, 1999. Attention modulates contextual influences in the primary visual cortex of alert monkeys, *Neuron*, 22:593–604.
- Jones, B. H., 1970. Responses of single neurons in cat visual cortex to a simple and a more complex stimulus, *Am. J. Physiol.*, 218:1102–1107.
- Jones, H. E., K. L. Grieve, W. Wang, and A. M. Sillito, 2001. Surround suppression in primate V1, *J. Neurophysiol.*, 86:2011–2028.
- Kapadia, M. K., M. Ito, C. D. Gilbert, and G. Westheimer, 1995. Improvement in visual sensitivity by changes in local context: parallel studies in human observers and in V1 of alert monkeys, *Neuron*, 15:843–856.
- Kapadia, M. K., G. Westheimer, and C. D. Gilbert, 2000. Spatial distribution of contextual interactions in primary visual cortex and in visual perception, *J. Neurophysiol.*, 84:2048–2062.
- Kastner, S., H. C. Nothdurft, and I. N. Pigarev, 1997. Neuronal correlates of pop-out in cat striate cortex, *Vis. Res.*, 37:371–376.
- Knierim, J. J., and D. C. Van Essen, 1992. Neuronal responses to static texture patterns in area V1 of the alert macaque monkey, *J. Neurophysiol.*, 67:961–980.
- Komatsu, H., I. Murakami, and M. Kinoshita, 1996. Surface representation in the visual system, *Cogn. Brain Res.*, 5:97–104.
- Kovacs, I., 1996. Gestalten of today: early processing of visual contours and surfaces, *Behav. Brain Res.*, 82:1–11.
- Lamme, V. A. F., 1995. The neurophysiology of figure-ground segregation in primary visual cortex, *J. Neurosci.*, 15:1605–1615.
- Lamme V. A. F., 2000a. Neural mechanisms of visual awareness; a linking proposition. *Brain Mind*, 1:385–406.
- Lamme, V. A. F., V. Rodriguez, and H. Spekreijse, 1999. Separate processing dynamics for texture elements, boundaries and surfaces in primary visual cortex, *Cereb. Cortex*, 9:406–413.
- Lamme, V. A. F., and P. R. Roelfsema, 2000. The distinct modes of vision offered by feedforward and recurrent processing, *Trends Neurosci.*, 23:571–579.
- Lamme, V. A. F., and H. Spekreijse, 1998. Neuronal synchrony does not represent texture segregation, *Nature*, 396:362–366.
- Lamme, V. A. F., H. Supér, R. Landman, P. R. Roelfsema, and H. Spekreijse, 2000b. The role of primary visual cortex in visual awareness, *Vis. Res.*, 40:1507–1521.
- Lamme, V. A. F., H. Supér, and H. Spekreijse, 1998a. Feedforward, horizontal, and feedback processing in the visual cortex, *Curr. Opin. Neurobiol.*, 8:529–535.
- Lamme, V. A. F., B. W. Van Dijk, and H. Spekreijse, 1992. Texture segregation is processed by primary visual cortex in man and monkey. Evidence from VEP experiments, *Vis. Res.*, 32:797–807.
- Lamme, V. A. F., B. W. Van Dijk, and H. Spekreijse, 1993a. Contour from motion processing occurs in primary visual cortex, *Nature*, 363:541–543.
- Lamme, V. A. F., B. W. Van Dijk, and H. Spekreijse, 1993b. Organization of texture segregation processing in primate visual cortex, *Vis. Neurosci.*, 10:781–790.
- Lamme, V. A. F., B. W. Van Dijk, and H. Spekreijse, 1994. Organization of contour from motion processing in primate visual cortex, *Vis. Res.*, 34:721–735.
- Lamme, V. A. F., K. Zipser, and H. Spekreijse, 1998b. Figure-ground activity in primary visual cortex is suppressed by anaesthesia, *Proc. Natl. Acad. Sci. USA*, 95:3263–3268.
- Lamme, V. A. F., K. Zipser, and H. Spekreijse, 2002. Masking interrupts figure-ground signals in V1, *J. Cogn. Neurosci.*, 14:1044–1053.
- Landman, R., H. Spekreijse, and V. A. F. Lamme, 2003. Set size effects in monkey primary cortical cortex, *J. Cogn. Neurosci.*, in press.
- Landy, M. S., and J. R. Bergen, 1991. Texture segregation and orientation gradient, *Vis. Res.*, 31:679–691.
- Lee, T. S., R. Mumford, R. Romero, and V. A. F. Lamme, 1998. The role of the primary visual cortex in higher level vision, *Vis. Res.*, 38:2429–2454.

- Levitt, J. B., and J. S. Lund, 1997. Contrast dependence of contextual effects in primate visual cortex, *Nature*, 387:73–76.
- Li, W., P. Their, and C. Wehrhahn, 2001. Neuronal responses from beyond the classic receptive field in V1 of alert monkeys, *Exp. Brain Res.*, 139:359–371.
- Livingstone, M. S., and D. H. Hubel, 1988. Segregation of form, color, movement, and depth: anatomy, physiology, and perception, *Science*, 240:740–749.
- MacEvoy, S. P., W. Kim, and M. A. Paradiso, 1998. Integration of surface information in primary visual cortex, *Nat. Neurosci.*, 1:616–620.
- Maffei, L., and A. Fiorentini, 1976. The unresponsive regions of visual cortical receptive fields, *Vis. Res.*, 16:1131–1139.
- Malach, R., Y. Amir, M. Harel, and A. Grinvald, 1993. Relationship between intrinsic connections and functional architecture revealed by optical imaging and in vivo targeted biocytin injections in primate striate cortex, *Proc. Natl. Acad. Sci. USA*, 90:10469–10473.
- Marcus, D. S., and D. C. Van Essen, 2002. Scene segmentation and attention in primate cortical areas V1 and V2, *J. Neurophysiol.*, 88:2648–2658.
- Maunsell, J. H. R., and J. R. Gibson, 1992. Visual response latencies in striate cortex of the macaque monkey, *J. Neurophysiol.*, 68:1332–1344.
- Maunsell, J. H. R., and W. T. Newsome, 1987. Visual processing in monkey extrastriate cortex, *Annu. Rev. Neurosci.*, 10:363–401.
- Maunsell, J. H. R., and D. C. Van Essen, 1983. Functional properties of neurons in the middle temporal visual area of the macaque monkey. I. Selectivity for stimulus direction, speed and orientation, *J. Neurophysiol.*, 49:1127–1147.
- Mizobe, K., U. Polat, M. W. Pettet, and T. Kasamatsu, 2001. Facilitation and suppression of single striate-cell activity by spatially discrete pattern stimuli presented beyond the receptive field, *Vis. Neurosci.*, 18:377–391.
- Movshon, J. A., E. H. Adelson, M. S., Gizzi, and W. T. Newsome, 1986. The analysis of moving visual patterns, in *Pattern Recognition Mechanisms* (C. Chagas, R. Gatass, and C. Gross, eds.), New York: Springer-Verlag, pp. 117–151.
- Müller, J. R., J. Krauskopf, and P. Lennie, 1997. Mechanisms surrounding the classical receptive field in macaque V1, *Invest. Ophthalmol. Vis. Sci.*, 38:S969 (ARVO abstract 4489).
- Nelson, J. I., and B. Frost, 1978. Orientation selective inhibition from beyond the classic visual receptive field, *Brain Res.*, 139:359–365.
- Nelson, J. I., and B. Frost, 1985. Intracortical facilitation among co-oriented, co-axially aligned simple cells in cat striate cortex, *Exp. Brain Res.*, 6:54–61.
- Newsome, W. T., A. Mikami, and R. M. Wurtz, 1986. Motion selectivity in macaque visual cortex. III. Psychophysics and physiology of apparent motion, *J. Neurophysiol.*, 55:1340–1351.
- Newsome, W. T., R. H. Wurtz, M. R. Dürsteler, and A. Mikami, 1985. Deficits in visual motion perception following ibotenic acid lesions of the middle temporal visual area of the macaque monkey, *J. Neurosci.*, 5:825–840.
- Nothdurft, H. C., J. L. Gallant, and D. C. Van Essen, 1999. Response modulation by texture surround in primate area V1: correlates of “popout” under anesthesia, *Vis. Neurosci.*, 16:15–34.
- Nothdurft, H. C., 1985. Sensitivity for structure gradient in texture discrimination tasks, *Vis. Res.*, 25:1957–1968.
- Nothdurft, H. C., 1991. Texture segmentation and pop-out from orientation contrast, *Vis. Res.*, 31:1073–1078.
- Nothdurft, H. C., 1994. Common properties of visual segmentation, in *Higher-Order Processing in the Visual System* (R. Bock and J. A. Goode, eds.), Ciba Foundation Symposium 184, Chichester, UK: Wiley, pp. 245–268.
- Nothdurft, H. C., J. Gallant, and D. C. Van Essen, 2000. Response profiles to texture border patterns in area V1, *Vis. Neurosci.*, 17:421–436.
- Nowak, L. G., and J. Bullier, 1997. The timing of information transfer in the visual system, in *“Extrastriate Cortex” Cerebral Cortex*, vol. 12 (J. Kaas, K. Rockland, and A. Peters, eds.), New York: Plenum Press, pp. 205–241.
- Nowak, L. G., M. H. J. Munk, P. Girard, and J. Bullier, 1995. Visual latencies in areas V1 and V2 of the macaque monkey, *Vis. Neurosci.*, 12:371–384.
- Poggio, G. F., 1995. Mechanisms of stereopsis in monkey visual cortex, *Cereb. Cortex*, 3:193–204.
- Polat, U., K. Mizobe, M. W. Pettet, T. Kasamatsu, and A. M. Norcia, 1998. Collinear stimuli regulate visual responses depending on cell’s contrast threshold, *Nature*, 391:580–584.
- Ress, D., B. T. Backus, and D. J. Heeger, 2000. Activity in primary visual cortex predicts performance in a visual detection task, *Nat. Neurosci.*, 3:940–945.
- Roelfsema, P. R., V. A. F. Lamme, and H. Spekreijse, 1998. Object based attention in primary visual cortex of the macaque monkey, *Nature*, 395:376–381.
- Roelfsema, P. R., V. A. F. Lamme, H. Spekreijse, and H. Bosch, 2002. Figure-ground segregation in a recurrent network architecture, *J. Cogn. Neurosci.*, 14:525–537.
- Romani, A., G. Caputo, R. Callicco, E. Schintone, and V. Cosi, 1999. Edge detection and Surface “filling in” as shown by texture visual evoked potentials, *Clin. Neurophysiol.*, 110:86–91.
- Rossi, A. F., R. Desimone, and L. G. Ungerleider, 2001. Contextual modulation in primary visual cortex of macaques, *J. Neurosci.*, 21:1698–1709.
- Rossi, A. F., C. D. Rittenhouse, and M. Paradiso, 1996. The representation of brightness in primary visual cortex, *Science*, 273:1104–1107.
- Salin, P., and J. Bullier, 1995. Corticocortical connections in the visual system: structure and function, *Physiol. Rev.*, 75:107–154.
- Schiller, P. H., 1993. The effects of V4 and middle temporal (MT) area lesions on visual performance in the rhesus monkey, *Vis. Neurosci.*, 10:717–746.
- Schiller, P. H., B. L. Finlay, and S. F. Volman, 1976. Quantitative studies of single cell properties in monkey striate cortex. I–V, *J. Neurophysiol.*, 39:1288–1374.
- Schiller, P. H., and K. Lee, 1991. The role of the primate extrastriate area V4 in vision, *Science*, 251:1251–1253.
- Schmidt, K. E., R. Goebel, S. Lowel, and W. Singer, 1997. The perceptual grouping criterion of collinearity is reflected by anisotropies of connections in the primary visual cortex, *Eur. J. Neurosci.*, 9:1083–1089.
- Scholte, H. S., S. C. Witteveen, H. Spekreijse, and V. A. F. Lamme, 2002. Neural correlates of image segmentation are present during inattentive blindness. Submitted.
- Sillito, A. M., K. L. Grieve, H. E. Jones, J. Cudeiro, and J. Davis, 1995. Visual cortical mechanisms detecting focal orientation discontinuities, *Nature*, 378:492–496.
- Singer, W., and C. M. Gray, 1995. Visual feature integration and the temporal correlation hypothesis. *Annu. Rev. Neurosci.*, 18:555–586.

- Sugita, Y., 1999. Grouping of image fragments in primary visual cortex, *Nature*, 401:269–272.
- Supér, H., H. Spekreijse, and V. A. F. Lamme, 2001. Two distinct models of sensory processing observed in monkey primary visual cortex (V1), *Nat. Neurosci.*, 4:304–310.
- Treisman, A., 1993. The perception of features and objects, in *Attention: Selection, Awareness and Control: A Tribute to Donald Broadbent* (A. Baddeley and L. Weiskrantz, eds.), Oxford: Clarendon Press, pp. 5–35.
- Treisman, A., 1996. The binding problem, *Curr. Opin. Neurobiol.*, 6:171–178.
- Vidyasagar, T. R., 1998. Gating of neuronal responses in macaque primary visual cortex by an attentional spotlight, *Neuroreport*, 9:1947–1952.
- Wild, H. M., S. R. Butler, D. Carden, and J. J. Kulikowski, 1985. Primate cortical area V4 important for color constancy but not wavelength discrimination, *Nature*, 313:133–135.
- Wolfe, J. M., and S. C. Bennett, 1997. Preattentive object files: shapeless bundles of basic features, *Vis. Res.*, 37:25–43.
- Zeki, S. M., 1973. Colour coding in rhesus monkey prestriate cortex, *Brain Res.*, 53:422–427.
- Zeki, S. M., 1980. The representation of colours in the cerebral cortex, *Nature*, 284:412–418.
- Zipser, K., V. A. F. Lamme, and P. H. Schiller, 1996. Contextual modulation in primary visual cortex, *J. Neurosci.*, 16:7376–7389.

46 Contributions of Vertical and Horizontal Circuits to the Response Properties of Neurons in Primary Visual Cortex

THOMAS R. TUCKER AND DAVID FITZPATRICK

ONE OF THE FUNDAMENTAL challenges of visual neuroscience is to unravel how distinct components of cortical circuits contribute to the responses of individual cortical neurons. The complexity of the task remains daunting, but significant progress has come from the recognition of two types of connections: (1) vertical connections, which run perpendicular to the cortical surface, extend for short distances, and interconnect neurons in different layers, and (2) horizontal connections, which run parallel to the cortical surface, extend for long distances, and link together neurons that lie in the same layer. The functional contributions of these two types of connections have been most thoroughly studied in the superficial layers (layers 2/3) of primary visual cortex. The principal source of vertical inputs to layer 2/3 arises from lateral geniculate recipient neurons of layer 4. These inputs have traditionally been regarded as the driving force for layer 2/3 neurons; they are the primary determinant of receptive field size and shape, as well as stimulus selectivity (orientation preference, direction preference, etc.). In contrast, horizontal connections are viewed as modulators, the source of both receptive field surround effects and the fine-scale temporal patterning that underlies neural synchrony. In this chapter, we consider the origin of these functional distinctions, evaluate the evidence upon which they are based, and consider recent results that challenge this strict functional dichotomy.

The identification of vertical and horizontal connections

The work of Mountcastle in somatosensory cortex (Mountcastle, 1957, 1997; Powell and Mountcastle, 1959) and Hubel and Wiesel in visual cortex (Hubel and Wiesel, 1962, 1968, 1977) established one of the fundamental principles of cortical organization: the orderly arrangement of cells with similar functional properties into vertically oriented columns traversing the cortex from pia to white matter. In visual cortex, the similarity in the response properties of neurons (e.g., orientation preference, ocular dominance, position in visual space) recorded along a vertical electrode

penetration and the regular progression in response properties recorded along tangential penetrations led to the view that the elements of cortical circuitry critical for setting up these specific response properties are confined to the column (Hubel and Wiesel, 1962, 1968, 1977). Although the exact dimensions of the column were subject to some debate, the idea that response properties were generated from interactions within a relatively localized cortical region was consistent with the evidence from Golgi studies of Ramon y Cajal (1911), Lorente de No (1938), and Lund (1973; Lund and Boothe, 1975) showing a predominantly cylindrical arrangement of intracortical connections. Neurons in layer 4 of the macaque visual cortex, for example, give rise to axon arbors that ascend and produce terminal arbors that cover less than 1 mm of surface area in layer 2/3.

Fisken and colleagues (1975) were the first to recognize that some connections identified by degeneration techniques following cortical lesions extended for more than 1 mm across the cortical surface, but it was the work of Rockland and Lund (1982; Rockland et al., 1982) that provided the first clear picture of just how far this horizontal network could extend. Following injections of retrograde tracers into visual cortex in the tree shrew, these investigators demonstrated patches of labeled cells and terminals that were distributed over distances 3 to 4 mm from the injection site in cortical layer 2/3, covering a substantial fraction of V1 in this species. These initial observations were subsequently confirmed in other species (Matsubara et al., 1985, 1987; Rockland and Lund, 1983), and the elegant intracellular injection experiments of Gilbert and Wiesel (1983) and Martin and Whitteridge (1984) demonstrated that the bulk of these long-range connections originate from pyramidal neurons. Ultrastructural analysis also demonstrated that horizontal connections terminate on the dendritic processes of other pyramidal cells as well as smooth dendritic GABAergic neurons (McGuire et al., 1991). These anatomical observations received support from intracellular recordings in tissue slice experiments showing that electrical stimulation of

horizontal connections can evoke both excitatory and inhibitory postsynaptic potentials (EPSPs and IPSPs) at more distant sites (Hirsch and Gilbert, 1991; Weliky et al., 1995).

Reconciling horizontal connectivity with cortical receptive field properties

The demonstration that intracortical connections extend for distances far beyond the local column raised the question of how the selectivity in response properties that characterizes the column could be maintained in the face of such extra-columnar interactions. The answer to this question depends on the degree of functional specificity exhibited by horizontal connections, an issue that has been examined extensively with respect to the property of orientation selectivity. There is general agreement that horizontal connections are biased in their distribution toward sites that have similar preferred orientations. Evidence in support of this conclusion comes from experiments in which the distribution of labeled cell bodies or axon terminals resulting from small tracer injections has been compared to functional maps of orientation preference generated by 2-deoxyglucose (Gilbert and Wiesel, 1989) or intrinsic signal imaging techniques (Bosking et al., 1997; Kisvarday et al., 1994; Malach et al., 1993). With optical imaging techniques it has been possible to provide a quantitative assessment of specificity, generating orientation tuning curves of labeled boutons or cell bodies by assigning each labeled element the orientation preference for its location in the cortex (Fig. 46.1). The distribution of horizontal connections from a given site has a tuning function that peaks on the preferred orientation of the injection site (Bosking et al., 1997) and, for some cases, the width of the bouton tuning curve is comparable to that of the physiologically derived tuning curve for multiunit activity at the injection site. Given that measures of bouton tuning have been made from bulk injections of tracers, and that the injection sites themselves occupy some range of orientation preferences, these values may underestimate the degree of tuning present in the horizontal network. At the least, these results demonstrate a strong bias in the distribution of horizontal connections for sites that have similar orientation preferences.

The other feature of horizontal connections that had to be reckoned with was how their extent across the map of visual space relates to the receptive field size of V1 neurons. Defining the limits of the receptive field of neurons in visual cortex has never been a simple issue, but a common approach is to determine the *minimum discharge field* by presenting a small stimulus (usually a light or dark bar at the appropriate orientation) and delimiting the area of visual space that consistently elicits spike discharges above some background level (Barlow et al., 1967; Hubel and Wiesel, 1962). Surprisingly, the extent of visual field encompassed by the spread of horizontal connections was found to be two to three times the

size of minimum discharge fields of V1 neurons (Gilbert, 1992, 1998; Gilbert and Wiesel, 1983, 1989). For this reason, horizontal connections have been viewed as a potential substrate for receptive field surround effects—alterations in the response to presentation of a stimulus within the minimum discharge field produced by the presentation of stimuli in surrounding areas of visual space (Fiorani et al., 1992; Gilbert and Wiesel, 1990; Kapadia et al., 1995; Knierim and Van Essen, 1992; Maffei and Fiorentini, 1976; Nelson and Frost, 1985; Polat et al., 1998; Fig. 46.2A). As has been made clear by more recent intracellular recording experiments in cat visual cortex, receptive field surround effects reflect the fact that a cortical minimal discharge field is just the tip of the iceberg of a much larger region of subthreshold responsiveness (Bringuier et al., 1999). Although cortical neurons are most sensitive to a restricted region of visual space, subthreshold depolarizing and hyperpolarizing inputs can be detected from regions of visual space that are two to three times the size of the spike discharge zone (Fig. 46.2B). Based on latency measures and conduction velocity estimates, it has been argued that these subthreshold regions are mediated by monosynaptic connections conveyed by horizontal connections (Bringuier et al., 1999). This view is also consistent with the observation that activation of horizontal connections in tissue slice experiments elicits subthreshold responses significantly smaller in magnitude than those elicited by stimulation in layer 4 (Hirsch and Gilbert, 1991; Yoshimura et al., 2000).

In retrospect, the proposed functional dichotomy between horizontal and vertical connections arose as a natural consequence of accommodating an unexpected result (long-range horizontal connections) in an existing architectural framework in which receptive field properties were ascribed to interactions that occurred within a local column of cortical tissue. The simplicity of this relationship between distinct elements of cortical circuitry and features of neuronal responsiveness has significant appeal; however, there are a number of reasons to question this hypothesis, starting with a consideration of the considerable spatial overlap of the two sets of connections.

Horizontal connections are not strictly long-range

Compared with the arrangement of layer 4 inputs, horizontal connections extend for long distances across the cortical surface. However, horizontal connections are not exclusively long-range; the density of horizontal connections is actually greatest locally and diminishes with distance (Bosking et al., 1997; Gilbert and Wiesel, 1989; Kisvarday et al., 1997; Malach et al., 1993; Rockland and Lund, 1982; Rockland et al., 1982; Fig. 46.3A). At least some of these proximal connections originate as collaterals from the axons of pyramidal neurons that continue to more distal targets

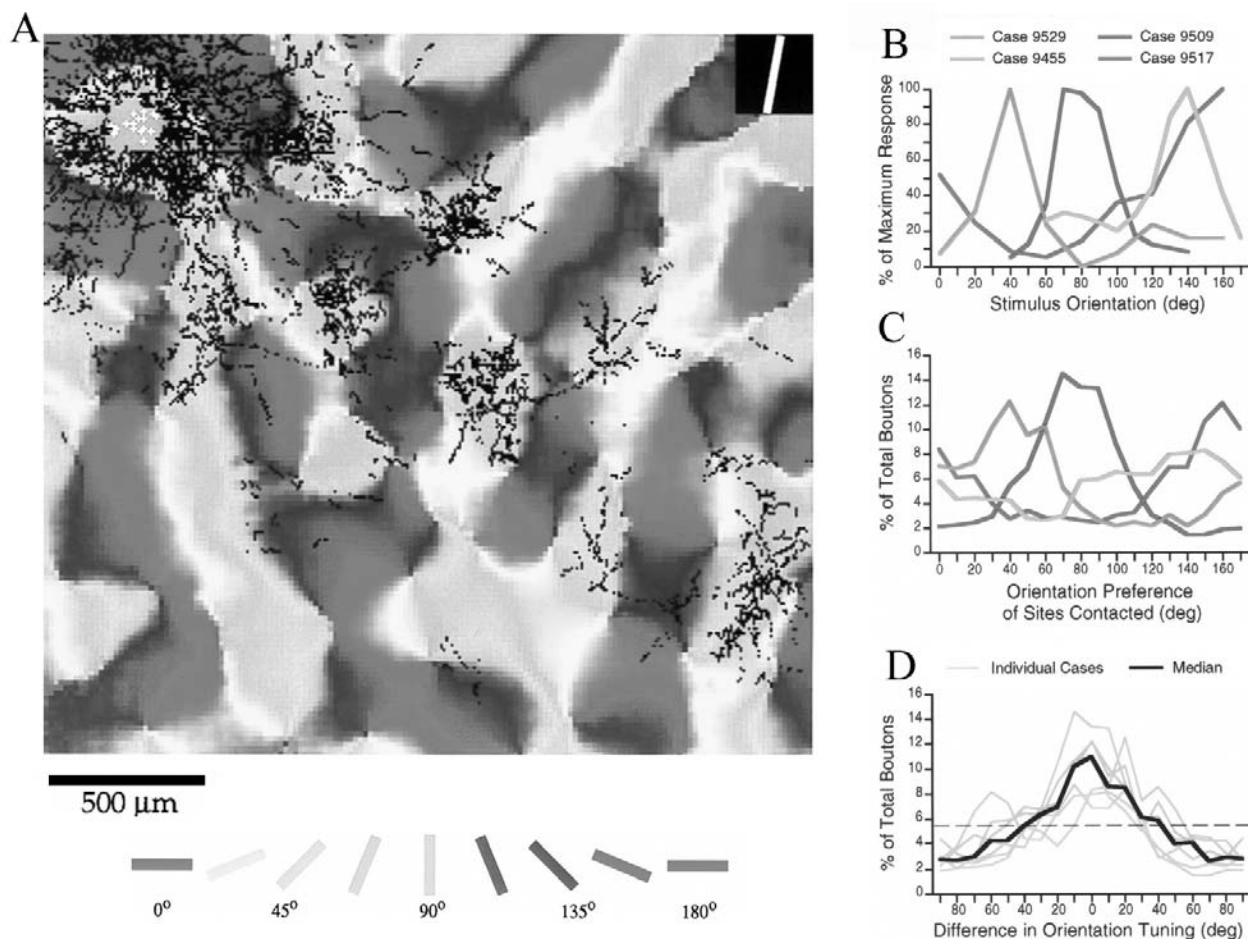


FIGURE 46.1. Relation of horizontal connections to maps of orientation preference derived with intrinsic signal optical imaging. *A*, Distribution of biocytin-labeled boutons (black dots) resulting from an injection of tracer into a site (white crosses) that responded preferentially to an 80 degree stimulus (just off vertical). Within 500 μm of the injection site the terminals are distributed over a wide range of orientations, while at longer distances the terminal patches are localized in regions that have orientation preferences similar to

that of the injection site. Orientation preference is color coded according to the key at the bottom of the panel. *B,C*, Comparison of the multiunit orientation tuning curves from four injection sites (*B*) with the bouton orientation tuning curves derived from the distribution of boutons on the optical maps (*C*). *D*, Summary of the orientation tuning of the bouton distribution relative to the preferred orientation of the injection site. (From Bosking et al., 1997, Copyright 1997 by the Society for Neuroscience.) (See color plate 28)

within the horizontal network (Gilbert and Wiesel, 1983; Kisvarday and Eysel, 1992; Martin and Whitteridge, 1984; Yabuta and Callaway, 1998), suggesting that the same signal is propagated throughout the cortical region that contributes to the minimum discharge field and the surrounding sub-threshold region. Thus, no parts of the receptive field escape the influence of the horizontal network; indeed, assuming a smooth and continuous mapping of visual space (see below), the impact of the horizontal network is likely to be as strong or stronger in the cortical region that contributes to the minimal discharge field.

Furthermore, the functional specificity that is a characteristic feature of long-range horizontal connections may not apply to the interactions mediated by these shorter-range horizontal connections. Although extracellular tracer injections reveal the modular specificity of long-range connec-

tions, with such connections terminating primarily in regions of orientation preference similar to that of the injection site, the pattern of termination within 500 μm of the injection site is diffuse and nonspecific, lacking the patchiness which is characteristic of the long-range horizontal connections (Bosking et al., 1997; Gilbert and Wiesel, 1989; Kisvarday et al., 1997; Malach et al., 1993). This pattern, suggestive of interconnections between cortical sites with a broad range of orientation preferences, is supported by the results of several recent physiological studies. For example, cross-correlation analysis suggests that there is a high degree of connectivity between pairs of neurons that are separated by distances of less than 500 μm , regardless of the orientation preference of the individual neurons (Das and Gilbert, 1999; DeAngelis et al., 1999; Hata et al., 1991; Michalski et al., 1983; Fig. 46.3*B*). Likewise, recent intracellular

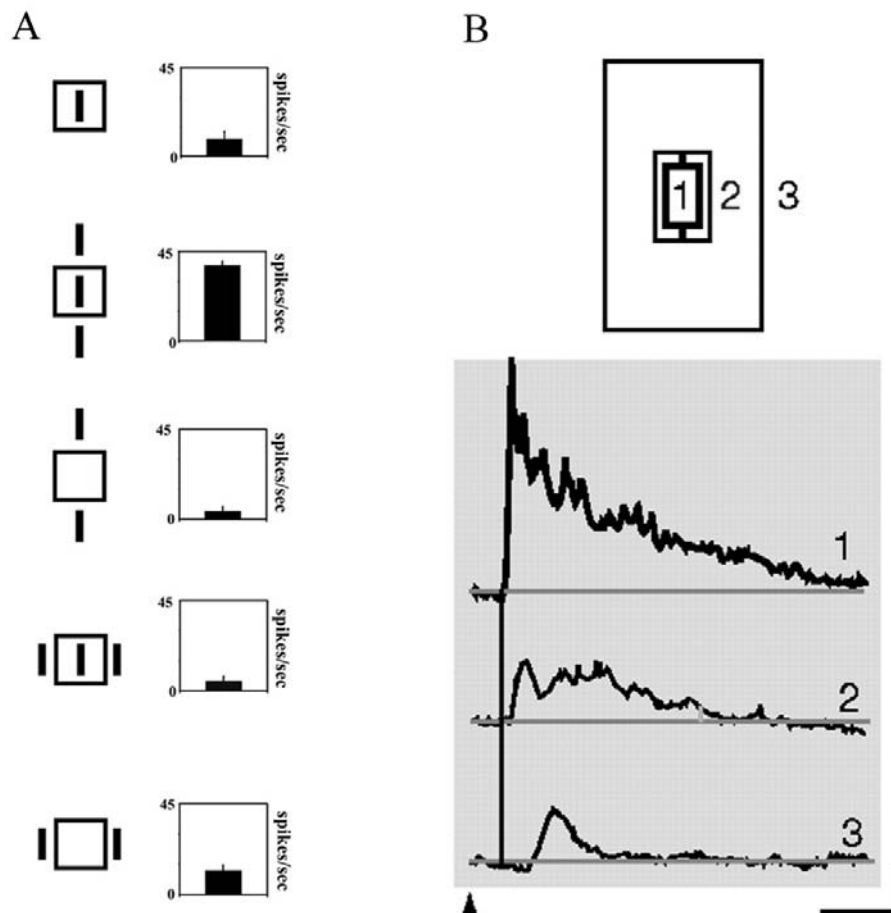


FIGURE 46.2. Receptive field center and surround. *A*, The black square indicates the boundaries of the minimum discharge field assessed by using a small bar the size of the receptive field to delimit the area of visual space that evokes spike discharge. Although presentation of stimuli in the region around the minimum discharge field does not evoke spikes, placement of stimuli in these regions can alter the response to stimuli presented in the minimum discharge field. In this case, a colinear arrangement of surround stimuli enhances the spike rate, while the noncolinear arrangement decreases the spike rate over that found with center stimulation

recording experiments show effects consistent with a uniform pattern of local connections whose tuning can be broad or narrow, depending on the properties of the orientation map. The subthreshold responses of neurons near pinwheel centers (regions where orientation preference changes rapidly across the cortical surface) are considerably broader in their orientation tuning than those that lie in regions where orientation is changing at a slower rate (Schummers et al., 2001).

Short-range horizontal interactions also include a significant contribution from the population of smooth dendritic, GABAergic neurons within layer 2/3. This is an extremely diverse class of neurons that differ in morphology and synaptic properties (Gupta et al., 2000; Miles, 2000). Most have axon arbors that do not extend over more than 500 μm , although one distinct class (the basket cell) spreads its axon

alone. *B*, Subthreshold responses from regions that surround the minimum discharge field. Intracellular records showing responses from flashed grating stimulation of the minimum discharge field (1) and annular stimulation with the minimum discharge field blocked by masks of different sizes (2, 3). Even stimulation with the largest mask several times the size of the minimum discharge field still evokes a significant subthreshold response. (*A* from Kapadia et al., 2000; *B* reprinted with permission from Bringuier et al., *Science* 283, 695, 1999. Copyright 2000 American Association for the Advancement of Science.)

arbor for distances that rival those of pyramidal cells (Kisvarday and Eysel, 1993; Kisvarday et al., 1993). Analysis of the distribution of boutons from inhibitory neurons (both short- and long-range) suggests that they are more broadly tuned than those of more distant pyramidal cell terminations (Kisvarday et al., 1994, 1997), and this observation is consistent with the results of photostimulation experiments in tissue slices (Roerig and Kao, 1999).

The functional significance of this dense system of local horizontal connections remains unclear, but two distinct hypotheses have been offered. One possibility is that these connections contribute to the minimum discharge field by adjusting response gain to match the range of contrasts that are present in the visual scene. Contrast-dependent shifts in the responsiveness of V1 neurons play a critical role in optimizing the representation of a wide range of stimulus

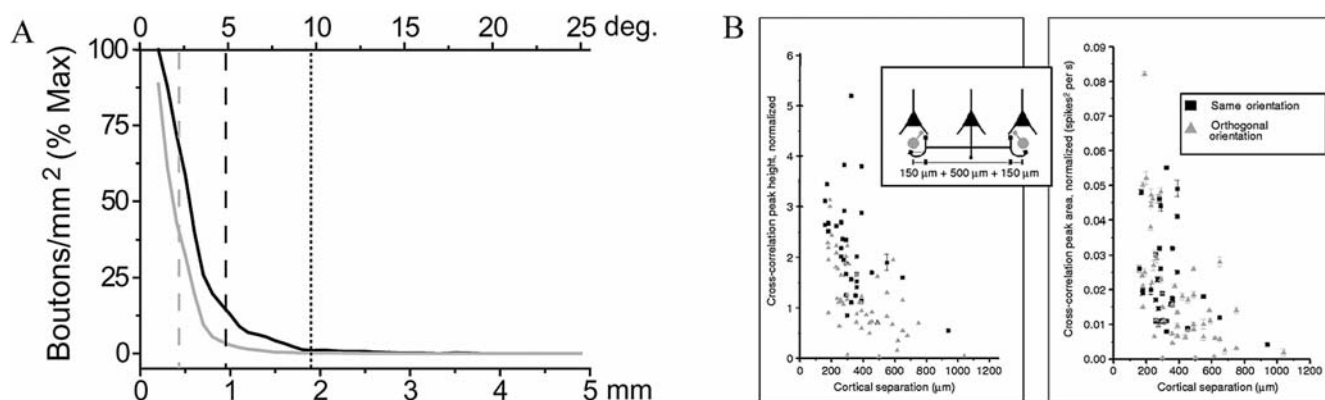


FIGURE 46.3. The properties of short-range horizontal connections. *A*, Number of boutons versus cortical distance along the axis of preferred orientation in the map of visual space (*black*) and along the orthogonal axis (*gray*). Horizontal connections are actually most dense locally, decreasing by an order of magnitude within a millimeter of the injection site center. Note greater extent and density of boutons along the axis of preferred orientation. *B*, Quantification of the degree of cross-correlation between neurons with different preferred orientations at short separation distances. *B*, Whether

using measures of peak height (*left*) or peak area (*right*), correlations are high regardless of whether the sampled pair have the same or orthogonal orientation preferences. These results are consistent with the view that short-range horizontal connections link cells with less specificity than their long-distance counterparts. (*A* from Chisum et al., 2003. Copyright 2003 by the Society for Neuroscience; *B*, reprinted by permission from *Nature* (Das and Gilbert, 1999, *Nature*, 399:655–661). Copyright 1999 Macmillan Publishers Ltd.)

contrasts within the limited range of cortical neuron spike discharge rates. Consistent with the nonspecific nature of local horizontal connections, the signal responsible for contrast gain control is thought to arise from a pool of neurons that respond to a wide range of stimulus orientations and whose receptive fields are limited to regions of visual space that correspond to the target neuron's receptive field (Bonds, 1989; DeAngelis et al., 1992; Heeger, 1992).

A second possibility is that a subset of these connections, though short-range, may link neurons with largely nonoverlapping receptive fields due to inhomogeneities in the mapping of visual space (Das and Gilbert, 1997). In cat visual cortex, localized jumps in the otherwise smooth mapping of visual space have been demonstrated to occur in association with discontinuities in the mapping of orientation preference known as *orientation pinwheel centers* (Das and Gilbert, 1999). As a result, for neurons that lie near pinwheel centers, local horizontal connections could mediate receptive field surround effects, linking cells with nonoverlapping receptive fields and different orientation preferences. Evidence in support of a contribution of short-range connections to receptive field surround effects comes from observations on the suppression of V1 responses that is induced by simultaneously presenting a line segment of the preferred orientation in the minimum discharge field and an orthogonally oriented line segment outside the minimum discharge field. These suppressive effects are most prominent for neurons located near pinwheel centers, where the stimulus configuration would be expected to activate nearby populations of cortical neurons linked by local horizontal connections. Although additional work needs to be done to confirm these results (Bosking et al., 2002; Fitzpatrick, 2000),

they suggest that local horizontal connections could contribute to either the minimum discharge field or the surround, depending on their location relative to orientation pinwheel centers.

Stimulation confined to the minimum discharge field activates a distributed population of layer 2/3 neurons linked by horizontal connections

The view that horizontal connections are responsible for the properties of the receptive field surround and not those of the minimum discharge field is also difficult to sustain if one considers the amount of cortical surface area that is activated by stimuli confined to the minimum discharge field. Stimuli confined to a receptive field activate a region of cortex that is large enough to include a significant fraction of a neuron's horizontal network (Fig. 46.4*A*). The relationship between the population of cortical neurons that is predicted to be activated by a stimulus filling the minimum discharge field of a layer 2/3 neuron in tree shrew visual cortex and the distribution of horizontal connections is illustrated in Figure 46.4*B*. In this example, the size of the receptive field has been convolved with the cortical map of visual space and with the point image size (the spread of activity expected for stimulation of a point in space) to arrive at an estimate of the area that would contain spiking neurons (Bosking et al., 2002). A similar estimate (without inclusion of point spread) is shown for results from the squirrel monkey visual cortex in Figure 46.4*C* (Sincich and Blasdel, 2001). These results indicate that stimulation of a neuron's minimum discharge field will be accompanied by spiking activity in a distributed population of layer 2/3 cortical

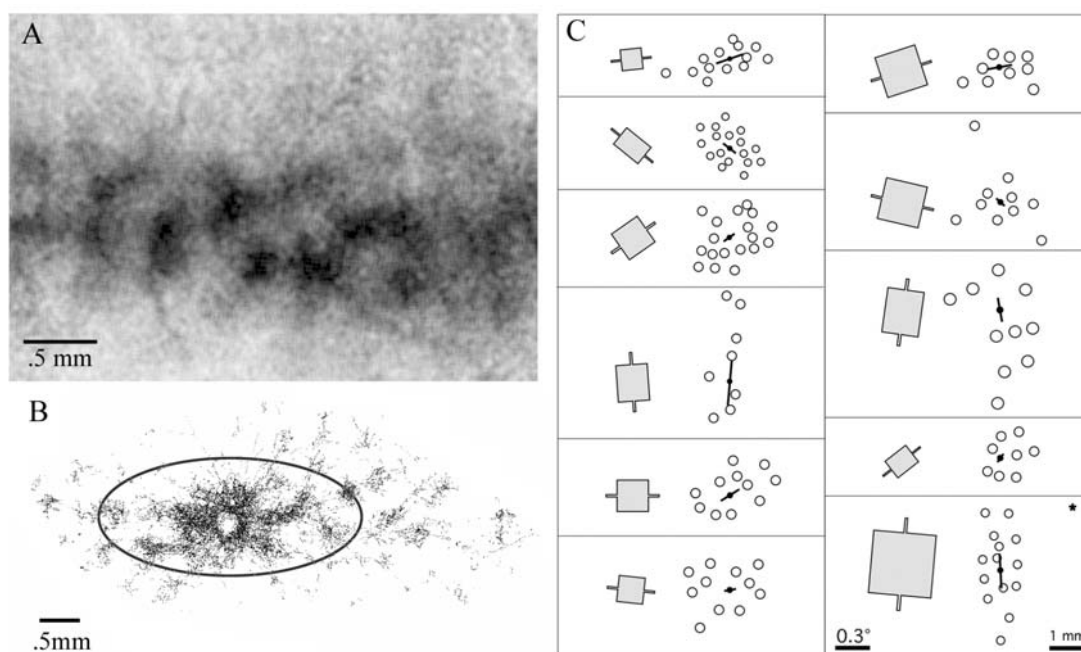


FIGURE 46.4. Horizontal connections and the minimum discharge field. *A*, Distribution of active neurons in V1 of the tree shrew resulting from the presentation of a single line $\frac{1}{4}$ degree in width (20 degrees in length) oscillating over 1 degrees of visual space. This stimulus results in a broad line of activated neurons (dark regions), with hot spots centered on regions that respond preferentially to the orientation of the stimulus. The average full width at half height of the active zone for such a stimulus is 1 mm. Movement of the stimulus to a new location 1 degree away results in systematic shifts of the activation peak of $200\mu\text{m}/\text{degree}$. Given that the average width of layer 2/3 cell receptive fields is 5 degrees, stimuli confined to the receptive field will activate a region of cortex

that includes a significant fraction of the neuron's horizontal network. *B*, Comparison of the region of cortex that would be activated by a stimulus that fills the receptive field of a layer 2/3 neuron (black oval) and the distribution of horizontal connections (black dots) in the tree shrew. *C*, Comparison of minimum discharge field size (gray squares) and horizontal connection extent (circles represent bouton patches in layer 2/3) in monkey visual cortex for 11 cases. Comparison of the receptive field plots and the anatomical plots (that have been scaled by the appropriate cortical magnification) reveals the potential contribution of horizontal connections to the minimum discharge field. (*C* from Sincich and Blasdel, 2001, Copyright 2001 by the Society for Neuroscience.)

neurons, neurons that are linked by the more proximal parts of the patchy horizontal network.

If the horizontal network contributes to the properties of the minimum discharge field, then anisotropies in the spatial arrangement of horizontal connections should be reflected in the shape of the minimum discharge field as well as the subthreshold surround. Horizontal connections in the superficial layers of tree shrew visual cortex exhibit striking anisotropy, extending preferentially along one axis of the cortical map of visual space. Furthermore, the axis of elongation is orientation specific, distributing so as to link cells whose receptive fields prefer similar orientations and are aligned along the axis of preferred orientation in visual space (Bosking et al., 1997). In the tree shrew, these connections extend roughly twice as far along the axis of preferred orientation (up to 20 degrees in the map of visual space) as along the orthogonal axis (Fig. 46.3*A*), and give rise to four times as many terminal boutons (Bosking et al., 1997; Chisum et al., 2003; Figs. 46.1*A*, 46.4*B*). This bias in the distribution of horizontal connections is consistent with the average shape of the minimum discharge field of layer

2/3 neurons (roughly 2:1) and with the size and shape of the subthreshold facilitatory zones that extend beyond the minimum discharge field for distances of up to 20 degrees (Chisum et al., 2003). These features appear to emerge in layer 2/3; layer 4 neurons in this species have receptive fields that are radially symmetric, poorly tuned for orientation, and either exhibit no sign of summation or show suppression for increases in stimulus length (Chisum et al., 2003). An orientation-specific anisotropy of horizontal connections also has been described in the cat and in squirrel and owl monkey visual cortex; however, the magnitude of elongation is less than that described in the tree shrew (Schmidt et al., 1997; Sincich and Blasdel, 2001), and this may reflect the less pronounced (or less homogeneous) elongation of layer 2/3 cell receptive fields in these species (Angelucci et al., 2002).

What is clear from these considerations is that the strict allocation of the minimum discharge field and subthreshold regions to the functions of vertical and horizontal circuits, respectively, must be tempered by the recognition of significant overlap in the spatial extent of these two types of con-

nections, as well as by the amount of the horizontal network that is activated by stimulation of the minimum discharge field. Indeed, based on the fact that their density falls with distance, the contribution of horizontal connections should be significant over the entire receptive field (supra- and subthreshold) and should be greatest in the region of the minimum discharge field. Furthermore, as the following sections indicate, the functional interactions between the minimum discharge field and the subthreshold regions that surround it are far from simple: they vary in sign (facilitatory or inhibitory) and in magnitude based on the nature of the visual stimulus and the context in which it is presented.

Intracortical circuits and receptive field dynamics: stimulus contrast and summation

The dynamics of receptive field center-surround interactions are well illustrated by considering the effects of varying stimulus contrast on the responses of V1 neurons to bars of varying lengths. Some of the earliest studies of the receptive fields of V1 neurons noted that many cells appeared to be tuned to the length of a bar moving through the receptive field. Increasing the length of a bar stimulus results in an increased neuronal response rate (*summation*) until an optimal bar length is reached, after which further increasing the bar length leads to a decrement in response often referred to as *endstopping*. More recently, it has become clear that the para-

meters of length tuning are highly dependent on stimulus contrast. For many cells in primate and cat V1, the length tuning curve for high-contrast stimuli plateaus at relatively short stimulus lengths, and many (but not all) tuning curves exhibit a reduction in response to the presentation of longer-length stimuli. At low-contrast values, however, the stimulus length over which summation occurs can be increased by two to four times over that found with high-contrast stimuli, and there is no sign of a reduced response to longer stimuli (Kapadia et al., 1999; Sceniak et al., 1999; Sengpiel et al., 1997; Fig. 46.5A). Thus, stimuli presented in the same region of visual space can exert a facilitatory effect, a suppressive effect, or have no effect, depending on stimulus contrast.

A similar contrast dependence is evident in center-surround interactions that have been probed with multiple discrete stimuli (Fig. 46.5B). For example, the effect produced by presentation of a colinear stimulus outside the minimum discharge field can often be changed from facilitation to suppression by increasing the contrast of the stimulus in the receptive field center (Henry et al., 1978; Kapadia et al., 2000; Levitt and Lund, 1997; Polat, 1999; Polat et al., 1998; Sengpiel et al., 1997). It is worth noting that there is considerable disagreement in the literature over the presence of facilitatory regions beyond the classical receptive field (DeAngelis et al., 1992, 1994; Kapadia et al., 1995, 1999; Levitt and Lund, 1997; Mizobe et al., 2001; Maffei and Fiorentini, 1976; Nelson and Frost, 1985; Polat et al., 1998;

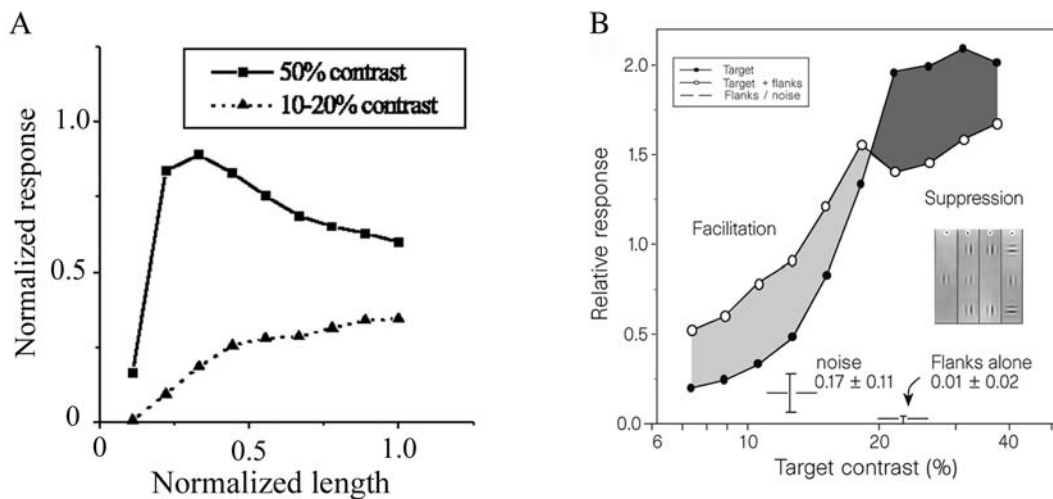


FIGURE 46.5. Dynamics of receptive field surround effects. *A*, Comparison of average length summation curves for a population of neurons in monkey visual cortex generated with stimuli of low and high contrast. For high-contrast stimuli, the length summation curve peaks at short stimulus lengths, and there is a decrease in response to longer stimulus lengths. For low-contrast stimuli, the peak of the length summation curve occurs at significantly longer lengths, and the reduction (endstopping) is often absent. *B*, Responses to arrays of Gabor stimuli exhibit contrast-dependent

facilitatory and suppressive effects. The neuronal response to Gabor stimuli centered in the minimum discharge field increases with increasing stimulus contrast (*filled circles*). The addition of colinear flanks (*open circles*) results in facilitation over single Gabor response at low contrast and suppression at high contrast. (*A* from Kapadia et al., 1999, Proc. Natl. Acad. Sci., USA, 96:12073–12078. Copyright 1999 National Academy of Sciences, USA. *B* reprinted by permission from *Nature* (Polat et al., 1998, *Nature*, 391:580–584). Copyright 1998 Macmillan Publishers Ltd.)

Sceniak et al., 1999; Sengpiel et al., 1997; Walker et al., 1999). Much of the discrepancy can be attributed to how the receptive field center is defined; facilitatory surround effects are likely to result from placement of discrete stimuli outside the minimum discharge field but within the regions that contribute to length summation with continuous stimuli (see Fitzpatrick, 2000 for discussion).

Length summation and surround facilitation are generally thought to arise from an increase in the activity of excitatory inputs, but endstopping and surround suppression have been attributed to a number of mechanisms, including recruitment of inhibition (Kapadia et al., 1999; Somers et al., 1998; Stemmler et al., 1995), withdrawal of excitation (Sceniak et al., 1999), or a combination of these factors (Anderson et al., 2001). In support of recruitment of inhibition, recordings from cortical slices show that weak electrical stimulation of intracortical circuits elicits purely EPSPs, while stronger stimulation elicits compound EPSP/IPSPs (Hirsch and Gilbert, 1991). Thus, by analogy, low-contrast stimuli which might be expected to evoke a relatively low level of activity in cortical circuits result in summation, while higher-contrast stimuli which reach the threshold for recruiting inhibitory inputs lead to endstopping. An alternative explanation suggests that endstopped responses are better explained by withdrawal of excitation than by increased inhibition. By quantifying the responses of cortical neurons to stimuli of different lengths at different contrasts and fitting the data with a difference of Gaussians model, Sceniak et al. (1999) found that length summation was relatively insensitive to changes in surround suppression but was well fit by changes in facilitation. Recent *in vivo* intracellular recordings provide evidence that supports both withdrawal of excitation and increased inhibition as contributors to the suppression: endstopping evoked during measurements of length tuning with high-contrast stimuli is associated with both increased inhibitory conductance and large decreases in excitatory conductance (Anderson et al., 2001).

In principle, the changes in excitatory and inhibitory currents that underlie the dynamics of length tuning could be explained solely by interactions between the network of long-range horizontal connections and short-range GABAergic neurons (Douglas and Martin, 1991; Douglas et al., 1995; Somers et al., 1998; Stemmler et al., 1995; Fig. 46.6). For low-contrast stimuli, the level of activity in the horizontal network is likely to be low; given that weak stimulation elicits only EPSPs (Hirsch and Gilbert, 1991), inhibition may not be recruited under these conditions. Increases in stimulus length recruit more and more of the horizontal network, leading to an increase in the average discharge rate of the neurons (Fig. 46.6*A*). This facilitation saturates at stimulus lengths that correspond to the cortical extent of horizontal connections. Indeed, recent analysis in macaque V1 shows that horizontal connections extend over

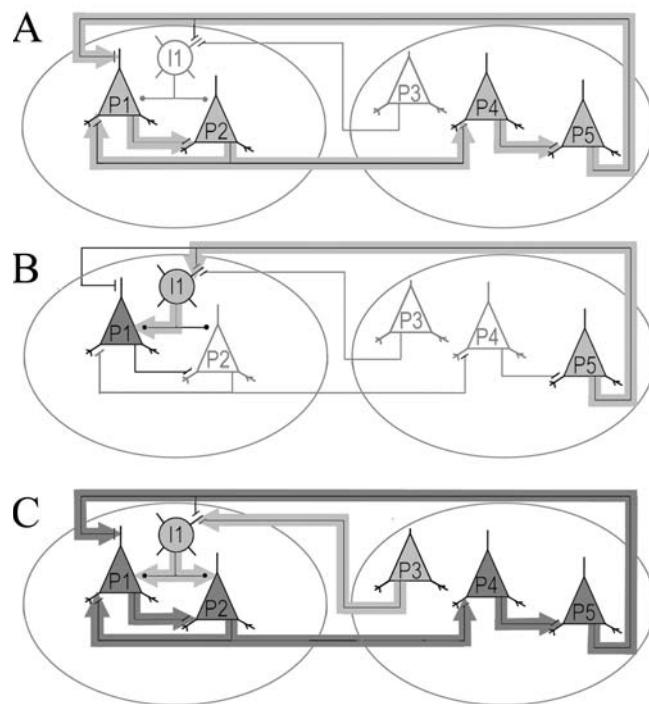


FIGURE 46.6. Changes in the level of activity of the horizontal network that may underlie length summation and endstopping. Populations of pyramidal cells are indicated by triangular symbols; networks of inhibitory cells are represented by a circular symbol with a smooth contour. Increases in activity are depicted by light gray, decreases by dark gray. Increases in the length of low-contrast stimuli recruit more of the excitatory horizontal network that synapses with P1 (*A*). Increases in the length of high-contrast stimuli lead to levels of activity in the horizontal network that are sufficient to recruit local inhibitory neurons, reducing the activity of P1 (*B*); concomitantly, the amount of excitatory activity in the horizontal network is reduced (*C*). (See color plate 29).

a distance that is in accord with the low-contrast measures of length summation (Angelucci et al., 2002; Cavanaugh et al., 2002). During presentation of high-contrast stimuli, in contrast, the high level of activity in the horizontal network permits the recruitment of inhibition. Thus, although increases in stimulus length still lead to recruitment of additional horizontal connections, at some point the level of activity in the horizontal network reaches the threshold of inhibitory neurons (Fig. 46.6*B*). At this point, the activity of local inhibitory neurons results in increased inhibitory conductances and, due to net reduction in the activity of the horizontal network, a concomitant decrease in excitatory conductances (Fig. 46.6*C*).

However, it seems likely that changes in the activity of vertical circuits could also play a significant role in the dynamics of length summation and endstopping, as layer 4 neurons themselves are known to exhibit summation. In addition, at low contrast, longer bars will recruit a larger percentage of the population of layer 4 neurons that converge onto a given layer 2/3 neuron, contributing to summation. Increasing the

length of high-contrast bars has a different effect: because layer 4 neurons are a significant source of the excitatory inputs to inhibitory neurons in layer 2/3, an increase in the length of a high-contrast bar produces more vigorous responses in layer 4 neurons and recruits GABAergic neurons in layer 2/3, contributing to endstopping in layer 2/3. Finally, because some layer 4 neurons in cat and monkey visual cortex exhibit endstopping themselves, increasing stimulus length can result in a decrease in the activity of vertical inputs, which is likely to contribute to the decrease in excitatory currents that accompanies the endstopped responses of layer 2/3 neurons. It has been suggested that a circuit involving either direct projections from a subpopulation of layer 6 neurons to layer 4 or projections from layer 6 neurons to the visual claustrum (a thin sheet of neurons in the rostral forebrain that projects back to cortical layer 4) may be the source of the endstopping of layer 4 neurons (Bolz and Gilbert, 1986; Sherk and LeVay, 1983). Indeed, inactivation of layer 6 neurons or lesions of the visual claustrum result in a reduction of endstopped responses in V1. Thus, while it is tempting to explain the dynamics of length summation as the result of interactions mediated largely by horizontal connections, a more complete explanation of these phenomena will require understanding how alterations in the activity of vertical inputs and inputs from extrinsic sources interact with horizontal interactions in shaping the responses of layer 2/3 neurons.

Intracortical circuits and receptive field dynamics: artificial scotoma

The response to presentation of stimuli within and outside the minimal discharge field is also sensitive to the neuron's stimulation history. Masking a limited region of the visual field for several minutes while stimulating the surrounding regions of visual space causes the receptive fields of cortical neurons in this *artificial scotoma* to expand to several times their original size (Gilbert and Wiesel, 1992; Kapadia et al., 1994; Pettet and Gilbert, 1992). The effect can be reversed by presenting visual stimuli within the masked region, causing the receptive fields to shrink to their original size.

It seems likely that an increase in the effectiveness of horizontal connections contributes to the expansion of the receptive field. During the creation of an artificial scotoma, the activity of pairs of layer 2/3 neurons that are separated by several millimeters across the cortical surface becomes more strongly correlated, consistent with an increase in the effective strength of horizontal connections (Das and Gilbert, 1995a). Although the precise synaptic basis for such an alteration in efficacy remains unclear, one possibility is that the change is largely a product of network dynamics—

alterations in the balance of excitation and inhibition that increase the responsiveness of layer 2/3 neurons to weaker, more distant inputs. For example, the local inhibitory network in layer 2/3 may be the source of tonic inhibition that regulates the sensitivity of layer 2/3 neurons to excitatory inputs. During the artificial scotoma paradigm, the local inhibitory network in the region of the cortex that represents the scotoma is less active than it would be if a stimulus was present, and the neurons are relatively more sensitive to horizontal inputs from the surrounding areas, resulting in an expanded receptive field. Changes in network excitability could be accompanied by potentiation of the synapses associated with horizontal connections during the masking period. In support of this proposal, *in vitro* experiments provide evidence that the strength of synapses in the horizontal network can be modified by stimulation (Hirsch and Gilbert, 1993).

An alternative possibility is that scotoma-induced changes in receptive field size depend less on network dynamics than on activity-dependent changes in intrinsic conductances, a possibility raised by studies of contrast gain control (Ohzawa et al., 1985). During sustained presentations of high-contrast visual stimuli, neuronal activity is high, but neuronal responsivity decreases due to the activation of intrinsic conductances which hyperpolarize the membrane potential (Carandini and Ferster, 1997; Sanchez-Vives et al., 2000a, 2000b). Conversely, during low-contrast visual stimulation, neuronal activity is low but responsivity increases due to the deactivation of intrinsic currents. The nature of these effects suggests that the efficacy of horizontal connections may be modulated, during changes in mean level of neuronal activation, through the control of membrane potential by intrinsic conductances. For example, during periods of full-field visual stimulation, the local inhibitory network receives direct activation through ascending afferents from layer 4 and local pyramidal cells receive tonic inhibition, rendering long-range horizontal connections relatively ineffective and shrinking receptive field area. However, during generation of an artificial scotoma, neuronal activity within the affected area is low, so the local inhibitory network is less active as afferents ascending from layer 4 are silenced. As a result, local pyramidal cells are released from tonic inhibition and neurons may depolarize enough to bring membrane potentials close to threshold, enabling horizontal connections to become more effective in driving spikes and yielding receptive field expansion. In this conception, activity-dependent changes in intrinsic conductance regulate the efficacy of horizontal inputs and establish the size of the minimum discharge field.

Although this discussion has focused on the impact of changes in the efficacy of horizontal connections, it is worth emphasizing that both network and conductance-induced changes in membrane potential operate simultaneously on

all of the inputs that a neuron receives, altering the efficacy of vertical as well as horizontal and feedback connections from extrastriate areas. The observation that artificial scotoma-induced changes in receptive field size are frequently accompanied by changes in the magnitude of response to the presentation of stimuli in the center of the receptive field, where vertical connections would be expected to be strongest, is consistent with an overall increase in responsiveness to the full spectrum of inputs that are centered on the cell's receptive field (Pettet and Gilbert, 1992). Furthermore, at least some of the increase in receptive field size following the artificial scotoma is likely to reflect the increased efficacy of those layer 4 inputs that lie most distant from the layer 2/3 neuron and contribute the fewest synaptic terminals. In addition, the proposed changes in intrinsic conductance would be expected to occur in layer 4 neurons themselves, altering the sizes of their receptive fields and thereby contributing to the changes of their targets in layer 2/3.

Intracortical circuits and neuronal synchrony

A prominent feature of neurons in visual cortex is their tendency to fire synchronously despite large cortical separation distances (Singer, 1999; Usrey and Reid, 1999). Most efforts to explain neuronal synchrony emphasize a prominent role for horizontal connections, and the orientation selectivity of long-range synchrony is certainly consistent with the properties of the horizontal network (Das and Gilbert, 1999; Gray et al., 1989; Hata et al., 1991; Toyama et al., 1981a, 1981b; Ts'o et al., 1986). However, two different synaptic mechanisms have been proposed to explain their involvement.

One possibility is that synchrony is largely the result of oscillations in the activity of a distinct class of pyramidal cells in superficial layers of cortex, termed *chattering cells*, that generates rhythmic bursts of action potentials at 20 to 70 Hz. The excitatory drive in this cell class is proposed to synchronize neuronal spiking, entrain neuronal populations, and generate gamma wave oscillations (Gray and McCormick, 1996). Supporting this theory, models show that neurons are most likely to fire action potentials when they receive multiple, coincident EPSPs (Softky and Koch, 1993; Stevens and Zador, 1998). Thus, concerted neuronal activation may arise from the ability of chattering cells to deliver bursts of EPSPs simultaneously to large neuronal populations (Fig. 46.7A). Although at least some chattering cells appear to give rise to horizontal connections, they represent only a small percentage of superficial pyramidal cells, raising the question of how this small number of cells could be the source of a signal that entrains large populations of neurons in widely separated orientation domains (Gray and McCormick, 1996). Some regular-spiking cells have intrinsic

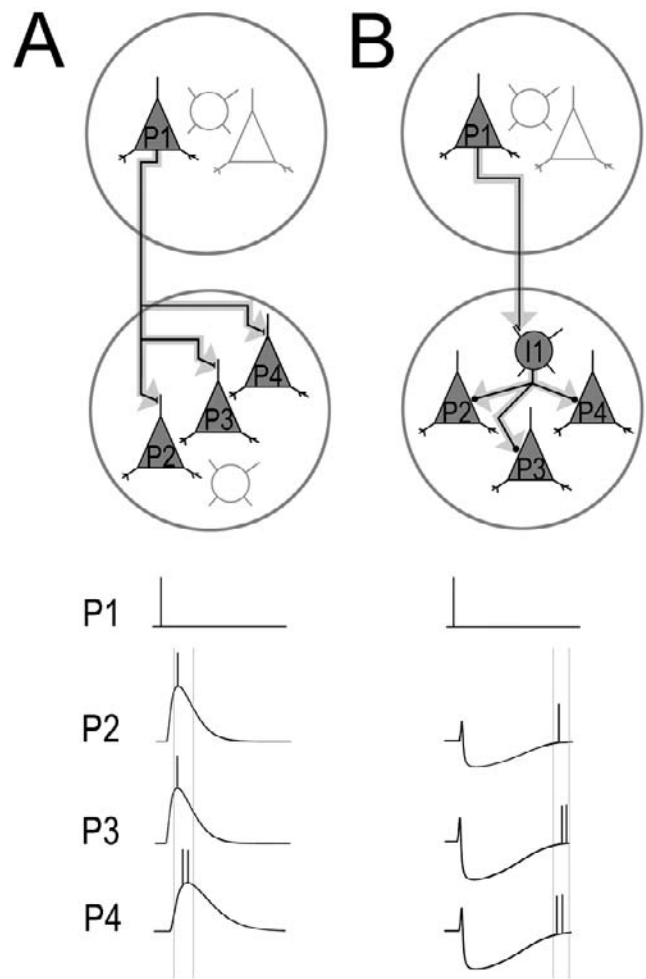


FIGURE 46.7. Horizontal connections and the generation of neuronal synchrony. *A*, Neuronal synchronization based on excitation driven by chattering cells. A chattering cell (P1) generates bursts of action potentials that are carried through long-range horizontal connections to pyramidal cells in neighboring orientation domains (P2 to P4); as shown below the circuit diagram, activity in P1 generates synchronous EPSPs in P2 to P4, resulting in synchronized firing patterns. *B*, Inhibition-based mechanism for generating neuronal synchrony. Through its horizontal connections, a regular-spiking pyramidal cell (P1) strongly activates the local inhibitory network (I1) in a neighboring domain, resulting in the generation of simultaneous IPSPs in local pyramidal cells (P2 to P4). As shown below the circuit diagram, as these pyramidal cells recover together from hyperpolarization, they fire synchronous action potentials, having a precise temporal relationship to P1.

sic membrane properties enabling them, when depolarized, to switch to a chattering mode (Brumberg et al., 2000), suggesting that an initially small group of chattering cells may recruit additional members; however, whether this is sufficient to produce temporal correlations over long distances remains to be shown.

An alternative view suggests that excitatory connections may be insufficient for generating synchronous activity, because EPSPs have relatively long durations and do not

constrain spike timing as effectively as does inhibition (Van Vreeswijk et al., 1994). Instead, synchronization may rely on the ability of inhibitory cells to control spike timing in pyramidal cells, as has been demonstrated in cortical slices (Cobb et al., 1995). By delivering IPSPs to numerous pyramidal cells, inhibitory cells cause pyramidal cells to hyperpolarize simultaneously and fire synchronous spikes during the rebound (Fig. 46.7*B*). While most inhibitory cell axons extend only several hundred microns, perhaps sufficient to synchronize activity within an orientation domain, there are two mechanisms by which they might evoke synchronization over longer cortical distances. First, large basket cells represent a small percentage of inhibitory cells in superficial layers, but they have arbors extending several millimeters (Kisvarday and Eysel, 1993; Kisvarday et al., 1993), raising the possibility that this cell type may contribute to synchronizing activity across long distances. Second, an alternative possibility is that the long axons of large basket cells are not required for long-range synchrony, because horizontal connections are very effective in driving inhibition (Hirsch and Gilbert, 1991). This possibility has received support from realistic neuronal models showing that the axons of pyramidal cells may generate synchrony over long distances by interconnecting the local inhibitory networks and driving inhibition in multiple orientation domains (Bush and Sejnowski, 1996; Traub et al., 1996).

While horizontally mediated synaptic interactions are no doubt critical to long-range synchronization (Wilson and Bower, 1991), the amplitude and timing of vertical inputs from layer 4 are also likely to play a significant role in these interactions. Neuronal synchrony originates at the earliest stages of visual processing, being evident in the retina and in the lateral geniculate nucleus, and may be further refined by corticothalamic feedback (Sillito et al., 1994; Singer, 1999; Usrey and Reid, 1999). The correlation in the activity of thalamic inputs to layer 4 neurons may serve as a seed for the coarse temporal patterning of responses in layer 2/3 that are then further refined by the actions of the horizontal network. Thus, the interplay between the timing and the amplitude of vertical and horizontal inputs is likely to be the source of the precise temporal synchrony that characterizes the responses of layer 2/3 neurons.

Summary and conclusion

We hope that this review has served to emphasize the continuing evolution of our conceptions of the cortical receptive field and the circuitry that underlies it. The cortical receptive field has become a dynamic entity, one in which context and history play significant roles in shaping its boundaries and altering its properties. With this has come the recognition that even small, simple stimuli activate large populations of cortical neurons whose interactions via

vertical and horizontal circuits are complex and whose functions are not so easily parsed into traditional functional categories such as center and surround. Understanding the neural basis for the response properties of layer 2/3 neurons will require a better understanding of the dynamic interplay between vertical and horizontal inputs that converge onto individual neurons, and how this interplay is altered by GABAergic inputs, intrinsic membrane properties, and the state of the cortical network. Perhaps it should come as no surprise that the properties of the neurons that mediate visual perception cannot be attributed to individual components of the network in which they are embedded. Like perception itself, the behavior of the circuit would appear to be more than the sum of its parts.

REFERENCES

- Anderson, J. S., I. Lampl, D. C. Gillespie, and D. Ferster, 2001. Membrane potential and conductance changes underlying length tuning of cells in cat primary visual cortex, *J. Neurosci.*, 21:2104–2112.
- Angelucci, A., J. B. Levitt, E. J. S. Walton, J.-M. Hupe, J. Bullier, and J. S. Lund, 2002. Circuits for local and global signal integration in primary visual cortex, *J. Neurosci.*, 22:8633–8646.
- Barlow, H. B., C. Blakemore, and J. D. Pettigrew, 1967. The neural mechanism of binocular depth discrimination, *J. Physiol. (Lond.)*, 193:327–342.
- Bolz, J., and C. D. Gilbert, 1986. Generation of end-inhibition in the visual cortex via interlaminar connections, *Nature*, 320:362–365.
- Bonds, A. B., 1989. Role of inhibition in the specification of orientation selectivity of cells in the cat striate cortex, *Vis. Neurosci.*, 2:41–55.
- Bosking, W. H., J. C. Crowley, and D. Fitzpatrick, 2002. Spatial coding of position and orientation in primary visual cortex, *J. Nat. Neurosci.*, 9:874–882.
- Bosking, W. H., Y. Zhang, B. Schofield, and D. Fitzpatrick, 1997. Orientation selectivity and the arrangement of horizontal connections in tree shrew striate cortex, *J. Neurosci.*, 17:2112–2127.
- Binguier, V., F. Chavane, L. Glaeser, and Y. Fregnac, 1999. Horizontal propagation of visual activity in the synaptic integration field of area 17 neurons, *Science*, 283:695–699.
- Brumberg, J. C., L. G. Nowak, and D. A. McCormick, 2000. Ionic mechanisms underlying repetitive high-frequency burst firing in supragranular cortical neurons, *J. Neurosci.*, 20:4829–4843.
- Bush, P., and T. Sejnowski, 1996. Inhibition synchronizes sparsely connected cortical neurons within and between columns in realistic network models, *J. Comput. Neurosci.*, 3:91–110.
- Carandini, M., and D. Ferster, 1997. A tonic hyperpolarization underlying contrast adaptation in cat visual cortex, *Science*, 276:949–952.
- Cavanaugh, J. R., W. Bair, and J. A. Movshon, 2002. Nature and interaction of signals from the receptive field center and surround in macaque V1 neurons, *J. Neurophysiol.*, 88:2530–2546.
- Chisum, H. J., F. Mooser, and D. Fitzpatrick, 2003. Emergent properties of layer 2/3 neurons reflect the collinear arrangement of horizontal connections in tree shrew visual cortex, *J. Neurosci.*, 20:2947–2960.

- Cobb, S. R., E. H. Buhl, K. Halasy, O. Paulsen, and P. Somogyi, 1995. Synchronization of neuronal activity in hippocampus by individual GABAergic interneurons, *Nature*, 378:75–78.
- Das, A., and C. D. Gilbert, 1995a. Receptive field expansion in adult visual cortex is linked to dynamic changes in strength of cortical connections, *J. Neurophysiol.*, 74:779–792.
- Das, A., and C. D. Gilbert, 1997. Distortions of visuotopic map match orientation singularities in primary visual cortex, *Nature*, 387:594–598.
- Das, A., and C. D. Gilbert, 1999. Topography of contextual modulations mediated by short-range interactions in primary visual cortex, *Nature*, 399:655–661.
- DeAngelis, G. C., R. D. Freeman, and I. Ohzawa, 1994. Length and width tuning of neurons in the cat's primary visual cortex, *J. Neurophysiol.*, 71:347–374.
- DeAngelis, G. C., G. M. Ghose, I. Ohzawa, and R. D. Freeman, 1999. Functional micro-organization of primary visual cortex: receptive field analysis of nearby neurons, *J. Neurosci.*, 19:4046–4064.
- DeAngelis, G. C., J. G. Robson, I. Ohzawa, and R. D. Freeman, 1992. Organization of suppression in receptive fields of neurons in cat visual cortex, *J. Neurophysiol.*, 68:144–163.
- Douglas, R. J., C. Koch, M. Mahowald, K. A. Martin, and H. H. Suarez, 1995. Recurrent excitation in neocortical circuits, *Science*, 269:981–985.
- Douglas, R. J., and K. A. Martin, 1991. A functional microcircuit for cat visual cortex, *J. Physiol.*, 440:735–769.
- Fiorani, M., M. G. P. Rosa, R. Gattass, and C. E. Rocha-Miranda, 1992. Dynamic surrounds of receptive fields in primate striate cortex: a physiological basis for perceptual completion?, *Proc. Natl. Acad. Sci. USA*, 89:8547–8551.
- Fisken, R. A., L. J. Garey, and T. P. Powell, 1975. The intrinsic, association and commissural connections of area 17 on the visual cortex, *Philos. Trans. R. Soc. Lond. B. Biol. Sci.*, 272:487–536.
- Fitzpatrick, D., 2000. Seeing beyond the receptive field in primary visual cortex, *Curr. Opin. Neurobiol.*, 10:438–443.
- Gilbert, C. D., 1992. Horizontal integration and cortical dynamics, *Neuron*, 9:1–13.
- Gilbert, C. D., 1998. Adult cortical dynamics, *Physiol. Rev.*, 78:467–485.
- Gilbert, C. D., and T. N. Wiesel, 1983. Clustered intrinsic connections in cat visual cortex, *J. Neurosci.*, 3:1116–1133.
- Gilbert, C. D., and T. N. Wiesel, 1989. Columnar specificity of intrinsic horizontal and corticocortical connections in cat visual cortex, *J. Neurosci.*, 9:2432–2442.
- Gilbert, C. D., and T. N. Wiesel, 1990. The influence of contextual stimuli on the orientation selectivity of cells in primary visual cortex of the cat, *Vis. Res.*, 30:1689–1701.
- Gilbert, C. D., and T. N. Wiesel, 1992. Receptive field dynamics in adult primary visual cortex, *Nature*, 356:150–152.
- Gray, C. M., P. Konig, A. K. Engel, and W. Singer, 1989. Oscillatory responses in cat visual cortex exhibit inter-columnar synchronization which reflects global stimulus properties, *Nature*, 338:334–337.
- Gray, C. M., and D. A. McCormick, 1996. Chattering cells: superficial pyramidal neurons contributing to the generation of synchronous oscillations in the visual cortex, *Science*, 274:109–113.
- Gupta, A., Y. Wang, and H. Markram, 2000. Organizing principles for a diversity of GABAergic interneurons and synapses in the neocortex, *Science*, 287:273–278.
- Hata, Y., T. Tsumoto, H. Sato, and H. Tamura, 1991. Horizontal interactions between visual cortical neurones studied by cross-correlation analysis in the cat, *J. Physiol.*, 441:593–614.
- Heeger, D. J., 1992. Normalization of cell responses in cat striate cortex, *Vis. Neurosci.*, 9:181–197.
- Henry, G. H., A. W. Goodwin, and P. O. Bishop, 1978. Spatial summation of responses in receptive fields of single cells in cat striate cortex, *Exp. Brain. Res.*, 32:245–266.
- Hirsch, J. A., and C. D. Gilbert, 1991. Synaptic physiology of horizontal connections in the cat's visual cortex, *J. Neurosci.*, 11:1800–1809.
- Hirsch, J. A., and C. D. Gilbert, 1993. Long-term changes in synaptic strength along specific intrinsic pathways in the cat visual cortex, *J. Physiol.*, 461:247–262.
- Hubel, D. H., and T. N. Wiesel, 1962. Receptive fields, binocular interaction and functional architecture in the cat's visual system, *J. Physiol.*, 160:106–154.
- Hubel, D. H., and T. N. Wiesel, 1968. Receptive fields and functional architecture of monkey striate cortex, *J. Physiol.*, 195:215–243.
- Hubel, D. H., and T. N. Wiesel, 1977. Ferrier Lecture. Functional architecture of macaque monkey visual cortex, *Proc. R. Soc. Lond. B. Biol. Sci.*, 198:1–59.
- Kapadia, M. K., C. D. Gilbert, and G. Westheimer, 1994. A quantitative measure for short-term cortical plasticity in human vision, *J. Neurosci.*, 14:451–457.
- Kapadia, M. K., M. Ito, C. D. Gilbert, and G. Westheimer, 1995. Improvement in visual sensitivity by changes in local context: parallel studies in human observers and in V1 of alert monkeys, *Neuron*, 15:843–856.
- Kapadia, M. K., G. Westheimer, and C. D. Gilbert, 1999. Dynamics of spatial summation in primary visual cortex of alert monkeys, *Proc. Natl. Acad. Sci. USA*, 96:12073–12078.
- Kapadia, M. K., G. Westheimer, and C. D. Gilbert, 2000. Spatial distribution of contextual interactions in primary visual cortex and in visual perception, *J. Neurophysiol.*, 84:2048–2062.
- Kisvarday, Z. F., C. Beaulieu, and U. T. Eysel, 1993. Network of GABAergic large basket cells in cat visual cortex (area 18): implication for lateral disinhibition, *J. Comp. Neurol.*, 327:398–415.
- Kisvarday, Z. F., and U. T. Eysel, 1992. Cellular organization of reciprocal patchy networks in layer III of cat visual cortex (area 17), *Neuroscience*, 46:275–286.
- Kisvarday, Z. F., and U. T. Eysel, 1993. Functional and structural topography of horizontal inhibitory connections in cat visual cortex, *Eur. J. Neurosci.*, 5:1558–1572.
- Kisvarday, Z. F., D. S. Kim, U. T. Eysel, and T. Bonhoeffer, 1994. Relationship between lateral inhibitory connections and the topography of the orientation map in cat visual cortex, *Eur. J. Neurosci.*, 6:1619–1632.
- Kisvarday, Z. F., E. Toth, M. Rausch, and U. T. Eysel, 1997. Orientation-specific relationship between populations of excitatory and inhibitory lateral connections in the visual cortex of the cat, *Cereb. Cortex*, 7:605–618.
- Knierim, J. J., and D. C. Van Essen, 1992. Neuronal responses to static texture patterns in area V1 of the alert macaque monkey, *J. Neurophysiol.*, 67:961–980.
- Levitt, J. B., and J. S. Lund, 1997. Contrast dependence of contextual effects in primate visual cortex, *Nature*, 387:73–76.
- Lorente de No, R., 1938. The cerebral cortex: architecture, intracortical connections and motor projections, in *Physiology of the Nervous System* (J. F. Fulton ed.), London: Oxford University Press, pp. 291–339.
- Lund, J. S., 1973. Organization of neurons in the visual cortex, area 17, of the monkey (*Macaca mulatta*), *J. Comp. Neurol.*, 147:455–496.

- Lund, J. S., and R. G. Boothe, 1975. Interlaminar connections and pyramidal neuron organization in visual cortex, area 17 of the macaque monkey, *J. Comp. Neurol.*, 159:305–334.
- Maffei, L., and A. Fiorentini, 1976. The unresponsive regions of visual cortical receptive fields, *Vis. Res.*, 16:1131–1139.
- Malach, R., Y. Amir, M. Harel, and A. Grinvald, 1993. Relationship between intrinsic connections and functional architecture revealed by optical imaging and in vivo targeted biocytin injections in primate striate cortex, *Proc. Natl. Acad. Sci. USA*, 90:10469–10473.
- Martin, K. A., and D. Whitteridge, 1984. The relationship of receptive field properties to the dendritic shape of neurones in the cat striate cortex, *J. Physiol.*, 356:291–302.
- Matsubara, J. A., M. S. Cynader, and N. V. Swindale, 1987. Anatomical properties and physiological correlates of the intrinsic connections in cat area 18, *J. Neurosci.*, 7:1428–1446.
- Matsubara, J., M. Cynader, N. V. Swindale, and M. P. Stryker, 1985. Intrinsic projections within visual cortex: evidence for orientation-specific local connections, *Proc. Natl. Acad. Sci. USA*, 82:935–939.
- McGuire, B. A., C. D. Gilbert, P. K. Rivlin, and T. N. Wiesel, 1991. Targets of horizontal connections in macaque primary visual cortex, *J. Comp. Neurol.*, 305:370–392.
- Michalski, A., G. L. Gerstein, J. Czarkowska, and R. Tarnecki, 1983. Interactions between cat striate cortex neurons, *Exp. Brain Res.*, 51:97–107.
- Miles, R., 2000. Perspectives: neurobiology. Diversity in inhibition, *Science*, 287:244–246.
- Mizobe, K., U. Polat, M. W. Pettet, and T. Kasamatsu, 2001. Facilitation and suppression of single striate-cell activity by spatially discrete pattern stimuli presented beyond the receptive field, *Vis. Neurosci.*, 18:377–391.
- Mountcastle, V. B., 1957. Modality and topographic properties of single neurons of cat's somatic sensory cortex, *J. Neurophysiol.*, 20:408–434.
- Mountcastle, V. B., 1997. The columnar organization of the neocortex, *Brain*, 120:701–722.
- Nelson, J. I., and B. J. Frost, 1985. Intracortical facilitation among co-oriented, co-axially aligned simple cells in cat striate cortex, *Exp. Brain Res.*, 61:54–61.
- Ohzawa, I., G. Sclar, and R. D. Freeman, 1985. Contrast gain control in the cat's visual system, *J. Neurophysiol.*, 54:651–667.
- Pettet, M. W., and C. D. Gilbert, 1992. Dynamic changes in receptive-field size in cat primary visual cortex, *Proc. Natl. Acad. Sci. USA*, 89:8366–8370.
- Polat, U., 1999. Functional architecture of long-range perceptual interactions, *Spat. Vis.*, 12:143–162.
- Polat, U., K. Mizobe, M. W. Pettet, T. Kasamatsu, and A. M. Norcia, 1998. Collinear stimuli regulate visual responses depending on cell's contrast threshold, *Nature*, 391:580–584.
- Powell, T. P. S., and V. B. Mountcastle, 1959. Some aspects of the functional organization of the cortex of the postcentral gyrus of the monkey: a correlation of findings obtained in a single unit analysis with cytoarchitecture, *Bull. Johns Hopkins Hosp.*, 105:133–162.
- Ramon y Cajal, S., 1911. *Histologie de système nerveux de l'homme et des vertèbres* (L. Azoulay, trans.), Paris: Maloine.
- Rockland, K. S., and J. S. Lund, 1982. Widespread periodic intrinsic connections in the tree shrew visual cortex, *Science*, 215:1532–1534.
- Rockland, K. S., and J. S. Lund, 1983. Intrinsic laminar lattice connections in primate visual cortex, *J. Comp. Neurol.*, 216:303–318.
- Rockland, K. S., J. S. Lund, and A. L. Humphrey, 1982. Anatomical banding of intrinsic connections in striate cortex of tree shrews (*Tupaia glis*), *J. Comp. Neurol.*, 209:41–58.
- Roerig, B., and J. P. Kao, 1999. Organization of intracortical circuits in relation to direction preference maps in ferret visual cortex, *J. Neurosci.*, 19:RC44.
- Sanchez-Vives, M. V., L. G. Nowak, and D. A. McCormick, 2000a. Cellular mechanisms of long-lasting adaptation in visual cortical neurons in vitro, *J. Neurosci.*, 20:4286–4299.
- Sanchez-Vives, M. V., L. G. Nowak, and D. A. McCormick, 2000b. Membrane mechanisms underlying contrast adaptation in cat area 17 in vivo, *J. Neurosci.*, 20:4267–4285.
- Sceniak, M. P., D. L. Ringach, M. J. Hawken, and R. Shapley, 1999. Contrast's effect on spatial summation by macaque V1 neurons, *Nat. Neurosci.*, 2:733–739.
- Schmidt, K. E., D. S. Kim, W. Singer, T. Bonhoeffer, and S. Lowel, 1997. Functional specificity of long-range intrinsic and inter-hemispheric connections in the visual cortex of strabismic cats, *J. Neurosci.*, 17:5480–5492.
- Schummers, J. M., J. Marino, and M. Sur, 2001. Orientation tuning of intracellular potentials and spike responses at pinwheel centers and iso-orientation domains in primary visual cortex, *Soc. Neurosci. Abstr.*, 27:619.19.
- Sengpiel, F., A. Sen, and C. Blakemore, 1997. Characteristics of surround inhibition in cat area 17, *Exp. Brain Res.*, 116:216–228.
- Sherk, H., and S. LeVay, 1983. Contribution of the cortico-claustral loop to receptive field properties in area 17 of the cat, *J. Neurosci.*, 3:2121–2127.
- Sillito, A. M., H. E. Jones, G. L. Gerstein, and D. C. West, 1994. Feature-linked synchronization of thalamic relay cell firing induced by feedback from the visual cortex, *Nature*, 369:479–482.
- Sincich, L. C., and G. G. Blasdel, 2001. Oriented axon projections in primary visual cortex of the monkey, *J. Neurosci.*, 21:4416–4426.
- Singer, W., 1999. Neuronal synchrony: a versatile code for the definition of relations?, *Neuron*, 24:49–65.
- Softky, W. R., and C. Koch, 1993. The highly irregular firing of cortical cells is inconsistent with temporal integration of random EPSPs, *J. Neurosci.*, 13:334–350.
- Somers, D. C., E. V. Todorov, A. G. Siapas, L. J. Toth, D. S. Kim, and M. Sur, 1998. A local circuit approach to understanding integration of long-range inputs in primary visual cortex, *Cereb. Cortex*, 8:204–217.
- Stemmler, M., M. Usher, and E. Niebur, 1995. Lateral interactions in primary visual cortex: a model bridging physiology and psychophysics, *Science*, 269:1877–1880.
- Stevens, C. F., and A. M. Zador, 1998. Input synchrony and the irregular firing of cortical neurons, *Nat. Neurosci.*, 1:210–217.
- Toyama, K., M. Kimura, and K. Tanaka, 1981a. Cross-correlation analysis of interneuronal connectivity in cat visual cortex, *J. Neurophysiol.*, 46:191–201.
- Toyama, K., M. Kimura, and K. Tanaka, 1981b. Organization of cat visual cortex as investigated by cross-correlation technique, *J. Neurophysiol.*, 46:202–214.
- Traub, R. D., M. A. Whittington, I. M. Stanford, and J. G. Jefferys, 1996. A mechanism for generation of long-range synchronous fast oscillations in the cortex, *Nature*, 383:621–624.

- Ts'o, D. Y., C. D. Gilbert, and T. N. Wiesel, 1986. Relationships between horizontal interactions and functional architecture in cat striate cortex as revealed by cross-correlation analysis, *J. Neurosci.*, 6:1160–1170.
- Usrey, W. M., and R. C. Reid, 1999. Synchronous activity in the visual system, *Annu. Rev. Physiol.*, 61:435–456.
- Van Vreeswijk, C., L. F. Abbott, and G. B. Ermentrout, 1994. When inhibition, not excitation, synchronizes neural firing, *J. Comput. Neurosci.*, 1:313–321.
- Walker, G. A., I. Ohzawa, and R. D. Freeman, 1999. Asymmetric suppression outside the classical receptive field of the visual cortex, *J. Neurosci.*, 19:10536–10553.
- Weliky, M., K. Kandler, D. Fitzpatrick, and L. C. Katz, 1995. Patterns of excitation and inhibition evoked by horizontal connections in visual cortex share a common relationship to orientation columns, *Neuron*, 15:541–552.
- Wilson, M., and J. M. Bower, 1991. A computer simulation of oscillatory behavior in primary visual cortex, *Neural Comput.*, 3:498–509.
- Yabuta, N. H., and E. M. Callaway, 1998. Cytochrome-oxidase blobs and intrinsic horizontal connections of layer 2/3 pyramidal neurons in primate V1, *Vis. Neurosci.*, 15:1007–1027.
- Yoshimura, Y., H. Sato, K. Imamura, and Y. Watanabe, 2000. Properties of horizontal and vertical inputs to pyramidal cells in the superficial layers of the cat visual cortex, *J. Neurosci.*, 20:1931–1940.

47 Nonlinear Properties of Visual Cortex Neurons: Temporal Dynamics, Stimulus Selectivity, Neural Performance

DUANE G. ALBRECHT, WILSON S. GEISLER, AND ALISON M. CRANE

Introduction

ANALYSIS OF VISUAL CORTX NEURONS The primary visual cortex plays a very important role in vision and visual perception. To begin with, consider the fact that without area V1, all of the many visual cortical areas (which constitute approximately half of the cerebral cortex in the macaque monkey) are deprived of the visual information relayed through the thalamus from the retina. It has been known for more than a century that damage to this area produces almost total blindness. However, area V1 is not merely a relay station between the thalamus and the other cortical regions. On the contrary, V1 clearly transforms the lateral geniculate nucleus input: in comparison to the relatively simple center-surround receptive fields of geniculate cells, the receptive fields of V1 neurons are considerably more complex and, as will be emphasized in this chapter, the cells are considerably more selective for specific visual features. Finally, consider the anatomical size of the region and the complexity of the neural tissue. In the macaque monkey, V1 constitutes approximately 10% of the entire cerebral cortex, and in comparison to all of the other cortical areas, the primary visual cortex has about twice as many neurons per unit volume, with perhaps half a billion neurons per hemisphere. Given all of these facts, analysis of both the structures and the functions of the primary visual cortex stands as an important challenge to visual neuroscientists in their quest to understand vision and visual perception.

Beginning with the work of Hubel and Wiesel (1962), measurements of the responses of V1 neurons (in the form of action potentials) have provided a wealth of information concerning both the potential biophysical and biochemical mechanisms as well as the ultimate visual information processing functions of these neurons. Nonetheless, in spite of this wealth of scientific information that has accumulated over the decades, in many respects we have taken only a very small step toward a complete understanding of how the visual cortex contributes to visual perception.

In an attempt to analyze the structures and the functions of visual cortex neurons, many researchers have used the well-developed conceptual and mathematical techniques of what can be termed a *systems analysis*. This quantitative approach was introduced to visual neuroscience in principle by Hartline, who was studying the *Limulus* visual system (e.g., Ratliff et al., 1974); it has since been used to study the retina, lateral geniculate nucleus, and visual cortex of the primate and related species (e.g., De Valois et al., 1982; Enroth-Cugell and Robson, 1966; Movshon et al., 1978; Ohzawa et al., 1985; Shapley and Victor, 1979; for reviews see Carandini et al., 1999; De Valois and De Valois, 1988; Ferster and Miller, 2000; Geisler and Albrecht, 2000; Palmer et al., 1991; Robson, 1975; Shapley and Lennie, 1985).

Over the past several decades, much research has been devoted to describing both the linear and the nonlinear properties of V1 neurons using a systems analysis. Within this framework, one begins by assessing what aspects of the behavior can be accounted for by simple linear equations and what aspects require nonlinear equations. In this chapter, we describe linear and nonlinear response properties that have been measured within V1 neurons. We then discuss these measurements (and others) within the context of functional transformations of the visual information that ultimately produce high degrees of reliable stimulus selectivity. Finally, we consider several models, at different levels of analysis, of the neural operations that can potentially account for the linear and nonlinear behaviors that have been measured.

STIMULUS SELECTIVITY: FEATURES, FILTERS, AND FUNCTIONS Research over the past several decades indicates that stimulus selectivity plays a fundamental role in the analysis of visual information within the visual systems of humans, primates, and related species. Within the visual cortex, each neuron is quite selective for a specific *visual feature*. Currently, there is no agreed-upon intuitive name that adequately captures the presumed function associated with this selectivity

(e.g., *edge detector*, *line detector*, *spatial frequency detector*, and so forth). Nonetheless, it is possible to summarize and quantify the selectivity by measuring the responses as a function of many different stimulus dimensions that describe visual stimuli: for example, spatial position, spatial orientation, spatial frequency, temporal frequency, direction of motion, contrast, color, and so forth. These stimulus dimensions are relatively easy to manipulate within the laboratory to measure stimulus selectivity in a systematic, quantitative, and replicable fashion. Further, it is possible to develop descriptive mathematical equations that can adequately describe and summarize the measured responses along these various dimensions. Finally, these descriptive equations can be combined with other equations and analyses to assess the performance characteristics of visual cortex neurons within this multidimensional space and to investigate the ultimate functional consequences of the measured stimulus selectivity.

Rather than attempting to characterize the function of visual cortex neurons using simple intuitive visual feature detection (e.g., edge detection), it is possible to conceptualize the function of each neuron, in a somewhat more neutral fashion by thinking of the function as a filtering operation. A neuron in the primary visual cortex only responds to a specific range of values within a complex (and not necessarily intuitive) multidimensional feature space. In so doing, the neuron filters out the overwhelming majority of unique subsets within the total set and only passes (or signals) the presence of a very small and unique subset. It seems reasonable to assume that whatever this particular type of stimulus selectivity might be, it will probably be closely related to the statistics of natural images (Barlow, 1961).

The observation that cortical neurons are selective for a specific subset of possible visual stimuli has important implications for the overall performance capabilities of cortical neurons: because of this stimulus selectivity, the response of each neuron contains specific information about the presence or absence of a particular feature within the visual stimulus that could be used by a subsequent brain mechanism to detect, discriminate, and identify that specific visual feature. For example, the response magnitude could be used to identify, with a high level of confidence, a specific oriented spatial contour, demarcated by a specific color contrast, moving across a particular location in space, at a particular rate, in a particular direction, and so forth.

This high degree of stimulus selectivity at the level of the visual cortex has led to several different hypotheses regarding the ultimate functional significance of the selectivity. One hypothesis is that the selectivity reflects a sparse code that is well matched to the statistics of natural images (Field, 1987; Olshausen and Field, 1987). A second hypothesis is that the selectivity for local image feature/attributes is a critical step toward the goal of object segregation (Geisler and

Albrecht, 2000). A third hypothesis is that the selectivity reflects the sequential hierarchical progression toward neurons within higher cortical regions that are selective for real-world objects (Barlow, 1995). As noted some time ago, sequential filtering is functionally equivalent to pattern recognition (Craik, 1966).

Regardless of whether one, or all, of these hypotheses proves to be accurate, it seems clear that the stimulus selectivity of cortical neurons plays an important role in visual information processing. With this observation in mind, the major focus of this chapter will be those linear and nonlinear properties (and mechanisms) that could potentially have a beneficial influence, or a deleterious influence on stimulus selectivity.

SPATIOTEMPORAL FILTERS AND SYSTEMS ANALYSIS In an attempt to characterize both the structures and the functions of visual cortex neurons, from the subcellular level to the behavioral level, many neuroscientists have used the well-developed techniques of systems analysis. The basic principles of this analytical approach have been fully described for the physical sciences as well as the life sciences (e.g., Marmarelis and Marmarelis, 1978; Schwarz and Friedland, 1965) and need not be formally described in this chapter. Stated simply, one attempts to identify and characterize the linear as well as the nonlinear properties of a complex system with the goal of developing a quantitative model that can potentially describe the behavior of the system under a wide range of diverse circumstances. Within this framework, visual cortex neurons can be conceptualized as spatiotemporal filters that respond selectively along several different stimulus dimensions.

There are different methodologies that can be used to investigate a physical system of interest: for example, one can use a frequency domain analysis, a space and/or time domain analysis, a white noise domain analysis, and so forth (see Marmarelis and Marmarelis, 1978). All of these methods have been applied to visual cortex neurons. As noted above, this quantitative systems approach was initially introduced to visual neuroscience by Hartline (and colleagues), but over the past three decades many different laboratories have adopted this approach, and as a consequence we have a rich understanding of both the linear and nonlinear properties of visual cortex neurons (for recent reviews of this literature, see Carandini et al., 1999; Ferster and Miller, 2000; Geisler and Albrecht, 2000).

To simplify this chapter, the frequency domain analysis will be the major focus, although other analyses will be discussed when appropriate. In a frequency domain analysis of visual cortex neurons, the visual stimulus is a spatiotemporal sine wave grating pattern, which can be systematically varied along many different stimulus dimensions. These measurements, and the equations that can be used to

describe the responses along the various stimulus dimensions, have provided a quantitative description of the stimulus-response characteristics of visual cortex neurons across a wide and diverse set of circumstances.

LINEAR SYSTEMS ANALYSIS CAN REVEAL BOTH LINEAR AND NONLINEAR PROPERTIES Over the past half century, linear systems analysis has played a major role in the quantitative analysis of the visual system. As will be described in this chapter, there is overwhelming evidence that visual cortex neurons exhibit a variety of nonlinear properties. Although specific mathematical methods have been developed to study nonlinear systems (e.g., Victor and Knight, 1979; Victor et al., 1977; see also Marmarelis and Marmarelis, 1978), we have learned a great deal about the nonlinear properties of visual cortex neurons by applying linear systems techniques and analyzing the deviations from what would be expected from a linear system.

In a linear system, the response to the sum of several inputs is equal to the sum of the responses to each input individually, and as the amplitude of the stimulus increases the response increases proportionately. There are many standard techniques for characterizing a linear system that could be applied (see Schwarz and Friedland, 1965), and have been applied, to characterize visual cortex neurons. For example, one could measure either the spatiotemporal receptive field or the spatiotemporal transfer function (e.g., DeAngelis et al., 1993; Palmer et al., 1991). If a system is linear, then all of the different techniques give equivalent results and the measurements made with any one of the techniques can be used to predict the responses of the system to arbitrary inputs. However, when a system is nonlinear, two different techniques may give different results; in this case, it becomes essential to use several different techniques and then compare what is similar and what is not. For example, in the case of visual cortex neurons (as will be described below), the spatiotemporal receptive field and the spatiotemporal transfer function are not exactly equivalent. Finally, note that oftentimes, a specific nonlinear mechanism can only be revealed, isolated, and studied using a specific technique. In the case of visual cortex neurons, different nonlinear properties have been discovered and characterized by using different linear systems techniques.

TEMPORAL DYNAMICS, STIMULUS SELECTIVITY, NEURAL PERFORMANCE During natural viewing, eye movements create a rapid progression of diverse images, and because of this, the spatiotemporal contrast can change rapidly over the course of a few hundred milliseconds (for a comprehensive review see Carpenter, 1991). The average duration of a single fixation (during normal saccadic inspection of a visual scene) is approximately 200 msec. This is an important observation to keep in mind when considering the potential

effects of a specific linear or nonlinear mechanism on stimulus selectivity and neural performance. If the temporal dynamics of the mechanism are relatively fast, then the mechanism might be able to influence selectivity and performance during a single fixation, based on the spatiotemporal contrast contained within that single fixation. On the other hand, if the temporal dynamics are relatively slow, then the mechanism will not be able to influence stimulus selectivity during a single fixation, based on the spatiotemporal contrast within that fixation.

Over the past several decades, many different laboratories have measured the responses of V1 neurons using drifting spatial frequency gratings, across a wide array of stimulus dimensions, using stimulus durations that are relatively long, to approximate a steady-state condition. These measurements, along with other measurements, have revealed some of the fundamental linear and nonlinear properties of V1 neurons (e.g., De Valois et al., 1982; Movshon et al., 1978; for recent reviews see Carandini et al., 1999; Ferster and Miller, 2000; Geisler and Albrecht, 2000).

The drifting steady-state measurements can be supplemented by measurements of the responses to transient stationary stimuli, where the stimulus durations approximate the fixation durations during natural viewing. Consider using a stationary grating that is presented for a brief interval (200 msec) to measure the responses as a function of some stimulus dimension of interest (e.g., contrast). The measured poststimulus time histograms offer a unique opportunity to examine the temporal dynamics of specific linear and nonlinear properties on a fine time scale. With such a set of measurements, one can ask a wide range of different experimental questions and compare the results of the experiments to what we have learned from the steady-state experiments. Consider the following, somewhat overlapping, subset of possible questions:

- In general, are the basic response properties that have been measured using drifting steady-state stimuli similar under transient stationary conditions?
- What is the temporal onset of the stimulus selectivity along each of the fundamental stimulus dimensions?
- Do the selectivities change over the course of the brief interval?
- How long does it take for the nonlinear properties (e.g., contrast-set gain control) to build up through time?
- How do the temporal dynamics compare to the average fixation duration during natural viewing?
- Does the well-established relationship between the mean and the variance of the responses of cortical neurons hold under these transient stationary conditions?
- Does the discrimination performance change?

Recently, several different laboratories have measured the responses to brief stimuli and analyzed the time course of

some of the fundamental properties (e.g., Albrecht et al., 2002; Frazor et al., 1997; Gillespie et al., 2001; Muller et al., 2001; Ringach et al., 1997). Within this chapter, we will consider measurements using drifting steady-state stimuli and measurements using stationary transient stimuli. The results of both types of measurements will be discussed within the context of the effects of the various nonlinearities on stimulus selectivity within a time frame that is comparable to natural viewing.

Linear and nonlinear properties

SOME LINEAR PROPERTIES OF SIMPLE CELLS Hubel and Wiesel (1962) described two basic types of neurons in the visual cortex: *simple cells* and *complex cells*. Since then, some investigators have elaborated the original binary classification with subsidiary and supplementary subclassifications (e.g., Henry, 1977) and others have argued that simple and complex cells reflect opposite ends of a virtual continuum (Chance et al., 1998; Geisler and Albrecht, 2000; Mechler and Ringach, 2002). However, the basic distinction between simple and complex cells remains an important part of the published literature. Stated simply, simple cells have a variety of linear properties that are not generally seen in most complex cells. Specifically, in their original report, Hubel and Wiesel (1962) described four basic linear properties of simple cells:

- Distinct excitatory and inhibitory subregions within the receptive field
- Spatial summation within a given subregion
- Mutual antagonism between subregions
- Responses to novel stimuli can be predicted (qualitatively) on the basis of the arrangement of the subregions

These four properties are what one would expect from a linear spatiotemporal filter. Complex cells, on the other hand, failed to display these properties and were therefore defined by exclusion. For example, a typical complex cell will produce excitatory responses to both white and black stimuli in the same spatial location. This is clearly not what one would expect from a linear spatiotemporal filter. Nonetheless, it is important to emphasize that notwithstanding the various linear and nonlinear properties of simple and complex cells, both types of neurons are highly selective for specific stimulus attributes (e.g., orientation).

Many different laboratories have measured a variety of properties of simple cells using many different types of stimulus protocols. On the basis of this research, it is possible to list a set of linear properties that have been reported in simple cells. Note that in each case, the implied comparison is between (1) the measured neural response behavior of simple cells and (2) the known theoretical behavior of a linear spatiotemporal filter. Finally, bear in mind that the

comparison between the measured behavior of the neurons and the known behavior of a linear filter is always approximate, and never exact.

The receptive field and the optimal stimulus. The receptive field can be mapped using flashing white and black spots (or bars/lines). This map (which is analogous to the impulse response of a linear spatial filter) provides one characterization of the stimulus selectivity for the dimension of space. Thus, for example, one can qualitatively predict the optimal spatial position (say, 2 degrees above the optic axis), spatial orientation (say, horizontal), and spatial configuration of the contrast (say, one narrow white line flanked by two narrow black lines). This observation suggests that the spatial variations in luminance contrast are summed in a linear fashion.

Responses to drifting gratings. When a linear spatiotemporal filter is stimulated with a drifting sine wave, the response is a sinusoidal modulation in synchrony with the temporal frequency of the stimulus. Similarly, when a simple cell is stimulated with a drifting sine wave, the response of the cell modulates in synchrony with the temporal frequency of the input. However, the shape of the temporal response (i.e., the poststimulus time histogram) is not sinusoidal. Specifically, all of the negative values of the sine wave are absent. This observation is not particularly surprising given that simple cells generally have little or no maintained activity (and, of course, there are no *negative action potentials*). In sum, the responses of simple cells to drifting sine waves are similar to what one would expect from a linear filter followed by half-wave rectification.

Responses as a function of spatial phase. Using a stationary spatial frequency sine wave grating whose contrast is modulated in time (i.e., a counterphase flickering grating), it is possible to measure the responses as a function of spatial phase. If this measurement is performed on a linear spatiotemporal filter, the response is a sinusoidal function of spatial phase. Similarly, if this measurement is performed on a simple cell, the response (i.e., the poststimulus time histogram) is approximately a sinusoidal function of spatial phase. There is a specific relationship between the direction selectivity of a linear filter and the responses as a function of spatial phase. The responses of simple cells follow these linear expectations to a first approximation (Albrecht and Geisler, 1991; Reid et al., 1991; Tolhurst and Dean, 1991).

Spatiotemporal transfer function. There are several strong constraints that are implied by the linear model for the spatiotemporal receptive field (e.g., amplitude symmetry and phase additivity), and many of these constraints hold, to a

first approximation, for simple cells. Because these constraints hold, it is possible to describe the spatiotemporal phase transfer function using a simple four-parameter linear equation (Albrecht, 1995; Dawis et al., 1984; Hamilton et al., 1989).

Null phase position. Enroth-Cugell and Robson (1966) introduced a clever method to test for linear spatial summation in retinal ganglion cells whose center-surround receptive fields are approximately circularly symmetric. The logic of this test is simple. A white-black edge is positioned on the center of the receptive field and then flashed on and off. If the cell sums its inputs in a linear fashion, then the response of the cell should be unaffected by the flashing edge because the increased luminance over half of the receptive field is canceled by an equivalent decrease in the luminance over the other half. The method is clever for the following reason: No response is evoked, and hence the linearity of spatial summation can be tested even if there are response nonlinearities. This method for testing the linearity of spatial summation has been applied to simple cells, and the linear prediction holds to a first approximation (e.g., De Valois et al., 1982; Movshon et al., 1978).

Receptive field and spatial frequency tuning. It is possible to characterize the properties of a complex unknown system by measuring either the *impulse response* or the *frequency response*. If the system is linear, either set of measurements would provide a complete description of the system, and further, one would be able to predict the impulse response from the frequency response (and vice versa). Measurements of the spatial receptive field and the spatial frequency tuning are analogous to the impulse response and frequency response. Movshon et al. (1978) have demonstrated that it is possible to predict the shape of the spatial receptive field profile on the basis of the measured spatial frequency response function to a first approximation.

Spatiotemporal receptive field and motion. If the receptive field is measured as a function of both space and time using stationary flashed bars or spots, and if the cell behaves in a linear fashion, it is possible to use the resulting spatiotemporal receptive field to determine (1) whether the cell is direction selective, (2) the optimal direction of motion, and (3) the degree of direction selectivity.

It has been demonstrated that these linear expectations hold for simple cells to a first approximation (DeAngelis et al., 1993; McLean and Palmer, 1989).

SOME NONLINEAR PROPERTIES OF BOTH SIMPLE AND COMPLEX CELLS

Response refractory period. As the firing rate of a given neuron increases, the absolute and relative refractory periods will

produce response saturation that is solely determined by the magnitude of the firing rate, regardless of what particular stimulus produced the high rate of firing. The temporal dynamics for this nonlinearity are on the order of a few milliseconds or less. It is worth noting that from the perspective of neural performance there are potential costs and benefits associated with this nonlinearity. In particular, response saturation that is caused by the absolute or relative refractory period is deleterious on stimulus selectivity because it makes the neuron less selective at high firing rates. Interestingly, however, the regularization in the spike trains that occurs during this type of saturation has beneficial consequences for detection, discrimination, and identification performance because, for most cells, the regularization decreases the variance in the firing pattern relative to the mean (Geisler et al., 1991). One might speculate that these two factors could potentially offset each other to some extent.

Response rectification. Hubel and Wiesel (1962) were the first to observe the effects of rectification: they reported that many complex cells responded in an excitatory fashion to both white and black lines (or bars) in the same spatial location throughout all positions of the receptive field. Similarly, as illustrated in Figure 47.1A, when stimulated with a counterphase flickering sine wave grating pattern, excitatory responses are observed regardless of whether the luminance is increasing or decreasing over a particular spatial region (e.g., De Valois et al., 1982; Movshon et al., 1978). This type

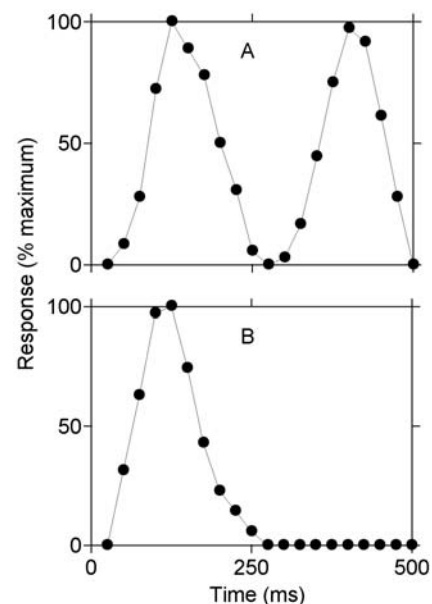


FIGURE 47.1. Responses (poststimulus time histograms) of two monkey cells to a counterphase flickering sine wave grating pattern, to illustrate response rectification in complex cells (A) and simple cells (B). (Adapted from De Valois et al., 1982.)

of behavior can be described as full-wave rectification. When a sine wave is passed through a linear filter followed by full-wave rectification, the output is the absolute value of the input.

In comparison, as illustrated in Figure 47.1B, when simple cells are stimulated with a drifting or flickering sine wave grating, only half of the modulation appears in the response waveform (e.g., Albrecht and De Valois, 1981; Movshon et al., 1978). This type of nonlinear behavior can be described as half-wave rectification: when a linear filter, followed by half-wave rectification, is stimulated with a sine wave, the output does not contain any of the values of the sine wave that are below zero. As will be described below, rectification, in both simple and complex cells, appears to be fully operational within 200 msec, and thus it can exert its influence within the time frame of a single fixation.

Half-wave rectification could, in part, be a simple consequence of the fact that cortical cells tend to have little or no maintained spontaneous discharge; the net result can be thought of as a threshold nonlinearity. Although half-wave rectification forces a doubling of the number of elements that are required to transmit both the positive and the negative values, it does have beneficial consequences. First, it conserves metabolic energy within the cortex by reducing the number of action potentials produced, the amount of neurotransmitter substance released, and so forth. Second, it increases the stimulus-specific identification performance of a neuron: given that the cell produces no action potentials unless a very specific stimulus is present at a very specific location within the visual field, just a few action potentials can strongly constrain the most likely set of potential visual features at that location (Barlow et al., 1987; Geisler and Albrecht, 1995, 1997). Third, full-wave rectification can be useful for computing *motion energy* (Adelson and Bergen, 1985; Watson and Ahumada, 1985) and *texture energy* in the stimulus (Bergen, 1991).

Response expansion. Measurements of the responses as a function of luminance contrast using drifting gratings have shown that, in general, as the contrast increases from zero, the response increases in an accelerating fashion (e.g., Albrecht and Hamilton, 1982; Sclar et al., 1990). Figure 47.2 shows measurements of the contrast response function from a representative cell to illustrate the response expansion that can be seen at the lower values of contrast. The smooth curve shows the fit of a Naka-Rushton equation:

$$r_i(c) = \frac{c^n}{c^n + c_{50}^n}$$

where n is the response exponent, c_{50} is the half-saturation contrast, and c is luminance contrast. Many studies have shown that this function provides a good fit to the contrast response function of striate cortex neurons (e.g., Albrecht

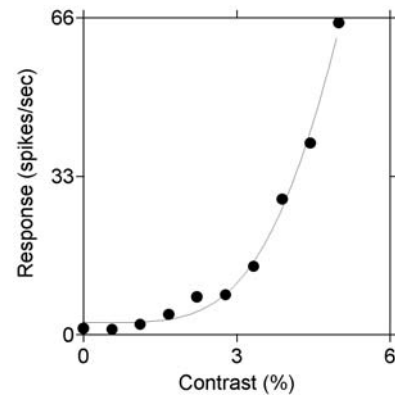


FIGURE 47.2. Responses (mean firing rate) as a function of contrast for a representative neuron to illustrate the response expansion that can be seen in the contrast response function at lower contrasts, prior to the compression and saturation that are induced by the contrast-set gain control. (D. G. Albrecht and W. S. Geisler, unpublished observations.)

and Hamilton, 1982; Albrecht et al., 1984; DeAngelis et al., 1993; Geisler and Albrecht, 1997; McLean and Palmer, 1996; Sclar et al., 1990; Tolhurst and Heeger, 1997). The exponent of this equation can be used to quantify the response expansion. The average value in the primary visual cortex is approximately 2.5.

Note that in measurements of the contrast response function, the acceleration is most easy to visualize at the lower values of contrast (prior to any compression and saturation). However, it would be incorrect to conclude that the effects of the accelerating nonlinearity are expressed only at low contrasts. Indeed, there are many other types of experimental observations, which demonstrate that the response acceleration operates across the full range of contrast and response, even after the response is fully saturated. For example, as noted above, the responses of simple cells as a function of spatial phase are approximately sinusoidal, but not exactly. Specifically, the responses as a function of spatial position appear more narrow and peaked than a sine wave across the full range of contrasts, even contrasts that evoke fully saturated responses. A linear filter that is followed by an accelerating nonlinearity produces exactly this sort of behavior. Interestingly, if the value of the expansive exponent, determined from the measured contrast response function for a given cell, is taken into consideration (i.e., by applying the acceleration to a sinusoidal function), the predicted responses provide a reasonably good fit to the measured responses of that cell.

There are other observations that cannot be predicted by a linear filter alone, but can be accounted for reasonably well if a linear filter is followed by an accelerating nonlinearity. Several of these observations are listed below. In each case, the accelerating nonlinearity diminishes the discrepancy between the linear prediction and the measured properties.

- The measured spatial frequency selectivity is narrower than expected, based on the measured receptive field (e.g., De Valois et al., 1985; Tadmor and Tolhurst, 1989).
- The measured direction selectivity is greater than expected, based on the responses as a function of spatial phase (Albrecht and Geisler, 1991; Murthy et al., 1998; Reid et al., 1991; Tolhurst and Dean, 1991).
- The measured direction selectivity is greater than expected, based on the spatiotemporal receptive field (DeAngelis et al., 1993; McLean and Palmer, 1994).
- The measured orientation selectivity is greater than expected, based on the measured receptive field (Gardner et al., 1999).
- Vernier acuity is greater than expected, based on measurements of length summation (Swindale and Cynader, 1989).
- Direction selectivity is greater when action potentials are measured and compared to intracellular synaptic potentials (Jagadeesh et al., 1997).

Response saturation. Measurements of the contrast response function have shown that cortical neurons generally have a limited dynamic response range followed by response saturation. Figure 47.3 plots the responses as a function of contrast to illustrate response saturation. Measurements illustrated below (Figs. 47.7 to 47.10) have demonstrated that the saturation can occur well within the time frame of a single fixation. In a later section (“Contrast Response Nonlinearities”) we will consider the potential effects of saturation on stimulus selectivity.

Contrast-set gain control. As shown in Figure 47.3, the responses of cortical cells saturate as the contrast increases, oftentimes at very low contrasts. This saturation could be determined by either (1) the magnitude of the response or (2) the magnitude of the contrast. Measurements performed over the past several decades have shown that this saturation is only one manifestation of a scaling of the response based on the magnitude of the contrast: a contrast-set gain control. Recent measurements (e.g., the section “Contrast Response Nonlinearities”) have shown that this nonlinearity is operational well within the time frame of a single fixation. Interestingly, this contrast-set gain control affords the maintenance of stimulus selectivity and high differential sensitivity along many dimensions; however, this beneficial consequence comes at the expense of differential sensitivity along the dimension of contrast.

Consider the effect of response-set saturation determined by the absolute and relative refractory periods: in this case, the saturation would diminish stimulus selectivity because at contrasts that produce response saturation, optimal and nonoptimal stimuli could produce equivalent responses. However, measurements of the contrast response function

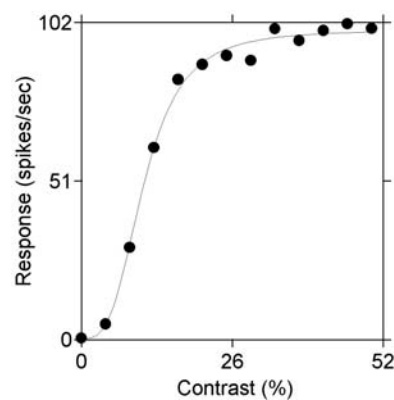


FIGURE 47.3. Responses (mean firing rate) as a function of contrast for a representative neuron recorded from the monkey cortex to illustrate response saturation. (D. G. Albrecht and W. S. Geisler, unpublished observations.)

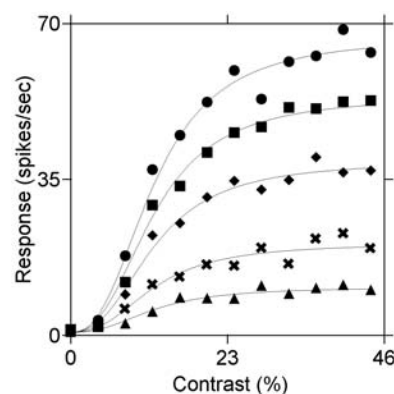


FIGURE 47.4. Contrast response functions measured at five different spatial frequencies to illustrate contrast-set gain control. The smooth curves through the measured responses show the fit of a single, scaled Naka-Rushton equation (with the same half-saturation contrast and the same expansive exponent). The fact that the shape of the contrast response function remains invariant with spatial frequency indicates that the scaling (including the saturation) is determined by the magnitude of the contrast and not the magnitude of the response. (D. G. Albrecht and W. S. Geisler, unpublished observations.)

using optimal and nonoptimal stimuli have shown that the saturation is not determined by the magnitude of the response (e.g., Fig 47.4); instead, the saturation is determined by the magnitude of the contrast (Albrecht and Hamilton, 1982; Sclar and Freeman, 1982; for a review see Carandini et al., 1999; Geisler and Albrecht, 2000). Further, the saturation is just one manifestation of an overall scaling of the entire contrast response function by the magnitude of the contrast.

Latency shift. As contrast increases and the response magnitude increases, there is a decrease in the latency of the response. This latency shift could be determined by either

(1) the magnitude of the response or (2) the magnitude of the contrast. Measurements have demonstrated that the shift is determined by the contrast, and not the response (Albrecht, 1995; Carandini and Heeger, 1994; Carandini et al., 1997; Dean and Tolhurst, 1986; Gawne et al., 1996; Reich et al., 2001). Figure 47.5 shows the shift for a representative cell at an optimal and a nonoptimal spatial frequency. The magnitude of the response to the optimal stimulus was approximately three times the magnitude of the response to the nonoptimal stimulus. Therefore, if the latency was determined by the magnitude of the response, then the latency shift should be greater for the optimal stimulus. However, as can be seen, the shift appears to be equivalent for both the optimal and the nonoptimal stimulus.

Contrast adaptation. When a V1 neuron is presented with a high-contrast grating for an extended period of time (e.g., 30 seconds), the response magnitude decreases, as illustrated in Figure 47.6 (Albrecht et al., 1984; McLean and Palmer, 1996; Movshon and Lennie, 1979; Saul and Cynader, 1989). The temporal dynamics of this nonlinearity are too slow to have an influence on stimulus selectivity within a single fix-

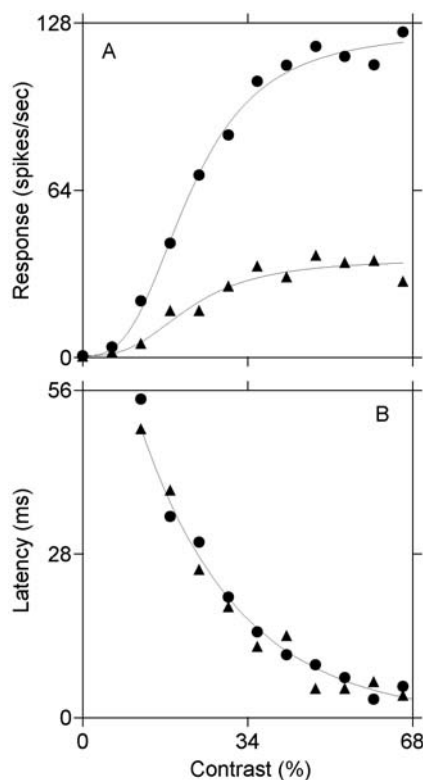


FIGURE 47.5. Response amplitude (*A*) and response latency (*B*) plotted as a function of contrast, to illustrate that the latency shift is determined by the magnitude of the contrast and not the magnitude of the response. (D. G. Albrecht and W. S. Geisler, unpublished observations.)

ation, based on the level of stimulus contrast within that single fixation. To the extent that there is some degree of contrast adaptation during a single fixation, this adaptation has been induced over the course of many fixations.

Other types of nonlinear behaviors

- Nonlinear spatial summation (Movshon et al., 1978)
- Spatial frequency inhibition (De Valois and Tootell, 1983)
- Surround effects, outside the classic receptive field (Cavanaugh et al., 2002a, 2002b; De Valois et al., 1985)
- Non-Fourier envelope responses (Zhou and Baker, 1994)
- Supersaturation (Bonds, 1991; Li and Creutzfeldt, 1984)
- Cross-orientation inhibition (Bonds, 1989)
- Nonspecific suppression (e.g., Carandini et al., 1997; DeAngelis et al., 1992; Nelson, 1991).

Temporal dynamics

It is worthwhile to consider the temporal dynamics of the various nonlinear properties, described above, within the context of the potential effects upon stimulus selectivity and neural performance during natural viewing. For example, if the onset of a specific nonlinear mechanism is slow relative to the duration of a single fixation, then it will not affect the selectivity and neural performance within a single fixation based on the spatiotemporal contrast within that fixation.

RAPID AND SLOW NONLINEARITIES It is clear that some of the nonlinearities operate rapidly enough to exert their influence on stimulus selectivity and performance based on the response to a stimulus during a single fixation. It is equally

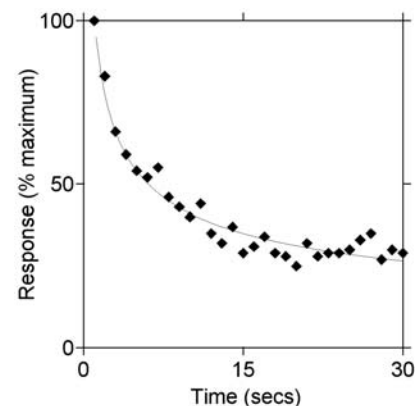


FIGURE 47.6. Responses (mean firing rate) of a cortical cell to a high-contrast spatial frequency grating drifting over the course of 30 sec, to illustrate contrast adaptation. (Adapted from Albrecht et al., 1984.)

clear that other nonlinearities could not have a significant influence on the selectivity and performance, based on the stimulus within a single fixation, because the onset occurs over the course of many seconds. Consider the temporal dynamics of the absolute refractory period, half-wave rectification, the latency shift, and contrast adaptation.

- *Response refractory period:* Any refractory effects on selectivity and performance would surely be fully expressed within the time frame of a single fixation, given that they would operate on the order of a few milliseconds.

- *Response rectification:* To the extent that rectification is based on the transduction from the voltage within the neuron to the production of action potentials, any rectification effects would also be fully expressed within a single fixation.

- *Latency shift:* The average value of the contrast-induced latency shift is approximately 45 msec (Albrecht, 1995; Carandini and Heeger, 1994; Carandini et al., 1997; Dean and Tolhurst, 1986). Therefore, the effects of the latency shift can be expressed within the time frame of a single fixation, and the shift will be based on the contrast within that fixation.

- *Contrast adaptation:* It takes approximately 15 seconds for contrast adaptation to achieve two-thirds of its full strength (e.g., Albrecht et al., 1984). Therefore, the effects of contrast adaptation cannot be expressed within the time frame of a single fixation.

CONTRAST RESPONSE NONLINEARITIES Most of the nonlinear properties described above can be seen in the steady-state measurements of the contrast response function. However, the steady-state measurements are not well suited for analysis of the temporal dynamics that occur on the time frame of a single fixation. As described in the preceding section “Temporal Dynamics, Stimulus Selectivity, Neural Performance,” the responses to transient stationary gratings are useful for examining the temporal dynamics of linear and nonlinear properties. Recently, several different laboratories have been measuring the responses to brief stimuli and analyzing the time course of some of the fundamental properties (e.g., Albrecht et al., 2002; Frazor et al., 1997; Gillespie et al., 2001; Muller et al., 2001; Ringach et al., 1997).

In this section we show the responses as a function of contrast when the stimulus is a stationary grating, presented for a brief interval (200 msec), in order to illustrate how the contrast response function develops over the course of the first 200 msec after stimulus onset. Further, we consider some of the general questions posed in the Introduction, within the context of this specific set of transient stationary measurements. For example, one can ask: How long does it take for the two nonlinearities, response expansion and contrast-set gain control, to build up? If the expansion and

gain control take more than a few hundred milliseconds, they will have little or no influence on the responses during a single fixation, based on the level of contrast within that fixation. Therefore, these two nonlinearities will have little or no influence on stimulus selectivity during a single fixation.

Poststimulus time histogram as a function of contrast. Figure 47.7 shows the responses of a neuron recorded from within the monkey visual cortex to stationary gratings that were presented for a 200 msec interval at 10 different levels of contrast. Each set of data points plots the responses as a function of time, every 4 msec (i.e., the poststimulus time histogram), for 10 different levels of contrast (from 0% to 90% in linear increments). The smooth curves through the data points plot the average poststimulus time histogram that has been scaled for the amplitude of the response at a given level of contrast and shifted for the latency of the response at a given level of contrast. For ease of viewing the rapid variations across time and contrast, only 100 msec of the responses are plotted and the contrast-induced latency shift has been removed, such that the responses at each level of contrast are optimally aligned (i.e., they begin at the same time, peak at the same time, and so forth). There are several trends that are easy to see when the responses are plotted in this fashion:

- The magnitude of the response increases rapidly from the base rate to the maximum firing rate in approximately 20 msec and then declines to approximately one-third of the maximum firing rate within approximately 30 msec after the peak.
- The overall shape of the poststimulus time histogram appears to be relatively similar across the different levels of contrast.
- Simply scaling and shifting the average temporal response profile accounts for much of the variation in the data (over 95% on average across a population of cells).

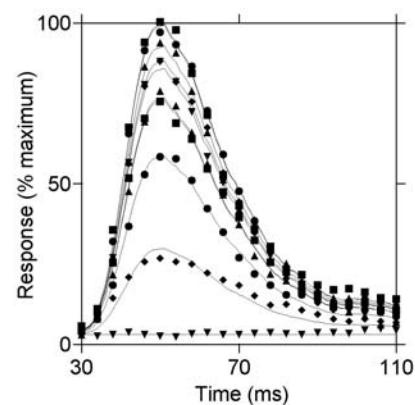


FIGURE 47.7. Responses (poststimulus time histograms) of a neuron recorded from the monkey visual cortex as a function of time and contrast. (Adapted from Albrecht et al., 2002.)

- Although the stimulus remains on for 200msec, the response is considerably more transient.

It is important to note that there is a great deal of heterogeneity from cell to cell (Albrecht et al., 2002).

Responses as a function of contrast through time. Figure 47.8 plots the responses as a function of contrast for six different times during the course of the responses shown in Figure 47.7: 58 (◆), 62 (■), 70 (▲), 78 (●), 86 (▼), and 102msec (✕). The smooth curves through each set of data points plot the parameter-optimized fits of a single, scaled Naka-Rushton equation, with the same half-saturation contrast (29.6%) and the same expansive response exponent (3.1); the equation was simply scaled in amplitude for the different time intervals. There are several trends that are easy to see when the responses are plotted in this fashion:

- A single, scaled Naka-Rushton equation accounts for a large percentage of the variation in the data (over 95% across a population of cells).

- The expansive response exponent and the contrast-set gain control appear to be present in every time interval, even the first interval, which occurs only 8msec after the onset of the response.

- The saturation does not appear to be determined by the magnitude of the response given that the saturation occurs at the same contrast, independent of the magnitude of the response.

Responses during the first 16msec. Figure 47.9 plots the responses as a function of contrast during the first 16msec after the onset of the response to a transient stationary grating. Each set of data points plots the responses in sequential 2msec time bins after the onset of the response. The sequential order of the symbols is as follows: (■), (▲), (◆), and (●), with dashed lines, and (■), (▲), (◆), and (●),

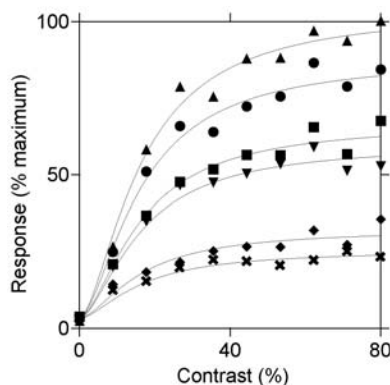


FIGURE 47.8. Responses (from the poststimulus time histograms shown in Figure 47.7) as a function of contrast during the first 50msec after the onset of the response to a stationary grating. (Adapted from Albrecht et al., 2002.)

with solid lines. The curves through each set of points show the parameter-optimized fit of a single, scaled Naka-Rushton equation, with the same expansive response exponent (3.1) and half-saturation contrast (31.0). There are several trends that are easy to see in this plot:

- The responses are quite systematic and appear to be qualitatively similar across the different time intervals.

- A single, scaled Naka-Rushton equation accounts for a large percentage of the variation in the responses across contrast and through time (over 95%); this demonstrates quantitatively that the shape of the contrast response function is relatively invariant through time.

- The two important nonlinearities (expansive response exponent and contrast-set gain control) appear to be fully operational at the onset of the response (well within 10msec after the onset of the response).

Responses to optimal and nonoptimal stimuli during the first 20msec. Figure 47.10 plots the responses as a function of contrast

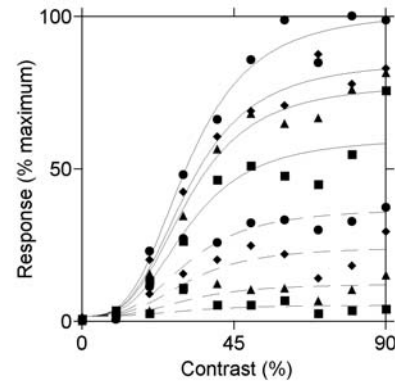


FIGURE 47.9. Responses (mean firing rate) as a function of contrast during the first 16msec after the onset of the response to a stationary grating. (Adapted from Albrecht et al., 2002.)

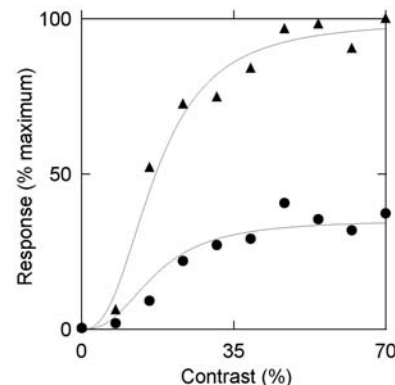


FIGURE 47.10. Responses (mean firing rate) as a function of contrast during the first 20msec of the response for an optimal (▲) and a nonoptimal (●) spatial phase. (Adapted from Albrecht et al., 2002.)

during the first 20 msec after the onset of the response for an optimal and a nonoptimal spatial position. The smooth curves through the data points plot the fit of a single Naka-Rushton equation that is simply scaled for each spatial position (i.e., the same exponent and half-saturation contrast). The single, scaled equation indicates that the scaling is determined by the magnitude of the contrast and not the magnitude of the response.

Response expansion and contrast-set gain control. In summary, using transient stationary gratings, it is possible to track the temporal dynamics of various linear and nonlinear properties to assess whether these properties could, or could not, play a role in shaping stimulus selectivity and performance on the time frame of single fixations during natural viewing. Based on the measurements illustrated in Figures 47.7 to 47.10, it appears as though the two nonlinearities revealed within the measurements of the contrast response function operate rapidly enough to have a significant impact on stimulus selectivity and neural performance. The functional implications of these virtually instantaneous nonlinearities are discussed in greater detail below.

TEMPORAL NONLINEARITIES The temporal properties of V1 neurons have been measured using drifting gratings as well as stationary gratings; in addition, the stimuli have been presented for relatively prolonged durations (several seconds, to approximate a steady-state condition) as well as for relatively brief durations (to approximate natural viewing more closely). The results of these different types of measurements do not always conform to what would be expected within the framework of a linear system. Further, these discrepancies are not easily explained, even when the other known nonlinearities are taken into consideration.

Steady-state stimuli versus impulsive stimuli. Consider several discrepancies between the properties that are measured using drifting steady-state stimuli as opposed to transient stationary stimuli:

- The responses to transient stationary stimuli decay more rapidly than expected from the steady-state temporal frequency transfer function (Muller et al., 2001; Tolhurst et al., 1980).
- The steady-state temporal frequency tuning changes substantially as contrast increases (e.g., Albrecht, 1995; Hawken et al., 1992; Holub and Morton-Gibson, 1981), whereas the temporal response profile for transient stationary gratings is relatively invariant as contrast increases (Albrecht et al., 2002).
- Under steady-state conditions, the variability of cortical neurons is approximately proportional to the mean firing rate (e.g., Geisler and Albrecht, 1997; Softky and Koch, 1993; Tolhurst et al., 1983), whereas this relationship does

not hold for the initial transient response to stationary gratings (Muller et al., 2001).

Transient stationary stimuli versus transient drifting stimuli. There are several discrepancies between the responses measured for transient drifting stimuli versus transient stationary stimuli (Albrecht et al., 2002; Frazor et al., 1997; Muller et al., 2001):

- Responses to stationary gratings are more transient than responses to drifting gratings.
- Both detectability and discriminability are better for drifting gratings than for stationary gratings.
- Transient stationary gratings generally produce large off-responses, whereas transient drifting gratings generally do not.
- Transient stationary gratings often evoke complex secondary oscillations, whereas transient drifting gratings generally do not.

SELECTIVITY ALONG OTHER DIMENSIONS Figures 47.7 to 47.10 indicate that the properties of the contrast response function are fully established at the very onset of the response and remain relatively invariant throughout the entire time course of the response, during an interval comparable to natural fixation (i.e., a 200 msec interval). These findings lead one to ask whether the response properties along other stimulus dimensions are similar. For example, is the stimulus selectivity along other stimulus dimensions fully established at the onset of the response? Similarly, is the stimulus selectivity along other stimulus dimensions relatively invariant throughout the entire time course of the response during an interval comparable to natural fixation?

With these questions in mind, it is important to note that several different lines of evidence appear to indicate that this type of behavior (i.e., rapid development and invariance through time) may not generalize to other stimulus dimensions. However, it is equally important to note that this is an emerging line of research and that the results across laboratories are not yet entirely reconcilable. In brief, it appears as though some important aspects of stimulus selectivity develop over the course of the first 50 msec after the onset of the response.

Spatial frequency and orientation selectivity measured with a reverse correlation procedure. Ringach et al. (1997) have measured the temporal dynamics of orientation tuning using a new *reverse correlation* procedure (where gratings are presented for very brief intervals: 20 msec). Their measurements indicate that orientation tuning changes through time for some V1 neurons: specifically, the preferred orientation changes and the selectivity increases (however, see Gillespie et al., 2001; Mazer et al., 2002; Muller et al., 2001).

Bredfeldt and Ringach (2002) used a similar procedure to measure the temporal dynamics of spatial frequency selectivity. Their measurements indicate that spatial frequency selectivity also changes through time. Specifically, the measurements indicate that (1) the preferred spatial frequency shifts from low frequencies to high frequencies and (2) the selectivity increases (however, see Albrecht et al., submitted).

Spatial frequency and orientation selectivity measured in an awake, behaving monkey. Mazer et al. (2002) have measured the responses of V1 neurons using the awake, behaving preparation, in which a monkey is trained to fixate while visual stimuli are presented (for a duration longer than 20 msec). Unlike the measurements of Ringach et al. (1997), their measurements indicate that orientation selectivity is relatively invariant through time. However, similar to Bredfeldt and Ringach (2002), the measurements of Mazer et al. indicate that the preferred spatial frequency increases through time.

Spatial frequency selectivity measured with transient stationary stimuli. We have measured spatial frequency selectivity using stationary gratings that are turned on for 200 msec and off for 300 msec (Albrecht et al., submitted). In agreement with Bredfeldt and Ringach (2002) and Mazer et al. (2002), we find that spatial frequency selectivity changes through time. Specifically, our measurements indicate that the latency of the response increases as spatial frequency increases. This latency shift causes the peak of the spatial frequency response function to shift through time, and it also causes the spatial frequency selectivity to decrease as the responses are integrated over the course of 200 msec: the spatial frequency peak and the bandwidth change as the responses are integrated over the first 50 msec, and then they both become relatively stable and remain invariant thereafter.

Spatial frequency, spatial phase, and direction selectivity during natural fixation. Given that all three laboratories discussed in the preceding sections, using very different measurement techniques, have reported that spatial frequency tuning changes through the course of an interval comparable to natural fixation, it is important to consider the functional consequences of these changes. Although these changes may help us understand the underlying structural components that produce high degrees of stimulus selectivity, it seems unlikely that these changes will have important functional consequences for the discrimination and identification performance, if one assumes that subsequent neurons integrate the responses over more than just a few milliseconds. Specifically, if the response to a given stimulus is integrated through time following the onset of the response, the stimulus selectivity should become relatively stable within 50 msec.

In addition, it is important to keep in mind the effect of the integration interval on the signal-to-noise ratio when

considering neural discrimination and identification performance. We know from signal detection theory that performance should improve as the integration interval increases. In the case of V1 neurons, as the integration interval increases, the number of action potentials increases, and because the variance is proportional to the mean of the response, the longer the integration interval the larger the signal-to-noise ratio. We have found that, on average, it takes approximately 50 msec to reach 50% of the total number of action potentials when a stationary grating is presented for 200 msec (Albrecht et al., 2002, submitted). Thus, for example, integrating over the entire 200 msec would, on average, double the number of action potentials, which would increase the signal-to-noise ratio by approximately 50% (assuming a variance proportionality constant of 1.3).

Even if stimulus selectivity is dynamic over the first 50 msec of the response, measurements indicate that if the integration interval is extended to 200 msec (comparable to natural fixation), the selectivity for many stimulus dimensions is stable and essentially equivalent to the selectivity that is measured with steady-state stimuli (Frazor, 2002; Frazor et al., 1997). This observation holds not only for spatial frequency, but also for direction selectivity and spatial position selectivity. Figure 47.11 illustrates the responses as a function of spatial frequency and the direction of stimulus

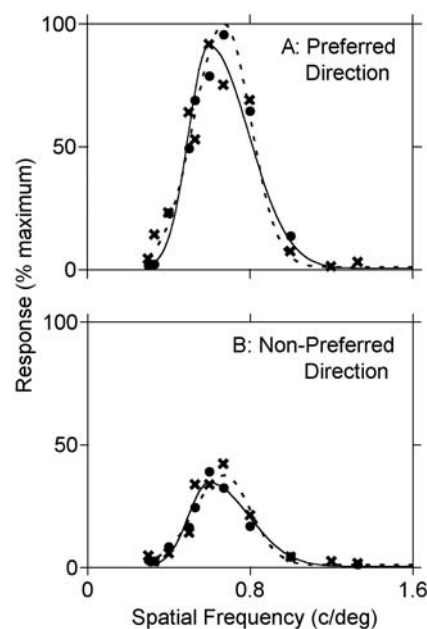


FIGURE 47.11. Responses (mean firing rate per 200 msec) as a function of spatial frequency for the preferred direction of motion (A) and the nonpreferred direction of motion (B). The responses and fitted curve for steady-state stimuli are shown with the \times and solid curve; the responses and fitted curve for transient stimuli are shown with the \bullet and dashed curve. (Adapted from Frazor, 2002.)

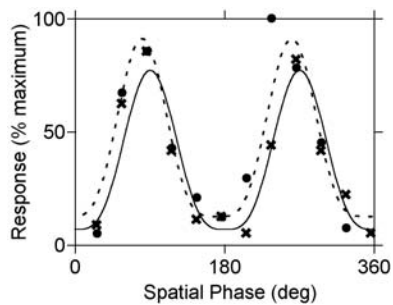


FIGURE 47.12. Responses (mean firing rate per 200msec) as a function of spatial position. The responses and fitted curve for steady-state stimuli are shown with the \times and solid curve; the responses and fitted curve for transient stimuli are shown with the \bullet and dashed curve. (Adapted from Frazor, 2002.)

motion for transient and steady-state methods of stimulus presentation; Figure 47.12 illustrates the responses of the selectivity for spatial position. In sum, the stimulus selectivity for these three dimensions for integration over 200msec is very similar to the stimulus selectivity that has been measured using steady-state stimuli.

Conclusion

MODELS AT DIFFERENT LEVELS OF ANALYSIS There are many different laboratories measuring the properties of visual cortex neurons and developing models at many different levels of analysis. In preparation for writing this chapter, we searched the literature to learn more about the different types of models that have been proposed for neurons in the visual cortex. We tried to be as inclusive as possible. As one might expect, there are hundreds of unique types of models that have been proposed over the past several decades to account for a variety of different linear and nonlinear properties of visual cortex neurons, at many different levels of analysis. In order to organize this vast literature (which cannot be reviewed here), we have found that it is useful to distinguish three different levels of models: *descriptive models*, *functional models*, and *structural models*.

Descriptive models. Consider performing systematic measurements of the responses across a large population of visual cortex neurons as a function of some important stimulus dimension; say, for example, the dimension of contrast. At this stage of the investigation (i.e., after performing the measurements), it is useful to have a *descriptive model*. The goal of a *descriptive model* is to summarize and interpolate the measured responses using an atheoretical mathematical equation. For example, the Naka-Rushton equation provides a reasonably accurate description of the contrast response function for the overwhelming majority of visual cortex neurons using only three free parameters.

If the *descriptive model* provides an accurate description of the trends in the data across the entire sample of neurons, it becomes a very powerful tool that can be used in many different applications. To begin with, the function can be used to describe important characteristics of the responses across the entire sample of cells in a unified and quantitative fashion. Oftentimes, the parameters of the equation directly quantify the property of interest (e.g., the exponent of the Naka-Rushton equation). Even if the parameters themselves are not useful, it is easy to use the equation to solve for the value of interest, as long as the equation provides an accurate description.

In addition to providing this initial summary of the data, a *descriptive model* can be used in many other applications. Consider the following applications of the Naka-Rushton equation:

- To test quantitatively the hypothesis that response saturation is determined by the magnitude of the response or the magnitude of the contrast (see above).
- To test quantitatively the hypothesis that the contrast-set gain control and the expansive response exponent are present virtually instantaneously (see above).
- To test quantitatively the hypothesis that the latency shift is determined by the magnitude of the contrast or the magnitude of the response (see above).
- To assess the degree to which the variation in the measured responses is more likely a result of systematic variation, as opposed to the inherent stochastic variation of cortical neurons, by performing randomization tests of specific null hypotheses (e.g., Albrecht et al., 2002).
- As one final example, the equation has been effectively incorporated into many different higher-level models, at both the functional level and the structural level (e.g., Albrecht and Geisler, 1991; Carandini et al., 1999; Heeger, 1991, 1992a, 1992b).

Several examples of *descriptive models* are given in Albrecht et al. (2002).

Functional models. Upon completing systematic measurements and the quantitative description and summary using a *descriptive model* (or models), it then becomes useful, at this stage of the investigation, to consider analyzing the systematic trends within a functional context and to develop a *functional model*. The goal of a *functional model* is to characterize the response properties within the context of a visual information processing algorithm.

Consider, for example, systematic measurements of the responses of a simple cell as a function of contrast (in both directions of motion) and spatial position. The responses can be summarized using the Naka-Rushton equation. Then, as trends are observed, analyzed, and quantified, one can begin to speculate about possible functions that are revealed within

a given set of measurements. Given the measurements described in this example, several important trends reveal possible functions.

- The contrast response function reveals an accelerating nonlinearity.
- The contrast response function reveals a saturating nonlinearity.
- The responses scale and saturate at the same contrasts for both optimal and nonoptimal spatial positions, even though the response magnitude is very different for these two positions.
- The cell is direction selective.
- The responses as a function of contrast saturate at the same contrast for the two directions of motion, even though the response amplitudes are very different for the optimal versus nonoptimal direction of motion.
- The degree of direction selectivity is related to the responses as a function of spatial phase, but the selectivity is much larger than would be expected.
- The phase response function is approximately sinusoidal.
- There is a null phase position even though the cell is direction selective.
- The phase response function is more narrow and peaked than a sine wave.

Within the context of the *descriptive model*, these are all separate facts that are quantified with the Naka-Rushton equation. However, these apparently disparate facts can be unified within the context of a relatively simple *functional model*: a linear spatial filter, whose gain is set by the overall magnitude of the contrast, followed by an expansive response exponent (e.g., Albrecht and Geisler, 1991; Carandini and Heeger, 1994; Ferster, 1994; Heeger, 1991, 1992a, 1992b; for reviews see Carandini et al., 1999; Geisler and Albrecht, 2000). The linear filter accounts for (1) the sinusoidal responses as a function of spatial position, (2) the direction selectivity, and (3) the relationship between the two. The contrast-set gain control accounts for the saturation at the same contrast, independent of response amplitude. The expansive exponent accounts for (1) the mismatch between the direction selectivity and the responses as a function of spatial phase as well as (2) the narrow and peaked pattern. Several examples of *functional models* are given in Albrecht et al. (2002).

Structural models. Upon completing systematic measurements and analyzing the systematic trends within a functional context, it is then useful to develop a *structural model*. The goal of a *structural model* is to characterize the biophysical and biochemical neural mechanisms that are responsible for some specific property. Consider, for example, two of the nonlinear properties that have been identified in many

different laboratories in many different stimulus situations: contrast-set gain control and the expansive response exponent. Many different laboratories are currently working to understand these nonlinearities within the context of various structural models.

Structural models for response expansion and contrast-set gain control include: expansive voltage-spike transduction, noisy membrane potential, recurrent excitation, intracortical inhibition, correlation-based inhibition, synaptic depression, nonspecific suppression, shunting inhibition, tonic hyperpolarization, strong push-pull inhibition, and changes in membrane conductance. Some models rely on feed-forward inputs, others rely on feedback inputs, and still others rely on lateral inputs through local connections and through the far-reaching interconnectivity among cortical neurons. For recent discussions and reviews of this literature, and related issues, see the sources listed in Table 47.1.

CONTRAST-SET GAIN CONTROL

Gain control, amplifiers, light adaptation. The gain control that occurs within electrical systems in general, and electronic amplifiers in particular, has provided a useful analogy for the type of gain control that occurs at various levels of the visual system. Consider, for example, the ammeter analogy discussed by Craik (1938), or consider a simple amplifier. The purpose of a traditional amplifier is to take a small input voltage and make it larger by multiplying the input by a con-

TABLE 47.1
Examples of contemporary *structural models*

Abbott et al. (1997)
Adorjan et al. (1999)
Anderson et al. (2000)
Carandini et al. (1999)
Chance et al. (1998)
Douglas et al. (1995)
Ferster and Miller (2000)
Gilbert et al. (1990)
Hirsch et al. (1998)
Kayser et al. (2001)
Miller et al. (2001)
Murthy and Humphrey (1999)
Nelson et al. (1994)
Somers et al. (1995)
Stetter et al. (2000)
Troyer et al. (1998)
Wieland et al. (2001)
Worgotter et al. (1998)

stant factor. The *gain* of an amplifier refers to this multiplicative factor: it relates the magnitude of the output to the magnitude of the input. To optimize the limited dynamic response range of the amplifier, across a wide range of input values (while attempting to minimize distortions), *gain control* systems can be introduced to adjust the magnitude of the multiplicative factor based on the magnitude of the input, the output, or both: if the input values are small, the gain is adjusted to be large, whereas if the input values are large, the gain is adjusted to be small.

The amplifier analogy and terminology have been applied to the light adaptation characteristics of the visual system (e.g., Hood, 1998; Shapley and Enroth-Cugell, 1984). Conceptually, within this analogy, the gain of the system is adjusted based on the prevailing, ambient range of luminance intensities available within the visual stimulus at any point in time. The gain control in this case shifts the sensitivity to light, based on the average amount of light available. The goal is to use effectively the limited response range so as to optimize high differential sensitivity (to luminance increments and decrements) and other such performance characteristics. The amplifier analogy and terminology have also been applied to the contrast response characteristics of visual cortex neurons.

Cortical contrast-set gain control. It seems reasonable to take the traditional notions of gain control that have been applied to light adaptation and brightness discrimination and apply the same basic concepts to the virtually instantaneous type of contrast-set gain control that occurs within the visual cortex. However, one must apply the analogy carefully because the direct application to the dimension of contrast and contrast discrimination performance is not particularly useful. It may lead one to think that the contrast-set gain control has the beneficial consequence of improving contrast discrimination. It does not. In fact, it is deleterious in the sense that the responses as a function of contrast saturate at low contrasts (due to the contrast-set gain control).

In the light adaptation analogy, one might suppose that the gain control in the cortex is designed to position the limited dynamic response range of V1 neurons around the ambient level of contrast for optimal contrast discrimination performance. If one attempts to apply the analogy, as formulated above, one is immediately confronted with a number of properties of the gain control that are to some extent counterintuitive. Specifically, the gain control produces response saturation that is virtually instantaneous, oftentimes at very low levels of contrast, for both optimal and nonoptimal stimuli, even though the latter do not produce large amplitude responses. These properties have a deleterious effect on contrast discrimination: obviously, when the cell saturates, contrast discrimination is eliminated.

Gain control in a multidimensional feature space. As emphasized many times within this chapter, one hallmark of cortical neurons is stimulus selectivity. To characterize this selectivity, visual neuroscientists measure the responses along many different stimulus dimensions. Although these measurements are fundamental in our analysis of V1 neurons, it is important not to lose sight of the fact that the stimulus selectivity of any given neuron reflects many stimulus dimensions simultaneously. We study the selectivity within the multidimensional feature space, varying each stimulus dimension individually, but the visual feature itself is the simultaneous combination along all of the dimensions.

The traditional notions of gain control can be applied to cortical contrast-set gain control; however, it is necessary to consider more than the single stimulus dimension of contrast. Specifically, one must consider all of the *other* stimulus dimensions. Within this framework, the gain control does improve discrimination performance, but not along the dimension of contrast. Instead, the gain control improves performance within a multidimensional feature space. The contrast gain of the cell's dynamic response range is set such that the optimal stimulus (within this feature space) will always produce the maximum response, and the nonoptimal stimuli will simply scale down accordingly, independent of the overall ambient prevailing level of contrast. In so doing, the discrimination performance is optimized along all of the stimulus dimensions within this feature space, with the exception of contrast, and deviations from the optimum will produce maximum discriminability. Further, when the cell produces saturated responses, it identifies the presence of a specific feature with a high degree of certainty.

In sum, for the traditional analogy of gain control to be useful, the dimension of luminance needs to be compared to a multidimensional feature space: the contrast-set gain control scales the responses, based on the average prevailing contrast, such that differential sensitivity is optimized within the multidimensional feature space.

REFERENCES

- Abbott, L. F., K. Sen, J. A. Varela, and S. B. Nelson, 1997. Synaptic depression and cortical gain control, *Science*, 275:220–224.
- Adelson, E. H., and J. R. Bergen, 1985. Spatiotemporal energy models for the perception of motion, *J. Opt. Soc. Am. A*, 2:284–299.
- Adorjan, P., J. B. Levitt, J. S. Lund, and K. Obermeyer, 1999. A model for the intracortical origin of orientation preference and tuning in macaque striate cortex, *Vis. Neurosci.*, 16:303–318.
- Albrecht, D. G., 1995. Visual cortex neurons in monkey and cat: effect of contrast on the spatial and temporal phase transfer function, *Vis. Neurosci.*, 12:1191–1210.
- Albrecht, D. G., and R. L. De Valois, 1981. Striate cortex responses to periodic patterns with and without the fundamental harmonics, *J. Physiol. (Lond.)*, 319:497–514.

- Albrecht, D. G., S. B. Farrar, and D. B. Hamilton, 1984. Spatial contrast adaptation characteristics of neurones recorded in the cat's visual cortex, *J. Physiol. (Lond.)*, 347:713–739.
- Albrecht, D. G., and W. S. Geisler, 1991. Motion selectivity and the contrast-response function of simple cells in the visual cortex, *Vis. Neurosci.*, 7:531–546.
- Albrecht, D. G., W. S. Geisler, R. A. Frazor, and A. M. Crane, 2002. Visual cortex neurons of monkeys and cats: temporal dynamics of the contrast response function, *J. Neurophysiol.*, 88:888–913.
- Albrecht, D. G., W. S. Geisler, R. A. Frazor, and A. M. Crane, 2003. Visual cortex neurons of monkeys and cats: temporal dynamics of spatial frequency selectivity. Submitted.
- Albrecht, D. G., and D. H. Hamilton, 1982. Striate cortex of monkey and cat: contrast response function, *J. Neurophysiol.*, 48:217–237.
- Anderson, J. S., M. Carandini, and D. Ferster, 2000. Orientation tuning of input conductance, excitation, and inhibition in cat primary visual cortex, *J. Neurophysiol.*, 84:909–926.
- Barlow, H. B., 1961. Three points about lateral inhibition, in *Sensory Communication* (W. A. Rosenblith, ed.), New York: Wiley, pp. 782–786.
- Barlow, H. B., 1995. The neuron doctrine in perception, in *The Cognitive Neurosciences* (M. S. Gazzaniga, ed.), Cambridge, MA: MIT Press, pp. 415–435.
- Barlow, H. B., T. P. Kaushal, M. Hawken, and A. J. Parker, 1987. Human contrast discrimination and the threshold of cortical neurons, *J. Opt. Soc. Am. A*, 3:1443–1449.
- Bergen, J. R., 1991. Theories of visual texture perception, in *Vision and Visual Dysfunction 10B* (D. Regan, ed.), New York: Macmillan, pp. 114–134.
- Bonds, A. B., 1989. The role of inhibition in the specification of orientation selectivity of cells of the cat striate cortex, *Vis. Neurosci.*, 2:41–55.
- Bonds, A. B., 1991. Temporal dynamics of contrast gain in single cells of the cat striate cortex, *Vis. Neurosci.*, 6:239–255.
- Bredfeldt, C. E., and D. L. Ringach, 2002. Dynamics of spatial frequency tuning in macaque V1, *J. Neurosci.*, 22:1976–1984.
- Carandini, M., and D. J. Heeger, 1994. Summation and division by neurons in primate visual cortex, *Science*, 264:1333–1336.
- Carandini, M., D. J. Heeger, and J. A. Movshon, 1997. Linearity and normalization in simple cells of the macaque primary visual cortex, *J. Neurosci.*, 17:8621–8644.
- Carandini, M., D. J. Heeger, and J. A. Movshon, 1999. Linearity and gain control in V1 simple cells, in *Cerebral Cortex*, vol. 13, *Models of Cortical Circuits* (P. S. Ulinski, E. G. Jones, and A. Peters, eds.), New York: Kluwer Academic/Plenum, pp. 401–443.
- Carpenter, R. H. S., ed., 1991. *Eye Movements*, vol. 8: *Vision and Visual Dysfunction*. Boca Raton, FL: CRC Press.
- Cavanaugh, J. R., W. Bair, and J. A. Movshon, 2002a. Nature and interaction of signals from the receptive field center and surround in macaque V1 neurons, *J. Neurophysiol.*, 88:2530–2546.
- Cavanaugh, J. R., W. Bair, and J. A. Movshon, 2002b. Selectivity and spatial distribution of signals from the receptive field surround in macaque V1 neurons, *J. Neurophysiol.*, 88:2547–2556.
- Chance, F. S., S. B. Nelson, and L. F. Abbott, 1998. Synaptic depression and the temporal response characteristics of V1 cells, *J. Neurosci.*, 18:4785–4799.
- Craik, K. J. W., 1938. The effect of adaptation on differential brightness discrimination, *J. Physiol. (Lond.)*, 92:406–421.
- Craik, K. J. W., 1966. *The Nature of Psychology*, Cambridge: Cambridge University Press.
- Dawis, S., R. Shapley, E. Kaplan, and D. Tranchina, 1984. The receptive-field organization of X-cells in the cat: spatiotemporal coupling and asymmetry, *Vis. Res.*, 24:549–564.
- Dean, A. F., and D. J. Tolhurst, 1986. Factors influencing the temporal phase of response to bar and grating stimuli for simple cells in the cat striate cortex, *Exp. Brain Res.*, 62:143–151.
- DeAngelis, G. C., I. Ohzawa, and R. D. Freeman, 1993. Spatiotemporal organization of simple-cell receptive fields in the cat's striate cortex. II. Linearity of temporal and spatial summation, *J. Neurophysiol.*, 69:1118–1135.
- DeAngelis, G. C., J. G. Robson, I. Ohzawa, and R. D. Freeman, 1992. The organization of suppression in receptive fields of neurons in cat visual cortex, *J. Neurophysiol.*, 68:144–163.
- De Valois, R. L., D. G. Albrecht, and L. G. Thorell, 1982. Spatial frequency selectivity of cells in macaque visual cortex, *Vis. Res.*, 22:545–559.
- De Valois, R. L., and K. K. De Valois, 1988. *Spatial Vision*, New York: Oxford University Press.
- De Valois, R. L., L. G. Thorell, and D. G. Albrecht, 1985. Periodicity of striate-cortex-cell receptive fields, *J. Opt. Soc. Am. A*, 2:1115–1123.
- De Valois, K. K., and R. B. H. Tootell, 1983. Spatial frequency-specific inhibition in cat striate cortex cells, *J. Physiol. (Lond.)*, 336:359–376.
- Douglas, R. J., C. Koch, M. Mahowald, K. A. C. Martin, and H. H. Suarez, 1995. Recurrent excitation in neocortical circuits, *Science*, 269:981–985.
- Enroth-Cugell, C., and J. G. Robson, 1966. The contrast sensitivity of retinal ganglion cells of the cat, *J. Physiol. (Lond.)*, 187:517–552.
- Ferster, D., 1994. Linearity of synaptic interactions in the assembly of receptive fields in cat visual cortex, *Curr. Opin. Neurobiol.*, 4:563–568.
- Ferster, D., and K. D. Miller, 2000. Neural mechanisms of orientation selectivity in the visual cortex, *Annu. Rev. Neurosci.*, 23:441–471.
- Field, D. J., 1987. Relations between the statistics of natural images and the response properties of cortical cells, *J. Opt. Soc. Am. A*, 4:2379–2394.
- Frazor, R. A., 2002. Cat and monkey V1 neurons: comparison of the responses to sustained and transiently presented stimuli. Ph.D. dissertation, University of Texas.
- Frazor, R. A., D. G. Albrecht, W. S. Geisler, and A. M. Crane, 1997. Response of V1 neurons during intervals similar to normal fixation, *Invest. Ophthalmol. Vis. Sci. (Suppl.)*, 38:S15.
- Gardner, J. L., A. Akiyuki, I. Ohzawa, and R. D. Freeman, 1999. Linear and nonlinear contributions to orientation tuning of simple cells in the cat's striate cortex, *Vis. Neurosci.*, 16:1115–1121.
- Gawne, T. J., T. W. Kjer, and B. J. Richmond, 1996. Latency: another potential code for feature binding in striate cortex, *J. Neurophysiol.*, 76:1356–1360.
- Geisler, W. S., and D. G. Albrecht, 1995. Bayesian analysis of identification in monkey visual cortex: nonlinear mechanisms and stimulus uncertainty, *Vis. Res.*, 35:2723–2730.
- Geisler, W. S., and D. G. Albrecht, 1997. Visual cortex neurons in monkeys and cats: detection, discrimination, and identification, *Vis. Neurosci.*, 14:897–919.
- Geisler, W. S., and D. G. Albrecht, 2000. Spatial vision, in *Handbook of Perception and Cognition, Seeing*, 2nd ed. (K. K. De Valois, ed.), New York: Academic Press, pp. 79–128.

- Geisler, W. S., D. G. Albrecht, R. J. Salvi, and S. S. Sanders, 1991. Discrimination performance of single neurons: rate and temporal-pattern information, *J. Neurophysiol.*, 66:334–362.
- Gilbert, C. D., J. A. Hirsch, and T. N. Wiesel, 1990. Lateral interactions in visual cortex, *Cold Spring Harbor Symp. Q. Biol.*, 55:663–667.
- Gillespie, D., I. Lampl, J. S. Anderson, and D. Ferster, 2001. Dynamics of the orientation-tuned membrane potential response in cat primary visual cortex, *Nat. Neurosci.*, 4:1014–1019.
- Hamilton, D. B., D. G. Albrecht, and W. S. Geisler, 1989. Visual cortical receptive fields in monkey and cat: spatial and temporal phase transfer function, *Vis. Res.*, 29:1285–1308.
- Hawken, M. J., R. M. Shapley, and D. H. Grosof, 1992. Temporal frequency selectivity in monkey lateral geniculate nucleus and striate cortex, *Vis. Neurosci.*, 13:477–492.
- Heeger, D. J., 1991. Nonlinear model of neural responses in cat visual cortex, in *Computational Models of Visual Processing* (M. S. Landy and J. A. Movshon, eds.), Cambridge, MA: MIT Press, pp. 119–133.
- Heeger, D. J., 1992a. Normalization of cell responses in cat striate cortex, *Vis. Neurosci.*, 9:181–197.
- Heeger, D. J., 1992b. Half-squaring in responses of cat simple cells, *Vis. Neurosci.*, 9:427–443.
- Henry, G. H., 1977. Receptive field classes in the striate cortex of the cat, *Brain Res.*, 133:1–28.
- Hirsch, J. A., J. M. Alonso, R. C. Reid, and L. M. Martinez, 1998. Synaptic integration in striate cortical simple cells, *J. Neurosci.*, 18:9517–9528.
- Holub, R. A., and M. Morton-Gibson, 1981. Response of visual cortical neurons of the cat to moving sinusoidal gratings, *J. Neurophysiol.*, 46:1244–1259.
- Hood, D. C., 1998. Lower-level visual processing and models of light adaptation, *Annu. Rev. Psych.*, 49:503–535.
- Hubel, D. H., and T. N. Wiesel, 1962. Receptive fields, binocular interaction, and functional architecture in the cat's visual cortex, *J. Physiol. (Lond.)*, 160:106–154.
- Jagadeesh, B., H. S. Wheat, L. L. Kontsevich, C. W. Tyler, and D. Ferster, 1997. Direction selectivity of synaptic potentials in simple cells of the cat visual cortex, *J. Neurophysiol.*, 78:2772–2789.
- Kayser, A., N. J. Priebe, and K. D. Miller, 2001. Contrast-dependent nonlinearities arise locally in a model of contrast invariant orientation tuning, *J. Neurophysiol.*, 85:2130–2149.
- Li, C., and O. Creutzfeldt, 1984. The representation of contrast and other stimulus parameters by single neurons in area 17 of the cat, *Pflügers Arch.*, 401:304–314.
- Marmarelis, P. Z., and V. Z. Marmarelis, 1978. *Analysis of Physiological Systems*, New York: Plenum, pp. 1–487.
- Mazer, J. A., W. E. Vinje, J. McDermott, P. H. Schiller, and J. L. Gallant, 2002. Spatial frequency and orientation tuning dynamics in area V1, *Proc. Natl. Acad. Sci USA*, 99:1645–1650.
- McLean, J., and L. A. Palmer, 1989. Contribution of linear spatiotemporal receptive field structure to velocity selectivity of simple cells in area 17 of cat, *Vis. Res.*, 29:675–679.
- McLean, J., and L. A. Palmer, 1994. Organization of simple cell responses in the three-dimensional (3-D) frequency domain, *Vis. Neurosci.*, 11:295–306.
- McLean, J., and L. A. Palmer, 1996. Contrast adaptation and excitatory amino acid receptors in cat striate cortex, *Vis. Neurosci.*, 13:1069–1087.
- Mechler, F., and D. L. Ringach, 2002. On the classification of simple and complex cells, *Vis. Res.*, 42:1017–1033.
- Miller, K. D., D. J. Pinto, and D. J. Simons, 2001. Processing in layer 4 of the neocortical circuit: new insights from visual and somatosensory cortex, *Curr. Opin. Neurobiol.*, 11:488–497.
- Movshon, J. A., and P. Lennie, 1979. Pattern-selective adaptation in visual cortical neurons, *Nature*, 278:850–852.
- Movshon, J. A., I. D. Thompson, and D. J. Tolhurst, 1978. Spatial summation in the receptive fields of simple cells in the cat's striate cortex, *J. Physiol. (Lond.)*, 383:53–77.
- Muller, J. R., A. B. Metha, J. Krauskopf, and P. Lennie, 2001. Information conveyed by onset transients in responses of striate cortical neurons, *J. Neurosci.*, 21:6978–6990.
- Murthy, A., and A. L. Humphrey, 1999. Inhibitory contributions to spatiotemporal receptive-field structure and direction selectivity in simple cells in cat area 17, *J. Neurophysiol.*, 81:1212–1224.
- Murthy, A., A. L. Humphrey, A. B. Saul, and J. C. Feidler, 1998. Laminar differences in the spatiotemporal structure of simple cell receptive fields in cat area 17, *Vis. Neurosci.*, 15:239–256.
- Nelson, S. B., 1991. Temporal interactions in the cat visual system I. Orientation-selective suppression in visual cortex, *J. Neurosci.*, 11:344–356.
- Nelson, S., L. Toth, B. Sheth, and M. Sur, 1994. Orientation selectivity of cortical neurons during intracellular blockade of inhibition, *Science*, 265:774–777.
- Ohzawa, I., G. Sclar, and R. D. Freeman, 1985. Contrast gain control in the cat's visual system, *J. Neurophysiol.*, 42:833–849.
- Olshausen, B. A., and D. J. Field, 1987. Sparse coding with an overcomplete basis set: a strategy by V1?, *Vis. Res.*, 37:3311–3325.
- Palmer, L. A., J. P. Jones, and R. A. Stepnoski, 1991. Striate receptive fields as linear filters: characterization in two dimensions of space, in *The Neural Basis of Visual Function* (A. G. Leventhal, ed.), Boca Raton, FL: CRC Press, pp. 246–265.
- Ratcliff, F., B. W. Knight, Jr., F. A. Dodge, Jr., and H. K. Hartline, 1974. Fourier analysis of dynamics of excitation and inhibition in the eye of *Limulus*: amplitude, phase and distance, *Vis. Res.*, 14:1155–1168.
- Reich, D. S., F. Mechler, and J. D. Victor, 2001. Temporal coding of contrast in primary visual cortex: when, what, and why, *J. Neurophysiol.*, 85:1039–1050.
- Reid, R. C., R. E. Soodak, and R. M. Shapley, 1991. Directional selectivity and spatiotemporal structure of receptive fields of simple cells in cat striate cortex, *J. Neurophysiol.*, 66:505–529.
- Ringach, D. L., M. J. Hawken, and R. Shapley, 1997. Dynamics of orientation tuning in macaque visual cortex, *Nature*, 387:281–284.
- Robson, J. G., 1975. Receptive fields: spatial and intensive representations of the visual image, in *Handbook of Perception*, vol. 5, *Vision* (E. C. Carterette and M. P. Friedman, eds.), New York: Academic Press, pp. 81–112.
- Saul, A. B., and M. S. Cynader, 1989. Adaptation in single units in the visual cortex: the tuning of aftereffects in the spatial domain, *Vis. Neurosci.*, 2:593–607.
- Schwarz, R. J., and B. Friedland, 1965. *Linear Systems*, New York: McGraw-Hill, pp. 1–521.
- Sclar, G., and R. D. Freeman, 1982. Orientation selectivity in the cat's striate cortex is invariant with stimulus contrast, *Exp. Brain Res.*, 46:457–461.
- Sclar, G., J. H. R. Maunsell, and P. Lennie, 1990. Coding of image contrast in central visual pathways of macaque monkey, *Vis. Res.*, 30:1–10.
- Shapley, R. M., and C. Enroth-Cugell, 1984. Visual adaptation and retinal gain controls, *Prog. Ret. Res.*, 3:263–346.

- Shapley, R., and P. Lennie, 1985. Spatial frequency analysis in the visual system, *Annu. Rev. Neurosci.*, 8:547–583.
- Shapley, R. M., and J. D. Victor, 1979. Nonlinear spatial summation and the contrast gain control of cat retinal ganglion cells, *J. Physiol. (Lond.)*, 290:141–161.
- Sofky, W. R., and C. Koch, 1993. The highly irregular firing of cortical cells is inconsistent with temporal integration of random EPSPs, *J. Neurosci.*, 13:334–350.
- Somers, D. C., S. B. Nelson, and M. Sur, 1995. An emergent model of orientation selectivity in cat visual cortical simple cells, *J. Neurosci.*, 15:5448–5465.
- Stetter, M., H. Bartsch, and K. Obermayer, 2000. A mean-field model for orientation tuning, contrast saturation, and contextual effects in the primary visual cortex, *Biol. Cyber.*, 82:291–304.
- Swindale, N. V., and M. S. Cynader, 1989. Vernier acuities of neurons in area 17 of cat visual cortex: their relation to stimulus length and velocity, orientation selectivity, and receptive-field structure, *Vis. Neurosci.*, 2:165–176.
- Tadmor, Y., and D. J. Tolhurst, 1989. The effect of threshold on the relationship between the receptive-field profile and the spatial-frequency tuning curve in simple cells of the cat's striate cortex, *Vis. Neurosci.*, 3:445–454.
- Tolhurst, D. J., and A. F. Dean, 1991. Evaluation of a linear model of directional selectivity in simple cells of the cat's striate cortex, *Vis. Neurosci.*, 6:421–428.
- Tolhurst, D. J., and D. J. Heeger, 1997. Comparison of contrast-normalization and threshold models of the responses of simple cells in cat striate cortex, *Vis. Neurosci.*, 14:293–309.
- Tolhurst, D. J., J. A. Movshon, and A. F. Dean, 1983. The statistical reliability of signals in single neurons in the cat and monkey visual cortex, *Vis. Res.*, 23:775–785.
- Tolhurst, D. J., N. S. Walker, I. D. Thompson, and A. F. Dean, 1980. Non-linearities of temporal summation in neurones in area 17 of the cat, *Exp. Brain Res.*, 38:431–435.
- Troyer, T. W., A. E. Krukowski, N. J. Priebe, and K. D. Miller, 1998. Contrast-invariant orientation tuning in cat visual cortex: thalamocortical input tuning and correlation-based intracortical connectivity, *J. Neurosci.*, 18:5908–5927.
- Victor, J. D. and B. W. Knight, 1979. Nonlinear analysis with an arbitrary stimulus ensemble, *Q. Appl. Math.*, 37:113–136.
- Victor, J. D., R. M. Shapley, and B. W. Knight, 1977. Nonlinear analysis of cat retinal ganglion cells in the frequency domain, *Proc. Natl. Acad. Sci. USA*, 74:3068–3072.
- Watson, A. B., and A. J. Ahumada, 1985. Model of human visual-motion sensing, *J. Opt. Soc. Am. A*, 2:322–341.
- Wielaard, D. J., M. Shelley, D. McLaughlin, and R. Shapley, 2001. How simple cells are made in a nonlinear network model of the visual cortex, *J. Neurosci.*, 21:5203–5211.
- Worgotter, F., E. Nelle, B. Li, L. Wang, and Y. Diao, 1998. A possible basic cortical microcircuit called “cascaded inhibition.” Results from cortical network models and recording experiments from striate simple cells, *Exp. Brain Res.*, 122:318–332.
- Zhou, X. Y., and C. L. Baker, Jr., 1994. Envelope-responsive neurons in areas 17 and 18 of cat, *J. Neurophysiol.*, 72:2134–2150.

48 Binocular Interaction in the Visual Cortex

RALPH D. FREEMAN

THERE ARE TWO MAJOR physiological transformations that occur in central pathways in the primary visual cortex. The first is that the receptive field (RF) structure, which consists of concentric center-surround patterns for ganglion and lateral geniculate nucleus (LGN) cells, becomes elongated, rectangular, and orientation specific in striate cortex. The second transformation is that input from left and right eyes, which is essentially segregated in peripheral pathways, becomes integrated at the level of V1, which is therefore the first stage of binocular visual processing.

This review provides selected coverage of the physiological elements of binocular vision. An attempt is made to identify central areas that have been addressed and to consider certain problems with some experimental approaches. For the most part, theoretical investigations are not covered. The most functionally relevant application of binocular function, that is, stereoscopic depth discrimination, is not dealt with here except in a cursory fashion. These topics are covered in other chapters in this volume (e.g., Chapters 49, 87, and 88).

Finally, it should be stated at the outset that this review is heavily influenced by the work on this subject that has been conducted in my laboratory. No attempt is made to give equal weight to all reports in the literature. An attempt is made to discuss work that is directly relevant to the topics that are covered here.

Background

The mixing of inputs from left and right eyes in the visual cortex is not complete, but it does provide the basis for the physiological fusion of monocular images. There are minor species differences in this regard since the population of cells in input layers of the primate is more monocular than that of the cat (Hubel and Wiesel, 1962, 1968). Monocular pathways clearly support a two-dimensional analysis of the visual world. The image from each eye projects to regions that produce two-dimensional maps of object space. These maps are interpreted in monocular pathways. Because the two eyes have slightly different views of visual space, their respective images are displaced on the retinas. This retinal disparity is the necessary and sufficient condition for stereoscopic depth discrimination. It allows the two-dimensional projection of visual space to become a three-dimensional percept.

Disparity-based stereopsis was demonstrated in early psychophysical studies (Wheatstone, 1838).

Details of the anatomical pathways that subserve binocular vision are covered in other chapters (see Chapter 37). The primary relevant physiological finding is that neurons in the striate cortex or V1 are responsive binocularly. The original demonstration of this, from studies of area 17 in the cat, was mainly by procedures in which tests were conducted alternately between left and right eyes. In other words, conclusions about binocular function were made from monocular tests. This is problematic because, as shown below, monocular tests can produce faulty assessments of the degree of binocularity of a cell. To be fair, the landmark study of binocular interaction in the cat (Hubel and Wiesel, 1962) included tests of both eyes simultaneously. It was also noted that some cells responded only when both eyes were activated simultaneously. However, subsequent to the early study, most experiments in which binocularity has been assessed have used only monocular tests (see below).

One other factor should be noted in connection with the physiological study of binocular vision. In the early investigations, the suggestion was made that binocular interaction in the visual cortex could be connected to the physiological basis of stereoscopic depth discrimination (Hubel and Wiesel, 1962). However, the way in which this might be accomplished was not specified. In subsequent investigations, direct attempts were made to identify neurons that responded to stimuli positioned at different depths. The factor referred to above is that essentially all the early work was conducted under the assumption that cortical neurons are depth detectors. This is, of course, a reasonable approach, and it follows the work of a long line of investigators who were interested in *trigger features* as they applied to a particular animal (for example, Lettvin et al., 1959). One limitation of this approach is that a given experiment and the main results are linked to a specific interpretation. In the case of *depth-detecting* neurons, it is possible that the disparity selectivity of cortical cells is a result of RF organization. There may be no direct linkage to a perceptual process. It is very important to establish this link, and recent work on alert, behaving monkeys enables a firm connection to be made between RF response characteristics and behavioral performance (Cumming and Parker, 2000; DeAngelis and Newsome, 1999).

It is possible to approach the physiological study of binocular vision without the assumption that neurons in the primary visual cortex are depth detectors. In this case, the question addressed is: how do binocular cells combine inputs from right and left eyes? The approaches used to answer this question are similar to those that have been undertaken for investigations of monocular pathways. In the most general sense, the purpose is to establish how a cell integrates light within its RF. This approach offers the potential of establishing the mechanisms of monocular and binocular processing in a unified manner.

Before describing the studies in which this approach has been applied, it is useful to summarize the classical work on the physiological basis of stereoscopic depth discrimination. The first direct study was performed in anesthetized paralyzed cats (Barlow et al., 1967). Neurons in area 17 were found to be selectively responsive to different retinal disparities corresponding to spatial depth ranges from near to far distances, as depicted in Figure 48.1. Preferences were found for a large range of both crossed and uncrossed disparities. However, the reported range of disparities was three times larger for horizontal compared to vertical disparities. This has a functional advantage because the horizontal displacement of the two eyes means that this orientation is required for stereopsis. Subsequent studies did not confirm this observation (Ferster, 1981; LeVay and Voigt, 1988; Nikara et al., 1968), but some hint of this asymmetry was found in other work (Joshua and Bishop, 1970; von der Heydt et al., 1978). By analysis of phase (shape) differences between the RFs of left and right eyes (to be described below), it has been shown that there are clear disparity-processing dissimilarities between horizontal and vertical orientations (DeAngelis et al., 1991).

Following the initial results of studies on disparity-sensitive cells in the cat's visual cortex, an attempt was made to replicate these findings in monkey striate cortex. The first

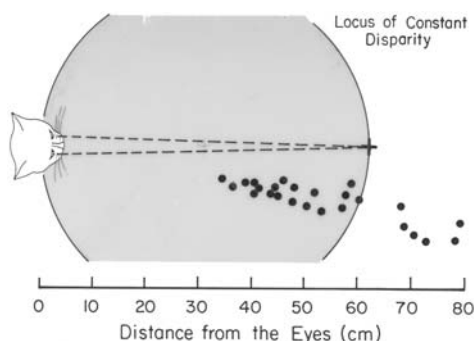


FIGURE 48.1. In this conventional view of disparity-selective neurons, the cat fixates a position on an arc tangent screen which traces the locus of contrast disparity. The data points represent cells tuned to relative retinal disparities corresponding to different depths in space.

result of this attempt was remarkable because the claim was made that there were no disparity-sensitive cells in V1 but there were in V2 (Hubel and Wiesel, 1970). This conclusion was wrong, of course, but it took studies in the awake, behaving monkey to sort out the issue. A series of experiments by Poggio and collaborators established conclusively that neurons in V1 and V2 are sensitive to relative changes in stereoscopic depth (Poggio and Talbot, 1981; Poggio and Fischer, 1977; Poggio et al., 1988).

The awake, behaving monkey setup is illustrated in Figure 48.2. An animal is trained to fixate a location on a screen that can be positioned at different depths. During fixation, individual cortical cells are recorded. In the initial study, four types of depth-sensitive neurons were identified: tuned excitatory, tuned inhibitory, near, and far cells. Response curves for these categories are shown in Figure 48.3. This scheme was modified subsequently (Poggio et al., 1988). However, it is reasonably clear from other work (LeVay and Voigt, 1988) that a four- or six- or n -category system is not adequate and not correct. The reasons for this inadequate classification system are explained in detail in a previous review (Freeman and Ohzawa, 1990).

In none of the early studies was an attempt made to develop a functional mechanism within which a disparity encoding and detecting system might fit. The problems with a disparity processing system based on four or six categories of cell types may be solved by the use of an encoding scheme that is scaled to the size or spatial frequency selectivity of cortical neurons. To do this, we need to analyze RF shape (phase) as well as relative position. In this way, we can determine if binocular disparity information is coded and represented in the visual cortex by phase-disparity selective neurons at different size or spatial frequency scales. The basis of this approach is detailed below.

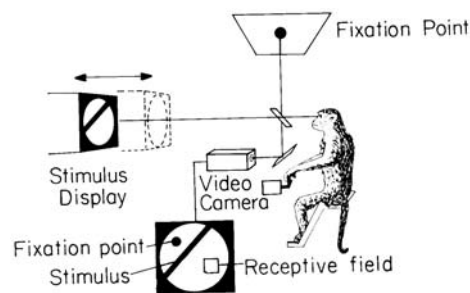


FIGURE 48.2. An experimental arrangement is shown for behavioral and neurophysiological testing of a primate. The monkey views a fixation point on a stimulus display and, through a beam splitter, on a second screen. The stimulus display may be moved fore and aft to change the relative depth. RFs of cortical cells are projected onto the stimulus display. The monkey presses a key when the fixation spot is illuminated. Visual targets used to explore neural activity are projected to the monkey's eye via the beam splitter.

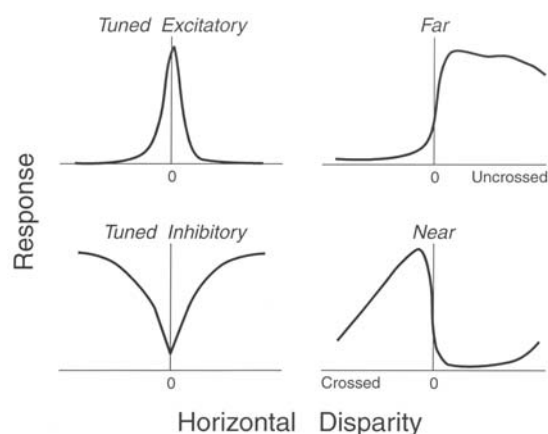


FIGURE 48.3. Four cortical cell types are illustrated according to their response patterns. Horizontal disparity is indicated on the abscissas, and response is represented on the ordinates. Crossed and uncrossed disparities are located to the left and right, respectively, of the zero position. Tuned excitatory and inhibitory cells respond or are suppressed, respectively, at zero disparity. Near and far cells respond to close or far distances, respectively.

Ocular dominance: the wrong way to assess binocularity

As mentioned above, the early studies of binocular interaction in the visual cortex resulted in a subjective ranking scale of ocular dominance (Hubel and Wiesel, 1962). This scale includes seven categories: groups 1 and 7 represent neurons that are entirely monocular, group 4 denotes equally balanced input from left and right eyes, and groups 2, 3, 5, and 6 indicate binocular cells with varying degrees of contralateral or ipsilateral dominance. In the original description of these categories, there is a footnote for groups 2 and 6 which states that for these cells, the non-dominant eye may be ineffective in activating the cell but it could influence the response to stimulation of the dominant eye (Hubel and Wiesel, 1962). No data were given to substantiate this statement, and no further mention is made of it in the original paper or in subsequent work.

In studies that followed, other investigators were apparently unaware of the footnote. An entire literature resulted in which binocular status was measured and assessed using monocular tests to derive ocular dominance histograms. Most of the experiments in the study of development and plasticity of vision use ocular dominance histograms, subjectively obtained, to draw conclusions concerning the effects of a given protocol. In the examples described below, it is shown that the reliance on subjective ocular dominance histograms can underestimate the degree of binocularity of a population of cells in the visual cortex. It seems unlikely that the conclusions of many studies in which this was the sole basis of assessment are incorrect. However, it is possible that for some investigations, especially those concerning the effects of monoc-

ular deprivation, there may have been more binocularity than was reported.

As noted above, estimation of this parameter is the primary measurement of a very large body of literature. In nearly every study, subjective measurements have been made of ocular dominance by using tests of response strength through each eye and then assigning an ocular dominance rating. This rating is then taken as a statement about the binocular status of the cell even though, in nearly every case, no binocular tests were performed. There are many studies on the development and plasticity of vision in which ocular dominance histograms, for different conditions of rearing, are derived for a sample of cells. Different protocols, mainly of a phenomenological nature, have been used to make inferences about mechanisms. In most of these studies, the shape of the ocular dominance histogram is the sole basis for conclusions about how a given rearing condition interferes with the development of normal binocular vision. Brief descriptions of these studies are presented below and in other reviews (e.g., Mitchell and Timney, 1984).

The main problem with this experimental process is that the method of estimating ocular dominance histograms is not entirely accurate. Specifically, it tends to make the cell under study appear to be more monocular than it actually is if tested binocularly. This is because of a threshold non-linearity in which a subthreshold input from an eye that appears to be silent can be expressed under binocular viewing and testing conditions. In other words, cells may appear to be monocular when each eye is tested individually, but they exhibit clear binocular interaction when tested dichoptically (Freeman and Ohzawa, 1988, 1992; Ohzawa et al., 1996). This interaction may be phase specific or it may be a general suppressive effect. In any case, these considerations make it clear that the use of subjective estimates of ocular dominance designations is not the correct way to determine binocular status. Instead, dichoptic tests should be run by which one may derive a binocular interaction index, such as that described below which specifies depth of modulation (Freeman and Ohzawa, 1992).

Binocular interaction measured by phase-shifted gratings

In a classical study of the retina, gratings with sinusoidal luminance profiles were used to determine spatial summation characteristics of RFs of ganglion cells (Enroth-Cugell and Robson, 1966). A number of similar investigations were then carried out at different levels of central and peripheral visual pathways. We used a related approach to study the binocular system and sought to determine the rules by which signals from left and right eyes are combined (Freeman and Robson, 1982; Ohzawa and Freeman, 1986a, 1986b). To do this, we used dichoptically presented, phased-varying gratings with sinusoidal luminance distributions. The stimuli are

depicted in Figure 48.4. In Figure 48.4A, a relative phase shift between two sinusoidal gratings is represented on the left. On the right, phase shifts in actual gratings are shown in a dichoptic presentation. In Figure 48.4B, RFs of simple cells are represented by Gabor functions. The abscissas for these curves denote retinal position, and the ordinate gives sensitivity to a luminance increment. In this case, negative positions of each curve represent OFF (dark-excitatory) subregions and positive positions denote ON (bright-excitatory) subregions. Dashed curves represent Gaussian envelopes of the idealized RFs. The curves give a full range of RF shape representations for phase shifts around the clock. Figure 48.4C depicts how relative dichoptic phase shifts appear to a viewer.

Before describing specific results, it is worthwhile to consider how signals from left and right eyes may be combined in the visual cortex. Inputs, which may be symmetrical, could be combined in a linear manner. This is represented in Figure 48.5A. Inclusion of a threshold mechanism, which follows binocular convergence, may be added to this rule of combination. In Figure 48.5B, multiplicative convergence is depicted. A good example of this is when a cortical cell is unresponsive to input through either eye but responds to stimulation of both eyes simultaneously (Hubel and Wiesel, 1962; Barlow et al., 1967). Figures 48.5C and 48.5D depict conditions in which there are symmetrical inputs that are modified by postsynaptic (C) or presynaptic (D) inhibition. For a great deal of the data that we and others have collected, results may be accounted for by a process of linear summation combined with a threshold mechanism. For other data, multiplicative binocular interaction is a major component both for simple and for complex cells (Anzai et al., 1999a, 1999b).

The unique characteristic of simple cells in the visual cortex is that they have discrete ON and OFF adjacent regions in their RFs. Therefore, dichoptic presentation of phase-varying gratings should result in regular increments and decrements of a neuron's response corresponding to the relative stimulation of ON and OFF areas of the RF. This is in fact what occurs for nearly all cells. Data from the detailed study of cortical cells, using this technique, are shown in Figures 48.7, 48.8, and 48.9. For comparison, results from tests of an LGN cell are shown first (Fig. 48.6).

To do these tests, qualitative estimates are made initially of the preferred stimulus parameters of each cell. For cortical

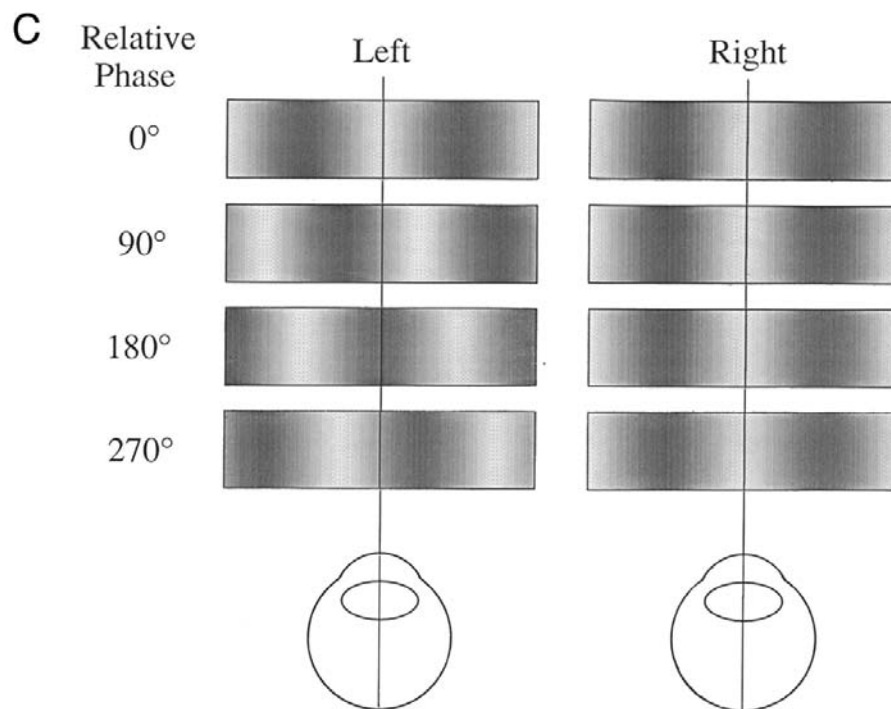
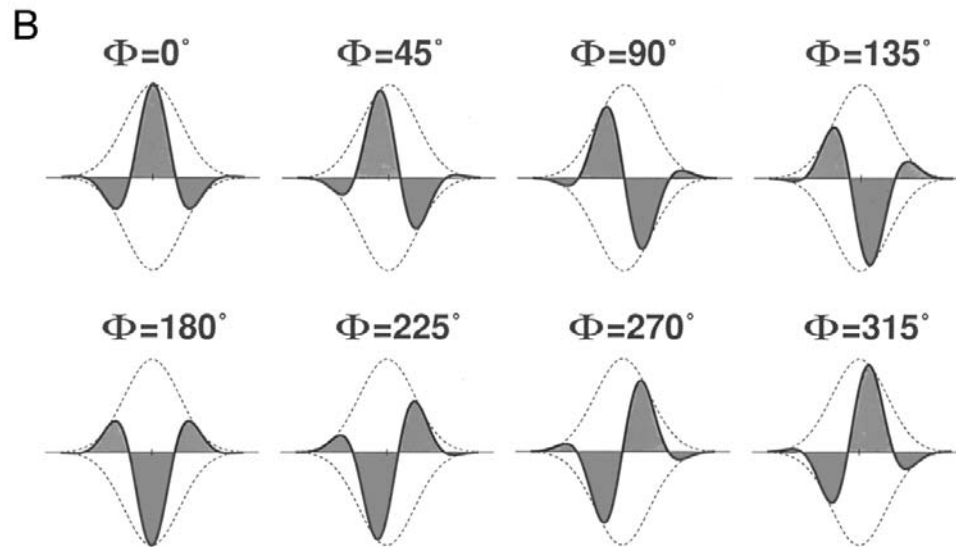
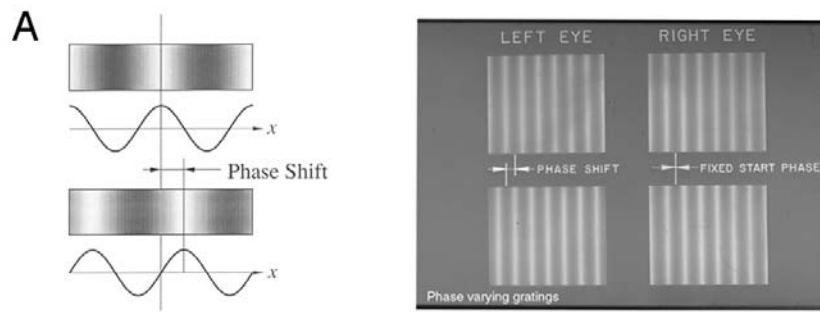
cells, this includes orientation and spatial frequency preferences. Since cortical cells are broadly tuned temporally, nearly all tests are run at 2 Hz. Contrast is arbitrarily set to elicit strong responses without causing excessive saturation. Generally, values of 50% are used. After each eye is tested monoptically, dichoptic presentations are made with relative interocular phase varied randomly, generally in 30-degree or 45-degree steps.

Responses from an LGN cell are illustrated in Figure 48.6. Results of monocular tests are shown in Figures 48.6A and 48.6B for orientation and spatial frequency, respectively. A typical pattern is seen, that is, responses are monocular (left eye driven in this case) and nonorientation specific. Clear spatial frequency selectivity is exhibited by the responsive eye. Phase-specific responses are shown in Figure 48.6C for randomly interleaved steps of 45 degrees. Monocular and blank (null) conditions are interleaved with the dichoptic tests. As expected, dichoptic tests elicit clearly modulated bursts corresponding to ON areas and silent sections in which ON and OFF regions counterbalance each other. The null condition shows a substantial level of spontaneous activity, and this is also observed in the monocular run of the nonresponsive right eye. Since binocular interaction at the level of the LGN is minimal, with the exception of a very mild suppressive influence from the nonresponsive eye, presumably mediated through intralaminar connections (Xue et al., 1987), dichoptic relative phase shifts are not expected to alter response levels. As seen in Figure 48.6D, there are minimal changes in response for the LGN cell illustrated. Response amplitudes shown in Figure 48.6D are obtained by harmonic analysis of each histogram in Figure 48.6C at the temporal frequency of the grating drift. The average spontaneous level is shown by the dashed line at the bottom of Figure 48.6D.

Data for a simple cell, in the same format as those for the LGN unit described above, are shown in Figure 48.7. Clear orientation and spatial frequency tuning functions are seen in Figure 48.7A and 48.7B, respectively, for monoptic runs. The PSTH histogram of Figure 48.7C shows a typical modulated discharge with bursts of firing at the first harmonic of the temporal frequency of the stimulus grating. Responses from right eye stimulation are stronger than those from the left eye. Note that at a relative interocular phase of 180 degrees, the neuron is silent. Phase positions on either side yield increased response levels. This is shown clearly in the harmonic analysis of Figure 48.7D. This

FIGURE 48.4. Phase shift grating conditions are illustrated. In *A*, a relative phase shift between an upper and a lower sinusoidal grating pair is depicted on the left. On the right, a fixed phase position is maintained for the right eye. For the left eye, the grating phase is varied. In *B*, various phase angles are indicated for Gabor functions that represent receptive field profiles for simple cells. The

abscissa for each curve gives retinal position, and the ordinate represents sensitivity. Dashed curves are Gaussian envelopes of the model receptive fields. In *C*, the appearance of phase-shifted, dichoptically viewed gratings is illustrated with fixed phase positions for the right eye.



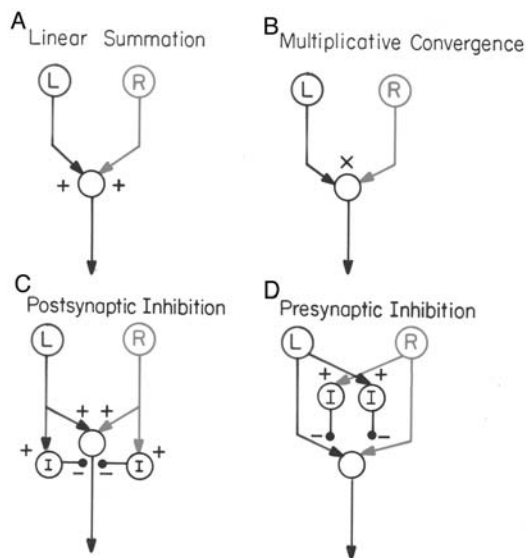


FIGURE 48.5. Four schematic models are illustrated that might underlie the rules of combination of signals from left and right eyes. L and R represent left and right eyes, respectively. Inhibitory interneurons are labeled I.

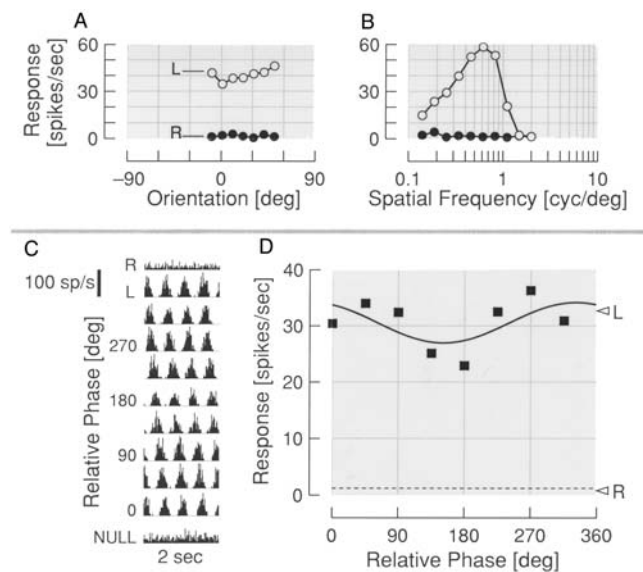


FIGURE 48.6. Responses are shown for an LGN neuron stimulated with drifting sinusoidal gratings. *A* and *B* represent orientation and spatial frequency tuning curves, respectively, for monocular tests. Dichoptic tests, run with phase-varying gratings, result in the PSTH data of *C*. The null condition is for a luminance screen with no pattern. Harmonic analysis is performed on the histograms of *C*, resulting in the function of *D*, in which responses are indicated for different relative phases.

phase-varying function is equivalent to a retinal disparity tuning curve.

An example of a typical complex cell response is represented in Figure 48.8. Once again there is clear, although relatively broad, tuning for orientation and spatial frequency

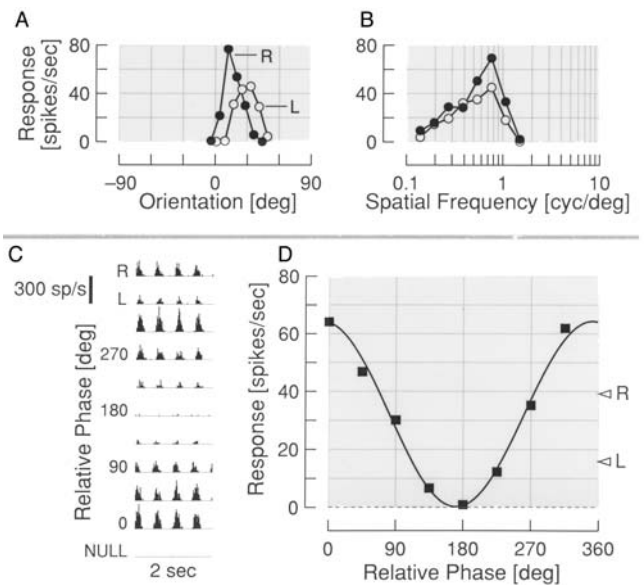


FIGURE 48.7. Responses are shown for monoptic and dichoptic tests of a cortical simple cell. The same format as that in Figure 48.7 is used.

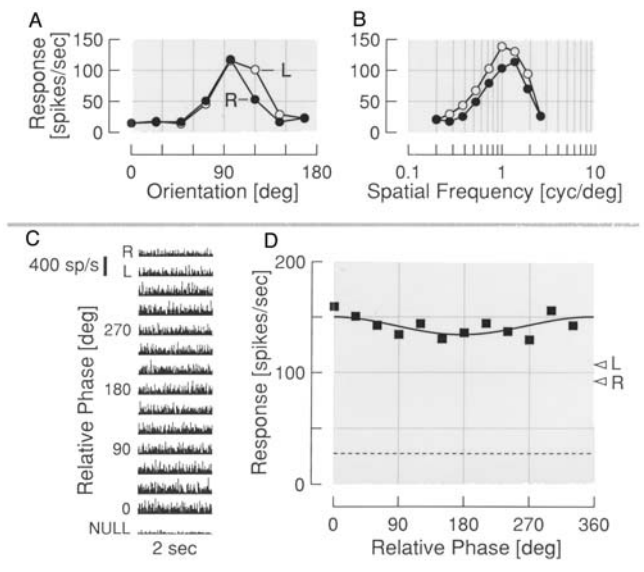


FIGURE 48.8. Responses are shown for monoptic and dichoptic tests of a cortical complex cell for which responses are phase insensitive. The same format as that in Figure 48.7 is used.

in the monoptic testing mode. The PSTH histograms shown in Figure 48.8C exhibit typical uniform discharge rates across the entire range of relative phase. As a result, the harmonic analysis yields a relatively flat response function, as presented in Figure 48.8D.

What is unexpected, however, is the other example of responses from a complex cell, as shown in Figure 48.9. As in the previous case, monoptic tuning functions for orientation and spatial frequency are clear and fairly broad. The PSTH histograms in Figure 48.9C exhibit nonmodulated

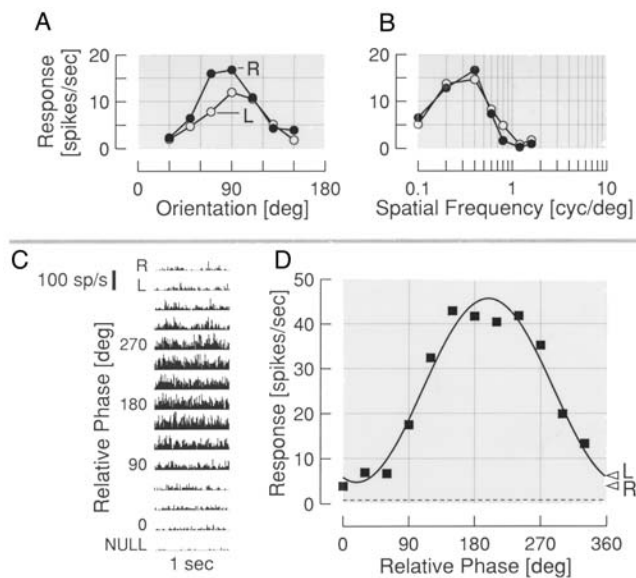


FIGURE 48.9. Responses are shown for monoptic and dichoptic tests of a cortical complex cell for which responses are phase specific. The same format as that in Figure 48.7 is used.

discharge patterns, but there are prominent differences for relative phase values. Monocular responses are relatively weak, and relative phases around 210 degrees are very strong. Phase values near 0 degrees are also weak. The result, as shown in the harmonic analysis of Figure 48.9D, is a clear phase-tuned response function. Since ON and OFF regions of complex cells are mixed so that the position of a stimulus in the monocular mode is not critical, relative phase tuning is not expected to be found in the dichoptic condition.

A possible explanation of this type of response is that the subunits of complex cells which exhibit phase-sensitive binocular interaction are either simple cells or are organized

like simple cell RFs. One prediction of this arrangement is that the subunits, which are phase specific, retain this characteristic at the output level of the neuron which would account for the pattern seen in Figure 48.9. It is possible to probe this conjecture by creating a special testing protocol, as illustrated in Figure 48.10. In each case illustrated (*A*, *B*, and *C*), a complex cell is depicted from which PSTH histograms are being collected in response to different stimulus protocols. In Figure 48.10A, a sinusoidal grating with optimal parameters of orientation, spatial frequency, and temporal frequency is drifted in a given direction across the RF. Stimulation in this case is monoptic, and the right eye is occluded. The resulting PSTH data at the bottom depict a typical mean discharge elevation without modulation. Figure 48.10B represents the result of another monoptic stimulation protocol with a grating of optimal parameters. In this case, the grating is not drifted. Instead, it is counterphased in place, that is, it flickers, with dark and bright components exchanging places sinusoidally. The typical response of a complex cell to this stimulus is different from the maintained discharge represented in Figure 48.10A. A flickering grating stimulus causes a modulated discharge at twice the temporal frequency of the counterphase, that is, there are two bursts of discharge per cycle of flicker (Movshon et al., 1978). The PSTH in Figure 48.10B represents a frequency-doubled response in accordance with previous results.

An interesting test concerning the organization of the subunit may be conducted by noting a relationship in wave theory. Traveling and standing sine waves are related to each other as follows. If two identical sine waves are drifted in opposite directions at the same drift rate, the combination results in a single flickering sine wave with twice the peak amplitude of each drifting wave.

With this relationship in mind, the question of subunit organization may be addressed in the following manner. A

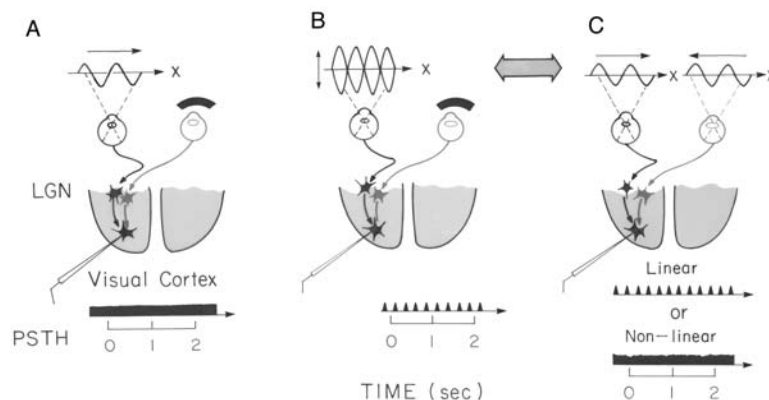


FIGURE 48.10. A schematic illustration is shown of predicted responses of a complex cell according to different stimulus configurations. In *A*, a drifting grating is presented to the left eye only, resulting in an average increase in mean discharge. In *B*, a counterphase grating is shown to the left eye only, resulting in a modu-

lated, frequency-doubled response. In *C*, gratings are drifted in opposite directions in front of each eye, resulting in either a frequency-doubled (linear combination) response or an average increase in mean discharge (nonlinear combination).

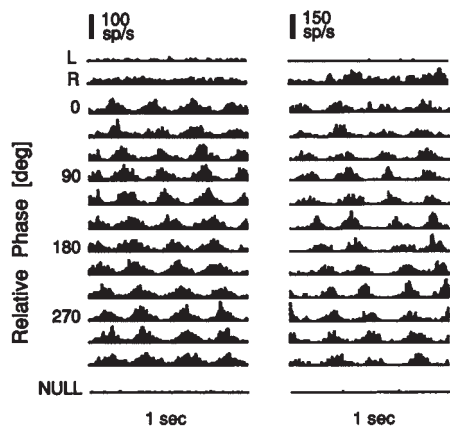


FIGURE 48.11. PSTH histograms are presented for two complex cells stimulated by sinusoidal gratings of optimal parameters drifting at the same rate in opposite directions before left and right eyes. The right eye dominates in each case. The drift rate of 2 Hz yields four bursts of discharge per second, that is, the response is frequency doubled.

sinusoidal grating of optimal parameters is drifted across the RF of each eye in opposite directions, as depicted in the upper part of Figure 48.10C. If the drifting gratings are combined neurally, then the cells' response would be equivalent to that for a counterphased grating, that is, the discharge would be modulated bursts at twice the drift frequency. This would occur if the subunits of the complex cell carried out a linear summation of the inputs from each eye. The alternative is for a nonlinear combination to occur in which the response to a drift pattern is the dominant factor. In this case, the response of the complex cell would be a mean discharge with no modulation. These alternative possibilities are depicted in Figure 48.10C.

Examples of responses to the stimulus configuration shown in Figure 48.10C are given for two complex cells in Figure 48.11. Monocular responses are indicated in the top two histograms. For both cells, stimulation of the right eye causes an increase in mean discharge. The left eye does not respond in either case, that is, both cells are almost completely direction selective. Again in both cases, there is a striking modulated discharge pattern at virtually all relative phase values dichoptically tested. The temporal scale shows 1 second of response time, and the drift rate of each moving grating is 2 Hz. Therefore, the response of each cell is a frequency-doubled discharge, as predicted for a linear combination of signals from left and right eyes. In these cases, and in many others we have observed, the silent eye during monoptic testing exerts a clear influence on the cell's response during dichoptic activation (Ohzawa and Freeman, 1986a, 1986b; Freeman and Ohzawa, 1988, 1992).

Binocular processing of contrast

How do the above findings apply to standard variables of a visual stimulus? Of all the parameters of visual processing,

contrast is one of the most fundamental. It is perhaps the most straightforward variable to observe with respect to changes of response strength in central visual pathways. This is because alterations in contrast levels presumably affect a relatively uniform population of neurons. Many investigations have been carried out regarding the advantages in sensitivity of binocular compared to monocular vision. Most of these are psychophysical studies. In some of this work, it is suggested that binocular summation is not simply a statistical effect by which there are two chances to observe a given stimulus. Instead, it is thought to involve an active process in which there is neuronal interaction between signals from left and right eyes (e.g., Blake and Fox, 1973; Blake et al., 1981).

Although most of the work in this area has been done from a behavioral perspective, there are relevant physiological data on binocular summation. There has also been an attempt to relate directly the behavioral and physiological approaches. The neural basis of binocular summation in behaviorally determined contrast detection may be studied by measuring contrast response functions of cells in central visual pathways. By comparing results of tests from monoptic and dichoptic stimulation and applying receiver operating characteristic (ROC) analysis to the data, it is possible to derive monocular and binocular neurometric functions for each cell (Bradley et al., 1985). From this analysis, contrast thresholds and slopes for each neurometric function may be determined. Taken together, these data provide a bridge between behavioral and physiological studies.

Examples of responses from cells tested over a wide range of contrasts from 1% to $\approx 30\%$ are presented in Figure 48.12. In Figure 48.12A, data are shown for a simple cell for which left and right eye response strengths are approximately equal. The response rates for the left eye, right eye, and both eyes (*open circles*, *filled circles*, and *open triangles*, respectively) increase almost linearly with log contrast above an apparent contrast threshold level. There is some evidence of saturation in the binocular run at the higher contrast levels. Response strengths of the binocular tests are substantially stronger than the monocular counterparts at all but the lowest contrast levels. For the complex cell, whose data are shown in Figure 48.12B, right eye responses are stronger than those of the left eye, and binocular tests yield higher discharge rates than either. Monocular runs have steeper slopes than those for the simple cell of Figure 48.12A, and there is only a slight hint of saturation in the binocular function. Although these examples are representative of a relatively large population, there is considerable variability in response functions among the cells.

There are a number of aspects to the analysis of these data. Two elements are presented in Figure 48.13. Contrast thresholds are estimated by analysis of neurometric functions and ROC curves by which estimates are made of slope

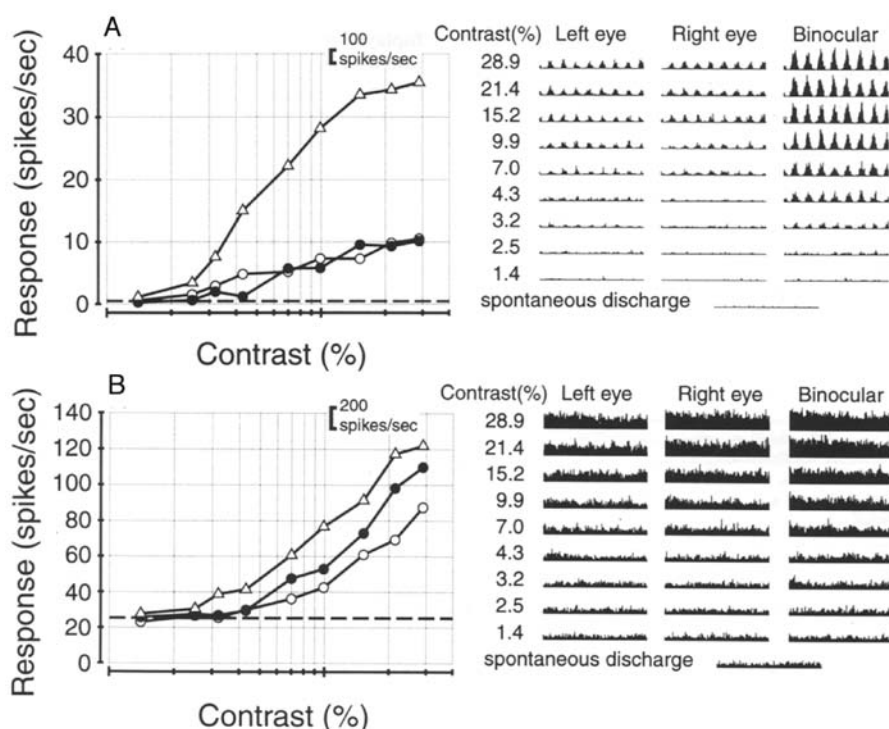


FIGURE 48.12. Contrast response functions are shown for a cortical simple cell (A) and a complex cell (B). Open circles, filled circles, and open triangles represent mean discharge rates for the left eye, right eye, and binocular stimulation, respectively. Dashed lines indicate spontaneous levels.

intercepts. In this case, contrast threshold is defined as the contrast which gives a response probability of 0.75. This is an operational criterion response probability of a neuro-metric function. Details of the procedures used to drive these estimates are given elsewhere (Anzai et al., 1995). Distributions of estimated contrast thresholds for a population of cortical cells are given in Figure 48.13A. Values for the left eye, right eye, and both eyes are given, respectively, in the histograms from top to bottom. The geometric means, indicated by arrows above each histogram, are 6.8%, 6.2%, and 4.2%, respectively, for the left, right, and both eyes. Mean monocular thresholds of left and right eyes are significantly greater than that for both eyes together.

If the ratio of monocular contrast threshold to binocular contrast threshold is computed for each cell, it is possible to derive an index of binocular advantage for the population of cells under study. This commodity, which may be called a *binocular advantage ratio*, is plotted in Figure 48.13B. Open and filled arrows indicate geometric means of the binocular advantage ratios for left/binocular and right/binocular distributions, respectively. The values for left and right eyes are very similar (1.86 and 1.82, respectively). These values are significantly greater than a ratio of 1, indicating that individual neurons have a clear binocular advantage in processing visual information.

Contrast differences between left and right eyes

Just as the retina adapts to prevailing absolute luminance levels (Kuffler, 1953), the visual cortex adjusts its response range according to ambient contrast. This adaptive mechanism, contrast gain control (Ohzawa et al., 1985; Sclar et al., 1985), is a very effective way of maintaining high sensitivity over a large range of contrasts. Although this mechanism is transferable from one eye to the other (Sclar et al., 1985), interocular contrast mismatches suggest independent control of monocular pathways. Direct comparisons of monocular and binocular contrast encoding indicate that the primary mechanism occurs at a monocular site (Truchard et al., 2000).

Suppose that the contrast of a visual stimulus is relatively weak in one eye and strong in the other. This may happen in cases of anisometropia, amblyopia, or strabismus in which one eye has reduced function. It may also occur in rare cases in individuals with normal binocular vision when specular reflection from a surface effectively reduces the contrast of one eye's view more than the other. In any case, it is reasonable to assume that the eye through which a weak signal is generated will have little overall influence on the visual process. The results of psychophysical studies are consistent with this conjecture (Halpern and Blake, 1988; Legge and Gu, 1989; Schor and Heckmann, 1989; Westheimer and McKee, 1980). These studies show that relatively small

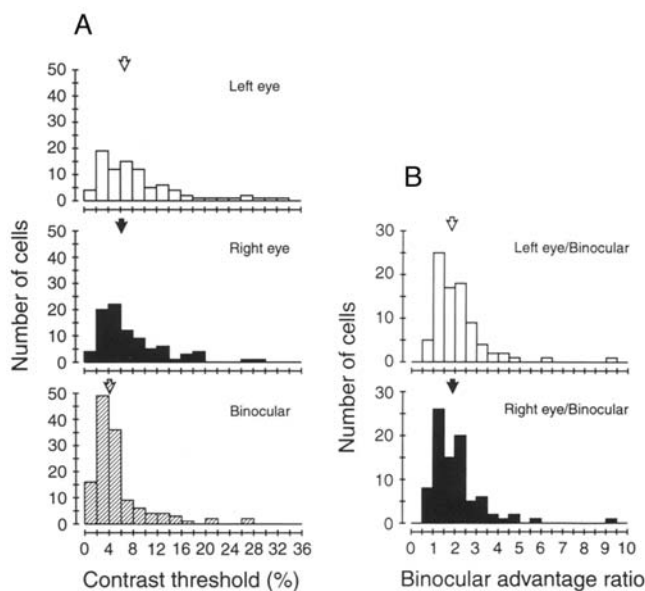


FIGURE 48.13. In *A*, contrast thresholds are shown for left eye, right eye, and binocular stimulation. Arrows indicate geometric means of contrast thresholds. The mean binocular threshold is significantly lower than either monocular value. In *B*, binocular advantage ratios are shown for left and right eyes. Arrows indicate geometric means of the binocular advantage ratios. Considered together, these data indicate that individual neurons have a significant binocular advantage.

contrast mismatches between the two eyes result in severely reduced stereo acuities. However, physiological investigations of interocular contrast differences yield different results. In particular, binocular interaction studies in which interocular phase is varied between gratings with different contrast values for each eye, demonstrate a compensation mechanism which acts to effectively boost the signal from the weak eye.

Examples of results from this physiological test are given in Figure 48.14. In Figure 48.14*A*, data are shown for a vigorously responding phase-specific complex cell tested with 50% contrast gratings presented to left and right eyes. The clear phase-specific response is typical of about half the population of complex cells (Ohzawa and Freeman, 1986a, 1986b). The same test was run again, but in this case, grating contrast to one eye was reduced by nearly a log unit to 6.3%. The result, shown in Figure 48.14*B*, is remarkably similar to the previous finding, that is, there is a clear phase-specific response pattern, with only a slightly reduced peak discharge rate around a relative phase of 180 degrees. A second complete run was made with another set of contrasts, that is, 50% to one eye and 12% to the other, and a very similar result was obtained. To quantify the degree of binocular interaction, one cycle of a sinusoid is fit to the phase-specific response curve. Using this fit, a *depth of modulation* index is derived allowing quantification of the degree of binocular interaction. The depth of modulation is equal to the ratio of amplitude of the fitted sinusoid over the mean of the binocular responses. In general, the larger the index,

the stronger the degree of binocular interaction. The flatter the interaction curve, the closer the index is to zero. In this case, stimuli presented to a given eye has no effect on the other eye's response pattern. In other words, the depth of modulation index provides a quantified assessment of the effect one eye has on a cell. Excitation through the other eye is used as the reference for this index.

In Figure 48.14*C*, depth of modulation is plotted on the left vertical axis and the response of the neuron to different contrasts is plotted for one eye (the left) on the right vertical axis. For the two contrast difference levels, depth of modulation is nearly the same as that for the identical contrast runs (50% for each eye). The contrast response curve for the left eye is standard and has a steep slope, that is, it is a monotonically increasing function. A second example, this time for a simple cell, is illustrated in Figure 48.14*D–F*. The same format as for the preceding example is used, and the data show a very similar pattern. Once again, the depth of modulation is essentially flat and the contrast response function for the left eye is also a steep, monotonically increasing curve, as in the previous example. For both of the cells shown in Figure 48.14, there is essentially no reduction in the depth of modulation even with relatively enormous differences in contrast levels between left and right eyes. This pattern may be compared with the monocularly elicited responses to stimulation of one eye (the left in both cases). In both monoptic cases, there is a sharp decline in response as contrast is reduced. These examples are clearly representative of a larger sample. For 21 cells tested in similar ways, mean depth of modulation values are given in Figure 48.14*G*. Once again, contrast differences between left and right eyes appear to have little effect on depth of modulation. These results may be interpreted in the context of a contrast gain reduction system that is mainly operational at monocular sites in the visual pathway (Truchard et al., 2000).

The compensatory mechanism for unequal signal strength in right and left eyes

What is the main implication of the results from the dichoptic experiments employing a strong stimulus to one eye and a weak one to the other? The data presented above for dichoptic stimulation with phase-varying gratings having different contrast levels for left and right eyes show clearly that a compensatory mechanism provides relative constancy of interaction. Since the use of a low-contrast grating implies a raised threshold, there must be a synaptic gain of signals from the eye receiving weak input. The gain must be high when input contrast is low and relatively low when input contrast is high. This suggests two mechanisms in the compensatory process. The first is a threshold mechanism that follows the convergence of inputs from both eyes. Strong inputs from either or both eyes raise the threshold level for spike discharge. Because monocular input can raise the threshold, and both eyes are affected, this may account for

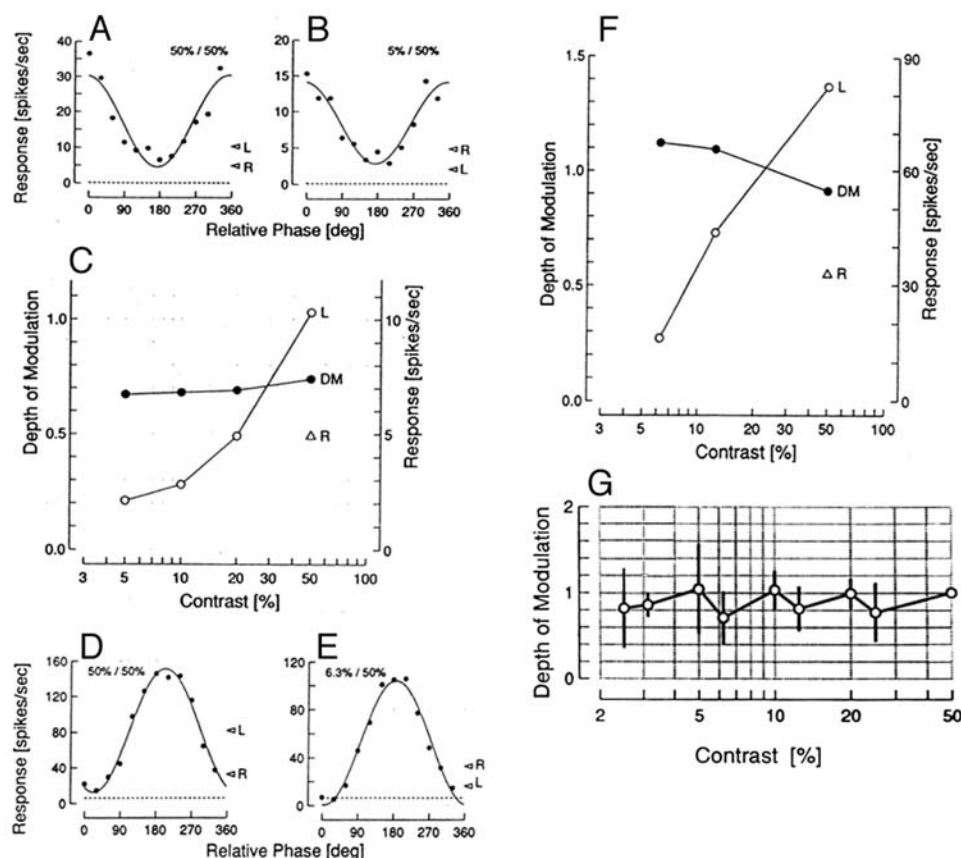


FIGURE 48.14. Data are shown for dichoptic tests in which the contrast of the grating presented to one eye is considerably lower than that for the other eye. Results are given for equal right and left eye contrasts (*A*) and unequal contrasts (*B*). In *C*, depth of modulation is shown for four contrast difference values (filled symbols).

the interocular transfer of contrast gain control. The second mechanism is also a type of contrast gain control. In this case it is a monocular function, and it operates at the synaptic contact between a given eye and a cortical target cell. This second mechanism can account for the observed constancy of binocular interaction when low- and high-contrast gratings are used for left and right eyes, respectively.

Interocular contrast differences create artificial changes in ocular dominance

We have considered how the assessment of binocular status should not be made. It is now possible to address ocular dominance from a different perspective. Note that the binocular presentation of unequal contrast gratings is a way to alter ocular dominance artificially. This is because contrast is a stimulus variable that directly affects the input strength that cortical cells receive. Ocular dominance is determined by the relative gain of inputs to a given cell from left and right eyes. Although the gain control mechanism is not readily available for experimental manipulation, net input to a given cortical cell from each eye may be altered by changes in input strength. This, in effect, changes the ocular dominance of

The same graph contains a contrast response function for the left eye with the discharge rate on the right. *D*, *E*, and *F* contain the same type of data for another cell. *G* is a summary graph for a population of cells showing that contrast differences between left and right eyes do not change the depth of modulation.

the neuron. This change is, of course, an artificial one and temporary. It should not be confused with previous attempts to change the intrinsic ocular dominance of a neuron as it is studied (Tsumoto and Freeman, 1981).

With the artificial changes in ocular dominance, instituted by the unequal contrast experiments, there is a somewhat surprising constancy in binocular response. This constancy occurs over a very wide range of input strength variation between the eyes. An eye with relatively reduced strength, by as much as a full log unit, still modulates the response of a given neuron. How does this apply to the case of actual variations in ocular dominance, as expressed in the full range of values that are reported in histograms? A gain imbalance in a normal visual cortex may be compensated for by mechanisms such as those discussed above. The wide range of ocular dominance values that are observed may be the result of a genetic compromise because it may be relatively difficult to program every cortical cell so that it has exactly balanced input from left and right eyes. However, because of the compensatory mechanisms described here, ocular dominance variability may not be important for binocular visual function under real conditions. Therefore, the subject of

ocular dominance of cortical cells may be of interest in laboratories but of little consequence in the real world of binocular vision.

Development and plasticity of binocular vision

Quantitative investigations of development of binocular vision have shown that the physiological apparatus that underlies this function is operational as early as one can effectively measure it. This applies to the kitten's visual system (Freeman and Ohzawa, 1992) as well as that of the primate (Chino et al., 1997). Although the subject of development and plasticity of vision is not part of the topic of this chapter, it is of interest here because it provides an opportunity to emphasize how estimates of binocular function can differ, depending on how measurements are made. Two examples are instructive, and they are illustrated in Figure 48.15.

The first example is for a cortical neuron recorded from a normally reared kitten at 3 weeks' postnatal. Note the standard tuning curves for orientation and spatial frequency for the left eye (Figs. 48.15*A* and 48.15*B*). For the right eye the curves are completely flat because there is no response for orientation and spatial frequency runs. In the dichoptic mode in which gratings are presented at various relative interocular phases, there are clear modulated responses (Fig. 48.15*C*). The monoptic response, for the left eye, is slightly modulated and the discharge is vigorous. Once again, in this sequence, the right eye is completely silent. What is striking is that harmonic analysis (Fig. 48.15*D*) reveals a clear overall suppressive effect. The eye which is silent when tested monoptically exerts a clear and substantial overall suppression of the response. There are two functions in Figure 48.15*D*. Data for one curve (*filled symbols*) were obtained 20 minutes after completion of the first run. Data from the second run are nearly superimposed on those from the first, so the overall suppression is clear and consistent. The conclusion here is that an eye that appears completely silent in the monocular mode is clearly connected to the neuron under study when tests are conducted dichoptically. The point is that an inaccurate picture is presented if only monocular tests are performed.

A similar situation applies for the other cell for which data are presented in Figure 48.15*E–H*. In this case, the neuron was recorded from a cat that had been monocularly deprived for nearly 3 years starting at the age of 3 weeks' postnatal. As the data in Figures 48.15*E* and 48.15*F* show, the nondeprived (left) eye drives the cell vigorously and the deprived (right) eye is completely ineffective. The PSTH data in Figure 48.15*G* again show a strong discharge from the nondeprived eye and greatly reduced responses for the dichoptic relative phase runs. Plots of the response amplitude (DC

component) obtained from harmonic analyses of the histograms in Figure 48.15*G* are presented as a function of relative phase in Figure 48.15*H* (*open symbols*). As the graph shows, there is a very strong non-phase-specific, uniform depression of responses compared to response levels for the nondeprived (left) eye alone. The neuron's activity is nearly shut off. A second curve (*filled symbols*) is also shown. These data, nearly superimposed on the first curve, are for a second interocular relative phase run in which the grating for the deprived (right) eye is rotated by 90 degrees so that it is orthogonal to the optimal grating orientation. As the data show, the suppressive influence of the deprived (right) eye is nonoriented. Once again, monocular tests alone do not capture the response characteristics of this neuron. There are many similar examples, and these have been documented elsewhere (e.g., Freeman and Ohzawa, 1988, 1992). Considered together, these data demonstrate that binocular tests are required to establish complete characteristics of neuronal responses in the visual cortex.

Conclusions

This review considers some of the essential factors in the physiological combination of signals from left and right eyes. The integration of monocular pathways in striate cortex produces the neural substrate for stereoscopic depth discrimination. This function is considered only briefly here. The focus instead is on the underlying features of the neural elements of binocular function. One of the key points is that the long-standing use of monocular tests to estimate binocular function in the form of ocular dominance measurements is not adequate. Instead, dichoptic techniques should be employed. Standard parameters and results of dichoptic tests involving phase-varying sinusoidal gratings are considered. The binocular processing of contrast information is dealt with in order to consider the physiological advantage of binocular compared to monocular vision. For gratings presented dichoptically, differences in contrast between left and right eye gratings result in surprisingly constant binocular interaction profiles. Gain control mechanisms, primarily at monocular sites, are responsible for this effect. Differences in left and right eye grating contrast also permit artificial manipulation of effective ocular dominance. The findings from these experiments suggest that ocular dominance differences among a population of cortical cells may be of laboratory interest only. It is possible that compensatory mechanisms offset ocular dominance variability in perceptual vision. Finally, brief consideration is given to the development and plasticity of vision to illustrate that monocular tests do not expose subthreshold input from an eye. In this case, binocular function is not adequately determined.

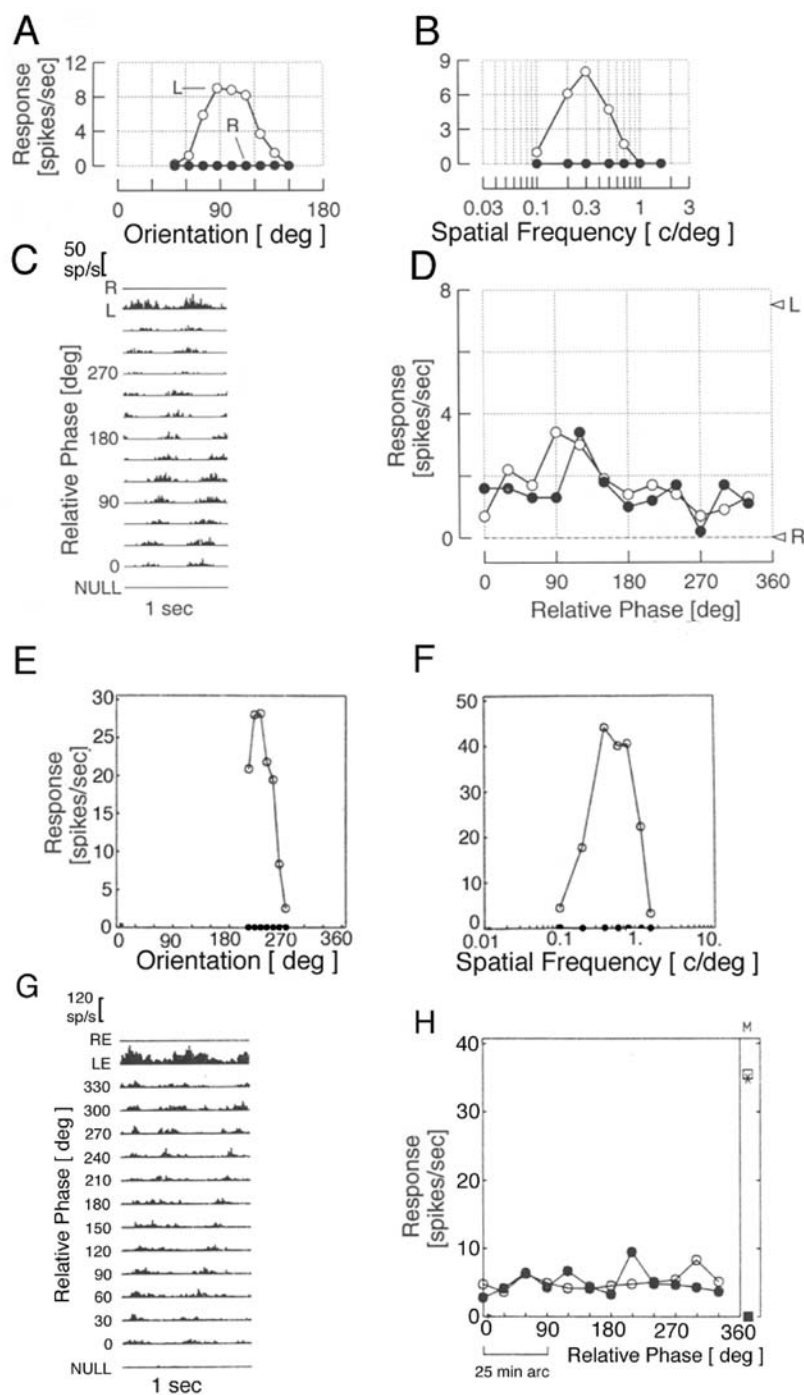


FIGURE 48.15. Results of monoptic and dichoptic tests are presented for a kitten at 3 weeks postnatal (A–D) and for an adult reared with right eye monocular deprivation (E–H). The format is the same as that in Figures 48.7 to 48.10. The second curve in D (filled symbols) is from a complete dichoptic test, identical to the first,

run 20 minutes after completion of the initial sequence. There are also two sets of data in H. One curve (filled symbols) is for a condition in which the grating presented to the deprived eye is rotated 90 degrees during the dichoptic test.

REFERENCES

- Anzai, A., M. A. Bearnse, Jr., R. D. Freeman, and D. Cai, 1995. Contrast coding by cells in the cat's striate cortex: monocular vs. binocular detection, *Vis. Neurosci.*, 12(1):77–93.
- Anzai, A., I. Ohzawa, and R. D. Freeman, 1999a. Neural mechanisms for processing binocular information I. Simple cells, *J. Neurophysiol.*, 82(2):891–908.
- Anzai, A., I. Ohzawa, and R. D. Freeman, 1999b. Neural mechanisms for processing binocular information II. Complex cells, *J. Neurophysiol.*, 82(2):909–924.
- Barlow, H. B., C. Blakemore, and J. D. Pettigrew, 1967. The neural mechanism of binocular depth discrimination, *J. Physiol.*, 193(2):327–342.
- Blake, R., and R. Fox, 1973. The psychophysical inquiry into binocular summation, *Percept. Psychophys.*, 14:161–185.
- Blake, R., M. Sloane, and R. Fox, 1981. Further developments in binocular summation, *Percept. Psychophys.*, 30(3):266–276.
- Bradley, A., B. C. Skottun, I. Ohzawa, G. Sclar, and R. D. Freeman, 1985. Neurophysiological evaluation of the differential response model for orientation, and spatial-frequency discrimination, *J. Opt. Soc. Am. A*, 2(9):1607–1610.
- Chino, Y. M., E. L. Smith 3rd, S. Hatta, and H. Cheng, 1997. Postnatal development of binocular disparity sensitivity in neurons of the primate visual cortex, *J. Neurosci.*, 17(1):296–307.
- Cumming, B. G., and A. J. Parker, 2000. Local disparity not perceived depth is signaled by binocular neurons in cortical area V1 of the macaque, *J. Neurosci.*, 20(12):4758–4767.
- DeAngelis, G. C., and W. T. Newsome, 1999. Organization of disparity-selective neurons in macaque area MT, *J. Neurosci.*, 19(4):1398–1415.
- DeAngelis, G. C., I. Ohzawa, and R. D. Freeman, 1991. Depth is encoded in the visual cortex by a specialized receptive field structure, *Nature*, 352(6331):156–159.
- Enroth-Cugell, C., and J. G. Robson, 1966. The contrast sensitivity of retinal ganglion cells of the cat, *J. Physiol.*, 187:515–552.
- Ferster, D., 1981. A comparison of binocular depth mechanisms in areas 17, and 18 of the cat visual cortex, *J. Physiol.*, 311:623–655.
- Freeman, R. D., and I. Ohzawa, 1988. Monocularly deprived cats: binocular tests of cortical cells reveal functional connections from the deprived eye, *J. Neurosci.*, 8(7):2491–2506.
- Freeman, R. D., and I. Ohzawa, 1990. On the neurophysiological organization of binocular vision, *Vis. Res.*, 30(11):1661–1676.
- Freeman, R. D., and I. Ohzawa, 1992. Development of binocular vision in the kitten's striate cortex, *J. Neurosci.*, 12(12):4721–4736.
- Freeman, R. D., and J. G. Robson, 1982. A new approach to the study of binocular interaction in visual cortex: normal and monocularly deprived cats, *Exp. Brain Res.*, 48(2):296–300.
- Halpern, D. L., and R. R. Blake, 1988. How contrast affects stereoacuity, *Perception*, 17(4):483–495.
- Hubel, D. H., and T. N. Wiesel, 1962. Receptive fields, binocular interaction, and functional architecture in the cat's visual cortex, *J. Physiol.*, 160:106–154.
- Hubel, D. H., and T. N. Wiesel, 1968. Receptive fields and functional architecture of monkey striate cortex, *J. Physiol.*, 195(1):215–245.
- Hubel, D. H., and T. N. Wiesel, 1970. Stereoscopic vision in macaque monkey. Cells sensitive to binocular depth in area 18 of the macaque monkey cortex, *Nature*, 225(227):41–42.
- Joshua, D. E., and P. O. Bishop, 1970. Binocular single vision and depth discrimination. Receptive field disparities for central and peripheral vision and binocular interaction on peripheral single units in cat striate cortex, *Exp. Brain Res.*, 10(4):389–416.
- Kuffler, S., 1953. Discharge patterns and functional organization of mammalian retina, *J. Neurophysiol.*, 16:37–68.
- Legge, G. E., and Y. C. Gu, 1989. Stereopsis and contrast, *Vis. Res.*, 29(8):989–1004.
- Lettvin, J. Y., H. R. Maturana, W. S. McCulloch, and W. H. Pitts, 1959. What the frog's eye tells the frog's brain, *Proc. Inst. Radio Eng.*, 47:1940–1951.
- LeVay, S., and T. Voigt, 1988. Ocular dominance and disparity coding in cat visual cortex, *Vis. Neurosci.*, 1(4):395–414.
- Mitchell, D. E., and B. Timney, 1984. Postnatal development of function in the mammalian visual system, in *Sensory Processes, Part I*, vol. 3 (I. Darian-Smith, ed.), Bethesda, MD: American Physiological Society, pp. 507–555.
- Movshon, J. A., I. D. Thompson, and D. J. Tolhurst, 1978. Receptive field organization of complex cells in the cat's striate cortex, *J. Physiol.*, 283:79–99.
- Nikara, T., P. O. Bishop, and J. D. Pettigrew, 1968. Analysis of retinal correspondence by studying receptive fields of binocular single units in cat striate cortex, *Exp. Brain Res.*, 6(4):353–372.
- Ohzawa, I., G. C. DeAngelis, and R. D. Freeman, 1996. Encoding of binocular disparity by simple cells in the cat's visual cortex, *J. Neurophysiol.*, 75(5):1779–1805.
- Ohzawa, I., and R. D. Freeman, 1986a. The binocular organization of simple cells in the cat's visual cortex, *J. Neurophysiol.*, 56(1):221–242.
- Ohzawa, I., and R. D. Freeman, 1986b. The binocular organization of complex cells in the cat's visual cortex, *J. Neurophysiol.*, 56(1):243–259.
- Ohzawa, I., G. Sclar, and R. D. Freeman, 1985. Contrast gain control in the cat's visual system, *J. Neurophysiol.*, 54:651–667.
- Poggio, G. F., F. Gonzalez, and F. Krause, 1988. Stereoscopic mechanisms in monkey visual cortex: binocular correlation and disparity selectivity, *J. Neurosci.*, 8(12):4531–4550.
- Poggio, G. F., and W. H. Talbot, 1981. Mechanisms of static and dynamic stereopsis in foveal cortex of the rhesus monkey, *J. Physiol.*, 315:469–492.
- Poggio, G. F., and B. Fischer, 1977. Binocular interaction and depth sensitivity in striate and prestriate cortex of behaving rhesus monkey, *J. Neurophysiol.*, 40:1392–1405.
- Schor, C., and T. Heckmann, 1989. Interocular differences in contrast and spatial frequency: effects on stereopsis and fusion, *Vis. Res.*, 29(7):837–847.
- Sclar, G., I. Ohzawa, and R. D. Freeman, 1985. Contrast gain control in the kitten's visual system, *J. Neurophysiol.*, 54(3):668–675.
- Truchard, A. M., I. Ohzawa, and R. D. Freeman, 2000. Contrast gain control in the visual cortex: monocular versus binocular mechanisms, *J. Neurosci.*, 20(8):3017–3032.
- Tsumoto, T., and R. D. Freeman, 1981. Ocular dominance in kitten cortex: induced changes of single cells while they are recorded, *Exp. Brain Res.*, 44(3):347–351.
- von der Heydt, R., C. Adorjani, P. Hanny, and G. Baumgartner, 1978. Disparity sensitivity and receptive field incongruity of units in the cat striate cortex, *Exp. Brain Res.*, 31(4):523–545.
- Westheimer, G., and S. P. McKee, 1980. Stereogram design for testing local stereopsis, *Invest. Ophthalmol. Vis. Sci.*, 19(7):802–809.
- Wheatstone, C., 1838. Contributions to the physiology of vision. Part the first: on some remarkable, and hitherto unobserved phenomena of binocular vision, *Philos. Trans. R. Soc. Lond. B Biol. Sci.*, II:371–394.
- Xue, J. T., A. S. Ramoa, T. Carney, and R. D. Freeman, 1987. Binocular interaction in the dorsal lateral geniculate nucleus of the cat, *Exp. Brain Res.*, 68(2):305–310.

49 From Binocular Disparity to the Perception of Stereoscopic Depth

ANDREW J. PARKER

THE AIM OF THIS CHAPTER is to give a modern neurobiological account of the perception of stereoscopic depth. *Stereopsis* is understood here in its present-day usage as being the sense of depth created by binocular disparities. There are two main components to the chapter. First, there is a review of the role of V1 neurons in the initial registration and processing of binocular disparities. It is concluded that V1 has an important role but falls short in several respects in providing a full account of stereopsis. Second, there is a shift in focus to extrastriate cortex in a search for neuronal activity that can better explain some of the key characteristics of stereoscopic depth perception. This section reviews our current understanding of the ways in which single cortical neurons selective for binocular disparity may contribute to the perception of stereoscopic depth. Finally, there is a brief concluding section that aims to highlight gaps in our current knowledge and point out directions for future research. This chapter is inevitably highly selective and incomplete. Its purpose is to focus on recent developments and to identify some issues that may be within our grasp during the next 10 years or so.

The groundwork of any account of stereoscopic depth is the perceptual and psychophysical investigations initiated in the nineteenth century by Wheatstone, inventor of the mirror stereoscope (Wheatstone, 1838, 1852). Although others, notably Leonardo da Vinci, had previously understood that the right and left eyes obtain slightly different views of the visual scene, Wheatstone appreciated that presenting images to the left and right eyes in a way that mimicked the natural viewing geometry could create a sense of binocular depth. This set off a string of nineteenth-century investigations, which are summarized in von Helmholtz (1909/1962). Figure 49.1 summarizes how objects at different depths give rise to binocular disparities.

A critical concept is *binocular correspondence*. Locations at the same distance on the retinas from the left and right foveas are said to be in *anatomical correspondence*. Psychophysically, the concept of correspondence is more complex: one commonly adopted definition is pairs of points on the left and right retinas that generate the same sense of visual direction when stimulated monocularly (see Howard and Rogers, 1995, for a summary of these issues). Importantly, the perception of

an object with binocular depth in front of or behind the binocular fixation point depends on the visual stimulation of *noncorresponding* points on the left and right retinas (Fig. 49.1*B,C*).

Our understanding of how single neurons support this visual function began in the 1960s, when Hubel and Wiesel (1962) discovered binocular summation within the striate cortex. Soon afterward, it was established that some of these striate cortical neurons possess receptive fields that are not in exact correspondence between the two eyes (Barlow et al., 1967; Bishop et al., 1971; Nikara et al., 1968). The connections of some of these binocular cortical neurons from the left and right eyes are organized such that the neuron responds best when an object is further than the binocular fixation point (Fig. 49.1*B*). Other neurons respond best when the object is nearer than the binocular fixation point (Fig. 49.1*C*). The small inset panels in Figure 49.2 show a collection of tuning curves measured for single V1 neurons in the macaque monkey. Each curve shows the firing rate of one neuron plotted against the disparity of the stimulus. The curves have been chosen to illustrate the range of tuning types encountered in V1.

Neurons with this type of receptive field are candidates for a physiological mechanism that is responsible for binocular stereopsis. Deviations from exact correspondence have two possible forms (Fig. 49.3). In one form (position encoding), the centers of the receptive fields occupy noncorresponding locations on the left and right retinas (Barlow et al., 1967; Ohzawa et al., 1990). Figures 49.1*B* and *C* show the shifts in retinal locations of a binocular object at different distances: this mechanism matches these shifts in retinal stimulation with an equivalent shift in the centers of the left and right eyes' receptive fields. In the other form (phase encoding), the centers are in corresponding locations but the exact profile of the receptive field differs between the left and right eyes (Ohzawa et al., 1997). Either type of difference endows the binocular visual system with a fundamental sensitivity to stereoscopic depth by making the neuron's response stronger at some disparities than others (Fig. 49.3). A detailed discussion of these properties is presented in Chapter 48 of this volume.

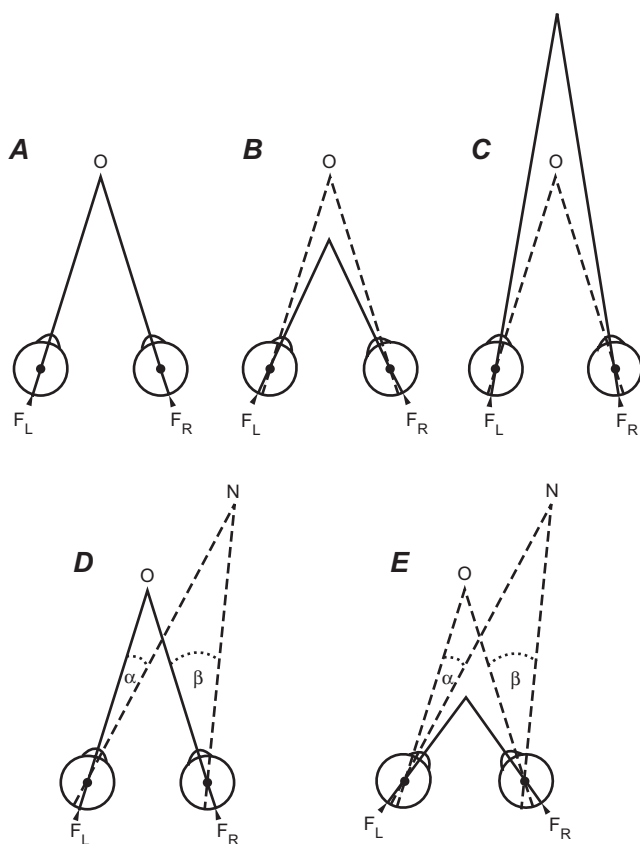


FIGURE 49.1. Diagrams illustrating the definitions of binocular disparity used in this chapter. In all diagrams, the optic center of each eye is shown with a solid circle •, the positions of the left and right foveas (F_L and F_R , respectively) are shown with solid arrows, the directions of binocular gaze are indicated with solid lines, and the visual directions of nonfixated objects are indicated with dashed lines. *A*, The simplest case, in which the two eyes fixate a single object, *O*. *B*, Object *O* remains in the same location, but the eyes have rotated inward toward the midline to fixate a new point closer to the observer than *O*. The projection lines of *O* now fall on noncorresponding retinal points. The retinal projection of *O* is to the right of the fovea in the left eye and to the left of the fovea in the right eye. *C*, Object *O* is again in the same location, but the eyes have rotated outward away from the midline to fixate a point farther away from the observer. The retinal projection of *O* is now to the left of the fovea in the left eye and to the right of the fovea in the right eye. *D*, The eyes now fixate object *O* with a second object, *N*, at a different depth from the observer. The angles α and β between *O* and *N* are unequal in the two eyes, and the difference $\beta - \alpha$ is the relative disparity between *N* and *O*. The value $\beta - \alpha$ is also the absolute disparity of *N* because the observer is fixating *O*. *E*, When the binocular gaze is shifted to a nearer point, *O* and *N* both have different absolute disparities. However, the relative disparity between *O* and *N* is unaltered.

Disparity selectivity

Whichever of these two forms of selectivity is present (or a mixture of them), a system of binocular disparity based on retinal noncorresponding points is firmly locked to the coordinate frames for each retina. As Figure 49.1 illustrates, when the eyes converge or diverge to inspect a new target, mechanisms locked to noncorresponding points register a new disparity value for an object *O* that remains at a fixed distance from the observer. The geometric projection lines for object *O* alter as the binocular fixation point moves closer or farther in depth. By fixating *O*, the visual system brings the object to corresponding points on the left and right retinas, hence a disparity of zero (Fig. 49.1*A*). Converging closer than *O* gives *O* a *far* disparity, and converging farther than *O* gives *O* a *near* disparity. Thus, when the disparity of *O* is measured in terms of retinal noncorresponding points, its disparity is subject to fluctuation as the eyes move, despite the fact that it is actually at a constant distance from the observer. Most physiological studies of disparity selectivity have explored within this framework, which may be termed *absolute disparity* (Cumming and Parker, 1999).

Another way of describing binocular disparity has been current in the literature on the psychology of depth perception. Here the emphasis has been not primarily on noncorresponding points in retinal coordinates but on the difference in the retinal projections of two visible objects at different depths from the observer, for example, points *O* and *N* in Figure 49.1*D*. The angles that are subtended by the gap between *O* and *N* are, of course, different in the left and right eyes. Figure 49.1*E* shows that this difference is not substantially affected by the vergence angle of the eyes (at least to the extent that the eyes may be assumed to rotate around their true optical centers, which is reasonable for small rotation angles). This measure of disparity has been termed *relative disparity* and is in fact equal to the difference in the absolute disparities of the two visible points under consideration.

An estimate of relative disparity can only be achieved by the nervous system if there are at least two features that can be seen in the visual field. By comparison, the nervous system can estimate the absolute disparity of a single point in an otherwise empty visual field. Absolute and relative disparity are associated with different visual and oculomotor functions. Absolute disparity is an important parameter in controlling disparity-driven vergence movements (Rashbass and Westheimer, 1961), whereas the finest stereoacuties are obtained with stimulus arrays that include relative disparity (Andrews et al., 2001; Westheimer, 1979). Most compelling is a demonstration by Erkelens and Collewijn (1985) and Regan et al. (1986). Observers view a display with two depth planes defined by a relative disparity between them. A

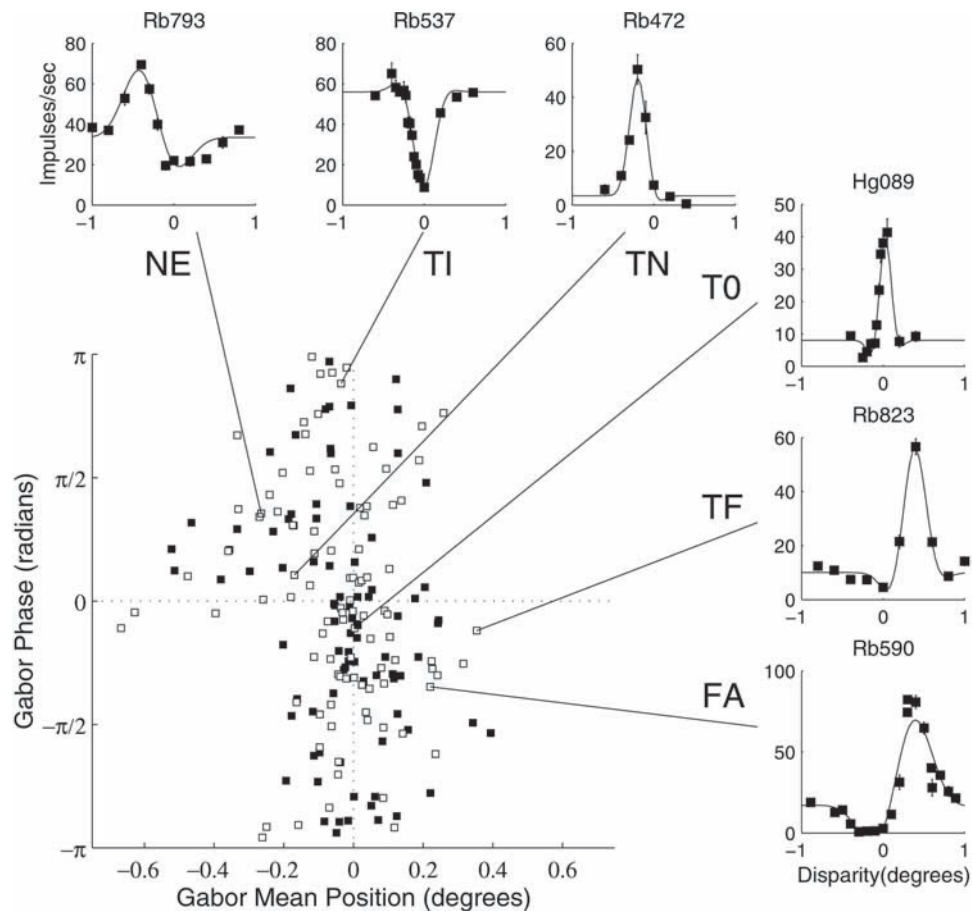


FIGURE 49.2. The small inset panels show six examples of disparity-tuning curves recorded from single neurons in macaque V1. The smooth curves through the data points are Gabor functions (Gaussian multiplied by sinusoid). The main plot shows the values of position disparity (in degrees of disparity, reflecting the esti-

mated position of the peak of the Gaussian) and phase disparity (in phase angle, reflecting the estimated phase of the sinusoidal component of the Gabor function). Data are shown for 180 neurons recorded from V1 of two macaque monkeys. (From Prince et al., 2002a.)

change in the absolute disparity of the entire display causes a human observer to track the change with vergence movements of the eyes, but no perceptible change of depth is generated. On the other hand, movement of one of the planes in depth relative to the other gives rise to a vivid sense of motion in depth.

Disparity-selective neurons have been identified not just within the striate cortex but also throughout the visual areas of the extrastriate cortex (Cumming and DeAngelis, 2001). This makes it clear that the discovery of a specialized set of neurons responsible for stereoscopic depth perception has to go beyond the identification of disparity selectivity in single neurons. We need a specific comparison between the perceptual properties of stereoscopic vision and the properties of single neurons studied in neurophysiological experiments. Considerable progress toward this goal has been made in recent years.

V1 and its response properties

Cortical area V1 is the first site in the brain at which information from the two eyes is brought together by means of specific excitatory connections designed to create high precision for binocular disparity. Some of these single neurons carry highly accurate signals. Such neurons can encode an alteration in the disparity of a stimulus with an accuracy that rivals that of psychophysical observers (Prince et al., 2000). This is remarkable given that psychophysical observers should be potentially able to access information from all the neurons in the relevant cortical areas at their disposal in performing the same task.

Recent quantitative measurements provide a basis for estimating the total range of disparities processed by V1 neurons and how the resources of V1 are applied, in terms of both numbers of neurons and the signaling capability of neuronal firing. Figures 49.2 and 49.4 show the distribution

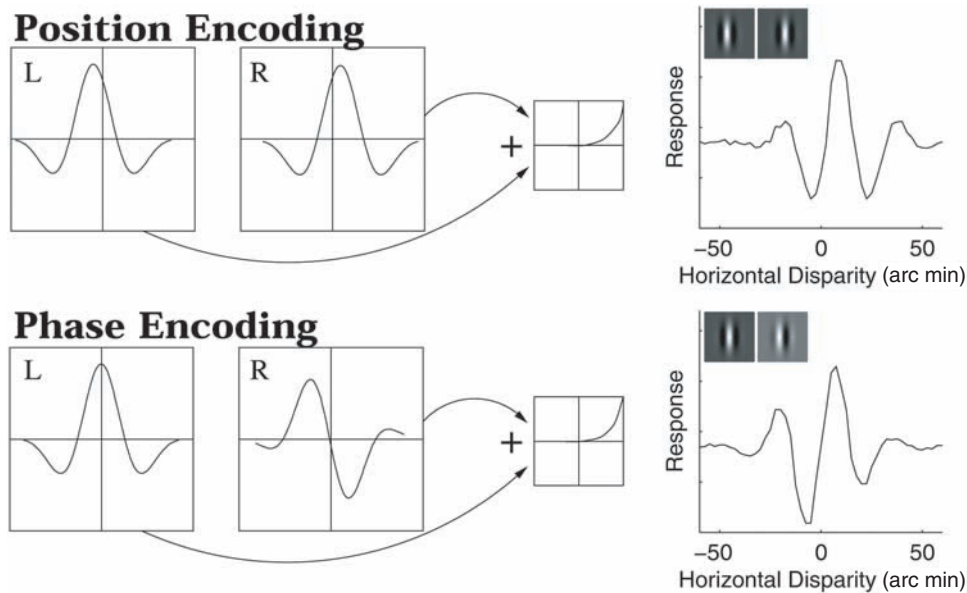


FIGURE 49.3. The disparity-tuning curves at the right are generated by a computational model of the binocular receptive field (Ohzawa et al., 1990). The random-dot stereo image is received and filtered by the receptive field structures for the left and right eyes, illustrated by the receptive field profiles marked L and R and the gray inset panels in which ON regions of the receptive field are white and OFF regions are dark. The outputs of the left and right eyes' receptive fields are added linearly and then passed through a half-wave rectifier. The computational model simulates the repeated presentation of dynamic random-dot stereograms by presenting many different patterns of dots at one disparity and taking the overall average response to each disparity. Each disparity-tuning curve plots these computed responses on the ordinate against the disparity of the stimulus (in arbitrary units) on the abscissa. The top row shows the shapes of tuning curve predicted by the position-shift model (Ohzawa et al., 1990). In this case, the left eye and right eye have the same arrangement of ON and OFF zones

and are related by a simple translation. The disparity-tuning curve has even symmetry. The bottom row shows an alternative way of generating disparity tuning. Here the location of the ON and OFF zones is different in the left and right eyes, whereas the overall centers of the receptive fields remain in the same position with respect to one another. This type of disparity tuning is called *phase disparity* because when the left eye and right eye receptive fields are described by a Gabor function (the product of a Gaussian multiplied by a sinusoid, as seen in the figure), the rearrangement of the ON and OFF zones is achieved by means of a shift in the phase of the sinusoidal component that describes the receptive field. The resultant tuning curves for disparity are odd-symmetric rather than even-symmetric. Binocular receptive fields that contain a mixture of both position-shift and phase-shift mechanisms generate disparity-tuning curves that are intermediate between odd and even symmetry (see Fig. 49.2 for examples). (From Prince et al., 2002a.)

of peak disparities for neurons recorded at eccentricities within 5 degrees of the fovea. The data are from Prince et al. (2002a) and are plotted separately for the two types of mechanism identified earlier in this chapter and in Chapter 48 of this volume. The horizontal axis (position disparity) shows the scatter of peak disparities for interocular differences in receptive field location, while the vertical axis (phase shift) shows the scatter of peak disparities generated by interocular differences in the profile of the receptive field. To allow a direct comparison, Figure 49.4 expresses the phase shifts in units of visual angle equivalent to position disparities (see Prince et al., 2002a, for details). The scatter of peak disparities for V1 receptive fields is approximately Gaussian, with a total range of just over 0.5 degree.

Figure 49.5 shows the neuronal activity pooled across 180 disparity-tuned neurons from cortical area V1 in the near-foveal part of the visual field as a function of the stimulus disparity. The neuronal activity has been pooled in a way that reflects the statistical reliability of the signals from indi-

vidual neurons. These data have again been analyzed separately for the two types of interocular difference in receptive fields (position and phase). Taken as a whole, the population of V1 neurons has the greatest potential for discrimination near the fixation plane at zero disparity, a finding that is consistent with a wide range of psychophysical data. The V1 population remains functionally effective in disparity discrimination over a range of about ± 1 degree of disparity. This is consistent with the largest values of stereoscopic disparity that can be processed psychophysically by human and macaque observers with random-dot stereograms (Glennerster, 1988; Prince et al., 2002a).

Despite these close correspondences between the properties of the neuronal population in V1 and psychophysical measures of the range and sensitivity of binocular disparity mechanisms, there are several respects in which the properties of V1 neurons are fundamentally inconsistent with many of the perceptual properties of binocular stereoscopic vision. We will therefore now focus on some important

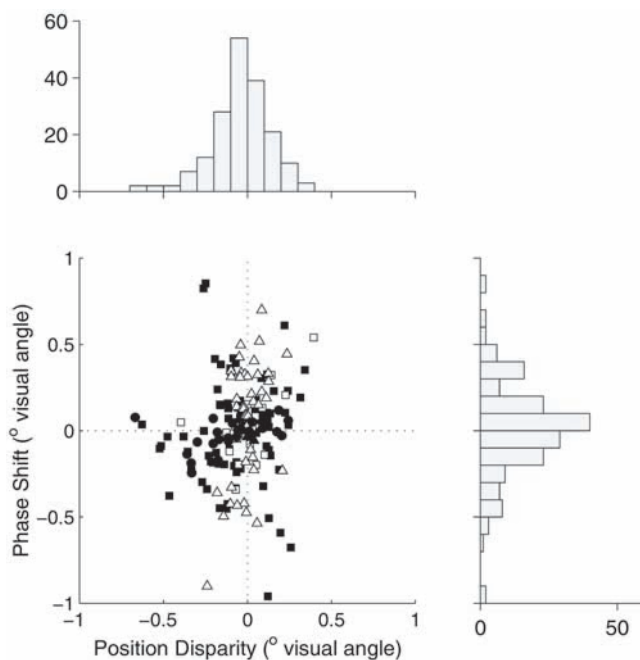


FIGURE 49.4. The scatter plot shows the same data as Figure 49.2, except that the phase shifts have been converted to an equivalent visual angle rather than a phase angle. This allows a direct comparison of the relative importance of phase and position disparity, which may be viewed by inspecting the histograms above and to the right. The different symbols in the scatter plot indicate whether the binocular receptive fields are best characterized by an interocular difference in receptive field location (position disparity) or receptive field profile (phase shift): \triangle , phase shift only; \bullet , position shift only; \blacksquare , position and phase shift; \square , either phase or position but not both; \blacktriangle , neither phase nor position. (From Prince et al., 2002a.)

discrepancies between the behavior of V1 neurons and stereo-depth perception.

V1 NEURONS RESPOND TO ABSOLUTE, NOT RELATIVE, DISPARITY As mentioned above, psychophysical judgments of stereoscopic depth by humans and macaques are most sensitive when relative disparity information is included in the visual stimulus. By contrast, V1 neurons respond to absolute disparity (Cumming and Parker, 1999). Disparity-tuning curves of V1 neurons were measured with a stimulus that contained relative disparity information, so that if there were any receptive field structures sensitive to relative disparity, they would be adequately stimulated. The V1 tuning curves were examined in two conditions. Each condition included a different amount of absolute disparity that was added to the entire stimulus array (including the binocular fixation point) with a tightly controlled feedback loop that took into account the state of convergence of the eyes. The extra absolute disparity mimics the sensory effect of a convergent or divergent eye movement away from the binocular fixation point. Hence it is important to monitor vergence and adjust

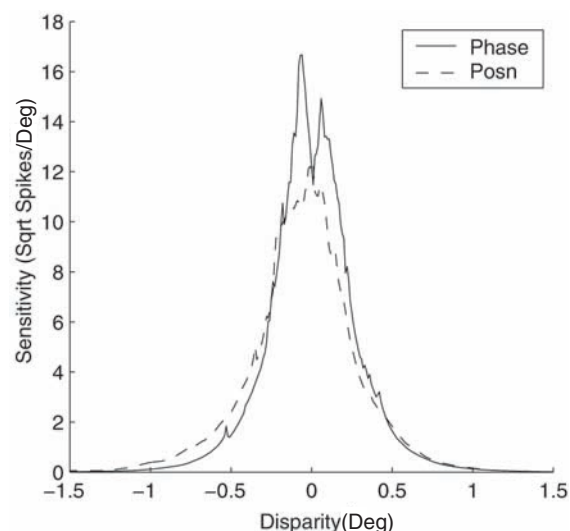


FIGURE 49.5. Sensitivity of the population of V1 neurons to changes in disparity. The abscissa plots the disparity of the dynamic random-dot stimulus, while the ordinate shows the ability of the population of V1 neurons to signal a change from the tested disparity. The neuronal sensitivity is estimated by first taking the square root of the neuronal firing and pooling across neurons the absolute value of the slope of the disparity-tuning curve (the ordinate scale is the square root of spikes per second per degree of disparity). The plot shows separately the contributions of phase shift and position disparity mechanisms, which are similar.

The justification for taking the square root of the neuronal spike counts is that the variance of neuronal spike counts tends to rise more or less proportionately with the mean spike count. Without a square root transform, the firing rates pooled across neurons would be biased toward those neurons with high mean firing rates. Such neurons are inherently also highly variable. Thus a square root transform gives a more equal weighting to all statistically significant signals, regardless of the mean firing rate of the neurons (see Appendix A in Prince et al., 2002b, for details).

the visual stimulus appropriately to keep the added absolute disparity at the desired value.

When an extra amount of absolute disparity is added to the display, a receptive field that is fundamentally responsive to absolute disparity should simply respond on the basis of the absolute disparities in the display. A mechanism that is fundamentally responsive to relative disparity should respond entirely on the basis of the relative disparities in the display. The situation is like that in Figure 49.1E, where the relative disparity between O and N is not affected by the vergence angle of the eyes. For a neuron that is selective for relative disparity, its response should not be affected by the addition of extra absolute disparities to the display. For neurons in V1, the results are unambiguous: all disparity-selective neurons in V1 are fundamentally responsive to absolute disparity (Cumming and Parker, 1999). Thus these neurons code disparity in terms of retinal correspondence.

V1 NEURONS RESPOND TO LOCAL DISPARITY, NOT STEREOSCOPIC DEPTH The way in which the visual system sorts out which features on the left retina correspond to those on the right retina and how the visual system derives depth signals from these binocular matches has been a topic of considerable research, both psychophysically and computationally. A fairly simple stimulus array highlights the main issues. Consider the case of a simple stimulus consisting of four dots in a horizontal row presented to both the left and right eyes in a stereoscope (Fig. 49.6). The human subject perceives a horizontal row of four dots all in the same depth plane. This appears unremarkable until one appreciates that, since every dot is identical to every other, there is actually no particular factor within the stimulus that forces this specific perceptual interpretation (Julesz, 1971; Marr and Poggio, 1976). Numerous other patterns of pairing between left and right eyes are possible, even if one applies the constraints that there should be no unmatched dots left over and that each dot should match only once. The latter constraint is doubtful for human vision in view of the possibility of multiple matching of features in Panum's limiting case, in which two similar dots in one eye and a single dot in the other lead to a sensation of stereoscopic depth.

Computational arguments have been made based on a number of principles, two of which are (1) that the visual system tends to select the smoothest possible disparity field and/or (2) that the visual system allows only unique, rather than multiple, matches between a feature in one eye and a feature in the other. In practice, we are not certain which of these is more significant for the mammalian visual system, although undoubtedly they are close to the truth since the principles reflect the geometric structure of natural scenes.

Without needing to understand exactly which principles are most significant, we can use a stimulus with multiple repeating features to probe different levels of stereoscopic depth processing in the cerebral cortex to discover whether true stereoscopic matching of features has been achieved at any particular neuronal site. For example, in macaque V1, a variant of the four-dot stimulus has been used to examine whether V1 neurons respond primarily to local disparity or binocular depth. In the stimulus used by Cumming and Parker (2000), a drifting sinusoidal grating was placed within a sharp circular window, with both grating and window having the same disparity (Fig. 49.6). This stimulus has the appearance of a flat surface with the bars of the grating at the same depth as the window. However, V1 neurons that are tuned to binocular disparity respond whenever there are appropriate contours in the left and right eye receptive fields of the neuron, even though the disparity that generates the response actually corresponds to a binocular match that forms no part of the psychophysical observer's percept. In other words, V1 neurons behave as if they are sensitive to

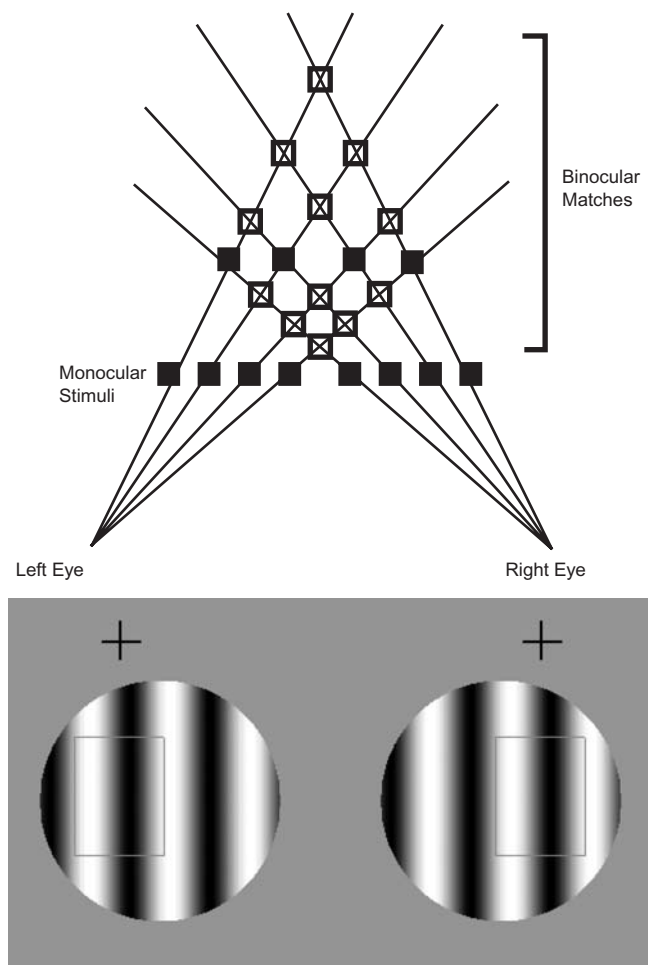


FIGURE 49.6. The upper diagram shows the 16 possible pairings of 4 identical dots presented to the left and right eyes. The lower diagram shows the windowed sinusoidal grating stimuli used by Cumming and Parker (2000) to test whether V1 neurons can identify globally correct stereoscopic matches. The crosses represent the binocular fixation point, and the rectangular boxes placed within the grating patches indicate a binocular cortical receptive field tuned to zero disparity. Even though a psychophysical observer perceives the grating patch to be at a nonzero disparity, V1 neurons tuned to zero disparity respond well to this stimulus because the local luminance information over the receptive field is also consistent with a stimulus of zero disparity.

all 16 possible pairings of the dots in Figure 49.6 rather than just the 4 pairings that correspond to the percept. In this sense, V1 neurons do not extract the global stereoscopic percept from this configuration.

V1 NEURONS RESPOND TO DISPARATE STIMULI THAT DO NOT GENERATE A SENSE OF STEREOSCOPIC DEPTH In normal viewing of a natural three-dimensional scene, features that are visible in both the left and right eyes' images generally have the same contrast polarity in each image. Thus a bright feature in one eye corresponds geometrically to a bright feature in the other eye and similarly for dark features. The

major exception to this occurs with a specular highlight, where the mirror-like reflection may send light directly along the line of sight to one eye and not to the other. This unusual circumstance creates a condition in which very different contrast values are presented to the two eyes. When artificial stereoscopic images are viewed under laboratory conditions, the presence of features that are of opposite contrast polarity (a bright dot in one eye paired with a dark dot in the other eye) has either a deleterious or a completely disruptive effect on stereo processing as measured psychophysically. If the feature of opposite contrast in the two eyes is a pair of isolated bars or dots, then the thresholds for detecting stereoscopic depth are raised substantially (Cogan et al., 1993, 1995; Cumming et al., 1998). Notably, when the features are binocularly fused, the percept is classically described as *lustrous* (von Helmholtz, 1909/1962), consistent with an association with specular highlights. In the case of random-dot stereograms that have a moderately dense packing of dots, the sense of stereopsis is completely destroyed by binocular anticorrelation: psychophysically the depth threshold is immensurable, and there is no segregation of one region from another purely on the basis of a difference in disparity.

These psychophysical responses are in contrast to the behavior of a simple disparity-detecting mechanism that gives a reasonable model for V1 neurons by computing the correlation between spatially localized regions in the left and right eyes' images. When two features have the same contrast and shape in the left and right eyes' images, the local correlation between the images will be highly positive. Introducing binocular anticorrelation by inverting the contrast of just one of these features does not simply reduce the correlation between the left and right images to zero but actually makes the correlation highly negative. Any model like the binocular energy model of Ohzawa et al. (1990), which is based on multiplication of spatially filtered versions of the left and right eyes' images, shows an inversion of its disparity tuning under binocular anticorrelation (Cumming and Parker, 1997). Disparities that are maximally effective with correlated images become maximally suppressive with anticorrelated images and vice versa.

When the disparity tuning of V1 neurons to binocularly correlated images is compared with the tuning to anticorrelated images, many neurons show an inversion of the tuning curve, as predicted by the binocular energy model (Cumming and Parker, 1997). However the amplitude of the anticorrelated response is often smaller than that of the correlated response, and indeed, some tuning curves do not show a simple inversion. At the behavioral level, ultra-short-latency vergence movements show an inverted response with binocularly anticorrelated patterns. Thus a large field of binocularly anticorrelated random dots with far disparities actually causes a transient convergence rather

than the divergence that would be generated with binocularly correlated random-dot patterns (Masson et al., 1997). Hence, these fast vergence eye movements may be driven directly from sensory detectors that register a simple correlation over a large region of the left and right eye' images. A particularly close match has been observed between the characteristics of these vergence movements and the tuning properties of neurons in the extrastriate medial superior temporal area (MST) (Takemura et al., 2001). However, some of the disparity-tuning properties of MST neurons may be derived from neurons at earlier stages in the visual pathways.

Psychophysically, it is possible to identify a stage in binocular processing at which disparity-detecting mechanisms invert their response under binocular anticorrelation (Neri et al., 1999). This observation is in sharp contrast with the perceptual effect of anticorrelated stimuli placed at nonzero disparities. As mentioned above, anticorrelated stimuli with spatially isolated features such as single bars or edges do give rise to a sense of depth. In the case of random-dot stereograms, a sense of binocular depth is generated at low dot densities and is absent at moderate to high dot densities (Cogan et al., 1993; Cumming et al., 1998). The critical observation is that when anticorrelated disparities do generate a sense of binocular depth, the perceived depth is always in the direction predicted by the geometric arrangement of the features (Cumming et al., 1998; Read and Eagle, 2000). Thus a binocularly anticorrelated bar with near disparities gives rise to the perception of a feature that is closer to, not farther from, the subject than the binocular fixation point.

This response is not predicted from a disparity detector based on simple correlation and appears to require the initial generation of a monocular response to contour that is independent of contrast sign before stereoscopic processing (Ziegler and Hess, 1999). Stereopsis from such responses are confined to single isolated features, and the visual system appears to be unable to derive any sense of depth from the more crowded and complex arrangements of dots in anticorrelated random-dot stereograms with the same facility.

In summary, V1 neurons show evidence of disparity-specific responses to stimuli that are ineffective in generating a percept of stereoscopic depth. We may conclude that it is insufficient simply to activate disparity-specific neurons in V1 to perceive stereo depth: there must be a further stage at which the pattern of activation of neurons within V1 is evaluated and tested for consistency prior to the generation of a stereoscopic depth percept.

The role of extrastriate cortex

The evidence that has been reviewed at this point indicates that V1 is important for the initial registration and analysis

of binocular disparity. There are some close matches between the performance of the V1 population of neurons and the psychophysical capabilities of the visual system. However, for a complete explanation of many of the perceptual qualities of binocular stereoscopic depth, it is necessary to look outside V1 in the extrastriate cortex. Evidence concerning the responses of the various extrastriate areas is sparse at the moment, although identification of sites is now of critical importance.

The satisfactory identification of sites will require the application of multiple techniques (single-unit recording, electrical microstimulation, functional magnetic resonance imaging (fMRI) and other imaging methods, visual psychophysics) in combination with tests for the perceptual significance of cortical responses of the kind discussed above for V1. Such experiments are aimed chiefly at providing a neuronal basis for the perceptual psychology of binocular stereopsis. However, the outcome will have implications reaching beyond this issue. For example, early developmental experience has been thought to induce normal binocular function, primarily due to actions upon the striate cortex. Thus, the effect of disrupted visual experience has been interpreted principally in terms of changes in striate connectivity, with extrastriate sites being affected only consequentially due to alterations within V1. Since we can now determine that there must be extrastriate sites that act importantly upon striate signals to generate a complete sense of binocular depth, the discovery of these sites becomes a priority, not only for perceptual psychology but also for the developmental neurobiology of binocular vision.

THE BEGINNINGS OF RELATIVE DISPARITY Since we know that cortical area V1 responds fundamentally to absolute disparity, while psychophysically humans and monkeys are most sensitive to stimuli that include relative disparities, one criterion for interesting extrastriate sites is that they show a specific sensitivity to relative disparity. In both cortical areas V2 and the lateral division of the middle superior temporal area (MSTl), there are reports of neurons that are sensitive to the manipulation of relative disparity as a parameter (Eifuku and Wurtz, 1999; Thomas et al., 2002). Since the evidence from each study is of a rather different nature, they will be described separately before being compared.

There are a number of possible experimental designs for testing for the presence of sensitivity to relative disparity. At the heart of one class of these designs is an approach that establishes criteria for designating a region of the receptive field that may be reasonably termed the *center* and then designating a region immediately adjacent to it that may be termed the *surround*. The experiment then places pairs of stimuli of different disparity in the center and surround and looks for an interaction between the responses of the center and the surround, such that the response to center stimula-

tion is differentially altered by stimuli of different disparity in the surround. The center is generally defined either with respect to the *minimum response field* (Henry et al., 1969) or by obtaining an estimate of the summation area of the center with a stimulus of uniform disparity that is centered on the receptive field and then measuring the neuron's response as a function of stimulus diameter.

With this approach, Thomas et al. (2002) observed, for a proportion of neurons in cortical area V2, that the disparity preference of the center region of the receptive field can be shifted to a different value by changing the disparity of the surround. The direction of the shifts is consistent with a sensitivity to relative disparity. Thus when the disparity of the surround is altered to indicate a surface closer to the subject, the disparity preference of the center shifts in the same direction. The ability to modulate the disparity preference of the center is greater when the surround stimulus is given a disparity close to the tuning preference of the center. In other words, the effect of the surround is strongest when its disparity is close to the natural tuning profile for the center mechanism. This may reflect the fact that psychophysical sensitivity for relative disparity is most acute for small differences in disparity between the two regions to be compared. Only rarely did the neurons studied by Thomas et al. (2002) show magnitudes of shift in the disparity preference of the center consistent with a tuning curve wholly dominated by relative disparity. Nonetheless, in comparison with neurons in V1 (Cumming and Parker, 1999), those in V2 show an impressive transformation of neuronal sensitivity to disparity.

Using a different approach, Eifuku and Wurtz (1999) also examined the modulation of center responses by the disparity of the surround. These authors studied the MSTl. They concentrated on varying the disparity difference between center and surround and examining the effect on firing rate rather than the tuning preference of the neurons. They found that the firing pattern of some neurons was more strongly affected by the relative disparity between the center and surround rather than the absolute disparity of either alone. Although there were strong changes in firing in these experiments, it is not entirely clear that these results represent the same kind of sensitivity to relative disparity found by Thomas et al. (2002).

First, in Eifuku and Wurtz (1999), the range of disparities over which modulation takes place is very large, up to 3 degrees of disparity. At such large disparities, the perceptual sensitivity to relative disparity is weak and the stimuli would very likely be diplopic. Second, while the observations are consistent with a shift in disparity preference of the type found by Thomas et al. (2002), they are also consistent with simpler forms of interaction such as a simple modulation of the gain of the center response by the disparity of surround. Demonstration of a true selectivity for relative disparity (as

opposed to merely a change in response when relative disparity is manipulated) requires a measurable multiplicative interaction between the disparities of the center and the surround upon the response of the neuron rather than an additive effect of each alone. A multiplicative interaction provides the ability to respond invariantly to relative disparity over a range of absolute disparities.

There are other ways in which sensitivity to relative disparity may be significant. Neurons in a number of extrastriate cortical areas are sensitive to the shapes of contours defined by disparity alone (von der Heydt et al., 2000). Some of these neurons exhibit the same selectivity for the orientation of the contour whether they are stimulated with luminance-defined or disparity-defined contours. The mechanisms by which this is achieved are unknown, but sensitivity to relative disparity (Thomas et al., 2002) could feasibly be involved. However, to achieve a segregation of one region from another for contour requires no specific signal about whether one region is in front of or behind another. In this respect, segregation is different from relative disparity (see Fig. 49.7 for a stereogram that illustrates how binocular information can yield segregation without a specific depth difference).

Another role for neuronal signals about relative disparity is in the generation of neuronal receptive fields that are sensitive to the three-dimensional structure of the disparity fields. Some way further forward from V2, in the inferotemporal cortex, there are neurons whose firing rate codes

the curvature of disparity fields (Janssen et al., 2000). The curvature preference of these neurons is maintained over a range of absolute depth values and two-dimensional locations within the visual field. However, it should be emphasized that even these neurons also have some sensitivity to the parameters of two-dimensional location and absolute depth, like the neurons found in V2.

Issues relating to the processing of relative disparity have also recently been addressed in human subjects using fMRI of the brain. Interpretation of the BOLD (blood oxygenation level dependent) response is more complex since it is an indirect measure of pooled neuronal activity, some of which may be nonspiking activity. For this reason, it is harder to link BOLD responses to changes in a sensory parameter such as disparity: the BOLD response has inherently less precision because the cortical signal is pooled over spatial location and time and reflects the metabolic demands of neuronal processing. It is hard to determine which aspects of the stimulus are responsible for the measured response and relate them to the signals in single neurons. For example, it is clear that there are measurable cortical activations generated by contours between spatial regions of the visual field that differ in depth (Mendola et al., 1999). Like the single-unit physiology of von der Heydt et al. (2000), some of these activations probably reflect a generalized response to visual contours rather than to the difference in depth (as in Fig. 49.7).

Backus et al. (2001) used a pair of binocular depth planes whose separation in depth was varied parametrically. The upper and lower limits for the perception of binocular depth were measured psychophysically, and the cortical activation of several extrastriate areas was assessed by comparing the specific activation generated by the two-plane stimulus relative to the general activation created by the one-plane stimulus. Backus et al. argued that cortical areas with specific sensitivity to relative disparity would be more strongly activated by the two-plane rather than the one-plane stimulus and, indeed, the limits of the psychophysical performance correspond rather well with the range of disparities that generate the specific activation. The degree of specific activation for the two-plane stimulus was strongest in cortical area V3A, but several other visual cortical areas also showed signs of specific activation.

Indices of perceptual signals

Another approach to examining the coding of disparity and binocular depth involves studies in which awake, behaving macaques perform a specific binocular depth task while single neurons are recorded simultaneously. The trial-by-trial neuronal responses can then be compared individually with the psychophysical responses of the animal. A general overview of this approach and its application to perceptual

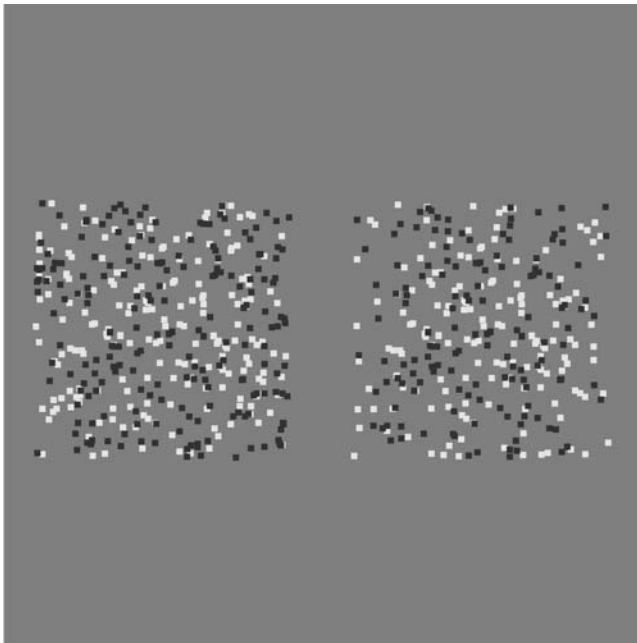


FIGURE 49.7. Random-dot stereogram showing the ability of binocular correlation without a sensation of depth to generate segregation of one image region from another.

processing is available elsewhere (Parker and Newsome, 1998). With one exception already discussed (Prince et al., 2000), the majority of studies that have used this approach to study binocular depth have been performed in middle temporal cortical area V5.

Cortical area V5/MT has been associated for a number of years with a significant role in the perception of visual motion (Movshon et al., 1986; Newsome et al., 1989; Salzman et al., 1990). Although the presence in V5/MT of neurons with selectivity for binocular disparity was discovered at an early stage (Maunsell and Van Essen, 1983) in the exploration of this area, only recently has this knowledge been consolidated through a detailed quantitative study (DeAngelis and Newsome, 1999). It appears that (1) about two-thirds of the neurons in this area show significant selectivity for binocular disparity, (2) the tuning curves are typically odd symmetric in their tuning characteristics about the fixation plane, and (3) there is evidence for a functional clustering of different tuning types, such that neurons preferring “near” or “far” disparities appear to be encountered together.

As previously acknowledged, the presence of neurons with particular tuning properties, even the organization of those tuning properties into a columnar structure, does not constitute adequate evidence for the direct involvement of those neurons in perceptual processing. However, there are now several compelling lines of evidence for a link between the activation of these disparity-specific neurons in V5/MT and binocular depth perception. Such a link does not necessarily mean that a unique role for V5/MT in the perception of binocular depth has been established. The current evidence allows for the possibility of similar links being established for other cortical areas. Even so, it is somewhat surprising to learn that the evidence linking the activity of V5/MT neurons to particular perceptual processes is as strong for binocular depth as it is for visual motion.

There are three main lines of evidence, two of which indicate strong correlations between neuronal activity and perceptual state and the third of which seeks evidence of a more causative nature. The first line of evidence compares the basic sensitivities of the individual neurons against the psychophysical performance of the macaque monkey: this is the comparison of neurometric and psychometric performance (Parker and Newsome, 1998). This comparison has been made for two binocular depth tasks.

In the first of these tasks, the sensitivity to binocular disparity is probed by exploiting the fact that the perceptual ambiguity of structure-from-motion stimuli can be resolved by adding a controlled amount of binocular disparity to the figure. Consider the side view of a transparent cylinder that rotates about its principal axis and is depicted by dots randomly placed on the surface of the cylinder (Fig. 49.8). This cylinder is ambiguous in its direction of rotation if the cylin-

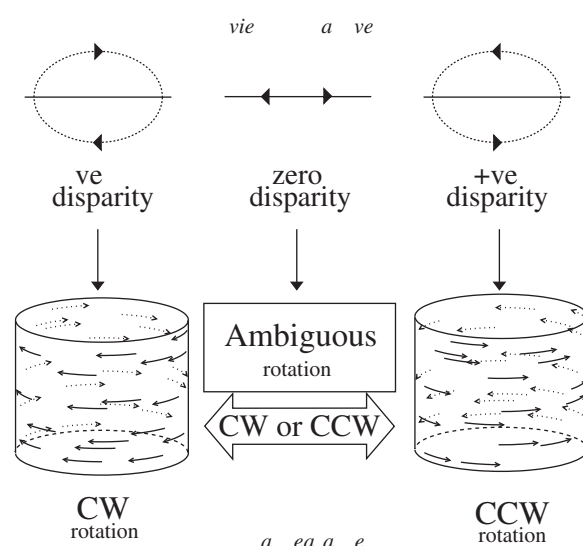


FIGURE 49.8. Diagram of a cylinder depicted by moving patterns of dots. When all the dots have the same binocular disparity (zero) as in the center panel, the direction of rotation of the pattern is inherently ambiguous (see Ullman, 1979, for discussion). Addition of a pattern of disparities that separates the front and rear surfaces of the cylinder fixes the direction of rotation, either as clockwise (left) or counterclockwise (right).

der is viewed monocularly or all the dots are at the same binocular depth plane. This ambiguity is inherent in the motion information, which is insufficient to fix the direction of rotation (Treue et al., 1991). The addition of a binocular disparity that separates the front and rear surfaces determines the direction of rotation. Thus psychophysical observers can be trained to report the direction of rotation of a cylinder stimulus with small amounts of binocular disparity present. The sensitivity of a psychophysical observer to binocular disparity can therefore be assessed in terms of the smallest amount of disparity that makes the direction of rotation unambiguous.

V5/MT neurons respond vigorously to these cylinder stimuli (Bradley et al., 1998; Dodd et al., 2001). In the majority of cases, the neurons' firing changes monotonically as stereoscopic depth is used to separate the front and rear surfaces of the cylinder. This response is much as would be expected for neurons that are conjointly selective for both the visual motion and the binocular disparity in the stimulus, with an odd-symmetric tuning curve for binocular disparity. Analysis of the performance of the neurons in discriminating one direction of rotation of the cylinder from the other shows that single neurons in V5/MT are highly sensitive to binocular disparity. The average neuron was only 1.24 times less sensitive than the psychophysical performance of the macaque monkeys that carried out simultaneous judgments on the stimuli used to test the neurons (Krug et al., 2001).

A broadly similar conclusion has been reached for a quite different form of depth task. In this task, a plane of binocular dots is presented at a relatively coarse disparity, either closer to or farther from the fixation plane. The presence of the plane is disguised by the addition of binocularly uncorrelated dots. The task for the macaque monkey is to identify on any individual trial whether the correlated dots are in the closer or the farther depth plane. The psychophysical performance is assessed by finding the proportion of binocularly correlated dots that are required to sustain this judgment (DeAngelis et al., 1998). A recent study (Uka and DeAngelis, 2001) has compared the sensitivity of single neurons against psychophysical performance on this task. In this case the single neurons were, on average, close in sensitivity to the psychophysical observer.

The second line of evidence that links the activity of V5/MT neurons to the perception of stereoscopic depth arises from an analysis of the trial-by-trial covariation between neuronal firing and behavioral choice in a psychophysical experiment (Parker and Newsome, 1998). This covariation is expressed in terms of a measure called *choice probability*, which takes a value of 0.5 when there is a random association between the neuronal response and behavioral choice and increases to 1 if the neuronal response predicts every psychophysical response. It is a measure of how well an ideal observer would perform in predicting the behavioral response from the firing pattern of a single neuron (Fig. 49.9).

In the earlier work on the sensitivity of V5/MT neurons to visual motion, the choice probability in a direction discrimination task was 0.56 (Britten et al., 1996). This value

was statistically different from 0.5, but it represents a relatively weak association between behavioral choice and neuronal activity. In the same brain area, when macaque monkeys are making perceptual judgments about the direction of rotation of an ambiguous cylinder stimulus, the choice probability is much stronger (0.67; see Dodd et al., 2001). For the task used by DeAngelis et al. (1998), which involves the detection of the depth of a plane of binocularly correlated dots, the choice probability was 0.59 (DeAngelis and Uka, 2001).

Choice probability is inherently a measure of correlation rather than causation, so these differences in measured values must be interpreted with some caution. For example, it would be a mistake to assume that activity in V5/MT is necessarily more strongly associated with binocular depth than with motion analysis simply because the observed choice probabilities are stronger. There are a number of cognitive factors, such as attention, task difficulty, degree of training on the task, and so on, that might affect the measures of choice probability. Equally, at the neuronal level, there are important factors such as the size and connectivity of the neuronal populations activated by these different stimuli, the strength of neuronal activity generated by different stimuli, and the degree of correlation in firing patterns between different members of the active population (Shadlen et al., 1996).

One study has investigated evidence for a causal link between the activation of V5/MT neurons and perceptual decisions about binocular depth (DeAngelis et al., 1998). In this case, electrical microstimulation of a small region of cortex was applied at the same time as a visual stimulus was

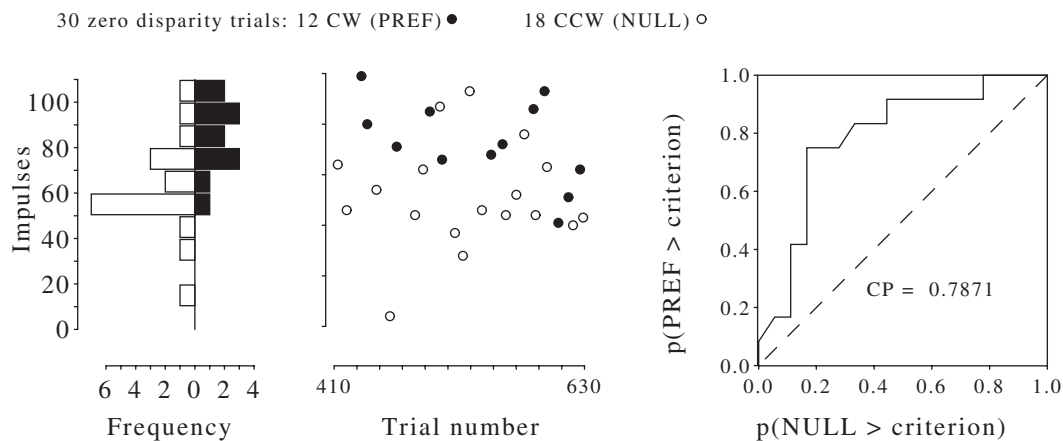


FIGURE 49.9. The firing of a single V5/MT neuron to 30 trials in which the macaque monkey was required to judge the direction of rotation of the ambiguous zero-disparity stimulus shown in the middle of Figure 49.8. The impulse counts on each trial are coded with solid symbols when the monkey made a clockwise (CW) judgment about the ambiguous cylinder and open symbols when the monkey made a counterclockwise (CCW) judgment. This neuron fired more strongly to CW rotations with unambiguous cylinders.

The left-hand panel shows histograms of impulse counts, the middle panel shows the individual impulse counts coded by choice on individual trials, and the right-hand panel shows the calculation of choice probability (CP) as the area under the solid curve. The solid curve is constructed using the same principle as the analysis of receiver operating characteristic (ROC) curves in signal detection theory (see Britten et al., 1996; Dodd et al., 2001, for details). (From Dodd et al., 2001.)

presented. When the electrical stimulation was applied in a region of the cortex where the typical neuronal preference was for near disparities, the macaque monkey's perceptual decisions were shifted to generate more "near" decisions. Interestingly, the effects of electrical microstimulation on this task were strongest in those regions of the cortex that had the strongest tuning for binocular disparity. Note, however, that the stimulus and psychophysical task used in these experiments is unlikely to make demands on fine-grained stereoscopic acuity, since the paradigm involves the detection of a minimum level of binocular correlation of dots that have coarse disparities and are located either closer to or farther from the binocular fixation point.

In summary, the evidence linking activity in V5/MT to some aspects of binocular depth judgments must be considered impressively strong. The responses of neurons in this area are individually reliable enough to sustain binocular depth judgments. Their responses sometimes covary tightly on a trial-by-trial basis with perceptual decisions about binocular depth. Artificial activation of this region of cortex influences binocular depth judgments. On the other hand, many V5/MT neurons respond to binocularly anticorrelated patterns in a way broadly similar to the behavior of V1 neurons, even though these patterns do not result in a coherent depth percept. Specifically, it is clear that there are neurons with statistically significant choice probabilities that also modulate strongly to the binocular disparity of anticorrelated random-dot patterns. The first criterion is generally regarded as evidence in favor of a link between neuronal activity and perceptual judgments, while the second criterion suggests that the same neurons carry signals that are not associated with psychophysical depth perception (Krug et al., 2000). It may be that the links between neuronal activity and perceptually relevant signals can be dynamically formed and broken in ways that remain to be determined. Clearly, further experimental investigations are required to resolve these issues. Comparative data from several extrastriate cortical areas will be needed before a more complete picture will emerge.

Concluding remarks

Our understanding of how binocular vision yields a sense of stereoscopic depth is in a time of transformation. We have acquired a solid understanding of the contribution of V1 neurons to this process, and we have a good working model of the functional organization of the binocular receptive fields of these neurons. No doubt our picture of the binocular mechanisms of V1 neurons will continue to be refined and amended. However, it is clear that a bigger task is to gain a deeper understanding of the roles of neurons in the extrastriate visual cortex. Present work has established several aspects of binocular processing that still require a full

explanation at the neuronal level. For example, it is still unclear which neuronal sites support the unambiguous resolution of matching of binocular features from the left and right inputs. In other cases, such as the emergence of a representation of relative disparity, we can already identify an important role for V2, which may be enhanced and further processed by other extrastriate areas.

A speculative argument can be advanced for a binocular pathway concerned with three-dimensional shape, perceptual segregation of different regions of the visual field, and relative disparity judgments that originates in V2 and projects presumably via V4 to regions of inferior temporal cortex. Processing in this pathway depends strongly on accurate establishment of binocular corresponding features between the eyes and on the ability to process fine-grained stereoscopic depth differences.

A different pathway may be concerned with integration of motion and stereo information. This includes V5 (MT), MST, and potentially V3 or V3A. This pathway includes the capability of responding more rapidly to stimuli that change in depth. It may therefore make use of signals based on simpler measures such as interocular correlation (as explored by DeAngelis et al., 1998) and therefore show inversion of disparity tuning curves with binocularly anticorrelated stimuli. A faster responding sensory pathway would also be more naturally selected for the control of binocular eye movements, particularly fast, stereotyped responses (Masson et al., 1997).

The distinction being drawn here has its roots in similar distinctions about fine and coarse stereoscopic processing that have been advanced at various times on the basis of psychophysical and computational arguments (e.g., Mallot et al., 1996). The current evidence suggests that both pathways may have a role to play in perceptual judgments about stereoscopic depth, although the involvement of each pathway is almost certainly task dependent. Mapping these various distinctions onto a coherent neuronal framework remains a task for the future.

Acknowledgments

I thank Kristine Krug for a critical reading of this chapter. Work in our laboratory is supported by the Wellcome Trust and the Royal Society.

REFERENCES

- Andrews, T. J., A. Glennerster, and A. J. Parker, 2001. Stereoacuity thresholds in the presence of a reference surface, *Vis. Res.*, 41:3051–3061.
- Backus, B. T., D. J. Fleet, A. J. Parker, and D. J. Heeger, 2001. Human cortical activity correlates with stereoscopic depth perception, *J. Neurophysiol.*, 86:2054–2068.

- Barlow, H. B., C. Blakemore, and J. D. Pettigrew, 1967. The neural mechanism of binocular depth discrimination, *J. Physiol.*, 193:327–342.
- Bishop, P. O., G. H. Henry, and C. J. Smith, 1971. Binocular interaction fields of single units in the cat striate cortex, *J. Physiol.*, 216:39–68.
- Bradley, D. C., G. C. Chang, and R. A. Andersen, 1998. Encoding of three-dimensional structure-from-motion by primate area MT neurons, *Nature*, 392:714–717.
- Britten, K. H., W. T. Newsome, M. N. Shadlen, S. Celebrini, and J. A. Movshon, 1996. A relationship between behavioral choice and the visual responses of neurons in macaque MT, *Vis. Neurosci.*, 13:87–100.
- Cogan, A. I., L. L. Kontsevich, A. J. Lomakin, D. L. Halpern, and R. Blake, 1995. Binocular disparity processing with opposite-contrast stimuli, *Perception*, 24:33–47.
- Cogan, A. I., A. J. Lomakin, and A. F. Rossi, 1993. Depth in anticorrelated stereograms—effects of spatial density and interocular delay, *Vis. Res.*, 33:1959–1975.
- Cumming, B. G., and G. C. DeAngelis, 2001. The physiology of stereopsis, *Annu. Rev. Neurosci.*, 24:203–238.
- Cumming, B. G., and A. J. Parker, 1997. Responses of primary visual cortical neurons to binocular disparity without depth perception, *Nature*, 389:280–283.
- Cumming, B. G., and A. J. Parker, 1999. Binocular neurons in V1 of awake monkeys are selective for absolute, not relative, disparity, *J. Neurosci.*, 19:5602–5618.
- Cumming, B. G., and A. J. Parker, 2000. Local disparity not perceived depth is signaled by binocular neurons in cortical area V1 of the macaque, *J. Neurosci.*, 20:4758–4767.
- Cumming, B. G., S. E. Shapiro, and A. J. Parker, 1998. Disparity detection in anticorrelated stereograms, *Perception*, 27:1367–1377.
- DeAngelis, G. C., B. G. Cumming, and W. T. Newsome, 1998. Cortical area MT and the perception of stereoscopic depth, *Nature*, 394:677–680.
- DeAngelis, G. C., and W. T. Newsome, 1999. Organization of disparity-selective neurons in macaque area MT, *J. Neurosci.*, 19:1398–1415.
- DeAngelis, G. C., and T. Uka, 2001. Contribution of MT neurons to depth discrimination II Correlation of response and behavioral choice, *Soc. Neurosci.*, 680:13.
- Dodd, J. V., K. Krug, B. G. Cumming, and A. J. Parker, 2001. Perceptually bistable figures lead to high choice probabilities in cortical area MT, *J. Neurosci.*, 21:4809–4821.
- Eifuku, S., and R. H. Wurtz, 1999. Response to motion in extrastriate area MSTl: disparity sensitivity, *J. Neurophysiol.*, 82:2462–2475.
- Erkelens, C. J., and H. Collewijn, 1985. Eye-movements and stereopsis during dichoptic viewing of moving random-dot stereograms, *Vis. Res.*, 25:1689–1700.
- Glennerster, A., 1998. d(max) for stereopsis and motion in random dot displays, *Vis. Res.*, 38:925–935.
- Henry, G. H., P. O. Bishop, and J. S. Coombs, 1969. Inhibitory and subliminal excitatory receptive fields of simple units in cat striate cortex, *Vis. Res.*, 9:1289–1296.
- Howard, I. P., and B. J. Rogers, 1995. *Binocular Vision and Stereopsis*, New York and Oxford: Oxford University Press.
- Hubel, D. H., and T. N. Wiesel, 1962. Receptive fields, binocular interaction and functional architecture in the cat's striate cortex, *J. Physiol. (Lond.)*, 160:106–154.
- Janssen, P., R. Vogels, and G. A. Orban, 2000. Three-dimensional shape coding in inferior temporal cortex, *Neuron*, 27:385–397.
- Julesz, B., 1971. *Foundations of Cyclopean Perception*, Chicago: University of Chicago Press.
- Krug, K., B. G. Cumming, and A. J. Parker, 2000. The role of single MT(V5) neurons in stereo perception in the awake macaque, *Eur. J. Neurosci.*, 12:285 (Supplement).
- Krug, K., J. V. Dodd, B. G. Cumming, and A. J. Parker, 2001. Highly sensitive MT/V5 neurons correlate more closely with the reported percept in a 3-D structure-from-motion task, *Soc. Neurosci. Abstr.*, 27:680–7.
- Mallot, H. A., P. A. Arndt, and H. H. Bülthoff, 1996. A psychophysical and computational analysis of intensity-based stereo, *Biol. Cybern.*, 75:187–198.
- Marr, D., and T. Poggio, 1976. Cooperative computation of stereo disparity, *Science*, 194:283–287.
- Masson, G. S., C. Busettini, and F. A. Miles, 1997. Vergence eye movements in response to binocular disparity without depth perception, *Nature*, 389:283–286.
- Maunsell, J. H. R., and D. C. Van Essen, 1983. Functional properties of neurons in middle temporal visual area of the macaque monkey. 2. Binocular interactions and sensitivity to binocular disparity, *J. Neurophysiol.*, 49:1148–1167.
- Mendola, J. D., A. M. Dale, B. Fischl, A. K. Liu, and R. B. H. Tootell, 1999. The representation of illusory and real contours in human cortical visual areas revealed by functional magnetic resonance imaging, *J. Neurosci.*, 19:8560–8572.
- Movshon, J. A., E. H. Adelson, M. S. Gizzi, and W. T. Newsome, 1986. The analysis of moving visual patterns, in *Pattern Recognition Mechanisms* (C. Chagas, R. Gattass, and C. G. Gross, eds.), New York: Springer-Verlag, pp. 117–151.
- Neri, P., A. J. Parker, and C. Blakemore, 1999. Probing the human stereoscopic system with reverse correlation, *Nature*, 401:695–698.
- Newsome, W. T., K. H. Britten, and J. A. Movshon, 1989. Neuronal correlates of a perceptual decision, *Nature*, 341:52–54.
- Nikara, T., P. O. Bishop, and J. D. Pettigrew, 1968. Analysis of retinal correspondence by studying receptive fields of binocular single units in cat striate cortex, *Exp. Brain Res.*, 6:353–372.
- Ohzawa, I., G. C. DeAngelis, and R. D. Freeman, 1990. Stereoscopic depth discrimination in the visual cortex—neurons ideally suited as disparity detectors, *Science*, 249:1037–1041.
- Ohzawa, I., G. C. DeAngelis, and R. D. Freeman, 1997. The neural coding of stereoscopic depth, *Neuroreport*, 8:R3–R12.
- Parker, A. J., and W. T. Newsome, 1998. Sense and the single neuron: probing the physiology of perception, *Annu. Rev. Neurosci.*, 21:227–277.
- Prince, S. J. D., B. G. Cumming, and A. J. Parker, 2002a. Range and mechanism of encoding of horizontal disparity in macaque V1, *J. Neurophysiol.*, 87:209–221.
- Prince, S. J. D., A. D. Pointon, B. G. Cumming, and A. J. Parker, 2000. The precision of single neuron responses in cortical area V1 during stereoscopic depth judgments, *J. Neurosci.*, 20:3387–3400.
- Prince, S. J. D., A. D. Pointon, B. G. Cumming, and A. J. Parker, 2002b. Quantitative analysis of the responses of V1 neurons to horizontal disparity in dynamic random-dot stereograms, *J. Neurophysiol.*, 87:191–208.
- Rashbass, C., and G. Westheimer, 1961. Independence of conjugate and disjunctive eye movements, *J. Physiol. (Lond.)*, 159:361–364.
- Read, J. C., and R. A. Eagle, 2000. Reversed stereo and motion direction with anticorrelated stimuli, *Vis. Res.*, 40:3345–3358.
- Regan, D., C. J. Erkelens, and H. Collewijn, 1986. Necessary conditions for the perception of motion in depth, *Invest. Ophthalmol. Vis. Sci.*, 27:584–597.

- Salzman, C. D., K. H. Britten, and W. T. Newsome, 1990. Cortical microstimulation influences perceptual judgments of motion direction, *Nature*, 346:174–177.
- Shadlen, M. N., K. H. Britten, W. T. Newsome, and J. A. Movshon, 1996. A computational analysis of the relationship between neuronal and behavioral responses to visual motion, *J. Neurosci.*, 16:1486–1510.
- Takemura, A., Y. Inoue, K. Kawano, C. Quaia, and F. A. Miles, 2001. Single-unit activity in cortical area MST associated with disparity-vergence eye movements: evidence for population coding, *J. Neurophysiol.*, 85:2245–2266.
- Thomas, O. M., B. G. Cumming, and A. J. Parker, 2002. A specialisation for relative disparity in V2, *Nat. Neurosci.*, 5:472–477.
- Treue, S., M. Husain, and R. A. Andersen, 1991. Human perception of structure from motion, *Vis. Res.*, 31:59–75.
- Uka, T., and G. C. DeAngelis, 2001. Contribution of MT neurons to depth discrimination. I Comparison of neuronal and behavioral sensitivity, *Soc. Neurosci. Abstr.*, 27:680–12.
- Ullman, S., 1979. *The Interpretation of Visual Motion*, Cambridge, MA: MIT Press.
- von Helmholtz, H., 1909/1962. *Handbook of Physiological Optics*, 3rd ed., New York: Dover.
- von der Heydt, R., H. Zhou, and H. S. Friedman, 2000. Representation of stereoscopic edges in monkey visual cortex, *Vis. Res.*, 40:1955–1967.
- Westheimer, G., 1979. Co-operative neural processes involved in stereoscopic acuity, *Exp. Brain Res.*, 36:585–597.
- Wheatstone, C., 1838. Contributions to the physiology of vision: I. On some remarkable, and hitherto unobserved, phenomena of binocular vision, *Philos. Trans. R. Soc. Lond.*, 128:371–394.
- Wheatstone, C., 1852. Contributions to the physiology of vision: II. On some remarkable, and hitherto unobserved, phenomena of binocular vision (continued), *Philos. Trans. R. Soc. Lond.*, 142:1–17.
- Ziegler, L. R., and R. F. Hess, 1999. Stereoscopic depth but not shape perception from second-order stimuli, *Vis. Res.*, 39:1491–1507.

VII DETECTION AND SAMPLING

50 Formation and Acquisition of the Retinal Image

DAVID R. WILLIAMS AND HEIDI HOFER

THE QUALITY OF VISION ultimately rests on the properties of both the eye and the brain. For complex visual tasks such as inferring the objects in a three-dimensional visual scene, mechanisms in the brain are obviously paramount in establishing visual performance. However, for simpler tasks such as visual resolution, fundamental constraints on performance often arise in the eye itself. This chapter evaluates the roles for spatial and color vision of early stages of visual processing, beginning with the formation of the retinal image and followed by the acquisition of that image by the photoreceptor mosaic. The chapter focuses on foveal vision, where visual resolution is highest. Discussions of the off-axis optical and neural performance of the eye can be found elsewhere (Jennings and Charman, 1981; Navarro et al., 1993; Packer and Williams, 2003; Thibos, 2000; Williams et al., 1996).

Retinal image formation

Though its optical components are made of living tissue instead of glass, the eye forms a remarkably good retinal image. The quality of this image depends on diffraction at the pupil, aberrations in the cornea and lens, light scatter in the optical media, and the optical properties of the retina. Fourier optics succinctly describes the effects of diffraction and aberrations. For an excellent treatment of Fourier optics in imaging systems generally, see Goodman (1996). See Thibos (2000) or Packer and Williams (2003) for treatments pertaining to the eye.

THE WAVE ABERRATION Figure 50.1*A* shows a perfect and an aberrated eye forming a retinal image of a distant object such as a star. The parallel light rays arriving at the eye from the star can be described alternatively as a series of planar wave fronts. The wave front is always perpendicular to each ray at the point of intersection. The optics of a perfect eye transform this planar wave front into a spherical wave front which collapses to form a compact light distribution on the retina. The perfect eye delays light traveling through different parts of the pupil so that all the light takes exactly the same time to reach the retinal location where the image of the star is formed.

In the aberrated eye shown in Figure 50.1*B*, the wave front is not delayed by the proper amounts and the wave front inside the eye departs from its ideal spherical shape. It fails to collapse to a compact point at the retina, and blurring is inevitable. Aberrations arise from several sources, such as a misshapen cornea or lens, and these errors add. The contributions of the cornea and lens to these errors are often compensatory, especially in young eyes, so that the overall optical quality of the eye is superior to that of either element alone (Artal et al., 2001). We can sum all the errors experienced by a photon passing through the cornea and lens and assign the sum to the point in the entrance pupil of the eye through which the photon passed. It is convenient to express the total error in a unit of distance, such as micrometers (μm), indicating how far the distorted wave front departs at each point in the entrance pupil from the ideal wave front. A map of the eye's entrance pupil that plots the error at each entry point is the eye's wave aberration. The wave aberration captures in one function all the aberrations for a particular wavelength of light that ultimately influence image quality at a particular location on the retina. Figures 50.2*A–D* are wave aberrations for four typical human subjects. Like a fingerprint, the wave aberration is different in different people, though there is often some degree of mirror symmetry between eyes of the same person (Liang and Williams, 1997; Porter et al., 2001). Figure 50.2*E* shows the wave aberration for an ideal eye, which is zero at every point in the pupil.

DECOMPOSING THE WAVE ABERRATION INTO INDIVIDUAL ABERRATIONS To understand more clearly what is wrong with the optics of an individual eye, one can decompose the wave aberration into a number of component aberrations. A Zernike decomposition is used in much the same way that Fourier analysis is used to decompose an image into spatial frequency components. Zernike polynomials are defined on the unit circle, which approximates the natural shape of the eye's pupil. Figure 50.3 shows the pyramid of Zernike modes, akin to the periodic table of elements. Three modes, piston, tip, and tilt, that cap the pyramid have been omitted because these modes do not influence image quality. Modes are characterized by their *radial order*, which refers to the

exponent that describes how the function behaves in the radial direction from the center of the pupil.

Figure 50.4 shows the average magnitude of these modes in a normal population (Porter et al., 2001, see also Castejon-Mochon et al., 2002). The higher-order monochromatic aberrations were measured with a Shack-Hartmann wave front sensor in a population of 109 normal subjects for a 5.7 mm pupil size. The magnitude corresponds to the absolute value of the Zernike coefficient associated with each Zernike mode. Each Zernike coefficient is the root mean square deviation of the wave front from the ideal wave front for each particular Zernike mode expressed in microns. The largest monochromatic aberration of the eye is typically defocus, followed by astigmatism. These are the only aberrations that conventional spectacles and contact lenses correct. However, normal eyes have many monochromatic aberrations besides defocus and astigmatism (Berny and Slansky, 1969; Howland and Howland, 1977; Liang and Williams, 1997; Liang et al., 1994; Sergienko, 1963; Smirnov, 1961; van den Brink, 1962; Walsh and Charman, 1985; Walsh et al., 1984; Webb et al., 1992). Generally speaking, Figure 50.4 shows that aberrations corresponding to more rapidly varying errors across the pupil (i.e., higher radial order) have smaller amplitudes and make a smaller contribution to the total wave aberration for normal eyes.

THE PUPIL FUNCTION The retinal image is made up of light that arrives from many different locations in the pupil. In addition to depending on the eye's aberrations, the quality of the retinal image depends on how much light entering

each location in the pupil actually gets caught by the retinal receptors. The pupil function succinctly captures both the wave aberration and the variation of the effectiveness of light at different points in the pupil. The pupil function is

$$P(\eta, \zeta) = P_0(\eta, \zeta) \cdot \exp\left(i \frac{2\pi}{\lambda} W(\eta, \zeta)\right)$$

where (η, ζ) are two-dimensional spatial coordinates in the entrance pupil and λ is the wavelength of light used to measure the eye's wave aberration, $W(\eta, \zeta)$. $P_0(\eta, \zeta)$ is the amplitude transmittance across the eye's optics, the truncating effect of the iris being the most important. The

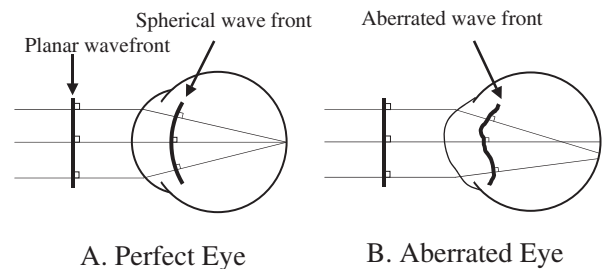


FIGURE 50.1. *A*, Retinal image formation for an aberration-free eye. Parallel rays from a distant point source converge inside the eye to a single point on the retina. If light is described as a wave, image formation consists of a planar wave front incident on the cornea that is transformed into a spherical wave front, which collapses to a single point on the retina. *B*, In the case of all real eyes, aberrations deviate the rays so that they do not converge to a point. Alternatively, the wave front is distorted from the ideal spherical shape, and the retinal image is blurred.

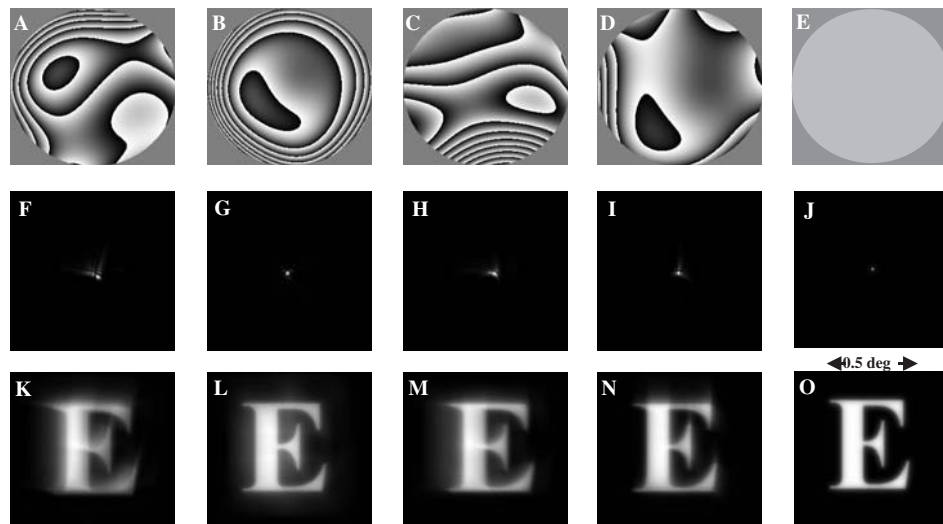


FIGURE 50.2. *A–E*, Wave aberrations of real eyes are shown in *A–D*; the flat wave aberration of an ideal, aberration-free eye is shown in *E*. The pupil diameter was 5.7 mm. *F–J*, The point spread functions computed from the wave aberrations shown in *A–E*. *K–O*, The result of convolving the point spread function with the letter

E, which subtended 0.5 minute of arc. Note the increased blur in the real eyes compared to the diffraction-limited eye. The calculations were performed assuming white light, axial chromatic aberration in the eye, and that a wavelength of 555 nm was in best focus on the retina.

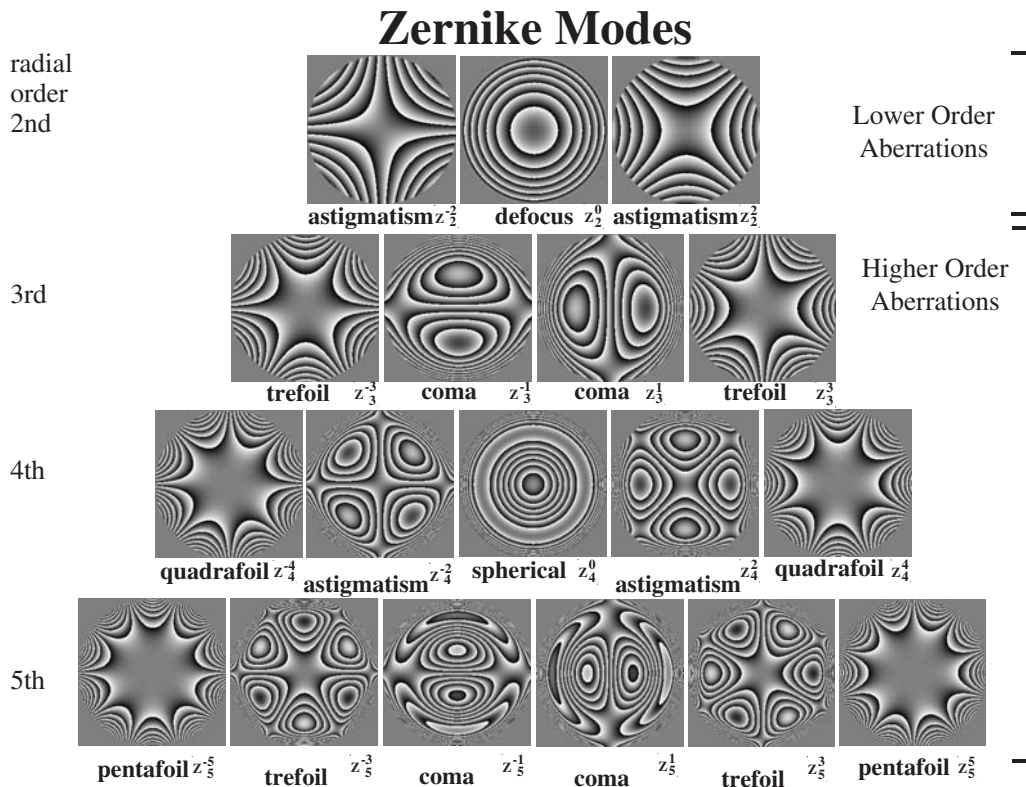


FIGURE 50.3. The pyramid showing each of the Zernike modes in radial orders 2 through 5, along with their names and their designation (OSA Standard). Tip, tilt, and piston, which would normally cap the pyramid, have been excluded because they do not influence image quality.

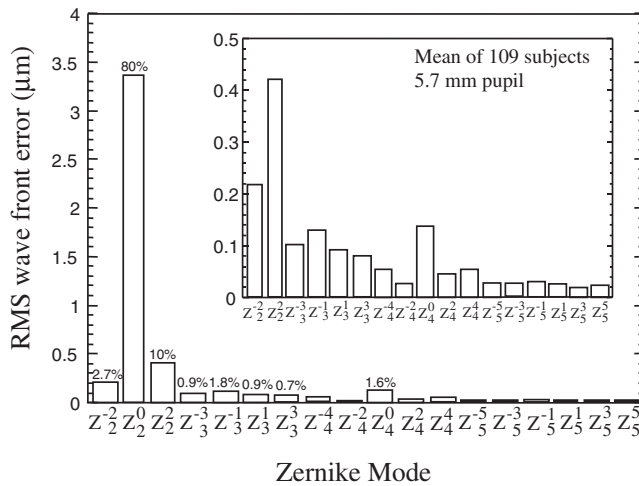


FIGURE 50.4. Mean absolute root mean square (RMS) values for 18 Zernike modes as measured from a population of 109 normal human subjects for a 5.7 mm pupil. The percentages above some modes indicate the percentage of the total wave aberration variance accounted for by each mode. The inset excludes the first Zernike mode corresponding to defocus and has an expanded ordinate to illustrate the magnitudes of higher-order aberrations.

variation in the absorption of the cornea and lens across the pupil is small enough in the normal eye that it can usually be ignored. However, because of the antenna properties of cones, the quantum efficiency of the retina depends on the entry point of light in the pupil. Though this effect, known as the *Stiles-Crawford effect*, is caused by the optics of the retina, it is equivalent to reducing the amplitude transmittance toward the margin of the entrance pupil (see Chapter 53). Therefore, the generalized pupil function for the eye includes the directional sensitivity of the retina in $P_0(\eta, \zeta)$.

THE POINT SPREAD FUNCTION In evaluating the quality of an imaging system such as the eye, it is often useful to characterize the system's point spread function (PSF). The PSF describes the distribution of light in the retinal image when the eye is viewing a distant point source, such as a star, and provides a complete description of image quality at that retinal location for a given wavelength of light. Figures 50.2*F–J* show the PSFs corresponding to the wave aberrations of Figures 50.2*A–E*, respectively. Because of aberrations in real eyes, the PSFs are broader and more irregular than the aberration-free PSF for the same 6 mm pupil size, shown in Figure 50.2*J*.

The PSF is the squared modulus of the Fourier transform of the pupil function. That is,

$$\begin{aligned} PSF(x, y) &= |\mathfrak{F}(P(\lambda d \eta, \lambda d \xi))|^2 \\ &= \mathfrak{F}(P(\lambda d \eta, \lambda d \xi)) \cdot \mathfrak{F}(P(\lambda d \eta, \lambda d \xi))^* \end{aligned}$$

where the Fourier transform is given by

$$\mathfrak{F}(f(\eta, \xi)) = \iint f(\eta, \xi) \cdot \exp[+i2\pi(x\eta + y\xi)] d\eta d\xi$$

This is of fundamental importance, because it allows us to compute the retinal image of a particular object, a single point of light, based on knowledge of the pupil function. Knowledge of the retinal image of a single point of light allows us to compute the retinal image of any object, as we describe later. This is a very powerful result, because it provides a firm quantitative link between aberrations in the eye and their impact on the retinal image.

DIFFRACTION An analysis based solely on geometrical optics might lead one to suppose that the PSF in the aberration-free eye of Figure 50.2*f* would be a single point. But even in this case, the light is spread out somewhat across the retina due to diffraction at the pupil, an inevitable consequence of the wave nature of light. The PSF shown in Figure 50.2*f* has a bright central core, called the *Airy disk*,

surrounded by dimmer rings. The PSF can be described quantitatively by

$$I(r) = [2\mathcal{J}_1(\pi r)/\pi r]^2$$

where $I(r)$ is normalized intensity as a function of distance r from the peak and \mathcal{J}_1 is a Bessel function of the first kind. The radius of the PSF, r_0 , expressed in radians and measured from the peak to the first point at which the intensity is zero, is given by

$$r_0 = 1.22\lambda/\alpha$$

where λ is the wavelength of light and α is the diameter of the circular pupil. Because the width of the diffraction-limited PSF is proportional to wavelength and inversely proportional to pupil diameter, the retinal image quality of this ideal eye is optimum at large pupil sizes and short wavelengths. Figure 50.5 illustrates the inverse relationship between PSF diameter and pupil size for an aberration-free eye.

LIGHT SCATTER In addition to blurring by diffraction and aberrations, the eye's PSF is blurred by light scatter in the anterior optics and retina (Vos, 1963). The sources of intraocular scattered light are (1) forward scatter from the

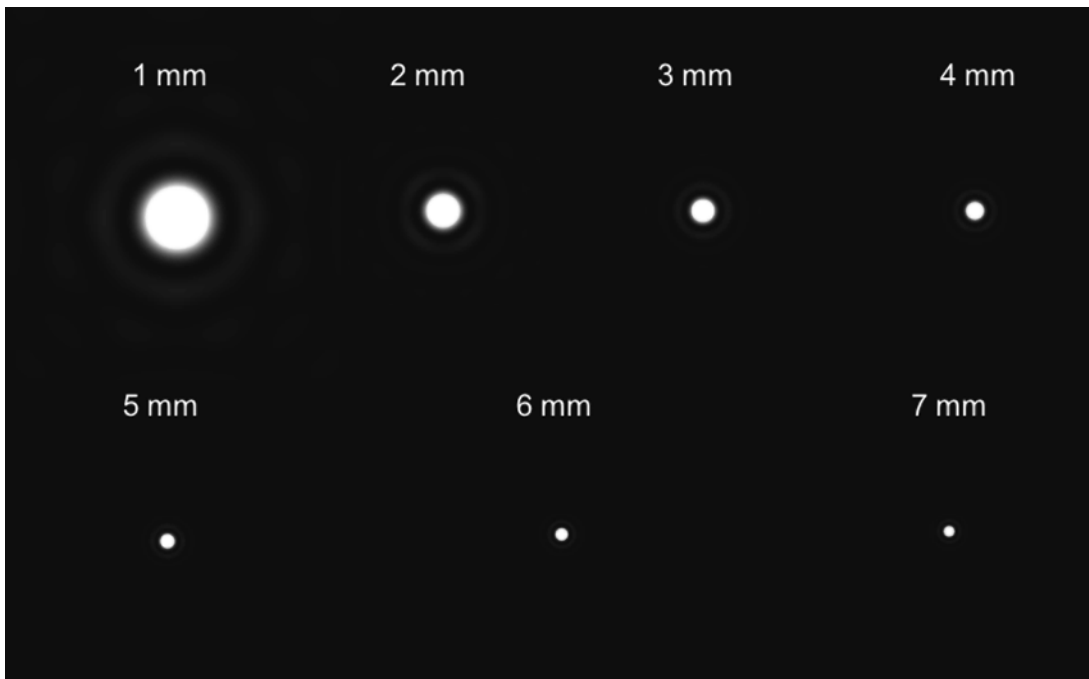


FIGURE 50.5. PSFs for an ideal, aberration-free eye limited only by diffraction for various pupil diameters. Note that the diameter of the PSF is inversely proportion to pupil diameter. (Courtesy of Austin Roorda.)

cornea, (2) forward scatter from the lens, (3) forward scatter from the retina, and (4) back scatter from the fundus. Roughly a quarter of the scatter comes from the cornea, another quarter from the retina, and the remaining half from the lens. Since most of the forward scattering is by relatively large particles, the scattered light in the eye does not show a strong wavelength dependence (Wooten and Geri, 1987).

Scatter tends to contribute predominantly to broaden and increase the skirt of the PSF. This has the effect of adding a veiling illumination to the retinal image, reducing image contrast at relatively low as well as high spatial frequencies. In the young eye, scatter is not a major source of image blur. It becomes important primarily in the aging eye (Guirao et al., 1999; Westheimer and Liang, 1995), or in the young eye when the observer is required to detect a relatively dim object in the vicinity of a much brighter object. The PSF due to scatter can be summed with the PSF due to diffraction and aberrations, at which point the retinal image can be computed for any object, as described below.

COMPUTING RETINAL IMAGES Once we have the PSF, the retinal image for any arbitrary object can be computed either in the spatial domain or in the frequency domain. In the spatial domain, the intensity distribution of the image, $I(x, y)$, is the convolution of the PSF with the intensity distribution of the object, $O(x, y)$. That is,

$$I(x, y) = \text{PSF}(x, y) \otimes O(x/M, y/M)$$

where M is the magnification between the object and image planes. The convolution of two functions $f(x, y)$ and $g(x, y)$ is

$$f(x, y) \otimes g(x, y) = \iint f(x, y) \cdot g(r - x, s - y) dx dy$$

In practice, the computation of the retinal image is more efficient in the spatial frequency domain. In that case, the intensity distribution of the object, $O(x, y)$, is Fourier transformed to provide the object Fourier spectrum, $\sigma(f_x, f_y)$. That is,

$$\sigma(f_x, f_y) = \mathfrak{F}(O(x, y))$$

The object Fourier spectrum is then multiplied by the optical transfer function (OTF) of the eye to give the image Fourier spectrum:

$$i(f_x, f_y) = \text{OTF}(f_x, f_y) \cdot \sigma(Mf_x, Mf_y)$$

By taking the inverse Fourier transform of the image spectrum, one obtains the retinal image

$$I(x, y) = \mathfrak{F}^{-1}(i(f_x, f_y))$$

The OTF is the autocorrelation of the pupil function. Alternatively, the OTF can be computed by taking the Fourier transform of the PSF. The OTF is complex, consisting of two parts, a modulation transfer function (MTF) and a phase transfer function (PTF). The MTF indicates how faithfully the contrast of each spatial fre-

quency component of the object is transferred to the image. The PTF indicates how individual spatial frequency components of the object have been translated in the retinal image.

ESTIMATES OF THE POINT SPREAD FUNCTION AND MODULATION TRANSFER FUNCTION Figure 50.6 illustrates how the PSF changes with pupil diameter for a typical human eye when both aberrations and diffraction are taken into account. At small pupil sizes, aberrations are insignificant and diffraction dominates. The PSF takes on the characteristic shape of the Airy pattern, with a wide core and little light in the skirt around it. At larger pupil sizes, aberrations dominate. The PSF then has a small core but reveals an irregular skirt that corresponds to light distributed over a relatively large retinal area. A pupil size of roughly 3 mm in diameter represents a good compromise between blur due to diffraction and aberrations (Campbell and Gubisch, 1966). In this case, the full width at half height of the PSF is approximately 0.8 minute of arc, corresponding to nearly twice the width of a cone at the foveal center.

Retinal image quality is often represented by the MTF instead of the PSF, mainly because only relatively recently has it been possible, with the advent of wave front sensing, to recover the PSF. Only the MTF was accessible with earlier methods of measuring the optical quality of the eye, such as laser interferometry and the double pass technique (Artal et al., 1995). The MTF by itself is not as complete a description of the eye's optics as the PSF, because it does not include the PTF. Image quality in the human eye depends on the PTF when the pupil is large (Charman and Walsh, 1985). Furthermore, accurate phase information is important for the perception of complex scenes (Piotrowski and Campbell, 1982). Nonetheless, the MTF has its uses, especially in situations where the contrast sensitivity of the eye is involved. In that case, knowledge of the MTF of the optics allows the segregation of optical and neural factors in visual performance.

The solid curves in Figure 50.7 show MTFs for a diffraction-limited eye with pupil diameters ranging from 2 to 7 mm calculated for a wavelength of 555 nm.

Figure 50.7 also shows the mean monochromatic MTFs (*dashed lines*) computed from the wave aberration measurements for 14 eyes made with a Shack-Hartmann wave front sensor (Liang and Williams, 1997). For small pupil sizes, the MTF is high at low spatial frequencies owing to the absence of light in the skirt of the PSF. For large pupil sizes, however, the MTF is reduced at low spatial frequencies due to the large skirt in the PSF that aberrations produce. However, at high frequencies, the MTF is higher than that for small pupils due to the narrower core of the PSF. The implication of this is that although a 2 to 3 mm pupil is commonly said to represent the best trade-off

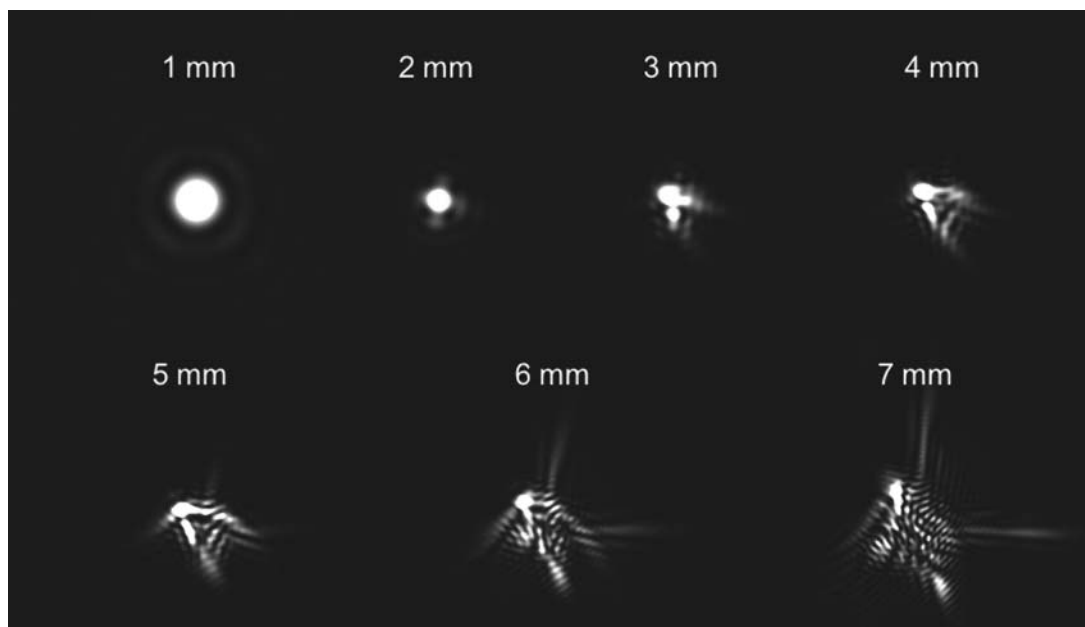


FIGURE 50.6. PSFs for a typical real eye for various pupil diameters. Defocus and astigmatism have been zeroed. Note that diffraction controls the PSF shape for small pupils, whereas aberrations dominate for large pupils. (Courtesy of Austin Roorda.)

between diffraction and aberrations, there is no single optimum pupil size. The optimum size depends on the task. Smaller pupils minimize optical aberrations for visual tasks involving low spatial frequencies. Larger pupils transmit high spatial frequencies for tasks that involve fine spatial detail even though they suffer more aberrations. If the goal is to resolve very fine features in images of the retina, then larger pupils transfer more contrast. With increasing pupil diameter, the difference between the diffraction-limited and real MTFs grows due to the decrease in the contribution of diffraction to retinal blur and the increase in the role of aberrations.

RETINAL IMAGES IN POLYCHROMATIC LIGHT In everyday viewing situations, the eye is confronted with broadband light instead of monochromatic light. The assessment of retinal image quality then demands that the effects of chromatic aberration be taken into account. Chromatic aberration arises because the refractive index of the ocular medium increases with decreasing wavelength. Consequently, any light rays incident on the cornea will generally be bent more if the wavelength is short than if it is long. See Thibos (1987) for a review of chromatic aberration in the eye. There are two kinds of chromatic aberration, axial and transverse. The main effect of axial chromatic aberration is to cause the

Zernike polynomial corresponding to defocus to vary with wavelength. All the other aberrations retain roughly the same amplitudes when expressed in microns (Marcos et al., 1999). Across the visible spectrum from 400 to 700 nm, the difference of focus caused by axial chromatic aberration is about 2.25 diopters. Transverse chromatic aberration can manifest itself either as a lateral displacement of a single point in a scene or as a magnification difference of an extended object. In the typical human eye, transverse chromatic aberration does not reduce image quality very much in the fovea.

The blur produced by chromatic aberration does not have especially important effects on spatial vision. The largest aberrations in human eyes are defocus and astigmatism, followed by the aggregate effect of all the remaining, higher-order monochromatic aberrations. Chromatic aberration is not as large as the combined effect of the higher-order aberrations, and its influence on vision is less pronounced. Campbell and Gubisch (1967) found that contrast sensitivity for monochromatic yellow light was only slightly greater than contrast sensitivity for white light. Visual performance on spatial tasks usually depends very little on the S cones, the cone class that would generally experience the greatest retinal image blur due to axial chromatic aberration. Moreover, the proximity of the L and M absorption spectra means

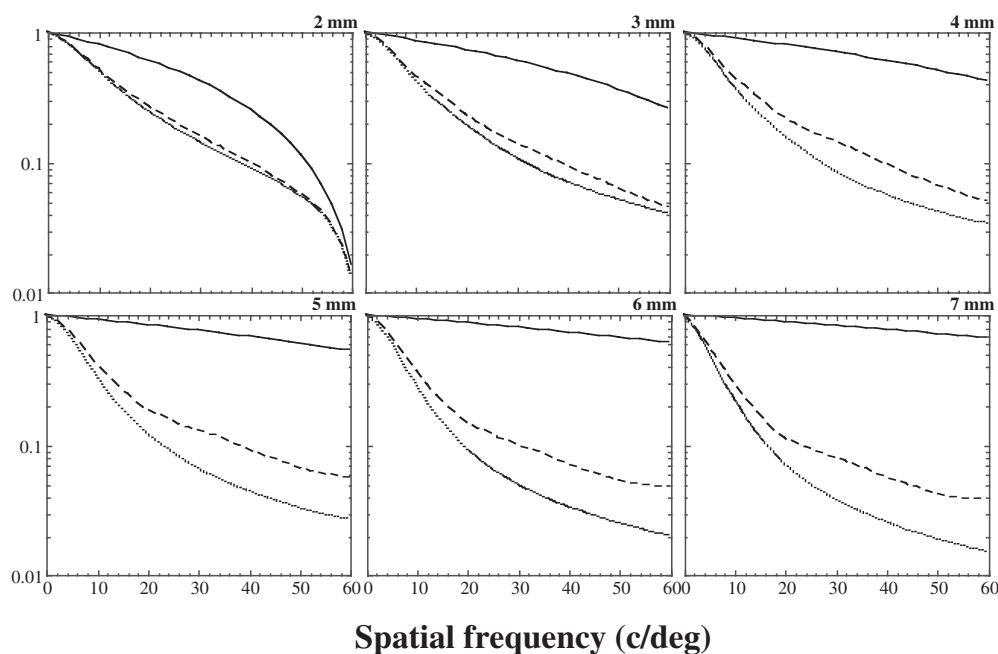


FIGURE 50.7. MTFs calculated for eyes with pupils ranging from 2 to 7 mm. In each panel, the solid line shows the MTF for an eye whose optics suffer only from diffraction, $\lambda = 555$ nm. The dashed lines show the mean monochromatic MTFs of 14 normal human eyes. MTFs were computed from wave aberration measurements obtained with a Hartmann-Shack wave front sensor and a 7.3 mm pupil (Liang and Williams, 1997). The dotted lines show the MTFs expected in white light, taking into account the axial but not the transverse chromatic aberration of the eye. The eye was assumed

to be accommodated to 555 nm, and its spectral sensitivity was assumed to correspond to the photopic luminosity function. The MTFs were calculated without defocus and astigmatism by setting the appropriate Zernike terms in the wave aberration to zero. This is not quite the same as finding the values of defocus and astigmatism that optimize image quality, as one does in a conventional clinical refraction. Had such an optimization been performed, the white light and monochromatic MTFs would have been more similar.

that the deleterious effects of axial chromatic aberration will be similar for both cone types. The reduced spectral sensitivity of the eye at short and long wavelengths also reduces the deleterious effects of chromatic aberration. In fact, the 2 diopters of defocus produced by chromatic aberration will have an effect on image quality similar to that of 0.15 diopter of monochromatic defocus, an amount that is close to the limit of what can be detected (Bradley et al., 1991). A less widely recognized reason that chromatic aberration is not more deleterious is that it is overwhelmed by the numerous monochromatic aberrations. These aberrations, most of which spectacles fail to correct, dilute the impact of axial chromatic aberration (Marcos et al., 1999; Yoon and Williams, 2002).

Figure 50.7 compares the MTFs in monochromatic (*dashed curves*) and broadband (*dotted curves*) light. These curves were obtained by computing the separate MTFs at each wavelength and then computing from these the mean MTF, weighting the influence of each separate MTF by the photopic luminosity function.

Retinal image acquisition

SPATIAL FILTERING BY THE CONE APERTURE Once light passes through the optics of the eye, it must pass through the retina on its way to the photoreceptors that transduce the retinal image. Foveal cones enjoy relatively unperturbed access to the retinal image because the inner retina and its associated vasculature have been swept aside to form the foveal pit. The photoreceptors themselves blur the retinal image by averaging light within their collection area (Miller and Bernard, 1983). The size of the human foveal cone aperture has been estimated psychophysically in humans to correspond to about half of the anatomical diameter (MacLeod et al., 1992). This estimate probably represents the lower bound of its true size. Even under the assumption that the cone aperture corresponds to the size of a foveal cone ($\sim 2.5 \mu\text{m}$), it is half the size of the eye's optical PSF for an aberrated eye with a 3 mm pupil. Therefore, under normal viewing conditions, the spatial resolution of the eye is not limited by the spatial frequency bandwidth of the cone aperture (Williams, 1985).

PHOTORECEPTOR TOPOGRAPHY Color and spatial vision at high light levels is subserved by 4 to 5 million cones (Curcio

et al., 1990; Osterberg, 1935) that are distributed unevenly across the retina. Cone density peaks at an average of 200,000 cones/mm² at the center of the fovea, then falls sharply to one-half maximum at less than 0.2 degree of eccentricity, to one-tenth maximum at 1 degree of eccentricity, and to 5000 cones/mm² or less near the edge of the retina. Foveal cones are set in a lattice which has an approximately triangular packing arrangement, as illustrated in Figure 50.8. The mean center-to-center spacing of the most central cones has been measured anatomically at 2.24 μ m (27 seconds of arc) (Curcio et al., 1990) and interferometrically (see below) in the living human eye at 2.7 μ m (32 seconds of arc) (Williams, 1988).

OBSERVATIONS WITH LASER INTERFEROMETRY An especially effective way to investigate image acquisition by the retina is with the use of laser interferometry. Interference fringes are formed on the retina by passing all the light through two small point sources imaged near the eye's pupil. Because the eye's wave aberration is constant at the small spatial scale of these point sources, the blurring effects of the eye's optics are avoided (Arnulf and Dupuy, 1960; Campbell and Green, 1965; Le Grand, 1935; Williams, 1985). When the two beams from a single laser overlap at the retina, they interfere with each other, producing an interference fringe with a sinusoidal luminance profile whose spatial frequency is proportional to the beam separation. The spatial frequency of the interference fringe is limited only by the size of the pupil. In the case of an 8mm pupil, the cutoff exceeds 200 c/deg in visible light. Normal observers viewing inter-

ference fringes can resolve the regular stripes of the fringe up to frequencies in the range from 45 to 70 c/deg, depending on the observer and whether steps have been taken to reduce laser speckle, which otherwise masks interference fringes (Williams, 1985). At higher spatial frequencies, many observers report seeing a scintillating pattern of irregular stripes that are not present in the original image (Byram, 1944; Campbell and Green, 1965; Williams, 1985). Perhaps the first report of this phenomenon was that of Bergmann (1858), who reported seeing similar effects when viewing gratings without the benefit of interferometry. Figure 50.9 shows drawings of the appearance of high-frequency fringes from several sources.

Figure 50.10 demonstrates the origin of this phenomenon using a simulation first suggested by Yellott (1982). When the spatial frequency exceeds the resolution limit of about 60 c/deg, a lower-frequency, distorted moiré pattern occurs that is indistinguishable from the regular, higher-frequency pattern that is actually imaged on the mosaic. This moiré pattern can be exploited to study the topography of the photoreceptor mosaic in the living human fovea (Williams, 1988).

The subjective observations of interference fringes that exceed the limit of visual resolution can be well described by a two-stage model (Tiana et al., 1991). The first stage samples the continuous retinal image with the photoreceptor mosaic, and the second stage reconstructs the sampled image with a postreceptoral, low-pass spatial filter that accepts spatial frequencies up to the resolution limit and rejects those above it. At spatial frequencies above about 60 c/deg, the spatial filter rejects the original

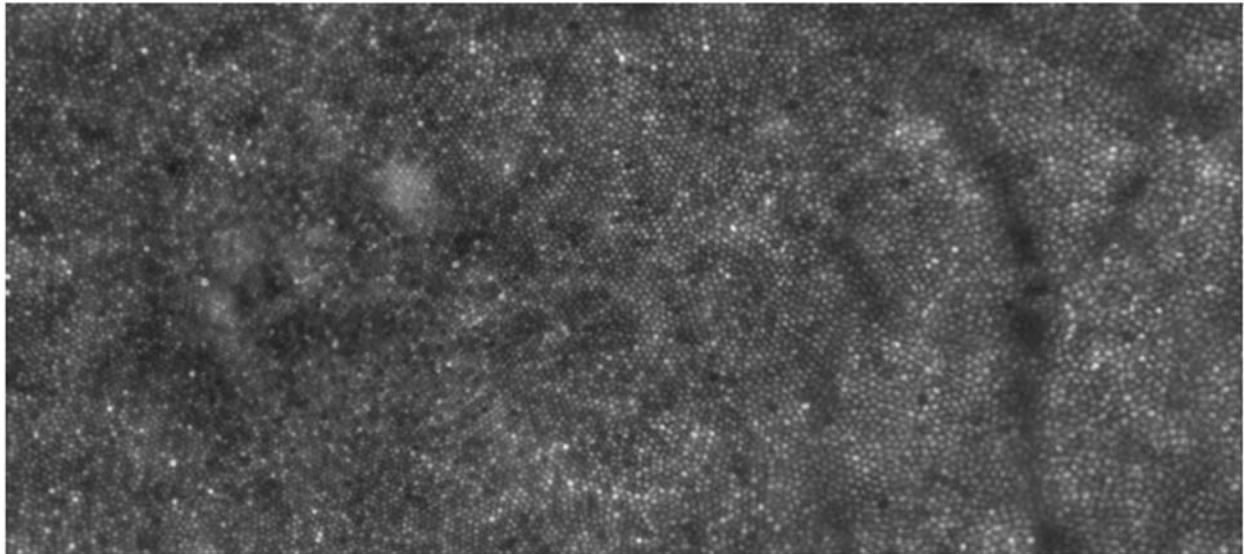


FIGURE 50.8. Image of the center of the living human fovea obtained with the Rochester Adaptive Optics Ophthalmoscope. Because of the 1 degree field of view of the instrument, this larger image was constructed by merging a number of overlapping images centered at different locations. The height of the image is 0.98

degree and its width is 2.2 degrees, extending from 0.7 degree temporal to 1.5 degrees nasal retina. Note the increase in cone spacing with increasing distance from the foveal center. (Courtesy of Matt MacMahon and Heidi Hofer.)

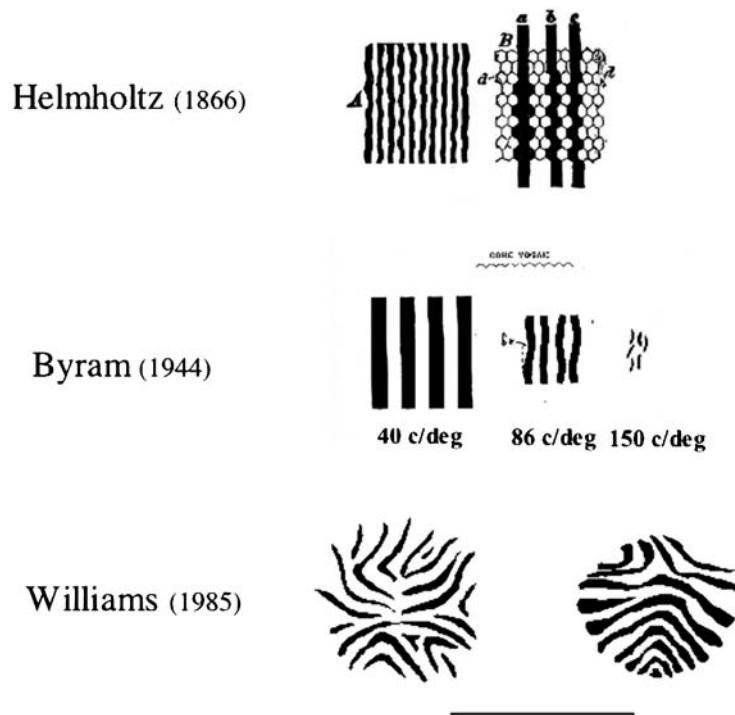


FIGURE 50.9. Drawings from three different authors of the appearance of high-frequency gratings, illustrating distortions in the appearance of the gratings caused by aliasing.

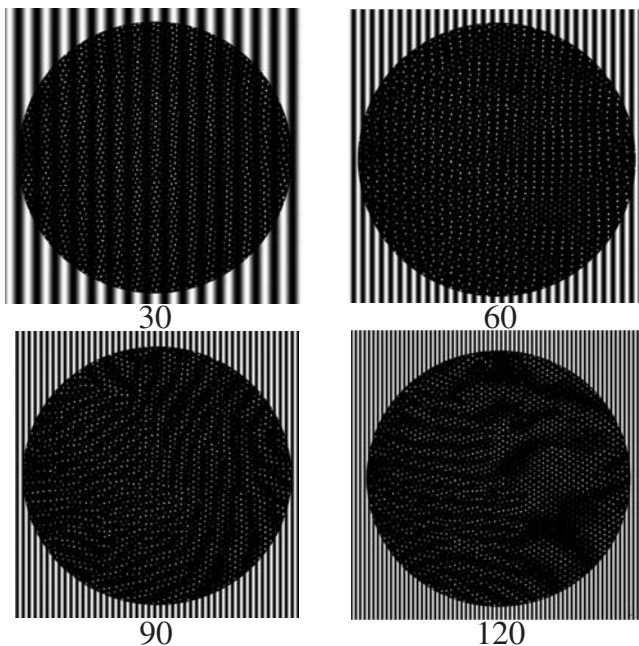


FIGURE 50.10. Simulation of aliasing in which a 30, 60, 90, and 120 c/deg fringe is superimposed on the foveal cone mosaic. Cone locations, taken from a tangential section of primate fovea, are represented as points. The 30 c/deg grating is adequately sampled by the mosaic, and the 60 c/deg grating is near the Nyquist limit. When the limit is exceeded, the reader interprets the image as a low-frequency, distorted moiré pattern instead of a high-frequency grating. At 120 c/deg, the grating period roughly equals the cone spacing, which produces a very coarse alias.

grating and passes the moiré patterns generated by the cone mosaic.

This phenomenon is closely related to the sampling theorem (Shannon, 1949). In its simplest form, to reconstruct a one-dimensional signal from a set of regularly spaced samples, the sampling rate must be equal to or greater than twice the highest frequency in the signal. Put another way, the highest spatial frequency that is adequately sampled, known as the *Nyquist limit*, is half the sampling frequency. Aliasing, which is essentially the creation of a low-frequency moiré pattern, results from exceeding the Nyquist limit. The sampling theorem is often applied to the cone mosaic, despite the fact that the mosaic is neither regular nor one-dimensional. The cone mosaic is a disordered two-dimensional sampling array. See Peterson and Middleton (1962) for a discussion of two-dimensional sampling. In the case of the foveal cones, the packing geometry is regular enough to produce moiré patterns that look like zebra stripes, while outside the fovea, aliasing takes on the appearance of two-dimensional spatial noise.

The optical quality of the eye plays a major role in preventing foveal cone aliasing from disrupting visual experience under normal viewing conditions. Figure 50.11 shows the relationship between the eye's MTF for various pupil sizes and the foveal cone Nyquist limit. The optics of the eye filter out those spatial frequencies above ~ 60 c/deg that exceed the Nyquist limit of the foveal cone mosaic, and these

are the frequencies that could produce aliasing. This relationship between optics and mosaic is often described as one in which they are matched, first articulated by Helmholtz (1896). While this is approximately true for the fovea, the optics are substantially superior to the grain of the peripheral mosaic and especially that of subsequent neural sampling arrays en route to the brain. The spatial frequency spectra of natural visual scenes generally have amplitudes that decline as the inverse of spatial frequency (Field, 1987). This allows the optics to provide higher contrast in the retinal image at sub-Nyquist frequencies without encountering aliasing. Snyder et al. (1986) argued convincingly that evolution should drive the cutoff frequency of the eye's optics to frequencies higher than the Nyquist limit. This is because the resulting improvement in image contrast at spatial frequencies below the Nyquist limit more than offsets the deleterious effects of any aliasing of spatial frequencies above the Nyquist limit.

The Nyquist limit is not an impenetrable barrier beyond which the eye cannot possibly resolve (Ruderman and Bialek, 1992; Williams and Coletta, 1987). Spatial sampling does not obliterate contrast in the retinal image above the Nyquist frequency in the same way that spatial filtering drives the contrast to zero above the cutoff frequency set by diffraction. The sampling process by itself usually has no effect on image contrast. Instead, by reducing the dimensionality of the image, it introduces ambiguity simply because the signal between the sample points is unknown. The original object becomes only one of an infinite number of objects that could have generated the observed distribution of quantum catches. It is then up to postreceptoral processes, probably involving the use of a priori information, to interpret the ambiguous image. Experimental support for the idea that the Nyquist limit is not impenetrable comes from Williams and Coletta (1987), who showed that observers could reliably discriminate the orientation of gratings at spatial frequencies 50% greater than the Nyquist limit in the parafoveal retina. Subsequent unpublished experiments by David Brainard in my laboratory showed that spatial frequency discrimination was exceedingly poor for frequencies above the Nyquist limit. Nonetheless, limited orientation information is preserved at supra-Nyquist spatial frequencies.

Appealing solely to the Nyquist limit of the sampling theorem oversimplifies the mechanisms that actually set the resolution limit. Strictly speaking, the retina and brain as well as the cone mosaic share the responsibility for setting the visual resolution limit. This point has been made with intriguing experiments that show perceptual consequences of interference fringes that exceed the resolution limit (He and MacLeod, 2001; Macleod and He, 1993). If foveal grating resolution were determined by cone sampling alone, then one would expect the highest spatial frequency inter-

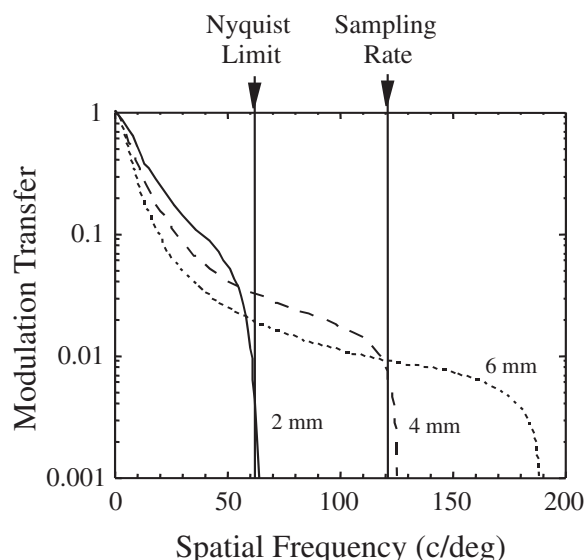


FIGURE 50.11. The relationship between the eye's modulation transfer function for 2, 4, and 6 mm pupils and the foveal cone Nyquist limit and sampling rate. Because the modulation transfer is greatly reduced at frequencies in excess of the Nyquist limit, the eye's optics protect vision from aliasing under normal viewing conditions.

ference fringe that can be resolved to increase with increasing contrast until the Nyquist barrier is reached and remain constant thereafter. Surprisingly, this is not always the case. In a previously unpublished experiment in my laboratory, an observer adjusted the spatial frequency of a fixed-contrast interference fringe to find the highest spatial frequency at which a grating could be seen in foveal vision. Figure 50.12 shows these settings with filled-circle symbols for various fringe contrasts. Also shown are forced-choice contrast sensitivity measurements (filled-square symbols), in which observers could detect gratings at very high spatial frequencies due to aliasing by the cone mosaic (Williams, 1985) and nonlinear distortion (He and MacLeod, 1996; Sekiguchi et al., 1991). The striking thing about the acuity settings is that, for contrasts above about 15%, acuity declines significantly with increasing contrast. Very high contrast stimuli near the resolution limit have a dazzling appearance, including a change of hue that is diminished at reduced contrast.

The nervous system is not able to represent these stimuli, faithfully, possibly because such high spatial frequencies at such high contrast are not experienced in normal viewing. We know that adults reared with cataracts have impressively poor visual performance even when their optics are restored (Fine et al., 2002; Gregory, 1990). Amblyopia demonstrates how restricted visual experience during development can lead to permanent neural deficits. It is plausible that the data in Figure 50.12 illustrate a kind of amblyopia in normal eyes, an amblyopia that is revealed only when the normal optics are improved. It would be of some interest to know whether

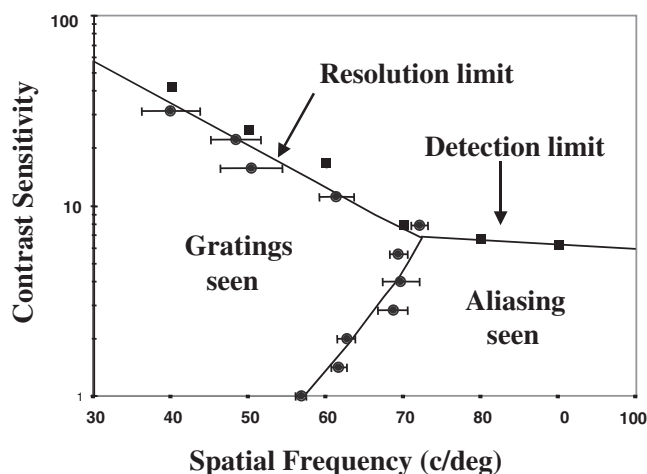


FIGURE 50.12. Forced-choice contrast sensitivity for laser interference fringes (632.8 nm) (*squares*). Fringes can be detected beyond the resolution limit due to nonlinearities in the retina as well as aliasing by the cone mosaic. *Circles* show acuity for resolving regular stripes in interference fringes obtained with the method of adjustment. The highest settings slightly exceed the Nyquist limit for this observer of about 56 c/deg, which may be an example of supra-Nyquist resolution. As fringe contrast is increased above about 15%, acuity actually declines rather than increases. This may be due to the fact that the visual system of this observer developed without exposure to such high-contrast stimuli at such high spatial frequencies and lacks the capacity to represent such stimuli.

extended experience with high-frequency interference fringes can improve resolution.

TRICHROMATIC SAMPLING AND CHROMATIC ALIASING So far, we have considered sampling by the cone mosaic without distinguishing between different classes of cone. The normal cone mosaic is composed of three submosaics of cones, L, M, and S, as shown in Figure 50.13. Unlike color film, which samples each location in the image with three emulsions, the retina samples the image with only one spectral sensor at each location. This means that at a local spatial scale, the retina is color blind. Because the sampling density of each submosaic is necessarily lower than the sampling density of the mosaic as a whole, chromatic aliasing can arise at lower spatial frequencies than the Nyquist limit for the mosaic as a whole.

Holmgren (1884) noticed that the hue of stars varied from instant to instant, a fact he attributed to selective excitation of different cone classes as the point of light moved across the mosaic. This observation is a form of chromatic aliasing and has led to a number of investigations that probe the cone mosaic with small spots (cf. Cicerone and Nerger, 1989; Krauskopf, 1978; Vimal et al., 1989). This color fluctuation is never very salient, because the optics of the eye blur the point of light across several cones. It has recently become possible to use adaptive optics (Liang et al., 1997) to reduce

the diameter of the spots of light to less than the diameter of an individual cone. Under these conditions, Heidi Hofer at the University of Rochester has shown that the chromatic fluctuations are greatly increased.

Chromatic aliasing can also be observed when viewing spatially extended stimuli as well as sharply focused points of light. High-contrast patterns such as black and white lines with spatial frequencies between 10 and 40 c/deg sometimes appear to contain splotches of desaturated color (Brewster, 1832; Erb and Dallenbach, 1939; Luckiesh and Moss, 1933; Skinner, 1932). Williams et al. (1991) have named this effect *Brewster's colors* after the first person to have described them. The visual system is remarkably resistant to the effects of chromatic aliasing. In those cases in which it can be detected at all, it is subtle and fleeting. The visual system has apparently evolved the capacity for color discrimination without any substantial cost for spatial vision under natural viewing conditions. The statistics of natural scenes make high-contrast, high spatial frequency signals rare events, optical blurring in the eye reduces the potential for aliasing, and clever postreceptoral processing based on prior information about natural visual scenes may also tend to hide the apparently haphazard organization of the trichromatic mosaic.

S cones are of particular interest because they sample the foveal retinal image especially coarsely, accounting for less than 10% of the cone population (Ahnelt et al., 1987; Bumsted and Hendrickson, 1999; Curcio et al., 1991; de Monasterio et al., 1981, 1985; Roorda and Williams, 1999; Wikler and Rakic, 1990; Williams and Collier, 1983; Williams et al., 1981b). Correspondingly, the resolution of gratings seen only by S cones is one-fourth to one-sixth that of the luminance mechanism fed by L and M cones (Stromeyer et al., 1978; Williams and Collier, 1983), and S cone aliasing is seen above the resolution limit. In the human fovea, S cones are randomly arranged, at least in local patches of retina, so that aliasing appears as spatial noise instead of the more regular zebra stripe-like patterns seen in foveal vision with interference fringes. A widely accepted explanation for the sparse sampling by S cones is that chromatic aberration blurs the short-wavelength retinal image enough that the sparse sampling is adequate to capture the retinal image seen by the S cone mosaic (Yellott et al., 1984).

In most though perhaps not all human foveas, S cones are absent in the central 20 minutes of arc (Williams et al., 1981a). It is especially striking that this is not subjectively obvious since it renders us tritanopic within the most acute portion of our visual field. The brain must be equipped with sophisticated mechanisms capable of hiding this gaping chromatic blind spot from us (Brainard and Williams, 1993; Magnussen et al., 2001). A priori information presumably plays a role.

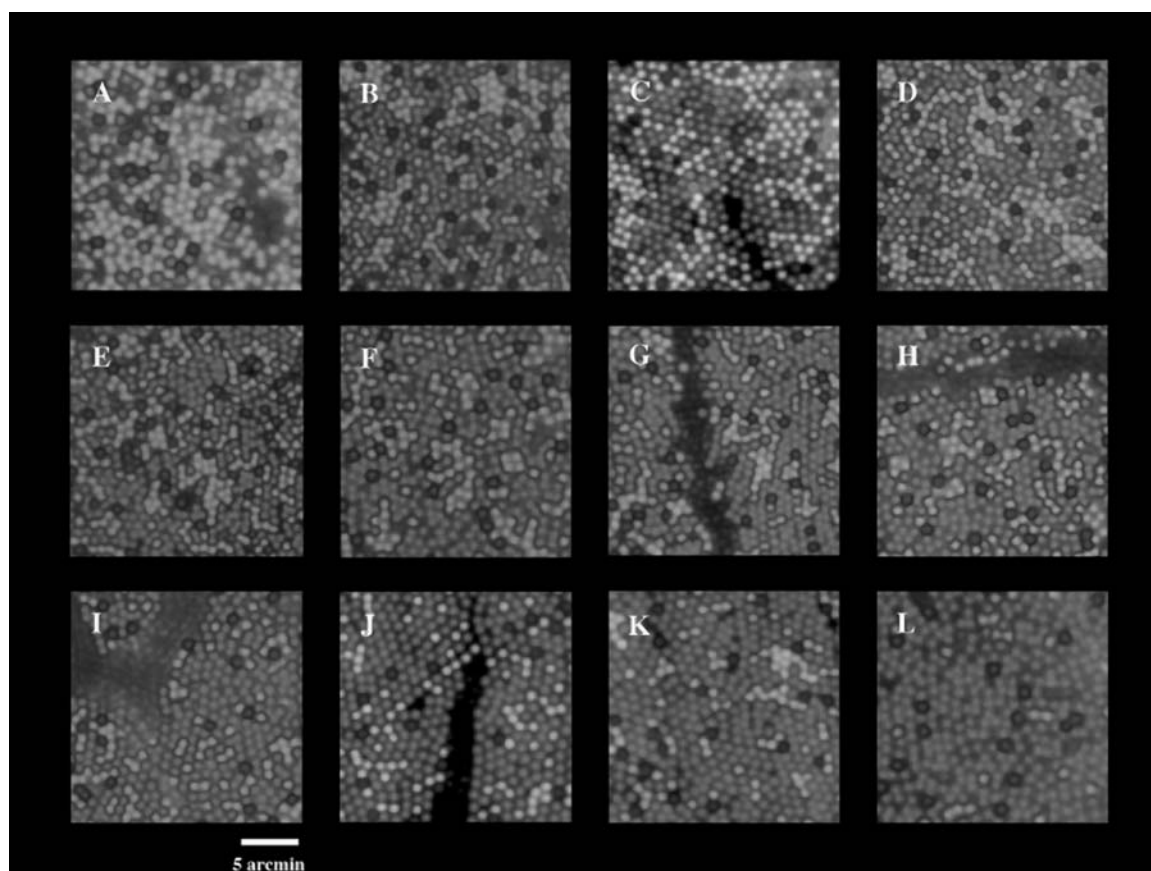


FIGURE 50.13. Images of the cone mosaics of 10 subjects with normal color vision, obtained with the combined methods of adaptive optics imaging and retinal densitometry. The images are false colored so that blue, green, and red are used to represent the S, M, and L cones, respectively. (The true colors of these cones are yellow, purple, and bluish-purple). The mosaics illustrate the enormous variability in L/M cone ratio. The L/M cone ratios are *A*, 0.37, *B*, 1.11, *C*, 1.14, *D*, 1.24, *E*, 1.77, *F*, 1.88, *G*, 2.32, *H*, 2.36, *I*, 2.46, *J*, 3.67, *K*, 3.90, *L*, 16.54. The proportion of S cones is relatively

constant across eyes, ranging from 3.9% to 6.6% of the total population. Images were taken either 1 or 1.25 degrees from the foveal center. For two of the 10 subjects, two different retinal locations are shown. Panels *D* and *E* show images from nasal and temporal retinas respectively for one subject; *J* and *K* show images from nasal and temporal retinas for another subject. (Images *C*, *J*, and *K* are from Roorda and Williams, 1999. All other images were made by Heidi Hofer.) (See color plate 30).

Because the sampling densities of the L and M cone submosaics are lower than the density of the mosaic as a whole, one might expect to find a reduction in the acuity of the separate L and M cone submosaics. However, there is no measurable difference in contrast sensitivity or acuity when the L and M cones are isolated compared to conditions in which they operate together (cf. Brindley, 1953; Williams, 1991). This is true even when laser interference fringes are used to exclude blurring by the optics of the eye. To be sure, resolution declines when the density of cones in the submosaic becomes sparse enough. The S cone submosaic is a case in point. Nonetheless, relatively large density losses have no obvious effects on grating acuity (Geller et al., 1992). This is almost certainly due to the disordered arrangement of L and M cones, which creates small clumps of like-type cones whose spacing is much less than the average spacing of that submosaic. These clumps may

be sufficiently large and common to subserve better than expected acuity, especially with extended stimuli such as large patches of grating. Only when one cone class is greatly underrepresented, as in some heterozygous carriers for congenital X-linked protanopia, is resolution clearly affected in cone-isolating conditions (Miyahara et al., 1998). Presumably, visual stimuli that are more localized, such as vernier targets, would be better suited to reveal a deficit due to the coarser grain of the separate L and M cone submosaics.

VARIATION IN CONE RATIO AND COLOR VISION A wealth of evidence shows that the ratio of L to M cones is highly variable in the normal population (Bowmaker and Dartnall, 1980; Dartnall et al., 1983; Hagstrom et al., 1997; Jacobs and Deegan, 1997; Jacobs et al., 1993; Roorda and Williams, 1999; Rushton and Baker, 1964; Vimal et al., 1989;

Yamaguchi et al., 1997). This is illustrated in Figure 50.13, which shows images of the cone mosaic obtained with adaptive optics in the retinas of ten different eyes. The L/M cone ratio ranges from 0.37 to 19.5. Gunther and Dobkins (2002) found evidence that chromatic contrast sensitivity was depressed slightly in subjects with extreme ratios of L to M cones estimated with flicker photometry. Nonetheless, it is striking how little difference the ratio of L to M cones makes for vision, except when the ratio becomes extreme. Due to the similarity of the M and L cone spectra, the photopic luminosity function changes relatively little with large changes in the L/M cone ratio (cf. Jacobs and Deegan, 1997). Color appearance, at least for large stimuli where aliasing is not an issue, seems not to depend on the L/M ratio (Brainard et al., 2000; Miyahara et al., 1998; Neitz et al., 2002). The subjective boundaries between hues are apparently set by factors other than cone numerosity. As Pokorny and Smith (1977) proposed, the balance point of color opponent mechanisms may be determined by the average chromaticity in natural scenes. This would be a more efficient choice for the visual system since it would minimize the metabolic cost of transmitting neural signals about the most common colors in the world, reserving resources for departures from the average. Neitz et al. (2002) have recently reported some experimental support for this view, showing that the color boundary between red and green, unique yellow, can undergo modification over a period of many days of exposure to an altered chromatic environment. Presumably, this same mechanism explains the constancy of color vision despite the large spectral changes in the lens with age (Werner, 1996).

THE LIMITS OF HUMAN VISION An optical engineer, undertaking to design the human eye, would not have chosen the same parameters for optical quality and sampling that evolution has created in the eye. The coarse and random sampling performed by the three cone submosaics would generally be unacceptable in a digital camera that has the optical quality of the eye. It must be that central mechanisms for object recognition are especially good at rejecting sampling artifacts, and it seems likely that experience with visual scenes during development is used to create representations that hide the grain of the neural visual system from us under ordinary viewing conditions.

Given the tolerance the visual system has for undersampling, it is natural to wonder how much normal vision could be improved by improving the optics of the eye (Charman, 2000; Williams et al., 2001). Laser interferometry shows that grating resolution does not improve much. In practice, interferometry is limited to the presentation to the retina of a small number of monochromatic gratings of different spatial frequency and orientation. Adaptive optics, on the other

hand, can increase the retinal image contrast of any arbitrary stimulus with any spectral properties. Adaptive optics, unlike interferometry, is subject to blurring by diffraction. Nonetheless, it can be used to correct the eye's higher-order monochromatic aberrations as well as defocus and astigmatism. Correcting higher-order aberrations in normal eyes increases contrast sensitivity by roughly a factor of 2 on average at high frequencies (Yoon and Williams, 2002). In the average eye, correcting higher-order aberrations will produce a benefit only when the pupil is large. With a 6 mm pupil, the higher-order aberrations are roughly equivalent to one-third of a diopter of defocus (Guirao et al., 2002). Of course, this benefit is highly variable, depending on the amount of higher-order aberrations in the eye. There are large individual differences in higher-order aberrations, just as there are for astigmatism.

It is advantageous to correct higher-order aberrations in eyes that have large amounts of these aberrations, and the recent excitement in wave front sensing and wave front correction with customized contact lenses and refractive surgery offers the possibility of substantial benefit in these people. However, in eyes with good optical quality already, the benefit of correcting higher-order aberrations comes with some costs in addition to the possibility of aliasing. Color artifacts associated with chromatic aberration are increased. It is possible to detect the chromatic fringing caused by chromatic aberration in normal viewing conditions, and the accommodative mechanism can sometimes use this effect to pick the direction with which to accommodate (Fincham, 1951; Kruger and Pola, 1986). Correcting monochromatic aberrations in broadband light makes chromatic aberration even more visible. White targets seen through adaptive optics reveal quite pronounced blue-green fringes when the eye is slightly myopic and reddish fringes when the eye is slightly hyperopic. Long-term exposure to chromatic fringes makes them less visible (Held, 1980), and it is possible that adaptation could reduce the visibility of this effect as well.

Another possibly negative effect of correcting the monochromatic aberrations of the eye is that the depth of field is reduced. This is illustrated in Figure 50.14, which shows the Strehl ratio of the eye's PSF as a function of light vergence. These data were calculated from wave aberration measurements of 13 eyes, assuming an equal energy spectrum and axial chromatic aberration in the eyes. Pupil size was 6 mm. Note that correcting monochromatic aberrations increases image quality over a range of about 1.25 diopters, but outside this region, image quality is actually lower with correction than without it. If the eye's chromatic aberration is also corrected, the benefits when focus is optimized are even greater but the depth of focus is even smaller. The true cost of this loss of depth of field in everyday vision has not been explored.

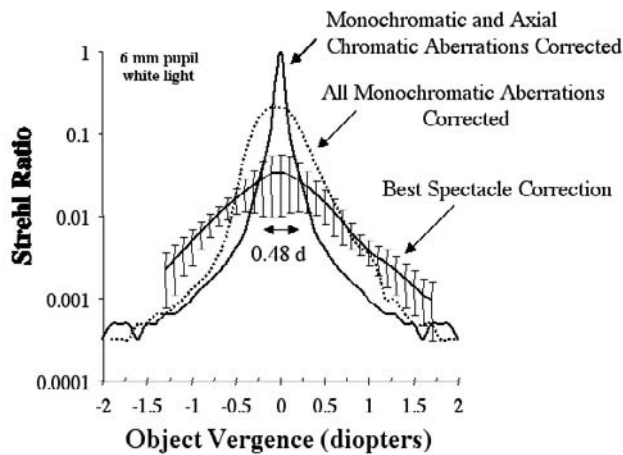


FIGURE 50.14. The Strehl ratio of the eye's PSF as a function of light vergence.

The parameters that the eye has evolved for image formation and image acquisition seem to be well balanced in the best human eyes so that improvement in any single parameter does not create large improvements in visual performance and can even come at a cost.

Acknowledgments

The authors wish to thank Antonio Guirao, Jason Porter, and Geunyoung Yoon for their contribution to the chapter. Williams' laboratory is supported by National Institutes of Health Grants EY01319 and EY07125 and the National Science Foundation Science and Technology Center for Adaptive Optics, managed by the University of California at Santa Cruz under cooperative agreement No. AST-9876783.

REFERENCES

Ahnelt, P. K., H. Kolb, and R. Pflug, 1987. Identification of a subtype of cone photoreceptor, likely to be blue sensitive, in the human retina, *J. Comp. Neurol.*, 255:18–34.

Arnulf, A., and O. Dupuy, 1960. La transmission des contrastes par le système optique de l'œil et les seuils des contrastes rétinien, *C.R. Acad. Sci. (Paris)*, 250:2757–2759.

Artal, P., A. Guirao, E. Berrio, and D. R. Williams, 2001. Compensation of corneal aberrations by the internal optics in the human eye, *J. Vision*, 1:1–8.

Artal, P., S. Marcos, R. Navarro, and D. R. Williams, 1995. Odd aberrations and double-pass measurements of retinal image quality, *J. Opt. Soc. Am. A*, 12:195–201.

Bergmann, C., 1858. Anatomisches und Physiologisches über die Netzhaut des Auges. *Zeitschrift für ration. Medizin*, 2:83–108. Translated by D'Zmura, M., 1996. Bergmann on visual resolution, *Perception*, 25:1223–1234.

Berny, F., and S. Slansky, 1969. Wavefront determination resulting from foucault test as applied to the human eye and visual instruments (offprint), *Opt. Instruments Tech.*, 1:375–386.

Bowmaker, J. K., and H. J. Dartnall, 1980. Visual pigments of rods and cones in a human retina, *J. Physiol. (Lond.)*, 298:501–511.

Bradley, A., X. X. Zhang, and L. N. Thibos, 1991. Achromatizing the human eye, *Optom. Vis. Sci.*, 68:608–616.

Brainard, D. H., A. Roorda, Y. Yamauchi, J. B. Calderone, A. Metha, M. Neitz, J. Neitz, D. R. Williams, and G. H. Jacobs, 2000. Functional consequences of the relative numbers of L and M cones, *J. Opt. Soc. Am. A*, 17:607–614.

Brainard, D. H., and D. R. Williams, 1993. Spatial reconstruction of signals from short-wavelength cones, *Vis. Res.*, 33:105–116.

Brewster, D., 1832. On the undulations excited in the retina by the action of luminous points and lines, *Philos. Mag. J. Sci.*, 1–174.

Brindley, G. S., 1953. The effects on colour vision of adaptation to very bright lights, *J. Physiol.*, 122:332.

Bumsted, K., and A. Hendrickson, 1999. Distribution and development of short-wavelength cones differ between *Macaca* monkey and human fovea, *J. Comp. Neurol.*, 403:502–516.

Byram, G. M., 1944. The physical and photochemical basis of visual resolving power. Part II. Visual acuity and the photochemistry of the retina, *J. Opt. Soc. Am.*, 34:718–738.

Campbell, F. W., and D. G. Green, 1965. Optical and retinal factors affecting visual resolution, *J. Physiol. (Lond.)*, 181:576–593.

Campbell, F. W., and R. W. Gubisch, 1966. Optical Quality of the Human Eye, *J. Physiol. (Lond.)*, 186:558–578.

Campbell, F. W., and R. W. Gubisch, 1967. The effect of chromatic aberration on visual acuity, *J. Physiol. (Lond.)*, 192:345–358.

Castejon-Mochon, J., N. Lopez-Gil, A. Benito, and P. Artal, 2002. Ocular wave-front aberration statistics in a normal young population, *Vis. Res.*, 42:1611–1617.

Charman, N., 2000. Ocular aberration and supernormal vision, *Optician*, 220:20–24.

Charman, W., and G. Walsh, 1985. The optical phase transfer function of the eye and the perception of spatial phase, *Vis. Res.*, 25(4):619–623.

Cicerone, C. M., and J. L. Nerger, 1989. The relative numbers of long-wavelength-sensitive to middle-wavelength-sensitive cones in the human fovea centralis, *Vis. Res.*, 29:115–128.

Curcio, C. A., K. A. Allen, K. R. Sloan, C. L. Lerea, J. B. Hurley, I. B. Klock, and A. H. Milam, 1991. Distribution and morphology of human cone photoreceptors stained with anti-blue opsin, *J. Comp. Neurol.*, 312:610–624.

Curcio, C. A., K. R. Sloan, R. E. Kalina, and A. E. Hendrickson, 1990. Human photoreceptor topography, *J. Comp. Neurol.*, 292:497–523.

Dartnall, H. J., J. K. Bowmaker, and J. D. Mollon, 1983. Human visual pigments: microspectrophotometric results from the eyes of seven persons, *Proc. R. Soc. Lond. B Biol. Sci.*, 220:115–130.

de Monasterio, F. M., E. P. McCrane, J. K. Newlander, and S. J. Schein, 1985. Density profile of blue-sensitive cones along the horizontal meridian of macaque retina, *Invest. Ophthalmol. Vis. Sci.*, 26:289–302.

de Monasterio, F. M., S. J. Schein, and E. P. McCrane, 1981. Staining of blue-sensitive cones of the macaque retina by a fluorescent dye, *Science*, 213:1278–1281.

Erb, M. B., and K. M. Dallenbach, 1939. "Subjective" colors from line patterns, *Am. J. Psych.*, 52:227.

Field, D. J., 1987. Relations between the statistics of natural images and the response properties of cortical cells, *J. Opt. Soc. Am. A*, 4:2379–2394.

- Fincham, E., 1951. The accommodation reflex and its stimulus, *Br. J. Ophthalmol.*, 35:381–393.
- Fine, I., H. S. Smallman, P. Doyle, and D. I. MacLeod, 2002. Visual function before and after the removal of bilateral congenital cataracts in adulthood, *Vis. Res.*, 42(2):191–210.
- Geller, A. M., P. A. Sieving, and D. G. Green, 1992. Effect on grating identification of sampling with degenerate arrays, *J. Opt. Soc. Am. A*, 9:472–477.
- Goodman, J. W., 1996. *Introduction to Fourier Optics*, New York: McGraw-Hill.
- Gregory, R., 1990. *Eye and Brain: The Psychology of Seeing*, 5th ed., Princeton, NJ: Princeton University Press.
- Guirao, A., C. Gonzalez, M. Redondo, E. Geraghty, S. Norrby, and P. Artal, 1999. Average optical performance of the human eye as a function of age in a normal population, *Invest. Ophthalmol.*, 40(1):203–213.
- Guirao, A., J. Porter, D. R. Williams, and I. Cox, 2002. Calculated impact of higher-order monochromatic aberrations on retinal image quality in a population of human eyes: erratum, *J. Opt. Soc. Am. A*, 19(3):620–628.
- Gunther, K., and K. Dobkins, 2002. Individual differences in chromatic (red/green) contrast sensitivity are constrained by the relative number of L- versus M-cones in the eye, *Vis. Res.*, 42:1367–1378.
- Hagstrom, S. A., J. Neitz, and M. Neitz, 1997. Ratio of M/L pigment gene expression decreases with retinal eccentricity, in *Colour Vision Deficiencies XIII* (C. R. Cavonius, ed.), Dordrecht, the Netherlands: Kluwer Academic, pp. 59–66.
- He, S., and D. MacLeod, 1996. Local luminance nonlinearity and receptor aliasing in the detection of high frequency gratings, *J. Opt. Soc. Am. A*, 13:1139–1151.
- He, S., and D. MacLeod, 2001. Orientation-selective adaptation and tilt after-effect from invisible patterns, *Nature*, 411:473–476.
- Held, R., 1980. The rediscovery of adaptability in the visual system: effects of extrinsic and intrinsic chromatic dispersion, in *Visual Coding and Adaptability*, Hillsdale, NJ: Bell Laboratories, pp. 69–94.
- Helmholtz, H., 1896. *Helmholtz's Treatise on Physiological Optics* (trans. from the 3rd German ed.; J. P. C. Southall, ed.), 3rd ed., New York: Dover, 1962.
- Holmgren, E., 1884. Über den Farbensinn, in *Compte rendu du congrès international de science et médecine* (vol. 1, *Physiology*), Copenhagen: International Medical Congress, pp. 80–98.
- Howland, H. C., and B. Howland, 1977. A subjective method for the measurement of monochromatic aberrations of the eye, *J. Opt. Soc. Am.*, 67:1508–1518.
- Jacobs, G. H., and J. F. Deegan 2nd, 1997. Spectral sensitivity of macaque monkeys measured with ERG flicker photometry, *Vis. Neurosci.*, 14:921–928.
- Jacobs, G. H., J. Neitz, and M. Neitz, 1993. Genetic basis of polymorphism in the color vision of platyrrhine monkeys, *Vis. Res.*, 33:269–274.
- Jennings, J. A., and W. N. Charman, 1981. Off-axis image quality in the human eye, *Vis. Res.*, 21:445–455.
- Krauskopf, J., 1978. On identifying detectors, in *Visual Psychophysics and Physiology* (J. C. Armington, J. Krauskopf, and B. R. Wooten, eds.), New York: Academic Press.
- Kruger, P. B., and J. Pola, 1986. Stimuli for accommodation: blur, chromatic aberration and size. *Vis. Res.*, 26(6):957–971.
- Le Grand, Y., 1935. Sur la mesure de l'acuité visuelle au moyen de franges d'interférence, *C.R. Acad. Sci., Paris*, 200:490–491.
- Liang, J., B. Grimm, S. Goelz, and J. Bille, 1994. Objective measurement of the wave aberrations of the human eye using a Hartmann-Shack wavefront sensor, *J. Opt. Soc. Am. A*, 11:1949–1957.
- Liang, J., and D. R. Williams, 1997. Aberrations and retinal image quality of the normal human eye, *J. Opt. Soc. Am. A*, 14:2873–2883.
- Liang, J., D. R. Williams, and D. T. Miller, 1997. Supernormal vision and high resolution imaging through adaptive optics, *J. Opt. Soc. Am. A*, 14:2884–2892.
- Luckiesh, M., and F. K. Moss, 1933. A demonstrational test of vision, *Am. J. Psych.*, 45:135.
- MacLeod, D., and S. He, 1993. Visible flicker from invisible patterns, *Nature*, 361:256–258.
- MacLeod, D. I. A., D. R. W. Williams, and W. Makous, 1992. A visual nonlinearity fed by single cones, *Vis. Res.*, 32:347–363.
- Magnussen, S., L. Spillmann, F. Stürzel, and J. S. Werner, 2001. Filling-in of the foveal blue scotoma, *Vis. Res.*, 41:2961–2967.
- Marcos, S., S. A. Burns, E. Moreno-Barriuso, and R. Navarro, 1999. A new approach to the study of ocular chromatic aberrations, *Vis. Res.*, 39(26):4309–4323.
- Miller, W. H., and G. D. Bernard, 1983. Averaging over the foveal receptor aperture curtails aliasing, *Vis. Res.*, 23:1365–1369.
- Miyahara, E., J. Pokorny, V. C. Smith, R. Baron, and E. Baron, 1998. Color vision in two observers with highly biased LWS/MWS cone ratios, *Vis. Res.*, 38:601–612.
- Navarro, R., P. Artal, and D. R. Williams, 1993. Modulation transfer of the human eye as a function of retinal eccentricity, *J. Opt. Soc. Am. A*, 10:201–212.
- Neitz, J., J. Carroll, Y. Yamauchi, M. Neitz, and D. R. Williams, 2002. Color perception is mediated by a plastic mechanism that is adjustable in adults, *Neuron*, 35:783–792.
- Osterberg, G. A., 1935. Topography of the layer of rods and cones in the human retina, *Acta Ophthalmol.*, 6(Suppl 13):1–102.
- Packer, O., and D. Williams, 2003. Light, the retinal image, and photoreceptors, in *The Science of Color*, 2nd ed. (S. K. Shevell ed.), Washington, DC: OSA. In press.
- Pettersen, D. P., and D. Middleton, 1962. Sampling and reconstruction of wave number limited functions in N -dimensional euclidean space, *Information Control*, 5:279–323.
- Piotrowski, L. N., and F. W. Campbell, 1982. A demonstration of the visual importance and flexibility of spatial-frequency amplitude and phase, *Perception*, 11:337–346.
- Pokorny, J., and V. C. Smith, 1977. Evaluation of single pigment shift model of anomalous trichromacy, *J. Opt. Soc. Am.*, 67:1196–1209.
- Porter, J., A. Guirao, I. Cox, and D. R. Williams, 2001. Monochromatic aberrations of the human eye in a large population, *J. Opt. Soc. Am. A*, 18(8):1793–1803.
- Roorda, A., and D. R. Williams, 1999. The arrangement of the three cone classes in the living human eye, *Nature*, 397:520–522.
- Ruderman, D. L., and W. Bialek, 1992. Seeing beyond the nyquist limit, *Neural Comput.*, 4(5):682–690.
- Rushton, W. A. H., and H. D. Baker, 1964. Red/green sensitivity in normal vision, *Vis. Res.*, 4:75–85.
- Sekiguchi, N., D. R. Williams, and O. Packer, 1991. Nonlinear distortion of gratings at the foveal resolution limit, *Vis. Res.*, 31(5):815–831.
- Sergienko, N. M., 1963. On the resolving power of the eye, *Vestnik Ophthalmol.*, 3:39–44.
- Shannon, C. E., 1949. Communication in the presence of noise, *Proc. IRE*, 37:10.

- Skinner, B. F., 1932. A paradoxical color effect, *J. Gen. Psychol.*, 7:481.
- Smirnov, M. S., 1961. Measurement of wave aberration in the human eye, *Biophysics*, 6:776–795.
- Snyder, A. W., T. R. Bossomaier, and A. Hughes, 1986. Optical image quality and the cone mosaic, *Science*, 231:499–501.
- Stromeyer, C. F., 3d, R. E. Kronauer, and J. C. Madsen, 1978. Apparent saturation of blue-sensitive cones occurs at a color-opponent stage, *Science*, 202:217–219.
- Thibos, L. N., 1987. Calculation of the influence of lateral chromatic aberration on image quality across the visual field, *J. Opt. Soc. Am. A*, 4:1673–1680.
- Thibos, L. N., 2000. Formation and sampling of the retinal image, in *Seeing* (K. K. De Valois ed.), London: Academic Press, pp. 1–54.
- Tiana, C. L. M., D. R. Williams, N. J. Coletta, and P. W. Haake, 1991. A model of aliasing in extrafoveal human vision, in *Computational Models of Visual Processing* (M. Landy and A. Movshon, eds.), Cambridge, MA: MIT Press, pp. 36–56.
- van den Brink, G., 1962. Measurements of the geometrical aberrations of the human eye, *Vis. Res.*, 2:233–244.
- Vimal, R. L., J. Pokorny, V. C. Smith, and S. K. Shevell, 1989. Foveal cone thresholds, *Vis. Res.*, 29:61–78.
- Vos, J. J., 1963. Contribution of the fundus oculi to entoptic scatter, *J. Opt. Soc. Am.*, 53:1449.
- Walsh, G., and W. N. Charman, 1985. Measurement of the axial wavefront aberration of the human eye, *Ophthalmol. Physiol. Opt.*, 5:23–31.
- Walsh, G., W. N. Charman, and H. C. Howland, 1984. Objective technique for the determination of monochromatic aberrations of the human eye, *J. Opt. Soc. Am. A*, 1:987–992.
- Webb, R. H., C. M. Penney, and K. P. Thompson, 1992. Measurement of ocular wavefront distortion with a spatially resolved refractometer, *Appl. Opt.*, 31:3678–3686.
- Werner, J. S., 1996. Visual problems of the retina during ageing: compensation mechanisms and colour constancy across the life span, in *Progress in Retinal and Eye Research*, vol 15/2 (N. N. Osborne and J. Chader, eds.), Oxford: Pergamon Press, pp. 621–645.
- Westheimer, G., and J. Liang, 1995. Influence of ocular light scatter on the eye's optical performance, *J. Opt. Soc. Am. A*, 12: 1417–1424.
- Wikler, K. C., and P. Rakic, 1990. Distribution of photoreceptor subtypes in the retina of diurnal and nocturnal primates, *J. Neurosci.*, 10:3390–3401.
- Williams, D. R., 1985. Aliasing in human foveal vision, *Vis. Res.*, 25:195–205.
- Williams, D. R., 1988. Topography of the foveal cone mosaic in the living human eye, *Vis. Res.*, 28:433–454.
- Williams, D. R., 1991. The invisible cone mosaic, in *Advances in Photoreception: Proceedings of a Symposium on Frontiers of Visual Science*, Washington, DC: National Academy Press, pp. 135–148.
- Williams, D. R., P. Artal, R. Navarro, M. J. McMahon, and D. H. Brainard, 1996. Off-axis optical quality and retinal sampling in the human eye, *Vis. Res.*, 36:1103–1104.
- Williams, D. R., and N. J. Coletta, 1987. Cone spacing and the visual resolution limit, *J. Opt. Soc. Am.*, 4:1514–1523.
- Williams, D. R., and R. Collier, 1983. Consequences of spatial sampling by a human photoreceptor mosaic, *Science*, 221:385–387.
- Williams, D. R., D. I. A. MacLeod, and M. M. Hayhoe, 1981a. Foveal tritanopia, *Vis. Res.*, 21:1341–1356.
- Williams, D. R., D. I. A. MacLeod, and M. M. Hayhoe, 1981b. Punctuate sensitivity of the blue sensitive mechanism, *Vis. Res.*, 21:1357–1376.
- Williams, D. R., N. Sekiguchi, W. Haake, D. Brainard, and O. Packer, 1991. The cost of trichromacy for spatial vision, in *From Pigments to Perception* (A. Valberg and B. B. Lee, eds.), New York: Plenum.
- Williams, D. R., G. Y. Yoon, A. Guirao, H. Hofer, and J. Porter, 2001. How far can we extend the limits of human vision? in *Customized Corneal Ablation: The Quest for SuperVision* (S. M. MacRae, R. R. Krueger, and R. A. Applegate, eds.), Thorofare, NJ: Slack, Inc., pp. 11–32.
- Wooten, B. R., and G. A. Geri, 1987. Psychophysical determination of intraocular light scatter as a function of wavelength, *Vis. Res.*, 27(8):1291–1298.
- Yamaguchi, T., A. G. Motulsky, and S. S. Deeb, 1997. Visual pigment gene structure and expression in the human retinae, *Hum. Mol. Genet.*, 6:981–990.
- Yellott, J. I., 1982. Spectral analysis of spatial sampling by photoreceptors: topological disorder prevents aliasing, *Vis. Res.*, 22:1205–1210.
- Yellott, J., B. Wandell, and T. Cornsweet, 1984. The beginnings of visual perception: the retinal image and its initial encoding, in *Handbook of Physiology Section 1—The Nervous System III* (I. Darian-Smith, ed.) *Am. Physiological Society Published*, Bethesda, MD. Part 2, pp. 257–316.
- Yoon, G. Y., and D. R. Williams, 2002. Visual performance after correcting the monochromatic and chromatic aberrations of the eye, *J. Opt. Soc. Am. A*, 19(2):266–275.

51 Thresholds and Noise

THEODORE E. COHN

A NATURAL WAY TO describe the quality of a visual detection system is to specify the least amount of light that can be seen. This concept was formalized by Fechner (1860) in the mid-nineteenth century and persists with us today. The concept was given a name, *threshold*, which has evolved in meaning as understanding of threshold phenomena has increased. Most importantly, we have begun to understand the nature of the threshold and its relation to noise.

The title of this chapter is redundant. In vision there cannot be thresholds without noise. With noise, vision is limited. Without noise, the only limit is the grain of light itself; a single photon is the irreducible threshold. And while the concept of *noise* has only recently crept into our thinking about threshold, it is central to the discussion. Noise is ubiquitous. It is intrinsic to all light sources, it arises as a result of pupil instability, and it is characteristic of all cell membranes, including those of neurons, and of all chemically mediated synapses.

In this chapter I trace the concept of the threshold to its most recent embodiment. Related topics will be examined: physiological thresholds and psychophysical thresholds, dependence of threshold upon adaptation level, target size, duration and color; threshold models, and key unexplored problems. The discussion begins with three different definitions of threshold: the classical one due to Fechner, the traditional concept that replaced it, and finally the modern version.

The classical (Fechnerian) threshold

Fechner is said to have borrowed a concept from Hebart, that of a *limen* or limit below which intensity is too small to be seen (Boring, 1942). Thus energy at or below the limen is unseen, while that above the limen is seen. This concept is shown schematically in Figure 51.1A. Measurement, by techniques that Fechner himself introduced, disproved the elegance of this concept immediately. No such unique limit can be found experimentally. Instead, the limit gives the appearance of whimsy: it is sometimes at one value, sometimes at another, and always both changing and unpredictable. Figure 51.1B illustrates this modified classical threshold for three different instances: low, medium, and high. The evidence for this modified theory is that some intensity that is not (reported as) “seen” on one occasion may be seen on the next, and one that was seen might not be seen later.

One can imagine that for repeated examples, the measured frequency seen will equal the fraction of occasions on which threshold, defined in this way, is exceeded. Thus, the measured frequency seen averages over a multiplicity of instances, and the result is a curve that rises from zero or a few instances seen and asymptotes at 100% seen. Instances of reports of seen intensity when no stimulus has been delivered have been known since the time of Fechner. Thus the frequency of reports seen may rise from a nonzero value at zero contrast. As will be seen below, there are two different ways of dealing with such events. One assumes that they are guesses and then modifies all seen events by a putative guess rate. The other approach treats these as noise-caused events and uses them to gain a greater understanding of the relevant noise.

Figure 51.2 shows an example of such a frequency seen curve (also termed a *psychometric function*—see the later section “The Psychometric Function”) and, on the same abscissa, the putative probability density of the threshold value. In a sense, then, this traditional concept of the threshold incorporates a sort of noise, a random variability of the value of the threshold. The conclusion that Fechner and the entire vision community reached, and that held for 100 years, was that of a randomly varying limen or threshold. The inclusion of randomness in this model may have been the first acknowledgment that noise had to play a role in threshold, though this was not explicit. How then to quantify or estimate the threshold?

The traditional threshold

A threshold that varies randomly over time is best described by its typical value, hence the search for a mean or average. In a yes/no task, the probability with which a presented stimulus will be judged to be present usually varies monotonically with the stimulus intensity. This function is called the *psychometric function*. The (traditional) threshold is defined by convention. It is taken as the intensity that leads to a probability of detection of some prescribed value that is usually, though not always, 0.50. That intensity can be determined by a number of means. The most obvious method is to fit the psychometric function with a reasonably smooth curve and to interpolate. More modern approaches abound, and all have the merit of shortening the time it takes to conduct an experiment to make the determination. Usually these

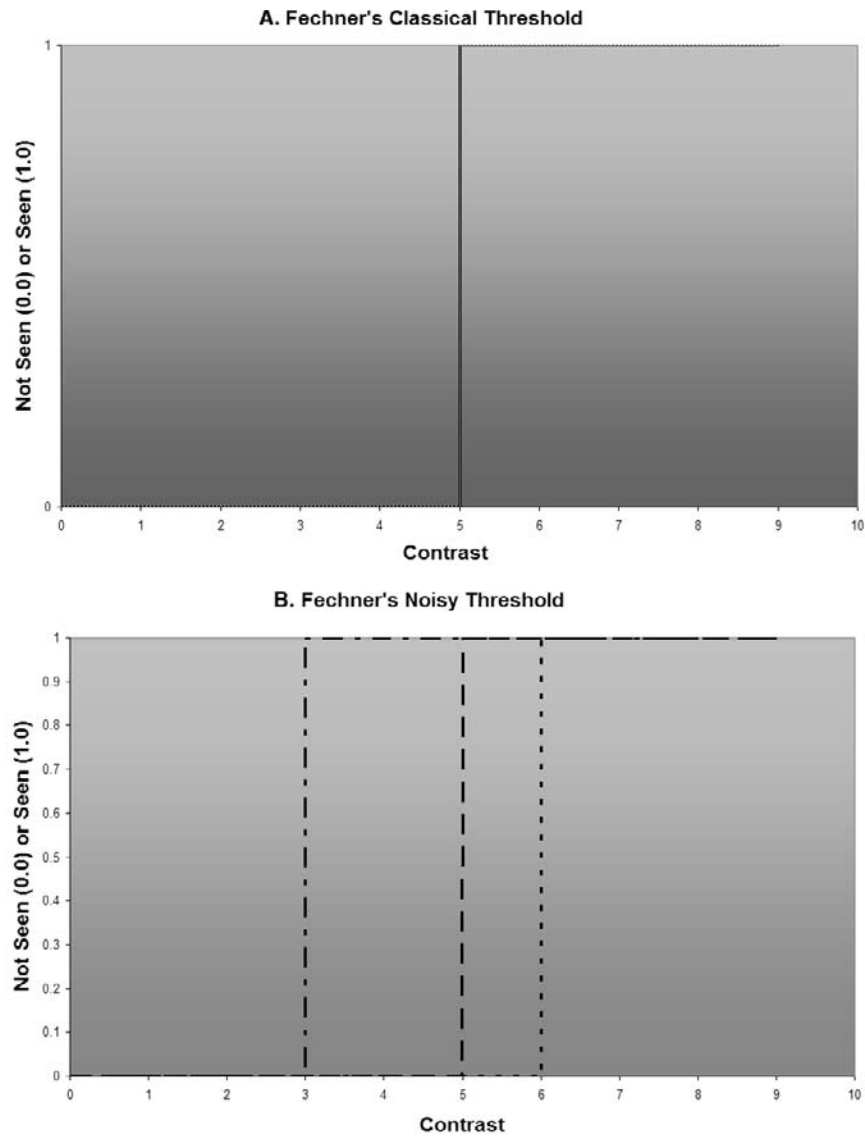


FIGURE 51.1. *A*, Schema for Fechner's idea of (classical) threshold. The abscissa is contrast, and the ordinate is a dichotomous variable indicating "seen" or "not seen." A contrast above the threshold level is seen; otherwise it is not seen. *B*, Modified threshold schema for the case where the threshold can vary from time to time. Coordinates are as in *A*. Three arbitrary instances are illustrated. The (traditional) threshold theory holds that the level of contrast above which a target is seen varies at random.

techniques, called *adaptive staircases*, lead rapidly to a threshold estimate by using information gained during the trials to structure subsequent trials. The reader is referred to studies by Watson and Pelli (1983) and by King-Smith et al. (1994) and to a review by Klein (2001) for details.

The modern threshold

The traditional threshold concept described above rests on the premise that it is the manifestation of a noise-limited process wherein the noise is randomness in the location along the intensity (or contrast) continuum of the intensity limen. This conceptualization is what scientists call a *model*. It supplants Fechner's classic threshold model of a static

barrier that intensity has to exceed in order for a stimulus to be seen. The premise may be false. Tanner and Swets (1954) disproved the premise of a threshold below which no information was available with two elegant experiments. One showed that false alarms, assertions by the observer that a stimulus had been seen when none was present, cannot be guesses in the sense that some information must have guided the choice. The other showed that a second choice in a multialternative detection task could be accomplished with better than chance success when the first choice was wrong. Under the threshold assumption, a wrong first choice implies that the threshold could not have been exceeded, so the success of a second choice could not have been better than chance. That other sources of noise might enter into the

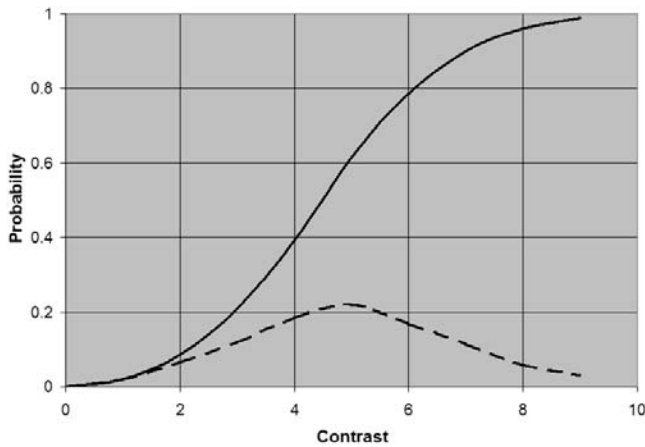


FIGURE 51.2. Frequency of the seen curve (solid) for a traditional threshold observer. Another name for this function is *psychometric function*. The abscissa is target contrast. The ordinate is frequency seen, the fraction of trials on which the observer reports that the target is seen. The dashed curve shows the presumed underlying probability distribution of the threshold level that would have led to the solid frequency seen curve.

picture (e.g., that another model might supply a better description) illustrates a general approach to threshold matters. Suppose that for a given visual system one could specify a set of noises and transformations that limit the ability to perceive light. Then one could define the threshold intensity as that intensity which enabled the observer to achieve a specified level of performance in a detection task.

Theory—thresholds implied by the irreducible noise implicit in light

Instead of asking what the magnitude of the threshold is, it has been argued (Barlow, 1958; Rose, 1948) that one should first ask what it should be. Here's the logic. Suppose that we could develop an analytic approach to finding the level of performance that a given stimulus could allow. This performance level would assume that processing is ideal and that the only limitation on detection comes from noise that accompanies or is intrinsic in the stimulus. If that calculation could be achieved, then we would have a benchmark against which to compare the performance of any observer, whether human or machine, animal or neuron. In Rose's and Barlow's terms, the disparity between real measured performance and the superior ideal performance defines the *logical space* (Rose's term) within which models may be constructed or mechanisms sought. This strategy has been deployed during recent years and has led to some very powerful advantages, which include (1) the ability to model quantitatively the internal noise sources of real observers, (2) the ability to ascribe sensory deficiency to one or more candidate causes, and (3) the ability to define processing efficiency, which is a measure of performance that can be

largely independent of stimulus contrast. In order to illustrate these matters, I present below a development of ideal observer processing of a light stimulus plus degradations of that ideal observer that may serve to help model real observers. The development begins with an irreducible source of noise that exists in all visual detection situations. This is the point of departure for several seminal papers in the area of thresholds and noise, those of Hecht et al. (1942), Rose (1948), Barlow (1956), and Sakitt (1972).

THE QUANTUM FLUCTUATION LIMIT Consider a detection task in which an increment in intensity, ΔI [quanta/DEG²/SEC/NM], is to be detected in the presence of a background, I [quanta/DEG²/SEC/NM]. Assume a duration T [SEC], an area, A [DEG²], and a rectangular window in the wavelength domain of width Γ [NM]. Predicted performance can be formulated for the quantum fluctuation-limited ideal observer (Cohn, 1976a; Tanner and Clark-Jones, 1960). The derivation of this relationship is straightforward. Detectability is conventionally defined (Tanner and Birdsall, 1958) as the difference of means of two hypothesis distributions divided by a common standard deviation. In the present case, the distributions are approximately Gaussian (see below). Adding the approximation that for ΔI small compared to I , the standard deviations are nearly the same ($\sim \sqrt{ATI\Gamma}$), this detection problem reduces to one in which means are different by $\Delta IAT\Gamma$. Then

$$d' = \frac{\Delta IAT\Gamma}{\sqrt{ATI\Gamma}} \quad (1)$$

The means and standard deviation used in this computation are real numbers without units.

A note on units: In equation 1 the numerator and denominator are without units, the former being the difference of Poisson means (which are not necessarily integers) and the latter being the square root of the Poisson variance, which is also without units. In later equations, variables have been manipulated to isolate ΔI on one side of the equation. Its dependence on such variables as A , T , and so on should be viewed as numerically correct, with each such variable retaining its original units. A scale change (e.g., specifying T in minutes instead of seconds) would be reflected by a constant in the expression related to the square root of the scaling constant.

Graham (1989) has pointed out the useful insight that the factor that multiplies ΔI can be thought of as the sensitivity of the observer. This is because it is the inverse of the threshold (see development below that leads to equation 3).

Anticipating conclusions that real data to be described below will compel, I also present a modified ideal photon detector prediction for an observer with two imperfections likely in human eyes: a nonzero dark light, D [events/DEG/SEC], and an imperfect quantum efficiency, p ($0 < p < 1$).

1.0). Hecht et al. (1942) anticipated the latter, and the former was anticipated by Barlow (1956). The dark light, D , reflects events that exist, by assumption, at the level of the photopigment. It can also be expressed in units of quanta at the locus of the cornea by accounting for the attenuation from cornea to photopigment (reflection, absorptions, scatter, and imperfect catching) that is conveniently summarized as quantum efficiency (Rose, 1948).

Quantum efficiency is taken here as the fraction of quanta incident at the cornea used by the observer. Thus, a number of factors including corneal reflection, media absorption (Hecht et al., 1942), macular pigment absorption (Hammond et al., 1998), photopigment depletion (Reeves et al., 1998), photoreceptor optical cross-section (Curcio et al., 1990; Øesterberg, 1935), and photopigment catching (Hagins, 1955) all are subsumed under this single parameter. The predicted detectability, d' , is given by

$$d' = \frac{p\Delta IAT\Gamma}{\sqrt{pAT\Gamma(I + D + p)}} \quad (2)$$

For an ideal observer ($p = 1.0$; $D = 0$), this reduces to equation 1.

In order to formulate the predicted threshold increment, ΔI , one adopts a convention for detectability at threshold. A convenient choice is $d' = 1.0$, which corresponds to an error rate in a yes/no task of close to 24%. Then

$$\Delta I = \sqrt{\{(I + D + p)/(pAT\Gamma)\}} \quad (3)$$

which, for the ideal observer (for whom $D = 0$ and $p = 1.0$), is

$$\Delta I = \sqrt{I + AT\Gamma} \quad (4)$$

PREDICTED SQUARE-ROOT LAWS Equation 4 expresses jointly what have come to known as the *square-root laws of quantum fluctuation-limited detection performance*. Each such law is obtained by examining the relation between ΔI and one of the independent variables, I (DeVries-Rose), A (Piper's), T (Piéron's), or Γ (unnamed). Each of these will be considered in turn and compared to empirical evidence that relates to it. First, however, a variety of other traces of quantum fluctuation limitations will be described as they figure in the quest for evidence that the human approaches the limit set by the variability in light itself.

THE QUANTUM FLUCTUATION FINGERPRINT Quantum fluctuations, variability in the number of arriving quanta that can be caught in a given space-time-wavelength interval, present the fundamental limitation for thresholds and as such, need to be better understood. While the matter of their importance at absolute threshold has been known since the classic work of Hecht et al. (1942), their importance above absolute threshold has not. The fingerprints devolve from the quantum nature of light. The primary fingerprint is the set of four square-root laws that are developed above. Others

come about in detection situations, and all have their origin in the variable nature of light.

The number of photons caught in a fixed space-time-wavelength interval is random, and its probability distribution can be shown for most light sources to be described as Poisson. The Poisson distribution has one free parameter, the mean. All other higher-order moments are simple functions of the mean, the variance being numerically equal to it. In a detection task as described above, an increment, ΔI , will raise the mean and thus the variance. A convenient way to appraise theoretical detection predictions is to use the receiver operating characteristic (ROC) of signal detection theory (Tanner and Swets, 1954). The ROC curve plots hit rate versus false alarm rate for a detection situation. Theoretical curves for the simplest case of a deterministic signal in additive Gaussian noise are straight lines of unity slope in coordinates for which z -scores corresponding to hit and false alarm rates are plotted.

As Poisson ROC curves are well approximated by Gaussian curves (Thibos et al., 1979), one can picture the effects of this added variance. One effect is that the photon count distribution for the increment stimulus has more variance and the increment is thus less detectable than the decrement, which has lower variance. This translates to a higher increment threshold for the same contrast or modulation. Thus, the approximation that led us to equation 4 obscures this feature.

A second-order effect is that the ROC curve changes shape in response to that extra variance for increments. Variance affects slope, and the result is that the ROC slope (on z -coordinates) is less than 1.0 for increments and greater than 1.0 for decrements. Finally, a tertiary effect is seen in the last fingerprint, an elusive one that has been seen only in physiological preparations involving single cells. The quantal nature of light means that only discrete integer values can be coded. Nonetheless, the nervous system may superimpose a more fine-grained code (for example, with more than one action potential per photon). The result is that some adjacent categories of response are indistinguishable and will show concave cusps. Examples may be seen in both Cohn et al. (1975) and Cohn (1983). To sum up, quantum fingerprints are as follows:

- (First-order) Square-root laws
- (First-order) Increment threshold larger than decrement threshold. Thibos et al. (1979) give this expression:

$$d' = \left| \frac{\Delta I}{I} \right| \frac{\sqrt{IAT\Gamma}}{(1 - (\Delta I/I))^{1/4}} \quad (5)$$

where $\Delta I < 0$ for decrement contrast

- (Second-order) ROC slope >1.0 for decrements and <1.0 for increments. Thibos et al. give this expression:

$$\text{Slope} \cong \left(1 + \frac{\Delta I}{I}\right)^{1/6} \quad (6)$$

- (Third-order) ROC cusps

Figure 51.3 shows theoretical ROC curves for increment and decrement detection that reveal each of the quantum fluctuation fingerprints save for the square-root laws.

Measurement of the square-root laws

In this section I describe, in order, studies that bear on the approach of human observers to the predictions of the square-root laws. It will be seen that obedience to these laws is not ubiquitous. More significantly, no conditions have yet been described in which all of these laws can be shown to hold (Barlow, 1958). Nonetheless, the point where human performance approaches that predicted by these laws proves to be a useful starting point to understand what forces influence visual thresholds and, in particular, what noise might be limiting.

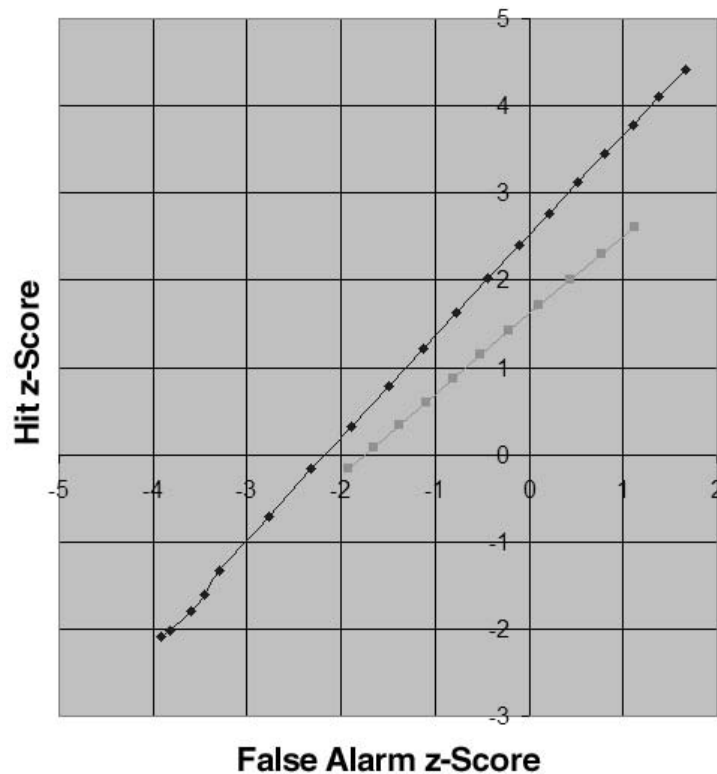


FIGURE 51.3. Quantum fluctuation fingerprint. ROC curves on probability coordinates are presented. The ordinate is the z -score transform of the probability of a hit (target presented and seen) for an ideal photon detector. The abscissa is the z -score transform of the false alarm probability. A background of 10 quanta with contrast of +6 or -6 quanta is assumed. The upper curve is for the six-photon decrement. The lower curve for the six-photon increment. Elements of the fingerprint manifest here include (1) decrement

THRESHOLD VERSUS INTENSITY: THE DEVRIES-ROSE LAW Evidence for this square-root law has been described since the two named investigators derived it (DeVries, 1943; Rose, 1948). The attempt to verify it empirically has always failed in a global sense (Fig. 51.4), although it is equally true that a small range of low backgrounds always presents a good fit.

Figure 51.4 displays data that are typical of a number of studies. The resulting data are alternatively referred to as *Threshold versus Intensity (TVI) curves*, as *increment threshold curves*, or as *Stiles curves*. These data are taken from Barlow (1977). The threshold on the ordinate ($I = 0$) is actually the absolute threshold. Under some conditions (Baumgardt and Smith, 1965), the threshold declines from the absolute threshold for values of I near the absolute threshold (this behavior is seen in other settings, such as masking, where the function is termed the *dipper*; see “The Psychometric Function”). At low backgrounds the increment threshold rises, often with a slope (log-log coordinates) near 0.5. At higher backgrounds the slope increases to approximately 1.0, and

threshold (detectability 2.5) less (greater) than increment threshold (detectability 1.6); (2) decrement ROC slope > 1.0 ; (3) increment ROC slope < 1.0 ; (4) cusps can occur when the precision of coding exceeds that of the target (see the lower left of the decrement curve). The primary quantum fluctuation fingerprint, the several square-root laws, would be seen if the ROC curves had been parameterized in any of the independent variables, A , T , Γ , or I .

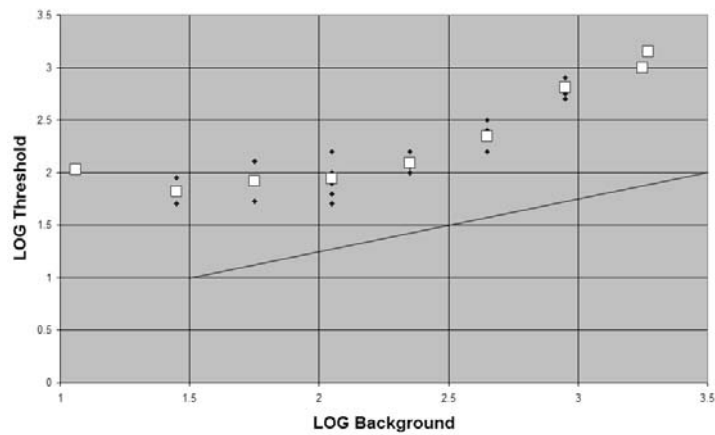


FIGURE 51.4. TVI curves. The abscissa is log background intensity, $\log I$. The ordinate is log threshold, $\log \Delta I$. The TVI function shows a slight threshold reduction below absolute threshold at very low backgrounds, then a threshold rise roughly corresponding to

the DeVries-Rose law (line). Squares are averages of the several thresholds at a given background. (Data transcribed from Barlow, 1977).

this is the Weber law domain. Aguilar and Stiles (1954) showed conditions (blue test on a red background) in which the slope becomes asymptotically infinite for a narrow range of backgrounds above the Weber regime, and this has been interpreted as evidence for saturation of the photoreceptor elements (rods) responsible for the detection. Ultimately, when cones become engaged, and this is a strong function of both stimulus conditions and retinal locus, at least the early elements of the sequence of domains are repeated.

In order to interpret this behavior, it is most convenient to study the relation of these empirical data to the data expected of the ideal observer that are shown as a solid line in Figure 51.4. It is apparent that ideal performance lies closest to the empirical thresholds in the DeVries-Rose domain. Thus, one wants to find physiological explanations for the shortfall there first, for under those conditions it is logical to assume that the deficiencies, as compared to the ideal, are the least complex (Barlow, 1977). Other phenomena are certain to be at play, for the threshold increases further beyond what an extrapolation would lead one to expect, both at lower and higher backgrounds.

EXPLAINING THRESHOLDS IN THE DEVRIES-ROSE REGIME
Start with an assumption. Suppose that the only limit on sensitivity in this domain is due to quantum fluctuations, as DeVries and Rose thought. Then the shortfall in the DeVries-Rose regime is explained most parsimoniously by an inability to use all of the available quanta (Barlow, 1957a,b; Rose, 1948). This deficiency may arise from one or more of several physical processes (e.g., reflection, absorption, scattering, imperfect photon catching in photopigment), and possibly physiological ones, and was very clearly anticipated by Hecht et al. (1942; see their “corrections”) in their landmark paper on absolute threshold. It is quantified as the ratio of photons apparently used in the task to the number of those

presented at the cornea. This ratio is termed *detective quantum efficiency* and is given the designation F . Values of F determined by Barlow are not so low as to defeat a formulation that rests solely on quantum fluctuations, but they are close. Complete concordance would require that the detective quantum efficiency determined by psychophysical means approached approximately the quantum losses calculated (or measured) by physiological-optical means. Barlow (1977) estimated that 30% of photons incident at the cornea were absorbed in photopigment, considerably more than what Hecht et al. thought (10%). But the highest reported detective quantum efficiency in a psychophysical task thus far is Barlow’s for rods and is about 7%. This leaves room for other sources of noise or information loss. Hallett’s (1987) refinement, which assumes a slowly changing response characteristic, places the value closer to 10%.

DECREMENT THRESHOLDS IN THE DEVRIES-ROSE REGIME

Two studies (Patel and Jones, 1968; Short, 1966) measured both increment and decrement thresholds at backgrounds just above absolute threshold. Their findings were quite similar. At the lowest backgrounds, the decrement threshold was smaller than the increment threshold. Example data are shown in Figure 51.5. Prior to understanding the quantum fluctuation fingerprint, there were two ways to think about such a finding. One could imagine either that OFF neurons in the visual pathway were more sensitive (had a higher quantum efficiency) or that ON neurons were noisier (manifested their own internal noise). The former cannot be true for optical reasons because both pathways use the same photoreceptors. However, OFF neurons might indeed receive input from more photoreceptors.

DARK LIGHT: ANOTHER NOISE AT ABSOLUTE THRESHOLD

Barlow (1956) advanced an explanation for the low back-

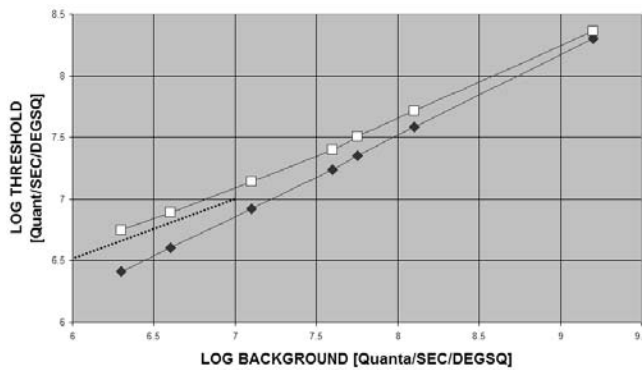


FIGURE 51.5. Thresholds for increments and equal-contrast decrements. The abscissa is log background intensity, and the ordinate is log threshold. Filled symbols incate decrements and open symbols represent increments. Stimuli were $\frac{1}{4}$ degree in diameter and 50msec duration. The dashed line shows the DeVries-Rose square-root law. At higher backgrounds increment thresholds are virtually equal to decrement thresholds, and data are better fit by a curve of higher slope tending toward Weber's law. (After Patel and Jones, 1968.)

ground inefficiency which he termed *dark light*. As is apparent in Figure 51.4, some factor besides quantum loss must be at play at the lowest backgrounds, where the noise inherent in the background cannot be expected to pose a significant barrier to detection. Traditionally, vision researchers have thought of the zero background condition as a unique circumstance, concerning which they have referred to the *absolute threshold problem*. This means that some process has caused threshold to be finite, and not infinitesimal, and the researchers in the field have since wondered what this process is. Barlow supplied a prescient answer. He hypothesized the existence of thermally caused spontaneous isomerization of photopigment that presented a “background” of neural activity (indistinguishable from that caused by light) which added to the real-light background, I . If so (and much contemporary evidence, including that obtained from photoreceptor recording, is consistent with this view), it is as if the background against which the stimulus must compete is the sum of the dark light, D , and the real light, I . Then the absolute threshold cannot be infinitesimal (as the extrapolation of the DeVries-Rose law would imply), but rather finite, and determined by the magnitude of the dark light. That magnitude has been estimated by a number of means and amounts, on average, to a fraction of a photon-like event per second per photoreceptor (Sakitt, 1972).

There is a subtlety involved in the units of dark light. If, as often is the case, it is estimated as the background, I , for which a curve fitting asymptotic low background performance intersects with one that fits asymptotic high background performance, then its units are specified as if at the input (e.g., at the cornea where I is estimated). But this must

be corrected by another estimated parameter, that of the quantum efficiency, p . This is because events due to light compete (or are intermingled) with those due to dark light in the photopigment. And because quantum efficiency may have a physiological component, comparing rods to cones can be hazardous (Barlow, 1957a) because rods may differ from cones in that regard.

APPLICATIONS OF THE DARK LIGHT CONCEPT A number of researchers have used the simple model of processing described above to infer the cause of less than normal sensitivity as occurs in ocular disease. Suppose, for example, that an observer suffered from excessive dark light, D , but her quantum catching was ideal ($p = 1.0$). In that case, thresholds would be higher, as shown in equation 3, which is repeated here:

$$\Delta I = \sqrt{\{(I + D \div p) \div (pAT\Gamma)\}} \quad (3)$$

For $I \sim D$, thresholds are elevated. For high backgrounds, $I \gg D$ and thresholds are normal. Now, in contrast, assume that $D = 0$ and consider the effect of a quantum catching inefficiency, as evidenced by $p \neq 1.0$. Equation 3 becomes

$$\Delta I = \sqrt{\frac{I}{AT\Gamma}} \quad (4)$$

Whether for small or large I , thresholds are raised by a multiplicative factor ($1 / \sqrt{p}$). Thus the first situation is manifest in a TVI curve that is elevated over the normal but only for low backgrounds. The second one is elevated for all backgrounds.

Hood (1988) has pointed out that one's model of how the TVI curve becomes shaped determines how one interprets the shape changes that occur in conditions of abnormality. While he focused on the development of normal thresholds through childhood and while his model contained no quantum fluctuation noise, his point is well taken.

HIGH BACKGROUND INEFFICIENCY Now consider the high background condition which leads to Weber's law. Here thresholds are markedly higher than predicted for an ideal photon detector, even one with a quantum efficiency less than unity. What could explain this deficiency of processing? An attractive explanation is found in the very earliest work of Rose (1948). He appreciated that physiological elements couldn't possibly match their dynamic range to the span of energy that impinges on the eye between noon and night. He thus hypothesized gain control in neural elements and pointed out that internal noise processes might become more prominent as the background level goes up and thus gain goes down. Shapley and Enroth-Cugell (1984) formalized this notion. With fairly simple assumptions, it causes a system that is dominated by quantal noise at low levels to become dominated by internal noise at high levels.

Suppose for simplicity that the system gain is set by a photon counter that estimates the background intensity level by averaging the photon catch over a sufficiently long period of time, say several minutes. Let this average level be given by \bar{I} [unitless]. One convenient gain would normalize the photon input at any given moment by this average. If an internal noise follows the gain control, then a new performance prediction would be

$$d' = \left(\frac{\Delta I}{\bar{I}} \right) \frac{AT\Gamma}{N} \quad (7)$$

where N is the standard deviation of the (late) noise process in units of quanta. Solving for ΔI when $d' = 1.0$ leads to Weber's law. Hence, we may view the increased thresholds in this range of backgrounds as being due both to quantum inefficiency and to a combination of internal noise and gain control that together lessen the influence of the externally originating quantum fluctuations. It follows that under some conditions both quantal and internal noise may be manifest in performance.

Hornstein et al. (1999) nicely illustrated this principle for a photoreceptor operating at a single adaptation level. They showed that the gain is so low at high temporal frequencies that internal noise dominates even at a low enough background, one for which quantal noise dominates for low frequencies. The evidence for this conclusion relates to the statistical nature of the neural responses, which are treated above (see "The Quantum Fluctuation Fingerprint") in the general case.

To this point we have seen that only two types of inefficiency suffice to explain low background thresholds, and the addition of a third type, the combination of proximal internal noise and gain control, suffices to explain performance at higher backgrounds.

THE LOW BACKGROUND SENSITIZATION A number of early studies reported that low background increment thresholds were in some cases less than the absolute threshold. Barlow's data in Figure 51.4 show a subtle form of this effect. The theory immediately advanced to explain this phenomenon (Baumgardt and Smith, 1965) was little more than a repetition of its description. The term, *facilitation*, given to this phenomenon was intended to convey the idea that a bit of light would drive neurons into a more receptive state, thereby requiring fewer photons to achieve a criterion change in response. The problem with such a theory is that it leaves out the symmetrical requirement that false alarms, positive responses in the absence of a stimulus, also should rise. If so, it is not clear that sensitivity can be improved.

Nachmias (1966) pointed out that this was not the only possible answer and argued that it was possible that the additional photons from the background merely had the effect of showing an observer where to look for those from the

target. Data described by Baumgardt and Smith showing that the smaller the size of the background light the greater the advantage of turning it on support Nachmias' conjecture. This historical sidelight is nonetheless of contemporary relevance because of its similarity to dipper phenomena (see the section "The Psychometric Function" below).

The reader will appreciate that an absolute threshold experiment is conducted in the dark. While there may be a small central fixation mark of sufficient luminance to stimulate cones (for the purpose of allowing steady central fixation), observers are not generally equipped to handle an instruction of the sort "expect the stimulus 17 degrees to the right of fixation." But a weak background can illuminate elements of the background plane that would allow an observer to remember where to look and to actually use that information. Sensitization, as a concept, is similar to the concept of the transducer nonlinearity that arises in the context of departures from ideal observer performance in simple detection tasks at any background. This will be elaborated below. Suffice it to say here that a definitive study to separate these two explanations of sensitization has not been reported. A simple one would be to replicate the phenomenon while measuring ROC curve parameters. Uncertainty can leave a trace on the ROC curve. This could lead to an unequivocal finding.

AREA AND THRESHOLD Another of the square-root laws of quantum limited performance implicit in equation 2 arises from quantum fluctuations. This law relates area to threshold. Perhaps the most complete account can be found in Barlow's early paper on increment threshold (1957b). The empirical relation is shown in Figure 51.6. Threshold falls in inverse proportion to area for small areas and for large areas is constant with area. Adopting the same rationale as for the TVI function, one imagines the ideal photon detector theoretical relation as lying below that of the real detector and being a line on log-log coordinates with slope $-1/2$. Then one can see that the measured threshold is closest to that predicted at the part of the empirical curve where the function bends from one of slope $= -1$ to one of slope $= 0$. The most economical explanation of the departure from theory is the quantum (in)efficiency which is represented in these coordinates as simply a constant added to the curve at all areas. If so, the question becomes: what forces cause the threshold to escalate so rapidly with area for low areas and to remain fixed for high areas? Before answering this question, it is well to examine the classical treatment of the empirical function at small areas.

LOW AREA THRESHOLDS Low area thresholds depart strongly from those extrapolated from performance at middle areas. This function, of slope -1.0 on log-log coordinates, has been referred to as *Ricco's law* after its first dis-

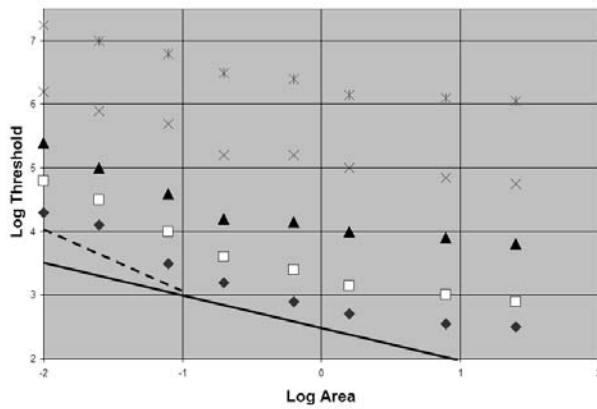


FIGURE 51.6. Area-threshold relationship. The abscissa is the log target area, and the ordinate is log threshold. Successive curves indicate successively higher backgrounds. The solid line (slope = -0.5) is the square-root law for the ideal photon detector, Piper's law. The dashed line (slope = -1.0) shows Ricco's law. Measured human thresholds lie closest to predicted thresholds in the Piper's law range. It is thus assumed that human processing is most efficient there, and the next step is to identify causes for larger than extrapolated thresholds at both lower and higher areas.

coverer (Riccó, 1877) and is said to be consistent with “perfect” or “total” summation because of reciprocity between area and threshold. The largest area for which Ricco's law holds is said to be the *Ricco area* or the *area of complete summation*, and for the record, this area declines as the adaptation level increases. That Ricco's is a law of perfect summation appears to be a contradiction to the quantum fluctuation model, in which performance is perfect by assumption and threshold varies with the square root of the background. How can this apparent contradiction be resolved?

Thus one has to contend not only with the question of why Ricco's law is not a law of ideal performance, but also with what brings it about. It will be seen that the explanation for the latter is also the explanation for the former. Barlow (1958, 1964) was careful to outline the key implicit assumption in the formulation of the square-root laws that may have broken down in this case. The assumption is that the human observer integrates only those photons that fall in the area, A , designated for the target. Suppose that the assumption is not true (Rosell and Wilson, 1973) and that, in fact, the observer is unable to sum photons over areas smaller than a particular area, A_{\min} (Barlow termed this deficiency a *mismatching loss*). One might think of this area as that of the smallest receptive field. The consequence of such an inability is that more photons are gathered from the background than is necessary or desirable. Those photons, and their Poisson fluctuations, constitute noise that makes detection of the target more difficult than it would otherwise have been. This consequence is embodied in a modified detection equation

$$d' = \frac{\Delta I A T \Gamma}{\sqrt{A_{\min} T \Gamma}} \quad (8)$$

from which Ricco's law immediately follows. Then A_{\min} , which is essentially Ricco's area, is actually *the smallest area of complete summation*, not the largest. There is a more modern way of viewing this phenomenology. In considering that the early vision is characterized by filters, one might ask what effect these filters should have on ideal detection performance. The answer is that filters in the spatial domain at low backgrounds are low-pass. This means that high-frequency information fails to gain admission to the signaling pathway. A low-pass system is one that approximately integrates high frequencies. If the area over which it integrates is too large, it collects too many background photons; thus, the threshold is compromised and is higher than it would otherwise be. It is worth mentioning at this point that Ricco's law ensues at zero background in the dark, and one might wonder how this phenomenon is embraced by a modified ideal observer theory. The answer, as described above, is due (as so many are) to Barlow (1958). A too-large integration area will gather dark light from photoreceptors untouched by the target. This raises the threshold because of the noise or variability of the photoreceptors due to the dark light.

Application of this insight is useful. It has been reported that senescence leads to increased Ricco's areas (Scheffrin et al., 1998). On the interpretation that Ricco's area reflects a deficiency of processing, one then interprets such a finding as indicating the possibility of an increased minimum summing area.

THRESHOLDS AT LARGE AREAS A comparable argument can be made for the processing deficiency that is measured at high areas. Suppose that there is an area beyond which the eye cannot integrate. Such an area is not apparent in practice unless one considers that there is an upper limit on receptive field size, which appears to be finite. If one accepts that argument, then constant threshold as area increases is expected. If one does not, the filter explanation provides some respite. At even low backgrounds, the spatial contrast sensitivity function is bandpass. For large areas with their predominantly low spatial frequencies, the eye acts not as an integrator but as a differentiator, seeking contrast in distinction to light. It is as if there is a maximum area, A_{\max} , over which photon integration can occur. If so, equation 1 becomes

$$d' = \frac{\Delta I A_{\max} T \Gamma}{\sqrt{I A_{\max} T \Gamma}} \quad (9)$$

The result is independence of performance, and thus of threshold, from area A , for areas greater than A_{\max} .

At high backgrounds, different phenomenology emerges. If backgrounds are high enough that internal gain controls

effectively minimize the quantum fluctuations in comparison to internal noise processes, \mathcal{N} , performance measures have different dependence upon area. In this instance, Ricco's law emerges for low areas because it is only the noise in the proximal neuron(s) that matters, and that noise, an internal noise arising at or near that level, would not depend on area. At high areas, there would be no areal dependence by the same arguments advanced above: the brain is simply unable to integrate photons over areas larger than A_{\max} .

DURATION AND THRESHOLD The situation for duration is quite similar to that for area. In a sense, each is the dual of the other. Empirical threshold-versus-duration curves are shown in Figure 51.6 as adapted from Barlow (1958). The prediction of the ideal photon detector is again a line with slope = $-1/2$ on log-log coordinates termed *Piéron's law*. Thresholds of the human observer lie closest to those of the ideal where the empirical data themselves fall close to a slope of $-1/2$. Explaining the shortfall in processing quality evidenced by thresholds elevated from those extrapolated from middle durations requires two separate explanations, one at low duration and one at high duration.

At low duration we must ask why ideal performance has failed, and the attractive possibility is that the human observer is simply unable to fix her attention upon epochs shorted than a minimum duration, T_{\min} . If so, and by analogy to the area-threshold relationship, too many background quanta are summed and equation 1 becomes

$$d' = \frac{\Delta I T \Gamma}{\sqrt{A T_{\min} I \Gamma}} \quad (10)$$

This expression is the embodiment of the ubiquitous Bloch's law, which, like Ricco's law, is not a law of perfect integration under conditions where quantum fluctuations are the main limitation on performance. Thus it is important to avoid the temptation to refer to the largest duration for which Bloch's law holds as the integrating time of the eye. The integrating time is more properly the largest duration for which Pieron's law holds.

The physiological concept of a receptive field, so useful above in appraising low area thresholds, is not duplicated in the temporal domain. Instead one can rest on the concept of the *temporal impulse response*, which is especially long for small receptive fields.

At large durations, we have a situation likewise similar to that in the area-threshold relation. Most often, threshold is fixed at high durations, although there is evidence in some studies of a minimum threshold at middle durations (e.g., Swanson et al., 1987) which appears to be related to biphasic photoreceptor impulse responses (or, equivalently, the bandpass frequency response).

CHROMATIC EXTENT AND THRESHOLD The following description refers to phenomena that have not, to this author's knowledge, been explicitly studied. Consider the relation implicit in equation 4 between threshold, ΔI , and wavelength extent, Γ . As with area and duration, an increase in wavelength extent should lower the threshold according to a square-root law. The task would be to detect an increment of area A , of duration T , and of a specified wavelength extent and specified center wavelength superimposed on a white background. Can we imagine limitations similar to those for area or for duration that might limit the observer and thus raise thresholds? Consider first scotopic vision. In the case of small values of wavelength extent, because rod photoreceptors are the initial receptive elements and because they are broadband, they will have to sum wavelengths from beyond the band of interest. According to the concept of *univariance*, an absorbed photon is treated the same way irrespective of its wavelength. In this case, we could say that we have a minimum band limitation. If that minimum band extent is G , then G will replace Γ in the denominator of the performance prediction and a linear law, not a square-root law, would be expected. In the case of stimuli with large wavelength extent, the picture does not change. So for rods we predict a linear law, showing no sign (e.g., no square-root relationship) of quantum-limited behavior.

Cones may present a different picture. Even though the receptive elements are broadband, computation that takes advantage of different absorption in different cones could be used to exclude wavelengths beyond those in the stimulus band. In that case, and if the photon count is low, it might be possible to observe square-root law behavior. While some authors have argued that quantum fluctuations have little bearing on behavior above absolute threshold (Hecht, 1942; Massof, 1987), that assertion has not been proven. In fact, quantum fluctuation fingerprints may be seen in detection data where cones are involved. Two simple examples are these: both first- and second-order quantum fluctuation effects have been described for cones. Cohn (1976a) has shown that decrement threshold is less than increment threshold in rod-free fovea and when the color of the target can be seen, and has also shown that the decrement ROC curve slope is greater than unity.

The psychometric function

Perhaps the most fundamental relation that appears explicitly in the relations described above (equations 1, 2, and 5 to 9) is the psychometric function. The more traditional definition is that of the frequency-seen (which is but one component of d') versus the contrast. [The reader is referred to Klein's (2001) extensive recent review of the recent psychometric function literature.] The psychometric function is

defined here as the relation between observer performance, d' , and signal contrast as expressed by ΔI . As can be seen, the prediction for the ideal observer or for a nonideal observer with a number of different possible flaws (e.g., dark light, quantum inefficiency, internal noise) is simple proportionality between ΔI and contrast. The constant of proportionality is dependent on all of the aforementioned parameters, including especially observer parameters of efficiency and dark light and signal parameters of area, duration, background, and wavelength extent.

The first test of this proportionality prediction was that of Tanner and Swets (1954), and the result was a marked failure. Instead of simple proportionality between d' and contrast, measured d' was better described as a power function of contrast $\sim(\Delta I)^r$, where $r > 2.0$. (A value of $r = 1.0$ would have exactly matched the prediction.) In other words, weak signals were disproportionately hard to see. A subsequent test (Nachmias and Kocher, 1970), however, was intriguing. Placing the signal to be detected on top of a contrast pedestal of identical time course and spatial extent (which would not alter the prediction) did indeed lead to a proportional relationship.

Two major classes of explanation (Cohn and Lasley, 1985) have been advanced to explain this difference between predicted and measured performance for human observers. At the same time, some investigators have explored the relation for single neurons. Below I describe both the explanations and the physiological findings and their interrelation.

THE NONLINEAR TRANSDUCER EXPLANATION Nachmias and Sansbury (1964) were the first to describe this possibility. They reasoned that a physiological nonlinearity early in the system attenuated weak signals and that the psychometric function shape merely mirrored the shape of the transducer nonlinearity. Taking equation 5 as a point of departure is necessary because one needs a late internal noise source to make this explanation work (Lasley and Cohn, 1981). Suppose that contrast was attenuated by a nonlinearity:

$$f(\Delta I) = (\Delta I)^r \quad (11)$$

Then the relation becomes

$$d' = \left(\frac{\Delta I}{I} \right)^r \frac{AT\Gamma}{N} \quad (12)$$

Equation 12 applies only to low-contrast signals. It is not meant to convey a prediction for large-contrast signals for those should lead to saturation. But even for small signals, it is intriguing beyond its ability to fit data. Suppose that one sought the predicted area- or duration-threshold relationship for near-threshold increments. Rearrangement in equation 12 leads to a relationship in which threshold is predicted to be proportional to area or duration to the $1/r$ power. Since many authors have estimated r to be 3 and above (cf.

Graham, 1989), the ubiquitous existence of Ricco's and Bloch's laws would tend to refute this nonlinearity hypothesis should it emerge under the same conditions.

THE UNCERTAINTY EXPLANATION Tanner (1961) proposed that observer uncertainty, analogous to a similar phenomenon observed in radar detection apparatus, could be the cause of an accelerating psychometric function. The uncertainty explanation, in brief, suggests that the observer does not know which of a number of directions to attend to, or to which of a number of possible times (equally, the observer may have been told these particulars but may be unable to use the information fully). In recent years, vision scientists have been more explicit about what it means to be looking in various places or at various times, referring to relevant (signal-containing) and irrelevant neural channels or mechanisms (cf. Pelli, 1985). In either case, it has been shown theoretically (Peterson et al., 1954) and empirically (see Cohn and Lasley, 1985, for a summary) that weak signals will suffer disproportionately (presumably because strong signals point themselves out both for time and for location.)

A line of research that extends from Tanner's (1961) paper to the present day has sought to demolish one or the other of these opposing theories of the nonlinear psychometric function. Dispassionate reading of these papers leads to the conclusion that despite pronouncements as to the demise of one or the other theory (cf. Foley and Legge, 1981; Lasley and Cohn, 1981) consensus has not been achieved.

PHYSIOLOGICAL PSYCHOMETRIC FUNCTIONS (NEUROMETRIC FUNCTIONS) As both alternative explanations for the nonlinear psychometric function may point to visual pathway elements, one is naturally led to inquire how those elements behave. Data exist for photoreceptors, for retinal ganglion cells, and for cortical neurons. Photoreceptors are known to exhibit a nonlinear (saturating) response characteristic (Cohn, 1983; Lillywhite and Laughlin, 1979; Schnapf et al., 1990), but that does not necessarily translate to a nonlinear neurometric function. It is worthwhile to distinguish these two response indicators. The magnitude of the response is not the only determinant of the sensitivity of response. Response magnitude must be compared with response variability, or noise, this being the rule for threshold problems.

Both the near linearity of the predicted neurometric function and the disparity between increment and decrement detectability have been observed in neurometric functions for photoreceptors and for retinal ganglion cells. Locust photoreceptors do not exhibit a linear response characteristic. Instead, they show marked saturation, as would be expected. Nonetheless, for contrasts where saturation occurs, detectability is still nearly proportional to contrast (Cohn, 1983). Also, increment detectability is inferior to decrement

detectability, and by an amount that is predicted from the number of quanta that the photoreceptor is catching (Hornstein et al., 1999). But photoreceptors are the first neural element in the perceptual chain. One might wonder if this phenomenology persists at higher levels where nonlinearities and other sources of noise and information loss may be important. Half of the answer was shown early (Cohn et al., 1975), where class IV dimming retinal ganglion cells of *Rana pipiens* showed both the second-order quantum fluctuation fingerprint (ROC slope > 1.0 for contrast decrements) and the first-order (De Vries-Rose) square-root law.

OFF-center (brisk, sustained) cat retinal ganglion cells also showed these results and, in addition, showed a first-order fingerprint, that increment threshold (for stimuli confined to the receptive field center) is greater than decrement threshold (Levick et al., 1983). Of course, one might think that such a finding reflects little more than a preference of the OFF-center neuron for negative contrast in the receptive field center. But two findings argue against that possibility. First, the same finding emerges, paradoxically, in the receptive field center of the ON-center neuron. For that neuron, decrement stimuli are seen with higher detectability than equal-contrast increment stimuli. This result suggests that ON cells are more sensitive to OFF stimuli than to ON stimuli owing to quantum fluctuations. The second finding is that the neuron in question uses so many of the quanta available in its receptive field that there is no statistical room for a source of variance greater than, or even approximately equal to, that due to quantum fluctuations to determine the threshold of the cell. Two surprising but robust conclusions follow from this. Under the conditions of test, and for those very sensitive cells, the “spontaneous activity” of the cell is

actually the code of the background quantum catch and is not spontaneous in any sense. Moreover, quantum utilization is high, (close to the quantal attenuation determined densitometrically (Bonds and Macleod, 1974) that it is necessary to conclude that each photoreceptor in the receptive field sends signals to the neuron.

Cortical neurons are generally thought to respond in a highly nonlinear fashion, and it might seem impossible to expect that any could even approximate the linear neurometric function prediction. The primary reason is that many such cells show no spontaneous activity and thus show no response for weak stimuli, an extreme version of *weak signal suppression*. Nonetheless, the available literature shows the existence of neurons that do obey the proportionality prediction. Tolhurst et al. (1983) have published response summaries for a number of complex cells. Figure 51.7 shows some data from one such cell which exhibited a significant spontaneous discharge. Such a cell is a candidate for processing a low-contrast stimulus, as cells with no spontaneous firing cannot do so. Despite a tendency for the literature to pronounce cortical neurometric functions to be nonlinear, departures from simple proportionality in a cell such as this are so small as to be unconvincing.

Added external noise as an analytic tool

Since the deployment of signal detection methods in the 1950s, scientists have found that using external noise (noise that is generated in the stimulus domain) has analytic and strategic advantages in the search for an accurate characterization of the system under study. The most fundamental of these approaches pits external noise against internal

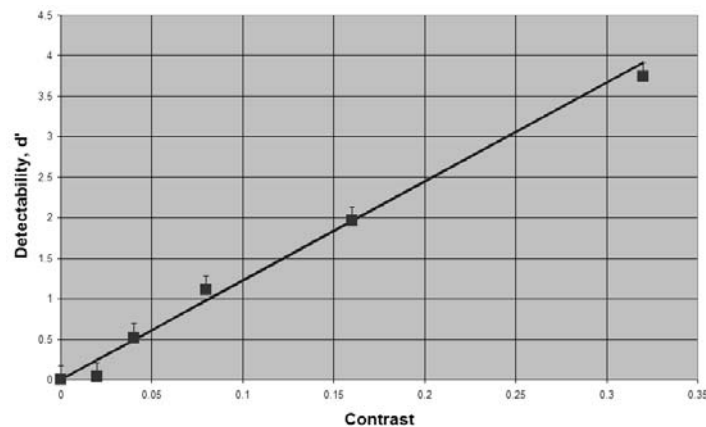


FIGURE 51.7. Neurometric function for a complex cell. The abscissa is target contrast for a sinusoidal grating moving across the receptive field of a complex cell. The ordinate is the detectability as extracted from ROC curves fitted to measured distributions of action potentials counted following the stimulus, a single cycle passing one point on the retina. The line is the prediction of proportionality between detectability and contrast of an ideal photon

detector. It is fit by eye with the constraint that detectability must be identically zero for zero contrast. Photoreceptors (Cohn, 1983) and retinal ganglion cells (Cohn et al., 1975; Levick et al., 1983) show nearly identical proportional behavior, except that at low backgrounds, the quantum fluctuation causes a slight reduction of increment detectability, and amplification of decrement detectability can be measured. (Data from Tolhurst et al., 1983.)

noise. When external noise of sufficient magnitude is introduced, the threshold is, of course, raised. When raised enough, by enough noise, the threshold that remains is limited solely by the external noise, and internal noise may be eliminated from formulations. The noise power at which performance is halved (or threshold is doubled) is the one for which the internal noise can be viewed as equivalent to the external noise when it is referred to the input (Cohn, 1976b; Nagaraja, 1964; Pelli and Farell, 1999). External noise can also be used to strategic advantage. Cohn and Macleod (1999) showed a noise probe technique that allowed them to characterize the summation properties of the visual system.

Threshold behavior as an indicator of sensory deficiency

While the identification of the components of normal human vision is far from complete, a number of these components are agreed upon. It is clear that quanta available at the cornea are not fully utilized and that dark light dominates real backgrounds at low light levels. It is also likely that the combination of gain control and proximal internal noise sets the detection limit at higher backgrounds. Considerable evidence suggests that intrinsic uncertainty as to stimulus parameters characterizes normal visual behavior (Cohn and Lasley, 1985; Pelli, 1985; Tanner, 1961). This specificity of knowledge places scientists in a position of good leverage. If the question is why a particular human visual nervous system is deficient compared to normal, each of the information-losing components in the extant model becomes a candidate for the locus of a site-specific deficiency. Then a strategic series of measurements is capable of revealing the nature of a given deficit. Hood (1988) has employed this strategy to study the nature of the deficiency that is erased by development using electroretinographic thresholds. Werner et al. (2001) have employed it to examine the nature of the age-related deficiency in psychophysical thresholds. It should be apparent that the accuracy of the model directly determines the validity of the conclusions drawn from its use. In particular, a model of threshold that ignores noise is not complete and thus cannot be expected to fully capture behavior.

REFERENCES

- Aguilar, M., and W. S. Stiles, 1954. Saturation of the rod mechanism of the retina at high levels of stimulation, *Optica Acta*, 1:59–65.
- Barlow, H. B., 1956. Retinal noise and absolute threshold, *J. Opt. Soc. Am.*, 46:634–639.
- Barlow, H. B., 1957a. Intrinsic noise of cones, in *National Physical Laboratory Symposium on the Visual Problems of Colour*, vol. 2, London: Her Majesty's Stationery Office, pp. 617–630.
- Barlow, H. B., 1957b. Increment thresholds at low intensities considered as signal/noise discriminations, *J. Physiol. (Lond.)*, 136: 469–488.
- Barlow, H. B., 1958. Temporal and spatial summation in human vision at different background intensities, *J. Physiol. (Lond.)*, 141:337–350.
- Barlow, H. B., 1964. The physical limits of visual discrimination, in *Photophysiology* (A. C. Giese, ed.), New York: Academic Press, pp. 163–202.
- Barlow, H. B., 1977. Retinal and central factors in human vision limited by noise, in *Vertebrate Photoreception* (H. B. Barlow and P. Fatt, eds.), New York: Academic Press.
- Baumgardt, E., and S. W. Smith, 1965. Facilitation effect of background light on target detection: a test of theories of absolute threshold, *Vis. Res.*, 5:299–312.
- Bonds, A. B., and D. I. A. Macleod, 1974. The bleaching and regeneration of rhodopsin in the cat, *J. Physiol. (Lond.)*, 242:237–253.
- Boring, E. G., 1942. *Sensation and Perception in the History of Experimental Psychology*, New York: Appleton-Century-Crofts.
- Cohn, T. E., 1976a. Quantum fluctuation limit in foveal vision, *Vis. Res.*, 16:573–579.
- Cohn, T. E., 1976b. Detectability of a luminance increment: effect of superimposed random luminance fluctuation, *J. Opt. Soc. Am.*, 66:1426–1428.
- Cohn, T. E., 1983. Receiver operating characteristic analysis of photoreceptor sensitivity, *Proc. IEEE*, 873–881.
- Cohn, T. E., D. G. Green, and W. P. Tanner, Jr., 1975. Receiver operating characteristic analysis. Application to the study of quantum fluctuation effects in optic nerve of *Rana pipiens*, *J. Gen. Physiol.*, 66:583–616.
- Cohn, T. E., and D. J. Lasley, 1985. Visual sensitivity, *Annu. Rev. Psychol.*, 37:495–521.
- Cohn, T. E., and D. I. A. Macleod, 1999. Flash masking by nearby luminance noise probes, *J. Opt. Soc. Am. A*, 16:750–754.
- Curcio, C. A., K. R. Sloan, R. E. Kalina, and A. E. Hendrickson, 1990. Human photoreceptor topography, *J. Comp. Neurol.*, 22:292(4):497–523.
- DeVries, H. L., 1943. The quantum character of light and its bearing upon threshold of vision, the differential sensitivity and visual acuity of the eye, *Physica*, 10:553–564.
- Fechner, G. T., 1860. *Elemente der Psychophysik*, vol. 2, Leipzig: Breitkopf und Härtel, p. 559 (reprinted Bristol: Thoemmes Press, 1999).
- Foley, J. M., and G. E. Legge, 1981. Contrast detection and near-threshold discrimination in human vision, *Vis. Res.*, 21:1041–1053.
- Graham, N. V. S., 1989. *Visual Pattern Analyzers*, Oxford Psychology Series No. 16, New York: Oxford University Press.
- Hagins, W. A., 1955. The quantum efficiency of bleaching of rhodopsin in situ, *J. Physiol. (Lond.)*, 129:22–23P.
- Hallett, P. E., 1987. Quantum efficiency of dark-adapted human vision, *J. Opt. Soc. Am. A*, 4:2330–2335.
- Hecht, S., 1942. The quantum relations of vision, *J. Opt. Soc. Am.*, 32:42.
- Hecht, S., S. Shlaer, and M. H. Pirenne, 1942. Energy, quanta and vision, *J. Gen. Physiol.*, 25:819–840.
- Hood, D. C., 1988. Testing hypotheses about development with electroretinographic and increment-threshold data, *J. Opt. Soc. Am. A*, 5:2159–2165.
- Hornstein, E., D. Pope, and T. E. Cohn, 1999. Noise and its effects on photoreceptor temporal contrast sensitivity at low light levels, *J. Opt. Soc. Am. A*, 16:718–727.

- King-Smith, P. E., S. S. Grigsby, A. J. Vingrys, S. C. Benes, and A. Supowit, 1994. Efficient and unbiased modifications of the QUEST threshold method: theory, simulations, experimental evaluation and practical implementation, *Vis. Res.*, 34:885–912.
- Klein, S. A., 2001. Measuring, estimating, and understanding the psychometric function: a commentary, *Percept. Psychophys.*, 63(8):1421–1455.
- Lasley, D. J., and T. E. Cohn, 1981. Why luminance discrimination may be better than detection, *Vis. Res.*, 21:273–278.
- Levick, W. R., L. N. Thibos, T. E. Cohn, D. Catanzarro, and H. B. Barlow, 1983. Performance of cat retinal ganglion cells at low light levels, *J. Gen. Physiol.*, 82:405–426.
- Lillywhite, P. G., and S. Laughlin, 1979. Transducer noise in a photoreceptor, *Nature*, 277:569–572.
- Massof, R., 1987. Relation of the normal-deviate vision receiver operating characteristic curve slope to d' , *J. Opt. Soc. Am. A*, 4(3):548–550.
- Nachmias, J., 1966. Photosensitization and intrinsic noise in the visual system, *Vis. Res.*, 6:113–115.
- Nachmias, J., and E. C. Kocher, 1970. Visual detection and discrimination of luminance increments, *J. Opt. Soc. Am.*, 60:382–389.
- Nachmias, J., and R. V. Sansbury, 1974. Grating contrast: discrimination may be better than detection. *Vis. Res.*, 14:1039–1042.
- Nagaraja, N. S., 1964. Effect of luminance noise on contrast thresholds, *J. Opt. Soc. Am.*, 54:950–955.
- Øesterberg, G., 1935. Topography of the layer of rods and cones in the human retina, *Acta Ophthalmol. Kbh.*, Suppl. 6:1–102.
- Patel, A. S., and R. W. Jones, 1968. Increment and decrement visual thresholds, *J. Opt. Soc. Am.*, 58:696–699.
- Pelli, D., 1985. Uncertainty explains many aspects of visual contrast detection and discrimination, *J. Opt. Soc. Am. A*, 2:1508–1531.
- Pelli, D. G., and B. Farell, 1999. Why use noise? *J. Opt. Soc. Am. A*, 16:647–653.
- Peterson, W. W., T. G. Birdsall, and W. C. Fox, 1954. The theory of signal detectability, *Trans. IRE PGIT*, 4:171–212.
- Reeves, A., S. Wu, and J. Schirillo, 1998. The effect of photon noise on the detection of white flashes, *Vis. Res.*, 38:691–203.
- Riccó, A., 1877. Relazione fra il minimo angolo visuale e l'intensità luminosa, *Annali di Ottalmologia*, 6:373–479.
- Rose, A., 1948. The sensitivity performance of the human eye on an absolute scale, *J. Opt. Soc. Am.*, 38:196–208.
- Rosell, F. A., and R. H. Wilson, 1973. Recent psychophysical experiments and the display signal-to-noise ratio concept, in *Perception of Displayed Information*, (L. M. Biederman, ed.), New York: Plenum Press, pp. 167–232.
- Sakitt, B., 1972. Counting every quantum, *J. Physiol. (Lond.)*, 223:131–150.
- Schefrin, B. E., M. L. Bieber, R. McLean, and J. S. Werner, 1998. The area of complete scotopic spatial summation enlarges with age, *J. Opt. Soc. Am. A Opt. Image Sci. Vis.*, 15:340–348.
- Schnapf, J. L., B. J. Nunn, M. Meister, and D. A. Baylor, 1990. Visual transduction in cones of the monkey *Macaca fascicularis*, *J. Physiol. (Lond.)*, 427:681–713.
- Shapley, R., and C. Enroth-Cugell, 1984. Visual adaptation and retinal gain controls, in *Progress in Retinal Research*, vol. 3, New York: Pergamon, pp. 263–346.
- Short, A. D., 1966. Decremental and incremental visual thresholds, *J. Physiol. (Lond.)*, 185:646–654.
- Swanson, W. H., T. Ueno, V. C. Smith, and J. Pokorny, 1987. Temporal modulation sensitivity and pulse detection thresholds for chromatic and luminance perturbations, *J. Opt. Soc. Am. Ser. A*, 4:1992–2005.
- Tanner, W. P., Jr., 1961. Physiological implications of psychophysical data, *Ann. N.Y. Acad. Sci.*, 89:752–765.
- Tanner, W. P., Jr., and T. G. Birdsall, 1958. Definitions of d' and η as psychophysical measures, *J. Acoust. Soc. Am.*, 30:922–928.
- Tanner, W. P., Jr., and R. Clark-Jones, 1960. The ideal sensor system as approached through statistical decision theory and the theory of signal detectability, in *Visual Research Problems*, NAS-NRC Pub. No. 712, (A. Morris and E. P. Horne, eds.), Washington, DC: Armed Forces NRC Committee on Vision.
- Tanner, W. P., Jr., and J. A. Swets, 1954. A decision making theory of visual detection, *Psychol. Rev.*, 61:401–409.
- Thibos, L. N., W. R. Levick, and T. E. Cohn, 1979. Receiver operating characteristic curves for Poisson signals, *Biol. Cybern.*, 33:57–61.
- Tolhurst, D. J., J. A. Movshon, and A. F. Dean, 1983. The statistical reliability of signals in single neurons in cat and monkey visual cortex, *Vis. Res.*, 23:775–785.
- Watson, A. B., and D. G. Pelli, 1983. QUEST: a Bayesian adaptive psychophysical method, *Percept. Psychophys.*, 33:113–120.
- Werner, J. S., K. A. Schelble, and M. L. Bieber, 2001. Age-related increases in photopic increment thresholds are not due to an elevation in intrinsic noise, *Color Research and Application*, 26:48–52.

52 Ideal Observer Analysis

WILSON S. GEISLER

VISUAL SYSTEMS, AND the developmental and learning mechanisms that shape them during the life span, have evolved because they enhance performance in those tasks relevant to survival and reproduction, such as detecting and localizing predators or prey, navigating through the environment, identifying materials, estimating the three-dimensional geometry of the environment, recognizing specific objects encountered before, and so on. Thus, the proper study of a visual system must include an analysis of those specific tasks that the system evolved to perform. An ideal observer analysis provides a principled approach for understanding a visual task, the stimulus information available to perform the task, and the anatomical and physiological constraints that limit performance of the task.

The central concept in ideal observer analysis is the *ideal observer*, a theoretical device that performs a given task in an optimal fashion, given the available information and some specified constraints. This is not to say that ideal observers perform without error, but rather that they perform at the physical limit of what is possible in the situation. In general, ideal observers make mistakes because of the complexity and uncertainty that exist in the visual environment and because of the inherent noise in light or in whatever signal serves as input to the ideal observer. The fundamental role of uncertainty and noise in limiting possible performance implies that ideal observers must be derived and described in probabilistic (statistical) terms.

Ideal observer analysis involves determining the performance of the ideal observer in a given task and then comparing its performance to that of the biological system under consideration, which (depending on the application) might be the organism as a whole, some neural subsystem, or an individual neuron. In vision science, ideal observer analyses have been carried out for many different tasks, ranging from photon detection, to pattern discrimination, to information coding in neural populations, to shape estimation, to recognition of complex objects. Here the focus is on detection, discrimination, and identification, with an emphasis on what has been learned through ideal observer analysis about the retina, lateral geniculate nucleus (LGN), and primary visual cortex. Other applications of ideal observer analysis are described in other chapters within this volume (see also Knill and Richards, 1996; Simoncelli and Olshausen, 2001).

Basic concepts and formulas

The purpose of deriving an ideal observer is to determine the optimal performance in a task, given the physical properties of the environment and stimuli. Organisms generally do not perform optimally, and hence one should not think of an ideal observer as a potentially realistic model of the actual performance of the organism. Rather, the value of an ideal observer is to provide a precise measure of the stimulus information available for performing the task, a computational theory of how to perform the task, and an appropriate benchmark against which to compare the performance of the organism (Green and Swets, 1966). In addition, the ideal observer can serve as a useful starting point for developing realistic models (e.g., Schrater and Kersten, 2001). With an appropriate ideal observer in hand, one knows how the task should be performed. Thus, it becomes possible to explore in a principled way what the organism is doing right and what it is doing wrong. This can be done by degrading the ideal observer in a systematic fashion by including, for example, hypothesized sources of internal noise (Barlow, 1977), inefficiencies in central decision processes (Barlow, 1977; Green and Swets, 1966; Pelli, 1990), or known anatomical or physiological factors that would limit performance (Geisler, 1989).

Obviously, an ideal observer analysis is sensible only for objective tasks with well-defined performance goals, such as identifying as accurately as possible the physical category to which an object belongs or estimating some physical property of an object. Ideal observer analysis is neither possible nor sensible for subjective tasks such as judging the apparent hue of a stimulus or judging whether a stereoscopic display appears fused or diplopic.

BAYESIAN IDEAL OBSERVERS Most forms of ideal observer analysis are based on the concepts of Bayesian statistical decision theory. To illustrate the Bayesian approach, consider a categorization task where there are n possible stimulus categories, c_1, c_2, \dots, c_n , and the observer's task on each trial is to identify the category correctly, given the particular stimulus \mathbf{S} arriving at the eye.¹ If there is substantial stimu-

¹ Experts should note that in this example the utility/loss function is degenerate and does not appear; it will be introduced shortly.

lus noise or overlapping of categories, then the task will be inherently probabilistic. As might be expected intuitively, performance is maximized on average by computing the probability of each category, given the stimulus, and then choosing the category C that is most probable:^{2,3}

$$C = \arg \max_{c_i} [p(c_i|\mathbf{S})] \quad (1)$$

Note that “arg max” is just a shorthand notation for a procedure that finds and then returns the category that has the highest probability, given the stimulus.⁴ In practice, the probability of a category given the stimulus is often computed by making use of Bayes’ formula:

$$p(c_i|\mathbf{S}) = \frac{p(\mathbf{S}|c_i)p(c_i)}{p(\mathbf{S})} \quad (2)$$

where $p(c_i|\mathbf{S})$ is the *posterior probability*, $p(\mathbf{S}|c_i)$ is the *likelihood*, and $p(c_i)$ is the *prior probability*.⁵ The probability in the denominator, $p(\mathbf{S})$, is a constant that is the same for all the categories and hence plays no role in the optimal decision rule. Furthermore, it is completely determined by the likelihoods and prior probabilities:

$$p(\mathbf{S}) = \sum_{j=1}^n p(\mathbf{S}|c_j)p(c_j) \quad (3)$$

Substituting Bayes’ formula into equation 1, the optimal response is given by

$$C = \arg \max_{c_i} [p(\mathbf{S}|c_i)p(c_i)] \quad (4)$$

In other words, one can identify a stimulus with maximum accuracy by combining the prior probability of the different categories and the likelihood of the stimulus given each of the possible categories.

In the laboratory, maximizing accuracy is a common goal defined by the experimental design. For this goal, all errors are equally costly, because all errors have the same effect on the accuracy measure. However, this is rarely the case for natural situations, where the costs and benefits associated with different stimulus-response outcomes have a more complex structure. For example, if the goal is survival, then some errors are more costly than others—mistaking a

poisonous snake for a branch is more costly than mistaking a branch for a poisonous snake. Within the framework of Bayesian statistical decision theory, more complex goals are represented with a utility function, $u(\mathbf{r}, \mathbf{S})$, which specifies the cost or benefit associated with making response \mathbf{r} when the state of the environment is \mathbf{S} (e.g., Berger, 1985). In this more general case, the optimal decision is to make the response, \mathbf{R} , that maximizes the average utility over all the possible states of the environment (see footnote 3):

$$\mathbf{R} = \arg \max_{\mathbf{r}} \left[\sum_{\omega} u(\mathbf{r}, \omega) p(\mathbf{S}|\omega) p(\omega) \right] \quad (5)$$

In this decision rule, $p(\omega)$ is the prior probability of a given state of the environment, and $p(\mathbf{S}|\omega)$ is the stimulus likelihood given a state of the environment. Note that equation 4 is special case of equation 5, where the possible states of the environment are the stimulus categories, c_1, c_2, \dots, c_m , the possible responses are the category names, the benefits for all correct responses are equal, and the costs for all incorrect responses are equal.

CONSTRAINED BAYESIAN IDEAL OBSERVERS The class of Bayesian ideal observers considered so far operates directly on the stimulus \mathbf{S} that arrives at the eye. However, for many applications, it is useful to incorporate some biological constraints into an ideal observer analysis. For example, if good estimates are available for the optics of the eye, the spatial arrangement of the photoreceptors, and their spectral sensitivities, then these estimates can serve as plausible constraints on an ideal observer. In this case, the ideal observer would show the maximum performance possible in the given task, using the photons caught in the photoreceptors. Such an ideal observer must perform worse than one designed to use the photons arriving at the cornea. To the extent that the constraints are accurate, the difference in performance between the ideal observer at the cornea and the one at the level of photon absorptions would provide a precise measure of the information (relevant to the task) lost in the process of image formation and photon capture. Furthermore, the difference in the performance of the ideal observer at the level of photon capture and the performance of the organism as a whole would provide a precise measure of the information lost in the neural processing subsequent to photon capture (e.g., Geisler, 1989).

Another useful way to use constrained ideal observers is to allow some free parameters in the biological constraints and then determine what parameter values produce the best-performing ideal observer. For example, in an ideal observer at the level of photon absorptions, one can allow the peak wavelengths of the receptors to be free parameters and then determine what peak wavelengths would produce the best-performing ideal observer. This would be a precise

²In the case of ties at the highest probability, one can pick arbitrarily from those tied categories.

³Throughout this chapter, capital letters refer to random quantities and boldface letters refer to *vector* quantities, where the term *vector* refers to an ordered list of properties (generally, integer- or real-valued quantities).

⁴More simply, $\arg \max[f(x)]$ is the value of x (the argument) for which $f(x)$ reaches its maximum value.

⁵Bayes’ formula follows directly from the definition of conditional probability: $p(c_i|\mathbf{S}) = p(\mathbf{S}|c_i)p(c_i)/p(\mathbf{S})$

way of determining how close an organism's photoreceptors are to the optimum for the given task (Regan et al., 2001). Alternatively, the free parameters might represent the receptive field shapes (the configuration of weights placed on each receptor) for some given number of postreceptor neurons. This would be a precise way of determining how close an organism's receptive field shapes are to the optimum for the given task.

A general class of constrained Bayesian ideal observers can be represented by introducing a *constraint function*, $g_\theta(\mathbf{S})$, which maps (either deterministically or probabilistically) the stimulus \mathbf{S} at the cornea into an intermediate signal $\mathbf{Z} = g_\theta(\mathbf{S})$. For example, \mathbf{S} might be a vector representing the number of photons entering the pupil from each pixel on a display screen, and \mathbf{Z} might be a vector representing the number of photons absorbed in each photoreceptor; hence $g_\theta(\mathbf{S})$ would specify the combined effect of the optics, photoreceptor lattice, and photoreceptor absorption spectra. Alternatively, \mathbf{Z} might represent the spike count for each ganglion cell, and $g_\theta(\mathbf{S})$ would specify the combined effect of the optics and all retinal processing. Any free parameters, such as the peaks of the photoreceptor absorption spectra or the shapes of the receptive fields, are represented in the constraint function by a parameter vector θ .

For any given parameter vector, the optimal decision rule has the same structure as before:

$$\mathbf{R} = \arg \max_{\mathbf{r}} \left[\sum_{\omega} u(\mathbf{r}, \omega) p_\theta(\mathbf{Z} | \omega) p(\omega) \right] \quad (6)$$

The only difference is that the stimulus \mathbf{S} is replaced by the intermediate signal \mathbf{Z} . Applying this optimal decision rule typically requires determining the intermediate-signal likelihood $p_\theta(\mathbf{Z} | \omega)$, by combining the constraint function $g_\theta(\mathbf{S})$ with the stimulus likelihood distribution $p(\mathbf{S} | \omega)$. If there are free parameters, then the optimal parameter vector is given by the following formula (e.g., Geisler and Diehl, 2002):

$$\theta_{\text{opt}} = \arg \max_{\theta} \left[\sum_{\mathbf{Z}} \max_{\mathbf{r}} \left[\sum_{\omega} u(\mathbf{r}, \omega) p_\theta(\mathbf{Z} | \omega) p(\omega) \right] \right] \quad (7)$$

Using θ_{opt} in equation 6 gives the decision rule for the best-performing ideal observer over the free-parameter space.

The concepts and basic formulas of Bayesian ideal observer analysis are relatively straightforward. However, in specific applications, it can be very difficult to determine or compute the likelihoods, prior probabilities, utility functions, or sums over possible states of the environment. Indeed, there are many situations for which it is not yet possible to determine the performance of the ideal observer. Nonetheless, the number and range of successes have been growing over the years, and the prospects for continued success are good.

Detection, discrimination, and identification

Detection, discrimination, and identification are fundamental visual tasks that have been investigated extensively since the beginning of vision science. In the detection task, the observer is presented with either a background pattern or a background pattern plus a target pattern, and must decide whether or not the background pattern contains the target. The background pattern can range from a simple, uniform field of light to a complex natural scene. Similarly, the target can range from a simple, uniform patch of light to a complex natural object. In the discrimination task, the observer is presented with either a background plus a target or a background plus a modified target, and must decide whether the background contains the modified or unmodified target. Formally, detection and discrimination tasks are equivalent, because the discrimination task can be regarded as a detection task, where the "background" is the background plus the unmodified target and the "target" is the difference between the modified and unmodified targets. In the identification task, the observer is presented with a background plus one of n possible targets and must decide which target is contained in the background. Thus, the discrimination task is a special case of the identification task where the number of possible targets is two.

During the last half century, ideal observer analysis has played an important role in the development of our understanding of the physical, physiological, and cognitive factors that underlie detection, discrimination, and identification performance. Before discussing these applications of ideal observer analysis, I introduce the ideal observer for detection and discrimination tasks, where all sources of information that the ideal observer receives are statistically independent. Many of the results described later are based on this simple kind of ideal observer.

OPTIMAL DISCRIMINATION GIVEN STATISTICALLY INDEPENDENT SOURCES OF INFORMATION On each trial of a detection or discrimination task, a stimulus, \mathbf{S} , from one of the two categories is received by the ideal observer, and it must pick a category. From equation 4, we see that the optimal decision rule is to compute the likelihood ratio, $p(\mathbf{S} | c_2) / p(\mathbf{S} | c_1)$, and compare this ratio to a criterion, $p(c_1) / p(c_2)$, which is the ratio of the prior probabilities of the two categories. If the likelihood ratio exceeds this criterion, then the ideal observer picks c_2 ; otherwise, it picks c_1 . For present purposes, suppose that the prior probabilities are equal (criterion = 1.0).

Consider a situation where the stimulus consists of a set of stimulus components or information sources, $\mathbf{S} = \langle S_1, \dots, S_n \rangle$. For example, S_i might represent the number of photons entering the pupil from the i th pixel on a video monitor or the number of spikes generated by the i th ganglion cell in the retina. If all the components are statistically

independent, then the probability of the whole stimulus is the product of the probabilities of the individual components. In this case, the performance of the ideal observer can be determined by considering the performance of the ideal observer separately for each component. Assuming approximate normality, an ideal observer that uses only the i th component will perform with an accuracy (percent correct) of

$$PC_i = \Phi\left(\frac{d'_i}{2}\right) \quad (8)$$

where

$$d'_i = \frac{|E(S_i|c_2) - E(S_i|c_1)|}{\sqrt{\frac{Var(S_i|c_2) + Var(S_i|c_1)}{2}}} \quad (9)$$

and $\Phi(\cdot)$ is the standard normal integral function. The quantity in equation 9 is called *d-prime*, and it is the absolute value of the difference in the expected values (means) for the two categories divided by the square root of the average of the variances for the two categories. Intuitively, *d-prime* is a signal-to-noise ratio; the signal is the difference in the means, and the noise is the square root of the average variance. These formulas for ideal observer performance are often quite accurate, even when the probability distributions for components deviate substantially from the normal distribution (although formulas become inaccurate for severe deviations).

It can be shown (e.g., Green and Swets, 1966) that the accuracy of an observer that optimally combines all the stimulus components is given by

$$PC_{\text{ideal}} = \Phi\left(\frac{d'_{\text{ideal}}}{2}\right) \quad (10)$$

where

$$d'_{\text{ideal}} = \sqrt{\sum_{i=1}^n (d'_i)^2} \quad (11)$$

In words, the *d-prime* for an ideal observer combining independent sources of information is simply the square root of the sum of the squared *d-primes* for each source alone.

In psychophysical experiments, the measured performance accuracy can be converted into a *d-prime* value, d'_{real} . One useful measure of the difference between real and ideal performance is the “efficiency” η , which is defined as the square of the ratio of the real and ideal values of *d-prime* (Tanner and Birdsall, 1958):⁶

$$\eta = \frac{(d'_{\text{real}})^2}{(d'_{\text{ideal}})^2} \quad (12)$$

PHOTON NOISE The first useful applications of ideal observer analysis in vision were directed at understanding the limits to visual performance imposed by the randomness of light and then determining how closely the human visual system approaches those limits (Barlow, 1957, 1958b; DeVries, 1943; Hecht et al., 1942; Rose, 1948). It was well known at the beginning of the twentieth century that the number of photons emitted by a light source (or absorbed by a material) in a fixed time interval is generally described by the Poisson probability density:

$$p(z) = \frac{e^{-a} a^z}{z!} \quad (13)$$

where z is the specific number of photons emitted (or absorbed) and a is the mean number of photons emitted (or absorbed).

In one of the earliest studies of how photon noise might affect visual performance, Hecht et al. (1942) measured threshold for detection of a spot of light in the dark. In this detection task, one stimulus category (c_1) is a completely dark background and the other (c_2) is a spot of light against the dark background. The investigators chose conditions likely to yield the lowest possible thresholds: a small spot with a wavelength at the peak of the rod spectral sensitivity function (507 nm), presented briefly at the eccentricity where rod receptor density is greatest. They found that threshold for this stimulus was approximately 100 photons at the cornea. Depending on one’s estimates of the transmittance of the ocular media, light collection area of the rods, optical density of the rod photopigment, and isomerization probability given photon absorption, this threshold translates into something like 10 to 20 effective photon absorptions scattered among a few hundred rods (Barlow, 1977; Hecht et al., 1942). If this is the average number of effective photon absorptions at detection threshold, then the probability of absorbing no photons is quite small, and hence the human observer must be performing considerably below the level of the ideal observer (whose performance is given by combining equations 4 and 8). Nonetheless, this threshold is small enough to imply that photon noise may be an important factor limiting human vision.

It was realized that if photon noise does limit human vision, then intensity discrimination (i.e., contrast detection) should follow the square-root relation implied (approximately) by the photon-noise-limited ideal observer (DeVries, 1943; Rose, 1948):

$$\Delta a = ka^{0.5} \quad (14)$$

⁶This is a generalization of Tanner and Birdsall’s definition.

where a is the average number of photons received from the background, $\Delta a + a$ is the average number of photons received from the background plus target, and k is a constant determined by the percentage of correct responses used to define threshold. The symbols in Figure 52.1 show the exact performance of the photon-noise-limited ideal observer for a number of background intensities expressed in units of quanta. The symbol at a background of 0.0 shows the absolute threshold of the ideal observer. The *straight line* is the approximation to the ideal observer given by equation 14, which is accurate for backgrounds above a few quanta. The *solid curve* is the approximation to the ideal observer obtained using the normality assumption described in the section "Optimal Discrimination Given Statistically Independent Sources of Information."

A number of human psychophysical studies have demonstrated that there is a substantial range of background intensities and target shapes where contrast detection follows the square-root relation both under rod-dominated (scotopic) conditions (e.g., Barlow, 1957; Blakemore and Rushton, 1965) and under cone-dominated (photopic) conditions (e.g., Banks et al., 1987; Barlow, 1958a; Kelly, 1972). For example, the symbols in Figure 52.2 show the contrast sensitivity (1/contrast threshold) measured in the human fovea as a function of the spatial frequency of sine wave

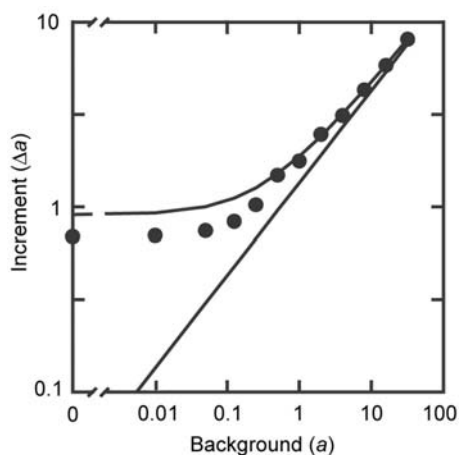


FIGURE 52.1. Performance of the photon-noise-limited ideal observer in a single-interval, two-alternative, forced-choice intensity discrimination task where the presentation probabilities for background and background plus target are equal and the criterion for threshold is 75% correct. The *solid symbols* show the exact predictions for a number of background energies (in units of quanta). The lumpiness of the predictions is due to the discrete nature of the Poisson probability density. The *solid straight line* shows the prediction of equation 14, which is reasonably accurate for background energies above a few quanta. The *solid curve* is based on the normal approximation that is commonly used in computing ideal observer predictions. It is quite accurate for background energies above 0.5 quanta, and for most purposes it is sufficiently accurate down to absolute threshold.

targets for three background intensity levels. The spacing between the solid curves equals the value ($\sqrt{10}$) predicted by the square-root law.

There is additional evidence that photon noise may play a role in contrast detection. For example, in psychophysical studies, the shape of the receiver operating characteristic (ROC) for increment and decrement targets is often consistent with photon noise (Cohn and Lasley, 1986), and in electrophysiological studies, individual primate rods (Baylor et al., 1984) and cat ganglion cells (Barlow et al., 1971) produce reliable responses to the absorption of single photons. However, none of this evidence is definitive. Humans generally perform considerably worse than the photon-noise-limited ideal observer, making it quite possible that other factors (e.g., Poisson-like neural noise) are responsible for those visual performance characteristics that appear to be consistent with photon noise (Graham and Hood, 1992; Kortum and Geisler, 1995).

OPTICS AND PHOTORECEPTORS The optics of the eye, photoreceptor lattice, and absorption spectra of the photopigments are relatively well understood in humans and macaques, making possible a relatively rigorous ideal

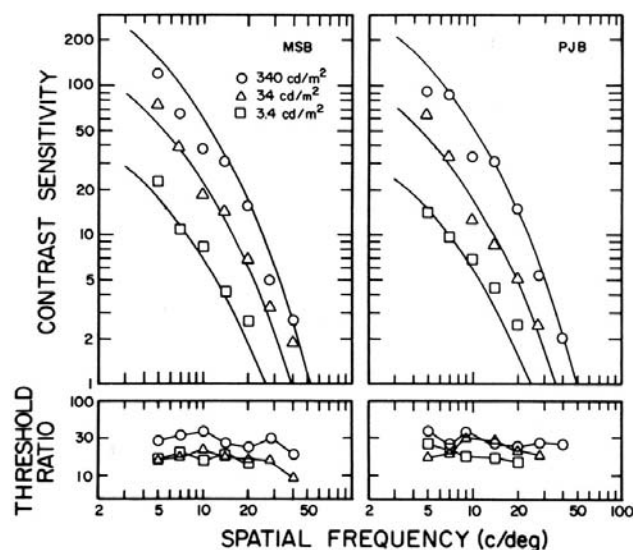


FIGURE 52.2. Contrast sensitivity functions measured in two human observers at three background intensity levels for sine wave targets having a fixed number of cycles. The targets were presented for 0.1 second in the center of the fovea. The solid curves are the performances of an ideal observer limited by photon noise, the optics of the eye, the photoreceptor lattice, and the absorption spectra of the cone photopigments. The quantum efficiency of the ideal observer has been adjusted so that the solid curves align optimally with the data. The spacing between the solid curves is due to photon noise and corresponds to the square-root law. The lower panels show the ratio of ideal threshold to real threshold, when there is no adjustment of quantum efficiency. (Adapted from Banks et al., 1987).

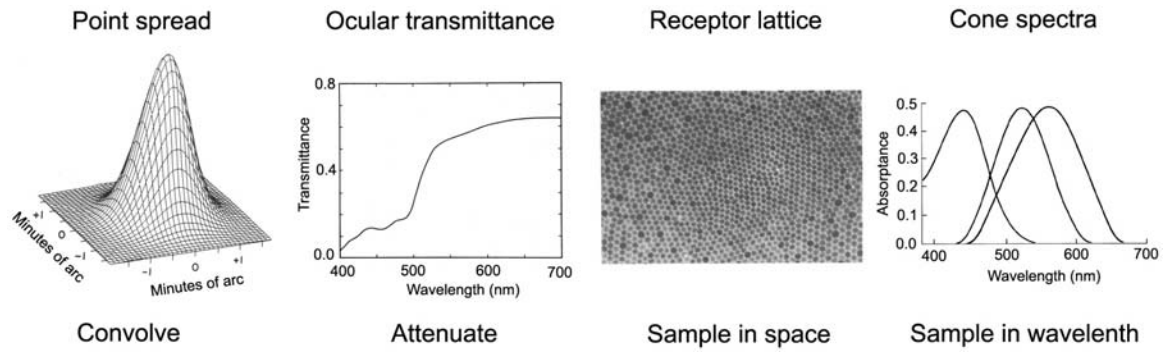


FIGURE 52.3. Computing the mean number of photons absorbed in each photoreceptor. First, the image is convolved with appropriate point spread functions. Second, the chromatic spectral energy distribution at each image location is attenuated by the ocular transmittance function. Third, the blurred and attenuated

spectral energy distribution is summed over the aperture of each photoreceptor. Fourth, the spectral energy distribution entering each photoreceptor is multiplied by the effective absorption spectrum for that receptor; integrated, and converted to units of quanta.

observer analysis of how these factors limit detection and discrimination performance (Banks and Bennett, 1988; Banks et al., 1987; Beckmann and Legge, 2002; Geisler, 1984, 1989). The number of photons absorbed in a photoreceptor is described by a Poisson probability density (equation 8), and the number of photons absorbed in each receptor is statistically independent of the number absorbed in any other receptor (across presentations of the same stimulus). Thus, performance of the ideal observer can be easily calculated using the formulas in the section “Optimal Discrimination Given Statistically Independent Sources of Information” if the parameter (mean) of the Poisson distribution is known for each photoreceptor for the two stimuli being discriminated.

Typical steps for calculating the mean number of photons absorbed in each photoreceptor are illustrated in Figure 52.3: (1) convolve with the optical point spread function, (2) attenuate across wavelength using the ocular transmittance function, (3) sum the light across the aperture of each photoreceptor in the lattice, and (4) multiply by each photoreceptor’s absorption spectrum and integrate across the wavelength. In terms of the general terminology of the section “Constrained Bayesian Ideal Observers,” these processing steps constitute a constraint function $g_0(\mathbf{S})$ that maps the stimulus into an intermediate signal—the pattern of photon absorptions in the photoreceptors—although in this case without any free parameters.

Suppose that after applying these steps the mean number of photon absorptions in the i th photoreceptor is a_i for stimulus a and is b_i for stimulus b . Since the variance of the Poisson probability distribution is equal to its mean, the d -prime for the ideal observer using only the i th photoreceptor is

$$d'_i = \frac{|b_i - a_i|}{\sqrt{\frac{b_i + a_i}{2}}} \quad (15)$$

and hence, by equation 11, d -prime for the full ideal observer is

$$d'_{\text{ideal}} = \sqrt{2 \sum_{i=1}^n \frac{(b_i - a_i)^2}{b_i + a_i}} \quad (16)$$

To determine the discrimination threshold for the ideal observer, the difference between stimulus a and stimulus b is varied (along the dimension of interest) until the d'_{ideal} reaches a value corresponding to the chosen criterion level of accuracy (typically 75% correct).⁷ The solid curve in Figure 52.1 shows the thresholds obtained with equation 16 for an intensity discrimination task where stimulus a and stimulus b are identical except for intensity (i.e., a scale factor). Ideal observer analyses at the level of the photoreceptors in humans have been carried out for a number of different detection, discrimination, and identification tasks.

One area that has received considerable attention is spatial vision. Banks et al. (1987) measured the high-frequency limb of the contrast sensitivity function in the fovea for briefly presented sine wave targets with a fixed number of spatial cycles. The symbols show the contrast sensitivities measured at three background intensities. The solid curves in Figure 52.2 show the performance of the ideal observer shifted vertically on the log contrast axis. (The vertical shifting, which is done to compare the shapes of the real and ideal threshold functions, corresponds to scaling the efficiency of the ideal observer down by a constant factor.⁸) The lower panels show the actual ratios of real to ideal

⁷For most stimulus conditions, these formulas for the ideal observer at the level of the photoreceptors are slightly less accurate than those described in Geisler (1989), but they are sufficiently accurate for most purposes, and are simpler and more intuitive.

⁸For a photon-noise-limited ideal observer, scaling the efficiency down by a constant factor is equivalent to placing a neutral density filter in front of the eye.

thresholds. The fact that the ratios are approximately constant as a function of spatial frequency and contrast suggests that much of the measured variation in human performance may be due to preneural factors. The fact that the ratios are high (approximately 20) implies that the overall efficiency of the neural processing subsequent to photon absorption in the receptors is relatively low (less than 1%).

Banks and Bennett (1988) performed a similar analysis of contrast sensitivity in human infants and found that a substantial fraction of the difference between adult and infant contrast sensitivity is consistent with the optical and photoreceptor immaturities that have been measured in the infant eye. Davila and Geisler (1991) showed that detection thresholds measured for spot targets as a function of target area vary in a similar fashion, for human and ideal observers, for targets up to several hundred square minutes of arc (Fig. 52.4). These results are consistent with the measurements of the contrast sensitivity function measured by Banks et al. (1987); cf. Figure 52.2.

Geisler (1984) and Geisler and Davila (1985) showed that some of the dramatic differences in performance observed across different types of acuity tasks are qualitatively consistent with the performance of an ideal observer operating at the level of the photoreceptors. In traditional acuity tasks, humans (with normal vision) can resolve changes of approximately 45 to 60 seconds of arc in the spatial position of two overlapping image features. This corresponds to a change in spacing of two foveal cone diameters. However, in *hyperacuity* tasks, humans can resolve changes in spatial position of a few seconds of arc if the features are slightly separated (e.g., Westheimer, 1979). The ideal observer shows similar differences in acuity because of differences in the nature of the discrimination information when features overlap on the retina as opposed to when they do not. This difference in the nature of the information also leads to rather different performance as a function of intensity: the performance of the ideal observer shows that the physical limit for resolving two overlapping features decreases with the fourth root of intensity, whereas the physical limit for resolving changes in the position of two spatially separated features decreases with the square root of intensity. This difference is also seen qualitatively in psychophysical studies (Geisler and Davila, 1985).

Another area that has received considerable attention is color vision. Once again, there are a number of examples in which human performance is qualitatively, and sometimes quantitatively, similar to that of an ideal observer at the level of the photoreceptors. Wavelength discrimination functions of humans are similar in shape to that of the ideal observer (Geisler, 1989; Vos and Walraven, 1972). The high spatial frequency limb of the chromatic contrast sensitivity function in humans is similar in shape to that of the ideal observer (Geisler, 1989; Sekiguchi et al., 1993). Some of the deficits

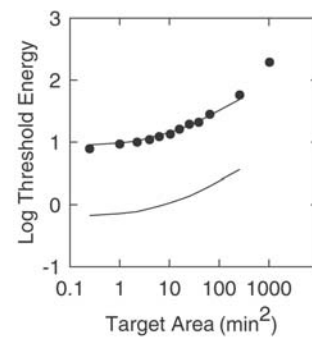


FIGURE 52.4. Detection threshold for spot targets in the central fovea as a function of target area. The data points are thresholds for a human observer, and the solid curves are the thresholds for an ideal observer operating at the level of photon absorptions in the receptors. The *lower solid curve* shows the thresholds of the ideal observer; the *upper solid curve* is the same curve translated vertically for the purpose of comparing shapes. (Adapted from Davila and Geisler, 1991.)

in color discrimination performance in human infants are consistent with the performance of an ideal observer that incorporates the known immaturities in the infant's optics and photoreceptors (Banks and Bennett, 1988).

The examples described above demonstrate that there are many tasks where human discrimination performance parallels the performance of an ideal observer limited by preneural factors. Thus, some of the variation in human performance in these tasks would seem to be explained by preneural factors in the sense that subsequent neural mechanisms must be extracting the available information from the photoreceptors with relatively constant efficiency. The importance of this observation is that it moves physiological research forward from the question of what mechanisms are responsible for the variations in discrimination performance for the stimuli entering the eye to the question of what mechanisms are responsible for achieving the nearly constant discrimination performance for the signals exiting the photoreceptors.

Of course, there are many tasks where human performance does not parallel the performance of the ideal observer limited by preneural factors. For example, even though the density of cones and the quality of the optics of the eye decline with eccentricity from the fovea, the decline in contrast sensitivity at high spatial frequencies is much more precipitous than predicted by the ideal observer (Banks et al., 1991). Similarly, the decline in letter identification performance drops much more quickly than that predicted by the ideal observer (Beckman and Legge, 2002). In these cases, most (or all) of the variation in performance must be due to neural mechanisms. These are also important results because they localize the relevant mechanisms beyond the photoreceptors.

NEURAL FACTORS IN THE RETINA AND PRIMARY VISUAL CORTX The neural mechanisms in the early stages of the visual pathway are less well understood than the preneural factors (optics, receptor lattice, photopigments); nonetheless, there is sufficient knowledge to carry out limited ideal observer analyses, with the caveat that the analyses may change substantially as new anatomical and physiological knowledge accumulates. Banks et al. (1991) extended the earlier ideal observer analysis of Banks et al. (1987) to include a more complete description of the preneural factors, as well as a description the spatial pooling (summation) implied by the density of the ganglion cells and the sizes of their center mechanisms. They found that the performance of the ideal observer paralleled human performance in several detection and discrimination tasks measured as a function of retinal eccentricity. For example, Figure 52.5 shows grating acuity (*solid squares*) and vernier acuity (*solid circles*) as a function of retinal eccentricity. The *left panel* shows human performance reported by Westheimer (1982), and the *right panel* shows the performance of the ideal observer. The *open symbols* show the performance of an ideal observer that is limited only by preneural factors. As can be seen, the ideal observer that includes retinal spatial pooling parallels human performance considerably better than one that does not. Further, the retinal ideal observer displays the interesting property that vernier acuity declines more rapidly than grating acuity as a function of eccentricity. This is a counterintuitive prediction that further illustrates the value of ideal observer analysis for understanding the information processing consequences of the stimulus, task, and physiological/anatomical factors. As Banks et al. point out, there are aspects of the variation in human visual acuity with eccentricity unlikely to be explained by retinal factors; however, an ideal observer analysis (or something equivalent) is essential for determining those aspects.

Arnold and Geisler (1996) performed an ideal observer analysis similar to that of Banks et al., but they included some additional retinal factors based on the receptive field properties of ganglion cells in the macaque monkey (Croner and Kaplan, 1995; Croner et al., 1993). They found that ideal observer contrast sensitivity, at the level of the ganglion cell responses, parallels human contrast sensitivity fairly well as a function of target spatial frequency, eccentricity, and size (see also Geisler and Albrecht, 2000).

There are detection and discrimination tasks where human performance does not parallel the performance of the ideal observer at the level of the ganglion cell responses. These tasks include contrast discrimination and spatial frequency masking. Geisler and Albrecht (1997) performed an ideal observer analysis of contrast discrimination and spatial frequency discrimination at the level of the responses of neurons in primary visual cortex. However, this analysis is

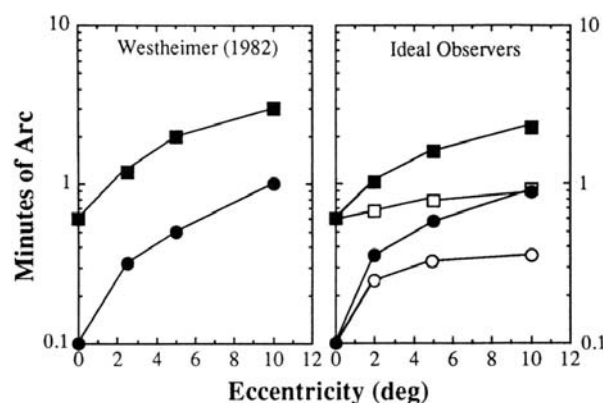


FIGURE 52.5. Grating acuity (*squares*) and vernier acuity (*circles*) as a function of retinal eccentricity. The *left panel* shows human performance (Westheimer, 1982). The *right panel* shows the performance of an ideal observer at the level of the photoreceptors (*open symbols*) and an ideal observer that also incorporates spatial summation consistent with the center sizes and spatial density of the retinal ganglion cells. (Adapted from Banks et al., 1991.)

more tentative because of the vast number of neurons in V1, their highly heterogeneous receptive field properties, and the potential for long-range interactions within V1 and from other cortical areas. The strategy was to measure (with single-unit electrophysiology) the spatial frequency tuning functions, contrast response functions, and noise characteristics of a large population of cortical neurons. From these response functions and noise measurements, Geisler and Albrecht determined the ideal contrast discrimination performance and spatial frequency discrimination performance of each cortical neuron in the population using equation 9. Finally, they determined the ideal performance for the whole population under the assumption of statistical independence equation 11. The solid curves in Figure 52.6 show the shapes of the contrast discrimination and spatial frequency discrimination functions from the ideal observer analysis. The open symbols show the data from several different studies in humans and monkeys (see figure caption). For comparison, note that the contrast discrimination function of an ideal observer at the level of the photoreceptors is flat; that is, contrast threshold is constant independent of the background contrast.

PIXEL NOISE, NEURAL NOISE, AND CENTRAL EFFICIENCY In the tasks considered so far, photon noise was the only source of stimulus noise (other than the random selection of the stimulus category on each trial). However, in natural and artificial environments, signals of interest are often embedded in complex, randomly varying background patterns which act as a source of stimulus noise. Thus, an important class of ideal observer analyses is those directed at tasks where pixel noise is added to the stimulus display. For

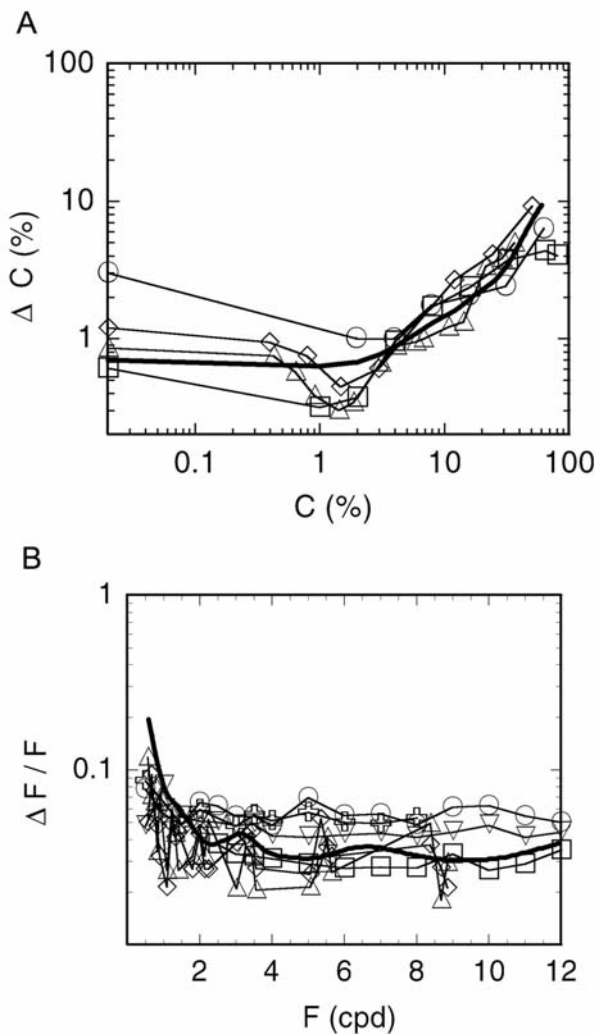


FIGURE 52.6. *A*, Contrast discrimination threshold as function of base contrast. Open symbols are data from psychophysical studies (several in humans and one in monkey). *B*, Spatial frequency discrimination threshold as a function of base frequency. Open symbols are data from several psychophysical studies in humans. The solid curves show the relative performance of an ideal observer that combines the responses of a population of neurons whose contrast-response functions, spatial-frequency-tuning functions, and noise characteristics were measured one at a time in monkey V1. The efficiency of the ideal observer was reduced by the same factor in both plots to allow comparison of shapes.

example, Figure 52.7 shows human and ideal performance for amplitude discrimination of small targets (spots and grating patches) in white noise as a function of noise spectral power density (Burgess et al., 1981). The solid line of slope 1.0 shows the absolute performance of an ideal observer operating at the level of the cornea. Thus, the difference between real and ideal performance represents all losses of information within the eye, retina, and central visual pathways. For these conditions, efficiency ranges from about 20% to 70%, much higher than the efficiency for similar targets in uniform backgrounds ($<1\%$). In other

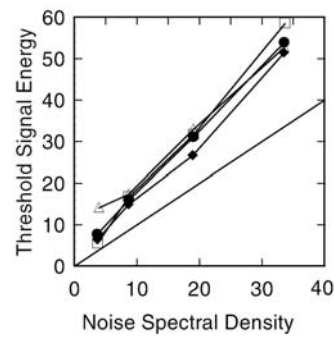


FIGURE 52.7. Comparison of real and ideal performance for the discrimination of simple localized targets in white noise. The diagonal line of slope 1.0 shows the performance of the ideal observer; the symbols show the performances of human observers for several different spot and sine wave grating targets. (Adapted from Burgess et al., 1981.)

words, the human observers are performing much more closely to ideal in the pixel noise tasks. One possible explanation for this difference between tasks is that the pixel noise dominates the photon noise, and other sources of noise in the early levels of the visual system, effectively sidestepping inefficiencies of the peripheral visual system. Thus, the difference in performance between real and ideal observers in Figure 52.7 may reflect primarily the inefficiencies of central decision mechanisms (e.g., Barlow, 1978).

Pixel noise experiments, in conjunction with appropriate ideal observer analyses, have been used to isolate and measure central mechanisms that limit discrimination performance (Barlow, 1978; Burgess et al., 1981; Kersten, 1987; Pelli, 1990), to evaluate neural noise levels in the early visual system (Legge et al., 1987; Pelli, 1990), and to develop models relevant for understanding the detection and discrimination of targets in the noisy images created by radiological devices and image enhancers (Barrett et al., 1992; Burgess et al., 1982; Myers and Barrett, 1987; Myers et al., 1985).

Recently, new insights into the efficiency of central pooling and decision mechanisms have been gained by analyzing the samples of noise on each experimental trial, contingent upon the observer's response on that trial (Abbey et al., 1999; Ahumada, 1996; Beard and Ahumada, 1999; Gold et al., 2000). Specifically, suppose that there are two possible targets, a and b , and that on each trial one of the targets is randomly selected and then added to a random sample of white noise. By averaging together all samples of noise when the observer responded " b ," averaging together all the samples of noise when the observer responded " a ," and then subtracting these two average noise images, one obtains a *classification image*. If a sufficient number of such trials are run, the classification image provides a detailed map indicating the weight the observer placed on each pixel location in making the decision. This classification image

can be compared with the one generated by the ideal observer to give detailed information about inefficiencies in the real observer's central pooling and decision mechanisms. Measurements of classification images show that observers tend to make use of only a subset of the pixel locations that contain useful information, and sometimes use locations that contain no useful information (e.g., locations where target contours are occluded; Gold et al., 2000).

Natural scene statistics and natural selection

The introduction to this chapter began with the truism that the proper study of a visual system must include an analysis of those specific tasks that the system evolved to perform. However, as we have seen, ideal observer analyses have been largely confined to tasks involving relatively simple stimuli generated in the laboratory. Recently, measurements of statistical properties of natural environments have become available, allowing ideal observer analyses for tasks involving more naturalistic stimuli. This is an important direction for research because the results can speak more directly to the relationship between the statistics of natural environments and the design of perceptual systems.

One topic that has received considerable interest is color identification. For example, Regan et al. (1998, 2001) measured the wavelength distributions of primary food sources (fruits) of several New World monkeys and the wavelength distributions of the surrounding foliage. They then used an ideal observer analysis to determine optimal placement of the M and L cones for identifying food sources in the surrounding foliage. Interestingly, optimal placement corresponds fairly well with actual placement, although, as Regan et al. pointed out, other factors (such as minimizing chromatic aberration) may also contribute to actual placement. Osorio and Vorobyev (1996) have made a similar case for placement of the cone photopigments in Old World primates. Similarly, the two cone pigments in dichromatic mammals appear to be nearly optimally placed for discriminating between natural leaf spectra (Chiao et al., 2000; Lythgoe and Partridge, 1989).

Another topic that has received some attention is contour detection (Elder and Zucker, 1998; Geisler et al., 2001; Sigman et al., 2001). For example, Geisler et al. (2001) extracted edge elements from images of diverse natural scenes and then computed co-occurrence probabilities for different possible geometrical relationships between the edge elements. (Note that the geometrical relationship between a pair of edge elements is described by a vector in three dimensions: distance, direction, and orientation difference.) Two different co-occurrence probability distributions were measured: one for edge elements that belong to the same physical contour (i.e., the same surface boundary, shadow/lighting boundary, or surface-marking boundary)

and one for edge elements that belong to different physical contours. Using these two probability distributions, Geisler et al. derived an ideal observer for detecting contours embedded in complex backgrounds and compared its performance to human performance on the same tasks. Remarkably, the performance of the ideal observer based on natural image statistics was quite similar to human performance across all conditions—the correlation between human and ideal detection accuracy was approximately 0.9. This result suggests that there is a close relationship between contour grouping mechanisms in humans and the statistics of contours in natural images.

These two examples, and a number of the examples described earlier, demonstrate that there can be a close correspondence between real and ideal observers. Nonetheless, there are many reasons to expect real observers not to reach the performance of the ideal observer:

1. In the laboratory, the task (including the stimulus likelihoods and prior probabilities) is defined by the experimenter, and may not correspond well with the tasks that the organism has evolved or learned to perform in the natural environment.
2. Organisms evolve or learn to perform many different tasks, and hence there may be compromises in design that lead to nonideal performance in a given task.
3. There are limits to the range of materials that organisms can synthesize and exploit, and limits on the possible structure of organic molecules, but there are not similar limits on the ideal observer.
4. Perceptual systems (and the learning mechanisms that shape them) are designed through natural selection, and thus the intrinsic utility function is fitness (birth and death rates), which may imply an ideal observer rather different from the one implied by the utility function specified in a laboratory task.
5. Evolution through natural selection is an incremental process in which each change must produce an increase in fitness; thus, the real observer may correspond to a local maximum in the space of possible solutions, whereas the ideal observer corresponds to the global maximum in the space of possible solutions.
6. In general, evolution lags behind changes that occur in environmental likelihoods and prior probabilities; thus, a real observer may not even correspond to a local maximum in the space of possible solutions.

MAXIMUM FITNESS IDEAL OBSERVERS One way to begin understanding the differences between real observers and ideal observers is to measure properties of the natural environment (e.g., natural scene statistics) and, from these, design more naturalistic laboratory tasks. The most appropriate ideal observers for analyzing such tasks are those where the measure of utility is fitness (birth and death rates), although

this may often not be practical. The fitness utility function can be represented as a growth factor function, $\gamma(\mathbf{r}, \omega)$, which equals 1 plus the birth rate minus the death rate for each possible response and state of the environment (Geisler and Diehl, 2002). Thus, given a particular stimulus \mathbf{S} , the maximum-fitness ideal observer will make the response that maximizes the growth factor averaged across all possible states of the environment. In other words, the maximum-fitness ideal observer will make the response

$$\mathbf{R} = \arg \max_{\mathbf{r}} \left[\sum_{\omega} \gamma(\mathbf{r}, \omega) p(\mathbf{S} | \omega) p(\omega) \right] \quad (17)$$

This equation is identical to the standard Bayesian ideal observer equation 5, except that the utility function is the growth-factor function.

Geisler and Diehl (2002) have demonstrated that utility functions based on fitness can yield ideal observers that behave quite differently from those based on more traditional utility functions. For example, Figure 52.8 compares the decision criterion of an ideal observer that maximizes accuracy with one that maximizes fitness. In the hypothetical scenario they considered, a predator species is trying to detect prey (its only food source). All other things being equal, natural selection favors mutations that result in an increase in the birth rate of the predator. However, when birth rate increases, the result is a decline in the number of prey and hence a reduction in the prior probability that a prey is in the immediate vicinity. If the utility function of the ideal observer corresponds to maximizing prey detection accuracy (the typically utility function in laboratory experiments), then the optimal decision criterion equals the ratio of the prior probabilities, which is shown by the *dashed curve* in Figure 52.8. On the other hand, if the goal is to maximize fitness, then the optimal decision criterion is relatively invariant with birth rate (*solid curve*), because the decrease in target prior probability is balanced by the increase in payoff when a prey is captured. This example demonstrates the potential importance of considering fitness utility functions when evaluating the performance of real observers.

BAYESIAN NATURAL SELECTION A complementary approach to understanding the differences between real observers and ideal observers is to measure properties of the natural environment and incorporate those into a model that represents the process of natural selection, which, unlike the ideal observer, does not necessarily find the global optimum. It is possible to formulate a quantitative version of the theory of natural selection that incorporates the same terms—prior probability distributions, stimulus likelihood distributions, and utility functions—as those in a Bayesian ideal observer (Geisler and Diehl, 2002). This Bayesian formulation of natural selection provides a convenient conceptual frame-

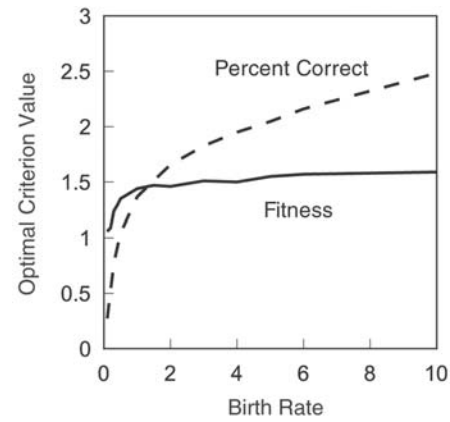


FIGURE 52.8. Comparison of an ideal observer having a utility function based on maximizing growth rate (1 + birth rate – death rate) versus a more standard ideal observer having a utility function based on maximizing detection accuracy. The *dashed curve* shows the decision criterion of an ideal predator that is maximizing prey detection accuracy as a function of the predators' birth rate (which causes a decrease in the prior probability of a prey being within the local vicinity). The *solid curve* shows the decision criterion of the ideal predator that is maximizing growth rate. The lumpiness of the solid curve is due to noise in the simulation process. (Adapted from Geisler and Diehl, 2002.)

work for understanding how natural scene statistics, and other properties of the environment, influence the evolution and hence design of a perceptual system.

Briefly, the fundamental equation of Bayesian natural selection shows how the expected number of organisms of a given species carrying a given vector of alleles \mathbf{a} at time $t + 1$ is related to the number of organisms carrying the same allele vector at time t , the prior probability of a state of the environment at time t , the likelihood of a stimulus given the state of the environment, the likelihood of a response given the stimulus, and the growth factor given the response and the state of the environment:

$$\bar{O}_a(t+1) = O_a(t) \sum_{\omega} p_a(\omega | t) \sum_{\mathbf{r}} \gamma_a(\mathbf{r}, \omega) \sum_{\mathbf{s}} p_a(\mathbf{r} | \mathbf{s}) p_a(\mathbf{s} | \omega) \quad (18)$$

The actual number of organisms at time $t + 1$ is a random number, $O_a(t + 1)$, that is obtained by sampling from appropriate probability distributions for births, deaths, mutations, and sexual recombination. A separate fundamental equation is set up for each allele vector in each species under consideration, and the process of natural selection is represented by iteration of these fundamental equations in parallel over time. (Note that mutations and sexual recombination may create new allele vectors and, hence, new fundamental equations, and that extinction of alleles or species will remove fundamental equations.)

Using this formulation of natural selection and the corresponding maximum fitness ideal observer, Geisler and Diehl (2002) explored the coevolution of receptor spectral

sensitivities in a hypothetical predator species and camouflage in a hypothetical prey species. They found that there are many starting conditions where the spectral sensitivities (and decision criterion) of the predator species converge to that of the maximum-fitness ideal observer. Further, they found that there are different stable coevolutionary end states, and that these different end states are not equally good in terms of the average growth rate (fitness) for either the predator or the prey. This may seem contradictory (how can two different solutions both represent maximum fitness?), but in fact, it is expected because in realistic evolutionary scenarios the prior probability distributions change over time, and hence the maximum-fitness ideal observer changes over time. If the stable end-state prior probabilities are different, then the maximum-fitness ideal observer may be different. This example demonstrates the potential importance of measuring natural scene statistics, and of considering the incremental process of natural selection, when evaluating the performance of real observers.

Conclusion

This chapter outlined the basic concepts and formulas of ideal observer analysis as it has been applied in studies of biological vision, and then illustrated the application of ideal observer analysis in a number of cases involving detection, discrimination, and identification tasks. Although real visual systems are never ideal, deriving the performance of an ideal observer can be very useful for understanding the computational requirements of a task and the limits to performance imposed by specific anatomical and physiological factors. The range of situations where ideal observer analysis can be usefully applied has grown over the years, and it is likely to become an even more central tool as we attempt to understand natural scene statistics and their relationship to the design and evolution of visual systems.

REFERENCES

- Abbey, C. K., M. P. Eckstein, and F. O. Bochud, 1999. Estimation of human-observer templates in two-alternative forced-choice experiments, *SPIE*, 3663:284–295.
- Ahumada, A. J., 1996. Perceptual classification images from vernier acuity masked by noise, *Perception*, 25:18.
- Arnou, T. L., and W. S. Geisler, 1996. Visual detection following retinal damage: predictions of an inhomogeneous retino-cortical model. *SPIE Proc. Hum. Vis. Electr. Imaging*, 2674:119–130.
- Banks, M. S., and P. J. Bennett, 1988. Optical and photoreceptor immaturities limit the spatial and chromatic vision of human neonates. *J. Opt. Soc. Am. A*, 5:2059–2079.
- Banks, M. S., W. S. Geisler, and P. J. Bennett, 1987. The physical limits of grating visibility, *Vis. Res.*, 27:1915–1924.
- Banks, M. S., A. B. Sekuler, and S. J. Anderson, 1991. Peripheral spatial vision: limits imposed by optics, photoreceptors, and receptor pooling, *J. Opt. Soc. Am. A*, 8:1775–1787.
- Barlow, H. B., 1957. Increment thresholds at low intensities considered as signal/noise discriminations, *J. Physiol. (Lond.)*, 136:469–488.
- Barlow, H. B., 1958a. Intrinsic noise of cones, in *National Physical Laboratory Symposium on Visual Problems of Colour*, vol. 2, London: Her Majesty's Stationery Office, pp. 617–630.
- Barlow, H. B., 1958b. Temporal and spatial summation in human vision at different background intensities, *J. Physiol. (Lond.)*, 141:337–350.
- Barlow, H. B., 1977. Retinal and central factors in human vision limited by noise, in *Vertebrate Photoreception* (H. B. P. Fatt, ed.), London: Academic Press, pp. 337–358.
- Barlow, H. B., 1978. The efficiency of detecting changes of density in random dot patterns, *Vis. Res.*, 18:637–650.
- Barlow, H. B., W. R. Levick, and M. Yoon, 1971. Responses to single quanta of light in retinal ganglion cells of the cat, *Vis. Res.*, 11(suppl. 3):87–102.
- Barrett, H. H., T. Gooley, K. Girodias, J. Rolland, T. White, and J. Yao, 1992. Linear discriminants and image quality, *Image Vis. Comput.*, 10:451–460.
- Baylor, D. A., B. J. Nunn, and J. L. Schnapf, 1984. The photocurrent, noise and spectral sensitivity of rods of the monkey *Macaca fascicularis*, *J. Physiol. (Lond.)*, 357:575–607.
- Beard, B. L., and A. J. Ahumada, 1999. Classification images for detection, *Invest. Ophthalmol. Vis. Sci.*, 40:3015.
- Beckmann, P. J., and G. E. Legge, 2002. Preneural limitations to identification performance in central and peripheral vision, *J. Opt. Soc. Am. A*, 19:2349–2362.
- Berger, J. O., 1985. *Statistical Decision Theory and Bayesian Analysis*, 2nd ed., New York: Springer-Verlag.
- Blakemore, C. B., and W. A. H. Rushton, 1965. The rod increment threshold during dark adaptation in mornal and rod monochromat, *J. Physiol.*, 181:629–640.
- Burgess, A. E., R. F. Wagner, and R. J. Jennings, 1982. Human signal detection performance for noisy medical images. In O. Nalcioglu, and M. S. Prewitt (eds.), *Proceedings of International Workshop on Physics and Engineering in Medical Images*: New York: IEEE.
- Burgess, A. E., R. F. Wagner, R. J. Jennings, and H. B. Barlow, 1981. Efficiency of human visual signal discrimination, *Science*, 214:93–94.
- Chiao, C., M. Vorobyev, T. W. Cronin, and D. Osorio, 2000. Spectral tuning of dichromats to natural scenes, *Vis. Res.*, 40:3257–3271.
- Cohn, T. E., and D. J. Lasley, 1986. Visual sensitivity, *Annu. Rev. Psychol.*, 37:495–521.
- Croner, L. J., and E. Kaplan, 1995. Receptive fields of P and M ganglion cells across the primate retina, *Vis. Res.*, 35:7–24.
- Croner, L. J., K. Purpura, and E. Kaplan, 1993. Response variability in retinal ganglion cells of primates, *Proc. Natl. Acad. Sci. USA*, 90:8128–8130.
- Davila, K. D., and W. S. Geisler, 1991. The relative contributions of pre-neural and neural factors to areal summation in the fovea, *Vis. Res.*, 31:1369–1380.
- De Vries, H. L., 1943. The quantum character of light and its bearing upon threshold of vision, the differential sensitivity and visual acuity of the eye, *Physica*, 10(7):553–564.
- Elder, J. H., and S. W. Zucker, 1998. Evidence for boundary-specific grouping, *Vis. Res.*, 38(1):143–152.
- Geisler, W. S., 1984. Physical limits of acuity and hyperacuity, *J. Opt. Soc. Am. A*, 1:775–782.
- Geisler, W. S., 1989. Sequential ideal-observer analysis of visual discriminations, *Psychol. Rev.*, 96:267–314.

- Geisler, W. S., and D. G. Albrecht, 1997. Visual cortex neurons in monkeys and cats: detection, discrimination, and identification, *Visual Neurosci.*, 14:897–919.
- Geisler, W. S., and D. G. Albrecht, 2000. Spatial vision. In *Seeing* (2nd ed.) (K. K. De Valois, ed.), New York: Academic Press, pp. 79–128.
- Geisler, W. S., and K. D. Davila, 1985. Ideal discriminators in spatial vision: two-point stimuli, *J. Opt. Soc. Am. A*, 2:1483–1497.
- Geisler, W. S., and R. Diehl, 2002. Bayesian natural selection and the evolution of perceptual systems, *Philos. Trans. R. Soc. Lond. B*, 357:419–448.
- Geisler, W. S., J. S. Perry, B. J. Super, and D. P. Gallogly, 2001. Edge co-occurrence in natural images predicts contour grouping performance, *Vis. Res.*, 41:711–724.
- Gold, J. M., R. F. Murray, P. J. Bennett, and A. B. Sekuler, 2000. Deriving behavioural receptive fields for visually completed contours, *Curr. Biol.*, 10:663–666.
- Graham, N., and D. C. Hood, 1992. Quantal noise and decision rules in dynamic models of light adaptation, *Vis. Res.*, 32:779–787.
- Green, D. M., and J. A. Swets, 1966. *Signal Detection Theory and Psychophysics*, New York: Wiley.
- Hecht, S., S. Schlaer, and M. H. Pirenne, 1942. Energy, quanta, and vision, *J. Gen. Physiol.*, 25:819–840.
- Kelly, D. H., 1972. Adaptation effects on spatio-temporal sine-wave thresholds, *Vis. Res.*, 12:89–101.
- Kersten, D., 1987. Statistical efficiency for the detection of visual noise, *Vis. Res.*, 27:1029–1040.
- Knill, D. C., and W. Richards, eds. 1996. *Perception as Bayesian Inference*, Cambridge: Cambridge University Press.
- Kortum, P. T., and W. S. Geisler, 1995. Adaptation mechanisms in spatial vision II: flash thresholds and background adaptation, *Vis. Res.*, 35(11):1595–1609.
- Legge, G. E., D. Kersten, and A. E. Burgess, 1987. Contrast discrimination in noise, *J. Opt. Soc. Am. A*, 4(2):391–404.
- Lythgoe, J. N., and J. C. Partridge, 1989. Visual pigments and the acquisition of visual information, *J. Exp. Biol.*, 146:1–20.
- Myers, K. J., and H. H. Barrett, 1987. Addition of a channel mechanism to the ideal-observer model, *J. Opt. Soc. Am. A*, 4:2447–2457.
- Myers, K. J., H. H. Barrett, M. M. Borgstrom, D. D. Patton, and G. W. Seeley, 1985. Effect of noise correlation on detectability of disk signals in medical imaging, *J. Opt. Soc. Am. A*, 2:1752–1759.
- Osorio, D., and M. Vorobyev, 1996. Colour vision as an adaptation to frugivory in primates, *Proc. R. Soc. Lond. B*, 263:593–599.
- Pelli, D. G., 1990. The quantum efficiency of vision. in *Vision: Coding and Efficiency* (C. Blakemore, ed.). Cambridge: Cambridge University Press, pp. 3–24.
- Regan, B. C., C. Julliot, B. Simmen, F. Vienot, P. Charles-Dominique, and J. D. Mollon, 1998. Frugivory and colour vision in *Alouatta seniculus*, a trichromatic platyrrhine monkey, *Vis. Res.*, 38:3321–3327.
- Regan, B. C., C. Julliot, B. Simmen, F. Vienot, P. Charles-Dominique, and J. D. Mollon, 2001. Fruits, foliage and the evolution of primate colour vision, *Philos. Trans. R. Soc. Lond. B*, 356:229–283.
- Rose, A., 1948. The sensitivity performance of the human eye on an absolute scale, *J. Opt. Soc. Am.*, 38:196–208.
- Schrater, P. R., and D. Kersten, 2001. Vision, psychophysics and Bayes, in *Statistical Theories of the Brain* (R. P. N. Rao, B. A. Olshausen, and M. S. Lewicki, eds.), Cambridge, MA: MIT Press.
- Sekiguchi, N., D. R. Williams, and D. H. Brainard, 1993. Efficiency in detection of isoluminant and isochromatic interference fringes, *J. Opt. Soc. Am. A*, 10:2118–2133.
- Sigman, M., G. A. Cecchi, C. D. Gilbert, and M. O. Magnasco, 2001. On a common circle: Natural scenes and Gestalt rules, *Proc. Natl. Acad. Sci. USA*, 98:1935–1940.
- Simoncelli, E. P., and B. A. Olshausen, 2001. Natural image statistics and neural representation, *Annu. Rev. Neurosci.*, 24:1193–1215.
- Tanner, W. P., Jr., and T. G. Birdsall, 1958. Definitions of d' and n as psychophysical measures, *J. Acoust. Soc. Am.*, 30:922–928.
- Vos, J. J., and P. L. Walraven, 1972. An analytical description of the line element in the zone-fluctuation model of color vision: 1. Basic concepts, *Vis. Res.*, 12:1327–1344.
- Westheimer, G., 1979. The spatial sense of the eye, *Invest. Ophthalmol. Vis. Sci.*, 18:893–912.
- Westheimer, G., 1982. The spatial grain of the perifoveal visual field, *Vis. Res.*, 22:157–162.

53 Scotopic Vision

WALTER MAKOUS

THE WORD *SCOTOPIC* STEMS from the Greek root *skotos* (σκοτος), with a suffix denoting kinds of vision, as in myopic, protanopic, amblyopic, and diplopic. Skotos means “darkness,” so scotopic vision is vision in the dark. Although this calls to mind what is sometimes referred to as *Leibowitz’s law* (“You can’t see a damn thing in the dark”), the term is generally understood to denote vision adapted for the darkness of night.

Those interested in scotopic vision are especially referred to the book *Night Vision* (Hess et al., 1990), containing many thoughtful and thorough chapters on this topic. Those that relate specifically to the present chapter are “Rod-Mediated Vision: Role of Post-Receptor Filters” and “Post-Receptor Sensitivity of the Achromat,” by Hess; “The Light-Adaptation of the Human Rod Visual System,” by Sharpe; “Dark Adaptation: A Re-Examination,” by Lamb; “The Photoreceptors in the Achromat,” by Sharpe and Nordby; and “Absolute Sensitivity,” by Makous. Since the publication of this book, much work not covered here has been done on interactions between rod and the cone signals and on dark adaptation, covered in Chapters 54 and 55.

This chapter, then, is devoted to the properties of those mechanisms that are specifically adapted for dim or night vision. As scotopic vision is distinguished from the rest of vision primarily insofar as it differs from photopic vision, some of the properties of photopic vision are described in what follows so as to point to those differences. This chapter also is concerned primarily with human vision and treats other species only insofar as they shed light on human vision. No effort is made here to supply a compendium of all that is known about scotopic vision. Rather, some of the salient properties and issues are discussed and analyzed here, leaving the underlying anatomy and physiological mechanisms to other chapters, notably Chapter 17.

Conversion tables

To compare psychophysics with electrophysiological experiments and to interpret the findings in terms of underlying anatomical structures and physiological mechanisms, it is useful to have convenient means of converting back and forth between photometric quantities and such things as the density of retinal illumination, or the rate of quantal absorptions within the receptors. Tables 53.1 and 53.2 provide such information. These tables and the rationale for the entries

have been published previously (Makous, 1997), but they are reproduced here for readers’ convenience and to correct errors in the original.

Spectral sensitivity

The shape of the curve expressing the proportion of incident light (I_i) absorbed ($I_i - I_t$) as opposed to transmitted (I_t) as it passes through an absorbing medium is determined by Beer’s law ($-\log I_t/I_i = cd\epsilon_\lambda$) and therefore depends on the optical density, that is, on the negative logarithm of the product of the concentration of the absorbing pigment (c), the length of the path through the medium (d), and the spectral extinction coefficient (ϵ_λ) of the pigment. The sensitivity of the isolated rods of *Macaca fascicularis* closely match the spectral absorption of rhodopsin, with an optical density of 0.29 to 0.41, which includes the range of the best estimates of its density in human rods made by other means (Baylor et al., 1984). Psychophysically, the spectral sensitivity of aphakic observers (those from whom the lens of the eye has been removed) also matches the absorption spectrum of rhodopsin (Griswold and Stark, 1992), which, in turn, acceptably matches the (CIE) scotopic luminous efficiency function once preretinal absorption is taken into account.

The sensitivity of the scotopic system to variations and mixtures of wavelengths renders it the prototypical *single-channel* system: its response to any two wavelengths can be equated by suitable adjustment of intensity; that is, the system is *univariant* (cf. Chapter 17), a term introduced by Rushton (1972). Depending on the stimulation of cones, either simultaneously or in the recent past, stimulation of rods can elicit a great variety of color responses, but under neutral conditions the result of rod excitation is usually described as white or bluish white (see Chapter 55).

Lower limits

The first step here is to define the boundaries of scotopic sensitivity: its lower and upper limits and its spatial and temporal limits.

The lower limit of stimuli that can be detected by a human observer, that is, the *absolute threshold*, depends on the spatial and temporal extent of the test stimulus, and on its wavelength and location on the retina. Wavelength, and to a large extent retinal location as well, simply affect the

TABLE 53.1

Rod conversions.

	Troland	cdm^{-2} , 2 mm p.	cdm^{-2} , dmm p.	qstr s^{-1} on ret.	qdeg s^{-1} on ret.	$\text{qmm}^{-2} \text{s}^{-1}$ on ret.	$\text{q}\mu\text{m}^{-2} \text{s}^{-1}$ on ret.	q s^{-1} Rod, Abs.	q s^{-1} Rod, Act.	mac. Td	Cat Td
1 Troland =	1	0.318	1.273 d ⁻²	8.99E+8	2.74E+5	3.23E+6	3.230	6.460	4.310	0.588	0.600
1 cdm^{-2} , 2-mm p. =	3.142	1	0.250 d ²	2.82E+9	8.60E+5	1.01E+7	10.147	20.295	13.540	1.848	1.885
1 cdm^{-2} , d-mm p. =	0.785 d ²	4 d ⁻²	1	1.14E+9 d ²	3.49E+5 d ²	4.11E+6 d ²	4.11 d ²	8.22 d ²	5.49 d ²	0.749 d ²	0.76 d ²
1 $\text{qstr}^{-1} \text{s}^{-1}$ =	1.11E-9	3.54E-10	8.77E-10 d ⁻²	1	3.05E-4	3.59E-3	3.59E-9	7.19E-9	4.79E-9	6.54E-10	6.67E-10
1 $\text{qdeg}^{-2} \text{s}^{-1}$ =	3.65E-6	1.16E-6	2.87E-06 d ⁻²	3.28E+3	1	1.18E+1	1.18E-5	2.36E-5	1.57E-5	2.15E-6	2.19E-6
1 $\text{qmm}^{-2} \text{s}^{-1}$ =	3.10E-7	9.85E-8	2.43E-07 d ⁻²	2.78E+2	8.48E-2	1	1.00E-6	2.00E-6	1.33E-6	1.82E-7	1.86E-7
1 $\text{q}\mu\text{m}^{-2} \text{s}^{-1}$ =	0.310	0.099	0.243 d ⁻²	2.78E+8	8.48E+4	1.00E+6	1	2.000	1.334	0.182	0.186
1 $\text{q s}^{-1}/\text{rod abs.}$ =	0.155	0.049	0.188 d ⁻²	1.39E+8	4.24E+4	5.00E+5	0.500	1	0.667	0.091	0.093
1 $\text{q s}^{-1}/\text{rod, act.}$ =	0.232	0.074	0.182 d ⁻²	2.09E+8	6.35E+4	7.49E+5	0.749	1.499	1	0.136	0.139
1 mac. Td =	1.700	0.541	1.335 d ⁻²	1.53E+9	4.66E+5	5.49E+6	5.491	10.982	7.327	1	1.020
1 cat Td =	1.667	0.531	1.308 d ⁻²	1.50E+9	4.56E+5	5.38E+6	5.383	10.767	7.183	0.980	1

TABLE 53.2

Cone conversions.

	Troland	cdm^{-2} , 2 mm Pupil	cdm^{-2} , dmm Pupil	$\text{qstr}^{-1} \text{s}^{-1}$ on Retina	qdeg s^{-1} on Retina	$\text{qmm}^{-2} \text{s}^{-1}$ on Retina	$\text{q}\mu\text{m}^{-2} \text{s}^{-1}$ on Retina	q s^{-1} Cone Abs.	q s^{-1} Cone, Act.	Mac. Td	Cat Td
1 Troland =	1	0.318	1.273 d ⁻²	2.62E+9	7.98E+5	9.41E+6	9.410	16.610	11.080	0.588	0.600
1 cdm^{-2} , 2 mm p. =	3.142	1	0.250 d ²	8.23E+9	2.51E+6	2.96E+7	29.562	52.182	34.809	1.848	1.885
1 cdm^{-2} , dmm p. =	0.785 d ²	4 d ⁻²	1	3.33E+9 d	1.02E6 d	1.20E+7 d	11.98 d	18.81 d ²	12.55 dd ²	0.749 dd ²	0.76 dd ²
1 $\text{qstr}^{-1} \text{s}^{-1}$ =	3.82E-10	1.22E-10	3.00E-10 d ⁻²	1	3.05E-4	3.59E-3	3.59E-9	6.34E-9	4.23E-9	2.25E-10	2.29E-10
1 $\text{qdeg}^{-2} \text{s}^{-1}$ =	1.25E-6	3.99E-7	9.84E-07 d ⁻²	3.28E+3	1	1.18E+1	1.18E-5	2.08E-5	1.39E-5	7.37E-7	7.52E-7
1 $\text{qmm}^{-2} \text{s}^{-1}$ =	1.06E-7	3.38E-8	8.43E-08 d ⁻²	2.78E+2	8.48E-2	1	1.00E-6	1.77E-6	1.18E-6	6.25E-8	6.38E-8
1 $\text{q}\mu\text{m}^{-2} \text{s}^{-1}$ =	0.106	0.034	0.083 d ⁻²	2.78E+8	8.48E+4	1.00E+6	1	1.765	1.177	0.063	0.064
1 $\text{q s}^{-1}/\text{cone, abs.}$ =	0.060	0.019	0.053 d ⁻²	1.58E+8	4.80E+4	5.67E+5	0.567	1	0.667	0.035	0.036
1 $\text{q s}^{-1}/\text{cone, act.}$ =	0.090	0.029	0.080 d ⁻²	2.36E+8	7.20E+4	8.49E+5	0.849	1.499	1	0.053	0.054
1 mac. Td =	1.700	0.541	1.335 d ⁻²	4.45E+9	1.36E+6	1.60E+7	15.997	28.237	18.836	1	1.020
1 cat Td =	1.667	0.531	1.308 d ⁻²	4.36E+9	1.33E+6	1.57E+7	15.683	27.683	18.467	0.980	1

probability that the quanta in the test flash will be absorbed, and they disappear as variables if the threshold is specified in terms of number of quanta absorbed (cf. Table 53.1). Moreover, once one knows the sensitivity to the smallest, briefest test stimuli, one can infer the main effects of the spatial and temporal variables.

NOISE Noise is treated in detail in Chapter 51 and requires only the briefest mention here. As was pointed out by Denton and Pirenne (1954), Barlow (1956), and others, absolute sensitivity is limited by noise that originates within the visual system, and an understanding of absolute sensitivity requires estimates of that noise. However, many of the early experiments on absolute sensitivity, such as the classic one by Hecht et al. (1942), were primarily concerned with measuring the number of quanta delivered by a threshold stimulus. This information leaves open questions about the amount of noise in the system and the related question of the observer's criterion for responding. The experiment of Hecht et al., for example, does not provide narrowly constrained estimates of noise because the rate of false-positive responses is not reported. Moreover, single yes-no responses, such as those used by Hecht et al., do not constrain estimates of noise as much as responses on a rating scale (Makous, 1990).

Sakitt (1972) reported the preferred rating-scale responses under excellent conditions for estimating internal noise. If one conceptually refers this internal noise to an external source of spurious quanta that are otherwise identical to those in the stimulus but that have effects equivalent to those of internal noise (see Chapters 51 and 54), then one can say that her three observers performed as though every stimulus was accompanied by noise quanta that resulted in an average of 4 to 9 activations for one observer, 8 to 13 for another, and 9 to 17 for the third (Makous, 1990). These estimates correspond well with direct measurements from macaque rods (Schneeweis and Schnapf, 1995).

THRESHOLDS Sakitt's threshold results were comparable to those of Hecht et al.: they found that 54 to 148 quanta delivered to the cornea yielded detections on 60% of the trials, and she found that 55 to 66 quanta at the cornea yielded middle ratings (those closest to a threshold judgment) on about 50% of the trials. Trained observers with good night vision, tested under identical conditions, have highly similar absolute thresholds (Makous, 1997): an root mean square (rms) standard deviation of 0.13 on a log scale (33 observers in 8 studies).

These experiments were done to ensure that all the quanta were used effectively, that is, that they fell within the retinal area and time interval within which the spatial and temporal distributions of the quanta are irrelevant: Hecht et al. flashed a 10' disk for 1 msec, and Sakitt flashed a 29'

disk for 16 msec. These experiments answered the question: what are the fewest quanta that one can detect in a single stimulus?

A different question was answered by an experiment of Denton and Pirenne (1954): what is the dimmest surface that one can see? To test this, they viewed a 45 degree disk for approximately (sic) 5 seconds, binocularly with natural pupils. Their mean threshold (computed on a log scale) was $-6.07 \log \text{cdm}^{-2}$, an increase in sensitivity over that in the experiment of Hecht et al. by 6.23 log units and over that in Sakitt's experiment by nearly 4 log units.

Great as these differences are, a few arithmetic calculations show that they are mutually consistent. Binocular vision may confer an advantage as great as a factor of 2 (Makous, 1990). A factor of 12 was gained through use of the natural pupil (square of the ratio of 7 to 2 mm). By increasing the duration of the stimulus from the 1 and 16 msec durations used by Hecht et al. and Sakitt, respectively, to a duration well beyond the 100 msec limit on temporal integration (Hood and Finkelstein, 1986), Denton and Pirenne gained sensitivity by factors of about 100 and 6, respectively. The analogous increase in size from 10' and 29' to 45 degrees might have gained another a factor of 144 and 8, respectively. That is, no matter where the observer fixated (fixation was not controlled in this experiment), the 45 degree field would have covered retinal eccentricities exceeding 22.4 degrees from the fovea, where spatial summation at absolute threshold is 2 degree or more (Hood and Finkelstein, 1986). Hence, the relative increase in the area over which quanta were summed in Denton and Pirenne's experiment over that in Hecht et al. and Sakitt's would be $(120/10)^2 = 144$ and $(120/29)^2 = 17$, respectively. Finally, the large area and long duration of Denton and Pirenne's stimuli offer the advantage of probability summation over a large number of semi-independent opportunities for detection at different locations in the visual field and at different times; however, no matter how many such opportunities occur, probability summation operates only over the range of intensities covered by the psychometric function, increasing its slope. From the psychometric functions shown by Denton and Pirenne, it seems that the benefits of probability summation amounted to no more than a factor of 2.

Putting these results together, then, one finds that the proportional increase in sensitivity one might expect for the experiment of Denton and Pirenne over that of Hecht et al. is $2 \cdot 12 \cdot 100 \cdot 144 \cdot 2 = 7 \cdot 10^5$, or 5.8 log units, and $2 \cdot 12 \cdot 6 \cdot 17 \cdot 2 = 5 \cdot 10^3$, or 3.7 log units over that of Sakitt. These are within 0.4 and 0.3 log unit of the observed differences and well within the uncertainty of the estimates, so it follows that the thresholds of Denton and Pirenne are mutually consistent with those of Hecht et al. and Sakitt, in spite of the enormous quantitative differences between them.

CONE THRESHOLD By convention, the upper limit of scotopic vision is the lower limit of photopic vision. One can measure this by finding the absolute threshold during the cone plateau of a dark adaptation curve (Stabell and Stabell, 1981), by finding the lowest Troland value at which color discriminations can be made (Walkey et al., 2000), or by finding the lowest Troland value at which the Stiles-Crawford effect shows signs of cone input (cf. the section below on the Stiles-Crawford effect): the three methods yield absolute cone thresholds of 0.2, 0.3, and 0.3 phot Td at the fovea, respectively. The first method shows an approximately linear increase of threshold with eccentricity, on a logarithmic scale, with a 1.8 log unit decrease at 65 degrees temporal. The agreement of the cone plateaus with one another and with the other estimates may be partly fortuitous, for the cone plateaus of different observers, measured under identical conditions, are themselves rather variable (Makous, 1997): the rms standard deviation of 0.59 on a log scale (15 observers in 7 studies). This variability may be related to the high variability of cone density in the central retina, where cone sensitivity tends to be measured: the coefficient of variation (standard deviation over the mean) is 46% at the fovea (Curcio et al., 1990). This is to be compared with 8% to 15% at 10 degrees of eccentricity and beyond. That rod sensitivity varies less across observers (above) than cone sensitivity may be related to the lower variation in receptor density at the sites where their sensitivity typically is measured, which is comparable to that of peripheral cones.

The luminance of white paper under a full moon is about 0.2 cdm^{-2} , or about twice the cone threshold with a 2 mm pupil. Compared to the range of some 12 orders of magnitude spanned by visual sensitivity, and compared to the variability of these two quantities, the upper limit of scotopic vision comes stunningly close to the maximal light level encountered at night under natural conditions.

Nevertheless, under ideal conditions, bright, saturated colors probably should be visible from the light of the moon alone (although I have never seen them myself in 35 years of casual observation). It is perhaps noteworthy that it is possible to read newspaper print at night without difficulty and without awareness of the scotoma caused by the absence of rods in the central fovea. This rod-free area ranges from 0.85 degrees (Ahnelt et al., 1987) to 1.25 degrees (Curcio et al., 1990) anatomically. The central scotoma of an achromat has been reported to be 0.3 degree but it may be smaller than in a trichomat's retina, in which the rods must compete for space with cones. In both cases, the scotoma causes an involuntary shift of fixation from the central fovea to a neighboring region containing rods (Barash et al., 1998).

ROD SATURATION Where cones enter is not where the rods exit. In spite of some interference by the cones in the passage of rod signals to the brain (see Chapter 55), rods continue to contribute to vision well above the cone threshold, up to the level of light that drives them to their maximal output. Any further modulation of light above that level elicits the same response—or at least changes in response that are too small to be detected—so the rod system is blind to such modulation. This condition of maximal output has come to be called *rod saturation*, perhaps by analogy to the saturation of an electronic amplifier. (See also Chapter 54.) Rod saturation corresponds to the maximum signal that the rods can deliver to the proximal nervous system, not necessarily the upper limit to activation of any rod processes. Afterimages have been used to show that saturated rods nevertheless can preserve a record of their history of excitation even while saturated (Sakitt, 1967), and stimuli more intense than those that saturate the rods prolong the period of saturation (Penn and Hagins, 1972); hence the limit lies between the processes that respond to light and those that generate the signal propagated from the rods to the brain.

The range of conditions over which the rods and cones both contribute to vision is called the *mesopic range*; the range where rods do not contribute is called the *photopic range*. Then, as rods continue to respond to variations of stimulation up to the highest luminances available under natural conditions, strict use of this definition limits photopic vision to the central fovea, where rods are absent, and to special conditions arranged in the laboratory.

Even though the rods and cones share the same pathway to the brain, so adroit is the visual system at blending the two signals into a seamless visual experience that the separate contributions of the two systems can be disentangled only by special experimental manipulations (covered in Chapter 55).

As the visual response of the rod system is often described by a function that approaches an asymptotic limit, it might seem difficult to specify a precise luminance, or Troland value, at which saturation occurs, and one might suppose that some other parameter, such as the semisaturation coefficient, might be easier to pin down, but just the opposite is true. Saturation is achieved not by driving the rods to their asymptotic limit, but by driving them close enough to that limit so that any further modulation of output is below threshold. This turns out to be a sharply defined value for a given test stimulus. However, there are two impediments to its measurement: (1) sufficient stimulus intensity is necessary to ensure that the rods have been driven to saturation, and (2) the cone system intrudes by detecting the test stimulus before rod-saturating levels can be reached. The first problem is merely technical, but it has marred several attempts to measure rod saturation. The second problem can be solved by the use of achromatic observers, who lack

functioning cones, but that approach depends on the assumption that rod saturation in a retina lacking cones is the same as rod saturation in a trichromat, an assumption that may not be true.

These technical problems lend impetus to the search for an alternative way of measuring or defining rod saturation, perhaps one based on the entire threshold-versus-intensity function, such as the semisaturation coefficient. However, the low end of that function is dominated by the properties of the proximal rod network, not by the rods themselves, and to separate the contributions of the network from those of the rods requires a theory. Until a consensus on such a theory is reached, it is better to take an empirical approach. In 1982, Adelson ended his paper on rod saturation with the statement “the story on rod saturation and adaptation seems incomplete,” and that story has changed little in 20 years.

Quite aside from these conceptual difficulties, the data simply are not clear. A close reading of the classic paper by Aguilar and Stiles (1954), shows that the statements in the text do not agree with the data they show. Owing to the difficulties discussed in the preceding paragraph, statements about the Troland value at which saturation occurs are difficult to interpret.

However, the *data* from several studies are shown in Figure 53.1. As the test stimuli differ, and as some reports provided only relative thresholds, the curves have been shifted vertically by eye to bring them into coincidence (arbitrarily) at about $1.5 \log \text{Td}$.

Each curve has a region at high background levels at which the thresholds abruptly increase; the background level at which no test flash can be seen, no matter how intense—that is, where the slope approaches unity—is defined as the saturating background. The figure shows that the rods of the achromat, KN (heavy, continuous curve), saturate at a higher retinal illuminance than those of the other observers (Sharpe, 1990). This might be attributed to KN’s lack of cones, for Alexander and Kelly (1984) have reported that excitation of cones moves rod saturation to lower values. This effect of cones could be due to the leakage of cone signals into rods through gap junctions (Schneeweis and Schnapf, 1995): the addition of cone signals to those originating within the rods themselves may well drive the output of the rods to its maximum at lower stimulus intensities than would occur without the contribution from cones. However, this explanation of KN’s data is complicated by the fact that Blakemore and Rushton’s observer (circles) also was an achromat (rod monochromat), and this observer’s rods seem to saturate at lower intensities than any of the other observers (Blakemore and Rushton, 1965), at about the same level as those of the observer of Fuortes et al. (1961), who was “deficient in cone vision.” The four trichromatic observers of Aguilar and Stiles (1954) and that of Adelson (1982) fall in between. The flattening of their curves at the highest background levels is convincingly attributed to detection of the test flash by cones. Where the rods might saturate within this region governed by cone sensitivity is hard to guess. However, the lower end (2000 Td) of the range

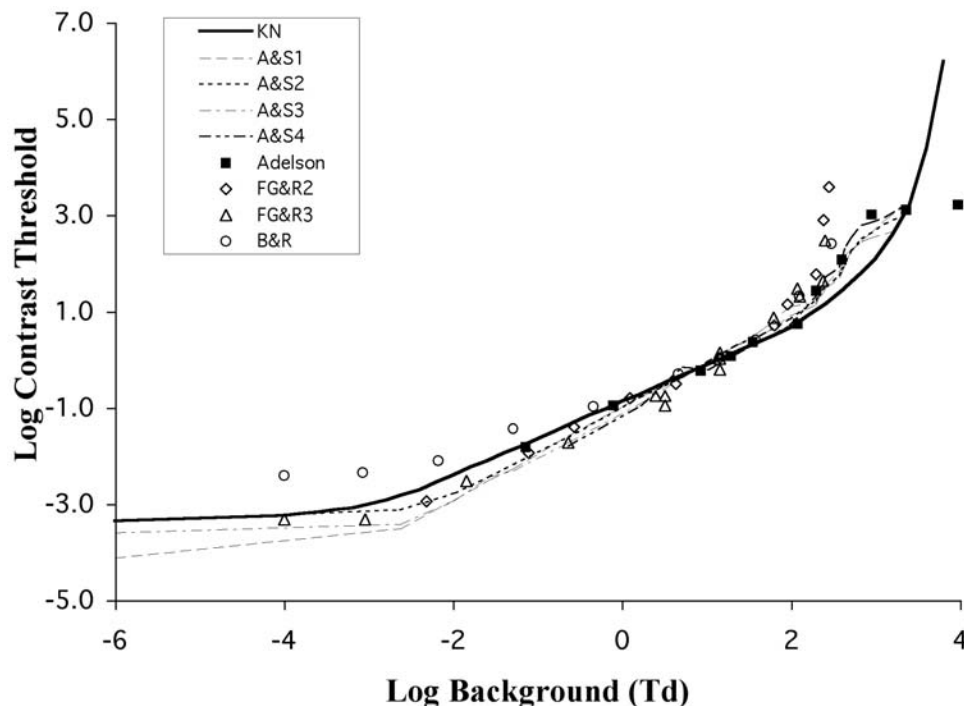


FIGURE 53.1. Rod saturation from six studies.

for rod saturation cited in Aguilar and Stiles's paper and so frequently quoted (2000 to 5000 Td), is simply the highest background value that Aguilar and Stiles tested, well into the cone domain of the data. From these data one can conclude that rod saturation by steady background fields falls somewhere in the range 280 to 6300 Td.

Flashing the background pushes rod saturation to even lower values (Adelson, 1982). This is nevertheless consistent with a site of saturation within the rods, for the flux density of a steady background must be as much as 0.65 log unit greater than that of a flashed background to produce the same membrane current in the outer segment of a human rod (Kraft et al., 1993), and the voltage response in the inner segment, which drives the neurotransmitter release at the rod synapse, shows a large transient, or *nose*, at stimulus onset (Schneeweis and Schnapf, 1995) that pushes saturation to even lower values.

Adaptation

The main features of adaptation are covered by Reeves (Chapter 54) and the adaptation of receptors by Burns and Lamb (Chapter 16). However, some properties of adaptation specific to the human scotopic system and not covered in those chapters deserve comment here.

Most important, primate rods do not adapt in the sense of changing their gain. This is perhaps because no such adaptation is required, for over the entire range of scotopic vision, no rod is activated by more than a single quantum within the time during which it sums signals (discounting the effects of random fluctuations). That is, at 0.3 Td, the upper limit of scotopic vision (see above), the mean rate of quantum activations per rod is about 3/sec (from Table 53.2). As the interval between quantal activations (one-third of a second) is comparable to the integration time of primate rods (Schneeweis and Schnapf, 1995), this is the minimum signal that can be delivered to a rod. Hence, adaptation would confer no benefits on the rods under scotopic conditions.

Rushton (1963) showed that the adaptive changes that occur within the retina must occur proximal to the rods themselves, at a site he dubbed the *adaptation pool*, where the signals from many rods converge. Some such mechanism is required to avoid saturation of the cells on which the rod signals converge, and the best place to do that is at the site of convergence itself. This convergence follows from the presence of some 90 million rods in a human eye (Curio et al., 1990), with only about 1.25 million optic nerve fibers to carry their signals to the brain (Rodieck, 1998, p. 256). The actual amount of convergence, or size of the pools, is no doubt greater than the ratio of these two numbers, but it has proved difficult to measure psychophysically (Andrews and Butcher, 1971; Barlow and Andrews, 1973; Makous, 1997).

That little of the adaptation observed is attributable to the rods follows from the observation (Rushton, 1965b) that quanta from a background light that hit no more than 1% of the rods raise the threshold by 300%. If the quanta completely inactivated every rod they hit, the background would raise thresholds by no more than 1%, not the 300% actually observed.

Primate rods differ fundamentally, in both size and function, from those of the cold-blooded vertebrates that have been most extensively studied. Depending on the species, such a rod is 6 to 11 μm in diameter (Pugh and Lamb, 1993), compared to 2 μm for a human rod (Young, 1971). This means that the rate of quantal absorptions at a given light level is 9 to 30 times greater for the rod of a cold-blooded animal than for a human rod, but its semisaturation constant is about five to six times lower (Fain et al., 2001) (i.e., 5 to 10 as opposed to 30 to 50 quanta/sec). Hence, it takes a luminance 45 to 180 times lower to saturate an amphibian rod than a primate rod, so amphibian rods require protection against saturation that primates can do without.

Spatial sensitivity

The spatial aspects of scotopic vision were superbly reviewed and discussed by Hess (1990), to which the reader is referred. Here it seems necessary only to reproduce, in Figure 53.2, the scotopic contrast sensitivity curves measured 10 degrees in the temporal retina by D'Zmura and Lennie (1986). The corresponding photopic curves are also shown to ease comparison of the two sensitivities under comparable conditions.

Scotopic contrast sensitivity shows a modest but clear drop from a maximum of 50 as spatial frequency drops below 1 c/deg. The spatial antagonism this represents is comparable in magnitude to that observed in the cone system under comparable conditions. As the two share the same neural pathway beginning with the ganglion cells (see Chapter 17), they share any mechanisms producing spatial antagonism within the shared pathway. As these effects are of similar magnitude, any mechanisms serving spatial antagonism where the rod and cone pathways are separate must have equal effects.

Figure 53.2 also shows that scotopic grating acuity is, at best, about 6 c/deg in normal trichromats, which compares well with 7 c/deg in an achromat (Hess and Nordby, 1986). The low cutoff presumably reflects an adaptation of the rod system to the low signal-to-noise ratio in small areas of the retinal image; that is, the rod system improves the signal-to-noise ratio by averaging the signal and noise over larger retinal areas than the cone system, and as the noise in different receptors tends to be independent and the signal correlated, such averaging increases the signal-to-noise ratio in the elements that perform the averaging (see Chapter 51).

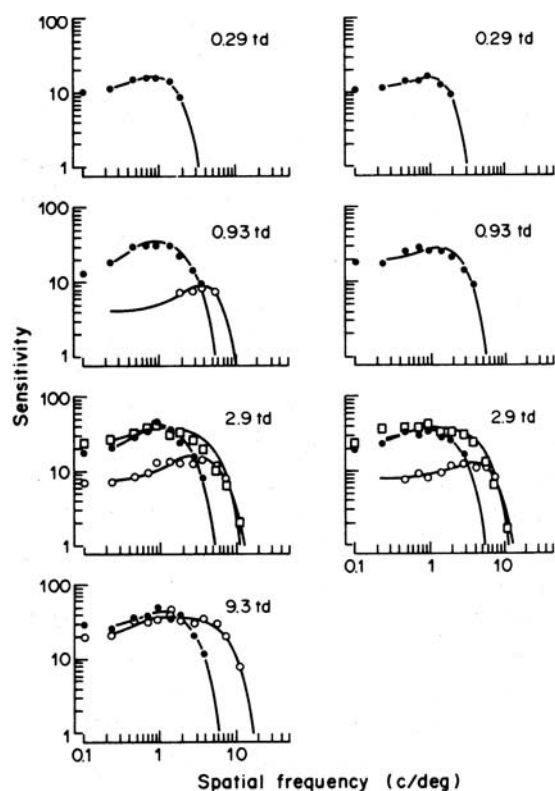


FIGURE 53.2. Scotopic (black circles) and photopic (white circles) contrast sensitivity. The squares are measured with achromatic gratings.

Vernier acuity, which depends more upon cortical processing than grating acuity does, is about 10 times greater than grating acuity in both scotopic and photopic vision when measured under comparable conditions, reaching a maximum in scotopic vision of 1.5 arc minutes for three observers (Livingstone and Hubel, 1994). This presumably also reflects the common cortical processing that signals from the two systems must share, but it shows that the greater low-pass filtering by the rod pathway has no differential effect on Vernier acuity relative to grating acuity.

Temporal sensitivity

Unlike the spectral and spatial properties of the scotopic system, its temporal properties show an unexpected complexity: there are at least two pathways through the retina, a fast and a slow one, and perhaps a third, relatively insensitive one (see also Chapter 17). These produce different contrast sensitivity functions (CSFs), a discontinuity in the function expressing the dependence of temporal resolution on luminance, and mutual cancellation of their respective signals. As rod signals have been observed in primate cones (Schneeweis and Schnapf, 1995), the fast pathway is likely to be through the retinal network serving the cones (Sharpe and Stockman, 1999; Stockman et al., 1995).

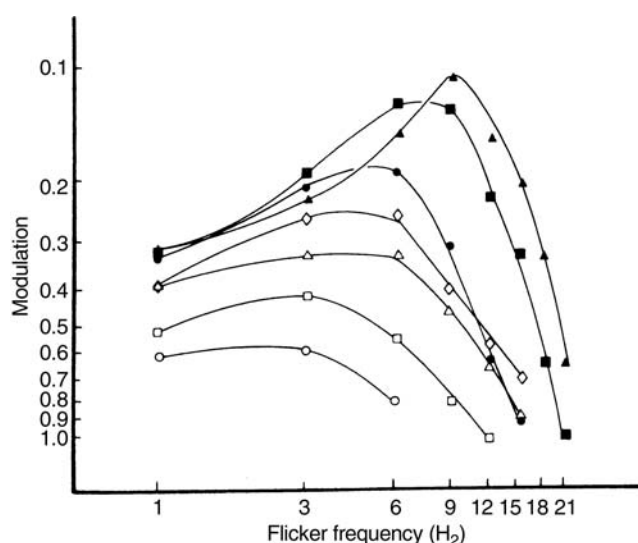


FIGURE 53.3. Scotopic contrast sensitivity at different mean levels. White symbols, scotopic; black symbols, photopic. The mean illuminances increase in log unit steps from 0.00025 to 21.4 scot. Td, and the highest value is 45.7 scot. Td.

CONTRAST SENSITIVITY Figure 53.3 shows the temporal CSFs over the scotopic range of intensity, including those passing through both the slow and the fast pathways (Conner, 1982), and three photopic curves. The bandpass shape of the curves observed above 3.7 scot. Td here and elsewhere (Sharpe et al., 1989) corresponds to a biphasic impulse response characteristic of the fast (cone) pathway; and the low-pass shape of the curves observed below that value corresponds to a monophasic impulse response characteristic of the slow (rod) pathway. This change, between a monophasic and a biphasic impulse response, takes about 1 second (Takeuchi et al., 2001), even though *sensitivity* can change between scotopic and photopic levels in less than 100 msec (Crawford, 1947). Note that wherever curves cross, raising the light level causes a paradoxical decrease in sensitivity at certain frequencies.

One consequence of the attenuation of high temporal frequencies relative to that of the photopic system is that perceived motion is slower when the motion stimulates only rods than when only cones are stimulated under otherwise identical conditions (Gegenfurtner et al., 2000).

MAXIMAL FREQUENCY The maximal frequency of the temporal CSF, otherwise known as the *critical flicker frequency*, at varying Troland values is shown in Figure 53.4 (Hess and Nordby, 1986).

The maximum for the rod pathway itself is about 15 Hz, as reported in the classic paper on the topic by Hecht and Shlaer (1936), but the fast pathway responds up to 26 Hz, both in the achromat, as shown here, and in the trichromat (Conner, 1982). That Hecht and Shlaer's data show no sign

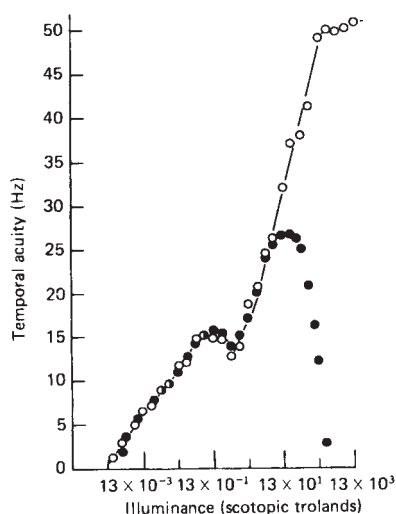


FIGURE 53.4. Critical flicker frequency in an achromat (*white symbols*) and a trichomat (*black symbols*).

of the fast pathway reflects the fact that its contribution is masked by the cone response unless special methods are used to make it visible, such as use of a long-wave background and the Stiles-Crawford effect. Nevertheless, under mesopic conditions, rod signals presumably mix with signals originating within the cones and pass together with the cone signals through the cone pathway.

As shown in Figure 53.4, even the signals from rods that pass through the cone pathway are limited to lower frequencies than those from the cones, owing presumably to limits within the rods themselves. These limits, within the rod pathway and within the rods themselves, are likely to serve a function in temporal vision analogous to that in spatial vision (discussed above), which improves the signal-to-noise ratio by limiting the frequencies passed by the rod system at low luminances.

CANCELLATION If the two pathways take different amounts of time to reach the same ganglion cells, then they should arrive out of phase with respect to one another at some temporal frequency and so interfere with or cancel one another. Such cancellation does occur at 15 Hz (Conner, 1982; Sharpe et al., 1989): as the amplitude (and mean luminance) of 15 Hz flicker increase above threshold, the flicker first becomes noticeable and then increases in apparent amplitude; but as the amplitude increases further, the apparent flicker amplitude diminishes and ultimately disappears, and finally it reappears as the amplitude increases even further. Thus, there is a dead zone, or range of amplitudes, within which the flicker is not visible. This dead zone is scotopic, for the threshold for detecting flicker during the cone plateau of a dark adaptation curve lies well above it. Changes in the phase of the rod flicker response can be measured by observ-

ing its interference with cone flicker of fixed phase; this technique confirms that the phase lag required for cancellation occurs when the frequency is 15 Hz (Sharpe et al., 1989). Such cancellation is perhaps the strongest evidence for the dual pathway, for an alternative explanation of the dead zone is difficult to summon.

A THIRD PATHWAY Evidence for a third pathway for rod signals through the retina has recently been summarized by Sharpe and Stockman (1999). This pathway is via direct contacts between rods and off-bipolar cells, but it has been observed only in rodents (so far) and may be one of several peculiarities of their eyes.

Central processing

As has been mentioned several times above, the rods and cones share the same pathway to the brain (see Chapter 17). Consequently, they share the same cortical mechanisms. However, the cortex and afferent pathways contain filters that might block passage of rod signals, excluding rod signals from certain kinds of processing. Such filters include high-pass spatial and temporal filters and those filters that pass only opponent color signals.

Among those mechanisms that in fact are shared by both rod and cone signals, for example, are the opponent motion channels (Gegenfurtner et al., 2000) and motion processing in general (van de Grind et al., 2000), as well as the three temporal frequency channels (Hess et al., 1996). However, the increasing attenuation of high frequencies as luminance decreases eventually leaves mechanisms selective for the highest speeds (van de Grind et al., 2000) and highest temporal frequencies (Takeuchi and De Valois, 2000) unexcited, shifts the response curves of the remaining mechanisms to lower frequencies, and decreases the apparent speed of moving objects.

Another consequence of the shared pathway is that one cannot distinguish a grating that stimulates only rods from one that stimulates only cones once differences in apparent contrast are eliminated (D'Zmura and Lennie, 1986); that is, the signals are indistinguishable once they reach the common pathway. An exception, widely appreciated among those who have done experiments on dark adaptation with small, brief test flashes, is that one can identify the rod-cone break on the basis of the appearance of the flashes: they change suddenly from small, sharply defined stimuli that are clearly seen or not to larger, diffuse stimuli, the presence of which is often much more uncertain. However, this difference in appearance presumably is due to attenuation by the rod system of the high spatial frequencies in the small spots, before the signals reach the common pathway, and so no separate central pathway need be invoked.

Much of the research on scotopic vision in the past decade concerns changes over time at opposite ends of the life span.

INFANTS In the same year that *Night Vision* was published, Brown (1990) wrote a comprehensive review of the development of visual sensitivity in infants, to which the reader is referred for work published before 1990. She reported that absolute threshold and contrast sensitivity begin 1.5 to 3 log units lower than adult levels but approach adult levels by 6 months, much earlier than photopic vision. However, quantitative comparisons between adults and younger infants on both measures are complicated by other differences, such as the extent of spatial and temporal integration. The spatial scale of scotopic vision of 10-week-olds in the presence of adapting backgrounds is four times that of the adult, as measured by spatial summation (Hansen et al., 1992) and by spatial sensitization, that is, center-surround organization (Hansen and Fulton, 1994); and full temporal summation in 10-week-olds extends to 1 second, the longest durations tested (Fulton et al., 1991).

If one describes the progress of development by means of the logistic growth curve (formally identical to the Nakaguchi-Rushton curve, well known among vision scientists), then the age at half height (the semisaturation constant) for the sensitivity and maximal response of both the scotopic electroretinographic (ERG) a-wave and b-wave and for psychophysically measured scotopic sensitivity in the periphery of the visual field (30 degrees), all cluster around 10 weeks (Fulton and Hansen, 2000). Parafoveal sensitivity (10 degrees) lags by about 10 weeks, corresponding to the delay in retinal development.

One way in which 3-month-old infants and adults are nearly identical is in the transition from scotopic to photopic vision with increasing luminance, as measured by the eye movements elicited by moving gratings (Chien et al., 2000).

AGING That scotopic sensitivity diminishes with aging is universally accepted. The causes of the decline are less certain. Part is due to a 12% mean reduction in pupil area per decade (Birren et al., 1950; Lowenstein and Lowenstein, 1969) and to an increase in the optical density of the lens at short wavelengths: a mean of 0.20 density unit per decade of life, increasing after age 60 to 0.67 density unit per decade; however, there are enormous individual differences among persons of the same age, amounting to as much as a factor of 10 (Pokorny et al., 1987). In addition to these factors, the scotopic system itself loses sensitivity. Jackson and Owsley (2000) report a mean rate of loss of 20% per decade, twice as fast as they observed in the cone system. This may correspond to the finding that the human retina

loses some 34,000 rods per year, while no cone loss has yet been detected. The rate at which sensitivity is lost does not depend on retinal location or age (from the 20s to the 80s) but does depend on spatial frequency (Scheffrin et al., 1999), being more than twice as fast (13% to 14% per decade) at low spatial frequencies ($= 1.2 \text{ c/deg}$) as at higher spatial frequencies (1.8 and 2.4 c/deg). Why the rates differ between studies is not known, but as the rate does depend on stimulus properties, perhaps the difference has to do with differences in the stimuli or the background luminances used ($-0.85 \log \text{ scot. Td}$ for Scheffrin et al. and unspecified by Jackson and Owsley). Although the change of absolute threshold does depend on spatial frequency, there is also an increase of increment threshold (against a background of $-3.29 \log \text{ scot. Td}$) that is independent of the size (spatial frequency) of the test spot over the range of diameters, 0.4 to 4.6 degrees (Scheffrin et al., 1998).

The area over which light is summed to reach threshold, that is, *Ricco's area*, increases 15% per decade (Scheffrin et al., 1998), so that it follows a U-shaped function—well, perhaps a backward-J-shaped function—over the entire life span, from four times that of a young adult at 10 weeks, to twice that of a young adult at 75 years (Hansen et al., 1992). The spatial frequency specific effects described in the preceding paragraph exclude an explanation based on a preferential loss of sensitivity to high spatial frequencies and leave only neural reorganization as an explanation for the change in spatial summation.

Dark adaptation also changes with aging. The time constant of scotopic dark adaptation, exponential on semilogarithmic coordinates, increases 20.4 sec/decade (Jackson et al., 1999), and these rate changes are unrelated to asymptotic sensitivity, that is, to the absolute threshold (Jackson and Owsley, 2000).

The quantitative effects of aging on rates of sensitivity change are cited here with a caution against overinterpretation, for the values depend on stimulus conditions.

There is an intrinsic problem in understanding the effects of aging on any form of visual sensitivity. One would like to separate the visual effects of specific pathologies, such as age-related maculopathy (ARM) and glaucoma, from the natural processes of aging that are independent of disease, such as the changing mean pupillary aperture. Many diseases of the eye that compromise vision are incurable, so their incidence must increase with age. In a recent study of patients 65 to 79 years old who were given a comprehensive eye exam and declared by the eye care specialist performing the exam to be free of any disease that might affect their vision, 60% were found to have early signs of ARM (Jackson et al., 1998). Some diseases can degrade visual performance in careful laboratory tests long before they can be detected clinically. For example, some 25% to 35% of the ganglion cells have been lost before the loss is clinically detectable

(Kerrigan-Baumrind et al., 2000). Hence, there is no way to ensure that the subjects in an aging population are free of disease, and certainly some proportion of them have early forms of disease that affect their test performance and depress the average scores without being diagnosed. The question is, what proportion they are, how much of the age-related loss they account for, and if there is any such loss that cannot be attributed to incipient disease. Curcio et al. (1993) argue that the photoreceptor losses with increasing age cannot be attributed to ARM, at least, for the disease affects rods and cones equally, but the photoreceptor loss is predominantly rods.

Even longitudinal studies are affected by this conundrum, for there is an endpoint to the data on each individual, and it is difficult to determine whether any preceding decline of visual function is due to disease that had not yet progressed to the clinically detectable stage by the time of death.

If there is no loss of sensitivity except from disease, and if there are some individuals at any given age who are free of any such disease, and if the incidence and severity of the disease increase with the age of the cohort (as it must), then the variance of sensitivity within the population should increase. No such increase in variance has been established. The absence of such evidence leaves open the possibility that all neural losses of sensitivity associated with aging reflect pathological processes, not the natural processes of aging in the absence of pathology.

Some unresolved issues

STILES-CRAWFORD EFFECT Figure 53.5 shows the relative sensitivity to light entering the eye at varying distances from the center of the pupil (Crawford, 1937), that is, the Stiles-Crawford effect. The different curves represent sensitivity at varying background luminances. Sensitivity, of course, is greatest when the backgrounds are dimmest. The black symbols are assumed to represent the sensitivity of the rod system and the white symbols the sensitivity of the cone system. (These curves were measured 5 degrees from the fovea with 50 msec flashes of a 0.46 degree disk.)

Note the near absence of a Stiles-Crawford effect at the lowest (scotopic) luminances. This has been confirmed by many others, as summarized by Enoch and Lakshminarayanan (1991); however, the light to which rods are sensitive is absorbed by the lens, which varies in thickness with pupillary eccentricity. When this is taken into account, the rods do show a Stiles-Crawford effect, although clearly much smaller than that of the cones (Alpern et al., 1983; Sharpe and Nordby, 1990).

The reason for the diminished Stiles-Crawford effect in rods is unknown. It may relate at least partially to a difference in the size and shape of rods as opposed to cones. However, as fovea cones have about the same size and shape

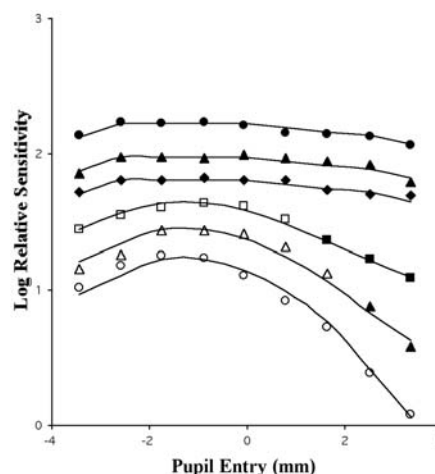


FIGURE 53.5. Stiles-Crawford effect at varying Troland values. Background luminances are, from the top: 0, 0.000060, 0.00107, 0.0102, 0.096, and 22 cdm^{-2} .

as rods, the foveal Stiles-Crawford effect should be about the same as that of the rods. The foveal Stiles-Crawford effect does seem to be shallower than it is in the parafovea (Westheimer, 1967), and there is some evidence that this might be as shallow as the rod's Stiles-Crawford effect if the foveal Stiles-Crawford effect is tested with small enough spots and if changes in the test spots caused by varying pupil entry are avoided by varying the entry position of the background light instead of that of the light in the test spot (Starr et al., 1979).

Another possible reason for the difference between rod and cone Stiles-Crawford effects is that the cones, and not rods, are sheathed by processes derived from pigment epithelial cells (Blanks et al., 1988). The refractive indices of these sheaths may differ from the rest of the intercellular space between the receptors and so cause differences between the waveguide properties of the rods and cones. In any case, the reason for the differences between the Stiles-Crawford effects of rods and cones remains unknown.

A related phenomenon that is not understood is the progressive changes in the shapes of the curves in Figure 53.5. Changes in sensitivity caused by a change in the pathway of the light through the pupil must depend on the properties of either the rods or the cones or on a combination of the two. A widely held assumption is that in threshold experiments, the threshold is determined by the most sensitive mechanism excited by the test stimulus or, in this case, the more sensitive mechanism, the overall sensitivity curve representing the envelope of the sensitivities of the participating mechanisms. In Figure 53.5, the top curve (measured in complete darkness), is taken as representing the rod Stiles-Crawford effect and the bottom curve (measured on a background of 69 cdm^{-2}) as representing the cone Stiles-Crawford effect. However, any such envelope

must have a discontinuity—or *kink*, in Rushtonian terms—where the two curves intersect. No such kink is visible in any of these curves.

Often when two mechanisms are nearly equally sensitive, the overall sensitivity of the observer is determined by summation of the probabilities of detection by each of the two mechanisms (Pirenne, 1943; Tyler and Chen, 2000). This tends to smooth out the discontinuity where the sensitivity profiles of the two mechanisms intersect, as can be seen at the rod-cone breaks of many dark adaptation curves (Hecht et al., 1937; Makous et al., 1976). However, such summation is restricted to the range of test intensities spanned by the psychometric function, and such summation drops rapidly with a drop in the probability of detection by either mechanism. These considerations render probability summation an unsatisfactory explanation of the deviations of the data in Figure 53.5 from the envelopes of the underlying curves. Take, for example, the white triangle at a pupil entry of 0.8 mm: it lies too high by 0.30 unit on the log axis, and the sensitivity of the rods is about 0.62 unit below that of the cones. If one describes the psychometric function as Gaussian on a log scale, then changing the threshold by 0.3 unit through probability summation requires a standard deviation (of the psychometric function) greater than 1 log unit, more than 10 times what is typical (Makous, 1990).

To describe these data, full, algebraic summation of the signals from rods and cones is required. The curves passing through the data represent the sums of rod and cone sensitivities: the assumed rod sensitivity is the mean of the top three curves, and the shape of the assumed cone sensitivity adjusted to minimize the squared deviation from the bottom three curves. The ratio of cone to rod signals at the respective maxima of the two curves (12:1 for the squares and 40:1 for the triangles) likewise has been adjusted to minimize the residual error.

DUAL RETINAL PATHWAYS Presumably the signals from rods follow dual pathways through the retina in all experiments, whether temporal, spatial, or any other variables are under study. The fact that they have been detected in temporal and not in spatial experiments may be due to the fact that the rod pathway does not pass all the signals issuing from the rods themselves, but the cone pathway does, and so the difference between pathways is more evident than it is in spatial experiments, where the filtering performed by the syncytium of rod gap junctions may more nearly match the passband of the afferent pathway (Savage and Banks, 1992). If the spatial signal originating in the rod matrix passes through both pathways without further filtering in either one, the signals arriving at the ganglion cell layer will be identical, and those passing through separate pathways will be difficult to disentangle experimentally.

Acknowledgments

This work was supported by U.S. Public Health Service Grants EY-4885 and EY-1319. I thank Steven L. Buck, John S. Werner, Adam Reeves, and an anonymous reviewer for valuable comments on an earlier version of this chapter, and I especially thank Jean-Pierre Raynauld for pointing out the errors in the original versions of Tables 53.1 and 53.2.

REFERENCES

- Adelson, E. H., 1982. Saturation and adaptation in the rod system, *Vis. Res.*, 22:1299–1312.
- Aguilar, M., and W. S. Stiles, 1954. Saturation of the rod mechanism of the retina at high levels of stimulation, *Optica Acta*, 1:59–65.
- Ahnelt, P. K., H. Kolb, and R. Pflug, 1987. Identification of a subtype of cone photoreceptor, likely to be blue sensitive, in the human retina, *J. Comp. Neurol.*, 255:18–34.
- Alexander, K. R., and S. A. Kelly, 1984. The influence of cones on rod saturation with flashed backgrounds. *Vis. Res.*, 24:507–511.
- Alpern, M., C. C. Ching, and K. Kitahara, 1983. The directional sensitivity of retinal rods, *J. Physiol. (Lond.)*, 343:577–592.
- Andrews, D. P., and A. K. Butcher, 1971. Rod threshold and patterned rhodopsin bleaching: The pigment epithelium as an adaptation pool, *Vis. Res.*, 11:761–785.
- Barash, S., A. Melikyan, A. Sivakov, and M. Tauber, 1998. Shift of visual fixation dependent on background illumination, *J. Neurophysiol.*, 79:2766–2781.
- Barlow, H. B., 1956. Retinal noise and absolute threshold, *J. Opt. Soc. Am.*, 46:634–639.
- Barlow, H. B., and D. P. Andrews, 1973. The site at which rhodopsin bleaching raises the scotopic threshold, *Vis. Res.*, 13:903–908.
- Baylor, D. A., B. J. Nunn, and J. L. Schnapf, 1984. The photocurrent, noise and spectral sensitivity of rods of the monkey *Macaca fascicularis*, *J. Physiol. (Lond.)*, 357:575–607.
- Birren, J. E., R. C. Casperson, and J. Botwinick, 1950. Age changes in pupil size, *J. Gerontol.*, 5:2216–2221.
- Blakemore, C. B., and W. A. H. Rushton, 1965. Dark adaptation and increment threshold in a rod monochromat, *J. Physiol. (Lond.)*, 181:612–628.
- Blanks, J. C., G. S. Hageman, L. V. Johnson, and C. Spee, 1988. Ultrastructural visualization of primate cone photoreceptor matrix sheaths, *J. Comp. Neurol.*, 270(2):288–300.
- Brown, A. M., 1990. Development of visual sensitivity to light and color vision in human infants: a critical review, *Vis. Res.*, 30:1159–1188.
- Chien, S. H.-L., D. Y. Teller, and J. Palmer, 2000. The transition from scotopic to photopic vision in 3-month-old infants and adults: an evaluation of the rod dominance hypothesis, *Vis. Res.*, 40:3853–3871.
- Conner, J. D., 1982. The temporal properties of rod vision, *J. Physiol. (Lond.)*, 332:139–155.
- Crawford, B. H., 1937. The luminous efficiency of light entering the eye pupil at different points and its relation to brightness threshold measurements, *Proc. R. Soc. Lond.*, 124B:81–96.
- Crawford, B. H., 1947. Visual adaptation in relation to brief conditioning stimuli, *Proc. R. Soc. Lond.*, 134B:283–300.
- Curcio, C. A., C. L. Millican, K. A. Allen, and R. E. Kalina, 1993. Aging of the human photoreceptor mosaic: evidence for

- selective vulnerability of rods in central retina. *Invest. Ophthalmol. Vis. Sci.*, 34:3278–3296.
- Curcio, C. A., K. R. Sloan, R. E. Kalina, and A. E. Hendrickson, 1990. Human photoreceptor topography, *J. Comp. Neurol.*, 292:497–523.
- Denton, E. J., and M. H. Pirenne, 1954. The absolute sensitivity and functional stability of the human eye, *J. Physiol. (Lond.)*, 123:417–442.
- D'Zmura, M., and P. Lennie, 1986. Shared pathways for rod and cone vision, *Vis. Res.*, 26:1273–1280.
- Enoch, J. M., and V. Lakshminarayanan, 1991. Retinal fibre optics, in *Visual Optics and Instrumentation* (W. N. Charman, ed.), Boca Raton, FL: CRC Press, pp. 280–309.
- Fain, G. L., H. R. Matthews, M. C. Cornwall, and Y. Koutalos, 2001. Adaptation in vertebrate photoreceptors, *Physiol. Rev.*, 81:117–151.
- Fulton, A. B., and R. M. Hansen, 2000. The development of scotopic sensitivity, *Invest. Ophthalmol. Vis. Sci.*, 41:1588–1596.
- Fulton, A. B., R. M. Hansen, Y. L. Yeh, and C. W. Tyler, 1991. Temporal summation in dark-adapted 10-week old infants. *Vis. Res.*, 31:1259–1269.
- Fuortes, M. G. F., R. D. Gunkel, and W. A. H. Rushton, 1961. Increment thresholds in a subject deficient in cone vision, *J. Physiol. (Lond.)*, 156:179–192.
- Gegenfurtner, K. R., H. M. Mayser, and L. T. Sharpe, 2000. Motion perception at scotopic light levels, *J. Opt. Soc. Am. A*, 17:1505–1515.
- Griswold, M. S., and W. S. Stark, 1992. Scotopic spectral sensitivity of phakic and aphakic observers extending into the near ultraviolet, *Vis. Res.*, 32:1739–1743.
- Hansen, R. M., and A. B. Fulton, 1994. Scotopic center surround organization in 10-week-old infants, *Vis. Res.*, 34:621–624.
- Hansen, R. M., R. D. Hamer, and A. B. Fulton, 1992. The effect of light adaptation on scotopic spatial summation in 10-week-old infants, *Vis. Res.*, 32:387–392.
- Hecht, S., C. Haig, and A. M. Chase, 1937. The influence of light adaptation on subsequent dark adaptation of the eye, *J. Gen. Physiol.*, 20:831–850.
- Hecht, S., and S. Shlaer, 1936. Intermittent stimulation by light. V. The relation between intensity and critical flicker frequency for different parts of the spectrum, *J. Gen. Physiol.*, 19:965–977.
- Hecht, S., S. Shlaer, and M. H. Pirenne, 1942. Energy, quanta, and vision, *J. Gen. Physiol.*, 25:819–840.
- Hess, R. F., 1990. Rod-mediated vision: role of post-receptoral filters, in *Night Vision: Basic, Clinical and Applied Aspects* (R. F. Hess and K. Nordby, eds.), Cambridge: Cambridge University Press, pp. 3–48.
- Hess, R. F., and K. Nordby, 1986. Spatial and temporal limits of vision in the achromat, *J. Physiol. (Lond.)*, 371:365–385.
- Hess, R. F., L. T. Sharpe, and K. Nordby, eds., 1990. *Night Vision: Basic, Clinical and Applied Aspects*, Cambridge: Cambridge University Press.
- Hess, R. F., S. J. Waugh, and K. Nordby, 1996. Rod temporal channels, *Vis. Res.*, 36:613–619.
- Hood, D. C., and M. A. Finkelstein, 1986. Sensitivity to light, in *Handbook of Perception and Human Performance*, vol. 1 (K. R. Boff, L. Kaufman, and J. P. Thomas, eds.), New York: Wiley, pp. 5–1 to 5–66.
- Jackson, G. R., and C. Owsley, 2000. Scotopic sensitivity during adulthood, *Vis. Res.*, 40:2467–2473.
- Jackson, G. R., C. Owsley, E. P. Cordle, and C. D. Finley, 1998. Aging and scotopic sensitivity, *Vis. Res.*, 38:3655–3662.
- Jackson, G. R., C. Owsley, and G. McGwin, 1999. Aging and dark adaptation, *Vis. Res.*, 39:3975–3982.
- Kerrigan-Baumrind, L. A., H. A. Quigley, M. E. Pease, D. F. Kerrigan, and R. S. Mitchell, 2000. Number of ganglion cells in glaucoma eyes compared with threshold visual field tests in the same persons. *Invest. Ophthalmol. Vis. Sci.*, 41:741–748.
- Kraft, T. W., D. M. Schneeweis, and J. L. Schnapf, 1993. Visual transduction in human rod photoreceptors, *J. Physiol. (Lond.)*, 464:747–765.
- Livingstone, M. S., and D. H. Hubel, 1994. Stereopsis and positional acuity under dark adaptation, *Vis. Res.*, 34:799–802.
- Lowenstein, O., and I. E. Lowenstein, 1969. The pupil, in *Muscular Mechanisms*, 2nd. ed., vol. 3 (H. Davson, ed.), New York: Academic Press, pp. 255–337.
- Makous, W., 1990. Absolute sensitivity, in *Night Vision: Basic, Clinical and Applied Aspects* (R. F. Hess and K. Nordby, eds.), Cambridge: Cambridge University Press, pp. 146–176.
- Makous, W. L., 1997. Fourier models and the loci of adaptation, *J. Opt. Soc. Am. A*, 14:2323–2345.
- Makous, W., D. Teller, and R. Boothe, 1976. Binocular interaction in the dark, *Vis. Res.*, 16:473–476.
- Penn, R. D., and W. A. Hagins, 1972. Kinetics of the photocurrent of retinal rods, *Biophys. J.*, 12:1073–1094.
- Pirenne, M. H., 1943. Binocular and unocular threshold of vision, *Nature*, 152:698–699.
- Pokorny, J., V. C. Smith, and M. Lutze, 1987. Aging of the human lens, *Appl. Opt.*, 26:1437–1440.
- Pugh, E. N., Jr., and T. D. Lamb, 1993. Amplification and kinetics of the activation steps in phototransduction, *Biochim. Biophys. Acta*, 1141:111–149.
- Rodieck, R. W., 1998. *The First steps in Seeing*. Sunderland, MA: Sinauer Associates.
- Rushton, W. A. H., 1963. Increment threshold and dark adaptation. *J. Opt. Soc. Am.*, 53:104–109.
- Rushton, W. A. H., 1965. The sensitivity of rods under illumination. *J. Physiol. (Lond.)*, 178:141–160.
- Rushton, W. A. H., 1972. Visual pigments in man, in *Photochemistry of Vision*, vol. VII/1 (H. J. A. Dartnall, ed.), New York: Springer, pp. 364–394.
- Sakitt, B., 1972. Counting every quantum, *J. Physiol. (Lond.)*, 223:131–150.
- Sakitt, B., 1976. Psychophysical correlates of photoreceptor activity, *Vis. Res.*, 17:129–140.
- Savage, G. L., and M. S. Banks, 1992. Scotopic visual efficiency: constraints by optics, receptor properties, and rod pooling, *Vis. Res.*, 32:645–656.
- Schefrin, B. E., M. L. Bieber, R. McLean, and J. S. Werner, 1998. The area of complete scotopic spatial summation enlarges with age, *J. Opt. Soc. Am. A—Opt. Image Sci. Vis.*, 15:340–348.
- Schefrin, B. E., S. J. Tregear, L. O. Harvey, Jr., and J. S. Werner, 1999. Senescent changes in scotopic contrast sensitivity, *Vis. Res.*, 39:3728–3736.
- Schneeweis, D. M., and J. L. Schnapf, 1995. Photovoltage of rods and cones in the macaque retina, *Science*, 268:1053–1056.
- Sharpe, L. T., 1990. The light-adaptation of the human rod visual system, in *Night Vision: Basic, Clinical and Applied Aspects* (R. F. Hess and K. Nordby, eds.), Cambridge: Cambridge University Press, pp. 49–124.
- Sharpe, L. T., and K. Nordby, 1990. The photoreceptors in the achromat, in *Night Vision: Basic, Clinical and Applied Aspects* (R. F. Hess and K. Nordby, eds.), Cambridge: Cambridge University Press, pp. 335–389.

- Sharpe, L. T., and A. Stockman, 1999. Rod pathways: the importance of seeing nothing, *Trends Neurosci.*, 22:497–504.
- Sharpe, L. T., A. Stockman, and D. I. A. MacLeod, 1989. Rod flicker perception: scotopic duality, phase lags and destructive interference, *Vis. Res.*, 29:1539–1559.
- Stabell, B., and U. Stabell, 1981. Absolute spectral sensitivity at different eccentricities, *J. Opt. Soc.*, 71:836–840.
- Starr, S. J., F. W. Fitzke, and R. W. Massof, 1979. The Stiles-Crawford effect in the central fovea, *Invest. Ophthalmol. Vis. Sci.*, 18(Suppl.):172.
- Stockman, A., L. T. Sharpe, K. Rüther, and K. Nordby, 1995. Two signals in the human rod visual system: a model based on electrophysiological data, *Vis. Neurosci.*, 12:951–970.
- Takeuchi, T., and K. K. De Valois, 2000. Velocity discrimination in scotopic vision, *Vis. Res.*, 40:2011–2024.
- Takeuchi, T., K. K. De Valois, and I. Motoyoshi, 2001. Light adaptation in motion direction judgments, *J. Opt. Soc. Am. A*, 18:755–764.
- Tyler, C. W., and C.-C. Chen, 2000. Signal detection theory in the 2afc paradigm: attention, channel uncertainty and probability summation, *Vis. Res.*, 40:3121–3144.
- van de Grind, W. A., J. J. Koenderink, and A. J. van Doorn, 2000. Motion detection from photopic to low scotopic luminance levels, *Vis. Res.*, 40:187–199.
- Walkey, H. C., J. L. Barbur, J. A. Harlow, and W. Makous, 2000. Chromatic sensitivity in the mesopic range, in *Proceedings: Colour and Visual Scales 2000*, Teddington, Middlesex, UK.: National Physical Laboratory.
- Westheimer, G., 1967. Dependence of the magnitude of the Stiles-Crawford effect on retinal location, *J. Physiol. (Lond.)*, 192:309–315.
- Young, R. W., 1971. Shedding of discs from rod outer segments in the rhesus monkey, *J. Ultrastruct. Res.*, 34:190–203.

54 Visual Adaptation

ADAM REEVES

THE VISUAL SYSTEM works effectively over a vast range of light intensities, from bright sunlight down to starlight—a range of over 1000 million to 1. Only a small part of this range can be encoded by the nervous system at any one time. Therefore, the eye must adjust its operating level to match the average ambient illumination. *Light adaptation* means the adjustment of the operating level of the eye to higher levels of illumination; dark adaptation, to lower levels. Adaptation is important theoretically and practically; without it, vision would be severely constrained.

Part of the adjustment to higher light levels is accomplished by constriction of the pupil. However, in humans the (round) pupil, which maximally is about 8 mm across, cannot constrict below 2 mm without sacrificing optical quality due to diffraction. Thus the effect of the pupil in regulating light is limited to about 16:1. (In species with slit eyes this effect is larger.) Thus the main mechanisms of adaptation in our eye lie within the receptors and neural structures of the retina. At the receptor level, pigment or receptor migration occurs in some species, but these do not occur in the human eye. Rather, our primary mechanism of adaptation is the *duplex* nature of the retina (Schultze, 1866). Our retinas (unlike those of rod-only or cone-only species) possess both a cone-driven photopic (daylight) system and a rod-driven scotopic (night) system. Adaptation is accomplished by a changeover from scotopic to photopic systems at dawn or dusk, as well as by adjustments of sensitivity within each system.

There are two distinct adaptive regimes. At the very lowest light levels every photon counts, so the ability of the visual system to detect individual photons in absolute darkness is critical. To the extent that this is possible, the dark-adapted eye may be compared meaningfully to an ideal detector of photons (Hecht et al., 1942). Rod photopigments can respond to individual quanta, and an enormously powerful amplification in the rod pathway permits such minute events to initiate neural responses. Over approximately 300 quanta/rod/sec, however, this amplification *saturates* the scotopic pathway, so it can no longer respond to further increases in light level. Such saturation is spatially localized; darker regions of the visual field will still be visible to the rods even when other regions are bright enough to saturate them. This is analogous to overexposure of photographic film, in that the film “whites out” only in those spots where the light is too bright.

At higher light levels the visual system has a different task, not to make every photon count—there are so many that this is pointless—but rather to encode the local contrasts (i.e., the variations around the mean light level) which specify the visible surfaces in the world. For example, the contrast of an achromatic object specifies its shade of gray; an object darker than the mean level appears dark gray or black, and an object lighter than the mean level appears light gray or white. Encoding contrast implies discounting the ambient illumination level: as long as there is enough light for the world to be visible, just how brightly it is illuminated is of no great consequence. (Still, one’s ability to distinguish a dull from a bright day means that the ambient level is not entirely discounted; in fact, it suffers a cube-root compression.) To the extent that the light-adapted eye can efficiently encode contrasts, one can say it is an ideal detector of surface variations, even though as a photon-counting device it is far from ideal.

These two adaptive regimes map approximately onto the rods (as photon counters) and cones (as contrast encoders) of Schultze’s (1866) duplicity theory. This mapping is imprecise, however: dark-adapted foveal cones can also respond to a few quanta, though not to single quanta, permitting some night vision even in the fovea (which has no rods). Moreover, even when the main rod pathway saturates, not-yet saturated (but strongly light-adapted) rods can still contribute to vision via a second, cone-dominated pathway. The precise nature of this second rod pathway is still controversial, but it may help the transition from fully rod- to fully cone-driven vision which occurs in the *mesopic* regime of light levels sandwiched between the scotopic and photopic regimes. Only at much higher (photopic) light levels do the rods themselves saturate and the cones take over completely.

The rest of this chapter delineates the two regimes and indicates the time courses involved. Dark adaptation is covered first, including the classic dark adaptation threshold curve and its more recently discovered “anomalies.” Light adaptation is then discussed in terms of the threshold versus intensity curve. The chapter chiefly considers adaptation as a shift of the operating level over decades of light intensity, but the last section briefly mentions rapid light adaptation, that visual sensitivity can to some small degree follow rapid changes in light intensity around a mean light level to which the eye has already been adapted.

Dark adaptation

DARK ADAPTATION: PHOTOPIC AND SCOTOPIC THRESHOLDS

Recovery of sensitivity in the photopic and scotopic systems during the course of dark adaptation can be illustrated by the solid-line curve in Figure 54.1. This classic curve (e.g., Hecht et al., 1937) is obtained by first exposing the eye to a large, uniform, bright light and then plunging it into total darkness. The threshold—the intensity of light just needed to detect a small, brief test flash—is determined at regular intervals as dark adaptation progresses. The threshold curve divides Figure 54.1 into two regions: test flash intensities below the threshold are invisible, while those above it are visible. The curve has two segments or limbs. In the first 2 minutes, detection thresholds drop rapidly and then taper off at the absolute photopic threshold. After a few more minutes the curve again drops, somewhat less rapidly, and reaches a final level, the *absolute* scotopic threshold, after about 45 minutes.

The progressive drops in threshold correspond to increases in visual sensitivity, first of the photopic system and then of the scotopic system. The change from one system to the other is called the *rod-cone break*, since in the duplicity theory scotopic vision is mediated exclusively by the *rod* photoreceptors and photopic vision by the three types of *cone* photoreceptors. Just-visible blue or green test lights appear colored if flashed before the break, indicating cone function, and colorless after it, indicating rod function. The ordinate in Figure 54.1 is in logarithmic units, so the threshold data illustrate a recovery in sensitivity on the order of 4 log units (or 10,000 to 1), of which the first log unit is due to recovery of cones, and the final three log units, of rods.

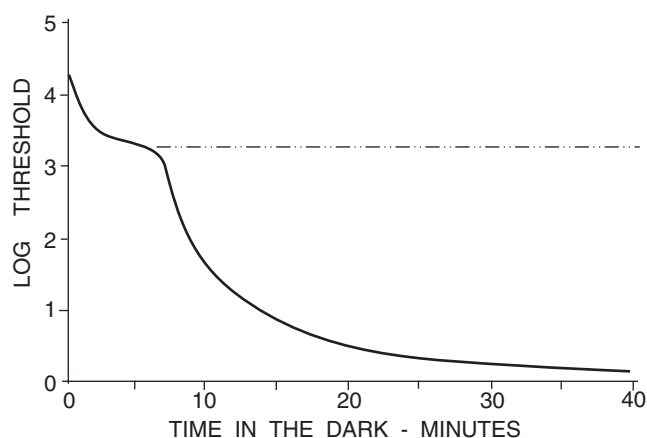


FIGURE 54.1. *Solid line:* Thresholds for brief blue or green parafoveal test flashes, expressed in logarithmic units relative to the scotopic absolute threshold. Abscissae are minutes in the dark following exposure to a bright, uniform adapting light. *Dotted line:* foveal flashes.

Figure 54.1 illustrates a dark adaptation curve produced by a blue or green test flash delivered to a peripheral retinal position where both rods and cones are numerous. When the dark adaptation curve is measured with long-wavelength (red) test flashes which are invisible to the rods, or with test flashes restricted to the rod-free foveal region, there is only a photopic limb, as indicated by the dashed line. All test flashes whose intensities fall between the dotted and the continuous line are detected by the rods alone. These curves simply illustrate duplicity. An enormously important practical application is due to Miles (1943), who first put on red goggles a half hour before night duty so that he could keep on reading (with his cones) while allowing his rods to regenerate; later, while on night duty, if he needed to go into a lit area, he put the goggles back on and preserved most of his dark adaptation.

THE PURKINJE SHIFT Relative brightness also changes at the rod-cone break. This change is called the *Purkinje shift*, after the Czech physician who noticed that differently hued flowers of similar brightness in daylight may differ in brightness in twilight. The shift can be quantified as a change in the peak spectral sensitivity of the eye from yellow-green or 555 nm (the photopic peak) before the break to blue-green or 507 nm (the scotopic maximum—the peak sensitivity of rhodopsin, the rod-photosensitive pigment) after it. While in daylight equally reflective yellow and blue-green flowers will seem about equally bright, as their spectral centroids straddle the photopic peak, in twilight the yellow flower will appear much dimmer, as its spectral centroid is far from the scotopic peak. In general, differently colored stimuli whose brightnesses match in daytime will differ in twilight unless the stimuli are restricted to the rod-free fovea (von Kries and Nagel, 1900). Fully appreciating the Purkinje shift frees the student from both the *stimulus error*—the assumption that a visual experience necessarily denotes a true state of affairs in nature—and the (often implicit) *idealist* belief that perception is purely mental, as the brightness matches are biophysically determined.

ADAPTIVE INDEPENDENCE The two limbs of the dark adaptation curves are not locked into place. They can be translated vertically (on a logarithmic scale of intensity) by altering the preadaptation light in wavelength composition or in intensity and by altering the test flash in wavelength, size, location on the retina, or duration (Barlow, 1972). These are all factors governing visual sensitivity; e.g., enlarging the test lowers the threshold due to summation in the retina. However, if the two limbs do appear, their time courses will be as shown. This invariance occurs because each class of photoreceptor recovers independently of the adaptive states of the other class of photoreceptor. Indeed, if the subject is a rod monochromat (i.e., has no photopic function), his dark

adaptation proceeds along the same time course as that of the rods of the normal subject (Rushton, 1981; Sharpe and Norby, 1990).

The principle of *adaptive independence* also holds in photopic vision to the extent that each class of cones recovers along a time course independent of the other classes of cones. Such independence may be explained by the electrical and chemical isolation of (mammalian) photoreceptors from each other. An exception to independence occurs at high light levels when electrical synapses between cones of different classes permit weak interactions. However, adaptation can occur not only in the cones but also at subsequent sites in the visual system, and recovery of these sites may also affect thresholds during dark adaptation. Thus threshold measurements may or may not demonstrate adaptive independence, depending on whether these subsequent sites of adaptation are involved. To illustrate, there are chromatically sensitive sites in the retina which receive opponent inputs from different cone classes (L versus M or S versus L and M). Adaptation of such sites can generate gross violations of the normal course of dark adaptation (see "Anomalies of Photopic Dark Adaptation" below).

BLEACHING AND RECOVERY FROM BLEACHING Vision starts with the capture of individual quanta of light by photopigment molecules located in the photoreceptors. Quantal captures *bleach* the photopigment molecule, which becomes transparent to light for some time after capture; only unbleached photopigment molecules are active—can respond to light. Bleaching plays a major role in regulating the sensitivity of the cones at the very highest light levels (10,000 cd/m² or above). After prolonged light adaptation to very high levels, even further increases in light intensity are balanced by decreases in the active cone photopigment, so the cones signal a steady level of light instead of an increase. This *protective* function of bleaching implies that the photopic system is not driven into saturation by intense sunlight. However, to restore sensitivity in the dark requires the photopigment to regenerate (recover from the bleached state). Regeneration is not instantaneous; rather, as dark adaptation continues, progressively more of the photopigment molecules regenerate and become actively available for capturing light.

The recovery of threshold with time in the dark following a bleach has been studied in great detail. Figure 54.2 shows 10 such recovery curves from 10 different light adaptations (from Hollins and Alpern, 1973). More intense adaptations (the rightward march of the curves) bleached more and more photopigment. The curves show how cone photopigment recovers exponentially during the first 5 minutes in the dark from the initial bleach. The close fit of the log thresholds (*symbols*) to the pigment recovery curves shows that as the fraction of active pigment molecules increases in the

dark, log threshold falls toward the absolute threshold. It is important that this agreement is obtained only when thresholds are plotted on a logarithmic scale.

It might seem that recovery from bleaching accounts for the recovery of threshold simply by increasing the number of photopigment molecules available to catch quanta. However, this is not so. A 50% bleach, for example, removes only half of the photopigment molecules available for catching quanta of light, but it raises thresholds by 100 times, not by 2 (open squares, middle of Fig. 54.2; note the log₁₀ scale for thresholds). Even after a mild bleach, when 90% of the cone photopigment is active, the threshold is still 10 times the cone absolute threshold (*inverted triangles*, far left of Fig. 54.2), not 1.1 times it. Similarly, rod thresholds can be 100 times the rod absolute threshold when 90% of the rhodopsin photopigment has recovered (Hecht et al., 1937). True, thresholds recover along the photopigment trajectory, at least after the stronger adaptations (Fig. 54.2), but this cannot be explained by the mere increase in the number of photopigment molecules available to catch quanta.

PHOTOPRODUCTS OF BLEACHING: THE VEILING EFFECT One explanation of data like those in Figure 54.2 is that photoproducts of bleaching remain in the receptors when the eye is in darkness, and these photoproducts act as an *equivalent light* which *veils* the incoming test flash and thus elevates the threshold. It is the progressive removal of these photoproducts which, by rending the veil (so to speak), reduces the equivalent to light and permits the threshold to recover. The term *veil* is used because thresholds for test flashes can also be elevated by glare sources—e.g., bright lights such as automobile headlamps, which, placed in the periphery of the visual field, generate a veil of real light across the eye. Stiles and Crawford (1937) showed psychophysically that, following bleaches, the human visual system behaves as though it were experiencing a veil equivalent to a real glaring light.

This metaphor may seem strained because, unlike the real light with which it can be equated, equivalent light is invisible. One typically sees a black field, not a visible afterimage, during the course of dark adaptation. However, real lights also become invisible if, like the equivalent light, they are retinally stabilized. Only if the edges of a field of light move on the retina is the retina able to signal its presence to the brain. Therefore, the assumption that an invisible equivalent to real light acts to raise the threshold is not as farfetched as it may appear.

The notion that photoproducts of bleaching account in part for recovery in the dark is tenable if the time course of their recovery matches up with the psychophysics. The next section discusses this point in detail and can be skipped without loss of continuity.

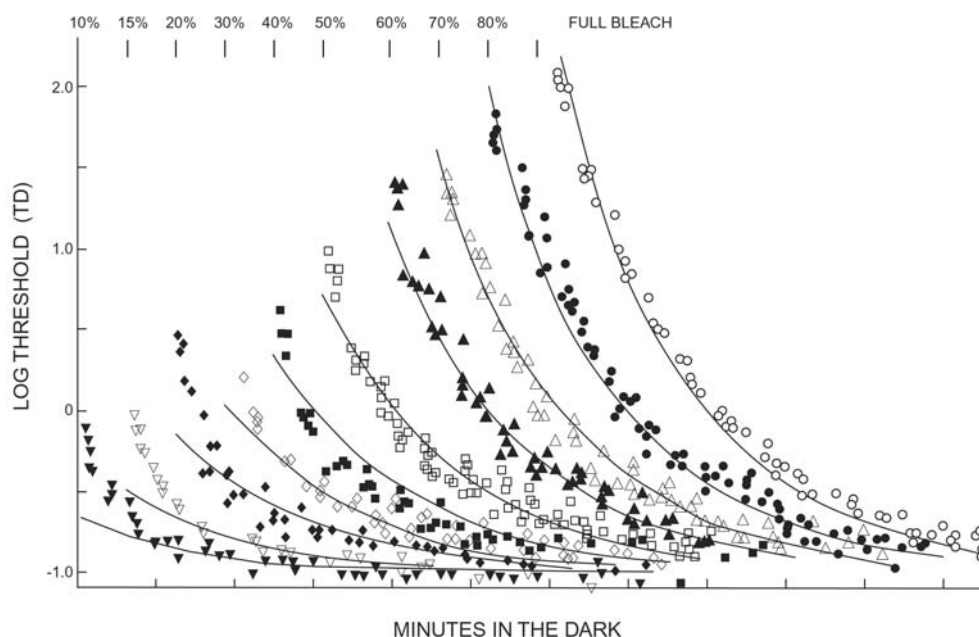


FIGURE 54.2. Symbols show recovery of L-cone-mediated foveal thresholds after 1 minute of light adaptation to bleaching lights. From right (*open circles*) to left (*filled inverted triangles*), 100%, 80%, 70%, 60%, 59%, 40%, 30%, 20%, 15%, and 10% of photopigment was bleached. Data are shifted to the right for clarity; each

time origin is indicated by a bar above. Curves show how cone photopigment recovers from the level determined by the light adaptation for the first 5 minutes in the dark. Agreement between data and curves shows that log threshold (not threshold per se) is related to the amount of photopigment. (After Hollins and Alpern, 1973.)

PHOTOPRODUCTS OF BLEACHING: THEORY A detailed theory of bleaching and equivalent light has been developed by Lamb and colleagues for scotopic dark adaptation in the toad retina (summarized in Leibrock et al., 1998, and Chapter 16, this volume). A physical basis for equivalent light is postulated to exist in the rod. The rod rhodopsin molecule, Rh, is activated to the form Rh* either by photon absorption—indicating light—or as a result of spontaneous thermal isomerization—a source of thermal noise that the visual system must somehow ignore (Barlow, 1988). Rh*, the virgin metarhodopsin II, or MII, then activates the G-protein cascade by catalyzing the conversion of inactive G to its active form, G*. Rh* is rapidly inactivated to the form MII-P-Arr, which is thought to be the main photoproduct generating the equivalent light.

II-P-Arr is thought to act via two mechanisms which generate rather different forms of equivalent light. First, a molecule of MII-P-Arr will very occasionally revert to Rh*. This mechanism will generate spurious events (noise) which are identical to real photon captures, thus producing *false alarms*—reports of light when none exists. Second, the ability of MII to activate the G-protein cascade is not totally eliminated by phosphorylation and arrestin binding; instead, MII-P-Arr can act directly on the phototransduction mechanism. The effects of this second mechanism will also resemble light in leading to steady activation of the cascade, although with less extreme fluctuations. At the start of dark adaptation, the scotopic threshold is controlled primarily by

the second mechanism, which initially generates far more equivalent light than the first. The second mechanism recovers relatively quickly, however, following the decay of MII-P-Arr (the human time constant of 2 minutes for this process agrees with that of the toad rod after correction for the toad's lower body temperature). This accounts for the relatively fast initial drop of threshold following the rod-cone break in Figure 54.1. The subsequent slow recovery of scotopic vision to absolute threshold, extending out to 45 minutes, is due to a slow reduction in the frequency of the photon-like noise events contributed by the first mechanism.

ROD-CONE INTERACTIONS DURING DARK ADAPTATION The distinctness of the rod-cone break seen at threshold in Figure 54.1 does not imply that vision is mediated by one or the other type of receptor; indeed, above threshold, both types of receptor may respond to a test flash. Whether this occurs depends both on the level of the original light adaptation and on the intensity of the test flash. After adaptation to bright lights, the rods or rod pathways will saturate, and rods will not contribute to vision until some time has passed in the dark. When recovered, however, unsaturated rods can contribute to the visibility of test flashes presented to the cones. One example in which rods and cones contribute to flicker perception is presented in Chapter 55 (Fig. 55.5). Another example is the progressive desaturation (apparent whitening) of colored test flashes which occurs as the rods increasingly recover in the dark. Judging the degree of

saturation is not easy, but it is easy (with practice) to adjust the intensity of a test flash until it appears just visibly colored (the hue *specific* threshold). As dark adaptation progresses, the specific threshold actually rises (as shown for a green test flash in Fig. 54.3 by *open circles*), contrary to the fall in detection threshold seen in Figure 54.1 and repeated in Figure 54.3 (*filled circles*), presumably to overcome the increasing achromatic response elicited from the recovering rods. Lie (1963) showed that this effect held for blue, green, yellow, and orange test flashes but not for red flashes, whose wavelengths were long enough to escape detection by the rods.

RETINAL OR CORTICAL ORIGINS OF SO-CALLED ROD-CONE INTERACTIONS Although the Lie effect, and others like it, are called *rod-cone interactions*, no direct interaction is necessarily implied. Rod signals must piggyback on those of cones (directly via electrical gap junctions or indirectly via AII amacrine cells) to access the ganglion cell axons which transmit signals to the mid-brain, from which they travel to the cortex. Ganglion cells which signal hue, whose inputs come entirely from cones, are distinct from ganglion cells which signal luminance, whose inputs come from both rods and cones. It is conceivable for cortical interactions between luminance-encoding and hue-encoding cells to give the appearance of rod-cone interactions (see Chapter 55).

It is sometimes possible to separate cortical from retinal interactions by comparing monocular and dichoptic stimulations. An example relevant to dark adaptation is provided by the *interocular light adaptation* effect (Landsford and Baker, 1969), in which the rod-cone break occurs 3 minutes later after light adaptation of the test eye alone than after an equal light adaptation of both eyes. This effect is illustrated in Figure 54.4, taken from Prestrude et al. (1978), who also showed that the Lie effect was similarly delayed. The difference in thresholds is considerable, a factor of about 5 times

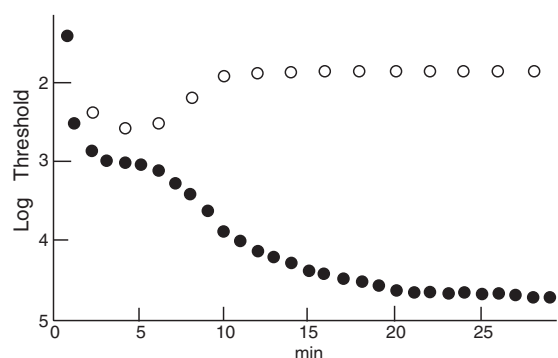


FIGURE 54.3. The specific threshold for just noticing hue (*open circles*) compared to the threshold for detection (*filled circles*), for a green test, during 30 minutes of dark adaptation. Flashes were 6 degrees parafoveal. The observer initially adapted to a large white 4000 mL field. (After Lie, 1963.)

after 15 minutes in the dark; it is still not known what causes the effect or why it is so large, but its interocular origin implies that it occurs cortically rather than in the retina.

Even the scotopic absolute threshold is affected by cortical interactions: one-eyed people have slightly *better* night vision than normals, and bleaching the cones of the nontest eye of a two-eyed person will slightly *lower* the scotopic absolute threshold (by $\sqrt{2}$) in the other eye for up to 10 minutes (Reeves et al., 1986). This can be explained if *dark light* from cones in a dark-adapted eye contributes noise to a central detection stage used to detect rod signals from either eye, assuming that enucleation or bleaching acts to improve vision by halving the noise at the detection stage.

ANOMALIES OF PHOTOPIC DARK ADAPTATION Photopic dark adaptation curve do not necessarily follow the first, descending, limb of Figure 54.1 (Stiles, 1949). Indeed, some violations of the rapid recovery are dramatic enough to have been termed *anomalies* of dark adaptation (Mollon, 1982).

The classic recovery curve shown in Figure 54.1 does occur if the observer attempts to *detect* the test flash, where detection can be based on any visual sensation at all. For example, detection of a long-duration red test flash may be based on its hue or its luminance; on a temporal transient at stimulus onset or a sustained spatial comparison between the test and the field; or even on an afterimage left behind when the flash is over. As *detection* is defined here, the choice is entirely up to the subject (and is generally not known by the experimenter).

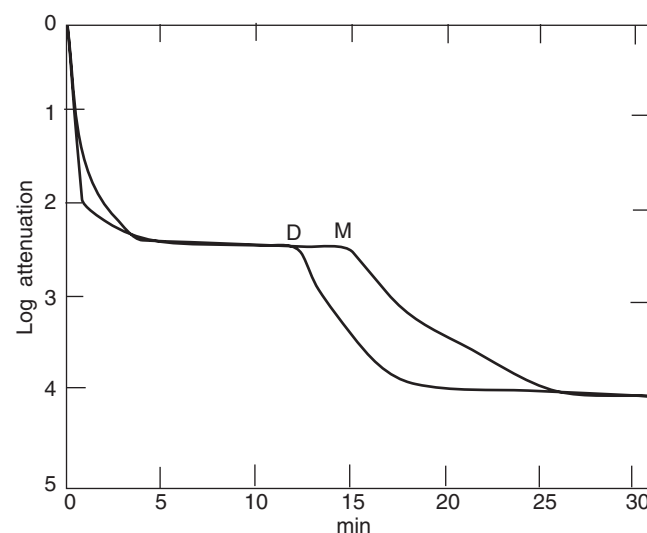


FIGURE 54.4. The interocular light adaptation effect. Test flashes were green and parafoveal. *M*, position of the rod-cone break following monocular adaptation to a bleaching light; *D*, position of the break following dichoptic adaptation to the same light in the test eye and an overlapping but dimmer light in the nontest eye. The delay (from *D* to *M*) is 3 minutes. (From Prestrude et al., 1978.)

However, the dark adaptation experiment can be repeated with test flashes whose thresholds are determined by sensitivity to one or another particular sensation. There are several methods for isolating specific sensations, which involve the choice of test stimulus or an instruction to the subject as to what property of the test to report. An example of the latter, already mentioned, is the specific threshold for just noticing a stimulus hue, which in fact rises after several minutes of dark adaptation. It is better, if possible, to design the test stimulus so as to elicit only one sensation, which removes the ambiguities inherent in the instruction. Thresholds for such special stimuli show that for some (but not all) light adaptations, the sensitivities of the photopic pathways which respond to fast luminance flicker (Reeves and Wu, 1997) and to hue (Mollon, 1982) may be abruptly *reduced* at the start of dark adaptation. Sensitivities may be reduced (and hence thresholds elevated) by a factor of 10 or 100, depending on conditions, so the anomalies are not minor. After such an abrupt desensitization, sensitivity typically recovers fairly slowly.

Illustrative data showing the loss of sensitivity for blue test flashes after exposure to yellow-adapting fields (termed *transient tritanopia*, meaning short-term blue blindness) were obtained in an extensive exploration by Augenstein and Pugh (1976). Whereas the green flash thresholds showed normal light adaptation (*filled circles, left half* of the plot of Fig. 54.5) and recovery (*filled circles, right half*), the blue test

flashes first rose at light onset, then stabilized close to absolute threshold, and then rose again at light offset before eventually recovering (*open circles*). The blue test flash thresholds were special (in the above sense) because the blue tests were detected by S cones, which elicit only hue sensations.

The next section (which may be skipped without loss of continuity) offers Pugh and Mollon's (1979) theory of the roller-coaster ride of the blue flash thresholds. The theory is of a *black box* nature, as this dramatic violation of the usual course of adaptation has not yet been explained at the physiological level. However, as it occurs only when test and adaptation fields are presented to the same eye, it is very likely a purely retinal effect—indeed, transient tritanopia was seen in the electroretinogram by Valeton and Van Norren (1979).

HUE-PATHWAY ANOMALIES: THEORY Pugh and Mollon (1979) theorized that an abrupt desensitization (followed by slow recovery) in early dark adaptation may be caused by a transient *rebound* of a polarized site. This theory was developed in the case of transient blue blindness (transient tritanopia) following onset and offset of an adapting yellow field (Fig. 54.5). This case is analytically special, since with the appropriate choice of stimuli, only S cones can detect the blue test flash and only L and M cones are light adapted by the yellow field. The S-cone test flashes can only be

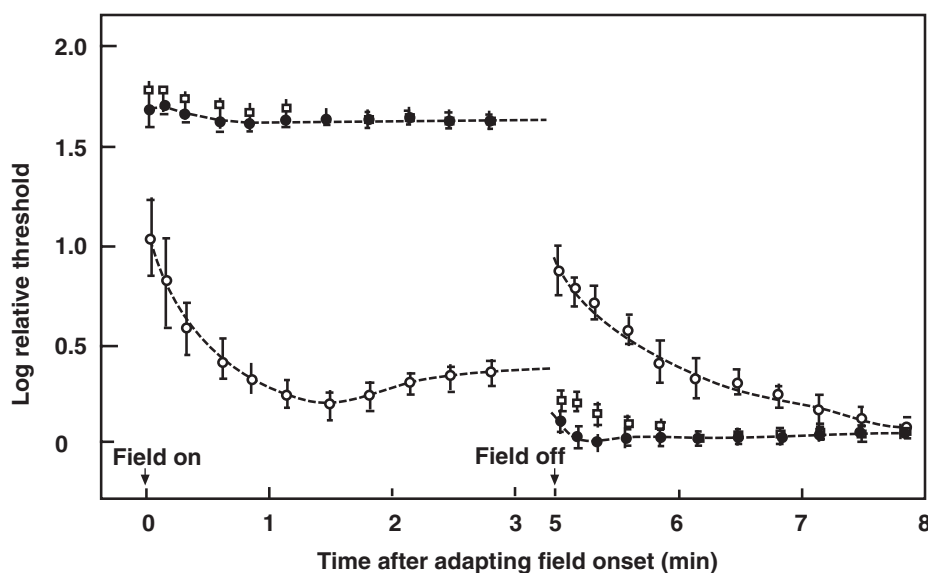


FIGURE 54.5. Thresholds for test flashes exposed during 5 minutes of light adaptation to a bright but nonbleaching yellow field (left half of the plot) and following offset of the field (right half of the plot). All thresholds are plotted in log units relative to absolute threshold. Light adaptation has a pronounced and continuous effect on green test flash thresholds, as the yellow field desensitizes M cones (*closed circles, upper left*). In contrast, light adaptation pro-

duced a smaller and temporary effect on blue test flash thresholds (*open circles, lower left*); this was necessarily mediated by an opponent site, as S cones were not adapted by the yellow field. The dark adaptation curves show normal recovery for the green test flash (*closed symbols, lower right*) but a surprising rise in threshold for the blue flash (*open circles, middle right*), illustrating rebound. (After Augenstein and Pugh, 1976.)

detected by their hue because S cones contribute virtually nothing to luminance. Thus, for the S-cone pathway to be desensitized when the yellow field is turned off, the rebound must occur at an opponent site which receives antagonistic inputs from S cones (blue) versus L and M cones (yellow).

This theory correctly implies normal recovery for blue test flash thresholds after turning off a 500 nm green field, as a 500 nm field is neutral, biasing the yellow-blue pathway neither toward yellow nor toward blue (unlike longer-wavelength fields, which polarize the pathway in the yellow direction), so turning it off does not generate a rebound (data not shown).

Pugh and Mollon postulated that the yellow/blue pathway is most sensitive when it is in a *neutral* state (adapted to white, gray, black, or green) and least sensitive when *polarized* (adapted to yellow or blue). They also hypothesized that during light adaptation to a polarizing field, such as yellow, a *force* develops fairly slowly (~15 second time constant) which opposes the polarizing signal and restores neutrality. Such a force works to make the yellow sensation generated by the field appear progressively whiter as light adaptation continues. Thus, at onset of the yellow field, blue test thresholds are initially driven high by the unopposed yellow polarization, but they fall progressively as the opposing force begins to neutralize the opponent site. After offset of the yellow field, the still active opposing force drives the site in the opposite (blue) direction, again making it less sensitive. The opposing force then decays with the same ~15 second time constant. The roller-coaster blue test flash thresholds in Figure 54.5 are entirely explained by a resistor-capacitor-circuit formulation of this idea (smooth curve).

This explanation does not refer to the appearance of the visual field once the yellow light has been turned off. One might think that after turning off of the field, the still active opposing force would generate a vivid blue afterimage, perhaps accounting for the difficulty in detecting blue flashes. However, subjects report seeing black, not blue. Nevertheless, if the yellow field is reduced in intensity by 10 times rather than being turned off, subjects do report a vivid blue afterimage (Reeves, 1983). Moreover, desensitization still occurs, is almost as large, and follows the same slow recovery process as when the eye is plunged into total darkness. Perhaps there always is a blue afterimage, which is kept visible (to the cortex) when the field is dimmed because the field constantly moves on the retina due to inescapable small eye movements but which fades to blackness when the field is off and there is no retinal motion to reevoke it.

The Pugh-Mollon theory is the best one available, but in its RC form it does not account for the abolition of transient tritanopia with light adaptation to 0.5 Hz flickering yellow fields (Reeves, 1983). Nor does it account for the reduction

in transient tritanopia, and the different spectral sensitivity of the residual effect, found when S cone decremental test flashes are employed instead of S cone incremental test flashes (Eskew and McLellan, 2000). These effects require postulating additional stages of integration and distinct S-ON and S-OFF opponently coded pathways.

A RED/GREEN ANOMALY The Pugh-Mollon theory, originally developed for the S-cone pathway, can also be applied to the red/green process. Sensitivity to red and green tests detected by the red/green opponent process is reduced at the start of dark adaptation if the light adaptation has been polarizing (in this case, red and green fields; white, black, and yellow are neutral). An analytical experiment in this case is tricky, because L and M cones also contribute to luminance, and luminance sensitivity recovers, permitting detection thresholds for red, yellow, or green test flashes to follow the descending photopic limb in Figure 54.1. However, it is possible to isolate the red/green hue pathway using hue flicker generated by alternating 580 nm and 640 nm test lights, whose hues are easily distinguishable, at rates of 4 to 6 Hz which are optimally visible for the hue pathway (Reeves, 1983). The lights were equated in luminance throughout dark adaptation to eliminate luminance flicker as a cue. Figure 54.6 shows the resulting *hue* (visible flicker) and detection thresholds as a function of time in the dark following offset of a 626 nm (polarizing) field.

Figure 54.6 (*top*) shows that thresholds for reporting hue flicker lie above those for detection throughout the period of dark adaptation. This effect is hard to see at the start, when the thresholds fall on top of each other, so the first 2 seconds have been stretched out in the *lower panel* for clarity. The first two data points in the lower panel (at the far left) indicate the two thresholds on the steady light-adapting field just before it was turned off. They are close, showing that almost as soon as one can detect the test at all, one can see it flicker. Only after the field is turned off do the thresholds diverge. The explanation in Pugh-Mollon terms is that the offset of the 626 nm (red) field produced a rebound in the red/green hue sensitive pathway. This rebound raised the hue flicker thresholds but did not affect the detections, which were based on luminance transients at test onset and offset rather than on seeing hue (Fig. 54.6). Indeed, after turning off a yellow field, which is neutral in the red/green pathway, both types of threshold recover equally (Reeves, 1983). There are other close correspondences between the yellow/blue and red/green pathways; in both cases there are no rebounds after offsets of bleaching fields (Mollon, 1982), and adapting to slowly flickering polarizing fields does not produce rebounds (Reeves, 1983). Since no gross divergences have since been discovered, the upshot appears to be that the dark adaptation of both yellow/blue and red/green pathways follows the same laws.

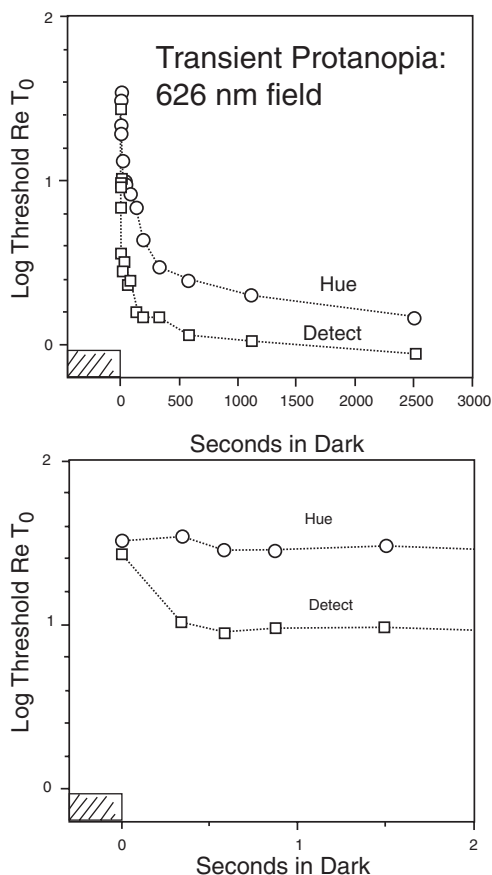


FIGURE 54.6. Thresholds for hue flicker and detection, plotted in logarithmic units relative to photopic absolute threshold (T_0). The *upper curves* show the entire time course of recovery; the *lower panel* shows just the first 2 seconds. *Open circles* show the hue flicker thresholds; *open squares*, thresholds for detection.

LUMINANCE ANOMALIES A transient tritanopia-like effect termed *transient lumanopia* has recently been discovered in the luminance pathway. Sensitivity to rapidly flickering white light (>12 Hz) may be reduced abruptly and dramatically, by up to 60 times, at the start of dark adaptation (Reeves and Wu, 1997). When this happens, sensitivity takes many seconds to start recovering. Although this might suggest a rebound in an opponent coded *black/white* pathway, analogous to the opponent pathway assumed by Pugh and Mollon (1979) to explain transient tritanopia, fast flicker in fact stimulates a nonopponent or additive luminance-sensitive channel. (Slower flickers stimulate other luminance-sensitive channels.) The additive channel can be approximated by a filter which is maximally sensitive to lower frequencies and progressively attenuates higher ones. The frequency at which attenuation is 50% (i.e., sensitivity is one-half of maximum) provides a benchmark called the *corner frequency*. Reeves and Wu postulated that the corner frequency is abruptly lowered at the start of dark adaptation. For example, immediately after turning off a 400 Td

white adapting field, the corner frequency drops from 20 Hz (the light-adapted level) to 10 Hz. The dramatic size of the lumanopia effect occurs because the luminance filter attenuates very rapidly, so that 18 Hz flicker, which is easily visible in the light, is attenuated 60-fold when the corner frequency drops to 10 Hz. According to this postulate, any test stimulus, even as a single flash, that can be detected via a relatively slow (<10 Hz) luminance-sensitive channel would not suffer lumanopia but rather would exhibit classical dark adaptation.

SUMMARY OF DARK ADAPTATION The classic recovery of photopic vision seen in Figures 54.1 and 54.2 is an important characteristic of the visual system and illustrates how adaptation occurs over a large range of light levels. Psychophysically it can be measured if the test flash stimulates a luminance channel sensitive to low temporal frequency components (these are present in a long-duration test flash or a flash which flickers at a low rate). Recovery in this channel may follow the time course of recovery of the cones themselves if veiling is taken into consideration. However, other channels, sensitive to hue or fast flicker, are typically desensitized at the start of dark adaptation. The physiological underpinnings for these large psychophysical desensitization effects are not known in detail, but in the case of hue they probably involve desensitization and recovery of retinal sites at which inputs from various classes of cones are opponent. The recovery of scotopic vision seen in the rod limb of Figure 54.1 is not subject to such anomalies and can be explained in terms of recovery of physiological mechanisms which create equivalent light.

Light adaptation

LIGHT ADAPTATION: THE SCOTOPIC AND PHOTOPIC INCREMENT THRESHOLD CURVES A classic measure of the extent of light adaptation is provided by the incremental threshold. This is the threshold for detecting a test flash superimposed on a large, steady, uniformly lit background to which the observer has been adapted for several minutes (see in insert in Fig. 54.8).

Some typical results are shown in Figure 54.7, which shows a plot of the incremental threshold as it depends on the luminance of the background. At low levels the background has no effect, but as the background is raised the threshold rises, at first gradually and then more rapidly. At higher levels there is a second plateau followed by a second rise. As in dark adaptation curves, the two limbs of the plot can be attributed to the participation of the rod and cone systems. When the eye is adapted to low levels, the rod system is more sensitive, but at higher adaptation levels scotopic sensitivity drops below that of the cones.

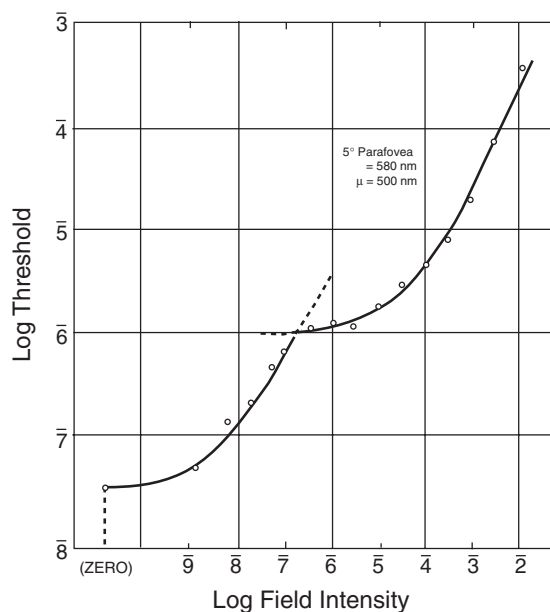


FIGURE 54.7. Rod and cone branches of the incremental threshold versus intensity curve measured in the parafovea. The test was yellow (580 nm) and the field green (500 nm) in order to expose both scotopic (*lower solid curve*) and photopic (*upper solid curve*) branches. Axes are in log units (the abscissa is in log ergs/deg/deg/sec). *Zero* refers to no background light at all, where the scotopic absolute threshold is measured. Dotted lines indicate when each system is less sensitive than the other. (From Wyszecki and Stiles, 1982.)

As in the dark adaptation curve, the limbs of the increment threshold curve depend on the testing conditions such as the size of the stimuli, their location on the retina, and their spectral composition. The example in Figure 54.7 is typical of yellow stimuli presented against a blue-green background in the parafoveal region. Other conditions result in a less conspicuous separation of the two retinal systems. A blue stimulus, which favors the scotopic system, presented against a red adapting field, which is effective in reducing the sensitivity of the photopic system, can produce an increment threshold curve in which the scotopic system is completely uncovered. When this is done, an abrupt rise in threshold above ~ 2000 Td indicates where the scotopic system begins to saturate, following the reasoning introduced by Stiles (e.g., Rodieck, 1973).

Theory of the increment threshold curve

Different sectors of the increment threshold curve may be distinguished for theoretical as well as descriptive purposes. Throughout the middle of the range the curve slope is 1.0 (for cones) or only slightly less than 1.0 for rods, approximating Weber's law that the ratio of increment threshold to background intensity is constant. At the upper end the rod curve swings steeply upward in the saturation region. (Bleaching protects the cones from saturation, so Weber's law

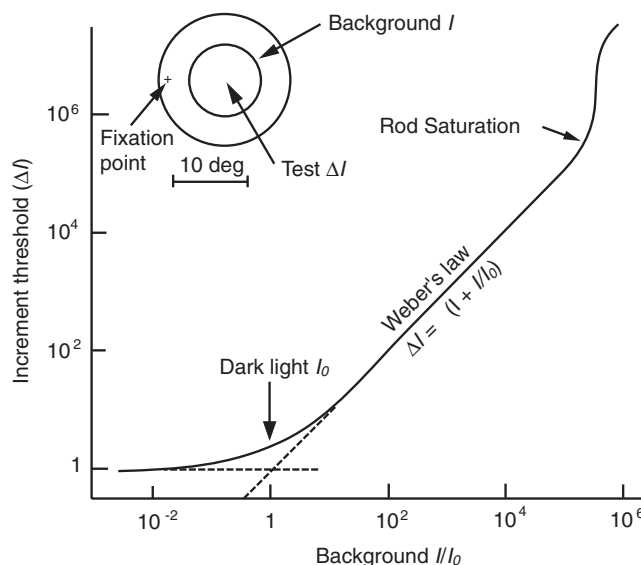


FIGURE 54.8. Theory of light adaptation curves. The increment threshold is plotted against the intensity of the field or background, expressed relative to the dark light (I_0) appropriate for the receptor class being studied. The dark light and Weber's law portions apply to rods and cones equally. The upper section illustrates saturation in rods, with cones just starting to take over at the very top. (Saturation is absent in cones.) Axes are in log units.

for the cones extends indefinitely.) At the lower end the curve bends and becomes horizontal, thus marking the region where the background is too weak to have an effect. The nineteenth-century philosopher and psychologist Fechner, the inventor of psychophysics, accounted for such data by invoking the concept of an intrinsic activity or *dark light* within the receptor systems that combines with the excitation produced by the background to raise the threshold. In his model, the increment threshold ΔI is related to the intensity of the field I by the equation

$$\Delta I = k(I + I_0) \quad (1)$$

where k is Weber's fraction and I_0 is the equivalent dark light. The curves shown in Figures 54.7, 54.8, and 54.9 are of this form, except where saturation occurs.

The reader will recall that the recovery of threshold in the dark is also explained by postulating a dark light, in this case an intrinsic excitation that persists after light adaptation. Although it does not give rise to visual sensation, dark light acts as a background against which the test flash must be seen during dark adaptation. Thus Fechner's idea lives on.

PHOTOPIC INCREMENT THRESHOLD CURVES The procedure of light adaptation is useful for investigating color processes. If, for example, incremental thresholds are measured with monochromatic test flashes presented against monochromatic backgrounds, the photopic sector shown in Figure

54.7 may break up, depending upon the particular wavelengths used, into two or more constituent limbs. By measuring the incremental threshold function systematically for a wide range of test and adaptation wavelengths, it is possible to determine the spectral sensitivities of these limbs and thus to define the color processes they represent (Stiles, 1953). Stiles showed that a slight variant of Fechner's equation applies separately to the rods and to each of the three cone classes (L, M, and S), each with its own dark light and k term). A sample of his results is presented in Figure 54.9, which illustrates light adaptation of two classes of cones, each over a factor of 10:1. In the experiment, test wavelength (475nm) and field wavelength (550nm) were held constant. In the dark, and on dim fields, the M cones are more sensitive to 475nm than are the S cones, so M cones detected the test, giving rise to the lower branch of the curve. However, the 550nm field is a more potent stimulus for M than S cones, so as the field was made more intense, it light-adapted the M cones more than the S cones. Thus, eventually, only the S cones could detect the test at threshold (upper branch).

This elegant scheme of Stiles is marred by the fact that light adaptation occurs not only at the receptor (cone) level but also at the opponent level. An opponent site can be adapted if light adaptation of the receptors is incomplete, so that a chromatically polarizing signal remains even after light adaptation. This was illustrated for the blue flash thresholds obtained after onset of a yellow field (*left side* of Fig. 54.5). Such opponent light adaptation also serves to raise threshold, typically by a only small factor (3 or less) in the red/green pathway (Stromeyer et al., 1999), but by up to 10 times in the yellow/blue pathway. (The reader may note

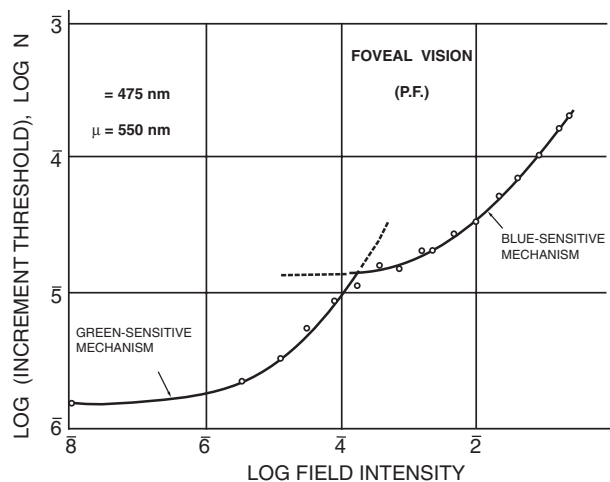


FIGURE 54.9. Increment threshold for a 475nm test flash superimposed on a steady 550nm field of the intensity shown (in log ergs/deg/deg/sec) on the abscissa. Curves obey equation 1. (From Stiles, 1953.)

that analogous effects in dark adaptation were larger; see the section "Anomalies of Photopic Dark Adaptation.") Despite detailed modeling and plentiful data (e.g., Stromeyer et al., 1999), a precise and *complete* scheme for understanding chromatic light adaptation still remains elusive.

In dark adaptation, the various types of threshold (detection versus hue or flicker) can diverge from each other markedly at light offset and, if they do, continue to diverge for several minutes. The picture at the start of light adaptation is less vivid. The author has found no evidence of transient lumanopia during light adaptation. Hue thresholds may illustrate a desensitization effect at the start of light adaptation, typically of 0.5 log unit or less, which decays away within 30 seconds or so (as seen in the left half of Fig. 54.5).

RAPID ADAPTATIONAL CHANGES The changes in visual sensitivity which accompany the onset of light and dark adaptation are also of considerable interest. These were first measured by superimposing a small, brief test flash on a large adaptation background that is switched on and off periodically. The experimental results, shown in Figure 54.10, indicate that the threshold for detecting the test flash begins to rise one-tenth of a second or so before the onset of the adaptation light. The threshold reaches a maximum near the time of onset, drops somewhat, and then climbs to a second but lower maximum at the time of offset. Sensitivity then returns within one-half of a second or so (Crawford, 1947).

The fact that the detection threshold starts to rise before the onset of the adaptation stimulus is surprising, and this effect has produced an enormous literature. Suffice it to say here that such masking can be obtained at almost full strength when the test is presented to one eye and the field to the other eye, indicating a primarily cortical origin for the

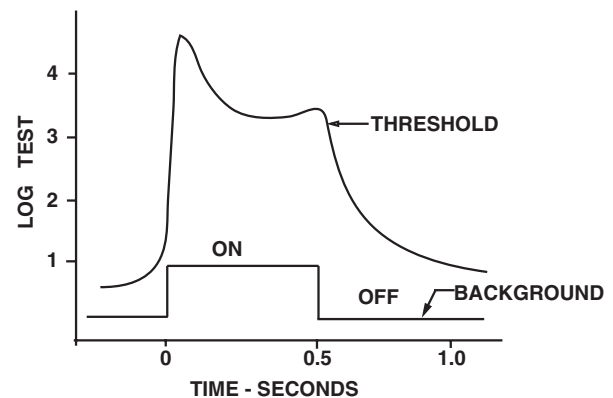


FIGURE 54.10. Log test thresholds just before, during, and after presentation of a 0.5 second adapting flash. A continuously present background desensitized rods and ensured photopic responding. (After Crawford, 1947.)

effect. In this case the adaptation stimulus acts in part as a mask, interfering with the visibility of the test (say, by distraction) rather than by altering the sensitivity of the visual pathway. However, it is possible to design stimuli which only raise thresholds monocularly and are therefore likely to indicate the time course of rapid retinal adaptation processes. The relevant literature can only be hinted at here. An elegant method was introduced by Boynton et al. (1961). They sinusoidally modulated the intensity of a spatially extended adapting field (rather than turning it on or off, as Crawford had done) and presented a smaller test flash at various times during the cycle. The mean light level was held constant. They found that visual sensitivity followed the modulation even when the modulation was too fast (30 Hz) or too low in amplitude to be visible, indicating that the method taps into adaptive sites prior to cortical awareness. How rapid light adaptation depends on flicker rate has been studied intensively since then; a detailed, primarily retinal, model has been fit to such data by Hood and Graham (1998).

LIGHT ADAPTATION AND TEMPORAL SENSITIVITY Modulation thresholds for sinusoidal or square-wave flicker have been studied to discover how the temporal response of the visual system depends on adaptation level. In this method there is only one stimulus, a field of light which flickers around a mean level to which the observer has been adapted. Briefly, slow flicker illustrates Weber law behavior in which modulation thresholds increase with mean light level, just as the flash thresholds do (Fig. 54.8). However, fast flicker illustrates linear behavior in which the mean level has almost no effect on the modulation threshold (as shown by the DeLange curves in Wyszecki and Stiles, 1982, p. 561). The fast flicker result violates the normal upward course of threshold and seems to cast doubt on the generality of the light adaptation phenomenon. However, fast flicker is difficult to see, so modulations must be high in order to attain threshold. An expression such as equation 1 can be employed to describe the experimental results if I_0 is presumed to increase at higher flicker rates.

Conclusions

The study of dark adaptation, initiated in the latter part of the nineteenth century, has come to exemplify the integration of physiology and behavior. What we see, and when, is determined by receptor processes whose physiology is now understood at a fairly deep level and by second-order effects—rod-cone and cone-cone interactions—which are beginning to yield to a more complete understanding.

REFERENCES

- Augenstein, E. J., and E. N. Pugh, Jr., 1976. The dynamics of the Pi-1 color mechanism: further evidence for two sites of adaptation, *J. Physiol. (Lond.)*, 272:247–281.
- Barlow, H. B., 1988. The thermal limit to seeing, *Nature*, 334:296–297.
- Barlow, H. B., 1972. Dark and light adaptation: Psychophysics, in *Handbook of Sensory Physiology*, vol. VII/4 (D. Jameson and L. M. Hurvich, eds.), New York: Springer-Verlag, pp. 1–29.
- Boynton, R. M., J. F. Sturr, and M. Ikeda, 1961. Study of flicker by increment threshold technique, *J. Opt. Soc. Am.*, 51:196–201.
- Crawford, B. H., 1947. Visual adaptation in relation to brief conditioning stimuli, *Proc. R. Soc. B*, 134:283–302.
- Eskew, R. T., and J. S. McLellan, 2000. ON and OFF S-cone pathways have different long-wave cone inputs, *Vis. Res.*, 40:2449–2465.
- Hecht, S., C. Haig, and A. M. Chase, 1937. The influence of light adaptation on subsequent dark adaptation of the eye, *J. Gen. Physiol.*, 20:831–850.
- Hecht, S., S. Schlaer, and M. H. Pirenne, 1942. Energy, quanta and vision, *J. Gen. Physiol.*, 25:819–840.
- Hollins, M., and M. Alpern, 1973. Dark adaptation and visual pigment regeneration in human cones, *J. Gen. Physiol.*, 62:430–447.
- Hood, D., and M. Graham, 1998. Threshold fluctuations on temporally modulated backgrounds: a possible physiological explanation based on a recent computational model, *Vis. Neurosci.*, 15:957–967.
- Landsford, T. E., and H. D. Baker, 1969. Dark adaptation: an interocular light adaptation effect, *Science*, 164:1307–1309.
- Leibrock, C. S., T. Reuter, and T. D. Lamb, 1998. Molecular basis of dark adaptation in rod photoreceptors, *Eye*, 12:511–520.
- Lie, I., 1963. Dark adaptation and the photochromatic interval, *Doc. Ophthalmol.*, 17:411–510.
- Miles, W. R., 1943. Red goggles for producing dark adaptation, *Fed. Proc.*, 2:109–115.
- Mollon, J., 1982. Color vision, *Annu. Rev. Psychol.*, 33:41–85.
- Prestrude, A. M., L. Watkins, and J. Waltskins, 1978. Interocular light adaptation effect of the Lie “Specific threshold,” *Vis. Res.*, 18:855–857.
- Pugh, E. N., and J. Mollon, 1979. A theory of the Pi1-Pi3 color mechanisms of Stiles, *Vis. Res.*, 19:293–312.
- Reeves, A., 1983. Distinguishing opponent and non-opponent detection pathways in early dark adaptation, *Vis. Res.*, 23:647–654.
- Reeves, A., N. Peachey, and E. Auerbach, 1986. Interocular sensitization to a rod-detected test, *Vis. Res.*, 26:1119–1127.
- Reeves, A., and S. Wu, 1997. Transient lumanopia: the invisibility of flicker in early dark adaptation, *J. Opt. Soc. Am. A*, 14:2509–2516.
- Rodieck, R. W., 1973. *The Vertebrate Retina*, San Francisco: W. H. Freeman.
- Rushton, W. A. H., 1981. Visual adaptation, in *Adler's Physiology of the Eye: Clinical Application*, 7th ed. (R. A. Moses, ed.), St. Louis: Mosby.
- Schultze, M., 1866. Zur Anatomie und Physiologie der Retina, *Arch. Mikro Anat.*, 2:175–286.
- Sharpe, L., and K. Norby, 1990. in *Night Vision* (R. F. Hess, K. Nordby, and L. T. Sharpe, eds.), Cambridge: Cambridge University Press.
- Stiles, W. S. and B. H. Crawford, 1937. The effect of a glaring light source on extra foveal vision. *Proc. Roy. Soc. (Lond.) B*, 123:90–118.

- Stiles, W. S., 1949. Increment thresholds and the mechanisms of colour vision, *Doc. Ophthalmol.*, 3:138–165.
- Stiles, W. S., 1953. Further studies of visual mechanisms by the two-color threshold method, *Col. Probl. Opt. Vis.* (U. I. P. A. P., Madrid) Vol. I, Reprinted in: W. S. Stiles, 1978. *Mechanisms of Color Vision*, London, Academic Press.
- Stromeyer, C. F., III, P. D. Gowdy, A. Chaparro, and R. E. Kronauer, 1999. Second-site adaptation in the red-green detection pathway: only elicited by low spatial frequency test stimuli, *Vis. Res.*, 39:3011–3023.
- Valeton, J. M., and D. Van Norren, 1979. Transient tritanopia at the level of the ERG b-wave, *Vis. Res.*, 19:689–693.
- von Kries, J., and W. A. Nagel, 1900. Weitere Mittheilungen ueber die functionelle Sonderstellung des Netzhautcentrums, *Z. Psych.*, 23:161–186.
- Wyszecki, G., and W. S. Stiles, 1982. *Color Science, Concepts and Methods, Quantitative Data and Formulae* (2nd ed.), New York: Wiley.

55 Rod-Cone Interactions in Human Vision

STEVEN L. BUCK

ALTHOUGH SITUATIONS can be arranged in which human vision is mediated by the activity of only one photoreceptor class, rods or cones, there is a broad range of environments and light levels in which both rods and cones are simultaneously active. Typically, it is only at the lowest (termed *scotopic*) or highest (termed *photopic*) light levels that rods alone or cones alone mediate our vision. The range of shared function varies with the wavelength of light but, as a rough generalization, rods and cones are active over a $4\log_{10}$ range of light levels (termed *mesopic*) that includes many modern indoor lighting environments. Historically, mesopic conditions have prevailed even in daytime for some parts of the year at northern latitudes (not just here in Seattle!) and at twilight or in fire-lit environments everywhere.

The phenomenology of rod-mediated and cone-mediated vision is as different as . . . well, night and day (dim, fuzzy, and achromatic vs. bright, crisp, and colorful), but our view of the world is unified. We don't see separate rod and cone views of the world, simultaneously, except perhaps through tricks of the visual psychophysicist. Put another way, both rod and cone signals contribute to the same set of visual processes that mediate our ability to detect color, spatial pattern, flicker, motion, and so forth.

With this joint contribution comes the occasion, perhaps even the inevitability, for rod- and cone-initiated signals to interact with each other to change both the sensitivities and perceptual qualities of our visual experience. The second part of this chapter examines the psychophysical and perceptual consequences or manifestations of these rod-cone interactions in human vision. The first part of the chapter highlights some features of the retinal processing of rod and cone signals that help us to understand why and how these interactions occur.

The duplex retina and shared neural pathways

OVERVIEW Three aspects of the retinal neural substrate are key for our understanding of rod-cone interactions. (This discussion will focus on primate retinal processing because of its direct relevance for human vision.) First, there appear to be no private rod pathways out of the retina. No retinal ganglion cells (the final retinal neural stage, whose axons form the optic nerve) have been found that transmit only rod-initiated signals. All rod signals appear to converge onto neural pathways that also transmit cone-initiated signals.

There are two fundamental consequences of this sharing of neural pathways. First, it is inevitable that rod and cone signals will contribute jointly to visual function, given their shared operating range of light levels. Second, the sharing of pathways provides the occasion for a wide range of combination effects: facilitation to suppression, superadditivity to subadditivity, and so on.

The second key feature is that there are multiple sites of interaction of rod and cone signals. Two sites that will be examined in more detail below are (1) the direct electrical (gap junction) synapses that are formed between rod and cone photoreceptors at the first stage of retinal neural processing and (2) the convergence of rod signals transmitted through the AII amacrine cells onto bipolar cells that receive signals from cones. The spotty evidence that we have already, the apparent multiplicity of subtypes of retinal neurons, and the complexity of their interconnections (especially those involving amacrine cells) all make it likely that there are many other points of convergence or interaction of rod and cone signals that are also important for vision in humans, primates, and probably most vertebrates.

The third key feature is that the strength, presence, and sometimes even direction of rod-cone interactions depend on functional network properties of the retina that can be exquisitely sensitive to states of adaptation and patterns of stimulation. These network properties are dynamic and can't be captured in a static wiring diagram. Gap junctions are likely to be important in the formation and state dependence of these network properties (Smith et al., 1986).

Given these features of retinal processing, it is not surprising that rod-cone interactions are found in most or perhaps all types of visual processing and that the properties of these interactions vary tremendously under different circumstances. Two of the better-documented pathways of rod-cone interaction in the retina are highlighted immediately below.

BEST KNOWN INTERACTION SITES

Rod-cone gap junctions. Although anatomical processes that appeared to connect the terminals of primate rod and cone photoreceptors (Fig. 55.1) had been described earlier (Cohen, 1965; Kolb, 1970), it was not until the 1970s that these were definitively identified as gap junctions (electrical synapses) (Raviola, 1976; Raviola and Gilula, 1973) in

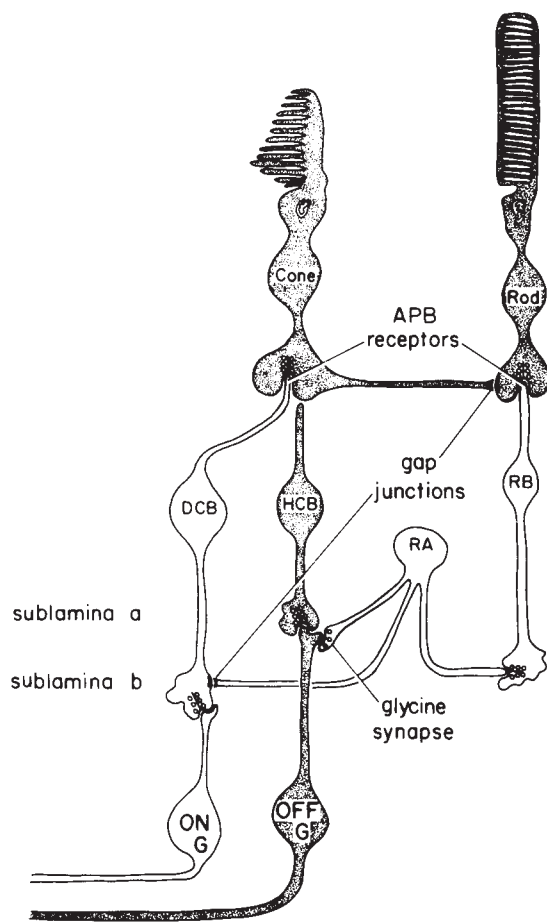


FIGURE 55.1. Diagram of two pathways for rod-cone interaction in primate retina. The classical rod pathway extends from rods to the rod bipolar (*RB*) and AII amacrine (*RA*) to depolarizing and hyperpolarizing cone bipolars (*DCB* and *HCB*). In the second pathway, rod signals enter cones directly via gap junctions. (Reprinted from *Trends in Neurosciences*, vol. 3, Daw, Jensen, and Brunken, Rod pathways in mammalian retinæ, pp. 110–1151, © 1990, with permission from Elsevier Science Publishers.)

several vertebrate species, including primates. Nelson showed that in cat retina, rod signals could be recorded from cone photoreceptors and from horizontal cell bodies, which had direct connections to cones but not to rods (Nelson, 1977; Nelson et al., 1976).

More recently, rod signals have also been recorded from cones (Schneeweis and Schnapf, 1995) and H1 horizontal cells (Verweij et al., 1999) in primate retina. As in the cat and other mammalian species, the rod signal recorded from primate horizontal cell bodies apparently reflects indirect rod input to cones and not direct rod input to the horizontal cell itself.

These two studies generally agree on several aspects of the relationship of rod and cone signals in this early retinal pathway. Rod and cone responses combine with the same direction of influence on the peak response of the cone or

horizontal cell and are independently adaptable. Cone responses are more transient, while rod responses contribute both to the initial peak response and to a more prolonged after-response (OFF response). Rod responses speed up and contribute more strongly to the transient peak as light level increases. The sensitivity of rod signals in cones and horizontal cells is only 1 to 2 log units greater than that of cone signals. Thus, this pathway seems well suited to transmit rod signals at mesopic light levels but is not sufficiently sensitive to mediate rod vision at low scotopic light levels (see also Chapter 17).

AII output to cone bipolars. As shown in Figure 55.1, the classical or primary pathway for rod photoreceptor signals is via rod bipolar cells and then the AII amacrine cells (Kolb, 1970), labeled *RA* in Figure 55.1. The outputs of these AII cells are mainly to ON (depolarizing) cone bipolar cells via gap junctions (Strettoi et al., 1994) and to OFF (hyperpolarizing) cone bipolars via conventional inhibitory synapses (Muller et al., 1988; Strettoi et al., 1992). (Thus, not only don't rod signals have private paths out of the retina, they don't even have private pathways to the retinal ganglion cells!) It is this AII pathway that appears to mediate rod vision at the lowest scotopic light levels. Rod signals in the AII pathway can be found over a 6 log unit range of stimulus intensities, including the lowest scotopic light levels (Buck et al., 1997c; Dacheux and Raviola, 1986). This means that the AII rod pathway is at least 3 log units more sensitive than the rod-cone gap-junction pathway (Verweij et al., 1999).

The interaction of rod and cone signals in the *cone bipolar cells* has not been studied systematically in primates. However, robust rod and cone signals can be recorded from *AII amacrine cells* in primates (Buck et al., 1997c; Dacey, 1996) and rabbit (Xin and Bloomfield, 1999). Both ON and OFF cone signals are found in AII cells and presumably come from cone bipolar cells. In primates, at least, sinusoidal stimulus modulation produces rod and cone responses in the AII of similar strength, but different latency, at higher light levels. These rod and cone signals can either add or cancel each other, depending on the frequency of stimulus modulation and the resulting phase relationship.

The accounts outlined above make the prediction that the cone bipolars should be the site of convergence of rod signals carried through two different retinal pathways, the rod-cone gap-junction pathway at high scotopic and mesopic light levels and the AII amacrine pathway over the entire range of rod response. This prediction has not been tested by intracellular recordings from cone bipolar cells in primates but is consistent with the results of human electroretinography (Stockman et al., 1995). In addition, Buck et al. (1997c) found that the temporal

sensitivity of rod signals was sluggish at low scotopic levels (peak sensitivity at 2 to 3 Hz with a 7 to 9 Hz cutoff) but appeared to speed up at mesopic light levels (allowing rod signals to be in canceling counterphase with cone signals at 10 Hz). Whether these brisker rod signals came through the rod-cone gap-junction pathway or the AII pathway was not clear.

Of great interest will be further work to determine (1) the different properties imposed on rod signals that pass through these two distinct retinal pathways and (2) what conditions favor transmission of rod signals by each pathway. Existing evidence and theory on these questions can be found in Chapter 17. The rod-cone gap-junction pathway and the AII amacrine pathway are currently the retinal pathways of rod-cone interaction that are best documented and of clearest relevance for primate vision. Other pathways have been identified in other species, such as the mouse (Tsukamoto et al., 2001), and may one day be determined also to be important for retinal processing in primates.

ROD INFLUENCE ON RETINAL OUTPUT PATHWAYS (GANGLION CELL TYPES) Fundamental questions also remain about what types of retinal ganglions transmit rod signals out of the retina, under what conditions each type of ganglion cell does so, how rod and cone signals interact to determine jointly the output of each type of ganglion cell, and how the later stages of the visual system use this information to mediate specific aspects of visual function.

Unfortunately, the literature is varied on the role of rod signals in the three best-understood classes of geniculate-projecting retinal ganglion cells in primates: the parvocellular-projecting midget ganglion cells, the magnocellular-projecting parasol cells, and the koniocellular-projecting small bistratified cells.

What seems most certain is that there is strong rod input to parasol cells, with the rod input of the same sign as the cone input to the cell's receptive field center (e.g., Virsu and Lee, 1983; Virsu et al., 1987; Wiesel and Hubel, 1966). Gouras and Link (1966) reported that rod and cone inputs interact at mesopic levels in phasic ganglion cells (presumed parasol cells). They also reported that rod signals arrive with longer latency than cone signals, so that the response of these phasic cells becomes cone dominated at mesopic and photopic light levels. Lee et al. (1997) also reported a longer latency for rod signals compared to cone signals in physiologically identified parasol cells and rod domination of the response of dark-adapted cells at all light level below 20 photopic trolands. Lee and colleagues found that rod and cone signals interacted in temporal-frequency-dependent ways which were consistent with superposition or summation of signals arriving with different latency. Similarly, Enroth-Cugell et al. (1977) showed that, in cat retina,

separately initiated rod and cone responses always summed, regardless of whether there was a latency difference.

Less certain is the role of rod signals in primate midget ganglion cells. Wiesel and Hubel (1966) reported finding rod input to 4 of 17 parvocellular lateral geniculate nucleus (LGN) cells (presumably reflecting inputs from midget ganglion cells). Rod input to these cells was always in the same direction of effect as the cone input to the receptive field center. Virsu and Lee (1983) and Virsu et al. (1987) also reported strong excitatory rod input to some parvocellular LGN cells, including most M-cone-center ON cells, and inhibitory rod inputs in some light-inhibited cells. L-cone-center cells rarely showed rod input, which was always weak.

In contrast, other studies have found little or no rod influence on the midget/parvocellular pathway. Purpura et al. (1988) found only a weak response of parvocellular-projecting (presumably midget) ganglion cells at mesopic and scotopic light levels. They concluded that primate pattern vision is mediated by magnocellular-projecting (presumably parasol) ganglion cells at scotopic levels: although midget cells may be able to convey information about coarse gratings (<0.6 c/deg), parasol cells display higher contrast gain even under these conditions at scotopic light levels. Most curiously, a sophisticated recent attempt to measure rod influence at scotopic and mesopic light levels in carefully identified macaque retinal ganglion cells found only weak rod input to midget ganglion cells (Lee et al., 1997). Overall, rod input was found in about 65% of midget cells at a scotopic light level of 2 trolands, but typically it never contributed more than a few spikes per second, even at maximum stimulus contrast. At a mesopic light level (20 trolands), rod influence may or may not have been present but was estimated to be less than 5% of the strength of the cone influence on these midget cells. In agreement with the general finding, rod influence, when found, was always in the same direction as the cone input to the center response of the ganglion cell. Lee et al. (1997) found no differences in frequency or strength of rod input between L-cone- or M-cone-center midget cells or between ON- or OFF-center midget cells, in contrast to the results of Virsu and Lee (1983) and Virsu et al. (1987).

We have the least information about the possibility of rod input to the small-bistratified ganglion cells and any other ganglion cells that also receive input from S cones. Virsu and Lee (1983) and Virsu et al. (1987) reported that most parvocellular LGN neurons with response patterns corresponding to B+Y-cells displayed a substantial rod excitatory input at about 2 trolands. D. M. Dacey (personal communication) has also found small-bistratified cells in the far periphery that display strong excitatory rod input at scotopic light levels. However, Lee et al. (1997) found no evidence of any rod input to any of 10 physiologically defined "blue-ON" cells

that correspond to the small-bistratified ganglion cells (Dacey and Lee, 1994).

The uncertain picture of rod influence on midget and bistratified ganglion cells that emerges from the above-mentioned studies stands in contrast to the considerable body of psychophysical evidence (surveyed later in this chapter) of rod influence on human color vision and the growing body of physiological and anatomical evidence that a mixture of rod and cone inputs is more the rule than the exception in earlier retinal pathways. At this point, one can only speculate that perhaps the variability among the ganglion cell studies is a result of the sensitivity of functional rod influence to adaptation states, light levels, and other stimulus variations that is evident in both the psychophysics surveyed below and the preganglion cell retinal physiology surveyed above.

Psychophysics of rod-cone interactions: consequences of shared retinal pathways

OVERVIEW The preceding review of our understanding of the retinal substrate of rod-cone interactions underscores that signals initiated in rods and cones share many of the same pathways through the retina and that they combine with the same direction of influence in those pathways. It should not be surprising, then, that a key principle in understanding the psychophysics of rod-cone interactions is that rod and cone signals mimic and reinforce each other in a wide variety of visual tasks under conditions in which both can contribute. However, just as visual processing under *isolated* cone or rod conditions manifests gain control and a variety of spatial, spectral, and temporal antagonisms, so too can rod-cone *interactions* produce increases or decreases in sensitivity and more or less salient percepts.

Psychophysically, in human vision the separate stimulations of rods and cones can be either partially or completely additive for (1) threshold detection of increments and spatial or temporal modulations and (2) suprathreshold brightness or luminosity judgments. More generally, though, background stimulation of either rods or cones tends to reduce (impair) spatial, temporal, and increment (intensity) sensitivity for vision mediated by the other system. Many of these rod-cone impairments show space/time/intensity dependencies that suggest that they are mediated by the same types of adaptive processes observed for isolated rod or cone vision. However, at least one, the rod impairment of cone-mediated flicker sensitivity, appears not to have a direct analog in either isolated rod or cone vision.

In the color domain, rod stimulation also affects suprathreshold hue, saturation, and brightness appearance and, at least in some cases, chromatic discrimination sensi-

tivity. Some of these effects can be understood in terms of differential rod influence on portions of the retinal pathways underlying chromatic processing.

SUMMATION OF ROD AND CONE SIGNALS

Threshold detection. One tradition in studying the quantitative combination rules for rod and cone signals involves the study of their joint contribution to the threshold for detecting the presence of a stimulus or a change from a background state. Early studies did not attempt to assess the additivity of signals from rods and a single cone type. For detection of spots of light, either at absolute threshold or on a background, initial studies found that rod and cone signals combined with less than perfect additivity (Benimoff et al., 1982; Drum, 1982; Frumkes et al., 1973; Ikeda and Urakubo, 1969). These studies found that the degree of additivity was less than perfect but better than that predicted either by probability summation of two independent systems or by orthogonal vector addition, which corresponds to an exponent of 2 in the much-used Minkowski metric or an angle of 90 degrees in vector addition (Graham, 1989).

Buck and Knight (1994) used chromatic adaptation and an increment-threshold paradigm to quantify the summation of rod signals with either M-cone signals or L-cone signals in isolation and found about the same degree of additivity as in the previous studies of aggregate or unspecified cone signals. In contrast, the additivity of rod and S-cone signals was less clear: Buck et al. (1997b) found only about as much additivity as might be expected from probability summation of two independent systems, while Naarendorp et al. (1996) found complete summation.

These studies leave unexplained the reason that these investigators most often found partial additivity between rod and cone signals. The answer was actually evident from the results of van den Berg and Spekreijse (1977) and was later confirmed by Kremers and Meierkord (1999) and Sun et al. (2001). Because rod and cone signals evoked by a single spot of light have different latencies in passing through the visual system, they do not completely overlap, evidently even for longer-duration flashes. This results in less than complete observed additivity. When rod- and cone-stimulating lights are flickered sinusoidally, observed additivity can be made perfect with an appropriate adjustment of the phase of the two flickering lights, provided that the flicker rate is high enough that detection is mediated by *achromatic* (inferred magnocellular) pathways. In *chromatic* (inferred parvocellular) pathways, rod signals show complete additivity with S-cone signals at low mesopic light levels but only probability summation with L- or M-cone signals (Sun, 2001; Sun et al., 2001).

Mesopic sensitivity/luminosity/brightness. Another tradition in studying the quantitative combination rules for rod and cone signals involves the study of their joint contribution to the brightness or effectiveness of suprathreshold lights.

So-called standard-observer functions have been constructed to express the average effectiveness or efficiency for human observers of suprathreshold lights throughout the visible spectrum. For the present discussion, the efficiency of a light can be considered a measure of how bright it would appear relative to lights of the same physical energy level but different wavelengths. Separate standard-observer functions have been established for photopic conditions mediated only by cones [CIE 1924 $V(\lambda)$ and CIE 1964 $V_{10}(\lambda)$] and for scotopic conditions mediated only by rods [CIE 1951 $V'(\lambda)$]. The photopic spectral efficiency function peaks at about 555 nm, while the scotopic spectral efficiency function peaks at about 505 nm. For stimuli presented outside the fovea at intermediate (mesopic) light levels, when both rods and cones mediate vision, human spectral efficiency falls somewhere in between. Figure 55.2 shows that the peak wavelength shifts from near 555 nm to near 505 nm as the light level is reduced. This shift from cone to rod spectral sensitivities underlies what is known as the *Purkinje shift*, an increase in the relative brightness of shorter-wavelength lights compared to longer-wavelength lights as the light level is reduced (see also Chapter 54).

At mesopic light levels, both rod and cone signals can contribute to the effectiveness, luminance, or brightness of lights. However, the exact contributions of rod and cone vision depend on stimulus parameters such as size, timing, and retinal location and the adaptation state of the observer, in addition to the overall light level. Despite these complexities, various attempts have been made to determine generalizable rules relating the rod and cone contributions to mesopic efficiency or brightness (the difference between these terms is not important for the present discussion). Palmer (1976) has suggested that the combined luminance of mesopic lights is approximated by the sum of the photopic luminance and the square root of the scotopic luminance times a parameter that varies with stimulus size. Under different conditions, Ikeda and Shimozono (1981) found that mesopic spectral brightness functions (expressed in log units) were approximated by the linear sum of weighted log scotopic and log photopic brightness functions. The weights on scotopic and photopic functions always summed to unity and varied inversely as the light level changed. Yaguchi and Ikeda (1984) showed that this relationship held over a 3 log unit range of light levels, with 0.1 troland purely scotopic and 100 trolands purely photopic. They also found that only the photopic function was needed to describe brightness matches of 100 trolands, regardless of the prior adaptation state of rods. Thus, 100 trolands

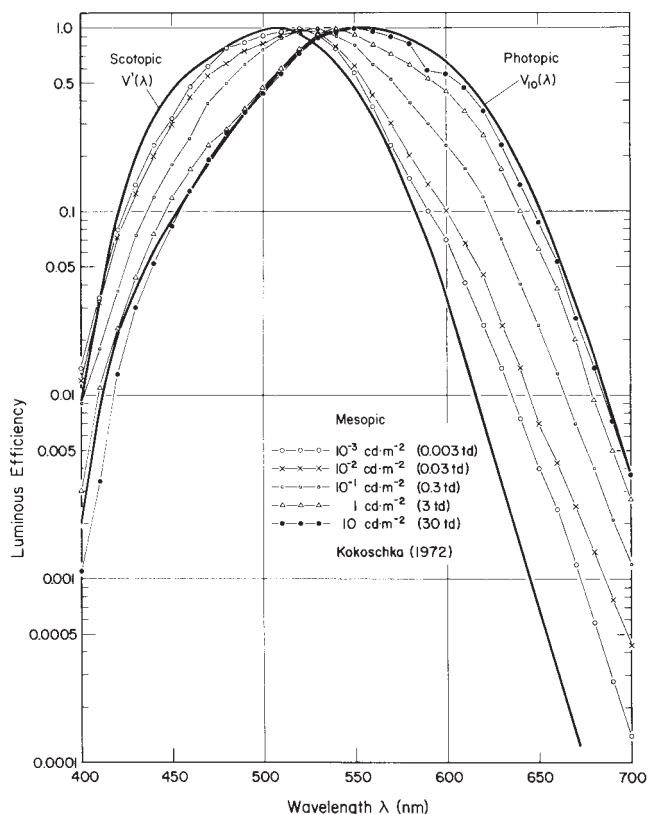


FIGURE 55.2. Mesopic spectral efficiency functions, compared to standard scotopic $V'(\lambda)$ and photopic $V_{10}(\lambda)$ functions. Data are the mean of three observers from Kokoschka (1972). The mesopic functions shift systematically from scotopic to photopic standards over a 4 \log_{10} light level range. (From Wyszecki and Stiles, *Color Science: Concepts and Methods, Quantitative Data and Formulae*, 2nd ed., © 1982. Reprinted by permission of John Wiley & Sons, Inc.)

appears to be a ceiling for rod contributions to brightness, at least for their stimuli.

Some investigators have argued that photopic luminance is mediated by parasol ganglion cells and magnocellular pathways (Lee et al., 1990). However, brightness has a complex relationship to luminance and is unlikely to have such a simple retinal substrate. In any case, the psychophysics of mesopic spectral sensitivity suggests that there should be some circumstances in which rod and cone contributions are additive in their influence on the output of primate parasol ganglion cells. Finally, there are some reports of suppressive brightness interactions between rod and cone signals (Drum, 1981). Although not fully understood, these reports are not necessarily at odds with the prevailing view of summation of rod and cone signals. Cone signals alone can interact to cause brightness reductions; rods may simply be adding to cone signals in pathways that lead to this suppression.

ROD-CONE INTERACTION IN DETECTION SENSITIVITY Sensitivity regulation processes operate under both scotopic and

photopic conditions. Signals from cones can either increase or decrease the sensitivity for detection of a spot of light by cones, and signals from rods can either increase or decrease the sensitivity for detection by rods. Examples of these processes include (1) the increase of increment threshold for a patch of light with an increase of background light level, (2) the decrease of increment threshold that can accompany the increase in the size of a background (termed *spatial sensitization*), and (3) the decrease of threshold that occurs during dark adaptation as the visual system recovers from higher light levels (see also Chapter 54).

As we have seen already, signals from rods and cones can operate together in retinal pathways and visual processing. It is not surprising, then, that either rod or cone signals can participate in many or most of the regulation processes that affect sensitivity for signals arising from the other photoreceptor type. In fact, this area attracted much early research interest as investigators found that rod-cone interactions play a role in the regulation of sensitivity for detection of spots of light during dark adaptation (recovery from a bleaching light) and on backgrounds that determine the state of light adaptation of a patch of retina.

One line of early work made use of procedures in which threshold for a briefly flashed test stimulus was measured as a function of the timing of a briefly flashed concentric disc

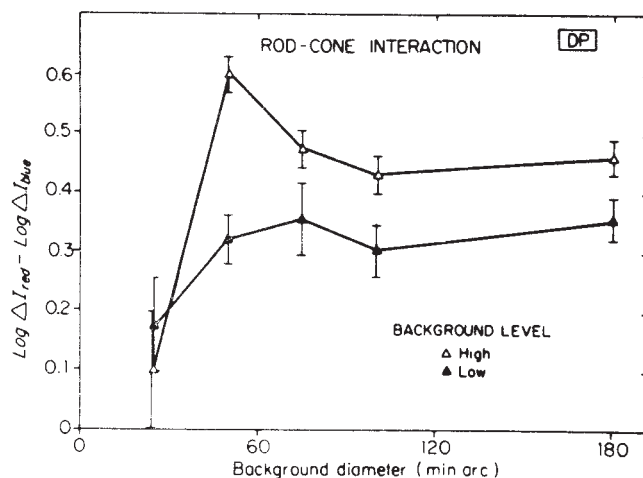


FIGURE 55.3. Elevation of rod-mediated increment thresholds varies with the size and light level of the cone-stimulating background disc. Each point represents the difference of rod threshold on red and blue backgrounds that are scotopically matched but that differ in excitation of cones. The magnitude of this rod-cone interaction increases with the level of cone stimulation on both smaller and larger backgrounds. At higher light levels, rod-cone interaction is typically larger for smaller backgrounds. Rod-cone interaction shows spatial sensitization analogous to that observed in isolated scotopic and photopic vision. (Reprinted from *Vision Research*, vol. 19, Buck, Peeples, and Makous, Spatial patterns of rod-cone interaction, pp. 775–782, © 1979, with permission from Elsevier Science Publishers.)

or annulus or an adjacent flanking patch. The results of these double-flash procedures (variously termed *contrast flash*, *after flash*, *backward masking*, or *metaconstrast*) were interpreted as showing that rod signals traveled through the visual system with up to 100 msec longer latency and that cone-stimulating flashes could raise (Foster, 1976; Frumkes et al., 1973) or lower (Barris and Frumkes, 1978) thresholds for rod-detected flashes, depending on the relative timing of the two flashes. Other studies suggested that rod flashes could also raise cone-mediated thresholds (Frumkes et al., 1972). Although interpretation of these double-flash procedures is complicated, they clearly demonstrate that rod and cone signals affect each other in ways similar to those found under isolated scotopic or photopic conditions.

Other early investigations focused on rod-cone interaction produced by steady background fields. Among the early reports, Makous and Boothe (1974) provided a particularly rigorous demonstration that steady cone background stimulation could raise rod thresholds, which had been previously suggested by Lennie and MacLeod (1973). They used multiple ways of varying the cone excitation provided by a background while keeping the rod background excitation constant. They found that, in all cases, backgrounds providing more cone excitation raised increment thresholds for a purely rod-detected test spot more than did backgrounds providing less cone excitation. Thus, rod and cone signals from the background worked together to determine the sensitivity of rod-mediated detection. Analogous to the reciprocal rod-cone interactions reported for the double-flash procedures, both directions of interaction were also reported on steady backgrounds. Increases of cone-mediated increment thresholds by rod-stimulating steady backgrounds were reported by Latch and Lennie (1977) and Temme and Frumkes (1977). These effects can be very large, with desensitizations of cone thresholds reported to be up to 2 log units, a factor of 100 (Buck, 1980).

Isolated scotopic and photopic vision display what is termed *spatial sensitization*: thresholds for a small test spot are highest for a somewhat larger steady background and then decline (become more sensitive) as background size increases (Westheimer, 1965, 1967). As illustrated in Figure 55.3, similar patterns are found for rod-cone interactions: the magnitude of the interaction is greatest on smaller backgrounds and decreases on larger backgrounds. This is true both for the desensitization of rod thresholds by background stimulation of cones, as shown in Figure 55.3 (Buck et al., 1979; Frumkes and Temme, 1977; Latch and Lennie, 1977) and for the reciprocal interaction (Buck, 1980; Latch and Lennie, 1977; Temme and Frumkes, 1977). Despite early reports to the contrary, both directions of rod-cone interaction are not confined to small background stimuli (Buck, 1985a, 1985b; Buck et al., 1979) and increase as the back-

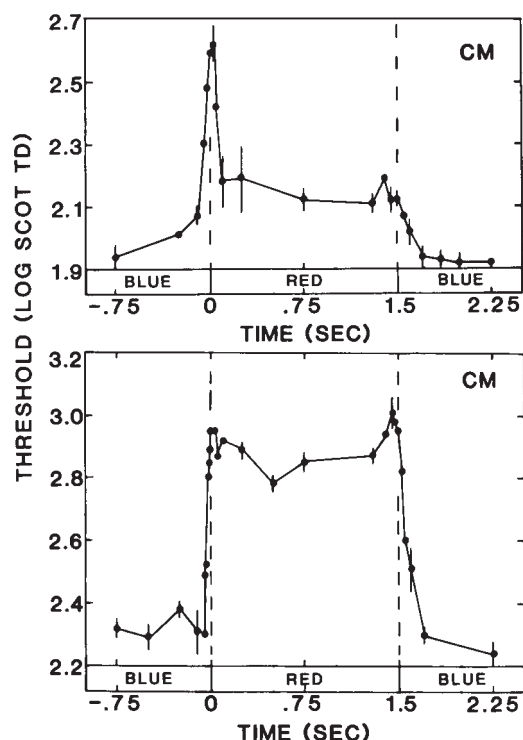


FIGURE 55.4. Time course of elevation of rod-mediated increment thresholds measured on alternating, scotopically equal, red and blue backgrounds. The red backgrounds stimulate cones more strongly than the blue backgrounds. Rod-cone interaction (threshold elevation) is greater and more sustained on smaller 0.6-degree-diameter backgrounds (*upper panel*) compared to larger 7.8-degree-diameter backgrounds (*lower panel*). Rod-cone interaction shows latency differences of center-surround antagonism analogous to that observed in isolated scotopic and photopic vision. (Reprinted from *Vision Research*, vol. 24, Buck, Stefurak, Moss, and Regal, Time course of rod-cone interaction, pp. 543–548, © 1984, with permission from Elsevier Science Publishers.)

ground light level increases (Buck, 1985a; Buck and Makous, 1981).

Another property of isolated scotopic and photopic vision that is shared by both directions of rod-cone interaction is that threshold elevation is greatest in response to background transients. Thus, rod-cone interaction often has been reported as greater when produced by flashed than by steady backgrounds (e.g., Ingling et al., 1977). As shown in Figure 55.4, both directions of rod-cone interaction can be greater at the onset (and sometimes offset) of a background than after the background has been on for even a few hundred milliseconds (Buck, 1985a, 1985b; Buck et al., 1984). Figure 55.4 also illustrates that such transients tend to be more prominent for large backgrounds, indicating that signals from large backgrounds operate with some latency to reduce the desensitization (effects of adaptation) of test thresholds.

These studies of increment-sensitivity regulation make it clear that rod and cone signals can work together both in

spatially localized adaptation processes and in the lateral interactions that work across the retina to regulate these adaptation processes. Questions persist, though, about which lateral pathways control which types of rod-cone interaction. Isolated rod and cone lateral interactions (inferred from spatial sensitization functions) have different size/distance parameter values for the same size and retinal location of stimuli. We don't know when both rod and cone pathways contribute to lateral interactions or when just one or the other contributes. The one clue we have is that lateral spatial interactions, as revealed by spatial sensitization functions, are quantitatively identical when purely scotopic annuli of varied size influence both rod test thresholds and cone test thresholds (Buck, 1985b). At least under the conditions tested, no such simple correspondence between either isolated rod or isolated cone lateral spatial interactions exists when background discs are used, suggesting that more than one lateral interaction mechanism is active in the latter situation.

ROD-CONE INTERACTION IN TEMPORAL SENSITIVITY Three fundamentally different types of rod-cone interactions can be observed for flickering stimuli.

The first rod-cone flicker interaction is familiar and ubiquitous: the manifestations of summation of rod and cone signals already discussed in the sections "Threshold Detection" and "Rod-Cone Interaction in Detection Sensitivity." Flicker signals originating in both rods and cones may either enhance or cancel each other, depending on their relative phase when they arrive at a common neural locus (e.g., Denny et al., 1990; van den Berg and Spekreijse, 1977). One of the first manifestations of this summative interaction was the report by MacLeod (1972) that cancellation can be obtained between rod and cone signals evoked by a single mesopic flickering stimulus, with appropriate adjustment of flicker frequency and light level. MacLeod reported that when a test stimulus was flickered at 7.5 Hz, it was visible at scotopic background light levels (when the rod response dominated) and at high background levels (when the cone response dominated), but flicker was invisible no matter how bright the test patch was at middle background levels (when rod and cone signals were approximately equal in magnitude and 180 degrees out of phase). MacLeod also showed that the test intensity needed to detect 7 Hz flicker increased as rods dark adapted, that 3.5 Hz flicker showed no such cancellation, and that the effects could be replicated with separate, superimposed rod- and cone-stimulating lights.

The second rod-cone flicker interaction is analogous to rod-cone interactions in increment detection. Knight and Buck (1993) and Sharpe et al. (1993) showed that cone excitation by a background raised the flicker threshold (amount of light needed to detect 15 Hz flicker) for one

psychophysical rod mechanism but had little effect on another. The relatively unaffected mechanism was the “slow” rod mechanism that is most evident at scotopic light levels and is likely a manifestation of rod signals passing through rod bipolar and AII amacrine cells. The affected mechanism was the “fast” rod mechanism that is most evident at mesopic levels (Connor and MacLeod, 1976) and is likely a manifestation of rod signals passing through direct gap junctions from rods to cones. The cone background presumably raises the rod flicker threshold by the same sensitivity regulation mechanisms that would operate on cone flicker signals.

However, some cone mechanisms may have more influence on rods than do others. For example, Shapiro (2002) has shown that rod flicker thresholds are more sensitive to variations of background L-cone stimulation influence than to variations of S-cone stimulation (M-cone variations were not tested).

The third rod-cone flicker interaction is a type not yet described in this chapter: the reduction of cone-mediated flicker sensitivity by signals from unstimulated, dark-adapted rods. (It will, however, have a counterpart in the next two sections.) This interaction was first described by Goldberg et al. (1983), Coletta and Adams (1984), and Alexander and Fishman (1984), with remarkable unanimity. As shown in Figure 55.5, during dark adaptation, the light level needed to detect flicker in a cone-detected test stimulus (say, at >15 Hz and long wavelength) initially falls as cones recover but then increases again, sometimes by more than a factor of 10, as rods recover sensitivity on their slower time scale.

The flicker-threshold elevation is independent of the degree of stimulation of rods by the test stimulus, and is instead controlled by the state of adaptation of rods in a large area surrounding the test (Alexander and Fishman, 1984; Coletta and Adams, 1984; Goldberg et al., 1983). Indeed, rod stimulation inside the test spot can be doubled with no change of cone threshold. However, the interaction can be removed by adding light to the area surrounding the test spot, with complete disappearance at surround light levels that saturate rods. Thus, the magnitude of this flicker-threshold elevation is directly related to the state of rod dark adaptation and inversely related to the state of rod light adaptation. The magnitude of the interaction is greatest for smaller test stimuli (less than 3 degrees in diameter) and higher flicker frequencies (15 to 40 Hz), as shown in Figure 55.6, and increases with increased retinal eccentricity (Alexander and Fishman, 1986). Consistent with control by the state of adaptation of distant rods, flicker threshold for test stimuli confined to the rod-free foveola is influenced by rods within a 2 degree radius (Coletta and Adams, 1986).

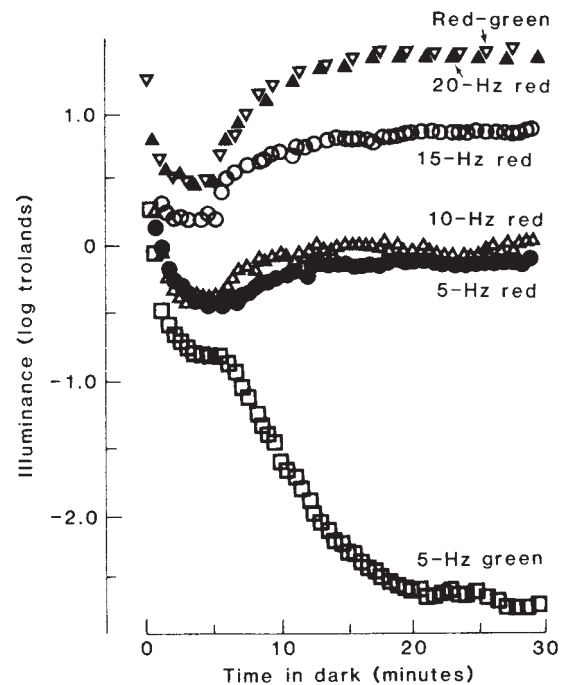


FIGURE 55.5. Elevation of cone-mediated flicker thresholds by dark-adapting rods, also known as *suppressive rod-cone interaction* (SRCI). Cone-mediated flicker thresholds first fell as cones gained sensitivity in the dark but then rose as rods also gained increased sensitivity. Cone thresholds are elevated by a tonic suppressive influence of unstimulated, dark-adapted rods in the vicinity of the test stimulus. A 5 Hz green flickering light (lowest trace) was detected by rods after about 5 minutes, so its threshold fell as rod sensitivity increased in the dark. (Reprinted with permission from Goldberg, Frumkes, and Nygaard 1983 (Inhibitory influence of unstimulated rods in the human retina: evidence provided by examining cone flicker, *Science*, 221:180–82), © 1983 American Association for the Advancement of Science.)

This type of rod-cone flicker interaction has been dubbed *suppressive rod-cone interaction* (SRCI) by Frumkes and Eysteins-son (1987), who argue that it arises from a tonic suppressive (possibly inhibitory) influence of dark-adapted rods on cone-mediated pathways that is removed by rod light adaptation. SRCI has been related to physiological processes observed in early retina in lower vertebrates and cat (Eysteins-son and Frumkes, 1989; Frumkes and Eysteins-son, 1988; Frumkes and Wu, 1990). The substrate for the interaction in humans is not known but is observable in the electro-retinogram (ERG) (Arden and Frumkes, 1986). Clinical patients who have a variety of disorders of the outer (distal) retina show little or no flicker interaction (Alexander and Fishman, 1985). Intriguingly, the effect is virtually absent in protanopes (who lack normal L cone pigment) but is evident in deuteranopes (who lack normal M-cone pigment) and color normals (Coletta and Adams, 1985; Frumkes et al., 1988). Similarly, in color-normal observers, the flicker interaction is accompanied by a selective loss of L-cone

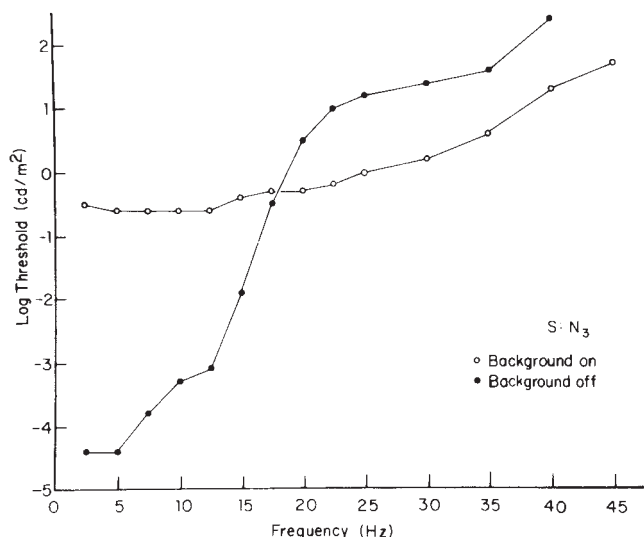


FIGURE 55.6. Flicker-frequency dependence of elevation of cone-mediated flicker thresholds by dark-adapted rods (SRCI). Above 18 Hz, flicker thresholds were always cone mediated but were lower when a background (*open symbols*) light-adapted rods in the vicinity of the test stimulus than when those rods were unstimulated and dark adapted (*closed symbols*). Saturation of the rods by the background presumably removes a tonic signal that suppresses cone flicker sensitivity. (Reprinted with permission from Alexander and Fishman 1984 (Rod-cone interaction in flicker perimetry. *Br. J. Ophthalmol.*, 68:303–309), © 1984 BMJ Publishing Group.)

sensitivity (Coletta and Adams, 1984). There is no obvious explanation from retinal anatomy and physiology for this striking cone specificity.

Coletta and Adams (1984, 1986) demonstrated a purely photopic analog of SRCI: the adaptive state of cones surrounding a flickering test patch also affected flicker sensitivity in the same way as SRCI. However, the retinal distances over which these interactions occurred differed by a factor of 3 or more. Thus, the pathways mediating the lateral spatial interactions responsible for flicker suppression may be different for rods and for cones. There is one report of an effect of cone adaptation state on rod-flicker sensitivity, analogous to SRCI, but it has not been studied further (Frumkes et al., 1986). In any case, there are no demonstrations of rod and cone signals working together (additively or otherwise) to mediate this sort of flicker interaction. The question of how these adaptation-state-dependent interactions are related to the more common rod-cone-combination interactions remains unanswered.

ROD-CONE INTERACTION IN SPATIAL SENSITIVITY There are many similarities between rod-cone interactions in the temporal and spatial domains, as well as some differences. We'll look at the similarities first. Resolution of the highest spatial and temporal frequencies is mediated by cones, rather than rods, even at low mesopic light levels. Resolution of the

lowest spatial and temporal frequencies may be possible at lower light levels for rod-mediated vision than for cone-mediated vision. In between, both rods and cones can work together to resolve both temporal and spatial patterns (Brown and Woodward, 1957; D'Zmura and Lennie, 1986; Long, 1978), although no one has quantified the degree of additivity between rod and cone contributions to grating resolution.

The adaptation state of rods influences cone-mediated spatial sensitivity in similar fashion to the influence on cone-mediated temporal sensitivity. Rod dark adaptation raises cone-mediated spatial thresholds and acuity (the highest spatial frequency or smallest detail resolvable). Adding a large rod-detected background increases cone spatial thresholds and acuity. The rod effects are smallest for low-spatial-frequency (large stripe) gratings but can be more than 1 log unit with high-spatial-frequency targets. Both spatial and temporal rod effects operate over the same range of light levels, near the high end of the scotopic/mesopic range (Naarendorp and Frumkes, 1991; Naarendorp et al., 1988). Furthermore, both temporal and spatial interactions increase with increased retinal eccentricity and decreased stimulus size (Lange et al., 1997), and both are reportedly absent in at least some protanopes (Frumkes et al., 1988). However, a variety of differences between the properties of the spatial and temporal interactions led Lange et al. (1997) to propose that different neural substrates mediate them. These differences include the occurrence of interocular transfer (yes for spatial but no for temporal) and the finding of the interaction with small stimuli confined to the fovea (yes for temporal but no for spatial).

Finally, rod and cone signals interact in the desensitization produced by prior adaptation to spatial patterns. Seminal early studies (e.g., Blakemore and Campbell, 1969) showed that, in photopic vision, adaptation to spatial contrast can raise spatial contrast thresholds for patterns of similar spatial frequency and orientation. Similar effects occur when the adapting pattern is seen by either rods or cones and the test pattern is seen by the other system (D'Zmura and Lennie, 1986). Furthermore, prior spatial adaptation of rods raised the light levels needed by cones for resolution of a low-frequency grating with specificities (measured as half-bandwidth at half-height) of 15 to 20 degrees on orientation and <1 octave of spatial frequency (Buck and Knight, 1986). These values are in the same domain as those reported in photopic vision, supporting the idea that rod and cone signals combine together distal from the site(s) at which spatial pattern adaptation produces desensitization to similar spatial patterns.

This spatial-contrast-adaptation interaction seems to be another example of rod and cone signals combining with the same sign in a common pathway before influencing visual performance in a similar way. In further support of this idea,

D’Zmura and Lennie (1986) found that moving spatial gratings visible to rods could be made indistinguishable from gratings visible to cones, with only adjustment of spatial contrast. However, this interaction also illustrates another general principle of rod and cone pathways: the properties of an early stage of rod or cone pathways may impart properties that exclude signals from portions of later pathways. In this case, the early limitations posed on rod-system acuity—up to about 6 to 7 c/deg at best (Brown and Woodward, 1957; Long, 1978)—keep rod signals from participating in the processing of higher spatial frequencies.

ROD INFLUENCE ON COLOR VISION Psychophysicists distinguish three perceptual aspects of color: brightness, saturation, and hue. There is a long-standing and relatively uncontroversial literature documenting rod influence on brightness (reviewed in the section “Mesopic Sensitivity/Luminosity/Brightness”) and saturation. In contrast, accounts of the influence of rods on hue have been often confusing and sometimes outright conflicting. Nevertheless, it is clear that rod excitation can influence all three perceptual dimensions of human color vision.

Rod influence does not, however, repeal the long-recognized trichromacy of normal human color vision. The *tetrachromacy* attributed to rod contributions to color vision (Trezona, 1970, 1974) refers only to the fact that rod signals can upset three-variable color matches when the adaptation level is changed. At any constant adaptation level, three variables (matching lights) suffice for color matches. Thus, the rod signals do not constitute an independent fourth channel for color vision. They must, instead, collapse onto the three-variable, cone-fed channels. How that may happen is discussed below.

Rod influence on hue. Several early studies suggested that there was a single rod hue, which was blue (e.g., Ambler, 1974; Trezona, 1970, 1974; Willmer, 1950). Despite the influence of these early reports, we know now that rod signals can evoke most or all hues, as first suggested by Stabell and Stabell (1971) over 30 years ago, but that they do so differentially, biasing the hues determined by cones. And despite over 50 years of scientific literature about rod influences on hue, textbooks at every level, from introductory psychology to advanced color vision, typically say only that rod vision is colorless or achromatic and that human color vision is based entirely on the output of the three types of cone photoreceptor. Certainly, no one has integrated rod influence into our current theoretical and quantitative models of human color vision. However, much progress has been made recently in this direction and in reconciling the diverse findings in the prior literature on rod influence on hue.

One group of studies of rod influence on hue investigated *scotopic color contrast*, in which a colored adapting field induces a hue into a simultaneously or successively presented, purely rod-detected test field. The overall conclusion of these studies is that rod signals can be associated with almost any hue but that there is an overall rod hue bias toward blue. Simultaneous scotopic color contrast was first reported by Willmer (1950), who showed that a purely rod-detected test field appeared bluish when presented adjacent to a red-appearing inducing field that was suprathreshold for both rod- and cone-mediated detection. During the 1960s and 1970s, Ulf and Bjorn Stabell studied both simultaneous and successive variants of scotopic color contrast. (In the latter case, the test field is presented immediately after an inducing field at the same retinal locus.) They concluded that by using a full range of hues of inducing field, a full range of scotopic-contrast hues could be produced, not just the blue hue found under the conditions tested by Willmer (Stabell, 1967). The Stabells further emphasized the close correspondence between the scotopic-contrast hue and the hue that is complementary (defined by cone-mediated color cancellation) to a given wavelength of inducing field (Stabell and Stabell, 1971, 1978).

The Stabells supported the hypothesis (1) that rod signals have access to all portions of the neural pathways that produce our color perceptions and (2) that the hue of both scotopic and photopic color contrast is determined by the differential adaptation of the color pathways resulting from stimulation of cones by the inducing field. Rod signals evoked by the rod-detected test field flow through the color pathways in essentially the same manner as the cone signals from an “achromatic” cone-detected test field. The resulting

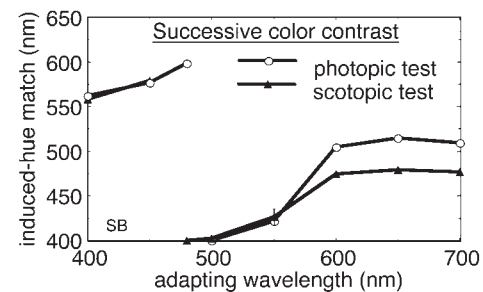


FIGURE 55.7. Comparison of scotopic and photopic successive contrast hues generated by the same adapting fields. Hue induced into the initially achromatic test stimulus is represented by the closest matching spectral wavelength (vertical axis) as a function of the adapting field wavelength (horizontal axis). Both photopic and scotopic contrast hues change in similar ways with adapting wavelength, indicating rod involvement in the full set of parallel color pathways. However, the increased blueness of scotopic contrast hues at longer wavelengths reveals a net rod blue bias. (Adapted from Buck and Ayers, 1997.)

color contrast hues, whether photopic or scotopic, are a reflection of the differential sensitivity (adaptive state) of the various portions of the color pathways caused by differential stimulation of cones by the inducing field.

Recent studies have explored the differences between scotopic and photopic color contrast hues (Buck, 1997; Buck and Ayers, 1997; Buck and Brandt, 1995; Stabell and Stabell, 1994). These differences suggest that, although rod signals may have access to all of the parallel color pathways, as the Stabells suggested, the rod signals have biased or differential effects in different portions of the color pathways. Thus, scotopic color contrast hues are not just determined by differential cone adaptation but are also influenced by differential effects of rod signals in different portions of the color pathways. In the case of successive scotopic color contrast, this differential effect is a net rod hue bias toward blueness (Buck, 1997; Stabell and Stabell, 1994), as illustrated in Figure 55.7.

Another group of studies assessed *rod influence during dark adaptation* on either the sensitivity for detecting hue or the qualitative perception of hue (i.e., whether red, green, blue, yellow, etc.). Analogous to what occurs with temporal and spatial sensitivity, sensitivity to hue decreases during dark adaptation (Lie, 1963; Spillmann and Conlon, 1972). This has been described in various ways in the literature. One way is to state that the *specific hue threshold* (the light level for just detecting the presence of hue) increases during dark adaptation. Another way is to state that the *photochromatic interval* (the difference in light level between absolute detection threshold and specific hue threshold) increases during dark adaptation. This is also equivalent to saying that during dark adaptation, achromatic thresholds decrease while chromatic thresholds increase. Interpretations of this phenomenon also vary. Lie (1963) has implied that rods increasingly contribute desaturating signals as they dark adapt. However, Ambler (1974) has suggested an explanation in terms of rods increasingly contributing a fixed blue signal that degrades the specificity of chromatic signals. In line with the latter interpretation, Frumkes has suggested that rod signals suppress chromatic cone signals differentially, with more suppression for red/green than for blue/yellow (McMullen et al., 1998). Whatever the ultimate resolution, there is no necessary relationship between the rod influence on hue detection and the rod influence on perceived suprathreshold hue quality. The threshold for hue detection seems likely to be more closely related to saturation than to hue quality.

One of the oft-cited studies supporting the idea that rod excitation is associated with a singular blue hue is that of Ambler (1974). He showed that below the specific hue (chromatic) threshold the dominant hue is blue, regardless of the wavelength of the light. Ambler reconciles his results with those of Lie (1963), who showed that the specific hue threshold increased during dark adaptation, by pointing out

that Lie's observers knew the suprathreshold hue associated with the wavelength they were viewing, so they may have discounted the anomalous rod blue hue. In contrast, Ambler's observers were blind to the wavelength they were viewing.

A third group of studies can be described as *rod-cone color-mixture studies*, in which the addition of rod stimulation causes a change from the hue that would result from the stimulation of cone photoreceptors alone. It was appreciated early on that color matches could be upset by rod influence if a large test field was used (for review see Shapiro et al., 1994). Richards and Luria (1964) and Trezona (1970, 1974) have argued from changes of color-matching functions with light level that rod stimulation adds blueness. For example, Trezona showed that progressively more B primary was needed, relative to the G and R primaries, to maintain a color match as light level dropped. However, the 445 nm B primary presumably appeared violet (red plus blue) rather than blue, and more G primary was needed as well, possibly to cancel the increased redness on the increased 445 nm light. However, these are inferences about the perceptual consequences of the primary lights that are not directly assessed in the color-mixture paradigm. (This is a general complication of making perceptual inferences from color-matching data.) Even though the evidence is inferential, these studies do suggest that rod stimulation enhances blueness. However, other rod influences on hue cannot be ruled out.

In fact, recent rod-cone mixture studies in my laboratory have used psychophysical manipulations to tease apart multiple rod influences on hue that affect different spectral regions and that operate with different time course and light-level dependence. A group of these studies consistently finds rod enhancements of the percepts of *blue*, *green*, and *short-wavelength red* (the red component in violet-appearing short-wavelength lights). These three rod hue enhancements are shown by studies of rod-induced shifts of the loci of unique (unitary or one-component) and binary (two-component) hues (Buck et al., 1997a, 2000), rod-induced shifts of the spectral distributions (hue scaling) of the four basic hues (Buck et al., 1998), as shown in Figure 55.8, and the time course and intensity dependence of rod-induced hue shifts (Knight and Buck, 2002). The use of narrowband spectral stimuli in all of these procedures permits separation of rod influences in different spectral regions that can be further distinguished by means of differences in temporal or intensity dependence.

These studies reveal that the blue and SW-red rod hue biases share several properties with each other (shorter-wavelength spectral locus, longer latency, greater light-level dependence) compared to the rod green bias. This is consistent with different rod influence on different portions of the neural pathways subserving hue perception. As schema-

tized in Figure 55.9, the green rod hue bias likely results from interaction of rod signals with retinal pathways processing signals from M and L cones, likely the pathways leading to midganglion cells. The blue and SW-red rod hue biases likely result from interaction of rod signals with retinal pathways processing signals from S cones, possibly the pathways leading to small-bistratified ganglion cells (Buck et al., 1998; Buck, 2001).

Appealing features of this account are that it is consistent with the general evidence that rod and cone signals act with the same sign on shared neurons and that rod signals must interact with signals from all three classes of cone and on both opponent-hue dimensions (red-green, blue-yellow). Following conventional color-vision and retinal-processing models (Dacey and Lee, 1994; De Valois and De Valois, 1993; Hurvich, 1981) that link cone excitations to hue percepts models, this scheme suggests that the green rod hue bias results from a stronger rod influence on M cone pathways than on L cone pathways, and that the blue and SW-red rod hue biases result from the additivity of rod signals with S cone signals.

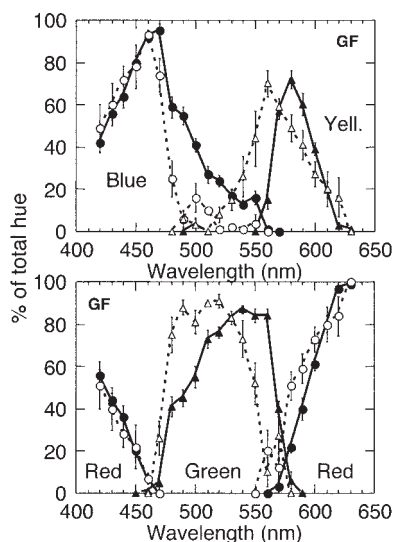


FIGURE 55.8. Rod influence changes the balance of hues seen across the spectrum. Shown are hue scaling functions for physically identical spectral stimuli of 1 second duration under two different adaptation states: cone-plateau (*open symbols and dashed lines*) and fully dark-adapted (*solid symbols and lines*). Under dark-adapted conditions, rod signals enhanced blue relative to yellow (*rod blue bias*) and green relative to long-wavelength red (*rod green bias*). Although not revealed in this figure, rod signals also enhanced short-wavelength red relative to green (*rod red bias*), thereby roughly canceling the rod green bias that would otherwise have been seen at short as well as long wavelengths. Similar hue scaling of very brief stimuli reveals that the rod green bias is complete very quickly, while the rod blue bias and rod red bias take longer to reach full magnitude. (Reprinted from *Vision Research*, vol. 38, Buck, Knight, Fowler, and Hunt, Rod influence on hue-scaling functions, pp. 3259–3263, © 1998, with permission from Elsevier Science Publishers.)

However appealing and simple this account of rod hue biases may be, it is clearly incomplete. At the physiological level, both the loci and mechanisms of the posited rod-cone interactions are unknown, and data on rod signals in retinal ganglion cells do little to explain the perceptual effects of rods on hue (see the section “Rod Influence on Retinal Output Pathways (Ganglion Cell Types)”). Psychophysically, the studies on which this account is based were designed to assess rod influence on hue at the lowest possible mesopic light levels, with constant rod excitation (and therefore differential photopic luminance) across wavelengths, and with a narrow range of stimulus sizes and retinal eccentricities. Studies from other laboratories indicate that when these conditions change, different patterns of rod hue influence are found (e.g., Nerger et al., 1995, 1998; Volbrecht et al., 2000). Even my own studies indicate that (1) variation of stimulus duration (Buck and Knight, in press) or duration of prior rod light adaptation (Knight and Buck, 2001) can determine whether rods enhance red or green, and (2) variation of light level can reverse the direction of the blue and SW-red rod hue biases (Buck et al., 2000). It is not yet clear how to reconcile the different results found under different conditions into a single account of rod influence on hue.

In any case, it is easy to understand why there is such a diversity of rod hue effects reported in the literature. Different tasks/stimuli may evoke different combinations of the separate rod influences.

Chromatic discrimination. The nature of the influence of rods on chromatic discrimination (distinguishing stimuli that differ in hue and/or saturation) is one of the most interesting aspects of rod influence on color vision. The ubiquitous desaturation that rods contribute to colored stimuli suggests that rods should *impair* chromatic discrimination by diluting the chromatic signals. Such results have indeed been reported for observers having normal color vision. Yet, studies of color-deficient observers, who lack one or more of the normal cone pigments, report circumstances in which rod signals appear to *enhance* chromatic discrimination.

For normal trichromatic observers, dark adaptation reduces wavelength discrimination for extrafoveal stimuli throughout most of the spectrum at mesopic light levels (Stabell and Stabell, 1984). Recent studies have shown that, for color-normal observers, rods impair both Rayleigh discriminations, which are mediated by L-M cone differences (Nagy and Doyal, 1993), and tritan discriminations, which are mediated by S cones (Knight et al., 2001). Using the Farnsworth-Munsell 100 hue test, Knight et al. (1998) found that rod-mediated impairment was considerably stronger along the tritan axis than along the Rayleigh axis. They also found that the rod impairment of tritan discrimination grew as the light level dropped. Thus, in color-

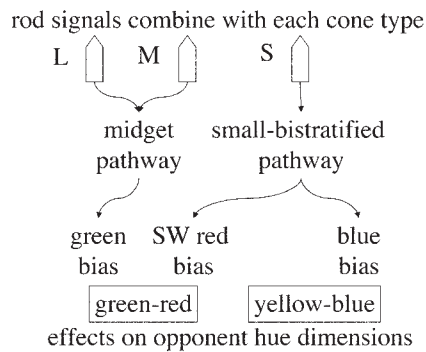


FIGURE 55.9. Retinal substrate scheme for rod influence on color pathways. Psychophysical results are consistent with the same-sign combination of rod signals with those of each cone type. Stronger rod influence on M-center than L-center midget ganglion cell pathways leads, by conventional color vision theory, to a midget-mediated *rod green bias*. Addition of rod signals to S-cone ganglion cell pathways (possibly small-bistratified) results, again by conventional color vision theory, to *rod blue bias* and *rod red bias*.

normal observers, rods impair chromatic discriminations mediated by either L-M-cone pathways or S-cone pathways in isolation.

Rods have quite the opposite effect in observers lacking one or more cone type. Smith and Pokorny (1977) studied the color matching and discrimination performance of protanopes and deuteranopes, who lack normal L- and M-cone pigments, respectively, and who cannot discriminate green or red from yellow for small foveal targets. However, when target size was increased so that rods were also stimulated, discrimination ability improved for both protanopes and deuteranopes. Protanopes and deuteranopes have two of the three normal cone types, but so-called blue-cone monochromats (also known as *X-chromosome-linked incomplete achromats*) have only S cones. Reitner et al. (1991) showed that in these individuals, rods can operate with S cones to mediate wavelength discrimination between 440 and 500 nm at mesopic light levels.

Thus, rod signals typically impair the chromatic discriminations mediated by cone signals in normal trichromatic observers. However, rod signals can restore at least some chromatic discrimination ability not supported by cone signals in color-deficient observers. Both results can be understood if it is assumed that rod signals have access to all three dimensions of normal trichromatic color vision. In color-normal observers, these rod signals reduce differences among the three signals, thereby reducing differential sensitivity. In color-deficient observers, rod signals substitute for cone signals to resuscitate one or more of the three dimensions of color vision that are otherwise lost because of missing cone types.

Final comments

Historically, rod-cone interactions were often regarded as unwanted artifacts in studies of spectral luminosity, color matching, and cone-mediated detection. Through half a century of research, we have come to appreciate the breadth of influence they have and how much they reveal about fundamental properties of human vision. We now recognize an expanding variety of demonstrated and possible substrates of interaction of rod and cone signals just within the primate retina. The challenge will be to identify the specific substrates of psychophysically observed rod-cone interactions that are important for human vision.

Harder to address empirically are issues of the utility and genesis of rod-cone interactions. Have they evolved because they confer particular advantages or because they are unavoidable concomitants of other useful aspects of our visual systems?

REFERENCES

- Alexander, K. R., and G. A. Fishman, 1984. Rod-cone interaction in flicker perimetry, *Bro. J. Ophthalmol.*, 68:303–309.
- Alexander, K. R., and G. A. Fishman, 1985. Rod-cone interaction in flicker perimetry: evidence for a distal retinal locus, *Doc. Ophthalmol.*, 60:3–36.
- Alexander, K. R., and G. A. Fishman, 1986. Rod influence on cone flicker detection: variation with retinal eccentricity, *Vis. Res.*, 26:827–834.
- Ambler, B. A., 1974. Hue discrimination in peripheral vision under conditions of dark and light adaptation, *Percept. Psychophys.*, 15:586–590.
- Arden, G. B., and T. E. Frumkes, 1986. Stimulation of rods can increase cone flicker ERGs in man, *Vis. Res.*, 26:711–721.
- Barris, M. C., and T. E. Frumkes, 1978. Rod-cone interaction in human scotopic vision—IV. Cones stimulated by contrast flashes influence rod threshold, *Vis. Res.*, 18:801–808.
- Benimoff, N. I., S. Schneider, and D. C. Hood, 1982. Interactions between rod and cone channels above threshold: a test of various models, *Vis. Res.*, 22:1133–1140.
- Blakemore, C., and F. W. Campbell, 1969. On the existence of neurones in the human visual system selectively sensitive to the orientation and size of retinal images, *J. Physiol.*, 203:237–260.
- Brown, K. T., and L. K. Woodward, 1957. Rod-cone interaction in the dark-adapted eye, *Optica Acta*, 4:108–114.
- Buck, S. L., 1980. Cones are desensitized by backgrounds they don't see, in *Recent Advances in Vision: Technical Digest*, Washington, DC: Optical Society of America, pp. FA11–FA13.
- Buck, S. L., 1985a. Cone-rod interaction over time and space, *Vis. Res.*, 25:907–916.
- Buck, S. L., 1985b. Determinants of the spatial characteristics of cone-rod interaction, *Vis. Res.*, 25:1277–1284.
- Buck, S. L., 1997. Influence of rod signals on hue perception: evidence from successive scotopic color contrast, *Vis. Res.*, 37:1295–1301.
- Buck, S. L., 2001. What is the hue of rod vision? *Color Res. Appl.*, 26(Suppl):S57–S59.

- Buck, S. L., and M. Ayers, 1997. Physical and sensory analysis of successive scotopic color contrast, in *Colour Vision Deficiencies XIII: Documenta Ophthalmologica Proceedings Series*, vol. 58 (C. R. Cavonius and J. D. Moreland, eds.), Dordrecht, the Netherlands: Kluwer, pp. 127–134.
- Buck, S. L., and J. Brandt, 1995. The range of scotopic contrast colors matches that associated with S-cone activation, in *Colour Vision Deficiencies XII: Documenta Ophthalmologica Proceedings Series*, vol. 57 (B. Drum, ed.), Dordrecht, the Netherlands: Kluwer, pp. 309–316.
- Buck, S. L., and R. Knight, 1986. Grating-adaptation aftereffects and cone-rod interaction, *J. Opt. Soc. Am. A*, 3:P27.
- Buck, S. L., and R. Knight, 1994. Partial additivity of rod signals with M- and L-cone signals in increment detection, *Vis. Res.*, 34:2537–2545.
- Buck, S. L., and R. Knight, in press. Stimulus duration affects rod influence on hue perception, in *Normal and Defective Colour Vision*, (J. Mollon, J. Pokorny, and K. Knoblauch, eds.), Oxford, Oxford University Press, pp. 179–186.
- Buck, S. L., R. Knight, and J. Bechtold, 1997a. Effect of rod stimulation on unique and binary hue judgments, in *IS&T/OSA Optics in the Information Age*, Springfield, VA: IS&T, pp. 11–15.
- Buck, S. L., R. Knight, and J. Bechtold, 2000. Opponent-color models and the influence of rod signals on the loci of unique hues, *Vis. Res.*, 40:3333–3344.
- Buck, S. L., R. Knight, G. Fowler, and B. Hunt, 1998. Rod influence on hue-scaling functions, *Vis. Res.*, 38:3259–3263.
- Buck, S. L., and W. Makous, 1981. Rod-cone interaction on large and small backgrounds, *Vis. Res.*, 21:1181–1187.
- Buck, S. L., D. R. Peeples, and W. Makous, 1979. Spatial patterns of rod-cone interaction, *Vis. Res.*, 19:775–782.
- Buck, S. L., E. Sanocki, and R. Knight, 1997b. Do rod signals add with S-cone signals in increment detection?, in *Colour Vision Deficiencies XIII: Documenta Ophthalmologica Proceedings Series*, vol. 58 (C. R. Cavonius and J. D. Moreland, eds.), Dordrecht, the Netherlands: Kluwer, pp. 451–458.
- Buck, S. L., D. L. Stefurak, C. Moss, and D. Regal, 1984. Time course of rod-cone interaction, *Vis. Res.*, 24:543–548.
- Buck, S. L., S. Stone, and D. Dacey, 1997c. Physiology of rod-cone interactions in the AII amacrine cell in macaque monkey retina, *Invest. Ophthalmol. Vis. Sci.*, 38(Suppl):S708.
- Cohen, A. I., 1965. Some electron microscopic observations on inter-receptor contacts in the human and macaque retinae, *J. Anat.*, 99:595–610.
- Coletta, N. J., and A. J. Adams, 1984. Rod-cone interaction in flicker detection, *Vis. Res.*, 24:1333–1340.
- Coletta, N. J., and A. J. Adams, 1985. Loss of flicker sensitivity on dim backgrounds in normal and dichromatic observers, *Invest. Ophthalmol. Vis. Sci.*, 26(Suppl):S187.
- Coletta, N. J., and A. J. Adams, 1986. Spatial extent of rod-cone and cone-cone interactions for flicker detection, *Vis. Res.*, 26:917–925.
- Connor, J. D., and D. I. A. MacLeod, 1976. Rod photoreceptors detect rapid flicker, *Science*, 195:698–699.
- Dacey, D. M., 1996. Morphology and physiology of the AII-amacrine cell network in the macaque monkey retina, *Soc. Neurosci. Abstr.*, 22:402.
- Dacey, D. M., and B. B. Lee, 1994. The blue-ON opponent pathway in primate retina originates from a distinct bistratified ganglion cell type, *Nature*, 367:731–735.
- Dacheux, R. F., and E. Raviola, 1986. The rod pathway in the rabbit retina. A depolarizing bipolar and amacrine cell, *J. Neurosci.*, 6:331–345.
- Daw, N. W., J. R. Jensen, and W. J. Brunken, 1990. Rod pathways in mammalian retinae, *Trends Neurosci.*, 3:110–115.
- Denny, N., T. E. Frumkes, and S. H. Goldberg, 1990. Comparison of summatory and suppressive rod-cone interaction, *Clin. Vis. Sci.*, 5:27–36.
- De Valois, R. L., and K. K. De Valois, 1993. A multi-stage color model, *Vis. Res.*, 33:1053–1065.
- Drum, B., 1981. Brightness interactions between rods and cones. *Percept. and Psychophys.*, 29:505–510.
- Drum, B., 1982. Summation of rod and cone responses at absolute threshold, *Vis. Res.*, 22:823–826.
- D’Zmura, M., and P. Lennie, 1986. Shared pathways for rod and cone vision, *Vis. Res.*, 26:1273–1280.
- Enroth-Cugell, C., G. Hertz, and P. Lennie, 1977. Cone signals in the cat’s retina, *J. Physiol.*, 269:273–296.
- Eysteinsson, T., and T. E. Frumkes, 1989. Physiological and pharmacological analysis of suppressive rod-cone interaction in *Necturus* retina, *J. Neurophysiol.*, 61:866–877.
- Foster, D. H., 1976. Rod-cone interaction in the after-flash effect. *Vis. Res.*, 16:393–396.
- Frumkes, T. E., T. Eysteinsson, 1987. Suppressive rod-cone interaction in distal vertebrate retina: intracellular records from *Xenopus* and *Necturus*, *J. Neurophysiol.*, 57:1361–1382.
- Frumkes, T. E., and T. Eysteinsson, 1988. The cellular basis for suppressive rod-cone interaction, *Visual Neurosci.*, 1:263–273.
- Frumkes, T. E., F. Naarendorp, and S. H. Goldberg, 1986. The influence of cone adaptation upon rod mediated flicker, *Vis. Res.*, 26:1167–1176.
- Frumkes, T. E., F. Naarendorp, and S. H. Goldberg, 1988. Abnormalities in retinal neurocircuitry in protanopes, *Invest. Ophthalmol. Vis. Sci.*, 29(Suppl):163.
- Frumkes, T. E., M. D. Sekuler, M. C. Barris, E. H. Reiss, and L. M. Chalupa, 1973. Rod-cone interaction in human scotopic vision—I. Temporal analysis, *Vis. Res.*, 13:1269–1282.
- Frumkes, T. E., M. D. Sekuler, and E. H. Reiss, 1972. Rod-cone interaction in human scotopic vision, *Science*, 175:913–914.
- Frumkes, T. E., and L. Temme, 1977. Rod-cone interaction in human scotopic vision.—II. Cones influence rod increment thresholds, *Vis. Res.*, 17:673–679.
- Frumkes, T. E., and S. M. Wu, 1990. Independent influences of rod adaptation on cone-mediated responses to light onset and offset in distal retinal neurons, *J. Neurophysiol.*, 64:1043–1054.
- Goldberg, S. H., T. E. Frumkes, and R. W. Nygaard, 1983. Inhibitory influence of unstimulated rods in the human retina: evidence provided by examining cone flicker, *Science*, 221:180–182.
- Gouras, P., and K. Link, 1966. Rod and cone interaction in dark-adapted monkey ganglion cells, *J. Physiol.*, 184:499–510.
- Graham, N., 1989. *Visual Pattern Analyzers*, New York: Oxford University Press.
- Hurvich, L. M., 1981. *Color Vision*, Sunderland, MA: Sinauer Associates.
- Ikeda, M., and H. Shimozone, 1981. Mesopic luminous-efficiency functions, *J. Opt. Soc. Am.*, 71:280–284.
- Ikeda, M., and M. Urakubo, 1969. Rod-cone interrelation, *J. Opt. Soc. Am.*, 59:217–222.
- Ingling, C. R., Jr., A. L. Lewis, D. R. Loose, and K. J. Myers, 1977. Cones change rod sensitivity, *Vis. Res.*, 17:555–563.
- Knight, R., and S. L. Buck, 1993. Cone pathways and the π_0 and π_0' rod mechanisms, *Vis. Res.*, 33:2203–2213.
- Knight, R., and S. L. Buck, 2001. Rod influences on hue perception: effect of background light level, *Color Res. Appl.*, 26 (Suppl):S60–S64.

- Knight, R., and S. L. Buck, 2002. Time-dependent changes of rod influence on hue perception, *Vis. Res.*, 42:1651–1662.
- Knight, R., S. L. Buck, G. Fowler, and A. Nguyen, 1998. Rods affect S-cone discrimination on the Farnsworth-Munsell 100-Hue Test, *Vis. Res.*, 38:3477–3481.
- Knight, R., S. L. Buck, and M. Pereverzeva, 2001. Stimulus size affects rod influence on tritan chromatic discrimination, *Color Res. Appl.*, 26(Suppl.):S65–S68.
- Kokoschka, 1972. Untersuchungen zur mesopischen Strahlungsbewertung, *Die Farb.*, 21:39–112.
- Kolb, H., 1970. Organization of the outer plexiform layer of the primate retina: electron microscopy of Golgi-impregnated cells, *Philos. Trans. R. Soc. Lond. B Biol. Sci.*, 258:261–283.
- Kremers, J., and S. Meierkord, 1999. Rod-cone-interactions in deuteranopic observers: models and dynamics, *Vis. Res.*, 39:3372–3385.
- Lange, G., N. Denny, and T. E. Frumkes, 1997. Suppressive rod-cone interactions: evidence for separate retinal (temporal) and extraretinal (spatial) mechanisms in achromatic vision, *J. Opt. Soc. Am. A*, 14:2487–2498.
- Latch, M., and P. Lennie, 1977. Rod-cone interaction in light adaptation, *J. Physiol.*, 269:517–534.
- Lee, B. B., J. Pokorny, V. C. Smith, P. R. Martin, and A. Valberg, 1990. Luminance and chromatic modulation sensitivity of macaque ganglion cells and human observers, *J. Opt. Soc. Am. A*, 7:2223–2236.
- Lee, B. B., V. C. Smith, J. P. Pokorny, and J. Kremers, 1997. Rod inputs to macaque ganglion cells, *Vis. Res.*, 37:2813–2828.
- Lennie, P., and D. MacLeod, 1973. Background configuration and rod threshold, *J. Physiol.*, 233:143–156.
- Lie, I., 1963. Dark adaptation and the photochromatic interval, *Doc. Ophthalmol.*, 17:411–510.
- Long, G. M., 1978. The unspecified role of cones and rods in grating detection: a theoretical note, *J. Opt. Soc. Am.*, 68:1009–1012.
- MacLeod, D., 1972. Rods cancel cones in flicker, *Nature*, 235:173–174.
- Makous, W., and R. Boothe, 1974. Cones block signals from rods, *Vis. Res.*, 14:2285–2294.
- McMullen, C. A., C. Caruso, and T. E. Frumkes, 1998. Dark-adapted rods suppress red-green opponency, *Invest. Ophthalmol. Vis. Sci.*, 39:S160.
- Muller, F., H. Wässle, and T. Voigt, 1988. Pharmacological modulation of the rod pathway in the cat retina, *J. Neurophysiol.*, 59:1657–1672.
- Naarendorp, F., N. Denny, and T. E. Frumkes, 1988. Rod light and dark adaptation influence cone-mediated spatial acuity, *Vis. Res.*, 28:67–74.
- Naarendorp, F., and T. Frumkes, 1991. The influence of short-term adaptation of human rods and cones on cone-mediated grating visibility, *J. Physiol.*, 432:521–541.
- Naarendorp, F., K. S. Rice, and P. A. Sieving, 1996. Summation of rod and S cone signals at threshold in human observers, *Vis. Res.*, 36:2681–2688.
- Nagy, A. L., and J. A. Doyal, 1993. Red-green color discrimination as a function of stimulus field size in peripheral vision, *J. Opt. Soc. Am. A*, 10:1147–1156.
- Nelson, R., 1977. Cat cones have rod input: a comparison of the response properties of cones and horizontal cell bodies in the retina of the cat, *J. Comp. Neurol.*, 172:109–136.
- Nelson, R., H. Kolb, E. V. Famiglietti, and P. Gouras, 1976. Neural responses in the rod and cone systems of the cat retina: intracellular records and procion stains, *Invest. Ophthalmol. Vis. Sci.*, 15:946–953.
- Nerger, J. L., V. J. Volbrecht, and C. J. Ayde, 1995. Unique hue judgments as a function of test size in the fovea and at 20-deg temporal eccentricity, *J. Opt. Soc. Am. A*, 12:1225–1232.
- Nerger, J. L., V. J. Volbrecht, C. J. Ayde, and S. M. Imhoff, 1998. Effect of the S-cone mosaic and rods on red/green equilibria, *J. Opt. Soc. Am. A*, 15:2816–2826.
- Palmer, D. A., 1976. Rod-cone mechanism underlying the Purkinje shift, *Nature*, 262:601–603.
- Purpura, K., E. Kaplan, and R. M. Shapley, 1988. Background light and the contrast gain of primate P and M retinal ganglion cells, *Proc. Natl. Acad. Sci. USA*, 85:4534–4537.
- Raviola, E., 1976. Intercellular junctions in the outer plexiform layer of the retina, *Invest. Ophthalmol.*, 15:881–894.
- Raviola, E., and N. B. Gilula, 1973. Gap junctions between photoreceptor cells in the vertebrate retina, *Proc. Natl. Acad. Sci. USA*, 70:1677–1881.
- Reitner, A., L. T. Sharpe, and E. Zrenner, 1991. Is colour vision possible with only rods and blue-sensitive cones? *Nature*, 352:798–800.
- Richards, W., and S. Luria, 1964. Color mixture functions at low luminance levels, *Vis. Res.*, 4:281–313.
- Schneeweis, D. M., and J. L. Schnapf, 1995. Photovoltage of rods and cones in the macaque retina, *Science*, 268:1053–1056.
- Shapiro, A. G., J. Pokorny, and V. C. Smith, 1994. Rod contribution to large-field color matching, *Color Res. Appl.*, 19:236–245.
- Sharpe, L. T., C. C. Fach, and A. Stockman, 1993. The spectral properties of the two rod pathways, *Vis. Res.*, 33:2705–2720.
- Smith, R. G., M. A. Freed, and P. Sterling, 1986. Microcircuitry of the dark-adapted cat retina: functional architecture of the rod-cone network, *J. Neurosci.*, 6:3505–3517.
- Smith, V. C., and J. Pokorny, 1977. Large-field trichromacy in protanopes and deuteranopes, *J. Opt. Soc. Am.*, 67:213–220.
- Spillmann, L., and J. E. Conlon, 1972. Photochromatic interval during dark adaptation and as a function of background luminance, *J. Opt. Soc. Am.*, 62:182–185.
- Stabell, B., 1967. Rods as color receptors in scotopic vision, *Scand. J. Psychol.*, 8:132–138.
- Stabell, U., and B. Stabell, 1971. Chromatic rod vision—III. Wavelength of pre-stimulation varied, *Scand. J. Psychol.*, 12:282–288.
- Stabell, U., and B. Stabell, 1978. Scotopic hues of simultaneous contrast, *Vis. Res.*, 18:1491–1496.
- Stabell, U., and B. Stabell, 1984. Color-vision mechanisms of the extrafoveal retina, *Vis. Res.*, 24:1969–1975.
- Stabell, U., and B. Stabell, 1994. Mechanisms of chromatic rod vision in scotopic illumination, *Vis. Res.*, 34:1019–1027.
- Stockman, A., L. T. Sharpe, K. R  ther, and K. Nordby, 1995. Two signals in the human rod visual system: a model based on electrophysiological data, *Vis. Neurosci.*, 12:951–970.
- Strettoi, E., R. F. Dacheux, and E. Raviola, 1994. Cone bipolar cells as interneurons in the rod pathway of the rabbit retina, *J. Comp. Neurol.*, 347:139–149.
- Strettoi, E., E. Raviola, and R. F. Dacheux, 1992. Synaptic connections of the narrow-field bistratified rod amacrine cell AII in the rabbit retina, *J. Comp. Neurol.*, 325:152–168.
- Sun, H., 2001. Rod-cone interactions. Ph.D. dissertation, University of Chicago.
- Sun, H., J. Pokorny, and V. C. Smith, 2001. Rod-cone interactions assessed in inferred magnocellular and parvocellular postreceptoral pathways, *J. Vis.*, 1:42–54.

- Temme, L. A., and T. E. Frumkes, 1977. Rod-cone interaction in human scotopic vision. III. Rods influence cone increment thresholds, *Vis. Res.*, 17:681–685.
- Trezona, P., 1970. Rod participation in the “blue” mechanism and its effect on color matching, *Vis. Res.*, 10:317–332.
- Trezona, P., 1974. Additivity in the tetrachromatic color matching system, *Vis. Res.*, 14:1291–1303.
- Tsukamoto, Y., K. Morigiwa, M. Ueda, and P. Sterling, 2001. Microcircuits for night vision in mouse retina, *J. Neurosci.*, 21:8616–8623.
- van den Berg, T., and H. Spekreijse, 1977. Interaction between rod and cone signals studied with temporal sine wave stimulation, *J. Opt. Soc. Am.*, 67:1210–1217.
- Verweij, J., D. Dacey, B. Peterson, and S. L. Buck, 1999. Sensitivity and dynamics of rod signals in macaque H1 horizontal cells, *Vis. Res.*, 39:3662–3672.
- Virsu, V., and B. B. Lee, 1983. Light adaptation in cells of macaque lateral geniculate nucleus and its relation to human light adaptation, *J. Neurophysiol.*, 50:864–878.
- Virsu, V., B. B. Lee, and O. D. Creutzfeld, 1987. Mesopic spectral responses and the Purkinje shift of macaque lateral geniculate nucleus cells, *Vis. Res.*, 27:191–200.
- Volbrecht, V. J., J. L. Nerger, S. M. Imhoff, and C. J. Ayde, 2000. Effect of the short-wavelength-sensitive-cone mosaic and rods on the locus of unique green, *J. Opt. Soc. Am. A*, 17:628–634.
- Westheimer, G., 1965. Spatial interaction in the human retina during scotopic vision, *J. Physiol.*, 181:881–894.
- Westheimer, G., 1967. Spatial interaction in human cone vision, *J. Physiol.*, 190:139–154.
- Wiesel, T. N., and D. H. Hubel, 1966. Spatial and chromatic interactions in the lateral geniculate body of the rhesus monkey, *J. Neurophysiol.*, 29:1115–1156.
- Willmer, E. N., 1950. Low threshold rods and the perception of blue, *J. Physiol.*, 111:17P.
- Wyszecki, G., and W. Stiles, 1982. *Color Science: Concepts and Methods, Quantitative Data and Formulae*, 2nd ed., New York: Wiley.
- Xin, D., and S. A. Bloomfield, 1999. Comparison of the responses of AII amacrine cells in the dark- and light-adapted rabbit retina, *Vis. Neurosci.*, 16:653–665.
- Yaguchi, H., and M. Ikeda, 1984. Mesopic luminous efficiency, *J. Opt. Soc. Am. A*, 1:120–123.

VIII BRIGHTNESS AND COLOR

56 Brightness and Lightness

ADRIANA FIORENTINI

THIS CHAPTER DEALS with sensations that are devoid of hue. The first part will introduce some basic terms used to define the perceptual qualities of *brightness*, relative to self-luminous objects, and of *lightness*, relative to opaque illuminated surfaces. A brief historical introduction about the role of simultaneous contrast in the perception of lightness will be followed by the description of a dual system that has been assumed to be responsible for the perception of brightness and darkness: the ON-center and OFF-center cells of the retina of mammals.

The subsequent section deals with lightness constancy, the fact that the perceived colors of objects remain substantially unvaried when illumination changes. It will be explained how lightness constancy can be tested experimentally, and the conditions will be described under which this “most noteworthy fact” in vision (Hering, 1964, p. 16) is verified and those in which departures from constancy have been found.

The third section is devoted to spatial contrast: area contrast and border contrast. Tentative theoretical interpretations and models that have been suggested to account for border contrast effects are discussed.

The last section introduces contrast induction for textures of light and dark elements. This is a perceptual process responsible for constancy of contrast perception under varying viewing conditions and is possibly related to neural mechanisms of contrast gain control.

Brightness and darkness

BASIC TERMS If the light flux reaching the eye from a region of the visual field generates a sensation devoid of hue, the source of this flux is an achromatic stimulus. *Hue* is the attribute of a color perception denoted by red, blue, yellow, green, and so on. Achromatic stimuli may differ substantially from each other in terms of their power spectra. This chapter deals with achromatic perceptions independent of the spectral distribution of the stimuli generating them. Achromatic perceptions, however, may differ from each other in brightness. For instance, two self-luminous, achromatic objects, separated from each other in a dark surround, differ in brightness if one emits more luminous flux than the other. *Brightness* is the attribute of visual perception according to which an area of the visual field appears to emit more or less light.

Achromatic sensations may also be produced by the surface of objects illuminated by daylight or other achromatic sources. The photometric quantity most relevant to this case is *luminance*. This is defined as the light flux emitted per unit of solid angle from the unit area of the surface of an object projected perpendicular to the viewing direction. The *reflectance* of an object having a matte surface is the ratio between the light flux reflected by the surface and the incident flux, both relative to the unit area. The luminance of a uniformly illuminated diffusing surface is proportional to its reflectance.

A single achromatic object, illuminated in an otherwise dark surround, always appears bright, its brightness depending on whether it is more or less strongly illuminated. Variations in brightness range from bright to dim. If, however, several objects with reflectance independent of wavelength are simultaneously present in the visual field next to each other, and are illuminated by an achromatic source, their achromatic colors may vary according to their reflectance, between white (objects with very high reflectance) and black (objects with very low reflectance), among various shades of gray. *Lightness* is the attribute of visual sensation according to which an object's surface appears to reflect more or less light with respect to an object that appears white. Lightness, therefore, may be understood as a quality of sensation that arises from the comparison of objects with surfaces of different reflectance, and is an attribute that characterizes the perceived surface separately from the intensity of the illuminating light (see the section “Lightness Constancy”).

The *objective contrast* relative to two regions of luminance, L_1 and L_2 , is the photometric quantity defined as the ratio between the luminance difference ($L_1 - L_2$) and the mean luminance $(L_1 + L_2)/2$.

The fact that a single illuminated object in a completely dark background always appears bright means that even a piece of coal would appear bright if illuminated in isolation, but the same piece of coal seen against a snow field would appear black (Gelb effect). This is an example of a large class of phenomena referred to as *simultaneous contrast effects*: an object of moderate reflectance may appear lighter or darker according to whether it is *surrounded* by a region that is considerably darker or brighter than the object itself (Fig. 56.1). More generally, if various objects of different reflectance are presented together and are illuminated from the same light source, the lightness of each object depends not only on the

reflectance of the others, but also on their spatial distribution and relative distances (see the section “Spatial Contrast”). In particular, for an object of very low reflectance to appear black, objects of higher reflectance must be present close to it.

The sensation of blackness may also result from *successive contrast*, produced by rapid changes of luminance in a given area of the visual field: a surface of a given luminance may appear lighter or darker according to whether the preceding luminance was lower or higher.

HISTORICAL BACKGROUND The perception of blackness was interpreted differently by the two great visual physiologists of the nineteenth century. According to Helmholtz (1867), blackness results from the absence of light: “a spot in the visual field that sends no light to the eye is seen black” (Helmholtz, 1962, p. 131). He maintained that blackness is a real sensation, to be distinguished from the lack of stimulation relative to objects located outside the field of view. However, he did not realize that blackness required the simultaneous (or immediately successive) presence of objects of different luminance.

A practical demonstration of how simultaneous contrast may affect the sensations of both lightness and color of juxtaposed surfaces was given by Chevreul (1839). Later, Hering (1878) stated clearly that the sensation of blackness results from simultaneous or successive contrast. Hering interpreted achromatic contrast in terms of the existence of an achro-

matic opponent mechanism, coding brightness and darkness by an antagonistic process similar to the opponent mechanisms that he assumed to code for blue-yellow and red-green color information (Hering, 1920). His hypothesis of the existence of separate mechanisms for processing of the achromatic and chromatic components of a visual stimulus subsequently received support from anatomical and electrophysiological findings in animals (see Chapter 30) but is also in agreement with psychophysical findings in humans. Consistent with Hering’s theory is the finding, by Shinomori et al. (1997) that the blackness of a color is inversely related to the luminance of its inducing field, independently of hue.

At very low light levels, when the eye is dark-adapted, the range of lightness variations is very restricted, and we perceive only faint variations of gray levels. With increasing illumination the range of lightness increases, and various shades of gray can be perceived, from white to black. Hering claimed that, with the increase in illumination, objects of higher reflectance appear increasingly whiter, but those of lower reflectance “appear increasingly darker, *blacker*, and finally dark black, even though their small light intensity has increased” (Hering, 1964, p. 75). This claim is disputable, as explained below. However, it was the increase in lightness differences with increased illumination that led Hering to assume the existence of two antagonistic mechanisms responsible for brightness and darkness sensations, respectively. Jung (1961) proposed that the two types of retinal ganglion cells, the ON-center and OFF-center cells, could have

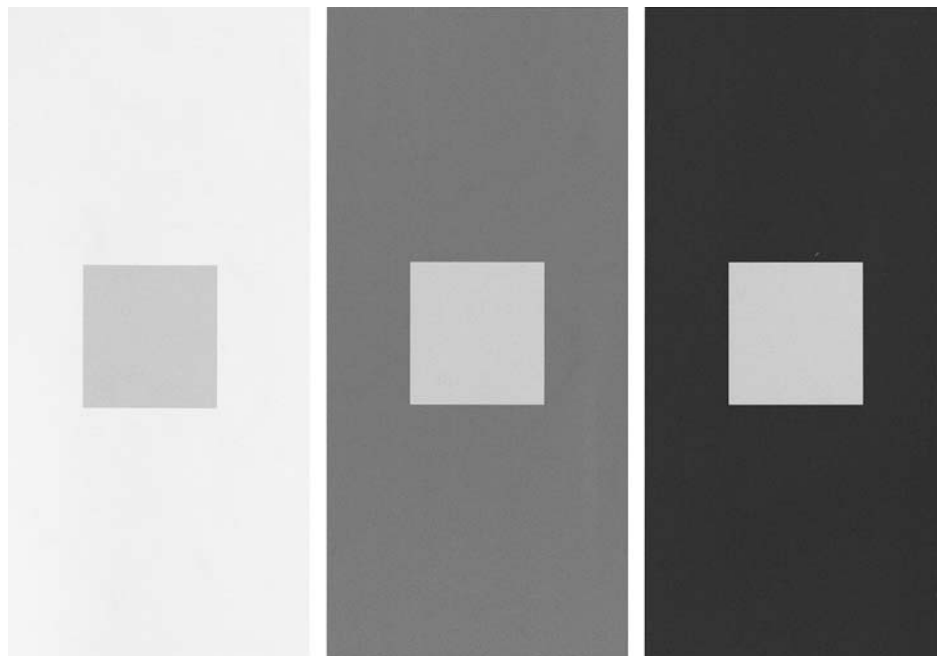


FIGURE 56.1. Example of simultaneous contrast (area contrast). The inner squares all have the same luminance, but they seem to be different: the darker the surround, the lighter the inner square, and vice versa.

this role (see the section “Lightness Constancy” and Chapter 18).

A DUAL SYSTEM FOR THE PERCEPTION OF BRIGHTNESS AND DARKNESS The possible role of ON-center and OFF-center cells in the perception of brightness and darkness, respectively, suggested by Jung (1961) and coworkers, was

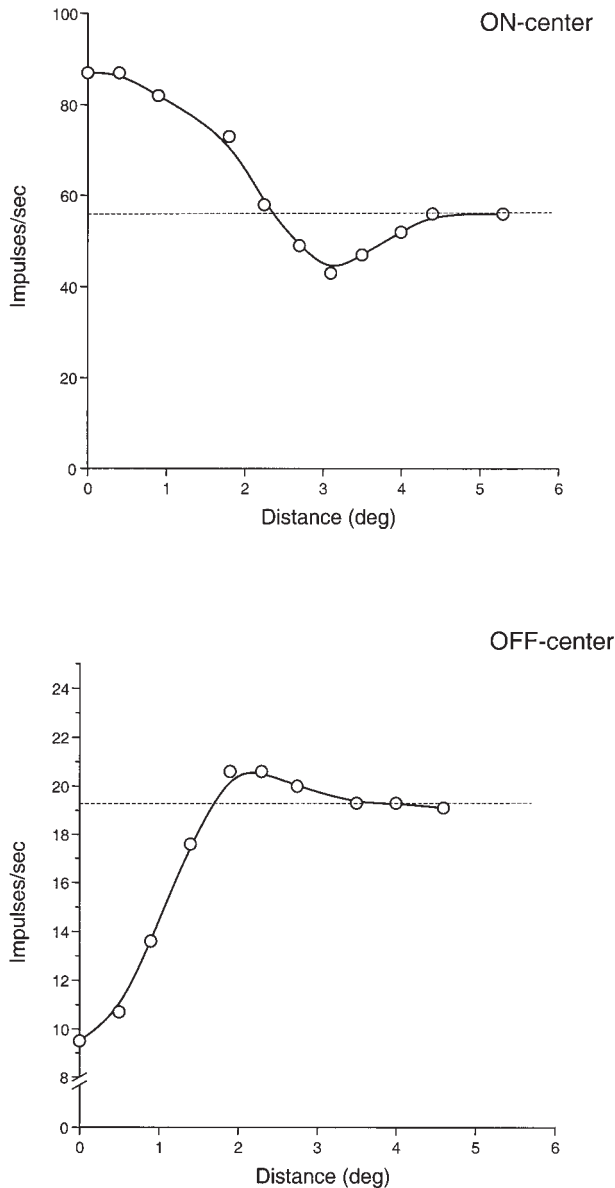


FIGURE 56.2. Responses of an ON-center and an OFF-center ganglion cell of the cat to a stationary light spot located in the center of the receptive field and modulated sinusoidally in luminance (0.5 Hz, mean luminance 2 cd/m^2) as a function of distance (in degrees of visual angle) from the receptive field center of a second spot of constant luminance (2 cd/m^2). Spot diameter 34 minutes of arc. Background 0.1 cd/m^2 . The ordinate indicates the rate of discharge of the cell averaged over a stimulus period. The horizontal dotted lines indicate the average discharge recorded in the absence of the stationary spot. (Adapted from Maffei, 1968.)

subsequently investigated both in animals and in humans (see Fiorentini et al., 1990, for review). It must be considered, however, that each retinal ganglion cell responds only to stimuli in a small area of the visual field, its receptive field, and that this field consists of two concentric regions with antagonistic responses to light, excitatory in the center and inhibitory in the surround, or vice versa (Fig. 56.2). Therefore, the optimal stimulus for a ganglion cell is not diffuse light, but a spot as large as the receptive field's center and either brighter (ON-center cells) or darker (OFF-center cells) than the background, that is, a contrast stimulus.

The two populations of ganglion cells form two parallel mosaics in separate layers of the retina, and in the central fovea of the monkey the number of ganglion cells is three to four times the number of cones, indicating that the two ON and OFF systems can use independently all of the information sampled by the photoreceptors (Wässle et al., 1990). The ON and OFF channels are kept separate at the lateral geniculate nucleus (LGN) and at the early stages of processing in the visual cortex. In line with the properties of the two classes of cells and their specialization for responding to contrast stimuli of opposite sign, it has been found that pharmacological blocking of ON-cell responses in the retina, LGN, and visual cortex, having no effect on OFF-cell responses, severely impairs the behavioral response of monkeys to spots brighter than the background while leaving the response to dark spots unaffected (Schiller et al., 1986). Thus, ON and OFF channels provide independent processing of localized increments and decrements of a light stimulus. Psychophysical experiments suggest that in humans the perception of temporal increments and decrements of luminance in a spatially uniform light stimulus is subserved by two independent systems (Krauskopf, 1980).

But what is the advantage of having these two independent systems? One channel could well signal both increments and decrements of the stimulus by modulations of the rate of discharge. However, a dual system is much more efficient in signaling relatively large variations of either sign in the input, responding to both input increments and decrements with an increase of discharge and avoiding the effects of discharge saturation.

In conclusion, the ON and OFF channels seem to be the neural substrate accounting for the perception of increments and decrements of light, localized spatially or temporally. However, whether and how the two systems can account for brightness and darkness perception under more general conditions of illumination and contrast is still largely unknown.

Lightness constancy

INVARIANCE OF PERCEIVED ACHROMATIC COLORS UNDER CHANGES OF ILLUMINATION It is a common experience that

the lightness of real objects illuminated in a natural environment is largely independent of the overall level of illumination. For instance, the page of this book looks white and the printed letters look black, whether or not the page is illuminated by bright sunlight or by a much weaker artificial source such as a desk lamp. This phenomenon is called *lightness constancy*. It is as if the visual system is able to keep the information about the relative amount of light coming from the surfaces of the various objects (determined by their reflectance) and disregard the amount of light physically reflected by the objects when this varies in the same proportion for all of them. Hering noted that “The approximate constancy of the colors of seen objects, in spite of large changes of general illumination, is one of the most noteworthy and most important facts in the field of physiological optics. Without this approximate constancy, a piece of chalk on a cloudy day would manifest the same color as a piece of coal does on a sunny day, and in the course of the day it would have to assume all possible colors that lie between black and white” (Hering, 1964, pp. 16–17).

Under uniform illumination, the luminance of surfaces depends only on their reflectance. Therefore, the relative luminance of an object with respect to its background depends only on the ratio of their reflectances and is independent of general illumination changes. Lightness constancy may be expected to occur so far as lightness is determined only by luminance (reflectance) *ratios*. This rule is valid for areas of different luminance adjacent to each other, such as displays consisting of disks surrounded by an annulus. In this case, the reflectance ratio is signaled by the gradient of luminance at the border between the two areas.

Lightness constancy can be tested psychophysically by presenting under various levels of illumination a pattern consisting of two or more patches of different reflectance and by matching the lightness of each of these patches to that of a comparison field of adjustable luminance. Hering’s (1920) suggestion that the bright portions of a pattern may become increasingly bright, and the dark portions increasingly dark, when illumination increases was not confirmed by psychophysical experiments (Jacobsen and Gilchrist, 1988), which indicate that under suitable testing conditions lightness constancy may hold under very large changes of illumination (Fig. 56.3).

LIMITS OF LIGHTNESS CONSTANCY Departures from lightness constancy have been found, and may depend on the experimental procedure used to test it and on the spatial configuration of the tested patterns. For instance, lightness constancy is nearly perfect if tested with complex Mondrian patterns, consisting of several adjacent rectangles of various reflectances, but less perfect for a disk surrounded

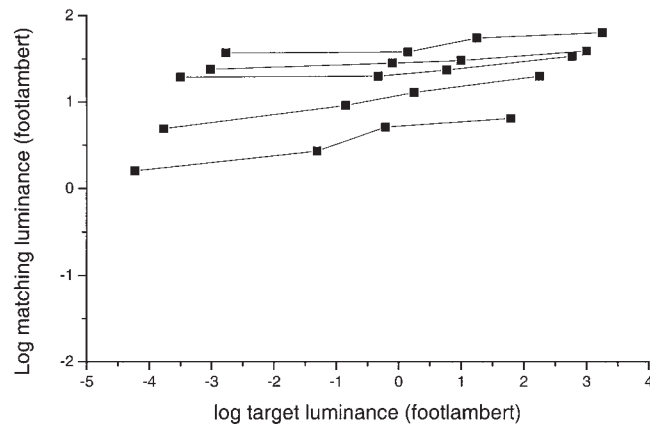


FIGURE 56.3. Lightness of five target squares of different reflectance, forming a cross-shaped pattern, and seen under four different illumination levels, covering a range of about 6 log units, as indicated on the abscissa. The ordinates indicate the matching luminance. The slope of each of the five functions corresponding to the five targets is very close to horizontal, indicating that the lightness is largely independent of illumination.

by an annulus of different reflectance (Arend and Goldstein, 1987). Failures to prove lightness constancy may be caused by a shift in the observer criterion from a match of lightness (opaque surface reflectance) to an evaluation of brightness (light intensity) (Arend and Goldstein, 1987; Whittle, 1991). In some cases, the normal perception of lightness for extended reflecting surfaces in a complex surround may be replaced by a perception of luminosity: rather than showing the expected white appearance of an opaque illuminated object, the object surface appears self-luminous.

Heggelund (1992) has proposed a bidimensional model to represent these various aspects of achromatic vision. From his data on the appearance of a test field of constant luminance surrounded by an annulus of variable luminance, he suggested that the achromatic colors are specified by their degree of similarity to the three qualities: white, black, and luminous. The two variables black and luminous are considered to be opponent, because they are mutually exclusive (like red and green in color-opponent processes) and are represented along one dimension of the bidimensional model. These variables are qualities of the light mode of appearance (aperture colors), although black requires contrast to be perceived. The black/white variables are qualities of the object mode of appearance and are not considered to be opponent, because they do not exclude each other (as opponent colors do, such as red and green or blue and yellow among the chromatic colors), but can be perceived as being both present in the grayness of a surface (as for instance, red and yellow are seen together in orange colors). These are represented in the model along a dimension orthogonal to the former. Under the simple conditions of his experiments (a disk of fixed luminance surrounded by an annulus of vari-

able luminance), Heggelund finds a shift between the two modes of appearance, the light mode and the surface or object mode, that occurs near zero contrast. He speculates that the luminous/black process, being related to simultaneous contrast, may be supported by neural units with antagonistic center-surround organization, while the white process could involve neural units without a center-surround organization.

The proposal of two separate processes for luminous/black perception and white perception is interesting. Obviously, the surface mode is important in ordinary vision, because these colors are seen as constant properties of the objects, largely independent of illumination and viewing conditions. However, under complex stimulus conditions the two modes can coexist to some degree, and it remains to be seen how these findings are extendable to vision in a normal environment.

A type of light constancy that contradicts the ratio rule is observed when a piece of gray paper is viewed successively against backgrounds of different reflectance, while the level of illumination is not changed. Although the luminance ratio at the edge varies considerably when passing from a lower to a higher background luminance, the gray paper may appear to change very little in lightness. This constancy with respect to background changes must therefore be distinguished from lightness constancy with respect to illumination (see, e.g., Gilchrist et al., 1999).

Moreover, lightness can be affected by higher-order perceptual factors, for instance, by depth perception (Gilchrist, 1977), by the apparent curvature of the surface (Knill and Kersten, 1991), or by perceived transparency or shading on the illuminated surfaces (Adelson, 1993) (see the section "Tentative Theoretical Interpretations and Models for Border Contrast Effects").

A cognitive theory of lightness perception, the anchoring theory, has been proposed recently (see Gilchrist et al., 1999, for review). This theory poses the problem of how the visual system ties relative luminance values extracted from the retinal image to specific values of black, white, and gray. Anchoring could be done, for instance, with reference to the highest luminance present in the field of view (Bruno et al., 1997) or to the average luminance. The model proposed by Gilchrist and coworkers is based on a combination of local and global anchoring of lightness values and seems to account satisfactorily for constancy failures, with respect to either illumination or background. An attempt to provide a neurophysiological basis for this model is a subject for future research (Paradiso, 2000).

Spatial contrast

AREA CONTRAST Simultaneous contrast, that is, the dependence of lightness of a uniform surface on the luminance of

the surrounding region, is not limited to a region around the border between two surfaces of different luminance. If an area of constant luminance is completely enclosed by the border, the effect of contrast on its lightness spreads over the area (as in Fig. 56.1). This contrast effect is called *area contrast*, to distinguish it from more localized contrast effects, the *border contrast* effects. In general, the lightness of an enclosed area is determined primarily by the average local contrast at the edges of the area.

The classical explanation of area contrast is in terms of reciprocal interactions between neural elements in the visual system. In particular, inhibitory interactions are exerted by elements strongly stimulated on elements more weakly stimulated, even at a relatively long distance from the former. The classical simultaneous contrast effect illustrated in Figure 56.1 is explained by assuming that, at some level of visual processing, neurons stimulated by a bright background inhibit the less stimulated neurons of the inner square, while a dark background does not have such an inhibitory effect on the square, which would therefore appear brighter than in the previous case. While local contrast effects at the edge between two areas of different luminance can be understood in terms of the properties of receptive fields of single neurons, as discussed below, the inhibitory interactions between differently stimulated neurons should extend for a relatively large distance in order to account for area contrast. Long-range lateral connections are known to exist in the visual cortex, and it is possible that border contrast information propagates at some distance from the edge, thus playing a role in area contrast (Spillmann and Werner, 1996).

BORDER CONTRAST EFFECTS Border contrast produced by a local modulation of luminance in an otherwise uniform surface can cause a difference in lightness between the two parts of the surface on either side of the local luminance modulation (Fig. 56.4). This illusory change in lightness, known as the *Craik-O'Brien-Cornsweet illusion*, spreads for a long distance on either side of the border and is an example of how border contrast can produce area contrast (Cornsweet, 1970; Craik, 1966; O'Brien, 1958). There are limits, however, to the ability of a local contrast to generate area contrast. For instance, the Craik-O'Brien-Cornsweet illusion is strong for luminance modulations of moderate contrast but decreases considerably at high local contrasts (Burr, 1987).

A well-known example of border contrast effects is the *Mach bands*, first described by the Austrian physicist Ernst Mach (1865). These are bright and dark lines that appear near the brighter and darker border, respectively, of a blurred edge between two uniform regions of different luminance (Fig. 56.5). The illusory lines sharpen the diffused border just as real lines would do (Fiorentini, 1972; Ratliff,

1965). Another illusory effect of contrast is the *Hermann grid illusion*, which consists in the appearance of dark blobs at the intersections of a grid of white bars on a black background (or, reciprocally, of light blobs at the intersections of a grid of black bars on a white background) (Hermann, 1870). Still another illusory effect is the *Chevreul illusion* (Chevreul, 1839) generated by a series of parallel stripes, each of constant luminance, but forming a staircase with luminance increasing regularly from one stripe to the next. The lightness of the stripes is not seen to vary in steps: each stripe looks brighter near the border with the lower luminance and darker near the border with the higher luminance, so that the whole pattern appears to have a sawtooth distribution of lightness.

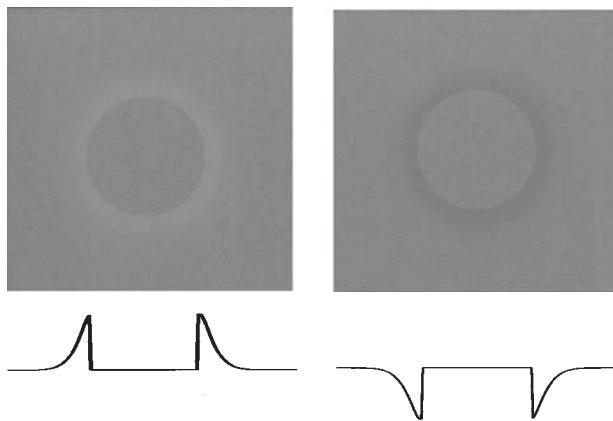


FIGURE 56.4. Craik-O'Brien-Cornsweet illusion: border-induced area contrast. The two discs have equal luminance, but appear of different lightness because of luminance modulations of opposite signs near the edges (see graphs).

TENTATIVE THEORETICAL INTERPRETATIONS AND MODELS FOR BORDER CONTRAST EFFECTS For all these border contrast effects, explanations were proposed in terms of the properties of the receptive fields of visual cells, with their antagonistic excitatory and inhibitory regions. Psychophysical evidence (Fiorentini and Maffei, 1968; Fiorentini and Mazzantini, 1966) shows that contrast stimuli near threshold may interact with each other within short distances and produce a spatial distribution of facilitatory and inhibitory effects qualitatively very similar to the response profiles of retinal ganglion cells of the cat and monkey (Fig. 56.6). These psychophysical data have been interpreted as reflecting the properties of *perceptive fields*, the perceptual counterpart of retinal receptive fields, and the perceptive field size has been shown to vary with retinal eccentricity in agreement with the variation of mean receptive field size in the monkey retina (Spillman et al., 1987). The perceptive field profile has also been found to depend on the orientation of the interacting line stimuli (Rentschler and Fiorentini, 1974), suggesting a relationship with the receptive fields of orientation neurons of the visual cortex, rather than merely with retinal receptive fields, which have circular symmetry.

If the antagonistic interactions revealed by these experiments justify the interpretation of border contrast effects in terms of properties of neuronal receptive fields, it should be noted that models based on the activity of single receptive fields (single-channel models) do not give a satisfactory account for most of the perceptual effects described above. In this type of model, all the receptive fields have the same form (concentric antagonistic regions), their size increases with distance from the visual field center, but each point in the visual field is served by a receptive field of only one size. It should be considered, by contrast, that at any given eccen-

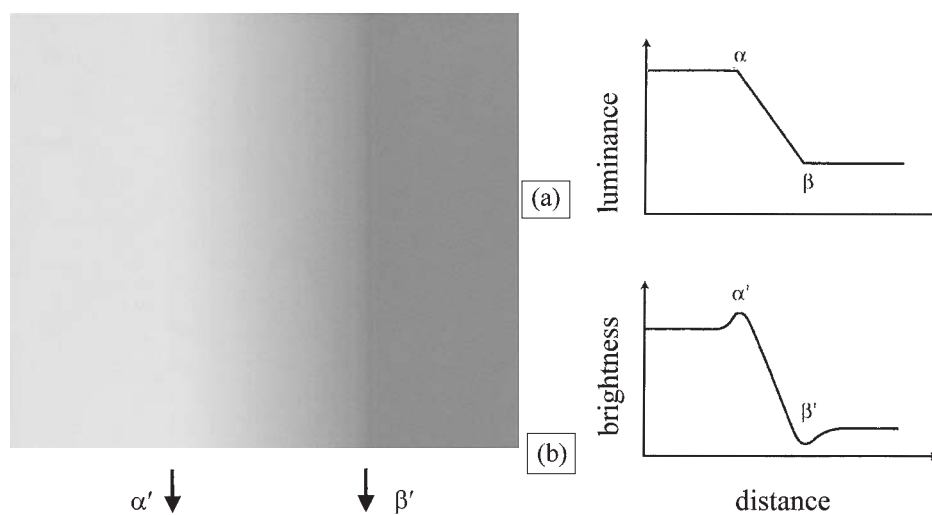


FIGURE 56.5. Mach bands. The luminance distribution (*left*) is constant vertically and varies horizontally from a constant upper level to a constant lower level through a linear ramp, extending from α' to β' , as indicated by the graph (*a*). Bright and dark illusory bands are perceived near the transitions from the ramp to the regions of constant luminance, as shown schematically in *b*.

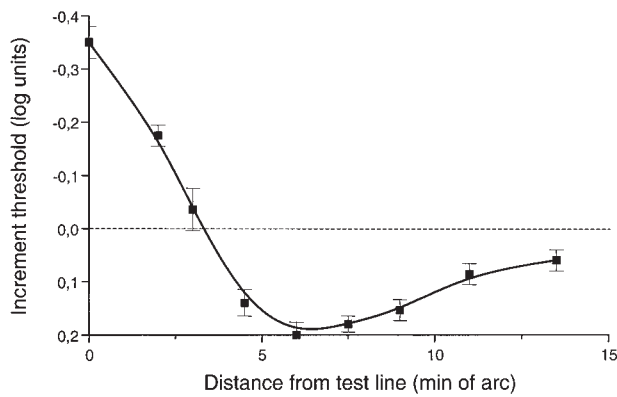


FIGURE 56.6. Excitatory and inhibitory subthreshold interactions between two thin lines superimposed on a uniform field (120 cd/m^2). Ordinates: log incremental threshold (just perceptible incremental luminance) of the test line (1 minute of arc width, 1 degree length) as a function of distance from the test line of a parallel line of the same size and of subliminal incremental luminance. The horizontal line indicates the threshold of the test line in the absence of the inducing line. Negative ordinates indicate facilitation, that is, a decrease in incremental test line threshold in the presence of the subthreshold parallel line, and positive ordinates indicate inhibition. (Adapted from Rentschler and Fiorentini, 1974.)

tricity there is a mosaic of cells with similar properties, but with somewhat different receptive field sizes and profiles. Not surprisingly, therefore, models based on the simultaneous contributions of a number of cells with different response profiles (multichannel models) have given more satisfactory accounts of border contrast effects (e.g., Marr and Hildreth, 1980; Watt and Morgan, 1985). Morrone and Burr (1988) have proposed a multichannel model, the local energy model, postulating the existence in the visual system of line and edge detectors with sensitivity profiles of even and odd symmetry, respectively, similar to those described for the receptive fields of a class of cortical neurons. The responses (both ON and OFF) of these fields are combined nonlinearly and signal the position of key features in the visual field, that is, lines and edges (according to whether the response of even or odd receptive fields prevails). The local energy model accounts successfully for Mach bands and other border contrast effects (Morrone and Burr, 1989; Morrone et al., 1994a). In particular, it explains satisfactorily the absence of Mach bands near a sharp luminance edge (Ross et al., 1989), something that was not easily justified, or even seemed to be contradicted, by previous Mach band interpretations.

Recently, a model of brightness perception, based on a modified version of the Watt-Morgan model and with filter properties assumed to be typical of retinal ganglion cells, has been used successfully to predict a number of border contrast effects (McArthur and Moulden, 1999). This offers further support to the earlier speculations that area and

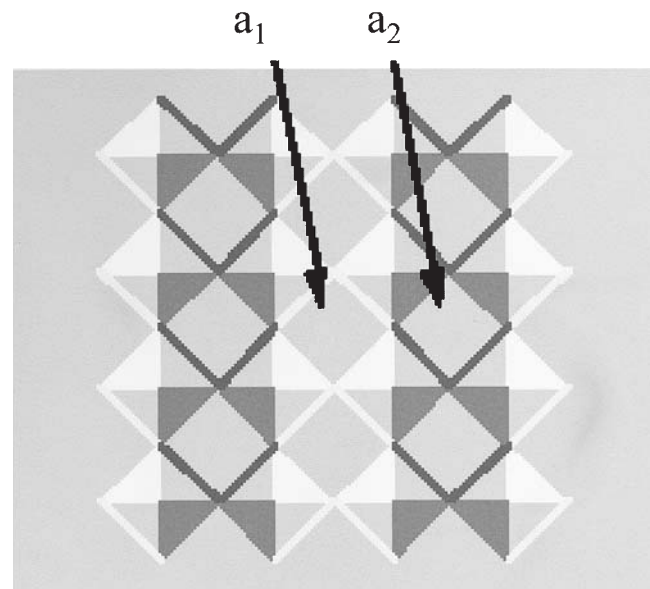


FIGURE 56.7. Argyle illusion. The two diamonds a_1 and a_2 have the same shade of gray, which is also the same as the background. They appear to have different lightness: a_1 looks darker than a_2 . The effect derives from the light and dark strips overlying the diamonds, which appear as light and dark transparent surfaces. The diamonds that seem covered by a more transparent strip look darker, and those that seem covered by a less transparent strip look lighter. (From Adelson, 1993.)

border contrast effects could be attributable at least in part to retinal processing. There is little doubt, however, that central neural mechanisms are also implied in simultaneous contrast area and border effects. Shevell et al. (1992) have shown that the classical effect of simultaneous contrast on the lightness of a central disk, when surrounded by an annulus of different luminance, does not occur if the disk and the annulus are presented separately to the two eyes. Thus, the effect can be explained in terms of retinal mechanisms. However, if a second ring now surrounds the previous one, the luminance of the second ring may affect the lightness of the first ring and also that of the disk. This effect of the second ring occurs at a level beyond the binocular fusion of the two monocular images, and this implies central processing. Adelson (1993) has provided interesting examples of lightness illusions, in which surfaces appear to have different lightness although they have the same luminance value. The illusions are due to a different interpretation of the surfaces in terms of either their apparent orientation in space or the effects of transparency (Fig. 56.7) and show how the perceptual organization of the stimuli can influence the judgement of lightness. Here again, the interpretation of junctions between surfaces as a change in depth and illumination may considerably affect the perception of surface lightness, other things being equal. Such effects can hardly be explained by low-level mechanisms and

have to be ascribed to high-level processing of the visual images.

Central processing must also be involved in the lightness effects produced by more complex patterns, for instance, patterns including not only reflectance edges, but also illumination edges produced by nonuniform illumination. Studying these type of patterns, Gilchrist et al. (1983) came to the conclusion that the visual system works to account fully for all gradients of light present on the retina, whether by the perception of changes in reflectance, changes in illumination, or both. In their view, this requires the assumption that the ratio of luminances on either side of an edge can contribute only relative information on the lightness of an area and its surround, while the integration of information contributed by other edges present in the field is required for perceiving absolute lightness. Integration of edges has also been invoked (Whittle, 1991) as an explanation of assimilation (Fig. 56.8), an effect apparently opposite to simultaneous contrast and such that a gray object on a black background will tend to appear darker than the same object on a white background. In their quantitative study of the relative contributions of physical contrast and assimilation to the perception of brightness, Shapley and Reid (1985, p. 5985) point out that “if the neural signal from the retina to the brain is only in terms of local contrast, then assimilation must be due to computational activity of the brain, acting on the contrast signals it receives from the retina.” The nature of the mechanism for assimilation, however, is still unknown.

A series of papers that offer a totally different interpretation of the perception of brightness, including simultaneous contrast and border contrast effects (such as Mach bands and the Craik-O’Brien-Cornsweet illusion), has appeared recently (see Paradiso, 2000, for a review). Perceptual experience based on the most common distributions of lightness

in the real world is responsible for the subjective interpretation of the various spatial luminance distributions, taking into account information about luminance gradients, perspective, orientation, and so on, and thus generating lightness perceptions and illusions. Obviously, this empirical strategy requires central processing, and in the view of the authors minimizes the role of low-level neural mechanisms in brightness perception (but see the section “Spatial Texture Interactions and Contrast Induction”).

Contrast gain control

SPATIAL TEXTURE INTERACTIONS AND CONTRAST INDUCTION

A perceptual phenomenon in some ways similar to simultaneous lightness contrast has been described for textures consisting of random elements of two different luminances (e.g., black and white) or for patterns with a spatially periodic one-dimensional variation of luminance (e.g., sinusoidal gratings). In such patterns, the *objective contrast* is proportional to the difference between the maximum and minimum luminance in the elements divided by the mean luminance. If a texture or grating patch of moderate objective contrast is surrounded by a similar texture of much higher contrast, the *apparent contrast* of the patch looks lower than that of the same patch when surrounded by a uniform background (Fig. 56.9).

This striking effect of contrast induction was first described by Chubb et al. (1989) for textures of black and white elements and was interpreted as resulting from a perceptual mechanism of *contrast gain control*. The visual system acts in such a way as to calibrate the local response to contrast, taking into account the average contrast of patterns and textures present in a large portion of the visual field, and thus provides for contrast constancy under various conditions in the visual environment. Interestingly, the contrast induction seems to be much stronger in the periphery of the visual field, than in the fovea (Fig. 56.9) (Xing and Heeger, 2000). Note that in the case of random textures, the mean luminance is equal for the inner patch and the background: there is no luminance gradient across the border. This is equivalent to saying that the effect is due to a second-order process (lack of the fundamental component in the Fourier spectrum of the pattern) and therefore cannot be explained in terms of linear mechanisms.

Subsequent research by a number of authors (see D’Zmura and Singer, 1999, for a review) showed that contrast induction is selective for various parameters of the stimuli, such as orientation, color, and spatial frequency content, and, for grating patterns, is sensitive to the relative spatial phase of the inner patch with respect to the background. Lu and Sperling (1996) described second-order contrast induction in patterns of constant luminance, where contrast varied with a spatial distribution that replicates one

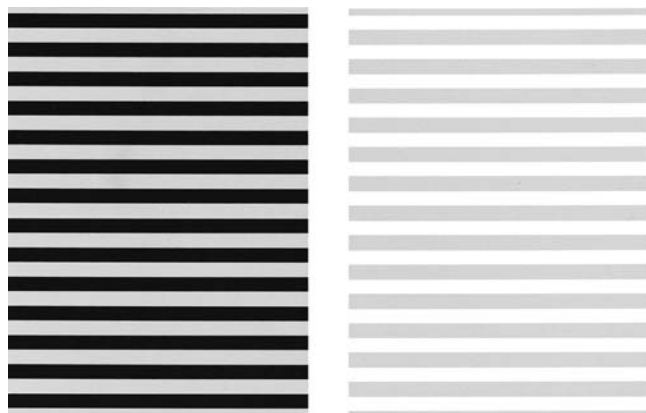


FIGURE 56.8. Example of assimilation: the gray background has the same luminance in the two parts of the figure, but it appears darker where the dark lines are superimposed (*left*) and brighter where the white lines are superimposed (*right*).

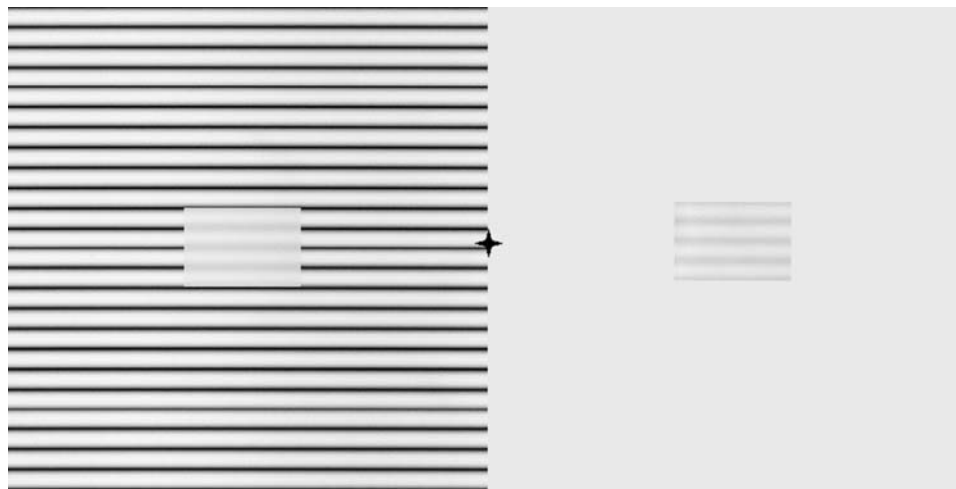


FIGURE 56.9. Example of contrast induction. The contrast of the two small gratings is physically the same, but it appears lower where it is surrounded by a high-contrast grating than where the surround is uniform. When the small cross at the center of the figure is fixated, so that the two small gratings are seen extrafoveally, contrast induction is substantially reinforced.

of those that, in the luminance domain, generate lightness illusions (Mach bands, Chevreul illusion Craik-O'Brien-Cornsweet illusion). The illusions are replicated in the apparent contrast domain, and this throws doubt on the purely empirical interpretation of Mach bands and other lightness illusions that has been suggested recently (see the section "Tentative Theoretical Interpretations and Models for Border Contrast Effects"): contrast modulations are rarely experienced.

The important question of whether the effects of contrast induction are purely monocular or may occur with dichoptic presentation of the central field and the surround has received opposite responses: Chubb et al. (1989) did not find any effect of a high-contrast surrounding annulus on the apparent contrast of an inner disk when these were flashed separately to the two eyes. With continuous presentation of the two stimuli, Singer and D'Zmura (1994) obtained dichoptic effects of approximately the same amount as with monocular presentation, both for achromatic and chromatic contrast induction. It seems likely therefore that, at least for steady stimuli, contrast induction has a cortical locus.

POSSIBLE NEURAL MECHANISMS FOR CONTRAST INDUCTION

Contrast induction may be explained in terms of lateral inhibition at some level of the visual system among mechanisms tuned to various spatial frequencies and orientations. Single cells both in the retina and in the visual cortex of cats and monkeys have been shown to present a contrast gain control that causes saturation of response amplitude for stimuli of high contrast (Carandini et al., 1997; Geisler and Albrecht, 1992; Shapley and Victor, 1981). These nonlinear response properties could result from a contrast gain control stage that pools shunting inhibition from a large population of surrounding cells (Carandini et al., 1997) or that scales

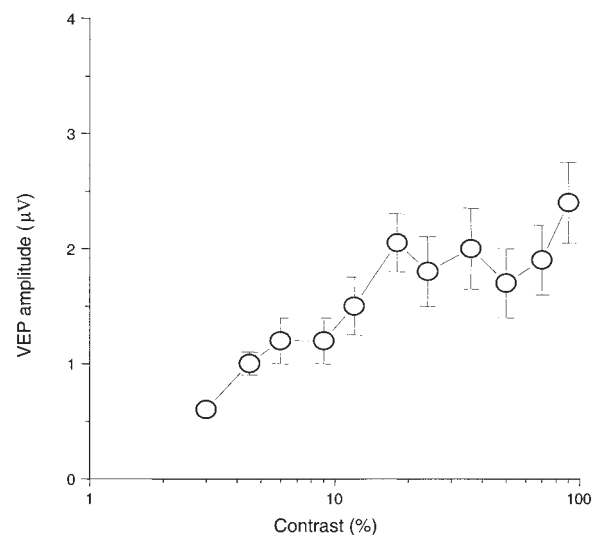


FIGURE 56.10. Pattern VEPs in response to sinusoidal gratings sinusoidally reversed in contrast at a fixed temporal frequency, for grating contrast varying in the range 3% to 100%. Ordinates: amplitude of the second harmonic of the averaged response. Mean VEP amplitudes (\pm s.e.) of 12 subjects for horizontal gratings of 2 c/deg, sinusoidally reversed in contrast at a temporal frequency optimal for each subject, in the range 4 to 10 Hz (replotted from Porciatti et al., 2000). Note that the amplitude increases with contrast in the range 3% to 20% and then remains practically constant up to the highest contrast.

the input contrast in relation to the average contrast in the surround (Geisler and Albrecht, 1992).

Electrophysiological evidence for contrast gain control in humans is provided by cortical visual evoked potentials (VEPs) in response to gratings alternated in contrast periodically at relatively low temporal frequencies. The amplitude of these pattern VEPs is found to increase linearly with log

contrast up to about 1 log unit above contrast threshold and then saturate (Fig. 56.10), while the latency of the response (evaluated from its temporal phase) shortens steadily with increasing contrast (Porciatti et al., 2000). By contrast, the pattern electroretinogram (PERG), that is, the retinal average response to contrast-alternating patterns, increases monotonically in amplitude (Hess and Baker, 1984) and does not vary in temporal phase when contrast increases from threshold to its maximum (100%) value (Morrone et al., 1994b). It has also been found that subjects with cortical hyperexcitability resulting in photosensitive epilepsy do not show amplitude saturation or latency decrease in their pattern VEP responses at high contrast (Porciatti et al., 2000). It seems, therefore, that the major contribution to contrast gain control in humans is provided by cortical mechanisms, although contrast gain control may also occur at more peripheral sites and its effects may add up at the cortical level. Whether these effects are interpretable in terms of the properties of contrast gain control in single cortical cells is obviously an open question. Still, it is interesting to note that the saturation index (a quantity measuring the amount of amplitude saturation) and the average latency decrement with increasing stimulus contrast of the human VEP responses (Porciatti et al., 2000) are in agreement with data obtained from simple cortical cells of the monkey under similar stimulus conditions (Carandini et al., 1997).

Summary

Some properties of achromatic color perception are well established psychophysically, and neurophysiological explanations have been suggested that can satisfactorily account for them. In particular, there is evidence that the ON and OFF systems are independently responsible for the suprathreshold perception of light increments and decrements. However, the role the two systems play in the perception of brightness and darkness under more general conditions is still to be assessed.

Models based on the properties of receptive fields of neurons with antagonistic excitatory and inhibitory regions in the retina and/or in the primary visual cortex can satisfactorily predict border contrast effects and some of the related brightness illusions. For other aspects of achromatic color perception, such as lightness constancy under general viewing conditions, area contrast, and contrast induction, long-range interactions seem to be required, possibly mediated by lateral connections that are known to be present in the primary visual cortex or by contributions from extrastriate cortical areas.

For a possible role of experience in the perception of brightness illusions, and for the effects of spatial arrangement and curvature in depth on lightness perception, expla-

nations in terms of neural mechanisms await future research.

REFERENCES

- Adelson, E. H., 1993. Perceptual organization and the judgment of brightness, *Science*, 262:2042–2044.
- Arend, L., and R. Goldstein, 1987. Simultaneous constancy, lightness and brightness, *J. Opt. Soc. Am.*, A4:2281–2285.
- Bruno, N., P. Bernardis, and J. Schirillo, 1997. Lightness, equivalent background and anchoring, *Percept. Psychophys.*, 59:643–654.
- Burr, D. C., 1987. Implications of the Craik-O'Brien illusion for brightness perception, *Vis. Res.*, 27:1903–1913.
- Carandini, M., D. Heeger, and J. A. Movshon, 1997. Linearity and normalization in simple cells of the macaque primary visual cortex, *J. Neurosci.*, 17:8621–8644.
- Chevreul, M. E., 1839. *De la Loi de Contraste Simultané des Couleurs*, Paris: Leon Laget.
- Chubb, C., G. Sperling, and J. A. Solomon, 1989. Texture interactions determine perceived contrast, *Proc. Natl. Acad. Sci. USA*, 86:9631–9635.
- Cornsweet, T. N., 1970. *Visual perception*, New York: Academic Press, pp. 270–273.
- Craik, K. J. W., 1966. *The Nature of Psychology. A Selection of Papers, Essays and Other Writings, by the Late K. J. W. Craik* (S. L. Sherwood ed.), Cambridge: Cambridge University Press.
- D'Zmura, M., and B. Singer, 1999. Contrast gain control, in *Color Vision: From Genes to Perception* (K. R. Gegenfurtner and L. T. Sharpe, eds.), Cambridge: Cambridge University Press, pp. 369–385.
- Fiorentini, A., 1972. Mach band phenomena, in *Handbook of Sensory Physiology*, vol. VII-4, *Visual Psychophysics* (D. Jameson and L. M. Hurvich, eds.), Berlin: Springer-Verlag, pp. 188–201.
- Fiorentini, A., G. Baumgartner, S. Magnussen, P. H. Schiller, and J. P. Thomas, 1990. The perception of brightness and darkness, in *Visual Perception: The Neurophysiological Foundations* (L. Spillmann and J. S. Werner, eds.), San Diego, CA: Academic Press, pp. 129–161.
- Fiorentini, A., and L. Maffei, 1968. Perceptual correlates of inhibitory and facilitatory spatial interactions in the visual system, *Vis. Res.*, 8:1195–1203.
- Fiorentini, A., and L. Mazzantini, 1966. Neural inhibition in the human fovea: a study of interactions between two line stimuli, *Atti Fond. G. Ronchi*, 21:738–747.
- Geisler, W. S., and D. G. Albrecht, 1992. Cortical neurons: isolation of contrast gain-control, *Vis. Res.*, 8:1409–1410.
- Gilchrist, A. L., 1977. Perceived lightness depends on perceived spatial arrangement, *Science*, 195:185–187.
- Gilchrist, A. L., S. Delman, and A. Jacobsen, 1983. The classification and the integration of edges as critical to the perception of reflectance and illumination, *Percept. Psychophys.*, 33:425–436.
- Gilchrist, A. L., C. Kossyfidis, F. Bonato, T. Agostini, J. Cataliotti, X. Li, B. Spehar, V. Annan, and E. Economou, 1999. An anchoring theory of lightness perception, *Psychol. Rev.*, 106:795–834.
- Heggelund, P., 1992. A bidimensional theory of achromatic color vision, *Vis. Res.*, 32: 2107–2119.
- Helmholtz, H. von, 1867. *Handbook der physiologischen Optik*, 1st ed. Leibnitz: Voss. English translation from the third German edition: 1962. *Treatise on Physiological Optics* (J. P. C. Southall ed.), New York: Dover, pp. 130–131.
- Hering, E., 1878. *Zur Lehre vom Lichtsinn*, Vienna: Gerald und Söhne.

- Hering, E., 1920. *Grundzüge der Lehre vom Lichtsinn*, Berlin, Springer. English translation: 1964. *Outlines of a Theory of the Light Sense* (L. M. Hurvich and D. Jameson, trans.), Cambridge: Cambridge University Press, pp. 16–17, 30–31, 74–75.
- Hermann, L., 1870. Eine Erscheinung des simultanen Kontrastes, *Pflügers Arch.*, 3:13–15.
- Hess, R. F., and C. L. Baker, Jr., 1984. Human pattern-evoked electroretinogram, *J. Neurophysiol.*, 51:939–951.
- Jacobsen, A., and A. L. Gilchrist, 1988. The ratio principle holds over a million-to-one range of illumination, *Percept. Psychophys.*, 43:1–6.
- Jung, R., 1961. Korrelationen von Neuronentätigkeit und Sehen, in *Neurophysiologie und Psychophysik des visuellen Systems* (R. Jung and H. H. Kornhuber, eds.), Berlin, Heidelberg, New York: Springer-Verlag, pp. 410–435.
- Knill, D., and D. Kersten, 1991. Apparent surface curvature affects lightness perception, *Nature*, 351:228–230.
- Krauskopf, J., 1980. Discrimination and detection of changes in luminance, *Vis. Res.*, 20:671–677.
- Lu, Z. and G. Sperling, 1996. Second-order illusions: Mach bands, Chevreul, and Craik-O'Brien-Cornsweet, *Vis. Res.*, 36:559–572.
- Mach, E., 1865. Ueber die Wirkung der räumlichen Verteilung des Lichtreizes auf die Netzhaut, I., *S. B. Akad. Wiss. Wien, math.-nat. Kl.*, 54:303–322 (F. Ratliff, trans., 1965).
- Maffei, L., 1968. Inhibitory and facilitatory spatial interactions in retinal receptive fields, *Vis. Res.*, 8:1187–1194.
- Marr, D., and E. Hildreth, 1980. Theory of edge detection, *Proc. R. Soc. Lond. B*, 207:187–217.
- McArthur, J. A., and B. Moulden, 1999. A two-dimensional model of brightness perception based on spatial filtering consistent with retinal processing, *Vis. Res.*, 39:1199–1219.
- Morrone, M. C., and D. C. Burr, 1988. Feature detection in human vision: a phase-dependent energy model, *Proc. R. Soc. Lond. B*, 235:221–245.
- Morrone, M. C., and D. C. Burr, 1989. The conditions under which Mach bands are visible, *Vis. Res.*, 29:699–715.
- Morrone, M. C., D. C. Burr, and J. Ross, 1994a. Illusory brightness step in the Chevreul illusion, *Vis. Res.*, 34:1567–1574.
- Morrone, M. C., V. Porciatti, A. Fiorentini, and D. C. Burr, 1994b. Pattern-reversal electroretinogram in response to chromatic stimuli: I, humans, *Vis. Neurosci.*, 11:861–871.
- O'Brien, V., 1958. Contour perception, illusion and reality, *J. Opt. Soc. Am.*, 48:112–119.
- Paradiso, M. A., 2000. Visual neuroscience: illuminating the dark corners, *Curr. Biol.*, 10:R15–R18.
- Porciatti, V., P. Bonanni, A. Fiorentini, and R. Guerrini, 2000. Lack of cortical contrast gain control in human photosensitive epilepsy, *Nat. Neurosci.*, 3:259–263.
- Ratliff, F., 1965. *Mach Bands*, San Francisco: Holden-Day.
- Rentschler, I., and A. Fiorentini, 1974. Meridional anisotropy of psychophysical spatial interactions, *Vis. Res.*, 14:1467–1473.
- Ross, J., M. C. Morrone, and D. C. Burr, 1989. The conditions under which Mach bands are visible, *Vis. Res.*, 29:699–715.
- Schiller, P. H., J. H. Sandell, and J. H. R. Maunsell, 1986. Functions of the ON and OFF channels of the visual system, *Nature*, 322:824–825.
- Shapley, R. M., and R. C. Reid, 1985. Contrast and assimilation in the perception of brightness, *Proc. Natl. Acad. Sci. USA*, 82:5983–5986.
- Shapley, R. M., and J. D. Victor, 1981. How the contrast gain control modifies the frequency responses of cat retinal ganglion cells, *J. Physiol.*, 318:161–179.
- Shevell, S. K., I. Holliday, and P. Whittle, 1992. Two separate neural mechanisms of brightness induction, *Vis. Res.*, 32:2331–2340.
- Shinomori, K., B. E. Scheffrin, and J. S. Werner, 1997. Spectral mechanisms of spatially-induced blackness: data and quantitative model, *J. Opt. Soc. Am., A*, 14:372–387.
- Singer, B., and M. D'Zmura, 1994. Color contrast induction, *Vis. Res.*, 34:3111–3126.
- Spillmann, L., A. Ransom-Hogg, and R. Oehler, 1987. A comparison of perceptive and receptive fields in man and monkey, *Hum. Neurobiol.*, 6:51–62.
- Spillmann, L., and J. S. Werner, 1996. Long-range interactions in visual perception, *Trends Neurosci.*, 19:428–434.
- Wässle, H., U. Grünert, J. Röhrenbeck, and B. B. Boycott, 1990. Retinal ganglion cell density and cortical magnification factor in the primate, *Vis. Res.*, 30:1897–1911.
- Watt, R. J., and M. J. Morgan, 1985. A theory of the primitive spatial code in human vision, *Vis. Res.*, 25:1661–1674.
- Whittle, P., 1991. Sensory and perceptual processes in seeing brightness and lightness, in *From Pigments to Perception* (A. Valberg and B. B. Lee, eds.), New York: Plenum Press, pp. 293–304.
- Xing, J., and D. J. Heeger, 2000. Centre-surround interactions in foveal and peripheral vision, *Vis. Res.*, 40:3065–3072.

57 Color Appearance

KENNETH KNOBLAUCH AND STEVEN K. SHEVELL

Light, neurons, and color

In the interest of clarity, the analysis of the chain of events from stimulus to perception requires a rigid distinction between *coding* and *perception*. At the earliest level, the visual system is confronted with images on the retina. *Coding* refers to the manner in which the information in the image is sampled, integrated, and transmitted in the visual system. For example, we can speak about the coding of light by photoreceptors. Subsequent transformations of the photoreceptors' signals also represent coding (or recoding) of the information in the retinal image. When discussing the relation between neural events and the stimulus, a fundamental question is how stimulus events are encoded by the responses of neurons.

In contrast, the term *color perception* ought to be reserved for what we actually experience: the hue, saturation, and brightness of color. In discussing the appearance of color, the term *representation* can be used to indicate how our experience of color is organized. This representation must have a correlate with neural activity at some level(s) of the visual system, so the coding should be related to the representation of color. The historically broad usage of the term *color* to refer to physical or physiological properties and events, rather than to perceived phenomena, continues to be a source of confusion that haunts the field. By restricting coding to the relation between neural activity and light, and perception to color appearance, many confusions in the literature are avoided, including ones implicit in misleading terms such as *red light*, *red cones*, *red genes*, and *red/green retinal pathway*. *Red* is only a percept.

In general, it is simplistic to expect the perception of color to be associated with the activity of single cells or even a single visual area. Early in the visual system, coding is highly local. At the ganglion cell and other precortical levels, activity is associated with the signals from small populations of photoreceptors and integrated over small regions of the visual field (Dacey, 1996). Progressing through the visual system, receptive fields grow to encompass larger and larger portions of the visual field (Zeki, 1993). This implies that at later stages of visual processing, the responses of cells are influenced by events occurring at locations quite distant from the centers of the receptive fields.

These physiological observations have a parallel in psychophysics. Metameric color matching (see below) can be

explained by local retinal coding in the visual system (Brindley, 1960; Schnapf et al., 1987). The colors that we attribute to lights and surfaces, however, are highly dependent on the spatial, temporal, and chromatic properties occurring elsewhere in the visual field (Spillmann and Werner, 1996). In fact, when color is considered under natural conditions, it seems to be an intrinsic property of objects, and not of the light in retinal images. Our visual system, having evolved in an environment characterized by certain regularities, is conjectured to take advantage of such regularities, to resolve an intrinsically ambiguous retinal stimulus into an invariant representation of the properties of objects (such as their spectral reflectances) (Shepard, 1994). The neural processes mediating color perception, therefore, are intertwined with those involved in object perception. The operation of such a complex process is likely to involve several stages of processing, as well as multilevel interactions, in order to integrate and extract information from locations throughout the visual scene.

Color appearance vs. color matching

Normal (and abnormal) color vision is defined by perceived matches between lights of different spectral composition (Wyszecki and Stiles, 1982). The matches must be perfect so that the two lights are not distinguishable. Such matches are referred to as *metameric matches*, as opposed to *isomeric matches* between physically identical lights. Normal human color vision is characterized as *trichromatic* because, in general, a metameric match between two fields of light can be obtained by adjusting three variables. These three variables are usually the radiances of three lights of different spectral composition (called *primaries*), but they need not be. For example, the three variables can be the wavelength and luminance of a monochromatic light (two variables) and the luminance of a superimposed broadband light (one variable). This matching configuration provides one way to assign three coordinates to a light. The wavelength of the monochromatic component is called the *dominant wavelength*; the ratio of the luminance of the monochromatic light to the sum of the luminances of the monochromatic and broadband components is the *colorimetric purity*; the sum of the luminances of the monochromatic and broadband components (the luminance of their mixture) gives the third component.

The analysis of lights based on their matching coordinates is called *colorimetry*. Matching, however, does not reveal how the lights appear, just that the matched fields do not differ in appearance. In other words, color matching specifies unequal physical lights that are not discriminable by human observers, without regard to the actual color appearance of the fields. Matching tells us what lights look alike but not what lights look like.

The color appearance of isolated lights also can be described with three dimensions: hue, saturation, and brightness. These dimensions refer to perceptual attributes of lights and surfaces, not to their neural representations. Unlike the color matching coordinates, attributes of color appearance depend on context (e.g., the state of visual adaptation and the spatial distribution of other lights in view). Thus, while metameric matches simplify our understanding of the coding of lights by representing many physical spectral distributions by the same point in a three-dimensional space, appearance complicates the situation because the same point in this space can correspond to many different appearances due to the effects of context. From the point of view of the observer, however, the neural processes mediating appearance simplify interactions with the environment because they work to assign the same percept to the same object in spite of the physical variations of its image on the retina.

Perceptual attributes of isolated lights

DIMENSIONALITY OF COLOR How many dimensions are required to specify the appearance of colors? There are at least two ways to interpret this question.

First, what is the minimum number of variables required to generate all the colors that we can experience? For isolated lights (i.e., lights presented on a dark background to the neutrally adapted eye), the answer is still three, as any manipulation of more than three will still be equivalent to some mixture of just three primary lights. However, the situation is more complex with lights presented in a context, as discussed below. An alternative interpretation is to ask, how many different perceptual attributes are required to describe the color of isolated lights? This question addresses the perceptual organization of color appearance. Given the three-dimensional space for coding light, can a simple perceptual organization be mapped onto it?

Color could be treated in a purely categorical fashion, with each region of the coordinate space assigned a different color name. Anthropological/linguistic (Berlin and Kay, 1969) and psychophysical evidence (Boynton and Olson, 1990) suggests that such a partition is possible, based on 11 basic color terms: red, yellow, green, blue, orange, brown, purple, pink, black, white, and gray. Nevertheless, there is ongoing debate as to the extent to which such an organiza-

tion reflects cultural-linguistic or physiological constraints on perception (Davidoff et al., 1999; Lindsey and Brown, 2002; Saunders and van Brakel, 1997). At least 3 of these 11 terms—brown, gray, and black—refer to colors that are perceived only in the presence of contrast with other lights, and not with any isolated light alone, so this scheme is more complex than is required to account for the appearance of isolated lights. Further, it fails to capture the richness of color perception, which is much more fine-grained than 11 categories. According to Judd and Kelly (1939), “there are about 10,000,000 surface-colors distinguishable in daylight by the trained human eye” (p. 359).

HUE, SATURATION, AND BRIGHTNESS The appearance of isolated lights may be described in a cylindrical coordinate frame with the dimensions of hue, saturation, and brightness. *Hue* is that aspect of color to which one refers when the color is given a specific name, such as red, green, orange, or purple. The hue of an isolated field changes systematically with its wavelength, but this does not generate the full gamut of hue percepts. Mixing together lights from the extreme long- and short-wavelength portions of the spectrum produces purplish hues. By including these mixtures, hues can be organized on a circle, and an angular position can be associated with each hue (Fig. 57.1A). The angle is only a marker, however, of which hue is associated with a particular wavelength or mixture of wavelengths.

A distinction is made between chromatic colors such as those just described and the achromatic color white, which has no hue. For isolated fields, the degree to which a color with hue differs from white is referred to as *saturation*. If hue is distributed around the perimeter of a circle, then saturation can be represented on the radii from the rim to the center, with the center assigned to an achromatic color (Fig. 57.1A). Finally, colors may vary in their perceived intensity or *brightness*. Brightness is represented on an axis perpendicular to the hue-saturation plane just described (Fig. 57.1B). These perceptual attributes can be measured using standard psychophysical scaling procedures (Gordon et al., 1994).

In general, the colorimetric coordinates of a light (e.g., dominant wavelength, colorimetric purity, and luminance) are not directly related to the perceptual coordinates of hue, saturation, and brightness. In particular, hue is not constant as the luminance of a fixed wavelength is varied (Bezold-Brücke effect) or as colorimetric purity is varied at fixed wavelength and luminance (Abney effect). Additionally, brightness is not constant at equiluminance for lights at different wavelengths (Helmholtz-Kohlrausch effect), and saturation is not constant for lights of equal purity.

HUE CANCELLATION A different perceptual representation is constructed by distinguishing unitary from binary colors.

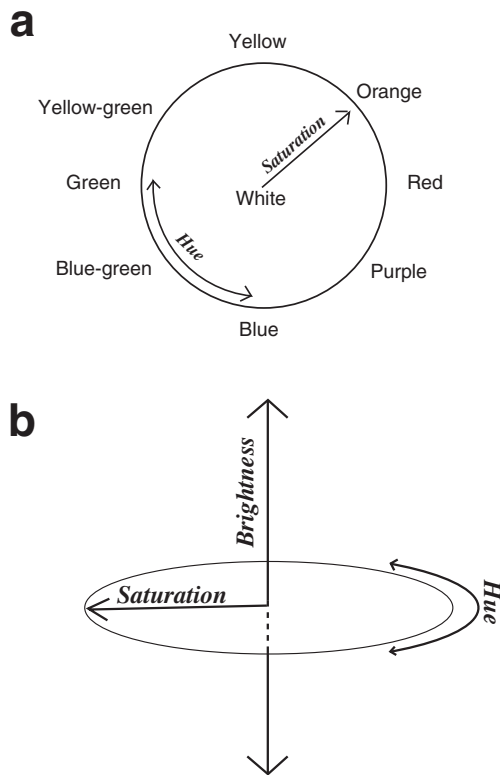


FIGURE 57.1. *A*, Representation of hue as an angular dimension around a circle and saturation as a radial distance from the central white. *B*, The addition of a brightness dimension perpendicular to the hue-saturation plane is used to represent the perceived intensity of a light.

Unitary colors—red, green, yellow, blue, white, and black—are psychologically elementary in that they cannot be decomposed perceptually into finer components. Colors such as orange and purple are binary because they can be described as combinations of unitary hues, for example, yellow-red and blue-red, respectively. Hering (1920/1964) noted that the unitary colors could be grouped into three pairs, the elements of which are in an antagonistic relation: red-green, yellow-blue, white-black. One criterion for this pairing is based on mutual exclusivity. While there are hues that are red-blue (violet), red-yellow (orange), green-yellow (lime green), and green-blue (aqua), there are no hues that are red-green or yellow-blue. The presence of one of these components excludes the other. On this basis, Hering proposed that opponent colors correspond to activity of opposite polarity within a single bipolar neural response. Thus, one process could signal either red or green but not both simultaneously; another could signal yellow or blue. One polarity can be arbitrarily assigned a positive sign, the other a negative sign. Thus, including white-black, three signed perceptual coordinates can be attributed to each light (and can be associated with its colorimetric coordinates), corresponding to the response of each of the underlying opponent-color processes (Fig. 57.2).

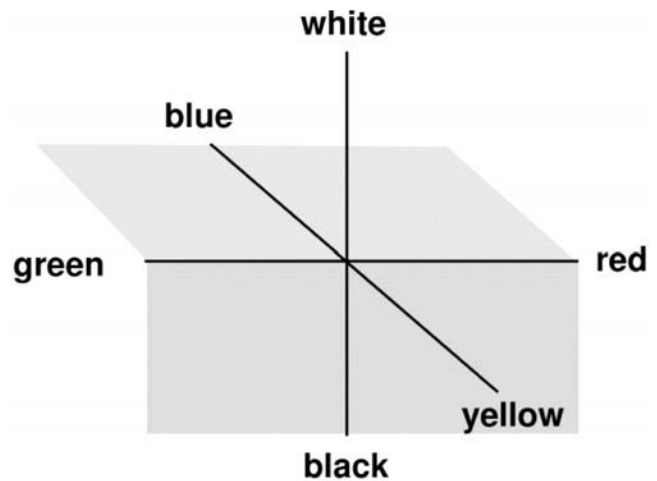


FIGURE 57.2. The three dimensions of opponent-colors theory—red-green, yellow-blue, and white-black—represented as a coordinate frame for describing the color of lights.

The hue cancellation task is used to determine opponent-colors coordinates. It is based on the mutual exclusivity of opponent hues. Because of this property, the mixture of lights containing opponent hues results in the counterbalancing or cancellation of the two hues. For example, mixing a small amount of a light that appears green with a light that appears red will result in a light that appears less reddish. Adding more of the green-appearing light will progressively reduce the redness until it disappears, at which point the light mixture is described as neither reddish nor greenish. Continuing to add green-appearing light will result in a greenish appearance of the mixture. At the *null* point of this continuum of mixtures (i.e., the point that appears neither reddish nor greenish), the mixture is a hue that is balanced or at equilibrium with respect to the red-green system. The possible residual hues—yellow, blue, white—are called *red-green equilibrium hues*. At equilibrium, it is hypothesized that the two lights of the mixture produce equal but opposite responses in the underlying red-green system. On the basis of this idea, the magnitude of redness (or greenness) of a given light is defined in terms of the energy of a standard green- or red-appearing light necessary to bring the mixture to red-green equilibrium. The same logic can be applied to yellow- and blue-appearing lights to measure their opponency by bringing their mixture to yellow-blue equilibrium, that is, to a mixture that appears red, green, or white. Figure 57.3 shows for one observer how the logarithm of the energy of a canceling standard varies across the spectrum in order to cancel the redness (*filled circles*), greenness (*unfilled circles*), blueness (*filled triangles*), and yellowness (*unfilled triangles*) of a 1 degree foveally viewed test field.

The activation of the red-green and yellow-blue systems also has been used to describe the hue of isolated lights of

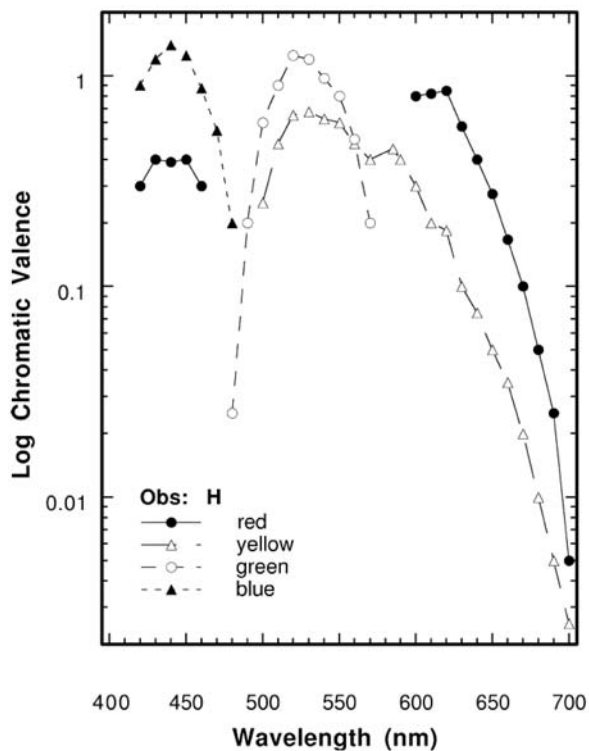


FIGURE 57.3. Hue cancellation data from one observer (replotted from Jameson and Hurvich, 1955). The points represent the energy of a standard light necessary to cancel a hue component at each wavelength. The canceling standards for this observer were 490 nm (greenish standard to cancel redness), 700 nm (reddish standard to cancel greenness), 467 nm (bluish standard to cancel yellowness), and 588 nm (yellowish standard to cancel blueness). Except for the reddish standard, the wavelengths were chosen to be at the unique hues for the observer.

different wavelength. Wavelengths at which one of the systems has a null response are equilibrium hues (also referred to as *unique hues*). Three unique hues appear in the spectrum, two for red-green (unique yellow and blue near 580 and 465 nm, respectively) and one for yellow-blue (unique green, near 505 nm). The yellow-blue equilibrium that appears unique red does not occur in the spectrum but requires the mixture of short-wavelength (blue- or bluish-red-appearing) and long-wavelength (yellowish-red-appearing) lights.

Hue cancellation functions were systematically measured in seminal studies that showed how these functions could be used as a coordinate frame that gives a coherent account for a large body of color-appearance observations (Hurvich and Jameson, 1955, 1956; Jameson and Hurvich, 1955, 1956). Two problems, however, arise. First, it is not obvious how to apply the logic of cancellation to the white-black system for isolated lights, because blackness results from only spatial and temporal interactions. For isolated lights, luminosity or brightness functions have been proposed as spectral sensitivities of whiteness. Neither of these is satisfying, however,

from a theoretical or an empirical point of view (see the section “Achromatic Appearance”). Second, how do hue cancellation coordinates relate to colorimetric specification from color matching? Since color matching functions are linearly related to the photon catch in cone photoreceptors, specifying the relation between hue cancellation and color matching would determine how hue perception depends on the light absorbed by photoreceptors.

The simplest relation possible would be a linear one. Some implications of linearity were appreciated early on. Schrödinger (1925/1994) understood that a linear relation implies that the spectral unique hues could not change wavelength with intensity, and that a locus of equilibrium lights will fall on a straight line in a chromaticity diagram. The invariance of the unique hues with light level was tested in several early studies (Dimmick and Hubbard, 1939; Hurvich and Jameson, 1951a; Purdy, 1931) though deviations from linearity, when found, were not developed theoretically until Krantz’s (1975) formal analysis was performed. Linearity implies two empirical properties: scalar invariance and additivity. Scalar invariance requires that a light perceived to be in hue equilibrium must remain in equilibrium when its radiance is changed. An invariant wavelength for each spectral unique hue would be consistent with this property. Additivity requires that the mixture of any two lights that are equilibrium hues from the same set must also be in that set. For example, a mixture of any two lights that individually appear unique blue or unique yellow must appear neither reddish nor greenish.

Several more recent studies indicate that linearity is satisfied for red-green but not for yellow-blue equilibria (Larimer et al., 1974, 1975; Valberg, 1971; Werner and Wooten, 1979). For example, Figure 57.4 shows that the wavelengths of the spectral unique hues (blue, green, and yellow) are approximately invariant with the level of retinal illumination, but the mixture ratio of two spectral lights that gives unique red is not (rightmost set of points for observers DB and AN). More extensive examinations revealed nonadditivity associated with both red-green and yellow-blue percepts (Ayama et al., 1985; Burns et al., 1984; Chichilnisky and Wandell, 1999; De Valois et al., 1997; Nagy, 1979). In some of these experiments a surround field was used, so technically they are not studies of isolated lights. The use of a surround field complicates the interpretation because it can introduce nonlinearity.

The relation between colorimetric coordinates and color appearance inspired what have been termed *zone models*, in which spectral information passes through two stages (or zones) of processing: spectral coding by three classes of photoreceptors, followed by excitatory and inhibitory recombination of the photoreceptor outputs to produce three postreceptoral responses. The postreceptoral responses are usually divided into two that are spectrally opponent and

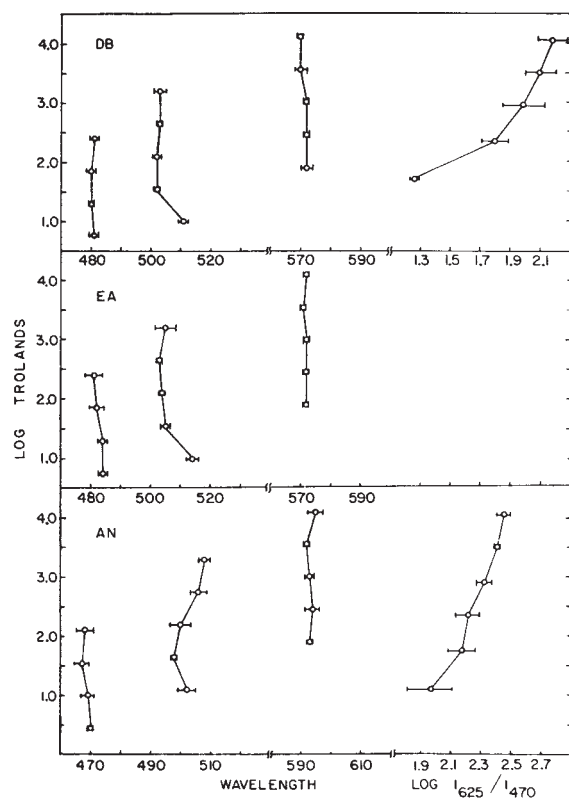


FIGURE 57.4. Test of the scalar invariance of unique hues for stimuli of 1 second duration (see text). (From Nagy, 1979. Reproduced with permission from Elsevier Science.)

one that is not. In the case of linearity, the postreceptoral responses are modeled by a system of linear equations:

$$\begin{aligned}(r-g)_\lambda &= a_1 L_\lambda + a_2 M_\lambda + a_3 S_\lambda \\ (y-b)_\lambda &= a_4 L_\lambda + a_5 M_\lambda + a_6 S_\lambda \\ (w-bk)_\lambda &= a_7 L_\lambda + a_8 M_\lambda + a_9 S_\lambda,\end{aligned}$$

where $r-g$, $y-b$, and $w-bk$ are the red-green, yellow-blue, and white-black responses; L_λ , M_λ , and S_λ are cone photoreceptor light absorptions; and a_i are constant weighting coefficients. Note that each cone distributes its signal to each hue channel and, because of the linearity with fixed coefficients, each cone signal contributes to only one polarity of each opponent channel. This implies that each cone signals a binary hue. Thus, in most models, L cones contribute to redness and to yellowness. Given the violations of linearity just discussed, however, this model must be modified. Several initial attempts considered photoreceptor signals to be a nonlinear function of light level (Elzinga and de Weert, 1984; Larimer et al., 1975; Werner and Wooten, 1979). As long as the nonlinearity is monotonic, this does not change the qualitative relation between cone signals and hue, that is, that cones signal a binary hue and that each cone signal contributes to only one polarity of a chromatic opponent mechanism. In addition, there has been some controversy

about how the cone responses affect color appearance. In the Jameson and Hurvich (1968) linear model, for example, M cones contribute to both greenness and yellowness, while some studies suggest that M cones can contribute to blueness (De Valois et al., 1997; Drum, 1989; Schirillo and Reeves, 2001).

Knoblauch and Shevell (2001) directly tested the contributions of cone responses to color percepts by measuring hue cancellation under conditions in which lights were constrained to vary along cone-isolation directions. In their experiment, the observer adjusted the level of excitation of only one cone class while setting a light to reach hue equilibrium (either red-green or yellow-blue, depending on the instructions given to the observer). The measurement was repeated for each of a series of increasing excitation levels of a second cone class while the excitation of the third cone class was held constant. If the cone excitation that the observer sets increases with an increase in the cone excitation of the second class, then the two cone classes contribute with opposite polarity to the color percept. If, on the other hand, the observer decreases cone excitation with an increase in the second class, then the two cone classes contribute with the same polarity.

For the range of conditions that Knoblauch and Shevell examined, red-green cancellation was linear, with L and S cones contributing with a polarity opposite to that of M cones. For example, Figure 57.5A shows that increasing L-cone excitation can be compensated by decreasing S-cone excitation in order to maintain a 0.8 degree field in red-green equilibrium. These results are consistent with standard models that have L and S cones contributing to redness and M cones to greenness. A more complex picture emerged when the observer adjusted lights to achieve yellow-blue hue equilibrium. The most striking result was that cone signals from one class of cones could vary nonmonotonically with respect to the level of another class to maintain a yellow-blue equilibrium percept. In the example in Figure 57.5B, increasing L-cone excitation is initially compensated for by an increase but eventually by a decrease in S-cone excitation in order to maintain a light in yellow-blue equilibrium. This implies not only nonlinearity, as previously found, but also that the polarity of input from a given cone class to an opponent-color response is not fixed. Another way to interpret this result is that there is no fixed hue signal associated with the output of a given cone class. Increasing the L-cone response, for example, may cause a light to appear either more yellowish or more bluish, depending on the levels of S- and M-cone stimulation. The same may be true of M cones, which would explain the conflicting reports of whether their signals contribute to blueness or yellowness. They may contribute to either, depending on the excitations of the other two cone classes.

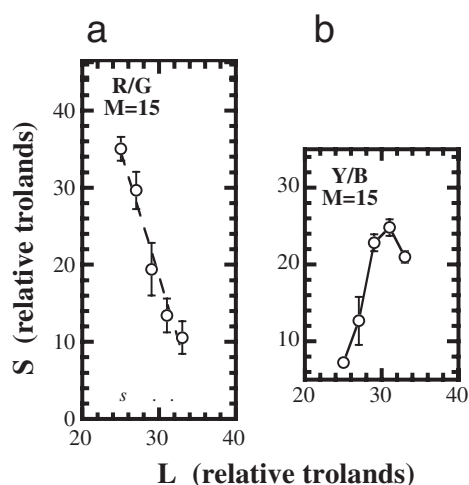


FIGURE 57.5. *A*, The S-cone excitation required to produce a red-green equilibrium percept, as a function of L-cone excitation and with a fixed level of M-cone excitation. *B*, The S-cone excitation required to produce a yellow-blue equilibrium percept, again as a function of L-cone excitation and with a fixed level of M-cone excitation. (From Knoblauch and Shevell, 2001.)

ACHROMATIC APPEARANCE The white-black dimension merits a treatment separate from that of the chromatic dimensions because it is organized differently. For example, isolated lights can appear white but not gray or black. The fact that only part of the perceptual dimension is accessible with isolated lights is a consequence of the fact that unlike red-green and yellow-blue opponency, white-black opponency arises from only spatial and temporal but not spectral interactions. This explains why a task like hue cancellation has not been attempted to measure this response for isolated lights. In the absence of a procedure based on perceptual antagonism to probe the white-black response, measures based on threshold, brightness, or luminosity have been used to represent the achromatic visual response (e.g., Hurvich and Jameson, 1955). Under many conditions, the first two of these measures are not free of contributions from chromatic mechanisms (Guth et al., 1969), while the perceptual significance of the last measure, based on luminance, is not obvious. Some insight into a solution to this problem can be gained by considering attempts to measure a spectral sensitivity for blackness.

The spectral efficiency of blackness has been estimated using spatial and temporal induction (Cicerone et al., 1986; Fuld et al., 1986; Volbrecht and Werner, 1989; Werner et al., 1984). As such, we are no longer speaking of isolated lights because the percept depends on contextual elements in space or time. These experiments determined the energy of an annular stimulus or a just-preceding stimulus required to render a test light black in appearance. Generally, these studies showed that the spectral sensitivity of blackness induction follows the luminosity function, which is based on

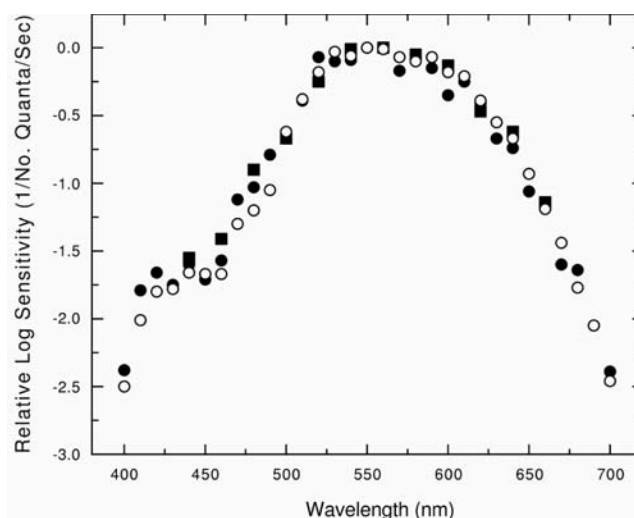


FIGURE 57.6. Comparison of spectral sensitivities based on heterochromatic flicker photometry (*unfilled circles*), temporal induction of blackness (*filled circles*) and spatial induction of blackness (*filled squares*) from a single observer. (Courtesy of J. S. Werner.)

flicker photometry (Fig. 57.6). If it is assumed that blackness should mirror whiteness in spectral efficiency, then these results support the idea that the luminosity function is the appropriate sensitivity function for the white-black response. The situation, however, is more complex. For example, Shinomori et al. (1997) found, as in the earlier studies, that the efficiency of a monochromatic annulus required to render a broadband central test disc black followed the standard luminosity function and that the judgments obeyed additivity. If the annulus was a fixed broadband light and the observer manipulated the energy of a monochromatic central test disc to obtain a black appearance, however, the spectral sensitivity showed evidence of contributions from chromatic mechanisms, and the judgments were nonadditive. These observations led the authors to propose that the induction mechanism from the surround was purely achromatic, while the perception of the central test disc was mediated by both achromatic and chromatic mechanisms.

In the presence of a surround field, Chichilnisky and Wandell (1999) found that observers could employ a cancellation criterion in estimating if a light was neither white nor black. With this configuration, they estimated the surface in color space on which lights are in white-black equilibrium. Conforming to the induction studies above, this surface is planar, indicating a linear white-black mechanism.

Another difficulty posed by the white-black dimension is that a rather large class of lights appears white when seen in isolation. For example, Hurvich and Jameson (1951b) showed that isolated lights of color temperatures ranging from 2842 to 10,000 K appeared hueless, and thus white, if their luminances were sufficiently high. The threshold

luminance for whiteness by this definition was found to be a U-shaped function of color temperature with a minimum between 20 and 40 cd/m² near 5500 K for two observers and near 7500 K for a third. Within the large range of color temperatures that appear white at relatively modest luminances, is there one that could be considered a neutral white? Jameson and Hurvich (1951) argued that a neutral white should be one that does not imbalance the underlying chromatic response functions by adaptation. Thus, adaptation to a neutral white would not cause shifts in the wavelengths of the spectral unique hues. The color temperature that satisfied this condition was at the minimum of the U-shaped whiteness threshold contour from the previous study, for each of the three observers (Hurvich and Jameson, 1951b).

RELATING PHYSIOLOGY TO APPEARANCE While the retina transmits visual information to several sites in the brain (Rodieck, 1998), the signals that pass from the retina via the lateral geniculate nucleus (LGN) to primary visual cortex (V1) and from there to ventral extrastriate areas are those that have been implicated in the coding of spectra and the perception of color (Dacey, 1996; Derrington et al., 1984; Gegenfurtner et al., 1996; Lennie et al., 1990; Shapley, 1990; Zeki, 1980, 1993). Early studies generated much excitement in showing antagonistic interactions between different cone classes in neurons from the retina to the cortex, as predicted from perception studies (De Valois, 1965; Wiesel and Hubel, 1966). The current view is to organize precortical coding into three pathways, M, P, and K, that are anatomically and functionally parallel (Chapter 30). There are suggestive resemblances between the characteristics of these pathways and those of the perceptual systems, white-black, red-green, and yellow-blue, respectively. The hope that there would be a simple correspondence between precortical cell classes and the perception of color, however, has not been borne out (Mollon and Cavonius, 1987; Valberg, 2001).

The retinal output of the M pathway originates in parasol ganglion cells, projecting to cells in the ventral magnocellular layers of the LGN which, in turn, project principally to layer 4c α of V1 (Rodieck, 1998). The cells in this pathway are characterized by high contrast gain and high sensitivity at low spatial and high temporal frequencies (Derrington and Lennie, 1984). The receptive fields of cells in this pathway are organized concentrically, with spatial antagonism between the center and the surround. The center and surround display similar spectral signatures, described by a weighted sum of the spectral sensitivities of the L and M cones (not to be confused with the M pathway). These characteristics recommend the pathway as a reasonable candidate for the substrate for the luminosity function (Lee et al., 1988) and a possible substrate for the white-black

system. Luminance information, however, is also transmitted along the P pathway.

The P pathway displays a number of features that are complementary to those of the M pathway. It has a lower contrast gain and is maximally sensitive at high spatial and low temporal frequencies (Derrington and Lennie, 1984). The retinal output originates in midget ganglion cells, projecting to cells in the dorsal parvocellular layers of the LGN which, in turn, project primarily to layer 4c β of V1 (Rodieck, 1998). In central vision, the receptive fields of P-pathway cells are activated by a single cone, typically an L or M cone (though there is also anatomical evidence for a small subset of P cells with S-cone centers; Calkins, 2001). There is ongoing controversy as to whether the surrounds of P cells are composed of only one cone class (M in the case of L centers and L in the case of M centers) or a mixture of M and L cones (Lennie et al., 1991; Martin et al., 2001; Reid and Shapley, 1992). In either situation, however, a spectral antagonism will be generated between the center and surround due to the differences in their spectral sensitivities (Lennie et al., 1991; Paulus and Kröger-Paulus, 1983). Thus, while a chromatic signal is transmitted along the P pathway, the spatial and spectral antagonisms are confounded in a manner that results in the coding of a mixture of luminance and chromatic information in the response. Algebraically, it has been shown that the mixture is multiplexed in such a way that the chromatic and luminance information could be recovered from different frequency bands by subsequent filtering (Ingling and Martinez-Uriegas, 1983).

There are several difficulties with the proposition that the P pathway is the substrate for red-green perception. First, the mechanism underlying red-green perception requires input from the S cones to account for redness at short wavelengths. The rare S-center P cells, however, are, on the basis of anatomical criteria, only of the OFF variety (Calkins, 2001). It remains to be shown that a small S-cone contribution of this nature would be sufficient to account for the role of S cones in red-green perception. Second, the fact that the pathway carries luminance signals would require that the red-green response be calculated at a cortical level beyond which the P pathway is no longer considered to be distinct from the M and K pathways. There are several possibilities. The excitation distributed across the several types of P cells, specified with respect to the spectral sensitivity of the center (L, M, or S) and whether the center is an ON or OFF response, could constitute the substrate of red-green perception. Alternatively, this information could be collected and integrated within a common class of cells at the cortex. The latter possibility does not exclude a contribution from other precortical pathways.

Recent studies have demonstrated a third precortical pathway transmitting chromatic signals, originating in a small bistratified ganglion cell (Dacey and Lee, 1994) and

projecting to a subset of cells in the interstitial koniocellular layers of the LGN which, in turn, project to cytochrome oxidase-rich regions of the supragranular layers of V1 (Hendry and Reid, 2000). The receptive fields in this pathway display nearly coextensive centers and surrounds with an ON signal from S cones and an OFF signal from L and M cones. Thus, the chromatic antagonism is not confounded with spatial antagonism, as in the P pathway. While their spectral sensitivity is consistent with a role in yellow-blue perception, they cannot function as its substrate alone. These cells show linear integration of spectral information (Chichilnisky and Baylor, 1999; Derrington et al., 1984). To accommodate the nonlinearities found in yellow-blue perception, these cells would have to interact with other cell types, such as from the P pathway, or perhaps with the recently reported monostriated S-OFF cells (Dacey et al., 2001). For example, models with combinations of rectified responses of ON and OFF pathways, within which cone signals interact antagonistically, would produce nonmonotonic hue cancellation behavior, as described above for yellow-blue perception (Chichilnisky and Wandell, 1999; De Valois and De Valois, 1993; Valberg, 2001).

Two new features in the classification of cells by their spectral sensitivities arise at the level of the cortex. First, some cells integrate spectral information nonlinearly (Lennie et al., 1990). The nonlinearity is demonstrated in cells whose spectral bandwidths are too narrow to have been produced by linear sums of cone signals. Second, while the distribution of the peak spectral sensitivities of the cells recorded *subcortically* displays three clusters, corresponding to the differences in cone inputs and interaction in the three subcortical streams (Derrington et al., 1984), this is no longer the case at the cortex. Instead, the spectral tuning of cells tends to a uniform distribution over color space. If one believes that the substrate of the perceptual-color representation is to be found in a specialized class of cells, then the goal of finding that substrate seems to have become even more elusive.

The transformation in spectral coding found at the cortex does not, at present, have a clear interpretation. The implications for perception probably require consideration of the significant changes in the spatial and temporal profiles that also occur in cortical neurons. Suggested roles for cortical recoding include finer representations of hue (Lennie et al., 1990), a contribution to the segmentation of contours on the basis of chromaticity and luminance differences (Gegenfurtner et al., 1996; Johnson et al., 2001), and the assignment of invariant colors to objects (color constancy; Zeki, 1980). To appreciate how cortical mechanisms underlie color appearance, however, will require taking account of how context affects color perception.

Perceptual attributes of lights in context

The color appearance of isolated lights reveals fundamental properties of neural coding that mediate hue, saturation, and brightness. The actual appearance of any given wavelength (or spectral distribution of wavelengths), however, depends on the context in which the light is viewed. In the natural world, nearly all colors that we experience are seen within a context of surrounding light and nearby objects, and this context strongly affects color appearance.

LIGHTNESS AND CHROMA Lights viewed in context can take on a color appearance that does not match any isolated light. Lights in context, therefore, can have percepts outside the range described by hue, saturation, and brightness. For example, no isolated light appears brown, burgundy, or gray. When a light is viewed in context, its appearance can be described *in relation* to other color percepts using two additional perceptual dimensions, lightness and chroma.

Lightness is the perceived magnitude of emitted light relative to a region that appears white. Lightness varies along a continuum from white to gray to black, in comparison to brightness, which varies from dazzling to very dim (Judd, 1940). This implies that a fixed light can change in lightness as its context is varied. For example, if a particular achromatic light has the highest luminance of any stimulus in view, it appears white. Its lightness is reduced by adding a nearby surrounding field of substantially higher luminance.

Chroma is the perceived difference between a particular color and an achromatic color of the same lightness. Thus, chroma depends on a reference color (usually a shade of gray), which varies with the lightness of the color sample. Saturation, by comparison, is the difference between a particular color and a constant white. Colors of fixed hue and lightness that vary in chroma are shown in Figure 57.7.

DARK COLORS An isolated light that appears achromatic will be seen as white, regardless of its luminance. Even a dim light barely above detection threshold appears white. By comparison, the same light can appear gray or even black when viewed in context. Context can result in color percepts that include a component of perceptual grayness or blackness (Evans, 1974). These color percepts, which include navy blue, maroon, and brown, are called *dark colors*. Brown, for example, is perceived when an isolated light that appears desaturated orange is surrounded by a "white" light of higher luminance, which induces grayness. Dark colors significantly expand the range of colors that we experience.



FIGURE 57.7. Colors that vary in chroma. (See color plate 31.)

CHROMATIC CONTRAST AND ASSIMILATION The change in color appearance caused by introducing nearby light is called *chromatic induction*. When the appearance of a light shifts away from the appearance of the nearby light, the shift is called *chromatic contrast*. For example, a light that appears yellow in isolation will appear greenish-yellow when surrounded by a long-wavelength light, which appears red. Shifts in color due to contrast can be substantial. Color shifts measured with nearby light that appears red, yellow, green, or blue are shown, respectively, in the top to bottom panels of Figure 57.8. Each panel shows the shifts, in CIE 1931 x, y chromaticity coordinates, caused by one of the inducing lights, presented in 18 minute wide stripes of a grating 2 degrees wide (the inducing chromaticity is indicated by the solid circle in each panel). Test stripes 6 minutes wide were presented between inducing stripes. Each arrow represents one test chromaticity: the tail indicates the appearance of the test alone (no inducing stripes), and the head shows the appearance with the inducing light. The measurements often show strong color shifts caused by induction, though smaller shifts would occur in natural viewing with normal eye movements, lights less similar in luminance, and typical chromatic aberration of the eye (optically corrected in this study). Theoretical explanations for chromatic contrast are considered in the next section (“Chromatic Adaptation”).

When the color appearance of a light shifts toward the context, the shift is called *chromatic assimilation*. A common example is the appearance of brick walls. The color of the brick shifts toward the appearance of the mortar. A demonstration of assimilation is shown in Figure 57.9 (view at arm’s length), where the backgrounds are physically identical but appear unequal because of an overlaying grid that appears yellow, red, or blue. Assimilation rather than contrast occurs with fields of relatively high spatial frequency. A transition from contrast to assimilation typically is found at about 3 to 6 c/deg (Fach and Sharpe, 1986), though factors other than spatial frequency also are relevant, including the relative size of inducing and test regions, the lights’ chromaticities, and the background field on which the test and inducing lights are viewed.

Assimilation results from optical factors and from neural processes. Blurred light on the retina, caused by chromatic aberration and diffraction, can contribute to assimilation, but optical factors cannot provide a full explanation (Fach and Sharpe, 1986; Shevell and Cao, 2003). This implies that

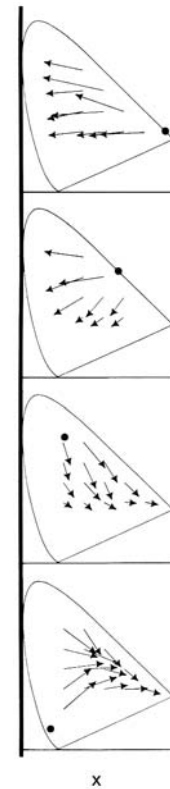


FIGURE 57.8. Shifts in color appearance caused by chromatic contrast (see text). (From Ware and Cowan, 1982. Reproduced with permission from Elsevier Science.)

neural processes also contribute to assimilation, in qualitative accord with the neural point spread function for chromatic pathways (Sekiguchi et al., 1993; Williams et al., 1993).

CHROMATIC ADAPTATION Classically, shifts in color appearance caused by chromatic adaptation were studied with uniform adapting fields. For example, a test light that appears yellow in isolation appears greenish-yellow when superimposed on a long-wavelength (red) adapting field. The test is superimposed on the long-wavelength adapting light, so physical admixture would drive the test to a more reddish appearance, but long-wavelength adaptation causes instead a shift toward greenness. Therefore, changes in color appearance with chromatic adaptation are due to neural processes.

The shift toward greenness is consistent with receptor desensitization caused by the long-wavelength field, which stimulates and (presumably) desensitizes L cones more than M cones. With the long-wavelength adapting field, the balance of neural responses from M and L cones for the test light is tipped toward the M cones, compared to the same light viewed without adaptation. A general form of this theory is expressed by the von Kries Coefficient Law (1905), which states that adaptation attenuates the neural signal from each type of cone by a fraction that depends on the

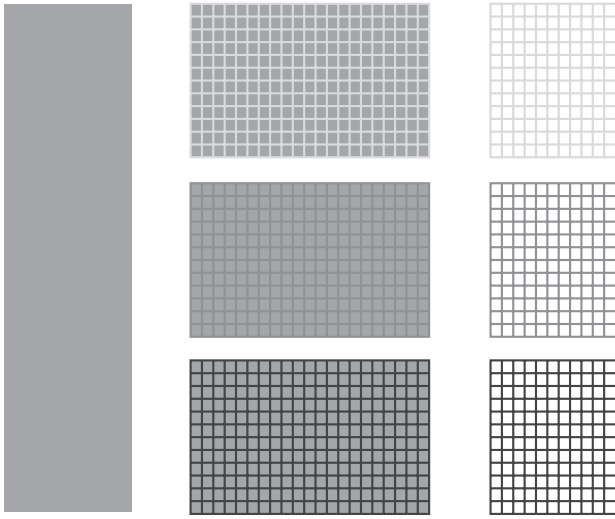


FIGURE 57.9. An example of chromatic assimilation. The three “orange” background regions in the center are physically identical at the chromaticity of the uniform bar on the left. Overlaying grids that appear yellow, red, or blue (shown alone on the right) shift the appearance of the orange background toward the appearance of the grids. (See color plate 32.)

degree to which each cone type is stimulated by the adapting field.

While the Coefficient Law gives a good empirical account of color appearance in some stimulus arrangements, several types of measurements are inconsistent with it. First, studies show that the attenuation for a given type of cone cannot be explained by only the adapting light absorbed by that particular cone type (Bauml, 1995; Cicerone et al., 1975). If the receptor gain-control framework is maintained, this implies that attenuation of signals from one cone type depends in part on light absorbed by one or both of the other two types. A more general failure of the Coefficient Law is revealed by color matching. Consider two different spectral distributions of light, $E_1(\lambda)$ and $E_2(\lambda)$, presented on distinct patches of retina exposed to different adapting lights. According to the coefficient law, lights $E_1(\lambda)$ and $E_2(\lambda)$ will be indistinguishable (i.e., match metamERICALLY) when they have identical neural responses from the L, M, and S cones:

$$\sum_{\lambda} [E_1(\lambda)q_L(\lambda)a_{L1}] = \sum_{\lambda} [E_2(\lambda)q_L(\lambda)a_{L2}]$$

(L-cone response)

$$\sum_{\lambda} [E_1(\lambda)q_M(\lambda)a_{M1}] = \sum_{\lambda} [E_2(\lambda)q_M(\lambda)a_{M2}]$$

(M-cone response)

$$\sum_{\lambda} [E_1(\lambda)q_S(\lambda)a_{S1}] = \sum_{\lambda} [E_2(\lambda)q_S(\lambda)a_{S2}]$$

(S-cone response)

The functions $q_L(\lambda)$, $q_M(\lambda)$, and $q_S(\lambda)$ are the spectral sensitivities of the L, M, and S cones, and a_{L1} , a_{M1} , and a_{S1} are the receptor gains for each cone type due to the adapting light in the retinal region of E_i ($i = 1, 2$). The sum is taken

over all visible wavelengths of light λ . According to these equations, if lights $E_1(\lambda)$ and $E_2(\lambda)$ are indistinguishable, then the lights should remain indistinguishable if both light levels are doubled to $2E_1(\lambda)$ and $2E_2(\lambda)$; more generally, any change of light level by proportion α to $\alpha E_1(\lambda)$ and $\alpha E_2(\lambda)$ should leave the lights indistinguishable. This implication of the von Kries Coefficient Law fails empirically (Hurvich and Jameson, 1958; Jameson and Hurvich, 1959).

The Coefficient Law also cannot explain the change in appearance of a single light viewed over an extended period of time (self-adaptation). Consider a light composed of a mixture of 546 and 670 nm, which at nonbleaching luminances are wavelengths that stimulate only the M and L cones (not the S cones). The Coefficient Law specifies that self-adaptation to the mixture may attenuate unequally the neural signals from M and L cones, so the appearance of the mixture may change over time according to the balance of the M-cone and L-cone responses. The appearance of the mixture after prolonged viewing, however, is actually matched to a briefly presented light that also stimulates S cones (Vimal et al., 1987). Perceptually, extended viewing causes desaturation, which is inconsistent with attenuation of only M- and L-cone receptor responses.

Generalizations of the Coefficient Law include a number of two-stage models, which incorporate a shift in the balance (neutral) point of a chromatically opponent neural response in addition to first-stage Coefficient-Law-style receptor attenuation (Jameson and Hurvich, 1972; Shevell, 1978; Ware and Cowan, 1982). Color-appearance shifts from chromatic induction (Ware and Cowan, 1982; Fig. 57.8), when modeled within the two-stage framework, cannot be explained without second-stage adaptation. For a fuller discussion of two-stage models, see Shevell (2003).

Up to this point, context has been limited to a uniform chromatic adapting field. A central issue in color appearance is whether the complex mosaic of real-world context can be understood within theoretical frameworks developed for uniform adapting light. Some studies support this view, at least as a first-order approximation. For example, consider the appearance of an array of *simulated* chromatic surfaces illuminated by some spectral distribution of light. While this visual stimulus is often used in experiments designed to assess *adaptation to the illuminant*, the typical stimulus for such studies is a mosaic of many different lights presented on an emissive video display, so the surface reflectances and the spectral illumination are only theoretical concepts rather than an actual feature of the physical stimulus. Adaptation to the light in this kind of display can be fairly well described by the Coefficient Law (Bauml, 1995; Brainard and Wandell, 1992), though this does not imply that the color shifts caused by adaptation are mediated by retinal neural processes (see Shevell and Humanski, 1984).

Another approach to considering whether adapting to complex chromatic context is “equivalent” to adapting to some uniform light is to measure appearance with a specifically designed background context composed of more than one luminance or chromaticity. One possibility is that the state of the visual system after adapting to a complex background is the same as for a uniform field at the spatial average of the light in the background. A more general proposal is that a complex context results in a state of the visual system identical to that for *some* uniform field (e.g., a distance-dependent weighted average of light, a nonlinear combination of chromaticities, or the region of peak luminance). Alternatively, a context composed of more than one chromaticity may establish a state of the visual system not attainable with any uniform field. For example, if a neural mechanism affecting color appearance is driven by only the chromatic contrast within the context, then a uniform field, which has no contrast by definition, cannot establish the same state attained with a complex field.

Several studies show that adaptation to patterns of light composed of more than one luminance or chromaticity cannot be explained by neural processes that mediate adaptation to a uniform field. Adaptation specifically to variation within a scene (contrast) alters both achromatic and chromatic appearance (Chubb et al., 1989; Singer and D’Zmura, 1994). Also, the quantitative relation between the perceived brightness of a test light and its luminance when the test is viewed within an inhomogeneous achromatic surrounding context is unlike the relation found with *any* luminance of uniform surround (Schirillo and Shevell, 1996). In the color domain, chromatic induction from a uniform surround is reduced by introducing chromatic variation (i.e., contrast) within a remote background area outside the surround; further, the reduction in induction varies with the magnitude and spatial frequency of the remote chromatic variation (Barnes et al., 1999; Shevell and Wei, 1998). Thus, adaptation to a complex chromatic context depends on neural processes that cannot be revealed with a uniform adapting light.

Color constancy

WHAT IS IT AND HOW IS IT POSSIBLE? In natural viewing, adaptation to complex scenes occurs continuously and with a powerful effect on color perception. While most objects that we see have stable spectral properties, the light from these objects reaching the eye changes markedly with the illuminating light. If the color appearance of each object were determined by the light from that object that enters the eye, the color of most objects would shift dramatically between sunrise and midday, and between outdoor viewing under sunlight and indoor viewing under lamp light. Such color shifts, however, are not experienced. Color constancy

is the perceived stability of the color of objects, despite changes of illumination. Constancy results from neural processes that mediate color perception.

The light from nearly every object outside the laboratory depends on both the object’s selective reflection of different wavelengths and the spectral energy distribution of the light illuminating the object (exceptions are colors of directly viewed light sources, such as traffic signals or television sets, i.e., colors that can be seen in the dark). A single surface seen in isolation in an otherwise dark field has an appearance determined directly by the light from that surface reaching the eye, which changes with the illumination. In this case, there is no color constancy because there is no biologically available information to separate the spectral distribution of illuminating light from the selective spectral reflectance of the surface. When the same surface is part of a complex scene, however, the visual system somehow takes account of the illumination to extract a neural representation of the surface color that is approximately invariant with changes in illumination. While the term *constancy* is somewhat misleading, because modest shifts in color appearance do occur with a change of illumination, color percepts are much closer to constancy than to the appearance predicted by the light reflected from an object.

How can color perception depend on the light absorbed by photoreceptors, while at the same time color constancy is the stable color appearance of objects despite changes in the light stimulating the receptors? The answer is that constancy depends on different spectral distributions of light from more than one region of the visual field. Color constancy fails if there is only a single isolated surface, as mentioned above, or if the illuminant is a monochromatic wavelength. In the latter case, the retinal stimulus from a complex scene is a single wavelength that varies only in magnitude, so there is no information about spectrally selective reflectance of the surfaces.

Color constancy is so effortless that the substantial color shifts that would occur without it are easily overlooked. Consider a standard set of chromatic reflecting surfaces that compose the Macbeth ColorChecker (Munsell Color Laboratory, New Windsor, NY), which is shown in the top panel of Figure 57.10 as it would appear in daylight. If color appearance depended on only the light reflected from each surface, without color constancy, then with illumination from an indoor tungsten (screw-in) light bulb the ColorChecker would appear as shown in the bottom panel. Of course, we do not experience such color shifts—a white shirt seen outdoors at noon appears to be the same color when seen indoors by lamplight—which implies the visual system adapts to the complex scene in order to discount the change in photoreceptor stimulation caused by a difference in illumination.

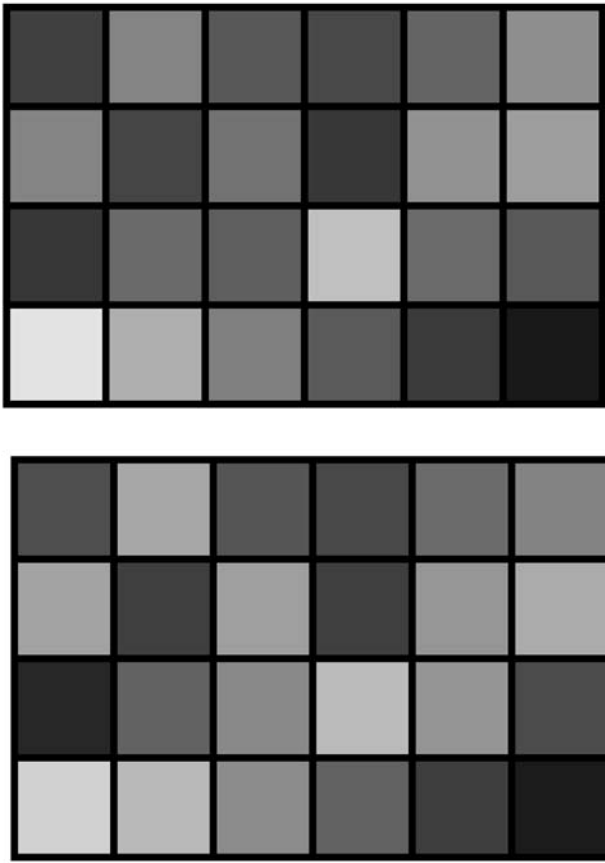


FIGURE 57.10. The chromatic surfaces of the Macbeth Color-Checker, rendered under illumination from approximate daylight (*D65, above*) or a tungsten lamp (*Illuminant A, below*). (See color plate 33.)

THEORETICAL ISSUES Classical theories hold that peripheral neural mechanisms cannot explain color constancy. Helmholtz (1866) proposed a learned, unconscious judgment process that takes account of the illuminant, and Hering's (1920/1964) theory includes the memory of an object's color built up from viewing it previously, in addition to receptor and retinal processes. Modern work supports the view that retinal processes alone cannot provide a complete explanation of constancy (Arend and Reeves, 1986; Cornelissen and Brenner, 1995).

Experimental evidence refutes any theory that explains constancy by an automatic, irreversible transformation of signals at a peripheral neural locus. Consider the color appearance of many papers composing a complex mosaic. When the papers are presented under some illumination (simulated on a video display), the color judged to match a particular region in the mosaic depends on the instructions given to the observer. Moderately good color constancy is found when the observer is told to adjust a patch (within a separate array of lights) to "look as if it were cut from the same piece of paper" as a region in the mosaic, though not when the same experiment is conducted but the observer is told to match the hue and saturation of the region in the mosaic (Arend and Reeves, 1986).

A theory of human color constancy can rely on only the information available to the nervous system. Theories that predict the appearance of an object from its physical spectral properties and the illumination falling on it are not theories of color constancy. These theories take as given the physical properties of the scene and specify the visual percept (Helson, 1938; Judd, 1940). A theory of constancy, on the other hand, should take as given the light captured by the retinal photoreceptors and specify the appearance of objects. The challenge for theories of constancy is that the light absorbed by receptors is not sufficient to uniquely determine the spectral reflectance of an object, and thus is not sufficient to give a stable representation of an object's color. Instead, the light captured by receptors is always ambiguous about the spectral reflectance of the object and the spectral distribution of illuminating light. The ambiguity is resolved in modern theories of constancy by modeling spectral illumination and reflectance after invoking specific assumptions about them, as described below.

MODELING ILLUMINATION AND REFLECTANCE When a surface with spectral reflectance function $R(\lambda)$ is illuminated by a light of spectral energy distribution $E(\lambda)$, the total number of quanta captured by each cone type, Q_S , Q_M , and Q_L , is given by $Q_i = \sum_{\lambda} [R(\lambda)E(\lambda)q_i(\lambda)]$, where $q_i(\lambda)$ is the spectral sensitivity of each type of cone ($i = S, M$, or L). With summation over the visible wavelengths λ from 400 to 700 nm, the total quanta captured by each type of cone can be written in matrix form:

$$\begin{bmatrix} Q_S \\ Q_M \\ Q_L \end{bmatrix} = \begin{bmatrix} q_S(400)E(400) & q_S(401)E(401) & q_S(402)E(402) & \dots & q_S(700)E(700) \\ q_M(400)E(400) & q_M(401)E(401) & q_M(402)E(402) & \dots & q_M(700)E(700) \\ q_L(400)E(400) & q_L(401)E(401) & q_L(402)E(402) & \dots & q_L(700)E(700) \end{bmatrix} \begin{bmatrix} R(400) \\ R(401) \\ R(402) \\ \vdots \\ R(700) \end{bmatrix}$$

The matrix, with 3 rows and 301 columns, relates the reflectance vector with 301 values [i.e., $R(400) - R(700)$] to the three quantal absorptions, Q_S , Q_M , and Q_L . The problem of color constancy is to determine the stable color of an object, characterized by its reflectance vector $R(\lambda)$, but, of course, three biologically available quantities Q_S , Q_M , and Q_L are insufficient to solve for the 301 reflectance values. The reflectance vector can be determined, however, by introducing specific assumptions about the spectral reflectance and/or the spectral distribution of the illuminant. Alternative theories of constancy are distinguished by the particular set of assumptions.

Suppose that the spectral distribution of the illuminant $E(\lambda)$ is assumed to be a weighted sum of three known spectral power distributions, $e_1(\lambda)$, $e_2(\lambda)$, and $e_3(\lambda)$; thus, $E(\lambda) = [a_1e_1(\lambda) + a_2e_2(\lambda) + a_3e_3(\lambda)]$, so only three parameters, a_1 , a_2 , and a_3 , must be determined to establish the illuminant $E(\lambda)$. Similarly, suppose that the spectral reflectance of an object is assumed to be a weighted sum of three known spectral reflectances, $r_1(\lambda)$, $r_2(\lambda)$, and $r_3(\lambda)$, so the spectral reflectance vector $R(\lambda)$ is given by $[b_1r_1(\lambda) + b_2r_2(\lambda) + b_3r_3(\lambda)]$; in this case, the problem of color constancy reduces to determining the weights b_1 , b_2 , and b_3 . Both assumptions are reasonable approximations to spectral reflectances and illuminants in the natural environment (Cohen, 1964; Judd et al., 1964). If the scene includes a standard reference patch of known spectral reflectance $R_{\text{Standard}}(\lambda)$, then the receptor quantal absorptions are sufficient to determine the spectral reflectance $R(\lambda)$ of an object in view (Buchsbbaum, 1980; Sallstrom, 1973; for a review see Shevell, 2003).

Other theories invoke different assumptions. For example, the illuminant $E(\lambda)$ can be any spectral distribution, not just a weighted sum of three fixed distributions, with three reference standards rather than one (Brill, 1978; Brill and West, 1986). Alternatively, the biologically awkward reference standard can be eliminated if the spectral reflectance of objects, $R(\lambda)$, is assumed to be a weighted sum of two rather than three known spectral reflectances (i.e., $R(\lambda) = [b_1r_1(\lambda) + b_2r_2(\lambda)]$; Maloney and Wandell, 1986). In general, the assumptions in these theories of constancy are fairly accurate but none is precisely correct, so the theories do not predict exact color constancy. Human color constancy, however, is not perfect, so the models have the potential to account also for the modest variation in color appearance with changing illumination.

MEASUREMENTS OF COLOR PERCEPTION WITH CHANGES IN ILLUMINATION Human color constancy is imperfect, which means that the color appearance of objects shifts to some degree with changes in illumination. Color perception is much closer to constancy than to the appearance predicted by the physical light from an object reaching the eye, but

how much closer? No single answer applies to all illuminants, objects, and viewing contexts.

Achromatic percepts (colorless white or gray) show excellent constancy when in a real three-dimensional scene viewed in an experimental room (Brainard, 1998). The chromaticity of a perceptually achromatic surface closely follows the chromaticity of the illuminant, as predicted by color constancy. When surfaces and illuminants are simulated and then presented on a video display (see, e.g., Arend et al., 1991), constancy is less good than with real objects and illuminants. Simulated scenes typically are restricted to lower light levels, a limited viewing angle, and a more restricted color gamut compared to natural viewing. Also, simulations rely on fairly simple physical models to determine the light from each object directed to the eye. Whether any or all of these factors contribute to poorer color constancy with video displays is an open question.

Measurements of color appearance using different spectral illuminants can test whether constancy is mediated by particular properties of a scene. Using cleverly designed stimuli in a real three-dimensional room, illumination can be changed while holding fixed the local light immediately surrounding a surface, the spatial average of the light over the whole scene, or the highest level of stimulation in the scene for each type of cone. If any of these three features of a complex scene completely mediates color constancy, then changing the illumination while holding that feature fixed should cause the color appearance of a surface to change with the illumination (i.e., color constancy should be eliminated). Experiments show that holding any of these three features fixed causes a reduction in constancy but does not eliminate it (Brainard, 1998; Kraft and Brainard, 1999). Therefore, color constancy cannot be linked to a state of the visual system established by only one of these features of the stimulus, a finding in accord with the mechanisms of chromatic adaptation revealed using simpler stimulus configurations (c.f. the section “Chromatic Adaptation”).

COLOR PERCEPTION, CONSTANCY, AND REPRESENTATION This chapter began by drawing a distinction between neural events in response to light (*coding*) and the colors we experience as a result of them (*perception*). The organization of the colors we experience is the *representation* of color. Color constancy concerns representation: varying the spectral composition of light from an object and (at least) early neural responses to it are represented by the same color percept.

Color constancy, however, points out that perception can involve more than one representation. For example, a uniformly painted wall seen partly in shadow is perceived to be a single color even though more careful examination immediately reveals a distinctly darker region. More generally, a spectrally uniform reflecting object can provide a variegated

retinal stimulus with substantial variation in chromaticity due, for example, to interreflections among surfaces and shadowing of one but not all simultaneous sources of illumination. With perfect color constancy, these variegations are ignored in a representation of object color but, perceptually, they are clearly visible when one attends to them. Another example occurs when a transparent colored filter overlays part of an image, in which case the observer perceives the color of the filter and of the underlying surfaces (D'Zmura et al., 1997); the perceived colors of the surfaces entirely under the filter approximate constancy (D'Zmura et al., 2000). Similarly, an object under (simulated) illumination can have either a perceived color approximating constancy or, with a difference only in instructions to the observer, a perceived color expected from the object's retinal image (Arend and Reeves, 1986). And in color memory, the color of a chromatic patch viewed within rich context and then recalled following 10 seconds of darkness is close to the physical stimulus of the learned patch, which includes the effect of illumination; when recalled following 10 minutes of darkness, however, the color is much less affected by the illuminant used during learning, as expected for constancy (Jin and Shevell, 1996). These observations indicate that more than one representation of color can result from the same retinal stimulus. Multiple neural codes in parallel pathways are well known to result from a particular visual stimulus; multiple perceptual representations of color can result as well.

Acknowledgment

We are grateful to many colleagues and students for comments on earlier drafts. This work was supported in part by MENRT Cognitique Grant COG 23b (K.K.) and PHS Grant EY-04802 (S.K.S.).

REFERENCES

Arend, L. E., and A. Reeves, 1986. Simultaneous color constancy, *J. Opt. Soc. Am. A*, 3:1743–1751.
 Arend, L. E., A. Reeves, J. Schirillo, and R. Goldstein, 1991. Simultaneous color constancy: papers with diverse Munsell values, *J. Opt. Soc. Am. A*, 8:661–672.
 Ayama, M., M. Ikeda, and T. Nakatsue, 1985. Additivity of red chromatic valence, *Vis. Res.*, 25:1885–1891.
 Barnes, C. S., J. Wei, and S. K. Shevell, 1999. Chromatic induction with remote chromatic contrast varied in magnitude, spatial frequency, and chromaticity, *Vis. Res.*, 39:3561–3574.
 Bauml, K. H., 1995. Illuminant changes under different surface collections: examining some principles of color appearance, *J. Opt. Soc. Am. A*, 12:261–271.
 Berlin, B., and P. Kay, 1969. *Basic Color Terms: Their Universality and Evolution*, Berkeley: University of California Press.
 Boynton, R. M., and C. X. Olson, 1990. Salience of chromatic basic color terms confirmed by three measures, *Vis. Res.*, 30:1311–1317.

Brainard, D. H., 1998. Color constancy in the nearly natural image 2. Achromatic loci, *J. Opt. Soc. Am. A*, 15:307–325.
 Brainard, D. H., and B. A. Wandell, 1992. Asymmetric color matching: how color appearance depends on the illuminant, *J. Opt. Soc. Am. A*, 9:1433–1448.
 Brill, M. H., 1978. A device performing illuminant-invariant assessment of chromatic relations, *J. Theoret. Biol.*, 71:473–478.
 Brill, M. H., and G. West, 1986. Chromatic adaptation and color constancy: a possible dichotomy, *Color Res. Appl.*, 11:196–204.
 Brindley, G. S., 1960. *Physiology of the Retina and Visual Pathway*, Baltimore: Williams & Wilkins.
 Buchsbaum, G., 1980. A spatial processor model for object colour perception, *J. Franklin Inst.*, 310:1–26.
 Burns, S. A., A. E. Elsner, J. Pokorny, and V. C. Smith, 1984. The Abney effect: chromaticity coordinates of unique and constant hues, *Vis. Res.*, 24:479–489.
 Calkins, D. J., 2001. Seeing with the S cones, *Prog. Retinal Res.*, 20:255–287.
 Chichilnisky, E. J., and D. A. Baylor, 1999. Receptive-field microstructure of blue-yellow ganglion cells in primate retina, *Nat. Neurosci.*, 2:889–893.
 Chichilnisky, E. J., and B. A. Wandell, 1999. Trichromatic opponent color classification, *Vis. Res.*, 39:3444–3458.
 Chubb, C., G. Sperling, and J. A. Solomon, 1989. Texture interactions determine perceived contrast, *Proc. Natl. Acad. Sci. USA*, 86:9631–9635.
 Cicerone, C. M., D. H. Krantz, and J. Larimer, 1975. Opponent-process additivity—III. Effect of moderate chromatic adaptation, *Vis. Res.*, 15:1125–1135.
 Cicerone, C. M., V. J. Volbrecht, S. K. Donnelly, and J. S. Werner, 1986. Perception of blackness, *J. Opt. Soc. Am. A*, 3:432–436.
 Cohen, J., 1964. Dependency of the spectral reflectance curves of the Munsell color chips, *Psychonom. Sci.*, 1:369–370.
 Cornelissen, F. W., and E. Brenner, 1995. Simultaneous colour constancy revisited: an analysis of viewing strategies, *Vis. Res.*, 35:2431–2448.
 Dacey, D. M., 1996. Circuitry for color coding in the primate retina, *Proc. Natl. Acad. Sci. USA*, 93:582–588.
 Dacey, D. M., and B. B. Lee, 1994. The “blue-on” opponent pathway in primate retina originates from a distinct bistratified ganglion cell type, *Nature*, 367:731–735.
 Dacey, D. M., B. B. Peterson, P. D. Gamlin, and F. R. Robinson, 2001. Retrograde “photofilling” reveals the complete dendritic morphology of diverse new ganglion cell types that project to the lateral geniculate nucleus in macaque monkey, *Invest. Ophthalmol. Vis. Sci.*, 42:S114.
 Davidoff, J., I. Davies, and D. Roberson, 1999. Colour categories in a stone-age tribe, *Nature*, 398:203–204.
 Derrington, A. M., J. Krauskopf, and P. Lennie, 1984. Chromatic mechanisms in lateral geniculate nucleus of macaque, *J. Physiol.*, 357:241–265.
 Derrington, A. M., and P. Lennie, 1984. Spatial and temporal contrast sensitivities of neurons in lateral geniculate nucleus of macaque, *J. Physiol.*, 357:219–240.
 De Valois, R. L., 1965. Analysis and coding of color vision in the primate visual system, *Cold Spring Harbor Symp. Quant. Biol.*, 30:567–579.
 De Valois, R. L., and K. K. De Valois, 1993. A multi-stage color model, *Vis. Res.*, 33:1053–1065.
 De Valois, R. L., K. K. De Valois, E. Switkes, and L. Mahon, 1997. Hue scaling of isoluminant and cone-specific lights, *Vis. Res.*, 37:885–897.

- Dimmick, F. M., and M. R. Hubbard, 1939. The spectral location of psychological unique yellow, green and blue, *Am. J. Psychol.*, 52:242–254.
- Drum, B., 1989. Hue signals from short- and middle-wavelength sensitive cones, *J. Opt. Soc. Am. A*, 6:153–157.
- D'Zmura, M., P. Colantoni, K. Knoblauch, and B. Laget, 1997. Color transparency, *Perception*, 26:471–492.
- D'Zmura, M., O. Rinner, and K. Gegenfurtner, 2000. The colors behind a transparent filter, *Perception*, 29:911–926.
- Elzinga, C. H., and C. M. M. de Weert, 1984. Nonlinear codes for the yellow/blue mechanism, *Vis. Res.*, 24:911–922.
- Evans, R. M., 1974. *The Perception of Color*, New York: Wiley.
- Fach, C., and L. T. Sharpe, 1986. Assimilative hue shifts in color gratings depend on bar width, *Percept. Psychophys.*, 40:412–418.
- Fuld, K., T. A. Otto, and C. W. Slade, 1986. Spectral responsivity of the white-black channel, *J. Opt. Soc. Am. A*, 3:1182–1188.
- Gegenfurtner, K. R., D. C. Kiper, and S. B. Fenstermaker, 1996. Processing of color, form and motion in macaque area V2, *Vis. Neurosci.*, 13:161–172.
- Gordon, J., I. Abramov, and H. Chan, 1994. Describing color appearance: hue and saturation scaling, *Percept. Psychophys.*, 56:27–41.
- Guth, S. L., N. J. Donley, and R. T. Marrocco, 1969. On luminance additivity and related topics, *Vis. Res.*, 9:537–575.
- Helmholtz, H. von, 1866. *Treatise on Physiological Optics* (J. P. C. Southall, trans.; 2nd ed., 1962), New York: Dover.
- Helson, H., 1938. Fundamental problems in color vision. I. The principle governing changes in hue, saturation, and lightness of non-selective samples in chromatic illumination, *J. Exp. Psychol.*, 23:439–476.
- Hendry, S. H. C., and R. C. Reid, 2000. The koniocellular pathway in primate vision, *Annu. Rev. Neurosci.*, 23:127–153.
- Hering, E., 1920/1964. *Outlines of a Theory of the Light Sense* (L. M. Hurvich and D. Jameson, trans.), Cambridge, MA: Harvard University Press.
- Hurvich, L. M., and D. Jameson, 1951a. The binocular fusion of yellow in relation to color theories, *Science*, 114:192–202.
- Hurvich, L. M., and D. Jameson, 1951b. A psychophysical study of white. I. Neutral adaptation, *J. Opt. Soc. Am.*, 41:521–527.
- Hurvich, L. M., and D. Jameson, 1955. Some quantitative aspects of an opponent-colors theory. II. Brightness, saturation and hue in normal and dichromatic vision, *J. Opt. Soc. Am.*, 45:602–616.
- Hurvich, L. M., and D. Jameson, 1956. Some quantitative aspects of an opponent-colors theory. IV. A psychological color specification system, *J. Opt. Soc. Am.*, 46:416–421.
- Hurvich, L. M., and D. Jameson, 1958. Further development of a quantified opponent-color theory, in *Visual Problems of Colour II*, London: HMSO, pp. 691–723.
- Ingling, C. R., and E. Martinez-Uriegas, 1983. The relationship between spectral sensitivity and spatial sensitivity for the primate r-g X-channel, *Vis. Res.*, 23:1495–1500.
- Jameson, D., and L. M. Hurvich, 1951. Use of spectral hue-invariant loci for the specification of white stimuli, *J. Exp. Psychol.*, 41:455–463.
- Jameson, D., and L. M. Hurvich, 1955. Some quantitative aspects of an opponent-colors theory. I. Chromatic responses and spectral saturation, *J. Opt. Soc. Am.*, 45:545–552.
- Jameson, D., and L. M. Hurvich, 1956. Some quantitative aspects of an opponent-colors theory. III. Changes in brightness, saturation and hue with chromatic adaptation, *J. Opt. Soc. Am.*, 46:405–415.
- Jameson, D., and L. M. Hurvich, 1959. Perceived color and its dependence on focal, surrounding, and preceding stimulus variables, *J. Opt. Soc. Am.*, 49:890–898.
- Jameson, D., and L. M. Hurvich, 1968. Opponent-response functions related to measured cone photopigments, *J. Opt. Soc. Am.*, 58:429–430.
- Jameson, D., and L. M. Hurvich, 1972. Color adaptation: Sensitivity control, contrast, afterimages, in *Handbook of Sensory Physiology*, vol. VII/4 (D. Jameson and L. M. Hurvich, eds.), Berlin: Springer-Verlag, pp. 568–581.
- Jin, E. W., and S. K. Shevell, 1996. Color memory and color constancy, *J. Opt. Soc. Am. A*, 13:1981–1991.
- Johnson, E. N., M. J. Hawken, and R. Shapley, 2001. The spatial transformation of color in the primary visual cortex of the macaque monkey, *Nat. Neurosci.*, 4:409–416.
- Judd, D. B., 1940. Hue saturation and lightness of surface colors with chromatic illumination, *J. Opt. Soc. Am.*, 30:2–32.
- Judd, D. B., and K. L. Kelly, 1939. Method of designating colors (Research Paper RP1239), *J. Res. Natl. Bureau Standards*, 23:355–366.
- Judd, D. B., D. L. MacAdam, and G. Wyszecki, 1964. Spectral distribution of typical daylight as a function of correlated color temperature, *J. Opt. Soc. Am.*, 54:1031–1040.
- Knoblauch, K., and S. K. Shevell, 2001. Relating cone signals to color appearance: failure of monotonicity in yellow/blue, *Vis. Neurosci.*, 18:901–906.
- Kraft, J. M., and D. H. Brainard, 1999. Mechanisms of color constancy under nearly natural viewing, *Proc. Natl. Acad. Sci. USA*, 96:307–312.
- Krantz, D. H., 1975. Color measurement and color theory: II. Opponent colors theory, *J. Math. Psychol.*, 12:304–327.
- Kries, J. von, 1903/1970. Influence of adaptation on the effects produced by luminous stimuli, in *Sources of Color Science* (D. L. MacAdam ed.), Cambridge, MA: MIT Press, pp. 120–126.
- Larimer, J., D. H. Krantz, and C. M. Cicerone, 1974. Opponent process additivity. I. Red-green equilibria, *Vis. Res.*, 14:1127–1140.
- Larimer, J., D. H. Krantz, and C. M. Cicerone, 1975. Opponent process additivity. II. Yellow/blue equilibria and nonlinear models, *Vis. Res.*, 15:723–731.
- Lee, B. B., P. R. Martin, and A. Valberg, 1988. The physiological basis of heterochromatic flicker photometry demonstrated in the ganglion cells of the macaque retina, *J. Physiol.*, 404:323–347.
- Lennie, P., P. W. Haake, and D. R. Williams, 1991. The design of chromatically opponent receptive fields, in *Computational Models of Visual Processing* (M. S. Landy and J. A. Movshon, eds.), Cambridge, MA: MIT Press.
- Lennie, P., J. Krauskopf, and G. Sclar, 1990. Chromatic mechanisms in striate cortex, *J. Neurosci.*, 10:649–669.
- Lindsey, D. T., and A. M. Brown, 2002. Color naming and the phototoxic effects of sunlight on the eye, *Psychol. Sci.*, 13:506–512.
- Maloney, L. T., and B. A. Wandell, 1986. Color constancy: a method for recovering surface spectral reflectances, *J. Opt. Soc. Am. A*, 3:29–33.
- Martin, P. R., B. B. Lee, A. J. White, S. G. Solomon, and L. Rüttiger, 2001. Chromatic sensitivity of ganglion cells in the peripheral primate retina, *Nature*, 410:933–936.
- Mollon, J. D., and C. R. Cavanious, 1987. The chromatic antagonisms of opponent process theory are not the same as those revealed in studies of detection and discrimination, in *Colour Vision Deficiencies VIII* (G. Verriest, ed.), Dordrecht: Junk, pp. 473–483.

- Nagy, A., 1979. Unique hues are not invariant at brief stimulus durations, *Vis. Res.*, 19:1427–1432.
- Paulus, W., and A. Kröger-Paulus, 1983. A new concept of retinal colour coding, *Vis. Res.*, 23:529–540.
- Purdy, D. M., 1931. Spectral hue as a function of intensity, *Am. J. Psychol.*, 43:541–559.
- Reid, R. C., and R. M. Shapley, 1992. Spatial structure of cone inputs to receptive fields in primate lateral geniculate nucleus, *Nature*, 356:716–718.
- Rodieck, R. W., 1998. *The First Steps in Seeing*, Sunderland, MA: Sinauer.
- Sallstrom, P., 1973. *Color and Physics: Some Remarks Concerning the Physical Aspects of Human Color Vision* (73-09), Stockholm: University of Stockholm, Institute of Physics.
- Saunders, B. A. C., and J. van Brakel, 1997. Are there nontrivial constraints on colour categorization? *Behav. Brain Sci.*, 20:167–228.
- Schirillo, J. A., and A. Reeves, 2001. Color naming of M-cone incremental flashes, *Color Res. Appl.*, 26:132–140.
- Schirillo, J. A., and S. K. Shevell, 1996. Brightness contrast from inhomogeneous surrounds, *Vis. Res.*, 36:1783–1796.
- Schnapf, J. L., T. W. Kraft, and D. A. Baylor, 1987. Spectral sensitivity of human cone photoreceptors, *Nature*, 325:439–441.
- Schrödinger, E., 1925/1994. The relationship of the four-color theory to the three-color theory, *Color Res. Appl.*, 19:37–47.
- Sekiguchi, N., D. R. Williams, and D. H. Brainard, 1993. Efficiency in detection of isoluminant and isochromatic interference fringes, *J. Opt. Soc. Am. A*, 10:2118–2133.
- Shapley, R., 1990. Visual sensitivity and parallel retinocortical channels, *Annu. Rev. Psychol.*, 41:635–658.
- Shepard, R. N., 1994. Perceptual-cognitive universals as reflections of the world, *Psychonom. Bull. Rev.*, 1:2–28.
- Shevell, S. K., 1978. The dual role of chromatic backgrounds in color perception, *Vis. Res.*, 18:1649–1661.
- Shevell, S. K., 2003. Color appearance, in *The Science of Color*, 2nd ed. (S. K. Shevell ed.), Oxford: Elsevier, pp 149–190.
- Shevell, S. K., and D. Cao, 2002. Chromatic assimilation. Evidence for a neural mechanism, in *Normal and Defective Colour Vision* (J. Mollon, J. Pokorny, and K. Knoblauch, eds.), Oxford: Oxford University Press, pp 114–121.
- Shevell, S. K., and R. A. Humanski, 1984. Color perception under contralateral and binocularly fused chromatic adaption, *Vis. Res.*, 24:1011–1019.
- Shevell, S. K., and J. Wei, 1998. Chromatic induction: border contrast or adaptation to surrounding light? *Vis. Res.*, 38:1561–1566.
- Shinomori, K., B. E. Scheffrin, and J. S. Werner, 1997. Spectral mechanisms of spatially-induced blackness: Data and quantitative model, *J. Opt. Soc. Am. A*, 14:372–387.
- Singer, B., and M. D’Zmura, 1994. Color contrast induction, *Vis. Res.*, 34:3111–3126.
- Spillmann, L., and J. S. Werner, 1996. Long-range interactions in visual perception, *Trends Neurosci.*, 19:428–434.
- Valberg, A., 1971. A method for precise determination of achromatic colours including white, *Vis. Res.*, 11:157–160.
- Valberg, A., 2001. Unique hues: an old problem for a new generation, *Vis. Res.*, 41:1645–1657.
- Vimal, R. L. P., J. Pokorny, and V. C. Smith, 1987. Appearance of steadily viewed lights, *Vis. Res.*, 27:1309–1318.
- Volbrecht, V. J., and J. S. Werner, 1989. Temporal induction of blackness. II. Spectral efficiency and test of additivity, *Vis. Res.*, 29:1437–1455.
- Ware, C., and W. B. Cowan, 1982. Changes in perceived color due to chromatic interactions, *Vis. Res.*, 22:1353–1362.
- Werner, J. S., C. M. Cicerone, R. Kleigl, and D. Dellarosa, 1984. Spectral efficiency of blackness induction, *J. Opt. Soc. Am. A*, 1:981–986.
- Werner, J. S., and B. R. Wooten, 1979. Opponent chromatic mechanisms: relation to photopigments and hue naming, *J. Opt. Soc. Am.*, 69:422–434.
- Wiesel, T. N., and D. H. Hubel, 1966. Spatial and chromatic interactions in the lateral geniculate body of the rhesus monkey, *J. Neurophysiol.*, 29:1115–1156.
- Williams, D., N. Sekiguchi, and D. Brainard, 1993. Color, contrast sensitivity, and the cone mosaic, *Proc. Natl. Acad. Sci. USA*, 90:9770–9777.
- Wyszecki, G., and W. S. Stiles, 1982. *Color Science: Concepts and Methods, Quantitative Data and Formulae*, 2nd ed., New York: Wiley.
- Zeki, S., 1980. The representation of colour in the cerebral cortex, *Nature*, 284:412–418.
- Zeki, S., 1993. *A Vision of the Brain*, London: Blackwell Scientific, pp. 297–299.

58 Chromatic Discrimination

JOEL POKORNY AND VIVIANNE C. SMITH

COLOR VISION REFERS to the ability of an organism to distinguish objects based on the variation in spectral reflectance. This ability has two aspects: discrimination of the objects and appreciation of their appearance. Chromatic discrimination is studied by traditional psychophysical methods. These methods can be adapted using behavioral techniques to the study of chromatic discrimination in the animal kingdom and can also be adapted to the physiological study of nonhuman primates. There are three requirements for an animal to have color vision. First, surfaces in the environment must show variation in spectral reflectance. Second, there must be multiple transducers (photoreceptors) that generate differential responses to light reflected from environmental surfaces. Third, there must be postreceptoral processes that compare receptor signals and generate codes that permit appreciation of spectral differences in the environment. Color vision is widespread in vertebrates (see Chapter 62). It is less developed in mammals with the exception of the primates. Old World primates such as the macaques have essentially the same retinal mechanisms to process spectral signals as humans. Thus, physiological study of their pathways has opened the door to understanding chromatic discriminative ability in humans.

Chromatic discriminative ability is an important feature of human life, as reflected in the number of studies of this ability in the scientific and engineering literature. In the laboratory, discrimination has typically been studied by determining the stimulus difference needed for an observer to see two stimulus patches as different. The two patches of light may be distinguished based on a difference in light level, a difference in spectral distribution, or a difference in the combination of light level and spectral distribution. The majority of chromatic discrimination studies have concentrated on conditions where discrimination is based solely on differences in spectral distribution.

This chapter reviews the properties of the human visual system that determine discriminative capacity, how chromatic discrimination varies with changes in stimulus conditions, and the modeling strategies that summarize discriminative capacity. The chapter draws freely on physiological studies in the macaque. There is now a good understanding of the retinal mechanisms that code and convey chromatic information to the brain. Results from the vast majority of chromatic discrimination studies can be characterized by retinal processes, including the photore-

ceptor spectral sensitivities, the postreceptoral interactions between signals from the photoreceptors, and sensitivity regulation within the retina. There are important cortical transformations of the information conveyed from the retina, but these determine the perception of complex scenes and do not limit discriminative capacity.

Background

THE PRIMATE RETINA

Photoreceptors. In humans, the cone photoreceptors provide the second requirement of color vision: three cone types of differing spectral sensitivity. Rod photoreceptors provide night vision and may interact with cone signals, but it is the cones that provide the basis of normal human color vision. There is now broad agreement on the spectral sensitivities of the long-wavelength-sensitive (L), middle-wavelength-sensitive (M), and short-wavelength-sensitive (S) cones. Figure 58.1A shows a representative set of spectral sensitivities expressed on an energy basis. The S cone has peak sensitivity near 435 nm. The M and L cones peak at mid-spectrum at 534 nm and 555 nm, respectively. The equal energy spectral sensitivities of the M and L cones are highly correlated, $r = 0.95$. For images encountered in everyday life, the correlation of M- and L-cone responses is 0.99 (Zaidi, 1997). Burns and Lamb (Chapter 16) give a more detailed review of the primate photoreceptors.

For chromatic discrimination, we are concerned with the relative responses of the three types of cones under conditions where light stimuli are presented at equal luminance. Figure 58.1B shows the cone spectral sensitivities expressed in terms of relative excitation for lights equated in luminance. The concept of luminance has its roots in the early-eighteenth-century scientific and industrial need for measurement and specification of the visual effectiveness of lights. The CIE 1924 standard luminous efficiency function and its successors were originally proposed for this purpose, but today they also represent the spectral sensitivity of one of the postreceptoral pathways (Lennie et al., 1993).

Based on the receptor spectral sensitivities alone, one would expect discrimination to be best at the wavelengths where the slopes of the sensitivity functions are steepest. This is qualitatively correct; wavelength discrimination is best in the spectral regions near 480 and 580 nm. However,

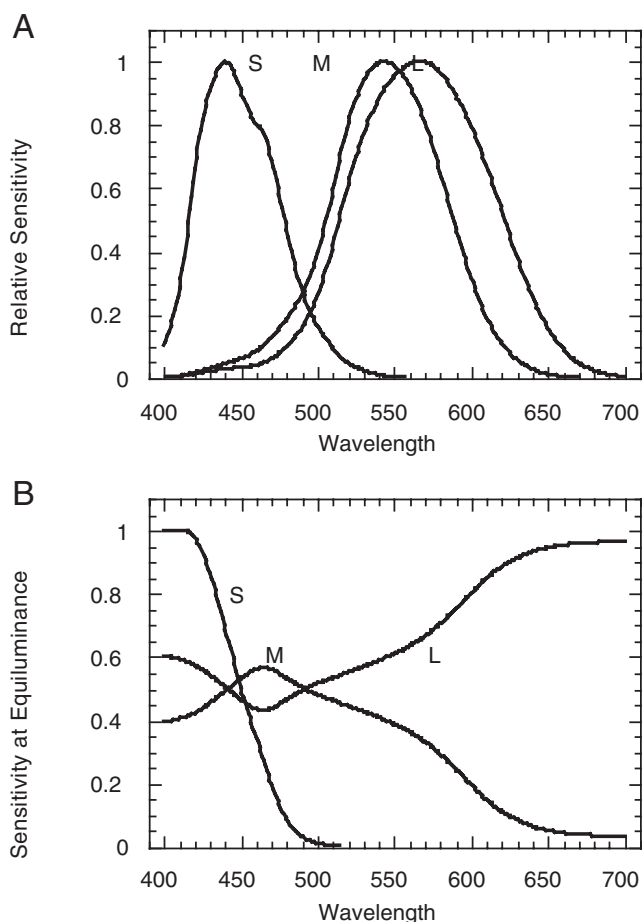


FIGURE 58.1. *A*, Relative cone spectral sensitivity functions (Smith and Pokorny, 1975) plotted as a function of wavelength. *B*, The cone spectral sensitivity functions plotted relative to luminance; the vertical scaling of the S-cone function is arbitrary.

changes in stimulus conditions cause chromatic discrimination to vary in complex ways that require incorporation of a representation of postreceptoral processing in current models.

Retinal pathways. Major advances in the understanding of retinal anatomy and electrophysiology in the past two decades (Dacey, 2000; Lee, 1996) have revealed three major pathways that convey photoreceptor signals to the brain. The common designations for these pathways arise from the layers of the lateral geniculate nucleus they traverse; the parvocellular (PC), koniocellular (KC), and magnocellular (MC) pathways. The circuitry for the three pathways consists of groups of cells which feed signals forward from the photoreceptor to the lateral geniculate nucleus, via bipolar and ganglion cells, with output to the visual cortex.

The PC pathway mediates spectral opponency of M and L cones and is responsive to luminance changes. PC ganglion cells show the classical center-surround receptive field organization, with a small center and a larger surround that

signals with opposite polarity. Four subgroups of PC cells show characteristic response patterns (Derrington et al., 1984; Lee et al., 1994), reflecting the center activity of the typical center-surround retinal ganglion cell. Like classically defined center-surround cells (Kuffler, 1952), ON-center cells respond to an increase and OFF-center cells to a decrease in luminance contrast on their centers (Derrington and Lennie, 1982). The cell types are further distinguished by their spectral properties. The L-ON-center and the M-OFF-center cells respond to an increase in L- versus M-cone contrast (reddish-appearing lights), and the M-ON-center and the L-OFF-center cell respond to an increase in M- versus L-cone contrast (greenish-appearing lights).

Another class of spectral opponency is shown by +S – (L + M) cells, which combine inputs from S, M, and L cones (Dacey and Lee, 1994). These ganglion cells have spatially coextensive centers and surrounds. The cells project to the KC pathway (Hendry and Reid, 2000; Martin et al., 1997). The parallel –S + (L + M) pathway is recognized in physiological studies (Valberg et al., 1986) but its detailed anatomy has not yet been described.

The third major pathway from retina to cortex is the nonopponent MC pathway, which sums inputs of M and L cones in either ON- or OFF-center receptive fields. M and L cones contribute to both centers and surrounds (De Valois et al., 1966; Lee et al., 1989; Wiesel and Hubel, 1966), which in most neurons have similar spectral sensitivities. It is not clear that S cones make any contribution to these receptive fields; if they do, it must be very small (Derrington et al., 1984; Kaiser et al., 1990). This pathway appears to form the physiological substrate for the psychophysical concept of luminance (Lee et al., 1988). Kaplan (Chapter 30) gives a more detailed review of the retinal postreceptoral pathways.

COLOR MATCHING When a photoreceptor absorbs light quanta, subsequent processing stages receive signals proportional to the number of quanta producing isomerizations. All quanta, once absorbed in a given photoreceptor, have identical effects, regardless of wavelength. This property, termed *univariance* (Rushton, 1972), forms the basis for modern colorimetry and for the systems for specifying chromaticity. Many different spectral distributions of light can evoke identical rates of quantal absorption in each of the three types of cones. Let us create an example, starting from the cone photopigment spectra expressed in terms of relative excitation for lights equated in luminance (Fig. 58.1*B*). For wavelengths above about 545 nm, S-cone sensitivity is sufficiently low that significant quantal absorptions occur in only the L and M cones. A stimulus field containing 580 nm light can appear identical to another field containing a mixture of two lights, such as 550 nm and 650 nm lights. An identity of quantal absorptions in the two fields can be

achieved because the 550 nm light produces a ratio of M- to L-cone absorptions that is higher than that of the 580 nm light, and the 650 nm light produces a ratio of M- to L-cone absorptions that is lower than that of the 580 nm light. A unique mixture ratio of 550 and 650 nm lights results in identical rates of quantal absorption in each of the cone types for the two fields. This is an example of a color match in which a test light (the 580 nm field) appears identical to a mixture of two primary lights (550 nm and 650 nm). Lights that appear identical but are composed of different spectral composition are called *metamers*.

This logic is the basis of color matching. Any arbitrary light exciting all three cone types can be matched using three primary lights. The term *trichromacy* is derived from this ability. Most humans make very similar matches and are called *normal trichromats*. When spectral lights are used for color matching, the test light and one primary light are mixed to match a mixture of the other two primaries.

The importance of the color match lies in the identity of appearance of the two mixture fields, not the actual appearance of the fields. The results of color mixture experiments reflect conditions where quantal catches in the three cone classes are equated. This is an important conclusion because it means that the color matching experiment is both very powerful and very limited. Neither the relative number of the three cone types nor the light level is important. When identity of appearance is attained at the quantal level, subsequent neural processing cannot undo the match. The color matching data are based on the spectral sensitivity of the photoreceptors, but that is all they tell us. Color matching obeys the properties of a linear system. Linearity holds for retinal locations that are cone-dominated (the fovea), and for light levels above cone threshold but below light levels that cause significant cone photopigment bleaching.

Chromaticity diagrams. The linearity property allows the results of color mixture experiments to be expressed in a variety of formats. A discussion of colorimetric transformation methods are beyond the scope of this chapter but may be found elsewhere (Brainard, 1995; Smith and Pokorny, 2003; Wyszecki and Stiles, 1982). One of the most useful formats is the chromaticity diagram, a two-dimensional representation of the results of a color mixture experiment. It is obtained by calculating the proportion of each primary in a match and then representing the proportions in a rectangular diagram formed by plotting two of the primaries.

The most commonly encountered chromaticity diagram is the CIE 1931 XYZ diagram and, for visual psychophysics, the more accurate Judd (1951b) modified XYZ diagram (Fig. 58.2A). The values for the spectral wavelengths plot on a horseshoe-shaped curve; broadband spectral distributions plot within the confines defined by the spectrum locus and the line joining the short and long wavelengths of the spec-

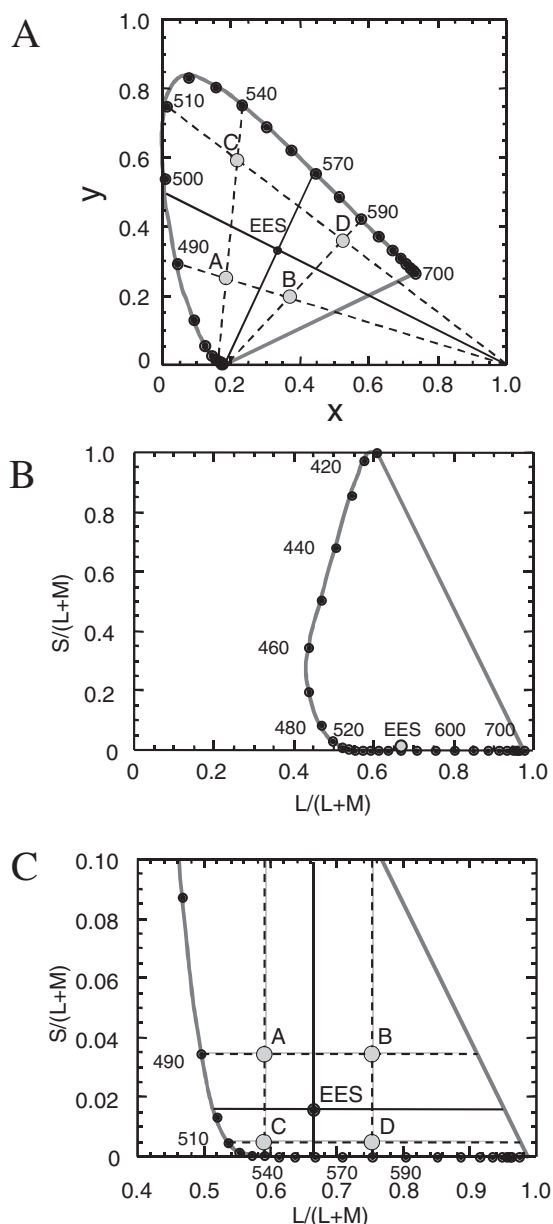


FIGURE 58.2. Chromaticity diagrams summarizing the 2 degree color matching data. *A*, The (x,y) diagram based on Judd's (1951b) revision of the 1931 CIE observer. The spectrum locus is the horseshoe shape with wavelengths noted. EES is the equal energy spectrum. The solid line and dashed lines converging on coordinate $(x = 1, y = 0)$ is a line in which the S-cone excitation is constant (L/M vary). The solid line and dashed lines converging on coordinate $(.1748, 0)$ is a line in which the L- and M-cone excitations are constant (S varies). The intersections of the dashed lines are shown as chromaticities A, B, C, and D. *B*, The (l,s) diagram of Boynton and MacLeod, representing cone excitations in an equiluminant diagram. *C*, The (l,s) diagram of panel *B* magnified to show the position of the EES. The horizontal lines represent chromaticities with constant S-cone excitation. The vertical lines represent chromaticities with constant L/M excitation. The coordinates A, B, C, and D are shown for comparison with panel *A*.

trum, the line of extraspectral purples. The chromaticity of the equal energy spectrum (EES) for the Judd (1951b) modified XYZ diagram plots at $x = 0.334$, $y = 0.336$. The line joining the EES chromaticity and a spectral wavelength represents a purity dimension, having excitation purity ranging from 0 at EES to 1 at the spectrum locus. The two solid lines drawn through the diagram are important in that they represent the chromaticities under neutral adaptation that theoretically reflect activity in only one of the postreceptoral PC or KC pathways while silencing the other. The pairs of dashed lines flanking the solid lines represent stimulus conditions in which the mechanism silenced for the stimuli represented by the solid lines produce steady but nonzero excitation on the other spectral opponent axis.

A physiological diagram. The CIE and Judd chromaticity diagrams have the disadvantage that they do not represent cone sensitivities directly. A more intuitive chromaticity space to present discrimination data was developed by MacLeod and Boynton (1979). This space is based on the photoreceptor sensitivities of Figure 58.1B, $L/(L + M)$, $S/(L + M)$. The MacLeod-Boynton chromaticity diagram represents a constant luminance plane. Since luminance is represented by a sum of L- and M-cone sensitivities, the proportions of L and M trade off on the horizontal axis. Figures 58.2B and 58.2C shows the MacLeod-Boynton chromaticity diagram. In this space, the ordinate and abscissa coordinates are proportional to L- and S-cone excitations for equiluminous colors. The abscissa is expressed in l-chromaticity (l), which is the proportion of L-cone excitation contributed by the total retinal illuminance ($L/L + M$). Since the luminous efficiency function is modeled as a linear sum of L- and M-cone contributions, a change in l-chromaticity is associated with a complementary change in m-chromaticity. Thus, a step “redward” is simultaneously an increment in L and a decrement in M. The ordinate value is in s-chromaticity ($S/(L + M)$), which is the proportion of S-cone excitation contributed by the total retinal illuminance. Therefore, the stimuli falling on the horizontal lines (L/M axis) show changes in M- and L-cone stimulation but constant S-cone stimulation. The stimuli falling along the vertical lines show changes in S-cone stimulation alone. Figure 58.2C shows the MacLeod-Boynton diagram with the solid and dashed lines through the diagram representing the same chromaticities as the lines in Figure 58.2A. Responses associated with the two postreceptoral spectral processing channels are now represented orthogonally, and it is straightforward to envision experimental designs that evaluate the discriminative capacities and possible interactions of the two major retinal pathways signaling spectral information.

Boynton and Kambe (1980) introduced an alternative normalization of the MacLeod-Boynton space with a scheme they called *cone trolands*. The L and M normalization

was retained; the S normalization was changed so that for an illumination metameric to the EES, S was set equivalent to (L + M) and called *S tds* (trolands). This normalization allows presentation of data either in (l, s) chromaticity units or in (L, S) cone troland units. Cone troland units are particularly useful in evaluating physiologically based models of chromatic detection and discrimination (Smith and Pokorny, 1996).

SENSITIVITY REGULATION The range of light levels encountered in the natural world is over a trillionfold, from a dark night in a forest to the snowfields of the Rocky Mountains. No single neuron can accommodate this range. A neuron has a threshold when its response is above the dark noise, increases with light level, and reaches a maximum response that is about 200 to 300 times the threshold response. At the maximum, the neuron is said to have *saturated*, since it cannot generate a differential response with a further increase in light level. Different organisms have adopted different strategies to cope with the range of light levels, including restricting the natural habitat and using pupil variation to control light admitted into the eye. One important strategy is the development of two receptor systems, a low-threshold system for lower levels (rods) and a high-threshold system for higher levels (cones). Even with these strategies, there remains a need for neural mechanisms to regulate sensitivity to the ambient illumination in order to avoid saturation. This behavior is sometimes called *adaptation*, although we prefer to restrict ourselves to the term *sensitivity regulation*. Sensitivity regulation means that the neuron resets its response range to the ambient level in order to match its 300-fold response range to that level. When light levels are high enough to bleach photopigment, receptors that have maintained response sensitivity are protected from saturation. Bleaching reduces the number of photopigment molecules available for absorption. It thus acts as a self-regulating sensitivity mechanism.

The classical psychophysical method used to study sensitivity regulation is the increment threshold (König and Brodhun, 1889). In an increment threshold experiment, a test stimulus is presented on a background of fixed luminance. The test stimulus radiance is adjusted to determine the detection threshold. The measurement is repeated at a series of background radiance levels, and a threshold versus radiance (TVR) function plotting the logarithm of threshold versus the logarithm of the background may be created.

Sensitivity regulation in rods. It is instructive to look at the TVR function for a single receptor pathway. We can do this for rods. Aguilar and Stiles (1954) isolated the rod system using a long-wavelength background to suppress the cone photoreceptors and a middle-wavelength test spot to stimulate the rod photoreceptors. Figure 58.3 shows the mean of

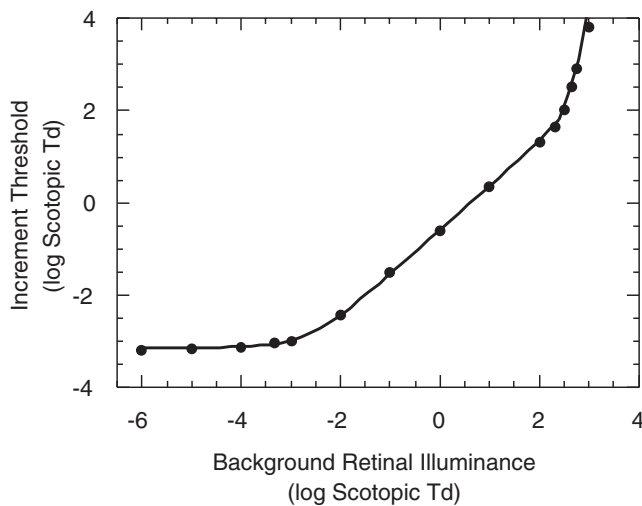


FIGURE 58.3. Increment thresholds for the rod system. (Data from Aguilar and Stiles, 1954.)

the thresholds from the four Aguilar-Stiles observers. The threshold is relatively constant at low scotopic levels (*scotopic* is the term used to describe light levels for rod-mediated vision), starts to increase near -4 log scotopic tds, and then rises linearly between background illuminances of -3.0 and 2.2 log scotopic tds. Above 2.2 log scotopic tds, the rod system begins to saturate, and the amplitude of the thresholds increases rapidly.

Below 2.2 log scotopic tds, the Aguilar-Stiles increment threshold value, ΔI , can be described for any scotopic illuminance, I , by an equation of the form

$$\Delta I = k(I^n + I_0) \quad (1)$$

I_0 is the so-called dark light. The exponent n and the constant k are defined for the asymptotic portion of the curve when I is much greater than I_0 but before saturation begins: n is the limiting slope of the TVR function plotted on log-log coordinates and, for $n = 1.0$, k is the Weber fraction, the fractional increment above the background light required for detection.

The TVR function is often characterized as composed of four segments. Starting from darkness, as background luminance is increased, the threshold does not differ from the absolute threshold for a dark background. This is called the *linear region* of the TVR function, and sensitivity in this section is hypothesized to be limited by neural (internal) noise (Barlow, 1958), the dark light. This neural noise is internal to the retina, and examples include thermal isomerizations of photopigment, spontaneous opening of photoreceptor membrane channels, and spontaneous neurotransmitter release. The second part of the TVR curve represents the transition between the linear region and the region where sensitivity regulation occurs. The linearly rising portion of the function is sometimes called the *Weber law*

region; ideally, it has a slope (n , in equation 1) of 1.0. This means that the sensitivity regulation is exactly compensating for the steady ambient illumination. Although the psychophysically observed Weber behavior with a slope of 1.0 is often attributed to adaptation in the rod receptors themselves, this cannot be the case since shallower slopes, of about 0.7, are found for some stimulus conditions different from those of Aguilar and Stiles (Shapiro et al., 1996; Sharpe et al., 1989). The rightmost portion of the TVR curve shows rod saturation at high background luminance. Sensitivity falls so drastically that no amount of increment light reaches detection threshold.

Sensitivity regulation in M and L cones. Sensitivity regulation in cones differs from that in rods. Saturation does not occur in the steady state for stimuli activating the M and L cones. At high background light levels, $>10,000$ tds, a significant amount of photopigment is depleted due to bleaching. Following the viewing of a bright light for a period of time, the loss of quantum catch ability reaches equilibrium and protects the cones from saturation.

Sensitivity regulation for stimulation of the M and L cones depends on the postreceptoral pathway in which measurements are made. In the MC pathway, the TVR function moves from threshold and attains Weber's law with a slope of unity. For foveal stimuli, threshold is near 0.1 td and Weber's law is achieved at 1 td (Hood and Finkelstein, 1986). In the PC pathway, the TVR function moves from threshold to a limiting slope near 0.6 to 0.7 until bleaching levels ($>10,000$ td) are reached. For foveal stimuli, threshold is near 1 td and the limited sensitivity regulation is achieved by 3 to 8 td. This pathway difference is evident both in psychophysical studies (Swanson et al., 1987) and in physiological studies (Lee et al., 1990).

Now, Weber's law requires $n = 1.0$ in equation (1). The finding that Weber's law occurs only in the MC pathway implies that sensitivity regulation is hierarchical. Some regulation is common to both pathways and may be in the cones themselves. Intracellular recordings from primate horizontal cells, one synapse removed from the receptors, show slopes of 0.6 to 0.7 (Smith et al., 2001) and independent sensitivity regulation in each cone type (Lee et al., 1999). The MC and PC pathways are differentiated at the first synapse, the cone-bipolar synapse. The additional regulation of the MC pathway thus occurs in the bipolar or ganglion cell complexes.

The linear slopes of 0.7 or 1.0 are sometimes referred to as *multiplicative regulation* (Hood and Finkelstein, 1986). The sensitivity regulation mechanism scales the response both to the background and to the test stimulus. The neural mechanisms that underlie multiplicative regulation are not delineated. In the photoreceptors, sensitivity regulation probably involves the complex interactions of the outer segment

photocurrent. Additionally time-dependent mechanisms, in which temporal resolution is traded for sensitivity, probably play a role both in the photoreceptor and in the MC-pathway mechanism.

There is another form of regulation in which the mechanism scales only the background (Hood and Finkelstein, 1986). This is called *subtractive regulation*. Subtractive regulation by itself is usually not considered an effective mechanism of light adaptation since it provides only a single scaling of the background light level. As the sole method of sensitivity regulation, it will delay but not protect the postreceptoral neurons from saturation. However, in combination with other mechanisms (e.g., following partial multiplicative regulation), it can be effective. Subtractive feedback is a possible neural substrate for subtractive sensitivity regulation. There is evidence that the PC pathway shows subtractive feedback (Krauskopf and Gegenfurtner, 1992; Smith et al., 2000). Subtractive feedback as a second form of hierarchical regulation in the PC pathway is attractive. It was stated that the L- and M-photopigment sensitivities are highly correlated. As a result, at a given luminance level the range of differential spectral stimulation is limited. There is only 0.3 log unit differential in M-cone to L-cone stimulation between 480 nm and 700 nm. This small range is easily handled by a subtractive feedback mechanism in place following the spectral opponent receptive field.

Sensitivity regulation in S cones. Sensitivity regulation in S cones differs considerably from that in L and M cones. In some ways, S-cone regulation is more similar to that in rods in that the S cones do show saturation (Mollon and Polden, 1977). They do not obey Weber's law. They may have some multiplicative regulation but with a limiting slope of 0.6 to 0.7. The S-cone system does show subtractive regulation. This has been termed *second-site* regulation in the literature (Pugh and Mollon, 1979). However, the range of S-cone stimulation relative to an adapting white stimulus is high, 60 to 1. Thus, the subtractive mechanism does not protect the S-cone system from saturation. There is still no final understanding of sensitivity regulation in the S-cone system.

Studies of chromatic discrimination

Chromatic discrimination is usually investigated at a constant luminance level. Originally, this tactic was chosen to ensure that the discrimination depended only on the presence of a spectral reflectance difference in the discrimination field. Classically, parametric chromatic discrimination data have been collected under three conditions: wavelength variation, purity variation, and chromaticity variation. A recent advance has involved sampling chromaticity along the theoretically significant axes shown in Figure 58.2, the two postreceptoral spectral opponent axes (Boynton and Kambe,

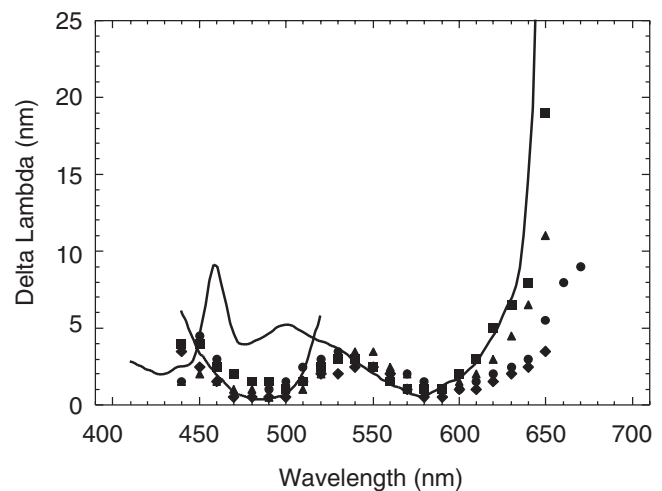


FIGURE 58.4. Wavelength discrimination. The threshold step $\Delta\lambda$ is plotted versus the standard λ . The data are for four observers of Pokorny and Smith (1970). The solid curves are predictions based on the model given in the section "A Modern Discrimination Theory Based on Retinal Physiology."

1980; Krauskopf and Gegenfurtner, 1992; Smith et al., 2000).

WAVELENGTH DISCRIMINATION For wavelength discrimination, the observer adjusts the test wavelength to achieve a just noticeable difference from a standard wavelength. In a typical experiment, the observer is instructed to view a stimulus field composed of two half-fields. The standard field is filled with a homogeneous light of narrow spectral band (λ), and the comparison field is filled with light that is slightly different from the standard ($\lambda + \Delta\lambda$). The fields are equiluminant so that the discrimination is not dependent on luminance information. The experiment is repeated for many standard wavelengths throughout the visible spectrum. Data obtained from several laboratories reveal similar results (e.g., Bedford and Wyszecki, 1958; Pokorny and Smith, 1970; Wright and Pitt, 1934, 1935). Figure 58.4 shows the measured $\Delta\lambda$ plotted as a function of the standard wavelength for four observers (Pokorny and Smith, 1970) viewing a 16 td field. The field was present for 5 seconds alternating with a 16 td white-appearing field. The typical wavelength discrimination curve has minima near 490 nm and 580 nm. Individual variance of the discrimination function appears greater below 460 nm (Wright and Pitt, 1934). The solid lines represent a model of wavelength discrimination detailed in the section "A Modern Discrimination Theory Based on Retinal Physiology."

COLORIMETRIC PURITY DISCRIMINATION *Colorimetric purity* refers to the continuum of lights that arise from the mixture of a spectral wavelength with an achromatic-appearing light of the same luminance. There are two important measure-

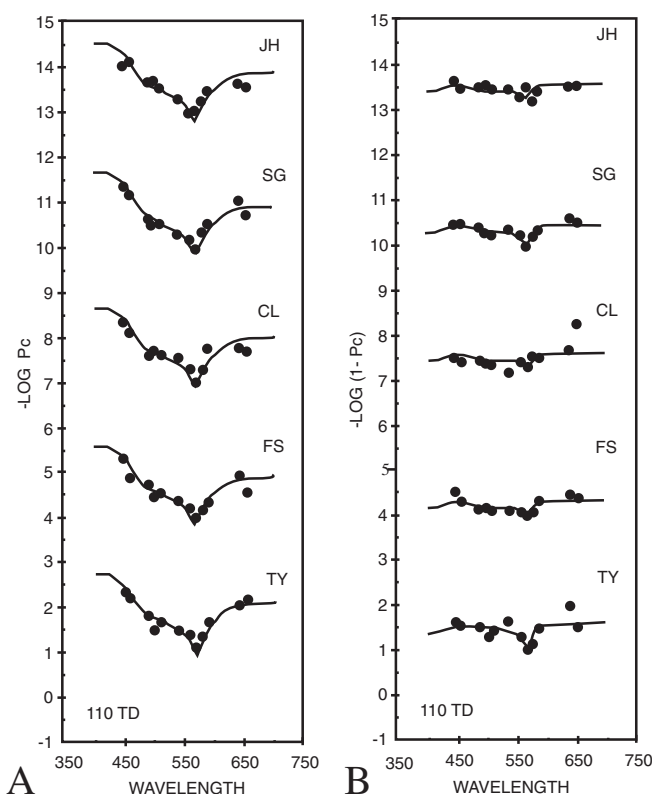


FIGURE 58.5. Colorimetric purity discrimination. *A*, The first step from white is plotted versus wavelength. *B*, The step from the spectrum is plotted versus wavelength. The data are for five observers of Yeh et al. (1993). The curves are predictions based on the model given in the section “A Modern Discrimination Theory Based on Retinal Physiology.”

ments. For least colorimetric purity, the observer compares a white-appearing light of fixed luminance with a mixture of the same white and a spectral wavelength to judge when the mixture is just tinged with color (Kraft and Werner, 1999; Yeh et al., 1993; see Pokorny and Smith, 1986, for a review of the earlier literature). Least colorimetric purity is defined as

$$P_c = L_\lambda / (L_w + L_\lambda) \quad (2)$$

where L_λ is the luminance of a spectral light and L_w is the luminance of the white-appearing light. For example, if 1 td of L_λ plus 99 td of L_w is discriminated from 100 td of L_w , the least colorimetric purity is 1%. Data are represented as sensitivity ($-\log(P_c)$), and show best discriminative ability at 400 nm and poorest ability at 570 nm. Figure 58.5A shows data for five observers of Yeh et al. (1993) collected at 100 td. For each observer, the range from best to poorest discrimination spans about 1.6 log units.

Colorimetric purity discrimination can also be estimated by adding a small amount of white-appearing light to a spectral light in comparison with the spectral light. For example, 20 td of $L_w + 80$ td of L_λ may be discriminated from 100 td of L_λ . This is the step from the spectrum, P_s .

$$P_s = L_w / (L_w + L_\lambda) = (1 - P_c) \quad (3)$$

The spectral colorimetric purity function, $(-\log(1 - P_c))$, shows little wavelength dependence (Kaiser et al., 1976; Yeh et al., 1993; see Pokorny and Smith, 1986, for a review of the earlier literature). Figure 58.5B shows data for five observers of Yeh et al. (1993) collected at 100 td. The solid lines in Figure 58.5 represent a model described in the section “A Modern Discrimination Theory Based on Retinal Physiology.”

CHROMATIC DISCRIMINATION An alternate representation of wavelength and colorimetric purity discrimination is on a chromaticity diagram such as that of Figure 58.2A. Wavelength discrimination will appear plotted as line segments on the horseshoe-shaped spectrum locus. Least colorimetric purity will be line segments radiating from the EES chromaticity toward the spectrum locus. Purity discrimination from the spectrum will appear as line segments pointing from the spectrum locus toward the EES chromaticity. The next logical advance was to assess chromatic discrimination from any point of the chromaticity diagram and in any direction. The production of arbitrary chromaticities and directions was not easy using a traditional colorimeter. Nonetheless, Wright (1941) recorded chromatic discrimination steps for various directions in the CIE space. The results were plotted as a series of short lines in the chromaticity space; the orientation of the line segment indicated the direction for discrimination, and the length of the line represented the just noticeable differences in chromaticity. Wright’s data showed that a given distance on the CIE chromaticity diagram represents different chromatic changes in discrimination ability. The discrimination step size is smallest near the short-wavelength region and largest near the 500 to 550 nm region in the CIE diagram. MacAdam (1942) developed another method to represent chromatic discrimination. He measured the standard deviations of repeated color matches at a set of arbitrary chromaticities and derived discrimination ellipses within the chromaticity diagram. Starting from the center of the ellipse, each ellipse represented the discrimination distance in all directions. Figure 58.6 shows some of the ellipses fitted to MacAdam’s data. The ellipses on the figure are 10 times larger than their actual size. MacAdam’s data generally agreed with the Wright (1941) data.

A number of studies have investigated the effect of luminance level on chromatic discrimination. The wavelength discrimination function is stable in the range of 100 to 2000 td (Bedford and Wyszecki, 1958). At lower luminance levels, wavelength discrimination deteriorates in the short-wavelength region (McCree, 1960; Stabell and Stabell, 1977; Weale, 1951). With decreasing field luminance, the major axes of chromatic discrimination ellipses rotate toward the

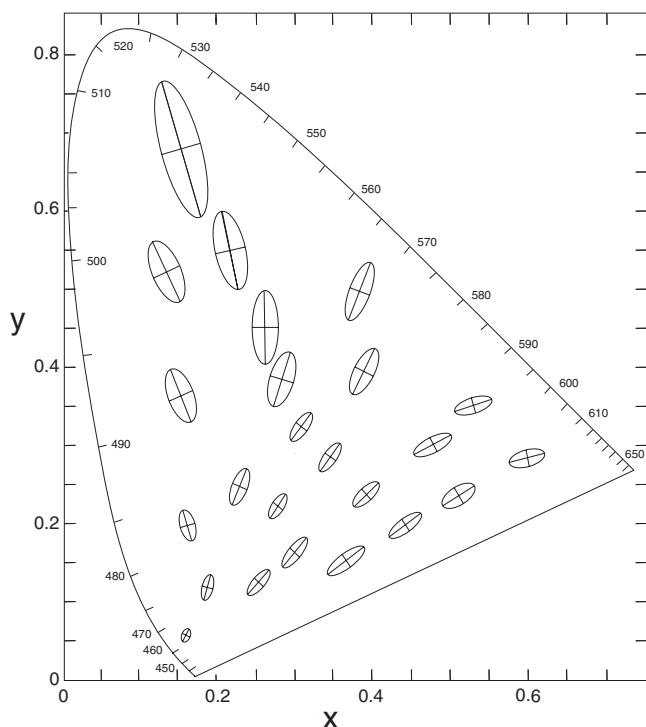


FIGURE 58.6. The MacAdam (1942) discrimination ellipses plotted in the (x,y) chromaticity diagram of the 1931 CIE observer. The ellipses are represented at 10 times their actual scale.

blue corner of the chromaticity diagram (Brown, 1951; Brown and MacAdam, 1949; Wyszecki and Fielder, 1971). Generally, it can be concluded that the discrimination sensitivity based on S cones declines more than that based on M and L cones at low luminance levels.

A clinical method of estimating chromatic discrimination is the Farnsworth-Munsell 100 hue test. The test was designed to measure hue discrimination among people with normal color vision and to measure the areas of color confusion in color-defective observers. The observer is required to arrange color samples by similarity in a sequential color series. The color samples are mounted in caps, which are numbered on the back and can be moved about freely during performance. The samples were chosen to represent perceptually equal steps of hue and to form a natural hue circle. Dean Farnsworth (1943) originally suggested that observers could be specified as showing only superior, average, or inferior chromatic discriminative ability, but more recent analysis techniques allow quantitative evaluation (Kitahara, 1984; Knoblauch, 1987; Smith et al, 1985; Victor, 1988).

MODERN APPROACHES Modern models include aspects of the classical approaches such as independent sensitivity regulation in the receptor types and opponent processes, but additionally account for discrimination under conditions where the discrimination stimuli are similar to the adapting chromaticity and under conditions where the discriminative

stimuli differ substantially from the adapting chromaticity. In the luminance domain, Craik (1938) found that discrimination was best when the discriminated stimuli were similar in luminance to the adaptation field, and that discrimination worsened as the luminance difference between the discriminated stimuli and the adaptation field increased. Krauskopf and Gegenfurtner (1992) extended this idea to the chromatic domain. They measured discrimination for a test field briefly displaced in chromaticity from a steady adapting field. When thresholds were measured in the same direction as the displacement ΔL for an L displacement or ΔS for an S displacement, thresholds rose in proportion to the difference between the test and adaptation chromaticities. When the threshold and the displacement were in different directions, ΔL for an S displacement or ΔS for an L displacement, thresholds were unchanged. A variety of experiments support the hypothesis that for discrimination threshold, the L- and S-cone axes are independent, or nearly independent, including habituation (Krauskopf et al., 1982) and noise masking (Sankeralli and Mullen, 1997) studies.

In a pioneering analysis, Le Grand (1949) analyzed the MacAdam (1942) data in terms of cone excitation. In making this calculation, he assumed that luminance was determined only by the sum of L- and M-cone responses. This simplification allowed him to calculate only the S- and L-cone excitation axes passing through each ellipse center; the M-cone excitation level was directly calculable from L. He then plotted the size of the arc through the ellipse as a function of the excitation at the center. The data for S cones had the shape of an increment threshold function. However, the data for L and M cones did not. Instead, there was a trade-off of L- and M-cone excitation. The data could be summarized by plotting the discrimination step as a function of the L/M ratio; discrimination was optimal when the cone excitations were balanced. Thus, for discriminations mediated by L and M cones, there is an intrinsic normalization near the EES chromaticity even when chromatic stimuli are presented continuously in an otherwise dark field, while for discriminations mediated by S cones, the data have the appearance of an increment threshold function. Boynton and Kambe (1980) confirmed and extended Le Grand's conclusions. They defined their stimuli in terms of S and L td. This allowed them to replot their chromatic discrimination data in a TVI format (log threshold versus log illuminance), where the abscissa is the amount of S-cone or L-cone stimulation and the ordinate is the discrimination threshold (ΔS and ΔL), at equiluminance.

Discrimination thresholds were gathered with a dark surround. At 120 td, discrimination ability dependent on S cones changed slowly with S-cone stimulation, then accelerated at high S-cone stimulation levels. On the other hand, discrimination ability along the L/(L + M) axis (Figs. 58.2A and 58.2B) showed a V shape with a minimum near white.

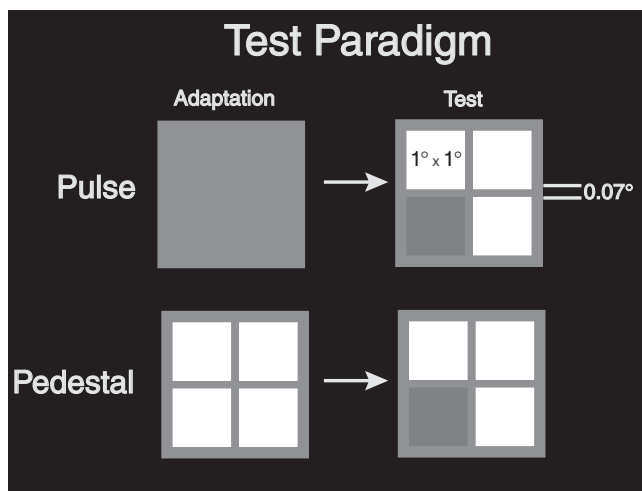


FIGURE 58.7. Display sequence for the Pulse (upper) and Pedestal (lower) Paradigms. The left figures show the display appearance during adaptation and intertrial intervals; the right figures show the appearance during a trial. (From Smith et al., 2000.) (See color plate 34).

With a white-appearing surround, discriminations mediated by S cones show a minimum at the background (Miyahara et al., 1993).

Smith et al. (2000) measured chromatic discrimination on the L/(L + M) axis for equiluminant stimuli in chromatic surrounds. They used two different stimulus presentation paradigms. The first was with pulsed stimuli like those of Krauskopf and Gegenfurtner (1992), in which there was a large temporal contrast step of the entire stimulus array. The second paradigm employed steadily presented discrimination stimuli, in which the stimulus array was continuously presented and only one of the test squares changed. Figure 58.7 shows the display sequences for the two paradigms. The paradigms differed only in the display preceding the trial; the trials presented identical stimuli. Chromatic discrimination was measured for steadily presented stimuli in order to evaluate conditions more nearly approximating those encountered in everyday experience. Figure 58.8 shows data collected under adaptation to three chromaticities along a constant S-cone line intersecting EES. The *open circles* represent thresholds for pulsed stimuli; the *closed squares* represent steadily presented test stimuli. The *solid lines* represent predictions from the model detailed in the section “A Modern Discrimination Theory Based on Retinal Physiology.” Arrows on the abscissa indicate the adapting chromaticities. For all conditions, discrimination is best when the test and adapting chromaticities are the same. There is little difference between thresholds for the pulsed and steadily presented test stimuli. Additional measurements showed that the discrimination steps were unchanged with variation of the background size. The pattern of results indicates that discrimination is determined at the border between test and surround. Chromatic alternation generates large signals in

Surround: $14.8^\circ \times 11.2^\circ$

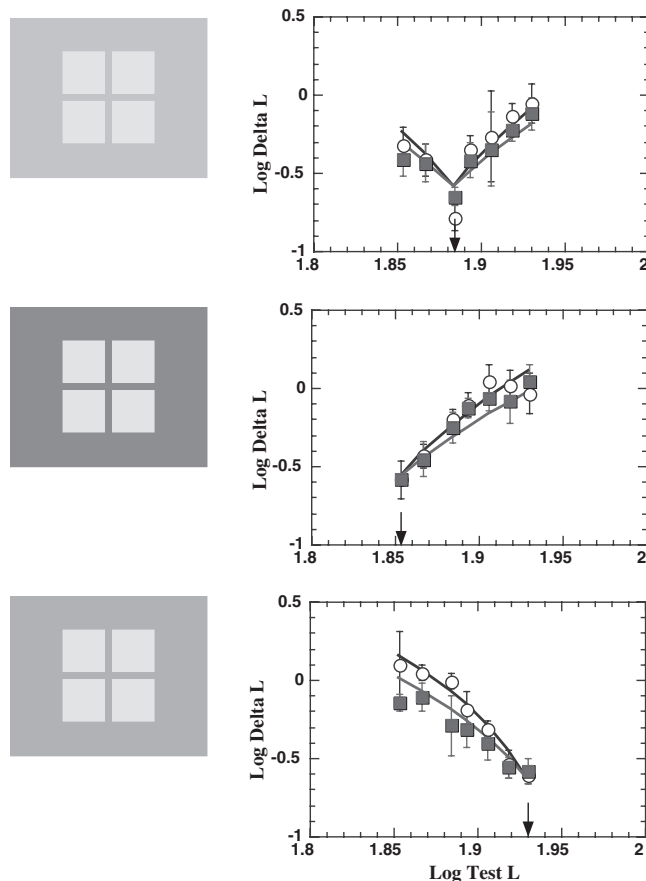


FIGURE 58.8. Discrimination data for a large rectangular surround comparing the Pulse and Pedestal Paradigms. The surround l-chromaticities are shown by arrows on the abscissa of each plot: 0.62 (*upper panel*), 0.665 (*middle panel*), and 0.74 (*lower panel*). Open circles show data for the Pulse Paradigm; closed squares show data for the Pedestal Paradigm. Icons on the left show the display appearance (not to scale) during adaptation and the intertrial interval for the Pedestal Paradigm. (From Smith et al., 2000.) (See color plate 35).

PC ganglion cells that do not adapt (Lee et al., 1990), and this situation may mimic that of blinking or of small eye movements sweeping a target back and forth across a small receptive field. In this case the adaptation state is maintained by the surround, and there is a continuous chromatic contrast across the border.

HOW DO THE L AND S AXES COMBINE? Boynton et al. (1986) developed a strategy to evaluate how response differences from the two chromatic mechanisms add to determine threshold. They plotted discrimination data in a normalized cone excitation space by setting the discrimination steps on the L-M- and S-cone axes equal. If signals from the two pathways were independent and combined by probability summation, data would have plotted as a circle. Diverse data sets plot as ellipses, with the major axis oriented at 135 degrees

in most cases (Nagy et al., 1987; Yebra et al., 1994). Though the ellipses typically did not deviate greatly from a circle, they did indicate an interaction. The data sets were gathered with diverse methodologies, so the finding is unlikely to be due to a procedural bias. When S- and L-cone excitation increase or decrease in tandem, there is some facilitation. When S- and M-cone excitation increase or decrease in tandem, there is independence or perhaps inhibition. On the other hand, studies designed to evaluate the interaction directly (Mullen et al., 1997) find only probability summation. Therefore, the presence of an interaction is controversial.

Models of chromatic discrimination

There have been two major traditions in theoretical accounts of color vision and color discrimination. One approach arose within the classical views of trichromacy. Color discrimination was thought to arise within the three independent cone pathways. This approach is called the *line element theory*. The second approach arose with Hurvich and Jameson's (1955) account of the Hering opponent process concept. Their model was proposed as an account of discrimination and color appearance. This *opponent colors theory* turned out to have the characteristics of so-called stage or zone theories that attempted to combine receptor trichromacy with postreceptor opponency. There were numerous stage or zone theories (reviewed by Judd, 1951a), but most were linear transforms of color mixture data. Vos and Walraven (1972a,b) proposed a well-developed stage theory that combined a trichromatic cone input stage with a subsequent cone ratio model of opponency. Although this model showed great predictive value, it has received little recent attention since it is inconsistent with modern electrophysiology. Both the line element and the opponent colors approaches have severe limitations, but it is nonetheless interesting to review them briefly.

LINE ELEMENT THEORY The line element was first proposed by Helmholtz (1891, 1892, 1896) and was developed by Schrödinger (1920) and later by Stiles (1946), among others (reviewed by Graham, 1965, and Stiles, 1972). In line element theory, the signals generated by three independent cone types, the S, M, and L cones, are subject to weights reflecting the radiance and quantal catch rate, the adaptational state, threshold noise, and a number of other considerations such as spatiotemporal parameters. Most versions of line element theory assume that the cones are in the Weber region at photopic levels of discrimination measurement. The cone excitations form three independent vectors. A discrimination threshold between two patches of color was envisioned as distance (dG) in this three-dimensional space. Helmholtz proposed the following equation to characterize a threshold difference between any two stimuli:

$$dG = \left[(dL/\sigma_L)^2 + (dM/\sigma_M)^2 + (dS/\sigma_S)^2 \right]^{1/2} \quad (4)$$

where dG is the discrimination threshold, dL , dM , and dS are the response differences in the three cone systems to the two colored patches, and σ_L , σ_M , and σ_S are weighting factors associated with sensitivity regulation. Starting at moderate luminance levels, the response of each cone sensitivity function was assumed to obey Weber's law and the Weber fraction of the three cone mechanisms was assumed to be equal. The Stiles (1946) modification of the Helmholtz line element allowed differences in the limiting Weber fractions of the cone mechanisms in the ratio (r:g:b) = (0.78:1:4.46).

The attraction of the line element approach lay in the fact that it treated chromatic discrimination in the same manner as increment thresholds in the luminance domain, thus providing a unified theory of detection and discrimination for the entire luminance range of photopic vision. The line element approach was proved wrong by the above-described Le Grand (1949) analysis, which showed that there was an antagonism between L- and M-cone responses. Subsequently Stiles (1972) noted that the existence of this minimum was inconsistent with line element theory even if a subtractive opponent process was added following a stage of cone-specific Weber sensitivity regulation. A major conclusion of the Stiles analysis was that Weberian sensitivity regulation (n , equation (1) is not solely a property of the cone photoreceptors).

OPPONENT COLORS THEORY Hurvich and Jameson (1955) updated the Hering concept of the opponent process. Their theory was based on some aspects of color appearance of spectral lights viewed in dark surrounds (see Chapter 57). Hurvich and Jameson pointed out that perceptually there are four unique hues—red, green, yellow, and blue—in the spectrum that represent unitary entities. Intervening hues appear to be mixtures of only pairs of these unique hues. Red could be paired with yellow (to give orange percepts) or blue (to give purple percepts) but not with green. In turn, green could be paired with yellow (to give lime percepts) or blue (to give aqua percepts) but not with red. Hurvich and Jameson measured what they called *chromatic opponent valences* to assess the spectral sensitivity of the two proposed chromatic opponent processes. They used a cancellation paradigm in which the amount of a unique hue needed to cancel its opposite was measured. For example, if the test was 620 nm (appearing orange), its redness content could be canceled by adding unique green and its yellowness content could be canceled by adding unique blue. The data could be plotted as energy-based red-green and blue-yellow valence curves with negative values (arbitrarily) assigned to the green and blue valences. It was necessary to use supplementary information to scale the red-green

and blue-yellow valence curves relative to each other. This was done by noting where the percept “orange” occurred in the spectrum. A valence chromaticity space at equiluminance with red-green and blue-yellow as the major axes could also be plotted. Although the paradigm sounds like an experiment in color appearance, it can also be conceived as memory color matching to an internally generated appearance standard. Hurvich and Jameson (1955) recognized that the data could be described by a linear transformation of color matching previously derived by Judd (1951a).

Hurvich and Jameson showed that the data of wavelength and least colorimetric purity discrimination were predicted by the chromaticity space formed by the valence curves. Wavelength discrimination was predicted by finding the wavelength excursion corresponding to constant angles around white. Least colorimetric purity was predicted by calculating the proportional distance of a fixed step from white to the spectrum locus. In other work, Jameson and Hurvich (1964) showed that many aspects of color appearance, such as hue scaling and color contrast, could be explained by their model (see Chapter 5).

Although the opponent colors model was successful in describing discrimination, it has problems as a color theory. The model assumes linearity, based in part on the supposition that hue cancellation data can be characterized as a linear transform of color matching data. However, this is not a critical test. Although the starting colors are spectral wavelengths, the end points expressed as chromaticity coordinates form clusters within the chromaticity diagram (Burns et al., 1984). There is no explicit statement of luminance or sensitivity regulation. The valence curves can be weighted to predict effects of luminance, but at the expense of generality of the model (Wyszecki and Stiles, 1982). In addition, the red-green valence has three lobes with positive red valence at short wavelengths. Although this aspect reflects color appearance, it is not seen in retinal spectral opponency. Aspects of color discrimination that primarily reflect the retinal opponency do not agree with the opponent colors model.

A MODERN DISCRIMINATION THEORY BASED ON RETINAL PHYSIOLOGY Here we present a model of spectral processing based on current physiological knowledge of the retinal pathways. The goal of the model is to incorporate both luminance gain and chromatic discrimination. It is based on modern physiology of retinal ganglion cells. The model for L- and M-cone discrimination, sketched in Figure 58.9A, is based on physiological data of the spectral opponent PC pathway of primates (Derrington et al., 1984; Lee et al., 1990, 1994). The model for S-cone discrimination is based on physiological data for the spectral opponency of the KC pathway (Fig. 58.9B). A conceptually similar version of this approach was proposed for by Zaidi et al. (1992).

A Spatiotemporal Contrast

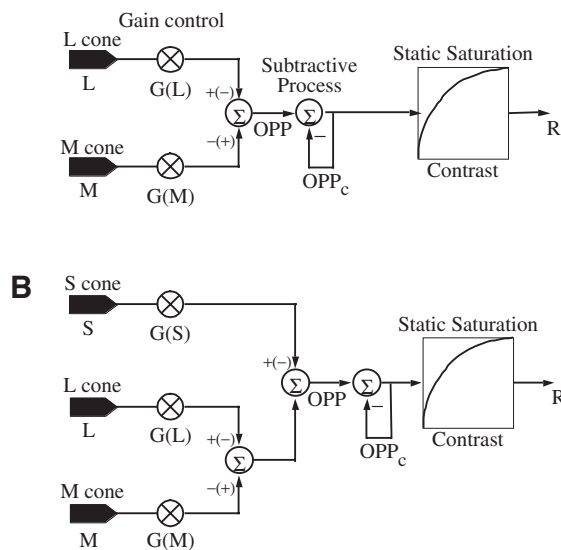


FIGURE 58.9. Schematic of a retinal model for equiluminant chromatic discrimination. *A*, the L/M cone system. *B*, the S-cone system.

Both models postulate an early stage of cone-specific multiplicative adaptation followed by a stage of spectral opponency between L and M cones for the L/M pathway or between S and L + M cones for the S pathway. Since gain control is not complete, the spectral opponent signal varies with wavelength and luminance. This signal is further controlled by subtractive feedback by the background. The signal then depends on the contrast between background and test chromaticity. All ganglion cells respond to their preferred contrast with a negatively accelerating function of contrast. This response follows a hyperbolic saturation function. Thus, four components determine contrast detection and discrimination: the absolute threshold, the gain function, the subtraction at the surround chromaticity, and the saturation function.

A given retinal ganglion cell responds best to a chromaticity change in its preferred direction (Kremers et al., 1993; Lee et al., 1994). Change in the nonpreferred direction will drive the cell below its resting level. The resting level is usually only about 15% of the maximal response rate. This is an intrinsic nonlinearity that renders the cell response asymmetric: the cell behaves as if partially rectified. For equiluminant chromatic pulses, $(+L - M)$ and $(-M + L)$ give redundant information, responding positively to “redward” changes from their adaptation point; similarly, $(+M - L)$ and $(-L + M)$ give redundant information, responding positively to “greenward” changes from their adaptation point (Lee et al., 1994). To achieve a response for the entire chromatic contrast range we require pairs of cells of opposite chromatic signatures, such as $(+L - M)$ and $(+M - L)$. A $(+L -$

M) cell predicts chromatic discrimination for pulses with redward direction ($L > L_A$) from the adaptation chromaticity, and a (+M – L) cell predicts chromatic discrimination for pulses with greenward direction ($L < L_A$) from the adaptation chromaticity. A similar argument may be made for the S-cone discriminations. All ganglion cells respond to their preferred contrast with a negatively accelerating function of contrast (Kaplan and Shapley, 1986).

The predictions were optimized for a condition in which the observer views a steady background field metameric to the EES (Smith et al., 2000). The discrimination target replaces the background for a trial. Both background and discrimination stimuli are maintained at equiluminance. The trial creates a chromatic spatiotemporal contrast event in the test array from the fixed adaptation level. An optimal test stimulus for chromaticity detection is of low spatiotemporal frequency, for example, a 2-degree diameter, 1 second duration pulse with blurred spatiotemporal edges. Use of a complex spatial pattern, a pseudoisochromatic plate design, with continuous view similarly raises thresholds by a constant (Watanabe et al., 1998).

The equations used to predict chromatic contrast detection and discrimination are detailed in the appendix. A simplified version of equation (A13) is

$$\log(\Delta L_c) = \log(L_0) - \log(G) + \log(O) \quad (5)$$

where L_0 depends on the criterion response, G refers to the multiplicative gain, and O refers to the opponent saturation function.

The absolute threshold L_{Th} is given by

$$\log(L_{Th}) = \log(L_0) + \log(S) \quad (6)$$

where S is a constant, characteristic of the parameters of the hyperbolic saturation function. When chromatic contrast detection is measured at the adapting chromaticity, the opponent signal is very small, and the chromatic contrast threshold approaches the shape of a TVI function rising from threshold:

$$\log(L) \sim \log(L_0) - \log(G) + \log(S) \quad (7)$$

where G refers to the multiplicative gain. This function is shown as a dashed line in Figure 58.10. Finally, chromatic contrast discrimination at various chromaticities (equation 5) describes a V-shaped function riding on the TVI function. The output of this model is shown in Figure 58.10A for fixed illuminations between 0.1 and 10,000 tds. The chromatic contrast discriminations are shown by V shapes.

A parallel equation can be derived for the S-cone pathway. A simplified version of equation (A17) is

$$\log(\Delta S_c) = \log(S_0) - \log(G) + \log(O) \quad (8)$$

The output of this model is plotted in Figure 58.10B with the assumption of adaptation to the EES. Again, the dashed

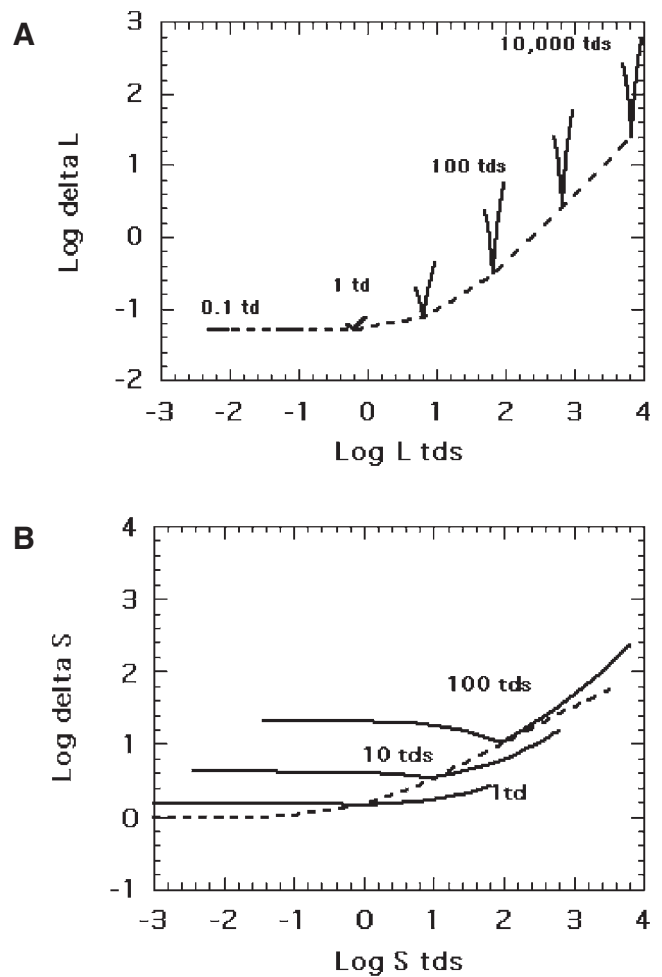


FIGURE 58.10. Discriminations predicted by the retinal model plotted as a function of retinal illuminance in trolands. A, The L/M cone system. B, The S-cone system. (From Smith and Pokorny, 1996.)

line shows the function predicted for a chromatic threshold measured on a “white” background.

Both models predict a V-shaped discrimination function at a constant retinal illuminance level. For the PC pathway, the V shapes are narrow, reflecting the small range of differential chromatic signal available at each illuminance. In comparison, the S-cone system shows broad functions since the range of S-cone stimulation relative to the “white” background is large. The V shapes are constant on the linear rising portion of the increment threshold function but gradually become shallow as illuminance drops.

This model can describe chromatic discriminations of many kinds. The model’s predictions for wavelength and colorimetric purity discrimination are shown in Figures 58.4 and 58.5. In these figures, the L/M and S-cone predictions are plotted independently. Model predictions for chromatic contrast discrimination are shown in Figure 58.7. The models allow prediction of the effect of using chromatic

backgrounds. The position of the V shape depends on the chromaticity of the background. Although the number of free parameters seems high at five, at a fixed retinal illuminance the threshold and gain terms are constant determining the vertical scaling constant. Thus, the V shape can be fit with only two parameters, a vertical scaling constant and the factor determining the slope of the V shape.

APPENDIX

Here we describe the equations used to derive the threshold predictions given in the main text as equations (5) and (6).

PC pathway

The L- and M-cone responses to a light of a given chromaticity and luminance are given by

$$R_l = I/l_{\max} = L/l_{\max} \quad (\text{A1})$$

$$R_m = mI/m_{\max} = M/m_{\max} \quad (\text{A2})$$

where l and m are the L and M cone chromaticities as in Figure 58.2B, I is the illumination level, and l_{\max} and m_{\max} are the maximal values of the L and M spectral sensitivities, scaled so that they sum to the total retinal illuminance. The L- and M-cone responses sum to the total luminance level, which is usually constant in any measurement of chromatic discrimination.

The cone sensitivities are subject to the multiplicative sensitivity regulation at the adapting chromaticities L_A and M_A provided by the background. Gain is described by a illuminance-dependent equation that is unity at absolute threshold and is a fraction at high illuminances. The terms $G(L_A/l_{\max})$ and $G(M_A/m_{\max})$ are multiplicative gain terms at the adapting chromaticity, given by an equation of the form

$$G(L) = 1/(1 + k_1 L_A/l_{\max})^{k_2} \quad (\text{A3})$$

$$G(M) = 1/(1 + k_1 M_A/m_{\max})^{k_2} \quad (\text{A4})$$

where L_A is in cone trolands and k_1 , k_2 are constants. Independent estimation of k_1 and k_2 requires evaluation of chromaticity discrimination as a function of radiance. The value of k_1 is about 1/3 tds and the value of k_2 is about 0.65. The value k_1 is such that in a simple gain system, a threshold at illuminance $1/k_1$ is twice the absolute threshold. At high illuminances, the product of the response and the gain term approaches a limiting value. For $L_A \gg 1$:

$$R \cdot G(L_A) = (L_A/l_{\max})/(1 + k_1 L_A/l_{\max})^{k_2} \quad (\text{A5})$$

The cone spectral opponent term can be derived for each of the four subtypes of PC-pathway cells, (+L – M–), (+M – L), (–L+M), and (–M+L). For a (+L – M) cell, the spectral opponent term at the test chromaticity would be given by

$$OPP_{(+L-M)} = [L_T/l_{\max} G(L_A/l_{\max}) - k_3 M_T/m_{\max} G(M_A/m_{\max})] \quad (\text{A6})$$

where the constant k_3 represents the surround strength of the spectral opponency. In retinal ganglion cell data, the surround strength for PC-pathway cells varies from 0.7 to 1.0 (Smith et al., 1992).

Next, we assume that the spectral opponent term is subject to subtractive feedback determined by the opponent signal at the adapting chromaticity.

$$OPP_C = OPP_T - k_4 OPP_A \quad (\text{A7})$$

where OPP_T is the spectral opponent term at the test chromaticity, OPP_A represents the spectral opponent term at the adapting chromaticity, and k_4 represents the subtractive feedback strength. Psychophysical studies of luminance thresholds have suggested that subtractive feedback can be as high as 0.9 (Hood and Finkelstein, 1986).

The response of a spectral opponent cell to a chromaticity change C from a fixed adapting chromaticity A follows the form of a hyperbolic saturation function (Kaplan and Shapley, 1986; Lee et al., 1990). This is given by

$$R_{OPP} = R_{\max}[OPP_C/(OPP_C + SAT)] \quad (\text{A8})$$

where OPP_C is a spectral opponent term and SAT is the static saturation.

If the subtractive term does not remove the entire effect of the adapting chromaticity, there will be some residual signal at the adapting chromaticity. Provided that the criterion for a threshold δ is small relative to R_{\max} , the chromatic discrimination threshold for an optimal spatiotemporal stimulus at the adapting chromaticity can be written based on the derivative to equation (5):

$$\log(\Delta L_A) = \log(\delta/R_{\max}) - \log[1/(G(L)/l_{\max}) + 1/(G(M)/m_{\max})] + \log[(OPP_A + SAT)^2/SAT] \quad (\text{A9})$$

This equation includes three terms: a threshold term, a gain term, and a saturation term. At absolute threshold, the gain is unity and the saturation term is zero. The first term, $\log(\delta/R_{\max})$, represents the absolute threshold. Above threshold at the adapting chromaticity, the value of OPP_A is very small and the third term approaches $\log[SAT]$. The equation then describes a regular TVI function as retinal illuminance is raised. The threshold at other test chromaticities will depend on the size of the contrast step, ΔOPP , between the adapting chromaticity and the new test chromaticity. This will introduce an additional term, ΔOPP , modifying equation (A9).

$$\log(\Delta L_C) = \log(\delta/R_{\max}) - \log[1/(G(L_A)/l_{\max}) + 1/(G(M_A)/m_{\max})] + \log[(\Delta OPP + OPP_A + SAT)^2/SAT] \quad (\text{A10})$$

A simplified version of this equation appears as equation (5) in the main body of the chapter.

S-cone pathway

A similar approach can be used to describe chromatic discrimination based on physiological data of the spectral opponent KC pathway of primates (Derrington et al., 1984; Lee et al., 1990, 1994). A major simplification occurs because at equiluminance, the (L+M) surround is constant. Discrimination is determined only by the S-cone stimulation. The initial equations are unchanged.

$$R_s = sI/s_{\max} = S/s_{\max} \quad (\text{A11})$$

where s is the S-cone chromaticities, as in Figure 58.2B, I is the illumination level, and s_{\max} is the maximal values of the S spectral sensitivities, scaled S tds (Boynton and Kambe, 1980). The cone term is subject to multiplicative sensitivity regulation:

$$G(S) = 1/(1 + k_1 S_A/s_{\max})^{k_2} \quad (\text{A12})$$

where S_A is the adapting signal in cone trolands and k_1 and k_2 are constants. The spectral opponent term can be derived for each of the two subtypes of S-cone-pathway cell, (+S (L+M) and (–S+(L–)+M). For a (+S–(L+M)) cell, the opponent term is given by

$$OPP_{(+S-)} = S_C/s_{\max} G(S_A/s_{\max}) - k_3 \quad (\text{A13})$$

The constant k_3 represents the surround strength of the spectral opponency. For the S-cone pathway, k_3 is set to give a null response for the cell at 500 nm (Pugh and Larimer, 1980).

The opponent term is again subject to subtractive feedback:

$$OPP_C = OPP - k_4 OPP_A \quad (A14)$$

where OPP_A represents the spectral opponent term at the adapting chromaticity and k_4 represents the subtractive feedback strength. The response of a given cell to a chromaticity, C , at a fixed adapting chromaticity is

$$R = R_{\max}[OPP_C/(OPP_C + SAT)] \quad (A15)$$

where OPP_C is the opponent signal at the adapting chromaticity. Provided that the criterion for a threshold, δ , is small relative to R_{\max} , the chromatic contrast detection threshold at the adapting chromaticity can be written based on the derivative to equation (10):

$$\log(\Delta S_A) = \log(S_{th}) - \log[(G(S)/S_{\max})] + \log[(OPP_A + SAT)^2/SAT] \quad (A16)$$

where the first term, S_{th} , represents δ/R_{\max} , the second term represents the luminance gain response, and the third term represents the opponent term. The thresholds for other starting chromaticities ΔOPP then include the extra term as described for the L/M pathway.

$$\log(\Delta S_C) = \log(S_{th}) - \log[(G(S)/S_{\max})] + \log[(OPP_A + \Delta OPP + SAT)^2/SAT] \quad (A17)$$

A simplified version of this equation appears as equation (8) in the main body of the chapter.

Acknowledgments

Preparation of this chapter was supported by U.S. Public Health National Eye Institute Research Grant EY00901. We thank Patrick Monnier for assistance with the figures.

REFERENCES

- Aguilar, M., and W. S. Stiles, 1954. Saturation of the rod mechanism of the retina at high levels of illumination, *Optica Acta* 1:59–65.
- Barlow, H. B., 1958. Intrinsic noise of cones, in: *Visual Problems of Colour*, Her Majesty's Stationery Office, London, pp. 617–630.
- Bedford, R. E., and G. W. Wyszecki, 1958. Wavelength discrimination for point sources, *J. Opt. Soc. Am.*, 48:129–135.
- Boynton, R. M., and N. Kambe, 1980. Chromatic difference steps of moderate size measured along theoretically critical axes, *Color Res. Appl.*, 5:13–23.
- Boynton, R. M., A. L. Nagy, and R. T. Eskew, Jr., 1986. Similarity of normalized discrimination ellipses in the constant-luminance chromaticity plane, *Perception*, 15:755–763.
- Brainard, D. H., 1995. Colorimetry, in *The Handbook of Optics*, 2nd ed., vol. I (M. Bass, E. W. V. Stryland, D. R. Williams, and W. L. Wolfe, eds.), New York: McGraw-Hill, pp. 26.1–26.54.
- Brown, W. R. J., 1951. The influence of luminance level on visual sensitivity to color differences, *J. Opt. Soc. Am.*, 41:684–688.
- Brown, W. R. J., and D. L. MacAdam, 1949. Visual sensitivities to combined chromaticity and luminance differences, *J. Opt. Soc. Am.*, 39:808–834.
- Burns, S. A., A. E. Elsner, J. Pokorny, and V. C. Smith, 1984. The Abney effect: chromaticity coordinates of unique and other constant hues, *Vis. Res.*, 24:479–489.
- Craik, K. J., 1938. The effect of adaptation on differential brightness discrimination, *J. Physiol. (Lond.)*, 92:406–421.
- Dacey, D. M., 2000. Parallel pathways for spectral coding in primate retina, *Annu. Rev. Neurosci.*, 23:743–775.
- Dacey, D. M., and B. B. Lee, 1994. The “blue-on” opponent pathway in primate retina originates from a distinct bistratified ganglion cell type, *Nature*, 367:731–735.
- Derrington, A. M., J. Krauskopf, and P. Lennie, 1984. Chromatic mechanisms in lateral geniculate nucleus of macaque, *J. Physiol. (Lond.)*, 357:241–265.
- Derrington, A. M., and P. Lennie, 1982. The influence of temporal frequency and adaptation level on receptive field organization of retinal ganglion cells in cat, *J. Physiol. (Lond.)*, 333:343–366.
- De Valois, R. L., I. Abramov, and G. H. Jacobs, 1966. Analysis of response patterns of LGN cells, *J. Opt. Soc. Am.*, 56: 966–977.
- Farnsworth, D., 1943. The Farnsworth-Munsell 100 hue and dichotomous tests for color vision, *J. Opt. Soc. Am.*, 33:568–578.
- Graham, C. H., 1965. Color: data and theories, in *Vision and Visual Perception* (C. H. Graham, ed.), New York: Wiley.
- Helmholtz, H. von, 1891. Versuch einer erweiterten Anwendung des Fechnerschen Gesetzes im Farbensystem, *Z. Psychol. Physiol. Sinnesorgane*, 2:1–30.
- Helmholtz, H. von, 1892. Versuch das psychophysische Gesetz auf die Farbenunterschiede trichromatischer Augen anzuwenden, *Z. Psychol. Physiol. Sinnesorgane*, 3:1–20.
- Helmholtz, H. von, 1896. *Handbuch der Physiologischen Optik*, 2nd ed., Hamburg: Voss.
- Hendry, S. H., and R. C. Reid, 2000. The koniocellular pathway in primate vision, *Annu. Rev. Neurosci.*, 23:127–153.
- Hood, D. C., and M. A. Finkelstein, 1986. Sensitivity to light, in *Handbook of Perception and Human Performance*, vol. I, *Sensory Processes and Perception* (K. R. Boff, L. Kaufman, and J. P. Thomas, eds.), New York: Wiley, pp. 5-1–5-66.
- Hurvich, L. M., and D. Jameson, 1955. Some quantitative aspects of an opponent-colors theory. II. Brightness, saturation and hue in normal and dichromatic vision, *J. Opt. Soc. Am.*, 45:602–616.
- Jameson, D., and L. M. Hurvich, 1964. Theory of brightness and color contrast in human vision, *Vis. Res.*, 4:135–154.
- Judd, D. B., 1951a. Basic correlates of the visual stimulus, in *Handbook of Experimental Psychology* (S. S. Stevens, ed.), New York: Wiley, pp. 811–867.
- Judd, D. B., 1951b. Colorimetry and artificial daylight, in Technical Committee No. 7 Report of Secretariat, United States Commission, International Commission on Illumination, Twelfth Session, Stockholm, pp. 1–60.
- Kaiser, P. K., J. P. Comerford, and D. M. Bodinger, 1976. Saturation of spectral lights, *J. Opt. Soc. Am.*, 66:818–826.
- Kaiser, P. K., B. B. Lee, P. R. Martin, and A. Valberg, 1990. The physiological basis of the minimally distinct border demonstrated in the ganglion cells of the macaque retina, *J. Physiol. (Lond.)*, 422:153–183.
- Kaplan, E., and R. M. Shapley, 1986. The primate retina contains two types of ganglion cells, with high and low contrast sensitivity, *Proc. Natl. Acad. Sci. USA*, 83:2755–2757.
- Kitahara, K., 1984. An analysis of the Farnsworth-Munsell 100-hue test, *Doc. Ophthalmol. Proc. Ser.*, 39:233–246.
- Knoblauch, K., 1987. On quantifying the bipolarity and axis of the Farnsworth-Munsell 100-Hue test, *Invest. Ophthalmol. Vis. Sci.*, 28:707–710.
- König, A., and E. Brodhun, 1889. Experimentelle Untersuchungen über die psychophysische Fundamentalformel in Bezug auf den

- Gesichtssinn, *Sitzungsberichte Preuss. Akad. Wissenschaften, Berl.*, 27:641–644.
- Kraft, J. M., and J. S. Werner, 1999. Aging and the saturation of colors. 1. Colorimetric purity discrimination, *J. Opt. Soc. Am. A*, 16:223–230.
- Krauskopf, J., and K. Gegenfurtner, 1992. Color discrimination and adaptation, *Vis. Res.*, 32:2165–2175.
- Krauskopf, J., D. R. Williams, and D. W. Heeley, 1982. Cardinal directions of color space, *Vis. Res.*, 22:1123–1131.
- Kremers, J., B. B. Lee, J. Pokorny, and V. C. Smith, 1993. Responses of macaque ganglion cells and human observers to compound periodic waveforms, *Vis. Res.*, 33:1997–2011.
- Kuffler, S. W., 1952. Neurons in the retina: organization, inhibition and excitation problems, *Cold Spring Harbor Symp. Quant. Biol.*, 17:281–292.
- Le Grand, Y., 1949. Les seuils différentiels de couleurs dans la théorie de Young *Rev. Opt.*, 28:261–278. (Color difference thresholds in Young's theory, *Color Res. Appl.*, 19:296–309, 1994; K. Knoblauch, trans.).
- Lee, B. B., 1996. Receptive field structure in the primate retina, *Vis. Res.*, 36:631–644.
- Lee, B. B., D. M. Dacey, V. C. Smith, and J. Pokorny, 1999. Horizontal cells reveal cone type-specific adaptation in primate retina, *Proc. Natl. Acad. Sci. USA*, 96:14611–14616.
- Lee, B. B., P. R. Martin, and A. Valberg, 1988. The physiological basis of heterochromatic flicker photometry demonstrated in the ganglion cells of the macaque retina, *J. Physiol. (Lond.)*, 404:323–347.
- Lee, B. B., P. R. Martin, and A. Valberg, 1989. Sensitivity of macaque retinal ganglion cells to chromatic and luminance flicker, *J. Physiol. (Lond.)*, 414:223–243.
- Lee, B. B., J. Pokorny, V. C. Smith, and J. Kremers, 1994. Responses to pulses and sinusoids in macaque ganglion cells, *Vis. Res.*, 34:3081–3096.
- Lee, B. B., J. Pokorny, V. C. Smith, P. R. Martin, and A. Valberg, 1990. Luminance and chromatic modulation sensitivity of macaque ganglion cells and human observers, *J. Opt. Soc. Am. A*, 7:2223–2236.
- Lennie, P., J. Pokorny, and V. C. Smith, 1993. Luminance, *J. Opt. Soc. Am. A*, 10:1283–1293.
- MacAdam, D. L., 1942. Visual sensitivities to color differences in daylight, *J. Opt. Soc. Am.*, 32:247–274.
- MacLeod, D. I. A., and R. M. Boynton, 1979. Chromaticity diagram showing cone excitation by stimuli of equal luminance, *J. Opt. Soc. Am.*, 69:1183–1185.
- Martin, P. R., A. J. White, A. K. Goodchild, H. D. Wilder, and A. E. Sefton, 1997. Evidence that blue-on cells are part of the third geniculocortical pathway in primates, *Eur. J. Neurosci.*, 9:1536–1541.
- McCree, K. J., 1960. Colour confusion produced by voluntary fixation, *Opt. Acta*, 7:281–291.
- Miyahara, E., V. C. Smith, and J. Pokorny, 1993. How surrounds affect chromaticity discrimination, *J. Opt. Soc. Am. A*, 10:545–553.
- Mollon, J. D., and P. G. Polden, 1977. An anomaly in the response of the eye to light of short wavelengths, *Philos. Trans. R. Soc. Lond. Ser. B: Biol. Sci.*, 278:207–240.
- Mullen, K. T., S. J. Cropper, and M. A. Losada, 1997. Absence of linear subthreshold summation between red-green and luminance mechanisms over a wide range of spatio-temporal conditions, *Vis. Res.*, 37:1157–1165.
- Nagy, A. L., R. T. Eskew, and R. M. Boynton, 1987. Analysis of color-matching ellipses in a cone-excitation space, *J. Opt. Soc. Am. A*, 4:756–768.
- Pokorny, J., and V. C. Smith, 1970. Wavelength discrimination in the presence of added chromatic fields, *J. Opt. Soc. Am.*, 69:562–569.
- Pokorny, J., and V. C. Smith, 1986. Colorimetry and color discrimination, in *Handbook of Perception and Human Performance*, vol. I, *Sensory Processes and Perception* (K. R. Boff, L. Kaufman, and J. P. Thomas, eds.), New York: Wiley, pp. 8-1–8-51.
- Pugh, E. N. J., and J. Larimer, 1980. Test of the identity of the site of blue/yellow hue cancellation and the site of chromatic antagonism in the p1 pathway, *Vis. Res.*, 20:779–788.
- Pugh, E. N. J., and J. D. Mollon, 1979. A theory of the p-1 and p-3 color mechanisms of Stiles, *Vis. Res.*, 19:293–312.
- Rushton, W. A. H., 1972. Visual pigments in man, in *Handbook of Sensory Physiology*, vol. VII/I (H. J. A. Dartnall, ed.), Berlin: Springer, pp. 364–394.
- Sankeralli, M. J., and K. T. Mullen, 1997. Postreceptoral chromatic detection mechanisms revealed by noise masking in three-dimensional cone contrast space, *J. Opt. Soc. Am. A*, 14:2633–2646.
- Schrödinger, E., 1920. Grundlinien einer Theorie der Farbenmetrik im Tagessehen, *Ann. Physik (Leipzig)*, 63:134–182. English translation in *Sources of Color Science* (D. L. MacAdam, ed.), Cambridge, MA: MIT Press, 1970.
- Shapiro, A. G., J. Pokorny, and V. C. Smith, 1996. An investigation of scotopic threshold-versus-illuminance curves for the analysis of color-matching data, *Color Res. Appl.*, 21:80–86.
- Sharpe, L. T., C. Fach, K. Nordby, and A. Stockman, 1989. The incremental threshold of the rod visual system and Weber's law, *Science*, 244:354–356.
- Smith, V. C., B. B. Lee, J. Pokorny, P. R. Martin, and A. Valberg, 1992. Responses of macaque ganglion cells to the relative phase of heterochromatically modulated lights, *J. Physiol. (Lond.)*, 458:191–221.
- Smith, V. C., and J. Pokorny, 1975. Spectral sensitivity of the foveal cone photopigments between 400 and 500 nm, *Vis. Res.*, 15:161–171.
- Smith, V. C., and J. Pokorny, 1996. The design and use of a cone chromaticity space, *Color Res. Appl.*, 21:375–383.
- Smith, V. C., and J. Pokorny, 2003. Color matching and color discrimination, in *The Science of Color* (S. Shevell, ed.), Optical Society of America, pp. 103–148.
- Smith, V. C., J. Pokorny, B. B. Lee, and D. M. Dacey, 2001. Primate horizontal cell dynamics: an analysis of sensitivity regulation in the outer retina, *J. Neurophysiol.*, 85:545–558.
- Smith, V. C., J. Pokorny, and A. S. Pass, 1985. Color-axis determination on the Farnsworth-Munsell 100-hue test, *Am. J. Ophthalmol.*, 100:176–182.
- Smith, V. C., J. Pokorny, and H. Sun, 2000. Chromatic contrast discrimination: data and prediction for stimuli varying in L and M cone excitation, *Color Res. Appl.*, 25:105–115.
- Stabell, U., and B. Stabell, 1977. Wavelength discrimination of peripheral cones and its change with rod intrusion, *Vis. Res.*, 17:423–426.
- Stiles, W. S., 1946. A modified Helmholtz line-element in brightness-colour space, *Proc. Phys. Soc. (Lond.)*, 58:41–65.
- Stiles, W. S., 1972. The line element in colour theory: a historical review, in *Color Metrics* (J. J. Vos, L. F. C. Friele, and P. L. Walraven, eds.), Soesterberg: AIC/Holland, pp. 1–25.
- Swanson, W. H., T. Ueno, V. C. Smith, and J. Pokorny, 1987. Temporal modulation sensitivity and pulse detection thresholds for chromatic and luminance perturbations, *J. Opt. Soc. Am. A*, 4:1992–2005.

- Valberg, A., B. B. Lee, and D. A. Tigwell, 1986. Neurons with strong inhibitory S-cone inputs in the macaque lateral geniculate nucleus, *Vis. Res.*, 26:1061–1064.
- Victor, J. D., 1988. Evaluation of poor performance and asymmetry in the Farnsworth-Munsell 100-hue test, *Invest. Ophthalmol. Vis. Sci.*, 29:476–481.
- Vos, J. J., and P. L. Walraven, 1972a. An analytical description of the line element in the zone-fluctuation model of colour vision—I. Basic concepts, *Vis. Res.*, 12:1327–1365.
- Vos, J. J., and P. L. Walraven, 1972b. An analytical description of the line element in the zone-fluctuation model of color vision—II. The derivation of the line element, *Vis. Res.*, 12:1345–1365.
- Watanabe, A., J. Pokorny, and V. C. Smith, 1998. Red-green chromatic discrimination with variegated and homogeneous stimuli, *Vis. Res.*, 38(21):3271–3274.
- Weale, R. A., 1951. Hue-discrimination in para-central parts of the human retina measured at different luminance levels, *J. Physiol. (Lond.)*, 113:115–122.
- Wiesel, T., and D. H. Hubel, 1966. Spatial and chromatic interactions in the lateral geniculate body of the rhesus monkey, *J. Neurophysiol.*, 29:1115–1156.
- Wright, W. D., 1941. The sensitivity of the eye to small colour differences, *Proc. Phys. Soc. (Lond.)*, 53:93–112.
- Wright, W. D., and F. H. G. Pitt, 1934. Hue-discrimination in normal colour-vision, *Proc. Phys. Soc. (Lond.)*, 46:459–473.
- Wright, W. D., and F. H. G. Pitt, 1935. The colour-vision characteristics of two trichromats, *Proc. R. Soc. (Lond.)*, 47:205–217.
- Wyszecki, G., and G. H. Fielder, 1971. New color-matching ellipses, *J. Opt. Soc. Am.*, 61:1135–1152.
- Wyszecki, G., and W. S. Stiles, 1982. *Color Science—Concepts and Methods, Quantitative Data and Formulae*, 2nd ed., New York: Wiley.
- Yebra, A., J. A. Garcia, and J. Romero, 1994. Color discrimination data for 2-degrees and 8-degrees and normalized ellipses, *J. Opt. Nouv. Rev. Opt.*, 25:231–242.
- Yeh, T., V. C. Smith, and J. Pokorny, 1993. Colorimetric purity discrimination: data and theory, *Vis. Res.*, 33:1847–1857.
- Zaidi, Q., 1997. Decorrelation of L- and M-cone signals, *J. Opt. Soc. Am. A*, 14:3430–3431.
- Zaidi, Q., A. Shapiro, and D. Hood, 1992. The effect of adaptation on the differential sensitivity of the S-cone color system, *Vis. Res.*, 32:1297–1318.

59 The Role of Color in Spatial Vision

KAREN K. DE VALOIS

COLOR VARIATION IS COMMON in nature, as is color vision in the animal kingdom. The ability to discriminate color differences without regard to luminance variations has apparently evolved independently multiple times. This, as well as the massive neural investment that primates make in color vision, suggests that it must provide significant advantages to the species that possess it. Color vision has traditionally been studied in splendid isolation, with only minimal attempts to examine the significance of spatial and temporal factors in color processing or the role of color in spatial or temporal vision. There have been compelling practical reasons for separating color and spatial vision experimentally, because before the advent of video displays it was difficult to produce complex spatiotemporal stimuli that varied in color without associated variations in luminance. Since the middle of the twentieth century, however, there has been an explosion of research on the characteristics of spatial vision based on color alone and on the role that color may play in spatial vision.

There are two general approaches to the study of color spatial vision. One is to determine the characteristics of spatial vision that is based solely upon color. This requires eliminating luminance variations from the stimuli to be used, then studying sensitivity to and analysis of spatial patterns when only color differences are present. This is technically quite demanding, in part because of the chromatic aberrations produced by the optical system of the eye. These introduce unwanted and sometimes unrecognized luminance artifacts into otherwise isoluminant stimuli. When it is successfully accomplished, however, using isoluminant stimuli has the advantage of isolating the color system so that its characteristics can be determined without the intrusion of the visual mechanisms that analyze luminance variations. This approach is based on the traditional assumption that the visual system can be neatly separated into a color vision subsystem and a quite separate luminance vision mechanism. If that assumption is unwarranted, and it may be, then interpretation of the results of such studies is not so straightforward. Nonetheless, a great deal of research has investigated the characteristics of spatial vision when only color variations are present. The general conclusion is that color differences alone can subserve reasonable spatial vision, though with somewhat lower resolution than is found with luminance variations. This work will be discussed further below.

The second major approach to studying the role of color in spatial vision is to consider the joint variation of color and luminance. The luminance mechanism as traditionally conceived is assumed to be insensitive to variations in chromaticity (see Lennie et al., 1993, for discussion). The interactions between the color vision system and the (presumed) single luminance mechanism have been widely studied. Alternative conceptions suggest that there may be additional mechanisms that are responsive to luminance-varying patterns but that are also selective for hue. Some research has been devoted to the study of the possible existence and characteristics of hue-selective mechanisms that respond to variations in effective intensity. This work will be discussed further below.

The ability to analyze the spatial variation of color across a scene confers certain marked advantages. Although color and luminance variations are often correlated in nature, they do not covary perfectly. Color provides a separate and often more reliable indication of the presence of reflectance differences in a visual scene, and thus may aid substantially in segregating the perceptual world into discrete objects. Color vision is also useful in foraging for food, for conspecific communication, and for identifying possible mates. A particular advantage for humans is that color can be readily categorized and thus efficiently coded in memory for later retrieval.

This chapter will consider only psychophysical approaches to the study of color spatial vision. For more information concerning the in this volume relevant physiological substrates, see Chapter 65.

Some important constraints on color spatial vision

There are many constraints on color vision. Two of these are especially significant in considering the role that color vision might play in spatial processing and will be briefly described here. First, color vision can operate only at relatively high light levels. There are three classes of cone photoreceptors, each with its own photopigment. The S cones are maximally sensitive in the short visible wavelengths; the M cones in the medium wavelengths; and the L cones in the longer wavelengths. The cones are responsible for transduction at moderate to high light levels and thus for color vision. The great majority of all cones are either L or M cones. Both absorb light over the entire

visible spectrum, and their spectral absorption functions differ only slightly. A different class of photoreceptors, rods, is responsible for vision at low light levels. They are not active at the high light levels at which color vision is prominent, and the cones are not responsive at very low light levels.

To estimate the amount of light present at a given position (more properly, the light coming from a given direction), the visual system need only count the number of photons it absorbs in the corresponding retinal region. (Here we ignore the added complexities resulting from differential sensitivity to different wavelengths and from nonlinear intensity-response functions.) This estimate can be based on the output of a single receptor type (the rods at low, or scotopic, light levels, for example) or on a combination of multiple receptor types in a specific region. To judge the chromaticity at a single point, however, the system must compare the number of photons absorbed in each of at least two photoreceptors that contain photopigments that differ in spectral sensitivity. To estimate luminance, thus, the critical information lies in the *sum* of the responses of the various photoreceptors present, but to judge color, it is the *difference* between receptors' outputs that is critical. Insofar as the receptor spectral sensitivities overlap, the signal from the sum will be larger than that from the difference. The L and M cones, which constitute some 90% or more of the cone population, have closely spaced spectral sensitivity peaks, only about 30nm apart, and thus give a much larger sum than the difference signal. In order to have a difference signal large enough to work with, the light level must be high and there must be at least two photoreceptor types with different spectral sensitivities. Thus, color vision cannot operate at all at scotopic levels and only poorly at low photopic light levels. Consequently, a spatial vision system that depended solely on color discriminations would be a major handicap for any species that is active in low light levels.

Spatial discriminations based on color differences have other constraints as well. A local luminance judgment can be based on the output of a single L or M cone. Detecting a variation in luminance across space can be accomplished by comparing the outputs of two such receptors at different retinal positions. Since the two receptors can be adjacent (representing adjacent visual directions), spatial resolution can in principle be as fine as the receptor spacing. To judge the *color* at any single point, however, requires a comparison between the outputs of two or more different photoreceptor types near one another in retinal location. To detect a variation in color across space, it is necessary to make at least two local color judgments, each of which requires a comparison of the outputs of at least two different cone types. This perforce limits spatial acuity for patterns that vary only in color.

Spatial vision at isoluminance

SPATIAL CONTRAST SENSITIVITY One of the most basic measures of spatial vision is the spatial contrast sensitivity function (CSF). To characterize the spatial CSF, the minimum amount of contrast required to detect a sinusoidal grating is measured at each of several spatial frequencies (where spatial frequency is defined in terms of cycles per degree visual angle, and contrast sensitivity is the reciprocal of the minimum detectable contrast). The spatial CSF for luminance, measured at photopic light levels in the central retina, is a bandpass function of spatial frequency (see De Valois and De Valois, 1988, for references). Sensitivity is highest for spatial frequencies in the range of about 2 to 5 c/deg and falls to zero by about 50 to 60 c/deg. There is a pronounced decline in sensitivity at the lower spatial frequencies as well.

When the grating to be detected contains only color variations, however, with luminance held constant, the spatial CSF is quite different. Contrast sensitivity is a low-pass function of spatial frequency, with no decline in sensitivity at lower spatial frequencies (Granger and Heurtley, 1973; Kelly, 1983; McKeefry et al., 2001; Mullen, 1985; van der Horst and Bouman, 1969; van der Horst et al., 1967). The fall-off in sensitivity at high frequencies is rapid. Contrast sensitivity falls to zero at lower spatial frequencies than is found with luminance-varying gratings. Both the high-frequency cutoff and the overall sensitivity level depend on the chromatic axis studied. When the pattern varies along a color axis in which there are equal and opposite variations in absorption by L and M cones, the high-frequency cutoff is lower than that seen for luminance-varying gratings, but it is reliably higher than that found with S-cone-varying gratings (McKeefry et al., 2001).

When the grating is defined solely by variations in absorption in the S cones (i.e., it lies along a tritanopic confusion axis), the high-frequency cutoff occurs below 10 c/deg (e.g., McKeefry et al., 2001). This can be understood by considering the small number of S cones (only about 7% of the total number of cones in the retina; Curcio et al., 1991) and their distribution. S cones are quite rare in the foveola, reach their peak density at an eccentricity of about 1 degree, and fall off very gradually as eccentricity increases. At no eccentricity is their density high enough to support fine spatial resolution.

Figure 59.1 illustrates the differences among the spatial CSFs for luminance and for two chromatic axes, one defined by the difference in absorption along an L-M cone axis (labeled *0 deg*) when S-cone absorption is held constant and the other by differences along an S-cone axis (labeled *90 deg*) when LM-cone absorption is held constant. In this illustration, the logarithm of contrast sensitivity is normalized such that all three functions are equated at their points of

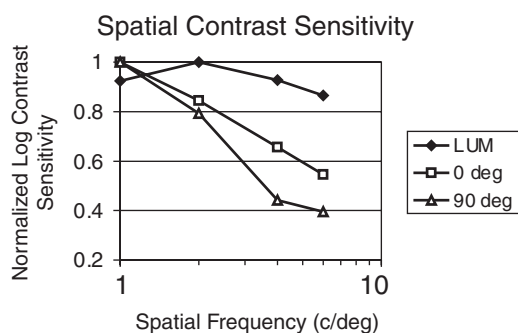


FIGURE 59.1. Normalized spatial contrast sensitivity functions. *Filled diamonds* show data from tests with luminance-varying gratings. *Open squares* represent an isoluminant axis differencing the output of L and M cones (labeled *0 deg*). *Open triangles* show data from tests in which gratings varied only in S-cone absorption (labeled *90 deg*). Note that the luminance function shows attenuation at the lowest spatial frequency, and that the S-cone function loses sensitivity at high spatial frequencies more rapidly than either of the other two functions.

maximum sensitivity. This allows a more direct comparison of their shapes. Note three things. First, the luminance CSF shows attenuation at the lowest spatial frequency. Had the function been extended to still lower frequencies, sensitivity would continue to decrease. Second, the two chromatic CSFs are low-pass. Both continue to increase in contrast sensitivity as the spatial frequency falls. Third, the fall-off in sensitivity at high spatial frequencies is more rapid for the S-cone axis than for the LM-cone axis.

The fact that we cannot detect isoluminant color-varying patterns of high spatial frequencies implies that the color system cannot contribute greatly to our perception of fine spatial detail. Reading fine print, for example, can only be done when there is sufficient luminance contrast between the letters and their background. This is less of a hindrance than might be supposed, since much of the most critical information in vision is carried in the medium and low spatial frequency components of scenes (e.g., Marron and Bailey, 1982). Thus, the color vision system that underlies vision at isoluminance could participate significantly in the detection and analysis of spatial pattern variations, despite its inability to encode high spatial frequency information.

The lack of a reduction in contrast sensitivity in the low spatial frequencies for isoluminant color-varying patterns can be understood by reference to the receptive field structure of color-opponent neurons in the retinogeniculate pathway (De Valois and De Valois, 1975; also see Chapter 65). The consequence is that as spatial frequency decreases beyond about 2 c/deg, the signal carried by the color system becomes increasingly strong while that from the luminance system becomes weaker. This can be best understood by reference to a diagram of the cone input map for a color-opponent cell.

The upper panel of Figure 59.2 illustrates the cone inputs to a typical color-opponent cell in the retina or the lateral geniculate nucleus (LGN) of the thalamus. In this neuron, there is an excitatory input from L cones in the receptive field (RF) center and an inhibitory input from M cones in the RF surround. The lower panel shows the separate RFs for color variations and for luminance variations. When the color changes from, say, white to an isoluminant red, the L cones absorb relatively more (producing excitation in the center mechanism), while the M cones absorb relatively less. Since the amount of inhibition produced by the M cones is a function of the number of photons they absorb, as the light

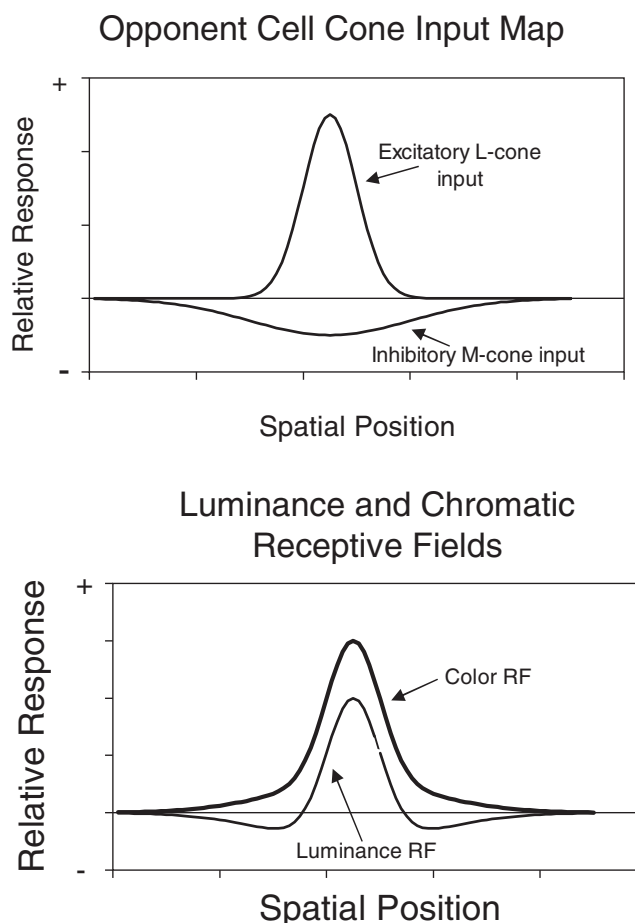


FIGURE 59.2. Color and luminance receptive fields. The *upper panel* shows the cone-input map from a +L center, -M surround opponent cell in the LGN. The L-cone input to the center mechanism is more powerful but restricted to a smaller region. The M-cone input to the concentric surround is weaker but covers a larger region. The center input here is excitatory to light increments, while the surround input is inhibitory to light increments. The *lower panel* illustrates the receptive fields for luminance variations (*thin line*) and for isoluminant color variations (*thick line*). Note that the color RF is excitatory across its entire extent. A color change produces the same kind of response at all locations. The luminance RF is excitatory for an increment in the center but inhibitory for an increment in the surround.

shifts from white to an isoluminant red, the amount of inhibition produced by the M-cone surround decreases. The net response of the neuron is the sum of its excitatory center response and its inhibitory surround response. Thus, anything that either increases the center response or decreases the surround response will cause a net increase in the neuron's excitatory output, and increasing the width of a red stimulus bar centered on the RF will increase total excitation all across the RF.

When the stimulus is a luminance increment, not a color change, however, the spatial receptive field is quite different. When a narrow bright bar is flashed on the RF center, it produces more excitation from the center mechanism *and* more inhibition from the surround mechanism. Since the center mechanism is more sensitive in the RF center, however, the net change in the neuron's response will be positive. Once the size of the bar exceeds that of the center mechanism, however, increasing its width even more will produce still more inhibition from the surround with no compensatory increase in excitatory response. Thus, the net response will decrease. Mapping the entire RF with a small spot would thus produce a center-surround function for a luminance change. This neuron would show its peak response to a luminance grating at some intermediate frequency, but its response to isoluminant chromatic gratings would be low-pass.

Although it is not entirely clear how best to compare color contrast and luminance contrast, Chaparro et al. (1993) have shown that on the basis of cone contrast comparisons, we are significantly more sensitive to color variations at low spatial frequencies than to luminance variations. Color vision thus assumes greater relative importance in the analysis of low spatial frequency information.

SPATIAL FREQUENCY AND ORIENTATION CHANNELS At early levels in the visual system, the luminance system performs parallel local spatial analyses using mechanisms (channels, for short) that are selective for spatial frequency (see De Valois and De Valois, 1988, for discussion). The luminance channels are bandpass for spatial frequency and orientation, as can be demonstrated with pattern adaptation (Blakemore and Campbell, 1969) or spatial masking (Legge and Foley, 1980). Adaptation to a luminance-varying grating of a single spatial frequency, for example, produces a temporary reduction in contrast sensitivity for similar gratings whose spatial frequencies lie within about ± 0.75 octave of the adaptation grating. A high-contrast mask of one spatial frequency will reduce the detectability of a simultaneously presented grating of a spatial frequency that is within about ± 1.25 octaves of the mask frequency. When stimuli vary only in color, not in luminance, similar adaptation and masking phenomena are seen. Adaptation to an isoluminant red-green sinusoidal grating of one spatial frequency produces a tem-

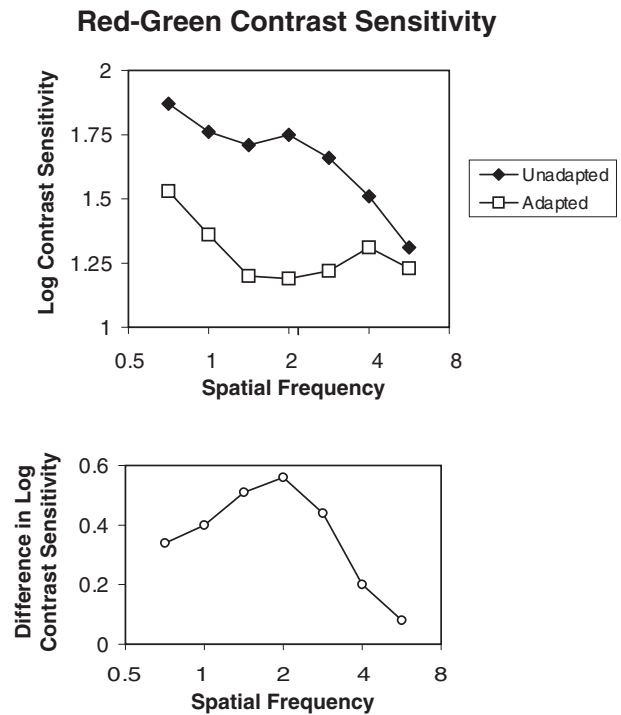


FIGURE 59.3. Pattern adaptation for an isoluminant grating. The *upper panel* shows spatial contrast sensitivity functions for isoluminant red-green gratings before and after adaptation to a 2 c/deg red-green grating. The *lower panel* plots the difference between the functions above. Note that the effect of adaptation is band-limited and centered on the adaptation frequency.

porary loss in contrast sensitivity to red-green test gratings of the same or similar frequencies but no loss in sensitivity to frequencies further removed (Bradley et al., 1988). The frequency spread of the adaptation effect for color is only slightly greater than that seen following adaptation to luminance-varying gratings. Similarly, adaptation to a vertical red-green isoluminant grating is followed by a temporary reduction in contrast sensitivity for similar vertical and near-vertical gratings but not for horizontal gratings (Bradley et al., 1988). As with spatial frequency, the spread in orientation is somewhat broader for adaptation to isoluminant chromatic gratings than to luminance-varying gratings, but the difference is not great.

The upper panel of Figure 59.3 shows spatial contrast sensitivity functions for a red-green grating measured before (filled symbols) and after (open symbols) adaptation to a 2 c/deg red-green grating. In the lower panel, the difference between the two functions is plotted. Note that the loss in sensitivity is band-limited and centered on the adaptation frequency.

Pattern masking results show a similar relationship between luminance and color vision. When a sinusoidal test grating is detected in the presence of a masking grating that is identical in every respect save contrast, the detection

contrast threshold for the test can be markedly affected. If the mask is at or below its own detection threshold, the contrast required to detect the presence of the test will be reduced (Legge and Foley, 1980), a result referred to as *sub-threshold summation*. If the mask contrast is well above threshold, however, the contrast required to detect the test will be increased. A similar relationship between mask contrast and test threshold holds when the mask and test are isoluminant chromatic gratings, identical except in contrast (Chen et al., 2000a; Losada and Mullen, 1994; Switkes et al., 1988). As with bandwidths estimated from adaptation studies, the frequency selectivity of spatial masking is similar for both color and luminance. These results, like those from the adaptation studies described earlier, demonstrate that the color vision system alone can support spatial analysis and that it is functionally similar to the luminance vision system.

Another indication of how well a particular mechanism can support spatial vision is the accuracy with which it can discriminate between two patterns that differ slightly in spatial frequency or orientation. When sinusoidal gratings vary in luminance, both spatial frequency and orientation discrimination are exquisitely fine (see De Valois and De Valois, 1988, or Webster et al., 1990, for relevant references). When the stimuli vary in chromaticity with no associated luminance variation, observers can still make surprisingly fine distinctions. A practiced subject can discriminate between two high-contrast isoluminant color-varying gratings that differ in spatial frequency by only 4% or in orientation by as little as 1 degree (Webster et al., 1990). When the grating spatial frequency is low and the contrast is high, the thresholds for discrimination of the spatial frequency or orientation of gratings that vary along an S-cone (tritanopic) axis do not differ significantly from those that vary along an L-M axis. Discrimination thresholds for both chromatic cardinal axes are slightly but reliably higher than comparable measures for gratings that vary in luminance.

Two primary conclusions can be drawn from these data. First, the mechanisms that process information about color variations in the absence of luminance are similar in organization to the luminance system, at least at intermediate levels in the visual system. They comprise a set of channels that are bandpass for both spatial frequency and orientation. Second, their selectivity along both spatial frequency and orientation dimensions is only slightly coarser than that of the comparable luminance mechanisms. This suggests that the color vision system is capable of significant spatial pattern analysis in the absence of luminance contrast. The requisite early-level processing is clearly available. These data do not, of course, provide any indication of the frequency with which naturally occurring spatial patterns differ in color with no associated luminance variations, or vice versa. It is unlikely that isoluminant patterns occur often in nature or extend greatly in either space or time.

DEPTH One important task for spatial vision is that of determining how far an object of interest is from the observer. Distance (depth) is critical in navigation, in determining whether or how to escape from a predator, capture prey, grasp food, and many other actions. The two-dimensional retinal image, however, reflects visual direction but does not directly represent depth. That must be derived.

There are both binocular and monocular cues to depth. The images of a scene in the two eyes are similar but not identical, and binocular disparity, the small differences between these two images, is the stimulus for stereopsis. Stereopsis has been widely studied by the use of random-dot stereograms (Julesz, 1971), patterns of randomly positioned dots in which some subset of target dots is slightly displaced horizontally in the pattern presented to one eye with respect to the same subset in the stimulus to the fellow eye. To an observer with normal stereopsis, the target dots will appear at a different depth (or distance) than those in the background, even though the image contains no monocular cues to depth.

The question of whether stereopsis occurs at isoluminance with random-dot stereograms has occasioned some dispute. Some studies (e.g., Livingstone and Hubel, 1987; Lu and Fender, 1972) have failed to find evidence for the perception of depth in random-dot stereograms at isoluminance. Others (e.g., de Weert and Sadza, 1983; Kingdom and Simmons, 1996; Scharff and Geisler, 1992; Simmons and Kingdom, 1995) have found that depth *can* be perceived in isoluminant random-dot stereograms. Kingdom et al. (1999) suggest that the specific impairment found with random-dot stereograms at isoluminance is more related to the perception of three-dimensional form than of depth per se.

Although stereopsis is perhaps the most widely studied cue to depth, it is often less important than the monocular depth cues in a scene. Many kinds of information in a visual image give information about the distance of objects, either absolute or relative. For example, if one object occludes the image of another, the occluding object must be closer to the observer than the partially hidden object. Although there have been reports that depth from monocular cues disappears at isoluminance (Livingstone and Hubel, 1987), other reports suggest that depth can be signaled at isoluminance by such monocular cues as texture gradients (Troscianko et al., 1991) and motion parallax (Cavanagh et al., 1995). The preponderance of the evidence suggests that the color vision system does carry some information about depth. However, the perception of depth in the absence of luminance contrast appears to be significantly compromised.

GEOMETRICAL ILLUSIONS Under many circumstances, the visual world as we perceive it differs significantly from the world as we measure it. One class of such anomalous per-

ceptions, known as *geometrical illusions*, has often been studied for the insights it provides into the visual processing mechanisms. Livingstone and Hubel (1988) examined several stimuli associated with geometrical illusions and concluded that the illusions either disappeared or were greatly reduced in magnitude when the stimuli were defined by color contrast in the absence of luminance contrast. Li and Guo (1995), on the other hand, measured illusion magnitudes for illusions of orientation (Zöllner), length (Müller-Lyer), and size (Delboeuf) and found no difference between patterns defined by luminance versus color contrast. However, they found that luminance contrast was necessary for the occurrence of various border and contour illusions such as the Kanisza triangle. The illusory figures disappeared completely at isoluminance. It is tempting to suggest that the resistance of the color vision system to such perceptual errors provides the observer with a useful check on the accuracy of perceptions of spatial patterns, but evidence for this argument is lacking.

RELATIVE POSITION One important task in spatial vision is the determination of the relative positions of different objects in the visual field. The precision with which this can be accomplished with luminance-varying targets is astonishing (e.g., Westheimer and McKee, 1977). Positional misalignments smaller than the diameter of a single cone can be reliably discriminated in the vernier acuity task, for example. Whether the color vision system can support fine judgments of relative position is an interesting question. The small, localized stimuli with which fine alignment hyperacuity is typically demonstrated are not appropriate for use at isoluminance, both because of the eye's chromatic aberration (which introduces unintended artifacts in such patterns) and because of the relative insensitivity of the chromatic system to high spatial frequencies. It is possible, however, to measure positional alignment using other kinds of targets that are more suitable for the color vision mechanisms, such as two-dimensional Gaussian blobs or Gabor patterns (a sine wave windowed by a Gaussian function) that vary only in color. When these stimuli are used and equated for detectability, comparable levels of performance are found whether the stimuli vary in luminance or in color (Kooi et al., 1991; Krauskopf and Farell, 1991). Within the range of targets to which it is sensitive, then, color vision appears to be able to support judgment of spatial alignment about as well as can luminance vision.

HIGHER-ORDER TASKS One of the most complex but important tasks the visual system faces is that of integrating contours across space. The detection of an isolated object against a homogeneous background can be accomplished by a simple system with minimal processing capability, but linking multiple spatially separated elements correctly and

determining the contour along which they lie are very difficult indeed. If the color vision system is to play a significant role in spatial vision, it should be capable of contour integration. The failure to see illusory figures such as the Kanisza triangle at isoluminance (Li and Guo, 1995), however, suggests that color vision might lack the ability to integrate across separated sections of a contour.

Mullen and her colleagues (McIlhagga and Mullen, 1996; Mullen et al., 2000) have examined contour integration using stimuli that varied along either isoluminant red-green or blue-yellow chromatic axes or in luminance. The task required the perceptual linking of a set of oriented Gabor patterns in order to extract the curving path along which they were placed. The target elements, which had orientations that varied by specified amounts, were presented in a background of similar Gabor patterns of randomly chosen orientations. Subjects performed similarly on contour integration over a range of curvatures, whether stimuli were defined by luminance variations or by variations along either of the two chromatic axes used. The effects of contrast and external noise were also comparable whether the stimuli varied in luminance or in color. However, perceptual linking was compromised by changing either the color (or luminance) axis or the phase of the pattern from element to element. The authors suggested that the three mechanisms use a common contour integration process but that this process is not blind to either color or phase.

Another task closely related to contour integration is pattern segregation—in effect, determining which parts of a complex scene belong together. There are many methods of studying pattern segregation. One is to determine how rapidly a target can be detected in a noisy background; another is to ask whether subjects can judge some aspect (e.g., position or orientation) of a region that is defined by a limited number of dimensions, again in a noisy background. When the target differs significantly from its background in color, detection and segregation can be accomplished quickly and efficiently (e.g., D'Zmura, 1991; Gegenfurtner and Kiper, 1992; Li and Lennie, 1997; Nothdurft, 1993; Webster et al., 1998). Webster et al. (1998) used cluttered backgrounds that varied in color in a manner similar to the variation found in natural scenes. They found that prior adaptation to the color distribution of the background significantly affected the speed with which a color-defined target could be detected, depending upon the similarity of the target color to the background distribution. They suggested that adaptation to natural scenes can be an important factor in determining how efficiently visual targets are detected.

Another way to examine pattern segregation is to determine the conditions under which the superimposition of two gratings of different orientations is seen as forming a single, coherent plaid as opposed to two separate surfaces. If the

two gratings are similar in spatial frequency, contrast, and color, they will most often appear to form a single plaid pattern. If, however, they differ in color—one red and one green, for example—they will appear to be two different objects (Rauschecker et al., 1973) and will alternate in perceptual rivalry. If a similar plaid pattern is set in motion, it will likely appear to be a single, coherent surface moving in one direction if the two gratings have the same color. If they differ in color, however, they will appear to be two transparent surfaces moving in different directions (Kooi et al., 1992).

These and many other studies have demonstrated that the color vision system has significant spatial abilities. It is organized in a manner similar to that of the luminance system, parsing a complex visual scene by multiple spatial frequency and orientation channels that operate in parallel. It can support many of the higher-level tasks important for a versatile visual system. However, in almost every case, performance is somewhat poorer when the stimuli are isoluminant than when they are defined by luminance contrast.

These demonstrations of the capabilities of the color vision system at isoluminance are useful because they reveal the extent to which color variations alone can be used to determine the spatial characteristics of the visual world. They reflect both the strengths and the limitations of color vision, and they reveal much about the manner in which the color system carries out spatial analyses. However, they are not necessarily relevant to vision as it normally operates. In nature, virtually all scenes contain both color contrast and luminance contrast. It is rare indeed to find any extended natural scene in which color varies but luminance is constant. So understanding the role that color actually plays in spatial vision requires a different approach.

Consider images drawn from nature. Objects typically differ from their backgrounds in both chromaticity and luminance, and a chromatic border will most often also contain luminance contrast. A joint color-luminance border is likely to indicate a change in surface reflectance and thus an object property of interest. The presence of a luminance border with no associated color change, however, is less often indicative of a reflectance border. Because we live in a three-dimensional world that is primarily illuminated by a directional light source (the sun), objects cast shadows. The luminance contrast across a shadow border can be quite high, often as high as the luminance contrast across reflectance borders. The presence of shading can be used as a cue to the three-dimensional structure of a scene (see, e.g., Cavanagh and Leclerc, 1989), but it can also be misleading with respect to object borders. The segregation of a complex scene into discrete objects and surfaces is among the first and most critical tasks the visual system faces at higher processing levels. If it is accomplished on the basis of contours regardless of how they are specified, then the presence of

shadow borders can lead to errors. Chromaticity is not strictly invariant across a shadow border, due to both Rayleigh scattering and reflection from nearby surfaces, but variations in chromaticity are usually small compared to the variations in luminance across shadow borders, and they are rarely apparent. Salient color borders thus may provide an alternative and more reliable indicator of how a visual scene should be segregated when both color and luminance vary.

Spatial vision with both color and luminance variations

It is useful to consider both what is known about the characteristics of spatial vision when both color and luminance variations are present and what advantages might accrue from the ability to discriminate color differences in the presence of luminance differences. Gur and Akri (1992), among others, have suggested that studies of isoluminant stimuli in isolation may fail to reveal the full contribution of color to spatial vision. Even if one assumes that the visual system treats color and luminance as separate dimensions, the question of how they interact, if at all, is important. It is well known, for example, that making brightness judgments between two stimuli that differ in hue is difficult (though subjects can do it reliably). This suggests that color differences might interfere with the coding of luminance information. Several studies have raised the question of how color- and luminance-coding systems might interact. Some of these will be reviewed briefly below.

ADAPTATION One way of addressing the question directly is to use the same adaptation and masking techniques that have been used to characterize mechanisms within a single dimension. For example, subjects can adapt to a high-contrast luminance-varying grating and then measure the detectability of a color-varying grating of the same spatial frequency, or vice versa. Bradley et al. (1988) compared the effects of cross-adaptation between color and luminance to adaptation and testing with the same stimuli. They found little transfer in either direction from one dimension to the other, even though the adaptation stimuli produced significant losses in sensitivity to test stimuli of the same contrast type (i.e., color or luminance). This result is compatible with a model of separate and largely independent dimensions for color and luminance, but other results (see below) suggest that the relationship is more complex.

SUPRATHRESHOLD MASKING When a suprathreshold grating masking paradigm is used, both color- and luminance-varying masking gratings reduce the detectability of superimposed test gratings of the other dimension (Chen et al., 2000a; De Valois and Switkes, 1983; Mullen and Losada, 1994; Switkes et al., 1988). In the case of a luminance mask and a color-varying test, however, the mask must be of

high contrast, significantly above its own detection threshold, before it begins to produce masking. An isoluminant color-varying mask, on the other hand, reduces the detectability of a superimposed luminance-varying test grating as soon as the mask is visible. Suprathreshold masking is consistent with either of two classes of models. If the mask and test gratings are detected by the same underlying mechanism, then cross-dimensional suprathreshold masking should occur in the same manner as masking when mask and test are drawn from the same contrast dimension (both luminance-varying, for example). However, if stimuli drawn from the two dimensions are processed by separate mechanisms, then cross-dimensional suprathreshold masking might reflect inhibitory interactions between the two mechanisms.

LOW-CONTRAST SUMMATION OR FACILITATION One way of examining these two models is to determine whether subthreshold summation occurs. If two stimuli are processed by the same underlying mechanism, then a half-threshold amount of one added to a half-threshold amount of the other should produce a threshold response. Consider, for example, a single receptor containing a single photopigment. The only information the receptor can report is the total number of photons it has absorbed. Suppose that it produces a criterion response when it absorbs 100 photons. If that receptor absorbs 10% of the incident photons at 600 nm and only 5% of the incident photons at 450 nm, then it should be possible to produce the same criterion response by either exposing it to 1000 photons of 600 nm light, or 2000 photons of 450 nm light, or a combination of 500 photons of 600 nm light and 1000 photons of 450 nm light. If the responses to the two wavelengths add linearly, then which combination of 600 nm and 450 nm light is used to produce a 100-photon absorption will be irrelevant.

A similar argument can be applied to the summation of subthreshold color-varying and luminance-varying stimuli. If they are processed by the same mechanism, the responses they produce should add and subthreshold summation should appear. The detection of a test stimulus should be facilitated by the presence of a low-contrast mask (or pedestal) irrespective of whether it varies in color or in luminance. Thus, it is instructive to determine what test contrast is required for detection when the mask pattern is below or near its own detection threshold. This question was first addressed by Switkes et al. (1988), using red-green isoluminant gratings and luminance-varying gratings matched in space-averaged chromaticity, luminance, and spatial frequency. When the mask varied in luminance and the test was isoluminant red-green, the contrast masking function was dipper-shaped—that is, it showed both facilitation with low-contrast pedestals and masking at high-mask contrasts. The contrast masking function, however, was not identical to that

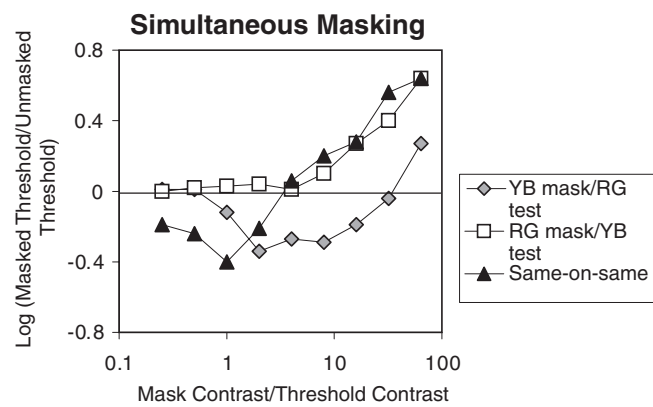


FIGURE 59.4. Simultaneous spatial masking. Mask and test gratings were either isoluminant red-green or luminance-varying yellow-black. When mask and test gratings were the same (i.e., both red-green or both yellow-black), the usual dipper-shaped function was seen (*filled triangles*). When the mask was yellow-black and the test was red-green, facilitation (increase in sensitivity) occurred over a broad range of contrasts (*gray diamonds*). When the mask was isoluminant red-green and the test was yellow-black, there was no facilitation (*open squares*). Masking increased with mask contrast once the mask exceeded its own detection threshold.

found when test and mask both varied in color or in luminance. Facilitation in the detection of the red-green isoluminant grating occurred over a broad range of low to medium pedestal contrasts but not when the pedestal was actually subthreshold. Only when the mask contrast was quite high did its presence impede the detection of the color-varying test grating.

When the mask was isoluminant red-green and the test was luminance-varying, however, a very different masking pattern appeared. A low-contrast red-green pedestal never reduced the contrast threshold for detecting a superimposed luminance-varying test grating, but once the color-varying mask exceeded its own threshold, it began to reduce the detectability of the luminance-varying test. This rather surprising result has been confirmed and extended to other chromatic axes (Chen et al., 2000a), though Mullen and Losada (1994), using different stimuli and presentation modes, found facilitation for detecting a luminance test at somewhat higher contrasts of a red-green mask.

Figure 59.4 illustrates simultaneous spatial masking functions for color and luminance gratings. The filled triangles show the dipper-shaped function obtained with either red-green masks and red-green tests or yellow-black masks and yellow-black test patterns. Both conditions produce essentially identical results, with facilitation at very low mask contrasts and reduction in sensitivity at higher mask contrasts. The gray diamonds show results from tests with yellow-black masks and red-green test gratings. There is facilitation over a broad range of mask contrasts, with a reduction in sensitivity to the test appearing only at quite high mask contrasts.

The open squares show the results of masking detection of a yellow-black test grating by a red-green mask. There is no increase in test detection sensitivity at any mask contrast. Once the mask exceeds its own detection threshold, it begins to make the test more difficult to detect, and the masking effect increases with mask contrast.

Chen et al. (2000b) have modeled the mechanisms underlying the full contrast range of cross-masking results and conclude that they are well fit by a model incorporating cross-mechanism divisive inhibition and a weak excitatory input from a luminance mechanism into the chromatic channels but no excitation from chromatic mechanisms into the luminance channel. Mullen et al. (1997), on the other hand, looked carefully for subthreshold summation between red-green and luminance mechanisms at detection thresholds, using a summation square analysis. They account for their results by a model positing chromatic and luminance mechanisms that are independent at threshold but that demonstrate probability summation.

HUE-SELECTIVE INTENSITY-CODING MECHANISMS Our discussion to this point has been cast in terms of two separate systems, one that encodes luminance variations and one that encodes chromatic variations. Another possibility is that there are mechanisms that respond to intensity variations, but that do so in a hue-selective manner. Hue selectivity implies that these are not traditional luminance mechanisms, hence the term *intensity coding*. There is a clear substrate of hue-selective neurons that respond vigorously to either color variation or luminance variation, from the midretinal ganglion cells to the parvocellular layers of the LGN and through various cortical regions. It would be surprising if the information they carry about intensity variations were simply discarded, but these color-selective neurons do not respond to luminance contrast in a hue-insensitive manner. For example, an LGN neuron that receives excitatory input from an L cone to its center mechanism and inhibitory input from M cones to its surround will respond with excitation to a full-field intensity increment if the stimulus is shifted toward longer wavelengths. If the intensity increment is shifted toward shorter wavelengths, however, the neuron will be inhibited, not excited (De Valois and De Valois, 1975). These neurons cannot be described as coding luminance per se, since their spectral sensitivity functions differ substantially from the photopic spectral luminous efficiency function, V_λ . They may nonetheless be involved in coding information about patterns that vary in intensity.

If hue-selective intensity coding mechanisms are important in spatial vision, their presence might be revealed in detection experiments. In macaque monkeys, the selective loss of the parvocellular LGN layers that contain color-selective neurons produces a reduction in contrast sensitivity for luminance-varying patterns (Merigan, 1989; Schiller

et al., 1990). If a human observer is asked to detect a small spot defined by an intensity increment upon a background, the hue of the stimulus can sometimes be reported at threshold luminance contrasts (Hood and Finkelstein, 1983). Guth and his colleagues (Guth, 1967; Guth et al., 1969) found significant failures of heterochromatic luminance additivity at threshold when the test was a luminance increment against a dark background. These observations all demonstrate that the detection of luminance-varying stimuli is mediated by hue-selective mechanisms under some conditions. On the other hand, selective masking experiments have argued against the existence of mechanisms selective for, say, bright red or dark green (Stromeyer et al., 1999).

A compelling clinical case study (Rovamo et al., 1982) also provides evidence for the existence of hue-selective channels that encode information concerning intensity differences. The individual concerned temporarily lost the ability to see achromatic patterns that varied in luminance, but she retained essentially normal contrast sensitivity for luminance-varying gratings viewed through either rose- or green-colored filters. Visually evoked potential measures confirmed the selective nature of the loss.

Several kinds of higher-order psychophysical adaptation studies (Hardy and De Valois, 2002; Mayhew and Anstis, 1972; McCullough, 1965; Virsu and Haapasalo, 1973) demonstrate color-selective encoding of intensity variations. For example, alternating adaptation to, say, a bright red-dark red grating of 4 c/deg and a bright green-dark green grating of 1 c/deg will shift the apparent spatial frequency of subsequently viewed 2 c/deg gratings in opposite directions, depending upon the hue (red or green) of the test pattern (Hardy and De Valois, 2002). This suggests that there may be a partial separation of mechanisms that encode information about intensity-varying patterns that differ in hue. A similar dissociation of adaptation aftereffects has also been used to argue for the separation of color and luminance coding mechanisms (e.g., Favreau and Cavanagh, 1981).

Figure 59.5 demonstrates encoding by color-selective luminance mechanisms. The subject's task was to determine which of two spatially separated Gabor patterns appeared to be higher in spatial frequency. In an unadapted state, subjects can make such judgments both accurately and reliably. In this experiment, however, the subject had first adapted to alternating red and green luminance-varying Gabor patterns. When the screen was red, the pattern on the left was 1 c/deg and the one on the right was 4 c/deg; when the screen was green, the pattern on the left was 4 c/deg and that on the right was 1 c/deg. During the test phase, a 2 c/deg pattern was always presented on the left, while the spatial frequency of the test pattern on the right varied. The data show that the apparent spatial frequency of the test patterns was a function of their color. Red 2 c/deg patterns

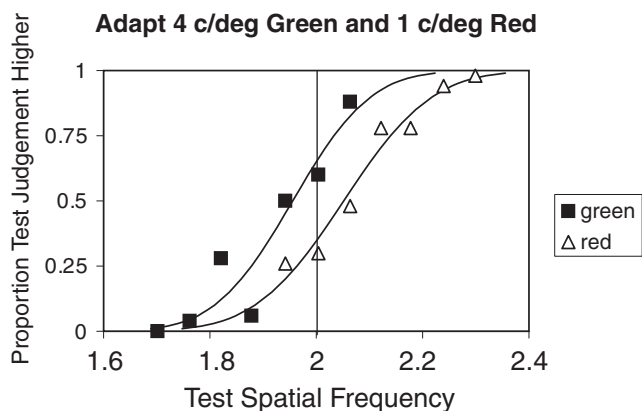


FIGURE 59.5. Color-selective change in apparent spatial frequency following differential adaptation to colored luminance-varying patterns. After adapting to a 1 c/deg bright red–dark red pattern alternating with a 4 c/deg bright green–dark green pattern, subsequently viewed 2 c/deg red test patterns (*open triangles*) appear shifted to higher spatial frequencies. Subsequently viewed 2 c/deg green test patterns (*filled squares*) appear shifted to lower spatial frequencies. Adaptation and test patterns were presented in the same retinal regions. See text for more details.

appeared to be shifted to still higher spatial frequencies, but green 2 c/deg patterns appeared to be shifted to lower spatial frequencies. Recall that all patterns, whether adaptation or test, varied only in luminance. They differed from each other (i.e., over time) in color, but at any given time, only one color was present on the screen. These data support the idea of color-selective luminance-encoding mechanisms.

The advantages of color for spatial vision

We have considered the extent to which the color vision system can support the tasks of spatial vision, the characteristics and limitations of spatial vision based solely upon color differences, the interactions between the traditionally conceived luminance system and the color vision mechanisms, and the possibility of hue-selective intensity encoding. However, a major puzzle remains. The primate visual system has made an extraordinarily large neural investment in color vision, which is among our finest visual abilities. Yet there is little agreement as to the basic functions that color vision serves. Color certainly adds beauty and interest to the visual world, yet it seems unlikely that we evolved such an elaborate mechanism primarily for aesthetic purposes. What then could be the advantages it confers upon those who possess it? Determining the presence, position, and nature of objects in the visual world—the essence of spatial vision—is surely among the most critical tasks of the visual system, and it seems highly likely that color vision plays a role in this most basic function. There are several ways in which adding color information could make spatial vision more effective.

Color vision can make foraging for food easier (Mollon, 1989). Frugivorous species, for example, must both detect their food and judge its state of ripeness. Since many fruits change color as they ripen, detecting them among foliage of a different color and accurately judging their state of ripeness is easier when color can be used as a cue. Any ability that increases one's success in foraging for food clearly provides an evolutionary advantage.

Another use for color vision is conspecific communication. Many species signal either gender or sexual receptivity by color. Finding a mate would in that case be simpler if the animal possesses color vision. Other species—notably humans—communicate emotion by color changes. Anger and embarrassment, for example, can be detected by the accompanying facial flush.

Color vision can be of significant assistance in the critical task of segmenting the visual world because color borders are more reliable indicators of reflectance edges than are luminance borders. Color differences profoundly affect the way in which we segregate moving patterns and thus how we perceive the motion direction (Kooi et al., 1992). Segregating objects on the basis of color differences reduces the ambiguities resulting from shadows in our three-dimensional world. Similarly, an object that differs significantly from its surround in color can be preattentively detected. Color then can be used to draw the attention of an observer. The effectiveness of color in drawing attention can be inferred from the existence of species that use color changes for purposes of camouflage.

Gegenfurtner and Rieger (2000) argue that color contributes both to the encoding of pattern information and to its retrieval in pattern recognition. They demonstrated that colored images of natural scenes are more accurately recognized than luminance-matched black-white images of the same scenes. They found that color provided an advantage in both the initial encoding stage and the later recognition of the same scenes. They suggest that the addition of color contributes to an enhancement of the memory representation of a complex scene. This interesting suggestion emphasizes the role of color in higher cognitive functions as well as in early pattern segmentation.

Color vision differs from luminance vision in certain respects that may be particularly important with respect to higher cognitive functions. Luminance is a one-dimensional continuum, and its perceptual aspect (brightness or lightness) is not easily categorized. Beyond the classification into bright, dark, and medium brightness, it is difficult to describe or to commit to memory the perceptual qualities associated with variations in luminance. Color is three-dimensional, comprising the perceptual aspects of hue, saturation, and brightness. Although two of these dimensions, saturation and brightness, are similar to luminance in being resistant to categorization in themselves, hue is different. A minimum of

four categories (red, green, blue, and yellow, the unique hues of Ewald Hering) are required to describe hues, and we possess other color names in abundance. Without prompting, normal observers typically use about 11 names to classify the colors of reflective objects (Berlin and Kay, 1969; Boynton and Olson, 1990). Some color names (orange, for example) represent a combination of basic hues; others reflect some combination of the three color dimensions (e.g., pink, a desaturated red). If information about a spatial pattern must be stored in memory for later retrieval, its color can be easily coded by reference to a common color category. This is surely easier than trying to encode its position along a continuum such as brightness. In addition, in a species possessing complex language, the communication involved in identifying information about objects is easier when spatial attributes can be joined with color attributes in the description. It sets the conditions necessary for identifying—in effect, recognizing—a previously unseen object.

Color vision thus serves many functions in the visual perception of spatial patterns. It supports the spatial analysis of patterns that contain only color contrast, though these are uncommon in nature. Color vision aids in the segregation of complex visual scenes, in the detection and identification of objects of interest, and in conspecific communication. It simplifies encoding and retrieving from memory information about objects and scenes, and it provides a means of categorizing and thus efficiently describing objects. Although we can analyze patterns without color vision, the addition of color to spatial vision enriches us.

Acknowledgments

The preparation of this chapter and much of the research on which it was based were supported by grants from the National Science Foundation, the National Eye Institute, the Nippon Telegraph and Telephone Corporation, and the University of California Committee on Research. I thank Wendy Davis and Michael Disch for assisting in the background research for the preparation of this chapter.

REFERENCES

- Berlin, B., and P. Kay, 1969. *Basic Color Terms: Their Universality and Evolution*, Berkeley: University of California Press.
- Blakemore, C., and F. Campbell, 1969. On the existence of neurones in the human visual system selectively sensitive to the orientation and size of retinal images, *J. Physiol. (Lond.)*, 203:237–260.
- Boynton, R. M., and C. X. Olson, 1990. Salience of chromatic basic color terms confirmed by three measures, *Vis. Res.*, 30:1311–1317.
- Bradley, A., E. Switkes, and K. K. De Valois, 1988. Orientation and spatial frequency selectivity of adaptation to colour and luminance gratings, *Vis. Res.*, 28:841–856.
- Cavanagh, P., and Y. Leclerc, 1989. Shape from shadows, *J. Exp. Psychol.: Hum. Percept. Perform.*, 15:3–27.
- Cavanagh, P., S. Saida, and J. Rivest, 1995. The contribution of color to depth perceived from motion parallax, *Vis. Res.*, 35:1871–1878.
- Chaparro, A., C. F. Stromeyer, E. P. Huang, R. E. Kronauer, and R. T. Eskew, 1993. Colour is what the eye sees best, *Nature*, 361:348–350.
- Chen, C.-C., J. M. Foley, and D. H. Brainard, 2000a. Detection of chromoluminance patterns on chromoluminance pedestals I: threshold measurements, *Vis. Res.*, 40:773–788.
- Chen, C.-C., J. M. Foley, and D. H. Brainard, 2000b. Detection of chromoluminance patterns on chromoluminance pedestals II: model, *Vis. Res.*, 40:789–803.
- Curcio, C. A., K. A. Allen, K. L. Sloan, C. L. Lerea, J. B. Hurley, I. B. Klock, and A. N. Milam, 1991. Distribution and morphology of human cone photoreceptors stained with anti-blue opsin, *J. Comp. Neurol.*, 312:610–624.
- De Valois, K. K., and E. Switkes, 1983. Simultaneous masking interactions between chromatic and luminance gratings, *J. Opt. Soc. Am.*, 73:11–18.
- De Valois, R. L., and K. K. De Valois, 1975. Neural coding of color, in *Handbook of Perception: Seeing*, vol. 5 (E. C. Carterette and M. P. Friedman, eds.), New York: Academic Press, pp. 117–166.
- De Valois, R. L., and K. K. De Valois, 1988. *Spatial Vision*, New York: Oxford University Press.
- de Weert, C. M. M., and K. J. Sadza, 1983. New data concerning the contribution of colour differences to stereopsis, in *Colour Vision* (J. D. Mollon, and L. T. Sharpe, eds.), London: Academic Press, pp. 553–562.
- D’Zmura, M., 1991. Color in visual search, *Vis. Res.*, 31:951–966.
- Favreau, O., and P. Cavanagh, 1981. Color and luminance: independent frequency shifts, *Science*, 212:831–832.
- Gegenfurtner, K. R., and D. C. Kiper, 1992. Contrast detection in luminance and chromatic noise, *J. Opt. Soc. Am. A*, 9:1880–1888.
- Gegenfurtner, K. R., and J. Rieger, 2000. Sensory and cognitive contributions of color to the recognition of natural scenes, *Curr. Biol.*, 10:805–808.
- Granger, E. M., and J. C. Heurtley, 1973. Visual chromaticity-modulation transfer function, *J. Opt. Soc. Am.*, 63:1173–1174.
- Gur, M., and V. Akri, 1992. Isoluminant stimuli may not expose the full contribution of color to visual functioning: spatial contrast sensitivity measurements indicate interaction between color and luminance processing, *Vis. Res.*, 32:1253–1262.
- Guth, S. L., 1967. Nonadditivity and inhibition among chromatic luminances at threshold, *Vis. Res.*, 7:319–327.
- Guth, S. L., N. J. Donley, and R. T. Marrocco, 1969. On luminance additivity and related topics, *Vis. Res.*, 9:537–575.
- Hardy, J. L., and K. K. De Valois, 2002. Color-selective analysis of luminance-varying stimuli, *Vis. Res.*, 42:1941–1951.
- Hood, D. C., and M. A. Finkelstein, 1983. A case for the revision of textbook models of color vision: the detection and appearance of small brief lights, in *Colour Vision: Physiology and Psychophysics* (J. D. Mollon and L. T. Sharpe, eds.), London: Academic Press, pp. 385–398.
- Julesz, B., 1971. *Foundation of Cyclopean Perception*, Chicago: University of Chicago Press.
- Kelly, D. H., 1983. Spatiotemporal variation of chromatic and achromatic contrast threshold, *J. Opt. Soc. Am.*, 73:742–750.
- Kingdom, F. A. A., and D. R. Simmons, 1996. Stereoacuity and colour contrast, *Vis. Res.*, 36:1311–1319.

- Kingdom, F. A. A., D. R. Simmons, and S. Rainville, 1999. On the apparent collapse of stereopsis in random-dot-stereograms at isoluminance, *Vis. Res.*, 39:2127–2141.
- Kooi, F. L., R. L. De Valois, and E. Switkes, 1991. Spatial localization across channels, *Vis. Res.*, 31:1627–1631.
- Kooi, F. L., K. K. De Valois, E. Switkes, and D. G. Grosf, 1992. High-order factors influencing the perception of sliding and coherence of a plaid, *Perception*, 21:583–598.
- Krauskopf, J., and B. Farell, 1991. Vernier acuity: effects of chromatic content, blur and contrast, *Vis. Res.*, 31:735–749.
- Legge, G. E., and J. M. Foley, 1980. Contrast masking of human vision, *J. Opt. Soc. Am.*, 70:1458–1471.
- Lennie, P., J. Pokorny, and V. Smith, 1993. Luminance, *J. Opt. Soc. Am. A*, 10:1283–1293.
- Li, A., and P. Lennie, 1997. Mechanisms underlying segregation of colored textures, *Vis. Res.*, 37:83–97.
- Li, C.-Y., and K. Guo, 1995. Measurements of geometric illusions, illusory contours and stereo-depth at luminance and colour contrast, *Vis. Res.*, 35:1713–1720.
- Livingstone, M., and D. H. Hubel, 1987. Psychophysical evidence for separate channels for the perception of form, color, movement, and depth, *J. Neurosci.*, 7:3416–3468.
- Livingstone, M., and D. H. Hubel, 1988. Segregation of form, color, movement, and depth: anatomy, physiology, and perception, *Science*, 240:740–749.
- Losada, M. A., and K. T. Mullen, 1994. The spatial tuning of chromatic mechanisms identified by simultaneous masking, *Vis. Res.*, 34:331–341.
- Lu, C., and D. H. Fender, 1972. The interaction of color and luminance in stereoscopic vision, *Invest. Ophthalmol. Vis. Sci.*, 11:482–490.
- Marron, J. A., and I. L. Bailey, 1982. Visual factors and orientation-mobility performance, *Am. J. Optom. Physiol. Opt.*, 59:413–426.
- Mayhew, J. E., and S. M. Anstis, 1972. Movement aftereffects contingent on color, intensity, and pattern, *Percept. Psychophys.*, 12:77–85.
- McCullough, C., 1965. Color adaptation of edge-detectors in the human visual system, *Science*, 149:1115–1116.
- McIlhagga, W. H., and K. T. Mullen, 1996. Contour integration with color and luminance contrast, *Vis. Res.*, 36:1265–1279.
- McKeefry, D. J., I. J. Murray, and J. J. Kulikowski, 2001. Red-green and blue-yellow mechanisms are matched in sensitivity for temporal and spatial modulation, *Vis. Res.*, 41:245–255.
- Merigan, W. H., 1989. Chromatic and achromatic vision of macaques: role of the P pathway, *J. Neurosci.*, 9:776–783.
- Mollon, J. D., 1989. “Tho’ she kneel’d in that place where they grew . . .,” *J. Exper. Biol.*, 146:21–38.
- Mullen, K. T., 1985. The contrast sensitivity of human colour vision to red-green and blue-yellow chromatic gratings, *J. Physiol. (Lond.)*, 359:382–400.
- Mullen, K. T., W. H. A. Beaudot, and W. H. McIlhagga, 2000. Contour integration in color vision: a common process for the blue-yellow, red-green and luminance mechanisms? *Vis. Res.*, 40:639–655.
- Mullen, K. T., S. J. Cropper, and M. A. Losada, 1997. Absence of linear subthreshold summation between red-green and luminance mechanisms over a wide range of spatio-temporal conditions, *Vis. Res.*, 37:1157–1165.
- Mullen, K. T., and M. A. Losada, 1994. Evidence for separate pathways for color and luminance detection mechanisms, *J. Opt. Soc. Am. A*, 11:3136–3151.
- Nothdurft, H.-C., 1993. The role of features in preattentive vision: comparison of orientation, motion and color cues, *Vis. Res.*, 33:1937–1958.
- Rauschecker, J. P., F. W. Campbell, and J. Atkinson, 1973. Colour opponent neurones in the human visual system, *Nature*, 245:42–43.
- Rovamo, J., L. Hyvärinen, and R. Hari, 1982. Human vision without luminance-contrast system: selective recovery of the red-green colour-contrast system from acquired blindness, *Doc. Ophthalmol. Proc. Ser.*, 33:457–466.
- Scharff, L. V., and W. S. Geisler, 1992. Stereopsis at isoluminance in the absence of chromatic aberrations, *J. Opt. Soc. Am. A*, 9:868–876.
- Schiller, P. H., N. K. Logothetis, and E. R. Charles, 1990. Role of the color-opponent and broad-band channels in vision, *Vis. Neurosci.*, 5:321–346.
- Simmons, D. R., and F. A. A. Kingdom, 1995. Differences between stereopsis with isoluminant and isochromatic stimuli, *J. Opt. Soc. Am. A*, 12:2094–2104.
- Stromeyer, C. F. III, R. Thabet, A. Chaparro, and R. E. Kronauer, 1999. Spatial masking does not reveal mechanisms selective to combined luminance and red-green color, *Vis. Res.*, 39:2099–2112.
- Switkes, E., A. Bradley, and K. K. De Valois, 1988. Contrast dependence and mechanisms of masking interactions among chromatic and luminance gratings, *J. Opt. Soc. Am. A*, 5:1149–1162.
- Troscianko, T., R. Montagnon, J. Le Clerc, E. Malbert, and P. L. Chanteau, 1991. The role of colour as a monocular depth cue, *Vis. Res.*, 31:1923–1929.
- Van der Horst, G. J., and M. A. Bouman, 1969. Spatiotemporal chromaticity discrimination, *J. Opt. Soc. Am.*, 59:1482–1488.
- Van der Horst, G. J., C. M. De Weert, and M. A. Bouman, 1967. Transfer of spatial chromaticity-contrast at threshold in the human eye, *J. Opt. Soc. Am.*, 57:1260–1266.
- Virsu, V., and S. Haapasalo, 1973. Relationships between channels for colour and spatial frequency in human vision, *Perception*, 2:31–40.
- Webster, M. A., K. K. De Valois, and E. Switkes, 1990. Orientation and spatial-frequency discrimination for luminance and chromatic gratings, *J. Opt. Soc. Am. A*, 7:1034–1049.
- Webster, M. A., V. E. Raker, and G. Malkoc, 1998. Visual search and natural color distributions, in *Human Vision and Electronic Imaging III* (B. Rogowitz and T. Pappas, eds.), Bellingham, WA: SPIE, pp. 498–509.
- Westheimer, G., and S. P. McKee, 1977. Spatial configurations for hyperacuity, *Vis. Res.*, 17:941–947.

60 Pattern-Selective Adaptation in Color and Form Perception

MICHAEL A. WEBSTER

... I used to think that the aftereffects of persisting stimulation of the retina obtained by prolonged fixation of a display could be very revealing. Besides ordinary afterimages there are all sorts of perceptual aftereffects, some of which I discovered. But I no longer believe that experiments on so-called perceptual adaptation are revealing, and I have given up theorizing about them. ...

J. J. Gibson, *The Ecological Approach to Visual Perception* (1979, p. 248)

J. J. Gibson was among the most influential perceptual psychologists of the twentieth century. Early in his career he reported a striking visual illusion—the tilt aftereffect (Gibson and Radner, 1937). After tilted lines are viewed for a brief period, a vertical line appears tilted in a direction opposite to the adapting orientation (Fig. 60.1). There are many similar examples of visual aftereffects. For example, to experience the motion aftereffect or *waterfall illusion*, stare at the water pouring down a fall for a few moments and then shift your gaze to the side. The static rocks will briefly appear to ooze upward. Such aftereffects are a consequence of perceptual adaptation. The visual system adapts or reduces its sensitivity in response to the currently viewed stimulus. These sensitivity changes are normally selective—they adjust to specific properties or patterns of the image—and thus the aftereffects are usually experienced as a bias toward the opposite or more novel image properties. The resulting illusions attest to the malleability of perception and have provided one of the most commonly used tools for probing visual coding. Indeed, adaptation is often referred to as the *psychologist's electrode*, for it is routinely used to try to detect and characterize visual mechanisms by measuring how their sensitivities change following adaptation.

However, while pattern adaptation has been central to the study of vision, it is less often thought to be important to the actual act of seeing and has even been regarded as an anomaly of perception, arising when the visual system is fatigued by exposure to situations it was never designed to handle. In later years, Gibson went on to found an entire school of perception that emphasized the importance of understanding vision within the context of the rich patterns of information provided by actively exploring the natural visual environment (Gibson, 1979). From this perspective, adaptation was no longer useful as a tool, because the very notion of intervening processes became irrelevant. But as the

quote above implies, he also felt that maintaining fixation on a tilted line (a typical procedure for inducing aftereffects) was itself an unnatural task, and thus was irrelevant to understanding the normal dynamics of perception. And in his final major treatise on vision, the aftereffects he helped reveal were relegated to a footnote.

The aim of this chapter is instead to emphasize the importance of adaptation, both as a method for understanding the processes mediating perception and as a principle for understanding why things look the way they do. Even brief exposures to a pattern can dramatically alter perception, and this is one reason adaptation remains such a popular paradigm. The following sections review the nature of these perceptual aftereffects and illustrate how they have been used to uncover the visual mechanisms encoding color and form. But if we can recast vision so easily in the lab, how is it being molded by the patterns we are routinely exposed to on the outside, as you walk through a forest or sit reading this page? The final sections take up this question by considering how visual perception is influenced by adaptation to the natural visual environment. The visual world is not random. Natural images have characteristic properties, and exposure to these *persisting patterns of stimulation* may therefore hold the visual system in specific states of adaptation. These states provide the relevant contexts for understanding natural vision.

Pattern adaptation and visual channels

What can an orientation-selective aftereffect tell us about the visual processes underlying form perception? Figure 60.2A shows the kinds of measurements one might record in a study of orientation adaptation. In this plot the angle corresponds to the pattern orientation, while the distance from the origin corresponds to the pattern contrast. Note that we could represent any stimulus within the plane by taking only two “measurements” (e.g., of the component contrasts along the horizontal and vertical axes) and that these could sample contrasts along any pair of axes within the plane. But how many measurements are actually used, and along which axes do they lie?

Adaptation experiments address this question by exploring how responses to stimuli are altered after observers are

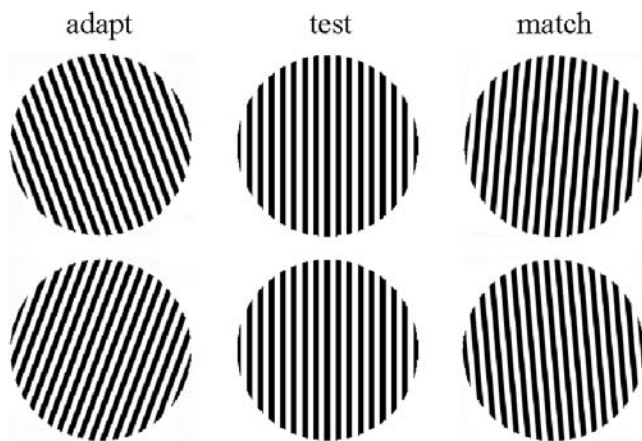


FIGURE 60.1. The tilt aftereffect. Adapting to a counterclockwise tilted line causes a vertical line to appear tilted clockwise, and vice versa.

exposed to and thus adapted by different stimuli. To induce a new state of adaptation, subjects typically view the adapting stimulus for a few minutes and then make judgments about a set of briefly presented test stimuli. Two common types of judgments are used. In one case, sensitivity is probed by finding the threshold for detecting or discriminating the test stimulus. In the second, the subjective appearance of the test is assessed. One way to do this would be to match the apparent orientation of the test by physically adjusting the orientation of a nearby comparison stimulus presented to a part of the retina maintained under neutral adaptation. This *asymmetric matching* task assumes that the effects of adaptation are confined to the regions of the retina (or their associated pathways) that were exposed to the stimuli. A second approach is to vary the test stimulus physically in order to cancel out a perceptual change. For example, the orientation of a test could be adjusted so that it always appears vertical. This *nulling* method assumes that any response changes

induced by adaptation are equivalent to the responses induced by a physical stimulus. Still other common measures include rating the perceived magnitude of an aftereffect or its perceived duration.

Figure 60.2A plots an idealized set of results after adapting to a bar tilted at a clockwise angle. Measures of sensitivity to different orientations would show that adaptation increases the threshold for detecting patterns that have orientations similar to the adapting pattern (Gilinsky, 1968). Measures of appearance would show that after adaptation a vertical line appears tilted counterclockwise. Both aftereffects are consistent with a selective loss in sensitivity to the adapting orientation, and thus imply that adaptation is altering the responses in something that can be selectively tuned for orientation. Results of this kind are usually explained in terms of visual channels—the notion that the visual system encodes information within a bank of *filters* that respond to different but overlapping ranges along the stimulus continuum (e.g., to different orientations, hues, or directions of motion). Any stimulus is thus represented by the distribution of activity across the set of channels. A further common assumption is that these channels are *labeled* for particular sensations, so that which stimulus is perceived (e.g., vertical or red) depends on which channels respond, while the magnitude of the stimulus (e.g., contrast or saturation) is encoded by the size of the response (Braddick et al., 1978).

Figure 60.2B shows one possible account of the tilt aftereffect based on changes in the distribution of activity across multiple channels. Suppose that adaptation reduces a channel's sensitivity according to how strongly the channel responded to the adapting stimulus. This would reduce the channel's responses to a subsequent test stimulus. The test orientations to which it is tuned would become harder to detect, and patterns that are above threshold would appear to have lower contrast. Moreover, the diminished signals

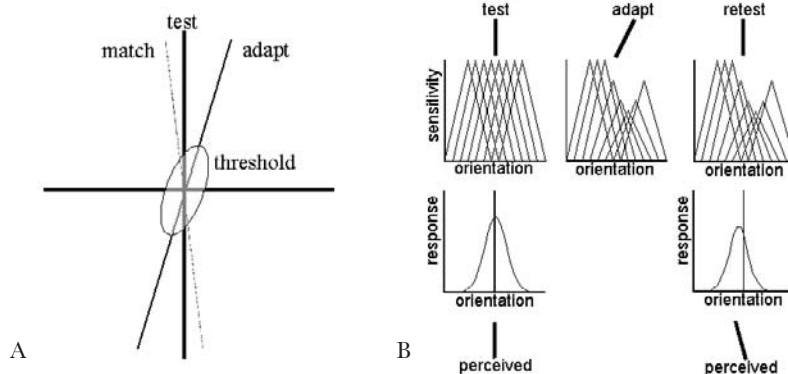


FIGURE 60.2. Multichannel accounts of the tilt aftereffect. *a*, Measurements of detection thresholds (elliptical contour) or perceived tilt of a vertical test after adapting to a clockwise bar. *b*, Both effects can be accounted for by adaptation in orientation-selective chan-

nels that reduces sensitivity in channels tuned to the adapter and thus skews the distribution of responses to the test away from the distribution of responses to the adapter.

would reduce its contribution to the collection of channel responses, and thus for nearby test orientations would skew the mean of the distribution away from the mean for the adapting orientation, inducing the perceived aftereffect. (However, this leaves the problem of how distortions in the pattern's features can be reconciled with their perceived retinal location; Meese and Georgeson, 1996.)

Often the studies using adaptation have not been interested in the processes of adaptation itself, but rather in the properties of the channels implied by the adaptation. One question of interest is the bandwidths or profiles of the channels. For example, an adaptation effect that influenced only a narrow range of orientations would imply that the channels are highly selective for orientation. A second commonly asked question concerns the number of channels. If the response changes are selective for the adapting axis, that implies a channel tuned to that axis. If selective aftereffects can be found for many axes, then that might imply many channels. We could thus repeat the measurements of Figure 60.2*A* for many adapting and test orientations in order to characterize how orientation is represented at the level at which the adaptation alters sensitivity. The results of such studies have shown that sensitivity changes appear selective for any orientation, suggesting that orientation is encoded effectively by a continuum of channels, with bandwidths (orientation range at which sensitivity falls to half the peak) on the order of roughly ± 10 degrees (Blakemore and Nachmias, 1971).

However, the interpretation of these results is complicated, precisely because any inferences about the underlying channels depends on assumptions about the nature of the adaptation. For instance, the model in Figure 60.2*B* assumes that each channel adapts independently. Yet suppose that adaptation instead reflects an interaction between channels (Barlow, 1990; Wilson, 1975). For example, Barlow suggested that adaptation involves reciprocal inhibition between two channels that builds up whenever their outputs are correlated. The effect of this mutual repulsion is to bias the channels' responses until they are statistically independent. An account of the tilt aftereffect based on this principle is shown in Figure 60.3. (For a comprehensive model, see Clifford et al., 2000.) In this example, orientation is encoded by pair of channels that, under neutral adaptation, are tuned to horizontal and vertical. Exposure to the clockwise adapter would produce covarying responses in both channels, leading to inhibition between them. This alters the response within each channel by subtracting a fraction of the response in the second channel. In turn, this reduces the responses to the adapting axis and tilts the tuning function for each channel away from the adapting axis, spherizing the response distribution. Thus, an important feature of this model is that adaptation could induce a selective change in sensitivity even to stimulus directions to which neither channel is tuned.

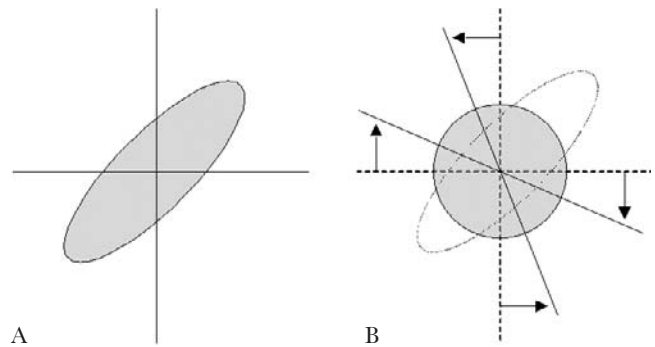


FIGURE 60.3. An alternative account of tilt aftereffects based on mutual inhibition between channels. *a*, Signals along an oblique axis produce correlated responses in channels tuned to horizontal and vertical. *b*, Inhibition between the channels leads to an oblique rotation of their response axes, decorrelating their outputs.

Consequently, adaptation effects alone do not conclusively reveal the specific channel structure.

The actual neural mechanisms underlying pattern-selective adaptation remain unresolved, though it is clear that the channels defined psychophysically do not reflect passive habituation in a neuron's responses. Physiological measurements of contrast adaptation in the cortex suggest that the response changes result from a tonic hyperpolarization imposed on a separate stimulus-driven response that is unaffected by adaptation (Carandini and Ferster, 1997). At least some components of the adaptation are extremely rapid (Muller et al., 1999), and can selectively adjust to the co-occurrence or contingencies between pairs of stimuli (Carandini et al., 1997) and alter the shape of an individual neuron's tuning curve (Movshon and Lennie, 1979; Muller et al., 1999).

The fact that very different models can lead to very similar explanations of visual aftereffects shows that the implications of contrast adaptation must be interpreted with caution. On the other hand, the models illustrated share important features. Both assume that stimuli are encoded by a set of channels that are (or can be) selectively tuned to many different directions, and that adaptation alters perception by altering the distribution of responses within these channels. Thus, the presence of a pattern-selective aftereffect remains a powerful source of evidence about the nature of visual representations.

The sites of adaptation

As Gibson noted, there are all sorts of perceptual aftereffects. Indeed, we can see the signs of adaptation literally everywhere we look. Neural adjustments begin at the earliest stages in the retina, where processes of light adaptation adjust sensitivity in order to match the ambient light level (Hood, 1998). At the other extreme, some perceptual adap-

tations are actually perceptual-motor adjustments, because they involve recalibration of sensorimotor signals. For example, many studies have examined the visual and behavioral changes that result when observers wear prisms that distort or even invert the visual field (Welch, 1986). Subjects show a remarkable capacity to adjust to these distortions so that they can move about and reach for objects appropriately. This relearning is distinct from a purely visual change because it requires active exploration of the world and primarily reflects changes in perceived body position.

At intermediate stages, the visual system adjusts not merely to the average light level, but also to the patterns of light or contrasts in the image (Webster, 1996). These patterns may be stimulus variations in space, time, or color. Classic examples include not only the tilt and motion aftereffects (Mather et al., 1998), but also numerous figural or size-selective aftereffects, in which adaptation to a particular shape or size biases the apparent shape or size of other images (Kohler and Wallach, 1944). Pattern adaptation can also selectively adjust to specific combinations or conjunctions of visual attributes, and in this case is known as *contingent adaptation* (Stromeyer, 1978). For example, color aftereffects can be induced that are contingent on the spatial orientation or direction of motion of a pattern, or vice versa. Contingent aftereffects are sometimes distinguished from simple pattern aftereffects by their long persistence and by the possibility that they must be actively extinguished rather than passively decaying, characteristics that have blurred the distinction between adaptation and learning.

The aftereffects of pattern adaptation primarily reflect sensitivity changes originating in visual cortex. Three lines of evidence support this. First, what is being affected is sensitivity to patterns—to tilted lines, tinted bars, or drifting gratings—and neurons in the primate visual system do not appear to have the requisite selectivity until striate cortex. For example, tuning for orientation, direction of motion, and spatial frequency are properties that first clearly emerge in striate cortex (De Valois and De Valois, 1988). The second source of evidence is that most visual aftereffects show substantial interocular transfer (Blake et al., 1981). That is, an adapting pattern that is viewed only by the right eye can influence a test pattern that is presented only to the left eye. Because signals from the two eyes first converge in the cortex, this is the earliest plausible site at which a sensitivity change could lead to binocular interactions. Finally, direct recordings from neurons along the visual pathway have shown that cortical cells are strongly adapted by patterns, while response changes in geniculate and retinal cells are weaker (Maffei et al., 1973; Ohzawa et al., 1982) though still substantial (Brown and Masland, 2001; Chander and Chichilnisky, 2001; Smirnakis et al., 1997).

While striate cortex may therefore be an important site of pattern adaptation, this does not preclude sensitivity changes

at higher levels. A number of aftereffects point to multiple cortical sites in pattern adaptation. For example, distinct motion aftereffects have been found for static versus dynamic test patterns and for simple gratings versus two-dimensional plaids, and these have been attributed to sensitivity changes at different sites or pathways (Mather et al., 1998). Moreover, functional magnetic resonance imaging (fMRI) studies have demonstrated response changes correlated with the motion aftereffect that are strongest in area MT, an extrastriate area specialized for motion (Tootell et al., 1995). Studies of orientation adaptation have provided intriguing clues about the sites of the sensitivity changes controlling the tilt aftereffect. Asymmetrical tilt aftereffects occur between real and illusory contours, and these may reflect differences between striate cortex and area V2 in the representation of subjective contours (Paradiso et al., 1989). Distinct tilt aftereffects can also be demonstrated for oriented contours versus oriented textures, with the former affecting sensitivity changes at relatively high levels of shape coding (Suzuki, 2001). Surprisingly, tilt aftereffects can also be induced by patterns that cannot be consciously perceived because they are too fine to be resolved (He and MacLeod, 2001). This suggests that at least some of the aftereffects arise at relatively early cortical levels before visual awareness.

Adaptation and color vision

We can readily distinguish distinct and qualitatively different stages of light adaptation and pattern adaptation in color vision, and can use these effects to characterize how information about color is transformed and represented at successive visual levels. Figure 60.4 shows a standard model of human color vision. At the first stage, light is encoded by the responses in three types of cone that have peak sensitivities at short, medium, or long wavelengths (S, M, or L). Subsequently the signals from the cones are combined to form postreceptoral channels. These channels may draw on receptor signals of the same sign to form luminance-sensitive or nonopponent channels, or may receive antagonistic inputs from different cones to form color-sensitive or opponent channels. The two color channels shown receive opposing signals from the L and M cones (L-M) or S opposed by both L and M cones (S-LM). These combinations represent the preferred color directions of cells in the retina and geniculate, and thus are thought to characterize postreceptoral color coding at precortical stages in the visual system (Derrington et al., 1984).

One could evaluate a model like Figure 60.4 by asking how a response change in the different channels might alter color perception. Alternatively, we could approach the question from the opposite direction, by measuring the effects of adaptation to a stimulus and then asking what set of channels is consistent with the observed aftereffects. For example,

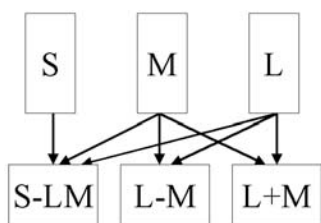


FIGURE 60.4. A standard two-stage model of color vision based on three classes of cones transformed into a luminance channel and two cone-opponent color channels.

Figure 60.5A shows a distribution of colors plotted in a space defined by the signals within the L-M and S-LM channels. In this plot different angles correspond to different hues, and saturation or contrast increases with the distance from the white origin. Note that this is very similar to the representation of contrast and orientation in Figure 60.2A. The stimulus distribution in Figure 60.5 is biased in two ways: the average color is not centered on white, and there is greater variance or contrast along the diagonal axis than along other axes of the space. Processes of light adaptation and contrast (pattern) adaptation selectively adjust to each of these properties (Webster and Mollon, 1995).

LIGHT ADAPTATION Light or chromatic adaptation induces dramatic changes in color vision that are easily demonstrated by the afterimages that are experienced when we fixate a pattern and then switch our gaze to a uniform field. The afterimages arise from lingering sensitivity changes that adjust each location of the retina according to the average light and color it is exposed to. In the example of Figure 60.5A the mean color would look purplish under neutral adaptation. However, adaptation readjusts sensitivity so that the average color appears more achromatic, producing corresponding shifts in the appearance of all colors in the distribution (Fig. 60.5B). To a large extent, the color appearance changes reflect multiplicative gain changes that occur independently within the cones or cone-specific pathways, a process known as *von Kries adaptation* (Chichilnisky and Wandell, 1995; Webster and Mollon, 1995; Wuerger, 1996). Thus, they represent adjustments at the first stage of color processing and, indeed, at the very beginning of vision.

In a classic series of experiments, Stiles (1959) examined the number and color selectivities of the mechanisms underlying chromatic adaptation. Thresholds for detecting a test light were measured in the presence of a uniform adapting background. As the background intensity increases, the processes that respond to the background become less sensitive or light adapt, so that performance follows a characteristic threshold versus intensity curve (Fig. 60.6). The test is detected by the mechanism(s) that are most sensitive on a given adapting background, with a switch between mechanisms revealed by separate branches in the curve. By varying

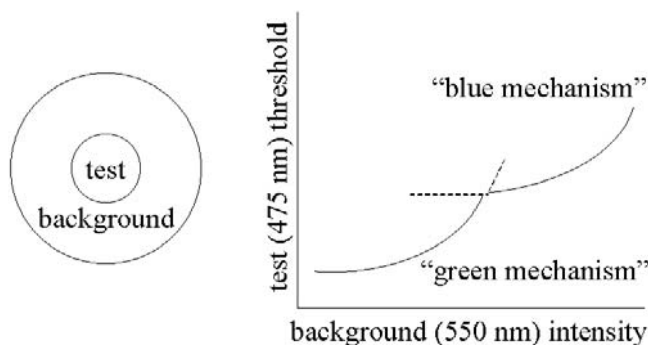


FIGURE 60.5. The two-color threshold method of Stiles. Thresholds for detecting a blue (475 nm) test on a yellow-green (550 nm) background follow two branches reflecting light adaptation in two different color mechanisms.

the wavelength of the test and adapting lights, Stiles showed that sensitivity was limited by a small number of discrete *pi* mechanisms with different sensitivities to wavelength, each adjusting independently to the adapting background.

The spectral sensitivities of the *pi* mechanisms are similar but not equivalent to those of the cones. Moreover, Stiles' work revealed more than three distinct mechanisms under different adapting conditions. These discrepancies have been resolved by showing that chromatic adaptation also depends on *second-site* adjustments in postreceptoral channels (Pugh and Mollon, 1979). One example of these is *transient tritanopia*, a loss in sensitivity to a short-wavelength test after turning off a long-wavelength background that is invisible to S cones (Mollon and Polden, 1977). Extinguishing the background should dark-adapt all of the cones and make them more sensitive, yet thresholds for an S cone detected test are temporarily elevated because the rebound from the yellow background saturates responses at a cone-opponent site. Such aftereffects provided an important source of evidence for color opponency. Second-site adjustments in light adaptation can also be seen in the ways that backgrounds influence sensitivity and appearance (Shevell, 1978; Walraven et al., 1990). A background light sets the gain of the visual mechanisms detecting a superimposed test but also physi-

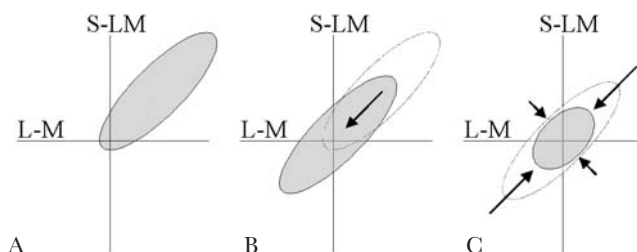


FIGURE 60.6. Adaptation in color vision. *a*, An elliptical distribution of colors plotted in terms of the two cone-opponent axes. Light adaptation adjusts to the mean of the distribution so that the average color appears white (*b*). Contrast adaptation instead adjusts to the variations in color around the average (*c*).

cally adds light to the test. However, this added light often has little effect on the test's appearance, because spatial and temporal filtering subtract the signals from the background, leaving the visual system to respond primarily to spatial and temporal transients. Differences in the time course of sensitivity changes suggest that chromatic adaptation may in fact depend on several sites of both multiplicative and subtractive adjustments (Fairchild and Reniff, 1995; Hayhoe et al., 1987).

CONTRAST ADAPTATION As Figure 60.5B shows, even if we renormalize for the average color in an image, there may often remain a bias in the variance or contrasts in the distribution. Visual mechanisms also adjust to these “patterns” of color through contrast adaptation. This produces changes in color vision that are very different from the effects of light adaptation. Chromatic adaptation in the cones is largely a process that readjusts the white point. Contrast adaptation instead alters the perceived contrasts relative to the average color and thus has very little effect on the mean color itself (Webster and Wilson, 2000). Many studies have examined color adjustments by measuring only the stimulus that looks achromatic. This is perhaps the best setting for detecting chromatic adaptation, but it is the least likely to reveal the presence of contrast adaptation.

The first investigators to explicitly study adaptation to color contrast were Guth (1982) and Krauskopf et al. (1982), both by measuring how color vision is affected by adapting to a background that flickered between two colors. An advantage of this approach is that the flickering field did not change the time-averaged luminance or chromaticity of the adapting field, and thus bypassed the early stages of chromatic adaptation to alter sensitivity at more central sites. In fact, like other forms of pattern adaptation, adaptation to color contrast primarily reflects sensitivity changes in the cortex (e.g., Engel and Furmanski, 2001; Lennie et al., 1990). Studies of contrast adaptation thus allow direct measurements of color coding at cortical levels.

Krauskopf et al. (1982) used contrast adaptation to explore the spectral sensitivities of cortical color channels and, in particular, to ask which directions in color space they are tuned for. To do this, they measured thresholds for detecting a color change from white after adapting to fields that were sinusoidally modulated in color along different axes within the plane of Figure 60.5. These threshold changes revealed two important properties of the adapted color channels. First, aftereffects were primarily selective for three *cardinal directions*: an achromatic axis and the L-M and S-LM chromatic axes. For example, after adaptation to an L-M modulation, an L-M test was much harder to see, while sensitivity to an S-LM or luminance-varying test remained largely unaffected. This suggested that the adapted channels are organized in terms of these dimensions, and not in terms

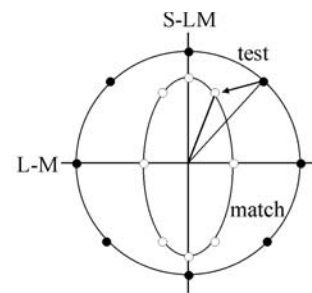


FIGURE 60.7. Contrast adaptation in color vision. Adaptation to flicker along the L-M axis reduces responses along this axis, compressing the circle of test stimuli into an ellipse. This biases the perceived hue of tests away from the adapting axis and toward the orthogonal axis.

of the red-green and blue-yellow dimensions predicted by subjective color experience. However, weak selectivity was also observed for adapting directions intermediate to the L-M and S-LM axes, suggesting the presence of additional channels tuned to these directions (Krauskopf et al., 1986). This raised the possibility that—like the representation of spatial patterns—the representation of color is elaborated in the cortex. Consistent with this, cells in striate cortex show a much wider range of preferred color directions than geniculate cells (Lennie et al., 1990).

Webster and Mollon (1994) extended this paradigm to examine how contrast adaptation alters color appearance. In their studies, subjects viewed adapting and test lights in a field above fixation and then matched the perceived color of the tests by adjusting the physical color in a comparison field presented below fixation. Color changes in the tests were strongly selective for the color axis of the adapting flicker, as illustrated schematically in Figure 60.7 by the matches made after adaptation to the L-M axis. This collapses perceived contrast along the L-M axis, and thus biases the perceived hue of test stimuli away from the L-M axis and toward the orthogonal (S-LM) axis (with a change in contrast but not hue along the adapting and orthogonal axes). Color shifts away from the adapting axis could be induced in any test direction, including the achromatic axis, suggesting that there is no axis that isolates a single type of channel (since the shifts presumably reflect a change in the distribution of responses across channels). These biases in perceived hue are analogous to the biases in perceived orientation in the tilt aftereffect and thus can be thought of as tilt aftereffects in color space. However, compared to orientation the hue shifts are many times larger, exceeding 30 degrees in some cases (compared to 5 degrees or less for typical tilt aftereffects). This difference may result because, when compared in a common metric like Figures 60.2 and 60.5, the color channels are much more broadly tuned than the channels coding orientation, so that the mean of the distribution shifts more with adaptation. The bandwidths of the color aftereffects

are in fact well fit by assuming that the channels are defined by different linear combinations of the cones.

Like orientation, these selective adjustments to color contrast could be achieved by very different routes. Specifically, to account for the selectivity for multiple directions, we could modify the second-stage mechanisms in Figure 60.4 either by adding many color channels that adapt independently or by allowing for adaptive interactions between them. Models based on each of these assumptions have been developed, and both provide a good fit of the observed color changes (Atick et al., 1993; Clifford et al., 2000; Lennie, 1999; Webster and Mollon, 1994; Zaidi and Shapiro, 1993). Thus, again, adaptation alone does not define the intrinsic number of color channels. However, other experimental approaches point to the presence of many chromatic mechanisms even in a single state of adaptation (Webster, 1996). This supports the idea that the cortex does encode color—like orientation—in a large number of channels, though it does not imply that these adapt independently.

Further adaptation effects have revealed a number of additional properties of cortical color channels. For example, adaptation to sawtooth modulations suggests that different populations of channels encode the opposite poles of luminance or chromatic axes (Krauskopf et al., 1982), and the axes may be even further subdivided into channels that code different ranges of contrast (Webster and Wilson, 2000). A number of studies have also explored a simultaneous analog of contrast aftereffects. The perceived contrast of a pattern can be strongly attenuated by embedding the pattern in a high-contrast surround (Chubb et al., 1989). This contrast induction again adjusts selectively to different chromatic axes (Brown and MacLeod, 1997; Singer and D’Zmura, 1994; Webster et al., 2002).

Adaptation has also proven useful for probing the spatial selectivities of color mechanisms. For example, adaptation to color spatial patterns (e.g., a red-green edge) makes color patterns with similar orientation and spatial frequency harder to detect (Bradley et al., 1988) and can induce tilt aftereffects in color patterns (Elsner, 1978). Moreover, the tilt aftereffects show selectivity for multiple color directions (Flanagan et al., 1990). Such results show that the affected channels can be tuned to both the color and the spatial properties of stimuli. A classic demonstration of this is the McCollough effect (McCollough, 1965). After viewing a red-vertical grating alternated in time with a green-horizontal grating, an achromatic-vertical grating looks greenish, while an achromatic-horizontal grating looks reddish. Thus, the color changes are contingent on the orientation of the adapting patterns. If we think of the bright-red adapting grating as an oblique direction within the color-luminance plane and the achromatic test as vertical, then this aftereffect can again be accounted for by a bias away from the adapting axis. That is, the color change in the test is a tilt

aftereffect in color-luminance space that is selective for spatial orientation (Webster and Malkoc, 2000).

The functions of adaptation

The preceding sections show that adaptation can exert a powerful hold over our perception. But if this influence reflects function rather than fatigue, then we should see tangible signs that it is helping us to see better in everyday contexts. The benefits of light adaptation seem clear. The response range of neurons is very limited, but must be used to encode visual signals over a staggering range of light intensities. Adjusting to the average light level allows the retina to use its full dynamic range to encode the information carried by stimulus contrasts (Craik, 1940; Walraven et al., 1990). Multiplicative adjustments within the cones further allow the visual system to maintain lightness and color constancy by factoring out changes in the mean illumination. Compared to light adaptation, the effects of pattern adaptation appear more subtle, and it has proven much more difficult to demonstrate improvements in visual performance. However, there are several potential benefits.

GAIN CONTROL One possibility is that adaptation protects against saturation in cortical responses in the same way that light adaptation protects retinal responses. Recordings in striate cells show that prior adaptation tends to center the cells’ contrast response functions around the adapting contrast, and this can allow cells to respond differentially to stimuli that before adaptation led to saturated and thus indistinguishable responses (Albrecht et al., 1984; Sclar et al., 1989). However, psychophysically, only a minority of studies have found that contrast adaptation can improve contrast discrimination (Greenlee and Heitger, 1988; Wilson and Humanski, 1993).

GAMUT MATCHING A related possibility is that contrast adaptation functions to match visual responses to the contrast gamut of the ambient environment to provide contrast constancy (Brown and MacLeod, 1997; Zaidi et al., 1998). In the case of color vision, an interesting example is provided by anomalous trichromats, who have M and L pigments with very similar spectral sensitivities. Because of this, the chromatic signal defined by the L-M difference is very weak, but adaptation might adjust the gain of postreceptoral channels to fill the available range (though whether this occurs in the retina or cortex is uncertain; MacLeod, 2002; Regan and Mollon, 1997).

NORMALIZATION The idea of gamut matching suggests that the visual system tends to settle around special states that may reflect expectations about the properties of the visual environment. Examples of these states include *white* for color

or *static* for motion. Many aftereffects can be seen as a consequence of renormalizations for these states, especially when the adapting stimulus itself appears more “neutral” over time. For example, with adaptation a background color appears less saturated, drifting patterns seem to slow down, and tilted bars may appear more vertical. These adjustments might compensate for mean biases in the world or correct for errors or distortions in the visual system of the observer (Andrews, 1964), thus providing a form of perceptual constancy. For example, we will see below that adaptive renormalizations could maintain constancy for image structure despite variations in retinal image blur.

DECORRELATION Pattern adaptation could plausibly improve not only coding within a channel but also coding across channels by removing redundancies between channel responses to provide more efficient representations (Barlow, 1990). Stimuli will often lead to correlated responses within a set of channels. By removing these correlations, adaptation could increase efficiency by allowing each mechanism to code independent information. Recent analyses of adaptation in cortical cells in fact support the role of adaptation in reducing redundancy (Carandini et al., 1997; Muller et al., 1999).

LEARNING Finally, by adjusting to the correlations between image properties, adaptation provides a mechanism for representing the stimulus associations in the environment and for learning about new ones (Barlow, 1990). This aspect of adaptation is considered further in the concluding section.

Adaptation and the natural visual environment

Whether adaptation is important to visual function hinges on whether it actually occurs in natural contexts. Again, there is no question of this for light adaptation. It is universally recognized that these adjustments are both a critical and an intrinsic part of the visual response to any stimulus. In fact, it would be meaningless to try to describe visual responses without assuming a particular state of light adaptation. But what of adaptation to tilted lines and waterfalls? Do the adjustments they reflect hold a similar status in perception? To assess this, it is important to ask how patterns of luminance and color vary within the kinds of natural images we normally encounter, and whether adaptation to these patterns can influence natural visual judgments.

EVOLUTIONARY ADAPTATIONS OF VISION Before exploring the rapid visual adjustments implied by visual aftereffects, it is worth remembering that the very structure of the visual system evolved as a long-term adaptation to the animal’s visual environment. Recent studies have provided powerful insights into visual coding by characterizing statistical prop-

erties of natural images and then asking how these could best be represented by the visual system. For example, color opponency can be seen as a means of removing redundancies across the different cones (Buchsbaum and Gottschalk, 1983), while the spatial structure of receptive fields removes redundancies across space (Srinivasan et al., 1982). In visual cortex, individual cells respond to different scales or spatial frequencies in the image. The response bandwidths increase roughly in proportion to the preferred frequency (e.g., as f), while the amplitude spectra of natural images instead characteristically vary as the inverse of frequency (e.g., as $1/f$) (Field, 1987). The tuning of cortical cells therefore compensates for the low-frequency bias in natural scenes so that response levels in the cortex are independent of spatial scale (see Chapter 70).

SHORT-TERM ADAPTATIONS TO VARYING ENVIRONMENTS However, the visual environment is not fixed and thus cannot be represented optimally by a visual system with fixed properties. Moreover, the visual system itself undergoes pronounced anatomical and physiological changes during development and aging. Some adjustments in the tuning are therefore important in order to match the system to the ambient environment and to provide stable perceptions despite variations in the observer. Exactly what kinds of natural stimulus patterns the visual system might adjust to is an intriguing but still largely unexplored question. Yet it is clear that natural images provide a powerful stimulus for pattern adaptation.

Webster and Mollon (1997) examined changes in color appearance induced by adaptation to the color contrasts characteristic of natural outdoor scenes. Color in natural images is highly constrained and tends to vary along a limited range of axes in color space, from blue-yellow for arid scenes to a greenish S-LM axis for lush scenes. In the former case there is often a very high correlation between the signals along the cardinal chromatic axes, so that color in these scenes is not efficiently represented in the geniculate. However, contrast adaptation might adjust to this bias in the cortex, and observers in different environments should then be adapted by the prevailing colors in different ways. Figure 60.8 shows tests of this by measuring color appearance after adaptation to a succession of colors drawn at random from a natural scene. Light adaptation adjusts to the average color, while contrast adaptation induces large, selective changes in sensitivity to the blue-yellow axis of the adapting distribution.

As noted above, natural images have characteristic amplitude spectra to which the visual system might normalize spatial sensitivity. However, image spectra are not entirely constant, but vary because of differences in both scenes and the observer. For example, optical blur steepens the spectrum by reducing finer details in the retinal image, and thus there

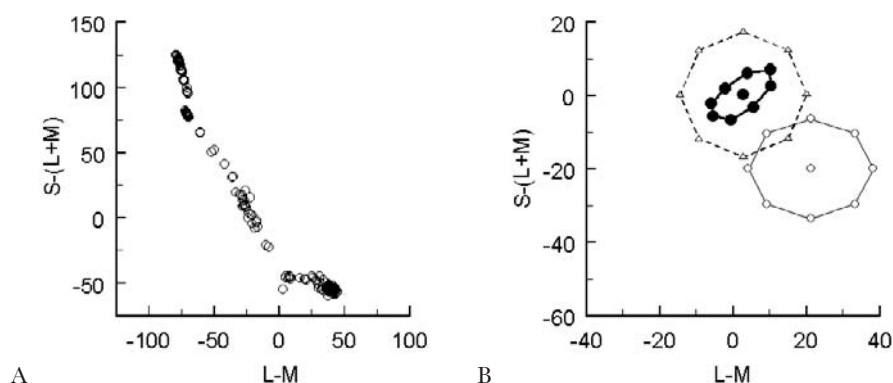


FIGURE 60.8. Adaptation to natural color distributions. Adaptation to the blue-yellow color variations in an arid scene (a) produces changes in color appearance that are strongly selective for the adapting axis (b). Test colors (unfilled circles) centered on the biased mean of the distribution are matched by colors centered around

white and compressed along the blue-yellow axis of the distribution (filled circles), showing the imprint of both light adaptation to the mean and contrast adaptation to the variations in the distribution. (Unfilled triangles plot the matches predicted by light adaptation alone.)

may be characteristic states of pattern adaptation associated with refractive errors. Visual acuity in fact increases after observers adapt for a period to optical defocus (Mon-Williams et al., 1998). Adaptation can also strongly affect the actual appearance of blur (Webster et al., 2002). Exposure to a blurred (sharpened) image causes a focused image to appear too sharp (blurred) (Fig. 60.9). Moreover, the blurred or sharpened adapting images themselves looked better focused the longer they are viewed, suggesting that adaptation is renormalizing perception of image focus. Figure 60.9 also shows a spatial analog of these effects induced by blurred or sharpened surrounds. Similar adaptation and induction effects also influence other judgments of the spatial statistics of images, such as the perception of texture density (Durgin and Huk, 1997). While these effects can be

very rapid, there may also be adjustments at much longer time scales. Fine et al. (2002) recently examined a subject who had had cataracts for decades. Even months after surgery, the world through his new lenses appeared overly sharpened.

The perceptual changes in blur adaptation are dramatic, possibly because the natural consequences of adaptation are best revealed by probing them with stimuli and tasks that are natural and relevant to the observer. Human face perception provides a clear example of such tasks. Observers are remarkably adept at recognizing and judging faces based on subtle differences in their configural properties and thus should be highly sensitive to any changes in configuration induced by adaptation. In fact, adaptation to a distorted face alters the appearance of subsequent faces (Webster and

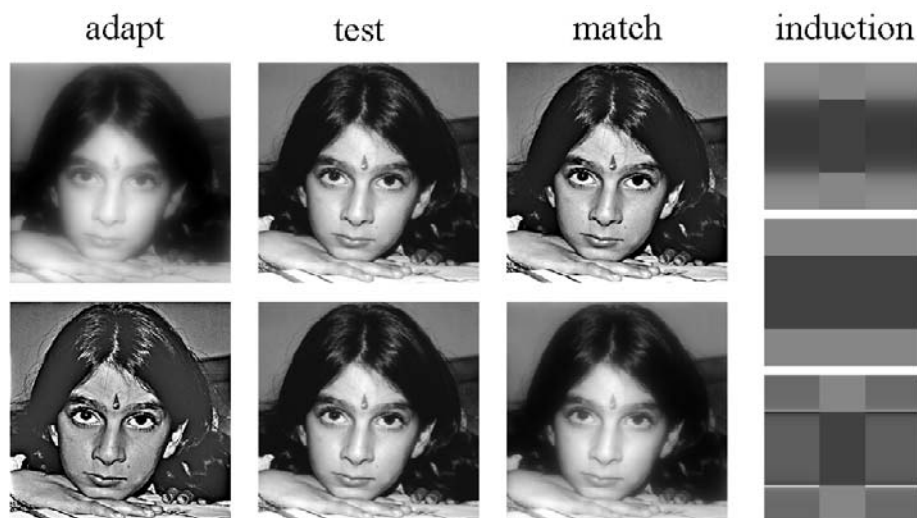


FIGURE 60.9. Adaptation to blur. A blurry adapting image causes a focused image to appear sharpened, or vice versa. Bars to the right show similar effects for induction. In each block the central

column of bars are all square edges. Yet the bars abutting the blurred edges appear too sharp, while the bars adjoining sharpened edges appear blurred.

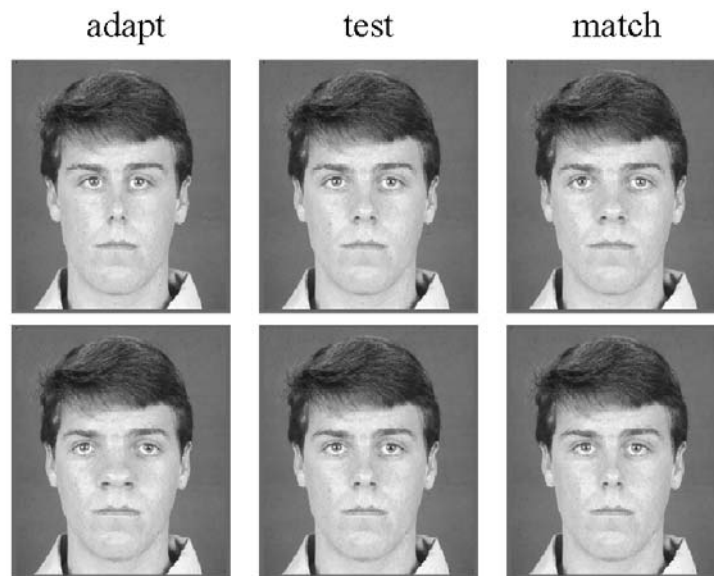


FIGURE 60.10. Adaptation to faces. Adaptation to a contracted face causes the original face to appear expanded, while an expanded face induces the opposite aftereffect.

MacLin, 1999) (Fig. 60.10). Large biases in recognition also occur for adapting and test images that are defined by the configurations characterizing real faces (Kaping et al., 2002; Leopold et al., 2001). Given that we are all exposed to a different diet of faces that are naturally “distorted” relative to the average human face, it seems likely that these adaptation effects influence many aspects of face recognition in everyday viewing. Recent studies have shown that face aftereffects are surprisingly unaffected by large changes in size or location between the adapting and test images (Leopold et al., 2001; Zhao and Chubb, 2001). This strongly suggests that the adaptation involves adjustments to the configural properties of the face, rather than to local, low-level features, and thus supports the possibility that the sensitivity changes reflect processes specialized for face coding. It seems probable that many other aspects of higher-level object recognition are similarly shaped by adaptation.

Adaptation and the phenomenology of perception

What are the implications of such adaptation effects for the subjective experience of seeing? One possible implication concerns whether we have shared or distinct perceptions (Webster, 2002). A long-standing philosophical question is what the world might look like if we could see it through the eyes of another. The private nature of our conscious experience may preclude a complete answer, but it is tempting to speculate that any answer will be constrained in important ways by the processes of adaptation. As the preceding sections illustrate, adaptation normalizes our perception according to properties of—or expectations about—the physical world. To the extent that two observers are adapted

to different environments, their visual systems will be normalized in different ways and their subjective experience should differ. For example, if you and I are exposed to a different population of faces, our perception (and not just our judgments) of the same physical facial characteristics are unlikely to agree. To the extent that two observers are exposed to a common environment, adaptation will tend to normalize their perception toward a convergent experience. For example, even if you and I have different refractive errors, our perceptions of image focus may converge because these differences are partially discounted by adaptation to the common spatial structure of scenes. Notably, in both cases, it is the similarities or differences in the environment—and not the intrinsic differences between observers—that determine how the visual system is normalized. Thus, at least some aspects of our private internal experience are controlled by public external variables that can be objectively measured.

The effects of adaptation also have important implications for the actual contents of visual awareness. The decorrelation model proposed by Barlow was built around the idea that adaptation serves to discount ambient information in order to enhance sensitivity to novel patterns. These novel patterns, or *suspicious coincidences*, may be the most important information to the observer, and thus processes that highlight them may be highly beneficial (Barlow, 1990). The role of adaptation in regulating visual salience remains largely unexplored, because most studies have focused on understanding how adaptation influences the encoding of the adapting pattern itself. However, the negative aftereffects characteristic of adaptation support this view, since they “draw attention” to the ways in which the test differs from

the adapter. In this regard, it is interesting to note that the consequences of adaptation are often much more striking in the test stimulus than in the stimulus to which we are adapted. Thus, the perceptual aftereffects of color and form are vivid imprints of sensitivity changes that often pass unnoticed during adaptation. If adaptation is part of our everyday visual experience, then perhaps most of what we notice about the world is a perceptual aftereffect.

Acknowledgments

This work was supported by Grant EY10834 from the National Eye Institute.

REFERENCES

- Albrecht, D. G., S. B. Farrar, and D. B. Hamilton, 1984. Spatial contrast adaptation characteristics of neurones recorded in the cat's visual cortex, *J. Physiol.*, 347:713–739.
- Andrews, D. P., 1964. Error-correcting perceptual mechanisms, *Q. J. Exp. Psychol.*, 16:104–115.
- Atick, J. J., Z. Li, and A. N. Redlich, 1993. What does post-adaptation color appearance reveal about cortical color representation? *Vis. Res.*, 33:123–129.
- Barlow, H. B., 1990. A theory about the functional role and synaptic mechanism of visual after-effects, in *Vision: Coding and Efficiency* (C. Blakemore ed.), Cambridge: Cambridge University Press, pp. 363–375.
- Blake, R., R. Overton, and S. Lema-Stern, 1981. Interocular transfer of visual aftereffects, *J. Exp. Psychol.: Hum. Percept. Perform.*, 7:367–381.
- Blakemore, C., and J. Nachmias, 1971. The orientation specificity of two visual aftereffects, *J. Physiol.*, 213:157–174.
- Braddick, O., F. W. Campbell, and J. Atkinson, 1978. Channels in vision: basic aspects, in *Handbook of Sensory Physiology VIII* (R. Held, H. W. Leibowitz, and H. Teuber, eds.), Berlin: Springer-Verlag, pp. 3–38.
- Bradley, A., E. Switkes, and K. K. De Valois, 1988. Orientation and spatial frequency selectivity of adaptation to color and luminance gratings, *Vis. Res.*, 28:841–856.
- Brown, R. O., and D. I. A. MacLeod, 1997. Color appearance depends on the variance of surround colors, *Curr. Biol.*, 7:844–849.
- Brown, S. P., and R. H. Masland, 2001. Spatial scale and cellular substrate of contrast adaptation by retinal ganglion cells, *Nat. Neurosci.*, 4:44–51.
- Buchsbaum, G., and A. Gottschalk, 1983. Trichromacy, opponent colours and optimum colour information transmission in the retina, *Proc. R. Soc. Lond. B*, 220:89–113.
- Carandini, M., H. B. Barlow, L. P. O'Keefe, A. B. Poirson, and J. A. Movshon, 1997. Adaptation to contingencies in macaque primary visual cortex, *Philos. Trans. R. Soc. Lond. B Biol. Sci.*, 52:1149–1154.
- Carandini, M., and D. Ferster, 1997. A tonic hyperpolarization underlying adaptation in cat visual cortex, *Science*, 276:949–952.
- Chander, D., and E. J. Chichilnisky, 2001. Adaptation to temporal contrast in primate and salamander retina, *J. Neurosci.*, 21:9904–9916.
- Chichilnisky, E.-J., and B. A. Wandell, 1995. Photoreceptor sensitivity changes explain color appearance shifts induced by large uniform backgrounds in dichoptic matching, *Vis. Res.*, 35:239–254.
- Chubb, C., G. Sperling, and J. A. Solomon, 1989. Texture interactions determine perceived contrast, *Proc. Natl. Acad. Sci. USA*, 86:9631–9635.
- Clifford, C. W. G., P. Wenderoth, and B. Spehar, 2000. A functional angle on some aftereffects in cortical vision, *Proc. R. Soc. Lond. B*, 267:1705–1710.
- Craik, K. J. W., 1940. The effect of adaptation on subjective brightness, *Proc. R. Soc. Lond. B*, 128:232–247.
- Derrington, A. M., J. Krauskopf, and P. Lennie, 1984. Chromatic mechanisms in lateral geniculate nucleus of macaque, *J. Physiol.*, 357:241–265.
- De Valois, R. L., and K. K. De Valois, 1988. *Spatial Vision*, Oxford: Oxford University Press.
- Durgin, F. H., and A. C. Huk, 1997. Texture density aftereffects in the perception of artificial and natural textures, *Vis. Res.*, 23:3273–3282.
- Elsner, A., 1978. Hue difference contours can be used in processing orientation information, *Percept. Psychophys.*, 25:451–456.
- Engel, S. A., and C. S. Furmanski, 2001. Selective adaptation to color contrast in human primary visual cortex, *J. Neurosci.*, 21:3949–3954.
- Fairchild, M. D., and L. Reniff, 1995. Time course of chromatic adaptation for color-appearance judgments, *J. Opt. Soc. Am. A*, 12:824–833.
- Field, D. J., 1987. Relations between the statistics of natural images and the response properties of cortical cells, *J. Opt. Soc. Am. A*, 4:2379–2394.
- Fine, I., H. S. Smallman, P. Doyle, and D. I. A. MacLeod, 2002. Visual function before and after the removal of bilateral congenital cataracts in adulthood, *Vis. Res.*, 42:191–210.
- Flanagan, P., P. Cavanagh, and O. E. Favreau, 1990. Independent orientation-selective mechanisms for the cardinal directions of color space, *Vis. Res.*, 30:769–778.
- Gibson, J. J., 1979. *The Ecological Approach to Visual Perception*, Boston: Houghton Mifflin.
- Gibson, J. J., and M. Radner, 1937. Adaptation, after-effect and contrast in the perception of tilted lines. I. Quantitative studies, *J. Exp. Psychol.*, 20:453–467.
- Gilinsky, A. S., 1968. Orientation-specific effects of patterns of adapting light on visual acuity, *J. Opt. Soc. Am. A*, 58:13–17.
- Greenlee, M. W., and F. Heitger, 1988. The functional role of contrast adaptation, *Vis. Res.*, 28:791–797.
- Guth, S. L., 1982. Hue shifts following flicker vs. fused adaptation reveal initial opponent mechanisms, *Invest. Ophthalmol. Vis. Sci. (Suppl.)*, 22:78.
- Hayhoe, M. M., N. I. Benimoff, and D. C. Hood, 1987. The time-course of multiplicative and subtractive adaptation process, *Vis. Res.*, 27:1981–1996.
- He, S., and D. I. A. MacLeod, 2001. Orientation-selective adaptation and tilt aftereffect from invisible patterns, *Nature*, 411:473–476.
- Hood, D. C., 1998. Lower-level visual processing and models of light adaptation, *Annu. Rev. Psychol.*, 49:503–535.
- Kapung, D., A. C. Bilson, and M. A. Webster, 2002. Adaptation and categorical judgments of faces [abstract], *J. of Vision*, 2:564a.
- Kohler, W., and H. Wallach, 1944. Figural aftereffects: an investigation of visual processes, *Proc. Am. Philos. Soc.*, 88:269–357.
- Krauskopf, J., D. R. Williams, and D. W. Heeley, 1982. Cardinal directions of color space, *Vis. Res.*, 22:1123–1131.
- Krauskopf, J., D. R. Williams, M. B. Mandler, and A. M. Brown, 1986. Higher order color mechanisms, *Vis. Res.*, 26:23–32.

- Lennie, P., 1999. Color coding in the cortex, in *Color Vision: From Genes to Perception* (K. R. Gegenfurtner and L. T. Sharpe, eds.), Cambridge: Cambridge University Press, pp. 235–247.
- Lennie, P., J. Krauskopf, and G. Sclar, 1990. Chromatic mechanisms in striate cortex of macaque, *J. Neurosci.*, 10:649–669.
- Leopold, D. A., A. J. O'Toole, T. Vetter, and V. Blanz, 2001. Prototype-referenced shape encoding revealed by high-level aftereffects, *Nat. Neurosci.*, 4:89–94.
- MacLeod, D. I. A., 2003. Colour discrimination, colour constancy and natural scene statistics, (the Verriest Lecture). In *Normal and Defective Color Vision*, J. D. Mollon, J. Pokorny, and K. Koblach (eds.), London: Oxford University Press, pp. 189–217.
- Maffei, L., A. Fiorentini, and S. Bisti, 1973. Neural correlate of perceptual adaptation to gratings, *Science*, 182:1036–1038.
- Mather, G., F. Verstraten, and S. Anstis, eds., 1998. *The Motion Aftereffect*, Cambridge, MA: MIT Press.
- McCollough, C., 1965. Color adaptation of edge-detectors in the human visual system, *Science*, 149:1115–1116.
- Meese, T. S., and M. A. Georgeson, 1996. The tilt aftereffect in plaids and gratings: channel codes, local signs and “patchwise” transforms, *Vis. Res.*, 36:1421–1437.
- Mollon, J. D., and P. G. Polden, 1977. An anomaly in the response of the eye to light of short wavelengths, *Philos. Trans. R. Soc. B*, 278:207–240.
- Mon-Williams, M., J. R. Tresilian, N. C. Strang, P. Kochhar, and J. P. Wann, 1998. Improving vision: neural compensation for optical defocus, *Proc. R. Soc. Lond. B*, 265:71–77.
- Movshon, J. A., and P. Lennie, 1979. Pattern-selective adaptation in visual cortical neurones, *Nature*, 278:850–852.
- Muller, J. R., A. B. Metha, J. Krauskopf, and P. Lennie, 1999. Rapid adaptation in visual cortex to the structure of images, *Science*, 285:1405–1408.
- Ohzawa, I., G. Sclar, and R. D. Freeman, 1982. Contrast gain control in the cat visual cortex, *Nature*, 298:266–268.
- Paradiso, M. A., S. Shimojo, and K. Nakayama, 1989. Subjective contours, tilt aftereffects, and visual cortical organization, *Vis. Res.*, 29:1205–1213.
- Pugh, E. N., and J. D. Mollon, 1979. A theory of the π_1 and π_2 color mechanisms of Stiles, *Vis. Res.*, 19:293–312.
- Regan, B. C., and J. D. Mollon, 1997. The relative salience of the cardinal axes of colour space in normal and anomalous trichromats, in *Colour Vision Deficiencies VIII* (C. R. Cavonius ed.), Dordrecht: Kluwer, pp. 67–76.
- Sclar, G., P. Lennie, and D. D. DePriest, 1989. Contrast adaptation in striate cortex of macaque, *Vis. Res.*, 29:747–755.
- Shevell, S. K., 1978. The dual role of chromatic backgrounds in color perception, *Vis. Res.*, 18:1649–1661.
- Singer, B., and M. D'Zmura, 1994. Color contrast induction, *Vis. Res.*, 34:3111–3126.
- Smirnakis, S. M., M. J. Berry, D. K. Warland, W. Bialek, and M. Meister, 1997. Adaptation of retinal processing to image contrast and spatial scale, *Nature*, 386:69–73.
- Srinivasan, M. V., S. B. Laughlin, and A. Dubs, 1982. Predictive coding: a fresh view of inhibition in the retina, *Proc. R. Soc. Lond. B*, 216:427–459.
- Stiles, W. S., 1959. Color vision: the approach through increment-threshold sensitivity, *Proc. Natl. Acad. Sci. USA*, 45:100–114.
- Stromeyer, C. F. I., 1978. Form-color aftereffects in human vision, in *Handbook of Sensory Physiology VIII* (R. Held, H. W. Leibowitz, and H. L. Teuber, eds.), New York: Springer-Verlag.
- Suzuki, S., 2001. Attention-dependent brief adaptation to contour orientation: a high-level aftereffect for convexity? *Vis. Res.*, 28:3883–3902.
- Tootell, R. B. H., J. B. Reppas, A. M. Dale, R. B. Look, M. I. Sereno, R. Malach, T. J. Brady, and B. R. Rosen, 1995. Visual motion aftereffect in human cortical area MT revealed by functional magnetic resonance imaging, *Nature*, 375:139–141.
- Walraven, J., C. Enroth-Cugell, D. C. Hood, D. I. A. MacLeod, and J. L. Schnapf, 1990. The control of visual sensitivity: receptor and postreceptor processes, in *Visual Perception: The Neurophysiological Foundations* (L. Spillmann and J. S. Werner, eds.), San Diego, CA: Academic Press, pp. 53–101.
- Webster, M. A., 1996. Human colour perception and its adaptation, *Network: Comput. Neural Syst.*, 7:587–634.
- Webster, M. A., 2002. Adaptation, high-level vision, and the phenomenology of perception, in *Human Vision and Electronic Imaging VII* (B. Rogowitz and T. Pappas, eds.), SPIE 4662:1–11.
- Webster, M. A., M. A. Georgeson, and S. M. Webster, 2002. Neural adjustments to image blur, *Nat. Neurosci.*, 5:839–840.
- Webster, M. A., and O. H. MacLin, 1999. Figural after-effects in the perception of faces, *Psych. Bull. Rev.*, 6:647–653.
- Webster, M. A., and G. Malkoc, 2000. Color-luminance relationships and the McCollough Effect, *Percept. Psychophys.*, 62:659–672.
- Webster, M. A., G. Malkoc, A. C. Bilson, and S. M. Webster, 2002. Color contrast and contextual influences on color appearance, *J. of Vision*, 2:505–519.
- Webster, M. A., and J. D. Mollon, 1994. The influence of contrast adaptation on color appearance, *Vis. Res.*, 34:1993–2020.
- Webster, M. A., and J. D. Mollon, 1995. Colour constancy influenced by contrast adaptation, *Nature*, 373:694–698.
- Webster, M. A., and J. D. Mollon, 1997. Adaptation and the color statistics of natural images, *Vis. Res.*, 37:3283–3298.
- Webster, M. A., and J. A. Wilson, 2000. Interactions between chromatic adaptation and contrast adaptation in color appearance, *Vis. Res.*, 40:3801–3816.
- Welch, R. B., 1986. Adaptation of space perception, in *Handbook of Perception and Human Performance*, vol. 1 (K. R. Boff, L. Kaufman, and J. P. Thomas, eds.), New York: Wiley, pp. 24.1–24.45.
- Wilson, H. R., 1975. A synaptic model for spatial frequency adaptation, *J. Theoret. Biol.*, 50:327–352.
- Wilson, H. R., and R. Humanski, 1993. Spatial frequency adaptation and contrast gain control, *Vis. Res.*, 33:1133–1149.
- Wuerger, S. M., 1996. Color appearance changes resulting from iso-luminant chromatic adaptation, *Vis. Res.*, 36:3107–3118.
- Zaidi, Q., and A. G. Shapiro, 1993. Adaptive orthogonalization of opponent-color signals, *Biol. Cybern.*, 69:415–428.
- Zaidi, Q., B. Spehar, and J. DeBonet, 1998. Adaptation to textured chromatic fields, *J. Opt. Soc. Am. A*, 15:23–32.
- Zhao, L., and C. F. Chubb, 2001. The size-tuning of the face-distortion aftereffect, *Vis. Res.*, 41:2979–2994.

61 Color Constancy

DAVID H. BRAINARD

COLOR IS USED TO RECOGNIZE and describe objects. When giving directions, we might provide the detail that the destination is a yellow house. When judging the ripeness of a fruit, we might evaluate its color. The ability to perceive objects as having a well-defined color is quite remarkable. To understand why, it is necessary to consider how information about object spectral properties is represented in the retinal image.

A *scene* is a set of illuminated objects. In general, the illumination has a complex spatial distribution, so that the illuminant falling on one object in the scene may differ from that falling on another. Nonetheless, a useful point of departure is to consider the case where the illumination is uniform across the scene, so that it may be characterized by its *spectral power distribution*, $E(\lambda)$. This function specifies how much power the illuminant contains at each wavelength. The illuminant reflects off objects to the eye, where it is collected and focused to form the retinal *image*. It is the image that is explicitly available for determining the composition of the scene.

Object surfaces differ in how they absorb and reflect light. In general, reflection depends on wavelength, the angle of the incident light (relative to the surface normal), and the angle of the reflected light (Foley et al., 1990). It is again useful to simplify and neglect geometric considerations, so that each object surface is characterized by a *spectral reflectance function*, $S(\lambda)$. This function specifies what fraction of incident illumination is reflected from the object at each wavelength.

The light reflected to the eye from each visible scene location is called the *color signal*. For the simplified imaging model described above, the spectral power distribution of the color signal $C(\lambda)$ is readily calculated from the illuminant spectral power distribution and the surface reflectance function:

$$C(\lambda) = E(\lambda)S(\lambda) \quad (1)$$

The retinal image consists of the color signal incident at each location after blurring by the eye's optics. In the treatment here, such blurring may be safely ignored.

The imaging model expressed by equation 1 assumes that the light source is spatially uniform, that the objects are flat and coplanar, and that the surface reflectances are Lambertian. It is sometimes referred to as the *Mondrian World* imaging model. The assumptions of the Mondrian World never hold for real scenes. A more realistic formulation would include a description of the spatial distribution of the

illuminant, the geometry of the scene, and how each object's spectral reflectance depends on the direction of the incident and reflected light (Foley et al., 1990; also see Fig. 61.2). Nonetheless, the Mondrian World is rich enough to provide a useful framework for initial analysis.

The form of equation 1 makes explicit the fact that two distinct physical factors, the illuminant and the surface reflectance, contribute in a symmetric way to the color signal. One of these factors, the surface reflectance, is intrinsic to the object and carries information about its identity and properties. The other factor, the illuminant, is extrinsic to the object and provides no information about the object.

Given that the color signal at an image location confounds illuminant and surface properties, how is it possible to perceive objects as having a well-defined color? Indeed, the form of equation 1 suggests that changes in illuminant can masquerade perfectly as changes in object surface reflectance, so that across conditions where the illuminant varies, one might expect large changes in the appearance of a fixed object. This physical process is illustrated by Figure 61.1. Each of the two patches shown at the top of the figure corresponds to a region of a single object imaged under a different outdoor illuminant. When the two patches are seen in isolation, their color appearance is quite different: there is enough variation in natural daylight that the color signal is substantially ambiguous about object surface properties.

When the two patches are seen in the context of the images from which they were taken, the variation in color appearance is reduced. This stabilization of appearance is by no means complete in the figure, where the reader views small printed images that are themselves part of a larger illuminated environment. For an observer standing in front of the home shown, however, the variation in perceived color is minimal and not normally noticed. This suggests that the visual system attempts to resolve the ambiguity inherent in the color signal by analyzing many image regions jointly: the full image context is used to produce a stable perceptual representation of object surface color. This ability is referred to as *color constancy*.

This chapter is about human color constancy. The literature on color constancy is vast, extending back at least to the eighteenth century (Mollon, in press), and this chapter does not attempt a systematic review. Rather, the goal is to provide an overview of how human color constancy can be studied



FIGURE 61.1. Same objects imaged under two natural illuminants. *Top*: The patches show a rectangular region extracted from images of the same object under different outdoor illuminants. *Bottom*: The images from which the patches were taken. Images were acquired

by the author in Merion Station, Pennsylvania, using a Nikon CoolPix 995 digital camera. The automatic white balancing calculation that is a normal part of the camera's operation was disabled during image acquisition. (See color plate 36.)

experimentally and how it can be understood. The next section presents an extended example of how constancy is measured in the laboratory. The measurements show both circumstances where constancy is good and those where it is not; a characterization of human color vision as either “approximately color constant” or “not very color constant” is too simple. Rather, we must characterize when constancy will be good and when it will not. The discussion outlines two current approaches.

Measuring constancy

This section illustrates how constancy may be measured by describing experiments conducted by Kraft and Brainard (1999; see also Brainard, 1998; Kraft et al., 2002). Before treating the specific experimental design, however, some general remarks are in order.

Several distinct physical processes can cause the illumination impinging on a surface to vary. The images in Figure 61.1 illustrate one such process. They were taken at different times, and the spectra of the illuminant sources changed. Color constancy across illumination changes that occur over time is called *successive color constancy*.

Geometric factors can also cause the illumination impinging on a surface to change. This is illustrated by Figure 61.2. All of the effects shown occur without any change in the spectra of the light sources but instead are induced by the geometry of the light sources and objects. Color constancy across illumination changes that occur within a single scene is called *simultaneous color constancy*.

The visual system's ability to achieve simultaneous constancy need not be easily related to its ability to achieve successive constancy. Indeed, fundamental to simultaneous constancy is some sort of segmentation of the image into regions of common illumination, while such segmentation is not obviously necessary for successive constancy (Adelson, 1999). Often results and experiments about successive and simultaneous constancy are compared and contrasted without explicit acknowledgment that the two may be quite different; keeping the distinction in mind as one considers constancy can reduce confusion. This chapter will focus on successive constancy, as many of the key conceptual issues can be introduced without the extra richness of simultaneous constancy. The discussion returns briefly to simultaneous constancy.

At the beginning of the chapter, constancy was cast in terms of the stability of object color appearance, and this is the sense in which the experiments presented below assess it. Some authors (Brainard and Wandell, 1988; D'Zmura and Mangalick, 1994; Foster and Nascimento, 1994; Khang and Zaidi, 2002) have suggested that constancy might be studied through performance (e.g., object identification) rather than through appearance per se. One might expect appearance to play an important role in identification, but reasoning might also be involved. Although the study of constancy using performance-based methods is an interesting direction, this chapter is restricted to measurements and theories of appearance.

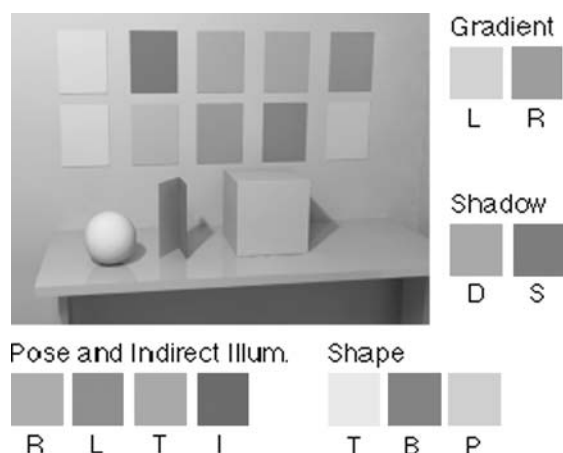


FIGURE 61.2. Image formation. Each set of square patches around the side of the image illustrates variation in the light reflected to the eye when surface reflectance is held fixed. *Gradient*: The two patches shown were extracted from the upper left (L) and lower right (R; above table) of the back wall of the scene. *Shadow*: The two patches were extracted from the tabletop in direct illumination (D) and shadow (S). *Shape*: The three patches shown were extracted from two regions of the sphere (T and B; center top and right bottom, respectively) and from the colored panel directly above the sphere (P; the panel is the leftmost of the four in the bottom row). Both the sphere and the panel have the same simulated surface reflectance function. *Pose and indirect illum*: The four patches were extracted from the three visible sides of the cube (R, L, and T; right, left, and top visible sides, respectively) and from the left side of the folded paper located between the cube and the sphere (I). The simulated surface reflectances of all sides of the cube and of the left side of the folded paper are identical. The image was rendered from a synthetic scene description using the RADIANCE computer graphics package (Larson and Shakespeare, 1998). There were two sources of illumination in the simulated scene: a diffuse illumination that would appear bluish if viewed in isolation and a directional illumination (from the upper left) that would appear yellowish if viewed in isolation. All of the effects illustrated by this rendering are easily observed in natural scenes. (See color plate 37.)

AN EXAMPLE EXPERIMENT Figure 61.3 shows the basic experimental setup used by Kraft and Brainard (1999). Subjects viewed a collection of objects contained in an experimental chamber. The chamber illumination was provided by theater lamps. The light from the lamps passed through a diffuser before entering the chamber, so that the overall effect was of a single diffuse illuminant. Each lamp had either a red, green, or blue filter, and by varying the intensities of the individual lamps, the spectrum of the chamber illumination could be varied. Because the light in the chamber was diffuse, the viewing environment provided a rough approximation to Mondrian World conditions.

The far wall of the experimental chamber contained a *test patch*. Physically, this was a surface of low neutral reflectance so that under typical viewing conditions it would have appeared dark gray. The test patch was illuminated by the

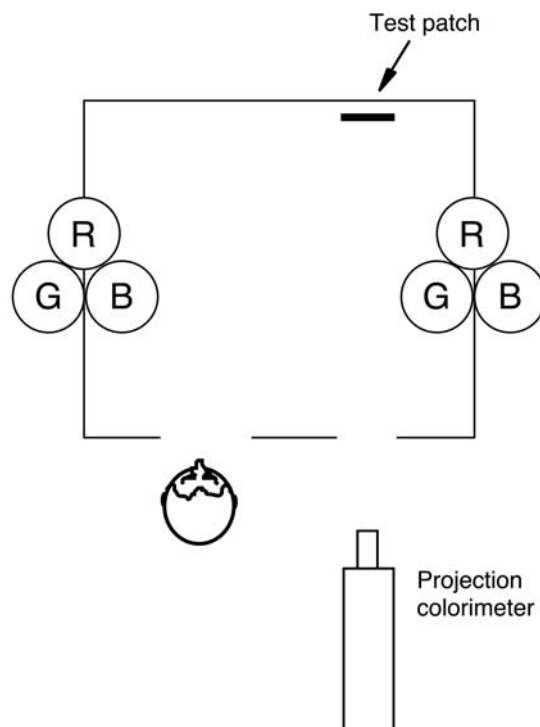


FIGURE 61.3. Schematic diagram of the experimental apparatus used in the experiments of Kraft and Brainard. An experimental chamber was illuminated by computer-controlled theater lamps. Different filters were placed over individual lamps, so that by varying their relative intensity the overall spectral power distribution of the chamber illumination could be varied. The light from the lamps was passed through a diffuser, producing a fairly homogeneous illumination. The observer viewed a test patch on the far wall of the chamber. The test patch was illuminated by the ambient chamber illumination and also by a beam from a projection colorimeter. The beam from the colorimeter was not explicitly visible, so that the perceptual effect of varying it was to change the apparent surface color of the test patch.

ambient chamber illumination and also by a separate projector. The projector beam was precisely aligned with the edges of the test patch and consisted of a mixture of red, green, and blue primaries. By varying the amount of each primary in the mixture, the light reflected to the observer from the test patch could be varied independently of the rest of the image. The effect of changing the projected light was to change the color appearance of the test, as if it had been repainted. The apparatus thus functioned to control the effect described by Gelb (1950; see also Katz, 1935; Koffka, 1935), wherein using a hidden light source to illuminate a paper dramatically changes its color appearance.

The observer's task in Kraft and Brainard's (1999) experiments was to adjust the test patch until it appeared achromatic. Achromatic judgments have been used extensively in the study of color appearance (e.g., Chichilnisky and Wandell, 1996; Helson and Michels, 1948; Werner and Walraven, 1982). During the adjustment, the observer controlled

the chromaticity of the test patch while its luminance was held constant. In essence, the observer chose the test patch chromaticity, which appeared gray when seen in the context set by the rest of the experimental chamber. Whether the test patch appeared light gray or dark gray depended on its luminance. This was held constant during individual adjustments but varied between adjustments. For conditions where the luminance of the test patch is low relative to its surroundings, Brainard (1998) found no dependence of the chromaticity of the achromatic adjustment on test patch luminance. This independence does not hold when more luminous test patches are used (Chichilnisky and Wandell, 1996; Werner and Walraven, 1982).

The data from the experiment are conveniently represented using the standard 1931 CIE chromaticity diagram. Technical explanations of this diagram and its basis in visual performance are widely available (e.g., Brainard, 1995; CIE, 1986; Kaiser and Boynton, 1996), but its key aspects are easily summarized. Human vision is trichromatic, so that a light $C(\lambda)$ may be matched by a mixture of three fixed primaries:

$$C(\lambda) \sim XP_1(\lambda) + YP_2(\lambda) + ZP_3(\lambda) \quad (2)$$

In this equation $P_1(\lambda)$, $P_2(\lambda)$, and $P_3(\lambda)$ are the spectra of the three primary lights being mixed, and the scalars X , Y , and Z specify the amount of each primary in the mixture. The symbol \sim indicates visual equivalence. When we are concerned with human vision, standardizing a choice of primary spectra allows us to specify a spectrum compactly by its *tristimulus coordinates* X , Y , and Z . The CIE chromaticity diagram is based on a set of known primaries together with a standard of performance that allows computation of the tristimulus coordinates of any light from its spectrum. The chromaticity diagram, however, represents lights with only two coordinates, x and y . These *chromaticity coordinates* are simply normalized versions of the tristimulus coordinates:

$$x = \frac{X}{X+Y+Z}, \quad y = \frac{Y}{X+Y+Z} \quad (3)$$

The normalization removes from the representation all information about the overall intensity of the spectrum while preserving the information about the relative spectrum that is relevant for human vision.

Figure 61.4 shows data from two experimental conditions. Each condition is defined by the scene within which the test patch was adjusted. The two scenes, labeled Scene 1 and Scene 2, are shown at the top of the figure. The scenes were sparse but had visible three-dimensional structure. The surface lining the chamber was the same in the two scenes, but the spectrum of the illuminant differed. The data plotted for each condition are the chromaticity of the illuminant (*open circles*) and the chromaticity of the observers' achromatic adjustments (*closed circles*).

The points plotted for the illuminant are the chromaticity of the illuminant, as measured at the test patch location when the projection colorimeter was turned off. These represent the chromaticity of the ambient illumination in the chamber, which was approximately uniform. The fact that the illuminant was changed across the two scenes is revealed in the figure by the shift between the open circles.

The plotted achromatic points are the chromaticity of the light reflected to the observer when the test appeared achromatic. This light was physically constructed as the superposition of reflected ambient light and reflected light from the projection colorimeter. Across the two scenes, the chromaticity of the achromatic point shifts in a manner roughly commensurate with the shift in illuminant chromaticity.

RELATION OF THE DATA TO CONSTANCY What do the data plotted in Figure 61.4 say about color constancy across the change from Scene 1 to Scene 2? A natural but misleading intuition is that the large shift in the achromatic locus shown in the figure reveals a large failure of constancy. This would be true if the data plotted represented directly the physical properties of the surface that appears achromatic. As noted above, however, the data plotted describe the spectrum of the light reaching the observer. To relate the data to constancy, it is necessary to combine information from the measured achromatic points and the illuminant chromaticities.

Suppose that the observer perceives the test patch as a surface illuminated with the same ambient illumination as the rest of the chamber. Introspection and some experimental evidence support this assumption (Brainard et al., 1997). The data from Scene 1 can then be used to infer the spectral reflectance of an *equivalent surface*. The equivalent surface would have appeared achromatic had it been placed at the test patch location with the projection colorimeter turned off.

Let the reflectance function of the equivalent surface be $\tilde{S}(\lambda)$. This function must be such that the chromaticity of $E_1(\lambda)\tilde{S}(\lambda)$ is the same as the chromaticity of the measured achromatic point, where $E_1(\lambda)$ is the known spectrum of the ambient illuminant in Scene 1. It is straightforward to find functions $\tilde{S}(\lambda)$ that satisfy this constraint. The inset to Figure 61.4 shows one such function. The function $\tilde{S}(\lambda)$ is referred to as the *equivalent surface reflectance* corresponding to the measured achromatic point.

The equivalent surface reflectance $\tilde{S}(\lambda)$ allows us to predict the performance of a color constant observer for other scenes. To a constant observer, any given surface should appear the same when embedded in any scene. More specifically, a surface that appears achromatic in one scene should remain so in others. Given the data for Scene 1, the chromaticity of the achromatic point for a test patch in Scene 2 should be the chromaticity of $E_2(\lambda)\tilde{S}(\lambda)$, where $E_2(\lambda)$

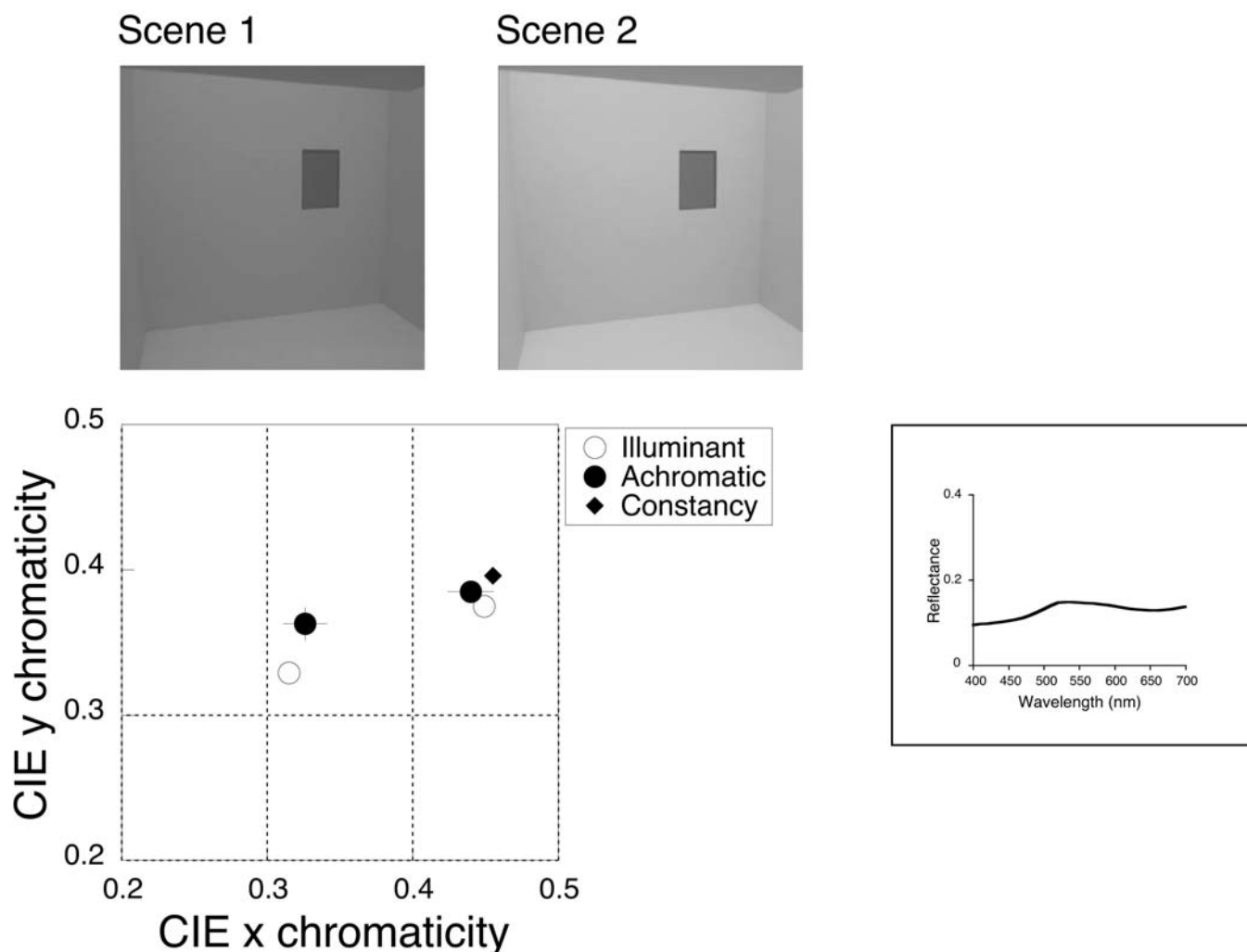


FIGURE 61.4. Basic data from an achromatic adjustment experiment. The images at the top of the figure show the observer's view of two scenes, labeled 1 and 2. The test patch is visible in each image. The projection colorimeter was turned off at the time the images were acquired, so the images do not show the results of observers' achromatic adjustments. The chromaticity diagram shows the data from achromatic adjustments of the test patch made in the context of the two scenes. The open circles show the chromaticity of the illuminant for each scene. The illuminant for Scene

1 plots to the lower left of the illuminant for Scene 2. The closed circles show the chromaticity of the mean achromatic adjustments of four observers. Where visible, the error bars indicate ± 1 standard error. The surface reflectance function plotted in the inset at the right of the figure shows the equivalent surface reflectance $\tilde{S}(\lambda)$ computed from the data obtained in Scene 1. The closed diamond shows the color constant prediction for the achromatic adjustment in Scene 2, given the data obtained for Scene 1. See the explanation in the text. (See color plate 38.)

is the spectrum of the illuminant in Scene 2. This prediction is shown in Figure 61.4 by the closed diamond.

Although the measured achromatic point for Scene 2 does not agree precisely with the constancy prediction, the deviation is small compared to the deviation that would be measured for an observer who had no constancy whatsoever. For such an observer, the achromatic point would be invariant across changes of scene. Thus, the data shown in Figure 61.4 indicate that observers are approximately color constant across the two scenes studied in the experiment.

Brainard (1998) developed a constancy index that quantifies the degree of constancy revealed by data of the sort

presented in Figure 61.4. The index takes on a value of 0 for no adjustment and 1 for perfect constancy, with intermediate values for intermediate performance. For the data shown in Figure 61.4, the constancy index is 0.83. This high value seems consistent with our everyday experience that the colors of objects remain stable over changes of illuminant but that the stability is not perfect.

A PARADOX AND ITS RESOLUTION The introductory section stated that illuminant and surface information is perfectly confounded in the retinal image. The data shown in Figure 61.4 indicate that human vision can separate

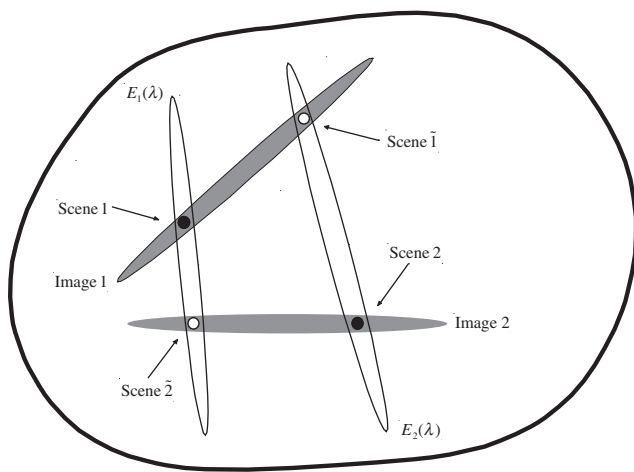


FIGURE 61.5. Schematic illustration of the ambiguity inherent in color constancy. The figure shows schematically the set of all scenes. Each point in the schematic represents a possible scene. Scenes 1 and 2 from the experiment described in text are indicated by closed circles. Each shaded ellipse encloses a subset of scenes that all produce the same image. The scenes represented by open circles, Scenes $\tilde{1}$ and $\tilde{2}$, produce the same images as Scenes 1 and 2, respectively. The open ellipses each enclose a subset of scenes that share the same illuminant.

these confounded physical factors and achieve approximate color constancy. This presents a paradox. If the information is perfectly confounded, constancy is impossible. If constancy is impossible, how can the visual system be achieving it?

The resolution to this paradox is found by considering restrictions on the set of scenes over which constancy holds. Figure 61.5 shows a schematic diagram of the set of all scenes, represented by the thick outer boundary. Each point within this boundary represents a possible scene, that is, a particular choice of illuminant and surface reflectances. The closed circles represent the two scenes used in the experiment described above. These are labeled Scene 1 and Scene 2 in the figure.

Denote the retinal image produced from Scene 1 as Image 1. Many other scenes could have produced this same image. This subset of scenes is indicated in the figure by the shaded ellipse that encloses Scene 1. This ellipse is labeled Image 1 in the figure. It also contains Scene $\tilde{1}$, indicated by an open circle in the figure. Scenes 1 and $\tilde{1}$ produce the same image and cannot be distinguished by the visual system.

Similarly, there is a separate subset of scenes that produce the same image (denoted Image 2) as Scene 2. This subset is also indicated by a shaded ellipse. A particular scene consistent with Image 2 is indicated by the open circle labeled Scene $\tilde{2}$. Like Scenes 1 and $\tilde{1}$, Scenes 2 and $\tilde{2}$ cannot be distinguished from each other by the visual system.

The open ellipse enclosing each solid circle shows a different subset of scenes to which it belongs. These are scenes that share a common illuminant. The open ellipse enclosing Scene 1 indicates all scenes illuminated by $E_1(\lambda)$, while the open ellipse enclosing Scene 2 indicates all scenes illuminated by $E_2(\lambda)$.

The figure illustrates why constancy is impossible in general. When viewing Image 1, the visual system cannot tell whether Scene 1 or Scene $\tilde{1}$ is actually present: achromatic points measured for a test patch embedded in these two scenes must be the same, even though the scene illuminants are as different as they are for Scenes 1 and 2. Recall from the data analysis above that this result (no change of achromatic point across a change of illuminant) indicates the absence of constancy.

The figure also illustrates why constancy can be shown across some scene pairs. Scenes 1 and 2 produce distinguishable retinal images, so there is no a priori reason for the measured achromatic points for test patches embedded in these two scenes to bear any relation to each other. In particular, there is no constraint that prevents the change in achromatic points across the two scenes from tracking the corresponding illuminant change. Indeed, one interpretation of the good constancy shown by the data reported above is that the visual system infers approximately the correct illuminants for Scenes 1 and 2. A mystery would occur only if it could also infer the correct illuminants for Scenes $\tilde{1}$ and $\tilde{2}$.

Figure 61.6 replots the results from achromatic measurements made for Scene 1 together with the results for a new scene, $\tilde{1}$. The illuminant in Scene $\tilde{1}$ is the same as that in Scene 2, but the objects in the scene have been changed to make the image reflected to the eye for Scene $\tilde{1}$ highly similar to that reflected for Scene 1; Scene $\tilde{1}$ is an experimental approximation to the idealized Scene $\tilde{1}$ described above. It would be surprising indeed if constancy were good when assessed between Scenes 1 and $\tilde{1}$, and it is not. The achromatic points measured for Scenes 1 and $\tilde{1}$ are very similar, with the constancy index between them being 0.11.

Discussion

CONSTANCY DEPENDS ON THE IMAGE ENSEMBLE STUDIED
The analysis and data presented above show that the degree of human color constancy depends on the choice of scenes across which it is assessed. Thus, it is not useful to summarize human performance through blanket statements about the degree of constancy obtained. Rather, questions about constancy must be framed in conjunction with a specification of the scene ensemble. Natural questions are (1) what ensembles of scenes support good constancy? and (2) how does constancy vary within some ensemble of scenes which

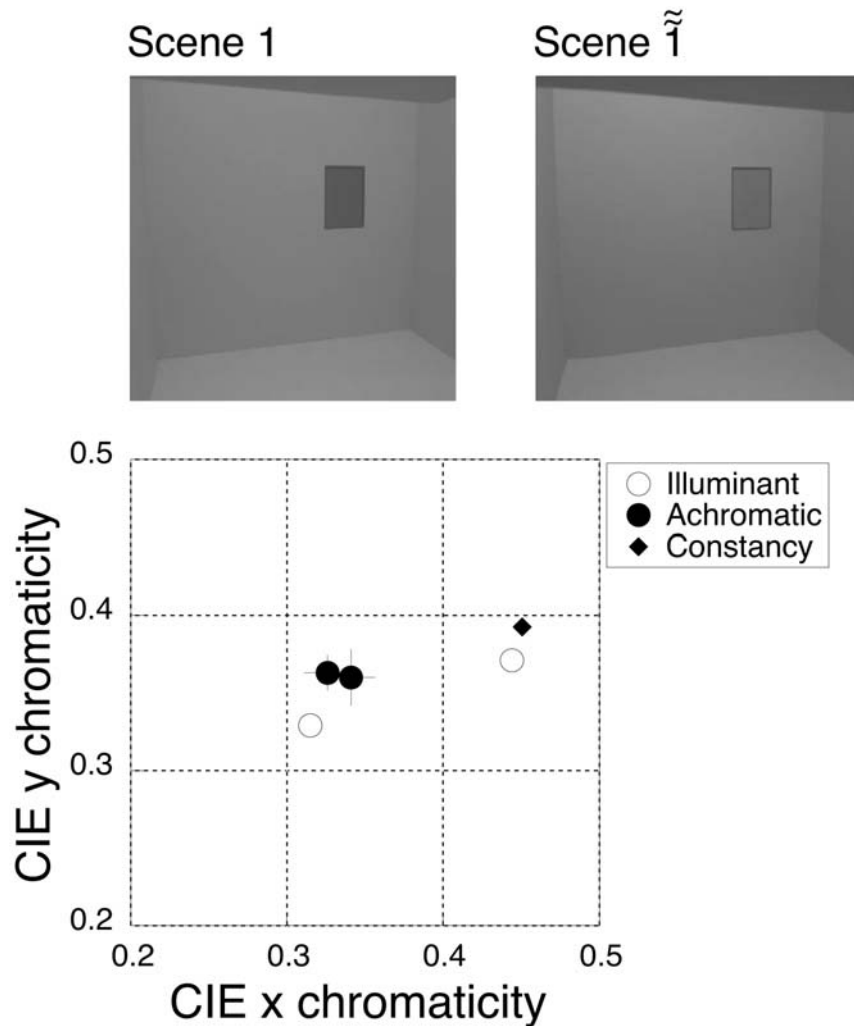


FIGURE 61.6. Achromatic data when both illuminant and scene surfaces are varied. The images at the top of the figure show the observer's view of two scenes, labeled 1 and $\tilde{1}$. The relation between these scenes is described in the text. The test patch is visible in each image. The projection colorimeter was turned off at the time the images were acquired, so the images do not show the results of

observers' achromatic adjustments. The chromaticity diagram shows the data from achromatic adjustments of the test patch made in the context of the two scenes. The format is the same as that of Figure 61.4. The equivalent surface reflectance $\tilde{S}(\lambda)$ computed from the data obtained in Scene 1 is shown in Figure 61.4. (See color plate 39.)

is intrinsically of interest? An example of the latter would be scenes that occur in natural viewing.

The choice of experimental scenes is a crucial aspect of the design of any constancy experiment. Without some a priori restriction the number of possible scenes is astronomical, and systematic exploration of the effect of all possible stimulus variables is not feasible. In choosing an ensemble of scenes for study, different experimenters have been guided by different intuitions. Indeed, it is this choice that most differentiates various studies. A common rationale, however, is to test specific hypotheses about how constancy might operate. The goal is to develop principles that allow generalization beyond the scenes studied experimentally.

Two broad approaches have been pursued. The *mechanistic approach* is based on the hope that constancy is mediated

by simple visual mechanisms and that these mechanisms can be studied through experiments with simple stimuli (e.g., uniform test patches presented on uniform background fields). The *computational approach* is to develop image processing algorithms that can achieve color constancy and to use insight gained from the algorithms to build models of human performance. This approach is often characterized by the use of stimuli closer to those encountered in natural viewing, as the algorithms are generally designed to take advantage of the statistical structure of natural images. The difference between the mechanistic and computational approaches is not always clear-cut: a mechanistic theory that explains human constancy can always be recast as a computational algorithm, while the action of a given algorithm can probably be approximated by the action of a series of

plausible neural mechanisms (see, e.g., Marr, 1982, chapter 1). Examples of both approaches are outlined below.

THE MECHANISTIC APPROACH Constancy is essentially a relative phenomenon; it can be assessed only by measuring appearance across two (or more) scenes. We cannot say from the data above that constancy is good for Scenes 1 and 2 but bad for Scene 1. Rather, constancy is good across the change from Scene 1 to Scene 2 but bad across the change from Scene 1 to Scene 1. Presumably it is possible to construct some other Scene 3 such that good constancy is revealed across Scenes 1 and 3.

What is it about the relation between Scenes 1 and 2 that supports the good constancy observed? A critical feature is that all that differs between them is the spectrum of the ambient illuminant. This design is common to most studies of constancy—stability of appearance is assessed under conditions where the surfaces comprising the scene are held fixed while the illuminant is varied (e.g., Arend and Reeves, 1986; Brainard and Wandell, 1992; Breneman, 1987; Burnham et al., 1957; Helson and Jeffers, 1940; McCann et al., 1976). It is probably the ubiquity of this surfaces-held-fixed design that leads to the oft-quoted generalization that human vision is approximately color constant (e.g., Boring, 1942).

When the surfaces in the image are held constant, it is easy to postulate mechanisms that could, qualitatively at least, support the high levels of observed constancy.

The initial encoding of the color signal by the visual system is the absorption of light quanta by photopigment in three classes of cone photoreceptors, the L, M, and S cones (for a fuller treatment see, e.g., Brainard, 1995; Kaiser and Boynton, 1996; Rodieck, 1998). The three classes are distinguished by how their photopigments absorb light as a function of wavelength. The fact that color vision is based on absorptions in three classes of cones is the biological substrate for trichromacy.

An alternative to using tristimulus or chromaticity coordinates to represent spectral properties of the light reaching the eye is to use cone excitation coordinates. These are proportional to the quantal absorption rates for the three classes of cones elicited by the light. The cone excitation coordinates for a light, \mathbf{r} , may be specified by using a three-dimensional column vector

$$\mathbf{r} = \begin{bmatrix} r_L \\ r_M \\ r_S \end{bmatrix} \quad (4)$$

It is well accepted that the signals initiated by quantal absorption are regulated by adaptation. A first-order model of adaptation postulates that (1) the adapted signals are determined from quantal absorption rates through multiplicative gain control; (2) at each retinal location the gains

are set independently within each cone class, so that (e.g.,) signals from M and S cones do not influence the gain of L cones; and (3) for each cone class, the gains are set in inverse proportion to a spatial average of the quantal absorption rates seen by cones of the same class. This model is generally attributed to von Kries (1905/1970). The three postulates together are sometimes referred to as *von Kries adaptation*. Von Kries recognized that models where some of the postulates hold and others do not could also be considered.

The first postulate of von Kries adaptation asserts that for each cone class, there is an adapted cone signal (a_L for the L cones, a_M for the M cones, and a_S for the S cones) that is obtained from the corresponding cone excitation coordinate through multiplication by a gain (e.g., $a_L = g_L r_L$). This may be expressed using the vector notation introduced in Eq. (4). Let the vector \mathbf{a} represent the magnitude of the adapted cone signals. Then

$$\mathbf{a} = \begin{bmatrix} a_L \\ a_M \\ a_S \end{bmatrix} = \begin{bmatrix} g_L & 0 & 0 \\ 0 & g_M & 0 \\ 0 & 0 & g_S \end{bmatrix} \begin{bmatrix} r_L \\ r_M \\ r_S \end{bmatrix} = \mathbf{D}\mathbf{r} \quad (5)$$

Because the adapted cone signals \mathbf{a} are obtained from the cone excitation coordinates \mathbf{r} through multiplication by the diagonal matrix \mathbf{D} , this postulate is called the *diagonal model for adaptation*. It should be emphasized that for the diagonal model to have predictive power, *all* of the effect of context on color processing should be captured by Eq. (5). In this model, two test patches that have the same adapted cone signals should have the same appearance.

In general, it is conceptually useful to separate two components of a model of adaptation (Brainard and Wandell, 1992; Krantz, 1968). The first component specifies what parameters of a visual processing model are allowed to vary with adaptation. The diagonal model provides this component of the full von Kries model. In the diagonal model, the only parameters that can vary are the three gains.

The second component of a full model specifies how the processing parameters are determined by the image. The diagonal model is silent about this, but the issue is addressed by the second two assumptions of the full von Kries model. Only cone excitation coordinates within a cone class influence the gain for that cone class, and the specific form of the influence is that the gain at a location is set inversely proportional to the mean excitation in a neighborhood of the location.

If the visual system implements von Kries adaptation, the adapted cone signals coding the light reflected from a surface are considerably stabilized across illuminant variation, provided that the other surfaces in the scene also remain fixed (Brainard and Wandell, 1986; Foster and Nascimento, 1994; Lennie and D’Zmura, 1988; see also Finlayson et al., 1994). Indeed, von Kries adaptation is the active ingredient

in later versions of Land's popular *retinex* account of successive color constancy. In the descriptions of the retinex algorithm, the adapted cone signals are called *lightness designators*, and these are derived from cone excitations through elaborate calculation. Nonetheless, for successive constancy the calculation reduces to a close approximation to classic von Kries adaptation (Land, 1986; see Brainard and Wandell, 1986; for early descriptions of Land's work see Land, 1959a, 1959b; Land and McCann, 1971).

Qualitatively, then, von Kries adaptation can explain the good constancy shown in experiments where the illuminant is changed and the surfaces in the scene are held fixed. Such adaptation also provides a qualitative account for the poor constancy shown by the data in Figure 61.6, where both the illuminant and surfaces in the scene were changed to hold the image approximately constant. On the basis of the data presented so far, one might sensibly entertain the notion that human color constancy is a consequence of early adaptive gain control.

Each of the postulates of von Kries adaptation have been subjected to sharply focused empirical test, and it is clear that each fails when examined closely. With respect to the diagonal model, a number of experimental results suggest that there must be additional adaptation that is not described by Eq. (5). These effects include gain control at neural sites located after signals from different cone classes combine and signal regulation characterized by a subtractive process rather than multiplicative gain control (e.g., Hurvich and Jameson, 1958; Jameson and Hurvich, 1964; Poirson and Wandell, 1993; Shevell, 1978; Walraven, 1976; see also Eskew et al., 1999; Webster, 1996).

The diagonal model fails when probed with stimuli carefully crafted to test its assumptions. Does it also fail for natural scenes? The illuminant spectral power distributions $E(\lambda)$ and surface spectral reflectance functions $S(\lambda)$ found in natural scenes are not arbitrary. Rather, these functions tend to vary smoothly as a function of wavelength. This constraint restricts the range of color signals likely to occur in natural scenes. Conditions that elicit performance in contradiction to the diagonal model may not occur for natural scenes. If so, the diagonal model would remain a good choice for studies of how adaptive parameters vary within this restricted domain.

The regularity of illuminant and surface spectral functions may be captured with the use of small-dimensional linear models (e.g., Cohen, 1964; Jaaskelainen et al., 1990; Judd et al., 1964; Maloney, 1986). The idea of a linear model is simple. The model is defined by N basis functions. These are fixed functions of wavelength, $E_1(\lambda), \dots, E_N(\lambda)$. Any spectrum $E(\lambda)$ is approximated within the linear model by a weighted sum of the basis functions

$$\tilde{E}(\lambda) = w_1 E_1(\lambda) + \dots + w_N E_N(\lambda) \quad (6)$$

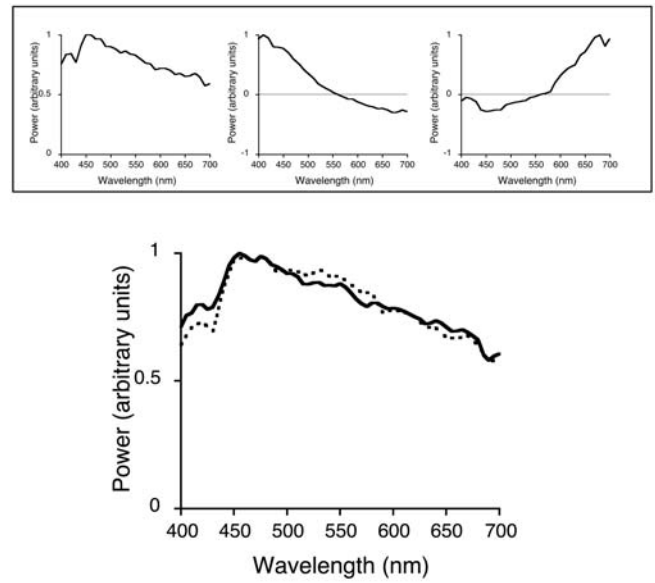


FIGURE 61.7. Linear model for natural daylights. *Top*: Three basis functions for the CIE linear model for daylights (CIE, 1986). *Bottom*: Linear model approximation to measured daylight. Solid line, measurement. Dotted line, reconstruction. The measured daylight was obtained from a database of measurements made available by J. Parkkinen and P. Silfsten on the World Wide Web at <http://cs.joensuu.fi/~spectral/databases/download/daylight.htm>.

where the weights are chosen to minimize the approximation error. Figure 61.7 plots the basis functions of a three-dimensional linear model for natural daylight and shows the linear model approximation to a measured daylight. The same approach can be used to express constraints on surface reflectance functions. The use of linear models has been central to computational work on color constancy (Brainard and Freeman, 1997; Brainard et al., in press; Maloney, 1999).

Mondrian World scenes where the illuminants and surface spectra are restricted to be typical of naturally occurring spectra can be referred to as *Restricted Mondrian World* scenes. When the experimental scenes are from the Restricted Mondrian World, the diagonal model seems to provide a good description of performance.

Brainard and Wandell (1992) tested the diagonal model using *asymmetric matching*. In asymmetric matching, the observer adjusts a matching patch, embedded in one scene, so that its appearance matches that of a test patch presented in another. In the context of the diagonal model, the match is taken to indicate two lights that elicit identical adapted cone signals. Let \mathbf{a}^t and \mathbf{a}^m represent the adapted cone signals for the test and matching patches. Equation (5) then yields

$$\mathbf{a}^t = \mathbf{D}^t \mathbf{r}^t = \mathbf{a}^m = \mathbf{D}^m \mathbf{r}^m \Rightarrow \mathbf{r}^m = [\mathbf{D}^m]^{-1} [\mathbf{D}^t] \mathbf{r}^t = \mathbf{D}^{t \rightarrow m} \mathbf{r}^t \quad (7)$$

where the diagonal matrix $\mathbf{D}^{t \rightarrow m}$ is

$$\mathbf{D}^{l \rightarrow m} = \begin{bmatrix} \frac{g_L^t}{g_L^m} & 0 & 0 \\ 0 & \frac{g_M^t}{g_M^m} & 0 \\ 0 & 0 & \frac{g_S^t}{g_S^m} \end{bmatrix} \quad (8)$$

If the diagonal model is correct, the cone excitation coordinates of the test and match patches are related by a diagonal matrix whose entries are the ratios of cone gains. A single asymmetric match determines the entries of the matrix $\mathbf{D}^{l \rightarrow m}$. Since Eq. (7) must hold with the same matrix $\mathbf{D}^{l \rightarrow m}$ for any choice of test patch cone coordinates, repeating the experiment with different test patches allows evaluation of the diagonal model.

In a successive matching experiment that employed simple synthetic scenes, Brainard and Wandell (1992) found that a large set of asymmetric matching data was in good agreement with the diagonal model. Similar results were obtained by Bauml (1995) also for successive matching and by Brainard et al. (1997) for simultaneous matching. To develop a theory of color constancy that applies to natural viewing, violations of the diagonal model may be small enough to neglect.

What about the other postulates of von Kries adaptation, which concern how the gains are set by image context? The notion that the gains are set as a function of a spatial average of the image has been tested in a number of ways. One approach is to examine the *equivalent background hypothesis*. In its general form, this hypothesis asserts that the effect of any image on the color appearance of a test light is the same as that of some uniform background. If the gains are set by a spatial average of the image, then the equivalent background hypothesis must also hold.

Precise tests of the equivalent background hypothesis where spatial variation of color is introduced into a uniform background, indicate that it fails (Brown and MacLeod, 1997; Shevell and Wei, 1998). The general logic is first to find a uniform field and a spatially variegated field that have an identical effect on the appearance of a single test light and then show that for some other test light these two contexts have different effects (Stiles and Crawford, 1932). Like the sharpest tests of the diagonal model, however, these studies did not employ stimuli from the Restricted Mondrian World.

Kraft and Brainard (1999) examined whether the spatial mean of an image controls the state of adaptation by constructing two illuminated scenes that had the same spatial mean. To equate the mean, both the illuminant and the scene surfaces were varied between the scenes. Kraft and Brainard then measured the achromatic loci in the two scenes. If the spatial mean were the only factor controlling adaptation, then the achromatic point in the two scenes

should have been the same. A more general constancy mechanism, however, might be able to detect the change in the illuminant based on some other aspect of the images. The achromatic points were distinct, with a mean constancy index of 0.39. Even for nearly natural scenes, control of the gains is not a simple function of the spatial mean of the image: the visual system has access to additional cues to the illuminant. Kraft and Brainard examined other simple hypotheses about control of adaptation in nearly natural scenes and found that none accounted for the data.

A key feature in Kraft and Brainard's (1999) design (see also Gilchrist and Jacobson, 1984; Kraft et al., 2002; McCann, 1994) is that both the illuminant and the surfaces in the scene were varied. When only the illuminant is varied, the data are roughly consistent with adaptation to the spatial mean of the image. Such data do not provide a sharp test, however, since essentially all plausible hypotheses predict good constancy when the surfaces in the image are held fixed across an illuminant change. Only by varying the surfaces and illuminants to differentiate predictions can strong tests be made. This point also applies to studies of the neural locus of constancy.

The current state of affairs for the mechanistic approach may be summarized roughly as follows. A gain control model provides a reasonable approximation to performance measured in scenes consisting of illuminated surfaces, but lacking is a theory that links the gains to the image. The agenda is to understand what image factors control the state of adaptation. In the lightness literature, this is sometimes referred to as the *anchoring problem* (e.g., Gilchrist et al., 1999). Within the mechanistic approach, one recent theme is to study the influence of image contrast (Brown and MacLeod, 1997; Golz and MacLeod, 2002; Krauskopf et al., 1982; Shevell and Wei, 1998; Singer and D'Zmura, 1995; Webster and Mollon, 1991) and spatial frequency content (Bauml and Wandell, 1996; Poirson and Wandell, 1993). Another approach (Bauml, 1995; Brainard and Wandell, 1992; Chichilnisky and Wandell, 1995) is to study rules of combination (e.g., linearity) that allow prediction of parameter values for many images on the basis of measurements made for just a few.

THE COMPUTATIONAL APPROACH The mechanistic approach is motivated by consideration of the physiology and anatomy of the visual pathways. The computational approach begins with consideration about how one could, in principle, process the retinal image to produce a stable representation of surface color. The computational approach focuses on the information contained in the image rather than on the specific operation of mechanisms that extract the information.

Computational algorithms often operate in two distinct steps (Maloney, 1999). The first step estimates the illuminant

at each image location, while the second step uses the estimate to transform the cone coordinates at each location to an illuminant-invariant representation. Given linear model constraints on natural surface reflectance functions, the second step is quite straightforward (Buchsbaum, 1980) and is well approximated by diagonal gain control (Brainard and Wandell, 1986; Foster and Nascimento, 1994). The deep issue is what aspects of the image carry useful information about the illuminant. This issue is completely analogous to the central issue within the mechanistic approach, namely, what aspects of the image control adaptation. Indeed, the idea linking the computational algorithms to measured human performance is that measured adaptation might be governed by the same image statistics that provide information about the illuminant (Brainard et al., in press; Maloney, 1999).

Many algorithms have been proposed for estimating the illuminant from the image (Brainard and Freeman, 1997; Buchsbaum, 1980; D’Zmura and Iverson, 1993; D’Zmura et al., 1995; Finlayson et al., 1997; Forsyth, 1990; Funt and Drew, 1988; Lee, 1986; Maloney and Wandell, 1986). A detailed review of the individual algorithms is beyond the scope of this chapter, but excellent reviews are available (Hurlbert, 1998; Maloney, 1999). Common across algorithms is the general approach of specifying assumptions that restrict the class of scenes and then showing how it is possible to estimate the illuminant within the restricted class. With reference to Figure 61.5, each algorithm is based on a rule for choosing one particular scene from within each shaded ellipse.

In practice, different proposed algorithms depend on different image statistics. For example, in Buchsbaum’s (1980) classic algorithm, the illuminant estimate was based on the spatial mean of the cone quantal absorption rates. As a model for human performance, this algorithm may be tested by asking whether adaptation is governed only by the spatial mean. As described above, experiments show that this is not the case. The detailed logic connecting this algorithm to human performance is described in a recent review (Brainard et al., in press).

Other computational algorithms depend on different aspects of the image. For example, Lee (1986; see also D’Zmura and Lennie, 1986) showed that specular highlights in an image carry information about the illuminant. This has led to tests of whether human vision takes advantage of the information contained in specular highlights (Hurlbert et al., 1989; Yang and Maloney, 2001).

In Yang and Maloney’s (2001) work, the stimuli consisted of realistic computer graphics renderings of synthetic scenes. That is, the locations, spectral properties, and geometric properties of the scene illuminants and surfaces were specified in software, and a physics-based rendering algorithm was used to generate the stimuli. In real scenes, the

information provided by separate cues tends to covary, which makes it difficult to separate their effects. By using synthetic imagery, Yang and Maloney teased apart the effects of independent cues. They were able to show that specular highlights can influence human judgments of surface color appearance and to begin to delineate the circumstances under which this happens. Delahunt (2001) employed similar techniques to study the role of prior information about natural daylights in successive color constancy. (For computational analysis of the use of such prior information, see Brainard and Freeman, 1997; D’Zmura et al., 1995). The methodology promises to allow systematic study of a variety of hypotheses extracted from the computational literature.

GENERALIZING TO SIMULTANEOUS CONSTANCY This chapter has focused on successive color constancy, and in particular on the case where the illuminant is approximately uniform across the scene. As illustrated by Figure 61.2, this idealized situation does not hold for natural scenes.

When an image arises from a scene with multiple illuminants, one can still consider the problem of successive color constancy. That is, one can ask what happens to the color appearance of an object in the scene when the spectral properties of the illuminant are changed without a change in scene geometry. Little, if any, experimental effort has been devoted to this question.

The case of spatially rich illumination also raises the question of simultaneous constancy—how similar does the same object appear when located at different places within the scene?

One thread of the literature has emphasized the role of scene geometry (Bloj and Hurlbert, 2002; Bloj et al., 1999; Epstein, 1961; Flock and Freedberg, 1970; Gilchrist, 1977, 1980; Hochberg and Beck, 1954; Knill and Kersten, 1991; Pessoa et al., 1996). Under some conditions, the perceived orientation of a surface in a scene can influence its apparent lightness and color in a manner that promotes constancy. The range of conditions under which this happens, however, is not currently well understood.

An interesting aspect of simultaneous constancy is that the observer’s performance can depend heavily on experimental instructions. In a study of simultaneous color constancy, Arend and Reeves (1986) had observers adjust the color of one region of a stimulus display until it appeared the same as another. They found that observers’ matches varied with whether they were asked to judge the color of the reflected light or the color of the underlying surface. More constancy was shown when observers were asked to judge the surface (see also Bauml, 1999; Bloj and Hurlbert, 2002). In a study of successive constancy, on the other hand, Delahunt (2001) found only a small instructional effect. It is not yet clear what conditions support the instructional dichotomy, or whether

the dichotomy indicates dual perceptual representations or observers' ability to reason from appearance to identity.

Recent theories of lightness perception have emphasized simultaneous constancy (Adelson, 1999; Gilchrist et al., 1999). At the core of these theories is that idea that perception of lightness (and presumably color) proceeds in two basic stages. First, the visual system segments the scene into separate regions. Second, image data within regions are used to set the state of adaptation for that region. (At a more detailed level, the theories also allow for some interaction between the states of adaptation in different regions.) The two-stage conception provides one way that results for successive constancy might generalize to handle simultaneous constancy: models that explain successive constancy for uniformly illuminated scenes might also describe the processes that set the state of adaptation within separately segmented regions within a single image (Adelson, 1999). To the extent that this hypothesis holds, it suggests that work on simultaneous constancy should focus on the segmentation process. At the same time, it must be recognized that the segment-estimate hypothesis is not the only computational alternative (see, e.g., Adelson and Pentland, 1996; Funt and Drew, 1988; Land and McCann, 1971; Zaidi, 1998) and that empirical tests of the general idea should also be given high priority.

Acknowledgments

I thank P. Delahunt, B. Wandell, and J. Werner for discussion and for comments on draft versions of this chapter. This work was supported by National Eye Institute Grant EY 10016.

REFERENCES

- Adelson, E. H., 1999. Lightness perception and lightness illusions, in *The New Cognitive Neurosciences*, 2nd ed. (M. Gazzaniga ed.), Cambridge, MA: MIT Press, pp. 339–351.
- Adelson, E. H., and A. P. Pentland, 1996. The perception of shading and reflectance, in *Visual Perception: Computation and Psychophysics* (D. Knill and W. Richards, eds.), New York: Cambridge University Press, pp. 409–423.
- Arend, L. E., and A. Reeves, 1986. Simultaneous color constancy, *J. Opt. Soc. Am. A*, 3:1743–1751.
- Bauml, K. H., 1995. Illuminant changes under different surface collections: examining some principles of color appearance, *J. Opt. Soc. Am. A*, 12:261–271.
- Bauml, K. H., 1999. Simultaneous color constancy: how surface color perception varies with the illuminant, *Vis. Res.*, 39:1531–1550.
- Bauml, K. H., and B. A. Wandell, 1996. Color appearance of mixture gratings, *Vis. Res.*, 36:2849–2864.
- Bloj, M. G., and A. C. Hurlbert, 2002. An empirical study of the traditional Mach card effect, *Perception*, 31:233–246.
- Bloj, M., D. Kersten, and A. C. Hurlbert, 1999. Perception of three-dimensional shape influences colour perception through mutual illumination, *Nature*, 402:877–879.
- Boring, E. G., 1942. *Sensation and Perception in the History of Experimental Psychology*, New York: D. Appleton Century.
- Brainard, D. H., 1995. Colorimetry, in *Handbook of Optics*, vol. 1, *Fundamentals, Techniques, and Design* (M. Bass ed.), New York: McGraw-Hill, pp. 26.1–26.54.
- Brainard, D. H., 1998. Color constancy in the nearly natural image. 2. Achromatic loci, *J. Opt. Soc. Am. A*, 15:307–325.
- Brainard, D. H., W. A. Brunt, and J. M. Speigle, 1997. Color constancy in the nearly natural image. 1. Asymmetric matches, *J. Opt. Soc. Am. A*, 14:2091–2110.
- Brainard, D. H., and W. T. Freeman, 1997. Bayesian color constancy, *J. Opt. Soc. Am. A*, 14:1393–1411.
- Brainard, D. H., J. M. Kraft, and P. Longère (in press). Color constancy: developing empirical tests of computational models, in *Colour Perception: From Light to Object* (R. Mausfeld and D. Heyer, eds.), Oxford: Oxford University Press.
- Brainard, D. H., and B. A. Wandell, 1986. Analysis of the retinex theory of color vision, *J. Opt. Soc. Am. A*, 3:1651–1661.
- Brainard, D. H., and B. A. Wandell, 1988. Classification measurement of color appearance, *Invest. Ophthalmol. Vis. Sci., Suppl.*, 29:162.
- Brainard, D. H., and B. A. Wandell, 1992. Asymmetric color-matching: how color appearance depends on the illuminant, *J. Opt. Soc. Am. A*, 9:1433–1448.
- Breneman, E. J., 1987. Corresponding chromaticities for different states of adaptation to complex visual fields, *J. Opt. Soc. Am. A*, 4:1115–1129.
- Brown, R. O., and D. I. A. MacLeod, 1997. Color appearance depends on the variance of surround colors, *Curr Biol.*, 7:844–849.
- Buchsbaum, G., 1980. A spatial processor model for object colour perception, *J. Franklin Inst.*, 310:1–26.
- Burnham, R. W., R. M. Evans, and S. M. Newhall, 1957. Prediction of color appearance with different adaptation illuminations, *J. Opt. Soc. Am.*, 47:35–42.
- Chichilnisky, E. J., and B. A. Wandell, 1995. Photoreceptor sensitivity changes explain color appearance shifts induced by large uniform backgrounds in dichoptic matching, *Vis. Res.*, 35:239–254.
- Chichilnisky, E. J., and B. A. Wandell, 1996. Seeing gray through the on and off pathways, *Vis. Neurosci.*, 13:591–596.
- CIE, 1986. *Colorimetry*, 2nd ed. (CIE Pub. 15.2), Vienna, Bureau Central de la CIE.
- Cohen, J., 1964. Dependency of the spectral reflectance curves of the Munsell color chips, *Psychon. Sci.*, 1:369–370.
- Delahunt, P. B., 2001. *An evaluation of color constancy across illumination and mutual reflection changes*. Unpublished Ph.D. thesis, University of California at Santa Barbara, Santa Barbara.
- D'Zmura, M., and G. Iverson, 1993. Color constancy. I. Basic theory of two-stage linear recovery of spectral descriptions for lights and surfaces, *J. Opt. Soc. Am. A*, 10:2148–2165.
- D'Zmura, M., G. Iverson, and B. Singer, 1995. Probabilistic color constancy, in *Geometric Representations of Perceptual Phenomena: Papers in Honor of Tarow Indow's 70th Birthday* (R. D. Luce, M. D'Zmura, D. Hoffman, G. Iverson, and A. K. Romney, eds.), Mahwah, NJ: Erlbaum, pp. 187–202.
- D'Zmura, M., and P. Lennie, 1986. Mechanisms of color constancy, *J. Opt. Soc. Am. A*, 3:1662–1672.
- D'Zmura, M., and A. Mangalick, 1994. Detection of contrary chromatic change, *J. Opt. Soc. Am. A*, 11:543–546.
- Epstein, W., 1961. Phenomenal orientation and perceived achromatic color, *J. Psychol.*, 52:51–53.

- Eskew, R. T., J. S. McLellan, and F. Giulianini, 1999. Chromatic detection and discrimination, in *Color Vision: From Molecular Genetics to Perception* (K. Gegenfurtner and L. T. Sharpe, eds.), Cambridge: Cambridge University Press, pp. 345–368.
- Finlayson, G. D., M. S. Drew, and B. V. Funt, 1994. Color constancy—generalized diagonal transforms suffice, *J. Opt. Soc. Am. A*, 11:3011–3019.
- Finlayson, G. D., P. H. Hubel, and S. Hordley, 1997. Color by correlation. Paper presented at the IS&T/SID Fifth Color Imaging Conference. Scottsdale, AZ: Color Science, Systems, and Applications.
- Flock, H. R., and E. Freedberg, 1970. Perceived angle of incidence and achromatic surface color, *Percept. Psychophys.*, 8:251–256.
- Foley, J. D., A. van Dam, S. K. Feiner, and J. F. Hughes, 1990. *Computer Graphics: Principles and Practice*, 2nd ed. Reading, MA: Addison-Wesley.
- Forsyth, D. A., 1990. A novel algorithm for color constancy, *Int. J. Comput. Vis.*, 5:5–36.
- Foster, D. H., and S. M. C. Nascimento, 1994. Relational colour constancy from invariant cone-excitation ratios, *Proc. R. Soc. Lond. B*, 257:115–121.
- Funt, B. V., and M. S. Drew, 1988. Color constancy computation in near-Mondrian scenes using a finite dimensional linear model. Paper presented at the IEEE Computer Vision and Pattern Recognition Conference, Ann Arbor, MI.
- Gelb, A., 1950. Colour constancy, in *Source Book of Gestalt Psychology* (W. D. Ellis ed.), New York: Humanities Press, pp. 196–209.
- Gilchrist, A., and A. Jacobsen, 1984. Perception of lightness and illumination in a world of one reflectance, *Perception*, 13:5–19.
- Gilchrist, A. L., 1977. Perceived lightness depends on perceived spatial arrangement, *Science*, 195:185.
- Gilchrist, A. L., 1980. When does perceived lightness depend on perceived spatial arrangement? *Percept. Psychophys.*, 28:527–538.
- Gilchrist, A. L., C. Kossyfidis, F. Bonato, T. Agostini, J. Cataliotti, X. Li, B. Spehar, V. Annan, and E. Economou, 1999. An anchoring theory of lightness perception, *Psychol. Rev.*, 106:795–834.
- Golz, J., and D. I. A. MacLeod, 2002. Influence of scene statistics on colour constancy, *Nature*, 415:637–640.
- Helson, H., and V. B. Jeffers, 1940. Fundamental problems in color vision. II. Hue, lightness, and saturation of selective samples in chromatic illumination, *J. Exp. Psychol.*, 26:1–27.
- Helson, H., and W. C. Michels, 1948. The effect of chromatic adaptation on achromaticity, *J. Opt. Soc. Am.*, 38:1025–1032.
- Hochberg, J. E., and J. Beck, 1954. Apparent spatial arrangement and perceived brightness, *J. Exp. Psychol.*, 47:263–266.
- Hurlbert, A. C., 1998. Computational models of color constancy, in *Perceptual Constancy: Why Things Look as They Do* (V. Walsh and J. Kulikowski, eds.), Cambridge: Cambridge University Press, pp. 283–322.
- Hurlbert, A. C., H. Lee, and H. H. Bulthoff, 1989. Cues to the color of the illuminant, *Invest. Ophthalmol. Vis. Sci.*, Suppl., 30:221.
- Hurvich, L. M., and D. Jameson, 1958. Further development of a quantified opponent-color theory, in *Visual Problems of Colour II*, London: HMSO, pp. 693–723.
- Jaaskelainen, T., J. Parkkinen, and S. Toyooka, 1990. A vector-subspace model for color representation, *J. Opt. Soc. Am. A*, 7:725–730.
- Jameson, D. B., and L. M. Hurvich, 1964. Theory of brightness and color contrast in human vision, *Vis. Res.*, 4:135–154.
- Judd, D. B., D. L. MacAdam, and G. W. Wyszecki, 1964. Spectral distribution of typical daylight as a function of correlated color temperature, *J. Opt. Soc. Am.*, 54:1031–1040.
- Kaiser, P. K., and R. M. Boynton, 1996. *Human Color Vision*, 2nd ed., Washington, DC: Optical Society of America.
- Katz, D., 1935. *The World of Colour* (R. B. MacLeod and C. W. Fox, trans.), London: Kegan, Paul, Trench Truber and Co.
- Khang, B. G., and Q. Zaidi, 2002. Cues and strategies for color constancy: perceptual scission, image junctions and transformational color matching, *Vis. Res.*, 42:211–226.
- Knill, D. C., and D. Kersten, 1991. Apparent surface curvature affects lightness perception, *Nature*, 351:228–230.
- Koffka, K., 1935. *Principles of Gestalt Psychology*, New York: Harcourt, Brace.
- Kraft, J. M., and D. H. Brainard, 1999. Mechanisms of color constancy under nearly natural viewing, *Proc. Natl. Acad. Sci. USA*, 96:307–312.
- Kraft, J. M., S. I. Maloney, and D. H. Brainard, 2002. Surface-illuminant ambiguity and color constancy: effects of scene complexity and depth cues, *Perception*, 31:247–263.
- Krantz, D., 1968. A theory of context effects based on cross-context matching, *J. Math. Psychol.*, 5:1–48.
- Krauskopf, J., D. R. Williams, and D. W. Heevely, 1982. Cardinal directions of color space, *Vis. Res.*, 22:1123–1131.
- Land, E. H., 1959a. Color vision and the natural image, part I, *Proc. Natl. Acad. Sci. USA*, 45:116–129.
- Land, E. H., 1959b. Color vision and the natural image, part II, *Proc. Natl. Acad. Sci. USA*, 45:636–644.
- Land, E. H., 1986. Recent advances in retinex theory, *Vis. Res.*, 26:7–21.
- Land, E. H., and J. J. McCann, 1971. Lightness and retinex theory, *J. Opt. Soc. Am.*, 61:1–11.
- Larson, G. W., and R. Shakespeare, 1998. *Rendering with Radiance: The Art and Science of Lighting Visualization*, San Francisco: Morgan Kaufman.
- Lee, H., 1986. Method for computing the scene-illuminant chromaticity from specular highlights, *J. Opt. Soc. Am. A*, 3:1694–1699.
- Lennie, P., and M. D’Zmura, 1988. Mechanisms of color vision, *CRC Crit. Rev. Neurobiol.*, 3:333–400.
- Maloney, L. T., 1986. Evaluation of linear models of surface spectral reflectance with small numbers of parameters, *J. Opt. Soc. Am. A*, 3:1673–1683.
- Maloney, L. T., 1999. Physics-based approaches to modeling surface color perception, in *Color Vision: From Genes to Perception* (K. T. Gegenfurtner and L. T. Sharpe, eds.), Cambridge: Cambridge University Press, pp. 387–416.
- Maloney, L. T., and B. A. Wandell, 1986. Color constancy: a method for recovering surface spectral reflectances, *J. Opt. Soc. Am. A*, 3:29–33.
- Marr, D., 1982. *Vision*, San Francisco: W. H. Freeman.
- McCann, J. J., 1994. Psychophysical experiments in search of adaptation and the gray world. Paper presented at the IS&T’s 47th Annual Conference, Rochester, NY.
- McCann, J. J., S. P. McKee, and T. H. Taylor, 1976. Quantitative studies in retinex theory: a comparison between theoretical predictions and observer responses to the “Color Mondrian” experiments, *Vis. Res.*, 16:445–458.
- Mollon, J. D., in press. The origins of modern color science, in *The Science of Color*, 2nd ed. (S. K. Shevell ed.), Optical Society of America.
- Pessoa, L., E. Mingolla, and L. E. Arend, 1996. The perception of lightness in 3-D curved objects, *Percept. Psychophys.*, 58(8): 1293–1305.
- Poirson, A. B., and B. A. Wandell, 1993. Appearance of colored patterns—pattern color separability, *J. Opt. Soc. Am. A*, 10:2458–2470.

- Rodieck, R. W., 1998. *The First Steps In Seeing*, Sunderland, MA: Sinauer.
- Shevell, S. K., 1978. The dual role of chromatic backgrounds in color perception, *Vis. Res.*, 18:1649–1661.
- Shevell, S. K., and J. Wei, 1998. Chromatic induction: border contrast or adaptation to surrounding light? *Vis. Res.*, 38:1561–1566.
- Singer, B., and M. D’Zmura, 1995. Contrast gain control—a bilinear model for chromatic selectivity, *J. Opt. Soc. Am. A*, 12:667–685.
- Stiles, W. S., and B. H. Crawford, 1932. Equivalent adaptation levels in localised retinal areas. Paper presented at the Report of Discussions of the Vision Physiology Society of London.
- von Kries, J., 1905/1970. Influence of adaptation on the effects produced by luminous stimuli, in *Sources of Color Vision* (D. L. MacAdam ed.), Cambridge, MA: MIT Press.
- Walraven, J., 1976. Discounting the background: the missing link in the explanation of chromatic induction, *Vis. Res.*, 16:289–295.
- Webster, M. A., 1996. Human colour perception and its adaptation, *Network: Comput. Neural Syst.*, 7:587–634.
- Webster, M. A., and J. D. Mollon, 1991. Changes in colour appearance following post-receptoral adaptation, *Nature*, 349:235–238.
- Werner, J. S., and J. Walraven, 1982. Effect of chromatic adaptation on the achromatic locus: the role of contrast, luminance and background color, *Vis. Res.*, 22(8):929–944.
- Yang, J. N., and L. T. Maloney, 2001. Illuminant cues in surface color perception: tests of three candidate cues, *Vis. Res.*, 41:2581–2600.
- Zaidi, Q., 1998. Identification of illuminant and object colors: heuristic-based algorithms, *J. Opt. Soc. Am. A*, 15:1767–1776.

62 Comparative Color Vision

GERALD H. JACOBS

FOR A WIDE RANGE of natural conditions, the overall photon flux and the distribution of spectral energies reaching the retina vary both spatially and temporally. These variations are the raw material that animals use in the conversion of light to sight. Depending on the nature of the recipient visual system, different features of the light signal can be exploited to yield vision. Specific organizations that allow nervous systems to analyze differences in the distribution of spectral energy have evolved in many different taxa. In most cases, the result is an animal that has some color vision. There are significant variations in the acuteness and nature of this capacity across species, and this chapter underlines that fact by considering the nature, distribution, evolution, and utility of color vision in different animals.

Studying animal color vision: an example

The defining conditions for formal descriptions of color vision, as well as many of the techniques used in testing, were developed from studies of human color vision. To provide a reminder of some of the basic features of color vision, and to illustrate how they can be evaluated in studies of color vision in nonhuman subjects, we consider first an example of such an investigation—a study of color vision in the domestic dog.

Human subjects can simply be asked to say whether lights, surfaces, or objects appear the same or different, or they can be directed to provide ordered descriptions of their perceptions. Establishing a dialog with a nonhuman subject typically requires either a training regimen, the goal of which is to establish a linkage between a visual stimulus and a response or, alternatively, the examination of some naturally occurring behavior in circumstances where the visual stimuli can be specified. With a compliant subject like the dog, effective communication can be easily initiated using operant conditioning procedures (Neitz et al., 1989).

Figure 62.1 summarizes results that characterize several features of dog visual performance. A basic feature is spectral sensitivity (Fig. 62.1A), in which sensitivity to lights of different wavelength content is established. In the dog, this was assessed by progressively decreasing the intensity of a monochromatic light until its presence could no longer be discriminated from a spectrally broadband light to which it had been added. This is not strictly a test of color vision, but the character of the function yields inferences about the

nature of the visual system that can, in turn, be linked to color vision. Here the appearance of a sharp decline in sensitivity at a point in the spectrum that separates two regions of higher sensitivity indicates the presence of two different kinds of photopigments in the eye, and it implies that signals initiated by these two have been combined in a spectrally opponent manner. The latter is a hallmark of the neural organization for color vision in a wide variety of species, so its characteristic signature in the dog's spectral sensitivity function is strongly suggestive of the presence of color vision (Chittka et al., 1992; Jacobs, 1981).

Color vision means that an animal can independently process wavelength and intensity information, and it is typically established by asking an animal to discriminate between lights that consistently differ only in their spectral energy distributions. A key in color vision tests of this sort is to make it impossible for animals to use any additional perceptual cues. The results of such a color vision test in which three dogs were required to discriminate between various monochromatic lights and spectrally broadband lights are shown in Figure 62.1B. For most such combinations discrimination performance was nearly perfect, so dogs must have color vision. Note, however, that they failed the test when they were asked to discriminate a narrow band of wavelengths centered at about 480 nm. Such failure means that their color vision is of a particular type. About 1% of all humans experience a similar failure and, like the dog, they are defined as having dichromatic color vision. Most people, however, can easily discriminate all of these spectral lights from the broadband light. These individuals are classified as trichromatic, and thus the normative color vision of humans and dogs is discretely different.

The failure of dogs to see a difference between a 480 nm light and one that contains all spectral wavelengths reveals a fundamental feature of color vision in all animals—that stimuli having quite different spectral energy distributions may appear the same. Such perceptual identities constitute color matches, and the analysis of such matches has proven central to understanding the nature of color vision. Another color matching experiment was conducted in which dogs were asked to discriminate various additive mixtures of 500 nm and 440 nm lights from a 480 nm light. The result was that, for most proportions, the mixture of 500 nm and 440 nm lights appeared different to dogs than 480 nm lights, but for a particular ratio of 500 nm and 440 nm there was a

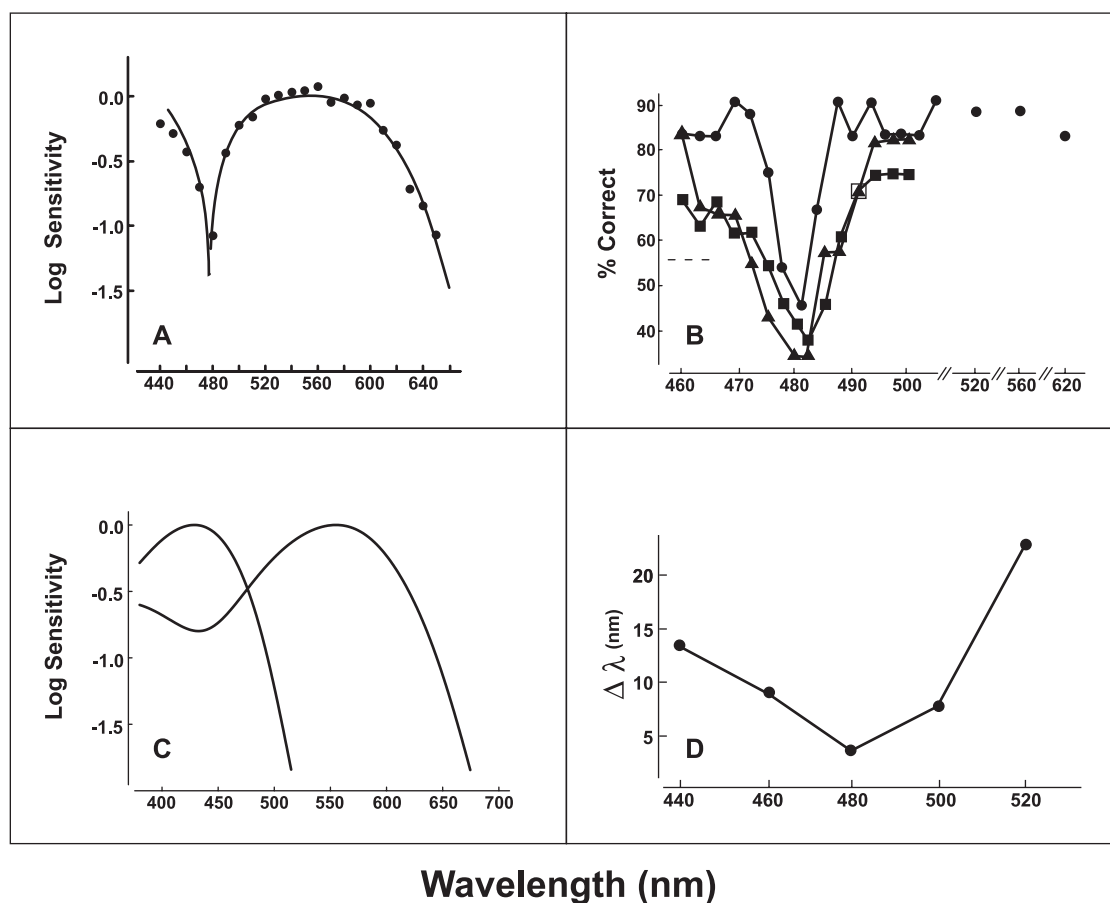


FIGURE 62.1. A compilation of measurements relevant to understanding dog color vision. *A*, spectral sensitivity. *B*, Color discrimination test. *C*, Cone pigment absorption spectra. *D*, Wavelength discrimination. The curves in *A* and *C* are normalized to have peak values of 1.0. The details of each of these curves are discussed in the text. (Data taken from Neitz et al., 1989.)

failure of discrimination, so that combination is said to match in color the 480 nm light. The relative amounts of the two mixture lights at this point define a color matching equation to the 480 nm light. These perceptual identities are conceptually powerful because from them inferences can be drawn about the spectral properties of the underlying cone photopigments. The nature of the color matches indicated that the two cone photopigments in the retina that support dichromatic color vision have spectral peaks at about 429 nm and 555 nm, respectively (Fig. 62.1*C*). Later direct measurements of dog cone pigments showed that these peak estimates were quite accurate (Jacobs et al., 1993).

The tests described established that the dog has color vision, identified its dimensionality (dichromatic), and yielded some strong indications of important features of the biology of vision in this species. But how acute is their color vision? The acuteness of color vision can be assayed in a number of different ways. Shown in Figure 62.1*D* are results from one such assessment, measurements of wavelength discrimination in which a determination was made of the size of the wavelength change ($\Delta \lambda$) required for successful discrimination at various locations in the spectrum. The results indi-

cate that at one point, around 480 nm, dogs have quite acute color vision, with differences of 5 nm or less required for successful discrimination. Away from that point discrimination quickly worsens, with the result that dogs are quite blind to wavelength differences over much of the middle and long wavelength portions of the spectrum. Human dichromats who behave in a similar fashion are often characterized as being “red/green color blind.”

This example illustrates how a number of basic features of color vision can be assessed in nonhuman species. These particular laboratory tests, which were easily accomplished for a common mammal, may be difficult or even impossible to apply to other species. In such cases, a range of other behavioral indices can be used. For example, insects like honeybees and wasps visit flowers to harvest nectar and pollen, and this natural behavior has often been exploited in controlled tests to examine insect color vision (Menzel and Backhaus, 1991). Whatever the technique, however, the goals of all animal color vision tests are usually quite similar: to assess the presence of color vision, to determine its dimensionality and acuteness, and to yield inferences about its biological basis and functional utility.

SOURCES OF INFORMATION The example just described shows that although nonhuman species may have color vision, it is not necessarily like ours. From a comparative perspective, then, a basic question is: who has color vision and what is it like? Given that there are millions of species of animals on the planet ranging in size from a few cells to a few tons, this is no small question. In a formal sense, color vision must be assayed behaviorally and, whereas it is true that many excellent behavioral studies have been conducted on representatives from some groups, for the vast majority of animals there is no information. This problem is ameliorated somewhat by our considerable understanding of the biological basis of color vision. For instance, there are strong linkages between the photopigments found in the eyes of animals and their potential for color vision. At minimum, an eye must have two or more types of photopigment that operate at common levels of illumination in order to provide the information required to support color vision, so any animal found to have only a single type of photopigment necessarily lacks color vision (strictly speaking, there may be some specialized cases where this is not true; for an example, see Neitz et al., 1999). Beyond the two pigment types required for color vision, there is significant correlation between the number of pigments present and the dimensionality of vision such that the presence of two pigments is associated with dichromacy, three pigments predicts trichromatic color vision, and so on. During the past quarter century, numerous methods have been developed to measure photopigments, so it is now usually much easier to do this than to undertake a direct examination of color vision, a task often arduous at best. The result is that photopigment measurements are now available for many species and, from these, predictions about color vision can be derived.

A second tool for inferring color vision comes from molecular biology. Single genes specify photopigment proteins (opsins), and enough has been learned about the structure of these genes to allow predictions about the properties of the photopigment specified by gene expression. Such analyses can be carried out on small tissue samples, and this provides the possibility of learning about photopigments in animals that may be unlikely targets for behavioral study (because of their size, ferocity, rareness, etc.). Information about photopigment genes is being generated very rapidly, and this too can serve as a useful adjunct to infer color vision. Beyond photopigments and their genes, there are a number of other biological markers that can be exploited to yield some predictions about color vision.

Even though there are other indices that can give indications of the presence and nature of color vision, it is clear that they cannot yield the same depth of insight obtained from direct studies of color vision. For example, knowledge

of the number of types of photopigment and their spectral properties may allow predictions about the dimensionality of color vision, but this by itself cannot predict the acuteness of the capacity, an aspect often more closely linked to the number and distribution of receptors containing the different cone types, as well as their nervous system wiring. Information about opsin genes can be even further removed from the realization of color vision because of the need to infer that the gene actually produces functional photopigment. In sum, although it is common to draw inferences about color vision from measurements of the types suggested, as I shall do freely here, it is important to remember that this is just what they are—inferences.

Considering both the direct examinations and those that document mechanisms, studies of animal color vision number in the hundreds, far too many to even list in a brief review. Instead, we consider a few topics that are intended to suggest the extent and nature of animal color vision. Further details on particular groups of animal can be found in the following review articles: insects (Briscoe and Chittka, 2001; Menzel and Backhaus, 1991); crustaceans (Marshall et al., 1999); lower vertebrates (Neumeier, 1998); fishes (Bowmaker, 1995); birds (Hart, 2001); mammals (Jacobs, 1993). Those interested in extinct vertebrates should see Rowe (2000).

DIMENSIONAL VARIATION Color vision results from neural comparisons of signals from receptor classes that have different spectral sensitivities. Increasing the number of receptor classes allows for an increase in the number of independent comparison channels and, correspondingly, in the potential dimensionality of color vision. Species that entirely lack a capacity for color vision stand at one extreme. Who are they? Not surprisingly, some of these are animals that live where photons are a scarce commodity. Deep-water environments certainly qualify in this regard and, indeed, both marine (Partridge, 1990) and freshwater (Bowmaker et al., 1994) fish that live at great depths often have only rod receptors that contain a single type of photopigment. Some species that live in brighter environments may also lack color vision; for example, cephalopods appear to be color blind (Wells, 1978; Messenger, 2001). Color vision is also absent in some mammals, but for a quite different reason. It has long been known that this condition occurs as an infrequent inherited or acquired defect in humans, but it is also a specieswide characteristic of some other mammals. In all of these animals, the retina has only a single class of cone containing middle-(MM) to long-wavelength-sensitive (L) pigment. A number of different mammalian species are like this, including some rodents (Cobb et al., 1999; Szel et al., 1996), nocturnal primates (Jacobs et al., 1996), and many—perhaps all—marine mammals (Fasick et al., 1998; Peichl et al., 2001; Levenson and Dizon, 2003). These animals have

the opsin genes required to produce a second, short-wave-length (S) cone pigment, but those genes contain fatal mutations. The implication is that ancestors to these species had color vision that was subsequently abandoned. Why this regressive step occurred in such a broad variety of species is a contemporary puzzle.

Minimal color vision requires at least two sets of photopigments, typically yielding dichromatic color vision. Like the dog, many other mammals apparently also have two pigments and dichromatic color vision (Jacobs, 1993). Dichromacy, however, does not seem to be a common arrangement. Beyond mammals, some fishes that live at midlevel depths have the photopigment potential for dichromacy (Bowmaker, 1995), as do some of the crustaceans (Marshall et al., 1999) and reptiles (Sillman et al., 2001), but most animals that have color vision seem to have escaped the confines of dichromacy.

Trichromacy is a much more common color vision arrangement. One reason for this is simply that insect species are abundant, and many of them seem to have trichromatic color vision. Although there is a great diversity of eye types among insects, there is nevertheless considerable commonality in their photopigments, with many species having three different types of photopigment, with respective peaks in the ultraviolet (UV), short (S), and middle (M) wavelengths (Briscoe and Chittka, 2001), although a long-wavelength-sensitive pigment may be added to this basic complement in many species of Lepidoptera. In some insect species, the total number of receptor types with differing spectral sensitivities is increased even further by the presence of screening pigments, photostable pigments that can serve to modify the spectral absorption properties of the photopigments. Although direct tests of color vision have not been done for most insects, the honeybee (*Apis mellifera*) has the best-studied color vision of any species outside of humans, and it is well documented that the three photopigments of the honeybee underlie acute trichromatic color vision (Backhaus, 1992). In addition to insects, some fishes (mostly living at shallower depths) are known to have three types of cone photopigments and putative trichromacy (Bowmaker, 1995), and, of course, many primates, including humans, are also trichromatic (Jacobs, 1996).

The addition of dimensions of color vision greater than trichromacy has occurred many times, or so it may seem, since many teleost fishes are known to have four types of cone pigment, as do a very large number of birds (Bowmaker, 1995; Hart, 2001). All of these animals are potential tetrachromats, as are other species, such as, turtles (Arnold and Neumeyer, 1987). It must be admitted, however, that of all the species that have four types of cone pigment, actual demonstrations that their operation gets translated into tetrachromatic color vision are very infrequent. Among the species in which tetrachromacy seems to have been

established are several common laboratory animals—goldfish, chickens, and pigeons. In the absence of appropriate tests, direct extrapolations from pigment complement to color vision dimensionality in other birds and fishes should be viewed with caution.

Considerable variation in color vision exists within each of these dimensional categories. For example, Figure 62.2 illustrates photopigment spectra and an index of color vision for two representative trichromatic species, an Old World monkey (*Macaca mulatta*) and the honeybee (*A. mellifera*), and a tetrachromat, the goldfish (*Carassius auratus*). The three have very different combinations of photopigment; for example, both honeybee and goldfish have UV-sensitive pigments that are not present in the monkey retina. Note too that the goldfish has an unusually long-wavelength-sensitive pigment. A consequence of these variations is that these species have strikingly different spectral sensitivities. Measurements of the capacity of each of these species to discriminate wavelength differences are illustrated in the right column of Figure 62.2. With a UV photopigment, both honeybee and goldfish have acute color vision at around 400 nm, a part of the spectrum to which the monkey is nearly blind to differences in color. The trichromats have in common two regions of most acute color discrimination, but in accord with differences in their photopigment complements, these regions are in different parts of the spectrum. Correspondingly, three regions of most acute discrimination, around 400, 500, and 610 nm, characterize wavelength discrimination in the tetrachromatic goldfish. The size of the wavelength change required for discrimination in the three species shown in Figure 62.2 suggests the possibility that there may also be real differences in the acuteness of color vision in these species. Comparisons like this illustrate the fact that dimensional characterization of color vision alone does not convey a very complete picture of animal color vision.

A simple count of the number of types of spectrally distinct photoreceptors shows that the potential for color vision with dimensionality even higher than tetrachromacy exists in a number of species. The reigning champions in this regard are the stomatopod crustaceans. The eyes of these diverse marine invertebrates contain a profusion of photopigments, with individual species having 11 to as many as 16 types of photopigment (Cronin and Marshall, 1989; Cronin et al., 2000)! And if that is not impressive enough, these eyes also contain a variety of spectral filters, so that the number of spectrally distinct receptors can be even higher than the number of photopigments. The result is a large number of receptors with narrowed spectral bandwidths. Behavioral experiments have shown that these animals in fact have color vision in that they can successfully discriminate a number of spectral stimuli from achromatic ones in the absence of a consistent brightness cue (Marshall et al., 1996). However, the nature of their color vision is unique, since the different

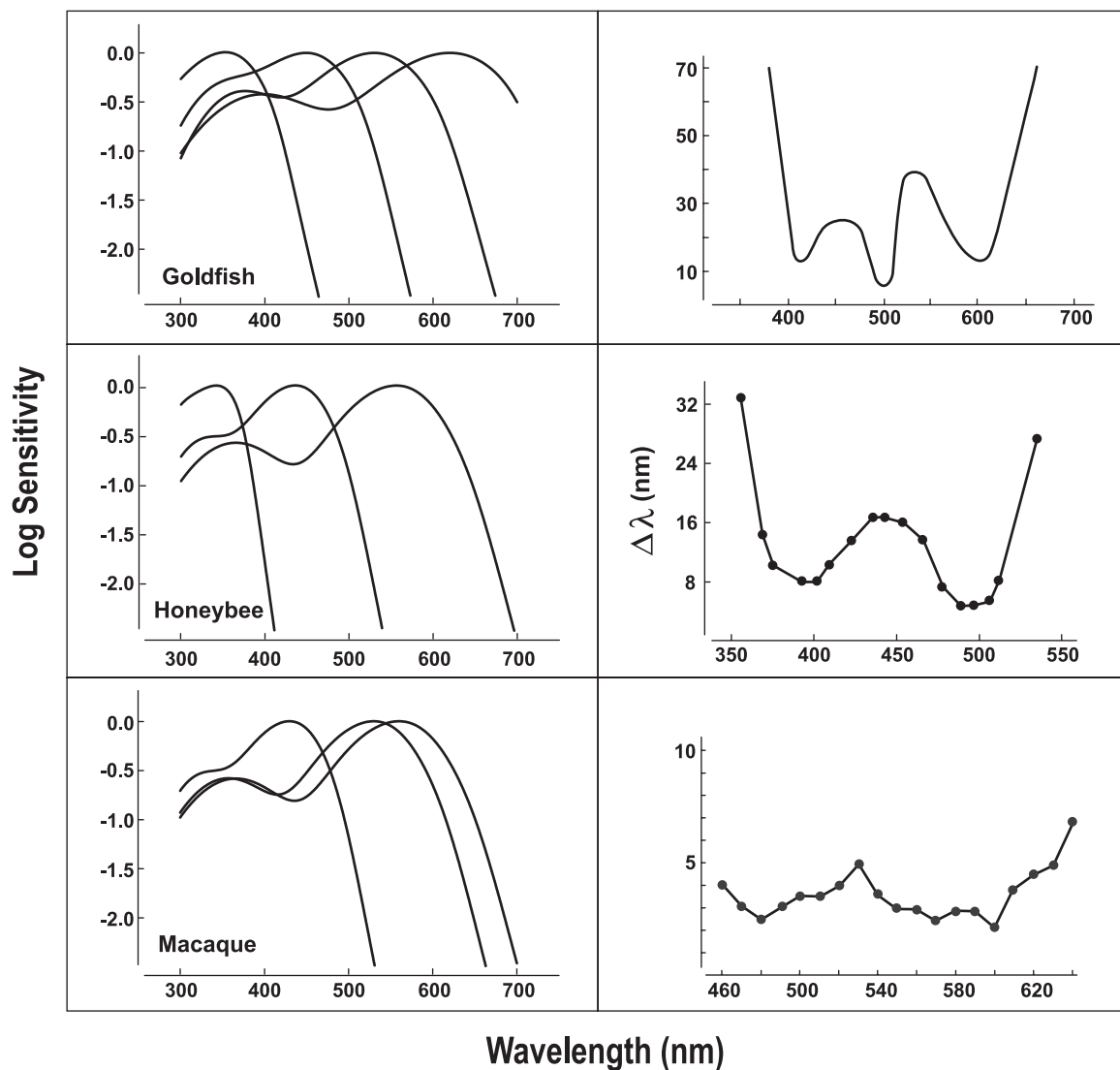


FIGURE 62.2. Photopigment absorption spectra (*left column*) and wavelength discrimination (*right column*) for three species. Honeybee and macaque monkey have trichromatic color vision; the goldfish is believed to be a tetrachromat. The sensitivity curves have been normalized as noted in Figure 62.1.

photoreceptor types found in stomatopods are separated into rows, and it is believed that the nervous system only allows for a series of spatially local dichromatic comparisons, that is, between pairs of receptors having differing spectral sensitivities. It may be that the stomatopod nervous system allows for further comparisons between these multiple dichromatic channels, but that is not established at present. It has been argued that a system of this kind could be used to enhance color constancy (see Chapter 61), a capacity that should be important, since stomatopods are often forced to make accurate absolute discriminations of the colors of objects (Osorio et al., 1997).

WAVELENGTH-SPECIFIC BEHAVIORS Although crustaceans like the stomatopods just described clearly have color vision

in a definitional sense, it has long been known that many invertebrates demonstrate a range of natural behaviors that somewhat resemble color vision yet do not satisfy the criteria usually associated with that capacity. These have been termed *wavelength-specific behaviors*, and they include stereotyped actions like egg laying, feeding, and escape, all behavioral sequences that can be reliably induced by stimulation of one or more spectrally distinct photoreceptors (Menzel, 1979). Wavelength-specific behaviors of this sort have been well documented in Lepidoptera and Hymenoptera, as well as in some Crustacea (Goldsmith, 1990; Marshall et al., 1996). Close examination of these cases often reveals the presence of the sorts of biological mechanisms associated with color vision, that is, more than one spectral class of receptor and neural interactions of inputs from these sep-

arate classes. However, these animals are typically unable to generalize this capacity so that it can be used in other situations. This absence of plasticity in making discriminations in novel situations is usually argued to separate wavelength-specific behaviors from color vision. The fact that animals that display wavelength-specific behaviors often have multiple types of photopigments and the requisite neural wiring for comparisons of their signals indicates that one needs to be particularly cautious in attributing color vision based solely on the presence of certain biological arrangements.

Evolution of color vision

An obvious conclusion drawn from the previous section is that most contemporary species have color vision and that the capacity appears in many different guises. How did this happen? Interest in the evolution of visual capacities is not new; in fact, that concern is a central theme in the most famous book on comparative vision, Gordon Walls' treatise on *The Vertebrate Eye and Its Adaptive Radiation* (1942). Although Walls and those who followed him offered plenty of speculation about the evolution of color vision, it is only in the past 15 years that our developing understanding of visual mechanisms has begun to allow some tentative answers to questions about color vision evolution.

SCENARIO FOR PHOTOPIGMENT EVOLUTION Two developments have led to a better appreciation of the evolution of color vision: more and better studies of color vision in contemporary species and the addition of information about the genes that specify photopigment opsins. The latter story starts in 1986 with the announcement of the sequence of the human cone opsin genes (Nathans et al., 1986). Since then there has been a steady accumulation of opsin gene sequences for many other species. Ideas about the evolution of photopigments, and by extension that of color vision, can be derived from comparisons of these sequences (Bowmaker, 1998; Nathans, 1999; Yokoyama and Yokoyama, 1989). One possible interpretation is that it may have begun with something similar to the eyespots found in green algae. These receptors contain pigments that are quite similar in structure to the opsins of both invertebrate and vertebrate photopigments, and that commonality suggests that motile microorganisms like the algae may have been the first to develop photopigments (Deininger et al., 2000). It is believed that in vertebrates a single cone opsin gene (and its photopigment product) emerged first. Later, somewhere between 400 and 1000 million years ago, this progenitor gene duplicated and then diverged in structure, yielding as offspring two types of cone pigment with respective peaks in the short and middle to long wavelengths (Bowmaker, 1998; Nathans et al., 1986; Neitz et al., 2001). The immediate utility of this added pigment is, of course, not known. One speculation is that

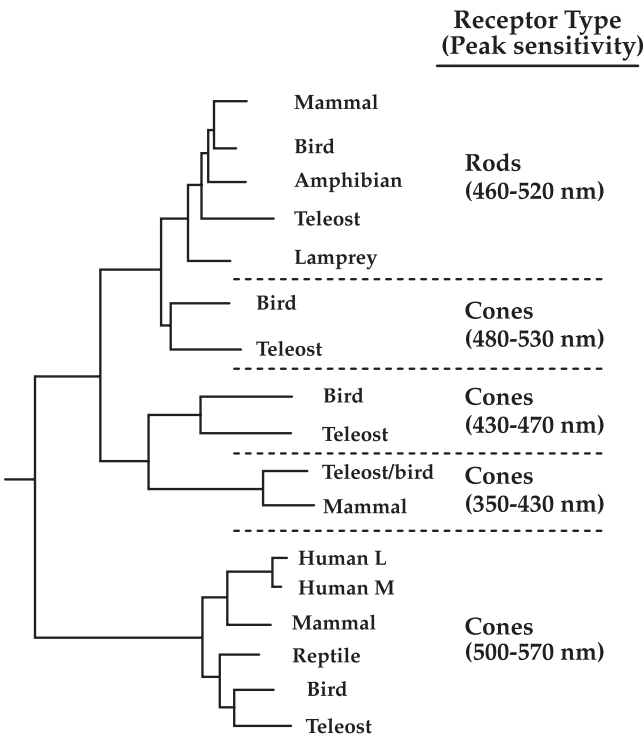


FIGURE 62.3. A simplified phylogeny for vertebrate photopigments. The interrelationships were inferred from comparisons of opsin gene structures. Illustrated are the relationships between four cone opsin gene families and a single rod opsin gene family. The peak sensitivities are ranges given for photopigments measured in contemporary representatives of each of the named groups. (Modified from Bowmaker, 1998.)

two cone pigments and the wiring requisite for extracting color information may actually have arisen as a device not for producing color vision per se, but rather as a means of eliminating the contaminating effects of flicker from the retinal image (Maximov, 2000).

Vertebrate rod photopigments arose from further changes in these original two cone pigments, and subsequently, the number of cone opsin gene families increased to four. Figure 62.3 shows a simplified phylogenetic tree for vertebrate photopigments as inferred from opsin gene structures (parallel structures for the phylogeny of invertebrate photopigments are available in Briscoe and Chittka, 2001). It is noteworthy that although vertebrate rod pigments all have very similar spectral properties, the cone pigments have spread their maximum sensitivities over a much larger portion of the spectrum. As we saw above, cone pigments reflective of the presence of all four families of cone opsin genes appear in many modern animals of several groups. Mammals are unusual in having cone pigments from only two of these families, implying that representatives of the other two gene families were lost sometime during mammalian evolution. One possibility is that this loss was associated with the dominant nocturnality and consequent supremacy of rod vision

in early mammals (Walls, 1942). Under those low-light conditions, neither cones nor color vision would likely be very useful.

Among mammals only the primates have added a third cone pigment to their retinal repertoire, and this has allowed them to become trichromatic. This happened uniformly for the catarrhines (Old World monkeys, apes, and humans) as a result of an X-chromosome gene duplication that occurred some 30 to 40 million years ago, an event that set the stage for the presence of separate M- and L-cone pigments (Nathans et al., 1986). The platyrrhine (New World) monkeys are very different. The vast majority of these species have polymorphic color vision, with individual animals having any of several versions of trichromatic or dichromatic color vision (Jacobs, 1998). This polymorphism, in turn, reflects individual variations in cone pigments and cone opsin genes. Like the catarrhines, these monkeys have an autosomal (chromosome 7) S-cone opsin gene, but unlike the catarrhines, they have only a single X-chromosome opsin gene. This gene is polymorphic, thus accounting for individual variations in cone pigments and color vision. How this works is illustrated in Figure 62.4 for the most common arrangement found in platyrrhine monkeys, one where there are three M/L opsin gene alleles and corresponding photopigments. An important consequence of this arrangement is that since males have only a single X chromosome, they necessarily have only a single type of M/L pigment and, thus, dichromatic color vision. With two X chromosomes, females can become heterozygous for their M/L opsin genes, and those that do have two types of M/L cone pigment and trichromatic color vision (Jacobs, 1984). The result of this arrangement is a striking array of different color vision capacities among conspecific animals.

One type of New World monkey departs notably from this polymorphic theme. Howler monkeys (*Alouatta*) have an opsin gene/photopigment arrangement that is very similar to that of the catarrhines (Jacobs et al., 1996). This would be expected to give them universal trichromatic color vision (although that fact has not yet been experimentally established). It would appear that something very similar to what happened in catarrhine history also occurred in the line to modern howler monkeys, that is an X-chromosome opsin duplication and subsequent divergence to permit separate M and L opsin genes and photopigments.

Until recently, it was believed that the third main group of primate, the more primitive strepsirrhines (lemurs, lorises, and their ilk), are unlike either catarrhines or platyrrhines in having only a single M/L photopigment with no polymorphic variations. This would make them similar to many non-primate mammals. It has now been discovered, however, that some diurnal strepsirrhines have M/L opsin gene and photopigment polymorphism similar to that described for the platyrrhines (Jacobs et al., 2002; Tan and Li, 1999), and

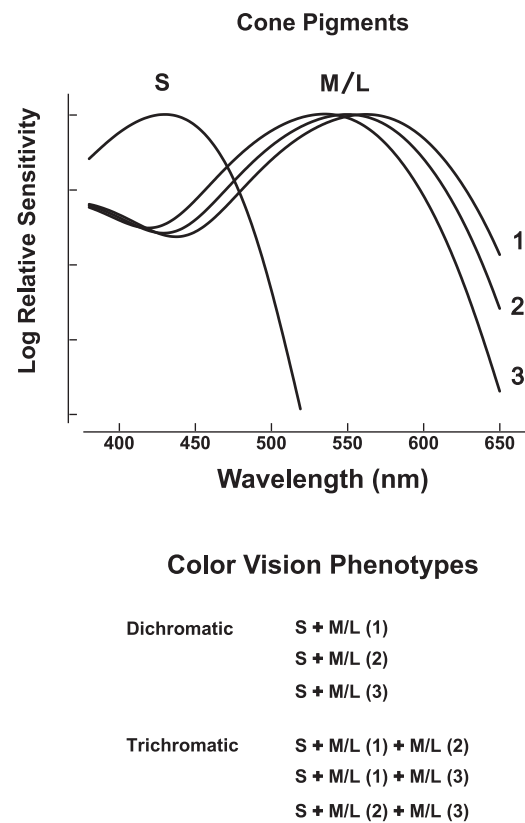


FIGURE 62.4. Schematic representation of the photopigment basis for the polymorphic color vision of most New World monkeys. Sketched at the top are the spectral sensitivities of four types of cone. The list at the bottom shows how these cone pigments are combined in individual animals to yield six different cone pigment and color vision phenotypes. (Modified from Jacobs, 1998.)

this means that some individuals in these species could also have trichromatic color vision. The strepsirrhines and platyrrhines are only distantly related, and it seems likely that the photopigment polymorphism seen in two groups arose independently.

OIL DROPLETS Animal eyes contain a variety of filters that serve to condition the light incident on photoreceptors. Many of these filters are spectrally selective, so they have long attracted attention for the possible role(s) they may play in vision (Douglas and Marshall, 1999). Among these filters, perhaps the most intriguing are the oil droplets located in the inner segments of cone photoreceptors of many birds, turtles, and lizards. Many of these oil droplets are densely pigmented and act as long-pass spectral filters, so that, depending on the location of the spectral cutoff, the droplets appear red, orange, or yellow in fresh tissue. Oil droplets influence the sensitivity of the photoreceptors, as illustrated in the curves of Figure 62.5 that compare the spectral sensitivity of the four classes of cone found in the pigeon retina with and without the influence of accompanying oil

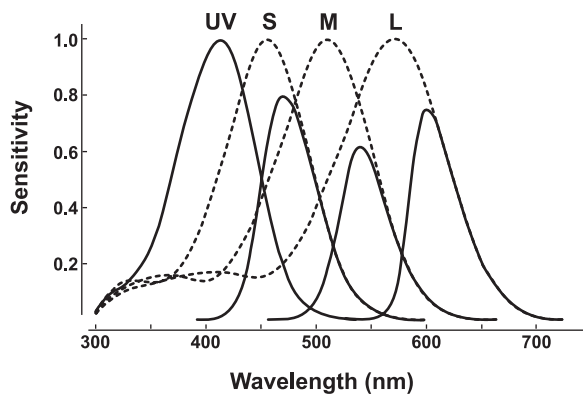


FIGURE 62.5. Spectral sensitivities of four types of cone found in the pigeon retina. The two sets of curves show sensitivity without (dashed) and with (continuous) filtering by the oil droplets that are found in each of these four receptor types. (Modified from Vorobyev et al., 1998.)

droplets. It can be seen that the effect of these oil droplets is to significantly narrow the cone absorption spectra, shift the locations of peak sensitivity, and decrease absorption efficiency.

In principle, a comparison of neural signals from a population of cones containing the same photopigments while having different types of oil droplets could provide a usable color signal, but there is no evidence that any animal has exploited that possibility. From a theoretical analysis, Vorobyev and colleagues have made a compelling argument to show that oil droplets found in bird retinas can potentially serve to enhance the animal's ability to discriminate important natural stimuli (such as plumage colors), and they may also serve to improve color constancy (Vorobyev et al., 1998). Whatever their specific roles, and these roles undoubtedly vary across different taxa, the presence of oil droplets in the retinas of many lineages implies that they are an ancient invention, possibly dating back to the ancestors of the earliest land vertebrates more than 400 million years ago (Robinson, 1994). If so, it is the absence of colored oil droplets in the retinas of some contemporary species that is notable. Viewed in this way, the absence of oil droplets reflects the loss of an ancestral adaptation, perhaps occasioned by a shift from a diurnal to a more nocturnal lifestyle.

IS COLOR VISION INEVITABLE? Color vision is present in the vast majority of all animals, and where it is absent, as in some mammals, its ancestral presence can often be inferred. The ubiquity of color vision raises the question of why this capacity evolved in so many different lineages. Part of the answer may come directly from a fundamental feature of photopigments. Photopigments have absorption bandwidths that are moderately narrow (half-bandwidths of about 50 to 70 nm) and fixed in size (Fig. 62.2). Consequently, any significant expansion of the spectral window through which an

animal senses its visual world requires that retinas contain populations of pigments with different absorption peaks. Discrete changes in the structures of pigment opsins (at the limit, a single amino acid substitution) that result from mutational changes in opsin genes can produce such new pigments (Asenjo et al., 1994; Merbs and Nathans, 1992). These new photopigments could be coexpressed in receptors along with a native pigment, as indeed they are in some contemporary species (Makino and Dodd, 1996; Rohlich et al., 1994), and this step alone will immediately yield a broadened spectral window (Jacobs et al., 1999). In most cases, however, pigment opsins get selectively transcribed into single receptors, and this allows both an expanded spectral window and a receptor basis for color vision.

Of course, multiple receptor types are necessary but not sufficient to yield color vision. What is also required is a nervous system organized to compare the rate of photon absorption in the different receptor types. This is typically accomplished by the presence of cells whose inputs are such that they generate output signals that are inhibitory/excitatory comparisons of photon capture in the different cone classes. These comparisons yield the spectral opponency property referred to above. Qualitatively similar comparisons are at the heart of the neural analysis of spatial information, in which case they are employed to compare the effects of stimulation at neighboring locations on the photoreceptor mosaic. A consequence is that any nervous system that has evolved to analyze spatial information in this fashion, which is to say virtually all visual systems, already has the basic organization required to set up spectral as well as spatial opponency. It is probably not unreasonable to suggest that virtually any visual system that adds a new type of photopigment will also gain some color vision.

Multiple types of photopigment and the appropriate neural comparisons set the stage for the presence of some color vision, but for these organizations to be maintained, to evolve, they must provide some adaptive advantage. The advantages of having color vision may seem self-evident, but is it possible to actually demonstrate the occurrence of such an advantage? One instance may be in the color vision of platyrrhine monkeys. We noted above that most of these species are polymorphic for M/L cone photopigments. The opsin genes specifying these alternative versions are only slightly different in structure, suggesting that they arose by discrete mutational changes (Neitz et al., 1991). The gene arrangement in these monkeys is such that a subset of the female monkeys, those that are heterozygous at the M/L opsin gene site, gain a dimension of color vision and become trichromatic (Fig. 62.4). How many females actually achieve trichromacy depends, in turn, on the relative frequencies of the three gene alleles. The results of a survey indicate that the three versions of these opsin genes are about equally frequent in the population, yielding an arrangement that will

maximize heterozygosity and, consequently, the incidence of female trichromacy (Jacobs, 1998). This outcome can best be explained as an example of overdominant selection, a circumstance in which a mutational change yields an advantage only to the heterozygous individual. The strong implication to be drawn from this example is that trichromatic color vision must be an adaptive trait for these monkeys.

One potential advantage of adding color vision capacity can be deduced from observations of human vision. At a given level of adaptation, a human observer can discriminate about 100 brightness steps. Because achromatic and chromatic dimensions of vision are orthogonal, adding a single dimension of color vision (i.e., becoming dichromatic) geometrically expands visual capacity (Neitz et al., 2001). So too does adding a third dimension, with the result that it is estimated that the trichromatic human can discriminate in excess of 2 million surface colors (Pointer and Attridge, 1998). This is a huge gain, and so in terms of sheer information-handling capacity, there can be considerable advantage to adding new dimensions of color vision.

If the acquisition of color vision may be close to inevitable, and if additional dimensions of color vision enhance discriminative capacity, then why isn't everyone, say, pentachromatic? The answer to this question about limitations on the dimensionality of color vision will no doubt differ for various lineages, reflective of the visual opportunities available in different environments. In general, however, it is true that there are inevitable costs associated with adding the new receptor types required for additional color vision capacity. For one thing, adding a new photopigment will reduce the number of receptors that contain earlier types of photopigment, and this may reduce the signal-to-noise ratio of each of the cone types, thus lowering overall color vision efficiency; this could be an important factor in limiting the number of cone types (Vorobyev and Osorio, 1998). Another potential problem is that in many visual systems the neural circuits for producing spectral opponency are quite specific, so acquiring a new color vision capacity may require elaborate nervous system changes as well as the simple addition of a photopigment. Adding new neural circuits is metabolically quite costly (Laughlin, 2001). Finally, model studies suggest that in terms of ability to discriminate many natural stimuli, there is probably little to be gained by having more than about four photopigments spread across the 300 nm spectral window available to most species (Menzel and Backhaus, 1991).

Utility of color vision

In considering why color vision exists at all, Gordon Walls questioned what it might do for animals that, he suggested, "certainly cannot appreciate sunsets and old masters" (Walls,

1942). It is conceivable that Walls was mistaken about the aesthetic lives of animals, but in any case his answer was similar to that given above: that color vision can considerably enhance the visibility of objects of interest. In recent years, some have tried to go beyond such generalities by asking how a particular type of color vision is suited to the visual tasks that an animal confronts. To give the flavor of these attempts, I briefly consider one of the best-studied examples.

HONEYBEES AND FLORAL COLORS Honeybees have trichromatic color vision. These insects are dependent on the pollen and nectar offered by flowers, and to obtain these, they have to make reliable discriminations among different flowers. On the other side of the coin, flowers achieve effective pollination by selectively attracting foraging bees. Since there is clear mutual gain for both bees and flowers in ensuring that efficient harvesting occurs, the relationship between floral coloring and bee color vision has been a natural focus for examining the utility of color vision (Kevan and Backhaus, 1998).

One step toward linking bee color vision to floral coloring can be made by considering the nature of the signals offered by flowers. Measurements of a large sample (>1000) of flowers drawn from several geographic locations reveal that their spectral reflectance patterns are not random—virtually all flowers can be placed in 1 of 10 categories, and only 5 of these are required to accommodate fully 85% of the entire sample (Chittka et al., 1994). Three such spectral reflectance patterns are illustrated in Figure 62.6. The potential visibility of these targets to honeybees can be crudely predicted by simply considering them in the context of the spectral absorption properties of bee photopigments (Fig. 62.2). For example, the flower whose reflectance spectrum is shown in Figure 62.6A should offer little or no color signal to the bee because its spectral reflectance is virtually constant across the entire spectral absorption range of the bee photopigments. At the same time, however, the pattern of reflectance of this flower does change very rapidly across the spectral absorption windows of the M and L pigments of Old World primates (Fig. 62.2), and so it would be predicted to offer a strong color signal to such observers and indeed it does, appearing red to a human viewer. Almost the reverse holds for the flower of Figure 62.6B. Here there is little reflectance change across the span of the primate cone photopigments, and flowers of this type appear white to a human observer. However, the reflectance pattern of this flower changes rapidly across the spectral bandwidths of the UV and S photopigments of the honeybee and thus offers a potentially strong color signal to the insect. The third reflectance pattern, shown in Figure 62.6C, is that measured for "green" foliage. Note that it shows only a small variation in reflectance pattern across the span of the honeybee photopigment absorption, and one would predict that it might

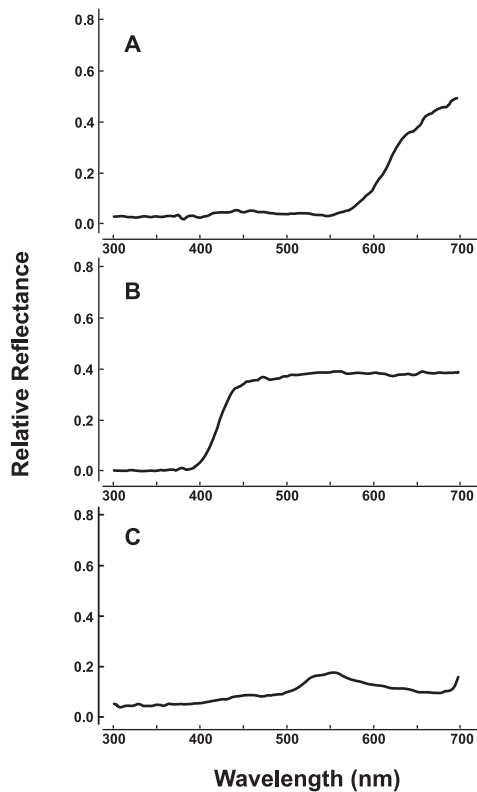


FIGURE 62.6. Reflectance spectra measured for three plants found in the visual environment of honeybees. *A*, A flower (*Justicia rizzinii*) that appears red to humans but is presumably uncolored to bees. *B*, A flower (*Bereroa incarnata*) that is white to humans but colored for honeybees. *C*, Green leaves. See text for further discussion. (Spectra taken from Chittka et al., 1994.)

appear essentially uncolored to the bee (Chittka et al., 1994). That fact is potentially important because it is from such foliage backgrounds that flower colors frequently need to be discriminated.

More quantitative predictions of the ability of bees to discriminate floral colors have been made by considering the spectral absorption and adaptational properties of bee photoreceptors in conjunction with some knowledge of the nature of color coding in the bee visual system (Chittka et al., 1994; Kevan and Backhaus, 1998). These efforts have led to the conclusion that bee visual systems and floral coloring are well matched for the efficient exchange of information (Chittka and Menzel, 1992). Whether or not this and other cases of insect color vision can be explained as evolutionary adaptations of photopigments to specific environmental opportunities is an issue of current debate (Briscoe and Chittka, 2001).

The discovery that flowers offer salient visual signals to insects in a portion of the spectrum that is invisible to humans led early investigators to conclude that UV might be special from ecological and evolutionary points of view (Goldsmith, 1994). The later discovery of UV receptors in

birds was similarly interpreted as implying that UV signals might be in some way unique. As the number of species known to have specific sensitivity to UV has expanded, and as understanding of the relationships between spectral cues and specific behaviors has broadened, it has become clearer that UV is probably not special (Hunt et al., 2001; Kevan et al., 2001). In concluding this discussion, no one is suggesting that UV signals are not important for some animals in some circumstances, but only that they should probably not be accorded any more significance than that given to other spectral signals.

THE ISSUE OF ANIMAL COLOR EXPERIENCE A fair conclusion from the material reviewed here is that behavioral experiments and biological inferences have taught us much about animal color vision. In many cases, one can now fairly confidently predict which spectral stimuli certain animals can or cannot discern and then go on to explain why this is so. But what has been learned about what animals may experience when they employ color vision? For instance, a foraging monkey may use color vision to quickly detect a fruit nestled in foliage, but in doing so, does it experience “yellow fruit” in “green foliage,” as a human observer might? There turns out to be precious little to indicate how animal color experiences may be similar to or different from our own or, indeed, if they even see colors in the sense that we do.

Transforming visual images so that they simulate for normal human trichromats the appearance of the world to human dichromats allows some insight into the color experiences of those with well-established alternative visual biology (Breitel et al., 1997). These predictions are based on a comparison of color discriminations of trichromats and dichromats and on reports of the perceptions of individuals whose color vision differs in the two eyes. One can never know for certain the color experiences of others, but this provides a reasonable approach to that end. It may be tempting to imagine that one could take color discrimination data and/or knowledge of photopigment complements and similarly deduce what color perceptions of other animals might look like to humans. The assumption in doing this is that the transformations between these indices and color experience are the same for different species. That assumption cannot be evaluated, and consequently such simulations may be enlightened fictions, but nevertheless they are fictions.

One higher-level aspect of human color vision is the ability to categorize colors by responding similarly to colors that can be discriminated. Such behavior is evidenced by the consistent use of color names, a process that seems nearly universal across cultural and linguistic boundaries (Abramov and Gordon, 1994). Categorical color perception has been demonstrated to occur in pigeons, and a range of observations suggest its occurrence in nonhuman primates (Jacobs, 1981; Zentall et al., 1986). This implies that at least some

animals are capable of deriving a generalized experience from their color vision abilities, but unfortunately, it does not tell us what that experience might be. In sum, although our personal experience of color makes it hard to believe that animals do not have some similar set of perceptual revelations, what these might be and how they differ across species remain a mystery.

Acknowledgments

Preparation of this chapter was supported by a grant from the National Eye Institute (EY02052). I thank Mickey Rowe for numerous helpful comments.

REFERENCES

- Abramov, I., and J. Gordon, 1994. Color appearance: on seeing red—or yellow, or green, or blue, *Annu. Rev. Psychol.*, 45:451–485.
- Arnold, K., and C. Neumeyer, 1987. Wavelength discrimination in the turtle *Pseudemys scripta elegans*, *Vis. Res.*, 27:1501–1511.
- Asenjo, A. B., J. Rim, and D. D. Oprian, 1994. Molecular determinants of human red/green color discrimination, *Neuron*, 12:1131–1138.
- Backhaus, W., 1992. Color vision in honeybees, *Neurosci. Biobehav. Rev.*, 16:1–12.
- Bowmaker, J. K., 1995. The visual pigments of fish, *Prog. Retinal Eye Res.*, 15:1–31.
- Bowmaker, J. K., 1998. Evolution of colour vision in vertebrates, *Eye*, 12:541–547.
- Bowmaker, J. K., V. I. Govardovskii, S. A. Shukolyukov, L. B. Zueva, D. M. Hunt, V. G. Sideleva, and O. G. Smirnova, 1994. Visual pigments and the photic environment: the Cottoid fish of Lake Baikal, *Vis. Res.*, 34:591–605.
- Breitel, H., F. Vienot, and J. D. Mollon, 1997. Computerized simulation of color appearance for dichromats, *J. Opt. Soc. Am. A*, 14:2647–2655.
- Briscoe, A. D., and L. Chittka, 2001. The evolution of color vision in insects, *Annu. Rev. Entomol.*, 46:471–510.
- Chittka, L., W. Beier, H. Hertel, E. Steinmann, and R. Menzel, 1992. Opponent colour coding is a universal strategy to evaluate the photoreceptor inputs in Hymenoptera, *J. Comp. Physiol. A*, 170:545–563.
- Chittka, L., and R. Menzel, 1992. The evolutionary adaptation of flower colours and insect pollinators' colour vision. *J. Comp. Physiol. A*, 171:171–181.
- Chittka, L., A. Shmida, N. Troje, and R. Menzel, 1994. Ultraviolet as a component of flower reflections, and the colour perception of hymenoptera, *Vis. Res.*, 34:1489–1508.
- Cobb, J. K., C. Bialozynski, J. Neitz, G. H. Jacobs, and M. Neitz, 1999. UV cone pigment genes from Syrian and Siberian hamsters, *Invest. Ophthalmol. Vis. Sci.*, 40:S353.
- Cronin, T. W., and N. J. Marshall, 1989. A retina with at least ten spectral types of photoreceptors in a mantis shrimp, *Nature*, 339:137–140.
- Cronin, T. W., N. J. Marshall, and R. L. Caldwell, 2000. Spectral tuning and the visual ecology of mantis shrimps, *Philos. Trans. R. Soc. Lond. B*, 355:1263–1268.
- Deininger, W., M. Fuhrmann, and P. Hegemann, 2000. Opsin evolution: out of the wild green yonder? *Trends Genet.*, 16:158–159.
- Douglas, R. H., and N. J. Marshall, 1999. A review of vertebrate and invertebrate ocular filters, in *Adaptive Mechanisms in the Ecology of Vision* (S. N. Archer, M. B. A. Djamgoz, E. R. Loew, J. C. Partridge, and S. Vallerga, eds.), Dordrecht: Kluwer Academic, pp. 95–162.
- Fasick, J. I., T. W. Cronin, D. M. Hunt, and P. R. Robinson, 1998. The visual pigments of the bottlenose dolphin (*Tursiops truncatus*), *Vis. Neurosci.*, 15:643–651.
- Goldsmith, T. H., 1990. Optimization, constraint, and history in the evolution of eyes, *Q. Rev. Biol.*, 65:281–322.
- Goldsmith, T. H., 1994. Ultraviolet receptors and color vision: evolutionary implications and a dissonance of paradigms, *Vis. Res.*, 34:1479–1487.
- Hart, N. S., 2001. The visual ecology of avian photoreceptors, *Prog. Ret. Eye Res.*, 20:675–703.
- Hunt, S., I. C. Cuthill, A. T. D. Bennett, S. C. Church, and J. C. Partridge, 2001. Is the ultraviolet waveband a special communication channel in avian mate choice? *J. Exp. Biol.*, 204:2499–2507.
- Jacobs, G. H., 1981. *Comparative Color Vision*, New York: Academic Press.
- Jacobs, G. H., 1984. Within-species variations in visual capacity among squirrel monkeys (*Saimiri sciureus*): color vision, *Vis. Res.*, 24:1267–1277.
- Jacobs, G. H., 1993. The distribution and nature of colour vision among the mammals, *Biol. Rev.*, 68:413–471.
- Jacobs, G. H., 1996. Primate photopigments and primate color vision, *Proc. Natl. Acad. Sci. USA*, 93:577–581.
- Jacobs, G. H., 1998. A perspective on color vision in platyrrhine monkeys, *Vis. Res.*, 38:3307–3313.
- Jacobs, G. H., J. F. Deegan II, M. A. Crognale, and J. A. Fenwick, 1993. Photopigments of dogs and foxes and their implications for canid vision, *Vis. Neurosci.*, 10:173–180.
- Jacobs, G. H., J. F. Deegan II, Y. Tan, and W.-H. Li, 2002. Opsin gene and photopigment polymorphism in a prosimian primate, *Vis. Res.*, 42:11–18.
- Jacobs, G. H., J. C. Fenwick, J. B. Calderone, and S. S. Deeb, 1999. Human cone pigment expressed in transgenic mice yields altered vision, *J. Neurosci.*, 19:3258–3265.
- Jacobs, G. H., M. Neitz, and J. Neitz, 1996. Mutations in S-cone pigment genes and the absence of colour vision in two species of nocturnal primate, *Proc. R. Soc. Lond. B*, 263:705–710.
- Kevan, P. G., and W. G. K. Backhaus, 1998. Color vision: ecology and evolution in making the best of the photic environment, in *Color Vision: Perspectives from Different Disciplines* (W. G. K. Backhaus, R. Kliegl, and J. S. Werner, eds.), Berlin: Walter de Gruyter, pp. 163–183.
- Kevan, P. G., L. Chittka, and A. G. Dyer, 2001. Limits to the salience of ultraviolet: lessons from colour vision in bees and birds, *J. Exp. Biol.*, 204:2571–2580.
- Laughlin, S. B., 2001. Energy as a constraint on the coding and processing of sensory information, *Curr. Opin. Neurobiol.*, 11:475–480.
- Levenson, D. H., and A. Dizon, 2003. Genetic evidence for the ancestral loss of SWS cone pigments in mysticete and odontocete cetaceans, *Proc. R. Soc. Lond. B*, 270:673–679.
- Makino, C. L., and R. L. Dodd, 1996. Multiple visual pigments in a photoreceptor of the salamander retina, *J. Gen. Physiol.*, 108:27–34.
- Marshall, J., J. Kent, and T. Cronin, 1999. Visual adaptations in crustaceans: spectral sensitivity in diverse habitats, in *Adaptive Mechanisms in the Ecology of Vision* (S. N. Archer, M. B. A. Djamgoz, E. R. Loew, J. C. Partridge, and S. Vallerga, eds.), Dordrecht: Kluwer Academic, pp. 285–327.

- Marshall, N. J., J. P. Jones, and T. W. Cronin, 1996. Behavioural evidence for colour vision in stomatopod crustaceans, *J. Comp. Physiol. A*, 179:473–481.
- Maximov, V. V., 2000. Environmental factors which may have led to the appearance of colour vision, *Philos. Trans. R. Soc. Lond. B*, 355:1239–1242.
- Menzel, R., 1979. Spectral sensitivity and color vision in invertebrates, in *Handbook of Sensory Physiology*, vol VII/6A (H. Autrum, ed.), Berlin: Springer-Verlag, pp. 503–580.
- Menzel, R., and W. Backhaus, 1991. Colour vision in insects, in *The Perception of Colour* (P. Gouras, ed.), Boca Raton, FL: CRC Press, pp. 262–293.
- Merbs, S. L., and J. Nathans, 1992. Absorption spectra of human cone pigments, *Nature*, 356:433–435.
- Messenger, J. B., 2001. Cephalopod chromatophores: Neurobiology and natural history, *Biol. Rev.*, 76:473–528.
- Nathans, J., 1999. The evolution and physiology of human color vision: insights from molecular genetic studies of visual pigments, *Neuron*, 24:299–312.
- Nathans, J., D. Thomas, and D. S. Hogness, 1986. Molecular genetics of human color vision: the genes encoding blue, green and red pigments, *Science*, 232:193–202.
- Neitz, J., J. Carroll, and M. Neitz, 2001. Color vision: almost reason enough for having eyes, *Opt. Photon. News*, 12:26–33.
- Neitz, J., T. Geist, and G. H. Jacobs, 1989. Color vision in the dog, *Vis. Neurosci.*, 3:119–125.
- Neitz, J., M. Neitz, J. C. He, and S. K. Shevell, 1999. Trichromatic color vision with only two spectrally discrete photopigments, *Nat. Neurosci.*, 2:884–888.
- Neitz, M., J. Neitz, and G. H. Jacobs, 1991. Spectral tuning of pigments underlying red-green color vision, *Science*, 252:971–974.
- Neumeyer, C., 1998. Color vision in lower vertebrates, in *Color Vision: Perspectives from Different Disciplines* (W. G. K. Backhaus, R. Kliegl, and J. S. Werner, eds.), Berlin: Walter de Gruyter, pp. 149–162.
- Osorio, D., N. J. Marshall, and T. W. Cronin, 1997. Stomatopod photoreceptor spectral tuning as an adaptation for colour constancy in water, *Vis. Res.*, 37:3299–3309.
- Partridge, J. C., 1990. The colour sensitivity and vision of fishes, in *Light and Life in the Sea* (P. J. Herring, A. K. Campbell, M. Whitfield, and L. Maddick, eds.), Cambridge: Cambridge University Press, pp. 167–184.
- Peichl, L., G. Behrmann, and R. H. H. Kroger, 2001. For whales and seals the ocean is not blue: a visual pigment loss in marine mammals, *Eur. J. Neurosci.*, 13:1520–1528.
- Pointer, M. R., and G. G. Attridge, 1998. The number of discernible colours, *Color Res. Appl.*, 23:52–54.
- Robinson, S. R., 1994. Early vertebrate colour vision, *Nature*, 367:121.
- Rohlich, P., T. van Veen, and A. Szel, 1994. Two different visual pigments in one retinal cone cell, *Neuron*, 13:1159–1166.
- Rowe, M. P., 2000. Inferring the retinal anatomy and visual capacities of extinct vertebrates, *Palaeontol. Electron.*, 3: <http://paleo-electronica.org/2000>
- Sillman, A. J., J. L. Johnson, and E. R. Loew, 2001. Retinal photoreceptors and visual pigments in *Boa constrictor imperator* *J. Exp. Zool.*, 290:359–365.
- Szel, A., P. Rohlich, A. R. Caffé, and T. van Veen, 1996. Distribution of cone photoreceptors in the mammalian retina, *Microsc. Res. Tech.*, 35:445–462.
- Tan, Y., and W.-H. Li, 1999. Trichromatic vision in prosimians, *Nature*, 402:36.
- Vorobyev, M., and D. Osorio, 1998. Receptor noise as a determinant of colour thresholds, *Proc. R. Soc. Lond. B*, 265:351–358.
- Vorobyev, M., D. Osorio, A. T. D. Bennett, N. J. Marshall, and I. C. Cuthill, 1998. Tetrachromacy, oil droplets and bird plumage colours, *J. Comp. Physiol. A*, 183:621–633.
- Walls, G. L., 1942. *The Vertebrate Eye and Its Adaptive Radiation*, Bloomfield Hills, MI: Cranbrook Institute of Science.
- Wells, M. J., 1978. *Octopus: Physiology and Behavior of an Advanced Invertebrate*, London: Chapman and Hall.
- Yokoyama, S., and R. Yokoyama, 1989. Molecular evolution of human visual pigment genes, *Mol. Biol. Evol.*, 6:186–197.
- Zentall, R. T., P. Jackson-Smith, J. A. Jagielo, and G. B. Nallan, 1986. Categorical shape and color coding by pigeons, *J. Exp. Psychol. Anim. Behav. Proc.*, 12:153–159.

63 Molecular Genetics of Human Color Vision and Color Vision Defects

MAUREEN NEITZ AND JAY NEITZ

THE TWO TYPES OF photoreceptor in the human eye, rods and cones, serve different functions. Rods serve vision only under conditions of very low light levels, such as at night when little light is available. In contrast, cones serve vision at relatively higher light levels. Most of our daily activities are performed in daylight and at room light levels above those where rods contribute significantly to vision but where cones are active. Thus, under most normal conditions, our vision is based on cone photoreceptors. The capacity to see color is a prominent component of cone-based vision, which requires multiple classes of cone photoreceptor. Most humans have trichromatic color vision mediated by at least three cone types, one from each of three well-separated spectral classes.

Photopigments are light-sensitive molecules that determine the spectral absorption characteristics of the cones. Thus, for each cone class, there is a corresponding class of cone pigment. The three classes are sometimes referred to as *blue*, *green*, and *red*. However, vision scientists usually refer to them according to their relative spectral sensitivities, *short*-, *middle*-, and *long-wavelength sensitive* (abbreviated *S*, *M*, and *L*). As far as we know, all humans with normal color vision have the same *S* pigment, and its absorption spectrum has a spectral peak near 415 nm (Bowmaker et al., 1980; Dartnall et al., 1983; Fasick et al., 1999). Traditionally it was assumed that human vision is characterized by a stereotyped set of *S*, *M*, and *L* pigments; however, recently it has become apparent that there is widespread variation in the *L* and *M* pigments that underlie normal vision (Dartnall et al., 1983; Merbs and Nathans, 1993; Neitz and Jacobs, 1986; Neitz et al., 1991, 1993; Winderickx et al., 1992a). The *L* pigments have spectral peaks near 560 nm (Dartnall et al., 1983; Schnapf et al., 1987), and the two most common variants are separated in spectral peak by approximately 3.5 nm (Merbs and Nathans, 1993; Neitz and Jacobs, 1986; Sharpe et al., 1998). Less common normal variants have spectral peaks that are shifted more than 8 nm shorter than the longest absorbing *L* pigment. *M* pigments peak near 530 nm (Dartnall et al., 1983; Schnapf et al., 1987), and normal variations also occur but with a lower frequency. Normal color vision requires the presence of the *S* pigment and at least one pigment from each of the *L* and *M* classes. Red-green color vision deficiencies are caused by the absence of expres-

sion or function of one class of pigment, either *L* or *M*. These color vision defects are extremely common, especially among people of Western European ancestry, for whom the frequency is about 8% in males and 0.4% in females.

Molecular genetic experiments have been combined with imaging, electrophysiology, and psychophysics to better understand the basic biology underlying color vision capacity, how the mechanisms arise during development, and how they have evolved. One of the most remarkable aspects of human color vision is the amazingly high degree of normal variation and the high frequency of defects. Color vision deficiency is one of the most frequent genetic anomalies in humans, and considerable progress has been made in understanding the molecular basis for it.

Background

TYPES OF COLOR VISION DEFECTS *Normal color vision* is the term used for the form of color vision shared by most humans. People with normal color vision can perceive four distinct (or unique) hues: red, yellow, green, and blue. Color information is extracted by neural circuits that compare the outputs of the cones. Red-green color vision is mediated by circuits that compare the outputs of the *L* and *M* cones. Blue-yellow color vision is mediated by circuits that compare the output of *S* cones to the summed outputs of the *L* and *M* cones. Together, these two neural systems provide the capacity to distinguish more than 100 different gradations of hue, which can be thought of as the sensations of the four unique hues individually or in combinations, such as shades of yellow-green, blue-green, purple (a red-blue color), and orange (a red-yellow color). People with congenital color vision defects see fewer hues than do people with normal color vision.

The term *protan* refers to color vision defects caused by the absence of functional *L*-cone pigment, and the term *deutan* refers to the absence of functional *M*-cone pigment. Together, protan and deutan defects are the most common inherited forms of color blindness, and they preferentially affect males. Their incidence varies with ethnicity (for a recent review see Sharpe et al., 1999). About 2% of Caucasian men suffer from a protan defect and 6% from a

deutan defect. Only about 1 in 230 females is affected by protan or deutan defects. Within the protan and deutan categories of color vision deficiency, there is variation in the degree to which color vision is impaired. The most severe forms are the dichromatic types, protanopia and deuteranopia, in which color vision is based on just two pigments in two types of cones, either S and M (protanopes) or S and L (deuteranopes). The milder forms are the anomalous trichromacies, protanomaly and deuteranomaly, in which the L or M pigment, respectively, is missing but is replaced by a pigment that allows a reduced form of trichromatic color vision. Understanding the nature of the pigments underlying anomalous trichromacy compared to normal color vision is complicated by the fact that there are normal variations in the L and M pigments. The L and M pigments can be thought of as forming two variable but mutually exclusive classes, illustrated in the lower part of Figure 63.1. Individuals with deuteranomaly, a form of anomalous trichromacy, lack an M pigment, but they have two different pigments from the L class. Individuals with protanomaly lack an L pigment, but they have two slightly different pigments from the M class. Within the anomalous trichromacies there is a wide range of phenotypic variation, with some affected individuals having hue perception approaching normal, while others have color vision almost as poor as a dichromat's.

A third class of congenital color vision deficiency, referred to as *tritan*, is associated with defects in the S-cone pigment. These defects occur in males and females with equal frequency and are extremely rare, affecting fewer than 1 in 10,000 people. Also extremely rare are the monochromatic color vision defects, the achromatopsias. These disorders are associated with normal rod photoreceptor function but reduced (incomplete achromatopsia) or absent (complete achromatopsia) cone function. One form of incomplete achromatopsia is blue cone monochromacy, which is generally characterized by the absence of both normal L- and M-cone function (Nathans et al., 1989). In the human retina, about 7% of the cones are S, and the remainder are L and M. Blue cone monochromats base their vision on S cones and rods and thus have diminished capacity for all aspects of vision mediated by cones, including color vision and acuity. Rod monochromacy is a form of complete achromatopsia. Affected individuals are completely color-blind and have very poor acuity. This disorder affects up to 1 in 30,000 people (Sharpe et al., 1999).

INHERITANCE PATTERNS OF COLOR VISION DEFECTS Protan and deutan defects are inherited as X-linked traits and are caused by mutation, rearrangement, or deletion of the genes encoding the L- and M-cone photopigments (Nathans et al., 1986a; Nathans et al., 1986b). These genes lie on the X chromosome, accounting for the pronounced gender differences in the frequency of red-green color vision

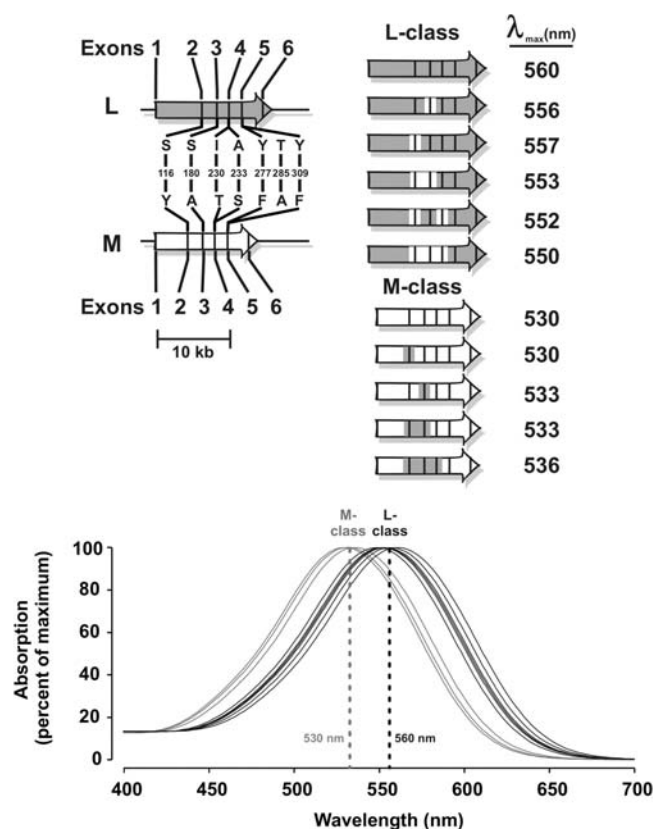


FIGURE 63.1. Spectral tuning in L and M photopigments. Shaded and unshaded arrows represent L- and M-photopigment genes, respectively. Thin black rectangles within the arrows represent the six exons, which are separated by five much larger introns. The relative sizes of introns and exons are drawn to scale. The seven spectral tuning sites encoded by exons 2 to 5 of the genes are indicated in the upper-left diagram along with the codon/amino acid number. The single-letter amino acid code is used to indicate the amino acid identities. When all seven amino acid residues are the ones shown for the schematic L gene (*upper left*), the pigment has the longest possible spectral peak (approximately 560 nm). When all the amino acids are those shown for the schematic M gene (*upper left*), the spectral peak is approximately 530 nm. Transposing the spectral tuning amino acids from L into M and vice versa produces pigments with intermediate spectral sensitivities. Amino acids 277 and 285, encoded by exon 5, produce the largest spectral shifts and define two major classes of pigments, M and L (*bottom*). Substitutions of amino acids encoded by exons 2, 3, and 4 are responsible for smaller spectral shifts that produce spectral subtypes within the L and M classes. The upper-right column shows the spectral variants of the L-class and M-class pigments encoded by genes that have been identified in humans. The shading surrounding individual exons indicates whether the spectral tuning site(s) specified by that exon encode the amino acids that shift the spectrum long (*shaded*) or short (*unshaded*). The wavelength of maximal sensitivity for each of variant pigments shown is an estimate derived by extrapolation from numerous studies (Asenjo et al., 1994; Merbs and Nathans, 1992; Neitz et al., 1995). The single-letter amino acid code is as follows: S, serine; Y, tyrosine; A, alanine; T, threonine; F, phenylalanine; I, isoleucine.

defects. Females have two X chromosomes; males have only one. There is a dosage compensation mechanism, termed *X inactivation*, to ensure that each cell in the female expresses only the required amount of each X-chromosome gene product. Female somatic cells retain one X chromosome as active; the other one is inactivated. In any given L- or M-cone photoreceptor cell, only one pigment gene from the array on the active X chromosome is expressed. The choice of which X chromosome will be active and which will be inactive is random, so on average, 50% of cells retain the paternal X-chromosome pigment genes as active and 50% retain the maternal pigment genes as active. X inactivation also ensures that the visual pigment genes from the maternal and paternal arrays are expressed in separate populations of cones. If a female carries the genes for color-blindness on one X chromosome and the genes for normal color vision on the other, she will have normal color vision. If she carries genes for color-blindness on both X chromosomes, but together her two X's specify at least one functional L and one functional M pigment, she will also have normal color vision. A female will be color-blind only if her two X chromosomes together do not specify both a functional L and a functional M pigment. In rare instances, females can exhibit skewed X inactivation, whereby the cells of a given tissue all have the same active X chromosome. This is usually seen only when expression of genes from one of the X chromosomes severely diminishes the survival of cells in which it is active. Thus, in rare circumstances, a female with the genes for color blindness on only one X chromosome could be color-blind if she had a severely skewed X inactivation such that all of her L and M cones expressed genes from the "color-blind" X chromosome.

Blue cone monochromacy is also inherited as an X-linked trait, and is caused by a variety of mechanisms including a combination of deletion and mutation of the X-linked visual pigment genes or deletion of cis-acting regulatory elements necessary for the expression of the L- and M-pigment genes (Nathans et al., 1989, 1993). In blue cone monochromats, neither L nor M genes are functionally expressed.

Tritan defects are caused by mutations in the S-pigment gene on chromosome 7 and display a dominant inheritance pattern, with incomplete penetrance (Weitz et al., 1992a; Weitz et al., 1992b). *Dominance* refers to the fact that only one mutant copy of the S-pigment gene is required to cause the color vision defect. *Incomplete penetrance* means that not everyone who carries the mutant S-pigment gene will exhibit a color vision deficiency.

Complete achromatopsia and forms of incomplete achromatopsia besides blue cone monochromacy are inherited as autosomal recessive traits. Defects in two different genes have been implicated in these vision disorders. Each gene encodes a subunit of the cone photoreceptor-specific cyclic-

GMP gated ion channel, the function of which is critical to the ability of cone photoreceptors to signal that light has been absorbed (Sundin et al., 2000; Wissinger et al., 2001).

Cone photopigments and their genes

Photopigments are members of the superfamily of G-protein coupled receptors. They are composed of two parts: an 11-*cis*-retinal chromophore and a protein component termed *opsin*. The chromophore is covalently bound to the opsin via a Schiff's base linkage to form the photopigment. The first step in vision is the absorption of light by the 11-*cis*-retinal chromophore, which isomerizes it to all-*trans* retinal, and this, in turn, causes the opsin to undergo a conformational change, converting the pigment to the activated form. The activated visual pigment triggers a biochemical cascade of events, the phototransduction cascade, which ultimately results in hyperpolarization of the photoreceptor cell via closure of cyclic-GMP gated ion channels (see also Chapter 16).

All G-protein coupled receptors are presumed to have evolved from a common ancestor. Likewise, all visual pigments are believed to have evolved from a common ancestor through the processes of gene divergence and duplication (Nathans et al., 1986a; Sharpe et al., 1999). The L and M genes each contain six exons, and each gene encodes an opsin of 364 amino acids (Nathans et al., 1986a). The genes encoding the L- and M-cone pigments share about 98% nucleotide sequence identity. Exons 1 and 6 of the L and M genes are identical; exons 2 through 5 contain nucleotide polymorphisms (Nathans et al., 1986a; Neitz et al., 1995; Winderickx et al., 1993). The S-pigment gene shares only about 45% nucleotide sequence identity with either the L or the M gene, and in evolution, it is estimated that the S gene diverged from the ancestor shared by the L and M genes more than 700 million years ago (Neitz et al., 2001). The S-pigment gene has five exons, which encode an opsin of 348 amino acids (Nathans et al., 1986a). A fraction of the amino acid differences among the opsins are responsible for differences in the relative absorption spectra of the pigments which make color vision possible.

SPECTRAL TUNING OF CONE PIGMENTS A common feature of G-protein coupled receptors is that they have seven transmembrane alpha helical segments. In visual pigments, the chromophore is nestled in a hydrophobic pocket that is created by the transmembrane domain of the opsin. Specific interactions between the chromophore and the side chains of amino acids that line the hydrophobic pocket tune the absorption spectra of the pigments, determining the wavelengths of light to which each pigment is sensitive. Our understanding of spectral tuning in the human S pigment is

incomplete, and spectral variation in this pigment has not been observed. In contrast, the amino acid substitutions responsible for the variation in spectral sensitivity between and among the human L and M pigments are relatively well understood.

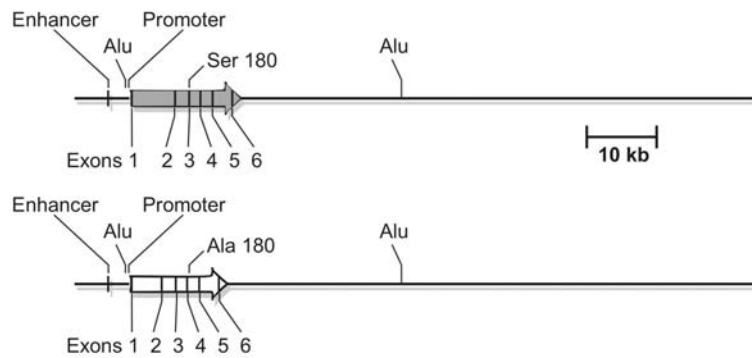
Eighteen amino acid dimorphisms have been identified among and between the human L and M pigments. The effects of amino acid substitutions on the absorption spectra of the pigments have been investigated using a wide variety of experimental approaches (Asenjo et al., 1994; Merbs and Nathans, 1992, 1993; Neitz et al., 1989, 1991; Sharpe et al., 1998; Yokoyama and Radlwimmer, 1998). In vitro, substitutions at seven amino acid positions are required to shift the spectrum from that of the longest absorbing L pigment to that of the shortest absorbing M pigment (Asenjo et al., 1994). These seven substitutions are indicated in Figure 63.1. Two substitutions together, at amino acid positions 277 and 285, produce the spectral separation between M and L classes. Substitutions at each of five other positions (116, 180, 230, 233, and 309) produce small shifts (1 to 4 nm). Thus, a gene can be defined as encoding an M-class or L-class pigment based on the amino acids specified by codons 277 and 285. M genes specify phenylalanine and alanine at positions 277 and 285, respectively, and peak near 530 nm. L genes specify tyrosine and threonine at positions 277 and 285, respectively, and peak near 560 nm. The other amino acid substitutions that produce small shifts in the wavelength of maximal sensitivity (λ_{\max}) can be thought of as producing spectral subtypes of M and L pigments (Fig. 63.1). There are fewer spectral subtypes of M than of L pigment, and the total range of variation in λ_{\max} is smaller in M than in L pigments. This appears to be the result of context-specific effects. For example, when a substitution is made at amino acid position 116 (encoded by exon 2) of the L pigment, it produces a shift of 2.5 nm. The same substitution made in the context of an M pigment does not produce a significant shift in spectral sensitivity. Similarly, a substitution at amino acid position 180 (encoded by exon 3) seems to produce a slightly smaller shift when introduced into an M pigment than into an L pigment. As will become apparent below, understanding the mechanism of spectral tuning in the human L and M pigments has provided insight into the molecular genetics of phenotypic variation in human color vision.

ARRANGEMENTS OF THE L- AND M-PHOTOPIGMENT GENES IN NORMAL COLOR VISION Among placental mammals, only primates have trichromatic color vision (Jacobs, 1993). There are two major primate lineages, Old World primates and New World primates. The Old World primates include African and Asian monkeys, apes, and humans. New World primates inhabit South and Central America. Color vision in these two lineages seems to be at different stages of evo-

lution. Most species of New World monkey have a single visual pigment gene on the X chromosome; however, in diurnal species there are multiple alleles of the X chromosome visual pigment gene, providing the basis for trichromacy in females (Jacobs, 1983). A female who receives two X chromosomes with different alleles encoding spectrally different pigments will express the two alleles in separate populations of cones because of X inactivation. The two cone populations produced by X inactivation in combination with the S cone provide heterozygous females with three spectrally distinct cone types, and they have trichromatic color vision. The males of these species and the homozygous females have dichromatic color vision. Old World primates, like humans, have both an L- and an M-pigment gene on the X chromosome (Hunt et al., 1998; Onishi et al., 1999). Thus, it appears that trichromacy like that found in humans arose after the split between New and Old World primates, estimated to have occurred some 60 million years ago (Neitz et al., 2001). One exception is the howler monkey, a species of New World monkey that has uniform trichromatic color vision in both females and males (Jacobs et al., 1996). Apparently, in this species a duplication of the X-chromosome photopigment gene occurred independently of that which occurred in the Old World primates (Dulai et al., 1999).

Human red-green color vision is believed to have its origins in an ancestral primate (or protoprimate) that was the predecessor of all modern Old World monkeys and apes. The photopigment genes in macaque monkeys have recently been examined (Onishi et al., 1999). The vast majority of macaques have one L- and one M-pigment gene that are adjacent to one another on the X chromosome, with the M gene downstream of the L gene. We assume that this is the gene arrangement in the ancestors of modern humans and that it came about because of a relatively recent gene duplication event. It is believed that all placental mammals except Old World primates and a select group of New World primates (Jacobs et al., 1996) have a single gene encoding a cone pigment on the X chromosome (Fig. 63.2A). Prior to the event that placed two photopigment genes on the X chromosome, our ancestors may have already reached a stage of color vision evolution in which they had multiple alleles of the X chromosome visual pigment gene similar to the situation that allows some New World monkey females, as described above, to enjoy trichromatic color vision. This is illustrated in Figure 63.2A, in which two single photopigment genes, L and M, are located on separate X chromosomes. Figure 63.2B illustrates how, in our ancient ancestor, a second photopigment gene could have been added to one X chromosome by an unequal crossover mechanism (Dulai et al., 1999). The length of the gene insertion extends from about 236 base pairs (bp) upstream of the start of the coding sequence of the M gene to about 18 kilobase pairs (kb) downstream of the last exon.

A. Single X-encoded pigment gene



B. Unequal recombination adds a gene

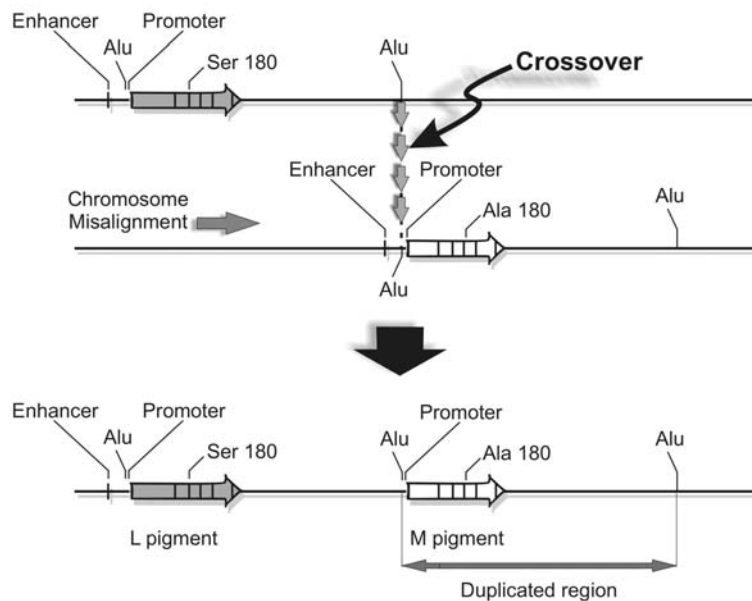


FIGURE 63.2. Trichromatic color vision arose in a primate ancestor by gene duplication. *A*, Ancestral arrays, like those found in most New World primate species, contain a single visual pigment. The human L- and M-photopigment gene array contains a large number of Alu sequences. From analysis of the DNA sequence of the array, it appears that the region between the Alu sequences indicated is responsible for duplicating the ancestral X chromosome visual pigment gene. *B*, The photopigment gene array responsible for uniform trichromacy arose when a second photopigment gene was added to the X chromosome. This is proposed to have occurred

by a favorable misalignment of two ancestral chromosomes containing a single pigment gene each. Recombination, possibly facilitated by Alu sequences, produced an X chromosome containing two visual pigment genes. In species that have just one pigment gene on the X chromosome, an enhancer element is present upstream of the gene and is required for expression of the gene. The enhancer was not duplicated when the second photopigment gene was added to the X chromosome. The enhancer has been termed the *locus control region* (LCR), and in humans it is required for expression of both L and M photopigments.

A feature of the region upstream of the human M gene is the presence of several Alu repeat elements. Human chromosomes contain about 1 million Alu repeat elements, and Alus have been implicated in unequal crossing over. It is possible that during meiosis, the two X chromosomes of a heterozygous female misaligned to bring Alu elements downstream of the L-like gene on one X chromosome into alignment with Alu elements just upstream of the M-like photopigment gene

on the other X chromosome, and these elements may have been involved in facilitating a crossover between the misaligned chromosomes. The result is the insertion of a primordial M-like gene downstream of a primordial L-like gene to form the predecessor of the modern human X chromosome photopigment gene array. This original unequal crossover should be considered to represent the occurrence of an extraordinarily improbable event. Normally, crossing

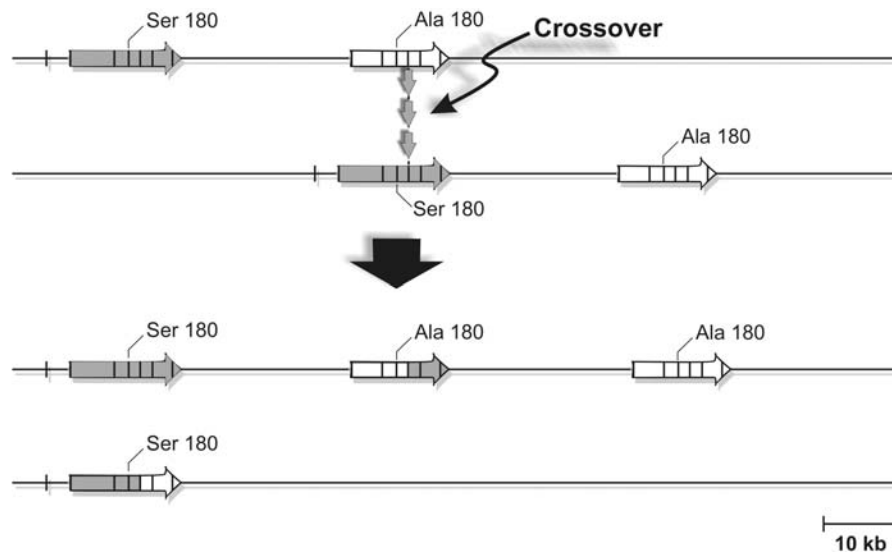


FIGURE 63.3 Intragenic crossovers alter the number of genes per array, intermix L- and M-gene sequences, and produce new arrays that cause color-blindness in males. Arrow diagrams for L and M genes are as indicated in Figure 63.1. Misaligned X chromosomes, each containing one L- and one M-pigment gene, undergo unequal homologous recombination within the L gene in one array and the M gene in the other array to produce two new arrays. The new

array with three genes contains a chimeric gene which contains exon 5 of the parental L gene and so encodes an L-class pigment. This type of array is common in males with deutan color vision defects. The other array has a single pigment gene that contains exon 5 from the parental M pigment gene, and so encodes an M pigment and is found in protanopes.

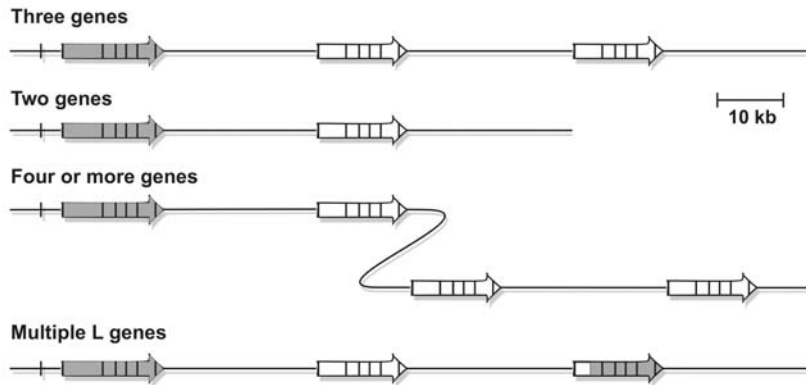
over requires the alignment of a long span of two homologous DNA sequences. Even though the presence of highly recombinogenic Alu sequences may have facilitated the event, it still must have been extremely unusual. Consider that Old World and New World monkeys have been separated in evolution by perhaps as long as 60 million years. Most New World species have not enjoyed the benefit of an unequal recombination event to provide them with uniform trichromacy despite the millions of meioses that occurred since they reached the stage where heterozygous females became trichromatic.

After the first unequal crossover which placed two highly homologous photopigment genes in tandem on the X chromosome, the probability of subsequent unequal crossovers must have increased dramatically. The repeat unit (Fig. 63.2B), including the gene and intragenic sequences, is nearly 40kb in length. This provides a large region of homology as the substrate for a crossover when the chromosomes misalign (Fig. 63.3). The combination of the tandem arrangement and their high degree of similarity has made the pigment gene array prone to unequal homologous crossovers, both within (intragenic) and between (intergenic) the genes. Both intra- and intergenic crossovers generate two new arrays, one with more and the other with fewer genes than the parental arrays. In addition, intragenic crossovers intermix the parental L- and M-gene sequences to produce chimeras (Fig. 63.3). The chimeric genes can encode pigments that differ in spectral sensitivity from either parental

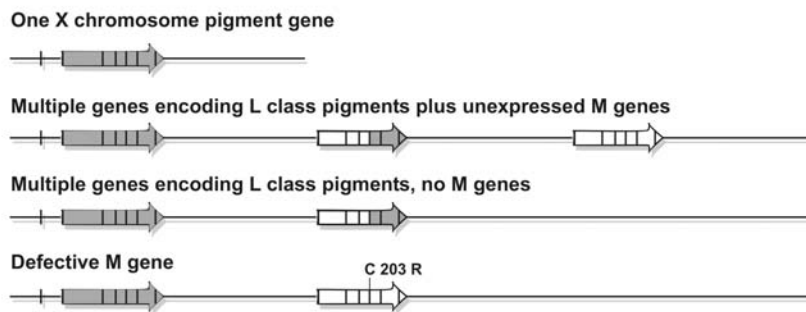
pigment, with the magnitude of the spectral difference being determined by the number of spectral tuning sites (Fig. 63.1) that differ in the chimeric pigment compared to the parental pigment of the same class. All intragenic crossovers between normal arrays with two pigment genes result in gene arrays that cause color vision defects; either product of the crossover illustrated in Figure 63.3, when inherited by a male, will confer a color-deficient phenotype.

Among humans, there is variation in the number of L and M genes per X chromosome array (Fig. 63.4) (Drummond-Borg et al., 1989; Hayashi et al., 1999; Nathans et al., 1986a; Neitz and Neitz, 1995). Presumably, modern humans descended from an ancestor with two visual pigment genes on the X chromosome, and unequal homologous recombination produced the variation in color vision genotype and phenotype in the present population. The variety of arrays seen in modern humans with normal color vision is illustrated in Figure 63.4A. The most common array contains one L gene followed by two M genes. This is quite different from Old World monkeys, in which there is usually one M and one L gene (Onishi et al., 1999), an array type that is seen in only one in five humans. Humans can and often do have more than three pigment genes per X chromosome (Neitz and Neitz, 1995). The differences between humans and monkeys are remarkable. Humans have more photopigment genes on average than monkeys, and there is tremendous widespread variation in the human gene sequences that is absent in monkeys (Tickner et al., 2002).

A. The L and M pigment gene arrangements of normal color vision



B. Deutan color vision defects



C. Protan color vision defects

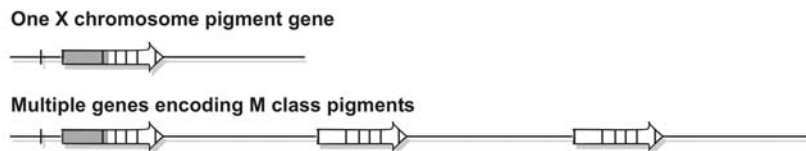


FIGURE 63.4 X-chromosome visual pigment gene arrays underlying normal color vision and color vision deficiencies in the modern human population. *A*, Arrays underlying normal color vision contain variable numbers of genes encoding L and M photopigments. An L gene is always in the first (5'-most) position. Additional L genes in normal arrays have most often been observed at the 3' end of the array. *B*, Arrays found in males with deutan color vision defects. Dichromats often have a single X chromosome pigment gene encoding an L-class pigment. Deuteranomalous

males have at least two different genes encoding spectral variants of L-class pigments and may or may not also have M-pigment genes. The M genes from deutan arrays are not expressed in the retina. In some cases deleterious mutations, such as one that substitutes the amino acid arginine for cysteine at position 203, causes the M pigment to be nonfunctional. *C*, Arrays found in males with protan color vision defects usually do not contain genes encoding L-class pigments but contain one or more genes encoding M-class pigments.

These differences are unexpected because both monkeys and humans arose from a common ancestor, and at present no satisfactory explanation has been offered.

Molecular genetics of common inherited color vision defects

DEUTAN DEFECTS Deutan defects are characterized by the absence of the M-cone contribution to vision. Deuteranopia

is the dichromatic form, and it affects about 1% of Caucasian males and about 1 in 4000 females. Most deuteranopes are missing all genes encoding M pigments. Usually they have just one visual pigment gene on the X chromosome, and it encodes an L pigment (Fig. 63.4*B*). Presumably, arrays with a single L gene have been produced by an unequal intergenic recombination between two normal arrays.

Deuteranopic males with normal-appearing arrays containing one L and one or two M genes have also been iden-

tified (Bollinger et al., 2001; Jagla et al., 2002). In these cases, when the M genes were sequenced, it was discovered that they contained a mutation that substituted the amino acid arginine for a cysteine at position 203 (C203R) of the pigment (Fig. 63.4B). This cysteine is highly conserved among all members of the superfamily of G-protein coupled receptors, and is involved in forming an essential disulfide bond in the pigment. The C203R mutation renders the pigment nonfunctional (Kazmi et al., 1997).

Deuteranomaly is the anomalous trichromatic deutan defect and is the most common inherited red-green color vision defect, affecting about 5% of Caucasian males. Although deuteranomaly is characterized by the absence of an M-cone contribution to vision, in about two-thirds of deuteranomalous males M genes are present in genomic DNA. These males also have genes to encode two pigments of the L class. Figure 63.4B illustrates an array with three genes: a parental L gene, a parental M gene, and between them, a chimeric gene. This gene arrangement is frequently observed in deuteranomalous males. The chimeric gene derives its 5' end from a parental M gene and its 3' end from a parental L gene, and encodes what has historically been termed the *anomalous pigment*. The pigment encoded by the chimeric gene will be of the L class because it has retained exon 5 from the parental L gene (Fig. 63.1). It may differ in spectral sensitivity from the parental L pigment, depending on differences in amino acids at the spectral tuning sites encoded by exons 2, 3, and 4. One long-standing hypothesis suggests that the phenotypic variation in deuteranomaly is directly related to variability in the magnitude of the spectral separation in the underlying X-encoded pigments (e.g., Alpern, 1981). The normal pigments from the L and M classes have overlapping absorption spectra, but they are well separated in spectral peak (Fig. 63.1). Two different wavelengths of light produce different rates of photon capture in the L versus M cones, and the relative difference in photon catch is the basis for color discrimination. In the case of deuteranomaly, color vision is based on two pigment variants from the L class, which are not very different in spectral peak. Thus, it takes a much larger difference in the wavelength of two lights to produce the equivalent relative difference in the rate of photon capture in the two L-cone variants, and color discrimination ability is reduced. This predicts that if the chimeric gene and the parental L gene in the same array encode pigments that differ in spectra, then the person will be deuteranomalous, but if the spectra do not differ, then the person will be a deuteranope. Further, the degree of color vision loss among deuteranomalous males should be greater with a smaller spectral separation between the underlying L-class pigments. In recent experiments to test this hypothesis, DNA sequencing of the genes that encode L-class pigment genes in deuteranomalous males was used to deduce the amino acid sequences of the

pigments, and spectral tuning data were used to predict the spectral separation between them. Color vision phenotypes for the deuteranomalous males were determined by performance on standard color vision tests (Neitz et al., 1996; Shevell et al., 1998). There is a very strong correlation between color vision behavior and the spectral separation between the underlying pigments. However, there are some exceptions in that some deuteranomalous males have much worse color discrimination than others with the same spectral separation between their L-class pigments. One explanation for the poorer performance in some deuteranomalous males is that they have a bias in the ratio of cones expressing their two L-pigment variants. A very large range of variation has been observed in the ratio of L to M cones among males with normal color vision (Carroll et al., 2000; Roorda and Williams, 1999; Vimal et al., 1989). One might expect a similar variation in the ratio of two spectral variants of L cones in deuteranomalous retinas. It may be that color discrimination based on two cones that are quite similar in spectral peak is very sensitive to the proportion of the two cone types. If the ratio is very biased, it might adversely affect the already reduced color discrimination of an anomalous trichromat.

The most typical gene arrays underlying deuteranomaly are ones with both M and L genes (Fig. 63.4B). The mystery has been why do men who inherit these arrays have a color vision defect? The C203R mutation has been found in the M genes of a few deuteranomalous males (Winderickx et al., 1992b), but many who have been examined have M genes with no identifiable defect. In a large-scale study to examine gene expression in retinas from male eye donors, Sjöberg et al. (1998) screened for the presence of mRNA from both M and L genes in a 6 mm² foveal sample from each of 150 male donors. For 6% of the retinas (9/150), no M-pigment mRNA was detected, identifying these as putative deutan retinas. Using a very sensitive assay, the relative amount of L- and M-pigment mRNA was quantified in these retinas, and it was found that M pigment mRNA was below the detection limit of the assay (Bollinger et al., 2000), which was 1 molecule of M-pigment mRNA in 50,000 molecules of L-pigment mRNA. The conclusion was that there is a complete absence of M-gene expression in deutan retinas. It appears that this absence of expression occurs because the last gene in an array with three or more genes is not expressed in the retina (Hayashi et al., 1999). Thus, a primary cause of deuteranomaly is the production of gene rearrangements, as illustrated in Figure 63.3, in which a gene encoding an L-class pigment displaces the M gene to the 3' end of the array where it is not expressed.

About one-third of deuteranomalous males lack M genes. As illustrated in Figure 63.3, an unequal crossover between ancestral two-gene arrays produces a deuteranomalous array that contains an M gene. However, some

deuteranomalous males (fewer than one-third) have two genes to encode L-class pigments but no M genes (Fig. 63.4B). To delete the M gene from a deuteranomalous array requires a second crossover event. The fact that two crossovers are required to produce a deuteranomalous array that lacks M genes might account for the relatively lower frequency of this array structure in deuteranomalous.

PROTAN DEFECTS Protan defects are characterized by the absence of an L-cone contribution to vision, and most males with a protan defect do not have genes encoding an L pigment (Fig. 63.4C). Protanopia is the dichromatic form, and protanomaly is the anomalous trichromatic form; each form affects about 1% of Caucasian men. They have X-chromosome arrays with genes for one or more M-class pigments. The recombination shown in Figure 63.3 generates an array with a single gene that is chimeric, with the 5' end from the parental L gene and the 3' end from the parental M gene. The gene encodes an M-class pigment because it derives exon 5 from the parental M gene (Fig. 63.1). A male with this array will be a protanope. Depending on the location of the crossover, the chimeric gene may encode a pigment that differs in amino acid sequence or in spectral sensitivity from the parental M pigment. Only rarely have protanopes who have an apparently intact L gene been identified, and the reason for the absence of L-cone function in these individuals is not known.

Among males with protanomalous color vision there is phenotypic variation, although it seems to be less pronounced than the variation among deuteranomalous males. This is perhaps expected since there are fewer spectral variants of the M-class pigments (Fig. 63.1). Some protanomalous males have multiple genes (Fig. 63.4C) that encode M-class pigments that are expected to differ in λ_{\max} because they differ at spectral tuning positions encoded by exons 3 and 4 of the genes. These small spectral differences are presumably the basis for a small amount of red-green color vision in protanomalous trichromats. However, some protanomalous males have genes encoding M-class pigments that do not differ at the M-pigment spectral tuning sites. There is evidence that in some of these subjects, the M-class pigments differ in optical density. The effect of increasing optical density is due to "self-screening." Two pigments that have the same spectral peak but differ in relative optical density will have spectral sensitivity curves in which the pigment with greater optical density has a broader spectral sensitivity curve, reflecting higher sensitivity to wavelengths on either side of the spectral peak. Near the peak and on the long-wavelength side of the peak, the difference in optical density between the two pigments qualitatively mimics a difference in spectral peak. We and our colleagues have suggested that amino acid polymorphisms encoded by exon 2 that shift the λ_{\max} of L but not of M pigments (Fig.

63.1) may alter the optical density of the M pigment, providing an effective difference in spectral sensitivity as the basis for a small amount of color discrimination (Neitz et al., 1999). However, some protan males who have genes encoding M-class pigments that differ at exon 2-encoded sites behave as dichromats, not anomalous trichromats (Jagla et al., 2002). There are at least two possible explanations for this observation. First, it seems likely that the optical density of a pigment may depend on the exact amino acid sequence of the pigment. As mentioned above, there are 18 dimorphic amino acid positions. Whether two pigments that differ by exon 2-encoded substitutions differ in optical density may depend on the complete amino acid sequences of the two pigments. If so, then it is expected that not every set of two pigments that differ by exon 2-encoded amino acids will also differ in optical density. Another explanation is that in order to support color discrimination, the ratio of two M-class cones in a protan retina must be within an optimal range, and that for some protanomalous males, the ratio of cones is not within the required range. The evidence that some protanomalous males have two M-class pigments that do not differ in λ_{\max} , but instead differ in optical density is clear (Neitz et al., 1999). The optical density differences correlate with the presence of exon 2-encoded amino acid differences; however, it has not been established that exon 2-encoded differences cause the optical density difference.

Conventionally, the diagnosis of color-defective individuals has been based on behavior in a color matching task, the Rayleigh color match, in which the subject is asked to discriminate mixtures of monochromatic red and green lights from a monochromatic yellow light. The clinical instruments used in color matching employ a small stimulus field subtending about 2 degrees. Interestingly, some subjects who cannot discriminate either a pure red or pure green light from yellow when the stimulus is small are able to do so if the stimulus is made large enough. One possible hypothesis had been that many dichromats might have had a very small number of *anomalous cones*, perhaps concentrated outside the macular region that they used for color vision if the stimulus was large enough. Recent results do not support this hypothesis; it has been shown that many of these people have only one pigment gene on the X chromosome and thus do not have the genetic basis for a second pigment absorbing in the middle to long wavelengths (Crognale et al., 1999). These people have exceedingly poor red-green color vision compared to normal individuals and even compared to most anomalous trichromats, discussed above, who can make red-green color discriminations when the stimulus is small. The basis for their minimal amount of red-green color discrimination is not known. It may be that they are able to use differences in the spectral absorption properties of different cones that occur because of inhomogeneities in the retina,

such as the optical density difference between cones in the fovea and those in the peripheral retina.

A WORD ABOUT ANOMALOUS PIGMENTS AND CONES Conventionally, it has been said that anomalous trichromacy occurs when either the normal M or L pigment is replaced by an “anomalous” pigment. These anomalous pigments have been thought of as being abnormal—different from the L and M pigments that underlie normal color vision and present only in people with color vision defects and in female carriers of color vision defects. It has long been understood that female carriers usually have normal color vision; thus, having anomalous pigments and normal pigments in the same retina (in separate cones) does not alter the person’s color vision phenotype from normal to abnormal. However, more recently, it has been realized that there is huge variation in the amino acid sequences and spectral sensitivities of the normal L and M pigments. DNA sequence analysis of the genes encoding pigments underlying deuteranomaly, protanomaly, and normal color vision (Neitz et al., 1995, 1996, 1999; Shevell et al., 1998; Winderickx et al., 1993) reveals that there is overlap between the highly variant sequences of normal L pigments and the anomalous pigments of deuteranomaly, and between normal M pigments and the anomalous pigments of protanomaly.

As described below, there is growing evidence for a stochastic model in which the identity of the cones as L versus M is defined solely by the spectral sensitivity of the expressed pigment. Since there is overlap in the spectral sensitivities of normal and anomalous pigments, in the context of the stochastic model, rather than being considered to have both a normal and an anomalous pigment, a deuteranomalous individual can be considered to have two spectral variants of L cones and protanomalous individuals can be considered to have two spectral variants of M cones. Thus, while the concept of normal versus anomalous pigments was useful in the context of earlier theories of color vision, it is somewhat inconsistent with what we now know about the biology underlying normal and color-defective vision.

Molecular genetics of rare inherited color vision defects

TRITANOPIA Inherited blue-yellow color vision defects are caused by mutations in the S-cone pigment gene. Tritanopes base color vision on L and M cones, and they lack functional S-cones. The S-pigment gene is on chromosome 7, and since humans are diploid, each S-cone photoreceptor cell has and expresses the S-pigment genes from both copies of chromosome 7. A genetic defect in only one S-pigment gene can be sufficient to cause tritanopia. Three different amino acid substitutions have been identified as causes of tritanopia. All three substitutions are nonconserved amino acid substitutions that occur in the membrane-spanning domain of the

S pigment (Weitz et al., 1992a; Weitz et al., 1992b) and are likely to interfere with protein folding.

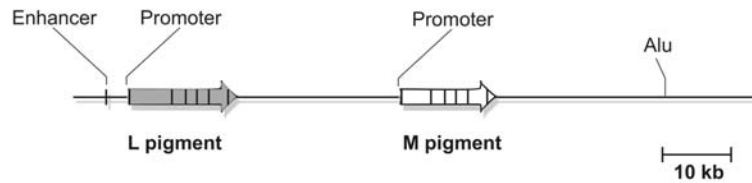
BLUE CONE MONOCHROMACY The genetic causes of blue cone monochromacy are heterogeneous, but all lead to a loss of function of both L and M cones. Two general causes of blue cone monochromacy have been identified (Nathans et al., 1989, 1993). One is the deletion of what has been termed the *locus control region* (LCR), a DNA element required for expression of both L- and M-pigment genes. The second is the presence of an inactivating point mutation, most commonly a C203R substitution, in an array with a single visual pigment gene. There are quite a few blue cone monochromats for whom the genetic cause has not been discovered. Some blue cone monochromats have been reported to have more than one class of functional cone (Smith et al., 1983). One possibility is that in cases in which the LCR has been deleted, there is still very low level expression of functional L or M pigment, enough to provide residual function of a second class of cone.

COMPLETE ACHROMATOPSIA AND FORMS OF INCOMPLETE ACHROMATOPSIA OTHER THAN BLUE CONE MONOCHROMACY Occasionally, populations with an extraordinarily high incidence of color blindness have been identified. This is true of autosomal recessive incomplete achromatopsia, which generally is extremely rare, but among the Pingelapese islanders in Micronesia, the incidence is about 5%. In that population, the genetic cause has been found: an amino acid substitution in the beta subunit of the cyclic-GMP gated ion channel. All three cone types, S, M, and L, use the same cyclic-GMP gated ion channel in phototransduction. The channel has two subunits, alpha and beta, each encoded by a separate gene. The beta subunit is encoded by a gene identified as *CNGB3*, which resides on chromosome 8. Mutations in the gene encoding the alpha subunit, *CNGA3*, which resides on chromosome 2, have also been found in families with rod monochromacy (Wissinger et al., 1998). Recently, *CNGA3* mutations were also found in patients with incomplete achromatopsia (Wissinger et al., 2001). The difference between complete and incomplete achromatopsia is that incomplete forms show residual cone function, whereas complete forms do not. One hypothesis is that some of the mutations in the ion channel subunits do not completely abolish function and give rise to the incomplete forms.

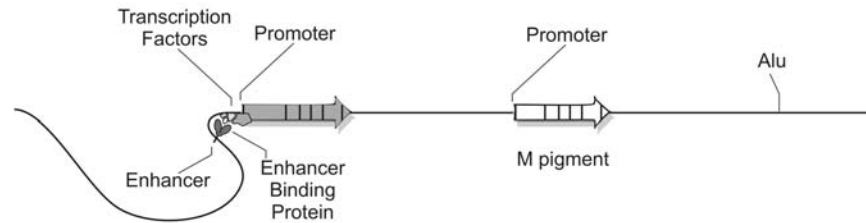
X-chromosome pigment gene expression and the identity of photoreceptors as M versus L cones.

GENE EXPRESSION FROM THE PIGMENT GENE ARRAY The rules and mechanisms that govern expression of the X-chromosome visual pigment genes remain largely unknown,

A. L/M gene array



B. L gene transcription



C. M gene transcription

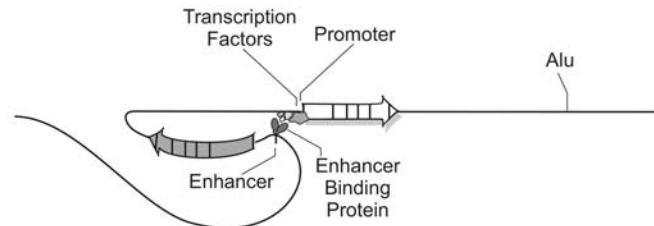


FIGURE 63.5. Transcription of L- and M-pigment genes. *A*, The L- and M-pigment gene array contains a single enhancer that is 5' (left) of the genes in the array. Each gene has its own promoter. The sequence of the promoter for the first gene in the array differs slightly from the promoter for other genes in the array. An interaction between the upstream enhancer and the promoter of an individual pigment gene is required for transcription of the gene.

B, In cones that express L pigment, the enhancer interacts only with the promoter for the L gene, and the promoters for the other genes in the array are excluded from interactions with the enhancer. *C*, In cones that express the M pigment, the enhancer interacts only with the promoter for an M gene, and other pigment gene promoters are excluded from interactions with the enhancer.

but what is known has been important for understanding the molecular genetics of inherited red-green color vision defects. Normal color vision requires at least one L and one M gene from the X-chromosome array to be functionally expressed in the retina, and the M and L genes must be expressed in separate populations of cones. Among humans with normal color vision there is variation in the number of both L and M genes. Most people have more than the two genes that are the minimum required for normal color vision (Fig. 63.4). Arrays with multiple M genes are most common; however, arrays with multiple L genes are not unusual (Drummond-Borg et al., 1989; Jørgensen et al., 1990; Nathans et al., 1986a; Neitz et al., 1995; Sjöberg et al., 1998). Each L- or M-cone photoreceptor expresses only one gene from the X-chromosome array (Hagstrom et al., 2000). Two questions that remain unresolved are (1) how does a photoreceptor choose which gene will be expressed and prevent expression of the other genes from the X-

chromosome pigment gene array? and (2) which of the genes from an individual array are expressed and which are not?

The approximately 200bp region immediately upstream of the coding sequence of each visual pigment gene on the X-chromosome contains promoter elements required for transcription (Fig. 63.5). Although highly homologous, the promoter for the gene in the 5' position in the array is not quite identical to the promoters for the other genes in the array (Nathans et al., 1986b). As a consequence of the tandem arrangement of the genes, the downstream genes added by unequal homologous recombination have the same promoter sequence as the parental M gene.

Transcription of the individual genes within the X-chromosome array also requires an upstream enhancer that lies 3.5kb upstream of the first gene in the array. An enhancer is a *cis*-acting DNA element that promotes transcription of a gene in a distance and orientation independent fashion. The X-chromosome visual pigment gene

enhancer is conserved across mammalian species, both in sequence and in location (Wang et al., 1992). As shown in Figure 63.2, the enhancer was not included when the second gene was added to create a gene array in our primate ancestor. Thus, all genes in the array must share the same enhancer (Fig. 63.5), the LCR (Wang et al., 1992).

A major unresolved issue is what determines the identity of a cone as L versus M. Two possibilities have been considered. The first is that the L and M cones each have a unique identity that is determined before the pigment genes are expressed. During development a cell adopts either an L- or an M-cone cell fate, and as a result, each expresses a unique subset of genes, including transcription factors to specifically activate transcription of an L- or M-pigment gene based on the predetermined identity of the cell. If this is indeed the case, then there can be aberrations in gene expression such that an L pigment could be misexpressed in an M cone and vice versa. In this model, the LCR is a powerful enhancer which may play a role in cell- and tissue-specific transcription but not in determining the identity of the cones as L versus M.

The second possibility is that L and M cones are identical until, by the action of a stochastic selection mechanism, each cell randomly makes a one-time choice of one X-chromosome visual pigment gene from the array for expression. In this scenario, termed the *stochastic model*, the identity of the cone is determined by the spectral sensitivity of the pigment that was randomly chosen for expression, and thus there is no possibility for an L cone to express an M pigment or vice versa.

The stochastic model can be considered to be very general, independent of the exact mechanism that makes the random choice. However, one specific theory has been postulated in which the LCR acts as the stochastic selector, forming a stable and irreversible complex with only one pigment gene promoter per cell, thereby ensuring that each cell expresses a single X-chromosome visual pigment gene (Hayashi et al., 1999; Wang et al., 1999) (Fig. 63.5). Our evolutionary ancestors had a single X-linked pigment gene. If for them the binding of the enhancer to the promoter (via DNA-protein and protein-protein interactions) was irreversible, then there would be no need to separately evolve a mechanism to direct mutually exclusive expression of multiple genes once the gene duplication occurred (Fig. 63.2). It is possible, as illustrated in Figure 63.2, that when the gene duplication occurred, our ancestors had already reached a stage in evolution in which there were multiple alleles at the X-chromosome photopigment gene locus. If so, the exclusive interaction of the enhancer with only one X-chromosome pigment gene promoter in each cell could have been exploited as the mechanism to direct the pigments into two separate subpopulations of cells. This allows the possibility that males and homozygous females could have

become trichromatic by the stroke of one highly favorable mutational event, which both added a gene and provided a mechanism for mutually exclusive expression.

Extremely attractive are both the idea that the identity of M versus L cones is determined by a stochastic process and the idea that the mutually exclusive expression of L and M genes is the result of exploiting a genetic mechanism that fortuitously preexisted in our ancestors with a single X-chromosome pigment gene. However, there is no direct experimental evidence for the formation of an irreversible enhancer-promoter complex, and as far as we know, there is no precedent for such an irreversible enhancer-promoter interaction in any other system. Even if the simple idea of a permanent binding of the enhancer to the promoter via a protein complex ultimately proves to be incorrect, the stochastic model and the idea of a one-step mutation providing both the photopigment basis for trichromacy and mutually exclusive expression for the new gene are important as general theories independent of the exact mechanisms that are envisioned to implement them.

As noted above, in the human retina there is tremendous individual variation in the L:M cone ratio, with an average 2:1 ratio of L to M cones (Carroll et al., 2000; Cicerone and Nerger, 1989; Miyahara et al., 1998; Roorda and Williams, 1999; Rushton and Baker, 1964; Wesner et al., 1991). Under the stochastic model, explaining the observed range of variation in the L:M cone ratio in people with normal color vision requires that the stochastic mechanism choose to activate transcription from L and M genes unequally and with different probabilities for different people. Also, in general, there must be a higher probability that, in normal arrays, an L gene will be chosen for expression. The structure of normal arrays, with an L gene in the first position, followed by M gene(s), suggests the possibility of a relationship between the proximity of a pigment gene to the LCR and the probability of being chosen for expression. Deeb and colleagues have proposed that only the first two genes in the array are expressed at levels significant for color vision, the third gene being effectively out of range of the LCR (Hayashi et al., 1999; Winderickx et al., 1992b). There is very clear evidence that the first gene in the array is preferentially expressed in humans (Balding et al., 1998; Sjöberg et al., 1998) and that the last gene in arrays with three or more genes is not expressed (Hayashi et al., 1999; Winderickx et al., 1992b). As introduced above, this absence of expression of the third gene in arrays with three genes is what causes the color vision defect in many deuteranomalous individuals. However, our understanding is incomplete. For example, there are reported cases in which expression of more than two of the genes from the X-chromosome array has been clearly demonstrated (Sjöberg et al., 1998). Finding exceptions implies that the rule that only two genes are expressed is not absolute. Recently, in a series of experiments using an

extremely sensitive, highly quantitative assay, mRNA from the last gene in the array from a series of male eye donors who each had three or more X-chromosome visual pigment genes, it was demonstrated that the 3'-most gene in each array was not expressed at a detectable level. The detection limit of the assay was sufficient to detect mRNA from the last gene in the array if it was expressed in a ratio of 1 in 50,000 copies of mRNA from other X-chromosome pigment genes (Bollinger et al., 2000). Our conclusion is that the absence of expression of these genes is complete. In the model where the LCR serves as the stochastic selector, it has been envisioned that the probability of a gene's being expressed in any cone is determined by its proximity to the LCR. In that model, it is conceived that the probability of expression could be markedly lower for the third gene but is probably not zero (Hayashi et al., 1999; Wang et al., 1999). Presently, research related to the expression of the L and M genes is very active. As more becomes known about this very puzzling process, the mechanisms that govern expression of the X-chromosome photopigment genes will be elucidated. This will, in turn, provide insight into the mechanism that produces the huge variation in L:M cone ratio across individuals. Ultimately, we will also know if the stochastic model is correct. If it is, it suggests that the only difference between an L and an M cone is the photopigment it expresses. This raises the question of how the neural circuits for red-green color vision, which compare the outputs of the L and M cones, arise.

Acknowledgments

We thank P. M. Summerfelt for technical assistance and J. Carroll, K. L. Gunther, and C. McMahon for valuable comments and suggestions. The writing of this chapter was supported by National Institutes of Health Grants EY09303, EY09620, & EY01931 and by Research to Prevent Blindness.

REFERENCES

- Alpern, M., 1981. Color blind color vision, *Trends Neurosci.*, 4:131-135.
- Asenjo, A. B., J. Rim, and D. D. Oprian, 1994. Molecular determinants of human red/green color discrimination, *Neuron*, 12:1131-1138.
- Balding, S. D., S. A. Sjöberg, J. Neitz, and M. Neitz, 1998. Pigment gene expression in protan color vision defects, *Vis. Res.*, 38:3359-3364.
- Bollinger, K., C. Bialozynski, J. Neitz, and M. Neitz, 2001. The importance of deleterious mutations of M pigment genes as a cause of color vision defects, *Color Res. Appl.*, 26:S100-S105.
- Bollinger, K., M. Neitz, and J. Neitz, 2000. Topographical expression of first vs. downstream L pigment genes in a retina from a male with two L and one M genes, *Invest. Ophthalmol. Vis. Sci.*, 41(Suppl):S807.
- Bowmaker, J. K., H. J. A. Dartnall, and J. D. Mollon, 1980. Microspectrophotometric demonstration of four classes of photoreceptor in an Old World primate, *Macaca fascicularis*, *J. Physiol.*, 298:131-143.
- Carroll, J., C. McMahon, M. Neitz, and J. Neitz, 2000. Flicker photometric electroretinogram estimates of L:M cone photoreceptor ratio in men with photopigment spectra derived from genetics, *J. Opt. Soc. Am. A*, 17:499-509.
- Cicerone, C. M., and J. L. Nergler, 1989. The relative numbers of long-wavelength-sensitive to middle-wavelength-sensitive cones in the human fovea centralis, *Vis. Res.*, 29:115-128.
- Crognale M. A., D. Y. Teller, T. Yamaguchi, A. G. Motulsky, and S. S. Deeb, 1999. Analysis of red/green color discrimination in subjects with a single X-linked photopigment gene, *Vis. Res.*, 39:707-719.
- Dartnall, H. J. A., J. K. Bowmaker, and J. D. Mollon, 1983. Human visual pigments: microspectrophotometric results from the eyes of seven persons, *Proc. R. Soc. Lond. B*, 220:115-130.
- Drummond-Borg, M., S. S. Deeb, and A. G. Motulsky, 1989. Molecular patterns of X-chromosome-linked color genes among 134 men of European ancestry, *Proc. Natl. Acad. Sci. USA*, 86:983-987.
- Dulai, K. S., M. von Dornum, J. D. Mollon, and D. M. Hunt, 1999. The evolution of trichromatic color vision by opsin gene duplication in New World and Old World primates, *Genome Res.*, 9:629-638.
- Fasick, J. I., N. Lee, and D. D. Oprian, 1999. Spectral tuning in the human blue cone pigment, *Biochemistry*, 38:11593-11596.
- Hagstrom, S. A., M. Neitz, and J. Neitz, 2000. Cone pigment gene expression in individual photoreceptors and the chromatic topography of the retina, *J. Opt. Soc. Am. A*, 17:527-537.
- Hayashi, T., A. G. Motulsky, and S. S. Deeb, 1999. Position of a "green-red" hybrid gene in the visual pigment array determines colour-vision phenotype, *Nat. Genet.*, 22:90-93.
- Hunt, D. M., K. S. Dulai, J. A. Cowing, C. Julliot, J. D. Mollon, J. K. Bowmaker, W. Li, and D. Hewett-Emmett, 1998. Molecular evolution of trichromacy in primates, *Vis. Res.*, 38:3299-3306.
- Jacobs, G. H., 1983. Within-species variations in visual capacity among squirrel monkeys (*Saimiri sciureus*): sensitivity differences, *Vis. Res.*, 23:239-248.
- Jacobs, G. H., 1993. The distribution and nature of colour vision among the mammals, *Biol. Rev.*, 68:413-471.
- Jacobs, G. H., M. Neitz, J. F. Deegan, and J. Neitz, 1996. Emergence of routine trichromatic colour vision in New World monkeys, *Nature*, 382:156-158.
- Jagla, W. M., H. Jägle, T. Hayashi, L. T. Sharpe, and S. S. Deeb, 2002. The molecular basis of dichromatic color vision in males with multiple red and green visual pigment genes, *Hum. Mol. Genet.*, 11:23-32.
- Jørgensen, A. L., S. S. Deeb, and A. G. Motulsky, 1990. Molecular genetics of X-chromosome-linked color vision among populations of African and Japanese ancestry: high frequency of a shortened red pigment gene among Afro-Americans, *Proc. Natl. Acad. Sci. USA*, 87:6512-6516.
- Kazmi, M. A., T. P. Sakmar, and H. Ostrer, 1997. Mutation of a conserved cysteine in the X-linked cone opsins causes color vision deficiencies by disrupting protein folding and stability, *Invest. Ophthalmol. Vis. Sci.*, 38:1074-1081.
- Merbs, S. L., and J. Nathans, 1992. Absorption spectra of the hybrid pigments responsible for anomalous color vision, *Science*, 258:464-466.

- Merbs, S. L., and J. Nathans, 1993. Role of hydroxyl-bearing amino acids in differentially tuning the absorption spectra of the human red and green cone pigments, *Photochem. Photobiol.*, 58: 706–710.
- Miyahara, E., J. Pokorny, V. C. Smith, R. Baron, and E. Baron, 1998. Color vision in two observers with highly biased LWS/MWS cone ratios, *Vis. Res.*, 38:601–612.
- Nathans, J., C. M. Davenport, I. H. Maumenee, R. A. Lewis, J. F. Hejtmancik, M. Litt, E. Lovrien, R. Weleber, B. Bachynski, F. Zwas, R. Klingaman, and G. Fishman, 1989. Molecular genetics of blue cone monochromacy, *Science*, 245:831–838.
- Nathans, J., I. A. Maumenee, E. Zrenner, B. Sadowski, L. T. Sharpe, R. A. Lewis, E. Hansen, P. Rosenberg, M. Schwartz, J. R. Heckenlively, E. Traboulsi, R. Klingaman, N. T. Bech-Hansen, G. R. LaRouche, R. A. Pagon, W. H. Murphy, and R. G. Weleber, 1993. Genetic heterogeneity among blue-cone monochromats, *Am. J. Hum. Genet.*, 53:987–1000.
- Nathans, J., T. P. Piantanida, R. L. Eddy, T. B. Shows, and D. S. Hogness, 1986a. Molecular genetics of inherited variation in human color vision, *Science*, 232:203–210.
- Nathans, J., D. Thomas, and D. S. Hogness, 1986b. Molecular genetics of human color vision: the genes encoding blue, green, and red pigments, *Science*, 232:193–202.
- Neitz, J., J. Carroll, and M. Neitz, 2001. Color vision: almost reason enough for having eyes, *Opt. Photon. News*, 12:26–33 (electronic copy available at <http://www.mcw.edu/cellbio/colorvision/>).
- Neitz, J., and G. H. Jacobs, 1986. Polymorphism of the long-wavelength cone in normal human color vision, *Nature*, 323: 623–625.
- Neitz, M. and J. Neitz, 1995. Numbers and ratios of visual pigment genes for normal red-green color vision, *Science* 267:1013–1016.
- Neitz, M., J. Neitz, and A. Grishok, 1995. Polymorphism in the number of genes encoding long-wavelength sensitive cone pigments among males with normal color vision, *Vis. Res.*, 35:2395–2407.
- Neitz, J., M. Neitz, J. C. He, and S. K. Shevell, 1999. Trichromatic color vision with only two spectrally distinct photopigments, *Nat. Neurosci.*, 2:884–888.
- Neitz, M., J. Neitz, and G. H. Jacobs, 1989. Analysis of fusion gene and encoded photopigment of colour-blind humans, *Nature*, 342:679–682.
- Neitz, M., J. Neitz, and G. H. Jacobs, 1991. Spectral tuning of pigments underlying red-green color vision, *Science*, 252:971–974.
- Neitz, J., M. Neitz, and G. H. Jacobs, 1993. More than three different cone pigments among people with normal color vision, *Vis. Res.*, 33:117–122.
- Neitz, M., J. Neitz, and G. H. Jacobs, 1995. Genetic basis of photopigment variations in human dichromats, *Vis. Res.*, 35:2095–2103.
- Neitz, J., M. Neitz, and P. M. Kainz, 1996. Visual pigment gene structure and the severity of human color vision defects, *Science*, 274:801–804.
- Onishi, A., S. Koike, M. Ida, H. Imai, Y. Shichida, O. Takenaka, A. Hanazawa, H. Komatsu, A. Mikami, S. Goto, B. Suryobroto, K. Kitahara, T. Yamamori, and H. Komatsu, 1999. Dichromatism in macaque monkeys, *Nature*, 402:139–140.
- Roorda, A., and D. R. Williams, 1999. The arrangement of the three cone classes in the living human eye, *Nature*, 397:520–522.
- Rushton, W. A. H., and H. D. Baker, 1964. Red/green sensitivity in normal vision, *Vis. Res.*, 4:75–85.
- Schnapf, J. L., T. W. Kraft, and D. A. Baylor, 1987. Spectral sensitivity of human cone photoreceptors, *Nature*, 325:439–441.
- Sharpe, L. T., A. Stockman, H. Jägle, H. Knau, G. Klausen, A. Reitner, and J. Nathans, 1998. Red, green, and red-green hybrid pigments in the human retina: correlations between deduced protein sequences and psychophysically measured spectral sensitivities, *J. Neurosci.*, 18:10053–10069.
- Sharpe, L. T., A. Stockman, H. Jägle, and J. Nathans, 1999. Opsin genes, cone photopigments, color vision, and color blindness, in *Color Vision: From Genes to Perception* (K. R. Gegenfurtner, and L. T. Sharpe, eds.), New York: Cambridge University Press, pp. 3–52.
- Shevell, S. K., J. C. He, P. M. Kainz, J. Neitz, and M. Neitz, 1998. Relating color discrimination to photopigment genes in deutan observers, *Vis. Res.*, 38:3371–3376.
- Sjoberg, S. A., M. Neitz, S. D. Balding, and J. Neitz, 1998. L-cone pigment genes expressed in normal colour vision, *Vis. Res.*, 38:3213–3219.
- Smith, V. C., J. Pokorny, J. W. Delleman, M. Cozinjensen, W. A. Houtman, and L. N. Went, 1983. X-linked incomplete achromatopsia with more than one class of functional cones, *Invest. Ophthalmol. Vis. Sci.*, 24:451–457.
- Sundin, O. H., Y. M. Yang, Y. Li, D. Shu, J. N. Hurd, T. N. Mitchell, E. D. Silva, and I. H. Maumenee, 2000. Genetic basis of total colourblindness among the Pingelapese islanders, *Nat. Genet.*, 3:289–293.
- Tickner, M. K., M. Neitz, and J. Neitz, 2002. Extreme polymorphism in L & M photopigment genes of humans but not monkeys, [Abstract] 2002 Annual Meeting Abstract and Program Planner [on CD-ROM]. Association for Research in vision and Ophthalmology. Abstract 3792.
- Vimal, R. L. P., J. Pokorny, V. C. Smith, and S. K. Shevell, 1989. Foveal cone thresholds, *Vis. Res.*, 29:61–78.
- Wang, Y., J. P. Macke, S. L. Merbs, D. J. Zack, B. Klaunberg, J. Bennett, J. Gearhart, and J. Nathans, 1992. A locus control region adjacent to the human red and green visual pigment genes, *Neuron*, 9:429–440.
- Wang, Y., P. M. Smallwood, M. Cowan, D. Blesh, A. Lawler, and J. Nathans, 1999. Mutually exclusive expression of human red and green visual pigment-reporter transgenes occurs at high frequency in murine cone photoreceptors, *Proc. Natl. Acad. Sci. USA*, 96:5251–5256.
- Weitz, C. J., Y. Miyake, K. Shinzato, E. Montag, E. Zrenner, L. N. Went, and J. Nathans, 1992a. Human tritanopia associated with two amino acid substitutions in the blue sensitive opsin, *Am. J. Hum. Genet.*, 50:498–507.
- Weitz, C. J., L. N. Went, and J. Nathans, 1992b. Human tritanopia associated with a third amino acid substitution in the blue sensitive visual pigment, *Am. J. Hum. Genet.*, 51:444–446.
- Wesner, M., J. Pokorny, S. Shevell, and V. Smith, 1991. Foveal cone detection statistics in color-normals and dichromats, *Vis. Res.*, 31:1021–1037.
- Winderickx, J., L. Battisti, Y. Hibibya, A. G. Motulsky, and S. S. Deeb, 1993. Haplotype diversity in the human red and green opsin genes: evidence for frequent sequence exchange in exon 3, *Hum. Mol. Genet.*, 2:1413–1421.
- Winderickx, J., D. T. Lindsey, E. Sanocki, D. Y. Teller, A. G. Motulsky, and S. S. Deeb, 1992a. Polymorphism in red photopigment underlies variation in colour matching, *Nature*, 356: 431–433.
- Winderickx, J., E. Sanocki, D. T. Lindsey, D. Y. Teller, A. G. Motulsky, and S. S. Deeb, 1992b. Defective colour vision associated with a missense mutation in the human green visual pigment gene, *Nat. Genet.*, 1:251–256.
- Wissinger, B., D. Gamer, H. Jägle, R. Giorda, T. Marx, S. Mayer, S. Tippmann, M. Broghammer, B. Jurklics, T. Rosenberg, S. G.

- Jacobson, E. C. Sener, S. Tatlipinar, U. Kellner, B. Lorenz, G. Wolff, C. Verellen-Dumoulin, M. Schwartz, F. P. M. Cremers, E. Apfelstedt-Sylla, E. Zrenner, R. Salati, L. T. Sharpe, and S. Kohl, 2001. *CNGA3* mutations in hereditary cone photoreceptor disorders, *Am. J. Hum. Genet.*, 69:722–732.
- Wissinger, B., H. Jägle, S. Kohl, M. Broghammer, B. Baumann, D. B. Hanna, C. Hedels, E. Apfelstedt-Sylla, G. Randazzo, S. G. Jacobson, E. Zrenner, and L. T. Sharpe, 1998. Human rod monochromacy: linkage analysis and mapping of a cone photoreceptor expressed candidate gene on chromosome 2q11, *Genomics*, 51:325–331.
- Yokoyama, S., and F. B. Radlwimmer, 1998. The “five-sites” rule and the evolution of red and green color vision in mammals, *Mol. Biol. Evol.*, 15:560–567.

64 Linking Retinal Circuits to Color Opponency

DAVID J. CALKINS

Mapping color perception to a physiological substrate

LINKING COLOR OPPONENCY WITH CONE ANTAGONISM We are able to perceive an amazingly diverse range of hue, or what we call in the vernacular *color*. The tremendous variability in the spectral composition of light reflected from surfaces lends itself to eliciting a daunting gamut of more than 100,000 discriminable colors, and the variation in the names we assign these colors is limited only by the scope of human experience. Yet, even with this variation, no demographic culture requires more than 11 color names to describe the quality of any hue (reviewed in Boynton, 1975). Of these 11, 5 can be described using either black or white in combination with the four unique hues—blue, green, yellow, and red (Bornstein, 1973). These four hues are themselves irreducible as percepts, and in that sense, each can be mapped at least conceptually to a perceptual channel whose activity correlates with that hue. The combined activity between channels presumably is what produces the rich variety of colors we experience.

The precise design of our visual system rigidly constrains how the activity of the color channels is mapped to hue sensation. Our ability to discriminate surfaces based on differences in spectral reflectance alone arises from a neural comparison of the rates of quantal absorption by the S-, M-, and L-cone photoreceptors (see Lennie and D’Zmura, 1988, for review). This neural comparison delimits color activity in the brain and has a characteristic signature that imposes upon hue perception a natural constraint. The four unique hues are organized into mutually exclusive or *opponent* pairs, blue/yellow (B/Y) and red/green (R/G). The members in each pair are opponent in the sense that we cannot perceive them simultaneously; their perceptive fields are spatially coextensive and cancellatory. We may perceive hue combinations *between* these pairs—for example, red and blue yielding a percept that is at once both (namely, violet)—but not combinations within a pair. Thus, there are no such hues as red-green or blue-yellow; we do not experience these percepts and therefore do not have names for them. This inherent phenomenology is explained in abstract terms by identifying each opponent pair with an independent color channel, B/Y and R/G, and through these channels all color perception is mediated.

A diverse body of psychophysical data implies that the B/Y and R/G channels each correlate with a neural *pathway* in which signals from the three cone types converge with one another in different *antagonistic* combinations (Hurvich and Jameson, 1957). The particular combination of cone antagonism bestows upon each channel a unique spectral sensitivity that correlates strongly with our perception of hue across the visible spectrum. For B/Y opponency, signals from S cones are combined antagonistically with an additive signal from M and L cones. This combination is abbreviated as $S/(M + L)$, where “/” indicates antagonism or subtraction. Very often the denotation $S-(M + L)$ is used instead, and the psychophysical spectral sensitivity of the channel (which by definition cannot be a negative number) is derived from the absolute value of the difference (Fig. 64.1). For R/G opponency, signals from L cones are combined antagonistically with those from M cones (abbreviated as L/M or $L-M$; Calkins et al., 1992). There is also a strong input from S cones into the R/G channel with the same polarity as the L-cone signal—the S signal can be canceled with appropriate stimulation of the M cones (Hurvich and Jameson, 1957; Stromeyer et al., 1998). Thus, much of the short-wavelength spectrum appears both blue and red, indicating activation of both the B/Y and R/G channels (DeValois et al., 2000a; Krauskopf et al., 1982; Wooten and Werner, 1979). The denotation “ L/M ” is a generalization that most visual scientists accept as a reasonable representation of the R/G channel but does not incorporate the S contribution. Each particular combination, $S/(M + L)$ or L/M , therefore represents the *minimal* condition that describes the defining opponency within a neural pathway consistent with the psychophysical properties of the appropriate color channel.

There are therefore two primary considerations in assigning an anatomical substrate to the cone-antagonism within the $S/(M + L)$ and L/M pathways: (1) the source of each pure cone signal prior to the site of antagonistic convergence and (2) the mechanism of antagonism itself. The first addresses the mechanism through which excitation from each cone type is collected or pooled and whether this pooling is indeed independent of the other photoreceptors (represented as “Stage 1” in Fig. 64.1). This stage accurately conveys the spectral sensitivity of the cone, including amplitude changes in cone sensitivity due to adaptation, and

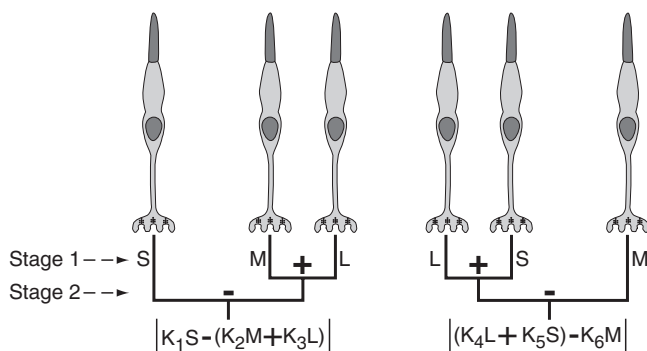


FIGURE 64.1. A two-stage cone-antagonistic model of color opponency. For B/Y opponency (*left*), signals from S cones are combined antagonistically (indicated by “−”) with the sum of signals from M and L cones (indicated by “+”); the net spectral sensitivity of the channel is given by the absolute value of the difference of the cone terms. Similarly, for R/G opponency (*right*), a combined signal from L and S cones is subtracted from signals from M cones. The K coefficients scale the spectral sensitivity of each cone and represent the combined effects for both stages in the model.

possibly modulates the cone signal further through its own intrinsic filters. In retinal terms, this stage likely corresponds to one or more types of bipolar cell that collect from cones and feed a glutamatergic excitatory signal forward to the ganglion cells. The second consideration addresses the anatomical site and mechanism through which signals from different cone types converge with opposite polarity, the so-called critical locus of opponency (“Stage 2” in Fig. 64.1; Teller and Pugh, 1983). This stage too could modulate or filter the collected cone signal through its own intrinsic properties. However, unlike the first stage, its output depends not on the spectral sensitivity of one cone type, but on the *difference* in sensitivity between two or more types. This difference signal forms the spectral signature of the color channel itself (for review, see Calkins and Sterling, 1999). In the primate retina, such antagonism between cones could arise through the convergence of an excitatory signal, say from a bipolar cell, with an inhibitory signal through lateral connections with horizontal cells (GABA-ergic) or amacrine cells (glycinergic), or more likely some combination of these. In the case of B/Y opponency, the antagonism is thought to involve the convergence of strictly excitatory signals from bipolar cells that respond to light with opposite polarity, that is, OFF cells versus ON cells. Thus, cone antagonism is not necessarily synonymous with physiological inhibition.

CHARACTERISTICS OF A COLOR PATHWAY There is great potential for spatial and temporal modulation of each cone’s signal through the two stages described in Figure 64.1 (e.g., Pugh and Mollon, 1979), the nature of which is well beyond the scope of this chapter. Because the sensitivity of each cone depends on ambient conditions, there is also the potential for spectral modulation (represented by the coeffi-

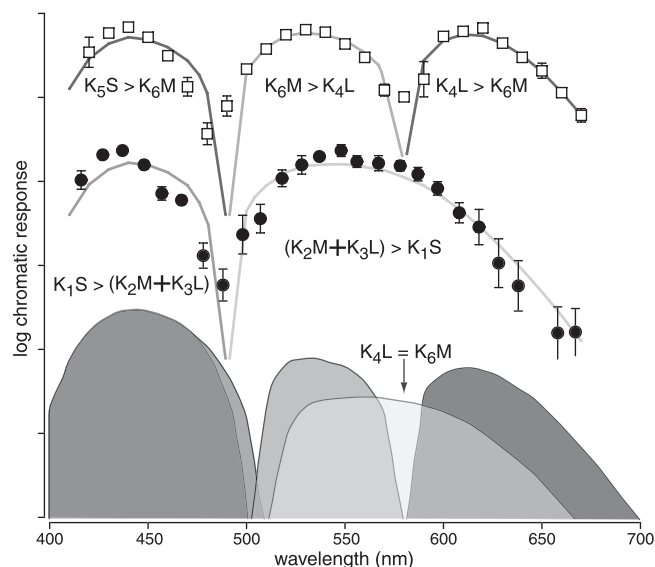


FIGURE 64.2. Data points represent the spectral sensitivity of the R/G (*open squares*) and the B/Y (*filled circles*) color channels estimated from chromatic scaling measurements (Romeskie, 1978). Solid curves were calculated from the model in Figure 64.1. The color of each curve represents the chromatic valence at each wavelength. The bottom traces represent the scaled sensitivity of the R/G and B/Y channels under typical psychophysical conditions. The color of the individual peaks represents the hue sensation of a monochromatic light at that wavelength. Threshold detection of monochromatic test lights would be mediated by the most sensitivity mechanism at each wavelength. Lights at and just above threshold elicit unique hues, while lights well above threshold generally fall and are detected through both R/G and B/Y channels. The location of unique yellow corresponds to the neutral point of the R/G channel, where detection is mediated solely by the B/Y channel (*arrow*). (See color plate 40).

cients K in Fig. 64.1). In effect, this modulation scales the amplitude of the cone sensitivities relative to one another, depending on the spectral composition and intensity of the ambient illumination. This shift greatly influences the resultant spectral sensitivity of the S/(M + L) and L/M pathways and therefore how the activity of the pathways partitions the visible spectrum into regions of dominant hue (Fig. 64.2). Thus, the color appearance of a monochromatic light under typical psychophysical conditions (i.e., a small spot on a larger adapting field) is directly related to the spectral sensitivity and activity of each channel.

This relationship between spectral sensitivity and hue perception allows some key predictions about the wiring of the S/(M + L) and L/M pathways. Most obviously, the output of a pathway should result in one hue and one hue alone, whose quality depends solely on the cone term dominating that output (as indicated in Fig. 64.2). Therefore the unique hues—blue, green, yellow, and red—ought to correlate closely with the activity of a pathway functioning in isolation. This is all to say that the S/(M + L) and L/M pathways should, in some measure, demonstrate separability and

TABLE 64.1
Some reviews of primate retinal circuitry and color vision

Review	Special Focus
Lennie and D’Zmura (1988)	Early visual pathways and color psychophysics
Kaplan et al. (1990)	P-cell physiology and receptive field characteristics
Wässle and Boycott (1991)	Retinal mosaics and circuitry
Lee (1996)	Ganglion cell receptive field types
Martin (1998)	Circuitry for receptive field formation
Dacey (1999)	Circuits for B/Y and R/G opponency
Calkins and Sterling (1999)	Midget ganglion cells and R/G color channel
Dacey (2000)	Cone contributions to ganglion and horizontal cells
Calkins (2001)	Circuitry from S cones, B/Y color channel

independence. As a corollary to this condition, the neutral points of each pathway (wavelengths where the cone terms cancel) ought to correspond to a locus of unique hue, where the other pathway solely mediates detection. For example, the wavelength at which the L- and M-cone terms in the L/M pathway cancel one another (570 to 580 nm under typical adaptive conditions) corresponds to unique yellow because detection is mediated only by the (M + L) envelope of the S/(M + L) pathway (Fig. 64.2). The chromatic neutral points are therefore closely dependent on the relative shift in cone sensitivity (reflected in the coefficients K in Figs. 64.1 and 64.2) prior to the stage of antagonistic convergence. The neutral points, then, represent the *chromatic signature* of the S/(M + L) and L/M pathways, and whatever circuitry in the visual system lends itself to establishing the critical locus of cone antagonism should in some measure support this signature.

The optics of the eye, the spatial sampling of retinal neurons, the ratio of rods to cones, and the relative numbers of L and M cones all change dramatically with increasing retinal eccentricity. Despite these variations, for normal trichromatic observers the S/(M + L) and L/M neutral points are remarkably invariant (Hibino, 1992; Kuyk, 1982; Nerger et al., 1995). Along these same lines, when appropriate stimuli are delivered to the peripheral retina, even as far out as 90 degrees, color is perceived with the same range of hues and with the same capacity to discriminate hues as in the fovea (Gordon and Abramov, 1977; Noorlander et al., 1983; Stabell and Stabell, 1982; van Esch et al., 1984). It is true that larger stimuli are required in the peripheral retina to produce comparable sensations, but this is not surprising given the decrease in spatial resolution of retinal mosaics and in the sensitivity of the color channels.

LINKING CIRCUITRY WITH CONE ANTAGONISM In short, the fundamental features of the color opponent channels are similar between the fovea and the peripheral retina—despite the common and mistaken belief that color discrimination

is a special function of the central retina. This consistency suggests two general possibilities for wiring the S/(M + L) and L/M pathways. The first possibility is that cone antagonism is established in the retina, within the presynaptic circuitry of one or more types of ganglion cell. In this case, the spectral signature of the color pathways begins with the particular circuitry producing the cone antagonism and is then conveyed to the cortex in a manner that is conserved across retinal eccentricity. This would place both stages of the generalized model in Figure 64.1 within the retina. The second possibility is that the cone antagonism inherent in color opponency is established later in the visual pathways, for example, in V1. In this instance, one or more types of ganglion cell could carry cone signals from the retina (Stage 1 in Fig. 64.1), and the antagonism (Stage 2) would be established in a central neuron where those signals converge with opposite polarity (e.g., ON-center vs. OFF-center cells). In this scheme, any antagonistic interactions within the ganglion cell receptive field, such as those between center and surround, would be ancillary to the critical spectral antagonism established at the central neuron. Spectral variations within the ganglion cell receptive field across retinal eccentricity (e.g., as the ratio of L to M cones changes) could then be washed out by cortical wiring.

Most visual scientists are willing to accept that color opponency at least begins in the retina for both B/Y and R/G opponency. This inference is supported by the vast physiological literature demonstrating cone antagonism within the receptive fields of many ganglion cells, mainly in those providing input to the parvocellular (P) region of the lateral geniculate nucleus (LGN; for reviews, see references in Table 64.1). This is especially so for the massive subset of these cells serving the central visual field. There, the net spectral sensitivity to full-field stimulation is generally (but not always) cone antagonistic, either S/(M + L) or L/M (Fig. 64.3), although many other combinations also have been found (de Monasterio and Gouras, 1975). The key issue is the circuitry for this antagonism and whether it is sufficient to explain the

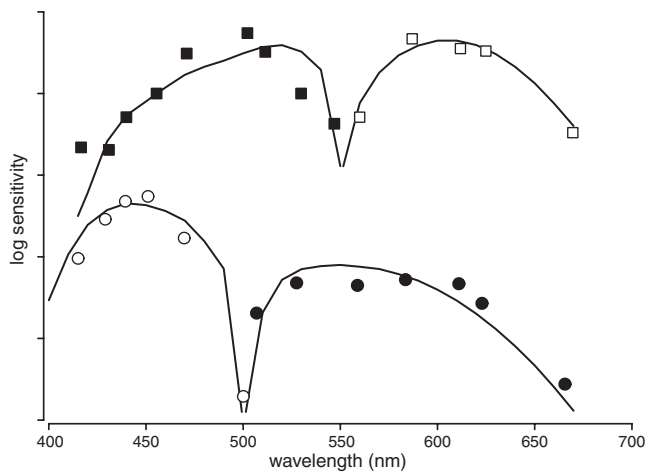


FIGURE 64.3. *Top*: spectral sensitivity of a nominal R/G opponent ganglion cell that responds with an increase in firing rate to long wavelengths (*open squares*) and with a decrease to middle and short wavelengths (*filled squares*). The curve was calculated from the R/G model in Figure 64.1. *Bottom*: spectral sensitivity of a B/Y opponent ganglion cell that responds with an increase in firing rate to short wavelengths (*open circles*) and with a decrease to middle and long wavelengths (*filled circles*). The curve was calculated from the B/Y model in Figure 64.1. (Data replotted from Zrenner, 1983b.)

spectral, spatial, and temporal properties of the opponent channels. Of particular interest for this chapter is whether the retinal circuitry is conserved across eccentricities or whether more central mechanisms are necessary to explain the consistent spectral signature of the opponent channels.

This chapter will explore two general schemes for wiring cone antagonism in a ganglion cell receptive field (Fig. 64.4). The first is through the simple convergence of signals from cones of different types via strictly excitatory cells that respond to light with opposite polarity, that is, OFF versus ON bipolar cells. This sort of wiring is likely to underlie the S/(M + L) spectral sensitivity of the *small bistratified* ganglion cell, and this chapter will discuss how the cell might contribute to B/Y opponency (see also Calkins, 2001). The second scheme involves the convergence of excitatory and inhibitory inputs in such a way to render the ganglion cell *color opponent*. For example, the excitatory center of a foveal P (or *midget*) ganglion cell is derived from a single cone via a *midget* bipolar cell, while its inhibitory surround is derived from a combination of cone inputs via GABA-ergic or glycinergic lateral connections (Calkins and Sterling, 1999). This chapter will discuss the mechanism through which the ganglion cell's spectral sensitivity reflects the difference between these signals across retinal eccentricities and the implications for R/G color opponency.

A retinal circuit for B/Y opponency

THE S-ON/(M + L)-OFF GANGLION CELL One of the purposes of color opponency, at least from the standpoint of

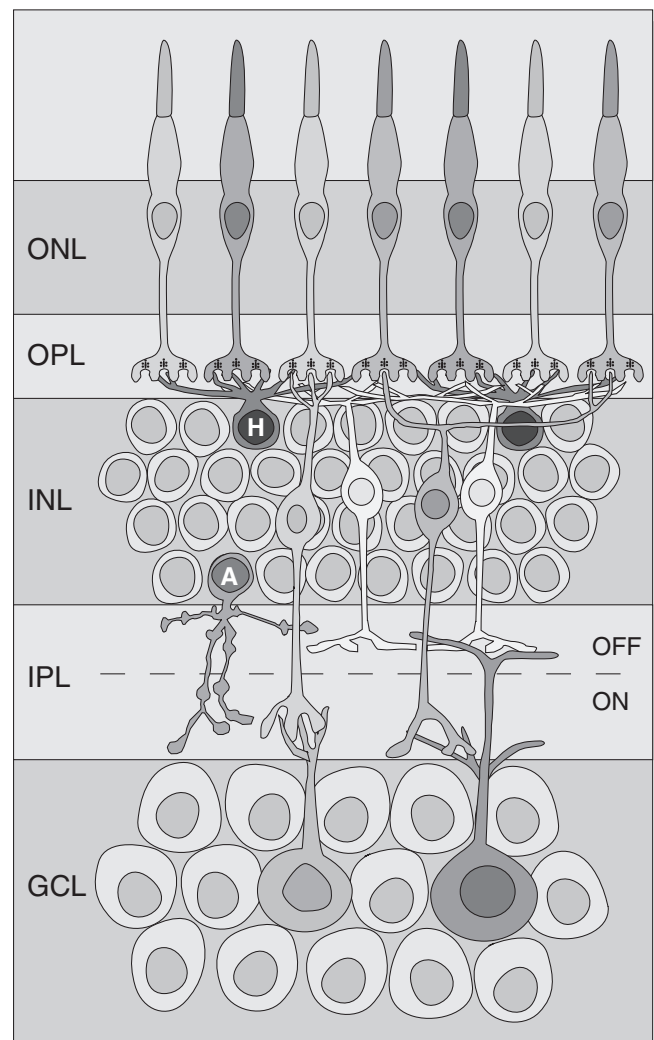


FIGURE 64.4. Two schemes for wiring cone antagonism in the receptive field of retinal ganglion cells. *Right*: antagonism for the S-ON/(M + L)-OFF ganglion cell (blue) established through converging ON and OFF bipolar cells. *Left*: antagonism for the midget cell (green) via convergence of excitation from a bipolar cell and inhibition via horizontal (H) and amacrine (A) cells. (See color plate 41.)

serving the efficiency of vision, is to optimize color information by reducing the redundancy resulting from the overlapping spectral sensitivities of the S, M, and L cones (Buchsbaum and Gottschalk, 1983; Derrico and Buchsbaum, 1991). To optimally fill the dynamic range of a ganglion cell with a pure cone-antagonistic signal, its receptive field ought to be spectrally but not spatially antagonistic (Calkins and Sterling, 1999). A small population of relay neurons in the LGN (Derrington and Lennie, 1984; Dreher et al., 1976; Marroco and DeValois, 1977; Wiesel and Hubel, 1966) and their corresponding ganglion cells in the retina (Dacey, 1996; de Monasterio, 1978; de Monasterio and Gouras, 1975; Zrenner, 1983a, 1983b) fulfill these criteria in a manner consistent with B/Y opponency (for

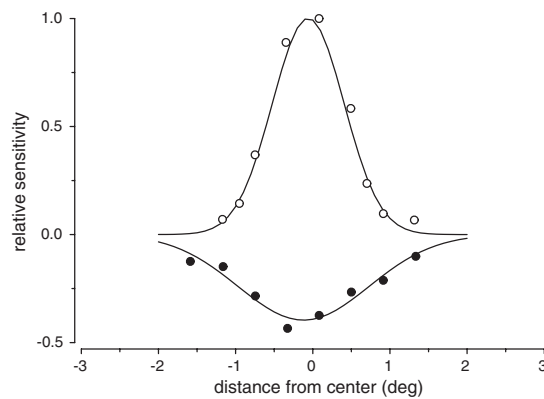


FIGURE 64.5. Spatially coextensive S-ON (*open symbols*) and (M + L)-OFF (*filled symbols*) responses of a small bistratified ganglion cell. [Data replotted from Dacey, 1996, and fit to a simple Gaussian (*solid curves*).]

review, see Calkins, 2001; Rodieck, 1991). These neurons have both the appropriate S/(M + L) spectral signature with a neutral point near 500 nm and the appropriate spatial response, in which the S and M + L components are coextensive (Fig. 64.5). Most of the so-called blue/yellow cells in the literature respond with excitation at the onset of S stimulation and at the offset of M + L stimulation, that is, S-ON/(M + L)-OFF; a small number of cells demonstrate the reverse configuration (this is discussed below).

A critical step forward in linking the S-ON/(M + L)-OFF cell with B/Y opponency was to correlate the physiological receptive field with the morphology of a ganglion cell and a particular synaptic circuitry. Intracellular recordings of spectral responses from macaque ganglion cells with subsequent staining of their dendritic trees revealed a small bistratified ganglion cell (Dacey and Lee, 1994). This ganglion cell has one dendritic arbor deep in the ON stratum of the inner retina and another dendritic arbor, cospatial with but slightly smaller than the first, in the OFF stratum (Calkins et al., 1998; Dacey, 1993b; Rodieck, 1991). The cell responds with excitation to the onset of short-wavelength light and to the offset of middle and long wavelengths, suggesting that the bistratified morphology correlates with segregated ON and OFF inputs in the inner retina.

BUILDING CONE ANTAGONISM IN THE S-ON/(M + L)-OFF RECEPTIVE FIELD What is the source of the different spectral contributions to the receptive field of the small bistratified cell (Stage 1 in Fig. 64.1)? In the ON stratum, dendrites of the cell intermingle with the axon terminals of the so-called blue cone or S bipolar cell. Excitation in the retina is conveyed through the release of glutamate, both at the cone → bipolar cell synapse and the bipolar cell → ganglion cell synapse (Massey, 1990). Other types of ganglion cell express *ionotropic* glutamate receptors, which open cation channels upon binding glutamate (Cohen and Miller, 1994;

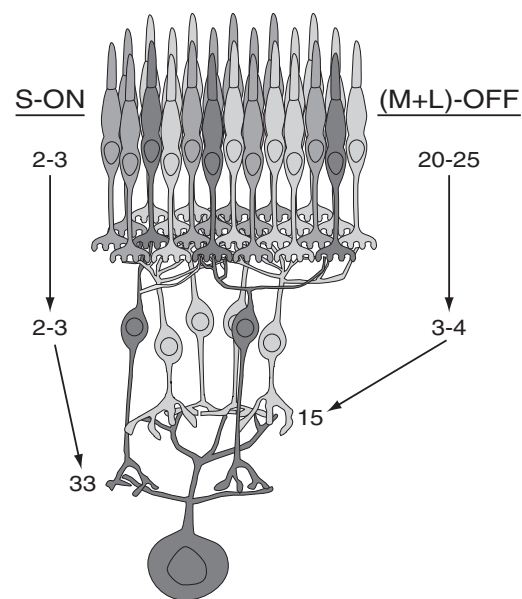


FIGURE 64.6. Summary of the presynaptic circuitry of the small bistratified ganglion cell in macaque fovea. The ganglion cell collects mostly from one S cone via 33 synapses from two or three S bipolar cells (blue) and from 20 to 25 M and L cones via 15 synapses from three or four DB2 and DB3 cells (yellow). Modified from Calkins (2001).

Lukasiewicz et al., 1997; Peng et al., 1995; Qin and Pourcho, 1995; Zhou et al., 1994). Thus, the S bipolar cell with light stimulation is likely to release glutamate that opens cation channels localized to the dendrites of the S-ON/(M + L)-OFF ganglion cell. Because increased light *decreases* the rate of glutamate release from photoreceptors, an ON bipolar cell must express a *metabotropic* glutamate receptor that uses a second-messenger cascade to invert the sign of polarization at the cone synapse (Shiells and Falk, 1995; Vardi et al., 1993). The S bipolar cell, like other ON bipolar cells in the mammalian retina, apparently expresses the L-AP4 or mGluR6 receptor (Euler et al., 1996; Hartveit, 1997; Nakajima et al., 1993; Vardi et al., 1998, 2000), indicating that the small bistratified cell's ON response to short wavelengths arises through excitation mediated by mGluR6 at the first synapse in the circuit.

The small bistratified cell also responds with excitation at the offset of yellow light that stimulates M and L cones (Chichilnisky and Baylor, 1999; Dacey and Lee, 1994). In the OFF stratum of the inner plexiform layer, the ganglion cell collects synapses from the DB2 and DB3 types of *diffuse* bipolar cell (Calkins et al., 1998), whose dendrites collect from each cone they span (Boycott and Wässle, 1999). There, at the cone terminal base, the dendrites of the DB2 and DB3 cells likely express ionotropic glutamate receptors (Haverkamp et al., 2001; Morigiwa and Vardi, 1999), which would *open* cation channels upon binding glutamate with the offset of M and L stimulation.

Thus, the actual cone antagonism in the S-ON/(M + L)-OFF circuit (Stage 2 in Fig. 64.1) is established through distinct, and strictly excitatory, bipolar cell circuits (Fig. 64.6). Through these circuits, S cones and M and L cones effect opposing currents in the small bistratified ganglion cell, and their joint stimulation produces concurrent S-ON and (M + L)-OFF responses. In the macaque fovea, the axon terminals of the S-cone bipolar cell provide 30 to 35 synapses to the ganglion cell in the ON stratum (Calkins et al., 1998). In the OFF stratum, the axon terminals of the DB2 and DB3 cells provide only about half as many synapses. Consequently, about 70% of the excitation in the receptive field is carried via the S-cone circuit. This difference in synaptic weight, when convolved with the number of converging cones, can account for the approximately 40% difference in amplitude between the S-ON and (M + L)-OFF components of the receptive field (Fig. 64.5). The difference may also explain the faster time to peak for the S component of the response (Chichilnisky and Baylor, 1999; Sterling, 1999).

Models of the S-ON/(M + L)-OFF receptive field generally are based solely on converging excitation from the parallel bipolar cell circuits. However, two levels of inhibition also contribute to the ganglion cell. In the inner plexiform layer, amacrine cells provide numerous synapses to the ganglion cell dendritic tree (Calkins et al., 1998; Dacey, 1993b; Ghosh and Grünert, 1999), while in the outer plexiform layer, horizontal cells provide a feedback signal to cones proportional to their mean activity and also are likely to directly inhibit bipolar cells (Sterling, 1999). Both levels of inhibition could contribute to a surround mechanism for the bipolar cells (Dacey, 1999). In particular, the H1 horizontal cell collects signals almost exclusively from M and L cones and lacks any substantial contact with S cones, while the H2 horizontal cell collects from and can provide feedback to all three cone types (Chan and Grünert, 1998; Dacey et al., 1996, 2000; Goodchild et al., 1996). Thus, both H1 and H2 cells would be able to contribute to the surround of the DB2 and DB3 bipolar cells, while the H2 cell could contribute to the surround for the S bipolar cell (for review, see Martin, 1998). Nevertheless, the ganglion cell apparently lacks a measurable *net* surround, and changing the size of a stimulus centered on the receptive field modifies very little the response of the cell (de Monasterio, 1978; Wiesel and Hubel, 1966). One simple explanation for this is that the reduction in activity in the OFF and ON bipolar circuits via horizontal cell feedback is about equivalent because of the overwhelming preponderance of input from M and L cones to both H1 and H2 cells (Rodieck, 1998). What is seen then in the ganglion cell response is only the difference between the excitatory S-ON and (M + L)-OFF components.

THE S-ON/(M + L)-OFF GANGLION CELL ACROSS RETINAL ECCENTRICITY The diameter of the dendritic arbor of the

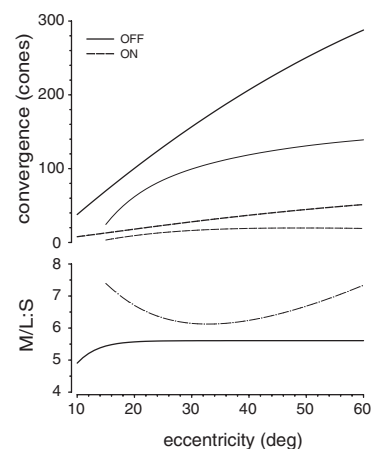


FIGURE 64.7. *Top*: convergence of M/L cones to the OFF dendritic tree and of S cones to the ON dendritic tree of the small bistratified ganglion cell in human (*thick lines*) and macaque (*thin lines*) retina. Convergence calculated as the product of dendritic tree area (polynomials in Fig. 64.9) with average density of S cones [(from Figs. 6A and 7A) or of M/L cones (from Curcio et al., 1990)]. *Bottom*: ratio of convergence of M/L cones to S cones in human (*stippled trace*) and macaque (*solid trace*) retina. The ratios are nearly constant across retinal eccentricity. Modified from Calkins (2001).

small bistratified cell in the OFF stratum is about 75% that of the ON arbor (Dacey, 1993b). The area encompassed by the OFF tree reflects this difference accordingly (see Figure 9 in Calkins, 2001). Nevertheless, because of their greater density, the estimated convergence of M and L cones is much higher than the convergence of S cones. In the macaque fovea, 20 to 25 M and L cones converge on the ganglion cell, compared to 3 to 4 S cones (Fig. 64.6). The convergence of M and L cones is systematically about five-fold higher than convergence of S cones across the human retina and six- or sevenfold higher across most of the macaque retina (Fig. 64.7). On the other hand, the great width of the spatial aperture of the receptive field of the S cone itself (Williams et al., 1983, 1993), combined with synaptic weighting, effectively molds the S-ON component of the S-ON/(M + L)-OFF receptive field into a continuous, smooth profile that is spatially coextensive with the (M + L)-OFF component (see Figure 1 in Calkins, 2001). Thus, both the spatial and spectral response profiles of the S-ON/(M + L)-OFF ganglion cell are consistent with cells involved in B/Y opponency.

The ratio of the convergence of M/L cones to S cones remains roughly constant across retinal eccentricity (Fig. 64.7). This consistency would contribute to a uniform spectral neutral point in the response of the S-ON/(M + L)-OFF cell to monochromatic stimulation. In the narrow range of eccentricities tested in the macaque retina, this is certainly the case (Zrenner, 1983a, 1983b). As alluded to earlier in the chapter, the neutral point of the B/Y channel in human observers is also remarkably uniform across a wide range of

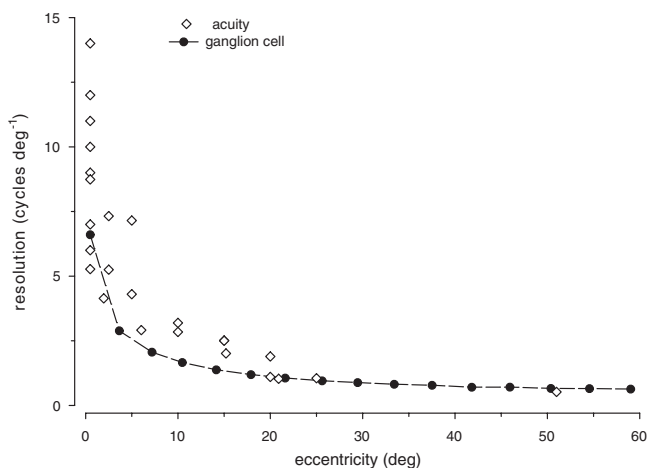


FIGURE 64.8. The sampling frequency of the small bistratified ganglion cell matches S acuity in the human retina. The sampling frequency of the ganglion cell is calculated as the corresponding Nyquist frequency, assuming triangular packing and based on the density measurements of Dacey (1993b) outside of the fovea and of Calkins et al. (1998) for the fovea. Acuity measurements were pooled from Daw and Enoch (1973), Green (1972), Mullen (1985), Stiles (1949), Stromeyer et al. (1978), and Williams et al. (1983) for the fovea and from Noorlander et al. (1983) and Hess et al. (1989) for the periphery. Modified from Calkins (2001).

eccentricities (see Figure 6 in Hibino, 1992). In the human retina, the relative number of M versus L cones likely varies with eccentricity (Hagstrom et al., 1998). It would be interesting to determine whether the synaptic weights of the S and M/L components of the ganglion cell receptive field also change with eccentricity to accommodate the M:L ratio.

It is difficult to extract from the early extracellular recordings the regularity with which either the S-ON/(M + L)-OFF geniculate cell or its ganglion cell counterpart samples the photoreceptor mosaic. This is important, because for a ganglion cell circuit to be associated with the critical locus of opponency, that circuit ought to sample the retinal mosaic with the same spatial resolution as the color channel in question. The mosaic of the S-ON/(M + L)-OFF small bistratified ganglion cell has been mapped by microinjection in the human and macaque retina for the parafovea and beyond (Dacey, 1993b). These injections provide precise measurement of the cell's dendritic arbor as a function of eccentricity. Assuming that adjacent arbors "tile" the retina, the average diameter of the dendritic tree provides an estimate of the cell's density and therefore of its spatial (or Nyquist) sampling rate (Dacey, 1993b). Individual differences between retinas are likely to be substantial, and the great variability between the size of dendritic arbors at a particular eccentricity confounds the estimate of density. Nevertheless, the estimated sampling rate of the small bistratified cell in the human retina agrees reasonably well with measurements of visual acuity based on discriminating S-cone isolating spatial

patterns (Fig. 64.8). Such psychophysical tasks are likely to tap the B/Y color channel, based on the color appearance of the pattern. The Nyquist rate for the fovea is based on identification of the ganglion cell in macaque retina using electron microscopy (Calkins et al., 1998). The finding in that retina was one small bistratified cell for every S cone, and there is little reason to doubt that the same holds for the human fovea. Thus, the small bistratified ganglion cell is likely dense enough to support the spatial acuity of the B/Y channel across eccentricity.

Reconstructions of the small bistratified cell with electron microscopy indicate that in the macaque fovea, the ganglion cell collects from about three S cones via 30 to 35 synapses from two or three S bipolar cells (Fig. 64.6; Calkins et al., 1998). Outside of the fovea, the dendritic tree of the ganglion cell in the ON stratum encompasses increasing expanses of retina as the cell's density declines (Dacey, 1993b). Based on anatomical measurements alone, a small bistratified cell at 10 to 20 degrees of eccentricity would collect from 5 to 10 S cones, while cells at 25 degrees of eccentricity and beyond, it would collect from 10 to 20 S cones. These numbers are consistent with highly sensitive multielectrode recordings from S-ON/(M + L)-OFF cells, which indicate a convergence of 5 to 15 S cones between 20 and 50 degrees of eccentricity (Chichilnisky and Baylor, 1999).

These same multielectrode recordings actually illustrate several important points. The signals from individual S cones to the receptive field of the ganglion cell sum *linearly*: their combined contribution predicts the net response of the cell to S stimulation. Also, the relative strength of the S signals varies greatly, with one S cone providing the dominant input. Conversely, a particular S cone may contribute to the receptive fields of neighboring small bistratified cells; however, that S cone provides the dominant input to only one ganglion cell (Chichilnisky and Baylor, 1999).

These physiological results match very well predictions based on circuitry. A single S cone provides about 70% of the synaptic input to an S bipolar cell. Similarly, a single S bipolar cell dominates in providing synapses to the small bistratified ganglion cell. The result of these two levels of synaptic weighting is that a single S cone outweighs its neighbors in providing excitation to a particular ganglion cell (Calkins, 2000; Calkins et al., 1998; Chichilnisky and Baylor, 1999). If every S cone is so represented, the density of the small bistratified cell ought to match the S cone density. This is clearly so in the primate fovea (Calkins et al., 1998). Outside of the fovea, in human retina, the disparity between the sampling of the small bistratified cell and the sampling of the S mosaic is small (compare Figures 6 and 10 in Calkins, 2001), too small to reject the hypothesis of 1:1 sampling given methodological differences and interretina variation. Therefore, it is reasonable to accept the idea that the spatial sampling of the small bistratified, S-ON/(M + L)-

OFF cell matches the acuity of the B/Y channel across retinal eccentricity (Fig. 64.8).

COMPLETING THE CIRCUIT: AN S-OFF CELL IN THE RETINA
The clear demonstration linking the morphology and circuitry of the small bistratified ganglion cell to the S-ON/(M + L)-OFF receptive field has reinforced the association of S cones with a single physiological pathway and therefore a single line into the B/Y channel. In many reviews, S cones are depicted as “skipping” contact with additional postsynaptic pathways (e.g., Martin, 1998). Along these lines, the lack of any regularity of physiological recordings from OFF cells with substantial S input has supported the view that S cones simply do not contact OFF pathways to the brain, including any that might support B/Y color vision. However, a careful survey of the literature reveals numerous physiological recordings from neurons with a pure S-OFF response (Calkins, 2001), and certain psychophysical experiments support S input to OFF channels (most recently, McLellan and Eskew, 2000; Shinomori et al., 1999). The physiological examples are relatively rare, compared to the S-ON/(M + L)-OFF cell, but nonetheless persist across multiple decades of investigation. These studies converge upon two distinct profiles of the receptive field. The first resembles the S-ON cell in that the S-OFF response is spatially coextensive with an (M + L)-ON response. The second resembles the textbook spatially and spectrally opponent cell in that the S-OFF response is localized to a center spatially concentric with an inhibitory M + L surround.

Complementary ON and OFF mosaics for a particular type of ganglion cell effectively partition the dynamic range of the pathway about the mean light level. Thus, each ganglion cell can use the full range of its spiking capacity to signal with excitation either graded increments or decrements from the mean. If such a strategy is used by the color channels, one might expect a ganglion cell with spatially coextensive S-OFF and (M + L)-ON regions (i.e., (M + L)-ON/S-OFF) to contribute to and complete the B/Y opponent channel (Zrenner, 1983a, 1983b; see the discussion of this topic in Sankeralli and Mullen, 2001). To make this argument convincing, though, requires identification of its morphological substrate and demonstration that its presynaptic circuitry optimizes a spectral signal at the price of spatial information, much like the small bistratified cell (Calkins and Sterling, 1999).

New views of R/G opponency

COMPARING R/G AND B/Y OPPONENCY Color opponency serves to optimize the information contained in the quantum catches of the S, M, and L cones through perceptive fields that are spectrally but not spatially antagonistic (Fig. 64.9). Cells involved in establishing the opponent channels at some level should eventually demonstrate receptive fields with the same so-called type II configuration (Calkins and Sterling,

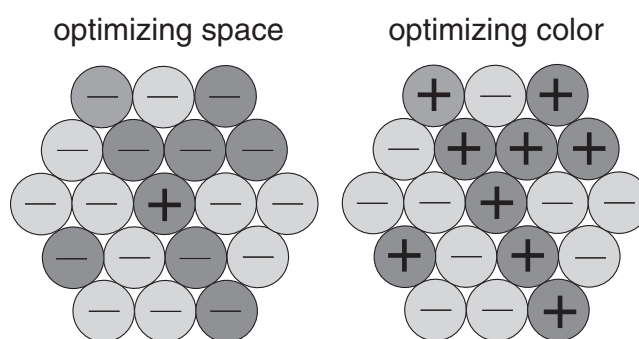


FIGURE 64.9. To optimize its spatial signal, a ganglion cell should remove the signal component shared with neighbors by subtracting a spatially weighted average of *all* surrounding cones. To optimize its spectral-difference signal, a ganglion cell should subtract all the signals of one cone type from all the signals of the other types. (Modified from Calkins and Sterling, 1999.)

1999). For B/Y opponency, spectral antagonism without spatial antagonism is established early on in the retina, in the receptive field of the small bistratified ganglion cell. For that cell, the difference in amplitude between the S-ON and (M + L)-OFF components is constant across the spatial extent of the receptive field (Rodieck, 1991). Thus, the only information available in the spike train of the cell is spectral and not spatial. Many cells in V1 demonstrate L/M antagonism in spatially coextensive domains of the receptive field—again, spectral without spatial antagonism. These cells are expected, therefore, to play some role in R/G opponency. Similarly, even earlier in the visual pathways, many cells in the parvocellular region of the LGN, and presumably their ganglion cell counterparts in the retina, also demonstrate type II receptive fields with spatially coextensive L-cone versus M-cone regions (de Monasterio, 1978; de Monasterio and Gouras, 1975; Dreher et al., 1976; Lee, 1996; Reid and Shapley, 1992; Wiesel and Hubel, 1966). These cells generally have the correct spectral signature, with the L/M neutral point near 570 to 600 nm (Rodieck, 1991), and the variability that is present can easily be attributed to different adaptive conditions. Based on these recordings, many investigators have proposed that the type II receptive fields may subserve a specialized pathway for R/G opponency (Hubel and Livingstone, 1990), and others have suggested a retinal circuit similar to that of the small bistratified ganglion cell as the critical locus for L/M antagonism (Calkins and Sterling, 1999; Rodieck, 1991).

For B/Y opponency, only 3% to 4% of the ganglion cells in the central fovea need be small bistratified cells to account for B/Y acuity (Calkins and Sterling, 1999). If the B/Y channel requires a corresponding S-OFF cell, this fraction increases by another 3% to 4%. Another 5% to 7% of the ganglion cells in the fovea are “parasol” ganglion cells, and 75% to 85% are midget cells (Boycott and Wässle, 1999). Other types of large and sparsely distributed ganglion cells that are likely uninvolved in color vision probably represent

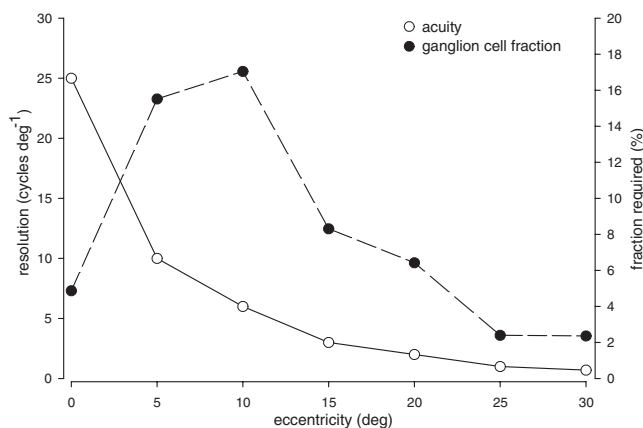


FIGURE 64.10. The fraction of all ganglion cells in the human retina necessary to account for psychophysically observed spatial acuity of the R/G channel. The fraction was calculated as the ratio of the Nyquist sampling density required, assuming triangular packing of ganglion cells, to the total ganglion cell density, using measurements of Curcio and Allen (1990) and assuming three or four ganglion cells per cone for the center fovea (Sjöstrand et al., 1994). Acuity measurements outside of the fovea are from Andersen et al. (1991), and those in the fovea are from Sekiguchi et al. (1993).

another 3% to 5%. Thus, at best, about 10% of the foveal ganglion cells remain that could include a dedicated R/G pathway from the retina. Figure 64.10 shows a plot of spatial acuity for R/G isolating patterns and the fraction of all ganglion cells necessary to account for the corresponding sampling rate. While there may be room for a dedicated R/G cell, the relatively large fraction of cells needed would make finding the cell at least as likely as encountering a small bistratified cell. Yet, in both anatomical and physiological studies, a clear mosaic of ganglion cells with L/M (or M/L) type II receptive fields has not been found. Moreover, if R/G opponency also demands complementary L-ON/M-OFF and M-ON/L-OFF mosaics, the fractions in Figure 64.10 must double, and there simply may not be enough ganglion cells to provide the necessary sampling rate. In the absence of a morphologically identified substrate in the retina, many now doubt the accuracy of L/M (or M/L) type II receptive fields derived from extracellular recordings in the retina or LGN.

THE P CELL HYPOTHESIS The early Golgi studies of the retina identified a densely populated ganglion cell with a small cell body and a narrow dendritic tree, with a corresponding bipolar cell providing it input (Polyak, 1941). Both cells were called *midget* because of their small size and morphology, and the ganglion cell is also called *P* because of its projections to the parvocellular layers of the LGN (for review, see Calkins and Sterling, 1999). Within the central 6 to 7 degrees or so, each midget ganglion cell collects from only a single cone via a single midget bipolar cell. Similarly,

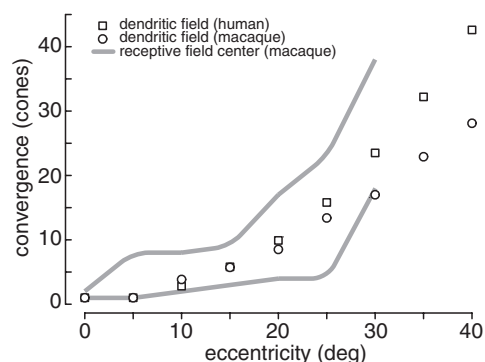


FIGURE 64.11. Cone convergence onto the P cell rises steadily with eccentricity for both macaque and human. Calculation for the region denoted by the shaded lines is based on the range of measurements of macaque P cell receptive field centers in retina and LGN (Croner and Kaplan, 1995; de Monasterio and Gouras, 1975; Derrington and Lennie, 1984) and of macaque cone spatial densities (Packer et al., 1989). This brackets the anatomical convergence calculated from the dendritic field areas and cone densities (calculated from Curcio et al., 1990; Dacey, 1993a; Packer et al., 1989; Watanabe and Rodieck, 1989). Modified from Calkins and Sterling (1999).

over most of the retina, the midget bipolar cell also collects from only a single cone. Conversely, within this region, each cone sends signals to both a single ON and a single OFF midget ganglion cell via an ON and an OFF midget bipolar cell. Outside of the fovea, the number of cones converging onto the midget ganglion cell via numerous midget bipolar cells increases as the dendritic tree of the ganglion cell expands. Nevertheless, at all retinal eccentricities, the midget cell is the most numerous and has the smallest anatomical sampling aperture of all ganglion cells, and therefore sets the limit for cone-mediated spatial acuity (see Dacey, 1993a).

The S-ON and (M + L)-OFF regions of the small bistratified cell's receptive field are spatially coextensive, and the cell lacks a measurable *net* surround. In contrast, the midget or P cell demonstrates a narrow receptive field center and a spatially concentric, inhibitory surround. The physiological center correlates closely in size with the sampling area of the dendritic tree (Fig. 64.11), while the surround is much broader and only about 55% to 60% the strength of the center (Croner and Kaplan, 1995). This *type I* receptive field structure is therefore optimized for spatial antagonism and the detection of high-frequency edges (Derrington and Lennie, 1984). While the circuitry for the center of the midget ganglion cell is relatively straightforward, the circuitry for the surround is more complex, probably involving feedback inhibition from both horizontal cells in the outer plexiform layer (OPL) and amacrine cells in the inner plexiform layer (IPL) (Fig. 64.12). As with other ganglion cells, much of the surround of midget cells is likely conveyed through its bipolar cell circuitry (Dacey, 1999; Dacey et al., 2000).

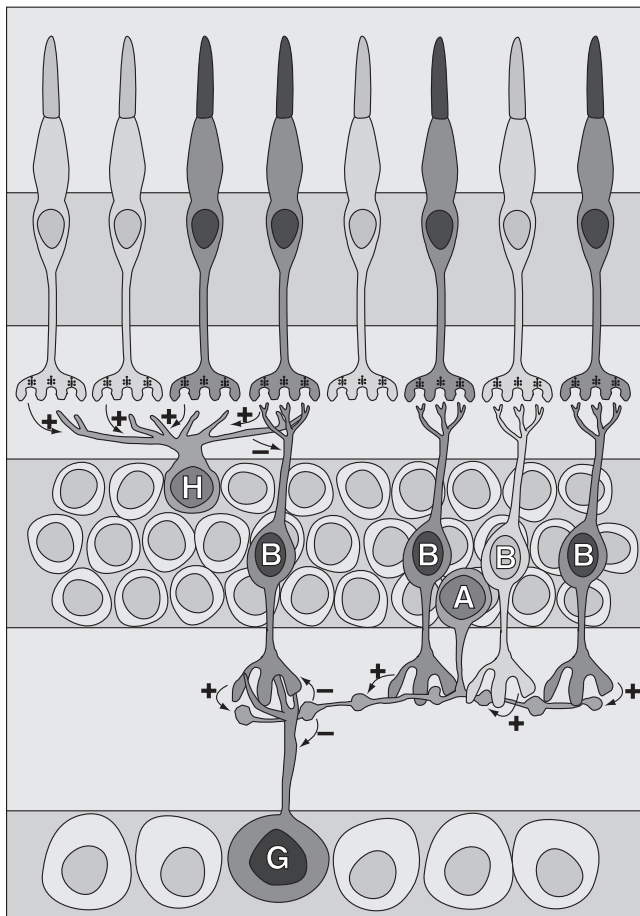


FIGURE 64.12. The horizontal cell (H) collects directly from both M and L cones and inhibits midwavelength bipolar cell dendrites; amacrine cells (A) also collect M and L input via bipolar cells (B) and inhibit the midwavelength bipolar cell axon terminal and the dendrites of the midwavelength P ganglion cell (G). Modified from Calkins and Sterling (1999). (See color plate 42).

By definition, the center mechanism for each midwavelength cell within the central 6 to 7 degrees is spectrally pure, either L or M. This is also likely to be the case for many midwavelength cells within the central 10 degrees, where convergence is still limited to a handful of cones and M and L cones distribute into small clusters of like type. Since recordings began in the early 1960s, nearly all of the physiological recordings from either P cells in the retina or their LGN counterparts have been from cells representing the central 10 to 15 degrees of the visual field. Most of these cells (but not all) demonstrated L/M or M/L cone-antagonistic receptive fields, and P cells were equated with color opponent cells (see Calkins and Sterling, 1999, for review). These recordings seemed to imply that the surround, like the center, must also be spectrally pure—but of the opposing cone type. While some data support this idea, careful physiological measurements indicate that horizontal cells are broadly tuned spectrally (Dacey et al., 1996; Dacheux and Raviola, 1990). Moreover, the anatomical connections to midwavelength cells from amacrine cells

are also spectrally mixed (Calkins and Sterling, 1996). Thus, there is little basis to support the idea that color opponency in the midwavelength cell of the central retina arises from antagonism between a pure center *and* a pure surround.

Simple models of the receptive field clearly show that random connections forming the surround can render the entire receptive field color opponent (Lennie et al., 1991). The reason is equally simple. Because the surround is so much weaker than the center, having about 60% of the center's strength (Croner and Kaplan, 1995), whatever cone contribution to the surround is common to the center is simply canceled by the dominant contribution of that cone type to the center. The net result is a more or less balanced antagonism between L and M cones, with resultant L-M or M-L spectral sensitivity yielding the appropriate neutral point (Lennie et al., 1991). In this model, the critical locus for R/G opponency is then placed at the point of convergence of excitatory (center) and inhibitory (surround) inputs forming the midwavelength cell receptive field.

With both an ON and an OFF midwavelength ganglion cell for each cone, in the fovea only 30% to 40% of all midwavelength cells need be opponent to account for the discrimination of R/G patterns. That is, if the R/G channel requires complementary L-ON/M-OFF and M-ON/L-OFF pairs, only 30% to 40% of the L and M cones need to contact midwavelength circuits in which the cone antagonism between center and surround is more or less balanced to a psychophysically appropriate spectral signature. Because of its center-surround organization, every midwavelength cell in the retina transmits information regarding spatial edges, regardless of its spectral sensitivity (Derrington and Lennie, 1984). However, because of the mixed surround, the amount of information concerning the difference between L- and M-cone activity will vary significantly across the mosaic of midwavelength cells. For cells in which the surround is biased in favor of the opposing cone type, the spectral antagonism will be strong. For cells in which the surround draws mainly from cones of the same type as the center, the antagonism will be weak or nonexistent. Indeed, physiological recordings verify this great variation in spectral sensitivity (Marroco and De Valois, 1977; Schiller and Colby, 1983; Zrenner and Gouras, 1983). The determinant factor is, of course, the distribution of L and M cones in the overlying cone mosaic, which is subject to spatial variation.

MIDWAVELENGTH CELLS IN THE PERIPHERAL RETINA Outside of the fovea, the convergence of cones to the midwavelength ganglion cell increases substantially (Fig. 64.12). Correspondingly, the probability that the receptive field center draws solely from either L or M cones diminishes with increasing retinal eccentricity. The first systematic recordings from morphologically identified midwavelength ganglion cells in the retinal periphery of the *Macaca* demonstrated that the majority of cells had

spectral sensitivity without any cone antagonism, that is, a net sensitivity best described as L + M (Dacey, 2000). This is to be expected from cells with centers drawing from increasingly expansive patches of the cone mosaic. On the other hand, the dendritic tree of the midget cell becomes increasingly asymmetric (anisotropic) with increasing retinal eccentricity (Dacey, 1993a; Wässle and Boycott, 1991). Since the mosaic of L and M cones is patchy, with irregular clusters of like type (Mollon and Bowmaker, 1992; Roorda and Williams, 1999), it is possible that the asymmetric geometry of the dendritic tree reflects selective connections with midget bipolar cells from only a single type of cone (but see the discussion of this possibility in Calkins and Sterling, 1999). Recent extracellular recordings from peripheral ganglion cells with P-cell-like receptive fields demonstrated a large contingency of L/M (or M/L) antagonistic responses (Martin et al., 2001). Though it does not follow *a priori* that these cells were all midget cells, it appears likely that the mosaic of midget cells across the retina includes both cells with and without strong spectral antagonism. To put this in psychophysical perspective, at 20 degrees of eccentricity, the R/G channel samples at 2 to 3 cycles/deg (Anderson et al., 1991). To account for this acuity, only 25% of the total midget population (110 cells/deg²) needs to demonstrate strong L/M (or M/L) antagonism.

IMPLICATIONS FOR R/G OPPONENCY The most widely accepted model for R/G opponency places the critical locus of cone antagonism within the midget cell's receptive field, embedded in the antagonistic interactions between the center and the surround. Because of the spatially concentric structure of these interactions, every midget cell transmits information about spatial edges (Derrico and Buchsbaum, 1991; Ingling and Martinez-Uriegas, 1983). On the other hand, the degree to which a midget cell also transmits information regarding spectral contrast (L vs. M) depends greatly on the composition of the center, since the surround is apparently mixed (Kingdom and Mullen, 1995; Mullen and Kingdom, 1996). In the central retina, most (but not all) midget cells are L/M or M/L antagonistic, and the strength of this antagonism depends on the composition of the *surround* (see above, Lennie et al., 1991). With increasing eccentricity the center size expands, and the degree of L/M antagonism is determined by the relative purity of the *center*. The point is that, across the entire retina the midget mosaic will demonstrate a highly variable spectral signature (L/M neutral point) from cell to cell, depending on the spatial structure of the overlying cone mosaic (Calkins and Sterling, 1999; Martin et al., 2001).

As a confounding factor, in the human retina the relative number of L and M cones varies across the retinal location, with L cones becoming more predominant with increasing eccentricity (Hagstrom et al., 1998). This is also consistent

with reports of L-dominant centers in P cells with increasing eccentricity (Shapley and Perry, 1986). Furthermore, there is great variability in the relative number of L and M cones between human observers (Hagstrom et al., 1998). Yet, the neutral point of the R/G channel is remarkably consistent not only from fovea to periphery (see above), but also between observers with known differences in their numbers of L and M cones (Miyahara et al., 1998). Thus, whatever information about R/G color vision is coming out of the retina via the midget ganglion cell is subject to a great deal of variability, not only because of the inherent circuitry of the cell, but also because of the highly diverse nature of the cone mosaic providing it input.

Building pathways for color vision: some remaining questions

S CONES AND COLOR CHANNELS It is a well-documented psychophysical fact that observers perceive not only "blue" with the stimulation of S cones, but also "red" (DeValois et al., 2000a; Krauskopf et al., 1982; Wooten and Werner, 1979). Thus, most short-wavelength lights are described as both, or as "violet," and S cones are assumed to provide input not only to the B/Y channel, but also to the R/G channel with the same polarity as the L cones. This explains in part why unique blue occurs with about equal stimulation of S and M cones—the "red" from S cancels the "green" from M (but see DeValois et al., 2000b). If the retinal substrate for the R/G channel is the midget system, then one might expect to find cells with L + S spectral sensitivity for their receptive field center, which is highly unlikely for cells within the central 6 to 7 degrees, where only a single cone provides the center. Only rare descriptions of any such cells exist, either in the retina or the LGN (see Calkins, 2001, for review). Our tendency as vision scientists is to try to correlate what cells we do find with a psychophysical channel, so the S input to the R/G channel is typically simplified out of physiological models—which is tantamount to the "tail wagging the dog." It is possible that whatever ganglion cells do have S input converge with L/M cells further along in the visual streams to produce the S contribution to the R/G channel (DeValois et al., 2000b).

THE ROLE OF THE CORTX IN R/G OPPONENCY Based on numbers alone (see above), it would seem unlikely that a circuit similar to that of the S-ON/(M + L)-OFF ganglion cell underlies R/G opponency. Yet, there are aspects of this idea that are far more parsimonious than the P cell hypothesis (see Calkins and Sterling, 1999). The receptive field of the midget/P cell is highly optimized for spatial contrast, and whatever spectral contrast exists in the receptive field is highly variable across the retina. It is, of course, possible that only a subset of midget cells, with the appropriate spectral

signature, carries R/G color information to the cortex, and that the cortex must “learn” during the development of the visual system to discriminate the output of “spatial” P cells from the output of “spectral” P cells. This might explain the highly regular spectral sensitivity of the R/G channel, and there are seemingly more than enough midget ganglion cells in the retina for a subset of those to represent a dedicated color pathway. Alternatively, the cortex could “demultiplex” whatever variable spectral contrast information is present in the spike train of each midget cell from the inherent spatial contrast (Ingling and Martinez-Uriegas, 1983; Kingdom and Mullen, 1995). A third possibility, though seemingly remote, is that because the spectral antagonism in the midget receptive field is simply an ancillary effect of the structure of the cone mosaic, it is completely irrelevant to the R/G color channel. The critical locus could represent a point in the visual streams where the output of ON and OFF midget cells converge, rendering all subsequent processing cone-antagonistic. In this case, only the spectral composition of the excitatory center would matter for creating receptive fields in higher cells with the appropriate L/M signature.

REFERENCES

- Anderson, S. J., K. T. Mullen, and R. F. Hess, 1991. Human peripheral spatial resolution for achromatic and chromatic stimuli: limits imposed by optical and retinal factors, *J. Physiol.*, 442:47–64.
- Bornstein, M. H., 1973. Color vision and color naming: a psychophysiological hypothesis of cultural difference, *Psych. Bull.*, 80:257–285.
- Boycott, B. B., and H. Wässle, 1999. Parallel processing in the mammalian retina. The Proctor Lecture, *Invest. Ophthalmol. Vis. Sci.*, 40:1313–1327.
- Boynton, R. M., 1975. Color, hue, and wavelength, in E. C. Carterette and M. P. Friedman (eds.), *Handbook of Perception*, vol. 5, New York: Academic Press.
- Buchsbaum, G., and A. Gottschalk, 1983. Trichromacy, opponent colours coding and optimum colour information transmission in the retina, *Proc. R. Soc. (Lond.) B*, 220:89–113.
- Calkins, D. J., 2000. The representation of cone signals in the primate retina, *J. Opt. Soc. Am. A*, 17:597–606.
- Calkins, D. J., 2001. Seeing with S cones, *Prog. Retinal Eye Res.*, 20:255–287.
- Calkins, D. J., and P. Sterling, 1999. Evidence that circuits for spatial and opponent color vision segregate at the first retinal synapse, *Neuron*, 24:313–321.
- Calkins, D. J., J. E. Thornton, and E. N. Pugh, 1992. Monochromatism determined at a long-wavelength/middle-wavelength cone-antagonistic locus, *Vis. Res.*, 32:2349–2367.
- Calkins, D., and P. Sterling, 1996. Absence of spectrally specific lateral inputs to midget ganglion cells in primate retina, *Nature*, 381:613–615.
- Calkins, D. J., Y. Tsukamoto, and P. Sterling, 1998. Microcircuitry and mosaic of a blue/yellow ganglion cell in the primate retina, *J. Neurosci.*, 18:3373–3385.
- Chan, T. L., and U. Grünert, 1998. Horizontal cell connections with short wavelength-sensitive cones in the retina: a comparison between new world and old world primates, *J. Comp. Neurol.*, 393:196–209.
- Chichilnisky, E. J., and D. A. Baylor, 1999. Receptive-field microstructure of blue-yellow ganglion cells in primate retina, *Nat. Neurosci.*, 2:889–893.
- Cohen, E. D., and R. F. Miller, 1994. The role of NMDA and non-NMDA excitatory amino acid receptors in the functional organization of primate ganglion cells, *Vis. Neurosci.*, 11:317–332.
- Croner, L. J., and E. Kaplan, 1995. Receptive fields of P and M ganglion cells across the primate retina, *Vis. Res.*, 35:7–24.
- Curcio, C. A., and K. A. Allen, 1990. Topography of ganglion cells in the human retina, *J. Comp. Neurol.*, 300:5–25.
- Curcio, C. A., K. R. Sloan, R. E. Kalina, and A. E. Hendrickson, 1990. Human photoreceptor topography, *J. Comp. Neurol.*, 292:497–523.
- Dacey, D. M., 1993a. The mosaic of midget ganglion cells in the human retina, *J. Neurosci.*, 13:5334–5355.
- Dacey, D. M., 1993b. Morphology of a small field bistratified ganglion cell type in the macaque and human retina, *Vis. Neurosci.*, 10:1081–1098.
- Dacey, D. M., 1996. Circuitry for color coding in the primate retina, *Proc. Natl. Acad. Sci. USA*, 93:582–588.
- Dacey, D. M., 1999. Primate retina: cell types, circuits and color opponency, *Prog. Retinal Eye Res.*, 18:737–763.
- Dacey, D. M., 2000. Parallel pathways for spectral coding in primate retina, *Annu. Rev. Neurosci.*, 23:743–775.
- Dacey, D. M., and B. B. Lee, 1994. The “blue-on” opponent pathway in primate retina originates from a distinct bistratified ganglion cell type, *Nature*, 367:731–735.
- Dacey, D. M., B. B. Lee, D. K. Stafford, J. Pokorny, and V. C. Smith, 1996. Horizontal cells of the primate retina: cone specificity without spectral opponency, *Science*, 271:656–659.
- Dacey, D. M., O. S. Packer, D. Brainard, B. Peterson, and B. Lee, 2000. Center-surround receptive field structure of cone bipolar cells in primate retina, *Vis. Res.*, 40:1801–1811.
- Dacheux, R. F., and E. Raviola, 1990. Physiology of H1 horizontal cells in the primate retina, *Proc. R. Soc. (Lond.) B*, 239:213–230.
- Daw, N. W., and J. M. Enoch, 1973. Contrast sensitivity, Westheimer function and Stiles-Crawford effect in a blue cone monochromat, *Vis. Res.*, 13:1669–1679.
- de Monasterio, F. M., and P. Gouras, 1975. Functional properties of ganglion cells of rhesus monkey retina, *J. Physiol.*, 251:167–195.
- de Monasterio, F. M., 1978. Properties of ganglion cells with atypical receptive-field organization in retina of macaques, *J. Neurophysiol.*, 41:1435–1449.
- Derrico, J. B., and G. Buchsbaum, 1991. A computational model of spatio-chromatic coding in early vision, *J. Vis. Commun. Image Represent.*, 2:31–38.
- Derrington, A. M., and P. Lennie, 1984. Spatial and temporal contrast sensitivities of neurones in lateral geniculate nucleus of macaque, *J. Physiol.*, 357:219–240.
- DeValois, R. L., N. P. Cottaris, S. D. Elfar, L. E. Mahon, and J. A. Wilson, 2000b. Some transformations of color information from lateral geniculate nucleus to striate cortex, *PNAS*, 97:4997–5002.
- DeValois, R. L., K. K. De Valois, and L. E. Mahon, 2000a. Contribution of S opponent cells to color appearance, *PNAS*, 97:512–517.
- Dreher, B., Y. Fukuda, and R. W. Rodieck, 1976. Identification, classification and anatomical segregation of cells with X-like and Y-like properties in the lateral geniculate nucleus of Old-World primates, *J. Physiol.*, 258:433–452.

- Euler, T., H. Schneider, and H. Wässle, 1996. Glutamate responses of bipolar cells in a slice preparation of the rat retina, *J. Neurosci.*, 16:2934–2944.
- Ghosh, K. K., and U. Grünert, 1999. Synaptic input to small bistratified (blue-ON) ganglion cells in the retina of a new world monkey, the marmoset *Callithrix jacchus*, *J. Comp. Neurol.*, 413:417–428.
- Goodchild, A. K., T. L. Chan, and U. Grünert, 1996. Horizontal cell connections with short-wavelength-sensitive cones in macaque monkey retina, *Vis. Neurosci.*, 13:833–845.
- Gordon, J., and I. Abramov, 1977. Color vision in the peripheral retina. II. Hue and saturation, *J. Opt. Soc. Am.*, 67:202–207.
- Green, D. G., 1972. Visual acuity in the blue cone monochromat, *J. Physiol.*, 196:415–429.
- Hagstrom, S. A., J. Neitz, and M. Neitz, 1998. Variations in cone populations for red-green color vision examined by analysis of mRNA, *NeuroReport*, 9:1963–1967.
- Hartveit, E., 1997. Functional organization of cone bipolar cells in the rat retina, *J. Neurophysiol.*, 77:1726–1730.
- Haverkamp, S., U. Grünert, and H. Wässle, 2001. The synaptic architecture of AMPA receptors at the cone pedicle of the primate retina, *J. Neurosci.*, 21:2488–2500.
- Hess, R. F., K. T. Mullen, and E. Zrenner, 1989. Human photopic vision with only short wavelength cones post-receptoral properties, *J. Physiol.*, 417:151–172.
- Hibino, H., 1992. Red-green and yellow-blue opponent color responses as a function of retinal eccentricity, *Vis. Res.*, 32:1955–1964.
- Hubel, D., and M. Livingstone, 1990. Color puzzles, in *Cold Spring Harbor Symposia on Quantitative Biology*, vol. LV, Cold Spring Harbor, NY: Cold Spring Harbor Laboratory Press, pp. 643–649.
- Hurvich, L. M., and D. Jameson, 1957. An opponent-process theory of color vision, *Psychol. Rev.*, 64:384–404.
- Ingling, C. R., Jr. and E. Martinez-Uriegas, 1983. The relationship between spectral sensitivity and spatial sensitivity for the primate r-g X-channel, *Vis. Res.*, 23:1495–1500.
- Kaplan, E., B. B. Lee, and R. M. Shapley, 1990. New views of primate retinal function, *Prog. Retinal Eye Res.*, 9:273–336.
- Kingdom, F. A. A., and K. T. Mullen, 1995. Separating colour and luminance information in the visual system, *Spatial Vis.*, 9:191–219.
- Krauskopf, J. D. R., M. B. Williams, and D. W. Heeley, 1982. Cardinal directions of color space, *Vis. Res.*, 22:1123–1131.
- Kuyk, T. K., 1982. Spectral sensitivity of the peripheral retina to large and small stimuli, *Vis. Res.*, 22:1293–1297.
- Lee, B. B., 1996. Receptive field structure in the primate retina, *Vis. Res.*, 36:631–644.
- Lennie, P., and M. D'Zmura, 1988. Mechanisms of color vision, *CRC Crit. Rev. Neurobiol.*, 3:333–400.
- Lennie, P., P. W. Haake, and D. R. Williams, 1991. The design of chromatically opponent receptive fields, in *Computational Models of Visual Processing* (M. S. Landy and J. A. Movshon, eds.), Cambridge, MA: MIT Press, pp. 71–82.
- Lukasiewicz, P. D., J. A. Wilson, and J. E. Lawrence, 1997. AMPA-preferring preceptors mediate excitatory synaptic inputs to retinal ganglion cells, *J. Neurophysiol.*, 77:57–64.
- Marroco, R. T., and R. L. DeValois, 1977. Locus of spectral neutral point in monkey opponent cells depends on stimulus luminance relative to the background, *Brain Res.*, 119:465–470.
- Martin, P. R., 1998. Colour processing in the primate retina: recent progress, *J. Physiol.*, 513:631–638.
- Martin, P. R., B. B. Lee, A. J. R. White, S. G. Solomon, and L. Rüttiger, 2001. Chromatic sensitivity of ganglion cells in the peripheral primate retina, *Nature*, 410:933–936.
- Massey, S. C., 1990. Cell types using glutamate as a neurotransmitter in the vertebrate retina, *Prog. Retinal Eye Res.*, 9:399–425.
- McLellan, J. S., and R. T. Eskew, Jr., 2000. ON and OFF S-cone pathways have different long-wave cone inputs, *Vis. Res.*, 40:2449–2465.
- Miyara, E., J. Pokorny, V. C. Smith, R. Baron, and E. Baron, 1998. Color vision in two observers with highly biased LWS/MWS cone ratios, *Vis. Res.*, 38:601–612.
- Mollon, J. D., and J. K. Bowmaker, 1992. The spatial arrangement of cones in the primate fovea, *Nature*, 360:677–679.
- Morigiwa, K., and N. Vardi, 1999. Differential expression of ionotropic glutamate receptor subunits in the outer retina, *J. Comp. Neurol.*, 405:173–184.
- Mullen, K. T., 1985. The contrast sensitivity of human color vision to red-green and blue-yellow chromatic gratings, *J. Physiol.*, 359:381–400.
- Mullen, K. T., and F. A. A. Kingdom, 1996. Losses in peripheral colour sensitivity predicted from “hit and miss” post-receptoral cone connections, *Vis. Res.*, 36:1995–2000.
- Nakajima, Y., H. Iwakabe, C. Akazawa, H. Nawa, R. Shigemoto, N. Mizuno, and S. Nakanishi, 1993. Molecular characterization of a novel retinal metabotropic glutamate receptor mGluR6 with a high agonist selectivity for L-2-amino-4-phosphonobutyrate, *J. Biol. Chem.*, 268:11868–11873.
- Nerger, J. L., V. J. Volbrecht, and C. J. Ayde, 1995. Unique hue judgments as a function of test size in the fovea at 20-deg temporal eccentricity, *J. Opt. Soc. Am. A*, 12:1225–1232.
- Noorlander, C., J. J. Koenderink, R. J. Den Ouden, and B. W. Edens, 1983. Sensitivity to spatiotemporal colour contrast in the peripheral visual field, *Vis. Res.*, 23:1–11.
- Packer, O., A. Hendrickson, and C. Curcio, 1989. Photoreceptor topography of the retina in the adult pigtail Macaque (*Macaca nemestrina*), *J. Comp. Neurol.*, 288:165–183.
- Peng, Y.-W., C. D. Blackstone, R. L. Hugarir, and K.-W. Yau, 1995. Distribution of glutamate receptor subtypes in the vertebrate retina, *Neuroscience*, 66:483–497.
- Polyak, S. L., 1941. *The Retina*, Chicago: University of Chicago Press.
- Pugh, E. N., Jr. and J. D. Mollon, 1979. A theory of the π_1 and π_3 color mechanisms of Stiles, *Vis. Res.*, 19:293–312.
- Qin, P., and R. G. Pourcho, 1995. Distribution of AMPA-selective glutamate receptor subunits in the cat retina, *Brain Res.*, 710:303–307.
- Reid, R. C., and R. M. Shapley, 1992. Spatial structure of cone inputs to receptive fields in primate geniculate nucleus, *Nature*, 356:716–718.
- Rodieke, R. W., 1991. Which cells code for color? In *From Pigments to Perception* (A. Valberg and B. Lee, eds.), New York: Plenum Press, pp. 83–93.
- Rodieke, R. W., 1998. *The First Steps in Seeing*, Sinauer Associates. Sunderland, MA.
- Romeski, M., 1978. Chromatic opponent-response functions of anomalous trichromats, *Vis. Res.*, 18:1521–1532.
- Roorda, A., and D. R. Williams, 1999. The arrangement of the three cone classes in the living human eye, *Nature*, 397:520–522.
- Sankeralli, M. J., and K. T. Mullen, 2001. Bipolar and rectified chromatic detection mechanisms, *Vis. Neurosci.*, 18:127–135.
- Schiller, P. H., and C. L. Colby, 1983. The responses of single cells in the lateral geniculate nucleus of the rhesus monkey to color and luminance contrast, *Vis. Res.*, 23:1631–1641.

- Sekiguchi, N., D. R. Williams, and D. H. Brainard, 1993. Efficiency in detection of insoluminant and isochromatic interference fringes, *J. Opt. Soc. Am. A*, 10:2118–2133.
- Shapley, R., and V. H. Perry, 1986. Cat and monkey retinal ganglion cells and their visual functional roles, *TINS*, 9:229–235.
- Shiells, R., and G. Falk, 1995. Signal transduction in retinal bipolar cells, *Prog. Retinal Eye Res.*, 14:223–247.
- Shinomori, K., L. Spillmann, and J. S. Werner, 1999. S-cone signals to temporal OFF-channels: asymmetrical connections to postreceptoral chromatic mechanisms, *Vis. Res.*, 39:39–49.
- Sjöstrand, J., N. Conradi, and L. Klarén, 1994. How many ganglion cells are there to a foveal cone? *Graefes Arch. Clin. Exp. Ophthalmol.*, 32:432–437.
- Stabell, U., and B. Stabell, 1982. Color vision in the peripheral retina under photopic conditions, *Vis. Res.*, 22:839–844.
- Sterling, P., 1999. Deciphering the retina's wiring diagram, *Nat. Neurosci.*, 2:851–853.
- Stiles, W. S., 1949. Investigation of the Scotopic and trichromatic mechanisms of vision by the two-color threshold technique, *Rev. d'Opt.*, 139–163.
- Stromeyer, C. F., K. Kranda, and C. E. Sternheim, 1978. Selective chromatic adaptation at different spatial frequencies, *Vis. Res.*, 8:427–435.
- Stromeyer, C. F. III, A. Chaparro, C. Rodriguez, D. Chen, E. Hu, and R. E. Kronauer, 1998. Short-wave cone signal in the red-green detection mechanism, *Vis. Res.*, 38:813–826.
- Teller, D. Y., and E. N. Pugh, Jr., 1983. Linking propositions in color vision, in *Colour Vision: Physiology and Psychophysics* (J. Mollon and L. Sharpe, eds.), New York: Academic Press, pp. 577–589.
- van Esch, J. A., E. E. Koldenhof, A. J. van Doorn, and J. J. Koenderink, 1984. Spectral sensitivity and wavelength discrimination of the human peripheral visual field, *J. Opt. Soc. Am. A*, 1:443–450.
- Vardi, N., R. Duvoisin, G. Wu, and P. Sterling, 2000. Localization of mGluR6 to dendrites of ON bipolar cells in primate retina, *J. Comp. Neurol.*, 423:402–412.
- Vardi, N., D. F. Matesic, D. R. Manning, P. A. Liebman, and P. Sterling, 1993. Identification of a G-protein in depolarizing rod bipolar cells, *Vis. Neurosci.*, 10:473–478.
- Vardi, N., K. Morigiwa, T.-L. Wang, Y.-Y. Shi, and P. Sterling, 1998. Neurochemistry of the mammalian cone “synaptic complex,” *Vis. Res.*, 38:1359–1369.
- Wässle, H., and B. B. Boycott, 1991. Functional architecture of the mammalian retina, *Physiol. Rev.*, 71:447–480.
- Watanabe, M., and R. W. Rodieck, 1989. Parasol and midget ganglion cells of the primate retina, *J. Comp. Neurol.* 289: 434–454.
- Wiesel, T. N., and D. H. Hubel, 1966. Spatial and chromatic interactions in the lateral geniculate body of the rhesus monkey, *J. Neurophysiol.*, 29:1115–1156.
- Williams, D. R., R. J. Collier, and B. J. Thompson, 1983. Spatial resolution of the short wavelength mechanism, in *Colour Vision: Physiology and Psychophysics* (J. Mollon and L. Sharpe, eds.), New York: Academic Press, pp. 487–503.
- Williams, D. R., N. Sekiguchi, and D. Brainard, 1993. Color, contrast sensitivity, and the cone mosaic, *Proc. Natl. Acad. Sci. USA*, 90:9770–9777.
- Wooten, B. R., and J. S. Werner, 1979. Short-wave cone input to the red-green opponent channel, *Vis. Res.*, 19:1053–1054.
- Zhou, Z. J., D. W. Marshak, and G. L. Fain, 1994. Amino acid receptors of midget and parasol ganglion cells in primate retina, *Proc. Natl. Acad. Sci. USA*, 91:4907–4911.
- Zrenner, E., 1983a. Neurophysiological aspects of colour vision in primates. Comparative studies on simian retinal ganglion cells and the human visual system. Monograph. *Studies of Brain Function*, vol. 9 (V. Braitenberg, H. B. Barlow, T. H. Bullock, E. Florey, O.-J. Grüsser, and A. Peters, eds.), Berlin, Heidelberg, New York: Springer.
- Zrenner, E. 1983b. Neurophysiological aspects of colour vision mechanisms in the primate retina, in *Colour Vision: Physiology and Psychophysics* (J. Mollon and L. Sharpe, eds.), New York: Academic Press, pp. 195–211.
- Zrenner, E., and P. Gouras, 1983. Cone opponency in tonic ganglion cells and its variation with eccentricity in rhesus monkey retina, in *Colour Vision: Physiology and Psychophysics* (J. Mollon and L. Sharpe, eds.), New York: Academic Press, pp. 211–223.

65 Neural Coding of Color

RUSSELL L. DE VALOIS

TO UNDERSTAND VARIOUS aspects of the neural organization underlying our color vision, it is essential to consider certain problems faced by the visual system in building a system to distinguish among objects on the basis of their chromaticity. Some problems are intrinsic to the physical characteristics of light and objects in the world; others are consequences of limitations in the anatomical and physiological properties of the visual nervous system. As a result, what may appear at first sight to be fairly straightforward problems turn out to be anything but. Let us begin by briefly considering some of these problems.

Confounds in the visual stimulus

SEPARATING THE REFLECTANCE FROM THE ILLUMINANT Most of the interesting objects in the world do not themselves emit light, but rather reflect some proportion of whatever light falls on them. To characterize such objects, one needs to determine their reflectance properties, but the amount of light reaching the eye from an object is a *product* of the illuminant and the reflectance of the object. Since one does not have any independent knowledge of the illuminant, this is one equation with two unknowns and thus formally unsolvable. That is to say, any visual stimulus is massively underspecified, there being an infinite number of possible combinations of surfaces and illuminants that could have produced any given number of photons coming from a particular direction. The severity of this problem is increased by the fact that variations due to the reflectance characteristics of objects are tiny compared to the huge variations in the illuminant. The reflectances of objects vary only over a range of about 20 to 1, with a white object reflecting about 90% of the incident light and a black object about 5%. The variation in light level in the course of a day, on the other hand, can be 1 billion to 1. The daunting task for the visual system is to capture the tiny variations due to objects and separate them from the massive variation due to the illuminant.

A related aspect of this problem is the need to separate the wavelength characteristics of objects from those of the illuminant, for the wavelength distribution of the light coming from an object is also a product of the wavelength distribution of the illuminant and the spectral reflectance characteristics of the object. The light reaching us from the sun is reddish at dawn and dusk and bluer at midday. Thus,

both the color and the lightness of objects are indeterminate in the absence of knowledge of the characteristics of the illuminant.

To solve these problems and others, the visual system must in effect make (educated) a priori assumptions about the nature of the world—for instance, about which variations in the stimulus are most likely due to the illuminant (and thus to be largely ignored) and which are likely due to visual objects (and thus to be further processed). Most of these assumptions have been acquired through evolution, others through experience with the environment in the course of development. Many of the characteristics of the neural processes can be seen as reflecting the particular assumptions the visual system makes about the world.

SEPARATING INTENSITY AND COLOR A second formally unsolvable problem for the visual nervous system is a consequence of the characteristics of the photopigments that constitute the first stage in the visual neural process. The photopigments have very broad spectral sensitivity; the two major cone types [the L (long-wavelength-sensitive) and M (middle-wavelength-sensitive) cones] absorb light of wavelengths across the whole visible spectrum. A given cone is more likely to absorb light of some wavelengths than of others, but an absorbed photon of any wavelength has precisely the same effect as one of any other wavelength. Thus, at the very first stage, wavelength and intensity information are totally confounded. This is known as the principle of *univariance*: a receptor is able to signal only one number—the number of photons absorbed; thus, it cannot separately report the wavelength and the intensity of the light incident upon it.

Multiple tasks and bottlenecks

An easy error to make when considering any single aspect of vision, such as color vision or space or motion detection, is to look at the process as if it were being carried out in isolation, as if that were the only task for which that part of the system was designed. There do appear to be separate processing units or regions for different aspects of vision, at least to some extent, in the later cortical processing centers. With billions of neurons available in the 35% or so of the cortex devoted to vision, it is perhaps possible to have one group processing only color, another only motion, and so on. This

is not a luxury available in the retina, however, where there are two severe bottlenecks that put a premium on multitasking.

RECEPTOR BOTTLENECK Although it is a rather odd use of the term, the physical dimensions of the receptors themselves can be considered an *information bottleneck*. Each receptor occupies a finite space in the array that samples the retinal image, thus excluding from that location a receptor with a different property. If we had some receptors just for color vision and other receptors just for high-acuity luminance vision, then our luminance visual acuity would be limited by the *luminance receptors* having *color receptors* interposed between them. As we discuss below, the fact that the same receptors support both color vision and high-acuity luminance vision can be seen to play a role in the locations of the spectral peaks of the different cone types, in the distributions of different cone types across the retina, and in the neural processing of the cone outputs.

The receptor bottleneck is probably also a factor in our having evolved a color vision system based on only three different cone types. Increasing the number of different cone types would necessarily result in a coarsening of the array of each variety of cone.

OPTIC NERVE BOTTLENECK A second bottleneck is in the optic nerve. Because the retina is inverted, the ganglion cell axons originate inside the eye and must produce a hole in the receptor layer in each nasal retina to exit the eye. The resulting 5 by 7 degree blind spot—large enough to encompass some 50 nonoverlapping images of the moon—is already an impediment to vision and would be even more so if there were more ganglion cells. A much larger optic nerve might also limit ocular mobility. There is thus a considerable advantage for neurons early in the visual path to multiplex information in order to carry out more than one type of analysis. Again, the consequence of this optic nerve bottleneck can be seen in the processing of color and luminance information in the retina.

Photopigments and receptors

A crucial initial stage in color processing is the possession by most humans and other Old World primates of three different cone types containing (at least) three different photopigments. The properties of the photopigments are discussed more completely in Chapter 16.

PHOTOPIGMENTS Critical factors for color vision are the spectral sensitivities of the different cone types. In fact, much of the psychophysical research in color vision in the first half of the twentieth century (e.g., Stiles, 1949) consisted of attempts to determine these functions. The reason is that the

extraction of color information is based on the differences between the spectral sensitivities of the different cone types, so the peaks and shapes of the spectral sensitivity functions are critical for understanding color vision.

The output of each individual cone, regardless of type, carries no color information, for it completely confounds intensity and wavelength information (the principle of univariance discussed above). Thus, an increase in photon capture by any given cone can result from an increment in the intensity of the light or from a shift toward a more favorable wavelength; a decrease in photon capture correspondingly does not allow one to tell whether there was a decrease in light at that location or a shift to a wavelength to which that cone was less sensitive. However, a long-wavelength light will always result in more photon captures by an L than by an M cone, regardless of its intensity. Increments and decrements in intensity with no change in wavelength will produce increases and decreases in photon capture by both L and M cones, but the ratio of their activities will remain constant. Changes in wavelength, on the other hand, will change the ratio of L to M activity. Intensity information thus lies in the sum of the activity of the different cone types, and color information lies in the differences between the activities of the different cone types. It is these two types of information that are extracted in the early retinal processing.

The spectral sensitivities of the human cone pigments have been well established from many different types of experiments, including psychophysical studies of normal and dichromatic human observers (Smith and Pokorny, 1975; von Kries, 1905; Vos and Walraven, 1971; and many others), microspectrophotometry of cone outer segments (e.g., Bowmaker and Dartnall, 1980), recordings of cone electroretinograms (Jacobs and Neitz, 1993), and recordings from individual cone outer segments (Schnapf et al., 1987). There are three things relevant to color vision to be noted in the cone pigment curves shown in Figure 65.1.

Broad spectral adsorption. One is that the absorption curves for the L- and M-cone pigments extend across the whole spectrum, making the L and M cones responsive to all wavelengths and intensities of light. It follows from the principle of univariance that the output of an L or M cone does not in any way specify either the color or the luminance of the light impinging on it. L and M cones thus should not be called or thought of as color receptors. Information about local color and luminance must be computed, as it is at multiple neural levels, by comparisons of the relative activities of several receptors in various combinations. Color and luminance information lies not in the outputs of individual receptors but in the differences and sums of the outputs of various receptors. The S (short-wavelength-sensitive) cones, on the other hand, differ from the L and M cones in this as in a number of other respects. They absorb primarily in the

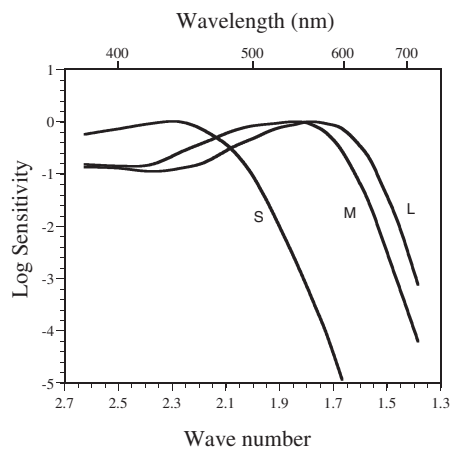


FIGURE 65.1. The spectral sensitivities of the three human cone photopigments. (Based on Stockman and Sharpe, 2000.)

short-wavelength range, and they appear to play a major role only in color vision.

Multiple photopigment alleles. A second point is that multiple alleles (varieties) of the L- and of M-cone photopigment genes are present in the normal as well as the color-defective human population. This was first postulated on psychophysical grounds by Alpern (Alpern, 1979; Alpern and Wake, 1977) and later verified by genetic studies (Neitz et al., 1993). While the S-cone photopigment gene, lying in isolation from the other pigment genes on an autosome, is quite uniform across the population, the L- and M-cone photopigment genes lie juxtaposed on the X chromosome (Nathans et al., 1986). One consequence of this is that the L and M genes are occasionally subject to exchange of parts during meiosis, leading to the aforementioned variability in the L and M photopigment spectral sensitivities.

Other consequences for color vision of the location of the L and M photopigment genes on the X chromosome derive from the fact that human males get only one X chromosome, while females get two. A very aberrant M or L photopigment gene will thus necessarily produce a significant color anomaly in males. As a consequence, some 8% of human males are either anomalous LM trichromats, with sufficiently deviant L or M photopigments to have color vision significantly different from that of normal observers, or they are LM dichromats, possessing either only an L or only an M photopigment and are thus reduced to a two-dimensional color vision system. Females, on the other hand, inheriting two X chromosomes, are far less likely (about 1% of the population) to have anomalous or dichromatic color vision, since that would entail inheriting the anomaly from each parent. An important corollary of this is that a significant number of females must have, in addition to the S photopigment, not just two but three or four L- and M-cone photopigments, having inherited, for example, slightly different L-

photopigment genes from their father and their mother. That is indeed the case (Neitz et al., 1993). However, such female observers are nonetheless trichromats; they do not have a four- or five-dimensional color system (Jordan and Mollon, 1993; Nagy et al., 1981). Contrary to the assumption from the time of Thomas Young (1802), the trichromatic limitation to our color vision lies not in the receptors but at some later processing stage.

Cone photopigment spacing. A third point to be made with respect to cone spectral sensitivities is that the peaks of the L- and M-cone photopigments are quite close together, about 30 nm apart on average, whereas the S-cone photopigment peak is some 90 and 120 nm away from the others. How are we to understand this arrangement, in particular the close spacing of the L- and M-cone peaks? As discussed above, color information lies in the difference between the spectral sensitivities of the cones, so it is clearly advantageous for color vision to have as wide a separation in spectral peaks as possible. One might thus expect a uniform and wide spacing of the three cone peaks. However, for high-acuity luminance vision, it would be advantageous if the peaks were all identical, that is, if there were only a single cone type to sample veridically the luminance distribution. The human arrangement can be seen as a compromise between these two opposing requirements. The L- and M-cone peaks are sufficiently close that the outputs of these cone types can be (and apparently are) treated as identical in the systems extracting information about intensity variations. However, the L and M peaks are sufficiently far apart to allow also for the extraction of considerable, although suboptimal, information about wavelength variations in the middle to long spectral range. Consistent with this supposition is the paucity of S cones in the central foveola (Ahnelt et al., 1987; Curcio et al., 1991), allowing for maximal sampling of the image by L and M cones in this region of highest acuity.

RECEPTORS The primary role of the receptors is to transduce faithfully increments and decrements in incoming light, or wavelength changes in one spectral direction or the other, into variations in neural activity. However, a straightforward linear transduction of photon capture into neural activity would not by itself be sufficient. Two problems, both of which demand an additional very nonlinear process, must also be tackled at very early stages in processing. One problem is that the dynamic range of light levels far exceeds the range that can be encoded in the nervous system. In the course of a day, light intensity can vary by more than 1 billion to 1. On the other hand, information is transmitted down ganglion cell axons by bursts of nerve impulses which, within the typical fixation period of about 250 msec, can span a range at most of about 50 to 1. There is thus a gross

mismatch between the dynamic range of light intensities and the dynamic range of signals that can be carried by cells in the visual nervous system. The other related problem is the need to maintain the color and brightness appearance of objects relatively constant in the presence of changing illumination. A given surface might reflect 80 photons to a receptor at one moment and 80 million at another moment when the illumination is brighter. For the surface to appear perceptually the same under these two conditions requires some nonlinear process. Major contributions to dealing with each of these problems are made by processes within the receptors themselves, as they must be to avoid saturating the later neural cells.

Linear transduction cascade. The receptor's outer segment membrane is held at an intermediate level of polarization by opposing forces of Na^+ inflow through ion pores in the membrane and metabolic effort expelling the Na^+ ions by means of ion pumps. Variations in the capture of light by the receptor photopigments located in the disks within the outer segment initiate a cascade of chemical reactions (described more fully in Chapter 16) resulting in changes in ion flow and thus changes in polarization of the membrane. Transient decrements and increments of various amounts in photon capture produce corresponding depolarizations and hyperpolarizations of the outer segment membrane, respectively, in a quite linear transduction process (Pugh and Lamb, 1990). The resulting currents are conducted to the synaptic region of the receptors, where they produce proportional variations in the release of the synaptic transmitter.

Nonlinear adaptational processes. This chemical cascade within the receptor's outer segment has two enzymatic sites, which provide for amplification of the small variations in photon capture that must be detected under dim light conditions. The photoisomerization of the *retinal* component of rhodopsin (or the similar cone opsins) turns the opsin into an enzyme that can potentially cleave, and thereby activate, numerous transducin molecules. Activated transducin, in turn, activates phosphodiesterase each molecule of which can hydrolyze many cGMP molecules. Since cGMP keeps the ion pores in the outer membrane open, their closure blocks Na^+ inflow, hyperpolarizing the membrane. A decrement in photon capture will correspondingly lead to a decrease in phosphodiesterase and thus an increase in cGMP, opening pores and depolarizing the membrane. As light levels increase and photon capture increases or decreases by thousands from instant to instant, the limited amount of available chemicals required in the cascade and the limited number of pores in the outer membrane will reduce the effectiveness of each photon capture by some fraction: it might take a change of 1000 photons under these

bright light conditions to have the same effect as a change of 1 photon in dim light.

A second adaptational nonlinearity at the initial stage of visual processing involves the inflow of Ca^{2+} as well as Na^+ ions through the outer membrane pores when they are opened by cGMP (Pugh and Lamb, 1990). The Ca^{2+} inflow acts as a negative feedback, since Ca^{2+} inhibits the production of cGMP. When elevated cGMP levels open more pores, the inflow cuts back on cGMP production; when cGMP levels fall, the decrease in Ca^{2+} inflow leads to more cGMP production.

These divisive gain control mechanisms have the desired effect of cutting down the dynamic range of the system from 1 billion to 1 to at most a few hundred to 1. They also provide a large initial step toward maintaining lightness constancy in the face of large changes in illumination. Since the adaptation occurs within each receptor, it is a major step toward maintaining color constancy as well. As the illumination becomes redder toward sunset, the L cones will be receiving relatively higher light levels than the M and S cones, and will thus adapt relatively more, thus compensating for the change in chromaticity of the illuminant. So, under steady-state adaptation (as is generally the case since illumination changes only very slowly during the day), the system functions in a quite linear fashion. A change in light level, however, triggers divisive nonlinearities within the receptors which allow the system to adjust to the new adaptation level.

Distribution across the retina. There are about 100 million rods and 3 to 5 million cones in the human (and macaque monkey) retina. The S cones are relatively few, only some 7% to 10% of the cone population (Curcio et al., 1991). L and M cones are very thin and densely packed in the center of the fovea. With increasing distance from the foveal center, they become thicker and separated increasingly farther from each other as a consequence of the appearance of S cones and then of rods. By a few degrees away from the foveal center, the cones are all surrounded by rods, which reach their highest concentration some 20 degrees away from the fovea. On the basis of receptor distribution alone, this must lead, as it does, to a loss of spatial acuity for chromatic as well as for photopic intensity-varying patterns with increasing retinal eccentricity. The primary changes with retinal eccentricity relevant to color vision, however, are related to how the retinal organization varies with eccentricity rather than with the distribution of receptors themselves.

Retinal and geniculate processing

One can see in the history of studies of vision, in particular of color vision, an increasing realization of the complexity of the problems faced by the visual system, and of the

number of processing levels that must be involved. The most influential early theory of color vision, that of Young (1802) and Helmholtz (1867), was essentially a one-stage model in which three receptors, each responsive to a different color region (red, green, and blue), fed up independent paths from the receptors to the brain to give us our color vision. The opponent-color model of Hering (1878), at least as modified by Schrödinger (1920) and by Jameson and Hurvich (1955), was essentially a two-stage model in which the three cone types were combined in various opposing combinations within the retina to form red-green, blue-yellow, and black-white opponent mechanisms that correspond to perceptual unique hues. The discovery of spectrally opponent cells in the monkey lateral geniculate nucleus (LGN) (De Valois et al., 1958), and the evidence that these cells fell into two spectrally opponent classes and one nonopponent class (De Valois, 1965; De Valois et al., 1966) seemed to provide evidence for such a two-stage opponent-color model.

In fact, it is now clear that not only are there three distinct principal cell types at each level beyond the receptors in the retinogeniculate path to the striate cortex (V1), but that these three cell types project down separate, largely independent paths through the retina and LGN to separate destinations in the visual cortex. We will briefly describe these three separate anatomical paths (discussed more fully in Chapter 30) and then describe the response characteristics and contribution to color vision of the cells in each. We will also present evidence, however, for further crucial color processing beyond the retina and LGN.

RETINO-GENICULATE-CORTICAL PATHS

Parvo (P_c) path. About 80% of the input from the retina to the visual cortex comes by way of the pathway originating largely from individual L and M cones and projecting through the four parvocellular (small cell) layers of the LGN to the cortex. Each L and M cone in the central 80 degrees or so of the retina is contacted by two midget bipolar cells, each of which contacts only this one cone (Wässle and Boycott, 1991). These paired midget bipolars respond in opposite ways to the receptor synaptic transmitter: one depolarizes to increments in photon capture, and the other depolarizes to decrements in photon capture (Famiglietti and Kolb, 1976). The midget bipolars also receive antagonistic input from the same and neighboring L and M cones by way of the feedback onto the cones by horizontal cells. These two inputs form the center and antagonistic surround of the receptive fields (RFs) of the bipolar cell, respectively. Each incremental and decremental midget bipolar feeds into a midget ganglion cell of the corresponding response type. The ganglion cells also receive input from surrounding areas by way of the amacrine cells.

In the central retina, input to the RF center of each midget ganglion cell comes mainly from a single midget bipolar and thus from a single L or M cone. With increasing retinal eccentricity, there is increasing bipolar-to-ganglion-cell convergence, and the midget ganglion cells get input into their RF centers from more than one midget bipolar and thus in most cases from a combination of L and M cones (Wässle et al., 1994).

The midget ganglion cells, in turn, project to one of the four parvocellular LGN layers and from there primarily to layer IVc β of the striate cortex (Hubel and Wiesel, 1972). The LGN on each side receives projections from the temporal half of the ipsilateral retina and from the nasal half of the contralateral retina, but the fibers from the two eyes go to different LGN layers. Thus outputs from the two eyes first come together in the striate cortex.

Magno (M_c) path. About another 10% of the input from the retina to the visual cortex also comes mainly from L and M cones, but with a very different sort of organization. Diffuse bipolar cells receive input even in the foveola from not one but a small group of L and M cones, with antagonistic input from a still larger number of cones in the region. There are again two types of bipolar cells, one which depolarizes to increments in photon capture by the small group of L and M cones and one which depolarizes to decrements in photon capture by the same group of cones. With retinal eccentricity, the number of cones feeding into the center and surround increases still further. There is no evidence that the diffuse bipolars show any selectivity among L and M cones, and thus presumably sum together the outputs of all L+M cones in a region. Although the anatomical origin of the input is not clear, there is physiological evidence that most cells in the magno path receive S-cone input as well (Cottaris et al., in prep.; Derrington et al., 1984). The two types of diffuse bipolars project to separate subregions of the inner plexiform layer, where they contact incremental and decremental parasol ganglion cells, respectively (with amacrine input as well). The axons of the parasol ganglion cells project to one of the two large-cell layers of the LGN and from there primarily to layer IVc α of V1.

Konio (K_c) path. As is the case with cells in the P_c and M_c paths, the RF centers of some S-opponent cells depolarize to increments in S-cone photon capture (+S) and those of others (−S) depolarize to S-cone decrements (Valberg et al., 1986). However, unlike the other paths, the S-opponent pathway is very unbalanced, there being about five times as many +S as −S cells. The +S path originates in a so-called S-cone bipolar that contacts one to three S cones, bypassing L and M cones in the region (Mariani, 1984). The S-cone bipolar synaptic region also gets input from H2 horizontal cells that make contact almost exclusively with S cones. The

S-bipolar contacts a bistratified ganglion cell in the plexiform layer in which incremental midwedge and parasol ganglion cells contact their respective bipolars. The other half of the bistratified ganglion cell's dendritic arbor contacts diffuse bipolars at a decremental synaptic level (Dacey and Lee, 1994). The bistratified ganglion cell thus receives a +S signal at one branch of its dendritic tree and a -LM signal at the other. With retinal eccentricity, the S cones become more widely spaced and the number of S cones that feed into each bistratified ganglion cell increases. However, the specificity of the inputs (with only S cones in the RF center) appears to be maintained out to the far retinal periphery (Kouyama and Marshak, 1992).

In addition to the six LGN layers that have long been recognized, additional thin layers of cells lying ventral to layers 1 to 4 of the LGN, forming the koniocellular path, have recently been described (Casagrande, 1994). A major component of that path consists of the S-opponent cells whose RF centers originate in the S cones (Hendry and Reid, 2000; Martin et al., 1997). The projection to the cortex of cells in the K_c layers is quite different from those in the main body of the LGN. Rather than projecting to layer IV of V1, these cells project to layers I and III, and mainly in the cytochrome-oxidase blob regions of each cortical module rather than uniformly over the whole cortical region.

RESPONSE PROPERTIES OF RETINOGENICULATE CELLS

Magno cells. Although M_c ganglion and LGN cells have been widely considered to be summing just the outputs of the L and M cones, and thus carrying a luminance signal (the human luminance function V_λ being well fit by $2L+M$), considerable evidence indicates that they receive significant input from S cones as well (Cottaris et al., in prep.; Derrington et al., 1984). However, since all three cone types feed into the RF centers of M_c cells with the same polarity, the magno pathway does constitute a largely *achromatic* channel. The RF surrounds of M_c cells also receive an antagonistic input from the sum of all the cone types. We can thus characterize the RFs of the incremental and the decremental M_c cells, respectively, as $(+LMS_c-LMS_s)$ and $(-LMS_c+LMS_s)$, where c and s refer to RF center and surround, respectively. Since it is equally important to detect and characterize dark and light objects, it is not surprising that the relative number of $+LMS_c$ and $-LMS_c$ magno cells is about the same.

The cells in the M_c path have a *spatially opponent* organization, with antagonistic input from RF center versus surround. They thus signal changes in the amount of light absorbed by a small group of cones relative to the amount absorbed by the cones in a larger, spatially overlapping area. With uniform illumination, largely irrespective of chromaticity, center and surround responses will tend to cancel,

but differential illumination within the RF will activate the cell. This organization begins to emphasize intensity information that is likely due to objects and minimize that related to the illuminant. The underlying "assumption" being made by the visual system is that if all the cones in a region absorb more light, or if they all absorb less, it is probably due to a change in the illumination (as when the sun goes behind a cloud or emerges from one). On the other hand, if one group of cones is activated more than its neighbors, this is likely the result of reflections from different objects or different parts of an object. Information about such local intensity variations is captured and carried to the cortex by cells in the M_c pathway. Since they sum together the outputs of different cone types, however, cells in this path carry little information about the chromaticity of patterns. If exactly the same proportions of L, M, and S cones fed into the centers and surrounds of M_c cells, they would respond only to achromatic patterns. However, most M_c cells receive more RF surround inputs from L cones than from M cones and thus have some degree of chromatic opponency (Derrington et al., 1984; Wiesel and Hubel, 1966). Because of this, because of their S-cone inputs, and because they give a small frequency-doubled response to isoluminant stimuli (Lee et al., 1989), it is a mistake to think that isoluminant stimuli would completely silence cells in the magno path.

The M_c cells respond with a shorter latency than the other cell types, give a biphasic, transient response to stimuli, and are maximally responsive to high temporal frequencies (de Monasterio and Gouras, 1975; Derrington and Lennie, 1984; Lee et al., 1989; Wiesel and Hubel, 1966). Because they sum over a group of cones in their RF centers rather than receiving input from a single cone, they are tuned to lower spatial frequencies than are cells in the other paths. However, they have a much higher contrast sensitivity than cells in the parvo and konio paths (Kaplan and Shapley, 1986). Despite their larger RF centers, they are thus responsive to quite high spatial frequencies.

Konio cells. While cells in the M_c path have mainly a spatially opponent organization, cells in the K_c path have primarily a *spectrally opponent* organization, signaling changes in the amount of light stimulating one or more S cones relative to the amount stimulating the neighboring L and M cones $(+S_c-LM_s)$ or $(-S_c+LM_s)$. Since the RF size of the antagonistic center and surround regions are approximately equal (Derrington et al., 1984; Wiesel and Hubel, 1966), these cells have spectral but little spatial opponency. We shall refer to these as *S-opponent cells*, or S_0 . Since the cone photopigments have broad and overlapping spectral sensitivity functions, one cannot identify the wavelength of a pattern by determining which cone is activated. However, differences in the relative activation of the different cone types *are* related to the spectral distribution of the light, and this information

is captured by a spectrally opponent organization. Short-wavelength light is absorbed relatively more by the S than by the L and M cones, regardless of its intensity. A shift in the light from middle toward short wavelengths will therefore excite a $+S_0$ cell in the K_i path, and a shift toward long wavelengths will excite a $-S_0$ cell.

Parvo cells. Finally, the ganglion and LGN cells in the P_c path (about 80% of the total) have both a *spatially* and a *spectrally opponent* organization. These cells, at least in the central retina, receive almost all their input from a single L or M cone in their RF center and from a small group of L and/or M cones in the surround. There are thus four varieties of these cells: $+L_c-M_s$ (or L_0), $-L_0$, $+M_0$, and $-M_0$. The $+L_0$ and $-M_0$ cells have the same spectral response characteristics (both $+L-M$), as do the $+M_0$ and $-L_0$ cells (both being $+M-L$). Since they encode the difference between the activity of L cones versus M cones in spectrally opponent organizations, they respond to color variations in the long-wavelength half of the spectrum. (It is the absence of these responses, because of a lack of either the L- or the M-cone pigment, that makes a protanope or deuteranope unable to discriminate red from yellow from green.) However, parvo cells also signal changes in activation of a single L or M cone relative to that in the surrounding L and M cones in a spatially opponent organization. The P_c cells thus carry both chromatic and achromatic information. Relative to M_c cells, cells in the parvo path are sensitive to higher spatial but lower temporal frequencies; they also have sustained monophasic responses and lower contrast sensitivity (de Monasterio and Gouras, 1975; Derrington and Lennie, 1984; Kaplan and Shapley, 1986; Lee et al., 1989; and others).

The RF organization of P_c cells, and the consequences of this organization for color, intensity, and spatial processing, are shown in Figures 65.2 and 65.3. The cone-input map of an idealized $+L_c-M_s$ opponent ganglion or LGN cell is diagrammed in Figure 65.2A. The cell receives input from an L cone in the RF center and opposing inputs from M cones in the surround (many P_c cells have a mixed L and M surround rather than a cone-specific surround, but the input from the “wrong” cone type in the surround would only somewhat dilute the strength of the center without eliminating the cone opponency). The critical point (De Valois and De Valois, 1975) is that a P_c cell with such a *cone-input* map has not one but two quite different *receptive field maps*, depending on the nature of the stimulus. A luminance change drives both L and M cones in the *same* direction, but they feed into the P_c cell in opposite directions, so a luminance increment would produce an RF with an excitatory center and an inhibitory surround (Fig. 65.2B). On the other hand, since a pure color change drives L and M cones in *opposite* directions, their inputs to the P_c cell become not antagonistic but synergistic. In the example shown in Figure

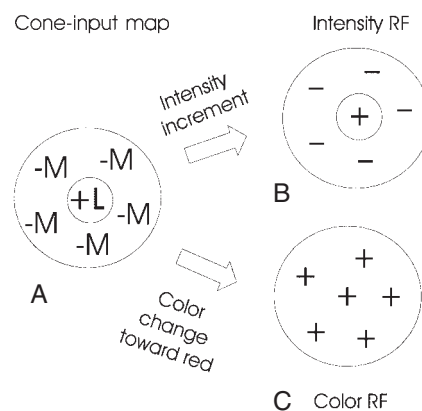


FIGURE 65.2. A cartoon demonstrating how color and intensity information is multiplexed by cells in the P_c pathway. Part *a* shows how L and M cones feed into a model $+L-M$ opponent cell. Part *b* shows how such a cell would respond to intensity increments. These drive L and M cones in the same direction, thereby producing an RF with center-surround antagonism. Part *c* shows how such a cell would respond to a color shift toward red, which drives L and M cones in opposite directions, thereby producing an RF with center-surround synergism.

65.2C, a color shift toward red produces excitation from the L cone in the RF center and a decrease in inhibition (and thus excitation) from the M cones in the surround as well.

As one would predict from the differing RFs for intensity and color changes shown in Figure 65.2, P_c cells show quite different spatial frequency tuning for chromatic versus achromatic stimuli. Figure 65.3 shows the average responses of four typical P_c cells (one of each RF center type, $+L_0$, $-L_0$, $+M_0$, $-M_0$) to isoluminant and to 50% contrast achromatic gratings. It can be seen that these cells respond to somewhat higher spatial frequencies, with spatially bandpass tuning, to achromatic patterns, whereas they show spatially lowpass tuning to pure chromatic patterns. They are most responsive to low-spatial-frequency chromatic stimuli and to high-spatial-frequency achromatic stimuli. (In terms of cone contrast, P_c cells are actually more responsive to chromatic

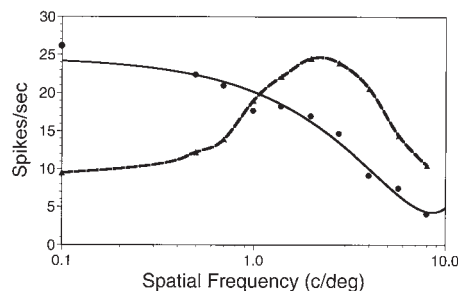


FIGURE 65.3. Averaged data from four L/M opponent LGN cells in response to grating patterns varying in intensity (diamonds) and in color (circles). It can be seen that these cells show bandpass spatial-frequency tuning to intensity variations, but lowpass tuning for color.

patterns across almost the whole spatial frequency range, since in the data shown in Figure 65.2, the cone contrasts of the 50% luminance gratings are about four times greater than those of the color gratings.) The chromatic and achromatic tuning functions of the LGN cells shown in Figure 65.3 look very similar to the corresponding contrast sensitivity functions of normal human observers for chromatic and achromatic gratings, as measured in psychophysical tests (e.g., van der Horst et al., 1967). This suggests that our relative sensitivities for chromatic and achromatic patterns of different spatial frequencies are determined by the response properties of P_c cells at the retinogeniculate level.

It appears, then, that P_c cells, with their combined spatial and chromatic opponency, carry both chromatic and achromatic information, but over somewhat different spatial frequency bands. The neural processing in the retina thus begins but does not complete the process of separating color and intensity information.

The presence of separate bipolar, ganglion, and LGN cells that respond to increments versus decrements of each cone type gives the parvo path the same advantage discussed above for M_c cells. It provides equal sensitivity to increments and decrements of light. In the case of parvo cells, it also provides for equal sensitivity to shifts in color toward red and toward green. There is one further advantage of this arrangement in the case of P_c cells: it leads to a simple cortical mechanism, discussed below, for eventually separating the color and luminance information that is multiplexed in this path to the cortex.

ENCODING OF COLOR SPACE A fundamental characteristic of our color vision, postulated by Thomas Young (1802) and first verified experimentally by Maxwell (1860), is that the multidimensional spectral space of natural images is collapsed to only a three-dimensional perceptual space: normal human observers are trichromats. Since early color processing of spatially uniform patterns is quite linear, color space can be transformed from one set of axes to another. A common system represents perceptual color space with the three axes of hue, saturation, and brightness. Another useful representation of color space, developed by MacLeod and Boynton (1979) and elaborated by Derrington et al. (1984), is based on the outputs of the three cone types as processed by the different LGN cell types (Fig. 65.4). The three axes in the MBDKL space correspond to the response properties of the P_c , K_c , and M_c LGN cells, respectively. The average responses of populations of each of the different varieties of P_c and K_c cells to shifts from white to various isoluminant chromatic stimuli around the circle in this color space are shown in Figure 65.5. It can be seen that the L–M and M–L P_c opponent cells fire maximally to 0 degrees and 180 degrees, respectively, with no response to 90 degree and 270 degree patterns, whereas the S-opponent K_c cells fire maxi-

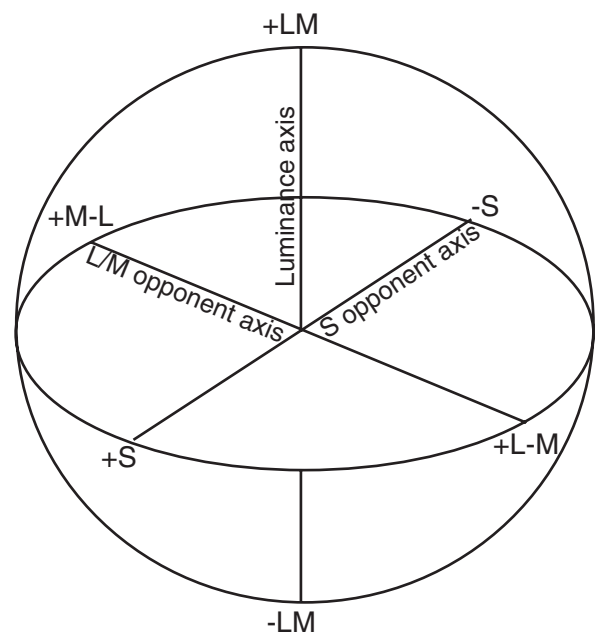


FIGURE 65.4. A diagram of the MBDKL color space based on the response properties of cells in the P_c , K_c , and M_c paths.

mally to 90 degrees and 270 degrees, with no response to 0 degree and 180 degree patterns. P_c and K_c cells thus form orthogonal chromatic axes in this color space. The paired +LMS and –LMS M_c cells fire to achromatic increments and decrements, respectively, along the third axis.

The chromatic response characteristics of cells, plus information about the time course of the responses, can also be obtained through reverse-correlation RF mapping with a rapidly presented sequence of isoluminant chromatic stimuli. Figure 65.6 shows such chromotemporal RFs of two representative LGN cells, a +M–L and a +S–LM opponent cell, respectively. Time with respect to stimulus onset is represented along the radii from the center out, and the different orientations represent different angles in the MBDKL isoluminant plane. The chromatic RF regions shown in red reflect a positive correlation between the response and the stimulus, and those shown in blue reflect a negative correlation. Thus, the +M–L cell (Fig. 65.6A), for instance, fires to stimuli from 90 degrees to 270 degrees, with maximum excitation at 180 degrees, and inhibits to stimuli from 270 degrees to 90 degrees, with maximum inhibition at 0 degrees. It can be seen that each of these cells has a response latency of about 50 msec and gives a monophasic, sustained response to the stimuli.

Both responses to chromatic flicker (Fig. 65.5) and chromotemporal RF mapping studies (Fig. 65.6) show that LGN cells' responses to isoluminant stimuli along various color angles not only are bimodally distributed, but they segregate into two distinct, nonoverlapping classes. It has long been thought that the three-dimensional limitation on our

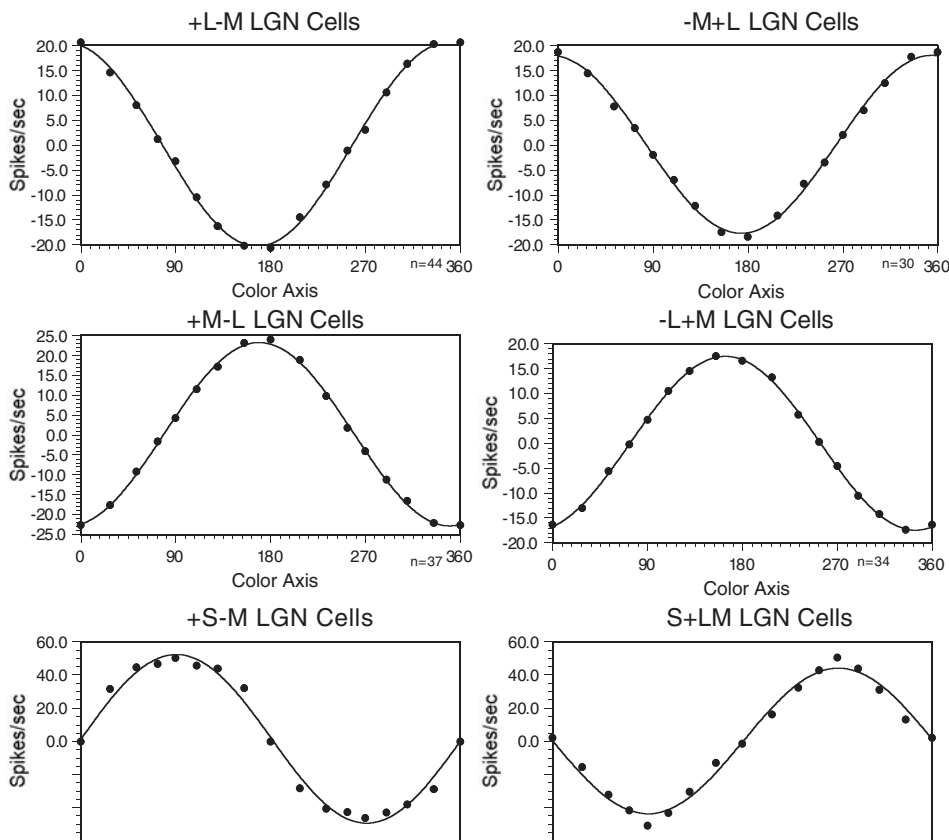


FIGURE 65.5. Averaged data from a large sample of LGN opponent cells of various response types. Shown are the responses to

full-field lights varying in various directions in MBDKL isoluminant color space.

color vision was set by the presence of only three cone pigments and receptors. However, it has been known for some time that we are trichromats even under mesopic conditions when rods as well as three cone types are active. Furthermore, as discussed above, females who inherit two different L-cone pigment alleles and thus have four cone pigments (with their rods making five receptor types) are still trichromats (Jordan and Mollon, 1993; Nagy et al., 1981). It therefore appears that the trichromatic limitation on our color vision is set not at the receptor level, but by the presence of just three retinogeniculate cell types projecting down the P_c , K_c , and M_c pathways.

One of the striking properties of color perception, emphasized by Hering (1878), is that various hues are not independent of each other but rather stand in an opponent relation. This can be seen in simultaneous and successive color contrast, in which, for instance, a red area induces the appearance of green in nearby regions and in the same region at the offset of the red. This opponent perceptual organization is also reflected in the fact that we can see combinations of red and yellow or blue and green in a single patch of color, but we do not see red and green or blue and yellow in the same place at the same time. Although the chromatic axes of LGN cells do not coincide with our per-

ceptual color axes, as we discuss below, the basic opponent nature of our perceptual color space reflects the opponent processing by the P_c and K_c cells in the retinogeniculate path.

Color processing in the striate cortex

MULTIPLICITY OF CHROMATICALLY RESPONSIVE CELLS Cells in the three main retinocortical paths (P_c , M_c , and K_c) project separately to layers IVc β , IVc α , and I and III of the striate cortex (V1), respectively, but within the cortex these paths no longer remain discrete. Rather, V1 cells combine the outputs of the different LGN cell types in various ways. As a consequence, the responses of V1 cells do not fall into a few discrete chromatic categories, as at the level of the LGN. Rather, their peak chromaticities are spread across the entire spectrum (Lennie et al., 1990; Thorell et al., 1984).

Most of the early cortical processing involves building RFs to detect various spatial aspects of the pattern (e.g., spatial frequency, orientation, motion, depth) within a local cortical region. Cells in these circuits may show some chromatic tuning just because almost all the input from the LGN is color-coded. The chromatic properties of these cells could be useful in circuits involved in identifying contours or characterizing shapes, but may make no contribution to color

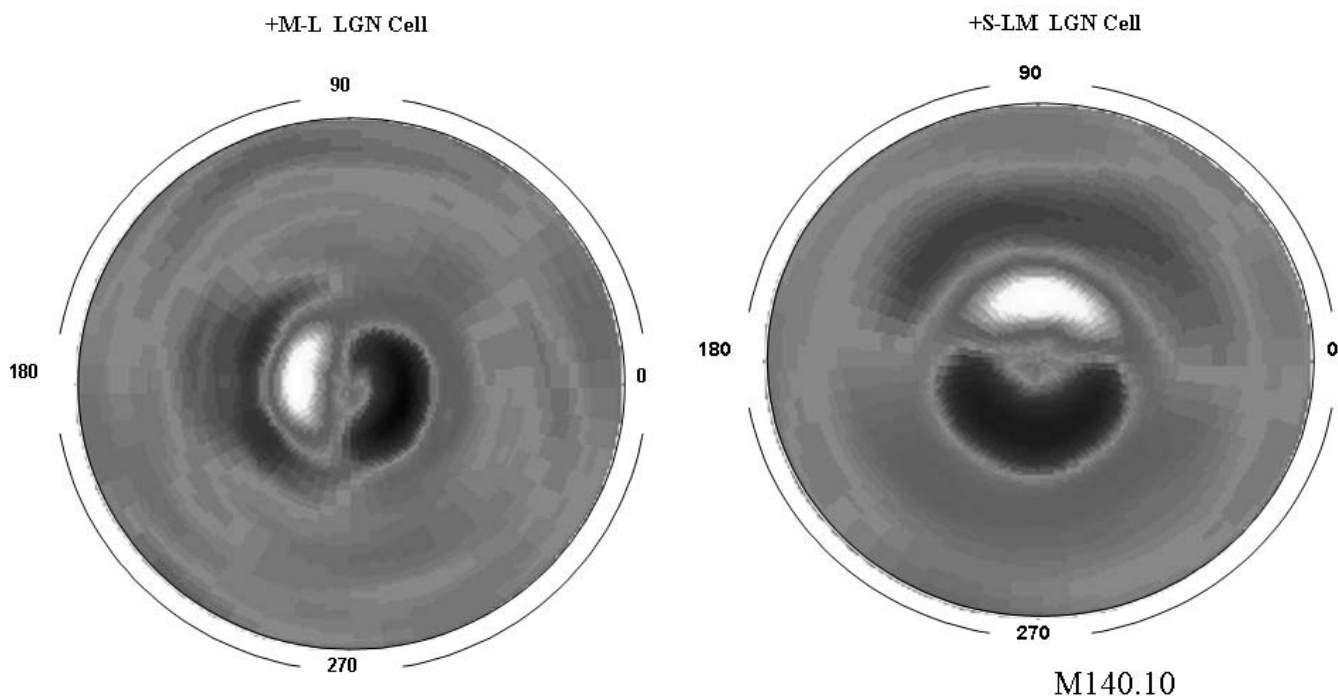


FIGURE 65.6. Shown are the chromo-temporal RFs of two LGN opponent cells, based on reverse-correlation mapping with the rapid presentation of full-field stimuli in various directions in MBDKL color space. In this representation, time from stimulus to response goes out from the center, and the orientation shows the color direction. Red shows positive correlation between stimulus and response of the cell; blue shows a negative correlation. *a*, The

RF of a +M-L cell. After an initial latency, this cell shows excitation to chromatic stimuli in the +M direction in the LM axis, with maximum response to 180 degrees, and inhibition to the +L direction, with maximum inhibition at 0 degrees. The +S-LM opponent cell whose RF is shown in *b* responds along the orthogonal color axis, with maximum excitation to 90 degrees and maximum inhibition to 270 degrees. (See color plate 43.)

perception per se. That such may be the case is indicated by the fact, discussed below, that individuals with certain cortical lesions may see no color in the world but still may be able to discriminate objects that differ from their background only in color (Mollon et al., 1980; Victor et al., 1989).

On the other hand, some cells found in V1 appear to be significant for color perception per se, in that their response properties reflect certain aspects of color processing which psychophysical evidence indicates must take place at some cortical level, and the chromatic response characteristics of these cells correspond to what one would expect from perception. With respect to color vision per se, the primary cortical processing involves separating color and luminance information, combining LGN cell types to produce cells whose color responses coincide with perceptual color categories, and further separating changes due to the illuminant from those due to visual objects by lateral interactions over large regions.

SEPARATION OF COLOR AND LUMINANCE As discussed above, some 80% of the cells in the retinogeniculate projection (those in the P_c path) multiplex color and luminance information. This is true also for many if not most cells in the striate cortex (Thorell et al., 1984). However, the presence

of four different types of P_c cells also allows for other cortical cells to separate luminance and long-wavelength color information by combining the outputs of P_c cells in two different ways (De Valois and De Valois, 1993; Lennie et al., 1991). When their outputs are summed in one way, the luminance components to their responses sum and the color components cancel. Summed in a different combination, the color components sum and the luminance components cancel. Consider a striate cortex cell that combines inputs from a number of + L_0 and + M_0 neurons in a region. Such a cell would respond to luminance variations but not to color variations, since both of the cell types that provide its inputs give excitatory responses to luminance increments in the RF center and to decrements in the surround. The color organizations of its inputs are opposite to each other (one being L-M and the other M-L), however, so the color information would cancel. Combined with input from a + S_0 cell, this would produce a V1 cell that fires to white and inhibits to black but does not respond to pure color variations. (Input from S cones contributes importantly to white; L+M alone gives yellow, not white.) This is represented in the top row of the model shown in Figure 65.7. Correspondingly, a cortical cell that combined inputs from - L_0 , - M_0 , and - S_0 cells in a region would fire to black, inhibit to white, and be quite

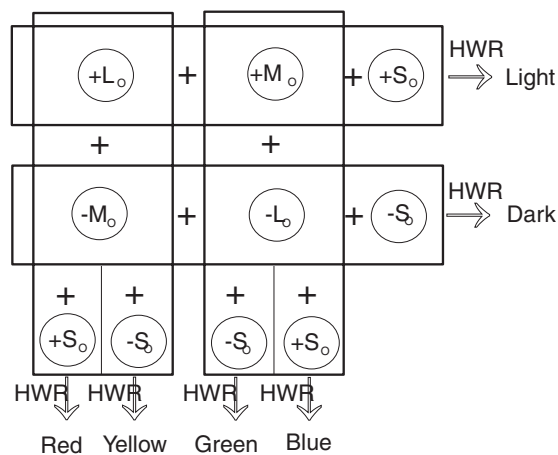


FIGURE 65.7. A model of how different types of LGN cells might be combined at the cortex to form the different perceptual color systems. (After De Valois and De Valois, 1993.)

unresponsive to pure chromatic patterns. On the other hand, a V1 cell receiving inputs from both $+L_0$ and $-M_0$ cells, or from both $+M_0$ and $-L_0$ cells (columns in Fig. 65.7), would respond to color changes but not to luminance variations, since their color responses would add, but their luminance RFs, which are opposite to each other, would cancel.

Rotation of color axes and sharpening of chromatic responses. The combination discussed above, in which LM opponent cells with common color characteristics but opposite luminance responses are combined, would separate out the chromatic component of the L/M-opponent cells, but it would not produce cells whose response characteristics correspond to perceptual red-green. The L/M-opponent LGN cells are often incorrectly referred to as forming as the red-green color system and S-opponent cells as constituting the blue-yellow color system. I first introduced this nomenclature (De Valois, 1965), but it has become increasingly clear that the peak responses of these LGN-opponent cells do not correspond to the location of the unique hues (De Valois et al., 1997, 2000b), see Figure 65.8. Thus, the region seen as blue does not correspond precisely to the response range of $+S-LM$ cells but is intermediate between these and the $+M-L$ cells; the MBDKL directions perceived as green do not correspond to that of $+M-L$ cells but are intermediate between that and $-S+LM$ cells; so also for yellow, although less so for red.

A second discrepancy between the spectral-response characteristics of LGN cells and color perception is that the responses of LGN cells to different chromatic directions that produce sinusoidally varying cone contrasts are also sinusoidal (Fig. 65.5), since their responses are quite linear. However, perceptual hue-scaling data are much more peaked (Fig. 65.8). For example, while there is a broad region around 270 degrees to which $-S+LM$ cells respond about

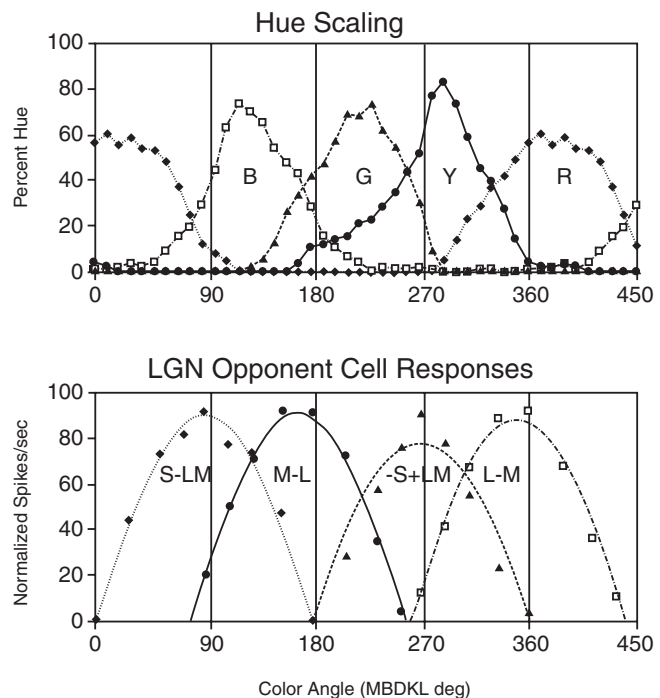


FIGURE 65.8. Comparison of perceptual hue scaling with responses of LGN cells. The top half of the figure shows judgments made by observers of the percentage of each color in stimuli at each of many different chromatic angles. The bottom half of the figure shows the averaged responses of a large population of LGN cells of different opponent cell types to similar stimuli. Note that the colors in the perceptual data are rotated with respect to the axes of the geniculate cells and that the perceptual functions are narrower, suggesting the existence of a stage of color processing past the geniculate.

equally, there is only a narrow region (around 290 degrees) which is perceived as being very yellow. Both of these discrepancies between LGN response characteristics and perception suggest that our basic color categorization reflects a cortical rather than an LGN level of processing. In fact, the response properties of some V1 cells correspond much more closely to the perceptual primary colors than do those of LGN cells (De Valois et al., 2000a). Figure 65.9 shows the chromatotemporal RF of two such V1 cells, each tuned to color axes intermediate to the LGN axes but closely corresponding to perceptual green (Fig. 65.9A) and perceptual blue (Fig. 65.9B), respectively. Furthermore, since most V1 cells show an expansive response nonlinearity, their chromatic tuning is typically more sharply peaked than is the case with LGN cells (De Valois et al., 2000a).

The relation between LGN and cortical cell responses and color perception has been modeled as (at least) a three-stage process (De Valois and De Valois, 1993); see Figure 65.7. L-M opponent cells excite to the so-called warm colors (red and yellow) and inhibit to the so-called cool colors (blue and green) and M-L cells fire to cool colors and inhibit to warm

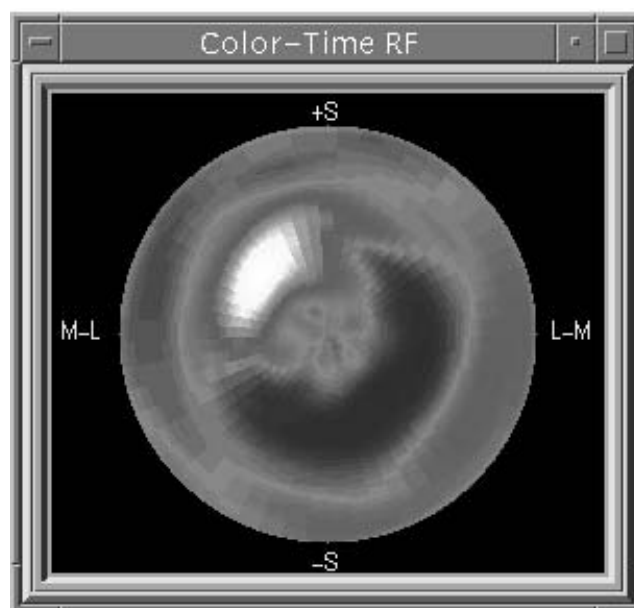
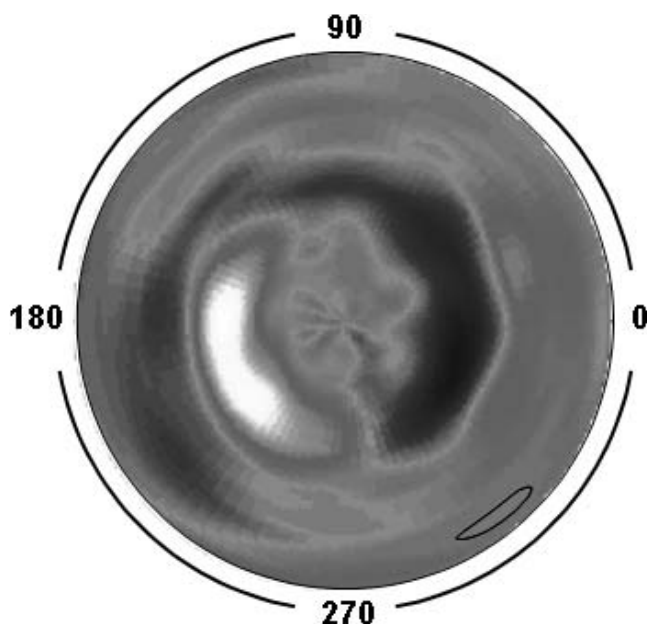


FIGURE 65.9. A comparison of responses of LGN cells to isoluminant stimuli (*left*) with the perceptual hue scaling of these same stimuli by human observers (*right*). Note that the perceptual colors

are shifted with respect to the LGN axes and are narrower, suggesting a further color processing step in V1. (See color plate 44.)

colors. The further addition of inputs from $+S_0$ or from $-S_0$ cells is required to split these classes into separate red and yellow and separate blue and green systems, respectively. The S-opponent retinogeniculate system, with its relative paucity of cells, essentially plays the role of a color modulator, being combined in various ways with the much more populous P_c cells to form three pairs of color systems.

Color processing beyond the striate cortex

For more than a century, there have been reports in the clinical literature of individuals who have lost the perception of color after a cortical lesion resulting from stroke or injury (see Meadows, 1974; Zeki, 1990, for reviews). This condition is called *achromatopsia*. A number of studies have shown that such individuals may still be able to make discriminations based on color alone, but they perceive no hue in the environment and are unable to identify the colors of objects (Mollon et al., 1980; Victor et al., 1989). It is also of interest that there has been one carefully studied case of a patient who, after a medical crisis, lost for some time the ability to see black-white patterns but retained color perception (Rovamo et al., 1982). She could see a color television program perfectly well, but a black-white program was invisible. Unfortunately, the site of the presumed cortical malfunction that led to this loss is unknown.

While the existence of at least one cortical region essential for color perception is clear from the clinical evidence, there is some dispute as to the precise anatomical location of this region, what its inputs from V1 and elsewhere might

be, and exactly what computations are carried out there. The output from V1 goes down several paths to later processing areas, including a path from V1 to V2 to V4 and from there to the inferotemporal cortex. There were early reports that area V4 seemed to be particularly involved with color. Almost all V4 cells were reported to be color selective and to be more chromatically selective than cells earlier in the path (Zeki, 1973). Area V4 was thus postulated to be the central *color center* and the likely site of injuries that produce achromatopsia. More recent studies, however, have found far fewer color-selective cells in V4 than were initially reported, and have found that V4 cells do not differ from LGN cells in their degree of color selectivity (e.g., Schein and Desimone, 1990; Schein et al., 1982). Furthermore, V4 lesions in macaques have been found to produce major deficits in form discrimination but to have minimal effect on color vision (Heywood et al., 1992; Walsh et al., 1992).

On the other hand, lesions in an inferotemporal lobe region that spared V4 were found to have a devastating effect on the macaque's color vision (Heywood et al., 1994). While it is difficult to determine homologous regions in monkey and human prestriate cortex, the clinical literature also indicates that a temporal lobe region anterior to the presumed homolog of monkey V4 is the location of those lesions that lead to achromatopsia (Meadows, 1974). Patients with achromatopsia are incapable of sorting chips by color in the Farnsworth-Munsell 100-hue test, and a functional magnetic resonance imaging study (Beauchamp et al., 1999) has shown that what is presumably this same temporal lobe region is specifically activated in normal observers when they

carry out this task. Several lines of evidence, then, appear to show that not V4 but rather some more anterior temporal lobe region is the cortical area which is crucial for color perception, with its destruction producing cerebral achromatopsia. While some agreement is emerging on the anatomical areas principally involved in processing color information beyond V1, exactly what further computations are being carried out is far from clear.

REFERENCES

- Ahnelt, P. K., H. Kolb, and R. Pflug, 1987. Identification of a subtype of cone photoreceptor, likely to be blue-sensitive, in the human retina, *J. Comp. Neurol.*, 255:18–34.
- Alpern, M., 1979. Lack of uniformity in colour matching, *J. Physiol. (Lond.)*, 288:85–105.
- Alpern, M., and T. Wake, 1977. Cone pigments in human deutan colour vision defects, *J. Physiol. (Lond.)*, 266:595–612.
- Beauchamp, M. S., J. V. Haxby, J. E. Jennings, and E. A. De Yoe, 1999. An fMRI version of the Farnsworth-Munsell 100-hue test reveals multiple color-selective areas in human ventral occipitotemporal cortex, *Cereb. Cortex*, 9:257–263.
- Bowmaker, J. K., and H. J. A. Dartnall, 1980. Visual pigments of rods and cones in a human retina, *J. Physiol. (Lond.)*, 298:501–511.
- Boycott, B. B., and H. Wässle, 1991. Morphological classification of bipolar cells of the primate retina, *Eur. J. Neurosci.*, 3:1069–1088.
- Casagrande, V. A., 1994. A third parallel visual pathway to primate area V1, *Trends Neurosci.*, 17:305–310.
- Cottaris, N. P., D. R. Elfar, and R. L. De Valois, Spatio-temporal receptive field profiles of macaque striate cortex simple cells. In preparation.
- Curcio, C. A., K. A. Allen, K. R. Sloan, C. L. Lerea, J. B. Hurley, I. B. Klock, and A. H. Milam, 1991. Distribution and morphology of human cone photoreceptors stained with anti-blue opsin, *J. Comp. Neurol.*, 312:610–624.
- Dacey, D. M., and B. B. Lee, 1994. The “blue-on” opponent pathway in primate retina originates from a distinct bistratified ganglion cell type, *Nature*, 367:731–735.
- de Monasterio, F. M., and P. Gouras, 1975. Functional properties of ganglion cells of the rhesus monkey retina, *J. Physiol. (Lond.)*, 251:167–195.
- Derrington, A. M., J. Krauskopf, and P. Lennie, 1984. Chromatic mechanisms in lateral geniculate nucleus of macaque, *J. Physiol. (Lond.)*, 357:241–265.
- Derrington, A. M., and P. Lennie, 1984. Spatial and temporal contrast sensitivities of neurones in lateral geniculate nucleus of macaque, *J. Physiol. (Lond.)*, 357:219–240.
- De Valois, R. L., 1965. Analysis and coding of color vision in the primate visual system, *Cold Spring Harbor Symp. Quant. Biol.*, 30:567–579.
- De Valois, R. L., I. Abramov, and G. H. Jacobs, 1966. Analysis of response patterns of LGN cells, *J. Opt. Soc. Am.*, 56:966–977.
- De Valois, R. L., N. P. Cottaris, S. D. Elfar, L. E. Mahon, and J. A. Wilson, 2000a. Some transformations of color information from lateral geniculate nucleus to striate cortex, *Proc. Natl. Acad. Sci. USA*, 97:4997–5002.
- De Valois, R. L., and K. K. De Valois, 1975. Neural coding of color, in *Handbook of Perception V* (E. C. Carterette and M. P. Friedman, eds.), New York: Academic Press, pp. 117–166.
- De Valois, R. L., and K. K. De Valois, 1993. A multi-stage color model, *Vis. Res.*, 33:1053–1065.
- De Valois, R. L., K. K. De Valois, and L. E. Mahon, 2000b. Contribution of S opponent cells to color appearance, *Proc. Natl. Acad. Sci. USA*, 97:512–517.
- De Valois, R. L., K. K. De Valois, E. Switkes, and L. Mahon, 1997. Hue scaling of isoluminant and cone-specific lights, *Vis. Res.*, 37:885–897.
- De Valois, R. L., C. J. Smith, S. T. Kitai, and S. J. Karoly, 1958. Responses of single cells in different layers of the primate lateral geniculate nucleus to monochromatic light, *Science*, 127:238–239.
- Famiglietti, E. V., and H. Kolb, 1976. Structural basis for On- and Off-center responses in retinal ganglion cells, *Science*, 194:193–195.
- Helmholtz, H. von, 1867. *Handbuch der Physiologischen Optik*, 1st ed., Hamburg: Voss. English translation: (1924) *Handbook of Physiological Optics*, 3 vols. (J. P. C. Southall ed.), Rochester, NY: Optical Society of America.
- Hendry, S. H. C., and C. M. Reid, 2000. The koniocellular pathway in primate vision, *Annu. Rev. Neurosci.*, 23:127–153.
- Hering, E., 1878. *Zur Lehre vom Lichtsinne*, Vienna: Carl Gerolds Sohn. English translation: (1964) *Outlines of a Theory of the Light Sense* (L. M. Hurvich and D. Jameson, trans.), Cambridge, MA: Harvard University Press.
- Heywood, C. A., A. Gadotti, and A. Cowey, 1992. Cortical area V4 and its role in the perception of color, *J. Neurosci.*, 12:4056–4065.
- Heywood, C. A., D. Gaffan, and A. Cowey, 1994. Cerebral achromatopsia in monkeys, *Eur. J. Neurosci.*, 7:1064–1073.
- Hubel, D. H., and T. N. Wiesel, 1972. Laminar and columnar distribution of geniculocortical fibers in the macaque monkey, *J. Comp. Neurol.*, 146:421–450.
- Jacobs, G. H., and J. Neitz, 1993. Electrophysiological estimates of individual variation in the L/M cone ratio, in *Colour Vision Deficiencies XI* (Documenta Ophthalmologica Proceedings Series 56) (B. Drum ed.), Dordrecht, Kluwer, pp. 107–112.
- Jameson, D., and L. M. Hurvich, 1955. Some quantitative aspects of an opponent-colors theory. I. Chromatic responses and saturation, *J. Opt. Soc. Am.*, 45:546–552.
- Jordan, G., and J. D. Mollon, 1993. A study of women heterozygous for colour deficiencies, *Vis. Res.*, 33:1495–1508.
- Kaplan, E., and R. M. Shapley, 1986. The primate retina contains two types of ganglion cells, with high and low contrast sensitivity, *Proc. Natl. Acad. Sci. USA*, 83:2755–2757.
- Kouyama, N., and D. W. Marshak, 1992. Bipolar cells specific for blue cones in the macaque retina, *J. Neurosci.*, 12:1233–1252.
- Lee, B. B., P. R. Martin, and A. Valberg, 1989. Sensitivity of macaque retinal ganglion cells to chromatic and luminance flicker, *J. Physiol. (Lond.)*, 414:223–243.
- Lennie, P., P. W. Haake, and D. R. Williams, 1991. The design of chromatically opponent receptive fields, in *Computational Models of Visual Processing* (M. S. Landy and J. A. Movshon, eds.), Cambridge, MA: MIT Press, pp. 71–82.
- Lennie, P., J. Krauskopf, and G. Sclar, 1990. Chromatic mechanisms in striate cortex of macaque, *J. Neurosci.*, 10:649–669.
- MacLeod, D. I. A., and R. M. Boynton, 1979. Chromaticity diagram showing cone excitation by stimuli of equal luminance, *J. Opt. Soc. Am.*, 69:1183–1186.
- Mariani, A. P., 1984. Bipolar cells in monkey retina selective for the cones likely to be blue-sensitive, *Nature*, 308:184–186.
- Martin, P. R., A. J. R. White, A. K. Goodchild, H. D. Wilder, and A. E. Sefton, 1997. Evidence that blue-on cells are part of the

- third geniculocortical pathway in primates, *Eur. J. Neurosci.*, 9:1536–1541.
- Maxwell, J. C., 1860. On the theory of compound colours, and the relations of the colours of the spectrum, *Philos. Trans. R. Soc. Lond.*, 150:57–84.
- Meadows, J. C., 1974. Disturbed perception of colour associated with localized cerebral lesions, *Brain*, 97:615–632.
- Mollon, J. D., F. Newcombe, P. G. Polden, and G. Ratcliff, 1980. On the presence of three cone mechanisms in a case of total achromatopsia, in *Colour Vision Deficiencies V* (G. Verriest ed.), Bristol: Hilger, pp. 130–135.
- Nagy, A. L., D. I. A. MacLeod, N. E. Heyneman, and A. Eisner, 1981. Four cone pigments in women heterozygous for color deficiency, *J. Opt. Soc. Am.*, 71:719–722.
- Nathans, J., D. Thomas, and D. S. Hogness, 1986. Molecular genetics of human color vision: the genes encoding blue, green and red pigments, *Science*, 232:193–202.
- Neitz, M., J. Neitz, and G. H. Jacobs, 1993. More than three different cone pigments among people with normal color vision, *Vis. Res.*, 33:117–122.
- Pugh, E. N., and T. D. Lamb, 1990. Cyclic GMP and calcium: the internal messengers of excitation and adaptation in vertebrate photoreceptors, *Vis. Res.*, 30:1923–1948.
- Rovamo, J., L. Hyvärinen, and R. Hari, 1982. Human vision without luminance-contrast system: selective recovery of the red-green colour-contrast system from acquired blindness, *Doc. Ophthalmol. Proc. Ser.*, 33:457–466.
- Schein, S. J., and R. Desimone, 1990. Spectral properties of V4 neurons in the macaque, *J. Neurosci.*, 10:3369–3389.
- Schein, S. J., R. T. Marrocco, and F. M. de Monasterio, 1982. Is there a high concentration of color-selective cells in area V4 of monkey visual cortex? *J. Neurophysiol.*, 47:193–213.
- Schnapf, J. L., T. W. Kraft, and D. A. Baylor, 1987. Spectral sensitivity of human cone photoreceptors, *Nature*, 325:439–441.
- Schrödinger, E., 1920. Grundlinien einer Theorie der Farbenmetrie im Tagesschen, *Ann. Physik Chem.*, 63:481–520.
- Smith, V. C., and J. Pokorny, 1975. Spectral sensitivity of the foveal cone photopigments between 400 and 500 nm, *Vis. Res.*, 15:161–171.
- Stiles, W. S., 1949. Increment thresholds and the mechanisms of colour vision, *Doc. Ophthalmol.*, 3:138–165.
- Stockman, A., and L. T. Sharpe, 2000. The spectral sensitivities of the middle- and long-wavelength-sensitive cones derived from measurements in observers of known genotype, *Vis. Res.*, 40:1711–1737.
- Thorell, L. G., R. L. De Valois, and D. G. Albrecht, 1984. Spatial mapping of monkey V1 cells with pure color and luminance stimuli, *Vis. Res.*, 24:751–769.
- Valberg, A., B. B. Lee, and D. A. Tigwell, 1986. Neurones with strong inhibitory S-cone inputs in the macaque lateral geniculate nucleus, *Vis. Res.*, 26:1061–1064.
- van der Horst, G. J. C., C. M. M. de Weert, and M. A. Bouman, 1967. Transfer of spatial chromaticity-contrast at threshold in the human eye, *J. Opt. Soc. Am.*, 57:1260–1266.
- Victor, J. D., K. Maiese, R. M. Shapley, J. Sidtis, and M. S. Gazzaniga, 1989. Acquired central dyschromatopsia: analysis of a case with preservation of color discrimination, *Clin. Vis. Sci.*, 4:183–196.
- von Kries, J., 1905. Die Gesichtsempfindungen, in *Handbuch der Physiologie des Menschen* (W. Nagel ed.), Braunschweig: Vieweg, pp. 109–282.
- Vos, J. J., and P. L. Walraven, 1971. On the derivation of the foveal receptor primaries, *Vis. Res.*, 11:799–818.
- Walsh, V., J. J. Kulikowski, S. R. Butler, and D. Carden, 1992. The effects of lesions of area V4 on the visual capabilities of macaques: colour categorization, *Behav. Brain Res.*, 52:81–89.
- Wässle, H., and B. B. Boycott, 1991. Functional architecture of the mammalian retina, *Physiol. Rev.*, 71:447–480.
- Wässle, H., U. Grünert, P. R. Martin, and B. B. Boycott, 1994. Immunocytochemical characterization and spatial distribution of midget bipolar cells in the macaque monkey retina, *Vis. Res.*, 34:561–579.
- Wiesel, T. N., and D. H. Hubel, 1966. Spatial and chromatic interactions in the lateral geniculate body of the rhesus monkey, *J. Neurophysiol.*, 29:1115–1156.
- Young, T., 1802. On the theory of light and colours, *Philos. Trans. R. Soc. Lond.*, 92:12–48.
- Zeki, S. M., 1973. Colour coding in rhesus monkey prestriate cortex, *Brain Res.*, 53:422–427.
- Zeki, S. M., 1990. A century of cerebral achromatopsia, *Brain*, 113:1721–1777.

66 The Processing of Color in Extrastriate Cortex

KARL R. GEGENFURTNER AND DANIEL C. KIPER

WHILE OUR UNDERSTANDING of the chromatic properties of cells in the early stages of the primate visual pathways has increased considerably in recent years, little is known about the processing of color information in the cerebral cortex. A number of experimenters have investigated the treatment of color information in the striate visual cortex (V1) of primates (Conway, 2001; Cottaris and De Valois, 1998; Dow and Gouras, 1973; Gouras, 1974; Hubel and Wiesel, 1968; Johnson et al., 2001; Lennie et al., 1990; Livingstone and Hubel, 1984; Michael, 1978a, 1978b, 1978c, 1979; Thorell et al., 1984; Ts'o and Gillbert, 1988; Yates, 1974) and in extrastriate area V4, which has been suggested to play an important role in the cortical analysis of color information (Schein and Desimone, 1990; Schein et al., 1982; Yoshioka et al., 1996; Zeki, 1973, 1980, 1983a, 1983b). However, the results of these studies are anything but equivocal, and the neuronal representation of color in the many other cortical areas has been little investigated.

Here we review the current state of knowledge about the processing of color signals in the primate extrastriate cortex. The questions raised by most studies can be grouped into three main classes: First, how is color encoded within particular cortical areas? Studies concerned with this question determine the chromatic properties of individual neurons, as well as the number of cells coding for color within a given cortical area. Second, how specific are the response properties of extrastriate neurons to different visual attributes? The aim of these studies is to determine whether or not color information is treated separately from other attributes, such as form or motion. Third, do the neuronal response properties support perceptual phenomena such as color constancy? In this chapter, our attention will center on these three fundamental aspects of color vision. The vast majority of data have been obtained from macaque monkeys, whose color vision is similar to that of humans (De Valois, 1965; Jacobs, 1993). Our review therefore focuses on this species and is complemented by results obtained from human subjects whenever possible.

To describe how color information is encoded within different cortical areas, we review what is known about the chromatic properties of cells and estimates of their proportion within these areas. Chromatic properties of cells are

largely captured by a description of their responses to stimuli varying in color. To determine whether color is treated independently of other visual attributes, we discuss how the chromatic properties of cells relate to other spatiotemporal properties of receptive fields, such as their selectivity to the orientation, direction of motion, or size of visual stimuli. Finally, we examine, whenever possible, the capacity of cells to maintain a stable response to a color stimulus in the face of changes in the stimulus illumination, in the chromatic composition of the background, or in different states of adaptation. Before considering in detail these various aspects of color processing in extrastriate cortex, it is necessary to briefly review the role of the primary visual cortex (V1), which provides the main inputs, directly or indirectly, to all extrastriate visual areas.

Primary visual cortex (V1)

In early studies of the primate primary visual cortex, the proportion of chromatically responsive cells was estimated to be relatively low (Hubel and Wiesel, 1968). A few years later, it was found that many cells that respond to luminance variations also respond to color variations, bringing the overall proportion of color-selective cells to about 50% in the striate cortex of macaque monkeys (Gouras, 1974; Dow and Gouras, 1973; Johnson et al., 2001; Thorell et al., 1984; Yates, 1974). These results are supported by studies using functional magnetic resonance imaging (fMRI), which showed a strong color-opponent response in the primary visual cortex of human subjects (Engel et al., 1997; Kleinschmidt et al., 1996).

The chromatic properties of V1 cells show both differences from and similarities with those at earlier stages of visual processing (retinal ganglion cells or parvo cells of the lateral geniculate nucleus, pLGN). A number of studies showed that in V1, unlike in the pLGN, the distribution of the cells' preferred colors does not obviously cluster around particular directions in color space (Lennie et al., 1990; Yoshioka et al., 1996). While most color-selective pLGN cells prefer stimuli modulated either along a roughly red-green or blue-yellow direction, those in the primary visual cortex can have preferences for many other directions. However, Lennie

et al. (1990) also found that pLGN and V1 cells have similar color tuning properties. They showed that a model that successfully describes the tuning properties of pLGN cells (Derrington et al., 1984) also fits the responses of most V1 neurons. This model postulates that the receptive field of cells can be summarized as a linear combination of the inputs from the three different cone classes. In other words, Lennie et al. showed that although V1 neurons, as a whole, sample color space more evenly than pLGN cells, individual cells in V1 are not more selective for color than pLGN cells. Other investigators have reported V1 cells with a narrow color selectivity that deviates significantly from the linear model (Cottaris and De Valois, 1998; Gouras, 1974; Yates, 1974), but overall, the proportion of such narrowly tuned cells appears to be small in V1.

A number of reports suggested that the color signals within V1 are carried by a special dedicated population of unoriented cells (Livingstone and Hubel, 1984; Roe and Ts'o, 1999; Ts'o and Gilbert, 1988). These results have been challenged more recently. In particular, Leventhal et al. (1995) found that most cells in the superficial layers of V1 are sensitive to both the orientation and color of a visual stimulus. In addition, many of these cells also signal the stimulus' direction of motion. More recently, Johnson et al. (2001) showed that V1 cells can simultaneously encode both the chromatic and spatial characteristics of a stimulus. These important findings raise serious doubts about the notion that color information is treated separately from other visual attributes within area V1.

While the contribution of V1 cells to color constancy has not been studied systematically, several results bear on that issue. In particular, a number of studies reported the existence of a population of double-opponent cells in the primary visual cortex of primates (Livingstone and Hubel, 1984; Michael, 1978a, 1978b, 1978c, 1979). These cells have a spatially and chromatically antagonistic center-surround organization, and their properties could lead them to play an important role in achieving color constancy (Zeki, 1980). Although some studies reported only a very low incidence of such cells in V1 (Lennie et al., 1990; Ts'o & Gilbert, 1988), their existence has been confirmed by more recent reports (Conway, 2001; Johnson et al., 2001). Finally, a possible role of V1 cells in color constancy is supported by their ability to adapt during prolonged exposure to a habituating stimulus (Lennie et al., 1994), while LGN neurons do not (Derrington and Lennie, 1984). Similar results have been reported by Engel and Furmanski (2001), who used fMRI to investigate the adaptability of the human primary visual cortex to chromatic stimuli. While these results suggest that the response properties of V1 cells could contribute to color constancy, they are by no means conclusive proof that color constancy is achieved in V1.

Color coding in extrastriate cortex

THE PROPORTION OF COLOR-SELECTIVE CELLS The proportion of cells capable of encoding color information appears to be remarkably stable across a number of extrastriate visual areas. Although the methods and criteria adopted by different authors render comparisons quite difficult, perusal of the literature suggests that, as in V1, a large proportion of cells in most extrastriate areas respond to color variations (Felleman and Van Essen, 1987). To obtain objective, quantitative estimates of the population of color coding neurons within V2, Gegenfurtner et al. (1996) measured the responses of cells to a set of drifting bars that span the color space around the isoluminant plane. These stimuli have a constant luminance contrast, and vary only in chromaticity (see Fig. 66.1, along with an example of a V2 cell's responses to these stimuli). For each cell, the authors computed a color responsivity (CR) index, defined as

$$CR = (R_{\text{col}} - b) / (R_{\text{white}} - b)$$

where R_{col} is the best response of the cell to any of the colored bars, R_{white} is the response to the white bar, and b is the cell's baseline firing rate.

Cells with CR exceeding 1.4 were classified as color-selective. For the cell shown in Figure 66.1B, CR was 6.03, meaning that the response to a green bar was six times as great as the response to a white bar (after subtracting the baseline). Using this criterion, Gegenfurtner et al. (1996) found that approximately 50% of V2 cells code for the color of a stimulus. This proportion is roughly similar across the various subdivisions of V2 defined by anatomical staining techniques (De Yoe and Van Essen, 1985; Hubel and Livingstone, 1987) and is in agreement with other quantitative studies (Baizer et al., 1977; Levitt et al., 1994; Peterhans and von der Heydt, 1993; Yoshioka et al., 1996).

Using the same methods and criteria, Gegenfurtner et al. (1997) found a similar proportion (~54%) of color cells in area V3. Earlier results yielded a lower estimate (Felleman and Van Essen, 1987), but the discrepancy disappears when the criteria used by the different authors are made comparable (Gegenfurtner et al., 1997).

Area V4 was proposed to be the main color-specialized area. Zeki (1983a, 1983b) presented cells with a Mondrian display and varied the wavelength composition of the individual rectangles making up the Mondrian pattern, as well as the wavelength composition of the illuminating lights. Using this arrangement, he was able to distinguish two categories of color-selective neurons in V4. A first class responded exclusively to the wavelength composition of the stimulus. A second class showed responses that correlated with the color appearance of the individual patches, as seen by a human observer. No estimates are available on the relative frequency of these two classes. The overall proportion

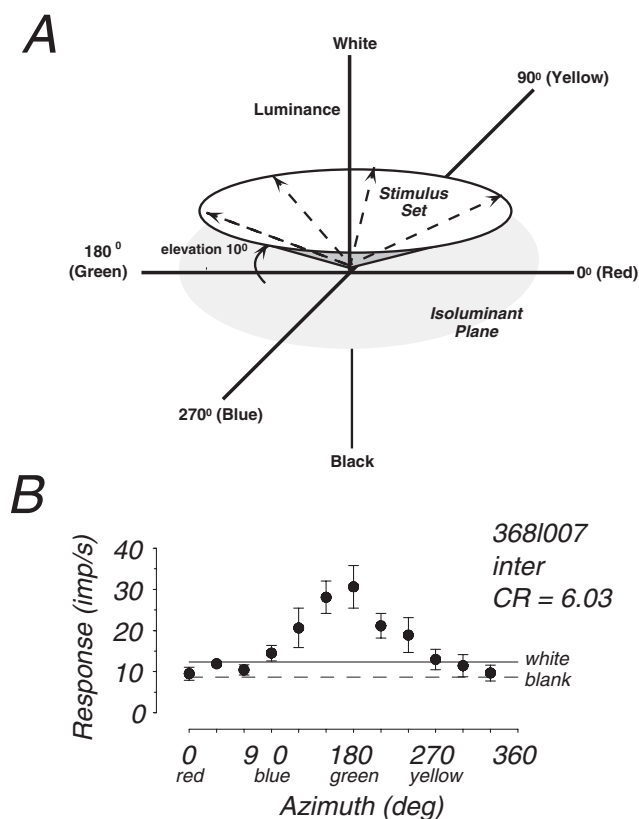


FIGURE 66.1. *A*, Schematic diagram illustrating the color space used by Gegenfurtner et al. (1996). At the origin of the color space is a neutral white. Along the L-M axis (red-green), the excitation of the L and M cones covaries to keep their sum constant. Along the S-(L + M) (blue-yellow) axis, only the excitation of the S cones varies. Along the luminance (black-white) axis, the excitation of all cone types varies in proportion to their excitation at the white point. The inverted cone represents a set of stimuli, here with an elevation of 10 degrees, and an azimuth varying between 0 and 360 degrees. Grating stimuli had colors modulated around the neutral white, thus lying on the surface of the cone. Examples of cell responses to such gratings are shown in Figure 66.3. The bar stimuli used to compute the color index (CR) had a single color, chosen on the outer rim of a cone like the one depicted here. *B*, Responses of V2 cells, located in a CO interstripe, to bars of varying color drifting on a dark background (see text). The solid horizontal line shows the response to white bars having the same luminance as the colored ones (37.5 cd/m²). The dashed horizontal line shows the cell's baseline firing rate.

of color-selective cells in V4 has varied considerably among authors, from less than 20% (Schein et al., 1982) to 100% (Zeki, 1973). Although a final consensual estimate is lacking, it is now widely agreed that the majority of V4 cells exhibit some color selectivity (Schein and Desimone, 1990). In inferotemporal (IT) cortex, which receives direct inputs from V4, the proportion of color-selective cells is believed to be high as well, and has been estimated between 48% (Gross et al., 1972) and 70% (Komatsu and Ideura, 1993; Komatsu et al., 1992).

Much less is known about the proportion of color-selective cells in areas that are known to be important for motion processing, such as MT and MST. Previously, these areas were assumed as lacking any color selectivity (Zeki, 1983c). However, using a combination of physiological and psychophysical techniques, Albright and collaborators have shown that color information does contribute to the responses of MT neurons (Croner and Albright, 1999; Dobkins and Albright, 1994; Thiele et al., 1999). Moreover, Gegenfurtner et al. (1994) showed that most MT neurons do respond to chromatic variations, although much less vigorously than to luminance modulation. In addition, they showed that most MT cells do not show the response properties that would qualify them as truly color-selective cells, and that their responses to color variations are too small to account for the animals' behavioral thresholds. Thus, although not totally absent, chromatic information seems to be poorly represented in area MT. These results agree quite well with fMRI responses in the human MT/MST complex (Tootell et al., 1995; Wandell et al., 1999).

THE PREFERRED COLOR OF CELLS In the retina and LGN, the preferred colors of cells cluster in specific directions of color space (Derrington et al., 1984). In V1, as mentioned above, the distribution of preferred colors is much more uniform, although a faint bias for the red-green and blue-yellow directions can be seen (Lennie, 1999; Lennie et al., 1990; Yoshioka et al., 1996), particularly in the populations of nonoriented and simple cells. In addition, most V1 cells prefer stimuli that vary in luminance compared to purely chromatic modulations.

These characteristics emerging in V1 hold true for V2 as well. Kiper et al. (1997) showed that the preferred colors of V2 cells do not cluster around particular directions in color space, and that most cells respond preferentially to luminance rather than to chromatic variations. The distribution of preferred color within the V2 population is shown in Figure 66.2*A*. In this graph, the preferred color of a cell is expressed by two values, azimuth and elevation, which are the polar coordinates of the cells' preferred direction in the color space depicted in Figure 66.1. An elevation of 90 degrees represents the purely luminance direction, and one of 0 degrees represents a preference for stimuli modulated in the isoluminant plane. In this plane, an azimuth of 0 degrees corresponds approximately to red, 90 degrees to blue, 180 degrees to green, and 270 degrees to yellow (see Derrington et al., 1984, for a complete description of this color space). In addition, Kiper et al. (1997) showed that the distribution of preferred colors holds true irrespective of the cells' location within any one of the three subcompartments that have been described within V2 (De Yoe and Van Essen, 1985) and irrespective of the cells' tuning in color space (see below).

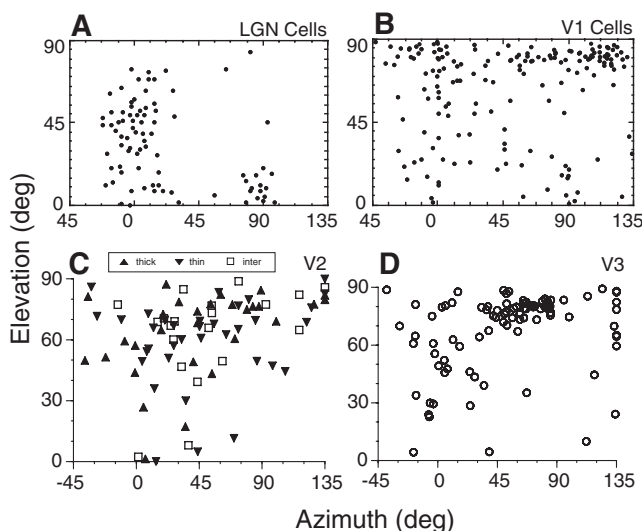


FIGURE 66.2. Scatterplots of the preferred azimuths and elevations of cells in the pLGN (A), V1 (B), V2 (C), and V3 (D). The V2 cells are subdivided into the different CO compartments. The azimuths and elevations were derived from the linear model proposed by Derrington et al. (1984).

In V3, the distribution of preferred directions is very similar to that of V2, except for an unusual number of cells giving strong responses for modulations in the blue-yellow direction (Gegenfurtner et al., 1997). These can be seen in Figure 66.2D as the cells clustering around an azimuth of 90 degrees.

For cells in area V4, Schein and Desimone (1990) determined the optimal wavelength using narrowband filters. They found that peak responses could be found at all wavelengths, as described above for V1, V2, and V3. Moreover, a small population of V4 cells exhibited several peaks in their wavelength tuning curves, with no systematic relationship between the location of the peaks. For cells in the IT cortex, Komatsu et al. (1992) also reported a rather uniform distribution of preferred colors. As in V4, a subpopulation of 20% of color-selective neurons preferred several colors. The functional significance of these multiple peaks of the wavelength tuning curves is presently not clear.

In area MT, Gegenfurtner et al. (1994) reported that although virtually all cells clearly prefer luminance variations, the preferred color of cells clustered in the red-green direction of color space. This is consistent with the notion that area MT derives its major inputs from the middle (M)- and long (L)-wavelength-sensitive cones via the magnocellular layers of the LGN (Gegenfurtner et al., 1994; Thiele et al., 1999). Note that short (S)-wavelength-sensitive cone inputs are not totally absent in area MT, as demonstrated by Seidemann et al. (1999) in monkeys and Wandell et al. (1999) in human subjects. Recent results, however, suggest that S cones contribute only to the luminance response of MT cells, and not to any color-opponent signal (Barberini et al., 2001).

THE TUNING OF CELLS IN COLOR SPACE Most V1 cells, like those in the LGN, have a rather broad selectivity for color, which is consistent with the hypothesis that they sum their cone inputs linearly, performing simple additions or subtractions between the signals originating in different classes of cones (Lennie et al., 1990). Although cells more selective than predicted by the linear model have been found in V1 (Cottaris and De Valois, 1998; Hanazawa et al., 2000; Lennie et al., 1990); their number seems to be small. In V2 they are much more numerous. Kiper et al. (1997) showed that the linear model failed to describe the tuning properties of a large group (~30%) of V2 color-selective cells. The tuning properties were determined by presenting sinusoidal gratings of different colors around the color circle illustrated in Figure 66.1A. A nonlinear function was used to interpolate between the data points, as shown by the dashed curve in Figure 66.3C. For linear cells, the predictions of both models are essentially identical, and they are not shown separately in Figures 66.3A, 66.3B, and 66.3D.

At a constant elevation of 10 degrees, bandwidth was defined as the angular difference between the color vector that gave the best response and the color vector where the response had decreased to 50% of the difference between the firing rate at the peak and 90 degrees away from it. This definition has the advantage that it predicts a constant bandwidth of 60 degrees, the angle whose cosine is 0.5 for linear cells, independently of their preferred azimuth and elevation. The resulting histogram of bandwidths for V2 neurons is shown in Figure 66.4A.

The distribution is bimodal, showing distinct subpopulations of narrowly tuned cells (like the one in Fig. 66.3C) and of cells with an approximately linear tuning (like that of Fig. 66.3B), which are clustered around a bandwidth of 60 degrees. To the right are cells for which the investigators could not reliably determine any color-specific tuning because they responded only to the luminance component of the stimuli. Using this measure of bandwidth, neurons could be classified into three categories: linear cells (bandwidth around 60 degrees), narrowly tuned cells (bandwidth lower than 45 degrees), and luminance cells (cells whose responses to the chromatic stimuli did not differ from that to the achromatic stimulus).

The resulting classification for a sample of V2 cells (Kiper et al., 1997) and of V3 neurons (Gegenfurtner et al., 1997) is shown in Figure 66.4B. In V2 there is a significant subpopulation of cells whose bandwidths are much narrower than that predicted by the linear model. This subpopulation is almost entirely missing from the V3 sample. Only a handful (5 of 90) of V3 cells showed an indication of narrow tuning in color space. Accordingly, the proportions of luminance and linear cells were slightly higher in V3. In area MT, the responses of nearly all cells are determined by the

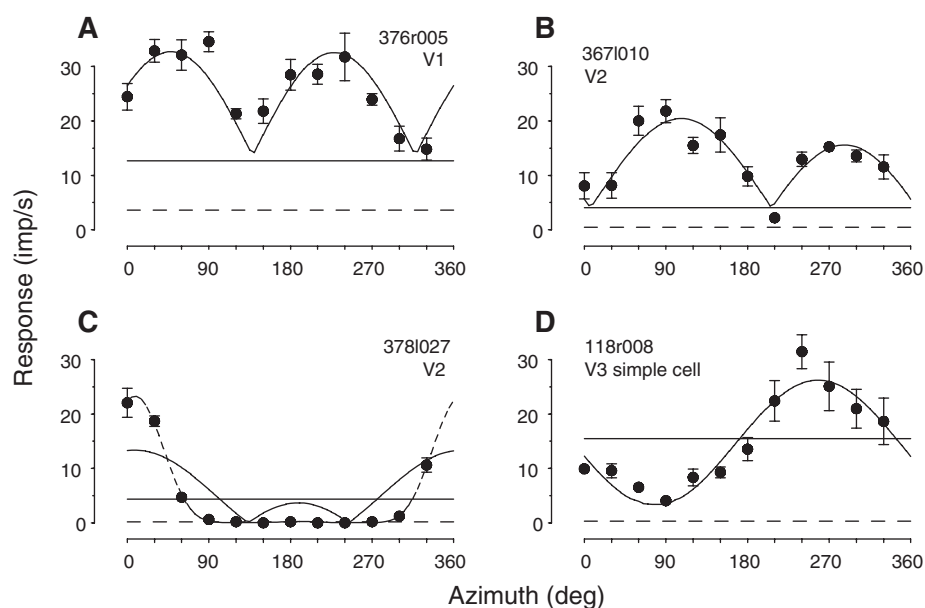


FIGURE 66.3. Responses of cells located in V1 (*A*), V2 (*B*, *C*), and V3 (*D*) to drifting sinusoidal gratings modulated around the white point, with varying azimuths and a constant elevation of 10 degrees as shown in Figure 66.1. The solid curve fitted through the data represents the prediction of the linear model (Derrington et al., 1984). The horizontal solid line shows the cells' response to a black-and-white grating having the same luminance contrast as the

colored gratings. The horizontal dashed line shows the response to a blank screen, with a luminance equal to the space-averaged luminance of the other stimuli. The dashed curve in *C* shows the prediction of the non-linear model. For the cells shown in *A*, *B*, and *D*, the predictions of the nonlinear model were almost identical to those of the linear model and are therefore not shown.

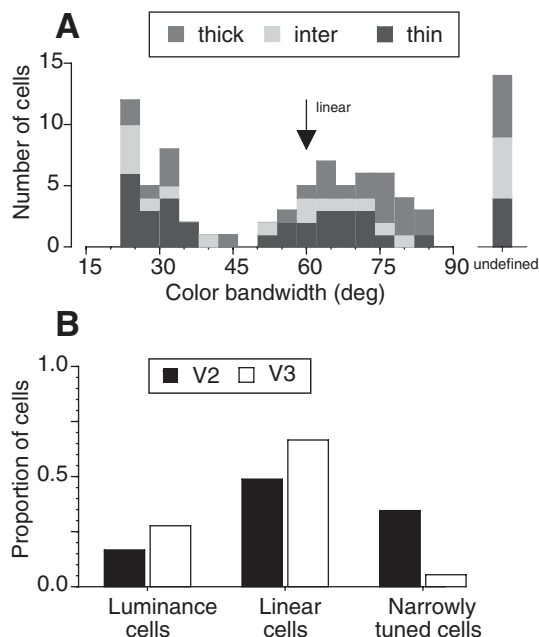


FIGURE 66.4. *A*, Histogram of the bandwidth of tuning in color space for 84 V2 cells. To the right ("undefined") are cells that responded only to luminance modulations. For each bandwidth bin, the cells located in different CO compartments are shown in various shades of gray. The linear model's prediction of a bandwidth of 60 degrees is indicated by the arrow. *B*, Distribution of luminance, chromatically linear, and chromatically narrowly tuned cells in V2 and V3 samples. Narrowly tuned cells were those with a bandwidth of less than 45 degrees.

luminance component of the stimuli alone (Gegenfurtner et al., 1994).

Perhaps even more than for the topics discussed above, the question of color selectivity of V4 cells is muddled by the use of different methods and criteria. Zeki (1980) reported a narrow wavelength selectivity of all V4 cells, a finding that contributed to the classification of V4 as a *color center* of the primate brain. However, the interpretation of these results has been questioned on methodological grounds (de Monasterio and Schein, 1982; Schein et al., 1982). Schein and Desimone (1990) showed that most V4 neurons are not more narrowly tuned in their wavelength selectivity than retinal ganglion or LGN cells, but that a subpopulation of narrowly tuned neurons also exists in V4. This result is not surprising if one considers that V4 lies between V2, where narrowly tuned neurons are numerous, and IT cortex, where neurons with a narrow wavelength selectivity have also been reported (Komatsu, 1997). To our knowledge, no systematic study of the chromatic tuning of cells exists for any other cortical area.

RESPONSES TO ISOLUMINANT STIMULI An important way to characterize the chromatic properties of cells is to study their responses to stimuli that vary only in chromaticity, so-called isoluminant stimuli. In V1, the majority of cells give stronger responses to stimuli that vary in luminance compared to purely chromatic modulations (Lennie et al., 1990), even

when the stimuli have been equated for cone contrast (Johnson et al., 2001). The same is true for areas V2 (Kiper et al., 1997) and V3 (Gegenfurtner et al., 1997). For the cells giving significant responses to isoluminant stimuli, it is of interest to determine the origin of the response and to compare the receptive properties derived from these stimuli to those obtained with luminance stimuli.

For 20 V2 cells and 9 V3 cells that gave robust responses to isoluminant chromatic stimuli, Gegenfurtner and his colleagues (Gegenfurtner et al., 1997; Kiper et al., 1997) measured the cells' tuning for orientation, spatial, and temporal frequency, as well as their contrast response function. Figure 66.5A shows a scatterplot of the optimal orientations determined using luminance and isoluminant chromatic stimuli. The correlation coefficient between these two measures was 0.98, and the mean difference in optimal orientation was 3.5 degrees. Similarly, selectivity for orientation as defined by an orientation index (Gegenfurtner et al., 1996) was not significantly different for the two types of stimuli ($t_{27} = 1.18$, $p > .1$) and was highly correlated ($\rho = 0.68$), as seen in Figure 66.5B. For 19 V2 cells the median optimal spatial frequency was 1.16 c/deg at isoluminance versus 1.03 c/deg for luminance stimuli; this small difference was not statistically significant ($t_{18} = 1.47$, $p > .05$), and the correlation between spatial frequency optima was high ($\rho = 0.87$). There was only a small difference in the optimal temporal frequency between the two stimulus types (2.25 Hz at isoluminance versus 2.69 Hz to luminance). There was no variation in the spatial or temporal bandwidths with stimulus type. Finally, there were no significant differences between the shape and steepness of the contrast response functions obtained with both types of stimuli.

These results show a strong similarity of the tuning for luminance and isoluminant stimuli, but responses at isoluminance do not necessarily have to be due to color-opponent inputs. Previous research (Dobkins and Albright, 1994; Gegenfurtner et al., 1994) had shown that the isoluminant point can vary slightly from cell to cell, and this can lead to a luminance-based response to nominally, that is, photometrically, isoluminant stimuli. To establish the relative magnitude of the response at or near isoluminance, Gegenfurtner and colleagues tested V2 and V3 cells with a range of stimuli at different elevations around zero (isoluminance). They could thus detect response minima or response nulls even in cells that do not strictly adhere to photometric isoluminance.

Two sets of stimuli were used: black and white achromatic gratings of increasing contrasts and heterochromatic gratings, which consisted of an isoluminant colored grating to which was added a black and white achromatic grating. The azimuths of the heterochromatic gratings were chosen to be the ones where the cells gave the best response. If a cell simply responds to the luminance component of the stimu-

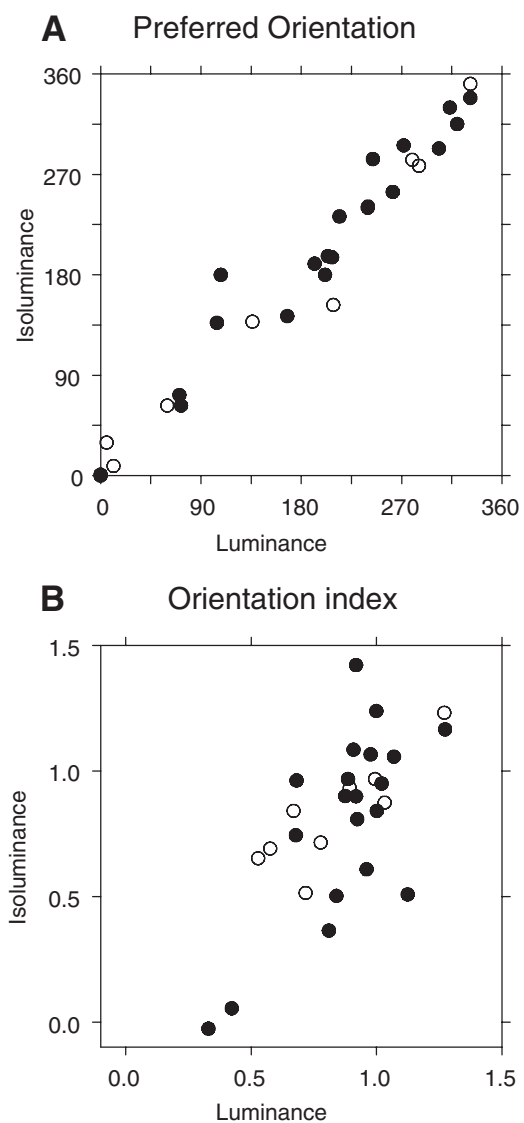


FIGURE 66.5. A, Scatterplot of the preferred orientation of 20 V2 cells (filled symbols) and 9 V3 cells (open symbols) for chromatic versus achromatic gratings. Preferred orientations were derived from fits of a smooth function to the data. B, Scatterplot of the orientation indices for the same cells.

lus, its response will be the same to the achromatic and heterochromatic gratings of the same luminance contrast. Thus, when the heterochromatic grating is isoluminant, the response will be zero. This zero response, or point of isoluminance for each cell, frequently did not correspond to that predicted by the human photopic luminance sensitivity curve $V(\lambda)$. For these cells, a small amount of luminance contrast needs to be added or subtracted to obtain a zero response. Their response curves for chromatic and achromatic stimuli will be identical but shifted horizontally. On the other hand, cells that receive color-opponent inputs should behave in a different way. They should respond well to all color stimuli, regardless of their luminance contrast.

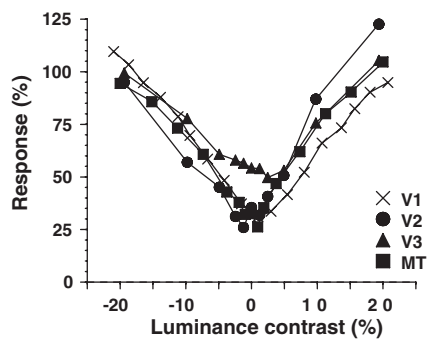


FIGURE 66.6. Averaged responses to stimuli with a fixed chromatic contrast but different luminance contrasts (see text). Each neuron's baseline firing rate was subtracted from the responses. The responses are plotted relative to the response to the gratings with a luminance contrast of 20%. Averaged population responses from simple and complex cells in V1 and V2 cells (averaged across CO compartments), V3, and MT are indicated by different symbols.

These cells should not have a null response for any of the chromatic stimuli in this experiment.

Since psychophysical experiments using isoluminant stimuli typically use photometrically isoluminant stimuli, it was of great interest to determine the overall response of cells for these particular stimuli. Cells were shown an isoluminant grating of about 10% root-mean-squared (RMS) cone contrast, and then luminance contrast of up to 20% was added to that grating. The population average response is shown for 319 V1 cells (Michael Hawken, personal communication), 33 V2 cells (Kiper et al., 1997), 71 V3 cells (Gegenfurtner et al., 1997), and 51 MT cells (Gegenfurtner et al., 1994). The surprising aspect of these data is the degree of similarity between the different areas. The response at isoluminance drops to about 30% of the maximal response in all areas (Fig. 66.6). The response does not go to zero. Even in magnocellularly dominated MT, there is a clear response. Moreover, the response is just as big as in V1 or V2, which share parvo- and magnocellular signals. Since all areas show a clear dip at isoluminance in the population average response, it is not surprising that many perceptual functions show a similar degradation at isoluminance.

INTERACTIONS BETWEEN COLOR AND OTHER VISUAL ATTRIBUTES

In addition to the description of individual cells' chromatic properties, several studies focused on the interactions between color signals and those coding other visual attributes. As described above, the notion that color signals in the cortex are strictly segregated from other attributes has been challenged in area V1 (Johnson et al., 2001; Leventhal et al., 1995). However, the existence of separate functional processing streams (Ungerleider and Mishkin, 1982) and the discovery of anatomically distinct compartments (the so-called thin stripes, thick stripes, and interstripes, revealed by stain-

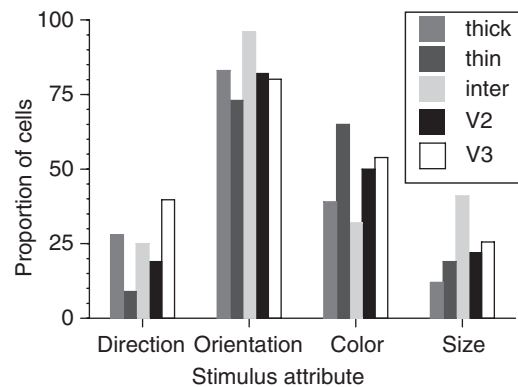


FIGURE 66.7. Proportion of neurons selective for the direction of motion, orientation, color, or size of a stimulus. As in Figure 66.4, different shades of gray indicate different CO compartments within V2. The proportion of cells in V2 taken as a whole is shown in black, that of V3 in white. The criteria used to classify the cells were identical for all samples.

ing the tissue for the metabolic enzyme cytochrome oxidase) within area V2 (De Yoe and Van Essen, 1985; Livingstone and Hubel, 1987) are still often taken as evidence for the *segregation* hypothesis in extrastriate visual areas.

This question was addressed directly by Gegenfurtner et al. (1996, 1997), who studied the selectivity of V2 and V3 cells to stimulus orientation, direction of motion, size, and color and investigated their interactions. After having quantified the selectivity of single cells for each particular attribute, using indices similar to the color index described above, they first reported on the distribution of these indices within the different subcompartments of area V2. If there is a functional segregation of different visual functions, the tuning properties of neurons in the different V2 compartments should reflect that fact. Although there is no anatomical evidence for the segregation of specialized pathways through area V3, it is of similar interest to determine physiologically whether single V3 neurons are selective for particular stimulus attributes in a way that might mirror anatomical specificity. Alternatively, there might be no functional segregation in the area; single V3 neurons might be selective along several stimulus dimensions.

Figure 66.7 shows the proportion of neurons selective for different stimulus attributes in each V2 compartment and in V3. There were some tendencies toward functional segregation: for example, color selectivity was most common in the thin stripes, size selectivity was most common in the interstripes, and orientation selectivity was somewhat less common in the thin stripes. However, despite the evidence for some degree of segregation, there was clearly no absolute segregation of selective sensitivity to color, form, or motion information into different pathways. Neurons showing selectivity to any attribute could be found in each of the compartments. Furthermore, these differences did not depend

on the particular criteria used to classify cells, and they were essentially the same in all cortical layers (Gegenfurtner et al., 1996). Figure 66.7 also compares the overall proportion of neurons in areas V2 and V3 that are selective for each of these stimulus attributes, using identical classification criteria in each area. It is clear that the only notable difference between V2 and V3 is the greater incidence of direction selectivity in V3 (roughly 40% vs. 20% in V2). In both areas, approximately 85% of the population was orientation-selective, 25% size-selective (endstopped), and 50% color-selective.

Another issue is the extent of integration and correlation among the response properties themselves; Gegenfurtner et al. (1996, 1997) investigated the relationships among the tuning characteristics of V2 and V3 neurons for different stimulus attributes. If different stimulus attributes were processed independently, one might expect neurons to show selectivity primarily to one stimulus attribute but not to several attributes simultaneously. Alternatively, it could be that each attribute has the whole range of other visual attributes associated with it. Figure 66.8 shows scatterplots of orientation, direction, and endstopping (i.e., size tuning) indices versus color responsivity for all V2 and V3 cells for which the investigators were able to measure these pairs of characteristics. The solid horizontal and vertical lines indicate the criterion values for classifying a cell as selective to that particular attribute. In both V2 and V3, there was no significant correlation between any of these selectivities. For example, in both areas there were cells that were highly selective for both stimulus color and orientation or for stimulus color and size. These are the cells that fall above and to the right of the criterion lines in Figure 66.8. Where V2 and V3 did seem to differ was in the association between color and direction selectivity. In V3, the investigators observed a population that was highly selective for both of these stimulus attributes; this group seemed to be absent from V2.

To quantify the degree of interaction between different attributes, Gegenfurtner et al. used Fisher's exact test for probabilities (see Hays, 1981, pp. 552–555) and confirmed that the probability with which a given neuron was color-selective did not depend on whether the cell was also selective for stimulus orientation, direction of motion, or size. In other words, these data do not support the hypothesis that the different stimulus attributes are processed in parallel in V2 and V3; rather, it seems that there are neurons tuned to any possible combination of attributes. The stimulus space spanned by color, orientation, direction, and size seems to be covered densely by the population of neurons in these areas.

Although such a detailed analysis of the interactions between different visual attributes is not available for other extrastriate areas, several results suggest that the situation is quite similar in a number of other visual areas. In V4,

Schein and Desimone (1990) reported that the selectivity of cells for orientation appears uncorrelated with their color properties. In that respect, V4 cells appear similar to the V1 and V2 populations, as supported by Yoshioka et al. (1996). In area MT, the few cells that code for color are also able to signal the direction of stimulus motion (Gegenfurtner et al., 1994), once more arguing against the idea that color signals are segregated from the others.

COLOR CONSTANCY The ability to perceive stable colors despite considerable changes in the illumination of a visual scene is considered a fundamental property of the human color vision system. The conditions necessary for efficient color constancy have been studied in numerous psychophysical studies and are still under scrutiny in many laboratories. Surprisingly, very little is known of the physiological basis of color constancy. The vast majority of the available neurophysiological data concerns area V4, and virtually nothing is known about the contribution of cells from other visual areas.

The pioneering work of Zeki in the early 1980s (1983a, 1983b, 1983c) described two populations of color-selective cells in area V4. One population (wavelength, or WL cells) responded to colored stimuli in a way that could be predicted by the wavelength composition of the stimulus. A second population (color-coded, or CC cells) gave responses that could not be predicted by the wavelength composition of the stimulus but correlated with its color appearance, as defined by human observers. In other words, CC cells exhibit *color-constant* responses; they code for the reflectance properties of an object irrespective of the illumination. Cells with this property seem absent in earlier stages of the visual pathways (Zeki, 1983a, 1983c), including area V2 (Moutoussis and Zeki, 2002), which provides a major input to V4. Unfortunately, most of these reports remain qualitative, and no estimate seems to be available about the frequency of WL and CC cells within V4 and the other cortical visual areas.

The notion that V4 plays an important role in color constancy received additional support from lesion studies (Walsh et al., 1993; Wild et al., 1985) showing that V4 lesions result in severe color constancy deficits despite well-preserved color discrimination abilities. These and more recent results using fMRI in humans led Zeki and his collaborators (Zeki and Marini, 1998; Zeki, 1993) to propose that V4 is the centerpiece of the second stage of color processing, concerned primarily with color constancy operations, but without regard for memory or more cognitive aspects of perception. Note, however, that both the electrophysiological results of Zeki and the conclusions drawn from the lesion studies have been challenged on methodological grounds (Lennie and D'Zmura, 1988). In particular, when comparing the responses of V4 neurons to those of V1, Zeki did not scale the spatial dimensions of the Mondrian stimuli to the

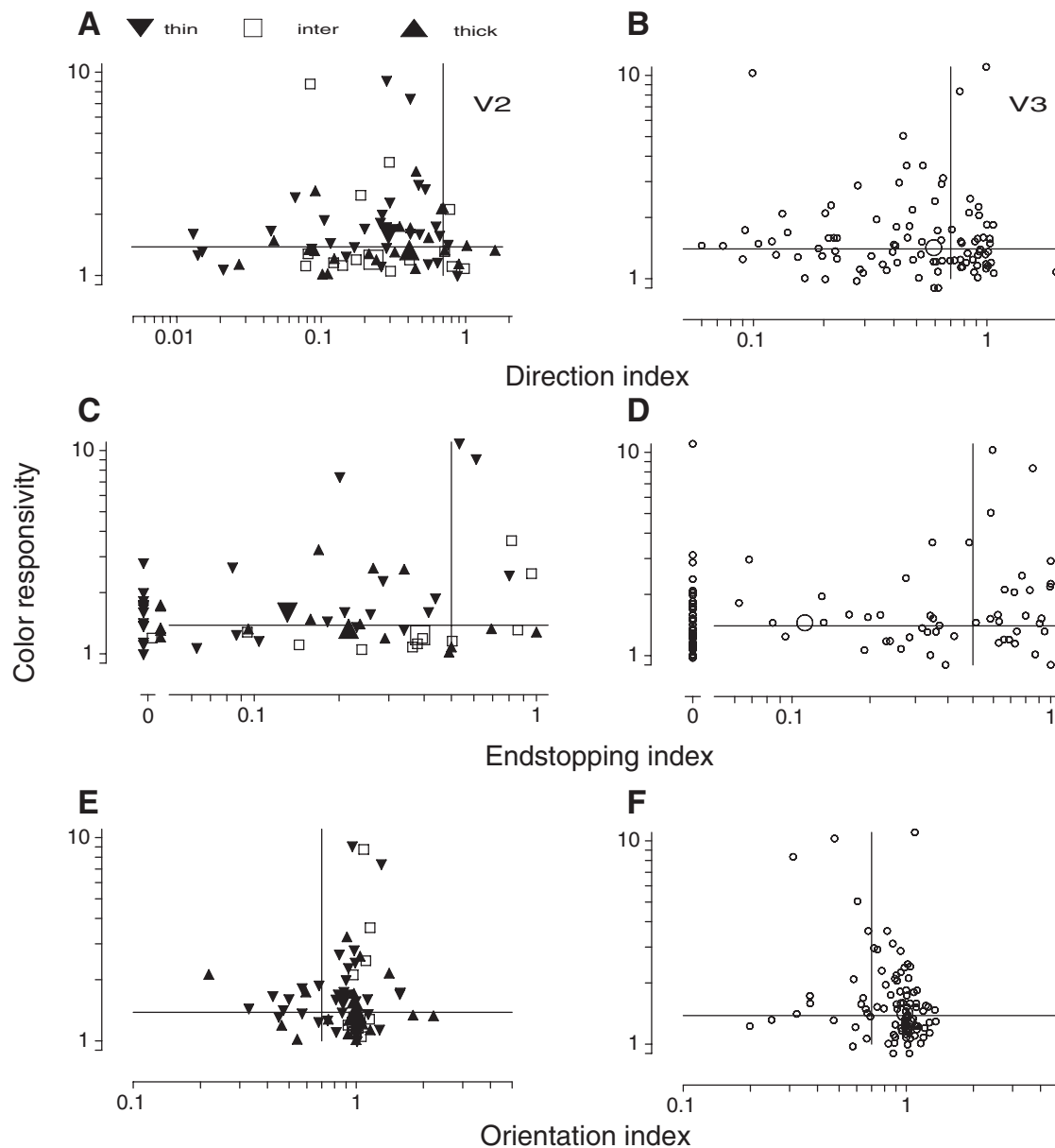


FIGURE 66.8. Association between different response selectivities for V2 (*A, C, E*) and V3 (*B, D, F*) cells. The scatterplots show the relations between color selectivity and direction selectivity (*A, B*), color versus size tuning (*C, D*), and color versus orientation selectivity (*E, F*). In *A, C*, and *E*, different symbols indicate the various CO compartments and the large symbols show the median values for each group of cells. In *B, D*, and *F*, the large symbols indicate the population mean.

neurons' receptive field size. It is well known that at corresponding eccentricities, receptive fields are much larger in V4 than in V1. Thus, the observed differences between V1 and V4 responses may be partly due to the larger sample of the Mondrian available to V4 than to V1 neurons. Moreover, the chromatic adaptation of the receptive fields was not controlled during these experiments, opening the door for another confounding dimension in the data. Finally, it is not clear whether the performance of animals with V4 lesions reflects a deficit in color constancy, in color discrimination, or in their ability to encode the spatial properties of the stimuli.

Despite all the debate about where in the brain color constancy is achieved, the physiological mechanisms of how we achieve color constancy are little understood. It is widely agreed that the light adaptation properties of cone photoreceptors play an important role. The recent rediscovery of double-opponent cells in area V1 (see above) has opened the debate about the possible role of these cells in color constancy. A potential additional mechanism may lie in the inhibitory surround exhibited by V4 cells. Indeed, Schein and Desimone (1990) found a large, spectrally sensitive surround outside the classical receptive field (CRF) of most V4

neurons. Although stimulation of the surround alone produced no responses, it could sometimes completely suppress the response to a stimulus in the CRF. For most V4 neurons, the surround's preferred color matched that of the CRF. This led the authors to propose that V4 could compute color contrast, and that the interactions between center and surround may play an important role in color constancy. Because the role of V4 in color constancy is not firmly established, and because so little is known about the contribution of cells from other areas, it is fair to state that the physiological basis of color constancy is still largely unknown and awaits further research.

IS THERE A COLOR CENTER IN THE BRAIN? The role of V4 as a color center of the primate brain is controversial. Early studies reported a very high incidence of color-selective cells in area V4, but later ones showed that this proportion is similar to that in other cortical areas of the ventral stream (Schein et al., 1982). As described above, the existence of V4 cells with a narrow tuning in color space is still debated, and so is the role of V4 cells in color constancy. For these reasons, many researchers question the qualification of V4 as the color center of the brain. In fact, some have proposed that other cortical areas play a more important role than V4 for color vision: studying monkeys with cortical lesions that spared V4, Heywood et al. (1995) suggested that it is lesions to the IT cortex, and not to V4, that mimic the human condition of cerebral achromatopsia (i.e., a specific loss of color vision). An analogous conclusion was reached by Hadjikhani et al. (1998), who, using fMRI in human subjects, described a color-selective area (which they called V8) anterior to the human equivalent of V4. These results were, however, challenged by Zeki et al. (1998), who argued that the "new" V8 is nothing but the human equivalent of V4, which had been described previously (McKeefry and Zeki, 1997). Other authors still (Gegenfurtner et al., 1996; Lennie, 1999) argue that color perception is not achieved in one particular cortical area, but that chromatic signals are treated, along with other visual attributes, in several cortical areas. The debate about the existence of a color center in the brain is ongoing, and further results are needed to resolve this issue.

Conclusions

The perception of colors is a central component of primate vision. Color facilitates object perception and recognition, and plays an important role in scene segmentation and visual memory. Moreover, it provides an aesthetic component to visual experiences that is fundamental to our perception of the world. But despite its enormous importance and the long history of color vision studies, little is known about the physiological basis of color perception. The treatment of color signals in the retina and LGN is relatively well documented,

but the existing data on cortical chromatic properties are scarce and often controversial.

The summary picture that emerges from our review is that different extrastriate areas differ very little from each other or from area V1 with respect to their chromatic properties. There are two possible conclusions one can draw. The first is that most of the processing for color vision is done early, at the stages of the retinal ganglion cells and the geniculate. The other one is that we need to study color in the cortex more closely and in more detail.

There are probably multiple reasons for the paucity of our knowledge on cortical processing of color. One is that some of the preferred models for the physiological investigation of the visual system involve animals with poor color vision, such as cats or ferrets. Another is that the color responses of individual neurons are often weak and, in extrastriate areas, might be severely degraded by anesthesia. Progress in investigating color vision physiology has probably also been slowed by the technical difficulty of producing and controlling suitable stimuli, and maybe even more by the impenetrable jargon used by color scientists! With the recent advances in display technology and brain imaging techniques, and increased communication between vision scientists from different disciplines, most of these obstacles should vanish, and new advances in our understanding of color perception should be made in the near future.

REFERENCES

- Baizer, J. S., D. L. Robinson, and B. M. Dow, 1977. Visual responses of area 18 neurons in awake, behaving monkey, *J. Neurophysiol.*, 40:1024–1037.
- Barberini, C. L., B. A. Wandell, and W. T. Newsome, 2001. S-cone inputs to area MT sum with L- and M-cone inputs, *Soc. Neurosci. (Abstr.)*, vol 27 no 165. 11.
- Conway, B. R., 2001. Spatial structure of cone inputs to color cells in alert macaque primary visual cortex (V-1), *J. Neurosci.*, 21(8):2768–2783.
- Cottaris, N. P., and R. L. De Valois, 1998. Temporal dynamics of chromatic tuning in macaque primary visual cortex, *Nature*, 395:896–900.
- Croner, L. J., and T. D. Albright, 1999. Segmentation by color influences responses of motion-sensitive neurons in the cortical middle temporal visual area, *J. Neurosci.*, 19(10):3935–3951.
- de Monasterio, F. M., and S. J. Schein, 1982. Spectral bandwidths of color-opponent cells of geniculostriate pathway of macaque monkeys, *J. Neurophysiol.*, 47:214–224.
- Derrington, A. M., J. Krauskopf, and P. Lennie, 1984. Chromatic mechanisms in the lateral geniculate nucleus of macaque, *J. Physiol.*, 357:241–265.
- Derrington, A. M., and P. Lennie, 1984. Spatial and temporal contrast sensitivities of neurones in the lateral geniculate nucleus of macaque, *J. Physiol.*, 357:219–240.
- De Valois, R. L., 1965. Analysis and coding of color vision in the primate visual system, *Cold Spring Harbor Symp. Quant. Biol.*, 30:567–579.

- De Yoe, E. A., and D. C. Van Essen, 1985. Segregation of efferent connections and receptive field properties in visual area V2 of the macaque, *Nature*, 317:8–61.
- Dobkins, K., and T. D. Albright, 1994. What happens if it changes color when it moves? The nature of chromatic input to macaque visual area MT, *J. Neurosci.*, 14(8):4854–4870.
- Dow, B. M., and P. Gouras, 1973. Color and spatial specificity of single units in rhesus monkey foveal striate cortex, *J. Neurophysiol.*, 36:79–100.
- Engel, S. A., and C. S. Furmanski, 2001. Selective adaptation to color contrast in human primary visual cortex, *J. Neurosci.*, 21(11):3949–3954.
- Engel, S. A., X. Zhang, and B. A. Wandell, 1997. Color tuning in human visual cortex measured using functional magnetic resonance imaging, *Nature*, 388:68–71.
- Felleman, D. J., and D. C. Van Essen, 1987. Receptive field properties of neurons in area V3 of macaque monkey extrastriate cortex, *J. Neurophysiol.*, 57:889–920.
- Gegenfurtner, K. R., D. C. Kiper, J. Beusmans, M. Carandini, Q. Zaidi, and J. A. Movshon, 1994. Chromatic properties of neurons in macaque MT, *Vis. Neurosci.*, 11:455–466.
- Gegenfurtner, K. R., D. C. Kiper, and S. B. Fenstemaker, 1996. Processing of color, form, and motion in macaque area V2, *Vis. Neurosci.*, 13:161–172.
- Gegenfurtner, K. R., D. C. Kiper, and J. B. Levitt, 1997. Functional properties of neurons in macaque area V3, *J. Neurophysiol.*, 77:1906–1923.
- Gouras, P., 1974. Opponent-colour cells in different layers of foveal striate cortex, *J. Physiol.*, 199:533–547.
- Gross, C. G., C. E. Rocha-Miranda, and D. B. Bender, 1972. Visual properties of neurons in inferotemporal cortex of the macaque, *J. Neurophysiol.*, 35:96–111.
- Hadjikhani, N., A. K. Liu, A. M. Dale, P. Cavanagh, and R. B. Tootell, 1998. Retinotopy and color sensitivity in human visual cortical area V8, *Nat. Neurosci.*, 1(3):235–241.
- Hanazawa, A., H. Komatsu, and I. Murakami, 2000. Neural selectivity for hue and saturation of color in the primary visual cortex of the monkey, *Eur. J. Neurosci.*, 12:1753–1763.
- Hays, W. L., 1981. *Statistics*, 3rd ed., New York: CBS College Publishing.
- Heywood, C. A., D. Gaffan, and A. Cowey, 1995. Cerebral achromatopsia in monkeys, *Eur. J. Neurosci.*, 7(5):1064–1073.
- Hubel, D. H., and M. S. Livingstone, 1987. Segregation of form, color, and stereopsis in primate area 18, *J. Neurosci.*, 4:309–356.
- Hubel, D. H., and T. N. Wiesel, 1968. Receptive fields and functional architecture of monkey striate cortex, *J. Physiol.*, 195:215–243.
- Jacobs, G. H., 1993. The distribution and nature of color vision among the mammals, *Biol. Rev.*, 68:413–471.
- Johnson, E. N., M. J. Hawken, and R. Shapley, 2001. The spatial transformation of color in the primary visual cortex of the macaque monkey, *Nat. Neurosci.*, 4:409–416.
- Kiper, D. C., S. B. Fenstemaker, and K. R. Gegenfurtner, 1997. Chromatic properties of neurons in macaque area V2, *Vis. Neurosci.*, 14:1061–1072.
- Kleinschmidt, A., B. B. Lee, M. Requart, and J. Frahm, 1996. Functional mapping of color processing by magnetic resonance imaging of responses to selective p- and m-pathway stimulation, *Exp. Brain Res.*, 110(2):279–288.
- Komatsu, H., 1997. Neural representation of color in the inferior temporal cortex of the macaque monkey, in *The Association Cortex—Structure and Function* (H. Sakata, A. Mikami, J. M. Fuster, eds.), Amsterdam: Harwood Academic.
- Komatsu, H., and Y. Ideura, 1993. Relationships between color, shape and pattern selectivities of neurons in the inferior temporal cortex of the monkey, *J. Neurophysiol.*, 70(2):677–694.
- Komatsu, H., Y. Ideura, S. Kaji, and S. Yamane, 1992. Color selectivity of neurons in the inferotemporal cortex of the awake macaque monkey, *J. Neurosci.*, 12(2):408–424.
- Lennie, P., 1999. Color coding in the cortex, in *Color Vision: From Genes to Perception* (K. R. Gegenfurtner and L. T. Sharpe, eds.), New York: Cambridge University Press.
- Lennie, P., and M. D’Zmura, 1988. Mechanisms of color vision, *Crit. Rev. Neurobiol.*, 3:333–400.
- Lennie, P., J. Krauskopf, and G. Sclar, 1990. Chromatic mechanisms in striate cortex of macaque, *J. Neurosci.*, 10:649–669.
- Lennie, P., M. J. M. Lankheet, and J. Krauskopf, 1994. Chromatically-selective habituation in monkey striate cortex, *Invest. Ophthalmol. Vis. Sci. Suppl.* 35, 1662.
- Leventhal, A. G., K. G. Thompson, D. Liu, Y. Zhou, and S. J. Ault, 1995. Concomitant sensitivity to orientation, direction, and color of cells in layers 2, 3, and 4 of monkey striate cortex, *J. Neurosci.*, 15:1808–1818.
- Levitt, J. B., D. C. Kiper, and J. A. Movshon, 1994. Receptive fields and functional architecture of macaque V2, *J. Neurophysiol.*, 71:2517–2542.
- Livingstone, M. S., and D. H. Hubel, 1984. Anatomy and physiology of a color system in the primate visual cortex, *J. Neurosci.*, 4:309–356.
- Livingstone, M. S., and D. H. Hubel, 1987. Psychophysical evidence for separate channels for the perception of form, color, movement, and depth, *J. Neurosci.*, 7:3416–3468.
- McKeefry, D., and S. Zeki, 1997. The position and topography of the human colour centre as revealed by functional magnetic resonance imaging, *Brain*, 120:2229–2242.
- Michael, C. R., 1978a. Color vision mechanisms in monkey striate cortex: dual-opponent cells with concentric receptive fields, *J. Neurophysiol.*, 41:572–588.
- Michael, C. R., 1978b. Color vision mechanisms in monkey striate cortex: simple cells with dual opponent-color concentric receptive fields, *J. Neurophysiol.*, 41:1233–1249.
- Michael, C. R., 1978c. Color-sensitive complex cells in monkey striate cortex, *J. Neurophysiol.*, 41:1250–1266.
- Michael, C. R., 1979. Color-sensitive hypercomplex cells in monkey striate cortex, *J. Neurophysiol.*, 42:726–744.
- Moutoussis, K., and S. Zeki, 2002. Responses of spectrally selective cells in macaque area V2 to wavelengths and colors, *J. Neurophysiol.*, 87:2104–2112.
- Peterhans, E., and R. von der Heydt, 1993. Functional organization of area V2 in the alert macaque, *Eur. J. Neurosci.*, 5:509–524.
- Roe, A. W., and D. Y. Ts’o, 1999. Specificity of color connectivity between primate V1 and V2, *J. Neurophysiol.*, 82:2719–2730.
- Schein, S. J., and R. Desimone, 1990. Spectral properties of V4 neurons in the macaque, *J. Neurosci.*, 10:3369–3389.
- Schein, S. J., R. T. Marrocco, and F. M. de Monasterio, 1982. Is there a high concentration of color-selective cells in area V4 of monkey visual cortex? *J. Neurophysiol.*, 47:193–213.
- Seidemann, E., A. B. Poirson, B. A. Wandell, and W. T. Newsome, 1999. Color signals in area MT of the macaque monkey, *Neuron*, 24(4):911–917.
- Thiele, A., K. R. Dobkins, and T. D. Albright, 1999. The contribution of color to motion processing of motion in macaque middle temporal area, *J. Neurosci.*, 19(15):6571–6587.
- Thorell, L. G., R. L. De Valois, and D. G. Albrecht, 1984. Spatial mapping of monkey V1 cells with pure color and luminance stimuli, *Vis. Res.*, 24:751–769.

- Tootell, R. B., J. B. Reppas, K. K. Kwong, R. Malach, R. T. Born, T. J. Brady, B. R. Rosen, and J. W. Belliveau, 1995. Functional analysis of human MT and related visual cortical areas using magnetic resonance imaging, *J. Neurosci.*, 15(4):3215–3230.
- Ts'o, D. Y., and C. D. Gilbert, 1988. The organization of chromatic and spatial interactions in the primate striate cortex, *J. Neurosci.*, 8:1712–1727.
- Ungerleider, L. G., and M. Mishkin, 1982. Two cortical visual systems, in *Analysis of Visual Behavior* (D. J. Ingle, M. A. Goodale, and R. J. W. Mansfield, eds.), Cambridge, MA: MIT Press.
- Walsh, V., D. Carden, S. R. Butler, and J. J. Kulikowski, 1993. The effects of V4 lesions on the visual abilities of macaques: hue discrimination and colour constancy, *Behav. Brain. Res.*, 53:51–62.
- Wandell, B. A., A. B. Poirson, W. T. Newsome, H. A. Baseler, G. M. Boynton, A. Huk, S. Gandhi, and L. T. Sharpe, 1999. Color signals in human motion-selective cortex, *Neuron*, 24(4):901–909.
- Wild, H. M., S. R. Butler, D. Carden, and J. J. Kulikowski, 1985. Primate cortical area V4 important for colour constancy but not wavelength discrimination, *Nature*, 313:133–135.
- Yates, J. T., 1974. Chromatic information processing in the foveal projection (area striata) of unanesthetized primate, *Vis. Res.*, 14:163–173.
- Yoshioka, T., B. M. Dow, and R. G. Vautin, 1996. Neuronal mechanisms of color categorization in areas V1, V2 and V4 of macaque monkey visual cortex, *Behav. Brain Res.*, 76:51–70.
- Zeki, S., 1973. Color coding in rhesus monkey prestriate cortex, *Brain Res.*, 53:422–427.
- Zeki, S., 1980. The representation of colours in the cerebral cortex, *Nature*, 284:412–418.
- Zeki, S., 1983a. Color coding in the cerebral cortex: the reaction of cells in monkey visual cortex to wavelengths and colors, *Neuroscience*, 9:741–765.
- Zeki, S., 1983b. Color coding in the cerebral cortex: the responses of wavelength-selective and color-coded cells in monkey visual cortex to changes in wavelength composition, *Neuroscience*, 9:767–781.
- Zeki, S., 1983c. The distribution of wavelength and orientation selective cells in different areas of the monkey visual cortex, *Proc. R. Soc. (Lond.)*, 217:449–470.
- Zeki, S., 1993. *A Vision of the Brain*. Cambridge, MA: Blackwell Scientific.
- Zeki, S., and L. Marini, 1998. Three cortical stages of colour processing in the human brain, *Brain*, 121:1669–1685.
- Zeki, S., D. J. McKeefry, A. Bartels, and R. S. J. Frackowiak, 1998. Has a new color area been discovered? *Nat. Neurosci.*, 1(5):335.

67 Improbable Areas in Color Vision

SEMIR ZEKI

COLOR VISION IS AN exciting subject that lends itself easily to theorizing. It is especially interesting to do so in relation to the human cerebral cortex, given the huge advances made in the past decade in imaging human brain activity in health and disease. It is also interesting to do so because understanding how the brain constructs colors promises to give significant insights into the cerebral processes underlying aesthetics in the ancient Greek sense, that is, the acquisition of knowledge through the senses. It is not surprising to find, therefore, that color has traditionally attracted the attention of all those who have been concerned with perception and knowledge, including philosophers and physicists. But theorizing, to have any value, must be based on reliable facts and interpretations. How reliable are the facts derived from imaging experiments relating to color vision? And how compelling are the interpretations based on these results?

This chapter deals with the quality of evidence that has been used to erect three cortical areas in the human brain—"VP," "V4v," and "KO"—all of them related directly or indirectly to color vision. How solid is the evidence for the existence of these areas, and how convincing is the interpretation of their functions? Let me emphasize that I am discussing the human brain, not the primate brain in general, though I shall refer, of course, to the evidence from monkeys from which some of the human areas are etymologically derived. Any conclusions reached about human visual areas must be derived from, and consistent with, evidence obtained from the human brain, without recourse to evidence from the monkey brain or from the brain of any other species. It is, of course, always good if the human evidence is supported by monkey evidence, but it should not have to rely on it. Too often in the recent past, there has been an attempt to hide behind a monkey in pleading for an interpretation, because that interpretation is not sustainable through human evidence alone. This chapter amounts, therefore, to an inquiry into the quality of evidence that we have come to accept in human imaging studies, a quality that I believe falls far short of what the instrumentation that we rely on is capable of delivering.

The location of the human cerebral color center and the visual field representation within it

The notion that color may be the function of a specialized cortical area was hinted at several times before Louis Verrey

(1888) published his paper entitled *Hémiachromatopsie droite absolue* (absolute right hemiachromatopsia). Verrey's advantage over his predecessors was that he had been able to examine the lesion that had led to the syndrome of acquired achromatopsia (cerebral color blindness). Apart from some involvement of the body of the corpus callosum, the lesion was confined to the fusiform and lingual gyri and was thus located in the inferior part of the occipital lobe (Fig. 67.1). Every word of Verrey's title, together with the figure representing the lesion in the brain of his achromatopsic patient, is worth studying. Together they tell a great deal about the organization of the visual brain even today, though much of this is not mentioned by Verrey and is read by me into his evidence with hindsight. Foremost among the lessons to be learned is something about the topographic organization of the human visual brain. Given that the lesion producing cerebral hemi-achromatopsia was located in the lingual and fusiform gyri, the title implies that a center located in the lower part of the occipital lobe controls color vision in both the upper and lower parts of the entire contralateral visual hemifield.

The discovery of a visual area lying outside the striate cortex was an embarrassment at the time (see Zeki, 1990, 1993, for reviews). Henschen and after him Holmes had concluded, correctly, that the lower part of the calcarine cortex (V1) represents the upper visual field and the upper part of the lower visual field. They had concluded, also correctly, that the calcarine cortex, which Henschen referred to as the "cortical retina" and Holmes as the "visuosensory" cortex, and which we now call the primary visual cortex or area V1, was coextensive with the striate cortex. This led both Henschen and Holmes to conclude, incorrectly, that V1 was the only visual center in the brain and therefore had to receive all visual "impressions," including color impressions (see Zeki, 1993, for a review).

From his single case of achromatopsia, Verrey had concluded, correctly, that there is a color center in the brain, but he had also supposed, incorrectly, that this is part of the "visuosensory" cortex. The implication was obvious: that the "visuosensory cortex" or "cortical retina" of the brain was larger than that supposed by Henschen and by Holmes, that is, it was not confined to the striate cortex. Verrey implied that the primary visual receptive cortex had a specialized subdivision dealing with color. Verrey's conclusions about the cortical site for color processing (*le centre du sensé*

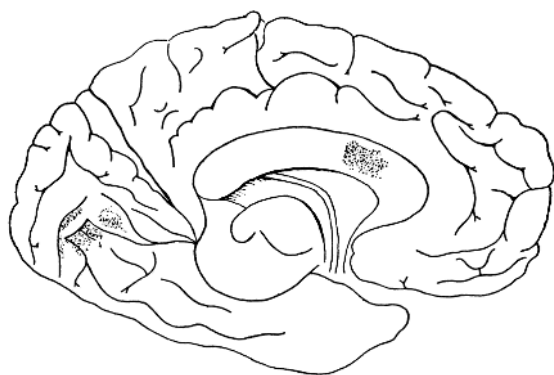


FIGURE 67.1. The sites of the lesions in the brain examined by Louis Verrey. (From Verrey, 1888.)

chromatique), together with his observation that both upper and lower contralateral quadrants were compromised in his unilaterally lesioned patient, implied that both quadrants are mapped in the lower part of the occipital lobe. Such an implicit supposition (which Verrey himself did not explicitly make) obviously cast a doubt on the way that Henschen and Holmes had supposed the visual field is mapped in the occipital lobe. Both Henschen and Holmes dealt with this in the same way, by brushing aside Verrey's evidence or ignoring it altogether, until it vanished from the literature (for reviews see Zeki, 1990, 1993).

There was a price to be paid for ignoring the significance of the finding that an area located in the lower occipital cortex controls color vision in both contralateral quadrants. That peril existed until well into the 1990s. Actually, it is probably with us even today. This is surprising because in 1980, Damasio alluded to it explicitly. He wrote: "one single area in each hemisphere controls color processing for the entire hemifield. This is so regardless of the fact that such an area is eccentrically located, in the lower visual association cortex, classically related to upper quadrant processing only. . . . The classic concept of a concentrically organized visual association cortex no longer appears tenable." No one took much notice of what Damasio said then, and I don't think that anyone takes much notice of it today either.

There is probably a good explanation for this intellectual scotoma. With time, and with the discovery that "areas 18 and 19" (Brodmann, 1905; von Bonin and Bailey, 1951), or areas V2 and V3 (Cragg, 1969; Zeki, 1969), form concentric rings around V1 (Fig. 67.2), it became customary to consider that the upper part of the visual field is represented in the lower occipital lobe and *vice versa*. A new habit developed of tagging on the letter "v" or "d" to areas to indicate that they are located in the lower occipital lobe ("v") and therefore represent upper fields or that they are located in the upper occipital lobe ("d") and therefore represent lower visual fields. This terminology begged for confusion and

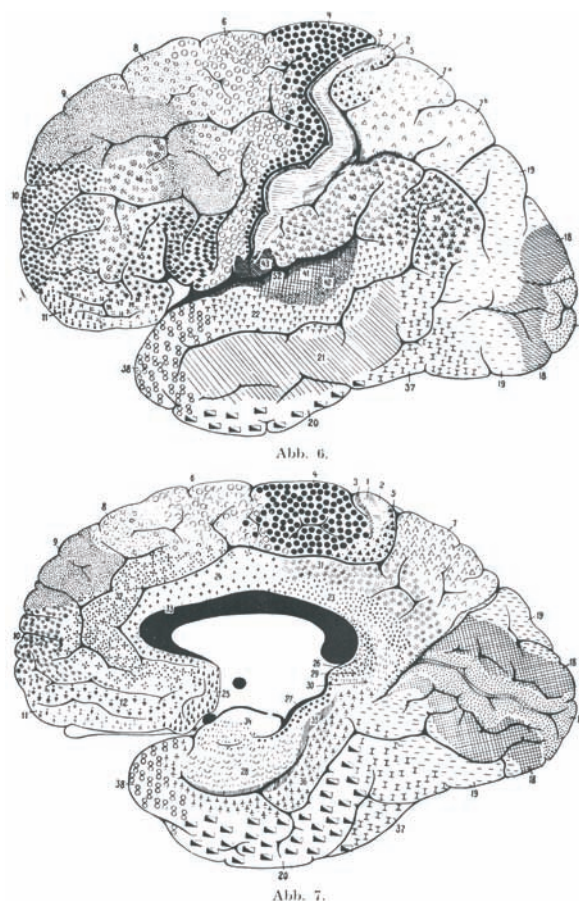


FIGURE 67.2. Brodmann's cytoarchitectonic map of the brain. Brodmann numbered the areas according to the sequence in which he studied them. Note how areas 18 and 19 form rings around area 17. (From Brodmann, 1909.)

trouble, which was not long in coming. It was based on an implicit assumption that had already been discounted, namely, that the upper contralateral quadrant is represented in the lower occipital lobe and *vice versa*. Verrey (1888) had shown that an area located in the lower occipital cortex must represent both contralateral quadrants (otherwise, how would one account for the complete contralateral hemiachromatopsia produced from a unilateral lesion in the lower occipital lobe?), and physiological evidence had shown that that an area located in the upper occipital lobe can represent both contralateral quadrants, as does area V3A (Van Essen and Zeki, 1978) or that it may be located somewhere between the two halves and still do the same, as does area MT in the owl monkey (Allman and Kaas, 1971). Indeed, Allman and Kaas had introduced the more neutral designations of + and - to indicate upper and lower field representation, respectively, without making either explicit or implicit assumptions about whether upper contralateral quadrants are represented only in the lower occipital lobe (Baker et al., 1981). It is unfortunate that their more sensi-

ble designations were not more widely used. If they had been, we might have avoided some of the present difficulties, though even that is not certain. At any rate, with implicit assumptions imposing themselves, if an area was found in the lower occipital cortex, “v” was hastily tagged on to it, irrespective of whether a dorsal counterpart could be found for it; if it was located in the upper occipital lobe, “d” was tagged on to it, again irrespective of whether a ventral counterpart could be found for it. It was but one step from this to describing what Jon Kaas (1993) has called “improbable” areas, ones that represent only one quadrant, with no representation for the other corresponding quadrant. But what kind of visual information is restricted to only one quadrant that it alone should have a cortical representation, without a companion area to represent the same information for the “unrepresented” quadrant? If the proponents of this bizarre terminology thought about it at all, they were not telling. A good example related to color vision is provided by area “VP.”

An improbable area: “VP”

Area V2 of the primate brain surrounds area V1 and is, in turn, surrounded by area V3. The latter has a dorsal and a ventral subdivision, just like V2 (Fig. 67.3). Throughout its dorsal and ventral extent, the representation of the horizontal meridian forms a common boundary between it and V2, and the representation of the vertical meridian is at its anterior border (Cragg, 1969; Zeki, 1969). In 1986 a number of papers from Van Essen’s group, summarized in Burkhalter et al. (1986), confirmed the manner in which the visual field is mapped in V3 (see also Shipp et al., 1995). They nev-

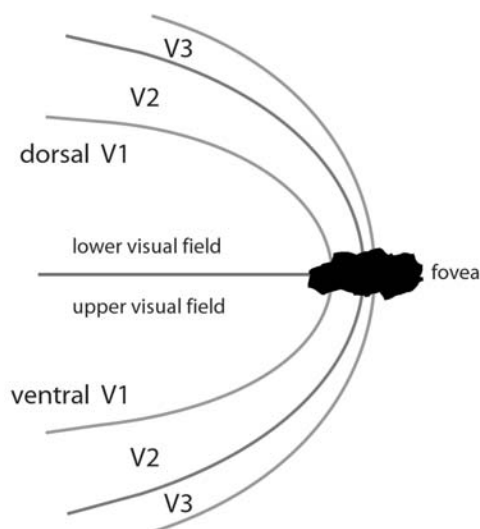


FIGURE 67.3. A schematic diagram of prestriate cortex and its relation to striate cortex. Red lines show the horizontal meridian, green lines the vertical meridian. (Redrawn from Zeki, 1969.) (See color plate 45.)

ertheless reported that the lower part of V3 does not receive a direct input from V1, unlike the upper part of V3. They also reported that the lower part of V3 contains a high concentration of color cells, again unlike upper V3. This led Van Essen to propose that the lower part of V3 is not part of V3 at all, but a distinct area that they called “VP.” This made “VP” one of Kaas’ “improbable areas,” for it implied that something happening in upper quadrants (in this case color, *inter alia*) is processed there, without a machinery for processing that same attribute when it occurs in lower quadrants. Also unaccounted for was why, among the areas that process color, “VP” alone should process this attribute in upper visual fields only. Such an asymmetric representation is not characteristic of V1 or V2 or V4—all of them involved in color processing. Burkhalter et al. (1986) gave a halfhearted explanation. They wrote unconvincingly: “any asymmetries relating to V3 and VP might well be cancelled by compensatory asymmetries in other areas. Thus, any perceptual consequences might be rather subtle, but nonetheless would be worth testing for.” Yet the term “VP” has survived unquestioningly and has made an appearance in the human imaging literature with even less evidence. In fact, all the evidence from the human literature speaks against such an asymmetry.

In the absence of any direct evidence in favor of a dichotomy between V3 and “VP” in the human, and evidence against it instead, there seems little doubt that the habit of naming the ventral part of human V3 “VP” is inherited from labeling in the macaque monkey. But how reliable is the macaque evidence? The negative anatomical evidence regarding the absence of a direct input from V1 to lower V3 in the macaque is not only doubtful but probably wrong. Such a projection has been found in *Cebus* (Rosa et al., 2000), and Lyon and Kaas (2001, 2002) have recently found the same not only in the marmoset monkey but also in the macaque monkey. It is instructive to compare the approach of Lyon and Kaas with the approach adopted by some in the imaging community. In their 2001 paper, Lyon and Kaas *postulated* that a V3 with upper and lower subdivisions would be characteristic of all primate visual brains. But they also tested the postulate by studying the macaque monkey (Lyon and Kaas, 2002). In the brisk world of human imaging experiments, this expensive and time-consuming luxury is seemingly not an option for everyone. Instead, what we have witnessed is the identification of a visual area in the human brain based on questionable evidence from the macaque. This is unfortunate. Given the real differences between species, the identification of human visual areas should be based on human measurements.

The anatomical evidence in favor of the absence of a direct input from lower V1 to lower V3 in the monkey is therefore far from convincing, and indeed, all the evidence speaks against it. The physiological evidence that, unlike V3,

there is a high concentration of color cells in “VP” is even less convincing; indeed, all human imaging studies speak against it too. These studies have succeeded in showing that there is an area lying anterior to V2, with the map characteristic of V3, but not a single one of them, even those that use the term “VP” for lower V3, has succeeded in showing any specialization in “VP” for color or any specific activation of “VP” with color stimuli (e.g., De Yoe et al., 1996; Sereno et al., 1995; Zeki et al., 1991). Where the question has been specifically addressed, it has been found that lower V3 is not specifically activated by color (Wade et al., 2002). On the other hand, studies have found that “VP” is activated in the same way as V3 (e.g., Smith et al., 1998). In spite of this, many persist in this *folie à plusieurs* of calling the lower part of V3 “VP,” oblivious to the fact that to have an area representing one quadrant without having a representation for the other quadrant makes it improbable. Improbable, but also possible. But if the latter, it needs a convincing explanation, which no one has yet provided. Instead, the precedent has been used to describe other improbable areas, as we shall see. Thus, the evidence from the human brain does not support a separation into VP and V3, but rather tells of an area V3 with upper and lower subdivisions, representing lower and upper visual fields, the two subdivisions being activated in the same way. It is, of course, right to record that not all have accepted this division into V3 and “VP” unquestioningly (e.g., Wandell, 1999).

Another improbable area: “V4v”

Our early imaging experiments showed that the color center in the human brain is located in the fusiform gyrus (Lueck et al., 1989; Zeki et al., 1991). It was called V4 without attaching a “v” or a “d” to it. At the time, this was not unreasonable. We had used full field stimulation and had no means of distinguishing upper from lower visual field representation within it. Unless one wanted to study its topography, which was not our aim, there was little need for us to do otherwise. We had read Verrey’s paper and remembered its title, which indicated that both upper and lower quadrants are mapped in the “color” center, located for him in the ventral part of the occipital lobe. This, we therefore supposed, was an area in which both quadrants are mapped, and there was little reason to add letters to its upper and lower parts. After all, neither we nor anyone else has bothered to add such letters to area V3A, located in the dorsal part of the occipital lobe, and in which upper and lower quadrants are separately mapped (Van Essen and Zeki, 1978; Zeki, 1978). Moreover, there was good reason to suppose that both upper and lower visual fields are separately mapped within the color center, because clinical evidence has shown more than once that the achromatopsia resulting from lesions there can be restricted to a quadrant.

Then came the method of visual field mapping in human prestriate cortex using phase encoding (Engel et al., 1994). The early data were interpreted to reveal an area called “V4v” (De Yoe et al., 1996; Sereno et al., 1995), but at the time, no one seemed much bothered by the fact that they did not reveal its dorsal counterpart, “V4d,” or if they did, they did not communicate their worries. This was strange. How could a sophisticated mapping method that stimulates the entire visual field activate the ventral subdivision of an area but not its dorsal counterpart? The studies of De Yoe et al. suggested that “V4v” overlapped, at least in part, our V4. They wrote: “The location of V4v corresponds to some of the locations identified in positron emission tomography studies as having color selective responses. However there is sufficient variability to make it difficult to be certain that such responses could not have come from VP.” The study of Sereno et al., however, did not mention any overlap with the color center that we had defined. Adding “v” to V4 and calling the area thus defined “V4v” nevertheless implied that this was the ventral part of V4, in which the upper contralateral quadrant alone is mapped. No one seemed to worry much about such an asymmetric representation, at least not in print. Indeed, why should anyone have thought about it at all? There was, after all, the precedent of “VP” to go by.

This was something of a puzzle. Could it be true that only upper visual fields are mapped in the part of the color center located in the fusiform gyrus, with lower visual fields mapped elsewhere, perhaps on the lateral surface of the occipital lobe? Though this seemed improbable, we decided to undertake another study in which we mapped the representation of the visual field using colored and achromatic Mondrians presented separately in the upper and lower hemifields. Compared to the sophistication of the phase encoding method, the approach that we used was hoary with age. But the results (McKeefry and Zeki, 1997) showed what we had suspected, and what the clinical evidence from Verrey on had implied, to us at least—that both upper and lower quadrants are separately mapped, side by side, within the color center and that therefore a center located in the lower occipital lobe is indeed responsible for the elaboration of color in both the upper and lower visual fields. This accounted for why lesions in the color center of one hemisphere can lead to a hemi-achromatopsia or even to an achromatopsia restricted to one quadrant (see Meadows, 1974, and Zeki, 1990, for reviews).

Old wine in new bottles

The repetition of our experiment, using phase encoding, and the confirmation of our results by Hadjikhani et al. (1998), represents perhaps one of the most surprising events in the history of mapping, not for the results obtained, which

were in fact identical to ours, but for the way in which these results were presented and for what has been read into them. They claimed to have found “a new retinotopic area that we call ‘V8,’ which includes a distinct representation of fovea and both upper and lower visual fields.” This previously undifferentiated cortical area “was consistently located just beyond the most anterior retinotopic area defined previously, area V4v” (emphasis of the “v” added). These claims gained added weight from an accompanying article by Heywood and Cowey (1998) which declared uncritically: “it is area V8, not the favorite candidate V4” that, when lesioned, produces cortical color blindness. Heywood and Cowey claimed that these results show that “the *human* color center is distinct from area V4. The *newlydefined* [sio] color area contains a complete retinotopic map of the contralateral visual half field, responds more robustly to color and, unlike V4, is activated by induction of color after effects” (emphasis added), which would seem to leave out of account the earlier discoveries of Sakai et al. (1995) on activation of the color center through color aftereffects.

The many uses of “v”

Anyone reading these articles casually may be forgiven for supposing that a new color area, distinct from what we had called human V4, had been found. But how “new” was this area? A slightly more careful reading of the results in Hadjikhani et al. (1998) shows that this “new” area is nothing more than a rediscovery of what we had defined, dressed up in a new name. Hadjikhani et al. wrote: “Based on the anatomical location and functional comparison used here, this collateral [sulcus] color selective patch appears equivalent to the previously reported [Lueck et al., 1998; Zeki et al., 1991] area involved in achromatopsia.” In fact, a comparison of their Talairach coordinates with those given by us in previous publications shows that the “new” color-

selective area, “V8,” is identical in position to the location of our human V4 (Fig. 67.4). Moreover, Hadjikhani et al. found that “When we averaged the Talairach coordinates of the color-selective area ‘V4’ described in previous studies . . . we found that it was about twice as close to the location of our retinotopically defined V8, compared to our retinotopically defined V4v” (emphasis on “v” added). But here comes the catch. Hadjikhani et al. write, in the very next sentence, “This supports all the other evidence that the color selective activity is located in area V8, rather than in ‘V4,’” which, presumably, is why they say that they had discovered a “previously undifferentiated” area. To any moderately careful reader, the first part of this sentence says that V8 is almost identical to V4, while the second part says that V8 is distinct and lies anterior to it. How is this feat achieved? Very simply, by dropping the *v* at the end of the sentence! This is no eristic quibble. The statement would have been unexceptionable if they had written “color selective activity is located in area V8, rather than in V4v” but, then, the claim of a “new,” “previously undifferentiated” visual area would have been difficult to sustain. The omission of the “v,” together with claims of a “new,” “previously undifferentiated” cortical area being discovered, have apparently convinced some of the innocent who work, or comment, on color vision that something new has indeed been discovered. Tootell and Hadjikhani (2001) have since written: “The Talairach coordinates of the original ventral color-selective region (“V8” or “V4” or “VO”) were never in dispute, although this has been a matter of apparent confusion.” The source of the confusion is not hard to trace. It lies in the claim that a “new,” “previously undifferentiated” color area located anterior to V4 has been discovered (Hadjikhani et al., 1998). The confused include even the experts, as witness the article by Heywood and Cowey (1998) about the “newly defined” color area and about the color center being “area V8, not the favorite candidate V4.”

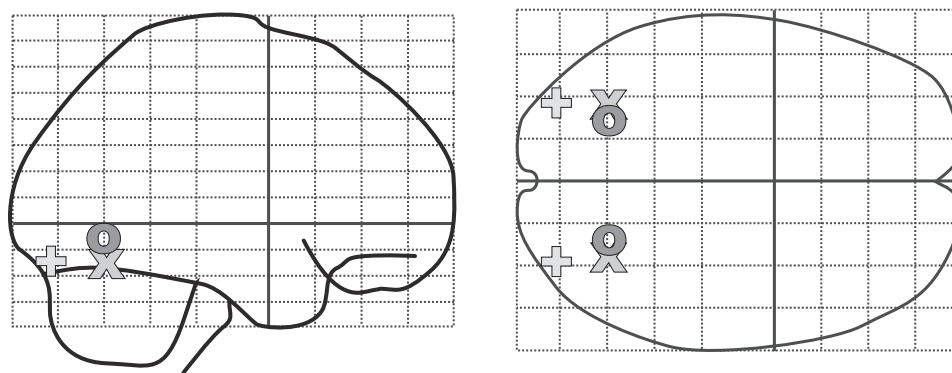


FIGURE 67.4. A glass projection of the brain showing three areas discussed in the text. The areas were located by using the Talairach coordinates of the three areas given in the paper by Hadjikhani et al. (1998). *O* corresponds to area V4 defined in Lueck et al. (1989; Zeki et al., 1991; and McKeefry and Zeki, 1997); *X* corresponds to the “new” area “V8” of Hadjikhani et al. (1998) and the + to area V4v defined by Sereno et al. (1995). (See color plate 46.)

Some of the comments made about the discovery of a “new,” “previously undifferentiated” color center are worth noting, for they speak volumes about the care with which papers are read, at least in the color vision and imaging communities. I restrict myself to one here, which says: “There is currently a heated debate about the location of the color center in the visual cortex” (Gegenfurtner, 2001). Actually, there isn’t, and there never was. The debate is about whether a new area has been discovered, and the admission of Tootell and Hadjikhani (2001) that it has not settles the issue. There is, of course, an additional debate not alluded to in the above quotation, which is about whether there is an area V4v, distinct from V4 (see below).

Cross-species comparisons

In trying to make claims for “V8” as being color selective as against V4 (although they are the same area), Tootell and his colleagues have taken refuge in a long debate about whether macaque V4 has any color selectivity. The argument is along two lines. The first one runs like this: “Zeki believed that monkey V4 is color selective. This is not so, and therefore the color-selective region in human prestriate cortex is not V4 but V8.” That debate, to which I shall return elsewhere, is irrelevant to the issue of whether a “new” color center has been discovered in the human brain, distinct from what was previously described by us. But it also helps to deflect attention from another problem, namely, the status of human “V4v.” The line of argument here is: “Macaque V4, as defined by Zeki, is the fourth visual map after V1. But in human there is a color *unselective* ‘V4v’ lying anterior to V3 and posterior to the color center called V4 by Zeki and his colleagues and recently rediscovered by us. It is therefore inappropriate to call this rediscovered area V4.” This argument is also irrelevant to whether a “new” color center has been discovered. But it raises an interesting question. Does human “V4v” exist, as an entirely separate and improbable area, which represents upper visual field only? There is no compelling evidence in its favor, which is not to say that there may not be some day. Tried though we have, we have found no evidence for an area “V4v” that is separate from area V4 as we have defined it, or from the same area rediscovered by Hadjikhani et al. (1998).

The most extensive and detailed retinotopic mapping experiments in the human visual brain to date have been done recently by Wandell and his colleagues at Stanford (Press et al., 2001; Wade et al., 2002). Their results show convincingly that there is no quarter field map corresponding to a putative “V4v” in ventral occipital cortex. There is thus no area “V4v,” which, given its improbability, is just as well. Their results also show that V4 is the fourth visual map and that it abuts lower V3. Thus, through this work, one of the arguments outlined in the above paragraph is emasculated

and loses its force. In sum, there is no current compelling evidence for the existence of area “V4v,” and the onus is on its proponents to demonstrate it convincingly and unequivocally. If they cannot do so, they should withdraw it. What is surprising, given the flimsy evidence for the existence of “V4v,” is the numerous papers that, in addressing other aspects of human visual brain organization, refer to it, thus leaving one with doubts about the quality of evidence that is deemed acceptable in the imaging community. It is hard to imagine that the more hard-nosed physiologists would ever have accepted the existence of a “V4v” based on the kind of evidence that is currently available.

There is a price to be paid for such uncritical acceptance of the evidence. An example is to be found in a paper by one of the coauthors of the Hadjikhani et al. (1998) paper. Cavanagh et al. (1998), in trying to account for why achromatopsic patients can see moving color stimuli, state, “In humans, the most recent fMRI studies [of Hadjikhani et al.] suggest a more anterior site, V8, for color analysis in a location consistent with the damage in the achromatopsic patients. The human homologue to V4 on the ventral surface (V4v) is probably also damaged in these patients but it includes only a representation of the upper visual fields.” But since V8 is nothing more than human V4 renamed, since Wade et al. (2002) have shown convincingly that there is no quarter field representation corresponding to the “V4v” of Hadjikhani et al. (1998), and since, therefore, the existence of “V4v” is in considerable doubt, the speculation is worse than useless. Such is the price that we pay for having, in the human imaging community, standards of evidence and of proof that fall well short of what is expected, and delivered, in other branches of neurobiology.

The human color center

The color center turns out to be more complex than was previously thought (Fig. 67.5). In our work, we have frequently referred to the V4 complex in both monkey and human, and in our most recent work we have described this complex in the human as comprising at least two subdivisions, which we refer to as V4 and V4a (Bartels and Zeki, 2000). V4 itself is topographically organized (Hadjikhani et al., 1998; McKeefry and Zeki, 1997; Wade et al., 2002), while V4a is not obviously so, which is not to say that more sophisticated mapping techniques may not reveal some topographic mapping within it in the future (Bartels and Zeki, 2000). It is important to realize that V4a lies anterior to V4 and therefore anterior also to the “newly discovered” color center of Hadjikhani et al. (1998). It is a part of the color center that they missed in their studies.

The topographic organization of V4 accounts well for why the achromatopsia induced by lesions in the fusiform gyrus may involve the whole of the contralateral hemifield

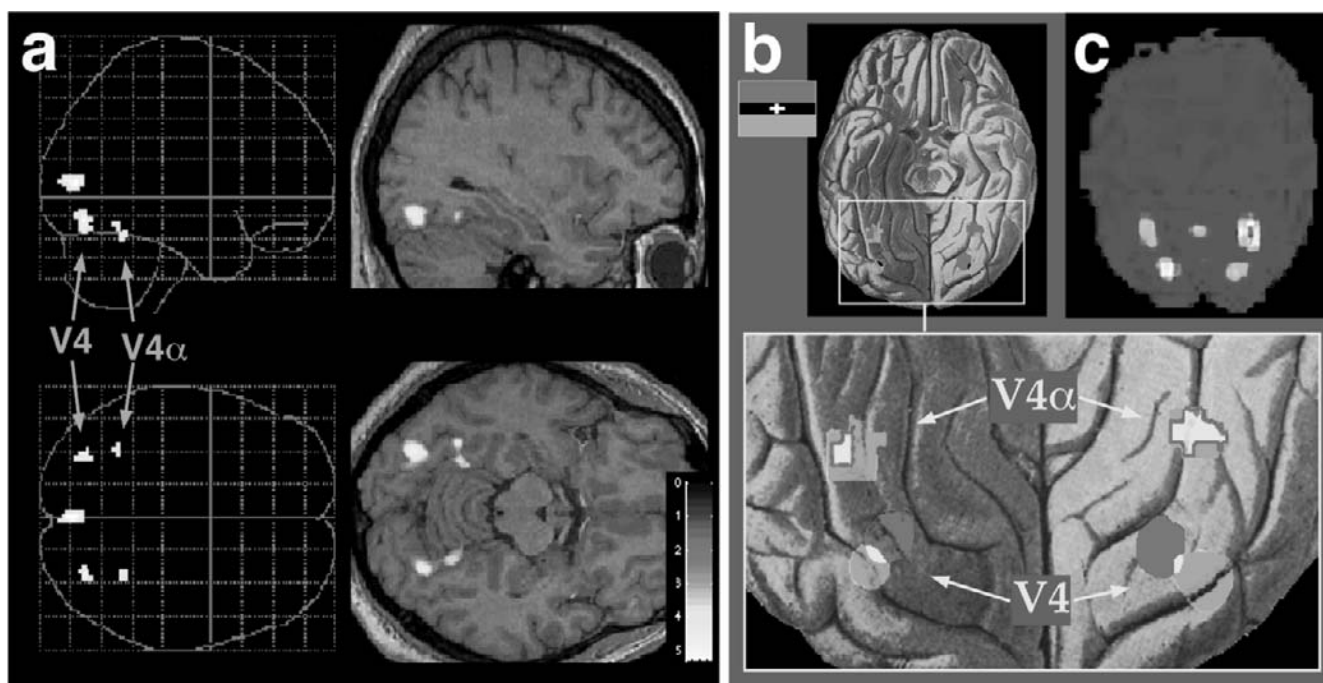


FIGURE 67.5. The segregation of the color-selective region in the fusiform gyrus (the V4 complex) into two areas, the posterior retinotopically organized area V4 and the anterior area V4a, as revealed by the reanalysis of the V4 mapping study (McKeefry and Zeki, 1997). *a, left*: Statistical parametric map (SPM) viewed in glass-brain projections of the comparison of all chromatic stimuli versus their achromatic counterparts for both upper and lower visual field stimulation (group of four subjects; threshold: $Z > 4.81$, $p < .05$, corrected for multiple comparisons, equivalent to $p < .000001$ uncorrected). *Right*: Slices taken through an SPM of a single subject superimposed on its structural image (slices at $x: -33$, $z: -14$ mm). *b*, Projection of the comparison of either upper field (in red) or lower field (in green) stimulation with color versus their achromatic counterparts onto a ventral view of a human brain

(overlapping regions are shown in yellow). For V4 (*bottom*), the SPM of the following comparison is projected onto the drawing: (superior colored vs. [superior achromatic + inferior colored + inferior achromatic]); (group of four subjects; threshold: $Z = 4.81$, $p < .05$ corrected). For V4a (*top*), SPMs of a comparison of color versus achromatic stimuli within the corresponding hemifield is projected onto the drawing (threshold: $Z = 3.09$, $p < .001$ uncorrected). *c*, An independent component analysis (ICA) separates spatially independent maps of brain activity without *a priori* knowledge about the stimulus conditions. ICA isolated the complete V4 complex, including the posterior (V4, *bottom*) and anterior (V4a) subdivisions in both hemispheres, shown here in the glass-brain view of a single subjects' brain. (From Bartels and Zeki, 2000.) (See color plate 47.)

(as in the patient of Verrey, 1888) or may be limited to a quadrant. Less certainly, the subdivisions of the color center into V4 and V4a may eventually help to account for what is problematic with the syndrome of cerebral achromatopsia. In some patients, the achromatopsia is transient, whereas in others it is more long-lasting and even permanent. Moreover, in some patients the achromatopsia is less severe than in others and can be described as a dyschromatopsia. In such patients, the color loss is not complete, being greater for some colors (usually the blues and the greens) than for others (see Zeki, 1990, for a review). Moreover, the color vision of some dyschromatopsic patients is very much wavelength based, in that they are not able to compensate for the predominance of one wavelength over another when the wavelength composition of the viewing conditions changes (Kennard et al., 1995). It is possible, but yet to be shown conclusively, that these variations depend upon the extent to which the lesions in the fusiform gyrus involve both subdivisions

of the human color center (see Bartels and Zeki, 2000, for a review).

Of course, there are those who believe that the whole notion of a cortical specialization for color vision is a fantasy and the search for it an outmoded folly. How convincing are their arguments? Here is one of the most forceful. Lennie (1999) writes: "The controls used in most functional imaging studies have involved comparing activity evoked by the presentation of an array of colored surfaces with the activity evoked by the presentation of the same elements at the same luminance, but now set to be gray. Visibility and salience can be quite different. Overall, the evidence for a specialized color pathway is not strong." Consider this statement carefully. It says essentially that the color center may be nothing more than a salience center. But color *does* make the visual world more salient. And so there is a color center after all, even after this denial, except that in this instance we call it the "salience center"! If there are good arguments against a

color center in the human brain, why resort to such wholly unconvincing arguments?

An improbable area in the making: "KO"

We are currently witnessing the making of another improbable area. It is known as the "kinetic occipital" area or area "KO," for which an alternative and, to me, more acceptable name is area V3B (Press et al., 2001; Smith et al., 1998). Area "KO" has been described as not only being "specialized in the processing of kinetic contours" but "genuinely specialized" in this task (Van Oostend et al., 1997). The acronym given it by Orban and his group reflects this belief (Dupont et al., 1997; Orban et al., 1995; Van Oostend et al., 1997). Its relation to color vision lies in the current attempts to homologize it with macaque V4 or, more accurately, with the dorsal part of macaque V4, dubbed "V4d" (Tootell and Hadjikhani, 2001), to which I return below. This would naturally make "KO" another improbable area, since all the evidence shows that cells in the upper part of V4 ("V4d") have their receptive fields in the lower contralateral quadrant (Pinon et al., 1998; Van Essen and Zeki, 1978). This, in turn, would imply that V4d processes kinetic contours in the contralateral lower field only, with no equivalent area for processing the same signals when they occur in the upper contralateral visual field, or at least no declared area.

Before going into such speculations, it is important to consider the evidence that "KO" is "genuinely . . . specialized in the processing of kinetic contours" (Van Oostend et al., 1997). The idea that there are brain areas specialized for the processing of forms derived from motion was actually first posited by Gulyas et al. (1994), but it was based on a faulty analysis of their imaging data which has attracted criticism (Frackowiak et al., 1996) and is therefore questionable. How reliable is the evidence of Orban's group?

In their work, Orban's group (Dupont et al., 1997; Orban et al., 1995; Van Oostend et al., 1997) compared the activity produced in "KO" when humans viewed bars produced from kinetic contours, from luminance differences, and from translational motion. They found that several areas are activated in these comparisons, including V3A, V5, and "KO," though the last was more active. This led them to conclude that the brain devotes a special area to the processing of kinetic contours. But there is a critical omission in these comparisons. What if "KO" is specialized for the extraction of shapes, no matter how derived, rather than the extraction of shapes from kinetic contours specifically? A critical comparison to distinguish between the two possibilities would be to study the activity in "KO" when contours are extracted from other attributes, for example, equiluminant colors. Color is generally agreed to be the most separate in its cortical representation from motion, even if there is much anatomical opportunity for cross-talk between the two systems and even

if such cross-talk does occur (Callaway, 1998). If "KO" is inactive when humans view visual stimuli in which simple shapes are extracted from equiluminant colors, then a fairly strong, though perhaps not definitive, case can be made for "KO"'s putative specialization. But if it is equally active when contours are extracted from equiluminant colors, as it is when the same contours are extracted from kinetic contours, then "KO" can be safely considered not to be specialized for the processing of kinetic contours. Our own studies show that area V3B, a better name for "KO," is in fact engaged when shapes are extracted, regardless of their provenance. This is not the place to go into this evidence, for what I am emphasizing is that claims for the specialization of "KO" have been made in the absence of critical comparisons which would establish whether it is specialized in the extraction of shapes from kinetic stimuli. At present, the evidence relating to the "genuine specialization" of "KO" for processing kinetic contours is so incomplete that it should raise considerable doubts in the neuroimaging community. Such evidence may, of course, be forthcoming in the future, but it is not available today. On the other hand, there is considerable evidence for "cue invariance" in the visual brain, by which is meant that cells in different areas of the brain respond to their preferred stimuli no matter how these stimuli are derived, that is, whether from luminance differences, kinetic boundaries, or equiluminant colors (Albright, 1992; Geesman and Andersen, 1996; Grill-Spector et al., 1998; Sary et al., 1993). To overwrite this evidence, it is not sufficient to keep repeating that "KO" is specialized for the processing of kinetic contours, as if every utterance establishes its role more solidly. What is needed is a solid experiment to establish its specialty. Such evidence is not currently available.

Precedence replaces evidence

The doubtful status of "KO" as an area that is specialized in the processing of kinetic contours is rendered more emphatic by the current attempts to make human "KO" the homolog of the dorsal part of macaque V4, or V4d (Tootell and Hadjikhani, 2001; see also the two contradictory abstracts by Orban's group—Fize et al., 2001, and Vanduffel et al., 2001), based on the argument that "KO" is the "topolog" of V4d. In replicating the findings of Orban's group, Tootell and Hadjikhani (2001) believe that they have confirmed that "KO" is indeed specialized for kinetic contours. But they used the same stimuli and paradigm as Orban's group and in essence replicated Orban's study. So complete was this repetition that the critical omission, the one that casts doubt on the conclusions of Orban's group, was not remedied at all. The critical comparison, to determine whether "KO" is also activated as well by shapes derived from other attributes, and especially from equilumi-

nant colors, was not done. The evidence of Tootell and Hadjikhani (2001) therefore adds nothing to the unconvincing evidence of Orban's group.

The issue is further compounded, and actually compromises the status of "KO" further, by the suggestion that it is the homolog of V4d. If so, then "KO" must be registering events occurring in the contralateral inferior quadrant only, since cells in V4d have their receptive fields there (Pinon et al., 1998; Van Essen and Zeki, 1978). This would make "KO" an area that is specialized for the processing of kinetic contours when these occur in the lower contralateral quadrant only, leaving the same activity occurring in the upper contralateral quadrant unrepresented in the cortex, or represented in another area, which would make that latter, yet to be discovered area, another improbable one. In fact, the evidence of Press et al. (2001) suggests otherwise, in showing that both upper and lower contralateral quadrants are mapped in V3B, the better name for "KO," a fact that appears to have been ignored in the headlong rush to homologize "KO" with V4d, since the latter represents lower contralateral quadrants only. Thus, a circle of confusion, consisting of increasing numbers of improbable areas, follows from the initial assumption that there is an improbable area, "VP." The best way of breaking that confusion is to get rid of the assumption, or at any rate to test it before accepting it. Where the assumption has been tested, it has not found to be true.

It is, of course, possible that this is exactly the way that the cortex is specialized and that, in thinking of areas that represent one quadrant only, Jon Kaas, and I after him, are being extremely unsophisticated in our approach to cortical mapping. Yet one cannot help feeling that the evidence in favor of these improbable areas is very weak at present. The danger is that once an improbable area is accepted on the basis of such weak evidence, one does not even have to produce strong evidence in favor of new improbable areas. Nor is this a hypothetical danger. In justifying their homology of "KO" with V4d, Tootell and Hadjikhani (2001) write: "Although such 'separated' quarter-field representations are conceptually unsatisfying, they are not unprecedented: the quarter-field representations in macaque 'V3' and 'VP' have long been considered separate areas by some investigators, based on empirical differences between V3 and VP" (Burkhalter et al., 1986; Felleman and Van Essen, 1991; Felleman et al., 1997; Van Essen et al., 1986). Yes, by some but not by all (see above). And even if it is accepted by all, the present evidence in favor of areas with just a quarter field representation is still not compelling. To date, at least two ("VP" and "V4v") have already been convincingly knocked out in both the human and the macaque brains (Lyon and Kaas, 2001, 2002; Wade et al., 2002). This does not auger too well for those who want to use the precedent of dubious quarter field representations to hastily erect new ones.

Conclusion

I have already reviewed extensively the early literature on the cortical involvement in color vision, and have tried to show to what extent it was dominated by preconceived notions (Zeki, 1990, 1993). Looking at what has happened since then, it seems that the considerable technological sophistication that is at our disposal for studying the human brain has not been matched by an equal sophistication in thinking about the brain. Where something is improbable, the evidence in its favor should be impeccable. The evidence of the past few years shows, instead, that in studies of cortical color vision, the improbable has imperceptibly become the acceptable and set the precedent for other improbables to become acceptable without the intervention of questioning.

The story of color vision as it relates to the cortex is thus a very sad one. In neurobiology it is indeed, to quote the title of Ford Maddox Ford's book, *The Saddest Story*.

There are, of course, also good things that have happened in our understanding of the role of the cortex in color vision. I will not relate these, but leave it to the commentators on discoveries in cortical color vision to do so.

Acknowledgment

The work of this laboratory is supported by the Wellcome Trust, London.

This review was concluded in January 2002 and has not been revised since.

REFERENCES

- Albright, T. D., 1992. Form-cue invariant motion processing in primate visual cortex, *Science*, 255:1141–1143.
- Allman, J. M., and J. H. Kaas, 1971. A representation of the visual field in the caudal third of the middle temporal gyrus of the owl monkey (*Aotus trivirgatus*), *Brain Res.*, 31:85–105.
- Baker, J. F., S. E. Petersen, W. T. Newsome, and J. M. Allman, 1981. Visual response properties of neurons in four extrastriate areas of the owl monkey (*Aotus trivirgatus*): a quantitative comparison of medial, dorsomedial, dorsolateral, and middle temporal areas, *J. Neurophysiol.*, 45:397–416.
- Bartels, A., and S. Zeki, 2000. The architecture of the colour centre in the human visual brain: new results and a review, *Eur. J. Neurosci.*, 12:172–193.
- Bonin, G. von, and P. Bailey, 1951. *The Isocortex of Man*. Urbana: University of Illinois Press.
- Brodmann, K., 1905. Beiträge zur histologischen Lokalisation der Grosshirnrinde. Dritte Mitteilung: Die Rindenfelder der niederen Affen, *J. Psychol. Neurol. Lpz.*, 4:177–276.
- Brodmann, K., 1909. *Vergleichende Lokalisationslehre der Grosshirnrinde in ihren Prinzipien dargestellt auf Grund des Zellenbaues*, Leipzig: J. A. Barth.
- Burkhalter, A., D. J. Felleman, W. T. Newsome, and D. C. Van Essen, 1986. Anatomical and physiological asymmetries related to visual areas V3 and VP in macaque extrastriate cortex, *Vis. Res.*, 26:63–80.

- Callaway, E. M., 1998. Local circuits in primary visual cortex of the macaque monkey, *Annu. Rev. Neurosci.*, 21:47–74.
- Cavanagh, P., M. A. Henaff, F. Michel, T. Landis, T. Troscianko, and J. Intriligator, 1998. Complete sparing of high contrast color input to motion perception in cortical color blindness, *Nat. Neurosci.*, 1:242–247.
- Cragg, B. G., 1969. The topography of the afferent projections in the circumstriate visual cortex of the monkey studied by the Nauta method, *Vis. Res.*, 9:733–747.
- Damasio, A., T. Yamada, H. Damasio, J. Corbett, and J. McKee, 1980. Central achromatopsia: behavioural, anatomic, and physiologic aspects, *Neurology*, 30:1064–1071.
- De Yoe, E. A., G. J. Carman, P. Bandettini, S. Glickman, J. Wieser, R. Cox, D. Miller, and J. Neitz, 1996. Mapping striate and extrastriate visual areas in human cerebral cortex, *Proc. Natl. Acad. Sci. USA*, 93:2382–2386.
- Dupont, P., B. DeBruyn, R. Vandenberghe, A. M. Rosier, I. Michiels, G. Marchal, L. Mortelmans, and G. A. Orban, 1997. The kinetic occipital region in human visual cortex, *Cereb. Cortex*, 7:283–292.
- Engel, S. A., D. E. Rumelhart, B. A. Wandell, A. T. Lee, G. H. Glover, E. J. Chichilnisky, and M. N. Shaden, 1994. fMRI of human visual cortex, *Nature*, 369:525.
- Felleman, D. J., A. Burkhalter, and D. C. Van Essen, 1997. Cortical connections of areas V3 and VP of macaque monkey extrastriate visual cortex, *J. Comp. Neurol.*, 379:21–47.
- Felleman, D. J., and D. C. Van Essen, 1991. Distributed hierarchical processing in the primate cerebral cortex, *Cereb. Cortex*, 1:1–47.
- Fize, D., W. Vanuffel, K. Nelissen, P. Van Hecke, J. B. Mandeville, R. B. H. Tootell, and G. A. Orban, 2001. Distributed processing of kinetic boundaries in monkeys investigated using fMRI, *Soc. Neurosci. Abstr.*, 11.9.
- Frackowiak, R. S. J., S. Zeki, J. B. Poline, and K. J. Friston, 1996. A critique of a new analysis proposed for functional neuroimaging, *Eur. J. Neurosci.*, 8:2229–2231.
- Geesaman, B. J., and R. A. Andersen, 1996. The analysis of complex motion patterns by form/cue invariant MSTd neurons, *J. Neurosci.*, 16:4716–4732.
- Gegenfurtner, K., 2001. Color in the cortex revisited, *Nat. Neurosci.*, 4:339–340.
- Grill-Spector, K., T. Kushnir, S. Edelman, Y. Itzhak, and R. Malach, 1998. Cue invariant activation in object-related areas of the human occipital lobe, *Neuron*, 21:191–202.
- Gulyas, B., C. A. Heywood, D. A. Popplewell, P. E. Roland, and A. Cowey, 1994. Visual form discrimination from color or motion cues—functional—anatomy by positron emission tomography, *Proc. Natl. Acad. Sci. USA*, 91:9965–9969.
- Hadjikhani, N., A. K. Liu, A. M. Dale, P. Cavanagh, and R. B. H. Tootell, 1998. Retinotopy and color sensitivity in human visual cortical area V8, *Nat. Neurosci.*, 1:235–241.
- Heywood, C., and A. Cowey, 1998. With color in mind, *Nat. Neurosci.*, 1:171–173.
- Kaas, J. H., 1993. The organization of the visual cortex in primates: problems, conclusions and the use of comparative studies in understanding the human brain, in *The Functional Organization of the Human Visual Cortex* (B. Gulyas, D. Ottoson, and P. E. Roland, eds.), Oxford: Pergamon Press, pp. 1–11.
- Kennard, C., M. Lawden, A. B. Morland, and K. H. Ruddock, 1995. Colour identification and colour constancy are impaired in a patient with incomplete achromatopsia associated with prestriate cortical lesions, *Proc. R. Soc. Lond.*, 260:169–175.
- Lennie, P., 1999. Color coding in the cortex, in *Color Vision* (K. R. Gegenfurtner and L. T. Sharpe, eds.), Cambridge: Cambridge University Press, pp. 235–247.
- Lueck, C. J., S. Zeki, K. J. Friston, M. P. Deiber, P. Cope, et al., 1989. The colour centre in the cerebral cortex of man, *Nature*, 340:386–389.
- Lyon, D. C., and J. H. Kaas, 2001. Connectional and architectonic evidence for dorsal and ventral V3, and dorsomedial area in marmoset monkeys, *J. Neurophysiol.*, 21:249–261.
- Lyon, D. C., and J. H. Kaas, 2002. Evidence for a modified V3 with dorsal and ventral halves in macaque monkeys, *Neuron*, 33:453–461.
- McKeefry, D., and S. Zeki, 1997. The position and topography of the human colour centre as revealed by functional magnetic resonance imaging, *Brain*, 120:2229–2242.
- Meadows, J. C., 1974. Disturbed perception of colours associated with localized cerebral lesions, *Brain*, 97:615–632.
- Orban, G. A., P. Dupont, B. DeBruyn, R. Vogels, R. Vandenberghe, and L. Mortelmans, 1995. A motion area in human visual cortex, *Proc. Natl. Acad. Sci. USA*, 92:993–997.
- Pinon, M. C., R. Gattass, and A. P. B. Sousa, 1998. Area V4 in *Cebus* monkey: extent and visuo-topic organization, *Cereb. Cortex*, 8:685–701.
- Press, W. A., A. A. Brewer, R. F. Dougherty, A. R. Wade, and B. A. Wandell, 2001. Visual areas and spatial summation in human visual cortex, *Vis. Res.*, 41:1321–1332.
- Rosa, M. P. G., M. C. Pinon, R. Gattass, and A. P. B. Sousa, 2000. “Third tier” ventral extrastriate cortex in New World monkey, *Cebus apella*, *Exp. Brain Res.*, 132:287–305.
- Sakai, K., E. Watanabe, Y. Onodera, I. Uchida, H. Kato, et al., 1995. Functional mapping of the human colour centre with echo-planar magnetic resonance imaging, *Proc. R. Soc. Lond. B*, 261:89–98.
- Sary, G., R. Vogels, and G. A. Orban, 1993. Cue-invariant shape selectivity of macaque inferior temporal neurons, *Science*, 260:995–997.
- Sereno, M. I., A. M. Dale, J. B. Reppas, K. K. Kwong, J. W. Belliveau, et al., 1995. Borders of multiple visual areas in humans revealed by functional magnetic resonance imaging, *Science*, 268:889–893.
- Shipp, S., J. D. G. Watson, R. S. J. Frackowiak, and S. Zeki, 1995. Retinotopic maps in human prestriate visual cortex: the demarcation of areas V2 and V3, *Neuroimage*, 2:125–132.
- Smith, A. T., M. W. Greenlee, K. D. Singh, F. M. Kraemer, and J. Hennig, 1998. The processing of first- and second-order motion in human visual cortex assessed by functional magnetic resonance imaging (fMRI), *J. Neurosci.*, 18:3816–3830.
- Tootell, R. B. H., and N. Hadjikhani, 2001. Where is “dorsal V4” in human visual cortex? Retinotopic, topographic and functional evidence, *Cereb. Cortex*, 11:298–311.
- Vanduffel, W., D. Fize, K. Nelissen, P. Van Hecke, J. B. Mandeville, R. B. H. Tootell, and G. A. Orban, 2001. Cue-invariant shape processing in the awake fixating monkey: a contrast-agent enhanced fMRI study, *Soc. Neurosci. Abstr.*, 11.10.
- Van Essen, D. C., W. T. Newsome, J. H. R. Maunsell, and J. L. Bixby, 1986. The projections from striate cortex to areas V2 and V3 in the macaque monkey: asymmetries, areal boundaries and patchy connections, *J. Comp. Neurol.*, 244:451–480.
- Van Essen, D. C., and S. M. Zeki, 1978. The topographic organization of rhesus monkey prestriate cortex, *J. Physiol.*, 277:193–226.
- Van Oostend, S., S. Sunaert, P. Van Hecke, G. Marchal, and G. A. Orban, 1997. The kinetic occipital (KO) region in man, an fMRI study, *Cereb. Cortex*, 7:690–701.

- Verrey, L., 1888. Hémichromatopsie droite absolue, *Arch. Ophthalmol. (Paris)*, 8:289–301.
- Wade, A. R., A. A. Brewer, J. W. Rieger, and B. A. Wandell, 2002. Functional measurements of human ventral occipital cortex: retinotopy and color, *Philos. Trans. R. Soc. Lond. B.*, 357:963–973.
- Wandell, B. A., 1999. Computational neuroimaging of human visual cortex, *Annu. Rev. Neurosci.*, 22:145–173.
- Zeki, S. M., 1969. Representation of central visual fields in prestriate cortex of monkey, *Brain Res.*, 14:271–291.
- Zeki, S. M., 1978. The third visual complex of rhesus monkey prestriate cortex, *J. Physiol.*, 277:245–272.
- Zeki, S., 1990. A century of cerebral achromatopsia, *Brain*, 113:1721–1777.
- Zeki, S., 1993. *A Vision of the Brain*, Oxford: Blackwell.
- Zeki, S., J. D. G. Watson, C. J. Lueck, K. J. Friston, C. Kennard, and R. S. J. Frackowiak, 1991. A direct demonstration of functional specialization in human visual cortex, *J. Neurosci.*, 11:641–649.

IX FORM, SHAPE
AND OBJECT
RECOGNITION

68 Spatial Scale in Visual Processing

ROBERT F. HESS

IN THE EARLY 1970s, our views about the nature of visual processing began to change. The default idea, that visual processing produced an image description based on a local feature representation, was being challenged. The new suggestion, which had its origins in visual psychophysics (Campbell and Robson, 1968), was that visual information is analyzed in terms of the amplitude of different Fourier components. According to this approach, information about spatial scale was available to the higher stages of perception and was used in a very specific way. Some found this latter view particularly objectionable because, unlike its applicability to physical optics, neural processes possessed a number of characteristics (nonlinearities and changes in spatial grain with eccentricity) that would potentially render such an analysis inappropriate (Petrov et al., 1980; Westheimer, 1973). However, the issue was developing into one of a more general nature. A slow transition occurred in thinking from the original Fourier proposal to a more general one involving the importance of a local, scale-based spatial analysis. This was essentially a debate about whether perception had access to information separately at each of a number of spatial scales or whether, at an early stage, visual information was rigidly combined across scales for a feature-based analysis. The emerging neurophysiology, which showed that neurons in the striate cortex have receptive fields that could be considered spatial or temporal filters (Campbell et al., 1968, 1969; Glezer et al., 1973; Maffei and Fiorentini, 1973), suggested that, at least at the level of the striate cortex, information could be separately accessed at a range of different spatial scales. Thus, the balance tipped toward the independent scale proposal. However, the more we learn about the properties of cells in extrastriate cortex (Kourtzi and Kanwisher, 2001), the more we realize that scale combination is an essential part of vision. Subsequent work reviewed here suggests a role for both types of analysis: an initial scale-independent process followed by, in some cases, scale combination. The relative roles of each depend on the particular task and stimuli.

History of the multiscale view

The emergence of spatial scale as an important aspect of visual processing came at about the same time from neurophysiological studies of animals and psychophysical studies of humans. In humans, following from the early aerial

reconnaissance work of Selwyn (1948) in England and the applied work of Schade (1956) in the United States, Campbell and Green (1965) began to develop and apply the measurement of contrast sensitivity to better specify human vision. This approach emphasized the importance of visual processing for object sizes larger than the resolution limit.

In particular, the contrast sensitivity function describes the relationship between the size of a stimulus and the contrast necessary to just detect it (i.e., its contrast threshold). The stimulus of choice is a sinusoidal grating (black and white bars with a sinusoidal luminance profile modulated about a mean light level) specified in units of spatial frequency (in cycles per degree subtended at the eye). Such a stimulus allows contrast to be altered without affecting the mean adaptational state of the eyes; the retinal image will also be sinusoidal in form. The form of this relationship is shown in Figure 68.1. Human sensitivity is best at intermediate object sizes (or spatial frequencies) and is reduced at both higher and lower spatial frequencies. Although the optics contributes to the reduction in contrast sensitivity at high spatial frequencies, the majority of the falloff at high spatial frequencies and all of the falloff at low spatial frequencies is due to the sensitivity of neural processes. The contrast sensitivity curve depicted in Figure 68.1 is for foveal viewing and photopic light levels. If stimuli are imaged on more peripheral parts of the field or under scotopic light levels, there is preferential loss of sensitivity at high spatial frequencies as a consequence of the reduced neural sensitivity under these conditions.

The next major advance came when Campbell and Robson (1968), Pantle and Sekular (1968) and Blakemore and Campbell (1969), provided evidence that the contrast sensitivity function was itself composed of a number of more narrowly tuned, independent spatial mechanisms. A series of psychophysical studies followed, outlining the degree to which these *spatial channels*, as they were called, were independent (Graham et al., 1978) and the ways in which they interacted (Graham and Nachmias, 1971).

During this same period, single-cell measurements from different parts of the visual pathway showed that neuronal receptive fields came in various sizes (Hubel and Wiesel, 1959, 1962) and that there was a systematic scaling of receptive field size with eccentricity in the retina and, to some extent, in the cortex (Hubel and Wiesel, 1968). Up to this

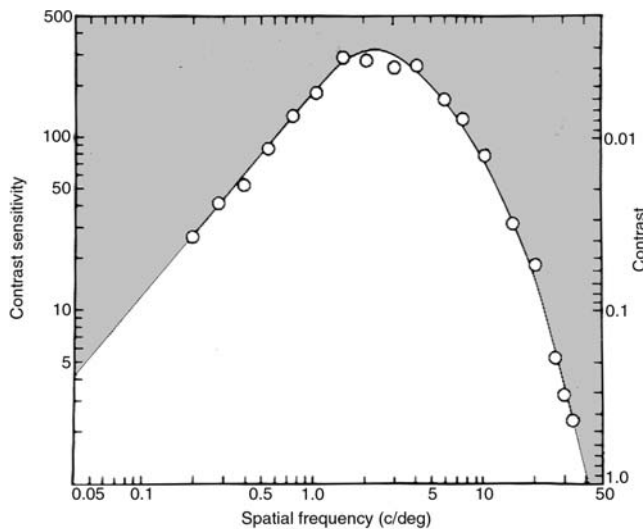


FIGURE 68.1. Contrast sensitivity function for foveal vision under photopic conditions. Contrast sensitivity (the reciprocal of the contrast needed for threshold detection) is plotted against the spatial frequency of a sinusoidal grating stimulus. This overall sensitivity function is itself composed of a set of more spatially restricted mechanisms termed *spatial channels*.

time, neurons were not really considered filters (in the sense that they only transmitted information of a particular spatial scale, just as a green filter attenuates blue and red light and only allows light of intermediate wavelengths to pass through); the prevailing idea was that they encoded certain stimulus features, and that they needed to do this at a range of different sizes. The idea that neurons could be sufficiently linear to be considered filters emerged from the retinal work of Enroth-Cugell and Robson (1966), which was very controversial at the time, beginning to have its main impact only a decade later. The primary visual cortex contains cells that are grouped together along a number of key processing dimensions: orientation, ocular dominance, and spatial frequency. Cells with similar spatial frequency preference are grouped together into domains whose map is locally continuous across V1. The distance between domains conforms to the hypercolumn description of cortical organization (Issa et al., 2000).

The impact of spatial scale on our thinking in vision research is reflected in the different computational approaches (Marr, 1982; Marr and Hildreth, 1980; Marr and Poggio, 1979; Morrone and Burr, 1988; Watt and Morgan, 1985; Wilson and Gelb, 1984; Wilson and Richards, 1989) that have developed subsequent to the work described above. All the models assume an initial spatial decomposition. They differ in the extent of this decomposition and in the level at which the information from these different spatial filters is combined and analyzed. The two extreme versions of this model were captured in Watt and Morgans' MIRAGE Model and Wilson's Line Element

Model. In the MIRAGE model, spatial filters were combined at an early stage, and only symbolic descriptors subsequent to this combination were used (Watt and Morgan, 1985). In the Wilson Line Element Model, later stages of processing had independent access to the output of individual spatial filters, and their outputs were flexibly combined to solve different tasks (Wilson and Gelb, 1984; Wilson and Richards, 1989).

In this chapter, I will give examples of the advantages of accessing information at different spatial scales; these include foveal specialization and visual stability under different light levels. After detailing the evidence for independent access to scale information, I will discuss the scale selection rules. Finally, I will give examples of situations where information at different scales is not kept separate but is combined in specific ways (the scale combination rules).

Scale and the functional specialization of central vision

The relationship between spatial scale and eccentricity has important consequences for visual processing, yet it is poorly understood. Our traditional view of this relationship has been dominated by the measurement of visual acuity and its relationship with eccentricity. Acuity is best at the fovea and deteriorates progressively at more peripheral loci. This is similar to how the receptive field size of retinal ganglion cells changes from fovea to periphery (Crook et al., 1988; de Monasterio and Gouras, 1975; Hubel and Wiesel, 1960). Small receptive fields are confined to the center of the visual field, and progressively larger ones are found in the periphery. In the cortex this situation changes. True, there is gradual enlarging of the average receptive field in regions of the cortex representing more peripheral parts of the visual field. However, at any eccentricity there is a range of sizes of receptive fields. Hubel and Wiesel's (1968) data suggest that this range is about 4/1 in the fovea. A better description is that in more peripheral parts of the visual field, the range of different-sized receptive fields, and by implication the range of spatial scales, is reduced because the number of cells with small receptive fields declines with eccentricity.

Our understanding of how spatial scale varies across eccentricity has been greatly extended by the use of contrast sensitivity measurements for targets of different spatial scale. Numerous investigators have contributed to this understanding. Particularly noteworthy was the study of Robson and Graham (1981), who used stimuli of fixed spatiotemporal bandwidth but well localized in space. They showed that for a wide range of spatial scales, the decline in sensitivity with eccentricity (plotted in absolute units, i.e., in degrees) was linear and depended on spatial scale; the finer the spatial scale, the more rapidly sensitivity fell off with absolute eccentricity. This result is seen in Figure 68.2A,

where contrast sensitivity is plotted against eccentricity in degrees for a range of different spatial frequencies. However, if a relative eccentricity metric (Fig. 68.2B) was used (i.e., measured in periods of the particular spatial scale), then all spatial frequencies within the range 1 to 20 c/deg exhibited a similar falloff; for the vertical meridian, this was found to be 60 periods per decade (contrast sensitivity fell by a decade at an eccentricity equal to 60 periods of a particular spatial frequency).

In a subsequent study, Pointer and Hess (1989) extended Robson and Grahams' approach to spatial frequencies below 1 c/deg. Their results showed that there were three different rules for how spatial scale varied with eccentricity, depending on the spatial range involved. At high to middle spatial frequencies (above 1.6 c/deg), they replicated the previous results of Robson and Graham (1981); the sensitivity gradient was 60 periods per decade. At middle to low spatial fre-

quencies (0.2 to 0.8 c/deg) the decline of sensitivity with relative eccentricity increases (30 periods per decade), and at very low spatial frequencies (0.1 c/degree and below), the decline in sensitivity is much more gradual (90 periods per decade).

From a purely psychophysical viewpoint, the relationship between spatial scale and eccentricity is fairly straightforward. At most spatial scales, sensitivity is best in the fovea, and the extent of this superiority depends on the spatial scale; the finer the spatial scale, the greater the superiority of the fovea. At very coarse scales, sensitivity is the same in the center of the field as it is in the periphery. There is no evidence for either peripheral superiority or foveal inferiority at coarse scales. Thus, at more eccentric loci, the range of spatial filters available to perception is reduced. Most neurophysiologists would not be comfortable with the above view. This is because this is not reflected in how the receptive field properties of neurons vary with eccentricity in primary cortex, where, as I have already said, the size of the average receptive field increases with eccentricity. This is best seen in the population response using functional imaging. Marrett et al. (1997), using an adaptation of the peripheral phase encoding method, showed that in human V1, spatial scale varies inversely with eccentricity; the fovea contains higher spatial scales, the periphery lower ones. However, what one needs to appreciate is that the psychophysical data reflect the potential contribution of all visual areas, not just V1. Area V2 in primate (and area 18 in cat) is known to contain neurons responding to lower spatial scales than V1 (Foster et al., 1985; Issa et al., 2000; Movshon et al., 1978). Extrastriate visual areas generally have larger receptive fields than V1 and sizable foveal representations. What this means is that, by virtue of the additional information provided by these different extrastriate areas, the fovea has access to additional levels of spatial processing at coarser scales, as well as at the extra-fine scales provided by V1. When we think of foveal specialization, we often think in terms of the magnified areal representation of the fovea in the primary visual cortex. Another way in which the fovea is specialized is that it has access, via the contribution of different visual areas, to a larger range of spatial filters than its peripheral counterpart. This provides a great deal of potential flexibility and computational power. It also represents an important economy in terms of processing bandwidth because not all scales need to be represented at all eccentricities.

Scale and light adaptation

One of the most impressive aspects of mammalian vision is the range of light levels over which it operates without greatly sacrificing sensitivity. The usual explanation for this is retinal: the duplex function of the photoreceptors together

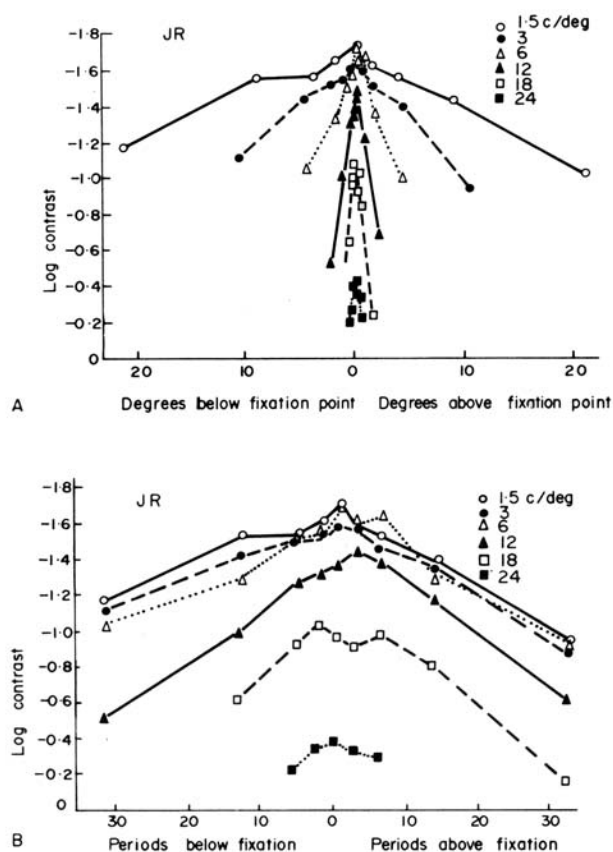


FIGURE 68.2. The regional variation of contrast sensitivity. In *A* and *B*, the results of Robson and Graham (1981) showing how contrast sensitivity for a range of spatial frequencies declines with eccentricity along the vertical meridian. In *A*, the results are plotted against eccentricity in degrees, whereas in *B*, eccentricity is in relative units (periods of the particular spatial frequency). Note that the relative slope (*B*) is the same for all spatial frequencies in the range tested. (Reproduced with permission from Robson and Graham, 1981.)

with gain control in postreceptoral retinal neurons. The fact that information is processed independently across scale, a mainly postretinal phenomenon, also helps extend our visual range and makes a significant contribution to perceptual stability across different light levels.

The relationship between spatial scale and mean light level is best seen in the results of Van Nes and Bouman (1967). They showed that at any one spatial scale there is a characteristic relationship between sensitivity and light level. At low light levels, sensitivity varies as the square root of the light level (so-called De Vries-Rose law) (De Vries, 1943; Rose, 1942, 1948), whereas at higher light levels, sensitivity is independent of the average light level (so-called Weber's law). The light level at which one behavior gives way to another varies with spatial scale. This is shown in Figure 68.3, in which, for a range of spatial frequencies, contrast sensitivity is plotted against the mean retinal illuminance (in trolands). These results suggest that neurons with smaller receptive fields reach this "transition" luminance at higher light levels than those with larger receptive fields. The psychophysics shows that this Rose-De Vries/Weber behavior occurs at all spatial scales.

At the level of the retina, the degree of spatial selectivity also varies with the light level. Enroth-Cugell and Robson (1966) showed that the position of peak responsivity of a neuron shifts to lower spatial frequencies at lower light levels. Curiously, the low-frequency limb of the response function can be in its Weber region when the high-frequency limb is in its De Vries-Rose region. In the cortex, this does not happen. Here the spatial tuning does not alter (either position of peak responsivity or bandwidth); only sensitivity varies with light level. Sensitivity varies in just the way Van

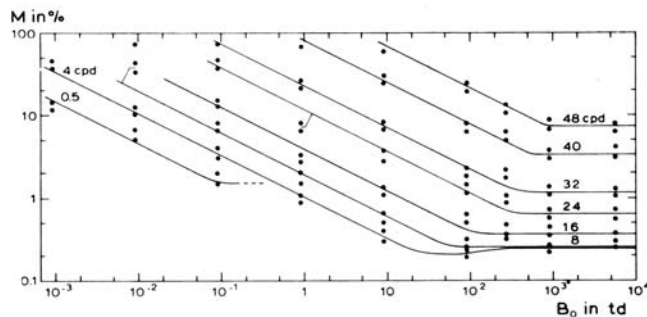


FIGURE 68.3. The scale-independent way in which contrast sensitivity varies with mean light level. The results have been replotted from Van Nes and Bouman (1967). Contrast sensitivity is plotted against the mean retinal illuminance in trolands for a range of different spatial frequencies (listed in the top inset). Each spatial frequency response exhibits two different rules, depending on the mean illuminance: a Weber rule at high light levels and a DeVries-Rose rule at low light levels. The transition from the former to the latter also depends on the mean light level. (Reproduced with permission from Van Nes and Bouman, 1967.)

Nes and Bouman (1967) described in humans. This is true for simple cells and complex cells in area 17 of cat (Hess, 1990; Kaufman and Palmer, 1990). Thus, by the time one gets to the cortex, reducing the light level seems to affect only sensitivity, not the individual spatial and temporal selectivity of neurons. To the extent that we process information independently at different spatial scales, this provides an opportunity for greater stability in our perceptions at reduced light levels. Our perception of spatial and temporal structure, information derived from the output of many filters, is not greatly affected by reducing the light level. For a change in the average light level by three to six orders of magnitude, our perceptions of spatial and temporal frequency are influenced as little as 10% (Hess, 1990). That sort of perceptual stability is remarkable and contributes significantly to our ability to operate effectively over a wide range of light levels.

Evidence for independent scale processing

SCALE AND SPACE

Contrast perception. Many studies have shown that the perceived contrast of a stimulus depends on the contrast of surrounding structures, a phenomenon known as *contrast induction* (Cannon and Fullenkamp, 1991; Chubb et al., 1989; Ejima and Takahashi, 1985; Ellemberg et al., 1998; Klein et al., 1974; Mackay, 1973). Two recent studies have shown that the magnitude of contrast induction depends on the spatial frequency difference between test and inducing stimuli (Chubb et al., 1989; Ellemberg et al., 1998). Chubb et al. (1989) showed that if the spatial frequency composition of test and inducing isotropic textures was 1 octave apart, the apparent contrast dropped from 40% to 15%. Ellemberg et al. (1998) showed a similar effect for single one-dimensional Gabor elements. Solomon et al. (1993) showed that this contrast induction is also tuned for orientation. Thus, it appears that the perceived contrast of an isolated region is determined in part by the contrast in adjacent regions and that this lateral influence is mediated within spatial scale. This is a curious result because one would intuitively expect contrast normalization to be mediated by a spatially and temporally broadband mechanism.

Contrast-defined structure. Objects can be defined in a variety of ways: by modulations in luminance, contrast, chromaticity, motion, and disparity. Human vision is best at detecting luminance modulation (so-called first-order modulation) but can also detect objects defined by contrast modulation (second-order modulation). Indeed, there is evidence that cortical cells can process both types of information at the level of the striate cortex (Baker, 1999; Zhou and Baker, 1993, 1994, 1996). Though there are different ways of mod-

eling the detection of contrast-defined objects, the standard model involves two stages: a linear first stage composed of bandpass spatial filters and a second stage of linear filtering preceded by a rectifying nonlinearity. It has been of interest to know the relationship between the first and second stages of linear filters; for example, do second-stage filters of a particular spatial scale receive the summed input of all first-stage filters? If they do, they would act as generic “texture grabbers” by detecting contrast modulation irrespective of the spatial composition of the texture. This would provide an obvious economy since fewer second-order neurons would be needed to cover all the possibilities of the first-order input. The results, however, suggest the opposite, namely, that spatial information is not collapsed prior to second-stage detection (Dakin and Mareschal, 2000; Graham et al., 1993; Langley et al., 1996). The current neurophysiology also supports this conclusion. Mareschal and Baker (1998) have shown that second-order detectors are tuned for the spatial frequency and, to a lesser extent, for the orientation of their input carrier frequencies. This means that more second-order detectors are required to cover all possibilities for the spatial tuning of their first-order input, but this may not be quite the problem it was once thought to be (Baker, 1999). This is an example of spatial scale being preserved through at least two different stages of visual analysis.

Contour. Recent attempts to understand contour processing have used spatially narrowband elements. Such stimuli allow tests of whether integration occurs between cells with different receptive field properties or between cells with similar receptive field properties. In one approach (Field et al., 1993), each presentation comprises an array of spatially and spatial frequency-localized elements. In one of the two presentations, a subset of these elements are arranged, by virtue of their orientation alignment, to define a contour. When subjects are asked to detect which presentation contains the contour, using a standard two alternate forced-choice psychophysical procedure, performance is found to be at ceiling for straight contours but declines as contour curvature increases (Field et al., 1993).

Another reason for using spatially narrowband elements and limiting the processing to just one scale is because of the properties of natural images (Field, 1993). Consider the orientation structure of a fractal edge at a number of different spatial scales. Unlike smooth edges, fractal edges do not exhibit the same consistency of local orientation across scale, making a number of previously proposed edge detection strategies (Canny, 1983; Lowe, 1988; Marr and Hildreth, 1980) problematic. A fractal edge is continuous at each scale, but the precise position and orientation of the edge change across scales. At any position, the edge may show a particular orientation at only one scale. This may be one good

reason for having cortical neurons with bandpass properties (Field, 1987, 1993; Hayes, 1989).

The above argument, based on the properties of natural images, suggests that it may be important for the visual system to solve the continuity problem separately at each scale, but is there any direct psychophysical support for this conclusion? The stimuli displayed in Figure 68.4*B* provide such a test. Here we are using the same paradigm as described above, except that the display is composed of equal numbers of Gabors and phase-scrambled edges. Phase-scrambled edges are micropatterns composed of $f + 3f + 5f$ compound Gabors in which the relative phases are randomized. When the components are phase-aligned, they produce local edge stimuli. The results in Figures 68.4*C* and 68.4*D* show that when contour elements alternated between Gabors and phase-scrambled edges (as is also the case for the background elements), good performance (*triangles*) was maintained across different spatial scales for the Gabor, scales that were common to the phase-scrambled elements. This suggests that the visual system solves the continuity problem independently at each of a number of spatial scales. Interestingly, this was not the case when Gabors were alternated with phase-aligned edges (*circular symbols*), suggesting the importance of phase alignment in broadband stimuli in determining whether scale combination occurs (Dakin and Hess, 1999). Textures composed of orientation flows have also been shown to exhibit spatial frequency selectivity. Kingdom and Keeble (2000) have shown that texture segmentation for such a task depends on the spatial frequency composition of the local elements, suggesting a scale-selective analysis.

SCALE AND MOTION Historically, there have been two different models of human motion detection, one using information within different spatial scales and the other involving information after it has been combined across spatial scales. The most popular example of the former is the motion energy model (i.e., the oriented energy in the spatiotemporal spectrum) utilizing neurons with receptive fields narrowly tuned for spatial frequency and orientation (Adelson and Bergen, 1985; van Santen and Sperling, 1985; Watson and Ahumada, 1985). A good test of this involves the motion of a spatially filtered broadband stimulus (spatial noise). For two-flash apparent motion, according to the first proposal above, the direction of displacement would be detected independently at a number of different spatial scales. D_{\min} (the smallest displacement detected) would be signaled by the detectors working at the finest spatial scale and ultimately would be limited by the signal-to-noise ratio within these detectors. D_{\max} (the largest displacement detected) would be signaled by the detectors working at the largest scale and ultimately would be limited by their half-cycle limit. An altogether different view (Morgan, 1992; Morgan and Mather,

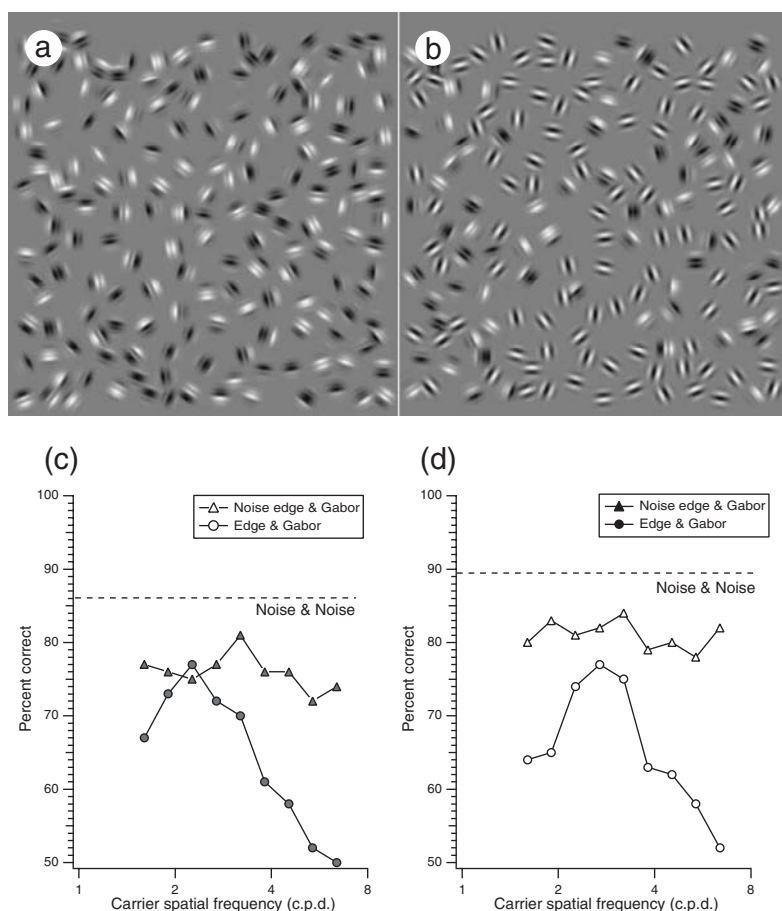


FIGURE 68.4. The scale-independent nature of contour integration. In *a* and *b*, an example of the stimuli are shown in which only a subset of the elements have their local orientation aligned along a notional curved contour. In *a*, all the elements are composed of phase-randomized $f + 3f + 5f$ compound Gabor micropatterns. In *b*, half of the elements are phase-randomized $f + 3f + 5f$ compound Gabor micropatterns and half are Gabor micropatterns having a spatial frequency corresponding to the abscissa in *c* and *d*. In *c* and *d*, psychophysical detection results are given for several different

stimulus conditions. Of particular note is the fact that performance is good across a range of spatial Gabor frequencies when the linking is between the phase-randomized $f + 3f + 5f$ compound Gabor micropatterns and Gabors of a single frequency, indicating that the task can be performed independently within each of several different spatial scales (*triangles*). Note that this is not the case when the compound Gabors exhibit phase coherence (i.e., edges and circles). (Results reproduced with permission from Dakin and Hess, 1999.)

1994) is that the visual system works on the displacements of image features that exist only when information across different spatial scales has been collapsed together by a single spatial filter prior to motion detection.

Initially, the independent scale model of motion was supported by the finding that, at least over part of the range (not at low spatial scales), D_{\max} scaled with the center frequency of bandpass-filtered noise images (Bischof and Di Lollo, 1990, 1991; Chang and Julesz, 1983, 1985; Cleary, 1990; Cleary and Braddick, 1990; Morgan, 1992; Morgan and Mather, 1994). However, this result was equally well described within the feature model of motion because the average separation between image features in bandpass-filtered images also scales with center frequency (Morgan, 1992; Morgan and Mather, 1994). The failure at very low spatial scales was due to the use of white rather than fractal

noise for the broadband stimuli. Fractal noise images (a $1/f$ amplitude spectrum), unlike white noise images (a flat amplitude spectrum) provide comparable energy for octavewide detectors tuned to different spatial scales (Field, 1987). Stimuli composed of white noise do not adequately stimulate visual detectors tuned to low spatial scales compared with those tuned to higher spatial scales. This resulted in the belief that high spatial frequencies interacted with low spatial frequencies for motion (Chang and Julesz, 1983, 1985; Cleary and Braddick, 1990).

Two recent findings, both involving differential spatial filtering between the two frames of a two-flash motion sequence, suggest that the detection of image motion occurs within rather than across spatial scale. The first is the finding that motion can be reliably detected between two image frames so long as there is motion energy within a common

spatial frequency band, suggesting that the visual system has equal access to information across spatial scale (Brady et al., 1997; Ledgeway, 1996). The second finding is that motion can be detected between motion sequences of fractal noise that are differentially low- or highpass filtered (Bex et al., 1995). One frame can be unfiltered; the other, either high-pass or lowpass filtered. This destroys the correlation between the edge structure but maintains information at common scales (Hess et al., 1998). These results are displayed in Figure 68.5 (in *A*, symbols show results for lowpass filtering of one frame; in *B*, symbols show results for high-pass filtering of one frame). The multichannel prediction was generated by assuming that D_{\max} is determined by information carried by the lowest scale supported by the stimulus within the constraints of the half-cycle limit. The spectral characteristics of the spatial noise are again important here. Initial attempts (Morgan and Mather, 1994) with white noise failed because low-frequency mechanisms were severely disadvantaged by the use of white noise stimuli. The use of fractal noise stimuli, which affords similar stimulation of spatial detectors tuned to fine and coarse scales, demonstrates that the detection of motion direction can occur independently at each of several spatial scales. This, of course, does not bear upon exactly what is computed within each of these scales. It could be motion energy (Adelson and Bergen, 1985) or some more scale-localized feature (Eagle, 1996). This is still an open question, one that may be resolved by investigating temporal summation aspects of motion detection.

SCALE AND STEREO The relationship between spatial scale and stereo processing, like that between spatial scale and motion processing, has been controversial. The initial recep-

tive field positional disparity model advanced by Barlow et al. (1967) and by Pettigrew et al. (1968) had no specific role for receptive fields of different size. A much later model, where disparity was encoded not by positional displacements of receptive fields but by phase disparities within receptive fields driven by the right and left eyes (Ohzawa and Freeman, 1986; Ohzawa et al., 1990, 1996), did have a specific link to the spatial properties of individual cells. It relied on high spatial frequency tuned cells processing only fine disparities and low spatial frequency tuned cells processing only coarse disparities (the so-called size-disparity correlation).

Support for such a size-disparity correlation in human stereo processing has not been clear-cut. For example, Schor and Woods (1983) provided the first psychophysical evidence for a size-disparity correlation by measuring the relationship between stereo sensitivity (D_{\min} and D_{\max}) and luminance spatial frequency. For D_{\min} (the lower disparity limit) below a spatial frequency of 2.4 c/deg, stereo thresholds depend directly on the peak luminance spatial frequency of the stimulus, representing a constant phase limit of around 1/36th of a spatial cycle (Fig. 68.6*A*). For D_{\max} (the upper disparity limit), Schor and Woods found a square-root relationship over approximately the same spatial frequency range with an asymptote at around 2.4 c/deg (Fig. 68.6*C*). This suggested that at least for D_{\min} , disparity may have been computed within each of a number of independent spatial scales (Schor et al., 1984).

Later work (Smallman and MacLeod, 1994, 1997) suggested that such a correlation may occur, at least for low-contrast targets, across the whole spatial frequency range including that above 2.4 c/deg. The interpretation of these results in terms of the role of spatial channels in stereo

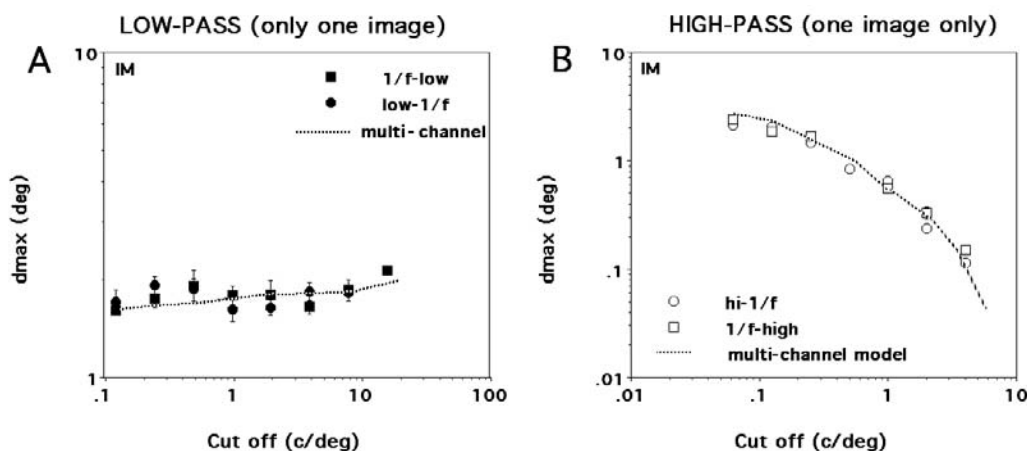


FIGURE 68.5. The effect of spatial scale on the discrimination of motion direction. *A*, Direction discrimination data (symbols) for fractal noise images are seen in two-flask apparent motion when only one of the two frames is subject to spatial filtering. *B*, Results are compared with a multichannel model in which motion direc-

tion is processed independently by channels at a number of different spatial scales and the channel with the highest signal-to-noise ratio determines performance. (Reproduced with permission from Hess et al., 1998.)

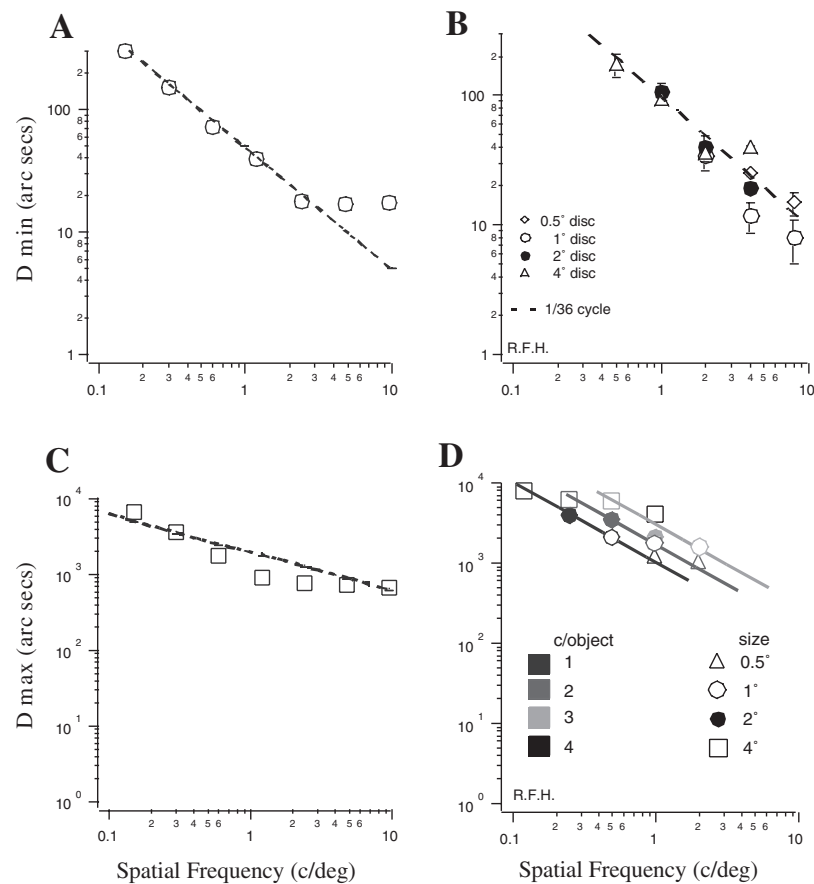


FIGURE 68.6. The scale-dependent nature of local stereo processing. In *A* and *C*, results are replotted from Schor and Woods (1983) for D_{\min} and D_{\max} , respectively, for a one-dimensional band-pass DOG stimulus in which the overall size and peak spatial frequency covary. In *B* and *D*, results for D_{\min} and D_{\max} , respectively,

for two-dimensional bandpass fractal noise stimuli in which overall size and peak spatial frequency have been decoupled (Hess et al., 2002). D_{\min} does scale with the peak spatial frequency of the image irrespective of stimulus size; D_{\max} does not. D_{\max} scales with object frequency, not retinal frequency (D).

processing has been controversial. The above interpretation, that there are spatial frequency mechanisms processing stereoscopic information only below 2.4 c/deg (Schor et al., 1984), has been challenged by the results of Yang and Blake (1991) and Kontsevich and Tyler (1994). Yang and Blake's (1991) masking results and Kontsevich and Tyler's (1994) modeling results argue that only spatial channels above 2.4 c/deg process stereo information. More recently, Glennerster and Parker (1997) questioned the conclusions of Yang and Blake's results, stating that they had not taken into account the overall visibility of the stimuli, and argued instead for multiple spatial mechanisms processing stereo information below 2 c/deg , a result supported by subsequent work (Prince et al., 1998).

In the majority of the above studies (e.g., Fig. 68.6*A*, *C*), the stimulus of choice was a one-dimensional spatially and spatial frequency localized stimulus, a difference of Gaussians (DOGs). One property of such a stimulus is that the peak spatial frequency and overall size of the stimulus covary, leaving one to wonder whether the relationship

described in Figure 68.6*A* is due to stimulus spatial frequency or size. A more general test of the size-disparity correlation would involve the use of broadband fractal stimuli for the reasons outlined above for the comparable case in motion. Such stimuli contain a range of different spatial scales and are not only representative of natural images but also optimal in stimulating different spatial frequency-tuned neurons (Field, 1987). Assuming that the visual system has independent access to an array of spatial frequency-tuned detectors, each responding up to its individual phase disparity limit, there are some clear predictions for how D_{\min} and D_{\max} should vary with low- and highpass filtering of such a broadband stimulus. D_{\min} should be determined by disparity neurons with the highest spatial frequency tuning (assuming that each spatial detector has comparable internal noise) and D_{\max} by the lowest. For D_{\min} , lowpass filtering should reduce stereo performance in a manner corresponding to some fixed fraction of a spatial cycle of the highest spatial frequency channel supported by the stimulus. This fraction will depend on factors such as stimulus contrast

because it represents not only a spatial limit but also a signal-to-noise limit. For the same reason, highpass filtering should have no effect on performance. D_{\max} , on the other hand, which is thought to be a predominantly spatial limit, should be limited by the half-cycle limit of the lowest spatial frequency channel supported by the stimulus. Therefore, it should display a falloff with filter cutoff frequency corresponding to a fixed phase relationship for highpass filtering but no effect for lowpass filtering. These predictions follow from possibly the simplest view of the relationship between spatial frequency-tuned disparity mechanisms: that the channel with the highest signal-to-noise ratio will determine performance. There are, of course, many other possibilities. For example, disparity mechanisms may receive input from the combined output of many spatial channels, and other factors may limit D_{\max} and D_{\min} (e.g., the type of local primitive derived from such a multiscale analysis).

The effect of various types of spatial filtering on stereopsis is seen in Figures 68.6B and 68.6D. Figure 68.6B shows how D_{\min} for a broadband fractal image varies with lowpass filtering (highpass filtering has no effect; data are not presented). Irrespective of the stimulus size (here, spatial frequency and stimulus size have been studied separately), D_{\min} gets progressively worse with progressive lowpass filtering (slope = 1/36th of the period of the highest frequency), bearing out the conclusions of Schor and Woods (1983). Figure 68.6D shows similar results for D_{\max} , but this time in terms of highpass filtering (lowpass filtering has no effect; data are not presented). However, the relationship is now much shallower (square root) than the independent scale prediction (slope of unity), and there is an effect of stimulus size. In fact, D_{\max} seemed to show the scale-dependent prediction (slope of unity) when we compared performance for stimuli not with the same spatial frequency (i.e., cycles/degree) but with the same object frequency (cycles/object), suggesting that it follows the information content of the stimulus rather than a spatial scale limit imposed by the visual system. Although D_{\min} can be thought of as reflecting the activity of the highest spatial frequency-tuned disparity neurons supported by a particular stimulus, D_{\max} cannot. It must involve information combined across scale. The Ohzawa-Freeman (1986) model would work for D_{\min} but not for D_{\max} . A combination of the models of both Ohzawa and Colleagues (1996) and Barlow et al. (1967) might be able to explain both limits.

There is more to stereopsis than the measures D_{\max} and D_{\min} . For example, local stereopsis can support the perception of complex three-dimensional surfaces (Tyler, 1974). Does spatial scale maintain its relevance at this higher level? The answer is yes, at least in some cases. Take the example of two identical sinusoidal surfaces defined by stereo added 180 degrees out of phase (Fig. 68.7). Such a stimulus is difficult to disambiguate when each surface is

made up of an array of micropatterns comprising the mixture of two spatial frequencies (Fig. 68.7A) an octave apart. Yet these surfaces can be disambiguated (Fig. 68.7B) when each surface contains its own exclusive spatial scale (Kingdom et al., 2001). This segregation by spatial scale has obvious ecological relevance because similar objects (e.g., foliage) at different depths will be represented at a different spatial scale, and this difference in scale by itself can aid segregation.

SCALE AND COLOR Any understanding of the relation between chromatic and achromatic processing necessitates an understanding of spatial scale. A comprehensive comparison of spatial processing in chromatic and achromatic vision was made using the contrast sensitivity function (Granger and Heurteley, 1973; Mullen, 1985; Sekiguchi et al., 1993). This showed that the overall spatial sensitivity of mechanisms that process red-green and blue-yellow is very different from that of the achromatic system. Chromatic sensitivity is lowpass, compared with the bandpass response of the achromatic system. Furthermore, although chromatic sensitivity is worse at higher spatial frequencies compared with its achromatic counterpart, its low spatial frequency sensitivity is better. These results are shown in Figure 68.8. Chromatic and achromatic processes work best at complementary spatial scales. Color vision does not provide the sort of detail that achromatic vision is capable of, but it does provide the ability to segment large regions based on subtle color differences.

The spatial properties of the individual mechanisms underlying human chromatic sensitivity are similar to those previously described for achromatic vision, namely, a more narrowly tuned bandpass mechanism extending over the entire range (Bradley et al., 1988; Losada and Mullen, 1994, 1995; Mullen and Losada, 1999). The scale-dependent rules for how sensitivity falls off across the visual field described above for the luminance grating are also relevant to chromatic sensitivity, with the proviso that red-green chromatic sensitivity falls off much more rapidly than its achromatic counterpart (Mullen, 1991). Blue-yellow and red-green cone opponency are distributed differently across the visual field, suggesting different underlying neural constraints (Mullen and Kingdom, 2002). However, this difference, like the above chromatic/achromatic difference, does not itself depend on spatial scale (K. T. Mullen, personal communication).

Scale selection

The ability to be able to process information independently at different scales has some obvious advantages. These involve situations where scales are differentially affected, for example, with reduced luminance levels, peripheral viewing,

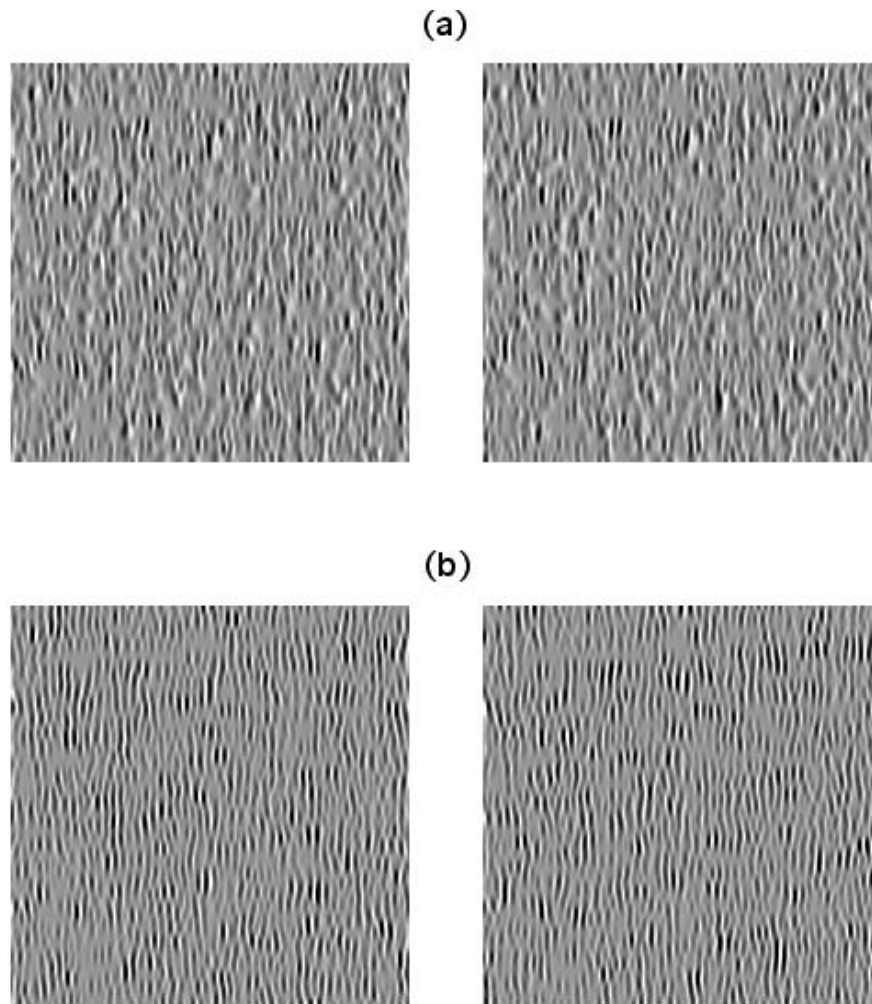


FIGURE 68.7. A scale-dependent example of transparency for global stereopsis. *a* and *b*, Example of dual-surface disparity gratings. Fusion of the two stereo pairs in *a* and *b* results in the percept of an obliquely oriented corrugated structure. This structure is actually composed of two interwoven sinusoidal disparity surfaces added out of phase. In *a*, each surface is composed of Gabor ele-

ments of a single scale, though there is an octave difference in the scale that represents each surface. In this case, the transparent nature of the two surfaces is perceived. In *b*, the Gabors of different scale are not segregated with respect to the surfaces. In this case, transparency is not perceived. (Reproduced with permission from Kingdom et al., 2001.)

motion, stereo, and color. Under these situations, common information derived from multiple scales will be less corrupted and, as a consequence, perceptions will be more stable. This benefit comes at a cost. Firstly, some of the more interesting image features occur only after scale combination; secondly, for information that is carried independently within multiple scales, one has to decide what scale to select and what scale to ignore: the problem of scale selection. Intelligent selection of spatial scale is always better than a dumb combination, but the question is, “What constitutes intelligent selection?” A number of rules have been proposed, each with application to a specific task. These range from selection of the scale with the best signal-to-noise ratio or the least variability to the tracking of filter output features across scale.

Initially, at least for texture tasks, rules were delineated for the selection of features for segregation (Julesz, 1981). Some of these feature rules for textures can be recast as filter selection, especially where the contrast polarity of features is important. A number of suggestions have been made for the selection of the appropriate scale of analysis. For example, within the image processing field, features such as zero crossing from the output of filters of different spatial scale were identified as important markers of image features. In one proposed scale selection rule, these zero crossings were tracked across scale and the highest scale at which they persisted was selected (Witkin and Tennenbaum, 1983). This initial approach, which was successful for one-dimensional features, ran into difficulty in its application to two-dimensional features (Yuille and Poggio, 1986). Another

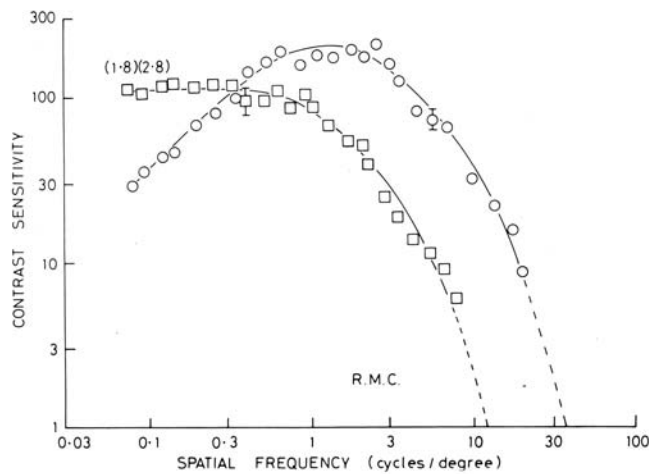


FIGURE 68.8. Spatial scale differences between achromatic and chromatic vision. Contrast sensitivity functions for achromatic and chromatic stimuli show that while the former excels at high spatial frequencies, the latter excels at low spatial frequencies. (Reproduced with permission from Mullen, 1985.)

suggestion was to use the scale with the best signal-to-noise ratio. A number of studies on motion (Bex et al., 1995; Brady et al., 1997; Eagle, 1996; Hess et al., 1998) and stereo (Hess et al., 2002) have assumed this. Malik and Perona (1990) proposed a “leader-takes-all” rule for a texture discrimination task. Elder and Zucker (1998) proposed the use of the minimum reliable scale for edge detection. Finally, Dakin (1997) proposed a statistical rule, the minimization of local orientation variance for a global orientation task.

Evidence for scale combination

Useful information in an image occurs at different scales within the one spatial region as well as at the one scale across different regions. Scale combination may help provide important object-based information in the presence of surface noise (Marr, 1982). Below is a discussion of specific situations where a rigid scale combination has been shown to occur. In some cases, it is not the stimuli but the task that determines whether the visual system combines information across scale or analyzes it separately at each of several scales. An example of the task-dependent nature of scale combi-

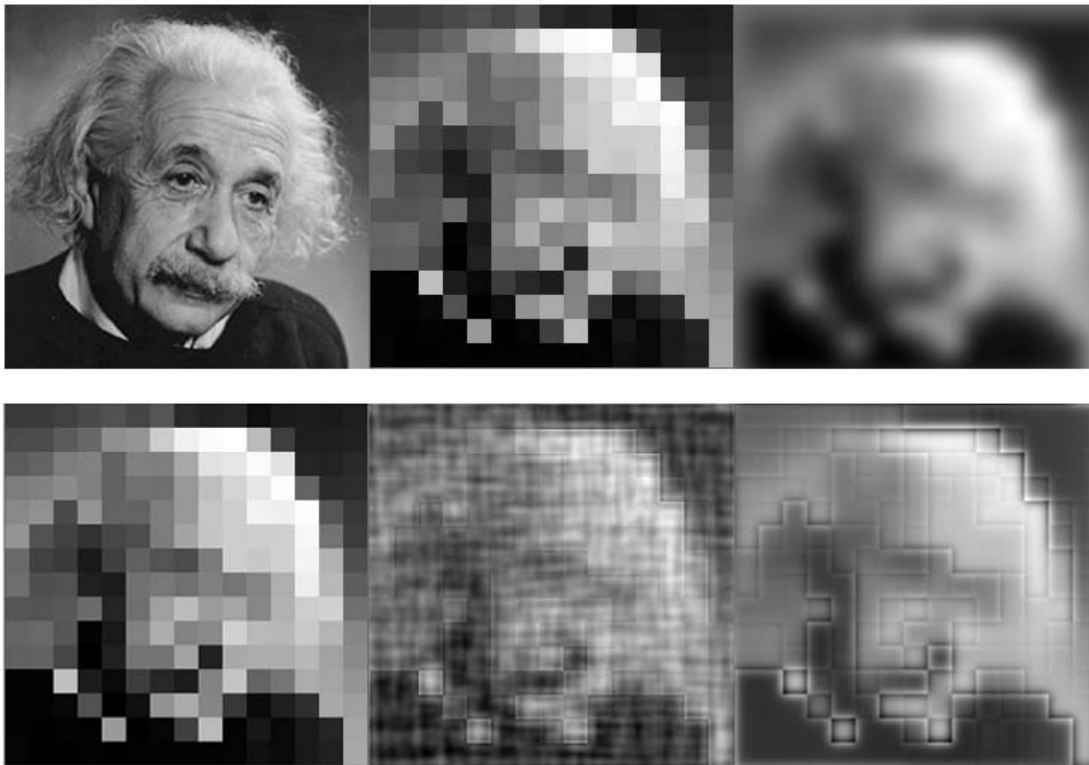


FIGURE 68.9. Object recognition does not occur independently within different scales. In the top frame, recognition is impaired when the image is block-quantized (*top, middle*) and to a much greater extent than expected on the basis of the available low spatial frequency information (*top, right*). This effect was originally thought to be due to critical band masking (Harmon and Julesz,

1973), but adding high frequencies (*bottom, middle*) does not impair performance (Morrone and Burr, 1983) to the same extent as block quantization (*bottom, left*). Flipping the luminance polarity (*bottom, right*) of the original block-quantized edges does aid recognition (Hayes, 1989). (Reproduced with permission from S. C. Dakin.)

nation is in *local* versus *global* discrimination tasks. For both spatial detection (Dakin and Bex, 2001) and motion detection (Bex and Dakin, 2000), it has been shown that at a local level elements are grouped in a scale-dependent way, but at a global level these local groupings are integrated across scale. On the other hand, proposals have been made for a rigid scale combination rule operating from coarse to fine scales. This was originally proposed to solve the correspondence problem for stereo (Marr and Poggio, 1979) but later was transformed into a model of spatiotemporal analysis where progressively finer scales are analyzed at progressively later times (Parker et al., 1997; Watt, 1987).

SPACE Harmon and Julesz (1973) were the first to show that images that are block-quantized are difficult to recognize. Compare Figure 68.9 (*top row*). The low spatial frequency

components shown in the right top figure are also present in the middle top figure but cannot be used to aid recognition. Though at first this was thought to be due to “masking” of the low spatial frequencies by the high spatial frequencies introduced by the quantization, it was later realized that it had more to do with phase continuity across scale (Canny, 1983; Hayes, 1989; Morrone and Burr, 1983). Compare Figure 68.9 (*bottom row*). In the middle bottom figure, additional high spatial frequencies similar to those introduced by blocking are added, but recognition is not so impaired as it is in the bottom left figure. Image identification is restored when the phase relationships are disrupted between the (blocking) high spatial frequencies and the (original) low spatial frequency components of the image. This is seen in Figure 68.9 (*bottom right*) where the phase of the

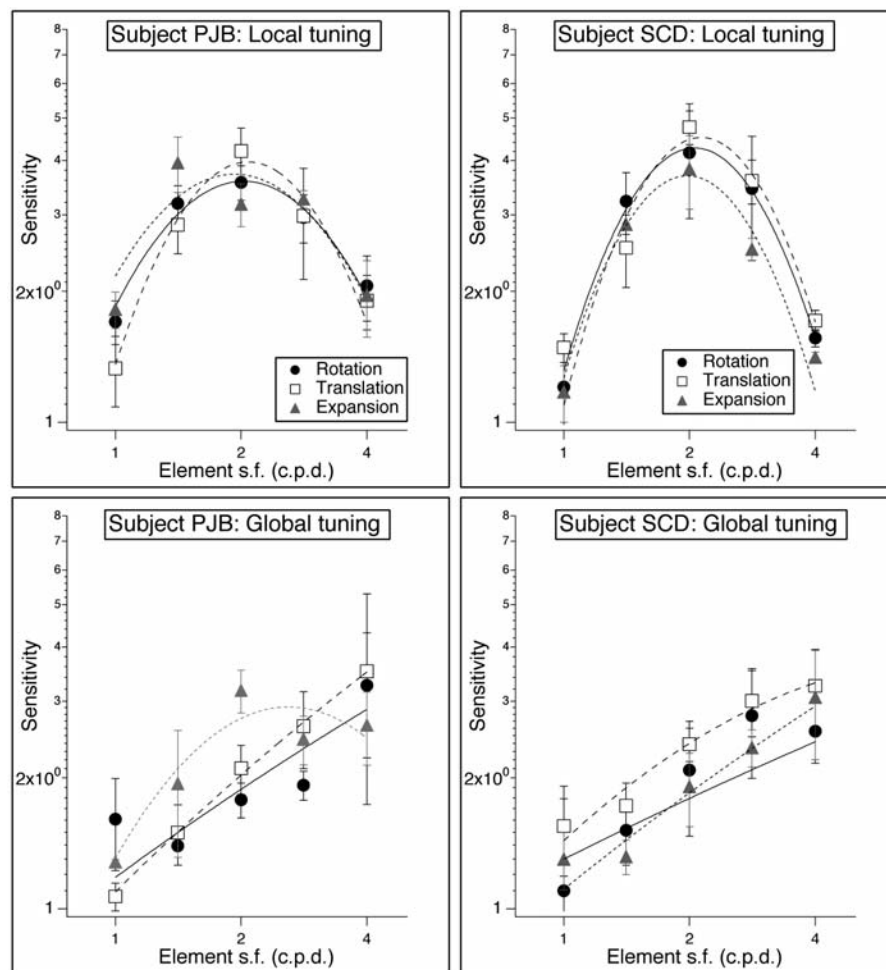


FIGURE 68.10. Spatial frequency tuning of local and global grouping for the recognition of structure in Glass patterns. In the top two frames, local sensitivity (the reciprocal of the signal-to-noise ratio at threshold) is plotted as a function of the spatial frequency of the element paired with a 2c/deg dipole element. Here sensitivity directly reflects the sensitivity of the underlying mechanism.

In the bottom two frames, global sensitivity is plotted as a function of the spatial frequency of a masking stimulus. Here sensitivity is related (inversely to the sensitivity of the underlying mechanism. Local grouping occurs within scale; global grouping occurs across scale. (Reproduced with permission from Dakin and Bex, 2001.)

high-frequency components introduced by blocking has been shifted by 180 degrees; now recognition is easier. If the visual system carried out an independent scale analysis without rigid combination, a block-quantized image should be recognizable via its low spatial frequency components. For example, faces that are blurred are not unrecognizable (Fig. 68.9 (*top right*)). That this is not the case suggests that although processing may initially occur within scale, it is only by combining information across scale that interesting image features can be revealed.

TEXTURE PERCEPTION Glass patterns are visual textures composed of a field of element pairs (dipoles) whose global orientation is determined by a simple geometric transformation (Glass, 1969). These patterns are ideal for looking at scale combination because it has been shown that this task can be performed equally well at a number of independent spatial scales (Dakin, 1997). To detect the global structure in these multielement arrays, observers must perform local grouping at the level of the dipoles in order to detect the local oriented structure and global grouping at the level of the array as a whole in order to combine these local orientation estimates to derive global structure. Dakin and Bex (2001) have shown that the local grouping operation occurs independently at each of a number of spatial scales (i.e., has bandpass tuning), whereas the global grouping combines information across spatial scale (i.e., has lowpass tuning). The spatial tuning results for these two processes are seen in Figure 68.10 for the geometric transformations of rotation, translation, and expansion.

BLUR PERCEPTION Our understanding of how we discriminate blur is still unresolved. There have been a number of different proposals. In some cases (Elder and Zucker, 1998; Field and Brady, 1997; Mather, 1997; Watt and Morgan, 1983), the neural mechanism involved would need to collapse information across spatial scale, whereas in others (Georgeson, 1994), multiscale or single-scale (Elder and Zucker, 1998) processing would suffice.

The straightforward suggestion that blur is signaled by the degree of activity at the highest spatial scale is not correct because we are better at discriminating a change in blur from a reference edge that is already blurred compared with a reference edge that is perfectly sharp (Watt and Morgan, 1983). This implies either that we cannot independently access the highest spatial frequency mechanisms that we possess to signal blur or that we choose not to use it for other reasons (i.e., if the finest scale is too noisy). Watt and Morgan (1983) proposed that there is a rigid combination of filter outputs (MIRAGE model) prior to blur analysis. They suggested that blur is signaled by the distance between adjacent peaks and troughs in the output of a second-derivative filter. Field and Brady (1997) and Mather (1997) proposed that

images look blurred when there is a change in the relative amplitude of detectable structure at different frequencies. To determine this would require a comparison of the activity across rather than solely within scales. Georgeson (1994) proposed (see also Kayargadde and Martens, 1994) another way of computing blur for aperiodic and periodic sinusoids based on a multiscale template model (Georgeson, 2001) in which blur is encoded by finding which of a set of multiscale Gaussian derivative templates best fits the second derivative profile of the edge; this model is simple, multiscale, fits well and (for one-dimensional edges) has no free parameters, and can be readily implemented by simple cells. An important contribution was also made by Elder and Zucker (1998), who used adaptive scale filtering; at each location, the system uses the *smallest reliable scale*, defined by signal-to-noise ratio.

MOTION VELOCITY Even though the early stages of visual processing involve the activity of spatiotemporal separable filters, there is evidence that human discrimination of image motion is in terms of velocity rather than temporal frequency. To achieve this, it is necessary to have filters with inseparable spatiotemporal properties (i.e., having sensitivity envelopes oriented in space-time), necessitating the combination of information across spatial and temporal scales prior to the processing of image velocity. Psychophysical studies have provided evidence for the importance of velocity in motion processing. Thompson (1981) showed that a common metric for motion adaptation was in terms of velocity rather than spatial and temporal frequency. McKee et al. (1986) showed the importance of velocity for the discrimination of image motion. More recently, it has been shown that the visual system integrates information across different orientation bands in a nonselective manner, leading to suboptimal performance in some situations (Schrater et al., 2000). Perrone and Thiele (2001) have provided neurophysiological support for the receptive field properties of neurons at the level of area MT in the extrastriate cortex being oriented in space-time. This suggests that information previously contained within individual spatial and temporal scales in area V1 has been combined at the level of MT to encode velocity.

Combination rules

At some stage within the visual process, for particular tasks, it is advantageous to combine information across spatial scale to derive interesting image features. The type of combination will depend critically on the nature of the image feature. Many different combination rules have been proposed, ranging from “blind” (i.e., indiscriminate) pooling to optimal pooling strategies. The main determinant is the particular feature involved.

For example, if the feature is the global orientation in an image, then it has been shown that information is first collapsed across scale or spatial frequency. Similarly, if the selected feature is the local spatial frequency structure, combination across orientation occurs (Dakin and Bex, 2001; Olzak and Thomas, 1991, 1992; Thomas and Olzak, 1996). There is also evidence that the visual system contains higher-level mechanisms that sum across spatial scale to process the orientation of image features but do not sum across scale to process either the spatial frequency or the contrast of image features (Olzak and Wickens, 1997). If the feature is local velocity, Schrater et al. (2000) have shown that the visual system uses a fixed combination rule over orientation rather than one adapted to the spatial properties of a particular stimulus. Their result is consistent with velocity-tuned detectors that measure the energy in fixed (i.e., blind pooling), orientationally broadband, planar regions of spatiotemporal frequency. If the feature is the global structure in either Glass (Dakin and Bex, 2001) or random-dot kinematograms (Bex and Dakin, 2000), information is combined across spatial scale, with greater weight given to lower spatial frequencies. If the feature is the global perception of plaids composed of two oblique sinusoidal gratings, information is collapsed across orientation prior to edge extraction (Georgeson and Meese, 1997).

A special case of interscale combination occurs for edge features where the combination process is phase sensitive. A number of computational schemes for edge detection exploit this by assessing the correlated activity between filter outputs across scale (Canny, 1983; Georgeson, 1992, 1994; Lowe, 1988; Marr, 1982; Marr and Hildreth, 1980; Morrone and Burr, 1988; Torre and Poggio, 1986). Georgeson and Meese (1997) report that the addition of a $3f$ component, if added in square wave phase to one component of their plaid stimuli, breaks down the previous combination across orientation. The perception of the plaid is now in terms of its components. This suggests that phase-sensitive combination of scale to extract edge features may be a special case and may take precedence over interorientation linking. Dakin and Hess (1999), using a contour integration task between elements with broad- and narrowband spatial properties, also argue that edge extraction may represent a special case and may occur concurrently with or prior to contour integration.

Conclusions

Some have argued that the visual system processes information only within scale, while others have stated that information is processed only across scale by the visual system. However, one can find examples of within- as well as across-scale analysis in vision, and this is quite task dependent. For

some tasks, scale combination occurs at a later stage in visual processing than for others. One example is efficient coding of edges. At the level of the striate cortex, humans have neurons with the appropriate spatial tuning properties to encode edge structure successfully via its harmonic components. However, if edges are an important feature of everyday images and if we want to achieve as sparse a code as possible (Olshausen and Field, 1996, 1997; see also Chapter 108 in this volume), it might be advantageous to also have some hardwired edge-detecting neurons (combination across scale) that would encode such common natural features more sparsely. Having such detectors would not preclude the use of multiscale processing for images with similar spatial frequency components (as edges) but where the phase relations are random (e.g., noise). This is an example of where within-scale and combined-scale analysis could coexist at the same stage of processing and even be capable of competing to accomplish similar tasks.

Initially, the within-scale processing idea was taken to extreme limits by assuming that the visual system did a formal Fourier analysis of the retinal image. This view has now given way to the more moderate proposal that visual information can be processed separately at each of a number of scales within the same region of the field, at least in early parts of the cortical pathway. Understanding this provides predictive power about what limits various types of visual processes. It is, of course, not the full story. In some cases, for example, image velocity encoding, spatial combination is a fundamental part of the extraction of the relevant visual information. Spatial scale is now a fundamental part of our thinking in vision. It is as hazardous to neglect it as it is to be unaware of its limitations.

Acknowledgments

I am grateful to all my collaborators throughout the years for their insight, patience, and understanding and to the Canadian Institutes of Health Research and National Science and Engineering Research Council of Canada for their support. I am grateful to Rebecca Achtman for helping with the illustrations.

REFERENCES

- Adelson, E. H., and J. R. Bergen, 1985. Spatio-temporal energy models for the perception of motion, *J. Opt. Soc. Am. A*, A2:284–299.
- Baker, C. L., Jr., 1999. Central neural mechanisms for detecting second-order motion, *Curr. Opin. Neurobiol.*, 9:461–466.
- Barlow, H. B., C. Blakemore, and J. D. Pettigrew, 1967. The neural mechanism of binocular depth discrimination, *J. Physiol. (Lond.)*, 193:327–342.
- Bex, P. J., N. Brady, et al., 1995. Energetic motion detection, *Nature (Lond.)*, 378:670–672.

- Bex, P. J., and S. C. Dakin, 2000. Narrowband local and broadband global spatial frequency selectivity for motion perception, *Invest. Ophthalmol. Vis. Sci. (Suppl.)*, 41:s545.
- Bischof, E. H., and V. Di Lollo, 1990. Perception of directional sampled motion in relation to displacement and spatial frequency: evidence for a unitary motion system, *Vis. Res.*, 9:1341–1362.
- Bischof, W. F., and V. Di Lollo, 1991. On the half-cycle displacement limit of sampled directional motion, *Vis. Res.*, 31:649–660.
- Blakemore, C., and F. W. Campbell, 1969. On the existence of neurones in the human visual system selectively sensitive to the orientation and size of retinal images, *J. Physiol. (Lond.)*, 203:237–260.
- Bradley, A., E. Switkes, and K. De Valois, 1988. Orientation and spatial frequency selectivity of adaptation to color and luminance gratings, *Vis. Res.*, 28:841–856.
- Brady, N., P. J. Bex, and R. E. Fredericksen, 1997. Independent coding across spatial scales in moving fractal images, *Vis. Res.*, 37:1873–1884.
- Campbell, F. W., and J. G. Robson, 1968. Application of Fourier analysis to the visibility of gratings, *J. Physiol. (Lond.)*, 197:551–566.
- Campbell, F. W., B. Cleland, and C. Enroth Cugell, 1968. The angular selectivity of visual cortical cells to moving gratings, *J. Physiol. (Lond.)*, 198:237–250.
- Campbell, F. W., G. F. Cooper, and C. Enroth Cugell, 1969. The spatial selectivity of the visual cells of the cat, *J. Physiol. (Lond.)*, 203:223–235.
- Campbell, F. W., and D. G. Green, 1965. Optical and retinal factors affecting visual resolution, *J. Physiol. (Lond.)*, 181:576–593.
- Cannon, W. M., and S. C. Fullenkamp, 1991. Spatial interactions in apparent contrast: inhibitory effects among grating patterns of different spatial frequencies, spatial positions and orientations, *Vis. Res.*, 31:1985–1998.
- Canny, J. F., 1983. Finding edges and lines in images. Boston: MIT AI Laboratory Technical Report.
- Chang, J. J., and B. Julesz, 1983. Displacement limits, directional anisotropy and direction versus form discrimination in random dot cinematograms, *Vis. Res.*, 23:639–646.
- Chang, J. J., and B. Julesz, 1985. Cooperative and non-cooperative processes of apparent motion of random dot cinematograms, *Spatial Vis.*, 1:39–41.
- Chubb, C., G. Sperling, and J. A. Solomon, 1989. Texture interactions determine perceived contrast., *Proc. Natl. Acad. Sci. USA*, 86:9631–9635.
- Cleary, R., 1990. Contrast dependence of short range apparent motion, *Vis. Res.*, 30:463–478.
- Cleary, R., and O. J. Braddick, 1990. Direction discrimination for bandpass filtered random dot cinematograms, *Vis. Res.*, 30:303–316.
- Crook, J. M., B. Lange-Malecki, B. B. Lee, and A. Valberg, 1988. Visual resolution of macaque retinal ganglion cells, *J. Physiol. (Lond.)*, 396:205–224.
- Dakin, S. A., 1997. The detection of structure in Glass patterns: psychophysics and computational models, *Vis. Res.*, 37:2227–2259.
- Dakin, S. A., and P. J. Bex, 2001. Local and global visual grouping: tuning for spatial frequency and contrast, *J. Vis.*, 1:99–112.
- Dakin, S. C., and R. F. Hess, 1999. Contour integration and scale combination processes in visual edge detection, *Spatial Vis.*, 12:309–327.
- Dakin, S. C., and I. Mareschal, 2000. Sensitivity to contrast modulation depends on carrier spatial frequency and orientation, *Vis. Res.*, 40:311–329.
- de Monasterio, F. M., and P. Gouras, 1975. Functional properties of ganglion cells in the rhesus monkey retina, *J. Physiol. (Lond.)*, 251:167–195.
- De Vries, H., 1943. The quantum nature of light and its bearing upon the threshold of vision, the differential sensitivity and visual acuity of the eye, *Physica*, 10:553–564.
- Eagle, R. A., 1996. What determines the maximum displacement limit for spatially broadband kinematograms, *J. Opt. Soc. Am. A*, 13:408–418.
- Ejima, Y., and S. Takahashi, 1985. Apparent contrast of a sinusoidal grating in the simultaneous presence of peripheral gratings, *Vis. Res.*, 25:1223–1232.
- Elder, J. H., and S. W. Zucker, 1998. Local scale control for edge detection and blur estimation, *IEEE Trans. Pattern Analysis Machine Intell.*, 20:699–716.
- Ellemberg, D., F. E. Wilkinson, H. R. Wilson, and A. S. Arsenault, 1998. Apparent contrast and spatial frequency of local texture elements, *J. Opt. Soc. Am. A*, 15:1733–1739.
- Enroth-Cugell, C., and J. G. Robson, 1966. The contrast sensitivity of retinal ganglion cells of the cat, *J. Physiol. (Lond.)*, 187:517–552.
- Field, D. J., 1987. Relations between the statistics of natural images and the response properties of cortical cells, *J. Opt. Soc. Am. A*, 4:2379–2394.
- Field, D. J., 1993. Scale-invariance and self-similar “wavelet” transforms: an analysis of natural scenes and mammalian visual systems, in *Wavelets, Fractals and Fourier Transforms* (M. Marge, J. C. R. Hunt, and J. C. Vassilicos, eds.), Oxford: Clarendon Press, pp. 151–193.
- Field, D. J., A. Hayes, and R. F. Hess, 1993. Contour integration by the human visual system: evidence for a local “association field,” *Vis. Res.*, 33:173–193.
- Field, D. J., and N. Brady, 1997. Visual sensitivity, blur and the sources of variability in the amplitude spectra of natural scenes, *Vis. Res.*, 37:3367–3384.
- Foster, K. H., J. P. Gaska, M. Nagler, and D. A. Pollen, 1985. Spatial and temporal frequency selectivity of neurones in visual cortical areas V1 and V2 of the macaque monkey, *J. Physiol. (Lond.)*, 365:331–363.
- Georgeson, M., 1992. Human vision combines oriented filters to compute edges, *Proc. R. Soc. Lond. B*, 249:235–245.
- Georgeson, M. A., 1994. From filters to features: location, orientation, contrast and blur, in *Higher-Order Processing in the Visual System* (CIBA Foundation Symposium 184) (M. J. Morgan ed.), Chichester, UK: Wiley.
- Georgeson, M. A., 2001. Seeing edge blur: receptive fields as multiscale neural templates, presented at the Vision Sciences Conference, Sarasota, FL.
- Georgeson, M. A., and T. S. Meese, 1997. Perception of stationary plaids: the role of spatial filters in edge analysis, *Vis. Res.*, 37:3255–3271.
- Glass, L., 1969. Moiré effects from random dots, *Nature*, 243:578–580.
- Glennerster, A., and A. J. Parker, 1997. Computing stereo channels from masking, *Vis. Res.*, 37:2143–2152.
- Glezer, V. D., A. M. Cooperman, V. A. Ivanov, and T. A. Tscherbach, 1973. Investigation of complex and hyper-complex receptive fields of visual cortex of the cat as spatial frequency filters, *Vis. Res.*, 13:1875–1904.
- Graham, N., and J. Nachmias, 1971. Detection of grating patterns containing two spatial frequencies: a comparison of single channel and multi-channel models, *Vis. Res.*, 11:251–259.

- Graham, N., J. G. Robson, and J. Nachmias, 1978. Grating summation in fovea and periphery, *Vis. Res.*, 18:815–825.
- Graham, N., A. Sutter, and H. Venkatesan, 1993. Spatial frequency and orientation selectivity of simple and complex channels in regional segregation, *Vis. Res.*, 33:1893–1911.
- Granger, E. M., and J. C. Heurley, 1973. Visual chromaticity-modulation transfer function, *J. Opt. Soc. Am.*, 63: 1173–1174.
- Harmon, L. D., and B. Julesz, 1973. Masking in visual recognition: effects of two dimensional filtered noise, *Science*, 180:1194–1197.
- Hayes, A., 1989. Representation by images restricted in resolution and intensity range. Ph.D. thesis, Department of Psychology, University of Western Australia.
- Hess, R. F., 1990. Vision at low light levels: role of spatial, temporal and contrast filters, *Ophthalmol. Physiol. Opt.*, 10:351–359.
- Hess, R. F., P. J. Bex, E. R. Fredericksen, and N. Brady, 1998. Is human motion detection subserved by a single or multiple channel mechanism? *Vis. Res.*, 38:259–266.
- Hess, R. F., H.-C. Liu, and Y. Z. Wang, 2002. Luminance spatial scale and local stereo-sensitivity, *Vis. Res.*, 42:331–342.
- Hubel, D. H., and T. N. Wiesel, 1959. Receptive fields of single neurons in the cat's striate cortex, *J. Physiol. (Lond.)*, 148:574–591.
- Hubel, D. H., and T. N. Wiesel, 1960. Receptive fields of optic nerve fibres in the spider monkey, *J. Physiol. (Lond.)*, 154:572–580.
- Hubel, D. H., and T. N. Wiesel, 1962. Receptive fields, binocular interaction and functional architecture in the cat's visual cortex, *J. Physiol. (Lond.)*, 160:106–154.
- Hubel, D. H., and T. N. Weisel, 1968. Receptive fields and functional architecture of monkey striate cortex, *J. Physiol. (Lond.)*, 195:215–243.
- Issa, N. P., C. Trepel, and M. P. Stryker, 2000. Spatial frequency maps in cat visual cortex, *J. Neurosci.*, 20(22):8504–8514.
- Julesz, B., 1981. Textons, the elements of texture perception, and their interactions, *Nature*, 290:91–97.
- Kaufman, D. A., and L. A. Palmer, 1990. The luminance dependence of the spatiotemporal response of cat striate cortical cells, *Invest. Ophthalmol. Vis. Sci. (Suppl.)*, 31:398.
- Kayargadde V. and J. B. Martens, 1994. Estimation of edge parameters and image blur using polynomial transforms. *CVGIP: Graphical models and image processing*, 56:442–461.
- Kingdom, F. A. A., and D. R. T. Keeble, 2000. Luminance spatial frequency differences facilitate the segmentation of superimposed textures, *Vis. Res.*, 40:1077–1087.
- Kingdom, F. A. A., L. R. Ziegler, and R. F. Hess, 2001. Luminance spatial scale facilitates depth segmentation, *J. Opt. Soc. Am. A*, 18:993–1002.
- Klein, S. A., C. F. Stromeyer, and L. Ganz, 1974. The simultaneous spatial frequency shift: a dissociation between the detection and perception of gratings, *Vis. Res.*, 14:1421–1432.
- Kontsevich, L. L., and C. W. Tyler, 1994. Analysis of stereothresholds for stimuli below 2.5 c/deg, *Vis. Res.*, 34:2317–2329.
- Kourtzi, Z., and N. Kanwisher, 2001. Representation of perceived object shape by the human lateral occipital complex, *Science*, 293:1506–1509.
- Langley, K., D. J. Fleet, and P. B. Hibbard, 1996. Linear filtering precedes non-linear processing in early vision, *Curr. Biol.*, 6:891–896.
- Ledgeway, T., 1996. How similar must the Fourier spectra of the frames of a random dot kinematogram be to support motion perception? *Vis. Res.*, 36:2489–2495.
- Losada, M. A., and K. T. Mullen, 1994. The spatial tuning of chromatic mechanisms identified by simultaneous masking, *Vis. Res.*, 34:331–341.
- Losada, M. A., and K. T. Mullen, 1995. Color and luminance spatial tuning estimated by noise masking in the absence of off-frequency looking, *J. Opt. Soc. Am. A*, 12:250–260.
- Lowe, D. G., 1988. Organization of smooth image curves at multiple spatial scales, in *Proceedings of the Second International Conference on Computer Vision*, New York: IEEE Computer Society Press.
- Mackay, D. M., 1973. Lateral interaction between neural channels sensitive to texture density, *Nature (Lond.)*, 245:159–161.
- Maffei, L., and A. Fiorentini, 1973. The visual cortex as a spatial frequency analyser, *Vis. Res.*, 13:1255–1267.
- Malik, J., and P. Perona, 1990. Preattentive texture discrimination with early visual mechanisms, *J. Opt. Soc. Am. A*, 7:923–932.
- Mareschal, I., and C. L. Baker, 1998. A cortical locus for the processing of contrast-defined contours, *Nat. Neurosci.*, 1:150–154.
- Marr, D., 1982. *Vision*, San Francisco: W. H. Freeman.
- Marr, D., and E. Hildreth, 1980. Theory of edge detection, *Proc. R. Soc. B*, 207:187–217.
- Marr, D., and T. Poggio, 1979. A computational theory of human stereo vision, *Proc. R. Soc. B*, 204:301–328.
- Marrett, S., A. M. Dale, J. D. Mendola, M. I. Sereno, A. K. Liu, and R. B. H. Tootell, 1997. Preferred spatial frequency varies with eccentricity in human visual cortex, *NeuroImage*, 3:157.
- Mather, G., 1997. The use of image blur as a depth cue, *Perception*, 26:1147–1158.
- McKee, S. P., G. H. Silverman, and K. Nakayama, 1986. Precise velocity discrimination despite random variations in temporal frequency and contrast, *Vis. Res.*, 26:609–619.
- Morgan, M. J., 1992. Spatial filtering precedes motion detection, *Nature*, 335:344–346.
- Morgan, M. J., and G. Mather, 1994. Motion discrimination in 2-frame sequences with differing spatial frequency content, *Vis. Res.*, 34:197–208.
- Morrone, M. C., and D. C. Burr, 1983. Added noise restores recognition of coarse quantized images, *Nature*, 305:226–228.
- Morrone, M. C., and D. C. Burr, 1988. Feature detection in human vision: a phase-dependent energy model, *Proc. R. Soc. B*, 235:221–245.
- Movshon, J. A., I. D. Thompson, and D. J. Tolhurst, 1978. Spatial and temporal contrast sensitivity in areas 17 and 18 of the cat's visual cortex, *J. Physiol. (Lond.)*, 283:101–130.
- Mullen, K. T., 1985. The contrast sensitivity of human colour vision to red-green and blue-yellow chromatic gratings, *J. Physiol. (Lond.)*, 359:381–400.
- Mullen, K. T., 1991. Colour vision as a post-receptoral specialization of the central visual field, *Vis. Res.*, 31:119–130.
- Mullen, K. T., and F. A. A. Kingdom, 2002. Differential distribution of red-green and blue-yellow cone opponency across the visual field, *Vis. Neurosci.*, 19:1–10.
- Mullen, K. T., and M. A. Losada, 1999. The spatial tuning of color and luminance peripheral vision measured with notch filtered noise, *Vis. Res.*, 39:721–731.
- Ohzawa, I., G. C. DeAngelis, and R. D. Freeman, 1990. Stereoscopic depth discrimination in the visual cortex: neurones ideally suited as disparity detectors, *Science*, 249:1037–1041.
- Ohzawa, I., G. C. DeAngelis, and R. D. Freeman, 1996. Encoding of binocular disparity by simple cells in cat's visual cortex, *J. Neurophysiol.*, 75:1779–1805.
- Ohzawa, I., and R. D. Freeman, 1986. The binocular organization of simple cells in cat striate cortex, *J. Neurophysiol.*, 56:221–242.
- Olshausen, B. A., and D. J. Field, 1996. Emergence of simple-cell receptive field properties by learning a sparse code for natural images, *Nature*, 381:607–609.

- Olshausen, B. A., and D. J. Field, 1997. Sparse coding with an overcomplete basis set: a strategy employed by V1? *Vis. Res.*, 37:3311–3325.
- Olzak, L. A., and J. P. Thomas, 1991. When orthogonal orientations are not processed independently, *Vis. Res.*, 31:51–57.
- Olzak, L. A., and J. P. Thomas, 1992. Configural effects constrain Fourier models of pattern discrimination, *Vis. Res.*, 32:1885–1898.
- Olzak, L. A., and T. D. Wickens, 1997. Discrimination of complex patterns: orientation information is integrated across spatial scale; spatial frequency and contrast information are not, *Perception*, 26:1101–1120.
- Pantle, A., and R. Sekular, 1968. Size detecting mechanisms in human vision, *Science*, 62:1146–1148.
- Parker, D. M., J. R. Lishman, and J. Hughes, 1997. Evidence for the view that spatiotemporal integration in vision is temporally anisotropic, *Perception*, 26:1169–1180.
- Perrone, J. A., and A. Thiele, 2001. Speed skills: measuring the visual speed analysing properties of primate MT neurons, *Nat. Neurosci.*, 4:526–532.
- Petrov, A. P., I. N. Pigarev, and G. M. Zenkin, 1980. Some evidence against Fourier analysis as a function of the receptive fields in cat's striate cortex, *Vis. Res.*, 20:1023–1025.
- Pettigrew, J. D., T. Nikara, and P. O. Beshop, 1968. Binocular interaction on single units in cat striate cortex: simultaneous stimulation by single moving slit with receptive fields in correspondence, *Exp. Brain Res.*, 6:394–410.
- Pointer, J. S., and R. F. Hess, 1989. The contrast sensitivity gradient across the human visual field: emphasis on the low spatial frequency range, *Vis. Res.*, 29:1133–1151.
- Prince, S. J. D., R. A. Eagle, and B. J. Rogers, 1998. Contrast masking reveals spatial-frequency channels in stereopsis, *Perception*, 27:1345–1355.
- Robson, J. G., and N. Graham, 1981. Probability summation and regional variation in contrast sensitivity across the visual field, *Vis. Res.*, 21:409–418.
- Rose, A., 1942. Quantum and noise limitations of the visual process, *J. Opt. Soc. Am.*, 43:715–725.
- Rose, A., 1948. The sensitivity performance of the human eye on an absolute scale, *J. Opt. Soc. Am.*, 38:196–208.
- Schade, O. H., 1956. Optical and photo-electric analog of the eye, *J. Opt. Soc. Am.*, 46:721–739.
- Schor, C. M., and I. C. Woods, 1983. Disparity range for local stereopsis as a function of luminance spatial frequency, *Vis. Res.*, 23:1649–1654.
- Schor, C. M., I. C. Woods, and J. Ogawa, 1984. Binocular sensory fusion is limited by spatial resolution, *Vis. Res.*, 24:661–665.
- Schrater, P. R., D. C. Knill, and E. P. Simoncelli, 2000. Mechanisms of visual motion detection, *Nat. Neurosci.*, 3:64–68.
- Sekiguchi, N., D. R. Williams, and D. H. Brainard, 1993. Aberration-free measurements of the visibility of isoluminant gratings, *J. Opt. Soc. Am. A.*, 10:2105–2117.
- Selwyn, E. W. H., 1948. The photographic and visual resolving power of lenses, *Photo. J.*, 88:6–12, 46–57.
- Smallman, H. S., and D. I. A. MacLeod, 1994. Size-disparity correlation in stereopsis at contrast threshold, *J. Opt. Soc. Am.*, 11:2169–2183.
- Smallman, H. S., and D. I. A. MacLeod, 1997. Spatial scale interactions in stereosensitivity and the neural representation of binocular disparity, *Perception*, 26:977–994.
- Solomon, J. A., G. Sperling, and C. Chubb, 1993. The lateral inhibition of perceived contrast is indifferent to on-center/off-center segregation, but specific to orientation, *Vis. Res.*, 33:2671–2683.
- Thomas, J. P., and L. A. Olzak, 1996. Uncertainty experiments support the roles of second order mechanisms in spatial frequency and orientation discriminations, *J. Opt. Soc. Am. A*, 13: 689–696.
- Thompson, P., 1981. Velocity after-effects: the effects of adapting to moving stimuli on the perception of subsequently seen moving stimuli, *Vis. Res.*, 21:337–345.
- Torre, V., and T. A. Poggio, 1986. On edge detection, *IEEE Trans. Pattern Analysis and Machine Intell.*, 8:147–163.
- Tyler, C. W., 1974. Depth perception in disparity gratings, *Nature (Lond.)*, 251:140–142.
- Van Nes, F. L., and M. A. Bouman, 1967. Spatial modulation transfer in the human eye, *J. Opt. Soc. Am.*, 57:401–406.
- van Santen, J. P. H., and G. Sperling, 1985. Elaborated Reichardt detectors, *J. Opt. Soc. Am. A*, 2:300–321.
- Watson, A. B., and A. J. Ahumada, 1985. Model of human visual motion sensing, *J. Opt. Soc. Am. A*, 2:322–341.
- Watt, R. J., 1987. Scanning from coarse to fine spatial-scales in the human visual system after the onset of the stimulus, *J. Opt. Soc. Am. A*, 4:2006–2021.
- Watt, R. J., and M. J. Morgan, 1983. The recognition and representation of edge blur: evidence for spatial primitives in human vision, *Vis. Res.*, 23:1465–1477.
- Watt, R. J., and M. J. Morgan, 1985. A theory of the primitive spatial code in human vision, *Vis. Res.*, 25:1661–1674.
- Westheimer, G., 1973. Fourier analysis of vision, *Invest. Ophthalmol. Vis. Sci.*, 12:86–87.
- Wilson, H. R., and D. Gelb, 1984. Modified line-element theory for spatial-frequency and width discrimination, *J. Opt. Soc. Am. A*, 1:124–131.
- Wilson, H. R., and W. A. Richards, 1989. Mechanisms of contour curvature discrimination, *J. Opt. Soc. Am. A*, 6:106–115.
- Witkin, A., and J. Tennenbaum, 1983. On the role of structure in vision, in *Human and Machine Vision* (J. Beck, B. Hope, and A. Rosenfeld, eds.), London: Academic Press.
- Yang, Y., and R. Blake, 1991. Spatial frequency tuning of human stereopsis, *Vis. Res.*, 31:1177–1189.
- Yuille, A. L., and T. Poggio, 1986. Scaling theorems for zero-crossings, *IEEE Trans. Pattern Analysis Machine Intell.*, 8:15–25.
- Zhou, Y. X., and C. L. Baker, Jr., 1993. A processing stream in mammalian visual cortex neurons for non-Fourier responses, *Science*, 261:98–101.
- Zhou, Y. X., and C. L. Baker, Jr., 1994. Envelope-responsive neurons in areas 17 and 18 of cat, *J. Neurophysiol.*, 72:2134–2150.
- Zhou, Y. X., and C. L. Baker, Jr., 1996. Spatial properties of envelope-responsive cells in area 17 and 18 neurons of the cat, *J. Neurophysiol.*, 75:1038–1050.

69 Spatial Channels in Vision and Spatial Pooling

HUGH R. WILSON AND FRANCES WILKINSON

THE CONCEPT OF SPATIAL channels in vision seems to have arisen from an early analogy to the auditory system. In audition it was known from the work of von Békésy (reviewed 1960) and others that the curve plotting auditory thresholds as a function of temporal frequency was in fact the envelope of many narrower tuning curves, each reflecting the response of hair cells at a particular locus along the basilar membrane. Once cosine gratings were introduced into vision by Schade (1958), it became possible to measure the spatial contrast sensitivity function (CSF; see Chapter 68), which plots the relationship between visual sensitivity (reciprocal of threshold contrast) and spatial frequency. The analogy then became obvious and begged to be tested: if spatial frequency in cycles per degree is analogous to auditory temporal frequency in hertz, then perhaps the CSF might also represent the envelope of many more narrowly tuned visual channels, just as in the case of auditory thresholds. Indeed, Campbell and Robson (1968), who pioneered the exploration of spatial channels in vision, set out to study vision by exploring this analogy to audition. As is now well known, they and others subsequently confirmed that the visual system contains multiple spatial channels, each tuned to a narrower range of spatial frequencies and orientations than the visual system as a whole. Furthermore, these channels can now be rather closely linked to responses of orientation-selective neurons in primary visual cortex (V1).

Early studies of spatial channels were based upon two assumptions. First, it was assumed that each channel was linear once the stimulus was strong enough to surpass a threshold value. Second, it was assumed that the channels processed visual information in parallel and independently of one another. Both of these assumptions have crumbled in recent years, and numerous studies have shown that linearity and independence are at best true only at the detection threshold. The demise of channel independence resulted from four major discoveries: contrast gain controls, collinear summation, low-level perceptual learning, and spatial pooling. Accordingly, this chapter will first review the major evidence leading to a characterization of spatial channels in vision. Against this background, modifications necessitated by these four major discoveries will be introduced.

The contemporary channel concept thus becomes one in which visual analyses on multiple spatial scales are integrated through nonlinearity and spatial pooling to begin the extraction of visual information relevant to texture, form, motion, and depth perception. The links to these different forms of perception cannot be developed fully here, but the interested reader will find these connections discussed elsewhere (Wilson and Wilkinson, 1997).

Evidence for spatial channels

Following the auditory analogy, Campbell and Robson (1968) measured detection thresholds for cosine gratings as a function of spatial frequency. At low temporal frequencies, the data (plotted as sensitivities which are reciprocals of threshold contrasts) describe a bandpass function, the CSF, with a peak at about 3 to 5 c/deg (Fig. 69.1). A convenient mathematical description of the CSF as a function of spatial frequency ω is given by Wilson and Giese (1977):

$$CSF(\omega) = M\omega^\alpha \exp(-\omega/f) \quad (1)$$

where the peak frequency can easily be shown to be $\omega = \alpha f$. For low temporal frequency presentations, $\alpha \sim 1$, $M = 150$, and $f = 5$ gives a good approximation to typical CSF data, and this function is plotted in Figure 69.1. Data obtained under transient or high temporal frequency conditions produce values of $\alpha \sim 0.4$.

To test the idea that the CSF might represent the envelope of many more narrowly tuned channels, Campbell and Robson (1968) conducted a summation experiment. Their logic was simple: measure the threshold for a complex spatial pattern composed of many widely separated spatial frequencies. If that threshold was simply a weighted sum of the thresholds for the individual components, the CSF must describe the properties of a single spatial channel that summed all spatial frequencies proportionately. If, however, the complex pattern reached threshold only when one of its spatial frequency components reached threshold independently, then the CSF must be the envelope of many spatial channels tuned to narrow ranges of spatial frequencies. The data, obtained using square wave gratings, were unambiguous: the visual system did not add up all spatial frequencies

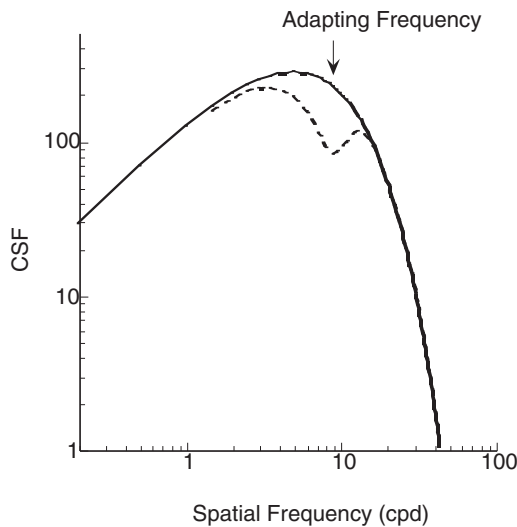


FIGURE 69.1. Typical CSF for sine wave gratings presented at low temporal frequency. The solid curve is from equation 1. The dashed notch depicts the effect of adaptation to the spatial frequency indicated.

equally but rather behaved like a bank of independent spatial channels, each sensitive to a different range of spatial frequencies.

In the wake of this discovery, which supported the analogy to audition, the race was on to characterize the spatial frequency bandwidths of individual channels. The earliest approach employed spatial frequency adaptation, and results were published almost simultaneously by Pantle and Sekuler (1968) and Blakemore and Campbell (1969). In this technique, subjects viewed a high-contrast grating of fixed spatial frequency ω for several minutes, moving their eyes across the bars to minimize conventional afterimage formation. Measurement of the CSF after this adaptation period revealed a notch of depressed sensitivities centered on ω , as illustrated in Figure 69.1. Bandwidth estimates based on the adaptation technique fell in the 1 to 2 octave range. (One octave is a factor of 2; 2 octaves are a factor of 4; so n octaves are a factor of 2^n .) Thus, adaptation studies suggested that spatial frequencies differing by a factor of 2 to 4 would be processed by independent spatial channels. Strong support for this range was provided by the classic study of Graham and Nachmias (1971), who showed convincingly that spatial frequencies differing by a factor of 3 (i.e., 1.6 octaves) were processed independently at threshold.

The subsequent 14 years saw many attempts to measure spatial channel bandwidths more precisely using a variety of techniques. Several approaches using a technique known as *subthreshold summation* produced bandwidth estimates as narrow as 0.33 octave (Kulikowski and King-Smith, 1973; Sachs et al., 1971). Subsequent work, however, showed that these figures were artifactually narrowed as a consequence of the spatial beat pattern that occurs when cosine gratings

of very similar spatial frequencies are added together (see Wilson, 1991, and Wilson and Wilkinson, 1997, for further discussion).

An oblique masking technique that was not subject to these problems was developed in our laboratory (Wilson et al., 1983). High-contrast masking gratings oriented at an angle of 15 degrees from vertical were superimposed on vertical test patterns with a 1 octave bandwidth (sixth spatial derivatives of Gaussians, D6s). In masking experiments the threshold elevation is defined as the ratio of the test pattern threshold in the presence of the masking grating to the test threshold measured with no mask present, so a threshold elevation of 1.0 would indicate that the mask had no effect on the test. In our experiments, the spatial frequencies of both test D6s and masking gratings were varied in half-octave steps from 0.25 up to 22.6 c/deg so that every test D6 was paired with a wide range of mask spatial frequencies. The resulting 14 threshold elevation curves, each obtained with a different D6 test spatial frequency, were fit quantitatively with a set of just six underlying visual channels tuned to peak frequencies of 0.8, 2.0, 2.8, 4.0, 8.0, and 16.0 c/deg (Wilson et al., 1983). The spatial frequency tuning curves for four of these visual channels are plotted in Figure 69.2. Note that the envelope of these curves describes the CSF fairly well. Although the notion of just six visual channels in the fovea remains controversial, it is nevertheless true that these six suffice to encode all of the spatial frequency information present in the stimulus; more than six channels would be redundant. Furthermore, shifting peak channel sensitivities to lower spatial frequencies in the visual periphery produces an effective continuum of channel tunings across the visual system (Swanson and Wilson, 1985).

In a subsequent experiment, Phillips and Wilson (1984) used masking to measure orientation bandwidths, and these were found to vary from ± 30 degrees at half amplitude for the lowest spatial frequencies down to ± 15 degrees for the highest spatial frequency mechanisms. These estimates of both spatial frequency and orientation bandwidths obtained by masking were in good quantitative agreement with bandwidths of single neurons in macaque area V1 as measured by De Valois et al. (1982). A graph comparing both spatial frequency and orientation bandwidths in macaques and humans can be found elsewhere (Wilson, 1991). The two-dimensional spatial receptive fields, $RF(x, y)$, of these visual channels could be well described using combinations of Gaussian functions

$$RF(x, y) = A\{\exp(-x^2/\sigma_1^2) - B\exp(-x^2/\sigma_2^2) + C\exp(-x^2/\sigma_3^2)\}\exp(-y^2/\sigma_y^2) \quad (2)$$

and a table of the various constants can be found in Wilson (1991). Furthermore, the fact that both spatial frequency and orientation bandwidths decrease with increasing peak frequency indicates that spatial processing by the visual system

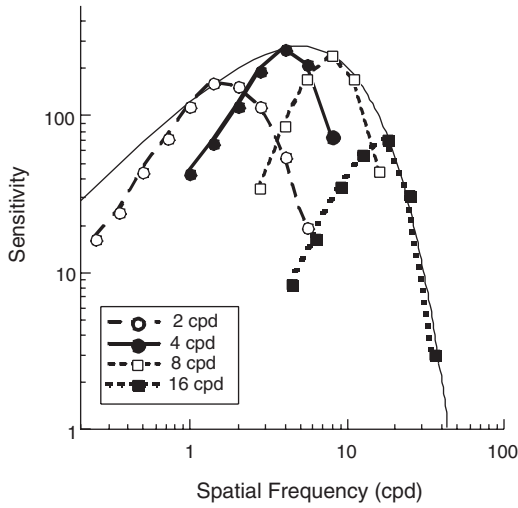


FIGURE 69.2. CSF with four underlying spatial frequency selective visual channels. The channels are most sensitive at 2, 4, 8, and 16 c/deg, and their envelope provides a good fit to the CSF above about 0.75 c/deg. (Data from Wilson et al., 1983.)

cannot be accurately described by a wavelet transform. Indeed, visual channels are performing neither a wavelet nor a Fourier transform (Wilson and Wilkinson, 1997). Rather, the data corroborate the early hypothesis of Thomas (1970) that visual channels reflect properties of cortical receptive fields of varying size and preferred orientation.

In order to infer the tuning curves in Figure 69.2, it was necessary to determine how masking varied with mask contrast. In a pioneering study, Nachmias and Sansbury (1974) had shown that threshold elevations due to masking were described by the “dipper-shaped” function of mask contrast depicted in Figure 69.3. As mask contrast increased from zero, test pattern thresholds initially decreased by a factor of about 2. At higher mask contrasts, however, test pattern thresholds rose substantially, resulting in large threshold elevations. Nachmias and Sansbury suggested that the masking dipper function reflected properties of a contrast nonlinearity in visual channels that was accelerating at subthreshold contrasts but compressive at suprathreshold contrasts. A suitable form for this function was found to be

$$F(C) = \frac{MC^{N+\epsilon}}{\alpha^N + C^N} \quad (3)$$

where M and α are constants. Typically, $2 \leq N \leq 4$, and $\epsilon \sim 0.5$ (Wilson, 1980; Wilson et al., 1983). Note that if $\epsilon = 0$, this is just a Naka-Rushton (1966) function of the type that has been successfully used to describe the responses of V1 cortical neurons (Albrecht and Hamilton, 1982; Sclar et al., 1990; see Chapter 47). This contrast nonlinearity generates the dipper function in Figure 69.3 on the assumption that contrast increments at threshold, Δ , are defined by the relation

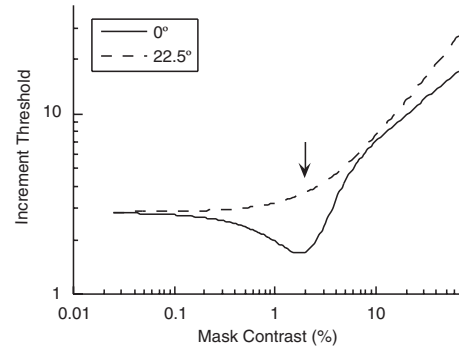


FIGURE 69.3. Typical contrast increment threshold functions. The solid curve illustrates grating contrast increment thresholds as a function of mask grating contrast when mask and test gratings are at the same orientation, 0 degrees. Note the characteristic dip at the location of the arrow, which was first reported by Nachmias and Sansbury (1974). The dashed line shows the effect of a masking grating at an angle of 22.5 degrees relative to the test grating. As reported by Foley (1994), the dip disappears in this case.

$$F(C + \Delta) - F(C) = 1 \quad (4)$$

Masking data were corrected for this contrast nonlinearity to obtain the tuning curves plotted in Figure 69.2 (Wilson et al., 1983).

This completes a brief historic review of visual channels as they were understood around 1990 (Graham, 1989; Wilson, 1991). To predict the response of an array of psychophysically defined cortical neurons, the receptive field description in equation 2 was first convolved with the luminance profile of the stimulus. Following this, the nonlinearity in equation 3 was applied pointwise to the convolution result to produce an estimate of neural responses to the pattern in question (see Wilson, 1991, for details). Thus, visual channels were assumed to process the retinal image entirely independently and in parallel. As we shall see, this formulation was radically altered by research during the subsequent decade.

Contrast gain controls

The first challenge to independent channels came from theoretical work on contrast gain controls by Heeger (1992). Heeger’s gain control model was originally designed to describe responses of V1 simple cells, but here we shall adapt it to the discussion of visual channels defined psychophysically. The first novel idea in this model is that the function in equation 3 does not represent a static nonlinearity in each independent channel. Instead, it represents a combination of two processes that evolve over time. The first of these is an accelerating nonlinear response of each channel to its optimal stimulus, which we shall take to be of the form C^N (Heeger focused on the special case $N = 2$). The second process is nonlinear feedback that produces the denomina-

tor in equation 3 when the system reaches the steady state. To see how this works in the simplest case, where only the i th channel is stimulated by a pattern of contrast C_i , consider the following pair of equations which describe the temporal response R_i of the i th channel as well as the response of the gain control signal G :

$$\begin{aligned}\frac{dR_i}{dt} &= -R_i + \frac{C_i^N}{\sigma^N} (M - G) \\ \frac{dG}{dt} &= -G + R_i\end{aligned}\quad (4)$$

These form a pair of coupled, nonlinear differential equations describing a feedback loop from R_i to G and then back to R_i . The first equation is cast in the form of conduction dynamics similar to those in the Hodgkin-Huxley equations (see Carandini et al., 1999; Wilson, 1999).

The dynamics in equation 4 are implicit in Heeger's (1992) model, which focused on the steady state or equilibrium solution. The steady state is obtained by setting $dR_i/dt = 0$ and $dG/dt = 0$ and then solving the simultaneous algebraic equations (Wilson, 1999). The solution to the second equation, $G = R_i$, can be substituted into the first to yield the following expression for R_i :

$$R_i = \frac{MC_i^N}{\sigma^N + C_i^N} \quad (5)$$

This is just a Naka-Rushton (1966) function with a form very similar to equation 3. In equation 5, however, the denominator arises as a result of the nonlinear feedback process described by equation 4, so the nonlinearity is dynamic rather than static.

The second, and even more important idea in Heeger's (1992) model is that the feedback should incorporate not just R_i , but also a sum of responses across orientations and a range of spatial frequencies. To implement this, Heeger postulated that the steady state of such a network would be

$$R_i = \frac{MC_i^{N+\epsilon}}{\sigma^N + \sum_j C_j^N} \quad (6)$$

where the summation ranges across all orientations and a range of spatial frequencies. In Heeger's cortical cell model $\epsilon = 0$, but as already noted, $\epsilon > 0$ for psychophysical channels. (It should be mentioned that this expression is easy to derive for the equilibrium of a feedforward network, but it is an approximation for feedback networks.) Equation 6 indicates that the response of each visual channel is normalized by the sum of the stimuli to a wide range of visual channels, hence the concept of a gain control. The implication is that *visual channels subject to a gain control are not independent*. Rather, they are coupled through the divisive nonlinearity in the denominator of equation 6.

A critical psychophysical test of equation 6 was performed by Foley (1994). Foley masked vertical cosine gratings with

cosine gratings at a range of different orientations. When vertical masks were used with vertical test gratings, threshold elevations as a function of mask contrast produced the characteristic dipper function illustrated by the solid line in Figure 69.3. When the masking grating orientation fell outside the bandwidth of the channel responding to the test grating, however, the dipper disappeared and the data assumed the shape of the dashed curve in Figure 69.3. This result is predicted by equation 6, and in fact, the curves in Figure 69.3 were generated from the equation. The static nonlinearity in equation 3, however, predicts that masks outside the orientation bandwidth should have no effect at all. Thus, Foley's (1994) study provided crucial support for the form of Heeger's (1992) contrast gain control mechanism embodied in equation 6, which links channels through a divisive pooling process.

Physiological support for contrast gain controls in V1 was first reported by Bonds (1989, 1991). He showed that V1 neurons could be actively inhibited by gratings outside their orientation bandwidth. Furthermore, this inhibition served to sharpen the orientation tuning of individual neurons. This implies that contrast gain controls in V1 play an active role in the formation of cortical-oriented receptive fields, a point to be amplified below.

Collinear facilitation

In addition to gain controls, another line of research has provided evidence for a different type of functional interaction among visual channels. This research was pioneered by Polat and Sagi (1993, 1994). Instead of masking a target pattern with a superimposed mask, they chose to separate the mask spatially from the target. Based on preliminary experiments, both test and mask patterns were Gabor functions with a space constant λ equal to the wavelength of the dominant spatial frequency:

$$G(x, y) = \cos(2\pi x/\lambda) \exp(-(x^2 + y^2)/\lambda^2) \quad (7)$$

Polat and Sagi (1993, 1994) used spatial configurations comprising two mask Gabors flanking a central target Gabor, as depicted in Figure 69.4. Threshold elevations for the central Gabor were then measured as a function of the separation of the masking Gabors in multiples of λ . For a value of $\lambda = 0.075$ degree (spatial frequency of 13.3 c/deg), Polat and Sagi (1993) found that the mask reduced the threshold of the target Gabor by about 50% when the mask was separated by 3λ to 4λ . This facilitation by the mask, however, was largely specific to the configuration in Figure 69.4A (separation of 4λ), as little or no target facilitation was found when the mask orientations were varied by 30 degrees, as in Figure 69.4B. A subsequent study showed that when both target and mask Gabors were oriented 45 degrees away from the line connecting the centers of the patterns, as in Figure 69.4C, there was again almost no facilitation of the

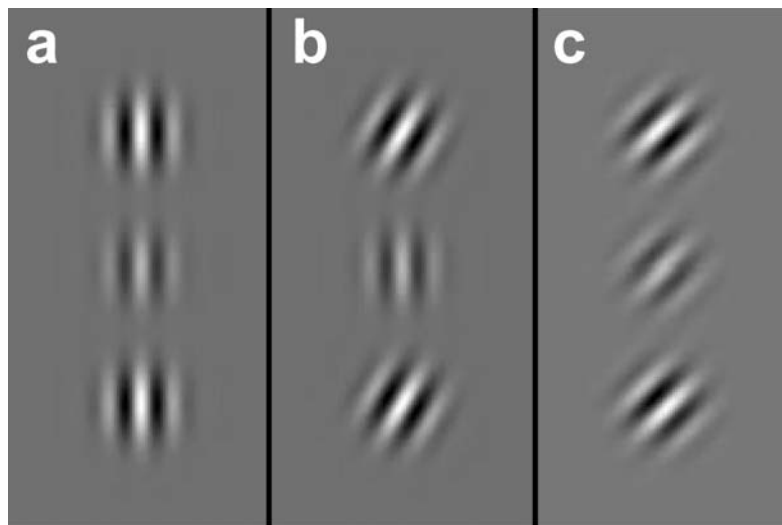


FIGURE 69.4. Spatial configurations of Gabor patches used in studies by Polat and Sagi (1993, 1994). Thresholds were measured for the central patch as a function of the orientation of the top and bottom flanking patches. Significant facilitation (threshold

decrease) was found in condition *a*, where the patches form a collinear configuration. Configurations *b* and *c*, which lack collinearity, failed to produce significant facilitation.

target Gabor (Polat and Sagi, 1994). Control experiments showed that this pattern of results did not depend on either the spatial frequency of the Gabors or their absolute orientations.

These experiments clearly indicate that there is lateral facilitation among orientation-selective visual channels that are spatially aligned along their preferred orientation, as in Figure 69.4A. Neither spatial alignment alone (Fig. 69.4B) nor orientation alignment away from the common spatial alignment (Fig. 69.4C) generates facilitation. This pattern of results provides clear evidence for *collinear facilitation*: lateral spatial facilitation along a line defined by a channel's preferred orientation.

Several further studies have also provided evidence for collinear facilitation. Field et al. (1993) studied contours defined by chains of Gabor functions embedded in a random field of Gabors. They showed that subjects could detect these contours only when the Gabors defining the contour were either collinear or tangent to smooth curves. From this they inferred the existence of a recurrent *association field* linking spatially adjacent visual channels with similar orientations (Chapter 70). Similarly, Kovács and Julesz (1993) argued that collinear facilitation could explain the salience of Gabor-defined circular contours in Gabor background noise. Finally, Wilson et al. (2001) demonstrated that dominance waves in binocular rivalry travel faster around an annulus of concentric contour than they do around an annulus of radial contour. This wave speed increase was interpreted as resulting from collinear facilitation. Anatomical and physiological evidence supports the existence of connections mediating collinear facilitation in primary visual

cortex. Studies on both cats and monkeys in several laboratories have shown that long-range excitatory connections preferentially occur between orientation columns having the same preferred orientation and an approximately collinear spatial arrangement (Das and Gilbert, 1995; Malach et al., 1993; Polat et al., 1998).

Collinear facilitation provides yet another indication that visual channels do not process the retinal image independently. Rather, they interact via long-range excitatory connections to enhance contour salience. Furthermore, collinear facilitation demonstrates that visual channels cannot be fully described by oriented visual filters such as that in equation 2. Rather, orientation selectivity itself is now thought to result in part from the action of recurrent collinear connections (Vidyasagar et al., 1996), and several recent V1 models have implemented this idea in detail (McLaughlin et al., 2000; Somers et al., 1998). The picture of visual channels that has emerged comprises a network of excitatory and inhibitory neurons like those diagrammed in Figure 69.5. Each gray patch represents a local neural ensemble containing multiple oriented units (only three are shown for clarity). All of these provide excitation to an inhibitory gain control neuron I, which in turn provides divisive feedback inhibition to the oriented units. In addition, oriented units in ensembles at different spatial locations form mutual long-range excitatory connections, provided that their locations are collinear. Several of these collinear connections are depicted by the double-headed arrows between identical orientations in different local networks. This figure captures the salient aspects of visual channel structure as understood today.

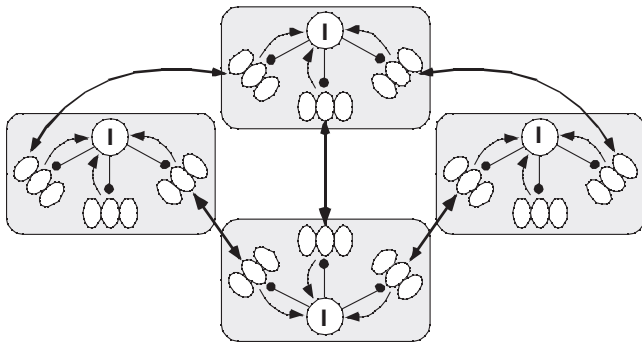


FIGURE 69.5. Schematic network for V1 channel interactions. Local modules enclosed by gray rectangles incorporate gain controls that link channels with different preferred orientations (only three are shown for clarity) via inhibitory feedback from neurons I. Facilitation is depicted by the arrows between modules linking channels with similar preferred orientations that are collinear in space. Both collinear facilitation and divisive gain control circuits contribute to channel orientation selectivity.

Perceptual learning

The description of visual channels in terms of oriented filters (equation 2) implies that these filters have fixed properties resulting from some combination of genetics and early visual development. As discussed in the previous two sections, however, visual filter characteristics are now known to reflect network interactions including contrast gain controls and collinear facilitation. If this is the case and connections (synapses) in these networks could be modified by experience, then it would be predicted that visual filters could be changed as a result of perceptual learning. A model of early synaptic modification resulting from perceptual experience was first proposed in the context of spatial frequency adaptation (Wilson, 1975), where it was shown that changes in inhibitory connection strengths based on a Hebbian correlation rule would produce appropriate changes in visual filter shapes.

Early experimental evidence for visual improvement resulting from perceptual learning was provided by Ball and Sekuler (1982). They trained subjects on discrimination of motion direction and found that subjects' performance improved over time. Furthermore, the improvements were specific to the direction of motion used during training and lasted for at least 10 weeks. These data are consistent with the hypothesis that bandwidths of direction-selective neurons become narrower as a result of training, thereby reducing direction discrimination thresholds.

The hypothesis that visual channel bandwidths are narrowed as a result of perceptual learning was tested directly by Saarinen and Levi (1995). McKee and Westheimer (1978) had already demonstrated that vernier acuity could be improved about twofold with extensive training. To deter-

mine whether such vernier improvements resulted from narrowing of orientation bandwidths, Saarinen and Levi first measured orientation bandwidths using a masking paradigm; then they trained subjects on a vernier task until perceptual learning occurred. Subsequent measurement of orientation bandwidths revealed that they had indeed become narrower by about a factor of 2, and the degree of narrowing correlated well with the extent of individual improvement on the vernier task.

Reference to Figure 69.5 suggests two ways in which synaptic modification might cause sharpening of channel bandwidths. One possibility would be an increase in the strength of synapses mediating collinear facilitation between oriented units that were simultaneously activated during training. However, such excitatory synaptic facilitation would have to be tempered by some form of inhibitory gain control increase to prevent runaway facilitation from triggering seizure-like activity such as migraine auras. An alternative model for the alteration of channel orientation bandwidths involves selective increases in the strength of inhibitory synapses in the local gain control circuits (Wilson and Humanski, 1993). Increases in inhibition from neighboring orientations in the model serve to sharpen the orientation tuning of the remaining units (which can also account for the tilt aftereffect). It is most likely, however, that a combination of excitatory and inhibitory synaptic modifications underlies perceptual learning, but further work will be required to elucidate the details.

Spatial pooling

While collinear facilitation may occur along nearly abutting contours in densely populated arrays of oriented elements, there is ample evidence that close juxtaposition of visual information may also interfere with the processing of individual elements. This problem is particularly marked in the visual periphery, where the phenomenon is known as *lateral masking*.

Early studies of lateral masking typically employed letters or other complex elements, and the loss of processing ability in the periphery under conditions of element proximity or crowding was viewed as masking or interference. Clearly, lateral interactions can interfere with perceptual processing in situations in which individual visual elements provide different and essential information (as in letter strings making up words). However, in the presence of an intact fovea, such a test situation is highly artificial in that an individual would normally fixate to place such stimuli on the fovea where such lateral interaction does not occur or is greatly reduced. Only in abnormal conditions such as amblyopia is crowding a problem in foveal vision. This raises the possibility that lateral masking in the periphery actually represents the

pooling or combination of information either as a means of economy of processing or for some other purpose. For example, when the elements are repetitive, lateral masking may reflect a trade-off of detailed local information in exchange for the encoding of global stimulus properties. Thus, a visual texture may, based on its global statistical properties, be appreciated as coarse or sparse, of high or low luminance and contrast, periodic or random without detailed knowledge of the fine structure of each component element. Wilkinson et al. (1997) demonstrated that discrimination thresholds in the periphery are elevated for three properties of a target Gabor element—contrast, spatial frequency, and orientation—when placed in the center of an array of similar elements, and proposed that their data could be explained if complex cells with large receptive fields pooled the input of several subunits. Consistent with the notion that this pooling might be involved in texture analysis were the later findings of this group (Ellemberg et al., 1998) that not only discrimination thresholds, but also the percept of Gabor contrast and spatial frequency were affected by proximity, again suggesting pooling. Altered perceived contrast and contrast discrimination thresholds have also been reported by Snowden and Hammett (1998) using gratings in an annular format; they too reported much stronger effects in the periphery than in the fovea. These authors proposed that this surround masking is just a more general case of pattern masking. However, a more recent study (Parkes et al., 2001) on orientation masking provided evidence that local orientation signals from target and surround stimuli are combined in a way that reflects contributions of the individual elements rather than suppression or masking of the central target information by the surrounding distractors. Thus, some form of weighted pooling is supported. Interestingly, these authors also demonstrated that pooling can occur in the fovea when the subject does not have prior information about the location of a target in an array, suggesting that focal attention may be able to drive a switch from pooling to nonpooling in foveal vision.

In this context, it is interesting to note that unpublished work on texture perception from our lab (Wilkinson and Peterson, 1989) provides evidence that the visual system may be organized to process global texture and local feature information in parallel from the parafovea and fovea, respectively. Textural judgments based on full-field stimuli were comparable to those based on parafoveal stimulation alone but not on foveal stimulation alone. This implies that when visually inspecting a textured surface, we may be encoding the contrast, granularity, and other global features through parafoveal pooling at the same time that we use our foveas to discern that nature of the texture's components. This possibility certainly merits further experimental investigation.

Higher-level pooling

Work in several laboratories over the past few years has provided strong evidence that as patterned input is channeled up through the visual pathways, there is increasing pooling of information across spatial channels. This is clearly the case in both the motion and form domains; here we restrict our summary to the latter. From the earliest work on the stimulus preferences of neurons in higher cortical areas such as inferotemporal cortex (Gross et al., 1972), it has been evident that information conveyed through the simple spatial channels of this discussion must be pooled in complex combinations at higher levels in order to represent objects of such complexity as faces. However, until recently there was little available evidence as to the stages of this process beyond the recognition of a hierarchical anatomical organization with abundant cross-talk between levels. In a series of recent psychophysical studies (Wilson and Wilkinson, 1998; Wilson et al., 1997), we have demonstrated that information is summed across orientations in highly specific configural ways to extract various global structures from the retinal input (ellipses, radial configurations). Functional imaging work from our laboratories (Wilkinson et al., 2000) provides converging evidence with human event-related potentials (Allison et al., 1999) and primate single unit electrophysiology (Gallant et al., 1993) pointing to cortical area V4 as a crucial intermediate level of processing where such pooling occurs.

Discussion

A decade ago, visual channels were viewed as a rigid basis set of oriented, spatial frequency tuned filters that processed the retinal image independently and in parallel. Over the past 10 years, channel independence has completely dissolved, to be replaced by a model in which channel properties emerge from a network of excitatory and inhibitory interactions epitomized by collinear facilitation and divisive contrast gain controls. These networks are also malleable in their connectivity, as manifested by perceptual learning. Furthermore, there is now evidence that spatial pooling of channel outputs at higher cortical levels represents a subsequent processing stage in which visual shapes are extracted from the input and measured.

Granted that excitatory and inhibitory interactions mediate channel properties, let us consider their functional significance. Contrast gain controls produced by divisive feedback serve to correct the neural representation of an image for variations in stimulus contrast. The fact that humans can recognize a face in sharp directional lighting as well as in diffuse, almost foggy conditions attests to the effectiveness of contrast gain controls. Collinear facilitation pro-

duced by weak long-range excitatory feedback serves to bind continuous contours together and enhance their salience as a prelude to further processing. Collinear facilitation does not, however, contribute to the *measurement* of object geometry. In peripheral vision, channel responses are pooled to extract statistical characteristics of visual textures. Finally, configural pooling extracts significant geometric shapes (ellipses, radial structure) from the retinal image and begins their measurement.

Current research is driven by the hypothesis that channel interactions evolved to perform important computations for shape analysis in form vision. In closing, we mention two challenging but unresolved issues concerning the role of multiple spatial frequency channels in vision. One likely function of interactions across spatial frequency scales is to maintain size constancy. It seems likely that pooling to extract shape information occurs in parallel on several spatial scales. Inhibition and subsequent pooling across scales could then produce neural units able to respond to a shape independent of size. A second possibility is that lower spatial frequencies provide context for the incorporation of object details encoded at higher spatial frequencies. These and other aspects of visual channel interactions provide a rich source of research hypotheses for the future.

REFERENCES

- Albrecht, D. G., and D. B. Hamilton, 1982. Striate cortex of monkey and cat: contrast response function, *J. Neurophysiol.*, 48:217–237.
- Allison, T., A. Puce, D. D. Spencer, and G. McCarthy, 1999. Electrophysiological studies of human face perception. I: potentials generated in occipitotemporal cortex by face and non-face stimuli, *Cereb. Cortex*, 9:415–430.
- Ball, K., and R. Sekuler, 1982. A specific and enduring improvement in visual motion discrimination, *Science*, 218:697–698.
- Blakemore, C., and F. W. Campbell, 1969. On the existence of neurones in the human visual system selectively sensitive to the orientation and size of retinal images, *J. Physiol.*, 203:237–260.
- Bonds, A. B., 1989. Role of inhibition in the specification of orientation selectivity of cells in the cat striate cortex, *Vis. Neurosci.*, 2:41–55.
- Bonds, A. B., 1991. Temporal dynamics of contrast gain in single cells of the cat striate cortex, *Vis. Neurosci.*, 6:239–255.
- Campbell, F. W., and J. G. Robson, 1968. Application of Fourier analysis to the visibility of gratings, *J. Physiol.*, 197:551–566.
- Carandini, M., D. J. Heeger, and J. A. Movshon, 1999. Linearity and gain control in V1 simple cells, in *Cerebral Cortex*, vol. 13, *Models of Cortical Circuitry* (P. S. Ulinski and E. G. Jones, eds.), New York: Plenum, pp. 401–443.
- Das, A., and C. D. Gilbert, 1995. Long range cortical connections and their role in cortical reorganization revealed by optical recording of cat primary visual cortex, *Nature*, 375:780–784.
- De Valois, R. L., D. G. Albrecht, and L. G. Thorell, 1982. Spatial frequency selectivity of cells in macaque visual cortex, *Vis. Res.*, 22:545–559.
- Ellemberg, D., F. Wilkinson, H. R. Wilson, and A. S. Arsenault, 1998. Apparent contrast and spatial frequency of local texture elements, *J. Opt. Soc. Am. A*, 15:1733–1739.
- Field, D. J., A. Hayes, and R. F. Hess, 1993. Contour integration by the human visual system: evidence for a local “association field,” *Vis. Res.*, 33:173–193.
- Foley, J. M., 1994. Human luminance pattern vision mechanisms: masking experiments require a new model, *J. Opt. Soc. Am. A*, 1710–1719.
- Gallant, J. L., J. Braun, and D. C. Van Essen, 1993. Selectivity for polar, hyperbolic, and Cartesian gratings in macaque visual cortex, *Science*, 259:100–103.
- Graham, N., 1989. *Visual Pattern Analyzers*, New York: Oxford University Press.
- Graham, N., and J. Nachmias, 1971. Detection of grating patterns containing two spatial frequencies: a comparison of single-channel and multiple-channel models, *Vis. Res.*, 11:251–259.
- Gross, C. G., C. E. Rocha-Miranda, and D. B. Bender, 1972. Visual properties of neurons in inferotemporal cortex of the macaque, *J. Neurophysiol.*, 35:96–111.
- Heeger, D. J., 1992. Normalization of cell responses in cat striate cortex, *Vis. Neurosci.*, 9:181–197.
- Kovács, I., and B. Julesz, 1993. A closed curve is much more than an incomplete one: effect of closure in figure-ground segmentation, *Proc. Natl. Acad. Sci. USA*, 90:7495–7497.
- Kulikowski, J. J., and P. E. King-Smith, 1973. Spatial arrangement of line, edge, and grating detectors revealed by subthreshold summation, *Vis. Res.*, 13:1455–1478.
- Malach, R., Y. Amir, M. Harel, and A. Grinvald, 1993. Relationship between intrinsic connections and functional architecture revealed by optical imaging and in vivo targeted biocytin injections in primary striate cortex, *Proc. Natl. Acad. Sci. USA*, 90:10469–10473.
- McKee, S. P., and G. Westheimer, 1978. Improvement in vernier acuity with practice, *Percept. Psychophys.*, 24:258–262.
- McLaughlin, D. C., R. Shapley, J. Shelley, and D. J. Wiesel, 2000. A neuronal network model for macaque primary visual cortex (V1): orientation selectivity and dynamics in the input layer 4Ca, *Proc. Natl. Acad. Sci. USA*, 97:8087–8092.
- Nachmias, J., and R. V. Sansbury, 1974. Grating contrast: discrimination may be better than detection, *Vis. Res.*, 14:1039–1042.
- Naka, K. I., and W. A. Rushton, 1966. S-potentials from colour units in the retina of fish, *J. Physiol.*, 185:584–599.
- Pantle, A., and R. Sekuler, 1968. Size detecting mechanisms in human vision, *Science*, 162:1146–1148.
- Parkes, L., J. Lund, A. Angelucci, J. A. Solomon, and M. Morgan, 2001. Compulsory averaging of crowded orientation signals in human vision, *Nat. Neurosci.*, 4:739–744.
- Phillips, G. C., and H. R. Wilson, 1984. Orientation bandwidths of spatial mechanisms measured by masking, *J. Opt. Soc. Am. A*, 1:226–232.
- Polat, U., K. Mizobe, M. W. Pettet, T. Kasamatsu, and A. M. Norcia, 1998. Collinear stimuli regulate visual responses depending on cell's contrast threshold, *Nature*, 391:580–584.
- Polat, U., and D. Sagi, 1993. Lateral interactions between spatial channels: suppression and facilitation revealed by lateral masking experiments, *Vis. Res.*, 33:993–999.
- Polat, U., and D. Sagi, 1994. The architecture of perceptual spatial interactions, *Vis. Res.*, 34:73–78.
- Saarienen, J., and D. M. Levi, 1995. Perceptual learning in vernier acuity: what is learned? *Vis. Res.*, 35:519–527.

- Sachs, M. B., J. Nachmias, and J. G. Robson, 1971. Spatial-frequency channels in human vision, *J. Opt. Soc. Am.*, 61: 1176–1186.
- Schade, O. H., 1958. On the quality of color television images and the perception of color detail, *J. Soc. Motion Pict. Television Eng.*, 67:801–819.
- Sclar, G., J. H. R. Maunsell, and P. Lennie, 1990. Coding of image contrast in central visual pathways of the macaque monkey, *Vis. Res.*, 30:1–10.
- Snowden, R. J., and S. T. Hammett, 1998. The effects of surround contrast on contrast thresholds, perceived contrast and contrast discrimination, *Vis. Res.*, 38:1935–1945.
- Somers, D. C., E. V. Todorev, A. G. Siapas, L. J. Toth, D. S. Kim, and M. Sur, 1998. A local circuit approach to understanding integration of long range inputs in primary visual cortex, *Cereb. Cortex*, 8:204–217.
- Swanson, W. H., and H. R. Wilson, 1985. Eccentricity dependence of contrast matching and oblique masking, *Vis. Res.*, 25:1285–1295.
- Thomas, J. P., 1970. Model of the function of receptive fields in human vision, *Psych. Rev.*, 77:121–134.
- Vidyasagar, T. R., X. Pei, and M. Volgushev, 1996. Multiple mechanisms underlying the orientation selectivity of visual cortical neurones, *TINS*, 19:272–277.
- von Békésy, G., 1960. *Experiments in Hearing* (E. G. Wever, trans.), New York: McGraw-Hill.
- Wilkinson, F., T. W. James, H. R. Wilson, J. S. Gati, R. S. Menon, and M. A. Goodale, 2000. An fMRI study of the selective activation of human extrastriate form vision areas by radial and concentric gratings, *Curr. Biol.*, 10:1455–1458.
- Wilkinson, F., and R. Peterson, 1989. Spatial limits to the perception of textural coherence, *Invest. Ophthalmol. Vis. Sci. Suppl.*, 30:254.
- Wilkinson, F., H. R. Wilson, and D. Ellefberg, 1997. Lateral interactions in peripherally viewed texture arrays, *J. Opt. Soc. Am. A*, 2057–2068.
- Wilson, H. R., 1975. A synaptic model for spatial frequency adaptation, *J. Theoret. Biol.*, 50:327–352.
- Wilson, H. R., 1980. A transducer function for threshold and suprathreshold human vision, *Biol. Cybernet.*, 38:171–178.
- Wilson, H. R., 1991. Psychophysical models of spatial vision and hyperacuity, in *Spatial Vision* (D. Regan ed.), London: MacMillan, pp. 64–86.
- Wilson, H. R., 1999. *Spikes, Decisions, and Actions: Dynamical Foundations of Neuroscience*, Oxford: Oxford University Press.
- Wilson, H. R., R. Blake, and S.-H. Lee, 2001. Dynamics of travelling waves in visual perception, *Nature*, 412:907–910.
- Wilson, H. R., and S. Giese, 1977. Threshold visibility of frequency gradient patterns, *Vis. Res.*, 17:1177–1190.
- Wilson, H. R., and R. Humanski, 1993. Spatial frequency adaptation and contrast gain control, *Vis. Res.*, 33:1133–1149.
- Wilson, H. R., D. K. McFarlane, and G. C. Phillips, 1983. Spatial frequency tuning of orientation selective units estimated by oblique masking, *Vis. Res.*, 23:873–882.
- Wilson, H. R., and F. Wilkinson, 1997. Evolving concepts of spatial channels in vision: from independence to nonlinear interactions, *Perception*, 26:939–960.
- Wilson, H. R., and F. Wilkinson, 1998. Detection of global structure in Glass patterns: implications for form vision, *Vis. Res.*, 38:2933–2947.
- Wilson, H. R., F. Wilkinson, and W. Asaad, 1997. Concentric orientation summation in human form vision, *Vis. Res.*, 37: 2325–2330.

70 Contour Integration and the Lateral Connections of V1 Neurons

DAVID J. FIELD AND ANTHONY HAYES

THERE IS AN OFTEN repeated claim that the only man-made object that can be seen from space is the Great Wall of China (Fig. 70.1): a structure that is in some sections over 2500 years old, and that snakes over some 6000 km of countryside. In reality, at the altitude of orbital flights, astronauts report seeing a variety of man-made structures, including roads and large seaway projects such as the Suez and Panama Canals. What characterizes many of these structures is the length and smooth continuity of the contours they create across the surface of the earth.

The notion that continuity is important to visual perception was a central idea of the Gestalt psychologists, who, in the first half of the twentieth century, described a set of perceptual grouping principles that included the *law of good continuation*. In formulating their laws, the Gestalt psychologists had rebelled against the belief that perception could be described as the consequence of simple accretion of visual elements.

Over the past 10 years, cognitive neuroscience has renewed its interest in the representation of contours and continuity. Researchers in visual anatomy, neurophysiology, computer science, and visual psychophysics have combined their approaches to develop models of how contours are perceived and integrated by the visual system. The reasons for this interest are several. Perhaps of primary importance is the fact that up to recently, much of the work on vision has concentrated on the properties of single neurons. Neuroscience data have provided considerable insight into the properties of the individual neurons that occur along the visual pathway. This work suggests that in the early stages of visual processing, the image of our visual environment is transformed into the responses of large arrays of neurons, each selective to properties such as orientation, position, spatial frequency, and direction of motion. Indeed, it has been argued that these basic properties of the visual system may produce a solution that is close to optimal for describing our natural environment (e.g., Field, 1987; see Chapter 108, for review). However, the question remains of how this information, encoded by different neurons, is integrated into the perception of whole objects and scenes. One common theme is that the visual system does so by building a hierar-

chy of ever more complex receptive fields through series of feedforward connections.

In this chapter, we review recent work that takes a different approach. This work suggests that, as early as primary visual cortex, neurons cannot be treated as simple feedforward devices that merely receive input from the retina. Their response properties depend on a complex relationship between the neighboring neurons and their input. In particular, this recent work demonstrates that neurons in primary visual cortex make use of long-range lateral connections that allow integration of information from far beyond the classical receptive field, and the evidence suggests that these connections are involved in associating neurons that respond along the length of a contour.

The classical description of a cortical neuron in primary visual cortex is that of a neuron, with feedforward inputs from the lateral geniculate nucleus, whose pattern of connections produces the receptive field profiles described in the 1960s by Hubel and Wiesel (see Hubel, 1988, for review). This classical receptive field of a visual neuron is defined as the area of the visual field that has the capacity to modify the resting potential of the neuron. However, while this basic feedforward linear model of the simple-cell receptive field has been invoked to explain a wide variety of perceptual phenomena—and is at the heart of a wide range of modeling studies—it is essentially wrong. Some of the earliest studies that measured receptive field properties of cortical neurons recognized that stimuli presented outside the classical receptive field can modify the activity of the neuron, even if those regions by themselves cannot effect a response (e.g., Maffei and Fiorentini, 1976).

The neurons in primary visual cortex show a variety of interesting nonlinearities, with many occurring within the classical receptive field. However, the nonlinearities that are of interest to us here are the responses to regions outside the classical receptive field. Stimulation of these areas typically does not produce a response but can modulate the activity of the neuron. This modulation in activity has commonly been described as inhibitory, and a variety of theories have been proposed (e.g., Allman et al., 1985). One popular account has argued that this inhibition can serve to



FIGURE 70.1. The Great Wall of China is one of a small number of man-made structures visible from space. The length and continuity of the contour etched on the surface of the earth by the wall allow the structure to be visible at considerable distances. The figure in *B* is an edge map of the picture of the Great Wall (*A*) using a simple (Sobel) edge detector. In the classical view, a neuron in

primary visual cortex responds to only a limited region of the visual field and responds to a restricted range of stimulus orientation. To see the contour formed by the wall as a single entity, some process must integrate the different pieces of the contour. (*Christopher Liu/ChinaStock, All Rights Reserved.)

normalize the neuron's response and make more efficient use of the neuron's limited dynamic range (Heeger, 1992; Schwartz and Simoncelli, 2001).

In this chapter, we concentrate on a new theory to account for some of these nonlinear effects. This theory proposes that the nonclassical surrounds of receptive fields are intimately involved in a process called *contour integration*. We do not mean to imply that contour integration is their only role; however, the evidence suggests that it is one role. Indeed, the evidence suggests that some of the effects that have given rise to the notion of nonclassical surrounds are generated by the active grouping or *association* of cells in neighboring regions of the visual field. In accord with the term *receptive field*, we have used the term *association field* to describe the region of associated activity (Field et al., 1993), while others have used the term *integration field* (e.g., Chavane et al., 2000) or *contextual field* (e.g., Phillips and Singer, 1997; see also Chapter 113).

In the following pages, we address four questions and explore some of the research that is providing answers. The questions are as follows: (1) What is contour integration, and why is it important? (2) What do the anatomy and physiology suggest about the underlying mechanism? (3) What does the behavior of individuals—humans and nonhuman primates—suggest about the underlying mechanism? (4) What insights are provided by computational models of the process?

We should note that when putting this review together, we discovered over 500 papers published in the past 10 years that bear directly on these issues of integration. Recently, a number of excellent reviews and discussions have been published on the topic or on associated topics. We recommend Fitzpatrick (2000), Gilbert (1998), and Callaway (1998) for discussions of anatomy and physiology; Polat (1999) and Hess and Field (1999) for reviews of psychophysics; and Li (1998) and Yen and Finkel (1998) for their comprehensive

discussions of the computational issues. In the limited space of this chapter, therefore, we will concentrate on a few issues which we feel have not received the primary attention of the above authors.

What is contour integration?

Consider the image shown in Figure 70.1A. Because reflection and illumination vary across the different surfaces, occlusions between surfaces commonly produce a luminance discontinuity (i.e., an edge), as shown in the edge map in Figure 70.1B. However, edges in scenes do not occur only at occlusions. They may also arise from textures within surfaces, as well as from shading discontinuities.

In the 1980s, a number of modeling studies were published that proposed computational strategies that would help to identify which of the edges in a scene made up the principal boundaries of an object. Under the assumption that boundary edges were likely to extend over large regions of the visual field, the computations were designed to extract only those edges that were continuous over an extended area. The algorithms that were developed were based on the assumption that the problem could be at least partially solved by integrating over neighboring regions that had similar orientations. However, although some of these integration models included, or were derived from, known physiology (e.g., Grossberg and Mingolla, 1985; Parent and Zucker, 1989), the evidence that an integration algorithm of this kind was actually performed by the visual system was not widely accepted.

Two lines of research have recently helped to support the plausibility of a scheme such as the one described above. The first line comes from a series of anatomical and physiological studies that used both cat and primate and suggest that there exist long-range connections between neurons in

primary visual cortex that link neurons with similar orientations. The second line consists of two types of psychophysical study that have provided evidence for the sorts of associations implied by the physiological and anatomical results (Field et al., 1993; Polat and Sagi, 1993, 1994). The results of these studies converge on an account that suggests that neurons in primary visual cortex integrate information from outside the classical receptive field in a way that promotes the integration of contours. Below we review some of these studies.

Physiology and anatomy of lateral connections

As noted above, a variety of early studies showed that stimuli outside of the classical receptive field of a neuron in visual cortex can modulate that neuron's activity. The sources of modulation potentially originate from feedforward connections, feedback connections from neurons farther along the visual pathway, lateral projections from neighboring neurons, or a combination of all three. Although we concentrate here on lateral connections, the modulation activity is almost certainly dependent on a more complex circuit involving all three. What has been remarkable over the past few years, however, has been the close ties found between lateral connections and visual behavior of humans and macaques when completing appropriate psychophysical tasks.

Early studies exploring the horizontal connections in visual cortex discovered that pyramidal neurons have connections that extend laterally for 2 to 5 mm parallel to the

surface and have terminations that are patchy and selective (Gilbert and Wiesel, 1979; Rockland and Lund, 1982). Studies on the extent and specificity of lateral projections have now been completed on the tree shrew (e.g., Bosking et al., 1997; Rockland and Lund, 1982), primate (e.g., Malach et al., 1993; Sincich and Blasdel, 2001), ferret (e.g., Ruthazer and Stryker, 1996), and cat (e.g., Gilbert and Wiesel, 1989), with largely good agreement between species but also some important differences.

Figure 70.2A provides an example of one of the impressive techniques that reveals the specificity of projections using a combination of optical imaging and anatomical data. These results from Bosking et al. (1997) show an overlay of the orientation columns revealed by optical imaging, with the lateral projections of pyramidal neurons near the injection site synapsing onto the surrounding regions. The lateral projections are revealed through extracellular injections of biocytin which label a small number of neurons near the injection site, along with their projections. The orientation tuning of a particular neuron is estimated by its location within an orientation column.

As the figure shows, the orientation column of the injection (shown by the dark areas) has the same orientation as those of the columns where the long range projections project (i.e., they synapse onto neurons that are also in the dark regions). The short-range projections do not show such specificity. Bosking et al. also found that in tree shrew the extent of the long-range projections was significantly greater along the axis corresponding to the orientation of the central neuron.

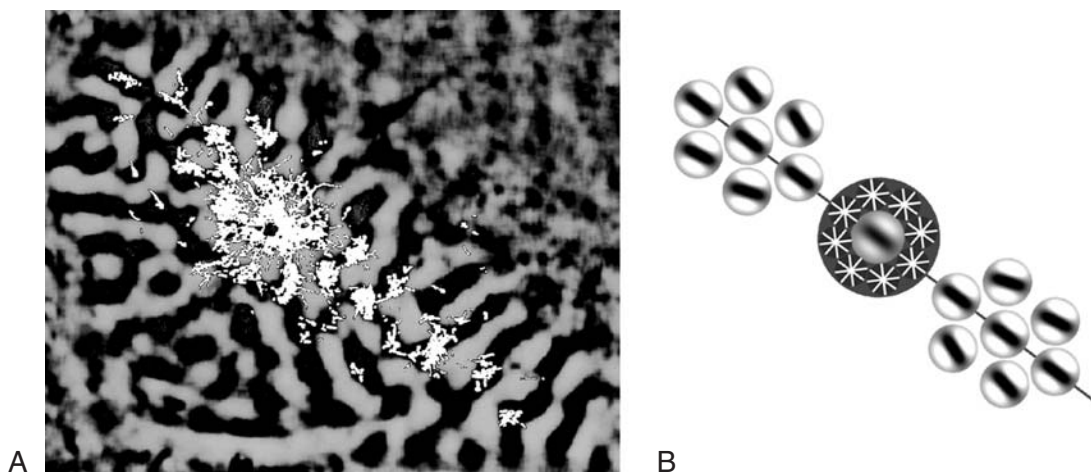


FIGURE 70.2. *A*, Results modified from Bosking et al. (1997) demonstrating the orientation-specific projections of a set of V1 neurons in the tree shrew. Optical imaging is used to reveal the orientation columns, while injections of biocytin are used to map the projections of a set of neurons taking up the biocytin (shown in white). As can be seen, the location of the orientation column of the injection is the same in most cases as the orientation column of

the projection. *B*, An experimentally and theoretically derived association field (Field et al., 1993) summarizing our beliefs regarding the underlying projections. Short-range connections are theorized to be largely inhibitory and independent of orientation, while long-range connections are theorized to be orientation specific and largely excitatory.

Work over the past decade has demonstrated that the lateral projections of these pyramidal neurons are quite specific, projecting to regions of the cortex with iso-orientation columns, as well as similar ocular dominance columns and cytochrome oxidase blobs (e.g., Malach et al., 1993; Yoshioka et al., 1996). Pyramidal cells that are tuned to an orientation aligned with the axes of the projections are shown to project primarily to iso-orientation columns. That is, neurons project primarily to neurons of similar orientation preference.

In some species, as exemplified in Figure 70.2A, the projections are considerably longer along the primary axis than orthogonal to the primary axis. For tree shrew (Bosking et al., 1997), owl monkey, and squirrel monkey (Sincich and Blasdel, 2001) the axis of projections is a factor of 2 to 4 longer along the primary axis than along the orthogonal axis. Cat and macaque show a similar specificity of projections (projecting to similar orientation columns). However, there is no clear evidence that the projections in these animals are elongated along the primary axis. As Sincich and Blasdel (2001) point out, the results from these highly binocular animals are confounded by the projections to related ocular-dominance columns and by the anisotropy of the visual field representation.

In addition to the anatomical studies, support for these results has come from single-unit studies that have explored the effects of co-oriented stimuli presented outside of the classical receptive field (Ito and Gilbert, 1999; Kapadia et al., 1995, 2000; Polat et al., 1998). The results demonstrate that when a neuron is presented with an oriented stimulus within its receptive field, a second collinear stimulus can increase the response rate of the neuron, while the same oriented stimulus presented orthogonal to the main axis (displaced laterally) will produce inhibition or at least less facilitation. Kapadia et al. (2000) attempted to map out these inhibitory and facilitatory effects in awake, behaving macaques, with the results showing good agreement with both the anatomy and human behavior, as described below.

Figure 70.2B shows our theoretical depiction of these lateral projections, which we have called an *association field* (Field et al., 1993). This depiction incorporates results from our psychophysical measurements with the particular example from Figure 70.2A. We will discuss these psychophysical results shortly. However, first we summarize what we see as some of the principal anatomical and neurophysiological findings that are important to our discussion of contour integration.

1. Long-range projections of pyramidal cells are “patchy,” projecting primarily to neurons in iso-orientation columns (i.e., with similar orientation tuning) (Gilbert and Wiesel, 1989; Malach et al., 1993).

2. Long-range projections commonly extend to distances two to four times the size of classical receptive fields, and extend primarily in a direction collinear with orientation tuning of the cell (Bosking et al., 1997; Sincich and Blasdel, 2001).

3. Long-range projections to collinear neurons appear to be largely facilitatory (Kapadia et al., 1995; Nelson and Frost, 1985; Polat et al., 1998); however, the neurophysiology results also suggest that facilitation is largely dependent on contrast, with excitation predominant at low contrasts (or with high-contrast, cluttered backgrounds) and inhibition predominant at high contrasts (Kapadia et al., 1999).

4. Long-range connections appear to be reciprocal (Kisvardy and Eysel, 1992).

5. Short-range projections appear to be largely independent of orientation and have been argued to be predominantly inhibitory (Das and Gilbert, 1999).

These conclusions are not unequivocal. For example, as noted above, not all species show elongation of projections along the primary axis. Furthermore, there is some debate as to whether these long-range connections are the source of facilitatory effects. Kapadia et al.’s (2000) results imply that regions orthogonal to the main axis will produce inhibitory modulation. However, Walker et al. (1999), using patches of gratings at positions adjacent to the classical receptive field, found little evidence for facilitation. Although they did find inhibition, that inhibition was rarely symmetric and was typically distributed unevenly. Kapadia et al. (1995) and Polat et al. (1998) have also shown that when a second line segment is presented collinearly outside of the classical receptive field and is aligned with the preferred orientation, a small majority of neurons produce a stronger response when the line segments are separated by a small gap. Their response is stronger to a discontinuous line than to a continuous line. These results might be expected if we assume that short-range inhibition could, in some neurons, cancel out facilitatory collinear effects.

The diagram in Figure 70.2B is a simplified representation of what we believe is the underlying mechanism of contour integration. We have made certain assumptions that lack clear support in the anatomy and neurophysiology. For example, in our model we imply that projections to regions offset from the primary axis will project to orientations that are offset in a regular manner. Figure 70.2A provides a weak suggestion that the off-axis projections are not as centered in the orientation column as those along the main axis, but this suggestion lacks quantitative physiological or anatomical data (the hypothesis has not been adequately tested). The motivation for the arrangement shown in the figure comes not from the anatomy and physiology, but from behavioral data discussed below.

Two lines of psychophysical research using different methodologies have demonstrated effects that correspond to the above-discussed anatomical and physiological data. The first line uses a contour integration task developed by Field et al. (1993), and the second explores the sensitivity of low-contrast, oriented elements as a function of the surrounding stimuli (Polat and Sagi, 1993).

An example of a stimulus used in the first line of research is demonstrated in Figure 70.3. Human observers are presented with arrays of high-contrast, oriented elements in which a subset has been aligned according to one of several alignment rules. Human observers attempt to identify the presence of this subset of elements as a function of the alignment. Figures 70.3A and B provide examples of two different rules. As the figure demonstrates, observers are more sensitive to collinear alignment than to orthogonal alignment, even though the stimuli are equated for their information content (Field et al., 1993).

A raft of studies using the contour integration task to investigate the conditions under which integration occurs have been published over the past 10 years. For example, studies have demonstrated that integration is possible with elements that have multiple depth planes (Hess and Field, 1995; Hess et al., 1997), with elements that have different phase or polarity (Field et al., 2000), with elements that have different bandwidths, and rather weakly with elements at multiple scales (Dakin and Hess, 1998, 1999). Hayes (2000) has demonstrated that when a local-motion signal induces an apparent displacement of each whole element, integra-

tion is stronger when the alignment corresponds to the elements' perceptual location as opposed to their physical location. Mullen et al. (2000) demonstrate that although integration across multiple hues is possible, integration between similar hues is more effective. Lee and Blake (2001) show a similar effect for movement. Hess and Dakin (1997) have suggested that there is a precipitous decline in contour integration in the periphery, although others have found that contour integration declines in the periphery at a rate similar to that of other visual functions, such as acuity (Nugent et al., 2001).

The second line of psychophysical research believed to be related to long-range cortical interactions explores the contrast threshold of low-contrast elements surrounded by flanking lines (Kapadia et al., 1995; Polat and Sagi, 1993). We refer the reader to Polat (1999) for a detailed review of this research. The results of these studies demonstrate that contrast thresholds for oriented stimuli are reduced (sensitivity is increased) when the stimuli are flanked by collinear stimuli. One of the difficulties in interpreting this research is that the effects are strongly contrast dependent. At the level of single neurons, Kapadia et al. (1999) demonstrated that at low contrasts the length summation area of a neuron increases on average by a factor of 4 relative to the summation area at high contrasts. The enlarged summation area also occurs when the central stimulus is surrounded by a texture of elements such as that shown in Figure 70.3. However, at high contrasts, the long-range effects appear to be largely inhibitory.

The above findings lead to an interesting question concerning whether both contrast-threshold effects and

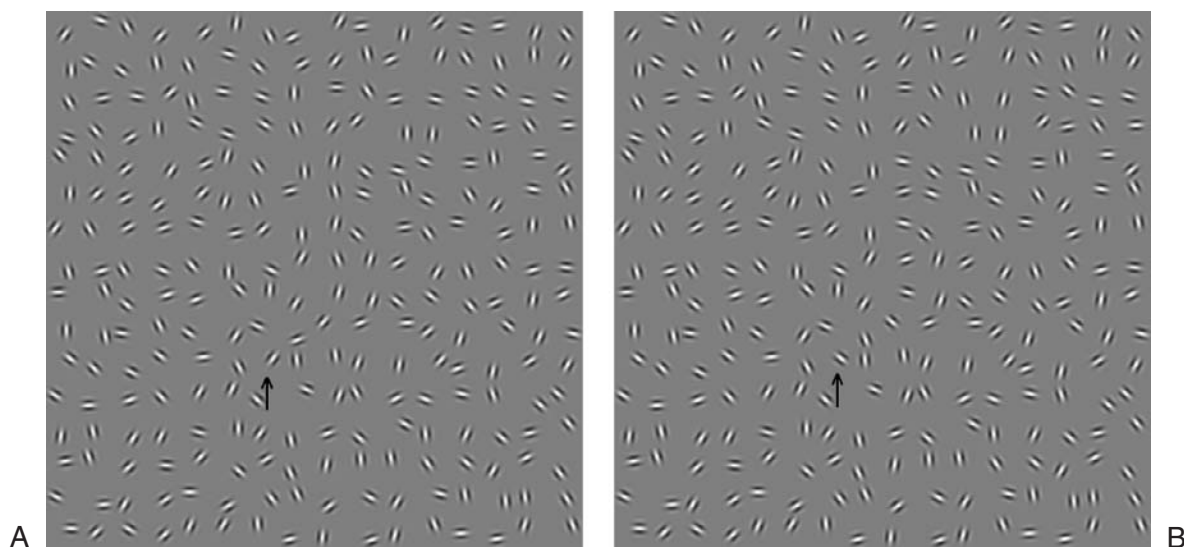


FIGURE 70.3. An example of two stimuli used to measure human sensitivity to contours. The two images contain a path at the same location in each image (as marked by *arrows*) but created according to two different rules (after Field et al., 1993). The reader should

be able to see that the contour or path contained in A is more visible than that in B. This figure is one example that demonstrates the human visual system's increased sensitivity to collinear arrangements.

contour-integration effects are due to dynamic changes to the classical receptive field. Do these effects simply reflect the expansion of the receptive field? This explanation may account for the effects of the contrast threshold, but there are three reasons why, for the contour integration task, it may not be an adequate explanation. First, the threshold effects are strongly dependent on the phase or polarity of flanks (Williams and Hess, 1998), while contour integration has little phase dependence (Field et al., 2000). Second, contour integration occurs between elements that differ by more than 30 degrees (Field et al., 1993) when the alignment is appropriate (Fig. 70.3A), but there is no evidence that the expansion of the receptive field's length would allow such integration. Third, there appears to be little evidence that perceived contrast is enhanced by flanking stimuli. We will return to this issue in the next section, but the reader can view Figure 70.3A and ask whether the elements in the path appear to be higher in contrast. Hess et al. (1998) found that large variations in contrast had no effect on the ability to detect the presence of the contour. Xing and Heeger (2001) also found no changes in perceived contrast when grating patches were surrounded by patches of similar contrast. Changes were noted only when the flanking patches were significantly higher in contrast.

Other psychophysical techniques have demonstrated intriguing results. Chavane et al. (2000) have demonstrated that the speed of an oriented element appears higher when it moves in a direction collinear to its axis than when it moves in a direction orthogonal to its axis. They argue that long-range connections may be responsible. Kapadia et al. (2000) have demonstrated that elements placed along the ends of a central element can induce a perceived change in the orientation of the central element toward the orientation of the central element. However, when the flanking elements are placed along the opposite axis (adjacent to the central element), the central element can be shifted away from the orientation of the flanking elements. They also demonstrated that the spatial distribution of this effect showed good agreement with the neurophysiology of cortical facilitation produced by the flanking lines. Mareschal et al. (2001) have also demonstrated that with a collinear arrangement, flanking grating patches can significantly increase the orientation discrimination thresholds of the central patch. Furthermore, the threshold increase is significantly higher in the collinear arrangement than when the orientation of the elements is perpendicular to the positions of the three patches.

Kovacs and Julesz (1993) demonstrated that when measuring the visibility of a path of elements as a function of the density of the surrounding elements, the path is significantly more visible if the contour forms a closed figure. Pettet et al. (1998) argue that this effect may be related to the directional smoothness of the contours (i.e., a circular

figure has all the elements changing orientation in a consistent direction). In either case, both results demonstrate that sensitivity depends on elements farther away than the immediate neighbors. The simple model, based on excitatory effects between neighbors, will not produce this effect. Of course, there is no reason to assume that these psychophysical effects necessarily occur in V1, and these psychophysical results may be an indication of the direction of attention toward features that undergo predictable change. Nonetheless, the results suggest that thresholds for perceiving contours depend on complex relationships.

We conclude this section on the psychophysical phenomena with a fascinating study by Kovacs et al. (1996). As noted earlier, Hess and Field (1995) demonstrated that it was possible to integrate contour fragments that had relatively large binocular disparities between them; Kovacs et al. went much further and presented to observers binocular image pairs that would be expected to produce rivalry. Consider the presentation of two completely different natural scenes to each eye. Under such conditions, one would expect one eye or the other to dominate much of the time. Kovacs et al. presented such images to observers and then broke up each pair so that each eye received patches from both images, such that the left eye received the complement of the right (e.g., the right eye gets 1,2,1,2,2,1 with the left eye receiving 2,1,2,1,1,2). As one can readily see by observing their demonstrations, Kovacs et al. found that observers commonly see complete images (1,1,1,1,1,1 or 2,2,2,2,2,2). The contours and other visual information were successfully integrated between the two eyes into a single perceptual whole. This result implies that the process involved in integrating contours is not eye specific.

Computational modeling

In some cases, computational models are simple reflections of the data found experimentally. They can be considered *existence proofs* demonstrating that it is at least possible to perform the desired task with the proposed architecture. They cannot demonstrate that the visual system necessarily uses the architecture of the model, but they can demonstrate that such a model would work if that architecture did underlie the task. However, at times, these models are most useful when they fail, and that may well be the case in the following studies we discuss.

To integrate contours, a variety of algorithms have been proposed that use the technique of integrating similar orientations along collinear directions. Part of the argument for using a collinearity algorithm appears to be that the nature of the task demands it. However, these early studies also went to some lengths to explain how such an algorithm might fit with the known physiology and anatomy (e.g., Grossberg and Mingolla, 1985; Parent and Zucker, 1989;

Shashua and Ullman, 1988). In the past 5 years, as our understanding of the underlying physiology has increased, so has the sophistication of computational models (e.g., Geisler and Super, 2000; Li, 1998, 2000; Yen and Finkel, 1998). These models have demonstrated that the architecture revealed by the physiology and anatomy can be used to provide an efficient means of extracting contours in natural scenes, and it can be used to account for a significant amount of the psychophysical data.

Our work on contour sensitivity (Field et al., 1993) was partly motivated by the belief that the properties of natural edges would be more efficiently coded by a linking process rather than by a high-level neuron tuned to the particular contour in question. The difficulty with the high-level neuron model is that the number of possible contours in the natural world, or even in our experiments, is much too large to have a neuron for every contour.

Geisler et al. (2001) and Sigman et al. (2001) have taken the ecological approach further and asked whether the contour integration model is an efficient means of coding natural scene contours. They measured the co-occurrence statistics of edge elements in natural scenes and found that the relative orientations of neighboring contour segments match well with those predicted physiologically, and with psychophysically defined association fields. Geisler et al.'s results are particularly interesting because of the requirements needed to measure these co-occurrence statistics. As they argue, these statistics are multidimensional in nature. Given an edge at a particular location with a particular orientation, the region around that location is a three-dimensional probability map of x -position by y -position by orientation. Only by mapping out this full probability map does one see the full set of statistical dependencies. And it is in these conditional probabilities that one finds the orientation dependencies that map onto the association field properties. The probability map is much higher in dimension if we include the additional dependencies across scale, chromaticity, motion, and disparity. Indeed, our own work (Hayes and Field, in prep.) suggests that both perceptual integration over scale and the structure of natural edges through scale follow similar rules.

A potential difficulty for all recent models (e.g., Geisler and Super, 2000; Li, 1998; Yen and Finkel, 1998), as well as for earlier models (e.g., Grossberg and Mingolla, 1985), is that they generally assume that recurrent activity increases the responses of the neurons along the contour. This assumption is supported by some neurophysiological results which show an increase in response rate with flanking collinear lines (Kapadia et al., 1995; Nelson and Frost, 1985). The difficulty is in understanding how the visual system untangles the relationship between neural activity and contrast. Responses increase with contrast, and they also increase with collinear arrangements. How does the visual

system decipher differences in contrast variation from differences in context (i.e., collinearity)?

Using human psychophysical techniques, Hess et al. (1998) found that contrast changes have little effect on the visibility of a contour. Consider the image shown in Figure 70.3. The contrast of the path elements is perceived to be the same as that of the background. Such results suggest that neurons must somehow carry the code for contrast separately from the code for the continuity of the contour. There are various possibilities for how this might be achieved. One possibility is that neurons that code contrast are different from those that code the contour. Under this hypothesis, we would need to assume that both neurons coding for contrast and neurons coding for continuity are present in V1.

A second approach proposes that continuity is represented by a temporal code, presumably tied to the synchronous activity of neighboring neurons. This approach to *binding* has received considerable recent attention and has some experimental support (Singer and Gray, 1995; see also Chapter 113). The difficulty with this model is that it requires a mechanism to detect the synchrony. Hess et al. (1998) suggest a rather different and more basic version of a temporal code. They suggest that contrast information is represented by the initial response generated by the feedforward activity, with the later response determined by the lateral connections and the context of the surrounding regions. The contrast signal could then be extracted from the collinearity signal by simply tracking the timing of the response. This hypothesis was derived from the neurophysiological work of Zipser et al. (1996). Using textures as stimuli, they found results consistent with this theory. However, Kapadia et al. (1999) provide data that are supportive in some ways but also make the story more complex. As noted in the previous section, Kapadia et al. found that collinear facilitation for neurons in V1 occurs only at low contrasts or at high contrasts in complex backgrounds. They also noted that this facilitation occurs after the initial transient response of the neuron during the *sustained* component of the response. This aspect of the response fits the model proposed by Hess et al. (1998). However, at high contrasts, the neurons do not show this sustained response, but only the sharp transient response. What sort of model predicts this high-contrast behavior? It may involve some degree of contrast normalization (e.g., Heeger, 1992), but at present we are not aware of any model that predicts both the timing of responses and the lack of facilitation at high contrasts.

There is also the question of whether lateral feedback has the appropriate timing to account for the neurophysiological findings. Along these lines, Van Rullen et al. (2001) provide an interesting alternative to the above models. They argue that models that iterate toward a solution using recurrent lateral feedback are too slow to explain reaction-time data and neurophysiological responses measured during

visual recognition. They suggest that the contours might be represented not by the magnitude of the neural response, but by the relative speed at which responses pass through the visual system. They argue that lateral connections may serve to facilitate the initial response allowing the collinear context to push the most “meaningful” information most quickly through the visual system.

However, all of the models fail to predict the smoothness constraint described by Pettet et al. (1998), whose results demonstrate that a contour which changes in a consistent direction is more visible than a contour which has multiple changes in direction. Such results suggest that sensitivity is a function of more than immediate neighborhood interactions. Contours changing orientation in a consistent angular direction provide for greater sensitivity. But whether this sensitivity is related to the lateral connections in V1, or to higher-level interactions or higher-level feedback, remains to be seen.

Some remaining questions

There remain a number of interesting and fruitful directions for research in this area, as well as a number of problems.

Psychophysical research, computational modeling, and measurements on natural scenes all support a particular mapping, such as that shown in Figure 70.2B. They suggest that off-axis projections will project to off-axis orientations along the lines of smooth curves. Our own eyeball estimates of the published anatomical data of Bosking et al. (1997) seem to suggest that the off-axis projections project to orientation columns that are slightly shifted from those along the primary axis. To our knowledge, though, no quantitative study has been conducted to support or dismiss this hypothesis.

Another question of interest is how contours are integrated across the midline. In V1, communication across the midline must pass across the corpus collosum, a pathway that is significantly longer and possibly less efficient. However, there appear to be no large differences between the integration across the midline or within a hemifield. Presumably, if integration occurs across the midline, this would show up as a delay in processing or a reduction in sensitivity. In our own unpublished work on this problem, no significant delay was found. Indeed, if no differences were found between contour integration across hemifields versus within hemifields, it would argue that much of the contour integration task (or at least the limiting factors in the task) must be performed by areas beyond V1.

There also remain questions regarding the relation between contour integration effects and the wide range of studies on illusory contours. A large number of studies that have investigated the perception of illusory contours, and have explored the conditions which produce the appearance

of an illusory surface partially bounded by illusory edges (e.g., see Leshner, 1995, for a review). The perception of the illusion depends on the *reliability* of the supporting contours (Kellman and Shipley, 1991), meaning that the supporting contours must fall along first-order curves, as shown in Figure 70.4A. However, the illusion also depends on the end junctions of the supporting contours (e.g., Rubin, 2001). Figure 70.4B shows an example where the illusion is blocked by converting the L-junctions inducing corners into T-junctions. Kapadia et al. (1995) have demonstrated that T-junctions can also reduce the sensitivity in a contour integration task when the elements are made of T-elements rather than simple line elements. Kapadia et al. also demonstrated that with single neurons, the effects produced by flanking collinear lines are also reduced with such flanking lines.

Although there are clearly some important relationships between illusory contours and contour integration, the illusion is certainly not a necessary component of the integration process. As readers may see for themselves, the perception of the contour in Figure 70.3A does not result in an illusion of luminance or the perception of structure between the elements. We should also note that while lateral connections presumed to underlie the contour integration task are found with V1 neurons, neural responses corresponding to illusory contours are not found earlier than V2 (Peterhans and von der Heydt, 1989; von der Heydt et al., 1984). Zhou et al. (2000) have also found that over half of the neurons in V2 and V4 also show selectivity to border ownership. Given the same local contour information (the same information within the classical receptive field), the majority of neurons were found to respond differentially to larger object properties. For example, a neuron responding to a vertical edge may produce a larger response, depending on whether the contour is part of an object to the left or to the right of the contour. In contrast to V2, only 18% of the neurons in the top layer of V1 show this differential response. Zhou et al. (2000) also noted that the differential response to border ownership occurred within 25 msec of

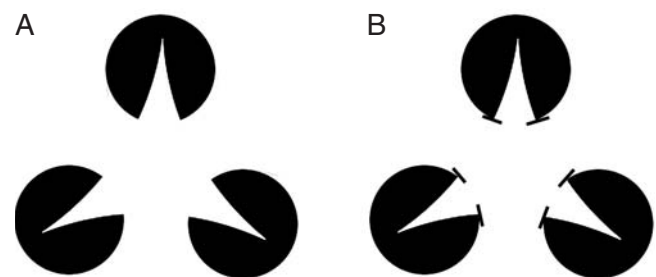


FIGURE 70.4. *A* shows a modified Kaniza figure that typically results in the perception of an illusory contour. *B* demonstrates the importance of the supporting endpoints in this illusion. The T-junction will typically reduce the strength of the illusory triangle.

response onset, arguing that the solution is generated within the visual cortex.

These results imply that lateral connections in V1 are important to the integration of contours, but they are not directly involved in the more complex “object” relationships portrayed by illusory figures and by object identity.

Summary

The anatomical, neurophysiological, psychophysical, and computational research of the past decade provides a compelling argument that neurons in area V1 integrate information from beyond the classical receptive field in a manner that assists in the integration of contours. Integrated contours represent a critical component of natural scenes important to early vision. They are important in defining the boundaries and extents of the objects in our world.

The lateral connections between neighboring neurons are certain to play a number of roles besides contour integration. As argued by a number of investigators, these connections are likely to play a role in contrast normalization, stereo, motion, and texture segregation, among others. Furthermore, the facilitation with single neurons is contrast dependent, and this may imply that the facilitation at collinear positions is a secondary effect to the inhibition found in much of the nonclassical surround. It is also likely that few of these computational problems are “solved” in V1. V1 neurons receive a large amount of input from higher visual areas, which undoubtedly plays a significant role. Indeed, there is ample evidence that both task outcome and the activity of these neurons can be modulated by attention (e.g., Ito and Gilbert, 1999) suggesting that our final model of V1 will be considerably more complex.

Overall, the studies reviewed here call into question the notion that V1 codes the visual world by breaking it down into an array of independent features. Although V1 neurons are differentially selective to a variety of visual features, their lateral connections, and the related perceptual phenomena, suggest that V1 should be considered as a complex web of interactions. Each neuron’s response depends in a complex way on its neighbors, on its inputs, and on feedback from higher levels. With the current surge of studies exploring these interactions, a clearer picture of their role is expected to develop over the next few years. At this time, however, the evidence suggests that the Gestalt psychologists of the early twentieth century had a profound insight with their law of good continuation. The integration of contours represents one task well served by the complex interactions found in early vision.

REFERENCES

- Allman, J., F. Miezin, and E. McGuinness, 1985. Stimulus specific responses from beyond the classical receptive field: neurophysiological mechanisms for local-global comparisons in visual neurons, *Annu. Rev. Neurosci.*, 8:407–430.
- Bosking, W. H., Y. Zhang, B. Schofield, and D. Fitzpatrick, 1997. Orientation selectivity and the arrangement of horizontal connections in tree shrew striate cortex, *J. Neurosci.*, 17:2112–2127.
- Callaway, E. M., 1998. Local circuits in primary visual cortex of the macaque monkey, *Annu. Rev. Neurosci.*, 21:47–74.
- Chavane, F., C. Monier, V. Bringuier, P. Baudot, L. Borg-Graham, J. Lorenceau, and Y. Fregnac, 2000. The visual cortical association field: a Gestalt concept or a psychological entity? *J. Physiol. (Paris)*, 94:333–342.
- Dakin, S. C., and R. F. Hess, 1998. Spatial-frequency tuning of visual contour integration, *J. Opt. Soc. Am. A*, 15:1486–1499.
- Dakin, S. C., and R. F. Hess, 1999. Contour integration and scale combination processes in visual edge detection, *Spatial Vis.*, 12:309–327.
- Das, A., and C. D. Gilbert, 1999. Topography of contextual modulations mediated by short-range interactions in primary visual cortex, *Nature*, 399:655–661.
- Field, D. J., 1987. Relations between the statistics of natural images and the response properties of cortical cells, *J. Opt. Soc. Am. A*, 4:2379–2394.
- Field, D. J., A. Hayes, and R. F. Hess, 1993. Contour integration by the human visual system: evidence for a local “association field,” *Vis. Res.*, 33:173–193.
- Field, D. J., A. Hayes, and R. F. Hess, 2000. The roles of polarity and symmetry in contour integration, *Spatial Vis.*, 13:51–66.
- Fitzpatrick, D., 2000. Seeing beyond the receptive field in primary visual cortex, *Curr. Opin. Neurobiol.*, 10:438–443.
- Geisler, W. S., J. S. Perry, B. J. Super, and D. P. Gallogly, 2001. Edge co-occurrence in natural images predicts contour grouping performance, *Vis. Res.*, 41:711–724.
- Geisler, W. S., and B. J. Super, 2000. Perceptual organization of two-dimensional patterns, *Psych. Rev.*, 107(4):677–708.
- Gilbert, C. D., 1998. Adult cortical dynamics, *Physiol. Rev.*, 78:467–485.
- Gilbert, C. D., and T. N. Wiesel, 1979. Morphology and intracortical projections of functionally characterised neurones in the cat visual cortex, *Nature*, 280:120–125.
- Gilbert, C. D., and T. N. Wiesel, 1989. Columnar specificity of intrinsic horizontal and corticocortical connections in cat visual cortex, *J. Neurosci.*, 9:2432–2442.
- Grossberg, S., and E. Mingolla, 1985. Neural dynamics of perceptual grouping: textures, boundaries, and emergent segmentations, *Percept. Psychophys.*, 38:141–171.
- Hayes, A., 2000. Apparent position governs contour-element binding by the visual system, *Proc. R. Soc. Ser. B*, 267:1341–1345.
- Heeger, D. J., 1992. Normalization of cell responses in cat striate cortex, *Vis. Neurosci.*, 9:181–197.
- Hess, R. F., and S. C. Dakin, 1997. Absence of contour linking in peripheral vision, *Nature*, 390:602–604.
- Hess, R. F., S. C. Dakin, and D. J. Field, 1998. The role of “contrast enhancement” in the detection and appearance of visual contours, *Vis. Res.*, 38:783–787.
- Hess, R. F., and D. J. Field, 1995. Contour integration across depth, *Vis. Res.*, 35:1699–1711.
- Hess, R., and D. Field, 1999. Integration of contours: new insights, *Trends Cogn. Sci.*, 12:480–486.

- Hess, R. F., A. Hayes, and F. A. A. Kingdom, 1997. Integrating contours within and through depth, *Vis. Res.*, 37:691–696.
- Hubel, D. H., 1988. *Eye, Brain, and Vision*, New York: Scientific American Library.
- Ito, M., and C. D. Gilbert, 1999. Attention modulates contextual influences in the primary visual cortex of alert monkeys, *Neuron*, 22:593–604.
- Kapadia, M. K., M. Ito, C. D. Gilbert, and G. Westheimer, 1995. Improvement in visual sensitivity by changes in local context: parallel studies in human observers and in V1 of alert monkeys, *Neuron*, 15:843–856.
- Kapadia, M. K., G. Westheimer, and C. D. Gilbert, 1999. Dynamics of spatial summation in primary visual cortex of alert monkeys, *Proc. Natl. Acad. Sci. USA*, 96:12073–12078.
- Kapadia, M. K., G. Westheimer, and C. D. Gilbert, 2000. Spatial distribution of contextual interactions in primary visual cortex and in visual perception, *J. Neurophysiol.*, 84:2048–2062.
- Kellman, P. J., and T. F. Shipley, 1991. A theory of visual interpolation in object perception, *Cogn. Psychol.*, 23:141–221.
- Kisvarday, Z. F., and U. T. Eysel, 1992. Cellular organization of reciprocal patchy networks in layer III of cat visual cortex (area 17), *Neuroscience*, 46:275–286.
- Kovacs, I., and B. Julesz, 1993. A closed curve is much more than an incomplete one: effect of closure in figure-ground segmentation, *Proc. Natl. Acad. Sci. USA*, 90:7495–7497.
- Kovacs, I., T. V. Papathomas, M. Yang, and A. Feher, 1996. When the brain changes its mind: interocular grouping during binocular rivalry, *Proc. Natl. Acad. Sci. USA*, 93:15508–15511.
- Lee, S. H., and R. Blake, 2001. Neural synergy in visual grouping: when good continuation meets common fate, *Vis. Res.*, 41:2057–2064.
- Leshner, G. W., 1995. Illusory contours: toward a neurally based perceptual theory, *Psychonom. Bull. Rev.*, 2:279–321.
- Li, Z., 1998. A neural model of contour integration in the primary visual cortex, *Neural Comput.*, 10:903–940.
- Li, Z., 2000. Pre-attentive segmentation in the primary visual cortex, *Spatial Vis.*, 13:25–50.
- Maffei, L., and A. Fiorentini, 1976. The unresponsive regions of visual cortical receptive fields, *Vis. Res.*, 16:1131–1139.
- Malach, R., Y. Amir, M. Harel, and A. Grinvald, 1993. Relationship between intrinsic connections and functional architecture revealed by optical imaging and in vivo targeted biocytin injections in primate striate cortex, *Proc. Natl. Acad. Sci. USA*, 90:10469–10473.
- Mareschal, I., M. P. Sceniak, and R. M. Shapley, 2001. Contextual influences on orientation discrimination: binding local and global cues, *Vis. Res.*, 41:1915–1930.
- Mullen, K. T., W. H. Beaudot, and W. H. McIlhagga, 2000. Contour integration in color vision: a common process for the blue-yellow, red-green and luminance mechanisms? *Vis. Res.*, 40:639–655.
- Nelson, J. I., and B. J. Frost, 1985. Intracortical facilitation among co-oriented, co-axially aligned simple cells in cat striate cortex, *Exp. Brain Res.*, 61:54–61.
- Nugent, A. K., R. Keswani, R. L. Woods, and E. Peli, 2001. Contour integration in the peripheral field of normal and low vision observers, *Invest. Ophthalmol. Vis. Sci.*, 42(4):5612.
- Parent, P., and S. Zucker, 1989. Trace inference, curvature consistency and curve detection, *IEEE Tran. Pattern Anal. Machine Intell.*, 11:823–839.
- Peterhans, E., and R. von der Heydt, 1989. Mechanisms of contour perception in monkey visual cortex II: contours bridging gaps, *J. Neurosci.*, 9:1749–1763.
- Pettet, M. W., S. P. McKee, and N. M. Grzywacz, 1998. Constraints on long range interactions mediating contour detection, *Vis. Res.*, 38:865–879.
- Phillips, W. A., and W. Singer, 1997. In search of common foundations for cortical computation, *Behav. Brain Sci.*, 20:657–722.
- **Polat, U., 1999. Functional architecture of long-range perceptual interactions, *Spatial Vis.*, 12:143–162.
- Polat, U., K. Mizobe, M. W. Pettet, T. Kasamatsu, and A. M. Norcia, 1998. Collinear stimuli regulate visual responses depending on cell's contrast threshold, *Nature*, 391:580–584.
- Polat, U., and D. Sagi, 1993. Lateral interactions between spatial channels: suppression and facilitation revealed by lateral masking experiments, *Vis. Res.*, 33:993–999.
- Polat, U., and D. Sagi, 1994. The architecture of perceptual spatial interactions, *Vis. Res.*, 34:73–78.
- Rockland, K. S., and J. S. Lund, 1982. Widespread periodic intrinsic connections in the tree shrew visual cortex, *Science*, 215:1532–1534.
- Rubin, N., 2001. The role of junctions in surface completion and contour matching, *Perception*, 30:339–366.
- Ruthazer, E. S., and M. P. Stryker, 1996. The role of activity in the development of long-range horizontal connections in area 17 of the ferret, *J. Neurosci.*, 16:7253–7269.
- Schwartz, O., and E. P. Simoncelli, 2001. Natural signal statistics and sensory gain control, *Nat. Neurosci.*, 4(8):819–825.
- Shashua, A., and S. Ullman, 1988. Structural saliency: the detection of globally salient structures using 2 locally connected network. In *Proc. Int. Conf. Comput. Vis. (ICCV) Tampa, FL*, 482–488.
- Sigman, M., G. A. Guillermo, C. D. Gilbert, and M. O. Magneasco, 2001. On a common circle: natural scenes and Gestalt rules, *Proc. Natl. Acad. Sci. USA*, 98:1935–1940.
- Sincich, L. C., and G. G. Blasdel, 2001. Oriented axon projections in primary visual cortex of the monkey, *J. Neurosci.*, 21:4416–4426.
- Singer, W., and C. M. Gray, 1995. Visual feature integration and the temporal correlation hypothesis, *Ann. Rev. Neurosci.*, 18:555–586.
- Van Rullen, R., A. Delorme, and S. J. Thorpe, 2001. Feed-forward contour integration in primary visual cortex based on asynchronous spike propagation, *Neurocomputing*, 38:1003–1009.
- von der Heydt, R., E. Peterhans, and G. Baumgartner, 1984. Illusory contours and cortical neuron responses, *Science*, 224:1260–1262.
- Walker, G. A., I. Ohzawa, and R. D. Freeman, 1999. Asymmetric suppression outside the classical receptive field of the visual cortex, *J. Neurosci.*, 19:10536–10553.
- Williams, C. B., and R. F. Hess, 1998. Relationship between facilitation at threshold and suprathreshold contour integration, *J. Opt. Soc. Am. Ser. A*, 15:2046–2051.
- Xing, J., and D. J. Heeger, 2001. Measurement and modeling of centre-surround suppression and enhancement, *Vis. Res.*, 41:571–583.
- Yen, S. C., and L. H. Finkel, 1998. Extraction of perceptually salient contours by striate cortical networks, *Vis. Res.*, 38:719–741.
- Yoshioka, T., G. G. Blasdel, J. B. Levitt, and J. S. Lund, 1996. Relation between patterns of intrinsic lateral connectivity, ocular

- dominance, and cytochrome oxidase-reactive regions in macaque monkey striate cortex, *Cereb. Cortex*, 6:297–310.
- Zhou, H., H. S. Friedman, and R. von der Heydt, 2000. Coding of border ownership in monkey visual cortex, *J. Neurosci.*, 20:6594–6611.
- Zipser, K., V. A. F. Lamme, and P. H. Schiller, 1996. Contextual modulation in primary visual cortex, *J. Neurophysiol.*, 16:7376–7389.

71 Shape Dimensions and Object Primitives

CHARLES E. CONNOR

THE RETINAL IMAGE produced by an object is infinitely variable due to changes in viewpoint and illumination. Somehow, this infinity of images must be mapped to a single internal representation in order to identify the object consistently. Moreover, this feat must be accomplished for a virtual infinity of different objects. Neurobiological systems handle this object recognition problem on a fast time scale with apparent ease. In primates, including humans, object recognition is carried out by the ventral pathway of extrastriate visual cortex. The general structure and function of this pathway are reviewed in Chapters 76 and 77. This chapter addresses a particular solution to the object recognition problem—structural representation—and evaluates the evidence that this solution is utilized in the primate ventral pathway.

Neural representation schemes can be broadly divided into two classes, local and distributed. In local (or *labeled-line*) representations, each stimulus is encoded by activity in a single neuron or neural group that functions only to represent that stimulus. In distributed representations, each stimulus is encoded by a pattern of activity across a population of neurons, and each neuron participates in representing multiple stimuli. Distributed representation schemes are thus much more efficient, and they seem to be the rule in sensory systems, where individual neurons typically respond to a range of stimuli. The greater efficiency of distributed representations is critical for encoding object shape, because the infinite space of potential stimuli makes a local scheme impractical.

If shape representation is distributed, then how exactly is shape information decomposed and parceled out across neurons? In other words, what elements of shape information do individual neurons represent? At the receptor level in the retina, shape information is partitioned across space. Each neuron represents information about luminance and/or color at a discrete spatial location in the visual image. In this form, shape information is far too implicit to be useful. Moreover, as discussed above, the spatial patterns of luminance produced by a given object are constantly changing. The visual system must transform this pixelated, spatiotopic representation into another type of distributed representation—one in which the pattern for a given object is relatively consistent (facilitating recognition) and patterns for similar objects are themselves similar (facilitating

comparison and categorization; this property is known as *second-order isomorphism*; Edelman, 1999).

Structural representation: theory

According to many theories (Milner, 1974; Selfridge, 1959; Sutherland, 1968), this transformation is based on an alphabet of simple shape elements or *primitives* that correspond to common real-world object components. Each neuron would represent one type of primitive, responding whenever that primitive was present within its receptive field. A given object would be represented by the combined activity of a number of such neurons, each signaling one of the primitives constituting the object. A complete representation would also require information about the relative position and connectivity between primitives.

This is a *structural* representation in the sense that neurons explicitly encode the geometric composition of the object. The idea is also referred to as *representation by parts* or *representation by components* (Biederman, 1987), since the object is described in terms of its parts or primitives. Parts-based representation satisfies the requirement for consistency, since the list of parts making up an object does not change when the retinal image changes. The particular parts that are visible may change when the object rotates (due to self-occlusion), but a familiar object is recognizable from a subset of its parts. Structural or parts-based representation also satisfies the requirement for similarity or second-order isomorphism: Explicitly encoding the geometrical structure of objects ensures that similar objects will have similar neural representations. Finally, parts-based coding has the efficiency and capacity required to represent the infinite space of object shape. A finite number of neurons encoding basic shape elements can represent any combination of those elements in the same way that letters of the alphabet can represent any word.

The discrete form of the theory described above is convenient for conveying the basic coding principle, and it analogizes to letters encoding words and DNA triplets encoding proteins. But the notion of stereotyped shape primitives signaled by all-or-nothing neural responses is a simplification. The shapes of real-world object components vary continuously. Correspondingly, visual neurons respond in a graded fashion across a range of shapes. Thus, the shape

alphabet is really a set of shape dimensions suitable for describing object components—a *multidimensional feature space* (Edelman, 1999; Edelman and Intrator, 2000). [Some authors would reserve the label “structural” for the discrete form of the theory (Edelman and Intrator, 2000); I use it here to encompass all schemes in which part identity and position are explicitly represented.] Neurons with graded tuning in those dimensions would provide an analog signal (in spikes per second) related to how closely shape elements in the current image match their tuning peaks. Neural tuning peaks would be distributed across shape dimensions, so that any value could be represented. A given object would be represented by a constellation of population activity peaks corresponding to its constituent parts.

EXAMPLE: CONTOUR FRAGMENTS What would a structural representation look like? Figure 71.1 illustrates a structural scheme for encoding two-dimensional (2-D) outline and silhouette-like shapes such as alphanumeric characters. The shape to be represented is a bold numeral 2 (Fig. 71.1A). There are a number of ways in which this shape could be decomposed into parts. The decomposition shown here is based on curved contour fragments. (The theoretical and empirical reasons for proposing contour fragments as parts are discussed below.) The lowercase letters label contour fragments with different curvature values. These fragments can be represented in four dimensions, two describing shape (Fig. 71.1B) and two describing relative position (Fig. 71.1C).

The two shape dimensions shown here are curvature and orientation. Curvature (radial axis in Fig. 71.1B) can be either positive (convex, projecting outward) or negative (concave, indented inward). Curvature is defined mathematically as the rate of change in tangent angle per unit contour length. For a circle, curvature is inversely related to

radius. Thus, larger values signify tighter, sharper, more acute curvature. Extremely large values correspond to curvatures so tight that we perceive them as tangent discontinuities, that is, angles or corners. In Figure 71.1B, the curvature scale is squashed so that very sharp curves or angles have a value of 1.0 (convex) or -1.0 (concave). Thus, the sharp convex angle labeled *b* has a curvature value of 1.0, and the sharp concave angle *g* has a value of -1.0 . The broader-convexity *a* has a value near 0.5, and the broader-concavity *c* has a value near -0.5 . The straight contour segments (not labeled) would have curvature values of 0.

The other shape dimension is orientation (angular axis in Fig. 71.1B), which in this context means the direction in which the curved fragment “points.” More precisely, this is the direction of the surface normal—the vector pointing away from the object, perpendicular to the surface tangent—at the center of the curved contour fragment. Thus, the sharp-convexity *b* points toward the lower left (225 degrees), the broad-convexity *a* points toward the upper right (45 degrees), and so on. Note that this definition of orientation differs from the standard definition for straight lines or edges. The standard definition is orientation of the surface tangent rather than the surface normal. The orientation of the normal is more useful because it also indicates figure/ground direction. Under the convention used here, in which the surface normal points away from the figure interior, 45 degrees specifies a contour with the figure side on the lower left (e.g., *a*), while 225 degrees specifies a contour with the figure side on the upper right (e.g., *b*). The tangent in these two cases would be the same.

The relative position dimensions are shown in Figure 71.1C. The coordinate system used here is polar; the two dimensions are angular position and radial position with respect to the object center. (The radial position scale is relative to object height.) Polar coordinates are convenient

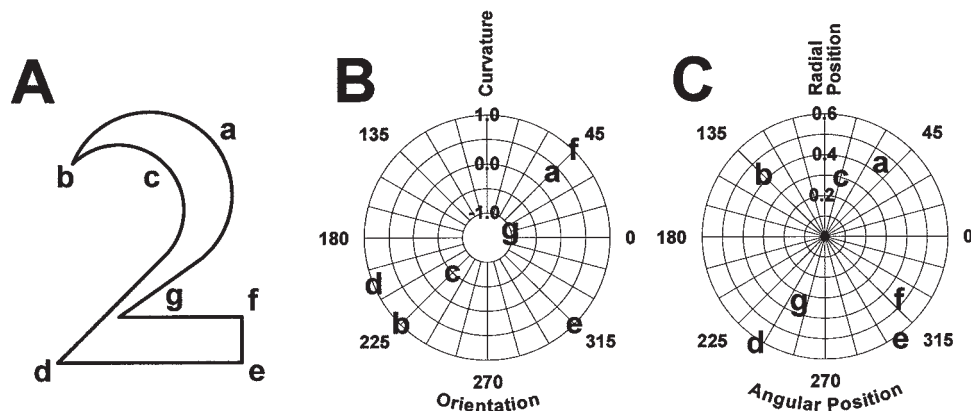


FIGURE 71.1. A structural (parts-based) shape-coding scheme based on contour fragments. *A*, The example shape, a bold numeral 2, can be decomposed into contour fragments (*a*–*g*) with different curvatures, orientations, and positions. *B*, The curvature and

orientation of each contour fragment is plotted on a 2-D domain. *C*, The positions of the contour fragments (relative to the object center) are plotted on a 2-D domain. Together, plots *B* and *C* represent a 4-D domain for describing contour fragments.

for representing shape because changes in object size do not affect angular position and produce a uniform scaling of radial position. Contour section *a* is at the upper right with respect to the object center, so it is plotted near 45 degrees; *b* is at the upper left and is plotted at 135 degrees. There are many other ways in which the necessary position information could be parameterized.

These four dimensions capture much of the information needed to specify a simple shape like the bold numeral 2. A few important shape dimensions, like contour fragment length and connectivity, have been left out for simplicity. Also, the bold 2 exemplifies just one class of 2-D objects. A much higher dimensionality would be needed to represent three-dimensional (3-D) objects, objects with internal structure, objects of greater shape complexity, and objects defined by color and texture variations.

In a neural representation, the four dimensions in Figure 71.1 would constitute the tuning space for a large population of cells. Figures 71.1*B* and 71.1*C* can be thought of as 2-D projections of a single four-dimensional (4-D) domain. Each cell would have a tuning peak somewhere in the 4-D space, and tuning peaks would be distributed across the entire space. Each contour fragment would be represented by an activity peak in the population response. In other words, if all the neurons' responses were plotted, using a color scale, at their tuning peak locations in Figures 71.1*B* and 71.1*C*, there would be hot spots at the points corresponding to the object's contour fragments. Fragment *a*, for example, would be represented by strong activity in the tuning range labeled *a* in Figures 71.1*B* and 71.1*C*, that is, strong activity in neurons tuned for broad convexity oriented near 45 degrees and positioned near the upper right of the object. The bold 2 as a whole would be represented by the constellation of peaks indicated by all the lowercase letters.

The population response pattern would consist not only of punctate peaks. Regions of constant or gradually changing curvature would be represented by continuous ridges in curvature space. For example, the broad convex region labeled *a* in Figure 71.1*A* would be represented by an arch-shaped ridge running clockwise from 135 to 315 in Figure 71.1*B*, because it would stimulate cells sensitive to broad convex curvature at all those orientations. The sharp angle at *b*, on the other hand, would be represented by a punctate peak. The entire pattern of ridges and peaks would characterize the sequence of gradual and abrupt curvature changes in the shape. Neural representations are often thought of as single population activity peaks, but one study of motion coding has shown that the visual system can be sensitive to aspects of the population response pattern other than peak position (Treue et al., 2000).

Neural representation in terms of contour fragments would have some of the important characteristics required

for object perception. It would be relatively robust to variations in an object's retinal image such as size and position changes. The population pattern would be stable in the orientation and angular position dimensions, and it would scale uniformly in the curvature and radial position dimensions. If curvature and radial position were represented relative to object size, the pattern would be stable in those dimensions as well.

Contour fragment coding would also meet the requirement of similar representations for similar objects (second-order isomorphism). The numeral 2 rendered in other fonts (2, 2, 2, 2, 2, 2) would retain key features in the curvature representation, such as the broad convexity near the upper right and the sharp convexity near the lower left. In other words, all 2s would evoke a ridge somewhere near *a* and a peak somewhere near *b* in the 4-D population response space (Fig. 71.1). In fact, it is that kind of curvature pattern that defines the numeral 2 and allows us to generalize across the entire category of printed and handwritten 2s. Learning a shape category is a process of finding the characteristic features that define that category. It is critical that the neural representations of those features be consistent or at least grouped in neural tuning space.

Finally, because of its combinatorial, alphabet-like coding power, the scheme shown in Figure 71.1 would have the capacity and versatility to represent a virtual infinity of shapes composed of standard contour fragments. This could be accomplished by a reasonable number of neurons with tuning functions spanning the 4-D contour curvature space. As noted above, however, a higher-dimensional space would be required to represent more complex objects.

SHAPE RECOGNITION MODELS The coding scheme in Figure 71.1 is just one way to parameterize shape. There are a number of theoretical ideas about shape primitives or shape dimensions (both of which can be grouped under the general heading of *shape descriptors*). Most theories posit a hierarchical progression of parts complexity, with each stage in the processing pathway receiving input signals for simpler parts and synthesizing them into output signals for more complex parts (Barlow, 1972; Hubel and Wiesel, 1959, 1968). In almost all models, the first level of shape description is local linear orientation (i.e., orientation of straight edges and lines). This choice is dictated by the overwhelming evidence that linear orientation is accurately and explicitly represented by cells at early stages in the ventral pathway (V1 and V2) (Baizer et al., 1977; Burkhalter and Van Essen, 1986; Hubel and Livingstone, 1987; Hubel and Wiesel, 1959, 1965, 1968).

Theories diverge concerning higher-level shape descriptors. Marr distinguished two general possibilities: boundary or surface-based descriptors and axial or volumetric descriptors (Marr and Nishihara, 1978). The contour

curvature scheme illustrated in Figure 71.1 is a surface-based description; it encodes the shape boundary, specifically the 2-D outline. This is a complete description of a flat silhouette shape like the numeral 2. It would also capture much of the important information about a 3-D shape and could even be used to infer 3-D surface shape (Koenderink, 1984). The potential importance of contour curvature was recognized by Attneave (1954), who pointed out that shape information is concentrated in contours at regions of high curvature, including angles. Angles may be particularly significant, because they are invariant to transformations in scale and can be easily derived by summing inputs from cells tuned for edge orientation (Milner, 1974). Contour curvature could serve as a final description level (Hoffman and Richards, 1984) or it could be used to infer the structure of more complex parts (Biederman, 1987; Dickinson et al., 1992; Hummel and Biederman, 1992).

Axial or volumetric descriptors constitute the ultimate level of representation in many theories. A volumetric primitive is a solid part, defined by the shape (straight or curved) and orientation (2-D or 3-D) of its medial axis. A complete object description in terms of medial axes is like a stick-figure drawing. That description can be refined with other parameters to represent how object mass is disposed about the axes—what the cross-sectional shape is and how width varies along the axis. A volumetric description of the bold numeral 2 would involve three medial axes, one curved and two straight, with corresponding width functions to specify the thick/thin structure of the font. (Cross-section would not be an issue for a flat 2-D shape.)

Volumetric primitives are also known as *generalized cones* (Marr and Nishihara, 1978; a generalized cone is constructed by sweeping a cross-section of constant shape but smoothly varying size along an axis) or *geons* (Biederman, 1987). Marr argued that a volumetric description would be more compact and stable than a surface-based description. For most alphanumeric symbols, the axis-defining dimensions would capture the stable, category-defining characteristics. More variable (e.g., font-specific) contour information would be segregated into the width and cross-sectional dimensions. However, medial axes must initially be inferred from surface or boundary information. This requires first segmenting the surface contour into parts (Marr and Nishihara, 1978), probably at regions of high concave curvature, because these represent joints between interpenetrating volumes (Hoffman and Richards, 1984). The medial axis for each part would then be derived from its contours. Some authors have proposed mechanisms for inferring 3-D volumetric structure from certain characteristic 2-D contour configurations (Biederman, 1987; Dickinson et al., 1992; Lowe, 1985).

As discussed above, a complete structural representation requires not just a list of primitives but also a description of

their spatial arrangement (as in Fig. 71.1C). Spatial information is initially available to the visual system in retinotopic coordinates. Because the retinal image of an object is so variable, it would be useful to transform spatial information into an object-centered reference frame (but see Edelman and Intrator, 2000, who argue that coarse retinotopy would suffice). At the least, the object could define the center of the reference frame, so that changes in position on the retina would not alter the neural representation. In other words, neural shape responses would be position invariant at the final level of representation. The object might also define the scale of the reference frame, meaning that shape responses would be size invariant at the final level. This would make the neural representation stable across changes in viewing distance.

Some theories would limit the spatial transformation to these two changes—position and scale (e.g., Fig. 71.1C). The orientation of the reference frame would still be defined by the retina or by the head, body, or world (which are usually aligned with the retina). If so, the neural representation would change when the object rotated in either 2-D space (around an axis pointing toward the viewer, e.g., turning upside down) or 3-D space (around any other axis, e.g., rotating around a vertical axis). Dealing with viewpoint changes of this kind is one of the most difficult aspects of shape recognition. One idea is that neural shape representations are viewpoint-dependent—different views of the same object are represented differently—and the visual system learns to recognize an object by storing a limited set of *canonical* views (Poggio and Edelman, 1990; Tarr and Pinker, 1989; Vetter et al., 1995). Intermediate views would be handled by neural mechanisms for interpolating between the canonical views (Poggio and Edelman, 1990). A more absolute solution to the viewpoint problem is to transform the structural description into a 3-D reference frame defined completely (in position, scale, and orientation) with respect to the object (Biederman, 1987; Dickinson et al., 1992). This would yield a more stable neural representation, but it would require complex mechanisms for inferring and synthesizing 3-D structure.

Mel and Fiser (2000) have described an alternative to encoding each part position in a single spatial reference frame. Units sensitive to part (or *feature*) conjunctions can represent not only identity but also local connectivity between parts. In the example in Figure 71.2, some neurons might be tuned for the conjunction of fragments *a* and *b*, others for *b-c*, others for *c-d*, and so on. The response pattern across a population of such units would constitute a unique representation for the bold numeral 2. In effect, the local conjunctions would be concatenated to specify the entire sequence of contour fragments. As discussed below, recent neurophysiological results provide support for this idea (Pasupathy and Connor, 2001).

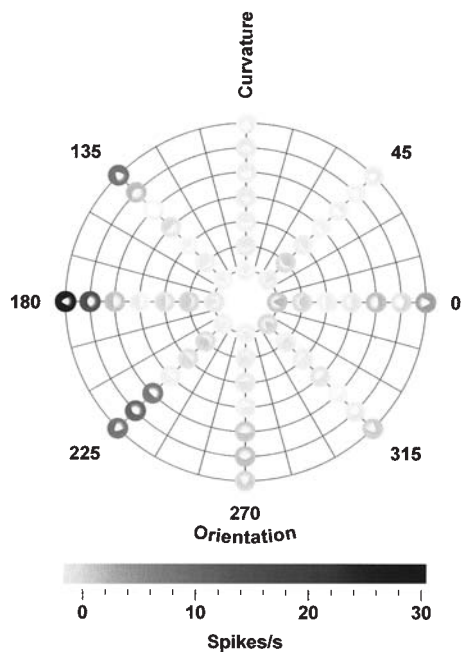


FIGURE 71.2. Tuning of a single macaque area V4 neuron in the curvature \times orientation domain. The gray circular backgrounds indicate the neuron's average responses to each of the stimuli (white icons). The scale bar shows that light backgrounds correspond to response rates near zero, dark backgrounds to response rates near 30 spikes per second.

The general alternative to parts-based or structural representation is holistic representation—coding schemes in which each signal carries information about an entire object or an entire scene rather than just one part. Fourier-like decomposition, with basis functions extending across the entire domain, is an example. Edelman proposes that shapes are represented in a multidimensional space defined by pointwise information across whole objects. The high dimensionality of a point-based representation can be reduced by describing a novel shape in terms of its distances from a limited number of learned reference shapes (Edelman, 1999). A recent extension of this theory posits that the reference shapes could be object fragments and that the positions of those fragments could be represented in retinotopic or object-centered space (Edelman and Intrator, 2000). This would constitute a flexible, learning-based (and explicitly continuous) version of structural representation. Ullman (1996) proposes that an object is recognized by virtual (neural) alignment of its complete retinal image (through appropriate translation, scaling, and rotation) and pointwise matching with a shape template stored in memory. He notes that this approach could also be integrated with structural decomposition mechanisms.

Structural representation: evidence

Much of the available neuroscientific evidence is at least consistent with structural representation of shape. There

are some results that directly support the theory. As in the first section, an example will be considered in detail before we move on to a general description of the literature.

EXAMPLE: CONTOUR FRAGMENT REPRESENTATION IN AREA V4
If the visual system explicitly encodes shape in terms of parts-level structural dimensions, as in Figure 71.1, at least three empirical results can be predicted:

1. Individual neurons should exhibit response rate tuning in those dimensions. There are other ways in which part structure might be encoded, but this would be the most explicit and useful.
2. Tuning function peaks should be distributed across the entire tuning space. This would be necessary for representing all possible part structures.
3. Tuning for parts-level structure should be consistent within different global shapes. For example, a cell tuned for sharp convex curvature oriented at 90 degrees and positioned at 90 degrees should respond to arrows (\uparrow), triangles (\blacktriangle), diamonds (\blacklozenge), and so on. This is the most novel prediction, since shape-tuning functions are usually conceived in terms of a single optimal global shape.

This section will describe how these three predictions are met for contour fragment representation in area V4.

V4 is an intermediate stage in the ventral, object-processing pathway of the primate visual system (Felleman and Van Essen, 1991; Ungerleider and Mishkin, 1982). It has been identified in humans through retinotopic mapping in functional magnetic resonance imaging (fMRI) experiments (DeYoe et al., 1996; Sereno et al., 1995). In the macaque monkey, V4 receives feedforward inputs from V1 and V2 and sends feedforward outputs to posterior and central parts of inferotemporal cortex (PIT and CIT) (Felleman and Van Essen, 1991). Because of its intermediate position in the shape-processing hierarchy, V4 has the potential to exhibit mechanistic details that may be obscured at higher levels. Many V4 neurons are tuned for linear orientation in the same way that V1 and V2 cells are (Desimone and Schein, 1987), but some are selective for more complex shape characteristics (Gallant et al., 1993, 1996; Kobatake and Tanaka, 1994). It is this latter group that is considered here.

Many V4 neurons are tuned for contour fragment shape, as hypothesized in Figure 71.1B (Pasupathy and Connor, 1999, 2001, 2002). The example cell in Figure 71.2 was studied in an awake macaque monkey performing a fixation task while contour stimuli were flashed in the cell's receptive field. The stimuli are depicted as small white icons against circular gray backgrounds. In the actual experiment, the

stimuli were presented in the optimal color for the cell against a uniform gray background covering the rest of the display screen. The stimuli were convex or concave contour fragments. The relevant contour fragment was defined by a sharp luminance transition, but the rest of the stimulus faded gradually into the background gray, as though one part of a larger object was illuminated with a spotlight. The stimuli are plotted on a polar curvature \times orientation domain, as in Figure 71.1*B*. Curvature gradually progresses from sharp concave (negative) at the center of the plot through flat (0) to sharp convex (positive) at the periphery. The average response to each stimulus is indicated by the gray level of its background circle (see the scale bar).

This neuron was tuned for acute convex curvature oriented toward the left. The sharpest convexity (outer ring) at 180 degrees evoked a response of 30 spikes per second. Stimuli nearby (in curvature space) evoked somewhat weaker responses, and distant stimuli evoked little or no response. Approximately one-third of V4 neurons exhibit this kind of graded tuning for curvature and orientation (Pasupathy and Connor, 1999). Tuning peaks are distributed across the entire extent of both dimensions, although there is a population-level bias toward sharper convex curvature.

These cells are also tuned for contour fragment position, as hypothesized in Figure 71.1*C*. The example cell in Figure 71.3 was shown in previous tests to be tuned for sharp convex curvature at orientations in the 0 to 270 degree range (lower right quadrant). Figure 71.3 shows how the cell responded to stimuli containing sharp convexities at a variety of positions relative to object center. Stimulus shape is again represented by the white icons, and average response is indicated by the surrounding gray circles (see the scale bar at the bottom). Relative position was varied by changing the configuration of the elliptical base from which the sharp convexity projected. Stimuli are plotted on a polar grid (as in Fig. 71.1*C*) according to the relative position of the sharp convexity. Relative position tuning was tested for three curvature orientations: 270 degrees (Fig. 71.3*A*), 315 degrees (Fig. 71.3*B*), and 0 degrees (Fig. 71.3*C*). In all three cases, the neuron displayed gradual position tuning with a peak near 315 degrees. Control tests in which the overall stimulus position was varied (not shown) proved that this kind of tuning depended on relative position, not absolute position on the retina. Also, the response pattern does not merely reflect a global shape preference. The optimum shape in the top plot is similar to a right apostrophe (’), while the optimum shape in the bottom plot is similar to a left apostrophe on its side. The consistent factor is the position of the sharp convexity relative to the object center. Most curvature-sensitive V4 neurons exhibit this kind of relative position tuning for contour fragments (Pasupathy and Connor, 2001). In the example in Figure 71.3, the curvature orientation and angular position peaks are similar (315 degrees), but exper-

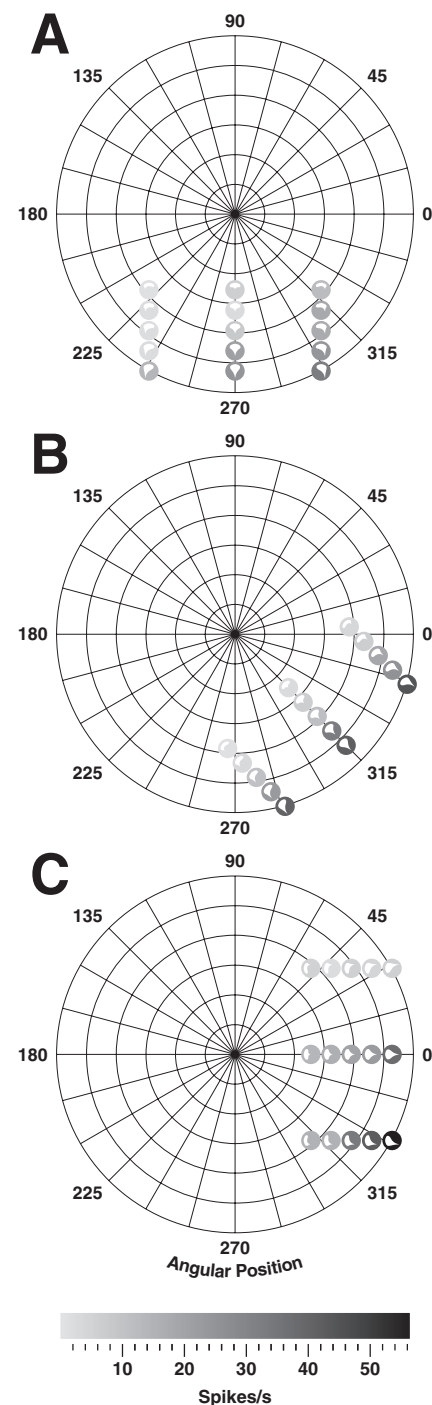


FIGURE 71.3. Tuning of a single macaque area V4 neuron for the position of a sharp convexity relative to object center. The convexities are oriented at 270 degrees (*A*), 315 degrees (*B*), and 0/360 degrees (*C*). The gray circular backgrounds indicate the neuron's average responses (see the scale bar) to each of the stimuli (white icons). The stimuli are plotted on a polar domain representing object-centered position.

iments with more complex shapes in PIT/CIT have shown that orientation and angular position can be dissociated. For example, a neuron can be tuned for curvature oriented at 90 degrees (pointing upward) but positioned at 0 degrees (to the right of object center; Brincat and Connor, 2001).

Thus, V4 neurons are tuned for contour fragment shape and position, and tuning peaks are distributed across shape space, fulfilling predictions 1 and 2. Moreover, this kind of tuning is consistent within different global shape contexts (prediction 3). The example cell in Figure 71.4 was responsive to sharp convex curvature oriented at 225 degrees. This cell was tested with a large set of shapes constructed by systematically combining contour fragments at various curvatures and orientations. Each stimulus is represented by a white icon within a gray circle indicating the average response of the cell (see the scale bar on the right). The stimuli are plotted in order of response strength. The stimuli that evoked the strongest responses all contained relatively acute convex curvature oriented at 225 degrees located near the lower left of the object (top rows). Stimuli without this feature evoked little or no response (bottom rows). The effective stimuli varied widely in global shape; the top row of Figure 71.4 includes crescents, triangles, raindrops, and so on. Similar results were obtained for the majority of curvature-sensitive cells in area V4 (Pasupathy and Connor, 2001), and population analysis revealed multi-peaked shape representations comparable to that hypothesized in Figure 71.1 (Pasupathy and Connor, 2002). Significantly, many cells were sensitive to conjunctions of two or three curvature fragments. The cell in Figure 71.4 was most responsive to sharp convexities conjoined in the counterclockwise direction to broader concavities (top rows). Shapes with sharp convexities conjoined to broad *convexities* evoked weaker

responses. The majority of V4 neurons (94/109) were significantly tuned for conjunctive curvature fragments. This could imply that spatial configuration is represented in terms of local connectivity (Mel and Fiser, 2000; see above).

Thus, V4 neurons have the basic response characteristics necessary to represent simple 2-D silhouette shapes in terms of their contour components. The precise choice of dimensions is arbitrary; the same tuning properties could be captured more or less effectively by a number of equivalent parameterizations (e.g., in terms of medial axis shape and width functions). Higher dimensionality might capture response properties more precisely, since some V4 cells appear to be tuned for contour fragments of greater complexity. The cell in Figure 71.4, for example, is most responsive to sharp convexities flanked by a concavity near the bottom of the shape (for further details, see Pasupathy and Connor, 2001). The important points, regardless of exact tuning dimensions, are that

1. Area V4 neurons are tuned for shape and relative position of object components.
2. Tuning functions are distributed across the entire range of shape and position.
3. Component-level tuning is consistent across different global shape contexts.

These properties imply that shape representation in area V4 is structural—that objects are represented in terms of their constituent parts.

STRUCTURAL REPRESENTATION IN THE VENTRAL PATHWAY
The ventral, object-processing pathway originates in primary visual cortex (V1) and continues (in the macaque monkey) through areas V2, V4, PIT (posterior inferotem-

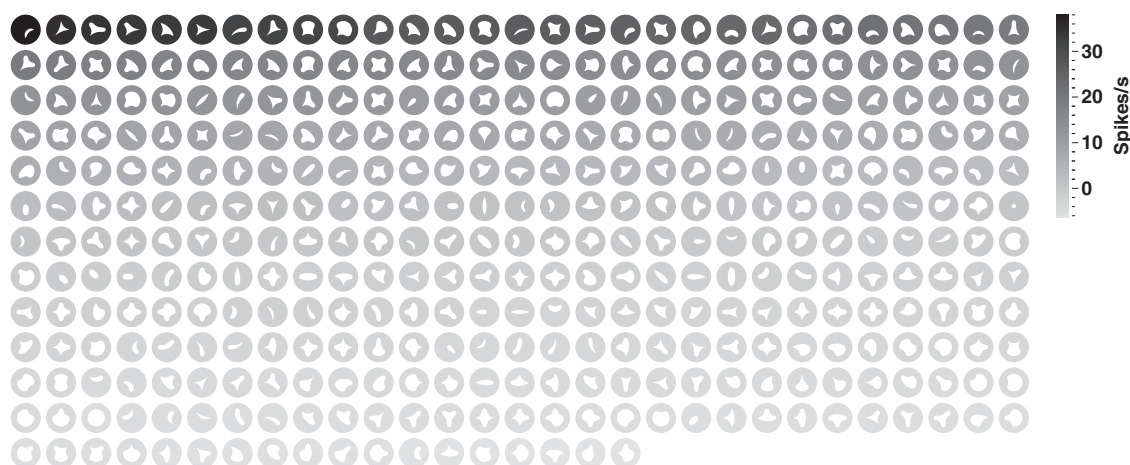


FIGURE 71.4. Tuning of a single macaque area V4 neuron for sharp convexity near the lower left (relative to object center) in a variety of global shape contexts. Shape stimuli (*white icons*) were constructed by systematically combining convex and concave frag-

ments into continuous closed contours. The gray circular backgrounds indicate the neuron's average responses (see the scale bar) to each of the stimuli.

poral cortex, also called TE), CIT, and AIT (central and anterior inferotemporal cortex, also called TE). Anatomical studies have shown that these areas are densely interconnected. The pattern of feedforward and feedback projections suggests a hierarchy in which V1 is the earliest processing stage and IT the latest and presumably most advanced (Felleman and Van Essen, 1991). Receptive field size and response complexity increase gradually through the pathway. These properties are consistent with the notion of hierarchical shape processing—the idea that simpler parts-level information is extracted at early processing stages, then synthesized at later stages to infer more complex parts structure (Barlow, 1972; Hubel and Wiesel, 1959, 1968).

If parts-based shape processing is hierarchical, it is clear that the first stage involves local orientation of lines, edges, and other extended image elements. This is the primary shape-related tuning dimension in V1 and V2 (Baizer et al., 1977; Burkhalter and Van Essen, 1986; Hubel and Livingstone, 1987; Hubel and Wiesel, 1959, 1965, 1968). It is also prominent at intermediate stages in the ventral pathway—V4 (Desimone and Schein, 1987) and PIT (Tanaka et al., 1991). Orientation tuning has often been interpreted as the first stage in a parts-processing hierarchy, though it has also been viewed as the first stage in a Fourier-like representation (Shapley and Lennie, 1985). If the parts-based hypothesis is correct, orientation signals could be combined to infer more complex contour information of the sort represented in area V4 (see above). Orientation tuning could also lead toward a medial axis-based representation. Lee and colleagues (1998) demonstrated a small but explicit signal for medial axes in area V1, and this could foreshadow more complex axial representation at later stages. According to some theories, orientation signals would be combined to infer the structure of complex 3-D primitives (Biederman, 1987; Dickinson et al., 1992). This has usually been envisioned as a process of detecting unusual configurations (*nonaccidental properties*) in the 2-D image that imply 3-D structure (Lowe, 1985). However, a recent study of area V4 revealed strong signals for 3-D orientation that could be used directly for deriving 3-D parts structure (Hinkle and Connor, 2002).

More complex contour fragments, such as angles and curves, could constitute a second level of structural complexity. The evidence for this in area V4 was discussed in the preceding section. Tuning for contour fragment shape and relative position appears to be even more prominent in PIT/CIT (Brincat and Connor, 2001). Selectivity for angles and curves has also been studied at earlier stages in the ventral pathway: V1 and V2 (Dobbins et al., 1987; Hammond and Andrews, 1978; Hegde and Van Essen, 2000; Heggelund and Hohmann, 1975; Hubel and Wiesel, 1965; Versavel et al., 1990). It should be noted that curvature tuning could also be consistent with holistic representation. Many V4 neurons are selective for curvilinear grating

stimuli (concentric, hyperbolic, and spiral), suggesting that curvature information may be summed in a global fashion (Gallant et al., 1993, 1996; Wilson, 1999).

Shape selectivity at higher stages in IT cortex is clearly complex and often related to behaviorally relevant object categories (Desimone et al., 1984). There are some results suggesting that this complex selectivity relates to part structure rather than global or holistic shape. Fujita and colleagues (1992) described a columnar (patchy) arrangement of responses to shape features. Examples presented in that report and others (Tanaka et al., 1991) show selectivity for parts-level features in a variety of global shape contexts (meeting prediction 3 in the previous section). Tsunoda et al. (2001) recently used optical imaging of surface cortex in IT to compare columnar activation by different stimuli. They presented striking examples in which shapes with partially overlapping part structures also evoked activity in partially overlapping sets of columns.

Perrett et al. (1982) tested cells in the fundus of the superior temporal sulcus (STS) that were selectively responsive to face stimuli. They found that many cells responded to multiple component facial features with very different shapes (e.g., eyes and hair), suggesting a parts-based synthesis (see also Chapter 78). Wang et al. (2000) used bicuculline to block inhibitory inputs to shape-selective IT neurons. This enhanced responses to previously effective shape stimuli, and in many cases also revealed responses to components of those stimuli. The revealed responses could reflect sub-threshold parts-related inputs that contribute to complex shape selectivity under normal conditions.

Several recent parametric studies of shape tuning in IT bear on the issue of structural representation. Sigala and Logothetis (2002) trained monkeys to discriminate two categories of cartoon faces. The two categories were distinguished by variations in eye separation and eye height. Mouth height and nose length also varied but were irrelevant to the categorization task. IT neurons showed higher selectivity for the two behaviorally relevant shape parameters. Thus, IT shape tuning functions seem to be modifiable at the level of object parts, suggesting a structural coding scheme. Yamane and colleagues (Yamane et al., 1988; Young and Yamane, 1992) parameterized photographic human faces in terms of distances between facial features. They found that STS and IT responses were best explained in terms of combinations of multiple distance measurements from various parts of the face, implying a holistic representation.

Op de Beeck and colleagues (2001) studied variations in silhouette shapes constructed by combining radial frequency components. Radial frequency functions are Fourier-like descriptors for variations in the radius of closed curves. Gradual changes in radial frequency component amplitudes produced parametric variations in overall stimulus shape.

Within groups of gradually varying stimuli, IT neurons showed smooth unimodal tuning along the dimensions defined by radial frequency amplitudes. The entire shape, not just single parts, varied along these dimensions. Thus, smooth tuning could be taken as evidence for global or holistic (rather than structural or parts-based) shape representation. However, smooth tuning might have depended on variations in specific parts of the shapes. Also, individual neurons tended to respond well to very different shapes from multiple groups, perhaps reflecting a common parts-level structure. At the population level, though, responses to the different shape groups were appropriately distinct. Notably, training monkeys to perform different categorization tasks (within groups) produced no discernible differences in neural representation. Baker et al. (2002) trained monkeys to discriminate abstract shapes formed by combining top and bottom parts in a factorial cross. Both parts-level and holistic tuning were enhanced for learned as compared to unlearned shapes, suggesting a mixed coding strategy.

Summary

Visual shape recognition is a daunting neurocomputational problem due to the virtual infinity of object shapes and the variability of a given object's retinal image. Both problems could be overcome by representing objects in terms of their constituent parts or primitives. This kind of structural coding scheme would depend on neurons tuned in a multidimensional space representing part shape and relative position. A number of recent studies of neural responses in the ventral (object-related) pathway of primate visual cortex are consistent with such a scheme. Other results imply a more holistic representation of global shape. Further parametric studies of shape tuning will be needed to fully elucidate the neural coding principles in the ventral pathway.

REFERENCES

- Attneave, F., 1954. Some informational aspects of visual perception, *Psychol. Rev.*, 61:183–193.
- Baker, C. I., M. Behrmann, and C. R. Olson, 2002. Impact of learning on representation of parts and wholes in monkey inferotemporal cortex, *Nat. Neurosci.*, 5:1210–1214.
- Baizer, J. S., D. L. Robinson, and B. M. Dow, 1977. Visual responses of area 18 neurons in awake, behaving monkey, *J. Neurophysiol.*, 40:1024–1037.
- Barlow, H. B., 1972. Single units and sensation: a neuron doctrine for perceptual psychology? *Perception*, 1:371–394.
- Biederman, I., 1987. Recognition-by-components: a theory of human image understanding, *Psychol. Rev.*, 94:115–147.
- Brincat, S. L., and C. E. Connor, 2001. Quantitative characterization of parts-based shape coding in IT cortex, *Soc. Neurosci. Abstr.*, 27.
- Burkhalter, A., and D. C. Van Essen, 1986. Processing of color, form and disparity information in visual areas VP and V2 of ventral extrastriate cortex in the macaque monkey, *J. Neurosci.*, 6:2327–2351.
- Desimone, R., T. D. Albright, C. G. Gross, and C. Bruce, 1984. Stimulus-selective properties of inferior temporal neurons in the macaque, *J. Neurosci.*, 4:2051–2062.
- Desimone, R., and S. J. Schein, 1987. Visual properties of neurons in area V4 of the macaque: sensitivity to stimulus form, *J. Neurophysiol.*, 57:835–868.
- DeYoe, E. A., G. J. Carman, P. Bandettini, S. Glickman, J. Wieser, R. Cox, D. Miller, and J. Neitz, 1996. Mapping striate and extrastriate visual areas in human cerebral cortex, *Proc. Natl. Acad. Sci. USA*, 93:2382–2386.
- Dickinson, S. J., A. P. Pentland, and A. Rosenfeld, 1992. From volumes to views: an approach to 3-D object recognition, *CVGP: Image Understanding*, 55:130–154.
- Dobbins, A., S. W. Zucker, and M. S. Cynader, 1987. Endstopped neurons in the visual cortex as a substrate for calculating curvature, *Nature*, 329:438–441.
- Edelman, S., 1999. *Representation and Recognition in Vision*, Cambridge, MA: MIT Press.
- Edelman, S., and N. Intrator, 2000. (Coarse coding of shape fragments) + (retinotopy) approximately = representation of structure, *Spatial Vis.*, 13:255–264.
- Felleman, D. J., and D. C. Van Essen, 1991. Distributed hierarchical processing in the primate cerebral cortex, *Cereb. Cortex*, 1:1–47.
- Fujita, I., K. Tanaka, M. Ito, and K. Cheng, 1992. Columns for visual features of objects in monkey inferotemporal cortex, *Nature*, 360:343–346.
- Gallant, J. L., J. Braun, and D. C. Van Essen, 1993. Selectivity for polar, hyperbolic, and Cartesian gratings in macaque visual cortex, *Science*, 259:100–103.
- Gallant, J. L., C. E. Connor, S. Rakshit, J. W. Lewis, and D. C. Van Essen, 1996. Neural responses to polar, hyperbolic, and Cartesian gratings in area V4 of the macaque monkey, *J. Neurophysiol.*, 76:2718–2739.
- Hammond, P., and D. P. Andrews, 1978. Collinearity tolerance of cells in areas 17 and 18 of the cat's visual cortex: relative sensitivity to straight lines and chevrons, *Exp. Brain Res.*, 31:329–339.
- Hegde, J., and D. C. Van Essen, 2000. Selectivity for complex shapes in primate visual area V2, *J. Neurosci.* (online), 20:RC61.
- Heggelund, P., and A. Hohmann, 1975. Responses of striate cortical cells to moving edges of different curvatures, *Exp. Brain Res.*, 23:211–216.
- Hinkle, D. A., and C. E. Connor, 2002. Three-dimensional orientation tuning in macaque area V4, *Nat. Neurosci.*, 5:665–670.
- Hoffman, D. D., and W. A. Richards, 1984. Parts of recognition, *Cognition*, 18:65–96.
- Hubel, D. H., and M. S. Livingstone, 1987. Segregation of form, color, and stereopsis in primate area 18, *J. Neurosci.*, 7:3378–3415.
- Hubel, D. H., and T. N. Wiesel, 1959. RFs of single neurones in the cat's striate cortex, *J. Physiol. (Lond.)*, 148:574–591.
- Hubel, D. H., and T. N. Wiesel, 1965. RFs and functional architecture in two nonstriate visual areas (18 and 19) of the cat, *J. Neurophysiol.*, 28:229–289.
- Hubel, D. H., and T. N. Wiesel, 1968. Receptive fields and functional architecture of monkey striate cortex, *J. Physiol. (Lond.)*, 195:215–243.
- Hummel, J. E., and I. Biederman, 1992. Dynamic binding in a neural network for shape recognition, *Psychol. Rev.*, 99:480–517.

- Kobatake, E., and K. Tanaka, 1994. Neuronal selectivities to complex object features in the ventral visual pathway of the macaque cerebral cortex, *J. Neurophysiol.*, 71:856–867.
- Koenderink, J. J., 1984. What does the occluding contour tell us about solid shape? *Perception*, 13:321–330.
- Lee, T. S., D. Mumford, R. Romero, and V. A. Lamme, 1998. The role of the primary visual cortex in higher level vision, *Vis. Res.*, 38:2429–2454.
- Lowe, D., 1985. *Perceptual organization and visual recognition*, Boston, MA: Kluwer Academic Publishers.
- Marr, D., and H. K. Nishihara, 1978. Representation and recognition of the spatial organization of three-dimensional shapes, *Proc. R. Soc. Lond. B Biol. Sci.*, 200:269–294.
- Mel, B. W., and J. Fiser, 2000. Minimizing binding errors using learned conjunctive features, *Neural Comput.*, 12:731–762.
- Milner, P. M., 1974. A model for visual shape recognition, *Psychol. Rev.*, 81:521–535.
- Op de Beeck, H., J. Wagemans, and R. Vogels, 2001. Inferotemporal neurons represent low-dimensional configurations of parameterized shapes, *Nat. Neurosci.*, 4:1244–1252.
- Pasupathy, A., and C. E. Connor, 1999. Responses to contour features in macaque area V4, *J. Neurophysiol.*, 82:2490–2502.
- Pasupathy, A., and C. E. Connor, 2001. Shape representation in area V4: position-specific tuning for boundary conformation, *J. Neurophysiol.*, 86:2505–2519.
- Pasupathy, A., and C. E. Connor, 2002. Population coding of shape in area V4, *Nat. Neurosci.*, 5:1332–1338.
- Perrett, D. I., E. T. Rolls, and W. Caan, 1982. Visual neurones responsive to faces in the monkey temporal cortex, *Exp. Brain Res.*, 47:329–342.
- Poggio, T., and S. Edelman, 1990. A network that learns to recognize three-dimensional objects, *Nature*, 343:263–266.
- Selfridge, O. G., 1959. Pandemonium: a paradigm for learning, in *The Mechanization of Thought Processes*, London: H. M. Stationary Office.
- Sereno, M. I., A. M. Dale, J. B. Reppas, K. K. Kwong, J. W. Belliveau, T. J. Brady, B. R. Rosen, and R. B. Tootell, 1995. Borders of multiple visual areas in humans revealed by functional magnetic resonance imaging, *Science*, 268:889–893.
- Shapley, R., and P. Lennie, 1985. Spatial frequency analysis in the visual system, *Annu. Rev. Neurosci.*, 8:547–583.
- Sigala, N., and N. K. Logothetis, 2002. Visual categorization shapes feature selectivity in the primate temporal cortex, *Nature*, 415:318–320.
- Sutherland, N. S., 1968. Outlines of a theory of visual pattern recognition in animals and man, *Proc. R. Soc. Lond. B Biol. Sci.*, 171:297–317.
- Tanaka, K., H. Saito, Y. Fukada, and M. Morioka, 1991. Coding visual images of objects in the inferotemporal cortex of the macaque monkey, *J. Neurophysiol.*, 66:170–189.
- Tarr, M. J., and S. Pinker, 1989. Mental rotation and orientation-dependence in shape recognition, *Cogn. Psychol.*, 21:233–282.
- Treue, S., K. Hol, and H. J. Rauber, 2000. Seeing multiple directions of motion-physiology and psychophysics, *Nat. Neurosci.*, 3:270–276.
- Tsunoda, K., Y. Yamane, M. Nishizaki, and M. Tanifuji, 2001. Complex objects are represented in macaque inferotemporal cortex by the combination of feature columns, *Nat. Neurosci.*, 4:832–838.
- Ullman, S., 1996. *High-Level Vision*, Cambridge, MA: MIT Press.
- Ungerleider, L. G., and M. Mishkin, 1982. Two cortical visual systems, in *Analysis of Visual Behavior* (D. G. Ingle, M. A. Goodale, and R. J. Q. Mansfield, eds.), Cambridge, MA: MIT Press, pp. 549–586.
- Versavel, M., G. A. Orban, and L. Lagae, 1990. Responses of visual cortical neurons to curved stimuli and chevrons, *Vis. Res.*, 30:235–248.
- Vetter, T., A. Hurlbert, and T. Poggio, 1995. View-based models of 3D object recognition: invariance to imaging transformations, *Cereb. Cortex*, 5:261–269.
- Wang, Y., I. Fujita, and Y. Murayama, 2000. Neuronal mechanisms of selectivity for object features revealed by blocking inhibition in inferotemporal cortex, *Nat. Neurosci.*, 3:807–813.
- Wilson, H. R., 1999. Non-Fourier cortical processes in texture, form, and motion perception, in *Cerebral Cortex*, vol. XIII (P. S. Ulinski & E. G. Jones, eds.), New York: Plenum, pp. 445–477.
- Yamane, S., S. Kaji, and K. Kawano, 1988. What facial features activate face neurons in the inferotemporal cortex of the monkey? *Exp. Brain Res.*, 73:209–214.
- Young, M. P., and S. Yamane, 1992. Sparse population coding of faces in the inferotemporal cortex, *Science*, 256:1327–1331.

72 Shape and Shading

JAN J. KOENDERINK AND ANDREA J. VAN DOORN

THE HUMAN OBSERVER is able to perceive the geometrical structure of objects, and many of their physical and chemical properties, from the radiation scattered toward the eye. The observer also perceives the *light field*, that is, the primary and secondary sources of radiation and how radiation pervades space. Although the dynamics of the interaction of the observer with the environment is very important, here we deal only with the monocular, static observer. Most of the optical structure available to such an observer is (approximately) available from pictures (photographs, computer graphics, paintings) of the environment. We abstract even further and will totally ignore spectral structure (*color*). We will not focus on the perception of material properties or on that of the light field, although these are interesting and highly relevant topics. Thus, we limit the discussion roughly to the domain of *pictorial shape from monochrome pictures*, photographs or renderings on computer screens. This has been a generic topic in visual psychophysics for over a century (Helmholtz, 1896; Hering, 1878; Kardos, 1934; Katz, 1911).

The light field

For the present purpose radiation is sufficiently described through *rays*, which are directed straight lines, or *photons*, which propagate via rectilinear orbits. These entities issue forth from *primary radiators* (the sun, light bulbs) and are scattered from objects that thereby become *secondary radiators*. Empty space (air will do) does not interact with the radiation. When rays or photons enter the eye, one “sees light” (or rather simply “sees”). *Light* is an aspect of consciousness; *radiation* is a physical entity that is never seen.

Consider empty space. It is filled with crisscrossing rays or swarms of photons. Consider some fiducial (and imaginary) volume element and add up the lengths of all rays that happen to cross it. When this total is divided by the volume, you obtain the volume (ray) density of radiation. Alternatively, you may count all photons that happen to be inside the volume within the span of 1 fiducial second of time. When this total is divided by the volume, you obtain the volume (photon) density. The two measures stand in a fixed ratio and need not be distinguished here. *Volume density* is important in *photo kinesis* of simple organisms but is rather irrelevant to the human observer.

One may also consider some fiducial (and imaginary) element of area and count all rays or photons that cross it (within 1 fiducial second, say). Add one for a crossing in one direction and subtract one for the crossing in the reverse direction (thus, you need an oriented area). The net count, divided by the area, depends upon the orientation of the area. For a small element, it is proportional to the cosine of the angle subtended by the surface normal and some direction that is characteristic of the light field. The magnitude and direction defined in this way comprise the *net flux vector*, which is an important descriptor of the light field (Gershun, 1939) (Fig. 72.1). It is the causal factor in the *photo taxis* of simple organisms. The net flux vector is the entity that photographers and interior designers (perhaps unknowingly) refer to when they discuss the “quality of the light.” Consider any closed loop in empty space. When you propagate the loop in the direction of the (local) net flux vector, you generate a tube. Area elements of the boundary of such tubes do not pass any net flux by construction (equally, many rays cross in either direction); thus, the light can be said to be transported by way of such *light tubes*. In contrast to light rays, light tubes are generally curved. They can even be closed. When a photographer refers to (diffuse) light “creeping around” an object, he or she is (unknowingly) referring to the tubes rather than the rays (Hunter and Fuqua, 1990) (Fig. 72.2). The human intuitive understanding of the behavior of diffuse light fields is based upon lifelong experience with net flux vector fields.

Finally (after volumes and surfaces), one may consider lines. How many rays go in a certain fiducial direction through some fiducial point? Clearly, *none*, for if the number of rays is finite, it is infinitely unlikely to meet with any specific possibility. In order to count a finite number of rays, one needs a finite “environment” of the fiducial ray, known as the *phase volume element* or *étendue* (Gershun, 1939; Moon and Spencer, 1981). The *étendue* is like a slender tube, characterized by the product of its (normal) cross-sectional area and its (solid) angular spread, for neighboring rays can be shifted in space or perturbed in direction. The number of rays in the tube divided by the *étendue* of the tube is the *radiance*. The radiance is the single most important entity for the human observer; what we refer to as the light field is simply the radiance distribution. Both the volume density and the net flux vector field can be derived (through suitably



FIGURE 72.1. This is one method used to observe (or even measure) the net flux vector field. Put a grease spot on a piece of bond paper. The spot appears lighter than the paper (*left*) if the back of the paper receives more irradiance than the front, whereas it appears darker than the paper (*right*) in the opposite case. The spot disappears (*center*) when the net flux vector lies in the plane of the paper. This way, you can easily map out the flux tubes in a room.

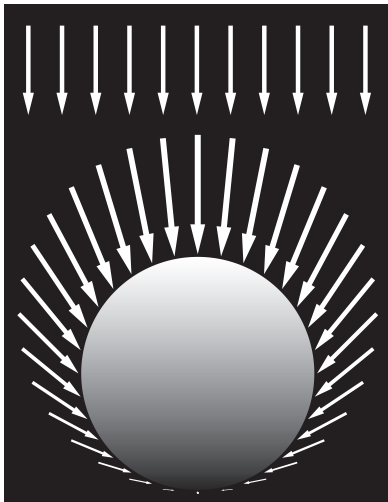


FIGURE 72.2. A uniform hemispherical diffuse beam is incident from above (the top row of arrows shows the direction of the incident net flux vector). The lower part of the figure shows how the net flux vector field is influenced by a black (fully absorbing) sphere. Both direction and magnitude are indicated. The illuminance on the surface of the sphere is indicated by shading. Notice that the whole surface is illuminated, also the part that faces away from the source. The obstacle influences both the magnitude and the direction of the net flux vector field: the light tubes “bend around the object.”

averaging over space and/or direction) from the radiance. In empty space the radiance is constant along straight lines. If you pick any point and consider all lines (directions) through the point, you obtain an extreme “fish-eye-like” picture: the radiance in all directions. Thus, the radiance contains all pictures you can shoot from any point in any direction. Indeed, an excellent (because very intuitive) way to think of the radiance is as an infinite filing cabinet [like Borges’s (1970) creepy library] of all possible pictures of your world. Such an intuitive grasp was, for instance, used by Gibson (1950) in his book on ecological optics. The concept of radiance has existed for centuries [Leonardo da Vinci (1927) understood it; the first to achieve some formal

understanding were Lambert (1760) and Bouguer (1729) in the eighteenth century]. Very nice introductions are Gershun’s (1939) paper and Moon and Spencer’s (1981) book (which unfortunately suffers from arcane terminology), but the literature tends to associate the notion with Adelson and Bergen’s (1991) *plenoptic function*.

Rays and light tubes originate from primary radiators and may end at absorbing (blackish) surfaces. They typically neither start nor end in empty space. The only exceptions are spatial *sources* or *sinks*. For instance, a volume of air may become a secondary source due to scattering of sunlight. This is important in *atmospheric perspective* [or *air light* (Koschmieder, 1924)]. Likewise, black smoke may cause the air to kill rays in midflight and thus form a sink. For the sake of simplicity, we will not consider such cases here.

Objects in the light field

Most objects in our ken are opaque and scatter photons at their surfaces. When a photon hits the surface from some direction, it is either absorbed or scattered in another direction. The probability of absorption depends on the direction of incidence, the probability of scattering depends on both the direction of incidence and the direction of exit. We are typically interested only in exit directions that send the ray to our eye; thus, we often refer to the exit direction as the *viewing direction*. The surface of any object is constantly bombarded by photons. The number of incident rays per surface area is the *irradiance* of the surface. The (scattered) radiance in the viewing direction divided by (because due to) the irradiance caused by rays from a certain direction of incidence is called the *bidirectional reflectance distribution function* (BRDF) (Koenderink and van Doorn, 1996a, 1996b, 1998; Koenderink et al., 1999; Nicodemus et al., 1977). The BRDF depends upon two directions and thus four angular parameters. For most common materials, the BRDF is a very complicated function indeed (CURET, 1997) (Figs. 72.3 and 72.4).

Wouldn’t it be nice if the radiance depended not on the viewing direction or on the direction of incidence, but only on the irradiance? Then the BRDF would be a constant instead of a four-parameter function. Alas, such surfaces don’t exist. They can be imagined, though, and were first conceived of by Lambert (1760), who noticed the remarkable fact that a whitewashed wall looks pretty much the same from all vantage points. Some matte surfaces (paper, plaster) actually come somewhat close. Virtually all theory and psychophysics on *shape from shading* (Horn and Brooks, 1989) applies to these imaginary surfaces (in psychophysics the stimuli are virtual—a computer screen—rather than real). Since actual surfaces are different, this should give rise to some concern.

A “white” Lambertian surface scatters all photons and absorbs none. It has a BRDF of $1/\pi$ and is said to possess

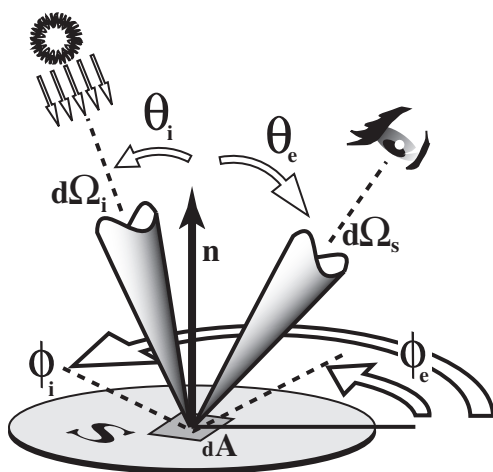


FIGURE 72.3. The definition of the BRDF. A narrow beam (angular spread indicated by the incident cone) irradiates the surface S (specified via its normal n). The surface is viewed from another direction. The BRDF is the radiance of the scattered beam divided by the irradiance caused by the incident beam. It depends on all the angles indicated in the diagram.



FIGURE 72.4. Two spheres on a desk illuminated by a window and several fluorescent overhead lights. Notice that the multiple sources are immediately apparent from the appearance of the metallic sphere, whereas the Lambertian sphere appears shaded by the “average source.” The cluttered objects in its environment largely cause the radiance pattern due to the metallic sphere, whereas that of the Lambertian sphere looks like a fairly standard textbook rendering. The BRDF of surfaces is just as important as the light field in shaping the radiance field.

unit *whiteness* (the technical term is *albedo*). If the surface receives unit irradiance (e.g., 1 mole—Avogadro’s number, or 6.0225×10^{23} —of photons per square meter in a second), the radiance of the beam scattered in all directions is $1/\pi$ mole photons per square meter, per second, and per unit solid angle (steradian). Since the photons are scattered into a half space (subtending a solid angle of 2π), there might be concern that a factor of 2 is missing here. It is not, though; the difference is due to the averaging over the slant of the

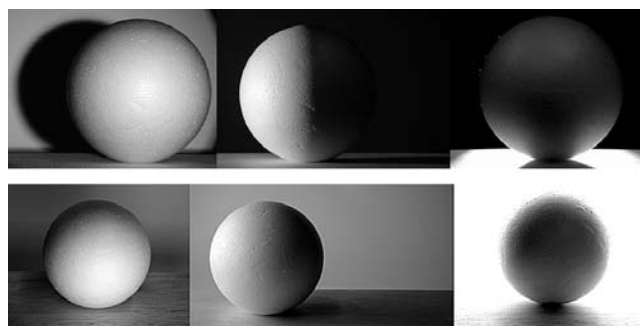


FIGURE 72.5. A white, matte sphere illuminated with a collimated (top row) and with a hemispherical diffuse (bottom row) beam. (Of course, the beam is vignetted by the support.) The direction of illumination is almost frontal (leftmost figures), from the left (center figures) and a *contre jour* (rightmost figures). Notice the nature of the body and the cast shadows. Because these are actual photographs, many additional effects (such as reflexes) are evident.

beams (the cosine factor), which reduces the “effective” solid angle by a factor of 2.

Consider a white Lambertian sphere in sunlight. Since sunlight is highly directional (*collimated*), only one hemisphere catches photons, whereas the other hemisphere is enveloped in an “attached” or *body shadow*. In the wake of the beam behind the object is the *cast shadow*, a cylindrical volume of vanishing volume density. The cast shadow becomes visible when you introduce a white object into it: it will not be illuminated, but it “catches” the shadow. The cast shadow volume extends for about 100 times the diameter of the object in the case of sunlight. Of the irradiated hemisphere, not every part catches an equal share of irradiance. When the surface is inclined with respect to the direction of the incident rays, the irradiance becomes less; it is proportional to the cosine of the inclination. This is usually referred to as *shading*; here we call it the (surface) *attitude effect*. The body shadow (and often the cast shadow too) tends to be far more visually striking than the shading, yet most of the literature has been devoted to shading alone. In terms of numbers, the hemisphere in shadow receives no radiation at all, whereas the average irradiance of the other hemisphere is one-half of the maximum (or *normal*) irradiance. In the visual field, the illuminated hemisphere (seen from the direction of the rays) appears as a disk with a dark rim [photographers speak of the *limb effect* (Adams, 1950)] (Fig. 72.5).

A *collimated beam*, like a sunbeam, is an extreme case. Apart from a sunbeam, it is not often encountered outside of the physics laboratory, although it figures prominently in theories on shading. In normal scenes, even in sunlight, the body shadow areas are rarely pitch black due to the effect of scattered radiation from the environment. Frequently encountered light fields are even more diffuse. Photographers (and visual artists in general) tend to avoid collimated beams (they fear *lunar effects*) and seek clearly directional yet diffuse fields

(da Vinci, 1927; Jacobs, 1988). An example is the *uniform hemispherical diffuse beam*, where the rays enter from one half-space. This is approximately realized by an overcast sky (Fig. 72.6) or a large, irradiated white wall on one side of the object, the environment on the other side being dark (common in the photographic studio). In such a light field (see Figs. 72.2 and 72.6), the cast shadow volume extends over less than the diameter of the object. There is no body shadow proper; all areas of the spherical object catch some radiation. Of course, the side of the object that faces the luminous half-space will be more strongly irradiated than the opposite side. This is due to the fact that the object occludes part of the extended source, technically referred to as *vignetting* [from *vignette*, an ornamental frame which “occludes” part of the framed picture, in the nineteenth century often stylized leaves of the grapevine (*Fr. vigne*)]. In the visual field the most strongly illuminated hemisphere still appears as a dark-rimmed disk, but the darkest part of the rim still receives one-half of the normal irradiance, and the average radiance seen from the direction of illumination is five-sixths of that of a normally irradiated planar disk.

Real sources are often between the range of the collimated beam (vanishing small angular spread), the hemispherical diffuse beam (all rays make at least some progress in the nominal direction) and the Ganzfeld, which is completely diffuse. Although the extremes are rare, they do occur in natural scenes (direct sunlight with hardly any scattering from environmental objects is almost collimated, whereas in a *polar whiteout* the Ganzfeld is closely approximated). Most beams are somewhere in between. Professionals (such as photographers) can judge the nature of beams quite accurately through their rendering properties. They look for body and cast shadows, specular reflexes, and especially the

nature of the edge of the body shadow where the rays grazing the surface interact strongly with local surface irregularities (e.g., the pores of the skin in the case of a human face) (Fig. 72.7).

The case of *multiple sources* is also of frequent importance. In the shading of Lambertian objects, only the irradiance of the surface is important, which means that multiple sources have the same effect as a virtual average source. Thus, the fact that the sources are multiple is apparent only due to vignetting. Each source causes particular body shadows and particular cast shadows because the occlusion geometry is different for the different sources. The radiance at the eye is simply the linear superposition of these sources. The professional looks for multiple cast shadows (often introducing a test body—hand or pencil—into the beams for the specific purpose of comparing cast shadows; see Fig. 72.8) and tell-tale specular reflections. In reflection the sources are often *resolved*. For instance, the portrait photographer will try to avoid multiple glints in the pupils of the eyes through careful placement of the sources (or will remove them by retouching at a later stage).

In much of the literature, the stimuli are due either to (simulated) collimated beams or to a collimated beam (often called *point source*, a rather unfortunate term) with ambient illumination. The reason is the structure of graphics rendering pipelines. Most programs cheerfully allow rays to enter from the wrong side (from the interior of the object), which yields a negative irradiance due to the attitude effect. The *ambient term* is simply a constant irradiance that cancels the negative value and returns one to the domain of physical possibilities. (If any negative value remains, it is simply clipped away.) This absurd procedure can be shown to yield (by a miraculous coincidence) the correct formula for the irradiance of a convex object in a uniform hemispherical diffuse field, and since it yields a fast algorithm, it is considered an intelligent implementation of the physics (Foley et al., 1990). It isn't, though; it works only for convex objects. If some corrugations are added to the surface, which should give rise to the all-important *texture*, the method yields



FIGURE 72.6. *Left*: A sunny day on the beach. The light field is the collimated sunbeam with secondary (scattered) radiation from the sky above and the sand below. Notice the pronounced body shadows (face) and cast shadows (of the figure on the sand); *Right*: This sculpture of grayish stone is illuminated from a heavily overcast sky (almost a perfect hemispherical diffuse beam). Most of the apparent shading is actually due to vignetting. There are no body or cast shadows.



FIGURE 72.7. A spherical candle with a rough surface finish, left in a collimated beam and center in a hemispherical diffuse beam. Note the local light directions with respect to the surface revealed by the surface irregularities. On the right, a pillar covered with rough plasterwork in direct sunlight. The edge of the body shadow reveals the nature of the source.



FIGURE 72.8. On the left, the cast shadows of the hand on the wall reveal the presence of two distinct (fairly collimated) beams. Notice that this is hardly apparent from the shading of the figure. On the right, cast shadows of objects at various distances from a wall are produced by a sunbeam (the hand and distant foliage behind the photographer). This is a single beam; the shadows look different due to the fact that the angular subtend of the sunbeam is about 0.5 degree.

nonphysical results (Koenderink and van Doorn, 1996a). Many psychophysical reports on shape from shading are rendered virtually worthless due to ignorance of these simple facts. (It would be too unkind to give references here; the reader is gently reminded to watch out for this.)

There exist a variety of implementations of the physics in graphics (software or hardware) pipelines. Some approximate the physics fairly closely, but most cut corners in various ways for the sake of computational efficiency at the cost of realism. When graphics renderings are to be used for stimuli, one should always check this out very carefully. A discussion of the various common implementations is beyond the scope of this chapter.

Important photometric effects

It is usually convenient to distinguish a number of important *levels of scale*. These are not to be taken in an absolute sense, but depend upon distance, size of the field of view or region of interest, and spatial resolution of the camera or eye. We distinguish (at least) the level of the *scene* or setting (insofar as it is of current interest), of the *object* (of present interest), and of significant *texture*. Texture is to be understood simply as *summarized* (incompletely described) structure. Anything below the level of texture is summarized in terms of average radiance at the eye. There may be a great deal of complicated physics at this level, but that is captured in terms of *material properties* (such as the BRDF). This means that material properties are level dependent; for instance, a treetop at a distance (leaves not resolved) is a material in this sense (CURET, 1997; Koenderink and van Doorn, 1996a, 1998; Koenderink et al., 1999). That is why objects often are perceived to have material attributes for which one finds no equivalents in physics textbooks. At the level of the object, one describes the structure in terms of shape and local *luminous atmosphere* (direction and diffuseness of the light field, any additional flare or air light). On the level of the scene, one

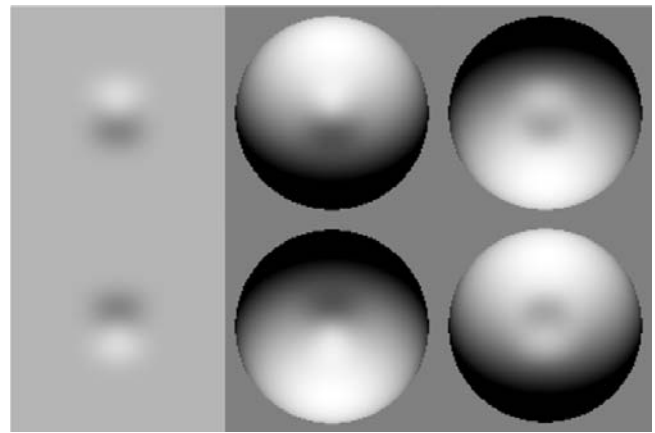


FIGURE 72.9. Context is all-important in shape due to shading. The left-hand column depicts abstract dipoles on a uniform field. An “up” dipole tends to look like a protrusion, a “down” dipole like an indentation due to an implicit “illumination from above” default assumption. The effect is weak and ambiguous. In the central and right-hand columns, the same dipoles are embedded in a context that suggests the actual direction of illumination (an illuminated sphere). The context works because a strong default assumption is that chunks of matter are generally convex. Both up and down dipoles look like protrusions in the central contexts and like indentations in the right-hand contexts. This perhaps suggests that extreme stimulus reduction might not be the best strategy in shape from shading studies. (Although most likely familiar, we haven’t encountered a simple figure like this in textbooks we know.)

distinguishes the general layout and global structure of the light field (sky, earth, clouds, sun, nearby whitewashed wall, etc.). Notice that the object is the context for the texture, and the scene is the context for the object. *Contexts* are visually all-important because they imply global surface attitude and light direction (Fig. 72.9). Psychophysics in context-free conditions tends to lead to sterile results (Erens et al., 1993a, 1993b). Examples include studies in shape from shading in the absence of occluding contours and/or indications of illumination direction.

The distribution of shadow and highlighted areas is the single most important cue in scenes. That is why the artist’s chiaroscuro thumbnail sketches, often made to decide on the global composition of paintings, tend to look like convincing, complete scenes. They fully specify layout and light field. Low-resolution images suffice or even surpass fully rendered scenes in visual realism. The artist is used to squinting or screwing up the eyes to see what is there (Baxandall, 1995; Gombrich, 1995).

Shading, shadow, and vignetting capture the shape of an object in its setting (Adams, 1950; Baxandall, 1995; Gombrich, 1995; Hunter and Fuqua, 1990; Jacobs, 1988). Typically, one side of objects is light and the other side is dark due to the directionality of the local light field. The nature of the edge of the body shadow reveals the diffuse-

ness of the light field. Texture is important here; if the light field is very directional, visual texture due to surface corrugations is almost completely limited to the edge of the body shadow (Fig. 72.10). When the light field is very diffuse, the edge is hardly apparent and visual texture is due mainly to vignetting. For this reason, cracks and pits in the surface appear dark. For instance, when one looks at humans, the clefts between fingers, the lips, an arm against the body, and so forth appear as dark lines. For the same reason, the eye sockets commonly appear as dark blotches in the face and cheekbones are accentuated due to dark concave areas, effects commonly accentuated by women using cosmetics. The darkness of a concavity is not due to the attitude effect, but to vignetting, that is, to the depth of the cavity reckoned in (solid) angular terms. (Thus, an optically deep pit may actually be only a minor depression in terms of distance. This leads to confusions in the psychophysical literature; the reader should beware.)

The pattern described above is often accentuated by specularities, which appear as a kind of “spicy addition” to the general shading pattern because often they are fairly localized (Fig. 72.11). Specularities commonly arise because the BRDF contains a *specular lobe* through Fresnel reflection at a smooth interface (Longhurst, 1986). Indeed, a diffuse (almost Lambertian) component due to photons scattered in the bulk material after passing the surface with a superimposed mirror-like reflection at the interface is common in most smoothly finished dielectrics such as polished woods, plastics, and polished stone (Klinker et al., 1987; Lu, 2000).

The distinctness of the specularities depends greatly on the diffuseness of the light field. This is because the specularities are simply *mirror images* of the light sources (or the environment in general), and thus are very broad (and therefore hardly noticeable) for diffuse light fields and almost punctate (extremely noticeable) for collimated ones. When the light field is collimated, the structure of the specularities depends mainly on the microstructure of the surface. Spectacular examples are offered by the reflection of the sun on rippled lakes. The difference in appearance between an orange and a tomato is largely due to the structure of their specularities.

When the scene contains more than one object (virtually all scenes do, except in psychophysical stimuli), the objects scatter photons toward each other and thus interact photometrically (Fig. 72.12). This is a very important effect, because it ties the object causally, in a visually obvious manner, to its environment. That is why reflexes are so highly prized by visual artists (and often exaggerated in paintings): they relate disjunct objects in a visually evident manner (Jacobs, 1988). If reflexes are left out (as in amateurish painting or many psychophysical stimuli), the scene isn’t easily integrated and tends to fall apart visually.

Although many objects are at least somewhat Lambertian, many deviations are common. We have already mentioned the specularities, which are ubiquitous. Other effects which are common enough to merit mention are backscatter, asperity scattering, and translucence.



FIGURE 72.10. Three photographs of a tree trunk taken only minutes apart on a clear day, early in the morning, with low sun. The shots were taken (*left to right*) with frontal illumination (note the cast shadow of the photographer), lateral illumination (note the cast and body shadow of the tree), and a *contre jour* (note the body and cast shadows of the tree). Texture due to three-dimensional

surface irregularities is mainly evident at the edge of the body shadow. This type of typical texture is worthless from the perspective of shape from texture theorists, yet it is an important cue both to global shape (the cylindrical tree trunk helps to determine the local light direction) and to local shape (the irregularities of the bark).

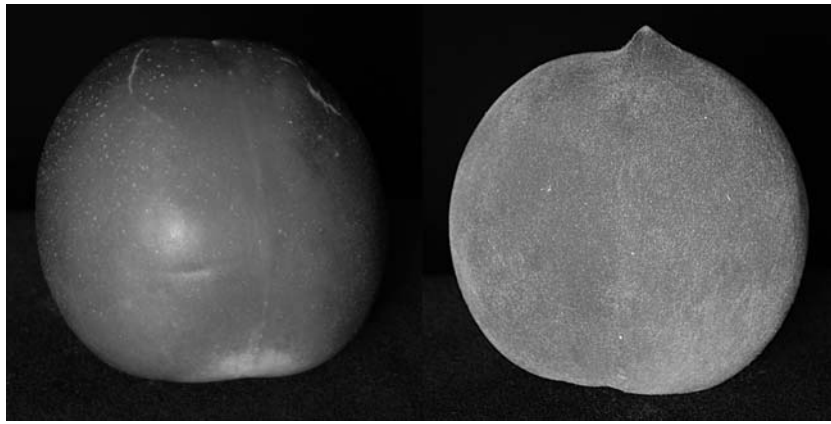


FIGURE 72.11. On the left a nectarine, on the right a peach, both irradiated with a collimated beam from the same direction. The nectarine is glossy, and the specularity and edge of the body shadow reveal the direction and nature of the beam. The nature of the specularity reveals much about the smoothness of the surface. Note the edge darkening [called the *limb effect* by Ansel Adams (1950)],

which together with the specularity makes the nectarine appear convex. The peach looks very flat in comparison. It misses the specularity, and the limb effect is effectively canceled through asperity scattering by the fibrous envelope of the peach (which indeed makes it look “peachy”).

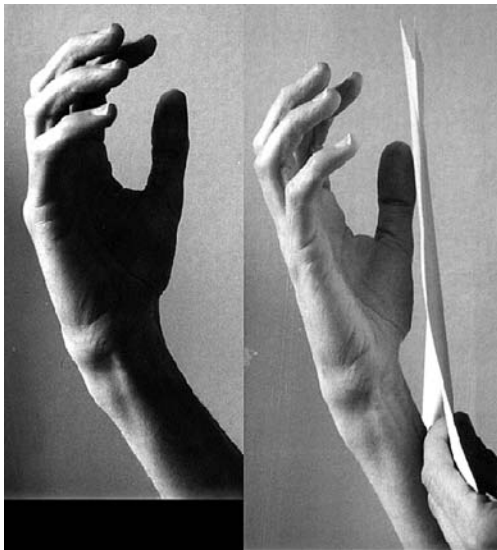


FIGURE 72.12. On the left, the back of a hand is illuminated by a distant window. The palm of the hand is turned away from the source and consequently appears quite dark. On the right, a piece of paper is held close to the inside of the hand. The paper “throws a reflex” on the hand, that is, acts like a secondary source, which sends a diffuse beam in the opposite direction from the primary beam. In actual scenes reflexes are always present and quite strong, though they go typically unnoticed by naive observers.

Backscatter is typical for rough surfaces that are close to Lambertian on the micro scale (Koenderink et al., 1999; Oren and Nayar, 1995). (Note that the Lambertian property itself is due to structure on a still finer scale.) Backscatter tends to be due to a combination of two important effects. One is occlusion, that is, the fact that near things may obstruct the view of far things. A rough surface will contain

many cast shadow areas when irradiated with a collimated beam. The shadowed areas make the surface appear darker, even when not resolved (thus *invisible*), for they simply decrease the average radiance. When one looks from the direction of the beam, the shadowed areas will be occluded by the (almost normally irradiated, thus very bright) structures that throw the shadows. In that case, the surface must appear quite bright. This is the *Richardson effect*. It can often be observed as a bright halo that appears around the shadow of one’s head when that shadow falls upon a rough surface such as grass or foliage. The second effect has to do with average surface attitude. On a rough surface there will be many areas almost orthogonal to the visual direction, even though the global surface is slanted. The parts that are slanted subtend small parts in the visual field due to foreshortening, whereas there is no foreshortening for the normally viewed (and thus irradiated) parts. Thus, a rough surface will be much brighter than a smooth, slanted surface when illuminated from the viewing direction simply because it contains an overdose of normally irradiated parts. Due to such effects, rough surfaces often have a very pronounced *backscatter lobe*. This lobe tends to decrease the limb effect due to shading and thus counteracts shading. It has the general effect of making things look flatter than they are.

Asperity scattering is very common in animals and plants, whose surfaces are often covered with hairs (Figs. 72.11, 72.13, and 72.14). In the case of furs, the hairs are aligned with the surface and, when in order (combed), lead to specularities with a very distinct pattern. When the hairs stand on end, asperity scattering proper occurs. The hair tips scatter photons and thus lighten up the surface, especially when there are many hair tips per unit area in the visual field. This happens especially at the occluding

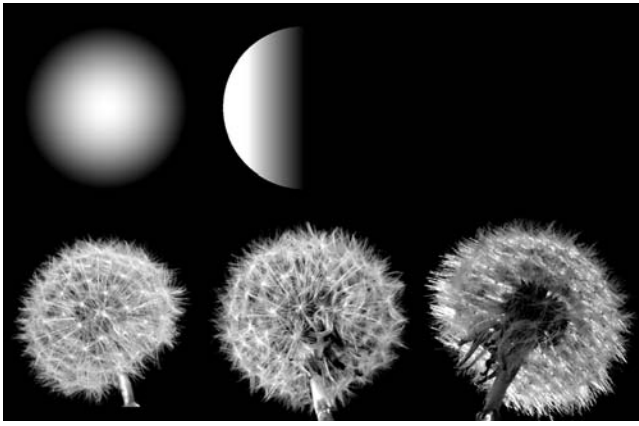


FIGURE 72.13. *Upper row*: a Lambertian sphere; *lower row*: a dandelion pappus. The columns are for frontal, lateral, and *contre jour* illumination. (Note that the Lambertian sphere is invisible against the dark background in the *contre jour* condition.) The dandelion pappus is not shaded but scatters photons to the camera by asperity scattering.



FIGURE 72.14. Asperity scattering is very common on plant and animal surfaces, including those of humans. Even young female faces are covered with downy, almost invisible hairs. Although the hairs on the cheeks are typically not apparent (often below resolution of the camera), they do influence the shading significantly, lightening up the contours and body shadow edges. Asperity scattering is the secret of “velvety” skin in female faces.

contours, where the surface is seen at a grazing angle and hair tip density is very high due to foreshortening. Thus, asperity scattering gives rise to a brightening of the contours. The effect can be seen in dark velvets and peaches (Lu, 2000). Asperity scattering gives surfaces a “peachy” or “soft” look. It counteracts the limb effect due to shading and thus tends to interact destructively with shape from shading processes.

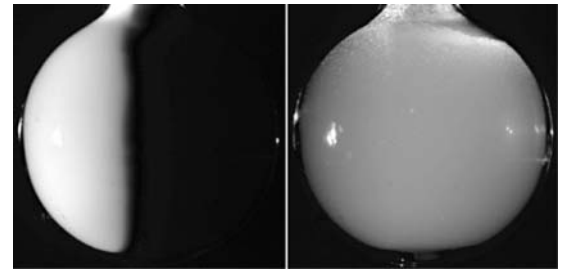


FIGURE 72.15. Shape from shading doesn’t properly apply to translucent objects. Here a spherical flask filled with milk has been immersed in clear water to eliminate refraction. It is illuminated with a collimated beam from the left. For concentrated milk (*left*) the sphere appears to have a proper body shadow, though photometric measurement reveals shading quite unlike that of a Lambertian object. When the milk is diluted with water (*right*), the body shadow disappears altogether because radiation is scattered from throughout the volume. The radiance that reaches the eye no longer depends only upon the local surface irradiance; the concept of shading does not apply to such cases.

Translucent materials are not at all rare. Most materials are translucent (or even transparent) at the micro scale. When a photon enters the bulk matter, it is repeatedly scattered and effectively performs a random walk until it escapes through the surface. This will typically happen at another location, though; thus, the BRDF description (which describes scattering at a surface point) does not work. The radiance you sample when you look at a point on the surface is due to photons that emerge from a column inside the material (Fig. 72.15). Photons in this column may have originated from any location. Thus, translucent materials look quite different from opaque ones, and concepts such as *shading* strictly do not apply (Koenderink and van Doorn, 2001) (Fig. 72.15). Scale is important here, for while many materials are translucent on the micro scale, the opaque approximation might suffice on a macro scale (think of human skin, for instance).

The structure of pictures

The radiance distribution at any point specifies all pictures one could possibly take (e.g., using a photographic camera, placing an eye) from that point. The actual pictures also contain features due to the camera or eye. Contrast will be affected by flare and the modulation transfer function (MTF) of the optical system. Resolution will be effectively limited, as will the dynamic range. The full range of radiances in a scene containing dark shadows and specular highlights cannot be rendered either photographically or on the computer screen. Thus, the stimuli used in psychophysical experiments almost certainly differ in a number of respects from the radiance field.

In pictures the field of view is necessarily limited, thus reducing the context. This may often introduce ambiguities,

such as reflexes thrown by objects from outside of the field of view. Such effects tend to look unnatural (they frequently lead to complaints by customers of photo finishing facilities), and even when unnoticed, they are likely to distort the visual perceptions of a scene.

Shape from shading

Shape is given a variety of meanings in the literature. The standard mathematical meaning of “invariant under a group of transformations” is the most useful one (Klein, 1893). In daily life, the shape of a thing is that which does not change when you rotate or displace the thing. Of course, this notion of shape depends on the choice of the transformation group. For instance, if you include magnifications, all spheres have the same shape, irrespective of their size. If you include arbitrary scalings in orthogonal dimensions, all triaxial ellipsoids have the same shape (and in fact are not different from spheres), and so forth. In shape from shading, the shape is the invariant under changes of illumination of a scene as evident from pictures of that scene. Here one needs to specify a variety of additional parameters—for example, that all pictures should be taken from the same point and with the same camera.

Shape by no means exhausts the realm of inferences that might be drawn from a picture. Apart from its shape, one might ask for other geometrical parameters (distance, spatial attitude, size, etc.), for material properties (glossy or matte, dry or wet, etc.), or for properties of the light field instead of the scene. Most often, a number of different properties must be expected to be mutually dependent. For instance, inferences concerning the light field, the material properties, and the shape can hardly be expected to be independent. Photographers straighten a crooked nose through suitable illumination, women apply cosmetics in order to change the visual shape of their faces, and so forth (Fig. 72.16).

Such interdependencies have been largely ignored in the literature. An exception that has attracted (perhaps too much) attention has been the concave-convex ambiguity (Kardos, 1934). The idea is that the pictures of a hemispherical concavity or a hemispherical boss on a plane are identical if illuminated from opposite directions. If this were true and if the stimulus yielded no cue (by context) concerning the direction of illumination, the observer would be at a loss to decide, and the responses would be completely idiosyncratic. The general consensus is that observers are biased toward the assumption that the illumination comes from above rather than from below. One problem with such experiments is that the stimuli are typically highly stylized; indeed, most often they represent unphysical situations. In actual scenes it is often difficult to obtain “clean” results, because the stimuli are not ambiguous at all; indeed, there



FIGURE 72.16. The dirt of decades has descended upon this statue, leading to apparent illumination from below (the dirt on top is dark and appears as shadow). The actual illumination is diffuse, though it appears fairly directional. The principle is the same as that used by women when they apply cosmetics to darken eye sockets or accentuate cheekbones.

are many differences. For instance, the concavity has no optical interaction with the plane at all, but the boss has. The boss throws a cast shadow on the plane and receives reflexes from it. The concavity vignettes the source and allows multiple scattering in its interior. All this leads to very different pictures. That does not mean that observers never experience convex-concave confusion, but the situations most likely to lead to such confusion are quite different from what the literature suggests. For instance, the most certain way to have observers report a convexity when a concavity exists is to illuminate the latter normally (thus, the above/below confusion doesn’t come up at all). In that case the center of the concavity appears brighter than the plane (due to internal reflexes), and it becomes very difficult to see the concavity as anything but convex (Fig. 72.17).

In the typical setting preferred by psychophysicists, pictures show isolated objects (very little context) in uniform light fields, either collimated (point source) or hemispherical diffuse (point source with ambient illumination). The surface finish tends to be either Lambertian or one of the BRDFs supported by standard graphics pipelines [such as Phong (1975) shading]. When texture is applied it tends to be flat (because the graphics engines allow easy texture mapping), which renders the texture cue worthless from the photometric point of view. In the majority of cases, the rendering fails to take either vignetting or multiple scattering into account. *Ray tracing* or *radiosity* renderings will allow for this, but these methods are computationally expensive and only approxi-

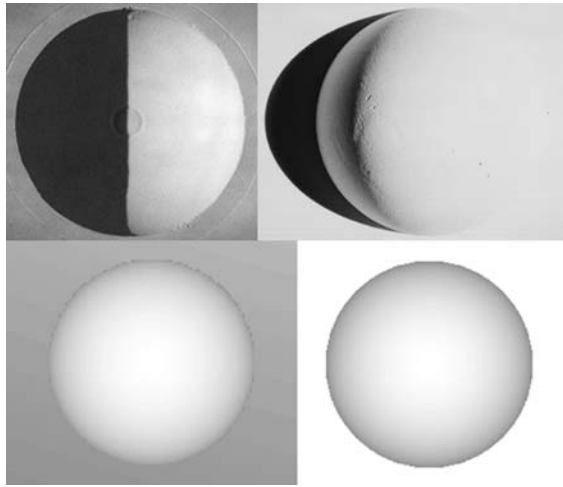


FIGURE 72.17. A hemispherical pit (*left column*) and boss (*right column*) on a plane. Illumination is with a collimated beam in all cases. The configurations are of matte white material. In the top row (actual photographs), the cast and body shadows and the reflexes evident in oblique illumination leave no doubt about which is which. The bottom row shows exact simulations of true Lambertian surfaces. Instead of a hemispherical boss (*right*), there is a full sphere against an infinitely distant white screen. Illumination is frontal. Note that the cavity at the bottom left looks much like a boss or a full sphere. The reason might be that the center is actually brighter than the plane due to internal reflexes in the cavity.

mately simulate the actual physics (Langer and Bülthoff, 2000).

In collimated light fields (sunlight), the most important cues are body shadow, the textural quality of the body shadow edge, the structure of the specularities, and the structure of the visual contour. An orange and a tomato both look spherical due to the overall shape of their contour and their body shadow; they differ in that the orange has a serrated contour, a broken-up specularity, and a roughly textured body shadow edge (Lu, 2000). Apart from the overall shape of the contour and the cast shadow, these cues typically are absent in commonly used paradigms.

In diffuse light fields the major cues are the overall shape of the contour, the textural effects due to vignetting, and the shading. Note that in this case the shading is not due to the attitude effect (thus, the standard shape from shading theories don't apply), but to vignetting. Vignetting makes the direction of the local light field at a surface element vary from place to place (and so does the degree of diffuseness), even if the global light field is nominally uniform (Koenderink and van Doorn, 1996a) (Fig. 72.18). The standard point source with ambient illumination fails to capture this.

Classical shape from shading theories assume that surfaces are perfectly Lambertian (thus, the radiance at the eye is perfectly proportional to the irradiance) and that each part

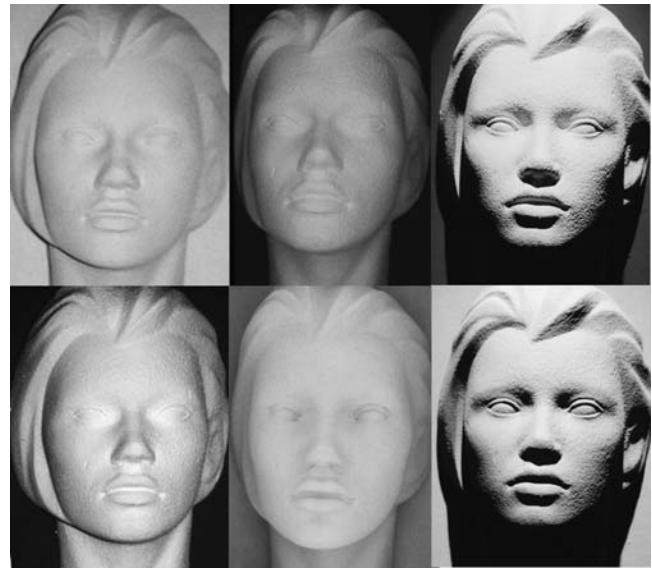


FIGURE 72.18. An artificial face painted matte dark gray (*bottom row*) and matte white (*top row*), illuminated frontally with a collimated beam (*left column*), a hemispherical diffuse beam (*center column*) and from high frontal with a collimated beam (*right column*). Note the differences, especially in the eye sockets and cleft between the lips, due to vignetting and reflexes. Vignetting occurs with the diffuse illumination (*center column*). Reflexes occur for the white material (*top row*) and hardly at all for the dark material (*bottom row*). Note the contrast of the texture due to the (three-dimensional) roughness of the material. The texture is strongest under collimated illumination, near the shadow boundary, on dark material. Texture contrast is less for diffuse illumination (due to the attitude effect), for light materials (due to reflexes), and for less oblique illumination (due to the attitude effect). Notice that classical shading is only one (and not necessarily the more important) cue.

of the surface is illuminated by the same source (no vignetting) (Horn and Brooks, 1989). Then the radiance received by the eye depends only upon the angle between the local surface normal and the net flux vector. In practice, this is approximately realized in the case of matte surfaces with shallow relief (no vignetting or reflexes). Then all surface elements with the same inclination with respect to the net flux vector will send the same radiance to the eye. For smooth surfaces such elements lie on curves, the *isophotes*. Shape from shading then derives the shape from the pattern of isophotes. Here *shape* can be defined locally as the relation between the surface normals of adjacent locations. When adjacent normals are not parallel, the surface is obviously curved. Because the irradiance of the surface depends only on the direction, not on the location, of the surface element, it is convenient to abstract from the locations altogether. The surface normals can be specified as unit vectors or, equivalently, as points on the unit sphere. Thus, one may conceive of the mapping of surface elements upon the unit sphere. This map is known as the *spherical image* or *Gauss map* (Gauss, 1827). Consider some Gauss maps: a plane obvi-

ously maps on a point (all its normals being parallel); thus, the Gauss map can be highly degenerate. Cylindrical and conical surfaces (more generally *developable surfaces*) map on curves. All other surfaces map on two-dimensional patches of the unit sphere. In that case, one can set up a one-to-one relation between the spherical image and the original surface, at least locally. This is extremely useful, because the irradiances of the unit sphere and the surface (in the same light field) must correspond (parallel normals by construction). Since the pattern of isophotes on the sphere is easy to construct (concentric small circles for a uniform light field), one immediately constructs the isophotes on the surface via the aforementioned map. Going in the other direction, the received radiance specifies the irradiance on the surface, thus on the unit sphere, and hence the local normal direction. The radiance distribution thus specifies the distribution of normals, which again (partly) specifies the shape (Koenderink and van Doorn, 1980, 1982).

Since the Gauss map may well be degenerated, complications arise. One point on the sphere may easily correspond to many points on the surface. One has to think of the spherical images as thoroughly “wrinkled,” with various folds and cusps, such that the sphere is multiply covered, the degree of covering varying from region to region (Fig. 72.19). This may be conceived of as either a curse or a blessing. It is a curse in the traditional theories because classical calculus is ill fit to deal with singularities. Indeed, many theories owe more to the straitjacket due to the method adopted by their originators than to the phenomenology of the field they are supposed to explain. In this case, the curse may be turned into a blessing, though, when one analyzes the structure of the field of isophotes near such folds. One finds that the wrinkles give rise to *critical points* (minima, maxima, and saddle points) of the irradiance field on the surface, even where the irradiance field on the sphere has no extrema or saddle points. Thus, such easily identifiable features of the radiance distribution signal the presence of folds of the spherical image. Folds of the Gauss map are due to inflections of the surface, the *parabolic curves*. These curves are important shape indicators. They are curves on the surface that bound convex, concave, and saddle-shaped regions. The pattern of parabolic curves can serve as a qualitative shape description. This pattern can be inferred from the detection of critical points of the radiance (maxima, minima, and saddle points, which are clearly apparent visually). This is a fairly robust way to make shape inferences, since one may relax a number of the strict assumptions underlying classical shape from shading. This is the case because the critical points are due more to the wrinkles than to the irradiance pattern on the sphere (Koenderink and van Doorn, 1980, 1982, 1993). Although these structures have proven useful in machine vision, they have not yet been researched in the case of human vision.

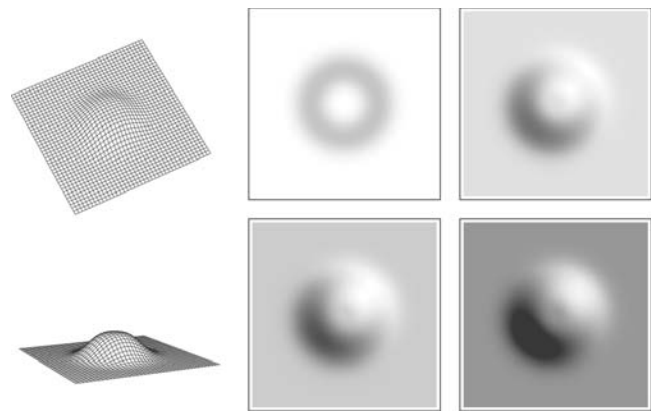


FIGURE 72.19. This shallow hill on a planar surface does not generate a contour except when viewed rather obliquely (*leftmost column*). Clearly, its summit has the same spatial attitude as the ground plane; thus, the Gauss map is multiply covered: there exists a *parabolic curve* at the locus of inflection of the curves of steepest descent from the hill; it is a closed loop that encircles the hill. When illuminated from above with a collimated beam, the parabolic curve shows up as a dark annulus, the top of the hill being as light as the plane (*top center*). For a slightly more oblique incidence, we still find an illuminance maximum near the summit but an additional one on the parabolic curve, as well as an additional minimum, also on the parabolic curve (*top right*). For a rather oblique incidence, the maximum near the summit is lost and we see a pair of extrema at opposite sides on the parabolic loop. When the direction of illumination is varied, these extrema travel along the parabolic curve but never “break loose.” Such dipole patterns are typical of the shading patterns of local protrusions on a surface and can be considered *textons* that specify protrusions. This is a robust cue because the precise illumination or shape is irrelevant.

Psychophysical results

There is remarkably little psychophysical material on shape from shading that might be considered in any way definitive. There are multiple reasons for this, but most in some way have to do either with extreme *stimulus reduction* or with *non-realistic stimuli*. The latter case is utterly trivial and will not be discussed here. It is by no means irrelevant, though. Perhaps unfortunately, much of the literature can safely be skipped unread due to the fact that the authors (no doubt cheerfully and in good faith) relied on graphics software that cut various corners for the sake of computational efficiency, but at the cost of physical realism. It is often impossible to establish the exact nature of the stimuli, since the authors either used the software without any real understanding or because it is impossible to establish the exact nature of the algorithms used in proprietary software. Some authors are apparently aware of possible problems but evade their responsibility by blaming them on computer graphics. This will not do. Worse still, others are blissfully unaware of the pitfalls. It is to be hoped that such problems will (in historical retrospect) turn out to be specific to the 1980s to 2010s period. The former problem is of scientific interest because it does reflect a con-

scious choice on the part of the authors. The idea is that the scientific method implies that one should eliminate as many irrelevant parameters as possible and study the system in as simple a representation as possible (e.g., in vitro). Thus, if the problem is shape from shading, then the stimulus should contain only shading and the response should address only shape. The problem with this simpleminded, dogmatic approach is that such stimuli never evoke a clear impression of shape (Erens et al., 1993a, 1993b) in the first place; thus, such measurements involve forced choices of the kind “Have you stopped beating your wife?” (Answer “yes” or “no”). The stimuli make no sense to the observers (nor do their responses), but the scientist is happy with both stimuli and results. The forced-choice paradigm guarantees scientific respectability. Such studies—which make up the bulk of the literature—can safely be skipped unread. There have been few counterforces in the history of experimental psychology, one notable exception being James Gibson (1950).

What is known is evident as much from the writings of professionals in the visual arts and of particularly perceptive art historians as from the technical psychophysical literature. It is clear that shape impressions derive from (Fig. 72.20)

- Pure contour (silhouettes);
 - Cartoon drawings (perhaps incomplete outline drawings with internal contours);
 - The mere indication of illuminated and shadowed areas;
 - And from pictures that contain all of these.
- It is also known that
- Specularities promote shape understanding;

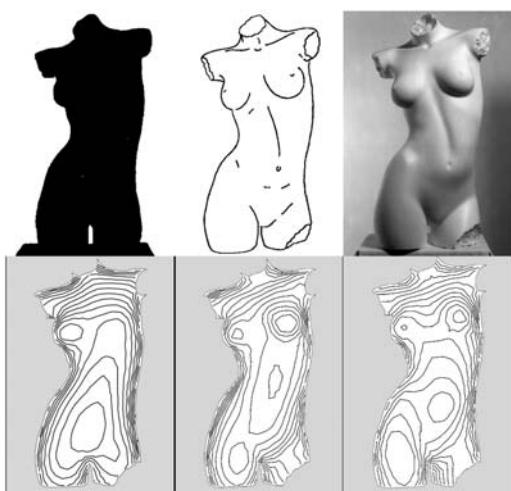


FIGURE 72.20. Three stimuli—a silhouette, a cartoon rendering, and a full-scale monochrome photograph—have identical geometry. The responses (depth contours) of a single subject show obvious differences. (The observer was confronted with the stimuli in this sequence.) Different observers vary greatly on the silhouette, much less so on the cartoon, and hardly at all on the photograph.

So do additional cues from texture, especially texture due to shadow and shading on a micro scale through three-dimensional surface corrugations (not so much from the “shape from texture” stimuli familiar from the psychophysical literature).

Shape impressions (we will discuss the operational definition of these entities later) of various observers only partly agree. Indeed, it cannot be otherwise because of the inherent cue ambiguity. Responses can never be expected to agree completely, for what is not specified by the stimulus has to be supplied by the observer when the task calls for it. This “beholder’s share” is by its very nature completely idiosyncratic. Ideally, the task should not call for the creative imagination of observers, but in practice this can hardly be avoided. To some extent (due to the inherent ambiguity), perception has to be “controlled hallucination.” But the responses of observers may be expected to agree (at best) only to the extent to which the shape is specified by the available cues. A rational comparison of responses should allow for this and disregard the beholder’s share. This has very important consequences for the interpretation of psychophysical data. The agreement of results obtained by different observers is a measure of the degree of the efficacy by which the cues are picked up by the observers, but only if one reckons *modulo* the cue ambiguity. It is indeed possible to show (Koenderink et al., 1996a) that the concordance becomes greater when the bouquet of available cues is enriched from mere silhouette to cartoon drawing and finally to fully shaded renderings. In that respect, human observers can be held to exploit the shape from shading cue. What is also clear is that observers’ shape impressions differ when the shading is varied (Koenderink et al., 1996b) (Fig. 72.21 and 72.22). Although to a first rough approximation constancy prevails (the perceived shapes don’t depend much on the direction of illumination, for instance), it can easily be shown that perceived shape nevertheless significantly and systematically depends upon the direction of illumination. This is nothing new, since visual artists have known for ages that faces illuminated from below are rendered quite unrecognizable. This is not only due to the fact that faces are special; it is the case for abstract sculpture as well.

Open problems

There remain numerous open problems in this particular domain; indeed, it is our firm conviction that most of the basic science in shape from shading remains to be done. Perhaps the majority of the literature is irrelevant due to incomplete description of the stimuli (the software problems mentioned above), extreme stimulus reduction (which transforms the task from one relating to the visual world into one involving only the visual field), or invalid paradigms due to

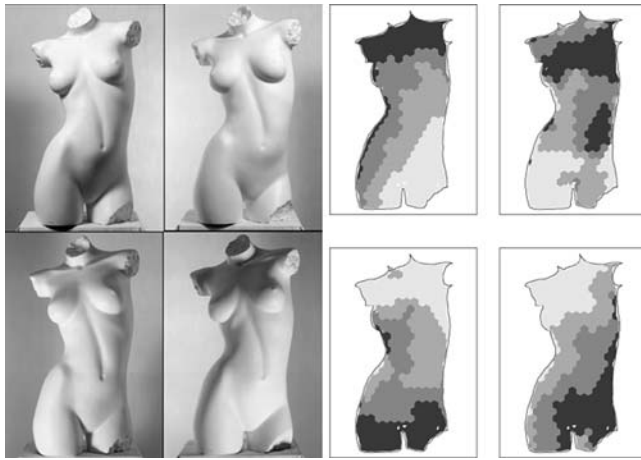


FIGURE 72.21. On the left, four geometrically identical photographs of an object with an illumination from four different directions. On the right are the residual depth maps (depth maps minus the average depth map for all four cases) of a single observer. Although the responses are very similar in all four cases (constancy), significant and systematic differences exist. It is as if the shape were “pulled out in the direction of the source.” (From Koenderink et al., 1996b.)

incomplete understanding of the relevant geometry and photometry.

It is important that stimuli be sufficiently complex to be considered natural, because only then can normal processing of the available cues be expected. This does not imply that single-cue studies are ruled out. One may use the standard engineering method of varying the cue structure in the neighborhood of a *set point* and correlating the resulting variations in the responses with those imposed upon the stimulus. When only a single parameter is varied, one effectively studies a single cue, but *in a natural setting*. Here lies a huge and very important field of endeavor.

It is important that stimuli be sufficiently complex to be reckoned generic. This involves an understanding of the ambiguities (Fig. 72.23) left by the cues. For instance, the majority of studies in shape from shading have involved Lambertian (or somewhat glossy) triaxial ellipsoids. These objects fail to be generic, because they are the only objects for which isophotes and shadow boundaries are planar curves. Any ellipsoid with the given contour is a “solution” if the lighting direction is unknown. Many shape from shading algorithms will simply not apply because these

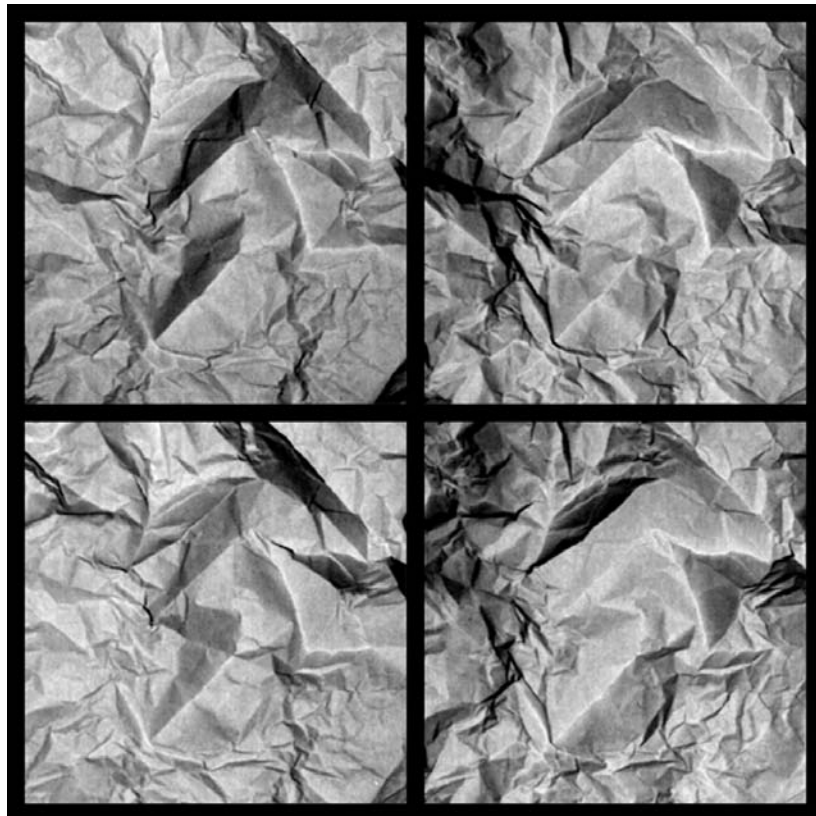


FIGURE 72.22. Crumpled paper illuminated from between the frontal and top left, top right, bottom left, and bottom right. Note how difficult it is to obtain a clear notion of the shape of this landscape—for instance, try to identify the hills and dales in all four images. In these examples the directions of illumination are not at all extreme.

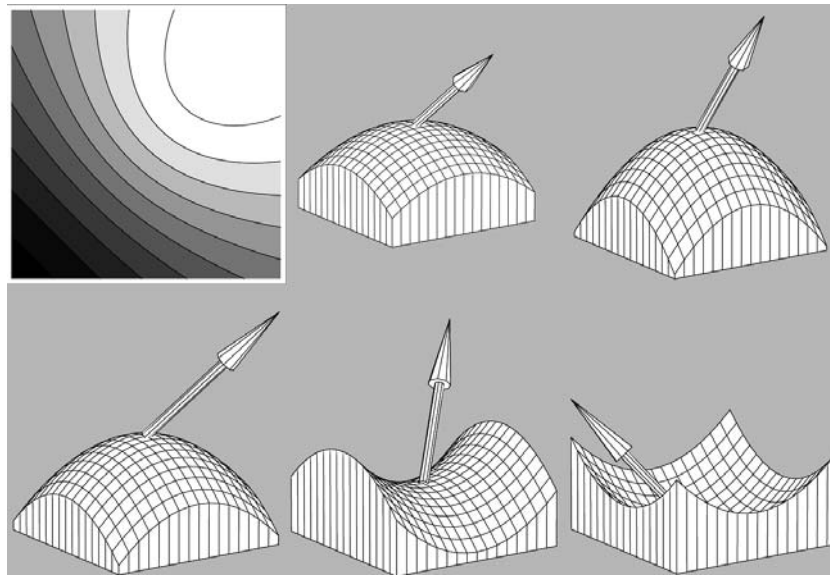


FIGURE 72.23. A single photograph (*top left figure*) can be “explained” via many different scenes. The depth of relief and obliqueness of illumination can be traded (*top right figures*), but even more complicated transformations (full and partial convex/concave inversions) are possible.

objects are degenerate. For instance, the Gauss map does not contain folds; thus, the powerful (because topological and thus robust) algorithms simply do not apply. Here stimulus reduction leads to severe constraints on the observer’s possibilities, perhaps excluding the use of the typical mechanisms. It is often thought that simple Euclidean objects (planes, ellipsoids, cylinders, regular polyhedra, etc.) make simple stimuli, but in fact these are often more complicated because they are degenerate and thus singular cases. Simple stimuli are generic and thus complicated from the perspective of high school geometry. There is little excuse to stop at such objects when modern computer techniques allow one to deal with generic cases with ease. Due to a scarcity of results, this represents another large and potentially fruitful field of endeavor.

It is important to understand that the very notion of *veridicality* depends upon the intrinsic ambiguities of the setting and thus on the precise nature of stimulus and response reduction. Part of the response has to be understood as completely idiosyncratic (the beholder’s share); part can at least conceivably be due to the cues. When observers agree in the latter part, they behave identically insofar as their responses are caused by the stimulus. This is the realm of psychophysics proper. When the notion of veridicality (all too often implicitly invoked in the evaluation of the response) depends on entities that are inherently ambiguous, the concept is void. The beholder’s share is a product of the creative imagination and (by definition) is not causally related to the stimulus, at least not in the immediate sense relevant to psychophysics. These topics are subtle and tricky and should be considered explicitly. This is a difficult topic

because the analysis of cue ambiguity remains incomplete for most of the relevant cues. Thus, the concept of veridicality should be used less lightly than is common in the literature. This is a very important and potentially rewarding field. It involves the simultaneous development of the theory and psychophysics.

How might one draw on the theories of shape from shading developed by the computer vision community for template theories of human shape from shading performance? The point is a very tricky one, yet typically is skipped (apparently it is thought to be a trivial issue or is not considered at all) in the literature on human vision. Most authors appear satisfied with trite remarks and indeed get away with it. The available material is typically an analysis of the physics (in a suitably simplified setting in order to render the problem soluble), eventually resulting in an algorithm. Ideally, one feeds the algorithm an image of some object; the algorithm crunches on it for a while and finally responds by yielding a three-dimensional description of the object in the image. The description could be a triangulation of the surface, for instance, a computer-aided design (CAD) file or a list of instructions to a computer-controlled machine that would yield a mechanical copy of the object. In order to turn this into a candidate theory for human performance, one needs to relate the algorithm to the observer’s input (the stimulus) and output (the response). The latter part seems difficult because few responses collected in psychophysical experiments are anywhere near triangulations, CAD files, or instructions to machine-controlled milling machines. The difficulties related to the former part should not be overlooked. Should one feed the pixel values of the

stimulus image or the local brightnesses perceived by the observer into the algorithm, for instance? Perceived brightness or lightness is a tricky area in its own right (Adelson, 2000; Gilchrist, 1994); the relation to radiances or albedos is at best nonlinear and quite likely not one-to-one. These are important topics (one would like to draw upon the no doubt highly relevant work of the computer vision community) that need much attention. The potential rewards are appreciable.

It should not be thought that all lightness gradients in artistic renderings are attempts to render shading in the photometric sense. Most artistic products are not so much (passive) renderings of a scene in front of the artist as attempts to create a work that will elicit certain responses in potential viewers. Shading in this latter sense was effectively used from the Stone Age on, and it is still a major component of artistic practice, even by artists who have been trained in photometric shading in art school. Of course, it would make no sense to run shape from shading algorithms on such pictures. Yet these pictures are often extremely effective in evoking vivid pictorial relief in human observers (Hogarth, 1981). Many “superrealistic” renderings are of this kind. Similar instances can often be observed in many images that result from a variety of scientific methods. A well-known example is scanning electron microscopic images. These tend to look very realistic (indeed, much like the products of superrealist draftsmen), though the process by which radiance modulations are obtained differs drastically from those that operate in the generic human environment. Here lies a wide field of potential study that has been completely ignored by the vision community.

Finally, it is very important that novel psychophysical tools be developed that allow one to probe *perceived shape* effectively. In the final analysis, perceived shape can only be defined operationally. In many cases, one evokes responses of observers that are (hopefully) mainly based on *shape impressions* these observers are believed to have, but these impressions themselves are never operationalized explicitly. This simply will not do. Shape impressions, though aspects of consciousness, are nevertheless *geometrical* entities that cannot be described via mere “yes/no” answers or magnitude estimations. One needs methods that yield responses that can be treated as geometrical objects, say triangulations, or other forms of surface description. Such descriptions necessarily involve data structures of finite geometry that will include hundreds or thousands of data points. (Think of the size of CAD files that are used to describe the shapes of industrial objects.) This again implies that psychophysical methods should yield at least 1000 bytes per hour instead of a few yes/no answers or 5-point scale ratings if the aim is to describe the structure of a perceived shape. Theories of shape from shading can only be assessed effectively when

such methods become readily available. There is no reason why this should be considered impossible, yet very little progress has been made. We consider this to be yet another open problem. Novel advances on this topic may well lead to considerable scientific progress in the future.

REFERENCES

- Adams, A., 1950. *Photography by Natural Light* (Basic Photo Series, Book 4), New York: Morgan and Lester.
- Adelson, E. H., 2000. Lightness perception and lightness illusions, in *The New Cognitive Neurosciences*, 2nd ed. (M. Gazzaniga ed.), Cambridge, MA: MIT Press, pp. 339–351.
- Adelson, E. H., and J. R. Bergen, 1991. The plenoptic function and the elements of early vision, in *Computational Models of Visual Processing* (M. Landy and J. A. Movshon, eds.), Cambridge, MA: MIT Press, pp. 3–20.
- Baxandall, M., 1995. *Shadows and Enlightenment*, New Haven, CT: Yale University Press.
- Borges, J. L., 1970. The library of Babel, in *Labyrinths, Selected Stories and Other Writings* (D. A. Yates and J. E. Irby, eds.), Harmondsworth, Middlesex, UK: Penguin Books.
- Bouguer, P., 1729. *Essai d'optique sur la Gradation de la Lumière*, Paris: Claude Jombert.
- CURET, Columbia-Utrecht Reflectance and Texture Database, 1997. <http://www.cs.columbia.edu/CAVE/curet>
- da Vinci, Leonardo, 1927. *Traité du Paysage* (Codex Vaticanus), Paris: Librairie Delagrave.
- Erens, R. G. F., A. M. L. Kappers, and J. J. Koenderink, 1993a. Perception of local shape from shading, *Percept. Psychophys.*, 54:145–156.
- Erens, R. G. F., A. M. L. Kappers, and J. J. Koenderink, 1993b. Estimating local shape from shading in the presence of global shading, *Percept. Psychophys.*, 54:334–342.
- Foley, J. D., A. van Dam, S. K. Feiner, and J. F. Hughes, 1990. *Computer Graphics, Principles and Practice*, 2nd ed., Reading, MA: Addison-Wesley.
- Gauss, C. F., 1827/1889. *Algemeine Flächentheorie* (German translation of *Disquisitiones generales circa Superficies Curvas*), Hrsg. A. Wangerin, Ostwald's Klassiker der exakten Wissenschaften 5, Leipzig: Engelmann.
- Gershun, A., 1939. The light field (P. Moon and G. Timoshenko, trans.), *J. Math. Phys.*, 18:51.
- Gibson, J. J., 1950. *The Perception of the Visual World*, Boston: Houghton Mifflin.
- Gilchrist, A., 1994. *Lightness, Brightness and Transparency*, Hillsdale, NJ: Erlbaum.
- Gombrich, E. H., 1995. *Shadows, the Depiction of Cast Shadows in Western Art*, London: National Gallery Publications.
- Helmholtz, H. von, 1896. *Handbuch der physiologischen Optik*, 2nd ed., Hamburg: Voss.
- Hering, E., 1878/1964. *Outlines of a Theory of the Light Sense* (L. M. Hurvich and D. Jameson, trans.), Cambridge, MA: Harvard University Press.
- Hogarth, B., 1981. *Dynamic Light and Shape*, New York: Watson-Guption.
- Horn, B. K. P., and M. J. Brooks, 1989. *Shape from Shading*, Cambridge, MA: MIT Press.
- Hunter, F., and P. Fuqua, 1990. *Light, Science and Magic: An Introduction to Photographic Lighting*, Boston: Focal Press.
- Jacobs, T. S., 1988. *Light for the Artist*, New York: Watson-Guption.

- Kardos, L., 1934. Ding und Schatten: eine experimentelle Untersuchung, *Zeitschrift für Psychologie* Erg.-Bd. 23, Leipzig: Barth.
- Katz, D., 1911. Die Erscheinungsweisen der Farben und ihre Beeinflussung durch die individuelle Erfahrung, *Zeitschrift für Psychologie* Erg.-Bd 7, Leipzig: Barth.
- Klein, F., 1893. Vergleichende Betrachtungen über neue geometrische Forschungen (Erlanger Programm), *Math. Ann.*, 43:63–100.
- Klinker, G. J., S. A. Shafer, and T. Kanabe, 1987. Using a color reflection model to separate highlights from object color, in *Proceedings of the First International Conference on Computer Vision (ICCV)*, (J. M. Brady and A. Rosenfeld, eds.), London: Computer Society Press, pp. 145–150.
- Koenderink, J. J., and A. J. van Doorn, 1980. Photometric invariants related to solid shape, *Opt. Acta*, 27:981–996.
- Koenderink, J. J., and A. J. van Doorn, 1982. Perception of solid shape and spatial layout through photometric invariants, in *Cybernetics and Systems Research* (R. Trappl ed.), Amsterdam, North Holland.
- Koenderink, J. J., and A. J. van Doorn, 1993. Illuminance critical points on generic smooth surfaces, *J. Opt. Soc. Am.*, A10:844–854.
- Koenderink, J. J., and A. J. van Doorn, 1996a. Illuminance texture due to surface mesostructure, *J. Opt. Soc. Am.*, A13:452–463.
- Koenderink, J. J., A. J. van Doorn, and M. Stavridi, 1996b. Bidirectional reflection distribution function expressed in terms of surface scattering modes, in *Computer Vision—ECCV’96*, vol. II (B. Buxton and R. Cipolla, eds.), Berlin: Springer.
- Koenderink, J. J., and A. J. van Doorn, 1998. Phenomenological description of bidirectional surface reflection, *J. Opt. Soc. Am.*, A15:2903–2912.
- Koenderink, J. J., and A. J. van Doorn, 2001. Shading in the case of translucent objects, in *Human Vision and Electronic Imaging VI*, (B. E. Rogowitz and T. N. Pappas, eds.), SPIE vol. 4299, Bellingham, Washington, pp. 312–320.
- Koenderink, J. J., A. J. van Doorn, C. Christou, and J. S. Lappin, 1996a. Shape constancy in pictorial relief, *Perception*, 25:155–164.
- Koenderink, J. J., A. J. van Doorn, C. Christou, and J. S. Lappin, 1996b. Perturbation study of shading in pictures, *Perception*, 25:1009–1026.
- Koenderink, J. J., A. J. van Doorn, K. J. Dana, and S. Nayar, 1999. Bidirectional reflection distribution function of thoroughly pitted surfaces, *Int. J. Comput. Vis.*, 31(2/3):129–144.
- Koschmieder, H., 1924/1968. see Middleton, W. E. K., *Vision Through the Atmosphere*, Toronto: University of Toronto Press.
- Lambert, J. H., 1760. *Photometria sive de mensura de gradibus luminis, colorum et umbræ*, Augsburg, Germany Eberhard Klett.
- Langer, M., and H. H. Bülthoff, 2000. Depth discrimination from shading under diffuse lighting, *Perception*, 29:649–660.
- Longhurst, R. S., 1986. *Geometrical and Physical Optics*, London: Longman.
- Lu, R., 2000. Ecological optics of materials, Ph.D. thesis, Utrecht University.
- Moon, P., and D. E. Spencer, 1981. *The Photoc Field*, Cambridge, MA: MIT Press.
- Nicodemus, F. E., J. C. Richmond, and J. J. Hsia, 1977. Geometrical considerations and nomenclature for reflectance, *Natl. Bur. Stand. (U.S.)*, Monograph 160.
- Oren, M., and S. K. Nayar, 1995. Visual appearance of matte surfaces, *Science*, 267:1153–1156.
- Phong, B.-T., 1975. Illumination for computer generated images, *Commun. ACM*, 18(6):311–317.

73 Visual Perception of Texture

MICHAEL S. LANDY AND NORMA GRAHAM

WHAT IS VISUAL TEXTURE, and how might a study of the visual perception of texture help us to better understand human vision? In this chapter we will attempt to give the reader a feel for how the study of texture perception is useful in understanding the impact of texture, as well as in providing a better understanding of basic visual mechanisms that respond not only to texture but to all visual stimuli. This review will be relatively brief and, of necessity, incomplete. We hope to give an overview of the different research areas concerned with texture perception and of the current issues. For a longer early review, we refer the reader to Bergen (1991).

Consider the scene in Figure 73.1. The border between the sky and the trees/grass involves a difference in luminance, one that would easily be signaled by a linear mechanism such as a simple cell in primary visual cortex. The boundary between the zebras and the background also involves a change in chromaticity (although not visible in the black-and-white image in Fig. 73.1), which might be signaled by color-opponent mechanisms. But the borders between pairs of zebras involve neither a difference in color nor a difference in average luminance. These borders include stretches of boundary that are black on one side and white on the other, stretches where the colors are reversed, and stretches where there is no local visual information to signal the boundary (where black abuts black or white abuts white). Nevertheless, we perceive a smooth, continuous occlusion boundary at the edge of each animal. It is as if the visual system possesses the capability of segmenting regions of the image based on a local textural property, such as separating “vertical stuff” from “horizontal stuff.”

Thus, texture is a property that is statistically defined. A uniformly textured region might be described as “predominantly vertically oriented,” “predominantly small in scale,” “wavy,” “stubby,” “like wood grain,” or “like water.” As Adelson and Bergen (1991) put it, texture is a property of *stuff* in the image, in contrast to visual features such as lines and edges, the *things* in the image (analogous to the linguistic difference between mass nouns like *water* and count nouns like *mouse*).

Another way of characterizing visual texture is by the uses to which it might be put. Texture is a property of an image region. Regions in the visual field can be characterized by differences in texture, brightness, color, or other attributes. Relatively early processes in the visual system can use texture

information to perform a tentative segmentation of the visual image into regions to ease the processing load on subsequent computational stages. The analysis of a single textured image region can lead to the perception of categorical labels for that region (“This looks like wood” or “This surface looks slippery”). The appearance of texture allows the observer to determine whether two textured regions appear to be made of the same or different stuff. If two abutting image regions have different surface texture, this may lead to the detection of the intervening texture border (like the border between adjacent zebras in Fig. 73.1). Such texture-defined boundaries may then be used to segment figure from ground and for two-dimensional shape identification. Finally, continuous changes in texture properties may result in the percept of three-dimensional shape (Gibson, 1950). A purpose of much research in this area is to define the mechanisms and representational schemes used to characterize texture, and thus to determine whether the same underlying mechanisms are responsible for each of the above perceptual capabilities.

Texture segregation

TEXTURE FEATURES Much of the work on perception concerns the ability of observers to discriminate certain texture pairs effortlessly. For example, Figure 73.2 shows rectangular regions of *Xs* and *Ts* on a background of *Ls*. Observers can perceive effortlessly that there is a region of *Xs* different from the background, that this region has smooth, continuous borders, and that these borders form a rectangular shape. This is referred to as the *segregation of figure from ground* or *segmentation of the image into multiple homogeneous regions*. At the same time, none of these observations may be made about the region of *Ts* without the use of effortful scrutiny of the individual texture elements one by one.

This sort of observation led a number of investigators to consider what aspects of image structure led to preattentive segregation of textures. Beck and Attneave and their colleagues (Beck, 1972, 1973; Olson and Attneave, 1970) hypothesized that textural segmentation is based on the distribution of simple properties of *texture elements*, where the simple properties are things like the brightness, color, size, the slopes of contours, and other elemental descriptors of a texture. Marr (1976) added contour terminations as an important feature.



FIGURE 73.1. Types of image borders. A natural image containing borders signaled by differences in luminance, color, and/or textural content.

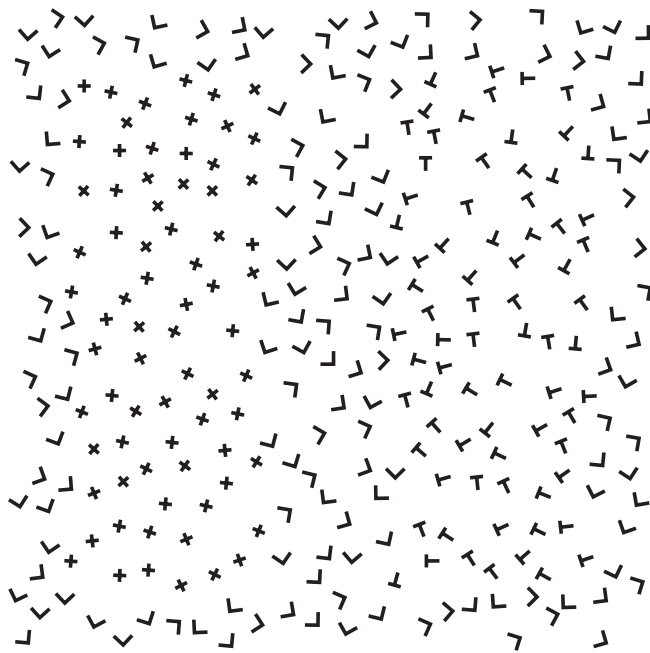


FIGURE 73.2. Texture segregation. Note that the region of Xs on the left is easily segregated from the background of Ls. One immediately perceives the borders between the two regions and the shape of the region containing the Xs. By contrast, the border between the Ts and Ls is difficult to see, and the shape of the region of Ts can only be discerned slowly, effortfully, and with item-by-item scrutiny.

Julesz's early efforts centered on image statistics. He first suggested (Julesz et al., 1973) that differences in dipole statistics were most important for texture pairs to segregate. (These are the joint image statistics of the gray levels found at the opposite ends of a line segment of a particular length and orientation, as it is placed at all possible image locations, gathered for all possible pairs of gray levels, dipole lengths, and orientations.) But counterexamples to this were found (e.g., Caelli and Julesz, 1978). It was then suggested that textures with identical third-order statistics would prove indiscriminable. (Analogous to dipole statistics, these are joint image statistics of the gray levels found at the three corners of a triangle with a particular size, shape, and orientation as it is placed at all possible image locations, gathered for all possible triplets of gray levels, triangle shapes, sizes, and orientations.) Again, counterexamples to this hypothesis were found (Julesz et al., 1978).

Julesz noted that the counterexamples were suggestive of an alternative explanation for texture segregation similar to those of Beck and Marr. Julesz found that texture pairs that segregated easily but had identical third-order statistics also differed in the amount of an easily discernible image feature (e.g., Caelli et al., 1978). The task then became one of identifying the list of image features, which Julesz (1981) dubbed *textons*, that were sufficient to explain segregation performance. The initial list of textons included such features as size, orientation, line terminations, and line crossings.

It has been noted that the third-order statistics used by Julesz were population statistics. That is, the counter-

examples to Julesz's various conjectures never had identical second- or third-order statistics within the actual finite images observed. Rather, the identity was over all possible images that could have been generated by the process that generated the particular instantiation of texture currently in view. In fact, for continuous images, image pairs with identical third-order statistics must be identical images, rendering that version of the conjecture trivial (Yellott, 1993), and finite, discrete images are determined by their dipole statistics (Chubb and Yellott, 2000). On the other hand, Victor (1994) makes the case for the appropriateness of the use of population statistics for theorizing about texture segregation.

The feature-based theories were echoed in research in the visual search field (Treisman, 1985). A target pattern in a field of distracter patterns was easily found whenever the target and distracters differed in a feature (e.g., size, orientation) similar to the texton features that led to effortless texture segregation. For example, a target **X** was effortlessly and immediately located in a field of distracter **L**s. However, when the target was a **T**, the task became effortful and required serial scrutiny of the texture elements, requiring more time with every additional distracter added to the stimulus (Bergen and Julesz, 1983). When the choice of target and distracters requires the observer to attend to a specific combination of two features, the search becomes difficult and observers often perceive *illusory conjunctions* between features of neighboring objects (Treisman and Schmidt, 1982). Somewhat analogous effects using texture elements having combinations of two features have been noted in texture segregation as well (Papathomas et al., 1999). However, Wolfe (1992) suggests that texture segregation and parallel visual search do not always follow the same rules.

A number of other observations have been made concerning when texture element stimuli do or do not segregate. Beck (1982) has pointed out that textures segregate based not only on the particular texture elements used but also on their arrangement, reminiscent of the Gestalt laws of figural goodness. As in the search literature (Treisman and Gormican, 1988), texture segregation may show asymmetries (Beck, 1973; Gurnsey and Browse, 1989). For example, a patch of incomplete circles will easily segregate from a background of circles, whereas the reverse pattern results in poor segregation. It has been suggested that this is due to a difference in the variability of responses of underlying visual mechanisms to the two possible texture elements (Rubenstein and Sagi, 1990).

Nothdurft (1985) suggested that finding an edge between two textures is analogous to finding a luminance-defined edge. To determine a luminance boundary involves locating large values of the derivative of luminance (the luminance gradient) across an image. Finding texture boundaries might involve the determination of other aspects of image struc-

ture (local scale, local orientation, etc.), and segregation would then result from large values of the *structure gradient*.

Finally, much of the literature assumes that effortless texture segregation and parallel visual search are truly effortless. That is, they require no selective attention to operate (demonstrated by, e.g., Braun and Sagi, 1990). However, Joseph et al. (1997) had observers perform an effortful secondary task and noted a large decrement in search performance in a search task that typically yields performance independent of the number of distracters. Thus, it is possible that even parallel search and, by extension, effortless texture segregation still require selective visual attention. Alternatively, texture segregation may not require focal visual attention, but attention may be used to alter the characteristics of visual mechanisms responsible for texture segregation (e.g., Yeshurun and Carrasco, 2000). Early literature also assumed that texture segregation was effortless in the sense of being immediate. However, at least some textures take substantial time to process (e.g., Sutter and Graham, 1995), thus undermining the notion that preattentive texture segregation is always immediate and effortless.

We have treated texture as if it is somehow an isolated cue that can signal the presence, location, and shape of an edge. However, texture can co-occur in a stimulus with other cues to edge presence such as luminance, color, depth, or motion. Rivest and Cavanagh (1996) showed that perceived edge location was a compromise between the position signaled by texture and by other cues (motion, luminance, color). In addition, localization accuracy was better for two-cue than for single-cue stimuli. Landy and Kojima (2001) found that different textural cues to edge location were combined using a weighted average, with greater weight given to the more reliable cues. This is analogous to the cue combination scheme that has been seen with multiple cues to depth (including depth from texture) by Landy et al. (1995), among others.

CURRENT MODELS OF TEXTURE SEGREGATION How might one model the aspects of texture segregation performance we have just surveyed? If an edge is defined by a difference in luminance (a typical light/dark edge), then a bandpass linear spatial filter similar to a cortical simple cell can detect the edge by producing a peak response at the location of the edge. But, a typical texture-defined edge (e.g., Figs. 73.2 and 73.4.4) has the same average luminance on either side of the edge and thus will not be detected by any purely linear mechanism.

Several early investigators (e.g., Beck, 1972; Julesz, 1981) suggested that observers calculate the local density of various image features, and that differences in these texton or feature statistics on either side of a texture-defined edge result in effortless texture segregation. However, it was never clearly described exactly what an image feature was and how

it would be computed from the retinal image. The image features discussed (e.g., lines of different slopes, line terminations and crossings) were clearly tied to the kinds of stimuli employed in most texture studies of the period (basically, pen-and-ink drawings) and would not be applied easily to natural gray-scale images.

An alternative line of modeling suggests that we need look no further than the orientation- and spatial frequency-tuned channels already discovered in the spatial vision literature through summation, identification, adaptation, and masking experiments using sine wave grating stimuli (De Valois and De Valois, 1988; Graham, 1989, 1992). For example, Knutsson and Granlund (1983) suggested that the distribution of power in different spatial frequency bands might be used to segregate natural textures, and ran such a computational model on patchworks of textures drawn from the Brodatz (1966) collection (a standard collection of texture images often used in the computational literature).

Bergen and Adelson (1988) pointed out that even the example of Xs, Ls, and Ts (Fig. 73.2) could be accounted for by the distribution of power in isotropic channels similar in form to cells found in the lateral geniculate nucleus (LGN) and layer 4 of primary visual cortex. Further, they showed that if the size of the Xs was increased to effectively equate the dominant spatial frequency or *scale* of the different texture elements, the segregation of Xs from a background of Ls could be made difficult. This was strong evidence against the texton or feature theories.

A plethora of similar models based on filters selective for spatial frequency and orientation have been investigated (Bovik et al., 1990; Caelli, 1985; Fogel and Sagi, 1989; Graham, 1991; Landy and Bergen, 1991; Malik and Perona, 1990; Sutter et al., 1989; Turner, 1986; for an alternative view, see Victor, 1988). These models are so similar in basic design that Chubb and Landy (1991) referred to this class as the *back pocket model of texture segregation*, as texture perception researchers pull this model from their back pocket to explain new phenomena of texture segregation.

The basic back pocket model consists of three stages (Fig. 73.3). First, a set of linear spatial filters, akin to the simple cells of primary visual cortex, is applied to the retinal image. Second, the outputs of the first-stage linear filters are transformed in a nonlinear manner (by half- or full-wave rectification, squaring, and/or gain control). Finally, another stage of linear filtering is used to enhance texture-defined contours. If this third stage consisted only of spatial pooling, the resulting outputs would resemble those of cortical complex cells. But often this linear filter is modeled as bandpass and orientation-tuned, so that it enhances texture-defined edges much as an orientation-tuned linear spatial filter enhances luminance-defined edges.

This process is illustrated in Figure 73.4. Figure 73.4A shows an orientation-defined texture border (Wolfson and

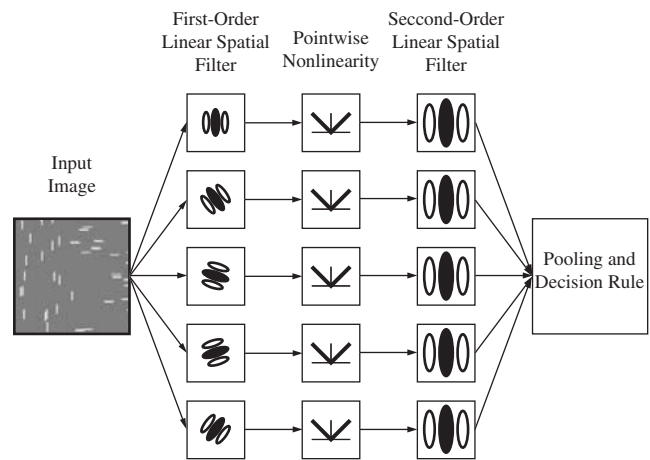


FIGURE 73.3. The back pocket model of texture segregation. The retinal image is first processed by a bank of linear spatial filters. Then some form of nonlinearity is applied. Here, a pointwise full-wave rectification is indicated. Next, a second stage of linear spatial filtering is applied to enhance the texture-defined edge. Subsequent decision processes are dependent on the particular psychophysical task under study.

Landy, 1995). In Figure 73.4B a vertically oriented spatial filter has been applied. The responses are larger to the vertically oriented portion of the image, but these responses are both strongly positive (when the filter is centered on a texture element) and negative (when the filter is positioned off to the side of a texture element). As a result, the average value of the output is identical on either side of the texture border, but on the left the response variability is greater. In Figure 73.4C the responses of Figure 73.4B have been rectified, resulting in larger responses in the area of vertically oriented texture. Finally, in Figure 73.4D, a second-order, larger-scale, vertically oriented spatial filter has been applied, resulting in a peak response at the location of the texture-defined edge. For a detection experiment (“Was there a texture-defined edge in this briefly-flashed stimulus?”) or “Were there two different texture regions or only one?”), a model would try to predict human performance by the strength of the peak response in Figure 73.4D as compared to peaks in responses to background noise in stimuli *not* containing texture-defined edges. For further examples, see Bergen (1991) and Bergen and Landy (1991).

A wide variety of terminology has been used to describe the basic model outlined in Figure 73.3, making the literature difficult for the neophyte. The basic sequence of a spatial filter, a nonlinearity, and a second spatial filter has been called the *back pocket model* (Chubb and Landy, 1991), an *LNL* (linear, nonlinear, linear) model, an *FRF* (filter, rectify, filter) model (e.g., Dakin et al., 1999), *second-order processing* (e.g., Chubb et al., 2001), or a *simple or linear channel* (the first L in LNL) followed by a *comparison-and-decision stage* (e.g., Graham et al., 1992).

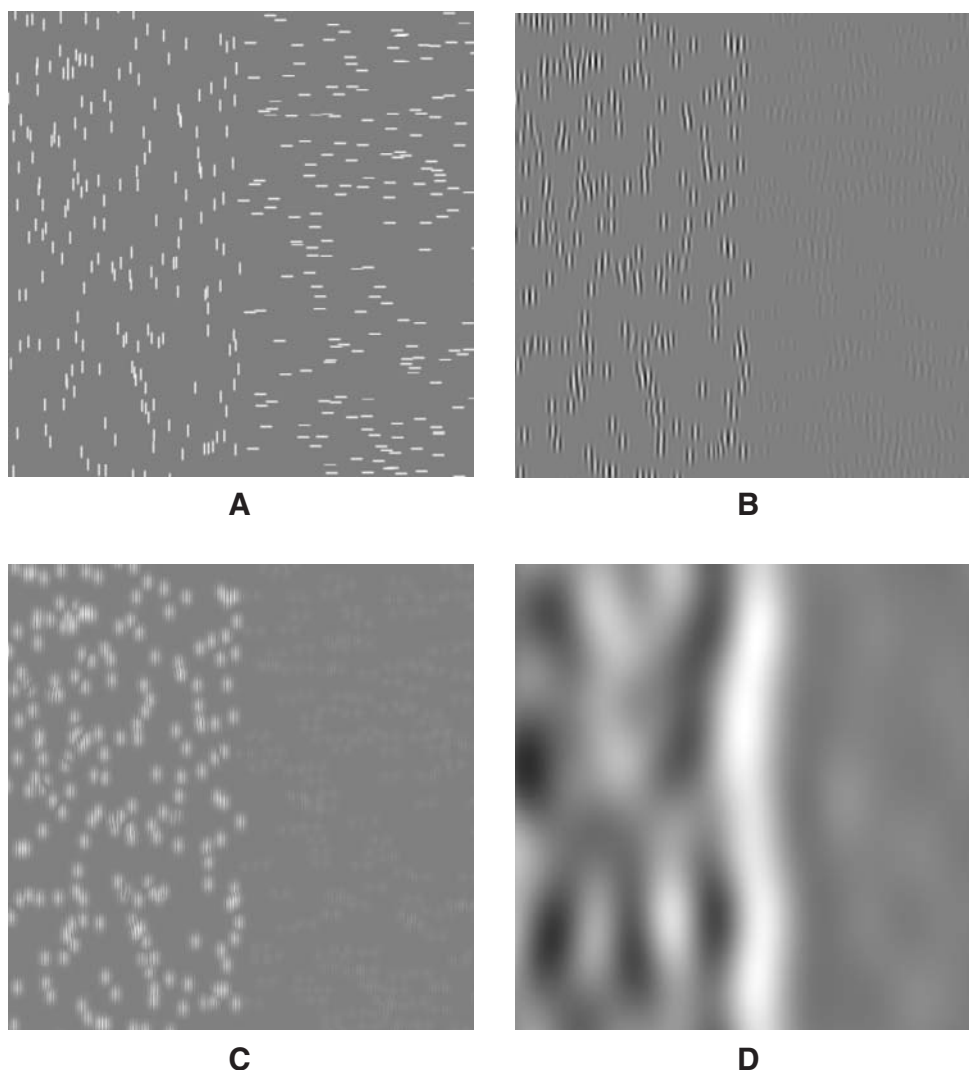


FIGURE 73.4. Back pocket model. *A*, An orientation-defined edge. *B*, The result of the application of a linear, vertically oriented spatial filter. *C*, The result of a pointwise nonlinearity (squaring). *D*, A second, large-scale, vertically oriented spatial filter yields a peak response at the location of the texture-defined border in *A*.

About the term “second-order” The term *second-order* can be particularly troublesome. In some hands, and as we will use it here, it merely refers to the second stage of linear filtering following the nonlinearity in a model like that of Figure 73.3. As such, it has been applied to models in a wide variety of visual tasks (Chubb et al., 2001). But *second-order* has another technical definition that has also been used in similar contexts. If the nonlinearity in Figure 73.3 is a squaring operation, then the pixels in the output image (after the second stage of linear filtering) are all computed as second-order (i.e., quadratic) polynomials of the pixels in the model input.

In this chapter, we will refer to the model of Figure 73.3 as a second-order model, meaning that it contains a second-order linear spatial filter. Of necessity, this second-order linear filter must follow an intervening

nonlinearity. Otherwise, there would simply be two sequential linear filters, which are indistinguishable from a single, lumped linear spatial filter. We will use this term regardless of the polynomial order of the intervening nonlinearity.

There is also a more general use of *second-order*. In this usage, a second-order entity (e.g., a neuron) pools, after some intervening nonlinearity, the responses from a number of other entities (called *first-order*) but, in this more general usage, the first-order entities do not form a linear filter characterized by a single spatial weighting function, as they do in Figure 73.3. Rather, the first-order entities can be an assortment of neurons sensitive to various things (e.g., different orientations or different spatial frequencies). See the introduction to Graham and Sutter (1998) for a brief review of such general suggestions.

Third-order models Second-order models are not the end of the story. For example, Graham et al. (1993) used an element-arrangement texture stimulus consisting of two types of elements, arranged in stripes in one region and in a checkerboard in another region. Consider the case where each texture element is a high-frequency Gabor pattern (a windowed sine wave grating) and the two types of elements differ only in spatial frequency. Consider a second-order model like that just described, with the first linear filter tuned to one of the two types of Gabor patches and the second linear filter tuned to the width and orientation of stripes of elements. This second-order model would yield a response to these element-arrangement textures that is of the same average level, although of high contrast in the striped region and low contrast in the checked region. To reveal the texture-defined edge between the checkerboard and striped regions, therefore, requires another stage of processing, which could be a pointwise nonlinearity followed by an even larger-scale linear spatial filter (another NL), thus producing a sequence LNLNL. For an illustration of such a model's responses, see Graham et al. (1993), Figure 4.

Here we will call this LNLNL sequence a third-order model. But, to avoid confusion, let us note that Graham and her colleagues refer to the first LNL as a complex channel or second-order channel and the final NL is an instance of what they call the comparison-and-decision stage.

About the terms "Fourier" and "non-Fourier" There is also possible confusion about the terms *Fourier* and *non-Fourier*. A stimulus like that in Figure 73.4A, in which the edge can be found by the model in Figure 73.3, has been referred to as *non-Fourier* (first applied to motion stimuli by Chubb and Sperling, 1988). The term was used because the Fourier spectrum of this stimulus does not contain components that correspond directly to the texture-defined edge. But some others (e.g., Graham and Sutter, 2000) have used the term *Fourier channels* for the first linear filters (the simple channels) in Figure 73.3 and reserved the term *non-Fourier* for the complex channels (the initial LNL) in what we called third-order models above (LNLNL).

This confusing terminology is the result of a difference in emphasis. In this chapter, we concentrate on models that localize (i.e., produce a peak response at) edges between two abutting textures. But, others (e.g., Graham and Sutter, 2000; Lin and Wilson, 1996) have emphasized response measures that can be used to discriminate between pairs of textures (whether simultaneously present and abutting or not) by any later, nonlinear decision process. Thus, finding the edge in an orientation-defined texture like that of Figure 73.3 is, in Graham and Sutter's terms, *Fourier-based*, as the power spectra of the two constituent textures differ, whereas finding the edge in a Gabor-patch element-arrangement texture like that of Graham et al. (1993) is *non-Fourier-based*,

as the power spectra of the two constituent textures do not differ.

MODEL SPECIFICATION The models of texture segregation just described are complicated, with many details that require elucidation. Are the initial linear filters of a second-order pathway the same spatial filters as the spatial frequency channels that have been described using grating experiments? What is the nature of the following nonlinearity? Are there fixed, second-order linear filters, and what is their form? This is an area of current active research, and most of these issues have not been convincingly decided.

Graham et al. (1993) and Dakin and Mareschal (2000) provide evidence that the initial spatial filters in a second-order pathway used to detect contrast modulations of texture are themselves tuned for spatial frequency and orientation. In the same article, Graham and colleagues also demonstrated that the initial spatial filters in a third-order pathway (their complex channels) were orientation- and spatial-frequency-tuned as well.

The back pocket model includes a nonlinearity between the two stages of linear spatial filtering that is required to demodulate the input stimuli. For small first-order spatial filters, Chubb et al. (1994) provided a technique called *histogram contrast analysis* that allowed them to measure aspects of the static nonlinearity, showing that it included components of higher order than merely squaring the input luminances. Graham and Sutter (1998) found that this nonlinearity must be expansive. They also (Graham and Sutter, 2000) suggested that a gain control mechanism acts as an inhibitory influence among multiple pathways of the types called second-order and third-order here.

First-order spatial frequency channels were first measured using sine wave grating stimuli and various experimental paradigms including adaptation, masking, and summation experiments (reviewed in Graham, 1989). Recently, researchers used analogous experiments to examine the second-order linear filters. To do so, researchers hope to deliver to the second-order filter something like the sine wave grating stimuli of classical spatial frequency channel studies. The usual ploy is to use a stimulus that has a sine wave (or Gabor) pattern to modulate some aspect of textural content across the stimulus. The assumed first-order filter and the subsequent nonlinearity demodulate this stimulus, providing as input to the second-order linear filter a noisy version of the intended grating or Gabor pattern.

Studies of texture modulation detection have revealed a very broadband second-order texture contrast sensitivity function (CSF) using a variety of texture modulations including contrast (Schofield and Georgeson, 1999, 2000; Sutter et al., 1995), local orientation content (Kingdom et al., 1995), and modulation between vertically and horizontally oriented, filtered noise (Landy and Oruç, 2002). This

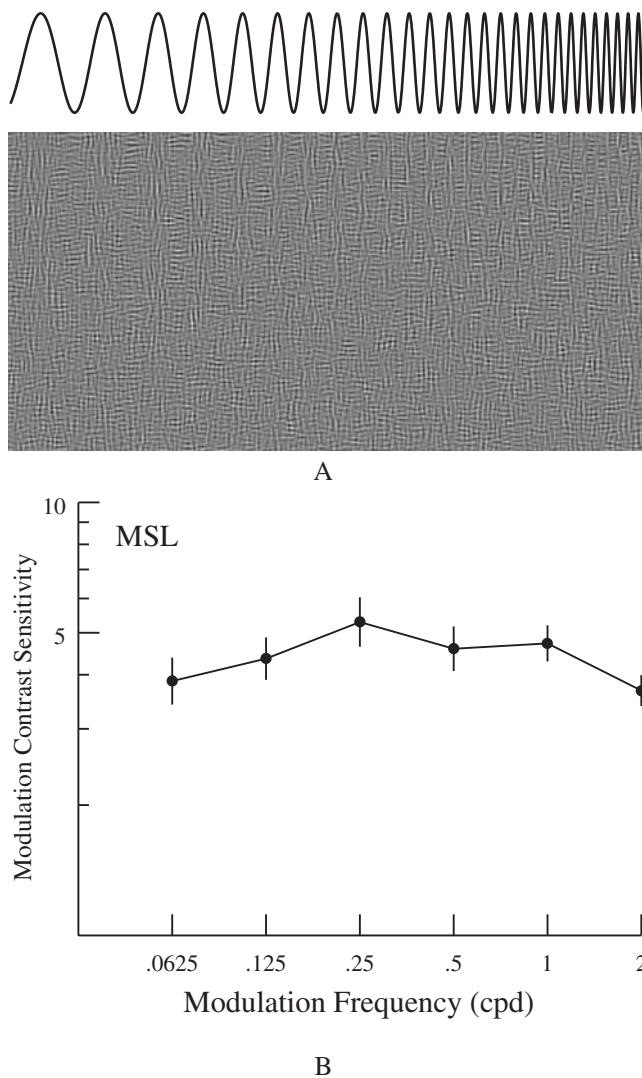


FIGURE 73.5. The second-order contrast sensitivity function. *A*, This figure is constructed using a modulator image to additively combine vertical and horizontal noise images (Landy and Oruç, 2002). The modulator, shown as a function above the texture, has a spatial frequency that increases from left to right, and its contrast increases from bottom to top. Large modulator values result in a local texture dominated by vertically oriented noise and small values by horizontally oriented noise. Note that threshold modulation contrast is nearly independent of spatial frequency. *B*, Example data from a forced-choice modulation contrast detection experiment using sine wave modulators of noise patterns.

function is far more broadband than the corresponding luminance CSF. A demonstration of this effect is shown in Figure 73.5*A*. A modulator pattern is used to combine additively a vertical and a horizontal noise texture. The modulator increases in spatial frequency from left to right and in contrast from bottom to top. As you can see, the texture modulation becomes impossible to discern at approximately the same level for all spatial frequencies. The sample data in Figure 73.5*B* confirm this observation.

Evidence for multiple second-order filters underlying this broad second-order CSF has been equivocal, with evidence both pro (Arsenault et al., 1999; Landy and Oruç, 2002; Schofield and Georgeson, 1999) and con (Kingdom and Keeble, 1996). Many studies have found texture discrimination to be scale-invariant, suggesting the existence of a link between the scale of the corresponding first- and second-order spatial filters (Kingdom and Keeble, 1999; Landy and Bergen, 1991; Sutter et al., 1995). It has also been suggested that the orientation preferences of the first- and second-order filters tend to be aligned (Dakin and Mareschal, 2000; Wolfson and Landy, 1995). This alignment of first- and second-order filters has also been supported for element-arrangement stimuli that require a third-order model to detect the texture-defined edges (Graham and Wolfson, 2001).

If there is an obligatory link between the scales of the first- and second-order filters, this suggests that the preferred second-order scale should depend on eccentricity. This was first demonstrated by Kehrner (1989), who noted that performance on an orientation-defined texture-segregation task at first improves as the target texture moves into the periphery and then worsens as the eccentricity increases further. The poor foveal performance was dubbed the *central performance drop* (CPD). This argument that the CPD is due to the relation between the scale of the second-order pattern and the local scale of the second-order filter was made by Yeshurun and Carrasco (2000), who, in addition, suggested that the second-order spatial filters are narrowed as a consequence of the allocation of selective attention.

The temporal properties of the first- and second-order filters are not well understood, although some information is available (Lin and Wilson, 1996; Motoyoshi and Nishida, 2001; Schofield and Georgeson, 2000; Sutter and Graham, 1995; Sutter and Hwang, 1999).

The possibility that the wiring between first- and second-order filters is more complicated than that shown in Figure 73.3 remains open as well (see, e.g., the appendix in Graham and Sutter, 1998; Mussap, 2001), with particular interest in possible lateral excitatory and inhibitory interactions among different positions within the same filter (Motoyoshi, 1999; Wolfson and Landy, 1999).

Early filters are not the only visual processes that play an important role in determining the conscious perception of textured stimuli. Consider He and Nakayama (1994), who constructed a series of binocular demonstration stimuli involving both texture and disparity. The foreground surface consisted of a set of textured squares. The background stimuli consisted of a region of I shapes surrounded by L shapes that, monocularly, segregated quite easily. However, when seen in depth with the squares (that abutted the Ls and Is) in front, both the Ls and Is were perceived as occluded by the squares. They underwent surface completion; that is, they were both perceived as larger rectangles

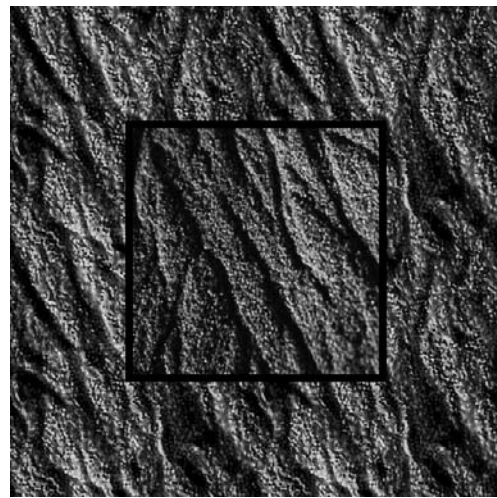
occluded by the squares, and texture segregation became effortful. This suggests that higher-level, surface-based representations are involved in judgments about the objects perceived on the basis of textured regions in the stimulus.

Texture appearance

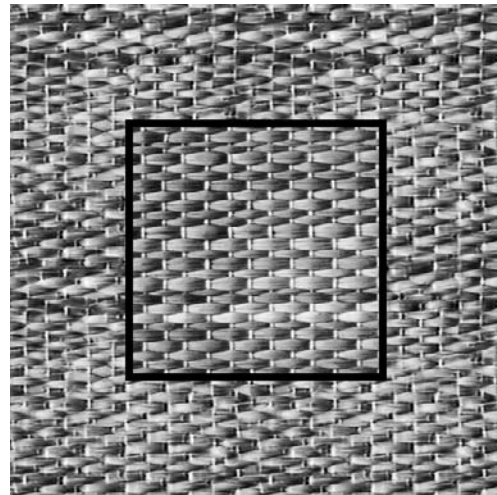
The previous section concentrated on research concerning observers' ability to detect borders between differing textures. Here we consider research more directly measuring the appearance of textures. If two images both appear to be a grassy field, then at some level of analysis, the representations of the two images must be similar. To understand the appearance of texture might involve developing such a representation, as well as a metric within that representation space so that textures are perceived as similar if their representations are close and dissimilar if far. Indeed, there is even evidence that texture appearance (or, at least, region-based) mechanisms can be responsible for texture segregation in some cases (Wolfson and Landy, 1998), as certain texture pairs can be discriminated just as well when they are separated as when they abut (forming an edge). Using region-based as well as edge-based mechanisms may be optimal for segregation processes (Lee, 1995).

One approach to this problem of measuring texture appearance is a classical one: elicit similarity judgments from observers and try to build a representation. Having done so, one can then ask whether the underlying dimensions have any semantic basis or whether dimensions satisfy any of the properties of other perceptual dimensions (such as the additivity and metamerism of color space). Three dimensions appeared to suffice for sets of natural textures (Rao and Lohse, 1996) as well as artificial ones (Gurnsey and Fleet, 2001; Harvey and Gervais, 1978). A texture analogy to color matching experiments with artificial one-dimensional textures provides satisfactory appearance matches with four texture primaries (Richards and Polit, 1974). As with color matching, this technique shows that one can account for texture matches with the four primaries, but it does not explain texture appearance. Color appearance depends on the particular metameric match, as well as on color context. Similarly, texture appearance can depend on context. For example, Durgin (2001) shows that the perceived texture density of a texture patch depends on the density of the surrounding texture.

An alternative approach is to analyze an instance of texture to estimate its representation and then use that representation to generate new instances of texture. The proposed representational scheme is considered successful if the newly generated textures are classified as "made of the same stuff as the original" by observers. The first such model, by Heeger and Bergen (1995), represented the input texture image as the histograms of values in each level of an



A



B

FIGURE 73.6. Texture appearance, representation, and extrapolation. In the technique of Portilla and Simoncelli (2000), a texture is first analyzed using a bank of linear spatial filters varying in preferred spatial frequency and orientation. A set of statistics, both first-order and correlational, on that set of filter responses becomes the representation of the given texture. This representation may be used to generate new instances of the texture. In each panel, the inset square is the original texture, and the rest of the image is new texture generated using the technique.

oriented pyramid representation of the image, that is, as the statistics of the responses from a collection of orientation- and spatial frequency-tuned spatial filters. The resulting newly generated texture images were occasionally striking in their similarity to the original. But, in other instances, especially those involving correlations between different image areas at long distances, the results were quite poor. More recent models incorporate higher-order statistics including correlations between pairs of filter responses across space,

spatial frequency, and orientation (De Bonet and Viola, 1998; Portilla and Simoncelli, 2000; Zhu et al., 1998). Figure 73.6 shows two sample textures (inset squares) that were extrapolated using the technique of Portilla and Simoncelli (2000). Clearly, the technique has captured a good deal of that which defines the appearance of these textures. The technique is somewhat less successful with purely periodic textures (tiles), binary or pen-and-ink textures, or with pseudotextures that are, for example, collections of small objects (e.g., a pile of jellybeans). It remains to be seen whether a metric (Euclidean, Minkowski, or other) applied to one of these texture representation spaces will correlate well with observers' judgments of the perceptual similarity of textures.

Few psychophysical tests of these new statistical characterizations of texture have been carried out. Kingdom et al. (2001), in an analogy to the work of Chubb and colleagues in the luminance domain (1994), found that observers were most sensitive to kurtosis in the histograms of wavelet (that is, multiscale, orientation-tuned) coefficients in artificial textures. Durgin (2001) has suggested that texture density is a separate dimension from either mean (luminance) or variance (root-mean-squared contrast).

The texture representation schemes just discussed are image-based. That is, all content of the representation is based on simple statistics based on responses of filters to the texture. A complete theory of texture perception might involve recognition that natural textures are associated with real-world materials, and the appearance of texture may well relate to perception of the particular material from which the image derived (wood, plastic, water, grassland, etc.) or properties of the real-world material that might relate to actions the observer might wish to take. This is the concept of an *affordance* (Gibson, 1979). Is this material sticky? Will it crumble in my hand? Will I be able to walk on it in bare feet? A great deal of work has been done, notably in the computer graphics world, to understand image properties of natural materials in order to simulate these materials in virtual displays. By contrast, very little research has been done on the perception of real-world textural properties. Recently, some effort has been made to understand the variety of images one can find of natural textures as viewpoint and lighting conditions are varied (Dana et al., 1999).

Shape from texture

Gibson (1950) pointed out that the perspective distortion of surface texture is a cue to surface layout. For example, consider a ground plane that is painted with randomly placed circles. As the surface recedes into the distance, three different *texture gradients* may be distinguished: size (farther-away texture elements are smaller in the retinal image), density

(farther-away texture elements are closer together in the retinal image), and compression (farther-away elements are more slanted relative to the line of sight and hence form more eccentric ellipses in the retinal image).

The computational literature is replete with suggested algorithms for the computation of shape from texture. These algorithms vary in how restrictive an assumption is made about the surface texture. The earliest algorithms (e.g., that of Witkin, 1981) assumed an isotropic texture (all orientations were equally represented on the surface, which is true of the above example). More recent algorithms (e.g., that of Aloimonos, 1988) only assume texture homogeneity (i.e., the texture is statistically the same at all positions on the surface). A particularly interesting algorithm is that of Malik and Rosenholtz (1997). This algorithm makes weak assumptions about the underlying surface texture. It looks for affine distortions in image statistics from one location to another, as seen in the responses of a bank of spatial filters varying in orientation and spatial frequency preference, much like the first stage in the current models of texture segregation.

Psychophysical research on the perception of shape from texture has followed a similar history. Cutting and Millard (1984) discussed the three possible texture gradients and manipulated them independently in their stimuli. They found that perception of slant for planar stimuli depended mainly on the size gradient, whereas perception of curved stimuli was almost completely determined by the compression gradient. Rosenholtz and Malik (1997) found texture isotropy to be unnecessary for human observers to estimate surface orientation, consistent with their computational theory. Li and Zaidi (2000) examined the types of surface texture that would give a veridical percept of shape when mapped onto a corrugated surface in perspective, and found that several aspects of the Fourier power spectrum were predictive of observer accuracy, corresponding to the availability of oriented energy along lines of maximum and minimum curvature in the surface.

A second line of psychophysical research has been to derive ideal (maximum a posteriori) observers and to compare the reliability of human observers' estimates of surface layout with those of the ideal observer. Blake et al. (1993) derived such a model with the assumption of isotropic, homogeneous surface texture and demonstrated that observers' estimates of surface curvature must use the compression gradient. Buckley et al. (1996) applied the same strategy to the estimation of surface slant, and found that texture compression dominates observer judgments even for fields of view large enough that, for the ideal, texture density should dominate. Finally, in a series of three papers, Knill (1998a, 1998b, 1998c) derived ideal observers for slant from texture that use the three texture gradient cues and derived the reliability of each cue as a function of slant and field

of view. He found that human observers became more reliable with increasing slant and field of view, just as did the ideal observers. Again, performance was so good that observers must have used texture compression and, at least in part, an assumption of isotropy.

Neurophysiology

The physiological substrate for the first-stage linear filters in texture segregation models is likely to be the spatial frequency and orientation-selective cells in cortical area V1. Further, V1 is sufficiently complicated that other attributes of the current models, such as the normalization or other nonlinearities and subsequent spatial pooling, could certainly also occur in V1. There are also lateral interactions between neurons in V1 (both excitatory and inhibitory) that go beyond the classical receptive field. There has been some controversy over the function of these lateral interactions in V1. Some have suggested that lateral interactions enhance responses to popout stimuli (Kastner et al., 1997, 1999; Nothdurft et al., 1999), to texture elements near texture borders (Nothdurft et al., 2000), to orientation contrast (Knierim and Van Essen, 1992; Sillito et al., 1995), and to figure rather than ground (Lamme, 1995; Zipser et al., 1996). Li (2000) even described a neural network model of segmentation that includes such processes.

However, the responses to orientation contrast stimuli are a complex function of the contrasts of the figure and ground (Levitt and Lund, 1997), suggesting that these V1 responses are primarily the result of a gain control mechanism that is only an initial stage of the computation of texture borders and figure-ground. Consistent with this view, several groups have found that input from outside the classical receptive field is mainly suppressive and suggest that it is not involved with figure-ground analysis (Freeman et al., 2001; Rossi et al., 2001; Sceniak et al., 2001; Walker et al., 2000). An in-depth review of a large range of results from areas V1 up through MT, and V4 (Lennie, 1998) concludes that it may be too much to attribute such functions as popout and figure-ground segregation to area V1, and that these functions probably occur in V2 through V4 or even at higher levels. Lennie suggests that "Spatial interactions in V1 probably have a less exotic role; they provide lateral inhibition in the domain of local structure so that, by analogy with lateral inhibition in the luminance domain, signals from regions of common structure are suppressed and contrasts in structure are made salient." In this view, it is not until area V4 that the system has even grouped regions of similar structure to find contours, regions, and surfaces and, perhaps, computed surface slant. And thus, in this view, many of the processes called into play by texture stimuli (e.g., the conscious perception of a surface as having a particular texture) would be determined predominantly by still higher-level cortical areas.

A recent functional magnetic resonance imaging study of static texture segregation (Kastner et al., 2000) concurs, finding little response to texture borders in V1 or V2/VP and increasing responses as one proceeds downstream from V3 to V4 and TEO.

Conclusions

The perception of texture is a rich and varied area of study. In the early coding of texture borders, there is some common ground between current psychophysical data and models and the physiology of primary visual cortex, such as the suggestion that texture border coding involves a succession of linear spatial filters and nonlinearities that include static nonlinearities as well as contrast gain control mechanisms. Less well understood, however, are such higher-level computations involving texture as the calculation of figure-ground, the coding of texture appearance, and the determination of depth and three-dimensional shape from texture cues.

Acknowledgments

Michael Landy was supported by National Eye Institute Grant EY08266 and Human Frontier Science Program Grant RG0109/1999-B. Norma Graham was supported by National Eye Institute Grant EY08459. We would like to acknowledge the helpful comments of Sabina Wolfson over a period of many years.

REFERENCES

- Adelson, E. H., and J. R. Bergen, 1991. The plenoptic function and the elements of early vision, in *Computational Models of Visual Processing* (M. S. Landy and J. A. Movshon, eds.), Cambridge, MA: MIT Press, pp. 3–20.
- Aloimonos, J., 1988. Shape from texture, *Artificial Intelligence*, 38:345–360.
- Arsenault, A. S., F. Wilkinson, and F. A. A. Kingdom, 1999. Modulation frequency and orientation tuning of second-order texture mechanisms, *J. Opt. Soc. Am. A*, 16:427–435.
- Beck, J., 1972. Similarity grouping and peripheral discriminability under uncertainty, *Am. J. Psychol.*, 85:1–19.
- Beck, J., 1973. Similarity grouping of curves, *Percept. Motor Skills*, 36:1331–1341.
- Beck, J., 1982. Textural segmentation, in *Organization and Representation in Perception* (J. Beck ed.), Hillsdale, NJ: Erlbaum, pp. 285–317.
- Bergen, J. R., 1991. Theories of visual texture perception, in *Vision and Visual Dysfunction*, vol. 10B (D. Regan ed.), New York: Macmillan, pp. 114–134.
- Bergen, J. R., and E. H. Adelson, 1988. Early vision and texture perception, *Nature*, 333:363–364.
- Bergen, J. R., and B. Julesz, 1983. Parallel versus serial processing in rapid pattern discrimination, *Nature*, 303:696–698.
- Bergen, J. R., and M. S. Landy, 1991. Computational modeling of visual texture segregation, in *Computational Models of Visual*

- Processing* (M. S. Landy and J. A. Movshon, eds.), Cambridge, MA: MIT Press, pp. 253–271.
- Blake, A., H. H. Buelthoff, and D. Sheinberg, 1993. Shape from texture: ideal observers and human psychophysics, *Vis. Res.*, 33:1723–1737.
- Bovik, A. C., M. Clark, and W. S. Geisler, 1990. Multichannel texture analysis using localized spatial filters, *IEEE Trans. Pattern Anal. Machine Intelligence*, 12:55–73.
- Braun, J., and D. Sagi, 1990. Vision outside the focus of attention, *Percept. Psychophys.*, 48:45–58.
- Brodatz, P., 1966. *Textures*, New York: Dover.
- Buckley, D., J. P. Frisby, and A. Blake, 1996. Does the human visual system implement an ideal observer theory of slant from texture? *Vis. Res.*, 36:1163–1176.
- Caelli, T., 1985. Three processing characteristics of visual texture segmentation, *Spatial Vis.*, 1:19–30.
- Caelli, T., and B. Julesz, 1978. On perceptual analyzers underlying visual texture discrimination: Part I, *Biol. Cybern.*, 28:167–175.
- Caelli, T., B. Julesz, and E. N. Gilbert, 1978. On perceptual analyzers underlying visual texture discrimination: Part II, *Biol. Cybern.*, 29:201–214.
- Chubb, C., J. Econopoulou, and M. S. Landy, 1994. Histogram contrast analysis and the visual segregation of IID textures, *J. Opt. Soc. Am. A*, 11:2350–2374.
- Chubb, C., and M. S. Landy, 1991. Orthogonal distribution analysis: a new approach to the study of texture perception, in *Computational Models of Visual Processing* (M. S. Landy and J. A. Movshon, eds.), Cambridge, MA: MIT Press, pp. 291–301.
- Chubb, C., L. Olzak, and A. Derrington, 2001. Second-order processes in vision: introduction, *J. Opt. Soc. Am. A*, 18:2175–2178.
- Chubb, C., and G. Sperling, 1988. Drift-balanced random stimuli: a general basis for studying non-Fourier motion perception, *J. Opt. Soc. Am. A*, 5:1986–2007.
- Chubb, C., and J. I. Yellott, Jr., 2000. Every discrete, finite image is uniquely determined by its dipole histogram, *Vis. Res.*, 40:485–492.
- Cutting, J. E., and R. T. Millard, 1984. Three gradients and the perception of flat and curved surfaces, *J. Exp. Psychol. Gen.*, 113:198–216.
- Dakin, S. C., and I. Mareschal, 2000. Sensitivity to contrast modulation depends on carrier spatial frequency and orientation, *Vis. Res.*, 40:311–329.
- Dakin, S. C., C. B. Williams, and R. F. Hess, 1999. The interaction of first- and second-order cues to orientation, *Vis. Res.*, 39:2867–2884.
- Dana, K. J., B. van Ginneken, S. K. Nayar, and J. J. Koenderink, 1999. Reflectance and texture of real-world surfaces, *ACM Trans. Graphics*, 18:1–34.
- De Bonet, J. S., and P. Viola, 1998. A non-parametric multi-scale statistical model for natural images, in *Advances in Neural Information Processing Systems 9* (M. I. Jordan, M. J. Kearns, and S. A. Solla, eds.), Cambridge, MA: MIT Press, pp. 773–779.
- De Valois, R. L., and K. K. De Valois, 1988. *Spatial Vision*, New York: Oxford University Press.
- Durgin, F. H., 2001. Texture contrast aftereffects are monocular; texture density aftereffects are binocular, *Vis. Res.*, 41:2619–2630.
- Freeman, R. D., I. Ohzawa, and G. Walker, 2001. Beyond the classical receptive field in the visual cortex, *Prog. Brain Res.*, 134:157–170.
- Fogel, I., and D. Sagi, 1989. Gabor filters as texture discriminator, *Biol. Cybern.*, 61:103–113.
- Gibson, J. J., 1950. *The Perception of the Visual World*, Boston: Houghton Mifflin.
- Gibson, J. J., 1979. *The Ecological Approach to Visual Perception*, Boston: Houghton Mifflin.
- Graham, N., 1989. *Visual Pattern Analyzers*, New York: Oxford University Press.
- Graham, N., 1991. Complex channels, early local nonlinearities, and normalization in perceived texture segregation, in *Computational Models of Visual Processing* (M. S. Landy and J. A. Movshon, eds.), Cambridge, MA: MIT Press, pp. 273–290.
- Graham, N., 1992. Breaking the visual stimulus into parts, *Curr. Dir. Psychol. Sci.*, 1:55–61.
- Graham, N., J. Beck, and A. Sutter, 1992. Nonlinear processes in spatial-frequency channel models of perceived texture segregation: effects of sign and amount of contrast, *Vis. Res.*, 32:719–743.
- Graham, N., and A. Sutter, 1998. Spatial summation in simple (Fourier) and complex (non-Fourier) texture channels, *Vis. Res.*, 38:231–257.
- Graham, N., and A. Sutter, 2000. Normalization: contrast-gain control in simple (Fourier) and complex (non-Fourier) pathways of pattern vision, *Vis. Res.*, 40:2737–2761.
- Graham, N., A. Sutter, and C. Venkatesan, 1993. Spatial-frequency- and orientation-selectivity of simple and complex channels in region segmentation, *Vis. Res.*, 33:1893–1911.
- Graham, N., and S. S. Wolfson, 2001. A note about preferred orientations at the first and second stages of complex (second-order) texture channels, *J. Opt. Soc. Am. A*, 18:2273–2281.
- Gurnsey, R., and R. A. Browse, 1989. Asymmetries in visual texture discrimination, *Spatial Vis.*, 4:31–44.
- Gurnsey, R., and D. J. Fleet, 2001. Texture space, *Vis. Res.*, 41:745–757.
- Harvey, L. O. Jr., and M. J. Gervais, 1978. Visual texture perception and Fourier analysis, *Percept. Psychophys.*, 24:534–542.
- He, Z. J., and K. Nakayama, 1994. Perceiving textures: beyond filtering, *Vis. Res.*, 34:151–162.
- Heeger, D., and J. R. Bergen, 1995. Pyramid-based texture analysis/synthesis, in *Proceedings of ACM SIGGRAPH 1995*. New York: Association for Computing Machinery, pp. 229–238.
- Joseph, J. S., M. M. Chun, and K. Nakayama, 1997. Attentional requirements in a “preattentive” feature search task, *Nature*, 387:805–807.
- Julesz, B., 1981. Textons, the elements of texture perception, and their interactions, *Nature*, 290:91–97.
- Julesz, B., E. N. Gilbert, L. A. Shepp, and H. L. Frisch, 1973. Inability of humans to discriminate between visual textures that agree in second-order statistics—revisited, *Perception*, 2:391–405.
- Julesz, B., E. N. Gilbert, and J. D. Victor, 1978. Visual discrimination of textures with identical third-order statistics, *Biol. Cybern.*, 31:137–140.
- Kastner, S., P. de Weerd, and L. G. Ungerleider, 2000. Texture segregation in the human visual cortex: a functional MRI study, *J. Neurophysiol.*, 83:2453–2457.
- Kastner, S., H. C. Nothdurft, and I. N. Pigarev, 1997. Neuronal correlates of pop-out in cat striate cortex, *Vis. Res.*, 37:371–376.
- Kastner, S., H. C. Nothdurft, and I. N. Pigarev, 1999. Neuronal responses to orientation and motion contrast in cat striate cortex, *Vis. Neurosci.*, 16:587–600.
- Kehrer, L., 1989. Central performance drop on perceptual segregation tasks, *Spatial Vis.*, 4:45–62.
- Kingdom, F. A. A., A. Hayes, and D. J. Field, 2001. Sensitivity to contrast histogram differences in synthetic wavelet-textures, *Vis. Res.*, 41:585–598.

- Kingdom, F. A. A., and D. R. T. Keeble, 1996. A linear systems approach to the detection of both abrupt and smooth spatial variations in orientation-defined textures, *Vis. Res.*, 36:409–420.
- Kingdom, F. A. A., and D. R. T. Keeble, 1999. On the mechanism for scale invariance in orientation-defined textures, *Vis. Res.*, 39:1477–1489.
- Kingdom, F. A. A., D. R. T. Keeble, and B. Moulden, 1995. Sensitivity to orientation modulation in micropattern-based textures, *Vis. Res.*, 35:79–91.
- Knierim, J. J., and D. C. Van Essen, 1992. Neuronal responses to static texture patterns in area V1 of the alert macaque monkey, *J. Neurophysiol.*, 67:961–980.
- Knill, D. C., 1998a. Surface orientation from texture: ideal observers, generic observers and the information content of texture cues, *Vis. Res.*, 38:1655–1682.
- Knill, D. C., 1998b. Discrimination of planar surface slant from texture: human and ideal observers compared, *Vis. Res.*, 38:1683–1711.
- Knill, D. C., 1998c. Ideal observer perturbation analysis reveals human strategies for inferring surface orientation from texture, *Vis. Res.*, 38:2635–2656.
- Knutsson, H., and G. H. Granlund, 1983. Texture analysis using two-dimensional quadrature filters, in *Proceedings of the IEEE Computer Society Workshop on Computer Architecture for Pattern Analysis and Image Database Management*, Silver Spring, MD: IEEE Computer Society, pp. 206–213.
- Lamme, V. A. F., 1995. The neurophysiology of figure-ground segregation in primary visual cortex, *J. Neurosci.*, 15:1605–1615.
- Landy, M. S., and J. R. Bergen, 1991. Texture segregation and orientation gradient, *Vis. Res.*, 31:679–691.
- Landy, M. S., and H. Kojima, 2001. Ideal cue combination for localizing texture-defined edges, *J. Opt. Soc. Am. A*, 18: 2307–2320.
- Landy, M. S., L. T. Maloney, E. B. Johnston, and M. J. Young, 1995. Measurement and modeling of depth cue combination: in defense of weak fusion, *Vis. Res.*, 35:389–412.
- Landy, M. S., and İ. Oruç, 2002. Properties of 2nd-order spatial frequency channels, *Vis. Res.*, 42:2311–2329.
- Lee, T. S., 1995. A Bayesian framework for understanding texture segmentation in the primary visual cortex, *Vis. Res.*, 35:2643–2657.
- Lennie, P., 1998. Single units and cortical organization, *Perception*, 27:889–935.
- Levitt, J. B., and J. S. Lund, 1997. Contrast dependence of contextual effects in primate visual cortex, *Nature*, 387:73–76.
- Li, A., and Q. Zaidi, 2000. Perception of three-dimensional shape from texture is based on patterns of oriented energy, *Vis. Res.*, 40:217–242.
- Li, Z., 2000. Pre-attentive segmentation in the primary visual cortex, *Spatial Vis.*, 13:25–50.
- Lin, L. M., and H. R. Wilson, 1996. Fourier and non-Fourier pattern discrimination compared, *Vis. Res.*, 36:1907–1918.
- Malik, J., and P. Perona, 1990. Preattentive texture discrimination with early vision mechanisms, *J. Opt. Soc. Am. A*, 7:923–932.
- Malik, J., and R. Rosenholtz, 1997. Computing local surface orientation and shape from texture for curved surfaces, *Int. J. Comput. Vis.*, 23:149–168.
- Marr, D., 1976. Early processing of visual information, *Philos. Trans. R. Soc. Lond. B*, 275:483–519.
- Motoyoshi, I., 1999. Texture filling-in and texture segregation revealed by transient masking, *Vis. Res.*, 39:1285–1291.
- Motoyoshi, I., and S. Nishida, 2001. Temporal resolution of orientation-based texture segregation, *Vis. Res.*, 41:2089–2105.
- Mussap, A. J., 2001. Orientation integration in detection and discrimination of contrast-modulated patterns, *Vis. Res.*, 41:295–311.
- Nothdurft, H. C., 1985. Sensitivity for structure gradient in texture discrimination tasks, *Vis. Res.*, 25:1957–1968.
- Nothdurft, H. C., J. L. Gallant, and D. C. Van Essen, 1999. Response modulation by texture surround in primate area V1: correlates of “popout” under anesthesia, *Vis. Neurosci.*, 16:15–34.
- Nothdurft, H. C., J. L. Gallant, and D. C. Van Essen, 2000. Response profiles to texture border patterns in area V1, *Vis. Neurosci.*, 17:421–436.
- Olson, R. K., and F. Attneave, 1970. What variables produce similarity grouping? *Am. J. Psychol.*, 83:1–21.
- Papathomas, T. V., A. Gorea, A. Feher, and T. E. Conway, 1999. Attention-based texture segregation, *Percept. Psychophys.*, 61:1399–1410.
- Portilla, J., and E. P. Simoncelli, 2000. A parametric texture model based on joint statistics of complex wavelet coefficients, *Int. J. Comput. Vis.*, 40:49–71.
- Rao, A. R., and G. L. Lohse, 1996. Towards a texture naming system: identifying relevant dimensions of texture, *Vis. Res.*, 36:1649–1669.
- Richards, W., and A. Polit, 1974. Texture matching, *Kybernetik*, 16:155–162.
- Rivest, J., and P. Cavanagh, 1996. Localizing contours defined by more than one attribute, *Vis. Res.*, 36:53–66.
- Rosenholtz, R., and J. Malik, 1997. Surface orientation from texture: isotropy or homogeneity (or both)? *Vis. Res.*, 16:2283–2293.
- Rossi, A. F., R. Desimone, and L. G. Ungerleider, 2001. Contextual modulation in primary visual cortex of macaques, *J. Neurosci.*, 21:1698–1709.
- Rubenstein, B. S., and D. Sagi, 1990. Spatial variability as a limiting factor in texture-discrimination tasks: implications for performance asymmetries, *J. Opt. Soc. Am. A*, 7:1623–1643.
- Sceniak, M. P., M. J. Hawken, and R. Shapley, 2001. Visual spatial characterization of macaque V1 neurons, *J. Neurophysiol.*, 85:1873–1887.
- Schofield, A. J., and M. A. Georgeson, 1999. Sensitivity to modulations of luminance and contrast in visual white noise: separate mechanisms with similar behavior, *Vis. Res.*, 39:2697–2716.
- Schofield, A. J., and M. A. Georgeson, 2000. The temporal properties of first- and second-order vision, *Vis. Res.*, 40:2475–2487.
- Sillito, A. M., K. L. Grieve, H. E. Jones, J. Cudeiro, and J. Davis, 1995. Visual cortical mechanisms detecting focal orientation discontinuities, *Nature*, 378:492–496.
- Sutter, A., J. Beck, and N. Graham, 1989. Contrast and spatial variables in texture segregation: testing a simple spatial-frequency channels model, *Percept. Psychophys.*, 46:312–332.
- Sutter, A., and N. Graham, 1995. Investigating simple and complex mechanisms in texture segregation using the speed-accuracy tradeoff method, *Vis. Res.*, 35:2825–2843.
- Sutter, A., and D. Hwang, 1999. A comparison of the dynamics of simple (Fourier) and complex (non-Fourier) mechanisms in texture segregation, *Vis. Res.*, 39:1943–1962.
- Sutter, A., G. Sperling, and C. Chubb, 1995. Measuring the spatial frequency selectivity of second-order texture mechanisms, *Vis. Res.*, 35:915–924.

- Treisman, A. M., 1985. Preattentive processes in vision, *Comput. Vis., Graphics Image Processing*, 31:156–177.
- Treisman, A. M., and S. Gormican, 1988. Feature analysis in early vision: evidence from search asymmetries, *Psychol. Rev.*, 95:15–48.
- Treisman, A. M., and H. Schmidt, 1982. Illusory conjunctions in the perception of objects, *Cogn. Psychol.*, 14:107–141.
- Turner, M. R., 1986. Texture discrimination by Gabor functions, *Biol. Cybern.*, 55:71–82.
- Victor, J. D., 1988. Models for preattentive texture discrimination: Fourier analysis and local feature processing in a unified framework, *Spatial Vis.*, 3:263–280.
- Victor, J. D., 1994. Images, statistics, and textures: implications of triple correlation uniqueness for texture statistics and the Julesz conjecture: comment, *J. Opt. Soc. Am. A*, 11:1680–1684.
- Walker, G. A., I. Ohzawa, and R. D. Freeman, 2000. Suppression outside the classical cortical receptive field, *Visual Neurosci.*, 17:369–379.
- Witkin, A. P., 1981. Recovering surface shape and orientation from texture, *Artificial Intelligence*, 17:17–45.
- Wolfe, J. M., 1992. “Effortless” texture segmentation and “parallel” visual search are *not* the same thing, *Vis. Res.*, 32:757–763.
- Wolfson, S. S., and M. S. Landy, 1995. Discrimination of orientation-defined texture edges, *Vis. Res.*, 35:2863–2877.
- Wolfson, S. S., and M. S. Landy, 1998. Examining edge- and region-based texture mechanisms, *Vis. Res.*, 38:439–446.
- Wolfson, S. S., and M. S. Landy, 1999. Long range interactions between oriented texture elements, *Vis. Res.*, 39:933–945.
- Yellott, J. I., Jr., 1993. Implications of triple correlation uniqueness for texture statistics and the Julesz conjecture, *J. Opt. Soc. Am. A*, 10:777–793.
- Yeshurun, Y., and M. Carrasco, 2000. The locus of attentional effects in texture segmentation, *Nat. Neurosci.*, 3:622–627.
- Zhu, S. C., Y. Wu, and D. Mumford, 1998. Filters, random fields and maximum entropy (FRAME)—towards a unified theory for texture modeling, *Int. J. Comput. Vis.*, 27:107–126.
- Zipser, K., V. A. F. Lamme, and P. H. Schiller, 1996. Contextual modulation in primary visual cortex, *J. Neurosci.*, 16:7376–7389.

74 Visual Segmentation and Illusory Contours

ROBERT SHAPLEY, NAVA RUBIN, AND DARIO RINGACH

THERE IS AN IMPORTANT transformation that takes place in visual perception between the analog representation of the visual image in the retina and surfaces and objects as they appear to us. The retinal image represents numerous different brightness levels and colors at a very large number of different points in space, with no explicit representation of which points belong together. But the image we perceive consists of a much smaller number of surfaces and objects that are segregated from the background and from each other. There are probably many stages of this transformation, but one stage of this process is known to be of great importance: visual segmentation. Segmentation is a process of parsing the different surfaces in an image, as well as grouping together the parts of the same surface that are separated from each other in the image by another, occluding surface. Segmentation therefore involves resolving the depth relationships between surfaces and objects in a scene.

Understanding segmentation will lead to insight about one of the major theoretical problems in visual neuroscience, namely, how neural signals about small, localized pieces of the visual image are combined into a complete representation of the spatially extended visual image. This is a particularly important example of a general problem in neuroscience: how to go from the local to the global level of object representation in the brain. In this chapter, we review some of the large body of work on visual segmentation in human subjects and animals. The aim is to present a coherent body of experimental results that all relate to the question How is fragmentary visual information completed and made into wholes? There is another significant body of work, on the theory of segmentation computations in perception, that is beyond the scope of this chapter. That would make another interesting separate chapter of visual neuroscience.

Illusory contours

As with many brain computations, we can understand segmentation better by observing its action when it deals with an exceptionally difficult task. Usually segmentation is done so efficiently by the brain that we (as observers) are unaware that it is happening. But for certain special visual images, the segmentation process becomes evident. This is the reason for the fascination with these special images, the so-called illusory contours (ICs). An example of such a visual image is

Figure 74.1, an image referred to as a *Kanizsa triangle*, named after the Italian Gestalt psychologist Gaetano Kanizsa, who made this image famous (Kanizsa, 1979). In this figure, the perception of a bright white triangle is very strong, but if one scrutinizes the boundaries of the triangle, it becomes evident that there is no difference in the amount of light coming to the eye from the regions inside and outside the perceived triangle. Yet we see the inside as a bright surface segmented from its background by sharp contours along the boundary of the triangle. In this sense, the boundary between the inside and outside of the triangle is an IC. This image is a classical example in favor of the basic concept of the Gestalt psychologists, also echoed in the work of Donald Hebb, that the brain is “searching” for meaningful patterns. In this case, the brain manufactures a perceptual triangle from fragmentary information because a meaningful pattern, an occluding triangle, is consistent with the available image information even though other perceptions are possible. It is reasonable to believe that the segmentation computations the visual system performs on these exceptional Kanizsa images are the same as for more typical images.

One of the main points of scientific investigation of ICs is the nature and location of the brain area that performs the segmentation of the illusory figure from its background. Some psychologists have favored an explanation in terms of perceptual problem solving and think of ICs as *cognitive contours* (e.g., Gregory, 1987). Such cognitive approaches do not usually specify or even speculate about the brain areas involved in the perception. However, we could speculate that such a cognitive explanation would involve both visual cortical areas in the posterior cerebral cortex, as well as frontal and temporal cortex. In opposition to the top-down cognitive approach, more bottom-up, stimulus-driven approaches have been proposed (e.g., Grossberg, 1997; Heitger and von der Heydt, 1993). The bottom-up explanation would seem to imply the involvement in IC perception of early visual areas in which visual signals are still arranged retinotopically. There are psychophysical as well as neurophysiological and brain imaging studies of the nature of IC processing and also of localization of IC-evoked signals. The results of these different studies provide a fairly compelling case for the concept that IC perception is the result of the combined and cooperative action of early and later, or more retinotopic and more abstract, visual cortical areas. In this chapter, we

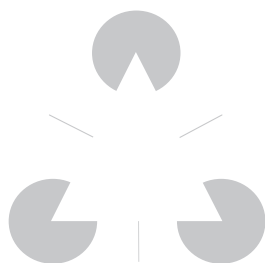


FIGURE 74.1. Kanizsa triangle. The occluding triangle that appears in front of the three circles and the three line segments has the same physical brightness as the surroundings. But it appears somewhat brighter, and appears to be a solid surface in front, because of perceptual processes.

begin by discussing psychophysical studies we have done on these problems, followed by a consideration of neurophysiological and brain imaging results on IC perception and segmentation.

Psychophysics of ICs

We have developed a psychophysical technique which was designed to provide an objective measure of the perceptual strength of ICs. This technique has yielded many new and interesting results that may enable us to forge a link between the perception and the neural mechanisms of perception related to segmentation. Figure 74.2 illustrates the technique: a shape discrimination task with ICs. The shapes are formed by Kanizsa-style Pacmen that are rotated around their centers by an angle α (see the figure legend for details). (*Pacman* is a term that refers to the shape of an agent in a video game from the early 1980s. The shape of Pacman was exactly the same as the cut-off circles used by Kanizsa in the IC figures he originated much earlier.) Two categories of shapes are formed: *thin* when $\alpha > 0$ and *fat* when $\alpha < 0$. The subject in the experiment must classify the shape. The pattern is flashed for about 100msec, and then a mask follows presentation. With a series of control experiments, we showed that performance on this task is facilitated significantly when the subject sees the ICs compared to her or his performance when it is based on the local inducers' orientation. One control experiment was done to measure discrimination performance when all the inducers face outward. Then performance on the task was quite poor. Another control experiment proved that it was contour completion in the blank spaces between the pacmen inducers that was crucial for task performance (rather than the symmetrical rotation of the inducers, for instance). This second control experiment involved the placement of lines arranged along the boundaries of a virtual square that overlapped the thin or fat illusory figures. Such masking that is remote from the inducers does degrade performance by a factor of 2 or more. Thus, a high level of performance on the shape

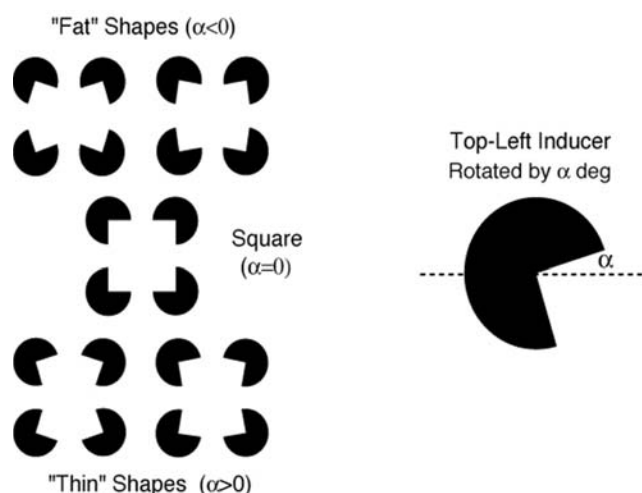


FIGURE 74.2. The thin-fat task used for psychophysics of ICs. *A*, A family of Kanizsa-like figures. The rotation parameter α specifies the angle of rotation of the upper-left inducer around its center, as shown in *B*. Adjacent inducers are rotated in opposite directions to achieve a consistent shape deformation of the illusory surface. (From Ringach and Shapley, 1996.)

discrimination task does, we believe, require perception of the illusory figures. We have used the task performance to answer quantitatively several important questions about illusory contours.

SPATIAL SCALE Ringach and Shapley (1996) found that ICs can span 15 degrees of visual angle, and thus must be formed by integration of neural signals over large distances in visual cortex. They also investigated the issue of spatial scale invariance. Scale-invariant properties of ICs were suggested by prior studies. Shipley and Kellman (1992) presented subjects with Kanizsa squares which varied in their absolute size and the radii of the inducing pacmen. They found that ratings of IC clarity were approximately scale invariant. In other words, the rating of a figure depended mainly on the ratio between the radius of the inducer and the side of the square. This ratio, termed the *support ratio*, is the crucial spatial parameter for ICs. In Ringach and Shapley's experiments on spatial scale, they collected shape discrimination data, as described above, with ICs at five different scales but always with the same support ratio. Figure 74.3 shows the variation in IC strength as a function of scale, and it is seen to be a relatively flat function. This is direct evidence for the spatial scale invariance of IC perception.

DYNAMICS Ringach and Shapley found that ICs can be formed by inducing elements that flash for a period of 100msec, but that neural integration must proceed for longer than 250msec for the contours to be completed. This is the conclusion of backward masking experiments in which

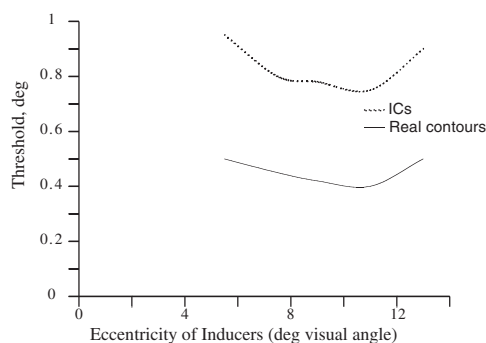


FIGURE 74.3. Scale invariance of IC perception. Thresholds for seeing ICs and real contours are plotted versus separation between the inducers. The real contours were drawn in the image connecting the corners of the inducers. Thresholds are expressed in terms of the rotation angle α that enables the observer to reach a criterion number of correct responses in the thin-fat task. (Figure derived from the data in Ringach and Shapley, 1996.)

the authors blocked the perception of a curved IC by the later presentation of a Kanisza square. Control experiments with real contours show that shape discrimination is much faster with real contours than with ICs. That more time is needed to create the ICs than is required to perceive shapes defined by luminance contours suggests that recurrent neural networks that require some time to compute the shapes may be involved in IC perception. Receptive field models like the ones proposed by Heitger and von der Heydt (1993) or Grossberg (1997) would produce ICs without any cost in time, and this seems to be disconfirmed by the behavioral data.

UPPER AND LOWER VISUAL FIELDS A prominent anatomical property of retinotopic visual areas such as V1/V2 is that the representation of the visual field is split into disjoint portions of the cortical sheet. There is the well-known anatomical break between the left and right hemispheres, each of which represents the contralateral visual fields in early visual areas, as discussed below. In addition, there is a wide separation between the upper and lower hemifield representations in extrastriate visual cortex such as V2 or V3. Introspectively, we are not aware of these discontinuities in the cortical retinotopic representation. Surfaces that cross the horizontal or vertical meridians appear unitary and whole. Nevertheless, under careful experimental conditions, it is possible to uncover behavioral effects that may be the result of the anatomical discontinuities of the cortex. Rubin et al. (1996) found such a behavioral effect: human observers exhibit a greater tendency to perceive ICs when the inducing stimuli fall on their lower visual field. There were two experiments that led to this conclusion, both illustrated in Figure 74.4. The stimulus used in the first experiment was a stereogram similar to that depicted in Figure 74.4A. When subjects fixated the upper cross in that figure, they perceived

a bright illusory horizontal stripe, bounded by ICs, linking the two filled rectangles. In contrast, when they fixated the lower cross, the illusory stripe “faded away” and the two filled rectangles were perceived to be disjoint. The stimulus is symmetric with respect to reflection about its horizontal midline, and therefore the only difference is that the (identical) stimulation falls on the upper versus lower visual hemifields. This is the first experimental result that indicates that ICs are perceived more easily in the lower visual field.

Rubin et al.’s second experiment utilized the thin-fat task to measure IC strength in the upper and lower visual fields, as depicted in Figure 74.4B with the data from a single subject. The left panels in Figure 74.4B show the results of an individual observer on the IC task, while the right panels show the results for a complete (or luminance) contour task. The upper and lower graphs show the subject’s psychometric functions as a measure of performance when the stimulus fell on the upper and lower hemifields, respectively. The lower hemifield shows a marked advantage for the performance of the IC task, as can be seen by examining the psychometric functions on the left side of Figure 74.4B. The psychometric function for the lower visual field is much steeper, indicating better performance. Also shown in this figure in the right-hand panels are the psychometric functions for filled-in Kanisza figures, for which the support ratio was 1.0—that is, these were real contours entirely defined by luminance difference. Defining threshold performance as the amount of rotation of the inducing elements needed for the subject to reach 82% correct discrimination, the thresholds for the IC figures were 2 degrees and 7.8 degrees for the lower and upper hemifields, respectively. For figures that were completely defined by luminance contours, the thresholds were not different in the different visual fields: thresholds for the lower and upper hemifields were, respectively, 1.1 and 0.9 degrees. Thus, a performance-based measure also showed that the lower visual field segmented the ICs more easily than the upper visual field.

VERTICAL MERIDIAN Perceptual completion can link widely separated contour fragments and interpolate ICs between them, but can it cross the “seams” in visual cortex, the vertical meridian representation that demarcates the boundary between the visual field representations in the left and right cerebral cortical hemispheres, and the horizontal meridian representation that separates upper and lower field representations? As illustrated in Figure 74.5, Pillow and Rubin (2002) answered this question using a variant of the thin-fat shape discrimination task, but with the variation that only one arm of the angle in an inducer was varied in a single presentation, either the arm that faced horizontally or the one that faced vertically. Thus, with inducers arranged symmetrically around the fovea, they could test whether hor-

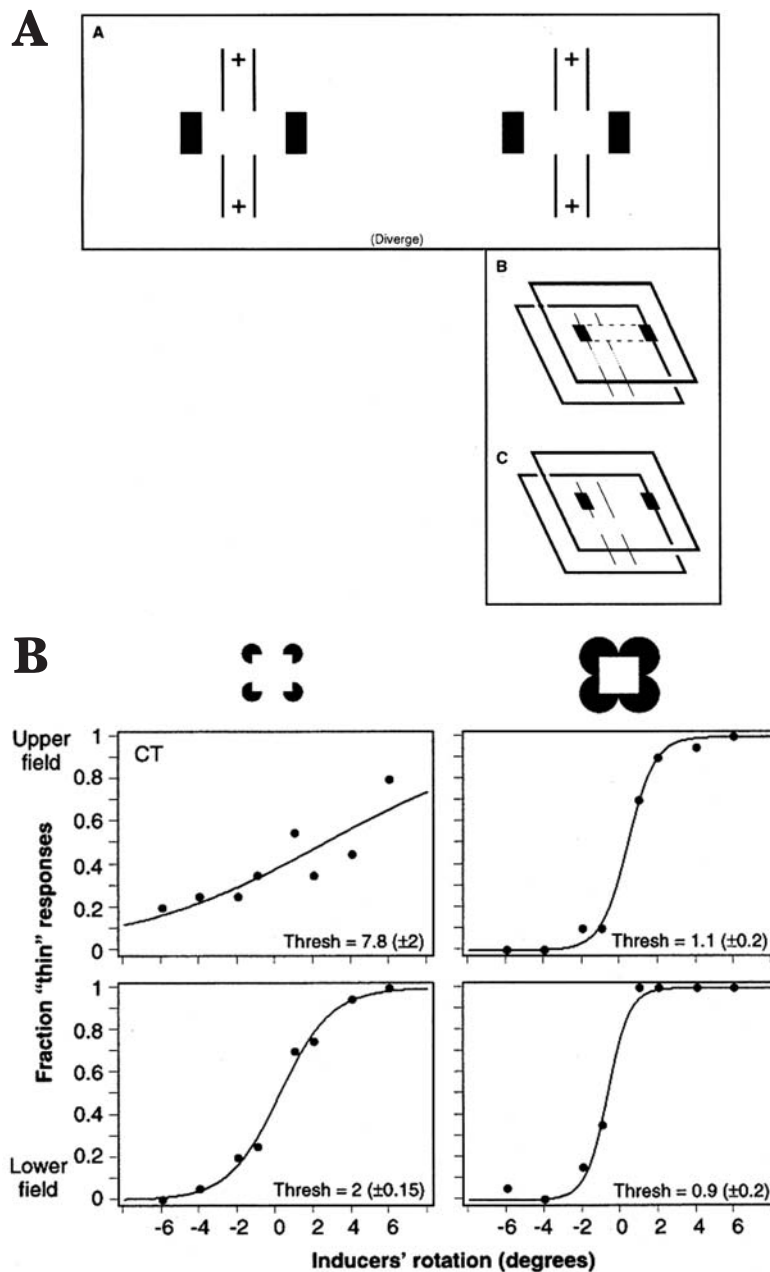


FIGURE 74.4. Upper/lower field asymmetry in IC perception. *A*, Stereogram that can be placed in the upper or lower visual field, depending on the placement of fixation. If the reader free-fuses the stereogram, she or he should observe a qualitative difference in the percept, as described in the text. *B*, Psychometric functions for the thin/fat task for ICs (*left panels*) and filled-in luminance contours (*right panels*). The inducer rotation angle α is the coordinate, is

labeled on the horizontal axis as “Inducer rotation.” The fraction of thin responses is plotted on the vertical axis. The upper panels are for the upper visual field; the lower panels are for the lower visual field. Steeper psychometric functions are indicative of better discrimination performance. The shallowest psychometric function is for IC perception in the upper visual field. (From Rubin et al., 1996.)

horizontal contours that crossed the vertical meridian could be perceived as well as contours that were contained within a single hemifield. They found that completion is much poorer when ICs cross the vertical meridian than when they reside entirely within the left or right visual hemifield and cross the horizontal meridian. This deficit reflects limitations in cross-hemispheric integration. The authors also showed that the

sensitivity to the interhemispheric divide is unique to perceptual completion: a comparable task which did not require completion showed no across-meridian impairment. Pillow and Rubin proposed that these findings support the existence of specialized completion mechanisms in early visual cortical areas (V1/V2), since those areas are likely to be more sensitive to the interhemispheric divide.

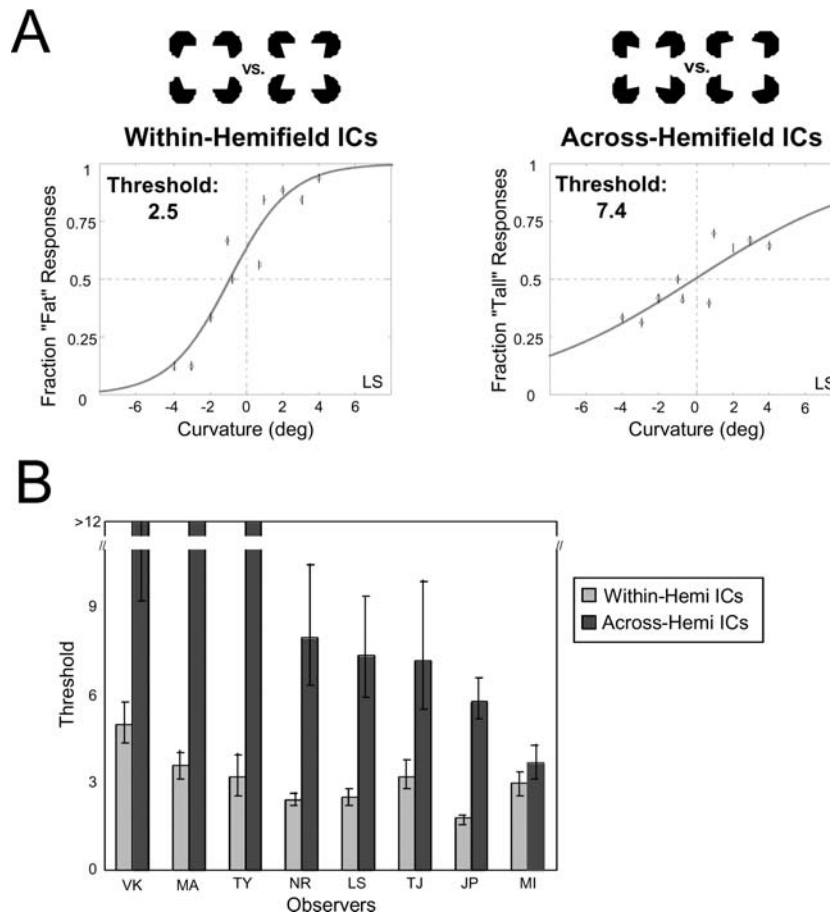


FIGURE 74.5. Meridional asymmetry in IC formation. *A*, Psychometric functions for the modified thin-fat task, as described in the text. Plotting conventions are as in Figure 74.4*B*. The steeper psychometric function for the within-hemifield IC (*left panel*)

indicates that performance is better for ICs that do not cross the vertical meridian. *B*, Summary of thresholds for within- and across-hemifield contour completion for all subjects tested. (From Pillow and Rubin, 2002.)

PERCEPTUAL LEARNING OF ICs Perceptual learning also has been used to investigate the cortical mechanisms of IC perception. From a study of human perceptual learning and IC perception, Rubin et al. (1997) concluded that the abrupt, insight-like perceptual learning observed in that study demanded that high-level visual areas, in which templates of remembered visual objects are stored, must interact with lower-level visual areas that have an analog representation of the visual image. Such multilevel interactions were needed to explain the stimulus size dependence of IC perceptual learning and at the same time its abrupt, insight-like onset. These results may help to reconcile psychophysical and neurophysiological results, which suggest that early retinotopic visual areas must be involved in IC perception, with brain imaging results that found IC-related activity in higher, nonretinotopic cortical regions. This issue is brought up again in the "Conclusions."

Neurophysiology of ICs

The first neurophysiology work we discuss tends to support a bottom-up, stimulus-driven explanation of IC perception. From electrophysiological single-cell recordings in awake monkeys, Peterhans and von der Heydt and their colleagues found that Kanizsa-type images and other IC images could excite spike activity in neurons in early visual cortex (see Chapter 76). Peterhans and von der Heydt (1989) recorded from single neurons in area V2 of the macaque visual cortex. Such a neuron responds with excitation to a luminance contour that crosses its receptive field. When an IC (as perceived by us) crosses its receptive field, the cell produces a slightly delayed excitatory response resembling the same cell's response to a real contour. As a control to ensure that the response is not merely a weak response to the remote features of the IC stimulus, the investigators made a small image manipulation (closing the inducing boundary), and this eliminated the neuron's response. Peterhans and von der Heydt also performed several quan-

tative studies on these IC-responsive V2 neurons, in particular measuring the orientation tuning for ICs and real contours on the same population of V2 neurons; they found that real contours and ICs produced similar orientation tuning in IC-responsive neurons in V2. Thus, these neurons seem to be a candidate neural substrate for IC perception. There also have been reports of IC responses in neurons in V1. This is a controversial point since von der Heydt and Peterhans and their colleagues maintained that they observed very few V1 neurons that produced IC responses. In part the discrepancy may occur perhaps because of the use of different stimuli and in part because of different views of what constitutes an IC. For our present purposes, it is enough to conclude that IC responses can be observed in retinotopic areas in the monkey's brain, areas that are traditionally thought of as stimulus driven.

The connection of the monkey V2 neurons with IC perception in humans needs to be established more firmly. We do not know the nature or quality of IC perception in monkeys because there are insufficient animal data using rigorous experiments to test for IC perception. Once we know that monkeys can exhibit behavior that proves that they see ICs in Kanizsa-type images, further experiments will be necessary to find out whether or not the V2 neurons have the same sort of parameter dependence on size, contrast, and retinal location as the behavior. One important question is, how do the V2 neurons respond to an IC that crosses the horizontal meridian? Humans respond as well to such ICs as they do to ICs that do not cross the horizontal meridian. The reader can observe this by fixating the middle of the Kanizsa triangle in Figure 74.1 and observing the robust lateral ICs that traverse the horizontal meridian in her or his visual field. But in V2 there is a marked separation between neurons that represent the visual field just above and just below the meridian (see Horton and Hoyt, 1991). So one might expect some deleterious effect on IC responses for meridian-crossing ICs in V2 neurons. If that dropoff in IC sensitivity in V2 neurons were observed, it might cast doubt on the role of V2 alone in IC perception. Moreover, as we will discuss below, the human brain imaging data point to other brain areas as the major processing sites for ICs in humans. The monkey results could be interpreted to indicate that similar IC-related activity is going on in human V2, but the functional magnetic resonance imaging (fMRI) and other techniques used on humans are too insensitive to measure it. A second possibility is that the V2 activity seen in monkeys is related to IC perception but that it is not the central mechanism involved in the percept. Another possibility is that human and monkey perception and neural mechanisms are fundamentally different at this midlevel stage of visual processing.

Human responses to ICs have been measured with fMRI techniques. Most fMRI studies have involved the measure-

ment of the activation of Kanizsa squares or diamonds compared with the same pacman-shaped inducers rotated outward or all in the same direction. An earlier study by Hirsch and colleagues (1995) found that there was activation of the occipital cortex lateral to V1 by Kanizsa-type figures, but they could not pinpoint the cortical location because the IC experiments were not combined with retinotopic mapping. Therefore, these studies established that signals related to segmentation were present in occipital cortex, but further work is needed to be more precise about localization.

The extensive research of Mendola and colleagues (1999) at Massachusetts General Hospital established that IC-related signals were observed in retinotopic area V3 and also in LO, the lateral occipital area previously discovered by Malach and colleagues (Malach et al., 1995). Figure 74.6 is an fMRI image from the Mendola paper indicating the large region of cortical activation evoked by the Kanizsa diamonds used as stimuli in that study. The early retinotopic areas V1 and V2 did not produce statistically significant activation, as seen in the figure. Mendola and her colleagues also used different inducers for ICs, such as aligned line endings, and found a similar pattern of brain activation in V3 and LO. These results are important in implicating extrastriate cortex in the process of visual segmentation in humans. But it is important to note the apparent conflict between these results and the findings of Peterhans and von der Heydt (1989) that implicated V2 in IC processing in monkeys. The brain imaging results on humans suggest that higher-level visual areas produce the major response to ICs.

Figure-ground and border ownership

While ICs are often chosen for studying visual segmentation, there are other visual phenomena that can also lead to an understanding of segmentation. The assignment of an image region as figure or ground is one such phenomenon. As Edgar Rubin, the famous perceptual psychologist, pointed out, such assignment is automatic and inescapable (Rubin, 1921). But ambiguous figures exist in which figure and ground assignments flip back and forth, and perception changes when that happens. Rubin's familiar face/vase figure is the most widely reproduced example, but there are other examples from E. Rubin that illustrate the consequences of figure-ground assignments even more. One of these is the Maltese cross figure in Figure 74.7. This example is described in Koffka's (1935) book but not depicted there. The diamond-shaped arms of the cross can appear to be grouped in fours, with a vertical and a horizontal pair grouped together as figures in front (resembling a propeller in shape) and then two diagonal pairs grouped together as figures in front (the vertical-horizontal pairs are then in back). The brightness contrasts in the figure are arranged

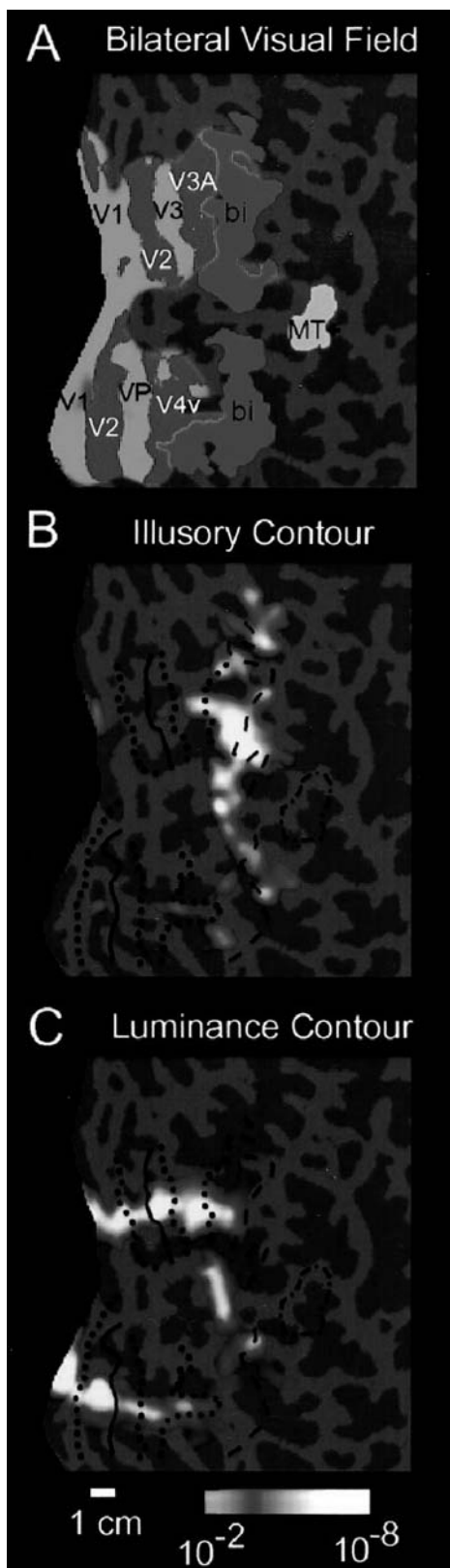


FIGURE 74.6. Mapping of IC responses in human cortex with fMRI. *A*, Map in human visual cortex of retinotopic visual areas and the interhemispheric region (labelled *bi* and colored green) using phase mapping. *B*, The region of differentially high activity when Kanizsa ICs are compared with activation produced by the unorganized pacman inducers. The main activation is in V3A and in the interhemispheric region. *C*, Activation produced by a square defined by luminance contours. (From Mendola et al., 1999, with permission.) (See color plate 48).



FIGURE 74.7. E. Rubin's Maltese cross figure. There are two sets of vanes, white and mid-gray. They group together to produce propeller figures that alternate front and back. When the propeller of a given color is seen in back, it tends to complete, into a gray diamond or a white square, respectively. Some observers report that the perceived value of the mid-gray changes, becoming darker when the gray regions form a propeller in front and lighter when they form a diamond in back. (Drawn from a description in Koffka, 1935.)

such that the vertical-horizontal propeller shape looks darker in front than it does when it is perceived in back, looking like a light gray diamond behind the white tilted propeller. This is because of the enhanced effect of brightness contrast across borders that define a figure and on the regions to which such borders are attached, as E. Rubin noted (cited in Koffka, 1935). Similar effects can be seen in color. This is only one of many illustrations of the deep consequences of figure-ground assignment. For instance, another consequence of the importance of figure-ground is that people remember the shapes of figures, not grounds. Thus, understanding the neural basis for this phenomenology is likely to be an important clue to the function of the visual system.

Figure-ground assignment is a special case of a more general problem in vision, the assignment of border ownership. Assignment of a region as figure or ground is all one

has to do if there is only one figure surrounded by the background. But if there are many figures, and if one is in front of another so that it partly occludes the shape of the second figure in the visual image, then the visual system must decide on the basis of image information which surface is in front along the boundary between the two figures in the image. Briefly, the brain has to decide which figural region owns the border between them; that is the front surface. Assignment of border ownership is a problem that must be solved in almost every visual image.

There have been only a few investigations of neural mechanisms for border ownership and figure-ground assignments. One study is by Zhou and colleagues (2000) on single cells in V1 and V2 cortex of macaque monkeys. By keeping local edge contrast the same but varying the global stimulus so that different regions own the boundary between them perceptually, Zhou et al. tested sensitivity to border ownership in single cortical neurons. The experimental design and results in an archetypal border-ownership cell are shown in Chapter 76 in this book from the work of Zhou et al. (2000). A substantial fraction of border-ownership cells like that cell are encountered in monkey V2 cortex. Baylis and Driver (2001) reported recently that many neurons in monkey inferotemporal (IT) cortex respond differentially to figure or ground, and thus these also must reflect signals about border

ownership. Since IT cortex is supposedly involved in object recognition, it is very reasonable that neurons in this area should be affected by border ownership that is necessary for accurate object recognition in the real world.

Studies in human cortex of figure-ground reversals using fMRI, by Kleinschmidt and his colleagues (1998) at the Wellcome Imaging Center in London, revealed activation over a number of areas in occipital, temporal, parietal, and even frontal cortex. The involvement of temporal, parietal, and frontal cortex seems to imply that activation of top-down influences from high-level cortical areas could be necessary for figure-ground reversal of border ownership. However, as in the case of ICs, it is also possible that there also may be signals associated with figure-ground assignment in “early” retinotopic areas like V1 or V2 that are undetectable with fMRI.

Amodal completion

An important part of segmentation in human visual perception is the phenomenon of amodal completion, that is, completion and grouping together of the parts of a partially occluded object that are visible. This completion process is crucial for normal object perception in the real world. Evidence that amodal completion affects the firing rates of

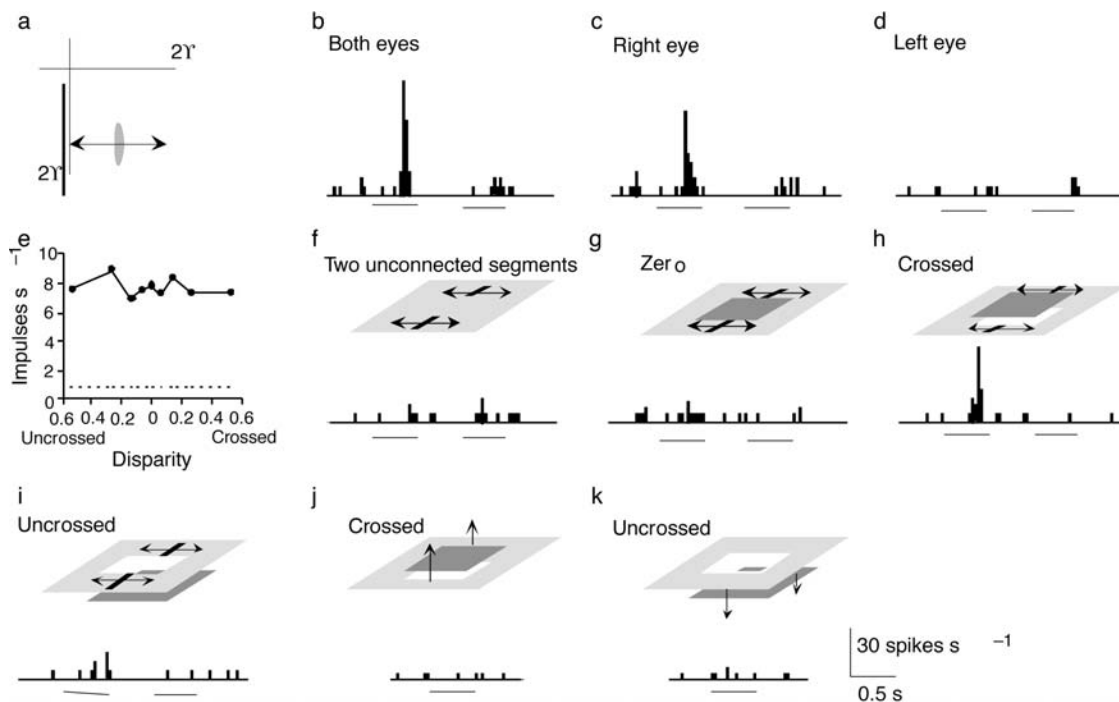


FIGURE 74.8. Sugita-amodal completion V1. Responses from a neuron in an awake, behaving monkey. The neuron responds to a long contour in its receptive field, as in *a*. It responds to both eyes (*b*) and to the right eye alone (*c*) but not to the left eye alone (*d*). The interesting manipulation is in *f* to *h*. In *f* the neuron does not

respond to two unconnected segments. In *g* it does not respond to the same two segments when they are perceived as being in front of a gray region. But there is a response when the retinal disparity is such that the gray region is in front, occluding the two line segments (*h*). (From Sugita, 1999, with permission.)

V1 neurons in macaque V1 was obtained by Y. Sugita by manipulating apparent occlusion using stereopsis, as shown in Figure 74.8. Only a small fraction of V1 neurons were affected by amodal completion, but still it is a significant result.

Amodal completion in human perception was studied by Ringach and Shapley (1996) using the thin-fat task. This was done by enclosing each pacman inducer with an annulus of the same gray scale as the inducer and investigating how accurately and with what speed the observers could perform the task. The accuracy of amodal completion was almost the same as for ICs. The speed of the processes leading to amodal versus IC completion was measured with a backward masking paradigm. The results of these experiments indicated that amodal completion was significantly slower than IC formation, up to 50 msec slower. However, the only masks that were used in this experiment were local pinwheel masks that overlapped spatially with the pacman, or modified pacman, inducers. This suggests that the difference in timing between amodal and IC completion may be caused by the neural computations that are used to define the junctions at the corners of the inducers. In other work not discussed here, psychophysical experiments on ICs and occlusion of the inducer corners indicated the great importance of neural signals about local junctions for global segmentation (Rubin, 2001).

Conclusions

Some of the psychophysical results reviewed here indicate that the process of segmentation requires recurrent networks for completion in early visual cortex. These are the results on dynamics, visual field dependencies, and the size specificity of perceptual learning of ICs. Such results tend to rule out models based simply on collection of signals by large receptive fields in higher visual areas. However, there are other results, such as size scale invariance and the abruptness of perceptual learning, that point to the necessary involvement of higher-level, more abstract representations only in higher-level visual areas. This duality is also reflected in the pattern of neurophysiological and brain imaging results.

The full spectrum of results about ICs and segmentation that we have reviewed here indicates that such perception is not simply the result of a single unitary process in the brain. A reasonable deduction from this pattern of results is that multiple visual areas collaborate on producing the IC percept and visual segmentation generally. Multistage processing and cooperation in vision have been suggested before in general terms, for instance, by Ullmann (1998). The picture that emerges from all the studies of segmentation we have reviewed is of a visual cortical network with intense feedback between higher-level visual areas and

lower-level areas that are exciting the higher-level areas. This cortical network acting as a feedback loop is hunting for structure in the visual image. Related ideas have been proposed more than once before, but now the weight of neurophysiological, brain imaging, and psychophysical evidence points more and more strongly to the visual cortex (that is, primary and extrastriate cortex taken altogether) as an array of feedback loops that cooperate in the segmentation of the visual image.

REFERENCES

- Baylis, G. C., and J. Driver, 2001. Shape-coding in IT cells generalizes over contrast and mirror reversal, but not figure-ground reversal, *Nat. Neurosci.*, 4:937–942.
- Gregory, R. L., 1987. “Illusory Contours and Occluding Surfaces,” in *The Perception of Illusory Contours* (S. Petry and G. Meyer, eds.), New York: Springer-Verlag, pp. 81–89.
- Grossberg, S., 1997. Cortical dynamics of three-dimensional figure-ground perception of two-dimensional pictures, *Psychol. Rev.*, 104:618–658.
- Heitger, E., and R. von der Heydt, 1993. A computational model of neural contour processing: figure-ground segregations and illusory contours, in *Proceedings of the International Conference on Computer Vision*, pp. 32–40.
- Hirsch, J., R. De La Paz, N. Relkin, J. Victor, K. Kim, T. Li, P. Borden, N. Rubin, and R. Shapley, 1995. Illusory contours activate specific regions in human visual cortex: evidence from functional magnetic resonance imaging, *Proc. Natl. Acad. Sci. USA*, 92:6469–6473.
- Horton, J. C., and W. F. Hoyt, 1991. Quadrantic visual field defects. A hallmark of lesions in extrastriate (V2/V3) cortex, *Brain*, 114:1703–1718.
- Kanizsa, G., 1979. *Organization in Vision*, New York: Praeger.
- Kleinschmidt, A., C. Buchel, S. Zeki, and R. S. Frackowiak, 1998. Human brain activity during spontaneously reversing perception of ambiguous figures, *Proc. R. Soc. Lond. B Biol. Sci.*, 265:2427–2433.
- Koffka, K., 1935. *Principles of Gestalt Psychology*, San Diego, CA: Harcourt, Brace.
- Malach, R., J. B. Reppas, R. R. Benson, K. K. Kwong, H. Jiang, W. A. Kennedy, P. J. Ledden, T. J. Brady, B. R. Rosen, and R. B. Tootell, 1995. Object-related activity revealed by functional magnetic resonance imaging in human occipital cortex, *Proc. Natl. Acad. Sci. USA*, 92:8135–8139.
- Mendola, J. D., A. M. Dale, B. Fischl, A. K. Liu, and R. B. Tootell, 1999. The representation of illusory and real contours in human cortical visual areas revealed by functional magnetic resonance imaging, *J. Neurosci.*, 19:8560–8572.
- Peterhans, E., and R. von der Heydt, 1989. Mechanisms of contour perception in monkey visual cortex. II. Contours bridging gaps, *J. Neurosci.*, 9:1749–1763.
- Pillow, J., and N. Rubin, 2002. Perceptual completion across the vertical meridian and the role of early visual cortex, *Neuron*, 33:805–813.
- Ringach, D., and R. Shapley, 1996. Spatial and temporal properties of illusory contours and amodal boundary completion, *Vis. Res.*, 36:3037–3050.
- Rubin, E., 1921. *Visuell wahrgenommene Figuren*, Copenhagen: Gylendal.

- Rubin, N., 2001. The role of junctions in surface completion and contour matching, *Perception*, 30:339–366.
- Rubin, N., K. Nakayama, and R. Shapley, 1996. Enhanced perception of illusory contours in the lower vs. the upper visual hemifields, *Science*, 271:651–653.
- Rubin, N., K. Nakayama, and R. Shapley, 1997. Abrupt learning and retinal size specificity in illusory contour perception, *Curr. Biol.*, 7:461–467.
- Shipley, T., and P. Kellman, 1992. Strength of visual interpolation depends on the ratio of physically specified to total edge length, *Percept. Psychophys.*, 48:259–270.
- Sugita, Y., 1999. Grouping of image fragments in primary visual cortex, *Nature*, 401:269–272.
- Ullmann, S., 1998. *High Level Vision*, Cambridge, MA: MIT Press.
- Zhou, H., H. S. Friedman, and R. von der Heydt, 2000. Coding of border ownership in monkey visual cortex, *J. Neurosci.*, 20:6594–6611.

75 Global Yet Early Processing of Visual Surfaces

YUKIYASU KAMITANI AND SHINSUKE SHIMOJO

FROM THE ECOLOGICAL optics viewpoint (Gibson, 1950), the input to the eyes is basically ambient light, that is, a lattice of lights that reflects geometry and perspectives between the observer and the environment. Since the lights are reflected from objects' surfaces, the lattice may be considered a summary of the environmental surfaces which is created according to the rules of optics. More importantly, the representation of visual surfaces is an essential step for the representation of visual objects, the materials the observer's action is aimed at and performed with. Thus, the task of the visual system is to retrieve from the retinal input the information about surfaces and objects that is ecologically relevant. It is primarily for this reason that understanding of visual surface representation is critical to our understanding of visual processing.

In spite of its functional significance, only recently has surface representation begun to be a subject of neurophysiological studies. This may be partly because the traditional view of visual processing derived from electrophysiological studies of single visual neurons is at odds with the fundamental nature of perceptual surfaces. In this chapter, we first illustrate the essential characteristics of perceptual surfaces, emphasizing the following points:

1. Local information given to limited areas of the visual field can lead to the global percept of surfaces, including the three-dimensional surface layout.
2. Surface representation occurs early in visual processing in the sense that it is not mediated by conscious/cognitive processes and even precedes other perceptual processes such as motion perception.

These characteristics may appear to be contradictory, but only if one takes the physiologically driven classical notion of visual processing as a hierarchical, unidirectional relay of signals through local feature detectors, whose size and complexity increase with the level in the hierarchy. According to the traditional view, global perception is achieved only at high/late stages of visual processing, involving even problem-solving processes. We attempt to reconcile these two seemingly incompatible characteristics of perceptual surfaces in the light of recent physiological evidence for dynamic and global processing in the early visual cortex.

From local inputs to global percept of surfaces

In classical illusions such as the Kanizsa figure (Fig. 75.1A) (Kanizsa, 1979) and the Varin configuration for neon color spreading (Fig. 75.1B) (Varin, 1971), we can observe completed surfaces even though the physical information is spatially limited. In the Kanizsa figure, in addition to illusory contours, the pacman-shaped stimuli create an illusory rectangular surface where the entire area appears slightly darker than the background. In the Varin figure, the color in the wedge-shaped portions appears to fill the square region. The term *filling-in* refers to the situation where a property such as brightness and color propagates beyond the region of physical stimulation to form a clear percept of a delineated surface. Filling-in phenomena are important because they provide a psychophysical paradigm to explore, as well as give insights into, the mechanism that integrates local inputs to form a global surface representation.

What is noteworthy is that filling-in effects often involve an impression of one surface in front of another (or others). An example may be seen in a white disc that appears to be partly occluded by the illusory rectangular surface in the Kanizsa figure (Fig. 75.1A). This is sometimes called *amodal* completion because the occluded surface is perceived but is not locally visible in the literal sense. In the same Kanizsa figure, the rectangular illusory surface can be considered *modally* completed because it is perceived as an entirely visible, occluding surface. Another example of modal completion is the illusory colored surface in the Varin figure (Fig. 75.1B). In this case, the colored portions are seen as parts of a single semitransparent colored surface through which the back surface is also visible, thus allowing visibility of two surfaces along the same line of sight. Thus, in short, filling-in and multiple surface layouts characterize visual surface perception from spatially sparse inputs.

Furthermore, it has been shown that minor changes in local visual inputs often lead to a drastic global change in surface perception. Figure 75.2 is an example demonstrating the effect of local disparity (Nakayama et al., 1989). The left-middle pair and the middle-right pair, which can fuse, contain opposite signs of local disparity, while the retinally stimulated areas are largely identical. Three discs through

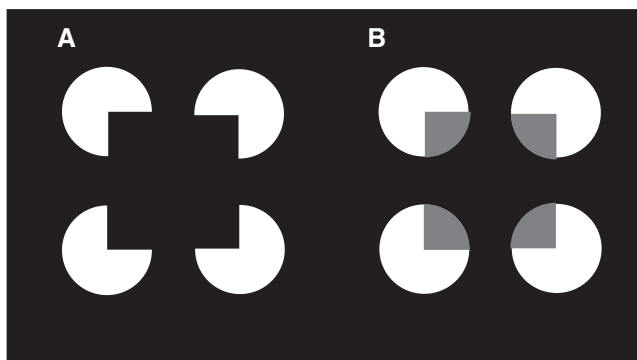


FIGURE 75.1. *A*, Kaniza square. In addition to illusory contours forming a square, the pacman-shaped stimuli give rise to the percept of an illusory surface in which the entire area appears slightly darker than the background, and amodally completed white discs. *B*, Varin figure for neon color filling-in. By adding colored wedge portions to *A*, a transparent, colored surface and white discs seen through it are induced. (See color plate 49.)



FIGURE 75.2. Effect of local disparity information on global surface layouts. The observer is expected to see either three discs through one window or one disc and three windows, depending on the direction of disparity. The converging fuser should fuse the left and middle images to see three discs through one window and the middle and right images to see one disc through three windows. The diverging fuser should fuse the opposite pairs. (From Nakayama et al., 1989.)

one window or one disc through three windows can be perceived, depending on the disparity, that is, on which pair is fused. Thus, the relationship between modal (occluding) and amodal (occluded) can be reversed by a local change in disparity. Nakayama et al. (1989) also showed that global surface layouts defined by local disparity influences recognition of a face occluded by stripes. The performance was better when the face was seen behind the stripes than in front, indicating that amodal completion of the face facilitated recognition.

Nakayama et al. (1990) studied the effect of local disparity on color filling-in using the Varin and other configurations. When the colored portions were defined as front (by a crossed disparity), color filling-in, subjective contours, and transparency were all enhanced. By contrast, when they were defined as behind, all these became amodal, thus suppressed.

Figure 75.3 presents examples of color filling-in derived from very limited colored areas (the original was developed by Ken Nakayama; an unpublished observation). Here,



FIGURE 75.3. Effect of local edges on global surface completion. The converging fuser should fuse the left and middle images; the diverging fuser should fuse the middle and right images. The difference in the small colored regions leads to remarkably different filled-in surfaces: a diamond in *A* and a cross in *B*. Note that one of the colored portions is given only for one eye (the colored region on the left of the middle image is missing). Global filled-in surfaces can be formed even in the absence of binocularly matched inputs. (Courtesy of Ken Nakayama.) (See color plate 50.)

colored areas, as well as disparity and collinearity cues, are presented very locally and sparsely. Note also that one of the colored areas is even unpaired between the left- and right-eye images (Nakayama and Shimojo, 1990). Yet, a microscopic difference in edge orientation alone gives rise to a global difference in the completed surface (compare the top and the bottom stereograms when fused). Whereas collinearity itself may be considered a global property, the information that defines this property is edge location and orientation, which are given only very locally.

Local changes in luminance-related cues, such as contrast at edges (Nakayama et al., 1990) and background luminance (Anderson, 1999), are also known to be critical in determining global surface properties. It should be noted that the local factors determining global surface properties, such as edge orientation, contrast at edges, disparity, and so on, are typical features that are detected in the early visual cortex (such as areas V1 and V2). Hence, the global aspects of surface perception do not exclude the critical role of local feature detection in the early visual cortex. As we will discuss later, one of the possible mechanisms underlying global surface representation is a propagation-like process starting from local features, which in effect can fill in a big gap in space to establish a surface representation. In such a mechanism, a local feature detector is local in the sense that it is activated by an isolated stimulus presented in a limited area (classical receptive field) but also global in the sense that the activity can be modulated by the global context outside the receptive field (Gilbert et al., 1990). Likewise, a local feature

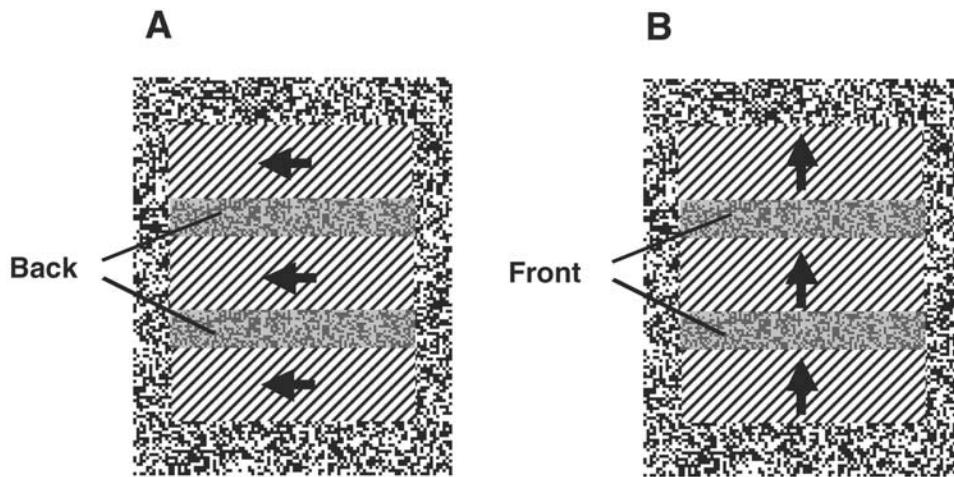


FIGURE 75.4. Effect of amodal completion on the barber pole illusion. In this illusion, the movement of stripes (moving orthogonal to their orientation) is seen through a window. They appear to move vertically (horizontally) through a vertically (horizontally) elongated frame. *A*, If the panels separating the diagonal stripes are seen in

back by adding disparity, the stripes, seen in three horizontally elongated regions, appear to move horizontally. *B*, If the panels are placed in front, the diagonal stripes are completed behind them, forming a vertically elongated region. Then the movement of the stripes is seen as vertical. (From Shimojo et al., 1989.)

is local in that it is given in a limited retinal area, but it can also be global in that it can modulate the activity of distant local feature detectors.

Surface formation in early visual processing

Surface completion may be considered an example of problem solving or reasoning. As an alternative, it may be achieved by bottom-up mechanisms based on local feature detection at the very early level of cortical processing. In the case of subjective contours (and surface), for example, top-down, cognitive theories (Gregory, 1972; Rock and Anson, 1979) and bottom-up mechanistic theories (Grossberg and Mingolla, 1985; Peterhans and von der Heydt, 1989) have been proposed.

More recent evidence indicates that the process of surface completion precedes other cognitive/perceptual processes. For example, Davis and Driver (1994) demonstrated that Kanizsa subjective figures can be detected without focal attention at parallel (thus early) stages of the human visual system. He and Nakayama (1994a) showed that visual search occurs only after the stage of amodal completion. Furthermore, a clinical study suggested that in a parietally damaged patient who suffered from *extinction* (a condition in which a visual stimulus is neglected when another stimulus is present in the intact visual field), the condition was less severe when bilateral stimuli formed a common surface, such as an illusory Kanizsa figure and a surface completed behind an occluder (Mattingley et al., 1997). Likewise, the perceived direction of ambiguous motion, both smooth (Shimojo et al., 1989) (Fig. 75.4) and apparent (He and Nakayama, 1994b; Shimojo and Nakayama, 1990), is affected by amodally com-

pleted surfaces, indicating the precedence of surface completion over at least some types of motion processing. For example, it is known that the perceived direction of a drifting grating is ambiguous when presented in a rectangular window, with the direction along the longer axis being dominant (the barber pole illusion; Wallach, 1935). This dominance is preserved even when the window is partly occluded such that the longer axis of the visible (nonoccluded) areas is different from that of the entire window (Shimojo et al., 1989) (Fig. 75.4B).

These results demonstrate that visual surface representation is established at a level earlier than cognitive and some perceptual processes as a result of preattentive or unconscious operations. On the other hand, it has been argued that surface perception can be regarded as a process of finding a statistically optimal solution to the inverse optics problem with regard to the real-world constraint (Nakayama and Shimojo, 1992; Poggio et al., 1985), thus analogous to cognitive inference at the functional level. It should be noted, however, that the early and inference-like aspects are not necessarily mutually exclusive. The real issue is whether the inference-like process is implemented at an early level, not mediated by conscious/cognitive processes, or at a late level, mediated by conscious/cognitive processes. The evidence above seems to support the former conclusion.

Aftereffects induced by perceptual surfaces

Aftereffects, visual sensations that persist after prolonged viewing of stimuli, have been widely used to characterize mechanisms underlying visual perception. The percept is thought to reflect adaptation of neural subunits which

respond to the adapting stimuli (see also Chapter 60). Aftereffects can be highly specific with respect to the features of adapting stimuli, such as orientation and spatial frequency, corresponding to the feature selectivity found in single neuronal responses in the visual system. Thus, aftereffects have been called the *psychologist's microelectrode* (Frisby, 1979), which can be used to probe the relationship between visual perception and underlying neural mechanisms. In this and the following sections, we highlight the global and early nature of visual surface representation in light of its role in the formation of aftereffects.

The orientation-contingent color aftereffect (the McCollough effect; McCollough, 1965) is one of the striking examples of highly specific sensory adaptation. In the paradigm of the McCollough effect, an observer views alternating horizontal and vertical stripes with different colors, such as red vertical stripes alternating with green horizontal stripes, for several minutes. After adaptation, a test stimulus consisting of achromatic horizontal or vertical stripes is perceived to be tinged with the color complementary to that of the adapting stripes with the same orientation. Watanabe et al. (1992) replaced the test stripes with a grid pattern that appears to consist of overlapping horizontal and vertical stripes due to its appropriate luminance combination for perceptual transparency and surface segregation. They found that the orientation-contingent color aftereffect is perceived in the subjective overlapping stripes. Watanabe (1995) also showed that a test pattern made of largely occluded but perceptually completed stripes can elicit the McCollough effect. These results demonstrate that the McCollough effect, which is generally thought to involve early visual processes specific to orientation and color (Stromeyer, 1978), can be mediated or preceded by the global processing of perceptual surfaces.

In the example described above, visual patterns inducing subjective surfaces were used as test stimuli on which the effects of adaptation were perceived. Is it possible to adapt to perceptually filled-in surfaces, resulting in aftereffects observed in the region that is not retinally stimulated during adaptation? It is known that prolonged viewing of a grating leads to a decrease in apparent contrast or to the elevation of threshold in a test grating with a similar orientation and spatial frequency (Blakemore and Campbell, 1969). Instead of a fully visible grating, Weisstein (1970) used a grating partially occluded by an object as an adapting stimulus and measured the apparent contrast of a small grating patch within the region where the occluding object had been presented during adaptation. The apparent contrast of the grating patch was significantly lower than that seen after adaptation to a blank screen or to the object alone. This suggests that the representation of amodally completed gratings can undergo adaptation in a manner similar to that of nonoccluded gratings.

Afterimages of filled-in surfaces

Afterimages are often distinguished from other aftereffects (tilt, motion, size, etc.) in that they do not require a particular test stimulus to observe the effect. Afterimages are modulation of the first-order visual features, luminance and color, which are defined at each point of an image. Thus, a homogeneous background, having first-order features (luminance/color), is sufficient to observe their modulation. By contrast, other aftereffects are modulation of higher-order visual features, such as orientation and motion, which are defined by the *relations* among more than one point, and thus require a patterned (higher-order) test stimulus to observe their modulation. Hence, afterimages have been considered to reflect the most primitive point-by-point visual processing, and their origin has been believed to arise from either bleaching of photochemical pigments or neural adaptation in other retinal cells (Brindley, 1962; Craik, 1940, 1966; Virsu and Laurinen, 1977).

Can afterimages, which have been thought to be concerned with primitive point-by-point processing, be created by adaptation to perceptually completed global surfaces? Shimojo et al. (2001) showed that perceptually filled-in surfaces can give rise to afterimages, using color filling-in displays such as the Varin figure (Figs. 75.1*B*, 75.5*A*). After prolonged adaptation, the adapting stimulus was replaced with a dark homogeneous background (Fig. 75.5*A*). The observers perceived not only the afterimages of the local inducers (pacmen/wedges or discs), but also a global afterimage of the perceptually filled-in surface (Fig. 75.5*B*). The global afterimage cannot be attributed to the general fuzziness and leaky edges of the afterimage, because adaptation to the inner wedge portions alone (without the outer pacmen) leads to the four parts corresponding to the wedges separately visible in the afterimage. The global afterimage is distinct from conventional afterimages in that it is visible at a portion that has not been retinally stimulated, but corresponds to a perceptually filled-in surface.

The observation described above, however, does not necessarily imply that the global afterimage arises from the adaptation of the neural mechanism producing the perceptually filled-in surface. It is possible that the global afterimage originates from local afterimages of the inducers: the color of the global afterimage may be merely a result of the ordinary filling-in mechanism that may equally treat real stimuli and signals due to local adaptation. Shimojo et al. (2001) performed a series of experiments to demonstrate that the global afterimage is indeed due to adaptation of the representation of the filled-in surface (surface adaptation hypothesis), as opposed to local adaptation followed by an ordinary filling-in process (element adaptation hypothesis).

First, the time course of the afterimage was analyzed. During the test period, different types of afterimage

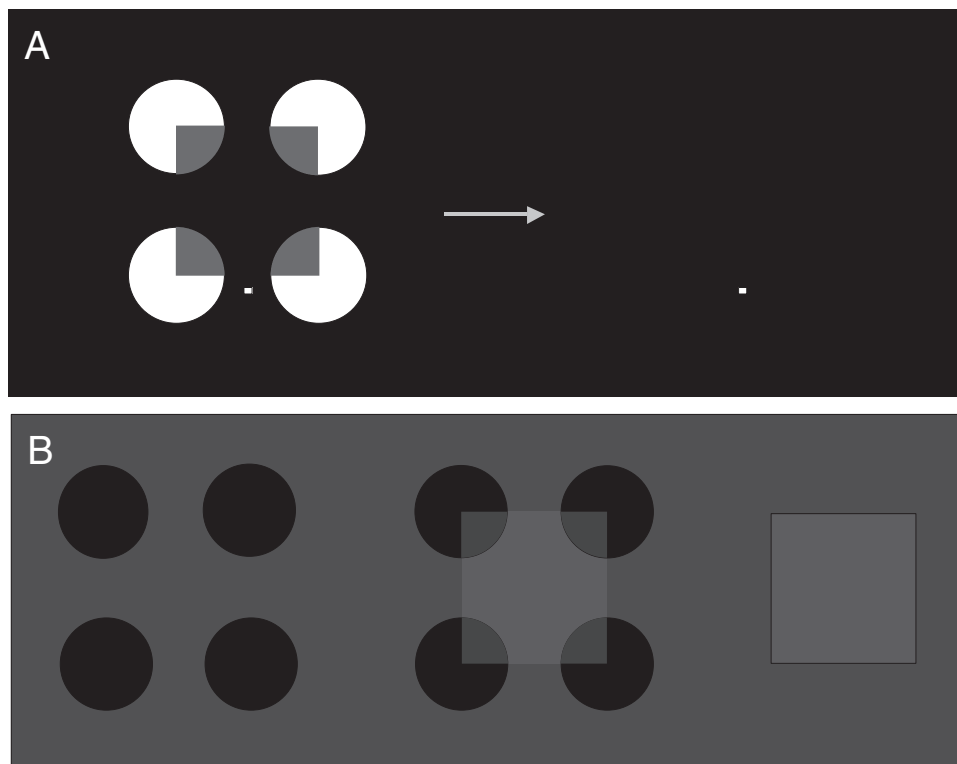


FIGURE 75.5. Afterimage formed by adaptation to a perceptually filled-in surface. *A*, After adaptation to the Varin figure for neon color filling-in (*left image*; fixating to the white dot for about 30 seconds), the afterimage is observed on a blank screen (*right*). *B*, Typical afterimages. During the observation period, the appearance of the afterimage changes dynamically. The afterimages for the discs (*left*), for the filled-in surface (*right*), and for both (*middle*) appear to alternate several times. (Adapted from Shimojo et al., 2001.) (See color plate 51.)

appeared and disappeared several times in different time courses. Subjects were asked to monitor the visibility of two types of afterimage separately using two buttons: the local afterimage, which corresponded to elements of the inducer (pacmen, wedges, discs, or their combinations), and the global afterimage, which extended out of them toward the central portion to form a color-filled rectangle (Fig. 75.5*B*). They pressed one button while the local afterimage was visible and another while the global afterimage was visible. The results show that there were significant time periods during which the subjects reported visibility of the global but not the local afterimages (average, 20% of the total test period of 20 seconds). Furthermore, the likelihood analysis for the global afterimage in the presence or absence of the local afterimage revealed that the global afterimage tended to be more visible when the local afterimage was *not* visible than when it was visible. These observations indicate that the visibility of the local afterimage is not a necessary or even a favorable condition for the visibility of the global afterimage, in disagreement with the element adaptation hypothesis.

One prediction of the surface adaptation hypothesis is that since the global afterimage is due to the perceptually filled-in surface during adaptation, the strength of the global

afterimage should be correlated with that of the perceptual filling-in during adaptation. The element adaptation hypothesis, on the other hand, predicts that the strength of the global afterimage should be determined solely by that of the local afterimages, and thus remain constant as long as the local afterimages are the same.

In another experiment, the strength of perceptual filling-in during adaptation was manipulated by alternating two frames (667 msec each) composed of complementary parts of the inducer, as shown in Figure 75.6*A* (except condition 5, where only the colored wedge portions were turned on and off). Since the strength of perceptual filling-in decreases approximately in the order of the conditions shown in Figure 75.6*A*, the surface adaptation hypothesis would predict that the strength of the global afterimage also decreases in the same order. On the other hand, since the total duration of adaptation was equal across portions of the stimulus in all the conditions except condition 5, the strength of the local afterimage should be the same across conditions 1 to 4. Thus, the element adaptation hypothesis would predict that the relative strength of the global afterimage would be approximately the same across conditions 1 to 4 (and perhaps weaker in condition 5). As shown in Figure 75.6*B* and 75.6*C*, both the estimated strength and the visible

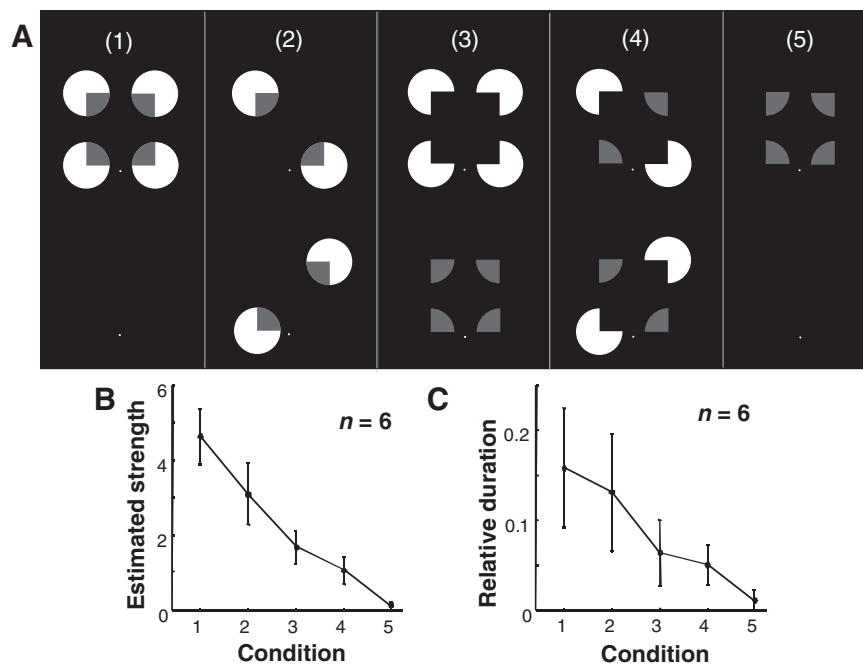


FIGURE 75.6. Surface versus element adaptation I. *A*, The inducer for the color filling-in was divided into complementary pairs (except in condition 5, where only the wedge portions were shown), and they were alternated (667 msec for each frame) for adaptation. The strength of perceptual filling-in during adaptation was varied (decreasing approximately in this order), while the total duration of adaptation to each portion of the inducer was held constant (except in condition 5). *B*, Estimated strength of the global afterimage for

the conditions depicted in *A*. The data for six subjects are pooled (error bar, standard error of the mean). The estimated value 10 corresponds to the strength of the global afterimage for the complete Vairn figure (no alternation or decomposition), which had been observed before this experiment. *C*, Duration of the global afterimage relative to the total test period. (From Shimojo et al., 2001.) (See color plate 52.)

duration of the global afterimage decreased according to the order of strength of perceptual filling-in, supporting the surface adaptation hypothesis but not the element adaptation hypothesis.

In the last experiment, a new type of dynamic stimulus for color filling-in was employed to further dissociate the predictions of these hypotheses. In the static condition (Fig. 75.7*A*), line segments were placed sparsely and statically, so that the impression of color filling-in would be minimal, while the local afterimage of the line segments formed strongly. In the dynamic condition (Fig. 75.7*B*), the line segments were displaced up and down to create an impression of motion, while the disc-shaped area within which the line segments were colored blue was fixed. It appeared as though a set of white line segments moved up and down behind a semitransparent, stationary colored disc. This condition was designed to enhance the impression of color filling-in during adaptation while minimizing the local afterimage of line segments by the constant displacement. The surface adaptation hypothesis predicts that the duration of the local afterimage would be reduced, whereas that of the global afterimage would be increased, relative to the static condition. The element adaptation hypothesis, on the other hand, predicts that both local and global afterimages would be attenuated in the dynamic condition, since the duration of the global

afterimage should depend strictly on that of the local afterimage. The results of the visible duration of the local and global afterimages clearly indicate the enhancement of the global afterimage in spite of the attenuation in the local afterimage, consistent only with the surface adaptation hypothesis.

These results support the idea that afterimages can arise from the adaptation of the neural mechanism representing perceptually filled-in surfaces. Since, unlike other aftereffects, afterimages are concerned with most primitive visual attributes, it may suggest that filled-in surfaces are represented at some very early stage of visual processing. In fact, Shimojo et al. (2001) also reported that interocular transfer of adaptation did not occur to induce the global afterimage in the unadapted eye, indicating that the adaptation occurred in monocular units, which exist only in the primary visual cortex or earlier (Hubel and Wiesel, 1962). In addition, when one eye was suppressed by pressure-blinding the retina after adaptation, the global as well as the local afterimages became invisible. Although these observations suggest contributions of retinal adaptation to the global afterimage, it is unlikely that retinal processing explicitly represents filled-in global surfaces, since each retinal cell deals with inputs only from a small area and lacks extensive long-range connections with other cells and projections from

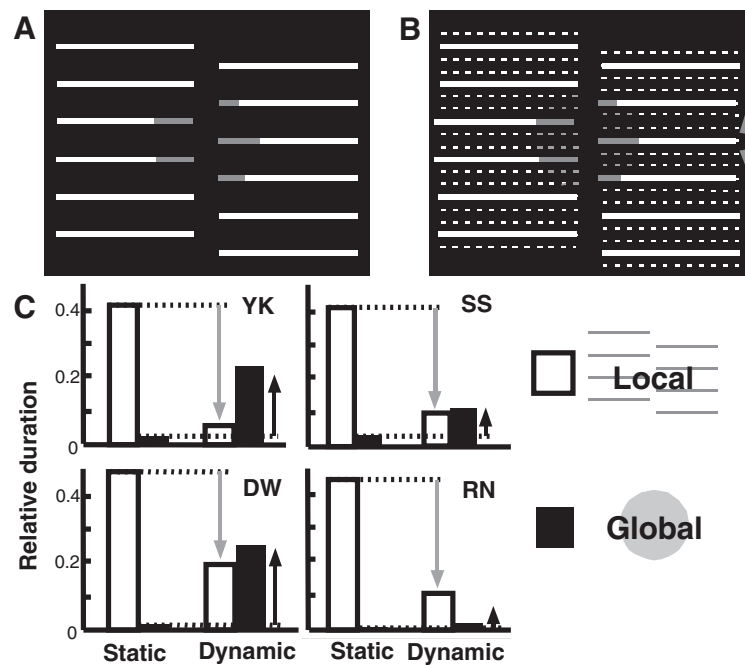


FIGURE 75.7. Surface versus element adaptation II. *A*, Static condition. The line segments were presented sparsely and statically. *B*, Dynamic condition. The line segments underwent vertical apparent motion while their portions in the fixed disc-shaped area were colored blue. The broken lines indicate positions for displacement and were invisible in the actual stimulus. The moving inducer pro-

duces more vivid filling-in but less local adaptation compared to the static condition. *C*, The duration of visible afterimages relative to the total observation time is plotted for the static and dynamic conditions in each subject. The white and black bars indicate local and global afterimages, respectively. (From Shimojo et al., 2001.) (See color plate 53.)

higher visual areas, which visual cortical neurons have. Therefore, the earliest level of visual cortical processing, which can handle both local primitive features and global connections, would need to be involved in the representation of perceptual surfaces and the adaptation that gives rise to the global afterimage. In the next section, we will discuss possible neural correlates in the early visual cortex.

Neural substrates for perceptual surfaces

It is challenging to explain the global aspects of surface perception in terms of topographically organized, small receptive fields of visual neurons (Barlow, 1953; Hubel and Wiesel, 1962; Kuffler, 1953). This is the case not only for illusory surfaces, which we have focused on in the previous sections, but also for real homogeneous surfaces whose edges and surface attributes are physically available, because visual neurons generally respond better to variation in luminance or color than to their absolute values (homogeneous surface attributes). It is now widely accepted, however, that the response of visual neurons can be substantially and selectively modulated by stimuli presented outside the classical receptive field (Allman et al., 1985; see also Chapter 45). Surface perception may be one of the global perceptual phenomena that require such long-range inter-

actions beyond classical receptive fields (Spillmann and Werner, 1996; see also Chapter 106).

Neural responses correlated with global surface perception have been demonstrated by manipulating the global context determining perceived surface attributes while holding the local features inside the receptive field constant. Rossi et al. (1996) studied the activity of neurons whose receptive field fell within a gray square surrounded by a background with changing luminance. This display produces illusory modulation of brightness of the central gray square: the brightness correlates negatively with the background luminance (brightness induction; Hering, 1964). They found that in many neurons in the primary visual cortex, the activity was modulated by the background luminance in accordance with the perceived brightness. Lamme (1995) showed that the activity of neurons in the primary visual cortex depends on the figure-ground context, that is, on which region appears as a surface in front of the other. A significantly larger response was observed when the receptive field was in the figure region than when it was in the background, while the local feature within the receptive field was constant. Zhou et al. (2000) (see also Chapter 76) reported another type of figure-ground selectivity of early visual cortical neurons. A local light-dark edge, for instance, could be the left side of a dark square or the right side of a light square. They found that neural responses to

the same edge can be modulated by the side to which the border belongs to (*border ownership*), while the context used to determine border ownership was provided outside the receptive field.

Neural responses to illusory or completed contours/lines that emerge in association with surface perception have also been found in early visual areas. Cells in area V1 as well as in V2 are known to be responsive to illusory contours, such as those perceived in the Kanizsa figure (e.g., Lee and Nguyen, 2001; von der Heydt et al., 1984; see also Chapter 76). Sugita (1999) demonstrated that cells in V1 respond to a bar occluded by a small patch (surface) when a disparity is given outside the receptive field such that the patch is seen in front. Bakin et al. (2000) also found that responses in the early visual areas (more in V2 than V1) are correlated with modally and amodally completed lines while depth cues for surface segregation are varied outside the receptive field.

Most of these electrophysiological data are consistent with the view that perceptual surfaces are topographically represented: the response of each cell reflects the perceived surface attributes at the point/area corresponding to its receptive field. The notion of topographical representation is often criticized for assuming “redundant processes of painting an internal screen” (Dennett, 1991). It is logically possible that perceptual surfaces are represented in a “symbolic” way, without being mediated by topographical representation. For instance, a neuron that is selectively activated by images of faces can be thought to represent faces symbolically, but such representation may not require a map of activity similar to faces formed in a visual cortical area. The coding of border ownership described above (Zhou et al., 2000) may be regarded as a semisymbolic representation in early visual areas, since it enables a determination of surface attributes and configuration by tracing the activity corresponding to the border without looking at the whole two-dimensional map of activity.

It has been argued, however, that in order to determine surface attributes from local ambiguous information given within receptive fields, the brain may make effective use of the topographically organized circuits in early visual areas (Pessoa et al., 1998). A solution to the problem of determination of surface attributes may be achieved by propagation of activity from cells receiving critical information such as edges through synaptic cascades of local connections. This propagation mechanism may be considered more consistent with the topographical as opposed to the symbolic representation. A recent human functional magnetic resonance imaging study provides further support for topographical representation of perceptual surfaces. When a color filling-in stimulus similar to the Varin figure was presented, clear activation was produced in the cortical region in the primary visual cortex corresponding to the filled-in area in the visual

field (Sasaki et al., 2001). Thus, perceptually filled-in surfaces could be represented by filling-in in the cortical map. This finding is highly consistent with the demonstration of global afterimages induced by filled-in surfaces, described in the previous section in detail. A similar implication comes from a totally different angle and method. Kamitani and Shimojo (1999) showed that by transcranial magnetic stimulation (TMS) of the human occipital cortex, a hole, or scotoma, can be created in a flashed, large-field visual pattern, in accordance with the anatomy of early cortical maps (Fig. 75.8). They also found distortion of the scotoma in grating patterns (Figs. 75.8*A* and 75.8*B*), which can be interpreted in terms of the local connection among orientation-detection units observed in the primary visual cortex (Kapadia et al., 1995). The distortion may reflect a completion process that operates against the inhibitory effect of TMS by propagation of activity through local synaptic connections (Fig. 75.8*D*).

While further studies must be done to determine whether, and to what degree, perceptual surfaces are topographically represented, functional characteristics of early visual cortical areas seem to be ideal to handle global as well as local information required for the processing of visual surfaces. It has been proposed that horizontal intrinsic connections within areas (Gilbert et al., 1990) and recurrent inputs from higher areas (Lamme and Roelfsema, 2000) result in dynamic changes in tuning in early visual areas, including the emergence of the global properties correlated with surface perception (Spillmann and Werner, 1996). It should be noted that recurrent inputs from higher areas are not necessarily derived from conscious/cognitive commands. They can be fast, automatic processes not mediated by conscious/cognitive processes. Furthermore, representation at early visual areas would remain early even after modulation by recurrent inputs, as long as it is available for later perceptual or cognitive processes. Although contributions of possible symbolic representation at higher areas, as well as global processing at subcortical levels (e.g., Pöppel, 1986), should not be excluded, the global and early aspects of visual surfaces discussed in the previous sections could be best explained by the global processing of early visual areas.

Conclusions

In this chapter, we have provided a framework to integrate psychophysical and physiological findings around the key concept of visual surface representation. We have shown that in light of recent findings, the classical view of visual processing as a serial relay of signals through local feature detectors with progressively increasing size and complexity needs to be fundamentally reconsidered. The classical view assumes certain analogies among the notions, such as local/global and early/late: local processing is early, and

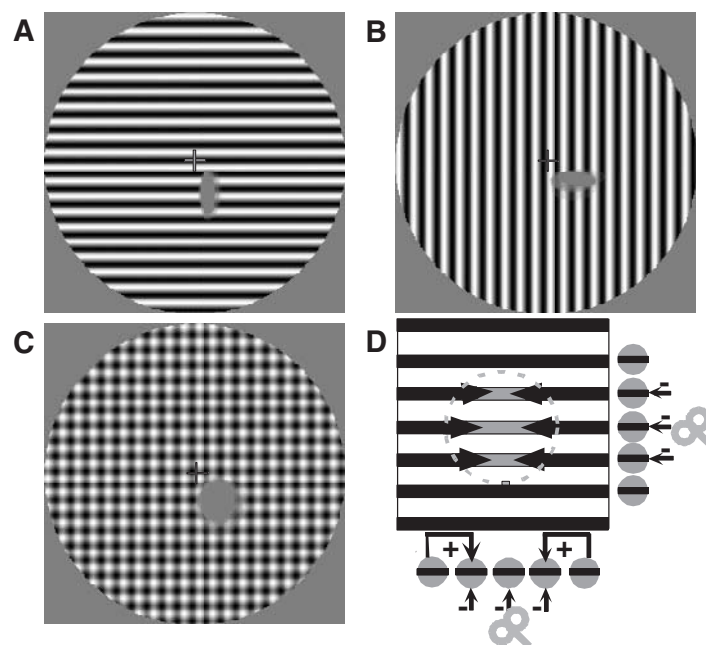


FIGURE 75.8. *A–C*, Reconstructed percepts of TMS-induced scotomas seen on flashed visual patterns: a horizontal grating (*A*), a vertical grating (*B*), and a grid pattern (*C*). The visual pattern was presented for 40 msec, and the magnetic stimulation was delayed for 106 msec. *D*, Hypothetical mechanism for the anisotropic distortion of the scotoma. A horizontal grating is shown with horizontally tuned neural units aligned vertically (*right*) and horizontally

(*bottom*). The central gray circle represents the visual space corresponding to the cortical area directly affected by the magnetic stimulation. Long-range facilitatory connections among collinearly aligned units (+ in the bottom row) mask inhibition by inputs caused by TMS (–); thus, the suppressed region appears compressed along the stripes. (From Kamitani and Shimojo, 1999.)

global processing is late. However, we have demonstrated that visual surface representation is achieved by global *yet* early processing.

We have also seen that the dichotomies of local versus global and early versus late themselves also need to be carefully applied to describe psychophysical phenomena and physiological processes involved in surface perception. For instance, a global surface representation can be created by local retinal inputs, and the activity of a neuron with a local receptive field is modulated by the global context. Early perceptual solutions look similar to late cognitive solutions based on inference, and recurrent processing in the visual cortex makes the distinction between early and late stages less meaningful. Such complications derive from the fact that that surface representation is beyond the scope of the classical view of visual processing as sequential, local-to-global feature detection.

REFERENCES

Allman, J., F. Miezin, and E. McGuinness, 1985. Stimulus specific responses from beyond the classical receptive field: neurophysiological mechanisms for local-global comparisons in visual neurons, *Annu. Rev. Neurosci.*, 8:407–430.
Anderson, B. L., 1999. Stereoscopic surface perception, *Neuron*, 24:919–928.

Bakin, J. S., K. Nakayama, and C. D. Gilbert, 2000. Visual responses in monkey areas V1 and V2 to three-dimensional surface configurations, *J. Neurosci.*, 20:8188–8198.
Barlow, H. B., 1953. Summation and inhibition in the frog's retina, *J. Physiol.*, 119:69–88.
Blakemore, C., and F. W. Campbell, 1969. On the existence of neurons in the human visual system selectively sensitive to the orientation and size of retinal images, *J. Physiol.*, 203:237–260.
Brindley, G. S., 1962. Two new properties of foveal afterimages and a photochemical hypothesis to explain them, *J. Physiol.*, 164:168–179.
Craik, K. J. W., 1940. Origin of visual after-images, *Nature*, 145:512.
Craik, K. J. W., ed., 1966. *The Nature of Psychology: A Selection of Papers, Essays and Other Writings by the Late K. J. W. Craik*, Cambridge: Cambridge University Press.
Davis, G., and J. Driver, 1994. Parallel detection of Kanizsa subjective figures in the human visual system, *Nature*, 371:791–793.
Dennett, D. C., 1991. *Consciousness Explained*, Boston: Little, Brown.
Frisby, J. P., 1979. *Seeing: Illusion, Brain, and Mind*, Oxford: Oxford University Press.
Gibson, J. J., 1950. *The Perception of the Visual World*, Boston: Houghton Mifflin.
Gilbert, C. D., J. A. Hirsch, and T. N. Wiesel, 1990. Lateral interactions in visual cortex, *Cold Spring Harb. Symp. Quant. Biol.*, 55:663–677.
Gregory, R. L., 1972. Cognitive contours, *Nature*, 238:51–52.
Grossberg, S., and E. Mingolla, 1985. Neural dynamics of form perception: boundary completion, illusory figures, and neon color spreading, *Psychol. Rev.*, 92:173–211.

- He, Z. J., and K. Nakayama, 1994a. Perceiving textures: beyond filtering, *Vis. Res.*, 34:151–162.
- He, Z. J., and K. Nakayama, 1994b. Perceived surface shape not features determines correspondence strength in apparent motion, *Vis. Res.*, 34:2125–2135.
- Hering, E., 1964. *Outlines of a Theory of the Light Sense*, Cambridge, MA: Harvard University Press.
- Hubel, D. H., and T. N. Wiesel, 1962. Receptive fields, binocular interaction and functional architecture in the cat's visual cortex, *J. Physiol.*, 160:106–154.
- Kamitani, Y., and S. Shimojo, 1999. Manifestation of scotomas created by transcranial magnetic stimulation of human visual cortex, *Nat. Neurosci.*, 2:767–771.
- Kanizsa, G., 1979. *Organization in Vision: Essays on Gestalt Perception*, New York: Praeger.
- Kapadia, M. K., M. Ito, C. D. Gilbert, and G. Westheimer, 1995. Improvement in visual sensitivity by changes in local context: parallel studies in human observers and in V1 of alert monkeys, *Neuron*, 15:843–856.
- Kuffler, S. W., 1953. Discharge patterns and functional organization of mammalian retina, *J. Neurophysiol.*, 16:37–68.
- Lamme, V. A., 1995. The neurophysiology of figure-ground segregation in primary visual cortex, *J. Neurosci.*, 15:1605–1615.
- Lamme, V. A., and P. R. Roelfsema, 2000. The distinct modes of vision offered by feedforward and recurrent processing, *Trends Neurosci.*, 23:571–579.
- Lee, T. S., and M. Nguyen, 2001. Dynamics of subjective contour formation in the early visual cortex, *Proc. Natl. Acad. Sci. USA*, 98:1907–1911.
- Mattingley, J. B., G. Davis, and J. Driver, 1997. Preattentive filling-in of visual surfaces in parietal extinction, *Science*, 275:671–674.
- McCollough, C., 1965. Color adaptation of edge-detectors in the human visual system, *Science*, 149:1115–1116.
- Nakayama, K., and S. Shimojo, 1990. DaVinci stereopsis: depth and subjective occluding contours from unpaired image points, *Vis. Res.*, 30:1811–1825.
- Nakayama, K., and S. Shimojo, 1992. Experiencing and perceiving visual surfaces, *Science*, 257:1357–1363.
- Nakayama, K., S. Shimojo, and V. S. Ramachandran, 1990. Transparency: relation to depth, subjective contours, luminance, and neon color spreading, *Perception*, 19:497–513.
- Nakayama, K., S. Shimojo, and G. H. Silverman, 1989. Stereoscopic depth: its relation to image segmentation, grouping, and the recognition of occluded objects, *Perception*, 18:55–68.
- Pessoa, L., E. Thompson, and A. Noe, 1998. Finding out about filling-in: a guide to perceptual completion for visual science and the philosophy of perception, *Behav. Brain Sci.*, 21:723–748.
- Peterhans, E., and R. von der Heydt, 1989. Mechanisms of contour perception in monkey visual cortex. II. Contours bridging gaps, *J. Neurosci.*, 9:1749–1763.
- Poggio, T., V. Torre, and C. Koch, 1985. Computational vision and regularization theory, *Nature*, 317:314–319.
- Pöppel, E., 1986. Long-range colour-generating interactions across the retina, *Nature*, 320:523–525.
- Rock, I., and R. Anson, 1979. Illusory contours as the solution to a problem, *Perception*, 8:665–681.
- Rossi, A. F., C. D. Rittenhouse, and M. A. Paradiso, 1996. The representation of brightness in primary visual cortex, *Science*, 273:1104–1107.
- Sasaki, Y., T. Watanabe, A. M. Dale, and R. B. Tootell, 2001. V1 involvement for color filling-in revealed by human fMRI, *Soc. Neurosci. Abstr.*, 12.11.
- Shimojo, S., Y. Kamitani, and S. Nishida, 2001. Afterimage of perceptually filled-in surface, *Science*, 293:1677–1680.
- Shimojo, S., and K. Nakayama, 1990. Amodal representation of occluded surfaces: role of invisible stimuli in apparent motion correspondence, *Perception*, 19:285–299.
- Shimojo, S., G. H. Silverman, and K. Nakayama, 1989. Occlusion and the solution to the aperture problem for motion, *Vis. Res.*, 29:619–626.
- Spillmann, L., and J. S. Werner, 1996. Long-range interactions in visual perception, *Trends Neurosci.*, 19:428–434.
- Stromeyer, C. F. I., 1978. Form-colour aftereffects in human vision, in *Handbook of Sensory Physiology: VIII. Perception* (R. Held, H. W. Leibowitz, and H. L. Teuber, eds.), Berlin: Springer-Verlag, pp. 97–142.
- Sugita, Y., 1999. Grouping of image fragments in primary visual cortex, *Nature*, 401:269–272.
- Varin, D., 1971. Fenomini di contrasto e diffusione cromatica nell'organizzazione spaziale del campo percettivo, *Rivista di Psicologia*, 65:101–128.
- Virsu, V., and P. Laurinen, 1977. Long-lasting afterimages caused by neural adaptation, *Vis. Res.*, 17:853–860.
- von der Heydt, R., E. Peterhans, and G. Baumgartner, 1984. Illusory contours and cortical neuron responses, *Science*, 224:1260–1262.
- Wallach, H., 1935. Über visuell wahrgenommene Bewegungsrichtung, *Psychol. Forsch.*, 20:325–380.
- Watanabe, T., 1995. Orientation and color processing for partially occluded objects, *Vis. Res.*, 35:647–655.
- Watanabe, T., G. L. Zimmerman, and P. Cavanagh, 1992. Orientation-contingent color aftereffects mediated by subjective transparent structures, *Percept. Psychophys.*, 52:161–166.
- Weisstein, N., 1970. Neural symbolic activity: a psychophysical measure, *Science*, 168:1489–1491.
- Zhou, H., H. S. Friedman, and R. von der Heydt, 2000. Coding of border ownership in monkey visual cortex, *J. Neurosci.*, 20:6594–6611.

76 Image Parsing Mechanisms of the Visual Cortex

RÜDIGER VON DER HEYDT

IN THIS CHAPTER, I WILL discuss visual processes that are often labeled as *intermediate-level vision*. As a useful framework, we consider vision as a sequence of processes, each of which is a mapping from one representation to another. Understanding vision, then, means analyzing how information is represented at each stage and how it is transformed between stages (Marr, 1982). It is clear that the first stage, the level of the photoreceptors, is an image representation. This is a two-dimensional (2-D) array of color values resembling the bitmap format of digital computers. Retinal processes transform this representation into a format that is suitable for transmission through the optic nerve to central brain structures. A radical transformation then takes place in the primary visual cortex. At the output of area V1 we find visual information encoded as a *feature map*, a representation of local features. The two dimensions of retinal position are encoded in the locations of the receptive fields of cortical neurons, but each neuron now represents not a pixel but a small patch of the image, and several new dimensions are added to the three color dimensions, such as orientation, spatial frequency, direction of motion, and binocular disparity.

While the local feature representation of V1 is known in detail, we still do not have a good understanding of the nature of processing in the extrastriate areas. At first glance, the visual properties of the neurons in area V2 are rather similar to those of their input neurons of V1, except that V2 neurons have larger receptive fields (Burkhalter and Van Essen, 1986; Zeki, 1978). Many neurons of area V4 again have properties that can be found in V1 and V2, such as selectivity for color, orientation, and spatial frequency (Desimone et al., 1985; Schein and Desimone, 1990; Zeki, 1978). Some neurons in the extrastriate areas show selectivity for increasingly complex features (see Chapter 71).

Here I will review evidence that the extrastriate areas provide a new stage of processing that may be described as *image parsing*. This stage appears as a mediator between the local feature representation of V1 and the processes of attentional selection and object recognition. From the enormous amount of information that streams in through the optic nerves at each moment, the visual system selects a small fraction, and in general precisely what is relevant for a given

task. This amazing performance indicates powerful mechanisms for organizing the incoming information. The Gestalt psychologists first pointed out that the visual system tends to organize elemental visual units (such as points and lines) into larger perceptual units, or figures, according to certain rules called *Gestalt laws* (see Chapter 106). Much of this organization occurs independently of what the subject knows or thinks about the visual stimulus. Gaetano Kanizsa illustrated this “autonomy of perception” with a painting that is supposed to show a knife behind a glass but is perceived instead as a transparent knife passing in front of the stalk of the glass (Kanizsa, 1979, Fig. 2.19).

Grouping together features that belong to an object is a general task of perception. Specific visual problems arise from the fact that vision is based on 2-D projections of a three-dimensional (3-D) world. Due to spatial interposition, parts of the scene are occluded and features of near and far objects are cluttered in the image. Projections of the same objects vary with the viewing angle, and the true 3-D shape of the objects and their relations in space can only be inferred from the images. In principle, any image has an infinite number of possible interpretations in 3-D; vision is an “ill-posed problem” (Poggio and Koch, 1985). In spite of this fundamental ambiguity, vision is the most reliable of our senses. Apparently, through evolution and experience, biological vision systems have learned to make efficient use of the regularities present in images and to infer the missing information (Attneave, 1954; Barlow, 1961; Helmholtz, 1866; Marr, 1982; Poggio and Koch, 1985; Ullman, 1996).

Illusory contours: creative mechanisms

A prominent example of this creative process is the phenomenon of illusory contours (Fig. 76.1). In *A*, the system “visibly” fills in the missing contours of an overlaying triangle. Note that the illusory contours are not just interpolations between given contrast borders, as they might seem to be in *A*, but form also in the absence of contrast borders that could be interpolated (*C*). In fact, when the corners of the overlying triangle are defined by lines which could be interpolated, illusory contours do not form (*B*). What all illusory contour figures have in common is the presence of occlusion

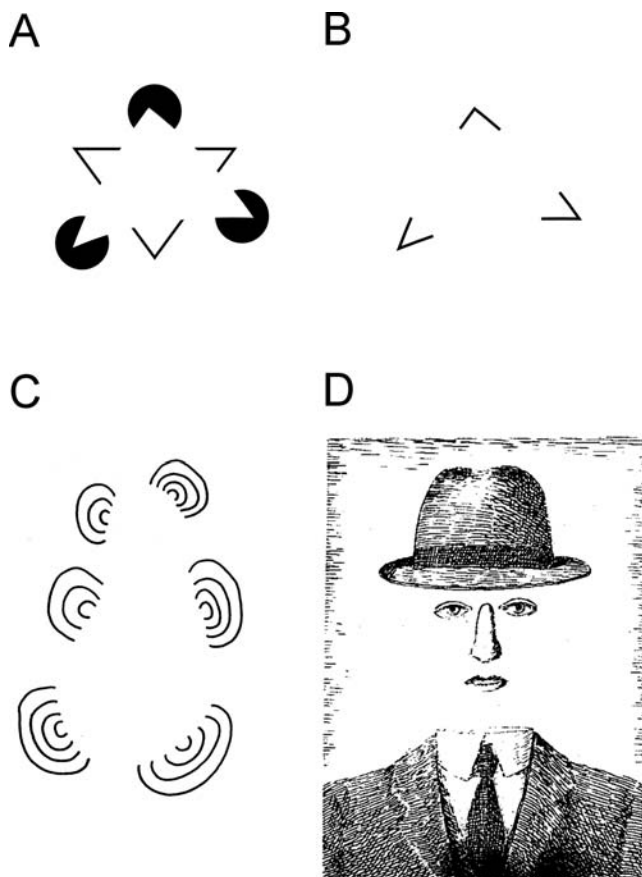


FIGURE 76.1. Perception of illusory contours. (*A* and *C*, after Kanizsa, 1979. *D*, René Magritte, *Paysage de Baucis*, etching, 1966.)

cues, such as terminations of lines and edges (Coren, 1972). Thus, the system seems to infer an occluding object. However, this is not an inference in abstract terms. The mere expectation of a contour does not lead to perception of illusory contours (Fig. 76.1*D*). Apparently, in forming the contours, the system combines evidence from occlusion cues with rules such as the Gestalt principle of good continuation.

Interestingly, illusory contours are represented in the visual cortex at a relatively early stage. In monkey area V2, many cells respond to illusory contour stimuli as if the contours were contrast borders (von der Heydt et al., 1984). Figure 76.2 shows an example of a cell that was tested with a moving illusory bar. The raster plot in *B* shows that the cell responds when the illusory contour traverses a small region that was determined before as the cell's minimum response field (ellipse; see legend). Figure 76.2*C* shows a control in which the two bars were moved exactly as in *B*, but the open ends were closed off with thin lines. Closing lines weaken the perceptual illusion (see the figure at the bottom), and they also reduce the responses of the neuron. Cells in V2 respond not only to figures with illusory bars,

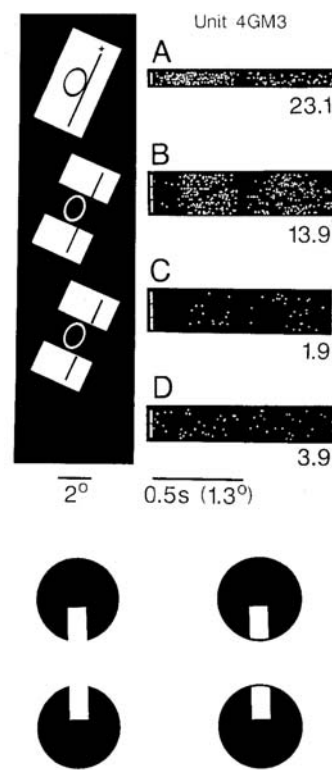


FIGURE 76.2. Illusory contour responses in a neuron of area V2. Each line of dots in the raster plots represents a sequence of action potentials fired in response to the stimulus shown on the left. *A*, Responses to a moving dark bar; *B*, to a figure in which a moving illusory bar is perceived; *C*, to a modified figure in which the illusion is abolished by adding line segments. Note the reduction of responses. The figures at the bottom illustrate the perceptual effect of adding lines. *D*, Spontaneous activity. Ellipses indicate the minimum response field of the neuron (i.e., the minimum region outside of which a bar does not evoke a response); the cross indicates the fixation point. (From Peterhans and von der Heydt, 1989, with permission.)

but also to other figures that produce illusory contours, such as a pattern of two abutting line gratings (Fig. 76.3*B*). It can be seen that the cell of Figure 76.3 responds at the same orientations for the illusory contour as for the bar stimulus; thus, it signals the orientation of an illusory contour. Using the criteria of consistent orientation tuning and response reduction by the closing lines, 30% to 40% of the cells of V2 were found to signal illusory contours of one or the other type, and the results obtained with the two types of contour were highly correlated (Peterhans and von der Heydt, 1989; von der Heydt and Peterhans, 1989).

As shown in Figure 76.2, illusory contour responses can be evoked by stimuli which are devoid of contrast over the excitatory center of the receptive field. The inducing contrast features can be restricted to regions from which an optimized bar stimulus would not evoke any response. The cells seem to integrate occlusion features over a region larger than the conventional receptive field (Peterhans et al., 1986).

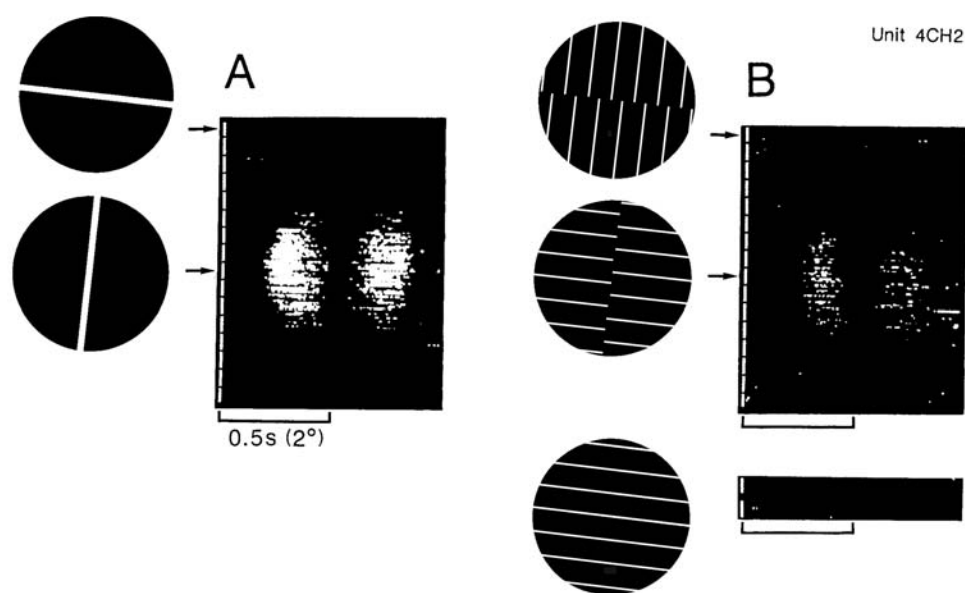


FIGURE 76.3. Illusory contour responses in another neuron of V2. In *A*, bars, and in *B*, the border between two gratings were moved across the receptive field at 16 different orientations spanning 180 degrees. The neuron responds at the same orientations for bars and illusory contours. *Bottom right, control*: grating without a border of discontinuity. (Modified from von der Heydt and Peterhans, 1989, with permission.)

Nevertheless, the extent of spatial integration is limited; for neurons with near-foveal receptive fields, the responses declined if the gap of the stimulus (Fig. 76.2*B*) was made wider than about 3 degrees visual angle.

V2 is one of the largest areas of the monkey cerebral cortex (Felleman and Van Essen, 1991), and the fact that so many cells in this area respond this way indicates that illusory contour stimuli probe a basic function of the visual cortex. V2 is an early stage of processing where responses are fast and highly reproducible. Illusory contour responses arise as early as 70 msec after stimulus onset (Lee and Nguyen, 2001; von der Heydt and Peterhans, 1989). This indicates that illusory contours are probably not the result of object recognition processes at higher levels but are generated within the visual cortex. Computational models have shown how such contours might be generated (e.g., Finkel and Sajda, 1992; Grossberg and Mingolla, 1985; Heitger et al., 1998).

PROCESSING STAGES Representation of illusory contours has also been demonstrated in V1 of cat (Redies et al., 1986; Sheth et al., 1996) and monkey (Grosf et al., 1993; Lee and Nguyen, 2001; Ramsden et al., 2001). However, it is not clear if cells in V1 also generalize over the various types of illusory contour figures and if they signal the contour orientation. Sheth et al. (1996) and Ramsden et al. (2001) used a combination of optical imaging and single-unit recording to identify the illusory contour representation with the abutting-grating type of stimulus. Sheth et al. found cells with consistent orientation tuning for illusory contours in V1

of the cat. In the monkey, Ramsden et al. found that the representation of illusory contours in V1 is different from that of V2. Illusory contours *reduced* activity in columns of the corresponding orientation but *increased* activity in columns of the orthogonal orientation, in contrast to V2, where the same columns were activated by illusory contours and contrast borders. They conclude that V1 deemphasizes illusory contours.

Studies that compared both areas invariably found marked differences between V1 and V2 in the frequency of cells that signaled illusory contours, the signaling of orientation, and the degree of cue invariance (Bakin et al., 2000; Leventhal et al., 1995; Ramsden et al., 2001; Sheth et al., 1996; von der Heydt and Peterhans, 1989).

CORRELATION OF PHYSIOLOGY AND PERCEPTION Varying the configurations and spatial parameters of the displays shows a tight correspondence between human perception and neural responses for illusory contours generated by abutting gratings (Fig. 76.3*B*) (Soriano et al., 1996). However, in discriminating the shape of illusory figures, the human visual system shows larger spatial integration than the neurons of monkey V2 (Ringach and Shapley, 1996). Because neurons that signal illusory contours are only a subset of the cells that signal contrast edges, orientation-dependent adaptation aftereffects should transfer from contrast-defined to illusory contours, but not in the reverse direction, and the discrimination of orientation should be less accurate for illusory contours than for contrast-defined contours. Both predictions were borne out in psychophysical experiments (Paradiso et

al., 1989; Westheimer and Li, 1996). Illusory contours are usually associated with perception of overlay (Coren, 1972), and some neurons in V2 are selective for the implied direction of occlusion of illusory contours (Baumann et al., 1997). Thus, the illusory contour mechanisms may be related to the coding of border ownership, discussed below.

ILLUSORY CONTOURS ARE UNIVERSAL Perception of illusory contours has been demonstrated in a variety of nonhuman species, including the cat, owl, and bee (Bravo et al., 1988; De Weerd et al., 1990; Nieder and Wagner, 1999; Srinivasan et al., 1987; for a review, see Nieder, 2002). Most elegant is the combination of behavioral experiments with single-cell recordings (Nieder and Wagner, 1999).

Border ownership: image context integration

Illusory contours and related visual phenomena are only the tip of an iceberg of cortical processes involved in perceptual organization. Kanizsa's figure (Fig. 76.1A) suggests that illusory contours are the product of mechanisms in figure-ground segregation. The system takes the peculiar arrangement of the black elements as evidence for an occluding triangle and hence creates a representation of its contours. In fact, it also creates the representation of a white opaque surface, as one can see from the subtle difference in brightness relative to the background. The illusory contours appear as the edges of this surface. Similar linking of contour and surface can also be observed for sharp contrast borders. Perception tends to interpret such borders as occluding contours and assigns them to a surface on one or the other side of the border. This compulsion of the visual system is demonstrated by Rubin's vase figure (Fig. 76.4A). The borders are perceived either as the contours of a vase or as the contours of two faces. Each border is perceived as belonging to one or the other side, but rarely to both. In the case of a simple figure such as the white square of Figure 76.4B, the contrast borders are "of course" perceived as the contours of the square. They seem to belong to the enclosed light-textured region. The surrounding gray, which does not "own" these borders, is perceived as extending behind the square, forming the background. Perception of border ownership is a subtle phenomenon that remained long unnoticed until it was discovered by the Gestalt psychologists (Koffka, 1935; Rubin, 1921).

One could argue that even the display of Figure 76.4B is ambiguous. With some effort, the square can also be perceived as a window, and the border then appears as the edge of the frame. Completely unambiguous displays can be produced by means of random-dot stereograms, as shown in Figure 76.4C. When binocularly fused by crossing the eyes (see the legend), the top pair shows a tipped square floating in front of a background plane, while the bottom pair shows

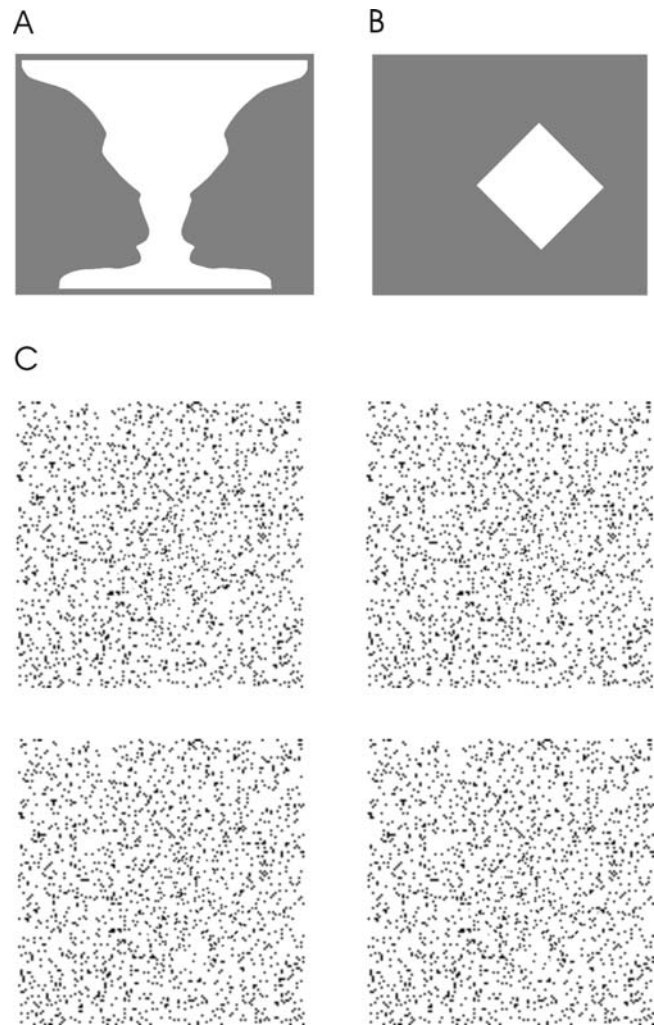


FIGURE 76.4. Perception of border ownership. *A*, Physiologist's version of Rubin's vase. The black-white borders are perceived either as contours of the vase or as contours of the faces. *B*, White square. The contrast borders are generally perceived as contours of the square. *C*, Stereograms. Left and right textured square fields can be fused, for example, by squinting (try crossing the lines of sight of the two eyes until three fields are perceived instead of two; the center field then shows the result of binocular fusion). On fusion with crossed eyes, the top pair shows a square figure, while the bottom pair shows a square window. In the former, the 3-D edges belong to the figure; in the latter, to the surround.

a square window through which a background plane can be seen. In the first case, the stereoscopic borders are perceived as the edges of the square; in the second case, as edges of the window frame. Perception of border ownership cannot be reversed in these stereograms.

In perceptual experiments we observe the tip of the iceberg. By recording signals in visual cortex, we should also be able to explore the depth of it. Contrast borders are represented in the visual cortex by signals of the orientation-selective cells discovered by Hubel and Wiesel. Do these signals also represent the relationship between border and

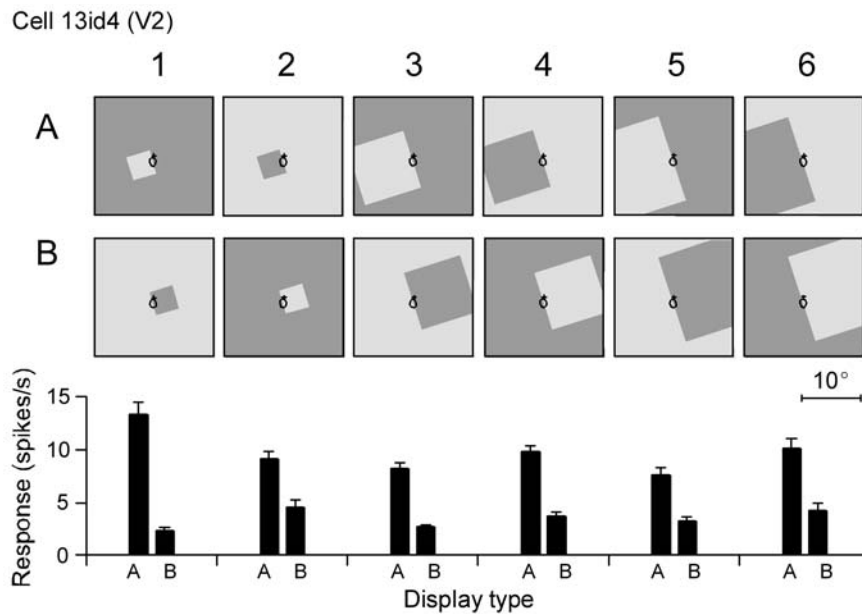


FIGURE 76.5. Selectivity for side of figure in a neuron of area V2. Edges of squares were tested so that the square was either on the left side (*A*) or on the right side (*B*) of the receptive field (ellipses show the minimum response field, cross marks the fixation point). Note that corresponding displays in *A* and *B* are identical over the

combined area of the two squares. Tests with square sizes of 4, 10, and 15 degrees are shown. The bar graph represents mean firing rates with the standard error. In every case, the neuron responds more strongly when the figure is on the left side, despite locally identical stimulation. (From Zhou et al., 2000, with permission.)

surface? This idea can be tested with a simple experiment (Zhou et al., 2000). Light-dark borders are placed in the receptive field of a neuron at optimal orientation (Fig. 76.5), and the same border is either presented as the right side of a light square (e.g., *A1*) or as the left side of a dark square (*B1*). *A2* and *B2* show a similar test with displays of reversed contrast, and columns 3 and 4 and 5 and 6 show the same kind of test with larger squares. The bar graph at the bottom represents the responses of a cell of V2. If we compare the responses to the corresponding displays in *A* and *B*, we see that in every case the neuron responds more strongly when the edge in the receptive field belonged to a square to the left than a square to the right, despite locally identical stimulation.

Note that the corresponding displays in rows *A* and *B* are identical over the entire region occupied by the two squares (as one can see by superimposing them). Thus, if a neuron responds differently, it must have information from outside this region. Therefore, by varying the size of the square, we can reveal the extent of image context integration. In this example, square sizes of 4, 10, and 15 degrees were tested, and in each case the responses differed, depending on the location of the figure. By contrast, the size of the minimum response field of this cell was only 0.4 degree, which is typical for V2 neurons of the foveal representation. Thus, although the cell can “see” only a small piece of contrast border through the aperture of its receptive field, its responses reveal processing of an area of at least 15 degrees in diameter.

What might be the mechanism of side-of-figure selectivity? For a single square figure on a uniform background, relatively simple algorithms would be able to discriminate figure and ground. The convexity of the figure area could be used, or simply the orientation of the L-junctions (corners) on either side of the receptive field, or the fact that the figure is a region of one color enclosed by a region of a different color (*surroundedness*). Any of these strategies would work for the isolated square. However, for other displays in which border ownership is also perceptually clear, mechanisms based on one simple strategy would fail to produce the right answer. We have used two other configurations besides squares to see how well the neural responses correlated with perception, a C-shaped figure shown in columns 3 and 4 of Figure 76.6, and a pair of overlapping squares as shown in columns 5 and 6 of the same figure. For the C shape, convexity is not valid, and the L-junctions next to the receptive field are reflected to the other side in comparison with the square, but surroundedness would still be a valid cue. For the overlapping squares, surroundedness is violated, while convexity and orientation of L-junctions are valid.

Figure 76.6 shows data from another neuron of V2. Columns 1 and 2 show the same test described in Figure 76.5. This cell was selective for contrast polarity, responding to light-dark edges as shown in *A1* and *B1* but hardly at all to dark-light edges as shown in *A2* and *B2* (the actual colors in the experiment were violet, shown here as light gray and

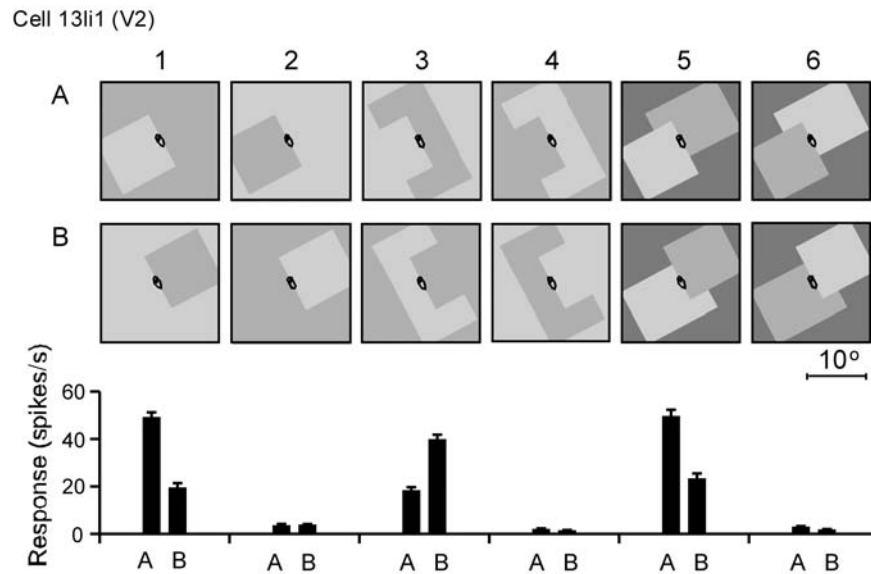


FIGURE 76.6. Example of a V2 neuron tested with squares, C-shaped figures, and overlapping figures. The neuron was color selective, with a preference for violet (depicted here as light gray). In the test with single squares (1 and 2) the neuron is selective for side of figure and local contrast polarity, responding best to the edge of a violet square located on the lower-left-hand side of the

receptive field (A1). With C-shaped figures (3 and 4), the neuron responds better to B3 than to A3, pointing to the lower left as the figure side, in agreement with perception. With overlapping figures (5 and 6), the neuron responds better to A5 than to B5, assigning the edge to the figure that is perceived as overlaying. (From Zhou et al., 2000, with permission.)

gray; the cell was strongly color selective). The cell was also side-of-figure selective, with a preference for figure location on the left side of the receptive field (display A1). Columns 3 and 4 show a test with a C-shaped figure. It can be seen that the cell “correctly” preferred the display in which the C-shaped figure was located on the left of the field (display B3), although the L-junctions next to the receptive field suggest a figure on the opposite side.

Columns 5 and 6 show a test with two overlapping figures. These displays are fairly symmetric about the receptive field as far as size of regions and distribution of colors are concerned, and neither of the figures is surrounded by uniform color. Nevertheless, the cell preferred display A5, in which the border in the receptive field belongs to the lower left figure. In this case, the T-junctions might account for the emergence of the occluding square as a figure (but convexity might also contribute because the overlapped region has a concavity, whereas the overlapping region does not). Thus, the responses of this cell are entirely consistent with the perception of border ownership. Not all cells tested showed this pattern, but the example is not unusual. About half of the cells with a side-of-figure effect for single squares exhibited the corresponding side preference for overlapping figures, while the others showed no significant response difference. Vice versa, the overlapping figure test predicted the single-figure result in about half of the cases. When tested with the concave side of C-shaped figures, about one-third of the cells with a side-of-figure effect for

single squares showed preference for the C on the same side; the others were indifferent. Cases in which the side preferences were “contradictory” (as judged by perception) were rare.

Cells with a response preference for one or the other side of the figure were found for any location and orientation of receptive field, and side-of-figure preference was invariant throughout the recording period. The responses of these cells seem to carry information not only about the location and orientation of the contours, but also about the side to which they belong. About half of the orientation-selective cells of areas V2 and V4 were found to be side-of-figure selective by the test of Figure 76.5. In 32% of the V2 cells, the ratio of the responses to preferred and nonpreferred sides was greater than 2, and ratios as high as 10 were not unusual. For comparison, by the same criterion, 29% of V1 cells are direction selective (De Valois et al., 1982) and 50% of upper-layer V1 cells are opponent color selective (from Fig. 76.9 of Leventhal et al., 1995). We found side-of-figure selectivity also in V1, but in a smaller fraction of the cells. These results show that the side-of-figure test probes an important aspect of the cortical representation.

Experiments as shown in Figures 76.5 and 76.6 suggest the existence of cortical mechanisms that use figure-ground cues to assign border ownership. In other words, the signals of orientation-selective cells in V2 might represent not only the location, orientation, and contrast of pieces of contour, but also the side of ownership.

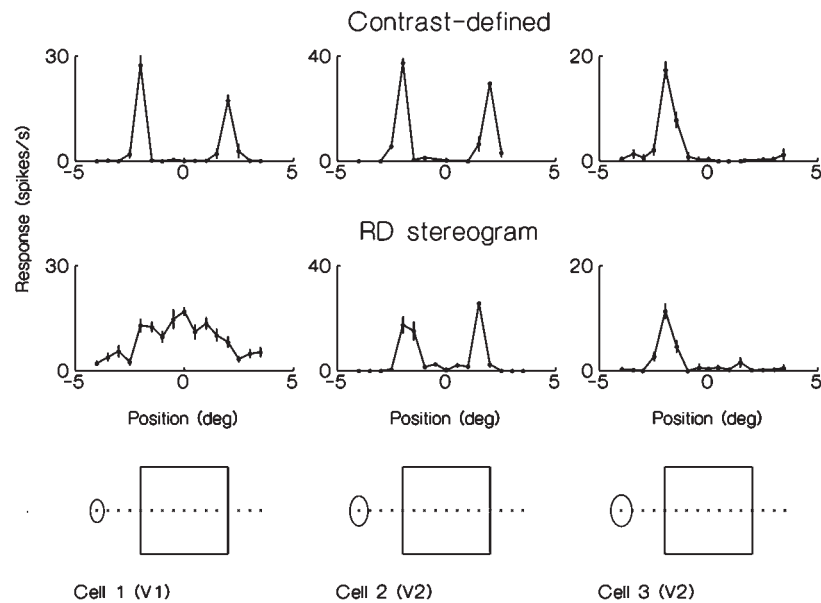


FIGURE 76.7. Stereoscopic edge selectivity. Responses of a neuron of V1 (*left*) and two neurons of V2. Contrast-defined squares are compared with squares portrayed in random-dot stereograms (Julesz, 1971). Each figure is presented at 16 different positions relative to the receptive field, as shown schematically at the bottom. Ellipses represent the minimum response fields; squares represent the test figures. Data points in the graphs correspond to the dotted

positions below. The plots show that cell 1 is edge selective for contrast-defined figures but responds all over the surface of the figure for random-dot stereograms, whereas cells 2 and 3 are edge selective for both types of figures. Most of these cells respond asymmetrically to the two sides, like cell 3. (From von der Heydt et al., 2000, with permission.)

Stereoscopic depth and monocular form cues

A crucial test of the hypothesis of border ownership coding is to examine the responses of orientation-selective cells to contrast-defined and disparity-defined figures. A contrast-defined square is generally perceived as a figure, with the borders assigned to the square (Fig. 76.4), while a corresponding region in a random-dot stereogram is perceived either as a figure, if its disparity is “near,” or as a window, if its disparity is “far,” relative to that of the surrounding region. In the stereogram, the nearer surface always owns the border. Thus, the random-dot stereogram is the “gold standard” of border ownership perception.

Binocular disparity is represented extensively in the monkey visual cortex (Cumming and DeAngelis, 2001; Poggio, 1995), and cells that signal edges in random-dot stereograms exist in area V2 (von der Heydt et al., 2000). These cells are orientation selective and respond to disparity-defined edges as well as to contrast borders (Fig. 76.7). Most of them are selective for the depth order of the stereoscopic edge, responding, for example, to a vertical edge if the front surface is on the right side, but not if the front surface is on the left side (cell 3 of Fig. 76.7).

If border ownership is represented in V2, then some of the cells there should combine monocular shape cues with binocular disparity information, and the side-of-figure pref-

erence should agree with the preferred depth order. That is, the preferred figure side should be the near side of the preferred step edge. This experiment is illustrated in Figure 76.8. With the random-dot stereogram, the cell is activated by the left edge of the figure and the right edge of the window, but not by the right edge of the square or the left edge of the window. From this we conclude that activation of this cell means border assignment to the surface on the right. Therefore, the responses to the contrast-defined square (*A* stronger than *B*) show that the cell “correctly” assigns the border to the square, so the square is interpreted as a figure. If the cell responded more strongly to *B* than to *A*, this would mean that it assigns the border to the frame and the square would be interpreted as a window.

Of 27 cells recorded in V2 that signaled depth order for random-dot edges and side of figure for contrast-defined figures ($p < .05$ in each case), 21 responded according to the “figure” interpretation and 6 according to the “window” interpretation (Qiu et al., 2001). This result is in agreement with the tendency in human perception to interpret compact, uniform regions in the image as objects.

We speculate that the minority of “window” responses might be not just aberrant signals, but the representation of a valid alternative parsing solution. Occasional dissident votes were also recorded when the side preferences for single squares were compared with those for overlapping figures.

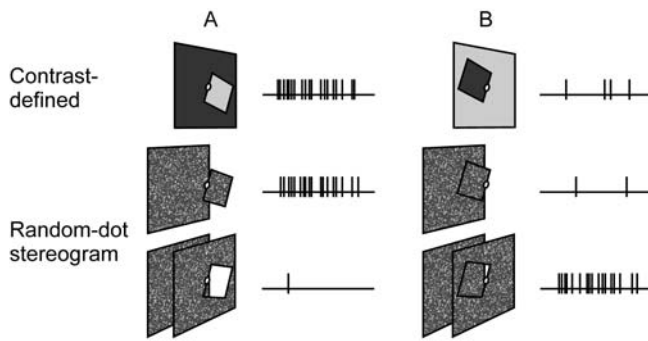


FIGURE 76.8. A critical test of the hypothesis of border ownership coding. Side-of-figure preference and stereo edge preference are assessed for each neuron. For contrast-defined squares, the “figure” interpretation is perceptually more compelling than the “window” interpretation. Therefore, if neurons code for border ownership, the preferred near side should be the preferred side of the figure. This fictitious neuron prefers the nearer surface to the right for the stereogram (regardless of whether a square or a window is displayed) and prefers the figure to the right (*A*) for the contrast-defined display, in accordance with the hypothesis.

Monocular form cues are usually ambiguous; a square can be perceived as a window, and even the display of two overlapping squares can alternatively be perceived as an L-shaped object adjacent to a square. It seems plausible that the visual cortex represents several alternative 3-D interpretations if the image is ambiguous.

LINKING CONTOUR AND SURFACE ATTRIBUTES The convergence of stereoscopic edge mechanisms and side-of-figure processing in single cells strongly supports the conclusion that side-of-figure selective cells code for border ownership. Figure 76.9 illustrates, for a pair of overlapping squares, how border ownership information is represented together with information about other contour features such as orientation, and color and luminance contrast. Each piece of contour is represented by two pools of neurons, one for each side of ownership. By analogy to the opponent coding of direction of motion, we assume that border ownership is encoded in the relative strength of activity in pairs of neurons of opposite side preference but otherwise identical receptive fields. This scheme of coding allows the linking of contour and surface attributes. Location and orientation of contour are coded by virtue of orientation selectivity and the small size of response fields. Color and brightness of object surface are coded by means of color and contrast polarity selectivity of cells with the corresponding border ownership pointer. Depth of surface is encoded similarly in the activity of stereo edge-selective cells.

A case for low-level mechanisms

An interesting point is the time course of the border ownership signals. Figure 76.10 compares the averaged neuronal

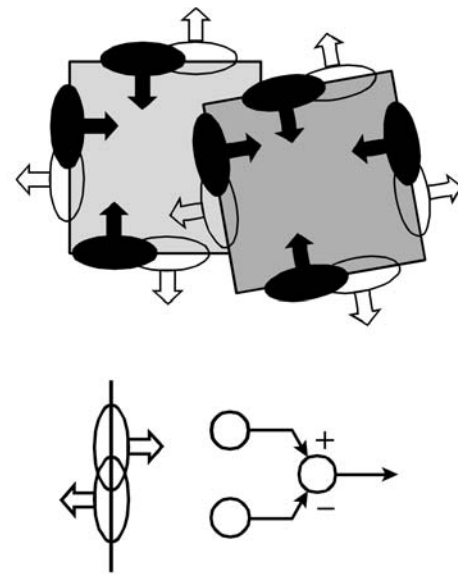


FIGURE 76.9. Schematic illustration of the cortical representation of a pair of overlapping squares. Ellipses indicate receptive fields. Each piece of contour is represented by two pools of orientation-selective neurons with opposite border ownership preference, as indicated by arrows. Filled symbols indicate the neurons whose activity would be enhanced for this stimulus. Border ownership is thought to be encoded in the relative activation of the two pools.

responses for a figure on the preferred side (thick line) and a figure on the nonpreferred side (thin line). Data from areas V1, V2, and V4 are shown. It can be seen that a differentiation of responses occurs soon after stimulus onset and well before the responses peak. Note also that the response difference in V2 neurons remains constant during the remainder of stimulus presentation. If the effect of side of figure were due to feedback from areas of much higher order, we would probably see a delay. The immediate differentiation suggests that the mechanisms reside in these lower-order visual areas. Also, Bakin et al. (2000), who studied neural correlates of contour salience, illusory contours, and depth capture in V1 and V2, found no increase of latency for these image-parsing processes. Lee and Nguyen (2001) found illusory contour responses in V2 with latencies as low as 50 msec, and differentiation between modal and amodal completion by 70 msec. All these results argue for fast processes, implicating highly parallel mechanisms in the lower-order cortical areas.

Because of the ambiguity of monocular form cues and the ill-posed nature of the vision problem in general, image segmentation is usually regarded as a task that cannot be solved by low-level computations but that requires the use of stored representations in memory. Why, then, would the visual system use low-level mechanisms at all to resolve figure-ground relationships? Since memory will eventually be used to recognize objects, one may wonder what is the advantage of low-level mechanisms.

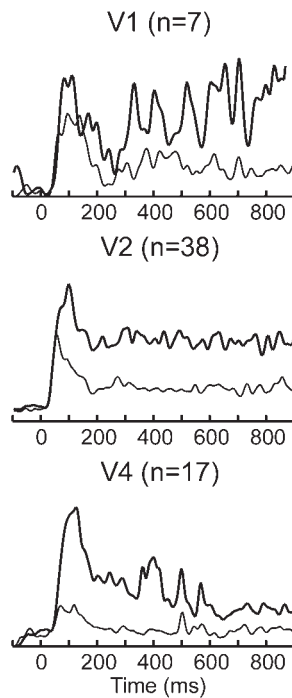


FIGURE 76.10. The time course of the border ownership signal. The figure shows the averaged normalized responses of neurons in three cortical areas. Squares of 4 or 6 degree size were presented, as in Figure 76.5. Zero on the time scale refers to the onset of the display. Thick and thin lines represent responses to preferred and nonpreferred sides, averaged over both contrast polarities. The delay between onset of response and differentiation of side of figure was less than 25 msec. (From Zhou et al., 2000, with permission.)

In the case of a single border, as in Figure 76.6, columns 5 and 6, assigning figure-ground direction reduces the number of shapes that have to be compared with memory from two to one (by eliminating the inverted L shape created by occlusion), which may not appear as a great saving. However, it is important to recognize that the problem is generally more complex. As an example, consider the display of Figure 76.11A, which might be perceived as two elongated objects occluding one another or, in keeping with the macaque perspective, as a branch in front of a tree stem. Contrast borders divide the display into seven regions of different shapes. Since the contrast borders may be occluding contours, most of these shapes are meaningless because they are surfaces of partly occluded objects, that is, regions that do not own the borders. There are 10 segments of borders (not counting the frame), each of which could belong to one of the adjacent regions, creating a total of $2^{10} = 1024$ possible depth configurations. Each depth configuration defines a different set of shapes. To help the reader to see this, I have illustrated two of the possible 3-D decompositions in Figure 76.11B. Most of these configurations are generally not perceived. The point is that there is a large number of shapes

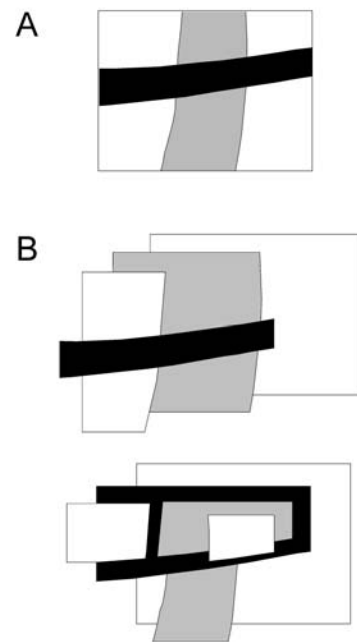


FIGURE 76.11. The interpretation of the overlay structure of images is highly ambiguous. *A*, Example of a display that would generally be perceived as two elongated objects occluding one another. *B*, Two of about 1000 possible interpretations of *A*.

that could give rise to an image like that of Figure 76.11A. All of these would have to be searched in memory if the system were not able to assign the borders beforehand. If borders are assigned, only the two bars in front of a white background have to be processed further. Thus, low-level border assignment reduces the load on the memory matching process enormously in this example; this is probably similar in images of natural scenes, which are generally complex.

Note that the advantage of low-level processes does not depend on their ability to find a unique solution for each parsing problem. On the contrary, the results on border ownership coding sketched above indicate that the visual cortex can simultaneously represent alternative solutions. A representation like that of area V2, which contains on the order of 100 million cells, has an enormous capacity. V1 and V2 can represent more than one orientation per image point (see, for example, simultaneous representation of two superimposed gratings in V1; Movshon et al., 1985). Therefore, it is plausible to hypothesize that the visual cortex can represent several alternative parsing results from which cognitive routines can select. Compared to the huge number of possible interpretations of an image, this would still be a very specific representation.

There are theoretical and empirical arguments for this hypothesis. On the theoretical side, it was pointed out that it would be a disadvantage if the system locked in on one solution, given the ambiguous information available at the

precognitive level (principle of least commitment; Marr, 1982). Experimental studies of binocular rivalry show that the duration of dominance of the stimulus in one eye depends on the suppressed stimulus in the other eye (Levelt, 1968). Accordingly, the unperceived stimulus in rivalry is represented in the neural activity in visual cortex (Leopold and Logothetis, 1996; Logothetis and Schall, 1989).

Conclusions

The studies reviewed above demonstrate a wealth of processes of visual organization in the cortex. While it was previously thought that contour mechanisms serve to make contrast borders explicit and “fill in the gaps,” recent findings indicate that cortical processing goes beyond representation and completion of contrast borders. The goal of this processing apparently is to make the 3-D structure of a scene explicit—specifically, to represent occluding contours and how they belong to surfaces. Assigning contours to surfaces is perhaps the most important first step on the way from image to object representation, because it specifies the surfaces in the scene and their ordering in depth. Three-dimensional surface organization influences perceptual grouping of elemental features in many ways and modulates responses of V1 and V2 neurons accordingly (Bakin et al., 2000; Sugita, 1999; Zipser et al., 1996). Changes in 3-D surface organization that alter perception of border ownership can also influence the perceived direction of motion, and this influence can be traced in the motion signals of area MT (Duncan et al., 2000).

The most surprising aspect of the new findings is that neural signals at early cortical levels, despite the small size of the conventional receptive fields of the cells, reflect information about the global image context. Assigning border ownership generally requires the application of algorithms that involve image regions of at least the size of the projection of the object to be processed. The same is true for labeling textured regions as figure or ground (Lamme, 1995; Lee et al., 1998; Zipser et al., 1996). These algorithms might implement Gestalt rules such as Prägnanz of form, contour closure, and common fate, as well as the rules that relate patterns of junctions to 3-D shape and layout of objects (Adelson, 1993; Nakayama et al., 1995; Waltz, 1975).

Thus, figure-ground segregation and assignment of border ownership are evidence for image parsing mechanisms and suggest networks of global scope. The organization of visual representations in terms of 3-D surfaces may be a first stage in the construction of object representations (Marr, 1982), or it may provide a structure for specific processing of selected detail information which is required by most visual tasks, when attention is directed to a specific object in a scene, or to a specific feature of an object (He and Nakayama, 1992; He and Ooi, 2000; Nakayama et al.,

1995; see also Egeth and Yantis, 1997). Perhaps the same networks that achieve image parsing serve also for the selection of information.

The exact nature of those image parsing mechanisms still needs to be clarified. What kinds of cues are used, and how are they combined? What is the output of this stage? Probably the output is not a globally coherent representation of 3-D relationships (because perception is not globally coherent; see the Penrose triangle and the work of the artist M. C. Escher), but rather a patchwork of coherent domains. How large are these domains? Does the parsing stage provide a unique solution for a given image (or domain) or multiple solutions? The mechanisms might either home in on the most likely interpretation of the given optical information or pass on several choices to the next stage. The results sketched out above on the combination of stereoscopic depth and monocular form cues suggest that V2 can represent multiple solutions in parallel, leaving the final decision to a later stage.

It has often been pointed out that vision (and any perception) is highly selective. An enormous amount of information streams in through the eyes, but little of it is used. A common demonstration is the “two pictures with 10 differences.” Viewers generally have to look back and forth many times between the two pictures before they find the differences. This shows that the amount of information the system can store and compare between two looks is only a small fraction of the total, even in those relatively simple drawings. This phenomenon of *change blindness*, which has been documented by formal experiments (Rensink et al., 1997; see also Chapter 102), has led to the conclusion that the visual system processes only the selected information and does not represent much more than the image. Whatever information is needed at a given moment, it is thought, can be retrieved from the image representation. However, psychological tests can only reveal processing that leads either to a motor response or to a retrievable representation in memory. As I have argued, this is only the tip of the iceberg. The recordings from the visual cortex reveal sophisticated processing of gigantic amounts of information. In the experiments on border ownership coding, for example, the animal was attending to a visual task at the fixation spot and thereby—probably—trying to ignore all other visual stimuli as much as possible, but border ownership processing was nevertheless obvious in half of the signals recorded in V2. Thus, it seems that many locations of the retinal image are processed automatically and in parallel all the time. Whenever our eyes saccade to a new point of fixation, area V2 recomputes the figure-ground relationships, parsing a new image into object-like chunks of information. All this occurs three or four times per second on average. Without this extensive preprocessing, the system would not be able to select information as efficiently as it does. The relatively

large size of the early visual areas V1, V2, and V4 is certainly related to the computational difficulty of the image parsing task, which still defies the power of supercomputers. The imperceptible function of these areas makes vision appear effortless.

REFERENCES

- Adelson, E. H., 1993. Perceptual organization and the judgment of brightness, *Science*, 262:2042–2044.
- Attneave, F., 1954. Some informational aspects of visual perception, *Psychol. Rev.*, 61:183–193.
- Bakin, J. S., K. Nakayama, and C. D. Gilbert, 2000. Visual responses in monkey areas V1 and V2 to three-dimensional surface configurations, *J. Neurosci.*, 20:8188–8198.
- Barlow, H. B., 1961. Possible principles underlying the transformations of sensory messages, in *Sensory Communication* (W. A. Rosenblith ed.), Cambridge, MA: MIT Press, pp. 217–257.
- Baumann, R., R. van der Zwan, and E. Peterhans, 1997. Figure-ground segregation at contours: a neural mechanism in the visual cortex of the alert monkey, *Eur. J. Neurosci.*, 9:1290–1303.
- Bravo, M., R. Blake, and S. Morrison, 1988. Cats see subjective contours, *Vis. Res.*, 28:861–865.
- Burkhalter, A., and D. C. Van Essen, 1986. Processing of color, form and disparity information in visual areas VP and V2 of ventral extrastriate cortex in the macaque monkey, *J. Neurosci.*, 6:2327–2351.
- Coren, S., 1972. Subjective contours and apparent depth, *Psychol. Rev.*, 79:359–367.
- Cumming, B. G., and G. C. DeAngelis, 2001. The physiology of stereopsis, *Annu. Rev. Neurosci.*, 24:203–238.
- De Valois, R. L., E. W. Yund, and N. Hepler, 1982. The orientation and direction selectivity of cells in macaque visual cortex, *Vis. Res.*, 22:531–544.
- De Weerd, P., E. Vandenbussche, B. Debruyn, and G. A. Orban, 1990. Illusory contour orientation discrimination in the cat, *Behav. Brain Res.*, 39:1–17.
- Desimone, R., S. J. Schein, J. Moran, and L. G. Ungerleider, 1985. Contour, color and shape analysis beyond the striate cortex, *Vis. Res.*, 25:441–452.
- Duncan, R. O., T. D. Albright, and G. R. Stoner, 2000. Occlusion and the interpretation of visual motion: perceptual and neuronal effects of context, *J. Neurosci.*, 20:5885–5897.
- Egeth, H. E., and S. Yantis, 1997. Visual attention: control, representation, and time course, *Annu. Rev. Psychol.*, 48:269–297.
- Felleman, D. J., and D. C. Van Essen, 1991. Distributed hierarchical processing in the primate cerebral cortex, *Cereb. Cortex.*, 1:1–47.
- Finkel, L. H., and P. Sajda, 1992. Object discrimination based on depth-from-occlusion, *Neural Comput.*, 4:901–921.
- Grosz, D. H., R. M. Shapley, and M. J. Hawken, 1993. Macaque-V1 neurons can signal illusory contours, *Nature*, 365:550–552.
- Grossberg, S., and E. Mingolla, 1985. Neural dynamics of form perception: boundary completion, illusory figures, and neon color spreading, *Psychol. Rev.*, 92:173–211.
- He, Z. J., and K. Nakayama, 1992. Surfaces versus features in visual search, *Nature*, 359:231–233.
- He, Z. J., and T. L. Ooi, 2000. Perceiving binocular depth with reference to a common surface, *Perception*, 29:1313–1334.
- Heitger, F., R. von der Heydt, E. Peterhans, L. Rosenthaler, and O. Kübler, 1998. Simulation of neural contour mechanisms: representing anomalous contours, *Image Vis. Comput.*, 16:409–423.
- Helmholtz, H. V., 1866. *Handbuch der physiologischen Optik*, Hamburg: Voss.
- Julesz, B., 1971. *Foundations of Cyclopean Perception*, Chicago: University of Chicago Press.
- Kanizsa, G., 1979. *Organization in Vision. Essays on Gestalt Perception*, New York: Praeger.
- Koffka, K., 1935. *Principles of Gestalt Psychology*, New York: Harcourt, Brace and World.
- Lamme, V. A. F., 1995. The neurophysiology of figure-ground segregation in primary visual cortex, *J. Neurosci.*, 15:1605–1615.
- Lee, T. S., D. Mumford, R. Romero, and V. A. F. Lamme, 1998. The role of the primary visual cortex in higher level vision, *Vis. Res.*, 38:2429–2454.
- Lee, T. S., and M. Nguyen, 2001. Dynamics of subjective contour formation in the early visual cortex, *Proc. Natl. Acad. Sci. USA*, 98:1907–1911.
- Leopold, D. A., and N. K. Logothetis, 1996. Activity changes in early visual cortex reflect monkeys' percepts during binocular rivalry, *Nature*, 379:549–553.
- Levelt, W. J. M., 1968. *On Binocular Rivalry*, The Hague: Mouton.
- Leventhal, A. G., K. G. Thompson, D. Liu, Y. Zhou, and S. J. Ault, 1995. Concomitant sensitivity to orientation, direction, and color of cells in layers 2, 3, and 4 of monkey striate cortex, *J. Neurosci.*, 15:1808–1818.
- Logothetis, N. K., and J. D. Schall, 1989. Neuronal correlates of subjective visual perception, *Science*, 245:761–763.
- Marr, D., 1982. *Vision. A Computational Investigation into the Human Representation and Processing of Visual Information*, San Francisco: Freeman.
- Movshon, J. A., E. H. Adelson, M. S., Gizzi, and W. T. Newsome, 1985. The analysis of moving patterns, *Exp. Brain. Res. Suppl.*, 11:117–151.
- Nakayama, K., Z. J. He, and S. Shimojo, 1995. Visual surface representation: a critical link between lower-level and higher-level vision, in *Invitation to Cognitive Science* (S. M. Kosslyn and D. N. Osherson, eds.), Cambridge, MA: MIT Press, pp. 1–70.
- Nieder, A., 2002. Seeing more than meets the eye: processing of illusory contours in animals, *J. Comp. Physiol. [A]*, 188:249–260.
- Nieder, A., and H. Wagner, 1999. Perception and neuronal coding of subjective contours in the owl, *Nat. Neurosci.*, 2:660–663.
- Paradiso, M. A., S. Shimojo, and K. Nakayama, 1989. Subjective contours, tilt aftereffects, and visual cortical organization, *Vis. Res.*, 29:1205–1213.
- Peterhans, E., and R. von der Heydt, 1989. Mechanisms of contour perception in monkey visual cortex. II. Contours bridging gaps, *J. Neurosci.*, 9:1749–1763.
- Peterhans, E., R. von der Heydt, and G. Baumgartner, 1986. Neuronal responses to illusory contour stimuli reveal stages of visual cortical processing, in *Visual Neuroscience* (J. D. Pettigrew, K. J. Sanderson, and W. R. Levick, eds.), Cambridge: Cambridge University Press, pp. 343–351.
- Poggio, G. F., 1995. Mechanisms of stereopsis in monkey visual cortex, *Cereb. Cortex*, 3:193–204.
- Poggio, T., and C. Koch, 1985. Ill-posed problems in early vision: from computational theory to analogue networks, *Proc. R. Soc. Lond. B*, 226:303–323.
- Qiu, F. T., T. J. Macuda, and R. von der Heydt, 2003. Neural correlates for Gestalt rules in figure-ground organization. *In press*.

- Ramsden, B. M., C. P. Hung, and A. W. Roe, 2001. Real and illusory contour processing in area V1 of the primate: a cortical balancing act, *Cereb. Cortex*, 11:648–665.
- Redies, C., J. M. Crook, and O. D. Creutzfeldt, 1986. Neuronal responses to borders with and without luminance gradients in cat visual cortex and dorsal lateral geniculate nucleus, *Exp. Brain Res.*, 61:469–481.
- Rensink, R. A., J. K. O'Regan, and J. J. Clark, 1997. To see or not to see: the need for attention to perceive changes in scenes, *Psychol. Sci.*, 8:368–373.
- Ringach, D. L., and R. Shapley, 1996. Spatial and temporal properties of illusory contours and amodal boundary completion, *Vis. Res.*, 36:3037–3050.
- Rubin, E., 1921. *Visuell wahrgenommene Figuren*, Copenhagen: Gyldendal.
- Schein, S. J., and R. Desimone, 1990. Spectral properties of V4 neurons in the macaque, *J. Neurosci.*, 10:3369–3389.
- Sheth, B. R., J. Sharma, S. C. Rao, and M. Sur, 1996. Orientation maps of subjective contours in visual cortex, *Science*, 274: 2110–2115.
- Soriano, M., L. Spillmann, and M. Bach, 1996. The abutting grating illusion, *Vis. Res.*, 36:109–116.
- Srinivasan, M., M. Lehrer, and R. Wehner, 1987. Bees perceive illusory contours induced by movement, *Vis. Res.*, 27:1285–1290.
- Sugita, Y., 1999. Grapings of image fragments in primary visual cortex, *Nature*, 401:269–272.
- Ullman, S., 1996. *High-level Vision*, Cambridge, MA: MIT Press.
- von der Heydt, R., and E. Peterhans, 1989. Mechanisms of contour perception in monkey visual cortex. I. Lines of pattern discontinuity, *J. Neurosci.*, 9:1731–1748.
- von der Heydt, R., E. Peterhans, and G. Baumgartner, 1984. Illusory contours and cortical neuron responses, *Science*, 224: 1260–1262.
- von der Heydt, R., H. Zhou, and H. S. Friedman, 2000. Representation of stereoscopic edges in monkey visual cortex, *Vis. Res.*, 40:1955–1967.
- Waltz, D. I., 1975. Understanding line drawings of scenes with shadows, in *The Psychology of Computer Vision* (P. H. Winston ed.), New York: McGraw-Hill, pp. 19–91.
- Westheimer, G., and W. Li, 1996. Classifying illusory contours by means of orientation discrimination, *J. Neurophysiol.*, 75:523–528.
- Zeki, S. M., 1978. Uniformity and diversity of structure and function in rhesus monkey prestriate visual cortex, *J. Physiol. (Lond.)*, 277:273–290.
- Zhou, H., H. S. Friedman, and R. von der Heydt, 2000. Coding of border ownership in monkey visual cortex, *J. Neurosci.*, 20: 6594–6611.
- Zipser, K., V. A. F. Lamme, and P. H. Schiller, 1996. Contextual modulation in primary visual cortex, *J. Neurosci.*, 16:7376–7389.

77 Inferotemporal Response Properties

KEIJI TANAKA

AREA TE OF THE INFEROTEMPORAL cortex represents the final purely visual stage of the occipitotemporal (or ventral visual) pathway (Fig. 77.1). The occipitotemporal pathway starts at the primary visual cortex (V1) and leads to TE after relays at V2, V4, and TEO. Although skipping projections also exist, such as those from V2 to TEO and those from V4 to the posterior part of TE, the step-by-step projections are more numerous. TE, in turn, projects to various polymodal brain sites, including the perirhinal cortex, prefrontal cortex, amygdala, and striatum of the basal ganglia. The projections to these targets are more numerous from TE, particularly from the anterior part of TE, than from areas at earlier stages. Therefore, there is a sequential cortical pathway from V1 to TE, and output from the pathway originates mainly from TE.

In monkeys, bilateral TE ablation or their complete deaf-ferentation by bilateral ablation of more than one stage in the occipitotemporal pathway resulted in severe and selective deficits in tasks that required visual discrimination or recognition of objects (Dean, 1976; Gross, 1973; Yaginuma et al., 1993). Thus, the occipitotemporal pathway is essential for object vision, and because TE is the final common stage of the pathway, it is expected that the mechanisms underlying flexible properties of primate object vision can be found in properties of neuronal responses in TE. In this chapter, I will discuss the properties of neuronal responses and the functional architecture of TE, the effects of learning in the adult on the response properties and functional architecture, and their relationship to object vision.

Moderately complex features

There is a principal difficulty in determining the stimulus selectivity of individual cells in TE. There is a great variety of object features in the world, and it remains to be determined how the brain scales down this variety. There have been studies that used mathematically perfect sets of shapes (Gallant et al., 1993, 1996; Richmond et al., 1987; Schwartz et al., 1983). However, the generality of these sets would hold only if the system were linear, which is hardly expected in higher visual centers.

We have used an empirical reduction method that involves the real-time modification of stimulus images on an image-processing computer system (Fujita et al., 1992; Ito et al., 1994, 1995; Kobatake and Tanaka, 1994; Tanaka et al.,

1991; Wang et al., 1998). After spike activities from a single cell were isolated, many three-dimensional animal and plant models were first presented manually to find the effective stimuli. Different aspects of the objects were presented in different orientations. Second, images of several most effective stimuli were taken with a video camera and displayed on a TV monitor by a computer to determine the stimulus that evoked the maximal response. Third, the image of the most effective stimulus was simplified step by step in the direction in which the maximal activation was maintained. Finally, the minimal requirement for maximal activation was determined as the critical feature for the cell, as exemplified in Figure 77.2. Even starting at the same object image, the effective direction of simplification varied from cell to cell. Thus, images used in the simplification procedure were made in real time while the activity of the cell was recorded. The procedure is time-consuming, and it usually takes 2 to 4 hours to determine the critical feature for one TE cell. The magnitude of responses often increased as the complexity of an image was reduced. This may be due to the adjustment of size, orientation, and shape, as well as the removal of other features, which may suppress the activation by the critical feature (Missal et al., 1997; Sato, 1989, 1995; Tsunoda et al., 2001).

Additional examples of the reduction of complexity of images for 12 other TE cells are shown in Figure 77.3. The pictures to the left of the arrows are the original images of the most effective object stimuli, and those to the right are the critical features determined after the reduction process. Some of the critical features are moderately complex shapes, while others are combinations of such shapes with color or texture. After determining the critical features for hundreds of cells in TE, we concluded that most cells in TE required moderately complex features for their maximal activation. The critical features for TE cells were more complex than just the orientation, size, color, or simple textures, which are known to be extracted and represented by cells in V1, but at the same time were not sufficiently complex to represent the image of a natural object through the activity of single cells. The combined activation of multiple cells, which represent different features contained in the object image, is necessary.

Although the reduction method appears to be the best among currently available methods of determining the stimulus selectivity of TE cells, it has limitations. The initial

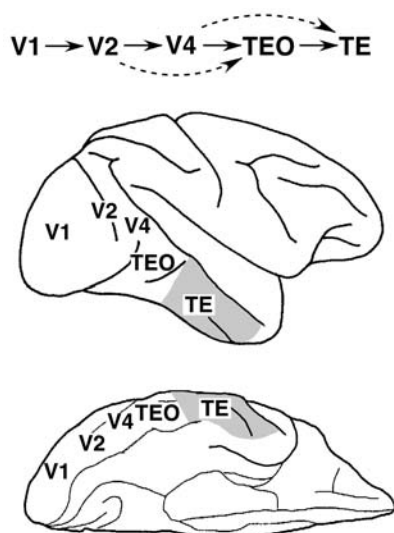


FIGURE 77.1. Occipitotemporal pathway (ventral visual pathway). Lateral view (*top*) and bottom view (*bottom*) of the monkey brain. The shadow indicates the extent of TE.

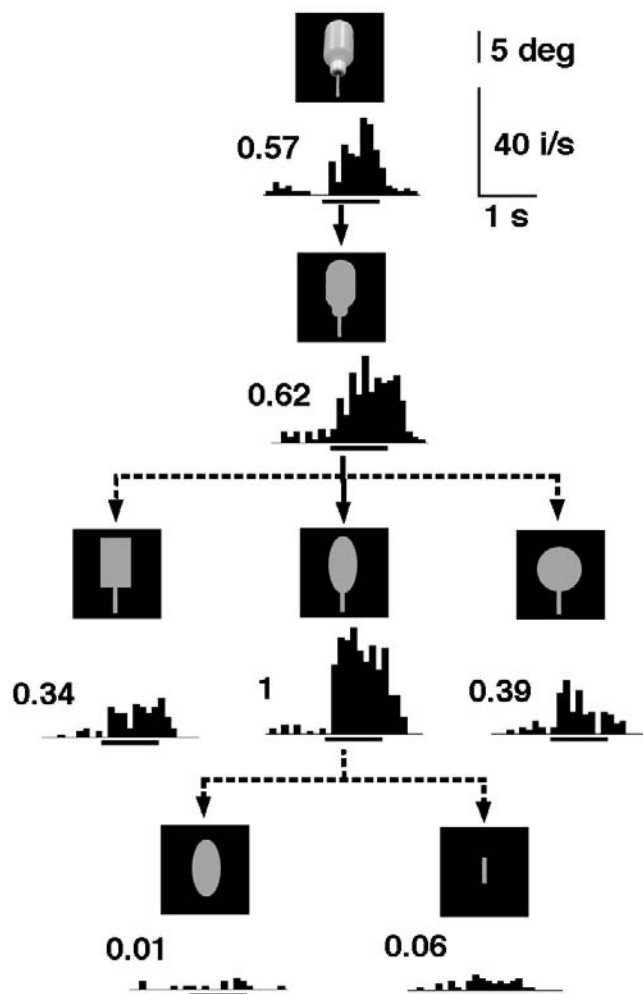


FIGURE 77.2. Example of reductive determination of optimal features for a cell recorded in TE.

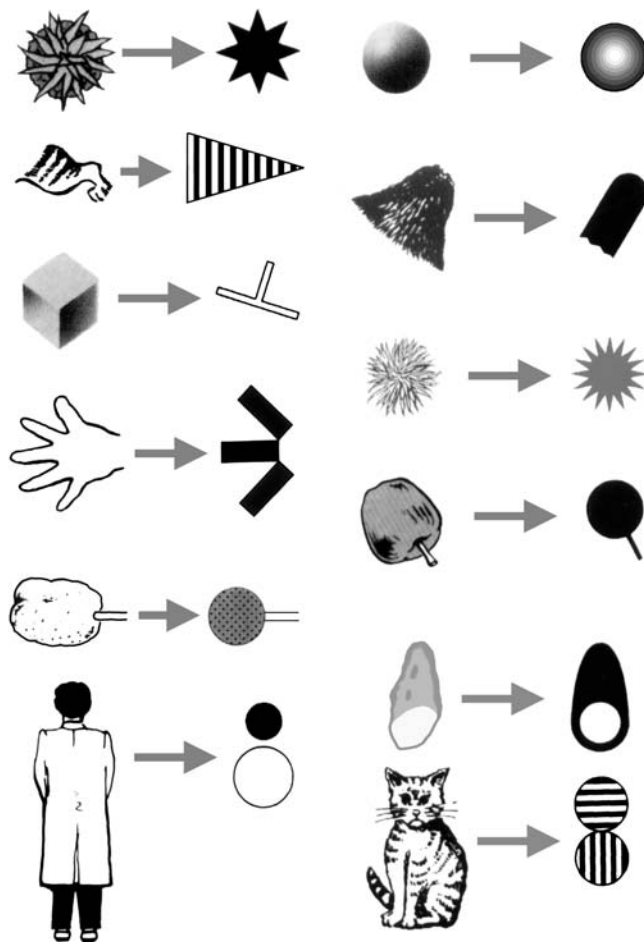


FIGURE 77.3. Further examples of reductive determination of optimal features for 12 other TE cells. The images to the left of the arrows represent the original images of the most effective object stimulus, and those to the right of the arrows represent the critical features determined by the reduction process. (See color plate 54).

survey of effective stimuli cannot cover the entire variety of objects existing in the world. We may miss some very effective features. In addition, the tested methods of reducing the complexity of effective object images are limited by the time of continuous recording from a single cell and also by the imagination of the experimenter. Because of these limitations, the objectiveness of the determined optimal features has sometimes been doubted. It is desirable that the reduction procedure be automated. Pasupathy and Connor (2001) have developed a method of presenting a large number of shapes made by combining several arcs of different curvatures. They have shown the usefulness of this method in studying the selectivity of V4 cells, but it may not be useful for TE cells, which respond to more complicated shapes than do V4 cells. Keyser et al. (2001) developed a method of analyzing responses to more than 1000 stimulus images in a fixation task. The stimulus images were presented individually for a short time (e.g., 100 msec) without an interstimulus

interval. The following stimulus presented may inhibit the response to the previous stimulus, but because the order of stimulus presentation is randomized and because TE cells tend to respond to a small part of the stimuli, there are no inhibitory interactions in the majority of repetitions. These two methods may be combined to explore systematically a large feature space of complex shapes—sufficiently complex for the activation of most TE cells.

Faces and other extensively learned objects

Although the critical features for the activation of TE cells are only moderately complex in general, there are cells that respond to faces and critically require nearly all the essential features of the face. Such cells were originally found deep in the superior temporal sulcus (Bruce et al., 1981; Perrett et al., 1982), but they were also found in TE (Baylis et al., 1987). Thus, there is more convergence of information to single cells for representations of faces than for those of nonface objects. This difference may be due to the fact that discrimination of faces from other objects is not the final goal, and further processing of facial images is needed to discriminate among individuals and expressions, while distinguishing a nonface object from other objects is close to the final goal. Optical imaging experiments showed that there is a cluster of such cells responding selectively to faces in a small region of TE (Wang et al., 1996, 1998).

There are suggestions that responses to whole objects will develop in TE if the subject is extensively trained in fine discrimination of similar objects. Logothetis et al. (1995) trained adult monkeys to recognize wire-frame objects against many other similar wire-frame objects, and recorded from cells in TE of the monkeys during the same task. About 20% of cells responded to wire-frame objects more strongly than to any other tested objects. Some of them responded to some parts of the objects as well as to the entire image of the objects, while others did not respond to parts of the objects (Logothetis, 1998). Based on these results, Logothetis (1998) proposed that some TE cells respond to whole objects with which the subjects have conducted fine discriminations, while a majority of TE cells respond to features present in images of multiple different objects. However, this remains to be studied further, because the examination of selectivity (described in Logothetis, 1998) for object parts was rather preliminary.

There are rare cases of brain-damaged patients whose capability of making fine discrimination among faces is specifically deteriorated (*prosopagnosia*). Their deficiency is specific in that they can normally discriminate a nonface object from other objects. They can also distinguish faces from other objects. Brain imaging studies showed that a region in the fusiform gyrus of normal human subjects is

more activated by faces than by other objects (*fusiform face region*) (Allison et al., 1994; Kanwisher et al., 1997; Puce et al., 1995). The damage of the prosopagnosic patients extends over the ventral surface of the occipitotemporal lobes. It includes the fusiform face region, although the damaged region is usually much larger. The fusiform face region may correspond to the small region of the monkey TE in which cells responding selectively to faces cluster. However, there is no consensus about the degree of stimulus selectivity of the fusiform face region (Haxby et al., 2001; Ishai et al., 1999; Kanwisher, 2000; Tarr and Gauthier, 2000), and its extent, as determined in previous studies, was larger (>5 mm) than the monkey face region (~1.5 mm). The nature of the fusiform face region should be studied further before we determine its relation with cells in the monkey TE responding selectively to faces.

Depth structure of object surfaces

Some of the critical features for the activation of TE cells include the gradient of luminosity (e.g., top right in Fig. 77.2). The gradient of luminosity often provides depth structure of object surfaces with an assumption of the direction of illumination. In this sense, the features represented by TE cells are not necessarily purely two-dimensional (2D). These features may be described in 2D space but reflect depth structures. Moreover, recent studies have found that some TE cells respond selectively to the horizontal disparity in addition to the 2D shape of stimuli.

The horizontal disparity between images projected to the left and right eyes is a strong cue for perception of depth. Although it was once assumed that the selectivity for disparity is more predominant in the occipitoparietal (or dorsal visual) pathway, which is responsible for visuomotor control or spatial vision, than in the occipitotemporal (or ventral visual) pathway, recent studies have shown that many cells in TE are selective to the disparity of stimuli, as well as to their 2D shapes in the frontoparallel plane.

Uka et al. (2000) recorded activity of TE cells in monkeys performing a fixation task and examined their responses to 2D shape stimuli presented at different depths. The depth was defined relative to that of the fixation point, as in other such experiments. They used 11 2D shapes, and cells that responded to at least one of them at zero disparity were examined for disparity selectivity. Responses of more than one-half (63%) of the cells showed statistically significant dependence on depth. Most of the disparity-selective cells were either near or far neurons according to the classification of Poggio and Fisher (1977). This is in contrast to the primary visual cortex and area MT, in which the tuned excitatory cells constitute a large part (2/3 in V1 and 2/5 in MT) of the disparity-selective cells (Maunsell and Van Essen, 1983; Poggio and Fisher, 1977).

The stimuli used by Uka et al. (2000) were flat in the depth direction, that is, there were no depth structures within their contours. Many objects in nature have surfaces tilted or curved in the depth direction, and such a depth gradient of the surface is an important feature of the object image. Janssen et al. (1999, 2000a, 2000b) used a stimulus set composed of stimuli having several different depth profiles in combination with several different 2D shapes. About one-half of the cells recorded from the ventral bank of the anterior part of the superior temporal sulcus exhibited selectivity for depth profile. Some of them responded to a linear gradient of depth, some to a combination of opposite linear gradients (or wedge profile), and others to a smooth concave or a convex depth curvature. These cells were selective for both 2D shape and depth profile. The selectivity for the depth profile was not explained by the selectivity for the depth position of a particular part of the stimulus, because the stimuli of the opposite depth profile did not activate the cells at any depth. The proportion of such cells was much lower in the ventrolateral surface (i.e., area TE) (about 10%) than in the ventral bank of the superior temporal sulcus.

Based on the cytoarchitectural criteria, the ventral bank of the anterior part of the superior temporal sulcus (TEa and TE_m) was distinguished from the ventrolateral surface (TE). However, H. Tanaka and I. Fujita (personal communication) found that cells in the ventral bank were as selective for complex 2D shapes as were cells in TE. Moreover, the cells in the ventral bank were much more sensitive to the direction of the disparity gradient or curvature (e.g., concave versus convex), than to the quantitative values of curvature or gradient (Janssen et al., 2000b). Therefore, responses of cells in the ventral bank of the superior temporal sulcus do not represent a full reconstruction of the three-dimensional (3D) structure of the objects. Rather, it may be the case that the representation in this area is still mainly 2D, and the qualitative information of disparity gradient or curvature simply renders the 2D representation richer.

INVARIANCE OF RESPONSES Our ability to recognize objects is retained even in the event of many different kinds of translation of the objects in space. These invariances can, in part, be explained by invariant properties of single-cell responses in TE. Using a set of shape stimuli composed of individually determined critical features and several other shape stimuli obtained by modifying the critical features, we have observed that the selectivity for shape is preserved over the receptive fields (Ito et al., 1995), which usually range from 10 to 30 degrees in a one-dimensional (1D) size. However, the maximum response is usually obtained around the geometrical center of the receptive field, and the magnitude of response decreases toward the edges of the receptive field (Ito et al., 1995; Op de Beeck and Vogels, 2000). The center of receptive fields is scattered around the fovea (Kobatake

and Tanaka, 1994; Op de Beeck and Vogels, 2000). Therefore, responses of individual TE cells carry coarse information on the position of stimuli as well as detailed information on their shape, color, and texture.

The effects of changes in stimulus size varied among cells (Ito et al., 1995; Tanaka et al., 1991). Twenty-one percent of the TE cells tested responded to a size range of more than 4 octaves of the critical features with more than 50% maximum responses, whereas 43% responded to a size range of less than 2 octaves. TE cells with considerable invariance for the location and size of stimuli were also found by Lueschow et al. (1994) and Logothetis et al. (1995). The tuned cells may be immature, and those with various optimal sizes may converge to yield the size-invariant responses. Alternatively, both size-dependent and -independent processing of images may occur in TE.

A definite number of TE cells tolerated reversal of the contrast polarity of the shapes. Contrast reversal of the critical feature evoked more than 50% of the maximum responses in 40% of tested cells (Ito et al., 1994). Sary et al. (1993) found that some TE cells responded similarly to shapes defined by differences in luminosity, direction of motion of texture components, and coarseness of texture while maintaining their selectivity for shape. Tanaka et al. (2001) found that about one-fourth of TE cells responded similarly to shapes defined by difference in horizontal disparity of texture components, to those defined by difference in the size of texture components, and to those defined by difference in luminosity.

Another kind of invariance of TE cells was found with regard to the aspect ratio of shapes. The aspect ratio is the ratio of the size along one axis of the stimulus to that along the orthogonal axis. When an object rotates in depth, the features contained in the image change their shapes. Unless occlusion occurs, changes occur mainly in the aspect ratio. For individual TE cells, we first determined the critical feature using the reduction method and then tested the effects of changes in the aspect ratio of the critical feature. We observed that one-half of cells responded to an aspect ratio range of more than 3 octaves with more than 50% of the maximum responses (Esteky and Tanaka, 1998).

In Figures 77.2 and 77.3 (and in our previous studies), we show the features determined to be critical for the activation of individual TE cells as 2D images. However, this is for the sake of description, and it does not necessarily mean that the cells were tuned to 2D images. Selectivity can only be defined as a list of tested stimulus deformations and their associated response reductions. The above-described invariances of TE cells suggest that they are actually more sensitive to certain types of deformation than others. The types of deformation that often occur when an object moves around appear to be better tolerated.

We examined the spatial distribution of the cells responding to various critical features in TE. By recording two TE cells simultaneously with a single electrode, we found that cells located close together in the cortex had similar stimulus selectivities (Fujita et al., 1992). The critical feature of one isolated cell was determined using the procedure described above, while the responses of another isolated cell, or non-isolated multiunits, were simultaneously recorded. In most cases, the second cell responded to the optimal and suboptimal stimuli of the first cell. The selectivities of the two cells differed slightly, however, in that the maximal response was evoked by slightly different stimuli, or the mode of the decrease in response differed when the stimulus was changed from the optimal stimulus.

To determine the spatial extent of the clustering of cells with similar selectivities, we examined the responses of cells recorded successively along long penetrations that were made vertical or oblique to the cortical surface (Fujita et al., 1992). The critical feature for a cell located in the middle of the penetration was first determined. A set of stimuli, including the critical feature for the first cell, its rotated versions, and ineffective control stimuli, was constructed, and cells recorded at different positions along the penetration were tested with the fixed set of stimuli. Cells recorded along the vertical penetrations commonly responded to the critical feature for the first cell or to some related stimuli. Such clusters of cells with similar stimulus selectivity covered nearly the entire thickness from layer 2 to layer 6. In the case of penetrations that were made oblique to the cortical surface, however, the cells that commonly responded to the critical feature of the first cell or to related stimuli were limited to within a short span around the first cell. The horizontal extent of the span was on average, 400 μm . Cells outside the span did not respond to any of the stimuli included in the set, or they responded to some stimuli that were not effective in activating the first cell and were included in the set as ineffective control stimuli. Based on these results, we proposed that TE is composed of columnar modules, cells in each of which respond to similar features (Fig. 77.4).

It should be noted that the precise determination of the optimal features is essential to observing the similarity of stimulus selectivities between neighboring cells clustered in a columnar region. Several studies, which used a fixed set of arbitrarily selected object images, failed to find the similarity. The optimal features for the activation of TE cells are complex and defined by many dimensions. The preference of cells within a column is similar in some dimensions but different in other dimensions. For example, cells in a column respond to star-like shapes or shapes with multiple protrusions. They are similar in that they respond to star-like shapes, but they may differ in the preferred number of pro-

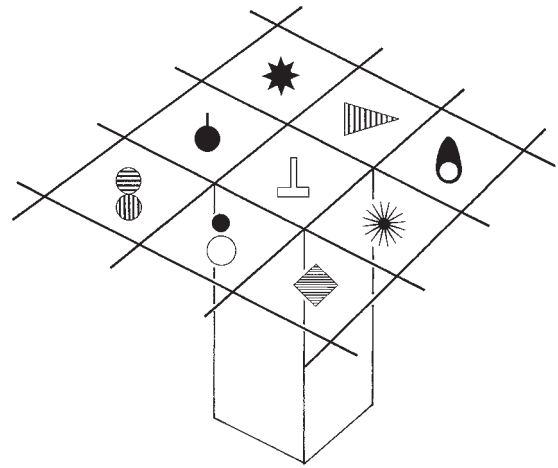


FIGURE 77.4. Schematic of the columnar organization in TE.

trusions or the amplitude of the protrusions. Therefore, if only a fixed set of object images is used, because star-like shapes with different numbers of protrusions appear in different objects, cells within the column will respond to different objects. The same is true for the primary visual cortex. Cells within an orientation column have the same preferred orientation, while they differ in the preferred width and length of stimuli, binocular disparity, and the sign of contrast. If a set of stimuli that vary not only in orientation but also in all other parameters is used, cells within an orientation column will not show clear similarity in selectivity.

Spatial arrangement of columns

To further study the spatial properties of the columnar organization in TE, we used optical imaging with intrinsic signals (Wang et al., 1996, 1998). The cortical surface was exposed and illuminated with red light tuned to 605 nm, and the reflected light image was recorded by a CCD video camera. The reflected images for different visual stimuli were compared. The region of the cortex with elevated neuronal activities appears darker than other regions in the reflected image.

We first recorded the responses of single cells with a microelectrode to determine the critical feature and then conducted optical imaging. In the experiment, the results of which are shown in Figure 77.5, the critical feature determined for a cell recorded at the cortical site indicated by a cross was the combination of white and black horizontal bars. The peri stimulus time (PST) histograms on the left side represent the responses of the cell. The combination evoked a strong response in the cell, but a white bar alone or a black bar alone did not activate the cell. The images on the right side were taken from the same 1×1.5 mm cortical region. A dark spot appeared around the penetration site when the monkey saw the combination of the two bars, whereas there

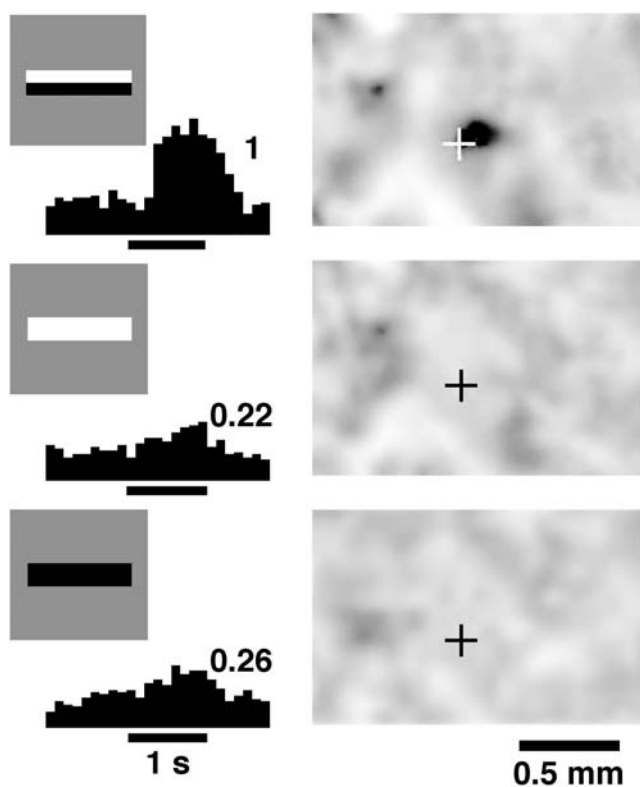


FIGURE 77.5. Correspondence of optical signals with neuronal activity. The histograms on the left show the responses of a cell recorded at the site indicated by the crosses in the optical images. The cell responded selectively to the combination of a white bar and a black bar. The white bar alone or the black bar alone evoked much smaller responses. Correspondingly, the optical image showed a black spot covering the recording site during the time the monkey was viewing the combination shape, whereas there were no dark spots for the control stimuli. (From Wang et al., 1996, with modification.)

were no dark spots around the site when the monkey saw the simpler features. Similar results were obtained in 11 out of 13 cases. Tsunoda et al. (2001) further confirmed the correlation of optical signals with neuronal responses in TE. Although the critical feature was determined for a single cell, a large proportion of cells in the region must be activated to produce an observable metabolic change. Therefore, the localized and specific occurrence of dark spots indicates a regional clustering of cells with similar stimulus selectivities.

However, when we observed a larger area of the cortical surface, we found that the presentation of a single feature activated multiple spots. In Figure 77.6, the spots activated by eight moderately complex features are indicated by different kinds of lines and superimposed, that is, spots activated by four features are shown in the upper half and those by the other four features in the lower half. For example, feature 1 evoked six spots, and feature 2 evoked two spots. A single feature is processed in multiple columns in TE.

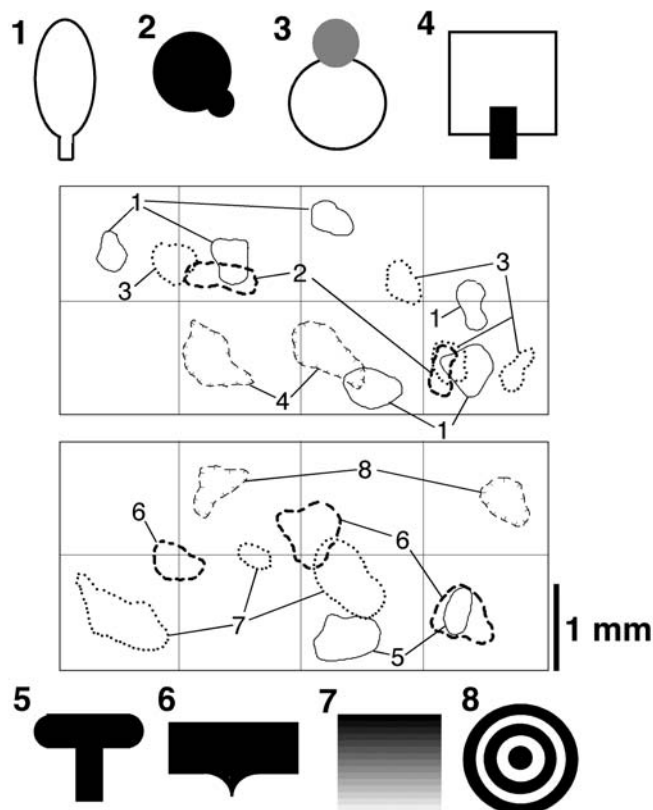


FIGURE 77.6. Map of activation evoked by the presentation of eight moderately complex features. To obtain the map, each image was subtracted by the reference image averaged over the images obtained for all the different stimuli combined in the experiment to remove the global darkening. The activation spots were delineated at $1/e$ of the maximum intensity in individual images, and the contours of spots in the images for different stimuli are indicated by different line types. (From Wang et al., 1998, with modification.)

Another interesting observation here is the partial overlapping between activation spots evoked by different features. Some of the overlapping regions, which were activated by many stimuli, likely represent columns of nonselective cells. However, others that were activated by only two of the stimuli may represent overlapping between selective columns. For many of these overlapping regions, we can find similarity between the two features, although the judgment of similarity is only subjective.

The partial overlapping of columns responding to different but related features was most clearly observed for faces presented in different views (Fig. 77.7). This experiment was performed using optical imaging guided by unit recording. We recorded five cells in one electrode penetration around the center of the imaged region, and all of them responded selectively to faces. Three of them responded maximally to the front view of the face, and the remaining two responded to the profile, that is, the lateral view of the face. In an optical imaging session, five different views of the face of the same

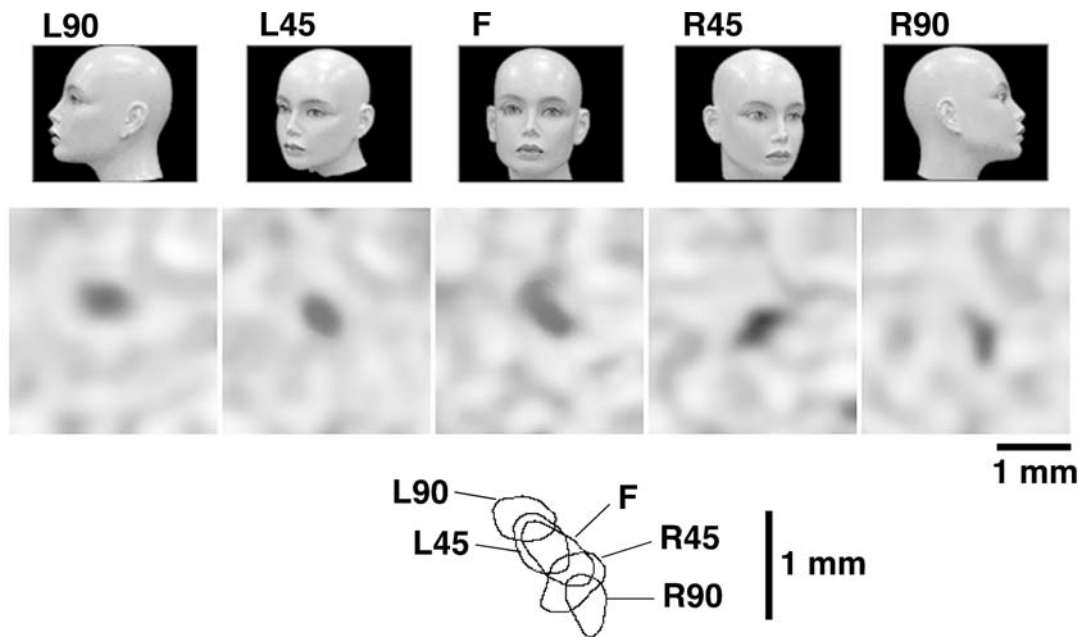


FIGURE 77.7. Systematic movement of the activation spot with rotation of the face. The images were obtained for five different views of the face of the same doll shown on top. The reference image obtained by averaging the five images was subtracted. The contours circumscribing the pixels with t -values at $p < .05$, compared with the reference image, are superimposed at the bottom. (From Wang et al., 1996, with modification.)

doll were presented in combination with 14 nonface features. All of the faces evoked activation spots around the center of the illustrated 3×3 mm region. However, their central positions were slightly different. The contours of the dark spots are superimposed at the bottom of Figure 77.7. The activation spot moved in one direction as the face was rotated from the left to the right profile through the front view of the face. Individual spots were 0.4 to 0.8 mm in diameter, and the overall region was 1.5 mm. These regions were not activated by the 14 nonface features.

Similar results, namely, selective activation by faces and systematic shift of the activation spot with the rotation of the face, were obtained for three other monkeys. In these three monkeys, optical imaging was not guided by unit recording. The recording chamber with an inner diameter of 18 mm was placed in the same region of TE, and the face-selective activation was found at approximately the same location (approximately the posterior third of TE on the lateral surface close to the lip of the superior temporal sulcus). The effects of rotating the face around a different axis (chin up and down) and of changing the facial expression were also determined in some of the experiments, but neither of these caused a shift in the activation spot. Only two faces were tested: a human face and a doll's face. The two faces activated regions that mostly overlapped. There are two possible interpretations of this result. One is that the variations other than those with horizontal rotation are represented at different sites not covered by the recording chamber in the

experiments. Alternatively, it is possible that only the variations along the horizontal rotation are explicitly mapped along the cortical surface as the first principal component, and other variations are embedded in overlapping cell populations.

Data for the nonface features are few, but I hypothesize that there are similar structures, and I propose a modified model of the columnar organization of neurons in TE as shown in Figure 77.8. The borders between neighboring columns are not necessarily distinct. Instead, multiple columns that represent different but related features partially overlap with one another and as a whole compose a larger scale unit. At least in some cases, some parameter of the features is continuously mapped along the cortical surface.

This systematic arrangement of related columns can be used for various computations necessary for object recognition. One simple possible computation is the generalization of activation by the horizontal excitatory connections to nearby columns representing related features. We may call it the *selective blurring of activation*. The blurring is selective in that the spread of activation in TE results in activation of related features but not blurring in the image plane. Another possible simple processing is the mutual inhibition among nearby columns for the winner-take-all-type selection.

The continuous mapping of different views of faces cannot be generalized to nonface objects. Because the critical features for TE cells are only moderately complex except for faces, the image of a nonface object has to be represented

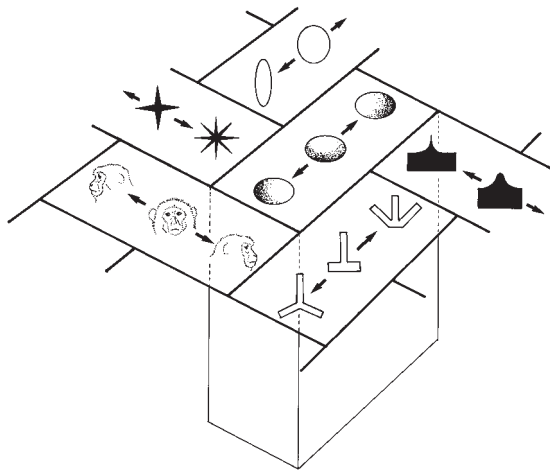


FIGURE 77.8. Revised schematic of the columnar organization in TE.

by a combination of activations at multiple cortical sites. Rotation of a nonface object causes changes in activation at multiple cortical sites, each of which corresponds to a partial change of a feature. The mechanisms underlying the view-invariant representation of nonface objects should be more widely distributed over a large region of TE than those for faces.

From features to objects

Since most inferotemporal cells represent features of object images but not the whole-object images, the representation of the image of an object requires a combination of multiple cells representing different features contained in the image of the object. This process of combination provides unique scientific problems. Objects often appear in a clutter. A part of features belonging to one object may be mistakenly combined with a part of features belonging to another object. This erroneous combination causes a false perception of an object that is not visually present. How does the brain avoid such an erroneous combination?

Previously, the synchronization of spiking activity between cells was proposed as the mechanism for binding the features belonging to one object. Some experiments found a correspondence between the synchronization and object borders (reviewed by Singer, 1999), while others did not (Lamme and Spekreijse, 1998). Another possible means of avoiding the erroneous combination is to have features partially overlapping with one another (Mel and Fiser, 2000). Suppose we are to represent four-letter strings. There will be an erroneous combination if we use only representation units coding single letters (e.g., ABCD is not discriminated from BADC, CDAM, and so on, if units code A, B, and C), while there will be no erroneous combinations if we use units specifying two consecutive letters and those specifying letters at the

beginning and end of three consecutive letters (e.g., ABCD is the only four-letter string that contains AB, CD, and A-C).

Tsunoda et al. (2001) compared activation of the inferotemporal cortex by object images and that by features included in the object images using a combination of optical imaging and single-cell recordings. The image of an object usually activated several spots within the imaged region (6×8 mm), and a feature contained in the object image activated part of the spots in some cases. This result was consistent with the idea that different spots were activated by different features contained in the object image. However, in other cases, the activation by a feature often included new spots that had not been activated by the whole-object image. Single-cell recordings revealed that cells within such spots were activated by a feature while inhibited by another feature included in the original object image. Previous single-cell recording studies had also shown that the response of inferotemporal cells to the optimal stimulus was suppressed by the simultaneous presentation of a second stimulus (Missal et al., 1997, 1999; Sato, 1989, 1995). These results indicate that the stimulus selectivity of inferotemporal columns should be described by both the simplest feature for the maximum activation and features that suppress the activation. Even with the same optimal feature for the excitation, the range of features that suppresses the excitation can vary from column to column and probably also from cell to cell. This complexity of the overall stimulus selectivity of inferotemporal columns and cells may help to reduce the chance of erroneous detection of nonexistent objects.

Yamane et al. (2001) also used a combination of optical imaging and single-cell recordings, and found that some of the columns activated by an object image were activated not by local features, but by a global feature of the object image. These columns were more sensitive to the global arrangement of object parts than to the properties of the parts. For example, one column responded to two vertically aligned black parts, regardless of the shape of either part. These columns representing global features also help reduce the possibility of erroneous detection of nonexistent objects.

Intrinsic horizontal connections within TE

Intrinsic horizontal connections span up to 8 mm in TE. Projection terminals are more or less continuously distributed within 1 mm from cells of origin, whereas they are clustered in patches in more distant regions (Fujita and Fujita, 1996; Tanigawa et al., 1998). The cells of origin of these horizontal connections contain inhibitory neurons within 1 mm, but they are composed exclusively of excitatory cells (mostly pyramidal cells) for longer connections (Tanigawa et al., 1998). Ionophoretic injection of bicuculline methiodide, an antagonist of an inhibitory synaptic transmitter GABA,

reduced the stimulus selectivity of TE cells; in particular, the stimuli optimal for nearby cells turned out to evoke excitatory responses during the blockage of inhibition (Wang et al., 2000). Inhibitory components of horizontal connections contribute to the formation of stimulus selectivity. The functional roles of excitatory components are not known. It is possible that they connect columns responding to similar features, as is the case in the primary visual cortex (Gilbert and Wiesel, 1989). The combination of optical imaging and anatomical tracing will provide insights into this issue.

Functions of TE columns

Representation by multiple cells in a columnar module, in which the precise selectivity varies from cell to cell while effective stimuli largely overlap, can satisfy two apparently conflicting requirements in visual recognition: one is the ability to disregard subtle changes in input images; the other is the preciseness of representation.

A cluster of cells having overlapping and slightly different selectivities may work as a buffer to absorb changes. Although single cells in TE tolerate some changes in size, contrast polarity, and aspect ratio, these invariant properties at the single-cell level are not sufficient to explain the entire range of flexibility of object recognition. In particular, responses of TE cells are generally selective for the orientation of the shape in the frontoparallel plane. Cells preferring different orientations and other parameters of the same three-dimensional shape may be packed in a column to provide invariant output. Whether signals from these selective cells converge to a group of single cells exhibiting invariant responses is a matter for further investigation. One possibility is that output of cells preferring different orientations, sizes, aspect ratios, and contrast polarities of the same shape overlaps in the target structure, thereby evoking the same effects. One of our anatomical studies involving injection of an anterograde tracer into a focal site in TE suggested that projections from TE to the ventrocaudal striatum of the basal ganglia exhibit this property (Cheng et al., 1997). Another possibility is that activation of cells may be transmitted to other cells within a column and to nearby columns that represent related features through horizontal excitatory connections in the presence of top-down signals from other brain sites, for example, the prefrontal cortex.

The representation by multiple cells with overlapping selectivities can be more precise than a mere summation of representations by individual cells. A subtle change in a particular feature, which does not markedly change the activity of individual cells, can be coded by differences in activities of cells with overlapping and slightly different selectivities. Projections from the ventroanterior part of TE to the perirhinal cortex extensively diverge (Saleem and Tanaka, 1996). Projection terminals from a single site of the ven-

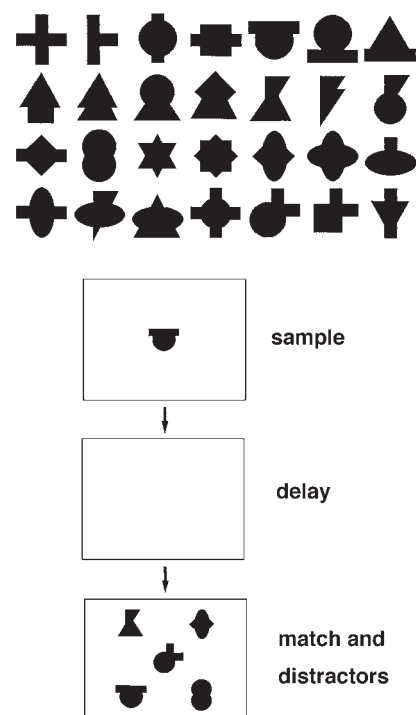


FIGURE 77.9. The 28 shapes used for the training (*top*) and the paradigm (*bottom*).

troanterior TE cover about one-half of the perirhinal cortex. This divergence in projections may distribute subtle differences in images over a larger area of the perirhinal cortex so that objects recognized at individual levels can be distinctively associated with other kinds of information. Subtle differences can also be emphasized by mutual inhibition between cells or nearby columns for winner-take-all-type selection. The inhibition may also be under top-down control.

Changes of selectivity in the adult

The selectivity of inferotemporal cells can be changed in adult animals by long-term training. We found this by training two adult monkeys to recognize 28 moderately complex shapes shown in the upper half of Figure 77.9 and recording from inferotemporal cells after the training (Kobatake et al., 1998). The training paradigm was a kind of delayed matching to sample shown in the lower half of Figure 77.9. One stimulus that was randomly selected from the set of 28 stimuli appeared on a television monitor as a sample, the monkey touched it, and the sample disappeared. After a delay period, the sample appeared again on the display, but this time together with four other stimuli that were randomly selected from the stimulus set. The monkey selected the sample and touched it to get a drop of juice as a reward. After an intertrial interval, the trial was repeated with a different sample. The monkey performed the task on a

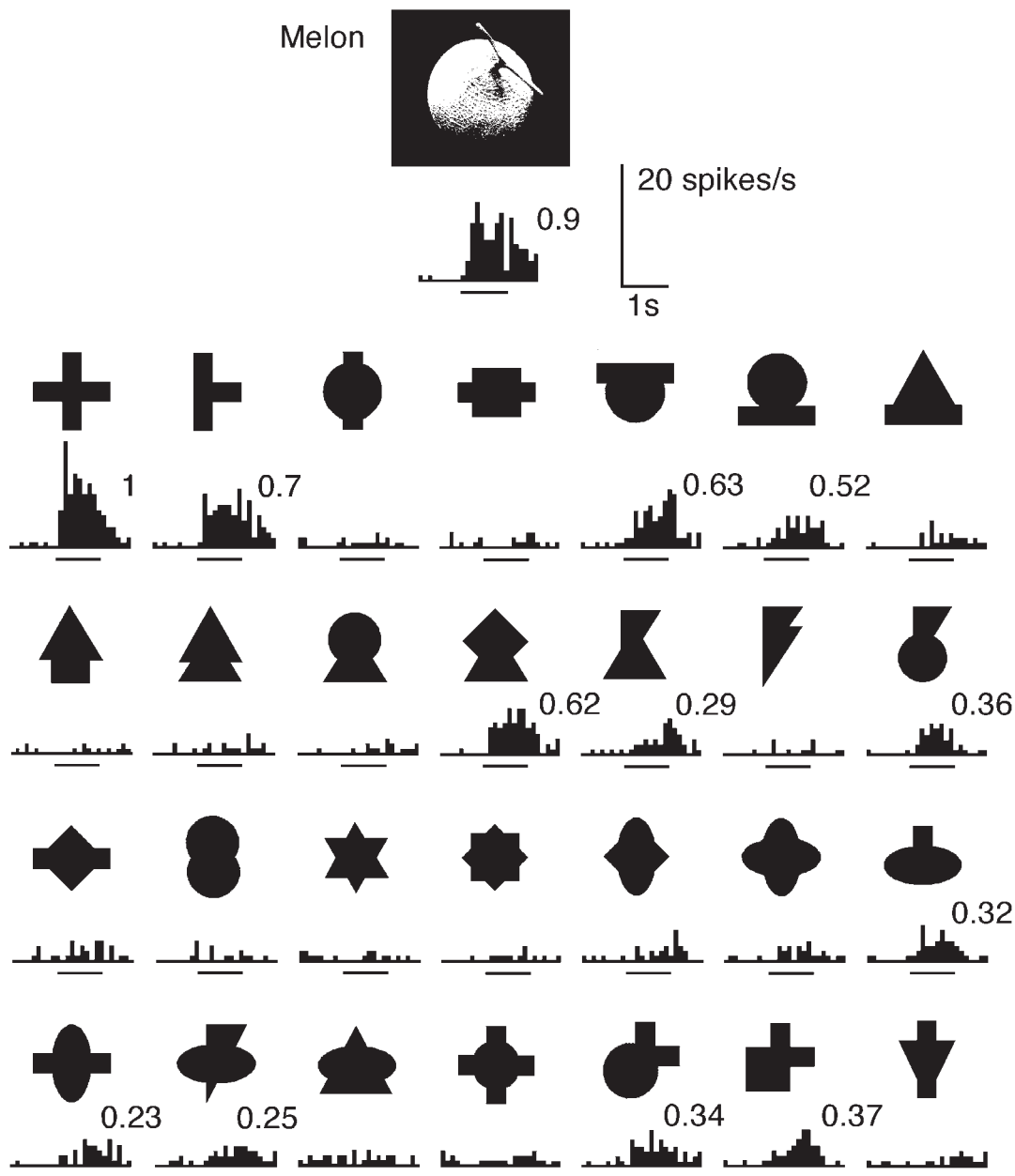


FIGURE 77.10. Responses of one TE cell to the image of the most effective stimulus of the object stimulus set (*top*) and its responses to the 28 shape stimuli used for the training. This cell was recorded from a monkey that had been trained with the 28 stimuli. Statistically significant responses ($p < .05$) are labeled with their relative response magnitudes. (From Kobatake et al., 1998, with modification.)

stand-alone apparatus placed in front of the home cage. The monkey came to the apparatus and practiced the task whenever it wanted. The training was performed starting with a 1 second delay, and the delay was increased gradually to 16 seconds. At the end of the training, the monkey performed 500 successful trials with greater than 80% performance.

After the training was completed, we prepared the monkeys for repeated recordings and conducted recordings from TE under anesthesia, once a week for 3 to 4 months. The training was continued on the days when the recordings were not conducted. We determined the most effective

stimulus for individual cells from the same set of animal and plant models that we used for the reduction experiment, and the response to this best object stimulus was compared with the responses of the same cell to the training stimuli. In this experiment, we did not conduct the reduction process, but just took the images of several most effective object stimuli with a video camera and presented them under computer control in combination with the training stimuli.

The cell illustrated in Figure 77.10 responded maximally to the sight of a watermelon among the object stimuli. However, the cell responded more strongly to the cross

shape, which was one of the training stimuli. There were also responses to several other training stimuli. Twenty-five percent of responsive cells recorded from the two trained monkeys responded more strongly to some of the training stimuli than to the best object stimulus, as in this example, but only 5% of responsive cells in the control monkeys responded maximally to some of the stimuli. These results indicate that the number of cells maximally responsive to training stimuli increased during the period of the discrimination training.

Sakai and Miyashita (1994) and Logothetis et al. (1995) had trained adult monkeys to discriminate among Fourier descriptors or wire-frame objects and found that many TE cells responded to the learned stimuli after the training. A unique contribution of our study is the demonstration that training increases the proportion of TE cells that respond to the learned stimuli as measured against untrained controls.

These results appear to be inconsistent with previous findings that responses of cells in TE and the perirhinal cortex decreased as the same stimuli were repeatedly presented. Miller et al. (1991) and Riches et al. (1991), by recording cells in TE and the perirhinal cortex during a serial delayed-matching-to-sample task, found that responses to the second (match) presentation of a stimulus were significantly smaller than those to the first (sample) presentation of the same stimulus in 10% to 30% of visually responsive cells. Miller et al. (1991) and Li et al. (1993) further found that, for stimuli that were new to the monkey at the beginning of the recording of a cell, the decrement of response did not recover from one trial to a sample presentation of the same stimulus in a new trial, even with several tens of intervening trials; thus, the decrement was accumulated through several trials repeatedly presenting the initially new, identical sample stimulus within a day. Riches et al. (1991) and Fahy et al. (1993) found that a definite proportion (about 15%) of TE and perirhinal cells responded to novel stimuli significantly more strongly than to familiar stimuli. This difference was found even when the individual familiar stimuli had not been presented since the previous day. These findings indicate that responses of TE and perirhinal cells decrease as stimuli become familiar, both within a day and across days.

The two sets of apparently conflicting findings can be explained as follows. As the familiarity of stimuli increases with repetition of their presentation, a small proportion of TE cells become more responsive to the stimuli, while responses of the remaining majority of TE cells to the same stimuli become weak. In other words, the representation of stimuli in the entire TE changes from a widely distributed one to a sparse one. Although sparse representations are not necessarily superior over distributed representations in discrimination accuracy, sparse representations have advan-

tages in memory capacity and connectional efficiency. Because the studies that found the decrease in the level of responses used a few arbitrarily selected stimuli (fewer than 10) for individual cells or did not pay much attention to the stimulus selectivity of cells, they found only the decrease that occurred in a majority of TE cells. In our study (Kobatake et al., 1998) and the study of Logothetis et al. (1995), only 10% to 25% of TE cells responded more strongly to some of the stimuli used in the training ($n = 28$ in our study) than to many reference stimuli.

It remains to be examined whether the columnar organization in TE changes in adults due to training. It is possible that the columns do not change once they are established in early development after birth. If this is the case, the changes in the selectivity of individual cells, like those observed in the previous studies, should occur in cells distributed across many columns, without emergence of columns specifically tuned to the stimuli used in the task training.

Relationship between task requirements and TE cells' selectivity

It is now established that the responsiveness of TE cells to particular stimuli changes according to long-term training with the stimuli even in adults. However, it is not yet clear whether the selectivity of TE responses reflects the behavioral requirements of the task in which the monkeys have been trained. To answer this question, the task should include something beyond a simple discrimination among stimuli. Sigala and Logothetis (2002) trained monkeys in a classification of many line drawings of faces into two groups. The monkeys reported their classification by pressing either the left or the right bar. Faces were varied by changing four parameters of the face: eye height, eye separation, nose length, and mouth height. The faces were thus distributed in a four-dimensional feature space. The two groups of faces were separated by a linear plane in the feature space, and the plane was defined by only two of the parameters (diagnostic parameters). Sigala and Logothetis (2002) recorded TE cells during the task after the monkeys had completely learned the classification. They found that responses of TE cells were statistically more selective for the two diagnostic parameters than for the other two parameters. The monkeys were also trained to classify line drawings of fishes, and similar results were obtained. These results may suggest that the selectivity of TE cells specifically develops through the task training to make the task requirement easier. In this study, however, the diagnostic parameters were not exchanged with the nondiagnostic parameters between monkeys. Therefore, it is possible that the parameters that were selected as diagnostic in the task happened to be more influential on responses of TE cells than the parameters

selected as nondiagnostic, even without the classification training.

Vogels (1999a, 1999b) pioneered the study of the relationship between the stimulus selectivity of TE cells and categorization behavior of monkeys. The monkeys were trained to distinguish trees from other objects and fishes from other objects. The ability of the monkeys to generalize the categorizations to novel trees and novel fishes was demonstrated (Vogels, 1999a). Vogels (1999b), by recording cells from TE after the monkey learned the categorization of trees versus nontrees, found that 10% of TE cells responded exclusively to subpopulations of trees and that none of them responded to all the trees. However, it is difficult to draw a conclusion from the data on whether TE cells as a whole were more sensitive to differences between trees and other objects than to variations within trees, or whether the TE cells responding only to trees emerged as a result of categorization training.

Sakai and Miyashita (1991) trained monkeys in a paired associate task. A trial of the task was composed of a sample presentation, delay, and choice periods, as in the delayed-matching-to-sample tasks. However, differences from the conventional delayed-matching-to-sample task were that two stimuli presented in the choice period did not include the sample stimulus, and the monkey had to select the one paired with the sample. Because the pairing was randomly determined by the experimenter, the paired stimuli were not more similar than unpaired stimuli. The pairing was consistent throughout the training, which lasted for several months. Sakai and Miyashita recorded activity of TE cells during the task after the monkeys had learned the associations and found that some TE cells responded selectively to both stimuli composing a single pair.

However, Higuchi and Miyashita (1996) found that this trace of associative memory in TE cells depended on the perirhinal cortex, to which TE projects. They first cut the anterior commissure to disconnect the left and right TE from each other. After the monkeys were trained in the paired associate task, the perirhinal cortex in one hemisphere was destroyed by injecting a toxic agent. TE cells on the lesioned side did not show the correlated responsiveness to paired stimuli, although their responses to individual stimuli were intact. These results indicate that the correlated responsiveness was generated in the perirhinal cortex and projected to TE through feedback input from the perirhinal cortex to TE.

In summary, it is now established that responsiveness of TE cells in an adult monkey to particular stimuli increases through training with the stimuli, but it is not clear whether the selectivity of individual TE cells reflects the behavioral requirements of the task in which the monkey has been trained. The trace of associative memory in TE found by Sakai and Miyashita (1991) was a reflection of a phenomenon that occurred primarily in the perirhinal cortex.

Conclusions

Neurons in area TE of the monkey inferotemporal cortex respond to moderately complex visual features of objects. Different TE cells respond to different features. Because the features to which individual TE cells respond are only moderately complex, combinations of several to several tens of cells responding to different features are necessary to specify particular objects. This coding of object images by combinations of features (combination coding) may underlie the generalization capability of our visual perception.

Cells with similar, but slightly different, stimulus selectivities cluster in local columnar regions. This clustering with certain variety suggests the presence of two schemes in representation of object images in TE. In one of them, an object image is represented by a combination of activated columns. In this coarse representation, the variety of selectivity within individual columns may work as a tool to disregard subtle changes in input images. The other representation depends on the distribution of activities among the cells within individual columns. Because cells within individual columns have overlapping and slightly different selectivities, the representation can be more precise than a simple summation of activities of the cells. These two types of representation may be working in parallel, with some graded emphasis changing in accordance to the behavioral context. There is some evidence for regularities in arrangement of columns at nearby positions, which may also have functional significance.

The stimulus selectivity of TE cells changes in adults as the monkey learns particular visual tasks with object images or complex patterns. These neuronal changes in the adult brain likely underlie the long-term memory of the monkey. By examining the relationship between neuronal changes and requirements of the tasks that the monkey has learned—or, in other words, changes in behavioral performance of the monkey through the learning—we will be able to clarify further the functional roles of the neuronal stimulus selectivity and columnar organization in TE.

REFERENCES

- Allison, T., H. Ginter, G. McCarthy, A. C. Nobre, A. Puce, M. Luby, and D. D. Spencer, 1994. Face recognition in human extrastriate cortex, *J. Neurophysiol.*, 71:821–825.
- Baylis, G. C., E. T. Rolls, and C. M. Leonard, 1987. Functional subdivisions of the temporal lobe neocortex, *J. Neurosci.*, 7:330–342.
- Bruce, C., R. Desimone, and C. G. Gross, 1981. Visual properties of neurons in a polysensory area in superior temporal sulcus of the macaque, *J. Neurophysiol.*, 46:369–384.
- Cheng, K., K. S. Saleem, and K. Tanaka, 1997. Organization of corticostriatal and corticoamygdalar projections arising from the anterior inferotemporal area TE of the macaque monkey: a *Phaseolus vulgaris* Leucoagglutinin study, *J. Neurosci.*, 17:7902–7925.

- Dean, P., 1976. Effects of inferotemporal lesions on the behavior of monkeys, *Psychol. Bull.*, 83:41–71.
- Esteky, H., and K. Tanaka, 1998. Effects of changes in aspect ratio of stimulus shape on responses of cells in the monkey inferotemporal cortex, *Soc. Neurosci. (Abstr.)*, 24:899.
- Fahy, F. L., I. P. Riches, and M. W. Brown, 1993. Neuronal activity related to visual recognition memory: long-term memory and the encoding of recency and familiarity information in the primate anterior and medial inferior temporal and rhinal cortex, *Exp. Brain Res.*, 96:457–472.
- Fujita, I., and T. Fujita, 1996. Intrinsic connections in the macaque inferior temporal cortex, *J. Comp. Neurol.*, 368:467–486.
- Fujita, I., K. Tanaka, M. Ito, and K. Cheng, 1992. Columns for visual features of objects in monkey inferotemporal cortex, *Nature*, 360:343–346.
- Gallant, J. L., J. Braun, and D. C. Van Essen, 1993. Selectivity for polar, hyperbolic, and Cartesian gratings in macaque visual cortex, *Science*, 259:100–103.
- Gallant, J. L., C. E. Connor, S. Rakshit, J. W. Lewis, and D. C. Van Essen, 1996. Neural responses to polar, hyperbolic, and Cartesian gratings in area V4 of the macaque monkey, *J. Neurophysiol.*, 76:2718–2739.
- Gilbert, C. D., and T. N. Wiesel, 1989. Columnar specificity of intrinsic horizontal and corticocortical connections in cat visual cortex, *J. Neurosci.*, 9:2432–2442.
- Gross, C. G., 1973. Visual functions of inferotemporal cortex, in *Handbook of Sensory Physiology*, vol. 7, part 3B (R. Jung, ed.), Berlin: Springer-Verlag, pp. 451–482.
- Haxby, J. V., M. I. Gobbini, M. L. Furey, A. Ishai, J. L. Schouten, and P. Pietrini, 2001. Distributed and overlapping representations of faces and objects in ventral temporal cortex, *Science*, 293:2425–2430.
- Higuchi, S., and Y. Miyashita, 1996. Formation of mnemonic neuronal responses to visual paired associates in inferotemporal cortex is impaired by perirhinal and entorhinal lesions, *Proc. Natl. Acad. Sci. USA*, 93:739–743.
- Ishai, A., L. G. Ungerleider, A. Martin, J. L. Schouten, and J. V. Haxby, 1999. Distributed representation of objects in the human ventral visual pathway, *Proc. Natl. Acad. Sci. USA*, 96:9379–9384.
- Ito, M., I. Fujita, H. Tamura, and K. Tanaka, 1994. Processing of contrast polarity of visual images in inferotemporal cortex of the macaque monkey, *Cereb. Cortex*, 5:499–508.
- Ito, M., H. Tamura, I. Fujita, and K. Tanaka, 1995. Size and position invariance of neuronal responses in monkey inferotemporal cortex, *J. Neurophysiol.*, 73:218–226.
- Janssen, P., R. Vogels, and G. A. Orban, 1999. Macaque inferior temporal neurons are selective for disparity-defined three-dimensional shapes, *Proc. Natl. Acad. Sci. USA*, 96:8217–8222.
- Janssen, P., R. Vogels, and G. A. Orban, 2000a. Selectivity for 3D shape that reveals distinct areas within macaque inferior temporal cortex, *Science*, 288:2054–2056.
- Janssen, P., R. Vogels, and G. A. Orban, 2000b. Three-dimensional shape coding in inferior temporal cortex, *Neuron*, 27:385–397.
- Kanwisher, N., 2000. Domain specificity in face perception, *Nat. Neurosci.*, 3:759–763.
- Kanwisher, N., J. McDermott, and M. M. Chun, 1997. The fusiform face area: a module in human extrastriate cortex specialized for face perception, *J. Neurosci.*, 17:4302–4311.
- Keysers, C., D.-K. Xiao, P. Foldiak, and D. L. Perrett, 2001. The speed of sight, *J. Cogn. Neurosci.*, 13:90–101.
- Kobatake, E., and K. Tanaka, 1994. Neuronal selectivities to complex object features in the ventral visual pathway of the macaque cerebral cortex, *J. Neurophysiol.*, 71:856–867.
- Kobatake, E., G. Wang, and K. Tanaka, 1998. Effects of shape-discrimination training on the selectivity of inferotemporal cells in adult monkeys, *J. Neurophysiol.*, 80:324–330.
- Lamme, V. A., and H. Spekreijse, 1998. Neuronal synchrony does not represent texture segregation, *Nature*, 396:362–366.
- Li, L., E. K. Miller, and R. Desimone, 1993. The representation of stimulus familiarity in anterior inferior temporal cortex, *J. Neurophysiol.*, 69:1918–1929.
- Logothetis, N. K., 1998. Object vision and visual awareness, *Curr. Opin. Neurobiol.*, 8:536–544.
- Logothetis, N. K., J. Pauls, and T. Poggio, 1995. Shape representation in the inferior temporal cortex of monkeys, *Curr. Biol.*, 5:552–563.
- Lueschow, A., E. K. Miller, and R. Desimone, 1994. Inferior temporal mechanisms for invariant object recognition, *Cereb. Cortex*, 5:523–531.
- Maunsell, J. H. R., and D. C. Van Essen, 1983. Functional properties of neurons in middle temporal visual area of the macaque monkey. II. Binocular interactions and sensitivity to binocular disparity, *J. Neurophysiol.*, 49:1148–1167.
- Mel, B. W., and J. Fiser, 2000. Minimizing binding errors using learned conjunctive features, *Neural Comput.*, 12:731–762.
- Miller, E. K., L. Li, and R. Desimone, 1991. A neural mechanism for working and recognition memory in inferior temporal cortex, *Science*, 254:1377–1379.
- Missal, M., R. Vogels, L. Chao-yi, and G. A. Orban, 1999. Shape interactions in macaque inferior temporal neurons, *J. Neurophysiol.*, 82:131–142.
- Missal, M., R. Vogels, and G. A. Orban, 1997. Responses of macaque inferior temporal neurons to overlapping shapes, *Cereb. Cortex*, 7:758–767.
- Op de Beeck, H., and R. Vogels, 2000. Spatial sensitivity of macaque inferior temporal neurons, *J. Comp. Neurol.*, 426:505–518.
- Pasupathy, A., and C. E. Connor, 2001. Shape representation in area V4: position-specific tuning for boundary conformation, *J. Neurophysiol.*, 86:2505–2519.
- Perrett, D. I., E. T. Rolls, and W. Caan, 1982. Visual neurones responsive to faces in the monkey temporal cortex, *Exp. Brain Res.*, 47:329–342.
- Poggio, G. F., and B. Fischer, 1977. Binocular interaction and depth sensitivity in striate and prestriate cortex of behaving rhesus monkey, *J. Neurophysiol.*, 40:1392–1405.
- Puce, A., T. Allison, J. C. Gore, and G. McCarthy, 1995. Face-sensitive regions in human extrastriate cortex studied by functional MRI, *J. Neurosci.*, 15:1192–1199.
- Riches, I. P., F. A. W. Wilson, and M. W. Brown, 1991. The effects of visual stimulation and memory on neurons of the hippocampal formation and the neighboring parahippocampal gyrus and inferior temporal cortex of the primate, *J. Neurosci.*, 11:1763–1779.
- Richmond, B. J., L. M. Optican, M. Podell, and H. Spitzer, 1987. Temporal encoding of two-dimensional patterns by single units in primate inferior temporal cortex. I. Response characteristics, *J. Neurophysiol.*, 57:132–146.
- Sakai, K., and Y. Miyashita, 1991. Neural organization for the long-term memory of paired associates, *Nature*, 354:152–155.
- Sakai, K., and Y. Miyashita, 1994. Neuronal tuning to learned complex forms in vision, *Neuroreport*, 5:829–832.
- Saleem, K. S., and K. Tanaka, 1996. Divergent projections from the anterior inferotemporal area TE to the perirhinal and entorhinal cortices in the macaque monkey, *J. Neurosci.*, 16:4757–4775.

- Sary, G., R. Vogels, and G. A. Orban, 1993. Cue-invariant shape selectivity of macaque inferior temporal neurons, *Science*, 260:995–997.
- Sato, T., 1989. Interactions of visual stimuli in the receptive fields of inferior temporal neurons in awake macaques, *Exp. Brain Res.*, 77:23–30.
- Sato, T., 1995. Interactions between two different visual stimuli in the receptive fields of inferior temporal neurons in macaques during matching behaviors, *Exp. Brain Res.*, 105:209–219.
- Schwartz, E. L., R. Desimone, T. D. Albright, and C. G. Gross, 1983. Shape recognition and inferior temporal neurons, *Proc. Natl. Acad. Sci. USA*, 80:5776–5778.
- Sigala, N., and N. K. Logothetis, 2002. Visual categorization shapes feature selectivity in the primate temporal cortex, *Nature*, 415:318–320.
- Singer, W., 1999. Neuronal synchrony: a versatile code for the definition of relations? *Neuron*, 24:49–65.
- Tanaka, K., H. Saito, Y. Fukada, and M. Moriya, 1991. Coding visual images of objects in the inferotemporal cortex of the macaque monkey, *J. Neurophysiol.*, 66:170–189.
- Tanaka, H., T. Uka, K. Yoshiyama, M. Kato, and I. Fujita, 2001. Processing of shape defined by disparity in monkey inferior temporal cortex, *J. Neurophysiol.*, 85:735–744.
- Tanigawa, H., I. Fujita, M. Kato, and H. Ojima, 1998. Distribution, morphology, and γ -aminobutyric acid immunoreactivity of horizontally projecting neurons in the macaque inferior temporal cortex, *J. Comp. Neurol.*, 401:129–143.
- Tarr, M. J., and I. Gauthier, 2000. FFA: a flexible fusiform area for subordinate-level visual processing automatized by expertise, *Nat. Neurosci.*, 3:764–769.
- Tsunoda, K., Y. Yamane, M. Nishizaki, and M. Tanifuji, 2001. Complex objects are represented in macaque inferotemporal cortex by the combination of feature columns, *Nat. Neurosci.*, 4:832–838.
- Uka, T., H. Tanaka, K. Yoshiyama, M. Kato, and I. Fujita, 2000. Disparity selectivity of neurons in monkey inferior temporal cortex, *J. Neurophysiol.*, 84:120–132.
- Vogels, R., 1999a. Categorization of complex visual images by rhesus monkeys. Part 1: behavioral study, *Eur. J. Neurosci.*, 11:1223–1238.
- Vogels, R., 1999b. Categorization of complex visual images by rhesus monkeys. Part 2: single-cell study, *Eur. J. Neurosci.*, 11:1239–1255.
- Wang, Y., I. Fujita, and Y. Murayama, 2000. Neuronal mechanisms of selectivity for object features revealed by blocking inhibition in inferotemporal cortex, *Nat. Neurosci.*, 3:807–813.
- Wang, G., K. Tanaka, and M. Tanifuji, 1996. Optical imaging of functional organization in the monkey inferotemporal cortex, *Science*, 272:1665–1668.
- Wang, G., M. Tanifuji, and K. Tanaka, 1998. Functional architecture in monkey inferotemporal cortex revealed by in vivo optical imaging, *Neurosci. Res.*, 32:33–46.
- Yaginuma, S., Y. Osawa, K. Yamaguchi, and E. Iwai, 1993. Differential functions of central and peripheral visual field representations in monkey prestriate cortex, in *Brain Mechanisms of Perception and Memory: From Neuron to Behavior* (T. Ono, L. R. Squire, R. E. Raichle, D. Perrett, and M. Fukuda, eds.), New York: Oxford University Press, pp. 1–33.
- Yamane, Y., K. Tsunoda, M. Matsumoto, A. Phillips, and M. Tanifuji, 2001. Decomposition of object images by feature columns in macaque inferotemporal cortex, *Soc. Neurosci. (Abstr.)*, 27:1050.

78 Invariant Object and Face Recognition

EDMUND T. ROLLS

INVARIANT OBJECT AND face recognition is a major computational problem that is solved by the end of ventral stream cortical visual processing in the primate inferior temporal visual cortex. The formation of invariant representations is crucial for the areas that receive from the inferior temporal visual cortex, so that when they implement learning based on one view, size, and position on the retina of the object, the learning generalizes later when the same object is seen in a different view, size, and position. Evidence that invariant representations are provided by some neurons in the inferior temporal visual cortex, and hypotheses about how these representations are formed, are described here. Some of the major properties of neurons in the primate inferior temporal visual cortex that will be described are summarized here.

Some neurons in the primate temporal cortical visual areas provide representations of faces and objects that are invariant with respect to position, size, and even view. These neurons show rapid processing and rapid learning. The particular face or object being seen is encoded using a distributed representation in which each neuron conveys independent information in its firing rate, with little information evident in the relative time of firing of different neurons. This ensemble encoding has the advantages of maximizing the information in the representation useful for discrimination between stimuli using a simple weighted sum of the neuronal firing by the receiving neurons, of generalization, and of fault tolerance. The invariant representations found may be produced in a hierarchically organized set of visual cortical areas with convergent connectivity from area to area, in which the neurons use a modified Hebb synaptic modification rule with a short-term memory trace to capture at each stage whatever can be captured that is invariant about objects as the objects change in retinal view, position, size, and rotation. The invariant representations formed in the temporal cortical visual areas are ideal as inputs to other brain regions involved in short-term memory, long-term episodic memory, and associative memory of the reward and punishment associations of the visual stimuli.

In addition to these neurons, there are separate face-selective neurons coding for face expression, face motion, and face view, which are likely to be involved in social interactions, in which explicitly encoded information of this type is useful.

Damage to these or related systems can lead to prosopagnosia, an impairment in recognizing individuals from the

sight of their faces, or in difficulty in identifying the expression on a face.

Neuronal responses found in different temporal lobe cortex visual areas

While recording in the temporal lobe cortical visual areas of macaques, Charles Gross and colleagues found some neurons that appeared to respond best to complex visual stimuli such as faces (Bruce et al., 1981; Desimone and Gross, 1979; see also Desimone, 1991). It was soon found that while some of these neurons could respond to parts of faces, other neurons required several parts of the face to be present in the correct spatial arrangement, and that many of these neurons did not just respond to any face that was shown, but responded differently to different faces (Desimone et al., 1984; Gross et al., 1985; Perrett et al., 1982; Rolls, 1984). By responding differently to different faces, these neurons potentially encode information useful for identifying individual faces. This early work showed that there is some specialization of function of different temporal cortical visual areas, and this specialization of function is described next.

The visual pathways project from the primary visual cortex V1 to the temporal lobe visual cortical areas by a number of intervening ventral stream cortical stages including V2 and V4 (Baizer et al., 1991; Rolls and Deco, 2002; Seltzer and Pandya, 1978). The inferior temporal visual cortex, area TE, is divided on the basis of cytoarchitecture, myeloarchitecture, and afferent input into areas TEa, TEm, TE3, TE2, and TE1. In addition, there is a set of different areas in the cortex in the superior temporal sulcus (Baylis et al., 1987; Seltzer and Pandya, 1978) (Fig. 78.1). Of these latter areas, TPO receives inputs from temporal, parietal, and occipital cortex; PGa and IPa from parietal and temporal cortex; and TS and TAa primarily from auditory areas (Seltzer and Pandya, 1978).

There is considerable specialization of function in these architectonically defined areas (Baylis et al., 1987). Areas TPO, Pga, and IPa are multimodal, with neurons that respond to visual, auditory, and/or somatosensory inputs. The more ventral areas in the inferior temporal gyrus (areas TE3, TE2, TE1, TEa, and TEm) are primarily unimodal visual areas. Areas in the cortex in the anterior and dorsal part of the superior temporal sulcus (e.g., TPO, IPa, and IPg)

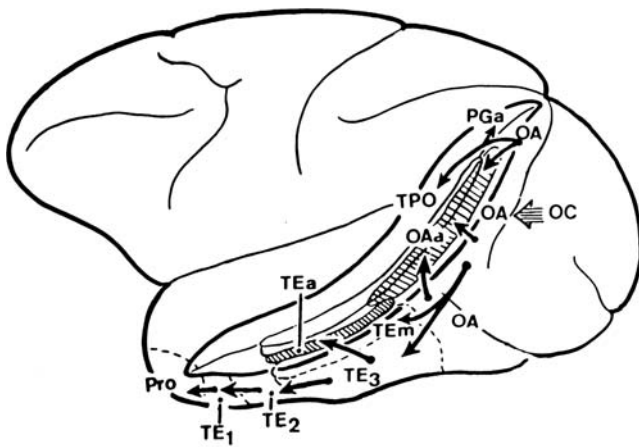


FIGURE 78.1. Lateral view of the macaque brain showing the different architectonic areas (e.g., TEa, TPO) in and bordering the anterior part of the superior temporal sulcus of the macaque (see text).

have neurons specialized for the analysis of moving visual stimuli. Neurons responsive primarily to faces are found more frequently in areas TPO, TEa, and TEm, where they comprise approximately 20% of the visual neurons responsive to stationary stimuli, in contrast to the other temporal cortical areas, in which they comprise 4% to 10%. The stimuli which activate other cells in these TE regions include simple visual patterns such as gratings and combinations of simple stimulus features (Baylis et al., 1987; Gross et al., 1985; Tanaka et al., 1990). Neurons with responses related to facial expression, movement, and gesture are more likely to be found in the cortex in the superior temporal sulcus, whereas neurons with activity related to facial identity are more likely to be found in the TE areas (see below and Hasselmo et al., 1989a).

The selectivity of one population of neurons for faces

Neurons with responses selective for faces respond 2 to 20 times more to faces than to a wide range of gratings, simple geometrical stimuli, or complex three-dimensional objects (Baylis et al., 1985, 1987; Rolls, 1984, 1992b). The responses to faces are excitatory, with firing rates often reaching 100 spikes per second, are sustained, and have typical latencies of 80 to 100 msec. The neurons are typically unresponsive to auditory or tactile stimuli and to the sight of arousing or aversive stimuli. These findings indicate that explanations in terms of arousal, emotional or motor reactions, and simple visual feature sensitivity are insufficient to account for the selective responses to faces and face features observed in this population of neurons (Baylis et al., 1985; Perrett et al., 1982; Rolls and Baylis, 1986). Observations consistent with these findings have been published by Desimone et al. (1984), who described a similar population of neurons

located primarily in the cortex in the superior temporal sulcus which responded to faces but not to simpler stimuli such as edges and bars or to complex nonface stimuli (see also Gross et al., 1985).

These neurons are specialized to provide information about faces in that they provide much more information (on average, 0.4 bit) about which (of 20) face stimuli is being seen than about which (of 20) nonface stimuli is being seen (on average, 0.07 bit) (Rolls and Tovee, 1995a; Rolls et al., 1997). These information theoretic procedures provide an objective and quantitative way to show what is “represented” by a particular population of neurons (Rolls and Deco, 2002; Rolls and Treves, 1998).

Masking out or presenting parts of the face (e.g., eyes, mouth, or hair) in isolation reveals that different cells respond to different features or subsets of features. For some cells, responses to the normal organization of cut-out or line-drawn facial features are significantly greater than to images in which the same facial features are jumbled (Perrett et al., 1982; Rolls et al., 1994b). These findings are consistent with the hypotheses developed below that, by competitive self-organization, some neurons in these regions respond to parts of faces by responding to combinations of simpler visual properties received from earlier stages of visual processing, and that other neurons respond to combinations of parts of faces and thus respond only to whole faces. Moreover, the finding that for some of these latter neurons the parts must be in the correct spatial configuration shows that the combinations formed can reflect not just the features present, but also their spatial arrangement. This provides a way in which binding can be implemented in neural networks (see also Elliffe et al., 2002). Further evidence that neurons in these regions respond to combinations of features in the correct spatial configuration was found by Tanaka et al. (e.g., 1990) using combinations of features that are used by comparable neurons to define objects.

Other neurons respond not to face identity but to face expression (Hasselmo et al., 1989a). The neurons responsive to expression were found primarily in the cortex in the superior temporal sulcus. Information about facial expression is of potential use in social interactions. A further way in which some of the neurons in the cortex in the superior temporal sulcus may be involved in social interactions is that some of them respond to gestures—for example, to a face undergoing ventral flexion (Hasselmo et al., 1989a; Perrett et al., 1989a). The interpretation of these neurons as being useful for social interactions is that in some cases these neurons respond not only to ventral head flexion, but also to the eyes lowering and the eyelids closing (Hasselmo et al., 1989b). These two movements (eye lowering and eyelid lowering) often occur together when one monkey is breaking social contact with another. It is also important when decoding facial expression to

retain some information about the direction of the head relative to the observer, for this is very important in determining whether a threat is being made in the observer's direction. The presence of view-dependent head and body gestures (Hasselmo et al., 1989b), and eye gaze (Perrett et al., 1985b), representations in some of these cortical regions where face expression is represented, is consistent with this requirement. In contrast, the TE areas (more ventral, mainly in the macaque inferior temporal gyrus), in which neurons tuned to face identity (Hasselmo et al., 1989a) and with view-independent responses (Hasselmo et al., 1989b) are more likely to be found, may be more related to an object-based representation of identity. Of course, for appropriate social and emotional responses, both types of subsystem would be important, for it is necessary to know both the direction of a social gesture and the identity of the individual in order to make the correct social or emotional response.

Outputs from the temporal cortical visual areas reach the amygdala and the orbitofrontal cortex, and evidence is accumulating that these brain areas use the representations of faces provided by the inferior temporal cortex visual areas to produce social and emotional responses to faces (Rolls, 1990, 1992a, 1992b, 1999). For example, lesions of the amygdala in monkeys disrupt social and emotional responses to faces, and we have identified a population of neurons with face-selective responses in the primate amygdala (Leonard et al., 1985), some of which respond to facial and body gestures (Brothers et al., 1990). Rolls et al. (2002b) have found a number of face-responsive neurons in the orbitofrontal cortex; these neurons are also present in adjacent prefrontal cortical areas (O'Scalaidhe et al., 1999; Wilson et al., 1993).

We have applied this research to the study of humans with frontal lobe damage to try to develop a better understanding of the social and emotional changes that may occur in these patients and that are related to the information these brain areas receive from the temporal cortical visual areas. Impairments in the identification of facial and vocal emotional expression were demonstrated in a group of patients with ventral frontal lobe damage who had behavioral problems such as disinhibited or socially inappropriate behavior (Hornak et al., 1996). A group of patients with lesions outside this brain region, without these behavioral problems, was unimpaired on expression identification tests. These findings suggest that some of the social and emotional problems associated with ventral frontal lobe or amygdala damage may be related to difficulty in identifying correctly facial (and vocal) expression and in learning associations involving such visual stimuli (Hornak et al., 1996, 2003; Rolls, 1990, 1999; Rolls et al., 1994a).

Neuroimaging data, while unable to address the details of what is encoded in a brain area or how it is encoded, do provide evidence consistent with the neurophysiology that

there are different face processing systems in the human brain. [Neurophysiology, at the single and multiple single neuron levels, rather than neuroimaging, is needed to understand issues such as the proportions of different types of neuron showing different types of response in a brain area; whether inputs from different sources or produced by different inputs activate the same neuron; the response latency in different areas; how long neurons in a given region must fire for perception to occur; whether the representation is fully distributed, sparse (and if so, how sparse it is and what the firing rate distribution is), or local; the amount of information provided by single neurons and how this scales with the size of the neuronal ensemble; the possibility of neuronal synchronization as a method of neural encoding; and, more generally, exactly how the information represented by the computing elements of the brain, and transmitted between the neurons, changes from stage to stage of neural processing in the brain. Answers to these issues are fundamental for understanding neural computation (Rolls and Deco, 2002).] For example, Kanwisher et al. (1997) and Ishai et al. (1999) have shown activation by faces of an area in the fusiform gyrus; Hoffman and Haxby (2000) have shown that distinct areas are activated by eye gaze and face identity; Dolan et al. (1997) have shown that a fusiform gyrus area becomes activated after humans learn to identify faces in complex scenes; and the amygdala (Morris et al., 1996) and orbitofrontal cortex (Blair et al., 1999) may become activated, particularly by certain face expressions.

The selectivity of a different population of neurons in the temporal cortex visual areas for objects

Other neurons in the inferior temporal visual cortex encode view-invariant representations of objects, including wire-frame objects (Logothetis and Sheinberg, 1996; Logothetis et al., 1994) and real objects (Booth and Rolls, 1998). For the neurons with view-invariant representations of real objects, it has been shown that no specific training is required to form the view-invariant representations and that experience with the objects in the home cage is sufficient (Booth and Rolls, 1998).

Distributed encoding of face and object identity

An important question for understanding brain function is whether a particular object (or face) is represented in the brain by the firing of one or a few (gnostic or *grandmother*) cells (Barlow, 1972), or whether instead the firing of a group or ensemble of cells, each with a different profile of responsiveness to the stimuli, provides a representation that is distributed across neurons. This issue is of considerable interest with respect to the inferior temporal visual cortex, for this

provides the main output from the ventral visual stream to brain areas such as the amygdala, orbitofrontal cortex, and hippocampal system, and influences how they make use of and read the code.

The actual representation found is distributed. Baylis et al. (1985) showed this with the responses of temporal cortical neurons that typically responded to several members of a set of five faces, with each neuron having a different profile of responses to each face. Hasselmo et al. (1989a) applied multidimensional scaling to populations of neurons recorded in the inferior temporal visual cortex and the cortex in the superior temporal sulcus, and indicated that the neural code read from the population indicated that these populations were coding for different aspects of the stimuli (see also Young and Yamane, 1992). In a more recent study using 23 faces and 45 nonface natural images, a distributed representation was found again (Rolls and Tovee, 1995a), with the average sparseness being 0.65. [The sparseness of the representation provided by a neuron can be defined as

$$a = (\sum_{s=1,S} r_s / S)^2 / \sum_{s=1,S} (r_s^2 / S)$$

where r_s is the mean firing rate of the neuron to stimulus s in the set of S stimuli (Rolls and Treves, 1998). If the neurons are binary (either firing or not firing to a given stimulus), then a would be 0.5 if the neuron responded to 50% of the stimuli and 0.1 if the neuron responded to 10% of the stimuli.] If the spontaneous firing rate was subtracted from the firing rate of the neuron to each stimulus, so that the changes of firing rate, that is, the *active responses* of the neurons, were used in the sparseness calculation, then the *response sparseness* had a lower value, with a mean of 0.33 for the population of neurons.

The distributed nature of the representation can be further understood by the finding that the firing rate distribution of single neurons when a wide range of natural visual stimuli are being viewed is approximately exponentially distributed, with a few stimuli producing high firing rates and increasingly large numbers of stimuli producing lower and lower firing rates (Baddeley et al., 1997; Rolls and Tovee, 1995a; Treves et al., 1999) (Fig. 78.2). This is a clear answer to the question of whether these neurons are grandmother cells: they are not, in the sense that each neuron has a graded set of responses to the different members of a set of stimuli, with the prototypical distribution similar to that of the neuron illustrated in Figure 78.2. On the other hand, each neuron does respond for more to some stimuli than to many others, and in this sense is tuned to some stimuli. The sparseness of such an exponential distribution of firing rates is 0.5. It has been shown that the distribution may arise from the threshold nonlinearity of neurons combined with short-term variability in the responses of neurons (Treves et al., 1999).

The distributed properties of the code used are further revealed by applying information theory (see Rolls and

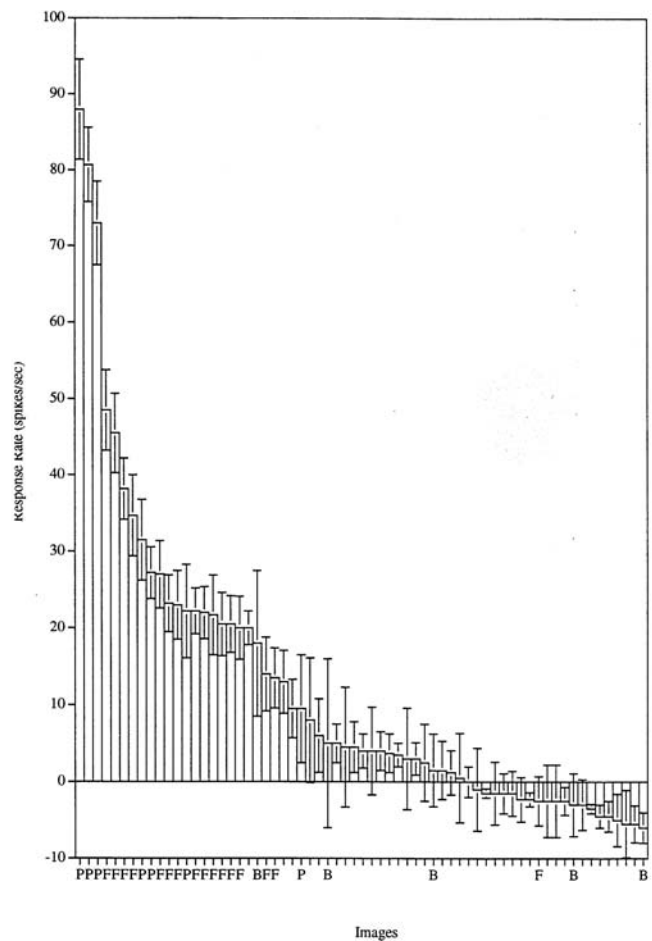


FIGURE 78.2. Firing rate distribution of a single neuron in the temporal visual cortex to a set of 23 face (F) and 45 nonface images of natural scenes. The firing rate to each of the 68 stimuli is shown. The neuron does not respond to just one of these stimuli. Instead, it responds to a small proportion of stimuli with high rates, to more stimuli with intermediate rates, and to many stimuli with almost no change of firing. This is typical of the distributed representations found in profile view; B, body parts (e.g., hands). (After Rolls and Tovee, 1995a.)

Deco, 2002; Rolls and Treves, 1998, Appendix 2; Shannon, 1948) to analyze how information is represented by a population of these neurons. The information required to identify which of S equiprobable stimuli were shown is $\log_2 S$ bits. The information about which of 20 equiprobable faces had been shown that was available from the responses of different numbers of these neurons is shown in Figure 78.3. First, it is clear that the information rises approximately linearly, and the number of stimuli encoded thus rises approximately exponentially, as the number of cells in the sample increases (Abbott et al., 1996; Rolls et al., 1997; see also Rolls and Treves, 1998). This direct neurophysiological evidence thus demonstrates that the encoding is distributed, that the responses are sufficiently independent

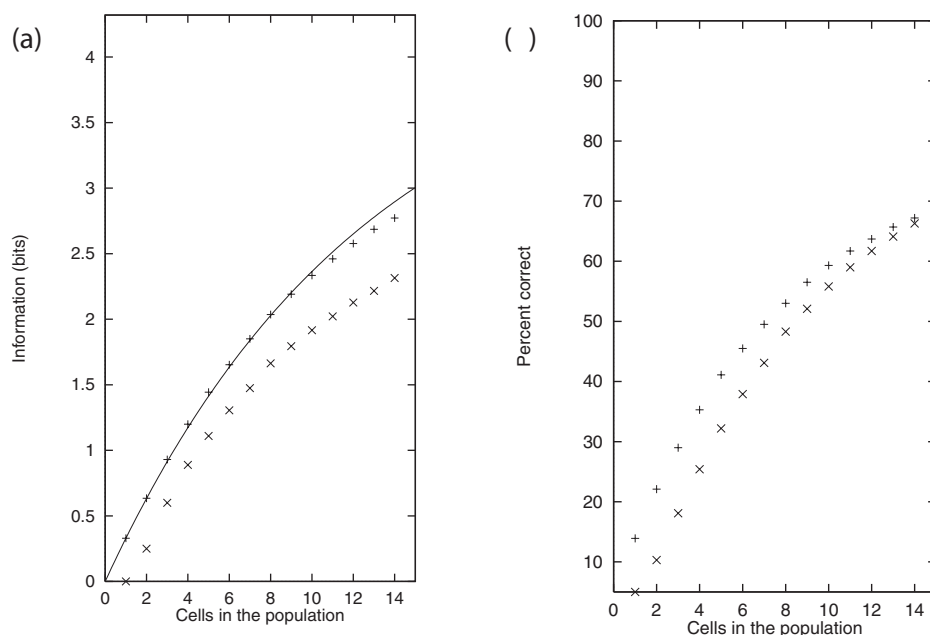


FIGURE 78.3. *a*, The values for the average information available in the responses of different numbers of these neurons on each trial about which of a set of 20 face stimuli has been shown. The decoding method was dot product (crosses) or probability estimation (pluses), and the effects obtained with cross-validation procedures utilizing 50% of the trials as test trials are shown. The remainder of the trials in the cross-validation procedure were used as training

trials. The solid line indicates the amount of information expected from populations of increasing size, assuming random correlations within the constraint given by the ceiling (the information in the stimulus set, $I = 4.32$ bits). *b*, The percentage correct (for estimating which stimulus was shown from the responses of different numbers of neurons using a decoding method) for the data corresponding to those shown in *a*. (After Rolls et al., 1997.)

and reliable, and that the representational capacity increases exponentially with the number of neurons in the ensemble. The consequence of this is that large numbers of stimuli, and fine discriminations between them, can be represented without having to measure the activity of an enormous number of neurons. [It has been shown that the main reason the information tends to asymptote, as shown in Figure 78.3 as the number of neurons in the sample increases, is that the ceiling on how much information is required to discriminate between the set of stimuli is being approached, which with 20 stimuli is $\log_2 20 = 4.32$ bits (Abbott et al., 1996; Rolls et al., 1997).] Second, it is clear that some information is available from the responses of just one neuron—on average, approximately 0.34 bit. Thus, knowing the activity of just one neuron in the population does provide some evidence about which stimulus was present, even when the activity of all the other neurons is not known. Rolls et al. (1997) also showed that information in the firing of individual neurons is made explicit in a way that allows neuronally plausible decoding, in which a receiving neuron simply uses each of its synaptic strengths to weight the input activity being received from each afferent axon and sums the result over all inputs. This is a dot product operation (between an input vector of the firing rates of different neurons and a synaptic weight vector, and the decoding is called *dot product decoding*).

It has also been shown that for the neurons in the inferior temporal visual cortex that encode view-invariant representations of objects, the same type of representation is found, namely, distributed encoding with independent information conveyed by different neurons (Booth and Rolls, 1998).

The analyses just described were obtained with neurons that were not simultaneously recorded, but similar results have now been obtained with simultaneously recorded neurons; that is, the information about which stimulus was shown increases approximately linearly with the number of neurons, showing that the neurons convey information that is nearly independent, with redundancy being on the order of 4% to 10% (Rolls et al., 2002a). Gawne and Richmond (1993) and Rolls et al. (2002a) showed that even adjacent pairs of neurons recorded simultaneously from the same electrode carried information that could be 90% independent. Panzeri et al. (1999a) and Rolls et al. (2003a) developed a method for measuring the information in the relative time of firing of simultaneously recorded neurons, which might be significant if the neurons became synchronized to some but not other stimuli in a set, as postulated by Singer and colleagues (e.g., Singer, 1999, 2000, Chapter 113). We found that for two different sets of inferior temporal cortex neurons, almost all the information was available in the firing rates (or number of spikes) of the cells, and almost no

information was available about which image was shown in the relative time of firing of different simultaneously recorded neurons (Panzeri et al. 1999a; Rolls et al. 2000a; 2000b). If significant cross-correlations between pairs of simultaneously recorded inferior temporal cortex neurons were present, these were usually not stimulus-dependent, and were associated with a small degree of redundancy between the cells. Thus, the evidence shows that most of the information is available in the firing rates (or number of spikes in a short time interval) of the neurons, and not in synchronization, for representations of faces and objects in the inferior temporal visual cortex (this is also the case for spatial neurons in the hippocampus and for olfactory neurons in the orbitofrontal cortex; see Rolls et al., 1996, 1998).

The information available from the number of spikes emitted by single neurons in short times is considerable, with the information available in a 50 msec time window being 75% of that available in a long window of 500 msec and 50% of that available in a 20 msec window (Tovee and Rolls, 1995; Tovee et al., 1993). Moreover, backward masking experiments show that sufficient information is available with 30 msec of inferior temporal cortex neuronal firing allowed for 50% correct recognition of the face shown (Rolls and Tovee, 1994; Rolls et al., 1994b; Rolls et al., 1999). Further, within a fraction of an interspike interval, with a distributed representation, much information can be extracted (Panzeri et al., 1999b; Rolls et al., 1997; Treves, 1993; Treves et al., 1997). In effect, spikes from many different neurons can contribute to calculating the angle between a neuronal population and a synaptic weight vector within an interspike interval. Given these facts, it is unnecessary, and indeed introduces a number of artificialities into the situation, to suppose that only the first spike of each neuron after a stimulus, and even the order in which spikes arrive from the different neurons, matters (Thorpe et al., 2001).

These results provide evidence that a cortical area can perform the computation necessary for the recognition of a visual stimulus in 20 to 30 msec and emphasizes just how rapidly cortical circuitry can operate. Although this speed of operation does seem fast for a network with recurrent connections (mediated, e.g., by recurrent collateral connections between pyramidal cells or by inhibitory interneurons), recent analyses of integrate-and-fire networks with biophysically modeled neurons which integrate their inputs and have spontaneous activity to keep the neurons close to the firing threshold show that such networks can settle very rapidly (Rolls and Treves, 1998; Treves, 1993; Treves et al., 1997). This approach has been extended to multilayer networks such as those found in the visual system, and again very rapid propagation (in 50 to 60 msec) of information through such a four-layer network with recurrent col-

laterals operating at each stage has been found (Panzeri et al., 2001).

The advantages of the distributed encoding actually found will now be discussed (see further Rolls and Deco, 2002; Rolls and Treves, 1998).

EXPONENTIALLY HIGH CODING CAPACITY This property refers to the fact that the information from a population of neurons rises linearly with the number of neurons, so that the number of stimuli that can be discriminated rises exponentially. This property arises from two factors: (1) the encoding is sufficiently close to independent by the different neurons (i.e., factorial), and (2) the encoding is sufficiently distributed.

EASE WITH WHICH THE CODE CAN BE READ BY RECEIVING NEURONS The code can be read with a neurally plausible, dot product, decoding method. All that is required of decoding neurons is the property of adding up postsynaptic potentials produced through each synapse as a result of the activity of each incoming axon (Abbott et al., 1996; Rolls et al., 1997) (Fig. 78.4).

GENERALIZATION, COMPLETION, GRACEFUL DEGRADATION, AND HIGHER RESISTANCE TO NOISE Because the decoding of a distributed representation involves assessing the activity of a whole population of neurons and computing a dot product or correlation between the set (or vector) of inputs and the synaptic weights (Fig. 78.4), a distributed representation provides more resistance to variation in individual components than does a local encoding scheme. This allows higher resistance to noise (Panzeri et al., 1996), graceful (in that it is gradual) degradation of performance when synapses or input axons are lost, and generalization to similar stimuli.

SPEED OF READOUT OF THE INFORMATION The information available in a distributed representation can be decoded by an analyzer more quickly than can the information from a local representation, given comparable firing rates.

Invariance in the neuronal representation of stimuli

One of the major problems that must be solved by a visual system is the building of a representation of visual information which allows recognition to occur relatively independently of size, contrast, spatial frequency, position on the retina, angle of view, and so on. This is required so that if the receiving regions such as the amygdala, orbitofrontal cortex, and hippocampus learn about one view, position, or size of the object, the animal generalizes correctly to other views, positions, and sizes of the object. The majority of face-selective neurons in the inferior temporal cortex have responses that are relatively invariant with respect to the size

Dot Product Multiple Cell Decoding

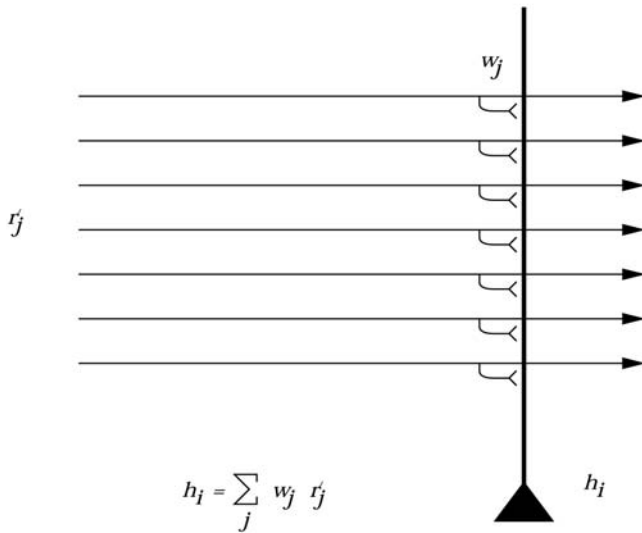


FIGURE 78.4. Neuronal activation and the dot product as used in models of associative memory. When a stimulus is present on the input axons, the total activation h_i of a neuron i is the sum of all the activations produced through each strengthened synapse w_{ij} by each active axon r'_j . We can express this as

$$h_i = \sum_j r'_j w_{ij}$$

where \sum_j indicates that the sum is over the C input axons (or connections) indexed by j . The synapse w_{ij} is the j th synapse (arising from axon j) onto neuron i . The multiplicative form indicates that activation should be produced by an axon only if it is firing and only if it is connected to the dendrite by a strengthened synapse. The sum of all such activations expresses the idea that summation (of synaptic currents in real neurons) occurs along the length of the dendrite to produce activation at the cell body, where the activation h_i is converted into firing r_i by a function that includes a threshold. Calculation of the neuronal activation by multiplying the vector of input firings by the vector of synaptic weights is an inner or dot product of two vectors which measures the similarity of the two vectors. It is this computation of similarity (very close to the correlation) between the two vectors that enables neurons to show the interesting properties of generalization, completion, graceful degradation, and resistance to noise, provided that the input representations r' are distributed (Rolls and Treves, 1998).

of the stimulus (Rolls and Baylis, 1986). The median size change tolerated with a response of more than half of the maximal response was 12 times. Also, the neurons typically responded to a face when the information in it had been reduced from a three-dimensional to a two-dimensional representation in gray on a monitor, with a response which was on average 0.5 of that to a real face. Another transform over which recognition is relatively invariant is spatial frequency, and it has been shown that the processing with respect to spatial frequency is not additive with respect to different bands of spatial frequency (Rolls et al., 1985, 1987).

Inferior temporal visual cortex neurons also often showed considerable translation (shift) invariance, not only under anesthesia (Gross et al., 1985), but also in the awake, behaving primate (Tovee et al., 1994). In most cases, the responses of the neurons were little affected by which part of the face was fixated, and the neurons responded (with a greater than half-maximal response) even when the monkey fixated 2 to 5 degrees beyond the edge of a face which subtended 8 to 17 degrees at the retina. Moreover, stimulus selectivity between faces was maintained this far eccentric within the receptive field.

Until recently, research on translation invariance considered the case in which there are only one or two images or objects in the visual field. What happens in a cluttered natural environment? Do all objects that can activate an inferior temporal neuron do so whenever they are anywhere within the large receptive fields of inferior temporal neurons? If so, the output of the visual system might be confusing for structures which receive inputs from the temporal cortical visual areas. To clarify this, Rolls et al. (2003a) recorded from inferior temporal cortex neurons while macaques searched for objects in complex natural scenes as well as in plain backgrounds, as normally used. They found that inferior temporal cortex neuron receptive fields are much smaller in natural scenes (mean radius = 15.7 degrees) than in plain backgrounds (mean radius = 33.7 degrees), and in complex backgrounds can reduce to close to the size of a 9×7 degree object. The peak firing rate of the neuron was little affected by whether the effective stimulus was a target to which attention should be shown or not in a complex scene or a plain background. In terms of responsiveness and selectivity, *background invariance* is thus a property of these neurons. Attention, as influenced by whether the object was to be searched for and was a target for action, had little effect in a complex scene. The main effect of object-based attention on inferior temporal cortex neurons was found in blank displays when it increased the receptive field size of objects that were the target for action. This increase was especially pronounced when there was only one object in a blank scene, but it was also found when there were two objects in a blank scene. It was concluded that inferior temporal cortex neurons, which provide the object-related output of the ventral visual processing stream, have receptive fields which shrink to approximately the size of an object when the object is shown in a natural scene. This helps the inferior temporal visual cortex to provide an unambiguous representation of a potential target, for the output reflects in a natural scene what is shown at the fixation point. The results also showed that attentional effects are mainly demonstrable in inferior temporal cortex neurons when stimuli are shown in an artificial plain background, and that normally the output of the inferior temporal cortex reflects what is shown at the fovea (see further Rolls and Deco, 2002; Trappenberg et al., 2002).

The translation invariance that is a property of these neurons may enable the visual system to compensate for small changes in the position of stimuli on the retina, and to adjust the receptive field size to that appropriate for receiving all the evidence relevant to diagnosing the presence of particular objects independently of their size (Rolls et al., 2003a). These findings are a step toward understanding how the visual system functions in a normal environment (see also Gallant et al., 1998; Stringer and Rolls, 2000) and are complemented by a finding of DiCarlo and Maunsell (2000) that inferotemporal cortex neurons respond similarly to an effective shape stimulus for a cell even if some distractor stimuli are present a few degrees away. A similar result was also found by Rolls and Tovee (1995b), who showed in addition that with two stimuli present in the visual field, the anterior inferior temporal neuronal responses were weighted toward the stimulus that was closest to the fovea.

In addition to these types of invariance, some temporal cortical neurons reliably respond differently to the faces of two different individuals independently of viewing angle, although in most cases (16/18 neurons) the response was not perfectly view-independent (Hasselmo et al., 1989b). Mixed together in the same cortical regions are neurons with view-dependent responses. Such neurons might respond, for example, to a view of a profile of a monkey but not to a full-face view of the same monkey (Perrett et al., 1985b). These findings, of view-dependent, partially view-independent, and view-independent representations in the same cortical regions are consistent with the hypothesis discussed below that view-independent representations are being built in these regions by associating together neurons that respond to different views of the same individual.

Further evidence that some neurons in the temporal cortical visual areas have object-based rather than view-based responses comes from a study of a population of neurons that responds to moving faces (Hasselmo et al., 1989b). For example, four neurons responded vigorously to a head undergoing ventral flexion, irrespective of whether the view of the head was full face, of either profile, or even of the back of the head. These different views could only be specified as equivalent in object-based coordinates. Further, the movement specificity was maintained across inversion, with neurons responding, for example, to ventral flexion of the head irrespective of whether the head was upright or inverted. In this procedure, retinally encoded or viewer-centered movement vectors are reversed, but the object-based description remains the same.

Neurons with view-invariant responses of objects seen naturally by macaques have also been described (Booth and Rolls, 1998). The stimuli were images of 10 real plastic objects which had been in the monkey's cage for several weeks to enable him to build view-invariant representations of the objects. After this visual experience, it was shown

that some inferior temporal cortex neurons have similar responses to views of the same object presented on a monitor and different responses to different objects. This invariance was based on shape in that it remained when the images of the objects were shown in gray scale (i.e., without color). Further evidence consistent with these findings is that some studies have shown that the responses of some visual neurons in the inferior temporal cortex do not depend on the presence or absence of critical features for maximal activation (e.g., Perrett et al., 1982; see also Tanaka, 1993, 1996). For example, Mikami et al. (1994) have shown that some TE cells respond to partial views of the same laboratory instrument(s) even when these partial views contain different features. Using a different approach, Logothetis et al. (1994) reported that in monkeys extensively trained (over thousands of trials) to treat different views of computer-generated wire-frame objects the same way, a small population of neurons in the inferior temporal cortex did respond to different views of the same wire-frame object (see also Logothetis and Sheinberg, 1996). However, extensive training is not necessary for invariant representations to be formed, and indeed, no explicit training in invariant object recognition was given in the experiment by Booth and Rolls (1998), as Rolls' (1992b) hypothesis is that view-invariant representations can be learned by associating together the different views of objects as they are moved and inspected naturally in a period that may be only a few seconds long.

Learning new representations in the temporal cortical visual areas

To investigate the idea that visual experience may guide the formation of the responsiveness of neurons, so that they provide an economical and ensemble-encoded representation of items actually present in the environment, the responses of inferior temporal cortex face-selective neurons have been analyzed while a set of new faces were shown. Some of the neurons studied in this way altered the relative degree to which they responded to the different members of the set of novel faces over the first few (one or two) presentations of the set (Rolls et al., 1989). This evidence is consistent with categorization being performed by self-organizing competitive neuronal networks, as described below and elsewhere (Rolls and Treves, 1998).

Further evidence that these neurons can learn new representations very rapidly comes from an experiment in which binarized black and white images of faces which blended with the background were used. These did not activate face-selective neurons. Full gray-scale images of the same photographs were then shown for ten 0.5 second presentations. In a number of cases, if the neuron happened to be responsive to that face, when the binarized version of the same face was shown next the neurons responded to it (Tovee

et al., 1996). This is a direct parallel to the same phenomenon which is observed psychophysically, and it provides dramatic evidence that these neurons are influenced by only a very few seconds (in this case 5 seconds) of experience with a visual stimulus. We have shown a neural correlate of this effect using similar stimuli and a similar paradigm in a positron emission tomography neuroimaging study in humans, with a region showing an effect of the learning found for faces in the right temporal lobe and for objects in the left temporal lobe (Dolan et al., 1997). Such rapid learning of representations of new objects appears to be a major type of learning in which the temporal cortical areas are involved.

Possible computational mechanisms in the visual cortex for object recognition

The neurophysiological findings described above, and wider considerations on the possible computational properties of the cerebral cortex (Rolls, 1989, 1992b; Rolls and Deco, 2002; Rolls and Treves, 1998), lead to the following outline working hypotheses on object (including face) recognition by visual cortical mechanisms.

Cortical visual processing for object recognition is considered to be organized as a set of hierarchically connected cortical regions consisting at least of V1, V2, V4, posterior inferior temporal cortex (TEO), inferior temporal cortex (e.g., TE3, TEa, and TE_m), and anterior temporal cortical areas (e.g., TE2 and TE1). There is convergence from each small part of a region to the succeeding region (or layer or stage in the hierarchy) in such a way that the receptive field sizes of neurons (e.g., 0.5 to 1 degree near the fovea in V1) become larger by a factor of approximately 2.5 with each succeeding stage (the typical parafoveal receptive field sizes

found would not be inconsistent with the calculated approximations of, e.g., 8 degrees in V4, 20 degrees in TEO, and 50 degrees in inferior temporal cortex; Boussaoud et al., 1991) (Fig. 78.5). Such zones of convergence would overlap continuously with each other (Fig. 78.5). This connectivity would be part of the architecture by which translation-invariant representations are computed.

Each stage in the hierarchy is considered to act partly as a set of local self-organizing competitive neuronal networks with overlapping inputs. The operation of competitive networks is described by Kohonen (1989), Rolls and Treves (1998), and Rolls and Deco (2002). They use competition implemented by lateral inhibition and associative modification of active inputs onto output neurons that are left firing after the competition. Competitive networks can be thought of as building feature analyzers, in that each neuron in a competitive network uses associative synaptic modification to learn to respond to a set or combination of coactive inputs to the neuron, which might represent a visual feature (Rolls and Milward, 2000; Rolls and Treves, 1998; Wallis and Rolls, 1997).

Increasing complexity of representations could also be built in such a multiple-layer hierarchy by similar competitive learning mechanisms. In order to avoid a combinatorial explosion, low-order combinations of inputs would be learned by each neuron. An important part of the theory is that some local spatial information is inherent in the features being combined. For example, cells might not respond to the combination of an edge and a small circle unless they were in the correct spatial relation to each other. [This is in fact consistent with the data of Tanaka et al. (1990), and with our data on face neurons, in that some faces neurons require the face features to be in the correct spatial configuration and not jumbled (Rolls et al., 1994b).] The local spatial

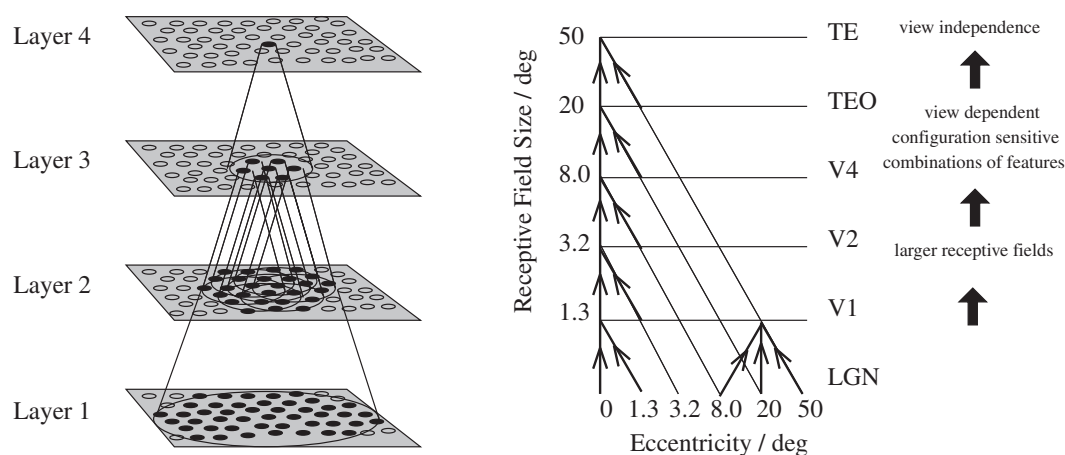


FIGURE 78.5. Schematic diagram showing convergence achieved by the forward projections in the visual system, and the types of representation that may be built by competitive networks operating at each stage of the system from the primary visual cortex (V1) to the inferior temporal visual cortex (area TE) (see text). LGN, lateral geniculate nucleus. Area TEO forms the posterior inferior temporal cortex. The receptive fields in the inferior temporal visual cortex (e.g., in the TE areas) cross the vertical midline (not shown).

information in the features being combined would ensure that the representation at the next level would contain some information about the (local) arrangement of features. Further low-order combinations of such neurons at the next stage would include sufficient local spatial information so that an arbitrary spatial arrangement of the same features would not activate the same neuron; this is the proposed, and limited, solution which this mechanism would provide for the feature binding problem (Elliffe et al., 2002). Once such a feature hierarchy scheme has been trained with exemplars in the early layers, training at only some locations is needed at the higher levels to achieve generalization to new locations of new objects trained at some locations (Elliffe et al., 2002).

Although hierarchical processing schemes have been investigated before (e.g., Fukushima, 1980, 1989, 1991), Rolls (1992b) suggested that translation, size, and view invariance could be computed in such a system by utilizing competitive learning that operates across short time scales to detect regularities in inputs when real objects are transforming in the physical world (Rolls, 1992a). The idea is that because objects have continuous properties in space and time in the world, an object at one place on the retina might activate feature analyzers at the next stage of cortical processing, and when the object is translated to a nearby position, because this would occur in a short period (e.g., 0.5 second), the membrane of the postsynaptic neuron would still be in its associatively modifiable state, and the presynaptic afferents activated with the object in its new position would thus become strengthened on the still-activated postsynaptic neuron. The neuronal mechanisms that might implement this short-term temporal averaging in modifiability are of interest and include lasting effects of calcium entry as a result of the voltage-dependent activation of NMDA receptors, as well as continuing firing of the neuron implemented by recurrent collateral connections forming a short-term memory. The short temporal window (e.g., 0.5 second) of associative modifiability helps neurons to learn the statistics of objects transforming in the physical world, and at the same time to form different representations of different feature combinations or objects, as these are physically discontinuous and present less regular correlations to the visual system. Foldiak (1991) has proposed computing an average activation of the postsynaptic neuron to assist with translation invariance. Rolls (1992a) suggested that other invariances, for example, size, spatial frequency, rotation, and view invariance, could be learned by mechanisms similar to those just described.

To test and clarify the hypotheses just described about how the visual system may operate to learn invariant object recognition, we have performed a simulation, VisNet, which implements many of the ideas just described, and is consistent with and based on much of the neurophysiology sum-

marized above. The network simulated can perform object recognition, including face recognition, in a biologically plausible way, and after training shows, for example, translation and view invariance (Rolls and Milward, 2000; Wallis and Rolls, 1997; Wallis et al., 1993). The network can identify objects shown in a cluttered environment (e.g., a natural scene) and can identify partially occluded objects (Stringer and Rolls, 2000). Parga and Rolls (1998) and Elliffe et al. (2000) incorporated the associations between exemplars of the same object in the recurrent synapses of an autoassociative (*attractor*) network so that the techniques of statistical physics could be used to analyze the storage capacity of a system implementing invariant representations in this way. They showed that such networks did have an "object" phase in which the presentation of any exemplar (e.g., a view) of an object would result in the same firing state as other exemplars of the same object, and that the number of different objects that could be stored is proportional to the number of synapses per neuron divided by the number of views of each object. Rolls and Milward (2000) and Rolls and Stringer (2001) explored the operation of the trace learning rule used in the VisNet architecture further, and showed that the rule operated especially well if the trace incorporated activity from previous presentations of the same object but no contribution from the current neuronal activity being produced by the current exemplar of the object. The explanation is that this temporally asymmetric rule (the presynaptic term from the current exemplar and the trace from the preceding exemplars) encourages neurons to respond to the current exemplar in the same way as they did to previous exemplars.

These results with a feature hierarchy network, VisNet, show that the proposed learning mechanism and neural architecture can produce cells with responses selective for stimulus type with considerable position or view invariance (Rolls and Deco, 2002). The network has recently been extended to incorporate back projections and interactions between a dorsal spatial processing stream and a ventral object processing stream, and is enabling extensive modeling of spatial and object attentional processes within a mean-field framework (Deco and Rolls, 2002; Rolls and Deco, 2002).

Conclusions

Neurophysiological investigations of the inferior temporal cortex are revealing at least part of the way in which neuronal firing encodes information about faces and objects and are showing that the representation implements several types of invariance. The representation found has clear utility for the receiving networks. These neurophysiological findings are stimulating the development of computational neuronal network models which suggest that part of the cellular processing involves the operation of a modified associative

learning rule with a short-term memory trace to help the system learn invariances from the statistical properties of the inputs it receives. It is a challenge to identify the cellular processes that could implement this short-term memory trace, as well as the processes that might help to maintain the total synaptic strength received by each neuron approximately constant, as is required for competitive networks (Rolls and Treves, 1998).

Acknowledgments

The author has worked on some of the investigations described here with P. Azzopardi, G. C. Baylis, M. Booth, P. Foldiak, M. E. Hasselmo, C. M. Leonard, T. J. Milward, D. I. Perrett, S. M. Stringer, M. J. Tovee, A. Treves, and G. Wallis, and their collaboration is sincerely acknowledged. Different parts of the research described were supported by the Medical Research Council, PG8513790 and PG9826105; by a Human Frontier Science Program grant; by an EC Human Capital and Mobility grant; by the MRC Oxford Interdisciplinary Research Centre in Cognitive Neuroscience; and by the Oxford McDonnell-Pew Centre in Cognitive Neuroscience.

REFERENCES

- Abbott, L. F., E. T. Rolls, and M. J. Tovee, 1996. Representational capacity of face coding in monkeys, *Cereb. Cortex*, 6:498–505.
- Baddeley, R. J., L. F. Abbott, M. J. A. Booth, F. Sengpiel, T. Freeman, E. A. Wakeman, and E. T. Rolls, 1997. Responses of neurons in primary and inferior temporal visual cortices to natural scenes, *Proc. R. Soc. B*, 264:1775–1783.
- Baizer, J. S., L. G. Ungerleider, and R. Desimone, 1991. Organization of visual inputs to the inferior temporal and posterior parietal cortex in macaques, *J. Neurosci.*, 11:168–190.
- Barlow, H. B., 1972. Single units and sensation: a neuron doctrine for perceptual psychology? *Perception*, 1:371–394.
- Baylis, G. C., E. T. Rolls, and C. M. Leonard, 1985. Selectivity between faces in the responses of a population of neurons in the cortex in the superior temporal sulcus of the monkey, *Brain Res.*, 342:91–102.
- Baylis, G. C., E. T. Rolls, and C. M. Leonard, 1987. Functional subdivisions of temporal lobe neocortex, *J. Neurosci.*, 7:330–342.
- Blair, R. J., J. S. Morris, C. D. Frith, D. I. Perrett, and R. J. Dolan, 1999. Dissociable neural responses to facial expressions of sadness and anger, *Brain*, 122:883–893.
- Booth, M. C. A., and E. T. Rolls, 1998. View-invariant representations of familiar objects by neurons in the inferior temporal visual cortex, *Cereb. Cortex*, 8:510–523.
- Boussaoud, D., R. Desimone, and L. G. Ungerleider, 1991. Visual topography of area TEO in the macaque, *J. Comp. Neurol.*, 306:554–575.
- Brothers, L., B. Ring, and A. S. Kling, 1990. Response of neurons in the macaque amygdala to complex social stimuli, *Behav. Brain Res.*, 4:199–213.
- Bruce, C., R. Desimone, and C. G. Gross, 1981. Visual properties of neurons in a polysensory area in superior temporal sulcus of the macaque, *J. Neurophysiol.*, 46:369–384.
- Deco, G., and E. T. Rolls, 2003. A neurodynamical cortical model of visual attention and invariant object recognition. In preparation.
- Desimone, R., 1991. Face-selective cells in the temporal cortex of monkeys, *J. Cogn. Neurosci.*, 3:1–8.
- Desimone, R., T. D. Albright, C. G. Gross, and C. Bruce, 1984. Stimulus-selective properties of inferior temporal neurons in the macaque, *J. Neurosci.*, 4:2051–2062.
- Desimone, R., and C. G. Gross, 1979. Visual areas in the temporal lobe of the macaque, *Brain Res.*, 178:363–380.
- DiCarlo, J. J., and J. H. R. Maunsell, 2000. Form representation in monkey inferotemporal cortex is virtually unaltered by free viewing, *Nat. Neurosci.*, 3:814–821.
- Dolan, R. J., G. R. Fink, E. T. Rolls, M. Booth, A. Holmes, R. S. J. Frackowiak, and K. J. Friston, 1997. How the brain learns to see objects and faces in an impoverished context, *Nature*, 389:596–599.
- Elliffe, M. C. M., E. T. Rolls, N. Parga, and N. Renart, 2000. A recurrent model of transformation invariance by association, *Neural Net.*, 13:225–237.
- Elliffe, M. C. M., E. T. Rolls, and S. M. Stringer, 2002. Invariant recognition of feature combinations in the visual system, *Biol. Cybern.*, 86:59–71.
- Foldiak, P. 1991. Learning invariance from transformation sequences, *Neural Comp.*, 3:193–199.
- Fukushima, K., 1980. Neocognitron: a self-organizing neural network model for a mechanism of pattern recognition unaffected by shift in position, *Biol. Cybern.*, 36:193–202.
- Fukushima, K., 1989. Analysis of the process of visual pattern recognition by the neocognitron, *Neural Net.*, 2:413–420.
- Fukushima, K., 1991. Neural networks for visual pattern recognition, *IEEE Trans.*, E74:179–190.
- Gallant, J. L., C. E. Connor, and D. C. Van-Essen, 1998. Neural activity in areas V1, V2 and V4 during free viewing of natural scenes compared to controlled viewing, *Neuroreport*, 9:85–90.
- Gawne, T. J., and B. J. Richmond, 1993. How independent are the messages carried by adjacent inferior temporal cortical neurons? *J. Neurosci.*, 13:2758–2771.
- Gross, C. G., R. Desimone, T. D. Albright, and E. L. Schwartz, 1985. Inferior temporal cortex and pattern recognition, *Exp. Brain Res. Suppl.*, 11:179–201.
- Hasselmo, M. E., E. T. Rolls, and G. C. Baylis, 1989a. The role of expression and identity in the face-selective responses of neurons in the temporal visual cortex of the monkey, *Behav. Brain Res.*, 32:203–218.
- Hasselmo, M. E., E. T. Rolls, G. C. Baylis, and V. Nalwa, 1989b. Object-centered encoding by face-selective neurons in the cortex in the superior temporal sulcus of the monkey, *Exp. Brain Res.*, 75:417–429.
- Hoffman, E. A., and J. V. Haxby, 2000. Distinct representations of eye gaze and identity in the distributed neural system for face perception, *Nat. Neurosci.*, 3:80–84.
- Hornak, J., E. T. Rolls, and D. Wade, 1996. Face and voice expression identification in patients with emotional and behavioural changes following ventral frontal lobe damage, *Neuropsychologia*, 34:247–261.
- Hornak, J., J. Bramham, E. T. Rolls, R. G. Morris, J. O'Doherty, P. R. Bullock, and C. E. Polkey, 2003. Changes in emotion after circumscribed surgical lesions of the orbitofrontal and cingulate cortices, *Brain* 126, in press.
- Ishai, A., L. G. Ungerleider, A. Martin, J. L. Schouten, and J. V. Haxby, 1999. Distributed representation of objects in the

- human ventral visual pathway, *Proc. Natl. Acad. Sci. USA*, 96: 9379–9384.
- Kanwisher, N., J. McDermott, and M. M. Chun, 1997. The fusiform face area: a module in human extrastriate cortex specialized for face perception, *J. Neurosci.*, 17:4302–4311.
- Kohonen, T., 1989. *Self-Organization and Associative Memory*, 3rd ed. (1984, 1st ed.; 1988, 2nd ed.), Berlin: Springer-Verlag.
- Leonard, C. M., E. T. Rolls, F. A. W. Wilson, and G. C. Baylis, 1985. Neurons in the amygdala of the monkey with responses selective for faces, *Behav. Brain Res.*, 15:159–176.
- Logothetis, N. K., J. Pauls, H. H. Bulthoff, and T. Poggio, 1994. View-dependent object recognition by monkeys, *Curr. Biol.*, 4:401–414.
- Logothetis, N. K., and D. L. Sheinberg, 1996. Visual object recognition, *Annu. Rev. Neurosci.*, 19:577–621.
- Mikami, A., K. Nakamura, and K. Kubota, 1994. Neuronal responses to photographs in the superior temporal sulcus of the rhesus monkey, *Behav. Brain Res.*, 60:1–13.
- Morris, J. S., C. D. Fritch, D. I. Perrett, D. Rowland, A. W. Young, A. J. Calder, and R. J. Dolan, 1996. A differential neural response in the human amygdala to fearful and happy face expressions, *Nature*, 383:812–815.
- O’Scalaidhe, S. P., F. A. W. Wilson, and P. S. Goldman-Rakic, 1999. Face-selective neurons during passive viewing and working memory performance of rhesus monkeys: evidence for intrinsic specialization of neuronal coding, *Cereb. Cortex*, 9:459–475.
- Panzeri, S., G. Biella, E. T. Rolls, W. E. Skaggs, and A. Treves, 1996. Speed, noise, information and the graded nature of neuronal responses, *Network*, 7:365–370.
- Panzeri, S., E. T. Rolls, F. Battaglia, and R. Lavis, 2001. Speed of information retrieval in multilayer networks of integrate-and-fire neurons, *Network: Comput. Neural Syst.*, 12:423–440.
- Panzeri, S., S. R. Schultz, A. Treves, and E. T. Rolls, 1999a. Correlations and the encoding of information in the nervous system, *Proc. R. Soc. B*, 266:1001–1012.
- Panzeri, S., A. Treves, S. R. Schultz, and E. T. Rolls, 1999b. On decoding the responses of a population of neurons from short time epochs, *Neural Comp.*, 11:1553–1577.
- Parga, N., and E. T. Rolls, 1998. Transform invariant recognition by association in a recurrent network, *Neural Comp.*, 10:1507–1525.
- Perrett, D. I., E. T. Rolls, and W. Caan, 1982. Visual neurons responsive to faces in the monkey temporal cortex, *Exp. Brain Res.*, 47:329–342.
- Perrett, D. I., P. A. J. Smith, A. J. Mistlin, A. J. Chitty, A. S. Head, D. D. Potter, R. Broennimann, A. D. Milner, and M. A. Jeeves, 1985a. Visual analysis of body movements by neurons in the temporal cortex of the macaque monkey: a preliminary report, *Behav. Brain Res.*, 16:153–170.
- Perrett, D. I., P. A. J. Smith, D. D. Potter, A. J. Mistlin, A. S. Head, D. Milner, and M. A. Jeeves, 1985b. Visual cells in temporal cortex sensitive to face view and gaze direction, *Proc. R. Soc. B*, 223:293–317.
- Rolls, E. T., 1984. Neurons in the cortex of the temporal lobe and in the amygdala of the monkey with responses selective for faces, *Hum. Neurobiol.*, 3:209–222.
- Rolls, E. T., 1989. Functions of neuronal networks in the hippocampus and neocortex in memory, in *Neural Models of Plasticity: Experimental and Theoretical Approaches* (J. H. Byrne and W. O. Berry, eds.), San Diego, CA: Academic Press, pp. 240–265.
- Rolls, E. T., 1990. A theory of emotion, and its application to understanding the neural basis of emotion, *Cogn. Emotion*, 4:161–190.
- Rolls, E. T., 1992a. Neurophysiology and functions of the primate amygdala, in *The Amygdala* (J. P. Aggleton ed.), New York: Wiley-Liss, pp. 143–165.
- Rolls, E. T., 1992b. Neurophysiological mechanisms underlying face processing within and beyond the temporal cortical visual areas, *Philos. Trans. R. Soc.*, 335:11–21.
- Rolls, E. T., 1999. *The Brain and Emotion*, Oxford: Oxford University Press.
- Rolls, E. T., N. C. Aggelopoulos, L. Franco, and A. Treves, 2002a. Information encoding in the inferior temporal cortex: contributions of the firing rates and correlations between the firing of neurons. Submitted for publication.
- Rolls, E. T., N. C. Aggelopoulos, and F. Zheng, 2003a. The receptive fields of inferior temporal cortex neurons in natural scenes, *J. Neurosci.*, 23:339–348.
- Rolls, E. T., and G. C. Baylis, 1986. Size and contrast have only small effects on the responses to faces of neurons in the cortex of the superior temporal sulcus of the monkey, *Exp. Brain Res.*, 65:38–48.
- Rolls, E. T., G. C. Baylis, and M. E. Hasselmo, 1987. The responses of neurons in the cortex in the superior temporal sulcus of the monkey to band-pass spatial frequency filtered faces, *Vis. Res.*, 27:311–326.
- Rolls, E. T., G. C. Baylis, M. E. Hasselmo, and V. Nalwa, 1989. The effect of learning on the face-selective responses of neurons in the cortex in the superior temporal sulcus of the monkey, *Exp. Brain Res.*, 76:153–164.
- Rolls, E. T., G. C. Baylis, and C. M. Leonard, 1985. Role of low and high spatial frequencies in the face-selective responses of neurons in the cortex in the superior temporal sulcus, *Vis. Res.*, 25:1021–1035.
- Rolls, E. T., H. D. Critchley, A. S. Browning, and K. Inoue, 2002b. Face-selective and auditory neurons in the primate orbitofrontal cortex. Submitted for publication.
- Rolls, E. T., H. D. Critchley, and A. Treves, 1996. The representation of olfactory information in the primate orbitofrontal cortex, *J. Neurophysiol.*, 75:1982–1996.
- Rolls, E. T., and G. Deco, 2002. *Computational Neuroscience of Vision*, Oxford: Oxford University Press.
- Rolls, E. T., L. Franco, N. C. Aggelopoulos, and S. Reece, 2003b. Application of an information theoretic approach to analysing the contributions of the firing rates and correlations between the firing of neurons, *J. Neurophysiol.*, 89:2810–2822.
- Rolls, E. T., J. Hornak, D. Wade, and J. McGrath, 1994a. Emotion-related learning in patients with social and emotional changes associated with frontal lobe damage, *J. Neurol. Neurosurg. Psychiatry*, 57:1518–1524.
- Rolls, E. T., and T. Milward, 2000. A model of invariant object recognition in the visual system: learning rules, activation functions, lateral inhibition, and information-based performance measures, *Neural Comput.*, 12:2547–2572.
- Rolls, E. T., and S. M. Stringer, 2001. Invariant object recognition in the visual system with error correction and temporal difference learning, *Network: Comput. Neural Syst.*, 12:111–129.
- Rolls, E. T., and M. J. Tovee, 1994. Processing speed in the cerebral cortex, and the neurophysiology of visual backward masking, *Proc. R. Soc. B*, 257:9–15.
- Rolls, E. T., and M. J. Tovee, 1995a. Sparseness of the neuronal representation of stimuli in the primate temporal visual cortex, *J. Neurophysiol.*, 73:713–726.
- Rolls, E. T., and M. J. Tovee, 1995b. The responses of single neurons in the temporal visual cortical areas of the macaque when more than one stimulus is present in the visual field, *Exp. Brain Res.*, 103:409–420.

- Rolls, E. T., M. J. Tovee, and S. Panzeri, 1999. The neurophysiology of backward visual masking: information analysis, *J. Cogn. Neurosci.*, 11:335–346.
- Rolls, E. T., M. J. Tovee, D. G. Purcell, A. L. Stewart, and P. Azzopardi, 1994b. The responses of neurons in the temporal cortex of primates, and face identification and detection, *Exp. Brain Res.*, 101:474–484.
- Rolls, E. T., and A. Treves, 1998. *Neural Networks and Brain Function*, Oxford: Oxford University Press.
- Rolls, E. T., A. Treves, R. G. Robertson, P. Georges-François, and S. Panzeri, 1998. Information about spatial view in an ensemble of primate hippocampal cells, *J. Neurophysiol.*, 79:1797–1813.
- Rolls, E. T., A. Treves, and M. J. Tovee, 1997. The representational capacity of the distributed encoding of information provided by populations of neurons in the primate temporal visual cortex, *Exp. Brain Res.*, 114:149–162.
- Seltzer, B., and D. N. Pandya, 1978. Afferent cortical connections and architectonics of the superior temporal sulcus and surrounding cortex in the rhesus monkey, *Brain Res.*, 149:1–24.
- Singer, W., 1999. Neuronal synchrony: a versatile code for the definition of relations? *Neuron*, 24:49–65.
- Singer, W., 2000. Response synchronisation: a universal coding strategy for the definition of relations, in *The New Cognitive Neurosciences*, 2nd ed. (M. Gazzaniga ed.), Cambridge, MA: MIT Press, pp. 325–338.
- Shannon, C. E., 1948. A mathematical theory of communication, *ATT Bell Labs. Tech. J.*, J27:379–428.
- Stringer, S. M., and E. T. Rolls, 2000. Position invariant recognition in the visual system with cluttered environments, *Neural Net.*, 13:305–315.
- Tanaka, K., 1993. Neuronal mechanisms of object recognition, *Science*, 262:685–688.
- Tanaka, K., 1996. Inferotemporal cortex and object vision, *Annu. Rev. Neurosci.*, 19:109–139.
- Tanaka, K., C. Saito, Y. Fukada, and M. Moriya, 1990. Integration of form, texture, and color information in the inferotemporal cortex of the macaque, in *Vision, Memory and the Temporal Lobe* (E. Iwai and M. Mishkin, eds.), New York: Elsevier, pp. 101–109.
- Thorpe, S. J., A. Delorme, and R. Van Rullen, 2001. Spike-based strategies for rapid processing, *Neural Net.*, 14:715–725.
- Tovee, M. J., and E. T. Rolls, 1995. Information encoding in short firing rate epochs by single neurons in the primate temporal visual cortex, *Visual Cogn.*, 2:35–58.
- Tovee, M. J., E. T. Rolls, and P. Azzopardi, 1994. Translation invariance and the responses of neurons in the temporal visual cortical areas of primates, *J. Neurophysiol.*, 72:1049–1060.
- Tovee, M. J., E. T. Rolls, and V. S. Ramachandran, 1996. Rapid visual learning in neurones of the primate temporal visual cortex, *Neuroreport*, 7:2757–2760.
- Tovee, M. J., E. T. Rolls, A. Treves, and R. P. Bellis, 1993. Information encoding and the responses of single neurons in the primate temporal visual cortex, *J. Neurophysiol.*, 70:640–654.
- Trappenberg, T. P., E. T. Rolls, and S. M. Stringer, 2002. Effective size of receptive fields of inferior temporal cortex neurons in natural scenes, in *Advances in Neural Information Processing Systems* (T. G. Dietterich, S. Becker, and Z. Ghahramani, eds.), Cambridge, MA: MIT Press, pp. 293–300.
- Treves, A., 1993. Mean-field analysis of neuronal spike dynamics, *Network*, 4:259–284.
- Treves, A., E. T. Rolls, and M. Simmen, 1997. Time for retrieval in recurrent associative memories, *Physica*, D107:392–400.
- Treves, A., S. Panzeri, E. T. Rolls, M. Booth, and E. A. Wackman, 1999. Firing rate distributions and efficiency of information transmission of inferior temporal cortex neurons to natural visual stimuli, *Neural Comput.*, 11:611–641.
- Wallis, G., and E. T. Rolls, 1997. Invariant face and object recognition in the visual system, *Prog. Neurobiol.*, 51:167–194.
- Wallis, G., E. T. Rolls, and P. Foldiak, 1993. Learning invariant responses to the natural transformations of objects, *Int. Joint Conf. Neural Networks*, 2:1087–1090.
- Wilson, F. A. W., S. P. O'Sclaidhe, and P. S. Goldman-Rakic, 1993. Dissociation of object and spatial processing domains in primate prefrontal cortex, *Science*, 260:1955–1958.
- Young, M. P., and S. Yamane, 1992. Sparse population encoding of faces in the inferotemporal cortex, *Science*, 256:1327–1331.

BIBLIOGRAPHY

- Ballard, D. H., 1993. Subsymbolic modelling of hand-eye coordination, in *The Simulation of Human Intelligence* (D. E. Broadbent ed.), Oxford: Blackwell, pp. 71–102.
- Baylis, G. C., and E. T. Rolls, 1987. Responses of neurons in the inferior temporal cortex in short term and serial recognition memory tasks, *Exp. Brain Res.*, 65:614–622.
- Bishop, C. M., 1995. *Neural Networks for Pattern Recognition*, Oxford: Clarendon Press.
- Eckhorn, R., and B. Popel, 1974. Rigorous and extended application of information theory to the afferent visual system of the cat, *Biol. Cybern.*, 16:191–200.
- Engel, A. K., P. Konig, A. K. Kreiter, T. B. Schillen, and W. Singer, 1992. Temporal coding in the visual system: new vistas on integration in the nervous system., *Trends Neurosci.*, 15:218–226.
- Hopfield, J. J., 1982. Neurons with graded responses have collective properties like those of two-state neurons, *Proc. Natl. Acad. Sci. USA*, 81:3088–3092.
- Koenderink, J. J., and A. J. Van Doorn, 1979. The internal representation of solid shape with respect to vision, *Biol. Cybern.*, 32:211–217.
- Kohonen, T., 1977. *Associative Memory: A System Theoretical Approach*, New York: Springer.
- MacKay, D. M., and W. S. McCullough, 1952. The limiting information capacity of a neuronal link, *Bull. Math. Biophys.*, 14:127–135.
- Maunsell, J. H. R., and W. T. Newsome, 1987. Visual processing in monkey extrastriate cortex, *Annu. Rev. Neurosci.*, 10:363–401.
- Miller, E. K., and R. Desimone, 1994. Parallel neuronal mechanisms for short-term memory, *Science*, 263:520–522.
- Miyashita, Y., 1993. Inferior temporal cortex: where visual perception meets memory, *Annu. Rev. Neurosci.*, 16:245–263.
- Olshausen, B. A., and D. J. Field, 1997. Sparse coding with an overcomplete basis set: a strategy employed by V1? *Vis. Res.*, 37:3311–3325.
- Perrett, D. I., A. J. Mistlin, and A. J. Chitty, 1987. Visual neurons responsive to faces, *Trends Neurosci.*, 10:358–364.
- Poggio, T., and S. Edelman, 1990. A network that learns to recognize three-dimensional objects, *Nature*, 343:263–266.
- Renart, A., R. Moreno, J. de la Rocha, N. Parga, and E. T. Rolls, 2001. A model of the IT-PF network in object working memory which includes balanced persistent activity and tuned inhibition, *Neurocomputing*, 38–40:1525–1531.
- Riesenhuber, M., and T. Poggio, 1998. Just one view: invariances in inferotemporal cell tuning, *Adv. Neural. Inf. Proc. Syst.*, 10:215–221.

- Rolls, E. T., 1991. Neural organisation of higher visual functions, *Curr. Opin. Neurobiol.*, 1:274–278.
- Rolls, E. T., 1996. A theory of hippocampal function in memory, *Hippocampus*, 6:601–620.
- Rolls, E. T., 2000. Neurophysiology and functions of the primate amygdala, and the neural basis of emotion, in *The Amygdala: A Functional Analysis* (J. P. Aggleton ed.), Oxford: Oxford University Press.
- Rolls, E. T., and M. J. Tovee, 1995. The responses of single neurons in the temporal visual cortical areas of the macaque when more than one stimulus is present in the visual field, *Exp. Brain Res.*, 103:409–420.
- Rolls, E. T., and A. Treves, 1990. The relative advantages of sparse versus distributed encoding for associative neuronal networks in the brain, *Network*, 1:407–421.
- Sato, T., 1989. Interactions of visual stimuli in the receptive fields of inferior temporal neurons in macaque, *Exp. Brain Res.*, 77:23–30.
- Thorpe, S. J., and M. Imbert, 1989. Biological constraints on connectionist models, in *Connectionism in Perspective* (R. Pfeifer, Z. Schreter, and F. Fogelman-Soulie, eds.), Amsterdam: Elsevier, pp. 63–92.
- Trappenberg, T. P., E. T. Rolls, and S. M. Stringer, 2002. Effective size of receptive fields of inferior temporal cortex neurons in natural scenes, in *Advances in Neural Information Processing Systems* (T. G. Diettrich, S. Becker, and Z. Ghahramani eds.), Cambridge, MA: MIT Press, pp. 293–300.
- Treves, A., and E. T. Rolls, 1991. What determines the capacity of autoassociative memories in the brain? *Network*, 2:371–397.
- Treves, A., and E. T. Rolls, 1994. A computational analysis of the role of the hippocampus in memory, *Hippocampus*, 4:374–391.
- Ullman, S., 1996. *High-Level Vision. Object Recognition and Visual Cognition*, Cambridge, MA: Bradford/MIT Press.
- Williams, G. V., E. T. Rolls, C. M. Leonard, and C. Stern, 1993. Neuronal responses in the ventral striatum of the behaving macaque, *Behav. Brain Res.*, 55:243–252.
- Willshaw, D. J., O. P. Buneman, and H. C. Longuet-Higgins, 1969. Nonholographic associative memory, *Nature*, 222:960–962.
- Xiang, J. Z., and M. W. Brown, 1998. Differential neuronal encoding of novelty, familiarity and recency in regions of the anterior temporal lobe, *Neuropharmacology*, 37:657–676.
- Yamane, S., S. Kaji, and K. Kawano, 1988. What facial features activate face neurons in the inferotemporal cortex of the monkey? *Exp. Brain Res.*, 73:209–214.

79 The Ventral Visual Object Pathway in Humans: Evidence from fMRI

NANCY KANWISHER

WE HUMANS CAN RECOGNIZE an object within a fraction of a second, even if we have never seen that exact object before and even if we have no advance clues about what kind of object it might be (Potter, 1976; Thorpe et al., 1996). The cognitive and neural mechanisms underlying this remarkable ability are not well understood, and current computer vision algorithms still lag far behind human performance. One promising strategy for attempting to understand human visual recognition is to characterize the neural system that accomplishes it: the ventral visual pathway, which extends from the occipital lobe into inferior and lateral regions of the temporal lobe. Here I describe research from neuroimaging on humans that has begun to elucidate the general organization and functional properties of the cortical regions involved in visually perceiving people, places, and things.

I will focus on two main questions in this review. First, what is the functional organization of the ventral visual pathway? This pathway has been characterized in some detail in the macaque using single-unit recording. However, very little was known about its organization in humans even a few years ago, when functional magnetic resonance imaging (fMRI) studies of this region began. Other chapters in this volume review the organization of this pathway in macaques, as well as the organization of earlier retinotopic regions in human visual cortex (see Chapters 32 and 34). This review will focus on the segment of the human ventral visual pathway that lies anterior to retinotopic cortex. I will argue that this pathway contains a small number of category-specific regions, each primarily involved in processing a specific stimulus class, in addition to a more general-purpose region that responds to any kind of visually presented object.

Second, what is the nature of the representations we extract from visually presented objects? This question is at the heart of any theory of object recognition and has long been addressed using behavioral methods such as priming. fMRI is beginning to provide some clues about the nature of the visual representations that are extracted in each region. The technique of fMRI adaptation (Grill-Spector et al., 2000; Naccache and Dehaene, 2001) enables us to determine the invariances and equivalence classes of neural representations of objects within each region of cortex scanned.

Other techniques are beginning to address the question of whether objects are represented in distributed neural codes that span much of the ventral visual pathway or whether some kinds of objects are represented in focal regions of cortex.

Functional organization: category-selective regions

This section describes work that has characterized three distinct regions in the human ventral visual pathway, each of which responds selectively to a single category of visual stimuli (Fig. 79.1).

FACES Faces are enormously rich and biologically relevant stimuli, providing information not only about the identity of a person but also about his or her mood, age, sex, and direction of gaze. Indeed, behavioral studies of normal subjects and neurological patients (see Farah, 2000, for a review), as well as event-related potentials in humans (Allison et al., 1999; Bentin et al., 1996) and single-unit recording in monkeys (Perrett et al., 1982; Chapter 78, this volume), provide evidence that face perception engages cognitive and neural mechanisms distinct from those engaged during the recognition of other classes of objects. Several brain imaging studies (e.g., Haxby et al., 1991; Puce et al., 1995, 1996; Sergent et al., 1992) described cortical regions that were most active during viewing of faces. However, these studies did not include the kinds of control conditions that are necessary for testing whether the activated regions are selectively involved in face perception.

Kanwisher et al. (1997) scanned subjects with fMRI while they viewed rapidly presented sequences of faces versus sequences of familiar inanimate objects. We found a region in the fusiform gyrus in most subjects, and a second region in the superior temporal sulcus in about half of the subjects, that produced a stronger MR response during face viewing than object viewing (see also McCarthy et al., 1997). A greater response to faces than to objects could be produced by processes that have nothing to do with face perception per se, including attentional engagement, which may be greater for faces than for nonfaces, a general response to anything animate or anything human, or a response to the

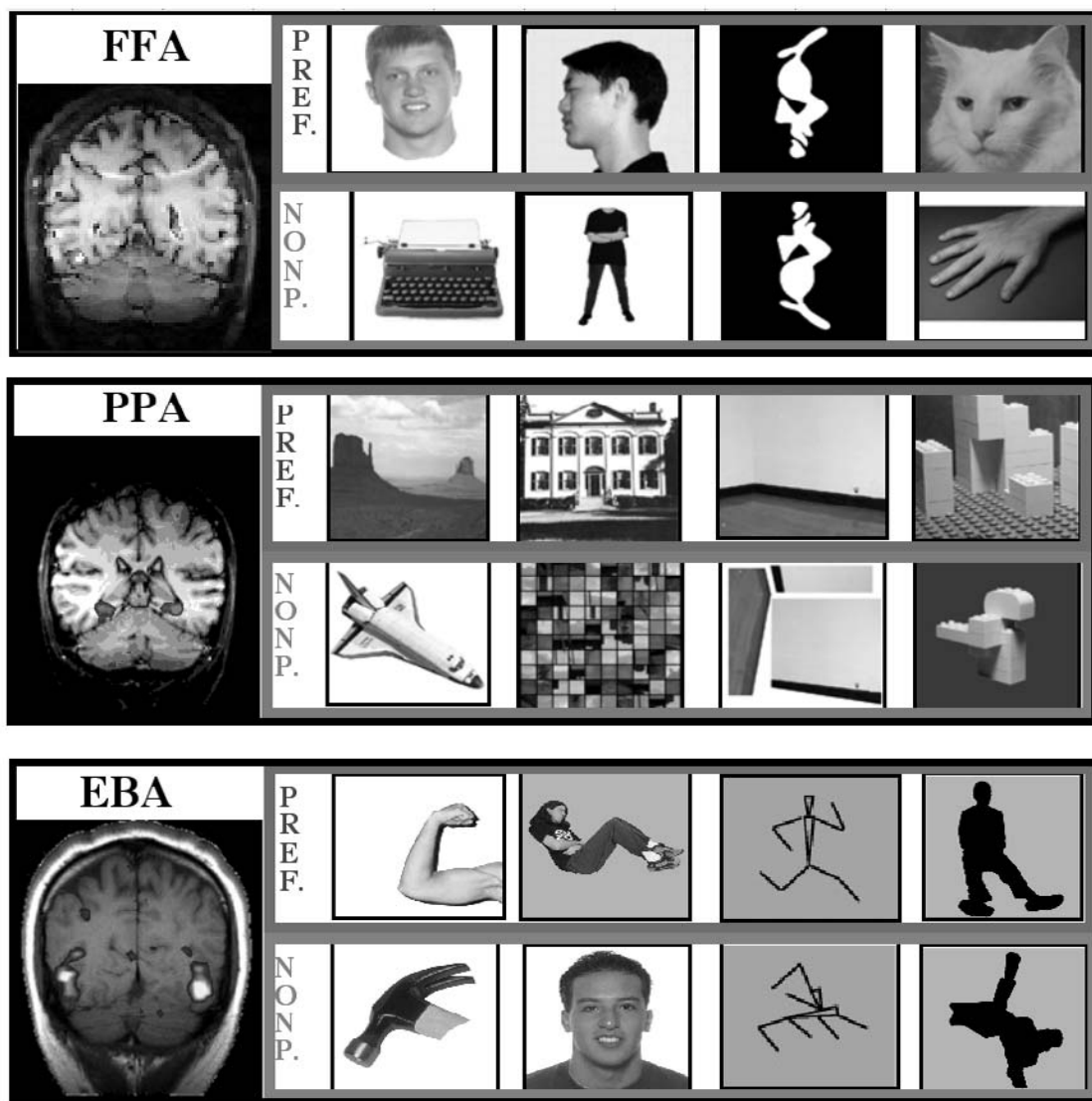


FIGURE 79.1. Three category-selective regions in human extrastriate cortex. The brain images at the left show coronal slices in individual subjects; overlaid in color are regions that responded significantly more strongly to faces than to objects (the FFA), to scenes than to objects (the PPA), and to body parts than to object parts (the EBA). Each region responds to a wide variety of exemplars of

the category; for each area, four examples of such preferred stimuli are shown in the blue box at the top. Examples of nonpreferred stimuli for each area (that elicit about half the response of preferred stimuli in terms of percent age signal increase from a fixation baseline) are indicated in the red box at the bottom. (See color plate 55.)

low-level visual features present in face stimuli. To test these and other hypotheses, we first identified the candidate face-selective fusiform region individually in each subject with the comparison of faces to objects, and then measured the response in this region of interest (ROI) to a number of subsequent contrasting conditions. After demonstrating that the same region responded at least twice as strongly to faces as to any of the other control stimuli, we concluded that this region is indeed selectively involved in face processing and named it the *fusiform face area* (FFA) (Fig. 79.1, top, and Fig. 79.2, bottom). The claim that the FFA responds selectively or specifically to faces does not mean that it responds *exclu-*

sively to faces. Although the FFA responds much more to faces than to objects, it responds more to objects than to a baseline condition such as a fixation point. The standard criterion for neural selectivity (Tovee et al., 1993), adopted here, is that the response must be at least twice as great for the preferred stimulus category as for any other stimulus category.

By now, the FFA has been studied extensively in many different experiments and labs. These studies generally agree that the FFA responds more strongly to a wide variety of face stimuli (e.g., front-view photographs of faces, line drawings of faces, cat faces, cartoon faces, and upside-down faces)

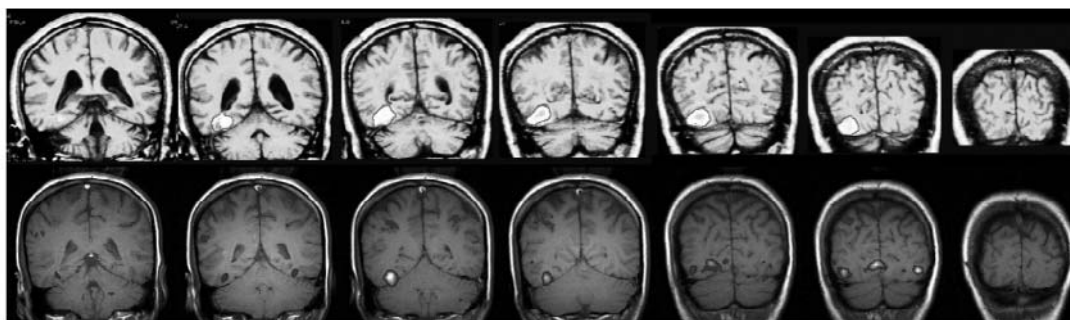


FIGURE 79.2. The top row (adapted from Figure 1 of Wada and Yamamoto, 2001) shows the site of a lesion (outlined in red for greater visibility) that produced a severe deficit in face recognition but not in object recognition. The bottom row shows the author's FFA (color indicates regions responding significantly more strongly during face viewing than object viewing). Note the similarity in the anatomical locus of the lesion and the FFA activation, suggesting that an intact FFA may be necessary for face but not object recognition. (See color plate 56.)

than to various nonface control stimuli, even when each of these (like faces) constitutes multiple similar exemplars of the same category, including houses (Haxby et al., 1999; Kanwisher et al., 1997), hands (Kanwisher et al., 1997), animals, provided that their heads are not visible (Kanwisher et al., 1999; but see Chao et al., 1999), flowers (McCarthy et al., 1997), or cars (Halgren et al., 1999). These effects are similar when the subject is merely passively viewing the stimuli or carrying out a demanding discrimination task on them (Kanwisher et al., 1997), suggesting that the response does not arise from a greater attentional engagement by faces than by other stimuli. Nor can the FFA response to faces be accounted for in terms of a low-level feature confound, as the response is higher when a face is perceived versus not perceived even when the stimulus is unchanged, as in binocular rivalry (Tong et al., 1998) and face-vase reversals (Hasson et al., 2001).

While the basic response properties of the FFA are generally agreed upon, the function of this region is not. The most basic question is whether the function of the FFA is truly specific to faces or whether it involves a domain-general operation that could in principle be applied to other stimuli (despite being more commonly carried out on faces). For example, in our original paper on the FFA, we suggested testing whether it could be activated by inducing holistic encoding on nonface stimuli. Rossion et al. (2000) found that although attending to whole faces, rather than parts of faces, enhanced the right (but not left) FFA response, attending to whole houses, rather than parts of houses, did not. These data argue against the domain-general holistic encoding hypothesis, instead implicating the right FFA in processing holistic/configural aspects of faces.

Gauthier and her colleagues have argued for a somewhat different domain-general hypothesis, according to which the right FFA is specialized for discriminating between any structurally similar exemplars of a given category for which the subject is an expert (Tarr and Gauthier, 2000). However, most of her evidence is based on studies using novel stimuli

called *Greebles*, a suboptimal choice for testing this hypothesis because they have the same basic configuration as a face (i.e., a symmetrical configuration in which two horizontally arranged parts are above two vertically aligned central parts, as in the configuration of eyes, nose, and mouth). Nonetheless, in one study, Gauthier et al. (1999) found that the FFA was activated by cars in car fanatics and birds in bird experts; this result was replicated by Xu et al. (Xu and Kanwisher, 2001). However, in both studies the effect sizes are small, and the response to faces remains about twice as high as the response to cars in car experts, a result that is consistent with both the face-specificity hypothesis and the subordinate-level-categorization-of-structurally-identical-exemplars-for-which-the-subject-is-expert¹ hypothesis. Stronger evidence on this debate comes from a double dissociation in neurological patients: face recognition impairments can be found in the absence of impairments in the expert discrimination of category exemplars (Henke et al., 1998) and vice versa (Moscovitch et al., 1997). These findings argue that different cortical mechanisms are involved in face perception and in the expert visual discrimination of structurally similar category exemplars (Kanwisher, 2000).

If the face specificity of the FFA is granted, the next question is what exactly the FFA does with faces. The FFA appears not to be involved specifically in discriminating the direction of eye gaze, because it is more active during attention to face identity than to gaze direction, while the face-selective region in the superior temporal sulcus responds more strongly in the opposite comparison (Hoffman and Haxby, 2000). Nor is the FFA likely to be specifically involved

¹Note that if any of these descriptors is removed, the hypothesis has already been disproved: the low FFA response to words shows that visual expertise is not sufficient, and the low FFA response during hand or house discrimination shows that subordinate-level discrimination of structurally identical exemplars is not sufficient to explain the high response to faces.

in extracting emotional expressions from faces, given the consistently high response of the FFA during viewing of expressionless faces. In studies directly manipulating the presence or absence of emotional expressions in face stimuli, the greatest activation is in the amygdala (Breiter et al., 1996) or anterior insula (Phillips et al., 1997), not the fusiform gyrus. Another hypothesis is that the FFA represents semantic rather than perceptual information (Martin and Chao, 2001). However, this too seems unlikely because (1) this region does not respond more to a familiar face, for which semantic information about the individual is available, than to an unfamiliar face, for which it is not (Gorno-Tempini and Price, 2001; Shah et al., 2001), and (2) this region does not appear to represent abstract semantic information about people in general, as it responds no more when subjects read paragraphs describing people than when they read paragraphs describing inanimate objects, though this same comparison produces robust activation in the superior temporal sulcus (R. Saxe and N. Kanwisher, unpublished data). Thus, the FFA appears not to be involved specifically in extracting information about gaze direction or emotional expression, or to be involved in representing semantic information about individual people.

Evidence that this area may be involved in simply detecting the presence of a face comes from the findings that activity in the FFA is strong even for inverted faces (Aguirre et al., 1999; Haxby et al., 1999; Kanwisher et al., 1998) and for line drawings of faces (A. Harris and N. Kanwisher, unpublished data; see also Halgren et al., 1999; Ishai et al., 1999), both of which support easy face detection but not face recognition. However, another study (K. Grill-Spector and N. Kanwisher, unpublished data) found that activity in the right FFA is correlated with both successful detection and successful categorization of faces (versus nonfaces) and in successful discrimination between individual faces, suggesting that it is involved in both of these abilities.

PLACES For navigating social primates like humans, one other visual ability is arguably as important as recognizing faces: determining our location in the environment. A region of cortex called the *parahippocampal place area* (PPA) appears to play an important role in this ability (Epstein and Kanwisher, 1998). The PPA responds strongly whenever subjects view images of places, including indoor and outdoor scenes, as well as more abstract spatial environments such as urban “scenes” made out of Legos, virtual spaces depicted in video games (Aguirre et al., 1996; Maguire et al., 1998), or close-up photographs of desktop scenes (P. Downing, R. Epstein, and N. Kanwisher, unpublished data). Remarkably, the visual complexity and number of objects in the scenes are unimportant; the response is just as high to bare empty rooms (two walls, a floor, and sometimes a door or window) as it is to complex photos of the same rooms completely fur-

nished. The PPA also responds fairly strongly to images of houses cut out from their background (though less than to full scenes), presumably because spatial surroundings are implicit in a depiction of a house. Thus, it is information about the spatial layout of the scene that is apparently critical to the PPA response (Fig. 79.1, *middle*).

Patients with damage to parahippocampal cortex often suffer from *topographical disorientation*, an impairment in wayfinding (Aguirre and D’Esposito, 1999; Epstein et al., 2001; Habib and Sirigu, 1987). The core deficit in these patients is an inability to use the appearance of places and buildings for purposes of orientation, perhaps implicating the PPA in place recognition. However, we tested a neurological patient with no PPA and largely preserved place perception but an apparent deficit in learning new place information, suggesting that the PPA may be more critical for encoding scenes into memory than for perceiving them in the first place (Epstein et al., 2001). This possibility is consistent with evidence from other laboratories suggesting that parahippocampal cortex is involved in memory encoding of words (Wagner et al., 1998) and scenes (Brewer et al., 1998).

The PPA is apparently not engaged in processes that rely on knowledge of the specific environment (such as planning a route to a particular location in one’s stored cognitive map of the world), as it responds with the same strength to familiar versus unfamiliar places: Epstein et al. (1999) presented MIT students and Tufts University students with scenes from the MIT and Tufts campuses, and found no difference in the response to the same images when they depicted familiar rather than unfamiliar places. Interestingly, however, a significantly higher response was found in the PPA to familiar than to unfamiliar buildings cut out from their background, perhaps because the spatial background was more likely to be inferred in a familiar scene.

One attractive idea is that the PPA may constitute the neural instantiation of a previously hypothesized system for spatial reorientation (Cheng, 1986; Hermer and Spelke, 1994). When disoriented rats and human infants must search for a hidden object, they rely largely on the shape of the local environment to reorient themselves and find the object (but see Gouteux et al., 2001; Learmonth et al., 2001). Strikingly, they completely ignore informative landmark cues such as the location of a salient visual object or feature. This led Cheng and others to hypothesize the existence of a *geometric module* that represents the shape (but not other features) of surrounding space for the purpose of reorientation. The exclusive use of spatial layout information, and not object/landmark information, is tantalizingly reminiscent of the much greater activation of the PPA by images of spatial layouts than images of objects.

How is the PPA related to the two other neural structures most commonly implicated in spatial encoding and navigation, the hippocampus and the parietal lobe? It has been

hypothesized that the hippocampus contains a cognitive map of the animal's environment (O'Keefe and Nadel, 1978). In contrast, the parietal lobe has been implicated in representing the specific spatial information that is relevant to guiding current action. In keeping with this division of labor, physiological recordings in animals indicate that the hippocampus contains allocentric (world-centered) representations of place, whereas the parietal lobes contain egocentric (body-centered) representations of spatial locations (Burgess et al., 1999). For example, *place cells* in the rat hippocampus respond when the animal is in a specific location in its environment, largely independent of which way the animal is facing, while *spatial view cells* in the primate hippocampus respond when the animal views a given spatial location (Georges-François et al., 1999). In contrast, neurons in the primate parietal cortex apparently represent space in a number of egocentric coordinates tied to the location of the retina, hand, or mouth (Colby and Goldberg, 1999). A recent study found that fMRI adaptation to repeated stimuli in the PPA occurs only when the same view of a scene is repeated, implicating the PPA in egocentric rather than allocentric representations of space (Epstein et al., 2003).

In sum, although it is now well established that the PPA responds selectively to information about spatial layouts and places, it remains unclear what exactly the PPA does with this information. Critical questions for future research concern the role of the PPA in reorientation and encoding of spatial information into memory, as well as the nature of the interactions between the PPA, the hippocampus, and the parietal lobe.

BODIES Our latest addition to the set of category-selective regions of cortex is the extrastriate body area (EBA) (Downing et al., 2001). This region responds about twice as strongly when subjects view images depicting human bodies or body parts (nothing too interesting!) as when they view objects or object parts (Fig. 79.1, *bottom*). The EBA is found in all subjects in the right (and sometimes also the left) lateral occipitotemporal cortex on the lower lip of the posterior superior temporal sulcus, just superior to area MT/MST. The EBA's response profile is unlikely to reflect low-level stimulus confounds, as the same region responded about twice as strongly to body as to nonbody stimuli even when the two stimulus sets were visually similar (e.g., stick figures versus rearranged versions of stick figures that no longer corresponded to body configurations; silhouettes of people versus slightly rearranged silhouettes). Further experiments showed that the EBA does not simply respond to anything living, animate, or known to be capable of motion, or to any object with parts that can move relative to each other: the EBA responds more to human bodies than to trees, mammals, or objects with movable parts such as scissors, staplers, and corkscrews. The one exception to the body

specificity of the EBA is the fact that this region responds no more to faces than to objects. As expected from this result, the EBA does not overlap much, if at all, with the face-selective region in the superior temporal sulcus.

At present, the function of the EBA is unknown. It may be involved in recognizing individuals (when their faces are hidden or far away), or in perceiving the body configuration of other people, or even in perceiving the location of one's own body parts. The EBA is suggestively close to area MT, perhaps implicating it in integrating information about body shape and motion (Grossman et al., 2000). The EBA is also close to other regions that have been shown to be activated during social perception, from discriminating the direction of eye gaze, to perceiving or inferring intentions, to perceiving human voices. Thus the EBA may be part of a broader network of nearby areas involved in social perception and social cognition.

WHAT ELSE? How many category-selective regions of cortex exist in the human visual pathway? Other categories including animals and tools have been reported to selectively activate focal regions of cortex (Martin and Chao, 2001). However, the evidence is not as strongly established in these cases. When only a few stimuli have been compared, apparent category selectivity must be treated cautiously. For example, we found a region that responded more strongly to chairs than to faces or places, replicating the findings of Ishai et al. (1999), but the same region responded just as strongly to pictures of food, animals, and flowers. In ongoing work in our lab, we have tested well over a dozen categories (P. Downing and N. Kanwisher, unpublished data); so far, we have found no other regions of cortex that exhibit the strong category selectivity typical of the FFA, PPA, and EBA. Thus, it appears that faces, places, and bodies may be unusual in the way they are processed and represented in the cortex. The apparent lack of other category-selective regions of cortex raises the question of how other kinds of objects are represented.

Functional organization: category-general regions

Considerable evidence suggests that in addition to the category-specific regions described previously, human visual cortex contains a region more generally involved in perceiving the shape of any kind of object. A large region of lateral and inferior occipital cortex just anterior to retinotopic cortex [the lateral occipital complex (LOC)] responds more strongly to stimuli depicting shapes than to stimuli with similar low-level features that do not depict shapes (Kanwisher et al., 1996; Malach et al., 1995; see Grill-Spector et al., 2001, for a review). Importantly, the response in this region was the same for familiar and unfamiliar shapes, so the response cannot be straightforwardly

accounted for in terms of matching to stored visual representations, or semantic or verbal coding of the stimuli. Common areas within this lateral occipital region are activated by shapes defined by motion, texture, and luminance contours (Grill-Spector et al., 1998a; Grill-Spector et al., 1998b). Several studies have implicated the LOC in visual object recognition by showing that activity in this region is correlated with success on a variety of object recognition tasks (Bar et al., 2001; Grill-Spector et al., 2000; James et al., 2000; Lerner et al., 2002). Thus, an investigation of the response properties of the LOC may provide important clues about the nature of the representations underlying object recognition.

Several studies have shown a reduction in the response of a particular region of the LOC (and other regions of cortex) when stimuli are repeated. Grill-Spector et al. (1999) further showed that in the LOC this effect (*fMRI adaptation*) can be observed even when the repeated shapes vary in size and position, demonstrating that the representations in this area are largely invariant with respect to changes in size and position. While this adaptation effect was not found across changes in object viewpoint or direction of illumination in this study, another recent study by Vuilleumier et al. (2002) found that the left fusiform gyrus (but not the right) exhibited invariance to viewpoint. Kourtzi and Kanwisher (2001) further demonstrated adaptation in this region between stimulus pairs that had different contours but the same perceived shape (because of changes in occlusion), but not between pairs with identical contours that differed in perceived shape (because of a figure-ground reversal). These findings suggest that neural populations in the LOC represent the perceived shape of an object in a fashion invariant to changes in position and size but not viewpoint (at least in the right hemisphere). Given the correlation of the MR signal in this region with successful recognition, representations with these properties are likely to play an important role in human object recognition.

Other studies have shown that the response in this region declines as images of familiar objects are cut into pieces and the positions of those pieces are rearranged. However, interestingly, most regions within the LOC do not show much decline in the magnitude of the MR response until images are broken into at least 16 fragments (Lerner et al., 2001), suggesting that neural populations in these regions are fragment-based rather than holistic. At the same time, the response of the LOC is strongly affected by more global factors such as object completion, with higher responses to partly occluded line drawings that can be completed compared to those that cannot (Lerner et al., 2002). Another intriguing recent study found that a small region within the LOC responds to objects compared to textures in both visual and haptic modalities, although most of the LOC responds preferentially to only visually presented objects (Amedi et al., 2001).

Anatomically, the LOC is close to and sometimes partly overlapping with the FFA (on the ventral surface) and the EBA (on the lateral surface). Note that such overlap does not imply any contradiction in the data; it simply indicates that some voxels respond significantly more strongly to faces than to nonface objects (and hence are included in the FFA) or to bodies than to objects (and hence are included in the EBA), while the same voxels also respond significantly more strongly to nonface objects than to scrambled objects (and hence are included in the LOC). However, such overlap does indicate that functional definitions of this sort do not serve to categorize uniquely each region of cortex. One account of this situation is that the FFA, EBA, and the LOC are in fact part of the same functional region, which is composed of a set of category-selective and/or feature-selective columns (Fujita et al., 1992) at such a fine scale that they cannot be resolved with fMRI, except for a few very large such regions such as the FFA. Another possibility is that the FFA and LOC (and the EBA and LOC) do not in fact overlap anatomically, with the apparent overlap due to limitations in the spatial resolution of fMRI.

In sum, it appears that the ventral visual pathway contains one region, the LOC, that responds strongly to object structure but that exhibits little selectivity for specific object categories, along with a small number of category-specific modules (for faces, places, bodies, and perhaps a few others yet to be discovered). Indeed, it would seem a sensible design for the cortex to supplement its general-purpose mechanisms for describing the shape of any kind of visually presented object (i.e., the LOC) with a small number of additional more specialized mechanisms, each of which may be designed to handle the unique computational challenges posed by stimuli of a specific kind.

Important open questions

As the previous sections suggest, neuroimaging in humans has taught us much about the functional organization of the ventral visual pathway and about the representations involved in object recognition. However, some of the most important and difficult questions remain to be tackled. Next, I outline some of these questions and the ongoing experimental work that is attempting to address them.

DISTRIBUTED VERSUS LOCAL REPRESENTATIONS OF OBJECTS
Many of the studies described in previous sections follow a common strategy in visual neuroscience of inferring the function of a cortical area, voxel, or neuron from the stimulus that drives it most strongly. However, this strategy is viable only to the extent that maximal responses carry most of the information in a neural representation.

Thus, an important unresolved question concerns the functional significance of the “nonpreferred” responses in

the cortical regions discussed above. For example, do the low but nonzero responses to nonfaces in the FFA reflect a critical involvement of the FFA in the detection or recognition of nonface objects? Haxby et al. (1999) have argued that the partial response to nonfaces is “problematic for [Kanwisher et al.’s] hypothesis that face-selective regions . . . constitute a ‘module specialized for face perception’” (p. 196). However, there are at least two reasons why it need not be problematic. First, because of limitations on the spatial resolution due to voxel size, blood flow regulation, and other factors, the MR signal intensity from a particular region should not be expected to reflect a pure measure of the activity in a single functional module, but will include contributions from functionally distinct adjacent (or interleaved) neural tissue. Second, there is no reason to expect even a strongly face-selective cortical area to shut itself off completely when a nonface is presented. Indeed, it is hard to imagine how this could occur without an additional gating mechanism that discriminates between faces and nonfaces and allows only face information into the region in question. In the absence of such a gating mechanism, it would be most natural to expect a low but positive response to nonfaces in a region of cortex specialized for face processing. Thus, the mere existence of nonpreferred responses does not argue against the functional specificity of the region they are recorded from. The critical questions we must answer to understand nonpreferred responses are (1) do they carry information? and (2) is this information used? A recent paper by Haxby et al. (2001) addresses the first question.

Haxby et al. (2001) used fMRI to scan subjects while they viewed eight different categories of stimuli. The data from each subject were then split in half, with the data from odd runs in one set and the data from even runs in the other set (the same stimuli were used in odd and even runs). In this fashion, two “partner” activation maps were generated for each of the eight stimulus categories (i.e., 16 activation maps per subject). Next, Haxby et al. carried out seven pairwise comparisons for each activation map, each testing whether that activation map was more similar to its partner (in the other data set) than to each of the activation maps from the other seven categories. In this fashion, the performance on activation map categorization was quantified as the percentage of these pairwise comparisons that were categorized “correctly,” that is, in which the target map was more similar to its partner than to the other map. Haxby et al. found high accuracy in activation map categorization, demonstrating that the patterns of activation for each category were highly replicable within individual subjects. More importantly, they argued that when only the region that responded maximally to a given category was included in the analysis, categorization performance in determining which of the nonpreferred categories had been presented was still well above chance. They therefore suggested that “regions such as the ‘PPA’ and

‘FFA’ are not dedicated to representing only spatial arrangements or human faces, but, rather, are part of a more extended representation for all objects.”

However, Haxby et al. did not carry out the analyses necessary to support this conclusion. Spiridon and Kanwisher (2002) replicated their main result, and also compared performance levels for discriminations involving faces and houses and discriminations between pairs of inanimate objects. We found that the FFA supports accurate discrimination between faces and nonfaces but performs at near-chance levels on discriminations between inanimate objects. Similarly, the PPA contains sufficient information for accurate discrimination of houses versus other objects but performs at near-chance levels on discriminations between nonpreferred stimuli. Further, on discriminations between small inanimate objects, neither the FFA nor the PPA outperforms retinotopic cortex, suggesting that any small amount of discriminative information concerning nonpreferred stimuli that may exist in these areas is likely to be based on low-level features that are confounded with stimulus category rather than on true abstract category information. Thus, although some object information may be distributed across the ventral visual pathway, we find no evidence that the FFA and PPA carry any real categorical information about nonpreferred stimuli.

Of course, these investigations are subject to two important limitations characteristic of all fMRI research. First, each voxel in the fMRI data contains hundreds of thousands of neurons, so it is possible that discriminative information for nonpreferred categories might exist in these regions at a finer spatial scale. Second, fMRI data (like neurophysiological recordings) are purely correlational, so even when information is present in a given cortical region, we cannot be sure that it forms a critical part of the representation.

A recent neuropsychological study addresses both problems for the case of the FFA. Wada and Yamamoto (2001) describe a neurological patient with an unusually circumscribed lesion restricted to the region of the right FFA (Fig. 79.2). This man was severely impaired on face recognition but had fully preserved object recognition. If we assume that his lesion included the right FFA, these data suggest that the FFA plays a necessary role in face but not object recognition (see also Barton et al., 2002). Thus, even if a small amount of category-discriminative information for nonfaces exists in the FFA of normal subjects (undetected in the Spiridon-Kanwisher study), this information appears not to play any necessary role in the recognition of those nonface objects.

WHAT DOES CORTICAL MODULARITY TELL US ABOUT VISUAL RECOGNITION? Even if we can determine that some categories of objects are primarily recognized within focal regions of cortex selectively responsive to those categories, will this tell us much about how visual recognition works?

Does the mere existence of a specialized cortical region for a given category imply that qualitatively distinct processing mechanisms are involved in recognizing stimuli from that category?

One might argue that special-purpose mechanisms for processing a particular stimulus class would be expected only if the recognition of stimuli from that class poses new computational problems that could not be handled by existing general-purpose mechanisms. Connectionist researchers have noted the computational efficiency gained by the decomposition of a complex function into natural parts (Jacobs, 1999), and cortical specializations for components of visual recognition are plausible candidates for such task decomposition. If visual cortex is organized in such a computationally principled fashion, then each of the modular components of the system we discover with functional imaging could be expected to instantiate a distinct set of computations.

However, an alternative hypothesis is that visual cortex contains a large number of stimulus-selective regions (such as the feature columns in inferotemporal cortex reported by Tanaka, 1997), but the computations that go on in each of these regions are very similar. On this view, cortical specialization might be found for virtually any stimulus class, yet these specializations might not imply qualitative differences in the processing of these stimulus classes. A critical goal for future research is to determine whether the functional organization of visual recognition is better characterized by this kind of *shallow specialization*, or whether it reflects a deeper form of functional decomposition in which each of a small number of functionally specific regions carries out a qualitatively distinct computation in the service of an evolutionarily or experientially fundamental visual process.

ORIGINS OF SPECIALIZED REGIONS WITHIN THE VENTRAL VISUAL PATHWAY Where do cortical specializations come from? Does functional differentiation within the ventral visual pathway arise from experience-dependent self-organization of cortex (Jacobs, 1997), or are these cortical specializations partly innately specified? For faces, places, and bodies, this question is hard to answer because both experiential and evolutionary arguments are plausible. Despite recent misattributions to me of innatist claims about the origins of the FFA (Pierce et al., 2001; Tarr and Gauthier, 2000), my view is that we have almost no relevant data on this question and are in no position to make any strong claims about the origins of the FFA.

On the one hand, experience must surely play some role in the development of face areas, given the ample evidence that neurons in the ventral visual pathway are tuned by experience. On the other hand, at least some aspects of face perception appear to be innately specified, as newborn infants preferentially track schematic faces compared to visually

similar scrambled faces (Johnson et al., 1991). However, these two observations leave open a vast space of possible ways that genes and environment could interact in the construction of a selective region of cortex such as the FFA.

What does seem pretty clear is that the development of normal adult face processing (and thus, by hypothesis, the development of the FFA) is heavily constrained both anatomically and chronologically. First, neuropsychological patients who selectively lose face recognition abilities as a result of focal brain damage are rarely if ever able to relearn this ability, suggesting that the remaining visual cortex (which is adequate for visual recognition of nonface objects) cannot be trained on face recognition in adulthood. Further, this inability to shift face mechanisms to alternative neural structures may be set very early in development, as evidenced by a patient who sustained damage to the fusiform region when only 1 day old, and who as an adult now has severe difficulties in the recognition of faces (and some other object categories) (Farah et al., 2000). Evidence that very early experience is also crucial in the development of normal adult face recognition comes from a remarkable recent study by Le Grand et al. (2001), who tested people born with dense bilateral cataracts. These people had no pattern vision until their cataracts were surgically corrected between 2 and 6 months of age. After surgery, pattern vision was excellent, if not quite normal. Surprisingly, these individuals never developed normal configural processing of faces. As adults, they are impaired at discriminating between faces that differ in the relative positions of facial features, despite being unimpaired at discriminating faces on the basis of individual face parts. (They are also unimpaired or on either task relative to normal controls when the face stimuli are presented upside down.) Thus, pattern vision in the first few months of life is necessary for the development of normal face processing as an adult; years of subsequent visual experience with faces are not sufficient.

One intriguing part of the puzzle comes from recent reports of *developmental prosopagnosic* patients, who have no brain damage discernible from MRI images or life histories but who are severely impaired at face recognition. These individuals generally do not have other cognitive impairments and often have few or no other impairments in other visual tasks (Duchaine, 2000; Nunn et al., 2001). Although many of these people report relatives with similar deficits, it is not known whether this syndrome is heritable. Thus, it is not yet clear whether it arises from subtle brain damage that cannot be detected on MRIs, or from alterations in genes that code specifically for the construction of a normal face recognition system, or from a failure of general developmental mechanisms that normally lead to the functional differentiation of neural tissue based on experience. Another clue comes from two recent studies showing that autistic subjects exhibit different patterns of cortical activation when

they view faces from those found in normal subjects (Pierce et al., 2001; Schultz et al., 2000). But as with developmental prosopagnosia, this finding can be explained in terms of either experience or genetic factors, or both.

One way to unconfound genetic and experiential factors in the development of category-specific regions of cortex is to consider a category for which a specific role of genes is unlikely: visual word recognition. People have been reading for only a few thousand years, which is probably not long enough for natural selection to have produced specialized machinery for visual word recognition. Thus, strong evidence for a region of cortex selectively involved in the visual recognition of letters or words would provide proof that experience alone with a given category of stimulus, without a specific genetic predisposition, can be sufficient for the construction of a region of cortex that is selectively involved in the recognition of stimuli of that category. Some evidence has been reported for cortical specializations for visually presented letters (Polk and Farah, 1998) and words (Cohen et al., 2000). However, preliminary work in our lab suggests otherwise: cortical regions that respond to visually presented words do not show the kind of selectivity seen in the FFA, PPA, and EBA (J. Jovicich and N. Kanwisher, unpublished data). Thus, for the case of visual recognition in humans, it is not yet clear whether it is the experience of the individual or the experience of the species (or both) that is critical for the construction of functionally distinct regions in the ventral visual pathway.

Conclusions

In just the past few years, functional neuroimaging has taught us a great deal about the organization of the ventral visual pathway in humans. Three new category-specific regions of cortex (the FFA, PPA, and EBA), as well as another category-general region (the LOC), have been discovered and described in some detail. But despite this rapid progress, fundamental questions remain unanswered. fMRI has taught us little or nothing about the perceptual functions each of these newly described regions is critical for, the connections between each of these areas and the rest of the brain, the developmental origins of these areas, or the actual mechanisms that occur in each and how they collectively accomplish object recognition.

On the other hand, new methods are being developed at a rapid rate and hold the promise of real progress in answering many of these questions. The integration of fMRI with event-related potential and magnetoencephalography data may provide the temporal resolution that will be critical for understanding how visual computations unfold over time. The ability to scan children and perhaps even infants should enable us to trace the appearance and function of each of these areas over development. Patient studies and transcran-

ial magnetic stimulation in normal subjects provide methods for testing the necessity of each region for different visual recognition tasks. Finally, in one of the developments I find most pleasing, the once one-way flow of information from primate visual neuroscience to visual cognitive neuroscience in humans has recently become bidirectional, with fMRI studies in macaques now motivated and informed by prior work on humans (Tsao et al., 2001; Vanduffel et al., 2001).

Acknowledgments

I thank Paul Downing, Russell Epstein, Winrich Freiwald, Miles Shuman, and Jonathon Winawer for comments on the manuscript and Ellen Goodman for help with the references. This work was supported by Grants MH59150 and EY13455 to N. Kanwisher.

REFERENCES

- Aguirre, G. K., and M. D'Esposito, 1999. Topographical disorientation: a synthesis and taxonomy, *Brain*, 122:1613–1628.
- Aguirre, G. K., J. A. Detre, D. C. Alsop, and M. D'Esposito, 1996. The parahippocampus subserves topographical learning in man, *Cereb. Cortex*, 6:823–829.
- Aguirre, G., R. Singh, and M. D'Esposito, 1999. Stimulus inversion and the responses of face and object-sensitive cortical areas, *Neuroreport*, 10:189–194.
- Allison, T., A. Puce, D. D. Spencer, and G. McCarthy, 1999. Electrophysiological studies of human face perception. I. Potentials generated in occipitotemporal cortex by face and non-face stimuli, *Cereb. Cortex*, 9:415–430.
- Amedi, A., R. Malach, T. Hendler, S. Peled, and E. Zohary, 2001. Visuo-haptic object-related activation in the ventral visual pathway, *Nat. Neurosci.*, 4:324–330.
- Bar, M., R. B. Tootell, D. L. Schacter, D. N. Greve, B. Fischl, J. D. Mendola, B. R. Rosen, and A. M. Dale, 2001. Cortical mechanisms specific to explicit visual object recognition, *Neuron*, 29:529–535.
- Barton, J. J., D. Z. Press, J. P. Keenan, and M. O'Connor, 2002. Lesions of the fusiform face area impair perception of facial configuration in prosopagnosia, *Neurology*, 58:71–78.
- Bentin, S., T. Allison, A. Puce, E. Perez, and G. McCarthy, 1996. Electrophysiological studies of face perceptions in humans, *JOCN*, 8:551–565.
- Breiter, H. C., N. L. Etcoff, P. J. Whalen, W. A. Kennedy, S. L. Rauch, R. L. Buckner, M. M. Strauss, S. E. Hyman, and B. R. Rosen, 1996. Response and habituation of the human amygdala during visual processing of facial expression, *Neuron*, 17:875–887.
- Brewer, J. B., Z. Zhao, J. E. Desmond, G. H. Glover, and J. D. E. Gabrieli, 1998. Making memories: brain activity that predicts how well visual experience will be remembered, *Science*, 281:1185–1187.
- Burgess, N., K. Jeffery, and J. O'Keefe, 1999. Integrating hippocampal and parietal functions: a spatial point of view, in *The Hippocampal and Parietal Foundations of Spatial Cognition* (N. Burgess, K. J. Jeffery, and J. O'Keefe, eds.), New York: Oxford University Press, pp. 3–29.
- Chao, L. L., A. Martin, and J. V. Haxby, 1999. Are face-responsive regions selective only for faces? *NeuroReport*, 10:2945–2950.

- Cheng, K., 1986. A purely geometric module in the rat's spatial representation, *Cognition*, 23:149–178.
- Cohen, L., S. Dehaene, L. Naccache, S. Lehericy, G. Dehaene-Lambertz, M. A. Henaff, and F. Michel, 2000. The visual word form area: spatial and temporal characterization of an initial stage of reading in normal subjects and posterior split-brain patients, *Brain*, 123(Pt 2):291–307.
- Colby, C. L., and M. E. Goldberg, 1999. Space and attention in parietal cortex, *Annu. Rev. Neurosci.*, 22:319–349.
- Downing, P., Y. Jiang, M. Shuman, and N. Kanwisher, 2001. A cortical area selective for visual processing of the human body, *Science*, 293:2470–2473.
- Duchaine, B. C., 2000. Developmental prosopagnosia with normal configural processing, *NeuroReport*, 11:79–83.
- Epstein, R., K. S. Graham, and P. E. Downing, 2003. Viewpoint-specific scene representations in human parahippocampal cortex, *Neuron*, 37:865–876.
- Epstein, R., E. De Yoe, D. Press, and N. Kanwisher, 2001. Neuropsychological evidence for a topographical learning mechanism in parahippocampal cortex, *Cogn. Neuropsychol.*, 18:481–508.
- Epstein, R., A. Harris, D. Stanley, and N. Kanwisher, 1999. The parahippocampal place area: recognition, navigation, or encoding? *Neuron*, 23:115–125.
- Epstein, R., and N. Kanwisher, 1998. A cortical representation of the local visual environment, *Nature*, 392:598–601.
- Farah, M. J., C. Rabinowitz, G. E. Quinn, and G. T. Liu, 2000. Early commitment of neural substrates for face recognition, *Cogn. Neuropsychol.*, 17:117–123.
- Fujita, I., K. Tanaka, M. Ito, and K. Cheng, 1992. Columns for visual features of objects in monkey inferotemporal cortex, *Nature*, 360:343–346.
- Gauthier, I., M. J. Tarr, A. W. Anderson, P. Skudlarski, and J. C. Gore, 1999. Activation of the middle fusiform “face area” increases with expertise in recognizing novel objects, *Nat. Neurosci.*, 2:568–573.
- Georges-François, P., E. T. Rolls, and R. G. Robertson, 1999. Spatial view cells in the primate hippocampus: allocentric view not head direction or eye position or place, *Cereb. Cortex*, 9:197–212.
- Gorno-Tempini, M. L., and C. J. Price, 2001. Identification of famous faces and buildings: a functional neuroimaging study of semantically unique items, *Brain*, 124:2087–2097.
- Gouteux, S., C. Thinus-Blanc, and J. Vauclair, 2001. Rhesus monkeys use geometric and nongeometric information during a reorientation task, *J. Exp. Psychol. Gen.*, 130:505–519.
- Grill-Spector, K., Z. Kourtzi, and N. Kanwisher, 2001. The lateral occipital complex and its role in object recognition, *Vis. Res.*, 41:1409–1422.
- Grill-Spector, K., T. Kushnir, S. Edelman, G. Avidan-Carmel, Y. Itzhak, and R. Malach, 1999. Differential processing of objects under various viewing conditions in the human lateral occipital complex, *Neuron*, 24:187–203.
- Grill-Spector, K., T. Kushnir, S. Edelman, Y. Itzhak, and R. Malach, 1998a. Cue-invariant activation in object-related areas of the human occipital lobe, *Neuron*, 21:191–202.
- Grill-Spector, K., T. Kushnir, T. Hendler, S. Edelman, Y. Itzhak, and R. Malach, 1998b. A sequence of object-processing stages revealed by fMRI in the human occipital lobe, *Hum. Brain Mapping*, 6:316–328.
- Grill-Spector, K., T. Kushnir, T. Hendler, and R. Malach, 2000. The dynamics of object-selective activation correlate with recognition performance in humans, *Nat. Neurosci.*, 3:837–843.
- Grossman, E., M. Donnelly, R. Price, D. Pickens, V. Morgan, G. Neighbor, and R. Blake, 2000. Brain areas involved in perception of biological motion, *J. Cogn. Neurosci.*, 12:711–720.
- Habib, M., and A. Sirigu, 1987. Pure topographical disorientation: a definition and anatomical basis, *Cortex*, 23:73–85, 1987.
- Halgren, E., A. M. Dale, M. I. Sereno, R. B. H. Tootell, K. Marinkovic, and B. R. Rosen, 1999. Location of human face-selective cortex with respect to retinotopic areas, *Hum. Brain Mapping*, 7:29–37.
- Hasson, U., T. Hendler, D. Ben Bashat, and R. Malach, 2001. Vase or face? A neural correlate of shape-selective grouping processes in the human brain, *J. Cogn. Neurosci.*, 13:744–753.
- Haxby, J. V., M. I. Gobbini, M. L. Furey, A. Ishai, J. L. Schouten, and P. Pietrini, 2001. Distributed and overlapping representations of faces and objects in ventral temporal cortex, *Science*, 293:2425–2430.
- Haxby, J. V., C. L. Grady, B. Horwitz, L. G. Ungerleider, M. Mishkin, R. E. Carson, P. Herscovitch, M. B. Schapiro, and S. I. Rapoport, 1991. Dissociation of object and spatial visual processing pathways in human extrastriate cortex, *Proc. Natl. Acad. Sci. USA*, 88:1621–1625.
- Haxby, J. V., L. G. Ungerleider, V. P. Clark, J. L. Schouten, E. A. Hoffman, and A. Martin, 1999. The effect of face inversion on activity in human neural systems for face and object perception, *Neuron*, 22:189–199.
- Henke, K., S. R. Schweinberger, A. Grigo, T. Klos, and W. Sommer, 1998. Specificity of face recognition: recognition of exemplars of non-face objects in prosopagnosia, *Cortex*, 34:289–296.
- Hermer, L., and E. S. Spelke, 1994. A geometric process for spatial reorientation in young children, *Nature*, 370:57–59.
- Hoffman, E. A., and J. V. Haxby, 2000. Distinct representations of eye gaze and identity in the distributed human neural system for face perception, *Nat. Neurosci.*, 3:80–84.
- Ishai, A., L. Ungerleider, A. Martin, J. L. Schouten, and J. V. Haxby, 1999. Distributed representation of objects in the human central visual pathway, *PNAS*, 96:9379–9384.
- Jacobs, R., 1997. Nature, nurture, and the development of functional specializations: a computational approach, *Psychological Bulletin and Review*, 4:299–309.
- Jacobs, R. A., 1999. Computational studies of the development of functionally specialized neural modules, *Trends in Cognitive Sciences*, 3:31–38.
- James, T. W., G. K. Humphrey, J. S. Gati, R. S. Menon, and M. A. Goodale, 2000. The effects of visual object priming on brain activation before and after recognition, *Curr. Biol.*, 10:1017–1024.
- Johnson, M. H., S. Dziurawiec, H. Ellis, and J. Morton, 1991. Newborns' preferential tracking of face-like stimuli and its subsequent decline, *Cognition*, 40(1–2):1–19.
- Kanwisher, N., 2000. Domain specificity in face perception, *Nat. Neurosci.*, 3:759–763.
- Kanwisher, N., J. McDermott, and M. Chun, 1997. The fusiform face area: a module in human extrastriate cortex specialized for face perception, *J. Neurosci.*, 17:4302–4311.
- Kanwisher, N., D. Stanley, and A. Harris, 1999. The fusiform face area is selective for faces, not animals, *NeuroReport*, 10:183–187.
- Kanwisher, N., F. Tong, and K. Nakayama, 1998. The effect of face inversion on the human fusiform face area, *Cognition*, 68:B1–B11.
- Kanwisher, N., R. Woods, M. Iacoboni, and J. Mazziotta, 1996. A locus in human extrastriate cortex for visual shape analysis, *JOCN*, 91:133–142.

- Kourtzi, Z., and N. Kanwisher, 2001. Shapes, not contours, determine fMRI responses in the human lateral occipital complex, *Science*, 293:1506–1509.
- Le Grand, R., C. J. Mondloch, D. Maurer, and H. P. Brent, 2001. Neuroprecognition. Early visual experience and face processing, *Nature*, 410:890.
- Learmonth, A. E., N. S. Newcombe, and J. Huttenlocher, 2001. Toddlers' use of metric information and landmarks to reorient, *J. Exp. Child Psychol.*, 80:225–244.
- Lerner, Y., T. Hendler, D. Ben-Bashat, M. Harel, and R. Malach, 2001. A hierarchical axis of object processing stages in the human visual cortex, *Cereb. Cortex*, 114:287–297.
- Lerner, Y., T. Hendler, and R. Malach, 2002. Object-completion effects in the human lateral occipital complex, *Cereb. Cortex*, 12: 163–177.
- Maguire, E. A., N. Burgess, J. G. Donnett, R. S. J. Frackowiak, C. D. Frith, and J. O'Keefe, 1998. Knowing where and getting there: a human navigational network, *Science*, 280:921–924.
- Malach, R., J. B. Reppas, R. B. Benson, K. K. Kwong, H. Jiang, W. A. Kennedy, P. J. Ledden, T. J. Brady, B. R. Rosen, and R. B. H. Tootell, 1995. Object-related activity revealed by functional magnetic resonance imaging in human occipital cortex, *Proc. Natl. Acad. Sci. USA*, 92:8135–8138.
- Martin, A., and L. L. Chao, 2001. Semantic memory and the brain: structure and processes, *Curr. Opin. Neurobiol.*, 112:194–201.
- McCarthy, G., A. Puce, J. C. Gore, and T. Allison, 1997. Face-specific processing in the human fusiform gyrus, *J. Cogn. Neurosci.*, 9:605–610.
- Moscovitch, M., G. Winocur, and M. Behrmann, 1997. What is special about face recognition? Nineteen experiments on a person with visual object agnosia and dyslexia but normal face recognition, *JOCN*, 9:555–604.
- Naccache, L., and S. Dehaene, 2001. The priming method: imaging unconscious repetition priming reveals an abstract representation of number in the parietal lobes, *Cereb. Cortex*, 1110:966–974.
- Nunn, J. A., P. Postma, and R. Pearson, 2001. Developmental prosopagnosia: should it be taken at face value? *Neurocase*, 7:15–27.
- O'Keefe, J., and L. Nadel, 1978. *The Hippocampus as a Cognitive Map*, Oxford: Oxford University Press.
- Perrett, D., E. T. Rolls, and W. Caan, 1982. Visual neurons responsive to faces in the monkey temporal cortex, *Exp. Brain Res.*, 47:329–342.
- Phillips, M. L., A. W. Young, C. Senior, M. Brammer, C. Andrew, A. J. Calder, E. T. Bullmore, D. I. Perret, D. Rowland, S. C. Williams, J. A. Gray, and A. S. David, 1997. A specific neural substrate for perceiving facial expressions of disgust, *Nature*, 389:495–498.
- Pierce, K., R. A. Muller, J. Ambrose, G. Allen, and E. Courchesne, 2001. Face processing occurs outside the fusiform "face area" in autism: evidence from functional MRI, *Brain*, 124(Pt 10):2059–2073.
- Polk, T. A., and M. Farah, 1998. The neural development and organization of letter recognition: evidence from functional neuroimaging, computational modeling, and behavioral studies, *Proc. Natl. Acad. Sci. USA*, 95:847–852.
- Potter, M. C., 1976. Short-term conceptual memory for pictures, *J. Exp. Psychol. Hum. Learning Memory*, 5:509–522.
- Puce, A., T. Allison, M. Asgari, J. C. Gore, and G. McCarthy, 1996. Differential sensitivity of human visual cortex to faces, letter-strings, and textures: a functional MRI study, *J. Neurosci.*, 16: 5205–5215.
- Puce, A., T. Allison, J. C. Gore, and G. McCarthy, 1995. Face perception in extrastriate cortex studied by functional MRI, *J. Neurophysiol.*, 74:1192–1199.
- Rossion, B., L. Dricot, A. Devolder, J. M. Bodart, M. Crommelinck, B. De Gelder, and R. Zoontjes, 2000. Hemispheric asymmetries for whole-based and part-based face processing in the human fusiform gyrus, *J. Cogn. Neurosci.*, 12:793–802.
- Schultz, R. T., I. Gauthier, A. Klin, R. K. Fulbright, A. W. Anderson, F. Volkmar, P. Skudlarski, C. Lacadie, D. J. Cohen, and J. C. Gore, 2000. Abnormal ventral temporal cortical activity during face discrimination among individuals with autism and Asperger syndrome, *Arch. Gen. Psychiatry*, 57:331–340.
- Sergeant, J., S. Ohta, and B. MacDonald, 1992. Functional neuroanatomy of face and object processing: a positron emission tomography study, *Brain*, 115:15–36.
- Shah, N. J., J. C. Marshall, O. Zafiris, A. Schwab, K. Zilles, H. J. Markowitsch, and G. R. Fink, 2001. The neural correlates of person familiarity. A functional magnetic resonance imaging study with clinical implications, *Brain*, 124(Pt 4):804–815.
- Spiridon, M., and N. Kanwisher, 2002. How distributed is visual category information in human occipito-temporal cortex? An fMRI study, *Neuron*, 35:1157–1165.
- Tanaka, K., 1997. Mechanisms of visual object recognition: monkey and human studies, *Curr. Opin. Neurobiol.*, 7:523–529.
- Tarr, M. J., and I. Gauthier, 2000. FFA: a flexible fusiform area for subordinate-level visual processing automatized by expertise, *Nat. Neurosci.*, 3:764–769.
- Thorpe, S., D. Fize, and C. Marlot, 1996. Speed of processing in the human visual system, *Nature*, 381:520–522.
- Tong, F., K. Nakayama, J. T. Vaughan, and N. Kanwisher, 1998. Binocular rivalry and visual awareness in human extrastriate cortex, *Neuron*, 21:753–759.
- Tovee, M. J., E. T. Rolls, A. Treves, and R. P. Bellis, 1993. Information encoding and the responses of single neurons in the primate temporal visual cortex, *J. Neurophysiol.*, 70:640–654.
- Tsao, D., Y. Sasaki, J. Mandeville, F. Leite, E. Pasztor, L. Wald, A. Dale, and G. Orban, 2001. fMRI reveals face-selective activity in awake behaving macaque, *Soc. Neurosci. Abstr.*, Program #122.2.
- Vanduffel, W., D. Fize, J. B. Mandeville, K. Nelissen, P. Van Hecke, B. R. Rosen, R. B. Tootell, and G. A. Orban, 2001. Visual motion processing investigated using contrast agent-enhanced fMRI in awake behaving monkeys, *Neuron*, 32:565–577.
- Vuillumier, P., R. N. Henson, J. Driver, and R. J. Dolan, 2002. Multiple levels of visual object constancy revealed by event-related fMRI of repetition priming, *Nat. Neurosci.*, 5:491–499.
- Wada, Y., and T. Yamamoto, 2001. Selective impairment of facial recognition due to a haematoma restricted to the right fusiform and lateral occipital region, *J. Neurol., Neurosurg., and Psychiatry*, 71:254–257.
- Wagner, A. D., D. L. Schacter, M. Rotte, W. Koutstaal, A. Maril, A. M. Dale, B. R. Rosen, and R. L. Buckner, 1998. Building memories: remembering and forgetting of verbal experiences as predicted by brain activity, *Science*, 281:1188–1191.
- Xu, Y., and N. Kanwisher, 2001. What is the magnitude and theoretical significance of the FFA response to expert stimuli? *Soc. Neurosci. Abstr.*, Prog. #417.9.

X MOTION, DEPTH, AND SPATIAL RELATIONS

80 Motion Cues in Insect Vision and Navigation

MANDYAM SRINIVASAN AND SHAOWU ZHANG

A GLANCE AT A FLY evading a rapidly descending hand or orchestrating a flawless landing on the rim of a teacup would convince even the most skeptical observer that many insects are not only excellent fliers and navigators, but also possess visual systems that are fast, reliable, precise, and exquisitely sensitive to motion. It is no wonder, then, that there has been considerable interest in trying to fathom how insects detect, evaluate, and use motion cues in their daily lives.

Early studies of the analysis of image motion by insects concentrated on the *optomotor response* (reviewed by Reichardt, 1969). An insect, flying tethered inside a striped drum, will tend to turn in the direction in which the drum is rotated. If the drum rotates clockwise, the insect will generate a yaw torque in the clockwise direction, and vice versa. This reaction helps the insect maintain a straight course by compensating for undesired deviations: a gust of wind that causes the insect to veer to the left, for example, would create rightward image motion on the eyes and cause the insect to generate a compensatory yaw to the right. Investigation of this optomotor response over several decades has provided valuable information on some of the characteristics of motion perception by the insect visual system (Borst and Egelhaaf, 1989; Buchner, 1984; Reichardt, 1969).

More recent studies, carried out primarily with freely flying honeybees, have revealed a number of additional contexts in which image motion is analyzed to coordinate flight and to obtain a useful percept of the world. It appears, for example, that bees analyze motion cues in a variety of different ways for negotiating narrow gaps, estimating the distances to objects, avoiding obstacles, controlling flight speed, executing smooth landings, and gauging the distance traveled. Here we describe some of these strategies and attempt to elucidate the properties of the underlying motion-sensitive mechanisms.

Unlike vertebrates, insects have immobile eyes with fixed-focus optics. Therefore, they cannot infer the distance of an object from the extent to which the directions of gaze must converge to view the object or by monitoring the refractive power that is required to bring the image of the object into focus on the retina. Furthermore, compared with human eyes, the eyes of insects are positioned much closer together and possess inferior spatial acuity. Therefore, even if an

insect possessed the neural apparatus required for binocular stereopsis, such a mechanism would be relatively imprecise and restricted to measuring ranges of only a few centimetres (Collett and Harkness, 1982; Horridge, 1987; Rossell, 1983; Srinivasan, 1993). Not surprisingly, insects have evolved alternative visual strategies for guiding locomotion and for seeing the world in three dimensions. Many of these strategies rely on using cues derived from the image motion that the animal experiences when it moves in its environment. Some of these cues are outlined below, and references to more complete accounts are provided.

Peering insects

Over 100 years ago, Exner (1891), pondering the eyestalk movements of crabs, speculated that invertebrates might use image motion to estimate object range. However, the first clear evidence to support this conjecture did not arrive until the middle of the twentieth century, when Wallace (1959) made the astute observation that a locust sways its head from side to side before jumping onto a nearby object (Fig. 80.1A). Wallace hypothesised that this *peering* motion, typically 5 to 10 mm in amplitude, was a strategy for measuring object range. To test this hypothesis, he presented a locust with two objects subtending the same visual angle. One object was relatively small and was placed close to the locust, while the other was larger and situated farther away. He found that the locust, after peering, jumped almost invariably to the nearer object. In a further series of elegant experiments, recently confirmed more quantitatively by Sobel (1990), a target was oscillated from side to side, in synchrony with the insect's peering movements. When the target was oscillated out of phase with the movement of the head, thereby increasing the speed and amplitude of the object's image on the retina, the locust consistently underestimated the range of the target (Fig. 80.1C). On the other hand, when the target was oscillated in phase with the head, it consistently overestimated the range (Fig. 80.1B). Thus, reduced image motion of the target caused the insect to overestimate the target's range, while increased motion had the opposite effect. These findings demonstrated convincingly that the peering locust was estimating the range of the target in terms of the speed of the

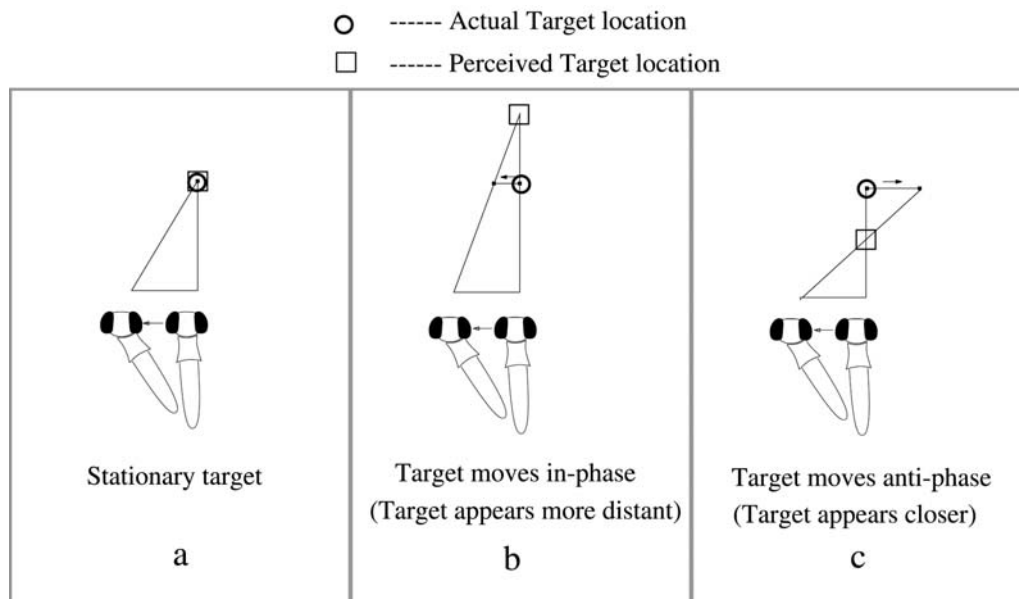


FIGURE 80.1. Experiments investigating how locusts measure the range of a target by peering, that is, moving the head from side to side. Range is estimated correctly when the target is stationary (A), overestimated when the target is moved in the same direction as the head (B), and underestimated when it is moved in the opposite direction (C). Thus, the range of the target is estimated in terms of the motion of the target's image during the peer. (Adapted from Sobel, 1990.)

image on the retina. It is now known that certain other insects, such as grasshoppers (Eriksson, 1980) and mantids (Horridge, 1986; Kral, 1998; Kral and Poteser, 1997; Poteser et al., 1998), also use peering to measure object range.

Flying insects

Peering, however, is practical only when an insect is not locomoting. Are flying insects capable of glean range information from image motion, and if so, how do they accomplish this? Stable flight in a straight line would seem to be a prerequisite for extracting information on range (Horridge, 1987; Srinivasan, 1993). Research over the past 50 years has uncovered a number of different ways in which insects use image motion to stabilize flight control and to extract useful information about the environment. We shall begin by considering strategies for visual control and stabilization of flight and then examine the ways in which image motion is used to glean information about the structure of the environment, and about the insect's movement within it.

STABILIZING FLIGHT For insects, vision provides an important sensory input for the stabilization of flight. If an insect flying along a straight line is blown to the left by a gust of wind, the image on its frontal retina moves to the right. This causes the flight motor system to generate a corrective yaw torque, which brings the insect back on course (reviewed by Reichardt, 1969). Similar control mechanisms act to stabilize pitch and roll (e.g., Srinivasan, 1977). This optomotor response (Reichardt, 1969) has provided an excellent exper-

imental paradigm with which to probe the neural mechanisms underlying motion detection. Largely through studies of the optomotor response in flies, we now know that the direction of image movement is sensed by correlating the intensity variations registered by neighboring ommatidia, or facets, of the compound eye (reviewed by Reichardt, 1969). Research over the past 30 years has uncovered the existence of a number of motion-sensitive neurons with large visual fields, each responding preferentially to motion in a specific direction (Hausen, 1993; reviewed by Hausen and Egelhaaf, 1989) or to rotation of the fly about a specific axis (Krapp and Hengstenberg, 1996). These neurons are likely to play an important role in stabilizing flight and providing the fly with a visually *kinesthetic* sense. Their properties have been reviewed extensively (e.g., Egelhaaf and Borst, 1993; Hausen, 1993; Hausen and Egelhaaf, 1989), and we shall not repeat them here.

HOVERING Hoverflies and certain species of bee display an impressive ability to hold a rigid position in midair, compensating almost perfectly for wind gusts and other disturbances. Kelber and Zeil (1997) investigated hovering in a species of stingless bee, *Tetragonisca angustula*. Guard bees of this species hover stably in watch near the entrance to their nest, protecting it from intruders. To investigate the visual stabilizing mechanisms, Kelber and Zeil acclimated the bees to the presence of a spiral pattern mounted on the vertical face of the hive, surrounding the entrance. When the spiral was briefly rotated to simulate expansion, the hovering guard bees darted away from the focus of apparent expansion;

when the spiral was rotated to simulate contraction, they moved toward the focus of contraction. These responses were always directed toward or away from the nest entrance, irrespective of the bee's orientation and therefore irrespective of the region of the eye that experienced the experimentally imposed pattern of image motion. Clearly, then, these creatures were interpreting expansion and contraction of the image as unintended movements toward or away from the nest entrance and were compensating for them.

NEGOTIATING NARROW GAPS When a bee flies through a hole in a window, it tends to fly through its center, balancing the distances to the left and right boundaries of the opening. How does it gauge and balance the distances to the two rims?

One possibility is that it does not measure distances at all, but simply balances the speeds of image motion on the two eyes as it flies through the opening. To investigate this possibility, Kirchner and Srinivasan (1989) trained bees to enter an apparatus that offered a reward of sugar solution at the end of a tunnel. Each side wall carried a pattern consisting of a vertical black-and-white grating (Fig. 80.2). The grating on one wall could be moved horizontally at any desired speed, either toward the reward or away from it. After the bees had received several rewards with the gratings stationary, they were filmed from above as they flew along the tunnel. When both gratings were stationary, the bees tended to fly along the midline of the tunnel, that is, equidistant from the two walls (Fig. 80.2*A*). But when one of the gratings was moved at a constant speed in the direction of the bees' flight—thereby reducing the speed of retinal image motion on that eye relative to the other eye—the bees' trajectories shifted toward the side of the moving grating (Fig. 80.2*B*). When the grating moved in a direction opposite to that of the bees' flight—thereby increasing the speed of retinal image motion on that eye relative to the other—the bees' trajectories shifted away from the side of the moving grating (Fig. 80.2*C*). These findings demonstrate that when the walls were stationary, the bees maintained equidistance by balancing the speeds of the retinal images in the two eyes. A lower image speed on one eye evidently caused the bee to move closer to the wall seen by that eye. A higher image speed had the opposite effect.

Were the bees really measuring and balancing image speeds on the two sides as they flew along the tunnel or were they simply balancing the contrast frequencies produced by the succession of dark and light bars of the gratings? This question was investigated by analyzing the flight trajectories of bees when the two walls carried gratings of different spatial periods. When the gratings were stationary, the trajectories were always equidistant from the two walls, even when the spatial frequencies of the gratings on the two sides—and therefore the contrast frequencies experienced

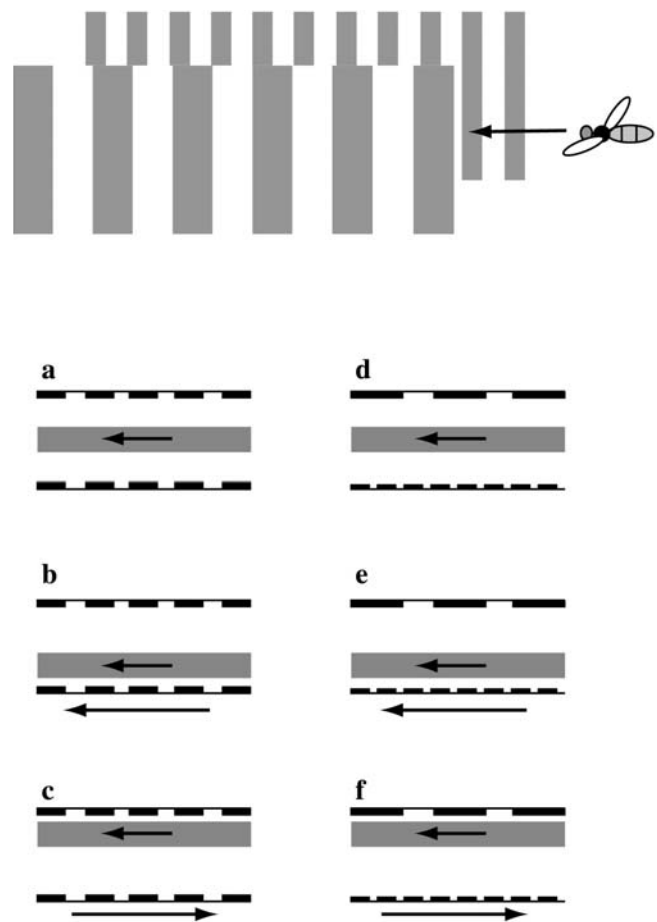


FIGURE 80.2. Experiment investigating how bees fly through the middle of a tunnel (the centering response). Bees are trained to fly through a tunnel 40 cm long, 12 cm wide, and 20 cm high to collect a reward placed at the far end. The flanking walls of the tunnel are lined with vertical black-and-white gratings with period of 5 cm. The flight trajectories of bees, as recorded by a video camera positioned above the tunnel, are shown in *A* to *F*. In each panel the shaded area represents the mean and standard deviation of the positions of the flight trajectories, analyzed from recordings of several hundred flights. The dark bars represent the black stripes of the patterns on the walls. The small arrow indicates the direction of bee flight and the large arrow the direction of pattern movement. When the patterns on the walls are stationary, bees tend to fly close to the midline of the tunnel (*A*, *D*). When the pattern on one of the walls is in motion, however, bees tend to fly closer to that wall if the pattern moves in the same direction as the bee (*B*, *E*) and farther away from that wall if the pattern moves in the opposite direction (*C*, *F*). These results indicate that bees balance the distances to the walls of the tunnel by balancing the speeds of image motion that are experienced by the two eyes, and that they are able to measure image speed rather independently of the spatial structure of the image. (Modified from Srinivasan et al., 1991.)

by the two eyes—differed by a factor of as much as 4 (Fig. 80.2D). When one of the gratings was in motion, the trajectories shifted toward or away from the moving grating (as described above) according to whether the grating moved with or against the direction of the bees' flight (Figs. 80.2E, 80.2F). These results indicate that the bees were indeed balancing the speeds of the retinal images on the two eyes and not the contrast frequencies. The above findings are true irrespective of whether the gratings possess square-wave intensity profiles (with abrupt changes of intensity) or sinusoidal profiles (with gradual intensity changes) and irrespective of whether the contrasts of the gratings on the two sides are equal or considerably different (Srinivasan et al., 1991). Further experiments have revealed that when the velocities of the bee and the pattern are known, it is even possible to predict the position of a bee's flight trajectory along the width of the tunnel, on the assumption that the bee balances the apparent angular velocities on either side of the tunnel (Srinivasan et al., 1991). These findings suggest that the bee's visual system is capable of computing the apparent angular speed of a grating independently of its contrast and spatial-frequency content.

Subsequent studies (Srinivasan and Zhang, 1997; Srinivasan et al., 1993) have investigated this *centering* response further by comparing its properties with those of the well-known optomotor response in an experimental setup which allows the two responses to be compared in the same individual under the same conditions. The results indicate that the centering response differs from the optomotor response in three respects. First, the centering response is sensitive primarily to the *angular speed* of the stimulus, regardless of its spatial structure. The optomotor response, on the other hand, is sensitive primarily to the *temporal frequency* of the stimulus; therefore, it confounds the angular velocity of a striped pattern with its spatial period. Second, the centering response is *nondirectional*, while the optomotor response is *directionally selective*. Third, the centering response is sensitive to higher temporal frequencies than is the optomotor response. Whereas the optomotor response exhibits a relatively low bandwidth (with half-magnitude points at 6 and 75 Hz), the centering response exhibits a relatively high bandwidth (with half-magnitude points at 3 Hz and well beyond 100 Hz). Thus, the motion-detecting processes underlying the centering response exhibit properties that are substantially different from those that mediate the well-known optomotor response (Srinivasan and Zhang, 1997; Srinivasan et al., 1993). Models of movement-detecting mechanisms underlying the centering response are described in Srinivasan et al. (1999).

Given that the role of the centering response is to ensure that the insect flies through the middle of a gap irrespective of the texture of the side walls, it is easy to see why this response is mediated by a movement-detecting system

which measures the angular speed of the image independently of its spatial structure. The movement-detecting system that subserves the optomotor response, on the other hand, does not need to measure image speed accurately: it merely needs to signal the *direction* of image motion reliably so that a corrective yaw of the appropriate polarity may be generated.

CONTROLLING FLIGHT SPEED Do insects control the speed of their flight, and, if so, how? Work by David (1982) and by Srinivasan et al. (1996) suggests that flight speed is controlled by monitoring the velocity of the image of the environment.

David (1982) observed fruitflies flying upstream in a wind tunnel, attracted by the odor of fermenting banana. The walls of the cylindrical wind tunnel were decorated with a helical black-and-white striped pattern so that rotation of the cylinder about its axis produced apparent movement of the pattern toward the front or the back. With this setup, the rotational speed of the cylinder (and hence the speed of the backward motion of the pattern) could be adjusted such that the fly was stationary (i.e., did not move along the axis of the tunnel). The apparent backward speed of the pattern then revealed the ground speed that the fly was "choosing" to maintain, as well as the angular velocity of the image of the pattern on the flies' eyes. In this setup, fruitflies tended to hold the angular velocity of the image constant. Increasing or decreasing the speed of the pattern caused the flies to move backward or forward (respectively) along the tunnel at a rate such that the angular velocity of the image on the eye was always "clamped" at a fixed value. The flies also compensated for headwind in the tunnel, increasing or decreasing their thrust to maintain the same apparent ground speed (as indicated by the angular velocity of image motion on the eye). Experiments in which the angular period of the stripes was varied revealed that the flies were measuring (and holding constant) the angular velocity of the image on the eye, irrespective of the spatial structure of the image.

Bees appear to use a similar strategy to regulate flight speed (Srinivasan et al., 1996). When a bee flies through a tapered tunnel, it decreases its flight speed as the tunnel narrows to keep the angular velocity of the image of the walls, as seen by the eye, constant at about 320 deg/sec (Fig. 80.3). This suggests that flight speed is controlled by monitoring and regulating the angular velocity of the image of the environment on the eye. (That is, if the width of the tunnel is doubled, the bee flies twice as fast.) On the other hand, a bee flying through a tunnel of uniform width does not change its speed when the spatial period of the stripes lining the walls is abruptly changed (Srinivasan et al., 1996). Thus, flight speed is regulated by a visual motion-detecting mechanism that measures the angular velocity of the image largely independently of its spatial structure. In

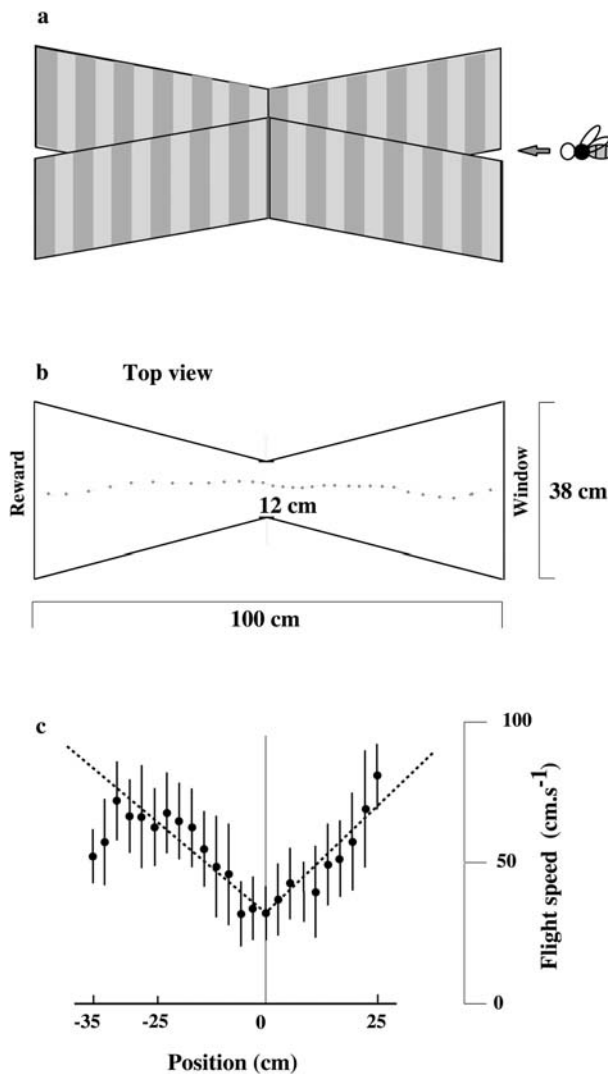


FIGURE 80.3. Experiment investigating visual control of flight speed. *A*, Bees are trained to fly through a tapered tunnel to collect a reward placed at the far end. The walls of the tunnel are lined with vertical black-and-white gratings with a period of 6 cm. *B*, A typical flight trajectory, as filmed from above by a video camera, where the bee's position and orientation are shown every 50 msec. *C*, Mean and standard deviation of flight speeds measured at various positions along the tunnel (data from 18 flights). The V-shaped line shows the theoretically expected flight speed profile if the bees were to hold the angular velocity of the images of the walls constant at 320 deg/sec as they fly through the tunnel. The data indicate that bees control flight speed by holding constant the angular velocity of the image of the environment. (Adapted from Srinivasan et al., 1996.)

this respect, the speed-regulating system is similar to the centering system. However, it is not known whether the regulation of flight speed in bees is mediated by a directionally selective movement-detecting mechanism or a nondirectional one.

An obvious advantage of controlling flight speed by regulating image speed is that the insect would automatically

slow down to a safer speed when negotiating a narrow passage.

ESTIMATING THE DISTANCE FLOWN It is well known that honeybees can navigate accurately and repeatedly to a food source. It is also established that bees communicate to their nestmates the distance and direction in which to fly to reach it through the famous *waggle dance* (von Frisch, 1993). But the cues by which bees gauge the distance flown to the goal have been a subject of controversy.

A few years ago, Esch and Burns (1995, 1996) investigated distance measurement by enticing honeybees to find food at a feeder placed 70 m away from a hive in an open field and recording the perceived distance as signaled by the bees when they danced to recruit other nestmates in the hive. When the feeder was 70 m away, the bees signaled 70 m—the correct distance. But when the feeder was raised above the ground by attaching it to a helium balloon, the bees signaled a progressively *shorter* distance as the height of the balloon was increased. This occurred despite the fact that the balloon was now *farther* away from the hive! Esch and Burns explained this finding by proposing that the bees were gauging distance flown in terms of the motion of the image of the ground below, rather than, for example, through the energy consumed to reach the feeder. The higher the balloon, the lower the total amount of image motion that the bees experienced en route to the feeder.

This hypothesis was examined by Srinivasan et al. (1996, 1997), who investigated the cues by which bees estimate and learn distances flown under controlled laboratory conditions. Bees were trained to enter a 3.2 m long tunnel and collect a reward of sugar solution at a feeder placed in the tunnel at a fixed distance from the entrance. The walls and floor of the tunnel were lined with black-and-white gratings perpendicular to the tunnel's axis (Fig. 80.4A). During training, the position and orientation of the tunnel were changed frequently to prevent the bees from using any external landmarks to gauge their position relative to the tunnel entrance. The bees were then tested by recording their searching behavior in an identical fresh tunnel that carried no reward and was devoid of any scent cues. In the tests, these bees showed a clear ability to search for the reward at the correct distance, as indicated by the search distribution labeled by the squares in Figure 80.4B.

How were the bees gauging the distance they had flown in the tunnel? Tests were carried out to examine the participation of a variety of potential cues, including energy consumption, time of flight, airspeed integration, and inertial navigation (Srinivasan et al., 1997). It turned out that the bees were estimating the distance flown by integrating, over time, the motion of the images of the walls on the eyes as they flew down the tunnel. The crucial experiment was one in which bees were trained and tested in conditions where

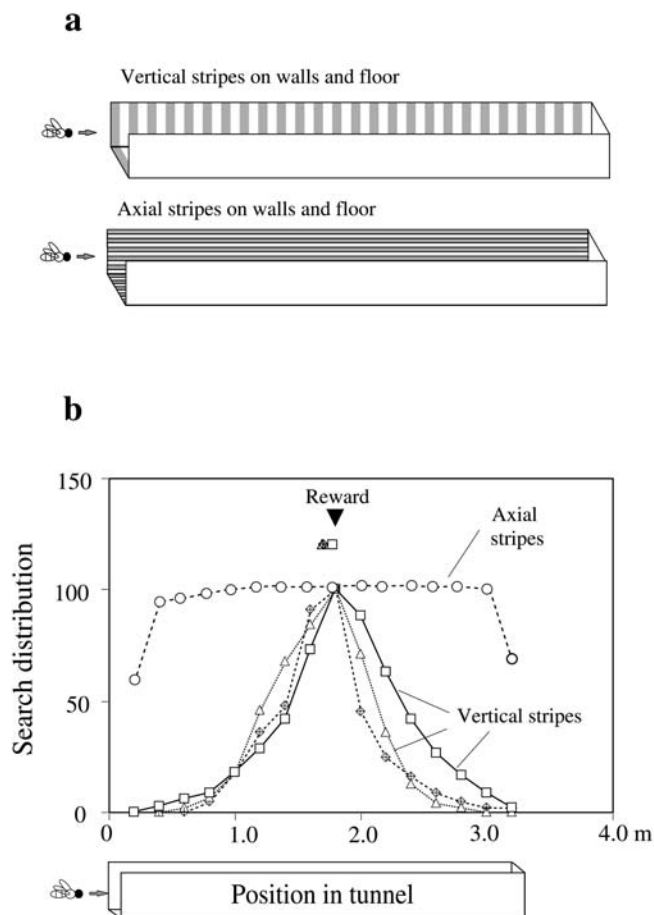


FIGURE 80.4. *A*, Experiment investigating how honeybees gauge distance flown to a food source. Bees are trained to find a food reward placed at a distance of 1.7 m from the entrance of a 3.2 m long tunnel 22 cm wide and 20 cm high. The tunnel is lined with vertical black-and-white gratings with a period of 4 cm. *B*, When the trained bees are tested in a fresh tunnel with the reward absent, they search at the former location of the feeder, as shown by the bell-shaped search distributions. This is true irrespective of whether the period of the grating is 4 cm (as in the training, *square symbols*), 8 cm (*triangles*), or 2 cm (*diamonds*). The inverted triangle shows the former position of the reward, and the symbols below it depict the mean values of the search distributions in each case. Bees lose their ability to estimate the distance of the feeder when image-motion cues are removed by lining the tunnel with axial (rather than vertical) stripes (*circles*). These experiments and others (Srinivasan et al., 1997) demonstrate that (1) distance flown is estimated visually by integrating over time the image velocity that is experienced during the flight, and (2) the honeybee's odometer measures image velocity independently of image structure. (Adapted from Srinivasan et al., 1997.)

image motion was eliminated or reduced by using axially oriented stripes on the walls and floor of the tunnel. The bees then showed no ability to gauge the distance traveled: in the tests, they searched uniformly over the entire length of the tunnel, showing no tendency to stop or turn at the former location of the reward (see the search distribution labeled by the circles in Fig. 80.4*B*). Trained bees tended to search for the feeder at the same position in the tunnel even if the period of the gratings lining the walls and floor was varied in the tests (search distributions labeled by triangles and diamonds in Fig. 80.4*B*). This indicates that the odometric system reads image velocity accurately over a four-fold variation in the spatial period of the grating.

These results, considered together with those of Esch and Burns (1995, 1996), indicate that the bee's "odometer" is driven by the image motion that is generated in the eyes during translatory flight. Evidently, bees use cues derived from image motion not only to stabilize flight and regulate its speed, but also to infer how far they have flown.

We have seen above that the balloon experiment caused bees to underestimate the distance they had flown, because they experienced less image motion than they normally would while cruising to a natural food source. What happens when bees encounter the opposite situation, namely, one in which image motion cues are artificially exaggerated? Srinivasan et al. (2000a) explored this question by training bees to fly directly from their hive into a short, narrow tunnel that was placed very close to the hive entrance. The tunnel was 6.4 m long and 11 cm wide. A feeder was placed 6 m from the entrance. The walls and floor of the tunnel were lined with a random visual texture. The dances of bees returning from this feeder were video-filmed. Incredibly, these bees signaled a flight distance of about 200 m, despite the fact that they had flown only a small fraction of this distance. Evidently, the bees were grossly overestimating the distance they had flown in the tunnel, because the proximity of the walls and floor of the tunnel greatly magnified the image motion that they experienced, in comparison with what would normally occur when foraging outdoors (Esch et al., 2001). This experiment again drives home the point that image motion is the dominant cue that bees use to gauge how far they have traveled.

EXECUTING SMOOTH LANDINGS How does a bee execute a smooth touchdown on a surface? An approach that is perpendicular to the surface would generate strong looming (image expansion) cues which could, in principle, be used to decelerate flight at the appropriate moment. Indeed, work by Wagner (1982) and Borst and Bahde (1988) has shown that deceleration and extension of the legs in preparation for landing are triggered by movement-detecting mechanisms that sense the expansion of the image. Looming cues are weak, however, when a bee performs a grazing landing on

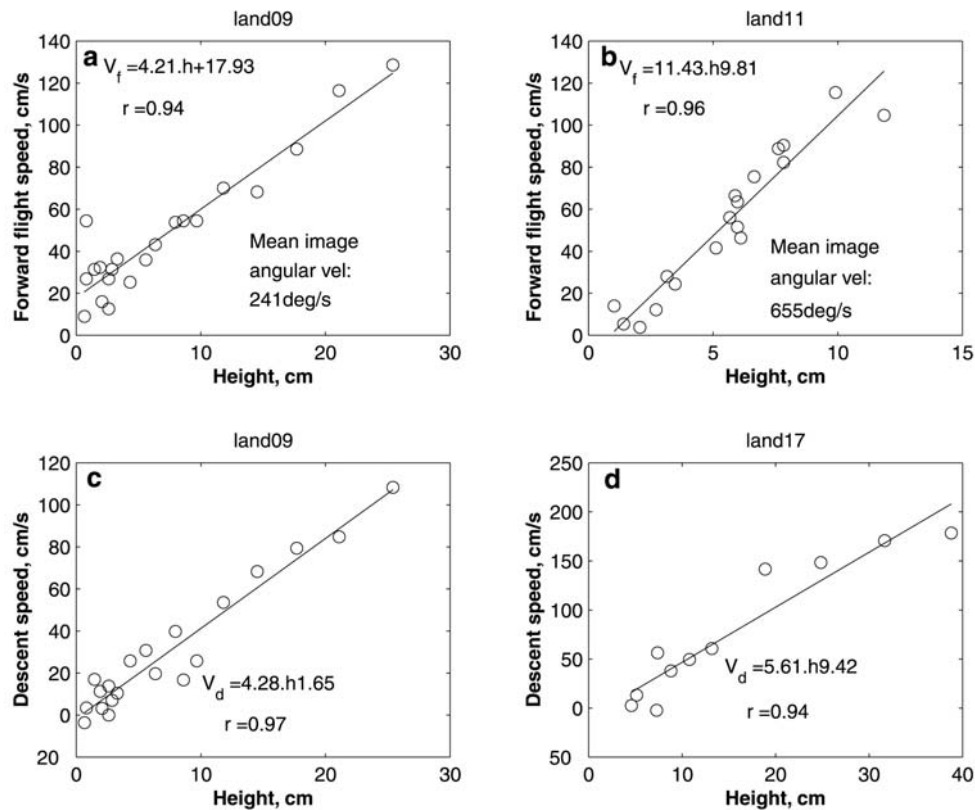


FIGURE 80.5. Typical results of an experiment investigating how bees make a grazing landing on a horizontal surface. *A, B*, Variation of forward flight speed (V_f) with height (h) above the surface for two landing trajectories. *C, D*, Variation of descent speed (V_d) with height (h) above the surface for two landing trajectories. The landing bee holds the angular velocity of the image of the ground

constant at 241 deg/sec in *A* and at 655 deg/sec in *B*, as calculated from the slopes of the linear regression lines. Also shown are the values of the correlation coefficient (r). Holding the image velocity of the ground constant during the approach automatically ensures that the landing speed is zero at touchdown. (Adapted from Srinivasan et al., 2000b.)

a surface. By *grazing landings* we mean landings whose trajectories are inclined to the surface at an angle that is considerably less than 45 degrees. In such landings, the motion of the image of the surface would be dominated by a strong translatory component in the front-to-back direction in the ventral visual field of the eye.

To investigate how bees execute grazing landings, Srinivasan et al. (1996, 2000b, 2001) trained bees to collect a reward of sugar water on a textured horizontal surface. The reward was then removed, and the landings that the bees made on the surface in search of the food were video-filmed in three dimensions.

Analysis of the landing trajectories revealed that the flight speed of the bee decreases steadily as it approaches the surface. In fact, the forward speed as well as the descent speed are approximately proportional to the height above the surface (Fig. 80.5), indicating that the bee is holding the angular velocity of the image of the surface approximately constant as the surface is approached. This strategy automatically ensures that both the forward and descent speeds are close to zero at touchdown. Thus, a smooth landing is achieved by an elegant and surprisingly simple process that

does not require explicit knowledge of the bee's instantaneous speed or height (Srinivasan et al., 2000b).

DISTINGUISHING OBJECTS AT DIFFERENT DISTANCES The experiments described above show that bees stabilize flight, negotiate narrow passages, and orchestrate smooth landings by using what seem to be a series of simple, low-level visual reflexes. But they do not tell us whether flying bees see the world in three dimensions in the way we do. Do bees perceive the world as being composed of objects and surfaces at various ranges? While this is a difficult question—one that a philosopher might even declare unanswerable—one can at least ask whether bees can be trained to distinguish between objects at different distances. Lehrer et al. (1988) trained bees to fly over an artificial meadow and distinguish between artificial flowers at various heights. The training was carried out by associating a reward with a flower at a particular height. The sizes and positions of the flowers were varied randomly and frequently during the training. This ensured that the bees were trained to associate only the height of the flower (or, more accurately, the distance from the eye), and not its position, or angular subtense, with the reward. Using

this approach—details of which are described in Srinivasan et al. (1989)—it was possible to train bees to choose either the highest flower, the lowest flower, or even one at an intermediate height. Clearly, then, the bees were able to distinguish flowers at different heights. Under the experimental conditions, the only cue that a bee could have used to gauge the height of each flower was the speed of the flower's image as the bee flew over it: the taller the flower, the faster the motion of its image.

Kirchner and Lengler (1994) extended this meadow experiment by training bees to distinguish the heights of artificial flowers that carried spiral patterns. Six flowers were presented at the same height, while a seventh was either higher (in one experiment) or lower (in another experiment). Bees trained in this way were tested with a constellation of three identical spiral-bearing flowers of the same height. One test flower was stationary, one was rotated to simulate expansion, and one was rotated to simulate contraction. Bees that had learned to find the higher flower in the training chose the “expanding” flower in the test, whereas bees that had learned to choose the lower flower in the training chose the “contracting” flower. For a bee flying above the flowers and approaching the edge of one of them, the expanding flower produced a higher image motion at its boundary than did the stationary one and was evidently interpreted to be the higher flower. The contracting flower, on the other hand, produced a lower image motion and was therefore taken to be the lower one. This experiment confirms the notion that image motion is an important cue in establishing the relative distances of objects.

DISCRIMINATING OBJECTS FROM BACKGROUNDS In all of the work described above, the objects that were being viewed were readily visible to the insects, since they presented a strong contrast—in luminance or color—against a structureless background. What happens if the luminance or color contrast is removed and replaced by motion contrast? To the human eye, a textured figure is invisible when it is presented motionless against a similarly textured background. But the figure pops out as soon as it is moved relative to the background. This type of relative motion, termed *motion parallax*, can be used to distinguish a nearby object from a remote background. Is an insect capable of distinguishing a textured figure from a similarly textured background purely on the basis of motion parallax?

In a series of pioneering experiments, Reichardt and his colleagues in Tübingen showed that a fly is indeed capable of such figure-ground discrimination (Egelhaaf et al., 1988; Reichardt and Poggio, 1979). A tethered, flying fly will show no sign of detecting a textured figure when the figure oscillates in synchrony with a similarly textured background. But it will react to the figure by turning toward it when the figure moves incoherently with respect to the background.

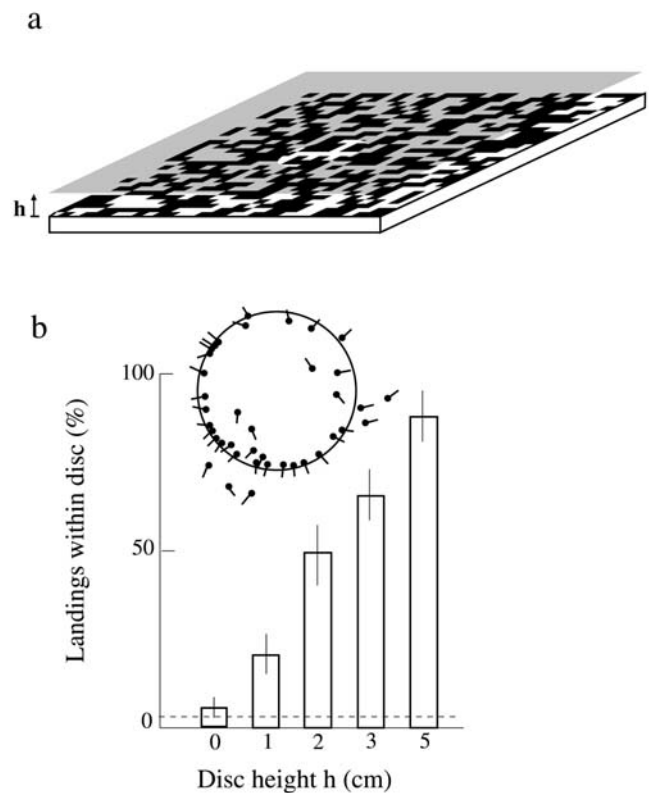


FIGURE 80.6. Experiment investigating the ability of bees to use motion parallax cues to distinguish a figure from a similarly textured background. *A*, The apparatus presents a textured disc 6 cm in diameter positioned under a sheet of clear perspex at a height h cm above a similarly textured background (42×30 cm; pixel size 5×5 mm). The disc is shown as being brighter than the background only for clarity. *B*, Bars show percentages of landings occurring within the disc for various heights (h) of the disc above the background. The detectability of the disc is reduced as h decreases, reaching the random-hit level (horizontal line) when $h = 0$, that is, when there is no motion parallax. The inset shows a sample of the distribution of landings of trained bees on the perspex sheet when $h = 5$ cm. (Adapted from Srinivasan et al., 1990.)

In antipodean Canberra, this question was approached in a different way. Srinivasan et al. (1990) examined whether freely flying bees could be trained to find a textured figure when it was presented raised over a background of the same texture. The figure was a disc bearing a random black-and-white Julesz texture (a texture composed of random black and white pixels, as shown in Fig. 80.6*A*). The disc was attached to the underside of a transparent perspex sheet which could be placed at any desired height above the background (Fig. 80.6*A*). It was found that bees could indeed be trained to find the figure and land on it, provided that the figure was raised at least 1 cm above the background (Fig. 80.6*B*). When the figure was placed directly on the background, the bees failed to find it (Srinivasan et al., 1990), demonstrating that the cue used to locate the figure is the relative motion between the images of the figure and the

background, caused by the bees' own flight above the setup. Video films of the bees' landings showed that when the disc was visible to the bees, they did not land at random on it: rather, they landed primarily near the boundary of the disc, facing the visual "cliff" (Fig. 80.6B). These experiments showed that the boundary has special visual significance and that bees are capable of detecting it reliably. Kern et al. (1997) have shown, through behavioral experiments and modeling, that the detectability of such boundaries can be well accounted for by a neural network which compares image motion in spatially adjacent receptive fields.

The ability to detect objects through the discontinuities in image motion that occur at the boundaries is likely to be important when an insect attempts to land on a leaf or a shrub. This is a situation where it may be difficult to distinguish individual leaves or establish which leaf is nearest, since cues based on contrast in luminance or color are weak. Visual problems of this nature are not restricted to insects. Over 130 years ago, Helmholtz (1866) speculated that humans might use cues derived from image motion in a similar way to distinguish individual trees in a dense forest.

Concluding remarks

Insects are prime subjects for studying the ways in which cues based on image motion are extracted and used by visual systems. This is because these creatures, possessing poor or no stereopsis, literally need to move in order to see the world in three dimensions. We now know that insects use information on image motion in a variety of visually mediated functions and behaviors that extend well beyond the classically studied optomotor response. Flying insects exploit such cues to stabilize flight, regulate flight speed, negotiate narrow gaps, infer the ranges to objects, avoid obstacles, orchestrate smooth landings, distinguish objects from backgrounds, and monitor the distance traveled. The emerging picture shows that there are a number of motion-sensitive pathways in the insect visual system, each with a distinct set of properties and geared to a specific visual function. It would seem unlikely, however, that all of these systems (and other, still undiscovered ones) are operative all of the time. Obviously, the optomotor system would have to be switched off, or its corrective commands ignored, when the insect makes a voluntary turn or chases a target (Heisenberg and Wolf, 1993; Kirschfeld, 1997; Srinivasan and Bernard, 1977). There is also evidence, for example, that the optomotor system is at least partially nonfunctional when insects fly through narrow gaps (Srinivasan et al., 1993). One major challenge for the future, then, is to discover the conditions under which individual systems are called into play or ignored, and to understand the ways in which these systems interact to coordinate flight. Another challenge is to uncover the neural mechanisms that underlie these visual capacities.

Acknowledgments

Some of the work described in this review was supported by the International Human Frontier Science Program (Grant RG-84/97), the U.S. Defense Advanced Research Projects Agency and the Office of Naval Research (Grant N00014-99-1-0506), and the Australian-German Joint Research Cooperation Scheme.

REFERENCES

- Borst, A., and S. Bahde, 1988. Visual information processing in the fly's landing system, *J. Comp. Physiol. A*, 163:167–173.
- Borst, A., and M. Egelhaaf, 1989. Principles of visual motion detection, *Trends Neurosci.*, 12:297–306.
- Buchner, E., 1984. Behavioral analysis of spatial vision in insects, in *Photoreception and Vision in Invertebrates* (M. A. Ali, ed.), New York: Plenum Press, pp. 561–621.
- Collett, T. S., and L. I. K. Harkness, 1982. Depth vision in animals, in *Analysis of Visual Behavior* (D. J. Ingle, M. A. Goodale, and R. J. W. Mansfield, eds.), Cambridge, MA: MIT Press, pp. 111–176.
- David, C. T., 1982. Compensation for height in the control of groundspeed by *Drosophila* in a new, "Barber's Pole" wind tunnel, *J. Comp. Physiol.*, 147:485–493.
- Egelhaaf, M., and A. Borst, 1993. Movement detection in arthropods, in *Visual Motion and Its Role in the Stabilization of Gaze* (F. A. Miles and J. Wallman, eds.), Amsterdam: Elsevier, pp. 203–235.
- Egelhaaf, M., K. Hausen, W. Reichardt, and C. Wehrhahn, 1988. Visual course control in flies relies on neuronal computation of object and background motion, *Trends Neurosci.*, 11:351–358.
- Eriksson, E. S., 1980. Movement parallax and distance perception in the grasshopper (*Phaulacridium vittatum*), *J. Exp. Biol.*, 86: 337–340.
- Esch, H., and J. E. Burns, 1995. Honeybees use optic flow to measure the distance of a food source, *Naturwissenschaften*, 82: 38–40.
- Esch, H., and J. Burns, 1996. Distance estimation by foraging honeybees, *J. Exp. Biol.*, 199:155–162.
- Esch, H. E., S. W. Zhang, J. Tautz, and M. V. Srinivasan, 2001. Honeybees share their world view with hive mates? *Nature (Lond.)*, 411:581–583.
- Exner, S., 1891. *The Physiology of the Compound Eyes of Insects and Crustaceans* (R. C. Hardie, trans.), Berlin and Heidelberg, Springer-Verlag, pp. 130–131.
- Frisch, K. von, 1993. *The Dance Language and Orientation of Bees*, Cambridge, MA: Harvard University Press.
- Hausen, K., 1993. The decoding of retinal image flow in insects, in *Visual Motion and Its Role in the Stabilization of Gaze* (F. A. Miles and J. Wallman, eds.), Amsterdam: Elsevier, pp. 203–235.
- Hausen, K., and M. Egelhaaf, 1989. Neural mechanisms of visual course control in insects, in *Facets of Vision* (D. G. Stavenga and R. C. Hardie, eds.), Berlin and Heidelberg: Springer-Verlag, pp. 391–424.
- Heisenberg, M., and R. Wolf, 1993. The sensory-motor link in motion-dependent flight control of flies, in *Visual Motion and Its Role in the Stabilization of Gaze* (F. A. Miles and J. Wallman, eds.), Amsterdam: Elsevier, pp. 265–283.
- Helmholtz, H. von, 1866. *Handbuch der physiologischen Optik*, Hamburg: Voss Verlag (J. P. C. Southall, trans., 1924; reprinted New York: Dover, 1962).

- Horridge, G. A., 1986. A theory of insect vision: velocity parallax, *Proc. R. Soc. Lond. B*, 229:13–27.
- Horridge, G. A., 1987. The evolution of visual processing and the construction of seeing systems, *Proc. R. Soc. Lond. B*, 230:279–292.
- Kelber, A., and J. Zeil, 1997. Tetragonisca guard bees interpret expanding and contracting patterns as unintended displacement in space, *J. Comp. Physiol. A*, 181:257–265.
- Kern, R., M. Egelhaaf, and M. V. Srinivasan, 1997. Edge detection by landing honeybees: behavioural analysis and model simulations of the underlying mechanism, *Vis. Res.*, 37:2103–2117.
- Kirchner, W. H., and J. Lengler, 1994. Bees perceive illusionary distance information from rotating spirals, *Naturwissenschaften*, 81:42–43.
- Kirchner, W. H., and M. V. Srinivasan, 1989. Freely flying honeybees use image motion to estimate object distance, *Naturwissenschaften*, 76:281–282.
- Kirschfeld, K., 1997. Course control and tracking: orientation through image stabilization, in *Orientation and Communication in Arthropods* (M. Lehrer ed.), Basel: Birkhäuser Verlag, pp. 67–93.
- Kral, K., 1998. Side-to-side head movements to obtain motion depth cues: a short review of research on the praying mantis, *Behav. Processes*, 43:71–77.
- Kral, K., and M. Poteser, 1997. Motion parallax as a source of distance information in locusts and mantids, *J. Insect Behav.*, 10:145–163.
- Krapp, H. G., and R. Hengstenberg, 1996. Estimation of self-motion by optic flow processing in single visual interneurons, *Nature (Lond.)*, 384:463–466.
- Lehrer, M., M. V. Srinivasan, S. W. Zhang, and G. A. Horridge, 1988. Motion cues provide the bee's visual world with a third dimension, *Nature (Lond.)*, 332:356–357.
- Poteser, M., M.-A. Pabst, and K. Kral, 1998. Proprioceptive contribution to distance estimation by motion parallax in a praying mantid, *J. Exp. Biol.*, 201:1483–1491.
- Reichardt, W., 1969. Movement perception in insects, in *Processing of Optical Data by Organisms and by Machines* (W. Reichardt ed.), New York: Academic Press, pp. 465–493.
- Reichardt, W., and T. Poggio, 1979. Figure-ground discrimination by relative movement in the visual system of the fly. Part I: experimental results, *Biol. Cybern.*, 35:81–100.
- Rossell, S., 1983. Binocular stereopsis in an insect, *Nature (Lond.)*, 302:821–822.
- Sobel, E. C., 1990. The locust's use of motion parallax to measure distance, *J. Comp. Physiol. A*, 167:579–588.
- Srinivasan, M. V., 1977. A visually-evoked roll response in the housefly: open-loop and closed-loop studies, *J. Comp. Physiol.*, 119:1–14.
- Srinivasan, M. V., 1993. How insects infer range from visual motion, in *Visual Motion and Its Role in the Stabilization of Gaze* (F. A. Miles and J. Wallman, eds.), Amsterdam: Elsevier, pp. 139–156.
- Srinivasan, M. V., and G. D. Bernard, 1977. The pursuit response of the housefly and its interaction with the optomotor response, *J. Comp. Physiol.*, 115:101–117.
- Srinivasan, M. V., M. Lehrer, and G. A. Horridge, 1990. Visual figure-ground discrimination in the honeybee: the role of motion parallax at boundaries, *Proc. R. Soc. Lond. B*, 238:331–350.
- Srinivasan, M. V., M. Lehrer, W. Kirchner, and S. W. Zhang, 1991. Range perception through apparent image speed in freely-flying honeybees, *Vis. Neurosci.*, 6:519–535.
- Srinivasan, M. V., M. Lehrer, S. W. Zhang, and G. A. Horridge, 1989. How honeybees measure their distance from objects of unknown size, *J. Comp. Physiol. A*, 165:605–613.
- Srinivasan, M. V., M. Poteser, and K. Kral, 1999. Motion detection in insect orientation and navigation, *Vis. Res.*, 39:2749–2766.
- Srinivasan, M. V., and S. W. Zhang, 1997. Visual control of honeybee flight, in *Orientation and Communication in Arthropods* (M. Lehrer ed.), Basel: Birkhäuser Verlag, pp. 67–93.
- Srinivasan, M. V., S. W. Zhang, M. Altwein, and J. Tautz, 2000a. Honeybee navigation: nature and calibration of the “odometer,” *Science*, 287:851–853.
- Srinivasan, M. V., S. W. Zhang, and N. Bidwell, 1997. Visually mediated odometry in honeybees, *J. Exp. Biol.*, 200:2513–2522.
- Srinivasan, M. V., S. W. Zhang, and J. S. Chahl, 2001. Landing strategies in honeybees, and possible applications to autonomous airborne vehicles, *Biol. Bull.*, 200:216–221.
- Srinivasan, M. V., S. W. Zhang, J. S. Chahl, E. Barth, and S. Venkatesh, 2000b. How honeybees make grazing landings on flat surfaces, *Biol. Cybern.*, 83:171–183.
- Srinivasan, M. V., S. W. Zhang, and K. Chandrashekara, 1993. Evidence for two distinct movement-detecting mechanisms in insect vision, *Naturwissenschaften*, 80:38–41.
- Srinivasan, M. V., S. W. Zhang, M. Lehrer, and T. S. Collett, 1996. Honeybee navigation en route to the goal: visual flight control and odometry, *J. Exp. Biol.*, 199:237–244.
- Wagner, H., 1982. Flow-field variables trigger landing in flies, *Nature (Lond.)*, 297:147–148.
- Wallace, G. K., 1959. Visual scanning in the desert locust *Schistocerca gregaria*, Forskal, *J. Exp. Biol.*, 36:512–525.

81

The Middle Temporal Area: Motion Processing and the Link to Perception

KENNETH H. BRITTEN

THE MIDDLE TEMPORAL area of the macaque monkey brain (MT, also known as V5) is one of the most studied parts of visual cortex. It has attracted great attention for very good reasons. By far the most important of these is that we have a very good idea of what it does—motion analysis. From the first description of the area (Dubner and Zeki, 1971), the remarkable preponderance of directional selectivity provided a good clue to function. Since then, the area has been the target of widely ranging experimental approaches: lesions, stimulation, anatomy, mapping, and imaging, to name but a few. The resulting large body of work has not overturned the primary conclusion that MT is a seminal area for motion analysis in cortex, but as one might expect, things have gotten more complicated. More complex properties have been elaborated, and new functions in addition to motion analysis have been suggested.

The study of MT and motion is a good example of how scientific progress should work. Early descriptive data allowed the formulation of clear functional hypotheses. Tests of these hypotheses allowed the formulation of more elaborate, more correct models that incorporate the principles of the first generation of hypotheses. This is where we stand now: the more complete, more complex second-generation ideas drive current experimental work.

In this chapter, I will first provide a brief overview of the classics, attempting, where possible, to fit these data into modern functional models of motion processing. Then I will review the body of work testing hypotheses relating activity in MT to perception. Cortical mechanisms of motion processing have been exhaustively reviewed (Albright and Stoner, 1995; Andersen, 1997; Battaglini et al., 1996; Duffy, 2000; Maunsell and Newsome, 1987; Orban, 1997; Parker and Newsome, 1998), and space does not allow this review to be encyclopedic. Instead, my goals are to capture current views on the function of this well-studied area and to illuminate the value of MT as a model system for studying the relationship between physiology and behavior.

Anatomy

MT got its name from its anatomical location in the owl monkey, a New World primate (Allman and Kaas, 1971).

The inappropriateness of this name for its location in the macaque brain (between the occipital and parietal lobes; Fig. 81.1) leads to its alternative, more neutral name, V5. Nonetheless, I will use the original term, MT, throughout, though V5 is entirely equivalent. There is little dispute at present that a homologous area is present in many species of primates and even prosimians (Krubitzer and Kaas, 1990). The area is jointly defined by two anatomical features: dense myelination and direct reciprocal connections with area V1 (Ungerleider and Mishkin, 1979; Van Essen et al., 1981; Zeki, 1974b). Figure 81.1 also schematizes some of the more important cortical and subcortical connections of MT. In addition to its input from V1, MT receives ascending input from V2, V3, and the lateral subdivision of the pulvinar complex. MT is connected with a wide variety of other cortical areas in the superior temporal sulcus (FST, STP, MST), the parietal lobe (VIP, LIP, 7a), and the frontal lobe areas (area 46, FEF, SEF) and by descending connections to the brainstem (dorsolateral pontine nuclei, DTN, and NOT) and midbrain (superior colliculus). In addition, it has extensive connections with the cerebellum.

This suite of connections places MT near the middle of a cortical hierarchy for motion processing sometimes called the *motion system* or *motion pathway* (Fig. 81.1). It starts in V1, where directionally selective neurons first appear, and heads toward posterior parietal cortex, where many of the structures participate in planning upcoming movements (Andersen et al., 1997). On this pathway, MT is the last area to have a clear retinotopy (Maunsell and Van Essen, 1987) and the first to be strongly connected to explicitly premotor structures. However, MT is not a bottleneck in this pathway by any means; V1 also connects to target areas in posterior parietal and frontal cortices by parallel routes that bypass MT.

One of the hallmark features of MT's anatomical organization is its retinotopy: it contains a fairly orderly map of contralateral visual space. The map varies from individual to individual, is often incomplete, and often contains spatial irregularities (Maunsell, 1986). The coordinates of the map are fairly consistent, with the fovea represented laterally and the vertical meridian representation running along the area boundaries. In addition to this overall retinotopy, MT

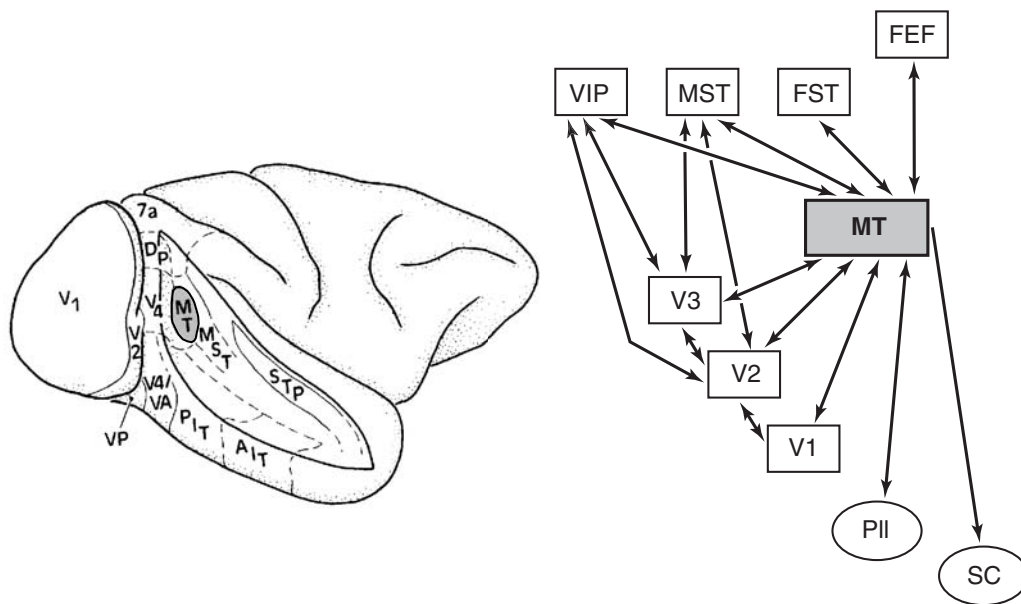


FIGURE 81.1. Summary of location and main connections of area MT. The left panel shows the superior temporal sulcus opened up to reveal the areas inside, including MT highlighted in yellow. The right panel shows the main connections of MT; subcortical structures are indicated by oval symbols. DTN, dorsal terminal nucleus; FEF, frontal eye fields; FST, fundus of the superior temporal sulcus;

MST, medial superior temporal; NOT, nucleus of the optic tract; PII, pulvinar nucleus, pars lateralis; SC, superior colliculus; SEF, supplementary eye fields; STP, superior temporal polysensory; VIP, ventral intraparietal. (Left panel from Maunsell and Newsome, 1987, with permission.)

contains organized maps for several different physiological response properties, discussed below.

Physiological response properties

DIRECTIONALITY Early reports on MT physiology emphasized the remarkable prevalence of directionally selective cells. The vast majority of MT cells are directionally selective, and most are strongly so. Figure 81.2 illustrates responses of a typical MT cell to a coherently moving random dot pattern, filling its receptive field. The polar plot relates the response of the cell (radial axis) to the direction of the stimulus (polar axis). This cell shows excitation in the preferred direction, as well as suppression in the opposite direction. (The maintained activity is indicated by the inner circle; it is about 17 impulses per second, a typical value.) The direction opposite the preferred is commonly referred to as the *null* direction and sometimes more precisely as the *antipreferred* direction. Responses in the null direction are not always suppressive; they range from strong suppression through no response to modest excitation (Albright, 1984; Britten et al., 1993; Maunsell and Van Essen, 1983a). Suppression by motion opposite the preferred direction (overt motion *opponency*) is widespread, though variable across cells, in MT; such responses are not typical of directionally selective cells at earlier stages on the motion pathway.

Directionality along this best (preferred–null) axis is frequently characterized by the *directionality index*, DI:

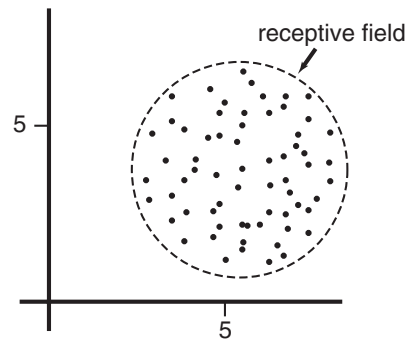
$$DI = 1 - \frac{N - m}{P - m}$$

where N is the null direction response, P is the preferred direction response, and m is the maintained activity. The average value for this index in MT ranges from about 0.85 to 1.0 in different studies, indicating that strong directionality is the norm. Although different laboratories apply different criteria in using this index to call a cell directionally selective, the fraction is always a large majority (Albright, 1984; Lagae et al., 1993; Maunsell and Van Essen, 1983a; Zeki, 1978).

Another clue to the importance of directionality in MT is that it is organized into a regular, columnar pattern (Albright et al., 1984). Direction is fairly consistent across cortical layers within a column, but changes systematically across the cortical surface (Figure 3), forming a fairly regular map of direction (see Fig. 81.3). While the map cannot be directly visualized in Old World primates owing to its location deep in a sulcus, in owl monkeys it lies exposed on the cortical surface. Optical imaging in this species has revealed a clear and consistent map (Geesaman et al., 1997). Direction columns in both species measure approximately one-half millimeter in dimension, and transitions between them may either be gradual or abrupt, where preferred direction reverses along a single axis of motion.

Equally important to the directional information carried by a directionally selective neuron, such as the one in Figure 81.2, is its precision, or directional *bandwidth*. Bandwidth describes the breadth of tuning of a single neuron and, by extension, the precision with which a neuronal population can encode the direction of stimulus movement. MT cells typically have fairly broad tuning for direction. Two related

a. Receptive field and stimulus



b. Single neuron response

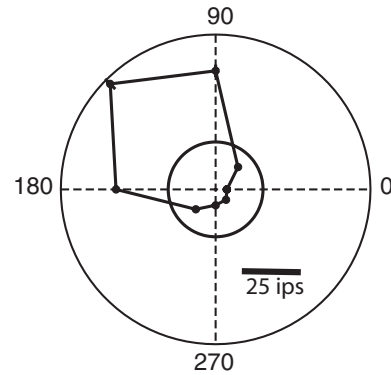


FIGURE 81.2. Directionality of an MT neuron. *a*, Stimulus geometry indicating the stimulus arrangement used in the experiment. The dynamic random dots filled the RF of the neuron under study, and was moved in eight different directions at 45 degree intervals. *b*, Polar plot showing neuronal responses. The polar angle indicates

the stimulus direction, and the radial dimension indicates the response magnitude. The inner circle indicates the maintained activity of the cell. Where standard errors are not visible, they are smaller than the symbols.

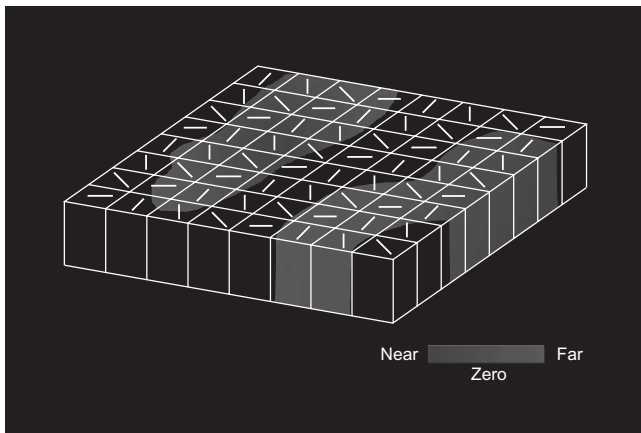


FIGURE 81.3. Schematic illustrating the map of direction and disparity in MT. Each box is a single column on the cortical surface (flattened for clarity). The white lines indicate the axis of the preferred direction of motion, and the colors indicate the stereo tuning of the region. (From DeAngelis and Newsome, 1999, with permission.) (See color plate 57).

measures are widely used to estimate bandwidth. One is the full width (or, frequently, half-width) at half-height, directly interpolated from the empirically measured tuning data. The other is the sigma parameter from Gaussian functions used to fit the directional tuning data. The sigma from a Gaussian fit is nearly identical to the half-width at half height. The best estimates from the literature give its average value as 50 to 60 degrees, or a full width at half-height of

100 to 120 degrees (Albright, 1984; Lagae et al., 1993; Maunsell and Van Essen, 1983a). This value depends to some extent on the stimulus; orientation selectivity modestly reduces the bandwidths for bar or grating stimuli.

SPATIAL PROPERTIES A striking correlate of position on a cortical hierarchy is increasing receptive field (RF) size, and MT RFs match their middle position in this regard. If eccentricity is expressed as E , then MT cells' RF diameters average approximately $0.8E$ (Maunsell and Van Essen, 1983a), about 10 times the diameter of a V1 cell of comparable eccentricity or 5 times that of a V2 cell. However, preferred spatial frequencies of MT cells do not scale with their larger RFs. These tend to peak near about 0.5 to 5 c/deg , not very different from their afferents, though they are somewhat more broadly tuned (J. A. Movshon, personal communication). This suggests that MT cells inherit their basic spatial tuning from their inputs.

A large fraction (approximately half) of MT cells demonstrate spatial interactions on a much larger spatial scale: they possess antagonistic surrounds (Allman et al., 1985; Born, 2000; Raiguel et al., 1995). These surrounds are "silent" when stimulated alone but exert a profound modulatory effect on the response to stimulation in the RF center. The modulation is typically directional and maximally suppresses the response when motion is in the preferred direction. In the extreme, surround stimulation *facilitates* center responses when it is in the opposite direction. Such center-surround organization is optimal for the detection and discrimination of object motion when an object moves relative to the

background. Cells that lack such antagonistic surrounds tend to respond optimally to wide-field motion, such as might be produced by self-motion through the environment. Interestingly, cells with and without antagonistic surrounds tend to be anatomically separated in columns or clusters (Born and Tootell, 1992). These columns clearly have distinct functional roles, since microstimulation in the two types of regions produced opposite effects on smooth pursuit eye movements (Born et al., 2000). This strongly suggests a role for the surrounds in the segregation of moving objects from their backgrounds. Another interesting feature of the surrounds in MT is that they are often spatially heterogeneous rather than smooth and radially symmetric (Raiguel et al., 1995). This arrangement can be useful and is exploited in some models of high-level motion processing (Royden, 1997).

TEMPORAL PROPERTIES Motion is as much about time as it is about space. The motion system in general is driven heavily by the magnocellular pathway (Nealey and Maunsell, 1994), which gives it characteristically rapid dynamics. Latencies in MT can be quite short, although the range is substantial. The minimum latency is as little as about 30 to 35 msec, and the median latency is approximately 90 msec (Heuer and Britten, 1999; Maunsell, 1986; Raiguel et al., 1999). Also characteristic of magnocellular-driven areas, MT cells respond to quite high temporal frequencies. Typically, they peak in the 3 to 10 Hz range, and most will have cut off by 30 to 50 Hz (J. A. Movshon, personal communication).

MT cells typically reduce their responses substantially at lower temporal frequencies, and they show profound adaptation to sustained input. When presented with the sudden onset of continuous motion, MT cells give a directional transient response, typically about twice as large as their sustained response, though this varies considerably (Lisberger and Movshon, 1999). This initial transient is informative about the acceleration of a moving target and may be useful in guiding pursuit eye movements (Krauzlis and Lisberger, 1994). Adaptation over a longer time period (seconds to tens of seconds) in a cell's preferred direction substantially reduces subsequent responses to any stimulus direction (Petersen et al., 1985; van Wezel and Britten, 2002).

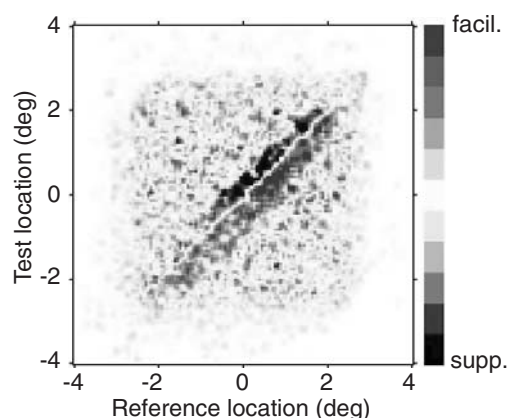
Another approach to investigating temporal properties of neurons is to analyze the distribution of spikes in a spike train. Because of its rapid kinetics and well-understood functional role, MT has been a fruitful target for such inquiry, and there is currently some debate about the statistics of MT spike trains. It is clear that MT rates can be modulated rapidly (see above) and that this rapid modulation captures substantial information about temporal variation in the stimulus (Bair and Koch, 1996; Buracas et al., 1998). What is less clear is the distribution of spikes under more sustained

stimulus conditions. Work at the Singer lab (Kreiter and Singer, 1996) has found very regular, stimulus-dependent peaks in MT spike-train autocorrelation functions. In certain models, this oscillatory behavior can carry substantial stimulus information (for review, see Maldonado et al., 1997). On the other hand, similar recordings from the Newsome laboratory showed substantial burstiness but little overt oscillatory behavior (Bair et al., 1992).

SPEED TUNING Speed tuning of MT neurons is much less studied than is directionality, and is somewhat more complex than it appears to be. Several investigations of MT used simple bar, grating, or random-dot stimuli to characterize the phenomenology of MT speed preferences. These experiments revealed that MT neurons are typically bandpass tuned for speed: their responses peak at medium speeds and decline at either faster or slower speeds (Albright, 1984; Lagae et al., 1993; Maunsell and Van Essen, 1983a). Preferred speeds are typically 5 to 30 deg/sec, scaling with eccentricity such that neurons with more peripheral RFs prefer higher speeds (Maunsell and Van Essen, 1983a). However, this relationship is fairly loose, and at any eccentricity there is a substantial range of preferred speeds. These preferred speeds are noticeably higher than those of V1 cells at corresponding eccentricities, raising an interesting question: Does MT merely inherit its speed tuning from a subset of selected V1 (or V2 and V3) afferents or does it perform additional computations to alter the preferences imposed by its inputs? There is some evidence to support each view.

Two approaches have been used to study the mechanisms underlying speed selectivity in MT, one based on distance and time and the other using a frequency-domain approach. One way to present stimuli rapidly at different locations and different delays is to present *white noise*, which contains elements randomly spaced in space and time. In Figure 81.44, we see the results of such an analysis of spatial interactions within an MT RF. In this experiment, bars were rapidly flashed at randomly chosen locations across an MT cell's RF. When two sequentially plotted points are located at an appropriate spatial and temporal interval for motion in the cell's preferred direction and speed, facilitation is observed ("hot" colors). When the interval is in the opposite direction, suppression occurs ("cool" colors). Thus, one may characterize the scale of the spatial interactions that give the cell its preferred direction and speed. These interactions occur over relatively local distances, much smaller than the overall dimensions of the RF. Indeed, the dimensions over which such directional interactions occur closely approach the dimensions of the RFs of V1 cells, suggesting that MT cells inherit their directionality from that of their afferents. These results are consistent with an earlier study using sequentially flashed bars rather than noise (Newsome et al., 1986).

a. Spatial interactions



b. Spatiotemporal profiles (2 cells)

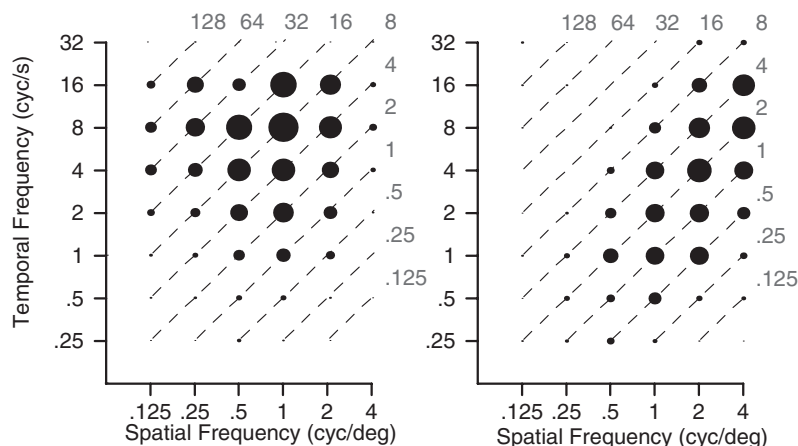


FIGURE 81.4. Two views of underlying mechanisms in MT RFs. *a* shows *two-bar interaction* profiles of a single MT RF. In this experiment, a pair of bars was presented at a short interval at different locations in the RF. The location of the first bar is shown on the horizontal axis, and that of the second bar is shown on the vertical axis. If the test bar is slightly ahead of the reference bar (along the cell's preferred-null axis), then the response to the test bar is facilitated (red colors). Conversely, if the offset is in the opposite direction, then the response is suppressed. The dimension of the red and blue profiles indicates the spatial extent of the interactions that lead to the cell's directionality. *b*, Spatiotemporal response profile of two MT cells seen in the frequency domain. Each dot

represents the measured response to a single grating of a specified spatial and temporal frequency. The diameter of the dot indicates the response magnitude of the cell. The cell on the left has independent preferences for certain spatial and temporal frequencies, while for the cell on the right, the preferred temporal frequency shifts with the spatial frequency. This implies that the cell actually prefers a particular velocity (indicated by the lines paralleling the diagonal; in this case about 2 deg/sec) regardless of the spatial composition of the stimulus. (*a* from Livingstone et al., 2000, with permission; *b* modified from Priebe and Lisberger, 2003, with permission.) (See color plate 58.)

The other approach, using the frequency domain, is illustrated in Figure 81.4*B*. Spatial frequency is the inverse of spatial interval, and temporal frequency is comparably the inverse of flash rate. Moving sine-wave gratings have just one spatial and one temporal frequency, and speed naturally varies with the combination. This figure shows the responses of two single MT cells to different spatial and temporal frequency combinations. Diagonal lines indicate different constant speeds. The circles indicate the response magnitude of two MT cells. The cell on the left gives responses at certain combinations of spatial and temporal frequencies, but these are independent of each other (*separable*). The cell on the right, however, shows something different—it responds better to higher temporal frequencies if the spatial frequency of the stimulus is higher. This produces the diagonal trend in the response profile. This trend toward the diagonal is a phenomenon never seen in V1 and clearly reflects summation of specific inputs to form a representation that is genuinely speed tuned. Some trend toward the diagonal is found in more than half of MT cells (Perrone and Thiele, 2001), but true speed tuning is clearly a minority phenomenon (Movshon et al., 1988; Priebe and Lisberger 2003). As we will see again in the next section on directional integration, this neither-fish-nor-fowl pattern of results is characteristic of MT. The representation clearly has a novel and interesting feature not seen at earlier levels—in this case, speed

tuning. Yet, many of the cells in MT do not show the emergent property, or only show its partial development.

MOTION INTEGRATION AND SEGREGATION Motions in the world are rarely discrete and uniform, as they are in the lab. Local motions from the individual contours of a single moving object are effortlessly unified into a single object motion vector. On the other hand, when multiple nearby objects move, their motions are perceptually well segregated. The dual phenomena of motion integration and segregation have perhaps received more attention from psychophysicists than any other aspect of motion processing (for review, see Braddick, 1993). They have also received some study, though considerably less, at the physiological level. Space does not allow an adequate treatment of this interesting and complex issue, but fortunately, many deeper treatments of the topic exist (Maunsell and Newsome, 1987; also see Chapter 82 in this volume).

When an object with contours of many different orientations moves, each contour, locally, is seen moving in a direction perpendicular to its orientation—the famous *aperture problem*. A simple stimulus to explore the mechanism by which these local contour orientations are combined consists of a plaid formed from two gratings moving in different directions. Perceptually, this will often cohere into a single *pattern* moving in a direction consistent with both individual

grating (*component*) motions. In one of the most frequently cited MT experiments, Movshon and colleagues (1985) demonstrated that about a third of MT cells integrated across the individual contours of a plaid stimulus and responded to the same pattern direction seen by human observers. Another third responded to the individual contours, and the rest were intermediate. Thus, a continuum of motion integration appeared to be present in MT. Importantly, the same measurement was made in V1, and no cells in V1 performed this integration. Therefore, once again, MT appears to be solving a problem not solved at earlier stages of processing.

More recently, additional work has elaborated on this point without calling the fundamental interpretation into question. MT is not unique in possessing neurons that can solve the aperture problem: similar observations have been made in other cortical and subcortical structures (Dumbrava et al., 2001; Gegenfurtner et al., 1997). Furthermore, pattern responses in MT appear to develop slowly over time—more slowly than the component responses (Pack et al., 2001)—and to depend on the anesthetic state of the animal (Pack and Born, 2001). Both of these observations are consistent with the idea that pattern responses in MT are not the result of a simple local calculation, but may depend on circuit dynamics, possibly including several cortical areas. However, the results are only suggestive at this point, and other interpretations are possible.

The converse problem of motion segregation has also received some study; this interacts with the representation of stereoscopic depth (see the next section). Earlier studies indicated that multiple different motions within the RF of a single MT cell may interact, even if perceptually they remain well segregated. The best demonstration of this effect uses “transparent” moving dot patterns—two groups of dots moving in different directions. Perceptually, these remain fairly distinct (though not completely; e.g., see Marshak and Sekuler, 1979). However, if the two motions are aligned with a neuron’s preferred-null axis, the motion in the cell’s null direction profoundly suppresses the response to motion in the preferred direction (Snowden et al., 1991). This suppression remains present when the two groups of dots are spatially nonoverlapping (but both are within the cell’s RF). This result makes it appear as if MT is averaging multiple motions within its RF and not maintaining separate representations. However, in an insightful series of experiments Qian, Andersen, and colleagues showed that the interaction depends critically on the depth planes in which the motions are presented. If the dots forming the two planes are separated from each other in depth, then the interaction between the two disappears (Qian and Andersen, 1994). This points to the fundamental importance of stereoscopic depth in how MT processes motion, but as we shall soon see, it also raises interesting problems.

Perceptually, motions can be segregated over quite short distances (van Wezel et al., 1994), much smaller than the dimensions of MT RFs. Even though MT is clearly capable of segregating motions in different depth planes, there is no similar documentation of MT supporting fine-scale segregation in a single depth plane. This is potentially a motion analysis problem where the limiting information is represented elsewhere than in MT. V1 is a likely candidate because of its finer-grained representation.

STEREOSCOPIC DEPTH Motion in the real world is rarely confined to the frontoparallel plane, where experimenters tend to place their stimuli. Furthermore, stereoscopic depth, like motion parallax, is a profound cue to spatial relationships in one’s surroundings. MT and other areas on the motion pathway provide the bulk of the visual inputs to posterior parietal cortex, where space is king. Therefore, it comes as little surprise that MT cells are tuned to stereoscopic depth as well as to motion. Originally, this was interpreted as true tuning for the three-dimensional (3D) motion of objects (Zeki, 1974a), but there was actually a related but subtly different mechanism: cells in MT are independently tuned both for two-dimensional (2D) motion *and* for the depth plane of the stimulus (Bradley et al., 1998; Maunsell and Van Essen, 1983b; Qian and Andersen, 1994). Tuning for stereo depth in MT is not unlike that found in V1; cells tend to be tuned for near-zero disparities or else have open-ended tuning for near or far disparities.

More recent experiments have demonstrated not only that MT cells are tuned for disparity, but also that MT contains an orderly topographic representation for stereo depth (DeAngelis and Newsome, 1999). Figure 81.3 shows a schematic depiction of how direction and stereo columns appear on the surface of MT. The oriented lines indicate the preferred axis of the direction columns, and the colored regions depict regions tuned for different stereoscopic depths. Interestingly, this map of depth is fractured; there are regions of stereo-tuned neurons interspersed with larger regions where the tuning is weak. These *untuned* regions still contain many individually selective cells; their tuning is scattered enough that they do not form a classic column. The regions of good tuning do show the hallmark of classic maps: progressive shifts of preferred disparity. Interestingly, there is no systematic relationship between the maps for disparity and the map for preferred direction. This again argues against the idea that MT is systematically organized into an orderly representation of 3D motion. However, as we shall see later, there is no doubt that the stereo signals are functional and contribute to the perception of the depth of moving objects.

MODULATION BY ATTENTION Selective attention allows observers to perceive an attended object or region of space

more rapidly and accurately, at the cost of other objects. Despite considerable research effort over several decades, the physiological underpinnings remain poorly understood (for a review, see Desimone and Duncan, 1995). Physiological studies in many extrastriate areas reveal profound attentional effects, and area MT is no exception.

Attention can be directed either to a specified spatial location or to a stimulus feature such as direction (color, orientation, and so on). The first experiments exploring attentional effects in MT used a design in which either space- or feature-based attention could have been at work. In these experiments (Treue and Maunsell, 1996), two stimuli moved through the RF of an MT cell, and attention was directed to one of the two. When the attended target moved through the RF in the preferred direction, the response was usually enhanced compared to the response when the nonattended target moved in the preferred direction. The effects were quite large, changing the response by almost a factor of 2 on average. Much smaller effects were seen when the response to attention directed with the cell's RF was compared with attention directed to a remote location. This result—attention exerting its strongest effects when two stimuli are within a single RF—appears to be typical of both dorsal and ventral stream areas.

In these experiments, attention was triggered by a cue that was delivered well before the data were collected. In closely related experiments, Recanzone and Wurtz (2000) saw much smaller attentional effects. The biggest difference was one of time; in the latter study, the monkey was cued to a particular target less than about 300 msec before the responses were measured. The difference between the two sets of results suggests that attentional signals need substantial time to exert their influence on neuronal responses.

Recent studies have allowed researchers to dissociate spatial and feature-based attentional modulation, and one may draw the tentative conclusion that directionally based attention is much more profound in its control of MT cell responses than is spatially directed attention. In one set of experiments, Seidemann and Newsome (1999) specifically cued a monkey to a particular spatial location within the RF. Such spatial attention produced only modest (10% to 15%, on average) modulation of the response. On the other hand, Treue and Martinez-Trujillo (1999) performed what was effectively the converse experiment: attention could be directed to either of two directions presented overlapping (transparently) within the RF. In this case, attention would profoundly affect the responses of the neuron, with magnitudes again approaching a factor of 2 in response amplitude. This response change, from related observations, appears to be a modulation of response *gain*, leaving the basic tuning of the neuron unchanged. In any case, attention clearly can profoundly modulate the responses of MT cells, and it appears that this modulation is based more

on the feature—direction—than on the spatial location of the stimulus.

The link to perception

From its physiological properties, MT appears remarkably specialized for the analysis of motion. Motion perception has also been extensively studied, and well-formed models exist for how motion *could* be analyzed in the brain. Therefore, it is natural that this area was fertile ground for tests of whether, and how, MT activity might support motion perception. This line of inquiry has used both correlative approaches and direct perturbations in a variety of motion tasks. For the most part, the results of all this work support the notion that signals in MT are critically involved in motion perception. However, it is equally clear that MT cannot be tied to motion perception in a one-to-one manner. The correlation with perception clearly is not perfect, suggesting that other structures must also play key roles in motion perception.

CORRELATION OF RESPONSE PROPERTIES WITH PERCEPTION
Correlation between neuronal properties and perceptual abilities is a powerful clue to function and forms one of the cornerstones of systems neuroscience. Correlation, of course, can mean any number of different things. I draw a distinction between two fundamentally distinct correlations: quantitative correlation of overall response properties with perceptual abilities and trial-by-trial correlation of neuronal responses with perceptual reports. This section only addresses the former, more abstract form of correlation. One good way to think about this approach is that it explores the *sufficiency* of the motion representation for the performance of motion tasks.

One such study involved the perception of moving plaid patterns. How one perceives such plaids depends on the brightness of the *nodes* of the plaid where the dark stripes intersect. If the luminance of these intersections is consistent with a transparent interpretation (i.e., one semitransparent grating occluding another), then the plaid is perceived as two distinct gratings slipping across one another (Stoner and Albright, 1992). Otherwise, observers see a single plaid pattern moving as described above in the section “Motion Integration and Segregation.” This observation sets up a clean test of physiological correlates of perception, because a single objective parameter (the luminance of the grating intersections) reliably controls observers' perception of motion. Therefore, one can ask whether MT cells show a similar phenomenon, and whether it depends on the luminance in a similar way. Interestingly, at the point at which human observers reported maximal transparency in the moving plaids, most MT *pattern cells* also tended to respond to the components of the grating rather than to the motion

of the plaid pattern as a whole. When the luminance of the intersections was adjusted to where the plaid pattern cohered, MT cells also tended to report the direction of the pattern rather than the components (reviewed in Albright and Stoner, 1995; Stoner and Albright, 1992).

This correlation is compelling, but a variety of interpretive difficulties lurk nearby. Most notably, one is comparing two species: subjective reports from humans against monkey physiology. This, of course, could be the explanation for the minor mismatch noted above. Naturally, one would then wish to perform the same experiment in the same species or, even better, on the same individuals (as quantitative measurements of perception vary from individual to individual as well). However, it is difficult to get monkeys to honestly report their perception of genuinely ambiguous stimuli, because there is no objectively right or wrong answer upon which to base a reward. Fortunately, some reassurance comes from the pattern of eye movements made by monkeys. When faced with large moving displays, monkeys made small-amplitude tracking eye movements. When presented with plaids such as the ones used in the human psychophysical experiments, the monkeys' eye movements tended to correlate with human perception of the direction of motion (Dobkins et al., 1998). These experiments have been extended using other stimulus manipulations (color, surrounding context) which influence the perception of motion direction (see Chapter 82 in this volume; see also Duncan et al., 2000). Across all of these manipulations, the signals in MT repeatedly demonstrate a correlation with the properties of human perception.

Another study explored the sufficiency of neuronal signals in MT for the perception of motion direction in the presence of noise (Britten et al., 1992). In this experiment, apparent motion was created by pairing dots in space and time; the strength of the motion was controlled by the fraction of dots so paired. The task of the monkey was to discriminate the direction of motion between two opposite alternatives. Where the motion was strong, the task was easy, but it could be made arbitrarily difficult. In this way, one can measure the limits of performance of either single neurons or the whole animal. One of the strengths of this experiment was that the measurements avoided the problem of comparing across species: the perceptual and physiological measurements were made at the same time using the same stimuli. The comparison was made more acute in one additional way as well. The monkey was trained to good performance on the task for a wide range of conditions—different speeds, eccentricities, stimulus sizes, and so on. The cells were studied with the task parameters adjusted to optimize the directionality of each cell. This is tantamount to finding the *best* neurons in MT for each configuration of the task. Thus, the sensitivity that was measured was not of a random sample of MT cells, but ones for which the task was ideal.

The canonical result of this experiment is that MT cells are nearly as sensitive to weak motion signals as is the monkey itself. Thresholds for individual cells [estimated using *receiver operating characteristic* (ROC) analysis] were only about 20% higher than thresholds of the monkey for the same stimuli. Some cells were in fact significantly more sensitive than the animal. Many assumptions entered this analysis, and it is worthwhile to examine these in some detail. First, both cells and monkey were given 2 seconds to examine the motion stimulus. While the analysis integrated the cells' signals perfectly over this relatively long duration, the monkey might not have been able to integrate as well. In fact, when the durations of the stimuli were shortened, both neuronal and behavioral sensitivity decreased as expected, but at somewhat different rates; the cells' thresholds were much worse than those of the monkey at a stimulus duration of 250 msec. Although this measurement was not made simultaneously, as were the others, it still hints at circumstances under which the relationship between MT neuronal activity and motion perception can be dissociated.

Further hints of this dissociation come from related experiments in which color is introduced into the stimulus. As this is discussed elsewhere in this volume (Chapter 82), I will mention the study only briefly. When the dots carrying the motion signal are colored so as to be distinct from the masking noise dots, they can be perceptually segmented, and thresholds fall dramatically (Croner and Albright, 1997). While MT signals are also improved, the perceptual improvement is much greater (Croner and Albright, 1999).

The same approach has been applied to other stimulus dimensions as well. When monkeys are trained on a stereoscopic depth discrimination task, one can use nearly identical stimulus manipulations and analyses to estimate the sensitivity of neurons and of the animal (Uka and DeAngelis, 2001). Stimuli were again optimized to the neurons' discriminative capacity, and the stereo signal indicating depth was degraded by the addition of noise. The nice thing about this experiment is that it is so similar to the motion experiments; the results can be directly compared across the two dimensions for direction and depth. In the depth experiment, a very similar result was obtained. Neurons in MT were again nearly identical in their sensitivity to the entire animal. Whether the same would be true of other dimensions is a fascinating question. At the very least, this finding suggests that MT does more than just analyze visual motion.

REAL-TIME CORRELATION WITH PERCEPTUAL DECISIONS
Another form of correlation is potentially more revealing in probing whether sensory signals are actually used by the animal during a perceptual task. Several laboratories have used this general approach to probe the link between MT activity and perception. One of the first demonstrations of

such a correlation came from the work of Logothetis and Schall (1989). These authors used perceptually ambiguous stimuli caused by binocular rivalrous motion. When opposite directions of motion are presented to the two eyes, the subject perceives, alternately, each of the two directions. While monkeys were reporting their percepts of such rivalry, the responses of MT cells were monitored. Many MT cells were modulated such that their firing rates depended on which of the two directions was being reported by the monkey at the time. Unfortunately, of the cells that were modulated, approximately equal numbers were correlated with the percept (i.e., increased their firing rate when the monkey reported their preferred direction) or the opposite. There are several possible interpretations of this a tantalizing finding. One is that the monkey may not have been honest in reporting its percept; the stimulus was intrinsically ambiguous, and there is in principle no way to reward the animal objectively. As in the Stoner and Albright experiment described above, eye movements help; small tracking eye movements tended to correlate with the reported percept, lending credence to the monkeys' reports of their experience. Rivalry is also, despite its usefulness in probing perception of ambiguous stimuli, a fairly nonphysiological stimulus. It is possible that the unpredictability of the modulation in MT relates to this fact.

Another stimulus manipulation to provoke perceptual ambiguity is closer to normal visual experience. Picture a transparent cylinder, with dots attached to its surface, rotating on its long axis. Under normal viewing conditions, with stereoscopic depth contributing, it is correctly and unambiguously viewed as rotating in a single direction. But if you remove the stereo depth from the image in the lab, it still appears vividly 3D (termed *structure-from-motion* or the *kinetic depth effect*), but the direction in which it rotates is ambiguous. Stare at it for a while, blink your eyes, and it will reverse in direction, with a different moving surface now seen as being in front. Two studies have explored correlates of this bistable percept in MT (Andersen et al., 1997; Dodd et al., 2001), and have found striking evidence that MT activity predicts the percept as it is occurring on a trial-by-trial basis. Dodd et al. quantified their results with a metric referred to as the *choice probability*—the probability with which an observer could infer what decision the monkey was about to make based only on the discharge of the neuron. This probability averaged a very significant 0.67 (0.5 would be chance). Thus, MT cells carry a distinct signature of the monkey's *upcoming* decision in their firing rates.

A very similar observation was made by the Newsome group in the context of the previously described direction discrimination task (Britten et al., 1996), where the monkey is discriminating between opposite directions of motion in the presence of masking noise. In this task, the alternatives can be made completely uncertain (pure noise), forcing the

monkey to guess. Even in this case, neuronal discharge predicts the monkey's decision to some degree. It should be noted that in this task, the percept is not clearly bistable, as it is in the cylinder task. Instead, there is weak, inconsistent, and unclear motion with no net direction. Interestingly, in this case, the average value of the choice probability was smaller (0.56) on average than that reported by Dodd et al. Thus, it appears that the value of this correlation depends on the task the animal is performing.

Further evidence for task dependence comes from the work of the Hoffmann group (Thiele and Hoffman, 1996). This experiment used variable contrast gratings in the context of a four-alternative discrimination task. Furthermore, the monkey reported its decision using a lever response rather than an eye movement. In this experiment, while there was a slight trend toward correlation between neuronal responses in MT and the monkeys' choices, it was not statistically significant. However, responses in two higher-order motion areas (MST and the superior temporal polysensory area) did show significant correlation.

Overall, the frequent presence of a trial-by-trial *signature* of directional decisions in neuronal firing rates is very revealing. Unquestionably, this indicates the intimate relationship between activity in the area and perceptually guided behavior. Two distinct mechanisms, however, are consistent with this family of observations. First, the correlation could reflect causation: when the cells are more vigorously reporting the presence of their preferred stimulus, the monkey is more likely to report it. Alternately, "top-down" influences might be in effect: when the monkey is biased toward or attending to a particular alternative on the task, this both raises the firing rates of the neurons and raises the chance of the decision. But either mechanism is consistent with a close quantitative relationship between neuronal activity and choice.

LESIONS TO TEST FUNCTION Lesions are frequently used to test the *necessity* of a specific structure for some function, and it is only natural that this approach has been brought to bear on the link between MT and the perception of motion. Necessity can be a bit of a slippery concept; it is rarely black and white in a system as complex as the cortical visual system. This is evident in the pattern of results emerging from a number of lesion studies on MT.

Lesions to MT and the surrounding cortical areas have been tested in a large number of labs, and the results are quite consistent across studies. Lesions restricted entirely to MT substantially elevate thresholds for the discrimination of opposed directions masked by noise (Newsome and Paré, 1986), the discrimination of small differences in speed (Orban et al., 1995; Pasternak and Merigan, 1994), and the discrimination of small differences in direction (Lauwers et al., 2000). Furthermore, these effects seem selective for motion where this has been tested. MT lesions did *not* affect

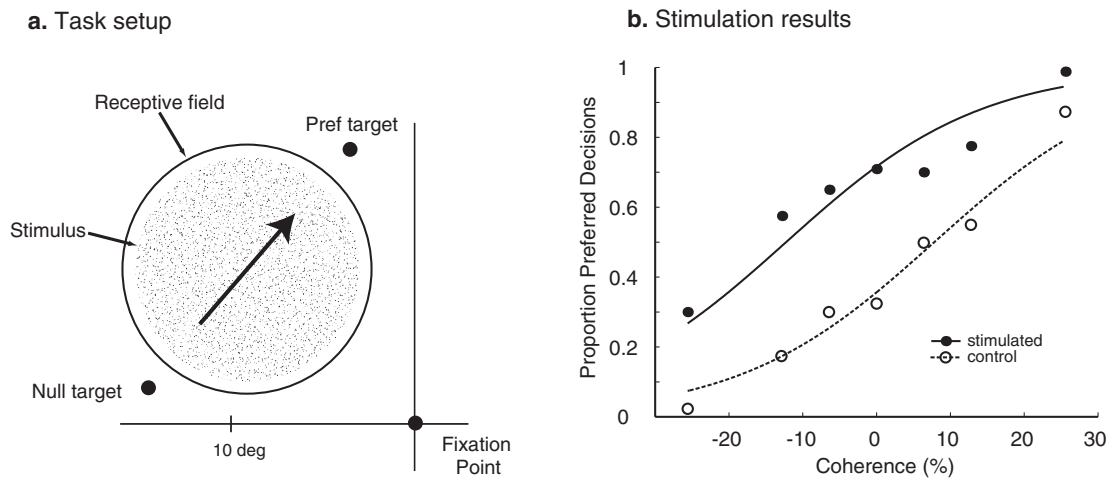


FIGURE 81.5. Results of an MT microstimulation experiment. The monkey is judging the direction of a random-dot stimulus filling the RF of a multiunit cluster in MT, as indicated in *a*. The coherence of the dots varies across a range spanning the psychophysical threshold, and on half of the trials microstimulation (200 Hz, 10 microamperes biphasic) is applied to the electrode.

b, Psychophysical results of the experiment showing the large shift in performance induced by the microstimulation. For all stimuli, microstimulation caused an increase in the proportion of preferred-direction decisions, showing that the current injection biased the monkey's performance.

contrast thresholds (Newsome and Paré, 1986) or the detection of color or texture differences (Schiller, 1993). Thus, these studies suggest a selective necessity of MT for motion-related tasks.

It is important to note that the necessity is not absolute: function will recover substantially given time after the lesion is placed. In the study of Newsome and Paré, thresholds recovered substantially or completely (for the more restricted lesions) after as little as 10 days. This recovery takes much longer and is less complete for larger lesions, and furthermore depends on the exact type of motion stimulus tested (Pasternak and Merigan, 1994; Rudolph and Pasternak, 1999). Interestingly, in most studies where recovery was incomplete, there was substantial involvement of the adjacent area, MST. This suggests that together the two areas are much more necessary for the normal discrimination of motion than is MT by itself. This is generally consistent with the anatomy of the motion pathway: parallel routes to the parietal lobe exist, but all pass through either MT or MST. However, it should be emphasized that even after complete removal of MT and MST, monkeys are not completely motion-blind. Other cortical areas clearly must contribute to the perception of motion.

Of course, another possibility for the recovery of function after more restricted lesions is reorganization of the representation in MT itself. Yamasaki and Wurtz (1991) explored reorganization in MT following lesions, and found the representation in the areas of the MT retinotopic map outside the lesion to be quite stable. From this, they concluded that the recovery from lesions was largely produced by mechanisms outside MT itself.

MICROSTIMULATION TO TEST FUNCTION Although lesions are a basic method for establishing the necessity of a structure, they do have some interpretive difficulties. Notably, they are subject to false negatives when redundant structures can fill in for the removed one. They also can be subject to false positives, because lesion effects can be indirect instead of direct. An alternative means of testing the involvement of a structure with a specified function, time-honored in the analysis of motor systems, is restricted activation. Stimulation is in some sense the converse of a lesion: one activates a particular circuit to see if the expected change in behavior ensues under one's functional hypothesis. This approach has been revealing in testing the function of MT in perception, and has provided the strongest case yet of this structure's multiple perceptual roles.

MT is organized in a columnar fashion, as is clear from the schematic in Figure 81.4, and this enables the application of intracortical microstimulation. If a single column carries a particular directional signal—say, leftward motion—then activation of this column should lead to an increased perception of leftward motion and more left choices in a left versus right discrimination task. Such a prototypical result is illustrated in Figure 81.5 from the work of Salzman and Newsome (Salzman et al., 1992). In this case, the stimulated performance curve is shifted upward (or leftward) from the control curve, indicating a large and statistically reliable increase in the proportion of choices in favor of the preferred direction of neurons at the stimulation location. This result, which was typical of the experiment, indicates that MT is directly and causally involved in the monkey's directional decisions. Another advantage of this

approach over the lesion approach is that one also gains some understanding of the nature of the involvement of the neurons in the decision. Parametric manipulations of this basic experiment have shown that in order to get a perceptual effect, the stimulus the monkey is judging must overlie the RF of the column of neurons being activated, and that using larger currents damages the directional specificity of the behavioral effects (Murasugi et al., 1993).

Microstimulation also has very good temporal specificity, as it can be applied at precise times within a trial relative to the visual stimulus and the monkey's behavioral choice. Interestingly, the time window in which microstimulation produces reliable effects appears to be task-dependent. In the original version of the task, the monkey is given one stimulus and then has all the information it will ever get to make its decision. In this case, microstimulation is effective only when it is temporally coincident with the visual stimulus; if it occurs either earlier or later, it is largely ineffective. However, if one changes the task to a delayed match-to-sample version, microstimulation becomes effective even when no stimulus is present in the interval between the sample and the match stimuli (Bisley and Pasternak, 2000).

Although no one has used microstimulation to test what modalities MT participates in, after the manner of the Schiller lesion experiment, we now have evidence from this approach that MT represents more than just motion. Because MT has columns representing stereoscopic depth as well as direction of motion, it is natural to test the role of MT in the judgment of stereoscopic depth as well. When MT is tested in this way, the perceptual effects of microstimulation on depth judgments are just as large and systematic as they are for judgments of motion direction (DeAngelis et al., 1998). This indicates that MT clearly contributes to perception of multiple stimulus dimensions. The involvement of MT in stereoscopic depth perception results makes sense for other reasons as well. Stereoscopic depth is similar to motion with respect to the nature of the computations involved, and both are powerful cues to spatial relationships in the world.

Concluding remarks

MT is the paragon of specialization in extrastriate cortex. No other area is as homogeneous in its response properties, nor have many areas received such depth of study. We know a lot about the mechanisms underlying MT responses, as well as the functional role of these responses in motion perception. A good case can be made—unusual in a complex network like extrastriate cortex—for both the *necessity* and the *sufficiency* of MT for motion perception. Yet, neither its necessity nor its sufficiency is complete from what we know. Clearly, MT does not work alone. The results of lesion experiments, as well as what we know of the anatomy of the

motion pathway, show that MT acts in concert with many other areas to support the perception of motion. Furthermore, MT carries information about visual features other than motion, such as stereo depth cues.

Sufficiency is an even more slippery concept: MT certainly has motion signals *sufficient* to guide perception in some cases. But no cortical structure can be sufficient in the strict sense of the word: perception must depend on the integrity of upstream and downstream areas, and probably on parallel areas carrying similar information. We can account for many qualitative and even quantitative features of motion perception using known aspects of physiology in MT. No one now seriously questions the linking hypothesis that MT is an integral part of how we see moving things.

The bad news is that our knowledge of this structure is still woefully inadequate in many regards. There are striking deficits in our knowledge of function at both at the descriptive and the mechanistic levels. To start with, motion psychophysics is complex, with many phenomena beyond simple direction or speed discrimination. Such perceptual phenomena as long-range apparent motion and second- or third-order motion are seeking good physiological correlates. Distinctions drawn between these phenomena by psychophysicists might reflect different neuronal substrates (e.g., Wilson and Ferrera, 1992), and this is subject to direct experimental test. Additionally, recent results on stereopsis suggest that the role of MT outside of motion might be wider than was previously thought. Stereo, like motion, is a good cue to the spatial structure of the scene, so one can easily imagine further experiments testing MT and other structures in the motion system as providing more general information on 2D and 3D space.

When it comes to questions of underlying physiological mechanisms, we are even more profoundly ignorant. There are good models largely consistent with the current experimental data but their predictions have not really been tested. To some extent, this is because the level of question makes the tests difficult. To cite just one of the many possible examples, consider velocity selectivity. A simple summation model such as the one proposed by Simoncelli and Heeger (1998) is consistent with the presence of truly velocity-selective cells, and furthermore suggests that the property of velocity selectivity emerges as a consequence of convergence of the appropriate inputs from V1 or other lower-order areas. Testing this hypothesis involves tracing patterns of cell-to-cell connectivity across multiple areas—a heroic experiment with current tools. Nonetheless, techniques that have been successfully applied to similar circuit-level questions in striate cortex could provide a wealth of valuable data to test and constrain present and future mechanistic models of MT processing.

Looking in the other direction, the field is well poised to form and test hypotheses regarding *how* information is read

out from MT and used in making decisions or guiding movements. Such work is well underway in several labs, and the next decade should be an exciting time in pursuing this level of question. Similarly, the question of how attention modulates sensory processing in MT is ripe for mechanistic study. We know that top-down influences have a profound effect on MT, but *how* this happens is still an question. Again, this is an issue that is best addressed at the circuit level.

Overall, then, we see that the past 25 years have been exciting ones in the study of the cortical mechanisms of perception, and MT is one of the poster children of how such questions can be addressed. Our ideas about its role in perception have evolved and will presumably continue to evolve. The next 25 years should be even more exciting.

REFERENCES

- Albright, T. D., 1984. Direction and orientation selectivity of neurons in visual area MT of the macaque, *J. Neurophysiol.*, 52:1106–1130.
- Albright, T. D., R. Desimone, and C. G. Gross, 1984. Columnar organization of directionally selective cells in visual area MT of macaques, *J. Neurophysiol.*, 51:16–31.
- Albright, T. D., and G. R. Stoner, 1995. Visual motion perception, *Proc. Nat. Acad. Sci. USA*, 92:2433–2440.
- Allman, J. M., and J. H. Kaas, 1971. A representation of the visual field in the caudal third of the middle temporal gyrus of the owl monkey (*Aotus trivirgatus*), *Brain Res.*, 31:85–105.
- Allman, J. M., F. Meizin, and E. McGuinness, 1985. Direction and velocity-specific responses from beyond the classical receptive field in the middle temporal visual area (MT), *Perception*, 14:105–126.
- Andersen, R. A., 1997. Neural mechanisms of visual motion perception in primates, *Neuron*, 18:865–872.
- Andersen, R. A., L. H. Snyder, D. C. Bradley, and J. Xing, 1997. Multimodal representation of space in the posterior parietal cortex and its use in planning movements, *Annu. Rev. Neurosci.*, 20:303–330.
- Bair, W., and C. Koch, 1996. Temporal precision of spike trains in extrastriate cortex of the behaving macaque monkey, *Neural Comput.*, 8:1185–1202.
- Bair, W., C. Koch, W. Newsome, and K. Britten, 1992. Power spectrum analysis of MT neurons from awake monkey, *Soc. Neurosci. Abstr.*, 18:12.
- Battaglini, P. P., C. Galletti, and P. Fattori, 1996. Cortical mechanisms for visual perception of object motion and position in space, *Behav. Brain Res.*, 76:143–154.
- Bisley, J. W., and T. Pasternak, 2000. The multiple roles of visual cortical areas MT/MST in remembering the direction of visual motion, *Cereb. Cortex*, 10:1053–1065.
- Born, R. T., 2000. Center-surround interactions in the middle temporal visual area of the owl monkey, *J. Neurophysiol.*, 84:2658–2669.
- Born, R. T., J. M. Groh, R. Zhao, and S. J. Lukasewycz, 2000. Segregation of object and background motion in visual area MT: effects of microstimulation on eye movements, *Neuron*, 26:725–734.
- Born, R. T., and R. B. Tootell, 1992. Segregation of global and local motion processing in primate middle temporal visual area, *Nature*, 357:497–499.
- Braddick, O., 1993. Segmentation versus integration in visual motion processing, *Trends Neurosci.*, 16:263–268.
- Bradley, D. C., G. C. Chang, and R. A. Andersen, 1998. Encoding of three-dimensional structure-from-motion by primate area MT neurons, *Nature*, 392:714–717.
- Britten, K. H., W. T. Newsome, M. N. Shadlen, S. Celebrini, and J. A. Movshon, 1996. A relationship between behavioral choice and the visual responses of neurons in macaque MT, *Vis. Neurosci.*, 13:87–100.
- Britten, K. H., M. N. Shadlen, W. T. Newsome, and J. A. Movshon, 1992. The analysis of visual motion: a comparison of neuronal and psychophysical performance, *J. Neurosci.*, 12:4745–4765.
- Britten, K. H., M. N. Shadlen, W. T. Newsome, and J. A. Movshon, 1993. Responses of neurons in macaque MT to stochastic motion signals, *Vis. Neurosci.*, 10:1157–1169.
- Buracas, G. T., A. M. Zador, M. R. DeWeese, and T. D. Albright, 1998. Efficient discrimination of temporal patterns by motion-sensitive neurons in primate visual cortex, *Neuron*, 20:959–969.
- Croner, L. J., and T. D. Albright, 1997. Image segmentation enhances discrimination of motion in visual noise, *Vis. Res.*, 37:1415–1427.
- Croner, L. J., and T. D. Albright, 1999. Segmentation by color influences responses of motion-sensitive neurons in the cortical middle temporal visual area, *J. Neurosci.*, 19:3935–3951.
- DeAngelis, G. C., B. G. Cumming, and W. T. Newsome, 1998. Cortical area MT and the perception of stereoscopic depth, *Nature*, 394:677–680.
- DeAngelis, G. C., and W. T. Newsome, 1999. Organization of disparity-selective neurons in macaque area MT, *J. Neurosci.*, 19:1398–1415.
- Desimone, R., and J. Duncan, 1995. Neural mechanisms of selective attention, *Ann. Rev. Neurosci.*, 18:193–222.
- Dobkins, K. R., G. R. Stoner, and T. D. Albright, 1998. Perceptual, oculomotor, and neural responses to moving color plaids, *Perception*, 27:681–709.
- Dodd, J. V., K. Krug, B. G. Cumming, and A. J. Parker, 2001. Perceptually bistable 3-D figures evoke high choice probabilities in cortical area MT, *J. Neurosci.*, 21:4809–4821.
- Dubner, R., and S. M. Zeki, 1971. Response properties and receptive fields of cells in an anatomically defined region of the superior temporal sulcus, *Brain Res.*, 35:528–532.
- Duffy, C. J., 2000. Optic flow analysis for self-movement perception, *Int. Rev. Neurobiol.*, 44:199–218.
- Dumbrava, D., J. Faubert, and C. Casanova, 2001. Global motion integration in the cat's lateral posterior-pulvinar complex, *Eur. J. Neurosci.*, 13:2218–2226.
- Duncan, R. O., T. D. Albright, and G. R. Stoner, 2000. Occlusion and the interpretation of visual motion: perceptual and neuronal effects of context, *J. Neurosci.*, 20:5885–5897.
- Geesaman, B., R. Born, R. Andersen, and R. Tootell, 1997. Maps of complex motion selectivity in the superior temporal cortex of the alert macaque monkey: a double-label 2-deoxyglucose study, *Cereb. Cortex*, 7:749–757.
- Gegenfurtner, K. R., D. C. Kiper, and J. B. Levitt, 1997. Functional properties of neurons in macaque area V3, *J. Neurophysiol.*, 77:1906–1923.
- Heuer, H. W., and K. H. Britten, 1999. Response normalization by middle temporal neurons. II: effects of contrast, *J. Neurophysiol.*, 88:3398–3408.
- Krauzlis, R., and S. Lisberger, 1994. Temporal properties of visual motion signals for the initiation of smooth pursuit eye movements in monkeys, *J. Neurophysiol.*, 72:150–162.

- Kreiter, A. K., and W. Singer, 1996. Stimulus dependent synchronization of neuronal responses in the visual cortex of the awake macaque monkey, *J. Neurosci.*, 16:798–828.
- Krubitzer, L. A., and J. H. Kaas, 1990. Cortical connections of MT in four species of primates: areal, modular, and retinotopic patterns, *Vis. Neurosci.*, 5:165–204.
- Lagae, L., S. Raiguel, and G. A. Orban, 1993. Speed and direction selectivity of macaque middle temporal neurons, *J. Neurophysiol.*, 69:19–39.
- Lauwers, K., R. Saunders, R. Vogels, E. Vandebussche, and G. A. Orban, 2000. Impairment in motion discrimination tasks is unrelated to amount of damage to superior temporal sulcus motion areas, *J. Comp. Neurol.*, 420:539–557.
- Lisberger, S. G., and J. A. Movshon, 1999. Visual motion analysis for pursuit eye movements in area MT of macaque monkeys, *J. Neurosci.*, 19:2224–2246.
- Livingstone, M. S., C. C. Pack, and R. T. Born, 2001. Two-dimensional substructure of MT receptive fields, *Neuron*, 30:781–793.
- Logothetis, N. K., and J. D. Schall, 1989. Neuronal correlates of subjective visual perception, *Science*, 245:761–763.
- Maldonado, P. E., I. Gödecke, C. M. Gray, and T. Bonhoeffer, 1997. Orientation selectivity in pinwheel centers in cat striate cortex, *Science*, 276:1551–1555.
- Marshak, W., and S. Sekuler, 1979. Mutual repulsion between moving visual targets, *Science*, 205:1399–1401.
- Maunsell, J. H. R., 1986. Physiological evidence for two visual systems, in *Matters of Intelligence* (L. Vaina ed.), Dordrecht: Reidel.
- Maunsell, J. H. R., and W. T. Newsome, 1987. Visual processing in monkey extrastriate cortex, *Annu. Rev. Neurosci.*, 10:363–401.
- Maunsell, J. H. R., and D. C. Van Essen, 1983a. Functional properties of neurons in the middle temporal visual area (MT) of the macaque monkey: I. Selectivity for stimulus direction, speed and orientation, *J. Neurophysiol.*, 49:1127–1147.
- Maunsell, J. H. R., and D. C. Van Essen, 1983b. Functional properties of neurons in the middle temporal visual area (MT) of the macaque monkey: II. Binocular interactions and the sensitivity to binocular disparity, *J. Neurophysiol.*, 49:1148–1167.
- Maunsell, J. H. R., and D. C. Van Essen, 1987. Topographic organization of the middle temporal visual area in the macaque monkey: representational biases and the relationship to callosal connections and myeloarchitectonic boundaries, *J. Comp. Neurol.*, 266:535–555.
- Movshon, J. A., E. H. Adelson, M. S. Gizzi, and W. T. Newsome, 1985. The analysis of moving visual patterns, in *Study Group on Pattern Recognition Mechanisms* (C. Chagas, R. Gattass, and C. Gross, eds.), Vatican City: Pontifica Academia Scientiarum, pp. 117–151.
- Movshon, J. A., W. T. Newsome, M. S. Gizzi, and J. B. Levitt, 1988. Spatio-temporal tuning and speed sensitivity in macaque visual cortical neurons, *Invest. Ophthalmol. Vis. Sci. Suppl.*, 29:327.
- Murasugi, C. M., C. D. Salzman, and W. T. Newsome, 1993. Microstimulation in visual area MT: effects of varying pulse amplitude and frequency, *J. Neurosci.*, 13:1719–1729.
- Nealey, T., and J. Maunsell, 1994. Magnocellular and parvocellular contributions to the responses of neurons in macaque striate cortex, *J. Neurosci.*, 14:2069–2079.
- Newsome, W. T., A. Mikami, and R. H. Wurtz, 1986. Motion selectivity in macaque visual cortex. III. Psychophysics and physiology of apparent motion, *J. Neurophysiol.*, 55:1340–1351.
- Newsome, W. T., and E. B. Paré, 1986. MT lesions impair discrimination of direction in a stochastic motion display, *Soc. Neurosci. Abstr.*, 12:1183.
- Orban, G. A., 1997. Visual processing in macaque area MT/V5 and its satellites (MSTd and MSTl), in *Cerebral Cortex* (K. S. Rockland, J. H. Kaas, and A. Peters, eds.), New York: Plenum, pp. 359–434.
- Orban, G. A., R. C. Saunders, and E. Vandebussche, 1995. Lesions of the superior temporal cortical motion areas impair speed discrimination in the macaque monkey, *Eur. J. Neurosci.*, 7:2261–2276.
- Pack, C. C., V. K. Berezovskii, and R. T. Born, 2001. Dynamic properties of neurons in cortical area MT in alert and anaesthetized macaque monkeys, *Nature*, 414:905–908.
- Pack, C. C., and R. T. Born, 2001. Temporal dynamics of a neural solution to the aperture problem in visual area MT of macaque brain, *Nature*, 409:1040–1042.
- Parker, A. J., and W. T. Newsome, 1998. Sense and the single neuron: probing the physiology of perception, *Annu. Rev. Neurosci.*, 21:227–277.
- Pasternak, T., and W. H. Merigan, 1994. Motion perception following lesions of the superior temporal sulcus in the monkey, *Cereb. Cortex*, 4:247–259.
- Perrone, J. A., and A. Thiele, 2001. Speed skills: measuring the visual speed analyzing properties of primate MT neurons, *Nat. Neurosci.*, 4:526–532.
- Petersen, S. E., J. F. Baker, and J. M. Allman, 1985. Direction-specific adaptation in area MT of the owl monkey, *Brain Res.*, 346:146–150.
- Priebe, N. J., M. M. Churchland, and S. G. Lisberger, 2003. Reconstruction of target speed for the guidance of smooth pursuit eye movements, *J. Neurosci.*, in press.
- Qian, N., and R. A. Andersen, 1994. Transparent motion perception as detection of unbalanced motion signals. II. Physiology, *J. Neurosci.*, 14:7367–7380.
- Raiguel, S., M. M. Van Hulle, D. K. Xiao, V. L. Marcar, and G. A. Orban, 1995. Shape and spatial distribution of receptive fields and antagonistic motion surrounds in the middle temporal area (V5) of the macaque, *Eur. J. Neurosci.*, 7:2064–2082.
- Raiguel, S. E., D. K. Xiao, V. L. Marcar, and G. A. Orban, 1999. Response latency of macaque area MT/V5 neurons and its relationship to stimulus parameters, *J. Neurophysiol.*, 82:1944–1956.
- Recanzone, G. H., and R. H. Wurtz, 2000. Effects of attention on MT and MST neuronal activity during pursuit initiation, *J. Neurophysiol.*, 83:777–790.
- Royden, C. S., 1997. Mathematical analysis of motion-opponent mechanisms used in the determination of heading and depth, *J. Opt. Soc. Am. A*, 14:2128–2143.
- Rudolph, K., and T. Pasternak, 1999. Transient and permanent deficits in motion perception after lesions of cortical areas MT and MST in the macaque monkey, *Cereb. Cortex*, 9:90–100.
- Salzman, C. D., C. M. Murasugi, K. H. Britten, and W. T. Newsome, 1992. Microstimulation in visual area MT: effects on direction discrimination performance, *J. Neurosci.*, 12:2331–2355.
- Schiller, P., 1993. The effects of V4 and middle temporal (MT) area lesions on visual performance in the rhesus monkey, *Vis. Neurosci.*, 10:717–746.
- Seidemann, E., and W. T. Newsome, 1999. Effect of spatial attention on the responses of area MT neurons, *J. Neurophysiol.*, 81:1783–1794.
- Simoncelli, E. P., and D. J. Heeger, 1998. A model of neuronal responses in visual area MT, *Vis. Res.*, 38:743–761.
- Snowden, R. J., S. Treue, R. G. Erickson, and R. A. Andersen, 1991. The response of area MT and V1 neurons to transparent motion, *J. Neurosci.*, 11:2768–2785.

- Stoner, G. R., and T. D. Albright, 1992. Neural correlates of perceptual motion coherence, *Nature*, 358:412–414.
- Thiele, A., and K.-P. Hoffman, 1996. Neuronal activity in MST and STPp, but not MT changes systematically with stimulus-independent decisions, *NeuroReport*, 7:971–976.
- Treue, S., and J. C. Martínez-Trujillo, 1999. Feature-based attention influences motion processing gain in macaque visual cortex, *Nature*, 399:575–579.
- Treue, S., and J. H. R. Maunsell, 1996. Attentional modulation of visual motion processing in cortical areas MT and MST, *Nature*, 382:539–541.
- Uka, T., and G. C. DeAngelis, 2003. Contribution of middle temporal area to coarse depth discrimination: comparison of neuronal and psychophysical sensitivity, *J. Neurosci.*, 23:3515–3530.
- Ungerleider, L. G., and M. Mishkin, 1979. The striate projection in the superior temporal sulcus of *Macaca mulatta*: location and topographic organization, *J. Comp. Neurol.*, 188:347–366.
- Van Essen, D. C., J. H. R. Maunsell, and J. L. Bixby, 1981. The middle temporal visual area in the macaque: myeloarchitecture, connections, functional properties and topographic representation, *J. Comp. Neurol.*, 199:293–326.
- van Wezel, R. J. A., and K. H. Britten, 2002. Motion Adaptation in area MT, *J. Neurophysiol.*, 88:3469–3476.
- van Wezel, R. J. A., F. A. J. Verstraten, R. E. Fredericksen, and W. A. van de Grind, 1994. Spatial integration in coherent motion detection and in the movement aftereffect, *Perception*, 23:1189–1195.
- Wilson, H. R., and V. P. Ferrera, 1992. A psychophysically motivated model for two-dimensional motion perception, *Vis. Neurosci.*, 9:79–97.
- Yamasaki, D. S., and R. H. Wurtz, 1991. Recovery of function after lesions in the superior temporal sulcus in the monkey, *J. Neurophysiol.*, 66:651–673.
- Zeki, S. M., 1974a. Cells responding to changing image size and disparity in the cortex of the rhesus monkey, *J. Physiol.*, 242:827–841.
- Zeki, S. M., 1974b. Functional organization of a visual area in the posterior bank of the superior temporal sulcus of the rhesus monkey, *J. Physiol.*, 236:549–573.
- Zeki, S. M., 1978. Uniformity and diversity of structure and function in rhesus monkey prestriate visual cortex, *J. Physiol.*, 277:273–290.

82 Merging Processing Streams: Color Cues for Motion Detection and Interpretation

KAREN R. DOBKINS AND THOMAS D. ALBRIGHT

THE BASIC TASK CONFRONTING a visual motion processor is that of detecting the continuity of image features as they are displaced in time and space. This process, referred to as the *motion correspondence* problem, involves “matching” features at one moment in time with the same objects, displaced in space, at a later moment in time. Although there exist several different types of image features that might be used for this matching process, here we focus on the role of *color* since this aspect of vision provides one of the most reliable means for discerning object boundaries.

Despite the appeal of utilitarian arguments, the degree to which the primate motion system makes use of object color has been an issue of long-standing debate in vision science. Indeed, it has been suggested that color information should exert little or no influence on motion detection, a notion that sprang from evidence for parallel processing of color versus motion in the primate visual system. Contrary to this once popular viewpoint, several new lines of evidence suggest that the motion system uses color information in ways that are both substantial and highly functional. Such findings, in turn, have inspired efforts to identify the mechanisms by which color information reaches motion processing areas of the brain.

In this chapter, we begin by presenting psychophysical evidence for the use of color in human motion perception. We then address evidence for neural correlates of these perceptual phenomena. In particular, we focus on a region of primate extrastriate cortex, known as the *middle temporal visual area* (area MT), which is thought to play a key role in motion perception. We then discuss the possible sources of input to area MT that may underlie the ability of neurons in this area to signal motion of chromatically defined patterns. To this end, we provide an overview of the three main retinogeniculate pathways of the primate visual system—parvocellular, koniocellular, and magnocellular—whose color responses are thought to be selective for red/green, blue/yellow, and luminance modulation, respectively. Finally, we describe the results of several neurophysiological experiments carried out using macaque monkeys as subjects, which address the extent to which these different pathways might contribute to chromatic responses observed in area MT. Note that parallels drawn between human psychophysical data and

macaque neural data are justified in light of the known similarities of visual system organization and function between these two primates (e.g., De Valois et al., 1974; Golomb et al., 1985; Newsome et al., 1989; Newsome and Paré, 1988).

Definitions of color channels

Before reviewing the psychophysical evidence for chromatic input to motion processing, it is necessary to review briefly the different dimensions of color vision. Theories of color vision posit the existence of three postreceptoral *channels*, which are derived from the sums and differences of the three cone types in the eye. The *achromatic* or *luminance* channel signals a weighted sum of long-wavelength-selective (L) and medium-wavelength-selective (M) cones (i.e., $L + M$, with some debate regarding the contribution of short-wavelength-selective (S) cones; e.g., Boynton et al., 1985; Eisner and Macleod, 1980; Stockman et al., 1991). Two *chromatic* channels signal weighted sums and differences of the cones. The *red/green* chromatic channel signals differences between L and M cones (i.e., $L - M$ or $M - L$). The *blue/yellow* chromatic channel signals differences between S-cones and the sum of L and M cones (i.e., $S(L + M)$). These three channels are referred to as *cardinal channels*, and the stimuli that isolate them are referred to as the *cardinal axes* of three-dimensional color space (Fig. 82.1). Note that stimuli varying along either the red/green or blue/yellow axis (or any axis within the plane of the two) do not vary in luminance; for this reason, stimuli modulated within this plane are referred to as *equiluminant*.

Psychophysical evidence for color input to motion processing

Over the past several decades, the reliance of motion detectors on signals arising within the luminance channel has been firmly established (see Nakayama, 1985, for review). By comparison, the use of red/green and blue/yellow chromatic information for motion processing has been far more controversial. Psychophysical studies probing the extent of chromatic influences on motion perception are numerous, and the results have been variously interpreted (see Dobkins and Albright, 1998; Gegenfurtner and Hawken, 1996, for

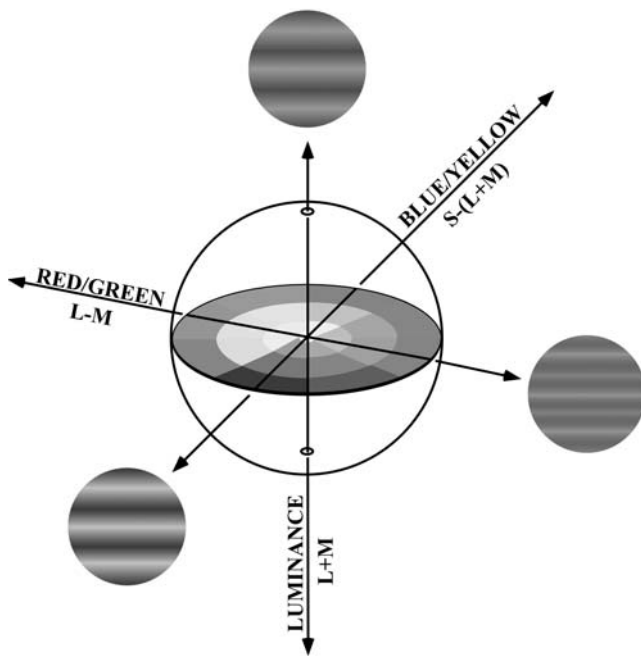


FIGURE 82.1. Three color channels. The *luminance* channel signals a weighted sum of long-wavelength-selective (L) and medium-wavelength-selective (M) cones, that is, $L + M$. The *red/green* chromatic channel signals differences between L and M cones, that is, $L - M$. The *blue/yellow* chromatic channel signals differences between short-wavelength-selective (S) cones and the sum of L and M cones, that is, $S - (L + M)$. (Reprinted from *Neuron*, vol. 25, Dobkins, K. R., *Moving Colors in the Lime Light*, Pages 15–18, Copyright 2000 with permission from Elsevier Science.) (See color plate 59.)

detailed reviews). One of the most direct ways in which researchers have investigated chromatic input to motion processing is to simply determine whether the direction of a chromatically defined moving stimulus can be discriminated. For *red/green* stimuli, studies employing sinusoidal gratings (e.g., Cavanagh and Anstis, 1991; Cavanagh et al., 1984; Cropper and Derrington, 1994, 1996; Derrington and Henning, 1993; Dobkins and Albright, 1993; Dobkins and Teller, 1996; Gegenfurtner and Hawken, 1995; Hawken et al., 1994; Lindsey and Teller, 1990; Metha et al., 1994; Mullen and Boulton, 1992; Palmer et al., 1993), random-dot kinematograms (Cavanagh et al., 1985; Morgan and Cleary, 1992; Morgan and Ingle, 1994; Simpson, 1990; Troscianko, 1987; but cf. Ramachandran and Gregory, 1978), and periodic dot displays (Agonie and Gorea, 1993; Dobkins and Albright, 1990; Gorea and Papathomas, 1989; Gorea et al., 1992; Green, 1989; Papathomas et al., 1991) have consistently shown that direction discrimination persists for chromatic stimuli, albeit often less reliably than for stimuli that contain luminance contrast. Far fewer studies have been conducted using stimuli that vary along the *blue/yellow* dimension of color. Similar to the case for red/green stimuli, motion of blue/yellow gratings can be discerned, yet the

motion typically appears relatively impoverished compared to moving stimuli containing luminance contrast (Cavanagh and Anstis, 1991; Cavanagh et al., 1984; Dougherty et al., 1999; Gegenfurtner and Hawken, 1995; Lee and Stromeyer, 1989; Moreland, 1982). In addition to the above-mentioned experiments, several studies have attempted to quantify precisely the degree to which chromatic information contributes to motion perception. One approach has been to employ a *motion nulling* paradigm in which a heterochromatic (red/green or blue/yellow) grating moving in one direction is superimposed upon an achromatic (i.e., luminance) grating moving in the opposite direction. This approach allows the sensitivity of motion detectors to chromatic contrast to be quantified and expressed relative to a benchmark of sensitivity for luminance contrast. Specifically, the amount of luminance contrast in the achromatic grating required to “null” the motion of the heterochromatic grating identifies the *equivalent luminance contrast* (EqLC) rendered by the chromatic contrast in the heterochromatic grating. For *red/green* gratings, EqLC has been shown to vary from 4% to 12%, depending on the spatial and temporal frequency of the stimulus (Cavanagh and Anstis, 1991; Teller and Palmer, 1996; Thiele et al., 2002; and see Agonie and Gorea, 1993, for similar values obtained using periodic dot displays). For *blue/yellow* gratings, EqLC values are a bit smaller, on the order of 2% to 5% (Cavanagh and Anstis, 1991; Teller et al., 1997). In sum, there exists a substantial amount of psychophysical evidence for both red/green and blue/yellow chromatic input to motion processing.

Neural correlates of color-based motion perception

Attempts to explore the neural substrates of chromatic contributions to motion perception have focused on the properties of cells in area MT of monkey extrastriate visual cortex. Area MT is recognized as a key component of the neural substrate for motion perception, with the vast majority of MT neurons exhibiting a high degree of selectivity for direction of motion (see Albright, 1993, for a review). Neurons in MT do not exhibit selectivity for object color (Albright, 1984; Baker et al., 1981; Maunsell and Van Essen, 1983b; Van Essen et al., 1981; Zeki, 1974). The absence of color selectivity in MT neurons has been heralded as evidence for the segregation of color and motion processing pathways. Only recently has attention been given to the possibility that directionally selective neurons can use information about object color to encode direction while possessing no selectivity for color per se. In support of this possibility, several studies have shown that neurons in MT are able to signal the direction of moving red/green and blue/yellow gratings, although responses are significantly weaker than, for moving luminance gratings (Dobkins and Albright, 1990, 1994; Gegenfurtner et al., 1994; Saito et al., 1989; Seidemann

et al., 1999; Thiele et al., 1999; and see Ffytche et al., 1995; Tootell et al., 1995; Wandell et al., 1999, for similar results obtained using brain imaging techniques in humans). These MT results thus mirror the impoverished, but not altogether absent, sensitivity to chromatic motion observed perceptually.

Sources of chromatic (red/green and blue/yellow) input to area MT

We next address the avenues by which area MT may have access to chromatic information. To this end, we turn to a discussion of the color selectivities of the three main retinogeniculate pathways of the primate visual system—parvocellular (P), koniocellular (K), and magnocellular (M)—and then discuss the potential for each pathway to reach motion processing regions such as MT. Details of the anatomy and physiology of these three pathways can be found in several previous reviews (e.g., Dobkins, 2000; Dobkins and Albright, 1998; Hendry and Reid, 2000; Kaplan et al., 1990; Merigan and Maunsell, 1993).

To begin, the names of these pathways are based on their anatomical distinction in the lateral geniculate nucleus (LGN) of the thalamus. Four LGN layers contain densely packed, small (*parvo* or *P*) cells, and two contain more sparsely placed, large (*magno* or *M*) cells. Just below each M and P layer exist layers (six in total) of extremely small dust-like cells, winning them the name *konio* or *K* cells. (Note that in the past, the K layers were referred to as *interlaminar* or *intercalated*.) The anatomical projections of these three pathways have been shown to remain entirely separate from the level of the retinal ganglion cells in the eye to primary visual cortex (area V1). Specifically, the P pathway originates within the *midget* retinal ganglion cells, which project selectively to the P layers of the LGN. The P layers, in turn, project selectively to layer 4C β of V1. In a parallel fashion, the M pathway originates within *parasol* ganglion cells of the retina, which project selectively to the M layers of the LGN. The M layers, in turn, send their projections to layer 4C α of area V1. The K pathway (or a portion thereof) originates within *blue-ON bistratified* ganglion cells of the retina, which project selectively to the middle two K layers of the LGN (i.e., layers K3 and K4). These K layers, in turn, send their projections to the *blobs* in the superficial layers of V1 (as well as sending sparse projections directly to extrastriate visual areas such as MT; see below).

COLOR RESPONSES OF P, K, AND M CELLS The color selectivities of cells within the P, K, and M pathways are thought to map roughly onto the red/green, blue/yellow, and luminance dimensions of color, respectively (see Chapter 30 for a discussion of other characteristics of the cells in these pathways). These differential color selectivities arise from the

different manner in which cone types feed into the three pathways. Specifically, midget ganglion cells of the P pathway receive opponent signals from L and M cones (i.e., $L - M$ or $M - L$), and thus respond preferentially to modulation along the *red/green* dimension (e.g., De Monasterio and Gouras, 1975; De Valois et al., 1966; Derrington et al., 1984; Gouras and Zrenner, 1979, 1981; Reid and Shapley, 1992; Wiesel and Hubel, 1966). For example, a given P cell may be activated when stimulated by red light yet inhibited when stimulated by green light (or vice versa). Blue-ON bistratified cells of the K pathway receive excitatory input from S-cones and inhibitory input from L and M cones, and thus respond best to modulation along the blue/yellow dimension (e.g., Calkins, 2001; Calkins et al., 1998; Dacey and Lee, 1994). Specifically, they are excited by blue light and inhibited by yellow light. There also appears to exist another class of ganglion cells, which are inhibited by blue light and excited by yellow light (e.g., Herr et al., 2003; Klug et al., 1993; and see Shinomori et al., 1999, for related psychophysical evidence); however, these cells are extremely scarce and may not be part of the K pathway. In sum, cells of both the P and K pathways exhibit selectivity for the *sign* of chromatic contrast (i.e., they are excited by one color and inhibited by another), a property that allows them to signal chromatic *identity*.

Parasol ganglion cells of the M pathway receive additive (i.e., $L + M$) cone signals and thus respond best to *luminance* modulation (e.g., De Monasterio and Gouras, 1975; Derrington et al., 1984; Wiesel and Hubel, 1966). Unlike cells of the P and K pathways, M cells do not exhibit *selectivity* for stimulus chromaticity. Despite their lack of chromatic selectivity, however, the majority of cells within the M pathway can signal chromatic (red/green) contrast in the following manner. First, they respond to borders defined by red/green contrast and to temporal changes between red and green, without regard for the sign of chromatic contrast (Dacey, 1996; Derrington et al., 1984; Gouras and Eggers, 1983; Hubel and Livingstone, 1990; Kaiser et al., 1990; Kruger, 1979; Lee et al., 1988, 1989a, 1989b, 1989c; Logothetis et al., 1990; Schiller and Colby, 1983; Shapley and Kaplan, 1989; Valberg et al., 1992). A second way in which M cells can signal chromatic contrast arises from the fact that the red/green luminance *balance point*—the contrast for which red and green phases of a stimulus elicit responses of equal magnitude—varies across the population of M cells. This variability ensures that, even at equiluminance, M cells as a population can never be truly silenced by heterochromatic stimuli (Logothetis et al., 1990). Whether M cells also respond to modulation along the blue/yellow dimension has been an issue of debate. Although early reports suggested negligible S-cone input to M cells (e.g., Dacey and Lee, 1994; Lee et al., 1988), more recently, substantial S-cone input has been reported (Calkins, 2001;

Chatterjee and Callaway, 2002). In particular, Chatterjee and Callaway found that S-cones contribute roughly 10% to the responsivity of M cells, a percentage that reflects the proportion of S-cones in the retina. They further found that all three cone types provide input of the same sign (i.e., L + M + S). This indicates that, similar to the case for red/green stimuli, M cells can respond to blue/yellow contrast, yet are not selective for the sign of chromatic variation.

In sum, the responses of M cells to both red/green and blue/yellow chromatic contrast can be said to be *unsigned*, that is, M cells provide information about chromatic contrast while not conveying information about chromatic identity per se. This unsigned chromatic signal can potentially allow for chromatic motion correspondence observed psychophysically and in area MT, an issue we return to later in this chapter.

P, K, AND M PATHWAY PROJECTIONS TO MT Although it was originally believed that only cells of the M pathway projected to MT, anatomical evidence now suggests that the P and K pathways also provide at least minimal input. The projections from the M pathway are the most clear and well studied. Specifically, projections from magnocellular-receptive layer 4C α of V1 project to layer 4B (Livingstone and Hubel, 1987), which in turn sends both direct and indirect (via area V2) projections to MT (DeYoe and Van Essen, 1985; Lund et al., 1975; Maunsell and Van Essen, 1983a; Shipp and Zeki, 1985). Direct evidence for P and K pathway input to area MT is far less abundant. In one study using an in vitro photostimulation technique, Sawatari and Callaway (1996) reported that many layer 4B neurons receive strong input from both magnocellular-receptive layer 4C α neurons and parvocellular-receptive layer 4C β neurons. Because layer 4B projects directly to area MT, such findings suggest that MT may receive a substantial amount of P-cell input. Most recently, Hendry and Reid (2000) reported direct (yet sparse) connections between K layers in the LGN and area MT (which bypass area V1 altogether).

In addition to these anatomical studies, other experiments have used neurophysiological methods to measure the amount of functional M and P pathway input to MT. In these studies, stimulus-evoked activity in MT was measured while specific LGN laminae were simultaneously inactivated. The results of these studies revealed large decrements in MT responsivity during magnocellular LGN inactivation but only small decrements in responsivity during parvocellular LGN inactivation (Maunsell et al., 1990). Based on these results, it appears that MT receives predominantly M pathway-driven input but a small amount of P pathway-driven input. Note that because their relevance was underappreciated at the time these experiments were conducted, inputs from the K pathway have not been considered.

Relative contributions of P, K, and M pathways to chromatic motion processing

With the knowledge that all three pathways (P, K, and M) send projections to area MT, there is the potential for each to contribute to the chromatic motion responses observed in this area. Several neurophysiological experiments have investigated the nature of chromatic motion responses in MT as a way of revealing the different pathways' contributions. The resulting evidence for M, K, and P pathway inputs are reviewed in sequence, below.

EVIDENCE FOR A M-PATHWAY CONTRIBUTION Two main studies have provided evidence that red/green chromatic responses originating in M cells may be sufficient to account for chromatic motion responses observed in area MT. In the first study, Dobkins and Albright (1994) employed a novel stimulus designed to test whether chromatic motion detection in MT is based on unsigned chromatic border information (reflective of signals carried within the M pathway) or chromatic identity per se (reflective of signals carried within the P pathway). The stimulus consisted of red/green heterochromatic sine-wave gratings that undergo repetitive chromatic contrast reversal with each spatial displacement (Fig. 82.2A). Under these conditions, motion correspondence based on unsigned chromatic borders is placed in direct opposition to correspondence based on conservation of the chromatic sign. If motion detectors in MT use M pathway-driven input, they should respond best to motion in the direction of the nearest chromatic border, regardless of chromatic sign (in the chromatically "unsigned" direction; solid arrow in Fig. 82.2A), since spatial proximity is itself a potent cue for motion correspondence (e.g., Ullman, 1980). If, on the other hand, MT neurons use P pathway-driven input, they should respond best to motion in the direction that preserves chromatic sign (in the chromatically "signed" direction; dashed arrow in Fig. 82.2A).

Representative data from one MT neuron tested with this stimulus are shown in Figure 82.2B. Data were obtained for both the signed (S) and unsigned (U) cues moving in the neuron's preferred direction at each of eight different luminance contrasts between the red and green stripes of the grating. These results show that for a small range of luminance contrasts near equiluminance, selectivity for direction of motion [as quantified by an *index of directionality*: $DI = (U - S)/(U + S)$] was such that the neuron responded best to motion of the unsigned chromatic cue ($DI > 0$). Away from equiluminance, the neuron was more sensitive to motion in the signed direction ($DI < 0$). This latter effect reflects a preference to preserve the sign of *luminance* contrast when it is also present in the stimulus (see Dobkins and Albright, 1994, Fig. 5). As outlined above, the larger responses to unsigned versus signed motion near equiluminance suggest that the

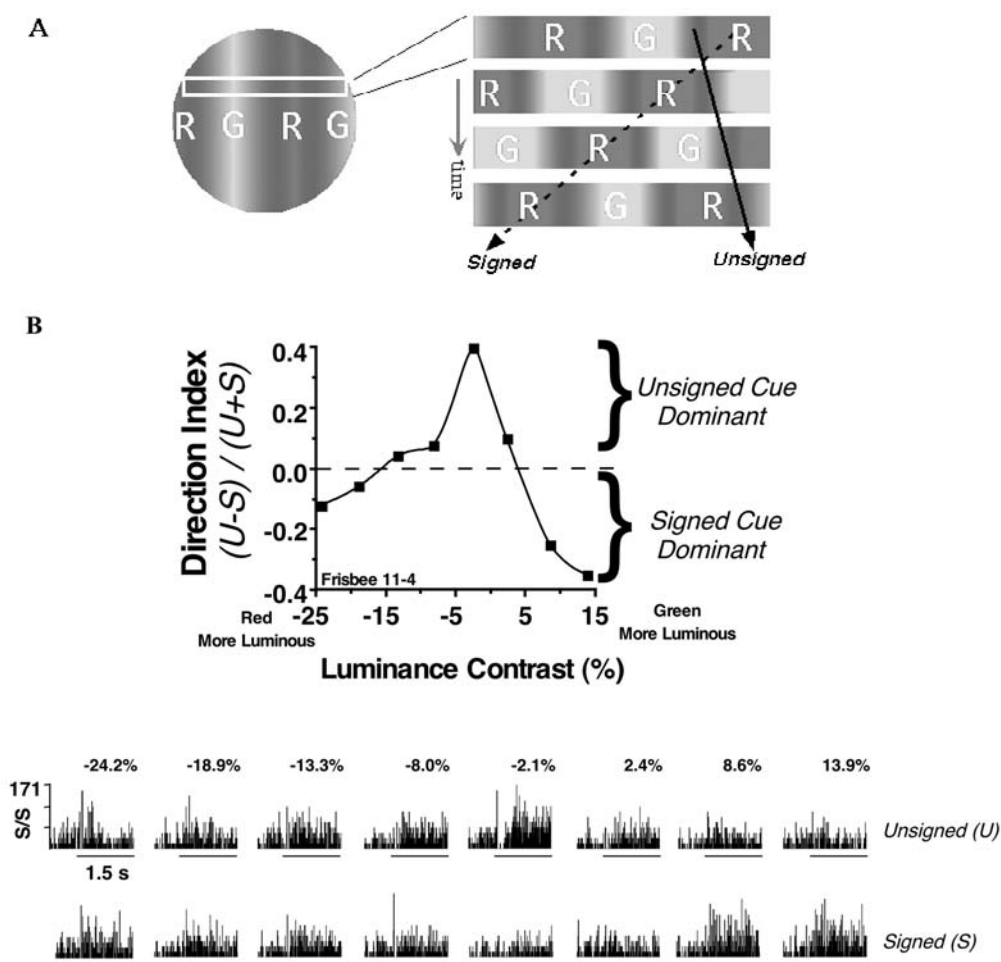


FIGURE 82.2. *A*, Heterochromatic gratings that undergo reversal of the sign of chromatic contrast coincident with each spatial displacement. The position in space of a one-dimensional slice of the grating is shown for four successive moments in time. Motion of the proximal unsigned chromatic border is rightward (*solid arrow*), while motion of the signed chromatic cue is leftward (*dashed arrow*). *B*, Data from one MT neuron presented with the moving contrast-reversed stimulus. Luminance contrast between the red and green phases of the grating was varied across eight different levels ranging in equal (5.4%) intervals from -24.2% (red more luminous) to +13.9% (green more luminous). Per-stimulus-time-histograms obtained in response to movement of the unsigned (*U*) and signed

(*S*) cues in the neuron's preferred direction are shown at the bottom for each red/green luminance contrast level tested ($S/S = \text{spikes/sec}$). Direction indices ($DI = (U - S)/(U + S)$), computed from responses elicited by the motion of unsigned and signed cues, are plotted as a function of luminance contrast (above). In line with the prediction based on M-cell responses (see text), near equiluminance (i.e., 0% luminance contrast), the neuron responded best to motion in the unsigned direction (i.e., DI s were positive). Away from equiluminance, DI s became negative, indicating that under these conditions, the neuron was more sensitive to motion in the direction that preserved the sign of both chromatic and luminance contrast. (See color plate 60.)

ability of MT neurons to signal the motion of chromatically defined stimuli can be accounted for by unsigned chromatic responses arising within the M pathway. In addition, the MT responses to heterochromatic gratings seen in Figure 82.2*B* are strikingly similar to those obtained in corresponding human psychophysical experiments (Dobkins and Albright, 1993), suggesting that MT provides the neural substrate for chromatic motion processing revealed perceptually.

In a second series of experiments, Thiele et al. (1999, 2001) adopted an EqLC paradigm (after Cavanagh and Anstis, 1991) in order to measure the strength of chromatic input to motion detectors in MT. As described earlier in this

chapter, the stimulus employed in this paradigm consisted of two sine-wave gratings—one heterochromatic (red/green), the other achromatic (yellow/black)—superimposed and moving in opposite directions (Fig. 82.3*A*). The amount of luminance contrast in the achromatic grating required to null the motion of the heterochromatic grating identifies the EqLC rendered by the chromatic contrast in the heterochromatic stimulus. In one experiment (Thiele et al., 2001), both MT neural responses and psychophysical data were obtained simultaneously from macaque monkeys, allowing for direct comparisons between psychophysical and neural estimates of EqLC. Representative data from one

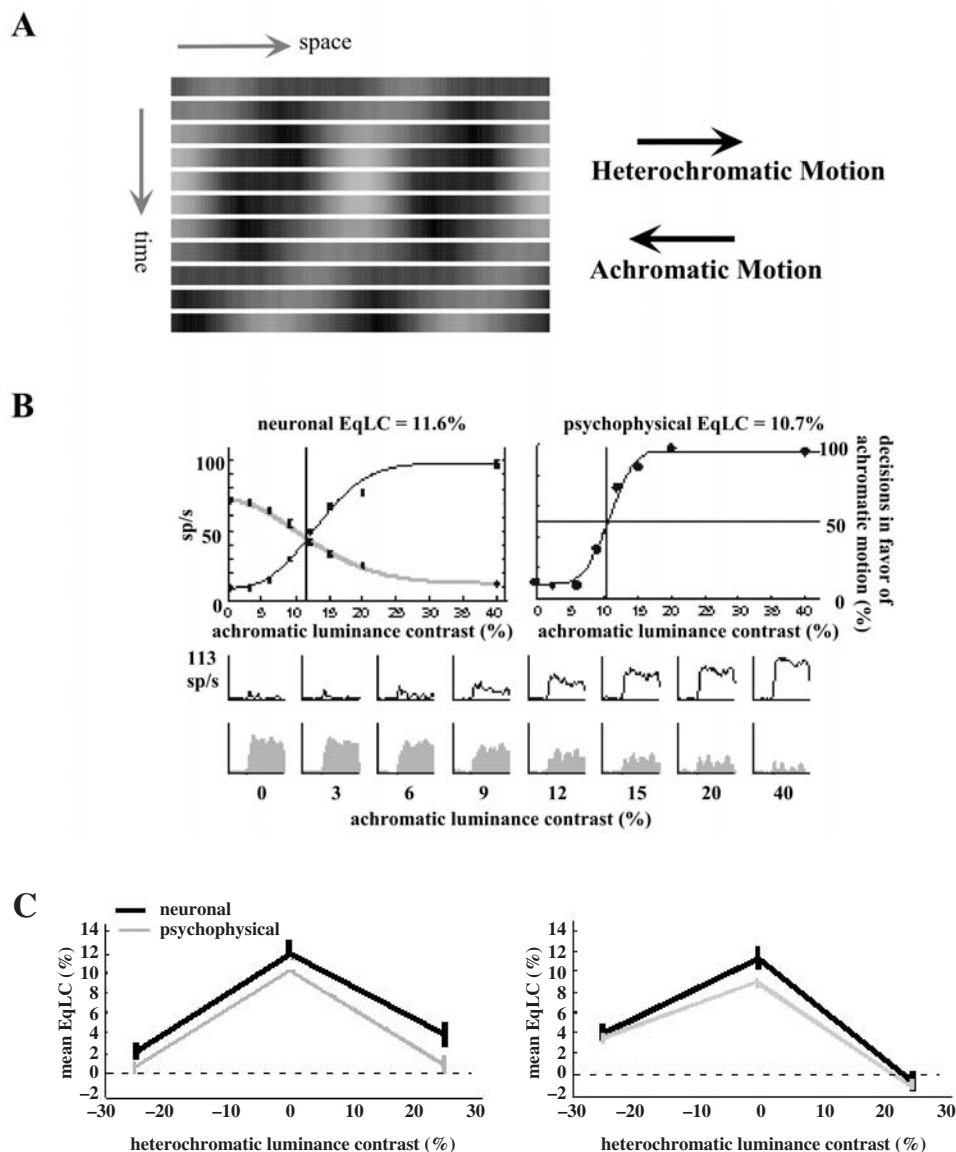


FIGURE 82.3. *A*, Space-time plot of the EqLC stimulus. This stimulus consists of two superimposed sinusoidal gratings—one achromatic (yellow/black), the other heterochromatic (red/green)—moving in opposite directions. The amount of luminance contrast in the achromatic grating required to null the motion of the heterochromatic grating identifies the EqLC rendered by the chromatic contrast in the heterochromatic grating. *B*, Representative neuronal and perceptual responses to the stimulus. In this example, the heterochromatic component was set to be equiluminant for the monkey. Gray per-stimulus-time-histograms (PSTHs) illustrate activity recorded when the heterochromatic component moved in the MT neuron's preferred direction (and thus, the achromatic component moved simultaneously in the antipreferred direction). Black-outlined PSTHs illustrate activity for the opposite directional polarity. Means and standard errors of neuronal responses (sp/s) are plotted as a function of achromatic luminance contrast (*above, left*). Neuronal EqLC was determined from intersections of curve fits to these data points. Corresponding psychophysical data are also plotted (*above, right*). Shown is the proportion of decisions in

favor of motion in the achromatic direction as a function of luminance contrast in achromatic grating. Psychophysical EqLC was determined from the null point (i.e., the point at which the perceived direction of motion was equally likely in favor of either stimulus component). *C*, Mean neuronal (black lines) and psychophysical (grey lines) EqLC values for two monkeys are plotted as a function of luminance contrast in the heterochromatic grating (0% = equiluminance, +25% = green more luminous, -25% = red more luminous). These results reveal a strong correspondence between neuronal and psychophysical estimates of EqLC, providing evidence that MT underlies chromatic motion processing revealed perceptually. In addition, in line with the M-cell model (see text), a marked decrease in EqLC was observed for heterochromatic gratings possessing 25% luminance contrast. (Reprinted from *Neuron*, vol. 32, Thiele, Dobkins and Albright, Neural Correlates of Chromatic Motion Perception, Pages 251–358, Copyright 2001 with permission from Elsevier Science.) (See color plate 61.)

testing session are presented in Figure 82.3B. Shown are simultaneously collected neural and psychophysical data for a condition in which the heterochromatic grating was set to be equiluminant for the monkey. These data reveal a strong correspondence between neural EqLC (11.6%) and psychophysical EqLC (10.7%), providing further evidence that MT underlies chromatic motion processing revealed perceptually.

In order to determine whether chromatic input to MT could be accounted for by chromatic responses originating in M cells, neural and psychophysical EqLC values obtained for equiluminant stimuli were compared to those obtained when the heterochromatic grating contained $\pm 25\%$ luminance contrast ($+25\%$ = green more luminous than red, -25% = red more luminous than green). Based on a model of the known scatter of red/green balance points across M cells, Cavanagh and Anstis (1991) demonstrated that EqLC should be greatest at equiluminance and should decline rapidly as luminance contrast is added to the heterochromatic grating (see also Thiele et al., 1999). That is, the effectiveness of the red/green portion of the heterochromatic grating is expected to diminish when luminance contrast is added to the grating. By contrast, a model based on chromatically selective P-cell responses predicts that EqLC should remain constant as luminance contrast is added to the heterochromatic grating, thus indicating an unvarying contribution of red/green contrast to motion processing with increases in luminance contrast.

In Figure 82.3C, mean neural and psychophysical EqLC values obtained for two monkeys are plotted as a function of luminance contrast in the heterochromatic grating. In line with the M-cell model, a marked decrease in EqLC was observed for heterochromatic gratings possessing 25% luminance contrast. Such findings lend further support to the notion that chromatic motion responses in MT can be accounted for by M-cell input. Interestingly, this pattern of results observed in monkey subjects is quite different from that obtained in human observers. In humans, EqLC is found to be *invariant* with increases in heterochromatic luminance contrast (Cavanagh and Anstis, 1991; Thiele et al., 2002). Such results conform to the P-cell model, leaving open the possibility that, in *humans*, there exists a relatively greater P-cell contribution to MT and/or that areas outside MT might contribute to chromatic motion processing.

EVIDENCE FOR K PATHWAY INPUT? The above-described experiments employed red/green stimuli and were aimed at revealing M versus P pathway contributions to chromatic motion processing in MT. Other recent neurophysiological studies in macaque monkeys have addressed the potential contribution of K pathway input by employing blue/yellow stimuli that isolate activity in S-cones (Seidemann et al., 1999). The results of these studies, shown in Figure 82.4,

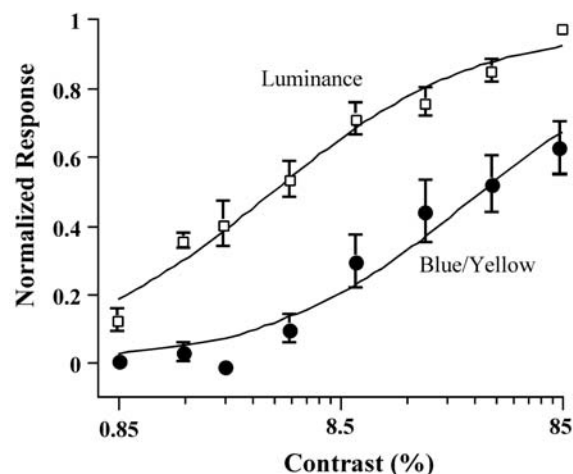


FIGURE 82.4. Mean responses and standard errors for a sample of MT neurons are plotted as a function of contrast, separately for luminance and blue/yellow (i.e., S-cone-isolating) stimuli. The response to blue/yellow stimuli may potentially result from either K- or M-pathway input to MT (see text). (Data from Seidemann, Poirson, Wandell and Newsome, *Neuron*, vol. 24, Color Signals in Area MT of the Macaque Monkey, Pages 911–917, Copyright 1999 with permission from Elsevier Science.)

reveal that blue/yellow stimuli elicit directionally selective responses in MT, although the contrast sensitivity of MT neurons is much lower for blue/yellow, compared to achromatic, moving gratings (see Wandell et al., 1999, for similar results obtained using functional magnetic resonance imaging in human subjects). This sensitivity to blue/yellow modulation may arise from the direct (yet sparse) connections known to exist between K layers in the LGN and area MT (Hendry and Reid, 2000). Alternatively, or in addition to this possibility, blue/yellow information might reach area MT via the M pathway, since recent evidence suggests that cells of the M pathway receive significant S-cone input (Calkins, 2001; Chatterjee and Callaway, 2002). Certainly, more extensive studies will be required to unequivocally establish the nature of blue/yellow input to MT.

EVIDENCE FOR A P-PATHWAY CONTRIBUTION While much of both the psychophysical and neurophysiological work has focused on the use of chromatic contrast as a cue for motion *correspondence*, other studies have demonstrated the influence of chromatic information on the *integration versus segmentation* of motion signals. Results from two different studies investigating this aspect of motion processing suggest that P-pathway input may underlie chromatic modulation of motion responses in area MT. In the first study, Dobkins et al. (1998) used moving plaid patterns (consisting of two superimposed component gratings whose motion directions differ from one another) to investigate whether motion integration in MT is influenced by chromatic information. In a previous psychophysical study, Kooi et al. (1992) showed

that when both component gratings that make up the plaid pattern are either red-bright/green-dark or green-bright/red-dark (referred to as *symmetric* plaids), the plaid is perceived to move coherently. Conversely, when one grating is red-bright/green-dark and the other is green-bright/red-dark (referred to as *asymmetric* plaids), the components appear to slide noncoherently across one another. Thus, depending on the color similarity of the component gratings, either *pattern* or *component* motion dominates motion perception (see also Cropper et al., 1996; Dobkins et al., 1992; Farell, 1995; Kooi and De Valois, 1992; Krauskopf and Farell, 1990; Krauskopf et al., 1996, for similar psychophysical results obtained with moving color plaids).

To reveal the neural basis of this perceptual phenomenon, Dobkins et al. (1998) measured responses in MT neurons elicited by symmetric versus asymmetric plaid patterns. In these experiments, they used a modified version of a plaid stimulus in which only one of the two component gratings moved, while the other remained stationary. In contrast to conventional plaids, this plaid design yields a *single* motion percept for *both* coherent and noncoherent plaid conditions (Fig. 82.5A). Example data from one MT neuron tested with symmetric plaids (perceived to move coherently) and asymmetric plaids (perceived to move noncoherently) are shown in Figure 82.5B. For each of these two plaid types, responses were obtained for both pattern motion and component motion presented in the neuron's preferred direction. When the plaid pattern was symmetric, the neuron responded better to pattern than to component motion. Conversely, when the plaid pattern was asymmetric, the neuron responded better to component motion. The responses of this neuron were thus remarkably similar to those observed in psychophysical experiments; that is, pattern motion dominated under symmetric conditions, while component motion dominated under asymmetric conditions.

This effect of color cues on motion integration in MT addresses the origin of the chromatic signals. It is highly unlikely that this modulatory effect could arise from signals originating within the M pathway, since the cells of this pathway lack chromatic selectivity and thus should not respond differentially to the red-bright/green-dark versus the green-bright/red-dark component gratings that make up the plaid stimuli. This is especially true given that the luminance contrast of the component gratings in these experiments was high enough (i.e., roughly 20%) to saturate the responses of M cells (Kaplan and Shapley, 1986). Thus, despite known variability in red/green balance points across the M-cell population (as described earlier), all M cells are expected to respond equally (and maximally) to the two component grating types. By contrast, the chromatic selectivity of P cells allows them to respond differentially to red-bright/green-dark versus green-bright/red-dark component gratings. For example, a *red-on* P cell (which is excited by red

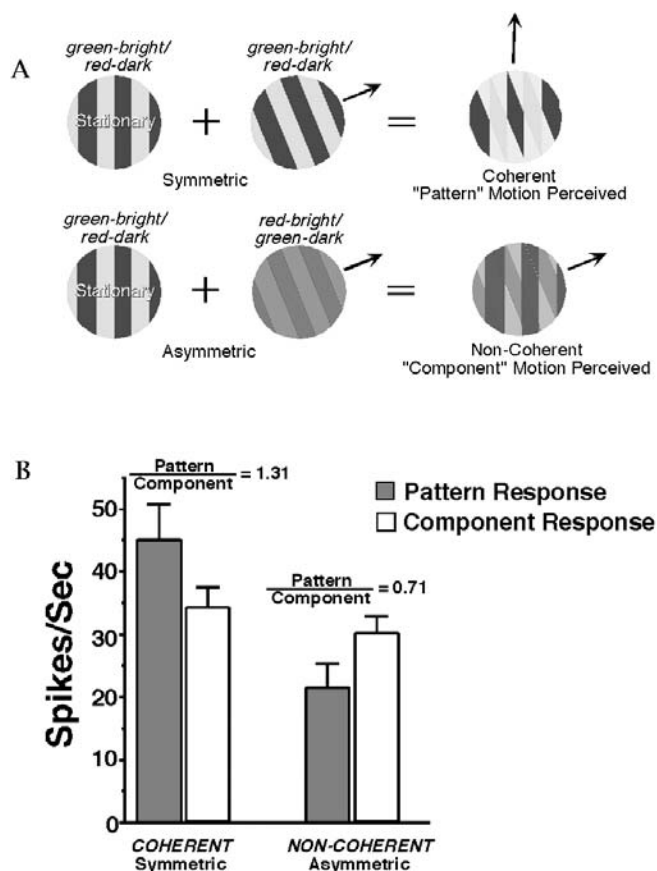


FIGURE 82.5. *A*, Color plaid stimuli in which one component moves while the other remains stationary. Under these conditions, both noncoherent and coherent motion are associated with a single motion percept. When the plaids are *symmetric* (top panel)—that is, both components are green-bright/red-dark—coherent pattern motion is perceived (in this example, moving upward). When the plaids are *asymmetric* (bottom panel)—that is, one green-bright/red-dark and one red-bright/green-dark component—noncoherent component motion is perceived (in this example, moving up to the right). *B*, Data from one MT neuron presented with color plaid stimuli. Responses are shown for both pattern motion (black bars) and component motion (white bars) presented in the neuron's preferred direction. When the plaid pattern was symmetric, the neuron responded better to pattern than to component motion. Conversely, when the plaid pattern was asymmetric, the neuron responded better to component motion. This influence of color information on motion integration suggests the existence of functional chromatic P pathway input to area MT (see text). (See color plate 62.)

light and inhibited by green light) is expected to respond more strongly to a red-bright/green-dark grating than to a green-bright/red-dark grating. A *green-on* P cell is expected to respond in a complementary fashion. Because P cells can distinguish the different component gratings, their input to MT has the potential to exert a modulatory influence on the integration of chromatic motion signals. Thus, in addition to the previously described evidence for an M-cell contribution to chromatic motion processing in MT, these color plaid

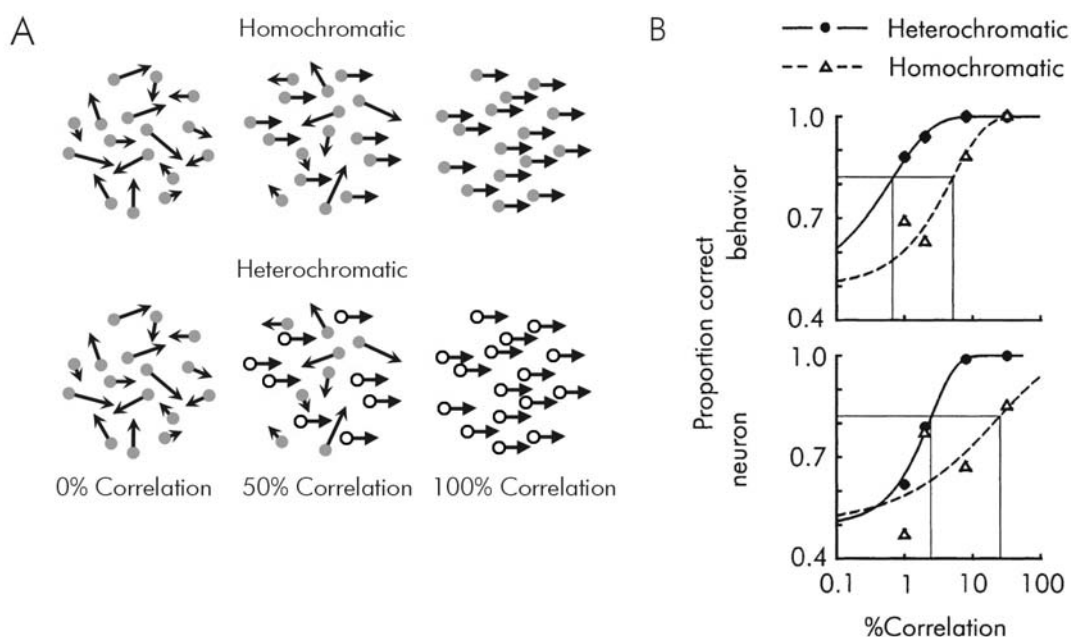


FIGURE 82.6. *A*, Homochromatic and heterochromatic stochastic motion stimuli. The stimulus consisted of a random array of small bright dots moving against a dark background. A varying proportion of the dots moved in the same direction, and thus constituted a motion signal, while the rest moved randomly and constituted motion noise. The proportion of signal dots, expressed as a percentage of the total and termed the *correlation*, is shown for three different levels of correlation: 0%, 50%, and 100%. In the homochromatic condition (*upper panel*), all of the dots had the same color. In the heterochromatic condition (*bottom panel*), the signal dots were red (open circles) while the noise dots were green (filled circles) or vice versa. *B*, Simultaneously obtained behavioral and neuronal performance functions obtained in one experiment using the

random-dot stimuli. Behavioral functions are shown at the top, and the corresponding neuronal functions obtained at the same time are shown below. Homochromatic, open triangles and dashed lines; heterochromatic, closed circles and solid lines. A large (~10-fold), statistically significant decrease in the behavioral heterochromatic threshold (thresholds: homochromatic = 5.0%, heterochromatic = 0.7%) was accompanied by a large (~10-fold), statistically significant decrease in the neuronal heterochromatic threshold (thresholds: homochromatic = 23.8%, heterochromatic = 2.4%). (Reprinted from *Neuron*, vol. 24, Croner and Albright, Seeing The Big Picture: Integration of Image Cues in the Primate Visual System, Pages 777–789, Copyright 1999 with permission from Elsevier Science.) (See color plate 63.)

experiments suggest that there also exists functional P-cell chromatic input to area MT.

In another set of experiments, Croner and Albright (1997, 1999) used a *stochastic motion stimulus* (after Newsome and Paré, 1988; Williams and Sekuler, 1984) to investigate the influence of color on motion segmentation both psychophysically and in area MT. This stimulus consisted of a random array of small bright dots moving against a dark background. A varying proportion of the dots moved in the same direction and thus constituted a motion signal, while the rest moved randomly and constituted motion noise. In the conventional configuration, all of the dots were of the same color (Fig. 82.6*A*, *upper panel*, “homochromatic”). When subjects reported the perceived direction of motion in these stimuli, their performance improved as the signal strength (the proportion of dots moving in a correlated fashion) increased (e.g., Newsome and Paré, 1988). To investigate the effects of color on motion segmentation, Croner and Albright simply made the signal and noise dots differ in color (Fig. 82.6*A*, *lower panel*, “heterochromatic”). When humans and monkeys were tested on these stimuli, their performance on the heterochromatic

stimuli was significantly better than their performance on the homochromatic stimuli (Fig. 82.6*B*; and see Croner and Albright, 1997), indicating that motion signals can be segmented—and their detection thus facilitated—on the basis of chromatic identity information.

To examine the neural basis of this effect, Croner and Albright (1999) recorded responses of MT neurons to the stimuli depicted in Figure 82.6*A* while monkeys performed a motion discrimination task. Approximately 20% of the MT neurons studied showed a significant improvement in their ability to discriminate direction when the signal and noise dots were of different colors. For many neurons (e.g., Fig. 82.6*B*), this change in neuronal discriminability closely paralleled changes in perceptual discriminability observed on the same trials. Thus, a subpopulation of MT neurons is strongly influenced by chromatic identity information, just as are observers’ perceptual judgments.

What kind of input is required to mediate this chromatic contribution to MT responses? As for the chromatic plaid studies described above, the dots in the stimuli diagrammed in Figure 82.6*A* were of high luminance contrast relative to

background. Since the responses of cells within the M pathway are not chromatically selective and because they saturate under these high-contrast conditions, it is unlikely that the relevant input comes from residual chromatic sensitivity of neurons in this pathway. Rather, chromatically selective information such as that carried by the P pathway must be involved. More specifically, Croner and Albright (1997) proposed that contextual cues for feature grouping lead to adjustments of the relative gain of the sensory signals reaching or passing through area MT. These gain adjustments, accordingly, enable motion signals bearing a common property (e.g., the color red) to be processed selectively, with minimal disruption by dynamic noise.

Concluding remarks

In conclusion, there now exists substantial evidence that all three color dimensions—luminance, red/green, and blue/yellow—influence motion processing revealed perceptually and in area MT. This color information appears to reach MT via input from the three subcortical pathways—magnocellular, parvocellular, and koniocellular, respectively. Moreover, contrary to previous views on the relationship between color and motion processing, the evidence reviewed here indicates that color augments motion processing in profound and functionally specific ways. We anticipate that future studies will address the neuronal circuitry and synaptic interactions that give rise to these functions.

Acknowledgments

We thank Greg Horwitz and Bart Krekelberg for thoughtful discussion and comments on the manuscript. T.D.A. is an Investigator of the Howard Hughes Medical Institute.

REFERENCES

- Agonig, C., and A. Gorea, 1993. Equivalent luminance contrast of red-green drifting stimuli: dependency on luminance-color interactions and on the psychophysical task, *J. Opt. Soc. Am. A*, 10:1341–1352.
- Albright, T. D., 1984. Direction and orientation selectivity of neurons in visual area MT of the macaque, *J. Neurophysiol.*, 52:1106–1130.
- Albright, T. D., 1993. Cortical processing of visual motion, in *Visual Motion and Its Use in the Stabilization of Gaze* (J. Wallman and F. A. Miles, eds.), Amsterdam: Elsevier, pp. 177–201.
- Baker, J. F., S. E. Petersen, W. T. Newsome, and J. M. Allman, 1981. Visual response properties of neurons in four extrastriate visual areas of the owl monkey (*Aotus trivirgatus*): a quantitative comparison of medial, dorsomedial, dorsolateral, and middle temporal areas, *J. Neurophysiol.*, 45:397–416.
- Boynton, R. M., R. T. Eskew, and C. X. Olson, 1985. Blue cones contribute to border distinctness, *Vis. Res.*, 25:1349–1352.
- Calkins, D. J., 2001. Seeing with S cones, *Prog. Retin. Eye Res.*, 20: 255–287.
- Calkins, D. J., Y. Tsukamoto, and P. Sterling, 1998. Microcircuitry and mosaic of a blue-yellow ganglion cell in the primate retina, *J. Neurosci.*, 18:3373–3385.
- Cavanagh, P., and S. Anstis, 1991. The contribution of color to motion in normal and color-deficient observers, *Vis. Res.*, 31:2109–2148.
- Cavanagh, P., J. Boeglin, and O. E. Favreau, 1985. Perception of motion in equiluminous kinematograms, *Perception*, 14:151–162.
- Cavanagh, P., C. W. Tyler, and O. E. Favreau, 1984. Perceived velocity of moving chromatic gratings, *J. Opt. Soc. Am. A*, 1:893–899.
- Chatterjee, S., and E. M. Callaway, 2002. S cone contributions to the magnocellular visual pathway in macaque monkey, *Neuron*, 35:1135–1146.
- Croner, L. J., and T. D. Albright, 1997. Image segmentation enhances discrimination of motion in visual noise, *Vis. Res.*, 37:1415–1427.
- Croner, L. J., and T. D. Albright, 1999. Segmentation by color influences responses of motion-sensitive neurons in the cortical middle temporal visual area, *J. Neurosci.*, 19:3935–3951.
- Cropper, S. J., and A. M. Derrington, 1994. Motion of chromatic stimuli: first-order or second-order? *Vis. Res.*, 34:49–58.
- Cropper, S. J., and A. M. Derrington, 1996. Rapid colour-specific detection of motion in human vision, *Nature*, 379:72–74.
- Cropper, S. J., K. T. Mullen, and D. R. Badcock, 1996. Motion coherence across different chromatic axes, *Vis. Res.*, 36:2475–2488.
- Dacey, D. M., 1996. Circuitry for color coding in the primate retina, *Proc. Natl. Acad. Sci. USA*, 93:582–588.
- Dacey, D. M., and B. B. Lee, 1994. The “blue-on” opponent pathway in primate retina originates from a distinct bistratified ganglion cell type, *Nature*, 367:731–735.
- De Monasterio, F. M., and P. Gouras, 1975. Functional properties of ganglion cells of the rhesus monkey retina, *J. Physiol. (Lond.)*, 251:167–195.
- De Valois, R. L., I. Abramov, and G. H. Jacobs, 1966. Analysis of response patterns of LGN cells, *J. Opt. Soc. Am.*, 56:966–977.
- De Valois, R. L., H. C. Morgan, M. C. Polson, W. R. Mead, and E. M. Hull, 1974. Psychophysical studies of monkey vision. I. Macaque luminosity and color vision tests, *Vis. Res.*, 14:53–67.
- Derrington, A. M., and G. B. Henning, 1993. Detecting and discriminating the direction of motion of luminance and colour gratings, *Vis. Res.*, 33:799–811.
- Derrington, A. M., J. Krauskopf, and P. Lennie, 1984. Chromatic mechanisms in lateral geniculate nucleus of macaque, *J. Physiol. (Lond.)*, 357:241–265.
- DeYoe, E. A., and D. C. Van Essen, 1985. Segregation of efferent connections and receptive field properties in visual area V2 of the macaque, *Nature*, 317:58–61.
- Dobkins, K. R., 2000. Moving colors in the lime light, *Neuron*, 25:15–18.
- Dobkins, K. R., and T. D. Albright, 1990. Color facilitates motion in visual area MT, *Soc. Neurosci. Abstr.*, 16:1220.
- Dobkins, K. R., and T. D. Albright, 1993. What happens if it changes color when it moves?: psychophysical experiments on the nature of chromatic input to motion detectors, *Vis. Res.*, 33:1019–1036.
- Dobkins, K. R., and T. D. Albright, 1994. What happens if it changes color when it moves?: the nature of chromatic input to macaque visual area MT, *J. Neurosci.*, 14:4854–4870.
- Dobkins, K. R., and T. D. Albright, 1998. The influence of chromatic information on visual motion processing in the primate visual system, in *High-Level Motion Processing—Computational*,

- Neurobiological and Psychophysical Perspectives* (T. Watanabe ed.), Cambridge, MA: MIT Press, pp. 53–94.
- Dobkins, K. R., G. R. Stoner, and T. D. Albright, 1992. Oculomotor responses to perceptually coherent and non-coherent plaids, *Soc. Neurosci. Abstr.*, 18:1034.
- Dobkins, K. R., G. R. Stoner, and T. D. Albright, 1998. Perceptual, oculomotor and neural responses to moving color plaids, *Perception*, 27:681–709.
- Dobkins, K. R., and D. Y. Teller, 1996. Infant motion: detection (M:D) ratios for chromatic-defined and luminance-defined moving stimuli, *Vis. Res.*, 36:3293–3310.
- Dougherty, R. F., W. A. Press, and B. A. Wandell, 1999. Perceived speed of colored stimuli, *Neuron*, 24:893–899.
- Eisner, A., and D. I. Macleod, 1980. Blue-sensitive cones do not contribute to luminance, *J. Opt. Soc. Am. A*, 70:121–123.
- Farell, B., 1995. Spatial structure and the perceived motion of objects of different colors, in *Early Vision and Beyond* (T. Papathomas, C. Chubb, A. Gorea, and E. Kowler, eds.), Cambridge, MA: MIT Press, pp. 121–131.
- Flytche, D. H., B. D. Skidmore, and S. Zeki, 1995. Motion-from-hue activates area V5 of human visual cortex, *Proc. R. Soc. Lond. B Biol. Sci.*, 260:353–358.
- Gegenfurtner, K. R., and M. J. Hawken, 1995. Temporal and chromatic properties of motion mechanisms, *Vis. Res.*, 35:1547–1563.
- Gegenfurtner, K. R., and M. J. Hawken, 1996. Interaction of motion and color in the visual pathways, *Trends Neurosci.*, 19:394–401.
- Gegenfurtner, K. R., D. C. Kiper, J. M. Beusmans, M. Carandini, Q. Zaidi, and J. A. Movshon, 1994. Chromatic properties of neurons in macaque MT, *Vis. Neurosci.*, 11:455–466.
- Golomb, B., R. A. Andersen, K. Nakayama, D. I. MacLeod, and A. Wong, 1985. Visual thresholds for shearing motion in monkey and man, *Vis. Res.*, 25:813–820.
- Gorea, A., J. Lorenceau, J. D. Bagot, and T. V. Papathomas, 1992. Sensitivity to colour- and to orientation-carried motion respectively improves and deteriorates under equiluminant background conditions, *Spatial Vis.*, 6:285–302.
- Gorea, A., and T. V. Papathomas, 1989. Motion processing by chromatic and achromatic visual pathways, *J. Opt. Soc. Am. A*, 6:590–602.
- Gouras, P., and H. Eggers, 1983. Responses of primate retinal ganglion cells to moving spectral contrast, *Vis. Res.*, 23:1175–1182.
- Gouras, P., and E. Zrenner, 1979. Enhancement of luminance flicker by color-opponent mechanisms, *Science*, 205:587–589.
- Gouras, P., and E. Zrenner, 1981. Color coding in primate retina, *Vis. Res.*, 21:1591–1598.
- Green, M., 1989. Color correspondence in apparent motion, *Percept. Psychophys.*, 45:15–20.
- Hawken, M. J., K. R. Gegenfurtner, and C. Tang, 1994. Contrast dependence of colour and luminance motion mechanisms in human vision, *Nature*, 367:268–270.
- Hendry, S. H. C., and R. C. Reid, 2000. The koniocellular pathway in primate vision, *Annu. Rev. Neurosci.*, 23:127–153.
- Herr, S., K. Klug, P. Sterling, and S. Schein, 2003. Inner S-cone bipolar cells provide all of the central elements for S cones in macaque retina. *J. Comp. Neurol.* (in press).
- Hubel, D. H., and M. S. Livingstone, 1990. Color and contrast sensitivity in the lateral geniculate body and primary visual cortex of the macaque monkey, *J. Neurosci.*, 10:2223–2237.
- Kaiser, P. K., B. B. Lee, P. R. Martin, and A. Valberg, 1990. The physiological basis of the minimally distinct border demonstrated in the ganglion cells of the macaque retina, *J. Physiol. (Lond.)*, 422:153–183.
- Kaplan, E., B. B. Lee, and R. M. Shapley, 1990. New views of primate retinal function, in *Progress in Retinal Research* (N. N. Osborne and G. J. Chader, eds.), New York: Pergamon Press, pp. 273–336.
- Kaplan, E., and R. M. Shapley, 1986. The primate retina contains two types of ganglion cells, with high and low contrast sensitivity, *Proc. Natl. Acad. Sci. USA*, 83:2755–2757.
- Klug, K., Y. Tsukamoto, P. Sterling, and S. J. Schein, 1993. Blue cones OFF-midget ganglion cells in macaque, *Invest. Ophthalmol. Vis. Sci. Suppl.*, 34:986.
- Kooi, F. L., and K. K. De Valois, 1992. The role of color in the motion system, *Vis. Res.*, 32:657–668.
- Kooi, F. L., K. K. De Valois, E. Switkes, and D. H. Grosf, 1992. Higher-order factors influencing the perception of sliding and coherence of a plaid, *Perception*, 21:583–598.
- Krauskopf, J., and B. Farell, 1990. Influence of colour on the perception of coherent motion, *Nature*, 348:328–331.
- Krauskopf, J., H. J. Wu, and B. Farell, 1996. Coherence, cardinal directions and higher-order mechanisms, *Vis. Res.*, 36:1235–1245.
- Kruger, J. K., 1979. Responses to wavelength contrast in the afferent visual systems of the cat and the rhesus monkey, *Vis. Res.*, 19:1351–1358.
- Lee, B. B., P. R. Martin, and A. Valberg, 1988. The physiological basis of heterochromatic flicker photometry demonstrated in the ganglion cells of the macaque retina, *J. Physiol. (Lond.)*, 404:323–347.
- Lee, B. B., P. R. Martin, and A. Valberg, 1989a. Amplitude and phase of responses of macaque retinal ganglion cells to flickering stimuli, *J. Physiol. (Lond.)*, 414:245–263.
- Lee, B. B., P. R. Martin, and A. Valberg, 1989b. Nonlinear summation of M- and L-cone inputs to phasic retinal ganglion cells of the macaque, *J. Neurosci.*, 9:1433–1442.
- Lee, B. B., P. R. Martin, and A. Valberg, 1989c. Sensitivity of macaque retinal ganglion cells to chromatic and luminance flicker, *J. Physiol. (Lond.)*, 414:223–243.
- Lee, J., and C. F. D. Stromeyer, 1989. Contribution of human short-wave cones to luminance and motion detection, *J. Physiol. (Lond.)*, 413:563–593.
- Lindsey, D. T., and D. Y. Teller, 1990. Motion at isoluminance: discrimination/detection ratios for moving isoluminant gratings, *Vis. Res.*, 30:1751–1761.
- Livingstone, M. S., and D. H. Hubel, 1987. Connections between layer 4B of area 17 and the thick cytochrome oxidase stripes of area 18 in the squirrel monkey, *J. Neurosci.*, 7:3371–3377.
- Logothetis, N. K., P. H. Schiller, E. R. Charles, and A. C. Hurlbert, 1990. Perceptual deficits and the activity of the color-opponent and broad-band pathways at isoluminance, *Science*, 247:214–217.
- Lund, J. S., R. D. Lund, A. E. Hendrickson, A. H. Bunt, and A. F. Fuchs, 1975. The origin of efferent pathways from the primary visual cortex, area 17, of the macaque monkey as shown by retrograde transport of horseradish peroxidase, *J. Comp. Neurol.*, 164:287–303.
- Maunsell, J. H., T. A. Nealey, and D. D. DePriest, 1990. Magnocellular and parvocellular contributions to responses in the middle temporal visual area (MT) of the macaque monkey, *J. Neurosci.*, 10:3323–3334.
- Maunsell, J. H., and D. C. Van Essen, 1983a. The connections of the middle temporal visual area (MT) and their relationship to a cortical hierarchy in the macaque monkey, *J. Neurosci.*, 3:2563–2586.

- Maunsell, J. H., and D. C. Van Essen, 1983b. Functional properties of neurons in middle temporal visual area of the macaque monkey. I. Selectivity for stimulus direction, speed, and orientation, *J. Neurophysiol.*, 49:1127–1147.
- Merigan, W. H., and J. H. Maunsell, 1993. How parallel are the primate visual pathways? *Annu. Rev. Neurosci.*, 16:369–402.
- Metha, A. B., A. J. Vingrys, and D. R. Badcock, 1994. Detection and discrimination of moving stimuli: the effects of color, luminance, and eccentricity, *J. Opt. Soc. Am. A*, 11:1697–1709.
- Moreland, J. D., 1982. Spectral sensitivity measured by motion photometry, *Doc. Ophthalmol. Proc. Ser.*, 33:61–66.
- Morgan, M. J., and R. Cleary, 1992. Effects of colour substitutions upon motion detection in spatially random patterns, *Vis. Res.*, 32:815–821.
- Morgan, M. J., and G. Ingle, 1994. What direction of motion do we see if luminance but not colour contrast is reversed during displacement? Psychophysical evidence for a signed-colour input to motion detection, *Vis. Res.*, 34:2527–2535.
- Mullen, K. T., and J. C. Boulton, 1992. Absence of smooth motion perception in color vision, *Vis. Res.*, 32:483–488.
- Nakayama, K., 1985. Biological image motion processing: a review, *Vis. Res.*, 25:625–660.
- Newsome, W. T., K. H. Britten, and J. A. Movshon, 1989. Neuronal correlates of a perceptual decision, *Nature*, 341:52–54.
- Newsome, W. T., and E. B. Paré, 1988. A selective impairment of motion perception following lesions of the middle temporal visual area (MT), *J. Neurosci.*, 8:2201–2211.
- Palmer, J., L. A. Mobley, and D. Y. Teller, 1993. Motion at isoluminance: discrimination/detection ratios and the summation of luminance and chromatic signals, *J. Opt. Soc. Am. A*, 10:1353–1362.
- Papathomas, T. V., A. Gorea, and B. Julesz, 1991. Two carriers for motion perception: color and luminance, *Vis. Res.*, 31:1883–1892.
- Ramachandran, V. S., and R. L. Gregory, 1978. Does colour provide an input to human motion perception? *Nature*, 275:55–56.
- Reid, R. C., and R. M. Shapley, 1992. Spatial structure of cone inputs to receptive fields in primate lateral geniculate nucleus, *Nature*, 356:716–718.
- Saito, H., K. Tanaka, H. Isono, M. Yasuda, and A. Mikami, 1989. Directionally selective response of cells in the middle temporal area (MT) of the macaque monkey to the movement of equiluminous opponent color stimuli, *Exp. Brain Res.*, 75:1–14.
- Sawatari, A., and E. M. Callaway, 1996. Convergence of magnocellular and parvocellular pathways in layer 4B of macaque primary visual cortex, *Nature*, 380:442–446.
- Schiller, P. H., and C. L. Colby, 1983. The responses of single cells in the lateral geniculate nucleus of the rhesus monkey to color and luminance contrast, *Vis. Res.*, 23:1631–1641.
- Seidemann, E., A. B. Poirson, B. A. Wandell, and W. T. Newsome, 1999. Color signals in area MT of the macaque monkey, *Neuron*, 24:911–917.
- Shapley, R., and E. Kaplan, 1989. Responses of magnocellular LGN neurons and M retinal ganglion cells to drifting heterochromatic gratings, *Invest. Ophthalmol. Vis. Sci.*, 30:323.
- Shinomori, K., L. Spillmann, and J. S. Werner, 1999. S-cone signals to temporal OFF-channels: asymmetrical connections to postreceptoral chromatic mechanisms, *Vis. Res.*, 39:39–49.
- Shipp, S., and S. Zeki, 1985. Segregation of pathways leading from area V2 to areas V4 and V5 of macaque monkey visual cortex, *Nature*, 315:322–325.
- Simpson, W. A., 1990. The use of different features by the matching process in short-range motion, *Vis. Res.*, 30:1421–1428.
- Stockman, A., D. I. MacLeod, and D. D. DePriest, 1991. The temporal properties of the human short-wave photoreceptors and their associated pathways, *Vis. Res.*, 31:189–208.
- Teller, D. Y., T. E. Brooks, and J. Palmer, 1997. Infant color vision: moving tritan stimuli do not elicit directionally appropriate eye movements in 2- and 4-month-olds, *Vis. Res.*, 37:899–911.
- Teller, D. Y., and J. Palmer, 1996. Infant color vision: motion nulls for red/green vs luminance-modulated stimuli in infants and adults, *Vis. Res.*, 36:955–974.
- Thiele, A., A. A. Rezac, and K. R. Dobkins, 2002. Chromatic input to motion processing in the absence of attention, *Vis. Res.*, 42:1359–1401.
- Thiele, A., K. R. Dobkins, and T. D. Albright, 1999. The contribution of color to motion processing in MT, *J. Neurosci.*, 19:6571–6587.
- Thiele, A., K. R. Dobkins, and T. D. Albright, 2001. Neural correlates of chromatic motion processing, *Neuron*, 32:1–20.
- Tootell, R. B., J. B. Reppas, K. K. Kwong, R. Malach, R. T. Born, T. J. Brady, B. R. Rosen, and J. W. Belliveau, 1995. Functional analysis of human MT and related visual cortical areas using magnetic resonance imaging, *J. Neurosci.*, 15:3215–3230.
- Troscianko, T., 1987. Perception of random-dot symmetry and apparent movement at and near isoluminance, *Vis. Res.*, 27:547–554.
- Ullman, S., 1980. The effect of similarity between line segments on the correspondence strength in apparent motion, *Perception*, 9:617–626.
- Valberg, A., B. B. Lee, P. K. Kaiser, and J. Kremers, 1992. Responses of macaque ganglion cells to movement of chromatic borders, *J. Physiol. (Lond.)*, 458:579–602.
- Van Essen, D. C., J. H. Maunsell, and J. L. Bixby, 1981. The middle temporal visual area in the macaque: myeloarchitecture, connections, functional properties and topographic organization, *J. Comp. Neurol.*, 199:293–326.
- Wandell, B. A., A. B. Poirson, W. T. Newsome, H. A. Baseler, G. M. Boynton, A. Huk, S. Gandhi, and L. T. Sharpe, 1999. Color signals in human motion-selective cortex, *Neuron*, 24:901–909.
- Wiesel, T. N., and D. H. Hubel, 1966. Spatial and chromatic interactions in the lateral geniculate body of the rhesus monkey, *J. Neurophysiol.*, 29:1115–1156.
- Williams, D. W., and R. Sekuler, 1984. Coherent global motion percepts from stochastic local motions, *Vis. Res.*, 24:55–62.
- Zeki, S. M., 1974. Functional organization of a visual area in the posterior bank of the superior temporal sulcus of the rhesus monkey, *J. Physiol. (Lond.)*, 236:549–573.

83 Functional Mapping of Motion Regions

GUY A. ORBAN AND WIM VANDUFFEL

MUCH OF WHAT WE know about motion processing comes from the many elegant single-cell studies in the nonhuman primate. This progress is reviewed in other chapters. Functional brain imaging, initially limited to positron emission tomography (PET), now includes functional magnetic resonance imaging (fMRI) as a neuroscientific tool for the study of motion regions. These mapping techniques have the advantage of being noninvasive and therefore are applicable to humans. They also provide a much wider-scale view of the system: one studies functional regions in the whole brain rather than recording single neurons in a given brain region.

Therefore, it is not surprising that during the past 15 years, with the advent of PET (Fox et al., 1986) and especially with fMRI (Belliveau et al., 1991; Kwong et al., 1992), there has been considerable progress in the understanding of the human visual system, particularly its motion processing component. Since functional imaging records the global activity of large groups of neurons indirectly, via a vascular response, the interpretation of these human measurements would have been impossible without the background of single-cell results. Progress was hampered by the fact that the two techniques were applied to different species, since it is generally not feasible to record single cells in humans and fMRI had not been performed in monkey. This situation has changed recently with the introduction of controlled fMRI experiments in the monkey (Logothetis et al., 1999) and especially in the awake monkey (Nakahara et al., 2002; Vanduffel et al., 2001). Indeed, the two species can now be compared using the same technique, paving the way for resolving long-standing debates concerning homologies. Furthermore, within the same species, single-cell recordings and fMRI can now be compared (Logothetis et al., 2001), providing insight into the origin of the fMRI signal. Additional comparisons with other physiological techniques such as optical imaging or double-label deoxyglucose have also become possible.

Two main paradigms have been used in human functional imaging, following the strategies established by single-cell studies. In one the subject is passive, fixating a point on the display, and activity evoked by different stimuli presented in the background is compared (Lueck et al., 1989). This provides information about the preattentive processing of motion information, an important initial stage. We might not be here reading this chapter without this capability, as we would probably not have survived previous unexpected

traffic situations. In the second paradigm, the subject is active and has his or her attention drawn to the moving stimuli, usually by being instructed to perform some task with them (Corbetta et al., 1991).

Since the cortex can process only motion occurring on the retina, eye movements will interfere with the interpretation of responses to moving stimuli. In initial imaging studies no eye movements were measured, but these measurements, either electro-oculographic recordings (Dupont et al., 1994) or infrared-based measurements (Tootell et al., 1997), were gradually introduced and are now standard.

The human motion complex of occipitotemporal cortex

Because of a lack of sensitivity in PET studies, or because of the use of surface coils in fMRI that restrict the part of the brain explored, the initial imaging studies concentrated on a motion-sensitive region, located in the temporo-parieto-occipital junction. Zeki et al. (1991) compared the brain activity when subjects passively viewed a random-dot pattern that was stationary to one that was moving in one of eight possible directions. One extrastriate region in the temporo-parieto-occipital cortex stood out by being significantly more active for moving than for stationary stimuli. Zeki et al. (1991) proposed that this region was the human homolog of monkey MT/V5. It should be noted that this result, like those of most imaging studies, was obtained by statistical analysis: the human motion complex of occipitotemporal cortex (hMT/V5) appeared as a set of voxels in which the difference in activity between motion and control was statistically significant.

This has two implications. First, much depends on the control condition, and here Zeki et al. (1991) introduced the static pattern as a control condition. This allows one to dissociate the effect of the stimulus pattern (which is removed) from its movement (which remains). However, by comparing just two closely matched conditions, one can conclude only that there is a relative difference in activity. By adding a further, lower-order condition, an empty fixation condition, as introduced by Tootell et al. (1995b) (see below), one can ascertain whether motion and stationary conditions differ in activation from some baseline level. One can then infer that the neuronal population, the activity of which is reflected by the MR signals, increases its activity above spontaneous activity, that is, shows an excitatory response.

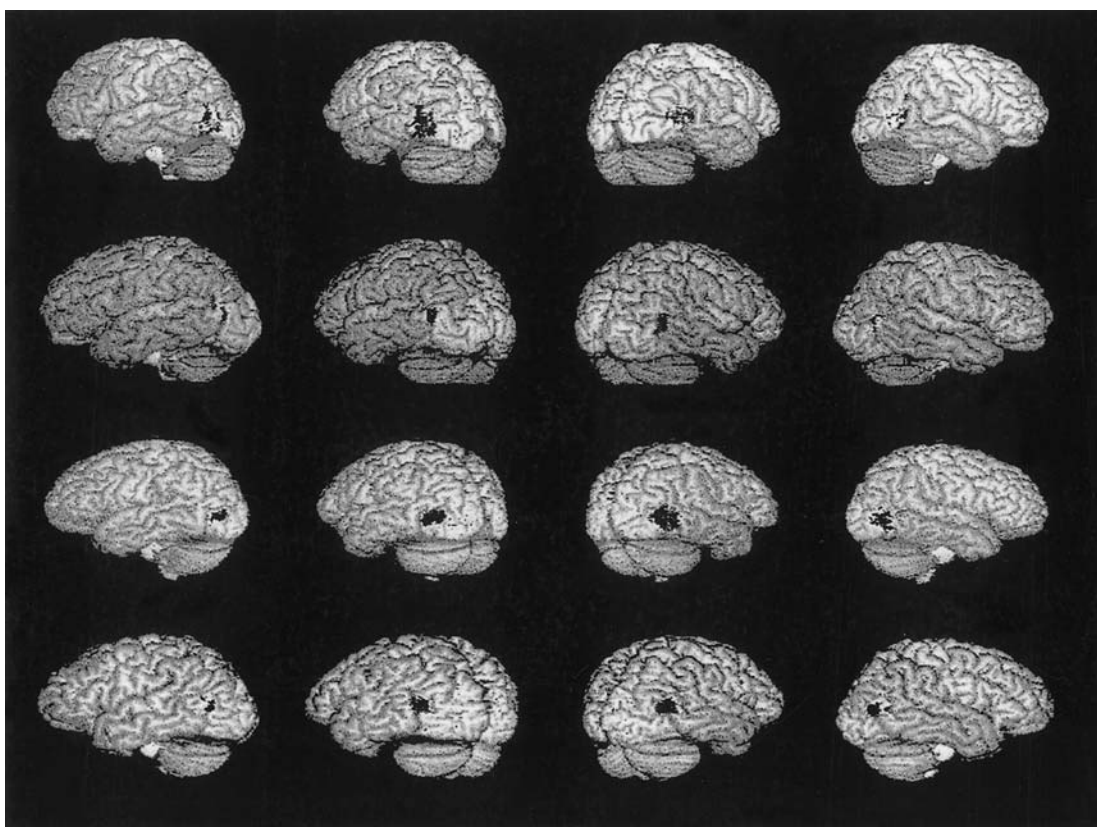


FIGURE 83.1. The cerebral hemispheres from four subjects, showing the hMT/V5+ of each as defined by PET activation experiments, superimposed on the individual's own MRI (rendered brain). Each subject occupies a row: the two hemispheres are shown as viewed at rotations of 50 and 90 degrees from the occipital pole. The Statistical Parametric Map (SPM) image is edited to leave only hMT/V5+. (From Watson et al., 1993.) (See color plate 64.)

Monkey fMRI has confirmed that this assertion indeed is valid for hMT/V5+ (see below). One does not know, however, to what extent this increased neuronal activity of the hMT/V5+ population reflects activity of inhibitory or excitatory neurons. The situation is analogous for single-cell studies, although some firing pattern criteria have been proposed to recognize inhibitory interneurons. Second, the statistical decision depends on the threshold chosen and the volume of search. The accepted standard is $p < .05$, but this can be applied to a region of interest (ROI) or to the whole brain. The ROI approach is the most sensitive, but it depends on the preliminary localizer scan to include all relevant voxels. Searching over the whole brain, on the other hand, requires correction for multiple comparisons and can be applied to a single subject or to a group of subjects. For a group analysis, one can use either a fixed-effect analysis (as in the Zeki et al., 1991, study), which allows one to draw conclusions only about the subjects tested, or a random effects analysis (Holmes and Friston, 1998), which allows inferences to be made about the general population.

In a subsequent study from the same laboratory (Watson et al., 1993) using a more sensitive camera, hMT/V5 was

studied in single subjects as well as across the group. This allowed the investigators to demonstrate the variability of its anatomical localization in the different subjects, at least when using a fixed reference such as the Talairach coordinates (Fig. 83.1). The authors noted that hMT/V5+ was closely associated with the ascending branch of the inferior temporal sulcus (ITS), a finding which has been amply confirmed by subsequent studies (Dumoulin et al., 2000; Tootell et al., 1995b). They noted that this region corresponds to a cortical field that is heavily myelinated from birth. A third PET study from our group provided the first independent confirmation of these observations with control of eye movements (Dupont et al., 1994).

The final identification of hMT/V5 was provided by Tootell et al. (1995b) using the greater spatial (5 to 10 mm rather than 15 to 20 mm in PET) and temporal resolution of fMRI. This technique not only has better resolution, but also allows a more complete functional investigation of a cortical region. Many tests can be performed on the same subject, because no radioactive tracer has to be injected. Tootell et al. provided evidence that hMT/V5 was not only motion sensitive, more so than V1 (Fig. 83.2), but also that

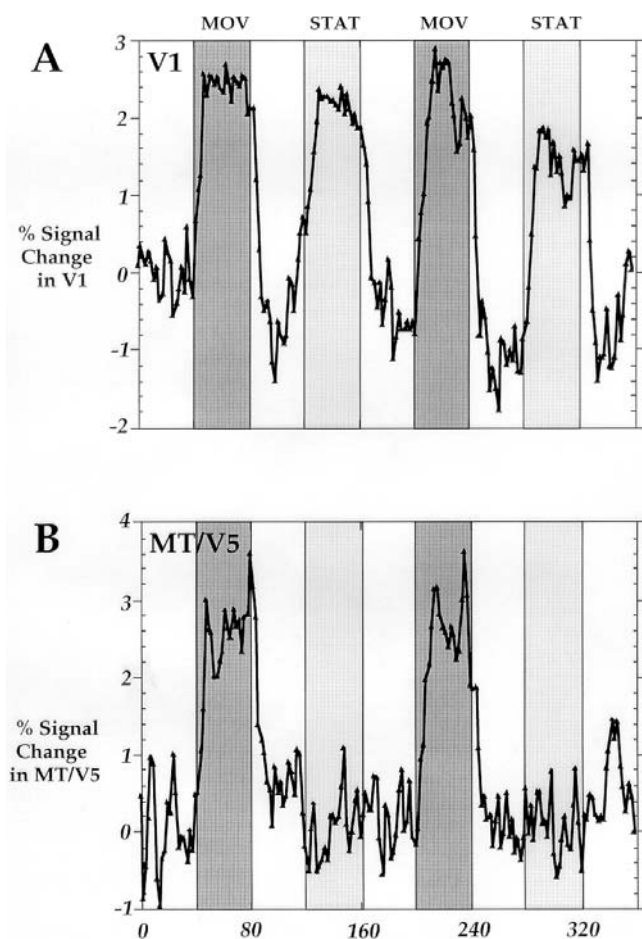


FIGURE 83.2. Time courses of the MRI signal amplitude from V1 (A) and hMT/V5+ (B) of the same subject, sampled every 2 seconds during a 6-minute scan (average of two presentations). (From Tootell et al., 1995b.)

it displayed three properties observed in monkey MT/V5: it was very sensitive to luminance contrast, it responded only weakly to equiluminant moving color stimuli, and it responded to ipsilateral stimulation. Because of the many functional similarities to monkey MT/V5, because of its localization with respect to retinotopic regions (Fig. 83.3), and owing to its distinct histological properties (Tootell and Taylor, 1995; see also Watson et al., 1993), this human cortical region was accepted as a distinct human cortical area. Work in the monkey has led to the consensus that several criteria need to be met for a region of cortex to be considered a separate area: retinotopic organization, connectivity, architectonics, and functional properties. Given the difficulty of obtaining detailed histological data in humans (but see Zilles et al., 1995), few visual cortical regions have achieved the status of distinct areas. hMT/V5, together with early regions V1, V2, V3, and V3A, is generally accepted as a separate cortical area.

However, even the identification of the motion-sensitive region in the ITS as the human homolog of MT/V5 may be premature. Monkey MT/V5 is joined by several satellites (Fig. 83.3) which are themselves selective for motion (Desimone and Ungerleider, 1986; for review see Orban, 1997). Thus, the human motion-sensitive region in the ITS may well correspond to the entire complex, including MT/V5 and its satellites, as suggested by DeYoe et al. (1996). This view has become generally accepted, and the region is referred to as hMT/V5+. Several authors have attempted to subdivide the complex using known properties of MST neurons: large ipsilateral overlap (Desimone and Ungerleider, 1986; Raiguel et al., 1997), responsiveness to optic flow patterns (Duffy and Wurtz, 1991; Lagae et al., 1994; Saito et al., 1986), and response during pursuit (Komatsu and Wurtz, 1988). hMT/V5+ responds to ipsilateral stimulation (Brandt et al., 2000; Ffytche et al., 2000; Tootell et al., 1998; Tootell et al., 1995b). Morrone et al. (2000) suggested that the parts of the hMT/V5+ complex that respond to translation and optic flow components are distinct entities. The part responsive to optic flow, presumed to be the homolog of MSTd, is located more ventrally and appears only when the flow stimuli are changing in time. This localization is in agreement with the results of an earlier passive study of optic flow by de Jong et al. (1994) and with these of a study from our group (Peuskens et al., 2001a) investigating the neural correlates of heading judgments based on optical flow. Both studies observed activity in a ventral satellite of hMT/V5+ related to expansion/contraction. On the other hand, Dukelow et al. (2001), using ipsilateral overlap and pursuit in the dark, reached a different conclusion: according to these authors, MSTd and MSTl are located anterior to MT/V5 proper in the human complex. This contradiction illustrates the difficulty of relating human imaging to monkey single-cell properties.

The recent study of Vanduffel et al. (2001) in the awake monkey makes this even more clear. Up to now, the hMT/V5 complex was believed to include homologs of the subregions of MST, in addition to MT/V5. Yet, when using the translating random-dot pattern typically used in human studies (Sunaert et al., 1999) in monkeys, Vanduffel et al. (2001) observed motion sensitivity in MT/V5, of course, as well as in MSTv and in FST, but not in MSTd (Figs. 83.3, 83.4). The advent of monkey fMRI has made it possible to identify the satellites in the human complex properly. One should scan the human complex at high resolution and test stimuli that differentiate the various parts of the motion complex in monkey fMRI. The aggregation of several functional regions into a single-motion complex may also explain some of the variability in its localization (Watson et al., 1993). As expected from single-cell studies, monkey MT/V5 was activated (above baseline) by both stationary and moving

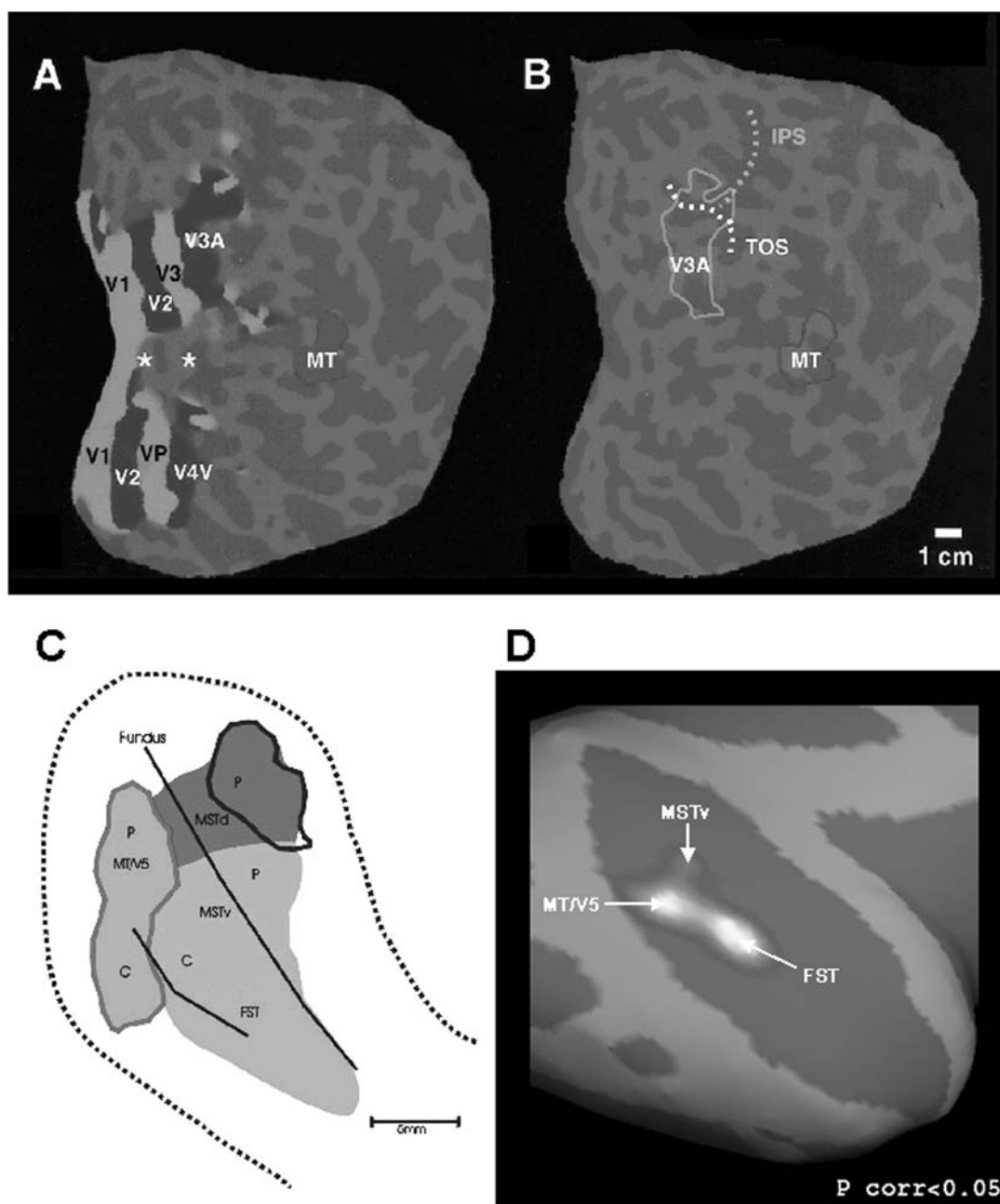


FIGURE 83.3. Location of hMT/V5+ with respect to the early retinotopic regions (*A*) and to the motion response of hV3A (*B*) on a flattened cortical surface from a single hemisphere. TOS, transverse occipital sulcus; IPS, intraparietal sulcus. *C*, *D*, Location of MT/V5 and satellites: schematic location of MT/V5, MSTv, MSTd, and FST in STS (modified from Orban, 1997) and actual

activation of MT/V5, MSTv, and FST by moving random dots in monkey M4 (Vanduffel et al., unpublished). In panel *C*, P and C indicate peripheral and central visual field representation; scale bar = 5 mm. In panel *D*, stimuli were restricted to the central 7 degrees of the visual field, corresponding to the central representations in panel *C*. (*A* and *B* from Tootell et al., 1997.) (See color plate 65.)

stimuli, but more so by motion. This activation translates into MR signals of opposite polarity in the standard BOLD (blood oxygen level dependent) fMRI and in contrast-enhanced fMRI, using MION (monocrystalline iron oxide nanoparticle) as the contrast agent (Fig. 83.4).

One should note that the definition of hMT/V5+ in humans reflects a difference in the activity level of the

hMT/V5+ population for the two types of stimuli. This is very different from the criterion used in single-cell studies, where regions are considered to be motion selective when they have large proportions of direction-selective cells. Even in monkey fMRI, which shows that the statistical definition of a motion-sensitive region indeed applies to MT/V5, this definition does not reflect the direction selectivity of the

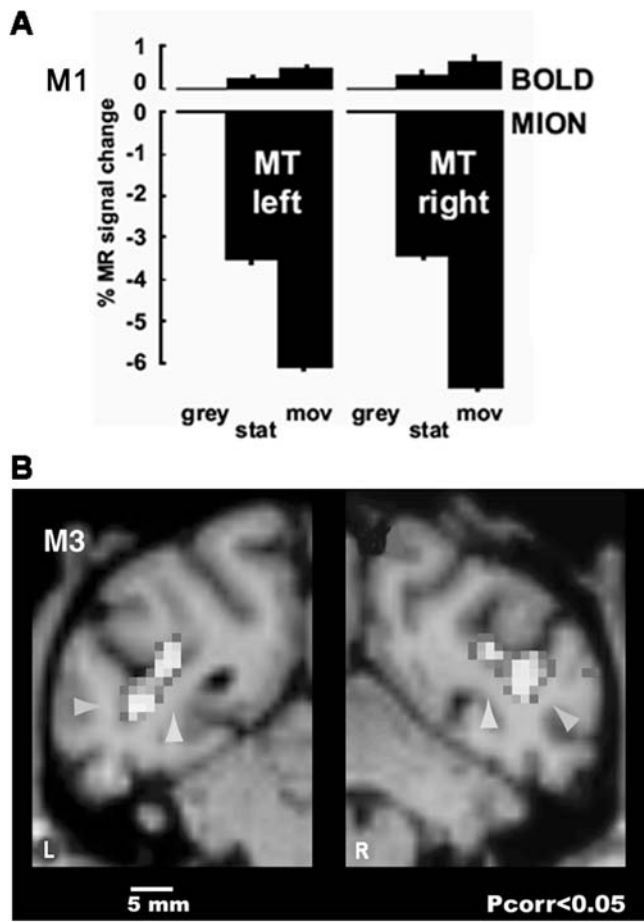


FIGURE 83.4. *A*, Comparison of BOLD and MION MR signals. Percent signal change in left and right MT/V5 (monkey M1) with respect to the no-stimulus (gray) condition for the three stimulus conditions: no stimulus, stationary, and moving random dots. Average of multiple time series with different order of conditions. Vertical lines indicate the standard error of the mean. Notice reversal of the MR signal sign in MION. *B*, SPMs of the two hemispheres of M3 on the coronal section through caudal superior temporal sulcus (STS) for the comparison of moving versus stationary dots. Voxel size $2 \times 2 \times 2$ mm. Lateral arrows, MT/V5; medial arrows, floor of STS; MSTv. (From Vanduffel et al., 2001.) (See color plate 66.)

underlying neuronal population. In fact, it probably reflects the speed tuning of the population. Because of the small eye movements that occur during fixation, even a stationary stimulus produces extremely slow speeds on the retina (on the order of 0.1 to 0.2 deg/sec) (Stavenski et al., 1975), and most MT/V5 neurons are much less sensitive to these slow speeds than to the 4 to 6 deg/sec speed used in the motion condition of the fMRI studies (Cheng et al., 1994; Churchland and Lisberger, 2001; Lagae et al., 1993; Mikami et al., 1986). This view has received support from the study of Chawla et al. (1999a), who reported that motion MR responses over hMT/V5+ and hV3A displayed an inverted U shape when speed was manipulated in the 1 to 32 deg/sec

range. Single-cell studies (Lagae et al., 1993; Orban et al., 1986) have suggested that speed tuning and direction selectivity tend to co-occur in neuronal populations. This may explain why Vanduffel et al. (2001) did observe a correlation, albeit a weak one, between motion sensitivity in the fMRI and the proportion of direction-selective neurons in the single-cell studies. Attempts have been made to use motion opponency as a direct indication of direction selectivity (Heeger et al., 1999), but this reflects the mutual inhibition between neurons tuned to opposite directions rather than direction selectivity as such. An alternative is to use unidirectional adaptation, as done by Tolias et al. (2001) in the anesthetized monkey. Because the reversal of direction after adaptation was not compared directly and statistically to the control event (phase shift in the same direction), this study remained inconclusive. Furthermore, Pack et al. (2001) have recently shown that responses of MT/V5 neurons to moving plaids are dependent on anesthesia.

Other motion-sensitive regions

Although hMT/V5+ is the most sensitive motion-responsive region, being active in both hemispheres of all subjects tested so far (over 100), many other regions are also responsive to motion.

PRIMARY VISUAL CORTX In the initial studies of Zeki et al. (1991) and Watson et al. (1993), primary visual cortex exhibited motion selectivity. Unilateral activation of V1 was also reported by Dupont et al. (1994). On the other hand, Tootell et al. (1995b) reported no difference in V1 MR responses between static and radially moving dots. Dupont et al. (1997), Goebel et al. (1998), and Dieterich et al. (1998) reported at least unilateral activation of V1. Sunaert et al. (1999) observed significant motion activation in V1 of half of the hemispheres studied. V1 activation in the monkey is also inconsistent (Vanduffel et al., 2001; Fig. 83.5), but this simply means that the activation of V1 by moving and stationary stimuli is not significantly different. The reason for the weakness of V1 activation may be the speed sensitivity of central V1 neurons more than the reduced proportion of direction-selective neurons (Hawken et al., 1988; Orban et al., 1986). Most neurons in the central representation of V1 are low pass for speed (Orban et al., 1986). In the anesthetized, paralyzed preparation, they respond well to very slow stimuli, corresponding to stationary stimuli in the awake subject, and this response decreases once speeds reach 3 to 10 deg/sec. Thus, for many of the V1 neurons in an awake subject, the stimulus moving at 4 to 6 deg/sec may be as effective as a stationary one. This explanation receives support from the interaction between size and motion sensitivity observed by Sunaert et al. (1999) in V1. Only the 14 degree wide stimuli produced consistent motion activation

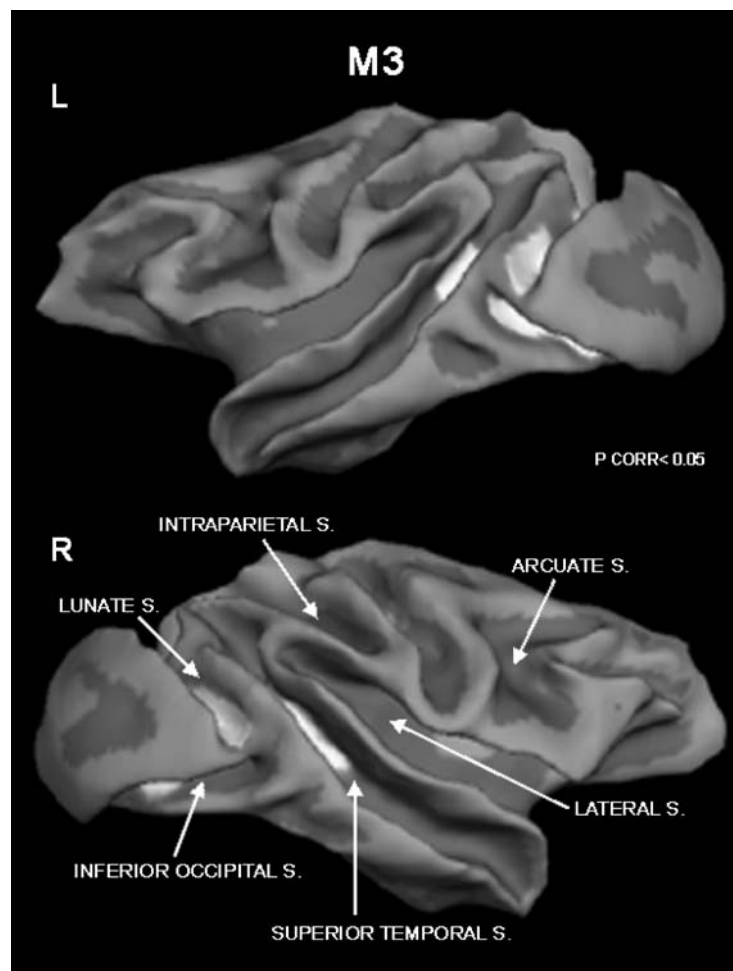


FIGURE 83.5. SPMs for moving versus stationary dots displayed on the partially unfolded hemispheres of monkey M3. The main sulci are indicated. (Adapted from Vanduffel et al., 2001.) (See color plate 67.)

in V1. More peripheral V1 neurons are less sensitive to slow speeds (Orban et al., 1986), being thus less active during fixation of static stimuli.

V3A Motion sensitivity in a part of the cuneus was noted by Watson et al. (1993) and Dupont et al. (1994). Watson et al. had suggested that this activation may correspond to V3, which in the monkey contains a fair proportion of direction-selective neurons (Gegenfurtner et al., 1997), but Tootell et al. (1995b) demonstrated that retinotopically defined V3 in humans exhibits little motion sensitivity. The cuneal motion-sensitive region was shown by Tootell et al. (1997) to correspond to retinotopically defined V3A and to be located near the transverse occipital sulcus (Fig. 83.2). This activation has since been observed by a number of authors (Ahlfors et al., 1999; Braddick et al., 2001; Chawla et al., 1999a; Cornette et al., 1998a; Goebel et al., 1998; Rees et al., 2000; Sunaert et al., 1999), although only Goebel et al. (1998) explicitly mapped the retinotopic regions. This suggests that there is a species difference here between

humans and monkeys. This was confirmed by the fMRI study of Vanduffel et al. (2001), who reported that monkey V3A displays no motion sensitivity.

PARIETAL CORTEX The initial studies of Watson et al. (1993), Dupont et al. (1994), and Tootell et al. (1995b) had noted a medial posterior parietal activation by moving compared to stationary stimuli. These parietal motion-sensitive regions were described in detail by Sunaert et al. (1999) using the resolution of fMRI applied to the whole brain. They described two regions in the occipital part of the intraparietal sulcus (IPS): one more ventral (VIPS) and one more dorsal at the junction with the parieto-occipital (PO) sulcus (POIPS). Similar regions were observed by Shulman et al. (1999) and by Goebel et al. (1998). More dorsally along the parietal part of the IPS (Fig. 83.6), Sunaert et al. (1999) distinguished an anterior region (DIPSA), also observed by Dupont et al. (1997) and Braddick et al. (2001), and a pair of more posterior regions that were difficult to distinguish from one another (DIPSM/L). This latter motion activation

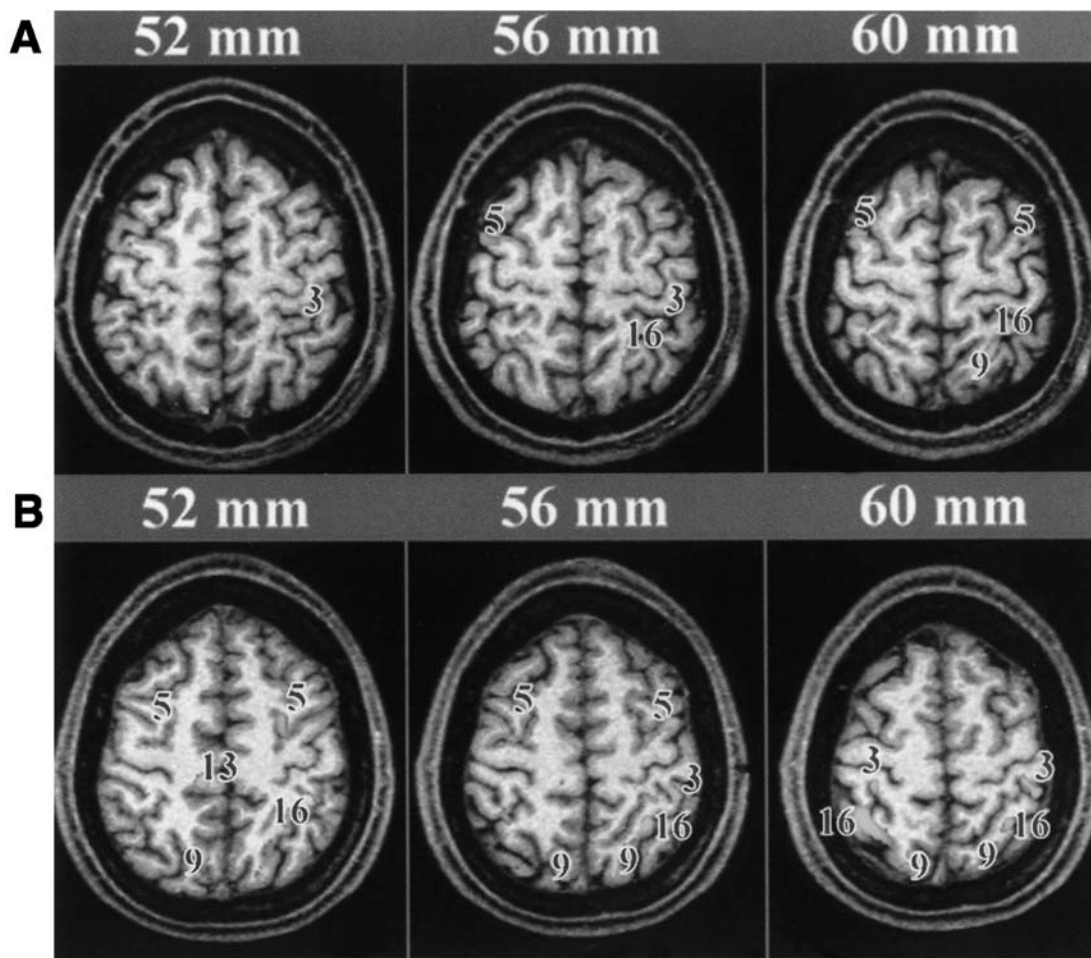


FIGURE 83.6. SPMs of two human subjects (*A* and *B*) corresponding to contrast motion minus stationary status superimposed on selected transversal sections. 3, DIPSA; 5, FEF; 9, DIPSM; 16, DIPSL; 13, cingulate motion-sensitive region. (See color plate 68.)

was observed by Dieterich et al. (1998). Strong activation of most of these parietal regions was observed in an attentive tracking task compared to a bouncing-ball control condition by Culham et al. (1998). They identified more or less segregated activation in regions roughly corresponding to VIPs, DIPSM/L, and DIPSA as described by Sunaert et al. (1999). The last region may correspond to what Bremmer et al. (2001) identified as the homolog of monkey VIP. Bremmer et al. used the multimodality of monkey VIP to trace the homologous region in humans. However, any multimodal region may correspond to the site identified by Bremmer et al., particularly since no specific motion contrast was used in the tactile and auditory modalities. Cross-modal activation in a visuoauditory speed discrimination task was observed more posteriorly by Lewis et al. (2000) in a region that seems to correspond to DIPSM/L. The same region was also engaged by a purely visual speed discrimination, as was a region close to VIPS.

In contrast to the rather extensive motion activation of IPS in humans, only one motion-sensitive region, probably

corresponding to VIP, was observed in the monkey fMRI by Vanduffel et al. (2001). This may suggest that the parietal cortex of humans and monkeys exhibits differences in motion sensitivity perhaps related to that noted for V3A.

In addition to the lateral parietal regions, there are indications that very large moving stimuli activate the PO cortex, possibly the homolog of monkey V6 (Cheng et al., 1995; Previc et al., 2000). The PO cortex is also responsive to motion reversals when their visibility is modulated (Cornette et al., 1998b).

VENTRAL CORTEX Watson et al. (1993) and Dupont et al. (1997), using PET, observed a motion-sensitive region in lingual cortex. This was confirmed in later fMRI studies by Sunaert et al. (1999), Rees et al. (2000), and Braddick et al. (2001). In keeping with Watson et al.'s early suggestion, Vanduffel et al. (2001) observed motion activation in ventral V2 and/or VP (Fig. 83.5). Occasionally, motion-related responses have been reported in fusiform cortex (Dupont et al., 1994; Rees et al., 2000).

Finally, motion responses have also been reported (Rees et al., 2000; Sunaert et al., 1999) in the cortex located behind hMT/V5+, which has been referred to as the *kinetic occipital* (KO) region (see below).

OTHER REGIONS Motion sensitivity of the frontal eye fields (FEF) has been reported in humans (Culham et al., 1998; Orban et al., 1999; Sunaert et al., 1999; Fig. 83.6) as well as in the monkey (Vanduffel et al., 2001; Fig. 83.5). FEF receives strong projections from MT/V5 and its satellites (Schall et al., 1995), and FEF in humans has been shown to be activated during visual pursuit (Petit and Haxby, 1999; Petit et al., 1997). Motion sensitivity has also been observed in the lateral sulcus at the retroinsular level (Braddick et al., 2001; Dupont et al., 1994; Sunaert et al., 1999). Sunaert et al. (1999) have suggested that this region is the homolog of the visual region bordering parietoinsular vestibular cortex (Grüsser et al., 1990). Vanduffel et al. (2001) observed motion sensitivity in this region in one of the their two animals (Fig. 83.5).

Finally, in humans, motion sensitivity has been reported in the superior temporal sulcus (STS) (Ahlfors et al., 1999; Braddick et al., 2001; Sunaert et al., 1999) in a region responding to facial movements (Puce et al., 1998) as well as in cingulate cortex (Braddick et al., 2001; Cornette et al., 1998a; Sunaert et al., 1999; Fig. 83.6).

Types of moving stimuli and stimulus parameters

STIMULUS PATTERNS A variety of stimulus patterns have been used to investigate motion sensitivity: Zeki et al. (1991) and most studies from the London group used translating random-dot patterns, as did Cornette et al. (1998a). We (Dupont et al., 1994, 1997; Sunaert et al., 1999; Van Oostende et al., 1997) have used translating random-textured patterns with small dots and 50% density, also used by Braddick et al. (2001). Tootell et al. (1997) and Tootell et al. (1995b) have used radially moving dots (i.e., alternating contraction and expansion), as did Goebel et al. (1998) and de Jong et al. (1994) (only expansion). Tootell et al. (1995b) also utilized moving gratings, as did Dupont et al. (1997, 2000). There has been no systematic study comparing motion responses for these different patterns.

Similarly, stimuli of various sizes have been used, often dictated by the MRI setting. Most groups have used stimuli about 30 degrees in diameter (Goebel et al., 1998; Tootell et al., 1995b; Zeki et al., 1991). We have routinely used smaller stimuli, the standard being 7 degrees for humans (Sunaert et al., 1999) and 14 degrees for monkeys (Vanduffel et al., 2001). However within the 3 to 14 degree range, diameter had little effect on motion sensitivity except in V1 (see above). Very large stimuli (80 to 100 degrees in diameter) were used by Cheng et al. (1995) and Previc et al. (2000).

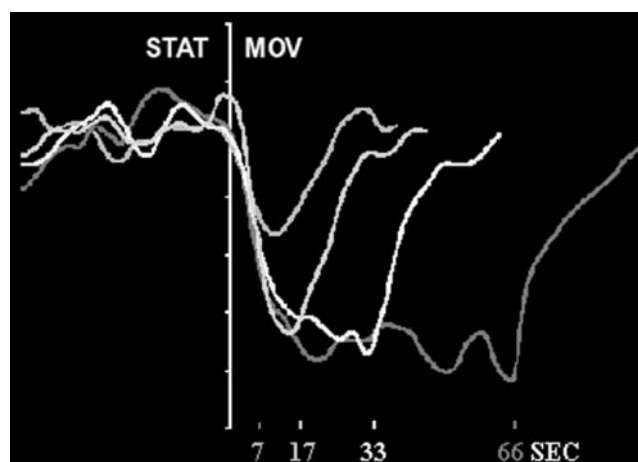


FIGURE 83.7. Time course of the MION MR signal from MT/V5 of a monkey subject for different durations of the motion epochs (indicated by color). (From Vanduffel et al., unpublished.) (See color plate 69.)

Previc et al. suggested that motion stimuli occupying a wide field of view are processed in the medial occipital pathways extending up to the PO sulcus, while smaller motion stimuli (less than 50 degrees in diameter) engage only lateral occipital pathways including hV3A and hMT/V5+.

STIMULUS PARAMETERS Other stimulus parameters have hardly been explored, except with regard to speed and contrast, as mentioned before. Cornette et al. (1998b) noted that reducing the number of motion axes from four, as used by Zeki et al. (1991) and our group, to one reduced the hMT/V5+ activation by 25%. A possible explanation of this decrease is adaptation by the use of a single axis (Tolias et al., 2001).

We tested the effect of epoch duration on MT/V5 activation in the monkey (Fig. 83.7). Epochs shorter than 15 seconds produced smaller activation in contrast agent-enhanced fMRI (using MION). We know that MT/V5 neurons respond to motion presentations as short as 10 msec (Orban, 1997). Hence the limitation on epoch duration arises at the vascular transduction stage of the fMRI, that is, within the changes in cerebral blood circulation occurring as a consequence of neuronal activity increase and which constitute the signal captured by the fMRI. In MION-enhanced fMRI, these changes are essentially changes in cerebral blood volume (Leite et al., 2002).

INCOHERENT MOTION AND DYNAMIC NOISE While incoherently moving dots (dots moving in random directions but at the same speed) activate hMT/V5+ more than coherently moving dots (all dots moving at the same speed and in the same direction) in passive subjects (McKeefry et al., 1997; see also Previc et al., 2000), the opposite has been reported under conditions of opposed motion discrimination (Rees

et al., 2000). The MR motion response over hMT/V5+ increased linearly with coherence in the latter study, mimicking, according to Rees et al., the behavior of MT/V5 neurons (Britten et al., 1992). Similar increases were noted over KO and hV3A.

In a dynamic noise stimulus or flicker, obtained by showing the motion frames in random order, both direction and speed are random, while incoherently moving dots still have the same speed and exhibit only random directions. Tootell et al. (1995b) reported that hMT/V5+ responds to flicker, albeit less than to moving dots. This was elaborated by Sunaert et al. (1999), who observed that while V1 responded very well to flicker (in fact, better than to motion), hV3A and especially hMT/V5+ responded less to flicker than to motion (Fig. 83.8), a finding in agreement with McCarthy et al. (1995) and Braddick et al. (2001). The difference in flicker versus motion response in V1 and hMT/V5+ closely matches the parallel observation by Heeger et al. (1999) that motion opponency occurs in hMT/V5+ but not in V1. Sunaert et al. (1999) observed that the flicker responses were abolished only at the level of parietal cortex (see also Orban et al., 1999). Braddick et al. (2001) confirmed that parietal cortex is significantly more activated by motion than by flicker, as are STS and lateral sulcus motion regions.

Preliminary results indicate that the same holds true in the monkey (Fig. 83.8). The decrease in flicker response over hMT/V5+ compared to V1 matches the properties of MT/V5 neurons which are less responsive to flicker than are their, direction-selective V1 counterparts (Qian and Andersen, 1994). This has been attributed to the increased mutual inhibition between neurons tuned to opposite directions (Heeger et al., 1999; Qian and Andersen, 1994). Thus, flicker suggests a distinction between lower-order motion regions such as hMT/V5+, hV3A, and lingual cortex and higher-order ones such as intraparietal sulcus, STS, lateral sulcus, and FEF.

NONLUMINANCE-DEFINED STIMULI Both random-dot patterns and gratings are luminance-defined stimuli, whose motion can be detected by a modified Fourier mechanism or energy detector. According to a number of psychophysical studies (Cavanagh, 1992; Chubb and Sperling, 1988), other stimuli can be detected only by higher-order mechanisms, although it is unclear how many higher-order mechanisms operate in the human visual system. Smith et al. (1998) have argued that second-order motion activates V3 and VP more than first-order motion, while both types of motion produce equal activation in hMT/V5+. It is difficult to derive any conclusion from this study, as the only comparisons made were between higher-order motion and either first-order motion or higher-order stationary stimuli. Subsequent studies, reported only in abstract form, have failed

to find any anatomical segregation between first-order and higher-order motion mechanisms (Dumoulin et al., 2001; Dupont et al., 2000; Somers et al., 1999). In the same vein, attentive tracking, in which subjects mentally follow one of many moving stimuli, and which has been presented as a higher-order motion mechanism (Cavanagh, 1992), activates many of the same regions as those ascribed to moving random dots or gratings (Culham et al., 1998; see above).

A related question is the extent to which the motion-responsive regions are activated by motion when that motion is defined by other attributes such as color. Tootell et al. (1995b) have shown that at equiluminance, moving gratings evoked little response over hMT/V5+, far less than luminance gratings. Ffytche et al. (1995) reported that no motion-from-hue responses (luminance motion signals were removed by a flicker masking strategy) could be observed, except over V1/V2 and over hMT/V5+ (only on the right side). In particular, no response was seen over V4 (the color region in the terminology of that group). Not only do motion signals arising from L and M cones reach hMT/V5+, but signals from S cones also do so in humans (Wandell et al., 1999) as well as in monkey (Seidemann et al., 1999). In the same vein, Seghier et al. (2000) reported that moving illusory contours induced by coherent rotation of pacman figures, compared to incoherent rotation that did not, evoked the percept of a moving Kanisza square, activated V1/V2, hMT/V5+, and the KO/LOS (lateral occipital sulcus) region. It was unclear whether these activations reflected the perception of the illusory contour or its motion. The view that seems to emerge is that all moving stimuli are processed in a single-motion processing pathway (but see Pinney and DeYoe, 2001, for stereo-defined motion and Previc et al., 2000, above), which may diverge farther up and reach multiple end stations (e.g., in STS, parietal cortex, and ventral cortex).

Perception of motion and hMT/V5+ activity

Initially, it was believed that there should be a close link between hMT/V5+ activity and the perception of motion, although the responsiveness to flicker noted by Tootell et al. (1995b) was an early indication of the oversimplification of this view.

The prolonged activity of hMT/V5+ during the motion aftereffect (waterfall illusion) and the similarity in time course of the two effects suggested a link between perception and hMT/V5+ activity, although Tootell et al. (1995a) cautioned that the aftereffect may also depend on areas upstream from hMT/V5+. The link was further stressed by the observation that the hMT/V5+ activity rebounded after adaptation only when a stimulus was visible, just like the perceptual effect (Culham et al., 1999), or when the stationary stimulus eliciting the aftereffect was in exactly the same

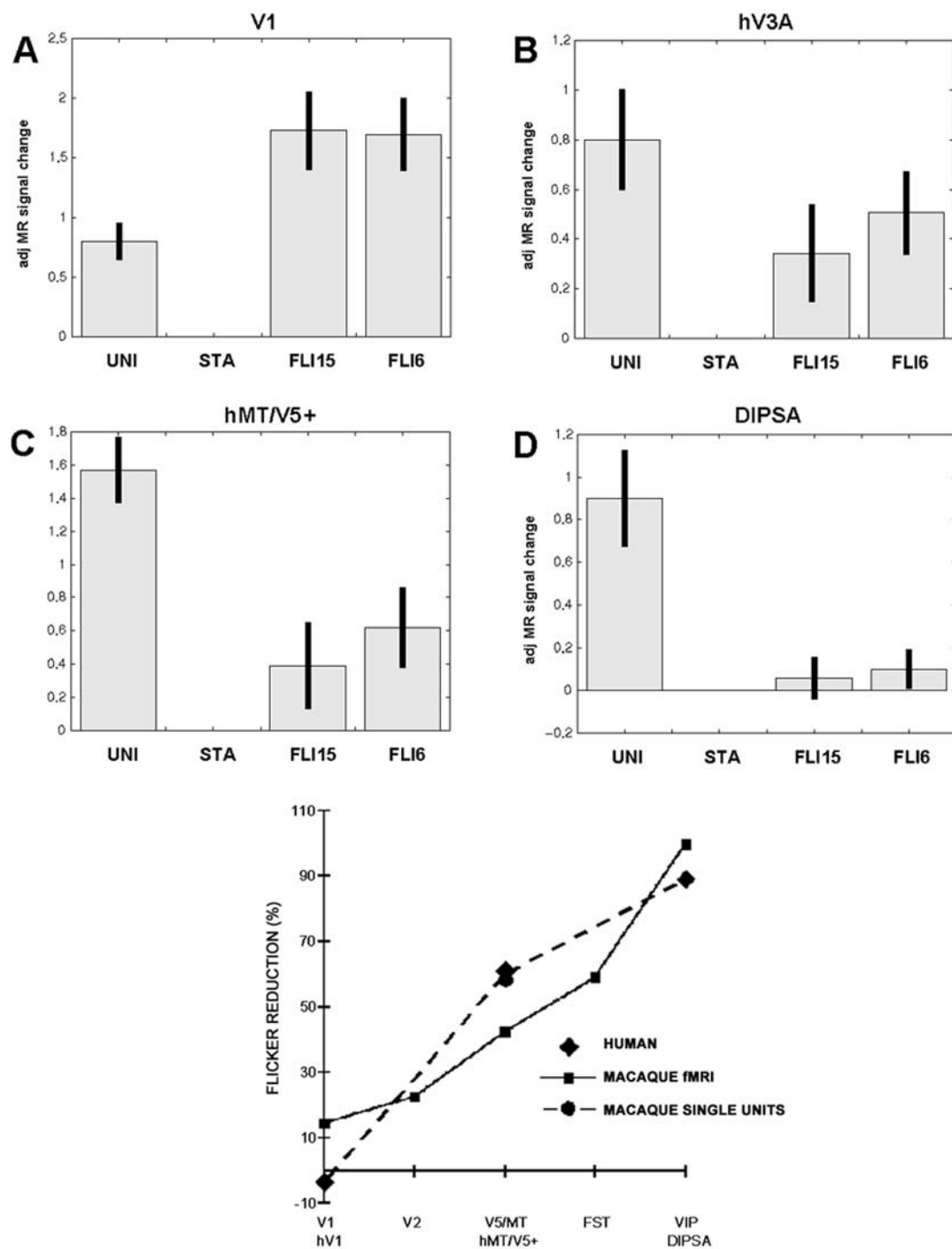


FIGURE 83.8. *A–D*, Activity profiles plotting adjusted MR signal change with respect to the stationary dots conditions for four conditions: moving (UNI), stationary (STA), and flickering at 15 and 6 Hz (FLI15 and FLI6) dots in four cortical regions (local maximum). Average of three human subjects. *E*, Flicker reduction (UNI-

FLI6/STA) plotted as a function of cortical area in human fMRI (Sunaert et al. 1999, but V1 sampled over same retinotopic parts as monkey data), monkey fMRI (bold) and for monkey single cells (Qian and Andersen, 1994). (*A–D*, from Sunaert et al., 1999; *E* from Vanduffel et al., unpublished.)

position as the adaptation stimulus (He et al., 1998). Huk et al. (2001) have recently challenged these studies (see also Hautzel et al., 2001; Taylor et al., 2000) and have noted that they were performed without attentional control. When Huk et al. controlled attention, the difference in activity evoked by a stationary stimulus after unidirectional or bidirectional adaptation vanished. The authors went on to show that directional adaptation occurs in hMT/V5+ by comparing responses to motion in the same or different directions to responses to the direction of adaptation while still controlling attention with a speed discrimination task. They observed large direction-selective adaptation in hMT/V5+ and in hV3A but not in early retinotopic areas (V1, V2, and V3).

Using a different stimulus, Enigma, in which many subjects see illusory motion, Zeki et al. (1995) tried to establish a relationship between hMT/V5+ activity and perception of motion even where no physical motion was present. The authors observed activity in or near hMT/V5+ during illusory motion control compared to a static control (obtained by a slight modification of the Enigma). The fact that the activity was slightly more inferior and anterior was interpreted as reflecting an origin in one of the satellites of MT/V5, perhaps MSTd. The authors also stress that only hMT/V5+ was active in the human brain during the illusory perception, but this may have simply reflected the ineffectiveness of the stimulus. It is difficult if not impossible to derive any conclusion from negative results in imaging.

Similar reasoning underlies the experiment by Kourtzi and Kanwisher (2000) showing that static images which imply motion, such as a picture of a diver, activate hMT/V5+ more than static images which do not imply motion. In two independent experiments, images of people as well as of animals and scenes were used, indicating the generality of the result. This small effect (a 2% increase compared to a 1.5% increase from the fixation baseline) was significant because only hMT/V5+, identified by a localizer scan, was tested, so that no correction for multiple comparisons was required. The technique of using the localizer is vulnerable to omissions, and Kourtzi and Kanwisher indicated that the effect extended to regions surrounding hMT/V5+. Senior et al. (2000), using similar stimuli, reported maximum activation in a region located behind hMT/V5+. Using somewhat different static stimuli portraying gestures, Peigneux et al. (2000) reported activation of the middle temporal gyrus extending from the STS region to hMT/V5+.

Thus, it seems that there is no simple relationship between hMT/V5+ activity and perception of motion. On the one hand, it is now well documented that hMT/V5+ can be active when no motion is perceived, such as during equiluminance and during flicker. On the other hand, conditions in which no motion is perceived can evoke the same level of

activity as those in which motion is perceived, such as after uni- and bidirectional adaptation, once attention is controlled. Finally, stimuli implying motion may have a wider representation than MT/V5+ itself. This does not mean that hMT/V5+ activity is not important for the perception of motion: perception may arise from differences in activity between subpopulations of MT/V5 neurons or from activity in areas upstream to hMT/V5+. Finally, it must be noted that MT/V5 has been implicated in functions other than motion perception, such as control of eye visual pursuit (Churchland and Lisberger, 2001; Lagae et al., 1993; Newsome et al., 1985), stereopsis (DeAngelis et al., 1998), and extraction of three-dimensional structure from motion (Xiao et al., 1997), and that activity over hMT/V5+ has been observed in dimming detection tasks (Claeys et al., 2001), which may relate to the flicker sensitivity and the high contrast sensitivity documented for hMT/V5+. Thus, the view that is emerging is that MT/V5, rather than being a unique "motion center," acts in concert with different sets of other regions to fulfill a wider variety of behavioral functions than motion perception alone.

Attention to motion

GLOBAL ATTENTION The effect of attention to motion in general was assessed by O'Craven et al. (1997). The clearest experiment was their second, in which subjects were asked to pay attention to the back dots, which were either moving among white stationary dots, stationary among white moving dots, or stationary without white dots. This attention manipulation allowed these investigators to disentangle the effect of motion, as such (and the effect of dot density) from the attention to motion, which amounted to about 30% of the sensory motion response. One should note, however, that since the subjects did not perform any task, we do not know how well they allocated their attention to the dots intended. Büchel et al. (1998) used a different strategy: they trained subjects to track increasingly small, brief changes in the speed of a continuously moving stimulus. During the scanning there were no actual changes, but the subjects still reported seeing some, and the attention effect was demonstrated behaviorally on the motion after-effect. The attention condition compared to the no-attention condition showed increased activity in hMT/V5+ (or slightly ventral to it) and hV3A, but also in V1/V2, an activation not observed by O'Craven et al. (1997). One should note, however, that the attention of the subject was drawn to the change in speed, not to motion in general. Büchel et al. also reported attention effects in parietal cortex in loci close to DIPSM/L and DIPSA (see above) and in FEF. O'Craven et al. could not observe these changes because of the limitations of a surface coil. Chawla et al. (1999b) compared attention-to-motion to attention-to-color in an event-related

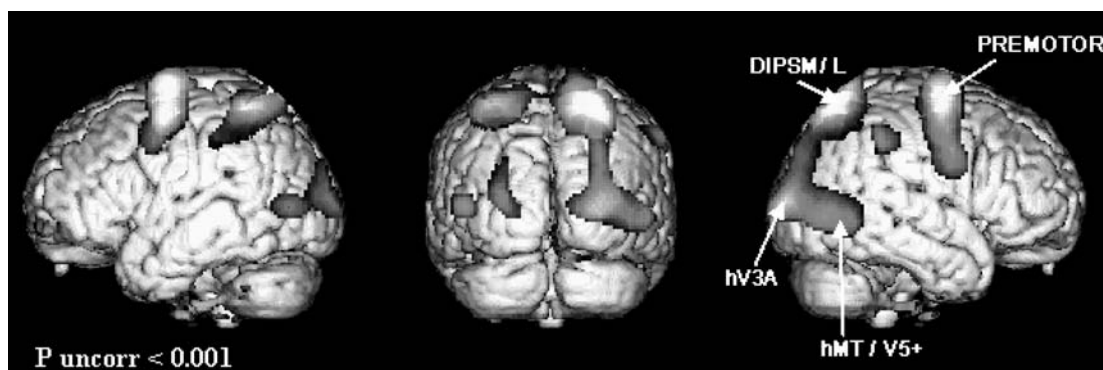


FIGURE 83.9. SPM for contrasting discrimination of the opposite direction of a moving grating to dimming detection. Average of nine human subjects (PET). The four main activations sites are indicated. (From Dupont et al., unpublished.) (See color plate 70.)

design and observed an increase in the hMT/V5+ response during attention-to-motion.

The converse effect, the drawing away of attention from motion, has been observed by Rees et al. (1997). The authors showed that attention to central visual stimulus substantially reduced the motion activity of hMT/V5. Rees et al. presented words in the center of the display and asked subjects to detect bisyllabic words compared to a low-load condition in which they detected uppercase words. We made similar observations in a control experiment for our initial monkey fMRI experiments, in which fixation was controlled by requiring the monkey to detect orientation changes of a very small, light bar. We measured the effect of a 32% reduction in the hMT/V5+ motion activation as the result of attention to this central bar (Sunaert et al., unpublished). Rees et al. (2001) subsequently showed that a similar task requiring attention to auditorily presented words had little effect on motion activation in hMT/V5+, hV3A, and KO.

ATTENTION TO DIRECTION OF MOTION Rather than asking subjects to attend to a moving versus stationary stimulus, one can draw the subjects' attention to a given aspect of motion, thus manipulating featural attention. This is usually done with a task requiring the subject to judge some aspect of motion (e.g., speed or direction). The manipulation of featural attention (Corbetta et al., 1991) should not be confused with task manipulation, in which the feature remains constant but the task performed with the attribute varies (Dupont et al., 1993; Fias et al., 2002; Orban et al., 1997). As O'Craven et al. (1997) noted, the use of a discrimination task does not allow for a pure attention manipulation, since either featural attention or decision factors can explain the differences in activation between the discrimination task and the control task. However, a conjunction analysis might provide that distinction (Peuskens et al., 2001a).

Figure 83.9 shows one of the most simple discrimination tasks, that of opposed motion discrimination, which has

been studied extensively in single-cell studies by Newsome and coworkers (Britten et al., 1992, Newsome and Paré, 1988). Compared to a dimming detection control task, discrimination of opposite directions of motion activates hMT/V5+ and hV3A but also parietal and premotor cortex. The parietal activation, and a fortiori the premotor one, may well reflect decision-related processes, according to single-cell studies (Shadlen and Newsome, 1996). In contrast, the activation of hMT/V5+ and hV3A most likely reflects featural attention. While the discrimination of opposite directions of motion does activate hMT/V5+, fine discriminations of direction, compared to the same dimming control task, fails to activate this area (Cornette et al., 1998a) but activates hV3A and parietal cortex. It is worth noting that the computations involved in these two tasks are very different. In the case of opposite direction of motion, direction-selective cells tuned to those directions are required (Britten et al., 1992). For fine discrimination, it may well be that the slope of the direction-tuning curve is important if one extrapolates from orientation discrimination (Schoups et al., 2001). For these fine discriminations, directional (tuned to a single direction) and nondirectional (tuned to opposite directions) cells then become equally useful.

Still related to direction processing is the heading task, in which the spatial distribution of directions contains the information about the direction of self-motion. This task, again with reference to the same dimming control task, activates hMT/V5+, as well as parietal and premotor cortex, but not hV3A (Peuskens et al., 2001a). Here the single-cell studies (Duffy and Wurtz, 1991; Lagae et al., 1994; Saito et al., 1986) have shown that neurons selective to expansion occur in MSTd, the homolog of which is included in the hMT/V5+ complex. Finally, expectations about the direction of motion elicited by a stationary cue (arrow) activate hMT/V5+ and also parietal motion-sensitive regions along the IPS (VIPS, DIPSM/L, and DIPSA; Shulman et al., 1999).

ATTENTION TO SPEED The aspect of motion which has received most attention is speed of motion. In their seminal study, Corbetta et al. (1991) compared same-different judgments of speed to a divided attention condition. They observed a strong activation over what is now known as hV3A, but also a weaker one over hMT/V5+. In a subsequent study, Beauchamp et al. (1997) compared hMT/V5+ activation by an identical stimulus, an annulus of coherently moving dots, under two attention conditions. Subjects either compared speeds in the two halves of the annulus or compared the colors in these halves, resulting in a 35% reduction of hMT/V5+ activity when attention was drawn away from the speed. Huk and Heeger (2000) again reported a 10% increase in activation of hMT/V5+, but not of V1 or hV3A, when comparing a speed discrimination to a contrast discrimination. In contrast, we (Orban et al., 1998; Sunaert et al., 2000b) observed an activation of hV3A (and V3) but not of hMT/V5+ when speed identification and a successive speed discrimination task were compared to a dimming control task. This result does not depend on the psychophysical performance level (Sunaert et al., 2000b). It remains unclear which of the small differences in stimulus and task explain the differences between these studies. It should be noted that in our last study (Sunaert et al., 2000b), we also observed a very small increase (5%) in the activity of hMT/V5+ in speed discrimination versus dimming detection. The frequently quoted observation that speed discrimination is impaired in monkeys after lesioning that includes MT/V5 (Orban et al., 1995b) simply indicates that MT/V5 is critical to speed discrimination, not that its activity level needs to be influenced by attention to speed. Finally, it is worthwhile to mention another peculiarity of speed discriminations. While all discriminations involving direction of motion engage parietal regions, this is not the case for speed discriminations (Sunaert et al., 2000a; but see Lewis et al., 2000).

Other behavioral functions of motion-sensitive regions

CONTROL OF MOVEMENTS Up to now, we have concentrated on the use of motion processing to judge motion in the outside world. Motion processing, however, has a much wider role (Nakayama, 1985). One additional function is the control of eye movements. It has been shown that optokinetic nystagmus, elicited by a rotating drum compared to fixating a stationary drum, activates hMT/V5+ but also V1 and FEF (Dieterich et al., 1998). Similarly, activation of hMT/V5+ has been observed during pursuit eye movements (Barton et al., 1996; O'Driscoll et al., 1998). In both cases, the effects of visual stimulation and of eye movements were difficult to distinguish. Finally, it has been shown that the FEF contains two subregions, the more lateral and inferior

of which is activated by pursuit rather than by saccades (Petit and Haxby, 1999; Petit et al., 1997).

It has been noted that hMT/V5+ is active when subjects view hand movements (Decety et al., 1994), even when this is compared to random motion (Bonda et al., 1996). Clearly, the role of motion regions in the control of eye and body movements needs more work, but the immobilization of the subject in the scanner, required for quality imaging, renders those studies more difficult.

KINETIC BOUNDARIES Motion processing can also be used to extract shape information from motion displays, both a two-dimensional (2D) (flat) shape that is extracted from the discontinuities in the velocity distribution and a three-dimensional (3D) shape derived from the speed gradients. Differences in motion direction produce the percept of kinetic boundaries, which are perceptually as sharp as luminance-defined boundaries. In comparing orientation discrimination using kinetic gratings rather than luminance-defined gratings, we (Orban et al., 1995a) observed an activation in a region posterior to hMT/V5+ rather than in hMT/V5+ itself. Subsequent studies (Dupont et al., 1997; Van Oostende et al., 1997) with passive subjects viewing kinetic gratings compared to luminance gratings, uniform motion (coherently translating dots), and transparent motion confirmed that this region, which we now refer to as the *kinetic occipital* (KO) region, is specifically involved in the processing of kinetic contours. It is located close to the lateral occipital sulcus, between hMT/V5+ anteriorly and hV3A and V3 posteriorly (Fig. 83.104). In this region, activation can be obtained by comparing scenes and objects to uniform textures (Malach et al., 1995), but this "lateral occipital" activation extends well beyond the KO region. Subsequent studies (Grill-Spector et al., 1998) have shown that LO is indeed activated by both luminance- and motion-defined objects. Using larger stimuli with radial kinetic contours, Reppas et al. (1997) failed to observe hMT/V5+ activation, as was the case in most of the subjects in our studies, but they did observe activation in early retinotopic regions rather than in KO. The activation of cortex representing the peripheral field observed by Reppas et al. may have been due to the fixed position of boundaries which, when compared to uniform motion, may induce differences in activity in neurons with surrounds (Jones et al., 2001). Failure to observe any activation over KO may have been due to the lack of resolvable contours in the center of the display, since KO responded to small kinetic gratings in our studies. A later study from the same laboratory using our stimuli did indeed observe KO activation along with hMT/V5+ activation (Tootell and Hadjikhani, 2001). It is worth noting that in all these studies the kinetic boundaries were stationary. This is very different from another type of

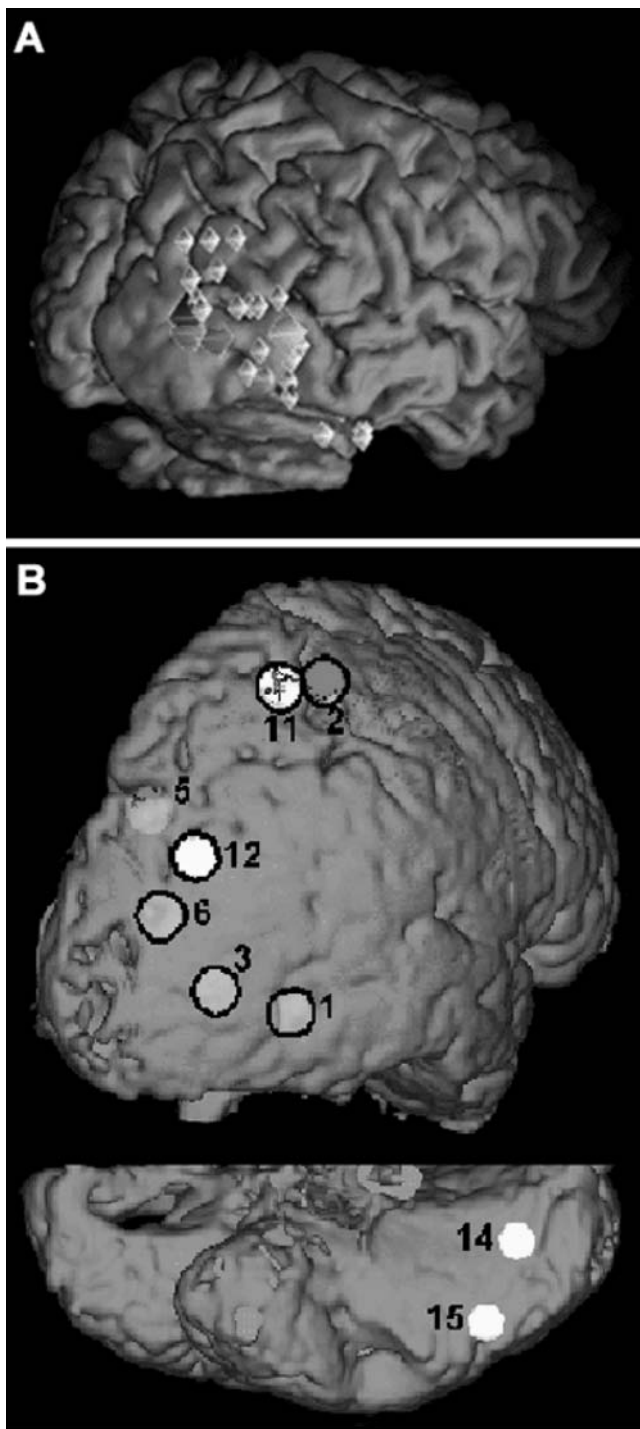


FIGURE 83.10. *A*, Location of the KO (red diamond) region compared to hMT/V5+ (green), V3A (blue), V3 dorsal (orange), and LO (yellow) diamonds. *B*, Nodes of the 3D from motion processing network on rendered brain; red, nodes from group and single-subject analysis; yellow, single-subject analysis; black circles, bilateral nodes; 1, hMT/V5+; 2, DIPSA; 3, lateral occipital sulcus; 5, POIPS; 6, TRIPS (junction transverse occipital and intraparietal sulci); 11, DIPSL; 12, VIPS; 14, lingual node; 15, fusiform node. (*A* from Van Oostende et al., 1997; *B* from Orban et al., 1999.) (See color plate 71.)

form-from-motion where the whole envelop (contour) moves. This has been shown to activate hMT/V5+ (Wang et al., 1999).

THREE-DIMENSIONAL STRUCTURE FROM MOTION Relatively little work has been done on the extraction of 3D shape from motion. Comparing 3D dynamic displays, in which 3D objects (random lines) are perceived, to 2D dynamic displays, in which flat objects are perceived, we (Orban et al., 1999) observed activation, across rigid and nonrigid conditions, of hMT/V5+, a lateral occipital region, and a series of regions along the IPS, as well as, in at least half of the subjects, lingual and fusiform cortex. Control experiments revealed that this activation was due neither to the differences in lower- and higher-order motion characteristics as such nor to attention. The activation of hMT/V5+ is in agreement with single-cell studies showing that MT neurons are selective for the direction of speed gradients, which correspond to the direction of tilt in depth (Xiao et al., 1997; see also Bradley et al., 1998). Using a different stimulus (a half-3D sphere created from random dots) and a different control (incoherently moving dots), Paradis et al. (2000) obtained quite a different result: activation of ventral lingual cortex and of a PO region. The reasons for this difference are unclear. On the one hand, their control condition is known to activate hMT/V5+ strongly; on the other hand, moving dots may not be as efficient for producing 3D motion activation as random lines (Sunaert et al., 2000a).

BIOLOGICAL MOTION A related phenomenon is biological motion, in which a set of moving dots create the impression of a moving human figure (Johansson, 1973). This stimulus compared to a scrambled control activates the STS motion region (Bonda et al., 1996; Grossman et al., 2000). This same STS region has been shown to be more strongly activated by facial movements than by simple, coherent motion of random dots (Puce et al., 1998). How specific that region is for biological motion compared to other complex motion displays is presently under investigation (Grèzes et al., 2001; Grossman and Blake, 2001; Peuskens et al., 2001b).

Conclusions

Many regions in human and monkey cortex are motion sensitive, the most prominent of these being the MT/V5 motion complex. This diversity is likely to reflect the different computations that can be performed on the retinal motion signals rather than distinct pathways for different types of motion stimuli. The different computations performed on the motion signals relate both to the many aspects of motion perception and to the many other behavioral functions of motion processing. Indeed, the most important function of the visual motion regions, like that of the visual system in general, is not to analyze the retinal motion signals,

and indirectly motion in the outside world, but to adapt the results of this analysis to the needs of other brain systems that have to make use of the visual information.

The advent of fMRI in the awake monkey holds the promise of rapid progress in understanding the function of the cerebral motion networks, which can now be studied at both the population and the single-neuron level

REFERENCES

- Ahlfors, S. P., G. V. Simpson, A. M. Dale, J. W. Belliveau, A. K. Liu, A. Korvenoja, J. Virtanen, M. Huottilainen, R. B. Tootell, H. J. Aronen, and R. J. Ilmoniemi, 1999. Spatiotemporal activity of a cortical network for processing visual motion revealed by MEG and fMRI, *J. Neurophysiol.*, 82:2545–2555.
- Barton, J. J. S., T. Simpson, E. Kiriakopoulos, C. Stewart, A. Crawley, B. Guthrie, M. Wood, and D. Mikulis, 1996. Functional MRI of lateral occipitotemporal cortex during pursuit and motion perception, *Ann. Neurol.*, 40:387–398.
- Beauchamp, M. S., R. W. Cox, and E. A. DeYoe, 1997. Graded effects of spatial and featural attention on human area MT and associated motion processing areas, *J. Neurophysiol.*, 78:516–520.
- Belliveau, J. W., D. N. Kennedy, R. C. McKinstry, B. R. Buchbinder, R. M. Weiskoff, M. S. Cohen, J. M. Vevea, T. J. Brady, and B. R. Rosen, 1991. Functional mapping of the human visual cortex by magnetic resonance imaging, *Science*, 254:716–719.
- Bonda, E., M. Petrides, D. Ostry, and A. Evans, 1996. Specific involvement of human parietal systems and the amygdala in the perception of biological motion, *J. Neurosci.*, 16:3737–3744.
- Braddick, O. J., J. M. O'Brien, J. Wattam-Bell, J. Atkinson, T. Hartley, and R. Turner, 2001. Brain areas sensitive to coherent visual motion, *Perception*, 30:61–72.
- Bradley, D. C., G. C. Chang, and R. A. Andersen, 1998. Encoding of three-dimensional structure-from-motion by primate MT neurons, *Nature*, 392:714–717.
- Brandt, T., T. Stephan, S. Bense, T. A. Yousry, and M. Dieterich, 2000. Hemifield visual motion stimulation: an example of inter-hemispheric crosstalk, *NeuroReport*, 11:2803–2809.
- Bremmer, F., A. Schlack, N. J. Shah, O. Zafiris, M. Kubischik, K. Hoffmann, K. Zilles, and G. R. Fink, 2001. Polymodal motion processing in posterior parietal and premotor cortex: a human fMRI study strongly implies equivalencies between humans and monkeys, *Neuron*, 29:287–296.
- Britten, K. H., M. N. Shadlen, W. T. Newsome, and J. A. Movshon, 1992. The analysis of visual motion: a comparison of neuronal and psychophysical performance, *J. Neurosci.*, 12:4745–4763.
- Büchel, C., O. Josephs, G. Rees, R. Turner, C. D. Frith, and K. J. Friston, 1998. The functional anatomy of attention to visual motion. A functional MRI study, *Brain*, 121:1281–1294.
- Cavanagh, P., 1992. Attention-based motion perception, *Science*, 257:1563–1565.
- Chawla, D., C. Buechel, R. Edwards, A. Howseman, O. Josephs, J. Ashburner, and K. J. Friston, 1999a. Speed-dependent responses in V5: a replication study, *NeuroImage*, 9:508–515.
- Chawla, D., G. Rees, and K. J. Friston, 1999b. The physiological basis of attentional modulation in extrastriate visual areas, *Nat. Neurosci.*, 2:671–676.
- Cheng, K., H. Fujita, I. Kanno, S. Miura, and K. Tanaka, 1995. Human cortical regions activated by wide-field visual motion: a H₂¹⁵O PET study, *J. Neurophysiol.*, 74:413–427.
- Cheng, K., T. Hasegawa, K. S. Saleem, and K. Tanaka, 1994. Comparison of neuronal selectivity for stimulus speed, length, and contrast in the prestriate areas V4 and MT of the macaque monkey, *J. Neurophysiol.*, 71:2269–2280.
- Chubb, C., and G. Sperling, 1988. Drift-balanced random stimuli: a general basis for studying non-Fourier motion perception, *J. Opt. Soc. Am. A*, 5:1986–2006.
- Churchland, M. M., and S. G. Lisberger, 2001. Shifts in the population response in the middle temporal visual area parallel perceptual and motor illusions produced by apparent motion, *J. Neurosci.*, 21:9387–9402.
- Claeys, K., P. Dupont, S. Sunaert, P. Van Hecke, E. De Schutter, and G. A. Orban, 2001. Human brain activations in a color discrimination task, *Soc. Neurosci. Abstr.*, 27:286.17.
- Corbetta, M., F. M. Miezin, S. Dobmeyer, G. L. Shulman, and S. E. Petersen, 1991. Selective and divided attention during visual discriminations of shape, color, and speed: functional anatomy by positron emission tomography, *J. Neurosci.*, 11:2383–2402.
- Cornette, L., P. Dupont, A. Rosier, S. Sunaert, P. Van Hecke, J. Michiels, L. Mortelmans, and G. A. Orban, 1998a. Human brain regions involved in direction discrimination, *J. Neurophysiol.*, 79:2749–2765.
- Cornette, L., P. Dupont, W. Spileers, S. Sunaert, J. Michiels, P. Van Hecke, L. Mortelmans, and G. A. Orban, 1998b. Human cerebral activity evoked by motion reversal and motion onset, *Brain*, 121:143–157.
- Culham, J. C., S. A. Brandt, P. Cavanagh, N. G. Kanwisher, A. M. Dale, and R. B. H. Tootell, 1998. Cortical fMRI activation produced by attentive tracking of moving targets, *J. Neurophysiol.*, 80:2657–2670.
- Culham, J. C., S. P. Dukelow, T. Vilis, F. A. Hassard, J. S. Gati, R. S. Menon, and M. A. Goodale, 1999. Recovery of fMRI activation in motion area MT following storage of the motion aftereffect, *J. Neurophysiol.*, 81:388–393.
- DeAngelis, G. C., B. G. Cumming, and W. T. Newsome, 1998. Cortical area MT and the perception of stereoscopic depth, *Nature*, 394:677–680.
- Decety, J., D. Perani, M. Jeannerod, V. Bettinardi, B. Tadary, R. Woods, J. C. Mazziotta, and F. Fazio, 1994. Mapping motor representations with positron emission tomography, *Nature*, 371:600–602.
- de Jong, B. M., S. Shipp, B. Skidmore, R. S. J. Frackowiak, and S. Zeki, 1994. The cerebral activity related to the visual perception of forward motion in depth, *Brain*, 117:1039–1054.
- Desimone, R., and L. G. Ungerleider, 1986. Multiple visual areas in the caudal superior temporal sulcus of the macaque, *J. Comp. Neurol.*, 248:164–189.
- DeYoe, E. A., G. J. Carman, P. Bandettini, S. Glickman, J. Wieser, R. Cox, D. Miller, and J. Neitz, 1996. Mapping striate and extrastriate visual areas in human cerebral cortex, *Proc. Natl. Acad. Sci. USA*, 93:2382–2386.
- Dieterich, M., S. F. Bucher, K. C. Seelos, and T. Brandt, 1998. Horizontal or vertical optokinetic stimulation activates visual motion-sensitive, ocular motor and vestibular cortex areas with right hemispheric dominance. An fMRI study, *Brain*, 121:1479–1495.
- Duffy, C. J., and R. H. Wurtz, 1991. Sensitivity of MST neurons to optic flow stimuli: I. A continuum of response selectivity to large-field stimuli, *J. Neurophysiol.*, 65:1329–1345.
- Dukelow, S. P., J. F. X. DeSouza, J. C. Culham, A. V. van den Berg, R. S. Menon, and T. Vilis, 2001. Distinguishing subregions of the human MT+ complex using visual fields and pursuit eye movements, *J. Neurophysiol.*, 86:1991–2000.

- Dumoulin, S. O., R. G. Bittar, N. J. Kabani, C. L. Baker, Jr, G. Le Goualher, G. Bruce Pike, and A. C. Evans, 2000. A new anatomical landmark for reliable identification of human area V5/MT: a quantitative analysis of sulcal patterning, *Cereb. Cortex*, 10:454–463.
- Dumoulin, S. O., R. F. Hess, C. L. Baker, Jr., and A. C. Evans, 2001. fMRI responses to first and second-order motion, *Invest. Ophthalmol. Vis. Sci.*, 42:S322.
- Dupont, P., B. De Bruyn, R. Vandenberghe, A. Rosier, J. Michiels, G. Marchal, L. Mortelmans, and G. A. Orban, 1997. The kinetic occipital region in human visual cortex, *Cereb. Cortex*, 7:283–292.
- Dupont, P., G. A. Orban, B. De Bruyn, A. Verbruggen, and L. Mortelmans, 1994. Many areas in the human brain respond to visual motion, *J. Neurophysiol.*, 72:1420–1424.
- Dupont, P., G. A. Orban, R. Vogels, G. Bormans, J. Nuyts, C. Schiepers, M. De Roo, and L. Mortelmans, 1993. Different perceptual tasks performed with the same visual stimulus attribute activate different regions of the human brain: a positron emission tomography study, *Proc. Natl. Acad. Sci. USA*, 90:10927–10931.
- Dupont, P., G. Sary, and G. A. Oran, 2000. Cerebral regions processing first and second order motion: a PET study, *Soc. Neurosci. Abstr.*, 26:2086.
- Flytche, D. H., A. Howseman, R. Edwards, D. R. Sandeman, and S. Zeki, 2000. Human area V5 and motion in the ipsilateral visual field, *Eur. J. Neurosci.*, 12:3015–3025.
- Flytche, D. H., B. D. Skidmore, and S. Zeki, 1995. Motion-from-hue activates area V5 of the human visual cortex, *Proc. R. Soc. Lond. B*, 260:353–358.
- Fias, W., P. Dupont, B. Reynvoet, and G. A. Orban, 2002. The quantitative nature of a visual task differentiates between ventral and dorsal stream, *J. Cogn. Neurosci.*, 14:646–658.
- Fox, P. T., M. A. Mintun, M. E. Raichle, F. M. Miezin, J. M. Allman, and D. C. Van Essen, 1986. Mapping human visual cortex with positron emission tomography, *Nature*, 323:806–809.
- Gegenfurtner, K. R., D. C. Kiper, and J. B. Levitt, 1997. Functional properties of neurons in macaque area V3, *J. Neurophysiol.*, 77:1906–1923.
- Goebel, R., D. Khorram-Sefat, L. Muckli, H. Hacker, and W. Singer, 1998. The constructive nature of vision: direct evidence from functional magnetic resonance imaging studies of apparent motion and motion imagery, *Eur. J. Neurosci.*, 10:1563–1573.
- Grezes, J., P. Fonlupt, B. Bertenthal, C. Delon-Martin, C. Segebarth, and J. Decety, 2001. Does perception of biological motion rely on specific brain regions? *NeuroImage*, 13:775–785.
- Grill-Spector, K., T. Kushnir, S. Edelman, Y. Itzhak, and R. Malach, 1998. Cue-invariant activation in object-related areas of the human occipital lobe, *Neuron*, 21:191–202.
- Grossman, E. D., and R. Blake, 2001. Brain activity evoked by inverted and imagined biological motion, *Vis. Res.*, 41:1475–1482.
- Grossman, E. D., M. Donnelly, R. Price, D. Pickens, V. Morgan, G. Neighbor, and R. Blake, 2000. Brain areas involved in perception of biological motion, *J. Cogn. Neurosci.*, 12:711–720.
- Grüsser, O.-J., M. Pause, and U. Schreier, 1990. Vestibular neurons in the parieto-insular cortex of monkeys (*Macaca fascicularis*): visual and neck receptor responses, *J. Physiol.*, 430:559–583.
- Hautzel, H., J. G. Taylor, B. J. Krause, N. Schmitz, L. Tellmann, K. Zimmern, N. J. Shah, H. Herzog, and H.-W. Müller-Gärtner, 2001. The motion aftereffect: more than area MT/V5?: evidence from 15O-butanol PET studies, *Brain Res.*, 892:281–292.
- Hawken, M. J., A. Parker, and J. S. Lund, 1988. Laminar organization of contrast sensitivity of direction selective cells in the striate cortex of the old world monkey, *J. Neurosci.*, 8:3541–3548.
- He, S., E. R. Cohen, and X. Hu, 1998. Close correlation between activity in brain area MT/V5 and the perception of a visual motion aftereffect, *Curr. Biol.*, 8:1215–1218.
- Heeger, D. J., G. M. Boynton, J. B. Demb, E. Seidemann, and W. T. Newsome, 1999. Motion opponency in visual cortex, *J. Neurosci.*, 19:7162–7174.
- Holmes, A. P., and K. J. Friston, 1998. Generalisability, random effects and population inference. *NeuroImage*, 7:S754.
- Huk, A. C., and D. J. Heeger, 2000. Task-related modulation of visual cortex, *J. Neurophysiol.*, 83:3525–3536.
- Huk, A. C., D. Ress, and D. J. Heeger, 2001. Neuronal basis of the motion aftereffect reconsidered, *Neuron*, 32:161–172.
- Johansson, G., 1973. Visual perception of biological motion and a model for its analysis, *Percept. Psychophys.*, 14:201–211.
- Jones, H. E., K. L. Grieve, W. Wang, and A. M. Sillito, 2001. Surround suppression in primate V1, *J. Neurophysiol.*, 86:2011–2028.
- Komatsu, H., and R. H. Wurtz, 1988. Relation of cortical areas MT and MST to pursuit eye movements. I. Localization and visual properties of neurons, *J. Neurophysiol.*, 60:580–603.
- Kourtzi, Z., and N. Kanwisher, 2000. Activation in human MT/MST by static images with implied motion, *J. Cogn. Neurosci.*, 12:48–55.
- Kwong, K. K., J. W. Belliveau, D. A. Chesler, I. E. Goldberg, R. M. Weiskoff, B. P. Poncelet, D. N. Kennedy, B. E. Hoppel, M. S. Cohen, R. Turner, B. Rosen, and T. J. Brady, 1992. Dynamic magnetic resonance imaging of human brain activity during primary sensory stimulation, *Proc. Natl. Acad. Sci. USA*, 89:5675–5679.
- Lagae, L., H. Maes, S. Raiguel, D. Xiao, and G. A. Orban, 1994. Responses of macaque STS neurons to optic flow components: a comparison of areas MT and MST, *J. Neurophysiol.*, 71:1597–1626.
- Lagae, L., S. Raiguel, and G. A. Orban, 1993. Speed and direction selectivity of macaque middle temporal neurons, *J. Neurophysiol.*, 69:19–39.
- Leite, F. P., D. Tsao, W. Vanduffel, D. Fize, Y. Sasaki, L. L. Wald, A. M. Dale, K. K. Kwong, G. A. Orban, B. R. Rosen, R. B. H. Tootell, and J. B. Mandeville, 2002. Repeated fMRI using iron oxide contrast agent in awake, behaving macaques at 3 Tesla, *NeuroImage*, 16:283–294.
- Lewis, J. W., M. S. Beauchamp, and E. A. DeYoe, 2000. A comparison of visual and auditory motion processing in human cerebral cortex, *Cereb. Cortex*, 10:873–888.
- Logothetis, N. K., H. Guggenberger, S. Peled, and J. Pauls, 1999. Functional imaging of the monkey brain, *Nat. Neurosci.*, 2:555–562.
- Logothetis, N. K., J. Pauls, M. Augath, T. Trinath, and A. Oeltermann, 2001. Neurophysiological investigation of the basis of the fMRI signal, *Nature*, 412:150–157.
- Lueck, C. J., S. Zeki, K. J. Friston, M.-P. Deiber, P. Cope, V. J. Cunningham, A. A. Lammertsma, C. Kennard, and R. S. J. Frackowiak, 1989. The colour centre in the cerebral cortex of man, *Nature*, 340:386–389.
- Malach, R., J. B. Reppas, R. R. Benson, K. K. Kwong, H. Jiang, W. A. Kennedy, P. J. Ledden, T. J. Brady, B. R. Rosen, and R. B. H. Tootell, 1995. Object-related activity revealed by functional magnetic resonance imaging in human occipital cortex, *Proc. Natl. Acad. Sci. USA*, 92:8135–8139.
- McCarthy, G., M. Spicer, A. Adrignolo, M. Luby, J. Gore, and T. Allison, 1995. Brain activation associated with visual motion

- studied by functional magnetic resonance imaging in humans, *Hum. Brain Mapping*, 2:234–243.
- McKeefry, D. J., J. D. G. Watson, R. S. J. Frackowiak, K. Fong, and S. Zeki, 1997. The activity in human areas V1/V2, V3, and V5 during the perception of coherent and incoherent motion, *NeuroImage*, 5:1–12.
- Mikami, A., W. T. Newsome, and R. H. Wurtz, 1986. Motion selectivity in macaque visual cortex: I. Mechanisms of direction and speed selectivity in extrastriate area MT, *J. Neurophysiol.*, 55:1308–1327.
- Morrone, M. C., M. Tosetti, D. Montanaro, A. Fiorentini, G. Cioni, and D. C. Burr, 2000. A cortical area that responds specifically to optic flow, revealed by fMRI, *Nat. Neurosci.*, 3:1322–1328.
- Nakayama, K., 1985. Biological image motion processing: a review, *Vis. Res.*, 25:625–660.
- Nakahara, K., T. Hayashi, S. Konishi, and Y. Miyashita, 2002. Functional MRI of macaque monkeys performing a cognitive set-shifting task, *Science*, 295:1532–1536.
- Newsome, W. T., and E. B. Paré, 1988. A selective impairment of motion perception following lesions of the middle temporal visual area (MT), *J. Neurosci.*, 8:2201–2211.
- Newsome, W. T., R. H. Wurtz, M. R. Dursteler, and A. Mikami, 1985. Deficits in visual motion processing following ibotenic acid lesions of the middle temporal visual area of the macaque monkey, *J. Neurosci.*, 5:825–840.
- O'Craven, K. M., B. R. Rosen, K. K. Kwong, A. Treisman, and R. L. Savoy, 1997. Voluntary attention modulates fMRI activity in human MT-MST, *Neuron*, 18:591–598.
- O'Driscoll, G. A., S. M. Strakowski, N. M. Alpert, S. W. Matthysse, S. L. Rauch, D. L. Levy, and P. S. Holzman, 1998. Differences in cerebral activation during smooth pursuit and saccadic eye movements using positron-emission tomography, *Biol. Psychiatry*, 44:685–689.
- Orban, G. A., 1997. Visual processing in macaque area MT/V5 and its satellites (MSTd and MSTl), in *Cerebral Cortex*, vol. 12, *Extrastriate Cortex in Primates* (K. S. Rockland, J. H. Kaas, and A. Peters, eds.), New York: Plenum Press, pp. 359–434.
- Orban, G. A., P. Dupont, B. De Bruyn, R. Vandenberghe, A. Rosier, and L. Mortelmans, 1998. Human brain activity related to speed discrimination tasks, *Exp. Brain Res.*, 122:9–22.
- Orban, G. A., P. Dupont, B. De Bruyn, R. Vogels, R. Vandenberghe, and L. Mortelmans, 1995a. A motion area in human visual cortex, *Proc. Natl. Acad. Sci. USA*, 92:993–997.
- Orban, G. A., P. Dupont, R. Vogels, G. Bormans, and L. Mortelmans, 1997. Human brain activity related to orientation discrimination tasks, *Eur. J. Neurosci.*, 9:246–259.
- Orban, G. A., H. Kennedy, and J. Bullier, 1986. Velocity sensitivity and direction selectivity of neurons in areas V1 and V2 of the monkey: influence of eccentricity, *J. Neurophysiol.*, 56:462–480.
- Orban, G. A., S. Sunaert, J. T. Todd, P. Van Hecke, and G. Marchal, 1999. Human cortical regions involved in extracting depth from motion, *Neuron*, 24:929–940.
- Orban, G. A., R. Saunders, and E. Vandenberghe, 1995b. Lesions of the superior temporal cortical motion areas impair speed discrimination in the macaque monkey, *Eur. J. Neurosci.*, 7:2261–2276.
- Pack, C. C., V. K. Berezovskii, and R. T. Born, 2001. Dynamic properties of neurons in cortical area MT in alert and anaesthetized macaque monkeys, *Nature*, 414:905–908.
- Paradis, A. L., V. Cornilleau-Peres, J. Droulez, P. F. Van De Moortele, E. Lobel, A. Berthoz, D. Le Bihan, and J. B. Poline, 2000. Visual perception of motion and 3-D structure from motion: an fMRI study, *Cereb. Cortex*, 10:772–783.
- Peigneux, P., E. Salmon, M. van der Linden, G. Garraux, J. Aerts, G. Delfiore, C. Degueldre, A. Luxen, G. Orban, and G. Franck, 2000. The role of lateral occipitotemporal junction and area MT/V5 in the visual analysis of upper-limb postures, *NeuroImage*, 11:644–655.
- Petit, L., V. P. Clark, J. Ingelholm, and J. V. Haxby, 1997. Dissociation of saccade-related and pursuit-related activation in human frontal eye fields as revealed by fMRI, *J. Neurophysiol.*, 77:3386–3390.
- Petit, L., and J. V. Haxby, 1999. Functional anatomy of pursuit eye movements in humans as revealed by fMRI, *J. Neurophysiol.*, 82:463–471.
- Peuskens, H., S. Sunaert, P. Dupont, P. Van Hecke, and G. A. Orban, 2001a. Human brain regions involved in heading estimation, *J. Neurosci.*, 21:2451–2461.
- Peuskens, H., S. Sunaert, J. Vanrie, K. Verfaillie, P. Van Hecke, and G. A. Orban, 2001b. Disentangling brain areas activated by biological motion, *Soc. Neurosci. Abstr.*, 27:165.35.
- Phinney, R. E., and E. A. DeYoe, 2001. fMRI investigation of purely stereoscopic (cyclopean) motion processing, *Soc. Neurosci. Abstr.*, 27:680.10.
- Previc, F. H., M. Liotti, C. Blakemore, J. Beer, and P. Fox, 2000. Functional imaging of brain areas involved in the processing of coherent and incoherent wide field-of-view visual motion, *Exp. Brain Res.*, 131:393–405.
- Puce, A., T. Allison, S. Bentin, J. C. Gore, and G. McCarthy, 1998. Temporal cortex activation in humans viewing eye and mouth movements, *J. Neurosci.*, 18:2188–2199.
- Qian, N., and R. A. Andersen, 1994. Transparent motion perception as detection of unbalanced motion signals, *J. Neurosci.*, 14:7367–7380.
- Raiguel, S., M. M. Van Hulle, D.-K. Xiao, V. L. Marcar, L. Lagae, and G. A. Orban, 1997. Size and shape of receptive fields in the medial superior temporal area (MST) of the macaque, *NeuroReport*, 8:2803–2808.
- Rees, G., K. Friston, and C. Koch, 2000. A direct quantitative relationship between the functional properties of human and macaque V5, *Nat. Neurosci.*, 3:716–723.
- Rees, G., C. D. Frith, and N. Lavie, 1997. Modulating irrelevant motion perception by varying attentional load in an unrelated task, *Science*, 278:1616–1619.
- Rees, G., C. Frith, and N. Lavie, 2001. Processing of irrelevant visual motion during performance of an auditory attention task, *Neuropsychologia*, 39:937–949.
- Reppas, J. B., S. Niyogi, A. M. Dale, M. I. Sereno, and R. B. Tootell, 1997. Representation of motion boundaries in retinotopic human visual cortical areas, *Nature*, 388:175–179.
- Saito, H., M. Yukie, K. Tanaka, K. Hikosaka, Y. Fukada, and E. Iwai, 1986. Integration of direction signals of image motion in the superior temporal sulcus of the macaque monkey, *J. Neurosci.*, 6:145–157.
- Schall, J. D., A. Morel, D. J. King, and J. Bullier, 1995. Topography of visual cortex connections with frontal eye field in macaque, *J. Neurosci.*, 15:4464–4487.
- Schoups, A., R. Vogels, N. Qian, and G. A. Orban, 2001. Practising orientation identification improves orientation coding in V1 neurons, *Nature*, 412:549–553.
- Seghier, M., M. Dojat, C. Delon-Martin, C. Rubin, J. Warnking, C. Segebarth, and J. Bullier, 2000. Moving illusory contours activate primary visual cortex: an fMRI study, *Cereb. Cortex*, 10:663–670.

- Seidemann, E., A. B. Poirson, B. A. Wandell, and W. T. Newsome, 1999. Color signals in area MT of the macaque monkey, *Neuron*, 24:911–917.
- Senior, C., J. Barnes, V. Giampietro, A. Simmons, E. T. Bullmore, M. Brammer, and A. S. David, 2000. The functional neuroanatomy of implicit-motion perception or representational momentum, *Curr. Biol.*, 10:16–22.
- Shadlen, M. N., and W. T. Newsome, 1996. Motion perception: seeing and deciding, *Proc. Natl. Acad. Sci. USA*, 93:628–633.
- Shulman, G. L., J. M. Ollinger, E. Akbudak, T. E. Conturo, A. Z. Snyder, S. E. Petersen, and M. Corbetta, 1999. Areas involved in encoding and applying directional expectations to moving objects, *J. Neurosci.*, 19:9480–9496.
- Smith, A. T., M. W. Greenlee, K. D. Singh, F. M. Kraemer, and J. Hennig, 1998. The processing of first- and second-order motion in human visual cortex assessed by functional magnetic resonance imaging (fMRI), *J. Neurosci.*, 18:3816–3830.
- Somers, D. C., A. E. Seiffert, A. M. Dale, and R. H. Tootell, 1999. fMRI investigations of motion aftereffects with 1st- and 2nd-order stimuli, *Invest. Ophthalmol. Vis. Sci.*, 40:S199.
- Stavenski, A. A., D. A. Robinson, R. M. Steinman, and G. T. Timberlake, 1975. Miniature eye movements of fixation in rhesus monkey, *Vis. Res.*, 15:1269–1273.
- Sunaert, S., G. Fesl, J. Todd, A. Rosier, P. Van Hecke, and G. A. Orban, 2000a. Human cortical regions involved in extracting 3D structure from motion depend on stimulus type and transparency, *Soc. Neurosci. (Abs.)*, 26:1583.
- Sunaert, S., P. Van Hecke, and G. Marchal, 1999. Motion-responsive regions of the human brain, *Exp. Brain Res.*, 127:355–370.
- Sunaert, S., P. Van Hecke, G. Marchal, and G. A. Orban, 2000b. Attention to speed of motion, speed discrimination, and task difficulty: an fMRI study, *NeuroImage*, 11:612–623.
- Taylor, J. G., N. Schmitz, K. Ziemons, M.-L. Grosse-Ruyken, O. Gruber, H.-W. Mueller-Gaertner, and N. J. Shah, 2000. The network of brain areas involved in the motion aftereffect, *NeuroImage*, 11:257–270.
- Tolias, A. S., S. M. Smirnakis, M. A. Augath, T. Trinath, and N. K. Logothetis, 2001. Motion processing in the macaque: revisited with functional magnetic resonance imaging, *J. Neurosci.*, 21:8594–8601.
- Tootell, R. B. H., and N. Hadjikhani, 2001. Where is “dorsal V4” in human visual cortex? Retinotopic, topographic and functional evidence, *Cereb. Cortex*, 11:298–311.
- Tootell, R. B. H., J. D. Mendola, N. K. Hadjikhani, P. J. Ledden, A. K. Liu, J. B. Reppas, M. I. Sereno, and A. M. Dale, 1997. Functional analysis of V3A and related areas in human visual cortex, *J. Neurosci.*, 17:7060–7078.
- Tootell, R. B. H., J. D. Mendola, N. K. Hadjikhani, A. K. Liu, and A. M. Dale, 1998. The representation of the ipsilateral visual field in human cerebral cortex, *Proc. Natl. Acad. Sci. USA*, 95:818–824.
- Tootell, R. B. H., J. B. Reppas, A. M. Dale, R. B. Look, M. I. Sereno, R. Malach, T. J. Brady, and B. R. Rosen, 1995a. Visual motion aftereffect in human cortical area MT revealed by functional magnetic resonance imaging, *Nature*, 375:139–141.
- Tootell, R. B. H., J. B. Reppas, K. K. Kwong, R. Malach, R. T. Born, T. J. Brady, B. R. Rosen, and J. W. Belliveau, 1995b. Functional analysis of human MT and related visual cortical areas using magnetic resonance imaging, *J. Neurosci.*, 15:3215–3230.
- Tootell, R. B. H., and J. B. Taylor, 1995. Anatomical evidence for MT and additional cortical visual areas in humans, *Cereb. Cortex*, 5:39–55.
- Van Oostende, S., S. Sunaert, P. Van Hecke, G. Marchal, and G. A. Orban, 1997. The kinetic occipital (KO) region in man: an fMRI study, *Cereb. Cortex*, 7:690–701.
- Vanduffel, W., D. Fize, J. B. Mandeville, K. Nelissen, P. Van Hecke, B. R. Rosen, R. B. H. Tootell, and G. A. Orban, 2001. Visual motion processing investigated using contrast-agent enhanced fMRI in awake behaving monkeys, *Neuron*, 32:565–577.
- Wandell, B. A., A. B. Poirson, W. T. Newsome, H. A. Baseler, G. M. Boynton, A. Huk, S. Gandhi, and L. T. Sharpe, 1999. Color signals in human motion-selective cortex, *Neuron*, 24:901–909.
- Wang, J., T. Zhou, M. Qiu, A. Du, K. Cai, Z. Wang, C. Zhou, M. Meng, Y. Zhuo, S. Fan, and L. Chen, 1999. Relationship between ventral stream for object vision and dorsal stream for spatial vision: an fMRI + ERP study, *Hum. Brain Mapping*, 8:170–181.
- Watson, J. D. G., R. Myers, R. S. J. Frackowiak, J. V. Hajnal, R. P. Woods, J. C. Mazziotta, S. Shipp, and S. Zeki, 1993. Area V5 of the human brain: evidence from a combined study using positron emission tomography and magnetic resonance imaging, *Cereb. Cortex*, 3:79–94.
- Xiao, D.-K., V. L. Marcar, S. E. Raiguel, and G. A. Orban, 1997. Selectivity of macaque MT/V5 neurons for surface orientation in depth specified by motion, *Eur. J. Neurosci.*, 9:956–964.
- Zeki, S., J. D. G. Watson, and R. S. J. Frackowiak, 1995. Going beyond the information given: the relation of illusory visual motion to brain activity, *Proc. R. Soc. Lond. B*, 252:215–222.
- Zeki, S., J. D. G. Watson, C. J. Lueck, K. J. Friston, C. Kennard, and R. S. J. Frackowiak, 1991. A direct demonstration of functional specialization in human visual cortex, *J. Neurosci.*, 11:641–649.
- Zilles, K., G. Schlaug, M. Matelli, G. Luppino, A. Schleicher, M. Qu, A. Dabringhaus, R. Seitz, and P. E. Roland, 1995. Mapping of human and macaque sensorimotor areas by integrating architectonic, transmitter receptor, MRI and PET data, *J. Anat.*, 187:515–537.

84 Optic Flow

WILLIAM H. WARREN

OPTIC FLOW IS THE PATTERN of motion present at the eye of a moving observer. Such flow patterns contain information about self-motion, moving objects, and the three-dimensional (3D) layout of the environment, and could potentially be exploited to control locomotion. The term was first used by Gibson (1950) to generalize Helmholtz's notion of *motion parallax* from single objects to the continuous environment surrounding the observer. He developed the concept during World War II while working on methods for pilot testing and training, after he concluded that the classical depth cues were inadequate to explain a pilot's practical ability to land an airplane. But little research was done on the subject until the 1980s, when its relevance to robot and vehicle guidance was recognized and computer animation made it amenable to study.

Optic flow is a key example of Gibson's (1979) *ecological approach* to perception and action. This functionalist approach emphasizes that the task of vision is to guide successful behavior in the natural environment, and stresses the importance of higher-order optical information that specifies complex properties of that environment and its relationship to the observer. The nervous system is viewed as providing causal support for the detection of informational variables and the modulation of action variables. Optic flow offers a case study of a higher-order variable that has been formally analyzed and empirically investigated in some detail. In what follows, we will trace optic flow through the cycle of perception and action.

The past 20 years have seen intensive research on the topic, with parallel developments in the domains of human perception, primate neurophysiology, and computational vision. This chapter aims to integrate these perspectives to address both mechanistic questions about how optic flow patterns are extracted by the visual cortex and functional questions about how this information is used to perceive self-motion and control behavior. (For related reviews see Lappe et al., 1999; Warren, 1998; regarding structure from motion, see Todd, 1995.)

The optic flow field

Optic flow is typically represented as an instantaneous velocity field in which each vector corresponds to the optical motion of a point in the environment, as in Figure 84.1A. It is immediately apparent that this flow field has a radial struc-

ture, with a *focus of expansion* (FOE) lying in the direction of self-motion. When one views the moving display, it is also apparent that the environment is a planar surface receding in depth. The radial pattern of vector directions depends solely on the observer's direction of translation, or *heading*, and is independent of the 3D structure. The magnitude of each vector, on the other hand, depends on both heading and depth and decreases quickly with distance. The radial flow pattern thus specifies one's current heading, whether or not the local FOE itself is visible. This was Gibson's fundamental hypothesis about the perception of self-motion from optic flow, and was the starting point for both psychophysical and neurophysiological experiments.

Although the velocity field description is compatible with the motion selectivity of cortical areas V1 and MT, it does not represent higher-order temporal components of the optic flow such as acceleration, or the trajectories of points over time. This appears to be a reasonable approximation, for the visual system is relatively insensitive to acceleration and relies primarily on the first-order flow to determine heading (Paolini et al., 2000; Warren et al., 1991a).

OBSERVER ROTATION However, the detection of optic flow by a moving eye is complicated by the fact that the eye can also rotate (Gibson, 1950, pp. 124–127). If the observer simply translates on a straight path, the flow pattern on the retina is radial (Fig. 84.1A). This is called the *translational component* of retinal flow, and recovery of heading from it is straightforward. A rotation of the observer, such as a pursuit eye or head movement, merely displaces the image on the retina, producing the *rotational component* of retinal flow.¹ Specifically, pitch or yaw of the eye create patterns of vertical or horizontal lamellar flow (Fig. 84.1B), and roll about the line of sight creates a pattern of rotary flow. But if the eye is simultaneously translating and rotating, which commonly occurs when one fixates a point in the world during locomotion, the retinal flow is the vector sum of these two components (Fig. 84.1C). The resulting flow field is more complex, without a qualitative feature corresponding to

¹To keep these distinctions clear, I will consistently use *translation* and *rotation* to describe observer movement and *lamellar* and *rotary* to describe flow patterns.

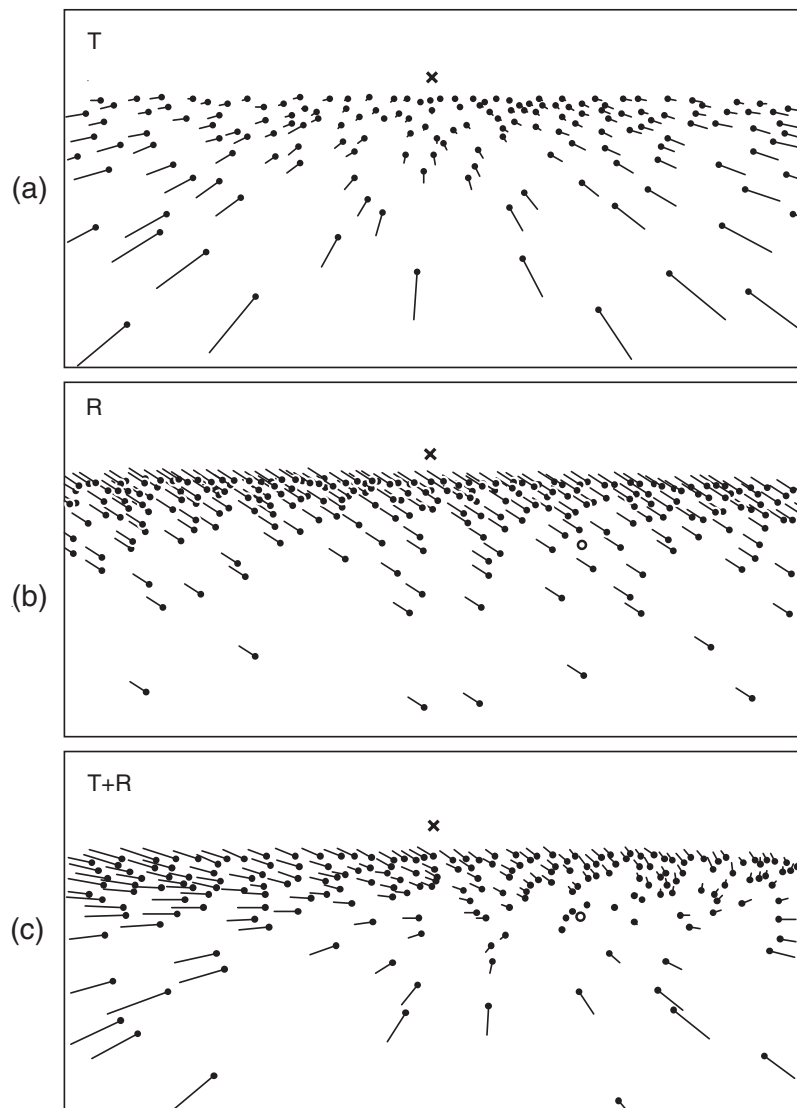


FIGURE 84.1. Retinal flow field for a ground plane with rotation about a diagonal axis. *a*, Translational component produced by observer translation toward the \mathbf{x} : radial flow from the heading point. *b*, Rotational component produced by eye rotation downward and to the right: lamellar flow upward and to the left. *c*, Flow field

produced by the sum of *a* and *b* due to heading toward the \mathbf{x} while rotating to track the \mathbf{O} on the ground plane. The singularity in the field is now at the fixation point. Note the motion parallax (differences in vector direction and length) at different distances across the surface.

one's heading; indeed, the singularity in the flow field is now at the fixation point.

Thus, to determine heading, the visual system must somehow analyze the translational and rotational components and recover the direction of self-motion. This has come to be known as the *rotation problem*. Fortunately, the retinal flow in a 3D scene contains sufficient information to solve this problem in principle. Specifically, *motion parallax between points at different depths corresponds to observer translation*, whereas *common lamellar motion across the visual field corresponds to observer rotation*.

THE PATH OF SELF-MOTION Even if the rotation problem can be solved, however, it only yields one's instantaneous

heading. A further problem is that the velocity field does not specify one's path over time—for instance, whether one is traveling on a straight or a curved path. In fact, the same flow field can be generated by a straight path together with eye rotation or by a circular path of self-motion. A particularly troublesome case appears in Figure 84.2, in which translation plus rotation about a vertical axis produces the same velocity field as a circular path on the ground plane. When presented with such flow displays, observers often report seeing a curved path of self-motion rather than a straight path plus rotation. How, then, can one determine whether one is traveling on a straight or a curved path? We will call this the *path problem*.

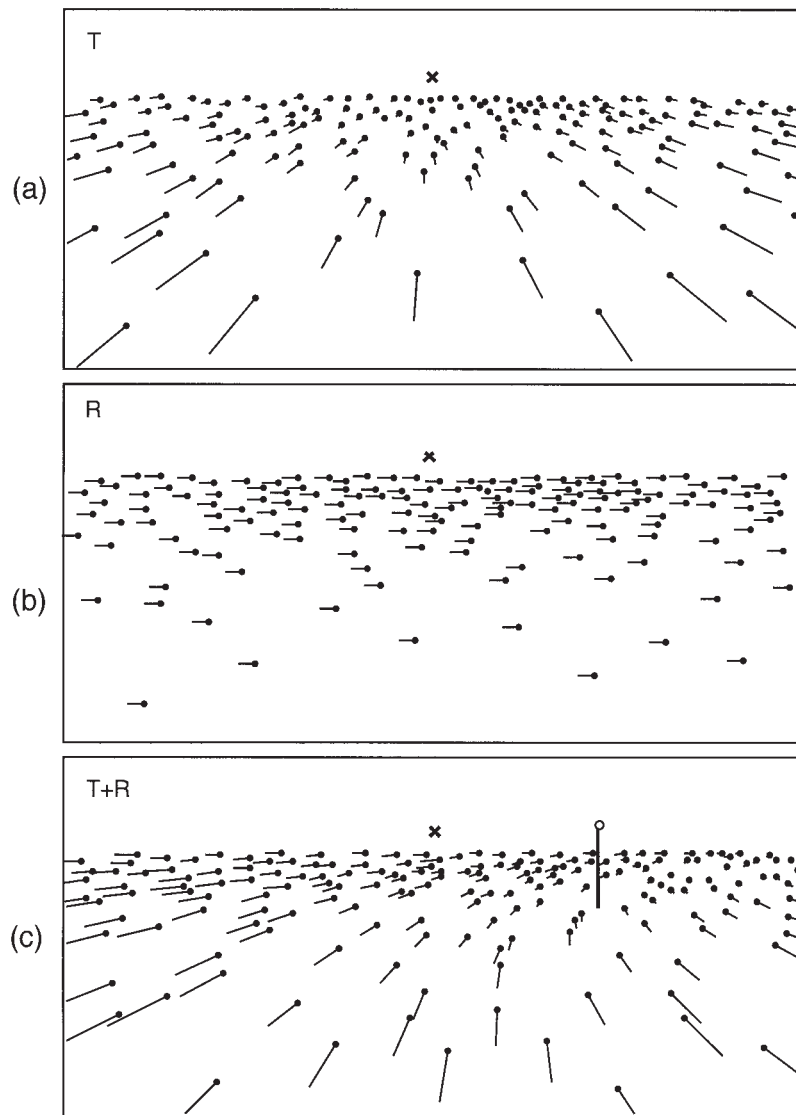


FIGURE 84.2. Retinal flow field for a ground plane with rotation about a vertical axis. *a*, *Translational component* produced by observer translation toward the **x**. *b*, *Rotational component* produced by eye rotation to the right. *c*, Flow field produced by the sum of *a* and *b* due to translating toward the **x** while rotating to track the **o** on the post, which is at eye level. An identical velocity field is generated by travel on a circular path to the right, with instantaneous heading along the tangent toward the **x**.

Before tackling these issues, let's consider the detection of optic flow patterns.

Detecting optic flow

From a mechanistic point of view, the basic question is how optic flow is detected by the visual system. It now appears that optic flow patterns are extracted in two steps, by first detecting local motion and then integrating it spatially in units sensitive to patterns of motion. This can be demonstrated psychophysically using random-dot displays in which the proportion of “signal” dots moving in a coherent flow pattern is varied relative to “noise” dots that jump to random positions on each frame. As the area of coherent motion in

the display increases, the direction of motion can be reported at a lower signal-to-noise ratio, providing evidence of spatial summation (Burr et al., 1998). Such coherence thresholds reveal summation for radial, rotary, and lamellar flow patterns over large visual angles up to 36 to 72 degrees. The data are closely predicted by an ideal integrator that pools local motion signals in units sensitive to pattern motion with large receptive fields.

FLOW-SELECTIVE UNITS IN MSTd Such findings converge with results from single-cell recordings in the dorsal region of the medial superior temporal area (MSTd) of macaque visual cortex (see Chapters 83 and 85, this volume). Saito et al. (1986) reported cells selective for expansion or con-

traction, clockwise or counterclockwise rotary flow, or directional lamellar flow, and proposed that they could be constructed by integrating input from velocity-selective cells in area MT. The MSTd cells are characterized by large receptive fields 15 to 65 degrees in diameter, distributed over the visual field to eccentricities of 50 degrees, with a higher concentration closer to the fovea (Raiguel et al., 1997). These cells exhibit stronger responses to larger stimulus patterns, consistent with spatial integration of local velocity signals (Duffy and Wurtz, 1991b; Tanaka and Saito, 1989).

About half of MSTd cells are selective for radial or rotary flow at various locations in their receptive fields, a property known as *position invariance*. Rigorous tests of position invariance ensure that a cell's response is not simply due to a coincidental match between the stimulus and a local region of the receptive field (Lagae et al., 1994). This finding is consistent with an architecture in which clusters of velocity-selective MT cells, each having a radial or rotary arrangement at different retinal loci, converge on one MSTd cell.

Such radial and rotary cells are also broadly tuned to the overall speed of motion, so that they may form a distributed representation of mean flow speed (Orban et al., 1995; Tanaka and Saito, 1989). There are also indications of sensitivity to speed gradients within the flow pattern, with some cells preferring an increasing gradient from center to periphery and others preferring a decreasing gradient (Duffy and Wurtz, 1997). However, the gradients tested were quite extreme, and MSTd cells are relatively insensitive to the fine speed gradients needed to distinguish 3D shape. Eliminating the pattern of vector directions has a far greater impact on a cell's response than eliminating the speed gradient (Tanaka et al., 1989).

MST projects to higher areas in the dorsal visual pathway, including parietal area 7a. Cells in this area are more narrowly tuned to radial, rotary, spiral, and lamellar flow patterns (Siegel and Read, 1997), indicating that the processing of optic flow continues beyond MSTd.

DECOMPOSITION OR TEMPLATES? There has been a great deal of interest in the hypothesis that specialized channels in MSTd form a basis set for the decomposition of optic flow. Koenderink and van Doorn (1975, 1981; Longuet-Higgins and Prazdny, 1980) showed that any optic flow field can be analyzed locally into lamellar motion plus three elementary components: *divergence* (div) or rate of local expansion, which together with surface slant can be used to estimate heading; *curl* or rate of local rotary flow; and *deformation* (def) or rate of shear along two orthogonal axes, which is specific to surface shape. This insight inspired a number of studies on sensitivity to radial, rotary, and lamellar flow in MSTd. However, there is often confusion between divergence and radial flow. Formally, div is a measure of the local rate of expansion, not the radial motion pattern or the FOE.

The balance of psychophysical research does not support decomposition into div, curl, def, and lamellar motion. For example, when the div is removed from an expansion pattern, resulting in radial flow with decelerating dot motion outward from the FOE, the detection thresholds for expansion in noise are unaffected (Kappers et al., 1996). Such results are contrary to a specialized divergence detector. Although the maximum of divergence can be located in visual displays (Regan and Beverly, 1982), there is no evidence that it is actually used to judge heading (Warren et al., 1988).

Similar conclusions have emerged from single-cell recordings in MSTd. When cells selective for radial or rotary flow are presented with a spiral flow pattern containing both div and curl components, the response is lower than with the equivalent radial or rotary pattern alone (Orban et al., 1992), indicating that the spiral flow is not decomposed. A majority of cells are not tuned to a single elementary component but respond to two or three individual components (Duffy and Wurtz, 1991a) or to combinations of radial and rotary flow (Graziano et al., 1994). There thus appears to be a continuum of cells selective not only for radial and rotary flow but also for intermediate spiral flow patterns.

Taken together, the evidence indicates that MSTd cells do not decompose optic flow into elementary components, but rather act as templates or filters for complex flow patterns. The advantage of a template mechanism is that, rather than simply recoding the information in the flow field, its response can signal the presence of meaningful patterns of stimulation.

Perception of translational heading

From a functional point of view, the primary question about optic flow is whether people can in fact perceive their self-motion from optic flow patterns. Cutting et al. (1992) estimated that a heading accuracy of about 1 to 3 degrees is required to guide ordinary locomotion such as running and skiing. When observers view a random-dot display of radial flow and judge whether they are heading to the left or right of a probe, they are highly accurate, with heading thresholds as low as 0.5 degree (Warren, 1976; Warren et al., 1988). Translational heading can thus be perceived from radial flow with sufficient accuracy to control locomotion.

SPATIAL INTEGRATION Heading judgments also reveal spatial integration, similar to simple coherence thresholds. In principle, a heading estimate could be obtained by triangulating just two motion vectors in a radial flow pattern. However, such a mechanism would be vulnerable to noise in local motion sensors, leading to large heading errors (Koenderink and van Doorn, 1987). Since each vector provides an estimate of the heading, pooling them allows this

redundancy in the flow pattern to reduce triangulation error. Consistent with such pooling, heading thresholds decrease as dots are added to a radial flow display, following a $1/\sqrt{N}$ rule, up to an asymptote with about 30 dots in a 40×32 degree display (Warren et al., 1988). Heading judgments are also highly robust to flow field noise created by perturbing vector directions (Warren et al., 1991a). Both of these properties are reproduced by a simple neural model of translational heading in which local motion signals are pooled in large-field radial flow templates (Hatsopoulos and Warren, 1991), consistent with the spatial integration observed in MSTd.

FLOW STRUCTURE AND SPEED GRADIENTS In line with the fact that the radial structure of flow is independent of depth, heading thresholds are similar in different 3D environments, including a ground plane, a frontal plane, and a cloud of dots. Judgments even remain accurate when speed gradients are removed by randomizing the magnitudes of local vectors, preserving their directions, but they become impossible when vector directions are randomized, preserving their magnitudes (Warren et al., 1991a). This result confirms the primary importance of the pattern of vector directions and is strikingly consistent with MSTd responses (Tanaka et al., 1989). However, heading judgments are influenced by large speed gradients. If vector magnitudes on one side of the FOE are greatly increased, perceived heading is biased toward the opposite side, and subjects report travel on a curved path (Dyre and Andersen, 1996). This is plausible because, in a homogeneous environment, the pattern of flow speeds is correlated with the path of travel. On a straight path, vectors tend to increase symmetrically from the FOE (Fig. 84.2A), whereas on a curved path, vectors on the outside of the path tend to be greater than those on the inside (Fig. 84.2C).

HEADING IN THE PRESENCE OF MOVING OBJECTS Most optic flow analyses presume a rigid scene, yet we locomote successfully in a dynamic environment with independently moving objects. A moving object can significantly alter the radial flow pattern, creating a local region of inconsistent motion. To cope with this, the visual system might segment the scene and make separate estimates of self-motion from the background flow and of object motion from the discrepant flow (Hildreth, 1992). A simpler solution would be to estimate the FOE by pooling all motion vectors, consistent with spatial integration in MSTd, although this would lead to predictable heading errors.

In fact, heading judgments exhibit just such errors when the object crosses the FOE (Warren and Saunders, 1995). If the object is moving in depth, it creates a piece of a radial flow pattern with a secondary FOE_o. This is enough to bias perceived heading *opposite* the direction of object motion by

a few degrees toward the FOE_o. Such an effect is consistent with spatial integration of all motion to locate the FOE. However, if the object is moving in the frontal plane, it creates a piece of lamellar flow, which biases perceived heading in the *same direction* as object motion (Royden and Hildreth, 1996). This effect is similar to an illusory shift in the FOE that occurs when a lamellar flow pattern is transparently superimposed on a radial flow pattern (Duffy and Wurtz, 1993) and could be a consequence of using lamellar flow to estimate observer rotation (Lappe and Duffy, 1999). On the other hand, both effects might also be explained as a result of pooling the motion parallax between the object and the background together with the local dot motions, which could be a consequence of using motion parallax to recover heading.

These results lead to the surprising conclusion that moving objects are not segmented in the course of perceiving heading, and suggest that self-motion relative to the environment may be determined by a task-specific mechanism that responds to any flow within its receptive field. MSTd cells might provide such a mechanism, for they respond selectively to a given flow pattern whether it is carried by a large field of random dots or the local boundary of a square (Geesaman and Andersen, 1996). This suggests that MSTd detects flow patterns produced by relative motion between the observer and the environment, without differentiating local object motion.

IS SELF-MOTION DETERMINED IN MSTd? Selectivity for large-field radial, rotary, and lamellar flow patterns and their combinations makes MSTd a likely candidate for extracting information about self-motion. Such global motion patterns are generated by observer translation, roll, and pitch/yaw with respect to the environment. As we have seen, there are a number of commonalities between the characteristics of MSTd cells and heading judgments: (1) large receptive fields suitable for global flow, (2) spatial integration, (3) dominance of vector directions but also (4) responses to large speed gradients, (5) speed tuning that could code the velocity of observer translation or rotation, and (6) failure to differentiate local object motion and global flow.

At first blush, the position invariance of MSTd cells appears inconsistent with this hypothesis, for heading detection by single cells implies a preferred locus for the FOE in the receptive field. However, this objection confuses response selectivity with response amplitude. Duffy and Wurtz (1995) found that 90% of expansion cells do have a preferred FOE and exhibit a graded response as the focus is shifted away from this position, which is well fit by a Gaussian tuning curve (Raiguel et al., 1997). A population of such cells is in principle sufficient for a precise distributed coding of heading direction. A second issue is that MSTd cells do not appear to form a contiguous retinotopic map of heading

direction. Nevertheless, similarly tuned cells tend to be clustered together in approximate cortical columns (Britten, 1998), which is not incompatible with distributed coding.

The most direct evidence that MSTd is involved in heading is that microstimulation in a cluster of cells biases radial flow localization judgments in the direction preferred by nearby cells in two-thirds of cases (Britten and von Wezel, 1998). The conclusion is reinforced by the finding that vestibular stimulation produced by physically translating the animal modulates the response amplitude and even the direction preference to radial flow in MSTd cells (Duffy, 1998). This strongly implies that MSTd is a site that integrates sensory stimulation about self-motion.

In humans, brain imaging studies indicate that a possible homolog of MSTd, an inferior satellite of MT/V5, is selective for radial and rotary flow patterns (Morrone et al., 2000). Using an active judgment task, Peuskens et al. (2001) found that attending to heading per se enhanced specific activity in this MT/V5 satellite, as well as in a posterior region of the dorsal intraparietal sulcus (a possible homolog of area 7a) and in dorsal premotor cortex. These results suggest that heading is detected in a pathway that is functionally similar to primate areas MSTd and 7a and directly related to motor behavior.

The rotation problem

Determining heading from radial flow during pure translation is relatively straightforward. But when the observer also makes a pursuit rotation of the eye or head, a component of lamellar flow is added, radically altering the retinal flow field (Fig. 84.2C). How, then, might the instantaneous direction of heading be determined during rotation? There are two general approaches to the rotation problem.

EXTRARETINAL THEORIES Extraretinal theories propose that internal signals about the rotational velocity of the eye and head, possibly including efferent, proprioceptive, and vestibular signals, are used to estimate the rotational component of self-motion (Banks et al., 1996; Royden et al., 1994). The rotational component can then be subtracted from the retinal flow pattern in order to recover the translational component and hence the instantaneous direction of heading. If any rotation remains in the flow pattern, it can be attributed to a curved path of self-motion. Note that the resulting heading estimate is in retinal coordinates, or an *oculocentric* frame of reference. Thus, extraretinal signals about the position of the eye and head may also be needed to transform the heading into *head-centric* and *body-centric* reference frames.

A possible mechanism for extraretinal theories is dynamic tuning of receptive fields in MSTd. During a pursuit eye movement, the preferred FOE tuning of most expansion

cells actually shifts on the retina in the direction of rotation, partially compensating for pursuit (Bradley et al., 1996). However, the mean shift is only half of what is needed to compensate fully for the eye movement. Some cells show no shift at all, but rather a modulation in the amplitude of their response, consistent with the notion of a *gain field* (Shenoy et al., 1999). On the other hand, Page and Duffy (1999) reported that a computed population vector fully compensates for pursuit rotation and might be “read out” by a higher area. Area 7a contains cells that are narrowly tuned to radial flow and show gain modulation by eye position (Read and Siegel, 1997), potentially converting an oculocentric heading estimate into a head-centric frame.

Physiological results would thus seem to support an extraretinal approach. However, Shenoy et al. (1999) found large receptive field shifts in response to the flow pattern alone, even when the eye was stationary. This suggests that partial compensation can occur on the basis of the retinal flow itself. Moreover, these experiments only tested planar (non-3D) flow patterns, and compensation might be greater with motion parallax in the display. This leads us to the second approach.

RETINAL FLOW THEORIES Gibson argued that the optical information available in natural environments is sufficient for visual perception, and was skeptical of the need for extraretinal signals. Retinal flow theories propose that heading can be determined from the pattern of retinal flow alone (Warren and Hannon, 1990). This is theoretically possible because observer rotation simply adds a common lamellar component to the flow field, such that the differential motion due to translation remains invariant. Numerous computational models have formally shown that instantaneous heading can be recovered from the velocity field during rotation (see Hildreth and Royden, 1998; Warren, 1998, for reviews). As before, this heading estimate is in an oculocentric frame of reference, so extraretinal position signals would seem to be necessary to convert it to head-centric and body-centric reference frames to recover one’s *absolute heading* in space. But such coordinate transformations could be bypassed by determining one’s *object-relative heading*, the direction of translation with respect to objects that are also registered in retinal coordinates. This is physiologically plausible because target position and optic flow analyses converge at least by area 7a.

There are three main classes of retinal flow theories. One class first estimates observer rotation from the lamellar flow, then subtracts the rotational component from the retinal flow pattern to recover the translational component (Perrone, 1992). In principle, the rotational component could be measured by integrating retinal velocities independently about three orthogonal axes (Koenderink, 1986). It is thus plausible that MSTd cells selective for horizontal,

vertical, and rotary flow patterns detect observer rotation; indeed, the preferred direction of pursuit eye movements in these cells is opposite the preferred direction of lamellar flow. Because the motion of more distant points is increasingly dominated by the rotational component (Fig. 84.2), depth information such as binocular disparity could also contribute to estimating the rotational component (van den Berg and Brenner, 1994).

A second class of theories determines the heading directly from motion parallax, which is also known as *relative* or *differential motion* (Longuet-Higgins and Prazdny, 1980; Rieger and Lawton, 1985). The relative motion between two points at different distances along a line of sight can be described by a difference vector. Remarkably, the set of difference vectors for a 3D scene forms a radial pattern centered on the heading. The rotation problem can thus be solved quite elegantly if there is sufficient depth structure in the environment. Moreover, relative motion and common motion could be extracted in parallel to decompose observer translation and rotation.

In theory, differential motion could be detected by an array of antagonistic center-surround units, with either circularly symmetric or bilateral center-surrounds (Royden, 1997). A majority of cells in area MT actually possesses such a bilateral opponent-motion organization, is sensitive to speed differences between center and surround, and is segregated in separate columns from classic MT velocity units (Born and Tootell, 1992; Xiao et al., 1997). Given that MT projects to MSTd, these two motion pathways could detect radial patterns of ordinary flow vectors and difference vectors in parallel, allowing the visual system to extract heading in both planar and 3D environments (Warren, 1998). Consistent with this idea, the responses of MSTd cells are enhanced by the addition of motion parallax in a radial flow display during fixation, and even more so during pursuit movements (Upadhyay et al., 2000). Thus, motion parallax signals contribute to activity in MSTd, especially during eye rotation, a finding that deserves further investigation.

A third class of theories is based on templates for the set of flow patterns produced by all possible combinations of observer translation and rotation (Lappe and Rauschecker, 1993; Perrone and Stone, 1994). The space of flow patterns is constrained by restricting rotations to pursuit of stationary points in the environment. Perrone and Stone (1998) showed that their model templates reproduce many properties of MSTd cells, including selectivity for radial, lamellar, and spiral flow, position invariance, and a preferred FOE.

PERCEIVING HEADING DURING ROTATION The psychophysical evidence on the rotation problem is mixed, and the issue remains controversial. In these experiments, displays are manipulated to dissociate retinal and extraretinal contributions. In the *actual rotation* condition, a radial flow pattern is

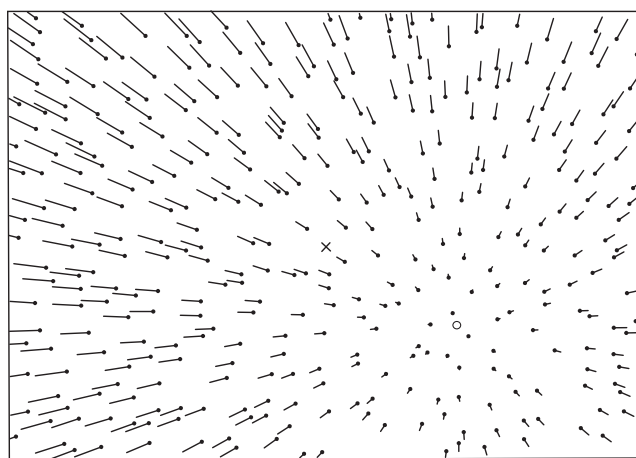


FIGURE 84.3. Retinal flow field for a frontal plane with rotation about a diagonal axis. The observer is translating toward the **x** while rotating to track the **O** on the plane downward and to the right. This produces a pseudo-FOE at the fixation point. Because the distance of the surface from the eye changes very little, only a little motion parallax is defined across a large display.

presented on the screen (Fig. 84.14) together with a moving fixation point that induces a pursuit eye movement; thus, extraretinal signals correspond to the rotation. In the *simulated rotation* condition, the flow pattern on the screen simulates the effect of forward translation plus a pursuit rotation (Fig. 84.1C) while the fixation point remains stationary, so extraretinal signals correspond to zero rotation. The flow pattern on the retina is thus the same in both conditions, while the extraretinal signal is manipulated. If judgments are equally accurate in the simulated and actual conditions, it implies that heading can be perceived from the retinal flow alone—even with conflicting extraretinal signals. On the other hand, if judgments are markedly less accurate in the simulated condition, it implies an extraretinal contribution.

Warren and Hannon (1988, 1990) reported that heading judgments with a random-dot ground plane (Fig. 84.1C) or 3D cloud were comparable in the two conditions, yielding heading thresholds below 1.5 degrees. On the other hand, with a frontal plane, which contains almost no motion parallax (Fig. 84.3), performance was at chance in the simulated condition but remained accurate in the actual condition. This pattern of results is consistent with retinal flow theories and confirms the importance of motion parallax. Observers even report an illusory eye rotation in the simulated condition corresponding to motion of the (stationary) fixation point away from the heading. But good performance with a frontal plane during actual eye rotation also indicates that extraretinal signals can contribute to heading judgments.

However, in these experiments the mean rotation rate over a trial was less than 1 deg/sec. At higher simulated rota-

tion rates (1 to 5 deg/sec),² heading judgments were subsequently found to be highly inaccurate (Banks et al., 1996; Royden et al., 1994). Constant errors rose to 15 degrees in the direction of simulated rotation but remained close to zero during actual eye rotation. This pattern of results is consistent with the extraretinal theory for high rotation rates. At the same time, other research supported a retinal flow theory (van den Berg, 1993; Wang and Cutting, 1999). Binocular disparity appeared to make heading judgments more reliable during simulated rotation (van den Berg and Breener, 1994), although Ehrlich et al. (1998) failed to replicate this effect.

Royden (1994) pointed out that observers frequently report a curved path of self-motion in the simulated rotation condition, and that heading errors in the direction of simulated rotation are consistent with the perception of a curved path. This might be expected from the ambiguity of the velocity field, for the same instantaneous field can be produced by a straight path plus rotation or by a circular path of self-motion with radius r (Fig. 84.2C), which are related by the ratio of translation and rotation speeds ($r = T/R$). Because extraretinal signals indicate that rotation is zero in the simulated condition, this could lead to the perception of a curved path. It is important to distinguish the concepts of *heading* and *path*, for although they are identical for a straight path, the instantaneous heading direction is tangent to a curved path. It is apparently difficult for observers to judge their instantaneous heading per se, for even when instructed to do so, they tend to report their perceived path. This leaves open the possibility that the oculocentric heading is accurately recovered during simulated rotation, but because the body-centric heading changes over time (literally drifting across the screen), subjects report a curved path.

One response to this dilemma was to try to elicit reports of instantaneous oculocentric heading by other means. When instructed to base heading judgments on the illusory motion of the fixation point, observers are more accurate than with path judgments of the same displays (van den Berg, 1996). This suggests that the visual system implicitly recovers heading during simulated rotation. When asked to judge the direction in which they are skidding while traveling on a circular path, observers' heading judgments also improve (Stone and Perrone, 1997), indicating that the instantaneous heading direction can be estimated.

Another response to the dilemma is to investigate the conditions for accurate path perception, since that is what observers tend to report.

The path problem

Observers can judge their prospective path of self-motion very accurately on a straight path, a circular path (Warren et al., 1991b), and even an elliptical path whose curvature changes with time (Kim and Turvey, 1998) from displays that simulate the view through the windshield of a turning car.³ A circular path can be parameterized by the instantaneous heading direction (\hat{T}), which is tangent to the path at the observation point, and the curvature of the path ($\kappa = 1/r$). Path curvature is equal to the rate of change in heading with respect to distance traveled ($\kappa = d\hat{T}/ds$), or with respect to time, scaled by translation speed ($\kappa = (d\hat{T}/dt)/T$). A higher-order path can be considered piecewise as a series of osculating circles, each of which is tangent to the path and defines a local path curvature.

We do not know how the visual system recovers curved paths of self-motion. The most straightforward solution is to determine the current body-centric heading and its rate of change, as just described. But contrary to this approach, path perception is quite accurate for windshield-like displays in which the body-centric heading doesn't change. This suggests a second solution: recovering the circular path directly from the flow field. A circular path on a ground plane generates a curved velocity field (Fig. 84.2C) that is stationary over time and uniquely corresponds to path curvature (for a constant eye height). The *locomotor flow line* that passes under the observer's feet specifies the oculocentric path (Lee and Lishman, 1977), and its location with respect to objects in the scene specifies the object-relative path. For higher-order paths, the flow field curvature changes over time with the path curvature. A third solution is to determine curvature from the ratio of rotation to translation speeds ($\kappa = R_p/T$), where R_p is the rotation attributed to path curvature after compensating for eye and head rotation (Ehrlich et al., 1998).

It is possible that spiral cells in MSTd code the path curvature from ground plane flow. It does not appear that extended paths are recovered by individual cells, for they respond similarly to a given flow pattern regardless of the one that precedes or follows it in a continuous sequence of stimulation (Paolini et al., 2000). Thus, single MSTd cells do not code for second-order temporal properties such as acceleration or changes in the flow pattern, but they could code the instantaneous path curvature.

RESOLVING THE PATH PROBLEM How, then, might one determine whether the path of self-motion is straight or curved from retinal flow alone? Li and Warren (2000) pro-

²A rotation rate of 1 deg/sec would be produced by fixating the ground plane 10 m ahead while walking at 1 m/sec and a 5 deg/sec rotation by fixating 4 m ahead.

³Specifically, the line of sight is along the tangent to the path, such that the instantaneous heading remains fixed on the screen.

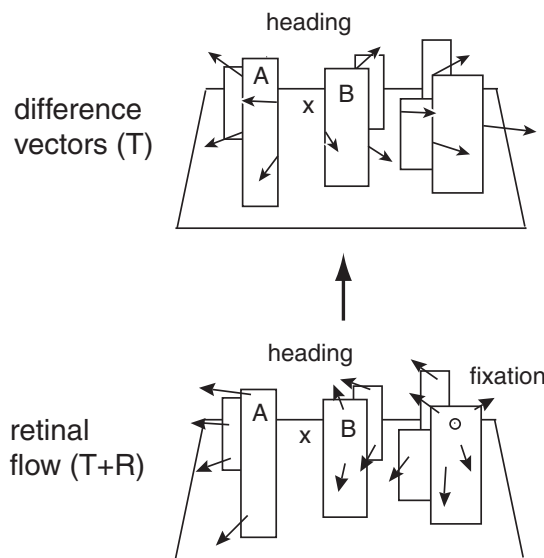


FIGURE 84.4. Object-relative heading. *Bottom*: Sketch of retinal flow in a complex scene. The observer is heading toward **x** while rotating rightward to track **o**. *Top*: Difference vectors from motion parallax specify the instantaneous heading. The current object-relative heading is a few degrees to the left of object B. If the path is straight, the heading will remain fixed in the scene over time; if the path is curved to the right, the heading point will shift rightward with respect to object B.

posed that the visual system updates the *object-relative heading* over time. Specifically, the visual system continually extracts the instantaneous heading with respect to objects in the scene, presumably on the basis of motion parallax (Fig. 84.4). The sequence of such headings over time traces out the observer's path through the environment. For example, if the path is straight, then the heading remains fixed in the scene, whereas if the path is curved, the heading shifts relative to objects over time.

This solution to the path problem requires sufficiently dense motion parallax for an accurate heading estimate and distinct reference objects in the scene that can be tracked over time. However, most previous research used random dots, which are necessarily sparse and not easily tracked. In contrast, when displays contain dense texture-mapped scenes with distinct objects, path judgments are reasonably accurate, with mean errors below 4 degrees at simulated rotation rates up to 7 deg/sec (Cutting et al., 1997; Li and Warren, 2000). This is also the case for active steering during simulated rotation (Li and Warren, 2002). Object-relative heading thus allows the visual system to determine the path of self-motion through the environment on the basis of retinal flow, even when it is in conflict with extraretinal signals.

The mixed results for heading judgments are probably a consequence of the cue conflict for path perception in the simulated rotation condition. Extraretinal signals

indicate that eye rotation is zero; hence, the rotational component of flow must be due to a curved path. But over time, the retinal flow specifies that object-relative heading is constant, so the observer must be traveling on a straight path through the depicted environment. If the visual system makes use of both retinal and extraretinal signals, it is not surprising that the data are inconsistent. But with distinct reference objects in the display, object-relative paths tend to dominate.

ROLE OF EXTRARETINAL SIGNALS The preceding evidence indicates that both retinal flow and extraretinal signals can contribute to heading and path perception. This raises the question of how retinal and extraretinal signals are related.

Recent results suggest that an extraretinal estimate of rotation is not simply subtracted from retinal flow; rather, the two interact nonlinearly (Crowell and Andersen, 2001; van den Berg et al., 2001). When real and simulated pursuit are in the same direction, extraretinal signals exert a partial influence, but when they are in opposite directions, there is little extraretinal influence. Moreover, if the retinal flow corresponds to a 3D scene (i.e., contains motion parallax or perspective), eye rotation is determined from the common lamellar flow, providing accurate pursuit compensation. Extraretinal signals merely indicate whether or not the eye is rotating, and gate the interpretation of lamellar flow as being due to a pursuit rotation or a curved path. This is consistent with the transparent motion illusion of Duffy and Wurtz (1993), which suggests that lamellar flow is used to estimate rotation when motion parallax is present. On the other hand, if the retinal flow is planar (not 3D), the rotation rate is quantitatively estimated from extraretinal signals, but with a gain of only 50%. This is consistent with the partial compensation for eye movements observed in MSTd cells with planar flow patterns (Bradley et al., 1996).

Furthermore, it appears that extraretinal signals begin to make a contribution half a second after the onset of flow (Grigo and Lappe, 1999). With simulated rotation displays shorter than 500 msec, heading toward a large frontal plane (Fig. 84.3) is judged accurately based on minimal motion parallax, whereas with longer displays heading is perceived erroneously at the fixation point. Given that fixations normally last for 300 to 500 msec, the results imply that under ordinary conditions the visual system may rely primarily on retinal flow.

Two neural models of MSTd incorporate extraretinal influences. Beintema and van den Berg (1998) assume flow templates with Gaussian tuning for combinations of radial and lamellar flow, similar to those of Perrone and Stone (1994). The model uses an extraretinal velocity signal to modulate the gain of a subset of units tuned to the corresponding rotation rate. Lappe (1998) assumes flow templates with sigmoidal tuning and uses an extraretinal velocity signal

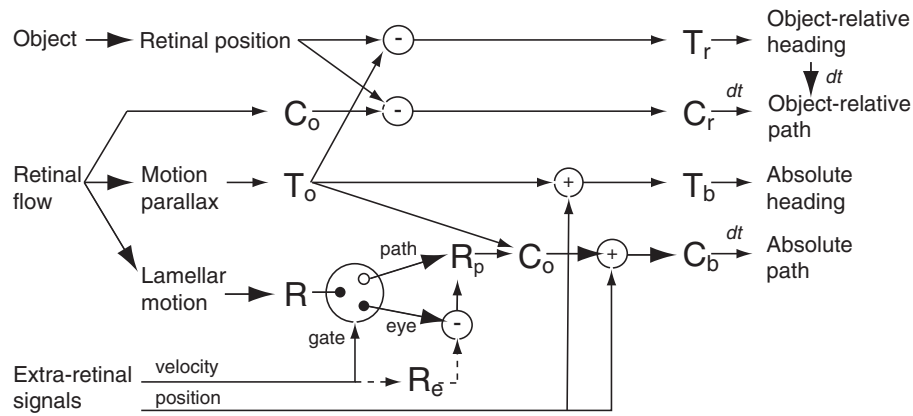


FIGURE 84.5. A heuristic summary of the flow of information in the visual system for recovering heading and path of self-motion. T , observer translation; R , total rotation; R_e , rotation attributed to eye and head pursuit; R_p , rotation attributed to path curvature; C , circular path. Subscripts a , b , and r indicate quantities in oculo-centric, body-centric, and object-relative reference frames, respectively.

to shift the tuning of individual cells so that the population response compensates fully for rotation. Given that a majority of expansion cells appear to have Gaussian-like tuning, and some evidence of gain modulation in MSTd, the first model would seem to be more plausible; on the other hand, the second model captures the observation that partial shifts in individual cells can yield full compensation in a population vector. However, both models assume that extraretinal signals provide an accurate measure of rotation rate, rather than gating the interpretation of retinal flow, and neither incorporates object-relative heading. Given the current state of knowledge, one must remain agnostic about such models, but they can help to guide further tests of MSTd.

A heuristic interpretation of the flow of information in the visual system, based on the results we have surveyed, appears in Figure 84.5. The lower part of the diagram illustrates the recovery of absolute heading and the upper part the recovery of object-relative heading. The evidence is generally consistent with the view that oculocentric translation (T_o) is determined from motion parallax and total rotation (R) from lamellar flow, either via parallel MT-MSTd pathways for differential and common motion or via compound templates in MSTd. The role of extraretinal velocity signals is largely limited to gating the total rotation R to eye and head pursuit or to path curvature (R_p), from which the instantaneous circular path (C_o) is determined. In the former case, they may provide a quantitative estimate of eye and head rotation (R_e), which is subtracted from R to estimate R_p when motion parallax is absent or fixation exceeds a half-second. To recover the absolute heading and path, extraretinal position information is needed to convert from oculocentric to body-centric frames. In contrast, objectrelative heading (T_r) is determined by merging the oculocentric heading (T_o) with an object's retinal position, bypassing the coordinate transformation. Similarly, to recover the object-relative path (C_r), the path determined from the curved flow field (C_o) is merged

with the object's position, or object-relative heading may be updated over time. Normally, the absolute and relative solutions are congruent, but during simulated rotation they are in conflict, and the object-relative solution tends to dominate.

Controlling locomotion with optic flow

We have now established that humans can perceive self-motion from optic flow under a variety of conditions and that specialized neural pathways exist to extract this information. Despite these findings, it is not a foregone conclusion that optic flow is actually used to control locomotor behavior, for other strategies are also available.

To locomote toward a stationary goal, an obvious strategy is simply to walk in the egocentric direction of the target, without using optic flow at all. For example, one could center the goal at the midline of the body and walk forward. Alternatively, optic flow from the scene could be used to steer toward a goal, using relations that are all within the visual domain. For example, one could walk so as to cancel the error between the FOE and the goal (Gibson, 1950) or between the perceived heading and the goal.

These hypotheses can be dissociated by using wedge prisms, which deflect the visual direction of the FOE from the direction of walking (Rushton et al., 1998). Thus, if participants guide walking by placing the deflecting FOE on the deflecting target, the "virtual" heading error between the FOE and the target will still be canceled, leading them to walk a straight path to the goal. But if they walk in the direction of the displaced image of the target, the virtual heading error will equal the prism deflection, and they will trace out a curved path to the goal. This is precisely what is observed with prisms in an open field, where there is minimal optic flow from fine grass texture, demonstrating that people can use egocentric direction to guide walking. On the other hand, we used a virtual reality lab to displace the FOE from

the direction of walking in a similar manner and manipulated the textured surface area in the display (Warren et al., 2001). In this setup, paths are significantly straighter and virtual heading error is reduced to near zero as optic flow and motion parallax are added to the display, consistent with an optic flow strategy. Similar improvements have also been reported with prisms as visual structure is added (Harris and Carre, 2001; Wood et al., 2000). Thus, both optic flow and egocentric direction contribute to the visual control of walking. Such redundancy provides robust locomotor control under a variety of environmental conditions.

In contrast, when walking to intercept a moving target, people rely solely on the visual direction of the target. Specifically, they walk with a direction and speed that keeps the bearing angle of the target constant, much like a sailor colliding with another boat (Fajen and Warren, 2002). This makes sense because radial flow from the whole scene is no longer informative about one's path toward a moving target.

We recently developed a dynamic theory of steering and obstacle avoidance that is based on object-relative heading with respect to goals and obstacles (Fajen et al., in press). Specifically, a goal acts like an attractor of heading, whose strength increases with its angle from the current heading and decreases with distance. In contrast, obstacles act like repellers of heading, whose strength decreases with both angle and distance. The resultant of these forces determines the current walking direction at a constant speed. The model closely fits human behavior for walking toward a goal, detouring around an obstacle, intercepting a moving target, avoiding a moving obstacle, and even predicts routes through an array of obstacles. In principle, such a model could be extended to include interactions among these basic behaviors, accounting for paths of locomotion in a complex dynamic environment.

Conclusion

We have followed optic flow through the cycle of perception and action, describing how information is generated by motion through the environment, detected to determine self-motion, and used to control behavior. Yet important questions remain unanswered. How, exactly, are translation and rotation determined from motion parallax and lamellar flow—in parallel pathways or compound templates? Can these processes account for the way moving objects bias perceived heading? How are curved paths of self-motion recovered and coded in this pathway? Precisely how do retinal and extraretinal signals interact? Are there distinct cortical representations of oculo-, head-, and body-centric heading or of object-relative heading? Is locomotion guided by perceived heading per se or by some other aspect of optic flow? And how is flow used in concert with proprioceptive and vestibular information to control locomotor behavior?

REFERENCES

- Banks, M. S., S. M. Ehrlich, B. T. Backus, and J. A. Crowell, 1996. Estimating heading during real and simulated eye movements, *Vis. Res.*, 36:431–443.
- Beintema, J. A., and A. V. van den Berg, 1998. Heading detection using motion templates and eye velocity gain fields, *Vis. Res.*, 38:2155–2179.
- Born, R. T., and R. B. H. Tootell, 1992. Segregation of global and local motion processing in primate middle temporal visual area, *Nature*, 357:497–499.
- Bradley, D. C., M. Maxwell, R. A. Andersen, M. S. Banks, and K. V. Shenoy, 1996. Mechanisms of heading perception in primate visual cortex, *Science*, 273:1544–1547.
- Britten, K. H., 1998. Clustering of response selectivity in the medial superior temporal area of extrastriate cortex of the macaque monkey, *Vis. Neurosci.*, 15:553–558.
- Britten, K. H., and R. J. A. von Wezel, 1998. Electrical microstimulation of cortical area MST biases heading perception in monkeys, *Nat. Neurosci.*, 1:59–63.
- Burr, D. C., M. C. Morrone, and L. M. Vaina, 1998. Large receptive fields for optic flow detection in humans, *Vis. Res.*, 38:1731–1743.
- Crowell, J. A., and R. A. Andersen, 2001. Pursuit compensation during self-motion, *Perception*, 30:1465–1488.
- Cutting, J. E., K. Springer, P. A. Braren, and S. H. Johnson, 1992. Wayfinding on foot from information in retinal, not optical, flow, *J. Exp. Psychol. Gen.*, 121:41–72.
- Cutting, J. E., P. M. Vishton, M. Flückiger, B. Baumberger, and J. D. Gerndt, 1997. Heading and path information from retinal flow in naturalistic environments, *Percept. Psychophys.*, 59:426–441.
- Duffy, C. J., 1998. MST neurons respond to optic flow and translational movement, *J. Neurophysiol.*, 80:1816–1827.
- Duffy, C. J., and R. H. Wurtz, 1991a. Sensitivity of MST neurons to optic flow stimuli. I. A continuum of response selectivity to large-field stimuli, *J. Neurophysiol.*, 65:1329–1345.
- Duffy, C. J., and R. H. Wurtz, 1991b. Sensitivity of MST neurons to optic flow stimuli. II. Mechanisms of response selectivity revealed by small-field stimuli, *J. Neurophysiol.*, 65:1346–1359.
- Duffy, C. J., and R. H. Wurtz, 1993. An illusory transformation of optic flow fields, *Vis. Res.*, 33:1481–1490.
- Duffy, C. J., and R. H. Wurtz, 1995. Response of monkey MST neurons to optic flow stimuli with shifted centers of motion, *J. Neurosci.*, 15:5192–5208.
- Duffy, C. J., and R. H. Wurtz, 1997. Medial superior temporal area neurons respond to speed patterns in optic flow, *J. Neurosci.*, 17:2839–2851.
- Dyre, B. P., and G. J. Andersen, 1996. Image velocity magnitudes and perception of heading, *J. Exp. Psychol. Hum. Percept. Perform.*, 23:546–565.
- Ehrlich, S. M., D. M. Beck, J. A. Crowell, T. C. A. Freeman, and M. S. Banks, 1998. Depth information and perceived self-motion during simulated gaze rotations, *Vis. Res.*, 38:3129–3145.
- Fajen, B. R., and W. H. Warren, 2002. Intercepting a moving target on foot. Submitted for publication.
- Fajen, B. R., and W. H. Warren, 2003. Behavioral dynamics of steering, obstacle avoidance, and route selection, *J. Exp. Psychol. Hum. Percept. Perform.*, 29:343–362.
- Geesaman, B. J., and R. A. Andersen, 1996. The analysis of complex motion patterns by form/cue invariant MSTd neurons, *J. Neurosci.*, 16:4716–4732.
- Gibson, J. J., 1950. *Perception of the Visual World*, Boston: Houghton Mifflin.

- Gibson, J. J., 1979. *The Ecological Approach to Visual Perception*, Boston: Houghton Mifflin.
- Graziano, M. S. A., R. A. Andersen, and R. J. Snowden, 1994. Tuning of MST neurons to spiral motions, *J. Neurosci.*, 14:54–67.
- Grigo, A., and M. Lappe, 1999. Dynamical use of different sources of information in heading judgments from retinal flow, *J. Opt. Soc. Am. A*, 16:2079–2091.
- Harris, M. G., and G. Carre, 2001. Is optic flow used to guide walking while wearing a displacing prism? *Perception*, 30:811–818.
- Hatsopoulos, N. G., and W. H. Warren, 1991. Visual navigation with a neural network, *Neural Networks*, 4:303–317.
- Hildreth, E., 1992. Recovering heading for visually-guided navigation, *Vis. Res.*, 32:1177–1192.
- Hildreth, E. C., and C. S. Royden, 1998. Computing observer motion from optical flow, in *High-Level Motion Processing* (T. Watanabe ed.), Cambridge, MA: MIT Press, 269–293.
- Kappers, A. M. L., S. F. te Pas, and J. J. Koenderink, 1996. Detection of divergence in optical flow fields, *J. Opt. Soc. Am. A*, 13:227–235.
- Kim, N.-G., and M. T. Turvey, 1998. Visually perceiving heading on circular and elliptical paths, *J. Exp. Psychol. Hum. Percept. Perform.*, 24:1690–1704.
- Koenderink, J. J., 1986. Optic flow, *Vis. Res.*, 26:161–180.
- Koenderink, J. J., and A. J. van Doorn, 1975. Invariant properties of the motion parallax field due to the movement of rigid bodies relative to an observer, *Opt. Acta*, 22:737–791.
- Koenderink, J. J., and A. J. van Doorn, 1981. Exterospic component of the motion parallax field, *J. Opt. Soc. Am.*, 71:953–957.
- Koenderink, J. J., and A. J. van Doorn, 1987. Facts on optic flow, *Biol. Cybern.*, 56:247–254.
- Lagae, L., H. Maes, S. Raiguel, D.-K. Xiao, and G. A. Orban, 1994. Responses of macaque STS neurons to optic flow components: a comparison of areas MT and MST, *J. Neurophysiol.*, 71:1597–1626.
- Lappe, M., 1998. A model of the combination of optic flow and extraretinal eye movement signals in primate extrastriate visual cortex: neural model of self-motion from optic flow and extraretinal cues, *Neural Networks*, 11:397–414.
- Lappe, M., F. Bremmer, and A. V. van den Berg, 1999. Perception of self-motion from visual flow, *Trends Cogn. Sci.*, 3:329–336.
- Lappe, M., and C. J. Duffy, 1999. Optic flow illusion and single neuron behaviour reconciled by a population model, *Eur. J. Neurosci.*, 11:2323–2331.
- Lappe, M., and J. P. Rauschecker, 1993. A neural network for the processing of optic flow from ego-motion in man and higher mammals, *Neural Comput.*, 5:374–391.
- Lee, D. N., and R. Lishman, 1977. Visual control of locomotion, *Scand. J. Psychol.*, 18:224–230.
- Li, L., and W. H. Warren, 2000. Perception of heading during rotation: sufficiency of dense motion parallax and reference objects, *Vis. Res.*, 40:3873–3894.
- Li, L., and W. H. Warren, 2002. Retinal flow is sufficient for steering during simulated rotation, *Psychol. Sci.*, 13:485–491.
- Longuet-Higgins, H. C., and K. Prazdny, 1980. The interpretation of a moving retinal image, *Proc. R. Soc. Lond. B*, 208:385–397.
- Morrone, M. C., M. Tosetti, D. Montanaro, A. Fiorentini, G. Cioni, and D. C. Burr, 2000. A cortical area that responds specifically to optic flow, revealed by fMRI, *Nat. Neurosci.*, 3:1322–1328.
- Orban, G. A., L. Lagae, S. Raiguel, D. Xiao, and H. Maes, 1995. The speed tuning of middle superior temporal (MST) cell responses to optic flow components, *Perception*, 24:269–285.
- Orban, G. A., L. Lagae, A. Verri, S. Raiguel, D. Xiao, H. Maes, and V. Torre, 1992. First-order analysis of optical flow in monkey brain, *Proc. Natl. Acad. Sci. USA*, 89:2595–2599.
- Page, W. K., and C. J. Duffy, 1999. MST neuronal responses to heading direction during pursuit eye movements, *J. Neurophysiol.*, 81:596–610.
- Paolini, M., C. Distler, F. Bremmer, M. Lappe, and K. P. Hoffman, 2000. Responses to continuously changing optic flow in area MST, *J. Neurophysiol.*, 84:730–743.
- Perrone, J. A., 1992. Model for the computation of self-motion in biological systems, *J. Opt. Soc. Am. A*, 9:177–194.
- Perrone, J. A., and L. S. Stone, 1994. A model of self-motion estimation within primate extrastriate visual cortex, *Vis. Res.*, 34:2917–2938.
- Perrone, J. A., and L. S. Stone, 1998. Emulating the visual receptive-field properties of MST neurons with a template model of heading estimation, *J. Neurosci.*, 18:5958–5975.
- Peuskens, H., S. Sunaert, P. Dupont, P. V. Hecke, and G. A. Orban, 2001. Human brain regions involved in heading estimation, *J. Neurosci.*, 21:2451–2461.
- Raiguel, S., M. M. van Hulle, D.-K. Xiao, V. L. Marcar, L. Lagae, and G. A. Orban, 1997. Size and shape of receptive fields in the medial superior temporal area (MST) of the macaque, *NeuroReport*, 8:2803–2808.
- Read, H. L., and R. M. Siegel, 1997. Modulation of responses to optic flow in area 7a by retinotopic and oculomotor cues in monkey, *Cereb. Cortex*, 7:647–661.
- Regan, D., and K. I. Beverly, 1982. How do we avoid confounding the direction we are looking and the direction we are moving? *Science*, 215:194–196.
- Rieger, J. H., and D. T. Lawton, 1985. Processing differential image motion, *J. Opt. Soc. Am. A*, 2:354–360.
- Royden, C. S., 1994. Analysis of misperceived observer motion during simulated eye rotations, *Vis. Res.*, 34:3215–3222.
- Royden, C. S., 1997. Mathematical analysis of motion-opponent mechanisms used in the determination of heading and depth, *J. Opt. Soc. Am. A*, 14:2128–2143.
- Royden, C. S., J. A. Crowell, and M. S. Banks, 1994. Estimating heading during eye movements, *Vis. Res.*, 34:3197–3214.
- Royden, C. S., and E. C. Hildreth, 1996. Human heading judgments in the presence of moving objects, *Percept. Psychophys.*, 58:836–856.
- Rushton, S. K., J. M. Harris, M. Lloyd, and J. P. Wann, 1998. Guidance of locomotion on foot uses perceived target location rather than optic flow, *Curr. Biol.*, 8:1191–1194.
- Saito, H., M. Yukie, K. Tanaka, K. Hikosaka, Y. Fukada, and E. Iwai, 1986. Integration of direction signals of image motion in the superior temporal sulcus of the macaque monkey, *J. Neurosci.*, 6:145–157.
- Shenoy, K. V., D. C. Bradley, and R. A. Andersen, 1999. Influence of gaze rotation on the visual response of primate MSTd neurons, *J. Neurophysiol.*, 81:2764–2786.
- Siegel, R. M., and H. L. Read, 1997. Analysis of optic flow in the monkey parietal area 7a, *Cereb. Cortex*, 7:327–346.
- Stone, L. S., and J. A. Perrone, 1997. Human heading estimation during visually simulated curvilinear motion, *Vis. Res.*, 37:573–590.
- Tanaka, K., Y. Fukada, and H. Saito, 1989. Underlying mechanisms of the response specificity of expansion/contraction and rotation cells in the dorsal part of the medial superior temporal area of the macaque monkey, *J. Neurophysiol.*, 62:642–656.
- Tanaka, K., and H. Saito, 1989. Analysis of motion of the visual field by direction, expansion/contraction, and rotation cells clus-

- tered in the dorsal part of the medial superior temporal area of the macaque monkey, *J. Neurophysiol.*, 62:626–641.
- Todd, J. T., 1995. The visual perception of three-dimensional structure from motion, in *Perception of Space and Motion*, 2nd ed. (W. Epstein and S. Rogers, eds.), San Diego, CA: Academic Press, pp. 201–226.
- Upadhyay, U. D., W. K. Page, and C. J. Duffy, 2000. MST responses to pursuit across optic flow with motion parallax, *J. Neurophysiol.*, 84:818–826.
- van den Berg, A. V., 1993. Perception of heading, *Nature*, 365: 497–498.
- van den Berg, A. V., 1996. Judgements of heading, *Vis. Res.*, 36: 2337–2350.
- van den Berg, A. V., J. A. Beintema, and M. A. Frens, 2001. Heading and path percepts from visual flow and eye pursuit signals, *Vis. Res.*, 41:3467–3486.
- van den Berg, A. V., and E. Brenner, 1994. Why two eyes are better than one for judgments of heading, *Nature*, 371:700–702.
- Wang, R. F., and J. E. Cutting, 1999. Where we go with a little good information, *Psychol. Sci.*, 10:71–75.
- Warren, R., 1976. The perception of egomotion, *J. Exp. Psychol. Hum. Percept. Perform.*, 2:448–456.
- Warren, W. H., 1998. The state of flow, in *High-Level Motion Processing* (T. Watanabe ed.), Cambridge, MA: MIT Press, pp. 315–358.
- Warren, W. H., A. W. Blackwell, K. J. Kurtz, N. G. Hatsopoulos, and M. L. Kalish, 1991a. On the sufficiency of the velocity field for perception of heading, *Biol. Cybern.*, 65:311–320.
- Warren, W. H., and D. J. Hannon, 1988. Direction of self-motion is perceived from optical flow, *Nature*, 336:162–163.
- Warren, W. H., and D. J. Hannon, 1990. Eye movements and optical flow, *J. Opt. Soc. Am. A*, 7:160–169.
- Warren, W. H., B. A. Kay, W. D. Zosh, A. P. Duchon, and S. Sahuc, 2001. Optic flow is used to control human walking, *Nat. Neurosci.*, 4:213–216.
- Warren, W. H., D. R. Mestre, A. W. Blackwell, and M. W. Morris, 1991b. Perception of circular heading from optical flow, *J. Exp. Psychol. Hum. Percept. Perform.*, 17:28–43.
- Warren, W. H., M. W. Morris, and M. Kalish, 1988. Perception of translational heading from optical flow, *J. Exp. Psychol. Hum. Percept. Perform.*, 14:646–660.
- Warren, W. H., and J. A. Saunders, 1995. Perception of heading in the presence of moving objects, *Perception*, 24:315–331.
- Wood, R. M., M. A. Harvey, C. E. Young, A. Beedie, and T. Wilson, 2000. Weighting to go with the flow? *Curr. Biol.*, 10:R545–R546.
- Xiao, D.-K., S. Raiguel, V. Marcar, and G. A. Orban, 1997. The spatial distribution of the antagonistic surround of MT/V5 neurons, *Cereb. Cortex*, 7:662–677.

85 The Cortical Analysis of Optic Flow

CHARLES J. DUFFY

GIBSON's (1950) description of optic flow shifted visual motion studies from the perspective of a stationary observer viewing moving objects to that of a moving observer navigating past stationary objects. He emphasized that optic flow is an important cue to heading direction and the three-dimensional layout of the visual environment.

Optic flow is analyzed in the context of other self-movement cues. Proprioceptive and vestibular sensations accompany all self-movement. Kineoceptive sensation and motor signals emerge during active self-movement. These cues are always available, but people moving with their eyes open in a lighted environment are greatly guided by vision.

Visual self-movement cues include optic flow and changes in the position, size, and shape of objects. There is no absolute boundary between optic flow and object motion, but the distinction highlights their interdependence: optic flow analysis can proceed without the burden of recognizing all of the objects in the flow field, and optic flow can assist in object recognition when objects create inconsistencies in the flow field.

This review of the cortical analysis of optic flow focuses on single-neuron studies in monkeys. Relevant studies of cat and human cortex are included for comparison but are not represented comprehensively. Behavioral and psychophysical studies are treated separately in this volume (Chapter 84). Informative studies of optic flow analysis in insects and birds (e.g., Krapp and Hengstenberg, 1996; Wylie et al., 1999) are omitted because their links to cortical motion processing are beyond the scope of this chapter.

Linking dorsal association cortex and spatial vision

The visual functions of parietotemporal cortex were revealed in electrical stimulation and lesion studies (Ferrier, 1876). These findings were overshadowed by the mapping of occipital visuotopy (Holmes, 1918; Inouye, 1909). Interest in extrastriate vision was sustained by experimental evidence of visual function after striate removal (Kluver, 1936) and by clinical evidence of differential parietal and temporal involvement in spatial and object vision (Kleist, 1935).

Updated approaches revealed visual evoked electrical activity in extrastriate cortex (Doty et al., 1964) and striate projections into these areas (Cragg, 1969; Zeki, 1969). Lesion analysis put these findings in the context of dorsal extrastriate specialization for spatial perception and con-

trasted it with ventral extrastriate specialization for object identification (Ungerleider and Brody, 1977; Ungerleider and Mishkin, 1982). Lesion studies suggested that the colliculo-pulvino-parietal visual pathway (Humphrey and Weiskrantz, 1967; Schneider, 1969) supports behavioral responses to visual motion (Doty, 1973; Pasik et al., 1969). Thus, converging dorsal geniculostriate and colliculo-pulvino-parietal pathways combine to serve vision for spatial orientation (Trevarthan, 1968).

The behavioral relevance of this system was seen in patients with striate lesions causing blindsight (Sanders et al., 1974) and extrastriate lesions causing spatial deficits (Botez, 1975). Posterior parietal neurons were found to combine visuosensory and visuomotor signals in a manner that suggested involvement in extrapersonal space perception (Mountcastle, 1976). These findings linked visual motion processing, visuospatial perception, and dorsal extrastriate cortex in a way that provided the theoretical foundation of efforts to understand the cortical analysis of optic flow.

Input to dorsal extrastriate areas

Converging projections from striate cortex to the posterior bank of the superior temporal sulcus (STS) are seen by anterograde fiber degeneration (Garey, 1968; Spatz et al., 1970; Zeki, 1971) and radiolabeled amino acid transport (Ungerleider and Mishkin, 1979). Combined anatomical and physiological studies identify a densely myelinated projection from striate cortex to the STS's middle temporal area (MT) with a distinct boundary at its lateral border with V4, an emphasis on movement responsiveness (Van Essen et al., 1981), and a visuotopic map of the contralateral hemifield (Maunsell and Van Essen, 1987). This projection extends from MT on the posterior bank of the STS to the floor and anterior bank of the STS, with central visual field more prominent posteriorly and peripheral vision more prominent anteriorly (Ungerleider and Desimone, 1986b).

MT is connected reciprocally to adjacent areas in the STS: dorsally to the medial superior temporal area (MST) and along the floor to the fundal superior temporal area (FST) (Desimone and Ungerleider, 1986; Kaas and Morel, 1993; Ungerleider and Desimone, 1986a). STS cortex also receives input from prestriate areas V2, V3, and V4 in the lunate sulcus (Baizer et al., 1991), projects ipsilaterally into posterior parietal cortex (Neal et al., 1988), and creates

patchy callosal connections (Van Essen et al., 1981). The STS's posterior parietal targets receive convergent somatosensory (Jones and Powell, 1970), frontal, and limbic (Mesulam et al., 1977) input. Horse-radish peroxidase (HRP) retrograde tracing and anterograde radio-amino acid tracing show reciprocal connections between the STS and the medial pulvinar thalamus. There are additional projections from pulvinar oralis, suprageniculate, and limitans thalamic nuclei to the inferior parietal lobule (IPL) (Yeterian and Pandya, 1985, 1989, 1991).

These findings support the notion of a gradient of geniculostriate and colliculopulvinar projections into dorsal extrastriate cortex. The geniculostriate projections are more prominent in the STS, whereas the colliculopulvinar projections are more prominent in posterior parietal cortex, where they are joined by a wide variety of other reciprocal connections that create a dense network of convergence (Elston and Rosa, 1997). The net effect is a highly interconnected, distributed system for visuospatial processing in this region (Felleman and Van Essen, 1991; Lewis and Van Essen, 2000).

Posterior dorsal stream motion processing

MT is the most posterior of the dorsal motion processing areas and the first motion-devoted area in that anteriorly directed stream. MT is roughly synonymous with the densely myelinated zone created by striate cortical projections to the posterior bank of the STS. Its neurons are selective for motion direction, but not object shape, with the columnar organization of direction preferences in a map of the contralateral visual field (Allman and Kaas, 1971; Dubner and Zeki, 1971; Zeki, 1974) MT has large receptive fields (~10 degrees square), with medial MT having larger peripheral receptive fields (MTp) and lateral MT having smaller foveal receptive fields (MTf) (Ungerleider and Desimone, 1986a, 1986b).

Direction, speed, and orientation tuning (Maunsell and Van Essen, 1983a) focus MT's activity on combinations of those properties (Albright et al., 1984; Mikami et al., 1986). Some MT neurons have opposite preferred directions in different parts of their receptive fields that may interact with distance cues to serve figure-ground discrimination (Allman et al., 1985; Maunsell and Van Essen, 1983b). These neurons are clustered in columns (Born and Tootell, 1992), with some showing center-surround directional organization and others showing asymmetrical arrangements (Xiao et al., 1997). Antagonistic receptive field neurons project preferentially to dorsal MST (MSTd), whereas synergistic receptive fields project preferentially to lateral MST (MSTl) and FST (Berezovskii and Born, 2000).

Anterior to MT is ventrolateral MST (MSTv or MSTl), with a mix of large and small receptive field neurons

(Komatsu and Wurtz, 1988a; Saito et al., 1986). An anterior subzone has small, peripheral receptive fields that do not include the fixation point (Tanaka et al., 1993). MSTl neurons show size- and speed-dependent direction selectivity. Small moving-dot patterns (<20 degrees in diameter) evoke one direction preference and larger patterns evoke the opposite preference. At intermediate sizes, speed modulates the responses, so opposite directions dominate at faster or slower speeds.

MSTl's size-dependent directionality is generally position invariant; size-direction relations are the same throughout the receptive field (Komatsu and Wurtz, 1988b). However, some MSTl neurons show receptive field specializations as size-dependent directional reversals requiring the occlusion of the central region. Increasing stimulus size without central occlusion suppresses all responses. Increasing size with central occlusion creates an annular stimulus that evokes reversed direction preferences (Tanaka et al., 1993). The center and the surround interact dynamically. Presenting the opposite direction in the surround enhances the center response; presenting a stationary texture in the surround causes still greater enhancement. The pronounced effect of the stationary surround distinguishes MSTl neurons from surround-sensitive neurons in MT and supports MSTl's role in object motion processing (Eifuku and Wurtz, 1998).

Object motion processing in MSTl is enhanced by sensitivity to the relative disparity of motion in the center and the surround. This is consistent with figure-ground discrimination of objects in the visual field (Eifuku and Wurtz, 1999). There are also interactions between moving objects in the receptive field, with the response to a spot moving in the preferred direction being enhanced by a second spot moving in the opposite direction and suppressed by a second spot moving in another direction. These interactions suggest an averaging of responses to paired stimuli, potentially summing signals that define an object and enhancing those responses by cues that distinguish the object from its background (Recanzone et al., 1997).

Anterior dorsal stream motion processing

Posterior parietal area 7a is at the anterior edge of the STS. The 7a neurons have very large receptive fields (>40 degrees square) (Yin and Mountcastle, 1977) that respond to moving stimuli regardless of their color, orientation, or shape (Robinson et al., 1978). These neurons are sensitive to the radial pattern of motion around the fixation point, preferring object motion either toward the fixation point or away from the fixation point. This opponent vector organization is accompanied by foveal sparing such that these neurons do not respond to stimuli at the fixation point (Motter and Mountcastle, 1981). Opponent vector neurons also possess

axial direction preferences and broadly tuned speed sensitivity, potentially enhancing their role in self-movement analysis (Motter et al., 1987; Steinmetz et al., 1987).

Neurons within the STS were first approached by the gradual encroachment of recording studies, first from the more anterior area 7a and then from the more posterior area MT. Recordings of visual tracking neurons in area 7a extended on to the anterior bank of the STS and revealed a combination of visual and pursuit responses. These neurons were activated by apparent target movement induced by the opposite direction of surround movement (the Dunker illusion) (Sakata et al., 1978). The preferred pursuit direction of these neurons was either the same as or the opposite of their preferred visual motion direction, suggesting that they receive both retinal (visual) and extraretinal (ocular proprioceptive or oculomotor corollary) input (Sakata et al., 1983).

This parietal transition zone in the STS also contains visual neurons that respond best to either object movement in the frontoparallel plane, object movement in depth (approaching or receding), or object rotation (clockwise or counterclockwise). This combination of response properties suggests that these neurons represent the complex movement of real objects in the environment (Sakata et al., 1985, 1986).

The complex direction selectivities of anterior STS neurons focused interest on MSTd. MSTd neurons were divided into three categories: 30% preferred small-object motion stimuli, 30% preferred large-field pattern motion stimuli, and the remainder were equally responsive to both (Tanaka et al., 1986). The large-field neurons were further classified by their direction selectivities: direction-selective neurons (~65%) responded best to dot patterns moving in the frontoparallel plane. Size neurons (~20%) responded best when the boundaries of an object moved to simulate symmetrical expansion or contraction. Rotation neurons (~15%) responded best when the pattern rotated clockwise or counterclockwise. The size and rotation stimuli showed position invariance, preferring the same type of movement at different locations in the receptive field such that simple local directionality did not readily explain their responses. These properties defined the DSR (direction, size, rotation) region, which is probably the same as MSTd (Saito et al., 1986).

Optic flow responses in MSTd

MSTd neuronal DSR responses were further characterized as preferring very large stimuli (circular diameters >40 degrees), with stronger responses to the movement of random-dot patterns than to small moving objects. Their direction selectivities are linked to the combination of local directionalities distributed throughout the stimuli, with less

critical contributions from the size and speed of visible elements in the pattern. These findings were the foundation of the notion that MSTd pattern motion responses were the product of an assembled pattern of MT-like local motion responses (Tanaka and Saito, 1989).

MSTd neurons were subsequently described as showing a continuum of selectivities for large (90 degrees square), planar, circular, and radial patterns of optic flow. This continuum was divided into three groups based on the statistical significance of responses to each type of optic flow: single-component neurons responded to one type, occurring as planar (10%), radial (9%), and circular (4%) neurons. Double-component neurons responded to two types with planocircular (17%) and planoradial (17%) neurons. Triple-component neurons responded to all three types as planocircularradial (29%) neurons (Duffy and Wurtz, 1991a).

These classes of neurons differed with respect to the position invariance of their optic flow selectivities, that is, their ability to maintain the same optic flow preferences when tested with small optic flow stimuli presented at different locations in the visual field. Some neurons show the same optic flow preferences throughout their receptive fields, whereas others show different optic flow preferences at different sites (Duffy and Wurtz, 1991b; Graziano et al., 1994; Lappe, 1996; Fig. 85.1). The site of greatest responsiveness to various optic flow stimuli also differed across a neuron's receptive field. One type of flow can have its greatest activation at one site, while another type of optic flow can have its greatest activation at a different site (Lagae et al., 1994).

Triple-component neurons show the least position invariance with different optic flow preferences at different locations in their receptive fields, consistent with their receptive fields being composed of local, planar directional subfields. In contrast, single-component neurons show the greatest position invariance with the same optic flow preferences at different locations in their receptive fields. Local directional subfields, or a mosaic of locally directional subfields, do not readily explain these responses. However, stronger inhibition in single-component neurons might resolve this conflict by suggesting that MSTd receptive fields are composed of partially overlapping, excitatory and inhibitory, planar directional subfields. From this perspective, stronger inhibitory subfields create the more selective single-component neurons, whereas weaker inhibitory subfields create the less selective triple-component neurons (Duffy and Wurtz, 1991b).

STS neurons were characterized by Orban et al. (1992) according to their selectivities for expansion/contraction, rotation, and deformation created by directional shear, noting that many were also responsive to planar motion. Neurons in areas MT and MST all responded to com-

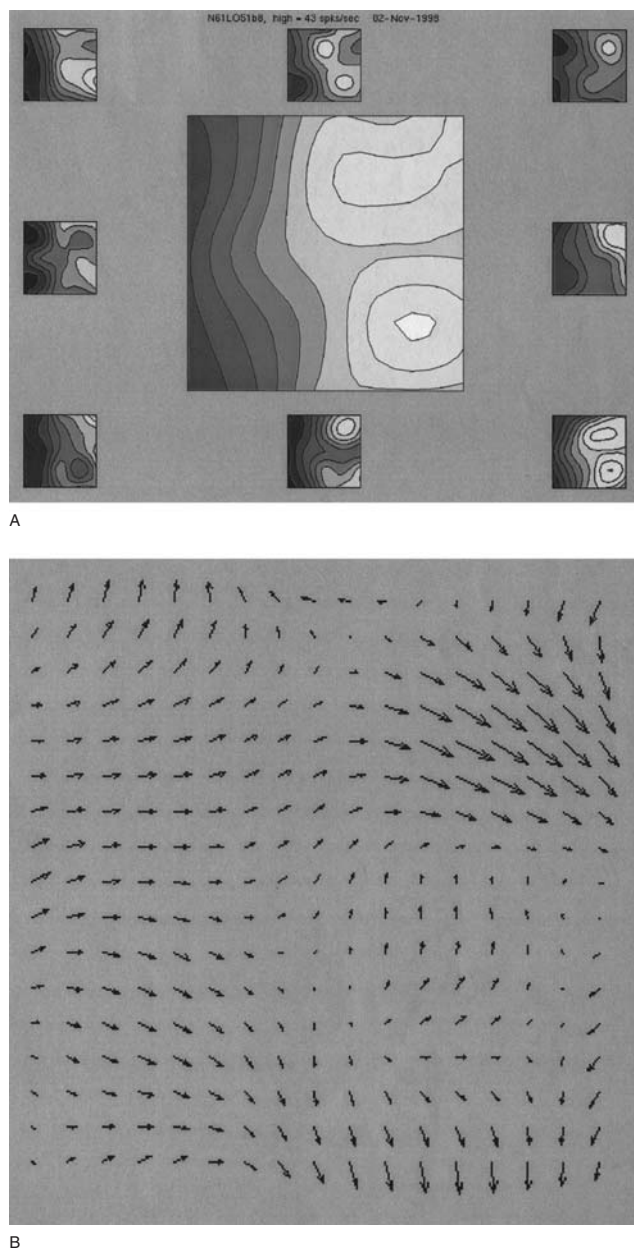


FIGURE 85.1. The complex receptive field organization of an MSTd neuron. Directional responses were tested at 25 positions across the central 100 degrees square of the visual field. *A*, Color contour map of the amplitude of the strongest responses across sites showing great excitatory effects at two separate sites in the right hemifield. Insets show maps of responses to the eight different directions tested. *B*, Vector plots of net directions of responses across sites in the same neuron showing a variable pattern of rightward motion selectivity. (From Logan and Duffy, 1998.) (See color Plate 72)

binations of planar motion and optic flow. However, tests of position invariance showed that MT neurons were all position sensitive in a manner consistent with simple planar directional receptive fields, in this regard, like the triple component neurons of adjacent area MSTd (Lagae et al., 1994).

Heading selectivity in MSTd

MSTd receptive field sizes average 33 degrees square, with substantial extension into the ipsilateral hemifield and no clear relationship between receptive field size and eccentricity (Raiguel et al., 1997). These large receptive fields are well suited to the task of estimating the heading of self-movement based on the large patterns of optic flow. Evidence for heading-selective neuronal activation in MSTd was obtained by comparing responses to various optic flow stimuli. These neurons were tested with optic flow simulating nine directions of forward self-movement as outward radial motion with different foci of expansion (FOEs). MSTd neurons respond selectively to particular FOE stimuli. The mapping of heading preferences revealed three patterns: (1) preferences for peripheral FOEs in one radial segment of the visual field, (2) preferences for FOEs at or near the fixation point, and (3) preferences for FOEs around, but not at, the fixation point. These FOE preferences might detect eccentric headings, gaze-aligned headings, and subtle deviations from gaze-aligned headings, respectively (Fig. 85.2; Duffy and Wurtz, 1995).

MSTd's heading selectivity has been thought to depend on local directional subfields and to match the predictions of neural network models of MST based on MT-like small, planar-directional receptive fields. These projections provide a weighted sampling of the optic flow field arranged to implement an algorithmic solution to heading determination (Heeger and Jepson, 1990). The MST-like layer shows sigmoidal relationships between FOE location and response amplitude that might support a population representation of heading (Lappe and Rauschecker, 1993).

An alternative neural network model of MST heading detection relies on directional template matching (Perrone and Stone, 1994). In this model, MT-like direction- and speed-tuned visual field subunits create a mosaic of sensors across the visual field. A subset of these direction-speed sensors project to each MST-like neuron to impart stimulus selectivity for optic flow. This model's units showed Gaussian distributions of FOE selectivity and replicated optic flow position invariance (Perrone and Stone, 1998).

A three-layered neural network might parse observer and object motion (Zemel and Sejnowski, 1995). The model can train on optic flow to modify the weights of network connections (Zhang et al., 1993) and implement an algorithmic approach to developing optic flow-selective unit responses (Nagel, 1987). The input layer has MT-like local directional units that project to an MST-like middle layer that then projects to an output layer for heading representation. This model responds to optic flow stimuli from observer movement and to small patterns created by object motion (Zemel et al., 1998).

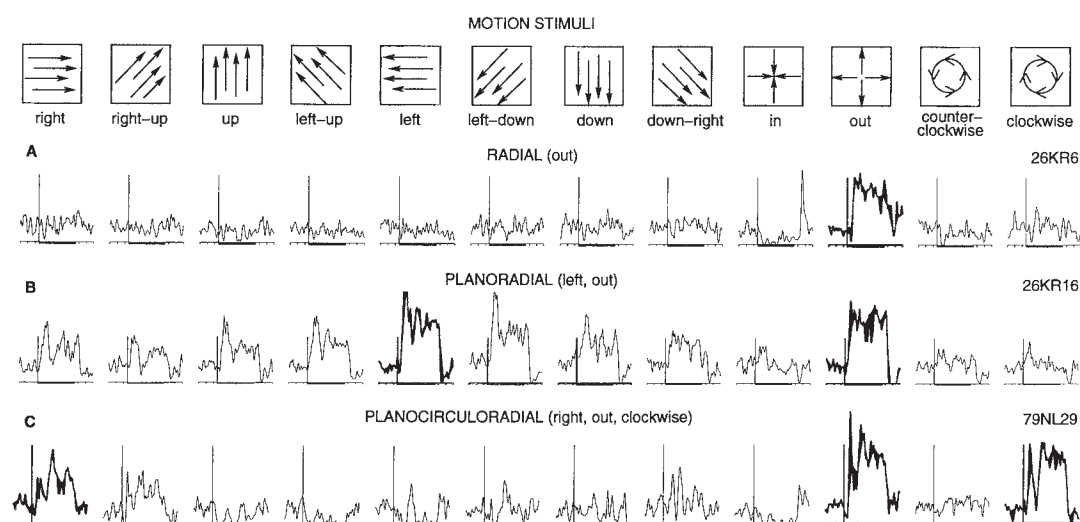


FIGURE 85.2. The continuum of optic flow selectivity in MSTd neurons. Icons along the top indicate the patterns of dot motion in the twelve 100 degree square optic flow stimuli used in this study. A–C, Spike density histograms of the firing rates of three neurons during the presentation of the optic flow stimuli. The vertical bar indicates the 75 spikes per second firing rate; horizontal bars indicate the 1 second stimulus duration. A, The responses of a single-

component radial neuron preferring outward radial optic flow. B, The responses of a double-component planoradial neuron preferring leftward planar and outward radial optic flow. C, The responses of a triple-component planocircularradial neuron preferring rightward planar, clockwise circular, and outward radial optic flow. (From Duffy and Wurtz, 1995.)

Another model might be derived by extending the overlapping gradient's view of MSTd's optic flow responses (Duffy and Wurtz, 1991b) to create a hierarchical processing model. Same-direction MT units covering a large part of the visual field could converge to create position-dependent triple-component neurons. Two triple-component neurons with different location and direction preferences could combine as the excitatory and inhibitory inputs to double-component planocircular or planoradial neurons with planar responses from the excitatory subfield and their radial or circular selectivity from directional inhibition. Adding another inhibitory directional input could take advantage of the orthogonality of circular and radial motion to create single-component responses.

The functional organization of MSTd

The functional organization of MSTd neuronal receptive fields has been explored by mapping direction selectivity across the central 100 degrees of the visual field. The resulting spatial-directional receptive field maps reveal several distinct subfields within each receptive field. The preferred directions of motion vary across subfields, with different subfields showing different proportions of excitatory and inhibitory responses. These subfields are differentially activated by different patterns of optic flow (Fig. 85.3; Logan and Duffy, 1998).

The columnar organization of MSTd has been examined by comparing neuronal response properties recorded along microelectrode penetration tracks. No clear visuotopic orga-

nization has been found; a clustering of similar optic flow selectivities has been observed in some penetrations but not others (Duffy and Wurtz, 1991b). Such inconsistency might reflect the different angles at which penetrations can cross MSTd along the curved path of the STS. Accounting for this curvature reveals some tendency for alternating clusters of expansion and rotation neurons across cortex (Lagae et al., 1994). Functional clustering reinforces this conclusion, with nearby neurons having more similar properties and distant neurons having dissimilar properties (Britten and van Wezel, 1998).

Radioactive isotope labeling reveals the distribution of expansion and rotation responsiveness. H^3 - and C^{14} -glucose administered during visual stimulation reveals an interdigitation of expansion-and rotation-dominated columns on the posterior bank and floor of the STS in the region of areas MT and MSTl. This interdigitation does not extend into MSTd on the anterior bank of the STS. It is not clear if the interdigitated labeling in MT and MSTl represents selective responsiveness to the patterns of optic flow or to the local planar motion components of the stimuli (Geesaman et al., 1997).

MSTd neuronal response mechanisms

Planar direction selectivity supports MSTd's responses to radial, circular, and spiral stimuli. MSTd neuronal heading specificity can be mimicked by overlapping radial or circular optic flow with planar motion stimuli. In less selective triple-component planocircularradial neurons, the underly-

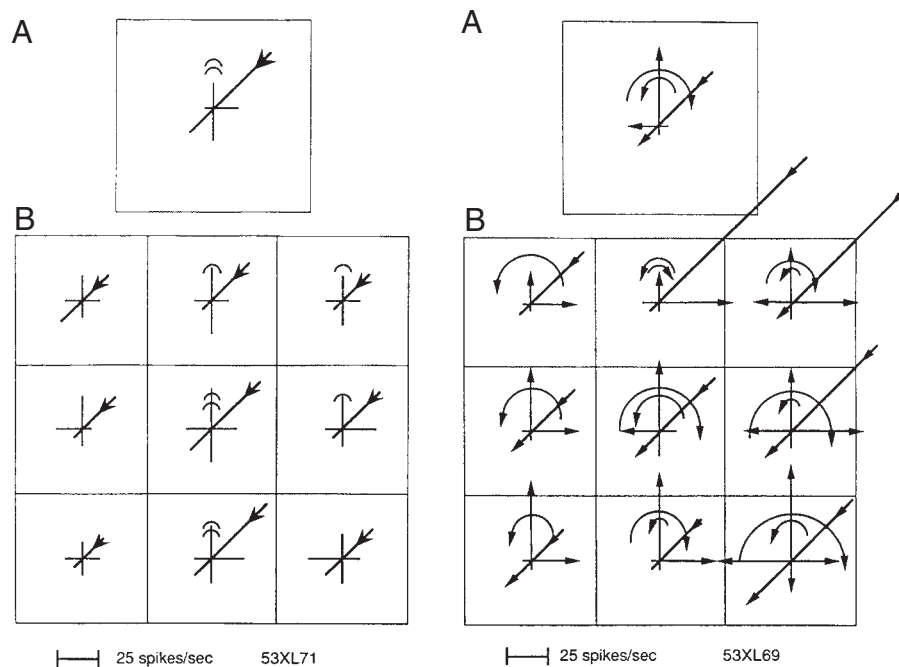


FIGURE 85.3. Polar plots of directional responses of two optic flow neurons in MSTd. Arrows are scaled to the amplitude of the neuronal response to the corresponding optic flow stimulus. Responses to four planar motion stimuli are represented by the horizontal and vertical limbs, responses to inward and outward radial stimuli are represented by the oblique limbs, and responses to the clockwise and counterclockwise circular stimuli are represented by arcs. The large frames indicate the directional responses to 100 degree square

stimulus; the small frames indicate the directional responses to the set of nine 33 degree square stimuli. *A*, Responses of a position-dependent triple-component neuron that showed substantially different optic flow selectivities at different locations. *B*, Responses of a position-invariant single-component inward radial-selective neuron that showed stable optic flow selectivities at different locations. (From Duffy and Wurtz, 1991b.)

ing planar response mechanism's relationship to local motion in the pattern stimuli is obvious. In more selective single-component circular or radial neurons, the underlying planar response mechanism is obscured by inhibitory interactions (Fig. 85.4). This does not mean that MSTd encodes heading by decomposing optic flow into its planar and other components. It only shows that MSTd derives heading from the available neural mechanisms of planar directional, excitatory, and inhibitory responsiveness (Duffy and Wurtz, 1997c).

The link between planar motion and optic flow responses in MSTd is supported by the form/cue invariance of their directional selectivity. Neuronal stimulus preferences evoked by random-dot optic flow are similar to the preferences evoked by a variety of discrete visual object motion stimuli. This similarity extends to preferences for radial, circular, and spiral stimuli but not to the strength of the responses or tuning width in that spiral stimulus space (Geesaman and Andersen, 1996). These results are consistent with a fundamental role for planar motion sensitivity: spiral stimulus space reflects local planar direction around 360 degrees, and both optic flow and moving objects present planar motion.

Further characterization of object motion responses in MSTd has focused on sensitivity to the direction and the three-dimensional orientation of the rotating object. These sensitivities are position invariant across changes in the object's position in the visual field. Speed gradients in these stimuli are critical cues for deriving structure-from-motion percepts, and MSTd neuronal responses reflect sensitivity to the same stimulus parameters (Sugihara et al., 2002). These responses appear to be a consequence of MSTd's direction and speed sensitivity, and obscure the functional distinction between MSTd and MSTl with respect to the analysis of self-movement and object motion.

MSTd neuronal motion selectivity varies during prolonged stimulation. Phasic responses in the first 200 msec of stimulation are less selective than those seen thereafter, but they are not entirely nonselective, their amplitude differing substantially with different optic flow stimuli. Later, tonic responses are more selective for certain optic flow patterns, with the degree of selectivity varying across neurons and continued activity measured for up to 15 seconds of optic flow stimulation. Thus, these responses may continue to represent heading during sustained observer motion (Duffy and Wurtz, 1997b).

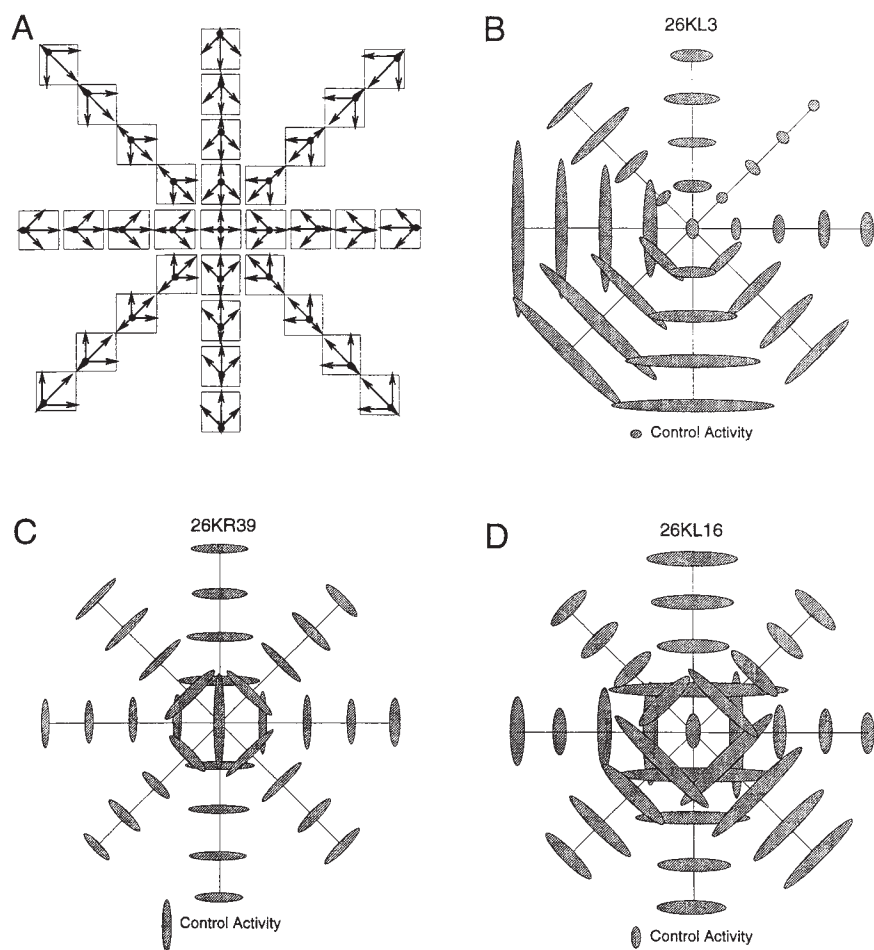


FIGURE 85.4. Patterns of FOF selectivity in three MSTd neurons. *A*, Arrows depict the patterns of dot motion in the 33 optic flow stimuli presented with FOFs at 10 degree intervals in the central visual field. *B–D*, Response amplitude indicated by the size of the oval at the position corresponding to that of the evoking

stimulus. *B*, A neuron that preferred down-left eccentric FOFs. *C*, A neuron that preferred central FOFs. *D*, A neuron that preferred central FOFs but not the centered FOF. (From Duffy and Wurtz, 1995.)

As with object motion responses, speed supplements direction as a primary stimulus parameter in MSTd's responses to optic flow. Speed tuning for complex optic flow patterns and planar motion most commonly show optimal responses over a range of speeds from 5 to 50 deg/sec. Slower or faster stimuli evoke successively smaller responses, with individual neurons having idiosyncratic speed-response profiles. Speed and direction tuning interact to create composite responsiveness to particular stimuli, leading to the suggestion that MSTd combines these signals to encode optic flow (Orban et al., 1995).

The notion that speed tuning might refine optic flow selectivity is supported by MSTd neuronal response sensitivity to the gradient of speeds in optic flow. Naturalistic optic flow contains speed gradients that reflect the three-dimensional layout of the visual environment, with distant features moving more slowly and nearer features more rapidly. MSTd neurons are sensitive to these speed gradients in optic

flow, so that some neurons respond best to stimuli simulating more distant features in the center of the visual field and nearer features in the periphery, as seen when moving down a corridor. Other neurons respond best to the reverse pattern, as seen when approaching an object in front of a distant background. MSTd neurons are also affected by the overlap of speed gradients that create motion parallax effects, with some neurons preferring greater simulated depth of field in optic flow stimuli (Duffy and Wurtz, 1997a).

The great majority of MSTd neurons (89%) are sensitive to binocular disparity, with 46% preferring crossed disparities (near), 38% preferring uncrossed disparities (far), and a few being tuned to a particular disparity. Almost half (40%) of the neurons reverse their preferred direction from crossed to uncrossed disparities. This does not depend on vergence angle, so that disparity relative to the plane of fixation affects responses across a range of absolute distances. This might

contribute to foreground-background discrimination as a moving observer fixates on a stationary point (Roy et al., 1992).

Together, these findings demonstrate that MSTd neurons are well suited to the analysis of optic flow during observer self-movement. Their response properties support sensitivity to the heading of self-movement, the structure of the environment, and the movement of discrete objects in the environment. Crossing the STS from MT to MSTl to MSTd, there is increasing complexity of visual motion responsiveness to both optic flow and object motion.

Temporal cortical responses to optic flow

Neuronal responses to optic flow are seen in STS cortex anterior to MSTd. About 1 cm ventroanteriorly along the STS is the superior temporal polysensory area (STP). Neurons in STP are diverse: 40% are exclusively visual, ~20% also respond to auditory stimuli, ~20% also respond to somatosensory stimuli, and ~20% respond to all three modalities. Their visual receptive fields are large, often including the entire visual field. Most are insensitive to the shape of visual stimuli, but 30%, such as neurons in inferotemporal cortex, are shape selective and prefer faces or facial features. Most are direction selective, with some preferring movement in depth and others preferring centrifugal or centripetal movement relative to the fixation point, such as opponent vector organization in posterior parietal cortex (Bruce et al., 1981).

The functional dichotomy of STP neuronal responsiveness extends to object motion responses that can be divided into two groups: those that are more selective for particular objects and those that are more selective for particular directions of movement. STP neurons that are more selective for particular objects respond only to the independent movement of those objects. The volitional movement of objects under the mechanical control of the animal's hand evokes only weak responses (Hietanen and Perrett, 1993, 1996a). The visual cues that define the object are critical to these responses, with some responding only to luminance-defined objects and other responding only to motion-defined objects (Anderson and Siegel, 1998).

STP neurons that are more selective for the direction of object motion most often prefer object motion along the cardinal axes of extrapersonal space: horizontal, vertical, and depth (Oram et al., 1993). These responses exhibit a body-independent motion discrimination such as the body-independent responses of object form neurons. That is, they respond to object movement when the animal is stationary, not when the animal is moving in a manner that might account for the apparent relative motion of the object (Hietanen and Perrett, 1996b).

The influence of relative movement on object responses suggests that these neurons might also respond to self-movement cues in optic flow. Optic flow responses are observed in 65% of STP neurons, half responding nonselectively to a variety of optic flow stimuli and half responding selectively to certain optic flow stimuli. More than half of these neurons respond to patterned optic flow but not to planar translational motion, whereas the remainder prefer planar motion. Responses to centered FOE stimuli comprise the majority of optic flow responses, although they too are accompanied mainly by translational movement responses (Anderson and Siegel, 1999).

Thus, STP neurons appear to intermix object form, object movement, and optic flow responses. The prevalence of radial expansion optic flow preferences, and the suppression of object motion responses by congruent background motion, suggest that this area may mediate the use of optic flow to detect the independent movement of animate objects seen during observer self-movement.

Parietal cortical responses to optic flow

Neuronal responses to optic flow occur in several areas in posterior parietal cortex (PPC). Neurons in the transition zone between MSTd and area 7a, in the upper-anterior bank of the STS and in the adjacent convexity cortex, have large receptive fields, often more than 90 degrees in diameter. Some respond to object movement in the frontoparallel or depth planes (Sakata et al., 1985) and others are activated object rotation, with weaker responses to planar motion or shear (the combination of two locally opposite directions). Many neurons prefer rotation in the depth plane and some respond to Ames window illusory rotation, suggesting a high-level link to object motion processing (Sakata et al., 1994).

Object motion responses in area 7a show opponent vector organization with preferences for movement toward or away from the fixation point, as well as superimposed preferences for a particular motion direction (Motter et al., 1987; Steinmetz et al., 1987). However, this radial organization of direction selectivity does not predict their responses to optic flow. Their optic flow responses can be selective for particular directions of radial or circular motion, or they can respond nonselectively to multiple directions of radial or circular motion (Siegel and Read, 1997). In addition, these neurons are sensitive to the speed of motion in optic flow, with interactions between speed tuning and optic flow selectivity, so neurons that respond to more than one type of optic flow may have different preferred speeds for those different optic flow stimuli (Phinney and Siegel, 2000).

Neurons in the floor of the intraparietal sulcus (IPS), in the ventral intraparietal area (VIP), have large visual receptive fields that respond selectively to optic flow. These

responses commonly combine radial or circular and planar motion preferences. The planar direction preferences are consistent across their receptive fields, suggesting that local planar motion preferences do not create templates favoring that neuron's preferred radial or circular stimuli (Schaafsma and Duysens, 1996).

The dorsal-medial extension of PPC includes area PEc, the caudal posterior parietal region. Neurons in this region are responsive to somatosensory stimuli and are thought to be involved in motor planning for reaching (Lacquaniti et al., 1995). They also have large visual receptive fields with robust direction selectivity. Most show simple directional responses to object motion, but some show opponent vector organization, preferring motion either inward to or outward from the fixation point. They also respond selectively to optic flow stimuli with different FOEs, with mixed object motion and optic flow responses similar to what has been observed elsewhere in the parietal lobe (Raffi et al., 2002; Squatrito et al., 2001).

In sum, optic flow responses can be elicited from a number of areas around the occipito-parieto-temporal junction. In all of these areas there is a range of preferences for optic flow stimuli simulating visual motion seen during observer self-movement. These optic flow responses are accompanied by selective responses to object motion stimuli, with both types of stimuli eliciting position invariance and speed sensitivity.

Optic flow responses in cat cortex

The dorsal association cortex of the cat includes extrastriate visual processing areas (Clare and Bishop, 1954) that receive input from the geniculo- and colliculocortical systems. The posteromedial (PMLS) and posterolateral (PLLS) regions in the lateral sulcus contain object motion direction-selective visual neurons with large binocular receptive fields that are broadly tuned for speed, with faster speeds preferred in more peripheral receptive fields. Most PLLS neurons and many PMLS neurons have receptive field locations and direction selectivities that create a preference for motion directed away from the fixation point, with fewer cells preferring motion toward the fixation point (von Grunau and Frost, 1983). Radial-selective neurons are combined with circular-selective neurons juxtaposing orthogonal directions in a potential substrate for optic flow analysis (Rauschecker et al., 1987).

Clare-Bishop neurons also respond to object motion: one-third prefer approaching stimuli, one-third prefer translational motion, and half as many prefer receding stimuli, with the remainder being nonresponsive or nonselectively responsive. These selectivities are partly attributable to size effects and partly to binocular distance cues. The posterior lateral sulcus shows more translational motion selectivity, and ante-

rior areas show more approach/recession selectivity and size effects (Toyama et al., 1990).

Anterior but not posterior lateral sulcus neurons show a centrifugal bias, as the preponderance of preferred object motion is directed away from the fixation point. In the posterior region, directional preferences are mainly orthogonal to a line from the receptive field center to the fixation point. This is consistent with a separation of radial and circular motion analysis, suggesting a large-scale organization of optic flow responses in cat lateral sulcus that has not been seen across the monkey STS (Sherk et al., 1995).

This large-scale organization may relate to differences in cortical projections, with the posterior predominance of corticotectal neurons and the anterior predominance of corticostriatal neurons. Corticotectal neurons have smaller receptive fields, slower speed preferences, centrifugal object motion, and a preference for contracting optic flow. Corticostriatal neurons have larger receptive fields, faster speed preferences, an absence of centrifugal bias, and a preference for expanding optic flow (Niida et al., 1997). Alternatively, regional differences in these responses may relate to receptive field size: posterior PMLS neurons with smaller, central receptive fields that prefer slower motion are less influenced by element size and speed gradients in optic flow. Anterior PMLS neurons with larger, peripheral receptive fields that prefer faster motion are more responsive to naturalistic element size and speed gradients (Brosseau-Lachaine et al., 2001).

The relationship between centrifugal bias and optic flow analysis was tested by raising kittens in darkness, except for timed exposure to either expanding or contracting optic flow stimuli presented either by controlled translational movement or by video simulation. Neither the direction nor the type of stimulation altered the centrifugal bias for object motion, although these animals did have more nonresponsive and nondirectional neurons. Thus, dark rearing altered the neuronal responses, but restricted exposure to certain patterns of optic flow did not change their object motion direction selectivity (Brenner and Rauschecker, 1990).

Lateral sulcus neurons prefer naturalistic optic flow stimuli as seen moving across a textured ground plane. Seventy percent of the neurons respond to optic flow, and most have stronger responses when the visual elements have distance-proportioned sizes and accelerate with simulated proximity. There is a preponderance of neurons that prefer optic flow stimuli simulating forward observer movement with mainly downward motion, compared to backward observer movement simulated with mainly upward motion (Kim et al., 1997). The optic flow selectivities of these neurons are not related to their object motion responses, with most neurons showing larger responses to the optic flow but no relationship between the preferred optic flow and object motion directions (Mulligan et al., 1997).

Radial, circular, and translational directionality differ between PMLS and PLLS. About 70% of the neurons in both areas respond to more than one type of optic flow, with an additional ~10% being unresponsive in both areas. The remaining neurons prefer one type of motion, more commonly favoring radial motion over circular or translational motion. In both areas, the nonselective neurons respond more strongly to object motion, whereas the selective neurons respond more strongly to optic flow (Li et al., 2000).

In sum, cat lateral sulcus neurons show many of the same response properties as monkey STS neurons. In cats, there may be greater regional separation of different response specializations and greater directional selectivity than in monkeys. Our understanding of optic flow analysis is still too incomplete to address the issue of whether cats and monkeys use the same neuronal processing mechanisms for optic flow analysis.

Optic flow evoked activity in human cortex

Neuroimaging has identified optic flow-responsive areas of human cerebral cortex. H_2O^{15} positron emission tomography (PET scanning) shows regional changes in cerebral blood flow (rCBF) with optic flow stimulation. Activation by random-dot motion is subtracted from that evoked by optic flow simulating observer movement across the ground plane to create a map of optic flow-selective rCBF that is matched to magnetic resonance images (MRI) used to identify cortical landmarks. Optic flow specific activation is localized to the right dorsal precuneus, right superior parietal lobule, and bilateral fusiform gyri, suggesting some right hemisphere lateralization of optic flow analysis in humans. The activated areas are roughly homologous with monkey areas V3, 7a, and TEO, respectively, but the homolog of MT/MST was not activated in this study (de Jong et al., 1994).

Complementary views of optic flow activation in humans come from combining H_2O^{15} rCBF PET imaging with blood oxygen level dependent (BOLD) functional MRI (fMRI). PET comparisons of rCBF during optic flow and stationary dot displays show multifocal optic flow specific activation in bilateral cuneus (V2, V3a), left-to-right MT/MST, bilateral dorsal IPS, bilateral dorsal premotor area, and right cerebellum. The presentation of similar stimuli during fMRI studies confirmed optic flow activation in bilateral MT/MST. Combining these data sets yielded an impression that the right MT/MST complex and the right dorsal IPS areas were most selectively responsive to optic flow (Peuskens et al., 2001).

BOLD-based fMRI has been used to distinguish between the human cortical homologs of monkey areas MT and MST. In these studies, activation of MT's purely contralateral receptive fields was compared to activation of MST's typically bilateral receptive fields. Full-field optic flow

showed activated sites selected as corresponding to human MT/MST, and also at sites in the IPS, parieto-occipital sulcus, and calcarine sulci. Contralateral hemifield stimulation activated only a more posterior segment of the MT/MST complex, with a more anterior segment activated by either contralateral or ipsilateral stimulation and considered to be homologous to monkey MSTd. Pursuit eye movements tracking a visual target also activated MT+, whereas pursuit of the imagined image of the subject's finger moving in darkness, eye movement without retinal slip, activated an anterolateral area that was considered homologous to monkey MSTl (Dukelow et al., 2001).

Neuroimaging shows the same dual roles of dorsal extrastriate cortex for optic flow and object motion analysis in humans that have been seen in single-neuron studies of monkeys. MRI shows selective activation of MT+ with intact objects versus the scrambled images of those objects. In addition, there is activation by both the movement and the shape of the objects, with synergistic interactions between movement and shape. Thus, MT+ may serve optic flow analysis and also contribute to the analysis of objects defined by movement or other cues (Kourtzi et al., 2002).

Eye position influences optic flow responses

The responses of posterior parietal visual fixation neurons are influenced by fixation position in the frontoparallel and depth planes (Sakata et al., 1980). Flashing a stationary stimulus at a constant receptive field location evokes different responses at different gaze angles. During active fixation, 61% of area 7a neurons show a substantial enhancement of visual responses at some gaze angles with no change in resting activity. In contrast, only 10% of the neurons show gaze angle effects during casual fixations between spontaneous saccades (Andersen and Mountcastle, 1983). As a result, additive models of visual gaze interactions have been rejected in favor of a multiplicative model that describes the area of preferred gaze as a gain field (Andersen and Braunstein, 1985).

Most fixation-responsive neurons (>90%) in areas 7a and MSTd show gaze angle gain fields that can be characterized as a three-dimensional function relating horizontal and vertical eye position to response amplitude. Usually, this function describes a plane, but in ~15% of the neurons this function peaks and falls off within the visual field (Squatrito and Maioli, 1996). Gaze angle interacts with visual and pursuit signals in MSTd, where 34% of pursuit neurons and 10% of visual motion neurons also show gaze angle effects (Squatrito and Maioli, 1997).

Gaze angle modulation of neuronal responses extends across cortical areas and functional response properties. Most neurons in areas MT (61%) and MST (82%) show gaze

angle effects that alter their fixation, pursuit, and visual responses without changing their direction selectivity. Gaze angle effects occur in fewer 7a (42%) and lateral intraparietal (LIP) (39%) neurons, but again, these effects alter responses to fixation, pursuit, and visual motion stimulus. In all of these areas, gaze angle response functions can be fit by a plane. In individual neurons, the same linear function could be applied to fixation, pursuit, and visual responses. This suggests that gaze angle modulates neuronal responses through a mechanism that is shared across response properties (Bremmer et al., 1997a; Bremmer et al., 1997b).

In area 7a, responses to optic flow depend on gaze angle, with more neurons (44%) showing good gaze angle fits to a linear response function than to a nonlinear function (28%). This is complicated by the observation that the function fitting the gaze angle effect often depends on the visual stimulus. This might be attributable to optic flow selectivity causing the response functions for different stimuli to extend over different ranges of response amplitude. Thus, stimulus-dependent differences in gaze angle functions might reflect nonlinear interactions with visual responses (Read and Siegel, 1997).

Pursuit eye movements and cortical motion processing

STS cortex participates in pursuit initiation and maintenance. Focal ibotenic acid lesions in MT create a retinotopic impairment of pursuit initiation in all directions, with saccade errors to moving, but not stationary, stimuli suggesting impaired motion analysis for eye movement control (Newsome et al., 1985). Foveal MT lesions cause pursuit maintenance deficits with movement toward the side of the lesion (Dursteler et al., 1987). Injections anywhere in MST cause pan-directional pursuit initiation deficits in the contralateral hemifield. Lesions in MSTl also cause directional pursuit maintenance deficits with target movement toward the side of the lesion whether the movement began in the contralateral or the ipsilateral hemifield (Dursteler and Wurtz, 1988). All of these lesion effects are temporary. The duration of MT lesion effects is proportional to the size of the lesion. When MT and most of MST is lesioned, recovery remains incomplete after 7 months, regardless of visual experience (Yamasaki and Wurtz, 1991).

Pursuit targets presented with feedback-controlled stabilization of the retinal image, or with blinking-off of the target during its movement, differentiate pursuit activation from retinal versus nonretinal input (e.g., efference copy of the movement command). Pursuit-related activity in MTf lapses during stabilization or blinking, suggesting a retinal origin. Pursuit-related activity in MSTd persists during stabilization and blinking, suggesting a nonretinal origin. Some MSTl neurons lapse and others persist. The combination of

retinal and nonretinal pursuit signals in MSTd suggests that these neurons sum retinal slip and eye velocity signals to drive pursuit (Newsome et al., 1988). Support for the retinal origin of V4 and MT pursuit responses, and for the nonretinal origin of MST pursuit responses, comes from comparisons of responses to retinal motion induced by object or ocular movement. V4 and MT neurons show the same responses to retinal motion regardless of whether it is the result of object or ocular movement, whereas MST neurons respond differently to the same retinal motion resulting from object motion or ocular movement (Erickson and Thier, 1991).

This view is supported by studies in which monkeys are trained to pursue an illusory target, the illusory intersection of incomplete lines in a regular figure. MT neurons that respond during the pursuit of a real object do not respond during pursuit of an illusory target. In contrast, some MST neurons respond during pursuit of real and illusory targets. This subset of MST pursuit-activated neurons do not stop their pursuit activity during a blinking-off of the target, seemingly identifying the subpopulation that accesses a nonretinal pursuit signal (Illg and Thier, 1997).

MT neurons prefer the same direction during pursuit and small spot movement. MSTd neurons reverse their visual motion direction preferences with stimulus size, typically across changes in stimulus dimensions from 20×20 to 30×30 degrees. The preferred pursuit direction is the same as that preferred with small visual stimuli and the opposite of that preferred with large visual stimuli. The largest responses are evoked by slow pursuit (<20 deg/sec) across a large, patterned visual stimulus moving in the opposite direction (Komatsu and Wurtz, 1988b). This suggests that the visual responses of STS neurons that prefer small spot movement (MT and some MSTl neurons) contribute to driving pursuit, whereas the large pattern responses (MSTd and some MSTl neurons) compensate for the perceptual consequences of pursuit.

Such a mechanism may operate to differentiate visual motion from environmental movement and from saccadic eye movements. In some MST and MT neurons, saccadic eye movements evoke a reversal of the preferred direction of visual motion. Thus, the population response to saccadic visual motion sums responses to subpopulations, yielding normal and reversed direction selectivity. These two signals combine to yield no net population response. This may account for the absence of perceived visual motion during the saccades that continuously interrupt fixations (Thiele, 2002).

The contribution of retinal and nonretinal signals in the generation of MT and MST pursuit responses has been tested by cueing a monkey to choose between two alternative pursuit targets. The great majority of MT (86%) and MST (74%) neurons responded only to the visual attributes

of the stimulus, but the remaining neurons responded to the color or the direction of the target that the monkey was cued to follow. The latency to pursuit initiation is increased by the addition of the second distractor target, but MT and MST neuronal responses did not show a comparable latency shift in this task. This supported the view that MT and MST process sensory signals for pursuit target selection but do not perform that target selection (Ferrera and Lisberger, 1997).

The dynamics of pursuit target selection are linked to MT and MST neuronal responses when the initial distance between two competing targets is varied. When they are far apart, both the eye movements and the neuronal responses show initial activity reflecting winner-take-all target selection. This suggests that the separate subpopulations activated by distant targets compete through inhibitory interactions to dominate pursuit initiation, whereas subpopulations activated by nearer targets average their activity to moderate pursuit initiation (Recanzone and Wurtz, 1999). Thus, the influence of STS neuronal responses on pursuit initiation is evident only when stimulus conditions distinguish between aspects of the underlying neural organization.

Optic flow evoked ocular following

Movement of a textured visual display in the frontoparallel plane creates an optic flow pattern that evokes fast, short-latency (50 msec) eye movements (Miles et al., 1986) with characteristics that are consistent with a role in stabilizing gaze during observer movement (Schwarz et al., 1989). Ocular following may be related to short-latency vergence responses to the onset of radial optic flow (Busetini et al., 1997) that interact with the translational vestibular-ocular reflex during self-movement (Paige and Tomko, 1991). Brainstem mechanisms serving these responses (Kawano et al., 1992) may derive visual activation from STS neurons.

MST neurons show strong responses with ocular following to patterned motion stimuli, with 59% responding at least 10 msec before the eye movement. Slowing the stimulus, blurring the pattern, or lowering its spatial frequency delays both the ocular and the neuronal responses. Most (73%) of these neurons discharge during the pursuit of a small target. Blinking-off the pursuit target decreases their activity before pursuit decelerates, suggesting visual regulation of pursuit acceleration. These neurons also respond during optokinetic stimulation, so that MST's projections to the dorsolateral pontine nucleus may involve it in pursuit, ocular following, and optokinetic eye movements (Kawano et al., 1994).

The speed and size of ocular following responses are inversely proportional to viewing distance; nearer stimuli

evoke larger responses (Busetini et al., 1991; Schwarz et al., 1989). This property is shared by only some (44%) of the MST neurons that are activated by ocular following to patterned motion (Inoue et al., 1998). MST's sensitivity to binocular disparity is shared by ocular following responses. The size and speed of ocular following are greatest at slightly crossed disparities (+4 degree) in which the patterned motion stimulus is just in front of the fixation plane. Ocular following decreases more steeply for uncrossed than for crossed disparities, with parallel effects in the relationship between disparity and MST response amplitude. Furthermore, differences between the ocular following responses of individual monkeys are reflected in corresponding differences in the MST population response. Thus, there is a good correlation between disparity effects on ocular following and MST neuronal responses (Takemura et al., 2000).

As previously noted, most (~75%) MST neurons form a continuum of disparity tuning curves, with peak responses at slightly crossed disparities. The remaining neurons peak at slightly uncrossed disparities. These responses sum to relate MST's population response to the average ocular following response based on their shared disparity dependence. Population response profiles across all MST neurons are directly related to ocular following responses ($r^2 = .93$ and $.98$ in two monkeys). Excluding neurons that responded best to slightly uncrossed disparities actually worsens the population fit. Thus, it seems that all disparity-sensitive ocular following neurons contribute to the eye movement response, not just a subpopulation of neurons that individually match ocular following's disparity profile (Takemura et al., 2001).

Vestibular influences on optic flow neurons

Visual-vestibular interactions dominate perception and action during self-movement (Israel et al., 1996; Loose et al., 1996; Telford et al., 1995). These interactions may be facilitated by the anatomical proximity of dorsal extrastriate visual areas and vestibular responsive areas in somatosensory cortical area 2v (Fredrickson et al., 1966; Schwarz and Fredrickson, 1971), posterior parietal area 7a (Faugier-Grimaud and Ventre, 1989; Ventre and Faugier-Grimaud, 1988), and the nearby parietoinsular and retroinsular areas (Akbarian et al., 1994; Grusser et al., 1990; Guldin et al., 1992). These interactions are most tangible in optic flow's influence on postural stability (Asten et al., 1988), reflecting brainstem (Henn et al., 1974) and cortical mechanisms (Buttner and Buettner, 1978) and linking optic flow, postural responses, and dorsal extrastriate cortex (Duffy and Wurtz, 1996).

Half of the pursuit neurons in area 7a (51%) respond to whole-body rotation around the animal's vertical axis in darkness. Most (36%) prefer the same direction of pursuit

and body rotation, with the remainder (15%) preferring opposite directions, possibly reflecting the directionality of convergent pursuit and vestibular inputs (Kawano et al., 1984). Areas 7a and MST also respond to vestibular signals about body tilt. Neurons with direction selectivity for the rotation of a visual object are inhibited by tilting the animal's body in the opposite direction. The tilt responses occur in complete darkness but are stronger when the animal is in a light. Such visual-vestibular interactions might distinguish between visual rotation from object motion or from body movement (Sakata et al., 1994).

MSTl neurons show similar preferred directions for pursuit, visual motion, and body rotation in darkness, although the body rotation responses are smaller (Thier and Erickson, 1992). Similarly, STP neurons respond to the looming of a moving visual object viewed by a stationary monkey, but not to the forward translational movement of the animal toward the stationary object (Hietanen and Perrett, 1996a). Together, these findings suggest that dorsal extrastriate areas integrate visual motion, body movement, and eye movement signals to distinguish between retinal motion from object versus observer movement.

Visual-vestibular interactions in MSTd neurons combine signals from optic flow and translation whole-body movement. Most neurons (70%) respond to optic flow stimuli simulating translational movement in the ground plane, and 48% show significant direction selectivity. Half of those neurons (24%) also show significant direction selectivity during translational movement in darkness. When optic flow is presented during the same direction of translational movement, the responses simply reflect optic flow's directionality. When optic flow is combined with the opposite direction of translational movement, there are many more significant interaction effects. This suggests that MSTd accesses visual and vestibular signals about translational self-movement to represent heading direction (Fig. 85.5; Duffy, 1998).

Optic flow responses during pursuit

Eye movements interact with optic flow analysis in several ways: as noted above, pursuit drives optic flow neurons, and optic flow evokes pursuit-like ocular following. In addition, pursuit complicates heading estimation by altering the retinal image of optic flow (Longuet-Higgins and Prazdny, 1980). Nevertheless, people can derive heading from the visual array during pursuit (Royden et al., 1992; Stone and Perrone, 1997; Warren and Hannon, 1990). This observation caused many to abandon the notion that the FOE is an important heading cue during self-movement and motivated much of the recent work on optic flow.

MSTd neurons show different FOE preferences for optic flow presented during fixation and pursuit. This reflects changes in the retinal image of the optic flow field caused

by eye rotation as well as direct responses to pursuit. About 27% of the neurons maintain similar FOE preferences during fixation and pursuit along the neuron's preferred pursuit axis. This effect is not seen when the retinal effects of pursuit are simulated in the optic flow display while the monkey remains fixated. This suggests that some MSTd neurons have pursuit responses that compensate for the effects of pursuit on the retinal image of optic flow. Alternatively, pairs of neurons with opposite pursuit-induced changes might combine to create pursuit-invariant FOE responses (Bradley et al., 1996).

Similar changes in the retinal image of optic flow can result from head rotation. MSTd neuronal responses to optic flow show different FOE preferences during fixation, pursuit, and head rotation. The changes induced by eye and head rotation are less than would be predicted by accounting for the impact of these movements on the retinal image of the optic flow. Some MSTd neurons seem to use pursuit and vestibular signals to maintain heading selectivity during eye or head rotation in either the preferred or antipreferred pursuit direction. Other neurons might form functional pairs to combine signals that could provide a veridical representation of heading and possibly support the responses of the pursuit-rotation invariant neurons (Shenoy et al., 1999).

Heading selectivity should be invariant with all pursuit directions. Three criteria for pursuit-invariant neurons are heading selectivity during fixation, stable responses to the fixation-preferred heading during pursuit, and no other heading becoming the preferred heading during pursuit (Fig. 85.6). Only 2 of 146 MSTd neurons satisfied all three criteria for eight pursuit directions, and both had purely inhibitory responses. The failure of individual neurons to maintain pursuit-invariant heading selectivity can be contrasted with the robust pursuit invariance of the population responses. MSTd population responses derived by vector summation (Georgopoulos et al., 1986) reliably indicate heading in optic flow during fixation and pursuit. This suggests that a population representation of heading in MSTd that might correspond to the behavioral capacity to interpret optic flow during fixation and pursuit (Fig. 85.7; Page and Duffy, 1999).

Heading estimation during pursuit is complicated by the presence of visible elements at various distances along the observer's line of sight (Longuet-Higgins and Prazdny, 1980). Nevertheless, human heading estimation improves with the addition of multiple depth planes in optic flow (Royden et al., 1992; Stone and Perrone, 1997; Warren and Hannon, 1990). MSTd neurons are sensitive to the presence of speed-defined depth planes in optic flow. These stimuli are created by dividing the moving flow elements into three groups with faster, moderate, and slower speeds simulating closer, intermediate, and farther distances, respectively, as a

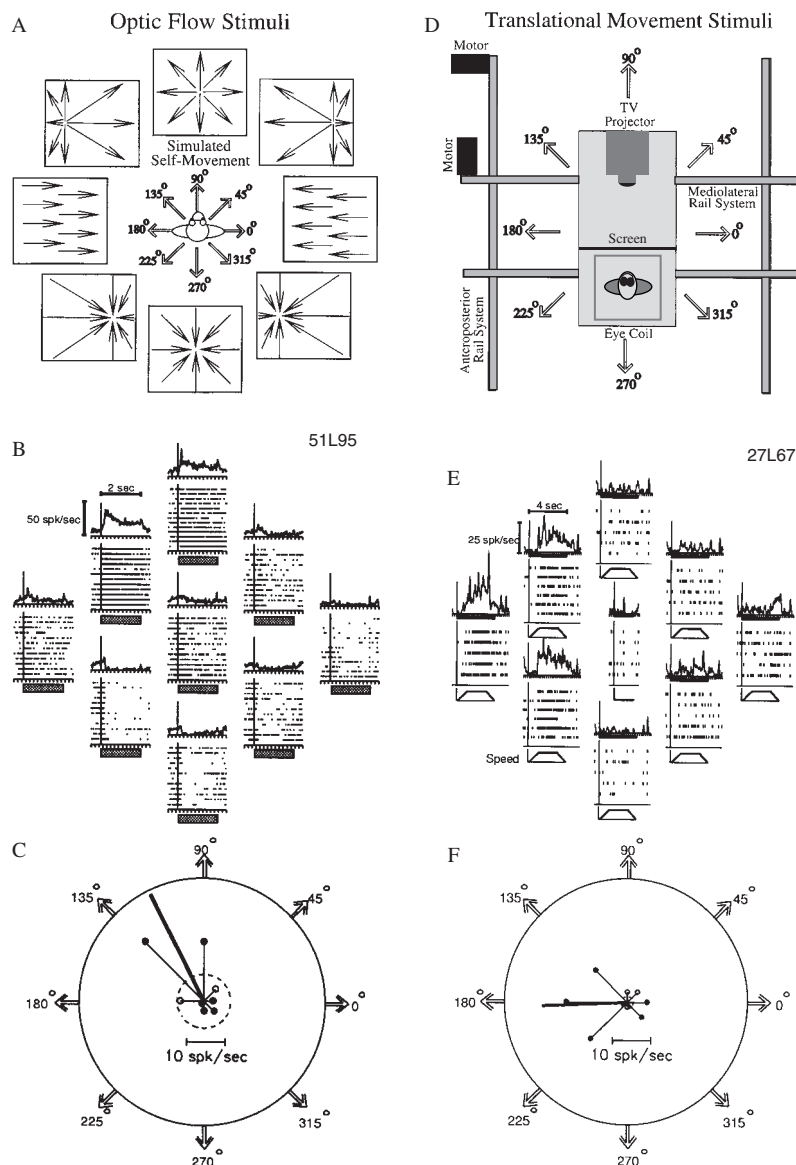


FIGURE 85.5. Responses of MSTd neurons to optic flow simulations of the self-movement scene (*left*) and to whole-body translational self-movement in darkness (*right*). *A*, Optic flow stimuli simulating movement in the ground plane. *B*, Spike density histograms and raster displays of optic flow responses. *C*, Polar plot

of responses showing a preference for leftward movement. *D*, Translational movement stimuli created by two-axis sled. *E*, Spike density histograms and raster displays of movement responses. *F*, Polar plots of responses showing a preference for leftward movement. (Modified from Duffy, 1998.)

motion parallax depth cue. Most neurons (70%) show stronger heading selectivity with multiple depth planes, with many (54%) showing a preference for a particular speed-defined depth plane. This suggests a solution to the creation of multiple FOEs during pursuit across multiple depth planes. MSTd neurons might use their speed sensitivity, possibly in conjunction with disparity sensitivity, to respond to only one of several depth planes in the stimulus. Thus, they might solve the depth planes problem by ignoring all but one depth plane, possibly with enhanced responses from the motion parallax cue (Upadhyay et al., 2000).

Interactions between pursuit effects and translational

vestibular responses alter MSTd neuronal heading selectivity for the direction of movement in the ground plane. Individual neurons show varying responses to optic flow, pursuit, and translational movement, with the vector addition of these response directionalities accounting for a large number of the responses to combined visual, pursuit, and movement stimuli. These interactions show prominent nonadditivities that cause each neuron's responses to combined stimuli to reflect idiosyncratically the contributions of optic flow, pursuit, and vestibular signals. Population vector summation again yields reliable heading responses whether the monkey maintains neutral gaze or pursues an earth-stationary

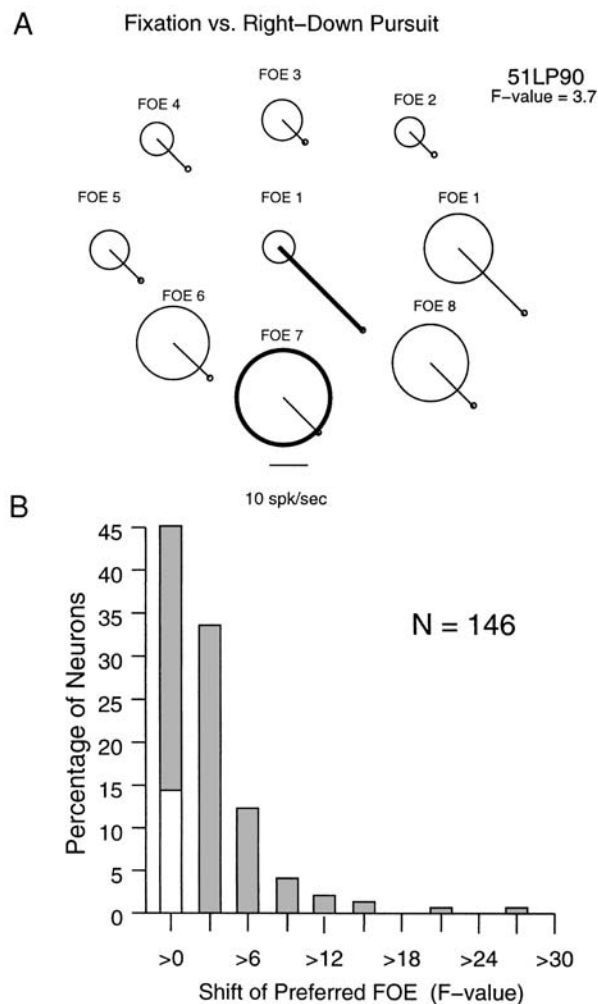


FIGURE 85.6. Responses of MSTd neurons to eight eccentric and the centered FOE outward radial stimuli during fixation and pursuit. *A*, Circles scaled to amplitude of fixation responses to the nine stimuli showing a preference for FOE no. 7. Polar limbs scaled to amplitude of responses during right-down pursuit show a centered FOE preference. *B*, *F* values from two-way analysis of variance of pursuit effects in 146 MSTd neurons showing that most had substantial changes in FOE preferences during pursuit (filled bars represent significant effects, $p < .05$). (From Page and Duffy, 1999.)

target. This supports the view that MSTd serves heading estimation by population encoding (Fig. 85.8; Page and Duffy, 2003).

Optic flow analysis, perception, and behavior

Motion perception is linked to activity in STS cortex (Pasternak and Merigan, 1994). MT and MST neuronal responses to their preferred and antipreferred motion directions are related to the monkey's motion coherence discrimination thresholds for those stimuli. The monkey's motion discrimination responses to near-threshold stimuli

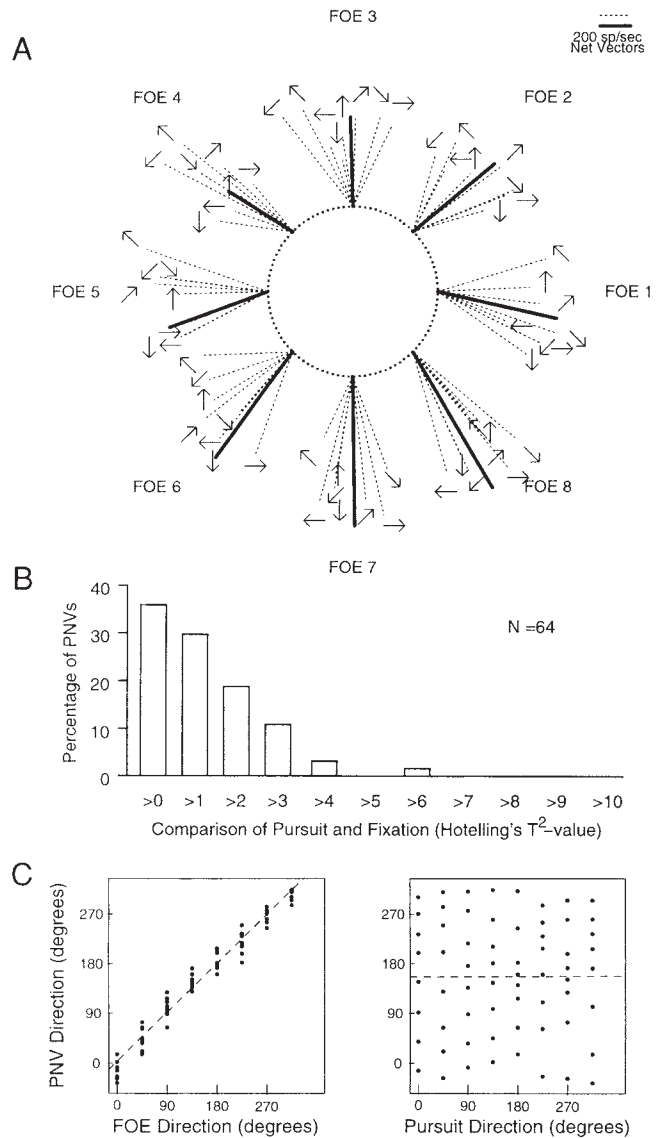


FIGURE 85.7. MSTd population responses to optic flow during fixation and pursuit. *A*, Net vectors of population responses to eccentric FOE stimuli during fixation (*bold lines*) and pursuit (*fine lines*; pursuit direction indicated by the *adjacent arrow*). *B*, Results of statistical comparisons between population responses during fixation and pursuit showing few significant differences. *C*, Direction of population net vector plotted against simulated heading (*left*) and pursuit direction (*right*) showing good agreement between the population response and the simulated heading. (From Page and Duffy, 1999.)

are correlated with neuronal response amplitudes on a trial-by-trial basis. Furthermore, both behavioral and neuronal responses show similar effects of varying motion parameters (Britten et al., 1992; Celebrini and Newsome, 1994). Monkeys trained in two-alternative forced-choice tasks make direction discriminations even when the stimulus is below the monkey's contrast detection threshold. In such cases, MST and STP neurons (but not MT neurons) show greater

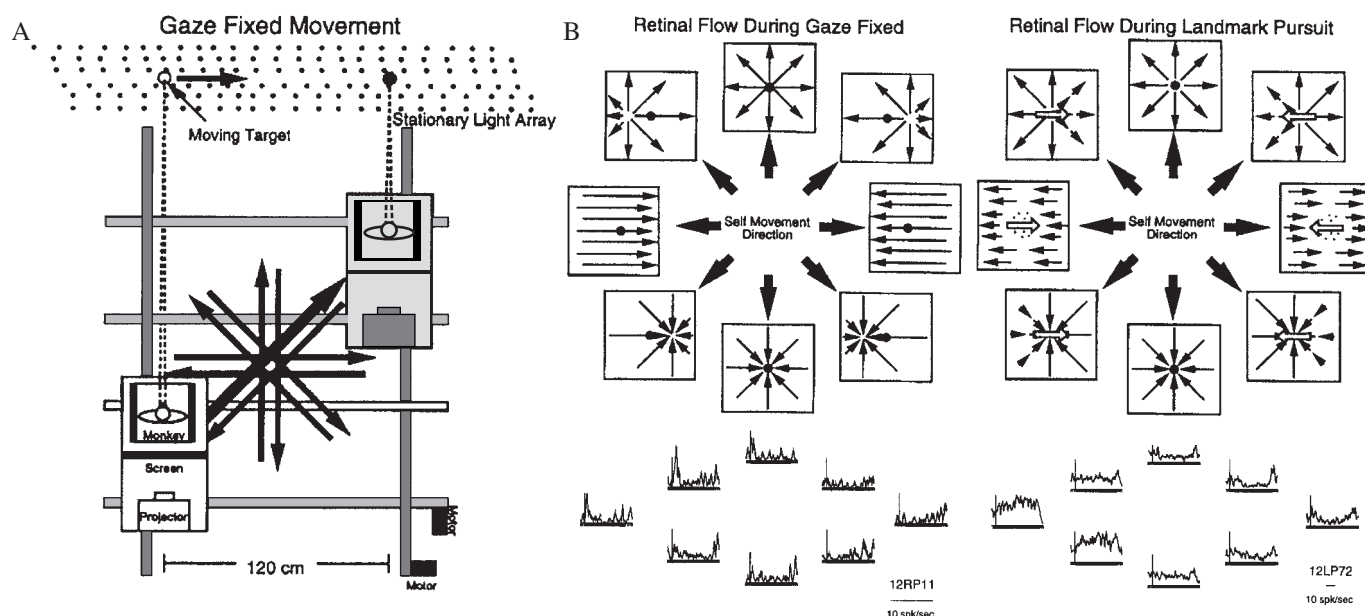


FIGURE 85.8. Interactions between optic flow, vestibular responses, and pursuit responses in MSTd neurons. *A*, Two oculomotor conditions are compared during eight directions of movement in light: gaze fixed straight ahead and landmark pursuit of

an earth-stationary target. *B*, Visual stimuli (*above*) and neuronal responses (*below*) showing strong responses with gaze fixed. Responses with landmark pursuit show very different directional preferences. (Modified from Page and Duffy, 2001.)

activity when the monkey chooses that neuron's preferred direction (Thiele and Hoffmann, 1996). These findings suggest a correspondence between neuronal activity in STS cortex and perceptual decisions about the direction of planar visual motion.

Microstimulation in MSTd alters the animal's ability to identify preferred versus antipreferred optic flow stimuli. Stimulation at a site where neurons prefer FOEs on one side promote the animal's responding to indicate the presence of the FOE on that side. Microstimulation interacts with pursuit effects, favoring behavioral responses indicating FOEs in the direction of the pursuit. This might reflect interference with mechanisms that compensate for pursuit effects on the retinal image of optic flow. These effects are not consistent across all sites in MSTd, but robust effects at some sites support the existence of links between neural activity in MSTd and optic flow perception (Britten and van Wezel, 1998).

MSTd neuronal activity has been linked to the illusory perception of optic flow. When a radial pattern of optic flow is superimposed on a uniform pattern of planar translational movement, the FOE appears to be displaced in the direction of the planar movement (Duffy and Wurtz, 1993). Some MSTd neurons show similar effects of overlapping radial and planar stimuli with responses that shift to match those evoked by radial stimuli with shifted FOEs (Duffy and Wurtz, 1997c). This behavior is mimicked by neurons

in a computational model of MSTd optic flow analysis, with that correspondence including the spectrum of neurons with and without the illusion-like shift of FOE tuning. This supports the notion that MSTd neuronal population encoding is linked to optic flow perception (Lappe and Duffy, 1998).

A link between optic flow analysis and the neural control of behavior is suggested by optic flow responses in motor cortex. In area 7a, 63% of the neurons respond to optic flow, with 38% responding to only one of eight stimuli. In motor cortex arm representation, only 21% of the neurons respond to optic flow but 74% are selective for only one of the eight stimuli. The large receptive fields of 7a neurons contrast with the absence of discernible receptive fields in motor cortical neurons. Motor cortical responses to optic flow might guide the interceptive targeting of arm movements to approaching objects and adjust arm movements to the kinematics of self-movement (Merchant et al., 2001).

Optic flow from natural observer movement presents a sequence of motion patterns that reflect heading changes. MSTd neurons respond to continuously changing optic flow patterns by transitioning their responses from those evoked by the preceding pattern to those evoked by the subsequent pattern (Duffy and Wurtz, 1997b). These transitions are not simple linear interpolations between responses. Rather, all MSTd neurons show nonlinear changes in activity during transitions between some stimuli. In most cases, those

changes constitute a response to the transition itself, with either linear, peaked, or stepwise response profiles. These effects are not attributable to the temporal context created by a sequence of optic flow stimuli. Rather, they reflect unique responses to particular motion patterns seen during the transition between other patterns (Paolini et al., 2000).

Stimulus sequence effects are more evident in MSTd neuronal responses to whole-body translational movement on clockwise (CW) and counterclockwise (CC) circular paths around a room while the animal views a wall-mounted light array. Heading selectivity is seen in 35% of the neurons as a preference for the same heading during CW and CC movement. Another 45% of the neurons show significant heading selectivity on only the CW or the CC path, and 20% of the neurons reverse their heading preference on the CC and CW paths (Fig. 85.9). The latter group responds at the same place in the room, regardless of the path to that place. A combination of heading sequence effects and location-specific activity contributes to these path-dependent heading responses and path-independent place responses. Thus, MSTd might contribute to spatial orientation by integrating self-movement cues over time (Froehler and Duffy, 2002). This could be achieved through interactions between MSTd and hippocampal place neurons for mapping extrapersonal space (McNaughton et al., 1994; O'Keefe and Nadel, 1978).

Behavioral influences on optic flow analysis

Behavior influences neural activity throughout extrastriate visual cortex, with evidence of spatial and nonspatial effects of attention and working memory that alter the amplitude and timing of neuronal discharges (Connor et al., 1997; Desimone, 1998; Fries et al., 2001). In humans, fMRI reveals attentional enhancement of visual responses (Kastner et al., 1998) and resting activity (Kastner et al., 1999), more so in extrastriate than striate areas. Spatial attention activates striate and extrastriate areas, with a correspondence between the spatial scale of the task and the retinotopic scale of cortical activation (Sasaki et al., 2001; Somers et al., 1999).

Spatial and featural attention influence fMRI-recorded activation in human STS cortex. The spatial allocation of attention enhances fMRI-measured activation by spot stimuli at corresponding sites in prestriate more than striate retinotopic maps. No retinotopic map is apparent in MT/MST using such stimuli, but greater activation is seen in the hemisphere that is contralateral to the attended location (Tootell et al., 1998). When subjects view visual motion during a direction or speed discrimination task, activation of MT+ is substantially greater than when they view the same stimuli passively or during a contrast or color discrimination task. When subjects direct attention to a centrally placed sta-

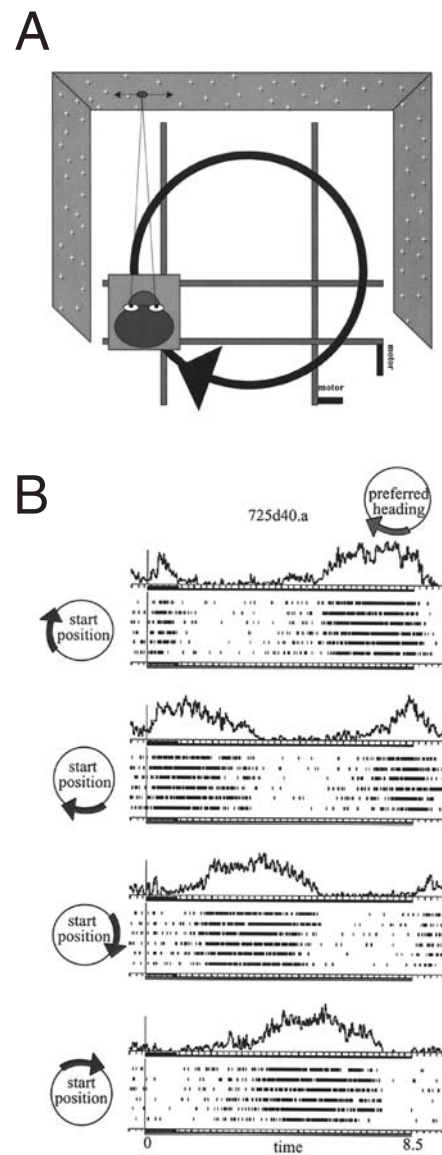


FIGURE 85.9. Responses of an MSTd neuron to movement on a circular path through the room. *A*, Sled movement was clockwise, (illustrated) or counterclockwise, with the monkey maintaining neutral gaze and head position toward the far wall (*top*). *B*, Responses of an MSTd neuron showing leftward movement selectivity that is phase-shifted across different starting positions of sled movement and is stronger during clockwise than counterclockwise movement. (Modified from Froehler and Duffy, 2000.)

tionary target rather than to the surrounding pattern of visual motion, MT+ activation is decreased (Beauchamp et al., 1997; Huk and Heeger, 2000). Even if an array of stationary dots fully overlaps the array of radial motion, MT+ activation is greater when the subject attends to the movement (O'Craven et al., 1997). Attention to tactile stimulation also decreases MT+ activation during the presentation of rotational patterns of visual motion (Haug et al., 1998).

Thus, the detailed characteristics of ongoing behavior can change the pattern of cortical activation that is created by optic flow stimuli.

Task demands influence single-neuron activity in areas MT and MST. These neurons are more responsive to spot movement in their receptive fields when attention is directed within their receptive fields, even when other nonattended stimuli are moving in the receptive field (Treue and Maunsell, 1996). Subtle changes in the task can alter the magnitude of spatial attentional effects on MT neuronal responses to moving stimuli. The spatial separation of moving stimuli and the timing of the monkey's discrimination responses play major roles in these effects (Seidemann and Newsome, 1999). Similarly, the impact of featural attention relies on task demands, with magnitude but not tuning effects on directional responses (Treue and Martinez Trujillo, 1999). Thus, spatial and featural attention can change STS neuronal responses to movement stimuli in a manner that depends on the detailed characteristics of the tasks.

Spatial attention alters the responses of area 7a neurons in a spatial match-to-sample task. The cue stimulus alters the resting activity of the neurons until the presentation of the next stimulus. Cue stimuli presented in the neuron's receptive field suppress responses to stimuli subsequently presented at that site (Constantinidis and Steinmetz, 1996; Steinmetz et al., 1994). Suppression at the cued location is not altered by presentation of the cue along with other distractor stimuli or by presentation of nonmatch stimuli prior to presentation of the match stimulus. This suggests that 7a neurons participate in the reorienting of spatial attention, preventing the entrapment of spatial attention at a cued location (Constantinidis and Steinmetz, 2001a, 2001b).

MSTd neuronal responses to optic flow are affected by spatial working memory and attention. The effects of spatial working memory are seen in a memory-guided saccade task in which optic flow is presented as a distractor between the spatial cue and the saccade. Both cue position and cue proximity effects occur: in some neurons, the absolute position of the cue enhances the optic flow responses. In other neurons, the distance from the cue to the FOE determines the cue's influence on the optic flow responses. The nonspatial effects of attention are seen when optic flow is alternately presented as the cue in an FOE-guided saccade task and as a distractor in a shape-guided saccade task (Fig. 85.10). The optic flow responses differ between the two tasks, mainly with greater response amplitude and narrower FOE tuning during trials in which optic flow guides the subsequent saccade (Dubin and Duffy, 2001). Thus, it appears that optic flow responses in MSTd are affected by both spatial working memory and attentional aspects of the task.

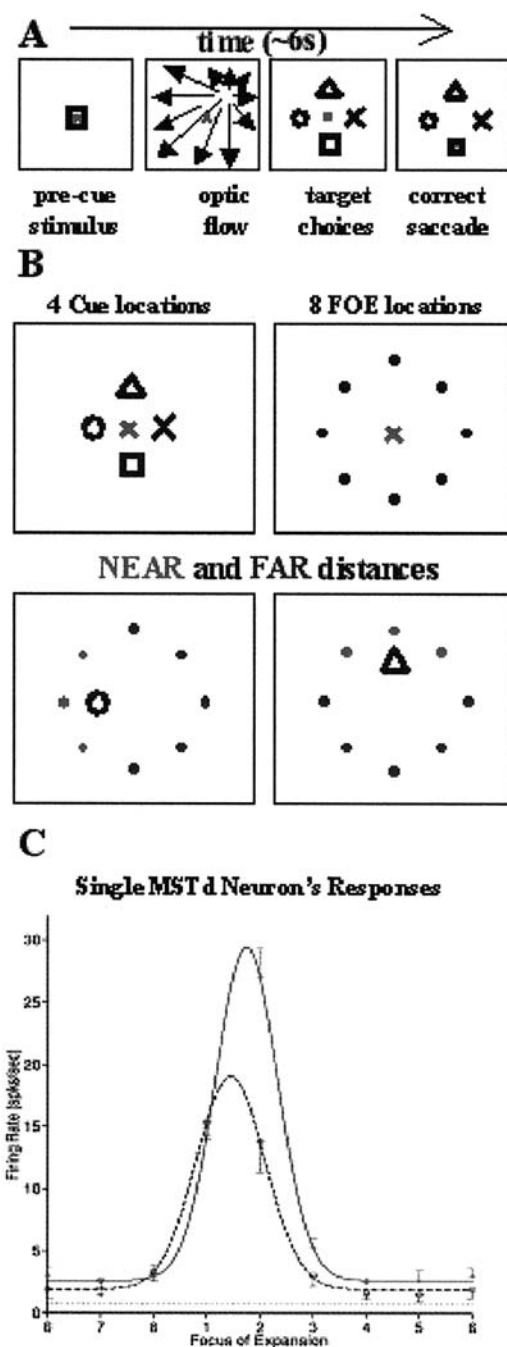


FIGURE 85.10. Spatial working memory effects on MSTd neuronal responses to optic flow. *A*, Stimulus paradigm in which a shape cue is first presented, followed by an optic flow stimulus and then by a target array that guides the monkey's response. *B*, Four shape cue locations and optic flow FOE locations presented in this study. *C*, Responses of an MST neuron to the FOE stimuli when the shape cue implied a location near (red) versus far (blue) from the FOE. Endogenous cueing of spatial working memory modifies the optic flow responses. (After Dubin and Duffy, 2001.) (See color Plate 73)

Conclusions

Optic flow analysis occurs in a distributed temporoparietal system that integrates a variety of sensory and motor signals about self-movement. Visual direction and speed are the most critical stimulus parameters contributing to optic flow–selective responses.

In the STS, area MT contains an array of local motion detectors that are modulated by motion in the surrounding segments of the visual field. Adjacent area MST supports the successive refinement of these signals across neurons to create optic flow–selective responses that are integrated with vestibular signals about self-movement. Posterior parietal and frontal motor cortices show optic flow responses that represent a heading signal that is seemingly extracted from its origins in receptive field–dependent visual mechanisms.

Oculomotor control mechanisms are intimately linked with optic flow analysis. The patterned motion of optic flow contributes to pursuit initiation and maintenance. Conversely, pursuit signals influence the neuronal population encoding of heading estimation to compensate for eye movement effects on the retinal image of optic flow. These mechanisms derive self-movement signals that are suitable to the task of guiding navigation through the visual environment. Such tasks influence optic flow analysis, potentially adapting to spatial and nonspatial aspects of ongoing behavior.

The cortical analysis of optic flow provides a model of multisensory integration and its inseparability from reciprocal interactions with behavior. Optic flow processing supports adaptation to the demands of complex environments and to the opportunities of a rich behavioral repertoire.

Acknowledgments

This chapter is dedicated to Dr. Katherine P. Duffy, whose support and tireless efforts to rewardingly occupy our sons facilitated the completion of this manuscript. This work was supported by grants from the National Eye Institute (EY10287) and the National Institute on Aging (AG17596). I am grateful to Drs. William K. Page, Marc J. Dubin, Michael T. Froehler, and David J. Logan for their comments and contributions to the work. I am grateful for the assistance of Jennifer Postle and Sherry Estes.

REFERENCES

- Akbarian, S., O. J. Grusser, and W. O. Guldin, 1994. Corticofugal connections between the cerebral cortex and brainstem vestibular nuclei in the macaque monkey, *J. Comp. Neurol.*, 339:421–437.
- Albright, T. D., R. Desimone, and C. G. Gross, 1984. Columnar organization of directionally selective cells in visual area MT of the macaque, *J. Neurophysiol.*, 51:16–31.
- Allman, J. M., and J. H. Kaas, 1971. A representation of the visual field in the caudal third of the middle temporal gyrus of the owl monkey (*Aotus trivirgatus*), *Brain Res.*, 31:85–105.
- Allman, J. M., F. M. Miezin, and E. McGuinness, 1985. Stimulus specific responses from beyond the classical receptive field: neurophysiological mechanisms for local-global comparisons in visual neurons, *Annu. Rev. Neurosci.*, 8:407–430.
- Andersen, G. J., and M. L. Braunstein, 1985. Induced self-motion in central vision, *J. Exp. Psychol. Hum. Percept. Perform.*, 11:122–132.
- Andersen, R. A., and V. B. Mountcastle, 1983. The influence of the angle of gaze upon the excitability of the light-sensitive neurons of the posterior parietal cortex, *J. Neurosci.*, 3:532–548.
- Anderson, K. C., and R. M. Siegel, 1998. Lack of selectivity for simple shapes defined by motion and luminance in STPa of the behaving macaque, *NeuroReport*, 9:2063–2070.
- Anderson, K. C., and R. M. Siegel, 1999. Optic flow selectivity in the anterior superior temporal polysensory area, STPa, of the behaving monkey, *J. Neurosci.*, 19:2681–2692.
- Asten, W. N. J. C., C. C. A. M. Gielen, and J. J. D. von der Gon, 1998. Postural adjustments induced by simulated motion of differently structured environments, *Exp. Brain Res.*, 73:371–383.
- Baizer, J. S., L. G. Ungerleider, and R. Desimone, 1991. Organization of visual inputs to the inferior temporal and posterior parietal cortex in macaques, *J. Neurosci.*, 11:168–190.
- Beauchamp, M. S., R. W. Cox, and E. A. DeYoe, 1997. Graded effects of spatial and featural attention on human area MT and associated motion processing areas, *J. Neurophysiol.*, 78:516–520.
- Berezovskii, V. K., and R. T. Born, 2000. Specificity of projections from wide-field and local motion-processing regions within the middle temporal visual area of the owl monkey, *J. Neurosci.*, 20:1157–1169.
- Born, R. T., and R. B. H. Tootell, 1992. Segregation of global and local motion processing in primate middle temporal visual area, *Nature*, 357:497–499.
- Botez, M. I., 1975. Two visual systems in clinical neurology: readaptive role of the primitive system in visual agnosic patients, *Eur. Neurol.*, 13:101–122.
- Bradley, D. C., M. Maxwell, R. A. Andersen, M. S. Banks, and K. V. Shenoy, 1996. Mechanisms of heading perception in primate visual cortex, *Science*, 273:1544–1549.
- Bremmer, F., C. Distler, and K. P. Hoffmann, 1997a. Eye position effects in monkey cortex. II. Pursuit- and fixation-related activity in posterior parietal areas LIP and 7A, *J. Neurophysiol.*, 77:962–977.
- Bremmer, F., U. J. Ilg, A. Thiele, C. Distler, and K. P. Hoffmann, 1997b. Eye position effects in monkey cortex. I. Visual and pursuit-related activity in extrastriate areas MT and MST, *J. Neurophysiol.*, 77:944–961.
- Brenner, E., and J. P. Rauschecker, 1990. Centrifugal motion bias in the cat's lateral suprasylvian visual cortex is independent of early flow field exposure, *J. Physiol.*, 423:641–660.
- Britten, K. H., W. T. Newsome, and R. C. Saunders, 1992. Effects of inferotemporal cortex lesions on form-from-motion discriminations in monkeys, *Exp. Brain Res.*, 88:292–302.
- Britten, K. H., and R. J. van Wezel, 1998. Electrical microstimulation of cortical area MST biases heading perception in monkeys, *Nat. Neurosci.*, 1:59–61.
- Brosseau-Lachaine, O., J. Faubert, and C. Casanova, 2001. Functional sub-regions for optic flow processing in the posteromedial lateral suprasylvian cortex of the cat, *Cereb. Cortex*, 11:989–1001.

- Bruce, C. J., R. Desimone, and C. G. Gross, 1981. Visual properties of neurons in a polysensory area in superior temporal sulcus of the macaque, *J. Neurophysiol.*, 46:369–384.
- Busetini, C., G. Masson, and F. A. Miles, 1997. Radial optic flow induces vergence eye movements with ultra-short latencies, *Nature*, 390:512–515.
- Busetini, C., F. A. Miles, and U. Schwarz, 1991. Ocular responses to translation and their dependence on viewing distance. II. Motion of the scene, *J. Neurophysiol.*, 66:865–878.
- Buttner, U., and U. W. Buettner, 1978. Parietal cortex (2v) neuronal activity in the alert monkey during natural vestibular and optokinetic stimulation, *Brain Res.*, 153:392–397.
- Celebrini, S., and W. T. Newsome, 1994. Neuronal and psychophysical sensitivity to motion signals in extrastriate area MST of the macaque monkey, *J. Neurosci.*, 14:4109–4124.
- Clare, M. H., and H. G. Bishop, 1954. Responses from an association area secondarily activated from optic cortex, *J. Neurophysiol.*, 17:271–277.
- Connor, C. E., D. C. Preddie, J. L. Gallant, and D. C. Van Essen, 1997. Spatial attention effects in macaque area V4, *J. Neurosci.*, 17:3201–3214.
- Constantinidis, C., and M. A. Steinmetz, 1996. Neuronal activity in posterior parietal area 7A during the delay periods of a spatial memory task, *J. Neurophysiol.*, 76:1352–1355.
- Constantinidis, C., and M. A. Steinmetz, 2001a. Neuronal responses in area 7a to multiple-stimulus displays: I. Neurons encode the location of the salient stimulus, *Cereb. Cortex*, 11:581–591.
- Constantinidis, C., and M. A. Steinmetz, 2001b. Neuronal responses in area 7a to multiple stimulus displays: II. Responses are suppressed at the cued location, *Cereb. Cortex*, 11:592–597.
- Cragg, B. G., 1969. The topography of the afferent projections in the circumstriate visual cortex, *Vis. Res.*, 9:733–747.
- de Jong, B. M., S. Shipp, S. Skidmore, R. S. J. Frackowiak, and S. Zeki, 1994. The cerebral activity related to the visual perception of forward motion in depth, *Brain*, 117:1039–1054.
- Desimone, R., 1998. Visual attention mediated by biased competition in extrastriate visual cortex, *Philos. Trans. R. Soc. Lond. B*, 353:1245–1255.
- Desimone, R., and L. G. Ungerleider, 1986. Multiple visual areas in the caudal superior temporal sulcus of the macaque, *J. Comp. Neurol.*, 248:164–189.
- Doty, R., 1973. Ablation of visual areas in the central nervous system, in *Handbook of Sensory Physiology* (R. Jung ed.), Berlin, Heidelberg, New York: Springer-Verlag, pp. 483–541.
- Doty, R., D. S. Kimura, and G. J. Mogenson, 1964. Photically and electrically elicited responses in the central visual system of the squirrel monkey, *Exp. Neurol.*, 10:19–51.
- Dubin, M. J., and C. J. Duffy, 2001. Nonspatial working memory effects in area MST, *Soc. Neurosci. Abstr.*, 27:165.
- Dubner, R., and S. M. Zeki, 1971. Response properties and receptive fields of cells in an anatomically defined region of the superior temporal sulcus, *Brain Res.*, 35:528–532.
- Duffy, C. J., 1998. MST neurons respond to optic flow and translational movement, *J. Neurophysiol.*, 80:1816–1827.
- Duffy, C. J., and R. H. Wurtz, 1991a. Sensitivity of MST neurons to optic flow stimuli. I. A continuum of response selectivity to large-field stimuli, *J. Neurophysiol.*, 65:1329–1345.
- Duffy, C. J., and R. H. Wurtz, 1991b. Sensitivity of MST neurons to optic flow stimuli. II. Mechanisms of response selectivity revealed by small-field stimuli, *J. Neurophysiol.*, 65:1346–1359.
- Duffy, C. J., and R. H. Wurtz, 1993. An illusory transformation of optic flow fields, *Vis. Res.*, 33:1481–1490.
- Duffy, C. J., and R. H. Wurtz, 1995. Response of monkey MST neurons to optic flow stimuli with shifted centers of motion, *J. Neurosci.*, 15:5192–5208.
- Duffy, C. J., and R. H. Wurtz, 1996. Optic flow, posture, and the dorsal visual pathway, in *Perception, Memory, and Emotion: Frontiers in Neuroscience* (H. Ono, B. L. McNaughton, S. Molotchnikoff, E. T. Rolls, and H. Nishijo, eds.), New York: Elsevier, pp. 63–77.
- Duffy, C. J., and R. H. Wurtz, 1997a. Medial superior temporal area neurons respond to speed patterns in optic flow, *J. Neurosci.*, 17:2839–2851.
- Duffy, C. J., and R. H. Wurtz, 1997b. Multiple components of MST responses to optic flow, *Exp. Brain Res.*, 114:472–482.
- Duffy, C. J., and R. H. Wurtz, 1997c. Planar directional contributions to optic flow responses in MST neurons, *J. Neurophysiol.*, 77:782–796.
- Dukelow, S. P., J. F. X. DeSouza, J. C. Culham, A. V. van den Berg, R. S. Menon, and T. Vilis, 2001. Distinguishing subregions of the human MT+ complex using visual fields and pursuit eye movements, *J. Neurophysiol.*, 86:1991–2000.
- Dursteler, M. R., and R. H. Wurtz, 1988. Pursuit and optokinetic deficits following chemical lesions of cortical areas MT and MST, *J. Neurophysiol.*, 60:940–965.
- Dursteler, M. R., R. H. Wurtz, and W. T. Newsome, 1987. Directional pursuit deficits following lesions of the foveal representation within the superior temporal sulcus of the macaque monkey, *J. Neurophysiol.*, 57:1262–1287.
- Eifuku, S., and R. H. Wurtz, 1998. Response to motion in extrastriate area MSTl: center-surround interactions, *J. Neurophysiol.*, 80:282–296.
- Eifuku, S., and R. H. Wurtz, 1999. Response to motion in extrastriate area MSTl: disparity sensitivity, *J. Neurophysiol.*, 82:2462–2475.
- Elston, G. N., and M. G. Rosa, 1997. The occipitoparietal pathway of the macaque monkey: comparison of pyramidal cell morphology in layer III of functionally related cortical visual areas, *Cereb. Cortex*, 7:432–452.
- Erickson, R. G., and P. Thier, 1991. A neuronal correlate of spatial stability during periods of self-induced visual motion, *Exp. Brain Res.*, 86:608–616.
- Faugier-Grimaud, S., and J. Ventre, 1989. Anatomic connections of inferior parietal cortex (area 7) with subcortical structures related to vestibulo-ocular function in a monkey (*Macaca fascicularis*), *J. Comp. Neurol.*, 280:1–14.
- Felleman, D. J., and D. C. Van Essen, 1991. Distributed hierarchical processing in the primate cerebral cortex, *Cereb. Cortex*, 1:1–47.
- Ferrera, V. P., and S. G. Lisberger, 1997. Neuronal responses in visual areas MT and MST during smooth pursuit target selection, *J. Neurophysiol.*, 78:1433–1446.
- Ferrier, D., 1876. *The Functions of the Brain*, London: Smith-Elder.
- Fredrickson, J. M., U. Figge, P. Scheid, and H. H. Kornhuber, 1966. Vestibular nerve projection to the cerebral cortex of the rhesus monkey, *Exp. Brain Res.*, 2:318–327.
- Fries, P., R. H. Reynolds, A. E. Rorie, and R. Desimone, 2001. Modulation of oscillatory neuronal synchronization by selective visual attention, *Science*, 291:1560–1563.
- Froehner, M. T., and C. J. Duffy, 2002. Cortical neurons encode path and place: where you go is where you are, *Science*, 295:2462–2465.
- Froehner, M. T., and C. J. Duffy, 2000. Heading and place effects on MST responses to self-movement, *Soc. for Neurosci. Abstr.*, 26:674.

- Garey, L. J., 1968. Interrelationships of striate and extrastriate cortex with primary relay sites of the visual pathway, *J. Neurol. Neurosurg. Psychiatry*, 2:135–157.
- Geesaman, B. J., and R. A. Andersen, 1996. The analysis of complex motion patterns by form/cue invariant MSTd neurons, *J. Neurosci.*, 16:4716–4732.
- Geesaman, B. J., R. T. Born, R. A. Andersen, and R. B. H. Tootell, 1997. Maps of complex motion selectivity in the superior temporal cortex of the alert macaque monkey: a double-label 2-deoxyglucose study, *Cereb. Cortex*, 7:749–757.
- Georgopoulos, A. P., A. B. Schwartz, and R. E. Kettner, 1986. Neuronal population coding of movement direction, *Science*, 233:1416–1419.
- Gibson, J. J., 1950. *The Perception of the Visual World*, Boston: Houghton Mifflin.
- Graziano, M. S. A., R. A. Andersen, and R. J. Snowden, 1994. Tuning of MST neurons to spiral motion, *J. Neurosci.*, 14:54–67.
- Grusser, O. J., M. Pause, and U. Schreier, 1990. Vestibular neurones in the parieto-insular cortex of monkeys (*Macaca fascicularis*): visual and neck receptor responses, *J. Physiol.*, 430:559–583.
- Guldin, W. O., S. Akbarian, and O. J. Grusser, 1992. Cortico-cortical connections and cytoarchitectonics of the primate vestibular cortex: a study in squirrel monkeys (*Saimiri sciureus*), *J. Comp. Neurol.*, 326:375–401.
- Haug, B. A., J. Baudewig, and W. Paulus, 1998. Selective activation of human cortical area V5A by rotating visual stimulus in fMRI; implication of attentional mechanisms, *NeuroReport*, 9:611–614.
- Heeger, D. J., and A. Jepson, 1990. Visual perception of three-dimensional motion, *Neural Comput.*, 2:129–137.
- Henn, V., L. R. Young, and C. Finley, 1974. Vestibular nucleus units in alert monkeys are also influenced by moving visual fields, *Brain Res.*, 71:144–149.
- Hietanen, J. K., and D. Perrett, 1993. Motion sensitive cells in the macaque superior temporal polysensory area I. Lack of response to the sight of the animal's own limb movement, *Exp. Brain Res.*, 93:117–128.
- Hietanen, J. K., and D. Perrett, 1996a. Motion sensitive cells in the macaque superior temporal polysensory area: response discrimination between self-generated and externally generated pattern motion, *Behav. Brain Res.*, 76:155–167.
- Hietanen, J. K., and D. I. Perrett, 1996b. A comparison of visual responses to object- and ego-motion in the macaque superior temporal polysensory area, *Exp. Brain Res.*, 108:341–345.
- Holmes, G., 1918. Disturbances of vision by cerebral lesions, *Br. J. Ophthalmol.*, 2:353–384.
- Huk, A. C., and D. J. Heeger, 2000. Task-related modulation of visual cortex, *J. Neurophysiol.*, 83:3525–3536.
- Humphrey, A. L., and L. Weiskrantz, 1967. Vision in monkeys after removal of the striate cortex, *Nature*, 215:595–597.
- Ilg, U. J., and P. Thier, 1997. MST neurons are activated by smooth pursuit of imaginary targets, in *Parietal Lobe Contributions to Orientation in 3D Space* (P. Thier and H.-O. Karnath, eds.), Heidelberg: Springer-Verlag, pp. 173–184.
- Inoue, Y. T. A., K. Kawano, T. Kitama, and F. A. Miles, 1998. Dependence of short-latency ocular following and associated activity in the medial superior temporal area (MST) on ocular vergence, *Exp. Brain Res.*, 121:135–144.
- Inouye, T., 1909. *Die Sehstörungen bei Schussverletzungen der kortikalen Sehphäre*. Leipzig: W. Engelmann.
- Israel, I., A. M. Bronstein, R. Kanayama, M. Faldon, and M. A. Gresty, 1996. Visual and vestibular factors influencing vestibular “navigation,” *Exp. Brain Res.*, 112:411–419.
- Jones, E. G., and T. P. S. Powell, 1970. An anatomical study of converging sensory pathways within the cerebral cortex of the monkey, *Brain*, 93:793–820.
- Kaas, J. H., and A. Morel, 1993. Connections of visual areas of the upper temporal lobe of owl monkeys: the MT crescent and dorsal and ventral subdivisions of FST, *J. Neurosci.*, 13:534–546.
- Kastner, S., P. De Weerd, R. Desimone, and L. G. Ungerleider, 1998. Mechanisms of directed attention in the human extrastriate cortex as revealed by functional MRI, *Science*, 282:108–111.
- Kastner, S., M. A. Pinsk, P. De Weerd, R. Desimone, and L. G. Ungerleider, 1999. Increased activity in human visual cortex during directed attention in the absence of visual stimulation, *Neuron*, 22:751–761.
- Kawano, K., M. Sasaki, and M. Yamashita, 1984. Response properties of neurons in posterior parietal cortex of monkey during visual-vestibular stimulation. I. Visual tracking neurons, *J. Neurophysiol.*, 51:340–351.
- Kawano, K., M. Shidara, Y. Watanabe, and S. Yamane, 1994. Neural activity in cortical area MST of alert monkey during ocular following responses, *J. Neurophysiol.*, 71:2305–2324.
- Kawano, K., M. Shidara, and S. Yamane, 1992. Neural activity in dorsolateral pontine nucleus of alert monkey during ocular following responses, *J. Neurophysiol.*, 67:680–703.
- Kim, J. N., K. Mulligan, and H. Sherk, 1997. Simulated optic flow and extrastriate cortex: I. Optic flow versus texture, *J. Neurophysiol.*, 77:554–561.
- Kleist, K., 1935. Über Form und Orstsbblindheit bei Verletzungen des Hinterhautlappens, *Dtsch. Z. Nervenheilk.*, 138:206–214.
- Kluver, H., 1936. An analysis of the effects of the removal of the occipital lobes in monkeys, *J. Psychology*, 2:49–61.
- Komatsu, H., and R. H. Wurtz, 1988a. Relation of cortical areas MT and MST to pursuit eye movements. I. Localization and visual properties of neurons, *J. Neurophysiol.*, 60:580–603.
- Komatsu, H., and R. H. Wurtz, 1988b. Relation of cortical areas MT and MST to pursuit eye movements. III. Interaction with full-field visual stimulation, *J. Neurophysiol.*, 60:621–644.
- Kourtzi, Z., H. H. Bulthoff, M. Erb, and W. Grodd, 2002. Object-selective responses in the human motion area MT/MST, *Nature*, 5:17–18.
- Krapp, H. G., and R. Hengstenberg, 1996. Estimation of self-motion by optic flow processing in single visual interneurons, *Nature*, 384:463–466.
- Lacquaniti, F., E. Guigon, L. Bianchi, S. Ferraina, and R. Caminiti, 1995. Representing spatial information for limb movement: role of area 5 in the monkey, *Cereb. Cortex*, 5:391–409.
- Lagae, L., H. Maes, S. Raiguel, D. K. Xiao, and G. A. Orban, 1994. Responses of macaque STS neurons to optic flow components: a comparison of areas MT and MST, *J. Neurophysiol.*, 71:1597–1626.
- Lappe, M., 1996. Functional consequences of an integration of motion and stereopsis in area MT of monkey extrastriate visual cortex, *Neural Comput.*, 8:1449–1461.
- Lappe, M., and C. J. Duffy, 1998. Neural mechanisms of an optic flow illusion: model and experiment, *Eur. J. Neurosci.*, 11:2323–2331.
- Lappe, M., and J. P. Rauschecker, 1993. A neural network for the processing of optic flow from ego-motion in higher mammals, *Neural Comput.*, 5:374–391.
- Lewis, J. W., and D. C. Van Essen, 2000. Corticocortical connections of visual, sensorimotor, and multimodal processing areas in

- the parietal lobe of the macaque monkey, *J. Comp. Neurol.*, 428:112–137.
- Li, B., B.-W. Li, Y. Chen, L.-H. Wang, and Y. F. Diao, 2000. Response properties of PMLS and PLLS neurons to simulated optic flow patterns, *Eur. J. Neurosci.*, 12:1534–1544.
- Logan, D. J., and C. J. Duffy, 1998. Local directionality in response fields of optic flow selective MST neurons, *Soc. Neurosci. Abstr.*, 24:649.
- Longuet-Higgins, H. C., and K. Prazdny, 1980. The interpretation of a moving retinal image, *Proc. R. Soc. Lond. B*, 208:385–397.
- Loose, R., T. H. Probst, and E. R. Wist, 1996. Perception of direction of visual motion. I. Influence of angular body acceleration and tilt, *Behav. Brain Res.*, 81:141–146.
- Maunsell, J. H., and D. C. Van Essen, 1983a. Functional properties of neurons in middle temporal visual area of the macaque monkey. I. Selectivity for stimulus direction, speed, and orientation, *J. Neurophysiol.*, 49:1127–1147.
- Maunsell, J. H., and D. C. Van Essen, 1983b. Functional properties of neurons in middle temporal visual area of the macaque monkey. II. Binocular interactions and sensitivity to binocular disparity, *J. Neurophysiol.*, 49:1148–1167.
- Maunsell, J. H. R., and D. C. Van Essen, 1987. Topographic organization of the middle temporal visual area in the macaque monkey: representational bias and the relationship to callosal connections and myeloarchitectonic boundaries, *J. Comp. Neurol.*, 266:535–555.
- McNaughton, B. L., S. J. Y. Mizumori, C. A. Barnes, B. J. Leonard, M. Marquis, and E. J. Green, 1994. Cortical representation of motion during unrestrained spatial navigation in the rat, *Cereb. Cortex*, 4:27–39.
- Merchant, H., A. Battaglia-Mayer, and A. P. Georgopoulos, 2001. Effects of optic flow in motor cortex and area 7a, *J. Neurophysiol.*, 86:1937–1954.
- Mesulam, M. M., G. W. Van Hoesen, D. N. Pandya, and N. Geschwind, 1977. Limbic and sensory connections of the inferior parietal lobule (area PG) in the rhesus monkey: a study with a new method for horseradish peroxidase histochemistry, *Brain Res.*, 136(3):393–414.
- Mikami, A., W. T. Newsome, and R. H. Wurtz, 1986. Motion selectivity in macaque visual cortex. I. Mechanisms of direction and speed selectivity in extrastriate area MT, *J. Neurophysiol.*, 55:1308–1351.
- Miles, F. A., K. Kawano, and L. M. Optican, 1986. Short-latency ocular following responses of monkey. I. Dependence on temporospatial properties of visual input, *J. Neurophysiol.*, 56:1321–1354.
- Motter, B. C., and V. B. Mountcastle, 1981. The functional properties of the light-sensitive neurons of the posterior parietal cortex studies in waking monkeys: foveal sparing and opponent vector organization, *J. Neurosci.*, 1:3–26.
- Motter, B. C., M. A. Steinmetz, C. J. Duffy, and V. B. Mountcastle, 1987. Functional properties of parietal visual neurons: mechanisms of directionality along a single axis, *J. Neurosci.*, 7:154–176.
- Mountcastle, V. B., 1976. The world around us: neural command functions for selective attention. The F. O. Schmitt Lecture in Neuroscience for 1975, *Neurosci. Res. Progr. Bull.*, 14:2–47.
- Mulligan, K., J. N. Kim, and H. Sherk, 1997. Simulated optic flow and extrastriate cortex. II. Responses to bar versus large-field stimuli, *J. Neurophysiol.*, 77:562–570.
- Nagel, H.-H., 1987. On the estimation of optical flow: relations between different approaches and some new results, *Artif. Intell.*, 33:299–324.
- Neal, J. W., R. C. Pearson, and T. P. Powell, 1988. The cortico-cortical connections within the parieto-temporal lobe of area PG, 7a, in the monkey, *Brain Res.*, 438:343–350.
- Newsome, W. T., R. H. Wurtz, M. R. Dursteler, and A. Mikami, 1985. Deficits in visual motion processing following ibotenic acid lesions of the middle temporal visual area of the macaque monkey, *J. Neurosci.*, 5(3):825–840.
- Newsome, W. T., R. H. Wurtz, and H. Komatsu, 1988. Relation of cortical areas MT and MST to pursuit eye movements. II. Differentiation of retinal from extraretinal inputs, *J. Neurophysiol.*, 60:604–620.
- Niida, T., B. E. Stein, and J. G. McHaffie, 1997. Response properties of corticotectal and corticostriatal neurons in the posterior lateral suprasylvian cortex of the cat, *J. Neurosci.*, 17:8550–8565.
- O'Craven, K. M., B. R. Rosen, K. K. Kwong, A. Treisman, and R. L. Savoy, 1997. Voluntary attention modulates fMRI activity in human MT-MST, *Neuron*, 18:591–598.
- O'Keefe, J., and L. Nadel, 1978. *The Hippocampus as a Cognitive Map*, Oxford: Clarendon Press.
- Oram, M. W., D. I. Perrett, and J. K. Hietanen, 1993. Directional tuning of motion-sensitive cells in the anterior superior temporal polysensory area of the macaque, *Exp. Brain Res.*, 97:274–294.
- Orban, G. A., L. Lagae, S. Raiguel, D. Xiao, and H. Maes, 1995. The speed tuning of medial superior temporal (MST) cell responses to optic-flow components, *Perception*, 24:269–285.
- Orban, G. A., L. Lagae, A. Verri, S. Raiguel, D. Xiao, H. Maes, and V. Torre, 1992. First-order analysis of optic flow in the monkey brain, *Proc. Natl. Acad. Sci.*, 89(7):2595–2599.
- Page, W. K., and C. J. Duffy, 1999. MST neuronal responses to heading direction during pursuit eye movements, *J. Neurophysiol.*, 81:596–610.
- Page, W. K., and C. J. Duffy, 2001. MST population encoding of heading during whole-body self-movement, *Soc. Neurosci. Abstr.*, 27:165.
- Paige, G. D., and D. L. Tomko, 1991. Eye movement response to linear head motion in the squirrel monkey: I. Basic characteristics, *J. Neurophysiol.*, 65:1170–1182.
- Paolini, M., C. Distler, F. Bremmer, M. Lappe, and K. P. Hoffmann, 2000. Responses to continuously changing optic flow in area MST, *J. Neurophysiol.*, 84:730–743.
- Pasik, P., T. Pasik, and P. Schilder, 1969. Extrageniculostriate vision in the monkey: discrimination of luminous flux-equated figures, *Exp. Neurol.*, 24:421–437.
- Pasternak, T., and W. H. Merigan, 1994. Motion perception following lesions of the superior temporal sulcus in the monkey, *Cereb. Cortex*, 4:247–259.
- Perrone, J. A., and L. S. Stone, 1994. A model of self-motion estimation within primate extrastriate visual cortex, *Vis. Res.*, 34:2917–2938.
- Perrone, J. A., and L. S. Stone, 1998. Emulating the visual receptive-field properties of MST neurons with a template model of heading estimation, *J. Neurosci.*, 18:5958–5975.
- Peuskens, H., S. Sanaert, P. Dupont, P. Van Hecke, and G. A. Orban, 2001. Human brain regions involved in heading estimation, *J. Neurosci.*, 21:2451–2461.
- Phinney, R. E., and R. M. Siegal, 2000. Speed selectivity for optic flow in area 7a of the behaving macaque, *Cereb. Cortex*, 10:413–421.
- Raffi, M., S. Squatrito, and M. G. Maioli, 2002. Neuronal responses to optic flow in the monkey parietal area PEc, *Cereb. Cortex*, 12:639–646.

- Raiguel, S., M. M. Van Hulle, D. Xiao, V. Marcar, L. Lagae, and G. A. Orban, 1997. Size and shape of receptive fields in the medial superior temporal area (MST) of the macaque, *NeuroReport*, 8:2803–2808.
- Rauschecker, J. P., M. W. von Grunau, and C. Poulin, 1987. Thalamo-cortical connections and their correlation with receptive field properties in the cat's lateral suprasylvian visual cortex, *Exp. Brain Res.*, 67:100–112.
- Read, H. L., and R. M. Siegel, 1997. Modulation of responses to optic flow in area 7a by retinotopic and oculomotor cues in monkey, *Cereb. Cortex*, 7:647–661.
- Recanzone, G. H., and R. H. Wurtz, 1999. Shift in smooth pursuit initiation and MT and MST neuronal activity under different stimulus, *J. Neurophysiol.*, 82:1710–1727.
- Recanzone, G. H., R. H. Wurtz, and U. Schwarz, 1997. Responses of MT and MST neurons to one and two moving objects in the receptive field, *J. Neurophysiol.*, 78:2904–2915.
- Robinson, D. L., M. E. Goldberg, and G. B. Stanton, 1978. Parietal association cortex in the primate: sensory mechanisms and behavioral modulations, *J. Neurophysiol.*, 41:910–932.
- Roy, J. P., H. Komatsu, and R. H. Wurtz, 1992. Disparity sensitivity of neurons in monkey extrastriate area MST, *J. Neurosci.*, 12:2478–2492.
- Royden, C. S., M. S. Banks, and J. A. Crowell, 1992. The perception of heading during eye movements, *Nature*, 360:583–585.
- Saito, H., M. Yukie, K. Tanaka, K. Hikosaka, Y. Fukada, and E. Iwai, 1986. Integration of direction signals of image motion in the superior temporal sulcus of the macaque monkey, *J. Neurosci.*, 6:145–157.
- Sakata, H., H. Shibutani, Y. Ito, and K. Tsurugai, 1986. Parietal cortical neurons responding to rotatory movement of visual stimulus in space, *Exp. Brain Res.*, 61:658–663.
- Sakata, H., H. Shibutani, Y. Ito, K. Tsurugai, S. Mine, and M. Kusunoki, 1994. Functional properties of rotation-sensitive neurons in the posterior parietal association cortex of the monkey, *Exp. Brain Res.*, 101:183–202.
- Sakata, H., H. Shibutani, and K. Kawano, 1978. Parietal neurons with dual sensitivity to real and induced movements of visual target, *NeuroScience*, 9:165–169.
- Sakata, H., H. Shibutani, and K. Kawano, 1980. Spatial properties of visual fixation neurons in posterior parietal association cortex of the monkey, *J. Neurophysiol.*, 43:1654–1672.
- Sakata, H., H. Shibutani, and K. Kawano, 1983. Functional properties of visual tracking neurons in posterior parietal association cortex of the monkey, *J. Neurophysiol.*, 49:1364–1380.
- Sakata, H., H. Shibutani, K. Kawano, and T. L. Harrington, 1985. Neural mechanisms of space vision in the parietal association cortex of the monkey, *Vis. Res.*, 25:453–463.
- Sanders, M. D., E. K. Warrington, J. Marshall, and L. Wieskrantz, 1974. "Blindsight": vision in a field defect, *Lancet*, 1(7860): 707–708.
- Sasaki, Y., N. Hadjikhani, B. Fischl, A. K. Liu, S. Marret, A. M. Dale, and R. B. H. Tootell, 2001. Local and global attention are mapped retinotopically in human occipital cortex, *PNAS*, 98: 2077–2082.
- Schaafsma, S. J., and J. Duysens, 1996. Neurons in the ventral intraparietal area of awake macaque monkey closely resemble neurons in the dorsal part of the medial superior temporal area in their responses to optic flow, *J. Neurophysiol.*, 76:4056–4068.
- Schneider, G. E., 1969. Two visual systems, *Science*, 163:895–902.
- Schwarz, D. W. F., and J. M. Fredrickson, 1971. Rhesus monkey vestibular cortex: a bimodal primary projection field, *Science*, 172:280–281.
- Schwarz, U., C. Busetini, and F. A. Miles, 1989. Ocular responses to linear motion are inversely proportional to viewing distance, *Science*, 245:1396.
- Seidemann, E., and W. T. Newsome, 1999. Effect of spatial attention on the responses of area MT neurons, *J. Neurophysiol.*, 81:1783–1794.
- Shenoy, K. V., D. C. Bradley, and R. A. Andersen, 1999. Influence of gaze rotation on the visual response of primate MSTd neurons, *J. Neurophysiol.*, 81:2764–2786.
- Sherk, H., J. N. Kim, and K. Mulligan, 1995. Are the preferred directions of neurons in cat extrastriate cortex related to optic flow? *Vis. Neurosci.*, 12:887–894.
- Siegel, R. M., and H. L. Read, 1997. Analysis of optic flow in the monkey parietal area 7a, *Cereb. Cortex*, 7:327–346.
- Somers, D. C., A. M. Dale, A. E. Seiffert, and R. B. H. Tootell, 1999. Functional MRI reveals spatially specific attentional modulation in human primary visual cortex, *Proc. Natl. Acad. Sci. USA*, 96:1663–1668.
- Spatz, W. B., J. Tigges, and M. Tigges, 1970. Subcortical projections, cortical associations, and some intrinsic interlaminar connections of the striate cortex in the squirrel monkey (*Saimiri*), *J. Comp. Neurol.*, 140:155–174.
- Squatrito, S., and M. G. Maioli, 1996. Gaze field properties of eye position neurones in areas MST and 7a of the macaque monkey, *Vis. Neurosci.*, 13:385–398.
- Squatrito, S., and M. G. Maioli, 1997. Encoding of smooth pursuit direction and eye position by neurons of area MSTd of macaque monkey, *J. Neurosci.*, 17:3847–3860.
- Squatrito, S., M. Raffi, M. G. Maioli, and A. Battaglia-Mayer, 2001. Visual motion responses of neurons in the caudal area PE of macaque monkeys, *J. Neurosci.*, 21:RC130.
- Steinmetz, M. A., C. E. Connor, C. Constantinidis, and J. R. McLaughlin, 1994. Covert attention suppresses neuronal responses in area 7A of the posterior parietal cortex, *J. Neurophysiol.*, 72:1020–1023.
- Steinmetz, M. A., B. C. Motter, C. J. Duffy, and V. B. Mountcastle, 1987. Functional properties of parietal visual neurons: radial organization of directionalities within the visual field, *J. Neurosci.*, 7:177–191.
- Stone, L. S., and J. A. Perrone, 1997. Human heading estimation during visually simulated curvilinear motion, *Vis. Res.*, 37:573–590.
- Sugihara, H., I. Murakami, K. V. Shenoy, R. A. Andersen, and H. Komatsu, 2002. Response of MSTd neurons to simulated 3D orientation of rotating planes, *J. Neurophysiol.*, 87:273–285.
- Takemura, A., Y. T. A. Inoue, and K. Kawano, 2000. The effect of disparity on the very earliest ocular following responses and the initial neuronal activity in monkey cortical area MST, *Neurosci. Res.*, 38:93–101.
- Takemura, A., Y. T. A. Inoue, K. Kawano, C. Quaia, and F. A. Miles, 2001. Single-unit activity in cortical area MST associated with disparity-vergence eye movements: evidence for population coding, *J. Physiol.*, 86:2245–2266.
- Tanaka, K., K. Hikosaka, H. Saito, M. Yukie, Y. Fukada, and E. Iwai, 1986. Analysis of local and wide-field movements in the superior temporal visual areas of the macaque monkey, *J. Neurosci.*, 6:134–144.
- Tanaka, K., and H. Saito, 1989. Analysis of motion of the visual field by direction, expansion/contraction, and rotation cells clustered in the dorsal part of the medial superior temporal area of the macaque monkey, *J. Neurophysiol.*, 62:626–641.
- Tanaka, K., Y. Sugita, M. Moriya, and H. Saito, 1993. Analysis of object motion in the ventral part of the medial superior tempo-

- ral area of the macaque visual cortex, *J. Neurophysiol.*, 69:128–142.
- Telford, L., I. P. Howard, and M. Ohmi, 1995. Heading judgments during active and passive self-motion, *Exp. Brain Res.*, 104:502–510.
- Thiele, A., P. Henning, M. Kubischik, and K.-P. Hoffmann, 2002. Neural mechanisms of saccadic suppression, *Science*, 295:2460–2462.
- Thiele, A., and K. P. Hoffmann, 1996. Neuronal activity in MST and STPp, but not MT changes systematically with stimulus-independent decisions, *NeuroReport*, 7:971–976.
- Thier, P., and R. G. Erickson, 1992. Vestibular input to visual-tracking neurons in area MST of awake rhesus monkeys, *Ann. N.Y. Acad. Sci.*, 656:960–963.
- Tootell, R. B. H., E. K. Hall, S. Marrett, W. Vanduffel, J. T. Vaughan, and A. M. Dale, 1998. The retinotopy of visual spatial attention, *Neuron*, 21:1409–1422.
- Toyama, K., K. Fujii, and K. Umetani, 1990. Functional differentiation between the anterior and posterior Clare-Bishop cortex of the cat, *Exp. Brain Res.*, 81:221–233.
- Treue, S., and J. C. Martinez Trujillo, 1999. Feature-based attention influences motion processing gain in macaque visual cortex, *Nature*, 399:575–579.
- Treue, S., and J. H. Maunsell, 1996. Attentional modulation of visual motion processing in cortical areas MT and MST, *Nature*, 382:539–541.
- Trevarthan, C., 1968. Two mechanisms of vision in primates, *Psychol. Forschung*, 31:229–337.
- Ungerleider, L. G., and B. A. Brody, 1977. Extrapersonal spatial orientation: the role of the posterior parietal, anterior frontal, and inferotemporal cortex, *Exp. Neurol.*, 56:265–280.
- Ungerleider, L. G., and R. Desimone, 1986a. Cortical connections of visual area MT in the macaque, *J. Comp. Neurol.*, 248:190–222.
- Ungerleider, L. G., and R. Desimone, 1986b. Projections to the superior temporal sulcus from the central and peripheral field representations of V1 and V2, *J. Comp. Neurol.*, 248:147–163.
- Ungerleider, L. G., and M. Mishkin, 1979. The striate projection zone in the superior temporal sulcus of *Macaca mulatta*: location and topographic organization, *J. Comp. Neurol.*, 188:347–366.
- Ungerleider, L. G., and M. Mishkin, 1982. Two cortical visual systems, in *Analysis of Visual Behavior* (D. J. Ingle, M. A. Goodale, and R. J. W. Mansfield, eds.), Cambridge, MA: MIT Press, pp. 549–586.
- Upadhyay, U. D., W. K. Page, and C. J. Duffy, 2000. MST responses to pursuit across optic flow with motion parallax, *J. Neurophysiol.*, 84:818–826.
- Van Essen, D. C., J. H. R. Maunsell, and J. L. Bixby, 1981. The middle temporal visual area in the macaque: myeloarchitecture, connections, functional properties and topographic representation, *J. Comp. Neurol.*, 199:293–326.
- Ventre, J., and S. Faugier-Grimaud, 1988. Projections of the temporo-parietal cortex on vestibular complex in the macaque monkey (*Macaca fascicularis*), *Exp. Brain Res.*, 72:653–658.
- von Grunau, M., and B. J. Frost, 1983. Double-opponent-process mechanism underlying RF-structure of directionally specific cells of cat lateral suprasylvian visual area, *Exp. Brain Res.*, 49:84–92.
- Warren, W. H., Jr., and D. J. Hannon, 1990. Eye movements and optical flow, *J. Opt. Soc. Am. A—Optics Image Sci.*, 7:160–169.
- Wylie, D. R., R. G. Glover, and J. D. Aitchison, 1999. Optic flow input to the hippocampal formation from the accessory optic system, *J. Neurosci.*, 19:5514–5527.
- Xiao, D. K., S. Raiguel, V. Marcar, and G. A. Orban, 1997. The spatial distribution of the antagonistic surround of MT/V5 neurons, *Cereb. Cortex*, 7:662–677.
- Yamasaki, D. S., and R. H. Wurtz, 1991. Recovery of function after lesions in the superior temporal sulcus in the monkey, *J. Neurophysiol.*, 66:651–673.
- Yeterian, E. H., and D. Pandya, 1985. Corticothalamic connections of the posterior parietal cortex in the rhesus monkey, *J. Comp. Neurol.*, 237:408–426.
- Yeterian, E. H., and D. Pandya, 1989. Thalamic connections of the cortex of the superior temporal sulcus in the rhesus monkey, *J. Comp. Neurol.*, 282:80–97.
- Yeterian, E. H., and D. Pandya, 1991. Corticothalamic connections of the superior temporal sulcus in rhesus monkeys, *Exp. Brain Res.*, 83:268–284.
- Yin, T. C., and V. B. Mountcastle, 1977. Visual input to the visuo-motor mechanisms of the monkey's parietal lobe, *Science*, 197:1381–1383.
- Zeki, S., 1969. Representation of central visual fields in prestriate cortex of monkey, *Brain Res.*, 14:271–291.
- Zeki, S., 1971. Convergent input from the striate cortex (area 17) to the cortex of the superior temporal sulcus in the rhesus monkey, *Brain Res.*, 28:338–340.
- Zeki, S., 1974. Functional Organization of a visual area in the posterior bank of the superior temporal sulcus of the rhesus monkey, *J. Physiol.*, 236:549–573.
- Zemel, R. S., P. Dayan, and A. Pouget, 1998. Probabilistic interpretation of population codes, *Neural Comput.*, 10:403–430.
- Zemel, R. S., and T. Sejnowski, 1995. Grouping components of three-dimensional moving objects in area MST of visual cortex, in *Advances in Neural Information Processing Systems 7* (G. Tesauro, D. S. Touretzky, and T. K. Leen, eds.), San Mateo, CA: Morgan Kaufmann, pp. 165–172.
- Zhang, K., M. I. Sereno, and M. E. Sereno, 1993. Emergence of position-independent detectors of sense of rotation and dilation with Hebbian learning: an analysis, *Neural Comput.*, 5:597–612.

86 The Perceptual Organization of Depth

ROLAND FLEMING AND BARTON L. ANDERSON

THE GOAL OF DEPTH perception is to identify the spatial layout of the objects and surfaces that constitute our surroundings. One important observation about the world around us that influences the way we see depth is that physical matter is not distributed randomly, with arbitrary depths at every location. On the contrary, the environment is generally well organized: the world consists mainly of tightly bound objects in a discernible layout. This order results from countless forces and processes (such as gravity and biological growth) which tend to organize matter into objects and place those objects in certain spatial relations. The central thesis of this chapter is that our perception of depth mirrors this organization. We argue that because the world consists of objects and surfaces, our perception of depth should likewise be represented in terms of the functionally valuable units of the environment, namely, surfaces and objects. As we shall see, this has profound consequences for the processing of depth information. In particular, there is more to depth perception than simply measuring the distance from the observer of every location in the visual field. Rather, the perception of depth is the *active organization* of depth estimates into meaningful bodies. Depth constrains the formation of perceptual units, and, reciprocally, the figural relations between depth measurements allow the visual system to parse its representation of depth into ecologically valuable structures.

There are many sources of information about depth from “pictorial” perspective to motion parallax. An exhaustive review of all these sources of information is beyond the scope of this chapter (although see Bruce et al., 1996; Palmer, 1999, for introductory reviews). Instead, we discuss three key domains in which the visual system “organizes” our perception of depth into meaningful units to emphasize the intimate relationship between depth processing and perceptual unit formation.

In the first section, we discuss how the visual system infers the layout of surfaces from local measurements of depth. We will argue that local estimates of depth are ambiguous but that the geometry of occlusion critically constrains the legal interpretations. Occlusion occurs when one opaque object partly obscures the view of a more distant object, as happens frequently under normal viewing conditions. Occlusion is important because it occurs at object boundaries, and therefore the depth discontinuities introduced by occlusion

provide ideal locations for the segmentation of depth into objects. Moreover, as we will show in the first section, the geometry of occlusion causes relatively near and relatively far depths to play different roles in the inference of surface structure.

In the second section we discuss the visual representation of environmental structures that are hidden from view. If the visual system is to organize depth into meaningful bodies, it must represent whole objects, not only those fragments that happen to be visible. In order to do this, the visual system must interpolate across gaps in the image to complete its representation of form. We argue that by considering the particular environmental conditions under which structures become invisible (specifically occlusion and camouflage), we can make predictions about the mechanisms underlying visual completion. We also discuss how visual completion influences the representation of depth.

Finally, we discuss what happens when the scene contains transparent surfaces, and thus multiple depths are visible along a single line of sight. We argue that this introduces a second segmentation problem in the perceptual organization of depth. The visual system not only needs to segment “perpendicular” to the image plane, such that neighboring locations are assigned to different objects; with transparency, the visual system also has to segment depth “parallel” to the image plane by separating a single image intensity into multiple depths, a process known as *scission* (Koffka, 1935). We discuss the conditions under which the visual system performs scission and how the ordering of the surfaces in depth is resolved.

We argue that the ambiguity of local depth measurements, the representation of missing structure, and the depiction of multiple depth planes are three of the major problems faced by a visual system if it is to organize depth into surfaces and objects. Through systematic explanations of example stimuli, we discuss some of the ways in which the visual system overcomes these problems.

Interpreting local depth measurements: the contrast depth asymmetry principle

In this section we discuss how occlusion constrains the interpretation of local depth estimates. Specifically, we show that

occlusion enforces a crucial asymmetry between relatively near and relatively distant structures that can have profound implications for the representation of surface layout. Although the principles are discussed in terms of binocular disparity, the fundamental logic relates to the geometry of occlusion and therefore applies to any local estimate of depth.

BINOCULAR STEREOPSIS AND THE CORRESPONDENCE PROBLEM
 Binocular stereopsis is the most thoroughly studied source of information about depth. Binocular depth perception relies on the fact that the two eyes receive slightly different views of the same scene. Because of the horizontal parallax between the two views, a given feature in the world often projects to two slightly different locations on the two retinas (Fig. 86.1). These small differences in retinal location, or binocular *disparities*, vary systematically with distance in depth from the point of convergence and can thus be used to triangulate depth. For a thorough treatment of stereopsis, see Howard and Rogers (1995) and Chapter 87.

In order to determine the disparity of a feature in the world, the visual system must localize that feature in the two retinal images. Once it has identified matching image features, the difference in retinal location is the binocular disparity, which can then be scaled to estimate depth. The visual system must not measure the disparity between features that do not belong together; otherwise, it will derive spurious depth estimates (Fig. 86.1). Because of this, the accuracy of the matching process is critical to binocular depth perception. The problem of identifying matching features in the two eyes' views (i.e., features that originate from a common source in the world) is known as the *correspondence problem*.

If the features that the visual system localizes in the two images are very simple, such as raw intensity values (or *pixels*), then in principle there could be many distracting features that do not in reality share a common origin in the world. Under these conditions the correspondence problem would be difficult, as the visual system would have to identify the one true match from among a large number of false targets.

However, there is considerable debate about what types of image features the visual system matches to determine disparity (Jones and Malik, 1992; Julesz 1960, 1971; Marr and Poggio, 1976, 1979; Pollard et al., 1985; Prazdny, 1985; Sperling, 1970). Psychophysically, at least, it now seems unlikely that the visual system matches raw luminances. Rather, the visual system seems to match local *contrast signals*, that is, localizable variations in intensity, such as luminance edges (Anderson and Nakayama, 1994; Smallman and McKee, 1995). This seems an almost inevitable consequence of early visual processing, which

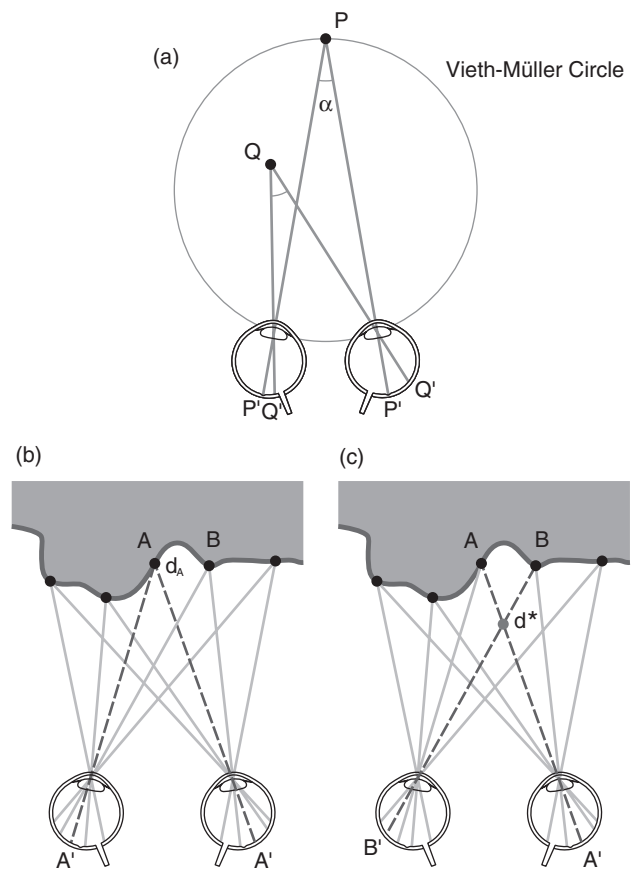


FIGURE 86.1. *a*, The two eyes converge by angle α on a point P . Therefore, by definition, P projects to the foveae of both eyes (P'). The Vieth-Müller circle is one of the geometrical horopters, that is, it traces a locus of points in space that project to equivalent retinal locations in the two eyes and thus carry no interocular disparity. Point Q is closer to the observer than P (as it falls inside the horopter). Therefore, it projects to different locations on the two retinas (Q). The difference in the locations of Q is the binocular disparity, which can be scaled by the vergence angle, α , to derive depth. *b*, When the visual field contains many points, there is a potential ambiguity concerning which image features correspond in the two eyes. Correct matches yield correct depth estimates, such as d_A . *c*, By contrast, false matches yield erroneous depth estimates. Here, the image of point A has been incorrectly matched with the image of point B , leading to an incorrect depth estimate, d^* .

maximizes sensitivity to contrasts rather than to absolute luminances (Cornsweet, 1970; Hartline, 1940; Ratliff, 1965; Wallach, 1948). By the time binocular information converges in V1, the visual field appears to be represented in terms of local measurements of oriented contrast energy (De Valois and DeValois, 1988; Hubel and Wiesel, 1962), and thus it is likely that these are the features from which disparity is computed.

If this is true, then the image features that carry disparity information are local contrasts such as luminance edges.

However, this poses a problem for the visual system, for in order to capture the functional units of the environment, the visual representation of depth should be tied to *surfaces and objects*, not to local image features. There is therefore a potential discrepancy between the image features that *carry* disparity information (i.e., local contrasts) and the perceptual structures to which depth is *assigned* (i.e., regions) in the ultimate representation of environmental layout. This discrepancy plays a critical role in the theoretical discussion that follows (see Anderson, in press).

A local image feature, such as an edge, has only one true match in the other eye's image. Therefore, the edge carries only one disparity. However, depth is ultimately assigned to the *two regions* that meet to form the edge. This results in a problem: in order to represent surface structure, the visual system must assign depth to *both sides* of an edge, even though the edge carries only one disparity (Fig. 86.2). How does the visual system infer the depths of two regions from every local disparity signal? We will show that the geometry of occlusion imposes an inviolable constraint on the interpretation of local disparity-carrying features. To anticipate, we show that the simple fact that near surfaces can occlude more distant ones, but not vice versa, has pro-

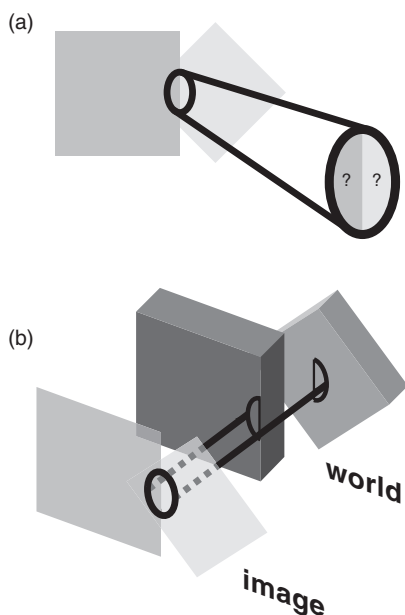


FIGURE 86.2. *a*, The image of a square occluding a diamond. A receptive field of limited extent (the ellipse) captures only local information about the scene, here a vertical luminance edge. This local information is ambiguous, as many different scenes could have resulted in the same image feature. *b*, If disparity is calculated by matching local contrasts, then the edge carries only a single disparity. However, in this case, the light and dark sides of the edge result from two distinct objects, and therefore different depths have to be assigned to the two sides of the edge.

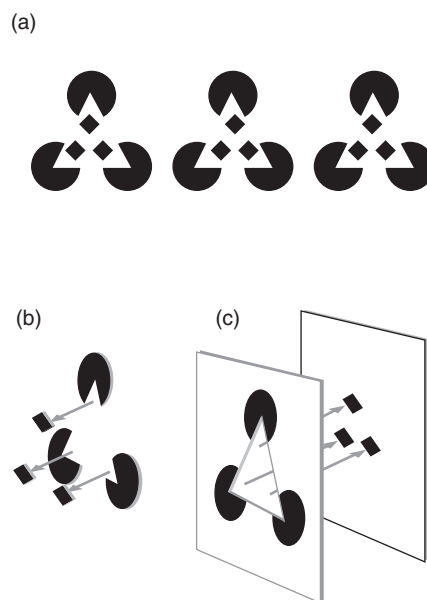


FIGURE 86.3. Asymmetries in depth interpolation. *a*, When the left stereopair is cross-fused, the diamonds appear to float independently in front of the Kanizsa triangle, as schematized in *b*. When the disparity of the diamonds is inverted (by cross-fusing the right stereopair), the diamonds drag their background with them, creating the percept of a triangular hole, even though only the disparity of the diamonds has changed (*c*). This asymmetrical change in surface structure can be explained by the contrast depth asymmetry principle (see text). (Adapted from Takeichi et al., 1992.)

found consequences for the assignment of depth to whole regions.

ASYMMETRIES IN DEPTH: A DEMONSTRATION By way of motivation for the theoretical discussion that follows, consider Figure 86.3, which is based on a figure developed by Takeichi et al. (1992). The figure consists of a Kanizsa illusory triangle and three diamonds. When disparity places the diamonds closer to the observer than the triangle and induces (by cross-fusing the stereopair on the left of Fig. 86.3), the diamonds appear to float independently in front of the background, and the Kanizsa triangle tends to be seen as a figure in front of the circular inducers; this percept is schematized in Figure 86.3*B*. The disparities in the display can be inverted simply by swapping the left and right eyes' views, as can be seen by cross-fusing the stereopair on the right side of Figure 86.3. In this case, what was previously distant becomes near and vice versa, such that the diamonds are placed *behind* the plane of the inducers. In both versions of the display, the triangle itself carries no disparity relative to the circular inducers; only the disparity of the diamonds changes from near to far. This simple inversion leads to a change in surface representation that is more

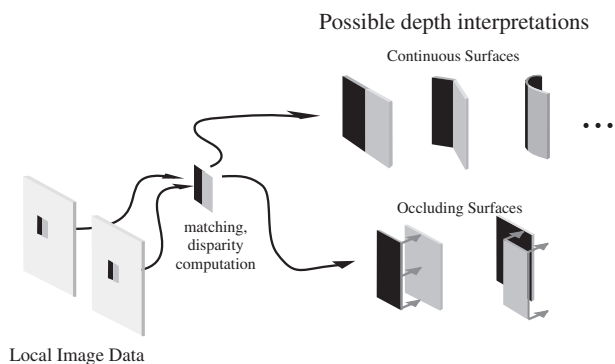


FIGURE 86.4. A contour which carries a depth signal (e.g., disparity) is inherently ambiguous. Two main classes of world states could have given rise to the contour: the contour could have originated from a single continuous surface (e.g., a reflectance edge or cast shadow), or it could have originated from an occlusion event. In the occlusion case, the border ownership of the contour (i.e., which side is the occluder) is ambiguous. Nonetheless, in all configurations, both sides of the contour are constrained to be at least as far as the depth signal carried by the contour. This introduces a fundamental asymmetry in the role of near and far contours in determining surface structure (see text for details). (Adapted from Anderson, in press; see also Anderson et al., 2002.)

complex than a simple reversal in the depth ordering of the perceptual units (as schematized in Fig. 86.3B). When the diamonds recede, they drag their background back with them, such that the triangle appears as a *hole* through which the observer can see a white surface; the three black diamonds lie embedded in the more distant white surface. This recession of the background has a secondary effect of increasing the strength of the illusory contour (the border of the triangle).

The important observations with regard to the theory are the following. First, when the diamonds are in front, they are freely floating and separate, while when they recede, they drag the background with them. Second, when the diamonds are forward, the Kanizsa triangle tends to be seen as a figure (rather than ground), but when the diamonds are more distant, the triangle is seen as a hole. And yet all that changed in the display was the disparity of the diamonds. Why does this simple reversal in depth lead to an asymmetric change in the surface representation? Why does the disparity of the diamonds influence the appearance of the triangle? These are the asymmetries of depth to which the following discussion pertains.

FROM FEATURES TO SURFACES: INTERPRETATION OF LOCAL DISPARITY SIGNALS Let us assume that the visual system has located a luminance edge and derived a disparity, d_0 , from that edge. What possible surface configurations are consistent with the local disparity measurement? Broadly, the legal interpretations fall into two classes, as shown in

Figure 86.4. The first class consists of surface events in which both sides of the edge meet at the depth of the edge, d_0 . There are many surface events for which this is the case: reflectance edges, cast shadows, and creases in the surface, to name just three. When the feature originates from a continuous manifold, as in these cases, interpretation is simple, as both sides of the edge are assigned the same depth, d_0 .

The second class of interpretations occurs when the edge corresponds to an object boundary and therefore represents a depth discontinuity (Fig. 86.4). In this case, one side of the edge lies at the depth of the occluding object, and the other side of the edge lies at the depth of the background. Therefore, the visual system must assign *different* depths to the two sides of the edge. How can the visual system assign two depths, when it is given only one disparity, d_0 ? The answer is that it only assigns a unique depth to the occluding side. The critical insight is the following: the depth measurement acquired at an occluding edge *only specifies the depth of the occluding surface*. The visual system assigns depth d_0 to the occluding surface. All that it knows about the other side is that it must be *more distant* than the occluding surface. If the more distant surface is untextured, then it could be at any depth behind the occluder and the local image data would remain the same. By contrast, if the depth of the occluding surface varies, the disparity carried by the object boundary must also change, because the occluding surface “owns” the contour (Koffka, 1935; Nakayama et al., 1989) and is therefore responsible for the disparity associated with the edge.

Although the visual system cannot uniquely derive the depth of the occluded side (i.e., the background) from the local disparity computation, there is one critical piece of information that it does have: the occluded side is *more distant* than the occluder. There is no way for an occluding object to be more distant than the background that it occludes. If the background is brought closer than the object, then the background *becomes the occluding surface* and carries the edge with it. In this way, occlusion introduces a fundamental asymmetry into the interpretation of disparity-carrying edges: the occluded side of the edge can be at any distance greater than d_0 , but neither side can be nearer than d_0 .

We can summarize the possible depth assignments (from the occlusion and nonocclusion classes just described) in the form of a constraint on the interpretation of local disparity-carrying contrasts, termed the *contrast depth asymmetry principle* (Anderson, in press; see also Anderson et al., 2002):

Both sides of an edge must be situated at a depth that is *greater than* or *equal to* the depth carried by that edge.

Although this geometric fact is simple in form, it can have pronounced effects on the global interpretation of images when the constraint applies to all edges simultaneously. We will now run through an example to show how the principle can explain the asymmetric changes in perceived surface structure that occur when near and far disparities are inverted.

APPLICATION OF THE CONTRAST DEPTH ASYMMETRY PRINCIPLE In order to demonstrate the explanatory power of the contrast depth asymmetry principle (hereafter CDAP), we will now use it to account for the demonstration in Figure 86.3. Recall that when the diamonds carry near disparity, they float freely in front of the background, and the illusory triangle tends to be seen as figure. When the disparity is reversed, however, the diamonds drag the background back with them, and the triangle appears as a hole. This asymmetry in surface layout is depicted in Figure 86.3B.

Let us first consider the case in which the diamonds appear to float in front. The visual system has to interpret the disparity signals carried by the edges of the diamonds. The CDAP requires both sides of the diamonds' edges (i.e., the black inside and the white outside of the diamonds) to be at least as distant as the edges. Now consider the "pacman" inducers, which are more distant than the diamonds. The constraint requires both sides of these edges to be at least as distant as their edges. This means that all of the black interior of the inducers must be at least this distant and, more importantly, *all of the white background* must be at least this distant, which is farther than the disparity of the diamonds. If all of the white background is farther than the diamonds, then the edges of the diamonds must be *occluding* edges, and the black interior of the diamonds must be an occluding surface. This explains why the diamonds are seen as independent occluders, floating in front of the large white background and black inducers: the edges of the "pacman" inducers drag the white background back, leaving the diamonds floating in front.

Now consider the case in which the diamonds are more distant than the inducers. Again, the CDAP requires both the inside and the outside of the diamonds to be at least as far back as their disparity dictates. This means that both the diamonds *and their white background* are dragged back to the more distant disparity. Now consider the "pacman" inducers, which carry a relatively near disparity. Because the white background behind the diamonds has been dragged back with the diamonds, the inducers and their white background must be occluding surfaces. This means that the background immediately surrounding the diamonds must be visible through a hole in the occluding surface. The edges of this hole are the illusory contours of the Kanizsa figure. Note again: the fact that both sides of every edge have to be

at least as far as the edge leads to asymmetrical surface structures when disparities are inverted.

This is just one example that shows how the CDAP can account for asymmetrical effects of relatively near and relatively far disparities on perceived surface layout. Because the CDAP is derived from the geometry of occlusion, it can account for a very large number of displays and can be used to generate surprising new displays (Anderson, 1999, Anderson, in press).

Occlusion and camouflage: hallucinating the invisible

The central thesis of this chapter is that the visual system does not merely record depth at each location in the visual field; rather, it actively organizes its depth measurements into functionally valuable units. In the previous section, we discussed how occlusion plays a key role in this organization. In this section, we discuss how the visual system handles what is arguably the hardest problem posed by occlusion: the visual representation of structures that are hidden and are therefore completely invisible. If seeing depth is about representing the actual layout of objects in the environment, then all portions of the objects must be represented, even those that are hidden from view: hidden portions do not disappear from the environment just because they do not appear in the image. Therefore, the visual system has to go beyond local image data to construct representations of hidden structures. We will now discuss how the environmental conditions of occlusion and camouflage predict properties of the construction process.

MODAL AND AMODAL COMPLETION We will consider two major ways in which parts of the scene can become invisible. The first is simple occlusion, in which an opaque object obscures part of a more distant object. When this happens, the occluded structures of the more distant object have no corresponding features in the image, and thus the visual system must somehow "reconstruct" the missing data. The second way that viewing conditions can lead to invisible structures is through camouflage. In camouflage it is the nearer, *occluding* surface that is rendered invisible because it happens to match the color of its background. Because the boundaries of the camouflaged object do not project any contrast, they have no corresponding features in the image, and thus the nearer object is effectively invisible. Under these circumstances, the visual system must actively "hallucinate" the invisible structures. In both cases, the visual system interpolates missing data, a process known as *visual completion*. This process is important to depth perception because it is one of the means by which the visual system organizes its depth measurements into meaningful bodies. We argue that depth perception and unit

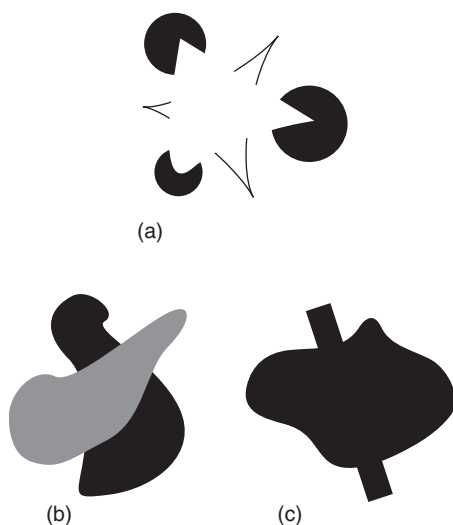


FIGURE 86.5. *a*, Modal completion. Most observers report seeing a vivid white triangle in front of three discs and a black triangular outline. The contours of the white triangle are subjectively distinct, resembling real contours, even though there is no corresponding image contrast, and hence the triangle is illusory. *b*, Amodal completion. Most observers report seeing a single continuous black shape, part of which is hidden from view by the gray occluder, even though the parts that are hidden from view are, by definition, invisible. *c*, A self-splitting object. Even though the shape is uniformly black, it tends to be seen as two forms, one in front of the other. Which form tends to complete modally, and which amodally, depends in part on the distance that must be spanned by the completion (Petter's law).

formation are intimately intertwined, for depth constrains the perceptual units that are formed, and perceptual organization influences the interpretation of local depth measurements.

The phenomenal quality of completed structures differs, depending on whether it is near (camouflaged) or far (occluded) structures that are interpolated. In the case of camouflage, the interpolation leads to a distinct impression of a contour or surface across the region of missing data. This is referred to as *modal completion* (Michotte et al., 1964/1991) because the experience is of the same phenomenal modality as ordinary visual experience. An illusory contour, for example, is crisp and subjectively similar to a real contour, as can be seen in Figure 86.5A. In contrast, the sense of completion experienced with occluded structures is less distinct. The black form in Figure 86.5B tends to be seen as a single object, part of which is hidden, rather than as two distinct objects, whose boundaries coincide with the boundary of the gray occluder. There is a compelling sense that the two visible portions of the black form belong to the same object and that that object continues in the space behind the occluder. However, this impression, although visual in origin, is not of the same phenomenal mode as normal and modal contours and is therefore referred to as

amodal completion (Michotte et al., 1964/1991). In general, the regions of the image which are visible, and lead to visual completion, are referred to as *inducers*.

THE IDENTITY HYPOTHESIS There is a vast literature on visual completion; a thorough discussion of all the issues is beyond the scope of this chapter. One important issue that is discussed in greater detail in Chapter 75 is whether visual completion occurs relatively early or late in the putative processing hierarchy. However, the perceptual organization of depth has a direct bearing on another current debate, specifically the extent to which modal and amodal completion are the consequences of a single process. This issue is intimately bound to depth perception because it determines the extent to which depth processing and perceptual organization are independent.

The debate runs roughly as follows. On the one hand, a strong claim has been made that a single mechanism is responsible for both modal and amodal completion. According to this account, perceptual organization (including visual completion) produces perceptual units, and an independent process places those units in depth. The theory states that psychological differences between modal and amodal completion result from the final depth ordering of the completed forms (Kellman and Shipley, 1991; Kellman et al., 1998; Shipley and Kellman, 1992) rather than a difference between the completion processes themselves. This is known as the *identity hypothesis*. On the other hand, the two processes could be largely independent, subject to different constraints and subserved by distinct neural mechanisms. A strong form of this *dual mechanism* hypothesis would be that the two processes are fundamentally different in nature—for example, that modal completion is largely data driven, while amodal completion is essentially *cognitive*. To anticipate, although we do not subscribe to the strongest form of the dual mechanism hypothesis, we will provide evidence that modal and amodal completion follow different constraints and argue that they are subserved by distinct neural processes. Central to the arguments that we present are the geometric and photometric conditions under which occlusion and camouflage actually occur in the environment.

The principal evidence for the identity hypothesis has been that subjects perform similarly with modally and amodally completed figures in a variety of tasks. In one task, Shipley and Kellman (1992) varied the spatial alignment of the inducing elements in both modally and amodally completed squares. Such misalignment is known to weaken the sense of completion, as the completed boundary is forced to undergo an inflection. Subjects were asked to rate the subjective strength of visual completion as a function of the degree of misalignment for modal and amodal versions of the display. Shipley and Kellman (1992) found that ratings

declined at the same rate as a function of misalignment for both modal and amodal figures. This has been interpreted as evidence that a single mechanism is responsible for both forms of completion.

Using a more rigorous method, Ringach and Shapley (1996) performed a shape discrimination task with modal and amodal versions of a Kanizsa figure. By rotating the inducing elements, the vertical contours of the completed square can be made to bow out (creating a “Fat” Kanizsa) or curve in (creating a “Thin” Kanizsa). Subjects were asked to discriminate between Fat and Thin versions of the display while the angle through which the inducers were rotated was varied. Ringach and Shapley found that discrimination performance as a function of rotation was nearly identical for modal and amodal versions of the display, a finding which is consistent with the identity hypothesis.

One problem with this type of evidence is that it relies on negative results, that is, a failure to detect a difference, which could be due to the method rather than to a fundamental property of the system being studied. If positive evidence could be provided that modal and amodal completion are subject to different constraints, or result in different perceptual units, then the identity hypothesis would no longer be tenable.

There are two major reasons for believing that modal and amodal completion should be subject to different constraints, both of which are related to the environmental conditions under which occlusion and camouflage occur. First, occlusion occurs over greater distances across images because it only requires that one object be in front of another. Camouflage, on the other hand, requires a perfect match in color between the near surface and its background, and thus occurs less frequently in general. This difference is reflected in a constraint on the image distances over which modal and amodal completion occur, which was first documented by Petter (1956). Petter used a class of stimuli now known as *spontaneously splitting objects* (SSOs), which consist of a single homogeneously colored shape, such as the one shown in Figure 86.5C, that tends to be interpreted as two independent shapes, one behind the other. Which object is seen in front tends to oscillate with prolonged viewing. However, which shape is seen in front first, and which tends to be seen in front for a greater proportion of the time, can be predicted rather well from the lengths of the contours that must be interpolated. Petter’s rule states that longer contours tend to be completed amodally, while shorter contours tend to be completed modally. Thus, which figure is seen in front can be predicted from the length of the contours that must be completed. If the two types of completion are subject to different constraints on the distances over which they occur, this opens the possibility that they are subserved by different mechanisms.

A second reason for believing that modal and amodal completion are subject to different constraints relates to the color conditions that are required for occlusion and camouflage to occur. Again, occlusion can happen between objects of any color. The reflectance of the near object is unrelated to the fact that it hides the more distant one from view. This suggests that amodal completion should not be sensitive to the luminance relations between the image regions involved. Camouflage, by contrast, requires a perfect match in luminance between the near and far surfaces. This implies that modal completion *should* be sensitive to the luminance relations between the image regions involved.

Recent experimental work has shown that this luminance sensitivity can lead to large differences between modal and amodal displays (Anderson et al., 2002). Anderson et al. created displays consisting of two vertically separated circles filled with light and dark stripes, as shown in Figure 86.6. The binocular disparity of the circles was kept constant, but the disparity of the light-dark contours inside the circles was altered to place the stripes behind or in front of the circular boundaries. When the stripes were further than the circles, the top and bottom stripes tended to complete amodally to form a single continuous dark and light surface, which appeared to be visible through two circular holes, as schematized in Figure 86.6D. This percept occurred irrespective of the luminance of the region surrounding the circles.

By contrast, when the disparity placed the contours *in front* of the circles, the dark and light stripes separated into different depth planes. The way in which the stripes separated from one another depended on the luminance of the surround. When the surround was the same color as the light stripes, the light stripes appeared to float in front and completed modally across the gap between the two circles. In this condition, the dark stripes completed amodally underneath the light stripes to form complete circles. This led to an impression of light vertical stripes in front of dark circles, as schematized in Figure 86.6E. However, when the surround was the same luminance as the dark stripes, the percept inverted, such that the dark stripes appeared to float in front of light discs. This demonstrates a fundamental dependence on luminance that was not present in the amodal version of the display. Furthermore, if the surround was an intermediate gray, then the display was not consistent with camouflage, as neither the light nor the dark stripes perfectly matched the luminance of the background. Under these conditions, there was no modal completion across the gap, and the percept was difficult to interpret. This demonstrates that modal completion is sensitive to luminance relations, while amodal completion is not.

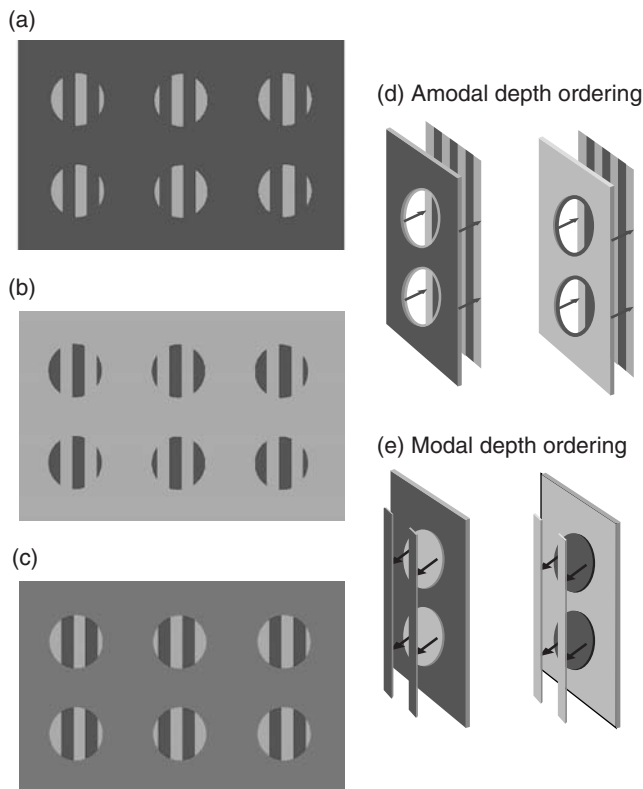


FIGURE 86.6. Demonstration of dependence of modal completion on surround luminance. When the left stereopairs of *a*, *b*, and *c* are cross-fused, the stripes tend to complete amodally between the gaps between the circular hole, creating the impression of a single striped surface (like wallpaper) viewed through two apertures, as depicted in *d*. This occurs irrespective of the luminance of the surround. However, when the right stereopairs are cross-fused, thus inverting the disparity, only two stripes appear to complete modally, and which stripes complete depends critically on the surround luminance, as depicted in *e*. When the surround is dark, as in *a*, the dark stripes complete modally; when the surround is light, as in *b*, the light stripes complete modally; and when the surround is intermediate, no completion is visible. This demonstrates that modal completion is luminance dependent, while amodal completion is not. (Adapted from Anderson et al., 2002.)

Anderson et al. showed that this luminance sensitivity could affect performance on basic visual tasks such as vernier acuity. The stripes in the top and bottom circles can be horizontally offset (i.e., misaligned slightly) without destroying the sense of completion. Subjects were asked to report in which of two displays the contours were slightly misaligned. Both modal and amodal completion facilitate performance in this task. However, in the amodal case, performance was unaffected by the luminance of the surround, while in the modal case, performance was much worse when the luminance of the surround was an intermediate gray (the condition in which the stripes do not complete across the gap). Thus, modal and amodal com-

pletion are subject to different constraints, both on the distance over which they occur and on the luminance conditions that are required to induce them. This positive evidence for a difference between modal and amodal completion uses essentially the same types of task as the negative evidence that had previously been used to support the identity hypothesis.

VISUAL COMPLETION AND THE PERCEPTUAL ORGANIZATION OF DEPTH The geometric and photometric differences between modal and amodal completion are derived directly from the environmental conditions of occlusion and camouflage. Because occlusion and camouflage occur under different circumstances, they have different consequences for the organization of depth into meaningful bodies. In fact, the differences can be exploited to generate stimuli in which modal and amodal completion lead to different shapes. This is important, as it shows that unit formation is intimately bound to the placement of structures in depth.

The greater “promiscuity” of amodal completion is the key in the generation of these displays. Figure 86.7 is a recently developed stereoscopic variant of the Kanizsa configuration in which the inducing elements are rotated outward (Anderson et al., 2002). When the straight segments (the “mouths” of the “pacmen”) are placed in front of the circular portions of the inducers, the impression is of five independent illusory fragments that float in front of five black discs on a white background. However, when the two eyes’ views are interchanged, and thus the straight contours are placed *behind* the circular segments, the impression is rather dramatically altered. With the disparity inverted, the impression is of a single amodally completed, irregularly shaped, black figure on a white background, which is visible through five holes in a white surface (these percepts are schematized in Figs. 86.7*B* and 86.7*C*). Thus, the former case consists of a total of 11 surfaces (5 fragments + 5 discs + white background), while the latter case consists of 3 (1 white surface with 5 holes + 1 black shape + white background). Clearly, the placement in depth has a considerable effect on what perceptual units are formed.

Anderson et al. also provided evidence that differences between modal and amodal interpolation can lead to differences in the very shapes of completed contours themselves. When the left-hand stereopair in Figure 86.8*A* is uncross fused, the resulting percept consists of six circular discs that are partly occluded by a jagged white surface on the right-hand side, as schematized in Figure 86.8*B*. However, when the disparities are inverted (by uncross-fusing the right pair of Fig. 86.8*A*), the modal completion across the regions between the four black blobs tends to take the form of a

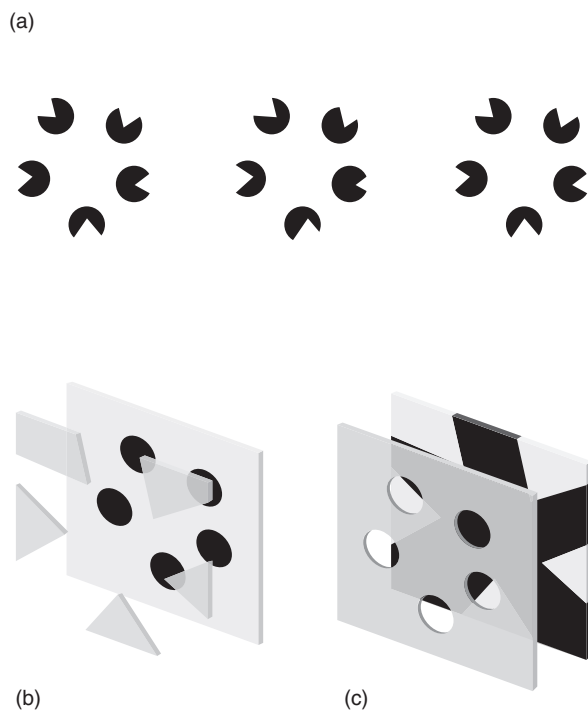


FIGURE 86.7. *a*, Relative depth alters perceptual organization. When the left stereopair is cross-fused, the figure tends to appear as five discs occluded by five distinct image fragments, as depicted in *b*; the transparency in *b* is included only so that both depth planes can be depicted simultaneously. When the depth ordering is reversed by cross-fusing the right stereopair, a single irregular black “star” appears to lie on a continuous white background, which is visible through five holes in a continuous overlying layer (*c*). In this depth ordering the black shape tends to appear as figure. (Adapted from Anderson et al., 2002.)

continuous wavy contour that runs down the center of the display. This percept is schematized in Figure 86.8C. The importance of this demonstration is that it shows that modal and amodal completion can not only result in different surface structures, but even in differently shaped contours. It is difficult to see what the concept of a single completion mechanism serves to explain if the two processes can result in different completed forms.

Ultimately, the identity hypothesis is a claim about mechanism and can therefore be assessed physiologically. There is a considerable body of evidence for extrastriatal units that are sensitive to illusory but not to amodally completed contours (see Chapter 76 for a review). A critical additional piece of evidence was provided recently by Sugita (1999), who found cells in V1 that respond to amodal completion across their receptive fields but not to modal completion. Cells responded weakly when presented with two unconnected edges; holes and occluding surfaces on their own; and stimuli in which two unconnected edges were separated by a hole. However, when the cells were presented with two edge fragments separated by an occluder (a

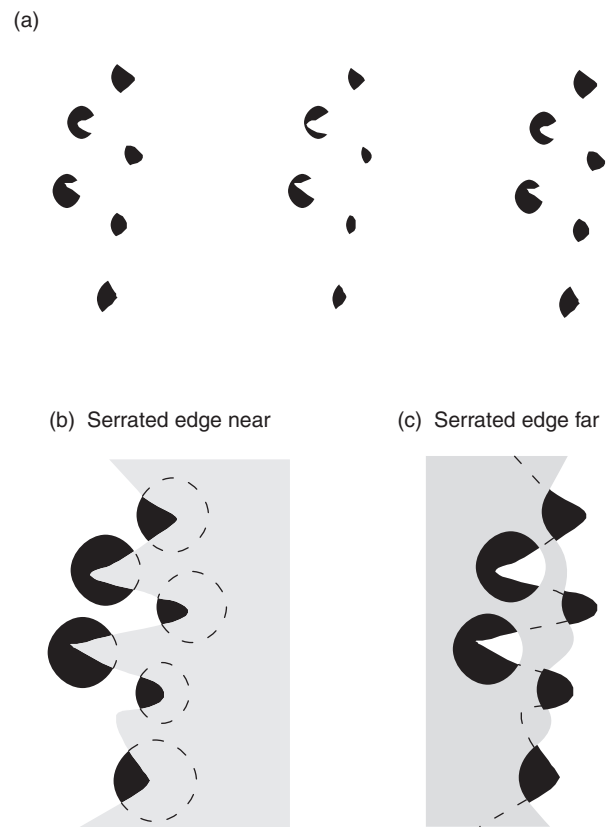


FIGURE 86.8. The serrated-edge illusion. When the left stereopair in *a* is uncross-fused, the resulting percept consists of six circular disks that are partly occluded by a jagged white surface on the right, as depicted in *b*. When the right stereopair is uncross-fused, the modal completion of these four black blobs tends to take the form of a single wavy contour that runs vertically down the center of the display, as depicted in *c*. Although other percepts are possible, this is an existence proof that depth inversion alone can alter the shape of modally and amodally completed contours. (Adapted from Anderson et al., 2002.)

stimulus that leads to amodal completion of the edge), the cells responded vigorously. This shows that at the earliest stages of cortical processing, there is a double dissociation between the representations of modal and amodal structures, a conclusion which supports the dual mechanism hypothesis.

Transparency, scission, and the representation of multiple depth planes

Transparency poses a particularly interesting problem in the perceptual organization of depth. With transparency, one object is visible *through* another, and thus two distinct depths lie along the same line of sight (Fig. 86.9). If the visual system is to represent depth in terms of the actual surfaces of the environment, it has to depict *two distinct depths* at a single location in the visual field. The process of projection compresses

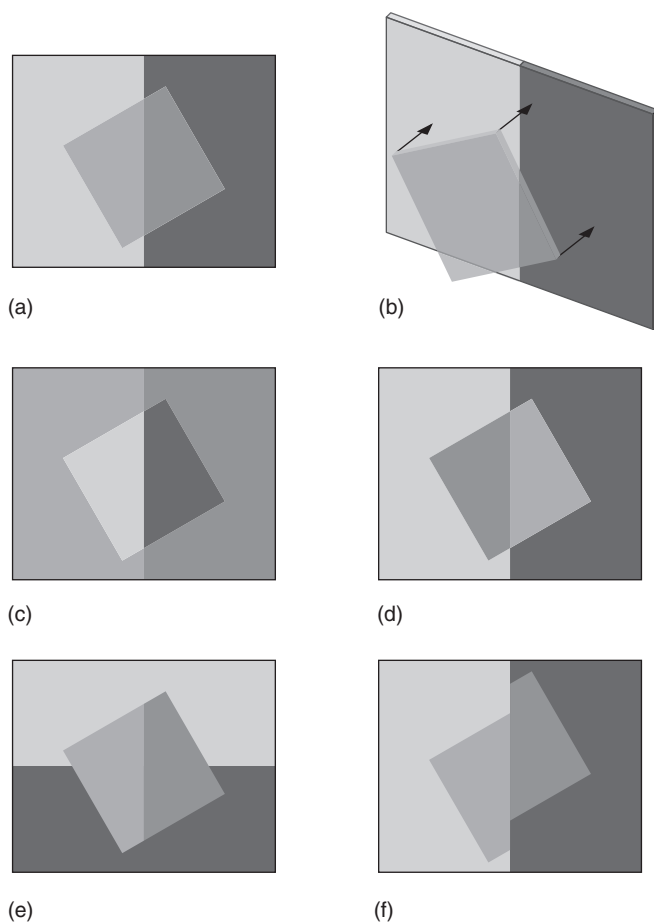


FIGURE 86.9. Perceptual transparency. The figure in *a* tends to be seen as a light gray transparent surface in front of a bipartite background, as depicted in *b*, and thus two distinct surfaces are visible along the same line of sight. Transparency is seen only when certain relations hold between the various regions of the display. In *c* the central region is higher in contrast than its surround and thus is not seen as transparent. In *d*, the polarity of the contrasts is reversed, and again transparency is not seen. In *e*, the contour of the underlying layer is not continuous inside and outside the central region, eliminating the percept of transparency. In *f*, the contour of the overlying layer is not continuous, which also reduces the percept of transparency.

the light arriving from the transparent surface and the light arriving from the more distant surface into a single image intensity on the retina. In order to represent both surfaces, the visual system has to separate a single luminance value into multiple contributions, a process known as *scission* (Koffka, 1935). We argue that scission is a type of perceptual segmentation, as it parses the representation of depth into distinct surfaces. However, rather than segmenting *neighboring* locations into distinct objects, scission separates depth into layers, or planes, and thus operates “parallel” to the image plane.

Scission poses the visual system with two principal problems. The first is to identify when a single luminance results

from two distinct depths. The second is to assign surfaces properties correctly at the two depths. By studying when and how we see transparency, we can learn how the visual system scissions depth into layers.

Much of the seminal work on perceptual transparency was conducted by Metelli (1970, 1974a, 1974b; see also Metelli et al., 1985), who provided a quantitative analysis of the color mixing that occurs when one surface is visible through another. When a background is visible through a transparent sheet, only certain geometrical and luminance relations can hold between the various regions of the display (Fig. 86.9). From these relations Metelli derived constraints that determine whether a region will look transparent or not, and how opaque it will appear if it does look transparent. This is important, as it determines the conditions under which the visual system scissions a single image intensity into multiple layers, and thus how the visual system stratifies its representation of depth.

Broadly, the conditions required for perceptual scission fall into two classes. The first are the photometric conditions for transparency, which detail the relations between the light intensities of neighboring regions that are necessary for scission. The second set of conditions for perceptual scission are geometrical, or figural. Depth separates into layers only when these relations hold between the various regions of the display.

PHOTOMETRIC CONDITIONS FOR SCISSION Consider the display shown in Figure 86.9A, which tends to be seen as a bipartite background that is visible through a transparent filter. The vivid separation of the central region into two depths occurs only when certain luminance relations hold. Metelli derived two constraints on the photometric conditions required for perceptual scission.

The intuition behind the first constraint, which we refer to as the *magnitude constraint*, is that a transparent medium cannot increase the contrast of the structures visible through it. The consequence of this constraint is that the central diamond must be lower or equal in contrast than its surround in order to appear transparent, as shown in Figure 86.9A. This constraint is important, as it restricts the conditions under which scission occurs: a region can scission only if its contrast is less than or equal to the contrast of its flanking regions. As can be seen in Figure 86.9C, infringement of this constraint with respect to the central diamond prevents the central region from undergoing scission. However, in this display, the constraint is satisfied for the region *surrounding* the diamond; thus, the display can be seen as a bipartite display viewed through a transparent filter with a diamond-shaped hole in the center.

The intuition behind the second luminance constraint, which we refer to as the *polarity constraint*, is that a transparent medium cannot alter the contrast polarity of the

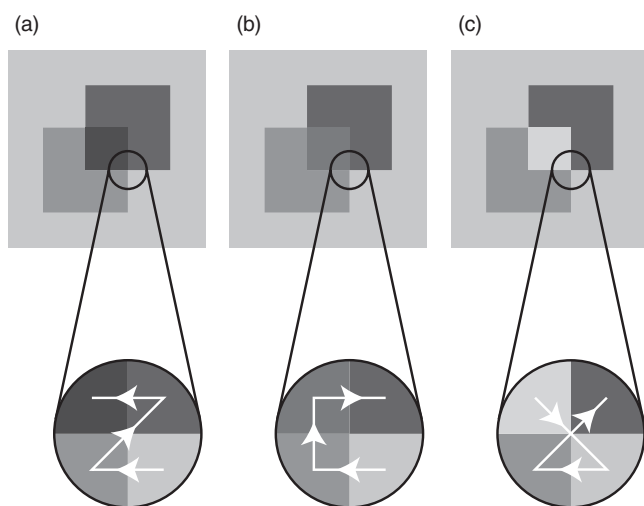


FIGURE 86.10. The polarity constraint means that transparency manifests itself in distinctive local ordinal relations in luminance. The only difference between the three figures is the luminance of the region of overlap. In *a*, the region is dark and the image is bistable, as either square can be seen in front. When this occurs, a line that passes progressively from brighter to darker regions creates a **Z** shape. In *b*, the overlap is intermediate, such that the line that joins regions of decreasing brightness is **C**-shaped. When this happens, exactly one of the surfaces appears transparent. In *c*, the overlap is light, creating a crisscross pattern. In this case, neither square appears transparent, as the polarity constraint is infringed for both squares. (Adapted from Beck and Ivry, 1988.)

structures visible through it. Put another way, if a dark-light edge passes underneath a transparent medium, the dark side will remain darker than the light side, no matter what the *absolute* luminances are. As can be seen in Figure 86.9D, infringement of this constraint prevents perceptual scission, demonstrating that the visual system respects this optical outcome of transparency. This constraint is particularly important in determining the depth ordering in transparent displays.

The polarity constraint enforces certain restrictions on the ordinal relationships between the luminances of neighboring regions. This means that, in principle, we can classify the locations where neighboring regions meet to determine whether scission is or is not possible in each region. This provides the visual system with a *local* signature of transparency. Beck and Ivry (1988) noted that if one draws a series of lines running progressively from the brightest to the darkest regions, there are three possible shapes that result, as shown in Figure 86.10. The only difference between the three figures is the luminance of the region of overlap between the two squares. In the first instance (Fig. 86.10A), the image is bistable, as either square can be seen as a transparent overlay. In these circumstances, the lines linking regions of

increasing luminance form a **Z** configuration. When the lines form a **C** shape (Fig. 86.10B), only one of the squares is seen as transparent, and when the lines crisscross (Fig. 86.10C), the polarity constraint is infringed for all regions and neither square scissions. Adelson and Anandan (1990) provided a similar taxonomy based on the number of polarity reversals. A number of lightness illusions demonstrate that scission can be predicted from the class of X-junctions in the display and that these X-junctions can have powerful effects on many qualities of our experience (see, e.g., Adelson, 1993, 1999).

The magnitude and polarity constraints can be unified as a single rule that describes a powerful local cue to scission. Anderson (1997) phrased the rule as follows: “When two aligned contours undergo a discontinuous change in contrast magnitude, but preserve contrast polarity, the lower-contrast region is decomposed into two causal layers.” There are two valuable consequences of this rule. The first is that it unifies the two Metelli constraints. The second is that it provides a *local* signature of transparency that can be applied to any meeting of contours. This includes those T-junctions that are in fact degenerate X-junctions, that is, those in which two neighboring regions happen to have exactly the same luminance. Anderson also demonstrated that a number of traditional lightness phenomena, including White’s effect and its variants, and neon color spreading, can be accounted for as cases of scission rather than as the consequence of traditional “contrast” or “assimilation” processes.

Having identified that a location contains two surfaces, the visual system has to partition the luminance at that location between the two depths. How much of the light is due to reflectance of the underlying surface, and how much is due to the properties of the overlying layer? The opacity of the overlying layer determines how the luminance is divided between the two depths. Metelli’s model makes explicit predictions about the perceived opacity and lightness of the transparent layer. The equations predict that two surfaces with identical transmittance should look equally opaque irrespective of their lightness. However, Metelli himself noted that dark filters tend to look more transparent than light filters with the same transmittance. Why does the visual system confuse lightness and transmittance in partitioning luminance between two depths?

In a series of matching experiments, Singh and Anderson (2002) recently resolved this issue. Subjects adjusted the opacity of one filter until it matched the perceived opacity of another filter with a different lightness. Singh and Anderson found that perceived transmittance is predicted almost perfectly by the ratio of *Michelson contrasts* inside and outside the transparent region, even though

such a measure is actually inconsistent with the optics of transparency. As discussed above, there is a general consensus that the early visual processing tends to optimize sensitivity to contrast rather than absolute luminance. Hence, in assigning transmittance, the visual system appears to use the readily available contrast measurements, even though they are not strictly accurate measurements of opacity.

FIGURAL CONDITIONS FOR SCISSION In addition to the luminance conditions, certain geometrical relations must hold between the various regions of the display in order for depth stratification to occur (Kanizsa, 1995/1979; Metelli, 1974a). These figural conditions fall into two broad classes. The first class requires good continuation of the *underlying* layer. Specifically, the contours that are in plain view should be continuous with the contours viewed through the region of presumed transparency. As can be seen in Figure 86.9E, infringement of this condition interrupts the percept of transparency. The second figural condition requires good continuation of the *transparent* layer. Figure 86.9F shows that infringement of this condition weakens or eliminates the percept of transparency.

There are conditions in which the figural cues to transparency are so strong that they can override the luminance cues. Beck and Ivry (1988) showed subjects displays like the one shown in Figure 86.10C, in which the region of overlap between the two figures is the wrong contrast polarity for either figure to be seen as transparent. Despite this, naive subjects did occasionally report seeing such figures as transparent, demonstrating that the sense of figural overlap is a central aspect of the percept of transparency. Certainly most observers are willing to agree that the region of overlap in Figure 86.10C appears to belong to two *figures* simultaneously, an impression that can be enhanced with stereo and relative motion. However, it should be noted that the gray of the overlap region does not appear to scission into two distinct sources, at least not in the same way as the overlap of a normal transparency display does (as in Figs. 86.10A and 86.10B). This leads to the possibility of two distinct neural processes in the perception of transparency. One is driven by relatively local cues and leads to phenomenal color scission. The other is driven by more global geometrical relations and leads to stratification in depth. Under normal conditions of transparency, the two processes operate in concert to produce the full impression of transparency. However, using carefully designed cue-conflict stimuli, such as those used by Beck and Ivry, these two factors in the representation of transparent surfaces can be distinguished. An open question, however, is how these processes are instantiated neurally. All we can conclude is that the representation of depth is much more

sophisticated than a mere two-dimensional map of depth values.

SCISSION AND THE PERCEPTUAL ORGANIZATION OF DEPTH Scission can have pronounced effects on perceptual organization. For example, Stoner et al. (1990) demonstrated that perceived transparency can alter the integration of motion signals into coherent moving objects. When a plaid is drifted at constant velocity across the visual field, it is typically seen as a single coherent pattern that moves at the velocity of the intersections between the two component gratings. However, with prolonged viewing, the plaid appears to separate into two component gratings that slide across each other, each of which appears to move in the direction perpendicular to its orientation. When the plaid is coherent, it appears to occupy a single depth plane, but when it separates into its components, the gratings tend to appear at different depths.

Stoner et al. varied the intensity of the intersections of the plaids and measured the proportion of time for which the plaid was seen as coherent. They found that when the color of the intersection was consistent with one grating being seen through the other (i.e., when the junctions were consistent with transparency), the proportion of the time for which the plaid appeared to separate into gratings was greatly increased. By contrast, when the color of the intersections infringed the polarity constraint, such that neither grating could be seen as transparent, the pattern tended to be seen as a coherent plaid rather than undergoing scission into distinct layers. This demonstrates that scission has important consequences for the representation of visual structure. When an image region scissions, the effects can spread to regions distant from the local cues to scission.

Scission acts as a nexus between depth and other visual attributes. Scission of depth can cause regions to change in apparent lightness; conversely, changes in luminance can cause changes in depth stratification. Figure 86.11 demonstrates this close relationship between luminance, scission, and the perceptual organization of depth. Three circular patches of a random texture were placed on a uniform background. Critical to the demonstration is that disparity is introduced between the circular boundaries and the texture inside the circles. When the disparity places the texture behind the circular boundaries, the circles appear as holes through which the texture is visible. The texture tends to appear as a single plane with continuously stochastically varying lightness. However, when the disparity places the texture in front of the circular boundaries, the percept changes considerably. The texture separates into two distinct layers: a near layer made up of clouds with spatially varying transmittance and a far layer that is visible through the

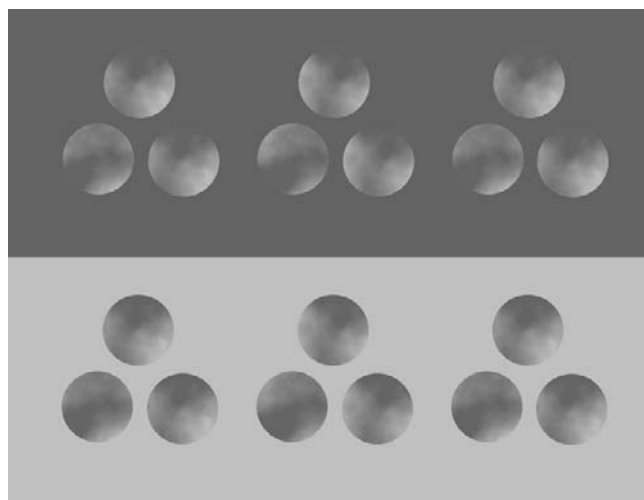


FIGURE 86.11. Scission and the perceptual organization of depth. The top and bottom figures are identical apart from the brightness of the surround. When the right stereopair is cross-fused, the figure appears as a single textured plane that is visible through three circular holes. This is seen irrespective of the luminance of the surround. However, when the disparity is reversed (by cross-fusing the left stereopair), the texture appears to separate into two depth planes. The near layer contains near clouds that vary spatially in thickness or opacity. Through these clouds can be seen three more distant discs, which appear more or less uniform in lightness. For this depth ordering, the structure completely reverses with a change in the luminance. In the top case, the dark portions of the texture form the clouds; in the bottom case, the light portions of the texture form the clouds. Scission makes these percepts possible by allowing the visual system to separate the intermediate grays into two distinct contributions. (Adapted from Anderson, 1999.)

clouds, which consists of uniform discs on a uniform background (see Anderson, 1999; Anderson, in press).

Another interesting property of this display is that the lightness and spatial structure of the clouds and discs reverse completely when the luminance of the surround varies. In Figure 86.11, the top and bottom displays are identical except for the lightness of the surround. When the surround is dark, the texture scissions into dark, smoke-like clouds in front of white discs. However, when the surround is white, it is the light portions of the texture that move forward, floating like mist in front of dark discs. One final observation about the display is that when the texture carries near disparity, and thus undergoes scission, the clouds that float in front tends to complete modally across the gaps in between the discs. This is in part due to the fact that the conditions for camouflage are satisfied, as discussed in the second section.

When the depth is reversed in the display, two asymmetries occur. The first is *geometrical* in that it alters the structure of the depths in the scene. In the near case the texture scissions into two layers, while in the far case the texture

appears relatively uniform in depth by comparison. The second asymmetry that occurs with depth inversion is *photometric* in that it is driven by the luminance of the surround and determines the lightness of the cloud and discs. When the texture is distant, the percept changes very little with changes to the luminance of the surround; by contrast, when the texture is near, the luminance of the surround critically determines how the scission occurs, as well as the lightness of the cloud and discs. In what follows, we will use the CDAP discussed in the first section and the concept of scission to explain these asymmetries. For a more thorough discussion, see Anderson (in press).

Let us first consider the case in which the texture carries far disparity relative to the circular boundaries. Because the texture is continuously varying in luminance, it carries localizable disparity signals at almost every location. Put another way, if disparity is carried by *contrast*, as argued in the first section, then patterns that are richly structured bear the densest distribution of disparities. Recall that the CDAP requires both sides of every contrast to be at least as distant as the disparity carried by the contrast. This means that when the texture is given far disparity (or, more precisely, when the *contrasts of the texture* are given far disparity), both the light and dark matter in the texture recede to this depth. In turn, the depth placement of the texture uniquely determines the border ownership of the boundaries of the discs, which carry relatively near disparity. If the *insides* of the discs (i.e., the texture) carry far disparity, then the *outsides* (i.e., the region surrounding the discs) must be at the depth carried by the circular boundary. Thus, the circles are seen as holes in the surrounding surface; it is through these holes that the texture is visible.

The situation is more complex when the depth is reversed, that is, when the contrasts of the texture are nearer than the contrast of the circular boundaries. Crucial to the following argument is that it is *contrasts* that carry disparity, while it is the light and dark regions that make up the contrasts to which depth is assigned. First, let us consider the circular boundary between the surround and the texture. When the surround is light, it is the dark portions of the texture (inside the circles) that contrast with the surround. Thus, the disparity of the circular boundary is carried by the contrast between the light matter of the surround and the dark portion of the textured disc. The CDAP requires both of these regions to be at least as distant as the disparity carried by the boundary. This means that the light surround is dragged back to this depth, and the dark matter of the texture is also dragged back to this depth. Now consider the contrasts between the dark and light portions within the texture. These contrasts carry relatively near disparity. But the contrast between the dark matter and the surround has already constrained the dark matter to be at least as distant

as the circular boundary. This means that it must be the *light matter of the texture* that is responsible for the near disparity of the texture, that is, the light matter is a near surface that partly obscures the dark matter. This explains why the texture splits into two depths: the dark matter is dragged back by forming a contrast that carries far disparity (i.e., the boundary of the disc) and the light matter floats in front, as its boundaries with the dark matter carry near disparity.

The final logical step in the explanation involves scission. The texture does not consist of only two luminances, but of a continuous range of luminances from light to dark. How can we explain the appearance of the intermediate luminances in the texture? Scission makes it possible to separate the intermediate luminances into two distinct components: dark “stuff” and light “stuff,” which have been compressed into a single luminance by the process of projection onto the retina. These two components lie in different depth planes. Put another way, scission allows the visual system to interpret the gray regions as *dark matter viewed through light matter*. The critical insight is that it is the dark stuff in the texture that forms the contrast with the surround. Therefore, all of the dark stuff belongs to the more distant depth, including the dark stuff within the grays. All of the remaining lightness in the grays belongs to the transparent clouds that float in front of the discs. In this way, the intermediate luminances are interpreted as varying degrees of transmittance of the overlying layer. The lighter the gray, the thicker the cloud; the darker the gray, the sparser. This explains why the disc appears as a uniform dark disc: all of the dark is “sucked out” of intermediate regions and is dragged back to form the disc. The “leftover” lightness is attributed to the transparent clouds.

The whole argument reverses when we change the surround from light to dark. When the surround is dark, it is the light portions of the texture that contrast with the surround, and therefore, it is the light portions of the texture that are dragged back. The near disparity of the texture must therefore be due to the dark regions, and thus dark clouds are seen to float in front of white discs. Again, as it is the *whiteness* of the texture that is dragged back, all of the whiteness in the intermediate luminances is attributed to the more distant discs. The remaining darkness in the grays is attributed to the dark clouds that float in front. In this way, changing the luminance of the surround changes which contrasts carry the disparities and thus which regions are dragged back by virtue of the CDAP. Scission enables the visual system to separate luminances into multiple contributions and thus segment the intermediate grays into two distinct depth planes.

This demonstration and others like it are important, as they show how multiple processes interface to determine our

percepts of depth and material quality. It is through the CDAP and scission that the visual system interprets local variations in luminance as meaningful surfaces located in depth. Depth stratification complements traditional segmentation as an important process through which the visual system organizes its representation of depth into ecologically valid structures.

Conclusions

It is common to think that depth perception involves little more than determining the depth at each location in the visual field. We have argued, to the contrary, that the visual system mirrors the structural organization of the environment by tying its representation of depth to surfaces and objects. Thus, depth perception is an active process of perceptual organization, as well as a passive process of acquiring depth estimates. We have argued that luminance, disparity, and contrast are some of the basic image features that carry local information about depth, while scission, visual completion, and the CDAP are some of the means by which depth is organized into surfaces.

In the first section, we introduced the CDAP and argued that

1. Disparity is carried by local contrasts (e.g., luminance edges) but depth is assigned to the regions that meet to form the contrasts.
2. Occlusion introduces a critical constraint on the interpretation of local disparity signals, the CDAP. This constraint requires that both sides of a contrast are at the depth specified by the contrast, or one side could be a more distant occluded surface. In the latter case, the disparity determines the depth of the *occluding* side.
3. The CDAP imposes a fundamental asymmetry between near and far structures. When simultaneously applied to all edges in a display, the CDAP can explain a number of asymmetrical changes in perceived surface layout that occur with simple inversion of the disparity field.

In the second section, we discussed how the visual system deals with structures that are invisible because they are hidden by occlusion or camouflaged against their background. We argued that

1. The visual system has to actively complete the missing data if it is to segment depth accurately into objects.
2. Consideration of the environmental conditions of occlusion and camouflage predicts (a) that modal completion is sensitive to luminance, while amodal completion is

not, and (b) that modal completion tends to occur over shorter distances than amodal completion.

3. As predicted from the environmental differences, distinct mechanisms are responsible for the two types of completion. The differences can be used to generate displays in which the completed forms differ when the disparity field is inverted.

Finally, in the third section, we discussed how scission allows the visual system to represent two depths along the same line of sight and thus organize depth into layer. We argued that

1. Certain luminance and figural relations must obtain in order for a region to undergo scission.

2. Scission can have pronounced effects on perceptual organization in regions distant from the local signatures of transparency.

REFERENCES

- Adelson, E. H., 1993. Perceptual organization and the judgment of brightness, *Science*, 262:2042–2044.
- Adelson, E. H., 1999. Lightness perception and lightness illusions, in *The New Cognitive Neurosciences* (M. Gazzaniga ed.-in-chief), Cambridge, MA: MIT Press.
- Adelson, E. H., and P. Anandan, 1990. Ordinal characteristics of transparency, Boston: AAAI-90 Workshop on Qualitative Vision, July 29.
- Anderson, B. L., 1997. A theory of illusory lightness and transparency in monocular and binocular images: the role of contour junctions, *Perception*, 26:419–453.
- Anderson, B. L., 1999. Stereoscopic surface perception, *Neuron*, 24:919–928.
- Anderson, B. L., in press. The role of occlusion in the perception of depth, lightness, and opacity, *Psychological Review*, (in press).
- Anderson, B. L., and K. Nakayama, 1994. Towards a general theory of stereopsis: binocular matching, occluding contours and fusion, *Psychol. Rev.*, 101: 414–445.
- Anderson, B. L., M. Singh, and R. W. Fleming, 2002. The interpolation of object and surface structure, *Cogn. Psychol.*, 44:148–190.
- Beck, J., and R. Ivry, 1988. On the role of figural organization in perceptual transparency, *Percept. Psychophys.*, 44:585–594.
- Bruce, V., P. R. Green, and M. A. Georgeson, 1996. *Visual Perception*, 3rd ed., Hove, East Sussex, UK: Psychology Press.
- Cornsweet, T. N., 1970. *Visual Perception*, New York: Academic Press.
- DeValois, R. L., and K. K. DeValois, 1988. *Spatial Vision*, New York: Oxford University Press.
- Hartline, H. K., 1940. The receptive fields of optic nerve fibres, *Am. J. Physiol.*, 130:690–699.
- Howard, I. P., and B. J. Rogers, 1995. *Binocular Vision and Stereopsis*, New York: Oxford University Press.
- Hubel, D. H., and T. N. Wiesel, 1962. Receptive fields, binocular interaction and functional architecture of monkey striate cortex, *J. Physiol.*, 160:106–154.
- Jones, J., and J. Malik, 1992. A computational framework for determining stereo correspondence from a set of linear spatial filters, *Image Vis. Comput.*, 10:699–708.
- Julesz, B., 1960. Binocular depth perception of computer generated patterns, *Bell Syst. Tech. J.*, 39:1125–1162.
- Julesz, B., 1971. *Foundations of Cyclopean Perception*, Chicago: University of Chicago Press.
- Kellman, P. J., and T. F. Shipley, 1991. A theory of visual interpolation in object perception, *Cogn. Psychol.*, 23:141–221.
- Kellman, P. J., C. Yin, and T. F. Shipley, 1998. A common mechanism for illusory and occluded object completion, *J. Exp. Psychol. Hum. Percept. Perform.*, 24:859–869.
- Kanizsa, G., 1955/1979. *Organization in Vision*, New York: Praeger.
- Koffka, K., 1935. *Principles of Gestalt Psychology*, Cleveland: Harcourt, Brace and World.
- Marr, D., and T. Poggio, 1976. Cooperative computation of stereo disparity, *Science*, 194:283–287.
- Marr, D., and T. Poggio, 1979. A computational theory of human stereo vision, *Proc. R. Soc. Lond B*, 204:301–328.
- Metelli, F., 1970. An algebraic development of the theory of perceptual transparency, *Ergonomics*, 13:59–66.
- Metelli, F., 1974a. The perception of transparency, *Sci. Am.*, 230:90–98.
- Metelli, F., 1974b. Achromatic color conditions in the perception of transparency, in *Perception: Essays in Honor of J. J. Gibson* (R. B. MacLeod and H. L. Pick, eds.), Ithaca, NY: Cornell University Press.
- Metelli, F., O. da Pos, and A. Cavedon, 1985. Balanced and unbalanced, complete and partial transparency, *Percept. Psychophys.*, 38:354–366.
- Michotte, A., G. Thines, and G. Crabbe, 1964/1991. Amodal completion of perceptual structures, in *Michotte's Experimental Phenomenology of Perception* (G. Thines, A. Costall, and G. Butterworth, eds.), Hillsdale, NJ: Erlbaum, pp. 140–167.
- Nakayama, K., S. Shimojo, and G. H. Silverman, 1989. Stereoscopic depth. Its relation to image segmentation, grouping, and the recognition of occluded objects, *Perception*, 18:55–68.
- Palmer, S. E., 1999. *Vision Science*, Cambridge, MA: MIT Press.
- Petter, G., 1956. Nuove ricerche sperimentali sulla totalizzazione percettiva, *Riv. Psicol.*, 50:213–227.
- Pollard, S. B., J. E. W. Mayhew, and J. P. Frisby, 1985. A stereo correspondence algorithm using a disparity gradient limit, *Perception*, 14:449–470.
- Prazdny, K., 1985. Detection of binocular disparities, *Biol. Cybern.*, 52:93–99.
- Ratcliff, F., 1965. *Mach Bands: Quantitative Studies on Neural Networks in the Retina*, San Francisco: Holden-Day.
- Ringach, D. L., and R. Shapley, 1996. Spatial and temporal properties of illusory contours and amodal boundary completion, *Vis. Res.*, 36:3037–3050.
- Shipley, T. F., and P. J. Kellman, 1992. Perception of partly occluded objects and illusory figures: evidence for an identity hypothesis, *J. Exp. Psychol. Hum. Percept. Perform.*, 18:106–120.
- Singh, M., and B. L. Anderson, 2002. Toward a perceptual theory of transparency, *Psychol. Rev.*, 109(3):492–519.
- Smallman, H. S., and S. P. McKee, 1995. A contrast ratio constraint on stereo matching, *Proc. R. Soc. Lond. B*, 260:265–271.
- Sperling, G., 1970. Binocular vision: a physiological and neural theory, *Am. J. Psychol.*, 83:461–534.

- Stoner, G. R., T. D. Albright, and V. S. Ramachandran, 1990. Transparency and coherence in human motion perception, *Nature*, 344:153–155.
- Sugita, Y., 1999. Grouping of image fragments in primary visual cortex, *Nature*, 401:269–272.
- Takeichi, H., T. Watanabe, and S. Shimojo, 1992. Illusory occluding contours and surface formation by depth propagation, *Perception*, 21:177–184.
- Wallach, H., 1948. Brightness constancy and the nature of achromatic colors, *J. Exp. Psychol.*, 38:310–324.

87 Stereopsis

CLIFTON M. SCHOR

STEREOPSIS IS ONE of our primary senses of spatial layout. Slightly different viewpoints of the two eyes produce binocular retinal image disparities that are used to perceive *relative depth* between objects as well as *surface slant* (orientation) and percepts of *object volume*. Stereopsis also provides information about forms hidden by texture camouflage (such as branches in tree foliage) and direction of object motion in depth relative to the head. Stereopsis is an extremely acute mechanism with one of the lowest visual thresholds—less than the width of a single retinal photoreceptor—which makes it one of the hyperacuities (Westheimer, 1979b).

Visual directions

Stereopsis is stimulated by horizontal disparity that results from the slightly different perspective views of the two eyes. Each eye views slightly more of the temporal than the nasal visual field and also sees more of the ipsilateral than the contralateral side of a binocularly viewed object. When viewed with one eye at a time, the retinal images of the three-dimensional (3D) scene have slightly different locations relative to the fovea of each eye, and they are seen in slightly different directions relative to the line of sight (oculocentric directions). However, each eye perceives the targets in a common direction relative to the head (egocentric direction). The perceived egocentric direction of an object is equal to the average of its oculocentric directions in the two eyes combined with the average of right and left eye positions (conjugate eye position). Movements of the eyes in opposite directions (convergence) have no influence on perceived egocentric direction. Thus, when the two eyes fixate on near objects that lie to the left or right of the midline (straight ahead) in asymmetrical convergence, only the conjugate component of the two eyes' positions (produced by movements of the two eyes in the same direction) contributes to perceived direction. Ewald Hering summarized these facets of egocentric direction as five rules of visual direction, and Howard (1982) has restated them. The laws are mainly concerned with targets imaged on corresponding retinal regions (i.e., stimulation of corresponding retinal points in the two eyes results in percepts in identical visual directions).

How are oculocentric visual directions of the two eyes combined in a common visual space, sometimes referred to as the *cyclopean eye*? When the target lies near the plane of fixation, its egocentric direction is based upon the similar

retinal image locations of the two eyes. When the target is slightly nearer to or farther from the plane of fixation, its monocular images are formed at different horizontal eccentricities from the foveas; however, its averaged direction is seen as single (allelotropia). The range of disparities that produce singleness is referred to as *Panum's fusional area* (Schor and Tyler, 1981). The consequence of averaging monocular visual directions of disparate targets is that binocular visual directions are perceived correctly from a reference point midway between the eyes (cyclopean eye). Binocular visual directions can be judged accurately only for targets with averaged visual directions. When targets are positioned far in front of or behind the plane of fixation, their retinal image disparity becomes large and the disparate targets appear diplopic (i.e., they are perceived in two separate directions). The directions of monocular components of the diplopic pair are perceived inaccurately as though each of the images had an invisible paired image formed on a corresponding retinal point in the other eye. There are ambiguous circumstances in which a target in the peripheral region of a binocular field is seen by only one eye because of partial occlusion of the other eye by the nose. The monocular target could lie at a range of viewing distances. However, its direction is judged as though it was located in the plane of fixation such that if it were seen binocularly, its images would be formed on corresponding retinal points.

Several violations of Hering's rules for visual direction have been observed in both abnormal and normal binocular vision. A common binocular abnormality is strabismus (an eye turn or deviation of one eye from the intended binocular fixation point). In violation of Hering's rules, people who have a constant turn of one eye (unilateral strabismus) can have constant diplopia, and they use the position of their preferred fixation eye to judge visual direction, regardless of whether they fixate a target with their preferred or deviating eye. People who have an alternating strabismus (either eye is used for fixation, but only one at a time) use the position of the fixating eye to judge the direction of objects (Mann et al., 1979). People with both types of strabismus use the position of only one eye to judge direction, whereas people with normal binocular eye alignment use the average position of the two eyes to judge direction with either eye alone.

Two exceptions in normal binocular vision involve monocular images, and a third exception involves judgment

of direction of binocular-disparate targets. Hering's rules predict that if a target is fixated with one eye while the other is covered, the target will appear to move in the temporalward direction (toward the ear nearest the open eye) if the eyes accommodate (focus on a near target), even if the monocular position of the open eye remains stationary. The perceived temporalward movement results from the nasalward movement of the covered eye caused by the cross-coupling between accommodation and convergence (Müller, 1843). When the open eye focuses on a near target, the covered eye automatically converges (i.e., turns nasalward) (cross-coupling). Hering's rules predict that the average horizontal position of the two eyes determines the egocentric direction of the foveated target. The first exception occurs when the apparently temporalward motion is greater during accommodation on a near target when one eye is occluded compared to when the other eye is occluded. This asymmetry between the eyes resembles the biased perception of egocentric direction in constant-unilateral strabismus, and it may be related to an extreme form of eye dominance.

The second exception to Hering's rules occurs when the retinal image of a target that is seen monocularly is imaged near a disparate target seen by both eyes (binocular view). Monocular views occur naturally in the peripheral visual field when one eye's view is occluded by the nose. The direction of the monocular target is judged as though it was positioned at the same depth as any nearby disparate binocular target rather than at the plane of fixation. The visual system assumes that there is an occluded counterpart of the monocular target in the contralateral eye that has the same disparity as the nearby binocular target, even though the image is seen only by one eye (Erkelens and van Ee, 1997).

The third exception to Hering's rules is demonstrated by the biased visual direction of a fused disparate target when its monocular image components have unequal contrast (Banks et al., 1997). Greater weight is given to the retinal locus of the image that has the higher contrast. The average location of the two disparate retinal sites is biased toward the monocular direction of the higher-contrast image. These are minor violations that occur mainly for targets lying nearer to or farther from the plane of fixation or distance of convergence. Since visual directions of off-horopter targets are mislocalized, even when Hering's rules of visual direction are obeyed, the violations have only minor consequences.

Binocular correspondence (the horopter)

We perceive space with two eyes as though they were merged into a single cyclopean eye located midway between them. This merger of the two ocular images is made possible by a sensory linkage between the two eyes that is based upon the anatomical combination of homologous regions of the two

retinas in the primary visual cortex. Unique pairs of retinal regions in the two eyes (corresponding points) must receive images of the same object so that these objects can be perceived as single, that is, in a common visual direction, and at the same depth as the point of fixation. This is made possible by the binocular overlap of the two eyes' visual fields. Hering defined binocular correspondence operationally as retinal locations in the two eyes which, when stimulated by real points in space, resulted in a percept in identical visual directions. For a fixed angle of convergence, optical projections into space, from corresponding retinal points located along the equator and midline of the each eye, intersect. In other cases, such as oblique eccentric (tertiary) locations on the retina, corresponding points have visual directions that do not intersect in real space. The horopter is the locus of object points in space whose images can be formed on corresponding retinal points. The horopter serves as a reference throughout the visual field for the same disparity as at the fixation point (zero disparity). To appreciate the shape of the horopter, consider a theoretical case in which corresponding points are defined as homologous locations on the two retinas (i.e., corresponding points are equidistant from and in the same direction relative to their respective foveas). Consider binocular combinations of points imaged on the horizontal retinal meridians or equators that pass through the foveas. The egocentric visual directions of corresponding points located on the retinal equator intersect in space at real points that define the longitudinal horopter. This theoretical horopter is a circle whose points will be imaged at equal eccentricities from the two foveas on corresponding points except for the small arc of the circle that lies between the two eyes (Ogle, 1962) (Fig. 87.1). While the theoretical horopter is always a circle, its radius of curvature increases with viewing distance. This means that its curvature decreases as viewing distance increases. At the limit, the theoretical horopter is a straight line at infinity that is parallel to the face and the interocular axis (frontoparallel). Thus, a surface representing zero disparity has many different shapes, depending on the viewing distance. The consequence of this spatial variation in horopter curvature is that the spatial pattern of horizontal disparities is insufficient information to specify depth magnitude or even depth ordering or surface shape and curvature. Additional information about target distance and direction relative to the head is needed to interpret surface shape and orientation (Garding et al., 1995).

Binocular matching (the correspondence problem)

Alignment of the two retinal images depends on eye position and the optical center of the eye (nodal point). The two separate components of eye position are the direction of gaze relative to the head (version) and the distance of gaze

Theoretical Longitudinal Horopter

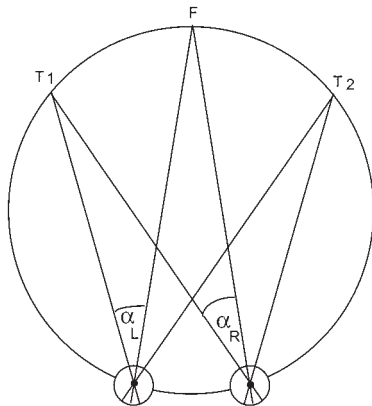


FIGURE 87.1. The theoretical horopter. The theoretical horopter or Vieth-Müller circle passes through the entrance pupils of the two eyes and the point of fixation (F). All points on this circle (e.g., $T1$ and $T2$) subtend equal angles at the entrance pupils of the two eyes ($\alpha_L = \alpha_R$). The Vieth-Müller circle represents the geometric locus of targets that subtend zero retinal image disparity.

where the two visual axes intersect (vergence). If both version and vergence eye position are known, the 3D scene can be reconstructed geometrically by projecting images from the retina through the nodal points of the two eyes, and the target lies at the points of intersection. However, the success of this exercise relies upon selecting image points that correspond to the same target in space. In complex natural scenes, there are many textured patterns that have similar shapes that lie in different locations, and potential binocular matches are possible between a given feature in one eye and several features in the other eye. This problem is exacerbated by camouflage surface texture such as tree foliage, where there is little spatial uniqueness of any particular texture element in the pattern. For example, false matches can occur when viewing a vertically oriented repetitive pattern (Fig. 87.2). The vertical bars in wallpaper patterns can appear to float out of the depth plane of the wall (the wallpaper illusion). The visual system utilizes several inferential shortcuts to limit the possible matches in natural textured patterns to a manageable number.

Disparities of the two retinal images could be analyzed in various ways. In a local analysis, individually perceived forms could be compared to estimate their binocular disparity. In this local analysis, form perception would precede depth perception (Helmholtz, 1909). In a global analysis, luminance properties of the scene, such as texture and other token elements, could be analyzed to code a disparity map from which depth was estimated. The resulting depth map would contribute to the perception of form. In this analysis, depth perception would precede form perception. In the

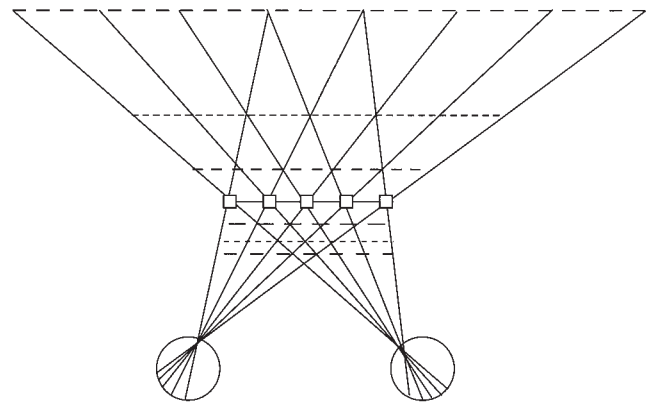


FIGURE 87.2. The wallpaper illusion. A repetitive pattern of vertical bars or an equally spaced horizontal row of dots can be matched in the two eyes to form one of many different depth planes.

local analysis, it is clear which monocular image components are to be matched binocularly because of their uniqueness. The global analysis is much more difficult since many similarly textured elements must be matched, and the correct pairs of images to match are not obvious. The matching problem is constrained by restricting matches to certain features of texture elements (types of primitives or tokens) and by prioritizing certain matching solutions over others. In addition, there is an interaction between the local and global analyses that simplifies the process. Local features are often visible within textured fields. For example, there are clumps of leaves in foliage patterns or target edges that are clearly visible prior to sensing depth. Vergence eye movements can align these unique monocularly visible patterns onto or near corresponding retinal points and reduce the overall range of disparity subtended by the textured object (Marr and Poggio, 1976). Once this has been done, the global system can begin to match tokens based upon certain attributes such as luminance spatial frequency and orientation.

Several serial processing models have been proposed to optimize solutions to the matching problem. These serial models utilize the spatial filters that operate at the early stages of visual processing. Center-surround receptive fields and simple and complex cells in the visual cortex have optimal sensitivity to limited ranges of luminance periodicity that can be described in terms of spatial frequency. The tuning or sensitivity profiles of these cells have been modeled with various mathematical functions (difference of two Gaussians, Gabor patches, Kauche functions, etc.), all of which have bandpass characteristics. They are sensitive to a limited range of spatial frequencies that is referred to as a *channel*, and there is some overlap in the sensitivity range of adjacent channels. These channels are also sensitive or tuned to limited ranges of different orientations. Thus, they encode both the size and orientation of contours in space. These filters serve to

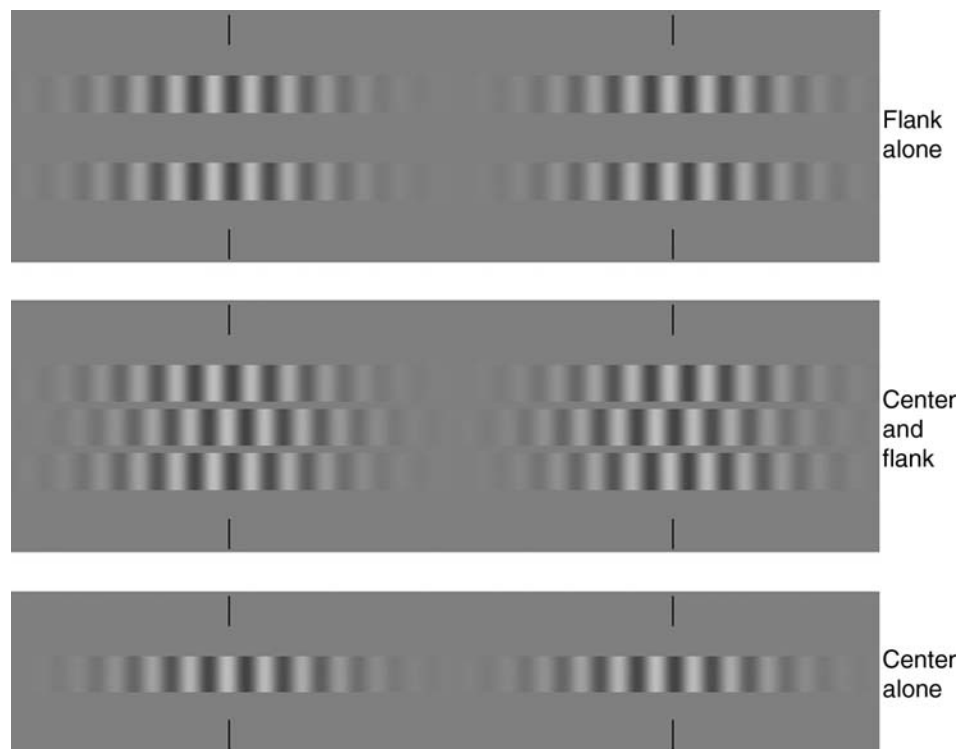


FIGURE 87.3. The center row in the middle panel has the same absolute disparity as the figure shown in the bottom panel, and the flanking rows in the middle panel have the same disparity as the rows shown in the upper panel. When the center panel is fused by crossing the eyes to merge the vertical lines on the left and right,

the depth ordering of the center panel is reversed from its counterparts in the upper and lower panels. This stereogram demonstrates that the minimum relative disparity has a higher priority than the minimum absolute disparity in the binocular matching process.

decompose a complex image into discrete ranges of its spatial frequency components. In the Pollard Mayhew and Frisby (PMF) model (Frisby and Mayhew, 1980), three channels tuned to different ranges of spatial frequency filter different spatial scale components of the image. Horizontal disparities are calculated between the contours having similar orientations and matched contrast polarities within each spatial scale. In addition, priority is given to similar matching solutions across several spatial scales. Most of these models employ both mutual facilitation and inhibition between disparity detectors; however, several stereo phenomena suggest a lesser role for inhibition. For example, we are able to see depth in transparent planes, such as views of a stream bed through a textured water surface, or views of a distant scene through a spotted window or intervening plant foliage. In addition, as the separation between two surfaces increases, their depth can be averaged, that is, seen as filled in, or they can be seen as two separate surfaces lying in different depth planes (Stevenson et al., 1989). Inhibition between dissimilar disparity detectors would obstruct these percepts.

Computational models of stereopsis employ a number of algorithms that constrain stereo matches to produce the smallest disparity offset from the plane of fixation (nearest neighbor match) or to minimize the disparity differences

between nearby features. In some natural scenes, such as a slanted textured plane, the nearest neighbor match and the minimum disparity difference match are in conflict when disparities in regions away from the point of fixation exceed one cycle of the texture spacing. In Figure 87.3, the center stimulus in the middle panel is surrounded by upper and lower flanking stimuli with the same disparity amplitude but the opposite depth sign. The flank and center are shown in isolation in the top and bottom panels, respectively. These patterns have multiple depth matches, as described above in the wallpaper illusion. The minimum depth difference (relative disparity) between the flank and center is smaller than the difference between the absolute disparities of the overall stimulus. When the top panel is fused by crossing the eyes (cross-fused), the flank appears nearer than the fixation lines. When the bottom panel is cross-fused, the center appears farther than the fixation lines. When the center panel is cross-fused, both the center and flanks appear either nearer to or farther from the fixation lines, and their depth ordering is reversed compared to the top and bottom panels. Figure 87.3 demonstrates a priority of minimum relative depth over minimum absolute disparity matching solutions.

Except for the edges, most textured areas of the plane have potential matching ambiguity, and their depth solution

will depend on the area, spatial separation, and disparity of adjacent textured regions. Binocular matches minimize the relative disparity between adjacent regions of the surface so that the textured surface is perceived as planar rather than fragmented (smoothness or continuity constraint) (Papathomas and Julesz, 1989; Zhang et al., 2001). The limited range of spatial interactions promotes matches that reduce abrupt changes in disparity while allowing large gradual increases in the disparity of slanted surfaces.

Disparity coded from edges and contrast information (second-order stereopsis)

Binocular matching is most difficult with repetitive textures that are presented in large fields located either in front of or behind the plane of fixation. A coarse-to-fine strategy reduces this matching ambiguity by first seeking matches of edge information (Mitchison and McKee, 1987). Edges or overall target shape can be described as a contrast variation of surface texture. Contrast variations are coded by a nonlinear or second-order process that is equivalent to rectifying the neural representation of the retinal image (Wilson et al., 1991b). Contrast-defined edges (contrast envelope) can be used to make coarse matches in stereo tasks involving large disparities that are near the upper disparity limits for stereopsis (Hess and Wilcox, 1994). These studies show that the upper disparity limit for stereopsis (maximum disparity that stimulated stereo depth) is not limited by first-order or luminance information such as the spatial frequency of a textured surface. Instead, the upper disparity limit for stereopsis increases with the size of the contrast envelope that contains the textured pattern (Hess and Wilcox, 1994). These results could be attributed to the disparity of edges coded by a nonlinear extraction of the contrast envelope (Wilcox and Hess, 1995).

Transient and sustained stereopsis

Second-order contrast cues stimulate both sustained and transient stereopsis. Sustained stereopsis is stimulated by small disparities (within the singleness range) that are presented for long durations. Transient stereopsis creates a brief (transient) impression of depth, and it is stimulated by briefly presented images (Kumar and Glaser, 1994) whose disparity can range from small values within the sensory fusion range (0.5 degree) to highly diplopic values (>8 degrees). Both sustained and transient stereopsis can be stimulated by first-order (luminance) and second-order (contrast) forms of spatial information. Transient stereopsis relies more heavily on second-order information than does sustained stereopsis. The transient system is more broadly tuned than the sustained system to differences between the texture (carrier) properties of the stimulus presented to the two eyes (i.e.,

spatial frequency, orientation, contrast, and contrast polarity) (Edwards et al., 1999; Schor et al., 1998).

Vivid stereoscopic depth can be perceived with brief stimuli, even when the detailed structure of the two retinal images differs markedly. Contrast envelope size (Schor et al., 2001) and, to a greater extent, temporal synchrony of the two eyes' stimuli (Cogan et al., 1995) are the primary means for selecting matched binocular inputs for transient stereopsis. Second-order stimuli work well in concert with first-order stimuli to assist the computation of binocular matches in a coarse-to-fine strategy. Second-order information from the contrast-defined edges provides coarse information to guide matches of small disparities in the luminance-defined texture by the fine system (Wilcox and Hess, 1997). This is not a function reserved exclusively for second-order stimuli because coarse first-order luminance information also guides disparity matches (Wilson et al., 1991a). This coarse-to-fine strategy utilizing contrast and luminance information is effective because spatial information represented by contrast and luminance is usually highly correlated in images formed in natural environments.

Stereo acuity

Stereopsis is the sense of relative depth between two or more features. It is stimulated by differences between absolute disparities subtended by these features (Westheimer, 1979a). Absolute disparity of an object quantifies its retinal disparity relative to the horopter. It is the difference in the locations of its retinal images in the two eyes from corresponding retinal points. Stereopsis is stimulated by differences between several absolute disparities, that is, relative disparity. Relative disparity describes the disparity difference between features. Relative disparity thresholds for stereopsis are lowest when targets are imaged on or near the horopter. Stereo sensitivity to relative disparity varies dramatically with the distance of these targets from the horopter or plane of fixation (Fig. 87.4). The average disparity of targets from the fixation plane is described as their *depth pedestal*. Stereo-depth discrimination thresholds, measured as a function of the depth pedestal, describe a depth discrimination threshold function that is summarized by a Weber fraction (stereo threshold/depth pedestal). The Weber fraction for stereopsis indicates that the noise or variability of the absolute disparities subtended by the targets is less than 5% over a range of disparity pedestals up to 0.5 degree (Badcock and Schor, 1985). Judgments of depth beyond this range of pedestals are clouded by the appearance of diplopia.

Spatial pooling and uncertainty

Stereo sensitivity can either be enhanced or reduced by nearby targets. The threshold for detecting depth corruga-

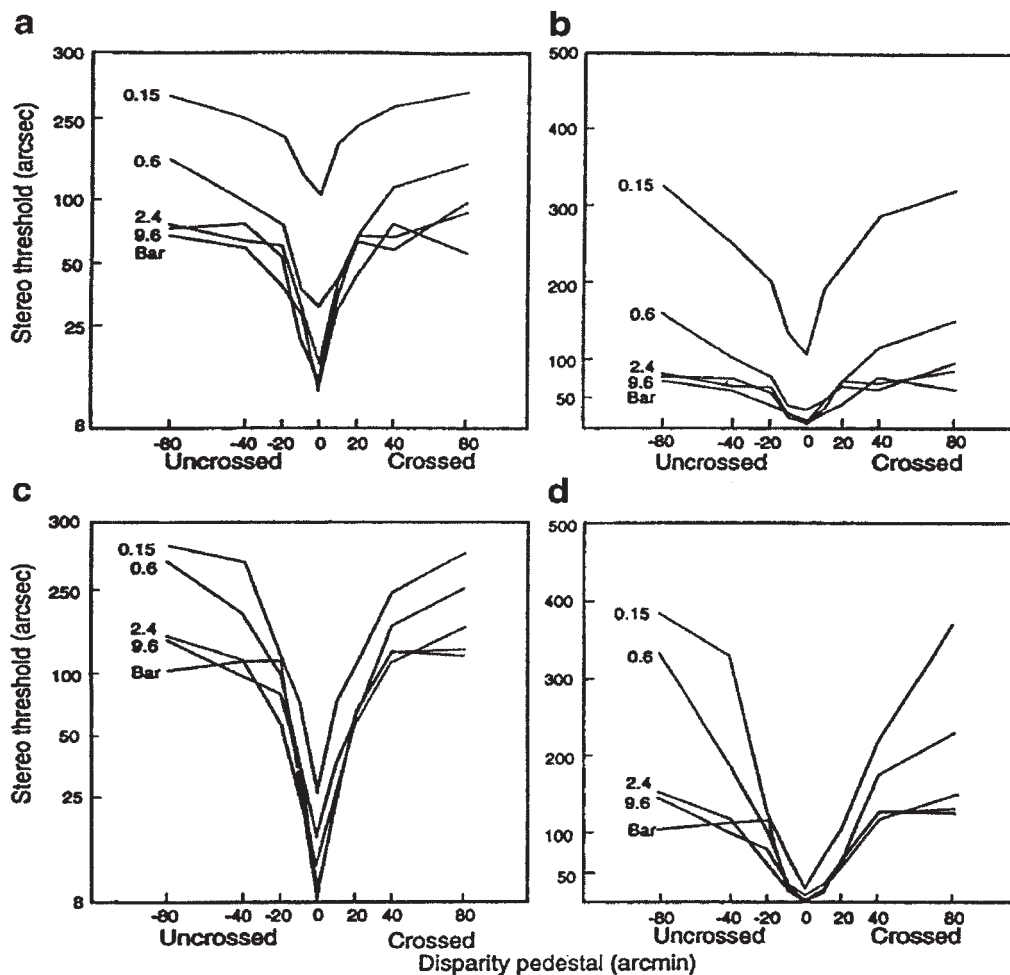


FIGURE 87.4. Threshold for depth discrimination between a test stimulus and a comparison stimulus as a function of the disparity offset (pedestal) of the comparison stimulus. Each curve shows the results using bandpass-filtered bar stimuli whose center spatial frequencies range from 0.15 to 9.6 c/deg. Stereo depth is most sensitive for targets located on the horopter, and threshold increases exponentially with disparity pedestal.

tions of a surface such as the folds in a hanging curtain decreases with depth-modulation frequency (reciprocal of spacing between the folds), up to 0.3 c/deg where the threshold is lowest (Tyler, 1975). At depth-modulation frequencies lower than 0.3 c/deg, the threshold for stereopsis is elevated and appears to be limited by a disparity gradient (i.e., a minimal rate of change in the depth/degree of target separation). At depth-modulation frequencies higher than 0.3 c/deg, the stereo threshold is elevated as a result of depth averaging of adjacent targets. Similar effects are seen with separations between point stimuli for depth (Westheimer, 1986; Westheimer and McKee, 1979).

When a few isolated targets are viewed foveally, changes in the binocular disparity of one target produce suprathreshold depth changes or depth biases in other targets when their separation is less than 4 arc min. This depth attraction illustrates a pooling of disparity signals (Parker and Yang, 1989).

When targets are separated by more than 4 to 6 arc min, the depth bias is in the opposite direction and features appear to repel one another in depth. Attraction and repulsion also occur with cyclopean targets (i.e., targets that can only be revealed by stereo depth, such as clumps of tree foliage) (Stevenson et al., 1991), showing that they are not based simply on positional effects at the monocular level. The enhancement of depth differences by repulsion might be considered a depth-contrast phenomenon that is analogous to Mach bands in the luminance domain (enhanced perceived contrast of edges) that are thought to result from lateral inhibitory interactions. Depth distortions that are analogous to Mach bands have been demonstrated with horizontal disparity variations between vertically displaced contours (Lunn and Morgan, 1996), demonstrating analogous spatial interactions in the horizontal disparity domain and the luminance contrast domain.

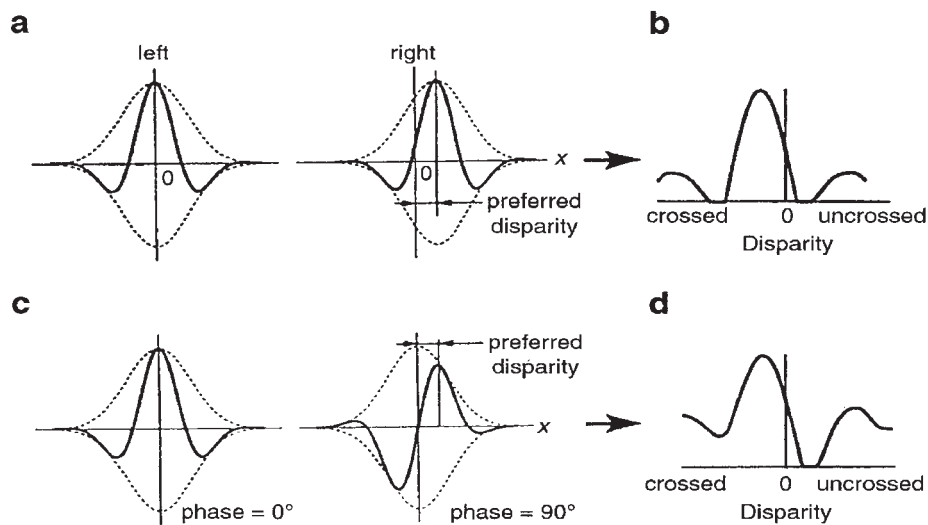


FIGURE 87.5. Position and phase encoding of disparity: two possible schemes of disparity encoding are shown. *Position coding:* *a*, Solid curves show the receptive field profile of left and right eye inputs to a binocular cell. The abscissa for each curve gives retinal position, and the ordinate gives the cell's sensitivity to luminance. *b*, The disparity tuning of the binocular cell that is sensitive to posi-

tional disparity. *Disparity coding:* *c*, Solid curves show the receptive field profile of left and right eye inputs to a binocular cell. The abscissa for each curve gives retinal phase, and the ordinate gives the cell's sensitivity to luminance. *d*, The disparity tuning of the binocular cell that is sensitive to phase disparity.

Frame of reference

Typically, stereo acuity is measured while looking straight ahead with respect to a flat (frontoparallel) frame of reference rather than the curved horopter. The frontoparallel frame of reference is an implicit or familiar frame of reference. Its pattern of disparities is usually symmetrical with respect to the gaze normal direction and the horopter. However, the frontoparallel plane is somewhat arbitrary since it contains disparities that do not lie on the zero-disparity surface of the horopter. A slanted plane can also be used as an arbitrary explicit frame of reference to make relative depth judgments. Indeed, depth discrimination off the plane of fixation is improved when the targets are presented within a reference surface of dots that have the same mean disparity as the pedestal (Andrews et al., 2001). However, with a frontoparallel reference plane, stereo thresholds increase with the distance in depth (disparity pedestal) of targets from the plane of fixation (Badcock and Schor, 1985). These observations suggest that the frame of reference for relative depth judgments is most effective when it is well defined by visual stimuli.

Disparity processing by early spatial filters

Stereo acuity depends upon spatial scale (range of spatial frequencies). The dependence of stereopsis on luminance spatial frequency suggests that disparity is processed early in the visual system by linear channels that are tuned to discrete bands of spatial frequency. When tested with a limited

range of spatial frequencies (narrowband luminance stimulus) (1.75 octaves) such as those produced by a difference of two Gaussians, the stereo threshold becomes lower as spatial frequencies increase up to 2.5 c/deg (Schor et al., 1984a; Smallman and MacLeod, 1994). When expressed as a phase disparity, stereo threshold is constant over this range of spatial frequencies. At spatial frequencies higher than 2.5 c/deg, stereo threshold has a constant position disparity. The constant position disparity at high spatial frequencies contradicts theories of disparity sensitivity based upon phase sensitivity within spatial channels. In addition to phase sensitivity, there may be other factors that limit disparity resolution, such as position sensitivity. Given the presence of both a phase and a position limit, the threshold is set by the limit that is higher. For low spatial frequencies, the constant phase limit would be higher than the position limit, and the converse would be true for high spatial frequencies. The higher limit would determine the threshold.

Disparity coding metrics (phase vs. position)

Physiologically, binocular receptive fields have two fundamental organizational properties (Fig. 87.5). The receptive fields that represent binocular disparity can be offset from a point of zero retinal correspondence (position disparity). They can also have zero positional disparity combined with a quadrature organization in which there is a 90 degree phase shift of the areas of excitation and inhibition in one eye's receptive field compared to the other (phase disparity) (DeAngelis et al., 1995). The position limit at high spatial

frequencies could result from positional jitter in all binocular receptive field sizes. Jitter would have a large influence on the disparity sensitivity of small receptive fields but only a minor influence on the sensitivity of large receptive fields. The same jitter is large relative to the phase coding ability of small (high-frequency) receptive fields. Jitter is responsible for the breakdown of the size-disparity correlation. At high spatial frequencies, stereo threshold is limited by positional uncertainty that causes the threshold to remain constant above 2.5 c/deg. For further discussion of neural mechanisms underlying stereopsis, see Chapter 48.

Other models of stereopsis assume that disparity processing is based solely upon positional information in spatial channels tuned to frequencies above 2.5 c/deg (Kontsevich and Tyler, 1994). In this model, elevated stereo thresholds at low spatial frequencies (below 2.5 c/deg) result from reduced effective contrast of low spatial frequencies passed by the lowest binocular spatial frequency channel that is tuned to 2.5 c/deg. The bandpass stereo tuning characteristics observed with interocular differences in low spatial frequencies (<2.5 c/deg) (Schor et al., 1984b) could result from the differences in effective contrast of these stimuli and interocular inhibition (Kontsevich and Tyler, 1994; Stevenson and Cormack, 2000).

Stereo-depth scaling (mapping from retinal angles to linear depth intervals)

Stereoscopic depth is stimulated by two-dimensional (2D) retinal disparities that can be described in angular units. Some information is lost from the 3D object when it is mapped optically to a 2D retinal image. A given 3D object maps to a specific 2D retinal image pattern; however, a given 2D retinal image pattern maps to many possible 3D scenes (the inverse mapping problem) (Pizlo, 2001). Horizontal retinal image disparity is insufficient to reconstruct a 3D space percept. The same horizontal retinal image disparity can correspond to 1 cm at an arm length and to 1 m at a remote 10 m viewing distance. Despite this growth of the linear depth interval with viewing distance for a fixed angular disparity, we perceive stereo depth veridically. A tennis ball appears to have the same thickness or volume at all viewing distances (depth constancy). Additional information is needed to map the disparity of two retinal images into absolute depth in head-centric (egocentric) space coordinates. In addition to retinal image disparity, stereo-depth perception depends upon the distance and direction (azimuth) of targets relative to the head. Three independent variables involved in mapping stereo depth into head-centric coordinates are retinal image disparity, viewing distance, and the separation in space of the two viewpoints (i.e., the baseline or interpupillary distance). In stereopsis, the relationship

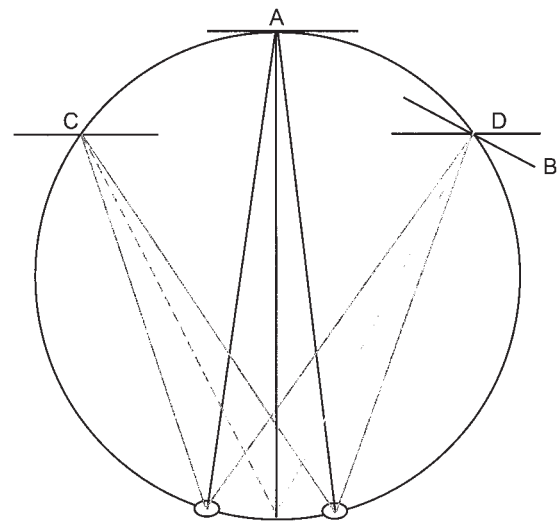


FIGURE 87.6. A top-down view of several slanted surfaces in different locations. Surfaces *A* and *B* are gaze normal. They subtend similar horizontal retinal image disparities, yet they have very different slant angles with respect to the head. Surfaces *A* and *C* both have the same head-centric frontoparallel orientation, but they subtend very different horizontal disparity patterns.

between the linear depth interval between two objects and their retinal image disparity pattern is approximated by the following expression:

$$\Delta d = \eta \times d^2 / 2a \quad (1)$$

where η is retinal image disparity in radians, d is viewing distance, $2a$ is the interpupillary distance, and Δd is the linear depth interval between two targets. The terms $2a$, d , and Δd are all expressed in the same units (e.g., meters). The formula implies that in order to perceive depth in units of absolute distance (e.g., meters), the visual system utilizes information about the interpupillary distance and the viewing distance. The equation illustrates that for a fixed retinal image disparity, the corresponding linear depth interval increases with the square of viewing distance and that information about viewing distance is used to scale the horizontal disparity into a linear depth interval.

Stereo-slant scaling

Disparity cues for surface shape and orientation also depend on target location relative to the head (distance and azimuth). For example, a surface that is parallel to the face has a similar horizontal retinal image disparity pattern when viewed straight ahead to a gaze normal surface that is tilted toward the right eye when viewed in rightward gaze (compare surfaces *A* and *B* in Fig. 87.6). Information about target distance and direction that is needed to discriminate between these two slant stimuli can be obtained from extraretinal and retinal cues. Extraretinal cues include infor-

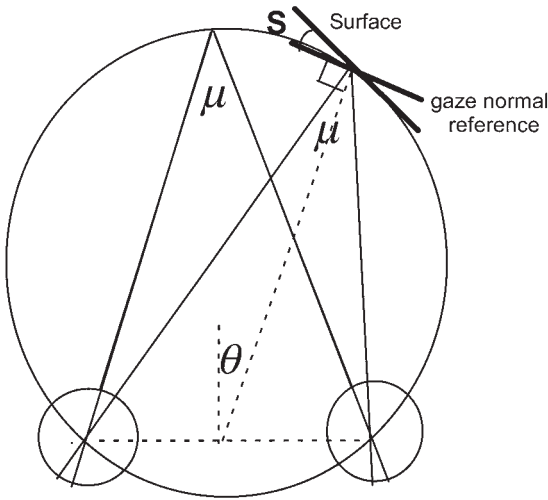


FIGURE 87.7. Slant (S) = $-\tan^{-1}(1/\mu \ln \text{HSR} - \tan \theta)$.

mation about version and horizontal vergence eye position. Surface orientation or slant can be estimated with a combination of horizontal disparity and eye position cues. Retinal image disparity for horizontal slant about a vertical axis can be described by the ratio of horizontal size of the two retinal images (left/right horizontal image size = HSR) (Ogle, 1962; Rogers and Bradshaw, 1995). For a single surface, the relationship between slant angle and combined cues of horizontal retinal image disparity (HSR), horizontal gaze angle (azimuth) (ϕ), and convergence angle (μ) is given by (Backus et al., 1999) (Fig. 87.7)

$$\text{Slant } (S) = -\tan^{-1}(1/\mu \ln \text{HSR} - \tan \phi) \quad (2)$$

Apart from extraretinal eye position signals, vertical disparity cues can also be used to estimate target azimuth when computing slant. Vertical disparities occur naturally with targets in tertiary directions from the point of fixation (Garding et al., 1995; Gillam and Lawergren, 1983; Liu et al., 1994) (Fig. 87.8). Vertical disparity can be described as the vertical size ratio of the two retinal images (left/right vertical image size = VSR) (Rogers and Bradshaw, 1995). The relationship between slant angle and combined cues of horizontal and vertical retinal disparity and convergence angle is given by (Backus et al., 1999)

$$\text{Slant } (S) = -\tan^{-1}(1/\mu \ln \text{HSR}/\text{VSR}) \quad (3)$$

This is a gaze normal description. Adding the azimuth (ϕ) yields slant relative to the head. The use of vertical disparity for slant perception is demonstrated by the tilt of an apparent frontoparallel plane that is induced by a vertical magnifier before one eye (i.e., the induced effect) (Ogle, 1962). The effect is opposite to the tilt produced by placing a horizontal magnifier before the same eye (the geometric effect). If both a horizontal and a vertical magnifier are placed before one eye in the form of an overall magnifier,

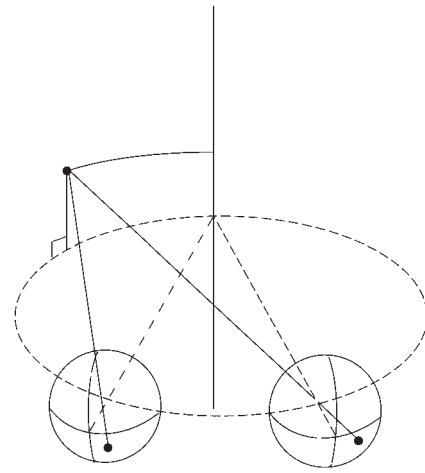


FIGURE 87.8. Vertical disparities occur naturally when targets are placed in tertiary positions while the eyes are aimed in another direction of gaze. Here the target is closer to the left than the right eye, and its image is larger in the left eye. Vertical disparity increases with target azimuth, elevation, and proximity to the observer.

no tilt of the plane occurs. In eccentric gaze, optical geometry causes the proximity of a target to one eye to produce an overall magnification of the image in the nearer eye. This could be sufficient to allow observers to make accurate frontoparallel settings in eccentric gaze. Together, vertical and horizontal magnification provide sufficient information to distinguish between a tilted plane that is viewed straight ahead and a frontoparallel plane viewed in eccentric gaze.

Simultaneous versus sequential stereopsis

One of the primary functions of the visual system is to provide a spatial sense of our surrounding environment. Tasks such as reaching or grasping involve motor interactions between ourselves and objects about us, and they require knowledge about the location and orientation of objects relative to ourselves in head-centric coordinates. Stereopsis is one of our primary senses of spatial layout. Stereopsis is most sensitive to relative disparity between two or more adjacent targets that can be imaged simultaneously within the high-resolution region of the central retina (Westheimer, 1979a, 1979b). Stereo-depth differences are more difficult to estimate when targets are imaged in the periphery, such as when comparing the depths of widely separated targets and only one target can be imaged on the fovea at a time. Under these conditions, stereoscopic depth discrimination is less sensitive than when both targets can be imaged on the fovea (McKee et al., 1990; Schor and Badcock, 1985). Perceiving the depth differences between several targets in different directions requires either that some of the objects be viewed peripherally at the same time (*simultaneous stereopsis*) or that the targets

be viewed sequentially with high-velocity gaze shifts (saccades), at different times, with successive saccadic-foveal fixations (*sequential stereopsis*).

With large target separations, simultaneous stereopsis is impaired by elevated thresholds for disparity discrimination in the retinal periphery. Similar effects are found for stereo-depth discrimination between targets that are presented sequentially in different directions (Enright, 1991; McKee et al., 1990). One target disparity is imaged briefly (150 msec) on the fovea, and when it is extinguished, another target disparity is imaged briefly on an eccentric retinal location while gaze remains fixed in one direction. The task is to compare differences in depth between sequential views of the two targets that are presented one at a time. Simultaneous and sequential stereopsis have identical thresholds when tested with large target separations (>2 degrees) during steady fixation (Enright, 1991; McKee et al., 1990). Thresholds increase proportionately with target eccentricity (Berry, 1948; McKee et al., 1990). Retinal position uncertainty is believed to increase with retinal eccentricity (Levi et al., 1984), and this source of noise is thought to account for the increase of stereo threshold with target separation (McKee et al., 1990).

Thresholds of both simultaneous and sequential stereopsis at 1.5 degrees of target separation are equal (approximately 0.5 to 1.0 arcmin) (Enright, 1991). Simultaneous stereopsis continues to improve at smaller separations down to a lower limit of a few seconds of arc; however, sequential stereopsis does not improve at separations of less than 2 degrees (McKee et al., 1990). With small target separations, the sequential stereo threshold is three to four times higher than for a single simultaneous view of the same target (Enright, 1991; Kumar and Glaser, 1994; McKee et al., 1990; Westheimer, 1979a). Eye position uncertainty, in the form of unregistered vergence fluctuations, is believed to account for the elevated threshold for sequential stereopsis (without eye movements) (McKee et al., 1990). Vergence noise would not impair simultaneous stereopsis because vergence jitter is common to binocular images seen simultaneously, and it is canceled in a presumed differencing process (Westheimer, 1979a).

Sensorimotor interactions

Saccadic gaze shifts in sequential stereopsis improve depth discrimination between widely spaced targets by imaging them near the fovea and horopter, where disparity resolution is most acute. Stereo sensitivity to depth differences between widely separated targets (>5 degrees) can be improved by as much as 50% with sequential gaze shifts that image the two targets sequentially onto the fovea compared to the same test without gaze shifts (Enright, 1991; Ogle, 1956; Wright, 1951). This improvement is thought to be due primarily to

the reduction of retinal position uncertainty when targets are imaged on the fovea (McKee et al., 1990).

Depth comparisons between targets in different locations are represented in head-centric coordinates, and stereo-depth perception depends upon target location relative to the head as well as horizontal retinal image disparity. In particular, vergence information is essential for estimating target distance from the head when vertical disparity information is sparse or absent (Brenner and van Damme, 1998; Wright, 1951). In the extreme case, vergence aligns the eyes precisely during fixation so that absolute retinal image disparity is reduced to zero. Yet depth differences between the sequentially fixated targets that subtend zero disparity can still be discriminated because efferent signals that align the eyes can be used to estimate target distance from the head (Brenner and van Damme 1998). Stereo threshold is limited by the uncertainty with which eye position is sensed (Backus et al., 1999), by the duration or dwell time of each fixation, and by time delays between sequential views (Kumar and Glaser, 1994) that are related to the dynamics of saccadic eye movements (Bahill et al., 1975). Even small to moderate saccades take 25 to 50 msec (Bahill et al., 1975), and this introduces an inter-stimulus interval (ISI) during which information about the first target depth may be lost or corrupted. The ISI could be extended beyond the duration of the saccade by saccadic suppression (reduced visual sensitivity during saccades) that occurs while changes in visual direction are updated to correspond to abrupt changes in eye position (Matin, 1986).

The minimum dwell time for fixating in a given direction of gaze is approximately the latency for a saccadic eye movement, or about 200 msec. The simultaneous stereo threshold is elevated by over fivefold when target duration is reduced from 1 second to about 7.5 msec (Harwerth and Rawlings, 1977). Thresholds for sequential stereopsis are reduced as the number of alternate saccadic fixations increases up to four to eight saccades (two to four cycles of alternate fixation) (Enright, 1991). Sequential stereo thresholds also become lower during the first four to six cycles of alternating sequential target presentations to the fovea without saccadic eye movements (Kumar and Glaser, 1994). Repeated fixations allow averaging to reduce the uncertainty of retinal disparity cues and target location sensed with eye position cues. In addition, the memory of sequential views could be refreshed by repeated gaze shifts (Hayhoe et al., 1998). Thresholds become elevated as stimulus onset asynchrony (SOA) increases (Kumar and Glaser, 1994). Increasing stimulus duration of sequential stimuli elevates the stereo threshold by lengthening the time between the onsets of the two stimuli (i.e., increase of SOA) (Kumar and Glaser, 1994). The improvement of sequential stereopsis appears to depend on the number of times the stimulus appears and the SOA, rather than the total presentation time. It is more

important to have short than long time intervals between sequential stereo stimuli.

Temporal masking

Temporal masking (Alpern, 1953) also elevates thresholds for sequential stereopsis (Butler and Westheimer, 1978; Tyler and Foley, 1974). Saccadic gaze shifts produce time delays between successively fixated targets. The transient onset of the second stimulus could mask the appearance of the first stimulus (backward masking) or vice versa, especially when the two stimuli are large textured surfaces (Kahneman, 1968). Backward masking has been shown to influence sensitivity to apparent motion with random-dot patterns (Braddick, 1973). An example of backward masking in stereopsis was reported by Butler and Westheimer (1978). They observed that the stereo threshold was elevated by adjacent contours presented 100 msec after the onset of the stereo test stimulus. The spatiotemporal masking is greatest when the mask and stereo stimulus have the same disparity. Masking is reduced by half when the disparity of the mask differs from that of the stimulus by only 15 sec arc.

Calibration errors

The magnitude of perceived depth difference between two targets may differ in simultaneous and sequential stereopsis. Calibration errors for retinal and extraretinal cues for stereo depth could have different emphasis or weights in these two forms of stereopsis. Retinal and extraretinal cues for stereo depth, including horizontal disparity, retinal eccentricity, and eye position signals, often have calibration errors that could produce perceived depth and slant biases (i.e., constant errors). Biases in horizontal disparity are related to uniform and nonuniform magnification effects for perceived direction, as described by Ogle (1962), that cause planar surfaces to appear curved and slanted. Biases in perceived visual direction are described by Ogle (1962) as partition errors. Perceived directions, stimulated by equal physical horizontal retinal eccentricities from the fovea (nasal vs. temporal), appear to have unequal perceived magnitudes (unequal oculocentric directions) in the nasal and temporal halves of the visual field (Kundt and Munsterberg asymmetries). These errors in perceived eccentricity of targets imaged on the two hemiretinas could cause directional biases of head-centric depth and slant estimates based on retinal eccentricity and gaze azimuth (θ) (see equation 2). Eye movement signal biases are related to minor muscle paresis or weakness within the oculomotor system that can cause over- or underestimation errors of sensed eye position that vary with direction of gaze. When foveal and peripheral targets are viewed simultaneously without eye movements, retinal position and disparity biases contribute to constant errors of depth and slant

estimates. When separated targets are fixated foveally with sequential gaze shifts, eye position biases will also contribute to constant head-centric errors of depth and slant estimates. Thus, the perceived depth difference between two widely spaced targets might appear different, depending on whether they were fixated sequentially with the fovea or viewed simultaneously at two different retinal locations.

Conclusions

Space perception is based on several sources of information that are estimated by the visual system. The perception of direction, distance, surface shape and orientation, and object volume can be obtained from monocular sources of information including motion parallax, texture gradients, perspective cues, and stimulus overlap (partial occlusion), and from the binocular source of retinal image disparity (stereopsis). The subject of stereopsis has been used to investigate spatial resolution limits of the visual system, to learn how 3D spatial information is represented in the brain, and to understand how perceptual systems reduce information content to a manageable level and also reduce information ambiguity of stimuli by employing ecological inferences as well as computational strategies.

Disparity by itself is an ambiguous depth cue since it is in retinal coordinates. To yield a depth percept, it must be mapped into head-centric coordinates using information about direction and distance to interpret relative depth magnitude and to reference depth in head-centric coordinates. Currently, a concentrated effort is being made to determine how this mapping occurs and the sensory and motor sources of information that are used to obtain information about distance and direction. Ultimately, these investigations will lead to an understanding of how we build up a 3D perceptual representation of space with sequential views such that our percept of space extends beyond any momentary field of view.

REFERENCES

- Alpern, M., 1953. Metacontrast, *J. Opt. Soc. Am.*, 43:648–657.
- Andrews, T. J., A. Glennester, and A. J. Parker, 2001. Stereoacuity thresholds in the presence of a reference surface, *Vis. Res.*, 41:3051–3061.
- Backus, B. T., M. S. Banks, R. van Ee, and J. A. Crowell, 1999. Horizontal and vertical disparity, eye position, and stereoscopic slant perception, *Vis. Res.*, 39:1143–1170.
- Banks, M. S., R. van Ee, and B. T. Backus, 1997. The computation of binocular visual direction: a re-examination of Mansfield and Legge (1997), *Vis. Res.*, 37:1605–1610.
- Badcock, D. R., and C. M. Schor, 1985. Depth-increment detection function for individual spatial channels, *J. Opt. Soc. Am. A*, 2(7):1211–1215.
- Bahill, A. T., M. R. Clark, and L. Start, 1975. The main sequence, a tool for studying human eye movements, *Math. Biosci.*, 24:191–204.

- Berry, R. N., 1948. Quantitative relations among vernier, real depth and stereoscopic depth acuities, *J. Exp. Psychol.*, 38:708–821.
- Braddick, O., 1973. The masking of apparent motion in random-dot patterns, *Vis. Res.*, 13:355–369.
- Brenner, E., and W. J. M. van Damme, 1998. Judging distance from ocular convergence, *Vis. Res.*, 38:493–498.
- Butler, T. W., and G. Westheimer, 1978. Interference with stereoscopic acuity: spatial, temporal and disparity tuning, *Vis. Res.*, 18:1387–1392.
- Cogan, A. I., L. L. Konstantovich, A. J. Lomakin, D. L. Halpern, and R. Blake, 1995. Binocular disparity processing with opposite-contrast stimuli, *Perception*, 24:33–47.
- DeAngelis, G. C., I. Ohzawa, and R. D. Freeman, 1995. Neuronal mechanisms underlying stereopsis: how do simple cells in the visual cortex encode binocular disparity? *Perception*, 24:3–31.
- Edwards, M., D. R. Pope, and C. M. Schor, 1999. Orientation tuning of the transient-stereopsis system, *Vis. Res.*, 39:2717–2727.
- Enright, J. T., 1991. Exploring the third dimension with eye movements: better than stereopsis, *Vis. Res.*, 31:1549–1562.
- Erkelens, C. J., and R. van Ee, 1997. Capture of the visual direction of monocular objects by adjacent binocular objects, *Vis. Res.*, 37:1193–1196.
- Frisby, J. P., and J. E. W. Mayhew, 1980. Spatial frequency tuned channels: implications for structure and function from psychophysical and computational studies of stereopsis, *Philos. Trans. R. Soc. Lond.*, 290:95–116.
- Garding, J., J. Porri, J. E. Mayhew, and J. P. Frisby, 1995. Stereopsis, vertical disparity and relief transformations, *Vis. Res.*, 35:703–722.
- Gillam, B. J., and B. Lawergren, 1983. The induced effect, vertical disparity and stereoscopic theory, *Percept. Psychophys.*, 34:121–130.
- Harwerth, R. S., and S. C. Rawlings, 1977. Viewing time and stereoscopic threshold with random-dot stereograms, *Am. J. Optom. Physiol. Opt.*, 54:452–457.
- Hayhoe, M. M., D. G. Bensinger, and D. Ballard, 1998. Task constraints in visual working memory, *Vis. Res.*, 38:125–137.
- Helmholtz, H. von., 1909. *Handbuch der Physiologischen Optik* (third German edition 1962; English translation by J. P. C. Southall, trans.)
- Hess, R. F., and L. M. Wilcox, 1994. Linear and non-linear filtering in stereopsis, *Vis. Res.*, 34:2431–2438.
- Howard, I. P., 1982. *Human Visual Orientation*, Chichester, UK: Wiley.
- Kahneman, D., 1968. Method, findings, and theory in the study of visual masking, *Psychol. Bull.*, 70:404–425.
- Kontsevich, L. L., and C. W. Tyler, 1994. Analysis of stereo thresholds for stimuli below 2.5 c/deg, *Vis. Res.*, 34:2317–2329.
- Kumar, T., and D. A. Glaser, 1994. Some temporal aspects of stereoacuity, *Vis. Res.*, 34:913–925.
- Levi, D. M., A. Kleins, and P. Actsebaomo, 1984. Detection and discrimination of the direction of motion in central and peripheral vision of normal and amblyopic observers, *Vis. Res.*, 24:789–800.
- Liu, L., S. B. Stevenson, and C. M. Schor, 1994. A polar coordinate system for describing binocular disparity, *Vis. Res.*, 34:1205–1222.
- Lunn, P. D., and M. J. Morgan, 1996. The analogy between stereo depth and brightness, *Perception*, 24:901–904.
- Mann, V. A., A. Hein, and R. Diamond, 1979. Localization of targets by strabismic subjects: contrasting patterns in constant and alternating suppressors, *Percept. Psychophys.*, 25:29–34.
- Marr, D., and T. Poggio, 1976. Cooperative computation of stereo disparity, *Science*, 194:283–287.
- Matin, L., 1986. Visual localization and eye movements, in Boff, K. R., *Handbook of Perception and Human performance*, vol. 1: *Sensory Processes and Perception* (K. R. Boff, L. Kaufman, and J. P. Thomas, eds.), New York: Wiley-Interscience, chapter 20, pp. 1–40.
- McKee, S. P., L. Welch, D. G. Taylor, and S. F. Bowne, 1990. Finding the common bond: stereoacuity and the other hyper-acuities, *Vis. Res.*, 30:879–891.
- Mitchison, G. J., and S. P. McKee, 1987. The resolution of ambiguous stereoscopic matches by interpolation, *Vis. Res.*, 27:285–294.
- Müller, J., 1843. *Elements of Physiology* (W. Baly, trans.), London: Taylor and Walton.
- Ogle, K. N., 1956. Stereoscopic acuity and the role of convergence, *J. Opt. Soc. Am.*, 46:269–273.
- Ogle, K. N., 1962. Spatial localization through binocular vision, in *The Eye*, vol. 4 (H. Davson ed.), New York: Academic Press, pp. 271–324.
- Papathomas, T. V., and B. Julesz, 1989. Stereoscopic illusion based on the proximity principle, *Perception*, 18:589–594.
- Parker, A. J., and Y. Yang, 1989. Spatial properties of disparity pooling in human stereo vision, *Vis. Res.*, 29:1525–1538.
- Pizlo, Z., 2001. Perception viewed as an inverse problem, *Vis. Res.*, 41:3145–3161.
- Rogers, B. J., and M. F. Bradshaw, 1995. Disparity scaling and the perception of frontoparallel surfaces, *Perception*, 24:155–179.
- Schor, C. M., and D. Badcock, 1985. A comparison of stereo and vernier acuity within spatial channels as a function of distance from fixation, *Vis. Res.*, 25:1113–1119.
- Schor, C. M., M. Edwards, and D. Pope, 1998. Spatial-frequency tuning of the transient-stereopsis system, *Vis. Res.*, 38:3057–3068.
- Schor, C. M., M. Edwards, and M. Sato, 2001. Envelope size tuning for stereo-depth perception of small and large disparities, *Vis. Res.*, 41:2555–2567.
- Schor, C. M., and C. W. Tyler, 1981. Spatio-temporal properties of Panum's fusional area, *Vis. Res.*, 21:683–692.
- Schor, C. M., I. C. Wood, and J. Ogawa, 1984a. Binocular sensory fusion is limited by spatial resolution, *Vis. Res.*, 24:661–665.
- Schor, C. M., I. C. Wood, and J. Ogawa, 1984b. Spatial tuning of static and dynamic local stereopsis, *Vis. Res.*, 24:573–578.
- Smallman, H. S., and D. I. MacLeod, 1994. Size-disparity correlation in stereopsis at contrast threshold, *J. Opt. Soc. Am. A*, 11:2169–2183.
- Stevenson, S. B., and L. K. Cormack, 2000. A contrast paradox in stereopsis, motion detection, and vernier acuity, *Vis. Res.*, 40:2881–2884.
- Stevenson, S., L. Cormack, and C. M. Schor, 1989. Hyperacuity, superresolution, and gap resolution in human stereopsis, *Vis. Res.*, 29:1597–1605.
- Stevenson, S. B., L. K. Cormack, and C. M. Schor, 1991. Depth attraction and repulsion in random dot stereograms, *Vis. Res.*, 31:805–813.
- Tyler, C. W., 1975. Spatial organization of binocular disparity sensitivity, *Vis. Res.*, 15:583–590.
- Tyler, C. W., and J. M. Foley, 1974. Stereomovement suppression for transient disparity changes, *Perception*, 3:287–296.
- Westheimer, G., 1979a. Cooperative neural processes involved in stereoscopic acuity, *Exp. Brain Res.*, 36:585–597.
- Westheimer, G., 1979b. The spatial sense of the eye, *Invest. Ophthalmol. Vis. Sci.*, 18:893–912.
- Westheimer, G., 1986. Spatial interaction in the domain of disparity signals in human stereoscopic vision, *J. Physiol.*, 370:619–629.

- Westheimer, G., and S. P. McKee, 1979. What prior uniocular processing is necessary for stereopsis? *Invest. Ophthalmol. Vis. Sci.*, 18:614–621.
- Wilcox, L. M., and R. F. Hess, 1995. D_{\max} for stereopsis depends on size, not spatial frequency content, *Vis. Res.*, 35:1061–1069.
- Wilcox, L. M., and R. F. Hess, 1997. Scale selection for second-order (nonlinear) stereopsis, *Vis. Res.*, 37:2981–2992.
- Wilson, H. R., R. Blake, and D. L. Halpern, 1991a. Coarse spatial scales constrain the range of binocular fusion on fine scales, *J. Opt. Soc. Am.*, 8:229–236.
- Wilson, H. R., V. P. Ferrera, and C. Yo, 1991b. A psychophysically motivated model for two-dimensional motion perception, *Vis. Neurosci.*, 9:79–97.
- Wright, W. D., 1951. The role of convergence in stereoscopic vision, *Proc. Phys. Soc. Lond. B.*, 64:289–297.
- Zhang, Z., M. Edwards, and C. M. Schor, 2001. Spatial interactions minimize relative disparity between adjacent surfaces, *Vis. Res.*, 41:2295–3007.

88 Binocular Rivalry

RANDOLPH BLAKE

WE VIEW THE WORLD through two laterally separated eyes, and yet we experience a single, stable visual world. The brain, in other words, manages to blend, or fuse, the two monocular images in a way that belies any hint of their dual origins, and it does so in a way that extracts stereoscopic information about the three-dimensional (3D) layout of objects in the environment. Several other chapters in this volume (Chapters 48, 49, and 87) cover material on binocular single vision and stereopsis.

The neural operations responsible for binocular single vision and stereopsis, however, are labile in the sense that they can be disrupted when dissimilar monocular stimuli are imaged on corresponding retinal locations. Under these conditions, the eyes transmit contradictory information to the brain. Faced with this contradiction, the brain lapses into an unstable state characterized by alternating periods of monocular dominance that persist as long as the eyes receive discordant stimuli—the phenomenon termed *binocular rivalry*. This chapter introduces the phenomenon, describes major characteristics of rivalry including conditions under which it does and does not occur, summarizes what is known about the neural bases of rivalry, and concludes with a section on the role of rivalry in normal vision. Because the literature on rivalry is so large, a comprehensive review is beyond the scope of this chapter. Interested readers are referred to any of several recent reviews of this literature (Blake, 2001; Fox, 1991; Howard and Rogers, 1995). For a very thorough, up-to-date bibliography on rivalry, take a look at Dr. Robert O'Shea's reference list on the World Wide Web at http://psy.otago.ac.nz/r_oshea/br_bibliography.html. Finally, readers are invited to visit the author's web page, which provides demonstrations of binocular rivalry and some of its major characteristics: <http://www.psy.vanderbilt.edu/faculty/blake/rivalry/BR.html>.

Binocular rivalry's characteristics

EXPERIENCING RIVALRY You can experience rivalry for yourself using each of the three pairs of pictures in Figure 88.1. You will need to follow the instructions in the caption to achieve the conditions for rivalry, and when you do, you will notice several of rivalry's hallmark characteristics. First, note that your visual experience is highly dynamic, with one figure dominating perception for several seconds, only to become phenomenally suppressed in favor of the competing

figure. Sometimes you may see bits and pieces of both figures, creating an impression of a dynamic patchwork. But often you'll see only one figure or the other for several seconds at a time, and neither figure will stay exclusively visible indefinitely (unless you have a strongly dominant eye). Note, too, that you cannot hold one eye's view dominant at will, even when one of the competing figures is a potentially interesting picture such as a female face; the alternations in dominance and suppression evidently are obligatory and may stem from neural adaptation of the currently dominant image (Lehky, 1988; Matsuoka, 1984; Mueller, 1990). You can, however, rescue one eye's figure from suppression prematurely by introducing an abrupt "transient" in the suppressed figure. In the laboratory, this can be accomplished by abruptly incrementing the contrast of a suppressed target (Blake et al., 1990; Wilson et al., 2001) or by introducing motion into a previously stationary, suppressed target (Walker and Powell, 1979). To demonstrate how these transient events can disrupt suppression, view rivalry between a pair of the rival figures in Figure 88.1. When one of the targets becomes suppressed, simply flick your finger in front of that figure; this maneuver will immediately restore the figure to dominance. If you were to repeatedly break suppression of that figure in this way—artificially forcing it to remain dominant—you would also find that it would stay dominant for shorter and shorter periods of time (Blake et al., 1990).

When considering binocular rivalry, it is important not to confuse it with Troxler's effect, the spontaneous fading of a visual figure that can occur when maintaining strict visual fixation. Troxler's effect does not require discordant stimulation to the two eyes, and it occurs readily in peripheral parts of the visual field and can be observed in central vision with targets of a few degrees in visual angle or larger. Troxler's effect is usually attributed to local retinal adaptation, whereas rivalry almost certainly arises from central neural events. It is important to distinguish Troxler's effect from rivalry suppression when studying the disappearance of rival targets viewed in the periphery (Levelt, 1965).

WHAT TRIGGERS RIVALRY Binocular rivalry can be instigated by differences between left- and right-eye views along almost any stimulus dimension, including contour orientation (Wade, 1974), spatial frequency (Fahle, 1982), and motion velocity (Breese, 1899; van de Grind et al., 2001).

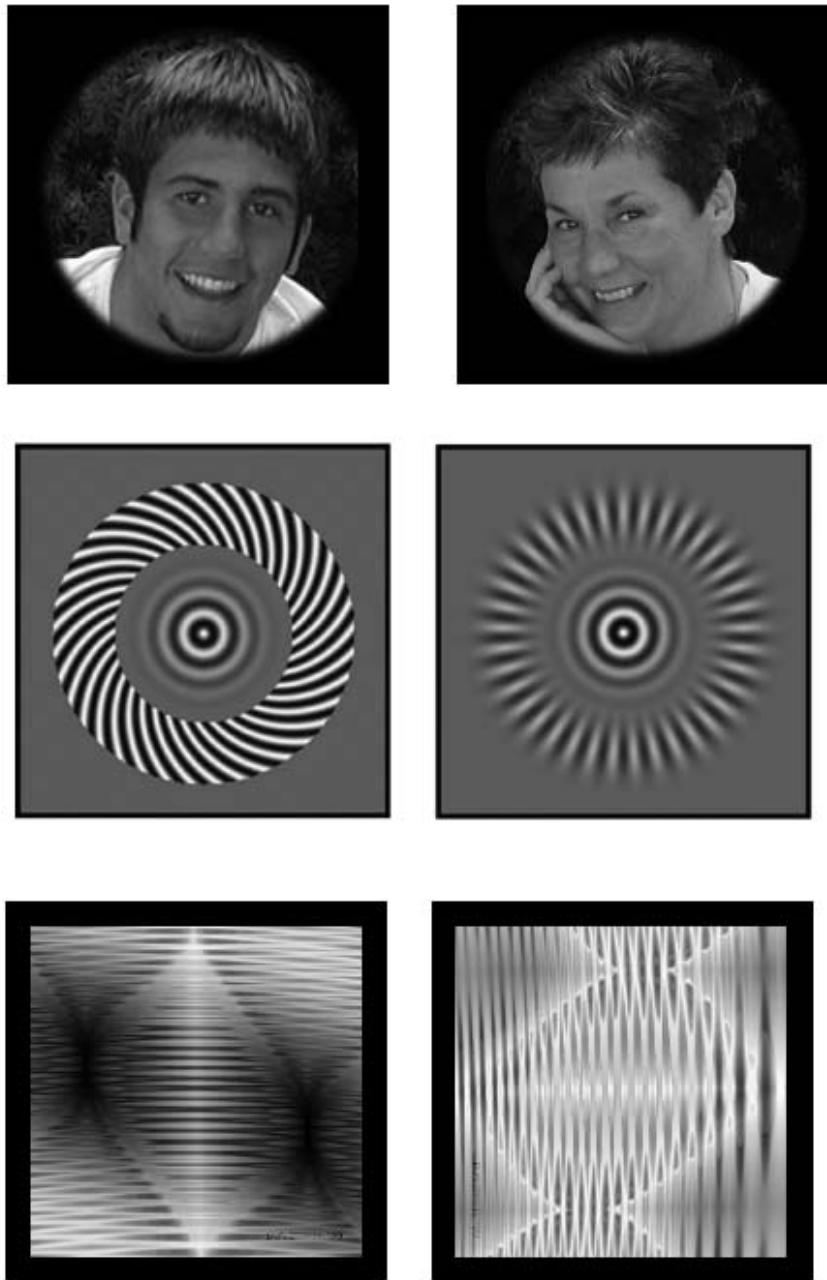


FIGURE 88.1. Provided here are three pairs of rival targets, each of which illustrates the alternations in dominance and suppression characterizing binocular rivalry. To achieve dichoptic stimulation (i.e., presentation of each figure to separate eyes), you must view these pairs either by crossing your eyes or by diverging your eyes, so that the fovea of each eye is seeing one image or the other. (Readers unable to “free-fuse” the targets may see anaglyphic examples of rivalry presented on the author’s web page: <http://www.psy.vanderbilt.edu/faculty/blake/rivalry/BR.html>.) While viewing the upper pair of rival targets—faces of two differ-

ent people—see if you can hold one face perceptually dominant indefinitely. Most people viewing rival targets find this to be impossible. The middle pair of rival targets were used by Wilson et al. (2001) to study *dominance waves* experienced as one portion of a previously suppressed figure emerges into dominance, quickly spreading to encompass the rest of the figure. To see these waves, fixate the central “bull’s-eye” portion of the figure and see what happens as the radial grating assumes dominance. The bottom pair of rival targets are computer-generated images created by David Bloom and used here with permission of the artist. (See color plate 74.)

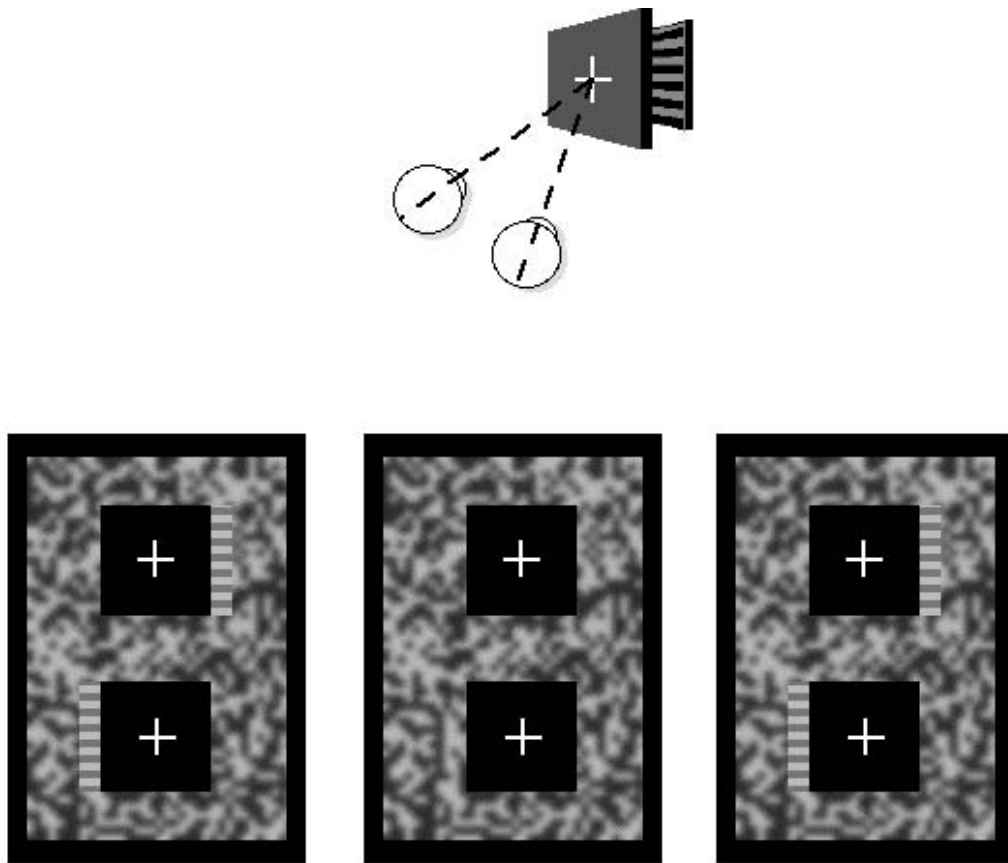


FIGURE 88.2. When one views binocularly a scene in which one object partially occludes another nearby object, one eye will see portions of the occluded object that are invisible to the other eye. This viewing situation—illustrated schematically in the upper part of this figure—creates a local region where dissimilar images stimulate corresponding retinal areas, conditions normally sufficient for binocular rivalry. When this condition is simulated in the laboratory, the incidence of rivalry is reduced (Shimojo and Nakayama, 1990). The pair of half-images in the lower part of the figure may be used to compare binocular rivalry for a “valid” binocular con-

figuration and an “invalid” binocular configuration. If you combine the two half-images by crossing your eyes, use the middle and left-hand figures; if you combine the two half-images by uncrossing your eyes, use the middle and right-hand figures. When the two half-images are appropriately fused, the gray squares will stand out in depth from the textured background, and the partially occluded striped object will be valid in the upper part of the figure and invalid in the lower part. Compare how frequently the striped region disappears in the upper versus the lower field.

There are several conditions, however, in which dissimilar stimulation to corresponding areas of the two eyes does *not* seem to trigger rivalry. One of these is when the two eyes view rapidly flickering rival targets (O’Shea and Blake, 1986; O’Shea and Crassini, 1984), and another is when the two rival targets are very low in contrast, near their threshold for visibility (Liu et al., 1992). In both instances, people describe seeing the binocular superimposition of the two dissimilar targets. It has been noted that these two stimulus conditions—rapid flicker and low contrast—both favor activation of the magnocellular pathway (see Chapter 30), which could mean that rivalry is more tightly coupled to neural activity in the parvocellular pathway (Carlson and He, 2000; Ramachandran, 1991).

Another interesting situation where dissimilar monocular stimulation does not yield rivalry has to do with the geome-

try of 3D space (Shimojo and Nakayama, 1990). Consider the two monocular images produced when you view a 3D scene in which one object (a gray rectangle in this example) partially occludes another (a striped rectangle), as illustrated by the drawing in the top part of Figure 88.2. In this situation, your right eye would be seeing parts of the occluded object that are invisible to your left eye. This means, in other words, that a region of the right eye’s image will contain a pattern of optical stimulation that is different from the optical stimulation falling on the corresponding region of the left eye’s image. (By the way, this geometrical consequence of looking at the world from two different perspectives was realized and discussed by Leonardo da Vinci.) Despite this conflicting stimulation to corresponding retinal areas, observers report that vision is relatively more stable when viewing pairs of images that mimic this situation, implying



FIGURE 88.3. Two stamps that are nearly identical in form but different in color. Free-fuse these two rival stamps and note the appearance of color. (See color plate 75.)

that the brain “understands” that the “conflict” is attributable to the 3D layout of objects in the world (Nakayama and Shimojo, 1990). Interestingly, when the images going to the two eyes are exchanged, observers experience more instances of binocular rivalry within this region of conflict. (Readers may experience the dependence of rivalry on scene interpretation using the pair of stereo images in the bottom part of Fig. 88.2.) These observations imply that the brain knows which eye is receiving which figure, which in turn determines whether one experiences stable fusion or unstable rivalry (see also Blake and Boothroyd, 1985).

Finally, there is some evidence that different “colors” viewed by the left and right eyes do not necessarily rival each other in the same way that different forms do. This can be seen in Figure 88.3, which presents a version of one of the stimulus conditions studied by Creed (1935) in his widely cited (and sometimes misinterpreted) study of binocular fusion and binocular rivalry. Note that the two stamps are identical in form except for the numerals and words signifying the stamps’ value; the colors, however, are distinctly different. When these two images are viewed in binocular combination, however, the color differences do not alternate in dominance; instead, people describe seeing a “washed-out” brown. Whatever the perceived color, it is clear—to put it in Creed’s words—that “we are not dealing with the common type of binocular rivalry in which the form that prevails brings with it the colour of its own object” (p. 383). Using these stamps, you might also try to compare the color of the numeral 1, when it is dominant, with the numeral 2, when it is dominant. Here, too, there is no sense that color changes over time, even though the form does. Again, to quote Creed, “Successive rivalry of forms is therefore not necessarily accompanied by successive rivalry of the corresponding colours” (p. 384).

TEMPORAL AND SPATIAL DYNAMICS The alternations in dominance and suppression during rivalry are not periodic, like the oscillations of a metronome; instead, successive durations of visibility are independent, random events that

collectively conform to a gamma distribution (Fig. 88.4). In other words, one cannot predict exactly how long a given duration of dominance will last (Fox and Herrmann, 1967; Lehky, 1995; Levelt, 1965). However, it is possible to influence the overall predominance of one figure over another, where *predominance* is defined as the total percentage of time that a given figure is dominant during an extended viewing period. Thus, for example, a high-contrast rival figure will tend to predominate over a low-contrast one (Mueller and Blake, 1989), and this increased predominance comes about mostly because the durations of suppression of a high-contrast figure are shorter, on average, than those of a low-contrast figure. It is as if a “stronger” stimulus manages to overcome suppression more quickly than does a “weaker” one (Blake, 1989; Fox and Rasche, 1969). When you stop and think about it, this also means that rivalry alternations should be faster, on average, between a pair of high-contrast rival targets than between a pair of low-contrast rival targets; this is, in fact, the case (Levelt, 1965). Besides contrast, other stimulus variables that “strengthen” a rival target and thereby enhance its predominance include spatial frequency (Fahle, 1982), motion velocity (Blake et al., 1998; Breese, 1899), and luminance (Levelt, 1965).

A rival figure embedded in a larger meaningful context also tends to predominate over one viewed in isolation, but in this case increased predominance arises from a lengthening of the durations of dominance, not an abbreviation of suppression durations (Sobel and Blake, 2001). This dissociation between the effect of a rival figure’s context and the effect of the strength of the figure itself suggests that rivalry dynamics have multiple determinants (Blake, 2001). There are also reports in the literature that meaningful or familiar rival targets predominate in rivalry over less meaningful or unfamiliar ones (for a review of this literature, see Walker, 1978; for an alternative interpretation of the role of meaning in rivalry, see Blake, 1988). It would be informative to replicate these results and, moreover, to learn whether increases in predominance with meaning, if reliably demonstrable, come about through lengthened dominance durations. To the extent that meaning influences other aspects of visual perception (Raftopoulos, 2001), it would not be surprising to find that meaning influences dominance periods of rivalry, for the dominance phases of rivalry appear to be functionally equivalent to normal monocular vision (Fox, 1991).

The potency of global context to influence the temporal dynamics of rivalry could reflect the involvement of higher-level visual processes in rivalry. Is there other evidence for the involvement of such processes? There are several published studies pointing to a role for attention in the control of rivalry dynamics. Several decades ago, Lack (1978) showed that observers could be trained to prolong one eye’s view during rivalry without resorting to tricks such as moving

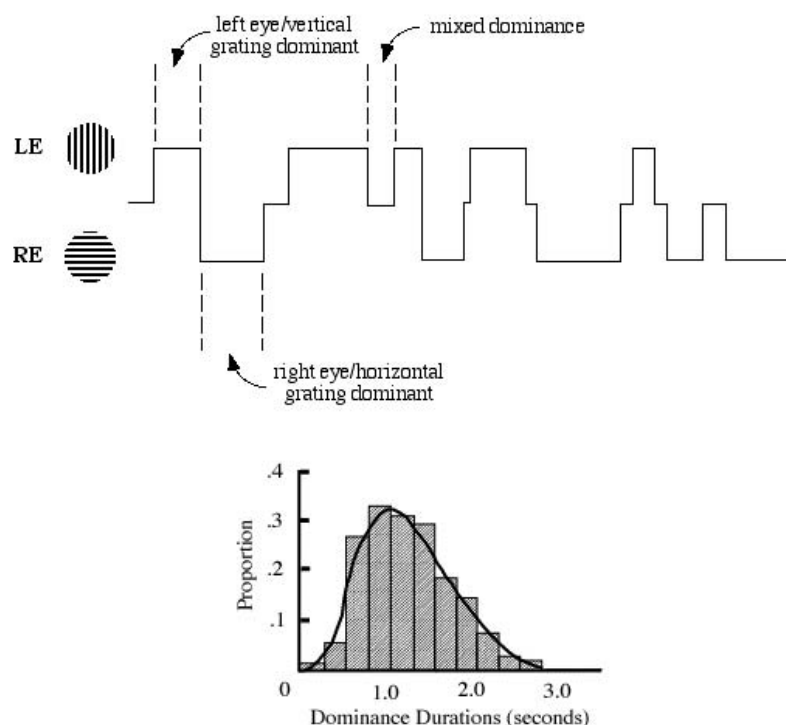


FIGURE 88.4. When an observer presses buttons to indicate successive periods of dominance of two rival targets, those successive durations are randomly distributed, independent variables (Levelt, 1965). The upper diagram shows a representative time line of successive periods of exclusive dominance of a vertical rival grating (viewed by the left eye in this case) and periods of exclusive dominance of a horizontal rival grating (viewed by the right eye). Intermixed among periods of exclusive dominance are occasional periods of “mixed” dominance during which portions of both rival

gratings are visible in a patchwork mosaic pattern. The incidence of mixed dominance tends to be greater with rival targets larger in angular subtense (Meenes, 1930). When dominance durations measured during extended tracking periods are plotted as a frequency histogram (lower portion of the figure), that distribution is well fit by a gamma distribution (solid line in the histogram). In general, the gamma distribution provides a close fit to rivalry alternation data when parameters are adjusted for individual differences (Fox and Herrmann, 1967; Logothetis, 1998).

the eyes in a manner that would favor that view. Instead, Lack’s observers purportedly directed attention to the favored target and thereby prolonged its visibility. It should be noted that rivalry alternations were not abolished under these conditions; despite focused attention, spontaneous reversals in dominance still occurred, albeit less frequently. More recently, Ooi and He (1999) showed that directing attention to a region of the visual field where a rivalry target is currently suppressed boosts the potency of visual motion at that region of the field to break suppression of that target.

What happens when one views multiple rival patterns distributed throughout the visual field? Take a look at the rival display presented in Figure 88.5, a pair of arrays of black and white Gaussian (i.e., blurred) blobs, with each white blob in one array pitted against a black blob in the other array. View the two arrays dichoptically using the free-fusion technique, hold your gaze steadily on the small fixation cross, and concentrate on the pattern of dominance throughout the visual field. Note how often all the black blobs or all the white blobs are simultaneously dominant. When observers actually track these periods of simultaneous dominance, the total incidence turns out to be greater than what would be

predicted if the individual blobs were rivaling independently on their own (Logothetis, 1998). There is a tendency, in other words, for dominance periods of coherent patterns to become perceptually entrained.

This tendency is even more pronounced in the color rival patterns shown in Figure 88.6, a variation of the display created by Diaz-Caneja (1928; see Alais et al., 2000). Here the addition of color further encourages grouping according to coherence, as you can confirm by comparing the rivalry associated with the gray-scale version and the color version.

In both Figures 88.5 and 88.6, periods of coherent dominance can be achieved only by very specific combinations of left-eye and right-eye components that are dominant simultaneously. This means, then, that one eye alone cannot be responsible entirely for dominance at any given moment. Instead, dominance may consist of a patchwork of visible features (Blake et al., 1992; Meenes, 1930), in this case collated from left- and right-eye views. Interocular grouping during rivalry has been nicely documented by Kovács et al. (1997), and it has been studied by others as well (Alais and Blake, 1999; Dörrenhaus, 1975).

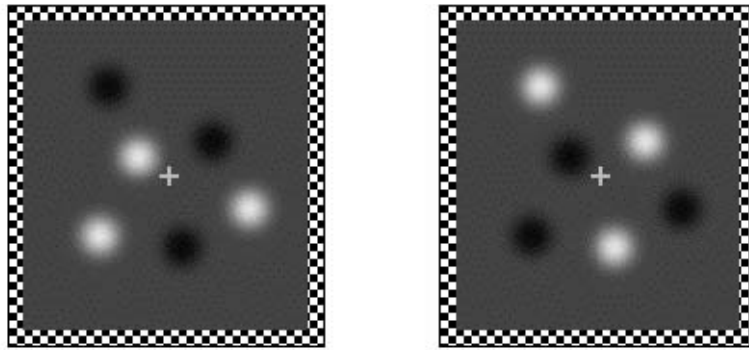


FIGURE 88.5. Rival display consisting of spatially distributed rival targets. Each eye's view consists of an array of blurred circles (Gaussian blobs) differing in contrast polarity between left- and

right-eye views. Free-fuse these two targets and note how often all blobs of a given contrast polarity are simultaneously dominant. (This display is a version of one described by Logothetis, 1998.)

One other intriguing characteristic of rivalry deserves mention, one having to do with the appearance of rival figures during transitions from suppression to dominance. Looking again at rivalry produced by the rival pair in the second row of Figure 88.1, pay particular attention to the emerging appearance of the rings as they assume dominance. You will probably notice that dominance originates

within a restricted region of a ring and spreads from there to encompass the entire figure. These “waves” of dominance are typical of rivalry produced by all sorts of rival figures; they imply the existence of neural “cooperativity” wherein interconnections among neighboring ensembles of neurons promote the spread of activation over spatially extended regions of cortical tissue. Wilson et al. (2001) estimated the

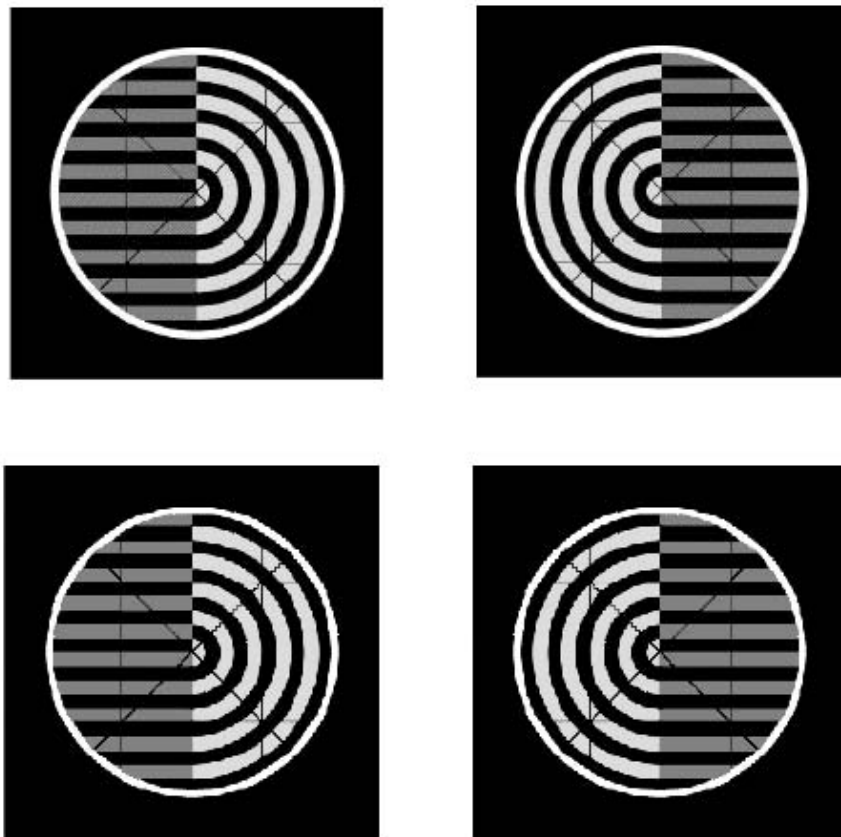


FIGURE 88.6. Two versions of the well-known display of Diaz-Caneja (1928). Upon viewing the gray-scale version (upper pair of rival targets), observers often see a complete bulls-eye pattern or a complete pattern of vertical lines. This implies that portions of

each eye's target are simultaneously dominant, presumably promoted by the spatial grouping that produces a coherent figure. This tendency toward grouping is even stronger in the color version of this figure shown at the bottom. (See color plate 76.)

speed with which dominance waves travel around the circumference of circular rival targets like those pictured in the second row of Figure 88.1, coming up with an average wave speed of about 4 degrees of visual angle per second. This estimated wave speed was even faster when the contours forming the rival target were collinear (i.e., the target was a concentric grating), presumably because waves of dominance travel more effectively along collinear contours. Wave speed (expressed in units of visual degrees per second) was also faster for larger rival targets whose contours were imaged in more peripheral regions of the retina. Expressed in units of cortical tissue (not degrees of visual angle), however, wave speed remained constant with retinal eccentricity, implying that these waves are being generated in a visual area whose magnification factor matches that for visual area V1 (i.e., the exaggerated neural representation of the fovea in the visual cortex).

With these spatial and temporal characteristics of binocular rivalry in mind, we turn next to a consideration of the source of interest in rivalry. Why have vision scientists been fascinated with this phenomenon for almost two centuries, and why in recent years have neuroscientists become intrigued with rivalry?

Binocular rivalry and visual awareness

Binocular rivalry was first systematically described by Sir Charles Wheatstone in his famous monograph on binocular stereopsis (Wheatstone, 1838). But it was Hermann von Helmholtz (1866/1925) and William James (1891) who brought rivalry to the forefront of psychology by treating it as a paradigm case for the study of attention. The noted British neurophysiologist Sir Charles Sherrington (1906) also exploited rivalry to make the case that the brain analyzed left- and right-eye views independently and merged the two views only after each had been fully elaborated. Expressed in contemporary terms, binocular rivalry was construed as a high-level cognitive activity involving competition between conflicting object descriptions. This conceptualization was maintained throughout much of the twentieth century (Walker, 1978), and it led to some unusual ideas about rivalry's practical applications. For example, some psychologists thought that rivalry might provide a revealing indirect tool for assessing intelligence (Crain, 1961), personality (Kohn, 1960), and a tendency to perceive violence (Toch and Schulte, 1961). Those psychometric applications never really caught on, although recent work by Pettigrew (2001) suggests that the issue is not dead.

What has caught on during the past decade or so is the idea that rivalry may provide a powerful tool for studying the neural concomitants of visual awareness (Blake, 1997; Crick and Koch, 1998; Logothetis, 1998). After all, a complex suprathreshold rival pattern can disappear from

visual awareness for seconds at a time, even though that pattern remains imaged on the eye; from a perceptual standpoint, a suppressed pattern temporarily ceases to exist. It should be possible, then, to find fluctuations in neural activity correlated with the intermittent appearance and disappearance of that pattern. And while the search for those neural events has not produced unambiguous answers, the initial results, summarized in the next paragraph, are tantalizing.

Brain imaging studies have discovered modulations in hemodynamic responses and, by inference, neural activity in visual areas of the brain that are tightly correlated with fluctuations in dominance and suppression during rivalry. These response modulations are observed in brain areas as early as primary visual cortex (Lee and Blake, 2002; Polansky et al., 2000; Tong and Engel, 2001), and they are even more pronounced in higher cortical areas in the temporal lobe (Tong et al., 1998) and in the parietal lobe (Lumer et al., 1998). Visual evoked potential measurements (Brown and Norcia, 1997) and neuromagnetic responses (Srinivasan et al., 1999) corroborate the involvement of occipital lobe regions in rivalry but do not pinpoint exactly where in the occipital lobe neural activity is varying with perception. Single-unit studies have recorded action potentials from neurons in awake monkeys trained to report rivalry alternations, and here the evidence points to an increasingly tight coupling between neural firing rate and perception as one moves from primary visual areas to higher cortical regions in the temporal lobe (Leopold and Logothetis, 1996; Logothetis and Schall, 1989; Sheinberg and Logothetis, 1997). Besides neural firing rate, temporal patterns of neural activity also may be correlated with dominance and suppression states during rivalry (Fries et al., 1997), a possibility that could tie rivalry to the larger issue of the role of synchronized neural discharges in perceptual grouping (Engel et al., 1999).

Although admittedly more indirect, perceptual data can also be used to draw inferences about the neural operations mediating binocular rivalry. Reiterating a point made earlier, a normally visible monocular stimulus is temporarily erased from sight during rivalry. To what extent does that stimulus remain visually effective despite its absence from phenomenal awareness? Answers to this question can shed light on the neural locus of rivalry relative to other visual processes (Blake, 1995). If suppression blocks input to a neural processing stage responsible for a given aspect of vision, that blockage should be reflected in visual perception. To illustrate this strategy in operation, consider the well-known motion aftereffect (MAE), that is, the illusory perception that a stationary object is moving produced by prolonged exposure, or adaptation, to real motion (see Chapter 83 for more on the MAE). It has been found that the MAE can be generated even when the adaptation motion itself is suppressed from awareness for a substantial portion of the adaptation

phase owing to binocular rivalry (Lehmkuhle and Fox, 1976; O'Shea and Crassini, 1981). The enduring effectiveness of motion signals in the face of suppression implies that the neural events underlying adaptation transpire prior to the site at which suppression occurs (or, alternatively, that the two occur within parallel pathways). In contrast, the cognitive process termed *picture priming* is disrupted by suppression, as evidenced by the failure of a normally effective picture presented to a suppressed eye to facilitate performance on a subsequent picture-naming task (Cave et al., 1998). This finding implies that suppression temporarily cuts off the flow of information to those neural mechanisms responsible for registering information crucial for object recognition. In general, suppression provides a potentially powerful inferential "landmark" for pinpointing the relative sites of neural processes within the hierarchical stages of visual information processing.

Perceptual measures also disclose other potentially revealing properties of the neural events underlying rivalry. It is well known, for example, that visually presented probe targets are harder to detect when those probes are presented to an eye during suppression, compared to detection during dominance (Wales and Fox, 1970). Evidently, the neural events mediating suppression of a given rival figure generalize to other, new information presented to the same region of the eye viewing that suppressed figure. However, the loss in sensitivity accompanying suppression phases is surprisingly modest in view of the fact that during suppression a complex high-contrast figure is being erased from conscious awareness for several seconds at a time. It remains to be learned how such a profound loss of vision can be accomplished by neural operations that produce only a very modest loss in overall visual sensitivity.

Is rivalry occurring all the time?

Binocular rivalry admittedly is experienced under rather artificial conditions that have no resemblance to those typifying everyday visual experience. Indeed, one leading authority on visual perception has characterized the conditions producing rivalry as "optical trickery" (Gibson, 1966). However, an enduring idea in vision science is that rivalry is occurring *all* the time, including during everyday viewing. Alternations in perception are not seen, the argument goes, because normally the two eyes are viewing the same visual scene and, therefore, these alternations are not visually conspicuous. Known as *suppression theory*, this idea, odd as it may seem, has been seriously advocated by a number of vision scientists over the years (Asher, 1953; Hochberg, 1964; Wolfe, 1986).

How can we know whether normal vision entails chronic, inconspicuous binocular rivalry? Recall from the previous section that periods of suppression are accompanied by

decreased visual sensitivity relative to an eye's sensitivity during dominance. If binocular vision always involves alternating suppression, even when the two eyes view the same scene, losses in visual sensitivity should be a symptom of that alternating suppression. Of course, during normal vision one would not know which eye was temporarily suppressed, but by chance alone, a series of brief test probes presented to one eye should find that eye in the suppression state approximately half of the time. Thus, probe sensitivity should suffer compared to a condition where viewing is monocular and, therefore, dominance is ensured. When these kinds of comparisons are made, however, normal single vision shows no evidence of being accompanied by intermittent losses in visual sensitivity (Blake and Camisa, 1978; O'Shea, 1987). For this and related reasons, it is generally recognized that binocular fusion takes precedence over binocular rivalry. Only when the two eyes view explicitly conflicting images does vision lapse into reciprocal periods of dominance and suppression. This is an important fact to know, for it implies that the neural concomitants of rivalry should be measurable only when a viewer is actually experiencing rivalry and not when experiencing stable binocular single vision.

While suppression cannot be the sole mechanism of binocular single vision, there are still everyday viewing situations where suppression probably does contribute to perception. It is true that left and right foveas rarely receive dissimilar stimulation for any length of time; the oculomotor system seeks to correct this situation by altering the vergence angle until matching features are imaged on the two foveas. There are, however, locations on the two retinas where dissimilar monocular images strike corresponding retinal areas, an inevitable consequence of the geometry of binocular vision. Objects located well in front of or well behind the horopter do cast images on distinctly different areas of the two eyes, and the resulting disparities will be too large for the stereoscopic system to resolve. Yet one ordinarily does not experience the consequences—confusion or diplopia—of this dissimilar monocular stimulation. Binocular single vision, then, may be accomplished by two processes, binocular fusion and binocular suppression (Ono et al., 1977). The potent inhibitory process revealed during rivalry, in other words, may contribute to normal binocular single vision.

For some individuals with chronic eye misalignment (i.e., the condition called *strabismus*, described in more detail in Chapters 12 and 14), suppression may indeed be operating all the time throughout the entire binocular visual field. After all, the stimulus conditions eliciting rivalry suppression and strabismic suppression are comparable: corresponding areas of the two eyes receive discrepant inputs. (In effect, the eyes "disagree" about the nature of the stimulus located at a given region of visual space.) Indeed, this assumption of

similarity of mechanisms appears in classic texts on ophthalmology (e.g., Duke-Elder, 1949). Moreover, there is some evidence suggesting that the two forms of suppression are comparable psychophysically (Blake and Lehmkuhle, 1976; Fahle, 1983; Holopigian, 1989). Inspired by this possible link, several laboratories are utilizing visual evoked potentials to examine the development of rivalry and binocular interactions in very young infants (Birch and Petrig, 1996; Brown et al., 1999), one motive being to relate those findings to the onset of strabismic suppression.

Is rivalry equivalent to other forms of multistable perception?

Binocular rivalry is not the only phenomenon where perceptual experience fluctuates even though the physical input remains unchanged, a behavior sometimes called *multistability*. Other compelling examples include bistable figures (wherein an ambiguous figure fluctuates between alternative figure/ground organizations or between alternative perspective interpretations; see Logothetis, 1998), monocular rivalry (in which two physically superimposed patterns dissimilar in color and form rival for dominance; see Campbell et al., 1973), and motion-induced blindness (wherein a normally visible stationary pattern is erased from awareness by a superimposed global moving pattern; see Bonnef et al., 2001). In all these cases, binocular rivalry included, the brain is confronted with conflicting or ambiguous information about the nature of an object at a given location in visual space. And descriptively speaking, the brain resolves this conflict by “entertaining” alternative perceptual interpretations over time. Several investigators have commented on the similarities in temporal dynamics among these various forms of perceptual instability and have concluded, therefore, that all may stem from common neural operations (Andrews and Purves, 1997; Pettigrew, 2001). This commonality certainly deserves closer examination, perhaps using some of the established techniques (e.g., test probes) that have been used to characterize binocular rivalry’s properties.

Conclusions

Binocular rivalry is inherently fascinating: visual experience fluctuates between alternative perceptual interpretations even though the input to vision remains unchanged. It is not surprising, then, that rivalry has enjoyed enduring interest over the past century and a half. But it’s really only during the past decade that the study of rivalry has become widely viewed as a serious, powerful “instrument” to be exploited by neuroscience in its attack on the mind/brain problem. Rivalry’s increased popularity has been accompanied by a number of clever psychophysical studies documenting the involvement of context, attention, and meaning in the pro-

motion of dominance. Indeed, concrete evidence of rivalry’s importance in visual neuroscience is the inclusion of a chapter on this subject in this volume.

Acknowledgment

Preparation of this chapter was supported, in part, by a research grant from the National Institutes of Health (EY013358).

REFERENCES

- Alais, D., and R. Blake, 1999. Grouping visual features during binocular rivalry, *Vis. Res.*, 39:4341–4353.
- Alais, D., R. P. O’Shea, C. Mesana-Alais, and I. G. Wilson, 2000. On binocular alternation, *Perception*, 29:1437–1445.
- Andrews, T. J., and D. Purves, 1997. Similarities in normal and binocularly rivalrous viewing, *Proc. Natl. Acad. Sci. USA*, 94:9905–9908.
- Asher, H., 1953. Suppression theory of binocular vision, *Br. J. Ophthalmol.*, 37:37–49.
- Birch, E. E., and B. Petrig, 1996. FPL and VEP measures of fusion, stereopsis and stereoacuity in normal infants, *Vis. Res.*, 36:1321–1327.
- Blake, R., 1988. Dichoptic reading: the role of meaning on binocular rivalry, *Percept. Psychophys.*, 44:133–141.
- Blake, R., 1989. A neural theory of binocular rivalry, *Psychol. Rev.*, 96:145–167.
- Blake, R., 1995. Psychoanatomical strategies for studying human vision, in *Early Vision and Beyond* (T. Papathomas, C. Chubb, E. Kowler, and A. Gorea, eds.), Cambridge, MA: MIT Press, pp. 17–25.
- Blake, R., 1997. What can be perceived in the absence of visual awareness? *Curr. Dir. Psychol. Sci.*, 6:157–162.
- Blake, R., 2001. A primer on binocular rivalry, including current controversies, *Brain Mind*, 2:5–38.
- Blake, R., and K. Boothroyd, 1985. The precedence of binocular fusion over binocular rivalry, *Percept. Psychophys.*, 37:114–124.
- Blake, R., and J. Camisa, 1978. Is binocular vision always monocular? *Science*, 200:1497–1499.
- Blake, R., and S. Lehmkuhle, 1976. On the site of strabismic suppression, *Invest. Ophthalmol.*, 15:660–663.
- Blake, R., R. P. O’Shea, and T. J. Mueller, 1992. Spatial zones of binocular rivalry in central and peripheral vision, *Vis. Neurosci.*, 8:469–478.
- Blake, R., D. Westendorf, and R. Fox, 1990. Temporal perturbations of binocular rivalry, *Percept. Psychophys.*, 48:593–602.
- Blake, R., K. Yu, M. Lokey, and H. Norman, 1998. Binocular rivalry and visual motion, *J. Cogn. Neurosci.*, 10:46–60.
- Bonnef, Y. S., A. Cooperman, and D. Sagi, 2001. Motion-induced blindness in normal observers, *Nature*, 411:798–801.
- Breese, B. B., 1899. On inhibition, *Psychol. Monogr.*, 3:1–65.
- Brown, R. J., T. R. Candy, and A. M. Norcia, 1999. Development of rivalry and dichoptic masking in human infants, *Invest. Ophthalmol. Vis. Sci.*, 40:3324–3333.
- Brown, R. J., and A. M. Norcia, 1997. A method for investigating binocular rivalry in real-time with the steady-state VEP, *Vis. Res.*, 37:2401–2408.
- Campbell, F. W., A. S. Gilinsky, E. R. Howell, L. A. Riggs, and J. Atkinson, 1973. The dependence of monocular rivalry on orientation, *Perception*, 2:123–125.

- Carlson, T. A., and S. He, 2000. Visible binocular beats from invisible monocular stimuli during binocular rivalry, *Curr. Biol.*, 10: 1055–1058.
- Cave, C., R. Blake, and T. McNamara, 1998. Binocular rivalry disrupts visual priming, *Psychol. Sci.*, 9:299–302.
- Crain, K., 1961. Binocular rivalry: its relation to intelligence, and general theory of its nature and physiological correlates, *J. Gen. Psychol.*, 64:259–283.
- Creed, R. S., 1935. Observations on binocular fusion and rivalry, *J. Physiol.*, 84:381–392.
- Crick, F., and C. Koch, 1998. Consciousness and neuroscience, *Cereb. Cortex*, 8:97–107.
- Diaz-Caneja, E., 1928. Sur l'alternance binoculaire, *Ann. Oculist*, October:721–731.
- Dörrenhaus, W., 1975. Musterspezifischer visueller wettstreit, *Naturwissenschaften*, 62:578–579.
- Duke-Elder, W. S., 1949. *Textbook in Ophthalmology*, St. Louis: Mosby.
- Engel, A. A. K., P. Fries, P. König, M. Brecht, and W. Singer, 1999. Temporal binding, binocular rivalry and consciousness, *Consciousness Cogn.*, 8:128–151.
- Fahle, M., 1982. Cooperation between different spatial frequencies in binocular rivalry, *Biol. Cybern.*, 44:27–29.
- Fahle, M., 1983. Non-fusible stimuli and the role of binocular inhibition in normal and pathologic vision, especially strabismus, *Doc. Ophthalmol.*, 55:323–340.
- Fox, R., 1991. Binocular rivalry, in *Binocular Vision and Psychophysics* (D. M. Regan ed.), London: Macmillan, pp. 93–110.
- Fox, R., and J. Herrmann, 1967. Stochastic properties of binocular rivalry alternations, *Percept. Psychophys.*, 2:432–436.
- Fox, R., and F. Rasche, 1969. Binocular rivalry and reciprocal inhibition, *Percept. Psychophys.*, 5:215–217.
- Fries, P., P. R. Roelfsema, A. K. Engel, P. König, and W. Singer, 1997. Synchronization of oscillatory responses in visual cortex correlates with perception in interocular rivalry, *Proc. Natl. Acad. Sci. USA*, 94:12699–12784.
- Gibson, J. J., 1966. *The Senses Considered as Perceptual Systems*, Boston: Houghton Mifflin.
- Helmholtz, H. von., 1866/1925. *Treatise on physiological optics* (J. P. Southall ed.), New York: Dover.
- Hochberg, J., 1964. Depth perception loss with local monocular suppression: a problem in the explanation of stereopsis, *Science*, 145:1334–1335.
- Holopigian, K., 1989. Clinical suppression and binocular rivalry suppression: the effects of stimulus strength on the depth of suppression, *Vis. Res.*, 29:1325–1334.
- Howard, I. P., and B. J. Rogers, 1995. *Binocular Vision and Stereopsis*, New York: Oxford University Press.
- James, W., 1891. *The Principles of Psychology*, London: Macmillan.
- Kohn, H., 1960. Some personality variables associated with binocular rivalry, *Psychol. Rep.*, 10:9–13.
- Kovacs, I., T. V. Papathomas, M. Yang, and A. Fehér, 1997. When the brain changes its mind. Interocular grouping during binocular rivalry, *Proc. Natl. Acad. Sci. USA*, 93:15508–15511.
- Lack, L., 1978. *Selective Attention and the Control of Binocular Rivalry*, The Hague: Mouton.
- Lee, S. H., and R. Blake, 2002. V1 activity is reduced during binocular rivalry, *J. Vis.*, 2:618–626 (online at: <http://journalofvision.org/2/9/4/>).
- Lehky, S. R., 1988. An astable multivibrator model of binocular rivalry, *Perception*, 17:215–228.
- Lehky, S. R., 1995. Binocular rivalry is not chaotic, *Proc. R. Soc. Lond. B*, 259:71–76.
- Lehmkuhle, S., and R. Fox, 1976. Effect of binocular rivalry suppression on the motion aftereffect, *Vis. Res.*, 15:855–859.
- Leopold, D., and N. Logothetis, 1996. Activity changes in early visual cortex reflect monkeys' percepts during binocular rivalry, *Nature*, 379:549–553.
- Levelt, W., 1965. *On Binocular Rivalry*, Soesterberg, the Netherlands: Institute for Perception RVO-TNO.
- Liu, L., C. W. Tyler, and C. M. Schor, 1992. Failure of rivalry at low contrast: evidence of a suprathreshold binocular summation process, *Vis. Res.*, 32:1471–1479.
- Logothetis, N. K., 1998. Single units and conscious vision, *Philos. Trans. R. Soc. Lond. B*, 353:1801–1818.
- Logothetis, N. K., and J. D. Schall, 1989. Neuronal correlates of subjective visual perception, *Science*, 245:761–763.
- Lumer, E. D., K. Friston, and G. Rees, 1998. Neural correlates of perceptual rivalry in the human brain, *Science*, 280:1930–1934.
- Matsuoka, K., 1984. The dynamic model of binocular rivalry, *Biol. Cybern.*, 49:201–208.
- Meenes, M., 1930. A phenomenological description of retinal rivalry, *Am. J. Psychol.*, 42:260–269.
- Mueller, T. J., 1990. A physiological model of binocular rivalry, *Vis. Neurosci.*, 4:63–73.
- Mueller, T. J., and R. Blake, 1989. A fresh look at the temporal dynamics of binocular rivalry, *Biol. Cybern.*, 61:223–232.
- Nakayama, K., and S. Shimojo, 1990. Da Vinci stereopsis: depth and subjective occluding contours from unpaired image points, *Vis. Res.*, 30:1811–1825.
- Ono, H., R. Angus, and P. Gregor, 1977. Binocular single vision achieved by fusion and suppression, *Percept. Psychophys.*, 21:513–521.
- Ooi, T. L., and Z. J. He, 1999. Binocular rivalry and visual awareness: the role of attention, *Perception*, 28:551–574.
- O'Shea, R. P., 1987. Chronometric analysis supports fusion rather than suppression theory of binocular vision, *Vis. Res.*, 27:781–791.
- O'Shea, R., and R. Blake, 1986. Dichoptic temporal frequency differences do not lead to binocular rivalry, *Percept. Psychophys.*, 39:59–63.
- O'Shea, R. P., and B. Crassini, 1981. Interocular transfer of the motion aftereffect is not reduced by binocular rivalry, *Vis. Res.*, 21:801–804.
- O'Shea, R. P., and B. Crassini, 1984. Binocular rivalry occurs without simultaneous presentation of rival stimuli, *Percept. Psychophys.*, 36:266–276.
- Pettigrew, J. D., 2001. Searching for the switch: neural bases for perceptual rivalry alternations, *Brain Mind*, 2:85–118.
- Polansky, A., R. Blake, J. Braun, and D. Heeger, 2000. Neuronal activity in human primary visual cortex correlates with perception during binocular rivalry, *Nat. Neurosci.*, 3:1153–1159.
- Raftopoulos, A., 2001. Is perception informationally encapsulated? The issue of the theory-ladenness of perception, *Cogn. Sci.*, 25:423–451.
- Ramachandran, V. S., 1991. Form, motion, and binocular rivalry, *Science*, 251:950–951.
- Sheinberg, D. L., and N. K. Logothetis, 1997. The role of temporal cortical areas in perceptual organization, *Proc. Natl. Acad. Sci. USA*, 94:3408–3413.
- Sherrington, C. S., 1906. *Integrative Action of the Nervous System*, New Haven, CT: Yale University Press.
- Shimojo, S., and K. Nakayama, 1990. Real world occlusion constraints and binocular rivalry, *Vis. Res.*, 30:69–80.

- Sobel, K., and R. Blake, 2001. How context influences binocular rivalry predominance. Presented at the annual meeting of the Visual Sciences Society, Sarasota, FL.
- Srinivasan, R., D. P. Russell, G. M. Edelman, and G. Tononi, 1999. Increased synchronization of neuromagnetic responses during conscious perception, *J. Neurosci.*, 19:5435–5448.
- Toch, H. H., and R. Schulte, 1961. Readiness to perceive violence as a result of polic training, *Br. J. Psychol.*, 52:389–393.
- Tong, F., and S. Engel, 2001. Interocular rivalry revealed in the cortical blind-spot representation, *Nature*, 411:195–199.
- Tong, F., K. Nakayama, J. T. Vaughan, and N. Kanwisher, 1998. Binocular rivalry and visual awareness in human extrastriate cortex, *Neuron*, 21:753–759.
- van de Grind, W. A., P. van Hof, M. J. van der Smagt, and A. J. Verstraten, 2001. Slow and fast visual motion channels have independent binocular-rivalry stages, *Proc. R. Soc. Biol. Sci.*, 268: 437–443.
- Wade, N. J., 1974. The effect of orientation in binocular contour rivalry of real images and afterimages, *Percept. Psychophys.*, 15: 227–232.
- Wales, R., and R. Fox, 1970. Increment detection thresholds during binocular rivalry suppression, *Percept. Psychophys.*, 8:90–94.
- Walker, P., 1978. Binocular rivalry: central or peripheral selective processes? *Psychol. Bull.*, 85:376–389.
- Walker, P., and D. J. Powell, 1979. The sensitivity of binocular rivalry to changes in the nondominant stimulus, *Vis. Res.*, 19: 247–249.
- Wheatstone, C., 1838. On some remarkable, and hitherto unobserved, phenomena of binocular vision, *Philos. Trans. R. Soc. Lond.*, 128:371–394.
- Wilson, H. R., R. Blake, and S.-H. Lee, 2001. Dynamics of travelling waves in visual perception, *Nature*, 412:907–910.
- Wolfe, J., 1986. Stereopsis and binocular rivalry, *Psychol. Rev.*, 93:269–282.

89 Sensorimotor Transformation in the Posterior Parietal Cortex

HANSJÖRG SCHERBERGER AND RICHARD A. ANDERSEN

THE POSTERIOR PARIETAL CORTEx (PPC) of the primate brain is an important structure for sensorimotor integration. One of its roles is the formation of intentions, or high-level plans for movement. The PPC can be subdivided into several subregions that represent maps of intentions for the planning of saccadic eye movements, reach movements, and grasping movements. These intention-related regions in the PPC appear to participate in the multisensory integration and coordinate transformations necessary for the generation of movements, and these functions seem to be facilitated by a unique distributed code for space representation. In at least two regions, the response fields of neurons are coded in eye-centered coordinates, independent of the sensory input modality (vision or audition) and the motor action that was performed (reach or saccade). Moreover, these retinal response fields in the PPC are gain-modulated by the position of the eye, head, and limb. Hence, space is not coded in a single-defined spatial reference frame in the PPC, but in a distributed fashion that allows other groups of neurons to read out spatial target locations in a variety of reference frames. The PPC also seems to participate in decision processes for movement generation, consistent with its role in sensorimotor transformation. Adaptation processes may constantly optimize the alignment of neural representations in the PPC, and the circuits are even flexible enough to allow the representation of new stimuli when they become relevant for behavior.

Knowing how intentions are encoded in the PPC could lead to a potential medical application. Intentions could be used to control a neural prosthesis for paralyzed patients. Such a device would read out the activity of PPC neurons, decode movement intentions with computer algorithms, and use the predictions to control an external device such as a cursor on a computer screen or a robotic limb. In preliminary investigations in healthy monkeys, the number of parietal recording sites needed to operate such a device has been estimated using single neurons and local field potentials. Recently, the intended movement activity in the PPC of monkeys was used to position a cursor on a computer screen without the actual movement of the monkey's arm. This was obtained without extensive training, which strongly suggests that the neural signals in PPC are

indeed highly cognitive and represent high-level plans for movement.

Coding of intention in the PPC

We define intention as a high-level plan for a movement that specifies the type and goal of the movement, such as the wish "I want to pick up my cup of tea." Such a high-level movement plan would not necessarily contain all the details of the movement, such as the movement path, muscle activation patterns, and joint angles, but it would encode the end-point location of the movement and what kind of movement is to be made. Intentions are derived from the integration of sensory input and may occur at the beginning of a sequence of ever more specific movement plans along the sensorimotor pathway. In the example of picking up a cup of tea, necessary specifications include which arm to use, the movement trajectory and speed, and the details of the muscle force pattern. These movement specifications may be included in the movement plan closer to the motor output stage and may not be present at the earlier, or higher-level, stages of movement planning.

Evidence that the PPC is involved in high-level cognitive functions for sensorimotor transformation first came from the observation of neurological deficits after PPC lesions (Balint, 1909). Patients with PPC lesions do not have a primary sensory or motor deficit; however, they have difficulties in estimating the location of stimuli in space or may be unable to plan movements appropriately (Geschwind and Damasio, 1985). The observations suggest that a disconnection occurs between the sensory and motor systems in the sensorimotor pathway (Goodale and Milner, 1992). Human functional magnetic resonance imaging (fMRI) experiments and monkey electrophysiological recordings further supported the concept that the PPC is neither strictly sensory nor motor, but encodes high-level cognitive functions related to action (Andersen, 1987; Goodale and Milner, 1992; Mountcastle et al., 1975). The monkey is a particularly good model for the study of the PPC, since its sophisticated eye-hand coordination is similar to that of humans and the PPC in both species seems to perform similar functions (Connolly et al., 2000; DeSouza et al., 2000; Rushworth et al., 2001).

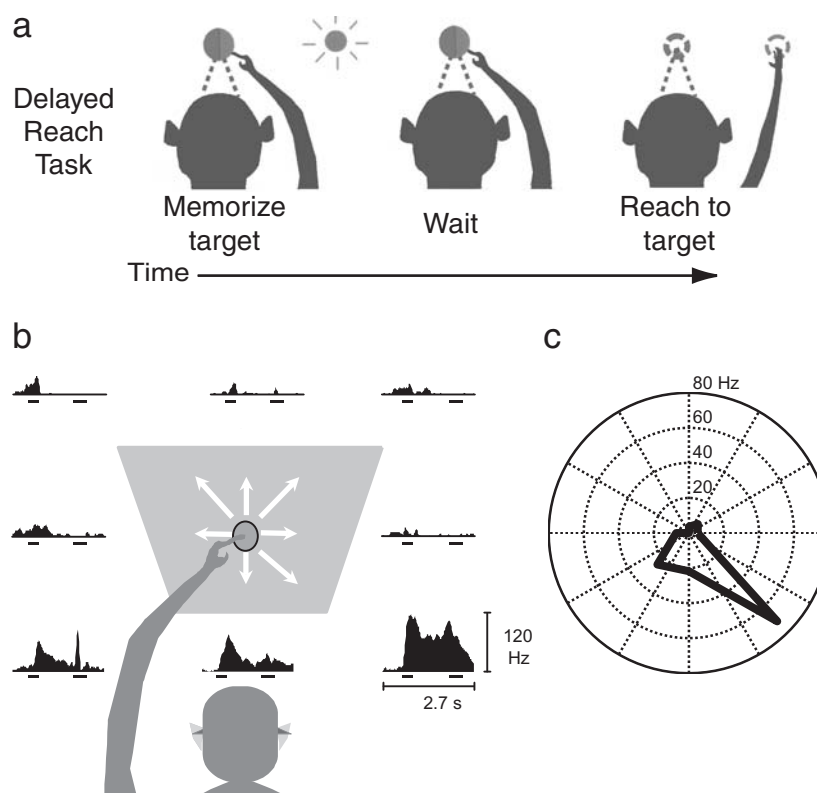


FIGURE 89.1. Spatial tuning of reach-related activity in PPC in a delayed reach task to separate sensory from motor components of behavior. *a*, Paradigm: animals memorized the location of a briefly flashed visual target, then waited in complete darkness for a go signal and made a reach to the remembered target location. *b*, Activity of a typical PPC cell with reach-related activity during stimulus presentation, waiting, and movement period of the task. Activity is maximal in the right-down direction for this cell. Each histogram depicts the cell's activity in one of eight tested reach

directions (white arrows; left-down direction occluded). Each histogram shows a spike density histogram representing the average action potential firing rate of all trials in the particular reach direction, and the short horizontal bars indicate the time of the target flash and the reach. *c*, Spatial tuning of the average firing rate during the waiting period (same cell as in *b*). Mean firing rate is plotted as amplitude along the movement direction, illustrating the strongest responses for right-down. (Data from Batista et al., 1999.)

PLANNING ACTIVITY IN THE PPC For separating sensory from motor components of behavior, the so-called memory task has been particularly useful (Hikosaka and Wurtz, 1983). In this task, a subject is first cued to the location of a movement by a briefly flashed stimulus, but must withhold the movement response until a go signal occurs (Fig. 89.1*A*). A typical PPC cell shows a burst of activity during the cue and at the movement period, indicating its relation to both sensory and motor components of the movement. During the memory period, cells in many parietal areas are also active, even in the dark (Gnadt and Andersen, 1988; Snyder et al., 1997). Figures 89.1*B* and 89.1*C* show the activity of a PPC neuron while the animal performed a delayed-reach task to targets in eight different directions (Fig. 89.1*B*). The histogram corresponding to each movement direction depicts the average firing rate of the neuron during the trial. The activity of the cell strongly increased during stimulus presentation, the waiting period, and the movement period of the task—in this example most strongly, in the right-down

direction. The increased activity during sensory, planning, and movement periods of the trial indicates that the PPC is neither a purely sensory nor a purely motor area but is involved in the high-level planning of movements, consistent with a role of this area in sensorimotor transformations.

The neuron in Figure 89.1 shows strongest activity for stimuli and movements down and to the right while being essentially silent for movements in the opposite direction. This *directional tuning* of activity is illustrated in the polar plot in Figure 89.1*C*, with the mean firing rate during the waiting period plotted as amplitude along the movement direction. Directional tuning is very common for many PPC neurons, with different neurons coding for different preferred directions. Hence, the combined activity of many neurons can code the direction of movements quite precisely.

To demonstrate that the activity during the delay period does not simply represent the sensory memory of the target, we used a paradigm in which the animals planned movements to two stimuli. For example, it has been shown that

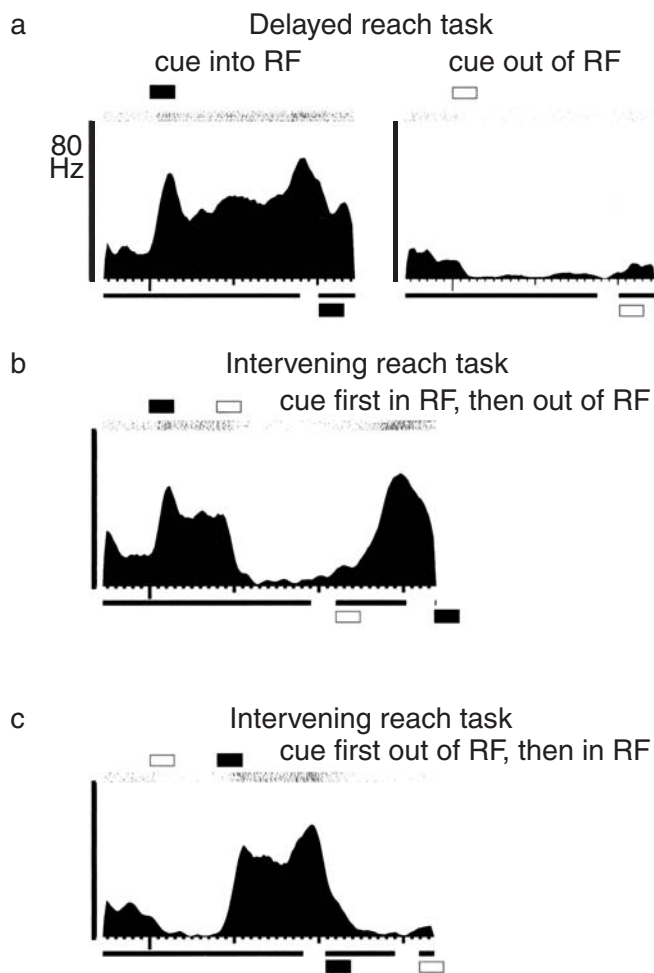


FIGURE 89.2. Example of a PRR neuron during the intervening reach task. Each panel in *a–c* shows, from top to bottom: timing of the cue stimulus into (filled bar) or out of (open bar) the response field (RF); spike rasters of 10 trials; spike density function (using a triangular kernel); timing of the button presses (horizontal bars) in one representative trial; and the acquired target (filled: in RF; open: out of RF). Vertical bar: calibration of firing rate. *a*, Delayed reach task with strong activity of the cell during the stimulus, delay, and movement periods when movements are planned inside the RF (left panel) and no activity when planned out of the RF (right panel). *b*, Activity of the same cell during an intervening reach task, when the first cue was shown in the RF and a second cue was presented out of the RF. *c*, Same cell with an intervening reach task, with the first cue out of the RF and the second cue in the RF. The cell was active when a reach was planned to the target location in the RF, but not when the animal was remembering that location and planning a reach to a location out of the RF. (Modified from Batista and Andersen, 2001.)

the delay period activity of neurons in the lateral intraparietal area (LIP) represents only the next planned eye movement, even though the animal had to hold two cued locations in memory (Mazzoni et al., 1996a). More recently, a similar result was also found for reach movements in the parietal reach region (PRR) (Batista and Andersen, 2001). Figure 89.2 shows a typical PRR neuron during this exper-

iment. In the delayed-reach task (Fig. 89.2A), the cell showed strong activity during the stimulus, delay, and movement periods when the movement was to a target inside of the response field of the cell (left panel) and no activity when the movement was to a target outside of the response field (right panel). On randomly chosen trials, an intervening reach task was used (Figs. 89.2B, C). In one task (B), a cue was first shown within the response field of the cell, and the animal began to plan, but not execute, a reach movement to that target. The activity of the cell was highly elevated. However, a second target was briefly shown outside the response field, and the animal had to change his plan to reach to the second target first. During this period, the cell was not active. After reaching to the second target, the animal had to reach to the remembered location of the first target that had been presented within the response field, and the cell became vigorously active again. The cell was active when a reach movement was planned to the target location within the response field of the cell, but was not active when the animal was remembering that location but planning a reach elsewhere. Corresponding results were found for the intervening reach task when the first cue was presented outside of the response field and the second in the response field of the cell (Fig. 89.2C). The delay period activity of PRR neurons therefore represents only the next planned reach movement, even though the animal had to remember two cued locations. The finding that nearly all PRR cells showed this behavior in these double movement task experiments rules out the coding of sensory memory in the delay period activity for most PRR neurons. This memory is most likely represented elsewhere or in a very small subpopulation of PRR cells.

TEMPORAL EVOLUTION OF PLANNING ACTIVITY Further evidence supporting the view that the PPC is involved in sensorimotor transformations comes from studies that elucidate the dynamic evolution of PPC activity during the task, changing in nature from sensory to cognitive to motor with the evolution of the task. For example, it was demonstrated in a delayed eye movement task (Platt and Glimcher, 1999) that the early activity of LIP neurons varied as a function of the reward probability or the probability that a stimulus location became a saccade target. However, during later task periods, the cells coded only the direction of the upcoming eye movement. In another study of LIP (Breznen et al., 1999; Sabes et al., 2002), monkeys were trained to make eye movements to specific locations cued on an object, and the object was rotated between the extinction of the cue and the saccade. At the beginning of the trial, LIP cells were found to carry information about the location of the cue and about the orientation of the object, both of which are important to perform the task. However, near the time of the eye movement, the same neurons encoded the direction of the

intended movement. Finally, in a study investigating the neural activity of PRR neurons when monkeys reached to auditory versus visual targets in a memory reach task (Cohen and Andersen, 2000), it was found that, during the cue period, visually cued trials carried more information about target location than did auditory cued trials. However, the amount of spatial information increased during the auditory trials, and the activity in the visual and auditory trials was not significantly different when the reach occurred. These studies emphasize the temporal evolution of activity in the PPC to reflect sensory, cognitive, and motor signals at different stages during a task.

DECISION PROCESSES FOR MOVEMENT PLANNING Recording experiments have found that the neural activity in LIP is related to the decision of a monkey to make an eye movement. Both the prior probability and the amount of reward associated with a particular movement influenced the neural representation of visual activity in LIP, which points to a role of this area in decision making (Platt and Glimcher, 1999). As monkeys accumulated sensory information for the planning of an eye movement, activity in LIP and the prefrontal cortex was found to increase, consistent with the idea that these areas are weighing decision variables for the purpose of eye movement planning (Coe et al., 2002; Gold and Shadlen, 2001; Shadlen and Newsome, 1996; Thompson et al., 1996).

Monkeys and humans have been shown to choose between two targets for a reach, depending on eye position and the stimulus locations in space, essentially favoring targets that tend to center the reach with respect to the head (Scherberger et al., 2003). We recently investigated the neural activity in PRR during this choice paradigm in the monkey and found that the neural activity of single PRR cells was only transiently related to the visual stimulus at the beginning of the trial, which was essentially identical for both choices. Later in the trial, the activity closely reflected the animal's choice of target for a reach (Scherberger and Andersen, 2001). This result suggests a role for PRR in decision processes for the generation of reach movements similar to that for LIP in decision processes for eye movements. Moreover, eye position gain effects have been shown in PRR and in LIP, and these gain effects may bias the decision of animals to choose targets based on the eye position. These and other findings suggest that decision making for movement planning is a distributed process that may involve many cortical areas including the PPC, and the particular areas involved may depend on the specific sensory input and motor actions considered.

INTENTION AND ATTENTION Given the fact that the PPC sits at the interface between sensory and motor systems, it is perhaps not surprising that the issue of how to distinguish intention from attention in this area has been of considerable research interest. To separate sensory from movement

processing, antisaccade and antireach paradigms have been used in which animals were trained to make movements in the opposite direction to a briefly flashed visual stimulus. Activity in the medial intraparietal area (MIP) has been shown to code mostly the direction of the movement plan, not the location of the stimulus (Eskandar and Assad, 1999; Kalaska, 1996). In LIP, the reverse has been reported for eye movements (Gottlieb and Goldberg, 1999); however, recently it has been reported that most LIP cells also code the direction of the planned eye movement after a brief transient response linked to the stimulus (Zhang and Barash, 2000). The antisaccade and antireach results suggest that the PPC contains both sensory- and movement-related responses and is involved in the intermediate stages of sensorimotor transformations.

In an experiment specifically designed to separate spatial attention from intention, monkeys were trained to attend to a flashed target and plan a movement to it during a delay period (Snyder et al., 1997). However, in one case the plan was for a saccadic eye movement, while in the other case the plan was for a reach. In other words, during the memory period, the only difference in the task was the type of movement the animal was planning. Figure 89.3 shows two intention-specific neurons from PPC, one from LIP (*A*) and one from PRR (*B*), while the animal planned an eye or arm movement to the same location in space. The activity of the LIP neuron showed a transient response due to the briefly flashed stimulus followed by activity during the delay period when the animal was planning an eye movement (left histogram) but not when the animal was planning an arm movement to the same location (right histogram). In contrast, the PRR neuron showed no elevated activity in the delay period when an eye movement was planned but a strong activity for the planning of an arm movement. Such results were typical in the PPC: LIP was much more active for the planning of eye movements, whereas PRR was more active during arm movement planning. PRR includes MIP, 7a, and the dorsal aspect of the parieto-occipital area (PO); however, MIP contains the highest concentration of reach-related neurons. These results from LIP and PRR strongly argue for a role of the PPC in movement planning.

INTENTIONAL MAPS The experiments mentioned above indicate a topographical separation of intentions within the PPC (Fig. 89.4). While area LIP seems to be specialized for the planning of saccades (Gnadt and Andersen, 1988), MIP and area 5 are more dedicated to the planning of reach movements (Buneo et al., 2002; Kalaska, 1996; Snyder et al., 1997). Other groups have identified areas PO, 7m, 7a, and PEc as additional reaching-related areas within the PPC (Battaglia-Mayer et al., 2000; Ferraina et al., 1997, 2001; MacKay, 1992). Furthermore, the anterior intraparietal area (AIP) seems to play a specialized role for grasping, as demon-

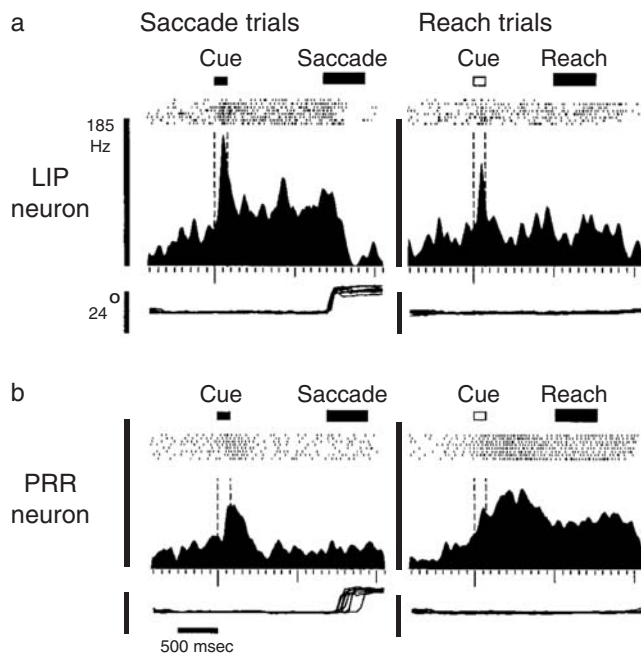


FIGURE 89.3. LIP and PRR neuron activity during a delayed saccade and delayed reach movement task. *a*, LIP cell showing elevated activity during the delay period (150 to 600 msec after the cue) before a saccade (*left*) but not before a reach movement (*right*). *b*, PRR cell showing no saccade activity (*left*) but showing reach activity (*right*) during the delay period with both movements planned to the same location in space. The neural activity in the delay period depended specifically on the movement intention. In all panels, short horizontal bars indicate the timing of the target flash (*filled*: saccade cue; *open*: reach cue), and long horizontal bars indicate the timing of the motor response (saccade or reach). Each panel shows a spike raster (eight trials aligned on cue presentation, every third action potential shown) and the corresponding spike density function (computed as in Fig. 89.2). Thin horizontal lines indicate the animal's vertical eye position during each trial. Vertical bars indicate calibration of firing rate and eye position. (Modified from Snyder et al., 1997.)

strated by Sakata and colleagues (1995). Cells in AIP respond to the shape of objects and the formation of the hand during grasping. Recent results of fMRI studies in humans were found to be consistent with the electrophysiological findings in the monkey. Rushworth et al. (2001) found that a peripheral attention task activated the lateral bank of the intraparietal sulcus, while the planning of manual movements involved activity in the medial bank. Connolly et al. (2000) reported a similar result using event-related fMRI. A specialized area for grasping has also been identified in the anterior aspect of the intraparietal sulcus in humans, which may be homologous to the monkey area AIP (Binkofski et al., 1998). Simon et al. (2002) also found a systematic anterior-posterior organization of activations associated with grasping, pointing, and eye movements. All this suggests that the parietal cortex is composed of distinguishable subregions both in monkeys and in humans.

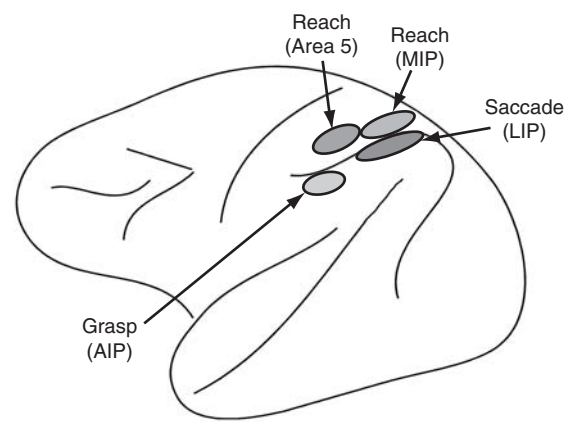


FIGURE 89.4. Anatomical map of intentions in the PPC. AIP, anterior intraparietal area; LIP, lateral intraparietal area; MIP, medial intraparietal area.

Sensory integration and space representation in the PPC

COORDINATE FRAMES Sensorimotor transformations include the integration of different sensory modalities, such as vision, sound, and touch, to develop movement plans. Since different sensory modalities represent space in different reference frames, for example, vision in retinal or eye-centered coordinates, sound in head-centered coordinates, and touch in body-centered coordinates, the question of how these senses are integrated becomes particularly important. On the motor output side, different motor actions similarly require the representation of target location in different reference frames according to the natural coordinates of the moving muscles. The surprising finding that several movement planning areas in the PPC represent space in an eye-centered coordinate frame independent of the sensory input and motor output may provide a unifying scheme for multimodal sensory integration and the development of high-level movement plans.

In area LIP, it was recently established that cells were involved in the planning of eye movements, regardless of whether the eye movements were triggered by a visual or an auditory stimulus (Grunewald et al., 1999; Linden et al., 1999; Mazzoni et al., 1996b). In further experiments directly addressing the question of the underlying reference frame, it was found that the majority of neurons coded auditory targets, similar to visual targets, in eye-centered coordinates, and with many response fields of LIP neurons gain-modulated by eye position (Stricanne et al., 1996). These findings suggest that LIP is involved in the sensory integration of visual and auditory signals and that many LIP neurons are encoding these signals in eye-centered coordinates. Earlier stages of auditory processing that project to LIP seem to encode auditory targets in head-centered coordinates, also with gain modulation by eye position (Wu and Andersen, 2001). Such a change of reference frame is con-

sistent with a current model of auditory target processing, where auditory signals are represented in head-centered coordinates, and gain-modulated by eye position, in order to transform them to an eye-centered representation at a subsequent stage (Xing and Andersen, 2000b).

Based on the findings in LIP, one wonders, how are sensory stimuli encoded for reach movements in PRR. One prediction would be that PRR codes sensory stimuli as motor error, that is, in limb coordinates; another possibility would be that PRR also codes in eye-centered coordinates. To test this hypothesis, monkeys were trained to reach to visual targets on a reach board from two different initial arm positions while their gaze was fixating in two different directions (Batista et al., 1999). Figure 89.5*A* depicts the four conditions: on the left side with the same eye position but different initial hand positions, and on the right side with the same initial hand position but different eye positions. The activity of one typical PPR neuron is shown in Figure 89.5*B*. Gray-scale values on each panel represent the cell's activity for reach movements from the illustrated initial hand position to the particular location on the board. As can be seen, the response field of the cell did not change with changes of the initial hand position (*left column*) but instead shifted with the gaze direction (*right column*). This finding was confirmed throughout the population of recorded neurons (Fig. 89.5*C*), where the response fields of the majority of neurons correlated better with the task when viewed in eye-centered as opposed to limb-centered coordinates. This result indicates that PRR codes intended limb movements to visual stimuli in eye-centered coordinates similar to how LIP codes for intended eye movements.

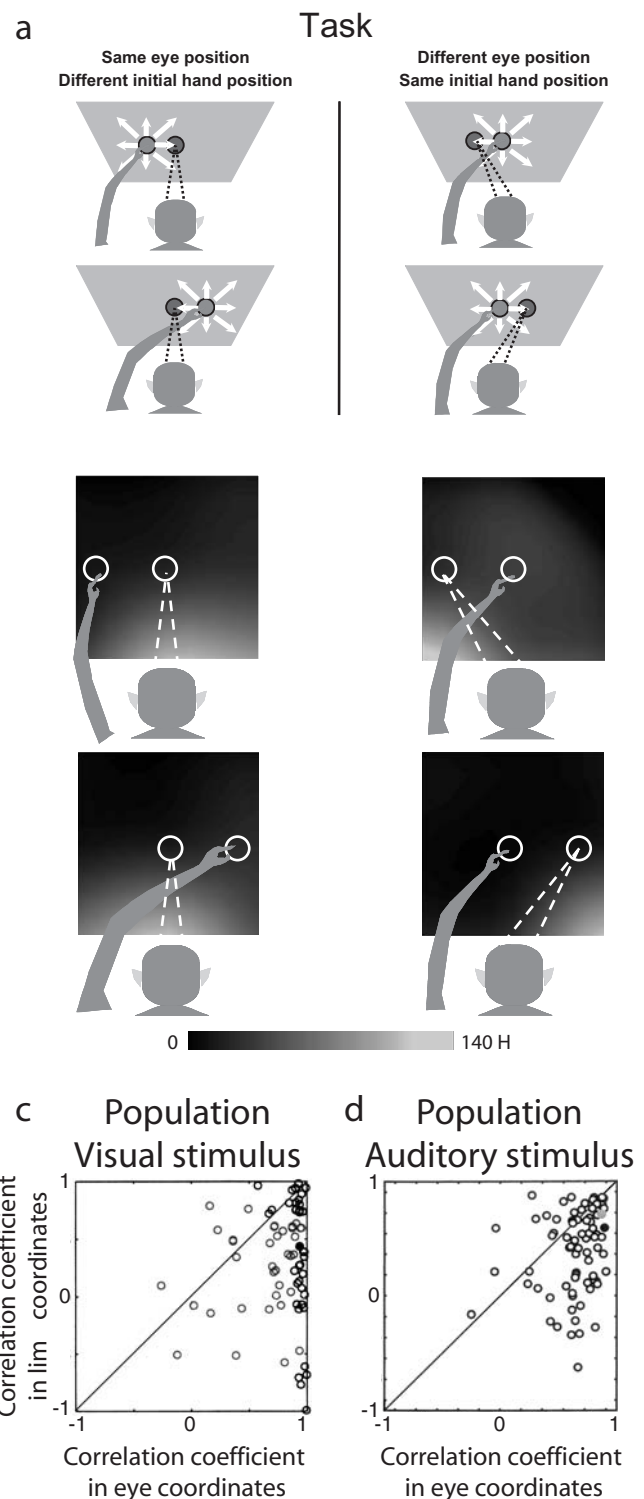


FIGURE 89.5. Encoding of reach target locations in eye-centered coordinates in PRR for visual and auditory stimuli. *a*, Delayed reach task in four conditions: same eye position but different initial hand positions (*left side*) and different eye position but same initial hand position (*right side*). *b*, Activity of one typical PPR neuron during the delayed reach task to a visual stimulus. On each panel, gray-scale values represent the cell's activity in the delay period for a reach from the illustrated initial hand position to the particular location on the board. The response field of the cell did not change with changes of the initial hand position (*left column*) but shifted with gaze direction (*right column*). *c*, Population response of the experiment in *b*, each circle represents one neuron. *x*-axis: correlation coefficient between responses for the same eye position but different hand positions (*a*, *left side*); *y*-axis: correlation coefficient between responses for the same initial hand position but different eye position (*a*, *right side*). Response fields of most neurons correlated better with eye-centered as opposed to limb-centered coordinates. *d*, Same experiment as in *b* and *c*, but with reaches made to auditory target locations in complete darkness. Axes and symbols as in *c*. Again, for most of the cells, the correlation was larger between response fields with the same eye position than between response fields with the same initial arm position. (*a–c* modified from Batista et al., 1999; *d* modified from Cohen and Andersen, 2000.)

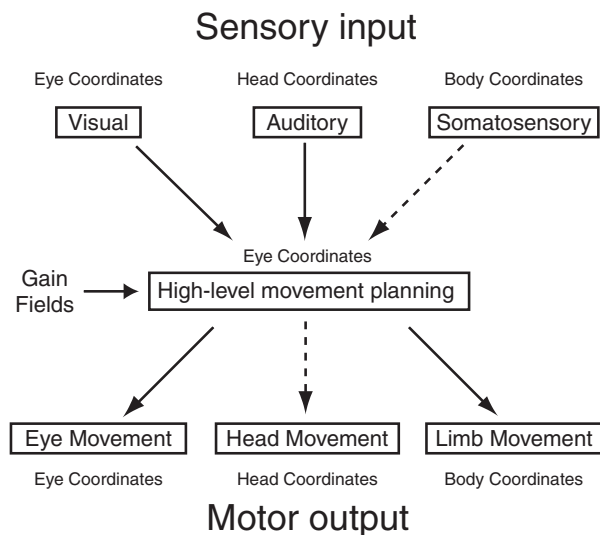


FIGURE 89.6. Multisensory integration and coordinate transformation in the PPC. Sensory input is transformed into a common eye-centered coordinate frame for high-level planning of movements that are subsequently transformed into various motor output coordinate frames. *Dotted arrows*: speculated transformations. Gain fields may provide a mechanism for coordinate transformations.

The possibility that PRR codes reach intentions independent of the sensory stimuli, similar to LIP, led to the counterintuitive prediction that many PRR neurons would encode reaches to auditory stimuli in eye-centered coordinates as well. This idea was tested in another study (Cohen and Andersen, 2000), where monkeys performed reach movements to auditory targets in complete darkness while the animal's initial hand position and gaze direction were systematically varied as described above (Fig. 89.5.4). Again, in the majority of cells, the correlation between response profiles with the same eye position was found to be much larger than between response fields with the same initial arm position (Fig. 89.5.5D). This result confirms that a majority of PRR neurons code reaches to auditory stimuli in eye-centered coordinates, even though the sensory stimulus, which is initially coded in head-centered coordinates, could easily be converted to body- and then limb-centered coordinates without the involvement of any eye-centered reference frame.

The above-mentioned results suggest that populations of LIP and PRR neurons both use a common eye-centered coordinate frame for space representation, independent of whether the sensory input is visual or auditory and regardless of whether the output is to move a limb or to make an eye movement. These findings lead to a general scheme of space representation in the PPC, where sensory input is converted to eye-centered representations in the PPC and high-level movement plans are formed that can be read out by motor output structures in their natural coordinates (Fig. 89.6). Currently, we do not know if somatosensory signals

coding the position of the hand are also coded in eye-centered coordinates in LIP and PRR and how head movements are coded in the PPC (*dotted arrows*). These are interesting questions for future research.

A possible reason for the use of a common reference frame in the PPC could be to facilitate the planning of coordinated movements, for example, during eye-hand coordination. A particular reason why an eye-centered representation has evolved in the PPC might be that vision is the most dominant and accurate spatial sense in primates.

There is a problem when using an eye-centered representation for the encoding of intentions in the PPC. Movement plans would need to be updated in eye coordinates every time an eye movement occurred before the movement plan was executed. This updating of movement plans during intervening saccades was indeed found in the superior colliculus (SC) (Mays and Sparks, 1980) and in LIP (Gnadt and Andersen, 1988) for eye movement plans, as well as for reach movement plans in PRR (Batista et al., 1999) and in human psychophysical reach experiments (Henriques et al., 1998).

GAIN FIELDS The gain modulations of the eye-centered response fields in LIP and PRR by eye, head, and limb position signals may provide a general mechanism for converting stimuli from various reference frames into eye-centered coordinates and, likewise, may allow other areas to read out signals from LIP and PRR in different coordinate frames, including eye, head, body, and limb-centered schemes (Fig. 89.6). It has been shown computationally that gain effects could be an effective mechanism for coordinate transformations in neural networks (Salinas and Abbott, 1995; Zipser and Andersen, 1988). Such a mechanism would also be very flexible, since the information of a group of eye-centered neurons that is gain-modulated by various body part positions could be subsequently read out in multiple frames of reference (Pouget and Snyder, 2000; Xing and Andersen, 2000b). The number of cells necessary for representing all possible combinations of eye, head, and body positions can remain within reasonable limits if, in each area, only those variables are encoded that are necessary to perform its specific functions (Snyder et al., 1998). Space representation in at least some areas of the PPC is thus distributed and composed of retinotopic response fields that are gain-modulated.

A similar gain mechanism could also provide the means for the remapping of eye-centered response fields in the PPC during intervening eye movements, which was demonstrated to occur during saccade planning in LIP in the double saccade paradigm (Gnadt and Andersen, 1988; Mazzoni et al., 1996a) and during reach planning in PRR in the intervening saccade paradigm (Batista et al., 1999). In a recent computational model, it was demonstrated that dynamical neural networks could be trained to perform the double saccade task (Xing and Andersen, 2000a). The model com-

prised eye-centered response fields that were gain-modulated by eye position and a shift of activity within eye-centered visual maps that corrected for intervening saccades, demonstrating that gain field mechanisms are sufficient for the saccade updating of eye-centered response fields in the PPC.

We highlighted the role of gain fields in the PPC for the updating of neural maps and for the coordinate transformations between different reference frames. It is clear, however, that gain mechanisms play an important role for other brain functions as well, such as decision making, attention, and object recognition (Salinas and Thier, 2000) and may be a general strategy of neural computation.

COORDINATE TRANSFORMATION Sensorimotor transformation in the PPC converts sensory input signals into motor plans for action. One essential step in achieving this goal is the transformation of the target location from the coordinates of its sensory input into the coordinates of the motor output. While we have highlighted a common eye-centered reference frame for the representation of intentions in the PPC and its possible role for multisensory integration, it is less well understood how intentions are transformed further downstream into motor commands (Fig. 89.6).

In the case of a reaching movement to a visual target, the target location of the reach has to be transformed from visual coordinates to the motor coordinates of the limb. This could be archived in various ways. In a *sequential* model, the eye-centered representation would be transformed sequentially first into a head-centered representation, then into a body-centered representation, and finally into the coordinates of the limb by sequentially considering the eye position, head position, and limb position. Alternatively, in a *combinatorial* model, the eye-centered target location could be combined at a single stage with the eye, head, body, and arm positions to compute the target in limb-centered coordinates (Battaglia-Mayer et al., 2000). However, such a combinatorial approach might require an unrealistically large number of cells for implementation in the PCC. In a third *direct* model, the current position of the limb is encoded in eye coordinates and compared with the eye-centered target position to directly generate the motor vector in the coordinates of the limb (Fig. 89.7A). This approach would require only a few computational stages and would rely only on variables in eye-centered coordinates.

This direct model is supported by findings of a recent study of area 5, a somatosensory cortical area within the PPC, where single neurons were found to encode target locations simultaneously in eye- and limb-centered coordinates (Buneo et al., 2002). Figure 89.7B–E shows the activity of a typical neuron for a reach movement with the same motor error in four conditions with different initial hand and eye fixation positions. The activity of the cell varied substantially

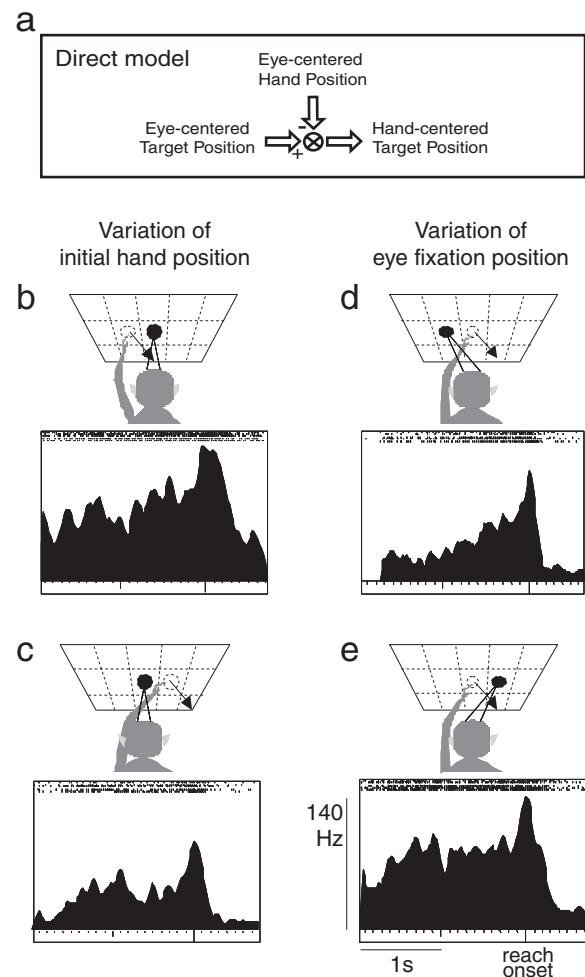


FIGURE 89.7. Direct visuomotor transformation for reaching in area 5. *a*, Direct transformation model. *b–e*, Activity of an area 5 neuron that simultaneously codes the target location in eye- and limb-centered coordinates, shown in a delayed reach movement task with different initial eye and arm positions. Each panel illustrates on top the different initial arm and eye positions for the same reach movement vector (arrow), and below the neural activity (spike rasters and spike density function). Thin bars (in *e*) calibrate time and firing rate. The activity of the cell varies substantially in the task when the initial arm position (*b*, *c*) or the eye position (*d*, *e*) is varied. However, the neural activity is very similar when the initial hand positions and target locations are identical in eye coordinates *b*, *e* and *c*, *d*. (Modified from Buneo et al., 2002.)

when either the initial hand position (*B*, *C*) or the eye fixation position (*D*, *E*) was varied, but was very similar between conditions with the same eye fixation and initial hand position relative to the target (*B*, *E* and *C*, *D*). Hence, the activity of the cell could be best described when both the target location in eye coordinates and the initial hand location in eye coordinates were taken into account. This finding is consistent with the PPC transforming target locations directly between these two reference frames.

Cells in PRR code the target location in eye-centered coordinates with a gain modulation by the initial hand

position, also in eye-centered coordinates (Buneo et al., 2002). Therefore, a convergence of input from cells in PRR onto area 5 could perform this direct transformation from eye- to limb-centered coordinates by using a simple gain field mechanism and without having to rely on intermediate coordinate frames or a large number of retinal, head, and limb position signals. On the other hand, psychophysical evidence has supported the above-mentioned sequential model (Flanders et al., 1992; McIntyre et al., 1997, 1998). The different results may reflect an underlying context dependence of the coordinate transformations for reaching, where direct transformations are preferred when both the target location and the hand are visible, while a sequential scheme may be preferred otherwise. Only future experiments can reveal the mechanisms for generating motor commands under different sensory conditions.

Plasticity: adaptation and behavioral significance

Plasticity is the ability of the brain to change the neural representation of a particular brain area either qualitatively or quantitatively. In the PPC, both learning and adaptation are important features in the context of sensorimotor transformations. An example for learning in the PPC was recently revealed in an electrophysiological study of LIP (Grunewald et al., 1999) where the responses of LIP neurons to auditory stimuli during a passive fixation task were investigated before and after the animals were trained to make saccades to auditory targets (Fig. 89.8). Before the saccade training, the number of cells responding to auditory stimuli in LIP was statistically insignificant; however, after training, about 12% of the cells showed significant responses to auditory stimuli, while the percentage of cells responding to visual stimuli (~45%) did not change (Fig. 89.8A). The amount of location information present in the neural responses for auditory stimuli before training was insignificant, but after training significant location information was present (Fig. 89.8B). The location information for visual stimuli was present before and after training. This indicates that at least some LIP neurons become active for auditory stimuli only after the animal has learned that these stimuli are relevant for oculomotor behavior.

Similar de novo representations of stimuli are suggested by the results of Sereno and Maunsell (1998). They reported that shapes of objects were encoded in LIP cells during a passive fixation task after the animals were trained to discriminate these objects in an eye-movement task. More recently, Toth and Assad (2002) showed that the activity of LIP cells represent color information of a visual stimulus during a delayed-saccade task if color information was behaviorally relevant to solve the task. These studies demonstrate the ability of the PPC to newly represent sensory stimuli that are behaviorally

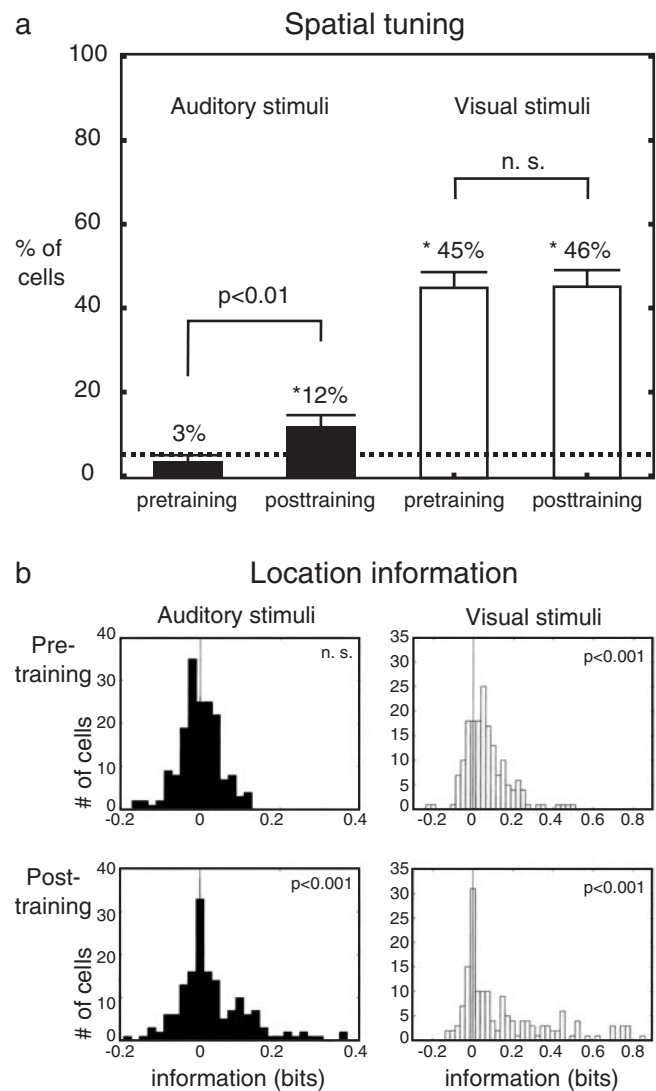


FIGURE 89.8. De novo representation of auditory stimuli in LIP. *a*, Proportion of cells that showed significant spatial tuning for auditory and visual stimuli in a fixation task before and after the animal had been trained to make auditory saccades. *x*-axis: pre- and post-training conditions for trials with auditory (filled bars) and visual stimuli (open bars); *y*-axis: number of cells with significant (Kruskal-Wallis test) tuning to auditory and visual stimuli. Error bars: standard deviation; *: significant difference from false-positive level (dotted line); *p* values above brackets indicate a significant difference in pairwise comparison (Fisher-Irwin test). *b*, Location information in each cell to auditory (left column) and visual targets (right column) before (top row) and after training (bottom row). Each panel shows a histogram of the location information (corrected for baseline) for each cell population. Vertical line: no location information present; *p* values: significance level (Wilcoxon test) that location information is present in the population. Spatial tuning and target location information for auditory stimuli was present after the animal was trained to make auditory saccades but not prior to training. (Modified from Grunewald et al., 1999.)

relevant, and point to a context-dependent flexibility in the neural representation of the PPC during sensorimotor transformation.

Neural plasticity also seems to be at work in the continuous fine-tuning of neural representations in the PPC to keep the various sensory and motor signals in register. An experiment specifically designed to disrupt this alignment is prism adaptation. Human subjects initially missreach to visual targets when wearing displacing prisms, but when provided with appropriate feedback about their errors, they gradually recover and reach correctly (Held and Hein, 1963). This suggests that a recalibration between sensory and motor coordinate frames has taken place. Clower et al. (1996) demonstrated in a positron emission tomography (PET) study that prism adaptation selectively activates the contralateral PPC to the reaching arm, which directly links the PPC to the adaptation effects, in perfect agreement with its role in sensorimotor transformation. The neural mechanisms underlying prism adaptation and associative learning in the PPC are largely unknown and likely involve other brain areas as well.

Neural prosthesis: reading out reach intentions

As we have seen, the activity in the PPC contains strong, reliable intention signals for eye and arm movements. Instead of demonstrating only correlations between the neural activity and behavior, it would be very important to test this relationship more directly. One type of experiment is illustrated in Figure 89.9, where the reach intentions of a monkey are recorded in PRR and then used to move a cursor on the display screen. The cursor location displays our prediction of where the animal is intending to reach based on the neural activity. This provides visual feedback to the animal, indicating where the reach will end up based purely on the animal's intention, that is, without the animal actually moving its arm. This sensory feedback provides a "closed loop" in the information flow of sensorimotor transformation, which enables the subject to learn and adapt its movement intentions in order to improve the accuracy of the reach predictions.

In a preliminary study, we used the PRR activity of two monkeys to predict in real time one out of two reach directions (Meeker et al., 2002). The animal performed a modified delayed-reach task in which a cursor was moved on the computer screen by interpreting the intended movement activity of the animal without its making an actual reach. This was achieved without extensive training of the animal, which suggests that PRR represents high-level reach intentions and is capable of adapting to this new behavior. A corresponding off-line analysis of single-cell recordings from PRR suggested that a reliable prediction of one out of eight movement directions is possible with only

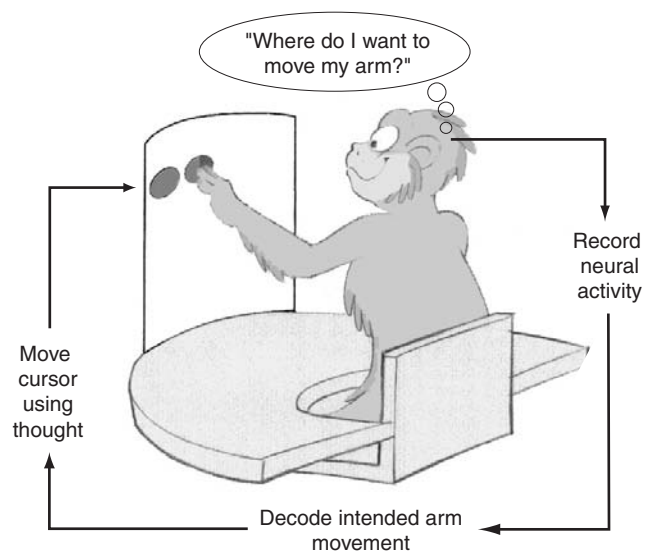


FIGURE 89.9. Schematic of an experiment to read out intentions. First, the activity of a single PRR neuron is recorded, and a database is constructed representing the neural activity for reaches in different directions. In test trials, the monkey then fixates and touches the center of a display screen, and a target is briefly flashed in either the preferred or the nonpreferred direction of the cell. Based on the response of the neuron in this single trial and the statistics of the cell's activity in the database, a prediction is made about whether the animal is intending to reach either in the preferred or in the nonpreferred direction of the cell, and a cursor is moved to the predicted location on the screen to give the monkey visual feedback. The animal is rewarded if the prediction corresponds to the cued target location, and it does not move its arm.

a very small number of simultaneously recorded neurons—on the order of 10 to 15 (Meeker et al., 2001; Shenoy et al., 2003).

The high-level movement planning activity in the PPC could, in theory, be used in paralyzed patients to control a neural prosthesis. Patients paralyzed by strokes, trauma, or neuropathies can often still think about making a movement but are unable to activate the appropriate muscles to execute it. A cortical prosthesis could record the movement intentions, interpret the intentions in real time using computer algorithms, and convert the decoded movement signals to control an external device. Useful devices could include a computer interface for communication, a robot limb, or muscle stimulators inside the patient's body that would ultimately restore the patient's to move paralyzed limbs.

Several groups are currently working to develop such a prosthesis, mainly using signals recorded from motor cortex (Chapin et al., 1999; Isaacs et al., 2000; Serruya et al., 2002; Taylor et al., 2002; Wessberg et al., 2000). While these groups certainly have demonstrated the possibility of using the movement signals in motor cortex for reading out movement plans, the use of more cognitive signals in PRR may

also have its advantages. First, the high-level cognitive nature of the signals in PRR may require only a few neurons to decode the end point of a reach movement (as opposed to decoding an entire movement trajectory). Next, sensory feedback is necessary for closing the loop and to facilitate learning and neural plasticity. Since many paralyzed patients have severed somatosensory feedback, which plays a prominent role in the primary sensory and motor cortical areas, visual feedback may become even more relevant. PRR is tightly linked to visual cortical areas, which provide perhaps its most dominant sensory inputs. Finally, after paralysis, motor cortex undergoes substantial degeneration, as has been shown in animal recording and human imaging studies (Bruehlmeier et al., 1998; Lotze et al., 1999; Wu and Kaas, 1999). Since the PPC is more closely related to the intact visual system, degeneration effects might be less severe in the PPC after paralysis. The field of neural prosthesis is young, and it is too early to tell whether a single part of the brain will afford the most optimal control. It is quite likely that the most effective prosthesis will be one that can tap into signals from multiple areas and take advantage of their different natural specializations.

Perhaps the most limiting factor for the success of a neural prosthesis is the lack of stability and reliability of chronically recorded neural signals, a problem that is largely independent of the brain area from which the neural signals are recorded. In this respect, it is noteworthy that we have recently found gamma band oscillations in the local field potential (LFP) signals during the delay period both in LIP when monkeys are planning an eye movement (Pesaran et al., 2002) and in PRR during reach planning (Scherberger et al., 2001). The spectral power in the gamma band of the LFP is tuned in both areas to the direction of the planned movement and changes its strength with the behavioral state, that is, it becomes stronger when the animal plans a movement and rapidly decreases during the movement execution. An “off-line” analysis of the LFP signal in PRR estimated that 50 to 100 recording sites would be sufficient to reliably predict one out of eight movement directions in a delayed reach movement task using the LFP signal alone (Scherberger et al., 2001). Since the LFPs reflect the activity of groups of cells in cortical columns rather than single cells, LFP activity is more stable and easier to record than that of single cells with chronic electrodes. Using the LFP to decode reach intentions in the PPC and perhaps elsewhere may therefore be an important step in the development of a neural prosthesis.

Conclusions

The PPC is an important area for sensorimotor integration and the formation of high-level cognitive plans for movement. The PPC is divided into a map of intentions, with dif-

ferent subregions representing the planning for saccades, reaches, and grasping movements. Each region contains a map of its working space and seems to be specialized for multisensory integration and coordinate transformation with respect to its particular action. In PRR and LIP, these maps are encoded in eye-centered coordinates independent of their sensory input and the motor plan. The activity in these maps is gain-modulated by eye, head, and limb position signals consistent with a distributed representation of space. This allows the direct transformation of spatial information into a variety of different reference frames. The distributed and abstract representation of intentions underscores the high-level, or cognitive nature of this area. The involvement of PPC in decision making and neural plasticity for space representation is consistent with its role in sensorimotor transformation. Efforts to read out and decode PPC signals to control a neural prosthesis will test our current theories of sensorimotor transformation as well as provide new leads to help paralyzed patients regain their motor integrity. These goals are central to this emerging field of *applied* systems neuroscience.

Acknowledgment

We thank the Christopher Reeve Paralysis Foundation, the James G. Boswell Foundation, the National Institutes of Health (NIH), the Defense Advanced Research Projects Agency (DARPA), the Sloan-Swartz Center for Theoretical Neurobiology, and the Office of Naval Research (ONR) for generous support.

REFERENCES

- Andersen, R. A., 1987. The role of the inferior parietal lobule in spatial perception and visual-motor integration, in *Handbook of Physiology—The Nervous System*, Bethesda, MD: American Physiological Society, pp. 483–518.
- Balint, R., 1909. Seelenlähmung des “Schauens,” optische Ataxie, räumliche Störung der Aufmerksamkeit, *Monatsschr. Psychiatr. Neurol.*, 25:51–81.
- Batista, A. P., and R. A. Andersen, 2001. The parietal reach region codes the next planned movement in a sequential reach task, *J. Neurophysiol.*, 85:539–544.
- Batista, A. P., C. A. Buneo, L. H. Snyder, and R. A. Andersen, 1999. Reach plans in eye-centered coordinates, *Science*, 285:257–260.
- Battaglia-Mayer, A., S. Ferraina, T. Mitsuda, B. Marconi, A. Genovesio, P. Onorati, F. Lacquaniti, and R. Caminiti, 2000. Early coding of reaching in the parietooccipital cortex, *J. Neurophysiol.*, 83:2374–2391.
- Binkofski, F., C. Dohle, S. Posse, K. M. Stephan, H. Hefter, R. J. Seitz, and H. J. Freund, 1998. Human anterior intraparietal area subserves prehension: a combined lesion and functional MRI activation study, *Neurology*, 50:1253–1259.
- Breznen, B., P. N. Sabes, and R. A. Andersen, 1999. Parietal coding of object-based saccades: reference frame., *Soc. Neurosci. Abstr.*, 25:1547.

- Bruehlmeier, M., V. Dietz, K. L. Leenders, U. Roelcke, J. Missimer, and A. Curt, 1998. How does the human brain deal with a spinal cord injury? *Eur. J. Neurosci.*, 10:3918–3922.
- Buneo, C. A., M. R. Jarvis, A. P. Batista, and R. A. Andersen, 2002. Direct visuomotor transformations for reaching, *Nature*, 416: 632–636.
- Chapin, J. K., K. A. Moxon, R. S. Markowitz, and M. L. Nicolelis, 1999. Real-time control of a robot arm using simultaneously recorded neurons in the motor cortex, *Nat. Neurosci.*, 2:664–670.
- Clower, D. M., J. M. Hoffman, J. R. Votaw, T. L. Faber, R. P. Woods, and G. E. Alexander, 1996. Role of posterior parietal cortex in the recalibration of visually guided reaching, *Nature*, 383:618–621.
- Coe, B., K. Tomihara, M. Matsuzawa, O. Hikosaka, 2002. Visual and anticipatory bias in three cortical eye fields of the monkey during an adaptive decision-making task, *J. Neurosci.*, 22:5081–5090.
- Cohen, Y. E., and R. A. Andersen, 2000. Reaches to sounds encoded in an eye-centered reference frame, *Neuron*, 27:647–652.
- Connolly, J. D., R. S. Menon, and M. A. Goodale, 2000. Human frontoparietal areas active during a pointing but not a saccade delay, *Soc. Neurosci. Abstr.*, 26:497.4.
- DeSouza, J. F., S. P. Dukelow, J. S. Gati, R. S. Menon, R. A. Andersen, and T. Vilis, 2000. Eye position signal modulates a human parietal pointing region during memory-guided movements, *J. Neurosci.*, 20:5835–5840.
- Eskandar, E. N., and J. A. Assad, 1999. Dissociation of visual, motor and predictive signals in parietal cortex during visual guidance, *Nat. Neurosci.*, 2:88–93.
- Ferraina, S., A. Battaglia-Mayer, A. Genovesio, B. Marconi, P. Onorati, and R. Caminiti, 2001. Early coding of visuomanual coordination during reaching in parietal area PFC, *J. Neurophysiol.*, 85:462–467.
- Ferraina, S., M. R. Garasto, A. Battaglia-Mayer, P. Ferraresi, P. B. Johnson, F. Lacquaniti, and R. Caminiti, 1997. Visual control of hand-reaching movement: activity in parietal area 7m, *Eur. J. Neurosci.*, 9:1090–1095.
- Flanders, M., S. I. Helms-Tillery, and J. F. Soechting, 1992. Early stages in a sensorimotor transformation, *Behav. Brain. Sci.*, 15:309–362.
- Geshwind, N., and A. R. Damasio, 1985. Apraxia, in *Handbook of Clinical Neurology* (P. J. Vinken, G. W. Bruyn, and H. L. Klawans, eds.), Amsterdam: Elsevier, pp. 423–432.
- Gnadt, J. W., and R. A. Andersen, 1988. Memory related motor planning activity in posterior parietal cortex of macaque, *Exp. Brain Res.*, 70:216–220.
- Gold, J. I., and M. N. Shadlen, 2001. Neural computations that underlie decisions about sensory stimuli, *Trends Cogn. Sci.*, 5:10–16.
- Goodale, M. A., and A. D. Milner, 1992. Separate visual pathways for perception and action, *Trends Neurosci.*, 15:20–25.
- Gottlieb, J., and M. E. Goldberg, 1999. Activity of neurons in the lateral intraparietal area of the monkey during an antisaccade task, *Nat. Neurosci.*, 2:906–912.
- Grunewald, A., J. F. Linden, and R. A. Andersen, 1999. Responses to auditory stimuli in macaque lateral intraparietal area. I. Effects of training, *J. Neurophysiol.*, 82:330–342.
- Held, R., and A. Hein, 1963. Movement produced stimulation in the development of visually guided behavior, *J. Comp. Physiol. Psychol.*, 56:872–876.
- Henriques, D. Y., E. M. Klier, M. A. Smith, D. Lowy, and J. D. Crawford, 1998. Gaze-centered remapping of remembered visual space in an open-loop pointing task, *J. Neurosci.*, 18:1583–1594.
- Hikosaka, O., and R. H. Wurtz, 1983. Visual and oculomotor functions of monkey substantia nigra pars reticulata. III. Memory-contingent visual and saccade responses, *J. Neurophysiol.*, 49: 1268–1284.
- Isaacs, R. E., D. J. Weber, and A. B. Schwartz, 2000. Work toward real-time control of a cortical neural prosthesis, *IEEE Trans. Rehabil. Eng.*, 8:196–198.
- Kalaska, J. F., 1996. Parietal cortex area 5 and visuomotor behavior, *Can. J. Physiol. Pharmacol.*, 74:483–498.
- Linden, J. F., A. Grunewald, and R. A. Andersen, 1999. Responses to auditory stimuli in macaque lateral intraparietal area. II. Behavioral modulation, *J. Neurophysiol.*, 82:343–358.
- Lotze, M., U. Laubis-Herrmann, H. Topka, and W. Grodd, 1999. Reorganization in the primary motor cortex after spinal cord injury—a functional magnetic resonance (fMRI) study, *Restor. Neurol. Neurosci.*, 14:183–187.
- MacKay, W. A., 1992. Properties of reach-related neuronal activity in cortical area 7A, *J. Neurophysiol.*, 67:1335–1345.
- Mays, L. E., and D. L. Sparks, 1980. Saccades are spatially, not retinocentrically, coded, *Science*, 208:1163–1165.
- Mazzoni, P., R. M. Bracewell, S. Barash, and R. A. Andersen, 1996a. Motor intention activity in the macaque's lateral intraparietal area. I. Dissociation of motor plan from sensory memory, *J. Neurophysiol.*, 76:1439–1456.
- Mazzoni, P., R. M. Bracewell, S. Barash, and R. A. Andersen, 1996b. Spatially tuned auditory responses in area LIP of macaques performing delayed memory saccades to acoustic targets, *J. Neurophysiol.*, 75:1233–1241.
- McIntyre, J., F. Stratta, and F. Lacquaniti, 1997. Viewer-centered frame of reference for pointing to memorized targets in three-dimensional space, *J. Neurophysiol.*, 78:1601–1618.
- McIntyre, J., F. Stratta, and F. Lacquaniti, 1998. Short-term memory for reaching to visual targets: psychophysical evidence for body-centered reference frames, *J. Neurosci.*, 18:8423–8435.
- Meeker, D., S. Cao, J. W. Burdick, and R. A. Andersen, 2002. Rapid plasticity in the parietal reach region demonstrated with a brain-computer interface, *Soc. Neurosci. Abstr.*, 28:357.7.
- Meeker, D., K. V. Shenoy, S. Cao, B. Pesaran, H. Scherberger, M. Jarvis, C. A. Buneo, A. P. Batista, S. A. Kureshi, P. P. Mitra, et al., 2001. Cognitive control signals for prosthetic systems, *Soc. Neurosci. Abstr.*, 27:63.6.
- Mountcastle, V. B., J. C. Lynch, A. Georgopoulos, H. Sakata, and C. Acuna, 1975. Posterior parietal association cortex of the monkey: command functions for operations within extrapersonal space, *J. Neurophysiol.*, 38:871–908.
- Peraran, B., J. S. Pezaris, M. Sahani, P. P. Mitra, and R. A. Anderson, 2002. Temporal structure in neuronal activity during working memory in macaque parietal cortex, *Nat. Neurosci.*, 5:805–811.
- Platt, M. L., and P. W. Glimcher, 1999. Neural correlates of decision variables in parietal cortex, *Nature*, 400:233–238.
- Pouget, A., and L. H. Snyder, 2000. Computational approaches to sensorimotor transformations, *Nat. Neurosci.*, 3(Suppl):1192–1198.
- Rushworth, M. F., T. Paus, and P. K. Sipila, 2001. Attention systems and the organization of the human parietal cortex, *J. Neurosci.*, 21:5262–5271.
- Sabes, P. N., B. Breznien, R. A. Andersen, 2002. Parietal representation of object-based saccades, *J. Neurophysiol.*, 88:1815–1829.
- Sakata, H., M. Taira, A. Murata, and S. Mine, 1995. Neural mechanisms of visual guidance of hand action in the parietal cortex of the monkey, *Cereb. Cortex*, 5:429–438.

- Salinas, E., and L. F. Abbott, 1995. Transfer of coded information from sensory to motor networks, *J. Neurosci.*, 15:6461–6474.
- Salinas, E., and P. Thier, 2000. Gain modulation: a major computational principle of the central nervous system, *Neuron*, 27:15–21.
- Scherberger, H., and R. A. Andersen, 2001. Neural activity in the posterior parietal cortex during decision processes for generating visually-guided eye and arm movements in the monkey, *Soc. Neurosci. Abstr.*, 27:237.8.
- Scherberger, H., M. A. Goodale, and R. A. Andersen, 2003. Target selection for reaching and saccades share a similar behavior reference frame in the macaque, *J. Neurophysiol.*, 89:1456–1466.
- Scherberger, H., M. Jarvis, and R. A. Andersen, 2001. Properties of the local field potential in the macaque posterior parietal cortex during arm-reaching movements. Paper presented at the 11th annual meeting of the Society for the Neural Control of Movement. Available at <http://www-ncm.cs.umass.edu>
- Sereno, A. B., and J. H. Maunsell, 1998. Shape selectivity in primate lateral intraparietal cortex, *Nature*, 395:500–503.
- Serruya, M. D., N. G. Hatsopoulos, L. Paninski, M. R. Fellows, and J. P. Donoghue, 2002. Brain-machine interface: instant neural control of a movement signal, *Nature*, 416:141–142.
- Shadlen, M. N., and W. T. Newsome, 1996. Motion perception: seeing and deciding, *Proc. Natl. Acad. Sci. USA*, 93:628–633.
- Shenoy, K. V., D. Meeker, S. Cao, S. A. Kureshi, B. Pesaran, C. A. Buneo, A. P. Batista, P. P. Mitra, J. W. Burdick, and R. A. Andersen, 2003. Neural prosthetic control signals from plan activity, *NeuroReport*, 14:591–596.
- Simon, O., J. F. Mangin, L. Cohen, D. Le Bihan, and S. Dehaene, 2002. Topographical layout of hand, eye, calculation, and language-related areas in the human parietal lobe, *Neuron*, 33:475–487.
- Snyder, L. H., A. P. Batista, and R. A. Andersen, 1997. Coding of intention in the posterior parietal cortex, *Nature*, 386:167–170.
- Snyder, L. H., K. L., Grieve, P. Brotchie, and R. A. Andersen, 1998. Separate body- and world-referenced representations of visual space in parietal cortex, *Nature*, 394:887–891.
- Stricanne, B., R. A. Andersen, and P. Mazzoni, 1996. Eye-centered, head-centered, and intermediate coding of remembered sound locations in area LIP, *J. Neurophysiol.*, 76:2071–2076.
- Taylor, D. M., S. F. Tillery, and A. B. Schwartz, 2002. Direct cortical control of 3D neuroprosthetic devices, *Science*, 296:1829–1832.
- Thompson, K. G., D. P. Hanes, N. P. Bichot, and J. D. Schall, 1996. Perceptual and motor processing stages identified in the activity of macaque frontal eye field neurons during visual search, *J. Neurophysiol.*, 76:4040–4055.
- Toth, L. J., and J. A. Assad, 2002. Dynamic coding of behaviourally relevant stimuli in parietal cortex, *Nature*, 415:165–168.
- Wessberg, J., C. R. Stambaugh, J. D. Kralik, P. D. Beck, M. Laubach, J. K. Chapin, J. Kim, J. Biggs, M. A. Srinivasan, and M. A. L. Nicolelis, 2000. Real-time prediction of hand trajectory by ensembles of cortical neurons in primates, *Nature*, 408:361–365.
- Wu, C. W.-H., and J. H. Kaas, 1999. Reorganization in primary motor cortex of primates with long-standing therapeutic amputations, *J. Neurosci.*, 19:7679–7697.
- Wu, S., and R. A. Andersen, 2001. The representation of auditory space in temporoparietal cortex, *Soc. Neurosci. Abstr.*, 27:166.15.
- Xing, J., and R. A. Andersen, 2000a. Memory activity of LIP neurons for sequential eye movements simulated with neural networks, *J. Neurophysiol.*, 84:651–665.
- Xing, J., and R. A. Andersen, 2000b. Models of the posterior parietal cortex which perform multimodal integration and represent space in several coordinate frames, *J. Cogn. Neurosci.*, 12:601–614.
- Zhang, M., and S. Barash, 2000. Neuronal switching of sensorimotor transformations for antisaccades, *Nature*, 408:971–975.
- Zipser, D., and R. A. Andersen, 1988. A back-propagation programmed network that simulates response properties of a subset of posterior parietal neurons, *Nature*, 331:679–684.

XI EYE MOVEMENTS

90 Gaze Control under Natural Conditions

ROBERT M. STEINMAN

Reason for studying the control of gaze

Little in visual neuroscience is of greater concern than a human being's ability to control the direction of *gaze* (the direction of the line of sight in spatial coordinates). Why? What could possibly make the human's control of gaze so important? The answer lies in the nature of the human *retina*, the receptor surface within the eye that *transduces* (translates) light, the *adequate* (most effective) stimulus for vision, into bio-electrical signals that are carried to the higher levels of the visual brain. These centers are responsible for our ability to see a world of colored objects, of various sizes and at various distances, moving or stationary with respect to each other, as well as moving or stationary with respect to ourselves. The retinal surface is very *heterogeneous* (diverse) with respect to its functional properties. A very small central depression (only about 1/40th of 1% of the retinal surface area), called the *fovea*, is responsible for our best visual acuity, that is, our ability to *discriminate* (distinguish) very fine details. The fovea is also responsible for our best color vision, while the regions outside of the fovea are particularly well suited for detecting very low levels of light and motion. The fact that the human retina had very heterogeneous functional properties was well established by the last quarter of the nineteenth century. (See Brindley, 1960, for many important older references and Oyster, 1999, for an up-to-date treatment of what is now known about the structure and function of the human eye.)

Why eye movements must be measured

One of the more intriguing aspects of human vision is the fact that the functional consequences of retinal heterogeneity are not experienced. Subjectively, our visual world is homogeneous. We perceive it as having good acuity and color representation throughout. Experiencing the visual world as homogeneous would not be possible if we could not move our eyes. Moving our eyes allows us to place selected visual objects in retinal regions specialized for processing different features. For example, we use the fovea for seeing colored details in brightly lighted environments, but shift to more peripheral retina when objects are too dim to be seen when they fall within the fovea (see Steinman and Cunitz, 1968, for the human oculomotor pattern near the absolute foveal threshold).

Two things were clear near the end of the nineteenth century, when the objective study of eye movements began. First, it was clear that the functional properties of the human retina were sufficiently heterogeneous to require the eye to move. Second, it had become clear from studies of reading, a particularly important and uniquely human eye movement behavior, that the way human beings move their eyes *cannot* be inferred from subjective impressions of what they were doing (Dodge and Cline, 1901; Huey, 1900; Javal, 1878). Objective measurement of human eye movements was required. This recognition encouraged the development of methods to measure human eye movements. These methods were developed and improved throughout the twentieth century, and a large body of knowledge about human eye movements was produced. See Collewyn (1998) for descriptions of many of the more popular contemporary methods of recording eye movements. See Hallett (1986), Steinman (1986), Kowler (1990), and Kowler (1991) for reviews of what has become a voluminous literature on human eye movements.

Why eye movements should be studied under ecologically relevant conditions

Virtually all of this knowledge was collected under unnatural, highly impoverished stimulating conditions. More often than not, the eye movements of only one eye were recorded. The head was immobilized on a biting board or a chin rest. The visual field was more often than not dark except for the fixation target, which was a tiny spot of light that lined up with the eye when it was centered in its orbit. Recordings were made while the single-point target remained stationary or moved during the recording. It is not clear, as we begin the second century of human eye movement research, that much of the knowledge we have, which is based on recordings made under such unnatural and highly impoverished conditions, applies to the way human beings actually control their gaze under more ecologically relevant conditions, that is, (1) when the human being's head and torso is free to move and (2) binocular gaze is recorded *accurately* as the human observes and manipulates (3) objects within arm's length in a (4) normally illuminated room. These conditions are particularly relevant for understanding the evolutionary success of our species. These are the conditions in which human beings fabricate and use tools, as well the conditions

in which they do most of their reading and other creative activities.

We have only just begun to study the way humans control their gaze under such natural conditions. I know of only five publications to date that meet the criteria listed above for studying human eye movements, *accurately* with respect to both space and time, under ecologically relevant conditions; namely, Epelboim (1998), Epelboim et al. (1995, 1997), Malinov et al. (2000), and Herst et al. (2001) (see Ballard et al. (1994), Land (1992), Land and Tatler (2001), Land et al. (1999), Smeets et al. (1996), and Land and Hayhoe (2001) for ecologically relevant experiments in which the eye movement recording methods were not sufficient to examine fine details of human performance). In addition, see Johansson et al. (2001) for an experiment in which objects were manipulated, condition (3) above, under less than ecologically relevant conditions. The authors recorded monocularly with a video-based eye-tracking system (effective bandwidth = 60 Hz) with the head immobilized on a biting board that “provided high stability of the head” (p. 6918). In short, we have just begun to study human eye movements accurately under the conditions in which humans evolved. At present, we still know very little about how gaze is actually controlled under natural conditions.

The first accurate, but unnatural, recordings of human fixation

It required half a century for investigators to get answers to two simpler questions, questions of interest ever since human eye movements were first recorded by Delabarre (1898): how well could gaze be kept on an attended target, and what kinds of eye movements were used to maintain gaze after fixation was achieved? Both of these questions had a bearing on a more fundamental question: how much does the image of an attended target move on the retina when the direction of gaze is maintained by rotations of the fixating eye within its orbit? This question was important because anatomical research early in the twentieth century revealed an even greater degree of retinal heterogeneity than was expected when human eye movement research began. There was a cellular specialization, called the *Central Bouquet* (Rochon-Duvigneaud, 1943) at the center of the fovea. It had a diameter of about only one-third of a degree of visual angle. This specialized region was filled with a densely packed group of rod-shaped cones. Clearly, the highest-quality human vision would require an exceptional ability to fixate an attended object. It had to be able to place the retinal image of the attended target exactly at the foveal center, and it had to be able to keep it there long enough for its finest details to be discriminated.

The problem encountered as soon as one tries to study the human being's control of gaze stems, in no small measure,

from the human's remarkable ability to control his or her gaze. Once it became possible to actually measure how good it was, free from artifacts, it became clear that gaze control was exquisite. Gaze could be placed and kept on an object with remarkably little variability, at least under the very unnatural conditions that were required to measure these minuscule behaviors. That is, the head had to be immobilized as much as possible, and the fixation target had to be placed on the line of sight when the eye was in its primary position in its orbit. Fixation did not seem nearly this good when measurements were first made by photographing light reflected from the curved surface of the cornea. This method, which was introduced by Dodge and Cline (1901), is called the *corneal reflex* method. It was used by Dodge, his collaborators, and many others, for 50 years, providing the bulk of the existing eye movement literature until 1950, when a new and much more accurate method came into vogue. Gaze during maintained fixation, as recorded with the corneal reflex method, was quite variable even when an experienced subject attempted to maintain gaze. But it was hard to know why because deviations in the direction of the beam reflected from the surface of the cornea could be caused by two motions: by a rotation of the eyeball or by a translation of the head. A translation of the head would bring the beam of light falling on the cornea to a different location on its curved surface. Changes in the position of the recording light falling on the photographic paper caused by rotations of the eyeball were of interest. Changes in position caused by head translations were not. They were artifacts. A technique was required to prevent them, or some way of recording them and subtracting them from the records was required (subtracting them was exceedingly difficult, perhaps even practically impossible; see Ratliff and Riggs, 1950). The human cornea is quite curved, which means that even a tiny translation of the head introduces a quite large artifact into the records. Clearly, the quality of human fixation, and the nature of retinal image motion, could not be known until this problem was solved. The very best biting board was not good enough to eliminate it (see Barlow, 1952, for a particularly heroic attempt to hold the head rigidly in place).

The first step toward the solution of this problem (known to the author) was made by Adler and Fliegelman (1934). They used the *optical lever technique* to measure human fixational eye movements. In this method, a very small, flat (plane) mirror is mounted on the eye, and eye movements are recorded when a beam of light, reflected from this mirror, falls onto photographic paper moving behind a slit at the front of a movie camera. The use of a *flat* mirror at the fulcrum of the optical lever, instead of the curved corneal surface, removes the head translation artifact from the records because the angle of incidence of the recording light beam does not change when the surface reflecting it to the photographic paper is flat. The angle of incidence does

change if the curved surface of the cornea is used, as had been the case in prior research. The optical lever technique easily produces records with very good spatial resolution because it has an inherent 2× magnification factor; that is, a 1 degree change in the angle of incidence results in a 2 degree change in the angle of reflectance (see Nachmias, 1959, for an explanation).

By 1934 it was also possible to record on rapidly moving photographic paper. This allowed a high degree of temporal as well as spatial resolution. Even the very smallest fixational eye movements could be seen in Adler and Fliegelman's (1934) records. They reported that when a human being maintained fixation, eye movements consisted of *rapid shifts* averaging about 15 min arc; *waves*—inconsistent in direction, extent, and duration with peak-to-peak (p-p) displacements of 2½ to 5 min arc; and *fine vibratory movements*—50 to 100 per second, with p-p extents of about 2¼ min arc. These were important results, but their validity was still in doubt because Adler and Fliegelman's subjects had been required to maintain fixation on a relatively nearby target (only 2 m away). With such a target, the slightest movement of the subject's head with respect to the fixation stimulus would confound head translations relative to the fixation stimulus with motions of the image of the fixation target on the retina. The sizes of the various fixational eye movements they reported were also questionable. These authors apparently did not understand that their optical lever magnified the extent of eye rotation. Their quantitative descriptions were twice as big as those that should have been reported. These facts made the significance of Adler and Fliegelman's results uncertain at best. Ratliff and Riggs (1950) solved these problems and, in doing so, provided a valid method for studying the finest features of the human eye movement pattern. Their improvements also made it possible for them to make inferences about the nature and extent of the retinal image motions of their fixation targets. Ratliff and Riggs' technique also laid the foundation for stabilizing retinal images in the presence of fixational eye movements, a type of research that engaged many investigators between 1950 and 1980. Their landmark paper began by summarizing the status of knowledge about high-frequency tremor during maintained fixation. In the authors' words:

The summary of the studies of physiological nystagmus [one of the terms used to describe the small high-frequency component of the eye movement pattern during maintained fixation; *high frequency tremor* was the other] indicates that there is . . . evidence to support three different positions . . . (1) the eye is in motion . . . and there are fine vibratory motions . . . (2) the eye is in motion, but there is little evidence of vibratory motions . . . (3) The eye is essentially motionless during short periods of fixation. (Ratliff and Riggs, 1950, p. 690)

Why were things so unclear in 1950, after 50 years of objective human eye movement research? The big problem

stemmed from the fact that it was not possible to separate motions caused by head movements from those caused by eye movements. Ratliff and Riggs (1950) introduced a simple way to get around this. Again, in their words:

Originally it was planned to use the simultaneous records of head and eye movements to determine the exact motions of the retinal image [during maintained fixation], because . . . both . . . must be known to determine the motions of the image on the retina. However, it became apparent . . . that the center of rotation of the head is not even approximately a fixed point. At times the center of rotation may be at the point of contact of the upper teeth with the biting board [a dental impression used to restrict head movement]. At other times it may be at the point of articulation of the vertebral column with the cranium. Since the center of the head cannot be determined with accuracy, the angular movements which are recorded are of little use in determining the linear extent of the movement of the eye due to head movements . . . a better method . . . was needed. (Ratliff and Riggs, 1950, pp. 692–693)

They avoided the problem of eye translations by using the optical lever technique, introduced by Adler and Fliegelman (1934). They improved it, however, by mounting their small, flat mirror in a tight-fitting scleral contact lens. (Adler and Fliegelman had stuck their mirror directly on the eye and held it in place with a dab of vegetable gum.) The contact lens allowed Ratliff and Riggs to record for much longer periods of time. The contact lens also eliminated the need for the subject to hold the eyelid up with a finger while recordings were made. Ratliff and Riggs' most important contribution, however, was the way in which they eliminated the confound produced by head translations relative to the target. Head movement artifacts were eliminated simply by using a collimating lens in front of the eye. This lens placed the fixation target at optical infinity. This arrangement allowed the head to translate on the biting board without causing the retinal image of the target to be displaced on the retina. The fixation target, once it was viewed through the collimating lens, was simply too far away for head translations to affect the position of its retinal image significantly.

Ratliff and Riggs' (1950) records were valid, but they were hardly representative of natural fixation. The target was fixated monocularly while the head was immobilized as much as possible on a biting board. Even under these very restricted conditions, valid measurements could only be made of eye rotations on a single meridian, usually the horizontal. Nachmias (1959) introduced the first convenient variant of the optical lever method that could be used to make simultaneous, valid, albeit still very unnatural measurements of eye rotations on both horizontal and vertical meridians without confounding vertical with torsional eye rotations. Many important human oculomotor characteristics were observed under such unnatural conditions, and some of their physiological underpinnings have been worked out in primate models by recording electrophysiological brain activity in the oculomotor systems of monkeys while

they performed a variety of oculomotor tasks. The bulk of this research was done with a magnetic eye movement recording method introduced by Robinson (1963).

Instrumentation continued to develop, and by the last decade of the twentieth century, it finally became possible to observe how a human being controlled gaze under relatively natural conditions, that is, with the head and torso free to move naturally as objects within arm's reach were observed and manipulated. Doing this required solving the problem Ratliff and Riggs (1950) had managed to get around by putting their targets at optical infinity. Observing gaze control with nearby objects requires measuring the smallest translations (<0.1 mm) of the head, as well as its roll, pitch, yaw, and two-dimensional binocular eye movements. All of these angles have to be measured to at least 1 arc min for the measurements of gaze to be at least twice as good as the performance of the oculomotor system, the biological system under study. See Epelboim et al. (1995) for a brief description of the instrumentation developed to do this. This unique instrumentation made possible the first accurate, natural studies of human gaze control. These studies have called into question the significance of many observations that had been made earlier under less natural conditions. These new naturalistic observations will be described after some highlights from earlier, somewhat less natural, research are reported. These observations clearly implied that studying the human being's control of gaze under unnatural conditions could be perilous. They could mislead the investigators. There were clear hints that this might be the case as early as 1953 when Riggs et al. published their pioneering study of stabilized retinal images. Their study reported a result whose significance was not appreciated for more than 25 years. This publication will be described in some detail after some necessary background and definitions are presented.

Background and definitions

Foveal creatures like ourselves make two very different kinds, or types, of eye movements. In the simplest classification, proposed by Steinman et al. (1990), these two kinds of eye movements are simply called *fast* and *slow*. This reduces the number of postulated oculomotor subsystems from five or more to only two (see Dodge, 1903; Hallett, 1986; Robinson, 1968, for descriptions of many more oculomotor subsystems). Steinman et al. (1990) justify their reduction by pointing out that the traditional classifications are based primarily on the stimulating conditions usually used to study one or another of these putative subsystems. The classifications do not seem to be based on any well-established differences in oculomotor performance, physiology, or anatomy. The simpler classification seems to be catching on, as evidenced by its adoption in a popular introductory perception text (Sekuler and Blake, 2002, pp. 364–370). In this

classification, eye movements are simply called either fast or slow on the basis of three oculomotor performance characteristics, namely, their (1) peak velocities, (2) acceleration characteristics, and (3) susceptibility to voluntary control. The initiation, size, and direction of the fast eye movements, which are called *saccades*, are under voluntary control. They accelerate very rapidly and attain their relatively high peak velocities early. Saccades do not require visual targets. Their peak velocities are somewhat lower, and the size of the smallest voluntary saccade is larger when no targets are visible, but their main performance characteristics are the same. As a consequence, humans can shift their gaze to look at something that may appear anywhere in a completely dark visual field almost as well as they can shift their gaze to look at something visible in peripheral vision. Said differently, saccades are not influenced by properties of the visual field. The eye will drift in an idiosyncratic direction in total darkness (often down) when the head is immobilized, however, because the low-velocity compensatory eye movements, called *slow control*, require input from a visible stimulus moving on the retina (Steinman et al., 1967, 1973).

Slow (or *smooth*) eye movements are different. They accelerate gradually, and their maximum velocity is less than half of that achieved by the fastest saccades. The susceptibility of these slow eye movements to voluntary control is also much more limited. Normally, they cannot be initiated voluntarily if nothing is moving on the retina. Smooth eye movements will respond reflexively to a moving object or frame in the visual field, *but only if* the observer is not provided with a stationary object which can be used to keep gaze in place. Objects or frames that are moving in the visual field can be ignored, but gaze can stay in place only if the visual field contains a visible stationary target. Head movements can also cause the retinal images of objects and frames to move, and if, *but only if*, the subject attends to these motions will they be tracked with smooth eye movements. If smooth eye movements are made by paying attention to a moving object, the response is called *smooth pursuit*. If smooth eye movements are made by paying attention to a large frame rather than to an object, many oculomotor researchers call these slow eye movements *optokinetic reflexes* (OKN), rather than smooth pursuits. This distinction seems to be based entirely on tradition, and not on the characteristics of the eye movements themselves or any known differences in their anatomical or physiological underpinnings. Note, however, that if the subject chooses to attend to a stationary object or frame, smooth eye movements will not be observed. Gaze will be maintained. So, what the person wants to attend to is under voluntary control, but when it comes to slow, or smooth, eye movements, properties of the attended stimulus determine the nature of the oculomotor response once the subject selects the stimulus. (See Kowler et al., 1984, for experimental results showing the degree to which selective atten-

tion determines the outcome when moving and stationary stimuli are present in the visual field at the same time, and see Kowler, 1990, for the most comprehensive treatment available of the importance of cognitive factors in controlling human eye movements.)

Head movements also provide another kind of input to the oculomotor system. The oculomotor system receives input from the hair cells in the semicircular canals of the vestibular system as well as from the retina. These hair cells respond to accelerations of the head, causing the eye to rotate in the direction opposite to the head's rotation. The eye's angular velocity, resulting from vestibular stimulation, is similar (~95%) to the head's angular velocity (Collewijn et al., 1983). These involuntary counterrolling eye movements, called the *vestibulo-ocular reflex* (VOR), can be canceled almost completely if the observer fixates an object attached to the head, such as the tip of the nose if it is illuminated and if it is long enough to be seen. The VOR cannot be made to operate voluntarily if the head is not allowed to move. Once it can move, what VOR does depends on what the subject is attending to. The velocity of the slow eye movements (smooth pursuits or OKN) that a subject uses to track a smoothly moving object or frame *can* be adjusted voluntarily to specified fractions of the target's velocity, but smooth eye movements *cannot* be made voluntarily without a target moving on the retina, and smooth pursuit velocity *cannot* exceed the velocity of the moving target. Subjects asked to get ahead of a smoothly moving target can do this, but only by making saccades ahead of the target. They cannot lead the target with smooth pursuits (Steinman et al., 1969).

Each type of eye movement accomplishes different things. The fast, voluntary eye movements, saccades, are used to fixate an attended object, that is, to place its retinal image within the fovea. Said differently, saccades are used to place gaze where, within the visual field, we want gaze to fall. Human saccades can attain peak velocities of about 550 deg/sec. Their peak velocity depends on their size. Larger saccades are faster. This velocity/amplitude relationship has been dubbed the *main sequence*, a term borrowed from star brightness magnitudes in astronomy which was probably introduced to impute some kind of special significance to this rather common phenomenon. Very small saccades, called *microsaccades* (smaller than 10 or 12 min arc), have velocities of only a few degrees per second. These tiny saccades are the smallest voluntary human behaviors (see Haddad and Steinman, 1973; Steinman et al., 1973, for a discussion of their nature and functional significance).

Saccades of all sizes are used to bring attended objects to fall at the *center of best vision* or *optimal locus* (Cornsweet, 1956) at the foveal center. Saccades of about 0.5 to 1.5 degrees of visual angle are used to read a line of ordinary text. Saccades can also be used to reestablish fixation quickly if an object suddenly moves away from the optimal locus.

Saccades can shift gaze among objects in the visual field very rapidly. We are not ordinarily aware of making these rapid gaze shifts, and it came as a surprise when it was discovered that such high-velocity jumps were used to read. Subjectively, one has the impression that our eyes glide smoothly across the text as we read each line of words. We can easily make ourselves aware of the relatively large gaze shift we use to move from the end of one line to the beginning of the next, but the jumps among the words are perceived as being smooth. They are not. The reading eye movement pattern is shown in Figure 90.1. This figure is somewhat unusual because it shows the reading eye movement pattern of a subject who is reading under relatively natural conditions. The subject is seated with the head and torso free as he reads a standard text located about 30 cm in front of his eyes. Only left eye movements are reproduced in this figure, but recording was binocular (the right eye movements were very similar to the left). Translations as well as rotations of the head are shown. The top graph in Figure 90.1 shows head rotations; the bottom graph shows rotations of the left eye. The pattern of head rotations varied during the trial. A 2 degree head rotation to the right was made during the third and fourth seconds as the eyes moved to the right across a line of text. There was a fast, large saccade (~25 degrees = about 10 cm on the page) that moved gaze to the left to the beginning of the next line of text near the middle of the fifth second, but the movement of the head was much slower, which meant that the head was still moving to the left as the eye was moving to the right as it read the new line of text. So, for about 0.5 second, the head and eye were moving in opposite directions.

Different head-eye coordinations were observed during other reading trials, and the second subject, who served in these experiments, also showed different kinds of head-eye coordination. Kowler et al. (1991) drew the following conclusions from this research:

Head rotations were larger when the head was free than when the head was on a the bite board [and] the S.D.s of head rotations with the head free are about twice what is observed when subjects try to hold the head as still as possible without artificial support during maintained fixation. . . . The head moves during reading but not in a stereotypical pattern . . . in some instances it moved in the same direction as the reading saccades; in other instances it moved in the opposite direction. Eye rotations compensated well for head movements, producing a fairly stable line of sight during intersaccadic intervals. (pp. 421–422)

None of these head and eye movements are perceived subjectively when one reads, a fact which seems as remarkable now as it did when it was first discovered a little over a century ago.

The human being's slow, or smooth, eye movements have velocities ranging from as little as 3 minutes of arc per second up to peak velocities of about 200 degrees of arc per second.

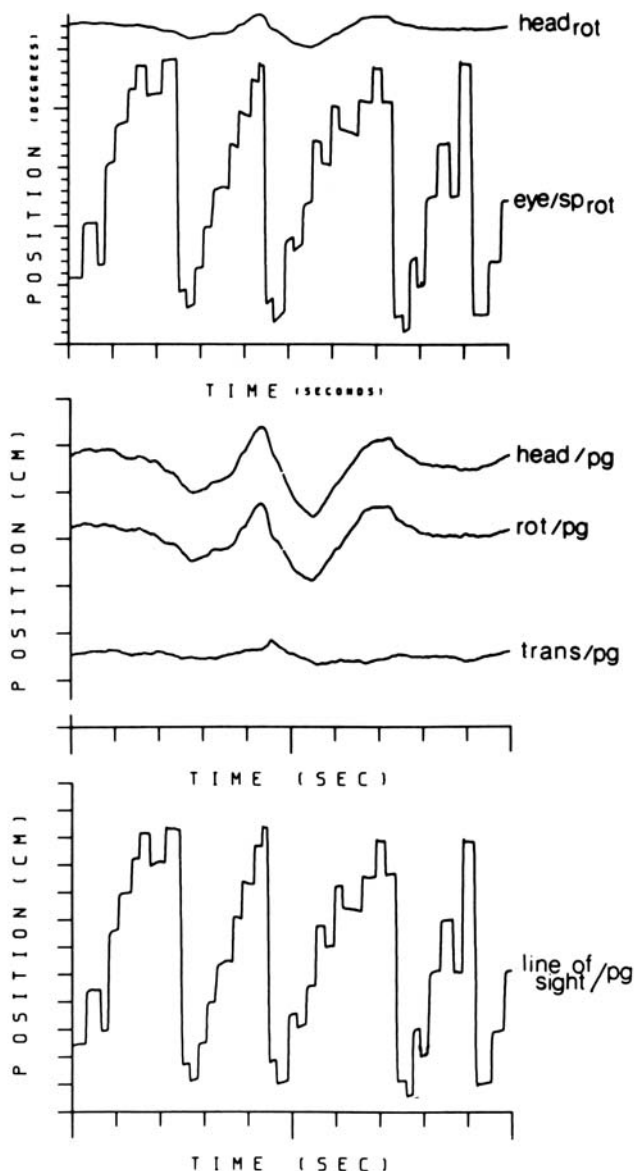


FIGURE 90.1. Results of a sample reading trial. *Top*: Horizontal rotation of the left eye and the head as a function of time during reading. Upward deflection of the traces indicates rightward eye or head motion. *Middle*: Total movement of the head (head/pg), the rotational component (rot/pg), and the translational component (trans/pg) on the page of text. These traces represent the positions of an imaginary line connecting the midpoint of the center of rotation of the left eye with the page. *Bottom*: Horizontal position of the line of sight of the left eye on the page of text. (From Kowler et al., 1991.)

They tend to be involuntary in the sense that normally they cannot be made by willing them in the absence of something moving in the visual field. They will, however, always be made in anticipation of a future target motion. These *anticipatory smooth eye movements* can be as fast as 60 deg/sec (see Steinman et al., 1990, for records showing very fast anticipatory smooth eye movements, and see

Kowler, 1990, for a review of her research on anticipatory smooth eye movements). We also speak of *involuntary* or *noisy drifts*. Adler and Fliegelman (1934) called these slow eye movements *waves*. They are involuntary slow shifts of gaze. They are observed in the intervals between small saccades, which are made when an adult subject maintains fixation on a stationary object with the head immobilized. The involuntary slow eye movements, which have been shown to correct such noisy drifts, have been described as smooth pursuit of a stationary object whose retinal image moves because of noisy drifts (Nachmias, 1959). Steinman et al. (1973) ascribed these compensatory fixational slow eye movements to the operation of an oculomotor subsystem they dubbed *slow control*.

Findings encouraging questions about the relevance of unnatural research

THE ROLE OF NATURAL AND UNNATURAL RETINAL IMAGE MOTION IN VISUAL PROCESSING Riggs et al. (1953), who initiated a long line of research on stabilized retinal images, reported an unexpected result whose significance would not be appreciated for 26 years. They used the contact lens optical lever technique to allow a subject to view a simple fixation target under three conditions. The first condition allowed what they called *normal* vision, in which the subject viewed the stimulus monocularly with the head fixed on a biting board. They called this vision normal because the retinal image displacements of the fixating eye were the same as the displacements present under the fixation conditions they normally used, that is, with the head immobilized on a biting board. In the second condition, a mirror path in the optical arrangements stabilized the retinal image of the fixation target. When the eye moved, the target moved with it by the same amount, so its retinal image did not move on the retina. In the third condition, called *exaggerated motion*, the mirror path was arranged so that an eye movement caused the fixation target to move on the retina twice as much as it moved during normal fixation. The subject indicated whether the fixation target was visible during fixation trials, which lasted for many seconds. As expected, the stabilized target disappeared often and remained invisible for the longest period of time. The target also disappeared occasionally during normal viewing. This was not surprising. Many observers had noticed periodic fading of fixation targets (and more complicated displays) when they stared at them for many seconds with the head immobilized artificially. Fading was least likely in the exaggerated retinal image motion condition. This result came as a surprise, but little was made of it at the time. It clearly meant that transient stimulation was useful for visual processing, but its implications were otherwise ignored. It became important 26 years later when Skavenski et al. (1979) published the first accurate monocular recordings of the head and eye movements

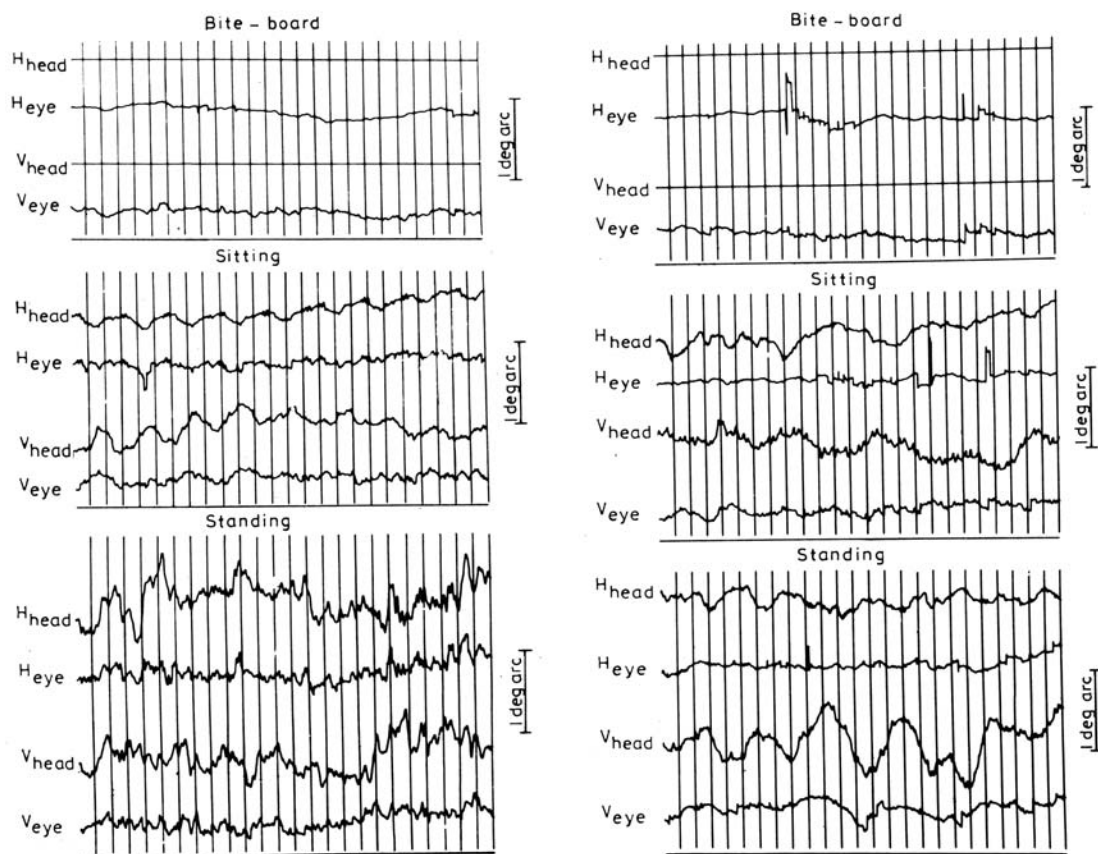


FIGURE 90.2. Representative horizontal (H) and vertical (V) head position and gaze of subject AAS (*left*) and RMS (*right*) while they fixated a target at optical infinity with their heads supported on a biting board or while they were standing as still as possible. Records

begin on the left. The vertical lines show 1 second intervals, and the vertical scales on the right show 1 degree of visual angle. Upward changes in these position traces signify rightward or upward rotations. (From Skavenski et al., 1979.)

of seated and standing subjects fixating a target located at optical infinity.

Figure 90.2 clearly shows that the head moves quite a lot when a human being tries to sit or stand as still as possible. A good deal of this head movement is compensated for by eye movements, but considerable retinal image motion remains. The eye traces in the records reproduced in Figure 90.2 show gaze. They would be horizontal straight lines if head movements were compensated for perfectly. There are very few instances where this can be seen in the records of both subjects when they sat or stood. Their gaze was considerably more stable when their heads had artificial support, as shown by the top two records in Figure 90.2. Note that in the two more natural conditions in which the subjects were sitting or standing still without artificial support, there was considerable uncompensated head motion. This led to considerable retinal image motion—enough to minimize, perhaps even to prevent, any fading of the fixation target. The retinal image velocities observed while they were sitting and standing were quite similar to those which had proved to be so effective in preventing fading in the exaggerated retinal image motion condition in the Riggs et al. (1953)

publication about stabilized images. The implications of these results, in the authors' words, were as follows:

[T]he gain of the compensatory machinery is tuned to guarantee that the retinal image will always move at some appreciable speed which would not be the case if the gain of compensation approached 1 when the amplitude of body rotation was small. . . . Note that subjects whose heads are supported on bite-boards occasionally report periods of target fading which means that retinal image speeds seen on a bite-board are only marginal for maintaining vision . . . [and] once we pay attention to the fact that compensation is mostly less than perfect . . . we are forced to consider how we see a perceptually clear world during such image motion. Oculomotorists have assumed that the quality of vision is a consequence of the stability of the retinal image [caused by the virtual perfection of oculomotor compensation]. The retinal image is not actually stable so perceptual clarity must depend in part on visual as well as on oculomotor activities. (Skavenski et al., 1979, pp. 681–682)

The significance of Figure 90.3 is quite similar to that of Figure 90.2. Here we see recordings made under even more natural conditions. Figure 90.3 shows head and *binocular* eye recordings of four subjects who attempted to maintain

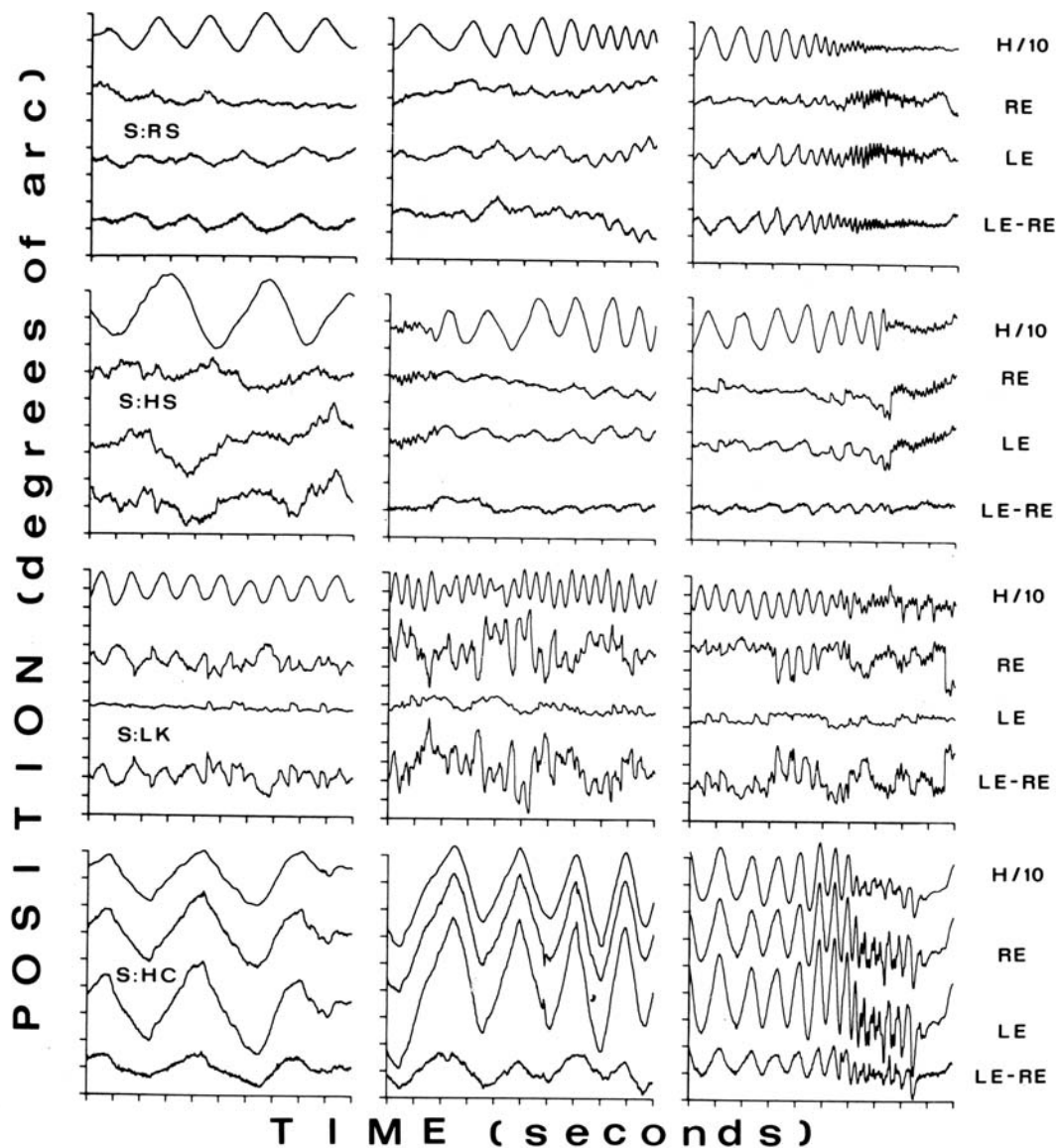


FIGURE 90.3. Representative horizontal eye and head movements of four subjects (R.S., H.S., L.K., and H.C.) while they fixated a distant object as they moved their heads. Records begins on the left, and the time-scale marks signify 1 second intervals. The head position trace (H/10) shows the position of the head to 1/10th of its actual value. Right eye position (RE) is just below the head, with

left eye position (LE) just below it, and the bottom trace in each graph (LE-RE) shows vergence. Upward changes in position traces in these records show rightward movements, and upward changes in vergence traces signify convergence. (From Steinman and Collewyn, 1980.)

fixation on distant targets (5000 or 35,000m away) as they actively oscillated their heads about their vertical axis at different frequencies and amplitudes. Once again we see considerable oculomotor compensation for head rotations, but it is far from perfect, which means that there was considerable residual retinal image motion. All four subjects reported seeing clearly throughout these trials. Some jitter of the visual field was reported at the highest head oscillation frequencies, but vision was always fused and clear despite such violent retinal image motions. Now that binocular record-

ings were finally made, a very surprising result can be seen: there was considerable difference in the degree of compensation by each of the subjects' eyes. This led to considerable variation in their vergence angles (the oscillations evident in the bottom trace in each subject's graphs, labeled "LE-RE," for "left eye-right eye"). This result was not expected. Such large variations in vergence angles should not have been observed when binocular fixation was maintained on such distant targets. The implications of these results, in the authors' words, were as follows:

It is not easy to study binocular eye movements accurately in freely moving subjects or to stabilize retinal images under such conditions. Furthermore, it was not believed to be necessary to study freely moving subjects. Almost all investigators . . . believed that natural visual and oculomotor performance, and their interaction, could be understood despite the fact that their subjects' heads were immobilized. Two assumptions underlie this belief. First, it is assumed that the oculomotor system compensates almost perfectly for motions of the body. . . . Second, it is assumed that compensatory oculomotor activities are almost perfectly yoked in the two eyes. Once these two assumptions are made, the fusion, stability and clarity of the visual world during normal activity can be explained. These explanations, however, rest on what we now know is an idealized view of the operation of the oculomotor system. (Steinman and Collewijn, 1980, pp. 427–428)

These results also suggest that much will be found under natural conditions that could not have been anticipated from what was known from research performed under the more common, much less natural conditions usually employed.

THE MICROSACCADE, FUNDAMENTAL OCULOMOTOR ACTION OR LABORATORY CURIOSITY The microsaccade has a long history in the study of human eye movements research. It first became prominent as what Adler and Fliegelman (1934) called *rapid shifts*, which were observed during attempts to maintain fixation. Adler and Fliegelman claimed that their extent was about “15 minutes of arc.” Once this value is corrected for their computational error (see above), these saccades would be 7.5 min arc, an acceptable value for what has been called a *microsaccade* since Zuber et al. (1965) introduced this term. Generally speaking, saccades smaller than 10 or 12 min arc along a single meridian have been placed in this category ever since accurate estimates of fixational eye movements began to be made about 50 years ago. Ditchburn (1955), who trained as a physicist and shifted his research interests to human vision after World War II, believed that transient stimulation provided by these microsaccades, which he called *flicks*, was essential for maintaining clear, high-quality color vision. Many subjects, but by no means all, whose fixational eye movements have been recorded since the optical lever technique came into vogue showed microsaccades in their eye movement pattern during maintained fixation. The status and significance of microsaccades came into question when Steinman et al. (1967) reported that simple instructions would reduce their frequency appreciably (by 50% or more) and even eliminate them completely. These reductions in microsaccade rates had no adverse effects on the quality of vision. This observation was followed by a series of publications, including some which showed that saccades as small as microsaccades were in the voluntary behavioral repertoire and others which showed that microsaccades could be used to track small target steps reliably. These experiments were summarized by Steinman et al. In 1973, by which time it was generally

accepted by most oculomotorists that microsaccades, which are present only in the behavior of adult human beings whose heads are being held artificially while they attempt to maintain fixation, were a laboratory curiosity rather than an important oculomotor behavior (Kowler and Steinman, 1979). Ditchburn (1980) preferred to believe otherwise, and his comment on one of the papers in this series led to an exchange of letters (Kowler and Steinman, 1980). This exchange should be of interest to anyone wondering about the significance of microsaccades. The significance of microsaccades for processing visual contrast and spatial detail was discussed in Steinman and Levinson (1990). This review also claims that microsaccades are not likely to contribute to any kind of visual processing. In addition, it reviews the extensive literature on stabilized images and also claims that microsaccades do not play a significant role in vision. When it first became possible to study the control of gaze under relatively natural conditions (Steinman and Collewijn, 1980), it became clear to the investigators that microsaccades were not common, perhaps even absent, in the fixational eye movement pattern once the head was free to move naturally. Nailing this down has become important now that microsaccades are beginning to be taken seriously in the primate oculomotor community (e.g., Bair and O’Keefe, 1998; Martinez-Conde et al., 2000; Rucci et al., 2000). For this reason, we randomly sampled 3375 saccades made by four subjects in two naturalistic sequential looking tasks and found that only 2 (0.06%) could be classified as microsaccades, that is, smaller than 12 min arc (Malinov et al., 2000). The implications of these results, in the authors’ words, were as follows:

We have another reportable, albeit expected result. Namely, microsaccades were extremely unlikely. . . . Those, who have studied human eye movements under natural conditions with instrumentation sufficiently sensitive (noise $\leq 2'$) to measure microsaccades, have rarely seen microsaccades (Steinman & Collewijn, 1980, were probably the first). But as far as we know, the actual likelihood of finding a microsaccade under natural conditions has never been reported, in part because: (i) other issues were under study; and microsaccades had lost their significance by 1980. They were laboratory curiosities, confined to human adults, whose head were supported artificially. (Malinov et al., 2000, p. 2089)

There is no reason to believe at this time that the situation has changed, so I would be cautious about accepting work imputing an important role to such behaviors in infrahuman primates, particularly inasmuch as it takes a lot of fixation training before monkeys even begin to show microsaccades in their fixational eye movement pattern (Skavenski et al., 1975; Steinman et al., 1973). We turn next to some relatively recent work on a subject that has forced a major revision of our thinking about the performance characteristics of one of the classical oculomotor subsystems: vergence.

NATURAL SMOOTH AND SACCADIC VERGENCE The oculomotor *vergence subsystem* was one of Dodge's (1903, 1907) five types of eye movement. He described these eye movements, which he called *type V*, in the following way:

The fifth type is in several respects unique. It consists, primarily, of movements of convergence and divergence . . . [when] the stimulus falls on disparate points of the two retinae, and the movements of the two eyes are consequently not in the same but in opposite directions. The most conspicuous of the differentiae of this type are the relative slowness of the movements. . . . Whereas movements of the first type [saccades] through 10° occupy about 40σ [msec]; eye movements of the fifth type . . . occupy about 400σ [msec]. (Dodge, 1903, pp. 327–328)

The slowness and smoothness of Dodge's type V eye movement were stressed in the oculomotor literature until quite recently, when Erkelens et al. (1989a) used the unique eye movement recording system developed at the University of Maryland to examine how vergence actually operated under much more natural conditions than had been possible before. These observations made it clear that studying human eye movements under unnatural conditions had given a very misleading impression of how the human oculomotor systems performs when it adjusts gaze in three dimensions. These experiments and the implications of their results, in the authors' words, were as follows:

We studied ocular vergence responses made under relatively natural viewing conditions as a first attempt to determine whether vergence responses obtained under such conditions could be predicted from descriptions of vergence responses to the isolated motion-in-depth cues that had been studied separately in previous experiments. We undertook to study vergence under relatively natural conditions because it has become increasingly clear in recent years that oculomotor performance, as well as its visual consequences cannot be predicted from studies undertaken under constraints that had been necessary and eventually became traditional in laboratory settings (Skavenski et al., 1979; Steinman and Collewijn, 1980; Collewijn et al. 1983; Steinman et al., 1985). . . . We found that ocular vergence in response to a target seen to be changing its position in depth in a normally lighted room, replete with natural cues to depth, had shorter delays and better dynamics than could have been expected from reports of previous experiments. . . . Changes in vergence often preceded changes in the distance of the target when the distance of the target was under control of the subject. The most accurate vergence tracking (smallest tracking error) was observed when voluntary movements of the upper torso . . . provided the changes in the distance of the target. (Erkelens et al., 1989b, pp. 418–419)

Figure 90.4 shows an example of one subject's slow or smooth vergence eye movements produced by changing the distance between the subject and the target in this experiment.

The next publication in this series of naturalistic experiments, by Erkelens et al. (1989a), yielded even more surprising results. Once again, the experiment and the

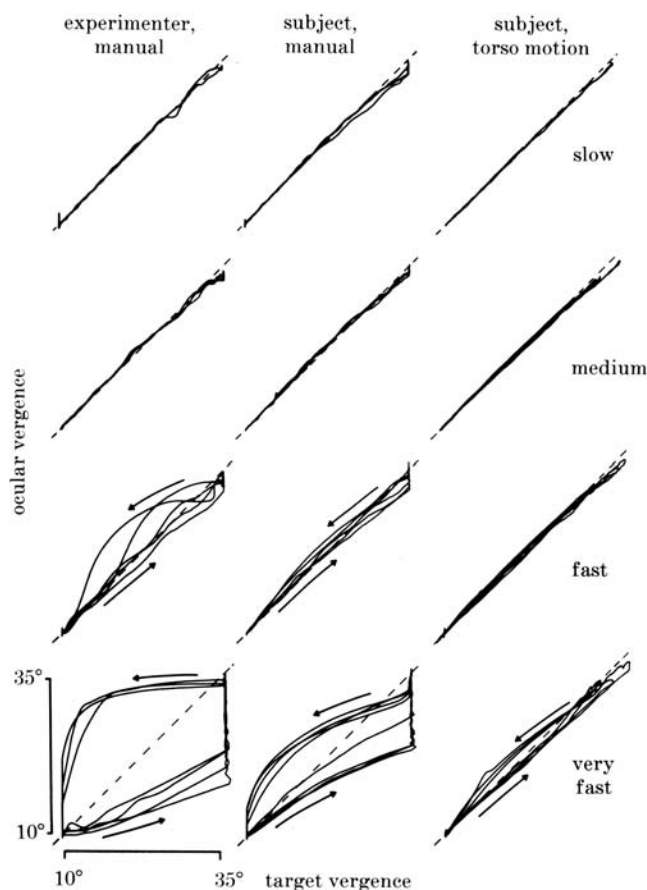


FIGURE 90.4. Typical relations between ocular-vergence and target-vergence angle of subject H.C. in response to slow (*first row*), medium (*second row*), fast (*third row*), and very fast (*bottom row*) changes in target distance. The three columns represent the three ways in which the distance of the target was varied. The diagonal dashed lines represent perfectly accurate vergence tracking. (From Erkelens et al., 1989b.)

implications of its results will be given in the authors' words:

In the preceding paper . . . we reported that the vergence subsystem makes timely and fast responses over a large dynamic range when it is provided with its 'natural input'. . . . We also showed that the vergence subsystem, like other oculomotor subsystems, is largely under voluntary control once it is provided with its natural input. . . . The present experiments . . . examined (1) shifts of gaze between stationary target objects . . . at different distances . . . along the median plane . . . and (2) shifts of gaze between objects that lay off to the side of the median plane as well as at different distances. . . . We examined . . . both [because they] are required for effective functioning in natural situations. We had no basis for predicting the quality of oculomotor performance. . . . We found that symmetrical vergence responses, as large as 30° , were largely smooth and attained maximum speeds as high as 200°s^{-1} . When . . . targets required asymmetrical vergence responses . . . vergence responses . . . were mediated almost exclusively by unequal saccades. . . . Such a dominant role for saccades in producing large vergence responses consistently has been rarely suspected. . . . We

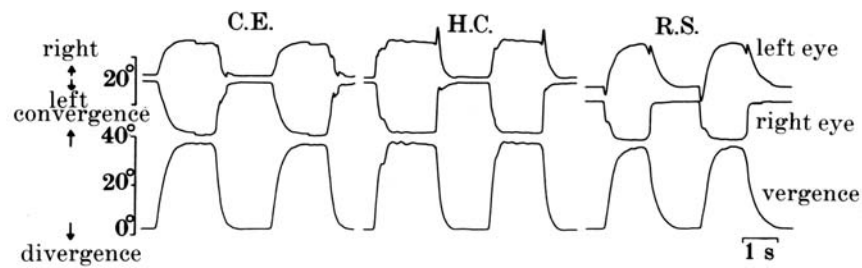


FIGURE 90.5. Representative binocular eye movements of three subjects (C.E., H.C., and R.S.) when they shifted gaze between light-emitting diodes (LEDs) located along each subject's median

plane. The small bar on the lower right shows a 1 second interval. The vergence shifts shown were mainly smooth. They were also very fast. (From Erkelens et al., 1989b.)

conclude that unequal saccades are generated normally in asymmetric vergence, and that traditional schemes . . . are incorrect. (pp. 442–443)

Figure 90.5 shows the very fast *smooth* vergence responses made by each of the three subjects, who shifted gaze between two targets located at different distances along their median plane. Figure 90.6 shows their asymmetrical *saccadic* vergence responses made when they shifted gaze between targets which were not located on their median plane. Note that under natural conditions, virtually all vergence changes are asymmetric and saccadic because targets are rarely located along the median plane and never stay there very long. The slightest movement of the body creates conditions favorable for saccadic rather than smooth vergence changes. Once this is appreciated, smooth vergence, like microsaccades, seems to be primarily a laboratory curiosity. It can be demonstrated, but it is hard to set up and almost impossible to maintain if the subject's head is not immobilized artificially.

The second paper on vergence under naturalistic conditions concluded as follows:

There is a great deal left to do now that we have shown that the control of vergence can be studied in the laboratory in ways that make sense with respect to the way vergence must operate in everyday life. We must now determine with our accurate, high-

bandwidth instrumentation, how the saccadic and slow subsystems function, synergistically, when gaze shifts between stationary objects . . . within the three-dimensional visual field in which human beings locate, track and manipulate objects of interest to them. We must refine our techniques to allow the subject's head to be free while he interacts with objects within reach of his hands. Once this is done, we will begin to have some idea of how cognitive, oculomotor and manual motor skills interact to guarantee our success as a species. (p. 464)

The reader should consult Judge (1991), who reviewed the status of vergence eye movements shortly after these two papers were published to gauge the novelty of these results with respect to how they fit with the traditional vergence literature, a literature that began with what Dodge (1903) called type V eye movements.

SUMMARY OF RECENT ECOLOGICALLY RELEVANT RESEARCH
The instrumentation developments required to study gaze under natural conditions were finished in 1992 and the first publication based on its use appeared in 1995, 3 years shy of the hundredth anniversary of the first publication reporting a method for recording human eye movements (Delabarre, 1898). In all, five papers meeting the requirements for studying gaze control under *natural* conditions have appeared so far (Epelboim, 1998; Epelboim et al., 1995, 1997; Herst et al., 2001; Malinov et al., 2000; see Steinman, 1995, for a detailed explanation of why and how the unique

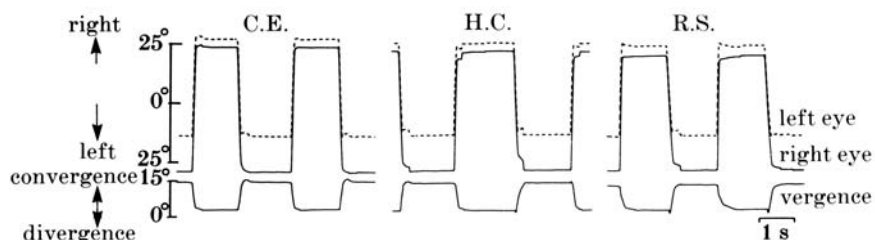


FIGURE 90.6. Representative binocular eye movements of three subjects (C.E., H.C., and R.S.) when they shifted gaze between a LED far away and to the right of the subject's median plane and a LED nearer and to the left of the subject's median plane. This target arrangement required asymmetrical vergence responses. The

dashed trace shows the position of the left eye; the solid trace shows the position of the right eye and vergence, that is, the difference between the positions of each eye. The small bar on the lower right shows a 1 second interval. The vergence shifts shown were mainly smooth. They were also very fast. (From Erkelens et al., 1989a.)

eye movement recording instrumentation at the University of Maryland was developed). In this series of experiments, the subject's head and torso were completely free as two-dimensional binocular gaze was recorded. The subject either looked at a sequence of targets in a specified order (look-only condition) or tapped a similar sequence of targets (tap condition). They were required to complete each sequence as rapidly as possible without making any errors. The targets were arranged in randomly selected locations on a work table in a well-illuminated chamber, which contained many objects and frames that provided excellent information about the location of the subject and targets within the three dimensions of the workplace. Data were also collected when the subject chose the order in which the targets would be fixated or tapped.

Only the main findings of these experiments will be summarized here. The source papers (listed just above) should be consulted for details. These results could not have been expected on the basis of prior work done under much less natural conditions. Highlights of the analyses completed and published so far are as follows: (1) just looking at a sequence of targets, solely to fixate each target accurately, and looking at a similar sequence to guide tapping, are fundamentally different tasks. The seemingly more complicated task, using vision to guide tapping, was easier, more pleasant, and took less time to complete than the task in which the subject did much less, namely, simply fixate each target in a sequence; (2) visual search (using a saccade to *find* the next target) is a separate and different saccadic activity from *looking from one target to the next in the sequence* in both looking and tapping tasks; (3) looking for its own sake, looking to guide tapping, and visual searching are synergistic, interacting in beneficial ways; (4) subjects almost *always* look at the target they are about to tap before tapping it, but are *convinced* that they do not do this often once a particular target pattern has been learned; (5) cyclopean gaze, on average, is more accurate than gaze from either eye, demonstrating that under natural conditions (6) subjects show no sign of a *dominant eye* when they use their eyes to perform visually guided motor tasks despite the fact that they do show a dominant eye when a conventional *phoria cover test* is performed; (7) microsaccades, when the head is free, are exceedingly rare (see the section "The Microsaccade, Fundamental Oculomotor Action or Laboratory Curiosity"); (8) vergence tends to be set 25% to 45% *beyond* the attended plane; in other words, subjects do *not* adjust binocular gaze to intersect at the attended target, but rather adjust their eyes to intersect much farther away; (9) subjects fixate no more accurately than a given task demands, implying that at least for ordinary visuomotor tasks, any part of the foveal floor which is good enough to do the job will be used; (10) the *main sequence*, like other characteristic oculomotor performance, is controlled from the top down, that is, high-level task demands, such as its objec-

tives or goals, set the control parameters in the oculomotor *plant* (its physiological machinery) automatically; it does this without any conscious effort; and (11) once the head, as well as the eye, is free from restraint, the head is most likely to begin to move before, or at the same time, as the eye. The way the four subjects of these experiments actually controlled their gaze when they only looked at and when they tapped sequences of targets can be visualized by going to the following web page: <http://brissweb.umd.edu>.

Some highlights of these publications, the first accurate reports of how human beings control gaze under ecologically relevant conditions, are reproduced in Figures 90.7 to 90.10. The reader should consult the source papers (cited above) for detailed explanations of how these data were collected and what they have been taken to mean. Examining the visualizations available at the web page (cited just above) after reading these source papers will also promote understanding of the significance of these figures.

The basis for achieving accurate gaze control lies in the human being's ability to call upon one or the other compensatory subsystem at different times and to varying degrees. This ability is built in. Choosing a particular behavioral objective (goal or purpose) sets the parameters in the oculomotor plant without any explicit, conscious efforts on the subject's part. Furthermore, under natural conditions, gaze control is lax, perhaps even lazy. One could just as easily call it *efficient*. Why should the oculomotor system set its parameters so as to make it do more work than is needed to get a particular job done? In short, it should not come as a surprise that gaze is not set to be as accurate as possible all the time. Evidence for this, as well as demonstrations of the human being's control of gaze by adjusting parameters of oculomotor subsystems, is clear when gaze is studied under conditions approximating those that are commonplace in the workaday world. It may be here, *and only here*, that the nature and extent of the human being's exquisite control gaze becomes apparent. Much of the oculomotor literature, which is based on research done with the head restrained and targets beyond arm's reach, has probably told us very little of lasting value despite a century of active research. Fortunately, methods are now available which make accurate, ecologically relevant research possible, so one can hope that a second century of oculomotor research will not be needed before we actually know how human beings control gaze as they do other things that are important for their success as a species.

Acknowledgments

This chapter is dedicated to the memory of Dr. Julie Epelboim (1964–2001), who contributed enormously to making the ecologically relevant research referred to in this chapter possible, as well as using this approach to collect the

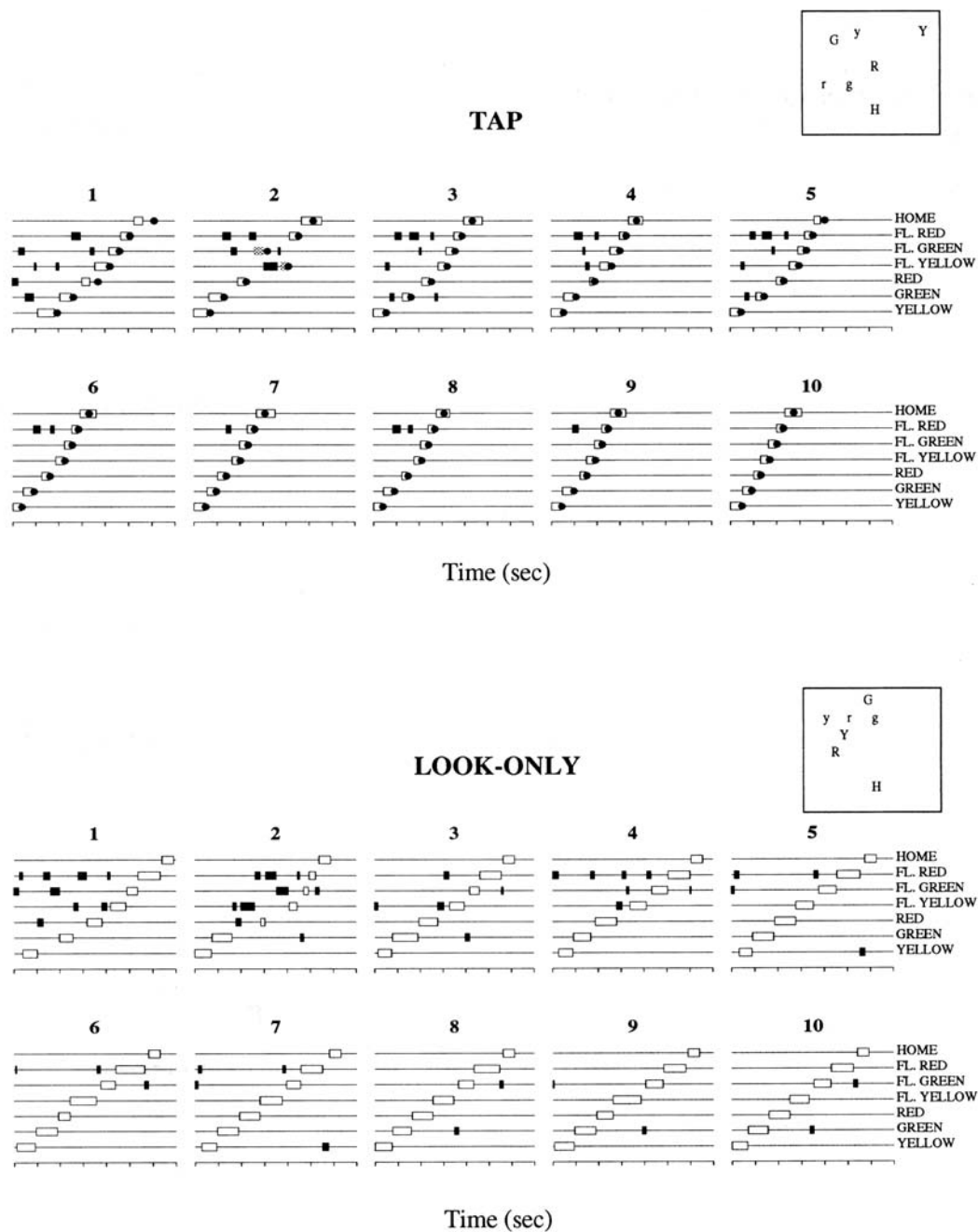


FIGURE 90.7. Look/tap diagrams for a 10 blocks of tapping trials and 10 blocks of looking-only trials. Each diagram represents one repetition with the same target configuration. The repetitions are numbered 1 to 10 above each diagram. The positions of targets on the work table for each block are shown in the rectangle signifying the colors of the six LED targets and a home button: Y, yellow; G, green; R, red; y, flashing yellow; g, flashing green; r, flashing red; H, home. Time is shown on the abscissa. Each horizontal line

the right. Boxes and dots on each horizontal line show when the subject looked at or tapped that target. Open boxes show sequence episodes, solid boxes show search episodes, and shaded boxes show looking episodes preceding tapping errors (see text). Widths of boxes show durations of looking episodes. Solid circles show the times of the taps. See the text for a full explanation, but it is clear that the visuomotor coordination during the two tasks was different. Looking for its own sake was not the same as looking to guide tapping. (From Epelboim et al., 1995.)

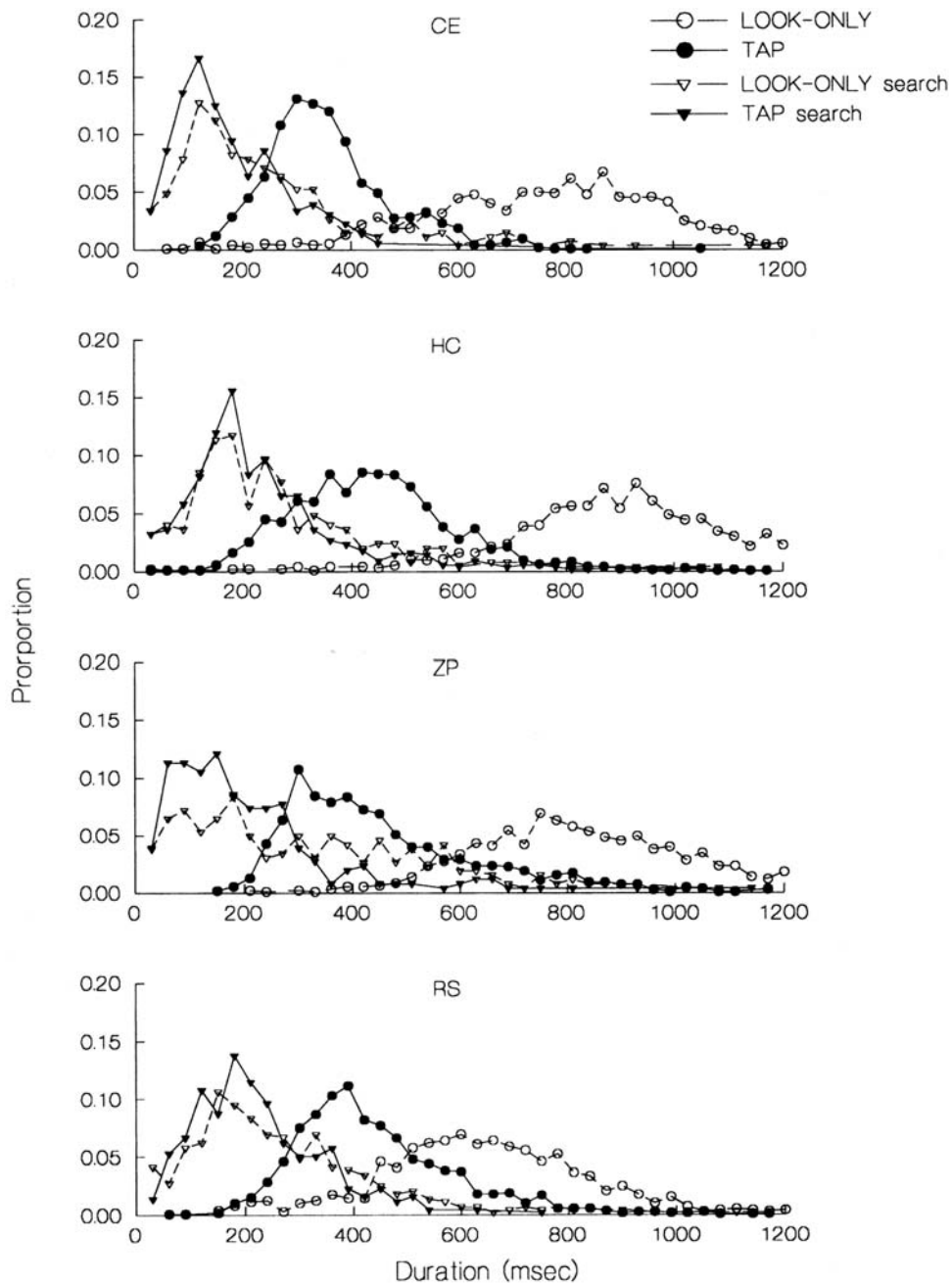


FIGURE 90.8. Distributions of sequence (*circles*) and search (*triangles*) episode durations (milliseconds). Data for tapping are shown as solid lines and solid symbols, and data for looking only are shown as dashed lines and open symbols. Bin width is 30 msec. Data for four subjects are shown in rows labeled C.E., H.C., Z.P., and R.S.. Each distribution is based on 950 to 1396 observations for sequence episodes and 247 to 552 observations for search episodes. All four

subjects showed that dwell-time distributions for search episodes were short and the same in both tasks, and dwell times were much longer during look-only trials. These results were taken to mean that saccades made to find targets are different from saccades made to move gaze through a sequence of targets. (From Epelboim et al., 1995.)

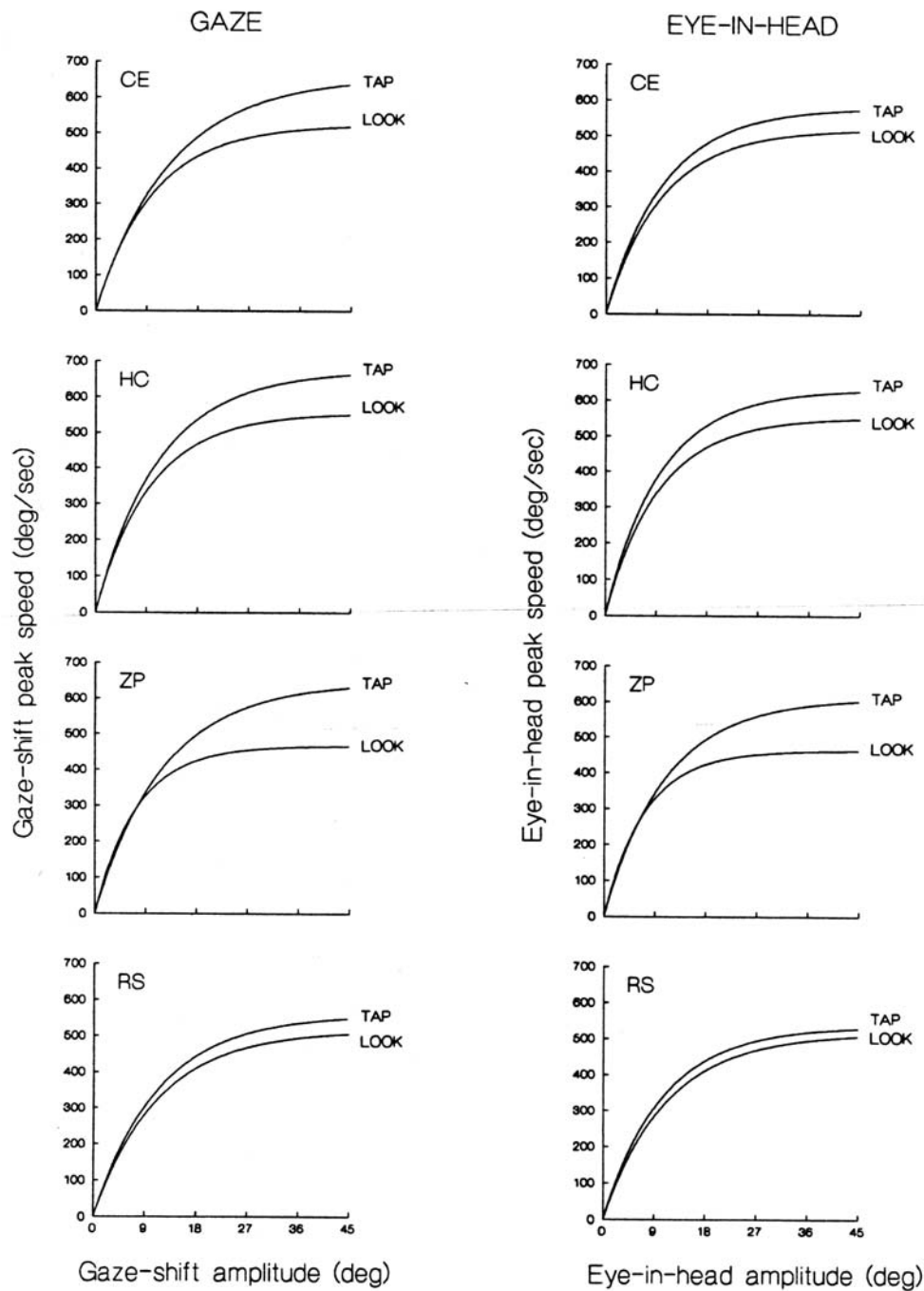


Figure 90.9. Gaze-shift peak speed (*left*) as a function of amplitude in space and eye-in-head peak speed (*right*) as a function of amplitude within the head of four subjects labeled C.E., H.C., Z.P., and R.S. These smooth curves are least square fits of the data. They show that the nature of the main sequence depends on the nature of the task, with higher velocities being found during

tapping than during looking only. The relatively small difference between the tasks shown by subject RS (bottom pair of graphs) can be explained by his age. He was 65 when these data were collected, so it was not surprising that his peak saccadic velocity was considerably lower than the highest velocities of the younger subjects. (From Epelboim et al., 1997.)

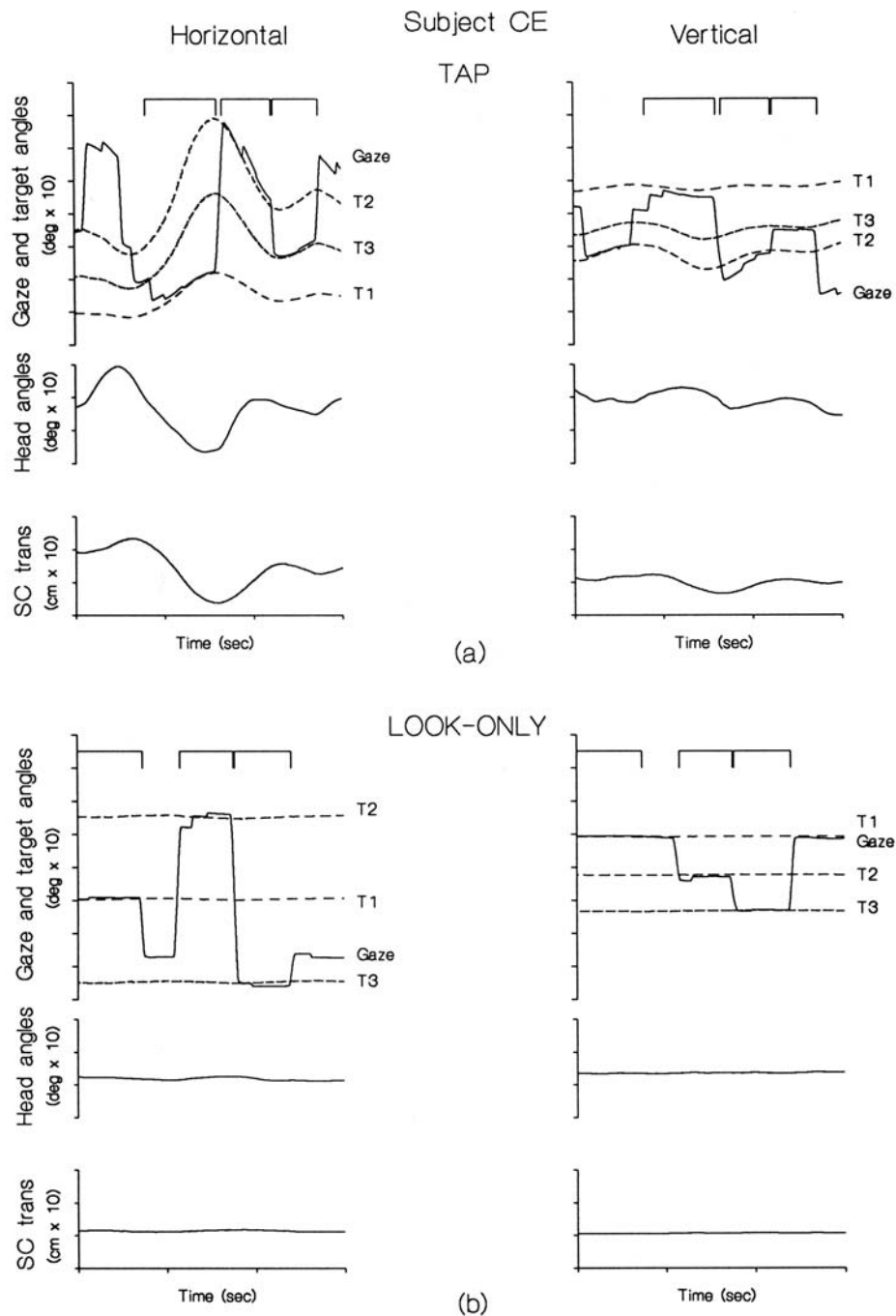


FIGURE 90.10. Analog records for subject C.E. during three segments of a tapping trial (a) and a looking-only trial (b). Horizontal components are shown on the left, and vertical components are shown on the right. The layout is the same for a and b. The top row shows gaze (solid lines) and target angles (dashed lines) for the right eye plotted as a function of time. Brackets above the graph show episodes during which CE was looking at each of the three targets

whose traces are shown. The second row shows head angles as a function of time. The bottom row shows translations of the sighting center of the right eye as a function of time. Gaze and head movements were used quite differently with respect to controlling the amount of retinal image motion when fixation was maintained during each task. (From Epelboim, 1998.)

data for her doctoral dissertation. Her obituary, including a list of her main publications, can be found in Herst et al. (2001). The research described in this chapter was supported, in part, by grants from the Chemistry and Life Sciences Directorate of the Air Force Office of Scientific Research, most recently, AFOSR Grant No. F496200210143.

REFERENCES

- Adler, F. H., and M. Fliegelman, 1934. Influence of fixation on the visual acuity, *Arch. Ophthalmol.*, 12:475–483.
- Bair, W., and L. P. O'Keefe, 1998. The influence of fixational eye movements on the response of neurons in area MT of the macaque, *Vis. Neurosci.*, 15:779–786.
- Ballard, D. H., M. M. Hayhoe, and J. B. Pelz, 1994. Memory representations in natural tasks, *J. Cogn. Neurosci.*, 7:68–82.
- Barlow, H. B., 1952. Eye movements during fixation, *J. Physiol. (Lond.)*, 116:290–306.
- Brindley, G. S., 1960. *Physiology of the Retina and the Visual Pathway*, London: Arnold.
- Collewijn, H., 1998. Eye Movement Recording in Carpenter, R. H. S., and J. G. Robson. *Vision Research: A Practical Guide to Laboratory Methods*, Oxford: Oxford University Press, pp. 245–285.
- Collewijn, H., A. J. Martins, and R. M. Steinman, 1983. Compensatory eye movements during active and passive head movements: fast adaptation to changes in visual magnification, *J. Physiol. (Lond.)*, 340:259–286.
- Cornsweet, T. N., 1956. Determination of the stimuli for involuntary drifts and saccadic eye movements, *J. Opt. Soc. Am.*, 46:987–993.
- Delabarre, E. B., 1898. A method for recording eye-movements, *Am. J. Psychol.*, 9:572–574.
- Ditchburn, R. W., 1955. Eye movements in relation to retinal action, *Opt. Acta*, 1:171–176.
- Ditchburn, R. W., 1980. The function of small saccades, *Vis. Res.*, 20:271–272.
- Dodge, R., 1903. Five types of eye movement in the horizontal meridian plane of the field of regard, *Am. J. Physiol.*, 8:307–327.
- Dodge, R., 1907. An experimental study of visual fixation. *The Psychological Review Monograph Supplements No. 35*, Lancaster, PA: Review.
- Dodge, R., and T. S. Cline, 1901. The angle velocity of eye movements, *Psychol. Rev.*, 8:145–157.
- Epelboim, J., 1998. Gaze and retinal-image-stability in two kinds of sequential looking tasks, *Vis. Res.*, 38:3773–3784.
- Epelboim, J., R. M. Steinman, E. Kowler, Z. Pizlo, C. J. Erkelens, and H. Collewijn, 1995. The function of visual search and memory in two kinds of sequential looking tasks, *Vis. Res.*, 37:2597–2607.
- Epelboim, J., R. M. Steinman, E. Kowler, Z. Pizlo, C. J. Erkelens, and H. Collewijn, 1997. Gaze-shift dynamics in two kinds of sequential looking tasks, *Vis. Res.*, 37:2597–2607.
- Erkelens, C., C. Steinman, and H. Collewijn, 1989a. Ocular vergence under natural conditions. II. Gaze-shifts between real targets differing in distance and direction, *Proc. R. Soc. Lond. B*, 236:441–465.
- Erkelens, C., J. Van der Steen, R. M. Steinman, and H. Collewijn, 1989b. Ocular vergence under natural conditions. I. Continuous changes of target distance along the median plane, *Proc. R. Soc. Lond. B*, 236:417–440.
- Haddad, G. M., and R. M. Steinman, 1973. The smallest voluntary saccade: implications for fixation, *Vis. Res.*, 13:1075–1086.
- Hallett, P. E., 1986. Eye movements, in *Handbook of Perception and Human Performance*, vol. I. (K. R. Boff, L. Kaufman, and J. P. Thomas, eds.), New York: Wiley, Section II, pp. 10–1–10–112.
- Herst, A. N., J. Epelboim, and R. M. Steinman, 2001. Temporal coordination of the human head and eye during a natural sequential tapping task, *Vis. Res.*, 41:3307–3319.
- Huey, E. B., 1900. On the psychology and physiology of reading, *Am. J. Psychol.*, 3:283–302.
- Javal, E., 1878. Essai sur la physiologie de la lecture, *Ann. Oculist*, 79:97–117, 240–274; 80:135–147.
- Johansson, R. S., G. Westling, Bäckström, and J. R. Flanagan, 2001. Eye-hand coordination in object manipulation, *J. Neurosci.*, 21:6917–6932.
- Judge, S. J., 1991. Vergence, in *Eye Movements* (R. H. S. Carpenter ed.), London: Macmillan, pp. 157–172.
- Kowler, E., 1990. The role of visual and cognitive processes in the control of eye movement, in *Eye Movements and Their Role in Visual and Cognitive Processes* (E. Kowler ed.), Amsterdam: Elsevier Science, pp. 1–70.
- Kowler, E., 1991. The stability of gaze and its implications for vision, in *Eye Movements* (R. H. S. Carpenter ed.), London: Macmillan, pp. 71–92.
- Kowler, E., Z. Pizlo, G. L. Zhu, C. Erkelens, R. M. Steinman, and H. Collewijn, 1991. Coordination of head and eyes during the performance of natural (and unnatural) visual tasks, in *The Head-Neck Sensory Motor System* (A. Berthoz, W. Graf, and P. P. Vidal, eds.), New York: Oxford University Press, pp. 419–426.
- Kowler, E., and R. M. Steinman, 1979. Miniature saccades: eye movements that do not count, *Vis. Res.*, 19:105–108.
- Kowler, E., and R. M. Steinman, 1980. Small saccades serve no useful purpose: reply to a letter by R. W. Ditchburn, *Vis. Res.*, 20:273–276.
- Kowler, E., J. Van der Steen, E. P. Tamminga, and H. Collewijn, 1984. Voluntary selection of the target for smooth pursuit in the presence of superimposed, full-field stationary and moving stimuli, *Vis. Res.*, 24:1789–1798.
- Land, M. F., 1992. Predictable eye-head coordination during driving, *Nature*, 359:318–320.
- Land, M. F., and M. Hayhoe, 2001. In what ways do eye movements contribute to everyday activities? *Vis. Res.*, 41:3559–3565.
- Land, M. F., N. Mennie, and J. Rusted, 1999. The roles of vision and eye movements in the control of activities of daily living, *Perception*, 28:1311–1328.
- Land, M. F., and B. W. Tatler, 2001. Steering with the head: the visual strategy of a racing driver, *Curr. Biol.*, 11:1215–1220.
- Malinov, I. V., J. Epelboim, A. N. Herst, and R. M. Steinman, 2000. Characteristics of saccades and vergence in two kinds of looking tasks, *Vis. Res.*, 40:2083–2090.
- Martinez-Conde, S., S. Macknik, and D. H. Hubel, 2000. Microsaccadic eye movements and firing of single cells in the striate cortex of macaque monkeys, *Nat. Neurosci.*, 3:251–258.
- Nachmias, J., 1959. Two-dimensional motion of the retinal image during monocular fixation, *J. Opt. Soc. Am.*, 49:901–908.
- Oyster, C. W., 1999. *The Human Eye: Structure and Function*, Sunderland, MA: Sinauer.
- Ratcliff, F., and L. A. Riggs, 1950. Involuntary motions of the eye during monocular fixation, *J. Exp. Psychol.*, 40:687–701.
- Riggs, L. A., F. Ratcliff, J. C. Cornsweat, and T. N. Cornsweat, 1953. The disappearance of steadily-fixated test objects, *J. Opt. Soc. Am.*, 43:495–501.

- Robinson, D. A., 1968. Eye movement control in primates, *Science*, 161:1219–1224.
- Robinson, D. R., 1963. A method of measuring eye movements using a search coil in a magnetic field, *IEEE Trans. Bio-Med. Electron.*, 10:137–145.
- Rochon-Duvigneaud, A., 1943. *Les yeux et al vision des vertèbres*, Paris: Masson.
- Rucci, M., G. M. Edelman, and J. Wray, 2000. Modeling LGN responses during free-viewing: a possible role of microscopic eye movements in the refinement of cortical orientation selectivity, *J. Neurosci.*, 20:4708–4720.
- Sekuler, R., and R. Blake, 2002. *Perception*, 4th ed., New York: McGraw-Hill.
- Skavenski, A. A., R. M. Hansen, R. M. Steinman, and B. J. Winterson, 1979. Quality of retinal image stabilization during small natural and artificial rotations in man, *Vis. Res.*, 19:678–683.
- Skavenski, A. A., D. A. Robinson, R. M. Steinman, and G. T. Timberlake, 1975. Miniature eye movements in rhesus monkey, *Vis. Res.*, 15:1269–1273.
- Smeets, J. B. J., M. M. Hayhoe, and D. H. Ballard, 1996. Goal-directed arm movements change head-eye coordination, *Exp. Brain Res.*, 109:434–440.
- Steinman, R. M., 1986. Eye movement, *Vis. Res.*, 26:1389–1400.
- Steinman, R. M., 1995. *Moveo ergo video*: Natural retinal image motion and its effect on vision, in *Exploratory Vision: The Active Eye* (M. S. Landy, L. T. Maloney, and M. Pavel, eds.), New York: Springer-Verlag, pp. 3–50.
- Steinman, R. M., and H. Collewyn, 1980. Binocular retinal image motion during active head rotation, *Vis. Res.*, 20:415–429.
- Steinman, R. M., and R. J. Cunitz, 1968. Fixation of targets near the absolute foveal threshold, *Vis. Res.*, 8:277–286.
- Steinman, R. M., R. J. Cunitz, G. T. Timberlake, and M. Herman, 1967. Voluntary control of microsaccades during maintained monocular fixation, *Science*, 15:1577–1579.
- Steinman, R. M., G. M. Haddad, A. A. Skavenski, and D. Wyman, 1973. Miniature eye movement, *Science*, 181:810–819.
- Steinman, R. M., E. Kowler, and H. Collewyn, 1990. New directions for oculomotor research, *Vis. Res.*, 30:845–1864.
- Steinman, R. M., and J. Z. Levinson, 1990. The role of eye movement in the detection of contrast and spatial detail, in *Eye Movements and Their Role in Visual and Cognitive Processes* (E. Kowler ed.), Amsterdam: Elsevier Science, pp. 115–212.
- Steinman, R. M., J. Z. Levinson, H. Collewyn, and J. van der Steen, 1985. Vision in the presence of known natural retinal image motion, *J. Opt. Soc. Am. A*, 2: 226–233.
- Steinman, R. M., A. A. Skavenski, and R. V. Sansbury, 1969. Voluntary control of smooth pursuit velocity, *Vis. Res.*, 9:1167–1171.
- Zuber, B. L., L. Stark, and G. Cook, 1965. Microsaccades and the velocity-amplitude relationship for saccadic eye movements, *Science*, 150:1459–1460.

91 Eye Movements in Daily Life

MICHAEL F. LAND

EYE MOVEMENT RESEARCH over the past 100 years has had two rather different goals. On the one hand, physiologists have directed their efforts at describing accurately the different types of eye movements—saccades, smooth pursuit, and so on, analyzing their mechanics and muscular physiology and searching for the neural machinery in the brain that generates them. On the other hand, many psychologists have been more concerned with the functions of eye movements, in particular with their roles in the execution of everyday activities (reading, driving, playing ball games, etc.). The main difference between the two traditions is that for the former, it is single eye movements that are the focus of interest, while for the latter, it is the sequences of eye movements, and more particularly the patterns of fixation that the eye movements produce, that are important. It is these sequences, and their relations to the actions they facilitate, that are the subject of this chapter.

While we are dimly aware that we look in the direction of the places where our actions are unfolding, we can get little further than this by introspection alone. What is required is a combination of objective eye movement recording synchronized to recordings of the actions to which the eye movements relate. Most of the studies reviewed here are of this type. The chapter is divided into two parts. The first part provides outline accounts of studies of real-life tasks. Drawing on these examples, the second part considers the nature of the eye movement strategies that accompany actions and other issues that relate to the joint control of eyes and motor behavior.

Part 1: The relations of eye movements to action in different activities

Activities involving the uptake of visual information can be divided into those that are basically sedentary—reading or typing, for example—and those such as carpentry or ball sports that involve more extensive movement. The former have been studied since eye movement recordings began (e.g., Dodge, 1900), but the latter have been open to investigation only since about 1960, when portable recording devices started to become available.

SEDENTARY ACTIVITIES: READING, MUSICAL SIGHT-READING, AND TYPING Although silent reading involves no overt action, it nevertheless requires a particular eye movement

strategy to enable the uptake of information in a way that allows meaning to be acquired. It is also one of best-studied (as well as the most atypical) examples of a clearly defined eye movement pattern. Erdman and Dodge (Dodge, 1900) first showed that the subjectively smooth passage of the eye across the page is in reality a series of saccades and fixations in which information is taken in during the fixations. Eye movements in reading are highly constrained to a linear progression of fixations to the right (in English) across the page, which allows the words to be read in an interpretable order. In this, reading differs from many other activities (such as viewing pictures), where order is much less important (Buswell, 1935). Reading is a learned skill, but the eye movements that go with it are not taught. Nevertheless, they are remarkably similar among normal readers. Eye movements during reading have been reviewed thoroughly recently, and only the principal facts need to be included here. Most of what follows is derived from an extensive review by Rayner (1998).

During normal reading, gaze (foveal direction) moves across the line of print in a series of saccades, whose size is typically seven to nine letters. Within limits this number is not affected by the print size, implying that the oculomotor system is able to make scaling adjustments to its performance. For normal print the saccade size is 1 to 2 degrees, and the durations of the fixations between saccades have a mean of 225 msec. In reading aloud, fixations are longer (mean, 275 msec). Most saccades (in English) are to the right, but 10% to 15% are regressions (right to left) and are associated in a poorly understood way with problems in processing the currently or previously fixated word. Words can be identified up to 7 to 8 letter spaces to the right of the fixation point, but some information is available up to 14 to 15 letter spaces; this is used in the positioning of subsequent saccade end points. From studies in which words were masked during fixations, it appears that the visual information needed for reading is taken in during the first 50 to 70 msec of each fixation. Adult readers typically read at a rate of about 300 words per minute or 0.2 second per word.

If changes are made to the text during the course of a fixation, both the duration of the current fixation and the size of the following saccade can be affected. This implies that the text is processed “on-line” on a fixation-by-fixation basis. Similarly, difficult words result in longer fixations, indicating that cognitive processes operate within single fixations. How

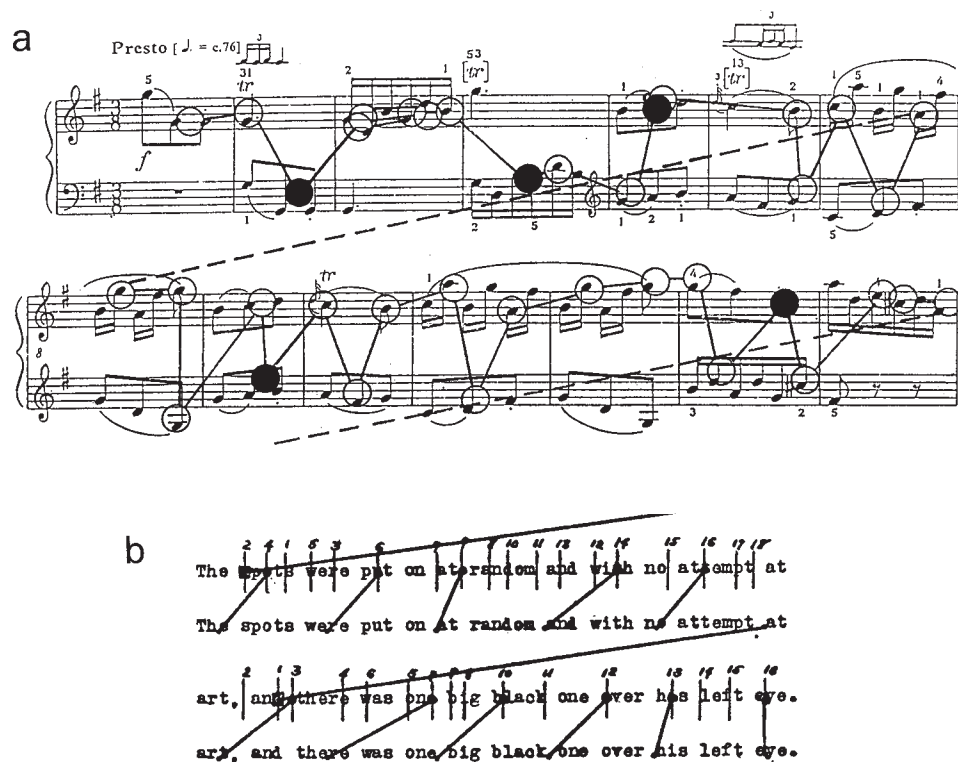


FIGURE 91.1. *a*, Fixations made by an expert accompanist while sight reading a passage from a sonata by Domenico Scarlatti at full speed. The shaded circles are fixations followed by glances down to the keyboard. Note that these have no detectable effect on the fixation sequence. *b*, Fixations during copy typing. The upper line of each pair shows the text being read, with fixations numbered in

order. The lower line shows the text as typed, and the diagonal lines show the letters being typed at the time of the indicated fixations on the upper row. The eye-hand span for this fast typist is about five letter spaces. (*a* from Land and Furneaux, 1997; *b* from Butsch, 1932.)

long it takes to process words all the way from vision to meaning is hard to assess, but in reading aloud, the time between fixating a word and speaking it (the eye-voice span) is about 1 second (Buswell, 1920).

Musical sight reading shares with text reading the constraint that gaze must move progressively to the right. It is, however, more complicated in that—for keyboard players—there are two staves from which notes must be acquired (Fig. 91.1*A*). Weaver (1943) recorded eye movements of trained pianists and found that they alternated fixation between the upper and lower staves, acquiring notes from the score at a rate of approximately 1.5 notes per fixation (making a note roughly equivalent to a word in text reading). This alternation means that notes that have to be played together are viewed at different times, adding the task of temporal assembly to the other cognitive tasks of interpreting the pitch and length of the notes. The time from reading a note to playing it (the eye-hand span) is similar to reading aloud: about 1 second. Furneaux and Land (1999) looked at the eye-hand span in pianists of differing abilities. They found that it did not vary with skill level when measured as a time interval, but that when measured in terms of the number of notes contained in that interval, professionals

averaged four compared with two for novices. Thus, the processing time is the same for everyone, but the throughput rate of the processor is skill dependent. The processing time did alter with tempo, however, with fast pieces having an eye-hand span of 0.7 second, increasing to 1.3 seconds for slow pieces.

Copy typing, like music playing, has a motor output, and according to Butsch (1932), typists of all skill levels attempt to keep the eyes 1 second ahead of the currently typed letter, which is much the same as in music reading. This represents about five characters (Fig. 91.1*B*). More recently, Inhoff and colleagues (Inhoff and Wang, 1992) found more variability in the eye-hand span and also showed that it was affected by the nature of the text. Using a moving window technique, they showed that typing starts to become slower when there are fewer than three letter spaces to the right of fixation, indicating a perceptual span about half the size of that used in normal reading. The potential word buffer is much bigger than this, however. Fleischer (1986) found that when typists use a read/check cycle of approximately 1 second each while typing continuously, they typically take in 11 characters during the read part of the cycle, and, exceptionally, strings of up to 30 characters can be stored.

These activities are all similar in that they involve the continuous processing of a stream of visual information taken in as a series of stationary fixations. This information is translated and converted to a stream of muscular activity of various kinds (or into meaning in the case of silent reading). In each case, the time within the processor is about 1 second. Once the appropriate action has been performed the original visual information is lost, so the process is more like a production line than a conventional memory system.

ACTIVITIES INVOLVING MOVEMENT The study of the gaze movements of head-free, fully mobile subjects required the development of eye trackers that were head- rather than bench-mounted. The first truly mobile apparatus for freely moving subjects was devised by Mackworth and Thomas (1962). It consisted of a helmet-mounted 8mm movie camera which viewed the scene ahead. Superimposed on this was a spot derived from the corneal reflex of one eye and conveyed to the camera by an inverted periscope arrangement. This device was successfully used to study eye movements in driving and flying, as well as during more stationary activities (Thomas, 1968). A decade later, small video cameras started to become available, making the recording process much simpler, and a number of video-based eye-movement cameras are currently available commercially. They typically consist of two cameras, one viewing the scene ahead and one viewing the eye. Commonly, the eye is illuminated with infrared light, which provides the eye camera with a “bright pupil” from infrared light reflected from the retina. This is tracked with appropriate software to provide the coordinates of eye direction, which can then be used to position a spot or a cross on the scene video, indicating the instantaneous direction of regard of the fovea. A variant of this design uses the outline of the iris to derive eye direction (Land, 1993). Such devices can be used for virtually any activity. Search-coil methods have also been used successfully to record gaze direction or eye and head direction separately (Collewijn, 1977). Their main limitation is that they can only be used within the magnetic field of the surrounding coils, which means that their versatility is not much greater than that of fixed-head methods.

EYE MOVEMENTS AND ACTIONS IN DOMESTIC TASKS Activities such as food preparation, carpentry, or gardening typically involve a series of different actions, rather loosely strung together by a “script.” They provide examples of the use of tools and utensils, and it is of obvious interest to find out how the eyes assist in the performance of these tasks.

Land et al. (1999) studied the eye movements of subjects while they made cups of tea. When tea is made with a teapot, this simple task involves about 45 separate acts (defined as “simple actions that transform the state or place of an entity through manual manipulation”; Schwartz et al.,

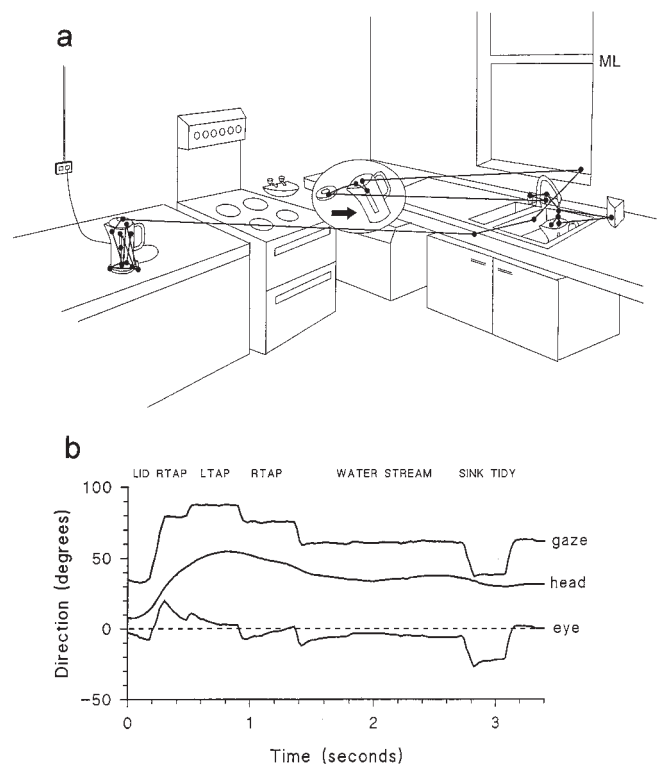


FIGURE 91.2. *a*, Fixations and saccades made during the first 10 seconds of the task of making a cup of tea (lifting the kettle and starting to fill it). Note that all but one of the fixations are on objects immediately relevant to the task. *b*, Plot of eye, head, and gaze movements toward the end of the task in *a*, showing the steady gaze fixations resulting from eye saccades and compensation for head movement by the vestibulo-ocular reflex. (From Land et al., 1999.)

1991). Figure 91.2 shows the 26 fixations made during the first 10 seconds of the task. The subject first examines the kettle (11 fixations), picks it up, and looks toward the sink (3 fixations), walks to the sink while removing the lid from the kettle (insert: 4 fixations), places the kettle in the sink and turns on the tap (3 fixations), then watches the water as it fills the kettle (4 fixations). There is only one fixation that is not directly relevant to the task (to the sink tidy on the right). Two other subjects showed remarkably similar numbers of fixations when performing the same sequence. The principal conclusions from this sequence are:

1. Saccades are made almost exclusively to objects involved in the task, even though there are plenty of other objects around to grab the eye.
2. The eyes deal with one object at a time. This corresponds roughly to the duration of the manipulation of that object and may involve a number of fixations on different parts of the object.

There is usually a clear “defining moment” when the eyes leave one object and move on to the next, typically with a combined head and eye saccade. These saccades can be used

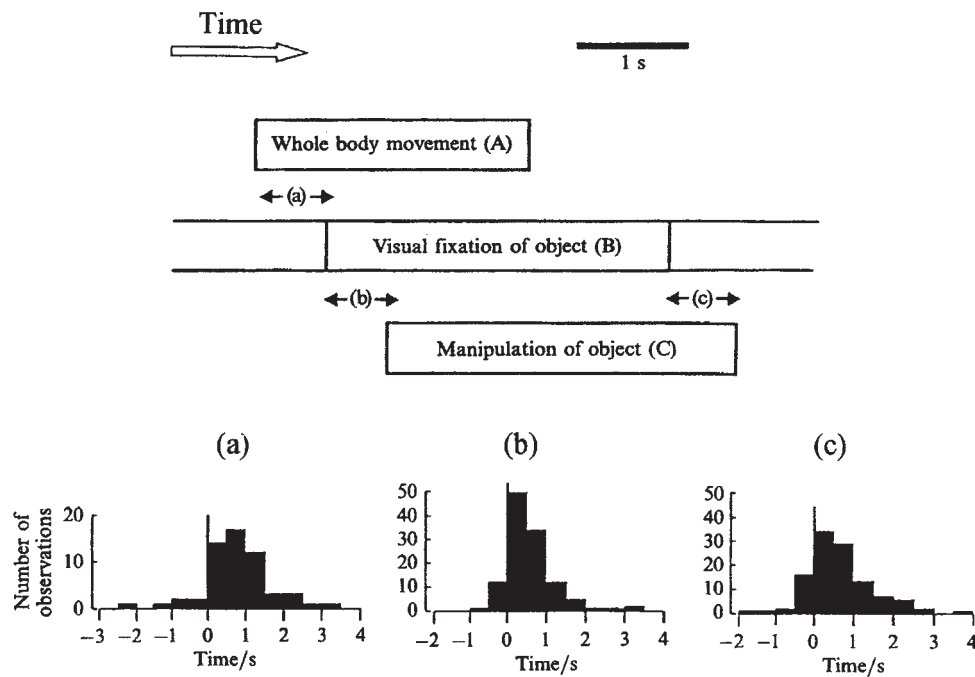


FIGURE 91.3. Timing of the relations of body, eye, and hand movements averaged from a total of 137 object-related actions during tea-making sessions by three different individuals. Movements of the whole body precede the first fixation by a mean of

0.61 second (a), and these precede the first signs of manipulation by 0.56 second (b). As each action draws to a close, fixation moves to the next object an average of 0.61 second before the end of the preceding action (c). (From Land and Hayhoe, 2001.)

to “chunk” the task as a whole into separate object-related actions, and they can act as time markers to relate the eye movements to movements of the body and manipulations by the hands. In this way, the different acts in the task can be pooled to get an idea of the sequence of events in a typical act. The results of this are shown in Figure 91.3. Perhaps surprisingly, it is the body as a whole that makes the first movement in an object-related action. Often the next object in the sequence is on a different work surface, and this may necessitate a turn or a few steps before it can be viewed and manipulated. About 0.5 second later, the first saccade is made to the object, and 0.5 second later still, the first indications of manipulation occur. The eyes thus lead the hands. Interestingly, at the end of each action, the eyes move on to the next object about 0.5 second before manipulation is complete. Presumably the information that they have supplied remains in a buffer until the motor system requires it.

Almost identical results were obtained by Hayhoe (2000) in a study of students making peanut butter and jelly sandwiches. She found the same attachment of gaze to task-related objects and the same absence of saccades to irrelevant objects. As with the tea making, gaze led manipulation, although with a somewhat shorter interval. This difference is probably attributable to the fact that the sandwich making was a sit-down task involving only movements of the arms. Two other differences that may have the same cause are the existence of more short-duration (<120 msec)

fixations than in the tea-making study and the presence of more unguided reaching movements (13%) mostly concerned with the setting down of objects. There was a clear distinction in both studies between within-object saccades, which had mean amplitudes of about 8 degrees in both, and between-object saccades, which were much larger, up to 30 degrees in sandwich making on a restricted table top and 90 degrees in tea making in the less restricted kitchen (Land and Hayhoe, 2001).

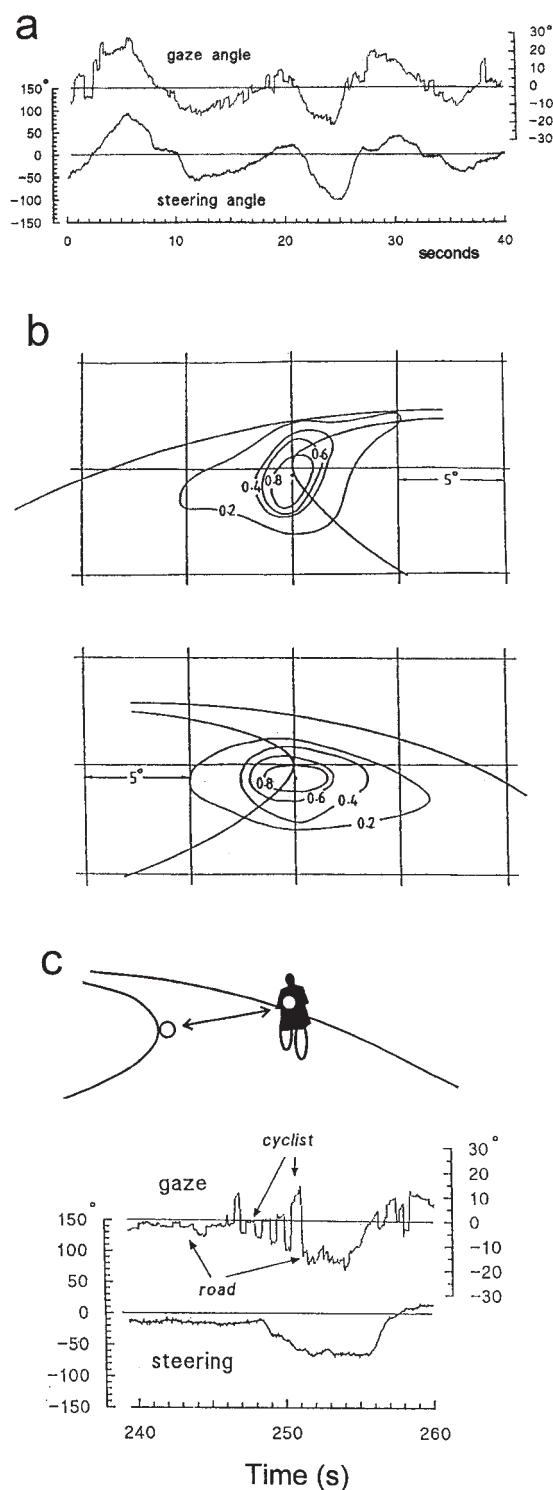
DRIVING Driving is a complex skill that involves dealing with the road itself (steering, speed control), other road users (vehicles, cyclists, moving and stationary pedestrians), and attention to road signs and other relevant sources of information. It is thus a multifaceted task, and one would expect a range of eye movement strategies to be employed. I will first consider steering, as this is a prerequisite for all other aspects of driving.

When steering a car on a winding road, vision has to supply the arms and hands with the information they need to turn the steering wheel the right amount. What is this control signal, and how is it obtained? As pointed out by Donges as early as 1978, there are basically two sorts of signal available to drivers: feedback signals (lateral and angular deviation from the road centerline, differences between the road’s curvature and the vehicle’s path curvature) and feedforward or anticipatory signals obtained

from more distant regions of the road up to 2 seconds ahead in time (corresponding to 90ft or 27m at 30mph). Donges (1978) used a driving simulator to demonstrate that each of these signals was indeed used in steering, although he did not discuss how they might be obtained visually.

Eye movement studies both on real roads (Land and Lee, 1994) and on a simulator (Land and Horwood, 1995) have confirmed Donges' two-level model of driving and have gone some way toward establishing how the eyes find the appropriate information. Earlier studies, mainly on U.S. roads that had predominantly low curvatures, had found only a weak relationship between gaze direction and steering (e.g., Zwahlen, 1993). However, on a winding road in Scotland, where continuous visual control was essential, a much more precise relationship was seen. Land and Lee (1994) found that drivers spent much of their time looking at the tangent point on the upcoming bend (Fig. 91.4*B*). This is the moving point on the inside of the bend where the driver's line of sight is tangential to the road edge; it is the point that protrudes into the road, and it is the only point in the flow field that is clearly defined visually. The angular location of this point relative to the vehicle's line of travel (effectively the driver's trunk axis if he or she is belted in) predicts the curvature of the bend: larger angles indicate steeper curvatures. Potentially, this angle is a signal that can provide the feedforward information required by Donges' analysis, and Figure 91.4*A* does indeed show that curves of gaze direction and steering wheel angle are almost identical. The implication is that this angle, which is equal to the eye-in-head plus the head-in-body angle when the driver is looking at the tangent point, is translated more or less directly into the motor control signal for the arms. Cross-correlating the two curves in Figure 91.4*A* shows that gaze direction precedes steering wheel angle by about 0.8 second. This provides the driver with a reasonable comfort margin, but the delay is also necessary to prevent steering from taking place before the bend has been reached.

FIGURE 91.4. Eye movements and steering. *a*, Simultaneous record of gaze direction and steering wheel angle during part of a drive on a winding road in Scotland. Note the extreme similarity of the two records. Cross-correlation shows that eye direction precedes steering by about 0.8 second. Brief glances off-road also occur. *b*, Contour plots showing the distribution of fixations by three drivers during right and left bends on a 1 km stretch of the same winding road as in *a*. Both are centred within 1 degree of the respective tangent points. Plots are normalized to the central value, which is approximately 0.12 fixations per $\text{deg}^2\text{s}^{-1}$. About 35% of fixations lie outside the 0.2 contour, and these are widely scattered. *c*, Time sharing between tasks. The driver's gaze alternates between the tangent point and the cyclist, spending approximately 0.5 second on each. Steering is linked to the road edge and suspended when looking at the cyclist. (From Land, 1998.)



Simulator studies showed that feedforward information from the distant part of the road was not sufficient on its own to provide good steering (Land and Horwood, 1995). When the near region of the simulated road was removed from view, curvature matching was still accurate, but position-in-lane control was very poor. To maintain good lane position required a view of the road only a few meters ahead, and this region provided much of the feedback information identified in the Donges model. Interestingly, this part of the road was rarely fixated compared with the more distant tangent point region, but it was certainly seen and used; it is typically about 5 degrees obliquely below the tangent point. Maurant and Rockwell (1970) had already concluded that lane position is monitored with peripheral vision. They also argued that learner drivers first use foveal vision for lane keeping, then increasingly move foveal gaze to more distant road regions and learn to use their peripheral vision to stay in the lane. Summala et al. (1996) reached similar conclusions. The principal conclusion from these studies is that neither the far-road feedforward input nor the near-road feedback input is sufficient on its own, but that the combination of the two allows fast, accurate driving (Land, 1998).

A feature of Figure 91.4A and similar records is that the eyes are not glued to the tangent point, but take time out to look at other things. These excursions are accomplished by gaze saccades and typically last between 0.5 and 1 second. The probability of these off-road glances occurring varies with the stage of the bend that the vehicle has reached, and they are least likely to occur around the time of entry into a new bend. At this point, drivers fixate the tangent point 80% of the time. It seems that special attention is required at this time, presumably to get the initial estimate of the bend's curvature correct. A confirmation of this came from Yilmaz and Nakayama (1995), who used reaction times to a vocal probe to show that attention was diverted to the road just before simulated bends and that sharper curves demanded more attention than shallower ones. The fewer and shallower the bends in the road, the more time can be spent looking off the road, and this probably accounts for the lack of a close relation between gaze direction and steering on studies of driving on freeways and other major roads.

Sometimes the eye must be used for two different functions at the same time, and as there is only one fovea and off-axis vision is poor, the visual system has to resort to time sharing. A good example of this is shown in Figure 91.4C, where the driver is negotiating a bend and so needs to look at the tangent point while passing a cyclist who needs to be checked on repeatedly. The record shows that the driver alternates gaze between the tangent point and cyclist several times, spending 0.5 second on each. The lower record shows that he or she steers by the road edge, which means that the coupling between eye and hand has to be turned off when

the driver views the cyclist (who would otherwise be run over!). Thus, not only does gaze switch between tasks, so does the whole visuomotor control system. Presumably, while looking at the cyclist, the information from the tangent point is kept "on hold" at its previous value.

This example has shown how the visual system is able to divide its time between different activities. In urban driving this is even more important, as each traffic situation and road sign competes for attention. To my knowledge, there has been no systematic study of where drivers look in traffic, but from our own observations, it is clear that drivers foveate the places from which they need to obtain information: the car in front, the outer edges of obstacles, pedestrians and cyclists, road signs and traffic lights, and so on. In general, speeds of 30 mph or less require only peripheral lane-edge (feedback) information for adequate steering. Thus, the necessity to use distant tangent points is greatly reduced, freeing up the eyes for the multiple demands of dealing with other road users. As with open-road steering, both foveal and peripheral vision are involved. Miura (1987) has shown that as the demands of traffic situations increase, peripheral vision is sacrificed to provide greater attentional resources for information uptake by the fovea.

BALL GAMES Some ball sports are so fast that there is barely time for the player to use his normal oculomotor machinery. Within less than 0.5 second (in baseball or cricket), the batter has to judge the trajectory of the ball and formulate a properly aimed and timed stroke. The accuracy required is a few centimeters in space and a few milliseconds in time (Regan, 1992). Half a second gives time for one or at most two saccades, and the speeds involved preclude smooth pursuit for much of the ball's flight. How do practitioners of these sports use their eyes to get the information they need?

Part of the answer is anticipation. Ripoll et al. (1987) found that international table tennis players anticipated the bounce and made a saccade to a point close to the bounce point. Land and Furneaux (1997) confirmed this (with more ordinary players). They found that shortly after the opposing player hit the ball, the receiver made a saccade down to a point a few degrees above the bounce point, anticipating the bounce by about 0.2 second. At other times, the ball was tracked around the table in a normal nonanticipatory way; tracking was almost always by means of saccades rather than smooth pursuit. The reason players anticipate the bounce is that the location and timing of the bounce are crucial in the formulation of the return shot. Until the bounce occurs, the trajectory of the ball as seen by the receiver is ambiguous. Seen monocularly, the same retinal pattern in space and time would arise from a fast ball on a long trajectory or a slow ball on a short one (Fig. 91.5A). (Whether either stereopsis or looming information is fast enough to provide a useful depth signal is still a matter of debate.) This ambiguity is

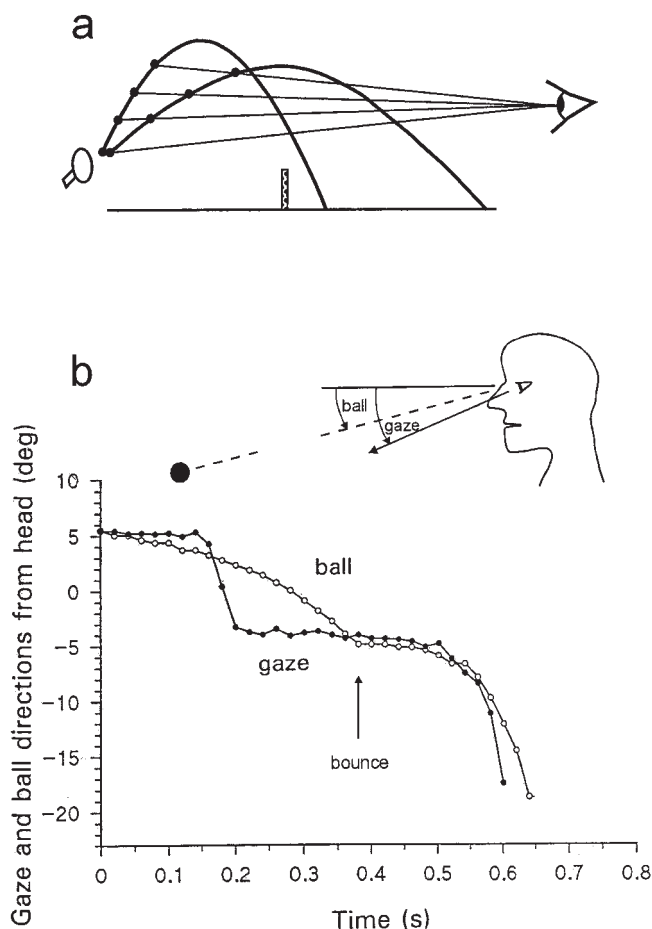


FIGURE 91.5. Anticipating the bounce in ball games. *a*, To the receiver of a table tennis stroke, there is little difference in the seen trajectory of a slow short ball and a faster long ball (ignoring stereopsis and looming). The position of the bounce is needed to disambiguate the real trajectory. *b*, Vertical gaze movements of a batsman in cricket facing a medium-pace ball from a bowling machine. He makes a downward saccade to the approximate bounce point about 140msec after the appearance of the ball, anticipating the bounce by almost 180msec in this case. He then tracks the ball for another 200msec. (From Land and McLeod, 2000.)

removed the instant the timing and position of the bounce are established. Therefore, the strategy of the player is to get gaze close to the bounce point (this cannot and need not be exact) before the ball does and lie in wait. The saccade that effects this is interesting in that it is not driven by a stimulus, but by the player's estimate of the location of something that has yet to happen.

In cricket, where—unlike baseball—the ball also bounces before reaching the batsman, Land and McLeod (2000) found much the same thing. With fast balls, the batsmen watched the delivery and then made a saccade down to the bounce point, the eye arriving 0.1 second or more before the ball (Fig. 91.5*b*). They showed that with a knowledge of the time and place of the bounce, the batsman had the infor-

mation he needed to judge where and when the ball would reach his bat. Slower balls involved more smooth pursuit. With good batsmen this initial saccade had a latency of only 0.14 second, whereas poor batsmen or nonbatsmen had more typical latencies of 0.2 second or more.

In baseball the ball does not bounce, and so that source of timing information is not available. Bahill and LaRitz (1984) examined the horizontal head and eye movements to batters facing a simulated fastball. Subjects used smooth pursuit involving both head and eye to track the ball to a point about 9ft from them, after which the angular motion of the ball became too fast to track (a professional tracked it to 5.5 ft in front; he had exceptional smooth pursuit capabilities). Sometimes batters watched the ball contact the bat by making an anticipatory saccade to the estimated contact point partway through the ball's flight. This may have little immediate value in directing the bat, because the stroke is committed as much as 0.2 second before contact (McLeod, 1987), but it may be useful in learning to predict the ball's location when it reaches the bat, especially as the ball often "breaks" (changes trajectory) shortly before reaching the batter. According to Bahill and LaRitz (1984), "The success of good players is due to faster smooth-pursuit eye movements, a good ability to suppress the vestibulo-ocular reflex, and the occasional use of an anticipatory saccade."

Part 2: issues and discussion

It is clear from the examples given in Part 1 that eye movements play a crucial role in the organization of actions, and that in general, the eyes begin to collect information before the action itself has begun (Fig. 91.3). Eye movements are thus a planned-in, proactive part of every action sequence and are not simply summoned up when more information is needed. In the discussions that follow, I explore how close are the relations, in space and time, between where we look and what we do, and what is the nature of the control structure that underlies both aspects of visually coordinated activity.

"DO IT WHERE I'M LOOKING" One of the first detailed studies of eye movements in relation to manipulative activity was performed by Ballard et al. (1992). They used a task in which a model consisting of colored blocks had to be copied using blocks from a separate pool. Thus, the task involved a repeated sequence of looking at the model, selecting a block, moving it to the copy, and setting it down in the right place (Fig. 91.6). The most important finding was that the operation proceeds in a series of elementary acts involving eye and hand, with minimal use of memory. Thus, a typical repeat unit would be as follows. Fixate (block in the model area); remember (its color); fixate (a block in the source area of the same color); pickup (fixated block); fixate

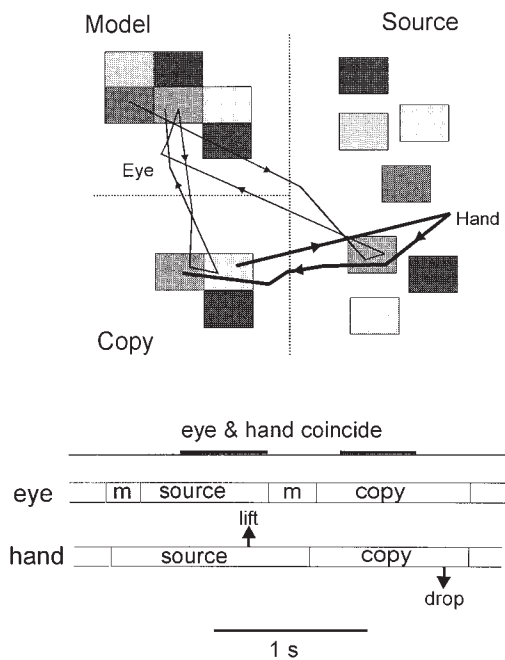


FIGURE 91.6. The block copying task. A copy of the Model is assembled from randomly positioned blocks located in the Source area. Typical movements of eyes and hand are shown, together with their timing in a typical cycle. The eyes not only direct the hands, but also perform checks on the Model to determine the color and location of the block being copied. (Modified from Ballard et al., 1992.)

(same block in the model area); remember (its relative location); fixate (corresponding location in the model area); move block; drop block. The eyes have two quite different functions in this sequence: to guide the hand in lifting and dropping the block and, alternating with this, to gather the information required for copying (the avoidance of memory use is shown by the fact that separate glances are used to determine the color and location of the model block). The only times that gaze and hand coincide are during the periods of about 0.5 second before picking up and setting down the block (as with other tasks, the eyes have usually moved on before the pickup or drop is complete).

The main conclusion from this study is that the eyes look directly at the objects they are engaged with, which in a task of this complexity means that a great many eye movements are required. Given the relatively small angular size of the task arena, why do the eyes need to move so much? Could they not direct activity from a single central location? Ballard et al. (1992) found that subjects could complete the task successfully when holding their gaze on a central fixation spot, but it took three times as long as when normal eye movements were permitted. For whatever reasons, the “do it where I’m looking” strategy is crucial for the fast and economical execution of the task. This strategy seems to apply universally.

HOW CLOSELY, IN SPATIAL TERMS, ARE EYE MOVEMENTS RELATED TO ACTIONS? In all the studies described in Part 1, the eyes look at points that are particularly informative for the ongoing action: in food preparation, it is the object being manipulated at the time; in steering, it is the tangent point; in ball games, the bounce point; and so on. How accurately these points are targeted by gaze depends on the spatial scale of the task. Thus, in reading, each fixation takes in about seven letter spaces, which with standard print at 40 cm means that saccades are about 1.33 degrees long, and so the maximum angular distance from any one detected letter is half this amount, 0.67 degree. At the other extreme, the average size of within-object saccades in both tea making and sandwich making was about 8 degrees, implying a maximum eccentricity of a viewed target of 4 degrees (Land and Hayhoe, 2001), which is six times greater than in reading. The difference is presumably due to the large size of culinary objects compared with letters.

Most other estimates are between these extreme values. For example, Johansson et al. (2001) used a high-precision eye tracker to study performance in a task in which a bar was grasped and lifted to make contact with a target switch, avoiding a projecting obstacle on the way (Fig. 91.7). They found that—as in other tasks—the eyes always fixated certain distinct landmarks (the grasp site, the target, and the surface to which the bar returned) and frequently but not always fixated the obstacle and the tip of the bar. They estimated the precision of fixation by determining the sizes of circles that enclosed 90% of the fixation points for all nine subjects: these were 3.3 degrees for the tip of the bar and 5.6 degrees for the obstacle. For the target itself, most fixations were within a 3 degree circle, and they regarded 3 degrees as the diameter of the “functional fovea” for this task. This implies a maximum target eccentricity of 1.5 degrees. (See also Chapter 90.)

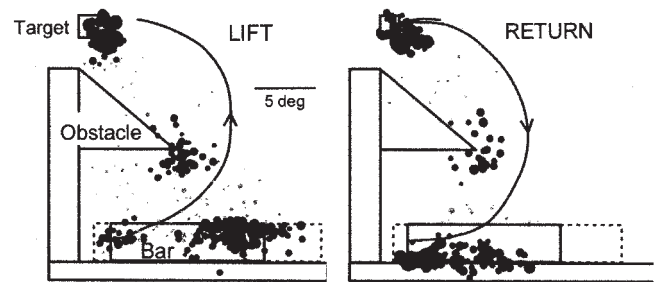


FIGURE 91.7. Accuracy of fixation during a task in which a bar is lifted past an obstacle to make contact with a target and then set it down again. All fixations of nine subjects. Five landmarks are consistently viewed: on the LIFT the grasp site, left tip of the bar, target, and tip of the obstacle. On the RETURN the support surface is viewed rather than the grasp site. Black circles are fixations within 3 degrees of one of these landmarks (more than 90%), and gray circles are fixations outside these regions. Areas of circles indicate fixation durations. (Modified from Johansson et al., 2001.)

How far from the fovea can useful information be obtained? Again, this is likely to depend on the scale of the task. Shioiri and Ikeda (1989) studied the extraction of information from pictures, using a window which was contingent on eye position. They found that the maximum area over which high-resolution pictorial information could be extracted was about 10 degrees across: larger windows provided no extra information. This implies that no further “useful resolution” is available outside about 5 degrees from the fixation point. However, this cannot be universally true. Land et al. (1999) found that subjects could make accurate single eye-and-head saccades to appropriate objects that were up to 50 degrees from the current fixation point. Clearly, some information that permitted object identification was available even in the far periphery.

TIMING AND THE ROLE OF BUFFERS In continuous activities such as reading aloud, sight-reading music, and copy typing, we have seen that there is an eye-action delay of about 1 second. Much of this is no doubt the time needed for the complex transformations that convert written symbols into the actions of muscles. In steering a car, there is also a delay of slightly less than 1 second between viewing the tangent point position and adjusting the steering. Besides allowing processing to occur, a second function of the buffer—at least in driving—is that it makes it possible for information for one action to be “put on hold” while the eye deals with something else. A particularly clear instance of this is the behavior of the motorist to the cyclist in Figure 91.4C.

In “one-off” actions such as those involved in food preparation, there is also evidence of a buffer in which information for action is stored. Figure 91.3 shows that at the beginning of a typical tea-making action, the eyes lead manipulative action by about 0.5 second, and at the end they move on to the next object about 0.5 second before the present action is complete. In that 0.5 second, the final manipulative acts must be guided by information held in a store. It seems likely that throughout each object-related action, visual information passes through a 0.5 second buffer, much as in the continuous actions just discussed.

INTRINSIC SALIENCE AND TOP-DOWN CONTROL In both tea making and sandwich making (Land and Hayhoe, 2001), we were particularly impressed by the way gaze moved from one task-relevant object to the next, ignoring all other objects that were not involved in the activity. The proportion of task-irrelevant objects viewed (other than during periods of waiting—for the kettle to boil, for example) was under 5% in both studies (see Fig. 91.2). The conclusion must be that, in real tasks, the eyes are driven much more by top-down information from the script of the activity than by the “intrinsic salience” of objects in the scene. In one sandwich-making experiment involving four subjects, 50% of the

objects on the table were irrelevant to the task (pliers, scotch tape, forks, etc.). In the interval before the task commenced, while the eyes were scanning the table, the proportion of irrelevant objects fixated was 52%. When the task started, this was reduced to 18%. Presumably this represented a shift from target selection based on intrinsic salience to one based on task instructions. Shinoda et al. (2001) reached similar conclusions with a driving task that required the detection of stop signs; they found that detection was heavily affected by both task instructions and the local context (they are rarely detected midblock, compared with at intersections).

Most recent ideas on the generation of saccades to new targets involve a *salience map*. This is a two-dimensional surface, tentatively located in the superior colliculus, in which peaks of excitation correspond to objects in the image. These peaks compete with each other in a winner-take-all manner to reach a threshold that triggers a saccade. Some versions of this salience map concentrate exclusively on bottom-up properties of the image, such as orientation, intensity, and color (e.g., Itti and Koch, 2000), while others allow a degree of top-down control to influence the state of the map (Findlay and Walker, 1999). The studies reported here emphasize this top-down influence, since it is clear that eye movements are very closely coupled to the script of the action as a whole. As Johansson et al. (2001) put it: “The salience of gaze targets arises from the functional sensorimotor requirements of the task.” (The only problem here is that the word *salience* loses its original meaning of conspicuity, and its definition becomes almost circular—an object is salient if it gets looked at, for whatever reason.)

It is not really a surprise to find a strong top-down influence on eye movements in real tasks. In Yarbus’ famous recording of eye movements when viewing a picture (“An Unexpected Visitor,” Fig. 91.8) in which observers were asked different questions about the picture, the influence of the instructions in determining the pattern of eye movements was striking (Yarbus, 1967). In real tasks, the instructions come not from the experimenter, but from the learned internal script for the activity. However, the effect in either case is that a large measure of control is imposed on the choice of the objects that are fixated.

THE FUNCTIONS OF INDIVIDUAL FIXATIONS To what extent is it possible to attribute particular functions in the execution of a task to individual fixations? In the block copying study of Ballard et al. (1992), shown in Figure 91.6, the logic of the task dictates that the first fixation on the model establishes a color, the fixation on the source locates an appropriately colored block, the next one on the model checks position, and the final fixation on the copy directs the block to the right place. There are some “supernumary” fixations (there are about seven fixations per cycle instead of the

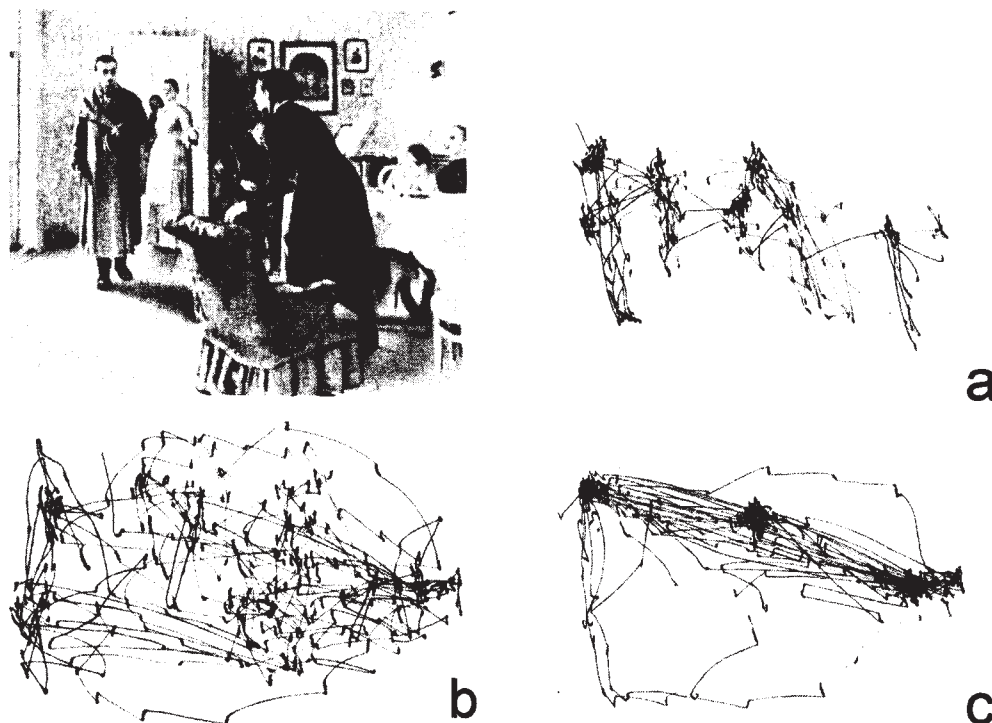


FIGURE 91.8. The painting “An Unexpected Visitor” (by I. E. Repin), with three of Yarbuss’ recordings of the eye movements of an observer looking at the picture with different questions in mind. The instructions were: (a) remember the clothes worn by the

people; (b) remember the positions of the people and objects in the room; (c) estimate how long the “unexpected visitor” had been away from the family. (Modified from Yarbuss, 1967.)

minimum of four required), so not all can have a neatly attributable function.

In tea making, Land et al. (1999) found that about one-third of all fixations could be clearly linked to subsequent actions. The remaining two-thirds were made after an action had been initiated, so that although they may well have had similar functions in guiding action, it was less clear how they were related to changes in motor behavior. [Of interest here was a subject, A.I., who had no eye movements, and who made head saccades instead (Land et al., 2002). These are slow and “expensive,” and in executing the task shown in Figure 91.2, A.I. made only one-third as many of these head saccades as normal subjects made eye saccades. As A.I. executed the task with normal speed and competence, the implication is that the rest of us make more saccadic eye movements than we really need.]

Land et al. (1999) found that the functions of fixations could be classified into just four categories, which were designated as locating, directing, guiding, and checking. *Locating* fixations are concerned with establishing the locations of objects, even though there was no associated motor activity at the time of the fixation. In a hand-washing task Pelz and Canoz (2001) also found a number of look-ahead fixations which anticipated future actions, and these are consistent with this category. *Directing* fixations accompany either a movement of the hand to contact an object (in which case

the object is fixated) or a movement of hand and object to a particular position (when the set-down position is fixated). Typically, only a single fixation is involved, and the eye usually moves away from the object or set-down point just before the hand reaches it. Thus, visual feedback is not involved in the last stage of the act. It seems that the main function of the directing fixation is to provide fovea-centered goal-position information to guide the arm. *Guiding* fixations are concerned with manipulations involving more than one object, for example, a kettle and its lid. Here both objects have to be guided relative to each other so that they dock in an appropriate way. Most tool use is of this nature (e.g., spanner and nut). It is more complicated than simple directing and usually involves a number of fixations that alternate between the two objects, and the action is normally completed under visual control. Some guided actions may involve more than two objects, for example, knife, bread, and butter. *Checking* fixations determine when some condition is met, for example, the kettle is full, the water boils, the top is off the bottle. These checking operations may require the eye to dwell on some appropriate region of an object, either in one long fixation or in a series of repeated fixations. When the specified condition is met, a new action is triggered. For example, when the kettle is full, the tap is turned off.

Interestingly, there are some things that are rarely if ever fixated during sequences of this kind. The hands themselves

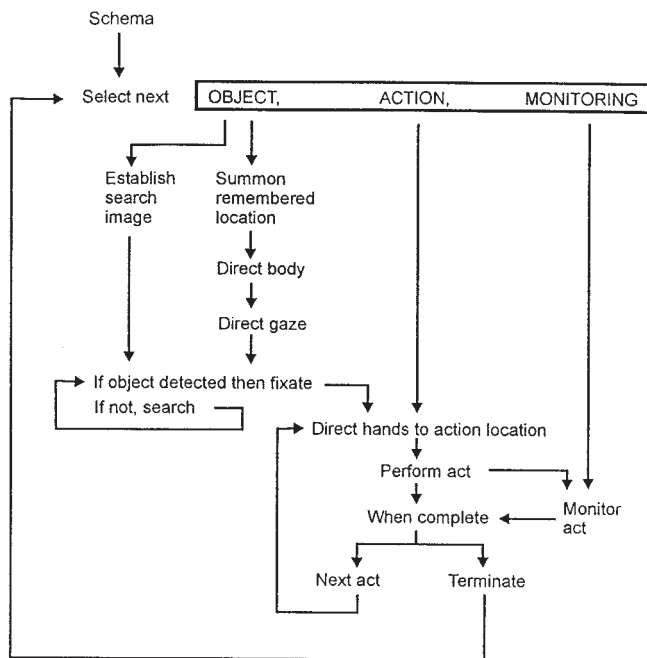


FIGURE 91.9. Scheme showing the flow of information in an object-related action. The eye movement system requires the identity and location of each object in the script or schema so that the eyes can guide the hands appropriately and monitor the results of the actions. Full explanation in text. (From Land and Hayhoe, 2001.)

are never fixated, and once objects have been acquired by the hands, they are not fixated either. The impression is that vision is a scarce and valuable resource, and is disengaged from action as soon as another sense can take over from it.

WHAT THE EYE-MOVEMENT SYSTEM NEEDS TO KNOW In a real-life task, the job of the eye movement system is to place the fovea in a position to obtain the information required for the next component of the activity. To do this, it must itself be supplied with appropriate information about where to look and what to look at.

Figure 91.9 is an attempt to identify the main information pathways during the performance of an object-related action during an action sequence like that of Figure 91.2. The most important function of gaze control is to shift the fovea from one object to the next in the “script” of the task as each action is completed. This means that the system must know which object to select and where it is located. This is far from simple. The object must be recognized somewhere in the visual periphery, which means that an appropriate search image must be activated across large parts of the visual field. Positional information is needed, and this can come from two sources: memory and immediate vision. In many instances, a subject would make an appropriate turn to the location of an object which was out of sight on the other side of the room, and it is a good assumption that the

object’s position was established in an earlier phase of the task in a locating fixation. There were several instances during tea making where an object was fixated 1 minute or more prior to its ultimate use, and when it was time to fetch the object, a memory saccade took gaze to within 20 degrees of it. This was then followed by one or two visually guided saccades finally resulting in fixation (Land et al., 1999). Object acquisition thus involves a complex interplay between object recognition, spatial memory, and vision.

When manipulation begins, the motor system of the arms and hands needs appropriate instructions about the action they must take. Vision may have a simple directing role here, or in the case of guiding, it may have a more active one, with gaze alternating between two objects as they approach each other. In addition, there are checking operations, and the eyes need to know where and what to check. This too must be part of the instructions that the gaze control system receives, presumably at the initiation of each new action.

In Figure 91.9, the script (schema) establishes the next action in the sequence. The gaze control system is supplied with information about the identity and location of the relevant object, and the motor system of the limbs with the manipulations to be performed on it. When the object is located manipulation begins, watched over by the eyes, which have been informed what to check to see that each operation is properly completed. When each sub-act is complete, a further manipulation of the same object may follow (lift milk jug, pour milk into cup, set down jug), or if there are no further sub-acts the action as a whole is terminated, the present set of instructions is abandoned, and those for the next action are sought.

Conclusions

In real-life tasks, the sequences of fixations that the eyes make are very closely bound in space and time to the actions they accompany. Eye movements generally precede manipulations, and they are proactive planned-in components of the action as a whole. There may be a delay of up to 1 second (sometimes longer) before the visual information manifests itself in action, and this implies the existence of a buffer within which transformations occur. Fixation patterns are specific to each activity, with the eyes reliably going to those points in the world from which the best information for that task can be obtained.

REFERENCES

- Bahill, A. T., and T. LaRitz, 1984. Why can’t batters keep their eyes on the ball? *Am. Sci.*, 72:249–253.
- Ballard, D. H., M. M. Hayhoe, F. Li, and S. D. Whitehead, 1992. Hand-eye coordination during sequential tasks, *Philos. Trans. R. Soc. Lond. B*, 337:331–339.

- Buswell, G. T., 1935. *How People Look at Pictures: A Study of the Psychology of Perception in Art*, Chicago: University of Chicago Press.
- Buswell, G. T., 1920. An experimental study of the eye-voice span in reading. *Suppl. Educational Monographs*, no. 17, Chicago: University of Chicago Press.
- Butsch, R. L. C., 1932. Eye movements and the eye-hand span in typewriting, *J. Ed. Psychol.*, 23:104–121.
- Collewijn, H., 1977. Gaze in freely moving subjects, in *The Control of Gaze by Brainstem Neurons* (R. Baker and A. Berthoz, eds.), New York: Elsevier, pp. 13–22.
- Dodge, R., 1900. Visual perception during eye movement, *Psychol. Rev.*, 7:454–465.
- Donges, E., 1978. A two-level model of driver steering behavior, *Hum. Factors*, 20:691–707.
- Findlay, J. M., and R. Walker, 1999. A model of saccade generation based on parallel processing and competitive inhibition, *Behav. Brain Sci.*, 22:661–721.
- Fleischer, A. G., 1986. Control of eye movements by working memory load, *Biol. Cybern.*, 55:227–238.
- Furneaux, S., and M. F. Land, 1999. The effects of skill on the eye-hand span during musical sight-reading, *Proc. R. Soc. Lond. B*, 266:2453–2440.
- Hayhoe, M., 2000. Vision using routines: a functional account of vision, *Vis. Cogn.*, 7:43–64.
- Inhoff, A. W., and J. Wang, 1992. Encoding of text, manual movement planning, and eye-hand coordination during copy-typing, *J. Exp. Psychol.: Hum. Percept. Perform.*, 18:437–448.
- Itti, L., and C. Koch, 2000. A saliency-based search mechanism for overt and covert shifts of visual attention, *Vis. Res.*, 40:1489–1506.
- Johansson, R. S., G. Westling, A. Bäckström, and J. R. Flanagan, 2001. Eye-hand coordination in object manipulation, *J. Neurosci.*, 21:6917–6932.
- Land, M. F., 1993. Eye head co-ordination during driving, *Proc. IEEE Syst. Man Cybern. Conf. Le Touquet.*, 3:490–494.
- Land, M. F., 1998. The visual control of steering, in *Vision and Action* (L. R. Harris and M. Jenkin, eds.), Cambridge: Cambridge University Press, pp. 163–180.
- Land, M. F., and S. Furneaux, 1997. The knowledge base of the oculomotor system, *Philos. Trans. R. Soc. Lond. B*, 352:1231–1239.
- Land, M. F., S. M. Furneaux, and I. G. Gilchrist, 2002. The organization of visually mediated actions in a subject without eye movements, *Neurocase*, 8:80–87.
- Land, M. F., and M. Hayhoe, 2001. In what ways do eye movements contribute to everyday activities? *Vis. Res.*, 41:3559–3565.
- Land, M. F., and J. Horwood, 1995. Which parts of the road guide steering? *Nature*, 377:339–340.
- Land, M. F., and D. N. Lee, 1994. Where we look when we steer, *Nature*, 369:742–744.
- Land, M. F., and P. McLeod, 2000. From eye movements to actions: how batsmen hit the ball, *Nat. Neurosci.*, 3:1340–1345.
- Land, M. F., N. Mennie, and J. Rusted, 1999. The roles of vision and eye movements in the control of activities of daily living, *Perception*, 28:1311–1328.
- Mackworth, N. H., and E. L. Thomas, 1962. Head-mounted eye-movement camera, *J. Opt. Soc. Am.*, 52:713–716.
- McLeod, P., 1987. Visual reaction time and high-speed ball games, *Perception*, 16:49–59.
- Miura, T., 1987. Behavior oriented vision: functional field of view and processing resources, in *Eye Movements: From Physiology to Cognition* (J. K. O'Regan and A. Lévy-Schoen, eds.), Amsterdam: North-Holland, pp. 563–572.
- Mourant, R. R., and T. H. Rockwell, 1970. Mapping eye-movement patterns to the visual scene in driving: an exploratory study, *Hum. Factors*, 12:81–87.
- Pelz, J. B., and R. Canoza, 2001. Oculomotor behavior and perceptual categories in complex tasks, *Vis. Res.*, 41:3587–3596.
- Rayner, K., 1998. Eye movements in reading and information processing: 20 years of research, *Psychol. Bull.*, 124:372–422.
- Regan, D., 1992. Visual judgments and misjudgments in cricket, and the art of flight, *Perception*, 21:91–115.
- Ripoll, H., P. Fleurance, and D. Caseneuve, 1987. Analysis of visual patterns of table tennis players, in *Eye Movements: From Physiology to Cognition* (J. K. O'Regan and A. Lévy-Schoen, eds.), Amsterdam: North-Holland, pp. 616–617.
- Schwartz, M. F., E. S. Reed, M. W. Montgomery, C. Palmer, and N. H. Mayer, 1991. The quantitative description of action disorganisation after brain damage: a case study, *Cogn. Neuropsychol.*, 8:381–414.
- Shinoda, H., M. M. Hayhoe, and A. Shrivastava, 2001. What controls attention in natural environments? *Vis. Res.*, 41:3535–3545.
- Shioiri, S., and M. Ikeda, 1989. Useful resolution for picture perception as a function of eccentricity, *Perception*, 18:347–361.
- Summala, H., T. Nieminen, and M. Punto, 1996. Maintaining lane position with peripheral vision during in-vehicle tasks, *Hum. Factors*, 38:442–451.
- Thomas, E. L., 1968. Movements of the eye, *Sci. Am.*, 219:88–95.
- Weaver, H. E., 1943. A study of visual processes in reading differently constructed musical selections, *Psychol. Monogr.*, 55:1–30.
- Yarbus, A., 1967. *Eye Movements and Vision*, New York: Plenum Press.
- Yilmaz, E. R., and K. Nakayama, 1995. Fluctuation of attention levels during driving, *Invest. Ophthalmol. Vis. Sci.*, 36:S940.
- Zwahlen, H. T., 1993. Eye scanning rules for drivers: how do they compare with actual observed eye-scanning behavior? *Transport. Res. Rec.*, 1403:14–22.

92 Selection of Targets for Saccadic Eye Movements

JEFFREY D. SCHALL

The perceptions of naked outlines, as in the diagrams of Euclid and the alphabetical characters, are to say the least of it, three parts muscular and one part optical. (Bain, 1855)

Vision is an active process. Primate visual behavior is organized around a fovea which provides high-acuity vision over a limited range of the central visual field (reviewed by Carpenter 1988, 1991). Consequently, to identify an object in the scene, the eyes must move so that the image of that object projects onto the fovea (Fig. 92.1). Saccadic eye movements are the rapid conjugate rotations of the eyes that redirect the focus of gaze to new points in the image. Saccades are produced in the context of ongoing behavior in a dynamic environment. For example, if the object of fixation is moving slowly, then fixation is maintained through production of pursuit eye movements. In addition, foveation of an object often precedes further action directed at the object, such as reaching and grasping (e.g., Biguer et al., 1984).

Gaze can be directed to only one item at a time, so some process must distinguish among possible locations to select the target for a saccade. Consequently, some items may be overlooked. The outcome of the selection process is purposeful in the context of visually guided behavior. Analyses of the pattern of eye movements have revealed certain regularities—such as concentrating on conspicuous and informative features of an image—in examining simple geometric stimuli (e.g., Findlay, 1997; Liversedge and Findlay, 2000; Motter and Belky, 1998; Zelinsky and Sheinberg, 1997), natural images (e.g., Melcher and Kowler, 2001; Viviani, 1990; Yarbus, 1967), or text (e.g., Liversedge and Findlay, 2000; O'Regan, 1990). When patterns of gaze are analyzed during performance of specific extended tasks (such as making a sandwich), certain regular patterns of saccades can be observed as well (e.g., Epelboim et al., 1995; Land and Hayhoe, 2001).

This chapter will review what is known about the neural basis of the process of selecting the target for a gaze shift. Although much is being discovered about the selection of targets for pursuit eye movements (e.g., Ferrera and Lisberger, 1997; Gardner and Lisberger, 2001; Kowler, 1990), space limits this chapter to the selection for saccadic eye movements.

Visual search, selection, and attention

To investigate how the brain selects the target for an eye movement, multiple stimuli that can be distinguished in some way must be presented. This experimental design is referred to as *visual search*. The visual search paradigm has been used extensively to investigate visual selection and attention (reviewed by Wolfe, 1998). In a visual search task, multiple stimuli are presented among which a target is discriminated. Search is efficient (with fewer errors and faster response times) if stimuli differ along basic visual feature dimensions, such as color, form, or direction of motion. In contrast, if the distractors resemble the target or if no single feature clearly distinguishes the stimuli, then search becomes less efficient (more errors, longer response times) (e.g., Duncan and Humphreys, 1989).

Saccade target selection cannot be discussed without consideration of the allocation of visual attention. In fact, it can be argued that visual target selection and the allocation of visual attention amount to the same thing. Visual attention is the topic of Chapters 101, 102, and 103. The focus of visual attention can be directed away from the focus of gaze. So the link between shifting gaze and directing attention is not obligatory (Crawford and Muller, 1992; Eriksen and Hoffman, 1972; Jonides, 1980; Klein et al., 1992; Posner, 1980; Remington, 1980; Reuter-Lorenz and Fendrich, 1992; Shepherd et al., 1986). Nevertheless, several lines of evidence indicate that covert orienting of visual attention and overt orienting of saccades depend on a common selection mechanism. First, perceptual sensitivity is reduced and saccade latency is elevated if attention is directed away from the target for a saccade (Deubel and Schneider, 1996; Hoffman and Subramaniam, 1995; Kowler et al., 1995). Second, directing attention in space can influence the trajectory of saccades (Kustov and Robinson, 1996; Sheliga et al., 1995). Third, bottom-up visual factors influence visual selection for attention and saccades in the same way. The visual conspicuousness of an oddball stimulus can drive covert (e.g., Theeuwes, 1991) and overt (Theeuwes et al., 1998) selection, and nontarget elements that resemble a designated target can get inadvertently selected covertly (e.g., Kim and Cave, 1995) and overtly (Bichot and Schall,

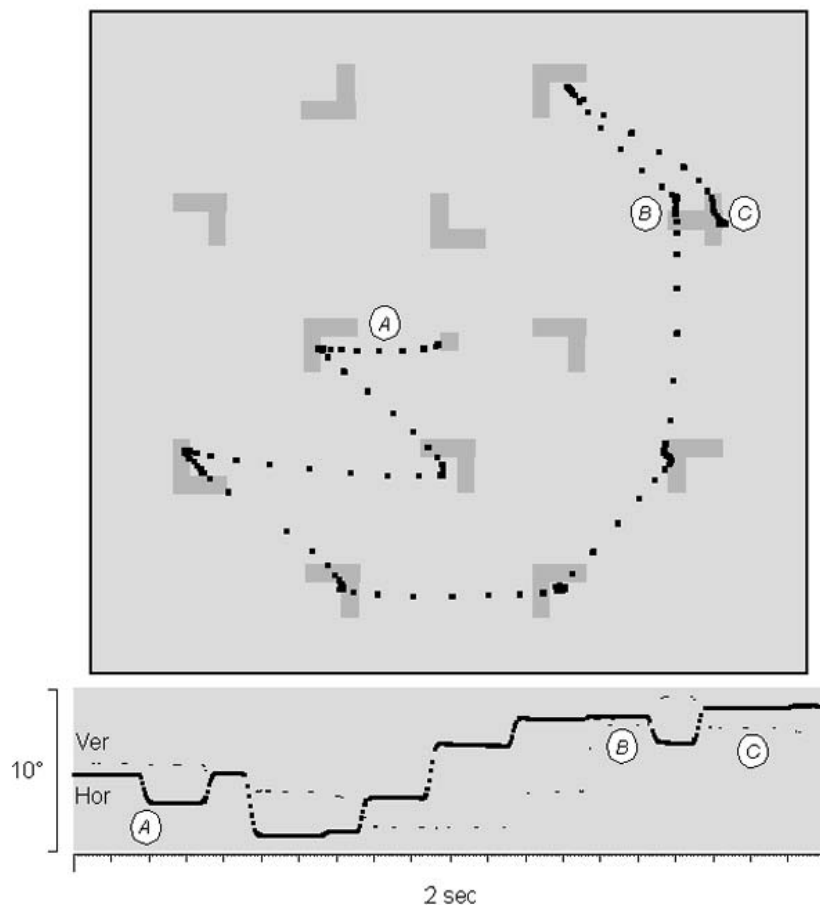


FIGURE 92.1. Gaze behavior of a monkey searching for a randomly oriented T among randomly oriented Ls. Each small dot plots the position of gaze sampled every 4 msec. The top panel plots eye position spatially. The bottom panel plots eye position in the horizontal (*thick*) and vertical (*thin*) axes as a function of time during the viewing period. The array appeared after the monkey fixated the central square. On this trial the monkey first shifted gaze to the left; this saccade corresponds to the first downward deflection in the plot of eye position in the horizontal axis (labeled *A*). Follow-

ing a sequence of eye movements around the perimeter of the array, the T was fixated for a brief period (labeled *B*), but the monkey made an errant saccade to another element. Following a shorter than usual fixation, gaze shifted back to the T, which was fixated for a sufficient period to earn reinforcement (labeled *C*). What neural processes led the monkey to foveate certain elements but not others in the array? What neural processes account for the variable amount of time spent foveating the various effectively identical elements? (Adapted from Schall and Thompson, 1999.)

1999b; Findlay, 1997; Motter and Belky, 1998; Zelinsky and Sheinberg, 1997). Fourth, cognitive strategies can override both covert (e.g., Bacon and Egeth, 1994) and overt (e.g., Bichot et al., 1996) oddball selection. Target selection is also influenced by implicit memory representations arising through short-term priming of location or stimulus features for covert (e.g., Maljkovic and Nakayama, 1994, 1996) and overt (Bichot and Schall, 1999b; McPeck et al., 1999, 2000; McPeck and Keller, 2001) orienting. In addition, experts are more likely than novices to fixate conspicuous but irrelevant parts of a visual image from their field of expertise (e.g., Chapman and Underwood, 1998; Nodine and Krupinski, 1998; Nodine et al., 1996). Finally, the pattern of visual fixation can be influenced by verbal instructions (Yarbus, 1967).

To explain observations like these, most models of visual search postulate the existence of a map of salience derived

from converging bottom-up and top-down influences (e.g., Cave and Wolfe, 1990; Itti and Koch, 2000; Koch and Ullman, 1985; Treisman, 1988; Wolfe, 1994). Other investigators have noted that the salience map is a useful construct to organize our understanding of how the brain selects the target for an eye movement (Findlay and Walker, 1999; Kusunoki et al., 2000; Thompson et al., 2001). *Salience* refers to how distinct one element of the image is from surrounding elements. This distinctness can occur because the element has visual features that are very different from those of its surrounding (a ripe red berry in green leaves). The distinctness can also occur because the element is more important than others (the face of a friend among strangers). The distinctness derived from visual features and importance confers upon that part of the image greater likelihood of receiving attention and a gaze shift. In the models of visual

search referred to above, one major input to the salience map is the maps of the features (color, shape, motion, depth) of elements of the image. Another major input is top-down modulation based on goals and expectations. The representation of likely targets that is implicit in and dependent on the feature maps becomes explicit in the salience map. Peaks of activation in the salience map that develop as a result of competitive interactions represent locations that have been selected for further processing, and thus covert orienting of attention and possibly but not necessarily a saccadic eye movement.

Preview of neural substrates

A network of structures in the brain produces and conveys the signals necessary to select a target and produce a saccade (Fig. 92.2). As readers of this volume know, visual processing begins in the retina but proceeds in earnest in primary visual cortex, where neurons respond selectively to stimuli possessing different features such as orientation or color (reviewed in Chapters 43, 44, 47, and 65). Visual processing is elaborated in a collection of distinct cortical areas that have various specializations (reviewed in Chapters 32, 33, 34, 66, 67, 76, 77, 78, 79, 81, 82, and 83). For example, area MT signals the motion of stimuli, and area V4 signals the color and form of stimuli. The extrastriate visual areas have been characterized as comprising separate processing streams. One stream passing into the temporal lobe is responsible for recognizing features and objects. Another stream passing into the parietal lobe is responsible for the sense of the body in space. Visual processing is not concluded in the parietal and temporal lobes; signals relay to and from the frontal lobes as well. For example, the frontal eye field is connected reciprocally with areas identified with both the dorsal and ventral processing streams (Baizer et al., 1991; Schall et al., 1995b; Stanton et al., 1995). Through this distributed network the characteristics of objects in the image can guide the direction of gaze, and goals and context can influence visual processing.

Movements of the eyes are produced by a network of neurons in the brainstem (reviewed by Scudder et al., 2002). This network shapes the pattern of activation of the ocular motor neurons that innervate the muscles generating the force that rotates the eyes to fixate the target. This network requires two inputs—where to shift gaze and when to initiate the movement. Key brain structures controlling the brainstem are the superior colliculus and the frontal eye field operating in a recurrent network through the basal ganglia and thalamus.

Pedagogically, it is easiest to review the experimental evidence by considering each part of the brain in turn. This style of presentation risks leaving the impression, most mistaken, that the various areas and structures operate in isola-

tion or sequence. In fact, the neural processes responsible for selecting a target and shifting gaze transpire concurrently in an interconnected network woven through the brain from front to back, top to bottom. Another caution involves summarizing information this way, for it is necessary to characterize the general properties of populations of neurons and impossible to describe the particularities of the diverse kinds of neurons actually observed. Moreover, because this is not an encyclopedia, the results of only a few of the many studies will be highlighted. The student is encouraged to consult the original research literature to gain a more realistic and critical understanding of the true diversity and complexity of the neuron populations that select the target for a saccade. In so doing, the alert reader will notice that the scope and depth of coverage of the various brain structures are proportional to this author's publications. Finally, the reader should be cautioned that many of the observations that will be described are the outcome of individual experiments in single laboratories that have not been independently replicated. This stipulation has two consequences. First, some of the observations and conclusions in this chapter will almost certainly need to be revised in light of new evidence. Second, many research opportunities exist to obtain such evidence that could make this chapter incomplete if not obsolete.

Superior colliculus

VISUAL RESPONSES The superior colliculus receives direct inputs from the retina, but it is also innervated by many cortical areas in the occipital, parietal, temporal, and frontal lobes (e.g., Fries, 1984). Visually responsive neurons in the superficial layers of the superior colliculus have spatially restricted receptive fields arranged in a precise retinotopic map (Fig. 92.3.4). They do not distinguish stimuli of different orientations, colors, or directions of motion (reviewed by Robinson and McClurkin, 1989). In experiments using macaque monkeys trained to fixate light spots for a fluid reward, the response of half of these neurons is enhanced if the stimulus is used by the monkey as a target for a saccadic eye movement (Goldberg and Wurtz, 1972; Wurtz and Mohler, 1976a). The enhancement can occur as either a larger initial response or an elevated activation after the initial visually evoked response. The enhanced activation can occur as well when a continuously visible stimulus is cued as the target for a saccade. This enhancement is a manifestation of the process that represents the location of a stimulus that will be the focus of a gaze shift. How this enhancement relates to selection of a target among alternative stimuli will be considered below.

SACCADE PRODUCTION The superior colliculus plays a central role in generating saccades guided by vision or other

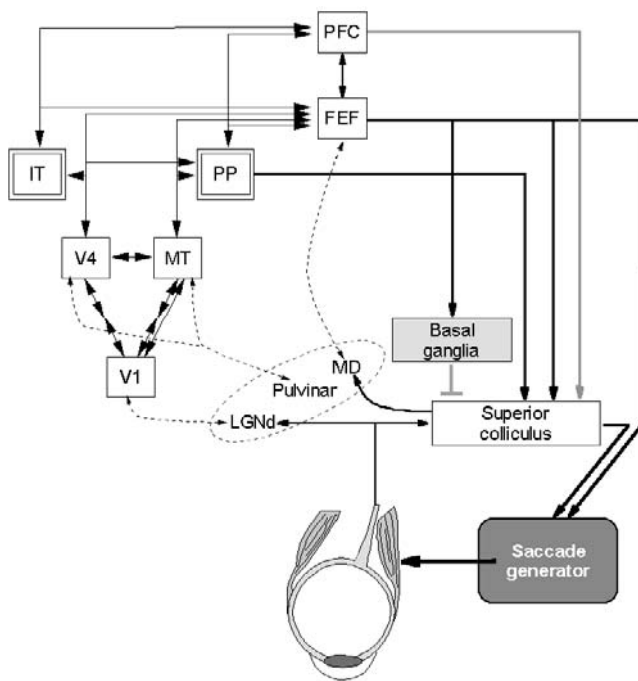


FIGURE 92.2. Overview of structures responsible for guiding and producing saccadic eye movements. Only a select few connections are shown, and the intrinsic organization of structures is ignored. Saccades are produced through the activation of a network in the brainstem saccade generator (*dark gray*). One input to the saccade generator is the superior colliculus; another is frontal eye field (FEF). FEF projects directly to superior colliculus as well as indirectly through the basal ganglia. Superior colliculus is under inhibitory control through the basal ganglia; FEF projections to the basal ganglia can release this inhibition. Signals from superior colliculus are relayed to FEF through the mediodorsal nucleus (MD) of the thalamus (enclosed in the oval). Activation arising concurrently through this interconnected network specifies where and when to shift gaze. The visual guidance of saccades originates in signals conveyed through retinal projections to superior colliculus and dorsal lateral geniculate nucleus (LGNd). LGNd innervates primary visual cortex (V1). Signals are routed from V1 to the network of extrastriate visual areas. Inputs to area V4 are relayed through other areas (symbolized by pairs of arrows). Inputs from V1 to MT are direct and relayed. The connections between cortical areas are reciprocated (*double arrowheads*). In addition to intracortical connectivity, extrastriate cortical areas communicate with the pulvinar nuclei of the thalamus. Signals from area V4 are sent to areas in the inferior temporal cortex (IT). Similarly, visual signals are routed to posterior parietal cortex (PP). A collection of rather distinct areas comprise IT and PP cortex (*outlined boxes*). The areas associated with IT cortex are responsible for the perception of features, forms, and objects. The areas associated with PP cortex are responsible for the perception of the body in space. Visual processing does not finish in the temporal and parietal lobes, though, because these areas project to the frontal lobe, in particular to FEF, as well as to superior colliculus. Like superior colliculus, FEF projects, albeit more weakly, to the saccade generator in the brainstem. The diverse visual inputs to FEF and superior colliculus convey an elaborate representation of the image to the centers that specify which saccade to produce. Through the connections of visual areas with FEF and superior colliculus, the features of an image can guide gaze. However, gaze can shift to inconspicuous but informative points in the image according to arbitrary rules. Connections of prefrontal cortex (pfc) with FEF and superior colliculus (although not as strong) (*gray line*) convey the influence of context, which can supplement or override the outcome of visual processing.

sensory modalities as well as self-generated saccades (reviewed by Munoz et al., 2000; Wurtz et al., 2000; Chapters 97 and 98). Neurons in the intermediate layers of the superior colliculus also discharge immediately before and during saccadic gaze shifts (reviewed by Sparks and Hartwich-Young, 1989). Neurons in the intermediate layers can be distinguished by the relative magnitude of activation following presentation of a stimulus and initiation of a saccade. Certain neurons respond to visual stimuli but have weak or no modulation associated with the saccade. Other neurons have weak if any visual response but exhibit high firing rates immediately before and during saccades; these are referred to as *burst neurons*. A third kind of neuron typically has a clear visual response, with activation sustained throughout an interval before the saccade and an elevated firing rate immediately before the saccade; these have been referred to as *buildup* or *prelude neurons* (Glimcher and Sparks, 1992; Munoz and Wurtz, 1995). The rostral end of the superior colliculus is populated by neurons that are active during fixation and exhibit a reduced firing rate before and during saccades (Munoz and Wurtz, 1993). These fixation neurons are in a push-pull relationship with the buildup neurons elsewhere in the superior colliculus. The balance of activation across the pools of fixation and buildup neurons controls saccade initiation (e.g., Dorris and Munoz, 1998; Dorris et al., 1997).

Each buildup and burst neuron is most active before saccades of a particular direction and amplitude and is progressively less active before saccades deviating from the optimal. In other words, each neuron has a receptive or movement field that is larger than the precision of saccades. Thus, before each saccade, neurons over a rather broad

extent of superior colliculus are activated in a graded manner (Fig. 92.3A). The space of saccade direction and amplitude is mapped in the intermediate layers in a topographic fashion corresponding to the map of visual space in the superficial layers of the superior colliculus. To produce a signal leading to a saccade of a particular direction and amplitude, the activations of many cells in a region of the motor map seem to be combined in a vector fashion (Lee et al., 1988; van Gisbergen et al., 1987).

When a pair of potential targets is presented close together, a larger zone of activation occurs across the map (Fig. 92.3B). A saccade resulting from the vector average of the zone of activation directs gaze to a location between the targets (Chou et al., 1999; Findlay, 1982; Ottes et al., 1984). This tendency is not exclusively automatic, though, because

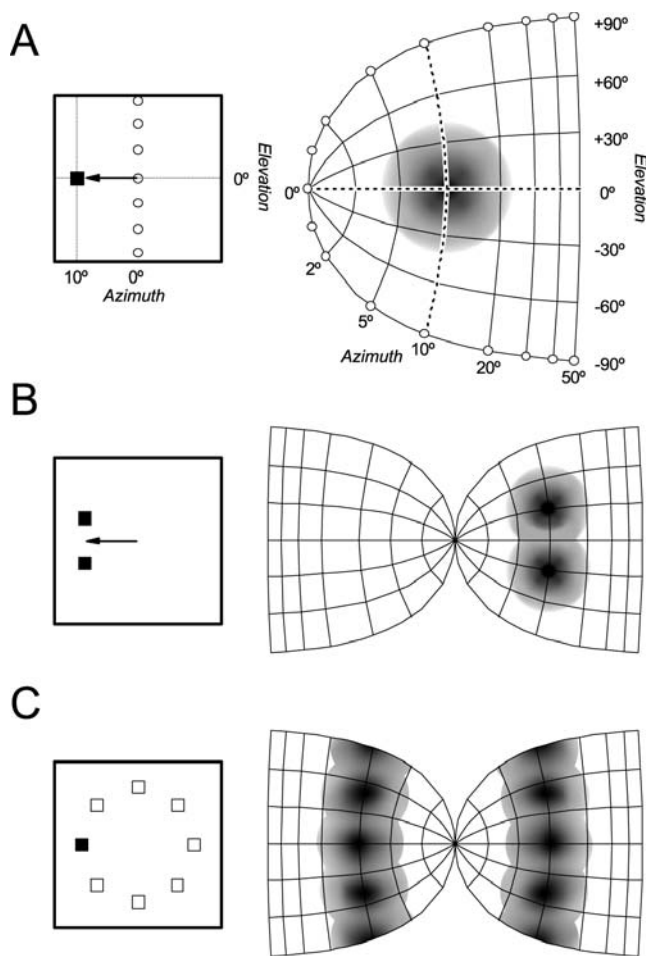


FIGURE 92.3. Pattern of activation in the superior colliculus. *A*, The left panel illustrates the visual field with a saccade (arrow) produced from the center to a target at 10 degrees azimuth and 0 degrees elevation. The vertical meridian is indicated by the row of circles. The right panel illustrates that the map of the superior colliculus as a mathematical formulation (Ottes et al., 1986) derived from a systematic survey of the direction and amplitude of saccades evoked by electrical stimulation of various parts of the superior colliculus (Robinson, 1972). A visually guided saccade to a point 10 degrees eccentric on the horizontal meridian is preceded by graded activation over an extended part of the superior colliculus map. The peak of activation (black) is centered at the appropriate point on the map, and surrounding neurons farther from the center of activation (gray) are progressively less active. The direction and amplitude of the saccade that is produced correspond to those specified by the location of the center of gravity of the activation in the superior colliculus map. *B*, Presentation of two nearby stimuli results in a broader zone of activation in the superior colliculus with two peaks. The center of gravity of the activation is a location between the two stimuli. This results in a saccade directing gaze to neither stimulus. The map of the superior colliculus representing each hemifield is shown. *C*, Presentation of eight stimuli produces activation in a large part of the superior colliculus map. The center of gravity of such balanced activation with multiple peaks amounts to a saccade with no amplitude. Thus, to produce a particular saccade, the activation in the superior colliculus map must evolve so that a single peak is present corresponding to the desired saccade direction and amplitude.

it can be influenced by cognitive factors (He and Kowler, 1989; Ottes et al., 1984, 1985).

If a circular array of stimuli is presented, then the spatial distribution of activation in the superior colliculus will be balanced around the map with multiple peaks (Fig. 92.3C). The vector combination of this distribution of activity amounts to a resultant with no length—not a very useful outcome. To produce a useful saccade, the activation in the map of the superior colliculus must be limited to the neurons contributing to generating just that saccade. Thus, if more than one location in the superior colliculus map becomes activated, then additional processing must resolve which of the peaks of activation should become dominant among the rest for an accurate saccade to just one among alternative stimuli. This additional processing is selection of the target.

TARGET SELECTION To learn how the superior colliculus contributes to selecting the target for a saccade, several investigators have presented monkeys with multiple stimuli among which to locate the target for an eye movement. In some studies, the target was identified by properties distinct from nontarget stimuli (Basso and Wurtz, 1998; Glimcher and Sparks, 1992; Olivier et al., 1999; Ottes et al., 1987). In other studies, the target location was specified by the properties of the stimulus at the central fixation point (Horwitz and Newsome, 2001; see also Kustov and Robinson, 1996) or by implicit cuing (Goldberg and Wurtz, 1972; Wurtz and Mohler, 1976a). The central observations were made primarily on the visually responsive prelude and buildup neurons. While the design of each study was different, the results can be summarized conveniently. Initially, when multiple stimuli are presented, activation arises at locations in the superior colliculus map corresponding to the potential saccade targets. Activation becomes relatively lower at locations that would produce saccades to nontarget elements and grows at locations corresponding to more conspicuous or important potential targets, ultimately yielding a burst that triggers the saccade produced by activation centered on just one location in the motor map.

One recent study presented monkeys with arrays of two, four, or eight stimuli among which one would be specified as the target (Basso and Wurtz, 1998). Visually responsive buildup neurons showed no difference in the initial response to target or nontarget stimuli in the response field (Fig. 92.4). The initial visual response decreased as the number of stimuli in the visual display increased from one to two, four, and eight. The attenuated activation following arrays with more potential targets was also seen in a delay period before the location of the target was cued. The modulation of the initial visual response was due in part to suppressive interactions across the visual field invoked by the multiple stimuli. However, some of the modulation of the visual response and all of the modulation of the delay period activity before the

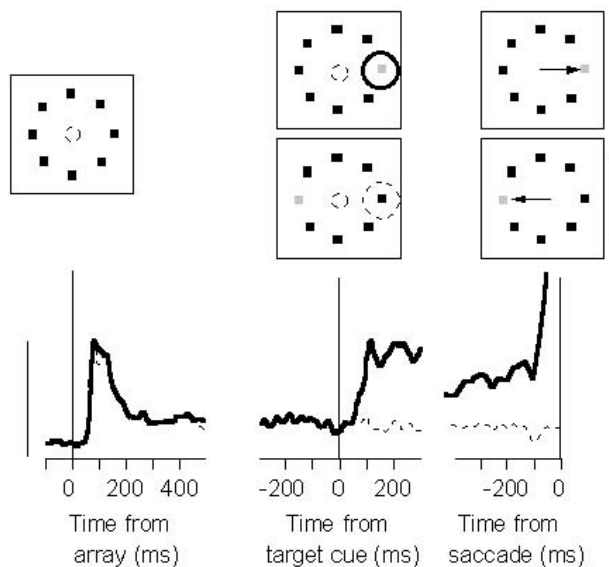


FIGURE 92.4. Activation of a visually responsive movement-related neuron in the superior colliculus of a monkey locating a target in an array of stimuli. The top panels illustrate the appearance of the stimuli and the production of the saccades under two conditions. The bottom panels illustrate the magnitude of activation of the neuron as a function of time from the indicated events. The activation when the stimulus in the response field was designated the target for the saccade (*thick*) is compared with the activation when a stimulus outside the response field is the target and the stimulus in the response field is ignored (*thin*). *Left*: the initial response to the array of identical stimuli is equivalent, regardless of whether the ultimate target or nontarget stimulus falls in the response field. During a succeeding delay, the activation was sustained at a moderate rate. *Center*: when one of the stimuli became visually distinct by dimming, the neural activity was modulated. If and only if the stimulus in the response field was specified as the target, the activation increased to a sustained higher level. The location of the response field is illustrated in the display panels; the line type corresponds to that used in the plot of activation. *Right*: the activation signaling whether the location in the response field was occupied by the target or a nontarget was sustained until the burst of activation immediately preceding the saccade. The plot of presaccadic activation when the saccade was into the response field was clipped for purposes of illustration. The scale bar for neuronal activation signifies 40 spikes per second. The scale bar for the visual display signifies 20 degrees. (Modified from Basso and Wurtz, 1998.)

target location was specified can be attributed to the predictability of the target location. This was tested by manipulating the probability of the target location in eight element arrays. When the particular location in arrays of eight elements that is in the response field is cued as the target on several successive trials, the visual response and delay period activity are greater than when the location in the response field is no more likely to be the target than any other location. Notably, this modulation based on recent experience takes some time across trials to develop, presumably constrained by the monkey's sense of expectancy. These data

indicate that the brain can develop a quotient of readiness to produce one or more saccades and that the degree of readiness are proportional to the experienced likelihood of target location (see also Dorris and Munoz, 1998; Glimcher and Sparks, 1992; Paré and Munoz, 1996).

Once the target location is specified by a change of appearance of one stimulus, the state of activation in the superior colliculus changes dramatically (Basso and Wurtz, 1998). Neurons with the specified target in their response field exhibit augmented activation, while the remaining neurons with nontarget stimuli in their response fields exhibit no change or a slight decrease in activity. This differential activation results in a concentration of activation centered on one point in the map corresponding to the saccade necessary to foveate the specified target. The process by which this activation becomes pronounced in just one region could arise through lateral inhibitory interactions within superior colliculus (Munoz and Istvan, 1998; Olivier et al., 1999; van Opstal and van Gisbergen, 1989) but probably also involve signals from cortical areas described below. Across the population of neurons, it took approximately 100 msec to represent uniquely the target in arrays of eight elements and approximately 50 msec in arrays with two elements. But once the target was selected, the magnitude of activity did not vary with the number of potential target locations. The prelude of additional activation representing the location of the target can be sustained for several hundred milliseconds until another stimulus signals the monkey to shift gaze. The pronounced saccade-related activation of the buildup neurons occurred when a saccade was generated into the response field, regardless of the stimulus configuration giving rise to that saccade, even if the saccade was to the nontarget.

SUMMARY The extensive evidence for the involvement of the superior colliculus in saccade target selection has led to the suggestion that superior colliculus can be understood in terms of a saliency map (reviewed by Findlay and Walker, 1999). However, we should not draw the unnecessary and mistaken conclusion that the superior colliculus performs this function uniquely and exclusively. In particular, because superior colliculus neurons do not discriminate visual features, inputs from the visual cortex must be used to select the target.

Primary visual cortex and the ventral stream

Selecting a particular element in an image requires the element to be distinguished from others. Such a distinction can be derived from differences in color, shape, motion, or depth. Therefore, selection of a target for a visually guided saccade must begin with neural signals that distinguish the features of elements in the image. A cornerstone of visual

neuroscience is the fact that neurons in the visual cortex respond selectively according to the color, shape, motion, and depth of stimuli. A signal sufficient to distinguish the features of visual objects is available in the first few spikes produced by neurons in primary and extrastriate visual cortex (Celebrini et al., 1993; Dinse et al., 1990; Muller et al., 2001; Oram and Perrett, 1992; Ringach et al., 1997; Sugase et al., 1999; Tovée et al., 1993; Vogels and Orban, 1991; von der Heydt and Peterhans, 1989).

Selectivity of neural responses for visual features forms the substrate for target selection; however, it is not sufficient because targets are distinguished only through a comparison to the features of other stimuli in the image. When more than one stimulus is presented, interactions occur between neurons responding to stimuli in neighboring parts of the scene. Modulation of responses by surrounding stimuli has been observed in neurons in primary visual cortex V1 (e.g., Blakemore and Tobin, 1972; Kapadia et al., 1995; Knierim and Van Essen, 1992; Polat et al., 1998; Rossi et al., 2001; Sillito et al., 1996; Zipser et al., 1996), as well as in areas MT and MST (Allman et al., 1985; Olavarria et al., 1992; Saito et al., 1986) and area V4 (Desimone and Schein, 1987). Note that this modulation does not occur for every neuron or in the same manner for all neurons, but space limits this description to the most general characteristics (see Chapters 45 and 46). The influence of surrounding stimuli on the response to a stimulus in the receptive field under most conditions takes some time to be expressed. Modulation of the response of neurons to a stimulus in the receptive field by stimuli present in the surrounding region provides the substrate for identifying the location of features that are conspicuously different from surrounding features.

AREA V4 Neural activity in extrastriate visual area V4 has been related to the guidance of saccades. Neurons in V4 exhibit modulated discharge rates before saccade initiation (Fischer and Boch, 1981) that seems to signal enhanced selectivity for the features of the stimulus at the location of the saccade (Moore, 1999). Also, the receptive fields of V4 neurons have been characterized as reducing in size to focus effectively around the target of the saccade (Tolias et al., 2001). This resembles a spatial shift of sensitivity within the receptive field in a spatial attention task (Connor et al., 1997).

Further information about how striate and extrastriate cortex select targets has been obtained in studies that present multiple stimuli to investigate the covert shift of attention. This is an extensive area of research that is reviewed in Chapters 101, 102, and 103. This line of research has been framed by the seminal observation that when two stimuli are presented in the receptive field of many neurons in area V4, the response to the preferred stimulus is modulated according to which of the two stimuli is selected for guiding a behavioral response (Chelazzi et al., 2001; Luck et al., 1997;

McAdams and Maunsell, 1999; Moran and Desimone, 1985; Reynolds et al., 1999). Similar observations have been made in area MT (Treue and Maunsell, 1999; but see Seidemann and Newsome, 1999). The common general conclusion is that when attention is allocated to one of the stimuli, the activation of the neurons selective for that stimulus becomes greater than the activation of the neurons selective for the nonselected stimulus.

For example, one study showed that neurons in V4 responded differentially to a stimulus in their receptive field, depending on whether the stimulus matched a cue stimulus presented in the fovea and so was selected for use in a perceptual judgment (Motter, 1994a, 1994b) (Fig. 92.5B). The initial visual response to the array was the same whether or not the stimulus in the receptive field matched the cue. After approximately 150 msec, the differential activation was manifest and persisted until the response was permitted. This selective activation did not depend on the feature specificity of neurons, did not require the continued presence of the foveal cue, and changed if the cue color was switched. Thus, neurons in prestriate areas produce signals sufficient for selecting among stimuli in the image according to the contrast among specific features.

INFERIOR TEMPORAL CORTEX Several studies have provided information on the role of inferior temporal cortex in selecting the target for a saccade. Chapters 77, 78, and 79 review the properties of neurons in inferior temporal cortex. Briefly, these neurons respond selectively to stimuli with particular combinations of features, ranging from conjunctions of color and shape to faces with specific identity or expression. The stimulus selectivity of neurons in inferior temporal lobe seems the same during both active scanning in a cluttered image and passive presentation (DiCarlo and Maunsell, 2000; Sheinberg and Logothetis, 2001), and investigators have described modulation of neurons to attended versus nonattended stimuli (e.g., Richmond and Sato, 1987; Sato, 1988). This chapter will concentrate on studies that have presented a target among multiple stimuli because it is under this condition that the process of target selection can be observed most directly.

The activity of neurons has been examined in inferior temporal cortex of monkeys making a saccade to the location of one stimulus in an array of stimuli that matched the appearance of a remembered cue stimulus (Chelazzi et al., 1998). One of the stimuli effectively activated the cell, and the other elicited little response. After the cue was presented, neurons discharged at a low rate throughout a delay period, although this activation was somewhat higher if the cue was an optimal stimulus. When the array of stimuli containing the target was presented with more than one stimulus in the large receptive field, the inferior temporal cortex cells exhibited an initial period of activation that did not vary with

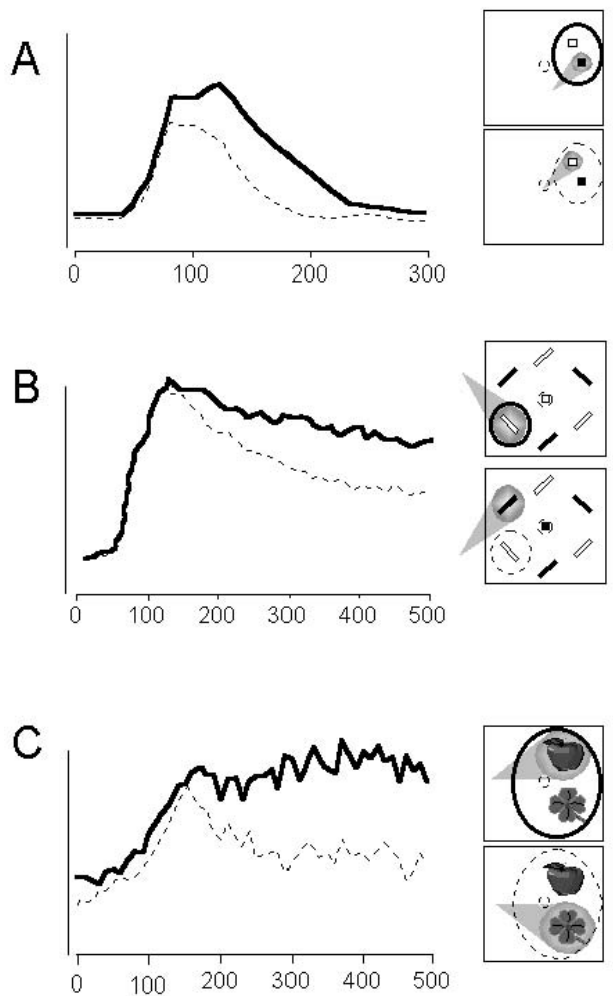


FIGURE 92.5. Target selection by neurons in the temporal lobe. *A*, Activation in area V4 related to spatial selection between two stimuli presented within the neurons' receptive field. Under identical stimulus conditions, activation when attention was directed to the location of the preferred stimulus (*thick solid*) was greater than activation when attention was directed to the location of the non-preferred stimulus (*thin dashed*). The difference in activation did not occur in the initial response. The scale bar for neuronal activation signifies 30 spikes per second. The scale bar for the visual display signifies 5 degrees. *B*, Activation in area V4 related to selection and identification of the orientation of stimuli matching the color of a sample in the center. Under identical stimulus conditions, when the stimulus in the receptive field matched the sample (*thick solid*) activation was greater than when the stimulus in the receptive field did not match the sample (*thin dashed*). The scale bar for neuronal activation signifies 50 spikes per second. The scale bar for the visual display signifies 5 degrees. *C*, Activation in IT cortex related to spatial selection between two stimuli presented within the neurons' receptive fields. The receptive fields of neurons in IT are much larger than those of neurons in area V4, and the neurons are selective for complex objects. Under identical stimulus conditions, activation when attention was directed to the location of the preferred stimulus (*thick solid*) was greater than activation when attention was directed to the location of the nonpreferred stimulus (*thin dashed*). The difference in activation did not occur in the initial response. The scale bar for neuronal activation signifies 20 spikes per second. The scale bar for the visual display signifies 5 degrees. (*A* modified from Luck et al., 1997; *B* modified from Motter, 1994a; *C* modified from Chelazzi et al., 1998.)

regardless of its features is necessary to guide saccadic eye movements. Such a representation seems to be present in the parietal and frontal lobes.

Posterior parietal cortex

Two areas in posterior parietal cortex—area 7A and the lateral intraparietal area (LIP)—have been distinguished on functional and anatomical grounds. The organization and functional properties of these areas are reviewed in Chapter 89. Area LIP is reciprocally connected with extrastriate areas such as V4 and MT that represent the features of elements in the image, as well as areas in inferior temporal cortex that signal more complex objects (e.g., Bullier et al., 1996; Morel and Bullier, 1990). Area LIP also projects to the superior colliculus (e.g., Lynch et al., 1985; Paré and Wurtz, 2001) and the frontal eye field (Baizer et al., 1991; Schall, et al., 1995b; Stanton et al., 1995), where it can influence saccade production.

A number of neurophysiological experiments have described properties of neurons in posterior parietal cortex related to target selection, as well as covert and overt orienting. Many studies have reported that the response to a stimulus is enhanced if it is to be the target for a saccade (e.g., Ben Hamed et al., 2002; Bushnell et al., 1981; Colby et al., 1996; Mountcastle et al., 1981, 1987; Robinson et al., 1978, 1995). In fact, this enhancement can occur if the

array configuration. However, 150 to 200 msec after presentation of the array, the activation of the neurons evolved to represent the identity of the target. If the optimal stimulus was the target, then neural activation remained elevated, discharging even more once the saccade brought the optimal stimulus into the fovea. However, if the nonoptimal stimulus was the target, then the activation was attenuated and remained so after fixation of the nonoptimal stimulus.

The general conclusion of these studies is that multiple stimuli compete for an explicit neural representation, and the competition among stimuli can be biased by other neural signals derived from experience or instruction (Desimone and Duncan, 1995). Consistent with this general hypothesis, if monkeys are given preferential experience with particular stimuli, the selection process observed in inferior temporal cortex neurons adapts to enhance the representation of the learned object (Jagadeesh et al., 2001). Ultimately, though, any enhanced activity in inferior temporal cortex represents the features characterizing the target and does not indicate that it is a target per se. This is so for all visual areas in which neurons respond selectively to stimuli with different features. A more general representation of the location of a target

peripheral stimulus instructs a manual response with no gaze shift; this observation is commonly interpreted as a neural correlate of the monkey's shifting attention covertly to the stimulus (Bushnell et al., 1981; Robinson et al., 1978; reviewed by Colby and Goldberg, 1999; for an alternative point of view, see Lynch et al., 1977; Mountcastle et al., 1975; Snyder et al., 2000; Chapter 89). Other studies have shown that the response to a stimulus is attenuated if the stimulus appears at a location where attention is already allocated (Constantinidis and Steinmetz, 2001b; Powell and Goldberg, 2000; Robinson et al., 1995; Steinmetz and Constantinidis, 1995; Steinmetz et al., 1994). The current hypothesis is that posterior parietal cortex represents the location of stimuli to which attention should or will shift. The aforementioned studies provide less insight into the contribution of posterior parietal cortex to target selection because they were conducted with the presentation of a single stimulus.

Recent studies have investigated the responses of neurons in posterior parietal cortex in monkeys confronted with displays consisting of a target and one or more distractors (e.g., Constantinidis and Steinmetz, 2001a, 2001b; Gottlieb et al., 1998; Platt and Glimcher, 1997). Neurons in area 7a signaled the location of a stimulus of one color among distractors of another color (Constantinidis and Steinmetz, 2001a). The initial response to the array was attenuated relative to the response to a single stimulus. The initial response to the array did not distinguish the location of the oddball, but within 100 to 150 msec the activation increased if the oddball was in the receptive field and decayed if only distractors were in the receptive field (Fig. 92.6A). This neural activity is clearly sufficient to represent the location of a conspicuous target.

Other studies have examined how neural activity in area LIP participates in target selection (Gottlieb et al., 1998). In one study, monkeys shifted gaze to the object in an array of eight distinct objects that matched a sample stimulus. If the object in the receptive field was designated the target, neurons exhibited a significant elevation of activity (Fig. 92.6B). When the sample was presented during fixation in the center of the array, the augmented activity for the target arose more than 200 msec after the target was specified. This time is longer than that observed in a similar condition in the study of superior colliculus described above, presumably because more time was needed to encode the properties of the sample and locate the matching element.

Taken together, the results indicate that the visual representation in posterior parietal cortex represents the location of conspicuous and relevant stimuli, that is, likely targets for orienting either covertly or overtly. Thus, as with superior colliculus, it appears that neurons in posterior parietal cortex embody the properties of units in a salience map (reviewed by Kusunoki et al., 2000). One complication, though, with

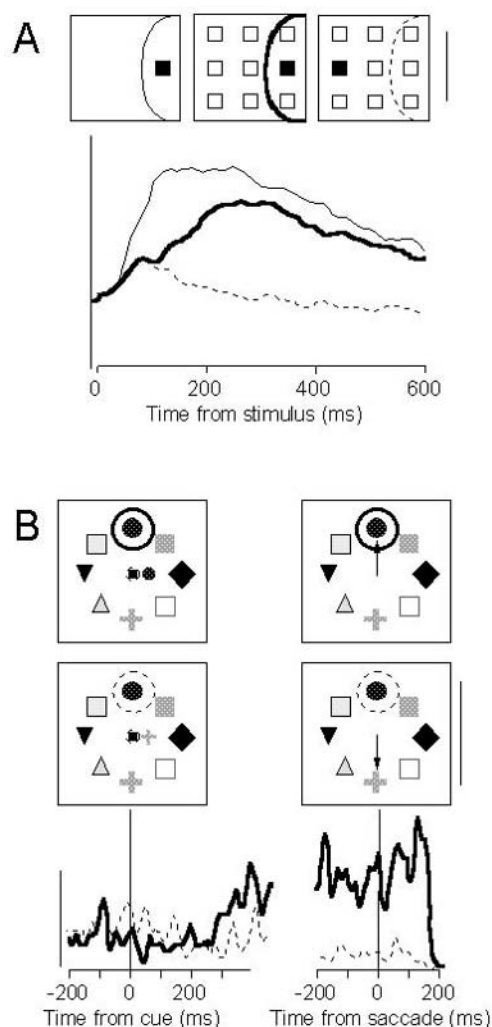


FIGURE 92.6. Target selection by neurons in the parietal lobe. *A*, Response of neurons in area 7a to a target presented alone in the receptive field (*thin solid*), the oddball stimulus of the array in the receptive field (*thick solid*), and the distractors in the receptive field (*thin dashed*). Compared to the response to the target alone, the response to the array is attenuated, especially in the initial 100 msec. Following presentation of the array, the initial response does not distinguish whether the oddball or only distractors were in the receptive field, but the activation evolved to represent whether or not the oddball was in the receptive field. The scale bar for neuronal activation signifies 40 spikes per second. The scale bar for the visual display signifies 50 degrees; note the difference in scale compared to that for the temporal lobe receptive fields. *B*, Activation of an area LIP neuron when a monkey must locate a target that matches a central cue. *Left*: while fixating in the center of the array, presentation of a cue for 200 msec signifies which element of the array is the target. Under identical stimulus conditions, the neuron began to discharge more if the stimulus in the receptive field is designated as the target (*thick solid*). No modulation was observed if the stimulus in the receptive field was not a target (*thin dashed*). *Right*: the activation was greatest before and after the saccade to the stimulus in the receptive field. The scale bar for neuronal activation signifies 20 spikes per second. The scale bar for the visual display signifies 40 degrees. (*A* modified from Constantinidis and Steinmetz, 2001a; *B* modified from Gottlieb et al., 1998.)

the hypothesis that LIP and area 7a correspond to a salience map concerns the quality of the map of the visual field and the topographic pattern of connections with the frontal eye field or superior colliculus. Given the orderly map of the visual field at the outset of visual processing and the orderly map of saccade direction and amplitude at the formation of saccade commands, it seems most expeditious if the locations of salient targets for orienting were represented in at least a roughly topographic map. Most physiological studies of parietal cortex have found very rough if any topographic mapping of the visual field (e.g., Blatt et al., 1990) and no clear pattern of mapping between LIP and the superior colliculus (Paré and Wurtz, 2001). However, more recent studies have detected rather rough topography by mapping receptive fields of neurons in the parietal cortex with denser sampling and exploring a wider extent of the intraparietal sulcus (Ben Hamed et al., 2001; Platt and Glimcher, 1998; see also Sereno et al., 2001). It remains to be seen how posterior parietal cortex contributes to the selection of targets near the center of gaze because shifts of gaze less than 10 degrees are by far the most common during natural vision (Bahill et al., 1975).

Frontal eye field

The frontal eye field is an area in prefrontal cortex that contributes to the transformation of visual signals into saccade commands (reviewed by Schall, 1997; Schall and Thompson, 1999; see Chapter 96). Thus, the frontal eye field has two facets, one motor and the other sensory. The frontal eye field is not as well known as the extrastriate visual areas in occipital, temporal, or parietal lobes, so some of its basic functional properties will be reviewed.

MOTOR FUNCTION The evidence for the motor function of frontal eye field is compelling. Low-intensity microstimulation of frontal eye field elicits saccades (e.g., Bruce et al., 1985). This direct influence is mediated by a population of neurons that discharge specifically before and during saccades (Bruce and Goldberg, 1985; Hanes and Schall, 1996; Hanes et al., 1998). The neurons in frontal eye field that generate movement-related activity are located in layer 5 and innervate the superior colliculus (Segraves and Goldberg, 1987; Sommer and Wurtz, 2000, 2001) and parts of the neural circuit in the brainstem that generate saccades (Segraves, 1992). These neurons, in concert with counterparts in the superior colliculus (Dorris and Munoz, 1998; Schiller and Koerner, 1971; Sparks, 1978; Wurtz and Goldberg, 1972), provide the signals necessary to produce saccadic eye movements. Neurophysiological data indicate the sufficiency of the activity of presaccadic movement-related neurons in frontal eye field to produce gaze shifts (Hanes and Schall, 1996; Hanes et al., 1998). Reversible inactivation

studies provide evidence for the necessity of frontal eye field in normal saccade production (Dias et al., 1995; Sommer and Tehovnik, 1997). These findings complement earlier observations that ablation of frontal eye field causes an initially severe impairment in saccade production that recovers in some but not all respects over time (e.g., Schiller and Chou, 1998; Schiller et al., 1987).

VISUAL FUNCTION The evidence that frontal eye field is involved in visual function is equally compelling. Frontal eye field is connected with a large number of visual cortical areas in both the dorsal and ventral streams (e.g., Barone et al., 2000; Schall et al., 1995b). In fact, quantitative analyses of the connectivity between cortical visual areas indicate that frontal eye field is a uniquely well-connected node in the network of visual cortical areas (Jouve et al., 1998). Lateral frontal eye field, which is responsible for generating shorter saccades, receives visual afferents from the foveal representation in certain retinotopically organized areas, such as V4 and MT, from areas that represent central vision in caudal parts of inferotemporal cortex and from other areas having no retinotopic order, such as LIP. In contrast, medial frontal eye field, which is responsible for generating longer saccades, is innervated by the peripheral visual field representation of retinotopically organized areas, from areas that emphasize peripheral vision or are multimodal, and from other areas that have no retinotopic order. The afferents from visual cortical areas to frontal eye field are reciprocated through feedback projections (Barone et al., 2000; Schall et al., 1995b). Another source of visual signals to frontal eye field is the thalamus through the lateral segment of the mediodorsal nucleus, as well as parts of neighboring thalamic nuclei (Huerta et al., 1986; Stanton et al., 1988). Neurons in these nuclei are visually responsive (Schlag and Schlag-Rey, 1984) and can convey visual signals to frontal eye field (Sommer and Wurtz, 1998). Frontal eye field is also connected with specific areas in prefrontal cortex (e.g., Stanton et al., 1993). These prefrontal connections can influence frontal eye field according to the context of history and goals.

Physiological recordings in monkeys trained to shift gaze to visual targets have found that most neurons in frontal eye field have visual responses (Bruce and Goldberg, 1985; Mohler et al., 1973; Schall, 1991). Consistent with the extensive convergence of visual inputs in frontal eye field, the neurons typically do not exhibit any selectivity for stimulus features such as orientation, color, or direction of motion. The time at which visual neurons in frontal eye field respond to flashed stimuli coincides with the latencies of visual responses in dorsal stream areas such as area MT; in fact, many neurons in frontal eye field respond to visual stimuli before some neurons in V1 do (Schmolesky et al., 1998). Like the response of their counterparts in superior colliculus and posterior parietal cortex, the visual response of many frontal

eye field neurons is enhanced if the stimulus in the receptive field is the target for a saccade (Goldberg and Bushnell, 1981; Wurtz and Mohler, 1976b).

VISUAL TARGET SELECTION A series of investigations has described neural correlates of target selection for visually guided saccades by recording the activity of neurons in the frontal eye field of monkeys trained to shift gaze to a target in visual search arrays (Bichot and Schall, 1999a; Bichot et al., 2001a; Bichot et al., 2001b; Murthy et al., 2001; Sato et al., 2001; Schall and Hanes, 1993; Schall et al., 1995a; Thompson et al., 1996). Following presentation of an array with a single conspicuous target among uniform distractors, visually responsive neurons in frontal eye field responded initially indiscriminately to the target or the distractors of the search array in their receptive field (Fig. 92.7). However, before a saccade to the conspicuous target was generated, a selection process proceeded by which visually responsive neurons in frontal eye field ultimately signaled the location of the oddball target stimulus. If the target of the saccade was in the response field, the frontal eye field activity was greatest. If nontarget distractors were in the response field, the activity was suppressed. Clearly, the visual selection observed in frontal eye field depends on the afferents from the various visual areas conveying feature selectivity. However, frontal eye field also provides extensive feedback connections to extrastriate visual cortex (Barone et al., 2000; Schall et al., 1995b), so the possibility that the state of neural activity in frontal eye field can influence neural processing in visual cortex should not be overlooked.

Frontal eye field is commonly regarded as an oculomotor area of the cerebral cortex. Accordingly, the target selection process observed in frontal eye field neurons may amount to no more than saccade preparation. Experiments have tested the alternative hypotheses that the selection observed in frontal eye field corresponds to visual selection or is identical to saccade preparation. In one study, activity of frontal eye field neurons was recorded while monkeys maintained fixation during presentation of a search array with a single conspicuous oddball (Thompson et al., 1997). Although no saccade was made to the oddball, frontal eye field neurons still discriminated the oddball from distractors at the same time and to the same degree as when a gaze shift was produced even though the absolute level of activity was reduced (Fig. 92.7*B*). Thus, the visual selection observed in frontal eye field does not require saccade execution.

Another experiment created a condition in which monkeys frequently shifted gaze to a location different from that occupied by the oddball target in a search array. Even when gaze shifted away from the popout oddball of a search array, visual neurons in frontal eye field represented the current location of the target (Murthy et al., 2001). Given the evidence that attention is usually allocated automatically

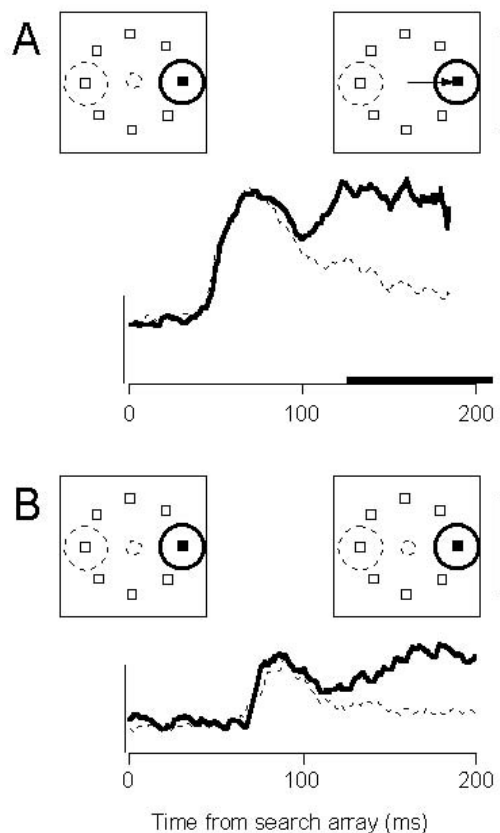


FIGURE 92.7. Target selection by neurons in the frontal lobe. *A*, Activation of a visually responsive neuron in frontal eye field following presentation of a popout search array when the monkey produced a saccade to the oddball when the oddball stimulus appeared in the receptive field (*thick solid*) and when distractors appeared in the receptive field (*thin dotted*). Unlike previous figures, the representation of the stimulus in the response field is collapsed into a single diagram. The initial response to the search array did not discriminate the target from a distractor, but after 100 msec the activation representing the location of the distractors was suppressed, and the activation representing the location of the target was sustained or elevated. The bar on the abscissa indicates the range of saccade initiation times. The scale bar for neuronal activation signifies 100 spikes per second. The scale bar for the visual display signifies 15 degrees. *B*, Activation of the same neuron when the monkey withheld a saccade to the oddball. The conventions are the same as in *A*. Although the discharge rate was lower, the neural activity signaled the location of the target at the same time and to the same degree as when the saccade was produced. The scale bar for neuronal activation signifies 100 spikes per second. The scale bar for the visual display signifies 15 degrees. (*A* modified from Thompson et al., 1996; *B* modified from Thompson et al., 1997.)

to the conspicuous oddball in a search array (e.g., Theeuwes, 1991), the fact that the visually responsive neurons in frontal eye field represented the location of the oddball whether or not it was the target of the gaze shift suggests that the activation of this particular population of neurons in frontal eye field corresponds to covert orienting of visual attention.

TIMING OF TARGET SELECTION AND SACCADIC INITIATION As illustrated in Figure 92.1, normal visual behavior is accomplished through a continuous cycle of fixation and visual analysis followed by another fixation and renewed visual analysis. The focus of gaze shifts two to five times every second. Curiously, the time spent fixating elements of an image varies to a degree that cannot be explained just by the properties of the image. Several studies have examined how fixation duration, the interval between saccades, varies (e.g., Hooge and Erkelens, 1996; Jacobs, 1987). In general, fixation duration seems to be adjusted according to the difficulty of finding the desired target, but moment-to-moment control of fixation duration based on the properties of the image does not seem to take place. Progress has been made in understanding the neural processes that control fixation duration.

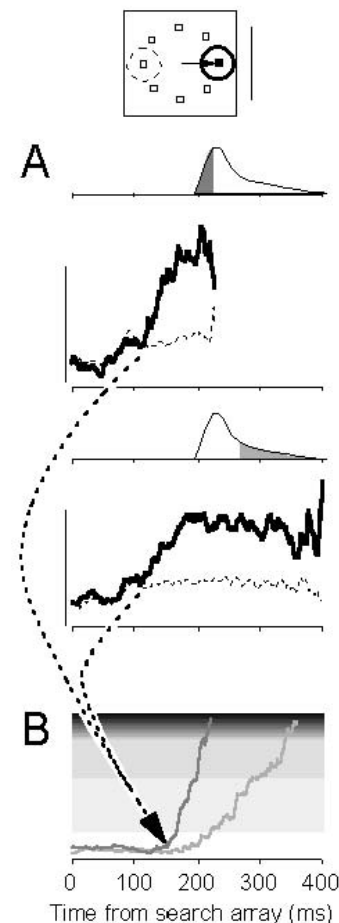
The neural process of target selection occupies a certain amount of time that can be measured with reasonable accuracy. This provides an opportunity to determine how the time of visual target selection relates to the time of saccade initiation. This work is motivated by the general hypothesis that behavioral response times are occupied by more or less distinct stages of processing (Donders, 1868; Miller, 1988; Sternberg, 1969). Recent studies have investigated how the

time taken to select a target relates to the time taken to initiate the saccade.

A key element of the design of these studies was allowing monkeys to shift gaze as soon as they could to the target. This contrasts with the design of most other studies of target selection that impose arbitrary delays between presentation of stimuli and permitting responses. The delays are introduced to distinguish neural modulation associated with different stages of processing. The disadvantage of this approach is that the delays change the way in which subjects perform tasks. In other words, the delay amounts to more than just the passage of time, because during the delay interval the state of the monkey is different from what it would have been had the delay not occurred.

During search for a single conspicuous target in a search array, the large majority of visually responsive neurons in frontal eye field discriminated the target from distractors at a rather constant interval after search array presentation (Sato et al., 2001; Thompson et al., 1996) (Fig. 92.8). However, at least under the conditions of very efficient search, the time taken to form a representation of the location of the target does not correspond to or predict when a saccade will be initiated. In other words, during the search for a conspicuous target, the delay and variability of saccade

FIGURE 92.8. Relationship between the time of target selection and the time of saccade initiation during search for a conspicuous target. *A*, The distribution of saccade latencies is illustrated above plots comparing activation when the target (*thick solid*) or distractors (*thin dashed*) fell in the receptive field. The top pair of panels shows the activation on trials in which the monkey made saccades with the shortest latencies (shaded early portion of the latency distribution). The bottom pair of panels shows the activation on trials in which the monkey made saccades with the longest latencies (shaded tail of the latency distribution). The dashed arrows originate at the time of target selection in each group of trials. The neuron discriminated the target from distractors following a relatively constant interval after presentation of the search array. The scale bar for neuronal activation signifies 100 spikes per second. The scale bar for the visual display signifies 15 degrees. *B*, The time at which a conspicuous target was selected by frontal eye field neurons does not predict when the saccade is initiated. Instead, the time of saccade initiation is specified most directly by the activation of another population of neurons in frontal eye field and other structures of the oculomotor system. Saccades are initiated when the activation in the pool of presaccadic movement neurons reaches a threshold (*shaded bar*). The premovement activation begins to increase at the time that the visual neurons select the target (*dotted arrows*). The variability of saccade reaction time can be accounted for by randomness in the time taken by the premovement activity to reach the threshold. Trials with the shortest reaction times occurred because the movement-related activation happened to reach the threshold sooner (*darker gray*), and the trials with the longest reaction times occurred because the movement-related activation happened to reach the threshold later (*lighter gray*). (Modified from Sato et al., 2001; Schall and Thompson, 1999.)



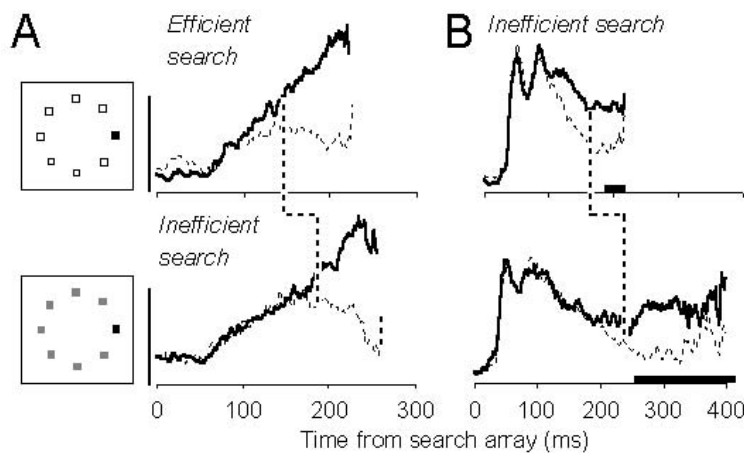


FIGURE 92.9. *A*, Effect of target salience on time of target selection. When the target is conspicuously different from the distractors, search is efficient, with shorter reaction times and fewer errors, and the target is selected earlier by frontal eye field neurons (*top*). When the target is more similar to the distractors, search is inefficient, with longer reaction times, and the target is selected later by frontal eye field neurons (*bottom*). The scale bar for neuronal activation signifies 100 spikes per second. Conventions are as in previous figures. *B*, Relationship between the time of target selection and the time of saccade initiation during the search for a less conspicuous target. The activity of another frontal eye field neuron is shown from the group of trials in which the monkey produced sac-

cadec with the shortest latencies (*top*) and from the group of trials with the longest latencies (*bottom*). The range of saccade latencies is indicated by the solid bar on the time axis. The stimulus conditions were identical but the time needed to locate the target varied, and saccade initiation was delayed until after the target was selected by the neuron. In other words, unlike efficient visual search, during inefficient visual search a significant fraction of the variability of reaction time is accounted for by variability in the time taken to achieve an explicit representation that locates the target among distractors. The scale bar for neuronal activation signifies 100 spikes per second. The scale bar for the visual display signifies 15 degrees. (Modified from Sato et al., 2001.)

latency cannot be accounted for by the delay of saccade target selection by frontal eye field neurons.

Frontal eye field neurons also exhibit activity mediating the selection of targets that are difficult to locate or may even be absent (Thompson and Schall, 1999, 2000). When the discrimination of the target is more difficult because the target more closely resembles the distractors, the time taken by neurons in frontal eye field to locate the target increases and accounts for a larger fraction but not all of the variability and duration of saccade latency (Bichot et al., 2001a; Sato et al., 2001) (Fig. 92.9).

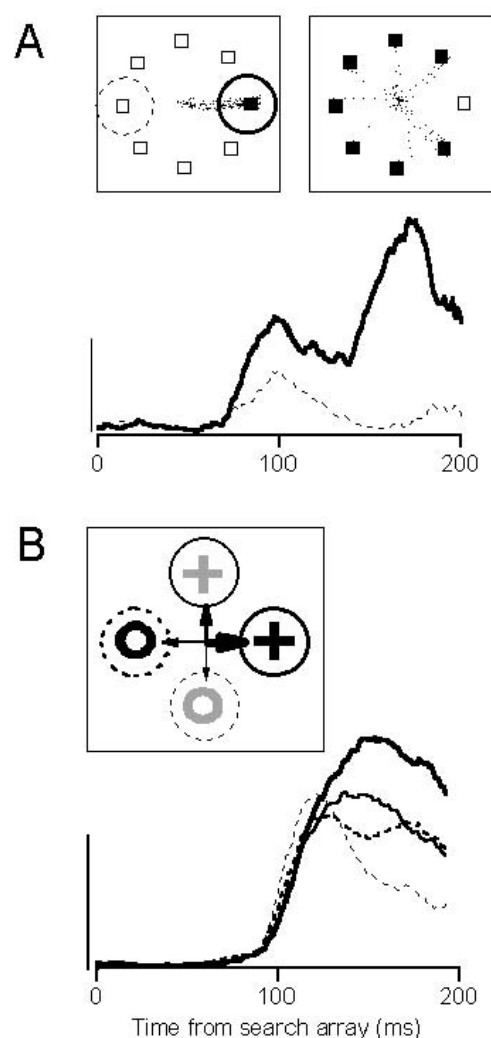
If the time of visual target selection during search does not account for the full duration and variability of saccade initiation times, then some other process must occur to prepare and produce the saccade. As described above, a population of neurons in frontal eye field and superior colliculus linked through the basal ganglia and thalamus provide the input to the brainstem network that produces the saccade. The activation of these particular neurons in frontal eye field and superior colliculus is necessary to produce a saccade; therefore, it is appropriate to identify the process of saccade preparation with the activation of these presaccadic movement neurons (also referred to as *buildup*, *prelude*, or *long-lead burst* neurons). Saccades are initiated when the activation in this network reaches a certain level that may vary across task conditions but appears to be constant within a condition (Hanes and Schall, 1996; Sparks, 1978). Most

of the variability of the latencies of saccades to a visual target can be accounted for by randomness in the rate of growth of activity to the threshold (Hanes and Schall, 1996) (Fig. 92.8).

Thus, the picture that emerges is that the process of visual selection occupies a certain amount of time that can be shorter and less variable if the target is conspicuous, or it can be longer and more variable if the target is less conspicuous. If subjects wish to prevent a saccade to a nontarget stimulus, then the preparation of the saccade can be delayed until the visual selection process has proceeded to a high degree of resolution. Neural activity mediating saccade preparation begins to grow as the selection process is completed, and (for reasons that are not clear) the rate of growth of activity leading to the movement varies apparently randomly such that sometimes gaze shifts sooner and sometimes later.

In higher primates, these two stages—visual selection and response preparation—are distinct and only loosely coupled. The variability of fixation duration during scanning behavior described earlier can be explained by variation in the movement preparation process independent of the visual selection process. In fact, occasionally it is possible for the saccade preparation process to become activated before identification of the currently fixated element and selection of the next target are completed. For example, during visual search, neurons in frontal eye field with no visual response

FIGURE 92.10. Visual selection of a learned target during popout search. *A*, The top displays show the saccades made by a monkey trained with only one instance of the visual search array—a red target among green distractors. When presented with an array in which the colors of the target and distractors were switched, instead of looking at the conspicuous green stimulus, this monkey looked only at one of the red distractors. The lower panel illustrates the activation of a single frontal eye field visual neuron in this monkey when the red target (*thick solid*) was in the receptive field and when green distractors (*thin dashed*) were in the receptive field. Unlike neurons recorded in monkeys that learned to perform generalized oddball search tasks, the initial visual response of this neuron discriminated the target from distractors. The scale bar for neuronal activation signifies 50 spikes per second. *B*, Visual selection of a remembered target during conjunction search. The top panel illustrates the pattern of gaze shifts produced by monkeys during conjunction search. The widths of the arrows indicate the incidence of correct saccades to the target (by far the most common of all) and of occasional errant saccades (much less common) to distractors having the same color or the same shape as the target (intermediate frequency) or having features opposite those of the target (least frequent). The wider arrow to the same shape distractors indicates more saccades to the distractor that had been the target in the previous experimental session. The bottom panel plots the activity of a frontal eye field neuron during conjunction search trials when the stimulus in its receptive field was the target (*red cross, thick solid*), the distractor with the same shape as the target (*thick dashed*), the distractor with the same color as the target (*intermediate dashed*), or the distractor sharing neither feature with the target (*thin dashed*). When this neuron was recorded, the target was the same shape as the target of the previous session. The scale bar for neuronal activation signifies 50 spikes per second. (*A* modified from Bichot et al., 1996; *B* modified from Bichot and Schall, 1999a.)



and only presaccadic movement activity can exhibit partial activation for nontarget stimuli that resemble the target (Bichot et al., 2001b). Such inappropriate activation of movement neurons can, if excessive, result in premature, erroneous saccades such as that shown in Figure 92.1. Independence of visual selection and response preparation is also necessary to explain the production of saccades that are not directed to the location of the selected target. For example, it is possible to shift gaze in the direction opposite a visual target, referred to as *antisaccade*. In monkeys producing antisaccades, visually responsive neurons in the superior colliculus and frontal eye field respond if the target falls in the receptive field, and movement neurons are active for saccades into the movement field whether it is a prosaccade or an antisaccade (Everling and Munoz, 2000; Everling et al., 1999).

EFFECTS OF LEARNING ON TARGET SELECTION As described at the beginning of the chapter, experts look at things differently from novices. This means that selection of targets for gaze shifts is influenced by experience. In one experiment to study the effects of experience on gaze behavior and associated neural activity in frontal eye field, monkeys were

trained exclusively with search arrays that contained a single item of a constant color among distractor items of another constant color (e.g., a red target among green distractors) (Bichot et al., 1996). As an experimental control, other monkeys were trained to produce a saccade to the oddball of both color configurations of the search arrays (i.e., a red target among green distractors and a green target among red distractors). The control monkeys shifted gaze to the oddball stimulus regardless of the feature that defined it, but the experimental monkeys persistently directed gaze to stimuli possessing the learned target color even if the target and distractor colors were switched (Fig. 92.10A). In other words, when experimental monkeys were presented with the search array complementary to that with which they were trained, they shifted gaze to the distractors (that were the color of the overlearned target) and not to the oddball target (that was the color of the overlearned distractors). As described above, frontal eye field neurons in control monkeys do not exhibit feature selectivity in the initial response, but their activity evolves to signal the location of the oddball stimulus. In monkeys trained exclusively on targets of one color, however,

about half of frontal eye field neurons show selectivity for stimuli of that color. This selectivity was manifest as a suppression of the initial visual response to the distractors (Fig. 92.10A).

How might this initial selective response arise in frontal eye field? One possibility is that appropriate bias signals are delivered to frontal eye field from other prefrontal areas. Other studies have demonstrated that the selective properties of prefrontal neurons can change according to rules or strategies (e.g., Wallis et al., 2001; White and Wise, 1999).

When objects of interest cannot be located only by their visual features, knowledge gained through experience is necessary. For example, visual search for a conjunction of features (such as a red cross among red circles, green crosses, and green circles) requires an explicit memory representation to identify the target (e.g., Bacon and Egeth, 1997; Treisman and Sato, 1990). A study of frontal eye field was conducted in monkeys trained to perform a visual search for a target defined by a unique combination of color and shape (e.g., a red cross). The color-shape combination that defined the target remained fixed during a data collection session but was changed randomly between sessions. Two separate contextual influences were exerted on gaze behavior and the neural selection process: visual similarity of distractors to the target and the history of target properties (Bichot and Schall, 1999a, 1999b) (Fig. 92.10B).

The evidence for the influence of visual similarity was revealed by the pattern of occasional erroneous saccades during conjunction search. Erroneous saccades tended to direct gaze to distractors that resembled the current target. Similar observations have been made with human observers during covert (Kim and Cave, 1995) and overt orienting (Findlay, 1997; Motter and Belky, 1998). When monkeys successfully shifted gaze to the target following the initial indiscriminate response, frontal eye field neurons not only discriminated the target from distractors but also discriminated among the nonselected distractors. More activation was present for distractors that were the same shape or color as the target than for distractors that shared neither feature of the target. One consequence of this observation is that stimuli that are not selected overtly may still influence subsequent processing because of the differential neural representation.

The history of stimulus presentation across sessions also affected the selection process during conjunction search. If an error was made, monkeys showed a significant tendency (in addition to the visual similarity tendency just described) to shift gaze to the distractors that had been the target in the previous session. Recordings from frontal eye field neurons during trials with correct saccades to the conjunction target revealed a corresponding discrimination among distractors with more activation for distractors that had been the target

during the previous session. This effect was evident across sessions that were more than a day apart and persisted throughout experimental sessions.

SUMMARY The extensive evidence for the involvement of frontal eye field in saccade target selection has led to the suggestion that superior colliculus can be understood in terms of a salience map (reviewed by Thompson et al., 2001). However, we should not draw the unnecessary and mistaken conclusion that frontal eye field performs this function uniquely and exclusively.

Dorsolateral prefrontal cortex

The source of the modulation observed in frontal eye field derived from experience is not known. It is reasonable to suppose that rostral areas of prefrontal cortex are involved given the evidence for prefrontal cortex instantiating rules (e.g., Miller and Cohen, 2001). The activity of neurons in prefrontal cortex areas rostral to frontal eye field has been described during tasks that required visual target selection (Constantinidis et al., 2001; Ferrera et al., 1999; Hasegawa et al., 2000; Rainer et al., 1998; see also Boussaoud and Wise, 1993; Kim and Shadlen, 1999). In some of these studies the selection of the target appeared as more of an all-or-none activation, largely because the responses began after the selection process was completed in visual areas of the cortex. However, a common feature of dorsolateral prefrontal cortex is the presence of activity during enforced delay periods in which monkeys must remember specific aspects of the stimuli to guide the eventual response. The characteristics of this delay period activation have been described in numerous studies.

One study presented monkeys with two stimuli, a bright target and a distractor with brightness that was varied across trials from that of the dim background to that of the bright target (Constantinidis et al., 2001). In this way, the discriminability of the target from the distractor was varied. After an instructed delay in which the stimuli were removed, monkeys shifted gaze to the location occupied by the brighter stimulus. The activation during the delay period varied according to the brightness of the stimulus in the receptive field and the performance of the monkeys. Neurons remained active during the delay period even if the stimulus in the receptive field had been the distractor. This result provides further evidence that nonselected stimuli are represented by differential activation (Bichot and Schall, 1999a; but see Rainer et al., 1998). This affords an opportunity for the properties of the nonselected stimuli to influence subsequent performance. Also, the magnitude of the activation varied such that if the distractor was more similar to the target, the activation evoked by the distractor was more similar to the activation evoked by the target. This was

observed when the properties of a cue stimulus outside the receptive field guided target selection (Kim and Shadlen, 1999) and also in an investigation of the tactile modality (Romo et al., 1999).

To summarize, the studies of dorsolateral prefrontal cortex have indicated that neurons may not participate directly in the target selection process but can encode the properties of selected and nonselected stimuli. Further work is needed to discover how the function of dorsolateral prefrontal cortex influences target selection in the more caudal parts of the brain.

General summary

Vision occurs naturally in a continuous cycle of fixations interrupted by gaze shifts. The guidance of these eye movements requires information about what is located where in the image. The identity of objects is derived mainly from their visible features. Single neurons in the visual pathway represent the presence of specific features by the level of activation. Each point in the visual field is represented by populations of neurons activated by all types of features. Topographic representations are found throughout the visual and oculomotor systems; neighboring neurons tend to represent similar visual field locations or saccades.

When confronted by an image with many possible targets, the visual system compares the features of elements across the visual field. The retinotopic maps of the visual field facilitate local interactions to implement such comparisons; in particular, a network of lateral inhibition can extract the locations of the most conspicuous stimuli in the visual field. The process of these comparisons can be influenced by knowledge so that inconspicuous but important elements in the image can be the focus of gaze. This selection process results in a state of activation in which neurons with potential targets in their receptive field are more active and neurons with nontargets in their receptive field are less active.

The outcome of this selection process can be represented at a level of abstraction distinct from the representation of the features themselves. This is why the hypothetical construct of a salience map is useful. The state of neural selection of a salient target relative to surrounding nontarget elements amounts to the covert allocation of attention that usually precedes overt shifts of gaze. The time taken for the brain to achieve an explicit representation of the location of a target varies predictably according to how distinct the target appears in relation to nontarget elements.

Coordinated with this visual processing is activation in a network including frontal eye field and superior colliculus that is responsible for producing the eye movement. A saccade is produced when the activation at one location within the motor map reaches a critical threshold. One job

of visual processing influenced by memory and goals is to ensure that only one site—the best site—within the map of movements becomes activated. This is done when the neurons signaling the location of the desired target develop enhanced activation while the neurons responding to other locations are attenuated. When confronted with ambiguous images having multiple potential targets, partial activation can occur in parts of the motor map representing saccades to nontarget elements that resemble the target. Saccade target selection converts an initially ambiguous pattern of neural activation into a pattern that reliably signals one target location in a winner-take-all fashion. However, the representation of likely targets for orienting does not automatically and unalterably produce a saccade. Sometimes potential targets are perceived without an overt gaze shift or gaze can shift to locations not occupied by salient stimuli. The explanation of this flexible coupling between target selection and saccade production requires separate stages or modules, one to select a target for orienting and another to produce gaze shifts. The flexible relationship between target selection and saccade production also affords the ability to emphasize speed or accuracy. Accuracy in fixating correctly can be emphasized at the expense of speed by allowing the visual selection process to resolve alternatives before producing a saccade. On the other hand, accuracy can be sacrificed for speed, allowing the visuomotor system to produce a saccade that may be inaccurate because it is premature relative to the target selection process.

This summary should be regarded as a signpost along a path and not as a destination. Much has been learned, but many questions remain. Throughout all the investigation, we should not lose a sense of marvel at the nimble and flexible manner of movements of the eyes. Is it any wonder that these shiny globes of gristle are called the windows to the soul?

Acknowledgments

I thank René Marois, Stephanie Shorter-Jacobi, and Veit Stuphorn for comments on the manuscript and Gale Fox, Jennifer Jewett, and Carol Wiley for manuscript preparation. Research in my laboratory has been supported by the National Eye Institute, the National Institute of Mental Health, and the McKnight Endowment Fund for Neuroscience.

REFERENCES

- Allman, J. M., F. Miezin, and E. McGuinness, 1985. Stimulus specific responses from beyond the classical receptive field: neurophysiological mechanisms for local-global comparisons of visual motion, *Annu. Rev. Neurosci.*, 3:532–548.
- Bacon, W. F., and H. E. Egeth, 1994. Overriding stimulus-driven attentional capture, *Percept. Psychophys.*, 55:485–496.

- Bacon, W. F., and H. E. Egeth, 1997. Goal-directed guidance of attention: evidence from conjunctive visual search, *J. Exp. Psychol. Hum. Percept. Perform.*, 23:948–961.
- Bahill, A. T., D. Adler, and L. Stark, 1975. Most naturally occurring saccades have magnitudes of 15 degrees or less, *Invest. Ophthalmol.*, 14:468–469.
- Bain, A., 1855/1879. *The Senses and the Intellect*, 3rd ed., New York: D. Appleton.
- Baizer, J. S., L. G. Ungerleider, and R. Desimone, 1991. Organization of visual inputs to the inferior temporal and posterior parietal cortex in macaques, *J. Neurosci.*, 11:168–190.
- Barone, P., A. Batardiere, K. Knoblauch, and H. Kennedy, 2000. Laminar distribution of neurons in extrastriate areas projecting to visual areas V1 and V4 correlates with the hierarchical rank and indicates the operation of a distance rule, *J. Neurosci.*, 20:3263–3281.
- Basso, M. A., and R. H. Wurtz, 1998. Modulation of neuronal activity in superior colliculus by changes in target probability, *J. Neurosci.*, 18:7519–7534.
- Ben Hamed, S., J. R. Duhamel, F. Bremmer, and W. Graf, 2001. Representation of the visual field in the lateral intraparietal area of macaque monkeys: a quantitative receptive field analysis, *Exp. Brain Res.*, 140:127–144.
- Ben Hamed, S., J. R. Duhamel, F. Bremmer, and W. Graf, 2002. Visual receptive field modulation in the lateral intraparietal area during attentive fixation and free gaze, *Cereb. Cortex*, 12:234–245.
- Bichot, N. P., S. R. Chenthal, and J. D. Schall, 2001a. Continuous processing in macaque frontal cortex during visual search, *Neuropsychologia*, 39:972–982.
- Bichot, N. P., and J. D. Schall, 1999a. Effects of similarity and history on neural mechanisms of visual selection, *Nat. Neurosci.*, 2:549–554.
- Bichot, N. P., and J. D. Schall, 1999b. Saccade target selection in macaque during feature and conjunction visual search, *Vis. Neurosci.*, 16:81–89.
- Bichot, N. P., J. D. Schall, and K. G. Thompson, 1996. Visual feature selectivity in frontal eye fields induced by experience in mature macaques, *Nature*, 381:697–699.
- Bichot, N. P., K. G. Thompson, S. R. Chenthal, and J. D. Schall, 2001b. Reliability of macaque frontal eye field neurons signaling saccade targets during visual search, *J. Neurosci.*, 21:713–725.
- Biguer, B., C. Prablanc, and M. Jeannerod, 1984. The contribution of coordinated eye and head movements in hand pointing accuracy, *Exp. Brain Res.*, 55:462–469.
- Blakemore, C., and E. A. Tobin, 1972. Lateral inhibition between orientation detectors in the cat's visual cortex, *Exp. Brain Res.*, 15:439–440.
- Blatt, G. J., R. A. Andersen, and G. R. Stoner, 1990. Visual receptive field organization and cortico-cortical connections of the lateral intraparietal area (area LIP) in the macaque, *J. Comp. Neurol.*, 299:421–445.
- Boussaoud, D. S., and P. Wise, 1993. Primate frontal cortex: neuronal activity following attentional versus intentional cues, *Exp. Brain Res.*, 95:15–27.
- Bruce, C. J., and M. E. Goldberg, 1985. Primate frontal eye fields I: single neurons discharging before saccades, *J. Neurophysiol.*, 53:603–635.
- Bruce, C. J., M. E. Goldberg, C. Bushnell, and G. B. Stanton, 1985. Primate frontal eye fields II: physiological and anatomical correlates of electrically evoked eye movements, *J. Neurophysiol.*, 54:714–734.
- Bullier, J., J. D. Schall, and A. Morel, 1996. Functional streams in occipito-frontal connections in the monkey, *Behav. Brain Res.*, 76:89–97.
- Bushnell, M. C., M. E. Goldberg, and D. L. Robinson, 1981. Behavioral enhancement of visual responses in monkey cerebral cortex. I. Modulation in posterior parietal cortex related to selective visual attention, *J. Neurophysiol.*, 46:755–772.
- Carpenter, R. H. S., 1988. *Movements of the Eyes*, 2nd ed., London: Pion.
- Carpenter, R. H. S., 1991. The visual origins of ocular motility, in *Eye Movements* (R. H. S. Carpenter ed.), *Vision and Visual Dysfunction* (J. Cronly-Dillon ed.), London: Macmillan, pp. 1–10.
- Cave, K. R., and J. M. Wolfe, 1990. Modeling the role of parallel processing in visual search, *Cogn. Psychol.*, 22:225–271.
- Celebrini, S., S. Thorpe, Y. Trotter, and M. Imbert, 1993. Dynamics of orientation coding in area V1 of the awake primate, *Vis. Neurosci.*, 10:811–825.
- Chapman, P., and G. Underwood, 1998. Visual search of driving situations: danger and experience, *Perception*, 27:951–964.
- Chelazzi, L., J. Duncan, E. K. Miller, and R. Desimone, 1998. Responses of neurons in inferior temporal cortex during memory-guided visual search, *J. Neurophysiol.*, 80:2918–2940.
- Chelazzi, L., E. K. Miller, J. Duncan, and R. Desimone, 2001. Responses of neurons in macaque area V4 during memory-guided visual search, *Cereb. Cortex*, 11:761–772.
- Chou, I. H., M. A. Sommer, and P. H. Schiller, 1999. Express averaging saccades in monkeys, *Vis. Res.*, 39:4200–4216.
- Colby, C. L., J. R. Duhamel, and M. E. Goldberg, 1996. Visual, presaccadic, and cognitive activation of single neurons in monkey lateral intraparietal area, *J. Neurophysiol.*, 76:2841–2852.
- Colby, C. L., and M. E. Goldberg, 1999. Space and attention in parietal cortex, *Annu. Rev. Neurosci.*, 22:319–349.
- Connor, C. E., D. C. Preddie, J. L. Gallant, and D. C. Van Essen, 1997. Spatial attention effects in macaque area V4, *J. Neurosci.*, 17:3201–3214.
- Constantinidis, C., M. N. Franowicz, and P. S. Goldman-Rakic, 2001. The sensory nature of mnemonic representation in the primate prefrontal cortex, *Nat. Neurosci.*, 4:311–316.
- Constantinidis, C., and M. A. Steinmetz, 2001a. Neuronal responses in area 7a to multiple-stimulus displays: I. neurons encode the location of the salient stimulus, *Cereb. Cortex*, 11:581–591.
- Constantinidis, C., and M. A. Steinmetz, 2001b. Neuronal responses in area 7a to multiple stimulus displays: II. responses are suppressed at the cued location, *Cereb. Cortex*, 11:592–597.
- Crawford, T. J., and H. J. Muller, 1992. Spatial and temporal effects of spatial attention on human saccadic eye movements, *Vis. Res.*, 32:293–304.
- Desimone, R., and J. Duncan, 1995. Neural mechanisms of selective visual attention, *Annu. Rev. Neurosci.*, 18:193–222.
- Desimone, R., and S. J. Schein, 1987. Visual properties of neurons in area V4 of the macaque: sensitivity to stimulus form, *J. Neurophysiol.*, 57:835–868.
- Deubel, H., and W. X. Schneider, 1996. Saccade target selection and object recognition: evidence for a common attentional mechanism, *Vis. Res.*, 36:1827–1837.
- Dias, E. C., M. Kiesau, and M. A. Segraves, 1995. Acute activation and inactivation of macaque frontal eye field with GABA-related drugs, *J. Neurophysiol.*, 74:2744–2748.
- DiCarlo, J. J., and J. H. Maunsell, 2000. Form representation in monkey inferotemporal cortex is virtually unaltered by free viewing, *Nat. Neurosci.*, 3:814–821.

- Dinse, H. R., K. Kruger, and J. Best, 1990. A temporal structure of cortical information processing, *Concepts Neurosci.*, 1:199–238.
- Donders, F. C., 1868/1969. On the speed of mental processes, in *Attention and Performance II* (W. G. Koster, trans.), Amsterdam: North-Holland, pp. 412–431.
- Dorris, M. C., and D. P. Munoz, 1998. Saccadic probability influences motor preparation signals and time to saccadic initiation, *J. Neurosci.*, 18:7015–7026.
- Dorris, M. C., M. Paré, and D. P. Munoz, 1997. Neuronal activity in monkey superior colliculus related to the initiation of saccadic eye movements, *J. Neurosci.*, 17:8566–8579.
- Duncan, J., and G. W. Humphreys, 1989. Visual search and stimulus similarity, *Psychol. Rev.*, 96:433–458.
- Epelboim, U., R. M. Steinman, E. Kowler, M. Edwards, Z. Pizlo, C. J. Erkelens, and H. Collewijn, 1995. The function of visual search and memory in sequential looking tasks, *Vis. Res.*, 35:3401–3422.
- Eriksen, C. W., and J. E. Hoffman, 1972. Temporal and spatial characteristics of selective encoding from visual displays, *Percept. Psychophys.*, 12:201–204.
- Everling, S., M. C. Dorris, R. M. Klein, and D. P. Munoz, 1999. Role of primate superior colliculus in preparation and execution of anti-saccades and pro-saccades, *J. Neurosci.*, 19:2740–2754.
- Everling, S., and D. P. Munoz, 2000. Neuronal correlates for preparatory set associated with pro-saccades and anti-saccades in the primate frontal eye field, *J. Neurosci.*, 20:387–400.
- Ferrera, V. P., J. K. Cohen, and B. B. Lee, 1999. Activity of prefrontal neurons during location and color delayed matching tasks, *NeuroReport*, 10:1315–1322.
- Ferrera, V. P., and S. G. Lisberger, 1997. Neuronal responses in visual areas MT and MST during smooth pursuit target selection, *J. Neurophysiol.*, 78:1433–1446.
- Findlay, J. M., 1982. Global visual processing for saccadic eye movements, *Vis. Res.*, 22:1033–1045.
- Findlay, J. M., 1997. Saccade target selection during visual search, *Vis. Res.*, 37:617–631.
- Findlay, J., and M. R. Walker, 1999. A model of saccade generation based on parallel processing and competitive inhibition, *Behav. Brain Sci.*, 22:661–674.
- Fischer, B., and R. Boch, 1981. Enhanced activation of neurons in prelunate cortex before visually guided saccades of trained rhesus monkeys, *Exp. Brain Res.*, 44:129–137.
- Fries, W., 1984. Cortical projections to the superior colliculus in the macaque monkey: a retrograde study using horseradish peroxidase, *J. Comp. Neurol.*, 20:55–76.
- Gardner, J. L., and S. G. Lisberger, 2001. Linked target selection for saccadic and smooth pursuit eye movements, *J. Neurosci.*, 21:2075–2084.
- Glimcher, P. W., and D. L. Sparks, 1992. Movement selection in advance of action in superior colliculus, *Nature*, 355:542–545.
- Goldberg, M. E., and M. C. Bushnell, 1981. Behavioral enhancement of visual responses in monkey cerebral cortex, II. Modulation in frontal eye fields specifically related to saccades, *J. Neurophysiol.*, 46:773–787.
- Goldberg, M. E., and R. H. Wurtz, 1972. Activity of superior colliculus in behaving monkey, II. Effect of attention on neuronal responses, *J. Neurophysiol.*, 35:560–574.
- Gottlieb, J. P., M. Kusunoki, and M. E. Goldberg, 1998. The representation of visual salience in monkey parietal cortex, *Nature*, 391:481–484.
- Hanes, D. P., W. F. Patterson, and J. D. Schall, 1998. The role of frontal eye field in counter-manding saccades: visual movement and fixation activity, *J. Neurophysiol.*, 79:817–834.
- Hanes, D. P., and J. D. Schall, 1996. Neural control of voluntary movement initiation, *Science*, 274:427–430.
- Hasegawa, R. P., M. Matsumoto, and A. Mikami, 2000. Search target selection in monkey prefrontal cortex, *J. Neurophysiol.*, 84:1692–1696.
- He, P. Y., and E. Kowler, 1989. The role of location probability in the programming of saccades: implications for “center-of-gravity” tendencies, *Vis. Res.*, 29:1165–1181.
- Hoffman, J. E., and B. Subramaniam, 1995. The role of visual attention in saccadic eye movements, *Percept. Psychophys.*, 57:787–795.
- Hooge, I. T. C., and C. J. Erkelens, 1996. Control of fixation duration in a simple search task, *Percept. Psychophys.*, 58:969–976.
- Horowitz, G. D., and W. T. Newsome, 2001. Target selection for saccadic eye movements: prelude activity in the superior colliculus during a direction-discrimination task, *J. Neurophysiol.*, 86:2543–2558.
- Huerta, M. F., L. A. Krubitzer, and J. H. Kaas, 1986. Frontal eye field as defined by intracortical microstimulation in squirrel monkeys, owl monkeys and macaque monkeys: I. Subcortical connections, *J. Comp. Neurol.*, 253:415–439.
- Itti, L., and C. Koch, 2000. A saliency-based search mechanism for overt and covert shifts of visual attention, *Vis. Res.*, 40:1489–1506.
- Jacobs, A. M., 1987. Toward a model of eye movement control in visual search, in *Eye Movements: From Physiology to Cognition* (J. K. O’Regan and A. Levy-Schoe, eds.), Amsterdam: Elsevier Science, pp. 275–284.
- Jagadeesh, B., L. Chelazzi, M. Mishkin, and R. Desimone, 2001. Learning increases stimulus salience in anterior inferior temporal cortex of the macaque, *J. Neurophysiol.*, 86:290–303.
- Jonides, J., 1980. Towards a model of the mind’s eye’s movement, *Can. J. Psychol.*, 34:103–112.
- Jouve, B., P. Rosenstiehl, and M. Imbert, 1998. A mathematical approach to the connectivity between the cortical visual areas of the macaque monkey, *Cereb. Cortex.*, 8:28–39.
- Kapadia, M. K., M. Ito, C. D. Gilbert, and G. Westheimer, 1995. Improvement in visual sensitivity by changes in local context: parallel studies in human observers and V1 of alert monkeys, *Neuron*, 15:843–856.
- Kim, M. S., and K. R. Cave, 1995. Spatial attention in search for features and feature conjunctions, *Psychonom. Sci.*, 6:376–380.
- Kim, J. N., and M. N. Shadlen, 1999. Neural correlates of a decision in the dorsolateral prefrontal cortex of the macaque, *Nat. Neurosci.*, 2:176–185.
- Klein, R., A. Kingstone, and A. Pontefract, 1992. Orienting of visual attention, in *Eye Movements and Visual Cognition: Scene Perception and Reading* (K. Rayner ed.), New York: Springer-Verlag, pp. 46–65.
- Knierim, J. J., and D. C. Van Essen, 1992. Neuronal responses to static texture patterns in area V1 of the alert macaque monkey, *J. Neurophysiol.*, 67:961–980.
- Koch, C., and S. Ullman, 1985. Shifts in selective visual attention: towards the underlying neural circuitry, *Hum. Neurobiol.*, 4:219–227.
- Kowler, E., 1990. The role of visual and cognitive processes in the control of eye movement, in *Eye Movements and Their Role in Visual and Cognitive Processes* (E. Kowler ed.), Amsterdam: Elsevier Science, pp. 1–70.
- Kowler, E., E. Anderson, B. Doshier, and E. Blaser, 1995. The role of attention in the programming of saccades, *Vis. Res.*, 35:1897–1916.

- Kustov, A. A., and D. L. Robinson, 1996. Shared neural control of attentional shifts and eye movements, *Nature*, 384:74–77.
- Kusunoki, M., J. Gottlieb, and M. E. Goldberg, 2000. The lateral intraparietal area as a salience map: the representation of abrupt onset, stimulus motion, and task relevance, *Vis. Res.*, 40:1459–1468.
- Land, M. F., and M. Hayhoe, 2001. In what ways do eye movements contribute to everyday activities? *Vis. Res.*, 41(25–26): 3559–3565.
- Lee, C., W. H. Rohrer, and D. L. Sparks, 1988. Population coding of saccadic eye movements by neurons in the superior colliculus, *Nature*, 332:357–360.
- Liversedge, S. P., and J. M. Findlay, 2000. Saccadic eye movements and cognition, *Trends Cogn. Sci.*, 4:6–14.
- Luck, S., J. L. Chelazzi, S. A. Hillyard, and R. Desimone, 1997. Neural mechanisms of spatial selective attention in areas V1, V2, and V4 of macaque visual cortex, *J. Neurophysiol.*, 77:24–42.
- Lynch, J. C., A. M. Graybiel, and L. J. Lobeck, 1985. The differential projection of two cytoarchitectural subregions of the inferior parietal lobule of macaque upon the deep layers of the superior colliculus, *J. Comp. Neurol.*, 235:241–254.
- Lynch, J. C., V. B. Mountcastle, W. H. Talbot, and T. C. Yin, 1977. Parietal lobe mechanisms for directed visual attention, *J. Neurophysiol.*, 40:362–389.
- Maljkovic, V., and K. Nakayama, 1994. Priming of pop-out: I. Role of features, *Memory Cognition*, 22:657–672.
- Maljkovic, V., and K. Nakayama, 1996. Priming of pop-out: II. The role of position, *Percept. Psychophys.*, 58:977–991.
- McAdams, C. J., and J. H. Maunsell, 1999. Effects of attention on orientation-tuning functions of single neurons in macaque cortical area V4, *J. Neurosci.*, 19:431–441.
- McPeck, R. M., and E. L. Keller, 2001. Short-term priming, concurrent processing and saccade curvature during a target selection task in the monkey, *Vis. Res.*, 41:785–800.
- McPeck, R. M., V. Maljkovic, and D. Nakayama, 1999. Saccades require focal attention and are facilitated by a short-term memory system, *Vis. Res.*, 39:1555–1566.
- McPeck, R. M., A. A. Skavenski, and K. Nakayama, 2000. Concurrent processing of saccades in visual search, *Vis. Res.*, 40:2499–2516.
- Melcher, D., and E. Kowler, 2001. Visual scene memory and the guidance of saccadic eye movements, *Vis. Res.*, 41:3597–3611.
- Miller, E. K., and J. D. Cohen, 2001. An integrative theory of prefrontal cortex function, *Annu. Rev. Neurosci.*, 24:167–202.
- Miller, J. O., 1988. Discrete and continuous models of human information processing: theoretical distinctions and empirical results, *Acta Psychol.*, 67:191–257.
- Mohler, C. W., M. E. Goldberg, and R. H. Wurtz, 1973. Visual receptive fields of frontal eye field neurons, *Brain Res.*, 61:385–389.
- Moore, T., 1999. Shape representations and visual guidance of saccadic eye movements, *Science*, 285:1914–1917.
- Moran, J., and R. Desimone, 1985. Selective attention gates visual processing in the extrastriate cortex, *Science*, 23:782–784.
- Morel, A., and J. Bullier, 1990. Anatomical segregation of two cortical visual pathways in the macaque monkey, *Vis. Neurosci.*, 4:555–578.
- Motter, B. C., 1994a. Neural correlates of attentive selection for color or luminance in extrastriate area V4, *J. Neurosci.*, 14:2178–2189.
- Motter, B. C., and E. J. Belky, 1998. The guidance of eye movements during active visual search, *Vis. Res.*, 38:1805–1815.
- Motter, B. C., 1994b. Neural correlates of feature selective memory and pop-out in extrastriate area V4, *J. Neurosci.*, 14:2190–2199.
- Mountcastle, V. B., R. A. Andersen, and B. C. Motter, 1981. The influence of attentive fixation upon the excitability of the light-sensitive neurons of the posterior parietal cortex, *J. Neurosci.*, 1:1218–1235.
- Mountcastle, V. B., J. C. Lynch, A. Georgopoulos, H. Sakata, and C. Acuna, 1975. Posterior parietal association cortex of the monkey: command functions for operations within extrapersonal space, *J. Neurophysiol.*, 38:871–908.
- Mountcastle, V. B., B. C. Motter, M. A. Steinmetz, and A. K. Sestokas, 1987. Common and differential effects of attentive fixation on the excitability of parietal and prestriate (V4) cortical visual neurons in the macaque monkey, *J. Neurosci.*, 7:2239–2255.
- Muller, J. R., A. B. Metha, J. Krauskopf, and P. Lennie, 2001. Information conveyed by onset transients in responses of striate cortical neurons, *J. Neurosci.*, 21:6978–6990.
- Munoz, D. P., M. C. Dorris, M. Paré, and S. Everling, 2000. On your mark, get set: brainstem circuitry underlying saccadic initiation, *Can. J. Physiol. Pharmacol.*, 78:934–944.
- Munoz, D. P., and P. J. Istvan, 1998. Lateral inhibitory interactions in the intermediate layers of the monkey superior colliculus, *J. Neurophysiol.*, 79:1193–1209.
- Munoz, D. P., and R. H. Wurtz, 1993. Fixation cells in monkey superior colliculus. I. Characteristics of cell discharge, *J. Neurophysiol.*, 70:559–575.
- Munoz, D. P., and R. H. Wurtz, 1995. Saccade-related activity in monkey superior colliculus. I. Characteristics of burst and buildup cells, *J. Neurophysiol.*, 73:2313–2333.
- Murthy, A., K. G. Thompson, and J. D. Schall, 2001. Dynamic dissociation of visual selection from saccade programming in frontal eye field, *J. Neurophysiol.*, 86:2634–2637.
- Nodine, C. F., and E. A. Krupinski, 1998. Perceptual skill, radiology expertise, and visual test performance with NINA and WALDO, *Acad. Radiol.*, 5:603–612.
- Nodine, C. F., H. L. Kundel, S. C. Lauver, and L. C. Toto, 1996. Nature of expertise in searching mammograms for breast masses, *Acad. Radiol.*, 3:1000–1006.
- Olavarria, J. F., E. A. DeYoe, J. J. Knierim, J. M. Fox, and D. C. Van Essen, 1992. Neural responses to visual texture patterns in middle temporal area of the macaque monkey, *J. Neurophysiol.*, 68:164–181.
- Olivier, E. M., C. Dorris, and D. P. Munoz, 1999. Lateral interactions in the superior colliculus, not an extended fixation zone, can account for the remote distractor effect, *Behav. Brain Sci.*, 22:694–695.
- Oram, M. W., and D. L. Perrett, 1992. Time course of neural responses discriminating different views of the face and head, *J. Neurophysiol.*, 68:70–84.
- O'Regan, J. K., 1990. Eye movements and reading, in *Eye Movements and Their Role in Visual and Cognitive Processes* (E. Kowler ed.), Amsterdam: Elsevier Science, pp. 395–453.
- Ottes, F. P., J. A. M. van Gisbergen, and J. J. Eggermont, 1986. Visomotor fields of the superior colliculus: a quantitative model, *Vis. Res.*, 26:857–873.
- Ottes, F. P., J. A. M. van Gisbergen, and J. J. Eggermont, 1984. Metrics of saccade responses to visual double stimuli: two different modes, *Vis. Res.*, 24:1169–1179.
- Ottes, F. P., J. A. M. van Gisbergen, and J. J. Eggermont, 1985. Latency dependence of colour-based target vs non-target discrimination by the saccadic system, *Vis. Res.*, 25:849–862.

- Ottes, F. P., J. A. M. van Gisbergen, and J. J. Eggermont, 1987. Collicular involvement in a saccadic colour discrimination task, *Exp. Brain Res.*, 66:465–478.
- Paré, M., and D. P. Munoz, 1996. Saccadic reaction time in the monkey: advanced preparation of oculomotor programs is primarily responsible for express saccade occurrence, *J. Neurophysiol.*, 76:3666–3681.
- Paré, M., and R. H. Wurtz, 2001. Progression in neuronal processing for saccadic eye movements from parietal cortex area LIP to superior colliculus, *J. Neurophysiol.*, 85:2545–2562.
- Platt, M. L., and P. W. Glimcher, 1997. Response of intraparietal neurons to saccadic targets and visual distractors, *J. Neurophysiol.*, 78:1574–1589.
- Platt, M. L., and P. W. Glimcher, 1998. Response fields of intraparietal neurons quantified with multiple saccadic targets, *Exp. Brain Res.*, 121:65–75.
- Polat, U., K. Mizobe, M. W. Pettet, T. Kasamatsu, and A. M. Norcia, 1998. Collinear stimuli regulate visual responses depending on cell's contrast threshold, *Nature*, 391:580–584.
- Posner, M., 1980. Orienting of attention, *Q. J. Exp. Psychol.*, 32:3–25.
- Powell, K. D., and M. E. Goldberg, 2000. Response of neurons in the lateral intraparietal area to a distractor flashed during the delay period of a memory-guided saccade, *J. Neurophysiol.*, 84:301–310.
- Rainer, G., W. F. Asaad, and E. K. Miller, 1998. Selective representation of relevant information by neurons in the primate prefrontal cortex, *Nature*, 393:577–579.
- Remington, R. W., 1980. Attention and saccadic eye movements, *J. Exp. Psychol. Hum. Percept. Perform.*, 6:726–744.
- Reuter-Lorenz, P., and A. R. Fendrich, 1992. Oculomotor readiness and covert orienting: differences between central and peripheral precursors, *Percept. Psychophys.*, 52:336–344.
- Reynolds, J. H., L. Chelazzi, and R. Desimone, 1999. Competitive mechanisms subserve attention in macaque areas V2 and V4, *J. Neurosci.*, 19:1736–1753.
- Richmond, B. J., and T. Sato, 1987. Enhancement of inferior temporal neurons during visual discrimination, *J. Neurophysiol.*, 58:1292–1306.
- Ringach, D. L., M. J. Hawken, and R. Shapley, 1997. Dynamics of orientation tuning in macaque primary visual cortex, *Nature*, 387:281–284.
- Robinson, D. A., 1972. Eye movements evoked by collicular stimulation in the alert monkey, *Vis. Res.*, 12:1795–1808.
- Robinson, D. L., E. M. Bowman, and C. Kertzman, 1995. Covert orienting of attention in macaques II. Contributions of parietal cortex, *J. Neurophysiol.*, 74:698–712.
- Robinson, D. L., M. E. Goldberg, and G. B. Stanton, 1978. Parietal association cortex in the primate: sensory mechanisms and behavioral modulations, *J. Neurophysiol.*, 41:910–932.
- Robinson, D. L., and J. W. McClurkin, 1989. The visual superior colliculus and pulvinar, in *The Neurobiology of Saccadic Eye Movements* (R. H. Wurtz and M. E. Goldberg, eds.), New York: Elsevier, pp. 337–360.
- Romo R., C. D. Brody, A. Hernandez, and L. Lemus, 1999. Neuronal correlates of parametric working memory in the prefrontal cortex, *Nature*, 399:470–473.
- Rossi, A., F. R. Desimone, and L. G. Ungerleider, 2001. Contextual modulation in primary visual cortex of macaques, *J. Neurosci.*, 21:1698–1709.
- Saito, H., M. Yukie, K. Tanaka, K. Kikosaka, Y. Fukada, and E. Iwai, 1986. Integration of direction signals of image motion in the superior temporal sulcus of the macaque monkey, *J. Neurosci.*, 6:145–157.
- Sato, T., 1988. Effects of attention and stimulus interaction on visual responses of inferior temporal neurons in macaque, *J. Neurophysiol.*, 60:344–364.
- Sato, T., A. Murthy, K. G. Thompson, and J. D. Schall, 2001. Search efficiency but not response interference affects visual selection in frontal eye field, *Neuron*, 30:583–591.
- Schall, J. D., 1991. Neuronal activity related to visually guided saccades in the frontal eye fields of rhesus monkeys: comparison with supplementary eye fields, *J. Neurophysiol.*, 66:559–579.
- Schall, J. D., 1997. Visuomotor areas of the frontal lobe, in *Cerebral Cortex*, vol. 12, *Extra striate Cortex of Primates* (K. Rockland, A. Peters, and J. H. Kaas, eds.), New York: Plenum Press, pp. 527–638.
- Schall, J. D., and D. P. Hanes, 1993. Neural basis of saccade target selection in frontal eye field during visual search, *Nature*, 366:467–469.
- Schall, J. D., D. P. Hanes, K. G. Thompson, and D. J. King, 1995a. Saccade target selection in frontal eye field of macaque I. Visual and premovement activation, *J. Neurosci.*, 15:6905–6918.
- Schall, J. D., A. Morel, D. J. King, and J. Bullier, 1995b. Topography of visual cortical afferents to frontal eye field in macaque: Functional convergence and segregation of processing streams, *J. Neurosci.*, 15:4464–4487.
- Schall, J. D., and K. G. Thompson, 1999. Neural selection and control of visually guided eye movements, *Annu. Rev. Neurosci.*, 22:241–259.
- Schiller, P. H., and I. H. Chou, 1998. The effects of frontal eye field and dorsomedial frontal cortex lesions on visually guided eye movements, *Nat. Neurosci.*, 1:248–253.
- Schiller, P. H., and F. Koerner, 1971. Discharge characteristics of single units in superior colliculus of the alert rhesus monkey, *J. Neurophysiol.*, 34:920–936.
- Schiller, P. H., J. H. Sandell, and J. H. R. Maunsell, 1987. The effect of frontal eye field and superior colliculus lesions on saccadic latencies in the rhesus monkey, *J. Neurophysiol.*, 57:1033–1049.
- Schlag, J., and M. Schlag-Rey, 1984. Visuomotor functions of central thalamus in monkey. II. Unit activity related to visual events, targeting, and fixation, *J. Neurophysiol.*, 51:1175–1195.
- Schmolesky, M. T., Y. Wang, D. P. Hanes, K. G. Thompson, S. Leutgeb, J. D. Schall, and A. G. Leventhal, 1998. Signal timing across the macaque visual system, *J. Neurophysiol.*, 79:3272–3278.
- Scudder, C. A., C. S. Kaneko, and A. F. Fuchs, 2002. The brainstem burst generator for saccadic eye movements: a modern synthesis, *Exp. Brain Res.*, 142:439–462.
- Segraves, M. A., 1992. Activity of monkey frontal eye field neurons projecting to oculomotor regions of the pons, *J. Neurophysiol.*, 68:1967–1985.
- Segraves, M. A., and M. E. Goldberg, 1987. Functional properties of corticotectal neurons in the monkey's frontal eye fields, *J. Neurophysiol.*, 58:1387–1419.
- Seidemann, E., and W. T. Newsome, 1999. Effect of spatial attention on the responses of area MT neurons, *J. Neurophysiol.*, 81:1783–1794.
- Sereno, M. I., S. Pitzalis, and A. Martinez, 2001. Mapping of contralateral space in retinotopic coordinates by a parietal cortical area in humans, *Science*, 294:1350–1354.

- Sheinberg, D. L., and N. K. Logothetis, 2001. Noticing familiar objects in real world scenes: the role of temporal cortical neurons in natural vision, *J. Neurosci.*, 21:1340–1350.
- Sheliga, B., M. L. Riggio, and G. Rizzolatti, 1995. Spatial attention and eye movements, *Exp. Brain Res.*, 105:261–275.
- Shepherd, M., J. M. Findlay, and R. J. Hockey, 1986. The relationship between eye movements and spatial attention, *Q. J. Exp. Psychol.*, 38A:475–491.
- Sillito, A. M., K. L. Grieve, H. E. Jones, J. Cudeiro, and J. David, 1996. Visual cortical mechanisms detecting focal orientation discontinuities, *Nature*, 378:492–296.
- Snyder, L. H., A. P. Batista, and R. A. Andersen, 2000. Intention-related activity in the posterior parietal cortex: a review. *Vis. Res.*, 40:1433–1441.
- Sommer, M. A., and E. J. Tehovnik, 1997. Reversible inactivation of macaque frontal eye field, *Exp. Brain Res.*, 116:229–249.
- Sommer, M. A., and R. H. Wurtz, 1998. Frontal eye field neurons orthodromically activated from the superior colliculus, *J. Neurophysiol.*, 80:3331–3335.
- Sommer, M. A., and R. H. Wurtz, 2000. Composition and topographic organization of signals sent from the frontal eye field to the superior colliculus, *J. Neurophysiol.*, 83:1979–2001.
- Sommer, M. A., and R. H. Wurtz, 2001. Frontal eye field sends delay activity related to movement, memory, and vision to the superior colliculus, *J. Neurophysiol.*, 85:1673–1685.
- Sparks, D. L., 1978. Functional properties of neurons in the monkey superior colliculus: coupling of neuronal activity and saccade onset, *Brain Res.*, 156:1–16.
- Sparks, D. L., and R. Hartwich-Young, 1989. The deep layers of the superior colliculus, in *The Neurobiology of Saccadic Eye Movements* (R. H. Wurtz and M. E. Goldberg, eds.), Amsterdam: Elsevier, pp. 213–255.
- Stanton, G. B., M. E. Goldberg, and C. J. Bruce, 1988. Frontal eye field efferents in the macaque monkey: I. Subcortical pathways and topography of striatal and thalamic terminal fields, *J. Comp. Neurol.*, 271:473–492.
- Stanton, G. B., C. J. Bruce, and M. E. Goldberg, 1993. Topography of projections to the frontal lobe from the macaque frontal eye fields, *J. Comp. Neurol.*, 330:286–301.
- Stanton, G. B., C. J. Bruce, and M. E. Goldberg, 1995. Topography of projections to posterior cortical areas from the macaque frontal eye fields, *J. Comp. Neurol.*, 353:291–305.
- Steinmetz, M. A., C. E. Connor, C. Constantinidis, and J. R. McLaughlin, Jr., 1994. Covert attention suppresses neuronal responses in area 7a of the posterior parietal cortex, *J. Neurophysiol.*, 72:1020–1023.
- Steinmetz, M. A., and C. Constantinidis, 1995. Neurophysiological evidence for a role of posterior parietal cortex in redirecting visual attention, *Cereb. Cortex*, 5:448–456.
- Sternberg, S., 1969. The discovery of processing stages: extensions of Donders' method, *Acta Psychol.*, 30:276–315.
- Sugase, Y., S. Yamane, S. Ueno, and K. Kawano, 1999. Global and fine information coded by single neurons in the temporal visual cortex, *Nature*, 400:869–873.
- Theeuwes, J., 1991. Cross dimensional perceptual selectivity, *Percept. Psychophys.*, 50:184–193.
- Theeuwes, J. A., F. Kramer, S. Hahn, and D. E. Irwin, 1998. Our eyes do not always go where we want them to go: capture of the eyes by new objects, *Psychol. Sci.*, 9:379–385.
- Thompson, K. G., N. P. Bichot, and J. D. Schall, 1997. Dissociation of target selection from saccade planning in macaque frontal eye field, *J. Neurophysiol.*, 77:1046–1050.
- Thompson, K. G., N. P. Bichot, and J. D. Schall, 2001. From attention to action in frontal cortex, in *Visual Attention and Cortical Circuits* (J. Braun, C. Koch, and J. Davis, eds.), Cambridge, MA: MIT Press, pp. 137–157.
- Thompson, K. G., D. P. Hanes, N. P. Bichot, and J. D. Schall, 1996. Perceptual and motor processing stages identified in the activity of macaque frontal eye field neurons during visual search, *J. Neurophysiol.*, 76:4040–4055.
- Thompson, K. G., and J. D. Schall, 1999. The detection of visual signals by macaque frontal eye field during masking, *Nat. Neurosci.*, 2:283–288.
- Thompson, K. G., and J. D. Schall, 2000. Antecedents and correlates of visual detection and awareness in macaque prefrontal cortex, *Vis. Res.*, 40:1523–1538.
- Tolias, A., S. T. Moore, S. M. Smirnakis, E. J. Tehovnik, A. G. Siapas, and P. H. Schiller, 2001. Eye movements modulate visual receptive fields of V4 neurons, *Neuron*, 29:757–767.
- Tovée, M. J., E. T. Rolls, A. Treves, and R. P. Bellis, 1993. Information encoding and the responses of single neurons in the primate temporal visual cortex, *J. Neurophysiol.*, 70:640–654.
- Treisman, A., 1988. Features and objects: The Fourteenth Bartlett Memorial Lecture, *Q. J. Exp. Psychol.*, 40A:201–237.
- Treisman, A., and T. Sato, 1990. Conjunction search revisited, *J. Exp. Psychol. Hum. Percept. Perform.*, 16:459–478.
- Treue, S., and J. H. Maunsell, 1999. Effects of attention on the processing of motion in macaque middle temporal and medial superior temporal visual cortical areas, *J. Neurosci.*, 19:7591–7602.
- van Gisbergen, J. A. M., A. J. van Opstal, and A. A. M. Tax, 1987. Collicular ensemble coding of saccades based on vector summation, *Neuroscience*, 21:541–555.
- van Opstal, A. J., and J. A. M. van Gisbergen, 1989. A nonlinear model for colliculus spatial interactions underlying the metrical properties of electrically elicited saccades, *Biol. Cybern.*, 60:171–183.
- Viviani, P., 1990. Eye movements in visual search: cognitive, perceptual and motor control aspects, in *Eye Movements and Their Role in Visual and Cognitive Processes* (E. Kowler ed.), Amsterdam: Elsevier Science, pp. 353–393.
- Vogels, R., and G. A. Orban, 1991. Quantitative study of striate single-unit responses in monkeys performing an orientation discrimination task, *Exp. Brain Res.*, 84:1–11.
- von der Heydt, R., and E. Peterhans, 1989. Mechanisms of contour perception in monkey visual cortex. I. Lines of pattern discontinuity, *J. Neurosci.*, 9:1731–1748.
- Wallis, J. D., K. C. Anderson, and E. K. Miller, 2001. Single neurons in prefrontal cortex encode abstract rules, *Nature*, 411:953–956.
- White, I. M., and S. P. Wise, 1999. Rule-dependent neuronal activity in the prefrontal cortex, *Exp. Brain Res.*, 126:315–335.
- Wolfe, J. M., 1994. Guided search 2.0: A revised model of visual search, *Psychol. Bull. Rev.*, 1:202–238.
- Wolfe, J. M., 1998. Visual search, in *Attention* (H. Pashler ed.), East Sussex, UK: Psychological Press. pp. 13–74.
- Wurtz, R. H., M. A. Basso, M. Paré, and M. A. Sommer, 2000. The superior colliculus and the cognitive control of movement, in *The New Cognitive Neurosciences*, 2nd ed. (M. S. Gazzaniga ed.), Cambridge, MA: MIT Press, pp. 573–587.
- Wurtz, R. H., and M. E. Goldberg, 1972. Activity of superior colliculus in behaving monkey: III. Cells discharging before eye movements, *J. Neurophysiol.*, 35:575–586.

- Wurtz, R. H., and C. W. Mohler, 1976a. Organization of monkey superior colliculus: enhanced visual response of superficial layer cells, *J. Neurophysiol.*, 39:745–765.
- Wurtz, R. H., and C. W. Mohler, 1976b. Enhancement of visual response in monkey striate cortex and frontal eye fields, *J. Neurophysiol.*, 39:766–772.
- Yarbus, A. L., 1967. *Eye Movements and Vision*, New York: Plenum Press.
- Zelinsky, G. J., and D. L. Sheinberg, 1997. Eye movements during parallel-serial search, *J. Exp. Psychol.: Hum. Percept. Perform.*, 23:244–262.
- Zipser, K. V., A. F. Lamme, and P. H. Schiller, 1996. Contextual modulation in primary visual cortex, *J. Neurosci.*, 16:7376–7389.

93 Visual Perception during Saccades

DAVID C. BURR AND M. CONCETTA MORRONE

WE FREQUENTLY REPOSITION our gaze by making rapid ballistic eye movements called *saccades* in order to focus the fovea on visual areas under scrutiny. While the strategy is highly efficient for the visual system, allowing it to analyze the whole visual field with the high resolution of the fovea, it poses several problems for perception. Saccades cause rapid large-field motion on the retina, potentially confusable with large-field motion in the external world. They also change the relationship between external space and retina position, confounding information about visual direction. Much effort has been made in recent years to attempt to understand the effects of saccades on visual function. Evidence suggests that saccades trigger two distinct neural processes: a suppression of visual sensitivity, specific to motion analysis, probably mediated by the magnocellular pathway, and a gross perceptual distortion of visual space just before the repositioning of gaze. While the evidence for these phenomena is strong, their functional role for perception is less clear, leaving several areas of inquiry still open.

Saccades are ballistic movements of the eyes made to reposition our gaze. They can be deliberate, but normally they are automatic and go unnoticed. Not only do the actual eye movements escape notice, but so does the image motion they cause and the fact that gaze itself has been repositioned. The first to document this problem was probably the Persian scholar Alhazen: "For if the eye moves in front of visible objects while they are being contemplated, the form of every one of the objects facing the eye . . . will move on the eye as the latter moves. But sight has become accustomed to the motion of the objects' forms on its surface when the objects are stationary, and therefore does not judge the object to be in motion" (Alhazen, 1083, p. 194; see Howard, 1996). Much later, Helmholtz (1866) argued that image motion caused by eye movements is *sensed* but not perceived. He further claimed that, together with "the effort of will involved in trying to alter the adjustment of the eyes," eye movement-induced retinal motion is used to maintain constancy of visual direction during and after saccades. Sperry (1950) and Von Holst and Mittelstädt (1954) expanded on Helmholtz's ideas in the 1950s with two closely related theories. They suggested that saccades were accompanied by a *corollary discharge* (Sperry, 1950) or an *effference copy* (Von Holst and Mittelstädt, 1954) of the motor signal and that this information was used to cancel image motion caused by saccades. This idea was popular, but it has become less

plausible with the realization that motion is probably analyzed by specialized mechanisms distinct from those signaling spatial position, and can therefore not simply be annulled by a contrary displacement signal (Burr and Ross, 1986).

An alternative potential source of extraretinal information about the eye position is proprioceptive signals from extraocular muscles: Sherrington's (1918) *inflow* theory. However, this theory has serious difficulty explaining perceptual effects that precede eye movement, given the latencies involved. Nevertheless, recent evidence suggests that proprioceptive feedback might contribute to stability, although the feedback loop has a high threshold and low gain (Bridgeman and Stark, 1991; Gauthier et al., 1988) and is certainly not sufficient to annul completely the effects of saccadic image motion. Historical accounts of early work and the debate between inflow and outflow theories are to be found elsewhere (e.g., Bridgeman et al., 1994; Carpenter, 1977).

Saccadic suppression

Another idea to emerge early in the twentieth century was that visual sensitivity is actively reduced during saccades. Holt (1903) concluded that saccades "condition a momentary visual central anaesthesia," a loss of sensitivity. However, evidence for suppression by saccades is contradictory. Many researchers (Krauskopf et al., 1966; Latour, 1962; Zuber and Stark, 1966) have reported weak threshold elevation for detecting spots of light flashed briefly during saccades (two- to threefold), and Krauskopf et al. (1966) found no threshold elevation at all. By contrast, Bridgeman et al. (1975) reported a strong reduction in sensitivity for detecting displacement during saccades when the displacement occurred at about the same time as the start of a saccade.

Dodge (1900) and Woodworth (1906) concluded that there was no requirement for a central change in visual functions, arguing that image motion during saccades was too rapid to be seen and caused what Campbell and Wurtz (1978) later termed a *grayout*. However, measurements of contrast sensitivity (during normal vision) show that this idea cannot be generally true. Although stimuli of high spatial frequency become unresolvable at saccadic speeds, stimuli of low spatial frequency can be seen only in motion but become considerably more visible at saccadic speeds (Burr and Ross,

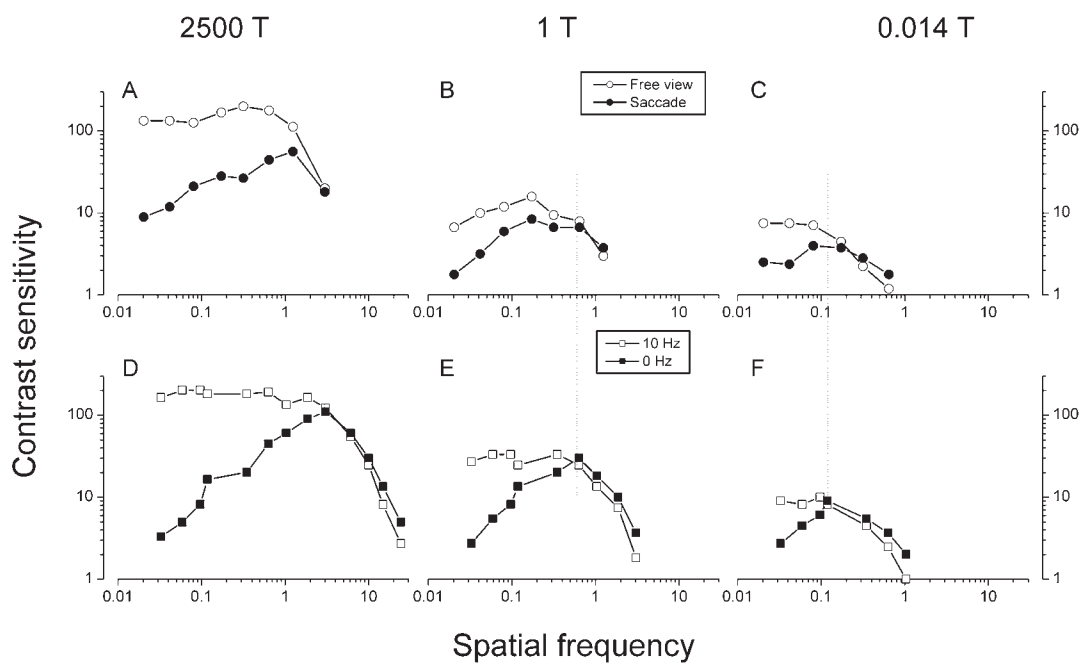


FIGURE 93.1. *A–C*, Contrast sensitivity for detecting a horizontal grating briefly displayed either at the beginning of a large (30 degrees) horizontal saccade (*filled circles*) or during free viewing (*open circles*). Measurements were made for 2500 trolands, 1 troland, and 0.014 troland. Sensitivity is greater during normal than saccadic viewing at low spatial frequencies, but the two curves converge at high frequencies; the point of convergence decreases steadily with retinal illuminance. Note that at the higher spatial frequencies of the lowest illuminance (*C*), contrast sensitivity was actually higher during saccades than during normal vision (see also Fig. 93.2). Measurements were not made above 3 c/deg, as the large

saccade would cause smearing of the grating. *D–F*, Contrast sensitivity for continuously displaced horizontal gratings, either stationary (*filled squares*) or drifting at 10 Hz (*open squares*). There is an advantage for drifting gratings at low spatial frequencies. The spatial frequency at which the motion curve peels away from the stationary curve changes with illuminance and corresponds very closely to the point at which the sensitivity during saccades (*above*) diverge from normal sensitivity, strongly suggesting that motion mechanisms are selectively suppressed during saccades. (Data reproduced with permission from Burr et al., 1982.)

1982). Thus, during saccades, the normally invisible low spatial frequencies that predominate in natural scenes (Field, 1987) should become abruptly salient, posing a potential problem for vision.

It seems that at least part of the reason motion is not seen during saccades is that the low spatial frequencies that would normally be so conspicuous are suppressed during saccades (Burr et al., 1982, 1994; Volkman et al., 1978). An example of this frequency-dependent suppression is shown in Figure 93.1*A–C*, which compares contrast sensitivity for detecting briefly flashed horizontal gratings during saccades (*filled symbols*) with that for fixation (*open symbols*). Sensitivity is very similar at the higher spatial frequencies, but at low spatial frequencies sensitivity during saccades is reduced sharply, reaching a tenfold reduction of sensitivity at 0.02 c/deg; these are the very frequencies that would otherwise be visible and highly conspicuous during saccades. The selectivity for spatial frequency might explain some of the conflicting data from earlier studies. Loss of sensitivity should depend on the spatial frequency content of the experimental stimuli, typically high (e.g., small spots of light) in the luminance threshold studies (Krauskopf et al., 1966;

Latour, 1962; Zuber and Stark, 1966) but low (large targets) in displacement studies (Bridgeman et al., 1975).

Burr et al. (1982) also reported qualitative changes in motion perception during saccades. Observers viewed at close distance a high-contrast scene back-projected through a deflectable mirror. Displacing the scene abruptly at saccadic speeds and amplitudes caused a strong sensation of motion that instantly commanded attention. However, if the displacements of the scene were the result of a saccade, the motion was sensed, but lacked the salience and the alarming sensation that usually accompany fast motion in normal viewing: subjects observed that the image had been displaced, but they did not report feeling startled. This qualitative impression, together with Bridgeman et al. (1975) demonstrations of large desensitization to displacement during saccades, suggested that the frequency selectivity of the suppression may reflect desensitization of motion mechanisms.

A good deal of evidence points to motion desensitization during saccades. However, it should be pointed out that it is difficult to test motion directly during saccades, for several important technical reasons. One is that, by definition,

motion requires moderately long stimulus durations, necessarily exceeding the duration of maximal saccadic suppression. Another is that the movement of the eyes will introduce image motion, which is difficult to take into account accurately in calculating the real retinal velocity of external motion. However, it is possible to infer the action of motion mechanisms using brief stimuli that contain a wide range of temporal frequencies and hence will excite motion mechanisms (tuned to all directions) as well as mechanisms that respond best to stationary stimuli.

An attempt to do this is shown in Figure 93.1. As mentioned earlier, sensitivity during saccades becomes progressively compromised at low spatial frequencies, while at higher spatial frequencies, above 3 c/deg, there is virtually no suppression at all. Figure 93.1D–F shows steady-state sensitivity measurements for stationary and drifting (10 Hz) gratings measured under comparable conditions. As had been well documented previously (Burr and Ross, 1982), gratings in motion are more conspicuous at low spatial frequencies. Importantly, the spatial frequency at which sensitivity for drifting gratings begins to exceed that of stationary gratings is very similar to the spatial frequency at which saccadic suppression begins (illustrated by the vertical dashed lines). As brief stimuli comprise a wide range of temporal frequencies, the similarity in frequency ranges suggests that it is the motion mechanism that is selectively impaired during saccades. To be certain that the correspondence in spatial frequency was not merely a coincidence, the measurements were repeated at two lower levels of illumination. At all three levels of illuminance, both sets of curves—sen-

sitivity to brief displays in normal and saccadic viewing and sensitivity to continuously drifting or stationary stimuli—peeled apart at about the same spatial frequency, consistent with the suggestion that the mechanisms suppressed during saccades are those responsible for the higher sensitivity to motion in normal viewing.

Despite the problems in examining motion perception directly during saccades, there have been several attempts to do so. For example, thresholds for detecting an abrupt change in the speed of a drifting grating are far poorer during saccades than during normal vision (Burr et al., 1982). The discrimination of motion of random-dot patterns is also severely impaired during saccades (Ilg and Hoffmann, 1993; Shiori and Cavanagh, 1989). And discrimination of two-frame motion sequences is severely impaired when one frame is presented near saccadic onset (Burr et al., 1999).

What may be the mechanism whereby motion sensitivity is reduced? Recent anatomical and physiological advances have shown that vision, at least in the early stages of visual analysis, is processed through two largely independent streams: the magno- and parvocellular systems (see Chapter 30). Although these two systems are not completely separate, parvocellular function can be probed by using equiluminant stimuli, which are modulated in color but not in luminance. The magno system there may respond spuriously to some equiluminant stimuli, but it is known to be incapable of color discriminations (Merigan, 1989). Figure 93.2 shows forced-choice discriminations of either the color of equiluminant red-green stimuli or the luminance of equichromatic yellow-

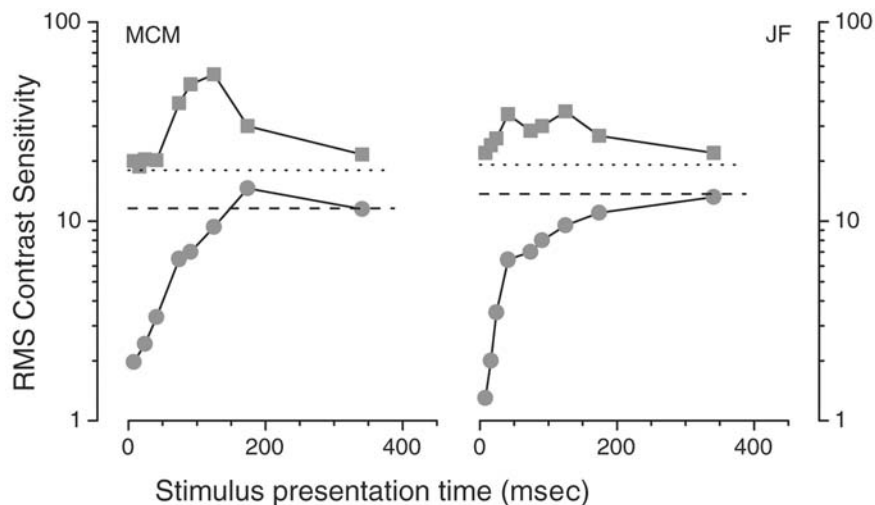


FIGURE 93.2. Contrast sensitivity for discriminating the color or the luminance of a broad horizontal bar briefly presented at a given time after the onset of a saccade (abscissa) for two subjects. Bars were modulated either in color (equiluminant red-green: *square symbols*) or in luminance (yellow-black: *circle symbols*). Sensitivity is expressed as the inverse of rms cone contrast. The dotted line

shows the chromatic sensitivity in free viewing, the dashed line the luminance sensitivity. Note that not only is there no desensitisation for chromatic discrimination just after the saccade, there is actually a marked increase in sensitivity for a period of up to 200 msec after the saccade. (Data reproduced with permission from Burr et al., 1994.)

black stimuli (both of very low spatial frequency) as a function of time after saccadic onset. Luminance discrimination (*filled circles*) was severely impaired just after saccadic onset, by one log unit, steadily improving to normal levels over a 200 msec period. Chromatic sensitivity (*filled squares*), on the other hand, was not at all impaired at around the time of the saccade, and actually improved over the period following the saccade, by approximately a factor of 2. This is an example of saccadic enhancement of contrast sensitivity, similar to that previously observed by Burr et al. (1982) for relatively high frequencies of luminance modulation (see Figure 93.1C) that presumably stimulate the same P-pathways.

These results, showing that equiluminant stimuli (irrespective of the spatial frequency) are not suppressed during saccades and can actually be enhanced, imply that saccadic suppression is specific to the magnocellular pathway. The parvocellular pathway, essential for chromatic discrimination, is left unimpaired. Using a different technique, Uchikawa and Sato (1995) arrived at a similar conclusion. They measured incremental spectral sensitivity for detecting monochromatic discs displayed against a white background during normal viewing and saccades. They showed that during saccades, the spectral sensitivity curve showed a marked decrease at ~570 nm (known as *Sloan's notch*), a clear signature of the spectrally opposed mechanisms of the parvocellular system. In normal viewing, this decrease was absent (for brief stimuli), suggestive of magnocellular function. Their results are replotted in Figure 93.3, together with representative measurements of responses of P and M retinal ganglion cells of macaque monkey. The psychophysical detection thresholds during normal viewing follow closely the responses of M cells, while during saccades they are more like those of P cells.

A fundamental question provoked by these studies was whether saccadic suppression results from a central signal, such as the corollary discharge proposed by Sperry (1950) and Von Holst and Mittelstädt (1954), or whether the visual motion caused by the eye movement itself masks vision during saccades (Campbell and Wurtz, 1978; Castet et al., 2001; MacKay, 1970, 1973). There is good evidence that image motion of the kind caused by saccades can mask brief stimuli (Campbell and Wurtz, 1978; Derrington, 1984; MacKay, 1973), but is this the only, or indeed the principal, mechanism at work? Diamond et al. (2000) simulated visual saccades by optically deflecting the display at suitable speed, amplitude, and acceleration, and measured contrast sensitivity to briefly displayed gratings. When the target gratings were displayed on an otherwise blank screen, simulated saccades had little effect on thresholds compared with real saccades. However, when a high-contrast random pattern was added to the display to provide a strong spurious visual motion signal, the simulated saccade produced a suppression

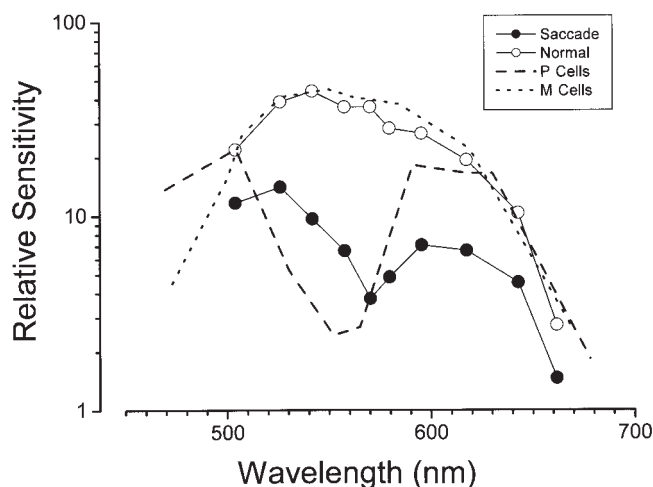


FIGURE 93.3. Sensitivity (in relative units) for detecting a monochromatic bar briefly presented on a white background in normal viewing (*open circles*) or at the onset of a 6 degree saccade. In normal viewing, the curve has a broad peak around 550 nm and closely follows the sensitivity of a sample of retinal M cells in the macaque monkey (taken from Zrenner, 1983). During saccades, however, the form of the curves changes dramatically to reveal Sloan's notch, a sharp dip in sensitivity at around 570 nm. The dashed lines show the average response of a population of P cells. While not following the human sensitivity data exactly, they show the same characteristic dip for middle wavelengths. This is very strong evidence for suppression of magnocellular activity during saccades. (Adapted with permission from Uchikawa and Sato, 1995, and Zrenner, 1983.)

that was comparable in magnitude to and lasted longer than that produced by the real saccade. This result suggests that visual masking can be important for vision at around the time of saccades but that it is not the only mechanism. There must also be a signal of nonvisual origin that accompanies each real saccade to decrease sensitivity to low-frequency, luminance-modulated stimuli. Other evidence for a non-visual suppression signal is that visual phosphenes generated by applying weak electrical signals to the eye in darkness are suppressed during saccades by a comparable amount to real light images (Riggs et al., 1974).

The similarity between the time course of saccadic suppression and visual masking observed by Diamond et al. (2000) could indicate that these two phenomena have a common site of action. This seems reasonable, given the evidence that saccadic suppression occurs early, preceding the site of contrast masking (Burr et al., 1994) and motion analysis (Burr et al., 1999). One interesting possibility is that both saccadic suppression and masking act on *contrast gain mechanisms* of cortical and/or geniculate cells. This idea predicts that saccades should not only decrease sensitivity, as shown in Figures 93.1 and 93.2, but should also cause the system to respond more rapidly. This is what occurs. During saccades, the temporal impulse response function

becomes more rapid (Burr and Morrone, 1996), as many models of contrast gain (e.g., Shapley and Victor, 1981) would predict.

The fact that the impulse response accelerates rather than decelerates during saccades suggests that although strongly attenuated, the magno system remains active during saccades (a parvo-dominated response should be slower). This is consistent with experiments demonstrating that under certain conditions, saccades in the direction of a rapidly moving, high-contrast grating can improve direction discrimination of that stimulus (Castet and Masson, 2000; Garcia-Perez and Peli, 2001). While these demonstrations clearly do not refute the existence of a centrally driven suppression mechanism, they do highlight the important point that centrally driven saccadic suppression only attenuates motion detection, not eliminating it completely, leaving an important role for other mechanisms, such as masking, in natural (usually visually rich) viewing conditions (Campbell and Wurtz, 1978; Derrington, 1984; Diamond et al., 2000; MacKay, 1973).

The studies discussed above all refer to moderate to large saccades and might not be applicable to the microsaccades that are normally made, together with slow drifts, around the fixation point. Most evidence suggests that small saccades cause little or no threshold elevation (Krauskopf et al., 1966; Sperling, 1990), indicating that the effects of the image tremor may be controlled by other means. Murakami and Cavanagh (1998, 2001) recently proposed that the retinal motion generated by microsaccades is eliminated by subtracting a baseline speed, estimated from the minimal retinal *jitter*, from the velocity signals of local-motion detectors. Evidence favoring this model is derived from the observation that if a region of the retina is adapted to jittering motion and a static pattern is subsequently inspected, the unadapted (but not the adapted) region appears to jitter. Murakami and Cavanagh claim that the reduction in motion sensitivity caused by adaptation reduces the estimate of the baseline jitter so that the motion caused by eye jitter becomes superthreshold in the unadapted region and hence visible. This idea is particularly interesting in the context of older theories that suggested that stabilization is achieved by subtraction of extraretinal signals. In such cases, there is subtraction of a speed scalar (not a spatial displacement vector) from velocity estimates that have been extracted by specialized motion detectors.

In conclusion, human psychophysical data clearly suggest an extraretinal suppression of early visual activity during saccades. There is also much neurophysiological evidence pointing to the underlying neural mechanisms of suppression, but there is no clear consensus on this: some studies show clear evidence of suppression, but others do not. Still others point to more complicated effects, such as an inversion of directional selectivity of MT cells during saccades

(Thiele et al., 2002). For a recent review of some of this literature, readers are referred to Ross et al. (2001).

Perceived position

Retinal motion is not the only problem introduced by saccades. A related problem is how the visual system manages to maintain a stable sense of visual direction while the retinal input is constantly changing. Helmholtz (1866) believed that the constancy of perceived position was maintained during and after saccades, because both extraretinal information (the *effort of will*) and retinal information (sensed but not perceived image motion) were used to recalibrate the direction of gaze.

Leonard Matin and colleagues (Matin, 1972; Matin and Pearce, 1965; Matin et al., 1969, 1970) and Bischof and Kramer (1968) were among the first to find errors in localization at the time of eye movements. Figure 93.4A replots data from Bischof and Kramer showing the perceived position of a stimulus briefly flashed at a variable interval after observers initiated a 16 degree saccade. There is a strong mislocalization immediately after the saccade onset in the direction of the saccade, about half of its amplitude. Halfway through the saccade, the direction of the misperception inverts before returning to veridical. This experiment has since been replicated by many observers, including Honda (1989, 1991, 1993), Schlag and Schlag-Rey (1995), and Dassonville et al. (1992). The curve in Figure 93.4 was replotted in a more recent study by Ross et al. (1997) that measured the perceived position of a bar briefly flashed at various times over a period preceding and following the saccade. The results are quite similar to those of Bischof and Kramer (except for the rebound after the saccade in this instance, although it has been observed under other conditions). They also show that the mislocalizations precede the saccade, before the eye has begun to move, reaching a maximum at around saccadic onset. The maximum shift is again about half the size of the saccade, suggesting a relative gain of 0.5, as observed by others (Bridgeman, 1995).

If the errors in localization are to compensate for eye movements, they should be in the same direction as the saccade. However, this is not always the case, as first observed by Bischof and Kramer (1968) and studied systematically by Ross et al. (1997). Figure 93.5A shows reports of perceived positions of visual targets presented just before a saccade as a function of the actual position of the bar. The small symbols show data on when the bars were flashed during control fixation conditions: localization was veridical and accurate. However, when the same bar was flashed to the stationary eye just prior to a saccade, it was seen to be displaced, but the direction of the displacement depended critically on its position. Bars flashed to the left of the

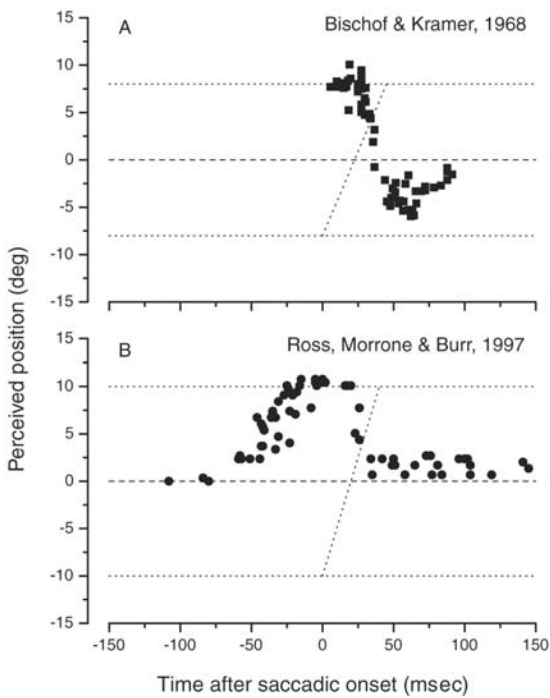


FIGURE 93.4. Perceived positions for stimuli briefly presented at various times relative to the onset of a rightward horizontal saccade (shown by the dotted lines). The dashed line shows the veridical position of the target. The upper curve show data reproduced from Figure 3 of Bischof and Kramer (1968), the lower curves from Figure 1 of Ross et al. (1997). Both data show a strong mislocalization of maximal strength near the onset of the saccade.

saccadic target were displaced rightward, in the direction of the saccade. However, bars flashed beyond the saccadic target were displaced leftward, against the direction of the saccade, resulting in a general compression. This compression is powerful enough to remove vernier offsets for line targets that are flashed at about the time of saccade onset and can create offsets for collinear line targets flashed at different times (75 msec apart). Compression can even cause four bars, flashed to straddle the saccadic target, to merge into a single bar and severely distorts natural scenes. Because the relative distance between objects does not depend on retinal coordinates in these conditions, this emphasizes how large the perceptual compression can be.

Compression does not always accompany saccades. For example, Cai et al. (1997) reported no compression occurring under the conditions of their experiment. The issue was at least partially resolved by Lappe et al. (2000), who reported compression only in conditions where visual referents were perceived after the saccade. Another major difference is that in order to remove visual referents, Lappe et al. performed their experiments at very low levels of illumination, near darkness, as did many of the previous investigations that report no compression (Cai et al., 1997).

As with saccadic suppression, it is important to understand if the apparent shifts and compression are caused by the visual events associated with the saccade or if they have a central origin. As before, simulating saccades by rapid

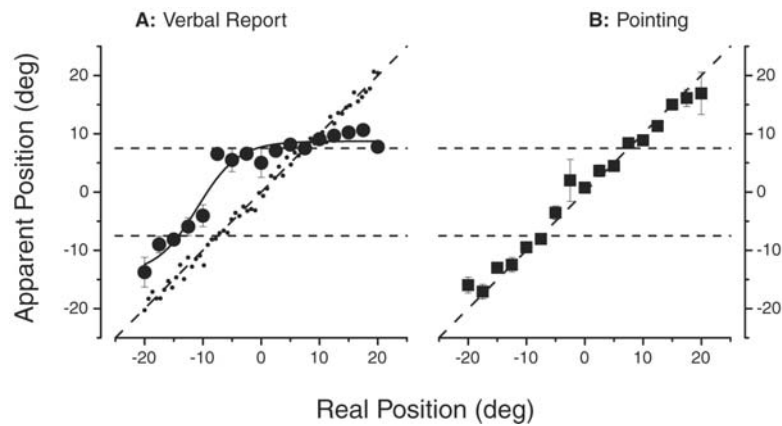


FIGURE 93.5. Perceived positions of bars briefly flashed to stationary eyes in the 40msec before observers made a 20 degree saccade. The large filled circles in A show results for verbal reports in which subjects called out a number from a remembered scale. In this example (taken from Burr et al., 2001), the subject closed her eyes immediately after making the saccade. The curve follow-

ing the data is the output of a model for the shift and compression effects (Morrone et al., 1997). The small circles show control data taken under identical conditions during fixation (from Ross et al., 1997). The filled squares in B show results for blind pointing to the remembered positions, again with the eyes shut. (Adapted with permission from Burr et al., 2001.)

rotation of a mirror provides crucial information. Mislocalizations can occur during simulated saccades, but they have a very different time course and magnitude than those during real saccades (Morrone et al., 1997). More significantly, no compression occurs with simulated saccades: all stimuli are displaced in the same direction and to the same extent, irrespective of their position in the visual field (Morrone et al., 1997).

There exists a good deal of evidence for the involvement of extraretinal eye position information in judging apparent visual direction, although some of it is contradictory. Helmholtz (1866) noted that causing the eye to move by applying pressure with the finger (creating an eye movement without an “intention to move” signal) caused an apparent displacement on the visual world. However, the inverse experiment, attempting to move the eyes under conditions of total paralysis, did not create a sense of apparent motion of the visual scene (Brindley et al., 1976; Stevens et al., 1976), even though there should have been a mismatch between the extraretinal signal and the retinal movement (or lack thereof). The issue has been readdressed by Matin et al. (1981), who showed that with partial systemic paralysis, observers make enormous errors in visual localization, on the order of 20 degrees. In darkness, partially paralyzed (but not normal) observers misperceive completely the median plane and make gross errors in pointing to visual targets. Most significantly, when using an auditory tone to localize a visual target, partially paralyzed observers grossly overestimate the eccentricity (Fig. 93.6). With full room illumination, the perception of the median plane and the pointing performance to visual targets return to normal, but the auditory-to-visual matches remain as distorted as they are in darkness (Fig. 93.6). This experiment provides clear evidence for the role of extraretinal eye position information in judging apparent visual direction. When the muscular response is weakened through partial paralysis, the motor command for a given response must be increased. The fact that the increase in gain of the motor command produces a commensurable increase in perceived eccentricity suggests that the extraretinal signal combines with retinal information in determining visual location. It seems that when present, visual information can dominate in determining the medial plane (possibly explaining the previous null results of Brindley et al., 1976, and Stevens et al., 1976); but the visual illumination is not sufficient to override the erroneous eccentricity estimates in the auditory-to-visual matches.

Motor responses during saccades

Although there is overwhelming evidence for perceptual mislocalizations during saccades, there is also good evidence that subjects maintain a veridical spatial map, and that this map can be used to guide motor activity such as second sac-

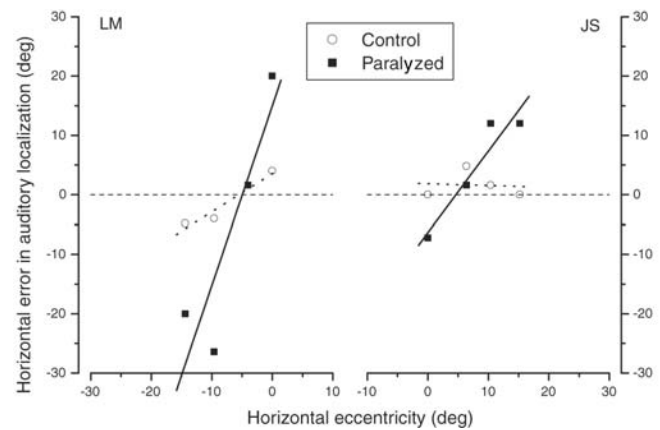


FIGURE 93.6. Error in auditory localizations of fixed visual targets in observers that have been partially paralyzed by curare (*filled squares*) compared with control measurements in the same observers (*open circles*). During paralysis, observers overestimated the distance of the light from the median by more than a factor of 2. These results suggest that extraretinal information used to control eye position is used in estimating eccentricity. These results were the same in darkness as in normal lighting conditions. (From Matin et al., 1981, with permission.)

cades and hammering (Hallett and Lightstone, 1976a, 1976b; Hansen and Skavenski, 1977, 1985). Bridgeman et al. (1975) also reported that subjects can point accurately to targets that were displaced perisaccadically, even though the subject did not perceive the change in target position. These results are intriguing because they imply that two visual representations exist: one that remains veridical during saccades and another that becomes transiently distorted. This is consistent with the long-standing (Trevarthen, 1968) and recently revived (Goodale and Milner, 1992) idea that separate systems are responsible for conscious perception and for direct interactions with our environment.

While the early evidence was clear, some recent experiments on pointing and secondary saccades have failed to replicate the original dissociation between motor accuracy and perceptual mislocalization during saccades, reporting localization errors for both tasks (Bockisch and Miller, 1999; Dassonville et al., 1992, 1995; Honda, 1991; Miller, 1996; Schlag and Schlag-Rey, 1995). However, it should be pointed out that localization errors for motor responses vary considerably both in size and in dynamics in different laboratories: some show errors as large as the perceptual errors, starting well in advance of saccadic eye movements (Dassonville et al., 1992, 1995; Schlag and Schlag-Rey, 1995); others show very small errors (4 to 5 degrees for 15 degree saccades), mainly for targets presented at the completion of the saccade (Bockisch and Miller, 1999; Miller, 1996). The errors have been reported to be similar for finger indication and for secondary saccades. Unfortunately, all these studies used different experimental paradigms, with various levels of dark adaptation, visual references from the eye recording systems,

and possible visual cues introduced from diffuse or reflected light from the apparatus (Bockisch and Miller, 1999; Dassonville et al., 1992; Miller, 1996).

We have recently revisited the problem to see whether the compression of visual space that occurs with verbal reports also occurs with blind pointing under matched conditions (Burr et al., 2001; see also Husain and Jackson, 2001). When asked to report verbally the position of a bar flashed just before a saccade, subjects made strong compression errors, as mentioned before and plotted in Figure 93.5A. This occurred even when all visual references were removed by obscuring the screen at the time of the report. However, when subjects were asked to point ballistically to the location where a bar had been seen (again with transient darkness caused by eye shutting), the pattern of pointing was virtually veridical (Fig. 93.5B). This supports the idea that there are two separate visual representations with separate remapping during saccades. Importantly, when subjects were asked to point with visual cues available (but the hands obscured from view), the pattern of errors was like that for verbal reports. This suggests that, when available, the perceptual representation can override the motor representation of visual space. It is also possible that this result explains the conflicting results in the literature. Hansen and Skavenski (1977, 1985) used the technique of transient darkness (with a light-adapted eye) to remove visual cues, and they reported accurate motor response, similar to those in Figure 93.5B. On the other hand, fully dark-adapted subjects, viewing stimuli through eye sensors that provided clear visual references (Schlag and Schlag-Rey, 1995), made substantial errors on secondary saccades in the direction of the primary saccade.

Other lines of evidence also suggest that veridical information might be available at the time of saccades and can be used under certain conditions. For example, Deubel et al. (1996) repeated Bridgeman et al.'s (1975) measurements of sensitivity to line displacements at the time of saccades. The saccade typically raises thresholds by more than a factor of 3. However, if a line is briefly blanked at the time of the saccade and reappears ~100 msec later, subjects can detect displacements with unimpaired accuracy. This suggests that information about position is not lost during the saccade and that mechanisms exist to maintain continuity between fixations. Interestingly, even under conditions where observers are unable to report correctly the direction of the displacement, they frequently make an accurate second saccade toward the displaced target (Deubel et al., 1998).

In conclusion, the bulk of the evidence suggests that veridical pointing and second saccades can occur with perisaccadic targets under conditions where perception is severely distorted. However, in order to demonstrate veridical motor responses, care must be taken to render the visual signals unreliable (that does not only entail removal of visual

references), or else vision will dominate. The results suggest the existence of separate representations for perception and action that are affected differently during saccades. However, there is clearly considerable interaction between the representations, and when there is conflict, the perceptual system seems to dominate.

Physiological mechanisms

In an important paper, Duhamel et al. (1992) showed that the receptive fields of some neurons in the lateral intraparietal area (LIP) of monkeys change position before each saccadic eye movement, effectively anticipating its consequences. Up to 80 msec before the onset of a saccade, LIP neurons start to respond to stimuli that will fall within their receptive field after the saccade is completed. This predictive effect might represent a mechanism by which the visual and oculomotor systems combine and calculate a spatially accurate image of the world in spite of the eye movement. This could enable neurons to respond immediately at the end of a saccade to stable stimuli that enter the receptive field by virtue of the saccade without having to “wait” for retinal reafference (Gottlieb et al., 1998).

Perisaccadic receptive field shifts are not unique to the LIP but have been found in other eye movement-related areas—for example, the superior colliculus (Walker et al., 1995) and the frontal eye field (Umeno and Goldberg, 1997), a medial parietal area that is associated with reaching (Batista et al., 1999)—and even in earlier stages in the cortical visual system, V4, V3a, and V2 (Nakamura and Colby, 2002). The remapping of receptive fields in all these areas is consistent with visual mislocalization in the direction of the saccade. It is not, however, obvious how it may explain the observed compression: compression requires a shift that is dependent on the position of the stimuli.

One possibility is that during the perisaccadic interval, not all LIP neurons (and other neurons in the parietal stream) show the predictive shift of receptive field in the direction of the saccade. Other neurons continue to respond to the pre-saccadic position, and some respond to stimuli in both positions (Kusunoki et al., 1997; Nakamura and Colby, 2000). Areas that receive input from the LIP (including the frontal eye field and the superior colliculus) might thus interpret stimuli arising over a large area (comprising pre- and post-saccadic receptive fields) as being in the same position, resulting in compression, particularly of the positions of stimuli that are flashed briefly during psychophysical experiments. The fact that many areas show anticipatory shifts in receptive fields, to a greater or lesser extent, could mean that multiple representations in all these areas in some way contribute to the observed compression.

Neural correlates of perisaccadic mislocalization have also been observed in MT and MST neurons. Using a

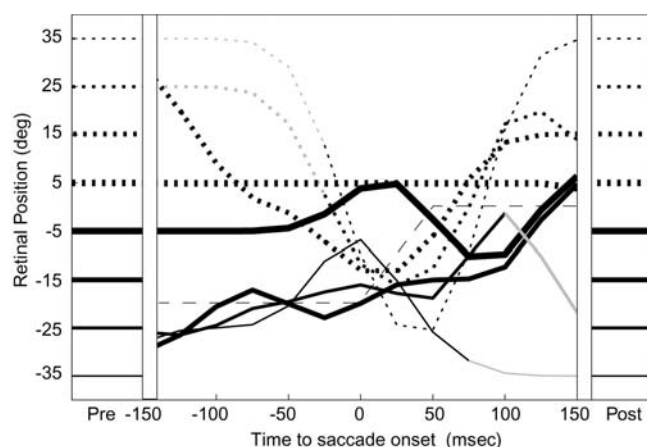


FIGURE 93.7. Perisaccadic compression of space in areas MT and MST. The curves of various widths and line types indicate the predictions of the perceived stimulus position of a population of MT and MST neurons, as a function of time relative to saccadic onset, for bars stimulated at various positions (actual positions are indicated at the left and right of the graph). The animal made 20 degree leftward saccades, as indicated by the faint dashed black curves. Well before and well after saccadic onset, the model prediction from the cell population is very close to veridical. However, at times near saccadic onset, the population code tends to converge near the saccadic target, implying compression. (From Krekelberg et al., 2003, with permission.)

Bayesian analysis, Krekelberg et al. (2003) show that a population of MT and MST cells can encode veridically the position of briefly flashed bars. However, analysis of the same neurons just prior to a saccade (using the weights derived from free viewing) shows a gross mislocalization in the population response, shown in Figure 93.7. The mislocalization is in the direction of compression, as observed with human observers. Interestingly, both the magnitude of the compression and the time course are very similar to those observed with human observers (Morrone et al., 1997; Ross et al., 1997).

While the work is new and very much in progress, it is fair to say that strong neural correlates exist between the psychophysical and electrophysiological single-unit findings, to account for both the systematic shift in the direction of the saccade and the compression toward the saccadic target. The areas involved include V3, LIP, VIP, MT, MST, and superior colliculus.

Future directions

At the time of saccades, vision is profoundly modified. There is a transient desensitisation of low-frequency stimuli modulated in luminance together with gross distortions of perceptual (but not motor) space. The time course of perceptual compression is very similar to that for loss of sensitivity: both begin more than 50 msec before saccades start, are maximal

at or shortly before the start of saccades, diminish during saccades, and disappear only after saccades have ended. These psychophysical findings, summarized in this chapter, have been confirmed in many laboratories and have spurred the successful search for neural correlates in the single neurons of nonhuman primates.

What is the functional role of these perisaccadic changes? How do they enable the visual system to perceive a steady world from input arriving from such unsteady sensory platforms? As discussed earlier, the transient suppression of low spatial frequency luminance information probably serves to dampen the motion system (or one part of the motion system), blunting the otherwise disturbing sensation of movement the rapid displacement should cause. But as we have seen, the suppression is very brief, lasting for only about 50 msec, and by no means total, 1 log unit at most. How can this brief, partial suppression obliterate the extended motion that occurs with each eye movement? Indeed, we know that motion is not totally suppressed in some cases (Castet and Masson, 2000) and that part of the magnocellular system remains operative at reduced gain (Burr and Morrone, 1996). One fruitful line for future research will be to simulate saccadic vision by large-field motion and spatial blur to investigate whether this transient partial attenuation of luminance, but not color, is sufficient to blunt the motion sensation or whether other factors are involved.

The perceptual distortions are even more perplexing: a shift in the direction of the saccade combined with gross compression of perceptual space toward the saccadic target. There is clear neural activity in the parietal pathway correlated with these two processes. But what is their function? Do the shift and compression facilitate directly the perceptual transitions from one fixation to another or is it an epiphenomenon of some more subtle, still not understood process?

Finally, there is now very good evidence that at the time of these gross perceptual distortions, veridical information remains available during saccades, information that can be used to guide ballistic motor acts and secondary saccades. What is the nature of the spatial representation used in this case? Why is this information normally unavailable to perception? Which visual pathway mediates the spatial map used by the action system? How can the retention of this ability be reconciled with the psychophysical and physiological demonstrations of massive suppression of the magno (dorsal) pathway's activity during saccade?

While much progress has been made in documenting the psychophysical and electrophysiological events that accompany saccades, many of the important questions about visual stability remain unsolved and will provide a fertile terrain for research for the next few decades.

Acknowledgments

This work was supported by grants from the Human Frontiers Science Program and the Italian Ministry of Education (MURST 40% 2000, 2001).

REFERENCES

- Alhazen, I., 1083/1989. Book of optics, *The Optics of Ibn al-Haytham* (A. I. Sabra, trans.), London: Warburg Institute.
- Batista, A., C. Buneo, L. Snyder, and R. Andersen, 1999. Reach plans in eye-centered coordinates, *Science*, 285:257–260.
- Bischof, N., and E. Kramer, 1968. Untersuchungen und Überlegungen zur Richtungswahrnehmung bei willkürlichen sakkadischen Augenbewegungen, *Psychol. Forsch.*, 32:185–218.
- Bockisch, C., and J. Miller, 1999. Different motor systems use similar damped extraretinal eye position information, *Vis. Res.*, 39:1025–1038.
- Bridgeman, B., 1995. Extraretinal signals in visual orientation, in *Handbook of Perception and Action* (W. Prinz and B. Bridgman, eds), London: Academic Press, pp. 191–223.
- Bridgeman, B., D. Hendry, and L. Stark, 1975. Failure to detect displacement of visual world during saccadic eye movements, *Vis. Res.*, 15:719–722.
- Bridgeman, B., and L. Stark, 1991. Ocular proprioception and efference copy in registering visual direction, *Vis. Res.*, 31:1903–1913.
- Bridgeman B., A. H. C. Van der Heijden, and B. M. Velichkovsky, 1994. A theory of visual stability across saccadic eye movements, *Behav. Brain Sci.*, 17:247–292.
- Brindley, G. S., G. M. Goodwin, J. J. Kulikowski, and D. Leighton, 1976. Proceedings: stability of vision with a paralysed eye, *J. Physiol.*, 258:65P–66P.
- Burr, D. C., J. Holt, J. R. Johnstone, and J. Ross, 1982. Selective depression of motion selectivity during saccades, *J. Physiol. (Lond.)*, 333:1–15.
- Burr, D. C., M. J. Morgan, and M. C. Morrone, 1999. Saccadic suppression precedes visual motion analysis, *Curr. Biol.*, 9:1207–1209.
- Burr, D. C., and M. C. Morrone, 1996. Temporal impulse response functions for luminance and colour during saccades, *Vis. Res.*, 36:2069–2078.
- Burr, D. C., M. C. Morrone, and J. Ross, 1994. Selective suppression of the magnocellular visual pathway during saccadic eye movements, *Nature*, 371:511–513.
- Burr, D. C., M. C. Morrone, and J. Ross, 2001. Separate visual representations for perception and action revealed by saccadic eye movements, *Curr. Biol.*, 11:798–802.
- Burr, D. C., and J. Ross, 1982. Contrast sensitivity at high velocities, *Vis. Res.*, 23:3567–3569.
- Burr, D. C., and J. Ross, 1986. Visual processing of motion, *Trends Neurosci.*, 9:304–306.
- Cai, R. H., A. Pouget, M. Schlag-Rey, Schlag, 1997. Perceived geometrical relationships affected by eye-movement signals, *Nature*, 386:601–604.
- Campbell, F. W., and R. H. Wurtz, 1978. Saccadic omission: why we do not see a greyout during a saccadic eye movement, *Vis. Res.*, 18:1297–1303.
- Carpenter, R. H. S., 1977. *Movement of the Eyes*, London: Pion.
- Castet, E., S. Jeanjean, and G. S. Masson, 2001. “Saccadic suppression”—no need for an active extra-retinal mechanism, *Trends Neurosci.*, 24:316–318.
- Castet, E., and G. S. Masson, 2000. Motion perception during saccadic eye movements, *Nat. Neurosci.*, 3:177–183.
- Dassonville, P., J. Schlag, and M. Schlag-Rey, 1992. Oculomotor localization relies on a damped representation of saccadic eye movement displacement in human and nonhuman primates, *Vis. Neurosci.*, 9:261–269.
- Dassonville, P., J. Schlag, and M. Schlag-Rey, 1995. The use of ego-centric and exocentric location cues in saccadic programming, *Vis. Res.*, 35:2191–2199.
- Derrington, A. M., 1984. Spatial frequency selectivity of remote pattern masking, *Vis. Res.*, 24:1965–1968.
- Deubel, H., B. Bridgeman, and W. X. Schneider, 1998. Immediate post-saccadic information mediates space constancy, *Vis. Res.*, 38:3147–3159.
- Deubel, H., W. X. Schneider, and B. Bridgeman, 1996. Postsaccadic target blanking prevents saccadic suppression of image displacement, *Vis. Res.*, 36:985–996.
- Diamond, M. R., J. Ross, and M. C. Morrone, 2000. Extraretinal control of saccadic suppression, *J. Neurosci.*, 20:3442–3448.
- Dodge, R., 1900. Visual perception during eye movements, *Psychol. Rev.*, 7:454–465.
- Duhamel, J.-R., C. L. Golby, and M. E. Goldberg, 1992. The updating of the representation of visual space in parietal cortex by intended eye movements, *Science*, 255:90–92.
- Field, D. J., 1987. Relations between the statistics of natural images and the response properties of cortical cells, *J. Opt. Soc. Am. A*, 4:2379–2394.
- Garcia-Perez, M. A., and E. Peli, 2001. Intrascaccadic perception, *J. Neurosci.*, 21:7313–7322.
- Gauthier, G., P. Normmay, and J. Vercher, 1988. Ocular muscle proprioception and visual localisation in man, *J. Physiol. (Lond.)*, 406:24.
- Goodale, M. A., and A. D. Milner, 1992. Separate pathways for perception and action, *TINS*, 15:20–25.
- Gottlieb, J., M. Kusunoki, and M. Goldberg, 1998. The representation of visual salience in monkey parietal cortex, *Nature*, 391:481–484.
- Hallett, P. E., and A. D. Lightstone, 1976a. Saccadic eye movements towards stimuli triggered by prior saccades, *Vis. Res.*, 16:99–106.
- Hallett, P. E., and D. A. Lightstone, 1976b. Saccadic eye movements to flashed targets, *Vis. Res.*, 16:107–114.
- Hansen, R. M., and A. A. Skavenski, 1977. Accuracy of eye position information for motor control, *Vis. Res.*, 17:919–926.
- Hansen, R. M., and A. A. Skavenski, 1985. Accuracy of spatial locations near the time of saccadic eye movements, *Vis. Res.*, 25:1077–1082.
- Helmholtz, H. von, 1866/1963. *Handbuch der Physiologischen Optik*, in *A Treatise on Physiological Optics* (J. P. C. Southall, trans.), New York 1963: Dover.
- Holt, E. B., 1903. Eye movements and central anaesthesia, *Psychol. Rev.*, 4:3–45.
- Honda, H., 1989. Perceptual localization of visual stimuli flashed during saccades, *Percept. Psychophys.*, 46:162–174.
- Honda, H., 1991. The time courses of visual mislocalization and of extra-retinal eye position signals at the time of vertical saccades, *Vis. Res.*, 31:1915–1921.
- Honda, H., 1993. Saccade-contingent displacement of the apparent position of visual stimuli flashed on a dimly illuminated structured background, *Vis. Res.*, 33:709–716.
- Howard, I. P., 1996. Alhazen’s neglected discoveries of visual phenomena, *Perception*, 25:1203–1217.

- Husain, M., and S. R. Jackson, 2001. Vision: visual space is not what it appears to be, *Curr. Biol.*, 11:R753–755.
- Ilg, U. J., and K.-P. Hoffmann, 1993. Motion perception during saccades, *Vis. Res.*, 33:211–220.
- Krauskopf, J., V. Graf, and K. Gaardner, 1966. Lack of inhibition during involuntary saccades, *Am. J. Psychol.*, 79:73–81.
- Krekelberg, B., M. Kubischik, K. P. Hoffmann, and F. Bremmer, 2003. Neural correlates of visual localization and peri-saccadic mislocalization, *Neuron* 37:537–545.
- Kusunoki, M., C. L. Colby, J.-R. Duhamel, and M. E. Goldberg, 1997. The role of the lateral intraparietal area in the control of visuospatial attention, in *In The Association Cortex: Structure and Function* (H. Sakata, A. Mikami, and J. M. Fuster, eds.), New York: Academic Press, pp. 191–206.
- Lappe, M., H. Awater, and B. Krekelberg, 2000. Postsaccadic visual references generate presaccadic compression of space, *Nature*, 403:892–895.
- Latour, P. L., 1962. Visual threshold during eye movements, *Vis. Res.*, 2:261–262.
- MacKay, D. M., 1970. Elevation of visual threshold by displacement of visual images, *Nature*, 225:90–92.
- MacKay, D. M., 1973. Visual stability and voluntary eye movements, in *Handbook of Sensory Physiology*, vol. VII/3 (R. Jung ed.), Berlin: Springer-Verlag pp. 307–331.
- Matin, L., 1972. Eye movements and perceived visual direction, in *Handbook of Sensory Physiology*, vol. VII/4: *Visual Psychophysics* (D. Jameson and L. M. Hurvich, eds.), Berlin: Springer-Verlag, pp. 331–380.
- Matin, L., E. Matin, and D. G. Pearce, 1969. Visual perception of direction when voluntary saccades occur: I. Relation of visual direction of a fixation target extinguished before a saccade to a subsequent test flash presented during the saccade, *Percept. Psychophys.*, 5:65–68.
- Matin, L., E. Matin, and J. Pola, 1970. Visual perception of direction when voluntary saccades occur: II. Relation of visual direction of a fixation target extinguished before a saccade to a subsequent test flash presented before the saccade, *Percept. Psychophys.*, 8:9–14.
- Matin, L., and D. G. Pearce, 1965. Visual perception of direction for stimuli flashed during voluntary saccadic eye movements, *Science*, 148:1485–1487.
- Matin, L., E. Picoult, J. K. Stevens, M. W. Edwards, D. Young, and R. MacArthur, 1981. Oculoparalytic illusion: visual-field dependent spatial mislocalizations by humans partially paralysed with curare, *Science*, 216:198–201.
- Merigan, W. H., 1989. Chromatic and achromatic vision of macaques: role of the P pathway, *J. Neurosci.*, 9:776–783.
- Miller, J., 1996. Egocentric localization of a perisaccadic flash by manual pointing, *Vis. Res.*, 36:837–851.
- Morrone, M. C., J. Ross, and D. C. Burr, 1997. Apparent position of visual targets during real and simulated saccadic eye movements, *J. Neurosci.*, 17:7941–7953.
- Murakami, I., and P. Cavanagh, 1998. A jitter after-effect reveals motion-based stabilization of vision, *Nature*, 395:798–801.
- Murakami, I., and P. Cavanagh, 2001. Visual jitter: evidence for visual-motion-based compensation of retinal slip due to small eye movements, *Vis. Res.*, 41:173–186.
- Nakamura, K., and C. L. Colby, 2002. Updating of the visual representation in monkey striate and extrastriate cortex during saccades, *Proc. Nat. Acad. Sci.*, 99:4026–4031.
- Riggs, L. A., P. A. Merton, and H. B. Morton, 1974. Suppression of visual phosphenes during saccadic eye movements, *Vis. Res.*, 14:997–1011.
- Ross, J., M. C. Morrone, and D. C. Burr, 1997. Compression of visual space before saccades, *Nature*, 384:598–601.
- Ross, J., M. C. Morrone, M. E. Goldberg, and D. C. Burr, 2001. Changes in visual perception at the time of saccades, *Trends Neurosci.*, 24:131–121.
- Schlag, J., and M. Schlag-Rey, 1995. Illusory localization of stimuli flashed in the dark before saccades, *Vis. Res.*, 35:2347–2357.
- Shapley, R. M., and J. D. Victor, 1981. How the contrast gain control modifies the frequency responses of cat retinal ganglion cells, *J. Physiol. (Lond.)*, 318:161–179.
- Sherrington, C. S., 1918. Observations on the sensual role of the proprioceptive nerve supply of the extrinsic ocular muscles, *Brain*, 41:332–343.
- Shiori, S., and P. Cavanagh, 1989. Saccadic suppression of low-level motion, *Vis. Res.*, 29:915–928.
- Sperling, G., 1990. Comparison of perception in the moving and stationary eye, in *Eye Movements and Their Role in Visual and Cognitive Processes* (E. Kowler ed.), Amsterdam: Elsevier, pp. 307–351.
- Sperry, R. W., 1950. Neural basis of the spontaneous optokinetic response produced by visual inversion, *J. Comp. Physiol. Psychol.*, 43:482–489.
- Stevens, J. K., R. C. Emerson, G. L. Gerstein, T. Kallos, G. R. Neufeld, C. W. Nichols, and A. C. Rosenquist, 1976. Paralysis of the awake human: visual perceptions, *Vis. Res.*, 16:93–98.
- Thiele, A., P. Henning, and P.-K. Hoffmann, 2002. Neural mechanisms of saccadic suppression, *Science*, 29S(5564):2460–2462.
- Trevarthen, C. B., 1968. Two mechanisms of vision in primates, *Psychol. Forsch.*, 31:299–348.
- Uchikawa, K., and M. Sato, 1995. Saccadic suppression to achromatic and chromatic responses measured by increment-threshold spectral sensitivity, *J. Opt. Soc. Am. A*, 12:661–666.
- Umeno, M., and M. Goldberg, 1997. Spatial processing in the monkey frontal eye field. I. Predictive visual responses, *J. Neurophysiol.*, 78:1373–1383.
- Volkman, F. C., L. A. Riggs, K. D. White, and R. K. Moore, 1978. Contrast sensitivity during saccadic eye movements, *Vis. Res.*, 18:1193–1199.
- Von Holst, E., and H. Mittelstädt, 1954. Das Reafferenzprinzip, *Naturwissenschaften*, 37:464–476.
- Walker, M. F., J. Fitzgibbon, and M. E. Goldberg, 1995. Neurons of the monkey superior colliculus predict the visual result of impending saccadic eye movements, *J. Neurophysiol.*, 73:1988–2003.
- Woodworth, R. S., 1906. Vision and localization during eye movements, *Psychol. Bull.*, 3:68–70.
- Zrenner, E., 1983. Neurophysiological aspects of colour vision mechanisms in the primate retina, in *Colour Vision: Physiology and Psychophysics* (J. D. Mollon and L. T. Sharpe, eds.), London: Academic Press, pp. 195–210.
- Zuber, B., and L. Stark, 1966. Saccadic suppression: elevation of visual threshold associated with saccadic eye movements, *Exp. Neurol.*, 16:65–79.

94 Smooth Pursuit Eye Movements: Recent Advances

STEPHEN J. HEINEN AND EDWARD L. KELLER

MOST OF THE WORK covered in previous reviews of the pursuit system (Eckmiller, 1987; Keller and Heinen, 1991; Leigh and Zee, 1999; Lisberger et al., 1987; Pola and Wyatt, 1991) describes the physiology and behavior of pursuit to a single small spot stimulus. The theoretical framework that guided this work was that the pursuit system used negative feedback to minimize the retinal-image motion introduced when an object moves (Krauzlis and Lisberger, 1989; Robinson et al., 1986). Much of current pursuit research involves functions that either modulate or override the negative feedback process in situations more closely aligned with object motion in the natural environment. The purpose of this review is to discuss how signals related to cognitive aspects of pursuit interact with signals arising in the visuomotor processing stream, and to summarize recent literature on a common neural substrate for pursuit and saccades that might support the more naturalistic cooperative response of these ocular subsystems. The outline of the chapter is as follows.

The first section discusses research on how pursuit operates under experimental conditions that more closely approximate natural scenes. Here we cover work on target selection, that is, how a single moving object is selected from among several objects. Literature on gain control in the pursuit system that occurs in these situations is also reviewed here. Next, work on the predictive mechanism that governs anticipatory pursuit is discussed. Finally, we address how the pursuit system responds to stimuli that are larger and more complex than a single spot. The second section speaks to the important emerging issue in pursuit research of how cognitive signals interact with signals in areas of the brain that process visual motion for pursuit. In this section, new developments in the cortical control of pursuit are discussed, including evidence that areas in the frontal lobe generate cognitive aspects of pursuit behavior. The cortical visual-motion processing areas in the superior temporal sulcus and parietal lobe, although not covered in detail, will be referenced here as components in a pathway that might be complementary to the frontal pathway. Also in this section, new developments in brainstem and cerebellar pursuit research will be discussed, including the exciting possibility that cognitive and visual-motion signals are processed in different regions at this level. In the third and final section, we sum-

marize recent evidence that the pathways subserving smooth pursuit and saccades overlap to a greater degree than was thought previously. Finally, we suggest that the reader refer to reviews by Leigh and Zee (1999) on pursuit deficits in the clinic and by Krauzlis (1994) on cortical visual-motion processing areas for pursuit, as these important topics are not covered in detail here.

Pursuit in the natural scene

The purpose of early smooth pursuit studies was to characterize the motor limb of the system without contamination by signals introduced by complex visual processing and cognition. To this end, most studies employed a single small spot to minimize the visual complexity of the stimulus and random-motion patterns to minimize target predictability. To understand fully how the pursuit system operates in a natural scene, recent research has been devoted to studying pursuit of visual stimuli that are more complex than the single spot and cognitive factors that contribute to pursuit control. This section will discuss recent research on target selection, gain control, and prediction, as well as work addressing how the pursuit system follows stimuli that are larger and visually more complex than the spot.

GAIN CONTROL AND TARGET SELECTION FOR PURSUIT It has been suggested that when the pursuit system is confronted with multiple objects, selective attention biases the observer to select a single one in a winner-take-all fashion (Kowler, 1990). Other work supports this contention for certain spatial and temporal target separations (Ferrera and Lisberger, 1997; Recanzone and Wurtz, 1999). Interestingly, during pursuit initiation, a weighted vector average of the speed and direction of both targets appears to describe the data better than does winner-take-all selection (Lisberger and Ferrera, 1997). Vector averaging during pursuit initiation occurs even when an animal is cued to track one of the targets before they move (Ferrera, 2000). In this study, the pre-motion cueing biased the subsequent pursuit response toward the cued target, yet the response remained influenced by the nonrewarded target motion. The results of microstimulation in area MT are consistent with the idea that

velocity signals that are read out from this structure are vector averaged for use by the pursuit system (Groh et al., 1997).

An increase in pursuit gain can occur after pursuit is engaged and the observer has selected an object to follow. Modulation of gain was first demonstrated in experiments where brief sinusoidal perturbations were superimposed upon step-ramp target motions (Goldreich and Lisberger, 1987). In this study, higher gain was observed when the perturbation occurred during pursuit than during fixation. Based on these data, the authors suggested that there is a neural “switch” that activates the pursuit system. Later work showed that the gain of the pursuit system with superimposed sinusoidal perturbations varied as a function of target speed (Keating and Pierre, 1996; Schwartz and Lisberger, 1994). Therefore, it appeared that a variable gain element, and not a switch, modified the pursuit system’s level of activation.

Normally, smooth pursuit to step-ramp target motion is initiated with a smooth eye acceleration followed by a saccade that places the fovea close to or on the target (Keller and Johnsen, 1990). Lisberger (1998) used the step-ramp paradigm to investigate the interaction between the smooth and saccadic components of pursuit initiation and found that eye velocity just after the saccade was greater than before it. He argued that this “postsaccadic enhancement” resulted from a boost of the gain in the visuomotor pathways. Specifically, the oculomotor system anticipates that the selected target will be near the fovea following the catchup saccade, and the system boosts pursuit gain to ensure that eye speed closely matches target speed at this time. The finding that when two targets are present, heightened eye velocity after the catchup saccade to the foveated target supports the idea that gain control is used during target selection (Gardner and Lisberger, 2001). These data are also evidence that postsaccadic enhancement of pursuit is spatially selective.

Recently, the frontal eye fields (FEF) have been implicated in pursuit gain control (Tanaka and Lisberger, 2001). These authors found that the magnitude of eye velocity induced by electrical stimulation here was greater during pursuit than during fixation. This difference was seen both with and without the sinusoidal perturbations used in earlier studies (e.g., Schwartz and Lisberger, 1994). Stimulation of the supplementary eye field (SEF) also facilitates eye velocity during pursuit (Missal and Heinen, 2001). In this study, stimulated eye velocity increased as a multiplicative function of initial eye velocity, suggesting that, as in the FEF, the current was interacting with a gain element. While the stimulation results in FEF and SEF are evidence that both of these areas are involved in a gain control process, a key difference in the results suggests that these regions have different specific roles in pursuit control. Stimulation in the FEF produces smooth eye movements even during fixation (Gottlieb et al., 1993;

Tanaka and Lisberger, 2001), but stimulation of the SEF does not (Missal and Heinen, 2001). This implies that the FEF is in the direct pathway for pursuit movement generation, while the SEF has a more general executive function, controlling the gain of intentional processes.

PURSUIT TO LARGER AND MORE COMPLEX VISUAL STIMULI
A stimulus larger than a spot will activate a population of motion detectors that tiles a spatially extended region. Since the pursuit system can generate only a single eye velocity vector, the outputs of multiple motion detectors must be combined in this situation to produce one signal. The motion perception system integrates signals that stimulate multiple motion detectors to eliminate noise and to better detect and discriminate spatially extended stimuli (Watamaniuk and Sekuler, 1992). When presented with a random-dot cinematogram (RDC) composed of multiple coherent-motion dots, the pursuit system also appears to integrate motion signals, since pursuit gain is higher, and there is less variability in the response than when a single-spot stimulus is pursued (Heinen and Watamaniuk, 1998) (Fig. 94.1). This finding suggests that the same motion processing substrate limits smooth pursuit and motion perception. The same conclusion was reached when psychophysical judgments and smooth pursuit responses were compared in motion direction discrimination tasks (Beutter and Stone, 1997; Krauzlis and Adler, 2001; Watamaniuk and Heinen, 1999). In all of these experiments, perceptual and motor performances were similar when directional noise was added to moving stimuli. Other work has demonstrated that human observers can integrate the local motion of line-figure objects to derive a global motion signal (Beutter and Stone, 2000). Global information was used similarly to both perceive and pursue these objects, even when partial occlusion made the resulting image motion vastly different from the underlying object motion.

An unresolved issue that surfaces when larger stimuli are used to study pursuit is the degree to which the function and the underlying neural architecture of the pursuit system are distinct from those that subserve other smooth eye movements. One system in question is the one that generates the optokinetic reflex (OKN). The OKN is a response to full-field motion that supplements the vestibulo-ocular reflex (VOR), a nonvisual reflex originating in the semicircular canals. The VOR serves to rotate the eyes to counter head rotation. The distinction between smooth pursuit and OKN is not clear in the literature. Typically, pursuit is studied with a small-spot stimulus and OKN with a large, textured field. However, pursuing a spot can produce eye movement behavior similar to that seen when large fields are used, that is, a recurring pattern of slow and fast phase responses (van den Berg and Collewyn, 1986). Conversely, stimuli larger than a spot can produce eye movements that look like smooth

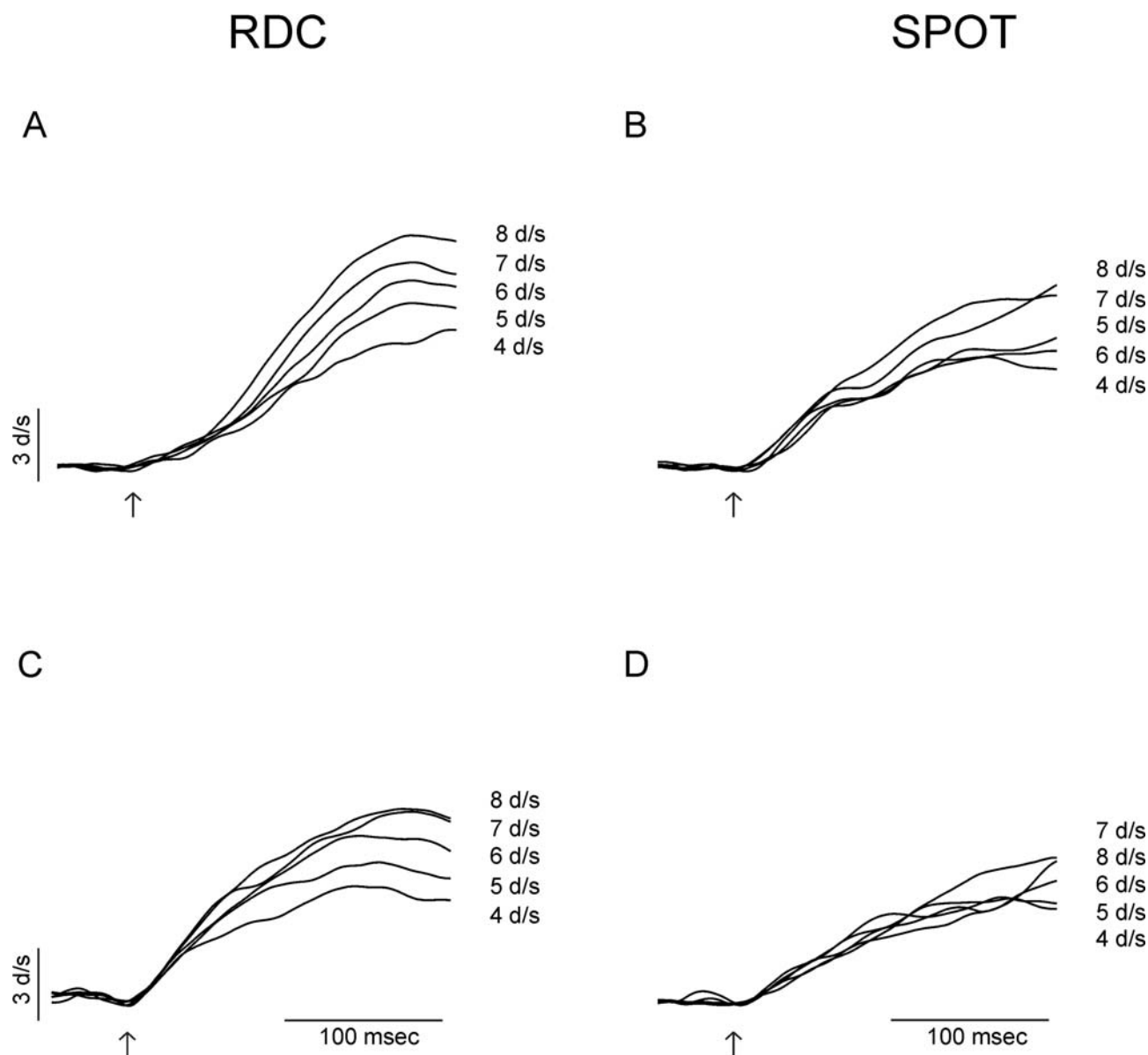


FIGURE 94.1. Eye speed during pursuit of single spots and random-dot cinematograms (RDCs) moving at different speeds. The left column (*A* and *C*) shows average eye speed during pursuit of 200 dot RDCs (dot size = 0.1 degree) that moved at 4, 5, 6, 7, and 8 deg/sec for one observer at the top (*A*) and for a second observer at the bottom (*C*); the right column (*B* and *D*) shows pursuit of a 0.1 degree spot moving at the same five speeds for each

of the two observers. Each trace is an average of approximately 10 trials. Traces are aligned on pursuit onset (*small vertical arrows*). Note that during pursuit of RDCs, observers showed higher gain as well as better speed discrimination, as evidenced by greater separation between the traces. (Modified from Heinen and Watamaniuk, 1998.)

pursuit (Beutter and Stone, 1997; Krauzlis and Adler, 2001; van den Berg and Collewyn, 1986; Watamaniuk and Heinen, 1999). Furthermore, the initial rapid OKN response to visual motion onset is thought to be controlled by the pursuit system (e.g., Cohen et al., 1977; Robinson, 1981), although this notion remains controversial (for a discussion, see Fuchs and Mustari, 1993).

A possible difference between OKN and pursuit is that OKN gain increases with stimulus size up to full field (e.g.,

Cheng and Outerbridge, 1975; Dubois and Collewyn, 1979; van Die and Collewyn, 1982), which does not appear to be the case for pursuit. In a preliminary study investigating the benefit that larger stimuli provide the pursuit system, it was found that increasing the size of a stimulus to ~12 degrees increased pursuit gain, but with further increases gain dropped (Watamaniuk and Heinen, 2000). Consistent with this, stimulating the retina beyond the ~12 degree central region with oppositely directed motion boosted the gain

again. These results implied that the receptive field for pursuit, that is, the *pursuit field*, has a center-surround architecture with an excitatory center and an inhibitory surround. Center-surround receptive fields are common in neurons throughout visual cortex, and neurons with similarly organized motion receptive fields have been found in area MT (Born and Tootell, 1992; Raiguel et al., 1995; Xiao et al., 1995) and could facilitate pursuit when an object moves in the world across a background.

Another type of smooth eye movement response that seems to overlap pursuit (and OKN) to a degree is ocular following. This response has been documented relatively recently and is present in both monkeys (Miles et al., 1986) and humans (Gellman et al., 1990). Ocular following is characterized by smooth eye movements that occur shortly after a large-field visual stimulus begins to move (latency of ~50 msec in monkeys). That a large stimulus is *required* to evoke ocular following suggests that it may be more similar to OKN than is pursuit, as pursuit movements can be made to a small spot stimulus. Nevertheless, the optimal retinal stimulation for ocular following appears to have a center-surround organization similar to that of the pursuit field but on a larger spatial scale, with a central excitatory region of ~20 degrees (Miles et al., 1986). Ocular following also has several properties that distinguish it from OKN as well as from smooth pursuit. First, ocular following is more pronounced when the stimulus is presented just after a saccadic eye movement (Kawano and Miles, 1986). Second, its gain is higher when the central field motion appears in the depth plane where the subject is attending and the motion in the periphery is presented with crossed disparity (Kawano et al., 1994a). This laboratory situation mimics the natural one that occurs when a moving observer attends to a central object and ignores the motion parallax induced by more distant ones.

Despite the differences in the optimal stimuli and responses for pursuit, OKN, and ocular following, the majority of neurons studied in cortical area MST (Kawano et al., 1994b), dorsolateral pontine nucleus (DLPN) (Kawano et al., 1992), and the cerebellum (Gomi et al., 1998) respond to all three types of eye movements. This observation suggests that these eye movement systems may share to a degree a common neural substrate.

PREDICTING OBJECT MOTION It is well established that the pursuit system can override reflexive behavior and predict target motion when it is periodic and continuous (Deno et al., 1995; Dodge et al., 1930; Stark et al., 1962; Westheimer, 1954; Winterson and Steinman, 1978). After an observer learns the periodicity of such a target, it can be pursued with zero phase lag or even phase lead. However, when that target first moves, the eyes lag behind initially because the first motion is unpredictable, and the pursuit system must rely on

a delayed signal arising from the retinal-image motion of the target. Pursuit in the step-ramp paradigm involves multiple discrete trials and can simulate the onset of multiple periodic target motions. Therefore, the step-ramp paradigm might be ideal for isolating signals related to retinal-image motion in the pursuit system. However, data obtained with the step-ramp paradigm must be interpreted carefully, because anticipatory pursuit can precede step-ramp motion even when motion parameters are randomized from trial to trial. Next we discuss some of the forces that guide anticipatory pursuit.

Anticipatory eye velocity is a function of target motion onset timing (Barnes and Asselman, 1991; Barnes and Grealy, 1992; Barnes et al., 1987) and target velocity (Kao and Morrow, 1994; Kowler and McKee, 1987; Kowler et al., 1984; Wells and Barnes, 1998), and can be enhanced by briefly blanking the fixation point (*gap paradigm*) before the target moves (Boman and Hotson, 1988; Heinen and Liu, 1997). Randomization does not necessarily eliminate anticipatory eye velocity, because the direction or speed of the target in trials that precede the one being studied are stored in short-term memory and can bias the pursuit response (Kowler and McKee, 1987; Kowler et al., 1984). There is also evidence that the timing of target motion onset is remembered from preceding trials and that this memory modifies anticipatory pursuit onset (Heinen et al., 2001). A cognitive expectation about the direction in which a target will move can override short-term memory and guide anticipatory pursuit (Kowler, 1989). As it does during continuous periodic motion, during step-ramp trials the predictive mechanism modulates eye velocity even while the target is moving (Kao and Morrow, 1994; Kowler and McKee, 1987; Kowler et al., 1984), including during the *open-loop period* which has been studied to understand visual-motion signals that drive pursuit.

There are other examples of cognitive influences on open-loop pursuit. In humans, pursuit speed declines when the subject's attention is directed away from the moving target (Khurana and Kowler, 1987). Also, initial eye acceleration is systematically higher for lower-speed trials inserted in a block of high-speed trials or lower for high-speed trials inserted in a block of lower-speed trials (Carl and Gellman, 1987; Kowler and McKee, 1987; Lisberger and Westbrook, 1985). This phenomenon might be related to short-term memory of previous target motion but, alternatively, could be due to a cognitive expectation about what the speed of the target will be if the observer determines that all the targets in the block have been set to move at the same speed.

Although previously thought to be a special property of the human oculomotor system (Fuchs, 1967), anticipatory pursuit occurs in monkeys as well (Fig. 94.2). Furthermore, as in humans, the predictive mechanism can modulate

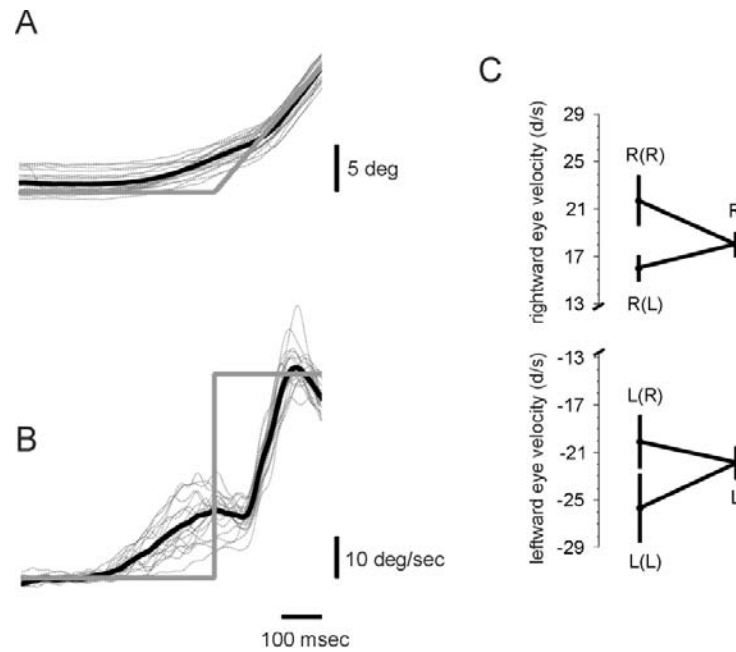


FIGURE 94.2. Predictive influences on monkey smooth pursuit. Eye and target position traces (*A*) and eye and target velocity traces (*B*) from a block of trials where the monkey tracked a target that always had the same constant velocity motion (50 deg/sec to the right). The target is shown as a solid gray line, individual eye traces as dashed gray lines, and mean eye traces as a solid dark line. Note that the anticipatory eye velocity began to build up before the target moved. Note also the sharp transition to rapid eye acceleration that occurs 100 msec after the target begins to move, consistent with activation by a retinal-image motion signal. *C*, The effect of target motion history on monkey open-loop pursuit. Data were taken during pursuit of a target that moved at a rate of 50 deg/sec, with

the direction randomly chosen on each trial as either left or right. The rightmost node of each plot indicates mean eye velocity for all trials where the target moved right (R) or left (L). The nodes on the left indicate the mean eye velocity of all trials with a given direction that are preceded by a trial with the same or opposite direction. For example, the point designated "R(L)" indicates the eye velocity of all trials where the target moved to the right, given that in the preceding trial target motion was to the left. Note that overall eye velocity was more rightward when the preceding target motion was to the right and more leftward when the preceding motion was to the left. The velocity of the eye was characterized at the end of the open-loop period.

open-loop pursuit in monkeys when target velocity is randomized (Fig. 94.2C). Since anticipatory and open-loop pursuit behave similarly during target randomization (Heinen et al., 2001), visual-motion processing and short-term memory might use the same neural substrate. This could occur if the activity of neurons in the motion pathway were altered by pursuit experience so that it biased the population response when new motion appeared. However, the visual stimulus can apparently generate a smooth response with different dynamics than anticipatory pursuit. It is often possible to identify two phases in the response, the first of which accompanies the onset of anticipation (Fig. 94.2B). Usually, an abrupt deflection of the eye velocity traces at ~80 to 100 msec after the target starts to move marks the onset of the second phase, which is characterized by higher acceleration than anticipation onset. That the onset of this second phase is time-locked to the onset of target motion suggests that it reflects the contribution of the visual signal to the pursuit response. In addition, eye acceleration during this second phase depends on retinal-image motion (e.g., Keller and Kahn, 1986; Lisberger and Westbrook, 1985).

Therefore, even if the visual-motion pathway is used to generate anticipatory pursuit, it might be possible to determine the relative contribution that the visual signal makes with the proper experimental design. A more detailed discussion of the interactions between processing streams for signals related to visual motion and cognition follows.

Extraretinal and retinal image motion substrates for smooth pursuit control

ARE VISUOMOTOR AND COGNITIVE PROCESSING SUBSERVED BY SEPARATE NEURAL PATHWAYS? Smooth pursuit eye movements usually cannot be generated without a moving target, suggesting that these eye movements are a sensorimotor reflex. This notion is supported by work in humans and monkeys demonstrating that pursuit depends on the visual properties of the stimulus—for example, its location with respect to the fovea and the direction and speed of its motion (Lisberger and Westbrook, 1985; Tychsen and Lisberger, 1986). These authors introduced the idea that the characteristics of eye acceleration during the open-loop period of pursuit to step-ramp target motion are determined by

retinal-image motion. However, a number of observations have raised doubts that the response of the pursuit system can be so simply explained.

Kowler (1990) has argued that visual-motion influences on pursuit cannot be studied in isolation from cognitive processes, because cognition is pervasive and affects every level of the system. Since physiological studies of the cognitive control of pursuit are relatively new, the question of whether cognition and visual motion are processed by separate neural subsystems is still largely open. Two alternative ways in which the pathways that carry these signals could be organized are presented in Figure 94.3. In the model shown at the top, cognitive and retinal-image signals are processed in the same pathway, and in the model shown at the bottom, they are processed independently. In the next several sections, we review recent studies that lay the groundwork for determining pathways that support the cognitive control of pursuit, and discuss how signals arising in these pathways interact with those generated by retinal-image motion.

AN ALTERNATIVE CORTICAL PATHWAY FOR SMOOTH PURSUIT

At the time we wrote our last review of the neurophysiology of the pursuit system (Keller and Heinen, 1991), a major pathway for pursuit from cortical motion processing areas in the superior temporal sulcus (STS), middle temporal (MT) area, and medial superior temporal (MST) area was well established. This pathway followed a classical cortico-ponto-cerebellar nexus with its relay in the DLPN. Since then, the FEF has been implicated in pursuit control with single-unit recordings (Fukushima et al., 2000; Gottlieb et al., 1994; MacAvoy et al., 1991), with imaging studies (Berman et al., 1999; O'Driscoll et al., 2000; Petit and Haxby, 1999; Petit et al., 1997), with electrical microstimulation (Gottlieb et al., 1993; Tian and Lynch, 1996), and with lesions (Keating, 1991; Lynch, 1987; MacAvoy et al., 1991; Shi et al., 1998). Single cells located in the floor and posterior bank of the arcuate sulcus discharge before pursuit onset and have directional tuning that, over the population, is rather uniformly distributed (Gottlieb et al., 1994). In contrast to the speed tuning of most MT cells, the response of FEF cells increases as a function of pursuit speed (Gottlieb et al., 1994). Electrical stimulation here produces a short-latency smooth eye movement, even when the animal is attempting to fixate a stationary target (Gottlieb et al., 1993). This is in contrast to what is observed in the STS, where stimulation fails to evoke significant smooth movements during fixation (Komatsu and Wurtz, 1989). Muscimol injections in the FEF suppress smooth pursuit in the same direction as that coded by cells recorded at the same sites (MacAvoy et al., 1991). The deficits these investigators observed were more severe and more lasting than the deficits produced by chemical lesions placed in isolated regions of the STS (Dürsteler and Wurtz,

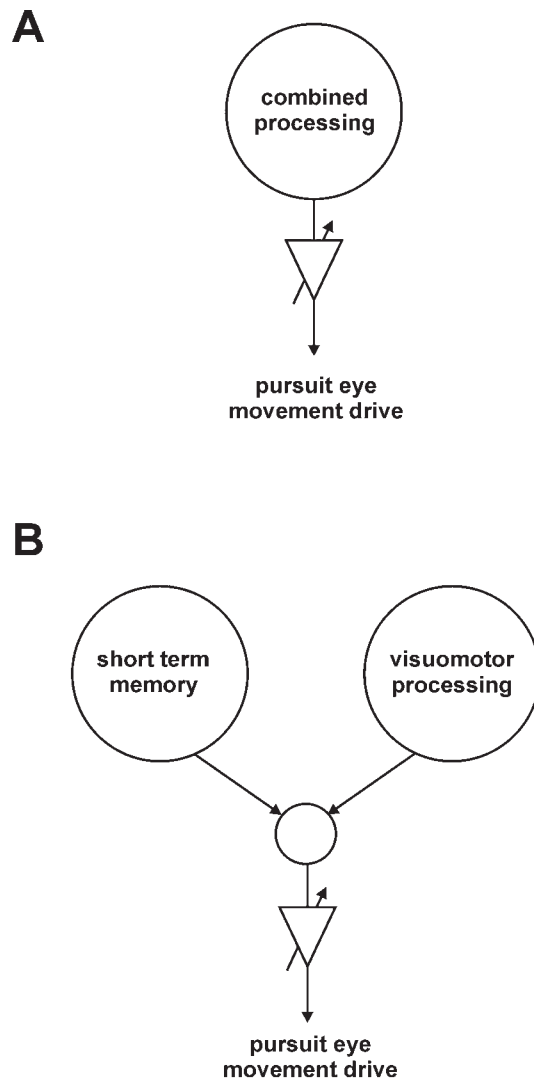


FIGURE 94.3. Functional organization schematics that hypothesize how retinal-image motion signals may be combined with a signal resulting from the memory of previous target motion to yield the pursuit eye movement drive signal. *A*, Short-term memory and retinal-image motion signals are processed in the same neural structures. The resulting signal is then passed through a variable gain element whose level is set by cognitive functions such as predictability of target motion and certainty of the target to be pursued. *B*, Signals resulting from short-term memory are processed separately from those resulting from direct retinal-image motion and are combined at a subsequent stage. Gain control is then exercised as in *A*.

1988; Dürsteler et al., 1987; Newsome et al., 1985) but comparable to those produced by larger injections that disrupted most of the motion processing cortex in the STS (Yamasaki and Wurtz, 1991). Ablations of the FEF that included the fundus of the arcuate sulcus produced milder deficits than those resulting from muscimol injections (Keating, 1993), perhaps because of neural adaptation that might have occurred given the longer recovery time that typically accompanies ablation studies.

Control of smooth pursuit by the frontal lobe is probably not limited to the FEF. The SEF, which had been implicated previously in saccade generation (Schlag and Schlag-Rey, 1987), also has neurons active during pursuit that are tuned for direction and speed (Heinen, 1995). The SEF receives projections from area MST (Huerta and Kaas, 1990), a structure that participates in visually guided pursuit (Newsome et al., 1988). The SEF also has strong reciprocal connections with the FEF (Huerta and Kaas, 1990). The SEF, in turn, projects to the nucleus reticularis tegmenti pontis (NRTP) (Shook et al., 1990), a brainstem region involved in the generation of pursuit movement commands (see below). Smooth eye movements have been evoked from the SEF in anesthetized cebus monkeys (Tian and Lynch, 1995) and more recently in behaving macaques (Missal and Heinen, 2001). Functional imaging studies suggest that activity in the SEF during pursuit is equal to or even greater than that which accompanies saccades (Berman et al., 1999; O'Driscoll et al., 2000; Petit and Haxby, 1999; Petit et al., 1997). In some respects, the pursuit eye movement-related physiology of the SEF appears similar to that of the FEF. However, neurons in the SEF have activity that rises to a peak which occurs close to the time when predictable target motion begins, stops, or reverses direction, implicating this structure in controlling the timing of predictive and anticipatory smooth pursuit (Heinen and Liu, 1997). Preliminary data suggest that stimulation of the SEF can also facilitate anticipatory eye velocity (Heinen et al., 2001). Furthermore, microstimulation experiments have implicated both the FEF (Tanaka and Lisberger, 2000) and the SEF (Missal and Heinen, 2001) in gain control for smooth pursuit, as was discussed earlier in this chapter.

NEW INSIGHTS INTO THE ROLES OF BRAINSTEM AND CEREBELLUM IN PURSUIT CONTROL Both the FEF and the SEF make stronger projections to the NRTP and the medial portion of the pontine nuclei than to the DLPN (Huerta and Kaas, 1990; Stanton et al., 1988). This suggests that these frontal cortical areas together form a cortico-reticular-cerebellar smooth pursuit pathway parallel to the cortico-ponto-cerebellar pathway that originates in the STS and courses mainly through the DLPN. Neurons in the NRTP are active during pursuit (Keller and Crandall, 1981; Suzuki et al., 1991), and stimulation here evokes smooth eye movements when the eyes are stationary, but without an active fixation target (Yamada et al., 1996). This behavior is more similar to that reported for stimulation of the FEF (Gottlieb et al., 1993) than that for stimulation of the STS or the DLPN (Komatsu and Wurtz, 1989; May et al., 1985). Deficits in pursuit also accompany reversible (lidocaine) or permanent (ibotenic acid) lesions of the NRTP (Suzuki et al., 1999). These authors suggested that the

NRTP is divided into a rostral region that is associated with pursuit eye movements and a caudal region that is involved in saccade control.

In our previous review, we discussed evidence that a posterior vermis to fastigial nucleus to vestibular nucleus pathway and a flocculus to ventral paraflocculus to vestibular nucleus pathway form parallel cerebellar pathways for pursuit. More recent single-unit recording studies support the role of the flocculus/ventral paraflocculus in smooth pursuit generation (Fukushima et al., 1999; Gomi et al., 1998; Suh and Kettner, 2000). Additional support has also accumulated for a parallel smooth pursuit pathway through the posterior vermis. Ablation of the cortex in lobules VI and VII significantly impairs pursuit function (Takagi et al., 2000). A recent paper suggested that most pursuit-related Purkinje cells in the posterior vermis are located in lobule VIII (Sato and Noda, 1992), and not in lobules VI and VII, as was previously reported (Suzuki and Keller, 1988a). This discrepancy has not been resolved. Lobules VI and VII project to the fastigial oculomotor region (FOR) (Yamada and Noda, 1987). Although the FOR was originally believed to be a saccade control region, more recently it has been shown to also participate in pursuit generation, the evidence being that single neurons here are active during pursuit (Büttner et al., 1991; Fuchs et al., 1994), and muscimol injections here lead to mild pursuit deficits (Robinson et al., 1997).

The output pathways for these putative parallel cerebellar pursuit pathways are different. The flocculus and paraflocculus have direct connections to the vestibular nuclei (VN) and the nucleus prepositus hypoglossi (PH), which are both established pursuit areas in the brainstem (Langer et al., 1985). In the only study with localized injections in the FOR using anterograde tracers (Noda et al., 1990), the caudal fastigial nucleus did not appear to project to the oculomotor region in the VN or to the PH; rather, these projections mostly terminated in the excitatory burst neuron (EBN), inhibitory burst neuron (IBN), and omnipause neuron (OPN) regions, which are thought to be involved in saccade control. However, some neurons located in the medial reticular formation near the abducens nuclei are modulated during pursuit (Eckmiller and Mackeben, 1980). More recently, saccadic burst neurons that are also modulated during pursuit have been identified in the EBN area (Missal and Keller, 2001).

Is there functional support for the anatomical evidence that two pursuit pathways course through the cerebellum? Some work suggests that these pathways differentially control predictive and visuomotor pursuit. One study used visual stimuli that allowed the authors to study activity accompanying pursuit responses to predictable target motion or to targets that made sudden, random changes in

motion direction and therefore could be followed better by relying on visual-motion signals (Suh and Kettner, 2000). They concluded that the floccular pathway is more concerned with predictive aspects of maintained pursuit than with the visually generated initiation of the randomly evoked pursuit. The pursuit pathway that courses through the posterior vermis to fastigial nucleus seems more concerned with direct visuomotor-driven pursuit (Takagi et al., 2000). These authors found that vermal lesions affected to a greater degree pursuit of random step-ramp motion during the open-loop period than during pursuit of a predictable target (triangle wave tracking). However, this point is controversial, because another study reached the conclusion that the flocculus was equally involved in predictive and visually guided pursuit (Stone and Lisberger, 1990).

In summary, the studies to date suggest that signals relating to retinal-image motion and cognition together determine the smooth pursuit response. However, only limited physiological data exist that address where these signals are processed and how they are combined to produce the pursuit movement.

Shared neural pathways for pursuit and saccades

The saccadic system reduces the retinal error between the image of an object and the fovea (Robinson, 1964). The pursuit system is thought to reduce retinal-image velocity that is produced by a moving object (Krauzlis and Lisberger, 1989; Robinson et al., 1986). Saccadic and smooth pursuit eye movements also have different temporal characteristics (Robinson, 1964, 1965). For the above reasons, it was thought that these eye movements are generated by separate neural systems, and neuroanatomical studies in the past supported this view (Leigh and Zee, 1999). However, evidence suggests that the pursuit and saccadic systems are not segregated absolutely. The saccadic system is sensitive to motion (de Brouwer et al., 2002; Keller and Johnsen, 1990), and the pursuit system can respond to positional error cues (Pola and Wyatt, 1980). Pursuit and saccades are coordinated in that the saccadic system appears to compensate for pursuit eye velocity (de Brouwer et al., 2002; Kim et al., 1998). This last section will cover research investigating neural substrates that may be shared by saccadic and pursuit ocular subsystems and that might support their cooperative behavior.

When an object moves in the natural scene, saccades and pursuit work together to foveate and track features of that object and to shift gaze to different objects. Recent evidence suggests that there is considerable overlap in the pursuit and saccade pathways. The superior colliculus (SC) was considered previously as involved exclusively in saccade control (see Guitton, 1991; Sparks and Hartwich-Young, 1989, for

reviews). In addition, rostral portions of the SC contain fixation neurons that are active during intersaccadic periods of fixation (Munoz and Guitton, 1991; Munoz and Wurtz, 1993; Peck, 1989). Recently, it was demonstrated that the rostral SC also contains neurons active during pursuit (Krauzlis et al., 1997, 2000). These same neurons are also active for small target displacements during fixation and for small saccades, and in both cases are more active for contralateral target displacements than for ipsilateral ones. Based on these results, it was suggested that neurons in the rostral colliculus code small motor errors, that is, mismatches between target and eye position that could be used to produce either corrective pursuit or corrective saccades (Krauzlis et al., 2000). This interpretation was supported by electrical stimulation and by similar effects on both types of eye movements following muscimol injections in the rostral SC (Basso et al., 2000).

Evidence for shared circuitry in the saccadic and pursuit systems has been reported in several other premotor structures that lie downstream from the SC. The posterior cerebellar vermis is one such structure. Early work showed that many Purkinje cells recorded in lobules VI and VII had both pursuit- and saccade-related activity, but the functional significance of this overlap was unclear (Suzuki and Keller, 1988b). This dual function of the vermis has been clarified recently by microstimulation experiments showing that the type of movement evoked depends on stimulation frequency and the behavioral state of the monkey, that is, whether it was engaged in a pursuit or saccade task (Krauzlis and Miles, 1998). Signals from lobules VI and VII reach the brainstem via projections to the caudal region of the fastigial nucleus (FN) (Noda et al., 1990). Some neurons in the caudal FN are active during saccades and some during pursuit, but none seem to be active for both types of eye movement (Fuchs et al., 1994).

OPNs lie in an anatomically distinct region of the raphe nucleus just rostral to the abducens nucleus, and receive projections from the FN and the region of the medial reticular formation where saccadic burst neurons are located (Langer and Kaneko, 1990; Noda et al., 1990). OPNs have been considered previously to gate exclusively the saccadic system by inhibiting these eye movements in the face of neural noise (see Keller, 1991, for a review). These neurons discharge at a high tonic rate during fixation but quiesce before and during all saccades. To prevent saccades from occurring, OPNs inhibit directionally selective burst neurons that in turn project directly to the ocular motoneurons. Recent evidence suggests that the activity of OPNs also decreases during smooth pursuit (Missal and Keller, 2002), and electrical stimulation in the OPN region slows ongoing pursuit movements (Missal and Keller, 2002). These findings suggest that OPNs inhibit the motor output signal for both pursuit

and saccades. Interestingly, EBNs do not seem to discharge at all during pursuit movements even when the inhibitory input from OPNs that project directly to them is reduced (Missal and Keller, 2001). Instead, a population of long-lead burst neurons (LLBNs) in the paramedian pontine reticular formation (PPRF) that fire for ipsilateral saccades also fire during ipsilateral pursuit (Missal and Keller, 2001). These authors hypothesized that LLBNs might be “latch” neurons that completely or partially silence OPNs during saccades or pursuit, respectively. In support of this, direct inhibitory projections from the PPRF to the OPNs have been demonstrated (Kamogawa et al., 1996). Pursuit/saccade cells which respond similarly for vertical movements have been reported in the interstitial nucleus of Cajal (Missal et al., 2000).

Two regions in the frontal cortex, the FEF and the SEF, are also involved in smooth pursuit and saccades. The FEF is an area where the distinction between pursuit and saccade control still appears to hold. This structure has nonoverlapping regions which contain either pursuit or saccade cells (Gottlieb et al., 1989) and in which only one of the two types of eye movement is evoked by electrical stimulation (Bruce et al., 1985; Gottlieb et al., 1993; Tian and Lynch, 1996). However, the anatomical projections of the pursuit and saccade areas in FEF appear to overlap in the brainstem reticular formation (Yan et al., 2001). The SEF also has neurons that are active during pursuit (Heinen, 1995; Heinen and Liu, 1997) and during saccades (Schall, 1991; Schlag and Schlag-Rey, 1987). Microstimulation here evokes saccades (Russo and Bruce, 2000; Schlag and Schlag-Rey, 1987; Tehovnik et al., 1994) and facilitates smooth pursuit (Missal and Heinen, 2001; Tian and Lynch, 1995). While the initial microstimulation experiments found saccade sites to be fairly equally distributed across the SEF (Schlag and Schlag-Rey, 1987), more recent work suggests that they lie in lateral subregions and that saccades cannot be evoked close to the midline (Russo and Bruce, 2000). Smooth pursuit sites appear to be distributed uniformly within the SEF and overlap to a degree the regions where saccades are evoked (Missal and Heinen, 2001).

Summary and future directions

Past research on the pursuit system using single-spot stimuli and linear systems analysis was essential in laying the groundwork to understand basic sensorimotor processing for pursuit and to determine the structures in the brain where this processing occurred. However, behavioral studies suggest that pursuit behavior has a complexity greater than that of a sensorimotor reflex and that cognitive factors are intrinsic to the pursuit response. Since the basic building blocks are now in place, it is timely to advance the level of stimulus complexity used in pursuit experiments and study

the neurophysiology of cognitive signals that modulate pursuit behavior in the natural scene. It is also important to consider that the pursuit and saccadic systems often operate together and therefore might use common signals that are processed in shared neural substrates. In conclusion, some of the challenging issues facing eye movement researchers in the future are how visual and cognitive signals interact and how ocular subsystems coordinate to view objects in the natural scene.

REFERENCES

- Barnes, G. R., and P. T. Asselman, 1991. The mechanism of prediction in human smooth pursuit eye movements, *J. Physiol. (Lond.)*, 439:439–461.
- Barnes, G. R., S. F. Donnelly, and R. D. Eason, 1987. Predictive velocity estimation in the pursuit reflex response to pseudo-random and step displacement stimuli in man, *J. Physiol. (Lond.)*, 389:111–136.
- Barnes, G. R., and M. A. Grealy, 1992. Predictive mechanisms of head-eye coordination and vestibulo-ocular reflex suppression in humans, *J. Vestib. Res.*, 2:193–212.
- Basso, M. A., R. J. Krauzlis, and R. H. Wurtz, 2000. Activation and inactivation of rostral superior colliculus neurons during smooth-pursuit eye movements in monkeys, *J. Neurophysiol.*, 84:892–908.
- Berman, R. A., C. L. Colby, C. R. Genovese, J. T. Voyvodic, B. Luna, K. R. Thulborn, and J. A. Sweeney, 1999. Cortical networks subserving pursuit and saccadic eye movements in humans: an fMRI study, *Hum. Brain Mapp.*, 8:209–225.
- Beutter, B. R., and L. S. Stone, 1997. Human motion perception and smooth eye movements show similar directional biases for elongated apertures, *Vis. Res.*, 38:1273–1286.
- Beutter, B. R., and L. S. Stone, 2000. Motion coherence affects human perception and pursuit similarly, *Vis. Neurosci.*, 17:139–153.
- Boman, D. K., and J. R. Hotson, 1988. Stimulus conditions that enhance anticipatory slow eye movements, *Vis. Res.*, 28:1157–1165.
- Born, R. T., and R. B. H. Tootell, 1992. Segregation of global and local motion processing in primate middle temporal visual area, *Nature*, 357:497–499.
- Bruce, C. J., M. E. Goldberg, M. C. Bushnell, and G. B. Stanton, 1985. Primate frontal eye fields. II. Physiological and anatomical correlates of electrically evoked eye movements, *J. Neurophysiol.*, 54:714–734.
- Büttner, U., A. Fuchs, G. Markert-Schwab, and P. Buckmaster, 1991. Fastigial nucleus activity in the alert monkey during slow eye and head movements, *J. Neurophysiol.*, 65:1360–1371.
- Carl, J., and R. Gellman, 1987. Human smooth pursuit: stimulus-dependent responses, *J. Neurophysiol.*, 57:1446–1463.
- Cheng, M., and J. S. Outerbridge, 1975. Optokinetic nystagmus during selective retinal stimulation, *Exp. Brain Res.*, 23:129–139.
- Cohen, B., V. Matsuo, and T. Raphan, 1977. Quantitative analysis of the velocity characteristics of optokinetic nystagmus and optokinetic after nystagmus, *J. Physiol. (Lond.)*, 270:321–344.
- de Brouwer, S., M. Missal, G. Barnes, and P. Lefevre, 2002. Quantitative analysis of catch-up saccades during sustained pursuit, *J. Neurophysiol.*, 87:1772–1780.

- Deno, D. C., W. F. Crandall, K. R. Sherman, and E. L. Keller, 1995. Characterization of prediction in the primate visual smooth pursuit system, *Biosystems*, 34:107–128.
- Dodge, R., R. C. Travis, and J. C. Fox, 1930. Optic nystagmus III. Characteristics of the slow phase, *Arch. Neurol. Psychiatry*, 24:21–34.
- Dubois, M. F. W., and H. Collewijn, 1979. Optokinetic reactions in man elicited by localized retinal motion stimuli, *Vis. Res.*, 19:1105–1115.
- Dürsteler, M. R., and R. H. Wurtz, 1988. Pursuit and optokinetic deficits following chemical lesions of cortical areas MT and MST, *J. Neurophysiol.*, 60:940–965.
- Dürsteler, M. R., R. H. Wurtz, and W. T. Newsome, 1987. Directional pursuit deficits following lesions of the foveal representation within the superior temporal sulcus of the macaque monkey, *J. Neurophysiol.*, 57:1262–1287.
- Eckmiller, R., 1987. The neural control of pursuit eye movements, *Physiol. Rev.*, 67:797–857.
- Eckmiller, R., and M. Mackeben, 1980. Pre-motor single unit activity in the monkey brain stem correlated with eye velocity during pursuit, *Brain Res.*, 184:210–214.
- Ferrera, V. P., 2000. Task-dependent modulation of the sensorimotor transformation for smooth pursuit eye movements, *J. Neurophysiol.*, 84:2725–2738.
- Ferrera, V. P., and S. G. Lisberger, 1997. The effect of a moving distractor on the initiation of smooth-pursuit eye movements, *Vis. Neurosci.*, 14:323–338.
- Fuchs, A. F., 1967. Periodic eye tracking in the monkey, *J. Physiol. (Lond.)*, 193:161–171.
- Fuchs, A. F., and M. J. Mustari, 1993. The optokinetic response in primates and its possible neuronal substrate, in *Visual Motion and Its Role in the Stabilization of Gaze* (F. A. Miles and J. Wallman, eds.), Amsterdam: Elsevier Science, pp. 343–369.
- Fuchs, A. F., F. R. Robinson, and A. Straube, 1994. Participation of the caudal fastigial nucleus in smooth-pursuit eye movements. I. Neuronal activity, *J. Neurophysiol.*, 72:2714–2728.
- Fukushima, K., J. Fukushima, C. R. S. Kaneko, and A. F. Fuchs, 1999. Vertical Purkinje cells of the monkey floccular lobe: simple-spike activity during pursuit and passive whole body rotation, *J. Neurophysiol.*, 82:787–803.
- Fukushima, K., T. Sato, J. Fukushima, Y. Shinmei, and C. R. S. Kaneko, 2000. Activity of smooth pursuit-related neurons in the monkey periarculate cortex during pursuit and passive whole-body rotation, *J. Neurophysiol.*, 83:563–587.
- Gardner, J. L., and S. G. Lisberger, 2001. Linked target selection for saccadic and smooth pursuit eye movements, *J. Neurosci.*, 21:2075–2084.
- Gellman, R. S., J. R. Carl, and F. A. Miles, 1990. Short latency ocular-following responses in man, *Vis. Neurosci.*, 5:107–122.
- Goldreich, D., and S. G. Lisberger, 1987. Evidence that visual inputs drive oscillations in eye velocity during smooth pursuit eye movements in the monkey, *Soc. Neurosci. Abstr.*, 13:170.
- Gomi, H., M. Shidara, A. Takemura, Y. Inoue, K. Kawano, and M. Kawato, 1998. Temporal firing patterns of Purkinje cells in the cerebellar ventral paraflocculus during ocular following responses in monkeys I. Simple spikes, *J. Neurophysiol.*, 80:818–831.
- Gottlieb, J. P., C. J. Bruce, and M. G. MacAvoy, 1993. Smooth pursuit eye movements elicited by microstimulation in the primate frontal eye field, *J. Neurophysiol.*, 69:786–799.
- Gottlieb, J. P., M. G. MacAvoy, and C. J. Bruce, 1989. Unit activity related to smooth pursuit eye movements in rhesus monkey frontal eye fields, *Soc. Neurosci. Abstr.*, 15:1203.
- Gottlieb, J. P., M. G. MacAvoy, and C. J. Bruce, 1994. Neural responses related to smooth pursuit eye movements and their correspondence with electrically elicited smooth eye movements in the primate frontal eye field, *J. Neurophysiol.*, 72:1634–1653.
- Groh, J. M., R. T. Born, and W. T. Newsome, 1997. How is a sensory map read out? Effects of microstimulation in visual area MT on saccades and smooth pursuit eye movements, *J. Neurosci.*, 17:4312–4330.
- Guittin, D., 1991. Control of saccadic eye and gaze movements by the superior colliculus and basal ganglia, in *Eye Movements* (R. H. S. Carpenter ed.), London: Macmillan, pp. 244–276.
- Heinen, S. J., 1995. Single-neuron activity in dorsomedial frontal cortex during smooth pursuit eye movements, *Exp. Brain Res.*, 104:357–361.
- Heinen, S. J., and M. Liu, 1997. Single-neuron activity in the dorsomedial frontal cortex during smooth pursuit eye movements to predictable target motion, *Vis. Neurosci.*, 14:853–865.
- Heinen, S. J., D. P. Munoz, G. R. Barnes, and M. Missal, 2001. Reflexive and cognitive aspects of sequential oculomotor behavior, *Proc. Neural Control Move.*, 6:11.
- Heinen, S. J., and S. N. J. Watamaniuk, 1998. Spatial integration in human smooth pursuit, *Vis. Res.*, 38:3785–3794.
- Huerta, M. F., and J. H. Kaas, 1990. Supplementary eye field as defined by intracortical micro-stimulation: connections in macaques, *J. Comp. Neurol.*, 293:299–330.
- Kamogawa, H., Y. Ohki, H. Shimazu, I. Suzuki, and M. Yamashita, 1996. Inhibitory input to pause neurons from pontine burst neuron area in the cat, *Neurosci. Lett.*, 203:163–166.
- Kao, G. W., and M. J. Morrow, 1994. The relationship of anticipatory smooth eye movement to smooth pursuit initiation, *Vis. Res.*, 34:3027–3036.
- Kawano, K., Y. Inoue, A. Takemura, and F. A. Miles, 1994a. Effect of disparity in the peripheral field on short-latency ocular following responses, *Vis. Neurosci.*, 11:833–837.
- Kawano, K., and F. A. Miles, 1986. Short-latency ocular following responses of monkey. II. Dependence on a prior saccadic eye movement, *J. Neurophysiol.*, 56:1355–1380.
- Kawano, K., M. Shidara, Y. Watanabe, and S. Yamane, 1994b. Neural activity in cortical area MST of alert monkey during ocular following responses, *J. Neurophysiol.*, 71:2305–2324.
- Kawano, K., M. Shidara, and S. Yamane, 1992. Neural activity in dorsolateral pontine nucleus of alert monkey during ocular following responses, *J. Neurophysiol.*, 67:680–703.
- Keating, E. G., 1991. Frontal eye field lesions impair predictive and visually-guided pursuit eye movements, *Exp. Brain Res.*, 86:311–323.
- Keating, E. G., 1993. Lesions of the frontal eye field impair pursuit eye movements, but preserve the predictions driving them, *Behav. Brain Res.*, 53:91–104.
- Keating, E. G., and A. Pierre, 1996. Architecture of a gain controller in the pursuit system, *Behav. Brain Res.*, 81:173–181.
- Keller, E. L., 1991. The brainstem, in *Eye Movements* (R. H. S. Carpenter ed.), London: Macmillan, pp. 200–223.
- Keller, E. L., and W. F. Crandall, 1981. Neural activity in the nucleus reticularis tegmenti in the monkey related to eye movements and visual stimulation, *Ann. N.Y. Acad. Sci.*, 374:249–261.
- Keller, E. L., and S. J. Heinen, 1991. Generation of smooth-pursuit eye movements: neuronal mechanisms and pathways, *Neurosci. Res.*, 11:79–107.
- Keller, E. L., and S. D. Johnsen, 1990. Velocity prediction in corrective saccades during smooth-pursuit eye movements in monkey, *Exp. Brain Res.*, 80:525–531.

- Keller, E. L., and N. S. Kahn, 1986. Smooth-pursuit initiation in the presence of a textured background in monkey, *J. Neurophysiol.*, 68:2147–2164.
- Khurana, B., and E. Kowler, 1987. Shared attentional control of smooth eye movement and perception, *Vis. Res.*, 27:1603–1618.
- Kim, Y. G., S. J. Heinen, and E. L. Keller, 1998. Coordination of smooth pursuit and saccadic systems during smooth pursuit initiation, *Soc. Neurosci. Abstr.*, 24:671.
- Komatsu, H., and R. H. Wurtz, 1989. Modulation of pursuit eye movements by stimulation of cortical areas MT and MST, *J. Neurophysiol.*, 62:31–47.
- Kowler, E., 1989. Cognitive expectations, not habits, control anticipatory smooth oculomotor pursuit, *Vis. Res.*, 29:1049–1057.
- Kowler, E., 1990. The role of visual and cognitive processes in the control of eye movement, in *Eye Movements and Their Role in Visual and Cognitive Processes* (E. Kowler ed.), Amsterdam: Elsevier, pp. 1–63.
- Kowler, E., A. J. Martins, and M. Pavel, 1984. The effect of expectations on slow oculomotor control—IV anticipatory smooth eye movements depend on prior target motions, *Vis. Res.*, 24:197–210.
- Kowler, E., and S. McKee, 1987. Sensitivity of smooth eye movement to small differences in target velocity, *Vis. Res.*, 27:993–1015.
- Krauzlis, R. J., 1994. The visual drive for smooth eye movements, in *Visual Detection of Motion* (R. J. Snowden and A. T. Smith, eds.), London: Academic Press, pp. 437–473.
- Krauzlis, R. J., and S. A. Adler, 2001. Effects of directional expectations on motion perception and pursuit eye movements, *Vis. Neurosci.*, 18:365–376.
- Krauzlis, R. J., M. A. Basso, and R. H. Wurtz, 1997. Shared motor error for multiple eye movements, *Science*, 276:1693–1695.
- Krauzlis, R. J., M. A. Basso, and R. H. Wurtz, 2000. Discharge properties of neurons in the rostral superior colliculus of the monkey during smooth-pursuit eye movements, *J. Neurophysiol.*, 84:876–891.
- Krauzlis, R. J., and S. G. Lisberger, 1989. A control systems model of smooth pursuit eye movements with realistic emergent properties, *Neural Comput.*, 1:116–122.
- Krauzlis, R. J., and F. A. Miles, 1998. Role of the oculomotor vermis in generating pursuit and saccades: effects of microstimulation, *J. Neurophysiol.*, 80:2046–2062.
- Langer, T. P., A. F. Fuchs, M. C. Chubb, C. A. Scudder, and S. G. Lisberger, 1985. Floccular efferents in the rhesus macaque as revealed by autoradiography and horseradish peroxidase, *J. Comp. Neurol.*, 235:26–37.
- Langer, T. P., and C. R. S. Kaneko, 1990. Brainstem afferents to the oculomotor omnipause neurons in monkey, *J. Comp. Neurol.*, 295:413–427.
- Leigh, R. J., and D. S. Zee, 1999. *The Neurology of Eye Movements*, New York: Oxford University Press.
- Lisberger, S. G., 1998. Postsaccadic enhancement of initiation of smooth pursuit eye movements in monkeys, *J. Neurophysiol.*, 79:1918–1930.
- Lisberger, S. G., and V. P. Ferrera, 1997. Vector averaging for smooth pursuit eye movements initiated by two moving targets in monkeys, *J. Neurosci.*, 17:7490–7502.
- Lisberger, S. G., E. Morris, and L. Tyschen, 1987. Visual motion processing and sensory-motor integration for smooth pursuit eye movements, *Annu. Rev. Neurosci.*, 10:97–129.
- Lisberger, S. G., and L. E. Westbrook, 1985. Properties of visual inputs that initiate horizontal smooth pursuit eye movements in monkeys, *J. Neurosci.*, 5:1662–1673.
- Lynch, J. C., 1987. Frontal eye field lesions in monkeys disrupt visual pursuit, *Exp. Brain Res.*, 68:437–441.
- MacAvoy, M. G., J. P. Gottlieb, and C. J. Bruce, 1991. Smooth-pursuit eye movement representation in the primate frontal eye field, *Cereb. Cortex*, 1:95–102.
- May, J. G., E. L. Keller, and W. F. Crandall, 1985. Changes in eye velocity during smooth pursuit tracking induced by microstimulation in the dorsolateral pontine nucleus of the macaque, *Soc. Neurosci. Abstr.*, 11:79.
- Miles, F., K. Kawano, and L. M. Optican, 1986. Short-latency ocular following responses of monkey I. Dependence on temporospatial properties of visual input, *J. Neurophysiol.*, 56:1321–1354.
- Missal, M., S. de Brouwer, P. Lefèvre, and E. Olivier, 2000. Activity of mesencephalic vertical burst neurons during saccades and smooth pursuit, *J. Neurophysiol.*, 83:2080–2092.
- Missal, M., and S. J. Heinen, 2001. Facilitation of smooth pursuit initiation by electrical stimulation in the supplementary eye fields, *J. Neurophysiol.*, 86:2413–2425.
- Missal, M., and E. L. Keller, 2001. Neurons active during both saccades and smooth pursuit suggest a convergence of oculomotor systems in the pontine reticular formation, *Soc. Neurosci. Abstr.*, 27:208.
- Missal, M., and E. L. Keller, 2002. Common inhibitory mechanism for saccades and smooth-pursuit eye movements, *J. Neurophysiol.*, 88:1880–1892.
- Munoz, D. P., and D. Guitton, 1991. Control of orienting gaze shifts by the tectoreticulospinal system in the head-free cat. II. sustained discharges during motor preparation and fixation, *J. Neurophysiol.*, 66:1624–1641.
- Munoz, D. P., and R. H. Wurtz, 1993. Fixation cells in monkey superior colliculus. I. Characteristics of cell discharge, *J. Neurophysiol.*, 70:559–575.
- Newsome, W. T., R. H. Wurtz, M. R. Dursteler, and A. Mikami, 1985. Deficits in visual motion processing following ibotenic acid lesions of the middle temporal visual area of the macaque monkey, *J. Neurophysiol.*, 53:825–840.
- Newsome, W. T., R. H. Wurtz, and H. Komatsu, 1988. Relation of cortical MT and MST to pursuit eye movements. II. Differentiation of retinal from extraretinal inputs, *J. Neurophysiol.*, 60:604–620.
- Noda, H., S. Sugita, and Y. Ikeda, 1990. Afferent and efferent connections of the oculomotor region of the fastigial nucleus in the macaque monkey, *J. Comp. Neurol.*, 302:330–348.
- O'Driscoll, G. A., A. L. Wolff, C. Benkelfat, P. S. Florencio, S. Lal, and A. C. Evans, 2000. Functional neuroanatomy of smooth pursuit and predictive saccades, *NeuroReport*, 11:1335–1340.
- Peck, C. K., 1989. Visual responses of neurones in cat superior colliculus in relation to fixation of targets, *J. Physiol. (Lond.)*, 414:301–315.
- Petit, L., V. P. Clark, J. Ingeholm, and J. V. Haxby, 1997. Dissociation of saccade-related and pursuit-related activation in human frontal eye fields as revealed by fMRI, *J. Neurophysiol.*, 77:3386–3390.
- Petit, L., and J. V. Haxby, 1999. Functional anatomy of pursuit eye movements in humans as revealed by fMRI, *J. Neurophysiol.*, 81:463–471.
- Pola, J., and H. J. Wyatt, 1980. Target position and velocity: the stimuli for smooth pursuit eye movements, *Vis. Res.*, 20:523–534.
- Pola, J., and H. J. Wyatt, 1991. Smooth pursuit: response characteristics, stimuli and mechanisms, in *Eye Movements* (R. H. S. Carpenter ed.), London: Macmillan, pp. 138–156.

- Raiguel, S., M. M. Van Hulle, D.-K. Xiao, V. L. Marcar, and G. A. Orban, 1995. Shape and spatial distribution of receptive fields and antagonistic motion surrounds in the middle temporal area (V5) of the macaque, *Eur. J. Neurosci.*, 7:2065–2082.
- Recanzone, G. H., and R. H. Wurtz, 1999. Shift in smooth pursuit initiation and MT and MST neuronal activity under different stimulus conditions, *J. Neurophysiol.*, 82:1710–1727.
- Robinson, D. A., 1964. The mechanisms of human saccadic eye movement, *J. Physiol. (Lond.)*, 174:245–264.
- Robinson, D. A., 1965. The mechanics of human smooth pursuit eye movement, *J. Physiol. (Lond.)*, 180:569–591.
- Robinson, D. A., 1981. Control of eye movements, in *Handbook of Physiology*, Section 1: *The Nervous System*, vol. II, part 2 (V. B. Brooks ed.), American Physiological Society, Bethesda, pp. 1275–1320.
- Robinson, D. A., J. L. Gordon, and S. E. Gordon, 1986. A model of the smooth eye pursuit eye movement system, *Biol. Cybern.*, 55:43–57.
- Robinson, F. R., A. Straube, and A. F. Fuchs, 1997. Participation of caudal fastigial nucleus in smooth pursuit eye movements. II. Effects of muscimol inactivation, *J. Neurophysiol.*, 78:848–859.
- Russo, G. S., and C. J. Bruce, 2000. Supplementary eye field: representation of saccades and relationship between neural response fields and elicited eye movements, *J. Neurophysiol.*, 84:2605–2621.
- Sato, H., and H. Noda, 1992. Posterior vermal Purkinje cells in macaques responding during saccades, smooth pursuit, chair rotation and/or optokinetic stimulation, *Neurosci. Res.*, 12:583–595.
- Schall, J. D., 1991. Neuronal activity related to visually guided saccadic eye movements in the supplementary motor area of rhesus monkeys, *J. Neurophysiol.*, 66:530–558.
- Schlag, J., and M. Schlag-Rey, 1987. Evidence for a supplementary eye field, *J. Neurophysiol.*, 57:179–200.
- Schwartz, J. D., and S. G. Lisberger, 1994. Initial tracking conditions modulate the gain of visuo-motor transmission for smooth pursuit eye movements in monkeys, *Vis. Neurosci.*, 11:411–424.
- Shi, D., H. R. Friedman, and C. J. Bruce, 1998. Deficits in smooth-pursuit eye movements after muscimol inactivation within the primate's frontal eye field, *J. Neurophysiol.*, 80:458–464.
- Shook, B. L., M. Schlag-Rey, and J. Schlag, 1990. Primate supplementary eye field: I. Comparative aspects of mesencephalic and pontine connections, *J. Comp. Neurol.*, 301:618–642.
- Sparks, D. L., and R. Hartwich-Young, 1989. The deep layers of the superior colliculus, in *The Neurobiology of Saccadic Eye Movements, Reviews of Oculomotor Research*, vol. III (R. H. Wurtz and M. E. Goldberg, eds.), Amsterdam: Elsevier Science, pp. 213–256.
- Stanton, G. B., M. E. Goldberg, and C. J. Bruce, 1988. Frontal eye field efferents in the macaque monkey. II. Topography of terminal fields in midbrain and pons, *J. Comp. Neurol.*, 271:493–506.
- Stark, L., G. Vossius, and L. R. Young, 1962. Predictive control of eye tracking movements, *IRE Trans. Hum. Factors Electron.*, 3:52–57.
- Stone, L. S., and S. G. Lisberger, 1990. Visual responses of Purkinje cells in the cerebellar flocculus during smooth-pursuit eye movements in monkeys. I. Simple spikes, *J. Neurophysiol.*, 63:1241–1261.
- Suh, M., and R. E. Kettner, 2000. Cerebellar flocculus and ventral paraflocculus purkinje cell activity during predictive and visually driven pursuit in monkey, *J. Neurophysiol.*, 84:1835–1850.
- Suzuki, D. A., and E. L. Keller, 1988a. The role of the posterior vermis of monkey cerebellum in smooth-pursuit eye movement control I. Eye and head movement-related activity, *J. Neurophysiol.*, 59:1–18.
- Suzuki, D. A., and E. L. Keller, 1988b. The role of the posterior vermis of monkey cerebellum in smooth-pursuit eye movement control. II. Target velocity-related Purkinje cell activity, *J. Neurophysiol.*, 59:19–40.
- Suzuki, D. A., T. Yamada, K. F. Betelak, and R. D. Yee, 1991. Smooth-pursuit eye movement related activity in monkey nucleus reticularis tegmenti pontis, *Soc. Neurosci. Abstr.*, 17:459.
- Suzuki, D. A., T. Yamada, R. Hoedema, and R. D. Yee, 1999. Smooth-pursuit eye-movement deficits with chemical lesions in macaque nucleus reticularis tegmenti pontis, *J. Neurophysiol.*, 82:1178–1186.
- Takagi, M., D. S. Zee, and R. J. Tamargo, 2000. Effects of lesions of the oculomotor cerebellar vermis on eye movements in primate: smooth pursuit, *J. Neurophysiol.*, 83:2047–2062.
- Tanaka, M., and S. G. Lisberger, 2000. Context-dependent smooth eye movements evoked by stationary visual stimuli in trained monkeys, *J. Neurophysiol.*, 84:1748–1762.
- Tanaka, M., and S. G. Lisberger, 2001. Regulation of the gain of visually guided smooth-pursuit eye movements by frontal cortex, *Nature*, 409:191–194.
- Tehovnik, E., K. Lee, and P. Schiller, 1994. Stimulation-evoked saccades from the dorsomedial frontal cortex of the rhesus monkey following lesions of the frontal eye fields and superior colliculus, *Exp. Brain Res.*, 98:179–190.
- Tian, J. R., and J. C. Lynch, 1995. Slow and saccadic eye movements evoked by microstimulation in the supplementary eye field of the cebus monkey, *J. Neurophysiol.*, 74:2204–2210.
- Tian, J. R., and J. C. Lynch, 1996. Functionally defined smooth and saccadic eye movement subregions in the frontal eye field of cebus monkeys, *J. Neurophysiol.*, 76:2740–2753.
- Tychsen, L., and S. G. Lisberger, 1986. Visual motion processing for the initiation of smooth-pursuit eye movements in humans, *J. Neurophysiol.*, 56:953–968.
- van den Berg, A. V., and H. Collewijn, 1986. Human smooth pursuit: effects of stimulus extent and of spatial and temporal constraints of the pursuit trajectory, *Vis. Res.*, 26:1209–1222.
- van Die, G., and H. Collewijn, 1982. Optokinetic nystagmus in man, *Hum. Neurobiol.*, 1:111–119.
- Watamaniuk, S. N. J., and S. J. Heinen, 1999. Human smooth pursuit direction discrimination, *Vis. Res.*, 39:70.
- Watamaniuk, S. N. J., and S. J. Heinen, 2000. Evidence for a structured receptive field subserving voluntary smooth eye movements, *Soc. Neurosci. Abstr.*, 26:1331.
- Watamaniuk, S. N. J., and R. Sekuler, 1992. Temporal and spatial integration in dynamic random-dot stimuli, *Vis. Res.*, 32:2341–2347.
- Wells, S. G., and G. R. Barnes, 1998. Fast, anticipatory smooth-pursuit eye movements appear to depend on a short-term store, *Exp. Brain Res.*, 120:129–133.
- Westheimer, G., 1954. Eye movement responses to a horizontally moving visual stimulus, *AMA Arch. Ophthalmol.*, 52:932–941.
- Winterson, B. J., and R. M. Steinman, 1978. The effect of luminance on human smooth pursuit of perifoveal and foveal targets, *Vis. Res.*, 18:1165–1172.
- Xiao, D. K., S. Raiguel, V. L. Marcar, J. J. Koenderink, and G. A. Orban, 1995. Spatial heterogeneity of inhibitory surrounds in

- the middle temporal visual area, *Proc. Natl. Acad. Sci. USA*, 92:11303–11306.
- Yamada, J., and H. Noda, 1987. Afferent and efferent connections of the oculomotor cerebellar vermis in the macaque monkey, *J. Comp. Neurol.*, 265:224–241.
- Yamada, T., D. A. Suzuki, and R. D. Yee, 1996. Smooth pursuit-like eye movements evoked by microstimulation in macaque nucleus reticularis tegmenti pontis, *J. Neurophysiol.*, 76:3313–3324.
- Yamasaki, D. S., and R. H. Wurtz, 1991. Recovery of function after lesions in the superior temporal sulcus in the monkey, *J. Neurophysiol.*, 66:651–673.
- Yan, Y. J., D. M. Cui, and J. C. Lynch, 2001. Overlap of saccadic and pursuit eye movement systems in the brain stem reticular formation, *J. Neurophysiol.*, 86:3056–3060.

95 Neural Control of Vergence

Eye Movements

LAWRENCE E. MAYS

EYE MOVEMENT CONTROL subsystems have evolved to serve different functions. For example, the vestibulo-ocular reflex mechanisms help stabilize images on the retina in the face of head motion, and the saccadic subsystem allows for very rapid changes in the direction of gaze. Binocular vision requires that the two eyes be aligned on an object of interest to within about 15 minutes of arc. A vergence subsystem has evolved to achieve this goal.

Vergence commands are those that rotate the two eyes simultaneously in the opposite direction. They are distinguished from *versional* commands, such as saccades and smooth pursuit, where the eyes move in the same direction. Often, the terms *disjunctive* and *conjugate* are used to refer to vergence and versional movements, respectively. Some authors (Ono, 1983) use *version* and *vergence* to refer to the underlying mechanisms, while using *disjunctive* and *conjugate* to refer to the actual eye movements. Vergence movements may be horizontal, vertical, or torsional (i.e., rotation around the line of sight). Vertical and torsional vergence are small, generally reflexive eye movements, and while they are important for aligning the two eyes upon a target, relatively little is known about these types of movements (Kertesz, 1983). Horizontal vergence movements can be reflexive or voluntary and are needed when gaze is shifted between targets at differing distances from the observer. *Convergence* refers to lines of sight moving toward each other; *divergence* to the reverse. Unless stated otherwise, *vergence* as used here will refer to *horizontal* vergence movements. The control of horizontal vergence movements by the extraocular motoneurons and their premotor inputs will be reviewed.

Horizontal vergence is part of what has been called the *near triad* or *near response* (Myers and Stark, 1990). The other components of the near response are pupillary constriction (*miosis*) and *accommodation* of the crystalline lens, which changes the focal length of the eye. The miosis associated with convergence is somewhat questionable (Stakenburg, 1991), but the relationship between accommodation and convergence is quite robust. Indeed, accommodation of the eye, as when switching from a far to a near target, invariably induces convergence, even if the target is viewed monocularly. This linkage is termed *accommodative convergence* and is measured clinically as the accommodative convergence/

accommodation (AC/A) ratio. Moreover, convergence of the eyes induces accommodation, and this effect, termed *convergence accommodation*, is equally robust. The strength of this relationship is the CA/C (convergence accommodation/convergence) ratio. Considering the linkage between accommodation and vergence, it may not be surprising that the premotor neurons that control vergence appear to control accommodation as well.

Hering (1868) observed that the two eyes act as if yoked, that is, they move either the same amplitude in the same direction (*version*) or the same amplitude in the opposite direction (*vergence*). *Hering's Law of Equal Innervation* implies that all eye movements should be generated by a linear combination of largely independent versional (*conjugate*) commands and vergence (*disconjugate*) commands. In this view, conjugate commands operate on a *cyclopean eye*, an imaginary eye located between the two actual eyes. Many, but not all, studies of vergence control have used symmetrical vergence movements, in which the subject looks between targets at different distances aligned with the cyclopean eye in order to eliminate versional demands. An alternative view to Hering's Law states that the brain has independent control of each eye. This has been debated for over a century, and the debate continues (Enright, 1984; Zhou and King, 1998). The focus is on how to interpret what appear to be unequal saccades in the two eyes when vergence movements are combined with saccades.

Finally, considerable attention has been directed to the analysis of higher-order brain mechanisms for vergence control. Recent evidence suggests roles for the parietal cortex (Gnadt and Mays, 1995), frontal eye fields (Gamlin and Yoon, 2000), and superior colliculus (Chaturvedi and Van Gisbergen, 1999). Since these areas are involved in other types of eye movements, they may help coordinate vergence movements with saccades or perhaps smooth pursuit.

Extraocular motoneurons

Medial and lateral rectus muscles, which are innervated by motoneurons in the oculomotor and abducens nuclei, respectively, are primarily responsible for convergence and divergence. Figure 95.1 is a schematic diagram of these

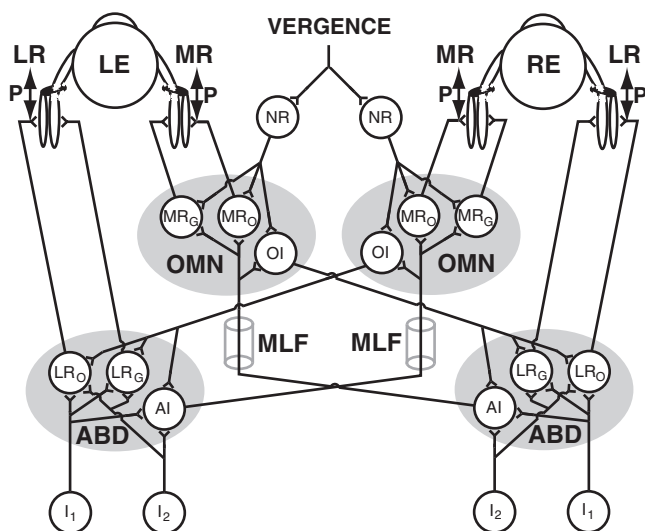


FIGURE 95.1. Schematic representation of horizontal oculomotor elements. Shaded ellipses indicate the oculomotor (OMN) and abducens (ABD) nuclei. The global layers of medial and lateral muscles are shown as inserting on the left (LE) and right eyes (RE). These layers are innervated by the subset of medial rectus (MR_G) and lateral rectus (LR_G) motoneurons. The orbital layers of these muscles are shown as inserting on muscle pulleys (P) and are innervated by the orbital subset of motoneurons (MR_O and LR_O). These MR_O and LR_O motoneurons appear to be responsible for moving the pulleys along an anterior-posterior axis (arrows). Abducens internuclear (AI) neurons are located in the abducens nucleus and send axons via the medial longitudinal fasciculus (MLF) to provide excitatory innervation to MR motoneurons and presumably oculomotor internuclear (OI) neurons as well. Many of the OI neurons are thought to project back to the ABD nucleus. Near response (NR) cells, which have a signal related to vergence and accommodation, appear to provide the needed vergence signal to MR motoneurons and probably provide the same signal to OI neurons. Two additional inputs (I₁ and I₂) are shown for ABD neurons. Hering's Law implies that I₁ and I₂ should be conjugate and vergence inputs, but recent work (Zhou and King, 1998) suggests that I₁ and I₂ are monocular ipsilateral and contralateral eye movement inputs.

motoneurons, as well as some of the premotor inputs to them. Extraocular motoneurons show a burst-tonic pattern of activity for saccades and have a linear relationship between firing rate and eye position (Robinson, 1970) for steady fixation.

NEURONS IN THE OCULOMOTOR NUCLEUS Two studies (Gamlin and Mays, 1992; Mays and Porter, 1984) showed that nearly all putative medial rectus (MR*) motoneurons increased their activity for symmetrical convergence. This observation refuted earlier speculation (Alpern and Wolter, 1956) that a distinct subset of motoneurons was uniquely responsible for vergence movements. The comparison between the slope of the tonic firing rate-to-position relationship of a motoneuron for conjugate eye movements (versional gain) and that for purely symmetrical convergence

movements (vergence gain) is of particular interest. Figure 95.2 illustrates this comparison for a sample of horizontal burst-tonic neurons in the medial rectus subdivisions of the oculomotor nucleus. Overall, the mean vergence gain of MR* motoneurons was essentially equal to that for changes in conjugate horizontal eye position, although the range of gains was much larger for convergence. Indeed, as Figure 95.2 shows, there is a very poor correlation between vergence gain and versional gain. If each motoneuron behaved in the same way for conjugate adduction as for convergence adduction, then all of the filled points in Figure 95.2 would fall along the line labeled "Ipsi eye." About 10% of MR motoneurons show little or no change in activity for convergence (points near the "Version only" line in Fig. 95.2), and another 10% have extremely high gains for vergence when compared to their versional gains. These recording studies may well have included some oculomotor internuclear (OI) neurons, which are located within the medial rectus subdivisions of the oculomotor nucleus but are not motoneurons (Fig. 95.1). An analysis of OIs (Clendaniel and Mays, 1994), identified by antidromic stimulation from the contralateral abducens nucleus, revealed activity profiles for versional and vergence eye movements which largely overlapped those of the larger sample of MR* motoneurons (Fig. 95.2). One possible difference is that none of the OI neurons had the very high vergence gains seen in some MR* cells, but this difference may be due to the very small sample of identified OIs. Interestingly, the activity of the OIs matched the activity of MR* motoneurons for both version and vergence, even though the OIs projected to the contralateral abducens nucleus. If OIs conveyed useful information about vergence movements to the contralateral abducens, one would expect these cells to be aligned with the "Contra eye" line in Figure 95.2, which is not the case. This indicates that the OIs coordinate versional movements and not vergence.

NEURONS IN THE ABDUCENS NUCLEUS The vast majority of abducens neurons decrease their activity for convergence (Gamlin et al., 1989a; Maxwell, 1991; Mays and Porter, 1984). Figure 95.3 shows the vergence and versional gains of abducens neurons and of horizontal burst-tonic fibers in the medial longitudinal fasciculus (MLF). The latter are presumed to be axons of abducens internuclear neurons (AIs), which have somata in the abducens nucleus and project, via the MLF, to provide excitatory input to medial rectus motoneurons (Steiger and Büttner-Ennever, 1979). The filled symbols in Figure 95.3 show data from abducens neurons that presumably represent both lateral rectus motoneurons and AIs. Open circles show data from antidromically identified AI neurons. Cells that exhibit the same behavior for versional and vergence abduction would fall along the "Ipsi eye" line, those that change their activity

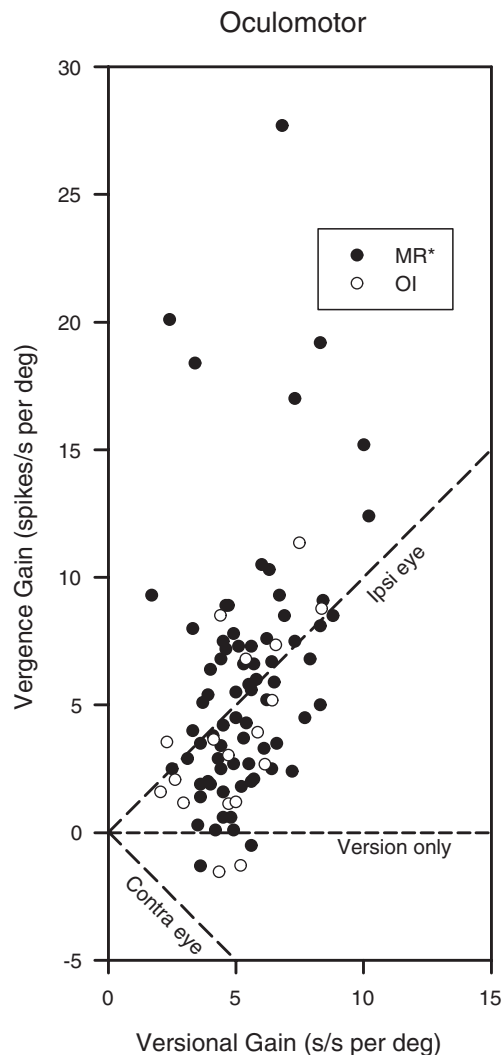


FIGURE 95.2. Distributions of static vergence and versional gains for neurons in the oculomotor nucleus displaying a burst-tonic firing pattern for conjugate adduction. Data are from Gamlin and Mays (1992). *Vergence gain* refers to the change in firing rate for each degree of adduction of the eye during symmetrical vergence movements. *Version gain* refers to the change in firing rate for each degree of adduction during conjugate saccades between distant targets. Positive values indicate increased activity for adduction. Open circles indicate oculomotor internuclear (OI) neurons, identified by antidromic stimulation from the contralateral abducens nucleus. Closed circles indicate cells with activity consistent with that of medial rectus (MR*) motoneurons but not positively identified as such. Data points falling along the dashed line labeled “Version only” represent cells that did not show any change in activity for symmetrical vergence movements. Data points on the “Ipsi eye” line showed the same change in activity for conjugate adduction as for symmetrical convergence. Any data points associated with the “Contra eye” line would have shown an increase in activity for conjugate adduction but a decrease for convergence, a pattern consistent with the innervation pattern for the contralateral eye. The overall activity pattern of OI neurons was very similar to that of putative MR* motoneurons. OI neurons did not have a Contra eye activity pattern, even though they project to the contralateral abducens nucleus. This suggests that OI neurons are used to coordinate horizontal conjugate movements and not vergence.

only for version would coincide with the “Version only” line, and those that fall along the “Contra eye” line would behave like contralateral MR motoneurons. Two important observations can be drawn from Figure 95.3. The first is that AIs (including MLF fibers) show the same pattern of responses as the overall population of abducens neurons, which presumably includes many lateral rectus (LR) motoneurons. The conclusion is that most LR motoneurons and AIs decrease their firing rate for convergence as well as for versional adduction. This is a critical observation since AIs provide powerful excitatory input to contralateral MR motoneurons. Since AIs decrease their activity for convergence, this means that they send an *inappropriate* signal to MR motoneurons during vergence movements. This implies that the AIs, like the OIs, coordinate conjugate horizontal eye movements and not vergence movements. The second observation is that, on average, abducens neurons do not reduce their firing rate as much for vergence adduction as for versional adduction. Indeed, most neurons in Figure 95.3 fall below the “Ipsi eye” line, which indicates equal firing rate change for version and vergence. This would suggest some degree of co-contraction of MR and LR muscles during convergence. However, recent measurements of LR and MR forces during convergence show no evidence of co-contraction (Miller et al., 2002). One possible reason for this apparent contradiction between muscle force measurements and motoneuron activity is that not all subsets of motor units develop equivalent forces for a given firing rate. Motoneurons responsible for larger decreases in muscle force during convergence may have been undersampled. Other explanations may involve the role of the trochlear motoneurons and muscle pulleys.

NEURONS IN THE TROCHLEAR NUCLEUS Although LR and MR muscles are primarily responsible for vergence eye movements, there is a well-known excyclotorsion of the eyes associated with convergence (Allen and Carter, 1967). The magnitude of this torsion depends on elevation of the eyes as well as the vergence angle, with greater excyclotorsion seen with ocular depression. A study of trochlear motoneurons (Mays et al., 1991) showed a systematic decrease in activity associated with convergence that was far larger than that expected from the values associated with conjugate abduction of the innervated eye. Moreover, the magnitude of the decrease in firing rate increased with ocular depression. These findings are consistent with the behavioral observation of excyclotorsion with convergence and with the lateral tilt of Listing’s plane during convergence (van Rijn and Van der Berg, 1993). The decreased superior oblique tension could aid adduction during convergence (Mays et al., 1991), but a recent analysis (Miller et al., 2002) of all muscle forces indicates that this cannot explain the discrepancy between the motoneuron and muscle force data.

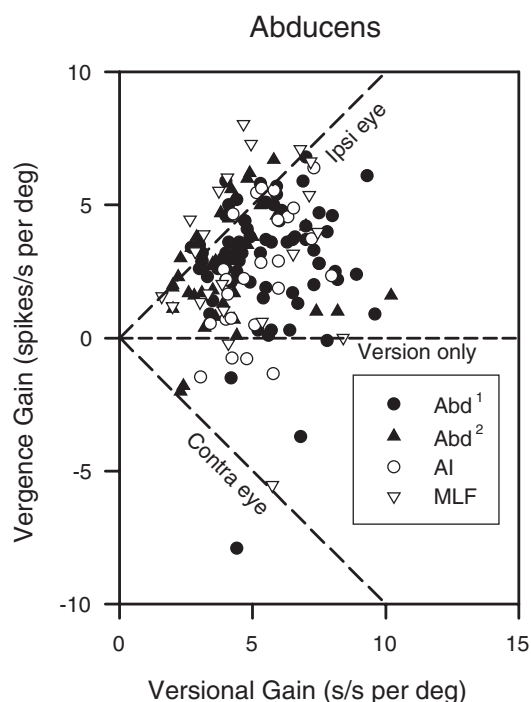


FIGURE 95.3. Distributions of static vergence and versional gains for neurons in the abducens nucleus displaying a burst-tonic firing pattern for conjugate abduction. *Vergence gain* refers to the change in firing rate for each degree of abduction of the eye for symmetrical vergence movements. *Version gain* refers to the change in firing rate for each degree of abduction during conjugate saccades between distant targets. Positive values indicate increased activity for abduction. Closed circles and triangles indicate cells with activity consistent with that of lateral rectus (LR) motoneurons but not positively identified as such. The closed circles (Abd^1), which are from Mays and Porter (1984) and Gamlin et al. (1989a), largely overlap the closed triangles (Abd^2) that were recorded by Maxwell (1991). Open circles indicate abducens internuclear (AI) neurons identified by antidromic stimulation of the medial longitudinal fasciculus (MLF) between the oculomotor and abducens nuclei. Open triangles are horizontal burst-tonic fibers recorded from the MLF, which are presumably axons of AI neurons. Data points falling along the dashed line labeled "Version only" represent cells that did not show any change in activity for symmetrical vergence movements. Data points on the "Ipsi eye" line showed the same change in activity for conjugate abduction as for symmetrical divergence. Most abducens neurons fell between the "Ipsi eye" and "Version only" lines, indicating that most decreased their activity for convergence and conjugate adduction, although the decrease for convergence was somewhat less. Any data points associated with the "Contra eye" line would have shown a decrease in activity for conjugate adduction but an increase for convergence, a pattern consistent with the innervation pattern for the contralateral eye. The overall activity pattern of AI neurons was very similar to that of the overall population of abducens neurons, which presumably included many LR motoneurons. Thus, most AI neurons decreased their firing rate for convergence, even though they project to the contralateral medial rectus (MR) motoneurons. This indicates that AI neurons send appropriate signals to the MR motoneurons to coordinate horizontal conjugate movements, but they do not provide the appropriate signals for vergence.

MUSCLE PULLEYS Recent evidence has shown that the effective origin of some eye muscles is altered by passing through slings or pulleys associated with Tenon's capsule (Demer et al., 1995). These pulleys are shown schematically in Figure 95.1 as rings labeled "P." It has been hypothesized that these pulleys provide a mechanical means for the eyes to obey Listing's Law. Indeed, it appears that the LR pulleys are moved posteriorly during convergence, while the MR pulleys shift anteriorly in such a way as to produce the lateral tilt of Listing's plane (Clark et al., 2000). Recent work (Demer et al., 2000) indicates that the orbital fiber layers of the LR and MR muscles insert on muscle pulleys and not on the globe itself. This implies that the activity of the motoneurons innervating orbital fibers in the pulley muscles (LR_O and MR_O in Fig. 95.1) may have very different activity patterns than the motoneurons innervating the global muscle fibers (LR_G and MR_G). Thus, the discrepancy between the LR motoneuron data and the absence of co-contraction may be due to recording a mixture of unidentified LR_O and LR_G motoneurons. To date, it has not been possible to distinguish between these motoneuron types with single-unit recording alone. The added biomechanical complexity of movable muscle pulleys makes it difficult to estimate muscle forces indirectly during convergence by observing the motoneuron firing rate from a combined motoneuron pool.

Premotor commands

NEAR RESPONSE CELLS AIs are a primary input to MR motoneurons for versional eye movements but not for vergence movements. This is implied by recording studies (Gamlin et al., 1989a) and convincingly demonstrated by clinical and experimental lesion studies (Gamlin et al., 1989b). Damage to the MLF, which carries AI axons, causes the clinical syndrome of internuclear ophthalmoplegia (Cogan, 1970), in which conjugate adduction is weakened or lost but convergence is preserved. This indicates that the MR motoneurons receive their vergence input from another source. Several studies (Judge and Cumming, 1986; Mays, 1984; Zhang et al., 1992) have conclusively demonstrated the presence of *near response* ("NR" in Fig. 95.1) cells in the midbrain reticular formation, just dorsal or lateral to the oculomotor nucleus, which carry signals related to vergence and accommodation but not version. Figure 95.4 shows the firing pattern of a near response cell for a symmetrical convergence movement. Most near response cells increase their activity for convergence (convergence cells). A smaller number of intermixed cells show the opposite response (divergence cells). For both types of cells, there is a nearly linear relationship between tonic firing rate and vergence angle and ocular accommodation. Many near response cells, including the one shown in Figure 95.4, also have a phasic

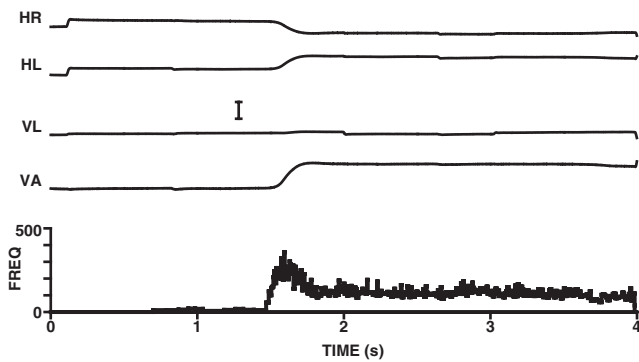


FIGURE 95.4. Activity pattern of a midbrain near response cell for symmetrical convergence. HR, horizontal right eye position; HL, horizontal left eye position; VL, vertical left eye position; VA, vergence angle, which is HL-HR. The firing rate is displayed as an instantaneous frequency histogram in spikes per second, which is the reciprocal of interspike interval. This neuron shows a linear tonic increase in activity for increasing convergence as well as a phasic increase related to convergence velocity. There is no change in firing rate for changes in conjugate eye position (not shown). Calibration bar = 5 degrees.

component to their activity that is related to vergence velocity. Some cells have *only* this phasic component for convergence (convergence burst cells) or divergence (divergence burst cells). For both types of burst cells, there is a nearly linear relationship between the number of spikes in the burst and the size of the vergence movement (Mays et al., 1986). Interestingly, this suggests that the vergence system, like the conjugate eye movement control systems, may be based on velocity commands and incorporates a vergence integrator to produce vergence position. Moreover, most MR motoneurons have both vergence position and vergence velocity signals (Gamlin and Mays, 1992). It has been possible to activate near response cells antidromically from the MR subdivisions of the ipsilateral oculomotor nucleus (Zhang et al., 1992). Based on the signals carried by these near response cells and the stimulation studies (Zhang et al., 1992), it seems very likely that the midbrain near response cells provide the needed vergence signals to the MR motoneurons.

Although the divergence and divergence burst cells have the signals needed by LR motoneurons, it has not yet been possible to determine if they project to the abducens nucleus. The most straightforward interpretation of Hering's Law would presume that conjugate (i.e., cyclopean) eye movement commands are provided to the abducens nucleus by one input (e.g., I_1 in Fig. 95.1), while a near response command, with the appropriate sign, is provided by a second input (I_2 in Fig. 95.1). This is in addition to the known near response input to MR motoneurons.

VERGENCE-ACCOMMODATION LINKAGE In order to understand the signals carried by the near response cells, the rela-

tionship between vergence and ocular accommodation has to be taken into account (Hung and Semmlow, 1980). Disparity-driven vergence can be considered as being under the control of a negative feedback servomechanism (Fig. 95.5). Referring to the top half of Figure 95.5, target distance determines convergence demand. The difference between the convergence demand and the convergence response is binocular disparity, which is the input to the vergence controller. The output of this controller goes eventually to the extraocular muscles (EOMs) to produce the convergence response. The goal of the vergence controller is to reduce disparity to an acceptably low level. A similar servomechanism is presumed to exist for the minimization of blur by an accommodation controller (lower half of Fig. 95.5). There is cross-coupling between these two control systems. In the absence of disparity, the accommodation system induces convergence with increases in accommodation. Similarly, increases in disparity-driven convergence result in increased accommodation. In normal viewing conditions, the two control systems function in a synergistic manner to provide the (covariant) appropriate amounts of accommodation and vergence.

An obvious question is whether the activity of midbrain near response cells (such as the one shown in Fig. 95.4) is related to accommodation or vergence. In terms of the model in Figure 95.5, a vergence-related near response cell would be located at the upper summing point (the small dashed ellipse labeled "VNR"), while an accommodation-related near response cell would be located at the lower summing point (the small dashed ellipse labeled "ANR"). For this analysis, it is necessary to dissociate the accommodative from the convergence responses. This can be done by attempting to vary accommodation while holding convergence constant or by varying convergence while holding accommodation constant. Although the two control systems are tightly coupled, some degree of dissociation of responses is possible. An early analysis of the activity of near response cells indicated that while a few cells could be classified as related to accommodation only, and another group appeared to be related to convergence only, the majority of near response cells were related to both (Judge and Cumming, 1986). A subsequent study of near response cells, including some that were activated by antidromic stimulation of the oculomotor nucleus and therefore in control of the vergence angle (Zhang et al., 1992), provided a model of how vergence (VNR) and accommodation (ANR) near response cells could be related both to accommodation and vergence.

Figure 95.6 shows the vergence and accommodation gains of 72 near response cells from the study by Zhang et al. (1992). Near response cells antidromically activated from the ipsilateral MR subdivisions of the oculomotor nucleus are shown as open circles; unidentified near response cells are

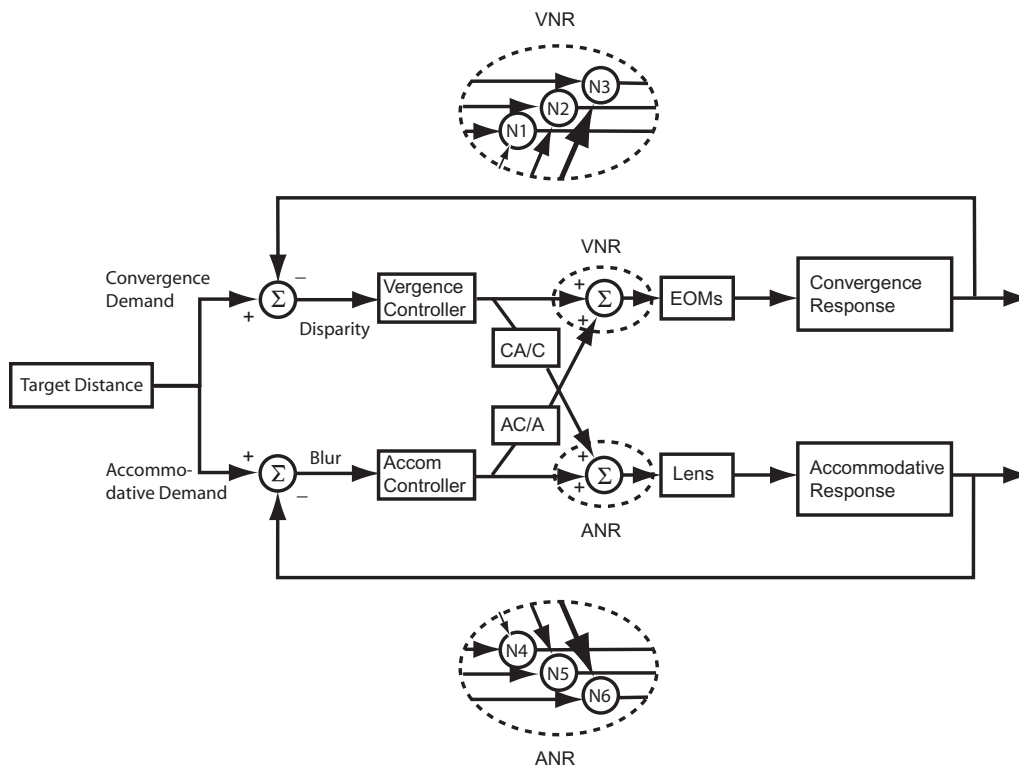


FIGURE 95.5. Dual interaction model of accommodation and vergence. Vergence and accommodation are controlled by their own negative feedback loops. In addition, part of the output of the accommodation controller is sent to the vergence subsystem. The gain of this cross-link is the AC/A ratio, and vergence near response (VNR) cells carry the summed signals. Part of the output of the vergence controller, with a gain corresponding to the CA/C ratio, is sent to the accommodation subsystem. The steady-state outputs of the accommodation and vergence controllers, and that of the cross-link components, can be calculated for any combina-

tion of convergence and accommodative demands as long as the CA/C and AC/A ratios are known. Accommodation near response (ANR) cells signal the sum of the output of the accommodation controller and the convergence accommodation signal. The large dashed ellipses represent a large number of near response cells, which receive direct and cross-link signals with different weights. The behavior of all recorded near response (N1 to N6) cells can be explained by assuming that different near response cells vary in the relative weights of their direct and cross-link inputs. EOMs, extraocular muscles.

shown as filled circles. The accommodation gain of a cell is the estimated change in firing rate for each diopter of accommodation if the vergence angle is held constant. The vergence gain is the estimated change in firing rate for each meter angle of convergence, if accommodation is held constant. The meter angle is a unit of angular measure that is comparable to the diopter (i.e., 1 M.A. is the angle between the eyes when viewing a target at 1 m). For the macaques used in this study, 1 M.A. is approximately 1.5 degrees. Any near response cell with activity related only to vergence angle, regardless of accommodation, would fall along the horizontal dashed line marked "Vergence Cell (N2)." Cells related exclusively to accommodation would fall along the vertical line marked "Accommodation Cell (N5)." Figure 95.6 shows that the majority of cells, whether identified as projecting to the oculomotor nucleus or not, are not uniquely related to accommodation or vergence alone but are related to both.

The model in Figure 95.5, at first glance, is incompatible with the distribution of the data in Figure 95.6. The ver-

gence near cells at the summing junction projecting to the oculomotor plant (dotted ellipse labeled "VNR") have exclusive control of the vergence angle. Similarly, the accommodation near cells at the summing junction projecting to the lens (dotted ellipse labeled "ANR") have exclusive control of the accommodation. Furthermore, there is no mixing of the outputs, implying that these signals are not shared between the extraoculomotor muscles and the ciliary muscle. The critical point associated with the results illustrated in Figure 95.6 is that both groups receive inputs from both the vergence and accommodation controllers, directly or through the cross-links. Consider the behavior of the model if one attempts to measure the accommodation gain of one of those cells by maintaining a constant level of convergence demand while increasing accommodation demand. Increasing accommodation demand will, accordingly, increase the accommodation level of the subject through the direct link between the accommodative controller and the accommodation near cells. At the same time, the increased accommodative signal will be sent to the vergence near cells

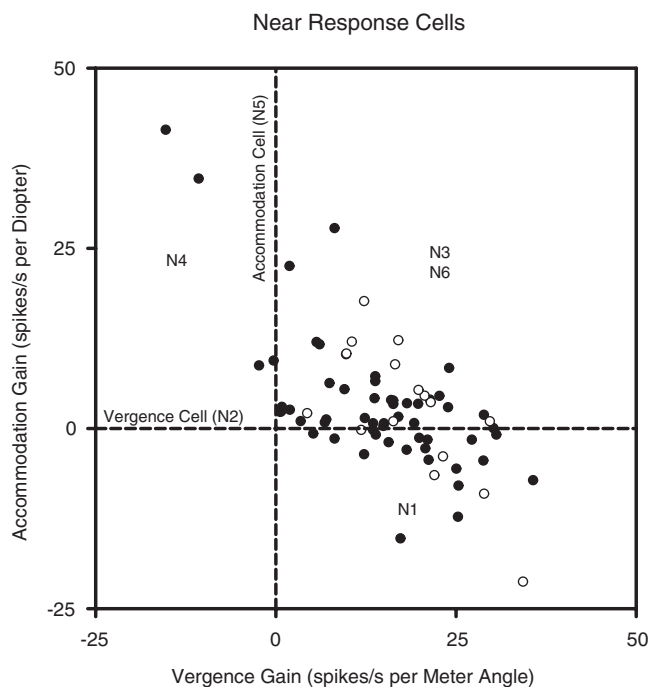


FIGURE 95.6. Relationship between vergence gain and accommodation gain for 72 near response cells. Data are from Zhang et al. (1992). Open circles represent a subset of these cells which were antidromically activated from the ipsilateral oculomotor nucleus and are presumed to be vergence near response (VNR) cells (see Fig. 95.5). *Accommodation gain* refers to the change in firing rate for each diopter of accommodation if the vergence angle remains constant. *Vergence gain* refers to the change in firing rate for each meter angle of convergence if accommodation remains constant. Note that, unlike Figures 95.2 and 95.3, vergence gain is calculated for total vergence angle in meter angles, which are comparable to diopters. Near response cells that have an accommodation gain of zero, and so have activity related exclusively to vergence angle, fall along the horizontal dashed line (Vergence Cell) and correspond to the vergence near response cells represented by N2 in Figure 95.5. Near response cells with activity related exclusively to accommodation (i.e., a vergence gain of zero) fall along the vertical dashed line and are represented in Figure 95.5 as N5 cells. Near response cells with a positive accommodation and vergence gain increase their activity for increases in either accommodation or convergence and are located in the upper right quadrant (N3 and N6 cells in Fig. 95.5). Near response cells with a negative accommodation gain and a positive vergence gain are located in the lower right quadrant. These cells *decrease* their activity with *increases* in accommodation, even though they otherwise increase their activity when accommodative and vergence demands increase appropriately (i.e., normal viewing conditions). This paradoxical behavior is due to the balance of direct and cross-link inputs as shown for N1 in Figure 95.5. Similarly, the cells in the upper left quadrant of Figure 95.6 have negative vergence gains, and so will decrease their activity for convergence if accommodation is held constant. These cells are represented by N4 in Figure 95.5.

through the AC/A cross-link to generate a covarying vergence change. This strategy is appropriate for what is normally needed in a natural environment, where vergence and accommodation are geometrically linked. However, in the situation where the vergence demand is left artificially unchanged, increasing accommodation will lead to over-convergence. This (negative) disparity error will engage the (di)vergence controller to reduce the vergence level of the subject to compensate for the unneeded vergence activation through the AC/A cross-link. This correction will also affect the accommodation level through the CA/C cross-link with additional (erroneous) changes in the accommodation level, and so on, but after a transitory period the subject will reach a steady-state condition. A similar sequence of events, starting with an increase in vergence demand, occurs when maintaining a constant level of accommodation demand while increasing vergence demand. How does this process affect the (steady-state) vergence and accommodation gains of a near response cell?

When the new steady state is reached, the vergence controller and the accommodation controller will have their output levels adjusted in such a way as to have the vergence and the accommodation levels matching the visual (dissociated) requirements in terms of vergence and accommodation. These adjustments at the controller level depend on the global AC/A and the CA/C ratios of the subject, but the important issue here is that these corrections are proportional to the variation imposed on the visual stimulus (i.e., the change in vergence demand for a fixed accommodation demand and vice versa). For example, keeping the vergence demand constant, larger changes in accommodation demands require larger changes in the output of the accommodation controller and proportional, but with a fixed ratio, negative changes in the output of the vergence controller to maintain an unchanged vergence level. The accommodative and vergence gains of each cell are determined by the relative amount of signal reaching the cell from the direct and cross-link inputs. These ratios will be determined by the global ratios of the subject, as well as by the individual weights of the direct and cross-link inputs to the cell. Depending on the resulting overall weights of the cell, we have three typical cases: (1) the ratio between the signal coming from the direct link and the cross-link is greater than 1; (2) it is exactly 1; (3) it is less than 1.

A vergence near cell with a ratio of exactly 1 (N2 in Fig. 95.5) will always receive equal and opposite signals from the direct and cross-link inputs during changes in accommodation only. The cell will appear insensitive to accommodation changes if they are not accompanied by vergence changes and so would be classified as a pure vergence cell. A cell with a ratio greater than 1 (i.e., a stronger direct link) will, under the same conditions, have a negative accommodation gain. This is because the negative direct corrective signal from the

vergence controller overcomes the positive accommodation signal from the cross-link (N1 in Fig. 95.5). A cell with a ratio less than 1 (i.e., stronger cross-link) will, in the same conditions, have a positive accommodation gain. The positive accommodation signal from the cross-link will overcome the negative direct corrective signal from the vergence controller (N3 in Fig. 95.5). The remarkable result is that all of these cells are, in terms of output, vergence cells, but depending on their weights, they can behave, at least partially, as “accommodation-related” cells. The same logic applies to the accommodation near cells (N5, N4, and N6, respectively) during changes in vergence with accommodation held constant, with, as a consequence, more or less “vergence-related” behavior. The overall schema does not change for vergence near cells during vergence changes with fixed accommodation demand or for accommodation near cells during accommodation changes with fixed vergence demand. The global AC/A and CA/C ratios of the subject are normally less than 1, when measured in comparable units (i.e., diopters and meter angles).

These theoretical considerations result in predictions that match the data in Figure 95.6 very closely. The two cells in the upper left quadrant of Figure 95.6 were not antidromically activated from the oculomotor nucleus. This is consistent with the model, since the N4 type cells would have to be in the accommodation output path. Vergence near response cells represented by N3 would show a positive vergence gain and a positive accommodation gain, but so would cells represented by N6 in the accommodation output path. Using plausible values for the AC/A and CA/C ratios, no near response cells that increase their activity for covariant convergence and accommodation should be seen in the lower left quadrant of Figure 95.6 using dissociated stimuli. Indeed, no cells were found with a negative accommodation gain and a negative vergence gain using the dissociated stimuli. This analysis shows that a biologically plausible distribution of differing direct and cross-link inputs to near response cells can account for the wide variety of vergence and accommodation gains, including negative gain values.

Saccade-vergence interactions

UNEQUAL HORIZONTAL SACCADSES Although the analysis of near response cells clearly demonstrates the presence of vergence-related signals, Hering’s Law suggests that we should also see premotor signals related exclusively to conjugate commands, that is, to movements of the cyclopean eye. Saccadic eye movements are assumed to be intrinsically conjugate. In other words, both eyes execute identical rotations of an amount related to the needs of the cyclopean eye. This assumption has been challenged by observations that horizontal saccades may be markedly unequal in amplitude if they are executed together with a vergence move-

ment. Figure 95.7A shows a smooth symmetrical convergence movement approximately 10 degrees in size made by a macaque. This movement was made between far and near targets aligned with the cyclopean eye and contained no saccades. The vergence velocity (VV) trace shows that the peak velocity of this movement was approximately 50 degrees. This is about an order of magnitude slower than the peak velocity of a conjugate saccade of similar size. Figure 95.7B shows a similar size convergence movement combined with a rightward saccade, indicated by an arrow. The rightward saccade made by the right eye appears to be two to three times smaller than the saccade made by the left eye. Careful analysis of saccades during vergence in both the human (Ono et al., 1978) and the macaque (Maxwell and King, 1992) has shown that the differences in saccade size between the two eyes cannot be attributed to the ongoing smooth vergence movement. That is, the difference in saccade size is larger than the one expected by the linear combination of the version and smooth vergence. This is more clearly shown by an inspection of the vergence velocity trace of Figure 95.7B, which shows an abrupt doubling of vergence velocity associated with the saccade. Hering’s Law would predict that the vergence velocity profile in Figure 95.7B would be the same as for smooth vergence in Figure 95.7A.

DO UNEQUAL SACCADSES IMPLY MONOCULAR CONTROL?

Markedly unequal horizontal saccades during vergence have been interpreted by some investigators (Enright, 1992) as a clear violation of Hering’s Law. Enright (1984) and others (Dell’Osso, 1994; Zhou and King, 1998) have suggested that the control mechanisms for the two eyes may be intrinsically independent. In this view, although many eye movements are conjugate, the underlying circuitry allows for independent control of the two eyes for smooth pursuit eye movements (King and Zhou, 1995) and for saccades (Enright, 1984). Any difference in the monocular commands to the two eyes would generate changes in the vergence profile that are not associated with the vergence system proper. Zee and colleagues (1992) have suggested alternative eye movement models that can produce unequal saccades without invoking monocular control. The critical observation for these models is that vertical saccades can also cause vergence to be speeded. An example of this can be seen in Figure 95.7C, which shows a small (2.5 degree) downward saccade which occurs during a 10 degree convergence movement. An examination of the vergence velocity trace in Figure 95.7C shows that its peak is more than doubled by the occurrence of the saccade (i.e., compare to VV in Fig. 95.7A). This indicates that the speeding of vergence depends on the occurrence of a saccade in any direction rather than the generation of unequal *horizontal* saccades.

Zee et al. (1992) have evaluated several models of saccade-vergence interactions, where vertical saccades can

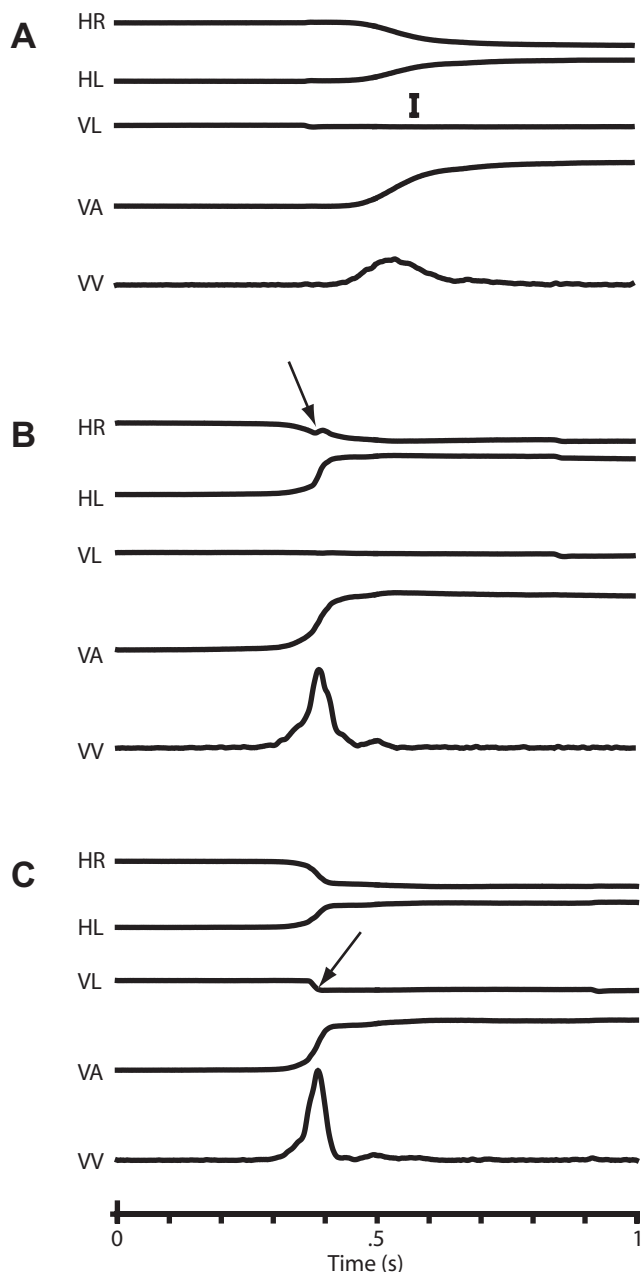


FIGURE 95.7. Saccade-vergence interactions. Convergence in the absence of a saccade (*A*), similar convergence with a horizontal (rightward) saccade (*B*), and similar convergence with a vertical (downward) saccade (*C*). The arrows in *B* and *C* indicate the occurrence of a saccade. The calibration bar corresponds to 5 degrees for eye position traces and 50 deg/sec for the vergence velocity (VV) trace. Eye position trace abbreviations are as in Figure 95.4. The occurrence of a saccade during the early phase of a vergence movement (either convergence or divergence) results in an immediate increase in vergence velocity, even if the saccade is purely vertical (*C*). This indicates that the mechanism by which vergence is speeded by a saccade does not depend on unequal horizontal saccadic rotations.

also speed vergence. Two related models, which are alternatives to the independent eye control hypothesis, allow for vergence-related neural activity to be gated by pontine omnipause neurons (OPNs) (Keller, 1974). Both models simulate saccade-vergence interactions reasonably well. One of these models, the OPN model, is consistent with two critical observations: (1) the enhancement of vergence velocity by vertical saccades (Enright, 1984; Zee et al., 1992), which could implicate the pontine OPNs (which are omnidirectional) in this interaction, and (2) the existence of midbrain vergence burst neurons which carry vergence velocity signals (Mays et al., 1986). These observations suggest that a vergence velocity signal could be modulated by saccade-related (i.e., OPN) activity.

The inputs to the OPN model are pure symmetric vergence and pure conjugate saccadic commands. Consider a convergence-saccade combination with a horizontal saccade that occurs near the beginning of the convergence. This situation typically produces markedly unequal horizontal saccades. In the absence of a saccade, a slow vergence command is relayed to convergence burst (CB) cells that are tonically, but weakly, inhibited by OPNs. Consequently, only slow vergence movements can occur in the absence of a saccade (Fig. 95.7*A*). The occurrence of a saccade is associated with the cessation of activity in the OPNs, which results in a release of the inhibition of the CB cells. The disinhibited CB cells produce an additional pulse of vergence activity that is processed through the vergence neural integrator, and the resulting position signal is combined with the vergence velocity signal at the CB-tonic cells. The output of these cells is added to the ongoing saccadic horizontal pulse and step commands communicated to the MR motoneurons by the AI neurons. The simple linear addition of these commands produces an accentuated pulse-step command for one eye and a diminished pulse-step command for the other eye, resulting in markedly unequal horizontal saccades in the two eyes (Fig. 95.7*B*). Since this depends on the omnidirectional OPN cells, saccades in all directions, including vertical saccades (Fig. 95.7*C*), will be equally effective in speeding vergence. Although this model requires more rigorous testing, it demonstrates that unequal horizontal saccades do not necessarily imply monocular saccadic control mechanisms for each eye.

Conjugate versus monocular commands

EXCITATORY BURST NEURONS The monocular control hypothesis suggested by Enright (1984) and the saccadic facilitation of vergence hypothesis described by Zee et al. (1992) imply very different ways of generating saccades and vergence eye movements. One way of resolving this issue would be to record premotor signals during these unequal horizontal saccades to determine if they are related to the

movement of the cyclopean eye (Hering's Law) or to the separate movements of the two eyes. This experiment has been reported by Zhou and King (1998), who recorded from putative excitatory burst neurons (EBNs), located in the pons near the abducens nucleus. EBNs project to the ipsilateral abducens nucleus and show a burst of activity that is related to the horizontal component of ipsilateral saccades. Specifically, the number of spikes in each burst is believed to be linearly proportional to the horizontal size of the saccade (Keller, 1974). Taking advantage of this relationship, Zhou and King counted the number of spikes recorded from EBNs during unequal-amplitude horizontal saccades. By comparing the number of spikes in the burst during unequal saccades with the number of spikes for conjugate saccades, Zhou and King determined if the burst was associated with the amplitude of the rotation of the ipsilateral eye, the contralateral eye, or the cyclopean eye. Although the activity of a few EBNs was associated with the cyclopean eye during unequal saccades, as expected by Hering's Law, the activity of the majority of EBNs was more closely associated with the rotation of either the ipsilateral or the contralateral eye.

OTHER MONOCULAR SIGNALS Zhou and King (1998) also reported that the majority of cells recorded in the nucleus prepositus hypoglossi, an area thought to produce horizontal eye position signals, were also monocular. McConville et al. (1994) recorded position-vestibular-pause cells in the vestibular nuclei of macaques during conjugate and vergence eye movements. They found that 18 out of 20 cells had monocular eye position signals.

HOW ARE MONOCULAR EYE COMMANDS USED? The results of Zhou and King are inconsistent with the idea that neurons in the abducens nucleus are provided with separate conjugate and vergence inputs, as required by Hering's Law. Instead, they strongly suggest that the inputs I_1 and I_2 in Figure 95.1 do not reflect conjugate and vergence inputs, but instead represent ipsilateral and contralateral eye commands. This new conjecture raises a puzzling question: how are these monocular commands used? A number of studies (Gamlin et al., 1989a; Maxwell, 1991; Mays and Porter, 1984), including data from Zhou and King, show that even if the inputs to the abducens nucleus represent monocular signals, the activity of the vast majority of abducens neurons is not monocularly coded. This can be seen in Figure 95.3. Abducens neurons with activity reflecting an ipsilateral monocular input would fall along the "Ipsi eye" dashed line, while those with activity related to the other eye would fall along the "Contra eye" line. While there are a number of cells with activity corresponding to a monocular ipsilateral eye input, there are very few with activity related to the contralateral eye. Indeed, most abducens neurons show an

activity pattern that is between the ipsi and contra eye lines. This indicates that if ipsilateral and contralateral eye movement signals are provided to neurons in the abducens nucleus, these signals are commingled and individual eye position information is lost on the abducens neurons. This finding is consistent with the AI and MLF recording data, as well as lesion studies (cited above), which demonstrate that neurons in the abducens nucleus do not provide an appropriate vergence signal to the MR motoneurons. Furthermore, monocular eye position and velocity signals do not appear to be used for the generation of vergence eye movements, at least via the abducens nucleus. This strongly implies that the vergence angle changes brought about by unequal horizontal saccades are not due to activity differences between abducens motoneurons and internuclear neurons.

It is possible that in primates these premotor monocular signals have lost their original function. From an evolutionary point of view, a fully developed vergence system with depth perception (stereopsis) is present only in primates. Primitive lateral-eye animals do not have a vergence system. In these animals, each eye is controlled independently; therefore, there is a need for appropriate monocular commands to be sent to each eye. This raises the possibility that the migration of the eyes from a lateral position to a frontal one with the development of an independent precise vergence system able to maintain the accurate binocular alignment needed by stereopsis was accompanied by the fusion of the original monocular signals into a single cyclopean structure. Disjunctive signals, generated independently by the vergence system, were simultaneously added to the motoneurons to allow precise disjunctive eye movements to be guided by disparity errors. These are also binocular from a sensory point of view. It should be noted that the precision required by the vergence system for stereopsis is much higher than that required by the versional systems (or the monocular ones in the evolutionarily primitive animals). This is even true in foveate animals, where the object of interest has to be projected over a small area of the retina for the best spatial resolution. Perhaps the inherent lack of precision achievable by a monocular arrangement pressed evolution toward a versional/vergence solution. The need for a positional vergence signal is also important in frontal-eye animals to estimate the viewing distance of the object of interest to program, accordingly, the gain of the vestibulo-ocular reflexes. For a review of this issue, see Miles (1995). An alternative possibility is that these monocular premotor signals were initially generated as versional signals, from which vergence signals were subtracted later on, perhaps to improve dynamic performance. At present, there is no way to distinguish between these alternatives.

Higher-order control

CEREBELLUM AND PONTINE AREAS There is some evidence that the cerebellum is involved in the near response. Westheimer and Blair (1973) reported transient vergence deficits after cerebellectomy in primates. Zhang and Gamlin (1998) found cells in the posterior interposed nucleus of the cerebellum related to vergence and accommodation. All of these cells increased their activity for divergence and so were described as *far response* cells. Gamlin and Clarke (1995) reported cells related to either near or far responses in the medial zone of the nucleus reticularis tegmenti pontis (NRTP), a precerebellar nucleus. Although these cells were often found near cells with saccade-related activity, the vergence-related cells did not change their activity in association with saccades or conjugate pursuit. The NRTP has reciprocal connections with the midbrain area containing the near response cells that, in turn, project to the oculomotor nucleus (May et al., 1992). Moreover, the NRTP is an area that receives cortical inputs and also has reciprocal connections with the cerebellum. It may be an important link providing vergence and accommodation signals to both the cerebellum and the midbrain near response areas.

SUPERIOR COLLICULUS The superior colliculus (SC) has long been implicated in the initiation of saccades and, more recently, in the control of gaze saccades (Freedman and Sparks, 1997) (i.e., combined rapid movements of the head and eyes). In the head-fixed animal, stimulation of most of the SC induces stereotyped conjugate contralateral saccades (Robinson, 1972). Stimulation of the rostral pole of the SC, which can inhibit saccades (Munoz and Wurtz, 1993), also partially inhibits convergence (Chaturvedi and Van Gisbergen, 2000), and stimulation of more caudal areas of the SC perturbs both ongoing saccades and vergence. Many neurons in the SC produce a burst of activity before specific contralateral saccades, but there have been no published reports of SC neurons firing for vergence in the absence of saccades. Preliminary data from our laboratory indicate that many saccade-related SC burst neurons fire less vigorously for saccades during both convergence and divergence than for conjugate saccades. This decrease in activity may be related to the report that saccades executed during vergence may be slower and longer than saccades of similar size without vergence (Collewijn et al., 1995). While there are some indications that the SC may be involved in saccade-vergence interactions, the significance of these observations remains unclear.

FRONTAL EYE FIELD The frontal eye field (FEF) area in macaques is located in the region of the arcuate sulcus. FEF cells fire in response to visual stimuli and also in relation to

saccades to visual stimuli (Bruce and Goldberg, 1985). Some neurons in the floor and posterior bank of the arcuate sulcus also discharge for smooth pursuit eye movements (Gottlieb et al., 1994). Recently, Gamlin and Yoon (2000) reported finding vergence- and accommodation-related cells just anterior to the arcuate sulcus. Most cells increased their activity for convergence, but some far response cells were observed as well. The activity of these cells appeared to be closely related to motor output, although several cells were responsive to the visual stimulus eliciting the near response. A small minority of cells were modulated during versional eye movements as well as during vergence. Microstimulation of an area anterior to the arcuate sulcus resulted in accommodation and convergence. The FEF projects to the NRTP, to the SC, and to brainstem oculomotor areas (Leichnetz, 1981; Leichnetz et al., 1984), and so may provide vergence and accommodation commands to these areas, as well as pursuit and saccadic commands.

PARIETAL CORTEX Many neurons in parietal cortex show a complex relationship between their activity and saccades, smooth pursuit, and fixation. A substantial number of neurons in the lateral intraparietal sulcus (LIP) discharge for saccades. A majority of these saccade-related neurons also show a modulation in activity associated with the vergence component when a saccade is combined with vergence (Gnadt and Mays, 1995). It appears that many cells are tuned for gaze shifts in three-dimensional space. More recently, Gnadt and Beyer (1998) antidromically activated a subset of LIP neurons with three-dimensional movement fields from the SC. This suggests a way in which vergence information, as well as saccadic signals, could be sent to the SC.

OTHER CORTICAL AREAS A number of other cortical areas have neurons that could provide information about the distance of an object from the viewer. Some neurons in ventral intraparietal cortex (VIP) (Colby et al., 1993) discharge most vigorously for visual stimuli near the face. Others fired for visual stimuli moving toward the animal. Areas MT (middle temporal) and MST (medial superior temporal) in the superior temporal sulcus have neurons that encode disparity and so may be important for tracking objects in three-dimensional space (Kawano et al., 2000). Other visual cortical areas, such as V1, contain neurons sensitive to binocular stimulation. Some of these neurons are particularly sensitive to targets near the plane of fixation (tuned-zero neurons), while others respond best to targets closer to (near cells) or beyond (far cells) the plane of fixation (Poggio, 1995). In short, there are many cortical areas with signals that could be used to control vergence movement. Whether or not signals in a particular area are, in fact, used for this purpose is unknown.

Summary

The activity patterns of extraocular motoneurons during versional and vergence eye movements have been well characterized. The biomechanical complexity of the oculomotor plant, especially with the recent discovery of movable muscle pulleys, has made the task of relating motoneuron activity to muscle forces quite difficult, as Miller et al. (2002) have pointed out. A better assessment of the role of the muscle pulleys, and of the mechanical coupling between the orbital and global muscle layers, is needed to resolve the discrepancy between muscle force data and motoneuron activity for vergence movements. This should be accompanied by recordings from motoneurons identified as innervating global or orbital muscle fibers.

There has been significant progress in understanding premotor near response commands and the role of near response cells in coordinating accommodation and vergence. Surprisingly, the nature of the commands used for conjugate eye movements needs further clarification. Recent work indicates that these premotor commands may be monocular, but it appears that these “monocular” signals are commingled to construct what is essentially a conjugate (cyclopean) signal at the level of the motoneurons. The evolutionary history of eye movement circuits may provide an explanation of why such a scheme should exist.

The debate as to whether the premotor commands are monocular or represent a combination of cyclopean and vergence signals has often centered on the nature of saccade-vergence interactions. The observation of horizontal saccades of different amplitudes does not, in itself, indicate that the control of the saccades is inherently monocular. A better understanding of the mechanism by which vergence speed is increased during saccades is needed.

The route by which vergence commands are generated and sent to near response neurons is unknown. Recent studies of the NRTP, the cerebellar interposed nucleus, and the FEF suggest several possibilities, but the details need to be provided. Visual cortical areas have an embarrassingly large number of disparity- and spatial frequency (blur)-sensitive neurons, but no direct linkage between the activity of these cells and the near response has been demonstrated.

Acknowledgment

I thank Dr. Claudio Busetini for his helpful comments on the manuscript and for his assistance in preparing the figures.

REFERENCES

- Allen, M. J., and J. H. Carter, 1967. The torsion component of the near reflex. A photographic study of the non-moving eye in unilateral convergence, *Am. J. Optom. Arch. Am. Acad. Optom.*, 44:343–349.
- Alpern, M., and J. R. Wolter, 1956. The relation of horizontal saccadic and vergence movements, *AMA Arch. Ophthalmol.*, 56:685–690.
- Bruce, C. J., and M. E. Goldberg, 1985. Primate frontal eye fields. I. Single neurons discharging before saccades, *J. Neurophysiol.*, 53:603–635.
- Chaturvedi, V., and J. A. M. Van Gisbergen, 1999. Perturbation of combined saccade-vergence movements by microstimulation in monkey superior colliculus, *J. Neurophysiol.*, 81:2279–2296.
- Chaturvedi, V., and J. A. M. Van Gisbergen, 2000. Stimulation in the rostral pole of monkey superior colliculus: effects on vergence eye movements, *Exp. Brain Res.*, 132:72–78.
- Clark, R. A., J. M. Miller, and J. L. Demer, 2000. Three-dimensional location of human rectus pulleys by path inflections in secondary gaze positions, *Invest. Ophthalmol. Vis. Sci.*, 41:3787–3797.
- Clendaniel, R. A., and L. E. Mays, 1994. Characteristics of antidromically identified oculomotor internuclear neurons during vergence and versional eye movements, *J. Neurophysiol.*, 71:1111–1127.
- Cogan, D. G., 1970. Internuclear ophthalmoplegia, typical and atypical, *Arch. Ophthalmol.*, 84:583–589.
- Colby, C. L., J. R. Duhamel, and M. E. Goldberg, 1993. Ventral intraparietal area of the macaque: anatomic location and visual response properties, *J. Neurophysiol.*, 69:902–914.
- Collewijn, H., C. J. Erkelens, and R. M. Steinman, 1995. Voluntary binocular gaze-shifts in the plane of regard: dynamics of version and vergence, *Vis. Res.*, 35:3335–3358.
- Dell’Osso, L. F., 1994. Evidence suggesting individual ocular motor control of each eye (muscle), *J. Vest. Res.*, 4:335–345.
- Demer, J. L., J. M. Miller, V. Poukens, H. V. Vinters, and B. J. Glasgow, 1995. Evidence for fibromuscular pulleys of the recti extraocular muscles, *Invest. Ophthalmol. Vis. Sci.*, 36:1125–1136.
- Demer, J. L., S. Y. Oh, and V. Poukens, 2000. Evidence for active control of rectus extraocular muscle pulleys, *Invest. Ophthalmol. Vis. Sci.*, 41:1280–1290.
- Enright, J. T., 1984. Changes in vergence mediated by saccades, *J. Physiol.*, 350:9–31.
- Enright, J. T., 1992. The remarkable saccades of asymmetrical vergence, *Vis. Res.*, 32:2261–2276.
- Freedman, E. G., and D. L. Sparks, 1997. Eye-head coordination during head-unrestrained gaze shifts in rhesus monkeys, *J. Neurophysiol.*, 77:2328–2348.
- Gamlin, P. D. R., and R. J. Clarke, 1995. Single-unit activity in the primate nucleus reticularis tegmenti pontis related to vergence and ocular accommodation, *J. Neurophysiol.*, 73:2115–2119.
- Gamlin, P. D. R., J. W. Gnadt, and L. E. Mays, 1989a. Abducens internuclear neurons carry an inappropriate signal for ocular convergence, *J. Neurophysiol.*, 62:70–81.
- Gamlin, P. D. R., J. W. Gnadt, and L. E. Mays, 1989b. Lidocaine-induced unilateral internuclear ophthalmoplegia: effects on convergence and conjugate eye movements, *J. Neurophysiol.*, 62:82–95.
- Gamlin, P. D. R., and L. E. Mays, 1992. Dynamic properties of medial rectus motoneurons during vergence eye movements, *J. Neurophysiol.*, 67:64–74.
- Gamlin, P. D. R., and K. Yoon, 2000. An area for vergence eye movement in primate frontal cortex, *Nature*, 407:1003–1007.

- Gnadt, J. W., and J. Beyer, 1998. Eye movements in depth: what does the monkey's parietal cortex tell the superior colliculus? *NeuroReport*, 9:233–238.
- Gnadt, J. W., and L. E. Mays, 1995. Neurons in monkey parietal area LIP are tuned for eye-movement parameters in three-dimensional space, *J. Neurophysiol.*, 73:280–297.
- Gottlieb, J. P., M. G. Macavoy, and C. J. Bruce, 1994. Neural responses related to smooth-pursuit eye movements and their correspondence with electrically elicited smooth eye movements in the primate frontal eye field, *J. Neurophysiol.*, 72:1634–1653.
- Hering, E., 1868. *Die Lehre vom binocularen Sehen*, [The Theory of Binocular Vision (B. Bridgeman and L. Stark, trans.), New York: Plenum Press; Leipzig: W. Engelmann].
- Hung, G. K., and J. L. Semmlow, 1980. Static behavior of accommodation and vergence: computer simulation of an interactive dual-feedback system, *IEEE Trans. BME*, 27:439–447.
- Judge, S. J., and B. G. Cumming, 1986. Neurons in the monkey midbrain with activity related to vergence eye movement and accommodation, *J. Neurophysiol.*, 55:915–930.
- Kawano, K., Y. Inoue, A. Takemura, Y. Kodaka, and F. A. Miles, 2000. The role of MST neurons during ocular tracking in 3D space, in *Neuronal Processing of Optic Flow* (M. Lappe ed.), San Diego, CA: Academic Press, pp. 49–63.
- Keller, E. L., 1974. Participation of medial pontine reticular formation in eye movement generation in monkey, *J. Neurophysiol.*, 37:316–332.
- Kertesz, A. E., 1983. Vertical and cyclofusional disparity vergence, in *Vergence Eye Movements: Basic and Clinical Aspects* (C. M. Schor and K. J. Ciuffreda, eds.), Boston: Butterworths, pp. 317–348.
- King, W. M., and W. Zhou, 1995. Initiation of disjunctive smooth pursuit in monkeys: evidence that Hering's law of equal innervation is not obeyed by the smooth pursuit system, *Vis. Res.*, 35:3389–3400.
- Leichnetz, G. R., 1981. The prefrontal cortico-oculomotor trajectories in the monkey, *J. Neurol. Sci.*, 49:387–396.
- Leichnetz, G. R., D. J. Smith, and R. F. Spencer, 1984. Cortical projections to the paramedian tegmental and basilar pons in the monkey, *J. Comp. Neurol.*, 228:388–408.
- Maxwell, J. S., 1991. The interaction of saccades and vergence eye movements and the effect of vergence angle on the discharge rate of abducens neurons in monkeys. Unpublished dissertation, University of Rochester.
- Maxwell, J. S., and W. M. King, 1992. Dynamics and efficacy of saccade-facilitated vergence eye movements in monkeys, *J. Neurophysiol.*, 68:1248–1260.
- May, P. J., J. D. Porter, and P. D. R. Gamlin, 1992. Interconnections between the primate cerebellum and midbrain near-response regions, *J. Comp. Neurol.*, 315:98–116.
- Mays, L. E., 1984. Neural control of vergence eye movements: convergence and divergence neurons in mid-brain, *J. Neurophysiol.*, 51:1091–1108.
- Mays, L. E., and J. D. Porter, 1984. Neural control of vergence eye movements: activity of abducens and oculomotor neurons, *J. Neurophysiol.*, 52:743–761.
- Mays, L. E., J. D. Porter, P. D. R. Gamlin, and C. A. Tello, 1986. Neural control of vergence eye movements: neurons encoding vergence velocity, *J. Neurophysiol.*, 56:1007–1021.
- Mays, L. E., Y. Zhang, M. H. Thorstad, and P. D. R. Gamlin, 1991. Trochlear unit activity during ocular convergence, *J. Neurophysiol.*, 65:1484–1491.
- McConville, K., R. D. Tomlinson, W. M. King, G. Paige, and E. Q. Na, 1994. Eye position signals in the vestibular nuclei: consequences for models of integrator function, *J. Vest. Res.*, 4:391–400.
- Miles, F. A., 1995. The sensing of optic flow by the primate optokinetic system, in *Eye Movement Research: Mechanisms, Processes and Applications* (J. M. Findlay, R. W. Kentridge, and R. Walker, eds.), Amsterdam: Elsevier, pp. 47–62.
- Miller, J. M., C. J. Bockisch, and D. S. Pavlovski, 2002. Missing lateral rectus force and absence of medial rectus co-contraction in ocular convergence, *J. Neurophysiol.*, 87:2421–2433.
- Munoz, D. P., and R. H. Wurtz, 1993. Fixation cells in monkey superior colliculus. II. Reversible activation and deactivation, *J. Neurophysiol.*, 70:576–589.
- Myers, G. A., and L. Stark, 1990. Topology of the near response triad, *Ophthalmic. Physiol. Opt.*, 10:175–181.
- Ono, H., 1983. The combination of version and vergence, *Vergence Eye Movements: Basic and Clinical Aspects* (C. M. Schor and K. J. Ciuffreda, eds.), Boston: Butterworths, pp. 373–400.
- Ono, H., S. Nakamizo, and M. J. Steinbach, 1978. Nonadditivity of vergence and saccadic eye movement, *Vis. Res.*, 18:735–739.
- Poggio, G. E., 1995. Mechanisms of stereopsis in monkey visual cortex [review], *Cereb. Cortex*, 5:193–204.
- Robinson, D. A., 1970. Oculomotor unit behavior in the monkey, *J. Neurophysiol.*, 33:393–404.
- Robinson, D. A., 1972. Eye movements evoked by collicular stimulation in the alert monkey, *Vis. Res.*, 12:1795–1808.
- Stakenburg, M., 1991. Accommodation without pupillary constriction, *Vis. Res.*, 31:267–273.
- Steiger, H. J., and J. A. Büttner-Ennever, 1979. Oculomotor nucleus afferents in the monkey demonstrated with horseradish peroxidase, *Brain Res.*, 160:1–15.
- van Rijn, L. J., and A. V. Van der Berg, 1993. Binocular eye orientation during fixations: Listing's law extended to include eye vergence, *Vis. Res.*, 33:691–708.
- Westheimer, G., and S. M. Blair, 1973. Oculomotor defects in cerebellectomized monkeys, *Invest. Ophthalmol.*, 12:618–621.
- Zee, D. S., E. J. Fitzgibbon, and L. M. Optican, 1992. Saccade-vergence interactions in humans, *J. Neurophysiol.*, 68:1624–1641.
- Zhang, H. and P. D. R. Gamlin, 1998. Neurons in the posterior interposed nucleus of the cerebellum related to vergence and accommodation, *J. Neurophysiol.*, 79:1255–1269.
- Zhang, Y., L. E. Mays, and P. D. R. Gamlin, 1992. Characteristics of near response cells projecting to the oculomotor nucleus, *J. Neurophysiol.*, 67:944–960.
- Zhou, W., and W. M. King, 1998. Premotor commands encode monocular eye movements, *Nature*, 393:692–695.

96 The Primate Frontal Eye Field

CHARLES J. BRUCE, HARRIET R. FRIEDMAN, MICHAEL S. KRAUS,
AND GREGORY B. STANTON

IN PRIMATES, A PARTICULAR region of frontal lobe neocortex, the frontal eye field (FEF), is prominently involved in the control of voluntary eye movements. FEF is principally concerned with eye movements that serve to image important aspects of the visual world on the most sensitive part of the retina, the fovea. Foveation is particularly important in primates because visual acuity at the primate fovea is far better than peripheral acuity. Because voluntary saccades are the most important and conspicuous eye movements of the foveation system, and because FEF has been most extensively studied in relation to saccades, the saccadic aspects of FEF will be emphasized in this chapter. However, smooth pursuit, fixation, and vergence eye movements also serve foveation, and FEF has a distinct subregion for smooth pursuit and is involved in vergence movements and fixation as well.

FEF and saccadic eye movements

DISCOVERY OF FEF AND OTHER CORTICAL EYE FIELDS David Ferrier (1876) was the first to discover that electrical stimulation of the frontal lobe neocortex deviated the eyes toward the contralateral side. It was subsequently found that all primates, including the great apes (Leyton and Sherrington, 1917) and humans (Penfield and Boldrey, 1937), possessed such an FEF. The top part of Figure 96.1 shows Ferrier's experimental mappings in a macaque monkey.

As also shown in Figure 96.1, FEF is not the only neocortical area involved in eye movements. In the macaque, there also is a parietal eye field (PEF), located in the lateral bank of the intraparietal sulcus (e.g., Shibutani et al., 1984), and a supplementary eye field (SEF), located in the dorsal frontal lobe near the midline (e.g., Mott and Schäfer, 1890; Schlag and Schlag-Rey, 1987). The FEF, PEF, and SEF are reciprocally interconnected (e.g., Huerta et al., 1987; Stanton et al., 1993, 1995). The FEF, however, seems to be the principal cortical eye field: FEF has the lowest thresholds for electrically elicited saccades (Russo and Bruce, 1993, 2000; Shibutani et al., 1984), oculomotor behavior is generally more impaired by FEF lesions than by lesions in the other eye fields (e.g., Schiller and Chou, 1998, 2000a, 2000b), and FEF is indispensable for visually guided saccades if the superior colliculus (SC) is damaged (Keating and Gooley, 1988; Schiller et al., 1980).

NATURE OF EYE MOVEMENTS ELECTRICALLY ELICITED FROM FEF Early FEF studies did not determine which type of eye movement caused the contralateral deviations produced by electrical stimulation. Nearly a century after Ferrier, Robinson and Fuchs (1969), using alert macaque monkeys as subjects and their search coil technique of transducing eye movements, unequivocally demonstrated that these electrically elicited eye movements were saccadic eye movements indistinguishable from naturally occurring saccades. When tested with the head unrestrained, FEF stimulation results in a combined eye-head movement (as does head-free stimulation in the SC as well as SEF and PEF). Thus, the elicited movement is actually a saccadic gaze shift, with the magnitude of the head component depending on circumstances including the size of the elicited movements at the FEF site (Tu and Keating, 2000; see also Sparks et al., 2001).

Still, the specific role of FEF remained unclear because FEF lesions do not abolish saccadic eye movements, nor do they produce oculomotor paralysis analogous to the skeletal paralysis following lesions of the upper motor neuron in area 4. Moreover, FEF neurons do not project directly to the oculomotor nuclei (Künzle and Akert, 1977), as was originally thought to be the case. However, extensive neurophysiological, anatomical, and behavioral evidence now establishes FEF as the principal cerebral cortex for voluntary movements of the eyes (Bruce, 1990; Bruce and Goldberg, 1984). Except for its smooth pursuit and vergence zones, each site in FEF yields saccades of a characteristic direction and amplitude, and the set of all possible contralaterally directed saccades is represented by each hemisphere's FEF (Bruce et al., 1985; Crosby et al., 1952; Robinson and Fuchs, 1969; Wagman et al., 1961). Figure 96.2 shows some of this topography, as well as examples of ipsiversive elicited smooth eye movements found in the depths of the arcuate sulcus; this smooth pursuit region of FEF is discussed near the end of this chapter.

Basic properties of saccadic eye movements. Thus, FEF provides a major efferent pathway from the neocortex for commanding voluntary saccadic eye movements, and so understanding this highly specialized aspect of the foveation system is key to understanding FEF function. Saccades are brief (usually <75 msec) and fast (usually >500 deg/sec) eye movements. Humans average about two saccades per second

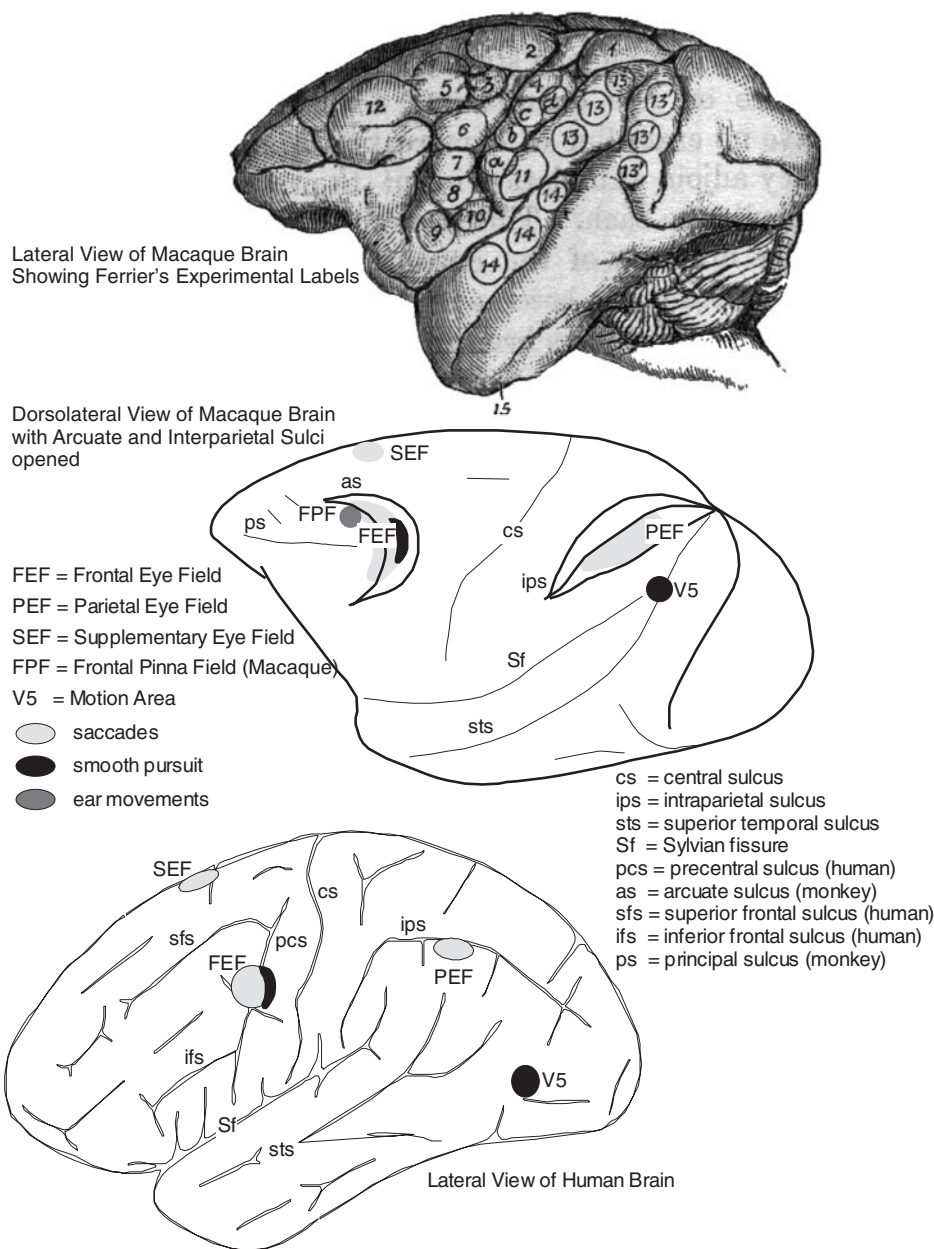


FIGURE 96.1. Cortex for eye movements in the human and the monkey. *Top*: left hemisphere of a macaque monkey mapped by Ferrier (1876). *Electrical irritation* at 12, 13, and 13' produced contralateral eye movements. The 12 region represents the FEF, although contemporary studies indicate that FEF is located principally in the anterior lip and anterior wall of the arcuate sulcus, and thus slightly posterior and lateral to Ferrier's location. Similarly, movements at 13 may be the PEF, but contemporary studies locate PEF in the LIP. Eye movements at 13' may reflect the seldom mentioned occipital eye field, also called the *posterior eye field*. *Bottom*:

Cortical regions important for saccade and smooth pursuit eye movements are highlighted on the monkey brain and the human brain. In both monkey and human, FEF is in front of premotor cortex for the hand and neck, and mostly lies within the sulcus marking the anterior limit of the precentral gyrus. In both species, the smooth pursuit region of FEF is just posterior to the saccadic region of FEF (particularly if the cortex was flattened). The monkey brain is shown from a dorsolateral viewpoint to minimize distortion of the arcuate sulcus.

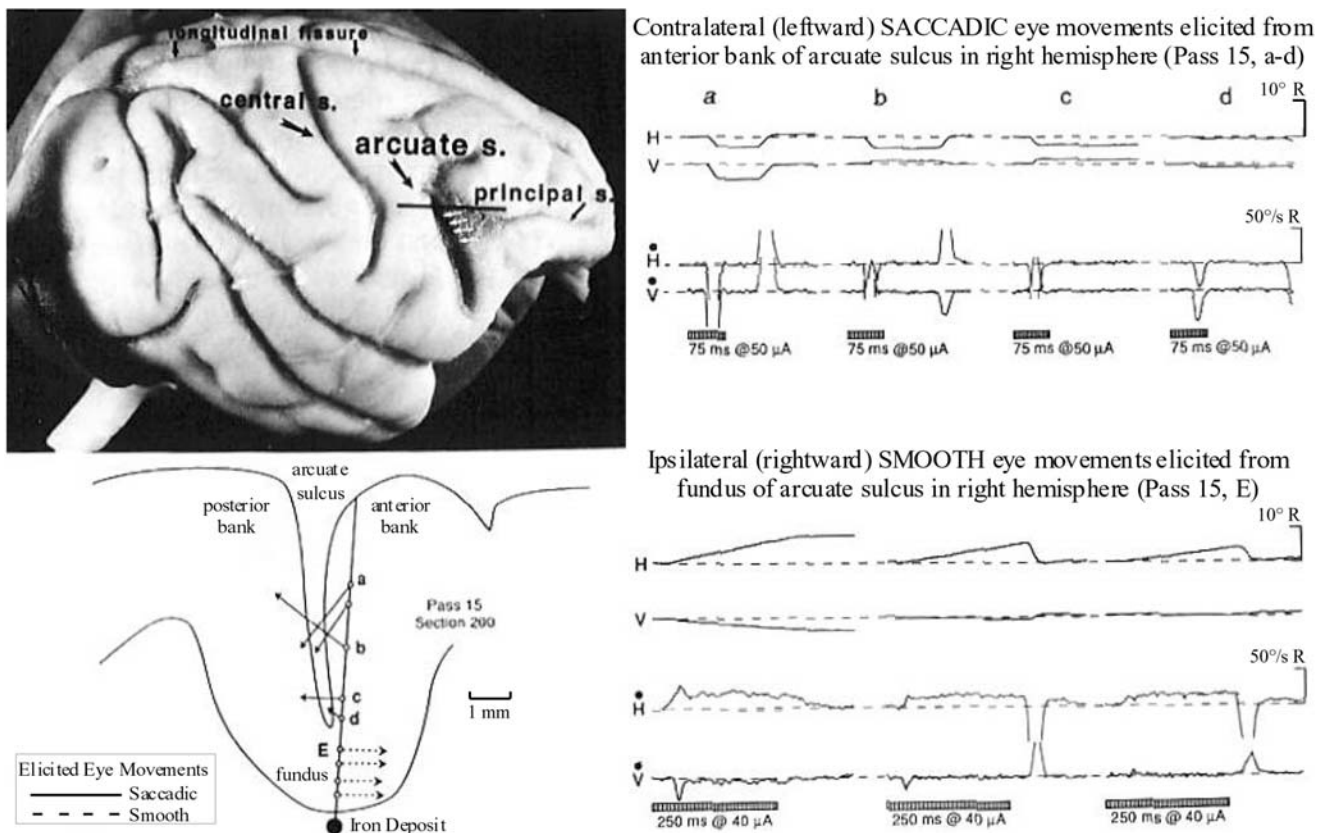


FIGURE 96.2. Reconstructed electrode pass down the anterior bank of arcuate through the saccadic FEF and encountering the smooth pursuit region of FEF. *Top left*: dorsolateral views of the right hemisphere. The small white arrows on the right hemisphere indicate additional locations where smooth eye movements were elicited. *Bottom left*: cross section of the arcuate sulcus showing reconstructions of electrode penetration down the anterior bank; sites that yielded saccadic and smooth eye movements are indicated. Note that contralaterally directed saccadic eye movements

were elicited first, whereas ipsilaterally directed smooth eye movements were elicited in the arcuate fundus. *Right*: representative eye movements at four saccadic sites (*a-d*) and three examples from a smooth movement site. In all cases, the electrical stimulation was applied while the monkey was attentively fixating a small stationary spot of light, and usually the monkey made a voluntary saccade back toward that spot after the electrical stimulation ceased. (Adapted from Figure 2 of MacAvoy et al., 1991.)

while awake, and so our day is spent in brief fixations of different small parts of the visual world, constantly, but only briefly, interrupted by saccades. This unremitting procession, the processing of foveal visual information during a fixation, as well as the planning of the next saccade, engages much of the human brain, as exemplified by brain-imaging studies of humans doing both simple and complex visuomotor tasks (e.g., Luna et al., 2001; O'Driscoll et al., 2000).

Saccades are open-loop (i.e., ballistic, preprogrammed) movements. In fact, less than 50 to 100 msec prior to its start, a saccade generally cannot be canceled or redirected on the basis of new sensory information. The saccadic waveform and its main parameters (duration, peak velocity, etc.) are largely determined by the dimensions of the movement being accomplished, and thus one cannot simply choose to make faster or slower saccades.¹ The saccadic objective is to effect the desired ocular displacement as quickly as possible and immediately return the eye to stationary fixation in the

new direction. In fact, vision during the saccade is poor or absent (*saccadic suppression*), meaning that the subject is nearly blind during saccades—more reason for their high speed and brief duration.

Saccadic launch is under voluntary control, and saccades have relatively long latencies (i.e., reaction times). For example, saccade latency, as measured from the time of the appearance of a visual target until the start of the saccadic movement to foveate the target, is usually 100 to 400 msec, with 200 msec being typical. By contrast, the vestibulo-ocular reflex has a 10 msec latency. Although saccades to quickly foveate suddenly appearing visual stimuli are somewhat reflexive; one can readily forgo making saccades to even highly salient stimuli. Furthermore, one can instead

¹ For example, saccade duration is roughly a linear function of the saccade size ($\sim 21 \text{ msec} + 2.2 \times \text{size}$; Carpenter, 1988).

make accurate and advantageous “predictive” or “anticipatory” saccades to the location where a stimulus is likely to appear in the future or even antisaccades in the opposite direction as a stimulus.

Thus, saccades are guided by our experience, guesses, objectives, and strategies,² as well as by overt visual stimulation, even though their motoric details are largely independent of their purpose. Overall, the saccadic plan is to consider judiciously whether to disengage the current foveated stimulus, select a new stimulus of interest, plan a movement based on the retinal locus that will foveate that new stimulus, execute the plan in a ballistic fashion, and then process the new foveal image for at least a few hundred milliseconds before considering a subsequent saccade.³ Reading is the prime example of the saccadic system fully engaged under voluntary control.

Neural basis of saccadic eye movements. Figure 96.3 summarizes the brain’s distributed network for triggering and carrying out voluntary saccades. All saccades are ultimately fashioned by a dedicated neural circuit in the brainstem called the *saccade generator* (e.g., Scudder et al., 2002). This network of several distinctive types of neurons in the pontine and mesencephalic reticular formation originally evolved to produce the quick-phase movements of vestibulo-optokinetic nystagmus that reflexively stabilize images on the retina. In primates, however, it serves as the final common pathway for all rapid eye movements, and so if the saccade generator is damaged, then all rapid eye movements, reflexive and voluntary, are disabled. Thus, the voluntary saccades of primates involve triggering a part of the phylogenetically older image stabilization circuitry for the purpose of foveation.

The output of the saccade generator is a displacement vector of the current direction of gaze and a *neural integrator* downstream of the saccade generator computes the tonic eye position signal needed to hold the eye steady in its new position following each saccade. Because it serves all eye movement commands, smooth/slow eye movements as well as rapid/saccadic movements, it is called the *common* neural integrator. Figure 96.3 details the brainstem locale of the saccade generator and neural integrator and illustrates how all saccadic eye movements rely on these two vital brainstem circuits.

Thus, FEF does not directly control the extraocular musculature, but instead achieves its purposes by triggering and

modulating the brainstem circuitry of the much older image stabilization system, that is, the circuits underlying the reflexive eye movements that serve to hold the whole visual world stationary on the retina. Without oculomotor stabilization during movements of the head or body, the retinal image is smeared and all vision, foveal and peripheral, is severely compromised. The stabilization system generally functions reflexively in parallel with the more voluntary foveation system (for a review, see Bruce and Friedman, 2002).

The superior colliculus and the visual-grasp response. The SC is the vertebrate brain’s prototype sensorimotor structure and occupies a key position in the saccade circuitry of Figure 96.3 above the saccade generator. The primate SC receives topographic visual projections from corresponding parts of both retinas that portray a precise map of the contralateral hemifield on each hemisphere’s SC. This visual map is found in the superficial layer of the SC and is in register with the map of the movement vectors for saccade-related neurons in the intermediate layer. This remarkable alignment of the sensory and motor maps underscores the principal role of the primate SC, which is to move the eyes so as to foveate quickly a stimulus seen anywhere in the visual periphery by commanding the saccade generator to fashion a rapid eye movement of the appropriate size and direction. This prepotent visually guided saccade has been called the *visual grasp reflex* and is the basic building block of the foveation system.

Probably the most important output from FEF for effecting saccades is its massive topographic projection to the intermediate layers of the SC (Huerta et al., 1986b; Stanton et al., 1988). Hanes and Wurtz (2001) found that FEF-elicited saccades were eliminated or distorted by temporary inactivation of parts of the SC map. Nevertheless, visually guided saccades and FEF-elicited saccades survive complete ablation of SC in primates because the primate also has a substantial neocortical network for saccades with access to the saccade generator independent of SC. Figure 96.3 also shows these cortical pathways and clarifies some effects of such lesions. For example, the sparing of visually guided saccades following SC lesions is mediated by FEF projections to the brainstem saccade generator that bypass the SC. The SC, however, normally provides a faster and more accurate pathway for visually guided saccades via its direct retinal projections and accurate retinotopic map, which explains why an increase in the latency of visually guided saccades is a lasting deficit of SC damage. Likewise, FEF lesions alone generally spare visually guided saccades; however, FEF lesions combined with SC lesions eliminate most visually guided saccades (Schiller et al., 1980). Thus, the primate SC and FEF provide both serial and parallel pathways for visual triggering of the brainstem saccade generator for the purpose of foveating saccades.

² Including social purposes for avoiding or making eye contact with others.

³ Saccades also have a refractory period; it is relatively difficult to initiate a saccade sooner than 100 to 200 msec after the previous saccadic movement ends.

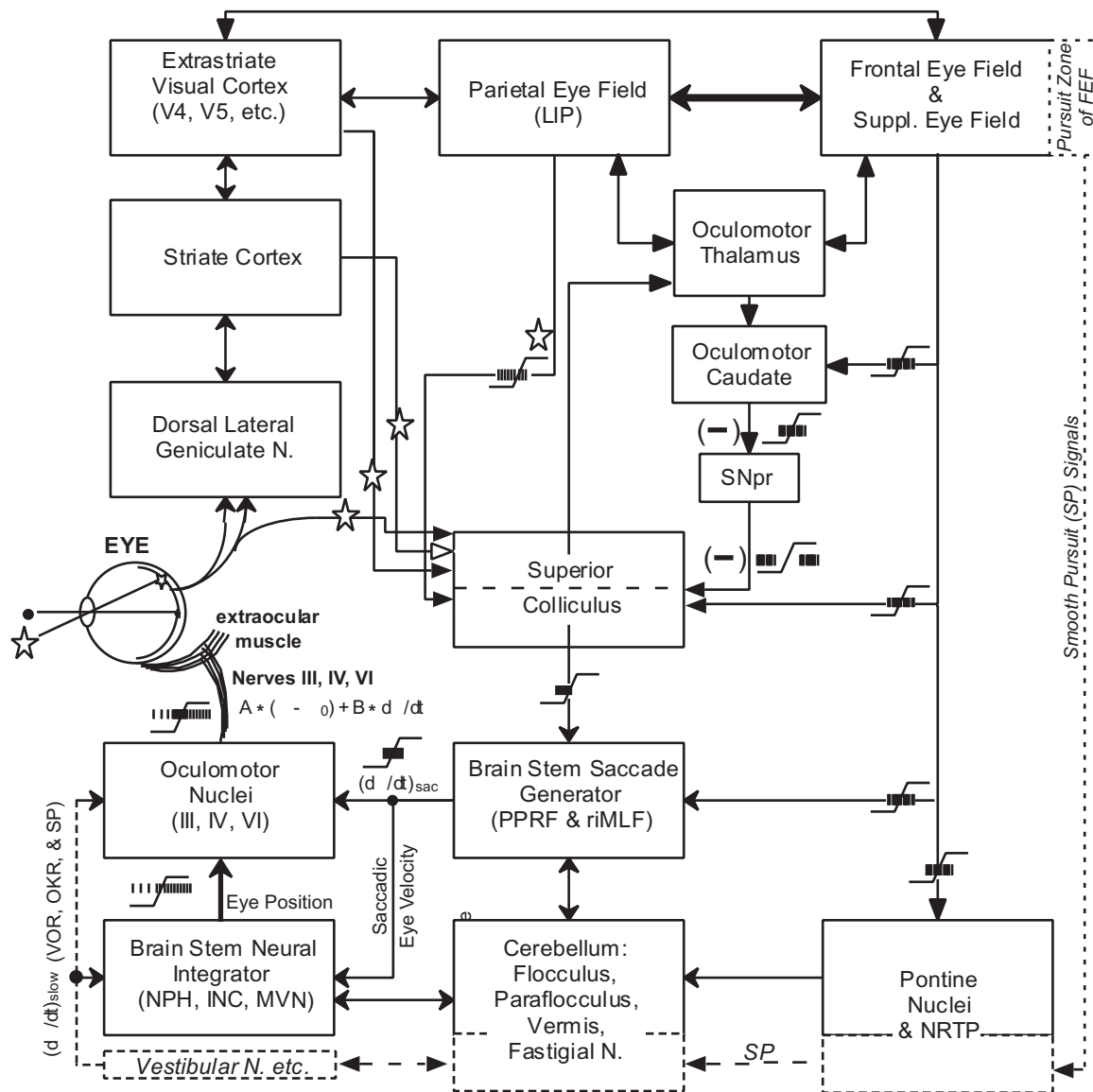


FIGURE 96.3. Pathways for voluntary and visually guided saccades and smooth pursuit. This diagram shows anatomical connections between cortical and subcortical structures involved in the control and generation of saccadic eye movements. The FEF receives visual information via pathways originating in the striate cortex, as do the PEF and the SEF. Note that all visual cortical areas project to the SC, with FEF, PEF, and SEF projecting primarily to its intermediate layers. By contrast, the superficial layers of SC receive direct visual projections from the retina and indirect visual projections from the striate and extrastriate cortices. Connections to locations marked with a star principally carry visual signals, whereas those marked by a saccade and burst are principally motoric.

The brainstem saccade generator is located in the paramedian pontine reticular formation (PPRF) and in the rostral interstitial nucleus of the medial longitudinal fasciculus (riMLF). The brainstem neural integrator is located in the medial vestibular nucleus (MVN), the adjacent nucleus prepositus hypoglossi (NPH), and the interstitial nucleus of Cajal (INC). The cerebellum controls the

gains of both the saccade generator and the common integrator, in addition to being a critical link in the pursuit pathway. The smooth pursuit pathways shown with dashed boxes, dashed lines, and italicized text is very basic; for example, V5 and other temporal and parietal areas, as well as the pursuit zone of FEF, project to the pursuit-related pontine nuclei. SNpr, substantia nigra pars reticulata; NRTP, nucleus reticularis tegmenti pontis; LIP, lateral intraparietal sulcus; Suppl, Supplementary; θ , eye position; $d\theta/dt$, eye velocity; $(d\theta/dt)_{\text{sac}}$, saccadic eye velocity; $(d\theta/dt)_{\text{slow}}$, slow (or smooth) eye velocity; VOR, vestibulo-ocular reflex; OKR, optokinetic reflex; SP, smooth pursuit; (-), inhibitory synapse; $A * (\theta - \theta_0) + B * d\theta/dt$, equation for spike rate of the general oculomotor neuron as a function of eye position and velocity; A and B, constants; θ , eye coordinate along the pulling direction of the extraocular muscle that is innervated; $d\theta/dt$, eye velocity along the same direction; θ_0 , eye position at which the oculomotor neuron is recruited.

EFFECTS OF FEF LESIONS ON SACCADIC EYE MOVEMENTS
Whereas FEF lesions spare most visually guided saccadic eye movements (unless combined with SC damage, as discussed above), there is a cluster of deficits indicating that FEF is important for many types of *purposive* saccades, particularly when no overt visual target is available. Gordon Holmes (1938) found that patients with frontal lesions had difficulty moving their eyes in response to verbal commands (“look right”), even though they could follow visual objects and understood the verbal commands. He concluded, “The frontal centers make possible the turning of gaze in any desired direction and the exploration of space, but they also keep under control, or inhibit, reflexes that are not appropriate.” Guitton et al. (1985) used the antisaccade paradigm to demonstrate just that, namely, that “Frontal lobe lesions in man cause difficulties in suppressing reflexive glances and in generating goal-directed saccades.” In other words, their subjects could not launch saccades in the direction opposite the visual target (antisaccades), even though they understood that to be the task. Instead, they often made inappropriate saccades toward the visual targets (prosaccades), exactly what they were instructed not to do. Humans with FEF lesions also have difficulty executing memory-guided saccades (Ploner et al., 1999). Similarly, monkeys have difficulty making memory saccades after FEF inactivation (Dias and Segraves, 1999; Dias et al., 1995; Sommer and Tehovnik, 1997). Monkeys with FEF lesions fail to generate predictive saccades during square-wave target motion (Bruce and Borden, 1986), as do humans with FEF lesions (Gaymard et al., 1999).

NEUROPHYSIOLOGY OF FEF IN RELATION TO SACCADIC EYE MOVEMENTS

Low-threshold FEF and presaccadic burst activity. Bruce et al. (1985) define FEF as cortex where saccades are elicited by microstimulation at 50 μ A or less with the electrode tip in gray matter. In the macaque monkey, this low-threshold (saccadic) FEF lies primarily in the anterior bank and anterior lip of the arcuate sulcus (see Figs. 96.1 and 96.2) and has a distinctive cytoarchitecture (see also Stanton et al., 1989).

When recording is restricted to the saccadic FEF, the vast majority of neurons have robust task-related changes in their discharge rate when a monkey performs almost any purposive saccadic eye movement task, such as a visually guided saccade task (see below), and a full range of saccade sizes and directions are tested for each cell. With appropriate control experiments, these functional activities can be parsed into several types, such as visual responses, auditory responses, presaccadic movement responses, postsaccadic responses, tonic gaze-direction responses, predictive movement activity, mnemonic visual activity, and so on (see below;

also see Bruce and Goldberg, 1985; Schall, 1991; Sommer and Wurtz, 2001).

Incidence and significance of presaccadic burst activity in FEF. One particular activity, a burst of increased spiking that starts immediately prior to saccades into a cell’s movement field, is the signature activity of the FEF. Approximately one-third of FEF neurons have this presaccadic burst (PSB) activity.⁴ A representative PSB from an individual FEF neuron is shown in Figure 96.4. PSB activity begins just prior to saccade initiation, usually ends approximately when the saccade is completed, and is always tuned, albeit fairly broadly, for a particular saccade vector (i.e., its movement field).

In many respects, FEF cells with PSB activity are remarkably similar to saccade-related bursters (SRBs), which are abundant in the intermediate layers of the SC (e.g., Glimcher and Sparks, 1993) and are even similar to vectorial *long-lead burst neurons* found in the rostral pontine reticular formation (e.g., Hepp and Henn, 1983). But there are significant differences in timing (Segraves and Park, 1993). Moreover, referring to the PSB activity in FEF as generic motor or movement activity (as in presaccadic movement responses, e.g., Bruce and Goldberg, 1985), although not incorrect, implies, by analogy with true motoneurons in the spinal cord and cranial nerve nuclei, a stronger relation between the FEF activity and the realized saccadic eye movements than is truly the case.

Most FEF neurons with PSB activity also have one or more other functional activities. Most conspicuously, approximately two-thirds of FEF cells with PSB also have significant visual activity in that they will respond to the appearance of simple visual stimuli, such as a spots of light, within a large peripheral receptive field (RF), even when no saccade is involved.⁵ Such was the case for the neuron of Figure 96.4. Conversely, a substantial fraction (~20%) of FEF cells have visual responses but lack PSB activity.

Relationship of PSB activity to electrically elicited saccades. PSB activity in the FEF correlates very strongly with the electrically elicited saccade phenomenon that has been used to discover, define, and map FEF. Bruce et al. (1985) found that thresholds for eliciting saccades were lowest at the sites of cells with PSB activity. When testing stimulation at the site of cells lacking PSB activity (usually these other cells were visually responsive, had postsaccadic activity, or both), far

⁴Bruce and Goldberg (1985) found 409 of 752 (54%) FEF cells to be presaccadic (their Table 1), and of a well-analyzed and classified subset of 115 presaccadic cells, 60% had presaccadic movement activity (Table 2) yielding ~33%, or approximately one-third.

⁵Bruce and Goldberg (1985) termed such cells *visuomovement* cells.

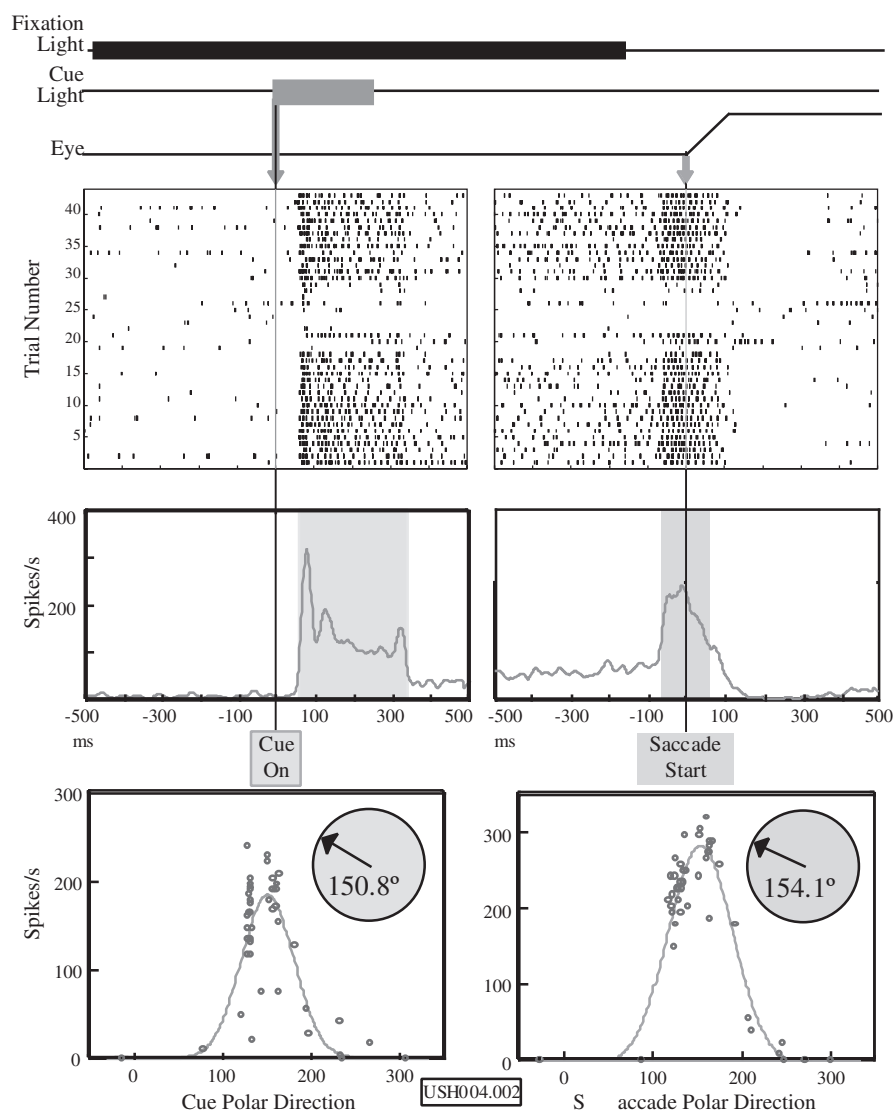


FIGURE 96.4. FEF neuron tested with the memory-saccade task. This neuron combined PSB with phasic-tonic visual activity and mnemonic continuation of the visual activity. *Top*: task events. Shortly after the monkey fixates a central light, a peripheral cue briefly appears. Then, after a delay period, the fixation light is extinguished and the monkey must saccade to the location where the peripheral cue had been shown earlier. The location was varied from trial to trial but was in the response field (RF), except for several trials in the middle of testing, when it was deliberately moved to locations outside the RF (see rasters and Gaussian-fit plots). *Top-middle*: rasters (by trial) and histograms of spike activity aligned on cue onset (*left*) show the burst of activity elicited by the

visual stimulus, and those aligned on the saccade onset (*right*) show the large burst of activity preceding the saccades. Note that the visual response has three components: a phasic high-rate burst to the initial appearance of the visual stimulus (latency ~50 msec), a robust tonic visual discharge while the cue remained on, and then, starting ~50 msec after the cue was extinguished, a medium-level tonic mnemonic response that was maintained above the cell's baseline level of activity throughout the delay interval. *Bottom-middle*: spike density histograms based on rasters. Blue and green indicate the intervals used for the Gaussian fits (*bottom*) of best direction for visual and PSB activity, respectively. (From M. S. Kraus et al., unpublished data.)

more electrical current was usually needed to elicit saccades. For example, low thresholds ($<50\mu\text{A}$) were found at the sites of 34 cells with both visual and PSB activity and 11 cells with PSB activity only, but only at the site of 3 cells with visual responses and no PSB activity. Conversely, high thresholds ($>150\mu\text{A}$) were found at the sites of 11 VIS + PSB cells and 2 PSB-only cells, but at the site of 21 visual-only

cells. Thus, recording PSB activity is highly indicative that electrically evoked saccades will be obtained with low currents.

Moreover, the dimensions of the evoked saccades at FEF sites are highly correlated, in both direction and amplitude, with the movement fields for PSB activity recorded from neurons at the same site (Bruce et al., 1985) (Figs. 96.3 and

96.4). Dimensions of both the PSB movement fields and the evoked saccades change together in a fairly systematic manner across the extent of the FEF (Bruce et al., 1985; Dias and Segraves, 1999).

Given this close relationship with the evoked saccades, it is not surprising that FEF cells with PSB activity are prevalent among those found to project to the SC and to the pontine reticular formation. Indeed, Segraves and Goldberg (1987) found that 59% of corticotectal neurons had presaccadic movement-related activity and that another 22% had foveal and fixation-related activity. The remaining 20% were miscellaneous FEF types. In fact, none of the 51 corticotectal cells in this study were primarily responsive to peripheral visual stimuli, even though this is an extremely common FEF cell type (~20%, as noted earlier; also see Fig. 96.6). A similar result was later found for FEF cells projecting to oculomotor regions of the pons (Segraves, 1992), with 48% of the corticopontine neurons firing in association with saccadic eye movements and 28% responsive to visual stimulation of the fovea combined with activity related to fixation.⁶

We infer from these data that the electrically evoked saccade phenomenon principally reflects the excitation of FEF cells with PSB activity that, in turn, activates the brainstem saccade generator via the corticotectal and corticopontine projections of FEF (Huerta et al., 1986; Stanton et al., 1988b). Thus, the functional involvement of the FEF in saccadic eye movements seems to involve naturally occurring PSB activity being sent to the saccade generator over the same FEF efferent pathways responsible for elicited saccades.

PSB activity is FEF's signature neuronal activity. In summary, the PSBs are a distinctive FEF activity. PSBs are manifest in ~33% of FEF neurons but are relatively rare in other neocortex, including the periprincipal prefrontal cortex anterior to the FEF/arcuate and the premotor cortex lying posterior to the arcuate/FEF. These two adjacent cortical regions both have abundant visual responses with large RFs fairly similar to those in FEF.⁷ Thus, although visual responses, both peripheral and central/foveal, are abundant in FEF, what truly distinguishes neural activity in FEF from activity in all other neocortical areas (except for the two other cortical eye fields, SEF and PEF) is FEF's abundance of neurons with robust PSBs. Moreover, the PSB activity is very strongly

associated with the low-threshold elicited saccade phenomenon used to discover, define, and map FEF.

An extremely strong line of evidence for the fundamental importance of the FEF's PSB activity for the production of saccadic eye movements comes from countermanding experiments. Hanes et al. (1998) find that FEF neurons with eye movement-related activity basically control the production of gaze shifts in this special paradigm where a signal to stop the saccade being prepared is sometimes given. Saccades were initiated if and only if the PSB activity of FEF neurons reached their threshold activation level, and not if their PSB activity decayed in response to the stop signal before reaching that level. In contrast, the spiking of FEF neurons with only visual activity was not critically related to the success of the stop signal.

PSB ACTIVITY IN FEF PRECEDES MOST TYPES OF PURPOSE SACCAD The PSB of FEF neurons occurs even in the absence of a visual target (e.g., in the learned-saccade and the memory-saccade paradigms); however, some FEF cells with PSBs in these tasks have little or no bursts in conjunction with "spontaneous" saccades made in the dark (Bruce and Goldberg, 1985; see their Figures 6 and 7). Moreover, as mentioned earlier, FEF lesions impair some categories of voluntary saccades but leave others (generally more reflexive) intact. Thus, it is an empirical question to know which of the many types of saccades (e.g., Table 3-1 in Leigh and Zee, 1999) that FEF PSB activity reliably precedes, and which types are not associated with PSB activity in FEF. Or, more quantitatively, how does the magnitude of PSBs in conjunction with different types of voluntary saccades, often made without a visual target, compare with the response magnitude on standard visually guided saccade tasks? Below we review data concerning the necessary and sufficient conditions for FEF's PSB activity, and, in conjunction with each type of saccade considered, we discuss which FEF activities and/or phenomena could underlie a target-appropriate PSB for that type of saccade.

FEF activity in conjunction with memory saccades. Single-cell examples of strong FEF activity in conjunction with memory saccades have been shown in many reports. Here we present the aggregate FEF response. Figure 96.5 shows the aggregate histograms from a primary database of 341 FEF cells that were (1) all deemed to have a significant presaccadic response and (2) all had their presaccadic responses parsed using the memory saccade task. The spike-density histogram on correctly performed trials in which the memory saccade was directed into its response field was computed for each neuron and then averaged across all 341 cells. Figure 96.6 shows the same data, but segregated into three basic FEF neuron types: 58 neurons with purely visual responses, 190 with both visual and PSB activity, and 93 with PSB activity but few or no visual responses.

⁶However, Sommer and Wurtz (2000, 2001) found FEF's corticotectal population to be more similar to the overall FEF (than did Segraves and Goldberg, 1987), and they emphasized that many corticotectal FEF cells were active during the delay period (on either a memory-saccade or a deferred-saccade task) as well as at the time of the saccade.

⁷Indeed, most macaque neocortex is visually responsive (e.g., Felleman and Van Essen, 1991).

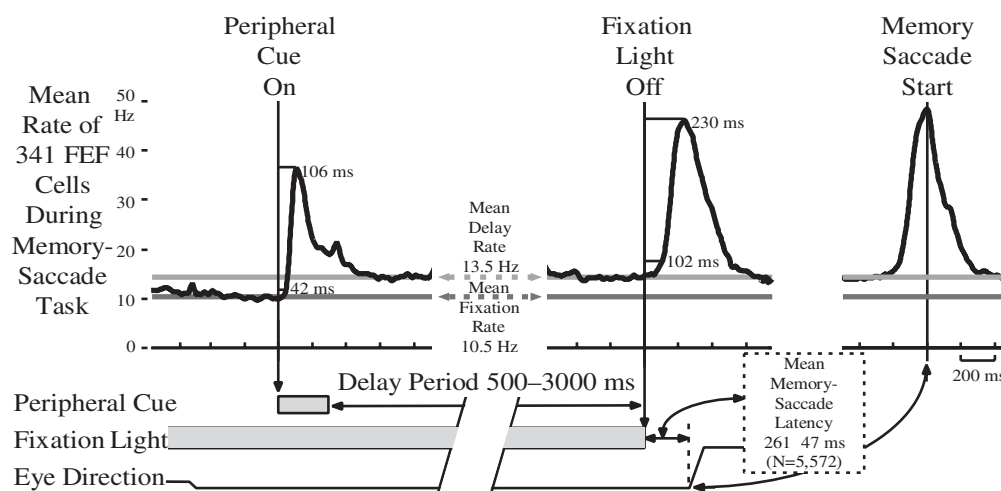


FIGURE 96.5. Aggregate FEF response on the memory-saccade task. Average activity of 341 FEF neurons (from six monkeys) tested on the memory-saccade task. Histograms of spike activity aligned on the cue onset (*left*) show the burst of activity elicited by the visual stimulus. The histograms aligned on the saccade onset (*right*) show the large burst of activity preceding and during the saccades. This same PSB of activity is shown in relation to the signal to saccade

in the *middle* histogram. Note that the visual response has three components: a phasic high-rate burst to the initial appearance of the visual stimulus (latency ~50 msec), a robust tonic visual discharge while the cue remained on, and then, starting ~50 msec after the cue was extinguished, a low-level tonic mnemonic response that was maintained throughout the delay interval. (Data from Friedman et al., 1997.)

These aggregate histograms indicate that overall spiking rate in the FEF is largest in conjunction with saccades, not with the visual target's appearance. Specifically, Figure 96.5 shows that the population PSB in conjunction with memory saccades has over twice as many spikes as the aggregate phasic response to the visual cues. The aggregate histograms in Figure 96.6 further make the case that the PSB is the more intense FEF activity: for the VIS + PSB cells, the PSB is much larger than the phasic visual burst. Moreover, the PSB for memory saccades of the PSB-only cells is larger than the phasic visual cue response of the VIS-only cells.

Memory-saccade PSBs versus PSBs for visually guided saccades. We compared the memory saccade activity of a subset of the cells shown in Figures 96.5 and 96.6 with their activity on two visually guided saccade tasks, namely, the deferred-saccade and step-saccade tasks. The deferred-saccade paradigm⁸ is identical to the memory-saccade paradigm except that the peripheral cue remains on and is thus still available to guide the saccade when the fixation light is eventually extinguished (which is the signal to saccade in both tasks). In the step-saccade task, the appearance of the peripheral spot coincides with the extinction of the fixation point (as if the fixation point quickly moved or "stepped"). Hence, there is no imposed wait (or delay) period, and the monkey can saccade as quickly as desired after the saccade target light appears.

Figure 96.7 shows that the aggregate PSB magnitude for the memory saccade is nearly identical to the PSB magni-

tude for the deferred saccades and is only slightly smaller than the PSB on the step-saccade task. This equality is particularly unexpected in light of a similar comparison recently carried out in the SC by Edelman and Goldberg (2001). They found that many SC burster cells did not respond in conjunction with memory saccades or responded much less than on their version of the deferred-saccade task. Thus, it would seem that FEF PSB activity is more reliable than SRB activity in the SC in conjunction with purposive memory-guided saccades performed without a visual target, even though the SRB activity in the SC is thought to be significantly more reliable than the PSB activity in FEF for most saccades, especially spontaneous saccades.

⁸Note regarding task terminology: both the deferred-saccade and memory-saccade tasks prominently feature a delay period, and indeed, both have been called *delay tasks* or *delayed-saccade tasks* in recent papers (e.g., Edelman and Goldberg, 2001; Sommer and Wurtz, 2000, 2001). However, to avoid confusion we do not use the term *delay* or *delayed* for either. Originally, *delayed* denoted a mnemonic task (e.g., *delayed saccade*: Hikosaka et al., 1989; *oculomotor delayed-response task*: Funahashi et al., 1989), and historically, it refers to the *delayed-reaction* task that Jacobsen (1936) used to test the memory of monkeys with frontal lesions. However, the deferred-saccade task does not involve memory, only a wait, so it is misleading to call it delay task. It was originally termed the *stable target saccade task* by Bruce and Goldberg (1985); later, Russo and Bruce (2000) termed it the *deferred-saccade task*.

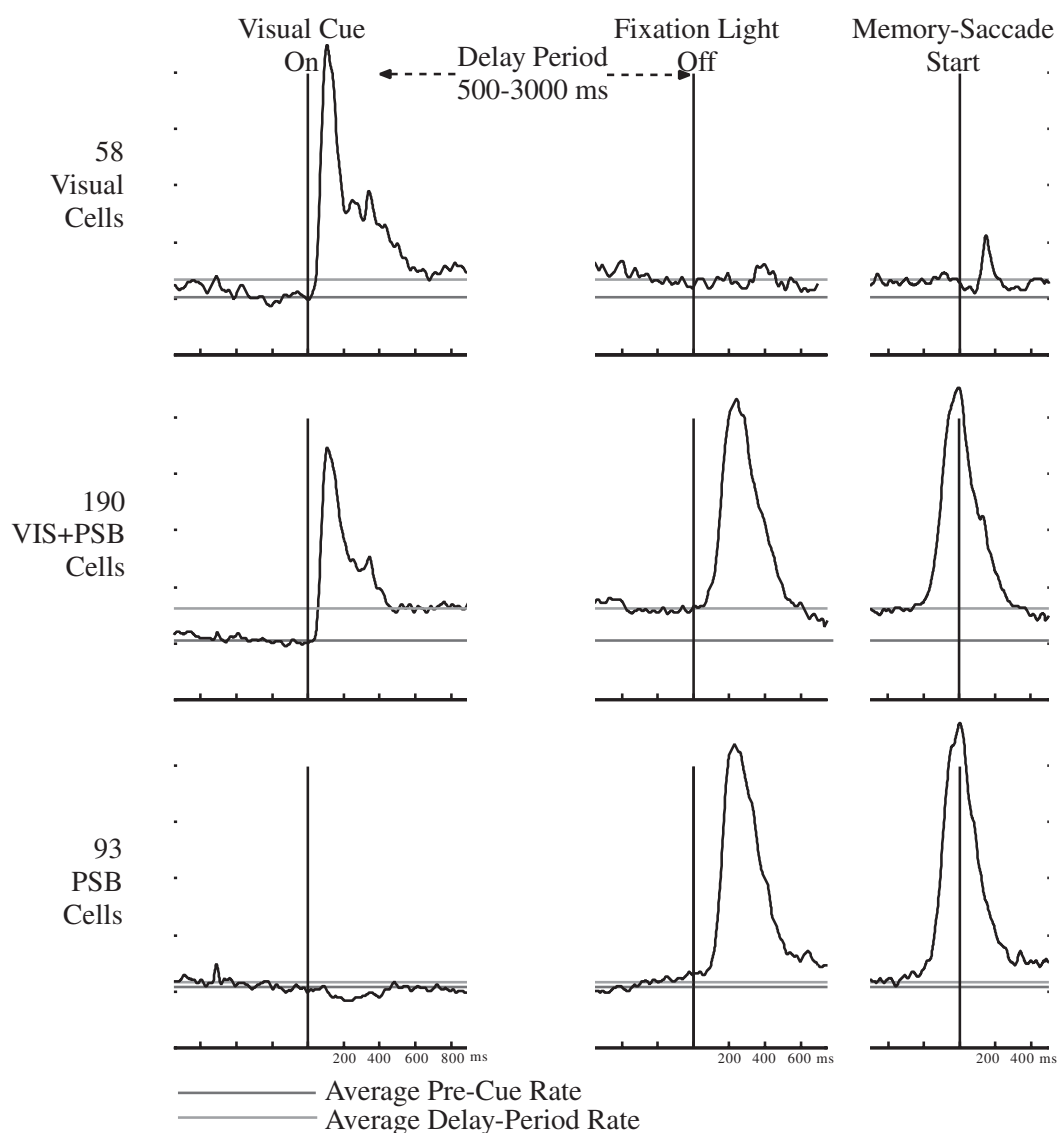


FIGURE 96.6. Aggregate FEF response on the memory-saccade task segregated by neuron type. This is the same experiment and data as in the previous figure, and presented in the same way except that the 341 neurons are separated into three categories: *Top*: neurons with only a visual response; *Middle*: neurons with both a visual (VIS) and a presaccadic burst (PSB); *Bottom*: neurons with a

PSB but no visual response. The red lines indicate the average baseline rate during fixation; the green lines are the average rate during the delay period after the cue is off. Note that PSB-only neurons do not have an elevated rate during the delay period and that VIS + PSB neurons have a higher elevation than VIS-only neurons. (Data from Friedman et al., 1997.)

BASIS OF PSBs FOR STEP, DEFERRED, AND MEMORY SACCADDES

FEF visual activity. As mentioned earlier, over half of the neurons in FEF are visually responsive. Typically, they have large RFs entirely or predominantly in the contralateral visual hemifield and respond promptly to the appearance of almost any visual stimulus within their RF, with little selectivity for color or form. FEF visual responses do not require overt attention to the stimulus or to the stimulus location, or that the visual stimulus have any functional significance. In general, the only requirement is that the stimulus be in the cell's RF.

Phasic, tonic, and mnemonic visual activities. The strongest visual responses in FEF are the short-lived phasic responses to the initial appearance of visual targets (e.g., Figs. 96.4 and 96.5). The intense phasic responses can serve as both target and trigger for FEF PSB activity in the step-saccade task. This reflects the fact that the initial appearance of a visual target sometimes immediately garners an unwelcome saccade in the deferred-saccade and memory-saccade tasks, and also the fact that saccades in the step-saccade task have significantly shorter latencies relative to tasks in which the trigger to saccade is given long after the initial visual response (e.g., a mean of 236 msec for the step saccades

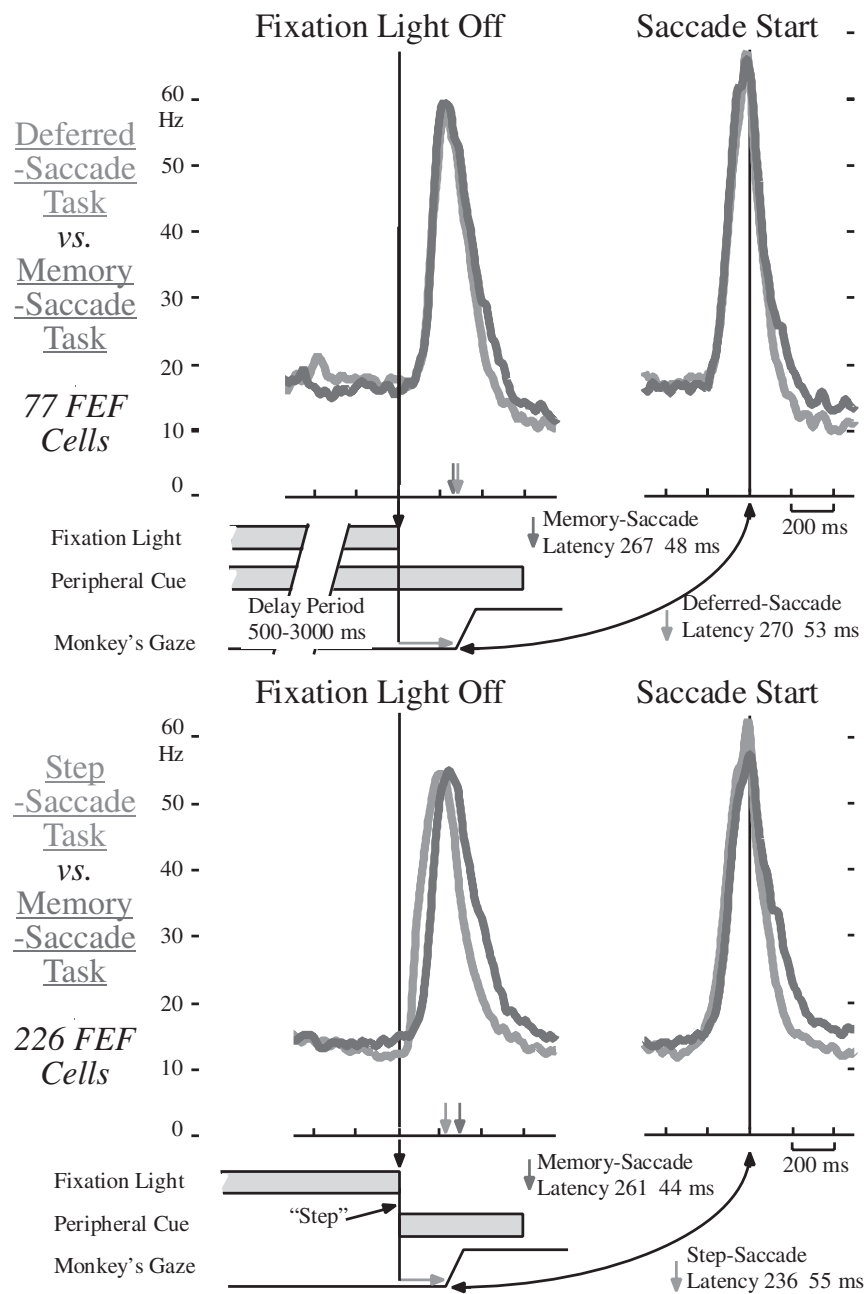


FIGURE 96.7. Comparison of PSB activity in FEF for visually guided saccades with PSB for memory-guided saccades. Histograms are aggregate activity of sets of FEF neurons recorded from six different monkeys during both tasks. *Top*: deferred-saccade task. Shortly after the monkey fixates a central light, a peripheral target appears in the neuron's response field. This target remains on for the remainder of the trial, but no saccade is permitted until the fixation light is extinguished at the end of the delay period. Thus, the target is an established presence at the time of the saccade. *Bottom*: standard step-saccade task. The fixation light is extinguished at the same time that the peripheral target appears. *Left*: histograms aligned on the fixation point's extinction. Note that the deferred-saccade PSB activity has the same latency as the memory-saccade PSB activity, but that the step-saccade response

slightly leads the memory-saccade response; however, the memory saccades themselves have a longer latency than the step saccades. *Right*: histograms aligned on the saccade start. Note that the deferred-saccade PSB has the same magnitude as the memory-saccade PSB activity, but that the step-saccade PSB activity is larger than the memory-saccade response; presumably this reflects the phasic visual response to the appearance of the peripheral target of the VIS + PSB cells in this sample. The number of neurons is smaller than that in the previous figures because (1) only a subset of the 341 cells were tested on both of these two visually guided saccade tasks, and (2) VIS-only cells were omitted from this comparison; only the PSB-only and the VIS + PSB cells were used. (Data from Friedman et al., 1997.)

vs. 270 msec for the deferred saccades for the behavior in Figure 96.5).

Some FEF cells respond phasically only to visual stimuli; however, assuming that a saccade to the stimulus's initial appearance does not occur, other visual cells then discharge tonically, usually at a relatively low rate, for as long as the stimulus remains in their RF (e.g., Fig. 96.4). This tonic FEF visual activity is available to target saccades to established visual targets on the deferred-saccade task when the signal to saccade is finally given.

After the visual cue is extinguished, many FEF cells still have significantly elevated activity during the delay period of the memory-saccade task (e.g., Figs. 96.4 and 96.5). This persistent mnemonic activity provides the targeting information that could underlie the spatially appropriate PSBs that materialize in FEF following the signal to saccade (usually extinction of the fixation light) at the end of the delay period. In Figure 96.6, note that the mnemonic/delay-period rate is most elevated for the combined visual-PSB cells, less elevated for the 58 visual-only cells, and nearly at the baseline level for the 93 PSB-only cells. Thus, FEF mnemonic activity is strongly associated with visual activity but is greatest in those visually responsive cells that also have PSB activity.

Alignment of visual and presaccadic movement fields. Visuomovement FEF cells have both visual and PSB activities, and their visual RF generally corresponds with the optimal saccade vector for their burst (i.e., movement field), as was shown for the cell of Figure 96.4. Moreover, the electrically elicited saccadic eye movement vector obtained at the cell's location generally matches its response fields as well. Thus, the FEF default is a foveating saccade. However, the PSB is independent of the location and/or presence of visual stimulation, particularly as shown by the antisaccade tasks and remapping experiments. Moreover, when carefully tested and fit as the cell in Figure 96.4, some visuomovement FEF cells turn out to be significantly discordant, with nonmatching, or even nonoverlapping, visual and movement fields (Friedman et al., 1998).

AURALLY GUIDED SACCADDES FEF activity also precedes saccades guided by sounds (aurally guided saccades). Russo and Bruce (1994) taught monkeys to make saccades directed to noise from one of eight speakers mounted along a horizontal hoop in front of the monkey. They then tested FEF cells in the dark after arranging the speaker hoop so that one of the speakers directed saccades into the cell's movement field. Figure 96.8 shows a representative FEF cell's response and a scatter plot of the data of all cells tested. In general, the magnitude of each cell's PSB for aurally guided saccades was comparable to its PSB for similar saccades directed to visual or visual-memory targets. Analogous

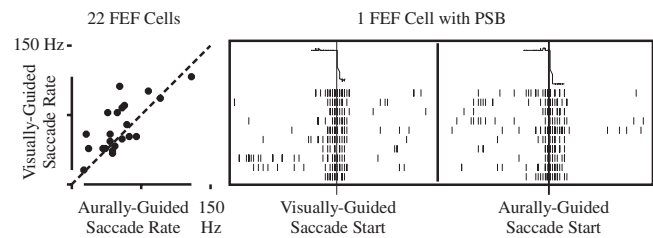


FIGURE 96.8. PSBs of FEF neurons in conjunction with aurally guided saccades. The rasters on the *right* show activity of an FEF neuron preceding visually guided saccades to an LED and preceding identical saccades guided to noise from a speaker at the LED location in the dark. The traces above the rasters show the waveform of representative visually and aurally guided saccades, and the raster lines are aligned on the saccade start. The scatter plot on the *left* shows, for all 22 FEF cells tested, PSB rates for aurally guided saccades versus those for visually guided saccades. (Adapted from Russo and Bruce, 1994.)

burst activity in the SC precedes aurally guided saccades (Jay and Sparks, 1987a).

Remapped FEF auditory activity. Although auditory responses in FEF are infrequent, some cells in and near the medial FEF do respond to sounds (Azuma and Suzuki, 1984; Bruce, 1990; Bruce and Goldberg, 1985; Russo and Bruce, 1989). However, the sound source location is initially given in head-centered coordinates, and it would seem inappropriate to generate PSBs in an oculocentric framework. Interestingly, these auditory RFs in frontal cortex are partially remapped from a craniocentric to an oculocentric framework (Russo and Bruce, 1993), similar to the remapping of SC auditory fields found by Jay and Sparks (1987b).

Such remapping should facilitate the production of appropriate PSB activity for aurally guided saccades. However, this production is complicated by the fact that the monkey's ears move substantially, and these pinna movements have a systematic relation to voluntary eye movements (Bruce et al., 1988). Since pinna orientation strongly affects the magnitude of the sounds reaching the inner ear, accurate remapping of the sound source location to oculocentric coordinates would have to take pinna position, as well as eye position, into account. Interestingly, the macaque has a small pinna movement region of cortex adjacent to the medial (large-saccade) region of the FEF (Burman et al., 1988).

ANTISACCADDES FEF neurons have robust PSBs in conjunction with antisaccades. For most FEF cells, the spiking rates are higher for prosaccades than for antisaccades (Everling and Munoz, 2000); however, a few FEF cells had significantly higher rates for antisaccades. Interestingly, several imaging studies have found that the human FEF is more active during antisaccades than in conjunction with prosac-

cares (e.g., O'Driscoll et al., 1995).⁹ As mentioned earlier, deficits in performing antisaccades are associated with FEF damage.

Everling and Munoz (2000) also found that saccade-related neurons in FEF had lower prestimulus and stimulus-related activity on antisaccade trials compared with prosaccade trials. This provides a plausible FEF mechanism for suppressing the prepotent prosaccade directly to the cue in the antisaccade situation. In fact, suppressing erroneous prosaccades is also a problem for patients with FEF damage (Guitton et al., 1985).

EXPRESS SACCADIC AND PREDICTIVE SACCADIC Dias and Bruce (1994) tested FEF neurons with the gap paradigm, which tends to trigger very short-latency *express* saccades. In the standard gap paradigm, the signal-to-saccade (e.g., fixation light off) precedes the peripheral target appearance by a 200 msec gap in time. It seemed possible that FEF cells might fail to burst *before* short-latency saccades on this paradigm, because Schiller et al. (1987) showed with experimental lesions that the SC is necessary for express saccades and that the FEF is not. However, Dias and Bruce found that all FEF cells with PSB activity still burst prior to short-latency saccades in the gap task. Moreover, approximately one-half of the FEF cells with PSB activity also responded to the gap event itself before the peripheral target came on. This *fixation-disengagement discharge* (FDD) is basically a prediction, as shown in Figure 96.9, because the target appeared in the cell's response field in only half of the trials. Thus, fixation-light extinction induces a moderate discharge of a large population of FEF cells representing a spectrum of possible saccades. This FDD could play a critical role in shortening saccade latency under the gap paradigm (the *gap effect*) by priming the SC (and the FEF) to respond more quickly and strongly upon the arrival of the peripheral visual signal informing which saccade to make. Moreover, these data indicate that FEF has a role in disengagement of fixation before saccades. It also indicates a powerful mechanism for quickly suppressing inappropriate FDD activity when a saccade outside the cell's movement field is called for, possibly the same mechanisms that terminate the buildup of PSB activity in order to stop a saccade from being made in the countermanding paradigm (Hanes et al., 1998).

The FDD is similar to the *anticipatory* discharge phenomenon: ~20% of FEF cells with PSB activity have an augmented discharge during fixation in a saccade task com-

pared to identical fixation in a nonsaccade task (Bruce and Goldberg, 1985). However, the FDD is a more robust response and is found on a much larger percentage of FEF cells. Furthermore, anticipatory activity is spatially selective in that it anticipates impending saccades into the cells' movement field, not just any impending saccade, whereas the FDD seems to involve disengagement of the current fixation prior to spatial specification of the saccade vector.

Fixation status signals (tonic foveation and eye position activity). The FEF cells that respond in relation to fixation or foveal stimulation could trigger both the FDD and PSB. One such type is excited by fixation (foveal) stimulation; these cells could play a role in suppressing activity in FEF and elsewhere in the interest of maintaining fixation. Another class has the inverse activity, being suppressed by foveal stimulation and spiking in response to extinction of the fixation light. Hanes et al. (1998) found that the discharge of FEF fixation neurons exhibited saccade-control properties in the countermanding situation. Moreover, fixation cells in FEF often project to the SC (Segraves and Goldberg, 1987), where their signals could play a role in triggering and suppressing SRB activity there.

Some of these fixation responses are modulated by the current eye position, and a few FEF cells simply respond tonically as a linear function of absolute eye position, for example, azimuth or elevation (Bruce and Goldberg, 1985). Both of these phenomena could be created by an efferent copy signal derived from the common neural integrator in the brainstem. This signal of current eye position may allow the FEF to be somewhat biased against calling for centrifugal saccades that move the eye to extreme orbital positions, and to be biased for centripetal saccades that move the eye closer to a central position in the orbit. An eye position signal could be used to remap sensory locations (see below).

REMAPPED SACCADIC (DOUBLE-STEP SACCADIC TASK) When peripheral lights at two separate locations are each briefly flashed in quick succession such that the second light is already extinguished before the eye has moved at all,¹⁰ primates naturally saccade to the physical location where the first light appeared and then, following a brief fixation period, make a second saccade to the physical location where the second light had appeared (Hallet and Lightstone,

⁹ However, a recent functional magnetic resonance imaging study (Connolly et al., 2000) located antisaccade activation in the human as being slightly anterior to the FEF, as identified by prosaccade activation.

¹⁰ Goldberg and Bruce (1990) typically used a 100 msec duration for the first light followed by a 50 msec duration for the second, as the latency of the first saccade was generally >150 msec.

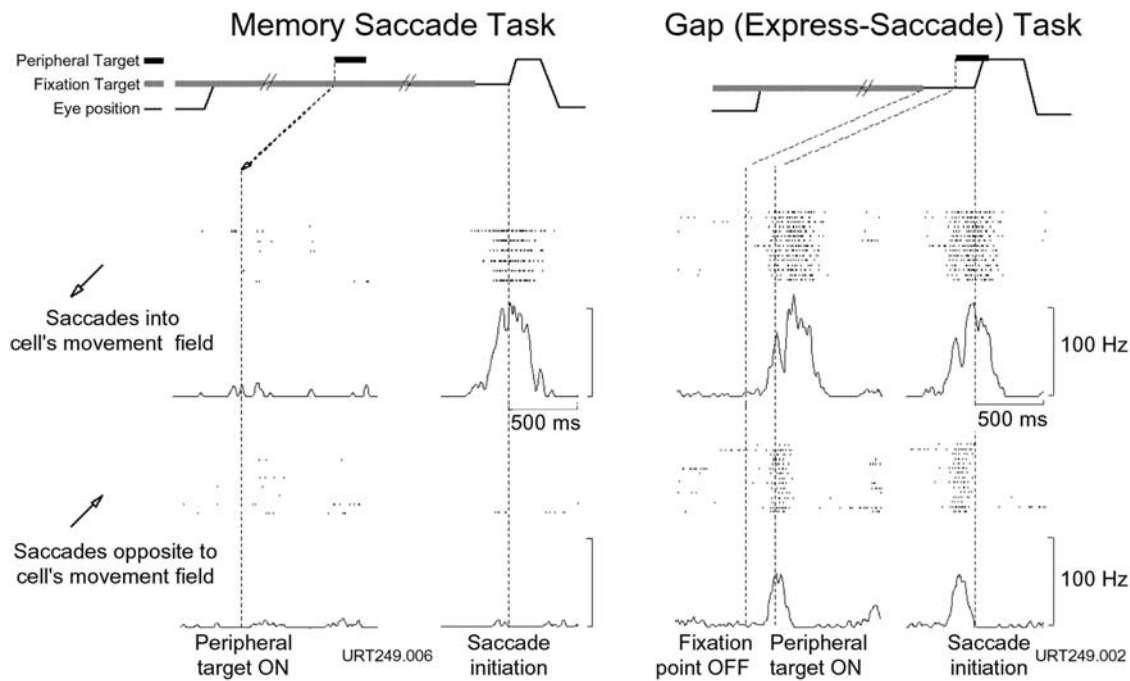


FIGURE 96.9. Activity of an FEF neuron with PSB activity on the memory-saccade task showing an FDD on the gap task. This neuron had no response to visual stimulation (PSB-only cell). *Left*: memory-saccade task. The paradigm is diagrammed at the top. The delay period is ~1 second, and two target locations were randomly interspersed: one in the center of the cell's response field—down and left—and the other opposite the cell's response field—up and right. Raster lines and spike density histograms on the left are aligned to the onset of the peripheral target. Those on the right are aligned to the beginning of the saccade; there is a strong PSB on all trials before saccades into the cell's movement field. *Right*: gap task. As diagrammed at the top, there is a 500-msec gap between the disappearance of the fixation target and the appearance of the peripheral saccadic target. Again, trials into and opposite to the cell's response field were randomly interspersed. The raster-histogram data on the left are aligned in relation to the task

events (disappearance of the fixation target and, 500msec later, appearance of the peripheral target). On the right, the same data are aligned on the saccade initiation. The median saccade latencies for this monkey in the gap task were ~80 msec quicker than for trials in a conventional step-saccade task without a gap (not shown) and over 100 msec quicker than its memory-saccade latency. In the gap task, the cell always had an FDD following the disappearance of the fixation target, but this FDD led into a PSB only when the saccade called for was into the cell's movement field and was sharply suppressed when the saccade was opposite to the cell's movement field. Note that there is no corresponding response to the disappearance of the fixation light in the memory-saccade task for trials opposite the cell's movement field, showing that the FDD is not simply a foveal off response. (Adapted from Dias and Bruce, 1994.)

1976).¹¹ This behavior is remarkable in that the vector of the second saccade is radically different from the vector from the fovea to the second light that the visual system registered. Mays and Sparks (1980) found that SC cells whose movement field matched the second saccade vector were usually very active in this situation, even though the visual cells in the superficial layers directly above them had not been visually activated. When FEF cells with PSB activity are tested (Goldberg and Bruce, 1990), a similar result obtains. Thus, PSBs in both FEF and SC "perform" the double-step saccade task.¹²

Remapped visual activity. Goldberg and Bruce (1990) hypothesized that a subtraction operation within FEF uses an efferent copy of the first saccade to remap FEF visual activity evoked by the second light to be suitable for guiding the second saccade (see also Bickle et al., 2000; Bruce, 1990;

Umeno and Goldberg, 1997, 2001). In other words, visual activity in FEF is initially given in retinal coordinates but is remapped by saccades to maintain its oculocentric validity. Similar remapping of visual activity is prominent in PEF (Colby and Goldberg, 1999), and PEF may be critical for the double-step situation (e.g., Duhmael et al., 1992).

¹¹ In early versions of the double-step saccade task, the second light appeared before the eye moved, but it remained on for the remainder of the trial. Westheimer, Wheelless, and others used this pulse-step version to study the ballistic nature of saccades. Hallet and Lightstone subsequently introduced the critical version wherein the second light flashes only briefly, and thereby completely disassociates the second visual vector from the second saccade vector.

¹² However, neither FEF nor SCs are critical for performing the double-step saccade task, and some reports indicate that PEF is the most important oculomotor structure for the remapping involved.

FEF postsaccadic activity codes the last saccade (efferent copy). Postsaccadic activity in FEF was first described by Bizzi (1967, 1968), and ~25% of FEF neurons are excited *after* particular saccadic eye movements (Bruce and Goldberg, 1985). This postsaccadic activity seems to represent an efferent copy of saccades actually executed, as it reliably follows all types of saccades made into the cell's postsaccadic movement field, even spontaneous saccades made in the dark or quick phases of nystagmus. An efferent copy of saccadic displacements, as coded by postsaccadic activity in FEF, is critical for several purposes. Interestingly, many FEF cells with presaccadic (visual, PSB, or both) activity often have postsaccadic activity for saccades directed opposite their presaccadic response fields. This reciprocity provides a mechanism for readily returning to the previous fixation (i.e., glances).

General suppression of presaccadic activities by saccade execution. A striking aspect of FEF presaccadic activity of all types (e.g., anticipatory, visual, mnemonic, and PSB) is that it quickly ends upon the execution of a saccade into the RF. Note in Figure 96.4 and in all the aggregate histogram figures that saccade execution actively ends the PSB shortly after the saccade, and often the postsaccadic rate goes well below baseline. Control experiments (Bruce, 1990) show postsaccadic suppression of both visual and mnemonic activities as well.

This suppression could come from the postsaccadic coding of prior saccades (efferent copy) just described. Such suppression is very important, because visual or mnemonic activity coding a peripheral cue location becomes misleading once the monkey foveates the peripheral location. Without prompt suppression, persistent activity could lead to multiple triggering of the same saccade, much like the "staircase" of saccades evoked by continued electrical stimulation in FEF. Bruce (1990) suggested that this suppression could be conceptualized as a single-step case of the efferent copy subtraction operation hypothesized to remap visual stimulus signals in FEF in the double-step paradigm, and thereby underlie double-step task behavior and physiology described earlier. Thus, the double-step behavior, the glance, and the virtue of not making multiple saccades in response to a single stimulus step may all reflect the same global transformation of FEF activity effected by the postsaccadic activity it receives following each saccade that is executed.

SACCADES TO MOVING TARGETS Saccades to rapidly moving targets are usually directed at a predicted target location, based on both the target's retinal position and its velocity as perceived 100 msec or so before the saccade starts. The PSBs of some FEF neurons evidence this velocity-predictive process, indicating that target motion information is being

utilized (Shi et al., 1995) and also that some visual activity in FEF was remapped by target velocity, which could provide targeting for the predictive PSB activity. Interestingly, the SC does not seem to provide such a predictive signal (Keller et al., 1996).

SACCADES BASED ON SELECTING FROM AMONG MULTIPLE TARGETS The paradigms discussed thus far show a single peripheral target at only one location (at a time), and therefore there is little ambiguity about the correct saccade vector. Testing FEF cells with paradigms that require a monkey to select the saccade target from among two or more concurrently seen peripheral targets shows profound effects of multiple targets and of target search and selection on visual activity in FEF (Schall and Hanes, 1993; Schall et al., 1995; Thompson et al., 1996, 1997). Nevertheless, FEF cells having PSBs respond reliably in relation to these complex volitional saccades matching the cell's movement field. Similarly, Shi et al. (1998b, 2000) found that FEF cells with PSB activity reliably burst before correctly performed saccades to targets in their response fields during a color match-to-sample memory task, even though the visual response to the RF target was far smaller whenever an alternative target simultaneously appeared in the opposite hemifield, as compared to control trials which presented only the correct target.

The oldest hypothesis is that FEF (and other structures) could select a stimulus to be a saccade target by somehow "enhancing" the intrinsic visual responses to that stimulus (e.g., Goldberg and Bushnell, 1991; Wurtz and Mohler, 1976). Moreover, when monkeys view a complex scene with natural scanning, enhanced visual responses effectively predict the next saccadic eye movement (Burman and Segraves, 1994). However, recent studies (Kodaka et al., 1997; Murthy et al., 2001) found that enhancement and selection of visual activity in FEF can be independent of eye movements and saccade programming. Similarly, Hanes et al. (1998) reported that FEF's visual activity did not predict or control the countermanding of saccades.

SUMMARY OF FEF SACCADE-RELATED ACTIVITIES AND PHENOMENON In conclusion, a diverse set of functional activities and cortical circuits underlie FEF's programming of purposive saccades in the monkey. These serve to facilitate the generation of appropriate PSBs in diverse situations and paradigms. In this respect, there is a more philosophical implication, beyond the realm of saccade latencies. Even though some FEF activity is firmly based on physical facts (visual stimuli, auditory stimuli, etc.), FEF PSB activity is neither a motor response nor a transformed or enhanced sensory response. It is more a motor prediction or guess based on the possibility and probability that a saccade into the cell's response field may or should soon happen

(Hasegawa et al., 2000). Human FEF is very active in conjunction with predictive saccades (O'Driscoll et al., 2000).

Bruce (1998) explored neural network models of FEF focusing on the generation of PSB activity. A small set of inputs represented FEF visual activity (eight peripheral and one foveal) in response to visual task events, and eight additional inputs provided postsaccadic corollary discharge input following saccadic events. These inputs went to a randomly connected two-layer Elman network with 32 hidden neurons. The network was trained using backpropagation, with the goal of having its eight output neurons learn to mimic PSB activity in FEF, each for a different optimal direction (0, 45, 90, 135, 180, etc.). The step-saccade, deferred-saccade, and memory-guided saccade paradigms were intermingled during training, with delays and target durations and locations varied over large ranges. This simple network learned to generate appropriate PSBs in the output neurons for all three paradigms. Hidden neurons had different combinations of visual, movement, and mnemonic activity with a variety of response fields. It is not known if such a simple network can learn to generate FEF-like PSBs for all the types of saccades reviewed earlier (e.g., express saccades, double-step saccades, antisaccades).

FEF and smooth pursuit eye movements

Smooth pursuit eye movements are the smooth, relatively slow (up to 100°/s) eye movements used to track moving targets. As was shown in Figure 96.2, the smooth pursuit zone of the macaque FEF (FEFsem) lies principally in the fundus of the arcuate sulcus. Microstimulation in FEFsem elicits smooth eye movements (usually ipsiversive) at fairly low thresholds. Discrete inactivation within FEFsem causes dramatic but reversible deficits in ipsiversive pursuit (Shi et al., 1998a), and unilateral FEF lesions that include the fundus cause profound and permanent pursuit deficits (Keating, 1991; Lynch, 1987; MacAvoy et al., 1991) even though the optokinetic reflex is not diminished by bilateral FEF ablation (Keating et al., 1996). Interestingly, schizophrenic patients show deficits in smooth pursuit (but normal optokinetic following); this deficit further implicates frontal lobe dysfunction as an underlying factor in schizophrenia (e.g., MacAvoy and Bruce, 1995; Sweeney et al., 1998).

As indicated in Figure 96.1, the smooth pursuit part of the human FEF is in the same relation to the saccadic FEF (Berman et al., 1999; Blanke et al., 2000; O'Driscoll et al., 2000; Petit et al., 1997; Rosano et al., 2002). Humans also show deficits in ipsiversive pursuit following damage to the FEF region.

SENSORY-TO-MOTOR TRANSFORMATION FOR SMOOTH PURSUIT
Neurons throughout the pursuit pathway have been studied

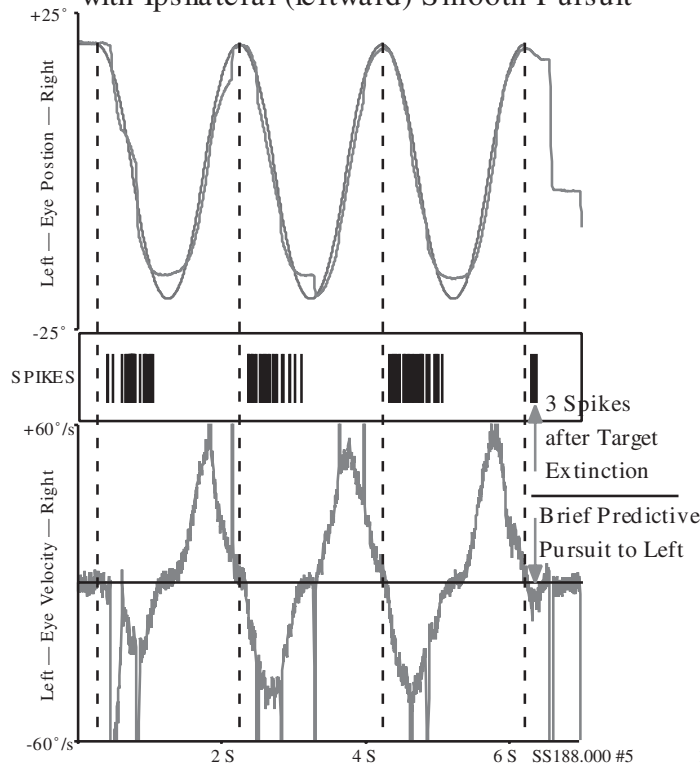
in the rhesus monkey. Similar to the saccadic system, neuronal activity in structures closer to the retina has obligatory responses to visual stimuli, but closer to the oculomotor nuclei the neural activity is more closely aligned with motor behavior. For example, most neurons in V5 are selective for the direction of stimulus motion that is not tracked. At the motor end, the smooth eye-velocity signal is elaborated in several pontocerebellar circuits, including the dorsolateral and the medial pontine nucleus and the nucleus reticularis tegmenti pontis, together with cerebellar pursuit areas: the flocculus, paraflocculus, and dorsal vermis. Many neurons in these structures respond as a fairly direct function of pursuit velocity.

The critical step in this sensorimotor transformation underlying pursuit is provided by neurons that respond to target motion, but *only* (or principally) when and if the target is *selected* for foveation/pursuit. The smooth pursuit zone of FEF is a candidate site. It lies downstream from V5 and other areas that provide most of the visual motion information for smooth pursuit but upstream from pontocerebellar and brainstem circuits that effect smooth pursuit movements (Fig. 96.3), (Stanton et al., 1998). Many FEF pursuit cells discharge to the motion of a pursuit target in a particular direction over nearly all of the visual field, but discharge remarkably little to targets moving in the same direction that are not pursued (Fukushima et al., 2000; Gottlieb et al., 1993, 1994; MacAvoy et al., 1991; Tanaka and Fukushima, 1998; Tanaka and Lisberger, 2001). Figure 96.10 shows such a neuron and the pursuit deficit caused by discrete inactivation at the site of that neuron. Interestingly, fMRI data in humans indicate that FEF and PEF are strongly activated by attentive tracking of moving targets (over their activation during passive viewing of the same visual motion), but the posterior temporal motion areas such as V5 are not rendered more active in the tracking condition (Culham et al., 1998).

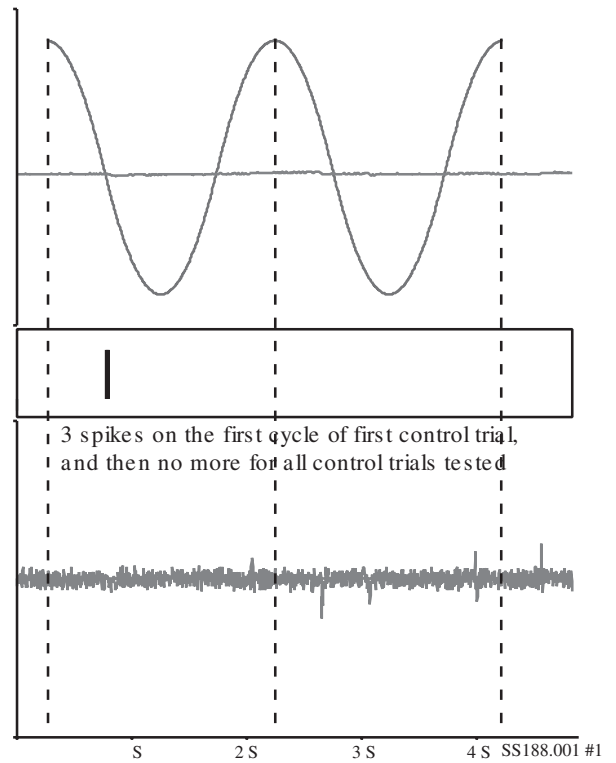
FEF and disjunctive eye movements

Gamlin and Yoon (2000) found elicited vergence eye movements and neuronal responses during natural vergence movements in a small region of macaque cortex between the posterior tip of the principal sulcus and the FEF boundary at the anterior lip of the arcuate sulcus. In general, these phenomena involved purely vergence movements without saccades, and the authors concluded that this region should be regarded as a vergence (and accommodation) zone of FEF. Ferraina et al. (2000) found that visual responses throughout FEF were generally selective for binocular disparity, with a range of crossed and uncrossed disparities coded across cells. Their finding raises the possibility that the FEF may command suitably disjunctive saccades whenever the target is at a different depth than the fixation point.

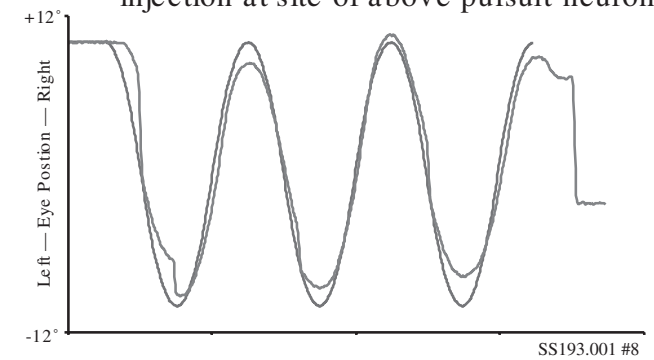
FEF Unit Responsive in conjunction with Ipsilateral (leftward) Smooth Pursuit



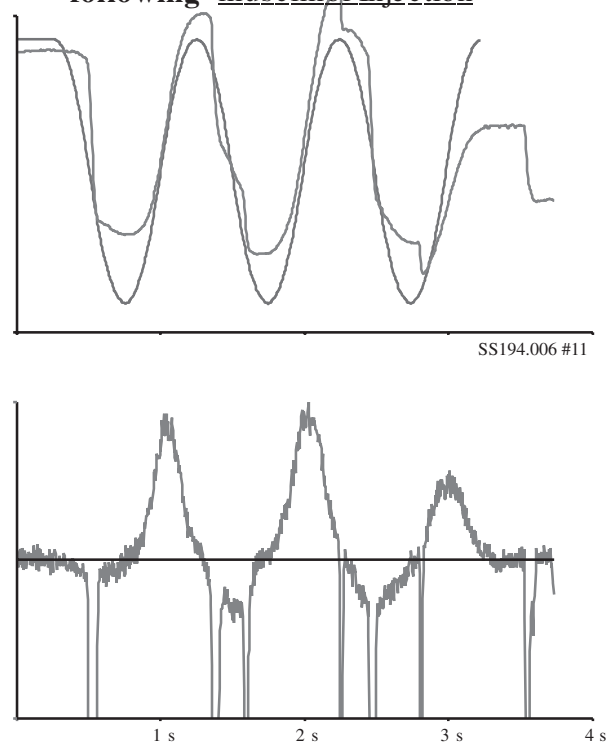
Not Responsive to Motion-only Control



Good Pursuit prior to muscimol injection at site of above pursuit neuron



Deficient Ipsilateral Pursuit following muscimol Injection



Summary

Eye movements require the integration of a diverse spectrum of physiological activities: sensory, motor, efferent copy, mnemonic, predictive, and cognitive. Physiological correlates of all of these activities have been identified in the primate FEF. This allows the FEF to serve as a model system of sensorimotor integration in the cerebral cortex. In humans, the frontal lobes are crucial for executing short- and long-range plans and complex coordinated behaviors by sustaining multiple specific and general goals while processing information, actions, and even thoughts directed at achieving. Parallels between such complex human behaviors and certain oculomotor behaviors suggest that understanding the physiological mechanisms of FEF function in such oculomotor situations could provide a basis for consideration of the neural mechanisms underlying more complex aspects of human frontal lobe function.

REFERENCES

- Azuma, M., and H. Suzuki, 1984. Properties and distribution of auditory neurons in the dorsolateral prefrontal cortex of the alert monkey, *Brain Res.*, 298:343–346.
- Berman, R. A., C. L. Colby, C. R. Genovese, J. T. Voyvodic, B. Luna, K. R. Thulborn, and J. A. Sweeney, 1999. Cortical networks subserving pursuit and saccadic eye movements in humans: an fMRI study, *Hum Brain Mapp.*, 8:209–225.
- Bickle, J., C. Worley, and M. Bernstein, 2000. Vector subtraction implemented neurally: a neurocomputational model of some sequential cognitive and conscious processes, *Conscious. Cogn.*, 9:117–144.
- Bizzi, E., 1967. Discharge of frontal eye field neurons during eye movements in unanesthetized monkeys, *Sci. Wash. DC*, 157:1588–1590.
- Bizzi, E., 1968. Discharge of frontal eye field neurons during saccadic and following eye movements in unanesthetized monkeys, *Exp. Brain Res.*, 6:69–80.
- Blanke, O., L. Spinelli, G. Thut, C. M. Michel, S. Perrig, T. Landis, and M. Seeck, 2000. Location of the human frontal eye field as defined by electrical cortical stimulation: anatomical, functional and electrophysiological characteristics, *NeuroReport*, 11:1907–1913.
- Bruce, C. J., 1990. Integration of sensory and motor signals for saccadic eye movements in the primate frontal eye fields, in *Signal and Sense, Local and Global Order in Perceptual Maps* (G. M. Edelman, W. E. Gall, and W. M. Cowan, eds.), New York: Wiley-Liss, pp. 261–314.
- Bruce, C. J., 1998. Neural network model of the frontal eye field capable of visually guided and memory-guided saccades, *Soc. Neurosci. (Abs.)*, 24:521.
- Bruce, C. J., and J. A. Borden, 1986. The primate frontal eye fields are necessary for predictive saccadic tracking, *Soc. Neurosci. (Abs.)*, 12:1086.
- Bruce, C. J., D. Burman, M. G. MacAvoy, and G. S. Russo, 1988. Changes in pinna orientation accompany shifts in direction of gaze in monkeys, *Soc. Neurosci. (Abs.)*, 14:957.
- Bruce, C. J., and H. R. Friedman, 2002. Eye movements, in *Encyclopedia of the Human Brain* (V. S. Ramachandran, ed.), New York: Academic Press.
- Bruce, C. J., and M. E. Goldberg, 1984. Physiology of the frontal eye fields, *Trends Neurosci.*, 7:436–441.
- Bruce, C. J., and M. E. Goldberg, 1985. Primate frontal eye fields. I. Single neurons discharging before saccades, *J. Neurophysiol.*, 53:603–635.
- Bruce, C. J., M. E. Goldberg, M. C. Bushnell, and G. B. Stanton, 1985. Primate frontal eye fields. II. Physiological and anatomical correlates of electrically evoked eye movements, *J. Neurophysiol.*, 54:714–734.
- Burman, D. D., C. J. Bruce, and G. S. Russo, 1988. Pinna movements elicited by microstimulation in the prefrontal cortex of monkeys, *Soc. Neurosci. (Abs.)*, 14:208.
- Burman, D. D., and M. A. Segraves, 1994. Primate frontal eye field activity during natural scanning eye movements, *J. Neurophysiol.*, 71:1266–1271.
- Carpenter, R. H. S., 1988. *Movements of the Eyes*, 2nd ed., London: Pion.
- Colby, C. L., and M. E. Goldberg, 1999. Space and attention in parietal cortex, *Annu. Rev. Neurosci.*, 22:319–349.
- Connolly, J. D., M. A. Goodale, J. F. Desouza, R. S. Menon, and T. Vilis, 2000. A comparison of frontoparietal fMRI activation during anti-saccades and anti-pointing, *J. Neurophysiol.*, 84:1645–1655.
- Crosby, E. C., R. E. Yoss, and J. W. Henderson, 1952. The mammalian midbrain and isthmus regions. II. The fiber connections. D. The pattern for eye movements on the frontal eye field and the discharge of specific portions of this field to and through midbrain levels, *J. Comp. Neurol.*, 97:357–383.
- Culham, J. C., S. A. Brandt, P. Cavanagh, N. G. Kanwisher, A. M. Dale, and R. B. Tootell, 1998. Cortical fMRI activation produced by attentive tracking of moving targets, *J. Neurophysiol.*, 80:2657–2670.
- Dias, E. C., and C. J. Bruce, 1994. Physiological correlate of fixation disengagement in the primate's frontal eye field, *J. Neurophysiol.*, 72:2532–2537.

FIGURE 96.10. Activity of FEF pursuit neuron and pursuit deficits after FEF deactivation. *Top left:* the pursuit neuron, recorded in the left hemisphere FEF, was active in conjunction with leftward (negative moving on the traces) smooth pursuit, responded throughout the leftward phase in all three cycles of sinusoidal motion (0.5 Hz), and discharged prior to leftward predictive pursuit that occurred at the end of each sinusoidal tracking trial. *Top right:* the neuron responded very little to visual motion that was not pursued and was completely silent, except for three spikes on the initial cycle, when

the monkey fixated a stationary point while viewing the same sinusoidally moving stimulus. *Bottom left:* normal sinusoidal (1.0 Hz) smooth pursuit of this monkey immediately before the injection. *Bottom right:* poor smooth pursuit immediately following a small muscimol injection at the site of the pursuit neuron shown above. Leftward smooth eye velocity was lower on every cycle, especially the first, and there was no more predictive pursuit after the target extinguished. (Adapted with permission from Shi et al., 1998a.)

- Dias, E. C., M. Kiesau, and M. A. Segraves, 1995. Acute activation and inactivation of macaque frontal eye field with GABA-related drugs, *J. Neurophysiol.*, 74:2744–2748.
- Dias, E. C., and M. A. Segraves, 1999. Muscimol-induced inactivation of monkey frontal eye field: effects on visually and memory-guided saccades, *J. Neurophysiol.*, 81:2191–2214.
- Duhamel, J.-R., M. E. Goldberg, E. J. FitzGibbon, A. Sirigu, and J. Grafman, 1992. Saccadic dysmetria in a patient with a right frontoparietal lesion. The importance of corollary discharge for accurate spatial behaviour, *Brain*, 115:1387–1402.
- Edelman, J. A., and M. E. Goldberg, 2001. Dependence of saccade-related activity in the primate superior colliculus on visual target presence, *J. Neurophysiol.*, 86:676–691.
- Everling, S., and D. P. Munoz, 2000. Neuronal correlates for preparatory set associated with pro-saccades and anti-saccades in the primate frontal eye field, *J. Neurosci.*, 20:387–400.
- Felleman, D. J., and D. C. Van Essen, 1991. Distributed hierarchical processing in the primate cerebral cortex, *Cereb. Cortex*, 1:1–47.
- Ferraina, S., M. Paré, and R. H. Wurtz, 2000. Disparity sensitivity of frontal eye field neurons, *J. Neurophysiol.*, 83:625–629.
- Ferrier, D., 1876. *The Functions of the Brain*, London: Smith, Elder, & Co.
- Friedman, H. R., D. D. Burman, G. S. Russo, E. C. Dias, G. B. Stanton, D. Shi, and C. J. Bruce, 1997. Neuronal activity in primate frontal eye field during memory-guided saccades, *Soc. Neurosci. (Abs.)*, 23:844.
- Friedman, H. R., D. D. Burman, D. Shi, and C. J. Bruce, 1998. Independence of visual and movement response fields of visuo-movement cells in monkey frontal eye field, *Soc. Neurosci. (Abs.)*, 24:522.
- Fukushima, K., T. Sato, J. Fukushima, Y. Shinmei, and C. R. S. Kaneko, 2000. Activity of smooth pursuit-related neurons in the monkey periarculate cortex during pursuit and passive whole-body rotation, *J. Neurophysiol.*, 83:563–587.
- Funahashi, S., C. J. Bruce, and P. S. Goldman-Rakic, 1989. Mnemonic coding of visual space in the monkey's dorsolateral prefrontal cortex, *J. Neurophysiol.*, 61:331–349.
- Gamlin, P. D., and K. Yoon, 2000. An area for vergence eye movement in primate frontal cortex, *Nature*, 407:1003–1007.
- Gaymard, B., C. J. Ploner, S. Rivaud-Pechoux, and C. Pierrot-Deseilligny, 1999. The frontal eye field is involved in spatial short-term memory but not in reflexive saccade inhibition, *Exp. Brain Res.*, 129:288–301.
- Glimcher, P. W., and D. L. Sparks, 1993. Representation of averaging saccades in the superior colliculus of the monkey, *Exp. Brain Res.*, 95:429–435.
- Goldberg, M. E., and C. J. Bruce, 1990. Primate frontal eye fields. III. Maintenance of a spatially accurate saccade signal, *J. Neurophysiol.*, 64:489–508.
- Goldberg, M. E., and M. C. Bushnell, 1981. Behavioral enhancement of visual responses in monkey cerebral cortex. II. Modulation in frontal eye fields specifically related to saccades, *J. Neurophysiol.*, 46:773–787.
- Gottlieb, J. P., C. J. Bruce, and M. G. MacAvoy, 1993. Smooth eye movements elicited by microstimulation in the primate frontal eye field, *J. Neurophysiol.*, 69:786–799.
- Gottlieb, J. P., M. G. MacAvoy, and C. J. Bruce, 1994. Neural responses related to smooth-pursuit eye movements and their correspondence with electrically elicited smooth eye movements in the primate frontal eye field, *J. Neurophysiol.*, 72:1634–1653.
- Guitton, D., H. A. Buchtel, and R. M. Douglas, 1985. Frontal lobe lesions in man cause difficulties in suppressing reflexive glances and in generating goal-directed saccades, *Exp. Brain Res.*, 58:455–472.
- Hallett, P. E., and A. D. Lightstone, 1976. Saccadic eye movements to flashed targets, *Vis. Res.*, 16:107–114.
- Hanes, D. P., W. F. Patterson, and J. D. Schall, 1998. Role of frontal eye fields in countermanding saccades: visual, movement, and fixation activity, *J. Neurophysiol.*, 79:817–834.
- Hanes, D. P., and R. H. Wurtz, 2001. Interaction of the frontal eye field and superior colliculus for saccade generation, *J. Neurophysiol.*, 85:804–815.
- Hasegawa, R. P., A. M. Blitz, N. L. Geller, and M. E. Goldberg, 2000. Neurons in monkey prefrontal cortex that track past or predict future performance, *Sci. Wash. DC*, 290:1786–1789.
- Hepp, K., and V. Henn, 1983. Spatio-temporal recoding of rapid eye movement signals in the monkey paramedian pontine reticular formation (PPRF), *Exp. Brain Res.*, 52:105–120.
- Hikosaka, O., M. Sakamoto, and S. Usui, 1989. Functional properties of monkey caudate neurons. III. Activities related to expectation of target and reward, *J. Neurophysiol.*, 61:814–832.
- Holmes, G., 1938. The cerebral integration of the ocular movements, *Br. Med. J.*, 2:107–112.
- Huerta, M. F., L. A. Krubitzer, and J. H. Kaas, 1986. Frontal eye field as defined by intracortical microstimulation in squirrel monkeys, owl monkeys, and macaque monkeys. I. Subcortical connections, *J. Comp. Neurol.*, 253:415–439.
- Huerta, M. F., L. A. Krubitzer, and J. H. Kaas, 1987. Frontal eye field as defined by intracortical microstimulation in squirrel monkeys, owl monkeys, and macaque monkeys. II. Cortical connections, *J. Comp. Neurol.*, 265:332–361.
- Jacobsen, C. F., 1936. Studies of cerebral function in primates. I. The functions of the frontal association areas in monkeys, *Comp. Psychol. Monogr.*, 13:3–60.
- Jay, M. F., and D. L. Sparks, 1987a. Sensorimotor integration in the primate superior colliculus. I. Motor convergence, *J. Neurophysiol.*, 57:22–34.
- Jay, M. F., and D. L. Sparks, 1987b. Sensorimotor integration in the primate superior colliculus. II. Coordinates of auditory signals, *J. Neurophysiol.*, 57:35–55.
- Keating, E. G., 1991. Frontal eye field lesions impair predictive and visually guided pursuit eye movements, *Exp. Brain Res.*, 86:311–323.
- Keating, E. G., and S. G. Gooley, 1998. Disconnection of parietal and occipital access to the saccadic oculomotor system, *Exp. Brain Res.*, 70:385–398.
- Keating, E. G., A. Pierre, and S. Chopra, 1996. Ablation of the pursuit area in the frontal cortex of the primate degrades foveal but not optokinetic smooth eye movements, *J. Neurophysiol.*, 76:637–641.
- Keller, E. L., N. J. Gandhi, and P. T. Weir, 1996. Discharge of superior collicular neurons during saccades made to moving targets, *J. Neurophysiol.*, 76:3573–3577.
- Kodaka, Y., A. Mikami, and K. Kubota, 1997. Neuronal activity in the frontal eye field of the monkey is modulated while attention is focused on to a stimulus in the peripheral visual field, irrespective of eye movement, *Neurosci. Res.*, 28:291–298.
- Künzle, H., and K. Akert, 1977. Efferent connections of cortical area 8 (frontal eye field) in *Macaca fascicularis*. A reinvestigation using the autoradiographic technique, *J. Comp. Neurol.*, 173:147–164.
- Leigh, R. J., and D. S. Zee, 1999. *The Neurology of Eye Movements*, New York: Oxford University Press.

- Leyton, A. S. F., and C. S. Sherrington, 1917. Observations on the excitable cortex of the chimpanzee, orang-utan, and gorilla, *Q. J. Exp. Physiol.*, 11:135–222.
- Luna, B., K. R. Thulborn, D. P. Munoz, E. P. Merriam, K. E. Garver, N. J. Minschew, M. S. Keshavan, C. R. Genovese, W. F. Eddy, and J. A. Sweeney, 2001. Maturation of widely distributed brain function subserves cognitive development, *NeuroImage*, 13:786–793.
- Lynch, J. C., 1987. Frontal eye field lesions in monkeys disrupt visual pursuit, *Exp. Brain Res.*, 68:437–441.
- MacAvoy, M. G., and C. J. Bruce, 1995. Comparison of the smooth eye tracking disorder of schizophrenics with that of nonhuman primates with specific brain lesions, *Int. J. Neurosci.*, 80:117–151.
- MacAvoy, M. G., J. P. Gottlieb, and C. J. Bruce, 1991. Smooth-pursuit eye movement representation in the primate frontal eye field, *Cereb. Cortex*, 1:95–102.
- Mays, L. E., and D. L. Sparks, 1980. Dissociation of visual and saccade-related responses in superior colliculus neurons, *J. Neurophysiol.*, 43:207–232.
- Mott, F. W., and E. A. Schäfer, 1890. On associated eye movements produced by cortical faradization of the monkey's brain, *Brain*, 13:165–173.
- Murthy, A., K. G. Thompson, and J. D. Schall, 2001. Dynamic dissociation of visual selection from saccade programming in frontal eye field, *J. Neurophysiol.*, 86:2634–2637.
- O'Driscoll, G. A., N. M. Alpert, S. W. Matthysse, D. L. Levy, S. L. Rauch, and P. S. Holzman, 1995. Functional neuroanatomy of antisaccade eye movements investigated with positron emission tomography, *Proc. Natl. Acad. Sci. USA*, 92:925–929.
- O'Driscoll, G. A., A. L. Wolff, C. Benkelfat, P. S. Florencio, S. Lal, and A. C. Evans, 2000. Functional neuroanatomy of smooth pursuit and predictive saccades, *NeuroReport*, 11:1335–1340.
- Penfield, W., and E. Boldrey, 1937. Somatic motor and sensory representation in the cerebral cortex of man as studied by electrical stimulation, *Brain*, 60:389–443.
- Petit, L., V. P. Clark, J. Ingeholm, and J. V. Haxby, 1997. Dissociation of saccade-related and pursuit-related activation in human frontal eye fields as revealed by fMRI, *J. Neurophysiol.*, 77:3386–3390.
- Ploner, C. J., S. Rivaud-Pechoux, B. M. Gaymard, Y. Agid, and C. Pierrot-Deseilligny, 1999. Errors of memory-guided saccades in humans with lesions of the frontal eye field and the dorsolateral prefrontal cortex, *J. Neurophysiol.*, 82:1086–1090.
- Robinson, D. A., and A. F. Fuchs, 1969. Eye movements evoked by stimulation of frontal eye fields, *J. Neurophysiol.*, 32:637–648.
- Rosano, C., C. M. Krisky, J. S. Welling, W. F. Eddy, B. Luna, K. R. Thulborn, and J. A. Sweeney, 2002. Pursuit and saccadic eye movement subregions in human frontal eye field: a high-resolution fMRI investigation, *Cereb. Cortex*, 12:107–115.
- Russo, G. S., and C. J. Bruce, 1989. Auditory receptive fields of neurons in frontal cortex of rhesus monkey shift with direction of gaze, *Soc. Neurosci. (Abs.)*, 15:1204.
- Russo, G. S., and C. J. Bruce, 1993. Effect of eye position within the orbit on electrically elicited saccadic eye movements: a comparison of the macaque monkey's frontal and supplementary eye fields, *J. Neurophysiol.*, 69:800–818.
- Russo, G. S., and C. J. Bruce, 1994. Frontal eye field activity preceding aurally guided saccades, *J. Neurophysiol.*, 71:1250–1253.
- Russo, G. S., and C. J. Bruce, 2000. Supplementary eye field: representation of saccades and relationship between neural response fields and elicited eye movements, *J. Neurophysiol.*, 84:2605–2621.
- Schall, J. D., 1991. Neuronal activity related to visually guided saccades in the frontal eye fields of rhesus monkeys: comparison with supplementary eye fields, *J. Neurophysiol.*, 66:559–579.
- Schall, J. D., and D. P. Hanes, 1993. Neural basis of saccade target selection in frontal eye field during visual search, *Nature*, 366:467–469.
- Schall, J. D., D. P. Hanes, K. G. Thompson, and D. J. King, 1995. Saccade target selection in frontal eye field of macaque. I. Visual and premovement activation, *J. Neurosci.*, 15:6905–6918.
- Schiller, P. H., and I. H. Chou, 1998. The effects of frontal eye field and dorsomedial frontal cortex lesions on visually guided eye movements, *Nature Neurosci.*, 1:248–253.
- Schiller, P. H., and I. H. Chou, 2000a. The effects of anterior arcuate and dorsomedial frontal cortex lesions on visually guided eye movements in the rhesus monkey: 1. Single and sequential targets, *Vis. Res.*, 40:1609–1626.
- Schiller, P. H., and I. H. Chou, 2000b. The effects of anterior arcuate and dorsomedial frontal cortex lesions on visually guided eye movements: 2. Paired and multiple targets, *Vis. Res.*, 40:1627–1638.
- Schiller, P. H., J. H. Sandell, and J. H. R. Maunsell, 1987. The effect of frontal eye field and superior colliculus lesions on saccadic latencies in the rhesus monkey, *J. Neurophysiol.*, 57:1033–1049.
- Schiller, P. H., S. D. True, and J. L. Conway, 1980. Deficits in eye movements following frontal eye-field and superior colliculus ablations, *J. Neurophysiol.*, 44:1175–1189.
- Schlag, J., and M. Schlag-Rey, 1987. Evidence for a supplementary eye field, *J. Neurophysiol.*, 57:179–200.
- Scudder, C. A., C. R. S. Kaneko, and A. F. Fuchs, 2002. The brainstem burst generator for saccadic eye movements: a modern synthesis, *Exp. Brain Res.*, 142:439–462.
- Segraves, M. A., 1992. Activity of monkey frontal eye field neurons projecting to oculomotor regions of the pons, *J. Neurophysiol.*, 68:1967–1985.
- Segraves, M. A., and M. E. Goldberg, 1987. Functional properties of corticotectal neurons in the monkey's frontal eye field, *J. Neurophysiol.*, 58:1387–1419.
- Segraves, M. A., and K. Park, 1993. The relationship of monkey frontal eye field activity to saccade dynamics, *J. Neurophysiol.*, 69:1880–1889.
- Shi, D., H. R. Friedman, and C. J. Bruce, 1995. Frontal eye field activity in conjunction with saccades made in response to step-ramp motion, *Soc. Neurosci. (Abs.)*, 21:1195.
- Shi, D., H. R. Friedman, and C. J. Bruce, 1998a. Deficits in smooth-pursuit eye movements after muscimol inactivation within the primate's frontal eye field, *J. Neurophysiol.*, 80:458–464.
- Shi, D., H. R. Friedman, and C. J. Bruce, 1998b. Neural activity associated with saccade target selection in the primate frontal eye field, *Soc. Neurosci. (Abs.)*, 24:1146.
- Shi, D., H. R. Friedman, and C. J. Bruce, 2000. Differentiated initial neural response in visual guided selection in frontal eye field of primate, *Soc. Neurosci. (Abs.)*, 26:0.
- Shibutani, H., H. Sakata, and J. Hyvärinen, 1984. Saccade and blinking evoked by microstimulation of the posterior parietal association cortex of the monkey, *Exp. Brain Res.*, 55:1–8.
- Sommer, M. A., and E. J. Tehovnik, 1997. Reversible inactivation of macaque frontal eye field, *Exp. Brain Res.*, 116:229–249.
- Sommer, M. A., and R. H. Wurtz, 2000. Composition and topographic organization of signals sent from the frontal eye field to the superior colliculus, *J. Neurophysiol.*, 83:1979–2001.

- Sommer, M. A., and R. H. Wurtz, 2001. Frontal eye field sends delay activity related to movement, memory, and vision to the superior colliculus, *J. Neurophysiol.*, 85:1673–1685.
- Sparks, D. L., E. G. Freedman, L. L. Chen, and N. J. Gandhi, 2001. Cortical and subcortical contributions to coordinated eye and head movements, *Vis. Res.*, 41:3295–3305.
- Stanton, G. B., C. J. Bruce, and M. E. Goldberg, 1993. Topography of projections to the frontal lobe from the macaque frontal eye fields, *J. Comp. Neurol.*, 330:286–301.
- Stanton, G. B., C. J. Bruce, and M. E. Goldberg, 1995. Topography of projections to posterior cortical areas from the macaque frontal eye fields, *J. Comp. Neurol.*, 353:291–305.
- Stanton, G. B., S.-Y. Deng, M. E. Goldberg, and N. T. McMullen, 1989. Cytoarchitectural characteristic of the frontal eye fields in macaque monkeys, *J. Comp. Neurol.*, 282:415–427.
- Stanton, G. B., H. R. Friedman, E. C. Dias, and C. J. Bruce, 1998. Cortical afferents to the smooth-pursuit eye movement region of the macaque frontal eye field, *Soc. Neurosci. (Abs.)*, 24:1146.
- Stanton, G. B., M. E. Goldberg, and C. J. Bruce, 1988b. Frontal eye field efferents in the macaque monkey: II. Topography of terminal fields in midbrain and pons, *J. Comp. Neurol.*, 271:493–506.
- Sweeney, J. A., B. Luna, N. M. Srinivasagam, M. S. Keshavan, N. R. Schooler, G. L. Haas, and J. R. Carl, 1998. Eye tracking abnormalities in schizophrenia: evidence for dysfunction in the frontal eye fields, *Biol. Psychiatry*, 44:698–708.
- Tanaka, M., and K. Fukushima, 1998. Neuronal responses related to smooth pursuit eye movements in the periarculate cortical area of monkeys, *J. Neurophysiol.*, 80:28–47.
- Tanaka, M., and S. G. Lisberger, 2001. Regulation of the gain of visually guided smooth-pursuit eye movements by frontal cortex, *Nature*, 409:191–194.
- Thompson, K. G., N. P. Bichot, and J. D. Schall, 1997. Dissociation of visual discrimination from saccade programming in macaque frontal eye field, *J. Neurophysiol.*, 77:1046–1050.
- Thompson, K. G., D. P. Hanes, N. P. Bichot, and J. D. Schall, 1996. Perceptual and motor processing stages identified in the activity of macaque frontal eye field neurons during visual search, *J. Neurophysiol.*, 76:4040–4055.
- Tu, T. A., and E. G. Keating, 2000. Electrical stimulation of the frontal eye field in a monkey produces combined eye and head movements, *J. Neurophysiol.*, 84:1103–1106.
- Umeno, M. M., and M. E. Goldberg, 1997. Spatial processing in the monkey frontal eye field. I. Predictive visual responses, *J. Neurophysiol.*, 78:1373–1383.
- Umeno, M. M., and M. E. Goldberg, 2001. Spatial processing in the monkey frontal eye field. II. Memory responses, *J. Neurophysiol.*, 86:2344–2352.
- Wagman, I. H., H. P. Krieger, C. A. Papatheodorou, and M. B. Bender, 1961. Eye movements elicited by surface and depth stimulation of the frontal lobe of *Macaca mulatta*, *J. Comp. Neurol.*, 117:179–188.
- Wurtz, R. H., and C. W. Mohler, 1976. Enhancement of visual responses in monkey striate cortex and frontal eye fields, *J. Neurophysiol.*, 39:766–772.

97 Changing Views of the Role of Superior Colliculus in the Control of Gaze

NEERAJ J. GANDHI AND DAVID L. SPARKS

LOCATED AT THE interface between sensory and motor processing, the superior colliculus (SC) serves as a useful model system for studying a number of important problems in integrative neuroscience. Based on traditional studies, the SC is known to contain maps of cells responsive to sensory stimuli, as well as a motor map of neurons involved in generating commands for saccades and short-duration and high-peak-velocity eye movements that rapidly change fixation between meaningful stimuli.

Since the last detailed review of the control of saccades by SC (Sparks and Hartwich-Young, 1989), our view of its participation in generating movements has changed significantly. Advances in understanding the role of the SC in the transformation of sensory signals into commands for orienting movements are reviewed here and in Chapter 98. The first two sections of this chapter briefly review progress in our knowledge of the anatomical organization and coding mechanisms of the SC. Subsequent sections discuss selected contemporary issues about collicular participation in achieving accuracy of saccades and in controlling other oculomotor and skeletomotor movements.

Anatomical organization in the SC

The superior and inferior colliculi form the roof of the midbrain. In mammals the SC is composed of seven alternating fibrous and cellular layers. On the basis of anatomical and behavioral data, these layers are grouped into two functional units: (1) superficial and (2) deep compartments. The superficial layers (*stratum zonale*, *stratum griseum superficiale*, and *stratum opticum*) receive inputs devoted almost exclusively to vision. Cells in the superficial layers of each colliculus are activated by stimuli appearing in the contralateral visual field and are topographically organized according to receptive field location (Cynader and Berman, 1972). Neurons with receptive fields near the center of the visual field are located anteriorly; those with receptive fields in the periphery are located posteriorly. Cells with receptive fields in the upper visual field are located medially; those with receptive fields in the lower visual field are located laterally. The perifoveal representation is enlarged, with over one-third of the collicular surface devoted to the central 10 degrees of the visual

field. The representation of the horizontal meridian runs from anterolateral to posteromedial. The visual signals observed are in retinal coordinates; cells respond to visual stimuli if, and only if, particular regions of the retina are activated. The outputs of the superficial layers are primarily ascending and terminate, for the most part, in various regions of the thalamus, including the pulvinar (see Sparks and Hartwich-Young, 1989, for a review).

In contrast, the intermediate (*stratum griseum intermedium*, *stratum album intermedium*) and deeper (*stratum griseum profundum* and *stratum album profundum*) layers—collectively, the deep layers—receive sensory inputs of several modalities (e.g., visual, auditory, and somatosensory) and contain neurons with motor properties. In their early description of SC neurons discharging before saccadic eye movements, Wurtz and Goldberg (1972) noted that the neurons have *movement fields*, that is, each neuron discharges before or during saccades having a particular range of directions and amplitudes. The size of the movement field is a function of the amplitude of the optimal movement. Some neurons that discharge prior to saccades also have visual receptive fields, while other neurons have only movement fields. Neurons discharging in response to visual stimuli and prior to eye movements have overlapping, but not necessarily coextensive, movement and receptive fields (Anderson et al., 1998; Wurtz and Goldberg, 1972).

Based on both neural recording and microstimulation experiments in head-restrained animals, it has been established that saccade direction and amplitude are topographically organized in the deep layers of the SC (Robinson, 1972; Schiller and Stryker, 1972). Neurons discharging prior to small saccades are located anteriorly, and those firing before large saccades are found posteriorly. Cells near the midline discharge prior to movements with up components, and those on the lateral side discharge maximally before movements with down components. Microstimulation of the deep layers produces a saccadic eye movement with an amplitude and a direction similar to those of the optimal vector encoded by the neurons near the tip of the electrode.

Despite the general correspondence between the motor and overlying sensory maps, there is no essential functional

linkage between retinotopically coded visual activity in the superficial layers and saccade-related premotor activity in the deep layers of the SC. Vigorous activity may occur in the superficial layers and may not be translated into saccade-related discharge in underlying cells in the deep layers. Conversely, saccade-related activity recorded from neurons in the intermediate and deeper layers may not be triggered by activity of the overlying visual neurons coding retinal error, that is, the distance and direction of the target image from the fovea. Thus, the activity of visual neurons in the superficial layers is neither necessary nor sufficient to produce activation of saccade-related neurons in the deep layers of the underlying colliculus (Mays and Sparks, 1980).

Yet, chemical inactivation in hamster SC (Mooney et al., 1992) and *in vitro* experiments in SC slices using whole-cell patch-clamp methods (Isa et al., 1998; Lee et al., 1997) have demonstrated synaptic transmission from superficial to intermediate layers. Excitatory postsynaptic potentials, evoked with mono- and polysynaptic latencies, were recorded from neurons in the intermediate layers when the overlying superficial layer was stimulated. In the presence of bicuculline, neurons in the intermediate layers even exhibited a burst upon stimulation of the superficial layers, suggesting that the signal transmission is suppressed by GABAergic inhibition. The burst property of intermediate layer neurons was also facilitated by activation of nicotinic acetylcholine receptors (Isa et al., 1998). Behaviorally, the occurrence of short-latency express saccades increased after microinjections of the acetylcholinergic agonist nicotine in the SC of awake, behaving monkeys (see Kobayashi et al., 2001, for a review). Thus, this interlaminar circuitry may play a critical role in reducing saccadic reaction time and triggering express saccades, which are absent following ablation of the SC (Schiller et al., 1987). A description of SC participation underlying saccadic initiation has been reviewed recently (Munoz et al., 2000; see Sparks et al., 2000, for a slightly different perspective).

Unlike the interlaminar organization, the neurons within the deep layers likely use local excitation and distant inhibition mechanisms to shape the evolution of the population activity that leads to the generation of each saccade. The electrophysiological (McIlwain, 1982; Munoz and Istvan, 1998) and pharmacophysiological (Meredith and Ramoa, 1998; Pettit et al., 1999) experiments that provide credence for such connectivity monitored extracellular activity while stimulation pulses were delivered to different parts of the collicular map. Thus, intracollicular connections likely shape the spatial and temporal profiles of activity, although a potential confound may be introduced by stimulation of fibers of passage. Before and during each saccade, neurons in approximately 25 to 30% of the collicular map discharge, and the size of the active area remains relatively invariant across saccades of all amplitudes and directions (Anderson

et al., 1998; McIlwain, 1975; Munoz and Wurtz, 1995b). The SC neurons project predominantly to brainstem structures that process the collicular commands to produce an appropriate movement.

Population coding

Each SC neuron in the deep layers discharging prior to a wide range of movement vectors translates into a large population of neurons active before and during any saccade. The large movement field characteristic of these cells led to population coding schemes for specifying the metrics of the desired movement (McIlwain, 1975, 1991; Sparks et al., 1976). Indeed, results of experiments in which a small subset of the population of neurons active before a saccade was reversibly inactivated support the hypothesis that each member of the active population participates in specifying the direction and amplitude of a saccade. The evidence indicates that saccadic accuracy results from the *averaging* of the movement tendencies produced by each unit in the active population (Lee et al., 1988; Sparks et al., 1990). Small changes in the direction or amplitude of saccades are produced by slight shifts in the location of the population of active cells within the motor map. Thus, the large movement fields of collicular neurons may contribute to, rather than detract from, the accuracy of saccadic eye movements (Baldi and Heiligenberg, 1988). Because the contribution of each neuron to the direction and amplitude of the movement is relatively small, the effects of variability or noise in the discharge frequency of a particular neuron are minimized.

Lesion data indicating that the SC is not essential for saccade generation (Schiller et al., 1987) do not necessarily indicate that it does not play a critical role in the initiation and execution of saccades in normal animals. Large deficits in saccade accuracy and latency are observed following reversible inactivation of SC (e.g., Aizawa and Wurtz, 1998; Hikosaka and Wurtz, 1985, 1986; Lee et al., 1988; Quail et al., 1998). Metrics of eye movements evoked by stimulation of the frontal eye fields following inactivation of the SC also support the hypothesis that collicular neurons play an important role in controlling the direction and amplitude of saccades (Hanes and Wurtz, 2001).

Neurons in the intermediate and deeper layers of SC also exhibit large receptive fields, and population coding schemes may also contribute to the accurate localization of sensory stimuli. Many neurons are responsive to auditory, somatosensory, or visual stimuli and are organized in anatomical maps (see Stein and Meredith, 1993, for a review). In anesthetized or paralyzed preparations, the visual, somatosensory, and auditory maps appear to be aligned, implying that the sensory signals have been translated into a common coordinate system. Before data from

alert animals were available, it was commonly assumed that this alignment allowed a general, modality-independent map of the external environment to be formed. In such a map, stimuli originating from a particular region of the external world, regardless of sensory modality, would activate a particular subset of multimodal neurons (neurons that respond to visual, auditory, or tactile stimuli). The activation of these sensory neurons, in turn, could initiate orienting responses by exciting adjacent cells with movement-related activity organized in a motor map aligned with the multimodal map of sensory space. But retinotopically organized visual signals, acoustic signals localized in head coordinates, and tactile signals organized in body coordinates will not be aligned when the eyes and limbs move with respect to the head.

A remapping is required to account for changes in the position of the relevant effector. For example, the spatial locations of the receptive fields of acoustically responsive cells shift with changes in eye position. This dynamic update of the site of acoustically driven activity encodes the direction and amplitude of the movement required to look to the auditory stimulus rather than the location of the target in space (Jay and Sparks, 1987; Peck et al., 1995; Populin and Yin, 1998). Groh and Sparks (1996) reported that the response of collicular neurons to tactile stimuli was significantly modulated by the position of the eyes in the orbits. Sensory signals in SC seem to be coding the direction and amplitude of the movement required to look to a stimulus rather than to the location of that stimulus in space. This transformation of sensory signals into a motor frame of reference is necessary because the motor map in the SC is organized in relative coordinates: the signals specify the change in gaze position required to look to a target. Input signals that initiate a movement must also specify the location of the target with respect to the current gaze position, not the location of the target in body or head coordinates.

Incorporation of feedback signals in the SC

As the short duration of saccades prevents visual feedback from contributing to their trajectory, these rapid eye movements once were considered ballistic. However, Robinson (1975) proposed a model in which a “local” feedback signal enables instantaneous control of saccades. While his original version has undergone various revisions, the skeleton of the models has remained the same: a corollary discharge signal is subtracted from the desired eye movement command to compute a dynamic motor error that specifies the metrics of the remaining eye movement; the ongoing eye movement continues until the feedback drives the motor error to zero.

According to some models (see Moschovakis et al., 1996, for a review), the command specifying the metrics of the

desired eye movement originates in the SC, the feedback signal stems from the pontomedullary reticular formation in the brainstem, and the neural comparator performing the subtraction resides downstream of the SC. Therefore, the SC is in the feedforward pathway of the neural circuit controlling saccadic eye movements. This traditional view, however, has been challenged by two nonexclusive hypotheses that place the SC inside the feedback loop. To maintain control of saccades, one theory employs the temporal dynamics of SC neuron discharge, while the other exploits the topographic organization of the SC. In this section, we describe the experiments used to support and dispute these hypotheses.

TEMPORAL CONTROL SCHEME Spikes were recorded as monkeys made saccades of the optimal amplitude coded by the movement field of the isolated neuron. The spike trains were converted into a continuous waveform representing spike rate by convolving each spike with a Gaussian kernel and then summing the individual signals as a function of time (Richmond et al., 1987). SC neurons in the intermediate and deeper layers were classified into one of three categories based on the level of activity at the end of the saccadic eye movement (Waitzman et al., 1991). Neurons with saccade-related bursts that ended completely by saccade offset were termed *clipped* cells. Neurons with saccade-related bursts that declined significantly but maintained low-level activity after the end of the saccade were considered *partially clipped* cells. Neurons that failed to discharge a burst during the saccade but exhibited low-level activity before, during, and after the movement were labeled *unclipped* cells. A quantitative index indicated that, in actuality, SC neurons formed a continuum across the three categories.

The discharge rate of clipped and partially clipped neurons decreased monotonically during the saccade and, therefore, was linearly related to the motor error of the eye movement. This evidence led to the hypothesis that saccade dynamics are controlled by the discharge profiles of the SC neurons (Waitzman et al., 1991). In this model, the locus of activity on the SC encodes the desired eye movement, and the level of activity represents the dynamic motor error. Thus, subtraction of the feedback signal from the desired movement command occurs at the level of the SC, placing it in the feedback loop.

How robust is the correlation between neural activity and dynamic motor error when the dynamics of saccades are altered from their stereotypical short duration? Interrupted saccades can be produced by stimulation of the omnipause neurons (OPNs), which gate the brainstem neurons that deliver the drive to the extraocular motoneurons to produce the saccade (see Moschovakis et al., 1996, and Scudder et al., 2002, for exhaustive reviews of brainstem physiology of

the saccadic system). The stimulation, triggered on the onset of a saccade directed to a briefly flashed target, halted the ongoing movement in midflight, and shortly after the offset of the stimulation train, a resumed saccade was generated to bring the eyes to the location of the extinct target (Keller et al., 1996). Since the dynamic motor error remains constant during the interruption duration (because the eyes are not moving), the temporal control scheme predicts that SC neurons encoding dynamic motor error should exhibit a sustained discharge rate during the interruption. To test this hypothesis, Keller and colleagues (Keller and Edelman, 1994; Keller et al., 2000) recorded activity of caudal SC neurons during saccades generated to the center of the movement field but interrupted by stimulation of the OPN region. As in the control condition, the cell exhibited a pre-motor burst prior to the onset of movement. Stimulation of the OPN region at the onset of the saccade attenuated SC activity, to various degrees in different cells, with the largest suppression observed in clipped and partially clipped neurons. During the interruption duration, the activity did not stabilize at a firing rate corresponding to the remaining motor error. At the onset of the resumed movement, the same neuron active for the initial saccade discharged again, provided that the interruption duration did not exceed approximately 100 msec; thus, for short interruption durations, the locus of collicular activity was not updated prior to the second eye movement. The peak activity associated with the second burst was significantly greater than the expected firing rate according to the temporal coding scheme. Also, the correlation between the firing rate and the motor error of the resumed movement was weaker than for control saccades. These results suggest that clipped and partially clipped neurons do not quantitatively code dynamic motor error. However, it is possible that stricter dynamic control may be exerted only toward the end of a saccade because the temporal relationship appears stronger for the later part of the movement, even in the case of interrupted saccades (compare the solid and dotted curves in Fig. 11 in Keller and Edelman, 1994). For larger interruption durations, the initial and resumed movements appeared to be treated as two separate saccades, as the population of neurons activated for the resumed saccades was the same ensemble of cells that discharged for a control eye movement of the same amplitude. Thus, the desired eye movement signal may be updated during the longer-duration interruption.

Another study delivered air puffs to the eye to perturb the saccadic trajectory and analyzed the corresponding activity in SC neurons (Goossens and Van Opstal, 2000). The dynamics of the eye movements were grossly perturbed. The motor error and neural activity were not correlated linearly for many neurons, arguing against the temporal control mechanism.

The activity of SC neurons was also evaluated when the stereotyped trajectories of saccades were altered by injection of muscimol in the OPN region (Soetedjo et al., 2002a). The resulting saccades, although accurate, exhibited lower peak velocity and longer duration. Corresponding activity of SC neurons consistently increased in duration, leading the authors to propose that the SC receives a feedback signal that regulates the duration of their discharge.

Soetedjo et al. (2002a) also analyzed the peak discharge rate of the SC neurons. The authors reasoned that the peak rate of SC neurons should remain the same for all saccades of the same metrics and, presumably, the same motor error. That less than half of the SC neurons in their sample of 11 cells showed a *decrease* in peak activity led them to conclude that the feedback signal does not result in collicular neurons coding dynamic motor error. Proponents of the temporal dynamic control scheme may argue with the expectation that the collicular firing rate should be the same after inactivation of OPNs. As reviewed above, microstimulation of OPNs produces dramatic alterations in the spatiotemporal pattern of collicular activity, and inactivation could similarly modify the discharge. A more direct test would have been to perform phase plane analyses of neural activity and dynamic motor error. Failure to demonstrate a linear relationship, particularly toward the end of the saccade, would be a more convincing argument against the temporal coding scheme.

SPATIAL CONTROL SCHEME Advocates of the spatial control hypothesis use a different nomenclature to classify SC cells (Munoz and Wurtz, 1995a). *Burst* neurons reside dorsally within the deep layers of the SC, have a circumscribed movement field, and discharge a sharp burst for saccades made to locations within the movement field. *Buildup* neurons typically reside ventral to the burst neurons and generally have movement fields without a peripheral boundary (but see Freedman and Sparks, 1997a). Fixation neurons constitute an extension of the buildup layer within the rostral pole of SC. They exhibit low-level activity during visual fixation and are silent during saccades (Munoz and Guitton, 1989; Munoz and Wurtz, 1993, 1995a; Peck, 1989). The region of the fixation neurons within the SC has been labeled the *fixation zone* and is hypothesized to inhibit the burst and buildup neurons in the saccade zone in the remainder of the SC.

According to the spatial encoding hypothesis (Munoz and Wurtz, 1995b; Munoz et al., 1991), a population of burst and buildup neurons within the caudal SC is active at around the onset of a large saccade. As the eye movement progresses, buildup neurons rostral to the initial site become activated *sequentially*. It has been hypothesized that the neural network in SC integrates the eye velocity feedback signal and shifts the population of active buildup neurons rostrally.

According to this proposal, the locus of activity within the buildup neuron layer of the SC map indicates dynamic motor error, while the site of activity of the burst neuron layer encodes desired movement. As the activity in the buildup layer reaches the rostral pole, fixation neurons are reactivated, which in turn inhibit the saccade zone of the SC as well as the premotor circuitry in the brainstem.

In reality, SC neurons fall along a continuum according to the presaccadic discharge parameter used to classify them into the burst or buildup category (Anderson et al., 1998). Also, a closer examination of the discharge properties of the so-called fixation neurons (Munoz and Wurtz, 1993) reveals that they pause only during ipsiversive saccades. Many fixation neurons typically discharge a presaccadic burst during small contraversive saccades generated to fixate parafoveal targets; some neurons increase their activity for movements as large as 15 degrees in amplitude. Thus, the concepts of the fixation zone and fixation neurons have been disputed. Instead, it has been suggested that fixation neurons are the rostral extension of buildup neurons and that the rostral SC still constitutes a saccade zone (Gandhi and Keller, 1999; Krauzlis et al., 1997). Alternatively, Bergeron and Guitton (2000) proposed that each fixation neuron has a characteristic motor error, which, when reached during a movement, will resume the cell's discharge. Consequently, some fixation neurons will not pause for saccades smaller than a particular amplitude, potentially explaining the lack of pause in fixation neurons during small contraversive saccades.

Support for the spatial encoding model was based on qualitative assessments of the population response of SC neurons in both cat (Munoz et al., 1991) and monkey (Munoz and Wurtz, 1995b). However, another evaluation of the evidence (Sparks, 1993) and other quantitative analyses have disputed the notion of a systematic and sequential shift from caudal to rostral SC. A basic requirement of this hypothesis is that a neuron must discharge for all saccades in the optimal direction and for all amplitudes larger than the one dictated by its location within the topographic map. Moreover, the closer the buildup neuron is to the rostral end of the SC, the later its activation must occur relative to saccade onset (and closer to saccade end).

Results of analyses that measured parameters of the neural discharge and correlated them with movement metrics have refuted the spatial encoding hypothesis (Anderson et al., 1998; Kang and Lee, 2000; Soetedjo et al., 2002b). When activity of pairs of buildup neurons, separated on average by over 1 mm along the rostrocaudal axis of the SC, was recorded during large saccades (Port et al., 2000), caudal-to-rostral activation was observed in approximately half of the pairs; several pairs exhibited the opposite, rostral-to-caudal, sequence of activation. This analysis, however, was limited to the rostrocaudal dimension, as it could not determine the spread of activity along the medi-

olateral extent. Examination of the population activity in both dimensions, across the surface of the SC, revealed a more complicated picture (Anderson et al., 1998). Activity spread medially, laterally, and rostrally during the saccade; no significant transition of activity was observed caudal to the initially active site. While the center of gravity of activity in the buildup layer showed a small, rostrally directed shift by the end of the saccade, the shift was random, not sequential, on a millisecond-by-millisecond basis. Another study (Moschovakis et al., 2001) used [^{14}C]deoxyglucose autoradiography to visualize the two-dimensional activity in the intermediate layers of the SC during saccades and observed no indication of a rostrally directed spread of activity, although whether this method has the sensitivity required to detect the proposed rostral spread of collicular activity remains unclear.

The spatial encoding mechanism has also been tested by chemical inactivation experiments (Aizawa and Wurtz, 1998; Quaia et al., 1998). It was reasoned that temporary inactivation by injections of muscimol to a local region of the SC would prevent or compromise the rostrally directed spread of activity during large saccades. Thus, the ongoing saccade was predicted to overshoot the target. The observed postlesion saccades either undershot or landed near the target location. Thus, the notion of a rostrally directed spread of activity as a dynamic control mechanism for saccades has been refuted by many studies.

STATIC FEEDBACK The two leading hypotheses concerning the role of SC in dynamic control of saccades have been tested extensively. Relevant experiments have raised various levels of doubt about each theory and, consequently, the controversy over a dynamic role of the SC in the control of saccades still exists. However, the notion of *static* feedback, one that does not compute the instantaneous motor error, has been supported by almost every experiment that has examined the activity of SC neurons during perturbations of the eye trajectory. Referring to the interrupted saccade experiments described above (Keller and Edelman, 1994; Keller et al., 2000), for example, the caudal region active at the onset of a large saccade discharges another burst at the onset of the resumed movement. If the SC does not receive feedback about the perturbation, that is, if the SC resides upstream of the feedback loop, a second burst would not be observed during the resumed movement. Of course, the *dynamics* of the movement need not be controlled by the temporal discharge pattern. Similar observations have been made when saccades were perturbed by stimulation of cortical (frontal eye fields: Schlag-Rey et al., 1992) and other subcortical (SC: Munoz et al., 1996; Sparks and Porter, 1983) structures.

Goossens and Van Opstal (2000) proposed a conceptual model in which the SC plays a feedforward role in the

control of saccades. They found that the number of spikes discharged by SC neurons during control and air-puff-induced perturbation trials was remarkably similar. Despite the altered burst dynamics, SC neurons executed the desired number of action potentials. Thus, these authors suggested that the role of the SC is to output an approximately fixed number of spikes to produce a desired change in the line of sight. But how does the SC know that its discharge has to be altered? A nonmetric-based feedback signal must be transmitted to the SC to account for the change in burst properties (Keller and Edelman, 1994; Soetedjo et al., 2002a), and intrinsic properties within the SC ensure that more than enough spikes are generated and transmitted to downstream structures (Goossens and Van Opstal, 2000).

Contribution of the SC during other orienting responses

In the past, experiments that explored the neurophysiological substrate of oculomotor systems typically investigated each oculomotor subsystem (e.g., saccades, smooth pursuit, vergence) in isolation. In addition, the head was restrained as animals performed eye-movement tasks. In the natural environment, however, we often orient from one target to another by integrating several types of movements. For instance, head movements can often accompany eye rotation, saccades and smooth pursuit are coordinated when tracking a moving object, and saccadic eye movements can have a vergence component.

As reviewed above and elsewhere (Sparks and Hartwich-Young, 1989), the SC is considered a key structure in sensorimotor processes that control saccades. More recently, the role of the SC has been examined during saccades coordinated with head movements (head-unrestrained gaze shifts), eye movements other than saccades (smooth pursuit, vergence, accommodation), and reaching movements of the arm. In the remainder of this chapter, we will review recent studies suggesting that the SC is involved in the generation of eye movements other than saccades, as well as movements of the head and arm.

COORDINATED EYE-HEAD MOVEMENTS When the head is free to move but the trunk is restrained in the straight-ahead position, coordinated movements of the eyes and head shift the direction of gaze, defined as the line of sight and computed as the sum of eye-in-head and head-in-space positions. Gaze shifts are usually characterized by the *amplitudes* of the gaze, eye, and head movements and by the *contributions* of the eye and head to the change in gaze. The onset and offset of gaze, eye, and head movements are typically determined by velocity criteria. Their amplitude values are computed by subtracting onset and offset positions, and eye and head contribution metrics are measured as the eye and head dis-

placements, respectively, during the duration of the gaze shift (Freedman and Sparks, 1997b). In general, the head continues to move for several hundred milliseconds after the end of a gaze shift, and the eyes counterrotate in the orbits during this period to maintain stability of gaze. Thus, the contribution component, particularly for the head movement, should be less than the amplitude measure.

The eye and head contributions for a desired change in gaze depend on the oculomotor range, which is species-dependent, as well as the initial eye-in-head and head-on-trunk positions. Because of their small oculomotor range (~25 degrees), cats have a higher propensity to generate head movements and, therefore, have been excellent subjects for examining the role of SC in controlling head-unrestrained gaze shifts. Stimulation of the SC produced effects that were dependent on the stimulation site, stimulation parameters, and initial position of the eyes in the orbits (Guitton et al., 1980; Paré et al., 1994; Roucoux et al., 1980). Electrical pulses delivered to the anterior SC primarily produced saccades, even when the head was free to move. Head movements, when they occurred, were initiated at around or after the end of saccades, thus minimizing their contribution to gaze shifts. Thus, the change in gaze evoked by stimulation of the anterior SC was similar in the head-restrained and head-unrestrained conditions. In contrast, gaze shifts evoked by stimulation of more caudal regions of the SC produced different effects in the head-restrained and head-unrestrained modes. When the head was prevented from moving, stimulation drove the eyes toward a specific orbital position. Thus, both contraversive and ipsiversive saccades were evoked when the initial eye position was ipsilateral or contralateral, respectively, to the desired orbital position. When the head was allowed to move, stimulation evoked relatively constant amplitude gaze shifts executed by a coordinated movement of the eyes and the head. The eye movement in the orbit, however, appeared similar to the movement observed in the head-restrained condition; that is, the eyes moved to specific orbital positions, independent of their initial positions (Paré et al., 1994; Roucoux et al., 1980).

To corroborate the microstimulation studies, the movement fields of feline SC neurons were compared in the head-restrained and head-unrestrained conditions (Munoz et al., 1991). The neural discharge was better modulated by gaze (eye-in-space) amplitude than by either eye-in-head or head-in-space components. Furthermore, the movement fields based on gaze parameters overlapped for the head-restrained and head-unrestrained conditions, suggesting that the phasic bursts of SC neurons encode gaze displacement. Collectively, the neural recording and microstimulation experiments have led to the hypothesis that SC encodes parameters of the gaze shift, as opposed to the eye-in-head or head-in-space components.

Unlike the nonprimate models, the SC in monkeys was traditionally considered to participate in the control of saccades only. The neural mechanism of the head component of coordinated eye and head movements was thought to be of extracollicular origin. This assumption was based on studies that examined the effects of stimulation of the anterior SC only (Stryker and Schiller, 1975), which primarily evoked saccades, and was further supported by neural recording experiments that failed to find head movement signals in the SC (Robinson and Jarvis, 1974). This topic was recently revisited (Cowie and Robinson, 1994; Freedman et al., 1996; Freedman and Sparks, 1997a; Seagraves and Goldberg, 1992), and it is now assumed that the primate SC also controls coordinated eye-head movements.

As in the feline SC, the properties of stimulation-evoked gaze shifts in nonhuman primates were a function of the site and parameters of stimulation (Freedman et al., 1996). Gaze amplitude initially increased with stimulation duration and then reached a plateau level dictated by the site of stimulation (site-specific maximal amplitude). The peak velocity of the gaze shift increased and the variability in the onset decreased as the frequency of stimulation was raised. Increases in stimulation intensity had modest effects on gaze peak velocity without changing the site-specific maximal amplitude, provided that the stimulation duration was extended to accomplish the entire movement. In general, the dynamics of stimulation-induced and visually guided gaze shifts were similar. [Stimulation parameters have similar effects on saccades evoked in the head-restrained monkey (Stanford et al., 1996; Van Opstal et al., 1990).]

The head component of stimulation-evoked gaze shifts was also dependent on the stimulation parameters. For stimulation of middle and caudal sites, the head continued to move for the duration of the stimulation and even after the end of the stimulation-evoked gaze shift (Freedman et al., 1996). Presumably, the head would have stopped moving once it reached its mechanical limits, although stimulation durations long enough to test this hypothesis were not applied. Head amplitude and duration were linearly related to stimulation duration within the tested range. Average head velocity also increased linearly with stimulation frequency, although the effect was modest compared to that on gaze velocity. Thus, the head movement did not exhibit any site-specific maximal amplitude for the tested range of stimulation durations. Even though a significant proportion of the head movement continued after gaze offset, the head contribution remained relatively independent of stimulation parameters (Freedman et al., 1996).

Changing the site of stimulation along the rostral-caudal dimension produced qualitatively similar effects in head-unrestrained monkey and cat. Stimulation of the anterior SC produced gaze shifts that were accomplished primarily by the eye (Freedman et al., 1996). Head movement, if

observed, was usually initiated at around gaze offset and, therefore, the head contribution was negligible. In contrast, stimulation of middle and caudal regions produced coordinated movements of the eyes and head (Freedman et al., 1996). Across all sites, however, the eye movements observed in the head-restrained and head-unrestrained conditions were similar—fixed vector for anterior sites and goal directed for caudal regions. Thus, it appears that the movements observed during SC stimulation in the head-restrained animal were reduced by the amount the head would contribute if stimulation were applied to the same site in the head-unrestrained condition. As a consequence, the amplitude axis of the (head-restrained) saccade motor map, particularly at the caudal end, is distorted by being more compressed than the map would be if it were constructed from head-unrestrained experiments (Freedman et al., 1996).

Analyses evaluating the effect of initial eye position in the head (IEP_h) have decomposed the vector of the stimulation-evoked movement and IEP_h into horizontal and vertical components (Freedman et al., 1996). Alternatively, Klier et al. (2001) transformed the coordinate system to analyze the orthogonal component of the movement and initial gaze position (IGP). Gaze amplitude, particularly the horizontal component, evoked by stimulation remained relatively constant, while eye and head contributions varied inversely as a function of IEP_h . [An assessment of Fig. 13A–C in Freedman et al. (1996), however, suggests that the gaze amplitude as well as its horizontal component may depend on IGP.] When the IEP_h was deviated in the direction of the stimulation-evoked gaze shift, head contribution increased and eye amplitude decreased for a given change in gaze. Conversely, if the IEP_h was contralateral to the direction of the stimulation-evoked movement, head contribution decreased and eye amplitude increased for a given gaze shift. Furthermore, head onset relative to gaze onset decreased (increased) as the IEP_h was ipsilateral (contralateral) to the direction of the ensuing gaze shift. Unlike the IEP_h , the effects of head position on stimulation-evoked gaze shifts and on eye and head contributions remain to be examined systematically.

Unlike the horizontal component, the vertical and orthogonal components of the stimulation-induced gaze shift were linearly related to the vertical IEP_h and orthogonal IGP, respectively. Suppose that stimulation of a specific SC site produced a gaze shift with an upward component when the eyes were initially centered in the orbits and the head was pointed straight ahead. Stimulation of the same site with an upward IEP_h or IGP generated a smaller upward, and sometimes even downward, component of gaze compared to the corresponding component produced with a downward IEP_h or IGP. Thus, varying the IEP_h while stimulating a caudal site and maintaining identical stimulation

parameters does *not* produce gaze shifts of same amplitude and direction.

The slope of the linear regression, describing the relationship between the orthogonal gaze shift component and orthogonal IGP, changed with the stimulation site (Klier et al., 2001). At rostral sites, the slope was near zero, indicating that the stimulation-evoked gaze shifts remained constant across all IGP and, presumably, IEP_h. As the stimulation electrode was positioned at increasingly caudal sites, the slope decreased gradually to negative one as the stimulation-evoked gaze shifts became goal-directed. The data obtained from stimulation of the rostral and caudal ends of the SC are consistent with the predictions of the constant gaze-displacement and desired gaze-position models, respectively. However, Klier et al. (2001) demonstrated that the distribution of the slopes is also consistent with another model that computes gaze displacement in *retinal*, as opposed to *spatial*, coordinates (see Crawford and Guitton, 1997, for a theoretical foundation). By accounting for the geometry of the eyeball, all gaze shifts evoked by microstimulation become constant vectors across all IGPs, thereby avoiding the need to explain the transition from gaze displacement to gaze position. Hence, the updated view is that the SC controls coordinated movements of the eyes and head and, furthermore, that the metrics of the gaze shifts are encoded in retinal coordinates.

These microstimulation experiments suggest that SC neurons issue a single signal to displace gaze by a desired displacement (*gaze-displacement* hypothesis). Alternatively, one population of SC neurons can provide eye displacement signals and another group of neurons may submit head displacement commands (*separate-channel* hypothesis). If these neurons are intermingled, stimulation could evoke gaze shifts similar to those expected from activation of neurons encoding gaze displacement. If stimulation selectively activated eye or head movement neurons, the movement would be isolated to just one of the pathways. Cowie and Robinson (1994) presented evidence hinting that stimulation of certain sites within the deep layers of the SC may produce head movements without an accompanying gaze shift. Recently, Corneil et al. (2002) and Pélisson et al. (2001) reported that stimulation of the SC with parameters sub-threshold to those required to produce gaze shifts can elicit head movements without changing the gaze position. While head movements evoked by stimulation of the SC support the separate-channel hypothesis, they are not inconsistent with the gaze-displacement hypothesis. For example, the stimulation-induced output could be a gaze command that was gated by OPNs in the eye pathway but not gated in the head pathway.

To differentiate between the gaze-displacement and separate-channel hypotheses, one might suggest correlating the neural activity with the metrics of gaze, eye, and head

components. However, this approach may not be definitive for two reasons. (1) Gaze, eye, and head amplitudes and directions do not vary independently and typically are highly correlated. (2) Based on a scales of measurements argument (Sparks and Gandhi, 2003), correlation analysis may not be an appropriate statistical test for neurons organized in a place code. Thus, conditions under which the three movement metrics can be dissociated, one held constant while the other two vary, are necessary to determine the representation of gaze in SC neurons (Freedman and Sparks, 1997a).

One behavioral dissociation (Fig. 97.14) emphasizes that for large gaze shifts, the eye amplitude saturates at ~35 degrees, even as the head and gaze components vary. The shaded regions in panel *B* show for three representative gaze shifts (*a-c*; vertical lines panel *A* and rows in panel *B*) how the encoding mechanism dictates the population of active SC neurons. The gaze-displacement hypothesis (“gaze” column, panel *B*) requires that, for gaze shifts of increasingly large amplitudes, the active ensemble of neurons shifts to more caudal locations. Thus, in recording from a neuron with an optimal vector larger than the three representative gaze shifts (*black dot*, panel *B*), an increase in firing rate would be associated with a larger gaze amplitude (“gaze” column, panel *C*). An increase in firing rate is also correlated with an increase in head amplitude (“head” column, panel *C*) because it covaries with gaze amplitude. In contrast, eye amplitude would remain relatively constant despite changes in the firing rate. According to the separate-channel hypothesis, the same population of neurons encoding eye displacement would remain active for all three gaze shifts, holding the shaded region constant (“eye” column, panel *B*). Hence, a neuron in the caudal SC would discharge at the same firing rate across a large range of gaze and head amplitude, as long as the eye movement remains relatively constant (“eye” column, panel *C*). Neurons encoding head displacement, on the other hand, will behave very much like SC neurons issuing gaze-displacement commands because head and gaze amplitude covary for large gaze shifts (compare the “head” and “gaze” columns in panels *B* and *C*). Note that while this behavioral dissociation allows an evaluation of the eye encoding scheme, it does not distinguish between gaze and head displacements. Thus, an analysis of only this subset of movements may not be sufficient to distinguish between the gaze-displacement and separate-channel hypothesis.

In the second dissociation condition, SC activity is analyzed for the subset of movements for which the head metrics are held constant while eye and gaze amplitude and direction vary (panel *D*). In this case, the population of neurons encoding gaze or eye displacements will shift for different gaze shifts, but the active ensemble of neurons encoding head displacement will remain constant (panel *E*).

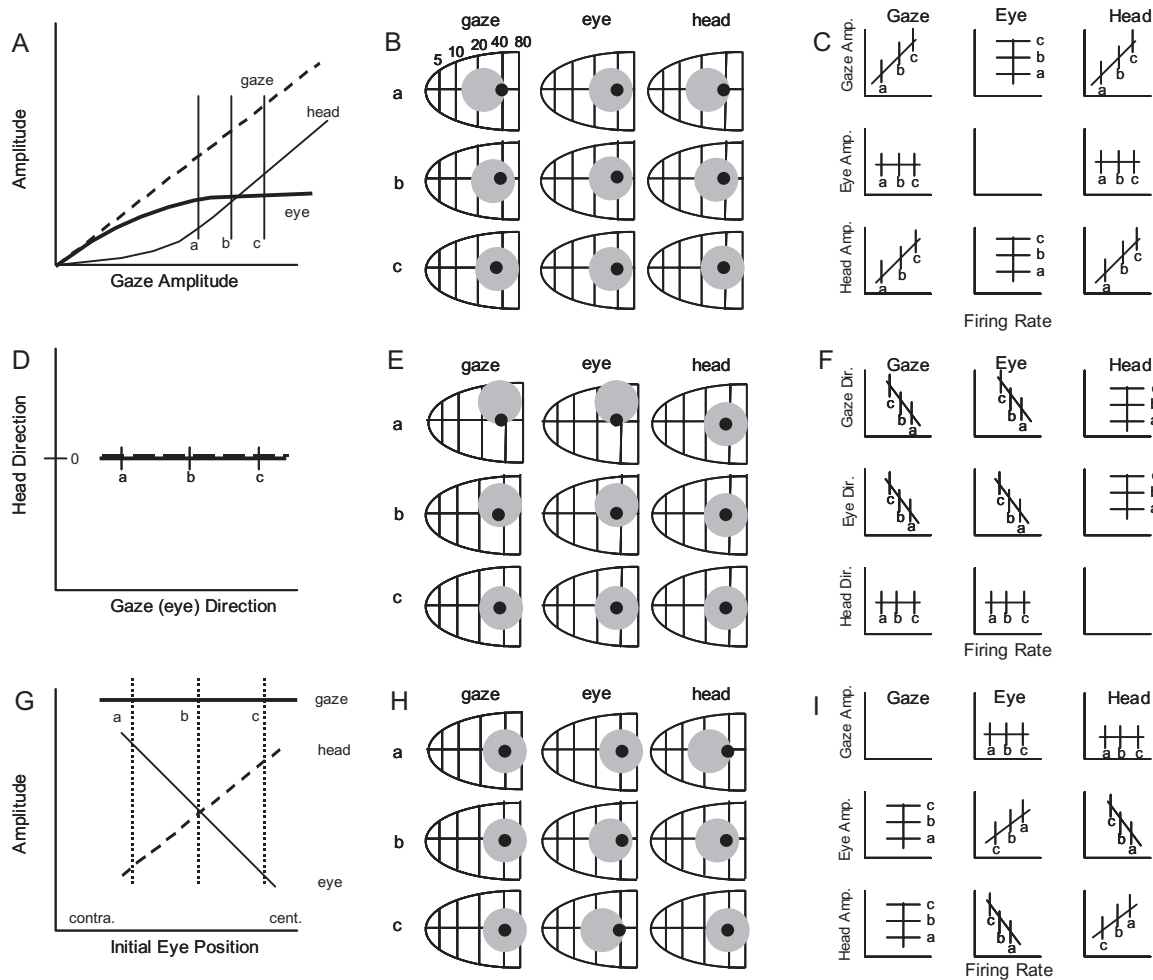


FIGURE 97.1. Strategy employed to determine whether the discharge of SC neurons supports the gaze-displacement or separate-channel hypothesis. *A*, *D*, *G*, Replotted schematic diagrams illustrating the behavioral dissociations of movement metrics. Analyses focused on the neural data of movements in which one of the eye, head, or gaze movements remained constant while the other two signals varied, as noted by the vertical lines marked *a–c*. *A*, Schematic of a behavioral dissociation in which eye amplitude is held constant while gaze and head amplitudes covary. *B*, Hypothetical locations of the active population of cells in the SC map as predicted by the alternative hypotheses during movements indicated in *A*, *a–c*; shaded region, active population; filled circle, location of the hypothetical (test) cell used to illustrate the specific predictions of the alternatives. The column labeled “gaze” outlines the locus of the active population according to the gaze-displacement hypothesis during movements (rows *a–c*). Similarly, the “eye” and “head” columns illustrate the loci of active populations according to the separate-channel hypothesis. *C*, Specific predictions of the hypotheses (columns) are outlined for the test cell

in *B*. Gaze, eye, and head movement amplitudes (rows) are plotted as functions of the hypothetical firing rate of the test cell. *D*, Schematic of a second behavioral dissociation, in which the head movement is constant while gaze and eye amplitudes covary. *E*, Loci of active populations in the SC map during three movements (*D*: *a–c*) according to the alternative hypotheses (columns labeled “gaze,” “eye,” and “head”). *F*, Specific predictions of gaze, eye, and head amplitude (rows) when plotted as a function of firing rate of test cell (filled circle in *E*). *G*, Schematic of a third behavioral dissociation in which gaze amplitude is held constant while eye and head contributions vary inversely as a function of horizontal initial eye position (IEP_h) in the head; contra., contralateral IEP_h ; cent., IEP_h close to zero. *H*, Loci of active populations in the SC map during three movements (*G*: *a–c*) according to the alternative hypotheses (columns labeled “gaze,” “eye,” and “head”). *I*, Specific predictions of gaze, eye, and head amplitude (rows) when plotted as a function of the firing rate of the test cell. (Figure and caption adapted from Freedman and Sparks, 1997a.)

Accordingly, the firing rate of a neuron encoding head displacement will not vary despite variations in gaze and eye directions (“head” column, panel *F*). Firing rates of neurons encoding gaze or eye displacements, on the other hand, will be related to gaze and eye directions, respectively, but not to head direction (“gaze” and “eye” columns, panel *F*). Thus, consideration of only this subset of movements allows a test of the head-displacement model, but it does not dissociate between the gaze- and eye-displacement models.

In the final dissociation condition, gaze amplitude is held constant while eye and head contributions vary inversely as a function of IEP_h (panel *G*). In this situation, the same population of neurons encoding gaze displacement is activated for the three representative movements (“gaze” column, panel *H*). The neural activity remains constant for the same gaze amplitude, despite various combinations of eye and head components (“gaze” column, panel *I*). As the IEP_h is deviated in the direction of the ensuing gaze shift, the eye amplitude decreases and the head amplitude increases. Thus, for constant gaze amplitude, the population of neurons encoding eye displacement and head displacement shift their center of activity in opposite directions as a function of IEP_h (“eye” and “head” columns, panel *H*). Consequently, the firing rate of a representative neuron encoding either eye or head displacement, while not related to gaze amplitude, would be inversely related to eye and head amplitudes (“eye” and “head” columns, panel *I*).

Freedman and Sparks (1997a) performed these analyses on 36 SC neurons recorded during head-unrestrained gaze shifts directed to visual targets. All neurons encoded gaze displacement; the relationship with gaze, eye, and head amplitudes to firing rate obeyed the predictions of the gaze-displacement hypothesis (“gaze” column, panels *C*, *F*, and *I*). Thus, these authors concluded that SC neurons encode desired gaze displacement, and that the single gaze command is separated into eye and head pathways downstream of the SC.

While the experimental design of Freedman and Sparks (1997a) is the most thorough and quantitative to date, their conclusion depends critically on the assumption that the vestibulo-ocular reflex (VOR) is inactive during gaze shifts. If the VOR is significantly active, their interpretation may be contaminated by the neural uncertainty problem (Sparks, 1999; Sparks and Gandhi, 2003). For instance, the neurons considered to encode desired gaze displacement may actually issue a desired eye movement command only. Other neural pathways may generate an accompanying head movement and, if the VOR gain is near unity, submit an ocular counterrotation signal of the amount that equals the head amplitude. Thus, the extraocular motoneurons incorporate the excitatory drive from the saccadic system and the inhibitory vestibular signal, resulting in a dissociation between the desired (encoded by SC neurons) and

executed eye movement (see Sparks and Gandhi, 2003, for simulations).

The results of Freedman and colleagues (Freedman and Sparks, 1997a; Freedman et al., 1996) can be accounted for by other hypotheses about the role of the SC in the control of gaze shifts. For example, the SC may contain separate populations of eye and head cells, but all neurons encode desired gaze displacement. Activation of either type of neuron sends signals to innervate muscles in the appropriate pathway. Downstream of the SC, the eye and head pathways can interact (via mechanisms such as cross-coupling, VOR, efference copy, or proprioception), producing a dissociation between the desired movement command and the executed movement amplitude (Sparks, 1999). Thus, a thorough understanding of collicular participation in the control of gaze shifts is likely to remain elusive until interactions between the eye and head pathways are elucidated.

SMOOTH PURSUIT Over the past decade the function of neurons in the rostral SC has come under considerable scrutiny. According to the traditional views, the cells in the rostral SC discharge prior to small saccades. A recent proposal that neurons in the rostral SC play a role in fixation was discussed in a previous section (“Spatial Control Scheme”). In the next three sections, we consider the possibility that neurons in the rostral SC participate in the control of eye movements other than saccades (smooth pursuit, vergence, and accommodation).

Behavioral experiments have demonstrated that small position errors (<3 degrees) induced by stepping a moving target produce changes in the speed of ongoing pursuit (Krauzlis and Miles, 1996; Morris and Lisberger, 1987; Segraves and Goldberg, 1994). Whether neurons in the rostral SC generate a general position error command that can be used to produce or modify smooth eye movements was the focus of a series of experiments by Krauzlis and colleagues (Basso et al., 2000; Krauzlis et al., 2000). They recorded the activity of neurons in the rostral SC during smooth pursuit eye movements and observed increases in discharge during contraversive pursuit movements, particularly when differences in target and eye speed created small position errors. Decreases in activity were observed during ipsiversive pursuit. Accordingly, one interpretation of the results is that neurons in the rostral SC issue commands used by the pursuit system. However, the same neurons also exhibited a burst of activity before small contraversive saccades. Thus, an alternative explanation is that the enhanced activity observed during pursuit eye movements could represent the *preparation* of catchup saccades—small saccades made to the moving target—that were not executed. To address this possibility, the activity of cells on trials in which catchup saccades were generated within 300 msec of the target motion (*early saccades*) was compared with the activity

of the same neuron during trials without early saccades (Krauzlis et al., 2000). If the neural activity on the trials without the early saccades reflects a saccade preparation signal, higher levels of activity should be present during the trials with early saccades because a rapid eye movement was actually produced. For most neurons, the discharge rate during the early pursuit phase was not significantly different for the trials with and without the early saccades. Thus, the authors concluded that the enhanced activity was associated with smooth pursuit, not saccades.

Artificial activation (microstimulation) and inactivation experiments were also conducted in an attempt to establish a more direct role of the rostral SC in producing ocular smooth pursuit (Basso et al., 2000). Microstimulation during fixation failed to elicit any smooth eye movements at currents above or below the threshold for evoking saccadic eye movements. This is in contrast to the smooth eye movements produced by stimulation of a small portion of the arcuate fundus and the neighboring posterior bank lying directly posterior to the principal sulcus in the frontal eye field area (Gottlieb et al., 1993; MacAvoy et al., 1991). Other studies, however, have reported that prolonged duration, high frequency, and large-intensity stimulation of the SC evoke a staircase of saccades, often interspersed with smooth eye movements during the intersaccadic intervals (Breznen et al., 1996; Missal et al., 1996; Moschovakis et al., 1998), although there is no consensus on whether these drift-like movements are actually smooth pursuit.

The failure to initiate pursuit movements with collicular microstimulation cannot be interpreted as evidence that the colliculus is not involved in pursuit eye movement. Behavioral experiments have shown that position errors introduced by jumping a moving target only affect ongoing pursuit movements (Krauzlis and Miles, 1996; Morris and Lisberger, 1987; Segraves and Goldberg, 1994). Furthermore, position steps in the direction of motion modestly facilitate pursuit, while steps in the opposite direction greatly suppress it. Thus, a stimulation-induced position error signal, which is the hypothesized output of the SC, should alter the kinematics of pursuit even if it does not initiate it. Ipsiversive pursuit should be suppressed by microstimulation, whereas contraversive pursuit should be facilitated. Basso et al. (2000) found that long-duration (300 to 400 msec) microstimulation of the rostral SC applied near the onset of a moving target produced large suppressive effects on ipsiversive smooth pursuit; these effects were significant and consistent with the predictions. The effect of microstimulation during contraversive smooth pursuit was minimal and inconsistent.

In a complementary experiment, the activity of neurons in the rostral SC was reduced by application of muscimol, a GABA agonist, and pursuit performance was assessed as animals tracked a moving target. A step-ramp task was used to assess, independently, the effects of the direction of the

pursuit and the location of the target in the visual field. Basso and colleagues (2000) observed a muscimol-induced reduction in pursuit velocity during contraversive pursuit initiation and an increase in pursuit velocity during ipsiversive pursuit. However, deficits were more dependent upon which part of the visual field pursuit targets were presented with than the direction of the pursuit movement. For example, with a right SC injection, pursuit velocities were reduced when the target was moving leftward in the left visual field, but not significantly reduced when the target was moving leftward in the right visual field. Also, with a right injection, increased pursuit velocity was observed if the target was moving rightward in the right visual field.

Collectively, these results were interpreted as support for the hypothesis that neurons in the rostral SC issue a general position error command that is used by both pursuit and saccadic subsystems (Basso et al., 2000; Krauzlis et al., 2000). According to this view, the rostral SC plays an important role in the control of pursuit eye movements. Although the data are suggestive, in our opinion a convincing case that the superior colliculus has a causative role in the initiation or maintenance of pursuit eye movements does not yet exist. A brief evaluation of the recording, microstimulation, and inactivation experiments follows.

With respect to the recording experiments, critical details of the analyses used to reject the hypothesis that increases in activity were related to the preparation of catchup saccades were not provided. For example, were the amplitudes of the movements in the early saccade trials within the center of the movement field of the neurons? Because neurons in the rostral SC have small movement fields, small changes in the saccade amplitude will result in a large change in the discharge characteristics. Furthermore, differences in firing rate in the two conditions would be easier to detect if the trials, in which saccades occurred, were aligned on saccade onset, not target motion. In the absence of information on these critical details, rejection of the hypothesis that changes in activity observed during pursuit movements are related to preparation of catchup saccades seems premature.

In the microstimulation experiments, contrary to the predictions, stimulation of many sites, particularly those represented within 1 degree of the fovea, significantly reduced pursuit velocity. This was observed during initial and maintained smooth pursuit in both contraversive and ipsiversive directions. These findings are compatible with an alternative interpretation of the data in which stimulation-evoked perturbations in pursuit movements are an indirect effect of activating OPNs. Stimulation of the OPNs in the pontine reticular formation is known to not only interrupt saccades but also attenuate ongoing pursuit (Missal and Keller, 2002). Thus, stimulation of the rostral SC, which has dense excitatory projections to the OPNs (Büttner-Ennever and Horn,

1994; Büttner-Ennever et al., 1999; Gandhi and Keller, 1997; Paré and Guitton, 1994), may increase the OPN response and, in turn, reduce pursuit velocity. This suggestion is consistent with the observation that stimulation of increasingly caudal regions, which has weaker projections to the OPNs, did not suppress smooth-pursuit (Basso et al., 2000).

The results of the inactivation experiment are puzzling. The finding that pursuit velocity effects were more dependent upon the region of the visual field in which the pursuit targets were presented than upon the direction of the pursuit movement is not the result expected if the inactivated cells are generating a motor command for a movement in a particular direction. This is the pattern of results that would be obtained if the inactivation were affecting visual motion processing in a particular region of the visual field or affecting the allocation of attention to particular parts of visual space.

Additional studies of the role of rostral SC in the control of smooth pursuit are necessary. A convincing argument can be made if a pathway from the SC to neurons in the traditional pursuit system is identified. Anatomical and functional connectivity experiments that use a combination of orthodromic and antidromic stimulation techniques may be appropriate. Furthermore, the experiments must show that the origin of the projections is limited to the rostral SC.

SACCADE-VERGENCE INTERACTIONS Eye movements to targets that are displaced in eccentricity and depth exhibit both *version* and *vergence* components, where version is the yoked, conjugate movement of both eyes and vergence refers to the nonconjugate movement of the eyes in opposite directions. In this section, we discuss the few studies exploring SC participation in these three-dimensional saccades (or saccade-vergence movements). It is reasonable to examine disparity coding and vergence movement signals in the SC since it receives projections from neurons in cortical areas that respond to spatial disparity or participate in producing vergence eye movements (e.g., Ferraina et al., 2000; Gnadt and Beyer, 1998; Gamlin and Yoon, 2000). In anesthetized cats, neurons in the superficial layers of the SC exhibit coarse disparity sensitivity, unlike the sharply tuned cells in striate cortex (Bacon et al., 1998; Dias et al., 1991). Activity of visuomotor neurons in the deeper layers of awake, behaving monkeys exhibited no systematic vergence- or disparity-related signals (Mays, 1996), although there may be a concentration of disparity-sensitive neurons located in the rostral SC (Berman et al., 1975; Jiang et al., 1996).

Recently, Chaturvedi and Van Gisbergen (1999) used microstimulation to investigate the role of the SC in saccade-vergence movements. Figure 97.2 shows the vertical component of versional (*left*) and vergence (*right*) components of

three-dimensional saccades when no stimulation was applied (V), when stimulation was delivered during fixation (E), and when stimulation was delivered during an ongoing movement (EV). Electrical stimulation (duration: 50 msec) delivered to the middle and caudal SC *during fixation* produced saccades (E; Fig. 97.2, *left*) *without* a vergence component (E; Fig. 97.2, *right*). However, effects on the vergence component were observed with stimulation of the same sites prior to or during target-directed three-dimensional saccades. As expected from previous studies (e.g., Gandhi and Keller, 1999; Schlag-Rey et al., 1989) stimulation of a SC site at *around the onset* of a visually guided saccade produced a version component (EV; Fig. 97.2, *left*) with a direction and an amplitude that were an average of those of the saccades encoded by the stimulation (E) and target-activated (V) sites. Following a brief interval, the animal compensated for the stimulation-evoked perturbation of the visually directed saccade by executing another saccade to the visual target.

During the interval when the stimulation-evoked movement was being executed, the stimulation-evoked vergence component (EV; arrow 1; Fig. 97.2, *right*) had a higher velocity than a control vergence movement without a version component (data not shown). When the stimulation-evoked version component ended (second vertical line), the vergence movement continued, albeit at a slower velocity (arrow 2), before reaccelerating during the saccadic movement made to compensate for the stimulation-induced perturbation (arrow 3).

When plotting amplitude as a function of *electrical latency*, defined as the difference between saccade and stimulation onsets, both initial saccade and intrasaccadic vergence components followed an averaging process that began when electrical latency was approximately -40 msec (stimulation led the visually guided saccade) and continued until roughly 40 msec after stimulation onset. The movement was guided primarily by the target-directed program for positive electrical latency but was dominated by the stimulation-evoked command for negative electrical latency; for electrical latency values around zero, the movement incorporated both target-directed and stimulation-evoked signals. The averaging process was highly correlated for the version and vergence components, both on a trial-by-trial basis and on average.

Because vergence movements could not be initiated without a saccadic component during the three-dimensional saccades, one conclusion that follows is that both types of movement are gated by the same mechanism (see Chapter 95). This conservative interpretation allows the commands for desired vergence movement to originate from an extracollicular source. But could vergence commands also be represented in the SC? Chaturvedi and Van Gisbergen (1999) entertained the notion that the premotor neural discharge of the SC specified both saccade and vergence metrics but that

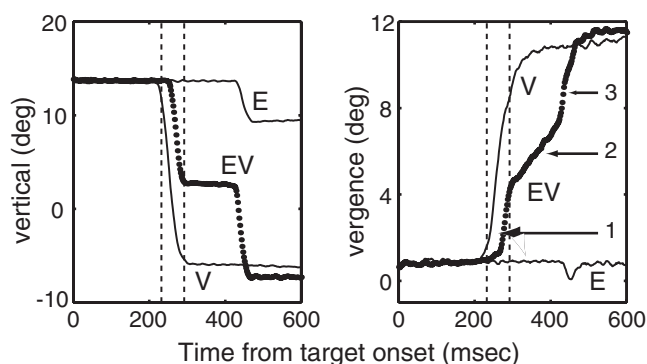


FIGURE 97.2. Example of a perturbation induced by stimulation of the SC during a three-dimensional saccade. Temporal traces of the vertical component of versional (*left*) and vergence (*right*) eye movements directed to a visual target (V), evoked by stimulation during fixation (E), or perturbed by microstimulation during a target-directed saccade (EV; *thick dotted trace*). The fixation and saccade targets were identical in both V and EV conditions. The vertical, dashed lines mark stimulation onset and offset. Arrows 1 to 3 are referred to in the text. Averaging of the movements encoded by the neurons at the stimulation-evoked and target-activated sites is sufficient to explain the observed behavior: the stimulation-evoked output encodes a vergence movement of zero amplitude and a saccade component of nonzero amplitude. (Modified from Chaturvedi and Van Gisbergen, 1999.)

stimulation of the SC output a zero vergence command, not a lack of vergence signal. Accordingly, stimulation delivered during fixation produced no vergence component, and stimulation applied at around saccade onset averaged the zero vergence command issued by the stimulation and the depth component programmed by the target-activated site. Focusing on the trials in which the visually guided three-dimensional saccades were initiated *prior* to stimulation onset (Fig. 97.2), Chaturvedi and Van Gisbergen assumed that the desired vergence signal must be fully encoded by the time of stimulation onset, as it presumably is for control conditions. If the vergence signal does not channel through the SC, then the intrasaccadic vergence components on stimulation and control trials should be similar. But the fact that averaging of the metric was observed led the authors to conclude that vergence signals are encoded in the SC output.

Stimulation of the rostral SC *after* the onset of three-dimensional saccades produced effects comparable to those observed for the middle and caudal SC (Chaturvedi and Van Gisbergen, 2000). With longer stimulation duration (500 msec), the resumed version component was often truncated and the vergence component often reversed direction, sometimes diverging beyond the initial fixation plane. When the stimulation was delivered prior to the onset of saccade-vergence movements, the onset of the version component was delayed until after stimulation offset. Unlike the middle and caudal SC, a small vergence component was observed during the microstimulation of the rostral SC. Thus, the

onset of saccade and vergence movements could be separated when stimulation was delivered to the rostral SC. Further differences between the rostral and posterior regions of SC were uncovered when stimulation interacted with pure vergence movements without a saccade component. A vergence, but not a version, component was initiated during stimulation of the rostral SC prior to the movement in depth (Chaturvedi and Van Gisbergen, 2000). Ongoing vergence movements stopped and reversed direction, often diverging the eyes beyond the initial fixation plane.

Chaturvedi and Van Gisbergen (1999, 2000) concluded that stimulation of the SC outputs zero vergence and desired saccade commands that interact with SC commands encoded for the three-dimensional saccade directed toward the visual target. The effect of the stimulation is to evoke a movement with version and vergence metrics reflecting an averaging process. While this concept makes a strong argument for participation of the SC in the control of vergence, additional experiments are required to support the hypothesis. A neural correlate of the vergence component within SC neurons has yet to be reported (Mays, 1996). Averaging effects observed during converging movements also need to be addressed during diverging movements with and without a saccade component.

ACCOMMODATION As our eyes converge or diverge, targets in the new depth plane become blurred. Accommodation is induced by contraction of the ciliary muscle, which changes the lens's radius of curvature. Thus, an important synkinesis exists between vergence and accommodation (Stark, 1983).

Stimulation of the rostral SC for prolonged periods and at fairly low intensities can alter accommodation in both eyes. Sawa and Ohtsuka (1994) found that after a latency of approximately 200msec, the dioptric power abruptly increased and then reached a plateau with prolonged microstimulation. The duration and maximum amplitude of the accommodative response were linearly correlated with stimulation duration and intensity, respectively. The low-threshold sites that produced accommodation were located within the superficial and intermediate layers of the rostral SC. Since the SC region that evoked accommodation overlaps, at least partially, with the location of fixation neurons, some neurons within the rostral SC may participate in active fixation as well as accommodation. Ohtsuka and Nagasaka (1999) injected different dyes into regions involved in controlling fixation (OPN region) and accommodation (e.g., posterior pretectal nucleus) and identified the retrogradely labeled cells in the SC. While double-labeled neurons were found throughout the SC, the population was highest in the rostral SC.

Given the close integration between the vergence and accommodation systems, it is important to understand

how vergence was perturbed by the stimulation; unfortunately, vergence eye movements were not recorded in these accommodation experiments. Further research is required to understand the role of SC in accommodation and vergence.

ARM MOVEMENT-RELATED NEURONS So far, we have addressed SC participation during saccades, eye movements other than saccades, and coordinated eye-head movements. Previous studies have also presented evidence that the SC participates in movements utilizing other skeletomotor systems. For example, stimulation of the cat SC evokes pinnae and vibrissae movements, and prolonged stimulation of the rat SC can evoke circling behavior (see Freedman et al., 1996, for a review). More recently, neurophysiological studies have suggested that the deeper layers of the SC and the underlying mesencephalic reticular formation in monkey may also participate in the control of arm movements (Stuphorn et al., 1999, 2000; Werner et al., 1997a; Werner et al., 1997b). These findings have important implications for our understanding of the neural control of integrated eye-hand movements.

Monkeys were trained to reach for targets in two conditions: one in which the subjects made a saccade to the target before touching it, and another in which the animals maintained fixation at the central stimulus while reaching for a target presented in the visual periphery. Arm movement-related discharge in SC neurons and electromyographic (EMG) activity from muscles of the shoulder, arm, trunk, and neck were recorded as the head-restrained animals performed the two tasks. The cross-correlations of discharge of many neurons and the EMG activity of several muscles, particularly those of the shoulder girdle, were highly significant. The discharge of most neurons and the EMG activity of many muscles led movement onset. For a small percentage of neurons, the average correlation coefficient between burst onset and movement onset was close to 1. Thus, the authors speculated that the neural discharge may provide the initiation signal for the arm movement.

The majority of these *reach* neurons did not discharge during saccades. Those that resided deeper than 4 mm below the surface of the SC and in the underlying mesencephalic reticular formation were not modulated by gaze position. Hoffman and colleagues (Stuphorn et al., 1999, 2000; Werner, et al., 1997a; Werner, et al., 1997b) proposed that these gaze-position-independent reach neurons may encode information more specific to the recruitment of appropriate muscles, although this notion needs to be tested.

Some dorsal neurons were intermingled within the saccade-related neurons of the SC, and many of them also exhibited visual, somatosensory, and/or saccade-related activity. Furthermore, the activity of reach neurons within

the SC was often modified by gaze position. Since the gaze-position-sensitive reach neurons were insensitive to the temporal profile of the reach movement, Hoffman and colleagues (Stuphorn et al., 1999, 2000; Werner, et al., 1997a; Werner, et al., 1997b) hypothesized that they might encode the amplitude and direction of the desired arm movement. It should be noted, however, that there is no evidence to support the hypothesis that either the location or firing rate of neurons with reach-related activity is related to either the amplitude or direction of an arm movement.

Although the extent of overlap in the saccade and reach movement fields still needs to be explored thoroughly, there appears to be a rough topography along the mediolateral extent—medial (lateral) regions encoding saccades and reach movements with upward (downward) movements. While saccades in the contralateral space were encoded by SC neurons, reach-related activity also included preferred movement directions into the ipsilateral hemifield. In this sense, the topography of the saccade and reach maps appears incongruent.

Summary

In this chapter, we evaluated several new lines of research that have emerged since the last detailed review of the role of SC in the control of orienting behavior (Sparks and Hartwich-Young, 1989). Over the past decade, significant research efforts have been devoted to understanding the role of collicular neurons in controlling the dynamics of saccades, determining whether the SC is inside or outside the feedback loop controlling saccade duration, and studying the participation of the SC in accommodation, fixation behavior, smooth pursuit, vergence, coordinated movements of the eyes and head, and reaching movements of the arms. We described problems in interpreting the results of experiments in which more than one movement system is active and issues that must be resolved before agreement can be reached on the expanded role of the SC in various movements.

Acknowledgments

We thank Drs. Edward Freedman and Jan Van Gisbergen for providing the figures. This research was supported by NIH Grants EY07009 (NJG) and EY01189 (DLS).

REFERENCES

- Aizawa, H., and R. H. Wurtz, 1998. Reversible inactivation of monkey superior colliculus. I. Curvature of saccadic trajectory, *J. Neurophysiol.*, 79:2082–2096.
- Anderson, R. W., E. L. Keller, N. J. Gandhi, and S. Das, 1998. Two dimensional saccade-related population activity in superior colliculus in monkey, *J. Neurophysiol.*, 80:798–817.

- Bacon, B. A., J. Villemagne, A. Bergeron, F. Lepore, and J. P. Guillemot, 1998. Spatial disparity coding in the superior colliculus of the cat, *Exp. Brain Res.*, 119:333–344.
- Baldi, P., and W. Heiligenberg, 1988. How sensory maps could enhance resolution through ordered arrangements of broadly tuned receivers, *Biol. Cybern.*, 59:313–318.
- Basso, M. A., R. J. Krauzlis, and R. H. Wurtz, 2000. Activation and inactivation of rostral superior colliculus neurons during smooth-pursuit eye movements in monkeys, *J. Neurophysiol.*, 84:892–908.
- Bergeron, A., and D. Guitton, 2000. Fixation neurons in the superior colliculus encode distance between current and desired gaze positions, *Nat. Neurosci.*, 3:932–939.
- Berman, N., C. Blakemore, and M. Cynader, 1975. Binocular interaction in the cat's superior colliculus, *J. Physiol.*, 246:595–615.
- Breznien, B., S. M. Lu, and J. W. Gnadt, 1996. Analysis of the step response of the saccadic feedback: system behavior, *Exp. Brain Res.*, 111:337–344.
- Büttner-Ennever, J. A., and A. K. Horn, 1994. Neuroanatomy of the saccadic omnipause neurons in nucleus raphe interpositus, in *Contemporary Ocular Motor and Vestibular Research: A Tribute to David A. Robinson* (A. F. Fuchs, T. Brandt, U. Büttner, and D. S. Zee, eds.), New York, Georg Thieme Verlag, pp. 488–495.
- Büttner-Ennever, J. A., A. K. Horn, V. Henn, and B. Cohen, 1999. Projections from the superior colliculus motor map to omnipause neurons in monkey, *J. Comp. Neurol.*, 413:55–67.
- Chaturvedi, V., and J. A. Van Gisbergen, 1999. Perturbation of combined saccade-vergence movements by microstimulation in monkey superior colliculus, *J. Neurophysiol.*, 81:2279–2296.
- Chaturvedi, V., and J. A. Van Gisbergen, 2000. Stimulation in the rostral pole of monkey superior colliculus: effects on vergence eye movements, *Exp. Brain Res.*, 132:72–78.
- Corneil, B. D., E. Olivier, and D. P. Munoz, 2002. Neck muscle activity evoked by stimulation of the monkey superior colliculus. II. Relationships with gaze shift initiation and comparison to volitional head movements, *J. Neurophysiol.*, 88:2000–2018.
- Cowie, R. J., and D. L. Robinson, 1994. Subcortical contributions to head movements in macaques. I. Contrasting effects of electrical stimulation of a medial pontomedullary region and the superior colliculus, *J. Neurophysiol.*, 72:2648–2664.
- Crawford, J. D., and D. Guitton, 1997. Visual-motor transformations required for accurate and kinematically correct saccades, *J. Neurophysiol.*, 78:1447–1467.
- Cynader, M., and N. Berman, 1972. Receptive-field organization of monkey superior colliculus, *J. Neurophysiol.*, 35:187–201.
- Dias, E. C., C. E. Rocha-Miranda, R. F. Bernardes, and S. L. Schmidt, 1991. Disparity selective units in the superior colliculus of the opossum, *Exp. Brain Res.*, 87:546–552.
- Ferraina, S., M. Paré, and R. H. Wurtz, 2000. Disparity sensitivity of frontal eye field neurons, *J. Neurophysiol.*, 83:625–629.
- Freedman, E. G., and D. L. Sparks, 1997a. Activity of cells in the deeper layers of the superior colliculus of the rhesus monkey: evidence for a gaze displacement command, *J. Neurophysiol.*, 78:1669–1690.
- Freedman, E. G., and D. L. Sparks, 1997b. Eye-head coordination during head-unrestrained gaze shifts in rhesus monkeys, *J. Neurophysiol.*, 77:2328–2348.
- Freedman, E. G., T. R. Stanford, and D. L. Sparks, 1996. Combined eye-head gaze shifts produced by electrical stimulation of the superior colliculus in rhesus monkeys, *J. Neurophysiol.*, 76:927–952.
- Gamlin, P. D., and K. Yoon, 2000. An area for vergence eye movement in primate frontal cortex, *Nature*, 407:1003–1007.
- Gandhi, N. J., and E. L. Keller, 1997. Spatial distribution and discharge characteristics of superior colliculus neurons antidromically activated from the omnipause region in monkey, *J. Neurophysiol.*, 78:2221–2225.
- Gandhi, N. J., and E. L. Keller, 1999. Comparison of saccades perturbed by stimulation of the rostral superior colliculus, the caudal superior colliculus, and the omnipause neuron region, *J. Neurophysiol.*, 82:3236–3253.
- Gnadt, J. W., and J. Beyer, 1998. Eye movements in depth: what does the monkey's parietal cortex tell the superior colliculus? *NeuroReport*, 9:233–238.
- Goossens, H. H., and A. J. Van Opstal, 2000. Blink-perturbed saccades in monkey. II. Superior colliculus activity, *J. Neurophysiol.*, 83:3430–3452.
- Gottlieb, J. P., C. J. Bruce, and M. G. MacAvoy, 1993. Smooth eye movements elicited by microstimulation in the primate frontal eye field, *J. Neurophysiol.*, 69:786–799.
- Groh, J. M., and D. L. Sparks, 1996. Saccades to somatosensory targets. III. Eye-position-dependent somatosensory activity in primate superior colliculus, *J. Neurophysiol.*, 75:439–453.
- Guitton, D., M. Crommelinck, and A. Roucoux, 1980. Stimulation of the superior colliculus in the alert cat. I. Eye movements and neck EMG activity evoked when the head is restrained, *Exp. Brain Res.*, 39:63–73.
- Hanes, D. P., and R. H. Wurtz, 2001. Interaction of the frontal eye field and superior colliculus for saccade generation, *J. Neurophysiol.*, 85:804–815.
- Hikosaka, O., and R. H. Wurtz, 1985. Modification of saccadic eye movements by GABA-related substances. I. Effect of muscimol and bicuculline in monkey superior colliculus, *J. Neurophysiol.*, 53:266–291.
- Hikosaka, O., and R. H. Wurtz, 1986. Saccadic eye movements following injection of lidocaine into the superior colliculus, *Exp. Brain Res.*, 61:531–539.
- Isa, T., T. Endo, and Y. Saito, 1998. The visuo-motor pathway in the local circuit of the rat superior colliculus, *J. Neurosci.*, 18:8496–8504.
- Jay, M. F., and D. L. Sparks, 1987. Sensorimotor integration in the primate superior colliculus. II. Coordinates of auditory signals, *J. Neurophysiol.*, 57:35–55.
- Jiang, H., D. Guitton, and K. E. Cullen, 1996. Near-response related neural activity in the rostral superior colliculus of the cat, *Soc. Neurosci. Abstr.*, 22:262.2.
- Kang, I., and C. Lee, 2000. Properties of saccade-related neurons in the cat superior colliculus: patterns of movement fields and discharge timing, *Exp. Brain Res.*, 131:149–164.
- Keller, E. L., and J. A. Edelman, 1994. Use of interrupted saccade paradigm to study spatial and temporal dynamics of saccadic burst cells in superior colliculus in monkey, *J. Neurophysiol.*, 72:2754–2770.
- Keller, E. L., N. J. Gandhi, and J. M. Shieh, 1996. Endpoint accuracy in saccades interrupted by stimulation in the omnipause region in monkey, *Vis. Neurosci.*, 13:1059–1067.
- Keller, E. L., N. J. Gandhi, and S. Vijay Sekaran, 2000. Activity in deep intermediate layer collicular neurons during interrupted saccades, *Exp. Brain Res.*, 130:227–237.
- Klier, E. M., H. Wang, and J. D. Crawford, 2001. The superior colliculus encodes gaze commands in retinal coordinates, *Nat. Neurosci.*, 4:627–632.
- Kobayashi, Y., Y. Saito, and T. Isa, 2001. Facilitation of saccade initiation by brainstem cholinergic system, *Brain Dev.*, 23:S24–27.

- Krauzlis, R. J., M. A. Basso, and R. H. Wurtz, 1997. Shared motor error for multiple eye movements, *Science*, 276:1693–1695.
- Krauzlis, R. J., M. A. Basso, and R. H. Wurtz, 2000. Discharge properties of neurons in the rostral superior colliculus of the monkey during smooth-pursuit eye movements, *J. Neurophysiol.*, 84:876–891.
- Krauzlis, R. J., and F. A. Miles, 1996. Transitions between pursuit eye movements and fixation in the monkey: dependence on context, *J. Neurophysiol.*, 76:1622–1638.
- Lee, C., W. H. Rohrer, and D. L. Sparks, 1988. Population coding of saccadic eye movements by neurons in the superior colliculus, *Nature*, 332:357–360.
- Lee, P. H., M. C. Helms, G. J. Augustine, and W. C. Hall, 1997. Role of intrinsic synaptic circuitry in collicular sensorimotor integration, *Proc. Natl. Acad. Sci. USA*, 94:13299–13304.
- MacAvoy, M. G., J. P. Gottlieb, and C. J. Bruce, 1991. Smooth-pursuit eye movement representation in the primate frontal eye field, *Cereb. Cortex*, 1:95–102.
- Mays, L. E., 1996. Activity of superior colliculus burst neurons during saccade-vergence interactions, *Soc. Neurosci. Abstr.*, 22:262.13.
- Mays, L. E., and D. L. Sparks, 1980. Dissociation of visual and saccade-related responses in superior colliculus neurons, *J. Neurophysiol.*, 43:207–232.
- McIlwain, J. T., 1975. Visual receptive fields and their images in superior colliculus of the cat, *J. Neurophysiol.*, 38:219–230.
- McIlwain, J. T., 1982. Lateral spread of neural excitation during microstimulation in intermediate gray layer of cat's superior colliculus, *J. Neurophysiol.*, 47:167–178.
- McIlwain, J. T., 1991. Distributed spatial coding in the superior colliculus: a review, *Vis. Neurosci.*, 6:3–13.
- Meredith, M. A., and A. S. Ramoa, 1998. Intrinsic circuitry of the superior colliculus: pharmacophysiological identification of horizontally oriented inhibitory interneurons, *J. Neurophysiol.*, 79:1597–1602.
- Missal, M., and E. L. Keller, 2002. Common inhibitory mechanism for saccades and smooth-pursuit eye movements. *J. Neurophysiol.*, 88:1880–1892.
- Missal, M., P. Lefèvre, A. Delinte, M. Crommelinck, and A. Roucoux, 1996. Smooth eye movements evoked by electrical stimulation of the cat's superior colliculus, *Exp. Brain Res.*, 107:382–390.
- Mooney, R. D., X. Huang, and R. W. Rhoades, 1992. Functional influence of interlaminar connections in the hamster's superior colliculus, *J. Neurosci.*, 12:2417–2432.
- Morris, E. J., and S. G. Lisberger, 1987. Different responses to small visual errors during initiation and maintenance of smooth-pursuit eye movements in monkeys, *J. Neurophysiol.*, 58:1351–1369.
- Moschovakis, A. K., Y. Dalezios, J. Petit, and A. A. Grantyn, 1998. New mechanism that accounts for position sensitivity of saccades evoked in response to stimulation of superior colliculus, *J. Neurophysiol.*, 80:3373–3379.
- Moschovakis, A. K., G. G. Gregoriou, and H. E. Savaki, 2001. Functional imaging of the primate superior colliculus during saccades to visual targets, *Nat. Neurosci.*, 4:1026–1031.
- Moschovakis, A. K., C. A. Scudder, and S. M. Highstein, 1996. The microscopic anatomy and physiology of the mammalian saccadic system, *Prog. Neurobiol.*, 50:133–254.
- Munoz, D. P., M. C. Dorris, M. Paré, and S. Everling, 2000. On your mark, get set: brainstem circuitry underlying saccadic initiation, *Can. J. Physiol. Pharmacol.*, 78:934–944.
- Munoz, D. P., and D. Guitton, 1989. Fixation and orientation control by the tecto-reticulo-spinal system in the cat whose head is unrestrained, *Rev. Neurol. (Paris)*, 145:567–579.
- Munoz, D. P., D. Guitton, and D. Pélisson, 1991. Control of orienting gaze shifts by the tectoreticulospinal system in the head-free cat. III. Spatiotemporal characteristics of phasic motor discharges, *J. Neurophysiol.*, 66:1642–1666.
- Munoz, D. P., and P. J. Istvan, 1998. Lateral inhibitory interactions in the intermediate layers of the monkey superior colliculus, *J. Neurophysiol.*, 79:1193–1209.
- Munoz, D. P., D. M. Waitzman, and R. H. Wurtz, 1996. Activity of neurons in monkey superior colliculus during interrupted saccades, *J. Neurophysiol.*, 75:2562–2580.
- Munoz, D. P., and R. H. Wurtz, 1993. Fixation cells in monkey superior colliculus. I. Characteristics of cell discharge, *J. Neurophysiol.*, 70:559–575.
- Munoz, D. P., and R. H. Wurtz, 1995a. Saccade-related activity in monkey superior colliculus. I. Characteristics of burst and buildup cells, *J. Neurophysiol.*, 73:2313–2333.
- Munoz, D. P., and R. H. Wurtz, 1995b. Saccade-related activity in monkey superior colliculus. II. Spread of activity during saccades, *J. Neurophysiol.*, 73:2334–2348.
- Ohtsuka, K., and Y. Nagasaka, 1999. Divergent axon collaterals from the rostral superior colliculus to the pretectal accommodation-related areas and the omnipause neuron area in the cat, *J. Comp. Neurol.*, 413:68–76.
- Paré, M., M. Crommelinck, and D. Guitton, 1994. Gaze shifts evoked by stimulation of the superior colliculus in the head-free cat conform to the motor map but also depend on stimulus strength and fixation activity, *Exp. Brain Res.*, 101:123–139.
- Paré, M., and D. Guitton, 1994. The fixation area of the cat superior colliculus: effects of electrical stimulation and direction connection with brainstem omnipause neurons, *Exp. Brain Res.*, 101:109–122.
- Peck, C. K., 1989. Visual responses of neurones in cat superior colliculus in relation to fixation of targets, *J. Physiol. (Lond.)*, 414:301–315.
- Peck, C. K., J. A. Baro, and S. M. Warder, 1995. Effects of eye position on saccadic eye movements and on the neuronal responses to auditory and visual stimuli in cat superior colliculus, *Exp. Brain Res.*, 103:227–242.
- Pélisson, D., L. Goffart, A. Guillaume, N. Catz, and G. Raboyeau, 2001. Early head movements by visual stimuli or collicular electrical stimulation in the cat, *Vis. Res.*, 41:3283–3294.
- Pettit, D. L., M. C. Helms, P. Lee, G. J. Augustine, and W. C. Hall, 1999. Local excitatory circuits in the intermediate gray layer of the superior colliculus, *J. Neurophysiol.*, 81:1424–1427.
- Populin, L. C., and T. C. T. Yin, 1998. Sensitivity of auditory cells in the superior colliculus to eye position in the behaving cat, in *Psychological and Physiological Advances in Hearing* (A. R. Palmer, A. Q. Summerfield, and R. Meddis, eds.), London: Whurr, pp. 441–448.
- Port, N. L., M. A. Sommer, and R. H. Wurtz, 2000. Multielectrode evidence for spreading activity across the superior colliculus movement map, *J. Neurophysiol.*, 84:344–357.
- Quaia, C., H. Aizawa, L. M. Optican, and R. H. Wurtz, 1998. Reversible inactivation of monkey superior colliculus. II. Maps of saccadic deficits, *J. Neurophysiol.*, 79:2097–2110.
- Richmond, B. J., L. M. Optican, M. Podell, and H. Spitzer, 1987. Temporal encoding of two-dimensional patterns by single units in primate inferior temporal cortex. I. Response characteristics, *J. Neurophysiol.*, 57:132–146.

- Robinson, D. A., 1972. Eye movements evoked by collicular stimulation in the alert monkey, *Vis. Res.*, 12:1795–1808.
- Robinson, D. A., 1975. Oculomotor control signals, in *Basic Mechanisms of Ocular Motility and Their Clinical Implications*, vol. 24 (P. Bach-y-Rita and G. Lennerstrand, eds.), Oxford: Pergamon Press, pp. 337–374.
- Robinson, D. L., and C. D. Jarvis, 1974. Superior colliculus neurons studied during head and eye movements of the behaving monkey, *J. Neurophysiol.*, 37:533–540.
- Roucoux, A., D. Guitton, and M. Crommelinck, 1980. Stimulation of the superior colliculus in the alert cat. II. Eye and head movements evoked when the head is unrestrained, *Exp. Brain Res.*, 39:75–85.
- Sawa, M., and K. Ohtsuka, 1994. Lens accommodation evoked by microstimulation of the superior colliculus in the cat, *Vis. Res.*, 34:975–981.
- Schiller, P. H., J. H. Sandell, and J. H. Maunsell, 1987. The effect of frontal eye field and superior colliculus lesions on saccadic latencies in the rhesus monkey, *J. Neurophysiol.*, 57:1033–1049.
- Schiller, P. H., and M. Stryker, 1972. Single-unit recording and stimulation in superior colliculus of the alert rhesus monkey, *J. Neurophysiol.*, 35:915–924.
- Schlag-Rey, M., J. Schlag, and P. Dassonville, 1992. How the frontal eye field can impose a saccade goal on superior colliculus neurons, *J. Neurophysiol.*, 67:1003–1005.
- Schlag-Rey, M., J. Schlag, and B. Shook, 1989. Interactions between natural and electrically evoked saccades. I. Differences between sites carrying retinal error and motor error signals in monkey superior colliculus, *Exp. Brain Res.*, 76:537–547.
- Scudder, C. A., C. R. S. Kaneko, and A. F. Fuchs, 2002. The brainstem burst generator for saccadic eye movements: a modern synthesis. *Exp. Brain Res.*, 142:439–462.
- Segraves, M. A., and M. E. Goldberg, 1992. Properties of eye and head movements evoked by electrical stimulation of the monkey superior colliculus, in *Head-Neck Sensory Motor Systems* (A. Berthoz, W. Graf, and P. P. Vidal, eds.), New York: Oxford University Press, pp. 292–295.
- Segraves, M. A., and M. E. Goldberg, 1994. Effect of stimulus position and velocity upon the maintenance of smooth pursuit eye velocity, *Vis. Res.*, 34:2477–2482.
- Soetedjo, R., C. R. S. Kaneko, and A. F. Fuchs, 2002a. Evidence that the superior colliculus participates in the feedback control of saccadic eye movements, *J. Neurophysiol.*, 87:679–695.
- Soetedjo, R., C. R. S. Kaneko, and A. F. Fuchs, 2002b. Evidence against a moving hill in the superior colliculus during saccadic eye movements in the monkey, *J. Neurophysiol.*, 87:2778–2789.
- Sparks, D. L., W. H. Rohrer, and Y. Zhang, 2000. The role of the superior colliculus in saccade initiation: a study of express saccades and the gap effect, *Vis. Res.*, 40:2763–2777.
- Sparks, D. L., 1993. Are gaze shifts controlled by a “moving hill” of activity in the superior colliculus? *Trends Neurosci.*, 16:214–218.
- Sparks, D. L., 1999. Conceptual issues related to the role of the superior colliculus in the control of gaze, *Curr. Opin. Neurobiol.*, 9:698–707.
- Sparks, D. L., and N. J. Gandhi, 2003. Single cell signals: an oculomotor perspective, in *Space Coding and Action Production: Progress in Brain Research*, vol. 142 (C. Prablanc, D. Pélisson, and Y. Rossetti, eds.), Amsterdam: Elsevier, pp. 35–53.
- Sparks, D. L., and R. Hartwich-Young, 1989. The deep layers of the superior colliculus, *Rev. Oculomot. Res.*, 3:213–255.
- Sparks, D. L., R. Holland, and B. L. Guthrie, 1976. Size and distribution of movement fields in the monkey superior colliculus, *Brain Res.*, 113:21–34.
- Sparks, D. L., C. Lee, and W. H. Rohrer, 1990. Population coding of the direction, amplitude, and velocity of saccadic eye movements by neurons in the superior colliculus, *Cold Spring Harb. Symp. Quant. Biol.*, 55:805–811.
- Sparks, D. L., and J. D. Porter, 1983. Spatial localization of saccade targets. II. Activity of superior colliculus neurons preceding compensatory saccades, *J. Neurophysiol.*, 49:64–74.
- Stanford, T. R., E. G. Freedman, and D. L. Sparks, 1996. Site and parameters of microstimulation: evidence for independent effects on the properties of saccades evoked from the primate superior colliculus, *J. Neurophysiol.*, 76:3360–3381.
- Stark, L., 1983. Normal and abnormal vergence, in *Vergence Eye Movements: Basic and Clinical Aspects* (C. M. Schor and K. J. Ciuffreda, eds.), Boston: Butterworths, pp. 3–13.
- Stein, B. E., and M. A. Meredith, 1993. *The Merging of the Senses. Cognitive Neuroscience Series*, Cambridge, MA: MIT Press.
- Stryker, M. P., and P. H. Schiller, 1975. Eye and head movements evoked by electrical stimulation of monkey superior colliculus, *Exp. Brain Res.*, 23:103–112.
- Stuphorn, V., E. Bauswein, and K. P. Hoffmann, 2000. Neurons in the primate superior colliculus coding for arm movements in gaze-related coordinates, *J. Neurophysiol.*, 83:1283–1299.
- Stuphorn, V., K. P. Hoffmann, and L. E. Miller, 1999. Correlation of primate superior colliculus and reticular formation discharge with proximal limb muscle activity, *J. Neurophysiol.*, 81:1978–1982.
- Van Opstal, A. J., J. A. Van Gisbergen, and A. C. Smit, 1990. Comparison of saccades evoked by visual stimulation and collicular electrical stimulation in the alert monkey, *Exp. Brain Res.*, 79:299–312.
- Waitzman, D. M., T. P. Ma, L. M. Optican, and R. H. Wurtz, 1991. Superior colliculus neurons mediate the dynamic characteristics of saccades, *J. Neurophysiol.*, 66:1716–1737.
- Werner, W., S. Dannenberg, and K. P. Hoffmann, 1997a. Arm-movement-related neurons in the primate superior colliculus and underlying reticular formation: comparison of neuronal activity with EMGs of muscles of the shoulder, arm and trunk during reaching, *Exp. Brain Res.*, 115:191–205.
- Werner, W., K. P. Hoffmann, and S. Dannenberg, 1997b. Anatomical distribution of arm-movement-related neurons in the primate superior colliculus and underlying reticular formation in comparison with visual and saccadic cells, *Exp. Brain Res.*, 115:206–216.
- Wurtz, R. H., and M. E. Goldberg, 1972. Activity of superior colliculus in behaving monkey. III. Cells discharging before eye movements, *J. Neurophysiol.*, 35:575–586.

98 The Dialogue between Cerebral Cortex and Superior Colliculus: Implications for Saccadic Target Selection and Corollary Discharge

MARC A. SOMMER AND ROBERT H. WURTZ

OUR SENSE OF VISION and our eye movements are intimately intertwined. Because high-acuity vision requires foveal inspection, we frequently make rapid or *saccadic* eye movements to shift images of interest onto the fovea. Visual perception provides information about where to look next and thus directs our saccades, and the resulting saccades move the retinas and therefore influence vision. Understanding how vision and saccades work together instead of in opposition to each other is critical for understanding how we see so effortlessly and efficiently.

It is becoming clear that cognitive processes play key roles in facilitating the cooperation between vision and saccades. By *cognitive processes*, we mean processes of information manipulation, in contrast to more rudimentary functions of sensory detection and movement execution. Cognitive processes range from the conscious and voluntary (e.g., rehearsal during short-term memory) to the unconscious and involuntary (e.g., procedural learning). In this chapter we concentrate on two cognitive processes important for visuosaccadic behavior and discuss some of the neuronal networks that mediate them.

The first cognitive process is the translation of generalized visual analysis into a specific decision about where to look next. We are usually aware of numerous objects in the visual scene, but we can make a saccade to only one object at a time. An efficient selection process is clearly needed. This first cognitive function, often conscious and voluntary in nature, might be thought of as a *forward* function in that information about the visual scene influences movement. We call it *saccadic target selection*, a term encapsulating multiple operations such as shifting attention, deciding where to look next, and preparing to move.

The second cognitive process is that which allows us to maintain a stable visual percept despite all the saccades we make. Saccades move the retinas at high velocity, and if our visual system did not have foreknowledge about these

sudden shifts, they would induce the alarming percept of a world constantly jumping around. Our visual system uses advance information about each upcoming saccade to lessen the imminent adverse effects of moving the retinas. This second cognitive function (an unconscious and involuntary one) might be thought of as a *reverse* function in that information about movement influences vision. We refer to it as a *corollary discharge* function (after Sperry, 1950), because it involves monitoring an internal correlate of a neuronal movement command. As will be discussed, corollary discharge has other uses as well, such as helping to produce a sequence of movements.

How does the brain accomplish these cognitive functions? We have known that both the cerebral cortex and the brainstem are important components of the visuosaccadic system for over a century (for a historical review see Tehovnik et al., 2000). Since about 1970, moreover, this research has benefited from a growing interest in exploring the neuronal bases of cognitive processes. Currently, it is well understood that many brain regions once thought to be primarily involved *either* in passive visual analysis *or* in eye movement generation are, in fact, involved in *both* and are additionally involved in the cognitive processes accompanying vision and eye movements. One such structure is the superior colliculus (SC), which lies on the roof of the midbrain, and other such structures lie in the cerebral cortex.

The cognitive functions that we consider are mediated by activity coursing in a network distributed throughout the brain; neither saccadic target selection nor corollary discharge arises from activity within a single brain area. As we will discuss, the projections from cerebral cortex to the SC have been studied in great detail, and the results indicate that saccadic target selection develops gradually from earlier, more visually related stages in cortex to later, more movement-related stages in the SC. Furthermore, there are at least two ascending pathways from the SC to cerebral

cortex. One seems to contribute to corollary discharge, and the other may contribute to spatial visual attention.

The interconnections between cerebral cortex and SC

Saccades are mediated by a system extending from the retina to the extraocular muscles that has been most extensively studied in the rhesus monkey, the animal model on which we will concentrate. The visuosaccadic system can be regarded as having three limbs, two of which are the afferent and efferent limbs (Fig. 98.1A). The afferent limb provides visual input from the retina. This pathway branches into two main routes, one coursing to the lateral geniculate nucleus and then to striate cortex (also known as V1) and another coursing to the superficial layers of the SC. The efferent limb provides motor output to the extraocular muscles. Motor commands are produced in the saccade generating circuitry in the brainstem, a collection of regions in the pons and midbrain that receives descending input from the SC and other structures.

The third limb is intermediary, connecting the afferent and efferent limbs (Fig. 98.1B). It is in this vast network of “in-between” areas that activity related to cognitive processes presumably resides, and interconnections between cerebral cortex and the SC are a major component of this network. Several regions of cerebral cortex project monosynaptically to the SC, and the SC reciprocates by projecting disynaptically up to many cerebral cortical regions via the thalamus (for reviews of the anatomy, see Leichnetz and Goldberg, 1988; Sparks and Hartwich-Young, 1989).

The SC and certain cortical regions are necessary for saccade generation. Reversible inactivation of the frontal eye field (Fig. 98.1B, FEF) causes severe deficits in the ability to make saccades to remembered targets (Chafee and Goldman-Rakic, 2000; Dias and Segraves, 1999; Sommer and Tehovnik, 1997), and similar effects have been reported for inactivation of the lateral intraparietal area (Fig. 98.1B, LIP) (Li et al., 1999). Reversible inactivation of the SC causes deficits in saccade production for all saccades made to either remembered or visual targets (Aizawa and Wurtz, 1998; Hikosaka and Wurtz, 1985; Lee et al., 1988; Schiller et al., 1987). Permanent ablation of either the SC or the frontal eye field causes serious deficits for a week or so, after which monkeys largely recover, but combined bilateral lesions of both the SC and the frontal eye field permanently devastate saccadic behavior (Schiller et al., 1980). The influence of many cortical regions seems to depend in large part on their projections to the SC; for example, the ability to evoke saccades electrically from the frontal eye field is severely impaired by inactivating the SC (Hanes and Wurtz, 2001), and the ability to evoke saccades electrically from the parietal and occipital lobes is abolished by ablating the SC

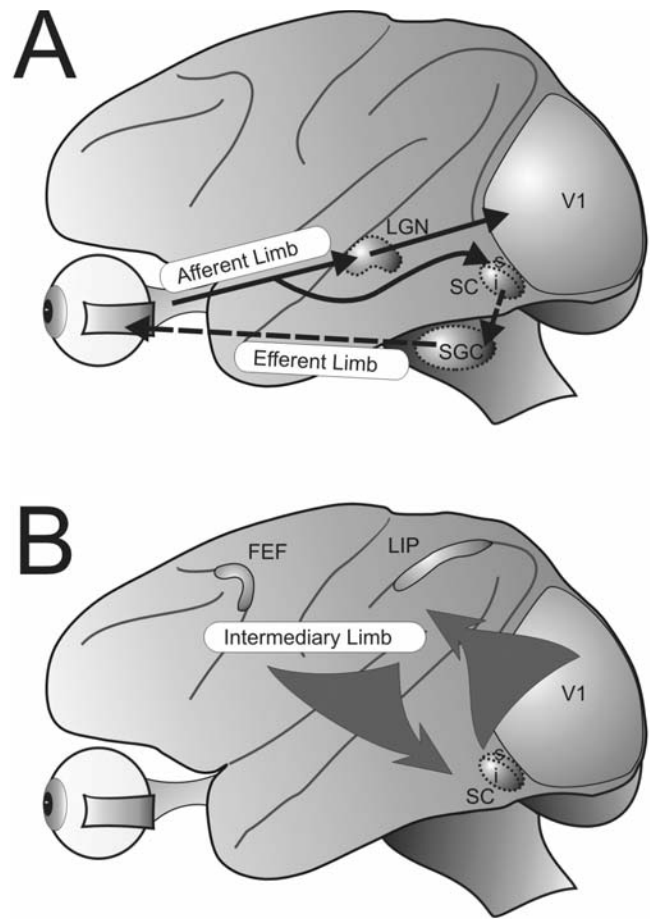


FIGURE 98.1. The three limbs of the visuosaccadic system in the monkey. *A*, The afferent limb, which provides visual input from the retina, and the efferent limb, which causes muscle contractions. Structures with dashed outlines are subcortical. There are other targets of retinal projections, too, but they are beyond the scope of this chapter. SC, superior colliculus (s, superficial layer; i, intermediate layer); LGN, lateral geniculate nucleus; V1, striate cortex; SGC, saccade generating circuitry. *B*, The intermediary limb, which connects the afferent and efferent limbs. This limb is a network of brain regions; prominent among them are the frontal eye field (FEF) and the lateral intraparietal area (LIP).

and the frontal eye field (Keating and Gooley, 1988; Schiller, 1977).

In sum, there is good reason to suspect that the overall network composed of the cerebral cortex and the SC is important for saccade generation. In the first half of this chapter, we will review what is known about the signals descending from cerebral cortex to the SC. Investigated so far have been three direct projections emanating from the frontal eye field, the lateral intraparietal area, and the striate cortex (Fig. 98.2A) and one indirect pathway, a basal ganglia route that relays signals from cortex to the SC via the substantia nigra pars reticulata (Fig. 98.2B). Then we will discuss the signals flowing in ascending pathways from the SC to cerebral cortex. Two such pathways are starting to be well

characterized, one that reaches the frontal cortex via the mediodorsal thalamus and another that reaches the parietal cortex via the pulvinar (Fig. 98.2C).

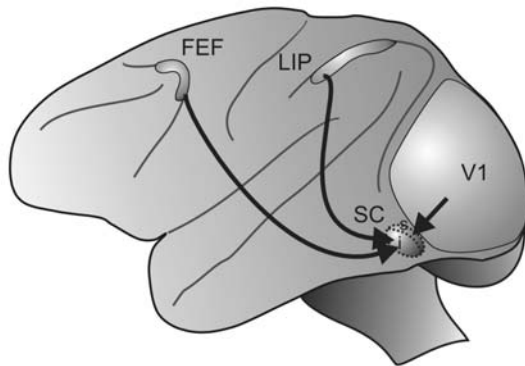
To eavesdrop on the dialogue between cerebral cortex and the SC, investigators have identified neurons that talk back and forth between the areas using two methods: antidromic and orthodromic activation. *Antidromic* activation is used to see if a recorded neuron in one region (e.g., a part of cortex) projects to another region (e.g., the SC). Figure 98.3A shows the logic. If electrical stimulation in region B causes a

recorded neuron in region A to fire at a fixed latency, and if other tests including one known as the *collision test* are successful (see the review by Lemon, 1984), then it is concluded that the neuron in region A is being activated through its own axon; therefore, the neuron projects to region B. *Orthodromic* activation is used to see if a recorded neuron in one region is receiving input from another region (Fig. 98.3B). If stimulation in region A causes a recorded neuron in region B to fire at a jittery latency and the collision test fails, then it is concluded that the neuron is being activated through synapses; therefore, this neuron receives input from region A. After a neuron's connections are identified with one or both of these methods, it is then analyzed to determine what signals it is carrying, as discussed next.

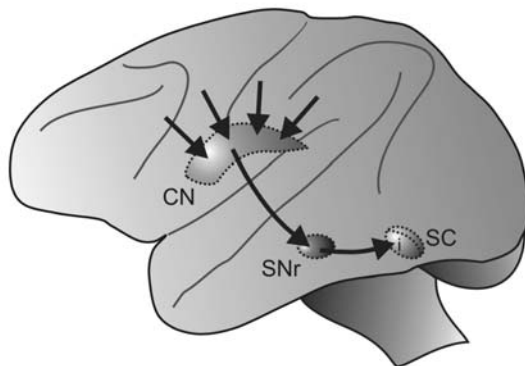
Descending projections from cortex to the SC

THE STAGES OF NEURONAL ACTIVITY RELATED TO VISUOSACCADIC BEHAVIOR Generating a saccade in response to visual stimulation involves a series of steps including analyzing the visual scene, attending to objects within it, remembering the locations of objects, deciding to look somewhere, preparing a saccade, and executing the movement. It is reasonable to presume that these steps are accompanied at the neuronal level by sequential stages of activity. Figure 98.4 illustrates examples of neuronal activity that may contribute to various stages of visuosaccadic behavior. These examples were recorded from two SC-projecting cortical neurons (a lateral intraparietal area neuron, Fig. 98.4B, *top*, and a frontal eye field neuron, Fig. 98.4B, *middle*), both identified using antidromic activation, and from a neuron within the intermediate layers of the SC (Fig. 98.4B, *bottom*). The neurons were studied while the monkey performed a visual delayed-saccade task (Fig. 98.4A, *left*). The monkey fixated a spot of light during a baseline period, and then a target flashed in the periphery (Fig. 98.4A, *top left*). The monkey was required to maintain fixation for an extended delay period (500 to 1000 msec) until the

A Direct Descending Projections



B Indirect Descending Pathway



C Ascending Pathways

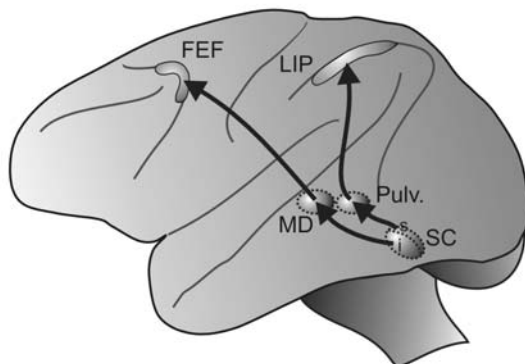


FIGURE 98.2. The descending projections and ascending pathways connecting cerebral cortex and the SC that have thus far been examined. *A*, Direct projections from cerebral cortex to the SC. The frontal eye field (FEF) and lateral intraparietal area (LIP) project to the SC intermediate layers, and the striate cortex (V1) projects to the SC superficial layers. *B*, Indirect route from cerebral cortex to the SC via the basal ganglia. Many regions of cerebral cortex project to the caudate nucleus (CN), which in turn projects to the substantia nigra. The substantia nigra pars reticulata (SNr) relays these signals to the intermediate SC. *C*, The ascending pathways from the SC to cerebral cortex. The intermediate SC projects to the mediodorsal thalamus (MD), which in turn projects to the frontal eye field and other prefrontal regions. The superficial SC projects to the pulvinar (Pulv.), which in turn projects to the lateral intraparietal area and other extrastriate regions.

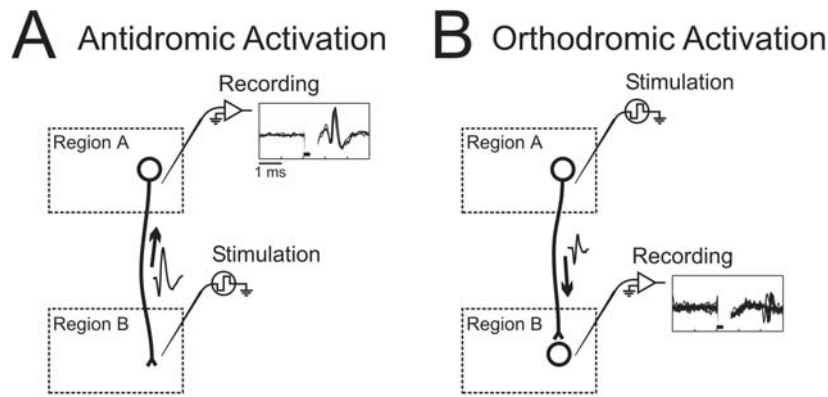
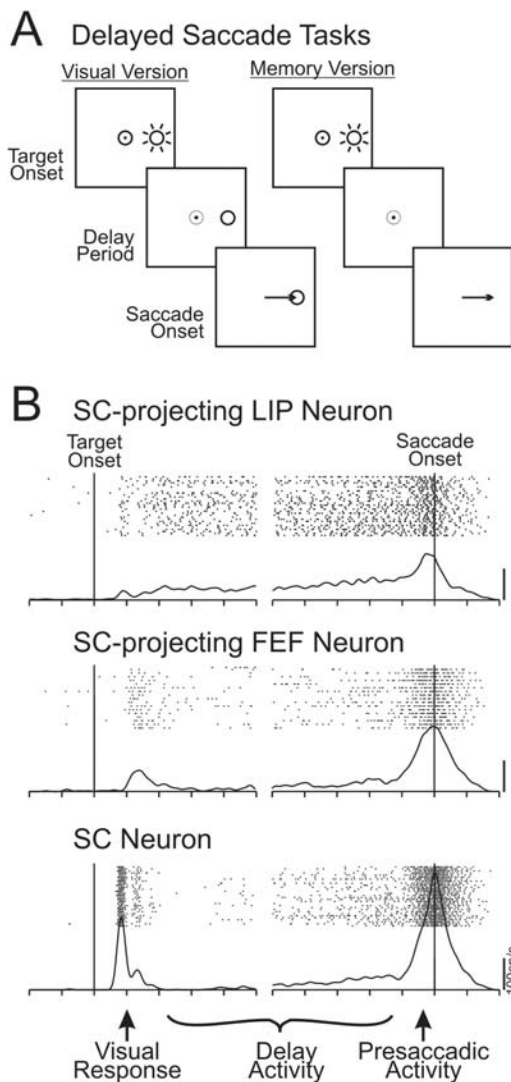


FIGURE 98.3. Methods for evaluating the signals sent between brain regions. *A*, In antidromic activation, one region, *B*, is stimulated while recording from a neuron in another region, *A*. Stimulation-evoked action potentials travel backward through the axon of the neuron and are recorded at the cell body. *B*, In orthodromic activation, one region, *A*, is stimulated while recording from a

neuron in another region, *B*. Stimulation evoked action potentials travel forward through projections and drive the neuron via synapses, and resultant postsynaptic action potentials are recorded at the cell body. (Spike waveform pictures modified from Sommer and Wurtz, 1998.)



fixation spot disappeared, which was the cue to move (Fig. 98.4*A*, middle left). Then the monkey was required to make a saccade to the location of the target (Fig. 98.4*A*, bottom left). Also used was a memory version of the task (Fig. 98.4*A*, right), which was identical to the visual version except that the target appeared only briefly so that its location had to be remembered during the delay period. These are classic delayed-response tasks similar to those introduced by Jacobsen (1935, 1936) for studying short-term memory deficits after frontal lobe damage, except that his experiments involved forelimb movements; the tasks were adapted for oculomotor research by Hikosaka and Wurtz (1983a). All the example neurons (Fig. 98.4*B*) were quiet during a baseline period before target onset and then, just after target onset, they exhibited a sudden increase of activity that probably represented detection of the target (Fig. 98.4*B*, visual response). Each neuron's activity then remained elevated above the baseline level during the delay period (Fig. 98.4*B*, delay activity). Just before saccade onset, the neurons exhibited

FIGURE 98.4. Visual, delay, and presaccadic neuronal activity. *A*, The signals carried by identified neurons typically are characterized using one or more versions of the delayed-saccade task. See text for details. *B*, Examples of activity recorded from an SC-projecting lateral intraparietal area (LIP) neuron, an SC-projecting frontal eye field (FEF) neuron, and an intermediate layer SC neuron while monkeys performed the visual version of the delayed-saccade task. In each panel the activity is aligned on target onset (left) and saccade onset (right). Rasters of dots show individual action potentials (each row is from a different trial). Curves show averaged firing rates (scale at the right). The time scale is 100 msec per tick on the abscissa. At the bottom, the visual responses, delay activity, and presaccadic activity are labeled. (Modified from Wurtz et al., 2001.)

increases in activity that probably represented commands to move the eyes (Fig. 98.4B, *presaccadic activity*).

It is the delay activity that is of particular interest to us because it occurs after the initial visual response and before a saccade is made, during the time when saccadic target selection should be occurring. Ever since the discovery of delay activity by Fuster and Alexander (1971), investigators have used a variety of methods to tease out what this activity represents. Studies of neurons throughout the brain have found that delay activity can be a correlate of nearly every cognitive function imaginable, including various types of memory, spatial attention, representation of task rules, operations linked to categorization (e.g., whether a viewed animal is a cat or dog), and movement preparation (for reviews see Fuster, 1997; Miller, 2000). Most of these studies examined neurons without identifying their connections, for example, without determining if they projected to the SC. In the following sections, we will discuss only those studies that examined neurons explicitly identified as sending delay activity and other signals to the SC.

SIGNALS SENT FROM FRONTAL CORTEX TO THE SC The first investigators to examine the signals sent from any cerebral cortical area to the SC in behaving monkeys were Segraves and Goldberg (1987), who used antidromic activation to identify SC-projecting frontal eye field neurons and studied their activity while monkeys performed a variety of tasks that included delayed saccade tasks. The results established that a variety of signals are transmitted from the frontal eye field to the SC, including visual responses, delay activity, and presaccadic bursts of activity. Segraves and Goldberg concluded, however, that the predominant output signal was a movement command represented by the presaccadic burst, implying that earlier visual detection and saccadic target selection functions are performed, for the most part, locally within the cerebral cortex.

To characterize more thoroughly the delay activity sent from frontal eye field to the SC, Sommer and Wurtz (2001a) studied SC-projecting frontal eye field neurons while monkeys performed a go/no-go delayed-saccade task. This task was similar to that diagrammed in Figure 98.4A, except that during the delay period the color of the fixation point changed. In half of the trials (go trials) the color changed to green, instructing the monkey to make a saccade to the target location after the delay period, and in the remaining trials (no-go trials) the color changed to red, instructing the monkey to maintain fixation after the delay period. This revealed whether delay activity was related to producing saccades. Separate visual and memory versions of the task revealed whether this delay activity was related more closely to working memory, to visual attention, or to movement preparation. They found, first, that delay activity was quite common in the SC-projecting frontal eye field neurons

(occurring in ~75% of the neurons) and, second, that the activity clearly did not represent only a single cognitive function. Most prevalent was delay activity related to working memory and to saccade preparation.

This study also revealed that the composition of signals sent from the frontal eye field to the SC was actually very diverse and included purely visual neurons as well as purely movement-related neurons (Sommer and Wurtz, 2000a). Reasons why these results differ from those of Segraves and Goldberg (1987), who found no purely visual neurons and a larger fraction of purely movement-related neurons, are discussed elsewhere (Sommer and Wurtz, 2000a). It is now well established that the signals carried by SC-projecting frontal eye field neurons are similar to those generally found in the frontal eye field (also noted by Everling and Munoz, 2000). This is true not only for the frontal eye field in monkey, but also for the homologous region (area 6) in cat (Weyand and Gafka, 1998a, 1998b).

Two other important signals are also transmitted from the frontal eye field to the SC. First, the projection carries fixation-related activity that starts when a monkey foveates a spot and continues even if the spot is briefly removed (Segraves and Goldberg, 1987). This activity seems to be sent to the entire SC (Sommer and Wurtz, 2000a), not just to the rostral SC where neurons with similar fixation-related signals are found (Munoz and Wurtz, 1993). Therefore, the descending fixation signals from the frontal eye field may work in parallel with rostral SC fixation signals to inhibit caudal, saccade-related SC neurons and keep the eyes steady. Second, the projection from the frontal eye field to the SC carries activity related to preparatory set (Everling and Munoz, 2000). In a task where the monkey was instructed by the fixation point color to make a saccade either toward or away from a suddenly appearing peripheral target, movement-related neurons projecting from the frontal eye field to the SC showed, on average, higher activity during the fixation period and just after target onset when the instruction was to make a saccade *toward* the target. Therefore, the projection may contribute to larger visual responses in the SC when stimuli are to be targeted for saccades, which may help shorten reaction times. These two issues, of fixation-related activity and preparatory set, are discussed further below.

Although the frontal eye field sends a multitude of signals to the SC, this does not prove that the signals affect the activity of SC neurons. To address this issue of causality, other studies used methods involving orthodromic stimulation. Guitton and Mandl (1974) showed, in paralyzed cats, that stimulating the frontal eye field can increase or decrease the activity of SC neurons. Schlag-Rey et al. (1992) examined the issue in behaving monkeys, stimulating the frontal eye field while recording from SC neurons during delayed-saccade tasks. They found that the sign of the stimulation-

evoked change in SC activity was a function of topography: when the frontal eye field and SC sites represented similar saccadic vectors, frontal eye field stimulation caused SC activity to increase, but if the vectors were mismatched, stimulation caused SC activity to decrease. Because the direct projection from the frontal eye field is presumably excitatory (glutamatergic), the decreases in activity seen in these studies likely were mediated by multisynaptic pathways, for example, via GABAergic interneurons within the SC.

In sum, the projection from the frontal eye field to the SC carries an abundance of signal types and is functionally potent. Besides the frontal eye field, other frontal regions such as the supplementary eye field also project to the SC and contain neurons having visual responses, delay activity, and presaccadic activity (reviewed by Schall, 1997). However, antidromic and orthodromic activation studies still need to be performed to determine precisely how these other areas influence the SC.

SIGNALS SENT FROM PARIETAL CORTEX TO THE SC Paré and Wurtz (1997) provided the first description of signals sent from any area of parietal cortex to the SC. They focused on the lateral intraparietal area, probably the most important parietal region for saccadic behavior. Using standard delayed-saccade tasks (Fig. 98.4.4), they demonstrated that SC-projecting lateral intraparietal area neurons carry visual, delay, presaccadic, and fixation-related activity. Not surprisingly, given the results already discussed in this chapter, the distribution of signals seemed quite similar to the distribution generally found in the lateral intraparietal area. A go/no-go task identical to that described above was used to study the delay activity in detail, revealing it to be highly diverse. In some neurons the activity seemed related to attending to or remembering the visual target, and in others it seemed more related to preparing the saccade. In all these ways, the SC-projecting lateral intraparietal area neurons were qualitatively similar to SC-projecting frontal eye field neurons. Differences could be detected only quantitatively (Wurtz et al., 2001), as discussed below.

At about the same time, Gnadt and Beyer (1998) showed that SC-projecting lateral intraparietal area neurons are tuned for binocular disparity, providing information about visual depth. This was expanded upon by Ferraina et al. (2002), who concluded that the disparity tuning was quite broad. Finally, the latter authors additionally found that some neurons in the adjacent ventral intraparietal area exhibiting strong sensitivity to visual motion also project to the SC (Paré et al., 1999).

SIGNALS SENT INDIRECTLY FROM CORTEX TO THE SC VIA THE BASAL GANGLIA In addition to the direct connections that carry signals from cerebral cortex to the SC, there is a crit-

ical indirect route through the basal ganglia. Many cerebral cortical areas project to the caudate nucleus, which in turn projects to the substantia nigra. Both of these projections are excitatory. The substantia nigra pars reticulata contains GABAergic neurons that project to and inhibit SC neurons. Unlike the signals sent from cortex to the SC, which usually take the form of elevations of activity above a quiet baseline level, the signals sent from the substantia nigra to the SC are usually manifested as decreases in activity below a steady, elevated baseline level (for review see Hikosaka et al., 2000).

Two studies examined SC-projecting substantia nigra neurons, and both found a great variety of signals transmitted. Hikosaka and Wurtz (1983b) concluded that every type of signal present in substantia nigra pars reticulata seems to be sent to the SC. This included visual signals, delay activity, and presaccadic activity. The delay activity was thought to be related to short-term visual memory, although it could have been related to movement preparation as well (experiments systematically manipulating whether a saccade occurred or not, i.e., go/no-go experiments, were not performed). They also found that the visual and presaccadic discharges of SC-projecting neurons often were influenced by the context of the task, being different when saccades were made to remembered as compared to visual targets.

Basso and Wurtz (2002) studied how the activity of substantia nigra pars reticulata neurons varied with the probability of making a saccade. In their task, multiple visual stimuli were presented simultaneously, and the probability that saccadic target selection had to occur for any one of the stimuli was manipulated by varying the number of stimuli (from one stimulus, corresponding to a 100% probability of saccadic target selection occurring for that stimulus, to eight stimuli, corresponding to only a 12.5% probability of saccadic target selection occurring for any particular stimulus). Only a minority of their substantia nigra neurons was identified as projecting to the SC, but they found no obvious differences in this subset as compared to the general sample of substantia nigra neurons examined. They previously had found that the delay activity of intermediate-layer SC neurons varied strongly with probability in this task: the greater the chance that saccadic target selection would occur for a target in the neuron's receptive field, the higher the level of delay activity (Basso and Wurtz, 1998). Surprisingly, however, this was not the case for substantia nigra neurons, which usually maintained the same level of delay activity regardless of the chance of saccadic target selection occurring for the target in the receptive field. This maintained level was only slightly different than the background firing rate. This suggests that one or more of the *direct* cortical projections to the SC, *not* the indirect route through the nigra, is primarily responsible for changes in SC delay activity

during saccadic target selection. Basso and Wurtz did find, however, that the short-latency visual responses of nigral neurons were strongly modulated by the probability of saccadic target selection. Taken together with the result of Hikosaka and Wurtz (1983b) that the visual responses of SC-projecting nigral neurons are sensitive to task context, these data suggest that the major cognitive-related influence of substantia nigra on SC is to cause visual-related changes in activity related to very early stages of saccadic target selection. Presumably these influences are primarily attentional in nature, as they are represented by altered visual responsiveness.

SIGNALS SENT FROM STRIATE CORTEX TO THE SC The final direct projection from cerebral cortex to the SC that has been investigated emanates from striate cortex. Unlike the other projections we have discussed, all of which target predominantly the intermediate layers of the SC, the projections from striate cortex target primarily the *superficial* layer (Kuypers and Lawrence, 1967; Ogren and Hendrickson, 1976). The SC superficial layer also receives direct projections from the retina (Cowey and Perry, 1980; Hendrickson et al., 1970), and neurons in this part of SC are visually responsive, with no presaccadic bursts of activity. Because it has been shown recently that striate cortical activity is influenced by attention (Haenny and Schiller, 1988; Motter, 1993; Posner and Gilbert, 1999) and may have delay activity related to short-term visual memory (Super et al., 2001), it is possible that signals in the projection from striate cortex might play some role in saccadic target selection. Whether this is true, however, remains unclear. The only study to examine this, in cat, found that SC-projecting striate cortical neurons often have enhanced visual responses when a visual stimulus is used as the target for a saccade as opposed to when it is viewed passively (Weyand and Gafka, 2001). In principle, this could represent spatial visual attention. It was not determined, however, whether the enhancement occurred only when saccades were made *toward* the target; for comparison, Wurtz and Mohler (1976a) showed that enhancement effects in monkey striate cortex are independent of saccade direction and therefore cannot represent a spatially localized shift of attention. The modulation might represent a general arousal or vigilance effect (or other effects beyond the scope of this discussion; see Weyand and Gafka, 2001).

Earlier studies of SC-projecting striate cortical neurons used anesthetized, paralyzed animals (cat: Palmer and Rosenquist, 1974; monkey: Finlay et al., 1976). These studies were valuable in describing the visual characteristics of SC-projecting striate cortical neurons (the neurons were typically binocular, complex, and orientation- and direction-tuned, with large receptive fields), but they did not address cognitive issues.

Also of interest in considering the relationship between visual cortex and the SC, at least with respect to cats, is the *Sprague effect* (Sprague, 1966): after ablation of visual cortex (including virtually all occipital visual areas, not just striate cortex), cats fail to orient to contralateral visual stimuli, but recovery occurs if the SC contralateral to the ablated cortex is lesioned or if the collicular commissure is cut. In a series of experiments, Rosenquist and colleagues showed that this recovery is likely due to disinhibition of the SC caused by interruption of fibers in the collicular commissure coming from the substantia nigra pars reticulata and from the pedunculo-pontine region (for a summary, see Durmer and Rosenquist, 2001). The Sprague effect has not been investigated in monkeys because the recovery of visual orienting is so fast following lesioning of visual cortex (in this case limited to striate cortex) that no subsequent interventions at the level of the SC are required for nearly complete recovery of orienting saccadic eye movements (Mohler and Wurtz, 1977).

GRADUAL PROGRESSION OF SACCADIC TARGET SELECTION FROM CORTEX TO THE SC As discussed above, neurons in the frontal eye field and the lateral intraparietal area send to the intermediate layers of the SC a wide range of signals related to visuosaccadic behavior, which leads to two questions. First, are the signals leaving these two cortical regions similar to each other or radically different from each other? And second, how do the signals sent from these cortical areas compare with signals in the recipient structure, the SC? To answer these questions, Wurtz and colleagues studied SC-projecting frontal eye field neurons, SC-projecting lateral intraparietal area neurons, and intermediate layer SC neurons using identical tasks, equipment, and analytical techniques (for detailed analysis, see Wurtz et al., 2001). They found that, qualitatively, the signals carried by SC-projecting neurons in both cortical areas were quite similar to each other and to the signals within the SC. Neurons in all three populations exhibited visual responses, delay activity, and presaccadic activity in nearly every possible combination.

When the signals were analyzed quantitatively, however, important differences were uncovered. First, the delay activity was examined to see if it was more strongly influenced by the visual target or by the upcoming movement. To gauge the influence of *visual stimulation* on the delay activity, the activity was compared in the visual and memory versions of the standard delayed-saccade task (Fig. 98.44). It was found that delay activity in the SC-projecting neurons of both cortical regions was strongly enhanced by visual input (to a similar degree in both regions), whereas delay activity in the SC intermediate layers was much less visually related, being equal whether a target remained in the receptive field or disappeared. To measure the influence

of *upcoming movement* on the delay activity, the activity was compared in the go and no-go trials of the go/no-go delayed-saccade task described above. Delay activity in the SC was much more strongly enhanced by upcoming movement than was delay activity in SC-projecting neurons of either cortical population.

Next, the visual responses and presaccadic activity of the neurons were compared. Visual responses in the three populations of neurons were not markedly different. The presaccadic activity, however, was much more intense in SC neurons (nearly always 200 to 600 spikes per second) than in cortical output neurons (rarely >200 spikes per second). Also, when the two populations of cortical output neurons were compared, SC-projecting frontal eye field neurons often were found to have presaccadic activity as their only signal (so-called pure movement neurons), whereas this was never seen in the SC-projecting lateral intraparietal area neurons.

In sum, this investigation answered both questions posed above. First, signals leaving the two cortical areas are not radically different from each other; they are similar, with only limited differences. Second, signals sent to the SC intermediate layers and signals within the SC intermediate layers are similar, except for important quantitative differences. Compared to the cortical output neurons, the SC neurons are more movement-related and less visually related. From cortex to the SC intermediate layers, there seems to be a gradual change in signal content corresponding to a progression in saccadic target selection processes from more visually related (i.e., processes of attention and visual memory) to more movement-related (i.e., processes of saccade preparation).

Other, less direct comparisons of cortical and SC activity support this idea. Everling and colleagues (Everling and Munoz, 2000; Everling et al., 1999), for example, examined neurons in the SC intermediate layers and in the frontal eye field using identical techniques. Here we consider their total sample of frontal eye field neurons, the projections of which were not identified except for a minority shown to project to the SC (results pertaining specifically to these SC-projecting neurons were discussed above). Neurons in both the frontal eye field and the SC had higher activity throughout trials when monkeys had to make saccades toward, as opposed to away from, a visual stimulus in the receptive field. Furthermore, activity in both areas predicted reaction time and the occurrence of errant saccades, indicating that the activity was strongly related to saccade production. The investigators concluded, however, that although these effects were similar in the two areas, they were weaker in the frontal eye field than in the SC.

Several other studies have examined cognitive-related activity in the SC intermediate layers as well (for detailed reviews see Basso, 1998; Wurtz et al., 2000). Glimcher and

Sparks (1992) were the first to examine systematically SC delay activity. They presented two peripheral visual stimuli, one within and one outside of the neuron's receptive field, and instructed monkeys by means of a central color cue which stimulus would be the saccadic target. They found that shortly after the monkeys were instructed to make their eventual saccade into a neuron's receptive field, activity of the neuron increased dramatically. Building on this result, Basso and Wurtz (1998) and Dorris and Munoz (1998) showed that the intensity of cognitive-related activity in SC neurons is directly correlated with the graded probability of making a saccade to a particular visual stimulus. In these and similar studies (Dorris et al., 1997; Everling et al., 1998, 1999), it was repeatedly found that cognitive-related SC activity predicted saccadic reaction times and the production of errant saccades, indicating that it was strongly movement-related. In contrast, Sommer and Wurtz (2001a) showed that delay activity sent from the frontal eye field to the SC does *not* seem to predict either reaction time or errant saccades. Taken together, these studies reinforce the model of a gradual progression in saccadic target selection processes that becomes more movement-related from cerebral cortex to the SC.

To see if delay activity in the SC really does influence saccadic target selection, Kustov and Robinson (1996) combined single-unit recordings with electrical stimulation to evoke saccades. They used tasks in which a peripheral or central cue elicited a shift of attention to one of two possible targets, one of which was located in the part of the visual field represented by the site studied in the SC. Monkeys exhibited decreased reaction times in making saccades to the cued targets, indicating that they shifted their attention as expected. The investigators found that delay activity in the SC increased during the attentional shifts and that when the SC was stimulated, evoked saccades were deviated toward the locus of attention. Hence, not only is the activity of SC neurons correlated with attentional shifts, but also it seems to affect the saccadic system such that electrically evoked saccades are altered. Similar conclusions were reached in a recent frontal eye field study (Moore and Fallah, 2001). In that experiment, subthreshold stimulation for evoking saccades in the frontal eye field caused enhanced performance in a spatial attention task, but only for attended targets located in the part of the visual field represented by the frontal eye field site. In summary, these studies confirm the underlying assumption that delay activity, at least in the SC and the frontal eye field, is in fact vital for the act of selecting a saccadic target.

Finally, Munoz and colleagues found neurons in the rostral pole of the SC that seem to inhibit, rather than facilitate, saccade production (for a review, see Wurtz et al., 2000). Whereas neuronal activity in more caudal SC is low during fixation and increases prominently just prior to

saccade production, activity in the rostral pole is high during fixation and decreases just prior to saccade production. Using orthodromic stimulation within the SC, they showed that the rostral pole's influence on neurons of the caudal SC is inhibitory (Munoz and Istvan, 1998). Therefore, some of the increased delay activity in caudal SC neurons during the experiments described above might be due in part to disinhibition caused by rostral SC afferents. Of course, this begs the question of what controls the rostral SC neurons; some of their input likely comes from cerebral cortex (Sommer and Wurtz, 2000a), but beyond that, little is known.

Ascending pathways from the SC to the cortex

The SC sends projections downstream, to the brainstem saccade-generating circuitry, and also *upstream*, to the thalamus. Ascending projections from the SC to the thalamus were identified anatomically decades ago (e.g., Benevento and Fallon, 1975), and it has long been presumed that these projections terminate on relay neurons that in turn project up to the cerebral cortex (e.g., Benevento and Rezak, 1976; Goldman-Rakic and Porrino, 1985). Very recently, these disynaptic pathways from the SC to cortex via the thalamus have been elucidated more directly using a novel anatomical method in which herpes viruses that pass retrogradely through synapses were injected into cerebral cortex. Primary and secondary labeling was detected in thalamic nuclei and the SC, respectively (Clower et al., 2001; Lynch et al., 1994).

Two major ascending pathways exist: one from the intermediate SC to the mediodorsal nucleus of the thalamus to the prefrontal cortex, and another from the superficial SC to the pulvinar region of the thalamus to extrastriate cortex. We will discuss the mediodorsal nucleus pathway in this section and the pulvinar pathway in the next.

THE ASCENDING PATHWAY THROUGH THE MEDIODORSAL NUCLEUS TO THE PREFRONTAL CORTEX Even before its presence was demonstrated explicitly by Lynch et al. (1994), a disynaptic pathway from intermediate SC to the prefrontal cortex was posited and there was much speculation regarding its possible function. Is it a *feedforward* route through which visual signals, some of which might be attentionally modulated, are relayed from the SC to prefrontal cortex (as hypothesized by Goldberg and Bushnell, 1981; Suzuki and Azuma, 1983; Wurtz and Mohler, 1976a)? Or is it a *feedback* route, through which prefrontal cortex is informed of the saccadic commands produced by the SC?

Evidence supporting both hypotheses was obtained in the first exploration of single neurons in primate visuomotor thalamus (Schlag and Schlag-Rey, 1984; Schlag-Rey and Schlag, 1984). Neurons located in or near the lateral edge of the mediodorsal thalamus, where SC-to-prefrontal cortex

relay neurons are found (Lynch et al., 1994), were shown to exhibit both visually related and saccade-related activity. The connections of these neurons were not physiologically identified, however, and thus it was unknown whether they actually projected to prefrontal cortex or received projections from the SC.

Recently, a set of studies used both identified neuronal recordings and reversible inactivation techniques to examine the pathway from SC to mediodorsal thalamus to frontal eye field (Sommer and Wurtz, 1998, 2000b, 2001b, 2002; Wurtz and Sommer, 2000). Every neuron in these experiments was shown with antidromic and/or orthodromic activation to be part of this ascending pathway. Three populations of neurons were studied: SC neurons projecting to the mediodorsal thalamus, mediodorsal thalamus relay neurons, and frontal eye field neurons targeted by the pathway. The conduction speed in this pathway is very fast: orthodromic and antidromic activation latencies confirmed that it only takes ~2.5 msec for signals to reach the frontal eye field from the SC through this route.

To characterize the signals carried by these neurons, delayed-saccade tasks were used, as described in previous sections. Neurons at every level of the pathway were active during these tasks, with most neurons having both a visual response and a presaccadic burst of activity and others having only one or the other signal. Therefore, both of the hypotheses noted above were supported in that the pathway definitely carries both visually related and movement-related discharges. Little delay activity was found in the ascending pathway, and therefore this activity was not characterized in detail using go/no-go or similar tasks.

Although the hypothesis that this pathway carries movement information was supported by the recording results, the results could not distinguish between two alternative possibilities regarding the function of these movement signals. Were they used as feedback, that is, corollary discharge, to inform the cerebral cortex about impending saccades, or were they used in a feedforward way to help in the execution of saccades? Both possibilities were supported by the characteristics of the neuronal activity in that the presaccadic bursts began ~100 msec prior to saccade onset and encoded specific vectors of saccades (i.e., the neurons usually had restricted movement fields).

To distinguish between these possibilities, reversible inactivation experiments were performed (Sommer and Wurtz, 2002) (Fig. 98.5A). The relay neurons were inactivated with the GABA agonist muscimol while monkeys performed either standard single-saccade tasks or else a double-step task that required corollary discharge information (Becker and Jürgens, 1979; Duhamel et al., 1992; Gaymard et al., 1994; Heide et al., 1995; Mays and Sparks, 1980). It was found that single saccades were not affected by inactivation, indicating that saccade-related signals in the ascending pathway

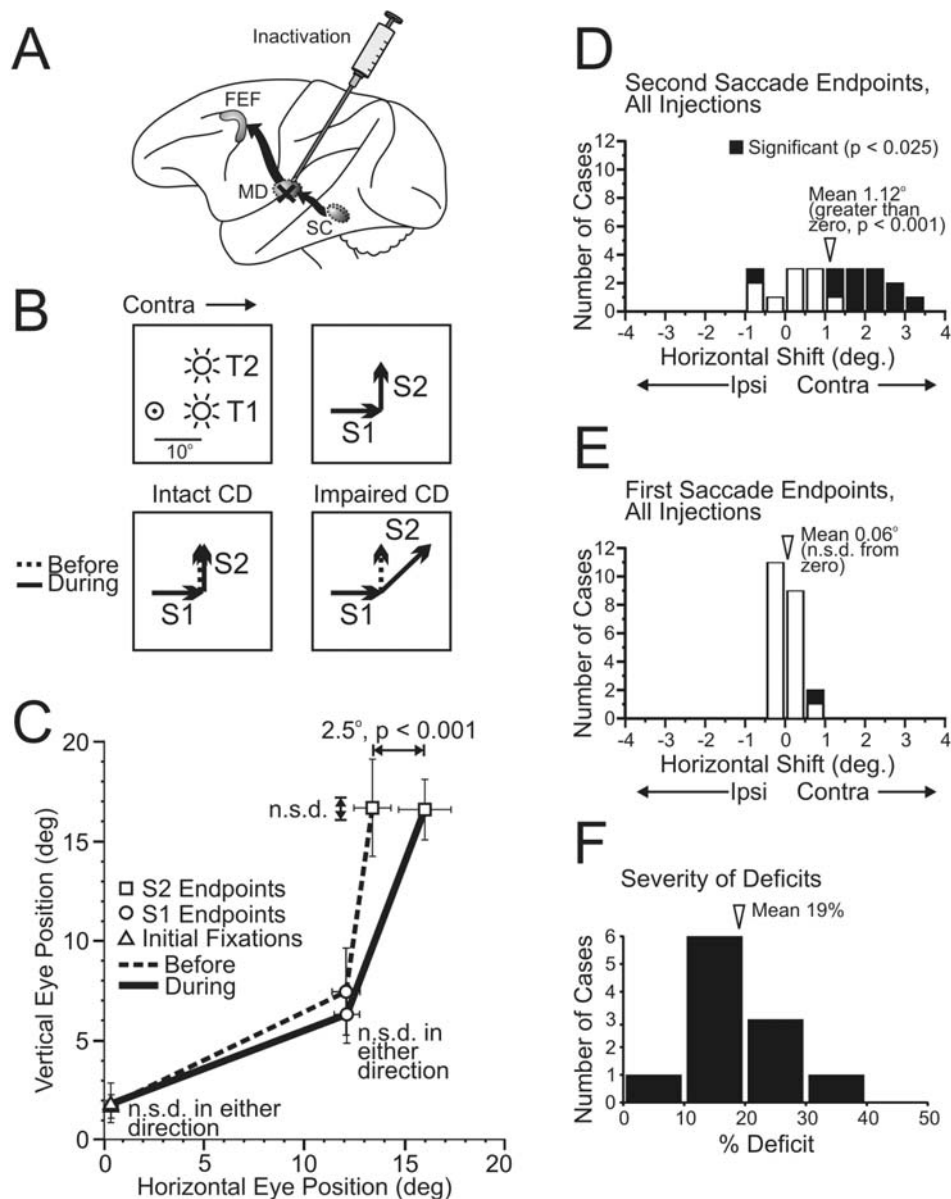


FIGURE 98.5. Test of the hypothesis that the ascending pathway through mediodorsal thalamus carries a corollary discharge signal. *A*, Muscimol was injected at the site of previously recorded mediodorsal thalamus relay neurons to inactivate them. *B*, Schematic of the double-step task. See text for details. T1, T2: first and second flashed targets, respectively; S1, S2: first and second saccades; CD, corollary discharge; Contra, contraversive to the injection site. *C*, Example results from a single injection. First saccades were shifted upward slightly as an artifact of being made in complete darkness (Gnadt et al., 1991). The differences in average locations, during versus before inactivation, were tested in both the horizontal and vertical directions for the initial fixation locations, the first saccade end points, and the second saccade end points. The only significant difference was a horizontal contraversive shift in second saccade end points as predicted by loss of corollary dis-

charge. n.s.d., not significantly different. *D*, Histogram of the horizontal shifts in second saccade end points for all cases (i.e., all the during vs. before pairs of saccadic sequences) in all injections. In nearly every case there was a contraversive shift. The mean shift was significantly greater than zero, as indicated, and many of the cases had an individually significant contraversive shift. The significance level is $p < .025$, which is Bonferroni-corrected from $p < .05$ because the data were tested in two directions. Ipsi, ipsiversive shift; Contra, contraversive shift. *E*, In contrast, first saccade end points were not shifted horizontally by inactivation (hence, the second saccade end-point shifts are not artifacts of prior first saccade end-point shifts). *F*, Histogram of the severity of deficits for all cases that had an individually significant shift. See text for a description of measuring severity of deficit. The mean deficit is indicated. (Adapted from Sommer and Wurtz, 2002.)

were not important for the general execution of saccades. However, consistent deficits were found during the double-step task, indicating that corollary discharge was impaired, as described next.

In the double-step task, a monkey fixated a spot and then two sequentially flashed targets were presented briefly in the periphery (Fig. 98.5*B*, *upper left*). The monkey had to look at the locations of the targets in the order in which they had appeared (Fig. 98.5*B*, *upper right*). Hence, to make the second saccade correctly, the monkey had to know whether it made the first saccade correctly. There was no visual feedback because the targets disappeared before saccades were initiated. Proprioception plays little or no role in the on-line control of saccades, so it could not help the monkey in keeping track of its first saccade (Bridgeman, 1995; Guthrie et al., 1983; Lewis et al., 2001; Steinbach, 1987). To perform the task, therefore, the monkey had to monitor a corollary discharge representation of the first saccade. If inactivation did not affect corollary discharge, then during the inactivation the monkey would make its first saccade and know that it did so; therefore, the second saccade would go straight up to the second target location from the end point of the first saccade, just as it did before inactivation (Fig. 98.5*B*, *lower left*). If inactivation totally eliminated corollary discharge, however, then during inactivation the monkey would make the first saccade and *not* know that it did so; hence, the second saccade would be made as if the monkey were still looking at the center of the screen, and it would go up at an angle so that its end point would be shifted contraversively (rightward) (Fig. 98.5*B*, *lower right*). This is in fact what happened: as shown in the example (Fig. 98.5*C*) and in the population data (Fig. 98.5*D*), there was a consistent contraversive shift in the end points of second saccades during inactivation. First saccade end points were not shifted on average, however (Fig. 98.5*E*), and neither were the initial fixation locations. In the vertical dimension there were no mean shifts in second saccade end points, first saccade end points, or initial fixation locations. Surprisingly, the deficits were partial, not total; in the example case, for instance, there was a 2.5 degree shift when a 10 degree shift had been expected, representing a 25% deficit. Overall there was a mean deficit of 19% (Fig. 98.5*F*), and thus although the effect was consistent, it was modest in magnitude. This suggests that other pathways, unaffected by the inactivations, also carry corollary discharge signals.

In summary, the results support two hypotheses regarding the function of this fast-conducting ascending pathway through mediodorsal thalamus. First, the pathway carries visual signals. Although the meaning of this finding is not yet fully understood, it demonstrates that visual signals in the frontal eye field do not arrive only in afferents from extrastriate cortex, as seems to be commonly believed. They also arrive from the intermediate layers of the SC, raising the

possibility that some interesting attributes of frontal eye field visual neurons (e.g., their ability to discriminate visual targets from distractors; reviewed by Schall, 1997) might be due in part to antecedent processing in the SC. Second, the pathway carries presaccadic discharges to frontal cortex, and reversible inactivation of the pathway demonstrated that these are corollary discharge signals. The corollary discharge signals contribute to the ability to make sequences of saccades. They may also contribute to visual scene stability during saccades, although this possibility has yet to be explicitly tested.

THE ASCENDING PATHWAY THROUGH THE PULVINAR TO THE VISUAL CORTEX While the SC intermediate layers have a prominent projection to cerebral cortex through mediodorsal thalamus, the superficial layers of the SC project to the cortex primarily through a pathway that includes the pulvinar nucleus of the thalamus (Clower et al., 2001). Neuronal activity in the SC layers that contribute to these two pathways also are different: neurons in both the superficial and intermediate layers exhibit short-latency responses to visual stimulation of the retina (about 40 to 60 msec; Wurtz et al., 1980) and nearly always have clear receptive fields (for reviews, see Sparks and Hartwich-Young, 1989; Wurtz and Albano, 1980), but in contrast to intermediate layer neurons superficial layer neurons show no presaccadic burst of activity. There is some overlap in the distribution of these visual and visual-movement neurons in that both are found in the lower levels of the superficial layers (the stratum opticum; Ma et al., 1991), but the extent to which neurons in this ventral superficial region contribute to one ascending pathway, to the other, or to both remains unknown. In this section, we will concentrate on the neurons with visual receptive fields but not presaccadic activity, and the term *SC neurons* in this section will refer to these superficial visual neurons.

The major inputs to these neurons are from the retina and striate cortex, as discussed above. It is reasonable to assume a priori that the signals sent from superficial SC up to cortex are visual in nature, but since recordings in the pulvinar of the monkey (Bender, 1981; Petersen et al., 1985) have not physiologically identified the source of any of the inputs to the neurons, and because there are inputs to pulvinar from visual cortex (Ogren and Hendrickson, 1976; Ungerleider et al., 1983, 1984), at this point we can only estimate the signal content in this pathway by reviewing studies of the general populations of neurons in the superficial SC, the pulvinar, and the parietal cortex.

This ascending pathway from the SC to cortex has been referred to as a *second visual pathway* or *second visual system* (Diamond and Hall, 1969; Schneider, 1969), and it has been considered important not only as a phylogenetically older pathway but also as one that may provide an alternative

route for visual information to reach cortex. Such an alternative route takes on particular importance in explaining the residual visual abilities (*blindsight*) (Stoerig and Cowey, 1997; Weiskrantz et al., 1974) and the residual visually related neuronal activity in extrastriate cortical areas (Girard et al., 1992; Rodman et al., 1989, 1990) that persist after removal of striate cortex.

Currently, there appear to be two major types of signals that could be conveyed through the pathway from the superficial SC to cortex via the pulvinar. One type is a visual response modulated by corollary discharge input, and this will be discussed first. The other is a visual response modulated by attention, discussed second.

One of the earliest investigations of the effect of a corollary discharge on visual processing in the primate was on superficial layer SC neurons (Robinson and Wurtz, 1976). The test for the effect of a corollary discharge was simply to determine if the neurons responded the same way when a saccadic eye movement swept their receptive field across a stationary stimulus as when the stimulus was swept across the receptive field while the eye was stationary. Many superficial layer SC neurons did not respond to the stimulus during the saccade, which was interpreted to be the effect of an extraretinal input to the SC present during the eye movement but not during the stimulus movement. This is in contrast to the lack of any such evidence for an extraretinal input to striate cortex neurons (Wurtz, 1969).

In principle, the extraretinal signal used by superficial SC neurons could have come either from a corollary discharge or from proprioceptive inflow from the eye muscles. To determine which, Richmond and Wurtz (1980) paralyzed the eye muscles and determined when eye movements were attempted by recording in the brainstem motor nuclei. Even in the absence of actual movement, modification of the visual response still occurred, leading the investigators to conclude that corollary discharge was sufficient for this modulation. Subsequent experiments on neurons in the pulvinar showed that their visual responses, too, were modified by eye movements (Robinson and Petersen, 1985). Given that the pulvinar receives afferents from the SC, this modulation could be a reflection of activity sent from the SC.

Thus, in the pathway from the superficial SC to the pulvinar, there is an indication of the influence of an extraretinal signal, which in the case of SC neurons has been demonstrated to involve corollary discharge. Note, however, that these neurons acted as if they *received* corollary discharge signals, as exhibited by changes to their visual responses. Where these particular corollary discharge signals come from remains unknown. In contrast, in the other ascending pathway, via mediodorsal thalamus, neurons carry a corollary signal *itself*, one sent up to the cerebral cortex, and we know that this signal comes from the SC intermediate layers.

Neuronal signals related to attention also have been studied in the SC-pulvinar pathway. When the monkey selects a target for its next saccade that lies in the receptive field of an SC neuron, the visual response of the neuron is frequently enhanced compared to the case in which the monkey selects a target well outside the receptive field of the neuron (Goldberg and Wurtz, 1972). This enhancement is consistent with a shift of attention to the visual target for the impending saccade, and such enhancement has been seen clearly in a number of regions including frontal cortex, parietal cortex, and the substantia nigra pars reticulata (for reviews, see Hikosaka and Wurtz, 1989; Wurtz et al., 1980). The relation of the enhancement to the generation of the saccade differs between the areas, however, as determined by comparing modulation of neuronal activity when the monkey must use the stimulus as the target for a saccade as opposed to holding its eyes steady and reaching out to touch the stimulus. This distinction was first made in the SC (Wurtz and Mohler, 1976b), where the enhancement accompanying saccades to a target was absent with a reach to the target. The same was true for neurons in the frontal eye field (Goldberg and Bushnell, 1981). In the parietal cortex, however, neurons showed an enhanced response with both saccades and reaching (Bushnell et al., 1981), suggesting that the modulation represented movement-independent visual attention. Enhancement found in the SC and the frontal eye field, in contrast, is more appropriately regarded as a correlate of target selection *specifically* related to saccade generation (Wurtz et al., 1980, 1982).

Gattass and Desimone (1996) tested whether enhancement of superficial SC visual neurons really was inextricably linked to saccade generation using a different method (as a caveat, they indicated that some of their neurons may have been in the pulvinar). They cued the monkey with a peripheral stimulus falling inside the visual receptive field of the neuron but required the monkey to make a visual discrimination at the site of the cued stimulus instead of making a saccade to the stimulus. The neurons showed an enhanced visual response when the cue was in the receptive field as opposed to when it was not. The enhancement was present even in the absence of the saccade, suggesting that it is dissociable from saccade generation. However, when they then used a symbolic cue at the fixation point, they found no such enhancement even though saccades still were not produced. This implies that the monkey may have been planning a saccade in response to the peripheral cue even though one was not executed; such a planned but withheld saccade would not be expected for symbolic cues at the fixation point. The results therefore do not seem to refute the idea that enhancement in the SC is devoted to saccade generation.

This link between enhancement of visual responses in the SC and saccade generation is further supported by the

observation that as the time at which a saccade is made shifts closer to the time of the visual response, the enhancement increases (Wurtz and Mohler, 1976b). It is as if the presaccadic activity in the SC intermediate layers acts on superficial layer neurons to facilitate the enhancement. This remains entirely hypothetical, however. No such connection has been verified either anatomically or physiologically, although connections from superficial to intermediate layers are now clearly established (e.g., Isa and Saito, 2001; Lee et al., 1997). At this point, the exact mechanism causing the enhancement remains unknown.

Many superficial SC neurons are known to convey visual information to the pulvinar, as shown using antidromic activation (Marrocco et al., 1981). Because that study used paralyzed monkeys, attentional effects on the visual responses leaving the SC could not be assessed. Attention has been studied, however, within the structure receiving these projections. The retinotopic maps of the inferior and lateral pulvinar regions have been clearly delimited (Bender, 1981, 1982), and neurons showing changes in activity related to saccadic eye movements or visual modulation have been found mainly in the inferior area (PI) and in another visually responsive area (Pdm) of the lateral pulvinar (Petersen et al., 1985; Robinson et al., 1986). These neurons showed visual enhancement for stimuli in the contralateral visual field similar to that seen in the SC, but with the striking difference that enhancement here occurred regardless of whether an eye movement to the target was made or a lever press was made (Petersen et al., 1985). Because the enhancement did not depend on the motor modality, it was an extremely sound candidate for mediating visual attention.

That these neurons contribute to shifts of attention made by the monkey was demonstrated conclusively by Petersen et al. (1987), who inactivated the region of the pulvinar where neurons were modulated by attention. First, they recorded neurons in this area and found that they were enhanced during an attentional task in which monkeys had to detect the dimming of a target in the neuron's receptive field. Then they inhibited the neurons with muscimol while monkeys performed a task in which a peripheral cue elicited attentional shifts, as measured by improvements in manual reaction time. In valid trials (Fig. 98.6A, *top*), the peripheral cue and the subsequently presented target appeared in the same hemifield and the reaction time to release a lever in response to target onset was relatively short, presumably because attention was drawn to the target location by the preceding cue (other experiments showed similar reaction time decreases when a central symbolic cue was used, demonstrating that these effects probably were not related to covertly preparing a saccade to the peripheral cue; Bowman et al., 1993). In invalid trials (Fig. 98.6A, *bottom*), the peripheral cue and the target appeared in opposite hemi-

fields and the reaction time was longer, presumably because attention was drawn away from the target location. During pulvinar inactivation, there was no effect on reaction time if both cue and target were presented ipsilaterally to the injection site (Fig. 98.6B, *top*: ipsilateral valid cue). However, if both the cue and target were presented contralaterally to the injection site, the reaction time was substantially increased (Fig. 98.6B, *bottom*: contralateral valid cue). The deficit appeared to represent an impairment in the ability to shift attention contraversively in response to the cue. On the other hand, injection of a GABA antagonist, bicuculline, did not seem to cause swifter attentional shifts (Fig. 98.6B, *bottom*); this may be a floor effect caused by the monkeys being so well trained that they could not possibly shift their attention faster. For brevity, results from invalid cue trials are not discussed here, but they further supported the conclusion that inactivation caused impairment of attentional shifts.

To summarize, currently we know that some pulvinar neurons show visual enhancement, that the enhancement is not dependent upon the execution of an eye movement, and that inactivation of the pulvinar impairs attention. While anatomy suggests that the regions of the monkey pulvinar studied lie on the pathway to cerebral cortex (Benevento and Fallon, 1975), a remaining caveat is that the extent to which various regions of pulvinar convey information from the SC to cortex is still unknown (e.g., Stepniewska et al., 1999).

Also not known is the extent to which the pulvinar-to-cortex projection modifies neuronal activity in cortex, particularly in the lateral intraparietal area considered previously in this chapter. As noted above, Bushnell et al. (1981) found movement-independent visual enhancement in parietal cortex similar to what was seen in the pulvinar. More recent experiments in parietal cortex (Robinson et al., 1995) showed enhancement using a peripheral cuing task similar to that used in the pulvinar inactivation experiments described above. Again, we do not know whether these parietal neurons received input from pulvinar, but anatomically this was quite possible. Another set of attention experiments in parietal cortex studied the effects of attentive fixation on the visual response of neurons (Mountcastle et al., 1981, 1987), and a recent study verified these observations and showed similar effects in the pulvinar (Bender and Youakim, 2001). Exactly what the SC-pulvinar pathway contributes to attentional activity in parietal cortex (and in other extrastriate areas; see reviews by Desimone and Duncan, 1995; Maunsell, 1995) remains a critical question.

In net, while the possible functional contributions of the pathway from the SC to cortex via the pulvinar have received more attention over a longer period (Diamond and Hall, 1969; Schneider, 1969) than has the pathway from the SC to cortex via the mediodorsal thalamus, the function of

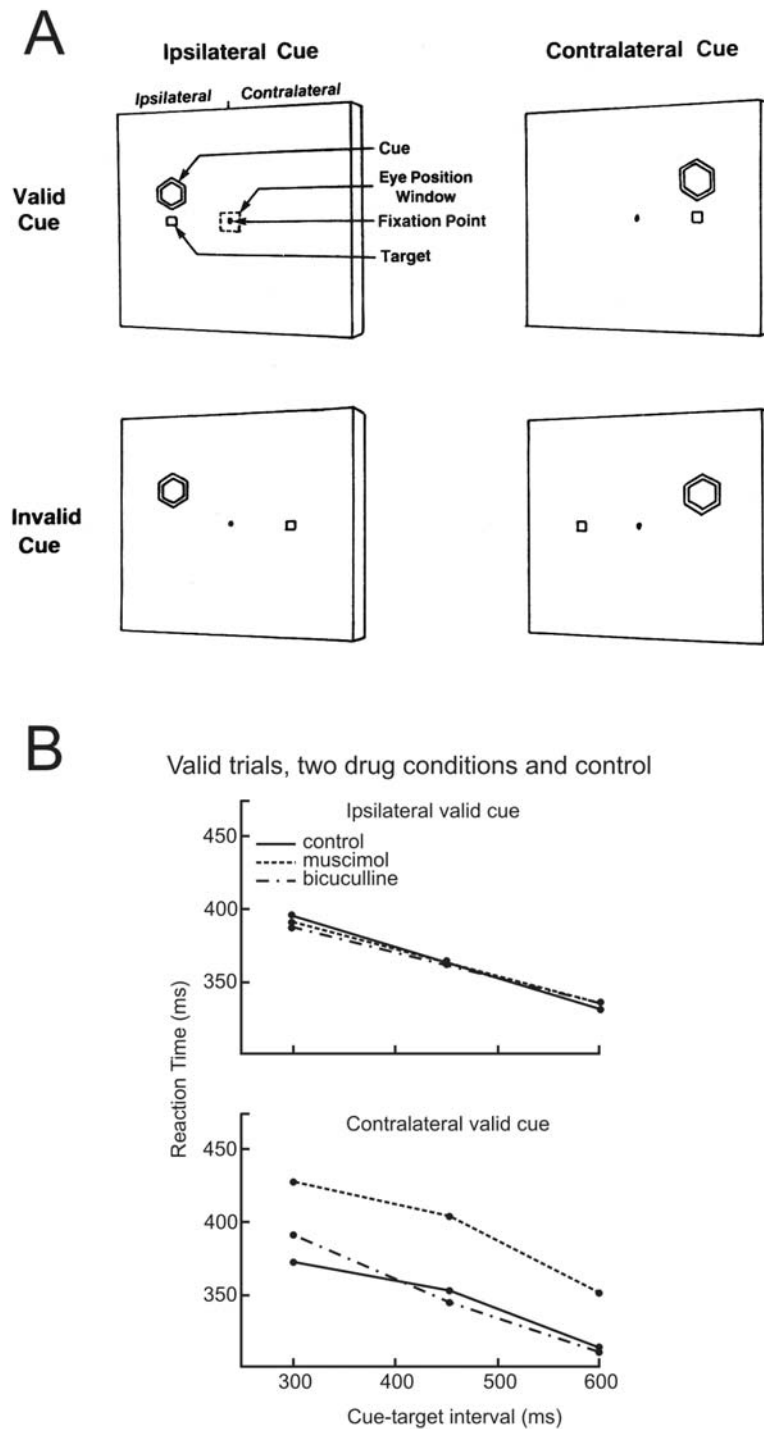


FIGURE 98.6. Test of the hypothesis that the ascending pathway through pulvinar carries an attention signal. *A*, Diagram of the task. The monkey foveated the fixation point and had to keep its eyes within the eye position window at all times. Then a cue stimulus was flashed, a cue-target interval ensued, and a target was presented. The monkey's task was to report detection of the target by manually depressing a lever. During valid cue trials (*top*), the cue and target appeared in the same hemifield; during invalid cue trials (*bottom*), they flashed in opposite hemifields. Ipsi- and contralateral

are with respect to the injection site. *B*, Effects of inactivating pulvinar on reaction times during valid cue trials. There was no effect of inactivation when the cue and target were presented ipsilaterally (*top*), showing that the monkey still could shift its attention in that direction. However, when the cue and target were presented contralaterally (*bottom*), the reaction time was abnormally slow during inactivation (muscimol data). Also shown are the results of bicuculline injection, which caused no deficits. (Adapted from Petersen et al., 1987.)

the pulvinar pathway is less well specified. Identified recordings in behaving animals are still needed to determine explicitly the signals conveyed in this pathway. The current data strongly suggest that neuronal activity all along the pathway is related to attention, changing from being more saccade-specific in SC to being more visual, that is, more motor modality-independent, in pulvinar and cortex.

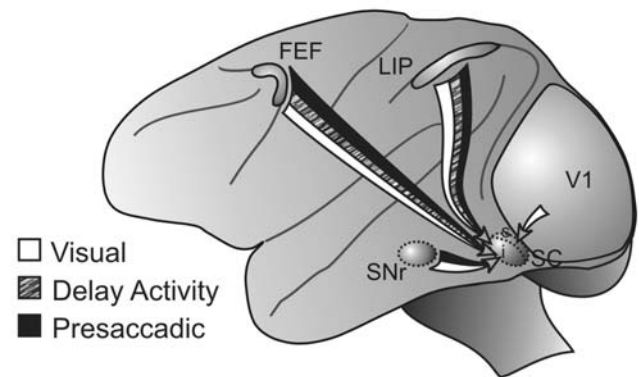
Finally, it should be noted that an additional ascending pathway appears to course from the superficial SC layer, reaching koniocellular neurons in the lateral geniculate nucleus that presumably project, in turn, to striate cortex (for a review, see Hendry and Reid, 2000). Visually related activity certainly must be relayed in this pathway, but as koniocellular neurons are extremely heterogeneous, it is difficult to speculate further about these ascending signals.

Conclusions

In this chapter, we described what is currently known about the dialogue between the cerebral cortex and the SC during visuosaccadic behavior. Figure 98.7 shows a summary diagram of the descending and ascending signals. Four descending routes have been investigated using antidromic activation techniques (Fig. 98.7A). The projections richest in signals related to saccadic target selection emanate from the lateral intraparietal area and the frontal eye field. Both projections send visual responses, cognitive-related delay activity, and presaccadic activity to the intermediate SC. The basal ganglia pathway via the substantia nigra relays strong visual and presaccadic signals to the intermediate SC, but delay activity in this projection seems related only weakly, if at all, to target selection. Striate cortex sends visual signals that are potentially interesting, but still poorly understood, to the superficial SC. Ascending pathways (Fig. 98.7B) are more challenging to study. Best characterized is the pathway from the intermediate SC to the frontal eye field (via mediodorsal thalamus), which carries visual signals and presaccadic activity that appears to serve a corollary discharge function. The pathway from the superficial SC to parietal cortex (via pulvinar) is presumed to carry mostly visual signals that are highly modulated by attention. We want to emphasize that there are numerous other descending and ascending connections between cerebral cortex and the SC, some of which might also be crucially important for saccadic target selection, corollary discharge, or other cognitive functions. This chapter focused only on interconnections for which there are currently at least some satisfactory physiological results related to cognitive issues.

Our goal has not been to consider just one particular brain region, but instead to determine what can be learned from analyzing the functional relation *between* areas, specifically between cerebral cortex and the SC. Our focus on visuosaccadic behavior provides only a limited glimpse of brain

A Descending Signals



B Ascending Signals

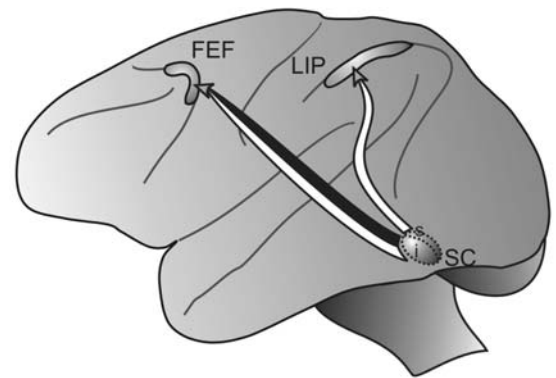


FIGURE 98.7. The dialogue between cerebral cortex and the SC. Each diagram depicts the signals transmitted between regions using arrows containing fills that correspond to the three main types of neuronal activity considered in this chapter; see the legend at the left. Only delay activity signals that were clearly shown to be involved in cognitive functions are included. *A*, Descending signals from cerebral cortex to SC. *B*, Ascending signals from SC to cerebral cortex. Relays in thalamus have been omitted for simplicity. Abbreviations as in Figure 98.2.

organization, but it does offer the opportunity to look at the neuronal basis of several cognitive functions using techniques that allow the functional identification of a part of the underlying circuit. A few general conclusions are worth pointing out explicitly.

First, when we compare the signals leaving cortex, within the SC, and in the ascending pathways, we never see a strict segregation of function between areas. There is no level of visuosaccadic processing in one area that is absent in the next. Instead, there is always an overlap between the signals seen in one area and those in the next, with a gradual shift in signal content. There appear to be progressive sensorimotor transformations rather than abrupt changes.

Second, the recognition that signals are conveyed up to cortex with very short latencies emphasizes that the neuronal

activity seen in cerebral cortex represents not just signal processing *within* the cortex but also processing directed *back* to the cortex from brainstem areas. The cortical and subcortical areas have to be regarded as a whole unit, not as a serial chain, just as is the case for cortical areas that also are reciprocally interconnected.

Finally, our most significant generalization concerns the nature of the information conveyed to cerebral cortex from the SC. What we find striking is that the information conveyed upstream is probably not critical for extracting information about the world. Instead, ascending information from the brainstem makes its important contribution to *interpreting* the visual input in the context of an animal's actions. The pulvinar pathway appears to inform the cortex of the relative behavioral importance of objects (as expressed by enhanced visual responses). In the mediodorsal thalamus pathway, signals inform the cortex about what saccade will be made next. This corollary discharge information probably allows the visual system to distinguish between actual full-field motion of the external world and full-field motion that is a trivial artifact of making a saccade. In sum, our perception of the visual world is a result of the visual input to cerebral cortex and the interpretation of that input, and key parts of that interpretation may depend upon information relayed up from the SC through the thalamus.

REFERENCES

- Aizawa, H., and R. H. Wurtz, 1998. Reversible inactivation of monkey superior colliculus: I. Curvature of saccadic trajectory, *J. Neurophysiol.*, 79:2082–2096.
- Basso, M. A., 1998. Cognitive set and oculomotor control, *Neuron*, 21:665–668.
- Basso, M. A., and R. H. Wurtz, 1998. Modulation of neuronal activity in superior colliculus by changes in target probability, *J. Neurosci.*, 18:7519–7534.
- Basso, M. A., and R. H. Wurtz, 2002. Neuronal activity in substantia nigra pars reticulata during target selection, *J. Neurosci.*, 22:1883–1894.
- Becker, W., and R. Jürgens, 1979. An analysis of the saccadic system by means of double step stimuli, *Vis. Res.*, 19:967–983.
- Bender, D. B., 1981. Retinotopic organization of the macaque pulvinar, *J. Neurophysiol.*, 46:672–693.
- Bender, D. B., 1982. Receptive field properties of neurons in the macaque inferior pulvinar, *J. Neurophysiol.*, 48:1–17.
- Bender, D. B., and M. Youakim, 2001. Effect of attentive fixation in macaque thalamus and cortex, *J. Neurophysiol.*, 85:219–234.
- Benevento, L. A., and J. H. Fallon, 1975. The ascending projections of the superior colliculus in the rhesus monkey (*Macaca mulatta*), *J. Comp. Neurol.*, 160:339–362.
- Benevento, L. A., and M. Rezak, 1976. The cortical projections of the inferior pulvinar and adjacent lateral pulvinar in the rhesus monkey (*Macaca mulatta*): an autoradiographic study, *Brain Res.*, 108:1–24.
- Bowman, E. M., V. J. Brown, C. Kertzman, U. Schwarz, and D. L. Robinson, 1993. Covert orienting of attention in macaques: I. Effects of behavioral context, *J. Neurophysiol.*, 70:431–443.
- Bridgeman, B., 1995. A review of the role of efference copy in sensory and oculomotor control systems, *Ann. Biomed. Eng.*, 23:409–422.
- Bushnell, M. C., M. E. Goldberg, and D. L. Robinson, 1981. Behavioral enhancement of visual responses in monkey cerebral cortex: I. Modulation in posterior parietal cortex related to selective visual attention, *J. Neurophysiol.*, 46:755–772.
- Chafee, M. V., and P. S. Goldman-Rakic, 2000. Inactivation of parietal and prefrontal cortex reveals interdependence of neural activity during memory-guided saccades, *J. Neurophysiol.*, 83:1550–1566.
- Clower, D. M., R. A. West, J. C. Lynch, and P. L. Strick, 2001. The inferior parietal lobule is the target of output from the superior colliculus, hippocampus, and cerebellum, *J. Neurosci.*, 21:6283–6291.
- Cowey, A., and V. H. Perry, 1980. The projection of the fovea to the superior colliculus in rhesus monkeys, *Neuroscience*, 5:53–61.
- Desimone, R., and J. Duncan, 1995. Neural mechanisms of selective visual attention, *Annu. Rev. Neurosci.*, 18:183–222.
- Diamond, I. T., and W. C. Hall, 1969. Evolution of neocortex, *Science*, 164:251–262.
- Dias, E. C., and M. A. Segraves, 1999. Muscimol-induced inactivation of monkey frontal eye field: effects on visually and memory-guided saccades, *J. Neurophysiol.*, 81:2191–2214.
- Dorris, M. C., and D. P. Munoz, 1998. Saccadic probability influences motor preparation signals and time to saccadic initiation, *J. Neurosci.*, 18:7015–7026.
- Dorris, M. C., M. Paré, and D. P. Munoz, 1997. Neuronal activity in monkey superior colliculus related to the initiation of saccadic eye movements, *J. Neurosci.*, 17:8566–8579.
- Duhamel, J.-R., M. E. Goldberg, E. J. FitzGibbon, A. Sirigu, and J. Grafman, 1992. Saccadic dysmetria in a patient with a right frontoparietal lesion: the importance of corollary discharge for accurate spatial behavior, *Brain*, 115:1387–1402.
- Durmer, J. S., and A. C. Rosenquist, 2001. Ibotenic acid lesions in the pedunculo-pontine region result in recovery of visual orienting in the hemianopic cat, *Neuroscience*, 106:765–781.
- Everling, S., M. C. Dorris, R. M. Klein, and D. P. Munoz, 1999. Role of primate superior colliculus in preparation and execution of anti-saccades and pro-saccades, *J. Neurosci.*, 19:2740–2754.
- Everling, S., M. C. Dorris, and D. P. Munoz, 1998. Reflex suppression in the anti-saccade task is dependent on prestimulus neural processes, *J. Neurophysiol.*, 80:1584–1589.
- Everling, S., and D. P. Munoz, 2000. Neuronal correlates for preparatory set associated with pro-saccades and anti-saccades in the primate frontal eye field, *J. Neurosci.*, 20:387–400.
- Ferraina, S., M. Paré, and R. H. Wurtz, 2002. Comparison of cortico-cortical and cortico-collicular signals for the generation of saccadic eye movements, *J. Neurophysiol.*, 87:845–858.
- Finlay, B. L., P. H. Schiller, and S. F. Volman, 1976. Quantitative studies of single-cell properties in monkey striate cortex. IV. Corticotectal cells, *J. Neurophysiol.*, 39:1352–1361.
- Fuster, J. M., 1997. *The Prefrontal Cortex. Anatomy, Physiology, and Neuropsychology of the Frontal Lobe*, Philadelphia: Lippincott-Raven.
- Fuster, J. M., and G. E. Alexander, 1971. Neuron activity related to short-term memory, *Science*, 173:652–654.
- Gattass, R., and R. Desimone, 1996. Responses of cells in the superior colliculus during performance of a spatial attention task in the macaque, *Rev. Bras. Biol.*, 56 Su. 1 Pt. 2:257–279.
- Gaymard, B., S. Rivaud, and C. Pierrot-Deseilligny, 1994. Impairment of extraretinal eye position signals after central thalamic lesions in humans, *Exp. Brain Res.*, 102:1–9.

- Girard, P., P. A. Salin, and J. Bullier, 1992. Response selectivity of neurons in area MT of the macaque monkey during reversible inactivation of area V1, *J. Neurophysiol.*, 67:1437–1446.
- Glimcher, P. W., and D. L. Sparks, 1992. Movement selection in advance of action in the superior colliculus, *Nature*, 355:542–545.
- Gnadt, J. W., and J. Beyer, 1998. Eye movements in depth: What does the monkey's parietal cortex tell the superior colliculus? *NeuroReport*, 9:233–238.
- Gnadt, J. W., R. M. Bracewell, and R. A. Andersen, 1991. Sensorimotor transformation during eye movements to remembered visual targets, *Vis. Res.*, 31:693–715.
- Goldberg, M. E., and M. C. Bushnell, 1981. Behavioral enhancement of visual responses in monkey cerebral cortex. II. Modulation in frontal eye fields specifically related to saccades, *J. Neurophysiol.*, 46:773–787.
- Goldberg, M. E., and R. H. Wurtz, 1972. Activity of superior colliculus in behaving monkeys. II. Effect of attention on neuronal responses, *J. Neurophysiol.*, 35:560–574.
- Goldman-Rakic, P. S., and L. J. Porrino, 1985. The primate mediodorsal (MD) nucleus and its projection to the frontal lobe, *J. Comp. Neurol.*, 242:535–560.
- Guittan, D., and G. Mandl, 1974. The effect of frontal eye field stimulation on unit activity in the superior colliculus of the cat, *Brain Res.*, 68:330–334.
- Guthrie, B. L., J. D. Porter, and D. L. Sparks, 1983. Corollary discharge provides accurate eye position information to the oculomotor system, *Science*, 221:1193–1195.
- Haenny, P. E., and P. H. Schiller, 1988. State dependent activity in monkey visual cortex. I. Single cell activity in V1 and V4 on visual tasks, *Exp. Brain Res.*, 69:225–244.
- Hanes, D. P., and R. H. Wurtz, 2001. Interaction of the frontal eye field and superior colliculus for saccade generation, *J. Neurophysiol.*, 85:804–815.
- Heide, W., M. Blankenburg, E. Zimmermann, and D. Kompf, 1995. Cortical control of double-step saccades: implications for spatial orientation, *Ann. Neurol.*, 38:739–748.
- Hendrickson, A., M. E. Wilson, and M. J. Toyne, 1970. The distribution of optic nerve fibers in *Macaca mulatta*, *Brain Res.*, 23:425–427.
- Hendry, S. H., and R. C. Reid, 2000. The koniocellular pathway in primate vision, *Annu. Rev. Neurosci.*, 23:127–153.
- Hikosaka, O., Y. Takikawa, and R. Kawagoe, 2000. Role of the basal ganglia in the control of purposive saccadic eye movements, *Physiol. Rev.*, 80:953–978.
- Hikosaka, O., and R. H. Wurtz, 1983a. Visual and oculomotor functions of monkey substantia nigra pars reticulata. III. Memory-contingent visual and saccade responses, *J. Neurophysiol.*, 49:1268–1284.
- Hikosaka, O., and R. H. Wurtz, 1983b. Visual and oculomotor functions of monkey substantia nigra pars reticulata. IV. Relation of substantia nigra to superior colliculus, *J. Neurophysiol.*, 49:1285–1301.
- Hikosaka, O., and R. H. Wurtz, 1985. Modification of saccadic eye movements by GABA-related substances. I. Effect of muscimol and bicuculline in monkey superior colliculus, *J. Neurophysiol.*, 53:266–291.
- Hikosaka, O., and R. H. Wurtz, 1989. The basal ganglia, in *The Neurobiology of Saccadic Eye Movements: Reviews of Oculomotor Research*, vol. III (R. H. Wurtz and M. E. Goldberg, eds.), Amsterdam: Elsevier, pp. 257–284.
- Isa, T., and Y. Saito, 2001. The direct visuo-motor pathway in mammalian superior colliculus; novel perspective on the inter-laminar connection, *Neurosci. Res.*, 41:107–113.
- Jacobsen, C. F., 1935. Functions of the frontal association area in primates, *Arch. Neurol. Psychiatry*, 33:558–569.
- Jacobsen, C. F., 1936. Studies of cerebral function in primates: I. The functions of the frontal association areas in monkeys, *Comp. Psychol. Monogr.*, 13:3–60.
- Keating, E. G., and S. G. Gooley, 1988. Disconnection of parietal and occipital access to the saccadic oculomotor system, *Exp. Brain Res.*, 70:385–398.
- Kustov, A. A., and D. L. Robinson, 1996. Shared neural control of attentional shifts and eye movements, *Nature*, 384:74–77.
- Kuypers, H. G. J. M., and D. G. Lawrence, 1967. Cortical projections to the red nucleus and the brain stem in the rhesus monkey, *Brain Res.*, 4:151–188.
- Lee, C., W. H. Rohrer, and D. L. Sparks, 1988. Population coding of saccadic eye movements by neurons in the superior colliculus, *Nature*, 332:357–360.
- Lee, P. H., M. C. Helms, G. J. Augustine, and W. C. Hall, 1997. Role of intrinsic synaptic circuitry in collicular sensorimotor integration, *Proc. Natl. Acad. Sci. USA*, 94:13299–13304.
- Leichnetz, G. R., and M. E. Goldberg, 1988. Higher centers concerned with eye movement and visual attention: cerebral cortex and thalamus, in *Neuroanatomy of the Oculomotor System* (J. A. Büttner-Ennever ed.), Amsterdam: Elsevier, pp. 365–429.
- Lemon, R., 1984. *Methods for Neuronal Recording in Conscious Animals*. IBRO Handbook Series: Methods in the Neurosciences, vol. 4, New York: Wiley, pp. 95–102.
- Lewis, R. F., D. S. Zee, M. R. Hayman, and R. J. Tamargo, 2001. Oculomotor function in the rhesus monkey after deafferentation of the extraocular muscles, *Exp. Brain Res.*, 141:349–358.
- Li, C. S., P. Mazzoni, and R. A. Andersen, 1999. Effect of reversible inactivation of macaque intraparietal area on visual and memory saccades, *J. Neurophysiol.*, 81:1827–1838.
- Lynch, J. C., J. E. Hoover, and P. L. Strick, 1994. Input to the primate frontal eye field from the substantia nigra, superior colliculus, and dentate nucleus demonstrated by transneuronal transport, *Exp. Brain Res.*, 100:181–186.
- Ma, T. P., A. M. Graybiel, and R. H. Wurtz, 1991. Location of saccade-related neurons in the macaque superior colliculus, *Exp. Brain Res.*, 85:21–35.
- Marrocco, R. T., J. W. McClurkin, and R. A. Young, 1981. Spatial properties of superior colliculus cells projecting to the inferior pulvinar and parabigeminal nucleus of the monkey, *Brain Res.*, 222:150–154.
- Maunsell, J. H. R., 1995. The brain's visual world: representation of visual targets in cerebral cortex, *Science*, 270:764–769.
- Mays, L. E., and D. L. Sparks, 1980. Dissociation of visual and saccade-related responses in superior colliculus neurons, *J. Neurophysiol.*, 43:207–232.
- Miller, E. K., 2000. The prefrontal cortex and cognitive control, *Nat. Rev. Neurosci.*, 1:59–65.
- Mohler, C. W., and R. H. Wurtz, 1977. Role of striate cortex and superior colliculus in visual guidance of saccadic eye movements in monkeys, *J. Neurophysiol.*, 40:74–94.
- Moore, T., and M. Fallah, 2001. Control of eye movements and spatial attention, *Proc. Natl. Acad. Sci. USA*, 98:1273–1276.
- Motter, B. C., 1993. Focal attention produces spatially selective processing in visual cortical areas V1, V2, and V4 in the presence of competing stimuli, *J. Neurophysiol.*, 70:909–919.
- Mountcastle, V. B., R. A. Andersen, and B. C. Motter, 1981. The influence of attentive fixation upon the excitability of the light-sensitive neurons of the posterior parietal cortex, *J. Neurosci.*, 1:1218–1235.

- Mountcastle, V. B., B. C. Motter, M. A. Steinmetz, and A. K. Sestokas, 1987. Common and differential effects of attentive fixation on the excitability of parietal and prestriate (V4) cortical visual neurons in the macaque monkey, *J. Neurosci.*, 7:2239–2255.
- Munoz, D. P., and P. J. Istvan, 1998. Lateral inhibitory interactions in the intermediate layers of the monkey superior colliculus, *J. Neurophysiol.*, 79:1193–1209.
- Munoz, D. P., and R. H. Wurtz, 1993. Fixation cells in monkey superior colliculus. I. Characteristics of cell discharge, *J. Neurophysiol.*, 70:559–575.
- Ogren, M. P., and A. E. Hendrickson, 1976. Pathways between striate cortex and subcortical regions in *Macaca mulatta* and *Saimiri sciureus*: evidence for reciprocal pulvinar connections, *Exp. Neurol.*, 53:780–800.
- Palmer, L. A., and A. C. Rosenquist, 1974. Visual receptive fields of single striate cortical units projecting to the superior colliculus in the cat, *Brain Res.*, 67:27–42.
- Paré, M., S. Ferraina, and R. H. Wurtz, 1999. Visual motion signals from the ventral intraparietal area to the saccadic system, *Soc. Neurosci. Abstr.*, 25:806.
- Paré, M., and R. H. Wurtz, 1997. Monkey posterior parietal cortex neurons antidromically activated from superior colliculus, *J. Neurophysiol.*, 78:3493–3497.
- Petersen, S. E., D. L. Robinson, and W. Keys, 1985. Pulvinar nuclei of the behaving rhesus monkey: visual responses and their modulations, *J. Neurophysiol.*, 54:867–886.
- Petersen, S. E., D. L. Robinson, and J. D. Morris, 1987. The contribution of the pulvinar to visual spatial attention, *Neuropsychologia*, 25:97–105.
- Posner, M. I., and C. D. Gilbert, 1999. Attention and primary visual cortex, *Proc. Natl. Acad. Sci. USA*, 96:2585–2587.
- Richmond, B. J., and R. H. Wurtz, 1980. Vision during saccadic eye movements. II. A corollary discharge to monkey superior colliculus, *J. Neurophysiol.*, 43:1156–1167.
- Robinson, D. L., E. M. Bowman, and C. Kertzman, 1995. Covert orienting of attention in macaques. II. Contributions of parietal cortex, *J. Neurophysiol.*, 74:698–712.
- Robinson, D. L., and S. E. Petersen, 1985. Response of pulvinar neurons to real and self-induced stimulus movement, *Brain Res.*, 338:392–394.
- Robinson, D. L., S. E. Petersen, and W. Keys, 1986. Saccade-related activity in the pulvinar nuclei of the behaving rhesus monkey, *Exp. Brain Res.*, 62:625–634.
- Robinson, D. L., and R. H. Wurtz, 1976. Use of an extraretinal signal by monkey superior colliculus neurons to distinguish real from self-induced stimulus movement, *J. Neurophysiol.*, 39:852–870.
- Rodman, H. R., C. G. Gross, and T. D. Albright, 1989. Afferent basis of visual response properties in area MT of the macaque. I. Effects of striate cortex removal, *J. Neurosci.*, 9:2033–2050.
- Rodman, H. R., C. G. Gross, and T. D. Albright, 1990. Afferent basis of visual response properties in area MT of the macaque. II. Effects of superior colliculus removal, *J. Neurosci.*, 10:1154–1164.
- Schall, J. D., 1997. Visuomotor areas of the frontal lobe, in *Cerebral Cortex*, vol. 12 (K. S. Rockland, J. H. Kaas, and A. Peters, eds.), New York: Plenum.
- Schiller, P. H., 1977. The effect of superior colliculus ablation on saccades elicited by cortical stimulation, *Brain Res.*, 122:154–156.
- Schiller, P. H., J. H. Sandell, and J. H. R. Maunsell, 1987. The effect of frontal eye field and superior colliculus lesions on saccadic latencies in the rhesus monkey, *J. Neurophysiol.*, 57:1033–1049.
- Schiller, P. H., S. D. True, and J. L. Conway, 1980. Deficits in eye movements following frontal eye field and superior colliculus ablations, *J. Neurophysiol.*, 44:1175–1189.
- Schlag, J., and M. Schlag-Rey, 1984. Visuomotor functions of central thalamus in the monkey. II. Unit activity related to visual events, targeting and fixation, *J. Neurophysiol.*, 51:1175–1195.
- Schlag-Rey, M., and J. Schlag, 1984. Visuomotor functions of central thalamus in monkey: I. Unit activity related to spontaneous eye movements, *J. Neurophysiol.*, 51:1149–1174.
- Schlag-Rey, M., J. Schlag, and P. Dassonville, 1992. How the frontal eye field can impose a saccade goal on superior colliculus neurons, *J. Neurophysiol.*, 67:1003–1005.
- Schneider, G. E., 1969. Two visual systems. Brain mechanisms for localization and discrimination are dissociated by tectal and cortical lesions, *Science*, 163:895–902.
- Segraves, M. A., and M. E. Goldberg, 1987. Functional properties of corticotectal neurons in the monkey's frontal eye field, *J. Neurophysiol.*, 58:1387–1419.
- Sommer, M. A., and E. J. Tehovnik, 1997. Reversible inactivation of macaque frontal eye field, *Exp. Brain Res.*, 116:229–249.
- Sommer, M. A., and R. H. Wurtz, 1998. Frontal eye field neurons orthodromically activated from the superior colliculus, *J. Neurophysiol.*, 80:3331–3335.
- Sommer, M. A., and R. H. Wurtz, 2000a. Composition and topographic organization of signals sent from the frontal eye field to the superior colliculus, *J. Neurophysiol.*, 83:1979–2001.
- Sommer, M. A., and R. H. Wurtz, 2000b. Activity in the pathway from superior colliculus to frontal eye field: mediodorsal thalamus relay neurons, *Soc. Neurosci. Abstr.*, 26:292.
- Sommer, M. A., and R. H. Wurtz, 2001a. Frontal eye field sends delay activity related to movement, memory, and vision to the superior colliculus, *J. Neurophysiol.*, 85:1673–1685.
- Sommer, M. A., and R. H. Wurtz, 2001b. Inactivation of mediodorsal thalamus causes saccadic deficits consistent with impairment of corollary discharge, *Soc. Neurosci. Abstr.*, 27:1503.
- Sommer, M. A., and R. H. Wurtz, 2002. A pathway in primate brain for internal monitoring of movements. *Science*, 296:1480–1482.
- Sparks, D. L., and R. Hartwich-Young, 1989. The deep layers of the superior colliculus, in *The Neurobiology of Saccadic Eye Movements: Reviews of Oculomotor Research*, vol. III (R. H. Wurtz and M. E. Goldberg, eds.), Amsterdam: Elsevier, pp. 213–256.
- Sperry, R. W., 1950. Neural basis of the spontaneous optokinetic response produced by visual inversion, *J. Comp. Physiol. Psychol.*, 43:482–489.
- Sprague, J. M., 1966. Interaction of cortex and superior colliculus in mediation of visually guided behavior in the cat, *Science*, 153:1544–1547.
- Steinbach, M. J., 1987. Proprioceptive knowledge of eye position, *Vis. Res.*, 27:1737–1744.
- Stepniewska, I., H. X. Qi, and J. H. Kaas, 1999. Do superior colliculus projection zones in the inferior pulvinar project to MT in primates? *Eur. J. Neurosci.*, 11:469–480.
- Stoerig, P., and A. Cowey, 1997. Blindsight in man and monkey, *Brain*, 120:535–559.
- Super, H., H. Spekreijse, and V. A. Lamme, 2001. A neural correlate of working memory in the monkey primary visual cortex, *Science*, 293:120–124.
- Suzuki, H., and M. Azuma, 1983. Topographic studies on visual neurons in the dorsolateral prefrontal cortex of the monkey, *Exp. Brain Res.*, 53:47–58.

- Tehovnik, E. J., M. A. Sommer, I.-H. Chou, W. M. Slocum, and P. H. Schiller, 2000. Eye fields in the frontal lobes of primates, *Brain Res. Rev.*, 32:413–448.
- Ungerleider, L. G., R. Desimone, T. W. Galkin, and M. Mishkin, 1984. Subcortical projections of area MT in the macaque, *J. Comp. Neurol.*, 223:368–386.
- Ungerleider, L. G., T. W. Galkin, and M. Mishkin, 1983. Visuotopic organization of projections from striate cortex to inferior and lateral pulvinar in rhesus monkey, *J. Comp. Neurol.*, 217:137–157.
- Weiskrantz, L., E. K. Warrington, M. D. Sanders, and J. Marshall, 1974. Visual capacity in the hemianopic field following a restricted occipital ablation, *Brain*, 97:709–728.
- Weyand, T. G., and A. C. Gafka, 1998a. Activity of neurons in area 6 of the cat during fixation and eye movements, *Vis. Neurosci.*, 15:123–140.
- Weyand, T. G., and A. C. Gafka, 1998b. Corticostriatal and corticotectal neurons in area 6 of the cat during fixation and eye movements, *Vis. Neurosci.*, 15:141–151.
- Weyand, T. G., and A. C. Gafka, 2001. Visuomotor properties of corticotectal cells in area 17 and posteromedial lateral suprasylvian (PMLS) cortex of the cat, *Vis. Neurosci.*, 18:77–91.
- Wurtz, R. H., 1969. Comparison of effects of eye movements and stimulus movements on striate cortex neurons of the monkey, *J. Neurophysiol.*, 32:987–994.
- Wurtz, R. H., and J. E. Albano, 1980. Visual-motor function of the primate superior colliculus, *Annu. Rev. Neurosci.*, 3:189–226.
- Wurtz, R. H., M. A. Basso, M. Paré, and M. A. Sommer, 2000. The superior colliculus and the cognitive control of movement, in *The New Cognitive Neurosciences*, 2nd ed. (M. S. Gazzaniga ed.), Cambridge, MA: MIT Press, pp. 573–587.
- Wurtz, R. H., M. E. Goldberg, and D. L. Robinson, 1980. Behavioral modulation of visual responses in the monkey: stimulus selection for attention and movement, in *Progress in Psychobiology and Physiological Psychology*, vol. 9 (J. M. Sprague and A. N. Epstein, eds.), New York: Academic Press, pp. 43–83.
- Wurtz, R. H., M. E. Goldberg, and D. L. Robinson, 1982. Brain mechanisms of visual attention, *Sci. Am.*, 246:124–135.
- Wurtz, R. H., and C. W. Mohler, 1976a. Enhancement of visual responses in monkey striate cortex and frontal eye fields, *J. Neurophysiol.*, 39:766–772.
- Wurtz, R. H., and C. W. Mohler, 1976b. Organization of monkey superior colliculus: enhanced visual response of superficial layer cells, *J. Neurophysiol.*, 39:745–765.
- Wurtz, R. H., B. J. Richmond, and S. J. Judge, 1980. Vision during saccadic eye movements. III. Visual interactions in monkey superior colliculus, *J. Neurophysiol.*, 43:1168–1181.
- Wurtz, R. H., and M. A. Sommer, 2000. Activity in the pathway from superior colliculus to frontal eye field: tectothalamic neurons, *Soc. Neurosci. Abstr.*, 26:969.
- Wurtz, R. H., M. A. Sommer, M. Paré, and S. Ferraina, 2001. Signal transformations from cerebral cortex to superior colliculus for the generation of saccades, *Vis. Res.*, 41:3399–3412.

99 Cerebellar Control of Eye Movements

DAVID S. ZEE AND MARK F. WALKER

THE CEREBELLUM PLAYS a pivotal role in the control of eye movements of all types. Its essential function is to optimize ocular motor performance so that images of objects of interest are brought to the fovea—where visual acuity is best—and kept there quietly—to give the brain time to analyze and interpret the visual scene. Patients with cerebellar disease report a number of disturbances of vision. These include (1) oscillopsia (illusory movement of the environment) during attempted fixation with the head still or with the head moving, (2) inability to focus on near objects, horizontal or vertical double vision, and impaired perception of the depth and orientation of objects, (3) inability to follow smoothly objects that are moving within the visual field, and (4) difficulty with tasks requiring accurate and rapid changes of fixation (e.g., reading).

Beginning with the landmark study of Westheimer and Blair (1973), who reported the effects of total cerebellectomy on eye movements in monkeys, knowledge of how the cerebellum contributes to the control of eye movements has burgeoned. Recent advances have been based on (1) the quantitative study and analysis of the functional disturbances in ocular motor performance caused by cerebellar lesions, both in human beings with cerebellar disease and in animals with enduring (surgical or electrolytic) or transient (with local anesthetics, cooling probes, or neurotoxins) experimental lesions; (2) physiological recordings of activity of single neurons during eye movements in awake, behaving primates; (3) artificial stimulation of the cerebellum, both transcranial magnetic stimulation in humans and direct electrical activation in experimental animals; (4) functional magnetic resonance imaging in intact humans; and (5) computational modeling. Taken together, these investigations have shown that the cerebellum participates in two fundamental aspects of ocular motor control: the *immediate*, “*on-line*” modulation of eye movement performance during ongoing behavior and *motor learning*, the long-term adaptive mechanisms by which motor performance is optimized. The anatomical and physiological basis of these functions is a major focus of contemporary neuroscience research.

Subclasses of eye movements

To understand how the cerebellum influences eye movements, it is useful to define the different subclasses of eye movements and to review ocular motor control signals and

their underlying anatomical substrate within the brainstem. It is on these circuits that the cerebellum exerts its influence (Leigh and Zee, 1999). *Saccades* are the rapid eye movements that quickly change the line of sight, placing the image of an object of interest on the fovea, where it can be scrutinized and its saliency determined (“fight or flight”). Saccades are characterized by their size, speed, and latency. The quick phases of nystagmus resemble saccades in their dynamic characteristics.

Vestibular slow phases are smooth eye movements that are generated by the vestibulo-ocular reflex (VOR); they act to stabilize images on the fovea when the head is rotating (rotational or r-VOR) or translating (translational or t-VOR). Vestibular slow phases are characterized by their amplitude, direction, and timing (or phase) relative to head motion. *Optokinetic* (OKN) slow phases are full-field visual following movements that can be elicited by rotation of the visual scene (e.g., with an optokinetic drum) around a subject. In natural circumstances, optokinetic slow phases act to supplement the r-VOR during sustained head rotation in the light. OKN slow phases, too, are characterized by amplitude, direction, and timing.

Pursuit is a smooth tracking eye movement that keeps the image of a moving object on the fovea. Pursuit movements are often characterized by their response to an abrupt change in target speed (*step-ramp* stimulus). The initial movement of the eye during the first ~100 msec of such tracking reflects the *open-loop* performance of the system (before visual feedback can be used to modify ongoing behavior). The acceleration of the eyes characterizes the response during this open-loop period. Sustained pursuit of a target moving at a constant-velocity is a measure of *closed-loop* behavior (which uses visual feedback to improve performance) and is characterized by a gain (eye velocity/target velocity). Predictive patterns of target motion, such as sinusoids, are also used to probe pursuit capabilities.

Vergence eye movements rotate the eyes by different amounts, usually in opposite directions, shifting gaze between objects at different distances and following objects moving in depth. This serves to maintain an image on both foveas at the same time and facilitates depth perception. Disparity (a difference between the location of an image on the two retinas), blur of images on the retina, and other features of the target (e.g., relative size) are cues that are used to signal its distance from the observer and to drive vergence.

Ocular motor control signals

The premotor commands that drive eye movements are understood best in terms of the active forces that must be generated to oppose the passive mechanical forces of the orbit (see Scudder et al., 2002, for a recent review). The major hindrance to rotation of the globe is orbital viscosity; the moment of inertia of the globe is relatively small. To move the eyes quickly, there must be a phasic increase in the frequency of neural discharge, which is roughly proportional to the velocity of the movement of the eye. In the case of saccades this is called the *pulse* of innervation. Once the eyes are brought to their new position, they must be held there against elastic-restoring forces of the orbital tissues, which would return the globe to the straight-ahead position. Preventing this centripetal drift requires a sustained tonic contraction of the extraocular muscles, called the *step* of innervation. Thus, to a first approximation, the premotor control signal for all types of eye movements is a *velocity position, phasic tonic, or pulse step* of innervation. This pattern of activity is reflected in the discharge of both ocular motoneurons and the eye muscles, whereas individual premotor neurons may show activity related to only one or another component of the ocular motor command.

The brainstem substrate

Premotor *eye velocity* commands are created by (largely) separate groups of neurons for each of the different types of eye movement. For example, premotor velocity commands for saccades and quick phases of nystagmus are generated in the pontine paramedian reticular formation (PPRF) by excitatory burst neurons (EBNs) for horizontal saccades, and in the rostral interstitial nucleus of the medial longitudinal fasciculus (riMLF) in the midbrain for vertical and torsional saccades. The eye position command or *step* of innervation is created by a common neural gaze-holding network or *neural integrator* that integrates, in the mathematical sense, eye velocity commands of all types to produce the appropriate position-coded information (the *step*) for the ocular motoneurons. Within the brainstem, the medial vestibular nucleus and the adjacent nucleus prepositus hypoglossi in the rostral medulla are important for the neural integration of horizontal ocular motor signals. For integration of vertical ocular motor signals, the interstitial nucleus of Cajal in the midbrain, coupled with activity in the vestibular and prepositus nuclei, is important. The cerebellum also has a key role in this critical gaze-holding function (see below).

Anatomical approach to the cerebellum and ocular motor control

Our approach to the contributions of the cerebellum to the control of eye movements will be based on *structural-functional* correlations, and we will discuss cerebellar influences on eye movements by anatomical regions. An important caveat is that the cerebellum has an important role in motor learning that permits adaptation and compensation for lesions that have occurred in other parts of the brain or in the motor effectors themselves. But almost certainly, the cerebellum also can compensate for lesions within it. Thus, a rigid compartmentalization of function, inferred from the enduring effects of lesions within the cerebellum, may not strictly apply to cerebellar contributions to the control of eye movements in intact subjects. With this limitation, our interpretation of the functions of the cerebellum will be based on the combination of the effects of acute and chronic lesions, as well as results of physiological studies. Here we will emphasize the areas within the cerebellum about which we know the most: the *flocculus/paraflocculus*, the *nodulus/ventral uvula* (lobules IX and X of the cerebellar vermis), and the dorsal *oculomotor vermis* (lobules V to VII) and its target in the posterior portion of the fastigial nucleus called the *fastigial oculomotor region* (FOR). There are other regions of the cerebellum, about which we know less, that are also concerned with eye movement control (e.g., posterior interposed nucleus, lateral cerebellar hemispheres). When possible, we will consider their ocular motor contribution. A comprehensive review of the cerebellar contribution to voluntary eye movements—saccades, pursuit, and vergence—including a review of electrophysiological studies, has recently appeared (Robinson and Fuchs, 2001).

The cerebellum has a distinctive anatomical organization. Purkinje cells of the cerebellar cortex project primarily to and *inhibit* cells within the underlying deep cerebellar nuclei; the projection of the vestibulocerebellum (flocculus, paraflocculus, nodulus, and uvula) is to the vestibular nuclei within the brainstem. Portions of the vestibular nuclei can be thought of as “displaced” deep cerebellar nuclei by their connections and embryological origin. There is a rich innervation to the cerebellar cortex from the inferior olive (as climbing fibers directly to Purkinje cells) and from various brainstem nuclei and the vestibular nerve (as mossy fibers to cerebellar granule cells and then onto Purkinje cells as parallel fibers). Purkinje cell discharges are of two types: simple spikes and complex spikes. Complex spikes occur at a relatively low frequency and arise from climbing fibers. Simple spikes discharge at a much higher frequency and originate from mossy fiber inputs. The discharge frequencies of complex and simple spikes are usually reciprocally related such that an increase in complex spike activity is associated

with a decrease in simple spike activity and vice versa. There are also direct climbing fiber and mossy fiber inputs to the underlying cerebellar nuclei, so that the cerebellar cortex can be thought of as a parallel pathway that can influence (via Purkinje cell projections) the direct flow of information, to and from the brainstem, through the deep nuclei.

Vestibulocerebellum: the flocculus/paraflocculus

The flocculus and paraflocculus, together with the caudal portions of the cerebellar vermis (nodulus and uvula), are part of the oldest portion of the cerebellum—the archicerebellum, also called the *vestibulocerebellum*. In rhesus monkeys, what had been called the flocculus has been divided on the basis of its afferent mossy fiber inputs into a caudal group of five folia, now called the *flocculus*, receiving its inputs primarily from the vestibular nucleus and nerve, the nucleus prepositus hypoglossi, the nucleus reticularis tegmenti pontis, and the mesencephalic reticular formation; and a rostral group of five folia, now considered part of the ventral paraflocculus, receiving their inputs largely from the pontine nuclei (Nagao et al., 1997a, 1997b; Rambold et al., 2002). The dorsal paraflocculus also receives visual information relayed via brainstem nuclei (Glickstein et al., 1994). Both the flocculus and paraflocculus receive climbing fiber inputs from the contralateral inferior olive. The flocculus also receives an input from the cell groups of the paramedian tracts, located in the midline near the medial longitudinal fasciculus in the pons and medulla (Büttner-Ennever and Horn, 1996). The main efferent pathways of the flocculus and paraflocculus are to the vestibular nuclei.

A number of investigators have recorded from neurons within the flocculus/paraflocculus and have related their activity to eye movements and to visual and vestibular stimuli. Neurons can be found that discharge in relation to various features of the stimulus, as well as to the position of the eye in the orbit and the movement of the eye during smooth pursuit, vergence, and the slow phases of nystagmus during various patterns of active and passive head motion (e.g., Belton and McCrea, 2000a, 2000b; Fukushima et al., 1999; Gomi et al., 1998; Hirata and Highstein, 2000; Kobayashi et al., 1998; Krauzlis, 2000; Leung et al., 2000; Suh et al., 2000; Takemura et al., 2001). This multiplicity of behaviors is not surprising considering the many type of abnormalities that can be produced by lesions in the flocculus/paraflocculus.

PURSUIT Lesions of the flocculus and paraflocculus lead to a characteristic ocular motor syndrome (Waespe et al., 1983; Zee et al., 1981). Smooth visual tracking of a moving target is impaired, either when the head is still (smooth pursuit) or moving (VOR suppression or cancellation) (Fig. 99.1). Both the initiation of pursuit and the response during sustained

tracking can be affected. Complete lesions of the flocculus/paraflocculus lead to a considerably decreased steady-state gain (eye velocity/target velocity), though pursuit does not appear to be as profoundly disturbed as it is after total cerebellectomy. Pursuit adaptation is also impaired after floccular/parafloccular lesions (Rambold et al., 2002). There is considerable recovery of pursuit function, even with relatively complete floccular/parafloccular lesions, implicating other parts of the cerebellum in the control of pursuit eye movements (see below). There may be differences in the role of the flocculus/paraflocculus in pursuit during combined eye-head tracking, depending upon whether the head is actively or passively rotated (Belton and McCrea, 2000a, 2000b). Likewise, there may be differences in the relative roles of the flocculus and paraflocculus in the generation of pursuit (Nagao and Kitazawa, 1998; Rambold et al., 2002). A number of investigators have recorded neural activity during pursuit and have shown a tight relationship between various parameters of eye motion and Purkinje cell discharge (Krauzlis, 2000; Takemura et al., 2001). No consensus, though, has been reached on the relative roles of the flocculus/paraflocculus in initiating versus sustaining pursuit or in responding to novel versus predictive patterns of target motion.

GAZE-HOLDING, POSTSACCADIC DRIFT, AND THE NEURAL INTEGRATOR A second cardinal feature of lesions of the flocculus/paraflocculus is *impaired gaze-holding*. After eccentric horizontal eye movements, the eyes drift centripetally (Fig. 99.2). This finding indicates that the flocculus/paraflocculus

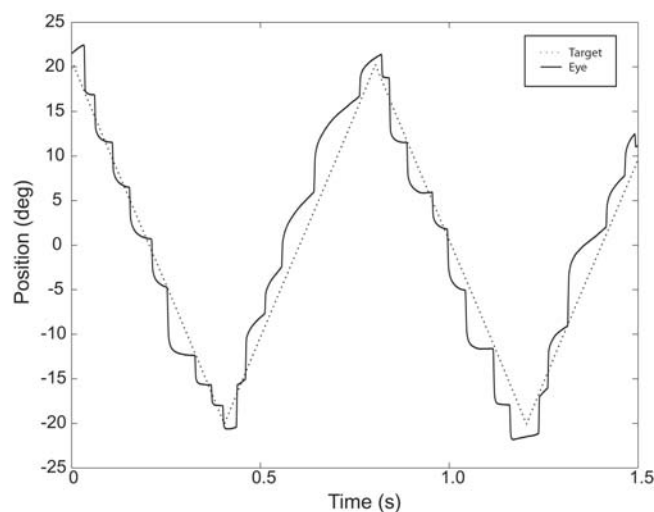


FIGURE 99.1. Horizontal eye position (*solid line*) during pursuit tracking of a small laser target moving at constant velocity (10 deg/sec) in a patient with spinocerebellar ataxia type 6. Note the reduced slow-phase gain, particularly for leftward pursuit, and the superimposed corrective quick phases (saccadic pursuit). Right is positive.

functions in the control of the brainstem neural integrators that convert velocity into position commands for all types of conjugate eye movements. The neural integrator cannot sustain its tonic output, and the eyes drift centripetally due to unopposed elastic restoring forces. Single-unit recordings within the flocculus/paraflocculus reveal that some Purkinje cells discharge in relation to the *position* of the eye in the orbit, as would be expected if the flocculus/paraflocculus contributes to the neural integrator (Miles et al., 1980).

A third distinctive feature of lesions in the flocculus/paraflocculus is *downbeat nystagmus*, in which the eyes drift up (slow phase) and are brought back to the fixation target by a corrective downward saccade (quick phase) (Fig. 99.3). This nystagmus seems to combine two types of defects produced by the removal of the flocculus/paraflocculus. The first is a tonic imbalance leading to an upward slow-phase drift even when the eyes are in the center of the orbit. The imbalance likely reflects a removal of inhibition from Purkinje cells in the flocculus/paraflocculus on vestibular pathways within the brainstem that mediate upward slow phases (Zee et al., 1981). This effect could be on pathways that mediate the r-VOR, the t-VOR, or pursuit, or at some point where these signals are already combined (Bohmer and Straumann, 1998). A second feature of the upward drift is that it can have either a decreasing or an increasing slow-phase velocity waveform (Fig. 99.3). The different velocity profiles can be explained by differences in the effect of the lesion on the vertical neural integrator. If the integrator is “leaky” such that its discharge decays with time, the velocity will decrease until reset by a quick phase. If the integrator is “unstable” (its discharge increases with time), an increasing velocity waveform will result. Some monkeys with experimental floccular and parafloccular lesions show downbeat nystagmus with a decreasing velocity waveform; others show an increasing velocity waveform. The effect of vertical eye position on the intensity of nystagmus varies with the waveform type. With an increasing

velocity waveform, intensity is greatest when looking up; with a decreasing velocity waveform, intensity is greatest when looking down.

A simple hypothesis to explain the effects of lesions of the flocculus/paraflocculus on gaze-holding is based upon the idea that there is an inherently poor, leaky ocular motor integrator within the brainstem (Zee et al., 1981). The neurons in the paramedian tracts and in the medial vestibular nucleus and the nucleus prepositus hypoglossi are probably important constituents of this integrator network (Aksay et al., 2001; Nakamagoe et al., 2000). In this scheme, the cerebellum improves the performance of this brainstem network by acting on a positive feedback loop around the brainstem neural integrator, acting to sustain the discharge of neurons in the absence of an ongoing external input. The flocculus/paraflocculus would then modulate the gain of this feedback loop. For the horizontal system, monkeys with floccular/parafloccular lesions always develop a gaze-evoked nystagmus with a velocity-decaying waveform, indicating that the flocculus/paraflocculus is critical for improving the performance of the inherently leaky horizontal brainstem neural integrator. The effect on the waveform of upward slow phases is less profound and more variable from animal to animal, suggesting that for the vertical integrator circuits the flocculus/paraflocculus has a more subtle modulatory role.

Another feature of the floccular/parafloccular syndrome is a brief drift of the eyes, lasting for several hundred milliseconds following saccades, called a *glissade*. Glissades occur in patients with cerebellar disease and in animals with experimental lesions in the flocculus/paraflocculus. This postsaccadic drift reflects a mismatch between the pulse (phasic) and the step (tonic) of innervation for saccades and is due to abnormal amplitude of the step output of the neural integrator relative to its velocity input, the pulse. Normally, these two premotor signals are precisely matched so that the eye stops abruptly at the end of the saccade. In monkeys with lesions of the flocculus/paraflocculus, the direction of the

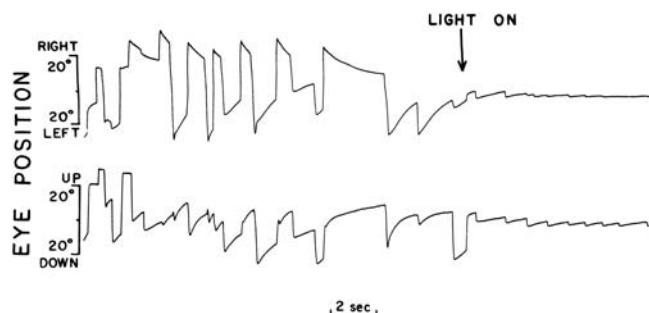


FIGURE 99.2. Eye movement recordings showing horizontal gaze-evoked nystagmus with centripetal drift and downbeat nystagmus in a monkey after bilateral removal of the flocculus and paraflocculus. (From Zee et al., 1981, with permission.)

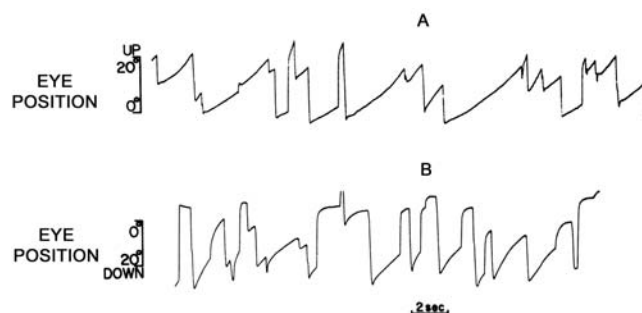


FIGURE 99.3. Eye movement recordings showing waveforms of vertical slow phases of downbeat nystagmus in darkness. Note both the exponentially increasing (A) and decreasing (B) waveforms. (From Zee et al., 1981, with permission.)

glissade, onward or backward, is variable from animal to animal.

VESTIBULAR-OCULAR REFLEXES The flocculus and parafofculus are not critical for the r-VOR in the sense that the r-VOR is still present in animals with lesions of the flocculus/parafofculus or even after complete ablation of the cerebellum. The amplitude, however, may be normal, increased, or decreased.

Patients with diffuse cerebellar lesions show abnormalities of the direction and conjugacy of the r-VOR (Fig. 99.4). In response to a high-acceleration horizontal rotation of the head (*head thrust*), a dynamic upward bias may appear so that the eyes move up as well as horizontally, producing a *cross-coupled* VOR (Walker et al., 2002). There are also inappropriate torsional components. Furthermore, the responses in the two eyes are disconjugate, with relatively more torsion in one eye and more vertical rotation in the other. Recent work has shown a similar type of abnormality in a monkey with a bilateral lesion of the flocculus (Zee et al., 2002).

Of particular current interest is the role of the cerebellum in the t-VOR, and the flocculus/parafofculus may be involved in its generation, though this is still unproven. The t-VOR itself can be measured alone (e.g., side-to-side or fore-and-aft motion on a linear sled) or in combination with the r-VOR (when the axis of rotation of the head is ahead of or behind the labyrinths, which leads to a combined rotation and translation). Patients with cerebellar lesions can have a profoundly impaired t-VOR even when the r-VOR is intact (Fig. 99.5) (Wiest et al., 2001; Zee et al., 2002). They also have defects in adjusting the r-VOR for the distance of the target of interest and for the displacement of the orbits from the axis of head rotation. These are necessary require-

ments for adequate gaze stabilization during head rotation, since virtually all head rotations are accompanied by some translation of the orbits. The flocculus/parafofculus has neurons that discharge in relation to vergence, and it is possible that this information is used to adjust the VOR for target distance, a necessary requirement whenever translation is a component of head motion (Snyder and King, 1996).

In patients with diffuse cerebellar disease, there also appears to be an association between deficits in the t-VOR and in smooth pursuit (Baloh et al., 1995). The t-VOR and pursuit normally work closely together; both act to stabilize on the fovea the images of objects that are moving across the visual field at a particular depth, either due to self-motion or to object motion. Thus, it is reasonable to speculate that the flocculus/parafofculus has a role in both pursuit and the t-VOR, and that both types of eye movement also share cerebellar circuitry, in accord with their close functional relationship. Other parts of the cerebellum, including the dorsal vermis and the underlying fastigial nuclei (see below), may also play a role in the t-VOR, as they do for pursuit.

Vestibulocerebellum: the nodulus/ventral uvula

The *nodulus* and adjacent *ventral uvula* are the most caudal aspects of the cerebellar vermis. They receive afferents from the vestibular nuclei, nucleus prepositus hypoglossi, inferior olive, and vestibular nerve. The nodulus/ventral uvula acts on the “low-frequency” components of the VOR via its projections to the velocity-storage mechanism within the vestibular nuclei (Sheliga et al., 1999). In the case of a constant-velocity rotation of the head, the velocity-storage mechanism acts to extend the duration of the VOR response

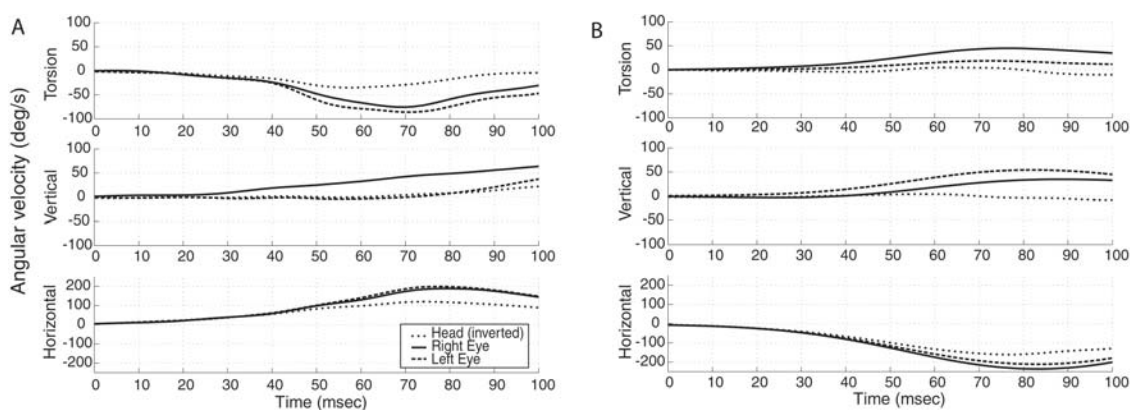


FIGURE 99.4. Binocular dual-axis scleral search coil recordings in a patient with cerebellar degeneration. Angular velocity components for both eyes and the head (inverted) are shown for head rotations in both horizontal directions. Note the increased horizontal gain, the upward vertical slow-phase component (cross-coupling) with horizontal head rotations in either direction, and the torsional

cross-coupling that changes direction with the direction of horizontal head rotation. The responses are also disconjugate. *A*, Rightward head rotation. *B*, Leftward head rotation. Right, up, and clockwise (relative to the patient) are positive. (From Walker et al., 2002, with permission.)

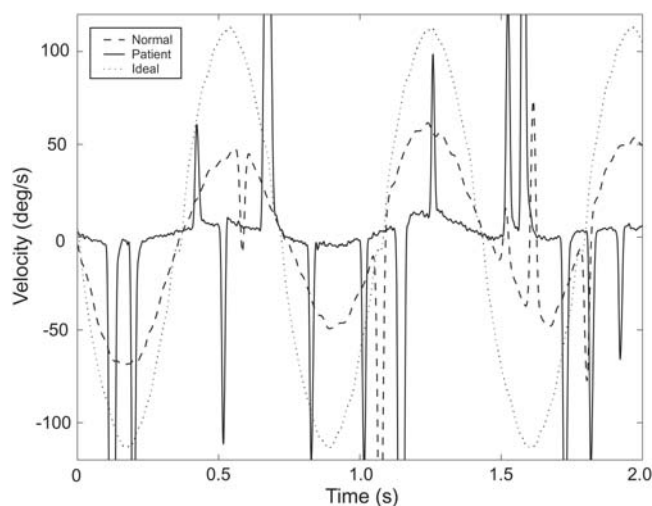


FIGURE 99.5. Horizontal eye velocity in response to interaural translation (0.7 Hz, peak acceleration 0.36g) in a normal subject (*dashed line*) and in a patient with cerebellar degeneration (*solid line*). Recordings were made in complete darkness except for a small center fixation target that flashed intermittently for 20 msec every 1000 msec to maintain orbital position and vergence angle. The dotted line shows the ideal eye velocity response based on the stimulus and target distance. The velocity “spikes” are quick phases. Note that the slow-phase gain is substantially reduced.

beyond that expected from the mechanical properties of the cupula-endolymph system within the semicircular canals. This perseverating action slows the decay of nystagmus during a constant-velocity rotation in the dark and improves the low-frequency performance of the reflex. Recordings of neural activity within the vestibular nerve during constant-velocity rotations in the dark reflect the time course of the change in the position of the cupula (which slowly returns to its neutral position after the onset of head rotation at a constant speed); recordings of activity within neurons in the vestibular nuclei reflect the additional action of the velocity-storage mechanism, and their activity outlasts the activity on primary afferents. During sustained “off-vertical axis” rotation of the head, when there is an imposed change in linear acceleration due to the continuous reorientation of the head relative to the pull of gravity, the velocity-storage mechanism modulates the *direction* of compensatory slow phases, reorienting the axis of eye rotation relative to the axis of head rotation.

Lesions of the nodulus have several effects. The duration of vestibular responses to a constant-velocity input is increased (the VOR time constant is increased). There is a loss of habituation to repetitive stimulation (the VOR time constant no longer decreases with repetitive stimulation). Tilt suppression of postrotary nystagmus, a phenomenon by which the decay of postrotary nystagmus is hastened by pitching the head down immediately following the end of a constant-velocity rotation, no longer occurs (Waespe et al.,

1985). With nodulus lesions, the VOR no longer shows the reorientation of the axis of eye rotation that normally occurs with an imposed linear acceleration (Angelaki and Hess, 1995; Wearne et al., 1998). Patients with diffuse cerebellar disease may show abnormally directed slow phases, or cross-coupling, even when there should be none, for example, during low-frequency head rotation around an earth-vertical axis, during sustained optokinetic stimulation with the head upright, and after horizontal head shaking (Walker and Zee, 1999). These abnormalities of VOR direction in response to low-frequency stimuli likely reflect dysfunction of the nodulus.

Periodic alternating nystagmus (PAN), a horizontal jerk nystagmus that changes direction every few minutes, may appear following lesioning of the nodulus. PAN reflects the combined actions of a (1) disinhibited brainstem vestibular velocity-storage mechanism (due to loss of inhibition from Purkinje cells in the nodulus that project to vestibular nuclei) and (2) an intact adaptive mechanism that acts to null any sustained unidirectional nystagmus, allowing PAN to change direction. This same adaptive mechanism produces the reversal phases of rotary and caloric nystagmus in normal subjects and the reversal phases of head-shaking-induced nystagmus in patients with labyrinthine lesions. Because Purkinje cell inhibition is mediated through GABA-b receptors, treatment with baclofen (a GABA-b agonist) disengages the velocity-storage mechanism and stops PAN.

The nodulus and uvula may have other ocular motor functions; lesions there also alter smooth pursuit and optokinetic nystagmus, but their exact contribution to these visual-following reflexes is unclear (Heinen and Keller, 1996).

FUNCTIONAL DIFFERENCES BETWEEN THE FLOCCULUS/ PARAFLOCCULUS AND THE NODULUS/UVULA The vestibulo-cerebellum has many functions, and lesions produce a variety of abnormalities. Can we extract any overriding principles about the functions of these two areas of the cerebellum? One simple hypothesis is that the flocculus and paraflocculus are more concerned with relatively immediate and fast-acting, foveally related ocular motor functions, such as smooth pursuit, the t-VOR, and steady gaze following saccades, all of which relate to holding images steady on the fovea. The nodulus and ventral uvula are more concerned with generating eye movements that determine the duration and axis of eye rotation in response to low-frequency vestibular stimuli and so determine the orientation of images on the entire retina (Sheliga et al., 1999). This idea remains speculative, and even within the flocculus/paraflocculus (Rambold et al., 2002) and nodulus/uvula there is likely a further segregation of function (Wearne et al., 1998).

Dorsal cerebellar vermis and the posterior fastigial nucleus

The dorsal vermis [lobules V to VII, called the *oculomotor vermis* (OMV)] and the underlying posterior fastigial nucleus (called the *fastigial oculomotor region*, FOR) are important in the control of saccades and pursuit. The OMV receives mossy fiber inputs from the paramedian pontine reticular formation, nucleus reticularis tegmenti pontis (NRTP), dorsolateral and dorsomedial pontine nuclei, vestibular nuclei, and nucleus prepositus hypoglossi; and climbing fiber inputs come from the inferior olive. The main projection of the Purkinje cells of the OMV is to the FOR. The FOR also receives axon collaterals of climbing fiber inputs from the inferior olive, and axon collaterals from mossy fibers projecting to the dorsal vermis from neurons within the pons. The main projection from the FOR crosses through the other fastigial nucleus and enters the uncinate fasciculus, which runs in the dorsolateral border of the superior cerebellar peduncle to reach the brainstem. The main targets of the FOR are the omnipause neurons and premotor saccadic burst neurons in the medulla, pons, and midbrain. In addition, the nucleus of the posterior commissure, the mesencephalic reticular formation, and the rostral pole of the superior colliculus receive inputs from the FOR. There are also projections to other structures including the NRTP, the dorsolateral pontine nuclei, vestibular nuclei, the superior

colliculus, and the nucleus prepositus hypoglossi. Thus, the OMV and FOR are poised to influence virtually all the critical neural structures within the brainstem that control saccade and pursuit eye movements.

SACCADES Considerable evidence points to the OMV and FOR playing an important role in the control of virtually every aspect of saccades. Lesions in the OMV lead to changes in the accuracy, latency, and dynamic properties of saccades (Fig. 99.6), as well as in the ability to undergo saccade adaptation (Barash et al., 1999; Takagi et al., 1998). Physiological studies in monkeys reveal that Purkinje cells in the OMV discharge before saccades, and stimulation of this same area can elicit saccades (Krauzlis and Miles, 1998; Thier et al., 2000). In humans, too, artificial stimulation using transcranial magnetic stimulation (Hashimoto and Ohtsuka, 1995) and functional magnetic resonance imaging scanning while subjects make saccades (Desmurget et al., 2000; Dieterich et al., 2000) confirm the participation of the OMV in the generation of saccades. Neurons in the FOR also discharge in relation to saccades. They supply a pre-saccadic burst for contraversive saccades (i.e., the right FOR bursts before leftward saccades) and a “braking” discharge, late during the saccade, for ipsiversive saccades (Robinson and Fuchs, 2001). Thus, each FOR acts to facilitate contraversive saccades and contributes to the termination of

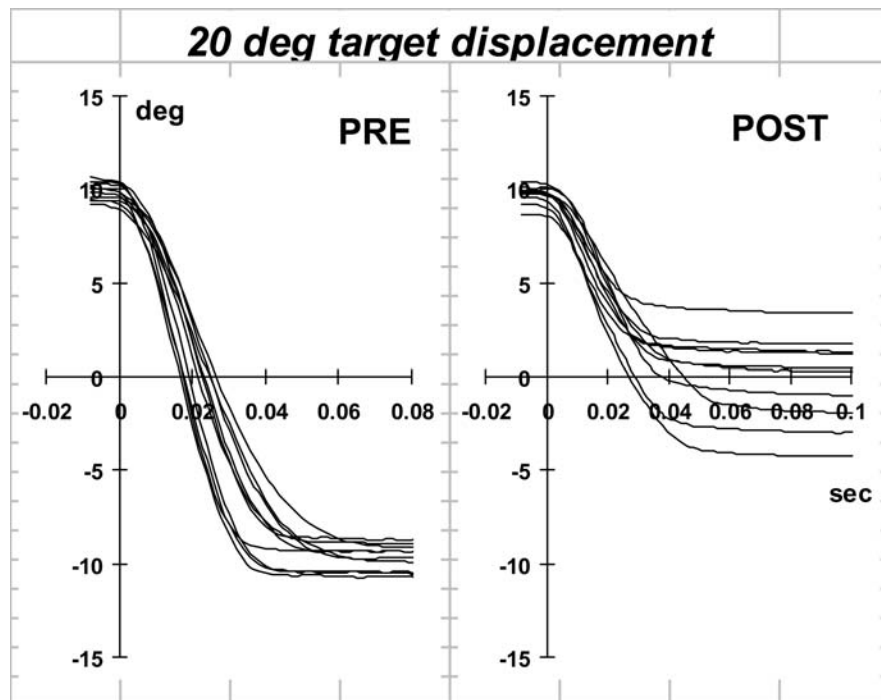


FIGURE 99.6. Representative traces of horizontal saccades in response to a leftward 20 degree target jump from a monkey with a lesion in the OMV. Ten consecutive trials were plotted. The left panel indicates prelesion data and the right panel early postlesion

data. Saccades were realigned to the same starting position. Note the hypometria and larger variability after lesioning. (From Takagi et al., 1998, with permission.)

ipsiversive saccades. Purkinje cells in the OMV behave in a similar way to those of the FOR, though, as predicted from their inhibitory nature, their “sign” is opposite. Thus, each side of the vermis acts to facilitate ipsiversive saccades and contributes to the termination of the contralateral saccades. Consequently, FOR lesions cause ipsiversive saccadic hypermetria (overshoot) and contraversive hypometria (undershoot). Bilateral FOR lesions cause bilateral hypermetria (Optican and Robinson, 1980). Since Purkinje cells of the OMV inhibit the ipsilateral FOR, the effects of OMV lesions are opposite to those of FOR lesions: hypermetric contraversive and hypometric ipsiversive saccades. Bilateral lesions in OMV cause hypometric saccades in both directions.

FUNCTIONAL LESIONS OF THE FOR The pattern of saccadic dysmetria that appears after unilateral inactivation of the FOR mimics an archetypical clinical neuro-ophthalmologic syndrome—*lateropulsion* of saccades—that occurs with vascular lesions in the dorsal lateral medulla (Wallenberg’s syndrome). With lateropulsion there is an inappropriate horizontal component *toward* the side of the lesion during attempted vertical saccades. Likewise, horizontal saccades overshoot when directed toward and undershoot when directed away from the side of the lesion. Together this pattern of saccadic dysmetria is called *ipsipulsion*. Why should a brainstem lesion produce lateropulsion of saccades? Here an understanding of basic cerebellar physiology suggests the answer (Waespe and Baumgartner, 1992). The lesion in the dorsolateral medulla interrupts, at the level of the inferior cerebellar peduncle, the climbing fiber projection to the Purkinje cells of the OMV. The removal of the climbing fiber input leads to an increase in the simple-spike discharge rate of the Purkinje cells because of the reciprocal relationship between the climbing fiber and simple-spike discharge rate of Purkinje cells. Consequently, there is an increased inhibition of the FOR on the side of the lesion. Hence, one can attribute ipsipulsion of saccades in Wallenberg’s syndrome to a loss of facilitation of contralateral saccades and a failure of inhibition of ipsilateral saccades. This is an example of a functional lesion of the FOR; the structural lesion is actually in the brainstem involving the inferior cerebellar peduncle.

HOW DOES THE CEREBELLUM INFLUENCE THE CIRCUITS WITHIN THE BRAINSTEM THAT GENERATE SACCADES? In spite of the considerable evidence relating the OMV and FOR to the control of saccades, many questions remain about how descending signals from the cerebral hemispheres and superior colliculus are transformed and shaped into the correct saccade premotor command. The FOR is clearly involved in this process, but not known are the precise source and timing of the signals that provide the input to the FOR.

Equally unclear is how the FOR, and the OMV through its projections to the FOR, influence the brainstem circuits that generate saccades. There are a number of possible targets by which the FOR could influence saccades. The early influence of the FOR on the initiation of saccades could be mediated through the excitatory burst neurons (EBN) within the brainstem reticular formation. The late influence of the FOR on stopping saccades could be through the inhibitory burst neurons (IBN) in the brainstem reticular formation. These neurons could act to “choke” or “brake” the saccade by strongly inhibiting the abducens nucleus that had been driving the agonist muscles during the saccade. Projections of the FOR to omnipause neurons (OPN), which inhibit premotor saccadic EBN—either directly or via projections to OPN from the fixation zone of the rostral pole of the superior colliculus—would be other routes by which the FOR could help bring the saccade to an end. Modulation of the trajectories of saccades on-line has also been suggested as a function of the FOR, with the OMV receiving information about performance during saccades and adjusting its inhibition upon the FOR to ensure saccade accuracy. In this scheme, the OMV would also recognize contexts (e.g., the position of the eye in the orbit) and adjust the output of the FOR to fit the particular circumstances in which the saccade must be generated. Though attractive, these speculations about cerebellar function in the control of saccades await experimental confirmation. (See Optican and Quaia, 2002; Robinson et al., 2002; and Scudder et al., 2002, for discussion of these issues.)

PURSUIT As with saccades, there is considerable evidence that the OMV and FOR participate in the generation of pursuit eye movements. Lesions in the OMV lead to changes in smooth pursuit as well as in the ability to undergo pursuit adaptation (Fig. 99.7) (Takagi et al., 2000). Electrical stimulation of the OMV can enhance ipsiversive or impair contraversive pursuit in monkeys (Krauzlis and Miles, 1998), and transcranial magnetic stimulation of the posterior cerebellum in humans can also evoke pursuit eye movements in the same pattern (Ohtsuka and Enoki, 1998). There are neurons in both the OMV and the FOR that discharge in relation to pursuit (Robinson and Fuchs, 2001). In the case of the FOR, neurons discharge early during contraversive pursuit and late for ipsilateral pursuit, analogous to activity associated with saccades. Thus, each FOR can act to facilitate contraversive pursuit and can contribute to the termination of ipsiversive pursuit. Purkinje cells in the OMV probably behave similarly to those of the FOR, though, as predicted from their inhibitory nature, their sign is opposite. Each side of the vermis acts to facilitate ipsiversive pursuit and contributes to the termination of contralateral pursuit.

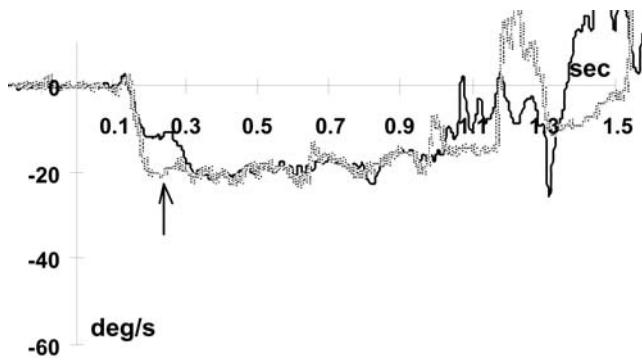


FIGURE 99.7. Step-ramp tracking for monkey (target velocity, 20 deg/sec) following lesioning in the OMV. Velocity traces are shown, with an average of 10 trials, pre- (gray line) and post- (black line) lesioning. Note the decrease in tracking velocity during the initial open-loop portion of visual tracking. The arrow indicates 100 msec after the onset of tracking (the open-loop period). (From Takagi et al., 2000, with permission.)

The pursuit deficits that have been reported after lesioning in the OMV and the FOR are largely in accord with the physiological findings. As expected, with a lesion in the FOR, contralateral pursuit is impaired. Bilateral FOR lesions would be expected to produce reasonably symmetrical and relatively intact pursuit, and this appears to be the case, though a detailed analysis of the open-loop behavior of such animals is not yet available. On the other hand, bilateral lesions of the OMV produce bilateral pursuit deficits.

One other remarkable finding after OMV lesioning in monkeys is that there are quantitative similarities in the effects of the lesions on saccade amplitude, and on pursuit velocity at the end of the open-loop initial period of pursuit tracking (the first 100 msec of tracking after a target has started moving or has changed its speed) (Takagi et al., 2000). This similarity suggests that the OMV functions in the control of the preprogrammed open-loop component of eye movements, and furthermore that saccades and the open-loop portion of pursuit share neural circuitry, not only in the cerebellum but also in the brainstem and superior colliculus. Compatible with this idea is the finding of neurons within the OMV that discharge for both pursuit and saccades, and that stimulation of the OMV can alter ongoing saccades or pursuit, depending on the parameters of the stimulus (Krauzlis et al., 1997).

WHY ARE THERE MULTIPLE AREAS WITHIN THE CEREBELLUM RELATED TO PURSUIT AND TO SACCADIC EYE MOVEMENTS? Before leaving the FOR and OMV, one must ask why there are multiple areas within the cerebellum that seem related to pursuit. For example, the uvula (Heinen and Keller, 1996) and the interposed nucleus (Robinson and Brettler, 1998), the flocculus/paraflocculus, and the FOR/OMV complexes

all have neurons that discharge with pursuit eye movements. Lesions in the uvula (Heinen and Keller, 1996) and within the lateral cerebellar hemispheres (Straube et al., 2001) also have been associated with pursuit deficits. One dichotomy to consider is that the OMV/FOR is more concerned with the initiation and termination of the preprogrammed, open-loop, initial portion of pursuit, and the flocculus/paraflocculus is more concerned with pursuit during sustained tracking. Such a strict segregation of function, however, is not yet proven. Furthermore, after partial lesioning in the cerebellar cortex there is considerable recovery of function, implying a striking ability for one part of the cerebellum to take over for another.

For saccades, too, there are neurons in areas of the cerebellum apart from the FOR/OMV that show saccade-related activity. They include the posterior portion of the interposed nucleus (Robinson, 2000), the basal interstitial nucleus (Takikawa et al., 1998), and the lateral cerebellar hemispheres (Mano et al., 1991). Both pursuit and saccades are commonly associated with other motor behaviors. Pursuit frequently works with (or against) the VOR during combined movements of the eyes and head or eyes and arms. Saccades, too, are associated with arm tracking and with leg movements during ambulation, and also form an important component of the compensatory response to translational movement of the head (Ramat and Zee, 2002; Wiest et al., 2001). Thus, one can envision a number of areas within the cerebellum associated with different motor behaviors that might want to “know” or use information about associated eye movements to help optimize their own performance.

Other abnormalities of ocular motor control associated with cerebellar dysfunction

ABNORMALITIES OF TORSION DURING FIXATION The torsional orientation of the eye during fixation is precisely controlled and is described by Donders’ and Listing’s laws (Fetter et al., 1997). Donders’ law states that during steady fixation, the torsional orientation of the eyes is fixed for a given eccentric (horizontal and vertical) eye position. Listing’s law describes the way in which Donders’ law is implemented; it defines the kinematic features of eye rotations that fix the torsional orientation of the globe for a given horizontal and vertical position of the eyes in the orbit. Listing’s law specifies a *primary position* of the eyes from which eccentric eye positions can be reached without a rotation of the eye about its line of sight. If the primary position is coincident with the straight-ahead reference position, all other positions can be reached from this position by rotation around an axis that lies in a plane (Listing’s plane) that is perpendicular to the primary position. How Listing’s law is implemented is a current area of intense investigation. Both

peripheral (mechanical) orbital and central factors likely play a role (Demer, 2002).

Patients with cerebellar lesions frequently show abnormalities of the torsional orientation of the eye during attempted steady fixation (Helmchen et al., 1997; Straumann et al., 2000). Listing's law can also be examined during pursuit by measuring the tilt of the axis of eye rotation when the orthogonal position of the eye is changed—for example, the amount of torsional eye velocity associated with horizontal tracking with the eye in elevated versus depressed positions (Walker et al., 2002). The pattern of torsion during pursuit is abnormal in patients with cerebellar disturbances and, together with the abnormalities of torsion during attempted fixation, implies that the cerebellum plays a role in the elaboration of Donders' and Listing's laws (Walker et al., 2002). Which part of the cerebellum serves this function is not yet known. The flocculus/paraflocculus might be involved, given its effect on three-dimensional orientation of the eyes during vestibular and optokinetic stimulation. The OMV could be involved, given the finding that lesions in the nucleus reticularis tegmenti pontis, which has strong projections to the OMV, lead to disturbances of the torsional orientation of the eye immediately following saccades (Van Opstal et al., 1996).

ABNORMALITIES OF TORSION DURING PURSUIT Another type of abnormality in the control of torsion occurs in patients with lesions involving the middle cerebellar peduncle (Fitzgibbon et al., 1996). In this case, there is inappropriate torsional eye velocity during vertical pursuit. The magnitude of the torsional velocity is proportional to the vertical velocity and the sign (clockwise or counterclockwise) changes, depending on whether the vertical component is up or down. The cause may be the interruption of fibers in the middle cerebellar peduncle that carry pursuit-related visual information between the pontine nuclei and the flocculus, paraflocculus, and OMV. Combined vertical-torsional eye velocities are also seen in the slow phases evoked by stimulation of individual vertical semicircular canals. This suggests that visual information for pursuit eye movements may be encoded in a vestibular (labyrinthine) coordinate frame and that the cerebellum may be important for the coordinate transformation that adjusts the axis of eye velocity. This interpretation emphasizes visual-vestibular interactions and the importance of the vestibular system in many aspects of the control of eye movements.

The cerebellum and binocular ocular motor control

Most of the findings relating the cerebellum to ocular motor control have dealt with conjugate eye movements. Much less is known about the role of the cerebellum in disconjugate ocular motor control, either of the relative positions of the

eyes during fixation (static alignment) or during movement (dynamic alignment or yoking of the eyes). Vestibular responses, especially those that take into account the translation of the head, must have a capability for disconjugate ocular motor control. Hence, it seems plausible that the cerebellum would have developed mechanisms for ensuring that each eye rotates by the correct amount during movement of the head. We have already discussed the finding that lesions within the flocculus produce disconjugate vestibular responses.

Physiological recordings from monkeys have identified neurons in several areas within the cerebellum that discharge in relation to vergence eye movements. The flocculus/paraflocculus (related to vergence angle), FOR (primarily related to convergence), and interposed nucleus (primarily related to divergence) all show activity related to vergence (Gamlin, 2002; Miles et al., 1980). Likewise, some of the pontine-cerebellar relay nuclei are also important for binocular control of eye movements (Gamlin et al., 1996).

DISORDERS OF STATIC ALIGNMENT WITH CEREbellar LESIONS

There is additional evidence from lesion studies implicating the cerebellum in binocular motor control (Versino et al., 1996). Patients with cerebellar damage sometimes show a skew deviation, a vertical misalignment of the eyes that cannot be attributed to an oculomotor or trochlear nerve palsy. The misalignment often changes its sense with horizontal eye position; most commonly, the abducting eye is higher. It has been suggested that this particular pattern of vertical misalignment of the eyes could arise from lesions in the vestibulocerebellum, perhaps the nodulus, and relate to phylogenetically old otolith-ocular reflexes in lateral-eyed animals, which produce a skew deviation that varies with horizontal eye position during fore and aft head tilt (Zee, 1996).

Patients with cerebellar abnormalities commonly have an esotropia (convergent squint in which the eyes turn inward), sometimes attributed to a divergence paralysis since the esodeviation is usually greater at distance. Patients with caudal cerebellar lesions may also have a divergence-beating nystagmus (convergent slow phases with divergent quick phases). These types of abnormalities hint at an excess of convergence tone with some cerebellar lesions.

Experimentally, too, there is evidence that cerebellar lesions lead to abnormalities of disconjugate eye movement control. Lesions of the FOR produce convergence failure, while lesions of the OMV produce esodeviations (Takagi et al., 2001). Alternating skew deviations have been reported in monkeys with large cerebellar lesions (Burde et al., 1975), and cooling of the midline deep cerebellar nuclei in monkeys produces dysmetric saccades with both a disconjugate and a conjugate component (Vilis et al., 1983). Patients with diffuse cerebellar atrophy also show disconjugate saccade dysmetria

in which the movements of the two eyes during and immediately after saccades are not yoked (Versino et al., 1996). Physiological studies also suggest a role for the interposed nucleus of the cerebellum in vergence and especially divergence control (Zhang and Gamlin, 1998). Taken together with the results of anatomical and physiological studies, there is compelling evidence for a role for the cerebellum in the disconjugate control of eye movements, though much needs to be learned about these particular aspects of cerebellar function.

Ocular motor learning and the cerebellum

Perhaps the most exciting aspect of cerebellar function is its role in motor learning. Considerable theoretical, experimental, and clinical effort has gone into understanding how this “neuronal learning machine” participates in this critical brain function. The flocculus/paraflocculus has a clear role in ocular motor learning (Ito, 2000; Lisberger et al., 1984; Optican et al., 1986; Rambold et al., 2002; Schultheis and Robinson, 1981). Monkeys or cats with complete floccular/parafloccular lesions cannot adaptively adjust the amplitude (gain) or the direction (relative to head motion) of the r-VOR or the pulse-step ratio for saccades. There is evidence that these same structures are also involved in pursuit adaptation (Kahlon and Lisberger, 2000; Nagao and Kitazawa, 2000; Rambold et al., 2002). The OMV, too, has a role in ocular motor learning. Adaptive modification of the initial acceleration of pursuit and of the amplitude of saccades is impaired with dorsal vermal lesions (Fig. 99.8) (Barash et al., 1999; Takagi et al., 1998, 2000). As expected, the FOR also plays a role in saccade (and presumably pursuit) adaptive control (Robinson et al., 2002). Disconjugate ocular motor control is also certainly subject to motor learning and is likely under cerebellar influence. One example is phoria adaptation, a mechanism by which ocular alignment is adaptively readjusted; phoria adaptation can be impaired with lesions in the cerebellum (Takagi et al., 2001). The particular areas within the cerebellum that participate in ocular motor learning have also been suggested from functional imaging studies (Desmurget et al., 2000), which complement findings from lesion and physiological studies.

The effect of lesions within the cerebellum on ocular motor function often varies from animal to animal. Examples discussed above include the pattern of postsaccadic drift (onward or backward), the amplitude of the gain of the VOR (up or down), and the waveform of the slow-phase velocity of downbeat nystagmus (velocity increasing or velocity decreasing), which appear after floccular/parafloccular ablation. While differences in the extent of lesions may explain some of this variability, another interpretation relates to the central role of the cerebellum in long-term ocular motor learning. In this formulation, the cerebellum

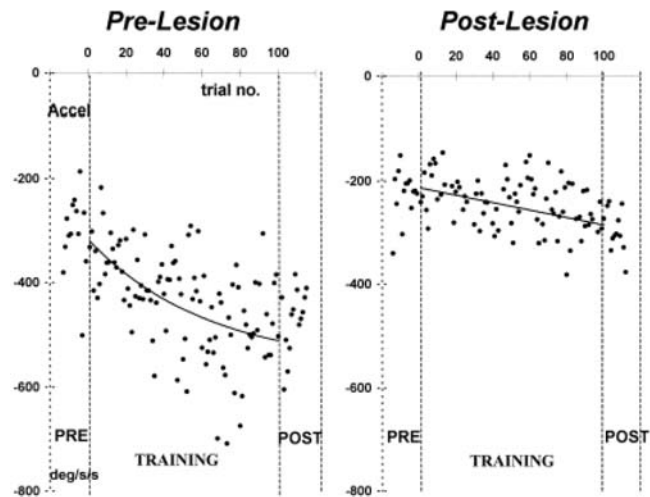


FIGURE 99.8. Trial-by-trial change in eye acceleration in the open-loop period during training in the increasing ($\times 2$) adaptation paradigm for a monkey following lesioning in the OMV. The abscissa indicates the trial number and the ordinate the average eye acceleration in the first 100 msec of tracking; this is a negative value, as tracking was leftward. One hundred trials were used in this training session and are demarcated by the inner vertical dashed lines. Note that after lesioning the increase (negative value) in average eye acceleration is attenuated. (From Takagi et al., 2000, with permission.)

acts to compensate for differences in motor performance that are idiosyncratic from animal to animal, depending on its particular genetic makeup and the “life history” of disease, trauma, as well as the interaction between inherent capabilities and environmental influences during development and aging. Consider, for example, human beings who become blind later in life. After a period of time, usually months to years, their eye movements begin to resemble those of a cerebellar patient with nystagmus and unsteady fixation (Leigh and Zee, 1980). In this case, the cerebellum has been deprived of the sensory error signals that it normally uses to keep the brainstem premotor circuits correctly calibrated for optimal visual and vestibular motor performance. The exact pattern of abnormality will depend on that patient’s particular life history. In other words, ocular motor learning is a dynamic process in which unwanted, spontaneous fluctuations in activity within brainstem ocular motor circuits must be detected and corrected. Without error signals, the cerebellum cannot “know about” and hence correct for this unwanted premotor activity, and there will be a slow, inevitable loss of calibration of ocular motor reflexes.

While there is no doubt that the cerebellum is important for ocular motor learning, the exact mechanisms are unclear, and their elucidation is a major focus of contemporary neuroscience. A number of uncertainties exist. For example, what are the precise *cellular and electrophysiological* mechanisms

of motor learning—for example, the role of climbing fiber versus mossy fiber inputs and the role of long-term depression (Anastasio, 2001; Frens et al., 2001; Hansel et al., 2001; Ito, 2001; Raymond and Lisberger, 2000)? What is the role of specific *neurotransmitters* such as nitrous oxide synthetase in motor learning (Li et al., 1995; Nagao and Kitazawa, 2000)? What are the relative roles of the cerebellar cortex and the deep cerebellar nuclei in *acquisition versus maintenance* of motor learning (Doyon et al., 2002; Robinson et al., 2002)? What are the differences in mechanisms between *short* (minutes to hours) and *long-term* (days to weeks) motor learning (Barash et al., 1999; Straube et al., 2001)? What are the differences in mechanisms between relatively simple motor learning (e.g., adjustment of the amplitude of the VOR for all head movements) and relatively complex, *context-specific motor learning* (e.g., adjustment of the amplitude of the horizontal VOR as a function of vertical eye position or adjustment of the same motor behavior, depending on internal or external cues (Gancarz and Grossberg, 1999; Straube et al., 2001; Thach, 1998)? What is the nature of the *error signals* that trigger motor learning? What are the relative roles of proprioceptive error signals (which may be important for disconjugate adaptation) (Lewis et al., 1995, 1999), visual error signals such as motion of images on the retina during head movement (Kahlon and Lisberger, 2000; Raymond et al., 1996), and efference copy error signals by which errors in performance are inferred based on monitoring of corrective ocular motor commands? What is the role of the cerebellum in generating *predictive* versus more *reflexive* motor behavior (Mauk et al., 2000; Miall and Reckess, 2002; Schultz and Dickinson, 2000)? What are the *pathways* through which cerebellar influences on adaptive control are mediated [e.g., the possible role of cerebral cortex in saccade adaptation via cerebello-thalamo-cortical pathways (Gaymard et al., 2001)]?

Summary

The cerebellum plays a central role in the coordination and calibration of all types of eye movements. Diseases and experimental lesions of the cerebellum result in a variety of ocular motor disturbances that impair vision by disrupting foveal stabilization during fixation, pursuit, or the VOR; making saccadic gaze-shifts inaccurate; and causing misalignment of the eyes. Long-term adaptive processes are disrupted. The control of torsion during fixation and eye movement is altered. A careful study of these abnormalities is contributing to a greater understanding of the function of the cerebellum in eye movement control and in the pathophysiology of cerebellar diseases.

REFERENCES

- Aksay, E., G. Gamkrelidze, H. S. Seung, R. Baker, and D. W. Tank, 2001. In vivo intracellular recording and perturbation of persistent activity in a neural integrator, *Nat. Neurosci.*, 4:184–193.
- Anastasio, T. J., 2001. Input minimization: a model of cerebellar learning without climbing fiber error signals, *NeuroReport*, 12:3825–3831.
- Angelaki, D. E., and B. J. Hess, 1995. Inertial representation of angular motion in the vestibular system of rhesus monkeys. II. Otolith-controlled transformation that depends on an intact cerebellar nodulus, *J. Neurophysiol.*, 73:1729–1751.
- Baloh, R. W., Q. Yue, and J. L. Demer, 1995. The linear vestibulo-ocular reflex in normal subjects and patients with vestibular and cerebellar lesions, *J. Vestib. Res.*, 5:349–361.
- Barash, S., A. Melikyan, A. Sivakov, M. Zhang, M. Glickstein, and P. Thier, 1999. Saccadic dysmetria and adaptation after lesions of the cerebellar cortex, *J. Neurosci.*, 19:10931–10939.
- Belton, T., and R. A. McCrea, 2000a. Role of the cerebellar flocculus region in cancellation of the VOR during passive whole body rotation, *J. Neurophysiol.*, 84:1599–1613.
- Belton, T., and R. A. McCrea, 2000b. Role of the cerebellar flocculus region in the coordination of eye and head movements during gaze pursuit, *J. Neurophysiol.*, 84:1614–1626.
- Bohmer, A., and D. Straumann, 1998. Pathomechanism of mammalian downbeat nystagmus due to cerebellar lesion: a simple hypothesis, *Neurosci. Lett.*, 250:127–130.
- Burde, R. M., M. H. Stroud, G. Roper Hall, F. P. Wirth, and J. L. O'Leary, 1975. Ocular motor dysfunction in total and hemi-cerebellectomized monkey, *Br. J. Ophthalmol.*, 59:560–565.
- Büttner-Ennever, J. A., and A. K. E. Horn, 1996. Pathways from cell groups of the paramedian tracts to the floccular region, in *New Directions in Vestibular Research* (S. Highstein, B. Cohen, and J. A. Büttner-Ennever, eds.), New York: Annals of the New York Academy of Sciences, pp. 532–540.
- Demer, J. L., 2002. The orbital pulley system: a revolution in concepts of orbital anatomy, *Ann. NY Acad. Sci.*, 956:17–32.
- Desmurget, M., D. Pelisson, J. S. Grethe, C. Prablanc, G. E. Alexander, and S. T. Grafton, 2000. Functional adaptation of reactive saccades in humans: a PET study, *Exp. Brain Res.*, 132:243–259.
- Dieterich, M., S. F. Bucher, K. C. Seelos, and T. Brandt, 2000. Cerebellar activation during optokinetic stimulation and saccades, *Neurology*, 54:148–155.
- Doyon, J., A. W. Song, A. Karni, F. Lalonde, M. M. Adams, and L. G. Ungerleider, 2002. Experience-dependent changes in cerebellar contributions to motor sequence learning, *Proc. Natl. Acad. Sci. USA*, 99:1017–1022.
- Fetter, M., T. Haslwanter, H. Misslisch, and D. Tweed, 1997. *Three-Dimensional Kinematics of Eye, Head and Limb Movements*, Amsterdam: Harwood.
- Fitzgibbon, E. J., P. C. Calvert, M. D. Dieterich, T. Brandt, and D. S. Zee, 1996. Torsional nystagmus during vertical pursuit, *J. Neuroophthalmol.*, 16:79–90.
- Frens, M. A., A. L. Mathoera, and J. van der Steen, 2001. Floccular complex spike response to transparent retinal slip, *Neuron*, 30:795–801.
- Fukushima, K., J. Fukushima, C. R. Kaneko, and A. F. Fuchs, 1999. Vertical Purkinje cells of the monkey floccular lobe: simple-spike activity during pursuit and passive whole body rotation, *J. Neurophysiol.*, 82:787–803.
- Gamlin, P. D. R., 2002. Neural mechanisms for the control of vergence eye movements, *Ann. NY Acad. Sci.*, 956:264–272.

- Gamlin, P. D. R., K. Yoon, and H. Y. Zhang, 1996. The role of cerebro-ponto-cerebellar pathways in the control of vergence eye movements, *Eye*, 10:167–171.
- Gancarz, G., and S. Grossberg, 1999. A neural model of saccadic eye movement control explains task-specific adaptation, *Vis. Res.*, 39:3123–3143.
- Gaymard, B., S. Rivaud-Pechoux, J. Yelnik, B. Pidoux, and C. J. Ploner, 2001. Involvement of the cerebellar thalamus in human saccade adaptation, *Eur. J. Neurosci.*, 14:554–560.
- Glickstein, M., N. Gerrits, I. Kralj-hans, B. Mercier, J. Stein, and J. Voogd, 1994. Visual pontocerebellar projections in the macaque, *J. Comp. Neurol.*, 349:51–72.
- Gomi, H., M. Shidara, A. Takemura, Y. Inoue, K. Kawano, and M. Kawato, 1998. Temporal firing patterns of Purkinje cells in the cerebellar ventral paraflocculus during ocular following responses in monkeys I. Simple spikes, *J. Neurophysiol.*, 80:818–831.
- Hansel, C., D. J. Linden, and E. D'Angelo, 2001. Beyond parallel fiber LTD: the diversity of synaptic and non-synaptic plasticity in the cerebellum, *Nat. Neurosci.*, 4:467–475.
- Hashimoto, M., and K. Ohtsuka, 1995. Transcranial magnetic stimulation over the posterior cerebellum during visually guided saccades in man, *Brain*, 118:1185–1193.
- Heinen, S. J., and E. L. Keller, 1996. The function of the cerebellar uvula in monkey during optokinetic and pursuit eye movements: single-unit responses and lesion effects, *Exp. Brain Res.*, 110:1–14.
- Helmchen, C., S. Glasauer, and U. Büttner, 1997. Pathological torsional eye deviation during voluntary saccades: a violation of Listing's law, *J. Neurol. Neurosurg. Psychiatry*, 62:253–260.
- Hirata, Y., and S. M. Highstein, 2000. Analysis of the discharge pattern of floccular Purkinje cells in relation to vertical head and eye movement in the squirrel monkey, *Prog. Brain Res.*, 124:221–232.
- Ito, M., 2000. Mechanisms of motor learning in the cerebellum, *Brain Res.*, 886:237–245.
- Ito, M., 2001. Cerebellar long-term depression: characterization, signal transduction, and functional roles, *Physiol. Rev.*, 81:1143–1195.
- Kahlon, M., and S. G. Lisberger, 2000. Changes in the responses of Purkinje cells in the floccular complex of monkeys after motor learning in smooth pursuit eye movements, *J. Neurophysiol.*, 84:2945–2960.
- Kobayashi, Y., K. Kawano, A. Takemura, Y. Inoue, T. Kitama, H. Gomi, and M. Kawato, 1998. Temporal firing patterns of Purkinje cells in the cerebellar ventral paraflocculus during ocular following responses in monkeys II. Complex spikes, *J. Neurophysiol.*, 80:832–848.
- Krauzlis, R. J., 2000. Population coding of movement dynamics by cerebellar Purkinje cells, *Neuroreport*, 11:1045–1050.
- Krauzlis, R. J., M. A. Basso, and R. H. Wurtz, 1997. Shared motor error for multiple eye movements, *Science*, 276:1693–1695.
- Krauzlis, R. J., and F. A. Miles, 1998. Role of the oculomotor vermis in generating pursuit and saccades: effects of microstimulation, *J. Neurophysiol.*, 80:2046–2062.
- Leigh, R. J., and D. S. Zee, 1980. Eye movements of the blind, *Invest. Ophthalmol. Vis. Sci.*, 19:328–331.
- Leigh, R. J., and D. S. Zee, 1999. *The Neurology of Eye Movements*, Oxford: Oxford University Press.
- Leung, H. C., M. Suh, and R. E. Kettner, 2000. Cerebellar flocculus and paraflocculus Purkinje cell activity during circular pursuit in monkey, *J. Neurophysiol.*, 83:13–30.
- Lewis, R. F., D. S. Zee, H. Goldstein, and B. Guthrie, 1999. Proprioceptive and retinal afference modify postsaccadic ocular drift, *J. Neurophysiol.*, 82:551–563.
- Lewis, R. F., D. S. Zee, M. X. Repka, D. L. Guyton, and N. R. Miller, 1995. Regulation of static and dynamic ocular alignment in patients with trochlear nerve palsy, *Vis. Res.*, 35:3255–3264.
- Li, J., C. S. Smith, and J. G. McElligott, 1995. Cerebellar nitric oxide is necessary for vestibulo-ocular reflex adaptation, a sensorimotor model of learning, *J. Neurophysiol.*, 74:489–494.
- Lisberger, S. G., F. A. Miles, and D. S. Zee, 1984. Signals used to computer errors in the monkey vestibuloocular reflex: possible role of the flocculus, *J. Neurophysiol.*, 52:1140–1153.
- Mano, N., Y. Ito, and H. Shibutani, 1991. Saccade-related Purkinje cells in the cerebellar hemispheres of the monkey, *Exp. Brain Res.*, 84:465–470.
- Mauk, M. D., J. F. Medina, W. L. Nores, and T. Ohyama, 2000. Cerebellar function: coordination, learning or timing? *Curr. Biol.*, 10:R522–R525.
- Miall, R. C., and G. Z. Reckess, 2002. The cerebellum and the timing of coordinated eye and hand tracking, *Brain Cogn.*, 48:212–226.
- Miles, F. A., J. H. Fuller, D. J. Braitman, and B. M. Dow, 1980. Long-term adaptive changes in primate vestibuloocular reflex. III. Electrophysiological evidence in flocculus of normal monkeys, *J. Neurophysiol.*, 43:1437–1476.
- Nagao, S., T. Kitamura, N. Nakamura, T. Hiramatsu, and J. Yamada, 1997a. Differences of the primate flocculus and ventral paraflocculus in the mossy and climbing fiber input organization, *J. Comp. Neurol.*, 382:480–498.
- Nagao, S., T. Kitamura, N. Nakamura, T. Hiramatsu, and J. Yamada, 1997b. Location of efferent terminals of the primate flocculus and ventral paraflocculus revealed by anterograde axonal transport methods, *Neurosci. Res.*, 27:257–269.
- Nagao, S., and K. Kitazawa, 1998. Differences of responsiveness to step-ramp smooth pursuit eye movements in the primate flocculus and ventral paraflocculus, *Neurosci. Res.*, SUPPL 22:316.
- Nagao, S., and H. Kitazawa, 2000. Subdural applications of NO scavenger or NO blocker to the cerebellum depress the adaptation of monkey post-saccadic smooth pursuit eye movements, *NeuroReport*, 11:131–134.
- Nakamagoe, K., Y. Iwamoto, and K. Yoshida, 2000. Evidence for brainstem structures participating in oculomotor integration, *Science*, 288:857–859.
- Ohtsuka, K., and T. Enoki, 1998. Transcranial magnetic stimulation of the posterior vermis during smooth pursuit eye movements in man, *Brain*, 121:429–435.
- Optican, L. M., and C. Quaia, 2002. Distributed model of collicular and cerebellar function during saccades, *Ann. NY Acad. Sci.*, 956:164–177.
- Optican, L. M., and D. A. Robinson, 1980. Cerebellar-dependent adaptive control of primate saccadic system, *J. Neurophysiol.*, 44:1058–1076.
- Optican, L. M., D. S. Zee, and F. A. Miles, 1986. Floccular lesions abolish adaptive control of post-saccadic drift in primates, *Exp. Brain Res.*, 64:596–598.
- Ramat, S., and D. S. Zee, 2002. TVOR responses to abrupt interaural accelerations in normal humans, *Ann. NY Acad. Sci.*, in press.
- Rambold, H., A. Churchland, Y. Selig, L. Jasmin, and S. G. Lisberger, 2002. Partial ablations of the flocculus and ventral paraflocculus in monkeys cause linked deficits in smooth pursuit eye movements and adaptive modification of the VOR, *J. Neurophysiol.*, 87:912–924.

- Raymond, J. L., and S. G. Lisberger, 2000. Hypotheses about the neural trigger for plasticity in the circuit for the vestibulo-ocular reflex, *Prog. Brain Res.*, 124:235–246.
- Raymond, J. L., S. G. Lisberger, and M. D. Mauk, 1996. The cerebellum: a neuronal learning machine? *Science*, 272:1126–1131.
- Robinson, F. R., 2000. Role of the cerebellar posterior interpositus nucleus in saccades I. Effect of temporary lesions, *J. Neurophysiol.*, 84:1289–1302.
- Robinson, F. R., and S. C. Brettler, 1998. Smooth pursuit properties of neurons in the ventrolateral posterior interpositus nucleus of the monkey cerebellum, *Soc. Neurosci. Abstr.*, 24:1405.
- Robinson, F. R., and A. F. Fuchs, 2001. The role of the cerebellum in voluntary eye movements, *Annu. Rev. Neurosci.*, 24:981–1004.
- Robinson, F. R., A. F. Fuchs, and C. T. Noto, 2002. Cerebellar influences on saccadic plasticity, *Ann. NY Acad. Sci.*, 956:155–163.
- Schultheis, L. W., and D. A. Robinson, 1981. Directional plasticity of the vestibulo-ocular reflex in the cat, *Ann. NY Acad. Sci.*, 374:504–512.
- Schultz, W., and A. Dickinson, 2000. Neuronal coding of prediction errors, *Annu. Rev. Neurosci.*, 23:473–500.
- Scudder, C. A., C. S. Kaneko, and A. F. Fuchs, 2002. The brainstem burst generator for saccadic eye movements: a modern synthesis, *Exp. Brain Res.*, 142:439–462.
- Sheliga, B. M., S. B. Yakushin, A. Silvers, T. Raphan, and B. Cohen, 1999. Control of spatial orientation of the angular vestibulo-ocular reflex by the nodulus and uvula of the vestibulocerebellum, *Ann. NY Acad. Sci.*, 871:94–122.
- Snyder, L. H., and W. M. King, 1996. Behavior and physiology of the macaque vestibulo-ocular reflex response to sudden off-axis rotation: computing eye translation, *Brain Res. Bull.*, 40: 293–301.
- Straube, A., H. Deubel, J. Ditterich, and T. Eggert, 2001. Cerebellar lesions impair rapid saccade amplitude adaptation, *Neurology*, 57:2105–2108.
- Straumann, D., D. S. Zee, and D. Solomon, 2000. Three-dimensional kinematics of ocular drift in humans with cerebellar atrophy, *J. Neurophysiol.*, 83:1125–1140.
- Suh, M., H. C. Leung, and R. E. Kettner, 2000. Cerebellar flocculus and ventral paraflocculus Purkinje cell activity during predictive and visually driven pursuit in monkey, *J. Neurophysiol.*, 84:1835–1850.
- Takagi, M., P. Trillenberg, and D. S. Zee, 2001. Adaptive control of eye movements in humans: control of smooth pursuit, vergence and eye torsion, *Vis. Res.*, 41:3329–3342.
- Takagi, M., D. S. Zee, and R. Tamargo, 1998. Effects of lesions of the oculomotor vermis on eye movements in primate: saccades, *J. Neurophysiol.*, 80:1911–1930.
- Takagi, M., D. S. Zee, and R. Tamargo, 2000. Effects of lesions of the oculomotor cerebellar vermis on eye movements in primate: smooth pursuit, *J. Neurophysiol.*, 83:247–262.
- Takemura, A., Y. Inoue, H. Gomi, M. Kawato, and K. Kawano, 2001. Change in neuronal firing patterns in the process of motor command generation for the ocular following response, *J. Neurophysiol.*, 86:1750–1763.
- Takikawa, Y., R. Kawagoe, N. Miyashita, and O. Hikosaka, 1998. Presaccadic omnidirectional burst activity in the basal interstitial nucleus in the monkey cerebellum, *Exp. Brain Res.*, 121:442–450.
- Thach, W. T., 1998. A role for the cerebellum in learning movement coordination, *Neurobiol. Learn. Mem.*, 70:177–188.
- Thier, P., P. W. Dicke, R. Haas, and S. Barash, 2000. Encoding of movement time by populations of cerebellar Purkinje cells, *Nature*, 405:72–76.
- Van Opstal, A. J., K. Hepp, Y. Suzuki, and V. Henn, 1996. Role of monkey nucleus reticularis tegmenti pontis in the stabilization of Listing's plane, *J. Neurosci.*, 16:7284–7296.
- Versino, M., O. Hurko, and D. S. Zee, 1996. Disorders of binocular control of eye movements in patients with cerebellar dysfunction, *Brain*, 119:1933–1950.
- Vilis, T., R. Snow, and J. Hore, 1983. Cerebellar saccadic dysmetria is not equal in the two eyes., *Exp. Brain Res.*, 51:343–350.
- Waespe, W., and R. Baumgartner, 1992. Enduring dysmetria and impaired gain adaptivity of saccadic eye movements in Wallenberg's lateral medullary syndrome, *Brain*, 115:1125–1146.
- Waespe, W., B. Cohen, and T. Raphan, 1983. Role of the flocculus and paraflocculus in optokinetic nystagmus and visual-vestibular interactions: effects of lesions, *Exp. Brain Res.*, 50:9–33.
- Waespe, W., B. Cohen, and T. Raphan, 1985. Dynamic modification of the vestibulo-ocular reflex by the nodulus and the uvula, *Science*, 228:199–202.
- Walker, M. F., H. Steffen, and D. S. Zee, 2002. Three-axis approaches to ocular motor control: a role for the cerebellum, in *Levels of Perception* (L. R. Harris and M. Jenkin, eds.), New York: Springer-Verlag.
- Walker, M. F., and D. S. Zee, 1999. Directional abnormalities of vestibular and optokinetic responses in cerebellar disease, *Ann. NY Acad. Sci.*, 871:205–220.
- Wearne, S., T. Raphan, and B. Cohen, 1998. Control of spatial orientation of the angular vestibuloocular reflex by the nodulus and uvula, *J. Neurophysiol.*, 79:2690–2715.
- Westheimer, G., and S. Blair, 1973. Oculomotor defects in cerebellectomized monkeys, *Invest. Ophthalmol.*, 12:618–621.
- Wiest, G., J. R. Tian, R. W. Baloh, B. T. Crane, and J. L. Demer, 2001. Otolith function in cerebellar ataxia due to mutations in the calcium channel gene CACNA1A, *Brain*, 124:2407–2416.
- Zee, D. S., 1996. Considerations on the mechanisms of alternating skew deviation in patients with cerebellar lesions, *J. Vestib. Res.*, 6:1–7.
- Zee, D. S., M. F. Walker, and S. Ramat, 2002. The cerebellar contribution to eye movements based upon lesions: binocular, three-axis control and the translational vestibulo-ocular reflex, *Ann. NY Acad. Sci.*, 956:178–189.
- Zee, D. S., A. Yamazaki, P. H. Butler, and G. Gücer, 1981. Effects of ablation of flocculus and paraflocculus of eye movements in primate, *J. Neurophysiol.*, 46:878–899.
- Zhang, H., and P. D. Gamlin, 1998. Neurons in the posterior interposed nucleus of the cerebellum related to vergence and accommodation. I. Steady-state characteristics, *J. Neurophysiol.*, 79:1255–1269.

XII ATTENTION AND COGNITION

100 Visual Perception and Cognition in Honeybees

SHAOWU ZHANG AND MANDYAM SRINIVASAN

DESPITE THE OBVIOUS optical differences between the “camera-type” eye of humans and the compound eye of the bee, research over the past two decades has begun to reveal that the fundamental principles of early visual processing in the two nervous systems may be quite similar, at least in a qualitative sense.

The worker honeybee carries a tiny brain. It occupies a volume of about 1 mm^3 , weighs about 1 mg, and contains fewer than 1 million neurons. Nevertheless, this creature, by virtue of its lifestyle, is a spectacularly suitable organism for studying the principles of pattern recognition and navigation, as well as those of learning in a more general sense (Menzel, 1990; Von Frisch, 1971). Gathering nectar and pollen is the *raison d'être* of a forager's existence. To forage successfully, a bee has to learn and remember not only the color and shape of flowers that are bountiful in these nutrients, but also how to get to them (Chittka et al., 1993; Lehrer et al., 1995; Vorobyev and Menzel, 1999; Wehner, 1981). Since the species or flowers that are in bloom one week are likely to be replaced by a different species at a different location the next week, the bee needs, and has indeed evolved, an impressive ability to learn colors, odors, shapes, and routes quickly and accurately. A bee can learn a new color in about half an hour (after it has made about 5 visits to collect a food reward), a new pattern in about half a day (after 20 to 30 rewarded visits), and a new route to a food source in about 3 to 4 visits (provided that the route is not through a complex labyrinth). The biology of the honeybee thus offers a tailor-made opportunity for studying the mechanisms by which sensory stimuli are recognized and navigational strategies are learned, remembered, and applied.

Over the past decade, work on the honeybee has begun to suggest that insects may not be the simple, reflexive creatures that they were once believed to be. Bees display perceptual and “cognitive” capacities that are surprisingly rich, complex, and flexible (Menzel and Müller, 1996; Srinivasan, 1994; Srinivasan and Zhang, 1998). This chapter reviews recent studies that have challenged the perceptual capacities of honeybees by posing question such as: Can bees learn abstract concepts? Do they generalize these concepts? Is sensory processing influenced by prior knowledge and

experience? Can bees learn complex tasks such as navigating through labyrinths? What information do bees acquire, memorize, and use when they learn how to tackle complex tasks?

This review is not intended to be exhaustive. Rather, it highlights important advances in our understanding of the processes underlying pattern recognition and perception, as well as the learning of complex tasks by the honeybee. The review will not cover some important areas in honeybee vision, such as the perception of color and motion. These topics have been discussed comprehensively in other reviews (Backhaus, 1998; Backhaus et al., 1987; Kevan et al., 2001; Menzel and Backhaus, 1989; Srinivasan et al., 1999; Chapter 80).

Three milestones in honeybee pattern recognition

The study of pattern recognition in the honeybee has seen three major milestones, or eras (Horridge, 1999; Srinivasan, 1994; Srinivasan and Zhang, 1998). The studies of the first era, by Karl Von Frisch (1915) and Hertz (1929), were carried out by cutting two or more patterns out of black paper, placing them flat on a horizontal table, and training a group of bees to collect a reward of sugar water at one of the patterns. The positions of the patterns were varied frequently to ensure that the bees learned to come to a specific pattern rather than to a specific location on the table. By analyzing the bees' performance in this task, they proposed the *flücker* hypothesis, which states that honeybees discriminate between visual patterns in terms of the frequency of on/off stimuli experienced by the compound eye as they cruise above the patterns (Hertz, 1933).

The next era commenced with the work of Wehner and Lindauer (1966), who began experimenting with patterns presented in the vertical plane. Although this may seem to be a simple modification at first glance, it opened up a whole new dimension in research on pattern recognition in bees. The reason was that one could now ask, for the first time, whether bees can distinguish between patterns that are rotated with respect to each other. This could not be done with patterns laid flat on a table, as the bees could approach such patterns from any direction. An interesting observation

made in these studies was that during training, the bees tended to hover stably in front of the training pattern for a second or two before landing on the entrance tube leading to the reward behind the pattern (Wehner and Flatt, 1977). This led Wehner to propose the *template* hypothesis, according to which bees fixate the pattern and memorize it in a photographic sense. When, after training, the bee is offered a choice between the rewarded pattern and another pattern, the bee evaluates the two patterns by comparing the extent to which each pattern matches the stored template that the bee has acquired of the rewarded pattern during training (Wehner, 1967, 1981). The template theory of pattern recognition was corroborated by the work of Gould (1985, 1986), who showed that bees could be trained to distinguish rather small differences between patterns, suggesting that recognition does indeed involve a fairly precise spatial evaluation of the extent to which the black and white regions in the viewed pattern match the corresponding regions in the template.

The third era of pattern recognition in honeybees began when investigators began to wonder whether bees could learn abstract features, or properties, of patterns instead of, or in addition to, memorizing them photographically (Van Hateren et al., 1990; Wehner, 1971). This was an important step toward gaining insights into the cognitive capacities of the honeybee brain. In the next section, we outline the progress made in this era.

Can bees abstract general properties of patterns?

There can be little doubt that bees use some kind of neural “snapshot” to remember and recognize patterns and landmarks (Collett and Cartwright, 1983; Judd and Collett, 1998). However, it is hard to imagine that this is all there is to pattern recognition. In their daily lives, bees are required to remember a number of different patterns and their properties. Examples include the shape of the nest or hive, shapes representing nectar-bearing flowers, and shapes of important landmarks on the way to the food source and back. If snapshots were the only mechanism for remembering shapes, bees would require a large memory to store all of these images. Given that the brains of bees contain far fewer neurons than do ours, it seems unlikely that they can afford the luxury of a large memory.

One would imagine, therefore, that bees also possess other, more economical means of representing patterns. Can bees abstract general features of a pattern—such as its orientation—without memorizing the pattern in its entirety? An early paper by Wehner (1971) hinted that bees could indeed abstract pattern orientation in this way. This question was pursued further by Van Hateren et al. (1990), who presented random gratings at two different orientations in a Y-maze apparatus (Fig. 100.1A, B). The stimuli were pre-

sented in the vertical plane, each at the end wall of one of the tunnels of the maze. The stimulus representing one of the orientations was associated with a reward of sugar water. The stimulus representing the other orientation offered no reward.

During training, the positions of the stimuli were interchanged frequently, and the reward was moved along with the positive stimulus, to prevent the bees from simply learning to fly to a specific tunnel. Two properties of the apparatus and the training paradigm prevented the bees from acquiring a template of the positive pattern. Firstly, the bees had to choose between the two stimuli at a considerable distance away from them; the stimuli could not be fixated at this distance. Secondly, the gratings were frequently replaced by other random gratings which were similarly oriented but had different spatial structures (Fig. 100.1B). Thus, to identify the positive stimulus correctly, the bees had to abstract its orientation, and not merely memorize a pattern in a photographic way.

Van Hateren et al. (1990) found that bees could be trained in this way to distinguish between vertical and horizontal orientations, as well as between two oblique directions (Fig. 100.1C–E). Furthermore, bees trained to distinguish between two mutually perpendicular orientations were able to discriminate the orientations of other patterns which they had never encountered previously (Fig. 100.2). Thus, bees are able to extract orientation information from patterns on which they are trained and to use this information to distinguish novel patterns.

How does the bee’s visual system extract the orientation of a pattern independently of its structure and without memorizing the pattern in a literal fashion? Srinivasan et al. (1993) provided evidence that the orientation of a pattern is discriminated by the geometrical cues that are intrinsic to the pattern and not by the cues derived from the direction of apparent image motion. Yang and Maddess (1997) found orientation detection neurons at lobula level in the bee with large fields and coarse orientation tuning. Recently, Horridge (1999) suggested that bees possess large-field filters that respond selectively to abstract stimulus properties such as symmetry, relative proportion of radial and tangential edges, angular size, orientation, and so on. The existence of filters is inferred when bees demonstrate that they can respond to a generalized cue extracted from a group of patterns that they encounter.

Recent work in our laboratory and elsewhere has revealed that bees can detect and learn other general properties of patterns, such as radial and circular symmetry (Horridge and Zhang, 1995). Bees can learn to detect bilateral symmetry and discriminate its axis as well (Giurfa et al., 1996; Horridge, 1996). Bees can also extract other abstract characteristics of objects, such as their color and size, without having to memorize the objects’

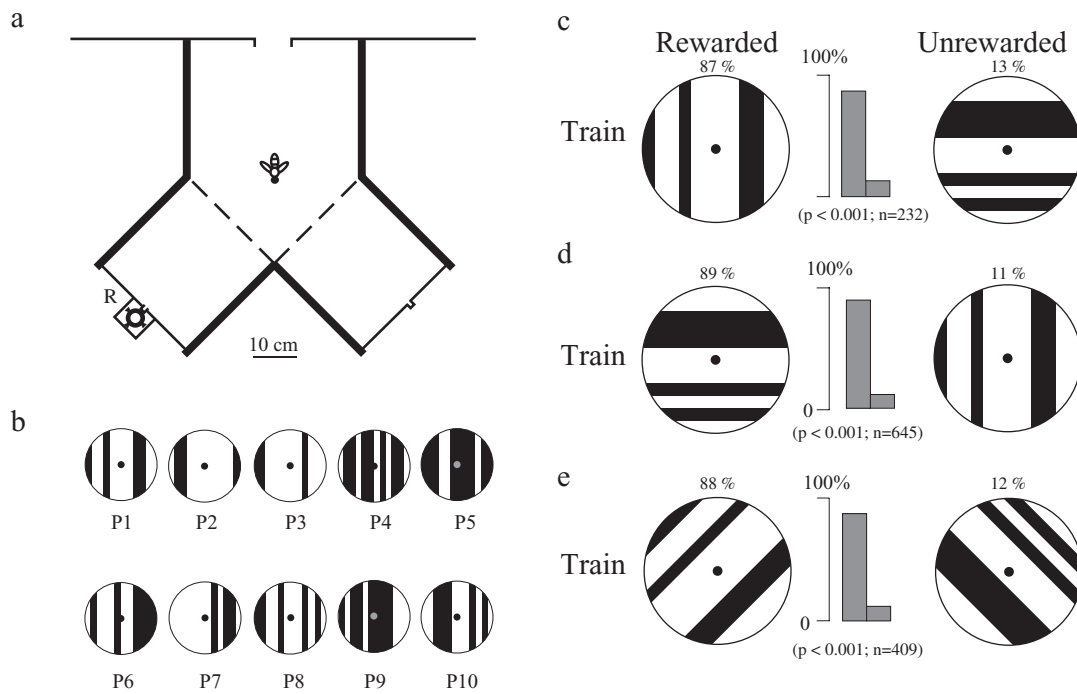


FIGURE 100.1. Discrimination of pattern orientation. In this and other figures, the vertical bars depict choice frequencies for the two stimuli in training or transfer tests, and n indicates the number of choices analyzed. Also shown is the probability value associated

with a t -test for examining whether the bees' preferences are significantly different from random choice. Details are given in the text. (Modified from Van Hateren et al., 1990).

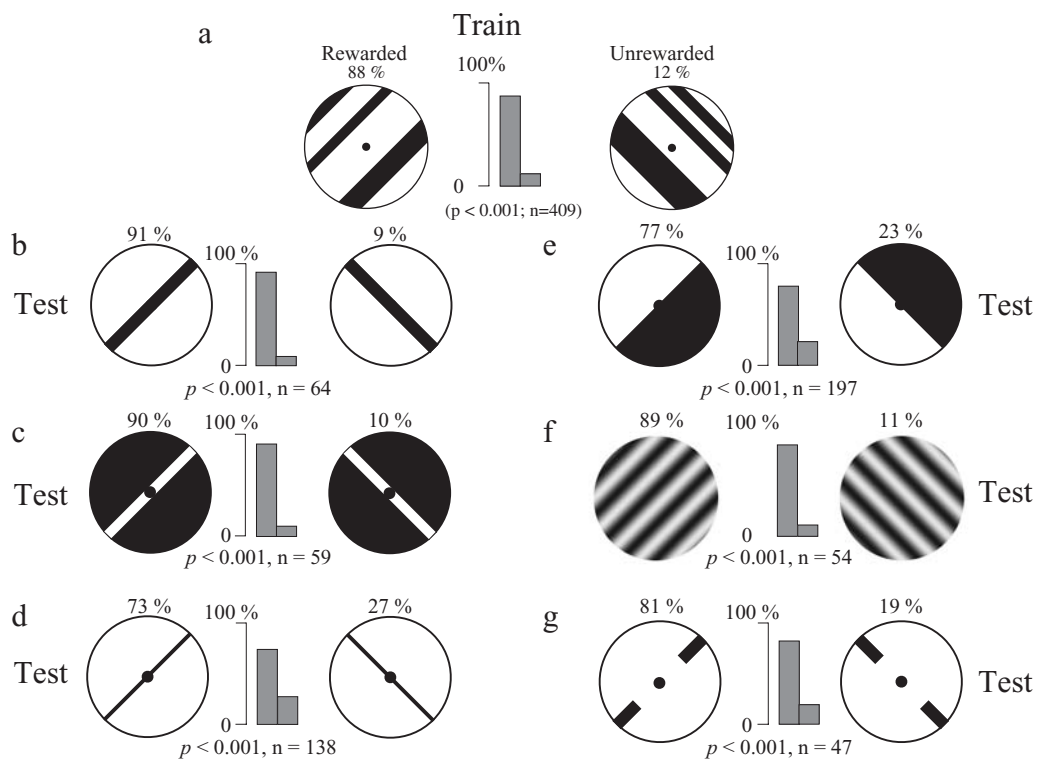


FIGURE 100.2. Bees, trained to distinguish between random gratings oriented at +45 degrees and -45 degrees (a), are able to extract the orientation information in these gratings and use it to discrim-

inate the orientations of other patterns (b-g) which they have never previously encountered. (Modified from Van Hateren et al., 1990).

images literally (e.g., Horridge et al., 1992a; Ronacher, 1992).

In all of the above-mentioned studies, bees clearly demonstrated that they are capable of extracting abstract cues of objects, then generalizing them and using the same criteria in novel discrimination tasks. It is important to emphasize that in all of the above experiments, the ability to generalize has been demonstrated by training bees to not one but a number of stimuli that differ individually in detail but share the property that is to be generalized. For example, the rewarded patterns all possessed the same orientation or the same kind of symmetry (e.g., left-right symmetry). These stimuli were shuffled randomly during the training. Such a training procedure ensures that the bees learn the critical cue that is associated with the reward (Horridge, 1999).

Top-down processing

It is well known that prior knowledge or experience aids us greatly in uncovering objects that are poorly visible, partially hidden, or camouflaged. Many of us who view the scene in Figure 100.3 for the first time do not see a familiar object, especially if we are unaware of the picture's content. Once the camouflaged dalmatian has been discovered, however, it is detected and recognized instantly every time the picture is encountered. Evidently, prior experience or knowledge aids the visual system significantly in the task of uncovering objects (Cavanagh, 1991; Goldstein, 1989; Lindsay and Norman, 1977).

Top-down processing of this kind can speed up the analysis of the retinal image when a familiar scene or object is encountered and can help fill in, or complete, details that are



FIGURE 100.3. A familiar but camouflaged object. (Readers experiencing difficulty in recognizing the dalmatian may wish to view the picture upside down.) (Photo courtesy R. C. James. Reprinted from Lindsay and Norman, 1977, with permission of the authors and publisher.)

missing in the optic array (Cavanagh, 1991). Is the ability to enhance processing in this way restricted to highly developed visual systems such as those of humans and higher mammals? Or does it extend to relatively simple visual systems such as those of invertebrates?

Zhang and Srinivasan (1994) approached this question by investigating whether bees are able to use prior experience to facilitate the detection of objects and the discrimination of their shapes. They first attempted to train bees to distinguish between two shapes—a ring and a disc—when each shape was presented in a camouflaged fashion as a textured figure positioned 6 cm in front of a similarly textured background (Fig. 100.4A). It turned out that bees were unable to learn to make this discrimination, despite lengthy training incorporating over 100 rewards per bee. Next, Zhang and Srinivasan examined whether bees could learn to distinguish the camouflaged patterns if they were first trained on a related but simpler discrimination: that of distinguishing between a black ring and a black disc, each presented 6 cm in front of a white background. The ring and the disc were of the same size and shape as their textured counterparts, and their spatial configuration in relation to the background was identical to that in the previous experiment. The bees were able to learn this new task (Fig. 100.4B). When these pretrained bees were tested on the task of Figure 100.4A, they could distinguish between the patterns immediately (Fig. 100.4C). Although the figures in Figure 100.4A are camouflaged, they can be detected by virtue of the relative motion between the images of the figure and the more distant background as the bee approaches the figure. Evidently, the bees were able to learn to use this motion parallax as a cue to break the camouflage—but only after they had been pretrained on uncamouflaged versions of the same shapes.

Thus, the bees were using knowledge acquired from the simpler black-white patterns of Figure 100.4C, to discern the camouflaged objects. Moreover, bees trained in this step-by-step fashion could learn to distinguish between other camouflaged objects that they had never previously encountered, such as two differently oriented bars (Fig. 100.4E), without any pretraining on black-and-white versions of the new shapes. This suggests that the enhancement in the bees' performance was not restricted to the specific training shapes, such as the camouflaged ring and disc. Rather, it appears that the bees were learning to look at the stimuli by extracting a novel cue—motion parallax—and using this cue to see and distinguish between novel shapes.

Honeybees perceive illusory contours

The human visual system possesses a remarkable ability to perceive and recognize objects even when they are partly occluded. An example of this is shown in Figure 100.5A.

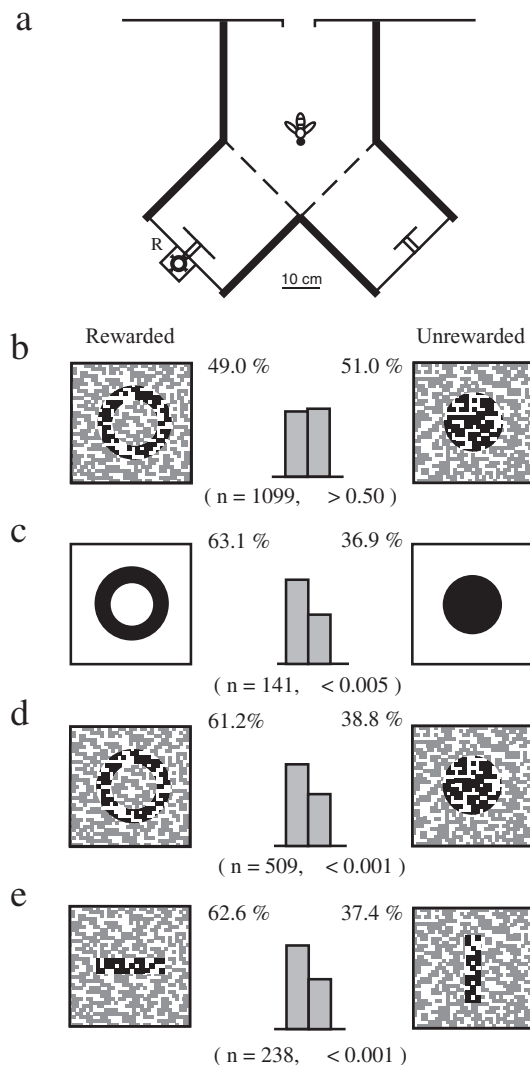


FIGURE 100.4. Investigation of top-down processing in honeybees. Details are given in the text. (Adapted from Zhang and Srinivasan, 1994.)

The figure shows one triangle, comprising the broken black lines. However, the gaps in the lines and the cutouts in the black circles create a strong impression of another triangle, laid upside down to occlude part of the original triangle. The *illusory contours* of this white triangle are particularly vivid. Interestingly, there are neurons in the visual cortex of the monkey that respond to such illusory contours (Von der Heydt and Peterhans, 1989; Von der Heydt et al., 1984).

Van Hateren et al. (1990) explored whether illusory contours such as those described above are also experienced by honeybees.

They trained bees to enter a Y-maze, as in Figure 100.1B, and to distinguish between randomly striped patterns that were oriented at +45 degrees and –45 degrees, by rewarding them on the +45 degree orientation. The bees were able

to learn this task well (Fig. 100.5B). When these trained bees were tested with rectangles oriented at +45 degrees and –45 degrees, they preferred the rectangle with the same orientation as the learned orientation (Fig. 100.5C). Thus, the bees were able to abstract the orientation information that they had learned in the training and apply it to the novel rectangular shapes. When the stripe-trained bees were tested with illusory rectangles oriented at +45 degrees and –45 degrees, they showed a significant preference for the +45 degree rectangle (Fig. 100.5D). This suggests that the bees were indeed perceiving the patterns in Figure 100.5D as rectangles. To examine this possibility further, the bees were confronted with the patterns in Figure 100.5E, where the illusion had been broken by scrambling the pacman-shaped figures. To us, the illusory rectangles are no longer visible: they have been destroyed. Interestingly, the bees behaved as if they could not distinguish between the two new patterns: they chose both patterns equally often (Fig. 100.5E).

There is evidence that insects experience many of the illusions that humans experience. Some other examples are the *waterfall illusion* (Srinivasan and Dvorak, 1979), the *Benham illusion* (Srinivasan et al., 1987), and the *Mueller-Lyer illusion* (Geiger and Poggio, 1975). Thus, the visual systems of insects may process information in ways akin to ours. Horridge et al. (1992b) have also reported the existence of neurons in the insect visual pathway that respond to illusory contours.

Learning to negotiate complex mazes

The ability to learn mazes has been investigated extensively in a number of higher vertebrates, notably rats, mice, and pigeons (Dale, 1988; Pick and Yanai, 1983). Relatively few studies, however, have explored the capacity of invertebrates to learn mazes. Can bees learn complex labyrinths requiring several correct decisions to be made to reach the goal?

Zhang et al. (1996) explored this question by attempting to train bees to fly through a variety of complex mazes to find a reward of sugar solution in the presence or absence of specific visual cues. The experiments were carried out in an All Weather Bee Flight Facility at the Australian National University's Research School of Biological Sciences. Each maze consisted of a 4 × 5 matrix of identical cubic boxes. Each wall of a box carried a hole in its center. The path through the maze was created by leaving open some of the holes between boxes and blocking others. Bees had to fly through a sequence of boxes to reach the goal, which was a feeder containing sugar solution. The experimental maze was placed on a movable table, and its position and orientation were varied frequently to prevent the bees from using landmarks external to the maze as navigational cues.

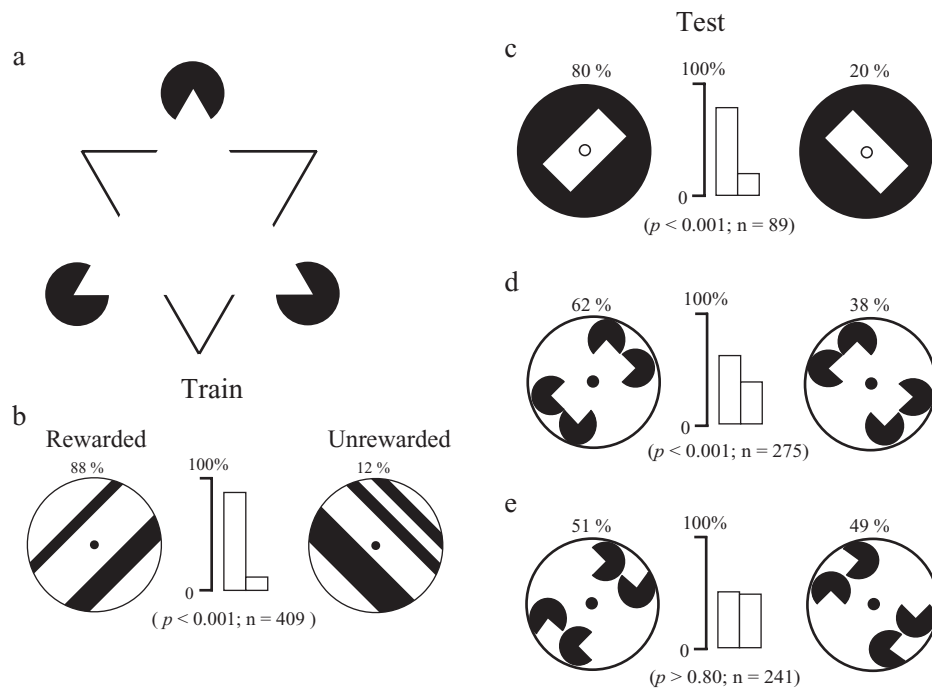


FIGURE 100.5. Like humans, honeybees perceive illusory contours. Details are given in the text. (Modified from Van Hateren et al., 1990.)

LEARNING TO NEGOTIATE A MAZE BY FOLLOWING A MARK
One series of experiments investigated the ability of bees to find their way through the maze by learning to *follow a color mark* that signaled the correct exit in each box. The mark was a 4×4 cm green square affixed immediately below the appropriate hole in each box to indicate the correct path (Fig. 100.6A). Bees were trained to enter the maze and take the correct path through it. This was accomplished by moving a feeder step by step along the correct path until it reached the third box in the path. During this period, the bees had the opportunity to learn that the mark in each box signaled the correct exit. After the bees had reached this stage, the feeder was moved directly to the last box on the path, left there briefly and then moved to its final destination, namely, the feeder cage behind the last box.

The bees' performance was tested immediately thereafter. During the test, only one bee at a time was allowed into the maze. Performance was scored by assigning each flight to one of four categories. Category 1 comprised flights in which a bee flew through the entire path and arrived at the goal without making any mistakes. Category 2 represented flights in which the bee turned back and retraced its path (once or many times) but remained on the correct path and arrived at the goal within 5 minutes. Category 3 comprised flights in which a bee made one or more wrong turns at the decision boxes but still arrived at the goal within 5 minutes. The last category, 4, represented unsuccessful searches, defined as flights in which the bee did not reach the goal within 5 minutes of entering the maze (regardless of whether it was

on the correct path or not). In some tests, the bees' performance was also evaluated by measuring the time required to reach the goal from the moment of entering the maze. Before each test, the boxes were swapped to remove possible olfactory cues.

The results show clearly that bees, trained initially to follow color marks through only a small initial part of the maze, are immediately able to "blaze a trail" by using the same cue to find their way through the rest of the maze (Test 1 in Fig. 100.6B). Performance continues to be good when the bees are tested on a new path, created by rearranging the boxes and marks (Test 2 in Fig. 100.6B). The control depicts the results of a test that measured the performance of the trained bees in following an unfamiliar route in an unmarked maze. This test represents a baseline against which the performance of the bees in the tests can be compared. Evidently, the trained bees had learned to follow the marks to the goal and were immediately able to use this rule to trace a novel path through the maze. The bees' performance in Tests 1 and 2 is significantly better than that in the control test.

LEARNING TO NEGOTIATE A MAZE BY USING A SYMBOLIC CUE
Another series of experiments examined whether bees could learn to negotiate mazes by *using a symbolic cue* (Zhang et al., 1996). Left and right turns were signaled according to a color placed on the back wall of each box where a turn had to be made (Fig. 100.6C). The training and testing procedures were similar to those described above. The results showed

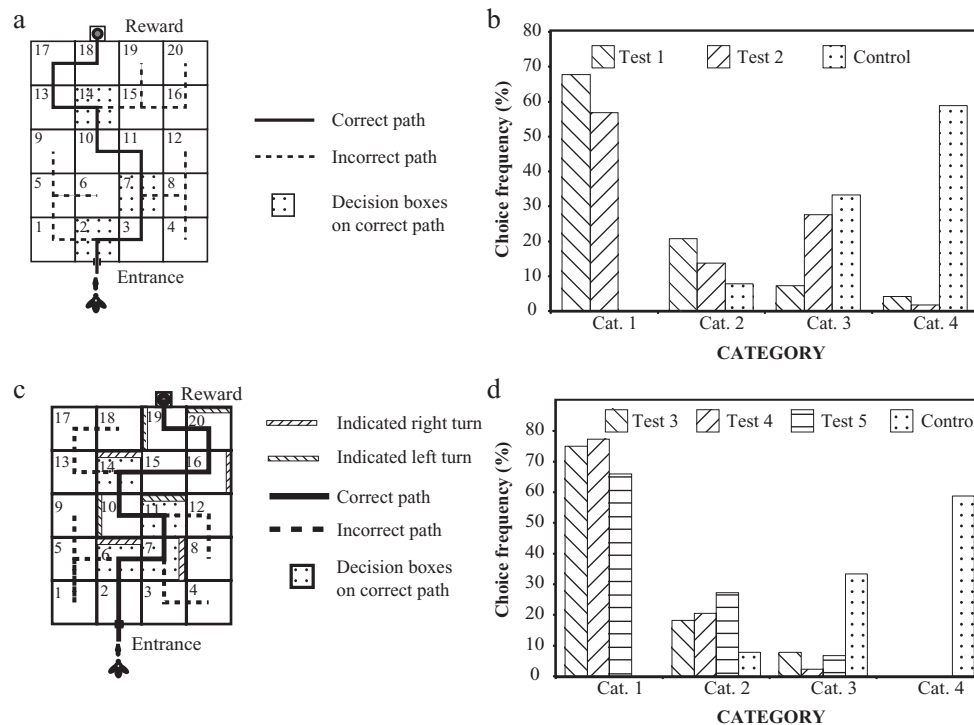


FIGURE 100.6. Learning to negotiate complex mazes by using visual cues. Details are given in the text. (Modified from Zhang et al., 1996.)

that bees learned this task very well too. In fact, their performance in this maze was just as impressive as in the mark-following maze.

Here again, bees trained to use the symbolic cue on a particular route were immediately able to use the cue to trace novel paths through the maze (Tests 4 and 5, Fig. 100.6D). The performance in all tests (Tests 4 to 6) was significantly better than that in the control test (Fig. 100.6D).

Walking honeybees are also capable of route-specific learning with respect to visual stimuli that function as navigational “signposts” (Zhang et al., 1998).

Context-dependent learning

The above maze experiments reveal that honeybees are capable of using symbolic color marks to make choices. Can bees learn tasks in a context-dependent way?

Gadagkar et al. (1995) examined whether honeybees could learn to associate environmental cues with rewards in a context-dependent manner. Two different contexts were set up, one at the hive and one at a feeder 12 m away. At the feeder, bees were offered a choice of two colors: blue and green. They had to choose the color green in order to gain access to the feeder. At the hive, they were again offered a choice between blue and green, but this time they had to choose blue—that is, make the opposite choice—to enter the hive. The bees were able to learn this task very well, showing a strong preference for green at the feeder and for blue at

the hive (Fig. 100.7, Exp. 1A). In a complementary experiment, a group of new bees was trained to choose blue at the feeder side but green at the hive side. They also learned this task very well (Fig. 100.7, Exp. 1B). Similar results were obtained using stimuli that consisted of gratings that were oriented vertically or horizontally (Fig. 100.7, Exp. 2A, B). Thus, bees can learn tasks in a context-dependent manner. In these experiments, the average flight time between the hive and the feeder was only 2 seconds, showing that bees can reverse their preference in a very short time.

Colborn et al. (1999) examined context-dependent learning by bumblebees. They investigated whether contextual cues can prevent interference during the acquisition of potentially competing visuomotor associations. Their findings are consistent with the hypothesis that different contextual signals are associated with approaching the nest or approaching the feeder, and that these contextual signals facilitate learned associations between orientation detectors and motor commands.

Learning principles of symbolic matching

One of the more complex tasks that has been used to investigate principles of learning and memory has been the *delayed match-to-sample* (DMTS). This task has been investigated in many different species such as the monkey (e.g., D’Amato et al., 1985), dolphin (e.g., Herman and Gordon, 1974), and pigeon (e.g., Roberts, 1972).

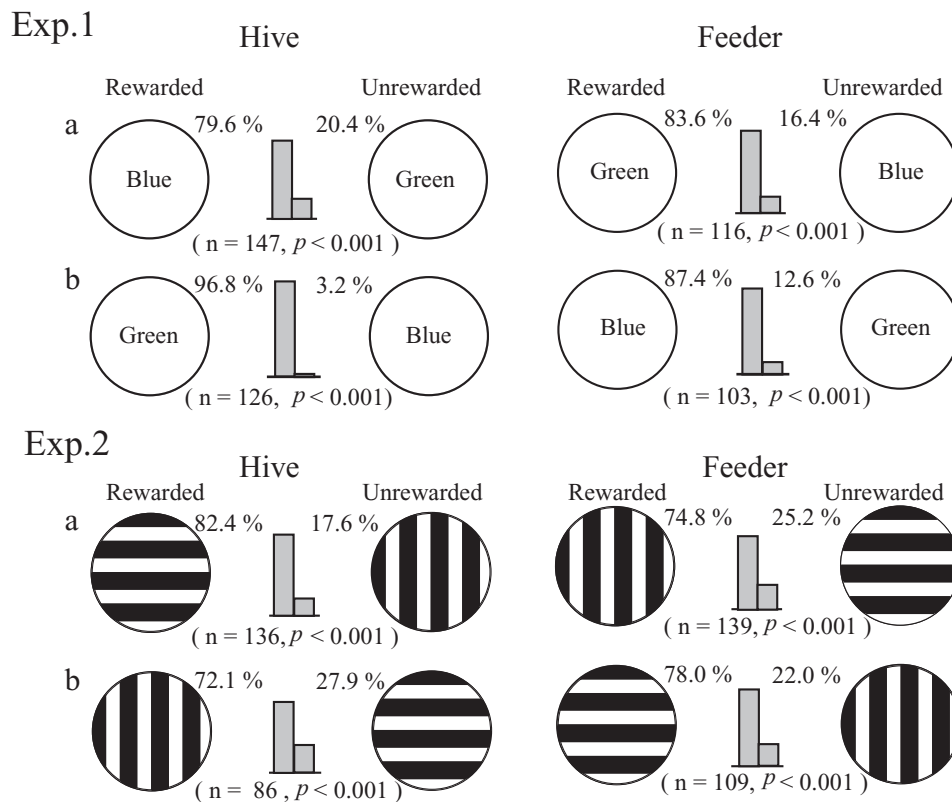


FIGURE 100.7. Context-dependent learning by honeybees. Details are given in the text.

Most DMTS tasks follow the same general procedure. Each trial begins with the presentation of a sample stimulus. The sample is followed by a delay or retention interval and then by the presentation of two or more test stimuli, one of which is identical to the sample stimulus. If the animal chooses the test stimulus that corresponds to the sample, then it obtains a reward (hence the name *delayed match-to-sample*). Most experiments use two or three sample stimuli, which are varied randomly from trial to trial.

A more complex variant of this task is the *symbolic delayed match-to-sample task* (SDMTS). In this task, none of the test stimuli physically match the sample: the experimenter arbitrarily designates the correct choice. Here the animal has to learn to associate the correct test stimulus corresponding to each sample stimulus.

Can bees learn such tasks? Their foraging behavior may give us some hints. Honeybees have evolved a number of navigational skills that enable successful foraging. Collett and Wehner have suggested that foraging insects traveling repeatedly to a food source and back to their homes navigate by using a series of visual images, or “snapshots,” of the environment acquired *en route* (Collett, 1996; Collett and Keblar, 1988; Collett et al., 1993; Judd and Collett, 1998; Wehner et al., 1990, 1996). By comparing the currently viewed scene with the appropriate stored image, the insect

is able to ascertain whether it is on the correct path and make any necessary corrections. Thus, successful foraging may require the bee to be able to solve tasks analogous to SDMTS tasks. Therefore, it is of interest to explore whether bees can learn DMTS and SDMTS tasks.

LEARNING THE SDMTS TASK IN THE VISUAL MODALITY
One series of experiments examined the bees’ ability to learn an SDMTS task in the visual modality (Zhang et al., 1999). Honeybees were trained to fly through a compound Y maze consisting of a series of interconnected cylinders (Fig. 100.8A). The first cylinder carried the sample stimulus. The second and third cylinders each had two exits. Each exit carried a visual stimulus, between which the bees had to choose. A bee, having made a correct choice in the second as well as in the third cylinder, arrived in a fourth cylinder, where it found a feeder with sugar solution. Thus, the second and third cylinders acted as decision stages: at each of these cylinders the bee had to choose between two stimuli. It was the single sample stimulus in the first cylinder that determined the choices the bees had to make in the subsequent decision stages.

During training, the sample stimulus was a black-and-white grating oriented either horizontally (Stimulus A) or vertically (Stimulus A’), respectively. The second cylinder (first decision stage) offered a choice between a blue square

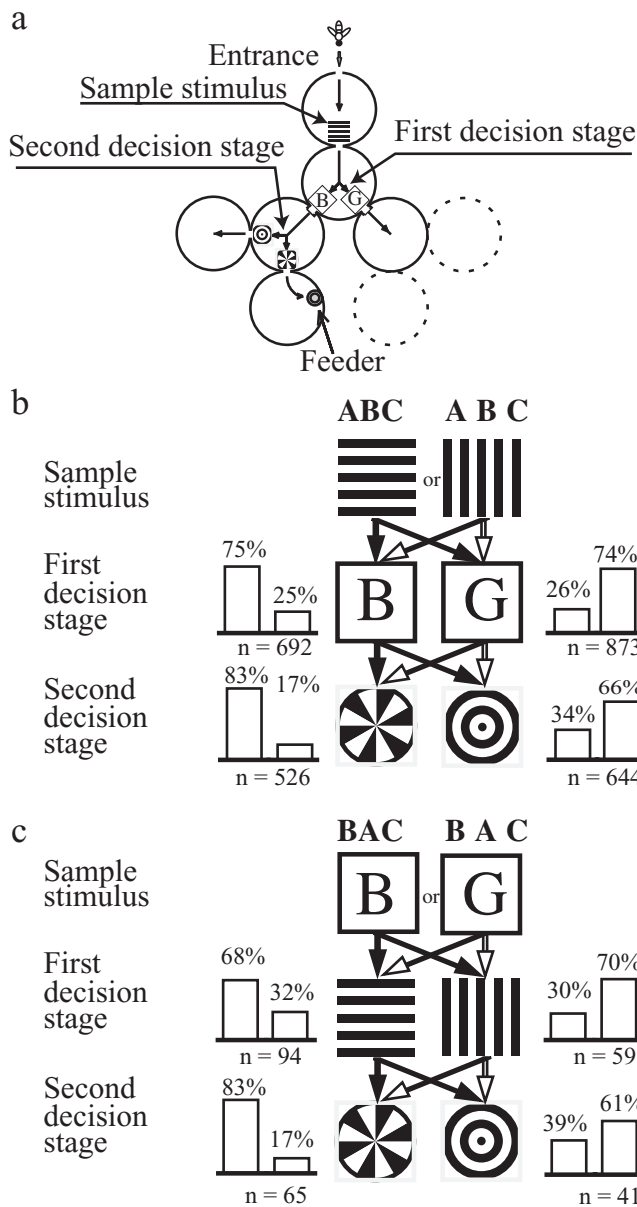


FIGURE 100.8. Learning a SDMTS task in the visual modality. Details are given in the text. (Modified from Zhang et al., 1999.)

(Stimulus B) and a green one (Stimulus B'), and the third cylinder a choice between a pattern consisting of a sectored disc (C) or of concentric rings (C') (Fig. 100.8B). When the sample stimulus was the horizontal grating, the feeder could only be reached if the bee chose blue in the second cylinder and the sectored disc in the third. However, when the sample was the vertical grating, the bee could reach the reward only if it chose green in the second cylinder and the ring pattern in the third.

After training, the bees were tested not only on the training sequences ABC and A'B'C' (learning tests) (Fig. 100.8B), but also in transfer tests which represented five other permutations of the training sequences. The results of tests

on one of the permuted sequences (BAC and B'A'C') are illustrated in Figure. 100.8C.

The results showed that bees are indeed capable of learning SDMTS tasks. Clearly, viewing the sample stimulus (horizontal or vertical grating) triggers recall of the stimulus that should be chosen in each of the subsequent stages (Fig. 100.8B). Furthermore, the trained bees continued to choose the appropriate stimulus at each stage of the maze even in the transfer test (Fig. 100.8C) as well as in tests using other permutations of the stimulus sequence (Zhang et al., 1999). These findings indicate that, in general, exposure to any one of the stimuli that were encountered in the training (A,B,C or A',B',C') was sufficient to trigger associative recall of all of the other stimuli belonging to that set. In all of the tests, changing the sample stimulus (from A to A', B to B', or C to C') caused the bees to change (and reverse) their preference for the stimuli that they encountered at subsequent stages of the maze. It should be noted that in this experiment, the bees were not specifically trained to distinguish between A and A', which were the sample stimuli in the training. Nevertheless, the bees distinguished between them in the transfer tests because they associated them with the stimulus sets ABC and A'B'C', respectively. It is also clear from this set of tests that the bees were capable of treating the stimulus pairs (B, B') (Fig. 100.8C) as well as (C, C') (not shown in the figure) as sample stimuli, even though these were never encountered as sample stimuli in the training.

The above findings suggest that bees solve the SDMTS task by mapping the six visual stimuli that they encounter in the training into two distinct sets, (A,B,C) and (A',B',C'), as illustrated in Fig. 100.9. After training, exposure to any stimulus belonging to a member of one of these sets triggers recall of the other two members belonging to that set. Thus, exposure to B, for example, triggers recall of A and C, whereas exposure to C' triggers recall of A' and B'.

LEARNING THE SDMTS TASK ACROSS SENSORY MODALITIES
Can bees learn an SDMTS task when they are required to make associations that span different sensory modalities? Clearly, humans display impressive cross-modal associative recall. It is a common experience that a smell or a sound can trigger a vivid recollection of an associated event in the past, even if it involves a different sensory modality and even if the episode occurred a long time ago (Baddeley, 1993).

Srinivasan et al. (1998) explored this capacity in bees by asking whether bees could learn to associate specific scents with specific colors. The apparatus consisted of a compound Y maze, as in the above experiments, but with a single decision stage. The sample stimulus, presented in the first cylinder, was a scent that was either lemon or mango. The decision stage offered a choice of two colors, blue or yellow. When the bees encountered lemon at the entrance, they had to learn to choose blue in the decision stage; when they

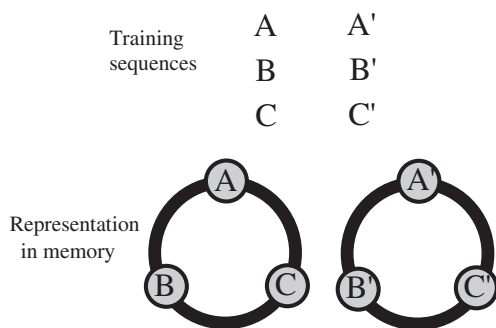


FIGURE 100.9. A model for associative grouping derived from the results of the SDMTS experiments. Details are given in the text.

encountered mango, they had to choose yellow. The bees learned this task very well. The scent of lemon evidently evoked recall of blue, whereas that of mango triggered recall of yellow. Bees could also be trained to make the opposite associations: lemon with yellow and mango with blue. They could also be trained to make symbolic matches in the opposite direction; that is, they could learn to associate a color in the entrance with a scent in the decision stage.

The evidence presented here clearly shows that honeybees are able to learn the SDMTS task, not only in the visual modality, but also across sensory modalities. Learning an SDMTS task requires that the bee be able, when presented with a sample stimulus, to recall other stimuli that are associated with the sample stimulus. For a foraging honeybee, cross-modal associative recall could facilitate the search for a food source. For example, detecting the scent of lavender could initiate a search for purple flowers.

Learning the concepts of sameness and difference

A related question is whether honeybees are able to group stimuli according to certain rules, or concepts, such as sameness or difference. In vertebrates, the capacity to acquire such concepts has been studied using two experimental procedures, the DMTS task and the DNMTS (*delayed nonmatch-to-sample*) task (Holmes, 1979; Zentall and Hogan, 1978). The DNMTS task is similar to the DMTS task except that the animal is required to respond to the stimulus that is different from the sample. It should be pointed out, however, that the ability to learn the concept of *sameness* or *difference* would be proven only if the animal is able to transfer the ability to choose correctly the matching (or nonmatching) stimulus to a completely novel set of stimuli which it had not experienced during training.

Giurfa et al. (2001) examined whether honeybees could learn the concepts of *sameness* and *difference*. The experiments were carried out at the Australian National University in Canberra as well as at the Free University in Berlin, independently and at the same time. The two laboratories

obtained the same results and decided to publish the study together.

The apparatus used in the experiments was similar to that used for the SDMTS tasks. Bees were trained on sector and ring patterns; that is, they had to learn to choose the sector or the ring pattern in the decision chamber, according to whether the sample stimulus at the entrance was the sector or the ring pattern. The bees learned this task well, showing a clear ability to choose the matching stimulus in each case (Fig. 100.10A, left-hand panel). The trained bees were then subjected to a transfer test, in which the stimuli were two colors, blue and yellow. The bees were immediately able to transfer the matching task to the colors, despite the fact that they had never been trained on them (Fig. 100.10A, right-hand panel). They were also able to transfer the matching ability to other novel stimuli, such as gratings oriented at +45 degrees and -45 degrees (data not shown).

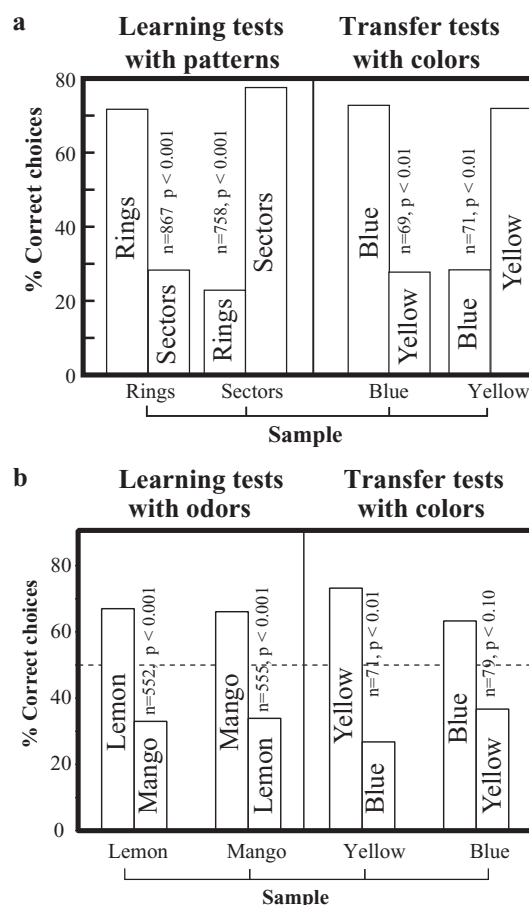


FIGURE 100.10. Learning the concept of *sameness*, and transferring it into novel stimuli in the same sensory modality and in different sensory modalities. *a*, Results of learning tests with sector and ring patterns (*left panel*) and transfer tests with colors (*right panel*). *b*, Learning tests with odors (*left panel*) and transfer tests with colors (*right panel*). Details are given in the text. (Modified from Giurfa et al., 2001.)

Bees can also learn to match odors, as shown in the left-hand panel of Figure 100.10B. Furthermore, bees trained on odors can immediately transfer the learned matching ability to colors, as shown in the right-hand panel of Figure 100.10B. Thus, the concept of *matching*, once learned, can be transferred even across sensory modalities.

Finally, bees can also learn the concept of *difference*. That is, they can be trained to choose the nonmatching stimulus rather than the matching one. Figure 100.11A shows learning curves obtained in two experiments investigating this capability. In one experiment, the training stimuli were colors (blue and yellow). Here bees had to learn to choose yellow in the decision chamber when they encountered blue at the entrance and *vice versa*. In another experiment, the training stimuli were linear gratings oriented horizontally and vertically. There bees had to learn to choose the verti-

cal grating in the decision chamber when they encountered a horizontal grating at the entrance and *vice versa*. It is evident from Figure 100.11A that the bees learned both nonmatching tasks well. Furthermore, in each case, the trained bees were immediately able to transfer the learned nonmatching concept to novel stimuli. Bees trained on the colors were able to perform nonmatching on the gratings and vice versa (Fig. 100.11B, C).

These findings demonstrate that honeybees can indeed learn rather abstract concepts, such as *sameness* and *difference*, and apply them to novel situations—situations on which they have not directly been trained.

Conclusions and discussion

Research over the past 30 years or so is beginning to suggest that learning and perception in insects are much more intricate and flexible than was originally assumed. Honeybees are capable of a variety of visually guided tasks that involve cognitive processes that operate at a surprisingly high level. Bees can abstract general properties of a stimulus, such as orientation or symmetry, and apply them to distinguish between other stimuli which they have never previously encountered. They can be taught to use new cues to detect camouflaged objects. Like humans, bees even experience visual illusions. They can learn to use symbolic rules to navigate through complex mazes and to apply these rules in flexible ways. Honeybees are able to form concepts, and to group and recall stimuli associatively. While the processes of learning and perception are undoubtedly more sophisticated in primates and mammals than in insects, there seems to be a continuum in these capacities across the animal kingdom rather than a sharp distinction between vertebrates and invertebrates. The abilities of an animal seem to be governed largely by what it needs in order to pursue its lifestyle, rather than whether or not it possesses a backbone.

The brain of the honeybee is tiny and carries about a millionfold fewer neurons than the human brain. However, like the brains of humans and higher mammals, the honeybee brain is highly compartmentalized and has evolved into an organ with specialized morphological and functional structures.

In recent years, much attention has been devoted to unraveling the functioning of the visual and olfactory pathways of the honeybee's brain. About half of the neurons in the brain belong to the optical lobes. Visual information is acquired by a pair of compound eyes that take up a substantial part of the head. The visual pathway comprises four distinct neuropils: the retina, lamina, medulla, and lobula. Like humans, honeybees possess trichromatic color vision, spatial vision, and motion-sensitive vision. Their trichromatic visual system features ultraviolet, blue, and green photoreceptors that are well suited to flower discrimination

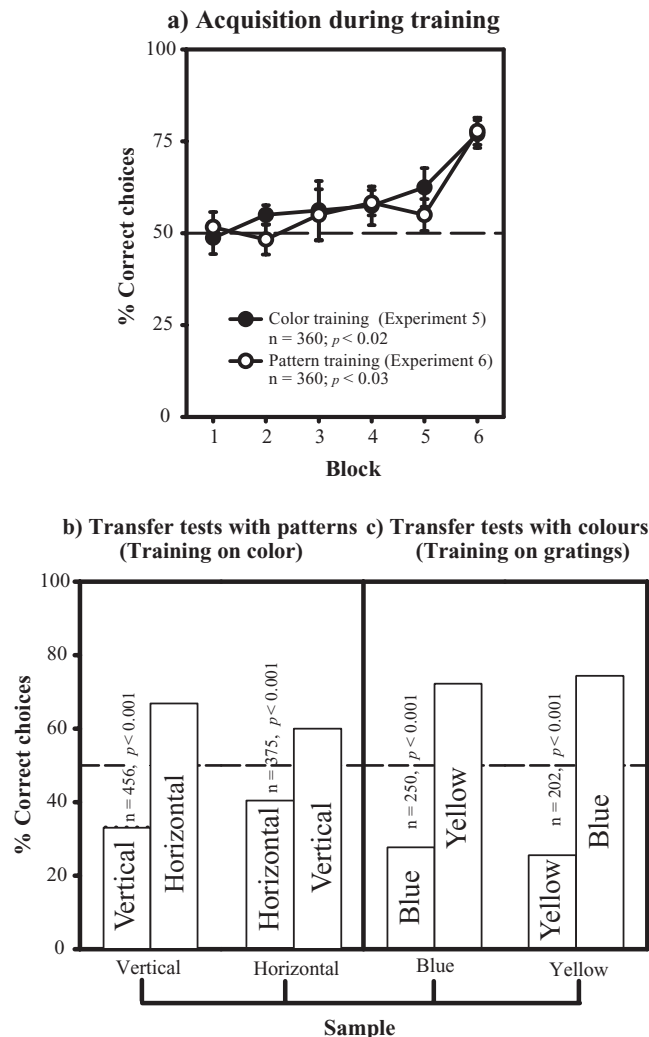


FIGURE 100.11. Learning the concept of *difference*. a, Learning curves for bees trained on colors (filled circles) and on gratings (open circles). b, c, Results of transfer tests. Details are given in the text. (Modified from Giurfa et al., 2001.)

(Vorobyev and Menzel, 1999). Shape perception in honeybees has evolved to respond innately to certain features of natural flowers, resulting in a spontaneous preference for flower-like patterns, such as radiating as well as symmetrical patterns (Lehrer et al., 1995). Bees also appear to have acquired the ability to extract a variety of abstract features, such as the orientation of edges or lines. There is evidence for the existence of orientation-analyzing mechanisms in the insect visual system that might be comparable functionally to those known to exist in the mammalian cortex (Srinivasan et al., 1993, 1994).

The antennal lobes receive their principal sensory input from olfactory receptors on the antennae (Hertel and Maronde, 1987; Winston, 1991). The *mushroom bodies* in the protocerebrum are believed to be the structures of the insect brain that are most closely associated with higher-order sensory integration, associative learning, and spatial memory (Mizunami et al., 1998; Withers et al., 1993). Thus, the mushroom bodies in insects may play a role similar to that played by the hippocampus in rats, birds, and higher mammals (Sherry and Healy, 1998).

The central nervous system of the honeybee is thus a promising system in which to explore the mechanisms that underlie the rich behavioral repertoire that can emerge from a relatively simple nervous system at a variety of levels: molecular, cellular, anatomical, electrophysiological, and computational.

REFERENCES

- Backhaus, W., 1998. Physiological and psychophysical simulations of color vision in humans and animal, in *Color Vision—Perspectives from Different Disciplines* (W. G. K. Backhaus, R. Kliegl, and J. S. Werner, eds.), Berlin: Walter de Gruyter, pp. 45–77.
- Backhaus, W., A. Werner, and R. Menzel, 1987. Color vision in honeybees: metric, dimensions, constancy, and ecological aspects, in *Neurobiology and Behavior of the Honeybee* (R. Menzel and A. Mercer, eds.), Berlin: Springer-Verlag, pp. 172–190.
- Baddeley, A., 1993. *Your Memory: A User's Guide*, London: Penguin Group, pp. 169–172.
- Cavanagh, P., 1991. What's up in top-down processing?, in *Representation of vision—Trends and Tacit Assumptions in Vision Research* (A. Gorea ed.-in-chief), Cambridge: Cambridge University Press, pp. 295–304.
- Chittka, L., M. Vorobyev, A. Shmida, and R. Menzel, 1993. Bee colour vision—The optimal system for the discrimination of flower colours with three spectral photoreceptor types? In *Sensory Systems of Arthropods* (K. Wiese ed.), Basel: Birkhaeuser Verlag/Switzerland Press, pp. 211–218.
- Colborn, M., A. Ahmad-Annuar, K. Fauria, and T. S. Collett, 1999. Contextual modulation of visuomotor associations in bumble-bees (*Bombus terrestris*), *Proc. R. Soc. Lond. B*, 266: 2413–2418.
- Collett, T. S., 1996. Insect navigation en route to the goal—multiple strategies for the use of landmarks, *J. Exp. Biol.*, 199:227–235.
- Collett, T. S., and B. A. Cartwright, 1983. Eidetic images in insects: their role in navigation, *Trends Neurosci.*, 6:101–105.
- Collett, T. S., S. N. Fry, and R. Wehner, 1993. Sequence learning by honeybees, *J. Comp. Physiol. A*, 172:693–706.
- Collett, T. S., and A. Kelber, 1988. The retrieval of visuo-spatial memories by honeybees, *J. Comp. Physiol. A*, 163:145–150.
- Dale, R. H. I., 1988. Spatial memory in pigeons on a four-arm radial maze, *Can. J. Psychol.*, 42:78–83.
- D'Amato, M. R., D. P. Salmon, and M. Colombo, 1985. Extent and limits of the matching concept in monkeys (*Cebus apella*), *J. Exp. Psychol. Anim. Behav. Proc.*, 11:35–51.
- Gadagkar, G., M. V. Srinivasan, and S. W. Zhang, 1995. Context-dependent learning in honeybees, *Pro. Austral. Neurosci. Soc.*, 6:226.
- Geiger, G., and T. Poggio, 1975. The Muller-Lyer figure and the fly, *Science*, 190:479–480.
- Giurfa, M., B. Eichmann, and R. Menzel, 1996. Symmetry perception in an insect, *Nature*, 382:458–461.
- Giurfa, M. S., W. Zhang, A. Jenett, R. Menzel, and M. V. Srinivasan, 2001. The concepts of “sameness” and “difference” in an insect, *Nature*, 410:930–933.
- Goldstein, E. B., 1989. *Sensation and Perception*, Belmont, CA: Wadsworth.
- Gould, J. L., 1985. How bees remember flower shapes, *Science*, 227:1492–1494.
- Gould, J. L., 1986. Pattern learning by honey bees, *Anim. Behav.*, 34:990–997.
- Herman, L. M., and J. A. Gordon, 1974. Auditory delayed matching in the bottlenose dolphin, *J. Exp. Anal. Behav.*, 21:19–26.
- Hertel, H., and U. Maronde, 1987. Processing of visual information in the honeybee brain, in *Neurobiology and Behavior of Honeybees* (R. Menzel and A. Mercer, eds.), Berlin: Springer-Verlag, pp. 141–157.
- Hertz, M., 1929. Die Organisation des optischen Feldes bei der Biene. II, *Z. Vergl. Physiol.*, 11:107–145.
- Hertz, M., 1933. Über figurale Intensitäten und Qualitäten in der optischen Wahrnehmung der Biene, *Biol. Zentbl.*, 53:10–40.
- Holmes, P. W., 1979. Transfer of matching performance in pigeons, *J. Exp. Anal. Behav.*, 31:103–114.
- Horridge, G. A., 1996. The honeybee (*Apis mellifera*) detects bilateral symmetry and discriminates its axis, *J. Insect Physiol.*, 42:755–764.
- Horridge, G. A., 1999. Two-dimensional pattern discrimination by the honeybee, *Physiol. Entomol.*, 24:197–212.
- Horridge, G. A., and S. W. Zhang, 1995. Pattern vision in honeybees (*Apis mellifera*): flower-like patterns with no predominant orientation, *J. Insect Physiol.*, 41:681–688.
- Horridge, G. A., S. W. Zhang, and M. Lehrer, 1992a. Bees can combine range and visual angle to estimate absolute size, *Philos. Trans. R. Soc. Lond. B*, 337:49–57.
- Horridge, G. A., S. W. Zhang, and D. O'Carroll, 1992b. Insect perception of illusory contours, *Philos. Trans. R. Soc. Lond. B*, 337:59–64.
- Judd, S. P. D., and T. S. Collett, 1998. Multiple stored views and landmark guidance in ants, *Nature* 392:710–714.
- Kevan, P. G., L. Chittka, and A. G. Dyer, 2001. Limits to the salience of ultraviolet: lessons from colour vision in bees and birds, *J. Exp. Biol.*, 204:2571–2580.
- Lehrer, M., G. A. Horridge, S. W. Zhang, and R. Gadakar, 1995. Shape vision in bees: innate preference for flower-like patterns, *Philos. Trans. R. Soc. Lond. B*, 347:123–137.
- Lindsay, P. H., and D. A. Norman, 1977. *Human Information Processing—An Introduction to Psychology*, New York: Academic Press.

- Menzel, R., 1990. Learning, memory and "cognition" in honey bees, in *Neurobiology of Comparative Cognition* (R. P. Kesner and D. S. Olton, eds.), Hillsdale, NJ: IEA, pp. 237–292.
- Menzel, R., and W. Backhaus, 1989. Color vision honey bees: phenomena and physiological mechanisms, in *Facets of Vision* (D. G. Stavenga and R. C. Hardie, eds.), Berlin: Springer-Verlag, pp. 282–297.
- Menzel, R., and U. Müller, 1996. Learning and memory in honeybees: from behavior to neural substrates, *Annu. Rev. Neurosci.*, 19:379–404.
- Mizunami, M., J. M. Weibrecht, and N. J. Strausfeld, 1998. Mushroom bodies of the cockroach: their participation in place memory, *J. Comp. Neurol.*, 402:520–537.
- Pick, C. G., and J. Yanai, 1983. Eight arm maze for mice, *Int. J. Neurosci.*, 21:63–66.
- Roberts, W. A., 1972. Short-term memory in the pigeon: effects of repetition and spacing, *J. Exp. Psychol. Anim. Behav. Proc.*, 6:217–237.
- Ronacher, B., 1992. Pattern recognition in honeybees: multidimensional scaling reveals a city-block metric, *Vis. Res.*, 32:1837–1843.
- Sherry, D., and S. Healy, 1998. Neural mechanisms of spatial representation, in *Spatial Representation in Animals* (S. Healy ed.), Oxford: Oxford University Press, pp. 133–157.
- Srinivasan, M. V., 1993. Even insects experience visual illusions, *Curr. Sci.*, 64:649–654.
- Srinivasan, M. V., 1994. Pattern recognition in the honeybee: recent progress, *J. Insect Physiol.*, 40:183–194.
- Srinivasan, M. V., and D. R. Dvorak, 1979. The waterfall illusion in an insect visual system, *Vis. Res.*, 19:1435–1437.
- Srinivasan, M., M. Lehrer, and R. Wehner, 1987. Bees perceive illusory colours induced by movement, *Vis. Res.*, 27:1285–1289.
- Srinivasan, M. V., M. Poteser, and K. Kral, 1999. Motion detection in insect orientation and navigation, *Vis. Res.*, 39:2749–2766.
- Srinivasan, M. V., and S. W. Zhang, 1998. Probing perception in a miniature brain: pattern recognition and maze navigation in honeybees, *Zoology*, 101:246–259.
- Srinivasan, M. V., S. W. Zhang, and H. Zhu, 1998. Honeybees link sights to smells, *Nature*, 396:637–638.
- Srinivasan, M. V., S. W. Zhang, and B. Rolfe, 1993. Is pattern vision in insects mediated by "cortical" processing? *Nature*, 362:539–540.
- Srinivasan, M. V., S. W. Zhang, and K. Witney, 1994. Visual discrimination of pattern orientation by honeybees: performance and implications of "cortical" processing, *Philos. Trans. R. Soc. Lond. B*, 343:199–210.
- Van Hateren, J. H., M. V. Srinivasan, and P. B. Wait, 1990. Pattern recognition in bees: orientation discrimination, *J. Comp. Physiol. A*, 167:649–654.
- Von der Heydt, R., and E. Peterhans, 1989. Cortical contour mechanisms and geometrical illusion, in *Neural Mechanisms of Visual Perception* (D. M. Lam and C. D. Gilbert, eds.), Houston, TX: Gulf Paul, pp. 157–170.
- Von der Heydt, R., E. Peterhans, and G. Baumgartner, 1984. Illusory contours and cortical neuron responses, *Science*, 224:1260–1262.
- Von Frisch, K., 1915. Der Farbensinn und Formensinn der Sienen, *Zool. Jahrb. Abt. Alg. Zool. Physiol. Tiere.*, 35:1–182.
- Von Frisch, K., 1971. *Bees: Their Vision, Chemical Senses, and Language*, Ithaca, NY: Cornell University Press.
- Vorobyev, M., and R. Menzel, 1999. Flower advertisement for insects: bees, a case study, in *Adaptive Mechanisms in The Ecology of Vision* (S. N. Archer, M. B. A. Djamgoz, E. R. Loew, J. C. Partridge, and S. Vallerga, eds.), Dordrecht: Kluwer Academic, pp. 537–553.
- Wehner, R., 1967. Pattern recognition in bees, *Nature*, 215:1244–1248.
- Wehner, R., 1971. The generalization of directional visual stimuli in the honey bee, *Apis mellifera*, *J. Insect Physiol.*, 17:1579–1591.
- Wehner, R., 1981. Spatial vision in arthropods, in *Vision in Invertebrates: Handbook of Sensory Physiology*, vol 7/6C (H. Autrum ed.), Berlin: Springer-Verlag, pp. 287–616.
- Wehner, R., S. Bleuler, and D. Shah, 1990. Bees navigate using vectors and routes rather than maps, *Naturwissenschaften*, 77:479–482.
- Wehner, R., and L. Flatt, 1977. Visual fixation in freely flying bees, *Z. Naturforsch.*, 32c:469–471.
- Wehner, R., and M. Lindauer, 1966. Zur Physiologie des Formensehens bei der Honigbiene. I, *Z. Vergl. Physiol.*, 52:290–324.
- Wehner, R., B. Michel, and P. Antonsen, 1996. Visual navigation in insects: coupling of egocentric and geocentric information, *J. Exp. Biol.*, 199:129–140.
- Winston, M. L., 1991. *The Biology of the Honey Bee*, Cambridge, MA: Harvard University Press.
- Withers, G. S., S. E. Fahrbach, and G. E. Robinson, 1993. Selective neuroanatomical plasticity and division of labour in the honeybee, *Nature*, 364:238–240.
- Yang, E. C., and T. Maddess, 1997. Orientation-sensitive neurons in the brain of the honeybee (*Apis mellifera*), *J. Insect Physiol.*, 43:329–336.
- Zentall, T. R., and D. E. Hogan, 1978. Same/different concept learning in the pigeon: the effect of negative instances and prior adaptation to transfer stimuli, *J. Exp. Anal. Behav.*, 30:177–186.
- Zhang, S. W., K. Bartsch, and M. V. Srinivasan, 1996. Maze learning by honeybee, *Neurobiol. Learn. Mem.*, 66:267–282.
- Zhang, S. W., M. Lehrer, and M. V. Srinivasan, 1998. Eye-specific route-learning and interocular transfer in walking honeybees, *J. Comp. Physiol. A*, 182:745–754.
- Zhang, S. W., M. Lehrer, and M. V. Srinivasan, 1999. Honeybee memory: navigation by associative grouping and recall of visual stimuli, *Neurobiol. Learn. Mem.*, 72:180–201.
- Zhang, S. W., and M. V. Srinivasan, 1994. Prior experience enhances pattern discrimination in insect vision, *Nature*, 368:330–333.

A Neural Basis for Human Visual Attention

SABINE KASTNER

IN EVERYDAY LIFE, the scenes we view are typically cluttered with many different objects. However, the capacity of the visual system to process information about multiple objects at any given moment in time is limited (e.g., Broadbent, 1958). Hence, attentional mechanisms are needed to select relevant information and to filter out irrelevant information from cluttered visual scenes. Selective attention is a highly flexible cognitive operation. Clearly, this capacity enables us to integrate easily information from many different sensory modalities and use it to guide behavior and motivation. Recent advances in functional brain mapping techniques have made it possible to study the neural basis of selective attention in the human brain. In this chapter, I will focus on mechanisms of selective attention that operate in the visual system—the best-understood sensory system of the mammalian brain.

Attention is a broad term that subsumes a variety of mechanisms mediating the selection of behaviorally relevant information. Attention can be drawn automatically to certain objects in cluttered scenes by means of *exogenous* or stimulus-driven mechanisms. For example, if you look at the display depicted in Figure 101.1A, the vertical line will be easily and effortlessly detected among the other lines because of its salience. In this case, the salience of the line stimulus is defined by the difference in orientation relative to the surrounding lines. Stimulus salience depends on various factors, including simple stimulus attributes or features, such as line orientation or color of the stimulus (e.g., Treisman and Gelade, 1980), perceptual grouping of stimulus features by Gestalt principles (e.g., Duncan, 1984; Lavie and Driver, 1996), and the dissimilarity between the stimulus and nearby distracter stimuli (e.g., Nothdurft, 1993). Another way to draw attention exogenously to a particular location of a visual scene is by providing a spatial cue, such as the dashed circle depicted in Figure 101.1B. Even though the vertical line does not stand out among the other lines in this display, it will be detected much faster if one is cued to the spatial location where it will be shown (Posner, 1980). In the display depicted in Figure 101.1C, none of the stimuli is particularly salient, and one must actively search through the display to identify the vertical line (e.g., Treisman and Gelade, 1980).

Hence, attention is directed voluntarily or *endogeneously* to the different items in the display until the vertical target line is found.

Selective attention to a spatial location has been shown to improve the accuracy and speed of subjects' responses to target stimuli that occur in that location (e.g., Posner, 1980). Attention also increases the perceptual sensitivity for the discrimination of target stimuli (Lu and Doshier, 1998), reduces the interference caused by distracters (Shiu and Pashler, 1995), and improves acuity (Carrasco and Yeshurun, 1998). In this chapter, I will describe mechanisms of selective attention that operate in the human visual cortex and may account for many of the known behavioral effects of attention. In particular, the emphasis will be on results of functional brain imaging studies in humans as they relate to results of single-cell recording studies in monkeys. Functional brain imaging measures hemodynamic changes, blood flow in the case of positron emission tomography, and blood oxygenation in the case of functional magnetic resonance imaging (fMRI), and these can be used as indirect measures of neural activity. In the following sections, I will first describe attention-related modulation of neural activity in visual cortical areas. Second, I will describe the evidence that source areas outside visual cortex generate attentional top-down signals that are transmitted via feedback projections to visual cortex and account for attentional response modulation.

Attentional response modulation in visual cortex

Convergent evidence from single-cell recording studies in monkeys and functional brain imaging and event-related potential (ERP) studies in humans indicates that selective attention can modulate neural processing in visual cortex. Attention may affect visual processing in several ways, such as facilitating neural processing by enhancing neural responses to attended stimuli, filtering of unwanted information by counteracting suppressive interactions induced by nearby stimuli, or biasing neural signals in favor of an attended location or stimulus attribute by increasing the baseline activity in the absence of visual input.

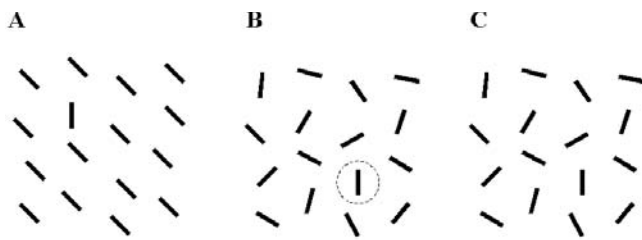


FIGURE 101.1. Cluttered visual scenes. Typical visual scenes contain many different objects, as outlined schematically here. The information from these multiple stimuli cannot be processed at the same time due to the limited processing capacity of the visual system. *A*, Salient objects may capture attention exogenously, that is, through bottom-up stimulus-driven mechanisms. In a condition in which no stimulus is particularly salient, the scene can be actively searched by directing attention voluntarily to the different items (*C*). This search may be facilitated if attention is directed to the spatial location at which a target stimulus (e.g., the *vertical line*) will appear by means of a cue (depicted by the *dashed circle* in *B*).

ATTENTION FACILITATES VISUAL PROCESSING AT ATTENDED LOCATIONS Functional brain mapping studies in the human visual cortex suggest that attentional mechanisms operate by enhancing neural responses to stimuli at attended locations, thereby facilitating information processing in favor of stimuli appearing at that location. In a typical functional brain imaging experiment, identical visual stimuli were presented simultaneously to corresponding peripheral field locations to the right and left of fixation while subjects were asked to direct attention covertly, that is, without executing eye movements to the right or the left. Directing attention to the left hemifield led to increased stimulus-evoked activity in extrastriate visual areas of the right hemisphere, whereas directed attention to the right hemifield led to increased activity in extrastriate visual areas of the left hemisphere (Heinze et al., 1994; Vandenberghe et al., 1997). Thus, responses to the stimuli were enhanced in the regions of extrastriate cortex containing the representations of the attended hemifield. In ERP studies that used a similar experimental design, it was shown that response enhancement in extrastriate cortex due to spatially directed attention may occur as early as 80 to 130 msec after stimulus onset (Heinze et al., 1994; Hillyard et al., 1998).

These results are in accordance with single-cell recording studies, which have shown that neural responses to a single stimulus presented within a neuron's receptive field (RF) are enhanced when the animal directs its attention to the RF compared to when the animal attends elsewhere. This effect, which increases with task difficulty (Spitzer and Richmond, 1991), has been demonstrated at many levels of visual processing, including areas V1 (Motter, 1993), V2 (Luck et al., 1997; Motter, 1993), V4 (Connor et al., 1997; Luck et al., 1997; McAdams and Maunsell, 1999; Moran and Desimone, 1985; Motter, 1993; Reynolds et al., 1999),

MT/MST (Recanzone and Wurtz, 2000; Treue and Maunsell, 1996), and LIP (Bushnell et al., 1981; Colby et al., 1996; Gottlieb et al., 1998). Not surprisingly, in human cortex, spatial attention effects have been found at similar levels of visual processing. Furthermore, it has been demonstrated that these attention effects are retinotopically organized, that is, response enhancement is seen only in the regions containing the sensory representation of an attended stimulus within a visual area (Brefczynski and DeYoe, 1999; Tootell et al., 1998). At the same time, the activity of neurons that represent unattended locations of the visual field appears to be attenuated. The exact nature of this response attenuation is not known.

Importantly, there is increasing evidence from single-cell physiology and functional brain imaging studies that neural responses can be modulated by attention as early as in V1 (Ito and Gilbert, 1999; Martinez et al., 1999; Motter, 1993; Roelfsema et al., 1998). Attentional response modulation in V1 appears to be more variable than in extrastriate cortex and may depend critically on a number of factors including task difficulty, competition from surrounding objects, and the need to integrate context. Attentional effects are typically smaller in early areas such as V1 and V2 compared to more anterior extrastriate areas such as V4 and TEO, indicating that attentional response enhancement increases from early to later stages of visual processing (e.g., Kastner et al., 1998). This finding suggests that attentional effects in early visual areas may be caused by reactivation from higher-order extrastriate areas. Single-cell recording studies support this idea by showing that attentional effects in area TE of inferior temporal cortex have a latency of about 150 msec (Chelazzi et al., 1998), whereas attentional effects in V1 have a longer latency of about 230 msec (Roelfsema et al., 1998). However, these latency differences may as well be attributed to local computations within areas.

In summary, spatial attention effects operate by enhancing neural responses evoked by visual stimuli at an attended location and have been demonstrated at all stages of visual processing, including primary visual cortex.

ATTENTION FACILITATES VISUAL PROCESSING OF ATTENDED STIMULUS ATTRIBUTES OR OBJECTS Attention modulates neural responses not only to visual stimuli at attended locations, but also to attended stimulus attributes. This has been shown in experiments that compared neural activity evoked within different visual cortical areas while subjects performed a task requiring selective attention to particular features of identical visual stimuli. In one such study, Corbetta et al. (1991) found that selective attention to either shape, color, or speed enhanced activity in the regions of extrastriate visual cortex that selectively process these same attributes. Attention to shape and color led to response enhancement in regions of the posterior portion of the

fusiform gyrus, including area V4. Attention to speed led to response enhancement in areas MT/MST. Other investigations have shown that attention to faces or houses led to response enhancement in the fusiform face area (FFA) or the parahippocampal place area (PPA), respectively (Wojciulik et al., 1998). These areas are located on the midanterior portion of the fusiform gyrus and are specialized for the processing of faces, houses, and other objects. Taken together, these results support the idea that selective attention to a particular stimulus attribute modulates neural activity in those extrastriate areas that preferentially process the selected attribute.

In typical visual scenes, many different stimulus attributes are combined in a particular object. How is the object as a whole processed if only one of its many attributes is attentionally selected? O'Craven and colleagues (1999) investigated this important question by presenting their subjects with a moving face superimposed on a house stimulus or with a moving house superimposed on a face stimulus. Subjects were instructed to attend selectively either to the face, the house, or the direction of motion. The activity evoked by these complex stimuli was investigated in the FFA, the PPA, and MT/MST, that is, in those areas that are specialized for the three different attributes contained in the stimuli. When the subjects attended to the direction of motion, the activity in the FFA was larger with moving face stimuli than with moving house stimuli. A complementary result was obtained in the PPA with moving house stimuli. These studies suggest that objects as a whole rather than single attributes of objects are the units of attentional selection, even when only one single attribute is behaviorally relevant.

ATTENTION HELPS TO FILTER OUT UNWANTED INFORMATION
Thus far, selective attention has been shown to operate by enhancing neural responses to a stimulus at an attended location or to an attended stimulus attribute. However, a typical visual scene contains multiple stimuli. Recent single-cell recording studies suggest that multiple stimuli in cluttered visual scenes compete for processing resources and that selective attention biases competitive interactions. In these studies, responses to a single visual stimulus presented alone in a neuron's RF were compared with the responses to the same stimulus when a second one was presented simultaneously within the same RF (Moran and Desimone, 1985; Recanzone et al., 2000; Reynolds et al., 1999). The responses to the paired stimuli were shown to be a weighted average of the responses to the individual stimuli when presented alone. For example, if a single good stimulus elicited a high firing rate and a single poor stimulus elicited a low firing rate, the response to the paired stimuli was reduced compared to that elicited by the single good stimulus. This result indicates that two stimuli present at the same time within a neuron's

RF are not processed independently, but rather interact with each other in a mutually suppressive way. This sensory suppressive interaction among multiple stimuli has been interpreted as an expression of competition for neural representation.

Single-cell recording studies have also shown that sensory suppressive interactions can be modulated by directed attention. In particular, in extrastriate areas V2 and V4, spatially directed attention to an effective stimulus within a neuron's RF eliminated the suppressive influence of a second stimulus presented within the same RF (Reynolds et al., 1999). Attentional effects were less pronounced when the second stimulus was presented outside the RF, suggesting that competition for processing resources within visual cortical areas takes place most strongly at the level of the RF. These findings imply that attention may resolve the competition among multiple stimuli by counteracting the suppressive influences of nearby stimuli, thereby enhancing information processing at the attended location. This may be an important mechanism by which attention filters out unwanted information from cluttered visual scenes (Desimone and Duncan, 1995).

Sensory suppression among multiple stimuli and its modulation by spatial attention has also been examined in the human cortex using fMRI (Kastner et al., 1998). In these studies, subjects were presented with images of colorful, complex stimuli in four nearby locations of the upper right quadrant of the visual field while they maintained fixation. Fixation was ensured by having subjects count the occurrences of Ts or Ls at fixation, an attentionally demanding task. The stimuli were presented under two different conditions, simultaneous and sequential. In the sequential condition, a single stimulus appeared in one of the four locations, then another appeared in a different location, and so on, until each of the four stimuli had been presented in the different locations. In the simultaneous condition, the same four stimuli appeared in the same four locations, but they were presented at the same time. Thus, integrated over time, the physical stimulation parameters were identical in the two presentation conditions, but sensory suppression among stimuli could take place only in the simultaneous presentation condition. It was therefore predicted that activation in the simultaneous presentation condition would be less than in the sequential presentation condition.

Activation of V1 and ventral stream extrastriate areas V2 to TEO was found under both stimulus presentation conditions compared to interleaved blank periods. Although the fMRI signal was similar in the two presentation conditions in V1 (Fig. 101.2A), the activation was reduced in the simultaneous condition compared to the sequential condition in V2, and this reduction was especially pronounced in V4 (Fig. 101.2A) and TEO, as predicted from the sensory suppression hypothesis. Importantly, the sensory suppression effect

appeared to be scaled to the RF size of neurons within visual cortical areas. That is, the small RFs of neurons in V1 and V2 would encompass only a small portion of the visual display, whereas the larger RFs of neurons in V4 and TEO would encompass all four stimuli. Therefore, suppressive interactions among the stimuli within RFs could take place most effectively in these more anterior visual areas.

The effects of spatially directed attention on multiple competing visual stimuli were studied in a variation of the paradigm used to examine sensory suppressive interactions among simultaneously presented stimuli, described above. In addition to the two different visual presentation conditions, sequential and simultaneous, two different attentional conditions were tested, unattended and attended. During the unattended condition, attention was directed away from the visual display by having subjects count Ts or Ls at fixation, exactly as in the original study. In the attended condition, subjects were instructed to attend covertly to the stimulus location closest to fixation in the display and to count the occurrences of one of the four stimuli, which was indicated before the scan started. Based on the results of monkey physiology studies, it was predicted that attention should reduce sensory suppression among stimuli. Thus, responses evoked

by the competing, simultaneously presented stimuli should be enhanced more strongly than responses evoked by the noncompeting sequentially presented stimuli (Luck et al., 1997; Moran and Desimone, 1985; Recanzone et al., 2000; Reynolds et al., 1999).

As illustrated in Figure 101.2*B* for area V4, directed attention to the display enhanced responses to both the sequentially and the simultaneously presented stimuli (gray-shaded blocks). This finding confirmed the effects of attentional response enhancement shown in numerous earlier studies in monkeys and humans, as cited previously. More importantly, and in accordance with the prediction from monkey physiology studies, directed attention led to greater increases in fMRI signals to simultaneously presented stimuli than to sequentially presented stimuli. Thus, attention partially canceled out the suppressive interactions among competing stimuli. The magnitude of the attentional effect scaled with the magnitude of the suppressive interactions among stimuli, with the strongest reduction of suppression occurring in areas V4 and TEO. These findings support the idea that directed attention enhances information processing of stimuli at the attended location by counteracting suppression induced by nearby stimuli, which compete for limited processing resources. In essence, unwanted distracting information is effectively filtered out. The degree to which distracting information can be eliminated depends on the load of the target task. For example, Rees et al. (1997) demonstrated that activation in area MT evoked by distracting moving stimuli was totally abolished when subjects performed a high-load linguistic task at fixation compared to a low-load version of the task. Thus, the greater the attentional resources devoted to the target, the less the processing of irrelevant distracting stimuli.

In summary, areas at intermediate levels of visual processing such as V4 and TEO appear to be important sites for the filtering of unwanted information by counteracting competitive interactions among stimuli at the level of the RF. This notion has recently been supported by studies in a patient with an isolated V4 lesion and in monkeys with lesions of areas V4 and TEO (De Weerd et al., 1999; Gallant et al., 2000). Subjects were asked to discriminate the orientation of a grating stimulus in the absence and in the presence of surrounding distracter stimuli. Significant performance deficits were observed in the distracter-present but not in the distracter-absent condition, suggesting a deficit in the efficacy of the filtering of distracter information.

ATTENTION AFFECTS NEURAL ACTIVITY EVEN IN THE ABSENCE OF VISUAL INPUT There is evidence that attentional top-down signals can be obtained not only by the modulation of visually driven activity, but also in the absence of any visual stimulation whatsoever. Single-cell recording studies have

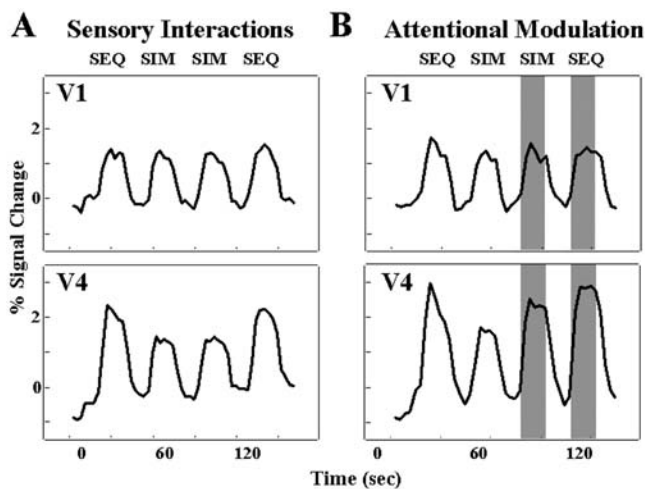


FIGURE 101.2. Sensory suppression and attentional modulation in human visual cortex. *A*, Sensory suppression in V1 and V4. As shown by the time series of fMRI signals, simultaneously presented stimuli (SIM) evoked less activity than sequentially presented stimuli (SEQ) in V4 but not in V1. This finding suggests that sensory suppressive interactions were scaled to the receptive field size of neurons in visual cortex. Presentation blocks were 18 seconds. *B*, Attentional modulation of sensory suppression. The sensory suppression effect in V4 was replicated in the unattended condition of this experiment when the subjects' attention was directed away from the stimulus display (unshaded time series). Spatially directed attention (gray-shaded time series) increased responses to simultaneously presented stimuli to a larger degree than to sequentially presented ones in V4. Presentation blocks were 15 seconds. (Adapted from Kastner et al., 1998).

shown that spontaneous (baseline) firing rates were 30% to 40% higher for neurons in areas V2 and V4 when the animal was cued to attend covertly to a location within the neuron's RF before the stimulus was presented there, that is, in the absence of visual stimulation (Luck et al., 1997). A similar effect was demonstrated in dorsal stream area LIP (Colby et al., 1996). This increased baseline activity, termed the *baseline shift*, has been interpreted as a direct demonstration of top-down feedback, biasing neurons representing the attended location and thereby favoring stimuli that will appear there at the expense of those appearing at unattended locations.

Attention-related top-down signals in the human visual cortex in the absence of visual stimulation were studied by adding a third experimental condition to the design used to investigate sensory suppressive interactions and their modulation by attention, as described above (Kastner et al., 1999). In addition to the two visual presentation conditions, sequential and simultaneous, and the two attentional conditions, unattended and attended, an expectation period preceding the attended presentations was introduced. The expectation period, during which subjects were required to direct attention covertly to the target location and instructed to expect the occurrences of the stimulus presentations, was initiated by a marker presented briefly next to the fixation point 11 seconds before the onset of the stimuli. In this way,

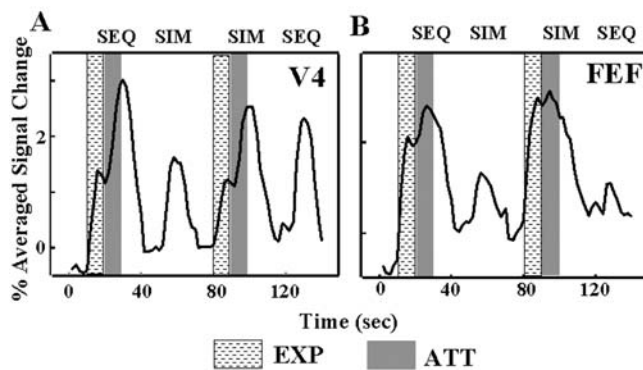


FIGURE 101.3. Increases of baseline activity in the absence of visual stimulation. *A*, Time series of fMRI signals in V4. Directing attention to a peripheral target location in the absence of visual stimulation led to an increase of baseline activity (EXP; textured blocks), which was followed by a further increase after the onset of the stimuli (ATT; gray-shaded blocks). Baseline increases were found in both striate and extrastriate visual cortex. *B*, Time series of fMRI signals in FEF. Directing attention to the peripheral target location in the absence of visual stimulation led to a stronger increase in baseline activity than in visual cortex; the further increase of activity after the onset of the stimuli was not significant. Sustained activity was seen in a distributed network of areas outside the visual cortex, including SPL, FEF, and SEF, suggesting that these areas may provide the source for the attentional top-down signals seen in visual cortex. (Adapted from Kastner et al., 1999).

the effects of attention in the presence and absence of visual stimulation could be studied.

It was found that during the expectation period preceding the attended presentations, regions within visual areas with a representation of the attended location were activated. This activity was related to directing attention to the target location in the absence of visual stimulation. Notably, the increase in activity during expectation was topographically specific, inasmuch as it was only seen in areas with a spatial representation of the attended location. As illustrated for area V4 in Figure 101.3A, the fMRI signals increased during the expectation period (EXP; textured epochs in the figure), before any stimuli were present on the screen. This increase of baseline activity was followed by a further increase of activity evoked by the onset of the stimulus presentations (ATT; gray-shaded epochs in the figure). The baseline increase was found in all visual areas with a representation of the attended location. It was strongest in V4 but was also seen in early visual areas. It is noteworthy that baseline increases were found in V1, even though no significant attentional modulation of visually evoked activity was seen in this area. This dissociation suggests that different mechanisms underlie the effects of attention on visually evoked activity and on baseline activity. Importantly, the increase in baseline activity in V1 has also been found to depend on the expected task difficulty. Ress and colleagues (2000) showed that increases in baseline activity were stronger when subjects expected a visual pattern that was difficult to discriminate compared to a pattern that was easy to discriminate. In areas that preferentially process a particular stimulus feature (e.g., color or motion), increases in baseline activity were shown to be stronger during the expectation of a preferred compared to a nonpreferred stimulus feature (Chawla et al., 1999).

The baseline increases found in human visual cortex may be subserved by increases in the spontaneous firing rate similar to those found in single-cell recording studies (Colby et al., 1996; Luck et al., 1997) but summed over large populations of neurons. The increases evoked by directing attention to a target location in anticipation of a behaviorally relevant stimulus at that attended location are thus likely to reflect a top-down feedback bias in favor of the attended location in human visual cortex.

Mechanisms of attentional control

Thus far, I have demonstrated that selective attention can modulate neural activity in visual cortex in the presence and in the absence of visual stimuli. There is evidence that attentional top-down signals derive from areas outside visual cortex and are transmitted via feedback projections to visual cortex. Studies in patients suffering from attentional deficits due to brain damage and functional brain imaging studies

in healthy subjects performing attention tasks have given insights into a distributed network of higher-order areas in frontal and parietal cortex. This network appears to be involved in attentional control.

VISUOSPATIAL NEGLECT: A DEFICIT OF SPATIAL ATTENTION

There is a long history demonstrating that unilateral brain lesions in humans often cause an impairment in spatially directing attention to the contralateral hemifield, a syndrome known as *visuospatial neglect*. In severe cases, patients suffering from neglect will completely disregard the visual hemifield contralateral to the side of the lesion (e.g., Rafal, 1994). For example, they will read from only one side of a book, apply makeup to only one half of their face, or eat from only one side of a plate. In less severe cases, the deficit is more subtle and becomes apparent only if the patient is confronted with competing stimuli, as in the case of visual extinction. In visual extinction, patients are able to orient attention to a single visual object presented to their impaired visual hemifield, but if two stimuli are presented simultaneously, one in the impaired and the other in the intact hemifield, the patients will only detect the one presented to the intact side, denying that any other object had been presented. These findings suggest that visual extinction reflects an attentional bias toward the intact hemifield in the presence of competing objects.

Visuospatial neglect may follow unilateral lesioning at very different sites, including the parietal lobe, especially its inferior part and the temporoparietal junction (Vallar and Perani, 1986), regions of the frontal lobe (Heilman and Valenstein, 1972), the anterior cingulate cortex (Janer and Pardo, 1991), the basal ganglia (Damasio et al., 1980), and the thalamus, in particular the pulvinar (Watson and Heilman, 1979). The finding that lesions of many different areas may cause visuospatial neglect has led to the notion that these areas form a distributed network for directed attention (Mesulam, 1999).

The classical view of inferior parietal cortex as the most typical lesion site in visuospatial neglect has recently been challenged by Karnath and colleagues (2001). They showed that the lesion site of patients with right hemispheric posterior lesions who suffered from visuospatial neglect and additional visual field defects was indeed located in the inferior parietal cortex including the region of the temporoparietal junction. However, in patients suffering from pure visuospatial neglect without additional visual field defects, the lesion site was located in the superior temporal gyrus (STG). Hence, the superior temporal cortex rather than the inferior parietal cortex may be the most important site for the control of spatial attention.

Neglect occurs more often with right-sided lesions than with left-sided lesions of the parietal or temporal cortex, suggesting a specialized role for the right hemisphere in directed

attention (Karnath et al., 2001; Vallar and Perani, 1986). Based on this hemispheric asymmetry, it has been proposed that the right hemisphere mediates directed attention to both sides of visual space, whereas the left hemisphere mediates directed attention only to the contralateral, right side of visual space (Mesulam, 1999). According to this view, in the case of a left hemisphere lesion, the intact right hemisphere would take over the attentional function of the damaged left hemisphere, whereas a right hemisphere lesion would result in a left-sided hemispatial neglect because of the bias of the intact left hemisphere for the right hemifield. This right hemispheric dominance of parietal cortex has been demonstrated only in cases of severe neglect; visual extinction appears to result as frequently from left- as from right-sided lesions (Rafal, 1994).

Importantly, stimulus-driven bottom-up mechanisms within visual cortex, such as figure-ground segmentation or perceptual grouping, which determine the salience of a stimulus, are preserved in the neglected hemifield and may influence the patient's behavior. For example, Mattingley et al. (1997) reported a patient with parietal damage whose extinction was less severe when bilateral stimuli were arranged to form an illusory Kanisza square, a percept based on automatic filling-in of illusory boundaries. This result shows that the patient could use the information from his neglected left hemifield to form the percept of a common surface. It therefore appears that following parietal damage, the competition among multiple stimuli can be biased equally well across the entire visual field by bottom-up processes, whereas mechanisms under top-down control, such as directing attention to a particular location, are biased toward the intact hemifield.

A DISTRIBUTED NETWORK FOR SPATIALLY DIRECTED ATTENTION

Results of functional brain imaging studies support the idea that top-down signals related to spatially directed attention may be generated by a distributed network of areas in frontal and parietal cortex. In addition to activations within visual cortex, activations of parietal and frontal cortex were investigated with the experimental design used to study competitive interactions and their modulation by spatial attention, as described above (Kastner et al., 1998). Results for a single subject are shown in Figure 101.4B. In this subject, the frontal eye fields (FEF) were activated bilaterally, together with the supplementary eye field (SEF) and the superior parietal lobule (SPL), when the subject directed attention to the peripheral target location compared to when the subject maintained fixation. Remarkably, none of these areas were activated to a significant degree when subjects were processing visual information in an unattended condition (Fig. 101.4A). A network consisting of areas in the SPL, FEF, and SEF was consistently activated across subjects. A similar network has been found to be activated in a variety

of visuospatial tasks (e.g., Corbetta et al., 1998; Nobre et al., 1997; Vandenberghe et al., 1997). In addition, but less consistently, activations in the inferior parietal lobule (IPL), the lateral prefrontal cortex in the region of the middle frontal gyrus (MFG), and the anterior cingulate cortex have been reported. A common feature among these visuospatial tasks is that subjects were asked to maintain fixation at a central fixation point and to direct attention covertly to peripheral target locations in order to detect a stimulus, to discriminate it, or to track its movement. Thus, there appears to be a general spatial attention network that operates independently of the specific requirements of the visuospatial task (for a meta-analysis and additional references, see Kastner and Ungerleider, 2000). Interestingly, the same areas of parietal cortex have been shown to be activated to a similar extent during different spatial and nonspatial attention tasks including peripheral shifts of attention, object matching, and nonspatial conjunction search (Wojciulik and Kanwisher, 1999). Hence, in parietal cortex, spatially and nonspatially based attentional selections may be mediated by a common neural substrate.

There are two notable differences in the results from patient studies and from functional brain imaging studies. First, the patient studies suggest a right parietal or temporal dominance in visuospatial attention; that is, directing attention to the left hemifield is presumed to be subserved exclusively by the right parietal or temporal cortex, whereas directing attention to the right hemifield is presumed to be subserved by both the left and the right parietal or temporal cortex. This notion has not been supported

unequivocally by functional brain imaging studies. Although some investigators have found a stronger or an even exclusive activation of areas in the right parietal lobe (Nobre et al., 1997; Vandenberghe et al., 1997), others have found largely symmetrical activations in the right and left parietal lobes (Kastner et al., 1999). Moreover, these symmetrical activations appeared to be independent of the visual hemifield attended (Vandenberghe et al., 1997). A second difference between the results from patient studies and from functional brain imaging studies concerns which portion of the parietal lobe plays a key role in attention. The patient literature has consistently identified the IPL, including the temporoparietal junction (Vallar and Perani, 1986), and the STG (Karnath et al., 2001) as critical lesion sites in neglect patients. By contrast, the majority of functional brain imaging studies point to the SPL rather than the IPL or the STG as the part of the parietal lobe that is involved in visuospatial attention. One possible explanation for this discrepancy is that many tasks used in the imaging studies involved a cue to indicate the location at which the visual stimulus would appear; these tasks thus had an expectancy component. Results of lesion studies suggest that the ability to maintain expectancy depends on the SPL rather than the IPL (Friedrich et al., 1998).

Evidence from fMRI studies (e.g., Hopfinger et al., 2000; Kastner et al., 1999) suggests that the attention-related activity in parietal and frontal areas does not reflect attentional modulation of visual responses; instead, the activity is due largely to the attentional operations themselves. Activations in frontal and parietal cortex during directed attention in the

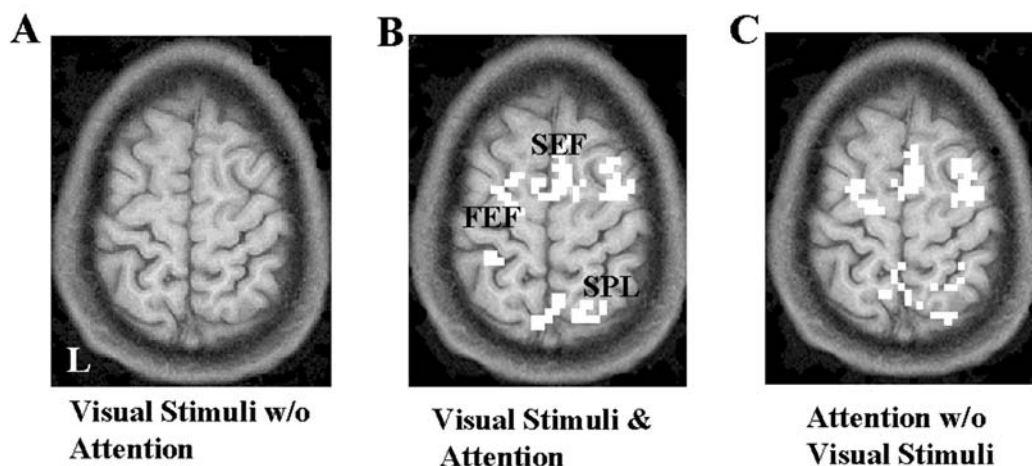


FIGURE 101.4. A frontoparietal network subserving biased competition and spatially directed attention. Axial slice through frontal and parietal cortex; same subject and experimental conditions as in Figure 101.3. *A*, Visual stimulation did not activate frontal or parietal cortex reliably when attention was directed elsewhere in the visual field. *B*, When the subject directed attention to a peripheral target location and performed an object discrimination task, a distributed frontoparietal network was activated including the SEF,

FEF, and SPL. *C*, The same network of frontal and parietal areas was activated when the subject directed attention to the peripheral target location in the expectation of the stimulus onset, that is, in the absence of any visual input whatsoever. This activity therefore may not reflect attentional modulation of visually evoked responses, but rather attentional control operations themselves. L, left hemisphere.

presence and in the absence of visual stimulation were investigated in the paradigm described above (Kastner et al., 1999). During directed attention in the absence of visual stimulation, the same distributed network for spatial attention as during directed attention in the presence of visual stimulation was activated, consisting of the FEF, the SEF, and the SPL (Fig. 101.4C). A time course analysis of the fMRI signals revealed that, as in visual cortical areas, there was an increase in activity in these frontal and parietal areas due to directed attention in the absence of visual input. However, first, this increase in activity was stronger in SPL, FEF, and SEF than the increase in activity seen in visual cortex (as exemplified for FEF in Fig. 101.3B); second, there was no further increase in activity evoked by the attended stimulus presentations in these parietal and frontal areas. Rather, there was sustained activity throughout the expectation period and the attended presentations (Fig. 101.3B). Taken together, these findings suggest that the activity reflected the attentional operations of the task and not visual processing. Hence, the distributed frontoparietal attention network may be the source of feedback that generates the top-down biasing signals seen in visual cortex. Because the magnitude of the activity in the parietal and frontal areas was the same during directed attention in the absence and in the presence of visual stimulation, it appears that this activity may be independent of the particular visual task, be it detection or discrimination. This would explain the finding that functional brain imaging studies using different visuospatial attention tasks have described very similar attentional networks.

The anatomical connections of SPL, FEF, and SEF put them in a position to serve as sources of top-down biasing signals within visual cortex. In the monkey, FEF and SEF are reciprocally connected with ventral stream areas (Webster et al., 1994) and posterior parietal cortex (Cavada and Goldman-Rakic, 1989), and posterior parietal cortex is connected with ventral stream areas via the lateral intraparietal (LIP) area (Webster et al., 1994).

The functional roles of these frontal and parietal areas in attentional selection and control are not well understood. In regions of parietal cortex, it has been shown that neural responses are enhanced during covert shifts of attention to peripheral visual stimuli (Bushnell et al., 1981; Colby et al., 1996). The strongest determinant of neural responsiveness in parietal cortex turned out to be the salience of the stimulus (Gottlieb et al., 1998). Therefore, it may be speculated that parietal cortex provides a *salience map* for exogenous stimuli that will capture attention rapidly. Recent functional brain imaging studies suggest that distinct parietal regions subserve different attentional processes. It was found that regions within the intraparietal sulcus were activated when

subjects voluntarily directed attention to a pre-cued location before the presentation of a visual target stimulus. In contrast, regions of the right temporoparietal junction were activated when target stimuli were detected at unattended locations (Corbetta et al., 2000). In the FEF and SEF, attentional response enhancement was originally shown in the context of activity related to the preparation of saccadic eye movements (e.g., Wurtz and Mohler, 1976), supporting the notion that covert shifts of attention precede overt shifts of gaze. More recent recording studies suggest, however, that the response enhancement in these frontal areas during covert shifts of attention to peripheral visual stimuli does not depend on the subsequent execution of saccades (Kodaka et al., 1997). The intimate functional relationship between covert shifts of attention and eye movements in frontal cortical areas has also been demonstrated in functional brain imaging studies. Areas including the FEF and SEF that were engaged by covert shifts of attention and by executing saccadic eye movements were shown to overlap greatly (e.g., Corbetta et al., 1998). Taken together, these studies have begun to define functional roles for distinct areas within frontal and parietal cortex in attentional control, which need further refinement in future research.

Thus far, results of single-cell recording studies and functional brain imaging studies clearly converge to support the idea that areas in parietal and frontal cortex are potential sources for generating and controlling attentional top-down signals. However, because results of functional brain imaging studies demonstrate only correlated activity of distributed brain areas and cannot establish the functional significance of a particular brain area in a given task, future studies using reversible lesion techniques such as cooling of brain tissue or transcranial magnetic stimulation are needed to test these ideas further.

Conclusion

The view that has been presented in this chapter is summarized in the simple attention model depicted in Figure 101.5. The representation of objects in visual cortex is determined by both bottom-up stimulus-driven factors and cognitive top-down influences such as selective attention. In visual cortex, target or distracter stimuli are not processed independently of each other; rather, they compete for limited processing resources by means of competitive interactions. Selective attention modulates neural activity in visual cortex both in the presence and in the absence of visual stimulation. The attention-related signals are generated from a distributed network of areas in frontal and parietal cortex and are transmitted via feedback projections to visual cortex.

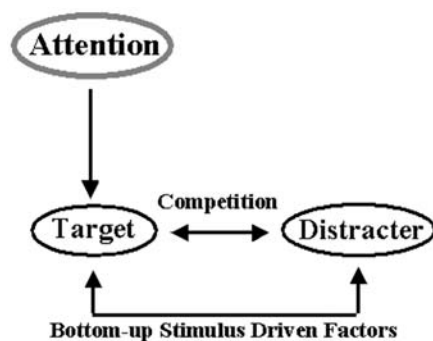


FIGURE 101.5 A model of selective visual attention. The representation of visual stimuli in visual cortex is determined by both bottom-up stimulus-driven factors and top-down cognitive influences such as attention. Visual stimuli are not processed independently of each other but interact competitively for limited processing resources.

REFERENCES

- Brefczynski, J. A., and E. A. DeYoe, 1999. A physiological correlate of the "spotlight" of visual attention, *Nat. Neurosci.*, 2:370–374.
- Broadbent, D. E., 1958. *Perception and Communication*, London: Pergamon Press.
- Bushnell, M. C., M. E. Goldberg, and D. L. Robinson, 1981. Behavioral enhancement of visual responses in monkey cerebral cortex, *J. Neurophysiol.*, 46:755–772.
- Carrasco, M., and Y. Yeshurun, 1998. The contribution of covert attention to the set-size and eccentricity effects in visual search, *J. Exp. Psychol. Hum. Percept. Perform.*, 24:673–692.
- Cavada, C., and P. S. Goldman-Rakic, 1989. Posterior parietal cortex in rhesus monkey: II. Evidence for segregated cortico-cortical networks linking sensory and limbic areas with the frontal lobe, *J. Comp. Neurol.*, 287:422–445.
- Chawla, D., G. Rees, and K. J. Friston, 1999. The physiological basis of attentional modulation in extrastriate visual areas, *Nat. Neurosci.*, 2:671–676.
- Chelazzi, L., J. Duncan, E. K. Miller, and R. Desimone, 1998. Responses of neurons in inferior temporal cortex during memory-guided visual search, *J. Neurophysiol.*, 80:2918–2940.
- Colby, C. L., J. R. Duhamel, and M. E. Goldberg, 1996. Visual, presaccadic, and cognitive activation of single neurons in monkey lateral intraparietal area, *J. Neurophysiol.*, 76:2841–2852.
- Connor, C. E., D. C. Preddie, J. L. Gallant, and D. C. Van Essen, 1997. Spatial attention effects in macaque area V4, *J. Neurosci.*, 17:3201–3214.
- Corbetta, M., E. Akbudak, T. E. Conturo, A. Z. Snyder, J. M. Ollinger, H. A. Drury, H. R. Linenweber, S. E. Petersen, H. E. Raichle, D. G. Van Essen, and G. L. Shulman, 1998. A common network of functional areas for attention and eye movements, *Neuron*, 21:761–773.
- Corbetta, M., J. M. Kincade, J. M. Ollinger, M. P. McAvoy, and G. L. Shulman, 2000. Voluntary orienting is dissociated from target detection in human posterior parietal cortex, *Nat. Neurosci.*, 3:292–297.
- Corbetta, M., F. M. Miezin, S. Dobmeyer, G. L. Shulman, and S. E. Petersen, 1991. Attentional modulation of neural processing of shape, color, and velocity in humans, *Science*, 248:1556–1559.
- Damasio, A. R., H. Damasio, and C. H. Chang, 1980. Neglect following damage to frontal lobe or basal ganglia, *Neuropsychologia*, 18:123–132.
- Desimone, R., and J. Duncan, 1995. Neural mechanisms of selective visual attention, *Annu. Rev. Neurosci.*, 18:193–222.
- De Weerd, P., M. R. Peralta III, R. Desimone, and L. Ungerleider, 1999. Loss of attentional selection after extrastriate cortical lesions in macaques, *Nat. Neurosci.*, 2:753–757.
- Duncan, J., 1984. Selective attention and the organization of visual information, *J. Exp. Psychol.*, 113:501–517.
- Friedrich, F. J., R. Egly, R. D. Rafal, and D. Beck, 1998. Spatial attention deficits in humans: a comparison of superior parietal and temporal-parietal junction lesions, *Neuropsychology*, 12:193–207.
- Gallant, J. L., R. E. Shoup, and J. A. Mazer, 2000. A human extrastriate area functionally homologous to macaque V4, *Neuron*, 27:227–235.
- Gottlieb, J. M., M. Kusunoki, and M. E. Goldberg, 1998. The representation of visual salience in monkey parietal cortex, *Nature*, 391:481–484.
- Heilman, K. M., and E. Valenstein, 1972. Frontal lobe neglect in man, *Neurology*, 22:660–664.
- Heinze, H. J., G. R. Mangun, W. Burchert, H. Hinrichs, M. Scholz, T. F. Muentel, A. Goes, M. Scherg, S. Johannes, M. Hunderhagen, and M. S. Gazzauiga, 1994. Combined spatial and temporal imaging of brain activity during visual selective attention in humans, *Nature*, 372:543–546.
- Hillyard, S. A., E. K. Vogel, and S. J. Luck, 1998. Sensory gain control (amplification) as a mechanism of selective attention: electrophysiological and neuroimaging evidence, *Philos. Trans. R. Soc. Lond. B*, 353:1257–1270.
- Hopfinger, J. B., M. H. Buonocore, and G. R. Mangun, 2000. The neural mechanisms of top-down attentional control, *Nat. Neurosci.*, 3:284–291.
- Ito, M., and C. D. Gilbert, 1999. Attention modulates contextual influences in the primary visual cortex of alert monkeys, *Neuron*, 22:593–604.
- Janer, K. W., and J. V. Pardo, 1991. Deficits in selective attention following bilateral anterior cingulotomy, *J. Cogn. Neurosci.*, 3:231–241.
- Karnath, H. O., S. Ferber, and M. Himmelbach, 2001. Spatial awareness is a function of the temporal not the posterior parietal lobe, *Nature*, 411:950–953.
- Kastner, S., P. De Weerd, R. Desimone, and L. G. Ungerleider, 1998. Mechanisms of directed attention in the human extrastriate cortex as revealed by functional MRI, *Science*, 282:108–111.
- Kastner, S., M. A. Pinsk, P. De Weerd, R. Desimone, and L. G. Ungerleider, 1999. Increased activity in human visual cortex during directed attention in the absence of visual stimulation, *Neuron*, 22:751–761.
- Kastner, S., and G. L. Ungerleider, 2000. Mechanisms of visual attention in the human cortex, *Annu. Rev. Neurosci.*, 23:315–341.
- Kodaka, Y., A. Mikami, and K. Kubota, 1997. Neuronal activity in the frontal eye field of the monkey is modulated while attention is focused on to a stimulus in the peripheral visual field, irrespective of eye movement, *Neurosci. Res.*, 28:291–298.
- Lavie, N., and J. Driver, 1996. On the spatial extent of attention in object-based visual selection, *Percept. Psychophys.*, 58:1238–1251.
- Lu, Z. L., and B. A. Doshier, 1998. External noise distinguishes attention mechanisms, *Vis. Res.*, 38:1183–1198.
- Luck, S. J., L. Chelazzi, S. A. Hillyard, and R. Desimone, 1997. Neural mechanisms of spatial selective attention in areas V1, V2, and V4 of macaque visual cortex, *J. Neurophysiol.*, 77:24–42.

- Martinez, A., L. A. Vento, M. I. Sereno, L. R. Frank, R. B. Buxton, D. J. Dubowitz, E. C. Wong, H. Hinrichs, H. J. Heinze, and S. A. Hillyard, 1999. Involvement of striate and extrastriate visual cortical areas in spatial attention, *Nat. Neurosci.*, 2:364–369.
- Mattingley, J. B., G. Davis, and J. Driver, 1997. Preattentive filling-in of visual surfaces in parietal extinction, *Science*, 275:671–674.
- McAdams, C. J., and J. H. R. Maunsell, 1999. Effects of attention on orientation-tuning functions of single neurons in macaque cortical area V4, *J. Neurosci.*, 19:431–441.
- Mesulam, M. M., 1999. Spatial attention and neglect: parietal, frontal and cingulate contributions to the mental representation and attentional targeting of salient extrapersonal events, *Philos. Trans. R. Soc. Lond. B Biol. Sci.*, 354:1325–1346.
- Moran, J., and R. Desimone, 1985. Selective attention gates visual processing in the extrastriate cortex, *Science*, 229:782–784.
- Motter, B. C., 1993. Focal attention produces spatially selective processing in visual cortical areas V1, V2, and V4 in the presence of competing stimuli, *J. Neurophysiol.*, 70:909–919.
- Nobre, A. C., G. N. Sebestyen, D. R. Gitelman, M. M. Mesulam, R. S. J. Frackowiak, and C. D. Frith, 1997. Functional localization of the system for visuospatial attention using positron emission tomography, *Brain*, 120:515–533.
- Nothdurft, H. C., 1993. The role of features in preattentive vision: comparison of orientation, motion and colour cues, *Vis. Res.*, 33:1937–1958.
- O’Craven, K. M., P. E. Downing, and N. Kanwisher, 1999. fMRI evidence for objects as the units of attentional selection, *Nature*, 401:584–587.
- Posner, M., 1980. Orienting of attention, *Q. J. Exp. Psychol.*, 32:3–25.
- Rafal, R. D., 1994. Neglect, *Curr. Opin. Neurobiol.*, 4:231–236.
- Recanzone, G. H., and R. H. Wurtz, 2000. Effects of attention on MT and MST neuronal activity during pursuit initiation, *J. Neurophysiol.*, 83:777–790.
- Rees, G., C. D. Frith, and N. Lavie, 1997. Modulating irrelevant motion perception by varying attentional load in an unrelated task, *Science*, 278:1616–1619.
- Ress, D., B. T. Backus, and D. J. Heeger, 2000. Activity in primary visual cortex predicts performance in a visual detection task, *Nat. Neurosci.*, 3:940–945.
- Reynolds, J. H., L. Chelazzi, and R. Desimone, 1999. Competitive mechanisms subserve attention in macaque areas V2 and V4, *J. Neurosci.*, 19:1736–1753.
- Roelfsema, P. R., V. A. F. Lamme, and H. Spekreijse, 1998. Object-based attention in the primary visual cortex of the macaque monkey, *Nature*, 395:376–381.
- Shiu, L. P., and H. Pashler, 1995. Spatial attention and vernier acuity, *Vis. Res.*, 35:337–343.
- Spitzer, H., and B. J. Richmond, 1991. Task difficulty: ignoring, attending to, and discriminating a visual stimulus yield progressively more activity in inferior temporal neurons, *Exp. Brain Res.*, 83:340–348.
- Tootell, R. B. H., N. Hadjikhani, E. K. Hall, S. Marrett, W. Vanduffel, J. T. Vaughan, and A. M. Dale, 1998. The retinotopy of visual spatial attention, *Neuron*, 21:1409–1422.
- Treisman, A. M., and G. Gelade, 1980. A feature-integration theory of attention, *Cogn. Psychol.*, 12:97–136.
- Treue, S., and J. H. R. Maunsell, 1996. Attentional modulation of visual motion processing in cortical areas MT and MST, *Nature*, 382:539–541.
- Vallar, G., and D. Perani, 1986. The anatomy of unilateral neglect after right-hemisphere stroke lesions: a clinical/CT-scan correlation study in man, *Neuropsychologia*, 24:609–622.
- Vandenberghe, R., J. Duncan, P. Dupont, R. Ward, J. Poline, S. Bormans, J. Michiels, L. Mortelmans, and G. A. Orban, 1997. Attention to one or two features in left or right visual field: A positron emission tomography study, *J. Neurosci.*, 17:3739–3750.
- Watson, R. T., and K. M. Heilman, 1979. Thalamic neglect, *Neurology*, 29:690–694.
- Webster, M. J., J. Bachevalier, and L. G. Ungerleider, 1994. Connections of inferior temporal areas TEO and TE with parietal and frontal cortex in macaque monkeys, *Cereb. Cortex*, 4:470–483.
- Wojciulik, E., and N. Kanwisher, 1999. The generality of parietal involvement in visual attention, *Neuron*, 23:747–764.
- Wojciulik, E., N. Kanwisher, and J. Driver, 1998. Covert visual attention modulates face-specific activity in the human fusiform gyrus: fMRI study, *J. Neurophysiol.*, 79:1574–1578.
- Wurtz, R. H., and C. W. Mohler, 1976. Enhancement of visual responses in monkey striate cortex and frontal eye fields, *J. Neurophysiol.*, 39:766–772.

102 Neural and Behavioral Measures of Change Detection

DANIEL J. SIMONS AND MICHAEL SILVERMAN

... [O]ur “experience,” is almost entirely determined by our habits of attention.

William James (1892), *Psychology* (p. 172)

Our visual world seems coherent and richly detailed. A single glance in any direction produces an abundance of visual sensations, and we readily see the objects and surfaces around us. This rich sensory input is effortlessly associated with a vivid perceptual experience, leading to the impression that all the visual details of our world are readily available to us. This inference is largely true. At any instant, we can direct our attention to any aspect of our environment, and when we do, we become aware of whatever is the focus of our attention. This fact, in conjunction with the stability and continuity of objects and their properties over time and space, can lead to the false impression that the immediacy of our visual experience derives from a rich, detailed *internal* representation. That is, we believe that we store the details of objects around us internally and that these representations underlie our rich visual experience.

Recent evidence from studies of change detection, however, raises the intriguing possibility that we lack such detailed representations. That, in reality, our visual experience derives not from a complete internal representation, but from two assumptions: (1) the world is stable over time, and (2) important events will draw attention and reach awareness. The first assumption reflects a basic principle of efficient design: if details in the world typically do not change and if they are not needed from one instant to the next, they need not be stored internally (Brooks, 1991; Gibson, 1966; O'Regan, 1992; Stroud, 1955). Interestingly, the second assumption, that salient events draw attention, is not always true. People often are unaware of surprisingly large, and potentially important, events in their visual world (Mack and Rock, 1998; Neisser, 1979; Rensink, 2000b; Rensink et al., 1997; Simons, 2000b; Simons and Chabris, 1999; Simons and Levin, 1997, 1998). The fact that an object or event is salient does not guarantee its detection; even fully visible and unusual objects and events sometimes go unnoticed when attention is allocated elsewhere (Mack and Rock, 1998; Simons and Chabris, 1999). For example, experienced pilots who were asked to use a head-up display

when landing a jet in a flight simulator sometimes proceeded with their landing without ever noticing that another aircraft was blocking their runway (Haines, 1991). Similarly, when observers are focusing their attention on a simple computer task, they often fail to notice unexpected objects appearing in the display, even when the objects appear at the point of fixation (Mack and Rock, 1998). Such effects of selective looking, or “looking without seeing,” have been noted for many years (e.g., Becklen and Cervone, 1983; Most et al., 2000, 2001; Neisser, 1979; Neisser and Becklen, 1975; Simons, 2000a; Simons and Chabris, 1999), and recent work has drawn closer links between this phenomenon and other failures of visual awareness.

If, as the chapter-opening quote from James suggests, awareness is limited to those items that are the focus of attention, then our experience of consciously perceiving all available details must be illusory. We cannot attend to all of the details of our environment, even if they are available to our visual system. If we are unaware of those things that are unattended, we cannot notice their absence from awareness. Consequently, our visual experience is richly detailed because we only notice the ways in which it is detailed, and we do not notice the ways in which it is sparse. This limited capacity of attention, which produces limits on conscious awareness, is revealed in our daily experiences. For example, many people will recognize the experience of looking repeatedly for car keys on a cluttered counter and simply not finding them, only to discover later that they were fully visible the entire time. The potential to see the keys is always present, but without attention, we do not become aware of their presence.

This explanation for visual experience raises two critical questions. First, what information, if any, is stored internally when observers fail to detect clearly visible objects such as the misplaced keys? Second, what mechanisms eventually lead to the conscious perception of these items? Change detection tasks provide a useful tool for the systematic exploration of both of these questions. Because successful detection requires both representations and comparisons (Simons, 2000b), when observers detect a change we can infer that they successfully represented the prechange information and

compared it (consciously or otherwise) to the postchange information. In the case of change detection failures, or *change blindness*, we can use additional measures to determine whether the failure resulted from a poor representation of the scene or from an insufficient comparison of the changed features. In other words, we can determine what, precisely, was represented from the initial display before the change was identified and how that representation differed from the internal representation when the change was eventually detected.

Failures of visual awareness such as change blindness result when visual events violate our expectations for what should happen or what typically happens—when they contravene our regular “habits of attention.” Such failures reveal the tenuous hold our visual representations have on our conscious experience of our environment. In this chapter, we discuss the relationship between attention, internal representations, and visual awareness by focusing on the phenomenon of change blindness—the inability to detect large changes to scenes when detection depends on comparing internal representations over time. Our discussion evaluates the information needed to detect changes successfully and considers the inferences that can be drawn from change blindness. We review recent evidence from behavioral, eye tracking, and neuroimaging studies of change detection, and we speculate about how further research in these areas might elucidate the mechanisms of change detection.

A brief history of evidence for change blindness

The literature on change blindness has a long history, dating back at least to the late 1970s (see Simons and Levin, 1997, for a review). Systematic work on change blindness largely began with studies of eye movements during reading (Blanchard et al., 1989; McConkie and Zola, 1979; Morris et al., 1990; Pollatsek and Rayner, 1992) and studies of displacement detection across saccades (Bridgeman et al., 1975; Li and Matin, 1990; Mack, 1970; Wallach and Lewis, 1965). Only more recently has the focus of change blindness research turned to the perception and representation of natural scenes. Early work on displacement detection focused primarily on the issue of whether or not the perception of the visual world is suppressed during eye movements and also whether information from consecutive fixations can be integrated into a single representation. In a typical experiment, observers might view a dot presented parafoveally and then, during a saccade to the location of the dot, the dot would be shifted in position. Typically, shifts of less than 10% of the extent of the eye movement are not noticed by the observer. Displacement detection is quite poor when saccades are long and the displacements are relatively short.

Unlike studies of displacement detection, change detection studies during reading have focused more on the identity than on the position of the changed item. When reading, changes that occur during saccades are rarely noticed. Observers continue reading at the same rate without noticing substantial changes to the appearance or even the presence of words that are not currently fixated. For example, if observers are asked to read text in AlTeRnAtInG cAsE, they do not notice when the case of each letter on the screen changes during every saccade (McConkie and Zola, 1979). In contrast, observers viewing the same displays with changes unconstrained by their fixation patterns cannot easily read the text because the now-visible changes produce massive transient signals throughout the display; it is difficult to read text that we see changing. The presence of a saccade during the change appears to prevent the automatic detection of changes by inhibiting or masking the transient signal that would otherwise be distracting. In order to detect case changes that occur during a saccade, observers must actively attend to the letter, memorize it, and then compare that letter before and after a saccade.

More recent studies of saccade-contingent change blindness have produced parallel results using natural scenes rather than text (Grimes, 1996; Hollingworth and Schrock, 2001; Hollingworth et al., 2001a; McConkie and Currie, 1996). For example, when studying a photograph for a subsequent memory test, observers often failed to notice when two central people in the scene swapped hats during a saccade (Grimes, 1996). Many even failed to notice when two people exchanged heads! Blindness for these scene changes disappeared entirely when the changes occurred during fixation, suggesting that something about the representation or comparison process was disrupted by the saccade.

In addition to studies of saccade-contingent change detection, a number of early experiments used change detection tasks to explore the limits of short-term visual memory (e.g., Pashler, 1988; Phillips, 1974). These experiments briefly presented an array of letters, dots, or other simple stimuli, followed by a brief delay interval and then by a slightly changed array. Unlike most of the saccade-contingent change studies, the observer's primary goal in these studies was to try to detect changes. Consequently, change blindness cannot be attributed to the unexpected nature of the change. Instead, failed change detection was attributed to the limits of short-term visual memory. Observers were unable to hold all of the information in the array in memory during the brief delay interval.

In a seminal study in the change blindness literature, Rensink et al. (1997) adapted these one-shot change detection tasks to explore prolonged search for change. They confirmed that change blindness is not specific to changes made across saccades; it can occur during fixation and even occurs

when observers actively search for changes. These failures of visual awareness result whenever the transient signal that would otherwise accompany a change is disrupted. In their visual search *flicker* task, observers view a rapid alternation of an original and a changed scene, with a brief blank screen following each image presentation. The blank screen, like a saccade, disrupts the localized transient signal that would otherwise be produced by the change, giving the display its flickering appearance. Even though they are actively searching, observers often require many alternations to detect large changes, sometimes searching unsuccessfully for up to a minute. Notably, the level of change blindness does not appear to diminish even when subjects have extra time to study the images or when they have practiced performing the task (Rensink, 2000c; Rensink et al., 1997). Perhaps more importantly, the nature of the change influences the speed of detection: changes to objects of central interest in the scene are detected more rapidly than changes to irrelevant or peripheral objects (Rensink et al., 1997). This *center of interest* effect reflects the importance of attention in change detection. Changes to objects in a scene that are more likely to be the focus of attention are detected more rapidly than those less likely to be attended. This finding suggests that attention plays a functional role in the eventual detection of changes and that change blindness occurs when observers fail to devote focused attention to the changing item both before and after the change.

However, other work suggests that attention to an object does not guarantee detection, particularly when changes occur unexpectedly (Levin and Simons, 1997; Levin et al., 2002; Simons and Levin, 1998; Simons et al., 2002). For example, nearly two-thirds of observers failed to report any change when the only actor in a motion picture unexpectedly was replaced by a different person across a cut from one camera angle to another (Levin and Simons, 1997). In fact, from 35% to 65% of observers typically fail to notice when a real-world conversation partner is surreptitiously replaced during the middle of an interaction (Levin et al., 2002; Simons and Levin, 1998). These studies suggest that attention to an object is necessary for change detection, but it is not sufficient to guarantee detection. Rather, successful detection requires attention to the specific features of the object that are changing so that observers can encode those features and then compare them following the change.

Given that successful change detection implies the existence of a representation, evidence for change blindness has sometimes been taken to imply the absence of any internal representation of the prechange feature—that our representation of the visual world is more sparse than we might otherwise believe (e.g., O'Regan and Noe, 2001; Rensink, 2000a; Simons and Levin, 1997). Although this conclusion might well be true, it does not follow logically from existing

evidence for change blindness. The absence of detection does not necessarily imply the absence of a representation. Change detection could fail even in the presence of a complete and detailed representation of the prechange scene, provided that observers do not compare that initial representation to the postchange scene (Scott-Brown et al., 2000; Simons, 2000b).

AN ASIDE: WHAT MAKES CHANGE BLINDNESS INTERESTING

Findings of change blindness are interesting not because they imply the absence of a representation, but because they run counter to our intuitive belief that unusual or unexpected events will draw our attention. These intuitions reflect an understanding that small, irrelevant changes will not capture attention. For example, nobody would be particularly surprised by the failure to notice a subthreshold change to the color of a single pixel in a photograph of a natural scene. However, people are surprised when the changes are large and supraliminal. To some degree, these intuitions are entirely reasonable based on our daily experiences. After all, most sudden changes in the world do produce a visible change signal and rarely occur quickly enough to start and finish during a saccade. Moreover, we do occasionally notice changes. For example, it is not uncommon to detect an occasional editing error in a motion picture. These examples of successful change detection are readily available, whereas, by definition, we do not become aware of those changes that we fail to notice. Given the tendency to judge the frequency of events based on the information that is most available in recollection (Tversky and Kahneman, 1982), estimates of successful change detection are likely to be inflated. Because some changes are noticed, we have the impression that all changes draw our attention, leading to awareness. Evidence for change blindness shows that this impression is false. Unexpected changes do not necessarily draw our attention.

This mistaken intuition can be demonstrated empirically (Levin et al., 2000). In one change detection study (Levin and Simons, 1997), observers viewed a brief motion picture of a lunch conversation in which an intentional change was made every time the camera cut instantaneously to a different angle. For example, a scarf worn by one of the actors disappeared and then reappeared from one shot to the next, plates changed from red to white and then back to red, and objects on the table switched locations. When unsuspecting observers were asked to view this film carefully, they typically did not report any of the changes (Levin and Simons, 1997). That is, they showed complete change blindness for these unexpected changes. To demonstrate the overestimation of change detection abilities, a different group of observers viewed still frames from the film and predicted how likely they would be to detect the various changes (Levin et al., 2000). These observers predicted far greater change detec-

tion for irrelevant changes than actually occurred: for example, approximately 90% of observers thought that they would notice the scarf change, and more than 75% thought they would notice the plate color change when, in reality, no subjects noticed either of these changes.

This massive overestimation of change detection rates reflects the intuitive assumption that important, unusual, or distinctive events will automatically draw attention. This assumption can have important implications, both for theoretical arguments about change detection and for practical applications of evidence for change blindness. Just as observers believe they will detect changes, product designers believe that the subtle change cues they provide will be sufficient to guide attention. One obvious situation in which change blindness can have dire consequences is driving. Brake lights are typically red, and when they come on, they simply brighten. The assumption that the brightening of brake lights will automatically draw attention even if we are focusing attention on some other aspect of the scene (or on other distracting events in the car such as a phone conversation) can have dire consequences. The change from dim to bright is an instantaneous change, and if the change itself does not attract attention, it sometimes will be missed. A more reasonable strategy for ensuring that motorists notice the onset of brake lights would be to have the change occur repeatedly, thereby increasing the probability that observers will be attending to the lights at some point when the change occurs. If drivers are aware of their own poor change detection abilities and the likelihood that other drivers will have mistaken intuitions about change detection of other drivers, then they can adjust. For example, if another car is following too closely and you need to brake, you can lightly pump the brake pedal to cause the brake light to flash repeatedly, thereby increasing the chances that the driver behind you will notice that you are stopping.

Studies of the mistaken belief in the absence of change blindness, something Levin et al. (2000) dubbed *change blindness blindness*, help reveal the potential consequences of change blindness. They also demonstrate that change blindness findings are surprising: not only are we blind to large changes in our visual world, but we remain largely unaware of this fact. This *meta-cognitive* failure might well have more real world consequences than the phenomenon of change blindness itself.

What is retained when changes are not reported?

Findings of change blindness have often been taken as support for the notion that we lack detailed internal representations of the visual world (O'Regan, 1992; O'Regan and Noe, 2001; Rensink, 2000a; Simons and Levin, 1997). Change blindness would be a natural consequence of sparse internal representations. Without an internal representation

of the prechange features, no comparison to the postchange scene would be possible and change detection would fail. However, as noted earlier, the failure to detect changes does not necessitate sparse representations. Observers might well retain much information about the prechange object even if they fail to report a change. Most studies of change detection rely on explicit reports to determine whether or not a change was detected, and many of these reports occur well after the change. Such measures may well underestimate the degree to which changes are detected. For example, in the person-change video described earlier (Levin and Simons, 1997), change detection was measured by obtaining written descriptions of the video after it ended. Observers might have detected a change but then immediately discounted it as implausible and forgotten it. And even if they did not detect the change, they might still have represented the details of the prechange object.

BEHAVIORAL MEASURES OF PRESERVED REPRESENTATIONS
Some behavioral work suggests the presence of preserved representations despite change blindness. In one study (Silverman, 2001), observers viewed letter matrices similar to those used in the classic partial report procedure (Sperling, 1960). On each trial, two matrices were presented in sequence, separated by a briefly displayed gray field. One, two, or all three of the letters in a randomly chosen row were replaced with different letters, and subjects were asked to report whether or not a change had occurred. They were then asked to identify a row of three letters that were degraded by removing 75% of their pixels. The letters were either novel or they were drawn from a changed row or an unchanged row from the previous arrays. Even when observers did not notice the change, they were better able to identify previously viewed letters than novel letters. Furthermore, they were equally good in identifying changed and unchanged rows from the matrices, suggesting that they had a fairly complete representation of the display. These findings are consistent with other work showing preserved representation of visual stimuli that could not be consciously reported (DeSchepper and Treisman, 1996; Mack and Rock, 1998; Moore and Egeth, 1997; Shapiro et al., 1997).

Additional evidence for preserved representations in the face of change blindness comes from a real-world study in which pedestrians were approached by an experimenter who, while carrying a red-and-white striped basketball, asked for directions to a gymnasium (Simons et al., 2002). During this interaction, a group of confederates walked down the sidewalk, and one of them surreptitiously took the ball away. The experimenter then asked the pedestrian a series of questions: "Did you notice anything unusual happen as the crowd of people passed between us? Did you notice anything change? Do you think anything has changed

about my appearance since the crowd went by?” Most observers responded no “to” all of these questions, indicating that they did not consciously detect the change. However, when the experimenter asked “Do you think that I had a basketball before the crowd went by?” more than 60% of the pedestrians responded “yes,” and they typically noted something about the ball’s unusual appearance when asked (e.g., that it was striped or unusually colored). This “discovered” memory (Schooler, 2001) suggests that observers had represented the presence of the ball and some of its features, but given that the disappearance of the ball did not change their interpretation of the scene or their immediate goal of giving directions, they did not spontaneously compare the current appearance of the scene to their initial representation. Rather, only when cued specifically about the ball did they make the necessary comparison. This finding suggests that change blindness can occur even when observers have an explicitly available representation of the prechange scene (see also Levin et al., 2002).

Together, these findings suggest that observers do form internal representations of some details of the prechange scene even when they do not explicitly report the presence of a change (see also Hollingworth et al., 2001b for evidence that observers sometimes detect changes many fixations after the change occurred). That observers can represent scenes without being aware of their representations is not surprising. Extensive evidence suggests that many aspects of perception occur without awareness (e.g., Chun and Jiang, 1998; Goodale and Milner, 1992; Kihlstrom et al., 1992; Maljkovic and Nakayama, 1994). Moreover, the fact that such representations are potentially accessible to awareness even when observers did not use the representation to detect a change further supports the idea that change blindness often results from a comparison failure (Scott-Brown et al., 2000; Simons, 2000b).

The finding that initial verbal reports of change detection underestimate the amount of information preserved in the face of change blindness raises the intriguing possibility that changes themselves might be detected without awareness. That is, observers might implicitly represent the prechange scene and then implicitly compare that representation to the changed scene. Therefore, a finding of implicit change detection would imply the existence of a representation of the prechange scene. Recent research on change blindness has explored the nature of our internal representations in the face of change blindness by testing whether more sensitive, on-line measures reveal change detection in the absence of awareness. This research has taken several forms. Some studies have relied on behavioral measures such as forced-choice guessing or measurements of response latency to look at change detection without awareness (Fernandez-Duque and Thornton, 2000; Smilek et al., 2000; Thornton and Fernandez-Duque, 2000; Williams and Simons, 2000).

Others have used measured eye movement patterns or fixation durations in the presence and absence of change detection (Hayhoe et al., 1998; Hollingworth et al., 2001b; Ryan and Cohen, 2002). And, in recent years, several laboratories have used neuroimaging measures such as event-related potentials (ERP) (Fernandez-Duque et al., 2002; Niedeggen et al., 2001) and functional magnetic resonance imaging (fMRI) (Beck et al., 2001; Huettel et al., 2001) to explore change detection with and without awareness. Note, of course, that all change detection, whether implicit or explicit, requires both a representation of the prechange scene and a comparison to the postchange scene. The existence of implicit change detection would require that the comparison process occur without awareness (Mitroff et al., 2002). However, if no such implicit comparison process exists, then change detection in the absence of a transient signal must depend on explicit comparisons (Mitroff et al., 2002). Given the dramatically different implications of these two possibilities for theories of change detection, the existence of implicit change detection has become a central question in the change blindness literature. Each of these approaches to exploring implicit change detection is discussed in detail below.

BEHAVIORAL EVIDENCE FOR AND AGAINST IMPLICIT CHANGE DETECTION Most attempts to measure implicit change detection use explicit reports of the occurrence of a change in order to identify detected and missed changes. Presumably, unreported changes were not explicitly detected. Any other evidence for change detection when the change was consciously missed would suggest the existence of implicit change detection and the corresponding representation of the prechange scene. For example, in one study (Fernandez-Duque and Thornton, 2000), observers were given a two-alternative forced-choice decision about which item had changed, and trials were separated into those for which observers did and did not report having seen the change. When observers had not seen the change, they presumably guessed which of the two alternatives had changed. Interestingly, their “guesses” were correct more than 50% of the time.

One concern with this finding, however, is that the observers’ reports of change detection might not exhaustively measure all of the explicit mechanisms that could have contributed to their performance (Holender, 1986; Merikle and Reingold, 1992); some unmeasured explicit factors might contribute to the guessing performance for unreported changes. One such mechanism is the explicit elimination of items known not to have changed (Fernandez-Duque and Thornton, 2000; Mitroff et al., 2002). If observers know that some items have not changed, they would guess correctly more than 50% of the time even if they did not see the change itself. In fact, this sort of

elimination strategy adequately accounts for the original data and even predicts performance on a modified version of this task (Mitroff et al., 2002). Thus, although forced “guessing” might provide a more sensitive measure of change detection than verbal reports, current evidence using this task is also consistent with the need for an explicit comparison mechanism for change detection.

Other claims of implicit change detection come from measures of response speed for missed changes. Observers sometimes take longer to respond “no change” when they miss a change than when there is actually no change (Williams and Simons, 2000). Such findings are consistent with the idea that the change was detected by the visual system and affected the response latency even though it did not reach awareness. However, as with forced-choice guessing, such studies do not exhaustively eliminate other explicit contributions to performance. For example, rated confidence in change present/absent decisions accounts for almost all of the increase in response latency for missed changes (Mitroff et al., 2002). To the extent that rated confidence reflects explicit detection, this finding raises doubts about the need to posit an implicit comparison process to explain differences in response latency.

Any study relying on verbal reports to distinguish between detected and undetected changes risks the possibility that criterion shifts can partially explain any implicit effects. Moreover, studies must carefully exclude any effects of explicit strategies that could influence performance even in the absence of change detection. For example, one recent study found evidence that the orientation of a changed item (horizontal or vertical) could influence orientation judgments about another item in a display, even if observers did not report noticing the change (Thornton and Fernandez-Duque, 2000). Observers were more accurate when the orientation of the changed item matched that of the judged item, and they were less accurate when the two were in conflict. This indirect measure of change detection holds promise because it does not require a response about the changed item. However, in this study, the relative positions of the changed item and the to-be-judged item were tightly linked: they were either the same item or diametrically opposite each other. Observers likely were aware of this contingency, and it could affect their strategy in performing the task. This change in strategy might well produce a congruence effect on orientation judgments even if observers did not detect the change. In fact, when the tight coupling of the positions of the changed and to-be-judged items was broken, the congruence effect was eliminated (Mitroff et al., 2002). This finding illustrates the difficulty of verifying the existence of implicit change detection. Not only must the experiment eliminate all explicit change detection, it must also rule out the contribution of other factors, be they implicit or

explicit, that could artificially inflate performance when changes are not reported.

Another example in which an explicit mechanism could account for findings of “implicit” change detection comes from measures of visual search speed in a flicker task (Smilek et al., 2000). Large changes to letter arrays are found more efficiently than small changes (i.e., they have shallower search slopes). Given that attention might be preattentively guided to the target of the search (Wolfe, 1994), the implicitly detected change might guide attention to the change location. Larger changes might exert a greater implicit influence on attention, leading to more efficient search. Although an implicit change detection mechanism could produce differences in search slopes, this difference is also consistent with evidence that larger changes are easier to detect explicitly with focused attention (Mitroff et al., 2002; Williams and Simons, 2000). In fact, when the possibility of implicit guidance is removed by randomizing the positions of each item in the search array for every alternation of the original and changed arrays, observers still show a search advantage for the larger changes (Mitroff et al., 2002). Under these conditions, implicit change detection could not produce the difference in search slopes because there is no stable information available to accumulate in a given location. The presumed basis for implicit accumulation did not exist in this study, but the results were comparable, thereby rendering the implicit accumulation hypothesis unnecessary.

The absence of compelling behavioral evidence for purely implicit change detection supports the intriguing possibility that changes are only detected via an explicit comparison mechanism. This hypothesis is consistent with theoretical frameworks in which the symbol comparison processes needed for change detection require explicit processing (Dulany, 1997). If true, this hypothesis predicts that change detection should never occur without some explicit awareness of the change. This prediction is readily testable: any evidence for implicit change detection in the absence of any explicit contamination will disprove the claim. This theoretical debate—whether or not comparisons of episodic representations can occur in the absence of awareness—is one that might well be aided by other on-line, indirect measures of change detection such as looking time or neuroimaging.

EYE MOVEMENTS AND IMPLICIT CHANGE DETECTION Over the past few years, several laboratories have explored the relationships between eye movements, fixation patterns, and change detection. As previously noted, much of the early work on change detection involved introducing changes during an eye movement. Other studies which measured fixation while introducing changes found that even when observers directly fixated the changed object, they sometimes failed to detect the change (O’Regan et al., 2000). That

is, fixation on the object does not guarantee detection (see also Levin and Simons, 1997; Simons and Levin, 1998). However, changes to the fixation pattern or to the duration of fixations on the changed object might provide evidence for the detection of unreported changes.

If observers implicitly detect changes, then the presence of a change in a scene might affect fixation patterns, regardless of whether or not observers were aware of the change. For example, they might fixate the changed region earlier or for a longer duration. Several studies provide some preliminary support for this sort of implicit change detection hypothesis (Hayhoe et al., 1998; Hollingworth et al., 2001b; Ryan and Cohen, 2002). For example, Hayhoe and colleagues (1998) measured eye movement patterns while participants attempted to recreate a pattern of colored blocks by selecting blocks from a stockpile and placing them appropriately in a workspace. When performing this task, participants often make a stereotyped sequence of eye movements, initially fixating the pattern, then fixating blocks in the stockpile, then returning to the pattern before finally fixating the appropriate location in the workspace. Saccade-contingent changes to the color of a block that was the target of the eye movement led to increases in fixation duration and often to an additional fixation on a neighboring block. Notably, these effects were stronger for saccades to the model pattern after subjects had already selected a block from the stockpile. Thus, eye movements provide a measure of change detection in this task, with longer fixation durations or additional fixations indicating some degree of change detection.

Whether or not increased fixation durations reflect implicit processing is not entirely clear, however. Subjects were only asked whether they had noticed changes at the end of the entire experiment, and postexperiment verbal reports are likely to be less sensitive than on-line eye movement measures. However, it would not be surprising if eye movement patterns were influenced by explicit processes. In fact, even if observers failed to detect the change altogether, they might look longer at a changed display than at an unchanged display. For example, if a subject had a block in hand from the stockpile and then saccaded to the pattern to verify its location, they might well notice that something was wrong when the saccade target was a different color than the held block. Given that they then could not place the held block without determining an appropriate location, they likely would spend more time fixating the pattern than they would have had the block not changed. Their awareness of having looked at the wrong block would influence fixation durations on the pattern even if they never explicitly or implicitly detected the change. Furthermore, even if they failed to notice the change happen, they might infer its occurrence from the fact that they were looking at the wrong color block after a saccade. Their

longer fixation could reflect their awareness of the need to change the focus of their fixation in order to complete the task.

In a more direct exploration of implicit change detection, Hollingworth et al. (2001b) compared fixation durations on a changed object when observers failed to report the change to fixation durations on the same critical region when no change was present. Subjects viewed a scene for 20 seconds in preparation for an upcoming memory test, and a change was introduced during a saccade away from the critical object (ensuring that they had viewed the object before the change). Observers explicitly reported noticing the change only 25% of the time. However, even when they missed the change, they tended to spend more time refixating the changed region. This difference in fixation durations might well reflect implicit detection of the change in the absence of awareness, but as for behavioral measures of implicit change detection, the result could also reflect explicit contributions to looking times. There is no way, given these data, to guarantee that subjects were entirely unaware of the change even though they did not report it (Hollingworth et al., 2001b). Without conclusive evidence for the complete absence of explicit change detection, differences in fixation patterns might well reflect below-criterion explicit detection. In other words, eye movements might simply be a more sensitive measure of explicit detection than are verbal reports or other overt responses.

One final study provides some converging evidence for the sensitivity of eye movement patterns to the presence of changes (Ryan and Cohen, 2002). Observers viewed one image and then, after a delay, they viewed either an identical image or a changed image. The images were counter-balanced such that an image that included a change for one participant was part of a no-change trial for another participant. Thus, by pooling data across observers, differences in the fixation patterns on a single image could be compared for trials with and without changes. When observers reported the change, they showed differences in fixation patterns for the changed scene compared to the same scene in no-change trials. Thus, change detection leads to differences in fixation patterns. Interestingly, several measures of the overall viewing pattern showed a difference between changed and unchanged scenes, regardless of whether or not observers reported the change. (However, measures of fixations to the changed region were different only when observers reported the change.)

Fixation patterns appear to provide a more sensitive measure of detection, but it is unclear whether they reveal implicit change detection. Even though observers did not verbally report the change, they might still have had some degree of awareness of it. Most observers in change detection studies adopt conservative response biases, reporting changes only when they are certain (Williams and Simons,

2000). It is possible that such response biases contributed to the effects for unreported changes in that some of these changes might have been explicitly rather than implicitly detected. This effect could be amplified in this analysis because data for a particular image were pooled across subjects in order to compare identical images from “aware” and “unaware” trials. More precisely, subjects who adopted more conservative biases likely would contribute more data to unaware trials, and those adopting more liberal biases would contribute more data to aware trials. If so, a larger subset of the unaware trials might involve changes that were detected but that did not surpass the subjects’ criterion for an explicit response. Claims of implicit change detection require that the measure of awareness exhaustively eliminate other explicit contributions to performance. Unless explicit reports of the presence or absence of a change are at chance, eye movement measures might reflect contributions of explicit detection rather than purely implicit detection.

Regardless of whether or not these findings indicate the presence of implicit change detection, they do raise a caution about the use of verbal reports as the sole measure of change detection. These findings suggest that observers maintain representations of the prechange scene, and that these representations contribute to fixation patterns even when observers do not report a change. Eye movement patterns do provide some preliminary support for the existence of implicit change detection, and further experiments are needed to determine whether these effects are truly implicit or whether other explicit factors such as criterion differences contribute to performance. In combination with the neuroimaging measures reviewed below, this approach could well serve to provide dissociations that otherwise would be unavailable via overt behavioral responses.

Neuroimaging and change detection

Only in the past few years have researchers begun to use on-line measures of the neural bases of change detection and change blindness. Here we briefly review all of the studies we are aware of—a total of four papers—by highlighting what they tell us about the mechanisms underlying change detection. Like the eye tracking studies, these papers focus on differences in the pattern of activation corresponding to conscious change detection and change blindness, as well as on evidence for implicit change detection. Two of these studies used event-related potentials (ERP), and two used functional magnetic resonance imaging (fMRI).

ERP STUDIES OF CHANGE DETECTION ERPs are a noninvasive measure of the magnetic impulses generated by nerve populations in the brain upon sensory stimulation. ERPs are measured by placing electrodes on the scalp and recording the amplitude of electrical activity at each electrode site.

Theoretically, the time course and regions of activation corresponding to the perception of a display can be inferred from changes in these signals. Of course, given that ERPs rely on a limited number of electrodes, spatial localization of activation requires summation across fairly large regions of cortex.

Although ERPs provide only coarse spatial resolution, in many respects they are optimal for measuring the time course of change detection and for dissociating brain activity in the presence and absence of changes. ERPs have excellent temporal resolution, often signaling the presence of a stimulus within 70 to 80 msec of visual stimulation. Thus, they can provide an on-line measure of neural functioning without any need for the subject to provide an overt response. That is, ERPs allow the measurement of differences in neural patterns of activation in response to changes that otherwise might not be measurable, thereby providing a way to dissociate neural activity in the presence of a change from neural activity in the absence of a change.

Recently, two studies using ERPs have looked at differences in neural activity when observers successfully and unsuccessfully search for changes (Fernandez-Duque et al., 2002; Niedeggen et al., 2001). Niedeggen and colleagues (2001) measured ERPs while observers searched for a change to the position or identity of one letter in an array of letters. They used a flicker task (limited to five cycles) in which the original and changed displays alternated repeatedly (1500 msec each), separated by a blank screen (200 msec). Most of the changes were detected within the five cycles allowed, and observers rarely reported a change when none was present. For the most part, the ERP measurements in this study were closely aligned with the behavioral ones. Averaged ERP traces showed a distinct positive deviation from 200 to 800 msec following the onset of the stimulus presentation during which observers reported the change. This positive deflection was significantly different from the control condition in which no change occurred. The finding that ERP traces differ for trials with a detected change and trials with no change is not terribly surprising. After all, differences in neural activity must exist in order for observers to produce different responses to these two types of trials.

The more interesting question is whether the ERP traces show any difference between trials in which a change is present, but not overtly detected, and trials in which no change is present. Such a difference would suggest that changes could be represented even if they were not overtly detected. However, the results revealed no difference in the ERP trace for undetected and absent changes. The absence of a difference is consistent with the idea that change detection requires at least the potential for an overt response. Of course, even if the ERP traces had differed, the interpretation of the difference would be subject to the same criticisms

and constraints noted earlier in the discussion of behavioral measures of implicit detection. As with any null result, the lack of an implicit effect could also be due to the insensitivity of the measure (e.g., not enough trials with missed changes).

Interestingly, the ERP trace from the image preceding the overt detection response also showed a positive deviation from 200 to 800 msec following stimulus onset. The deviation was somewhat smaller than for the stimulus presentation corresponding to the overt response, but it was present. At least three explanations for this result are possible. The positive deviation could correspond to some form of implicit detection that always precedes explicit detection. Note that it could not correspond to implicit detection more generally because the effect occurred only when observers did eventually make an overt change detection response. If observers failed to report the change, the ERP trace was no different from that in trials in which a change was absent. According to this account, favored by the authors, the brain registers the presence of a change, and the implicitly represented change guides focused attention to the change location, thereby allowing subsequent explicit detection.

A second possibility is that the positive deviations to earlier image presentations correspond to a gradual increase in the confidence of an explicit response. In other words, observers explicitly detect the change earlier, but they have not yet surpassed their criterion for responding. According to this view, the positive deviations to earlier images correspond to explicit but below-criterion change detection. A control experiment reported in the paper provided an initial attempt to eliminate this alternative: observers pressed one key when they “sensed” a change and then a different key when they detected the change. Presumably, if these observers lacked confidence in their change response, they should have reported sensing the change before reporting detection. On most trials, they did not report sensing the change during image presentations prior to the one for which they gave a detection response. However, they did report such sensing on approximately 15% to 20% of trials, which could contribute to the effect.

A related explanation for these positive deviations is that they correspond to explicit detection prior to an overt response and that the final, larger deviation corresponds to change certainty. Given that observers are biased to respond “no change” unless they are certain of the presence of a change, they might try to verify that they detected the change. To do so, they must view an additional image before responding. Thus, the positive deviation on earlier images might correspond to the initial explicit detection of a change, with the stronger positive deviation on the final image corresponding to a combination of detection, focused attention, and response preparation. This detection-plus-verification account is consistent with the lack of evidence

for an implicit effect of the presence of a change and suggests that the pattern of ERP deviations to all of the images corresponds to explicit detection.

Interestingly, this pattern of deviations in the ERP traces corresponds closely to behavioral work exploring change localization prior to overt responses (Mitroff and Simons, 2002). In these localization studies, observers were asked to try to localize a change following each change presentation, with presentations continuing until they succeeded or reached a maximum number of presentations. As in the ERP study (Niedeggen et al., 2001), localization performance was no more accurate in the presence of an undetected change than in the absence of a change; the presence of a change did not affect localization provided that observers never overtly reported the change. Observers showed some improvement in localization performance for the change presentation immediately before the change was explicitly reported. Prior to that, they showed no improvement in localization across consecutive guesses. This pattern is similar to the ERP finding of a positive deviation on the image presentation prior to the overt response. However, this finding can be explained without any need for implicit change detection. As observers search for changes, they likely focus on one area or item. Assuming that no change occurs at that location, they then immediately shift attention to a new location prior to the next presentation. Their change localization response at the end of each cycle likely corresponds to this new guess rather than to the location they have just eliminated as nonchanging. Then, when the change occurs at the guessed location, they report detecting it and localize it correctly. This pattern of guessing and then verifying is consistent with an entirely explicit change detection mechanism. The correspondence of the ERP pattern and the localization data leaves open the interesting question of whether the positive deviations on images prior to the detection response correspond to some form of verification or whether they represent implicit detection. Further exploration of this question, perhaps using both ERPs and localization responses, is needed to determine fully which of the three possible explanations best accounts for this brain activity prior to explicit reports of detection.

A second paper on ERP addressed the question of implicit change detection while exploring the mechanisms underlying search for change (Fernandez-Duque et al., 2002). This study also used a flicker task, but the cycled displays were complex photographs and each trial was separated into five sequential stages for analysis. Initially, observers searched for a change, but none was present for a variable number of cycles (stage 1). A change was introduced (stage 2), and once observers successfully identified the change, they monitored its location and reported when the item stopped changing (stage 3). Next, observers once again searched the display for a change (stage 4). This time,

however, the change occurred on only a small proportion of trials (sometimes it was a new change and sometimes it was the original change), and only the no-change trials were actually analyzed. Following stage 4, observers monitored the original change location and were asked to report if the change recurred (stage 5). Notice that in this paradigm, stages 1, 2, and 4 all involve search for a change, whereas stages 3 and 5 involve focused attention to the change location. This experiment addresses two distinct questions: (1) does searching through a scene differ from focused attention to a single location? and (2) does the absence of a change lead to different activation in the presence of an undetected change?

ERP patterns for focused attention to a single location (stage 5) and search through a scene (stage 4) were comparable, although a bilateral frontal negativity from 100 to 300 msec and a posterior-occipital positive deflection from 150 to 300 msec after stimulus onset were somewhat enhanced by sustained attention to a single location. Given that these differences are unrelated to change detection, they can be used to isolate the effect of change detection from any contributions of sustained attention to the change location. ERP patterns for focused attention on a detected change (stage 3) and search throughout a display for an undetected change (stage 2) were comparable to those involved in focused attention. The 150 to 300 msec negative deflection at frontal sites and the 100 to 300 msec positive deflection at posterior sites were comparable to those found in the comparison of stages 4 and 5. However, ERP traces in stage 3 also showed other differences from stage 2 that might correspond to awareness of the change, such as a greater positive deflection at central sites at delays of 350 to 600 msec. This finding represents one of the first attempts to measure the neural correlates of awareness of a change. Note, though, that differences in activation could also reflect differences in the tasks that subjects perform at each stage. For example, only stage 3 involves search for change removal which requires verification that a change is still present on every cycle. These task differences could induce changes in strategies that might affect ERP traces.

This experiment also considered whether the presence of an undetected change produces a different ERP trace than does the absence of a change (Fernandez-Duque et al., 2002). The design allowed a comparison of activation patterns for the same image when a change is present but not yet reported (stage 2) and when observers search for a change but none is present (stage 4). The presence of a change produced a significant bilateral positive deflection in anterior sites (more medial than lateral) between 240 and 300 msec after stimulus onset, suggesting neural registration of an unreported change. However, further work is needed to demonstrate conclusively that the differences correspond to the implicit registration of changes as opposed to explicit or

strategic influences. As for measures of awareness of the change, the demands of the two stages contributing to the comparison may be somewhat different. In stages 2 and 4, observers are given the same instruction to look for a change, and their subjective experience in both cases is likely that of trying to find a change and sometimes succeeding. However, in stage 2 they have already been searching for 12 to 22 flickers (the duration of stage 1), whereas stage 4 begins at the start of their search. If the initial stages of search differ from those occurring after a period of unsuccessful searching, then differences between stages 2 and 4 could result from changes in the search strategy. Changes also occur less frequently in stage 4 than in stage 2, a factor which might induce a different sort of attentional set. Finally, although subjects in both stages were told to search for a change, in stage 4 they knew that the change would either be the same one they saw earlier or a new one. This knowledge might contribute to the use of different search strategies. For example, subjects might initially devote more attention to the original change location, something they could not do in stage 2. In fact, the act of finding the first change might well influence the nature of the search for a subsequent change to the same image. Given that any of these factors could contribute to differences in patterns of neural activation even in the absence of implicit change detection, further studies are needed to clarify whether ERP measures reveal the existence of implicit change detection.

FUNCTIONAL MRI STUDIES OF CHANGE DETECTION Unlike ERP, fMRI has excellent spatial resolution but somewhat less precise temporal resolution. Consequently, it is better suited to studies of the anatomical locus of the mechanisms underlying change blindness and change detection, but does not provide as precise an estimate of the progression of change detection within a trial. Two published studies have explored change detection in the flicker task using event-related fMRI, one focusing primarily on identifying the anatomical regions involved (Huettel et al., 2001) and the other focusing on differences in activation for detected, undetected, and absent changes (Beck et al., 2001). Huettel and colleagues (2001) looked for brain regions that remained active throughout the search in a flicker task, as well as regions that showed phasic activity as a result of image onsets and offsets in this task. Regions including extrastriate visual cortex, frontal and supplementary eye fields, and inferior/insular frontal cortex in addition to several other regions were all active throughout the search task, suggesting that these areas contribute to visual search for change. This study provided some preliminary estimates of the areas involved in searching for changes, but it did not provide any experimental manipulations to test different aspects of change detection. Future studies can use their initial findings

by determining how activation in these regions varies as a function of changes to the nature of the displays or the task.

Beck and colleagues (2001) used fMRI techniques to address questions similar to those raised in ERP studies of change detection. As in the aforementioned ERP studies, neuroimaging was used to dissociate change detection from change blindness and also to look for differences in neural responses to the presence of an undetected change and the absence of a change (i.e., implicit change detection). This study also manipulated the nature of the changing images, using faces on some trials and outdoor scenes on others. These classes of stimuli typically lead to activity in discrete regions of the ventral visual pathway, faces activating what is now known as the *fusiform face area* (FFA) and outdoor scenes activating the *parahippocampal place area* (PPA) (Tong et al., 1998).

Not surprisingly, detection of face changes produced greater activation in the vicinity of the FFA, whereas detection of changes to outdoor scenes led to greater activation of areas near the PPA. Detection of changes to either type of stimulus also produced more activation in parietal and dorsolateral prefrontal cortex than did missed changes. These regions often are associated with attention and executive control, respectively. The finding of different patterns of activation for detected and missed changes is consistent with other evidence that responses in these regions are heightened by subjective awareness of the stimulus (Tong et al., 1998). Moreover, the finding that the FFA is more active when observers successfully detect a face change and that the PPA is more active when observers successfully detect a place change is consistent with these findings. These findings provide some neurological confirmation that attention is needed for successful change detection.

To examine the evidence for implicit change detection, activation to the absence of a change was subtracted from activation to the presence of an undetected change (Beck et al., 2001). An initial experiment revealed significant activation in the fusiform gyrus, the lingual gyrus, and the inferior frontal gyrus for undetected face changes. However, a second experiment that controlled for eye movement artifacts found no differences between activation in the presence of an undetected change and in the absence of a change. Consequently, these experiments do not provide conclusive evidence that changes are implicitly registered in the absence of conscious change detection. Further studies obviously are needed to verify this null result; however, the basic pattern is consistent both with ERP evidence (Niedeggen et al., 2001) demonstrating the similarity in activation patterns in the absence of a change and in the presence of an undetected change, and with behavioral evidence demonstrating that undetected changes do not influence localization performance (Mitroff and Simons, 2002). Although some of the on-line measures are consistent with implicit detection, none

incontrovertibly demonstrates the need for implicit detection. In fact, the findings described above may well be consistent with the idea that change detection occurs only via an explicit comparison mechanism.

Summary

Existing ERP and fMRI experiments provide contradictory evidence about the possibility of implicit change detection. Both ERP and fMRI results reveal no reliable differences between trials with missed changes and trials with no change (Beck et al., 2001; Niedeggen et al., 2001). However, the search for not-yet-detected changes does produce a different pattern of activation than the search for absent changes. For trials on which a change is subsequently detected, ERP signals to one or two images earlier in the sequence show weaker versions of the deviations that correspond to conscious report of a change (Niedeggen et al., 2001). This pattern is consistent with the idea that if changes are implicitly detected, they guide attention to the change. However, other interpretations that do not require an implicit change detection mechanism can still account for the results. Another study found similar differences in activation during the search for an absent second change to the scene and search for an initial change prior to its onset (Fernandez-Duque et al., 2002). This finding also provides some preliminary evidence for implicit change detection, but further studies are needed to eliminate all the potential explicit and strategic contributions from these ERP trace differences.

Neuroimaging is a useful tool for gaining new insights into the mechanisms of change detection. ERP and fMRI might well dissociate performance for detected and undetected changes in ways that would be impossible using solely behavioral measures, if only because behavioral measures typically require explicit responses. Despite the appeal of these new tools, however, they are still subject to the same assumptions and requirements underlying attempts to demonstrate implicit perception with strictly behavioral tasks. Any convincing demonstration of implicit perception must first confirm that explicit factors and strategies did not contribute to performance. The classic dissociation paradigm used to measure implicit processing requires that the explicit measure of performance show no sensitivity to the presence of a stimulus (Holender, 1986; Merikle and Reingold, 1992). Moreover, the measure must assess all possible explicit contributions to performance. That is, an insensitive measure of explicit change detection might reveal no discrimination of the presence of a change, but that would be unconvincing because stronger or more sensitive explicit measures might reveal discrimination. Only if the explicit measure is optimally sensitive and still shows no explicit discrimination can we be certain that any measured differences in performance

result from implicit processes (Holender, 1986). Given this stringent criterion, it might be impossible to demonstrate implicit change detection using solely direct measures based on subjective reports. Experimenters would first have to demonstrate a lack of explicit sensitivity to the presence of a change while still showing that performance for unreported changes was better than expected. However, if observers show no sensitivity, then aware and unaware trials cannot be distinguished, and it is unclear what trials to compare. In order to measure implicit detection behaviorally, it is necessary to separate trials on which observers saw the change from those on which they missed the change. However, to do so, the task must violate the conservative requirements of the dissociation paradigm.

Both neuroimaging and eye tracking might provide an escape from this catch 22 by dissociating patterns of activation in the presence and absence of a change even for tasks which exhaustively eliminate explicit change detection. To do so, an experiment would need to use a change detection task for which observers showed no explicit sensitivity to the presence of a change. That is, explicit reports of the presence or absence of a change would have to be no better than chance. The critical question, then, is whether looking times or neural activation in the presence of a change would differ from activation in the absence of a change. None of the experiments to date have applied such a stringent criterion, but given that they raise the possibility of an implicit comparison mechanism, strong tests of the hypothesis are needed. A difference in looking or in brain activity as a function of the presence of a change in a study meeting this criterion would provide the necessary evidence for the existence of an implicit representation of the change and would argue against the necessity of explicit comparisons in change detection. Such a finding would also raise the possibility that implicit detection plays a functional role in guiding attention as well as subsequent explicit detection. However, without such a controlled study, current findings of implicit change detection remain inconclusive, and existing results can be attributed to explicit processes and conscious strategies. In the absence of such counterevidence, current studies of change detection are consistent with the strong hypothesis that change detection, in the absence of a transient signal, occurs only through an explicit comparison mechanism.

Acknowledgments

Thanks to Diego Fernandez-Duque, Steve Mitroff, and Ian Thornton for helpful comments on earlier drafts of this manuscript. Thanks also to Neal Cohen, Diego Fernandez-Duque, Michael Niedeggen, Jennifer Ryan, and Ian Thornton for allowing us access to their not-yet-published experiments. Writing of this manuscript was supported

by grants from the NSF (BCS9905578) and the NIH (R01-MH63773-01) and by an Alfred P. Sloan Research Fellowship.

REFERENCES

- Beck, D. M., G. Rees, C. D. Frith, and N. Lavie, 2001. Neural correlates of change detection and change blindness, *Nat. Neurosci.*, 4:645–650.
- Becklen, R., and D. Cervone, 1983. Selective looking and the noticing of unexpected events, *Mem. Cogn.*, 11:601–608.
- Blanchard, H. E., A. Pollatsek, and K. Rayner, 1989. The acquisition of parafoveal word information in reading, *Percept. Psychophys.*, 46:85–94.
- Bridgeman, B., D. Hendry, and L. Stark, 1975. Failure to detect displacement of the visual world during saccadic eye movements, *Vis. Res.*, 15:719–722.
- Brooks, R. A., 1991. Intelligence without representation, *Artif. Intell.*, 47:139–159.
- Chun, M. M., and Y. Jiang, 1998. Contextual cueing: implicit learning and memory of visual context guides spatial attention, *Cogn. Psychol.*, 36:28–71.
- DeSchepper, B., and A. Treisman, 1996. Visual memory for novel shapes: implicit coding without attention, *J. Exp. Psychol. Learn. Mem. Cogn.*, 22:27–47.
- Dulany, D. E., 1997. Consciousness in the explicit (deliberative) and implicit (evocative), in *Scientific Approaches to Consciousness* (J. D. Cohen and J. W. Schooler, eds.), Mahwah, NJ: Erlbaum, pp. 179–211.
- Fernandez-Duque, D., G. Grossi, I. M. Thornton, and H. J. Neville, 2002. Representing change with and without awareness: an event-related brain potentials study. Manuscript in revision.
- Fernandez-Duque, D., and I. M. Thornton, 2000. Change detection without awareness: do explicit reports underestimate the representation of change in the visual system? *Vis. Cogn.*, 7:323–344.
- Gibson, J. J., 1966. *The Senses Considered as Perceptual Systems*, Boston: Houghton Mifflin.
- Goodale, M. A., and A. D. Milner, 1992. Separate visual pathways for perception and action, *Trends Neurosci.*, 15:20–25.
- Grimes, J., 1996. On the failure to detect changes in scenes across saccades, in *Perception (Vancouver Studies in Cognitive Science)*, vol. 2 (K. Akins ed.), New York: Oxford University Press, pp. 89–110.
- Haines, R. F., 1991. A breakdown in simultaneous information processing, in *Presbyopia Research: From Molecular Biology to Visual Adaptation* (G. Obrecht & L. W. Stark, eds.), New York: Plenum, pp. 171–175.
- Hayhoe, M. M., D. G. Bensinger, and D. Ballard, 1998. Task constraints in visual working memory, *Vis. Res.*, 38:125–137.
- Holender, D., 1986. Semantic activation without conscious identification in dichotic listening, parafoveal vision, and visual masking: a survey and appraisal, *Behav. Brain Sci.*, 9:1–66.
- Hollingworth, A., G. Schrock, and J. M. Henderson, 2001a. Change detection in the flicker paradigm: The role of fixation position within the scene, *Mem. Cogn.*, 29:296–304.
- Hollingworth, A., C. C. Williams, and J. M. Henderson, 2001b. To see and remember: visually specific information is retained in memory from previously attended objects in natural scenes, *Psychonom. Bull. Rev.* 8:761–768.
- Huettel, S. A., G. Güzelde, and G. McCarthy, 2001. Dissociating the neural mechanisms of visual attention in change detection using functional MRI, *J. Cogn. Neurosci.*, 13:1006–1018.

- James, W., 1892. *Psychology*, New York: Holt.
- Kihlstrom, J. F., T. M. Barnhardt, and D. J. Tataryn, 1992. Implicit perception, in *Perception without Awareness: Cognitive, Clinical, and Social Perspectives* (R. F. Bornstein and T. S. Pittman, eds.), New York: Guilford Press, pp. 17–54.
- Levin, D. T., N. Momen, S. B. Drivdahl, and D. J. Simons, 2000. Change blindness the metacognitive error of overestimating change-detection ability, *Vis. Cogn.*, 7:397–412.
- Levin, D. T., and D. J. Simons, 1997. Failure to detect changes to attended objects in motion pictures, *Psychonom. Bull. Rev.*, 4:501–506.
- Levin, D. T., D. J. Simons, B. L. Angelone, and C. F. Chabris, 2002. Memory for centrally attended changing objects in an incidental real-world change detection paradigm, *Bri. J. Psychol.*, 93:289–302.
- Li, W., and L. Matin, 1990. The influence of saccade length on the saccadic suppression of displacement detection, *Percept. Psychophys.*, 48:453–458.
- Mack, A., 1970. An investigation of the relationship between eye and retinal image movement in the perception of movement, *Percept. Psychophys.*, 8:291–298.
- Mack, A., and I. Rock, 1998. *Inattentional Blindness*, Cambridge, MA: MIT Press.
- Maljkovic, V., and K. Nakayama, 1994. Priming of pop-out: I. Role of features, *Mem. Cogn.*, 22:657–672.
- McConkie, G. W., and C. B. Currie, 1996. Visual stability across saccades while viewing complex pictures, *J. Exp. Psychol. Hum. Percept. Perform.*, 22:563–581.
- McConkie, G. W., and D. Zola, 1979. Is visual information integrated across successive fixations in reading? *Percept. Psychophys.*, 25:221–224.
- Merikle, P. M., and E. M. Reingold, 1992. Measuring unconscious perceptual processes, in *Perception without Awareness: Cognitive, Clinical, and Social Perspectives* (R. F. Bornstein and T. S. Pittman, eds.), New York: Guilford Press, pp. 55–80.
- Mitroff, S. R., and D. J. Simons, 2002. Changes are not localized before they are explicitly detected, *Vis. Cogn.*, 9:937–968.
- Mitroff, S. R., D. J. Simons, and S. L. Franconeri, 2002. The siren song of implicit change detection, *J. Exp. Psychol. Hum. Percept. Perform.*, 28:798–815.
- Moore, C. M., and H. Egeth, 1997. Perception without attention: evidence of grouping under conditions of inattention, *J. Exp. Psychol. Hum. Percept. Perform.*, 23:339–352.
- Morris, R. K., K. Rayner, and A. Pollatsek, 1990. Eye-movement guidance in reading: the role of parafoveal letter and space information, *J. Exp. Psychol. Hum. Percept. Perform.*, 16:268–281.
- Most, S. B., D. J. Simons, B. J. Scholl, and C. F. Chabris, 2000. Sustained inattention blindness: the role of location in the detection of unexpected dynamic events, *Psyche*, 6(14), <http://psyche.cs.monash.edu.au/v6/psyche-6-14-most.html>.
- Most, S. B., D. J. Simons, B. J. Scholl, R. Jimenez, E. Clifford, and C. F. Chabris, 2001. How not to be seen: the contribution of similarity and selective ignoring to sustained inattention blindness, *Psychol. Sci.*, 12:9–17.
- Neisser, U., 1979. The control of information pickup in selective looking, in *Perception and Its Development: A Tribute to Eleanor J. Gibson* (A. D. Pick ed.), Hillsdale, NJ: Erlbaum, pp. 201–219.
- Neisser, U., and R. Becklen, 1975. Selective looking: Attending to visually specified events, *Cogn. Psychol.*, 7:480–494.
- Niedeggen, M., P. Wichmann, and P. Stoerig, 2001. Change blindness and time to consciousness, *Eur. J. Neurosci.*, 14:1719–1726.
- O'Regan, J. K., 1992. Solving the “real” mysteries of visual perception: the world as an outside memory, *Can. J. Psychol.*, 46:461–488.
- O'Regan, J. K., H. Deubel, J. J. Clark, and R. A. Rensink, 2000. Picture changes during blinks: Looking without seeing and seeing without looking, *Vis. Cogn.*, 7:191–212.
- O'Regan, J. K., and A. Noe, 2001. A sensorimotor account of vision and visual consciousness, *Behav. Brain Sci.*, 24:939–1031.
- Pashler, H., 1988. Familiarity and visual change detection, *Percept. Psychophys.*, 44:369–378.
- Phillips, W. A., 1974. On the distinction between sensory storage and short-term visual memory, *Percept. Psychophys.*, 16:283–290.
- Pollatsek, A., and K. Rayner, 1992. What is integrated across fixations? In *Eye Movements and Visual Cognition: Scene Perception and Reading* (K. Rayner ed.), New York: Springer-Verlag, pp. 166–191.
- Rensink, R. A., 2000a. The dynamic representation of scenes, *Vis. Cogn.*, 7:17–42.
- Rensink, R. A., 2000b. Seeing, sensing, and scrutinizing, *Vis. Res.*, 40:1469–1487.
- Rensink, R. A., 2000c. Visual search for change: a probe into the nature of attentional processing, *Vis. Cogn.*, 7:345–376.
- Rensink, R. A., J. K. O'Regan, and J. J. Clark, 1997. To see or not to see: the need for attention to perceive changes in scenes, *Psychol. Sci.*, 8:368–373.
- Ryan, J. D., and N. J. Cohen, 2002. On-line representations of scenes. Manuscript under review.
- Schooler, J. W., 2001. Discovering memories in the light of metaconsciousness, *J. Aggression, Maltreatment, Trauma*, 4:105–136.
- Scott-Brown, K. C., M. R. Baker, and H. S. Orbach, 2000. Comparison blindness, *Vis. Cogn.*, 7:253–267.
- Shapiro, K. L., K. A. Arnell, and J. E. Raymond, 1997. The attentional blink: a view on attention and a glimpse on consciousness, *Trends Cogn. Sci.*, 1:291–296.
- Silverman, M., 2001. Priming from change blindness. Unpublished doctoral dissertation, New School University, New York.
- Simons, D. J., 2000a. Attentional capture and inattention blindness, *Trends Cogn. Sci.*, 4:147–155.
- Simons, D. J., 2000b. Current approaches to change blindness, *Vis. Cogn.*, 7:1–15.
- Simons, D. J., and C. F. Chabris, 1999. Gorillas in our midst: sustained inattention blindness for dynamic events, *Perception*, 28:1059–1074.
- Simons, D. J., C. F. Chabris, T. Schnur, and D. T. Levin, 2002. Preserved representations in change blindness, *Consciousness Cogn.*, 11:78–97.
- Simons, D. J., and D. T. Levin, 1997. Change blindness, *Trends Cogn. Sci.*, 1:261–267.
- Simons, D. J., and D. T. Levin, 1998. Failure to detect changes to people in a real-world interaction, *Psychonom. Bull. Rev.*, 5:644–649.
- Smilek, D., J. D. Eastwood, and P. M. Merikle, 2000. Does unattended information facilitate change detection? *J. Exp. Psychol. Hum. Percept. Perform.*, 26:480–487.
- Sperling, G., 1960. The information available in brief visual presentations, *Psychol. Monogr. Gen. Appl.*, 74:1–29.
- Stroud, J. M., 1955. The fine structure of psychological time, in *Information Theory in Psychology: Problems and Methods* (H. Quastler ed.), Glencoe, IL: Free Press, pp. 174–207.
- Thornton, I. M., and D. Fernandez-Duque, 2000. An implicit measure of undetected change, *Spatial Vis.*, 14:21–44.

- Tong, F., K. Nakayama, J. T. Vaughan, and N. Kanwisher, 1998. Binocular rivalry and visual awareness in human extrastriate cortex, *Neuron*, 21:753–759.
- Tversky, A., and D. Kahneman, 1982. Judgement under uncertainty: heuristics and biases, in *Judgement Under Uncertainty: Heuristics and Biases* (P. S. D. Kahneman and A. Tversky, eds.), Cambridge: Cambridge University Press, pp. 3–20.
- Wallach, H., and C. Lewis, 1965. The effect of abnormal displacement of the retinal image during eye movements, *Percept. Psychophys.*, 1:25–29.
- Williams, P., and D. J. Simons, 2000. Detecting changes in novel, complex three-dimensional objects, *Vis. Cogn.*, 7:297–322.
- Wolfe, J. M., 1994. Guided search 2.0: A revised model of visual search, *Psychonom. Bull. Rev.*, 1:202–238.

103 The Role of Attention in Visual Cerebral Cortex

JOHN H. R. MAUNSELL

THE DETECTION AND discrimination of sensory stimuli can be profoundly influenced by the amount of attention that a subject directs to them. Neurophysiological studies using a variety of approaches have shown that changes in an observer's state of attention are associated with changes in the processing of sensory signals. The effects of attention on the responses of neurons in visual cerebral cortex is the subject considered here.

Before addressing specific neuronal correlates of attention, it is important to define the type of attention that will be considered. *Attention* is used to refer to a variety of processes, and it is likely that some of these involve different brain mechanisms. For example, attention can refer to a level of arousal or wakefulness, or it can refer to the executive control that guides a task that evolves over the course of days or months. We will restrict our discussion to selective sensory attention: the process of focusing on one signal or stimulus to the exclusion of others. One example is spatial attention, where resources are concentrated on a particular location in visual or auditory space. Attention to particular stimulus features, such as color or orientation, is another form of selective sensory attention. Spatial attention and featural attention have both been shown to modulate the responses of visual neurons (Corbetta et al., 1991; McAdams and Maunsell, 2000; Treue and Martínez-Trujillo, 1999). Although spatial attention may produce stronger effects than featural attention, the two forms have not been shown to differ fundamentally, and they will not be distinguished here.

Although effects of selective attention have been demonstrated in the visual systems of many species, and using many neurophysiological techniques, we focus here on studies of individual neurons in the visual cerebral cortex of macaque monkeys.

Attention modulates the strength of neuronal responses

The most prominent effect of attention on the activity of neurons in visual cortex is a change in the strength of their response to a stimulus. Typically, a neuron's response to its optimal stimulus is stronger when the subject pays attention to it. Most observations suggest that attention alters

the sensitivity of neurons without affecting their stimulus preferences or selectivity, although exceptions will be discussed.

RANGE OF ATTENTIONAL EFFECTS WITHIN AND BETWEEN CORTICAL AREAS Attention has been found to modulate neuronal responses in every visual area examined, from V1 to the latest stages in the cortical hierarchy. However, the magnitude of attentional modulation varies greatly within and between areas and appears to be related to several factors.

Samples of neurons from individual visual areas invariably show a range of modulation by attention, even when the stimulus is optimized for each neuron. Some neurons respond robustly when the stimulus is attended and not at all when it is ignored. Others show no detectable effect of attention. Furthermore, occasional neurons have been found to have significant negative modulation by attention, so that they respond more strongly when a stimulus is ignored.

The reason for this range of effects is not understood. It is possible that neurons with response properties best suited to the current behavioral task are modulated most by attention. For example, when subjects perform a color discrimination task, neurons with greater color selectivity, or with color preferences well matched to the stimuli, might be more modulated by spatial attention than other neurons. However, no such correlation has been described, and the reason for the range of attentional modulations within cortical areas remains an important unanswered question.

Modulation by attention also differs between visual areas. The average strength of modulation is generally stronger in later stages of visual cortex. In V1, the average effect is weak, typically about a 10% increase in response (Crist et al., 2001; Haenny and Schiller, 1988; Luck et al., 1997; McAdams and Maunsell, 1999a; Mehta et al., 2000; Motter, 1993). Stronger effects are found in extrastriate areas. It is difficult to compare modulations from different studies quantitatively because they differ in stimulus conditions and task difficulty (see below), but some investigations have measured attentional modulation in different visual areas in the same subjects using consistent task conditions. Those studies

typically show greater modulations in successive stages of cortical processing. Figure 103.1 plots the averages for attentional modulation from experiments that measured responses in more than one visual area under equivalent conditions. Each symbol represents data from a different experiment. More modulation was found in later levels of visual cortex.

It is not known why attentional modulation should be stronger in later stages of visual cortex. One possibility is that attention acts to insert additional spikes at each level of visual cortex and that this additional activity accumulates, so that attentional modulation is greater at later stages. An alternative explanation is that attention acts to insert activity at the highest levels of visual cortex, and that this activity diminishes as it descends along feedback pathways. While either explanation might account for stronger modulations in later stages of cortex, they seem unlikely because they suggest that signals must grow or diminish uncontrollably as they propagate through cortex. No evidence suggests that sensory signals grow or diminish uncontrollably in this way. It seems more likely that there is an optimal amount of attentional modulation for sensory signals and that different optima exist for earlier and later sensory representations. Whatever the source, the reason for different degrees of modulation in different cortical areas is one of the most important questions to be answered about attentional modulations.

One consequence of the differences in attentional modulation between visual areas is to encourage investigators to focus more on certain areas. For example, area V4 has been extensively examined, in part because it is well positioned. It is early enough in cortical processing that its neurons

respond well to relatively simple stimuli that are easily controlled and manipulated, such as oriented bars or patches of color. It is also sufficiently advanced in cortical processing that attention modulations are fairly prevalent and easy to demonstrate. However, while V4 is a frequent subject for study in attention experiments, there is little reason to believe that it plays a special role in processes related to attention.

EFFECT OF TASK DIFFICULTY ON ATTENTIONAL MODULATION

Another factor affecting the magnitude of attentional modulation is task difficulty. Stronger responses are generally seen when animals must pay more attention to a stimulus (Spitzer et al., 1988). For example, responses of inferotemporal neurons grow progressively stronger as an animal goes from ignoring a stimulus, to attending it to detect a dimming, to attending it to discriminating its pattern (Spitzer and Richmond, 1991).

Changes in responses associated with task difficulty may be associated with vigilance, and therefore may be less specific than effects seen with attention to spatial locations or stimulus features. However, task difficulty can influence the magnitude of selective modulations associated with spatial attention. Modulation by spatial attention can be much stronger when animals perform a difficult version of a task in which they must detect changes in orientation (Boudreau and Maunsell, 2001).

Differences in a subject's level of effort cannot easily explain differences in attentional modulation between different cortical areas because in most relevant cases the same stimulus and task have been used in both areas, leaving no obvious basis for the subject to devote different levels of effort when recordings were made from different areas. Differences in effort might explain some of the range of modulations seen within areas, because the subject's effort might differ while data are collected from different neurons. However, an experiment that compared neuronal and behavioral effects of spatial attention found that the modulation of individual neurons by attention was uncorrelated with attentional modulation of behavior during the period when the neuron's responses were recorded (Cook and Maunsell, 2002). This suggests that the range of neuronal modulation within areas comes largely from sources other than vigilance.

Because task difficulty affects attentional modulation, the values reported by various studies cannot be taken as absolute, and comparisons between different experiments are problematic. Although the data in Figure 103.1 suggest that different experiments will find comparable average enhancement for a given visual area, those data are not representative of the differences between experiments because they were collected in the same laboratory using tasks of similar difficulty.

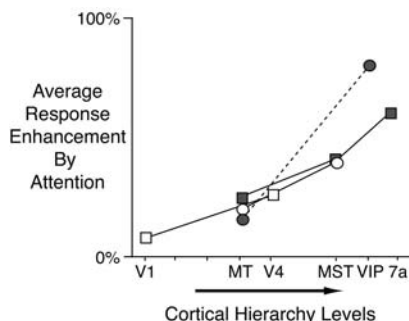


FIGURE 103.1. Attentional enhancement of neuronal responses increases as a function of position in the cortical hierarchy. Average attention modulation was taken from experiments that measured responses in at least two cortical levels using the same subjects and the same task. *Open squares* are data from McAdams and Maunsell (1999a); *open circles* are from Treue and Maunsell (1999); *filled squares* are from Ferrera et al. (1994); and *filled circles* are from Cook and Maunsell (2002). The cortical hierarchy levels are spaced according to the levels defined by Felleman and Van Essen (1991). (From Cook and Maunsell, 2002.)

The influence of the subject's effort also raises the question of whether much stronger modulations might be seen with particularly challenging tasks. Although some attention experiments have used near-threshold stimuli, many have used stimuli that were unlikely to have required much effort from the subjects. It is notable that particularly strong modulations were found by Mountcastle and his colleagues (1981), who compared responses during a visual task with responses to the same stimuli while the animals sat idle. Little work has been done to explore the limits of attention modulation. For example, responses to a visual stimulus might be much stronger when that stimulus is the subject of a challenging discrimination than to when it is irrelevant and attention is directed to a difficult auditory or somatosensory discrimination.

EFFECT OF ATTENTION WHEN NO STIMULUS IS PRESENT The effects of attention are often examined in terms of responses to visual stimuli, but attention can also affect neuronal activity when no stimulus is present. In early stages of visual cortex, modest increases in the spontaneous activity of neurons have been described when attention is directed to the part of the visual field containing a neuron's receptive field (Luck et al., 1997). This increased activity associated with spatial attention appears equivalent to increases in activity reported in the later stages of visual cortex, which are usually discussed in the context of short-term memory. For example, some inferotemporal neurons maintain an elevated level of activity during periods when the subject remembers a particular form or color, and not during periods when other stimuli must be remembered (Fuster, 1990; Fuster and Jervey, 1982; Miyashita et al., 1993; Yakovlev et al., 1998). Similarly, neurons in the lateral intraparietal area (LIP) remain active when animals pay attention to the motion of a stimulus that is briefly hidden from view (Assad and Maunsell, 1995; Eskandar and Assad, 1999). Thus, attentional modulations apply to undriven activity as well as stimulus-driven activity.

Some studies have not detected changes in undriven activity associated with attention. Because these changes are usually small (typically a few spikes per second), this may be a matter of statistical power. Alternatively, aspects of task design may make these changes less likely. McAdams and Maunsell (1999a) examined attentional modulation of driven and undriven activity in V4 and found that while responses to stimuli were modulated, activity immediately before the appearance of the stimulus was not affected by the location to which attention had been directed. The absence of modulation of undriven activity in this case may have been due to the timing of the stimulus presentations. Because the stimuli always appeared at predictable times and stayed on for relatively long periods, the animal had little motivation to direct its attention to the

cued location until after the stimulus appeared. Consistent with this, average attentional modulations increased during the stimulus presentation. Motter (1994) examined how quickly animals redirected their attention to different parts of the visual field after an instruction was given, and found that neuronal responses changed within a few hundred milliseconds. The dynamics with which attention can shift have not been well characterized, and there is no reason to believe that attention will be fixed during a behavioral trial or even during the course of an individual stimulus presentation.

Attention does not greatly affect underlying response properties

While attention changes the strength of neuronal responses, it does not appear to change profoundly the selectivity of neurons for particular stimuli. Testing whether attention changes the strength of responses can be done using a single fixed stimulus. A range of stimuli must be used to test whether attention affects selectivity. Only a handful of experiments have examined the effect of attention on neuronal selectivity.

EFFECT OF ATTENTION ON TUNING FOR STIMULUS ATTRIBUTES McAdams and Maunsell (1999a) examined how attention affects the orientation tuning of V4 neurons. Each neuron was tested with many orientations in each of two states of attention. Attention to the stimulus increased responses by an average of about 30%, but responses to all orientations were increased proportionally, so that on average there was no sharpening or broadening in orientation tuning. Data from the same study showed that attention increased responses of V1 neurons by a lesser amount, and again with no detectable change in the sharpness of tuning. Treue and Martinez-Trujillo (1999) tested the direction selectivity of neurons in the middle temporal (MT) visual area, and similarly found that attention increased responses without appreciably altering the sharpness of tuning for direction.

Earlier studies suggested that attention narrowed orientation or color tuning for V4 neurons (Haenny and Schiller, 1988; Spitzer et al., 1988). While there are several possible sources for this discrepancy, the most likely cause is the use of different measures for tuning bandwidth between the two sets of studies (McAdams and Maunsell, 1999a). At most, one of the measures could have remained constant across behavioral states. While there is no basis for arguing that either measure is superior, the fact that one measure showed no effect of attention on bandwidth suggests that attention acts primarily to increase sensitivity, not to alter selectivity. An effect of attention increasing the gain of neuronal responses is consistent with studies of attention in humans

using psychophysical methods, ERPs, or functional imaging (Hillyard et al., 1998; Lu and Doshier, 1998).

The variability of neuronal responses also appears to be largely unaffected by attention. When subjects are repeatedly presented with the same stimulus, their cortical neurons characteristically respond with different numbers of spikes on different presentations. The source of this variance is not understood, but the variance of the number of spikes produced is large, typically about the same magnitude as the mean number of spikes (e.g., Geisler and Albrecht, 1997). Although the mean number of spikes produced in response to a stimulus depends on whether the stimulus is attended by the subject, the relationship between the mean and the variance of the spike count is unchanged by attention (McAdams and Maunsell, 1999b). Similarly, no change is obvious in the distribution of interspike intervals.

Attention may change the spiking of cortical neurons in other ways, however. Recent studies have showed that attention is associated with increases in the synchrony of neuronal signals in both the visual and somatosensory cortex of monkeys (Fries et al., 2001; Steinmetz et al., 2000). It remains to be determined how these changes in the timing of neuronal signals interact with increases in the strength of neuronal responses.

EFFECTS OF ATTENTION ON RECEPTIVE FIELDS Attention does change the selectivity of neurons in some situations. Moran and Desimone (1985) found that when two small stimuli are placed within a V4 neuron's receptive field and the subject attends to just one, the neuron responds as if the receptive field had contracted around the stimulus that is the focus of attention. If one preferred and one nonpreferred stimulus are in the receptive field, attention to the preferred stimulus increases responses, while attention to the nonpreferred stimulus reduces responses, relative to attention directed elsewhere. Similar results have since been described in V4, MT, and the medial superior temporal (MST) area (Connor et al., 1996, 1997; Luck et al., 1997; Reynolds et al., 1999; Treue and Maunsell, 1996).

Changes in the efficacy of stimuli in different parts of the receptive field can be viewed as a change in neuronal selectivity. The response of the neuron as a function of position in the visual field (i.e., its receptive field profile) shifts and narrows as attention shifts to different locations. Thus, attention affects selectivity for spatial tuning, even if it has little effect on tuning for attributes like orientation or direction. However, such changes in selectivity may be an indirect consequence of effects of attention that do not alter selectivity directly (Maunsell and McAdams, 2001). Receptive fields large enough to hold two stimuli depend on converging inputs from neurons with smaller receptive fields at earlier

levels in the visual pathway. Imagine that attention acts at a level where receptive fields are sufficiently small that the two stimuli activate different neurons. Additionally, assume that at this level, the only effect of attention is to differentially modulate the strength of response of the two groups of neurons. A neuron in a later stage can have a receptive field large enough to contain both stimuli if it sums inputs from both sets of neurons at the earlier level. While attention does not alter the selectivity of neurons at the earlier level, the changes it causes at that level will change the spatial response profile (spatial selectivity) of the neuron at the later level. Thus, even if attention never changes the selectivity of sensory neurons directly, the convergence of inputs that have been differently affected by attention may lead to changes in selectivity. It should be noted that such changes might be largely limited to shifts in receptive fields, because receptive fields grow progressively larger at later stages in visual cortex. Tuning for stimulus dimensions such as orientation, direction, and color does not appear to broaden greatly in cortical processing and therefore may be less prone to this effect of attention.

ATTENTION AS INCREASED SALIENCE The effects of attention on neuronal responses are reminiscent of the effects of increasing stimulus salience when attention is kept constant. Changes in stimulus contrast or intensity, or other changes that make a stimulus better suited to the response properties of a neuron, typically increase the response of the neuron without altering its tuning for various stimulus attributes (Maunsell and McAdams, 2001; McAdams and Maunsell, 1999a). Most of the reported effects of attention on neuronal responses can be viewed as an effective increase in the intensity of the attended stimulus. For example, the effects of attention described above when two stimuli are in a neuron's receptive field are qualitatively the same as those expected if one stimulus became more intense while the other became less intense. Consistent with this, Reynolds et al. (2000) measured the effect of attention on the responses of V4 neurons using stimuli that covered a range of contrasts, and found that attention was equivalent to increasing stimulus contrast.

Other types of extraretinal inputs to visual cortex also appear to modulate responses without altering underlying selectivity. Signals related to the angle of gaze appear to scale receptive field profiles of neurons in posterior parietal cortex (Andersen et al., 1985). Behavioral differences between reward-associated and unrewarded stimuli scale orientation tuning curves in inferotemporal cortex (Vogels and Orban, 1994). Additionally, receptive field profiles of V4 neurons appear to scale multiplicatively when attention is directed to different points around the receptive field (Connor et al., 1996, 1997).

One of the goals of neurophysiological studies of attention is to understand how the changes it causes in neuronal responses relate to changes in behavioral performance. A general correlation exists in that attention makes neuronal responses to attended stimuli stronger and makes behavioral performance using attended stimuli better. A few studies have tried to relate quantitatively the effects of attention on neuronal responses to changes in behavioral performance.

McAdams and Maunsell (1999b) examined how a subject's attention influenced how well stimulus orientations were discriminated by the responses of individual V4 neurons. They used a d-prime measure, which estimated the orientation difference that would be needed before a neuron's responses to two orientations made it possible to tell which was which with 75% correctness in a two-alternative force-choice task. Attention improved neuronal performance: the median d-prime for unattended stimuli was 26.5 degrees, while that for attended stimuli was 20.4 degrees. The subject's behavioral performance was not measured in this experiment, however.

Recently, Cook and Maunsell (2002) compared neuronal and behavioral performance directly in a motion detection task in which stimuli spanned a range of motion strength and appeared in locations to which the subject directed greater or less attention. In this way, it was possible to assess whether the effects of attention on the neuronal response were commensurate with its effects on behavioral performance. For example, would a weak attended stimulus and a strong unattended stimulus that both produced the same level of neuronal performance also support the same level of behavioral performance?

Figure 103.2 plots average behavioral performance on detecting motion onset against average neuronal responses to the same stimuli parameterized by motion strength. Several motion strengths were tested while the animal attended to the receptive field location (*filled symbols*). One of these motion strengths was also presented in the receptive field when the animal was instructed to attend elsewhere (*open symbols*). Redirecting attention reduced both behavioral performance and neuronal responses. If the effect of attention was equivalent to changing stimulus strength, then the point for this other attentional condition should lie on the function defined by values obtained when the animal was attending to the receptive field location.

The results differed between visual areas. For neurons in MT (Fig. 103.2A, B), the average attentional modulation of neuronal responses was relatively weak, and was too small to explain the changes in behavioral performance associated with shifts in attention. In contrast, the average attentional modulation in the ventral intraparietal area (VIP) was more

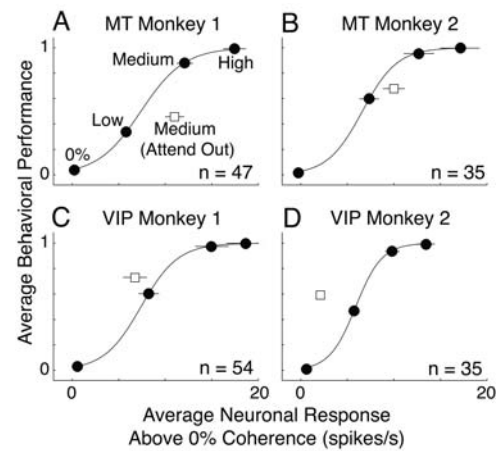


FIGURE 103.2. Average effects of attention on behavior and simultaneously recorded neuronal responses. *Filled symbols* plot behavioral performance and neuronal responses from trials where the animal was attending to the receptive field location. Different points are for stimuli with stronger or weaker motion signals. *Open symbols* plot behavioral and neuronal responses from trials where the medium motion strength appeared in the receptive field, but the animal's attention had been directed elsewhere. If changes in attention were equivalent to changes in stimulus strength, the *open symbols* would lie on the function defined by the *filled symbols*. Instead, for both animals, neuronal effects of attention were too weak in MT (A, B), and too strong in VIP (C, D). (from Cook and Maunsell, 2002.)

than what was needed to account for the changes in behavioral performance (Fig. 103.2C, D).

While there are several plausible explanations for these mismatches, one possibility is that a correspondence between neuronal and behavioral performance exists across attentional states only in those stages of cortex that are best suited for the detection or discrimination being done. As mentioned above, attentional modulations are greater in later stages of cortical processing. Consequently, a shift in attention that produces a particular change in behavioral performance will be associated with different amounts of attentional modulation in different cortical areas. In most visual areas, the average attentional modulation will not match the change in behavioral performance. The results from MT and VIP suggest that the average attentional modulation of neurons in a region intermediate between MT and VIP would be appropriate to account for the behavioral modulation.

More experiments will be needed to determine whether a correspondence between neuronal and behavioral performance persists across attentional states. If a correspondence were found, it would not say anything about the size of the pool of neurons that contributes to the behavior or whether the neurons were confined to a single area. However, it would raise important questions about how different levels of visual cortex contribute to different behaviors. For

example, it would be valuable to know whether neurons showing a correspondence across attentional states for a particular task had the greatest sensitivity for the stimulus attributes that were essential to the task being performed. It would also suggest that manipulating attention might be a valuable tool in exploring how individual neurons contribute to behaviors.

Concluding comments

The results described suggest a basic framework for understanding the function of attentional modulation in sensory processing. Images falling on the retinas activate subsets of neurons throughout visual cortex, with each neuron's activation determined by its more or less hardwired response properties and the content of the retinal image. This pattern of cortical activation is modified by attention. The responses of neurons with receptive fields in parts of the visual scene that are being attended by the subject, or with response properties consistent with stimulus features being attended, would be enhanced relative to others. Perception and behaviors would then be determined by the modified pattern of cortical activity, with the enhancement by attention leading to better discrimination and detection, and faster reaction times, for attended stimuli.

Many questions remain about attentional modulation of neuronal responses in visual cortex. Some of these are readily approachable and will likely be addressed in the near future. Others are more daunting and may need to wait for a more complete understanding of how sensory representations are used in guiding behaviors.

Among the more approachable issues is more information about how attention interacts with the sensory response properties of neurons. We have seen that the primary effect of attention appears to be an increase in sensitivity without much change in selectivity. That notion is based on only a few experiments, however. Other visual areas need to be examined using different tasks and a greater range of stimulus conditions. There is also a need for better information about differences in the amount of attentional modulation in different levels of cortical processing. The data point to a progressive increase in attentional modulation in cortical processing, but this has never been surveyed thoroughly.

Little is known about how selectively attention can act on neurons within visual cortex. For example, studies of spatial attention show that attention can enhance responses of neurons with receptive fields in one location while suppressing responses of neurons with receptive fields elsewhere, but it is not known whether attention can also adjust the enhancement neurons in earlier versus later stages of cortex, depending on task demands. While studies have shown greater modulation at later stages, no attempt has

been made to see whether attention to simpler or more complex stimuli might reverse or exaggerate the differences between levels. It would also be valuable to know whether attention can act differentially on areas in different streams of processing.

In the longer term, we must work toward understanding how attentional modulations of neuronal responses contribute to behavioral performance. It is a reasonable assumption that attentional modulations are optimizing some aspect of neuronal responses, but which one? The stronger responses associated with attention allow better neuronal performance (McAdams and Maunsell, 1999b), but this cannot be the complete explanation. If the performance of individual neurons were the entire story, there would be little reason for modulating responses: why not leave them in the state with better performance all the time? Stronger responses will generally give better performance, so why are neurons not always at the highest possible sensitivity? Presumably sensitivity is set to produce an appropriate balance between false alarms about the presence of a stimulus and failures to detect stimuli that are present. If so, the dynamic, differential modulation of neurons might work to adjust the criterion for neuronal responses in light of current information about the visual scene or the subject's motivation. We will not understand the role of attention in sensory processing until we can answer questions about the specific magnitudes of attentional modulation observed.

The sources of attentional modulation also remain to be determined. Functional imaging studies in humans have suggested that parietal cortex may be a good candidate (Corbetta et al., 1998; but see Duncan, 2001). Recently, Sereno and his colleagues (2001) described topographic maps associated with remembering the locations in the visual field in several sites in parietal cortex. Maps of this sort could provide the input needed to account for spatially selective enhancement of visual neurons with receptive fields in behaviorally relevant locations.

While much remains to be done, considerable progress is being made in understanding the role of attention in sensory processing. The past 5 years have seen the beginnings of a framework for quantitatively relating attentional modulation of neurons' responses to changes in behavioral performance, and the prospects for progress in the near future are excellent. Attention is proving to be among the most approachable cognitive processes for study at the level of responses of single units.

Acknowledgments

This research was supported by NIH Grant EY05911. John Maunsell is an Investigator with the Howard Hughes Medical Institute.

REFERENCES

- Andersen, R. A., G. K. Essick, and R. M. Siegel, 1985. The encoding of spatial location by posterior parietal neurons, *Science*, 230:456–458.
- Assad, J. A., and J. H. R. Maunsell, 1995. Neural correlates of inferred motion in primate posterior parietal cortex, *Nature*, 373:518–521.
- Boudreau, C. E., and J. H. R. Maunsell, 2001. Is spatial attention a limited resource for V4 neurons? *Soc. Neurosci. Abstr.*, 27:574–573.
- Connor, C. E., J. L. Gallant, D. C. Preddie, and D. C. Van Essen, 1996. Responses in area V4 depend on the spatial relationship between stimulus and attention, *J. Neurophysiol.*, 75:1306–1308.
- Connor, C. E., D. C. Preddie, J. L. Gallant, and D. C. Van Essen, 1997. Spatial attention effects in macaque area V4, *J. Neurosci.*, 17:3201–3214.
- Cook, E. P., and J. H. R. Maunsell, 2002. Attentional modulation of behavioral performance and neuronal responses in middle temporal and ventral intraparietal areas of macaque monkey, *J. Neurosci.*, 22:1994–2004.
- Corbetta, M., E. Akbudak, T. E. Conturo, A. Z. Snyder, J. M. Ollinger, H. A. Drury, M. R. Lineweber, S. E. Petersen, M. E. Raichle, D. C. Van Essen, and G. L. Shulman, 1998. A common network of functional areas for attention and eye movements, *Neuron*, 21:761–773.
- Corbetta, M., F. M. Miezin, S. Dobmeyer, G. L. Shulman, and S. E. Petersen, 1991. Selective and divided attention during visual discriminations of shape, color and speed: functional anatomy by positron emission tomography, *J. Neurosci.*, 11:2383–2402.
- Crist, R. E., W. Li, and C. D. Gilbert, 2001. Learning to see: experience and attention in primary visual cortex, *Nat. Neurosci.*, 4:519–525.
- Duncan, J., 2001. Frontal lobe function and the control of visual attention, in *Visual Attention and Cortical Circuits* (J. Braun, C. Koch, and J. L. Davis, eds.), Cambridge, MA: MIT Press, pp. 69–88.
- Eskandar, E. N., and J. A. Assad, 1999. Dissociation of visual motor and predictive signals in parietal cortex during visual guidance, *Nat. Neurosci.*, 2:88–93.
- Felleman, D. J., and D. C. Van Essen, 1991. Distributed hierarchical processing in the primate cerebral cortex, *Cereb. Cortex*, 1:1–47.
- Ferrera, V. P., K. K. Rudolph, and J. H. R. Maunsell, 1994. Responses of neurons in the parietal and temporal visual pathways during a motion task, *J. Neurosci.*, 14:6171–6186.
- Fries, P., J. H. Reynolds, A. E. Rorie, and R. Desimone, 2001. Modulation of oscillatory neuronal synchronization by selective visual attention, *Science*, 291:1560–1563.
- Fuster, J. M., 1990. Inferotemporal units in selective visual attention and short term memory, *J. Neurophysiol.*, 64:681–697.
- Fuster, J. M., and J. P. Jervey, 1982. Neuronal firing in the inferotemporal cortex of the monkey in a visual memory task, *J. Neurosci.*, 2:361–375.
- Geisler, W. S., and D. G. Albrecht, 1997. Visual cortex neurons in monkeys and cats: detection, discrimination and identification, *Vis. Neurosci.*, 14:897–919.
- Haenny, P. E., and P. H. Schiller, 1988. State dependent activity in monkey visual cortex. I. Single cell activity in V1 and V4 on visual tasks, *Exp. Brain Res.*, 69:225–244.
- Hillyard, S. A., E. K. Vogel, and S. J. Luck, 1998. Sensory gain control (amplification) as a mechanism of selective attention: electrophysiological and neuroimaging evidence, *Philos. Trans. R. Soc. Lond. B*, 353:1257–1270.
- Lu, Z. L., and B. A. Doshier, 1998. External noise distinguishes attention mechanism, *Vis. Res.*, 38:1183–1198.
- Luck, S. J., L. Chelazzi, S. A. Hillyard, and R. Desimone, 1997. Neural mechanisms of spatial selective attention in areas V1, V2, and V4 of macaque visual cortex, *J. Neurophysiol.*, 77:24–42.
- Maunsell, J. H. R., and C. J. McAdams, 2001. Effects of attention on the responsiveness and selectivity of individual neurons in visual cerebral cortex, in *Visual Attention and Cortical Circuits* (J. Braun, C. Koch, and J. L. Davis, eds.), Cambridge, MA: MIT Press, pp. 103–119.
- McAdams, C. J., and J. H. R. Maunsell, 1999a. Effects of attention on orientation-tuning functions of single neurons in macaque cortical area V4, *J. Neurosci.*, 19:431–441.
- McAdams, C. J., and J. H. R. Maunsell, 1999b. Effects of attention on the reliability of individual neurons in monkey visual cortex, *Neuron*, 23:765–773.
- McAdams, C. J., and J. H. R. Maunsell, 2000. Attention to both space and feature modulates neuronal responses in macaque area V4, *J. Neurophysiol.*, 83:1751–1755.
- Mehta, A. D., I. Ulbert, and C. E. Schroeder, 2000. Intermodal selective attention in monkeys. II: Physiological mechanisms of modulation, *Cereb. Cortex*, 10:359–370.
- Miyashita, Y., A. Date, and H. Okuno, 1993. Configurational encoding of complex visual forms by single neurons of monkey temporal cortex, *Neuropsychology*, 31:1119–1131.
- Moran, J., and R. Desimone, 1985. Selective attention gates visual processing in the extrastriate cortex, *Science*, 229:782–784.
- Motter, B. C., 1993. Focal attention produces spatially selective processing in visual cortical areas V1, V2, and V4 in the presence of competing stimuli, *J. Neurophysiol.*, 70:909–919.
- Motter, B. C., 1994. Neural correlates of feature selective memory and pop-out in extrastriate area V4, *J. Neurosci.*, 14:2190–2199.
- Mountcastle, V. B., R. A. Andersen, and B. C. Motter, 1981. The influence of attentive fixation upon the excitability of the light-sensitive neurons of the posterior parietal cortex, *J. Neurosci.*, 1:1218–1235.
- Reynolds, J. H., L. Chelazzi, and R. Desimone, 1999. Competitive mechanisms subserve attention in macaque areas V2 and V4, *J. Neurosci.*, 19:1736–1753.
- Reynolds, J. H., T. Pasternak, and R. Desimone, 2000. Attention increases sensitivity of V4 neurons, *Neuron*, 26:703–714.
- Sereno, M. I., S. Pitzalis, and A. Martinez, 2001. Mapping of contralateral space in retinotopic coordinates by a parietal cortical area in humans, *Science*, 294:1350–1354.
- Spitzer, H., R. Desimone, and J. Moran, 1988. Increased attention enhances both behavioral and neuronal performance, *Science*, 240:338–340.
- Spitzer, H., and B. J. Richmond, 1991. Task difficulty: ignoring, attending to, and discriminating a visual stimulus yield progressively more activity in inferior temporal neurons, *Exp. Brain Res.*, 83:340–348.
- Steinmetz, P. N., A. Roy, P. J. Fitzgerald, S. S. Hsiao, K. O. Johnson, and E. Niebur, 2000. Attention modulates synchronized firing in primate somatosensory cortex, *Nature*, 404:187–190.
- True, S., and J. C. Martínez-Trujillo, 1999. Feature-based attention influences motion processing gain in macaque visual cortex, *Nature*, 399:575–579.

- Treue, S., and J. H. R. Maunsell, 1996. Attentional modulation of visual motion processing in cortical areas MT and MST, *Nature*, 382:539–541.
- Treue, S., and J. H. R. Maunsell, 1999. Effects of attention on the processing of motion in macaque middle temporal and medial superior temporal visual cortical areas, *J. Neurosci.*, 19:7591–7602.
- Vogels, R., and G. A. Orban, 1994. Does practice in orientation discrimination lead to changes in the response properties of macaque inferior temporal neurons? *Eur. J. Neurosci.*, 6:1680–1690.
- Yakovlev, V. V., S. Fusi, E. Berman, and E. Zohary, 1998. Inter-trial neuronal activity in inferior temporal cortex: a putative vehicle to generate long-term visual associations, *Nat. Neurosci.*, 1:310–317.

104 Volition and the Prefrontal Cortex

EARL K. MILLER AND JONATHAN D. WALLIS

THE SOPHISTICATED sensory systems of advanced animals—a choice example being the primate visual system—provide a wealth of data about the external world. To take advantage of this, we humans have correspondingly evolved elaborate mechanisms for behavior. While virtually all animals can react to their immediate environment, the rich information we have about the world has allowed us to extend our behavioral repertoire beyond simple reflexive reactions. Primates and other advanced animals can learn to anticipate possible futures and coordinate thought and action in order to direct them toward achieving desired outcomes. This ability is the hallmark of intelligent behavior, and it is called *cognitive control*. A full understanding of visual processing can be achieved only through an appreciation of how the mechanisms for cognitive control can modulate visual processing and how visual information is used to constrain and guide behavior.

Because cognitive control necessarily involves the coordination of many different brain processes, it no doubt depends on circuits that extend over much of the cerebral cortex. However, one cortical region, the prefrontal cortex (PFC), seems to play a central role. It is the area that reaches its greatest elaboration in the human brain and is thus thought to be the neural instantiation of the mental qualities that we think of as “intelligent.” Accordingly, the PFC receives converging information from the visual system and, indeed, all other sensory systems, and it is interconnected with motor system structures needed for voluntary action.

Here we discuss anatomical, neuropsychological, and neurophysiological evidence for, and theories of, the role of the PFC in cognitive control. Much of this discussion will involve visually guided behaviors and other aspects of controlled visual processing such as focal attention, but because cognitive control is by nature supramodal, other modalities will also be considered. We will begin with a discussion of the characteristics of volitional, or controlled, processes, as they can provide predictions about the neural mechanisms likely to underlie them.

Controlled processing

All behavior varies along a continuum from mindless and automatic to willful and purposeful (i.e., controlled) behaviors (Barsalou, 1992). Automatic processes are reflexive. If a

car or a predator is bearing down on us, we leap out of the way before we have even had a chance to form the intention to do so. Automatic processes thus seem to depend on relatively straightforward, hardwired relationships between the brain’s input and output systems. In neural terms, it seems that they depend on strong, well-established neural pathways just waiting to be triggered by the right sensory cue. That is, automatic processes are driven in a bottom-up fashion: they are determined largely by the nature of the sensory stimuli and by whatever reaction they are most strongly wired to.

These relatively simple, hardwired, cue-response mappings are useful in many situations. Because they can simply be fired off by the environment, they are quick and can be executed without taxing the limited capacity of our conscious thoughts. But a creature that is at the mercy of its immediate environment is not well equipped to deal with the ambiguity, and exploit the opportunity, of a complex and dynamic world. Sometimes, the course of action is not obvious because cues are ambiguous (i.e., they activate more than one possible internal representation), or multiple behaviors might be triggered and the one that is optimal for a given situation is at a disadvantage relative to better-established (more automatic) alternatives. In these situations, ambiguity needs to be resolved by our internal states and intentions, by knowledge of possible and desired future outcomes (goals), and by knowledge of what means have been successful at achieving them in the past. This information is used to activate the same basic sensory, memory, and motor processes that are engaged during automatic behaviors. Only now, they are not triggered by cues from the environment. They are orchestrated in a top-down fashion by our expectations about goals and means. So, this mode of behavior is controlled in the sense that we (our knowledge and intentions) are in charge, not the environment.

A tenet of modern studies of behavior is that this knowledge is obtained by learning mechanisms that detect and store associations between cues, internal states, and actions that predict goal attainment (reward) (Dickinson, 1980). Insofar as primates are capable of navigating situations that involve diverse relationships across a wide range of informational domains, it follows that a neural system for cognitive control must have access to information from many brain systems and the ability to encode the goal-relevant relationships between them.

As implied above, the fundamental operation of a cognitive control system is selection, choosing which basic sensory, memory, and motor processes are activated at a given moment. Selection is central because of our very limited capacity to engage in controlled behaviors. This is evident to anyone who has tried to talk on the phone and answer e-mail at the same time; we can only think about a limited number of things at a time. This is in contrast to our high capacity for automatic processes. Because they can be triggered by the environment, any number of them can be fired off at once, as long as they do not come into direct conflict with one another.

It makes sense that brain mechanisms for cognitive control would evolve with this capacity limitation. First, there is the trade-off between amount of information and depth of analysis; focusing processing on a narrow band of information relevant to a current goal allows a much more elaborate analysis of a situation and available options. This single-mindedness also allows us to stay on track; processing information not relevant to a current goal increases the chance for distraction. In fact, in many views of cognition, *control* and *attention* are virtual synonyms. It follows that a neural system for cognitive control must have the infrastructure and mechanisms for selecting goal-relevant, and suppressing goal-irrelevant, processes throughout the cerebral cortex.

Also, as previously implied, the cognitive control system must be highly plastic. Virtually all voluntary, goal-directed behaviors are acquired by experience, and given that humans and other primates are capable of rapid learning of new volitional behaviors, the cognitive control system must have an equal capacity for rapid learning.

The cognitive control system must also have a way to deal with the gaps in time that are inevitable with goal-directed behaviors. Information about predicted goals and means must be brought on-line before the behaviors are executed and maintained until the current task is completed. Also, because goal-directed behaviors typically are extended over time, we often must wait for additional information or for a more opportune time to execute an action. The ability to keep goal-relevant information on-line and available for processing is called *working memory* (Baddeley, 1986). It is less critical for automatic processes because they are immediate: a stimulus triggers an already established circuit.

To bring the role of the cognitive control system into further focus, consider a model proposed by Norman and Shallice (1986). It illustrates a widely accepted view of the architecture of cognition (Fig. 104.1). At the lower level, there are the automatic processes (sensory analysis, memories, details of motor acts, well-learned skills, etc.). The system is in automatic mode when processing flows through the lower level, from input to output, along established pathways without any hindrance or modification: sensory inputs

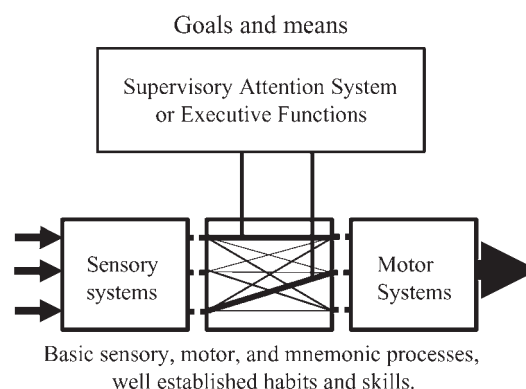


FIGURE 104.1. Two levels of cognitive processes proposed by Norman and Shallice (1986), among others. Represented here is the notion that specialized functions that acquire information about goals and means select and coordinate among innate and well-established routines.

trigger their analysis, which triggers long-term memories, actions, and so on.

A brain that contained only this lower level of processing, however, would belong to an automaton. It would only be capable of reacting reflexively to stimuli that happen to flow into it. To allow the system to engage in proactive, goal-directed behavior, most theories of cognition posit the need for “executive” functions specialized for acquiring and representing goals and means. These functions come on-line when a course of action is uncertain or if a reflexive, automatic reaction associated with a given input would produce an undesirable outcome. They send top-down signals that control the flow of processing through the lower (main) level by favoring goal-relevant processes and suppressing irrelevant ones. Because of this role, Norman and Shallice refer to the executive functions as the *Supervisory Attention System*. Another example of this two-level processing hierarchy is Baddeley’s *Working Memory* model, which posits an executive controller that selects the information that is held in lower-level short-term sketchpads (Baddeley, 1986).

To summarize, we have some expectations about the properties of a neural system for cognitive control. It should be a brain region where diverse information from other brain systems can converge and be synthesized into representations of goals and means. It should have a great capacity to learn from experience. It should have the ability to maintain that information on-line and a means for it to influence other brain systems. A rapidly accumulating body of evidence regarding the PFC suggests that it meets these requirements.

Anatomy of the PFC

The PFC consists of a collection of cortical areas that differ from one another on the basis of size, density, and

distribution of their neurons (Fig. 104.2). Generally, it is divided into 3 subdivisions (dorsolateral, ventrolateral, and orbital/medial), but these can be further subdivided into at least 18 distinct areas.

As we learned above, the theme of cognition (and learning and memory) is synthesis. While the brain's different sensory systems adopt a divide-and-conquer approach to analysis of the external world, it is the job of the learning and memory systems to put the results together to form the big picture. The anatomy of the PFC has long suggested such a role. Like other brain regions involved in learning (such as the basal ganglia and hippocampus), the PFC is a site of convergence of information from many different brain systems.

Different PFC regions have partially unique but overlapping connections with other brain areas. A major difference is between the lateral and orbitofrontal PFC. The lateral PFC is most directly connected with sensory and memory systems that deal with the outside world, while the orbitofrontal PFC is more associated anatomically with medial temporal limbic structures critical for long-term memory and "internal" information, such as affect and motivation (Barbas and Pandya, 1991).

The lateral PFC (dorsolateral and ventrolateral) receives projections from and sends projections to the visual, somatosensory, and auditory areas in the occipital, temporal, and parietal cortices (Barbas and Pandya, 1991; Pandya and Barnes, 1987). There is a good degree of multimodal convergence in these connections. Several lateral PFC areas receive overlapping inputs from at least two sensory modalities. Further, the lateral PFC is interconnected with areas such as the rostral superior temporal sulcus, which has neurons that can be activated by two or three modalities (visual, auditory, and somatosensory). The PFC is not directly connected with primary sensory areas but instead is interconnected with secondary or *association* sensory cortex. This suggests that the PFC operates on highly processed information.

The dorsal PFC (particularly dorsolateral area 46) is heavily interconnected with motor system structures and may be a primary output of the PFC to systems mediating voluntary behavior. It is interconnected with regions important for body and eye movements such as the supplementary motor area (SMA), the pre-SMA, and the rostral cingulate, premotor cortex, cerebellum, superior colliculus, and frontal eye fields (area 8). As with sensory cortex, there are no direct connections between the PFC and primary motor cortex; the PFC is instead connected with premotor areas that, in turn, send projections to primary motor cortex and the spinal cord.

There are also dense interconnections between the PFC and basal ganglia (BG), a set of subcortical structures that are highly interconnected with the motor system. Like the

PFC, the BG receives converging inputs from many cortical and subcortical regions. Unlike the PFC, however, the BG does not project back to the cortical regions that provide it with input; it projects primarily back to the motor cortex and the PFC (Graybiel, 2000; Houk and Wise, 1995). This suggests that the BG influences a wide range of brain functions, although its primary involvement may be with motor output. The anatomical "loops" between the PFC and BG suggest a close functional relationship. Passingham (1993) has suggested that the BG is a major conduit by which reward signals from dopaminergic midbrain ventral tegmental area neurons can influence the PFC.

The orbitofrontal and medial PFC are more strongly connected with limbic system structures than is the lateral PFC. They have direct and indirect (via the thalamus) connections with the hippocampus and associated neocortex, the amygdala, and the hypothalamus. They also have strong connections with olfactory and gustatory cortices, but relatively weaker connections than the lateral PFC to parietal and temporal cortices.

As in other parts of the neocortex, many PFC connections are local; the subdivisions are all reciprocally interconnected, as are their constituent areas (Barbas and Pandya, 1989). Thus, while different PFC subdivisions may have a somewhat privileged relationship with certain brain systems, the PFC also has the intrinsic circuitry to piece together this information as needed. Further, because the PFC is reciprocally connected with many different brain systems, it has the links to influence processing throughout the forebrain. Evidence that this infrastructure is used for cognitive control comes from the pattern of behavior deficits following PFC damage. This is discussed next.

Behavioral effects of PFC damage in humans

PFC damage does not result in simple deficits; there is relatively little overt impairment, at least on superficial examination. Sensory capabilities are intact, patients with PFC damage can remember events and facts, and they appear remarkably normal in casual conversation. Despite the superficial appearance of normality, however, PFC damage devastates a person's life. Patients have trouble staying employed, staying married, or even completing errands. This is due to a constellation of deficits, described next, that seems to reflect a selective loss of cognitive control, that is, a "dysexecutive" syndrome.

GOAL NEGLECT Humans with PFC damage seem to behave without any consideration for future consequences. They become *stimulus-bound*; they engage in whatever habitual behaviors happen to be triggered by cues in the immediate environment; they seem to lack any direction toward unseen goals or any weighing of the consequences of their

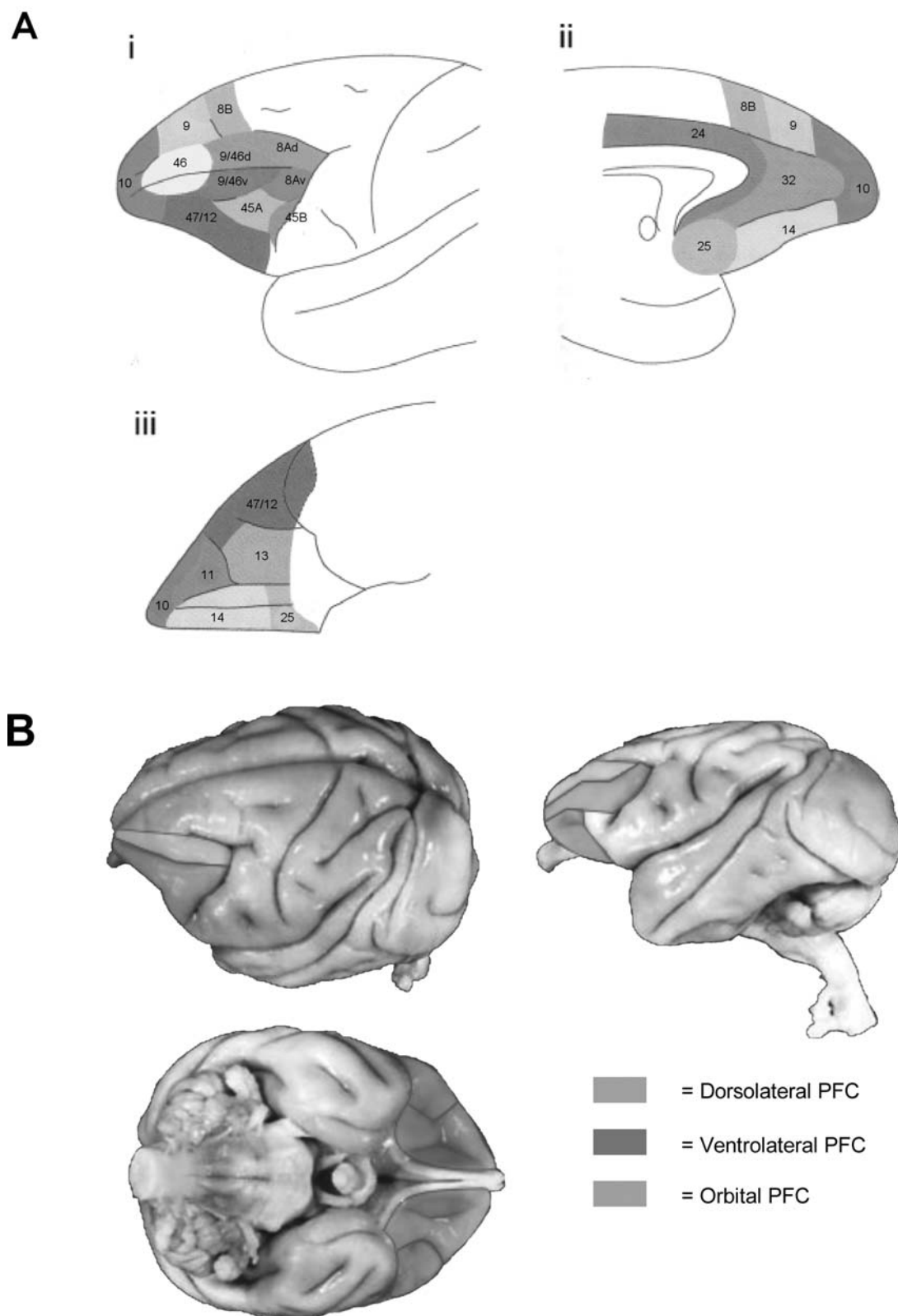


FIGURE 104.2. The prefrontal cortex of the macaque monkey. *A*, Cytoarchitectonic areas of the PFC from Petrides and Pandya

(1994). *B*, Major subdivisions of the PFC. Brain figures obtained from www.brainmuseum.org. (See color plate 77.)

actions. As you can imagine, people in this condition can be easily taken advantage of. There was the case of Elliot, a responsible, successful accountant, who, within a few years after PFC damage, got divorced, married and divorced again, fell in with a disreputable business partner, and lost his business (Eslinger and Damasio, 1985). Elliot became impulsive, lurching from one catastrophe to another based on his momentary whims and, apparently, the selfish suggestions of others who wished to take advantage of him.

This impulsiveness is well illustrated in what is known as *utilization behavior* (Shallice et al., 1989). A patient with PFC damage will habitually pick up and use nearby items. For example, if a doctor leaves a comb on the desk, the patient will pick up the comb and start combing his hair. In (hopefully) one case, the patient made use of a urinal that had been left on a desk. Formal tests of disinhibition include the Stroop Test (Fig. 104.3A), which requires a patient to name the color of the ink in which a word is written rather than read the word. The trick is that the word is the name of another color, and to perform the task it is necessary to suppress the reflexive reaction of reading the word. Following PFC damage, patients have difficulty with this. That is, they have trouble overcoming an automatic, reflexive response in order to emit one that is in accord with the task demand.

This inability to ignore irrelevant distractions and persist toward a goal has been termed *goal neglect* (Duncan et al., 1996). A more everyday example is the Multiple Errands Test of Shallice and Burgess (1991). The patient is required to perform various errands in a shopping center, such as obtaining a copy of the previous day's newspaper. Patients take much longer than control subjects. They habitually enter irrelevant shops just because they happen to be passing them and thus are repeatedly distracted from their principal goal.

PERSEVERATION Difficulties of PFC patients extend beyond overriding strong impulses and highly ingrained reflexes; they even have trouble overriding recently, and therefore weakly, established behaviors. Because other learning and memory systems are intact, they can learn to respond to specific cues in specific ways. But then they become “stuck” in that behavioral rut.

Consider a classic test of PFC impairment, the Wisconsin Card Sorting Test (WCST) (Fig. 104.3B). The patient is required to sort a deck of cards which contains a number of symbols. The cards differ from one another in the color, shape, and number of the symbols, and the patient must learn to sort them by trial and error, with only feedback about whether their responses are correct or not. Patients with PFC damage can learn an initial sorting

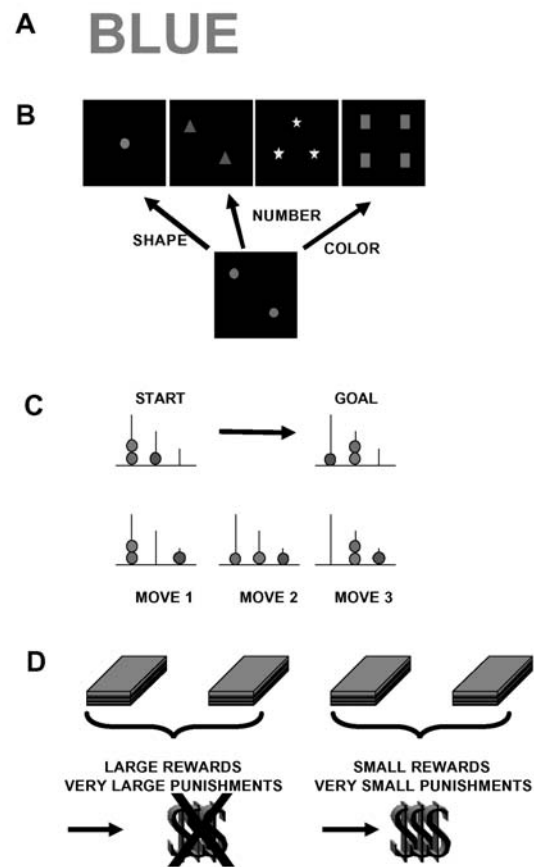


FIGURE 104.3. Tasks sensitive to PFC damage in humans. A, Stroop task. B, Wisconsin Card Sort. C, Tower of London task. D, Gambling task. See text for explanation of tasks. (See color plate 78.)

criterion, such as “sort by shape.” However, when the criterion is changed, for example, to “sort by number,” they cannot inhibit the previous rule in order to learn the new one (Milner, 1963). This is called *perseveration*, and it is seen in a wide variety of tasks. It seems that the remaining learning and memory mechanisms can potentiate straightforward responses to certain cues (like color), but without a specialized brain system for quickly figuring out goals and directing behavior toward them, the system can never acquire the experience necessary to draw behavior away from the previously rewarded one.

PLANNING In the examples described above, the basic units of behavior remain intact. What is lacking is the ability to organize them to pursue a goal. One patient, when making coffee, first stirred it and then added milk. Wilder Penfield’s sister had a large tumor removed (by Wilder) from her frontal lobes. She had been an excellent cook, and while her basic

skills remained, she seemed unable to organize the cooking of a meal. She moved haphazardly from preparing one part of the meal to another, so that some parts of the meal were burnt while others had hardly been started.

A formal test of planning is the Tower of London Test; it requires the patient to think several moves in advance (Fig. 104.3C). There are three vertical posts and three colored rings that can be placed on the posts. The three posts are of different lengths such that the first post can accommodate all three rings, the second post two, and the third post just one. From an initial starting position, the patient is asked to move the rings one at a time, from one post to another, to attain a specified goal pattern. This requires patients to use information about the goal state to anticipate which actions will move them progressively closer to it. Patients with PFC damage make many more moves than necessary to reach the final goal position, if they do at all.

EVALUATING CONSEQUENCES Learning new goal-directed behaviors depends on the capacity to evaluate the consequences of our actions so that, in the future, an optimal plan can be chosen. Evidence that certain types of PFC damage impair this process comes from a gambling task (Bechara et al., 1994) (Fig. 104.3D). The patient has to choose cards from four different decks in an effort to win “money.” Some cards win the patient some money, but others cause the patient to lose money. Unknown to the patient, cards from two decks will occasionally win large amounts of money, but they are also occasionally associated with very large losses, and choosing from them will result in a net loss. Choosing from the other two decks results in winning smaller amounts of money, but the losses are also smaller, and choosing from these two decks will result in a net profit. Control subjects quickly learn to limit their choices to the second two decks associated with smaller rewards but a profit, while patients with orbital PFC damage continually choose from the decks associated with large rewards and larger losses until they lose all their money.

WORKING MEMORY It has been suggested that many of the difficulties following PFC damage can be explained, at least in part, by a loss of working memory. This is the kind of short-term memory that one relies on when rehearsing a phone number. It is called *working memory* because the information is forgotten as soon as it is no longer relevant. The hypothesis that PFC damage impairs working memory stems from the observations that PFC damage in monkeys (see below) impairs a spatial delayed-response task that requires them (among other things) to remember the location of a stimulus or behavioral response over a brief delay of several seconds.

At first, an analogous impairment was not detected in humans, possibly because the patients verbalized the remem-

bered location (e.g., “it’s on the left”), which makes the task easier. But studies using abstract patterns that could not be easily encoded verbally revealed that the patient’s nonspatial working memory was impaired (Milner et al., 1985). Also, the *two-back* task has been shown to be sensitive to PFC damage or dysfunction. In this task, humans see a sequence of letters and must respond only if a current letter matches one seen two letters ago. Because this involves matching to a specific stimulus, it may rely on working memory rather than other, more passive, forms of immediate memory such as those that automatically detect repetition (Miller and Desimone, 1994). As will be discussed in the next section, however, PFC damage can impair performance on tasks that have no obvious working memory component.

Behavioral effects of PFC damage in monkeys

The PFC is not a single area, but a collection of cortical areas with unique patterns of inputs and outputs. Because PFC damage in humans happens by accident or illness, it is often diffuse and rarely limited to a specific area or subdivision. This makes it difficult to determine whether different PFC regions are specialized for different functions. The diffuse damage seen in humans can also lead to difficulty in assigning functions to the PFC in general; damage often encroaches on neighboring regions, such as the premotor cortex, the cingulate cortex, and the insular cortex. These problems can be circumvented by experimental induction of precise lesions in monkeys.

DELAYED-RESPONSE TASKS One of the most profound deficits following frontal lobe damage in monkeys occurs during delayed-response tasks. In a spatial version, the monkey sees a reward hidden at one of two locations. Then a screen is lowered and the monkey is made to remember the cued location by discouraging “cheating” strategies such as keeping its hand near the rewarded location. After a brief delay, the screen is raised and the monkey is allowed to choose a location (Fig. 104.4A). Monkeys with large PFC lesions behave as if they forgot where the reward was hidden, even after delays of just a few seconds. Later, it was shown that lesions restricted to the dorsolateral PFC alone could produce the same deficit.

Another type of delayed-response task, object matching, is impaired by damage to the neighboring ventrolateral PFC. In this task, monkeys are shown an object (the sample) and then, after a brief delay of several seconds, must choose the same object (the match) from one or more nonmatching objects (Fig. 104.4B). The most severe deficits are observed when the same two objects are used repeatedly, requiring the monkey to remember which of the two objects it has seen most recently.

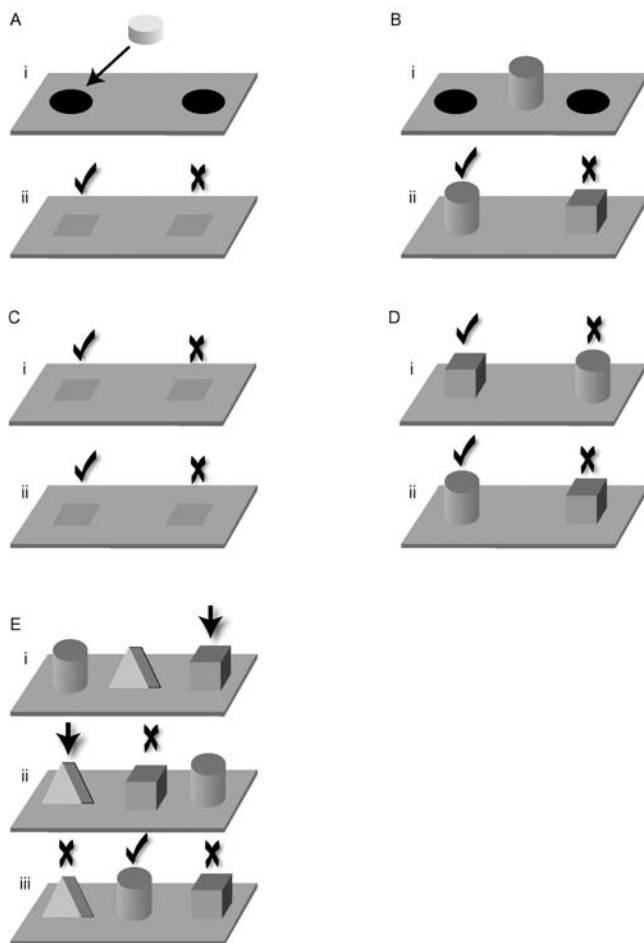


FIGURE 104.4. Tasks sensitive to PFC damage in monkeys. Check marks indicate correct choice; Xs indicate incorrect choices. The arrow in *E* indicates the monkey's choice in a self-ordered task. *A*, Spatial delayed response. *B*, Delayed matching-to-sample. *C*, Spatial reversal. *D*, Object reversal. *E*, Object self-ordered search task. (See color plate 79.)

These deficits are often explained by a loss of working memory. There are other interpretations, however. One possibility is that dysfunction is more broad than a specific deficit in working memory; it may reflect the type of goal neglect seen in humans with PFC damage. Consider the spatial delayed-response task. In an often-used oculomotor version, a cue is flashed at one of several possible locations in the visual periphery while monkeys maintain central gaze (Funahashi et al., 1989). After a brief delay, the monkeys are given a “go” cue and must move their eyes to the remembered location of the cue. Monkeys are impaired at this, but unimpaired when the memory delay is removed and they can simply look at the cue when it is flashed on. A loss of working memory to bridge the delay is a reasonable interpretation, but another possibility is that the “no delay” version of the task can be performed by reinforcing a reflexive orienting response to the onset of a stimulus (the cue) in the visual periphery. By contrast, when a delay is imposed,

there is nothing in the environment to indicate the correct response at the time of the action. The monkey's behavior must then be guided by internal information, not only by the memory of the cue but also by the knowledge of the formal demands of the task. In terms of the architecture pictured in Figure 104.1, the no-delay version of the task does not require the higher-order functions because the correct sensory cues can trigger the correct lower-level pathways at the correct time.

In fact, PFC damage in monkeys can impair performance on tasks that have no obvious working memory component. For example, monkeys with lesions of the ventrolateral PFC are impaired on a simultaneous color-matching task. In this task, the monkey is presented with a sample color and two test colors simultaneously. The monkey must choose the test color that matches the sample color. PFC lesioned monkeys were impaired despite the fact that the task involved contains no delays and therefore no working memory requirements. One possibility is that PFC damage produces impairments when, in the absence of a clear signal from the environment, monkeys must follow the logic of a task (e.g., “if the sample color is red, then choose the red stimulus” or “if the cue was on the left, then go to the left after the delay”). Support for this comes from studies showing that PFC damage produces impairments in conditional learning.

CONDITIONAL LEARNING TASKS Conditional learning tasks have been used to test the ability of animals to gain volitional control over behavior. They require learning of associative relationships that are arbitrary and extend beyond the simple one-to-one mappings that underlie reflexive reactions. Whether or not a given response is the correct response to a given cue depends on additional contextual information. For example, reaching for a beer can be rewarding, but only if one takes other information into account; if the beer belongs to another patron, the result could be disastrous. The need to take into account complex relationships in order to decide among alternative actions is presumably the reason cognitive control has evolved.

Monkeys with PFC damage are impaired at conditional learning tasks. For example, monkeys can be trained to learn associations between three distinct visual cues and three directional movements of a joystick. Each cue instructs a specific movement of the joystick. One means “up,” the other “down,” and so on. Bilateral damage to the ventrolateral and orbital PFC impairs this learning. Disconnecting the PFC from its inputs from high-order sensory cortex also results in conditional learning impairments. Humans with PFC damage are impaired on conditional learning tasks analogous to those conducted in monkeys. This deficit may depend on which PFC region is damaged; some studies report no conditional learning deficit following dorsolateral PFC damage in monkeys.

REVERSAL TASKS Perseveration in monkeys following PFC damage has been demonstrated using reversal tasks. In these tasks, reward is alternated between two locations (Fig. 104.4C) or between two objects (Fig. 104.4D), and monkeys must learn to choose the item that had not been rewarded most recently. This requires them to override a prepotent response (one that was just reinforced) in order to follow the task demands. Although deficits in reversal tasks can be seen following damage to several PFC regions, particularly large deficits occur after orbital (ventral) PFC damage. Monkeys perseverate, continuing to choose the location or object under which the reward had first been hidden. This has led to speculation that orbital PFC may be particularly important for inhibitory control (i.e., inhibiting prepotent responses).

OBJECT RECOGNITION TASKS Monkeys with lesions of the orbitofrontal PFC show impairments in visual recognition. This ability is tested using a delayed nonmatching-to-sample task. The monkey is presented with an object and then after a delay of a few seconds, is presented with that same object along with a novel object. New objects are used on each trial so that the monkey can perform the task by recognizing which of the two objects it has previously seen in order to pick the novel object. However, patients with damage to the homologous PFC region do not show this recognition deficit. One possibility for this discrepancy is that the deficit does not lie in recognition per se, but rather in the ability to learn the rules of the task. In particular, it has been suggested that the difficulty lies in making the association between the abstract quality of novelty and receiving a reward. This aspect of the task is not required in human patients, because the patients are explicitly told the rules of the task; monkeys have to learn them by trial and error.

FUNCTIONAL TOPOGRAPHY OF THE PFC A major question concerning prefrontal function is whether different processes can be mapped onto its different areas and subdivisions. The clearest example of a functional difference is the previously mentioned “external” versus “internal” emphasis of the lateral and orbitofrontal PFC, respectively. Observations from neuropsychological studies, such as those discussed above, have naturally led to attempts to assign more specific functions to different PFC areas. For example, the dorsal PFC has been suggested to be responsible for spatial memory, the ventral PFC for object memory, and the orbital PFC for inhibitory control in accord with their preferential connections with the parietal, inferior temporal, and limbic system structures, respectively. As subsequent studies have shown, however, PFC topography is not so simple and straightforward.

It is important here to discuss what constitutes evidence for a functional dissociation between two different brain

areas. In order to conclude that they perform, or at least emphasize, two different functions, it is necessary to demonstrate a double dissociation. A monkey with lesion X must be impaired at process A but not process B, while a monkey with lesion Y must be impaired at process B but not process A. A single dissociation, for example, showing that lesion X impairs process A but not process B, is insufficient evidence since this pattern of results could be achieved simply because the test used to assess process A is more sensitive than the test used to assess process B. It is often the case, however, that monkeys are tested on just one task, and any evidence for a double dissociation can only be inferred across different studies and (often) different laboratories. This complicates the interpretation because any differences in training and testing procedures and in the extent of the lesions are confounding factors. As a result, a clear double dissociation between different PFC regions has been difficult to establish.

Consider the hypothesis that different PFC regions mediate spatial versus object working memory. As mentioned above, some lesion studies have suggested that the dorsolateral PFC mediates visuospatial working memory, while the ventrolateral PFC mediates visual object memory tasks. This suggestion is based on (independent) observations that damage to the dorsolateral PFC impairs spatial delayed-response tasks but not object-matching tasks, while ventrolateral PFC lesions do impair object matching. However, further studies indicated that the story is not so straightforward.

For example, dorsal PFC lesions can impair performance on tasks that do not have a spatial component, such as object self-ordered search tasks. Here, the monkey is presented with three objects covering rewards and must choose each object in turn to get the reward, but after each choice a screen is lowered and the object's positions are shuffled (Fig. 104.4E). Thus, the monkey must continually remember which of the three objects it has already chosen. Also, monkeys with ventral (orbital) PFC lesions are impaired on both object and spatial reversal tasks. Furthermore, ventrolateral PFC lesions impair an auditory task in which monkeys must learn to respond to one tone and refrain from responding to another.

Neurophysiological studies paint a similar picture. There are examples of bias in the distribution of neurons that are sensitive to object identity or location in space (especially for the small population of highly specialized *face cells*) (Wilson et al., 1993). But there is also a good deal of intermixing of object and space (and other types of information). Up to half of lateral PFC neurons have been reported to be selective for both objects and their visual field location; many object-selective neurons have receptive fields just a few degrees in diameter (Rainer et al., 1998). Interestingly, most of the studies reporting integration of these (and other) types of

sensory (and motor) information have been conducted in monkeys trained on tasks in which their integration is needed for the task. By contrast, studies reporting areal segregation of information domains have used tasks in which object and space are separated into different tasks, or paradigms in which monkeys passively experience the stimuli and thus do not engage PFC functions. The great dependence of PFC neural properties on task demands will be discussed in greater detail below.

Likewise, the hypothesis that the orbital PFC is responsible for a monolithic function called *inhibitory control* is not straightforward. If more refined tests are used, inhibitory control deficits can also be observed in monkeys with lesions of the dorsolateral PFC. For example, marmosets were trained on a WCST-like task in which they had to choose stimuli on the basis of a rule, such as “choose by shape” and “choose by color.” When they were required to switch between different rules, monkeys with lesions of the dorsolateral PFC perseverated by continuing to choose on the basis of the previous rule, while monkeys with lesions of the orbital PFC were unimpaired (Dias et al., 1996). However, when the same stimuli were used in an object reversal task, in which the monkeys had to choose one object for a reward and then choose another object, monkeys with lesions of the orbital PFC perseverated by continuing to choose the object that had initially been rewarded. By contrast, the performance of monkeys with lesions of the dorsolateral PFC was normal. This suggests that both the dorsolateral and orbital PFC contribute to inhibitory control, but the dorsolateral PFC may be more engaged by inhibitory control over rules that involve shifts of attention between a stimulus dimension (e.g., color versus shape), while the orbital PFC may be more engaged by inhibitory control over choices based on associations between objects and rewards (Roberts and Wallis, 2000).

In short, the PFC is a complex brain region that cannot easily be split along simple lines. Its functional organization is an active area of research, particularly with the advent of functional imaging in humans. Although a clear picture has yet to emerge, we can make some general predictions. First, although broad categories or gradients of organization may exist, it is unlikely that different classes of information will be represented in a modular, or discretely localized, form. Complex behavior requires that we recognize and respond to relationships across diverse dimensions. Second, learning is likely to play an important role in the information represented in the PFC and hence in its organization.

COGNITIVE ARCHITECTURE AND PFC DAMAGE The pattern of deficits following PFC damage seems to reflect a selective loss of the higher-level functions from the bipartite cognitive architecture pictured in Figure 104.1. Well-established automatic routines on the lower level are intact and available to

be triggered by the appropriate sensory cues. But without the higher-level functions specialized to acquire and represent goals and means, the system would be at the mercy of the environment, ruled by whatever sensory inputs happen to flow into the system and by whatever thoughts, emotions, and actions are strongly associated with these inputs. Thus, behavior would seem impulsive and disinhibited and reactions inappropriate, because they would be emitted reflexively without any consideration of the future. Further, without the influence of predicted goals to continually drive task-appropriate processes, individuals would be distractible and would easily go “off track” when there are temporal gaps between sensory inputs or between those inputs and the individual’s responses. The system might be capable of learning to react to cues, but this learning would be inflexible. Without the ability to predict goals and means, the system would be stuck in a behavioral rut, always reacting to a cue with whatever behavior it was first associated; in other words, the system would perseverate.

To summarize, we have seen that the PFC is a brain area that has access to the diverse range of information that seems appropriate for a region that provides top-down control to other brain processes, and that its damage results in the goal neglect and impulsivity that would be predicted from a selective loss of the higher-order processes in a two-tier cognitive architecture. To begin to understand the neural mechanisms that help the PFC to play this role, we now turn to studies of its neural properties.

Neurophysiology of the PFC

The multimodal nature of inputs to the PFC is reflected in its neural activity. PFC neurons are activated by visual, auditory, tactile, and gustatory cues and by recalled memories, as well as voluntary limb and eye movements. In short, the PFC has access to the diverse informational domains needed to guide goal-directed behaviors. Its neurons have other properties that seem ideal for a system for cognitive control. PFC neural activity can reflect predicted rewards and learned task contingencies (i.e., goals and means) and keep them on-line during task execution.

REWARD-RELATED ACTIVITY Planning goal-directed behavior requires making predictions about goals and the consequences of events and actions. Evidence that PFC neurons participate in this process comes from studies showing that a large proportion of them encode information about expected rewards. For example, some neurons are activated by the delivery of a reward, while others respond when an expected reward is not delivered. After training, many PFC neurons show responses to visual cues that signal whether a reward will or will not be forthcoming and reflect the identity, size, and preference of an expected reward.

RULE REPRESENTATION Rules describe the logic of a goal-directed task. Conditional (if-then) associations (see “Behavioral Effects of PFC Damage in Monkeys”) are prime examples. As mentioned above, they must be acquired mechanisms that detect and store reward-predicting contingencies (associations) between events and actions. Many studies have shown that PFC neurons do just that. Because these studies have typically employed visual cues and either limb or eye movements, most of these studies have focused on the lateral PFC, which is directly connected with the visual and motor systems.

Asaad et al. (1998) recorded from the lateral PFC as monkeys learned associations between each of two visual cues and directional eye movements. Through trial and error, the monkeys learned to saccade to the right after one object was presented and saccade to the left after another object was presented. After this was learned (in about 10 to 15 trials) and practiced (for about 15 more trials), the associations were reversed and the monkeys learned the opposite contingencies: to saccade leftward after presentation of the object that had previously been associated with a rightward saccade and vice versa. Almost half (44%) of randomly selected lateral PFC neurons reflected the learned contingencies; they encoded specific associations between cues and saccades. For example, a given cell might be strongly activated only when object A instructed “saccade left” and not when object B instructed the same saccade or when object A instructed another saccade. This effect is not limited to associations between cues and actions. As noted above, many PFC neurons encode associations between a visual cue and a reward. Lateral PFC neurons can also reflect learned associations between visual and auditory stimuli and between two visual stimuli.

These studies suggest that PFC neurons represent relatively simple task contingencies. Others have shown that they can also encode more complex demands. For example, monkeys can be taught to alternate rapidly between different rules. Following a given cue, they can learn to direct a response to either the cue’s location (spatial matching rule) or an alternative location associated with the cue (associative rule), depending on which rule is currently in effect. When tested in this fashion, many PFC neurons show rule-specific activity (Asaad et al., 2000; White and Wise, 1999). A given PFC neuron might respond to a visual cue when the monkey is using an associative rule but exhibit weak or no activity under identical sensory and attentional conditions that differ only in that the monkey is instead using a spatial rule. Neurons also show reliable shifts in their baseline activity that may reflect a signal that keeps track of which rule is currently relevant.

CONCEPTS AND PRINCIPLES In the examples above, lateral PFC neurons were found to encode learned relationships

between specific cues and/or actions. However, it is not always advantageous for us to take the world so literally. A brain limited to recording each specific behavioral contingency that we encounter would need prodigious storage capacity and would bog us down with unnecessary details. Instead, we have evolved the ability to detect the commonalities across experiences and store them as abstract concepts and general principles. For example, knowing that a gadget is a camera imparts knowledge about parts and functions and spares us the need to learn it anew. Similarly, we have general principles for behavior such as dining in restaurants. This allows the navigation of many different situations with a minimal amount of storage and allows us to deal with novelty. By extracting the essential elements from our experiences, we can generalize to future situations that share some elements but may, on the surface, appear very different. Some recent studies have shown that the capacity of PFC neurons to reflect task demands extends to such abstracted representations.

One example comes from a study of perceptual categorization. Freedman et al. (2001) taught monkeys to categorize computer-generated images as cats and dogs. Three prototypical cats (a house cat, a tiger, and a cheetah) and three types of dogs (a German shepherd, a pointer, and a St. Bernard) were morphed, or blended, into single images that contained both cat and dog characteristics. Some images were 80% cat and 20% dog, or 60% dog and 40% cat. Monkeys were taught that if an image was more than half cat or more than half dog, it should be categorized as a cat or a dog, respectively. As many as a third of lateral PFC neurons reflected the category of the images. In other words, a given neuron might be activated in a similar fashion by all the cat images, even though the exact physical appearance of the different cats varied widely.

It is not only useful to group different sensory stimuli into perceptual categories, it is also useful to group different behavioral experiences according to common themes, that is, as abstract rules or generalized principles for behavior. To explore this, monkeys were trained to use two abstract rules; they indicated whether two successively presented pictures were either the same (match) or different (nonmatch), depending on which rule was currently in effect (Wallis et al., 2001). The monkeys could perform this task with novel pictures, thus demonstrating that they had learned two general principles that could be applied to stimuli that they had not directly experienced. The most prevalent neuronal activity observed in the three major PFC subdivisions (dorsolateral, ventrolateral, and orbital) were those that encoded the match and nonmatch rules. This suggests that rule representation may be a cardinal PFC function.

RAPID LEARNING IN THE PFC Insofar as primates can rapidly learn new behaviors, brain regions guiding them

must also have the ability to quickly change properties. PFC neurons do have this capacity. Monkeys can learn new conditional visuomotor associations in just a few trials, and as they do, PFC neural activity is rapidly modified to reflect the new contingencies. Striking examples of rapid experience-dependent neural plasticity come from studies of the frontal eye fields, part of Brodmann's area 8 that is important for voluntary shifts of gaze (Bichot and Schall, 1999). Normally, neurons in this area are selectively activated by saccade targets that appear in certain visual field locations. Monkeys were also trained to search for a target defined by a particular visual attribute (e.g., red). In this case, the neurons in the frontal eye fields acquired sensitivity to that attribute. Monkeys were also trained to search for a different target every day, and it was found that neurons discriminated not only the current target but also distracting stimuli that had been a target on the previous day relative to stimuli that had been targets even earlier. Monkeys were also more likely to make errors in choosing the distracting stimulus. It was as if the previous day's experience left an impression in the brain that influenced neural activity and task performance.

WORKING MEMORY The first observations that PFC neurons have the capacity to keep information on-line and available over multisecond delays were made in the 1970s by Fuster, Niki, and their colleagues. They demonstrated that during delayed-response tasks, many PFC neurons showed sustained activity that seemed to keep information about a cue or response available over multisecond delays. Goldman-Rakic and colleagues used an oculomotor version of the delayed-response task. In this task, monkeys were trained to maintain central gaze while a cue (a spot of light) was briefly flashed at one of eight locations in the visual periphery. Then, after a delay of 1 or more seconds, the monkeys were signaled to move their eyes to the remembered location of the cue. This allowed them to demonstrate that dorsolateral PFC neurons have precise tuning for memories of particular visual field locations (Funahashi et al., 1989). It also showed that PFC delay activity depends on dopamine (DA) receptors, neurotransmitters implicated in signaling reinforcements and thus central to acquiring and sustaining goal-directed behaviors.

PFC activity sustains brief memories of a wide range of behaviorally relevant cues: objects, colors, the frequency of a vibration to the hand, and forthcoming movements. Similar activity is also evident in the sensory and motor systems. This is not surprising; sustained activity is evident in many brain structures and must play a role in many neural processes ranging from sensory afterimages to holding a motor state. However, what separates more cognitive short-term memory processes such as working memory processes from such lower-level processes is specificity and robustness. Working memory selectively retains task-relevant informa-

tion (rather than just any stimulus) and does so over potential distractions. PFC neurons do have this ability. For example, when monkeys are required to sustain the memory of a sample object across a delay period filled with visual distractors that require attention and processing, sustained activity within the prefrontal cortex can still maintain a memory of the sample object (Miller et al., 1996). By contrast, sustained activity in visual cortical areas seems more labile; it is disrupted by the presence of distractors. Following a distracting stimulus, neural activity reflects the distractor rather than the stimulus the monkey is retaining in working memory. This particular ability is not unique to the PFC. Some neurons in the entorhinal cortex, a region critical for memory, can also maintain sample-specific delay activity across intervening stimuli.

The ability of PFC neurons to "latch onto" a behaviorally relevant input and maintain it robustly has been proposed to depend on gating signals that instruct the PFC network when to maintain a given activity state. This may come from reward-related signals from DA neurons in the midbrain and basal ganglia. These neurons are activated by reward or, importantly, by cues that predict that a reward is forthcoming (Schultz and Dickinson, 2000). In many behavioral tasks, presentation of the cue at the start of the trial is a good predictor that a reward is forthcoming. A burst of DA at this time could strengthen the current PFC representation, protecting it against interference from disruption by distracting information until another DA influx reinforces another representation (Braver and Cohen, 2000; Miller and Cohen, 2001). Local injection of DA antagonists in the PFC does block delay activity in the PFC. Further, the anatomical loops between the PFC and basal ganglia have been suggested to play a role here. Neural activity propagating around the loops may help sustain activity, and the basal ganglia have been suggested to provide a means by which DA signals can influence PFC activity (Passingham, 1993).

Theories of PFC and cognitive functions

The behavioral, anatomical, and neurophysiological observations reviewed above have naturally led to theories of PFC function. There is no model that encompasses all the mechanisms needed for cognitive control. Rather, different theorists have emphasized different aspects of PFC function.

WORKING MEMORY One view of PFC function emphasizes its role in maintaining behaviorally relevant cues on-line over brief (multisecond) temporal gaps (Goldman-Rakic, 1987). The PFC acts like a temporary scratch pad for the inputs it receives from other cortical systems. The importance of such a store for cognition was discussed above but is also appar-

ent to anyone who has tried to do math in her head; intermediate answers and operations must be buffered in a way that allows them to be kept “in mind.” Other deficits following PFC damage are thought to be sequelae of the working memory deficit. Patients may have difficulty planning or appear disinhibited because, without working memory, goal-relevant information is lost over all but the briefest delays, and thus their behavior takes its cue from the immediate environment.

As previously discussed, working memory is essential to controlled processing because goal-directed behaviors extend over time. Support for a role of the PFC in working memory comes from numerous studies showing sustained activity (or correlates of it) in the PFC during working memory tasks. But working memory cannot be the whole picture. It is difficult to explain voluntary behavior without positing additional mechanisms; for example, what determines what enters working memory and what is maintained? PFC involvement in working memory is likely part of a broader role in cognitive control.

SOMATIC MARKER HYPOTHESIS According to this hypothesis the orbitofrontal PFC is responsible for labeling cues or situations with *affective significance* (Damasio, 1994). It associates memories of past affect-laden events with a representation of the state of the autonomic nervous system that the event evoked. This tags the memory of the past event with a *somatic marker* that helps individuals make decisions. Similar events in the future can then evoke a “gut feeling” of the appropriate course of action by recall of the somatic marker. This is particularly helpful in very complex situations where it is difficult to evaluate all the pros and cons and their probabilities. Patients with damage to the orbitofrontal PFC may have difficulty reaching decisions, because no alternative will be obviously more emotionally preferable than others. They may make decisions randomly or impulsively and appear to be disinhibited. Support for this hypothesis comes from impairments on a gambling task (see “Behavioral Effects of PFC Damage in Humans”) following orbitofrontal damage in humans. This task is thought to depend on gut feelings because the probabilities associated with each deck of cards are too difficult to evaluate consciously. In addition, patients with orbitofrontal PFC damage do not show elevated skin conductance responses (a measure of autonomic function) preceding a choice from a risky deck, as normal subjects do.

MULTIPLE PROCESSING LEVELS This view of PFC function posits that there are different levels of cognitive processing that are localized in different PFC regions (Petrides, 1996). The lateral PFC is where information is first received by the PFC and processed. It is involved in simple functions such as maintenance and retrieval (recall) of information from

long-term storage in posterior cortex. For more elaborate processing, information is transferred to the middorsal PFC. This is where multiple behaviors are monitored and information is manipulated. For example, the lateral PFC can rehearse a phone number, but the middorsal PFC would be needed if you had to say it backward. Evidence supporting this hypothesis comes from neuroimaging studies in humans and lesion studies in monkeys. For example, when humans perform tasks that have manipulation requirements, there is greater blood flow into the middorsal PFC compared to the lateral PFC. By contrast, the reverse blood flow occurs if only simple maintenance is required.

RULE ACQUISITION AND REPRESENTATION Because knowledge about goals, means, and consequences is vital to planning and implementing complex goal-directed behavior, several investigators have suggested that the PFC is likely to play a central role in the acquisition and representation of rules. The PFC as a neural system for acquiring task contingencies was first proposed by Joaquin Fuster (1989). He suggested that the sustained and multimodal activity of PFC neurons was used to link together behaviorally associated but temporally separate events and actions.

Others have proposed hypotheses in the same vein. Passingham (1993) suggested that the pattern of deficits following PFC damage results from a loss of the ability to acquire specific types of associations, the conditional if-then rules (see “Behavioral Effects of PFC Damage in Monkeys”) that are used as a test of volitional control. Wise et al. (1996) proposed complementary roles for the PFC and the basal ganglia: the PFC acquires new rules, while the basal ganglia activates already familiar rules. Grafman (1994) suggested that the PFC contains managerial knowledge units (MKUs), sets of basic behavioral rules that can be combined into extended routines. A linked set of MKUs may describe the expected events and appropriate responses for dining in a restaurant, for example.

Miller and Cohen (2001) and their colleagues (Braver and Cohen, 2000; Miller and Asaad, 2002) have proposed models of PFC function that explain how it acquires rules and exerts control over other brain systems. They posit that cognitive control stems from the active maintenance of patterns of activity in the PFC that represent goals and their means. This activity feeds back to posterior cortex, providing bias signals whose net effect is to guide the flow of activity throughout the forebrain along neural pathways that establish the proper mappings between inputs, internal states, and outputs needed to perform the task at hand (Fig. 104.5A).

These representations are developed through the action of reinforcement signals on multimodal PFC circuitry. During learning, when a behavior is successful, reward signals augment the unique pattern of PFC activity evoked

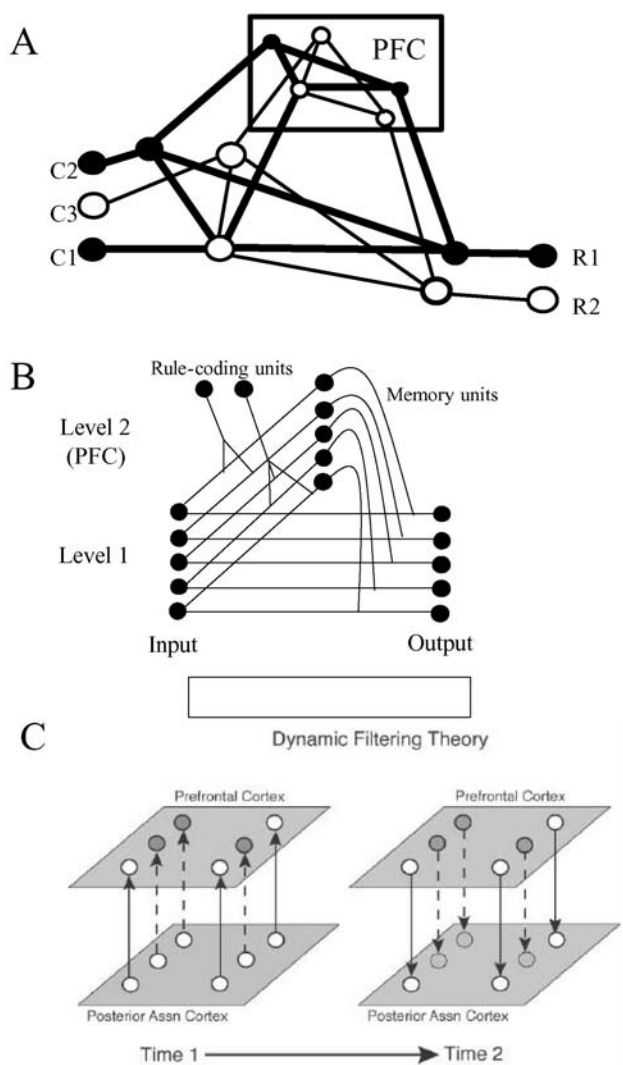


FIGURE 104.5. Models of PFC function. *A*, In the Miller and Cohen model, a task model is formed in the PFC when reward signals link together neurons activated by the events that led to the reward. A subset of cues can then activate the entire representation. Bias signals resulting from the maintenance of this pattern guide the flow of activity along neural pathways that establish the task-relevant mappings between representations of inputs (C1, C2, C3), internal states, and outputs (R1, R2) in posterior cortex. *Thick lines and filled circles* denote active processing lines. *B*, The models of Changeux and Dehaene include an executive level (level 2, thought to correspond to the PFC) with rule-coding units and working memory units that gate the flow of activity along lower-level input-output lines. *C*, Shimamura's dynamic filtering model (Shimamura, 2000). At Time 1, a region in PFC is activated by feedforward (i.e., bottom-up) projections from posterior cortex. This activity, along with influences such as task demands, sets up a pattern of activation in PFC (*light circles* = activation, *dark circles* = inhibition). At Time 2, posterior cortex is modulated by PFC via feedback (i.e., top-down) projections that enable both selection of task-relevant and inhibition of task-irrelevant neural activity. (*A* from Miller and Cohen, 2001; *B* modified from Changeux and Dehaene, 1993; *C* provided by Arthur Shimamura, 2000.)

by that situation, action, and consequence by strengthening connections between neurons activated by those events. These representations can begin quite modestly, but with time (and repeated iterations of this process), the PFC representation can “bootstrap” into further elaboration as combinations of events, contingencies between them, and the requisite actions are learned. Midbrain DA neurons have ideal properties for the reinforcement signal. They are activated by rewards and then, after learning, they are activated instead by the cues that predict those rewards and are inhibited when an expected reward is not delivered. As the aim of the organism is to predict the means to achieve a reward, this *reward prediction error* signal is ideal for instructing when the system should learn (Schultz and Dickinson, 2000).

The resulting pattern of PFC activity reflects the task's contingencies and, in neural terms, amounts to a “map” of the neural pathways between inputs, internal states, and outputs needed to perform the task. In short, the intermingling of diverse information in the PFC allows it to quickly plot a map of which neural pathways in the forebrain are successful at solving a task and then holds it on-line so that the rest of the neocortex can follow it. While the PFC may be critically involved in acquisition of this map, its long-term memory may be consolidated in other parts of the brain. The PFC, however, would retain the requisite links to retrieve the appropriate pattern and bring it on-line to guide behavior whenever stimuli are ambiguous (i.e., they activate more than one input representation) or when multiple responses are possible and the task-appropriate response must compete with stronger alternatives.

Similar models of prefrontal and executive function have been proposed. Network models of Changeux and Dehaene (1993) include an executive layer of “rule-coding” units (thought to correspond to the PFC) that controls the flow of information between the input and output layers (Fig. 104.5*B*). Shimamura (2000) proposed a dynamic filtering model of PFC function in which patterns of information sustained by the PFC select and reroute the flow of activity in posterior association cortex (Fig. 104.5*C*).

SELECTION BY BIASED COMPETITION AND SUSTAINED ACTIVITY

To understand how top-down signals from the PFC might select task-relevant neural pathways in other brain regions, consider Desimone and Duncan's (1995) biased competition model of visual attention. In the visual system, neurons processing different aspects of the visual scene (objects or locations) compete with each other for activation through mutual inhibitory interactions. This type of competition seems to occur at every level of the visual system and is thought to be important for enhancing contrast and separating figure from ground. The neurons that “win” the competition and remain active are those that incur a higher level of activity

and thus can suppress their competitors. The biased competition model posits that visual attention exploits this circuitry. In voluntary shifts of attention, a competitive advantage comes from excitatory signals (thought to originate from the PFC) that represent the to-be-attended stimulus. These signals enhance the activity of neurons in the visual cortex that process that stimulus and, by virtue of the mutual inhibition, suppress activity of neurons processing other stimuli.

This notion of excitatory bias signals that resolve local competition in the visual system can be readily adapted to cognitive control in many brain systems (Miller and Cohen, 2001). PFC bias signals can be viewed as the neural implementation of attentional templates, rules, or goals, depending on which brain system is the target of their biasing influence. Because top-down signals from the PFC are multimodal and include information about stimuli, actions, and so on that have become associated through experience, they can simultaneously select goal-relevant inputs, actions, and intervening representations, and thereby dynamically establish a set of neural circuits that would otherwise not exist.

O'Reilly and Munakata (2000) have pointed out that using sustained activation to provide these bias signals has advantages for cognitive control beyond the obvious ability to bridge temporal gaps. As mentioned above, long-term storage of information in the brain is widely thought to depend on structural changes between neurons that either increase or decrease the strength of their connection (i.e., by changing synaptic weights). This hardwiring has advantages for long-term storage and for automatic processes but disadvantages for cognitive control. First, changing synaptic weights has local effects; only the two neurons sharing the synapse are affected, and the information is expressed only when the circuit is fired. By contrast, the goals and means needed for cognitive control must be encoded in a fashion that allows it to influence other brain systems. Second, information encoded by hardwiring is relatively inflexible; well-established circuits will almost always fire off in the same way, and they do not generalize well to novel situations. Encoding the information needed for cognitive control in a pattern of ongoing activation solves these problems. The activity can be propagated across the brain to influence distant circuits, and it allows flexibility; if voluntary behavior stems from a pattern of information maintained in the PFC, changing behavior is as easy as changing the pattern (Miller and Cohen, 2001; O'Reilly and Munakata, 2000).

KNOWING WHEN TO ENGAGE COGNITIVE CONTROL A key question concerning cognitive control that we have not yet discussed is how the system knows when control is needed. Earlier, we noted that cognitive control is necessary when

cues are ambiguous or a reflexive reaction is disadvantageous. Brain systems must therefore exist for recognizing these situations and bringing control functions on-line.

A discussion of these mechanisms is beyond the scope of this review; besides, they are largely unknown. But worth noting here is the work of Cohen, Braver, and colleagues. They posit that the anterior cingulate detects a neural signature of when control is needed—conflict between incompatible representations (Botvinick et al., 2001)—and sends a signal to the PFC. Support for this hypothesis comes from observations of increased blood flow to the anterior cingulate when conflict between two behavioral responses occurs.

Summary

The ability to take charge of one's actions and direct them toward unseen aims is called *cognitive control*. Virtually all theories of cognition posit that cognitive control requires making predictions about available goals and what means might achieve them. This knowledge can then be used to select and coordinate among myriad lower-level, automatic sensory, memory, and motor functions.

The PFC, a brain structure that reaches its greatest complexity in the primate brain, seems to play a central role in cognitive control. It has access to, and the means to influence, processing in all major forebrain systems. Its damage in humans and monkeys results in goal neglect; individuals seem capable only of emitting habitual or innate reactions to the immediate environment, without any consideration or anticipation of future consequences and unseen goals. Neurophysiological studies indicate that PFC neurons seem to mediate the mechanisms essential for a cognitive control system: they are multimodal, they acquire and signal the formal demands of tasks, and they can sustain their activity to keep task-relevant information on-line and available during behavior.

Different theories of PFC function emphasize different contributions to cognitive control: maintenance and/or manipulation of information in working memory, the assignment of affective tags to events and choices, and the acquisition and on-line representation of task rules. None of these theories are mutually exclusive; each may reflect different facets of a system that is necessarily multivariate because of its role in guiding many different behaviors and interfacing with many other brain systems.

REFERENCES

- Asaad W. F., G. Rainer, and E. K. Miller, 1998. Neural activity in the primate prefrontal cortex during associative learning, *Neuron*, 21:1399–1407.
- Asaad W. F., G. Rainer, and E. K. Miller, 2000. Task-specific activity in the primate prefrontal cortex, *J. Neurophysiol.*, 84:451–459.
- Baddeley, A., 1986. *Working Memory*, Oxford: Clarendon Press.
- Barbas, H., and D. N. Pandya, 1989. Architecture and intrinsic

- connections of the prefrontal cortex in the rhesus monkey, *J. Comp. Neurol.*, 286:353–375.
- Barbas, H., and D. Pandya, 1991. Patterns of connections of the prefrontal cortex in the rhesus monkey associated with cortical architecture, in *Frontal Lobe Function and Dysfunction* (H. S. Levin, H. M. Eisenberg, and A. L. Benton, eds.), New York: Oxford University Press, pp. 35–58.
- Barsalou, L. W., 1992. *Cognitive Psychology: An Overview for Cognitive Scientists*, Hillsdale, NJ: Erlbaum.
- Bechara, A., A. R. Damasio, H. Damasio, and S. W. Anderson, 1994. Insensitivity to future consequences following damage to human prefrontal cortex, *Cognition*, 50:7–15.
- Bichot, N. P., and J. D. Schall, 1999. Effects of similarity and history on neural mechanisms of visual selection, *Nat. Neurosci.*, 2:549–554.
- Botvinick, M. M., T. S. Braver, D. M. Barch, C. S. Carter, and J. D. Cohen, 2001. Conflict monitoring and cognitive control, *Psychol. Rev.*, 108:624–652.
- Braver, T. S., and J. D. Cohen, 2000. On the control of control: the role of dopamine in regulating prefrontal function and working memory, in *Attention and Performance 18* (S. Monsell and J. Driver, eds.), Cambridge, MA: MIT Press.
- Changeux, J. P., and S. Dehaene, 1993. Formal models for cognitive functions associated with the prefrontal cortex, in *Exploring Brain Functions: Models in Neuroscience* (T. A. Poggio and D. A. Glaser, eds.), New York: Wiley.
- Damasio, A. R., 1994. *Descartes' Error: Emotion, Reason, and the Human Brain*, New York: G. P. Putnam.
- Desimone, R., and J. Duncan, 1995. Neural mechanisms of selective visual attention, *Annu. Rev. Neurosci.*, 18:193–222.
- Dias, R., T. W. Robbins, and A. C. Roberts, 1996. Dissociation in prefrontal cortex of affective and attentional shifts, *Nature*, 380: 69–72.
- Dickinson, A., 1980. *Contemporary Animal Learning Theory*, Cambridge: Cambridge University Press.
- Duncan, J., H. Emslie, P. Williams, R. Johnson, and C. Freer, 1996. Intelligence and the frontal lobe: the organization of goal-directed behavior, *Cogn. Psychol.*, 30:257–303.
- Eslinger, P. J., and A. R. Damasio, 1985. Severe disturbance of higher cognition after bilateral frontal lobe ablation: patient EVR, *Neurology*, 35:1731–1741.
- Freedman, D. J., M. Riesenhuber, T. Poggio, and E. K. Miller, 2001. Categorical representation of visual stimuli in the primate prefrontal cortex, *Science*, 291:312–316.
- Funahashi, S., C. J. Bruce, and P. S. Goldman-Rakic, 1989. Mnemonic coding of visual space in the monkey's dorsolateral prefrontal cortex, *J. Neurophysiol.*, 61:331–349.
- Fuster, J. M., 1989. *The Prefrontal Cortex*, New York: Raven Press.
- Goldman-Rakic, P. S., 1987. Circuitry of primate prefrontal cortex and regulation of behavior by representational memory, in *Handbook of Physiology: The Nervous System* (F. Plum ed.), Bethesda, MD: American Physiological Society, pp. 373–417.
- Grafman, J., 1994. Alternative frameworks for the conceptualization of prefrontal functions, in *Handbook of Neuropsychology* (F. Boller and J. Grafman, eds.), Amsterdam: Elsevier, p. 187.
- Graybiel, A. M., 2000. The basal ganglia, *Curr. Biol.*, 10:R509–R511.
- Houk, J. C., and S. P. Wise, 1995. Distributed modular architectures linking basal ganglia, cerebellum, and cerebral cortex: their role in planning and controlling action, *Cereb. Cortex*, 5:95–110.
- Miller, E. K., and W. F. Asaad, 2002. The prefrontal cortex: conjunction and cognition, in *Handbook of Neuropsychology* (J. Grafman ed.), New York: Elsevier.
- Miller, E. K., and J. D. Cohen, 2001. An integrative theory of prefrontal function, *Annu. Rev. Neurosci.*, 24:167–202.
- Miller, E. K., and R. Desimone, 1994. Parallel neuronal mechanisms for short-term memory, *Science*, 263:520–522.
- Miller, E. K., C. A. Erickson, and R. Desimone, 1996. Neural mechanisms of visual working memory in prefrontal cortex of the macaque, *J. Neurosci.*, 16:5154–5167.
- Milner, B., 1963. Effects of different brain lesions on card sorting, *Arch. Neurol.*, 9:90.
- Milner, B., M. Petrides, and M. L. Smith, 1985. Frontal lobes and the temporal organization of memory, *Human Neurobiology*, 4: 137–142.
- Norman, D. A., and T. Shallice, 1986. Attention to action: willed and automatic control of behavior, in *Consciousness and Self-Regulation: Advances in Research and Theory* (R. J. Davidson, G. E. Schwartz, and D. Shapiro, eds.), New York: Plenum, pp. 1–48.
- O'Reilly, R. C., and Y. Munakata, 2000. *Computational Explorations in Cognitive Neuroscience: Understanding the Mind*, Cambridge, MA: MIT Press.
- Pandya, D. N., and C. L. Barnes, 1987. Architecture and connections of the frontal lobe, in *The Frontal Lobes Revisited* (E. Perecman ed.), New York: IRBN Press, pp. 41–72.
- Passingham, R., 1993. *The Frontal Lobes and Voluntary Action*, Oxford: Oxford University Press.
- Petrides, M., 1996. Specialized systems for the processing of mnemonic information within the primate frontal cortex, *Philos. Trans. R. Soc. Lond. B Biol. Sci.*, 351:1455–1461.
- Petrides, H., and D. N. Pandya, 1994. Comparative architectonic analysis of human and macaque frontal cortex, in *Handbook of Neuropsychology* (F. Boller and J. Grafman, eds.), New York: Elsevier.
- Rainer, G., W. F. Asaad, and E. K. Miller, 1998. Memory fields of neurons in the primate prefrontal cortex, *Proc. Natl. Acad. Sci. USA*, 95:15008–15013.
- Roberts, A. C., and J. D. Wallis, 2000. Inhibitory control and affective processing in the prefrontal cortex: neuropsychological studies in the common marmoset, *Cereb. Cortex*, 10:252–262.
- Schultz, W., and A. Dickinson, 2000. Neuronal coding of prediction errors, *Annu. Rev. Neurosci.*, 23:473–500.
- Shallice, T., and P. W. Burgess, 1991. Deficits in strategy application following frontal lobe damage in man, *Brain*, 114:727–741.
- Shallice, T., P. W. Burgess, F. Schon, and D. M. Baxter, 1989. The origins of utilization behaviour, *Brain*, 112:1587–1598.
- Shimamura, A. P., 2000. The role of the prefrontal cortex in dynamic filtering, *Psychobiology*, 28:207–218.
- Wallis, J. D., K. C. Anderson, and E. K. Miller, 2001. Single neurons in the prefrontal cortex encode abstract rules, *Nature*, 411:953–956.
- White, I. M., and S. P. Wise, 1999. Rule-dependent neuronal activity in the prefrontal cortex, *Exp. Brain Res.*, 126:315–335.
- Wilson, F. A. W., S. P. O'Scalaidhe, and P. S. Goldman-Rakic, 1993. Dissociation of object and spatial processing domains in primate prefrontal cortex, *Science*, 260:1955–1958.
- Wise, S. P., E. A. Murray, and C. R. Gerfen, 1996. The frontal-basal ganglia system in primates, *Crit. Rev. Neurobiol.*, 10:317–356.

XIII THEORETICAL
AND
COMPUTATIONAL
PERSPECTIVES

105 The Evolution of the Visual System in Primates

JON H. KAAS

HUMANS HAVE LONG been impressed with both the similarities and the great differences they see in human behavior and those of the pets and other mammals around them. The obvious differences in behavior have led to interest in and speculation about brain size and structure, brain evolution, and the major functions of brains, especially consciousness. Some of this speculation has not been well informed, leaving the impression that we know little or can know little about brain evolution and that theories of brain evolution are necessarily unsupported and unscientific (for review, see Striedter, 1998). Moreover, we have inherited some misconceptions from the past, especially the belief that evolution is progressive and has a single direction of change (Preuss and Kaas, 1996). This has led to the view that complex human and monkey brains are composed of both old and new parts and that these can be distinguished by appearance. "Old" parts are supposed to look and act old by being poorly differentiated and having crude functions, while "new" parts look new by being well differentiated and having specialized functions (Kaas, 1987). However, evolution does not have a single direction of change, and brains can become smaller; parts can become less differentiated, and parts can be lost (Catania et al., 1999) as well as gained (Kaas, 1989). Old parts can be modified to perform new functions, and new parts modify other parts as they become integrated into existing systems.

Here we consider variations in the organization of the visual system of primates, and the close relatives of primates, as a result of adaptations subserving the differing opportunities and histories of various lines of descent within a framework of inherited and environmental constraints. Brains evolve through a process of "tinkering" with the course of development rather than extensive redesign (Jacob, 1977). Thus, the evolution of the complex human brain is one historical outcome of many possibilities, some of which have been realized by the other primates around us.

The visual system has many subcortical and cortical components, and it would be difficult to discuss them all. As cortex seems to be where mammals are especially variable, and as visual cortex mediates the important function of object vision, we focus here on visual cortex and the pathways leading to it.

How to study brain evolution

The study of brain evolution is a historical science, yet very little about brain evolution can be learned from the fossil record. Brains die and rot, and only the brain case, with luck, remains. Brain cases can tell us something about brain size, brain shape, and sometimes indicate major brain fissures. Brain size is easy to measure, and it is an important variable. Thus, much has been written about brain size (e.g., Jerison, 1973). Moreover, it is especially relevant to consider the implications of observed differences in brain size when studying the evolution of human brains, since our brains have greatly increased in size over the past 3 to 4 million years (Preuss and Kaas, 1999). But the great differences in the internal complexity of brains are not revealed by their external size and shape. Thus, most of what we learn about brain evolution will come indirectly through inferences based on observations made on the brains of the many extant (living) species (Kaas, 1997a). In studying human brain evolution, we have a rich opportunity in that living members of the primate order are highly varied in brain organization, and we have roughly 200 primate species to consider.

The comparative approach to studying brain evolution depends on examining the brains of the most relevant extant species, determining what feature or characters they share, and evaluating the probabilities that features are shared because they were inherited from a common ancestor or evolved independently (see Northcutt, 1984; Preuss, 2000; Striedter, 1998). To obtain a comprehensive understanding of the evolution of the human visual system and those of other primates will take much comparative research, but the approaches and methods of study are known. Fortunately, there has been considerable progress, and this progress allows some of the conclusions that follow here.

The basic premise of the evolutionary or phylogenetic approach is that the brain and other body parts of extant mammals are mixtures or mosaics of features that emerged at various times over the course of evolution. The distributions of any trait across the brains of extant mammals, and the phylogenetic relationships of these mammals, provide the critical sources of information about when a trait in any

particular line of evolution emerged. For example, all placental mammals have a corpus callosum. No other mammals or vertebrates do. Thus, the corpus callosum emerged after the ancestors of placental mammals diverged from marsupials. This cladistic approach (Hennig, 1966) sounds easy, and it is in concept, but the difficulty lies in recognizing brain characters. If current researchers disagree on the existence of V3 in primates, how can we deduce the evolution of V3? As a further complication, even if the existence of a corpus callosum or V3 can be determined with a high degree of certainty, this is only a start, since the features and functions of these structures will vary across and within lines of evolution. A serious problem here is that comparative studies can be time-consuming and costly, and thus the need to be practical will often compromise the plan of investigation. Finally, many relevant species are either unavailable for study or can be studied only after natural death. This includes most of the 200 or so species of primates that are potentially available for study. Fortunately, much can be learned from histological studies of the brains of a few available specimens, and interpretations of comparative studies can be guided by more extensive information from more fully studied species. Other important insights will come from our emerging understandings of the mechanisms of brain development and the “rules” of brain scaling (Finlay and Darlington, 1995; Kaas, 2000).

The origin and radiation of primates

Applying the comparative method to the study of brain evolution depends on knowing the phylogenetic relationships of the species under investigation. Molecular studies and statistical techniques have helped sort out such relationships over the past few years and have pushed back the probable times of divergence of major mammalian groups (e.g., Murphy et al., 2001). Early mammals arose from mammal-like reptiles approximately 200 million years ago and separated into six major lines that fractionated into the 20 or so orders of living mammals now commonly recognized (Fig. 105.1). Two early branches led to the present-day monotremes and marsupials. A third branch of placental or eutherian mammals divided into four major groups or superorders. The oldest of these superorders (Afrotheria) includes the surviving insectivore-like tenrecs of Madagascar, but also elephants and armadillos. Another early branch (Xenarthra) contains armadillos and sloths. The third group of placental mammals (Laurasiatheria) includes shrews and moles as well as bats, carnivores, pigs, and whales. The fourth superorder (Euarchontoglires) is the most relevant here, as it includes humans and the other primates, as well as the closest relatives of primates. Our closest nonprimate relatives are tree shrews (Scandentia) and flying lemurs (Dermoptera), which are included with primates in the

higher-order taxon, Archonta. Bats (Chiroptera) were once included in Archonta, but recent molecular evidence places them in the superorder Laurasiatheria. Although megachiropteran bats have well-developed visual systems that seem primate-like, humans are more closely related to rats, mice, and rabbits (Rodentia and Lagomorpha). To the extent that primates share brain traits with tree shrews and flying lemurs, these traits probably emerged before the time of divergence some 65 million years ago. Traits shared with rabbits and rodents evolved even earlier, perhaps 85 million years ago, while features shared with bats and cats go back even further (except for similar but independently evolved traits).

Early primates soon diverged into three main lines: a prosimian line leading to present-day lemurs, lorises, and galagos; a tarsier line with only a few surviving species; and a highly diverse line of anthropoid primates that split into New World monkeys, Old World monkeys, and apes. One line of apes gave rise rather recently (about 5 to 6 million years ago) to hominids and present-day bonobos and chimps. As the only remaining hominid, *Homo sapiens* appeared only within the past 200,000 years.

While much of what we infer about the organization of the human brain comes from studies on macaque monkeys, it is important to remember that we have evolved independently of Old World monkeys for at least 30 million years and that our brains have expanded by three to four times over those of our closest living relatives, the great apes, in less than 6 million years. Besides the great change in size over that time, what changes in structure, organization, and function occurred? Comparative studies of chimpanzee and human brains will help address this question, but much is beyond the scope of a comparative approach, as the intermediate brains that would bridge this huge gap are long gone.

What features of the visual system do primates share with other mammals?

The record of fossil brain endocasts (e.g., Jerison, 1973) indicates that early mammals were rather small and small-brained, with proportionately little neocortex. Such small-brained mammals remain in all four superorders of placental mammals, as well in the marsupial and, to some extent, monotreme groups (Krubitzer, 1998). Features that distantly related mammals share are those that were likely retained from the very first mammals (Kaas, 1995). If we consider hedgehogs and shrews from Laurasiatheria, rats and rabbits from Euarchontoglires, armadillos from Xenarthra, tenrecs (Fig. 105.2) from Afrotheria, opossums from Marsupialia, and perhaps the platypus from Monotremata, we find small eyes without a highly specialized area centralis, retinal projections to a dorsal lateral genicu-

Phylogeny of Living Mammals

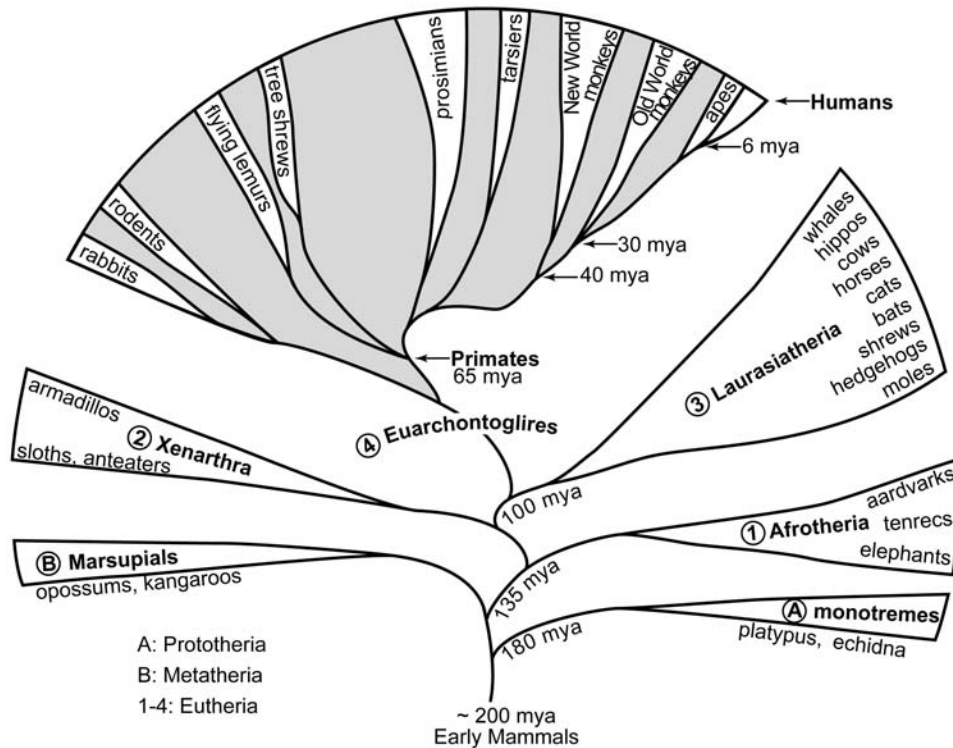


FIGURE 105.1. The evolutionary history of mammals. Recent molecular studies of mammalian phylogeny (e.g., Murphy et al., 2001) have reorganized the phylogenetic tree into four superordinal groups or superorders (1–4) of Eutherian (placental) mammals. Prototherian (A: Monotremes) and Metatherian (B: Marsupials) mammals diverged even earlier from the ancestors of placental mammals. Recent evidence is also pushing back the times of diver-

gences, so the values indicated here, in millions of years ago (mya), are approximate and controversial. Humans are placed with other primates in the superorder Euarchontoglires, with our closest relatives being tree shrews (Scandentia) and flying lemurs (Dermoptera). Rodents and lagomorphs (rabbits) are somewhat more distant.

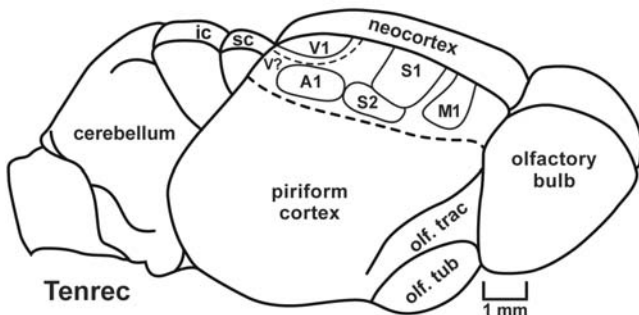


FIGURE 105.2. A dorsolateral view of the brain of a Madagascan tenrec (*Echinops telfairi*) showing the location of primary visual cortex (V1) and other sensory areas. A second visual area (V2) is presumed (dashed line along V1) from studies in other mammals. Note that there is very little neocortex and little space for visual areas (V?) in addition to V1 and V2. Tenrecs are distantly related to primates (Fig. 105.1). As mammals with little neocortex that are distantly related to each other have a V1 and a V2 but little room for other visual areas, we conclude that early mammals had V1 and V2 but few other visual areas. For reference, primary motor (M1) somatosensory (S1), and auditory (A1) areas are indicated. S2 is the second somatosensory area. (Based on Krubitzer et al., 1997.)

late nucleus (LGN) that is histologically rather uniform but with some segregation of inputs from the two eyes (Kahn and Krubitzer, 2002), and a superior colliculus that receives input from the entire retina of the contralateral eye and sparse but variable input from the temporal retina of the ipsilateral eye (Kaas and Preuss, 1993; Kahn and Krubitzer, 2002). A pulvinar (or lateral posterior) region of the thalamus is not large, and it does not have histologically distinct subdivisions, but portions do have inputs from the superior colliculus and visual cortex. In neocortex, there is a distinct but poorly differentiated primary visual area, V1 or area 17, with a retinotopic representation of the contralateral visual hemifield. The lateral border of V1 is largely formed by a strip-like second visual area V2 (Rosa and Krubitzer, 1999), and more laterally in temporal cortex there is a small amount of additional visual and multimodal cortex. The lack of a V2 and temporal visual cortex in the smallest of extant mammals, a 3 gram species of shrew, appears to be a consequence of an extreme reduction in body and brain size (Catania et al., 1999). A small strip of cortex medial to V1, area prostriata, may have visual functions, but this

subdivision of cortex has not been well studied. In brief, early mammals had poorly developed visual systems with only two to four subdivisions of visual cortex.

The visual system of early primates

The brains of early primates resembled those of the smaller present-day prosimians in approximate size and shape (Conroy, 1990). The temporal lobe was not as expanded as it is in living anthropoid primates, and the posterior parietal cortex was not as large. Since these regions of cortex are predominantly visual in function in primates, early primates had not yet expanded these regions of higher-order visual processing. Features of the skull suggest that early primates were nocturnal visual predators living on small prey and some fruit in the tropical rain forests. There would have been an emphasis on brain systems for visually detecting insects and other prey, and for visually guided reaching with the hand to grasp prey. Later, some prosimian primates and the newly emerged anthropoid primates shifted to diurnal life, with more emphasis on eating fruit (Ross, 1996, 2000). The ancestors of present-day tarsiers appear to have moved to a diurnal niche, which was then abandoned as they readapted to nocturnal life by evolving enormous eyes and a rod-dominated retina while retaining the diurnal adaptations of a fovea and two types of cones (Hendrickson et al., 2000; Ross, 1996). Present-day tarsiers have become such extremely specialized visual predators that they apparently eat no plant food. Primary visual cortex is proportionately large and exceptionally well differentiated into layers and sublayers in tarsiers (Collins et al., 2001a), much like the optic tectum of predatory birds.

We can make further deductions about the visual systems of early primates by comparing extant primates and determining what features they have in common (Weller and Kaas, 1982). Further comparisons with our closest nonprimate relatives, especially the closely related tree shrews and flying lemurs, will help indicate features that evolved with the first primates and those that evolved earlier.

An important change from related mammals as early primates emerged was forward rotation of the eyes. This created a larger binocular field and a shift of the retinal region of highest ganglion cell density near the margin of the temporal retina centrally toward the optic disc (Kaas and Preuss, 1993). Tree shrews have a binocular field of about 70 degrees, somewhat less than that of many mammals, but all extant primates have much larger binocular fields (Ross, 2000), and early primates probably had binocular fields of 130 degrees or more. The retina had the three major classes of ganglion cells that are found in all extant primates, the K, M, and P cells (Casagrande, 1994; Hendry and Yoshioka, 1994), named after the sizes of their target cells in the LGN (Kaas et al., 1978). Detailed vision depends greatly on the P-cell projections, and

in all primates most of the ganglion cells are P cells that project to the LGN. The fewer M cells may be important in motion detection. M cells relay to the LGN and superior colliculus, as do the smaller K cells that comprise 10% or so of the total in diurnal primates. K cells are more common in nocturnal primates, judging from the well-developed K-cell region of the LGN in nocturnal owl monkeys and the K-cell layers of the LGN of nocturnal prosimians (see below). Thus, early nocturnal primates likely had proportionately more K cells. These three basic classes of ganglion cells appear to have emerged earlier in mammalian evolution than with the first primates, but more comparative studies are needed.

The projections of the retinas to the superior colliculus in all examined primates (e.g., Lane et al., 1973) differ from all nonprimate patterns in that only the “hemiretinas” that are devoted to the contralateral visual hemifield project to each superior colliculus. In other mammals, the complete retina of the contralateral eye projects to the superior colliculus (Fig. 105.3). This pattern must have been present in the first primates, but not much before, because tree shrews, rats, and rabbits (close relatives of primates) all have the more generalized condition (Kaas et al., 1973). It was once thought that megachiropteran bats also had the primate pattern, and this was considered evidence that these bats might actually be

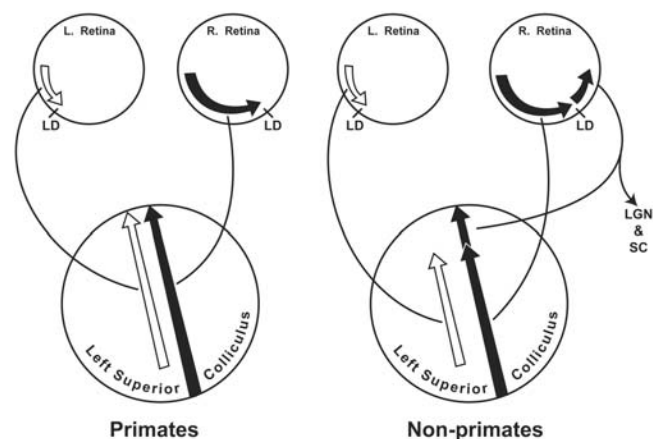


FIGURE 105.3. All primates share a unique type of retinotopic organization in the superior colliculus. In all primates, the left superior colliculus receives superimposed inputs from the nasal hemiretina of the right (R) eye and the temporal hemiretina of the left (L) eye, resulting in a representation of the right hemifield that is largely binocular. The right superior colliculus (SC) has a comparable pattern of inputs from the left and right eyes. In other studied mammals, the complete retina of the contralateral eye projects to the superior colliculus, even though the temporal retina also projects ipsilaterally to the LGN, as in primates. The temporal retina may also project weakly to the ipsilateral superior colliculus in a species-variable manner. Note that in nonprimate mammals, the superior colliculus represents the complete visual field of the contralateral eye, including the binocular part of the ipsilateral hemifield. LD, line of decussation of retinal projections to the two hemispheres.

primates (Pettigrew, 1986), but further study did not support this conclusion (Thiele et al., 1991). For other reasons, bats are no longer considered to be closely related to primates (Fig. 105.1). This primate specialization of only representing the contralateral hemifield in each superior colliculus likely relates to the emphasis on binocular vision that occurred in early primates. How this change altered superior colliculus function is uncertain.

The other major target of the retina, the dorsal LGN, also became specialized with the first primates. All primates have a laminated LGN that reflects a basic pattern of four main layers (Fig. 105.4). The two thinner ventral layers of large cells (the magnocellular layers) receive inputs from the M cells of the retina, while the two thicker dorsal layers of smaller cells (the parvocellular layers) receive inputs from the much more numerous P ganglion cells. The outer (external) layers of each pair receive inputs from the contralateral eye, and the inner (internal) layers receive inputs from the ipsilateral eye. However, there is some evidence for a modifica-

tion of this pattern in tarsiers so that the external magnocellular layer receives inputs from the ipsilateral eye (Pettigrew et al., 1989). The K cells project to a distinct pair of koniocellular layers of small cells in prosimian primates and to a scattering of small cells between layers in other primates. The P-cell layers divide to form additional sublayers in some of the New World monkeys, all of the Old World monkeys, and the great apes and humans. The closest relatives of primates, the tree shrews and flying lemurs, also have laminated LGNs, but with different arrangements of inputs from the two eyes than in primates. In addition, LGN layers in tree shrews segregate inputs from classes of ganglion cells in a different way than primates. Thus, distinctly laminated LGNs evolved independently and differently in tree shrews, flying lemurs, and primates. The early primates must have evolved a basic four-layer pattern from a more generalized LGN, with some segregation of inputs by eye of origin and little segregation by type of ganglion cell. Specialized layers for K-cell inputs were probably part of this early pattern,

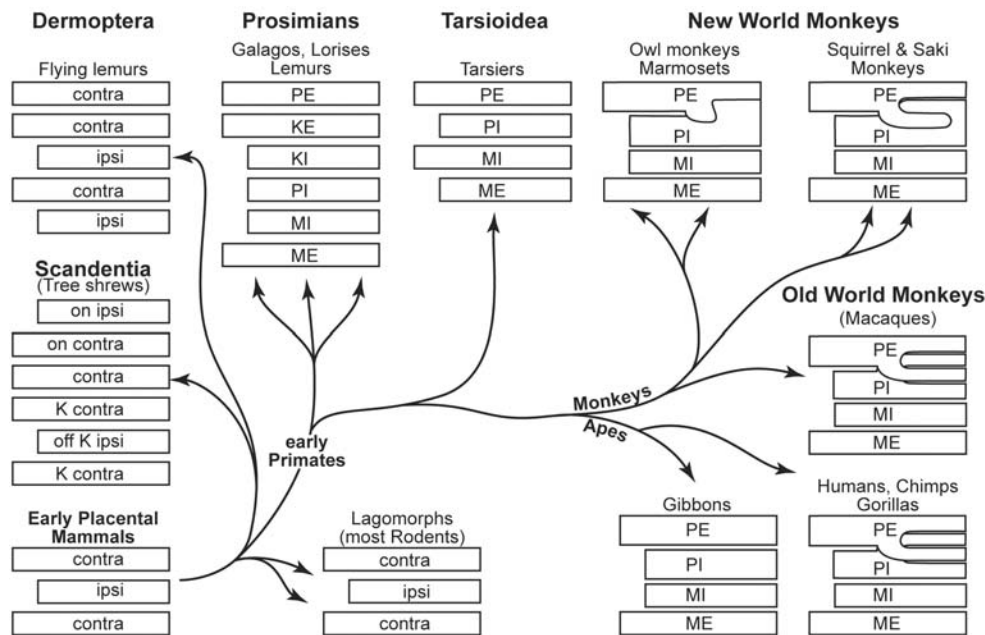


FIGURE 105.4. Laminar patterns of the dorsal LGN in primates. The schematics are of the laminar patterns in brain sections cut across layers that are stacked like slices of bread from ventral (or along the optic tract) to dorsal (near the pulvinar). Early mammals had a simple pattern of LGN lamination that segregated inputs from the ipsilateral retina in a central region between outer regions with inputs from the contralateral retina. All primates have a more elaborate pattern of four basic layers that evolved with the first primates. Close relatives of primates, tree shrews and flying lemurs, evolved different patterns of lamination. In flying lemurs, layers have been identified histologically and by having inputs from the contralateral (contra) or ipsilateral (ipsi) eye (Pettigrew et al., 1989). In tree shrews (Norton, 1982), microelectrode recordings suggest that M- and P-cell (termed Y and X) inputs are mixed in the same layers, unlike primates, while ON and OFF ganglion cell inputs are

segregated in different layers (Norton, 1982), unlike in primates. Other layers appear to have K-cell inputs. The basic primate pattern of lamination includes two parvocellular (P) and two magnocellular (M) layers, with the longer (for the monocular field) outer (external) layers receiving from the contralateral retina (PE, ME) and the shorter inner or internal layers (PI, MI) from the ipsilateral eye. Present-day tarsiers may have a modified pattern, as there is evidence that the two M layers have a reversed pattern of input in regard to eye of origin, so that ME receives input from the ipsilateral retina (Pettigrew et al., 1989). All prosimians have an extra pair of koniocellular layers (KE and KI). In other primates, K cells are scattered between layers where they do not form distinct layers. In many anthropoid primates, the parvocellular layers divide to form sublayers and leaflets of sublayers. (Based on Kaas et al., 1978.)

but these layers were lost as diurnal primates emerged. Tarsiers did not regain K layers with a return to nocturnal life, as tarsiers and the only nocturnal monkey, the owl or night monkey, evolved a thick K-cell region, but not distinct K-cell layers, between the P and M layers. In anthropoid primates, the emphasis on diurnal vision resulted in a great increase in the proportion of the LGN devoted to P-cell inputs. These layers became thicker, especially in parts representing central vision, and they subdivided to form four or more P “layers” (actually partial layers).

In all primates, the pulvinar complex appears to contain the major inferior, lateral, and medial divisions that interconnect with early (inferior and lateral pulvinar) and later (medial pulvinar) levels of the processing hierarchy in visual cortex. In anthropoid primates, the inferior pulvinar has distinct chemoarchitectonic subdivisions, two of which receive dense inputs from the superior colliculus (Stepniewska et al., 2000). All these subdivisions are not as obvious in prosimian primates, but at least some subdivisions of the inferior pulvinar exist (Symonds and Kaas, 1978). The pulvinar complex of tree shrews is quite differently organized (Kaas et al., 2000). Thus, a distinctive differentiation of pulvinar nuclei is part of the specialization of the visual system that occurred with early primates.

Visual cortex in early primates

Early primates were characterized by a large expanse of visual cortex that was divided into a number of visual areas, although the exact arrangement of the visual areas is uncertain. All primates have a large primary visual area, V1, which is rotated from its common position in other mammals to occupy the caudal pole of the hemisphere with much of the area on the ventral surface and medial wall, and in the calcarine sulcus, a fissure found only in primates. Primary visual cortex in extant primates is approximately two to three times larger than would be expected for mammals of a similar body size, but V1 is smaller in prosimian primates than in simian primates of similar size. Primates tend to devote a third to a half of V1 to the first 10 degrees of central vision, with this expansion of central vision being more pronounced in diurnal primates (Rosa et al., 1997). All primates have a similar projection pattern from LGN layers to V1 so that inputs from M layers terminate in a sublayer of layer 4 that is external to the sublayer with P layer inputs (Casagrande and Kaas, 1994). All primates appear to have modular subdivisions of layer 3, the dot-like pattern of cytochrome oxidase (CO) dense “blobs,” which receive afferents from the K cells of LGN (Casagrande, 1994), and the nonblob surrounds. Tree shrews do not have the CO blob pattern, although myelin stains reveal a dot-like pattern of myelin-poor blobs (Lyon et al., 1998). Both primates and tree shrews have orderly arrangements of orientation-selective

neurons in V1 (Humphrey et al., 1980). The major cortical outputs from V1 in all studied primates (Lyon and Kaas, 2002a, 2002b, 2002c) are in decreasing magnitude to V2, V3, MT, and DM (Fig. 105.5). Most of the projections to MT are from deep layer 3 (3C, incorrectly termed *layer 4B* in most studies; see Casagrande and Kaas, 1994, for review), while the middle of layer 3 (3B) provides most of the projections to the other cortical targets (Casagrande and Kaas, 1994).

In summary, early primates differed from their ancestors in having a large, rotated V1 that was disproportionately devoted to the central 10 degrees of vision. K, P, and M inputs from the LGN were already segregated into modules or sublayers. Outputs to MT and other extrastriate visual areas were largely from different sublayers of layer 3.

Most of the outer border of V1 is formed by the narrow belt-like second visual area, V2 in all extant primates. Most of the outer border of V1 represents the line of decussation of the retina (the vertical meridian), which corresponds to the full extent of the V1/V2 border. The rest of V1, corresponding to the temporal margin of monocular vision, is

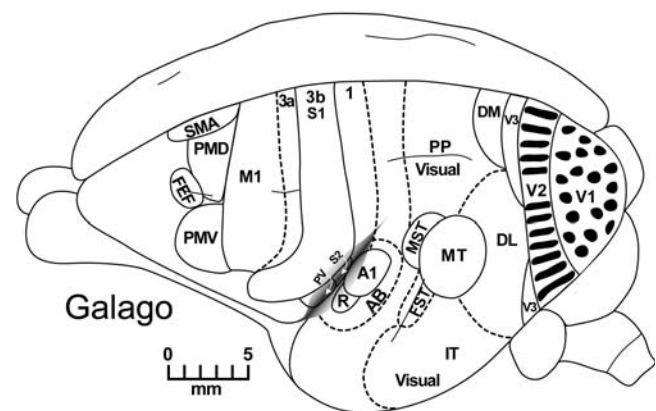


FIGURE 105.5. Subdivisions of visual cortex in a prosimian galago. Visual areas identified here likely emerged with the first primates. Visual areas include a primary area, V1, with CO dense modules (*dots*) and a second visual area, V2, with band-like CO dense (*bars*) and CO light modules with different connections and functions. V2 is bordered by a narrow third visual area, V3, with separate dorsal and ventral halves. A middle temporal visual area, MT, is found in the middle of the upper temporal lobe. Other visual areas include the dorsomedial visual area, DM, the dorsolateral visual area, DL (also known as V4), the fundal area of the superior temporal sulcus (FST), and the medial superior temporal area (MST). Posterior parietal cortex (PP) and inferior temporal cortex (IT) contain additional visual areas, but they have not been fully defined. In the frontal lobe, the frontal eye field (FEF) has visuo-motor functions. For reference, other areas common to all studied primates are included. Motor: SMA, supplementary motor area; PMD, dorsal premotor area; PMV, ventral premotor area; M1, primary motor cortex. Somatosensory: areas 3b (S1), 3a, and 1 (possibly 1 and 2), second area (S2), and parietal ventral area (PV). Auditory: A1, primary auditory area; R, rostral auditory area; AB, auditory belt.

bordered by a small, poorly understood area, the prostriata (Rosa et al., 1997). Nocturnal prosimians, and therefore early primates, devoted less of V1 to central vision. As a result, they devoted less of the border of V1 to the vertical meridian and a shared border with V2 (Rosa et al., 1997). Thus, V2 was less elongated than in diurnal primates. In monkeys, V2 is characterized by a modular organization that is revealed by stains for CO as alternating CO-dense and CO-light bands crossing V2. The CO-dense bands appear to be of two types, “thick” and “thin,” and each of the three types of bands is thought to have different connections with V1 modules and sublayers and with other visual areas (Krubitzer and Kaas, 1990). Such a pattern of modular organization is less apparent in prosimian primates, although CO-dense bands may be weakly apparent in favorable material (Preuss and Kaas, 1996; Preuss et al., 1993). However, modular differences in connections of V2 suggest that an anatomical framework for bands exists (Collins et al., 2001b). Tree shrews also have a banding pattern of V1 connections in V2, but the functional significance of this segregation is not clear (Lyon et al., 1998; Sesma et al., 1984). These observations suggest that V2 already had modular subdivisions in early primates, but the modules may have been less regular and distinct than in present-day simians. Nevertheless, a pattern of modular processing in V2 was part of the visual specialization of the primate branch of mammalian evolution.

The existence of V3 as a visual area in primates has long been in question (Kaas and Lyon, 2001). The dorsal half of V3 (V3d), representing the lower visual field, was defined by projections from V1, but the ventral half (V3v) appeared to have no such connections. This allowed for other interpretations of the V3 region. Some (e.g., Kaas, 1997b) favored the view that V3d was actually part of a larger area, the dorsomedial (DM) area, representing both the upper and lower visual quadrants. Alternatively, V3d was considered by others to be an incomplete visual area representing only the lower visual quadrant (e.g., Felleman and Van Essen, 1991). More recently, we have been able to demonstrate with injections of tracers in the less accessible ventral part of V1 that this part of V1 does project to the ventral V3 region in a range of primate species and that the overall projection pattern of V1 corresponds to that predicted for V3 (Lyon and Kaas, 2001, 2002a, 2002b, 2002c). Thus, compelling evidence exists for V3 in prosimian galagos, several species of New World monkeys, and Old World macaque monkeys. Given this broad distribution, early primates undoubtedly had a V3. However, there is no clear evidence yet for a V3 in tree shrews (Lyon et al., 1998), or in rodents and rabbits (Rosa and Krubitzer, 1999), so V3 does not appear to have been present in much earlier mammals that led to both primates and sister groups. This leads to the conclusion that V3 in primates and cats evolved

independently. This conclusion should be held cautiously, however, as further study could provide evidence for V3 in tree shrews and other mammals.

A similar conclusion relates to the evolution of the middle temporal (MT) visual area. This distinctive visual area has been found in galagos (Allman et al., 1973) and in all other studied primates, including humans, but not in tree shrews, rodents, or rabbits (Kaas, 1997b). MT is easily identified in primates by its projection pattern from V1, dense myelination, retinotopic organization, and neurons that are dominated by a relay of the M-cell pathway through V1 (Casagrande and Kaas, 1994). Because of this distribution, MT appears to be a visual area that first evolved with the early primates. Thus, cats are unlikely to have a homolog of MT, as is sometimes postulated.

In all primates, the dorsomedial (DM) visual area remains as a smaller area after its posterior border has been redefined to include a narrow V3d between DM and V1 (Fig. 105.5). Injections of tracers in different locations in V1 reveal a complete representation of the visual field in DM in addition to a separate representation of the lower field in V3d (Lyon and Kaas, 2001, 2002a, 2002b, 2002c). Because of its wide distribution in present-day primates, DM would have been present in the first primates. As yet, there is no obvious homolog of DM in tree shrews or rodents.

All primates have visual areas in addition to V1, V2, V3, MT, and DM, and some of these areas are likely to be widely shared and thus inherited from a common ancestor. There is already considerable evidence that this is the case for the dorsolateral visual (DL) area, which actually appears to consist of two parallel areas, one posterior to the other, in at least some primates (Stepniewska and Kaas, 1996). Likewise, there is good evidence for MST and FST (FST contains dorsal and ventral subdivisions; Kaas and Morel, 1993) in a range of primate species. The frontal eye field of monkeys and humans has been demonstrated in prosimian galagos (Fig. 105.5; Wu et al., 2000), suggesting that all primates have this visuomotor area. Other shared visual areas are likely to be identified in posterior parietal cortex, where regions have connections with other areas of visual cortex and with the superior colliculus, as well as premotor areas in all examined primates, and in inferotemporal cortex, which receives a massive input from the DL region in all examined primates (Weller and Kaas, 1987).

Evolution of the human visual system

Less is known about how the human visual system differs from that of the first primates. This is partly because it is not yet clear how much the visual systems of prosimians, New World monkeys, and Old World monkeys differ from each other (Kaas, 1997b). In addition, we are only in the early

stages of fully describing the organization of the human visual system, and we know little about the visual systems of apes. Members of the major branches of primate evolution cover a range of body and brain sizes (Fig. 105.6), and they are specialized in various ways, so we can expect variation within as well as across their groups. In Old World monkeys, over 30 visual areas have been proposed (Felleman and Van Essen, 1991), and these primates have greatly expanded regions of visual cortex in the temporal and parietal lobes compared to most New World monkeys and all prosimians. Quite possibly, Old World monkeys have more visual areas than New World monkeys. Further increases in overall brain size and the total extent of visual cortex undoubtedly occurred in the apes leading to our early hominid ancestors. Possibly there was a further increase in the number of visual areas, but this is uncertain. What is clear from the fossil record is that our ancestors of only 3 million years ago had brains only slightly larger (600 to 800 cc) than those of present-day African apes (Preuss and Kaas, 1999), and these brains may have resembled those of African apes in general organization. From that time, the brains of our ancestors increased rapidly in size to the present volume of about 1400 cc, but we know little about the structural changes in brain organization that occurred over that time. What is known from comparing human brains with those of apes and monkeys is that the easily identified primary visual area increased considerably in absolute size while occupying proportionately less of the total neocortex. This observation is consistent with the theory that the number of cortical areas, including visual areas, has increased.

The functions of cortical areas are altered as they increase or decrease in size due to distance constraints on single-

neuron capacities (Kaas, 2000). Small areas have intrinsic connections that cover more of the area and make them more suitable for global comparisons of receptive field centers with surrounds. While large areas are good for considering local detail, smaller areas are more broadly useful. This may be why the large human brain is not simply a larger version of a monkey brain. V1 and at least several other areas did not increase proportionately in size as brains became larger and new areas were likely added. As the complex human body has been made possible by the addition of gene copies that subsequently evolved new functions (Ohno, 1970), the addition of new cortical areas allowed both new and original areas to differentiate, specialize, and mediate new capacities (Allman and Kaas, 1974; Kaas, 1989).

Finally, understanding of brain evolution is still in its early stages. Much more can be learned about the evolution of complex visual systems from theoretical approaches that examine scaling issues related to brain size, as well as from our growing understanding of the modes of brain development and how development can be altered in evolution. Most important, much more can be learned about the brains of the living apes. As a recent example, the histochemistry of primary visual cortex of monkeys, apes, and humans has been compared, leading to the conclusions that some ancestral features of V1 were lost with the evolution of apes, while new features emerged after our ancestors diverged from the apes (Preuss et al., 1999). More specifically, humans do not show the band of dense CO staining of monkeys and apes that marks the outer (4A) stratum of P-geniculate afferent terminations. Furthermore, humans have a unique mesh-like pattern of dendrites and cells that appear to relate to the M-cell system in this sublayer. These observations suggest that the processing of P-cell information has been reduced and M-cell processing enhanced. As M cells respond well to motion and contrast in dim light, the human visual system may function better at dusk.

Presently, we know that human brains are about three times as large as those of the African apes, but we still know very little about how human and ape brains differ structurally. Histochemical and traditional architectonic approaches can help identify nuclei and cortical areas that apes and humans have in common (Hackett et al., 2001), specialized features of those areas (Preuss et al., 1999), and possibly nuclei and areas unique to humans. The goal of determining the similarities and differences in cortical organization across primates has been expressed from the time of Brodmann (1909), but now we have powerful modern methods to add force to such studies.

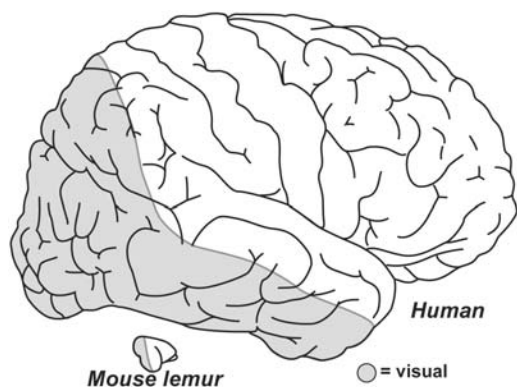


FIGURE 105.6. Size differences in primate brains. Our early primate ancestors were small, with small brains with few fissures, such as the mouse lemur brain (*lower left*). Smooth-brained members of the Euarchontoglires radiation (Fig. 105.1) gave rise to early primates with shallow lateral and calcarine fissures. The brain size and number of fissures increased dramatically in the course of evolving the human brain. The caudal regions of the lemur and human brain that are devoted to vision are shaded.

REFERENCES

- Allman, J. M., and J. H. Kaas, 1974. A crescent-shaped cortical visual area surrounding the middle temporal area (MT) in the owl monkey (*Aotus trivirgatus*), *Brain Res.*, 81:199–213.
- Allman, J. M., J. H. Kaas, and R. H. Lane, 1973. The middle temporal visual area (MT) in the bush baby (*Galago senegalensis*), *Brain Res.*, 57:197–202.
- Brodmann, K., 1909. *Vergleichende Lokalisationslehre der Grosshirnrinde*, Leipzig: Verlag Barth.
- Casagrande, V. A., 1994. A third parallel visual pathway to primate area V1, *Trends Neurosci.*, 17:305–310.
- Casagrande, V. A., and J. H. Kaas, 1994. The afferent, intrinsic, and efferent connections of primary visual cortex in primates, in *Cerebral Cortex*, vol. 10, *Primary Visual Cortex in Primates* (A. Peters and K. Rockland, eds.), New York: Plenum Press, pp. 201–259.
- Catania, K. C., D. C. Lyon, O. B. Mock, and J. H. Kaas, 1999. Cortical organization in shrews: evidence from five species, *J. Comp. Neurol.*, 410:55–72.
- Collins, C. E., A. E. Hendrickson, and J. H. Kaas, 2001a. Distribution of calbindin, parvalbumin and wisteria in primary visual cortex of tarsier, *Soc. Neurosci. Abstr.*, 27: Program No. 619.41.
- Collins, C. E., I. Stepniewska, and J. H. Kaas, 2001b. Topographic patterns of V2 cortical connections in a prosimian primate, *J. Comp. Neurol.*, 431:155–167.
- Conroy, G. C., 1990. *Primate Evolution*. New York: W. W. Norton.
- Felleman, D. J., and D. C. Van Essen, 1991. Distributed hierarchical processing in the primate cerebral cortex, *Cereb. Cortex*, 1:1–47.
- Finlay, B. L., and R. B. Darlington, 1995. Linked regularities in the development and evolution of mammalian brains, *Science*, 268:1578–1584.
- Hackett, T. A., T. M. Preuss, and J. H. Kaas, 2001. Architectonic identification of the core region in auditory cortex of macaques, chimpanzees, and humans, *J. Comp. Neurol.*, 441:197–222.
- Hendrickson, A., H. R. Djajadi, L. Nakamura, D. E. Possin, and D. Sajuthi, 2000. Nocturnal tarsier retina has both short and long/medium-wavelength cones in an unusual topography, *J. Comp. Neurol.*, 424:718–730.
- Hendry, S. H. C., and T. Yoshioka, 1994. A neurochemically distinct third channel in the macaque dorsal lateral geniculate nucleus, *Science*, 264:575–577.
- Hennig, W., 1966. *Phylogenetic systematics*, Urbana: University of Illinois Press.
- Huerta, M. F., L. A. Krubitzer, and J. H. Kaas, 1987. The frontal eye field as defined by intracortical microstimulation in squirrel monkeys, owl monkeys, and macaque monkeys. II. Cortical connections, *J. Comp. Neurol.*, 265:261–332.
- Humphrey, A. L., L. C. Skeen, and T. T. Norton, 1980. Topographic organization of the orientation column system of the tree shrew (*Tupaia glis*). II. Deoxyglucose mapping, *J. Comp. Neurol.*, 192:549–566.
- Jacob, F., 1977. Evolution and tinkering, *Science*, 196:1161–1166.
- Jerison, H. J., 1973. *Evolution of the Brain and Intelligence*, New York: Academic Press.
- Kaas, J. H., 1987. The organization and evolution of neocortex, in *Higher Brain Functions* (S. P. Wise ed.), New York: Wiley, pp. 347–378.
- Kaas, J. H., 1989. Why does the brain have so many visual areas? *J. Cogn. Neurosci.*, 1:121–135.
- Kaas, J. H., 1995. The evolution of neocortex, *Brain Behav. Evol.*, 46:187–196.
- Kaas, J. H., 1997a. What comparative studies of neocortex tell us about the human brain, *Rev. Brasil Biol.*, 35:315–327.
- Kaas, J. H., 1997b. Theories of visual cortex organization in primates, in *Cerebral Cortex*, vol. 12, *Extrastriate Cortex in Primates* (K. S. Rockland, J. H. Kaas, and A. Peters, eds.), New York: Plenum Press, pp. 91–125.
- Kaas, J. H., 2000. Why is brain size so important? Design problems and solutions as neocortex gets bigger or smaller, *Brain Mind*, 1:7–23.
- Kaas, J. H., J. K. Harting, and R. W. Guillery, 1973. Representation of the complete retina in the contralateral superior colliculus of some mammals, *Brain Res.*, 65:343–346.
- Kaas, J. H., M. F. Huerta, J. T. Weber, and J. K. Harting, 1978. Patterns of retinal terminations and laminar organization of the lateral geniculate nucleus of primates, *J. Comp. Neurol.*, 182:517–554.
- Kaas, J. H., and D. C. Lyon, 2001. Visual cortex organization in primates: theories of V3 and adjoining visual areas, *Prog. Brain Res.*, 134:285–295.
- Kaas, J. H., D. C. Lyon, N. Jain, and I. Stepniewska, 2000. Multiple subdivisions of tree shrew pulvinar revealed through AChE and Cat-301 chemoarchitecture and by connections with visual cortex, *Soc. Neurosci. Abstr.*, 26:1469.
- Kaas, J. H., and A. Morel, 1993. Connections of visual areas of the upper temporal lobe of owl monkeys: the MT crescent and dorsal and ventral subdivisions of FST, *J. Neurosci.*, 13:534–546.
- Kaas, J. H., and T. M. Preuss, 1993. Archontan affinities as reflected in the visual system, in *Mammal Phylogeny* (F. Szalay, M. Novacek, and M. McKenna, eds.), New York: Springer-Verlag, pp. 115–128.
- Kahn, D., and L. Krubitzer, 2002. Retinofugal projections in the short-tailed opossum (*Monodelphis domestica*), *J. Comp. Neurol.*, 447:114–127.
- Krubitzer, L., 1998. What can monotremes tell us about brain evolution? *Philos. Trans. R. Soc. (Lond.)*, Ser. B, 353:1127–1146.
- Krubitzer, L. A., and J. H. Kaas, 1990. Cortical connections of MT in four species of primates: areal, modular, and retinotopic patterns, *Vis. Neurosci.*, 5:165–204.
- Krubitzer, L. A., H. Kunzle, and J. H. Kaas, 1997. The organization of sensory cortex in a Madagascan insectivore, the tenrec (*Echinops telfairi*), *J. Comp. Neurol.*, 379:399–414.
- Lane, R. H., J. M. Allman, J. H. Kaas, and F. M. Miezin, 1973. The visuotopic organization of the superior colliculus of the owl monkey (*Aotus trivirgatus*) and the bush baby (*Galago senegalensis*), *Brain Res.*, 60:335–349.
- Lyon, D., N. Jain, and J. H. Kaas, 1998. Cortical connections of striate and extrastriate visual areas in the three shrew, *J. Comp. Neurol.*, 401:109–128.
- Lyon, D. C., and J. H. Kaas, 2001. Connectional and architectonic evidence for dorsal and ventral V3 and area DM in marmoset monkeys, *J. Neurosci.*, 21:249–261.
- Lyon, D. C., and J. H. Kaas, 2002a. Evidence for a modified V3 with dorsal and ventral halves in macaque monkeys, *Neuron*, 33:453–461.
- Lyon, D. C., and J. H. Kaas, 2002b. Evidence from V1 connections for both dorsal and ventral subdivisions of V3 in three species of New World monkeys, *J. Comp. Neurol.*, 449:281–297.
- Lyon, D. C., and J. H. Kaas, 2002c. Connectional evidence for dorsal and ventral V3, and other extrastriate areas in the prosimian primate, *Galago garnetti*. *Brain Behav. Evol.*, 59:114–129.

- Murphy, W. J., E. Eizirik, S. J. O'Brien, O. Madsen, M. Scally, C. J. Douady, E. Teeling, O. A. Ryder, M. J. Stanhope, W. W. DeJong, and M. S. Springer, 2001. Resolution of the early placental mammal radiation using Bayesian phylogenetics, *Science*, 294:2348–2351.
- Northcutt, R. G., 1984. Evolution of the vertebrate central nervous system: patterns and processes, *Am. Zool.*, 24:701–716.
- Norton, T. T., 1982. Geniculate and extrageniculate visual systems in the tree shrew, in *Changing Concepts of the Nervous System* (A. R. Morrison and P. L. Strick, eds.), New York: Academic Press, pp. 377–409.
- Ohno, S., 1970. *Evolution by Gene Duplication*, New York: Springer.
- Pettigrew, J. P., 1986. Flying primates? Megabats have the advanced pathway from the eye to midbrain, *Science*, 231:1304–1306.
- Pettigrew, J. P., B. G. M. Jamieson, S. K. Robson, L. S. Hall, K. I. McNally, and H. M. Cooper, 1989. Phylogenetic relations between microbats, megabats and primates, *Philos. Trans. R. Soc. Lond., Ser. B, Biol. Sci.*, 325:489–559.
- Preuss, T. M., 2000. Taking the measure of diversity: comparative alternatives to the model-animal paradigm in cortical neuroscience. *Brain Behav. Evol.*, 55:287–299.
- Preuss, T. M., P. D. Beck, and J. H. Kaas, 1993. Areal, modular, and connectional organization of visual cortex in a prosimian primate, the slow loris (*Nycticebus coucang*), *Brain Behav. Evol.*, 42:237–251.
- Preuss, T. M., and J. H. Kaas, 1996. Cytochrome oxidase “blobs” and other characteristics of primary visual cortex in a lemuriform primate, *Cheirogaleus medius*, *Brain Behav. Evol.*, 47:103–112.
- Preuss, T. M., and J. H. Kaas, 1999. Human brain evolution, in *Fundamental Neuroscience* (M. J. Zigmond, F. E. Bloom, S. C. Landis, J. L. Roberts, and L. R. Squire, eds.), San Diego, CA: Academic Press, pp. 1283–1311.
- Preuss, T. M., H. Qi, and J. H. Kaas, 1999. Distinctive compartmental organization of human primary visual cortex, *Proc. Natl. Acad. Sci. USA*, 96:11601–11606.
- Rosa, M. G. D., V. A. Casagrande, T. M. Preuss, and J. H. Kaas, 1997. Visual field representation in striate and prestriate cortices of a prosimian primate (*Galago garnetti*), *J. Neurophysiol.*, 77:3193–3217.
- Rosa, M. G. D., and L. A. Krubitzer, 1999. The evolution of visual cortex: where is V2? *Trends Neurosci.*, 22:242–248.
- Ross, C. F., 1996. Adaptive explanation for the origins of the Anthropoidea (primates), *Am. J. Primatol.*, 40:205–230.
- Ross, C. F., 2000. Into the light: the origin of anthropoidea, *Annu. Rev. Anthropol.*, 29:187–194.
- Sesma, M. A., V. A. Casagrande, and J. H. Kaas, 1984. Cortical connections of area 17 in tree shrews, *J. Comp. Neurol.*, 230:337–351.
- Stepniewska, I., and J. H. Kaas, 1996. Topographic patterns of V2 cortical connections in macaque monkeys, *J. Comp. Neurol.*, 371:129–152.
- Stepniewska, I., H. Qi, and J. H. Kaas, 2000. Projections of the superior colliculus to subdivisions of the inferior pulvinar in New World and Old World monkeys, *Vis. Neurosci.*, 17:529–549.
- Striedter, G. F., 1998. Progress in the study of brain evolution: from speculative theories to the stable hypotheses, *Anat. Rec. (New Anat.)*, 253:105–112.
- Symonds, L. L., and J. H. Kaas, 1978. Connections of striate cortex in the prosimian (*Galago senegalensis*), *J. Comp. Neurol.*, 181:477–512.
- Thiele, A., M. Vogelsang, and K. P. Hoffman, 1991. Pattern of retinotectal projection in the megachiropteran bat *Rousettus aegyptiacus*, *J. Comp. Neurol.*, 314:671–683.
- Weller, R. E., and J. H. Kaas, 1982. The organization of the visual system in Galago: comparisons with monkeys, in *The Lesser Bush Baby (Galago) as an Animal Model: Selected Topics* (D. E. Haines ed.), Boca Raton, FL: CRC Press, pp. 107–135.
- Weller, R. E., and J. H. Kaas, 1987. Subdivisions and connections of inferior temporal cortex in owl monkeys, *J. Comp. Neurol.*, 256:137–172.
- Wu, C. W. H., N. P. Bichot, and J. H. Kaas, 2000. Converging evidence from microstimulation, architecture, and connections for multiple motor areas in the frontal and cingulate cortex of prosimian primates, *J. Comp. Neurol.*, 423:140–177.

106 Gestalt Factors in the Visual Neurosciences

LOTHAR SPILLMANN AND WALTER H. EHRENSTEIN

It is now almost generally acknowledged that psychological facts have “correlates” in the biological realm. These correlates, the so-called psychophysical processes, are events in the central nervous system.

Wolfgang Köhler (1940)

A brain theory of visual perception

Gestalt psychology, best known for its richness of perceptual phenomena and rigor of observation, was more than just a school of phenomenology. It was an early and systematic approach to infer brain processes from percepts. In his seminal article on apparent motion between two successive stimuli, Max Wertheimer (1912) writes: “Es handelt sich um bestimmte, zentrale Vorgänge, physiologische ‘Querfunktionen’ besonderer Art, die als das physiologische Korrelat der Phi-Phänomene dienen” (We are dealing with certain, central processes, physiological lateral interactions of a special kind that serve as the physiological correlate of the phi phenomena). Accordingly, apparent motion was thought to be based on interactions between two brain states, resulting in a perceptual filling-in of the unstimulated interspace (*Felderfüllung*), not unlike an electrical short circuit. Thus, far from being content with his discovery of phi motion, Wertheimer was interested in the way in which it originated in the brain.

In 1923, using simple dot and line figures, Wertheimer further investigated the rules of perceptual organization, that is, the *Gestalt factors* or principles inherent in the visual system. Both of his papers had a lasting impact. They showed that our perception cannot be understood on the basis of stimuli alone, but also requires active mechanisms by which they are processed. More than 80 years later and notwithstanding passionate debates on linking propositions (Teller, 1990), we are now witnessing a physiology that aims to understand these principles in terms of interactions within neural networks.

Inspired by Wertheimer’s approach, Wolfgang Köhler (1920, 1923) systematically addressed the neural implications of the Gestalt concept. He postulated that the neuronal processes at the psychophysical level (*psychophysisches Niveau*), at which neuronal activity becomes conscious experience,

have isomorphic structural properties to perceptual *Gestalten*. Consequently, perceptual organization was assumed to rely on neuronal rather than on stimulus properties.

Although Gestalt psychologists studied perception in general, they often selected phenomena demonstrating that we are not free to perceive as we choose. No matter how hard we try or how often we look at a given stimulus pattern, we are always the victims of the constraints that the visual system imposes on us. The principles that determine why we see the way we do (Koffka, 1935) have become known as *laws of vision* (Metzger, 1936/1953). They are the reason why, in a multitude of possible “solutions,” only one percept typically materializes. When there are several solutions, the task for the visual system becomes a challenge (Fig. 106.1).

Instead of providing a full historical account of Gestalt factors (Spillmann, 1999a), we concentrate in this chapter on select examples to examine where we stand and where the future might lead us. Excellent treatises of visual perception within a Gestalt psychological context may be found in the handbook chapter of Teuber (1960), in the handbook volume edited by Metzger (1966), and in subsequent books and chapters by Hochberg (1971), Kanizsa (1979), Kubovy and Pomerantz (1981), Beck (1982), Rock (1984), Spillmann and Ehrenstein (1996), and Palmer (1999). Readers will also enjoy the recent papers by Sekuler (1996) and Westheimer (1999), which focus on Max Wertheimer’s early contributions and interpret them within the context of modern neuroscience.

Basic concepts of Gestalt psychology

What do we mean by *Gestalt*? According to the Austrian philosopher Christian von Ehrenfels (1890), the term *Gestalt* applies to perceptual unit formation and is characterized by two criteria: *Übersummativität* (superadditivity) and *Transponierbarkeit* (transposability). *Superadditivity*, denotes that the whole is different from (or more than) the sum of its parts and is perhaps best illustrated by Wertheimer’s (1912) phi motion, as already described. Two orthogonal lines presented briefly in the proper sequence will show phi motion (pure motion without object displacement) or appear as a single bar

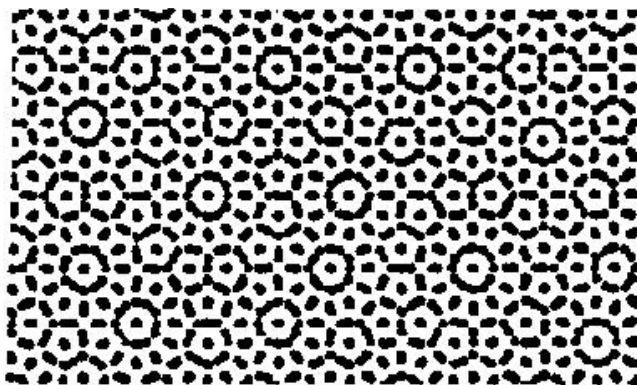


FIGURE 106.1. With prolonged inspection, continuous changes in perceptual grouping may be experienced. New “flowers” arise spontaneously from the “meadow” and disappear again, testifying to the instability of figure-ground segregation. (From Robinson, 1972; see also Spillmann and Ehrenstein, 1996.)

moving through a right angle (optimal motion). The perceived movement, including its direction and speed, cannot be reduced to the two static line events. It is an experience of its own (*sui generis*, Wertheimer, 1912; see also Steinman et al., 2000), “an emergent property that does not correspond with the piecemeal features of the stimuli” (Sharps and Wertheimer, 2000).

Another well-known example of superadditivity is a gray ring that lies on a ground half red, half green. As long as the ring is perceived as a whole, it looks uniformly gray (Koffka, 1935). However, if the two halves are separated by a thin border, simultaneous color contrast due to the red and green hemifields induces a distinct greenish and reddish color in the two semicircles. Koffka concluded that an intact, unified figure (*Gestalt*) will look uniform, while two semicircles produced by the same stimulus will look different. Thus, the whole has properties that are different from those of its parts.

The second Ehrenfels criterion, *transposition*, implies that the whole is preserved even if there are large changes to its components. What counts are the relations between stimuli rather than the specific stimulus attributes. A square may be small or large, black or colored, outline or surface, fully delineated or just defined by its apices: as long as there are four right angles connected by equilateral sides, it is a square. Transposition enables perceptual constancy or invariance (see the section “Perceptual Invariance Mechanisms” on page 1577).

In addition to these two criteria, *Gestalten* are distinguished by possessing an *equilibrium* that depends critically on the structural role of their components. For this reason, the same stimulus may appear differently, depending on the way in which it is embedded in a larger context. Conversely, different stimuli may elicit similar percepts as long as they have

similar structural properties. These observations were at the core of Köhler’s (1920) hypothesis that our perception does not depend on firm anatomical wiring (*Konstanzhypothese*), but rather on *dynamic self-organization* that aims at an energetic equilibrium.

Wertheimer (1923) proposed that this equilibrium expresses itself in the *Prägnanztendenz*, or the tendency toward a “good” *Gestalt*. The term implies that the simplest, most regular, and balanced organization “wins” in our perception. To account for *Prägnanz*, the Gestaltists assumed a number of *autochthonous* (i.e., inherent) factors responsible for grouping and figure-ground segregation. These factors determine the way in which we see.

PERCEPTUAL CONSTRAINTS Gestaltists considered perceptual organization as an active process, adding to rather than merely reflecting the stimulus. Typically, perceptual organization generates wholes and parts as well as groups and group members. Perception seems to us direct, undeniable, and veridical, helping us to get around in the world. But it is not always that simple.

This may be illustrated by three examples. (1) Sometimes we see what actually is not there. Take the Ehrenstein figure (Ehrenstein, 1941, 1954) or the Kanizsa triangle (Kanizsa, 1955, 1979), both of which stand out because of illusory contours and illusory surfaces for which there is no physical correlate in the stimulus (amodal contours; Fig. 106.2A, B). (2) At other times, we may be blind to what is actually in full sight. For example, a figure may require great effort to be discerned, because it is embedded (hidden) in a larger context that produces “wrong” figural groupings (Gottschaldt, 1926; Fig. 106.2C). (3) Finally, we may see the properties of a stimulus but not as they really are. This is evidenced by so-called geometric-optical illusions (Oppel, 1855; Hering, 1861; Fig. 106.2D, E). Shapes may appear distorted, and sizes, angles, and orientations may differ from their actual geometry and will remain this way, despite better knowledge of their true alignment. Such mismatches between stimulus and percept were taken by the Gestaltists as evidence of how the brain processes visual information. In this sense, illusory phenomena may be used as noninvasive tools to study the neural mechanisms underlying visual perception. Perceptual illusions thus reveal the limitations as well as the creative abilities of the visual system.

FIGURE-GROUND SEGREGATION AND PERCEPTUAL GROUPING A central issue of the Gestalt approach to perception is the distinction between figure and ground. The first person to address this distinction systematically was the Danish psychologist Edgar Rubin (1915), a student of G. E. Müller. His descriptions of the properties characterizing figure and ground are summarized as follows:

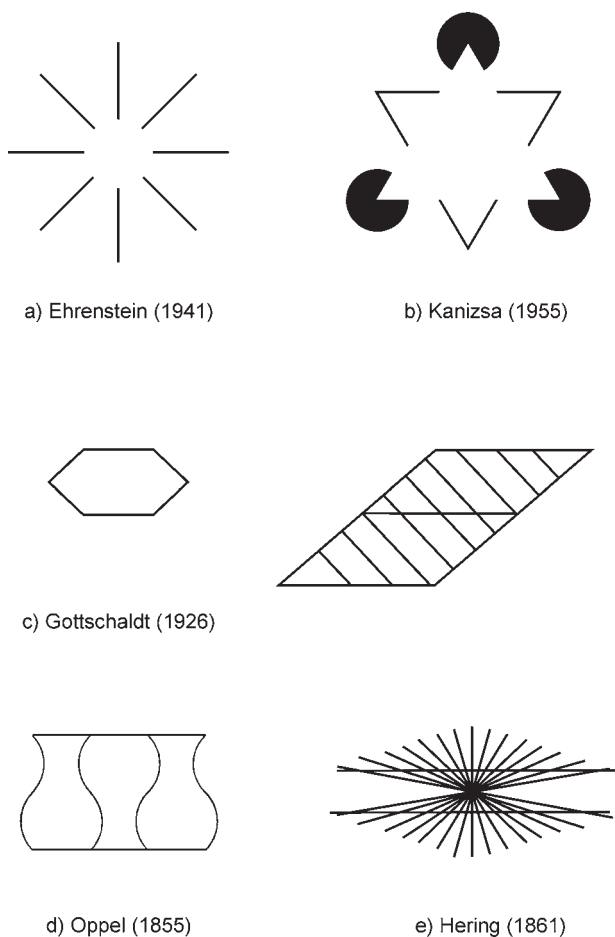


FIGURE 106.2. Demonstrations of Gestalt phenomena. *a*, Ehrenstein figure and *b* Kanizsa triangle displaying brightness enhancement, illusory contours, and amodal completion. *c*, Hidden figure by Gottschaldt; the hexagon on the left becomes nearly imperceptible when embedded in the parallelogram on the right. *d*, Geometric-optical illusions by Oppel; the “short” and “long” lines (on the top and bottom) are actually identical in length. *e*, The two “bowed” lines in the figure by Hering are, in fact, straight and parallel.

A figure possesses “Ding (thing) character;” it is spatially cohesive, delineated and appears to lie slightly above the ground. It is enclosed, i.e., demarcated by a contour, and fills the entire surface inside the border. A figure possesses a shape (frequently symmetrical) and is surrounded by a background, on which it rests. In contrast, the ground possesses *Stoff* (stuff, material) character; it appears farther away and is partially occluded by the figure. It is open (not delineated) and extends behind the figure. It has no conspicuous shape (e.g., a patch of sky between the clouds) and typically is larger than the figure.

The question of how we manage to parse a large stimulus field into figure and ground goes back to the Gestalt psychologists’ proposal that figures emerge on a ground due to so-called grouping factors (Wertheimer, 1923; see also

Bahnsen, 1928; Morinaga, 1941). Among these, similarity and common fate stand out as especially powerful for the formation of extended surfaces: sections of a stimulus pattern that have the same brightness, color, texture, or depth tend to become a surface in perception. Similarly, sections that move together in the same direction and with the same velocity assume surface properties. Taken together, these factors describe the lawful transformation of retinal stimuli into neural object representations. In the following subsections, we give a brief description of each of these factors (see also Palmer, 1999).

Symmetry. If faced with symmetrical and nonsymmetrical stimuli, perception follows symmetry as a figural organization principle. For example, spaces that are delineated by wavy, mirror-symmetric contours are perceived as figure, asymmetrical spaces as ground (Fig. 106.3A).

Parallelism. Similarly, undulating lines that are parallel and maintain their width (e.g., *Ebenbreite*) achieve the status of figure, whereas their nonparallel interspaces are delegated the role of ground (Fig. 106.3B).

Smooth (or “good”) continuation. Collinear stimulus parts tend to be linked together, whereas parts exhibiting sharp bends or corners are not (Fig. 106.3C). This observation calls for neurons sensitive to collinearity (see the section “Perceptive Neurons” on page 1579).

Closure. A closed stimulus is more readily organized into a figure than an open one (Fig. 106.3D). Closure also manifests itself in a tendency to complete perceptually a partly occluded object.

Proximity. All other factors being equal, closely adjacent stimuli are more likely to be grouped into perceptual units than are stimuli that are farther apart. An example is shown in Figure 106.3F, where neighboring dots are readily organized into pairs of dots. In comparison, the more widely spaced dots are almost impossible to group together. Proximity wins.

Similarity. Stimuli sharing the same brightness or color are more likely to be grouped than dissimilar stimuli. The same applies to size, shape, and orientation (Fig. 106.3G–I), as well as texture and depth.

Common fate. Stimuli that move simultaneously at the same speed and approximately in the same direction are seen as a group (Fig. 106.3J). This factor, common fate, ties together stimuli that are widely distributed in the visual field, producing the perception of coherent motion. Common fate is possibly the strongest of all classical grouping factors, overriding proximity and similarity. Stimuli that would not

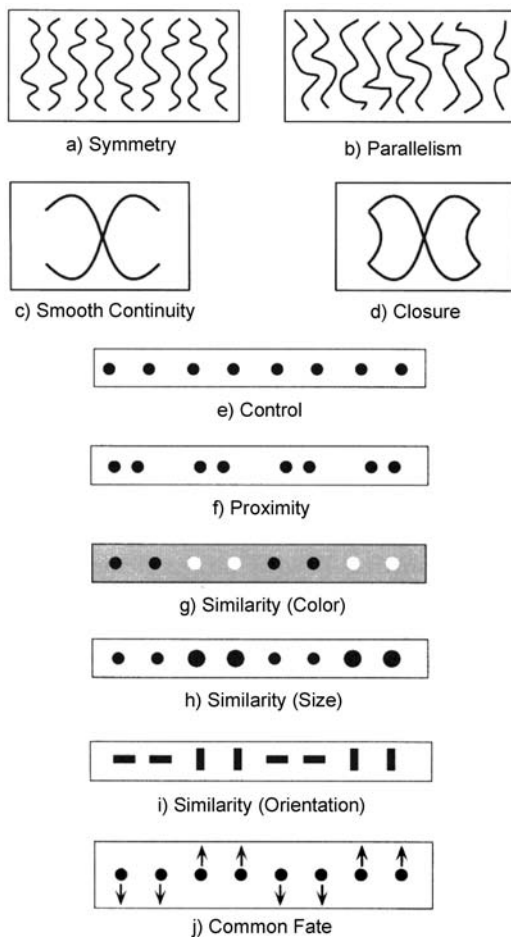


FIGURE 106.3. Schematic demonstration of Gestalt factors determining figural segmentation according to (a) symmetry (Bahnsen, 1928), (b) parallelism (Morinaga, 1941), (c) smooth continuation, (d) closure; and grouping of elements according to (f) proximity, (f–i) similarity, and (j) common fate. All but the first two factors are from Wertheimer (1923). (Adapted from Palmer, 1999.)

normally be grouped together in stationary displays will emerge as a group as soon as they begin to move in unison (i.e., covary in time and space).

Little was known at the time about the neuronal mechanisms underlying these perceptual segregations. However, recent psychophysical and neurophysiological studies have shed light on the processes that may be responsible for figure-ground organization. Among these, the spread of brightness and color information from an edge by long-distance filling-in are the best understood (see the sections “Surface Filling-in” on page 1582 and “Large-Scale Color Effects” on page 1583).

SUBJECTIVE FACTORS Although Gestalt psychologists were primarily concerned with the sensory (bottom-up) factors underlying figure-ground segregation and grouping, they also recognized that subjective (central or top-down) factors

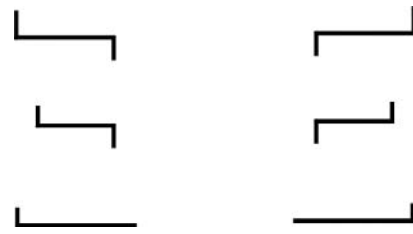


FIGURE 106.4. Demonstration of set (*Einstellung*) and past experience as factors in amodal completion. The meaningless assembly of lines on the left becomes a mirror-symmetric E after the capital letter E is discerned on the right. (From Ehrenstein, 2001.)

could modify perceptual organization. Such factors are an observer’s set (*Einstellung*) and past experience.

For example, the three pieces in Figure 106.4 (*left side*) may appear, at first glance, as a meaningless geometric arrangement of lines. However, when flipped over (Fig. 106.4, *right side*), they will—given appropriate knowledge—be easily recognized as a capital E with the missing contours amodally completed. Now, having the *Einstellung* of an E, if one looks back on Figure 106.4 (*left*), one immediately sees a mirror-symmetric E rather than a mere assembly of lines (Ehrenstein, 2001). Another example of the effect of past experience is the well-known Dalmatian dog (photographed by Ron C. James) which is perfectly hidden on a spotty surface due to its broken body lines, but once it has been discerned, it will be instantaneously visible on subsequent exposures.

In a natural setting, incomplete objects are the rule, rather than the exception, due to partial occlusion. Nonetheless, we have little difficulty seeing an incompletely given stimulus as complete because of the Gestalt factors of smooth continuation, closure, and completion. In this sense, it may be said that we perceive a stimulus correctly due to *active processes* in our brain. These processes complement and transform the visual input thereby producing percepts that match corresponding objects in the real world. Memory helps, but cognitive processes (e.g., unconscious inferences; Helmholtz, 1909–1911) are not needed. Figure 106.5 demonstrates that even impossible solutions are perceptually accepted, such as René Magritte’s rider on a horse (*Le blanc-seing*).

GESTALT FACTORS IN DYNAMIC DISPLAYS In addition to the (dynamic) factor of common fate, each of the other Gestalt factors has an equivalent in the realm of motion (Metzger, 1936/1953). For example, the factor of proximity finds its correlate in the factor of least displacement (*geringste Verschiebung*), while the factor of smooth continuation corresponds to the factor of a steady and uncrossed trajectory (*stetige Bewegungsbahn* and *kreuzungsfreier Verlauf*). Metzger (1935) showed that we can reconstruct depth from the trajectories of a cluster of vertical bars rotating on a platform and—when backprojected—casting their shadows on a two-



FIGURE 106.5. Magritte's rider on a horse requires scrutiny to appreciate the impossibility of the figure and scene. (*The Blank Signature*, 1965. National Gallery of Art, Washington, DC, Collection of Mr. and Mrs. Paul Mellon 1985.64.24; see Wenzel, 1998.)

dimensional screen. Despite different velocities and directions, as well as continuous transformations of the relationships between the shadows, the observer perceives a rigid three-dimensional assembly of bars—even monocularly—according to the Gestalt tendencies of persistence in shape and time (*Tendenz zur Formbeständigkeit, Gesetz der geringsten Veränderung*). The perceptual extraction of a moving shape in depth known as *kinetic depth effect* (Musatti, 1924; Wallach and O'Connell, 1953) is due to the same factors. Recent findings on depth from motion and motion transparency studies in the monkey place the neural mechanism of this phenomenon at the level of area MT (Bradley et al., 1998) (see Chapter 81).

Metzger's (1934, 1935) findings, together with earlier observations by Ternus (1926) on *phenomenal identity* (group vs. element motion), provided the basis for Michotte's (1946/1963) observations on *phenomenal causality*, where two moving stimuli are perceived to interact in various ways: entraining and launching, collision, traction, and passing each other. They may also be considered forerunners of Johansson's (1973) *biological motion*, showing that human figures dancing in the dark will be veridically perceived although the stimulus pattern consists of no more than a

small number of (coherently moving) lights attached to their joints. Neurons mediating biological objects from such motion have been found and studied in detail in monkey temporal cortex (Oram and Perrett, 1994).

GESTALT FACTORS IN THE ANIMAL KINGDOM Are Gestalt factors in visual perception unique to humans or do they influence the behavior of other species as well? In her pioneering work, Mathilde Hertz (1928) demonstrated that the perceptual organization of jaybirds' vision is similar to that of humans. Metzger (1936/1953) further showed in a variety of species (insects, birds, fish, mammals) that the same principles that make objects more conspicuous in human vision are used by nature to provide camouflage and concealment. Camouflaged animals blend in with their environment and may be perfectly hidden from even the most inquisitive eye. Camouflage reduces visibility by counteracting the very Gestalt principles that govern figure-ground segregation and grouping. Particularly effective in this regard are blobs and textures that interrupt existing boundaries or create new boundary contours and offset surfaces by suggesting "wrong" perceptual entities. If the animal remains still (or moves in unison with its surround), it becomes an integral part of its environment. On the other hand, a camouflaged animal will *pop out* as soon as it moves relative to its surround (factor of common fate).

Certain fish use countershading thereby being less visible against the water surface from below. Ramachandran et al. (1996) studied the mimicry of a bottom-dwelling flat fish (*Bothus ocellatus*) and found an amazing adaptability to the prevailing environment to minimize visibility from above. This species can even simulate on its skin a checkerboard pattern on which it is placed by the experimenter and will follow changes of check size with little delay. From such findings, we may conclude that the factors rendering an animal invisible are the same in predators and human observers, as they operate similarly and are equally effective in both.

The same assumption applies to geometric-optical illusions (Zöllner, Ebbinghaus, Ehrenstein) which have been demonstrated in goldfish, domestic chickens, starlings, finches, and guinea pigs (Dücker, 1966), thereby narrowing the number of possible explanations to one that is common to all.

PERCEPTUAL INVARIANCE MECHANISMS In addition to analyzing the figure-ground factors inherent in perception and perceptual processing, Gestaltists posed what is perhaps an even larger question: that of perceptual constancies (*Wahrnehmungskonstanzen*). Invariance mechanisms are of doubtless evolutionary survival value. Unless the retinal image of a stimulus that moves to and fro, translates, tilts, and rotates is attributed to the same object, we cannot derive experiences, as there is no object identity under different

stimulus conditions (Gibson, 1950). Furthermore, different illumination must be discounted in order for us to remain oriented in an ever-changing world (Neumeyer et al., 2002). Size, shape, and color constancy are thus fundamental perceptual mechanisms in human and nonhuman species, probably from birth on, as without them survival would be tenuous (Lorenz, 1959). The perceptual constancy of the ongoing stream of glimpses needed whenever we move our eyes (position constancy) and the distinction between object and subject movement (Ebenholtz, 2001) are genuine—but even less understood—problems of Gestalt psychology. Tentative answers to these basic questions concerning the underlying invariance mechanisms are just beginning to emerge from neurophysiological studies (Sary et al., 1993; for a review, see Spillmann, 2001).

Although we rely on invariance mechanisms all the time, they must be seen within the proper context (Spillmann, 1997). For example, in the case of color constancy, correct hue perception depends on the relational change of the entire scene acting as a reference system (*Bezugssystem*). A striking example is the well-known *Gelb effect* (Gelb, 1929). A black disc suspended in the dark is illuminated by the beam of a spotlight—it appears white. However, when a piece of white paper is placed on it, the disc immediately turns black. The Gelb effect demonstrates the importance of appropriate “anchors” (Gilchrist et al., 1999) for achieving and preserving color constancy and hence veridical perception. Relational perception (in the sense of Wertheimer and Köhler) is crucial not only for correctly perceiving brightness and color, but also for the transposition of paired differences between test and reference stimuli. For example, in Figure 106.3*F*, the widely spaced pairs of dots might group if surrounded by dots with even larger interspaces. Thus, a simple explanation of the Gestalt factor of proximity in terms of adjacency within localized receptive fields may not apply without also considering the context.

Although color constancy has been shown behaviorally in several species (e.g., bees and goldfish; Neumeyer, 1980; Ingle, 1985; Neumeyer et al., 2002), we know of only one study reporting color constancy neurons in area V4 of the primate (Zeki, 1980). Here neurons responded to a red patch in a multicolored Mondrian pattern regardless of changes in spectral illumination, suggesting that they were mediating invariant color. More studies of this kind are needed.

ISOMORPHISM A key concept of the Gestalt theory of brain processes is *isomorphism*. In the context of current neuroscience, isomorphism refers to the assumption of a structural resemblance between the proximal stimulus (retinal image) and its representation on the cortical surface.

Studies using radioactive tracers as well as functional magnetic resonance imaging (Tootell et al., 1982, 1998) have established a retinotopic but not isomorphic representation

of the stimulus on the surface of the cortex. Neighboring loci in the retinal image remain neighbors, although there is a complex logarithmic transformation between retinal and cortical images, as well as anisotropies along the horizontal and vertical meridians (Tootell et al., 1982; Schwartz, 1994; Wood and Schwartz, 1999). The cortical magnification factor (*M*) demonstrates that the size of receptive fields is inversely related to their spatial extent in the visual cortex. Stimuli of different eccentricity that are *M*-scaled therefore occupy the same space on the cortical surface (Wilson et al., 1990). For area V1 at least, *M* scales are the biologically correct perceptual metric. Numerous other areas are also concerned with visual processing, but none of them have the high magnification factor and high degree of retinotopic regularity of the primary (striate) cortical area. Understanding their role within the context of Gestalt psychology takes us to the forefront of neuroscience research today.

A second meaning of isomorphism, central to Gestalt theory, has received much less attention. It concerns the hypothesis according to which the experienced order in space is structurally identical to the functional order in the distribution of underlying brain processes (Köhler, 1947). Using metal electrodes applied to the back of the head, Köhler and Held (1949) set out to find the neuronal representation of a percept on the surface of the occipital cortex. For example, they tested the hypothesis by Köhler and Wallach (1944) that the figural aftereffect (an apparent displacement of a test pattern following prolonged exposure to an adaptation pattern) affected nearby stimulus contours more strongly, because their neural representations lay closer to each other on the cortical surface. The idea that perceptual as well as stimulus properties are the correlational counterparts of brain processes is now gaining acceptance as researchers begin to focus on the issue of conscious perceptions in the absence of stimulus correlates (e.g., Spillmann, 1999b; Engel and Singer, 2001; Kanwisher, 2001; see Chapter 114).

Gestalt concepts and neuroscience

In the past 40 years, neurophysiological research has produced a wealth of results that are obviously linked to Gestalt theory (Spillmann, 1997, 1999a, 2001). In the second half of this chapter, we will discuss these results because they not only advanced the field, but also promoted our understanding of the neural mechanisms underlying visual perception.

As to Wertheimer's (1912) apparent motion, it has been shown that movement-sensitive neurons in the frog respond to a pair of stimuli separated in space and time (apparent motion) as though they were responding to real motion (Grüsser-Cornehls, 1968). Meanwhile, single-cell recordings

in the monkey suggest that the neuronal substrate for apparent motion may be distributed over multiple cortical areas (V1, MT), in which neuronal responses depend critically upon the temporal and spatial intervals of the stimuli (Newsome et al., 1986). For high apparent speeds, physiological data from MT, but not V1, corresponded closely to the psychophysical data.

In today's field of neuroscience, we distinguish between three kinds of neuronal interactions: convergent/divergent (feedforward), horizontal (corticocortical), and reentrant (feedback from higher to lower areas). Wertheimer's (1912) *Querfunktionen* (lateral processes) would sensibly fall within the middle category, whereas the other two are now called *bottom-up* (sensory input) and *top-down* processes (attention, motivational states). Less tangible terms that have become popular over the years include *early* or *low-level*, *intermediate* or *mid-level*, and *late* or *high-level vision*.

RECEPTIVE FIELDS AS A FUNCTIONAL MICRO-GESTALT A concept now firmly established by single-cell neurophysiology is the *receptive field* (Kuffler, 1953) of a neuron, which includes excitatory and inhibitory regions of various shapes suited to encode different attributes of the physical stimulus. This concept has been used to support the idea of a hierarchical system for feature extraction by arguing that one class of neurons drives another, and as a consequence, stimulus selectivity and complexity of receptive field shapes increase from lower to higher levels of processing (Hubel, 1988). This concept was enthusiastically embraced by vision researchers but left Köhler incredulous (Teuber, 1967), as it was counter to his holistic theory of brain function based on electrochemical fields in the cortex. It also seemed to reintroduce atomism by dissecting the stimulus (and the subsequent percept) according to its local parameters (e.g., contrast, orientation, disparity).

Research has shown that there is a considerable degree of functional specialization—for example, cells in area V4 dedicated to color and cells in area V5 to motion (Livingstone and Hubel, 1987; Zeki, 1980, 1993, 2001). However, there is also evidence of multipurpose cells (Schiller, 1996) allowing for flexible and efficient interaction within distributed systems. Receptive field organization, with its various forms of center-surround antagonism and selective spatial and temporal sampling properties, integrates the initial receptor inputs in a superadditive way, thereby allowing for transposition of stimulus properties. In this sense, the receptive field may be considered a functional *micro-Gestalt* for processing visual stimuli (Spillmann and Ehrenstein, 1996). The extended wiring diagram of Felleman and Van Essen (1991) tracing hundreds of individual connections between a great many centers should not distract us from the obvious: that the visual brain is a highly interactive system of feedforward, feedback, and lateral loops that approaches a sort of func-

tional continuum despite (or even because of) the multitude of discrete pathways.

A major distinction between two processing streams (Mishkin et al., 1983), one to the temporal lobe ("what") and the other to the parietal lobe ("where"), is now generally accepted. According to this distinction, areas processing the shape of an object, including its brightness, color, orientation, and depth, are separated from cortical areas concerned with processing direction of motion and location in space. The question thus looms: how do all these attributes come together?

PERCEPTIVE NEURONS In 1970, Jung and Spillmann introduced the term *perceptive field* to denote the psychophysical correlate of the neuronal receptive field. Perceptive fields were understood to be organized analogously to receptive fields (i.e., center-surround), but to subserve many more neurons to achieve a percept (e.g., the Hermann grid illusion) or mediate a threshold response (the Westheimer paradigm). The sizes of *perceptive* fields defined and measured in this manner increased from the fovea to the periphery in close agreement with the size of single-cell *receptive* fields (Spillmann et al., 1987) (Fig. 106.6).

Twenty years later, Baumgartner (1990) proposed the term *perceptive neuron* for cells that respond as though they mediated the perception of illusory contours in Kanizsa-type figures. The Zurich group had found that neurons in area V2 responded to an *illusory* contour stimulus—the aligned top and bottom parts of a bar separated by an empty gap in the middle—in a way similar to a bar without a gap (Baumgartner et al., 1984; von der Heydt et al., 1984; Peterhans and von der Heydt, 1991). Since there was no physical stimulus activating the (local) receptive fields of

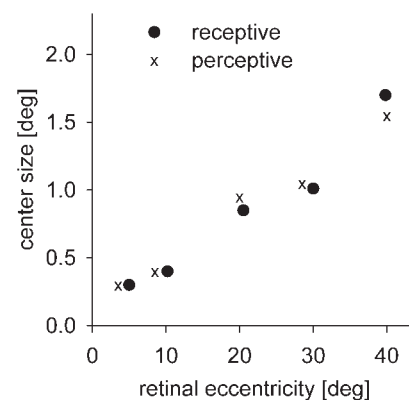


FIGURE 106.6. Comparison of receptive and perceptive field centers in the rhesus monkey. The sizes of the receptive field centers refer to retinal broadband cells and were taken from DeMonasterio and Gouras (1975). The sizes of the perceptive field centers were obtained using the Westheimer paradigm and are averages from the temporal and nasal retinas of two monkeys (Oehler, 1985). (From Spillmann et al., 1987.)

these neurons due to their location inside the gap, the authors inferred that there must have been an influence from a larger (global) response field in the outer surround, bridging the gap. When a thin orthogonal stop was attached to the inner end of each inducer, the neuronal response was abolished, as was the illusory contour. Since there was no physical stimulus activating the receptive fields of these neurons (as defined by bars and edges), the authors inferred that there must have been an influence from *beyond the classically defined receptive field*.

To account for the responses of these higher-order V2 neurons (or neuronal representations of the illusory contours), a gating mechanism was assumed that groups the signals of endstopped cells, each one detecting an attribute of the stimulus (line end or corner) (Peterhans et al., 1986). Stimulus alignment was critical: lines and corners that were out of register (or moved out of synchrony) no longer produced a response, a result that seems to follow from good continuation and collinearity (Peterhans and von der Heydt, 1991). Similarly, in psychophysics, it was found that a slight misalignment between the inducing stimuli and the test spot failed to reveal the subthreshold summation hypothesized to underlie the perception of illusory contours (Dresp and Bonnet, 1995). It is now known that context dependency of the neuronal response is not a privilege of area V2, but is already found in visual area V1 (see the section “Context-dependent Boundary Formation” on page 1582).

FACE CELLS Nowhere is the assumption of global rather than local processing more obvious than in face perception. The face is the most important visual stimulus in social interaction. Faces are global percepts that cannot be derived from individual features. Only holistic perception reveals the individuality of a face, as is evident from the clinical syndrome of *prosopagnosia*, or face blindness (Spillmann et al., 2000). Face-blind patients complain that they see the eyes, nose, mouth, ears, and hair but that “they don’t add up.”

In view of the biological preeminence of the facial stimulus, it should not be surprising that cells have evolved in the brain to encode faces. Such neurons have indeed been found. The early reports on neurons in the inferotemporal lobe (Rolls, 1984, 2000; Perrett et al., 1982, 1992) responding to intact faces more strongly than to their constituent parts have now been confirmed. “Face neurons” would be expected to allow for a certain amount of transposition and invariance for us to be able to recognize faces irrespective of illumination, distance, and viewpoint (Grüsser and Landis, 1991). Indeed, they must be capable of preserving the configural information of the face despite large transformations of the stimulus. Global or holistic perception enables perception of the identity as well as the physiognomic properties (emotional salience) of a face. However, as of yet, no type of neuron has been found to signal the facial expres-

sions of happiness or sadness, surprise or fear, anger or disgust, although brain lesions in the amygdala have been found to result in impaired recognition of fear and disgust (Calder et al., 2001). To show how the perception of emotional salience of a face is neurally encoded will be a major task of future research.

BINDING BY SYNCHRONIZATION: A MECHANISM FOR GESTALT FORMATION In the outside world, parts that belong to one object are situated next to each other. However, there are exceptions when it comes to the perception of groups and group members. Here the question arises of how we link up distant parts of a stimulus moving in the same or similar direction. The most widely discussed answer is: by response synchronization in cell assemblies. Neurons stimulated in a similar manner are hypothesized to adjust their firing patterns so as to discharge in unison (Eckhorn et al., 1988; Gray et al., 1989). Synchronization would then bind stimuli together in different loci by virtue of their common properties (e.g., orientation, color, size) and in this way achieve grouping. The advantage of such coupling by synchronized neuronal activity is obvious: it would enable cells and cell groups to change partners with which they share activity when the stimulus configuration changes. Binding by synchronization thus provides a flexible efficient neuronal mechanism for figure-ground segregation (see Chapter 113).

In addition to local features, binding plausibly underlies the detection of coherent motion according to the factor of *common fate*. How common must common fate be? Uttal et al. (2000) found that as few as 4 collinearly arranged dots moving on a random dynamic noise field of 100 dots suffice to be seen as a group. This low signal-to-noise ratio is astonishing, but even more remarkable is the fact that a similarly low ratio was found behaviorally in trained, alert monkeys and also when recording from individual neurons (Newsome et al., 1989; Britten et al., 1992).

Gestalt psychologists such as Köhler (1940) would have liked the idea of temporal binding because it generates percepts from the interaction of many neurons in different areas of the brain and because the same neurons can serve different percepts. Köhler wrote “A given visual field, for instance, is biologically represented by a certain distribution of processes in the occipital lobes of the brain; the correlates of other perceptual facts are located in various other lobes; and many psychological events are likely to concern the brain as a whole.” This foresight from the foremost theoretician of the Gestalt movement has proven to be remarkably close to today’s findings using neuroimaging methods. These findings suggest parallel stimulus processing within several retinotopically organized visual brain areas and cross-talk between these and nonvisual areas (Engel et al., 1997; Heeger, 1999; Kastner et al., 2000; Van Essen et al., 2001).

Examples of current Gestalt research

FIGURE-GROUND CORRELATES To account for stimulus integration and figure-ground segregation, new terms have emerged to convey the notion that a contour typically is unilateral: *belongingness* (Nakayama and Shimojo, 1990) and *border ownership* (Zhou et al., 2000). As a rule, the contour delineates the figure, not the ground. When figure and ground switch, as in bistable (reversible) figures, the assignment of the contour switches as well. This asymmetric assignment was central to Gestalt psychology and was referred to as the law of the inside (*Gesetz der Innenseite*; Metzger, 1936/1953).

Neurophysiological studies in monkey area V1 (Lee et al., 1998) as well as V2 provide evidence for this kind of figure-ground polarity. For example, neurons have been found that are selective for figure-ground direction (1) at illusory contours like those produced by Ehrenstein- or Kanizsa-type figures (Baumann et al., 1997; Heider et al., 2000; Peterhans and Heitger, 2001), (2) at luminance edges in overlapping squares and rectangles (Zhou et al., 2000), and (3) at stereo edges in random-dot stereograms (von der Heydt et al., 2000; Heider et al., 2002). This kind of neural activity would plausibly contribute to the perceptual segregation of figure and ground at these contours.

SMOOTH (OR “GOOD”) CONTINUATION In a series of experiments, contour processing was tested psychophysically by using a surface of Gabor patches with random orientations. Collinearly oriented but disconnected patches were added to

form a perceptual contour (Field et al., 1993; Kovács and Julesz, 1993). Figure 106.7 shows that these patches can easily be seen as a curvy line despite the fact that the distance between aligned patches is larger than the length of each patch and the elements in the background have a smaller average separation than those along the contour. This *popout* effect is even stronger when the patches form a closed circle. These results may be taken as evidence for a neuronal mechanism that perceptually connects individual stimuli with an *association field* (Field et al., 1993) according to the Gestalt factors of good continuation and closure. If one of the elements was rotated out of alignment, the chain broke up and a circle was no longer perceived. Kovács and Julesz (1994) also found that local contrast sensitivity within the virtual circle of orientated patches was enhanced relative to that on the outside, suggesting that the elements constituting the figure are privileged. Neurons coding collinearity (Peterhans and von der Heydt, 1991) may be involved in this task (see Chapter 70).

Stimuli beyond the classic receptive field have been shown to facilitate the response to a central bar in cat visual cortex when they are cooriented and coaxially aligned with the central stimulus (Nelson and Frost, 1985). In fact, when a jumbled target/background pattern was used for a stimulus, the response in area V1 of the alert monkey to an optimally oriented target bar increased when the immediately adjoining bars at either end of the target were rotated to become collinear with the central stimulus (Kapadia et al., 1995, Fig. 12). The combined response could even be higher than that

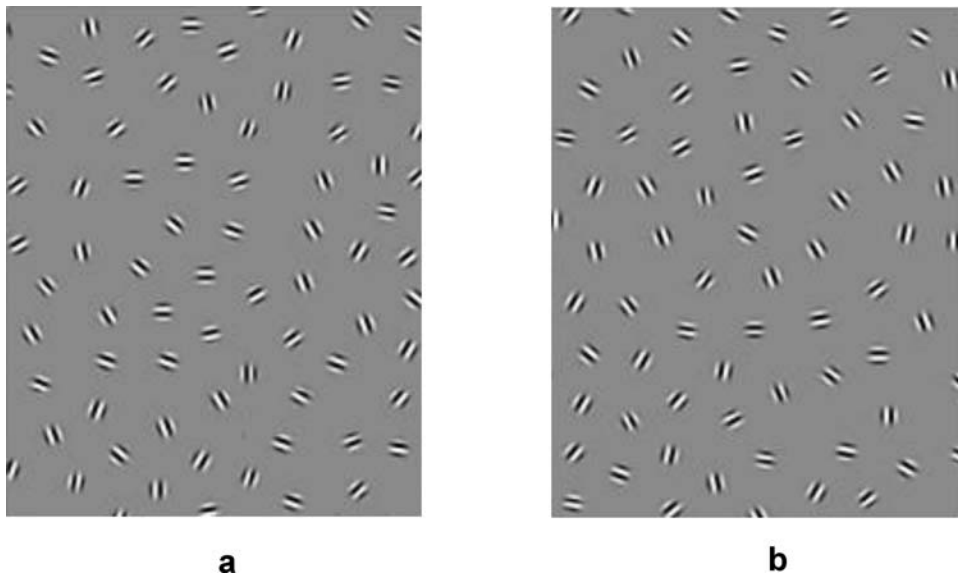


FIGURE 106.7. The figure of a circle in a random arrangement of Gabor patches becomes visible according to the Gestalt factor of good continuation. *a*, Partial curve; *b*, complete circular figure. Note that the number of patches and the overall distribution of

their orientations are equal in *a* and *b*, but the brain's response is not. (From Kovács and Julesz, 1993. Copyright 1993 National Academy of Sciences, USA.)

to the central bar alone. This increase suggests that surround inhibition was eliminated and replaced by collinear facilitation. Anatomical studies have shown that tangential connections in the primary visual cortex predominantly link neurons responding to contours that have similar orientation preferences and are aligned collinearly (Bosking et al., 1997; Schmidt et al., 1997). Together with neurophysiological evidence showing that these connections can mediate collinear facilitation, these results suggest that the neuronal circuitry underlying contour integration and perceptual salience is already present in area V1 (Löwel and Singer, 1992; Crook et al., 2002). The psychophysics of good continuation may thus find its neurophysiological correlate in the functional architecture of these connections (Palat and Sagi, 1994).

CONTEXT-DEPENDENT BOUNDARY FORMATION Boundaries typically result from stimulus differences at the edge between homogeneous but differing surfaces. Such differences may be luminance, wavelength, orientation, texture, motion, and depth contrast (Nothdurft, 1993; Bach and Meigen, 1997; for a review, see Regan, 2000). Even a phase lag (Leonards et al., 1996; Kandil and Fahle, 2001) or a difference in flicker frequency is sufficient to define an edge, and an edge owned by a space segregates figure from ground. Here it was found that the contour delineating a figure fuses at a flicker frequency as low as 4 to 5 Hz, whereas the enclosed surface area fuses at a much higher frequency (van de Grind et al., 1973). We may conjecture that this difference reflects processing by the parvo- and magnocellular systems, (Livingstone and Hubel, 1987): parvo-cells having low temporal and high spatial frequency resolution (edges); and magno-cells having high temporal and low spatial frequency resolution (surfaces).

Lateral neuronal effects of context-dependent contrasts were first reported by Nelson and Frost (1978) in area V1 of the cat and thereafter by others in the monkey (for a review, see Allman et al., 1985). Orientation and motion contrast were the phenomena most thoroughly studied (e.g., Knierim and Van Essen, 1992; Sillito et al., 1995; Sillito and Jones, 1996). Figure 106.8 shows that the response to a single orientation is best when there is a suitable center stimulus, and it becomes significantly weaker when flanker stimuli of like orientation are presented in the surround (Kastner et al., 1999; Nothdurft et al., 1999). Conversely, orthogonal stimuli restore the response. This result explains why a hatched square elicits a strong response when presented on a differently oriented background but a reduced response when the orientation contrast is eliminated (Lamme, 1995; Zipser et al., 1996). Thus, figure-ground segregation is likely to involve orientation-selective, context-sensitive neurons. A similar conclusion holds for neurons responding to motion and texture (see Chapter 45).

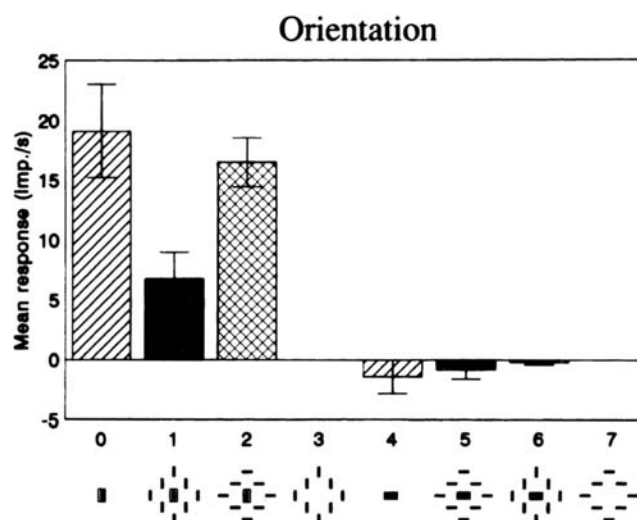


FIGURE 106.8. Neuron responses reflect orientation contrast in cat striate cortex. The response to the optimal stimulus (0) is much higher than to the same stimulus surrounded by like elements (1) but only slightly higher when surrounded by orthogonal stimuli (2). Little response is obtained when the orientations of the bars are rotated by 90 degrees (4–7). (From Kastner et al., 1997.)

SURFACE FILLING-IN While the neural representation of boundaries is fairly well understood, the cortical representation of surfaces is still a matter of conjecture. How do we account for the perception of uniform brightness, color, and texture on extended areas? As pointed out above, cortical neurons respond poorly to uniform stimuli. The question therefore arises of why and how we perceive a bright, colored area enclosed by a contour. Grossberg and Mingolla (1985) advocated two processing systems: a *boundary processing system* and a *feature processing system*. The latter produces perception of a uniform surface by diffusion of stimulus information extracted from the edge.

More specifically, Spillmann and Werner (1996) and Gilbert (1998) proposed that excitation (i.e., active filling-in) via horizontal connections accounts for area contrast and other large-scale effects. Indeed, when a large yellow disc is surrounded by an achromatic annulus and the luminance of the annulus is increased beyond that of the disc, the yellow color will change to brown and ultimately black: Hering's (1874) *Schwarzverhüllung*. This is definitely a surround effect, which requires that the luminance change is extracted at the contour and transmitted to the center of the disc.

These hypotheses are now receiving support from psychophysical experiments, suggesting that brightness and texture originate at the border and spread onto the delineated area until stopped by a black barrier (Paradiso and Nakayama, 1991). In this way, a homogeneous surface is created representing a figure on a ground (for a review, see Spillmann and DeWeerd, 2003).

LARGE-SCALE COLOR EFFECTS Filling-in of color represents a particular challenge to any explanation, as this is a large-scale effect driven by a small-cell input: color is processed predominantly by the parvocellular system, which is characterized by small receptive fields. Yet, a wide, uniform spread of perceived color has been evident at least since Goethe's (1810) description of colored shadows. Here subjectively saturated colors are induced and perceived on a large achromatic area when it is flanked by a chromatic surround. Recently, Kallmann et al. (2002) measured the induced color of these shadows and found in all cases a hue shift toward the complementary color of the surround. The effects were strongest for blue and yellow surrounds and under conditions where the luminance of the surround exceeded that of the "color-shadowed" area. This is a striking phenomenon that up to now has eluded physiological explanation, although results suggest involvement of the larger koniocellular or S-cone receptive fields.

There may be a relation to chromatic induction mechanisms. In an experimental setup similar to that producing colored shadows, Valberg (1974) measured the colors induced into an achromatic center by chromatic surrounds. The dependence of the induced colors on the hue and saturation of the inducing colors points to lateral processes within color opponent mechanisms. The finding that steady surrounds, remote from the receptive field center, affected the activity of parvocellular neurons in the macaque lateral geniculate nucleus (Valberg et al., 1985) further supported this suggestion. It thus appears that the global response field, far beyond the classical receptive field, controls cell response by means of simultaneous contrast, and it does not wait until the highest visual centers to do so. As daylight changes from dawn to dusk, these mechanisms presumably drive global gain control mechanisms and cause sensitivity shifts that ensure color and lightness discrimination for the objects encountered in a natural environment.

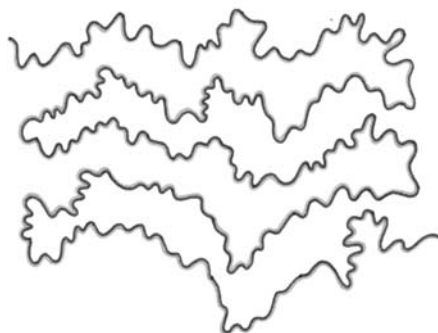


FIGURE 106.9. The watercolor effect as an example of large-scale color assimilation arising from thin color boundaries. A purple border flanked by an orange fringe produces a uniform orange coloration on the enclosed white surface area. The orange regions are segregated as figure from the other spaces, which are ground. (From Pinna et al., 2001.) (See color plate 80.)

A novel *watercolor effect* (Pinna et al., 2001) exhibits large-scale properties similar to those of Goethe's colored shadows, except that it is induced by a narrow fringe and is more subtle in appearance. Figure 106.9 shows a wavy line pattern consisting of a dark purple contour lined by an orange fringe. Clearly, the orange color is seen spreading uniformly over the entire surface area. This process is seemingly instantaneous and covers visual angles of up to 45 degrees. The watercolor effect may serve to enhance figure-ground segregation by imparting surface color to the enclosed area. It may also promote grouping between distant stimulus elements (Fig. 106.10). While diffuse and subtle, the color is not weak: when pitted against the classical Gestalt factors (see the section "Figure-Ground Segregation and Perceptual Grouping" on page 1574), watercolor invariably wins as the figural determinant (Pinna et al., 2003). The assimilative color spreading from the narrow fringe may arise in two steps: first, weakening of the contour by lateral inhibition between differentially activated edge cells (local diffusion); and second, unhampered flow of color onto the enclosed surface area (global diffusion).

Another spreading phenomenon that can fill-in large areas is *neon color spreading* (Bressan et al., 1997), where a veil of color covers the area of illusory brightness enhancement in the Ehrenstein and Kanizsa figures. Simple inducing stimuli, such as four short black lines connected by a colored cross, are sufficient to elicit the effect: a delicate glow in the color of the cross. However, spreading is not unique to color. Figure 106.11 demonstrates that spreading is also observed for texture (Watanabe and Cavanagh, 1991), suggesting that filling-in is a general mechanism by which the

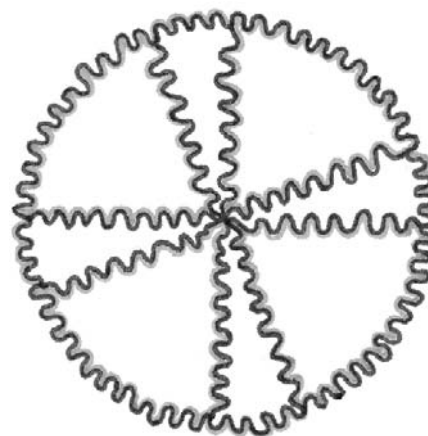


FIGURE 106.10. The watercolor effect is superior to the classical Gestalt factors (here, proximity) in conferring figure status on one space in preference to another. In this well-known variant of Rubin's (1915) sector disc (or Maltese cross), the narrow sectors are normally seen as the figure. However, if colored fringes are used for the figure's contours, then the watercolored sectors are seen as figures, regardless of whether their boundaries have proximity or not. (Courtesy of B. Pinna; see also Pinna et al., 2003.) (See color plate 81.)

visual system creates figures on a ground from sparse information.

GESTALT COMPLETION ACROSS SCOTOMATA The principles governing visual perception under normal circumstances would also be expected to be effective as a repair mechanism. From the work of Kaas et al. (1990) and Gilbert and Wiesel (1992), it appears that holes in the retina resulting in visual scotomata are compensated for by a massive reorganization of cortical receptive fields. The authors found that a deafferented cell quickly resumed firing when light fell on adjacent regions of the retina. One way to explain this reactivation is by assuming that collateral signals are fed to deafferented neurons through horizontal long-distance connections. Accordingly, patients rarely notice a dark spot in their visual field after laser coagulation of the retina. Instead, they report that the percept in the area of the lesion is largely undisturbed and complete, with color, brightness, and texture. There are limits, though, when the area to be bridged is too large and when the parts to be connected are

nonrelatable, for example, because of different orientation (Kellman and Shipley, 1991). In this case, no perceptual filling-in takes place. The interpolation required to bridge a scotoma, including the physiological blind spot (Fiorani et al., 1992; Durgin et al., 1995), may be analogous to that taking place in the formation of illusory contours in Ehrenstein- and Kanizsa-type figures (see the section “Perceptual Constraints” on page 1574).

APERTURE MOTION Preceded by Stumpf’s early observation in 1911 (see Todorovic, 1996), Hans Wallach (1935) was the first to analyze systematically the direction of perceived motion when moving contours are viewed through an aperture or a window (Wuerger et al., 1996). Here one observes a striking change in apparent motion direction dependent on the shape of the aperture. Normally, the perceived motion direction of a line with invisible end points would be at right angles to the line’s orientation. In a window, however, the direction of motion typically appears parallel to the contour of the window. For example, oblique lines viewed through a vertical rectangular slit are always seen to move vertically (*barber pole effect*). With an L-shaped aperture, the apparent direction of the moving lines changes from vertical to horizontal when the lines reach the base of the L. The *aperture problem* refers to a fundamental question of motion perception: how are local motion signals integrated to provide coherent motion percepts in a complex visual scene? The visual system itself faces the same difficulty: an aperture problem arises from the limited receptive field size of a single neuron (Adelson and Movshon, 1982; Hildreth, 1984).

To account for this problem, Movshon et al. (1985) proposed a two-stage model of motion processing. The information from first-order, direction-sensitive simple or complex cells of areas V1 and V2 is integrated in second-order *component* and *pattern* cells in area MT, whose neurons have large receptive fields and receive direction-selective inputs from areas V1 and V2. Component cells provide signals about the local motions of individual contours, similar to cells found in area V1. Pattern neurons, however, reflect integrated information about coherent motion that results from combined inputs of local motion signals from several different contours or orientations (Movshon et al., 1985). They occur only in area MT.

Recently, Grossberg et al. (2001) extended Movshon’s model, assuming directionally tuned transient short-range cells that respond to local image transients. Long-range cells in area MT pool their signals (multiple orientations, opposite contrast polarities, and depths). MT cells further activate a directional grouping network, proposed to occur within the adjacent cortical area MST, within which motion directions, generalized across space, compete to determine a local winner: coherent motion signals typically win over incoher-

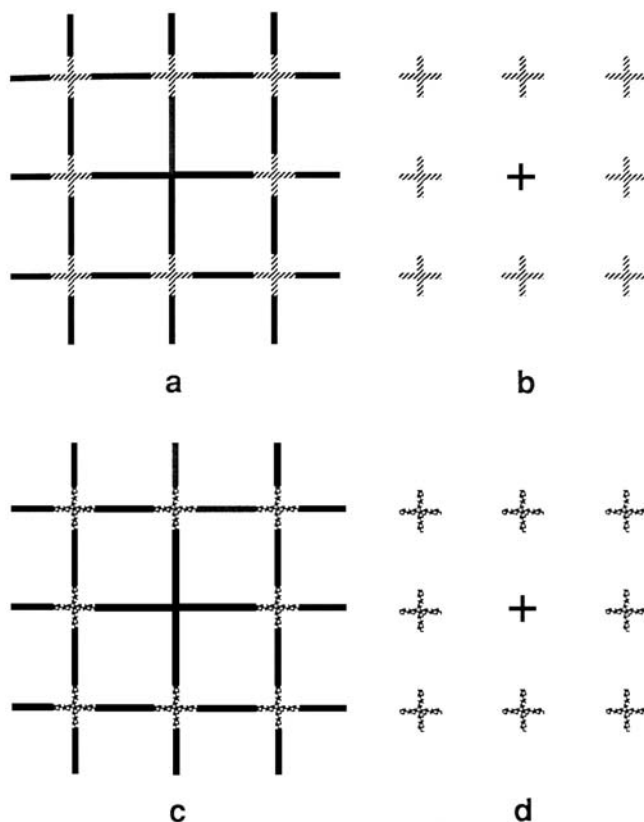


FIGURE 106.11. In addition to producing an illusory contour delineating a surface having illusory brightness, the brain is capable of filling the space with illusory texture. Illusory spreading of texture within the Ehrenstein pattern is shown for *a* hatched and *c* dotted crosses bridging the central gaps. *b*, *d* Crosses in isolation. The spreading effect is best observed in peripheral version; fixate at the center of the pattern. (From Watanabe and Cavanagh, 1991.)

ent ones. The winning direction coded by MST cells is fed back to MT cells, which enhance directionally consistent cell activities and suppress inconsistent activities.

Wallach's (1935) demonstrations of perceptual organization in seen motion have thus served to demonstrate local edge effects on whole-surface motion, and to inspire research and modeling of neuronal mechanisms in areas MT and MST that cast light on integrative mechanisms in motion perception.

Outlook

Gestaltists considered Gestalt factors in vision essentially as bottom-up mechanisms built into the visual system through evolution of the organism as it interacted with stimuli in a natural setting. In this sense, it may be said that illusory contours have evolved to support contour integration and contour completion in partially occluded stimuli (Dresp, 1997). In the words of Michael Wertheimer, "Gestalten are real phenomena in the natural world, not the whimsical, arbitrary creations of a mind" (Sharps and Wertheimer, 2000, p. 324). Today's attempts to match the visual features in natural scenes with the properties of known neuronal mechanisms will show how well we are equipped for the task: to encode the world around us (see Chapter 70).

Another question being asked today focuses on the relationship between vision and action. Gestalt psychologists restricted themselves to the study of perception (*reine Anschauung*). Yet, our sensory systems developed in close correspondence with our motor systems (Weizsäcker, 1947). Thus, one would expect that what we see has direct bearing on the way we act, and vice versa. Modern theories of visual function distinguish between different though interactive visual systems, one for the perception of objects, the other for the guidance of actions directed at those objects (e.g., Goodale and Humphrey, 1998). Evolutionary history suggests that these systems are based on the ventral stream (vision as a basis of cognition) and the dorsal stream (vision leading to motor control), respectively.

Perceptual constancy occurring despite translation and rotation of the eye, head, and trunk has now been added to the study of vision, as have changes of observation distance. Selective attention (Treue, 2001; see Chapter 103), fixation, guided saccades, and pursuit movement (Ebenholtz, 2001) have also been included. From these must emerge an understanding of how we construct maps of the space around us that are sufficiently accurate and stable for us to walk through them. Finally, cross-modal studies, already present in the older literature (e.g., Goldstein and Rosenthal-Veit, 1926; Schiller, 1932) are reentering the field (e.g., Ehrenstein and Reinhardt-Rutland, 1996; Stein, 1998; Lewald et al., 2001). They show, for example, that the direction of gaze

can influence the perceived auditory direction, an effect which can be linked to the (incomplete) transformation of spatial coordinates within auditory and visual neural representations in the primate midbrain and parietal cortex. Cross-modal sensory integration affords coherent space perception to enable proper action.

By its very nature, Gestalt psychology as a theoretical approach to vision and perception required the assumption of neural networks even before the term became ubiquitous. Perception is organization. It is implicit in every perceptual demonstration due to laterally interacting networks. Given today's knowledge, we realize that the questions then asked were far ahead of their time. Eighty years later, a biological basis for higher perceptual factors appears to be within our grasp. Seemingly effortlessly, our brains pick up information, process it, and enable us to maneuver in a complex environment. We negotiate our world far better and faster than any robot without stumbling. Why? Because Gestalt factors, the interface between the world and the percept, guide us along. A large number of neurons is not decisive, nor is the speed of processing. Gestalt-like interaction makes the difference.

Acknowledgments

Preparation of this chapter was supported by DFG Grant SP 67/6-2 (to LS) and DFG Grant Eh 91/4-4 (to WHE). Jerry Nelson helped with the conceptualization, and Ilona Kovács, Sigrid Löwel, Galina Paramei, Esther Peterhans, Viktor Sarris, Arne Valberg, John S. Werner, Mimsey West, and Michael Wertheimer provided valuable comments. Ute Lobisch prepared most of the figures. Baingio Pinna and Frank Stürzel assisted with the electronic data transfer. Simon and Anna cheered us up. We thank them all.

REFERENCES

- Adelson, E. H., and J. A. Movshon, 1982. Phenomenal coherence of moving visual patterns, *Nature*, 300:523–525.
- Allman, J., F. Miezin, and E. McGuinness, 1985. Stimulus specific responses from beyond the classical receptive field: neurophysiological mechanisms for local-global comparisons in visual neurons, *Annu. Rev. Neurosci.*, 8:407–430.
- Bach, M., and T. Meigen, 1997. Similar electrophysiological correlates of texture segregation induced by luminance, orientation, motion, and stereo, *Vis. Res.*, 37:1409–1414.
- Bahnsen, P., 1928. Eine Untersuchung über Symmetrie und Asymmetrie bei visuellen Wahrnehmungen, *Z. Psychol.*, 108:129–154.
- Baumann, R., R. van der Zwaan, and E. Peterhans, 1997. Figure-ground segregation at contours: a neural mechanisms in the visual cortex of the alert monkey, *Eur. J. Neurosci.*, 9:1290–1303.
- Baumgartner, G., 1990. Where do visual signals become a perception? in *The Principles of Design and Operation of the Brain* (J. C. Eccles and O. Creutzfeldt, eds.), Berlin: Springer, pp. 99–114.

- Baumgartner, G., R. von der Heydt, and E. Peterhans, 1984. Anomalous contours: a tool in studying the neurophysiology of vision, *Exp. Brain Res.*, suppl. 9:413–419.
- Beck, J., 1982. *Organization and Representation in Perception*, Hillsdale, NJ: Erlbaum.
- Bosking, W. H., Y. Zhang, B. Schofield, and D. Fitzpatrick, 1997. Orientation selectivity and the arrangement of horizontal connections in tree shrew striate cortex, *J. Neurosci.*, 17:2112–2127.
- Bradley, D. C., G. C. Chang, and R. A. Andersen, 1998. Encoding of three-dimensional structure-from-motion by primate area MT neurons, *Nature*, 392:714–717.
- Bressan, P., E. Mingolla, L. Spillmann, and T. Watanabe, 1997. Neon color spreading: a review, *Perception*, 26:1353–1363.
- Britten, K. H., M. N. Shadlen, W. T. Newsome, and J. A. Movshon, 1992. The analysis of visual motion: a comparison of neuronal and psychophysical performance, *J. Neurosci.*, 12:4745–4765.
- Calder, A. J., A. D. Lawrence, and A. W. Young, 2001. Neuropsychology of fear and loathing, *Nat. Rev. Neurosci.*, 2:352–363.
- Crook, J. M., R. S. Engelmann, and S. Löwel, 2002. GABA-inactivation attenuates colinear facilitation in cat primary visual cortex, *Exp. Brain Res.*, 143:295–302.
- DeMonasterio, F. M., and P. Gouras, 1975. Functional properties of ganglion cells of the rhesus monkey retina, *J. Physiol. (Lond.)*, 251:167–195.
- Dresp, B., 1997. On illusory contours and their functional significance, *Cahiers Psychol. Cogn.-Curr.-Psychol. Cogn.*, 16:489–518.
- Dresp, B., and C. Bonnet, 1995. Subthreshold summation with illusory contours, *Vis. Res.*, 35:1071–1078.
- Dücker, G., 1966. Untersuchungen über geometrisch-optische Täuschungen bei Wirbeltieren, *Z. Tierpsychol.*, 23:452–496.
- Durgin, F. H., S. P. Tripathy, and D. M. Levi, 1995. On the filling in of the visual blind spot—some rules of thumb, *Perception*, 24:827–840.
- Ebenholtz, S. M., 2001. *Oculomotor Systems and Perception*, Cambridge: Cambridge Univ. Press.
- Eckhorn, R., R. Bauer, W. Jordan, M. Brosch, W. Kruse, M. Munk, and H. J. Reitboeck, 1988. Coherent oscillations: a mechanism of feature linking in the visual cortex? Multiple electrode and correlation analysis in the cat, *Biol. Cybern.*, 60:121–130.
- Ehrenfels, C. von, 1890. Über Gestaltqualitäten, *Vjschr. wiss. Philos.*, 14:249–292. Translation in *Foundations of Gestalt Theory* (B. Smith ed.), Munich: Philosophia-Verlag, 1988, pp. 82–120.
- Ehrenstein, W., 1941. Über Abwandlungen der L. Hermannschen Helligkeitserscheinung, *Z. Psychol.*, 150:83–91.
- Ehrenstein, W., 1954. *Probleme der ganzheitspsychologischen Wahrnehmungslehre*, Leipzig: J. A. Barth.
- Ehrenstein, W. H., 2001. Perceptual organization, in *International Encyclopedia of the Social and Behavioral Sciences*, vol. 16 (P. B. Baltes and N. J. Smelser, eds.), Amsterdam: Elsevier Science, pp. 11227–11231.
- Ehrenstein, W. H., and A. H. Reinhardt-Rutland, 1996. A cross-modal aftereffect: auditory displacement following adaptation to visual motion, *Percept. Mot. Skills*, 82:23–26.
- Engel, A. K., and W. Singer, 2001. Temporal binding and the neural correlates of sensory awareness, *Trends Cogn. Sci.*, 5:16–25.
- Engel, S. A., G. H. Glover, and B. A. Wandell, 1997. Retinotopic organization in human visual cortex and the spatial precision of functional MRI, *Cereb. Cortex*, 7:181–192.
- Felleman, D. J., and D. C. Van Essen, 1991. Distributed hierarchical processing in the primate cerebral cortex, *Cereb. Cortex*, 1:1–47.
- Field, D. J., A. Hayes, and R. F. Hess, 1993. Contour integration by the human visual system: evidence for a local “association field,” *Vis. Res.*, 33:173–193.
- Fiorani, M., M. G. P. Rosa, R. Gattass, and C. E. Rocha-Miranda, 1992. Dynamic surrounds of RFs in primate striate cortex: a physiological basis for perceptual completion? *Proc. Natl. Acad. Sci. USA*, 89:8547–8551.
- Gelb, A., 1929. Die Farbenkonstanz der Sehdinge, in *Handbuch der normalen und pathologischen Physiologie*, vol. 12/1 (A. Bethe, G. V. Bergman, G. Emoden, and A. Ellinger, eds.), Berlin: Springer, pp. 594–678.
- Gibson, J. J., 1950. *The Perception of the Visual World*, Boston: Houghton Mifflin.
- Gilbert, C. D., 1998. Adult cortical dynamics, *Physiol. Rev.*, 78:467–485.
- Gilbert, C. D., and T. N. Wiesel, 1992. Receptive field dynamics in adult primary visual cortex, *Nature*, 356:150–152.
- Gilchrist, A., C. Kossyfidis, F. Bonato, T. Agostini, J. Cataliotti, X. J. Li, B. Spehar, V. Annan, and E. Economou, 1999. An anchoring theory of lightness perception, *Psychol. Rev.*, 106:795–834.
- Goethe, J. W. von, 1810. *Zur Farbenlehre*, Tübingen: J. G. Cotta. Translation in *Goethe's Color Theory* (R. Matthaei trans.), New York: Van Nostrand.
- Goldstein, K., and O. Rosenthal-Veit, 1926. Über akustische Lokalisation und deren Beeinflussbarkeit durch andere Sinnesreize, *Psychol. Forsch.*, 8:318–335.
- Goodale, M. A., and G. K. Humphrey, 1998. The objects of action and perception, *Cognition*, 67:181–207.
- Gottschaldt, K., 1926. Über den Einfluß der Erfahrung auf die Wahrnehmung von Figuren, *Psychol. Forsch.*, 8:261–317.
- Gray, C. M., P. König, A. K. Engel, and W. Singer, 1989. Oscillatory responses in cat visual cortex exhibit inter-columnar synchronization which reflects global stimulus properties, *Nature*, 338:334–337.
- Grind, W. A., van de, O.-J. Grüsser, and H. U. Lunkenheimer, 1973. Fusion frequency of Gestalt properties, in *Handbook of Sensory Physiology*, vol. VII/3A (R. Jung ed.), Berlin: Springer, pp. 463–464.
- Grossberg, S., and E. Mingolla, 1985. Neural dynamics of form perception: boundary completion, illusory figures, and neon color spreading, *Psychol. Rev.*, 92:173–211.
- Grossberg, S., E. Mingolla, and L. Viswanathan, 2001. Neural dynamics of motion integration and segmentation within and across apertures, *Vis. Res.*, 41:2521–2553.
- Grüsser, O.-J., and T. Landis, 1991. Visual agnosias and other disturbances of visual perception and cognition, in *Vision and Visual Dysfunction*, vol. 12 (whole volume) (J. Cronly-Dillon ed.), London: Macmillan.
- Grüsser-Cornehls, U., 1968. Response of movement-detecting neurons of the frog retina to moving patterns under stroboscopic illumination, *Pflügers Arch.*, 303:1–13.
- Heeger, D. J., 1999. Linking visual perception with human brain activity, *Curr. Opin. Neurobiol.*, 9:474–479.
- Heider, B., V. Meskenaitė, and E. Peterhans, 2000. Anatomy and physiology of a neural mechanism defining depth order and contrast polarity at illusory contours, *Eur. J. Neurosci.*, 12:4117–4130.
- Heider, B., L. Spillmann, and E. Peterhans, 2002. Stereoscopic illusory contours—cortical neuron responses and human perception, *J. Cogn. Neurosci.*, 14:1018–1029.
- Helmholtz, H. von, 1909–1911. *Handbuch der physiologischen Optik*, 3rd ed. Hamburg-Leipzig: G. Voss. Reprinted as *Helmholtz's*

- Treatise on Physiological Optics* (J. P. C. Southall trans.), Rochester, NY: Optical Society of America, 1924–1925.
- Hering, E., 1861. *Beiträge zur Physiologie I*, Leipzig: Engelmann.
- Hering, E., 1874. Zur Lehre vom Lichtsinne, Fünfte Mitteilung. Grundzüge einer Theorie des Lichtsinnes, *Sitzungsber. Kais. Akad. Wiss., Wien, math.-nat. Classe, Abt. III*, 69:179–217.
- Hertz, M., 1928. Wahrnehmungspsychologische Untersuchungen am Eichelhäher. 1, *Z. Psychol.*, 7:144–194; 2. 617–656. Reprinted as Figural perception in the jay bird, in *A Source Book of Gestalt Psychology* (W. D. Ellis trans.), London: Routledge and Kegan Paul, 1938.
- Hildreth, E. C., 1984. *The Measurement of Visual Motion*, Cambridge, MA: MIT Press.
- Hochberg, J., 1971. *Perception*, Englewood Cliffs, NJ: Prentice-Hall.
- Hubel, D. H., 1988. *Eye, Brain and Vision*, New York: W. H. Freeman.
- Ingle, D., 1985. The goldfish as a retiney animal, *Science*, 227:651–654.
- Johansson, G., 1973. Visual perception of biological motion and a model for its analysis, *Percept. Psychophys.*, 14:201–211.
- Jung, R., and L. Spillmann, 1970. Receptive-field estimation and perceptual integration in human vision, in *Early Experience and Visual Information Processing in Perceptual and Reading Disorders* (F. A. Young and D. B. Lindsley, eds.), Washington, DC: National Academy of Sciences, pp. 181–197.
- Kaas, J. H., L. A. Krubitzer, Y. M. Chino, A. L. Lanston, E. H., Polley, and N. Blair, 1990. Reorganization of retinotopic cortical maps in adult mammals after lesion of the retina, *Science*, 248:229–231.
- Kallmann, A. J., J. Schramme, and C. Neumeyer, 2002. Colored shadows—a quantitative analysis, *Invest. Ophthalmol. Vis. Sci.*, ARV abstract #3793 (available only on CD).
- Kandil, F. I., and M. Fahle, 2001. Purely temporal figure-ground segregation, *Eur. J. Neurosci.*, 13:2004–2008.
- Kanizsa, G., 1955. Margini quasi-percettivi in campi con stimolazione omogenea, *Riv. Psicol.*, 49:7–30.
- Kanizsa, G., 1979. *Organization in Vision*, New York: Praeger.
- Kanwisher, N., 2001. Neural events and perceptual awareness, *Cognition*, 79:89–113.
- Kapadia, M. K., M. Ito, C. D. Gilbert, and G. Westheimer, 1995. Improvement in visual sensitivity by changes in local context: parallel studies in human observers and in V1 of alert monkeys, *Neuron*, 15:843–856.
- Kastner, S., P. de Weerd, and L. G. Ungerleider, 2000. Texture segregation in the human cortex: a functional MRI study, *J. Neurophysiol.*, 83:2453–2457.
- Kastner, S., H. C. Nothdurft, and I. N. Pigarev, 1997. Neuronal correlates of pop-out in cat striate cortex, *Vis. Res.* 37:371–376.
- Kellman, P. J., and T. Shipley, 1991. A theory of visual interpolation in object perception, *Cogn. Psychol.*, 23:141–221.
- Knierim, J. J., and D. C. Van Essen, 1992. Neuronal responses to static texture patterns in area V1 of the alert macaque monkey, *J. Neurophysiol.*, 67:961–980.
- Koffka, K., 1935. *Principles of Gestalt Psychology*, New York: Harcourt, Brace.
- Köhler, W., 1920. *Die physischen Gestalten in Ruhe und im stationären Zustand*, Braunschweig, Germany: Vieweg.
- Köhler, W., 1923. Zur Theorie der stroboskopischen Bewegung, *Psychol. Forsch.*, 3:397–406.
- Köhler, W., 1940. *Dynamics in Psychology*, New York: Liveright.
- Köhler, W., 1947. *Gestalt Psychology*, New York: Liveright.
- Köhler, W., and R. Held, 1949. The cortical correlate of pattern vision, *Science*, 110:414–419.
- Köhler, W., and H. Wallach, 1944. Figural after-effects: an investigation of visual processes, *Proc. Am. Philos. Soc.*, 88: 269–357.
- Kovács, I., and B. Julesz, 1993. A closed curve is much more than an incomplete one: effect of closure on figure-ground segregation, *Proc. Natl. Acad. Sci. USA*, 90:7495–7497.
- Kovács, I., and B. Julesz, 1994. Perceptual sensitivity maps within globally defined visual shapes. *Nature (Lond.)*, 370:644–646.
- Kubovy, M., and J. R. Pomerantz, eds., 1981. *Perceptual Organization*, Hillsdale, NJ: Erlbaum.
- Kuffler, S. W., 1953. Discharge patterns and functional organization of mammalian retina, *J. Neurophysiol.*, 16:37–68.
- Lamme, V. A., 1995. The neurophysiology of figure-ground segregation in primary visual cortex, *J. Neurosci.*, 15:1605–1615.
- Lee, T. S., D. Mumford, R. Romero, and V. A. Lamme, 1998. The role of the primary visual cortex in higher level vision, *Vis. Res.*, 38:2429–2454.
- Leonards, U., W. Singer, and M. Fahle, 1996. The influence of temporal phase differences on texture segmentation, *Vis. Res.*, 36:2689–2697.
- Lewald, J., W. H. Ehrenstein, and R. Guski, 2001. Spatio-temporal constraints for auditory-visual integration, *Behav. Brain Res.*, 121:69–79.
- Livingstone, M. S., and D. H. Hubel, 1987. Psychophysical evidence for separate channels for the perception of form, color, movement, and depth, *J. Neurosci.*, 7:3416–3468.
- Lorenz, K., 1959. Gestaltwahrnehmung als Quelle wissenschaftlicher Erkenntnis, *Z. Exp. Angew. Psychol.*, 6:118–165.
- Löwel, S., and W. Singer, 1992. Selection of intrinsic horizontal connections in the visual cortex by correlated neuronal activity, *Science*, 255:209–212.
- Metzger, W., 1934. Beobachtungen über phänomenale Identität, *Psychol. Forsch.*, 19:1–60.
- Metzger, W., 1935. Tiefenerscheinungen in optischen Bewegungsfeldern, *Psychol. Forsch.*, 20:195–260.
- Metzger, W., 1936. *Gesetze des Sehens* (2nd. ed., 1953), Frankfurt: M: W. Kramer.
- Metzger, W., 1966. Figural-Wahrnehmung, in *Handbuch der Psychologie*, Bd. I, 1, Wahrnehmen und Erkennen (W. Metzger ed.), Göttingen: Hogrefe, pp. 693–744.
- Michotte, A., 1946. *La Perception de la Causalité*. Louvain: Institut Supérieur de Philosophie. Reprinted as *The Perception of Causality* (T. R. Miles and E. Miles, trans.), London: Methuen, 1963.
- Mishkin, M., L. G. Ungerleider, and K. A. Macko, 1983. Object vision and spatial vision: two critical pathways, *Trends Neurosci.*, 6:414–417.
- Morinaga, S., 1941. Beobachtungen über die Grundlagen und Wirkungen anschaulich gleichmäßiger Breite, *Arch. ges. Psychol.*, 108:310–348.
- Movshon, J. A., E. H. Adelson, M. S. Gizzi, and W. T. Newsome, 1985. The analysis of moving visual patterns, in *Pattern Recognition Mechanisms* (C. Chagas, R. Gattas, and C. Gross, eds.), New York: Springer, pp. 117–151.
- Musatti, C. L., 1924. Sui fenomeni stereocinetici, *Arch. Ital. Psicol.*, 3:105–120.
- Nakayama, K., and S. Shimojo, 1990. Toward a neural understanding of visual surface representation, *Cold Spring Harbor Symp. Quant. Biol.*, 55:911–924.
- Nelson, J. I., and B. J. Frost, 1978. Orientation-selective inhibition from beyond the classic visual receptive field, *Brain Res.*, 139: 59–65.
- Nelson, J. I., and B. J. Frost, 1985. Intracortical facilitation among co-oriented, co-axially aligned simple cells in cat striate cortex? *Exp. Brain Res.*, 61:54–61.

- Neumeyer, C., 1980. Simultaneous color contrast in the honeybee, *J. Comp. Physiol. A*, 139:165–176.
- Neumeyer, C., S. Dörr, J. Fritsch, and C. Kardelky, 2002. Colour constancy in goldfish and man: influence of surround size and lightness, *Perception*, 31:171–187.
- Newsome, W. T., K. H. Britten, and J. A. Movshon, 1989. Neuronal correlates of a perceptual decision, *Nature*, 341:52–54.
- Newsome, W. T., A. Mikami, and R. H. Wurtz, 1986. Motion selectivity in macaque visual cortex. 3. Psychophysics and physiology of apparent motion, *J. Neurophysiol.*, 55:1340–1351.
- Nothdurft, H. C., 1993. The role of features in preattentive vision: comparison of orientation, motion and color cues, *Vis. Res.*, 33:1937–1958.
- Nothdurft, H. C., J. L. Gallant, and D. C. Van Essen, 1999. Response modulation by texture surround in primate area V1: correlates of “popout” under anesthesia, *Vis. Neurosci.*, 16:15–34.
- Oehler, R., 1985. Spatial interactions in the rhesus monkey retina: a behavioural study using the Westheimer paradigm, *Exp. Brain Res.*, 59:217–225.
- Oppel, J. J., 1855. Über geometrisch-optische Täuschungen, *Jahresber. Physik. Verein Frankfurt*, 37–47.
- Oram, M. W., and D. I. Perrett, 1994. Responses of anterior superior temporal polysensory (SPa) neurons to “biological motion” stimuli, *J. Cogn. Neurosci.*, 6:99–116.
- Palmer, S. E., 1999. *Vision Science. Photons to Phenomenology*, Cambridge, MA: MIT Press.
- Paradiso, M. A., and K. Nakayama, 1991. Brightness perception and filling-in, *Vis. Res.*, 31:1221–1236.
- Perrett, D. I., J. K. Hietanen, M. W. Oram, and P. J. Benson, 1992. Organization and functions of cells responsive to faces in the temporal cortex, *Philos. Trans. R. Soc. Lond.*, B 335:23–30.
- Perrett, D. I., E. T. Rolls, and W. Caan, 1982. Visual neurons responsive to faces in the monkey temporal cortex, *Exp. Brain Res.*, 47:329–342.
- Peterhans, E., and F. Heitger, 2001. Simulation of neuronal responses defining depth order and contrast polarity at illusory contours in monkey area V2, *J. Comput. Neurosci.*, 10:195–211.
- Peterhans, E., and R. von der Heydt, 1991. Elements of form perception in monkey prestriate cortex, in *Representations of Vision: Trends and Tacit assumptions in Vision Research* (A. Gorea, Y. Frégnac, Z. Kapoula, and J. Findlay, eds.), Cambridge: Cambridge University Press, pp. 111–124.
- Peterhans, E., R. von der Heydt, and G. Baumgartner, 1986. Neuronal responses to illusory contour stimuli reveal stages of visual cortical processing, in *Visual Neuroscience* (J. D. Pettigrew, K. J. Sanderson, and W. R. Levick, eds.), Cambridge: Cambridge University Press, pp. 343–351.
- Pinna, B., G. Brelstaff, and L. Spillmann, 2001. Surface color from boundaries: a new “watercolor” illusion, *Vis. Res.*, 41:2669–2676.
- Pinna, B., J. S. Werner, and L. Spillmann, 2003. The watercolor effect: a new principle of grouping and figure-ground organization, *Vis. Res.*, 43:43–52.
- Polat, U., and D. Sagi, 1994. The architecture of perceptual spatial interactions, *Vis. Res.*, 34:75–78.
- Ramachandran, V. S., C. W. Tyler, R. L. Gregory, C. Rogers-Ramachandran, S. Duensing, C. Pillsbury, and C. Ramachandran, 1996. Rapid adaptive camouflage in tropical flounders, *Nature*, 379:815–818.
- Regan, D., 2000. *Human Perception of Objects*, Sunderland, MA: Sinauer.
- Robinson, J. O., 1972. *The Psychology of Visual Illusion*, London: Hutchinson.
- Rock, I., 1984. *Perception* (2nd ed., 1995), New York: W. H. Freeman.
- Rolls, E. T., 1984. Neurons in the cortex of the temporal lobe and in the amygdala of the monkey with responses selective to faces, *Hum. Neurobiol.*, 3:209–222.
- Rolls, E. T., 2000. Functions of the primate temporal lobe cortical visual areas in invariant visual object and face recognition, *Neuron*, 27:205–218.
- Rubin, E., 1915. *Synoplevede Figurer*. København: Glydendalske.
- Sary, G., R. Vogels, and G. A. Orban, 1993. Cue-invariant shape selectivity of macaque inferior temporal neurons, *Science*, 260:995–997.
- Schiller, P. von, 1932. Intersensorielle Transposition bei Fischen, *Z. vergl. Physiol.*, 19:304–309.
- Schiller, P. H., 1996. On the specificity of neurons and visual areas, *Behav. Brain Res.*, 76:21–35.
- Schmidt, K. E., R. Goebel, S. Löwel, and W. Singer, 1997. The perceptual grouping criterion of colinearity is reflected by anisotropies of connections in the primary visual cortex, *Eur. J. Neurosci.*, 9:1083–1089.
- Schwartz, E. L., 1994. Topographical mapping in primate visual cortex: history, anatomy and computation, in *Visual Science and Engineering: Models and Applications* (D. L. Kelly ed.), New York: Makel Dekker, pp. 293–359.
- Sekuler, R., 1996. Motion perception in a modern view of Wertheimer’s 1912 monograph, *Perception*, 25:1243–1258.
- Sharps, M. J., and M. Wertheimer, 2000. Gestalt perspectives on cognitive science and on experimental psychology, *Rev. Gen. Psychol.*, 4:315–336.
- Sillito, A. M., K. L. Grieve, H. E. Jones, J. Cudeiro, and J. Davis, 1995. Visual cortical mechanisms detecting focal orientation discontinuities, *Nature*, 378:492–496.
- Sillito, A. M., and H. E. Jones, 1996. Context-dependent interactions and visual processing in V1, *J. Physiol.*, 90:205–209.
- Spillmann, L., 1997. Colour in a larger perspective: the rebirth of Gestalt psychology, *Perception*, 26:1341–1352.
- Spillmann, L., 1999a. Gehirn und Gestalt I. Metzgers Gesetze des Sehens, *Psychol. Beitr.*, 51:458–493.
- Spillmann, L., 1999b. From elements to perception. Local and global processing in visual neurons, *Perception*, 28:1461–1492.
- Spillmann, L., 2001. Gehirn und Gestalt. II. Neuronale Mechanismen, *Kognitionswissenschaften*, 9:122–143.
- Spillmann, L., and P. DeWeerd, 2003. Mechanisms of surface completion: perceptual filling-in of texture, in *Filling-in: From Perceptual Completion to Cortical Reorganization* (L. Pessoa and P. DeWeerd, eds.), Oxford: Oxford University Press, pp 81–105.
- Spillmann, L., and W. H. Ehrenstein, 1996. From neuron to Gestalt: mechanisms of *Vi pe*, in *Comprehensive Human Physiology*, vol. 1. (R. Greger and U. Windhorst, eds.), Heidelberg: Springer, pp. 861–893.
- Spillmann, L., W. Laskowski, K. Lange, E. Kasper, and D. Schmidt, 2000. Stroke-blind for colors, faces and locations. Partial recovery after three years, *Restor. Neurol. Neurosci.*, 17:89–103.
- Spillmann, L., A. Ransom-Hogg, and R. Oehler, 1987. A comparison of perceptive and receptive fields in man and monkey, *Hum. Neurobiol.*, 6:51–62.
- Spillmann, L., and J. S. Werner, 1996. Long-range interactions in visual perception, *Trends Neurosci.*, 19:428–434.
- Stein, B. E., 1998. Neural mechanisms for synthesizing sensory information and producing adaptive behaviors, *Exp. Brain Res.*, 123:124–135.

- Steinman, R. M., Z. Pizlo, and F. J. Pizlo, 2000. Phi is not beta, and why Wertheimer's discovery launched the Gestalt revolution, *Vis. Res.*, 40:2257–2264.
- Teller, D. Y., 1990. The domain of visual science, in *Visual Perception: The Neurophysiological Foundations* (L. Spillmann and J. S. Werner, eds.), San Diego, CA: Academic Press, pp. 11–21.
- Ternus, J., 1926. Experimentelle Untersuchungen über phänomenale Identität, *Psychol. Forsch.*, 7:81–136.
- Teuber, H. L., 1960. Perception, in *Handbook of Physiology, Sect. 1: Neurophysiology*, (H. W. Field, V. E. Magoun, and J. Hall, eds.), Washington, DC: American Physiological Society, pp. 1595–1668.
- Teuber, H. L., 1967. Wolfgang Köhler 1887–1967, *Psychol. Forsch.*, 31:6–16.
- Todorovic, D., 1996. A gem from the past: Pleikart Stumpf's (1911) anticipation of the aperture problem, Reichardt detectors, and perceived motion loss at equiluminance, *Perception*, 25:1235–1242.
- Tootell, R. B. H., N. K. Hadjikhani, W. Vanduffel, A. K. Liu, J. D. Mendola, M. I. Sereno, and A. M. Dale, 1998. Functional analysis of primary visual cortex (V1) in humans, *Proc. Natl. Acad. Sci. USA*, 95:811–817.
- Tootell, R. B. H., M. S. Silverman, R. Switkes, and R. L. DeValois, 1982. Deoxyglucose analysis of retinotopic organization in primate striate cortex, *Science*, 218:902–904.
- Treue, S., 2001. Neural correlates of attention in primate visual cortex, *Trends Neurosci.*, 24:295–300.
- Uttal, W. R., L. Spillmann, F. Stürzel, and A. B. Sekuler, 2000. Motion and shape in common fate, *Vis. Res.*, 40:301–310.
- Valberg, A., 1974. Color induction: dependence on luminance, purity, and dominant or complementary wavelength of inducing stimuli, *J. Opt. Soc. Am.*, 64:1531–1540.
- Valberg, A., B. B. Lee, D. A. Tigwell, and O. D. Creutzfeldt, 1985. A simultaneous contrast effect of steady remote surrounds on responses of cells in macaque lateral geniculate nucleus, *Exp. Brain Res.*, 58:604–608.
- Van Essen, D. C., J. W. Lewis, H. A. Drury, N. Hadjikhani, R. B. H. Tootell, M. Bakircioglu, and M. I. Miller, 2001. Mapping visual cortex in monkeys and humans using surface-based atlases, *Vis. Res.*, 41:1359–1378.
- von der Heydt, R., E. Peterhans, and G. Baumgartner, 1984. Illusory contours and cortical neuron responses, *Science*, 224:1260–1262.
- von der Heydt, R., H. Zhou, and H. S. Friedman, 2000. Representation of stereoscopic edges in monkey visual cortex, *Vis. Res.*, 40:1955–1967.
- Wallach, H., 1935. Über visuell wahrgenommene Bewegungsrichtung, *Psychol. Forsch.*, 20:325–380.
- Wallach, H., and D. N. O'Connell, 1953. The kinetic depth effect, *J. Exp. Psychol.*, 45:205–217.
- Watanabe, T., and P. Cavanagh, 1991. Texture and motion spreading, the aperture problem, and transparency, *Percept. Psychophys.*, 50:459–464.
- Weizsäcker, V. von, 1947. *Der Gestaltkreis*, Stuttgart: Thieme.
- Wenzel, A., 1998. *Now You See It—Now You Don't. René Margritte*. Munich: Prestel.
- Wertheimer, M., 1912. Experimentelle Studien über das Sehen von Bewegung, *Z. Psychol.*, 61:161–265.
- Wertheimer, M., 1923. Untersuchungen zur Lehre von der Gestalt II, *Psychol. Forsch.*, 4:301–350.
- Westheimer, G., 1999. Gestalt theory reconfigured: Max Wertheimer's anticipation of recent developments in visual neuroscience, *Perception*, 28:5–15.
- Wilson, H. R., D. Levi, L. Maffei, J. Rovamo, and R. DeValois, 1990. The perception of form: retina to striate cortex, in *Visual Perception: The Neurophysiological Foundations* (L. Spillmann and J. S. Werner, eds.), San Diego, CA: Academic Press, pp. 231–272.
- Wood, R. J., and E. L. Schwartz, 1999. Topographic shear and the relation of ocular dominance columns to orientation columns in primate and cat visual cortex, *Neur. Networks*, 12:205–210.
- Wuerger, S., R. Shapley, and N. Rubin, 1996. "On the visually perceived direction of motion" by Hans Wallach: 60 years later, *Perception*, 25:1317–1367.
- Zeki, S. M., 1980. The representation of colors in the cerebral cortex, *Nature*, 284:412–418.
- Zeki, S. M., 1993. *A Vision of the Brain*, Oxford: Blackwell.
- Zeki, S. M., 2001. Localization and globalization in conscious vision, *Annu. Rev. Neurosci.*, 24:57–86.
- Zhou, H., H. S. Friedman, and R. von der Heydt, 2000. Coding of border ownership in monkey visual cortex, *J. Neurosci.*, 20:6594–6611.
- Zipser, K., V. A. Lamme, and P. H. Schiller, 1996. Contextual modulation in primary visual cortex, *J. Neurosci.*, 16:7376–7389.

107 Neural Mechanisms of Natural Scene Perception

JACK L. GALLANT

AN IMPORTANT GOAL of visual neuroscience is to understand the neural mechanisms mediating vision in the natural world. Natural vision is a difficult problem for two reasons. First, natural images are exceedingly complex, and their structure is not well understood. Second, natural visual behavior reflects the influence of a dynamic system controlling eye movements and attention and operating simultaneously at many levels of visual processing. These factors make it difficult to perform controlled experiments that isolate the specific attributes relevant to particular hypotheses about visual function. Therefore, most experiments in visual neuroscience address natural vision indirectly, using simple stimuli and tightly controlled visual behavior.

The degree to which theories developed from simple experiments can generalize to natural vision hinges on the linearity of visual neurons. In a linear system, the response to a complex stimulus is equal to the sum of the responses to its simpler constituents. This property is called *superposition*. If the visual system were linear, responses to complex stimuli such as natural scenes could be predicted based on a combination of responses to simple stimuli. However, the visual system does not generally obey superposition; responses to the sum of two simple stimuli often do not equal the sum of responses to each alone. The failure of superposition becomes markedly more pronounced at higher stages of visual processing. For example, neurons in the inferior temporal cortex often respond only to complex configurations of specific stimulus features and give no responses to the constituent parts. In such cases, experiments using very simple stimuli are likely to have limited utility.

A second common assumption of linear systems analysis is that the response to each stimulus is unaffected by previous stimuli. This is related to a property called *stationarity*. A stationary system does not change its characteristics over time and is therefore easy to analyze experimentally. However, nonstationary processes, such as visual adaptation, attention, learning, and memory, operate at all stages of visual processing and depend on the history of visual experience. To avoid the complexities of nonstationarity, conventional experiments are usually designed so that the system is held in one mode of operation. If this is not the natural mode of the system, then the results may not generalize to natural vision.

It is clear that the visual system at least partly violates the assumptions underlying many conventional neurophysiological experiments. This complicates both the conduct and the interpretation of experiments that use simple stimuli, especially for studies of higher visual processing. At the same time, the difficulty of quantifying and controlling natural vision limits our ability to address it directly using standard experimental procedures. Thus, the most difficult part of studying natural scene perception is developing appropriate experiments.

This chapter reviews current research on the neural mechanisms of natural scene perception. We begin with a brief review of the statistical properties of natural scenes insofar as they are currently known. Second, we review theoretical and experimental studies aimed at determining whether and how the visual system is optimized to process natural scenes. These studies have examined neural coding of natural scenes in retina, the lateral geniculate nucleus (LGN), and primary visual cortex (area V1). Third, we summarize recent experiments that use natural scenes to objectively characterize filtering properties of neurons in area V1 and in higher, extrastriate visual areas. Finally, we describe recent neurophysiological experiments on natural vision. These studies investigate both eye movements, which control how a natural scene is sampled, and attention, which affects how information is represented at various stages of visual processing. The review focuses on the ventral visual pathway and does not address natural scene perception in other visual subsystems (e.g., parietal cortex, frontal eye fields). The review also does not address perception of natural color images, an important area of current research.

Scene statistics

Natural images are obviously quite complex and may appear almost impossible to characterize. Fortunately, several reasonable assumptions simplify analysis of natural scenes. A *natural scene* can be broadly defined as any scene that is likely to be experienced in the normal evolution or development of an organism. This excludes many of the simple stimulus patterns, such as gratings and white noise, often used to study vision but rarely encountered in nature. It is also useful

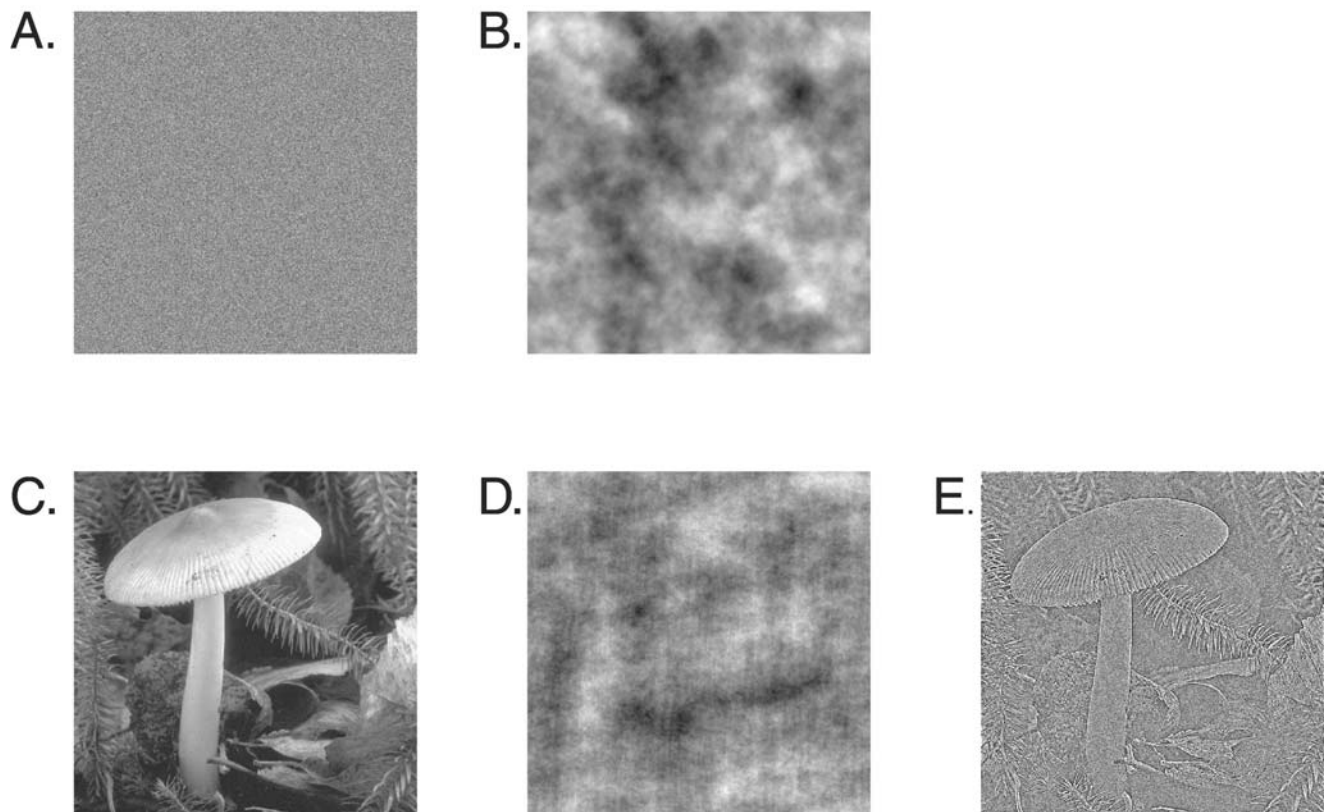


FIGURE 107.1. *A*, White noise. This stimulus has a flat power spectrum and no correlations between pixels. *B*, $1/f$ noise. This stimulus has a $1/f^2$ power spectrum like that of natural images but no correlations between pixels. *C*, A natural image. *D*, The natural image

shown in *C*, with a normal power spectrum and a scrambled phase spectrum. The image appears similar to the $1/f$ noise pattern shown in *B*. *E*, The natural image shown in *C*, but with a whitened power spectrum and a normal phase spectrum. The image is recognizable.

to ignore the structure of any single, specific image and focus instead on characterizing the statistical distribution of a large ensemble of scenes. Any specific regularities in this distribution could, in principle, be exploited by the visual system. Another simplifying assumption is *viewpoint invariance*, which reflects the fact that the camera (or eye) could observe a scene from any vantage point. Finally, it is useful to consider the spatial and temporal statistics of natural scenes in isolation insofar as this is possible. The spatial statistics of the scenes are determined by the structure of the world, while the temporal statistics are determined by several factors: the motion of objects in the world, the motion of the observer through the world, and the observer's eye movements.

The first-order spatial and temporal statistics of natural images are relatively well understood (Olshausen and Field, 2000; Ruderman, 1994). They describe the distribution of luminance values that might appear in any image. The second-order spatial statistics are more interesting; they describe the correlations between pairs of pixels. These correlations can be obtained from the spatial autocorrelation or from its Fourier transform, the power spectrum. Analysis of the autocorrelation matrix of the distribution of natural scenes reveals that nearby pixels tend to have similar bright-

ness values and that the strength of this correlation falls off with distance. Correspondingly, analysis of the power spectrum of this distribution shows that power decreases as $1/f^2$ (where f is spatial frequency; note that the power spectrum is the square of the amplitude spectrum). In other words, low spatial frequencies in natural scenes tend to have the most power, and power decreases with increasing spatial frequency (Field, 1987) (Fig. 107.1). These second-order statistics may reflect both scale invariance (Field, 1987; Ruderman, 1997) and the distribution of one- and two-dimensional image features such as edges, curves, line terminations, and so on (Balboa et al., 2001).

Natural scenes contain rich statistical structure beyond the two-point spatial correlations described by the power spectrum. Edges and lines, textures, surface patches, and objects all can contain correlations higher than second-order. A simple demonstration illustrates the importance of higher-order structure for natural scene perception: if the power spectrum of a white noise pattern is adjusted to match the $1/f^2$ spectrum of natural scenes, the resulting image will look like shapeless clouds (Fig. 107.1). This indicates that the appearance of a natural scene is not entirely (or even predominantly) determined by its power spectrum. Conversely,

if we weight the Fourier coefficients of a natural scene so that all frequencies have equal power (a process called *whitening*), the resulting image still contains substantial identifiable structure. Thus, the appearance of the scene is not determined solely by its power spectrum. Finally, it is easy to discriminate between scenes whose power spectra have been shuffled (i.e., the amplitudes of the spatial frequencies have been shuffled randomly). In contrast, it is impossible to discriminate between images whose phase spectra are randomized. This implies that much of the information about the meaning of specific natural scenes is carried in the spatial phase spectrum (Piotrowski and Campbell, 1982; Tadmor and Tolhurst, 1993; Thomson and Foster, 1997).

It is difficult to quantify the higher-order spatial statistics of natural scenes (Krieger et al., 1997; Thomson, 1999; Wegmann and Zetsche, 1990b) and their phase characteristics (Thomson, 2001). This is partly due to the common occurrence of surface and volume occlusions in natural scenes. Occlusion in natural images is a fundamentally nonlinear process, and few methods are available for quantifying the resulting distributions (Lee et al., 2001). Even so, useful image models can be obtained by using established statistical methods that do not explicitly consider occlusion.

One of the most useful statistical methods for discovering important structure in natural scenes has been independent components analysis (ICA) (Hyvarinen et al., 2001). Assume that each natural image reflects the combined influence of many independent factors that represent the structural elements of the image. Instead of identifying these elements according to some explicit theory, ICA extracts them directly from a large sample of images. ICA finds the independent factors that can be linearly combined to create any image from a distribution of natural scenes.

The theoretical importance of independent components (ICs) for image coding can be understood by considering the probability density function (PDF) of pixel correlations in natural images. If the PDF is Gaussian, then there are no privileged directions in correlation space and all linear coding strategies are equally efficient. However, if the distribution is not Gaussian, then image codes that are aligned with the most kurtotic dimensions will be most efficient. ICA allows one to discover these important non-Gaussian dimensions, even if they reflect image correlations beyond second-order.

Several different studies have now used ICA to characterize natural scenes (Bell and Sejnowski, 1997; Hyvarinen and Hoyer, 1999; Olshausen and Field, 1997) and have produced remarkably consistent results. In all cases the ICs are spatially localized, bandpass functions tuned for orientation and spatial frequency. Taken together these ICs can represent any natural scene, but very few of them appear in any specific scene. This form of representation is known as a *sparse code*.

The ICs of natural scenes are very similar to Gabor wavelets (each wavelet is a sinusoid weighted by a Gaussian envelope) that have been used as computational models of neurons in primary visual cortex (Daugman, 1988; Field, 1994; Navarro et al., 1996). When ICA is applied to videos of natural scenes containing moving objects (Szatmary and Lorincz, 2002; van Hateren and Ruderman, 1998), the ICs are localized in space-time, bandpass in spatial and temporal frequency, tuned for orientation, and direction selective. The close correspondence between the ICs of natural scenes (or movies) and the tuning properties of V1 neurons suggests that this area is optimized to process the sparsely distributed features in natural scenes. We discuss this issue more fully below.

Independence, as used in ICA, has a specific meaning: the presence of one IC predicts nothing about the presence or absence of any other element. However, there is no guarantee that the estimated ICs will indeed be completely independent. The ICA algorithm only ensures that they will be as independent as possible, given the data. The actual degree of independence is important; if the ICs of natural images are not entirely independent, further processing could recover additional information. The nonindependence of Gabor wavelet filters has been examined directly in theoretical studies by examining their responses to natural images (Simoncelli and Schwartz, 1999; Wegmann and Zetsche, 1990a; Zetsche et al., 1999). The filters are not completely independent; when one wavelet filter is triggered by an image, another filter is also likely to respond. These correlations reflect higher-order structure in natural images that might be exploited by further nonlinear processing.

Optimization

The question most commonly addressed in studies of natural scene perception has been whether the visual system is optimized to process natural scenes, and if so, what sort of optimization is involved. All species evolved in environments with specific physical properties and selective pressures should have favored those individuals that could most efficiently perceive their environment. Conversely, there is no reason to believe that natural selection would favor adaptation to arbitrary visual environments never experienced by an organism.

Theoretical considerations of signal processing suggest a clear strategy for optimally processing the information contained in natural scenes (Barlow, 2001; Zetsche and Krieger, 1999). First, the visual system should discard information that is not useful for processing a specific scene. Because the second-order correlations reflected in the $1/f^2$ power spectrum of natural scenes provide little useful information, the early stages of visual processing (retina, optic nerve, LGN, and possibly V1) might therefore reduce or eliminate them.

Second, the visual system should exploit the information remaining after decorrelation. This information is vital for identifying and processing the shapes in each specific scene. The Gabor-like sparse ICs of natural scenes represent one early aspect of information exploitation. More complex information is likely to be processed at later stages of processing in the inferior temporal processing stream (V1, V2, V4, and the inferior-temporal complex).

OPTIMIZATION IN RETINA AND LGN A basic form of decorrelation is to whiten the signal. Whitening produces a more efficient representation of the image because information is distributed more equally across the available channels (e.g., LGN afferents tuned to different spatial frequencies). Early studies on natural image processing concluded that spectral whitening is indeed implemented in the eye of the fly (Srinivasan et al., 1982). The contrast-response function of the fly eye effectively whitens the contrast distribution of natural scenes. This process is implemented by means of lateral inhibition between interneurons, which removes local spatial correlations. Theorists have argued that mammalian retinal ganglion cells and LGN neurons, both of which have a clear center-surround organization, might also decorrelate photoreceptor responses (Atick, 1992; Dong and Atick, 1995a; also see Barlow, 1961).

Because natural images vary over time, it is also likely that LGN neurons also whiten temporally varying signals (Dong and Atick, 1995a). The hypothesis that LGN whitens the temporal spectra of natural images has been tested directly in neurophysiological experiments (Dan et al., 1996). The experiments compared LGN responses obtained with movies of natural stimuli to those obtained with white noise. These two stimulus classes have substantially different temporal power spectra: natural movies have a complex $1/f^n$ power spectrum, while the power spectrum of white noise is flat. Thus, temporal decorrelation was assessed by comparing the power spectra of LGN responses obtained with the two stimulus classes. The temporal spectrum of LGN responses to natural movies was flat, even though the input had a complex temporal spectrum. This indicates that the LGN decorrelates natural temporal stimuli. In contrast, the power of LGN responses to white noise increased with temporal frequency. This shows that decorrelation is achieved by suppressing low temporal frequencies and enhancing high temporal frequencies. Taken together these results show that the LGN removes second-order temporal correlations in the input and that this whitening process is matched to the temporal statistics of natural vision.

OPTIMIZATION IN AREA V1 If V1 is optimized for processing natural scenes, then the receptive field properties of V1 cells should efficiently exploit information remaining after decorrelation by earlier stages of processing. We have

already seen that the ICs of natural scenes are spatially localized, tuned for orientation and spatial frequency, and sparsely distributed in each natural image (Bell and Sejnowski, 1997; Hyvarinen and Hoyer, 1999; Olshausen and Field, 1997; van Hateren and van der Schaaf, 1998). If primary visual cortex is optimized for processing such scenes, then V1 neurons might display these same key characteristics. This would permit efficient representation of natural scenes because the neural code would be aligned with the privileged axes of the stimulus space (Field, 1994; Zetzsche and Krieger, 1999). Many neurophysiological experiments conducted over the past 25 years have confirmed that V1 neurons are spatially localized bandpass filters tuned to orientation and spatial frequency (for review, see De Valois and De Valois, 1990). Thus, it appears that V1 cells are indeed optimized to detect the sparse components of natural scenes.

Several theoretical and experimental studies have investigated whether primary visual cortex uses a sparse code. The issue has been addressed by estimating *coding density* across the cell population (Barlow, 1961; Field, 1993; Vinje and Gallant, 2002). Coding density describes the fraction of neurons within a given visual area that participate in the representation of a natural scene. If a code is maximally dense, then information about a scene is completely distributed across all neurons and the decoder must integrate information from all cells to make sense of a scene. For this reason, dense codes tend to be robust to damage but difficult to decode. In contrast, a maximally sparse code represents each scene by the activity a single cell (e.g., one's grandmother would be represented by a single "grandmother cell"). Maximally sparse codes are easy to decode, but they are fragile and require enormous numbers of neurons.

The optimal coding density for representing natural scenes probably depends on both external (stimulus statistics) and internal (developmental and metabolic) factors. If the primary visual cortex is optimized for representing the sparse components of natural scenes, then the distribution of neural filters should match these components (Field, 1994; Olshausen and Field, 1996). Field (1987, 1994) first showed that when Gabor wavelets are adjusted to maximize their sparseness, they are most consistent with measured receptive field properties in primary visual cortex. Gabor wavelets are not the only type of filter that can form a sparse image representation. Many schemes that decorrelate pixels will produce a rather sparse code (Krieger and Zetzsche, 1996). It has been argued, however, that this representation produces an optimally sparse distribution for natural scenes (Field, 1987; Zetzsche and Krieger, 1999), consistent with the optimization hypothesis.

One open issue is how such a representation could come about, either through evolution or through learning.

Olshausen and Field (1996, 1997) demonstrated that an unsupervised neural network algorithm implementing ICA could learn a sparse distributed code for natural images. The resulting network elements were localized, oriented, and bandpass, much like the receptive field profiles of V1 simple cells (De Valois et al., 1982; Jones and Palmer, 1987). An important control condition demonstrated that the resulting elements did not look like V1 receptive fields when the model was trained on much simpler patterns (e.g., sinusoidal gratings). This result suggests that evolutionary and developmental processes could, in principle, have optimized area V1 to process natural scenes.

These theoretical studies demonstrate that Gabor wavelets can efficiently represent the sparse components of natural scenes. As noted above, such filters are not completely independent. They still possess significant correlations that reflect higher-order structure in natural scenes (e.g., corners and local curvature: Simoncelli and Schwartz, 1999; Zetzsche and Barth, 1990). This information is implicit, however, and can only be extracted by further, nonlinear processing (Krieger and Zetzsche, 1996; Zetzsche and Barth, 1990), which might occur within the nonclassical receptive field (nCRF) of neurons in primary visual cortex (Schwartz and Simoncelli, 2001; Simoncelli and Schwartz, 1999).

In a series of neurophysiological experiments, Vinje and Gallant (2000, 2002) investigated several hypotheses regarding sparse coding in primary visual cortex. Their stimuli simulated the stimulation neurons receive during free viewing of static natural scenes, including both fixations and saccadic eye movements. (This ensured that stimuli contained realistic spatial and temporal statistics.) They confirmed that natural stimulation of the nCRF increases kurtosis of the response distribution and decorrelates the responses of pairs of V1 neurons that receive similar stimulation (Vinje and Gallant, 2000). Using information theoretic analyses, they further found that nCRF stimulation also increases the information rate, the information per spike, and the efficiency of information transmission in individual neurons (Vinje and Gallant, 2002). Taken together these physiological results demonstrate that the nCRF increases the sparseness of the stimulus representation in V1, consistent with the hypothesis that the nCRF tunes V1 neurons to match informative components of the natural world.

Representation

The studies cited above confirm that vision scientists have achieved a good basic understanding of how shape is represented in primary visual cortex. Area V1 represents the visual world by means of a large bank of Gabor-like filters designed to match the sparse components of natural scenes. Much less is known about shape representation in the con-

stellation of over 30 extrastriate areas that make up the rest of the visual cortex (Gallant, 2000; Van Essen and Gallant, 1994). It is presently unclear if statistical analyses of natural scenes will provide new insights into scene structure beyond what is already known. Thus far, theoretical studies of shape have provided few clear, testable hypotheses about its potential neural representation.

Given these limitations, most neurophysiological experiments on shape coding in extrastriate cortex have sought to characterize neural responses along only a few specific stimulus dimensions (Desimone et al., 1984; Fujita and Tanaka, 1992; Gallant et al., 1993; Gross et al., 1972; Kobatake and Tanaka, 1994; Pasupathy and Connor, 1999). These studies suggest that higher visual areas implement banks of nonlinear, multidimensional filters for complex shape attributes. However, the fundamental principles of shape coding are still unknown. Experiments that use restricted stimulus spaces to test specific hypotheses are inevitably limited by the choice and size of the stimulus set. It is impossible to know, from these experiments alone, whether observed shape selectivity represents a fundamental coding property or merely reflects tuning along some other, unknown dimension. Therefore, some researchers have begun to address shape coding using natural scenes. Because a large sample of such images should include most relevant shape attributes, the stimulus selection bias can be minimized.

METHODS FOR INVESTIGATING SHAPE REPRESENTATION USING NATURAL SCENES Neurophysiological recordings can be made from single cells for only a limited time, usually a few hours at most. This constraint severely limits the number of images that can be used as stimuli in a real experiment. Under the best of circumstances, only a few thousand images can be sampled from the enormous universe of potential natural scenes. On the other hand, natural scenes are quite complex and contain rich statistical structure to which extrastriate neurons are presumably sensitive. These considerations suggest that the success of neurophysiological experiments will depend critically on procedures for data analysis and interpretation.

Despite the fact that many visual neurons are nonlinear, some insight can still be gained by the application of linear system identification methods. The fundamental idea behind linear system identification is that any system (in this case, a neuron) can be modeled as a filter that operates on the input and produces some output (DeBoer and Kuyper, 1968; Marmarelis and Marmarelis, 1978). This is conceptually equivalent to regression analysis. Instead of testing a specific hypothesis about shape coding, responses to complex stimuli are analyzed to determine how each stimulus component influences responses. These relationships are then summarized mathematically using a framework that describes both linear and nonlinear terms of the function relating

stimuli to responses. System identification uses a rich stimulus set and so requires few a priori assumptions about which specific stimulus attributes a neuron might encode.

In visual neurophysiology the mapping function that relates stimuli to responses is called the *spatiotemporal receptive field* (STRF). It describes both the spatial tuning of a cell and the evolution of tuning over time (Theunissen et al., 2001). STRFs are usually estimated by reverse correlation of recorded action potentials against preceding stimuli (DeAngelis et al., 1995; DeBoer and Kuypers, 1968), and several different algorithms have been proposed for performing this computation (Marmarelis and Marmarelis, 1978; Ringach et al., 2002; Theunissen et al., 2001). System identification methods have also been applied to other sensory systems (DeBoer and Kuypers, 1968; deCharms et al., 1998; DiCarlo et al., 1998; Klein et al., 2000; Theunissen et al., 2001).

STRF estimation works best when two conditions are satisfied: the stimulus is spectrally unbiased, and response nonlinearities can be described accurately. White noise is unbiased and so is theoretically optimal for such studies (Marmarelis and Marmarelis, 1978). However, white noise is an inefficient stimulus for characterizing neurons selective for complex shapes. One way to overcome this problem is to characterize cells with natural scenes rather than noise (Theunissen et al., 2001). Because the visual system evolved to process natural scenes, these stimuli should elicit robust responses from visual neurons. The disadvantage of this approach is that the STRF must be corrected to remove bias introduced by natural stimulus statistics, such as the $1/f^2$ spatial power spectrum and local spatiotemporal correlations. Procedures have recently been developed for removing these biases and for characterizing response nonlinearities, such as rectification, that have posed problems for previous system identification studies (David et al., 1999; Nykamp and Ringach, 2002; Ringach et al., 2002; Stanley et al., 1999; Theunissen et al., 2001).

One important decision that must be made before STRF estimation concerns which dimensions to use to characterize responses. Many studies using linear systems identification have simply performed reverse correlation in the spatial domain (i.e., pixel gray-scale values; DeAngelis et al., 1995; Jones and Palmer, 1987). However, some nonlinear neurons, such as complex cells in area V1, cannot be analyzed this way; the phase-invariant behavior of complex cells masks the structure of the spatial kernel. For this reason, researchers have computed STRFs using other parameter spaces such as the Fourier domain (Theunissen et al., 2001), the second-order response covariance matrix (Touryan and Dan, 2001), or nonlinear feature spaces (Ringach et al., 2002). Any decision about which parameter space to use during STRF estimation must inevitably reflect some spe-

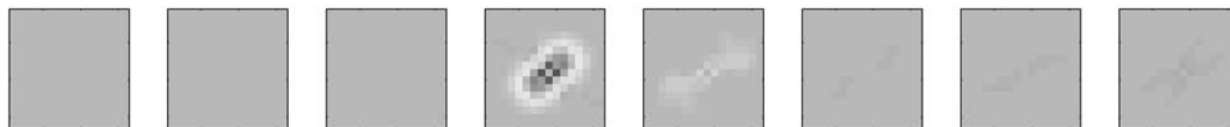
cific hypothesis about the nature of visual coding and nonlinear responses. When the chosen parameter space effectively linearizes the nonlinear response, it can significantly improve STRF estimates (Mazer et al., 2000; Theunissen et al., 2001).

STRF ESTIMATION IN AREA V1 System identification methods have been most often used to examine coding in the early visual system. The goal has usually been to determine whether computational models developed using simple stimuli account for responses to natural scenes. If the visual system is linear, then models developed using simple stimuli should generalize to natural vision. To the extent that the visual system is nonlinear, this may not occur. The practical influence of nonlinear processes is an empirical question that can only be investigated by comparing responses obtained using simple stimuli with those observed during natural vision (Theunissen et al., 2001). System identification provides a quantitative method for characterizing and comparing neural responses obtained under these different stimulus regimes.

One recent attempt to examine this issue compared STRFs of area V1 neurons in response to rapid sequences of random gratings and movies that simulated the stimulation received during natural vision (including the stimulation that occurs during eye movements; David et al., 1999; Theunissen et al., 2001) (Fig. 107.2). Each stimulus class was used to generate a separate STRF, giving two (potentially different) filter estimates per neuron. The accuracy of estimated STRFs was assessed by evaluating how well each one predicted neural responses. In general, STRFs generated from each stimulus class best predicted responses to the same class. For example, STRFs estimated from naturalistic stimulation best predicted responses to novel natural scenes (on average accounting for about 25% of the total variance in responses). These results demonstrate that area V1 is sensitive to the prevailing stimulus statistics. As these statistics vary, nonlinear mechanisms place the visual system into different operational modes.

To investigate what specific filtering properties were modulated by stimulus statistics, these experimenters examined the tuning profiles of recorded cells (David et al., 1999; Theunissen et al., 2001). Dynamic gratings evoked STRFs with simpler temporal responses and narrow tuning for orientation and spatial frequency. Natural stimuli tended to evoke STRFs with complex temporal profiles and broader spatial tuning for orientation and spatial frequency. STRFs obtained with natural stimuli were also less space-time separable than those obtained with dynamic stimuli (Mazer et al., 2002). These differences (and other data from the same study) indicate that temporal stimulus statistics have a substantial effect on both the temporal and spatial response properties of neurons in area V1.

A. Dynamic Grating Sequence



B. Natural vision movie

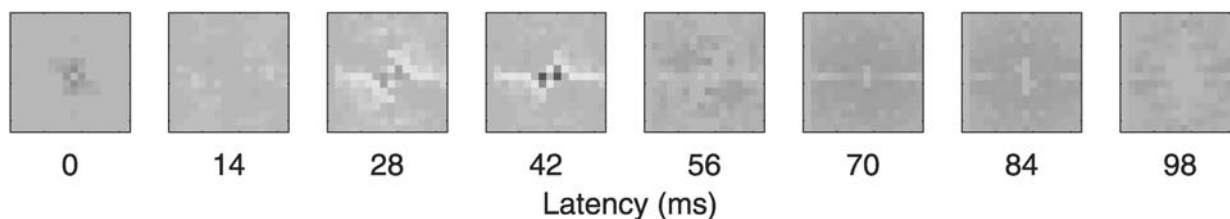


FIGURE 107.2. *A*, STRF of one V1 neuron obtained with a dynamic grating sequence. Each panel shows the Fourier power spectrum of the STRF at a single response latency (14 msec frame rate). The grating stimulus reveals good spatial tuning for left diagonal orientations and a simple temporal response with a latency of

about 40 msec. *B*, STRF of the same cell shown in *A*, obtained with a movie simulating natural vision. Although the spatial tuning of the STRF is relatively unaffected by stimulus statistics, the temporal response profile is quite different from that shown in *A*. (Adapted from Theunissen et al., 2001.) (See color plate 82.)

Eye movements and attention

Natural vision is an active process that operates in the context and service of behavior. Therefore, a complete description of natural vision must also address intention, attention, eye movements, and scene interpretation. These topics have been studied extensively using both behavioral and computational methods (for review, see Itti and Koch, 2001). Neurophysiological studies have been more limited and have tended to study specific components of natural vision (e.g., eye movements or attention) in isolation.

MODELS OF ATTENTION, EYE MOVEMENTS, AND CONTROL
Several computational models of how the visual system might function during natural vision have been proposed, and they share several core features (Deco and Zihl, 2001; Koch and Ullman, 1985; Lee et al., 1999; Niebur and Koch, 1996; Rao and Ballard, 1997; Schill et al., 2001; Sheinberg and Zelinsky, 1993). All treat sensory neurons as multidimensional filters. Within a given visual area, these filters collectively make explicit certain information about a visual scene. Other information is implicitly available and can be obtained by further processing. Although these neural filters have relatively stable tuning profiles, they are dynamically modulated by top-down attentional processes. These top-down influences reflect both immediate goals and prior knowledge about the structure of the visual world. By modulating filters appropriately, attention optimizes the visual system for a specific task.

As new stimuli are encountered, the neural filters respond in parallel. Because their responses are influenced both

bottom-up and top-down, they simultaneously represent both the structure of a scene and its behavioral relevance. In extrastriate areas that are retinotopically mapped, such as V4, the responses collectively form a saliency map indicating which spatial locations are most likely to contain behaviorally relevant patterns. Subsequent eye movements are then directed toward the point on the saliency map that is most active. Simultaneous with this, incoming neural responses are used to update continuously internal representations of the world.

There is ample behavioral evidence supporting this general model of active vision. Behavioral studies have shown that both humans (Binello et al., 1995; Mannan et al., 1995; Rao et al., 1996; Reinagel and Zador, 1999; Yarbus, 1967) and nonhuman primates (Burman and Seagraves, 1994; Gallant et al., 1998; Keating and Keating, 1982; Wilson and Goldman-Rakic, 1994) systematically sample complex scenes by moving their eyes toward points of interest. Indirect behavioral evidence suggests that selective attention is tightly coupled to these eye movements (Binello et al., 1995; Hoffman and Subramaniam, 1995; Kowler et al., 1995; Motter and Belky, 1998; Schill et al., 2001; Sereno, 1992).

There is also substantial neurophysiological support for the individual components of this model. Top-down attentional effects have been reported in most visual areas (for review, see Colby, 1991; Desimone and Duncan, 1995; Schall, 2001). It is clear that these attentional effects reflect task demands and internalized behavioral constraints (Chelazzi et al., 2001; Miller et al., 1993). Attention can modulate both the magnitude of neural responses to stimuli

at attended locations (spatial attention: McAdams and Maunsell, 1999) and selectivity for attended features or patterns (object attention: Motter, 1993, 1994; Olson and Gettner, 1996). It is also critical for scene segmentation (Desimone and Duncan, 1995; Moran and Desimone, 1985). In most cases, attention seems to alter the gain of neural filters (McAdams and Maunsell, 1999) or to gate inputs from earlier areas to facilitate scene analysis (Desimone and Duncan, 1995). However, it can also shift the spatial tuning profiles of V4 neurons somewhat (Connor et al., 1996, 1997). Other neurophysiological experiments support a close coupling between shifts of attention and eye movements, particularly in parietal areas 7a and LIP (Ben Hamed et al., 2002; Gottlieb et al., 1998; Steinmetz and Constantinidis, 1995). Eye movements and attention also appear to be coupled in area V4 (Mazer et al., 2001; Tolias et al., 2001).

NEUROPHYSIOLOGICAL STUDIES OF NATURAL SCENE PERCEPTION Neuroscientists have only recently begun to investigate the neural mechanisms mediating natural vision as an integrated system. In primary visual cortex, neural activity is substantially reduced during free viewing of natural scenes relative to what might be expected from studies using simple stimuli (Gallant et al., 1998). This effect appears to be due to two factors. First, natural scenes typically span the entire visual field and so drive suppressive mechanisms in the nCRF (Vinje and Gallant, 2000, 2002). Second, natural eye movements induce parasaccadic suppression, reflecting the combined influence of an efference copy of eye movements and direct suppression by high-velocity saccadic stimulation (Diamond et al., 2000; Judge et al., 1980).

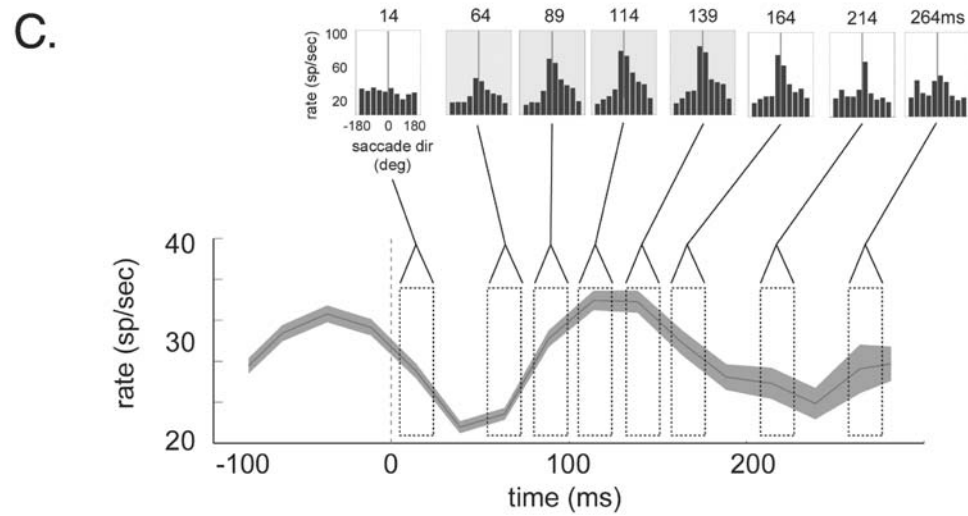
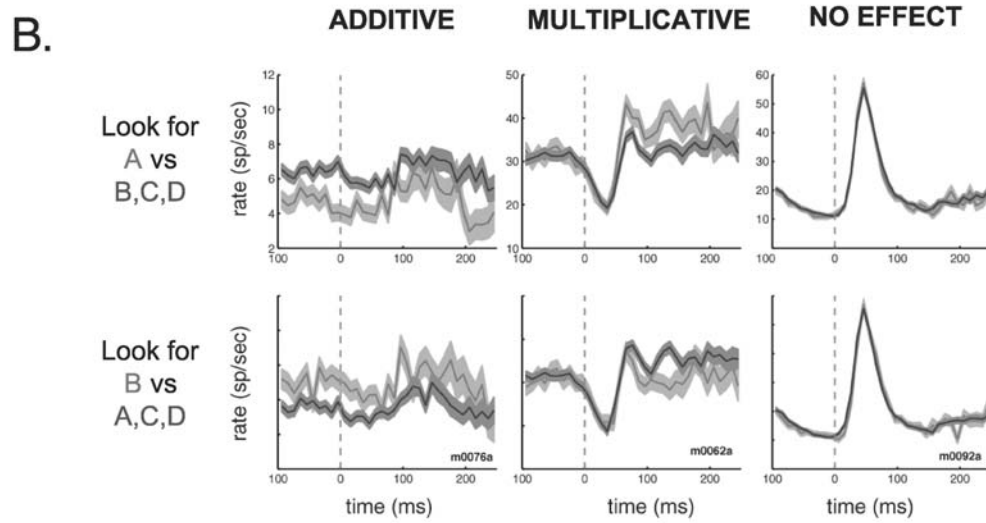
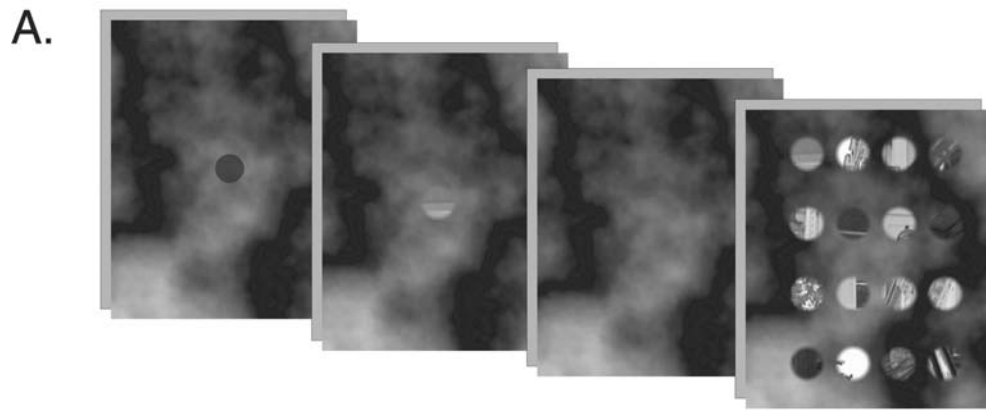
Recent experiments have examined V4 activity during free viewing visual search of natural stimuli (Mazer et al., 2001). Animals were trained to search for a natural image patch (3 to 10 degrees) hidden in a large array of similar patches (Fig. 107.3). Eye movements were permitted during search; both eye position and neural activity were recorded continuously. Search arrays were arranged so that whenever the animal fixated a patch, the receptive field of the recorded cell would be centered over a different patch. Several different modulatory effects were observed that were clearly related to the task. First, the overall activity of many V4 neurons was modulated by the search target. Some cells showed a persistent target-dependent enhancement or suppression of their activity throughout a trial, including during saccades. Others showed a target-dependent multiplicative enhancement or suppression of responses, consistent with a gain control mechanism. These effects occurred throughout each fixation and were independent of the image patch falling within the receptive field at any time. Therefore, they likely reflect top-down object-related attention. This suggests that V4 may contain several different classes of neurons that

participate in different aspects of natural vision. Second, some V4 neurons showed target-dependent modulation of their STRFs. In particular, Fourier domain STRF tuning profiles were modulated by the search target. This effect suggests that attention optimizes V4 neurons for a particular task by direct top-down modulation of spatial frequency and orientation tuning of individual cells. Finally, the activity of many neurons predicted the direction of subsequent eye movements: the larger the response of the cell, the more likely it was that the next saccade would place the fovea at the spatial location of the neuron's receptive field. Given that V4 neurons are affected by both task demands and stimulus properties, this suggests that V4 functions as a saliency map.

All of these observations are qualitatively consistent with the computational models of visual search reviewed above. Neurons in area V4 collectively implement a parallel bank of spatially localized multidimensional filters. The sensitivity and tuning profiles of these filters can be modulated by top-down influences to optimize performance in a specific task. During natural vision, the filters respond to local features in the scene according to their match with the stimulus characteristics. The output of the filter bank is then used to drive subsequent eye movements.

Natural vision experiments have also been used to examine object coding in the inferior temporal cortex (IT) during free viewing visual search for natural targets embedded in natural scenes (Sheinberg and Logothetis, 2001). Animals were required to locate a target in one of several images within which it might be embedded and were free to make eye movements as necessary to evaluate each image. IT cells were remarkably silent during the search task. However, they tended to give a burst of action potentials when animals recognized that a target was present in a particular image. Population analyses showed that these bursts tended to occur immediately before a saccade to the target item, consistent with the idea that IT activity correlates with recognition. Furthermore, larger bursts predicted faster response reaction times. Taken together these data indicate that IT activity encodes the probability that a behaviorally relevant target is present in a natural scene. These data also suggest that many aspects of visual processing, such as scene segmentation and grouping, are already completed by this stage of processing. IT cells may therefore be most involved in behavioral control and judgment.

Natural scene perception has also been examined using neurophysiological recordings in the frontal eye fields (FEF), which occupy a relatively late stage of visual processing. Neurons in this area form a representation of visual space but are also directly involved in the generation of eye movements to specific retinal coordinates (Schall, 2001). During free viewing of natural scenes, FEF neurons respond to natural scene patterns when they are the target for subse-



quent eye movements (Burman and Seagraves, 1994). However, these neurons do not respond to the same scenes when animals are required to follow a moving spot that retraces previous eye movements. Instead, during this rescan condition, neurons respond only to the target spot. Thus, during natural vision, FEF neurons appear to encode salient stimuli that are the targets for upcoming eye movements.

Future directions

Although vision is one of the oldest topics in systems neuroscience and psychology, study of the neural mechanisms mediating natural scene perception is quite young. Conventional experiments have been most productive in studies of the early stages of visual processing, where the system is quasi-linear. Experiments using natural scenes could provide a useful supplement to such studies, allowing us to evaluate current models and account for nonlinearities in early vision (Vinje and Gallant, 1998).

Computational and experimental neuroscientists are actively pursuing several lines of inquiry that are likely to reveal fundamental new functional and organizational principles of vision in the coming years. Most importantly, they are beginning to focus on characterizing the higher-order statistical structure of natural scenes (Schwartz and Simoncelli, 2001; Thomson, 1999; Zetzsche and Krieger, 1999). One important component of this research may be to develop nonlinear models of the way natural images are formed on the retina to account more accurately for occlusion and self-occlusion in natural scenes (Lee et al., 2001).

Better models of complex scene structure could substantially aid experimental studies of intermediate and late stages of visual processing. Because these neurons are highly nonlinear, conventional experimental methods employing simple stimuli and strong behavioral control may miss important functional characteristics. Linear system identification methods incorporating additivity and stationarity

assumptions may also have limited utility in these regions. Quantitative statistical analysis of natural scenes could simplify efforts to investigate these areas by enabling researchers to focus on their most important structural attributes.

Neural responses at higher stages of visual processing also depend strongly on behavioral state (Desimone and Duncan, 1995). Attention, learning, and memory are all increasingly influential at higher processing stages. Experiments designed to exploit natural visual behaviors can ensure that responses reflect the behavioral dependencies that actually occur during perception of natural scenes (Mazer et al., 2001).

Acknowledgments

James Mazer, William Vinje, Kate Gustavsen, Kathleen Bradley, and Stephen David provided extensive help in preparing this manuscript. In addition, James Mazer and Stephen David kindly allowed their data to be used in Figures 107.2 and 107.3. Bruno Olshausen, David Field, and Christoph Zetzsche also contributed many ideas about neural coding of natural images and about natural vision. Preparation of this chapter was supported by a grant from the NEI.

REFERENCES

- Atick, J. J., 1992. Could information theory provide an ecological theory of sensory processing? *Network Comput. Neural Syst.*, 3:213–251.
- Balboa, R. M., C. W. Tyler, and N. M. Grzywacz, 2001. Occlusions contribute to scaling in natural images, *Vis. Res.*, 41:955–964.
- Barlow, H. B., 1961. Possible principles underlying the transformation of sensory messages, in *Sensory Communication* (W. A. Rosenbluth ed.), Cambridge, MA: MIT Press, pp. 217–234.
- Barlow, H. B., 2001. Redundancy reduction revisited, *Network Comput. Neural Syst.*, 12:241–253.
- Bell, A. J., and T. J. Sejnowski, 1997. The “independent components” of natural scenes are edge filters, *Vis. Res.*, 37:3327–3338.

FIGURE 107.3. *A*, Free viewing visual search task. On each trial, one patch was designated as the target and the remaining patches were distracters. The target patch was presented at the center of the display and could be inspected freely. After a brief interval a grid of patches was presented, arranged so that each time a patch was fixated, another patch would appear in the receptive field of the recorded V4 neuron. (Several sample grids could appear sequentially on a single trial; only one grid is shown here.) The animal had to respond when the target patch was identified among the distracters. *B*, Top-down attentional modulation. The top row compares mean responses recorded during trials when patch A was the target with those obtained when B, C, or D were targets. The bottom row compares responses when patch B was the target with these when A, C, or D were targets. The left column shows data from one V4 neuron displaying persistent top-down attentional modulation. The middle column shows data from a different cell

with multiplicative modulation. The third column shows data from a cell with no attentional modulation. *C*, V4 activity predicts the direction of the next saccade. The bottom panel shows the average response of one V4 neuron during fixation (fixation onset at 0 msec). The time course of the response is typical of such cells: parasaccadic suppression followed by a transient response and then a lower sustained response. The upper panel breaks down responses according to the direction of the upcoming saccade. Upcoming saccades that will be directed toward the receptive field are at 0 degrees (center line in each box), while those that will be directed away are at –180 and +180 degrees (edges of box). Boxes represent different response epochs (noted above each box). Activity of this V4 neuron clearly predicts the direction of the next saccade; when activity is high, the next saccade is most likely to be directed toward the receptive field. (See color plate 83.)

- Ben Hamed, S., J. R. Duhamel, F. Bremmer, and W. Graf, 2002. Visual receptive field modulation in the lateral intraparietal area during attentive fixation and free gaze, *Cereb. Cortex*, 12:234–245.
- Binello, A., S. Mannan, and K. H. Ruddock, 1995. The characteristics of eye movements made during visual search with multi-element stimuli, *Spatial Vis.*, 9:343–362.
- Burman, D. D., and M. A. Seagraves, 1994. Primate frontal eye field activity during natural scanning eye movements, *J. Neurophysiol.*, 71:1266–1271.
- Chelazzi, L., E. K. Miller, J. Duncan, and R. Desimone, 2001. Responses of neurons in macaque area V4 during memory-guided visual search, *Cereb. Cortex*, 11:761–772.
- Colby, C. L., 1991. The neuroanatomy and neurophysiology of attention, *J. Child Neurol.*, 6:S90–S118.
- Connor, C. E., J. L. Gallant, D. C. Preddie, and D. C. Van Essen, 1996. Responses in area V4 depend on the spatial relationship between stimulus and attention, *J. Neurophysiol.*, 75:1306–1308.
- Connor, C. E., D. C. Preddie, J. L. Gallant, and D. C. Van Essen, 1997. Spatial attention effects in macaque area V4, *J. Neurosci.*, 17:3201–3214.
- Dan, Y., J. J. Atick, and R. C. Reid, 1996. Efficient coding of natural scenes in the lateral geniculate nucleus: experimental test of a computational theory, *J. Neurosci.*, 16:3351–3362.
- Daugman, J. G., 1988. Complete discrete 2-D Gabor transforms by neural networks for image analysis and compression, *IEEE Trans. Acoust. Speech Signal Proc.*, 36:1169–1179.
- David, S. V., W. E. Vinje, and J. L. Gallant, 1999. Natural image reverse correlation in awake behaving primates, *Soc. Neurosci. Abstr.*, 25:1935.
- DeAngelis, G. C., I. Ohzawa, and R. D. Freeman, 1995. Receptive field dynamics in the central visual pathways, *Trends Neurosci.*, 18:451–458.
- DeBoer, E., and P. Kuyper, 1968. Triggered correlation, *IEEE Trans. Biomed. Eng.*, 15:159–179.
- deCharmes, R. C., D. T. Blake, and M. M. Merzenich, 1998. Optimizing sound features for cortical neurons, *Science*, 280:1439–1443.
- Deco, G., and J. Zihl, 2001. A neurodynamical model of visual attention: feedback enhancement of spatial resolution in a hierarchical system, *J. Comput. Neurosci.*, 10:231–253.
- Desimone, R., and J. Duncan, 1995. Neural mechanisms of selective visual attention, *Annu. Rev. Neurosci.*, 18:193–222.
- Desimone, R., T. D. Albright, C. G. Gross, and C. Bruce, 1984. Stimulus-selective properties of inferior temporal neurons in the macaque, *J. Neurosci.*, 4:2051–2062.
- De Valois, R. L., D. G. Albrecht, and L. G. Thorell, 1982. Spatial frequency selectivity of cells in macaque visual cortex, *Vis. Res.*, 22:545–559.
- De Valois, R. L., and K. K. De Valois, 1990. *Spatial Vision*, New York: Oxford University Press.
- Diamond, M. R., J. Ross, and M. C. Morrone, 2000. Extraretinal control of saccadic suppression, *J. Neurosci.*, 20:3449–3455.
- DiCarlo, J. J., K. O. Johnson, and S. S. Hsiao, 1998. Structure of receptive fields in area 3b of primary somatosensory cortex in the alert monkey, *J. Neurosci.*, 18:2626–2645.
- Dong, D. W., and J. J. Atick, 1995a. Temporal decorrelation: a theory of lagged and nonlagged responses in the lateral geniculate nucleus, *Network Comput. Neural Syst.*, 6:159–178.
- Dong, D. W., and J. J. Atick, 1995b. Statistics of natural time-varying images, *Network Comput. Neural Syst.*, 6:345–358.
- Field, D. J., 1987. Relations between the statistics of natural images and the response properties of cortical cells, *J. Opt. Soc. Am. A*, 4:2379–2394.
- Field, D. J., 1993. Scale-invariance and self-similar “wavelet” transforms: an analysis of natural scenes and mammalian visual systems, in *Wavelets, Fractals, and Fourier Transforms* (M. Farge, J. C. R. Hunt, and J. C. Vascillicos, eds.), New York: Clarendon Press, pp. 151–193.
- Field, D. J., 1994. What is the goal of sensory coding? *Neural Comput.*, 6:559–601.
- Fujita, I., and K. Tanaka, 1992. Columns for visual features of objects in monkey inferotemporal cortex, *Nature*, 360:343–346.
- Gallant, J. L., 2000. The neural representation of shape, in *Seeing* (K. K. DeValois ed.), San Diego, CA: Academic Press, pp. 311–333.
- Gallant, J. L., J. Braun, and D. C. Van Essen, 1993. Selectivity for polar, hyperbolic, and Cartesian gratings in macaque visual cortex, *Science*, 259:100–103.
- Gallant, J. L., C. E. Connor, and D. C. Van Essen, 1998. Neural activity in areas V1, V2 and V4 during free viewing of natural scenes compared to controlled viewing, *NeuroReport*, 9:2153–2158.
- Gottlieb, J. P., M. Kusunoki, and M. E. Goldberg, 1998. The representation of visual salience in monkey parietal cortex, *Nature*, 391:481–484.
- Gross, C. G., C. E. Rocha-Miranda, and D. B. Bender, 1972. Visual properties of neurons in inferotemporal cortex of the macaque, *J. Neurophysiol.*, 35:96–111.
- Hoffman, J. E., and B. Subramaniam, 1995. The role of visual attention in saccadic eye movements, *Percept. Psychophys.*, 57:787–795.
- Hyvarinen, A., and P. Hoyer, 1999. Emergence of phase and shift variant features by decomposition of natural images into independent feature subspaces. *Neural Comput.*, 12:1705–1720.
- Hyvarinen, A., J. Karhunen, and E. Oja, 2001. *Independent Component Analysis*, New York: Wiley.
- Itti, L., and C. Koch, 2001. Computational models of visual attention, *Nature Neurosci. Rev.*, 2:194–203.
- Jones, J., and L. Palmer, 1987. An evaluation of the two-dimensional Gabor filter model of simple receptive fields in cat striate cortex, *J. Neurophysiol.*, 58:1233–1258.
- Judge, S. J., R. H. Wurtz, and B. J. Richmond, 1980. Vision during saccadic eye movements. I. Visual interactions in striate cortex, *J. Neurophysiol.*, 43:1133–1155.
- Keating, C. F., and E. G. Keating, 1982. Visual scan patterns of rhesus monkeys viewing faces, *Perception*, 11:211–219.
- Klein, D. J., D. A. Depireux, J. Z. Simon, and S. A. Shamma, 2000. Robust spectrotemporal reverse correlation for the auditory system: optimizing stimulus design, *J. Comput. Neurosci.*, 9:85–111.
- Kobatake, E., and K. Tanaka, 1994. Neuronal selectivities to complex object features in the ventral visual pathway of the macaque cerebral cortex, *J. Neurophysiol.*, 71:856–867.
- Koch, C., and S. Ullman, 1985. Shifts in selective visual attention: towards the underlying neural circuitry, *Hum. Neurobiol.*, 4:219–227.
- Kowler, E., E. Anderson, B. Doshier, and E. Blaser, 1995. The role of attention in the programming of saccades, *Vis. Res.*, 35: 1897–1916.
- Krieger, G., and C. Zetsche, 1996. Nonlinear image operators for the evaluation of local intrinsic dimensionality, *IEEE Trans. Image Proc.*, 5:1026–1042.
- Krieger, G., C. Zetsche, and E. Barth, 1997. Higher-order statistics of natural images and their exploitation by operators selective to intrinsic dimensionality, in *Proceedings of the IEEE Signal Processing Workshop on Higher-Order Statistics*, Los Alamitos, CA: IEEE, pp. 147–151.

- Lee, A. B., D. Mumford, and J. Huang, 2001. Occlusion models for natural images: a statistical study of a scale-invariant dead leaves model, *Int. J. Comput. Vis.*, 41:35–59.
- Lee, D. K., L. Itti, C. Koch, and J. Braun, 1999. Attention activates winner-take-all competition among visual filters, *Nat. Neurosci.*, 2:375–381.
- Mannan, S., K. H. Ruddock, and D. S. Wooding, 1995. Automatic control of saccadic eye movements made in visual inspection of briefly presented 2-D images, *Spatial Vis.*, 9:363–386.
- Marmarelis, P. Z., and V. Z. Marmarelis, 1978. *Analysis of Physiological Systems: The White Noise Approach*, New York: Plenum.
- Mazer, J. A., S. V. David, and J. L. Gallant, 2000. Spatiotemporal receptive field estimation during free viewing visual search in macaque striate and extrastriate cortex, *Soc. Neurosci. Abstr.*, 53:15.
- Mazer, J. A., S. V. David, and J. L. Gallant, 2001. Attentional modulation of macaque V4 neurons during free viewing visual search, *Soc. Neurosci. Abstr.*, 574.5.
- Mazer, J. A., W. E. Vinje, J. McDermott, P. H. Schiller, and J. L. Gallant, 2002. Efficient characterization of spatial frequency and orientation tuning dynamics in area V1 of awake behaving animals, *Proc. Natl. Acad. Sci. USA*, 99:1645–1650.
- McAdams, C. J., and J. H. R. Maunsell, 1999. Effects of attention on orientation-tuning functions of single neurons in macaque cortical area V4, *J. Neurosci.*, 19:431–441.
- Miller, E. K., L. Li, and R. Desimone, 1993. Activity of neurons in anterior inferior temporal cortex during a short-term memory task, *J. Neurosci.*, 13:1460–1478.
- Moran, J., and R. Desimone, 1985. Selective attention gates visual processing in the extrastriate cortex, *Science*, 229:782–784.
- Motter, B. C., 1993. Focal attention produces spatially selective processing in visual cortical areas V1, V2 and V4 in the presence of competing stimuli, *J. Neurophysiol.*, 70:909–919.
- Motter, B. C., 1994. Neural correlates of attentive selection for color or luminance in extrastriate area V4, *J. Neurosci.*, 14:2178–2189.
- Motter, B., and E. J. Belky, 1998. The zone of focal attention during active visual search, *Vis. Res.*, 38:1007–1022.
- Navarro, R., A. Taberner, and G. Cristobal, 1996. Image representation with Gabor wavelets and its applications, in *Advances in Imaging and Electron Physics* (P. W. Hawkes ed.), New York: Academic Press, pp. 1–84.
- Niebur, E., and C. Koch, 1996. Control of selective visual attention: modeling the “where” pathway, in *Advances in Neural Information Processing Systems* (D. S. Touretzky, M. C. Mozer, and M. E. Hasselmo, eds.), Cambridge, MA: MIT Press, pp. 802–808.
- Nykamp, D. Q., and D. L. Ringach, 2002. Full identification of a linear-nonlinear system via cross-correlation analysis, *J. Vis.*, 2:1–11.
- Olshausen, B. A., and D. J. Field, 1996. Emergence of simple-cell receptive field properties by learning a sparse code for natural images, *Nature*, 381:607–609.
- Olshausen, B. A., and D. J. Field, 1997. Sparse coding with an overcomplete basis set: a strategy employed by V1? *Vis. Res.*, 23:3311–3325.
- Olshausen, B. A., and D. J. Field, 2000. Vision and the coding of natural images, *Am. Sci.*, 88:238–245.
- Olson, C. R., and S. N. Gettner, 1996. Brain representation of object-centered space, *Curr. Opin. Neurobiol.*, 6:165–170.
- Pasupathy, A., and C. E. Connor, 1999. Responses to contour features in macaque area V4, *J. Neurophysiol.*, 82:2490–2502.
- Piotrowski, L. N., and F. W. Campbell, 1982. A demonstration of the visual importance and flexibility of spatial-frequency amplitude and phase, *Perception*, 11:337–346.
- Rao, R. P. N., and D. H. Ballard, 1997. Dynamic model of visual recognition predicts neural response properties in the visual cortex, *Neural Comput.*, 9:721–763.
- Rao, R. P. N., G. J. Zelinsky, M. M. Hayhoe, and D. H. Ballard, 1996. Modelling saccadic targeting in visual search, in *Advances in Neural Information Processing Systems* (D. S. Touretzky, M. C. Mozer, and M. E. Hasselmo, eds.), Cambridge, MA: MIT Press, pp. 830–836.
- Reinagel, P., and A. M. Zador, 1999. Natural scene statistics at the center of gaze, *Network Comput. Neural Syst.*, 10:341–350.
- Ringach, D. L., M. J. Hawken, and R. Shapley, 2002. Receptive field structure of neurons in monkey primary visual cortex revealed by stimulation with natural image sequences, *J. Vis.*, 2:12–24.
- Ruderman, D. L., 1994. The statistics of natural images, *Network Comput. Neural Syst.*, 5:517–548.
- Ruderman, D. L., 1997. Origins of scaling in natural images, *Vis. Res.*, 37:3385–3398.
- Schall, J. D., 2001. Neural basis of deciding, choosing and acting, *Nature Neurosci. Rev.*, 2:33–42.
- Schill, K., E. Umkehrer, S. Beinlich, G. Krieger, and C. Zetzsche, 2001. Scene analysis with saccadic eye movements: top-down and bottom-up processing, *J. Electron. Imag.*, 10:152–160.
- Schwartz, O., and E. P. Simoncelli, 2001. Natural signal statistics and sensory gain control, *Nat. Neurosci.*, 4:819–825.
- Sereno, A., 1992. Programming saccades: the role of attention, in *Eye Movements and Visual Cognition* (K. Rayner ed.), New York: Springer, pp. 89–107.
- Sheinberg, D. L., and N. K. Logothetis, 2001. Noticing familiar objects in real world scenes: the role of temporal cortical neurons in natural vision, *J. Neurosci.*, 21:1340–1350.
- Sheinberg, D. L., and G. J. Zelinsky, 1993. A cortico-collicular model of saccade target selection, in *Perception and Cognition* (G. dYdewalle, and J. V. Rensbergen, eds.), Elsevier, pp. 333–348.
- Simoncelli, E. P., and O. Schwartz, eds., 1999. Modeling surround suppression in V1 neurons with a statistically-derived normalization model, in *Neural information processing systems* (M. S. Kearns, S. A. Solla, and D. A. Cohn eds.), Cambridge, MA: MIT Press.
- Srinivasan, M. V., S. B. Laughlin, and A. Dubs, 1982. Predictive coding: a fresh view of inhibition in the retina, *Proc. R. Soc. Lond. Ser. B. Biol. Sci.*, 216:427–459.
- Stanley, G. B., F. F. Li, and Y. Dan, 1999. Reconstruction of natural scenes from ensemble responses in the lateral geniculate nucleus, *J. Neurosci.*, 19:8036–8042.
- Steinmetz, M. A., and C. Constantinidis, 1995. Neurophysiological evidence for a role of posterior parietal cortex in redirecting visual attention, *Cereb. Cortex*, 5:448–456.
- Szatmary, B., and A. Lorincz, 2002. Independent component analysis of temporal sequences subject to constraints by lateral geniculate nucleus inputs yields all the three major cell types of the primary visual cortex, *J. Comput. Neurosci.*, 11:241–248.
- Tadmor, Y., and D. J. Tolhurst, 1993. Both the phase and the amplitude spectrum may determine the appearance of natural images, *Vis. Res.*, 33:141–145.
- Theunissen, F. E., S. V. David, N. C. Singh, A. Hsu, W. E. Vinje, and J. L. Gallant, 2001. Estimating spatial temporal receptive fields of auditory and visual neurons from their responses to natural stimuli, *Network Comput. Neural Syst.*, 12:289–316.
- Thomson, M. G. A., 1999. Higher-order structure in natural scenes, *J. Opt. Soc. Am. A*, 16:1549–1553.

- Thomson, M. G. A., 2001. Beats, kurtosis and visual coding, *Network Comput. Neural Syst.*, 12:271–287.
- Thomson, M. G. A., and D. H. Foster, 1997. Role of second- and third-order statistics in the discriminability of natural images, *J. Opt. Soc. Am. A*, 14:2081–2090.
- Tolias, A. S., T. Moor, S. M. Smirnakis, E. J. Tehovnik, A. G. Siapas, and P. H. Schiller, 2001. Eye movements modulate visual receptive fields of V4 neurons, *Neuron*, 29:757–767.
- Touryan, J., and Y. Dan, 2001. Analysis of sensory coding with complex stimuli, *Curr. Opin. Neurobiol.*, 11:443–448.
- Van Essen, D. C., and J. L. Gallant, 1994. Neural mechanisms of form and motion processing in the primate visual system, *Neuron*, 13:1–10.
- van Hateren, J. H., and D. L. Ruderman, 1998. Independent component analysis of natural image sequences yields spatio-temporal filters similar to simple cells in primary visual cortex, *Proc. R. Soc. Lond. Ser. B Biol. Sci.*, 265:2315–2320.
- van Hateren, J. H., and A. van der Schaaf, 1998. Independent component filters of natural images compared with simple cells in primary visual cortex, *Proc. R. Soc. Lond. B*, 265:359–366.
- Vinje, W. E., and J. L. Gallant, 1998. Modeling complex cells in an awake macaque during natural image viewing, in *Advances in Neural Information Processing Systems 10* (M. I. Jordan, M. J. Kearns, and S. A. Solla, eds.), Cambridge, MA: MIT Press, pp. 236–242.
- Vinje, W. E., and J. L. Gallant, 2000. Sparse coding and decorrelation in primary visual cortex during natural vision, *Science*, 287:1273–1276.
- Vinje, B. V., and J. L. Gallant, 2002. Natural stimulation of the non-classical receptive field increases information transmission efficiency in V1, *J. Neurosci.*, 22:2904–2915.
- Wegmann, B., and C. Zetsche, 1990a. Visual system based polar quantization of local amplitude and local phase of orientation-filter outputs, in *Human Vision and Electronic Imaging: Models, Methods and Applications* (B. Rogowitz ed.), Bellingham, WA: SPJE pp. 306–317.
- Wegmann, B., and C. Zetsche, 1990b. Statistical dependence between orientation filter outputs used in a human vision based image code, in *Visual Communication and Image Processing* (M. Kunt ed.), Bellingham, WA: SPJE pp. 909–923.
- Wilson, F. A. W., and P. S. Goldman-Rakic, 1994. Viewing preferences of rhesus monkeys related to memory for complex pictures, colours and faces, *Behav. Brain Res.*, 60:79–89.
- Yarbus, A. L., 1967. *Eye Movements and Vision*, New York: Plenum.
- Zetsche, C., and E. Barth, 1990. Fundamental limits of linear filters in the visual processing of two-dimensional signals, *Vis. Res.*, 30:1111–1117.
- Zetsche, C., and G. Krieger, 1999. Nonlinear neurons and higher-order statistics: new approaches to human vision and electronic image processing, in *Human Vision and Electronic Imaging IV* (B. Rogowitz and T. V. Pappas, eds.), Bellingham, WA: SPJE pp. 2–33.
- Zetsche, C., G. Krieger, and B. Wegmann, 1999. The atoms of vision: Cartesian or polar? *J. Opt. Soc. Am. A*, 16:1554–1565.

108 Principles of Image Representation in Visual Cortex

BRUNO A. OLSHAUSEN

THE VISUAL CORTX is responsible for most of our conscious perception of the visual world, yet we remain largely ignorant of the principles underlying its function despite progress on many fronts of neuroscience. The principal reason for this is not a lack of data, but rather the absence of a solid theoretical framework for motivating experiments and interpreting findings. The situation may be likened to trying to understand how birds fly without knowledge of the principles of aerodynamics: no amount of experimentation or measurements made on the bird itself will reveal the secret. The key experiment—measuring air pressure above and below the wing as air is passed over it—would not seem obvious were it not for a theory suggesting why the pressures might be different.

But neuroscience cannot simply turn to mathematics or engineering for a set of principles that will elucidate the function of the cortex. Indeed, engineers and mathematicians themselves have had little success in emulating even the most elementary aspects of intelligence or perceptual capabilities, despite much effort devoted to the problem over the past 40 years. The lack of progress here is especially striking considering the fact that the past two decades alone have seen a 1000-fold increase in computer power (in terms of computer speed and memory capacity), while the actual “intelligence” of computers has improved only moderately by comparison.

The problem: pattern analysis

Although seldom recognized by either side, both neuroscientists and engineers are faced with a common problem: the problem of *pattern analysis*, or how to extract structure contained in complex data. Neuroscientists are interested in understanding how the cortex extracts certain properties of the visual environment—surfaces, objects, textures, motion, and so on—from the data stream coming from the retina. Similarly, engineers are interested in designing algorithms capable of extracting structure contained in images or sound—for example, to identify and label parts within the body from medical imaging data. These problems at their core are one in the same, and progress in one domain will likely lead to new insights in the other.

The key difficulty faced by both sides is that *the core principles of pattern analysis are not well understood*. No amount of experimentation or technological tinkering alone can overcome this obstacle. Rather, it demands that we devote our efforts to advancing new theories of pattern analysis and to directing experimental efforts toward testing these theories.

In recent years, a theoretical framework for how pattern analysis is done by the visual cortex has begun to emerge. The theory has its roots in ideas proposed more than 40 years ago by Attneave and Barlow, and it has been made more concrete in recent years through a combination of efforts in engineering, mathematics, and computational neuroscience. The essential idea is that the visual cortex contains a probabilistic model of images and that the activities of neurons are representing images in terms of this model. Rather than focusing on what features of “the stimulus” are represented by neurons, the emphasis of this approach is on discovering a good featural description of images of the natural environment, using probabilistic models, and then relating this description to the response properties of visual neurons.

In this chapter, I will focus on recent work that has attempted to understand image representation in area V1 in terms of a probabilistic model of natural scenes. The next section will provide an overview of the probabilistic approach and its relation to theories of redundancy reduction and sparse coding. The third section will then describe how this framework has been used to model the structure of natural images, and the fourth section will discuss the relation between these models and the response properties of V1 neurons. Finally, in the fifth section, I will discuss some of the experimental implications of this framework, alternative theories, and the prospects for extending this approach to higher cortical areas.

Probabilistic models

The job of visual perception is to infer properties of the environment from data coming from the sensory receptors. What makes this such a difficult problem is that we are trying to recover information about the three-dimensional world from

a two-dimensional sensor array. This process is loaded with uncertainty due to the fact that the light intensity arriving at any point on the retina arises from a combination of lighting properties, surface reflectance properties, and surface shape (Adelson and Pentland, 1996). There is no unique solution for determining these properties of the environment from photoreceptor activities; rather, some environments provide a more probable explanation of the data than others based on our knowledge of how the world is structured and how images are formed. Visual perception is thus essentially a problem of *probabilistic inference*.

In order to do probabilistic inference on images, two things are needed:

1. A model for how a given state of the environment (E) gives rise to a particular state of activity on the receptors (the observable data, D). This model essentially describes the process of image formation and can be characterized probabilistically (to account for uncertainties such as noise) using the conditional distribution $P(D|E)$.
2. A model for the *prior* probability of the state of the environment. This expresses our knowledge of how the world is structured—which properties of the environment are more probable than others—and is characterized by the distribution $P(E)$.

From these two quantities, one can make inferences about the environment by computing the posterior distribution, $P(E|D)$, which specifies the relative probabilities of different states of the environment given the data. It is computed by combining $P(E)$ with $P(D|E)$ according to Bayes's rule:

$$P(E|D) \propto P(D|E)P(E). \quad (1)$$

This simple equation provides a mathematical formulation of the essential problem faced by the cortex. By itself, it does not provide all the answers to how the cortex works. But it does provide a guiding principle from which we can begin to start filling in details.

REDUNDANCY REDUCTION The general idea of “perception as probabilistic inference” is by no means new, and in fact it goes back at least to Helmholtz (1867/1962). Attneave (1954) later pointed out that there could be a formal relationship between the statistical properties of images and certain aspects of visual perception. The notion was then put into concrete mathematical and neurobiological terms by Barlow (1961, 1989), who proposed a self-organizing strategy for sensory nervous systems based on the principle of *redundancy reduction*—that is, the idea that neurons encode information in such a way as to minimize statistical dependencies among them. Barlow reasoned that a statistically independent representation of the environment would make it possible to store information about prior probabilities, since the joint probability distribution of a particular state \mathbf{x}

could be easily calculated from the product of probabilities of each component x_i : $P(\mathbf{x}) = \prod_i P(x_i)$. It also has the advantage of making efficient use of neural resources in transmitting information, since it does not duplicate information in different neurons.

The first strides in quantitatively testing the theory of redundancy reduction came from the work of Simon Laughlin and M. V. Srinivasan. They measured both the histograms and spatial correlations of image pixels in the natural visual environment of flies and then used this knowledge to make quantitative predictions about the response properties of neurons in early stages of the visual system (Laughlin, 1981; Srinivasan et al., 1982). They showed that the contrast response function of bipolar cells in the fly's eye performs histogram equalization (so that all output values are equally likely) and that lateral inhibition among these neurons serves to decorrelate their responses for natural scenes, confirming two predictions of the redundancy reduction hypothesis.

Another advance was made 10 years later by Atick and Redlich (1992) and van Hateren (1992, 1993), who formulated a theory of coding in the retina based on whitening the power spectrum of natural images in space and time. Since it had been shown by Field (1987) that natural scenes possess a characteristic $1/f^2$ spatial power spectrum, they reasoned that the optimal decorrelating filter should attempt to whiten the power spectrum up to the point where noise power is low relative to the signal (since a signal with a flat power spectrum has no spatial correlations). The optimal whitening filter thus has a transfer function that rises linearly with the spatial frequency and then falls off where the signal power becomes equal to or less than the noise power. Interestingly, the inverse Fourier transform of such a spatial-frequency response function has a spatial profile similar to the center-surround antagonistic receptive fields of retinal ganglion cells and neurons in the lateral geniculate nucleus (LGN). Some experimental evidence for temporal whitening has also been found in the LGN of cats (Dan et al., 1996).

SPARSE, OVERCOMPLETE REPRESENTATIONS While the principle of redundancy reduction has been fairly successful in accounting for response properties of neurons in the retina and LGN, it would seem that other considerations come into play in the cortex. An important difference between the retina and cortex is that the retina is faced with a severe structural constraint, the optic nerve, which limits the number of axon fibers leaving the eye. Given the net convergence of approximately 100 million photoreceptors onto 1 million ganglion cells, redundancy reduction would appear to constitute a sensible coding strategy for making the most use of the limited resources of the optic nerve. V1, by contrast, *expands* the image representation coming from the

LGN by having many more outputs than inputs (approximately 25:1 in cat area 17—inferred from Beaulieu and Colonnier, 1983, and Peters and Yilmaz, 1993). If the bandwidth per axon is about the same, then the unavoidable conclusion is that redundancy is being *increased* in the cortex, since the total amount of information cannot increase (Field, 1994). The expansion here is especially striking given the evidence for wiring length being minimized in many parts of the nervous system (Cherniak, 1995; Chklovskii et al., 2002). What is being gained by spending extra neural resources in this way?

First, it must be recognized that the real goal of sensory representation is to *model* the redundancy in images, not necessarily to reduce it (Barlow, 2001). What we really want is a *meaningful* representation—something that captures the causes of images, or what’s “out there” in the environment. Second, redundancy reduction provides a valid probabilistic model of images only to the extent that the world can meaningfully be described in terms of statistically independent components. While some aspects of the visual world do seem well described in terms of independent components (e.g., surface reflectance is independent of illumination), most seem awkward to describe in this framework (e.g., body parts can move fairly independently but their movements are also often coordinated to accomplish certain tasks). Thus, in order to understand how the cortex forms useful representations of image structure, we must appeal to a principle other than redundancy reduction.

One way of potentially achieving a meaningful representation of sensory information is by finding a way to group things together so that the world can be described in terms of a small number of events at any given moment. In terms of a neural representation, this would mean that activity is distributed among a small fraction of neurons in the population at any moment, forming a *sparse code*. Such a representation is actually highly redundant, since the activity of any given unit is highly predictable (i.e., it spends most of its time at zero). But so long as it can provide a meaningful description of images, it is more useful than a dense representation in which redundancy has been reduced.

The first quantitative evidence for sparse coding in the visual cortex was provided by Field (1987), who examined the histograms of model V1 neuron activities in response to natural images. He modeled the receptive fields of these neurons using a Gabor function and showed that the settings of spatial-frequency bandwidth and aspect ratio which maximize the concentration of activity into the fewest number of units are roughly the same as those found for most cortical neurons—that is, around 1 to 1.5 octaves and with an approximately 2:1 length:width ratio. In other words, the particular shapes of V1 simple-cell receptive fields appear well suited for achieving a sparse representation of natural images.

In addition to these receptive field parameters, though, the cortex must choose how to *tile* the entire joint space of position, orientation, and spatial frequency in order to provide a complete representation of the image. Simoncelli et al. (1992) have argued that *overcompleteness* is a desirable property for tiling the input space in terms of these parameters, as it allows each output to carry a specific interpretation—that is, the amount of structure occurring at a particular position, orientation, and scale in the image. (An overcomplete representation is one where the number of outputs is greater than the dimensionality of the input.) By contrast, in a *critically sampled* representation (where there are just as many outputs as inputs), it is difficult to ascribe meaning to any one output value since it is corrupted by information from different positions, scales, and orientations. By expanding the representation, then, one achieves a better description of the structure in images.

One can achieve the best of both worlds by combining overcompleteness with sparseness. A technique now widely used in the field of signal analysis is to combine different families of wavelets—*time-frequency atom dictionaries*—in order to achieve the best combination of time and frequency localization for describing a particular signal (Mallat, 1999). Typically, one tries to obtain the sparsest possible representation of a signal by selectively drawing basis functions from different dictionaries according to how well they match the structure in the signal. The result is a highly concise description of the signal that reveals its true time-frequency structure (Chen et al., 2001; Mallat and Zhang, 1993).

Thus, by expanding the image representation and making it sparse, neurons in V1 could achieve a succinct description of images in terms of features specifically tailored to the structures occurring in natural scenes. For example, while an oriented edge element would require several neurons to be represented in the retina or LGN, this structure would be absorbed by the activity of a single unit within a local population in the cortex (Fig. 108.1). While nothing has been

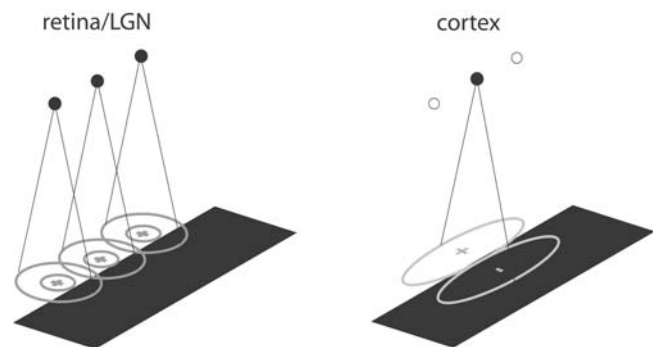


FIGURE 108.1. Sparse coding. By building oriented receptive fields, cortical neurons can represent image structures such as edges using fewer *active* units than in the retina or LGN. *Filled circles*, active units; *unfilled circles*, inactive units.

gained in the ability to describe the edge element per se—that is, there has been no gain in information—the description is now in a more convenient form. In other words, the activity of a single cortical unit conveys more *meaning* about what is going on in the image than does a single retinal or LGN neuron. Note, however, that although the code is sparse, it is still *distributed* in that multiple units still need to take responsibility for coding any given stimulus (Foldiak, 1995).

The conciseness offered by sparse, overcomplete coding is also useful for subsequent stages of processing. For example, once a scene is sparsely described in terms of local edge elements, it would be much easier to model the relationships among these elements to represent contours, since the activities of only a few neurons need to be taken into account. If we were to model these dependencies directly in terms of retinal ganglion cell activities, the number of associations and hence neural connections needed would be far greater. Sparseness is also desirable for pattern matching, since it lowers the probability of false matches among elements of a pattern (Baum et al., 1988; Jaekel, 1989; Willshaw et al., 1969; Zetsche, 1990).

As an aside, it is worth noting an example of where sparse, overcomplete coding is used in abundance: human communication. As pointed out by Zipf (1950), efficient communication involves a trade-off between the size of the vocabulary and its ease of use. One could have a small vocabulary where each word has various meanings, but the correct use of these words would rely heavily on careful choice of word order and establishing the proper context. At the other extreme, one could have an enormous vocabulary where each word is endowed with highly specific meaning, making its use very simple but requiring a large memory capacity to store all the words. Human communication balances this trade-off by having a large but manageable vocabulary. Thoughts are then conveyed by dynamically combining words into sentences. The code is overcomplete since there are many more words than phonemes used to form utterances (or letters to form words), and it is sparse in that any given sentence utilizes only a small fraction of the words in the vocabulary.

A simple probabilistic model of images

This section will describe specifically how the probabilistic approach has been used to model the structure of natural scenes, focusing on a sparse, overcomplete model of images. The next section will then discuss the relation between this model and the response properties of neurons in area V1.

LINEAR SUPERPOSITION MODEL A number of probabilistic models described in the literature have utilized a simple

image model in which each portion of a scene is described in terms of a linear superposition of features (Bell and Sejnowski, 1997; Lewicki and Olshausen, 1999; Olshausen, and Field, 1996a, 1997; van Hateren and van der Schaaf, 1998). It should be noted from the outset, however, that such a linear model of images cannot possibly hope to capture the full richness of the structures contained in natural scenes. The reason is that the true causes of images—light reflecting off the surfaces of objects—combine by the rules of occlusion, which are highly nonlinear (Ruderman, 1997). In addition, the retinal projection of an object will undergo shifts, rotations, and rescaling due to changes in viewpoint, and these types of variation also require more than a linear model to properly describe. However, at the scale of a local image patch (e.g., 12×12 pixels) it is possible that these factors are not very significant. Also, because the mathematics of linear systems are tractable, the linear model provides us with a convenient starting point for building a probabilistic model of images.

In the linear model, an image patch, $I(\mathbf{x})$, is described by adding together a set of basis functions, $\phi_i(\mathbf{x})$, with amplitudes a_i :

$$I(\mathbf{x}) = \sum_i a_i \phi_i(\mathbf{x}) + v(\mathbf{x}) \quad (2)$$

(\mathbf{x} denotes spatial position within the patch). The basis functions may be thought of as a set of spatial features for describing an image, and the coefficients a_i tell us how much of each feature is contained in the image. The variable v represents Gaussian noise, independent and identically distributed (i.i.d.), and is included to model structure in the images that is not well captured by the basis functions. The model is illustrated schematically in Figure 108.2.

Importantly, the basis set is assumed to be *overcomplete*, meaning that there are more basis functions (and hence more a_i s) than effective dimensions (number of pixels) in the

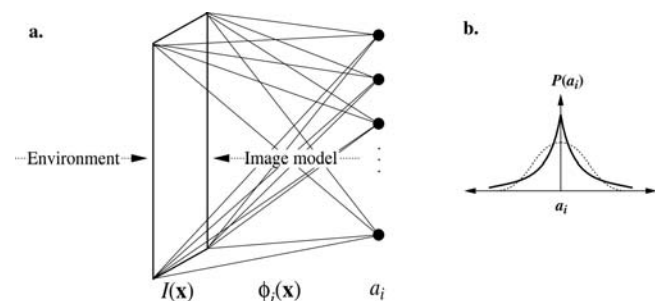


FIGURE 108.2. Image model. *a*, An image patch, $I(\mathbf{x})$, is modeled as a linear superposition of basis functions, $\phi_i(\mathbf{x})$. The image is thus represented, in terms of the model, by the coefficient values a_i . *b*, The prior probability distribution over the coefficients, $P(a_i)$, is peaked at zero, with heavy tails relative to a Gaussian of the same variance (shown as a *dotted line*) to encourage sparseness.

images. For example, in the instantiation described below, 200 basis functions are used to describe a 12×12 image patch, whereas 144 basis functions would suffice to form a complete representation. Because the representation is overcomplete, there is an infinite number of solutions for the coefficients in equation 2 (even with zero noise), all of which describe the image equally well in terms of mean squared error. In other words, there are multiple ways of explaining any given image in terms of the basis functions.

The degeneracy in the solution caused by overcompleteness is analogous to the ill-posed nature of visual perception discussed in the previous section. As before, two things are needed to infer a solution: a causal model for how the data are generated and a prior distribution over the causes (in this case, the coefficients). The first we have already specified in equation 2. Since the only uncertainty is the noise, which is Gaussian, the probability of an image given the coefficients is just a Gaussian distribution:

$$P(\mathbf{I}|\mathbf{a}, \theta) = \frac{1}{\mathcal{Z}_{\lambda_N}} e^{-\frac{\lambda_N}{2} \sum_{\mathbf{x}} [I(\mathbf{x}) - \sum_i a_i \phi_i(\mathbf{x})]^2}, \quad (3)$$

where $1/\lambda_N$ is the variance of the noise. The boldface notation is used to denote all elements of the corresponding variable (pixels or coefficients), and the symbol θ denotes all parameters of the model.

The prior probability distribution over the coefficients, a_i , is designed to enforce sparseness in the representation, and it is also (for now) factorial:

$$P(\mathbf{a}|\theta) = \prod_i \frac{1}{\mathcal{Z}_S} e^{-S(a_i)}. \quad (4)$$

S is a nonconvex function that shapes $P(a_i)$ to be peaked at zero with *heavy tails*, as shown in Figure 108.2B. For example, if $S(x) = |x|$, the prior corresponds to a Laplacian distribution, and if $S(x) = \log(1 + x^2)$, the prior corresponds to a Cauchy distribution. Note that although the joint prior over the coefficients is factorial, it need not stay that way, and in fact there are good reasons for making it nonfactorial, as discussed in the next section.

From the above two distributions (Eqs. 3 and 4), the relative probability of different explanations for an image sequence is computed via Bayes' rule, as before (Eq. 1):

$$P(\mathbf{a}|\mathbf{I}, \theta) \propto P(\mathbf{I}|\mathbf{a}, \theta) P(\mathbf{a}|\theta). \quad (5)$$

The posterior distribution, $P(\mathbf{a}|\mathbf{I}, \theta)$, rates the probability of each solution for the coefficients, but it still does not tell us how to *choose* a particular solution for a given image. One possibility is to choose the mean, $P(\mathbf{a}|\mathbf{I}, \theta) \mathbf{a}$ $d\mathbf{a}$, but this is difficult to compute because it requires sampling many values from the posterior. The solution we adopt here is to choose the coefficients that maximize the posterior distribution, the *Maximum A Posterior* (MAP) *estimate*:

$$\hat{\mathbf{a}} = \arg \max_{\mathbf{a}} P(\mathbf{a}|\mathbf{I}, \theta). \quad (6)$$

The MAP estimate $\hat{\mathbf{a}}$ may be computed via gradient descent on $-\log P(\mathbf{a}|\mathbf{I}, \theta)$. Thus, $\hat{\mathbf{a}}$ is given by the equilibrium solution to the following differential equation:

$$\tau \dot{a}_i = b_i - \sum_j C_{ij} a_j - S'(a_i) \quad (7)$$

where

$$b_i = \lambda_N \sum_{\mathbf{x}} \phi_i(\mathbf{x}) I(\mathbf{x})$$

$$C_{ij} = \lambda_N \sum_{\mathbf{x}} \phi_i(\mathbf{x}) \phi_j(\mathbf{x}).$$

The important thing to note here is that although the image model is linear, *the transformation from images to coefficients is nonlinear*. The reason is that the derivative of the *sparseness function*, S , is nonlinear. It essentially serves to self-inhibit the coefficients so that only those basis functions which best match the image are used. Thus, inferring the coefficients for an image sequence involves a process of selection, or *sparsification*, rather than simply filtering.

A neural circuit for sparsifying the coefficients according to Eq. 7 is shown in Figure 108.3. Each output unit (coefficient) is driven by the combination of a feedforward term (b_i), a recurrent term ($\sum_j C_{ij} a_j$), and a nonlinear self-inhibition term ($-S'(a_i)$). The feedforward contribution to each unit is computed by taking the inner product between its basis function and the image, akin to a classical receptive field model. The recurrent contribution is inhibitory and is computed by weighting the activities of other units according to their inner product with this unit's receptive field. Each unit is then subject to nonlinear self-inhibition, which discourages it from becoming active, thus encouraging sparse representations.

ADAPTING THE MODEL TO THE STATISTICS OF NATURAL IMAGES
So far, we have formulated a probabilistic model for describing images in terms of a sparse collection of additive fea-

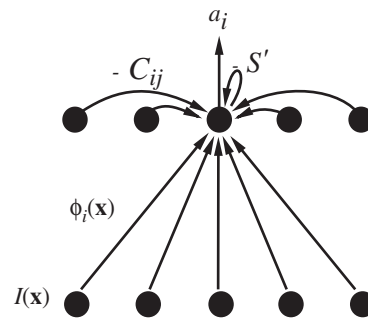


FIGURE 108.3. Neural circuit for computing the coefficients. Each coefficient, a_i , is driven by the combination of a feedforward term (inner product between its basis function and the image), a recurrent term (activities of other coefficients, weighted by the overlap of their basis functions), and a nonlinear self-inhibition term (derivative of the sparse cost function).

tures (basis functions). But what exactly should these features be? One could set them by hand to match the aforementioned Gabor function parameters which yield sparse representations of natural images (Field, 1987), but how do we know that there is not an even better, non-Gabor-like way to shape the basis functions that would lead to an even sparser description of images? We can find out by leaving the basis functions unparameterized and adapting them to best match the structure of natural images.

In general, any of the model parameters θ (which includes the basis functions $\phi_i(\mathbf{x})$, the sparseness function S , and the noise variance $1/\lambda_N$) may be adapted to best match the statistics of natural scenes by maximizing the average log likelihood of the model:

$$\hat{\theta} = \arg \max_{\theta} \langle \log P(\mathbf{I}|\theta) \rangle, \quad (8)$$

where the brackets $\langle \rangle$ mean “averaged over all images” and the likelihood of the model is defined as

$$P(\mathbf{I}|\theta) = \int P(\mathbf{I}|\mathbf{a}, \theta) P(\mathbf{a}|\theta) d\mathbf{a}. \quad (9)$$

A learning rule for the basis functions may therefore be obtained via gradient ascent on the average log likelihood:

$$\begin{aligned} \Delta \phi_i(\mathbf{x}) &\propto \frac{\partial \langle \log P(\mathbf{I}|\theta) \rangle}{\partial \phi_i(\mathbf{x})} \\ &= \lambda_N \langle \langle a_i e(\mathbf{x}) \rangle \rangle_{P(\mathbf{a}|\mathbf{I}, \theta)} \end{aligned} \quad (10)$$

where $e(\mathbf{x})$ is the residual image: $e(\mathbf{x}) = I(\mathbf{x}) - \sum_i a_i \phi_i(\mathbf{x})$.

Looking at Eq. 10, we can see that adapting the basis functions amounts to a simple Hebbian learning rule involving the coefficient activities and the resulting residual image averaged under the posterior distribution for each image. Instead of sampling from the full posterior distribution, though, we shall utilize a simpler approximation in which a single sample is taken at the posterior maximum, and so we have

$$\Delta \phi_i(\mathbf{x}) \propto \hat{a}_i e(\mathbf{x}). \quad (11)$$

In this case, however, we must rescale the basis functions after each update in order to ensure that they do not grow without bound (as described in Olshausen and Field, 1997).

When this procedure is carried out on hundreds of thousands of image patches extracted from natural scenes, the basis functions converge to a set of spatially localized, oriented, bandpass functions, as shown in Figure 108.4. Each basis function was initialized to random numbers, and this solution emerged purely as a result of maximizing the log likelihood of the model. Indeed, it seems reasonable that such functions would form a sparse description of natural images, since only a few of them would be needed to describe a line or contour passing through this patch of space. Why they become bandpass is less obvious, however, and some potential reasons are given in Olshausen and Field (1996b) and Field (1993). The learned basis functions are

well fit by Gabor functions, and the entire set of functions evenly tiles the joint space of position, orientation, and scale, as demonstrated in previous publications (Olshausen and Field, 1996a, 1996b, 1997).

TIME-VARYING IMAGES The model may be extended to the time domain by describing a sequence of images (i.e., a movie) in terms of a linear superposition of spatiotemporal functions, $\phi_i(\mathbf{x}, t)$. Here the basis functions are applied in a shift-invariant fashion over time, meaning that the same function is assumed to be repeated at each point in time. Thus, an image sequence is described by convolving the spatiotemporal basis functions with a set of time-varying coefficients, $a_i(t)$:

$$\begin{aligned} I(\mathbf{x}, t) &= \sum_i \sum_{t'} a_i(t') \phi_i(\mathbf{x}, t - t') + v(\mathbf{x}, t) \\ &= \sum_i a_i(t) * \phi_i(\mathbf{x}, t) + v(\mathbf{x}, t). \end{aligned} \quad (12)$$

The model is illustrated schematically in Figure 108.5.

Again, a sparse factorial prior is imposed on the coefficients over both space (i) and time (t), and the coefficients for an image sequence are computed via gradient descent on the negative log posterior:

$$\tau \hat{a}_i(t) = b_i(t) - \sum_j a_j(t) \star C_{ij}(t) - S'(a_i(t)) \quad (13)$$

$$\begin{aligned} \text{where } b_i(t) &= \lambda_N \sum_l \phi_i(l, t) \star I(l, t) \\ C_{ij}(t) &= \lambda_N \sum_l \phi_i(l, t) \star \phi_j(l, t), \end{aligned}$$

where \star denotes cross-correlation. Note, however, that in order to be considered a causal system, the value of a coefficient at time t' must be determined solely from image frames and other coefficient values prior to t' . For now, though, we shall not bother imposing this restriction, and in the next section we shall entertain some possibilities for making the model causal.

A learning rule for the spatiotemporal basis functions may be derived by maximizing the average log likelihood as before (for details see Olshausen, 2002). When the basis functions are adapted in this manner, using time-varying natural images as training data (van Hateren, 2000), they converge to a set of spatially localized, oriented bandpass functions that now *translate* over time. Shown in Figure 108.6 is a randomly chosen subset of the 200 basis functions learned, each 12×12 pixels and seven frames in time. Again, it seems intuitively reasonable that these functions would form a sparse representation of time-varying natural images, since only a few of them are needed to describe a contour segment moving through this patch of the image.

The tiling properties for velocity, as well as speed versus spatial frequency, are shown in Figure 108.7. The majority of

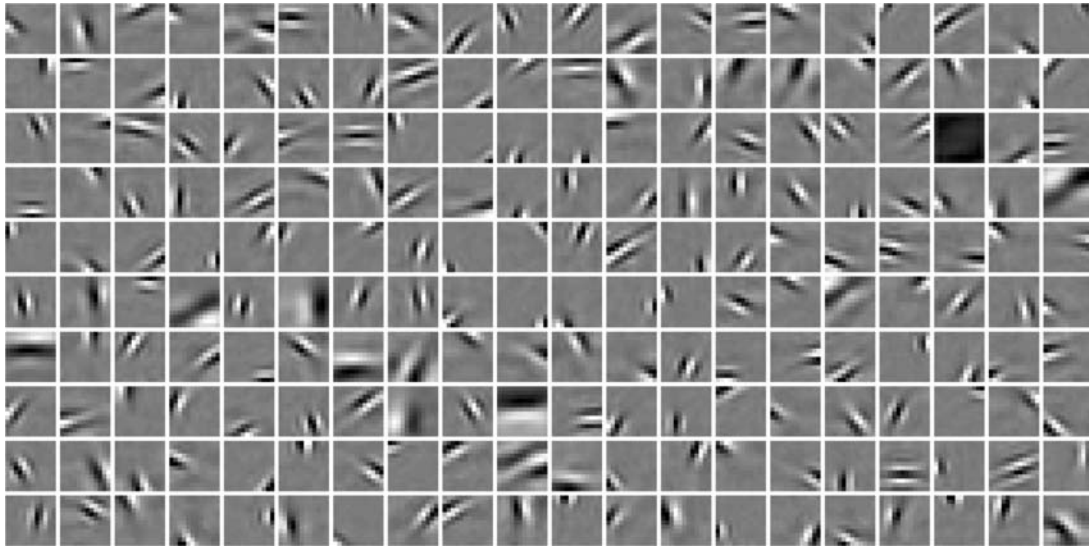


FIGURE 108.4. Basis functions learned from natural images. Shown is a set of 200 basis functions, each 12×12 pixels in size. Most have become localized well within the image patch, and all have become

oriented, with the exception of one function, which took on the DC component. The functions are also bandpass in spatial frequency, occupying different regions of the spatial-frequency domain.

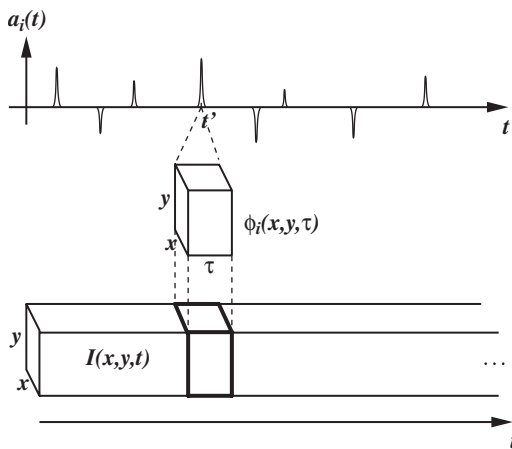


FIGURE 108.5. Spatiotemporal image model. A time-varying image patch, $I(\mathbf{x}, t)$, is modeled as a linear superposition of spatiotemporal basis functions, $\phi_i(\mathbf{x}, t)$, each of which is localized in time but may be applied at any point within the image sequence.

basis functions translate by less than one pixel per frame. (The frame rate is 25 frames per second, so a speed of one pixel per frame corresponds to 25 pixels per second.) The high-spatial-frequency basis functions are biased toward slow speeds, as expected, because at higher speeds they would give rise to temporal frequencies beyond the Nyquist limit. This limit is shown by the dashed line (e.g., a spatial frequency of 0.25 cy per pixel moving at two pixels per frame, or 50 pixels per second, would give rise to a temporal frequency of 12.5 Hz, which is equal to the Nyquist rate in this case).

Relation to V1 response properties

We now turn to the relation between the image model and the response properties of neurons in area V1. We shall first

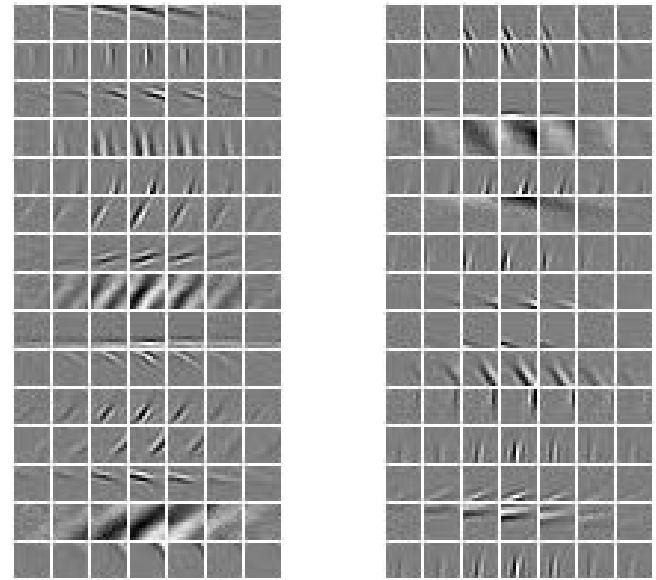


FIGURE 108.6. Space-time basis functions learned from time-varying natural images. Shown are 30 basis functions randomly selected from the entire set of 200 functions learned, arranged in columns. Each basis function is 12×12 pixels in space and seven frames in time. Each row shows a different basis function, with time proceeding from left to right.

focus on the response properties of simple cells and then discuss efforts to model the response properties of complex cells, as well as dependencies among them.

SIMPLE CELLS In the neural circuit implementation of the model, the basis functions correspond to the feedforward weighting functions that contribute to the final output value of each unit (Fig. 108.3). If we were to draw an analogy between the coefficients a_i of the model and neurons in V1,

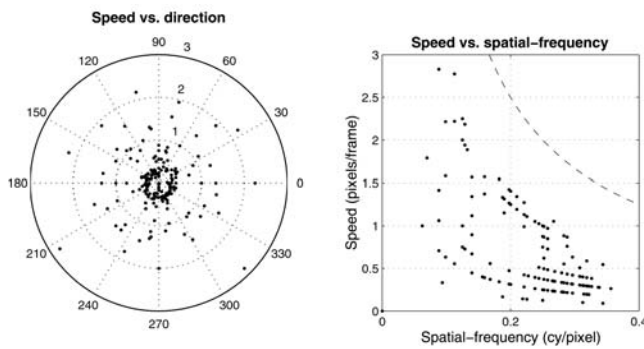


FIGURE 108.7. Basis function tiling properties. Each data point denotes a different basis function. In the polar plot at the left, radius denotes speed (in units of frames per second) and angle denotes the direction in which the basis function translates. In the plot at the right, the dashed line denotes the limit imposed by the Nyquist frequency (12.5 Hz). (The striated clustering is an artifact due to decimation in the spatiotemporal frequency domain.)

then it would seem most appropriate to compare the basis functions $\phi(\mathbf{x}, t)$ to the receptive fields of simple cells. These neurons behave in a somewhat linear manner in that in their response to a stimulus can be fairly well predicted from a weighted sum of inputs over space and time (although see Chapter 52 for a discussion of the response nonlinearities of these neurons). Their spatial receptive fields have been characterized as spatially localized, oriented, and bandpass, similar in form to the basis functions learned by the sparse coding model (spatial-frequency bandwidth of 1.1 octaves, length/width ratio of 1.3; Olshausen and Field, 1996a).

In terms of their temporal properties, simple cells tend to fall into two major categories—those that are separable in space and time and those that are inseparable (DeAngelis et al., 1995; McLean and Palmer, 1989). The latter tend to translate as a function of time, similar to the learned basis functions of the model, and it is this property that is thought to underlie the direction selectivity of V1 neurons (see also Chapters 44 and 48). If one assumes a size of 0.15 degree per pixel for the images used in training, then a speed of 1 pixel per frame (see Fig. 108.7) corresponds to 4 deg/sec, which is within the typical range of speed tuning found in simple cells (DeAngelis et al., 1993).

Given the similarities between the receptive field properties of V1 simple cells and the basis functions of the sparse coding model, it would seem that these neurons are well suited to form a sparse representation of natural images. It is also possible that the space-time separable simple cells could be fit within this framework, since one way to build neurons with space-time inseparable receptive fields is by summing a population of space-time separable units with different time constants. Thus, if the basis functions of the model were constrained such that they did not have access to inputs with arbitrary time delays, it may be possible to obtain both types of receptive field properties.

Ideally, one would like to compare not just the forms of individual basis functions, but also how the population as a whole tiles the joint space of position, orientation, spatial frequency, and velocity. However, to do such a comparison properly would require recording exhaustively from all neurons within a hypercolumn or so of visual cortex. From the partial assays of parafoveal neurons currently available, it would seem that there is an overabundance of neurons tuned to low spatial frequencies compared to the model (De Valois et al., 1982; Parker and Hawken, 1988; van Hateren and van der Schaaf, 1998). This discrepancy could be due to biases in sampling or to the fact that the model is currently ignoring many other stimulus dimensions that the cortex also cares about, such as color, disparity, and so on (Olshausen and Anderson, 1995). In addition, real neurons have a certain level of precision with which they can code information in amplitude and time, whereas in the model there is no limit in precision imposed upon the coefficient amplitudes (i.e., they have essentially infinite precision in amplitude). It seems likely that when such implementation details are taken into account, the bias toward low spatial frequencies could be explained, since the low spatial frequencies in natural scenes occupy a higher dynamic range than high spatial frequencies.

In addition to accounting for known receptive field properties, the model makes a prediction about the types of nonlinearities and interactions among neurons expected in response to natural images. In the neural implementation of the model (Fig. 108.3), each output unit is subject to nonlinear self-inhibition in addition to inhibition from neighbors whose receptive fields overlap with its receptive field. Figure 108.8 illustrates the effect of these output nonlinearities and interactions by comparing the time-varying value of one of the coefficients obtained by maximizing the posterior (sparsification) to that obtained by straightforward convolution (simply taking a feedforward weighted sum of inputs over space and time). The difference is striking in that the sparsified representation is characterized by highly localized punctate events, as opposed to the more graded and prolonged activations obtained with convolution. If we take the coefficients to be analogous to neurons in the cortex, then this would predict that the responses of neurons should be sparser than expected from simply convolving their feedforward weighting function with the image. Note also that the form of nonlinearity here is more complicated than the pointwise contrast response nonlinearity observed in simple cells (Albrecht and Geisler, 1991; Albrecht and Hamilton, 1982), as it involves interactions among units with overlapping receptive fields.

A recent study by Vinje and Gallant (2000, 2002) lends support to the idea of sparsification. They recorded from V1 neurons in an awake, behaving monkey while natural image sequences obtained from free viewing were played both in and around a neuron's receptive field. They showed that when neurons are exposed to progressively more context

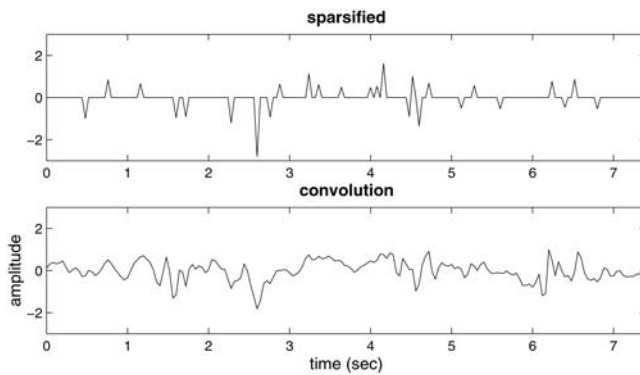


FIGURE 108.8. Coefficient signal computed by sparsification (*top*) versus convolving its corresponding basis function with the image sequence (*bottom*) for a 7.4 second image sequence (25 f/s).

around their classical receptive field, the responses become sparser. Importantly, the effect is not just an overall suppression of responses, but rather a combination of suppression and selective enhancement akin to the sparsification seen in Figure 108.8. In the model, this happens because units are effectively competing to describe the image at any given moment. With little or no context, there is more ambiguity about which basis functions are best suited to describe structure within the image, and so the activities would be expected to resemble more closely those predicted from convolution.

Before the sparse coding model can be taken seriously as a model of neural coding, however, one must address the issue of causality mentioned earlier. As it stands, the value of a coefficient at time τ is determined from image frames both prior to and after τ . But of course, real neurons cannot work this way. The model would thus need to be modified so that the value of a coefficient at time τ is determined only from image content prior to τ . This could be done by simply truncating the basis functions so that $\phi(\mathbf{x}, t) = 0$ for $t > 0$. However, it then becomes necessary to modify the dynamics of Eq. 13 so that the coefficients at time τ do not attempt to account for everything that has happened up to time τ . Otherwise, there will be no way for the basis functions to learn the continuity in images that exists from one frame to the next. More generally, there is a need to adopt a serious dynamical (differential equation) model rather than using fixed time delays, as currently formulated. These problems are the focus of current research.

COMPLEX CELLS While the receptive field of a simple cell can be mapped out in terms of its excitatory and inhibitory subfields, the receptive field of a complex cell can only be mapped out in terms of its feature selectivity—that is, orientation, spatial frequency, direction of motion, and so on. The reason is that complex cells by definition exhibit the striking nonlinearity of being locally position- or phase-

invariant. Since these neurons are insensitive to the exact alignment or polarity of an edge within their receptive fields, it is impossible to describe their responses in terms of a linear weighted sum of inputs.

Can these nonlinear response properties of complex cells also be accounted for in terms of a sparse coding model adapted to natural images? Hyvarinen and Hoyer (2000) have approached this question by assuming an architecture in which the basis function coefficients are grouped into local nonoverlapping pools. Another set of units—putative complex cells—then sums the squares of these units, one unit for each nonoverlapping pool. A sparse prior is then imposed on these units, and a set of basis functions is sought which best matches this model to natural images. After training, the “subunits” take on simple-cell-like receptive field properties (spatially localized, oriented, and bandpass), and all the units within a pool share the same orientation preference but have different phases or positions. Thus, the model seems to have learned the same sort of invariance exhibited by complex cells. On the other hand, the architecture of summing the squared outputs of subunits was assumed, and it is unclear what role this had in determining the outcome.

MODELING HORIZONTAL CONNECTIONS AND CONTEXTUAL EFFECTS Even though independence is assumed in the probabilistic models for both simple cells and complex cells above, there are still plenty of statistical dependencies among these units after adapting to natural images. Part of the reason for this is the existence of contours and other more global forms of structure in images which cannot be captured by localized receptive fields. Given that such dependencies exist among V1 neurons, what should be done?

Schwartz and Simoncelli (2001) have argued that the cortex should use its horizontal connections to remove dependencies via divisive normalization. They examined the pairwise dependencies between oriented bandpass filters and showed that although the outputs are decorrelated, they are heavily correlated in their magnitudes. They have proposed a model for reducing these magnitude correlations by dividing each output by the sum of squares of neighboring outputs. The resulting model seems to account well for contextual effects measured in V1 neurons using spatial frequency gratings.

An alternative approach is to use the horizontal connections to directly model the dependencies that exist, rather than removing them. In this scheme, units with colinear basis functions would actually reinforce each other’s activity rather than be suppressive. The idea of reinforcement is consistent with a substantial body of psychophysics (Field et al., 1993; Polat and Sagi, 1993) and physiology (Kapadia et al., 2000). There are also a number of computational models

which have been proposed along these lines for doing contour segmentation (Li, 2001; Parent and Zucker, 1989; Shashua and Ullman, 1988; Yen and Finkel, 1998), but the association connections in these models are usually set by hand and require substantial tweaking to work properly on natural images. Geisler et al. (2001) and Sigman et al. (2001) have measured the co-occurrence statistics of oriented filters on natural images and have shown that they follow a cocircularity structure, meaning that oriented units lying along the same circle are most correlated. It should be possible to incorporate these sorts of dependencies into the sparse, over-complete model by having a nonfactorial prior for the coefficients and adapting the model to images (Olshausen, 1997).

Discussion

Much of visual neuroscience has historically been guided by the question “how do neurons respond to the stimulus?” But what constitutes “the stimulus” in a natural scene is far from obvious. Indeed, years of research in machine vision have shown that the definition of a feature even as elementary as an edge or a contour is essentially an ill-posed problem, as it depends heavily on context and high-level knowledge. Nearly all of the properties of the world we experience are *inferred* from the data coming down the optic nerve, and as we have seen, inference depends on priors, and priors are built upon the statistics of natural scenes. If we accept the fact that these priors are embedded in the neural circuitry of the cortex, then modeling the structure of natural images and studying the response properties of neurons in terms of these models becomes of paramount importance to visual neuroscience.

I have described a simple probabilistic model of images based on sparse coding, and I have shown how the response properties of V1 neurons may be interpreted in terms of this model. Some support for this interpretation is provided by existing data, but the idea is still quite speculative and further tests are needed to rule completely in favor of this hypothesis. The type of experiments needed, though, are those which use natural scenes, or a reasonable facsimile thereof, as stimuli (see Chapter 107).

PROBABILISTIC MODELS AS EXPERIMENTAL TOOLS One of the objections to using natural images as experimental stimuli, often stated by neurophysiologists, is that they constitute an “uncontrolled” stimulus. But probabilistic models provide a principled way to describe the features contained in natural images, which we can then attempt to relate to the responses of neurons. One way this could be done, for example, is through the technique of *reverse correlation*. Rather than correlating neural activity directly with pixel values, as is commonly done, one could instead correlate activity with the sparsified basis function coefficients, a_i , that

are used to describe an image (i.e., the stimulus). Such an approach could potentially yield insights that could not have been obtained through reverse correlation in the pixel domain, because although the image model is linear, the coefficients are a nonlinear function of the image. Ringach et al. (2002) has recently utilized an approach along similar lines, yielding some novel findings about complex cell receptive fields.

It is also possible to run the probabilistic model in a generative mode in order to synthesize images to be used as stimuli. This is done by drawing coefficient values at random, according to the prior, and then generating either static or dynamic images according to Eqs. 2 or 12, respectively. Interestingly, even though the images being generated by this process are structured, the actual generative variables, a_i , are unstructured, so there is no need to correct for correlations in the stimulus (e.g., Theunissen et al., 2001). And in contrast to white noise, such structured images are more likely to be matched to what neurons are “looking for,” thus making it more likely that neurons will respond to a sufficient degree that they may be characterized. Comparing the results of reverse correlation obtained with synthetic images to those obtained with natural images would then enable one to determine which aspects of the latter are due to higher-order structure in natural scenes (beyond that captured by the model).

ALTERNATIVES TO SPARSENESS While sparseness has been the emphasis of this chapter, it should be mentioned that there are other optimality criteria for accounting for the response properties of visual neurons. For example, some have emphasized the role of statistical independence over sparseness and have pointed to the fact that similar results are obtained when independent component analysis (ICA) is applied to natural images (Bell and Sejnowski, 1997; van Hateren and Ruderman, 1998; van Hateren and van der Schaaf, 1998). However, the ICA algorithms used in these cases are also searching for a sparse description of data. For example, Bell and Sejnowski’s (1997) algorithm maximizes the same objective as Eq. 8, and they utilize a sparse (Laplacian) distribution for the prior when training on natural images (see Olshausen and Field, 1997, for a formal derivation of the equivalence). The algorithm used by van Hateren and van der Schaaf (1998) and van Hateren and Ruderman (1998) does not assume an explicit form for the prior but extremizes kurtosis (Hyvarinen and Oja, 1997). When trained on either static or dynamic natural images, the solution found by the algorithm has positive kurtosis, meaning that it is essentially maximizing kurtosis. Since kurtosis is also a measure of sparsity, it would thus be fair to interpret the algorithm as simply maximizing sparseness in this case.

Despite the fact that these previous applications of ICA have confounded the contributions of sparsity and indepen-

dence, it should still be possible to ascertain whether independence alone is sufficient to account for simple-cell receptive field properties. For example, Saito et al. (2000) has shown that when one constrains the basis functions to be orthonormal and minimizes the sum of marginal entropies (to maximize independence), the solution obtained is similar to that obtained by maximizing sparseness. However, the basis set was constrained here to be a member of a particular family of modulated cosine functions. When the bases are not constrained to be orthonormal, maximizing independence can lead to quite different solutions from those obtained by maximizing sparsity (for a spike process) (Saito, 2003).

Another objective that has been proposed for cortical neurons is *stability over time* (Einhauser et al., 2002; Hurri and Hyvarinen, 2003). The idea here is to impose stability on the representation in the hope that neurons will discover invariances in images. Einhauser et al. (2002) have constructed a network architecture similar to Hyvarinen and Hoyer's and have shown that when the derivative of activity is minimized, the receptive fields of subunits in the model resemble those of simple cells. Similarly, Hurri and Hyvarinen (2003) have shown that when the correlation of absolute values or squared outputs is maximized over time, the learned receptive fields also resemble simple-cell receptive fields. These results would seem to support the idea that simple-cell receptive fields also help to achieve invariant representations of time-varying natural images.

Finally, some have attempted to account for cortical receptive field properties purely from second-order statistics arising either from random activity during development (Miller, 1994) or in response to natural images (Li, 1996; Li and Atick, 1994). However, these approaches usually make some explicit assumption about the receptive field properties, such as localization or scale invariance (bandpass structure), in order to achieve properties similar to those of simple cells.

BEYOND V1 Perhaps the greatest promise of the probabilistic approach is its potential to be extended to multistage, hierarchical models of image structure (e.g., Dayan et al., 1995; Lee and Mumford, 2003; Mumford, 1994). Such models could possibly provide insight into the coding strategies used in higher visual areas such as V2 and V4. However, for the linear image model described here, nothing would be gained by simply stacking a number of such models together into a hierarchy, since they would form just another linear model. In order to gain descriptive power, some form of nonlinearity is needed. Hoyer and Hyvarinen (2002) have investigated building a two-stage hierarchical model using a complex cell type nonlinearity. They showed that when a sparse, overcomplete model is trained on the outputs of model complex cells, the learned basis functions become more elongated than those of units in the layer below. Thus, the model would appear to be grouping oriented Gabor-like

elements together into *contour units*. A different approach is taken by Karklin and Lewicki (2003), who use the second-layer units to model the variances of the first-layer units. Their model learns a number of higher-order groupings akin to Gabor functions, although the neurophysiological correlates of these functions are as yet unknown.

Beyond predicting ever more complex receptive fields, there is also the potential for hierarchical models to elucidate the role of two-way interactions that occur between levels of the visual cortical hierarchy via feedback pathways. For example, it has been proposed that feedback pathways may carry predictions from higher levels which are then subtracted from representations at lower levels (Mumford, 1994; Rao and Ballard, 1997). According to these models, the activity in lower levels would be expected to decrease when higher levels can successfully "explain" a stimulus. Recent functional magnetic resonance imaging studies lend support to this general idea, showing that activity in V1 decreases when local shape features are arranged so as to form a global percept of an object (Kersten et al., 1999; Murray et al., 2002).

Another proposed role for feedback pathways, also consistent with these findings, is that they serve to *disambiguate* representations at lower levels (Lee and Mumford, 2003; Lewicki and Sejnowski, 1997). According to this model, neural activity that initially results from the feedforward pass tends to be broadly distributed across a number of units. But as higher-level neurons provide context, activity in the lower level becomes concentrated onto a smaller number of units, similar to sparsification. Presumably, there are yet other possibilities to entertain, and so there is a strong need to develop hierarchical models that could form concrete predictions about what to look for in the cortex.

Summary

Understanding how the cortex performs pattern analysis is a central goal of visual neuroscience. In this chapter, I have presented a probabilistic approach to pattern analysis, and I have shown how it may help to explain a number of known properties of V1 receptive fields in addition to predicting certain nonlinearities (sparsification) in the responses of V1 neurons. The model described in this chapter should be viewed only as a starting point. The challenge ahead is to construct hierarchical models capable of describing higher-order structure in images (e.g., three-dimensional surfaces and occlusion) and to use these models to elucidate the types of representations employed in higher cortical areas, as well as the role of feedback projections.

Acknowledgments

I thank Marty Usrey for help with obtaining numerical estimates of cortical expansion, and I am grateful to an anonymous reviewer for helpful comments. This work was supported by NIMH Grant R29-MH57921.

REFERENCES

- Adelson, E. H., and A. P. Pentland, 1996. The perception of shading and reflectance, in *Perception as Bayesian Inference* (D. Knill and W. Richards, eds.), New York: Cambridge University Press, pp. 409–423.
- Albrecht, D. G., and W. S. Geisler, 1991. Motion selectivity and the contrast-response function of simple cells in the visual cortex, *Vis. Neurosci.*, 7:531–546.
- Albrecht, D. G., and D. B. Hamilton, 1982. Striate cortex of monkey and cat: contrast response function, *J. Neurophysiol.*, 48:217–237.
- Atick, J. J., and A. N. Redlich, 1992. What does the retina know about natural scenes? *Neural Comput.*, 4:196–210.
- Attneave, F., 1954. Some informational aspects of visual perception, *Psychol. Rev.*, 61:183–193.
- Barlow, H. B., 1961. Possible principles underlying the transformations of sensory messages, in *Sensory Communication* (W. A. Rosenblith ed.), Cambridge, MA: MIT Press, pp. 217–234.
- Barlow, H. B., 1989. Unsupervised learning, *Neural Comput.*, 1:295–311.
- Barlow, H. B., 2001. Redundancy reduction revisited, *Network: Comput. Neural Syst.*, 12:241–253.
- Baum, E. B., J. Moody, and F. Wilczek, 1988. Internal representations for associative memory, *Biol. Cybern.*, 59:217–228.
- Beaulieu, C., and M. Colonnier, 1983. The number of neurons in the different laminae of the binocular and monocular regions of area 17 in the cat, *J. Comp. Neurol.*, 217:337–344.
- Bell, A. J., and T. J. Sejnowski, 1997. The independent components of natural images are edge filters, *Vis. Res.*, 31:3327–3338.
- Chen, S. S., D. L. Donoho, and M. A. Saunders, 2001. Atomic decomposition by basis pursuit, *SIAM Rev.*, 43:129–159.
- Cherniak, C., 1995. Neural component placement, *Trends Neurosci.*, 18:522–527.
- Chklovskii, D. B., T. Schikorski, and C. F. Stevens, 2002. Wiring optimization in cortical circuits, *Neuron*, 34:341–347.
- Dan, Y., J. J. Atick, and R. C. Reid, 1996. Efficient coding of natural scenes in the lateral geniculate nucleus: experimental test of a computational theory, *J. Neurosci.*, 16:3351–3362.
- Dayan, P., G. E. Hinton, R. M. Neal, and R. S. Zemel, 1995. The Helmholtz machine, *Neural Comput.*, 7:889–904.
- DeAngelis, G. C., I. Ohzawa, and R. D. Freeman, 1993. Spatiotemporal organization of simple-cell receptive fields in the cat's striate cortex. I. General characteristics and postnatal development, *J. Neurophys.*, 69:1091–1117.
- DeAngelis, G. C., I. Ohzawa, and R. D. Freeman, 1995. Receptive-field dynamics in the central visual pathways, *Trends Neurosci.*, 18:451–458.
- De Valois, R. L., D. G. Albrecht, and L. G. Thorell, 1982. Spatial frequency selectivity of cells in macaque visual cortex, *Vis. Res.*, 22:545–559.
- Einhauser, W., C. Kayser, P. Konig, and K. P. Kording, 2002. Learning the invariance properties of complex cells from their responses to natural stimuli, *Eur. J. Neurosci.*, 15:475–486.
- Field, D. J., 1987. Relations between the statistics of natural images and the response properties of cortical cells, *J. Opt. Soc. Am. A*, 4:2379–2394.
- Field, D. J., 1993. Scale-invariance and self-similar “wavelet” transforms: an analysis of natural scenes and mammalian visual systems, in *Wavelets, Fractals, and Fourier Transforms* (M. Farge, J. Hunt, and C. Vascillicos, eds.), Oxford University Press, pp. 151–193.
- Field, D. J., 1994. What is the goal of sensory coding? *Neural Comput.*, 6:559–601.
- Field, D. J., A. Hayes, and R. F. Hess, 1993. Contour integration by the human visual system: evidence for a local “association field,” *Vis. Res.*, 33:173–193.
- Foldiak, P., 1995. Sparse coding in the primate cortex, in *The Handbook of Brain Theory and Neural Networks* (M. A. Arbib ed.), Cambridge, MA: MIT Press, pp. 895–989.
- Geisler, W. S., J. S. Perry, B. J. Super, and D. P. Gallogly, 2001. Edge co-occurrence in natural images predicts contour grouping performance, *Vis. Res.*, 41:711–724.
- Helmholtz, H. von, 1867/1962. *Treatise on Physiological Optics*, vol. III (trans. from the 3rd German ed.; J. P. C. Southall, trans.), New York: Dover.
- Hoyer, P. O., and A. Hyvarinen, 2002. A multi-layer sparse coding network learns contour coding from natural images, *Vis. Res.*, 42:1593–1605.
- Hurri, J., and A. Hyvarinen, 2003. Simple-cell-like receptive fields maximize temporal coherence in natural video, *Neural Comput.*, 15:663–691.
- Hyvarinen, A., and P. O. Hoyer, 2000. Emergence of phase and shift invariant features by decomposition of natural images into independent feature subspaces, *Neural Comput.*, 12:1705–1720.
- Hyvarinen, A., and E. Oja, 1997. A fast fixed-point algorithm for independent component analysis, *Neural Comput.*, 9:1483–1492.
- Jaeckel, L., 1989. A class of designs for a sparse distributed memory. *RIACS Technical Report 89.30*, NASA Ames Research Center, Mountain View, CA: Research Institute for Advanced Computer Science.
- Kapadia, M. K., G. Westheimer, and C. D. Gilbert, 2000. Spatial distribution of contextual interactions in primary visual cortex and in visual perception, *J. Neurophysiol.*, 84:2048–2062.
- Karklin, Y., and H. S. Lewicki, 2003. Learning higher-order structures in natural images, *Network: Computation in Neural Systems*, (in press).
- Kersten, D., L. Shen, K. Ugurbil, and P. Schrater, 1999. fMRI study of perceptual grouping using bistable stimulus, *Invest. Ophthalmol. Vis. Sci.*, 40:S820.
- Laughlin, S., 1981. A simple coding procedure enhances a neuron's information capacity, *Z. Naturforsch.*, 36:910–912.
- Lee, T. S. and D. Mumford, 2003. Hierarchical Bayesian inference in the visual cortex, *J. Opt. Soc. Am. A*, 20.
- Lewicki, M. S., and B. A. Olshausen, 1999. A probabilistic framework for the adaptation and comparison of image codes, *J. Opt. Soc. Am. A*, 16:1587–1601.
- Lewicki, M. S., and T. J. Sejnowski, 1997. Bayesian unsupervised learning of higher order structure, in *Advances in Neural Information Processing Systems*, 9, (M. Mozer, M. Jordan, and T. Petsche, eds.), Cambridge, MA: MIT Press.
- Li, Z., 1996. A theory of the visual motion coding in the primary visual cortex, *Neural Comput.*, 8:705–730.
- Li, Z., 2001. Computational design and nonlinear dynamics of a recurrent network model of the primary visual cortex, *Neural Comput.*, 13:1749–1780.
- Li, Z., and J. J. Atick, 1994. Towards a theory of striate cortex, *Neural Comput.*, 6:127–146.
- Mallat, S., 1999. *A Wavelet Tour of Signal Processing*, London: Academic Press.
- Mallat, S., and Z. Zhang, 1993. Matching pursuits with time-frequency dictionaries, *IEEE Trans. Signal Proc.*, 41:3397–3415.
- McLean, J., and L. A. Palmer, 1989. Contribution of linear spatiotemporal receptive field structure to velocity selectivity of simple cells in area 17 of cat, *Vis. Res.*, 29:675–679.
- Miller, K. D., 1994. A model for the development of simple cell receptive fields and the ordered arrangements of orientation

- columns through activity-dependent competition between ON- and OFF-center inputs, *J. Neurosci.*, 14:409–441.
- Mumford, D., 1994. Neuronal architectures for pattern-theoretic problems, in *Large Scale Neuronal Theories of the Brain* (C. Koch and J. L. Davis, eds.), Cambridge, MA: MIT Press, pp. 125–152.
- Murray, S. O., D. Kersten, B. A. Olshausen, P. Schrater, and D. L. Woods, 2002. Shape perception reduces activity in human primary visual cortex, *Proc. Nat. Acad. Sci. USA*, 99:15164–15169.
- Olshausen, B. A., 1997. A functional model of V1 horizontal connectivity based on the statistical structure of natural images, *Soc. Neurosci. Abstr.*, 23:2363.
- Olshausen, B. A., 2002. Sparse codes and spikes, in *Probabilistic Models of Perception and Brain Function* (R. P. N. Rao, B. A. Olshausen, and M. S. Lewicki, eds.), Cambridge, MA: MIT Press, pp. 257–272.
- Olshausen, B. A., and C. H. Anderson, 1995. A model of the spatial-frequency organization in primate striate cortex, in *The Neurobiology of Computation: Proceedings of the Third Annual Computation and Neural Systems Conference* (J. M. Bower ed.), Boston: Kluwer Academic, pp. 275–280.
- Olshausen, B. A., and D. J. Field, 1996a. Emergence of simple-cell receptive field properties by learning a sparse code for natural images, *Nature*, 381:607–609.
- Olshausen, B. A., and D. J. Field, 1996b. Natural image statistics and efficient coding, *Network*, 7:333–339.
- Olshausen, B. A., and D. J. Field, 1997. Sparse coding with an over-complete basis set: a strategy employed by V1? *Vis. Res.*, 37:3311–3325.
- Parent, P., and S. W. Zucker, 1989. Trace inference, curvature consistency, and curve detection, *IEEE Trans. Pattern Anal. Machine Intell.*, 11:823–839.
- Parker, A. J., and M. J. Hawken, 1988. Two-dimensional spatial structure of receptive fields in monkey striate cortex, *J. Opt. Soc. Am. A*, 5:598–605.
- Peters, A., and E. Yilmaz, 1993. Neuronal organization in area 17 of cat visual cortex, *Cereb. Cortex*, 3:49–68.
- Polat, U., and D. Sagi, 1993. Lateral interactions between spatial channels: suppression and facilitation revealed by lateral masking experiments, *Vis. Res.*, 33:993–999.
- Rao, R. P. N., and D. H. Ballard, 1997. Dynamic model of visual recognition predicts neural response properties in the visual cortex, *Neural Comput.*, 9:721–763.
- Ringach, D. L., M. J. Hawken, and R. Shapley, 2002. Receptive field structure of neurons in monkey primary visual cortex revealed by stimulation with natural image sequences, *J. Vis.*, 2:12–24.
- Ruderman, D. L., 1997. Origins of scaling in natural images, *Vis. Res.*, 37:3385–3398.
- Saito, N., 2003. The generalized spike process, sparsity, and statistical independence, in *Modern Signal Processing* (D. Rockmore and D. Healy, Jr. eds.), MSRI Publications, Cambridge University Press. [in press]
- Saito, N., B. M. Larson, and B. Benichou, 2000. Sparsity and statistical independence from a best-basis viewpoint, in *Wavelet Applications in Signal and Image Processing VIII, Proc. SPIE 4119* (A. Aldroubi, A. F. Laine, and M. A. Unser, eds.), Bellingham, WA: SPIE, pp. 474–486.
- Schwartz, O., and E. P. Simoncelli, 2001. Natural signal statistics and sensory gain control, *Nat. Neurosci.*, 4:819–825.
- Shaashua, A., and S. Ullman, 1988. Structural saliency: the detection of globally salient structures using a locally connected network, in *Proceedings of the International Conference on Computer Vision*, 2. Dec. 1988. Tarpon Springs, Florida.
- Sigman, M., G. A. Cecchi, C. D. Gilbert, and M. O. Magnasco, 2001. On a common circle: natural scenes and Gestalt rules, *Proc. Natl. Acad. Sci. USA*, 98:1935–1940.
- Simoncelli, E. P., W. T. Freeman, E. H. Adelson, and D. J. Heeger, 1992. Shiftable multiscale transforms, *IEEE Trans. Inf. Theory*, 38:587–607.
- Srinivasan, M. V., S. B. Laughlin, and A. Dubs, 1982. Predictive coding: a fresh view of inhibition in the retina, *Proc. R. Soc. Lond. B*, 216:427–459.
- Theunissen, F. E., S. V. David, N. C. Singh, A. Hsu, W. E. Vinje, and J. L. Gallant, 2001. Estimating spatio-temporal receptive fields of auditory and visual neurons from their responses to natural stimuli, *Network*, 12:289–316.
- van Hateren, J. H., 1992. A theory of maximizing sensory information, *Biol. Cybern.*, 68:23–29.
- van Hateren, J. H., 1993. Spatiotemporal contrast sensitivity of early vision, *Vis. Res.*, 33:257–267.
- van Hateren, J. H., 2000. *Natural Stimuli Collection*. <http://hlab.phys.rug.nl/archive.html>
- van Hateren, J. H., and D. L. Ruderman, 1998. Independent component analysis of natural image sequences yields spatio-temporal filters similar to simple cells in primary visual cortex, *Proc. R. Soc. Lond. B*, 265:2315–2320.
- van Hateren, J. H., and A. van der Schaaf, 1998. Independent component filters of natural images compared with simple cells in primary visual cortex, *Proc. R. Soc. Lond. B*, 265:359–366.
- Vinje, W. E., and J. L. Gallant, 2000. Sparse coding and decorrelation in primary visual cortex during natural vision, *Science*, 287:1273–1276.
- Vinje, W. E., and J. L. Gallant, 2002. Natural stimulation of the non-classical receptive field increases information transmission efficiency in V1, *J. Neurosci.*, 22:2904–2915.
- Willshaw, D. J., O. P. Buneman, and H. C. Longuet-Higgins, 1969. Nonholographic associative memory, *Nature*, 22:960–962.
- Yen, S. C., and L. H. Finkel, 1998. Extraction of perceptually salient contours by striate cortical networks, *Vis. Res.*, 38:719–741.
- Zetzsche, C., 1990. Sparse coding: the link between low level vision and associative memory, in *Parallel Processing in Neural Systems and Computers* (R. Eckmiller, G. Hartmann, and G. Hauske, eds.), Amsterdam: Elsevier Science, pp. 273–276.
- Zipf, G. K., 1950. *Human Behavior and the Principle of Least Effort*, Cambridge, MA: Addison-Wesley.

109 Local Analysis of Visual Motion

EERO P. SIMONCELLI

WE INHABIT AN EVER-changing environment in which sensing, processing, and acting on these changes can be essential for survival. When we move or when objects in the world move, the visual images projected onto our retinas change accordingly. The psychologist J. J. Gibson noted that important environmental information is embedded in this pattern of local retinal image velocities (Gibson, 1950), and thus initiated a scientific quest to understand the mechanisms that might serve to estimate and represent these velocities. Since that time, visual motion perception has been the subject of extensive research in perceptual psychology, visual neurophysiology, and computational theory.

There is an abundance of evidence that biological visual systems—even primitive ones—devote considerable resources to the processing of motion. A substantial proportion of the effort in the field of computer vision has also been devoted to the problem of motion estimation. Although the processing constraints in a biological system are somewhat different from those in an artificial vision system, each must extract motion information from the same type of brightness signal. This chapter adopts the philosophy that in order to understand visual motion processing in the brain, one should understand the nature of the motion information embedded in the visual world and the fundamental issues that arise when one attempts to extract that information (Marr and Poggio, 1977). I'll develop the most basic computational solution to the motion estimation problem, and examine the qualitative relationship between aspects of this solution and the properties of neurons in the motion pathway.

Local motion

Images are formed as projections of the three-dimensional world onto a two-dimensional light-sensing surface. This surface could be, for example, a piece of photographic film, an array of light sensors in a television camera, or the photoreceptors in the back of a human eye. At each point on the surface, the image brightness is a measurement of how much light fell on the surface at that spatial position at a particular time (or over some interval of time). When an object in the world moves relative to this projection surface, the two-dimensional projection of that object moves within the image. The movement of the projected position of each point in the world is referred to as the *motion field*.

The estimation of the motion field is generally assumed to be the first goal of motion processing in machine vision systems. There is also evidence that this sort of computation is performed by biological systems. The motion field must be estimated from the spatiotemporal pattern of image brightness. This is usually done by assuming that the brightness generated by points in the world remain constant over time. In this case, the estimated motion of these constant-brightness points (known as the *optical flow*) is also an estimate of the motion field. But as many authors have shown, the optical flow is *not* always a good estimate of the motion field (e.g., Horn, 1986; Verri and Poggio, 1989). For example, when a shiny object moves, specular highlights often move across the surface of the object. In this situation, the optical flow (corresponding to the highlight motion) does not correspond to the motion of any point on the object. Nevertheless, estimates of optical flow are almost universally used as approximations of the motion field.

In estimating optical flow, we cannot ask about the motion of an isolated point without considering the context surrounding it. That is, we can only recognize the motion of local *patterns* of brightness. But our ability to estimate a unique velocity at a given image location depends critically on the structure of the image in the neighborhood of that location. Consider first the simplest situation, in which an object is moving horizontally, perpendicular to the line of sight. Figure 109.1 depicts three prototypical situations that can arise. First, the local brightness might be constant. In this case, the local measurements places no constraint on the velocity. We will refer to this as the *blank-wall* problem.

Second, the local brightness might vary in only one direction—that is, the spatial pattern could be striped. In this case, only the velocity component that is perpendicular to the stripes is constrained. Any component along the stripes will not create a change in the image and thus cannot be estimated. This is typically known in the literature as the *aperture problem* (Fennema and Thompson, 1979; Marr and Ullman, 1981; Wallach, 1935). The expression refers to the fact that the motion of a moving one-dimensional pattern viewed through a circular aperture is ambiguous. The problem is not due to the aperture but arises from the one-dimensionality of the signal.

Finally, the local brightness may vary two-dimensionally, in which case the optic flow vector is uniquely constrained. But because of the occurrence of underconstrained regions

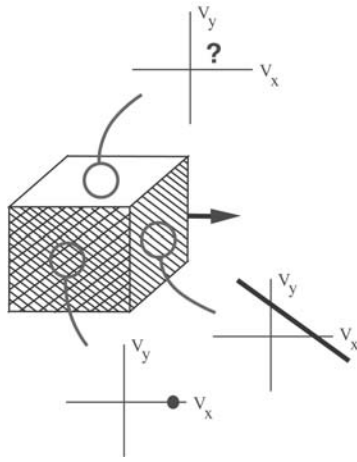


FIGURE 109.1. Conceptual illustration of motion estimation in three different regions of an image of a horizontally translating cube. In a region of constant brightness (top face of the cube), the local velocity is completely unconstrained since the observed image is not changing over time. We refer to this as the *blank-wall* problem. In a region where the brightness varies only along a unique spatial direction (striped side of the cube), the brightness changes are consistent with a one-dimensional set of velocities: one can determine the motion perpendicular to the stripes but *not* the motion along the stripes. This is known as the *aperture* problem. Finally, in a region where the brightness changes in all spatial directions (hatched side of the cube), a unique velocity is consistent with the observed brightness changes.

(blank-wall and aperture problems), a full solution for the motion problem in which all image points are assigned a velocity vector seems to require the integration of information across spatial neighborhoods of the image (and perhaps over time as well). This concept has been studied and developed for many years in computer vision (e.g., Hildreth, 1984; Horn and Schunck, 1981; Lucas and Kanade, 1981).

In addition to the blank-wall and aperture problems, in which the velocity is underconstrained, there are often locations in an image at which multiple velocity signals interact. In particular, this can occur at occlusion boundaries of objects, where any local spatial neighborhood must necessarily include some portion of both object and background, which are typically moving differently. Another example occurs in the presence of transparently combined surfaces or specular highlights. In each of these cases, the local motion description requires more than one velocity, along with some sort of assignment of which image content belongs to which velocity.

Solutions for the multiple-motion problem have been developed fairly recently. Specifically, a number of authors have proposed that one should simultaneously decompose the image into consistently moving layers of brightness content and estimate the motions within those layers (Ayer and Sawhney, 1995; Darrell and Pentland, 1995; Wang and Adelson, 1994; Weiss and Adelson, 1996). Some authors

have suggested that this sort of solution might be implemented biologically (Darrell and Simoncelli, 1994; Koehlin et al., 1999; Nowlan and Sejnowski, 1995).

We'll return to this point in the "Discussion" section, but for most of the chapter, we'll restrict our attention to the simple case of translational motion over a local patch of the image, ignoring the possibility of multiple motions. As in much of the computational motion literature, we view this as a building block that could be combined with further processing to provide a more complete solution for the analysis of motion. The goal of this chapter is to introduce a framework for thinking about motion and to interpret the components of that framework physiologically.

Computational framework

The problem of motion estimation may be formalized using well-developed tools of estimation theory. Specifically, we adopt a Bayesian framework, one of the simplest and most widely used in the engineering literature. Bayesian approaches have also been used to model various aspects of visual perception (e.g., see Knill and Richards, 1996).

BRIGHTNESS CONSTANCY In any estimation problem, the most essential ingredient is the relationship between the thing one is trying to estimate and the measurements that one makes. In most motion estimation schemes, this relationship comes from the *brightness constancy assumption* (Horn and Schunck, 1981): changes in image brightness are a result of translational motion in the image plane. When expressed mathematically, this gives a relationship between image values and the local velocity:

$$I(x + u\Delta t, y + w\Delta t, t + \Delta t) = I(x, y, t),$$

where u and w are the horizontal and vertical components of the image velocity at position (x, y) and time t . Assuming that the temporal interval Δt is small enough that the left side may be approximated by a Taylor series expansion up to first order, we can replace this with a differential version of the brightness constancy assumption:

$$I_x u + I_y w + I_t = 0, \quad (1)$$

where (I_x, I_y) are the spatial derivatives and I_t the temporal derivative of the image brightness. Note that this equation still corresponds to a particular position and moment in time: we've dropped the arguments (x, y, t) to simplify the notation.

Although the signal I is usually considered to represent the image brightness, the formulation may be generalized. In particular, one can use any function locally derived from the image brightness. For example, one could prefilter the image with a bandpass filter to enhance information at certain frequencies, one could use a point nonlinearity (e.g., logarithm) to reduce the dynamic range of the input, or one could compute a measure of local contrast by dividing by the local

mean. Under such modifications, equation 1 should be interpreted as expressing the constancy of some other (non-brightness) attribute. As such, the usual brightness-based motion estimator may be easily converted into a so-called second-order or “non-Fourier” motion estimator, as has been proposed by a number of authors (e.g., Chubb and Sperling, 1988; Fleet and Langley, 1994; Wilson and Kim, 1994).

Furthermore, the computation of derivatives of discretized images requires one to first perform some local integration by prefiltering with a lowpass filter. The differentiation and filtering operations may be combined, so that derivatives are effectively computed by convolution with the derivative of the prefilter (Simoncelli, 1993). In computer vision, for example, derivatives are often computed using the derivatives of a Gaussian function.

LOCAL COMBINATION OF CONSTRAINTS Equation (1) cannot be solved for the two components of velocity, since it imposes only a single linear constraint. This is simply a differential manifestation of the aperture problem: the derivative measurements characterize the local brightness values in terms of their variation along a single direction (the gradient direction), and thus only the component of velocity in this direction can be estimated. In order to estimate the velocity completely, we must impose further constraints on the problem. A simple solution is to assume that the velocity field is smooth (Horn and Schunck, 1981), or that it is constant over a small spatial neighborhood surrounding the location of interest (Lucas and Kanade, 1981), and to combine the constraints over that region. Alternatively, or in conjunction with the spatial combination, one can combine constraints arising from differently filtered versions of the image (e.g., Nagel, 1983). Many authors have described more sophisticated choices of combination rule (e.g., Black, 1992; Hildreth, 1984), but we will use this simplest form of spatial combination in this chapter.

MEASUREMENT NOISE Next, we assume that the derivative measurements are corrupted by a small amount of noise, as must be true in any real system. For computational convenience, we assume that the noise is additive and that the values are distributed according to a Gaussian probability density. Although this simple noise model is unlikely to be correct in detail (in particular, it is not a very accurate description of the noise in neural responses), it is sufficient to illustrate the fundamental issues of motion estimation.

Mathematically, we write

$$I_x u + I_y w + I_t = n,$$

where n is a random variable representing the noise. This enables us to write the probability of observing the spatiotemporal image structure assuming a given velocity:

$$P(I|u, w) \propto \exp\left[-(I_x u + I_y w + I_t)^2 / (2\sigma_n^2)\right],$$

where σ_n indicates the standard deviation of the noise variable n . Empirically, de Ruyter (2002) measured the relationship between gradient measurements and translational velocity in video footage gathered from a head-mounted camera, and found that it is roughly consistent with this formulation.

Now, as described previously, we combine the constraints over a small spatial region, in which we assume the velocity vector is constant and the noise variables are independent:

$$P(I|u, w) \propto \exp\left(-\sum (I_x u + I_y w + I_t)^2 / (2\sigma_n^2)\right) \quad (2)$$

where the sum combines the measurements at all locations within the neighborhood.

PRIOR PROBABILITY DISTRIBUTION ON VELOCITY Equation (2) describes the *likelihood function*: the probability of observing a spatiotemporal image pattern given a velocity (u, w) . In Bayesian estimation, one reverses this conditionalization using Bayes' rule in order to get the *posterior* distribution:

$$P(u, w|I) = \frac{P(I|u, w) P(u, w)}{\int du \int dw P(I|u, w) P(u, w)}. \quad (3)$$

The probability density $P(u, w)$ is known as the *prior*: it describes the probability of observing each velocity (independent of any particular image measurements).

For the prior probability distribution, we again make a choice of mathematical convenience: we assume that $P(u, w)$ is Gaussian with zero mean:

$$P(u, w) \propto \exp(-\|u^2 + w^2\| / 2\sigma_v^2). \quad (4)$$

As in the choice of the noise model, this may not be an accurate characterization of the distribution of image velocities that an organism would encounter in the world, but it suffices to capture the main aspects of a reasonable solution to the motion estimation problem. The intuition is that in the absence of any specific image information (e.g., in a dark room), one should assume that things are not moving. More generally, the model proposes that slow velocities occur more frequently than fast ones. This hypothetical property of the environment is mirrored by the long-standing hypothesis that the perceived motion of stimuli corresponds to the slowest motion consistent with the observed image information (see references in Ullman, 1979). In particular, Wallach (1935) proposed that humans tend to see line segments as moving in a direction normal to their orientation because the velocity associated with that direction is the slowest of all velocities consistent with the image information.

Combining equations 2 and 4, as specified in equation 3 gives the posterior distribution

$$P(u, w|I) \propto \exp\left[-(u^2 + w^2) / 2\sigma_v^2 - \sum (I_x u + I_y w + I_t)^2 / 2\sigma_n^2\right]. \quad (5)$$

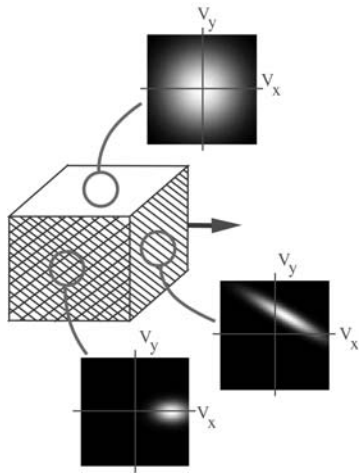


FIGURE 109.2. Illustration of posterior probability densities for the example shown in Figure 109.1.

This specifies a Gaussian distribution over (u, w) whose behavior is illustrated in Figure 109.2. Note that the distribution captures the uncertainties shown in the conceptual illustrations of Figure 109.1. In particular, the posterior density for the blank region is quite broad (it is identical to the prior). In the striped region, the density is elongated and lies along the line that defines the set of velocities consistent with the image constraints. The width along this line is determined by the prior variance, σ_v^2 . The width perpendicular to the line is determined by the noise variance, σ_n^2 , as well as the image contrast. And in the patterned region, the density is much more compact and centered on the correct horizontal velocity.

Physiological interpretation

A Bayesian model is appealing because of its generality and its construction from a relatively small number of realistic assumptions. It can be implemented in a distributed analog network (Stocker, 2001), and has been used in machine vision applications. In previous work, we have shown that the mean (equivalently, the maximum) of the Gaussian posterior distribution described by equation 5 provides a surprisingly good match to human perception of velocity for a variety of translating stimuli (Heeger and Simoncelli, 1993; Simoncelli, 1993; Weiss, 1998; Weiss et al., 2002). In this section, I'll describe the relationship between the elements of this framework and the functional properties of neurons that lie in the *motion pathway* of mammals such as cats or monkeys. This should not be thought of as a quantitative physiological model of motion processing, but rather as a more qualitative assignment of computational function to neural populations along the motion pathway.

We'll work backward through the system, starting from the posterior distribution of equation 5. If we hold the veloc-

ity (u, w) fixed, then this function is "tuned" for the velocity of the input image. That is, it is maximized when the underlying image structure is consistent with the velocity (u, w) , and it decreases as the image motion deviates from that velocity. We may identify this basic property with those neurons in visual area MT that are known as *pattern selective* (Movshon et al., 1986; Chapter 81). These neurons are tuned for retinal image velocity; they respond vigorously to a visual stimulus moving with a particular speed and direction, and are relatively indifferent to the stimulus' spatial pattern (Maunsell and van Essen, 1983; Movshon et al., 1986; Rodman and Albright, 1987).

A number of models posit that a population of such neurons provides a distributed representation of velocity (Grzywacz and Yuille, 1990; Heeger, 1987; Koch et al., 1989; Nowlan and Sejnowski, 1995; Simoncelli, 1993; Simoncelli and Heeger, 1998). Here we assume that the responses within this population correspond directly to samples of the posterior density. That is, the response of each neuron corresponds to equation 5 evaluated at a different "preferred" velocity (u, w) . Note that in this interpretation, no single neuron encodes the velocity of the stimulus, and an actual estimate of the velocity can be obtained only by combining information across the population. For example, one could compute the mean velocity by summing the preferred velocities of all of the neurons in the population, each weighted by the response of that neuron. Also note that in this interpretation, the prior distribution, $P(u, w)$, provides only a gain adjustment (multiplicative scale factor) on each of the neural response. The integral over (u, w) in the denominator of equation 3 corresponds to a sum over the responses of all neurons in the population. We have previously shown that this kind of divisive normalization operation is consistent with the response properties of MT neurons (Simoncelli and Heeger, 1998).

We can make a qualitative comparison of this model to typical neural responses in area MT. The lower left panel of Figure 109.3 shows polar plots of the response of a model MT neuron with preferred velocity $u = 0.3$, $w = 0$ pixels per frame as a function of the normal direction of a drifting sinusoidal grating. As with MT pattern cells (Movshon et al., 1986), the response is tuned for the direction of motion and is largest when this direction matches the preferred direction. The lower right panel shows the response as a function of direction for a "plaid" stimulus, constructed as the sum of two drifting gratings 120 degrees apart. The response is largest when this plaid stimulus is moving rightward, a configuration in which the two constituent gratings are moving at ± 60 degrees from rightward. This response to the direction of pattern motion (rather than to the two component directions) is a characteristic used to identify MT pattern cells (Movshon et al., 1986).

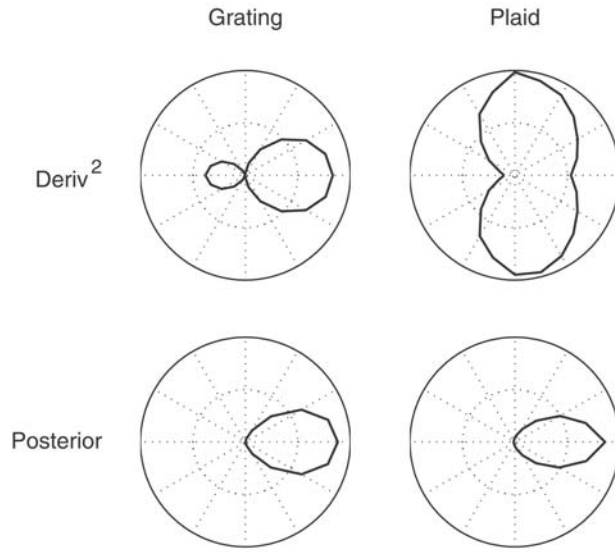


FIGURE 109.3. Direction tuning curves for model components. *Upper left*: model V1 neuron (squared directional derivative) response to a drifting sinusoidal grating; *upper right*: model V1 neuron response to a drifting sinusoidal plaid; *lower left*: model MT neuron (posterior probability) response to a grating; *lower right*: model MT neuron response to plaid.

Figure 109.4 shows the posterior function plotted as a function of stimulus speed (again for a drifting sinusoidal grating). The maximum response occurs at 0.3 pixel per frame, the speed corresponding to the chosen (u, w) . At half height, the curve spans a speed range of about 2 octaves, which is roughly comparable to the responses of some MT cells (Maunsell and van Essen, 1983).

Having identified the posterior distribution with MT pattern responses, we now want to consider the components

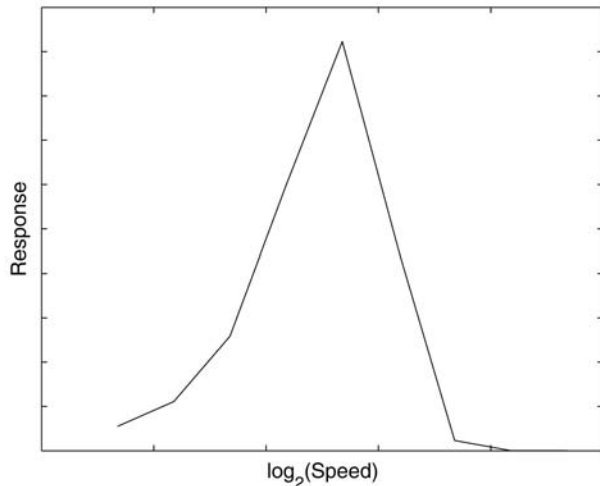


FIGURE 109.4. Speed tuning curve for posterior distribution (model MT neuron) to a drifting sinusoidal grating. The absolute scale of the horizontal axis is arbitrary, but the tick marks correspond to increments of speed by multiples of 2.

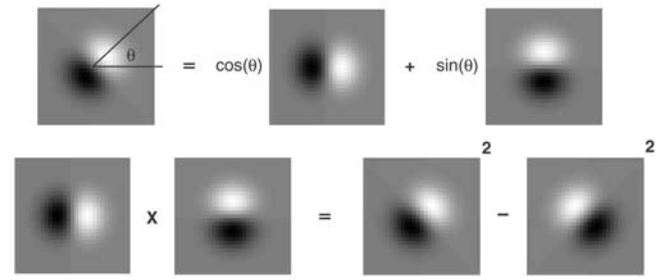


FIGURE 109.5. Illustration of two identities relating separable and oriented derivative operations. *Top*: A spatial derivative operator at any orientation may be computed as a linear combination of separable (axis-aligned) derivative operators (Eq. 7). *Bottom*: A product of X and Y derivatives may be computed as the difference of two squared, obliquely oriented derivatives (Eq. 6). Operators in both cases are Gaussian derivatives, but the identities hold for derivatives of other functions as well.

(i.e., the *afferents*) from which those responses are generated. The exponent of equation 5 may be expanded (dropping a factor of 2) as follows:

$$f(I, u, w) = - \sum [u^2 I_x^2 + 2uw I_x I_y + w^2 I_y^2 + 2u I_x I_t + 2w I_y I_t + I_t^2] / \sigma_n^2 + [u^2 + w^2] / \sigma_v^2,$$

where the sum is taken over a small spatial neighborhood. Many of the terms contain squared image derivatives, and those that contain products of image derivatives may be written as a difference of two squared derivatives. For example:

$$I_x I_y = [(I_x + I_y)^2 - (I_x - I_y)^2] / 4 = [I_{d1}^2 - I_{d2}^2] / 4, \quad (6)$$

where I_{d1} and I_{d2} are derivatives at angles 45 degrees and -45 degrees, respectively. In general, a derivative at any orientation may be constructed via a suitable combination of axis-aligned (separable) derivative operators (Freeman and Adelson, 1991):

$$I_\theta = \cos(\theta) I_x + \sin(\theta) I_y, \quad (7)$$

where I_θ is a derivative in direction θ . The mathematical relationships of equations 6 and 7 are illustrated in Figure 109.5.

An analogous transformation allows us to write the term containing $I_x I_t$ as a difference of two derivatives. Since one of the axes is now time, the result is a difference of space-time oriented derivatives, I_r and I_l , which are most responsive to vertically oriented structures that are moving rightward/leftward. This construction, known as an *opponent motion* computation, has been previously proposed as an explanation for a number of psychophysical phenomena (Adelson and Bergen, 1985). Similarly, the product $I_y I_t$ results in a difference of squared upward and downward derivatives I_u and I_d . Combining all of this allows us to write the exponent as

$$f(I, u, w) = -\frac{1}{\sigma_n^2} \sum u^2 (I_x^2 + \sigma_n^2 / \sigma_v^2) + uw (I_{d1}^2 - I_{d2}^2) / 2 \\ + w^2 (I_y^2 + \sigma_n^2 / \sigma_v^2) + u (I_r^2 + I_l^2) / 2 \\ + w (I_u^2 - I_d^2) / 2 + I_t^2. \quad (8)$$

The purpose of these transformations is to show that the computation of the posterior is based on a sum of terms that could arise in the responses of primary visual cortical neurons. The receptive fields of so-called *simple* cells in primary visual cortex (area V1) of cats and monkeys are selective for stimulus position and orientation (Hubel and Wiesel, 1962; Chapter 43). Many simple cells are also direction-selective: they give stronger responses for stimuli moving in one direction than in the opposite direction (Chapter 44). Many authors have characterized simple cell responses as the halfwave-rectified (and sometimes squared) responses of linear receptive fields (e.g., Campbell et al., 1968, 1969; Daugman, 1985; Heeger, 1992; Movshon et al., 1978). In these models, the neuronal response is derived from a weighted sum (over local space and recent past time) of the local stimulus contrast. This type of model can explain the primary properties of these cells, including selectivity for stimulus orientation, spatial frequency, temporal frequency, and direction.

The linear derivative filters used in our Bayesian motion estimator (as shown in Fig. 109.5) bear some similarity to the response properties of simple cells: they are tuned for spatial orientation, spatial frequency, temporal frequency, and direction. Example direction tuning curves of squared derivative operators for both gratings and plaids are shown in the top row of Figure 109.3. Note that, as in V1 neurons, the response to the plaid is bimodal: unlike the posterior response shown in the bottom row, the operator responds to each of the components of the plaid rather than to the pattern as a whole.

In general, tuning of first-derivative operators for most variables is significantly broader than that of most simple cells. We have shown in previous work that this inconsistency is easily corrected through the use of higher-order derivative operators (Heeger and Simoncelli, 1993; Simoncelli, 1993; Simoncelli and Heeger, 1998). The Bayesian solution given above may be rederived using such operators, and the form of the result is essentially the same despite the proliferation of terms in the equations.

Also prevalent in the primary visual cortex are *complex* cells, which exhibit similar selectivity for orientation, spatial, frequency temporal frequency, and direction but which are more nonlinear in their response properties. In particular, their responses are relatively insensitive to the precise location of stimuli within their receptive fields. Models of these cells have been based on local oriented *energy*, computed as the sum of squared responses of even- and odd-symmetric

oriented linear filters (e.g., Adelson and Bergen, 1985). In the Bayesian model of this paper, this type of construction could be achieved by combining the constraints obtained from differently filtered versions of the input image. Alternatively, this translation invariance of responses is approximately achieved with a sum of squared linear responses over a local spatial neighborhood, as in equation 8. Summarizing, the posterior distribution of our Bayesian model is constructed from building blocks that resemble direction-selective complex cells. This parallels the physiology, where it has been shown that the neurons that project from area V1 to MT are direction-selective complex cells (Movshon and Newsome, 1996).

Finally, we need to address the construction of the spatiotemporally oriented V1 responses from the primary afferents arriving from the lateral geniculate nucleus. These responses are generally not orientation-tuned and they are not directional (in cats and monkeys). Specifically, the receptive fields are described by a product of a spatial (center-surround) weighting function and a temporal weighting function (Chapter 35). In the context of the Bayesian model, spatial derivative computation (to produce orientation-selective receptive fields) can be obtained by spatial combination of lateral geniculate nucleus receptive fields, as has been suggested physiologically (Hubel and Wiesel, 1962; Reid and Alonso, 1995). A number of authors have suggested that directional responses may be constructed physiologically by superimposing an appropriate set of space-time separable responses (e.g., Adelson and Bergen, 1985; Fahle and Poggio, 1981; Watson and Ahumada, 1983). In the case of the directional derivatives used in this chapter, one need only sum a spatial and temporal derivative operator (with the correct weighting) to obtain a spatiotemporally oriented derivative operator selective for any desired orientation. This construction is made explicit in equation 7 and illustrated in the top panel of Figure 109.5.

Discussion

We have provided a Bayesian analysis for local motion based on a minimal set of assumptions: (1) brightness conservation, (2) a simple model of measurement noise, and (3) a prior preference for slower speeds. Given these assumptions, the components of the optimal solution can be seen to have properties qualitatively matching those of neurons in the mammalian motion pathway.

In previous work, we have shown that this model accounts for a surprising number of psychophysical results demonstrating nonveridical perception of motion stimuli (Weiss et al., 2002). We have also shown that an elaborated variant of this model can be fit more precisely to neural response properties (Simoncelli and Heeger, 1998). In that model, narrower V1 stage tuning curves are achieved through use

of higher-order derivatives, and nonlinear properties of V1 responses are incorporated using divisive normalization.

The particular Bayesian model described in this chapter is the simplest of its kind. A more correct model should include a more realistic model of uncertainty in photoreceptors, as well as in subsequent neural responses. It should also include a prior that more accurately reflects the velocity distribution in the visual environment (although this is quite difficult to model, given that it depends not just on the environment, but also on the motion of the organism). Such modifications are unlikely to lead to qualitatively different behaviors of the solution, but they may produce a more accurate account of the physiology.

Finally, the formulation of the motion estimation problem using brightness constancy is simplistic in assuming that a single translational velocity accounts for the motion in each local region. As described earlier, this assumption is violated in real scenes near occlusion boundaries and in the presence of transparent surfaces. Studies in computer vision have suggested that segmentation or grouping of the scene must be tightly integrated with the motion estimation solution, and a number of authors have proposed joint solutions (e.g., Ayer and Sawhney, 1995; Darrell and Pentland, 1995; Wang and Adelson, 1994; Weiss and Adelson, 1996). These solutions are invariably recurrent, perhaps suggesting that physiological implementations will require recurrent lateral or feedback projections between two neural populations computing velocity and grouping.

Acknowledgments

Thanks to J. Pillow and A. Stocker for helpful comments on the manuscript. The author is supported by the Howard Hughes Medical Institute and the Sloan-Swartz Center for Theoretical Visual Neuroscience at New York University.

REFERENCES

- Adelson, E. H., and J. R. Bergen, 1985. Spatiotemporal energy models for the perception of motion, *J. Opt. Soc. Am. A*, 2:284–299.
- Ayer, S., and H. Sawhney, 1995. Layered representation of motion video using robust maximum-likelihood estimation of mixture models and mdl encoding, in *Proceedings of the International Conference on Computer Vision*, Cambridge, MA: IEEE Computer Society.
- Black, M. J., 1992. A robust gradient method for determining optical flow, in *IEEE Conference on Computer Vision and Pattern Recognition*, Champaign-Urbana: IEEE Computer Society.
- Campbell, F. W., B. G. Cleland, G. F. Cooper, and C. Enroth-Cugell, 1968. The angular selectivity of visual cortical cells to moving gratings, *J. Physiol. (Lond.)*, 198:237–250.
- Campbell, F. W., G. F. Cooper, and C. Enroth-Cugell, 1969. The spatial selectivity of visual cells of the cat, *J. Physiol. (Lond.)*, 203:223–235.
- Chubb, C., and G. Sperling, 1988. Drift-balanced random stimuli: a general basis for studying non-fourier motion perception, *J. Opt. Soc. Am. A*, 5:1986–2006.
- Darrell, T., and A. Pentland, 1995. Cooperative robust estimation using layers of support, *IEEE Trans. Pattern Anal. Mach. Intell.*, 17:474–487.
- Darrell, T., and E. Simoncelli, 1994. Separation of transparent motion into layers using velocity-tuned mechanisms, in *European Conference on Computer Vision*, Springer-Verlag. Also available as MIT Media Laboratory Vision and Modeling Technical Report 244.
- Daugman, J. G., 1985. Uncertainty relation for resolution in space, spatial frequency, and orientation optimized by two-dimensional visual cortical filters, *J. Opt. Soc. Am. A*, 2:1160–1169.
- de Ruyter, R., 2002. Personal Communication.
- Fahle, M., and T. Poggio, 1981. Visual hyperacuity: spatiotemporal interpolation in human vision, *Proc. R. Soc. Lond. B*, 213:451–477.
- Fennema, C. J., and N. Thompson, 1979. Velocity determination in scenes containing several moving objects, *Computer Graphics and Image Processing*, 9:301–315.
- Fleet, D. J., and K. Langley, 1994. Computational analysis of non-fourier motion, *Vis. Res.*, 22:3057–3079.
- Freeman, W. T., and E. H. Adelson, 1991. The design and use of steerable filters, *IEEE Pattern Anal. Mach. Intell.*, 13:891–906.
- Gibson, J. J., 1950. *The Perception of the Visual World*, Boston: Houghton Mifflin.
- Grzywacz, N. M., and A. L. Yuille, 1990. A model for the estimate of local image velocity by cells in the visual cortex, *Proc. R. Soc. Lond. A*, 239:129–161.
- Heeger, D. J., 1987. Model for the extraction of image flow, *J. Opt. Soc. Am. A*, 4:1455–1471.
- Heeger, D. J., 1992. Half-squaring in responses of cat simple cells, *Vis. Neurosci.*, 9:427–443.
- Heeger, D. J., and E. P. Simoncelli, 1993. Model of visual motion sensing, in *Spatial Vision in Humans and Robots* (L. Harris and M. Jenkin, eds.), Cambridge: Cambridge University Press. Also available as MIT Media Laboratory Vision and Modeling Technical Report #191.
- Hildreth, E. C., 1984. Computations underlying the measurement of visual motion, *Artif. Intell.*, 23:309–355.
- Horn, B. K. P., 1986. *Robot Vision*. Cambridge, MA: MIT Press.
- Horn, B. K. P., and B. G. Schunck, 1981. Determining optical flow, *Artif. Intell.*, 17:185–203.
- Hubel, D., and T. Wiesel, 1962. Receptive fields, binocular interaction, and functional architecture in the cat's visual cortex, *J. Physiol. (Lond.)*, 160:106–154.
- Knill, D., and W. Richards, 1996. *Perception as Bayesian Inference*. Cambridge: Cambridge University Press.
- Koch, C., H. Wang, and B. Mathur, 1989. Computing motion in the primate's visual system, *J. Exp. Biol.*, 146:115–139.
- Koechlin, E., J. L. Anton, and Y. Burnod, 1999. Bayesian inference in populations of cortical neurons: a model of motion integration and segmentation in area MT, *Biol. Cybern.*, 80:25–44.
- Lucas, B. D., and T. Kanade, 1981. An iterative image registration technique with an application to stereo vision, in *Proceedings of the 7th International Joint Conference on Artificial Intelligence*. Vancouver: William Kaufman Inc., pp. 674–679.
- Marr, D., and T. Poggio, 1977. From understanding computation to understanding neural circuitry, *Neurosci. Res. Prog. Bull.*, 15:470–488.
- Marr, D., and S. Ullman, 1981. Directional selectivity and its use in early visual processing, *Proc. R. Soc. Lond. B*, 211:151–180.

- Maunsell, J. H. R., and D. C. van Essen, 1983. Functional properties of neurons in middle temporal visual area of the macaque monkey I. Selectivity for stimulus direction, speed, and orientation, *J. Neurophysiol.*, 49:1127–1147.
- Movshon, J. A., E. H. Adelson, M. S. Gizzi, and W. T. Newsome, 1986. The analysis of moving visual patterns, in *Experimental Brain Research Supplementum II: Pattern Recognition Mechanisms* (C. Chagas, R. Gattass, and C. Gross, eds.), New York: Springer-Verlag, pp. 117–151.
- Movshon, J. A., and W. T. Newsome, 1996. Visual response properties of striate cortical neurons projecting to area MT in macaque monkeys, *Vis. Neurosci.*, 16:7733–7741.
- Movshon, J. A., I. D. Thompson, and D. J. Tolhurst, 1978. Spatial summation in the receptive fields of simple cells in the cat's striate cortex, *J. Physiol. (Lond.)*, 283:53–77.
- Nagel, H. H., 1983. Displacement vectors derived from second order intensity variations in image sequences, *Comput. Vis. Pattern Recog. Image Proc.*, 21:85–117.
- Nowlan, S. J., and T. J. Sejnowski, 1995. A selection model for motion processing in area MT of primates, *J. Neurosci.*, 15:1195–1214.
- Reid, R. C., and J. M. Alonso, 1995. Specificity of monosynaptic connections from thalamus to visual cortex, *Nature*, 378:281–284.
- Rodman, H. R., and T. D. Albright, 1987. Coding of visual stimulus velocity in area MT of the macaque, *Vis. Res.*, 27:2035–2048.
- Simoncelli, E. P., 1993. Distributed analysis and representation of visual motion. Ph.D. thesis, Department of Electrical Engineering and Computer Science, Massachusetts Institute of Technology, Cambridge, MA.
- Simoncelli, E. P., and D. J. Heeger, 1998. A model of neuronal responses in visual area MT, *Vis. Res.*, 38:743–761.
- Stocker, A. A., 2001. Constraint optimization networks for visual motion perception—analysis and synthesis. Ph.D. thesis no. 14360, Swiss Federal Institute of Technology, Zürich, Switzerland.
- Ullman, S., 1979. *The Interpretation of Visual Motion*. Cambridge, MA: MIT Press.
- Verri, A., and T. Poggio, 1989. Motion field and optical flow: qualitative properties, *IEEE Pattern Anal. Mach. Intell.*, 11(5):490–498.
- Wallach, H., 1935. Über visuell wahrgenommene bewegungsrichtung, *Psychologische Forschung*, 20:325–380.
- Wang, J. Y., and E. H. Adelson, 1994. Representing moving images with layers, *IEEE Trans. Image Proc.*, 3:625–638.
- Watson, A. B., and A. J. Ahumada, 1983. A look at motion in the frequency domain, in *Motion: Perception and Representation* (J. K. Tsotsos ed.), New York: Association for Computing Machinery.
- Weiss, Y., 1998. Bayesian motion estimation and segmentation. Ph.D. thesis, Department of Brain and Cognitive Sciences, Massachusetts Institute of Technology, Cambridge, MA.
- Weiss, Y., and E. H. Adelson, 1996. A unified mixture framework for motion segmentation: incorporating spatial coherence and estimating the number of models, *Proceedings of the IEEE Conference on Computer Vision and Pattern Recognition*, pp. 321–326.
- Weiss, Y., E. P. Simoncelli, and E. H. Adelson, 2002. Motion illusions as optimal percepts, *Nat. Neurosci.*, 5:598–604.
- Wilson, H. R., and J. Kim, 1994. A model for motion coherence and transparency, *Vis. Neurosci.*, 11:1205–1220.

110 Visual Boundaries and Surfaces

STEPHEN GROSSBERG

Visual boundaries and surfaces and complementary cortical streams

Visual perception is highly context-sensitive. A visual scene cannot be easily understood by evaluating it just in terms of its local contrasts or individual pixels. It is better understood as a juxtaposition of objects which may mutually occlude one another in a scene or picture. Much evidence suggests that these objects are represented in terms of two types of information: boundaries and surfaces. This chapter reviews aspects of how and why this happens.

Where are visual boundaries and surfaces computed in the brain? Figure 110.1 summarizes three processing streams within the visual cortex that are activated by light impinging on the retina. One stream goes from the retina through the lateral geniculate nucleus (LGN) parvo stage (classified due to its parvocellular cell type) to the cortical processing stages V1 interblob, V2 interstripe, V4, and then to inferotemporal cortex. Another stream goes from retina through LGN parvo, V1 blob, V2 thin stripe, V4, and then again to inferotemporal cortex. A third stream goes from retina through LGN magno (classified due to its magnocellular cell type) to cortical processing layer 4B in area V1, V2 thick stripes, MT, and then parietal cortex. The interblob and blob streams are proposed to compute properties of visual boundaries and surfaces, respectively. Many experiments support this view (e.g., Elder and Zucker, 1998; Field et al., 1993; He and Nakayama, 1995; Lamme et al., 1999; Rogers-Ramachandran and Ramachandran, 1998).

The existence of such streams has led many scientists to conclude that our brains process perceptual qualities such as visual form, color, and motion using different *independent modules*. If the processing streams were independent modules, they could fully compute their particular processes on their own. In contrast, much perceptual data describe strong interactions between perceptual qualities. For example, changes in an object's perceived form or color can cause changes in its perceived motion, and vice versa, while changes in an object's perceived brightness can cause changes in its perceived depth, and vice versa (Egusa, 1983; Faubert and von Grünau, 1995; Kanizsa, 1974; Pessoa et al., 1996; Smallman and McKee, 1995). If geometrical properties like color, form, and depth are not computed indepen-

dently, then what is the geometry by which we really see the world?

Many data suggest that the brain's processing streams compute *complementary* properties (e.g., Grossberg, 2000). Each stream's properties are related to those of a complementary stream much as a key fits its lock or two pieces of a puzzle fit together. We are all familiar with complementarity principles in physics, such as the famous Heisenberg Uncertainty Principle of quantum mechanics, which notes that precise measurement of a particle's position forces uncertainty in measuring its momentum, and vice versa. As in physics, the mechanisms that enable each stream in the brain to compute one set of properties prevent it from computing a complementary set of properties. Each stream exhibits complementary strengths and weaknesses. How, then, do these complementary properties get synthesized into a consistent behavioral experience?

Neural models clarify how *interactions* between these processing streams overcome their complementary deficiencies and generate behavioral properties that realize the unity of conscious experiences. *Pairs* of complementary streams are the functional units that interact together in order to compute unambiguous information about the world. Such interactions may be used to explain many of the ways in which perceptual qualities are known to influence each other. Thus, although analogies like a key fitting its lock are suggestive, they do not fully capture the interactive dynamism of what complementarity means in the brain.

Each stream can possess multiple processing stages. For example, in Figure 110.1, the LGN inputs to cortical areas V1, V2, V4, and then inferotemporal and parietal cortices. Why is this so? One reason is that these stages realize a process of *hierarchical resolution of uncertainty*. *Uncertainty* here means that computing one set of properties at a given stage can suppress information about a different set of properties at that stage. Uncertainty principles are also familiar in physics. In the brain, these uncertainties are overcome by using more than one processing stage to form a stream. Overcoming informational uncertainty utilizes both hierarchical interactions within each stream and parallel interactions between streams that overcome their complementary deficiencies. The computational unit is thus not a single processing stage; it is, rather, an ensemble of processing stages

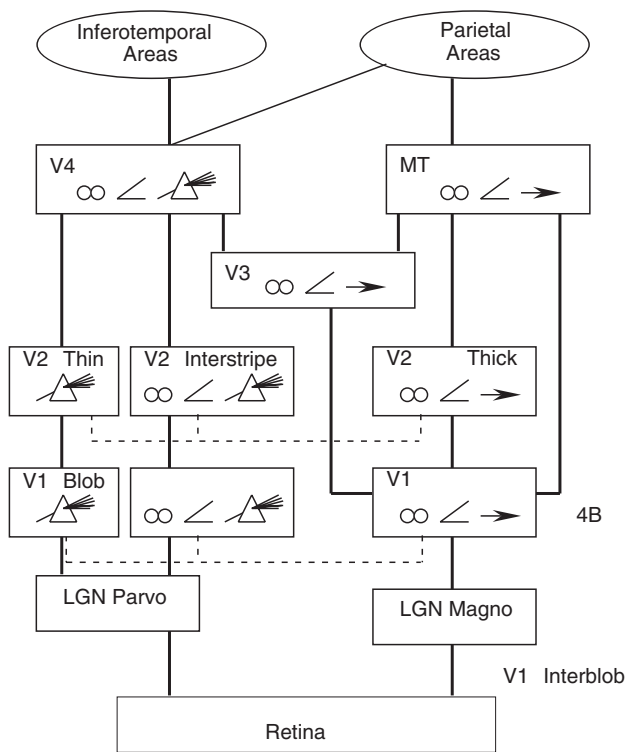


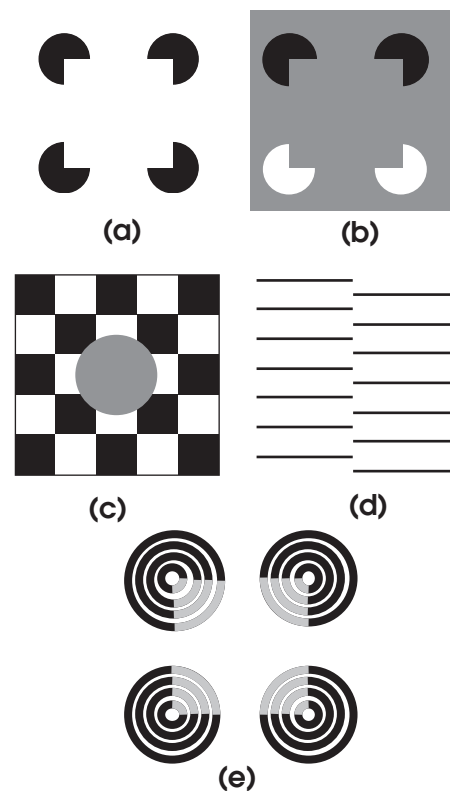
FIGURE 110.1. Schematic diagram of processing streams in visual cortex in the macaque monkey brain. Icons indicate the response selectivities of cells at each processing stage: rainbow, wavelength selectivity; angle symbol, orientation selectivity; spectacles, binocular selectivity; right-pointing arrow, selectivity to motion in a prescribed direction. (Adapted with permission from DeYoe and Van Essen, 1988.)

that interact within and between complementary processing streams.

Seeing versus recognizing: all boundaries are invisible

The boundary and surface streams obey complementary properties. One therefore needs to analyze both streams to fully understand how either stream normally functions. Figures 110.2*A* and 110.2*B* illustrate three pairs of complementary boundary and surface properties using visual illusions that are induced by variants of a Kanizsa square. In response to viewing Figure 110.2*A*, our brains construct a percept of a square even though the image contains only four black pacman, or pie-shaped, figures on a white background.

Why do our brains construct a square where there is none in the image? There are several reasons for this. One is that there is a *blind spot* in our retinas, a region where no light-sensitive photoreceptors exist. This region is blind because of the way in which the pathways from retinal photoreceptors are collected together to form the optic nerve that carries them from the retina to the LGN in Figure 110.1.



BOUNDARY COMPLETION

oriented inward
insensitive to contrast polarity

SURFACE FILLING-IN

unoriented outward
sensitive to contrast polarity

FIGURE 110.2. Visual boundary and surface interactions. *a*, A Kanizsa square. *b*, A reverse-contrast Kanizsa. *c*, An object boundary can form around the gray disc even though its contrast reverses relative to the background along its perimeter. *d*, An invisible, or amodel, vertical boundary. *e*, An example of neon color spreading. (See color plate 84)

We are not usually aware of this blind spot because our brains complete boundary and surface information across it (Kawabata, 1984). The actively completed parts of these percepts are visual illusions, because they are not derived directly from visual signals on our retinas. In fact, many of the percepts that we believe to be “real” are visual illusions whose boundary and surface representations just happen to look real. What we call a *visual illusion* is typically an unfamiliar combination of boundary and surface information.

Visual illusions provide many instructive examples of how boundaries and surfaces are formed. They also probe subtle relationships between what we can consciously see and recognize. The images in Figures 110.2*A* and 110.2*B* lead to percepts of a Kanizsa square, even though both images contain only four pacman inducers. To form the square, illusory contours form *inwardly* between cooperating pairs of

colinear pacman edges. (If boundaries were formed outwardly from a single inducer, then any speck of dirt in an image could crowd all our percepts with an outwardly growing web of boundaries.) Four such contours form the boundary of the Kanizsa square. This boundary completion process is *oriented* to form contours only between (almost) like-oriented and (almost) colinear inducers in the scene or image. Boundary completion can also complete “real” scenic contours which are not fully detected at the retina due to the blind spot.

The square boundary in Figure 110.2A can be both seen and recognized because of the enhanced illusory brightness within the square relative to the brightness of the background. An explanation of this brightness percept will be summarized below. In contrast, the square boundary in Figure 110.2B can be recognized even though it is not seen; that is, there is no brightness or color difference on either side of the illusory square boundary. Figure 110.2B shows that *some* boundaries can be consciously recognized even though they are perceptually unseen, or invisible. An emerging neural theory of how boundaries and surfaces are formed, called *FACADE* (Form-And-Color-And-DEpth) theory (e.g., Grossberg, 1994, 1997), predicts that *all boundaries are invisible* within the boundary system.

Why, and in what sense, are all boundaries invisible? This property enables boundaries to form around objects that are seen in front of textured backgrounds. For example, consider the boundary around the gray circular disc in Figure 110.2C. The gray disc lies in front of a black and white textured background whose contrasts with respect to the disc reverse along the disc’s perimeter. The brain can build a boundary around the entire disc, despite these contrast reversals. Perhaps the simplest example of a boundary that is completed from opposite contrasts is the reverse-contrast Kanizsa square in Figure 110.2B. Here a square boundary is formed between white and black pacmen on a gray background. The vertical boundaries form between black and white inducers that possess opposite contrast polarity with respect to the gray background: the black inducers have a black/gray, or dark/light, polarity, whereas the white inducers have a white/gray, or light/dark, polarity. Many observers can recognize this boundary without also seeing a contrast difference between the gray color inside and outside the square. Figure 110.2D illustrates yet another invisible boundary that can be consciously recognized.

Boundary formation: filtering and grouping

How does the brain build these boundaries? At an early stage of boundary processing, the brain pools, or adds, signals from cortical cells that are sensitive to opposite contrast polarities. In particular, at each position within the V1

interblobs, individual *simple cells* are most sensitive to a prescribed orientation at each position, but to only one contrast polarity. A simple cell can respond to either an oriented dark/light contrast or an oriented light/dark contrast, but not both. It thus behaves like a polarity-sensitive oriented filter. The outputs of simple cells that respond to the same position and orientation, but to opposite contrast polarities, are pooled at the next processing stage. This pooling process occurs at the *complex cells*.

Complex cells hereby become *insensitive* to the contrast phase, which is one of their defining characteristics (Hubel and Wiesel, 1977). They can detect an object boundary, whatever its relative contrast with respect to the background may be. Thus, a complex cell at any position along the edges of the white or black pacmen in Figure 110.2B, or anywhere along the circular boundary in Figure 110.2C, could be activated. By pooling dark/light and light/dark responses, the boundary system loses its ability to represent visible brightnesses or colors, since its output cannot signal the difference between dark and light. It is in this sense that “all boundaries are invisible.” Outputs from these complex cells activate the *inward* and *oriented* boundary completion process. Boundary completion occurs in, among other places, the V2 interstripe area (Von der Heydt et al., 1984). These three properties of boundary completion (inward, oriented, insensitive to contrast polarity) are summarized in Figure 110.2.

Boundary formation in the brain—also called *perceptual grouping*—is a key mechanism whereby we perceive geometrical objects such as lines, curves, and textured objects. Rather than being defined by such classical units as points and lines, boundaries arise as a coherent pattern of excitatory and inhibitory signals within a feedback network that includes retina, LGN, and V1 interblob and V2 interstripe areas. Grossberg (1984) and Grossberg and Mingolla (1985a, 1985b) introduced the first neural model of how boundary formation occurs in visual cortex. This Boundary Contour System (BCS) model clarifies how perceptual boundaries, or groupings, may be formed by several different types of “contoured” image properties, including edges, texture gradients, shading, and stereo differences. Since that time, steady progress in modeling the neural basis of perceptual grouping has been made (e.g., Gove et al., 1995; Grossberg, 1994; Li, 1998; Mumford, 1992), leading recently to models which clarify how the laminar circuits of visual cortex are designed to achieve perceptual grouping (see below). These models propose how spatially long-range excitatory interactions in cortical layer 2/3 build boundaries across space while interacting with shorter-range inhibitory interactions that suppress incorrect boundary groupings. These interactions select stronger boundary groupings from among many possible interpretations of a scene. A winning grouping may be represented by synchronous activity of the cells that

represent the boundary until it is reset to enable new boundaries to form.

Seeing by the surface stream

Given that boundaries are invisible, how do we see anything? Visible properties of a scene are predicted to be represented within the surface processing system (Grossberg, 1994) within the blob cortical stream between V1, V2, and V4 (Fig. 110.1). A key step in representing a visible surface is the *filling-in* process. What is filling-in, and why and how does it occur?

An early stage of surface processing compensates for variable illumination, or *discounts the illuminant*, in order to prevent illuminant variations from distorting all percepts. Discounting the illuminant attenuates color and brightness signals except near regions of sufficiently rapid surface change, such as edges or texture gradients. These *feature contours* are relatively uncontaminated by illuminant variations. After extracting these feature contours, later stages of surface formation use them to fill-in the attenuated regions with values that are less sensitive to illuminant changes. Filling-in is an example of hierarchical resolution of uncertainty, because the later filling-in stages overcome uncertainties about surface brightness and color that were caused by discounting the illuminant at an earlier processing stage.

How do the illuminant-discounted signals fill-in an entire region? Filling-in behaves like a diffusion of brightness or color across space. For example, consider the percept of *neon color spreading* that is elicited by Figure 110.2E. This figure consists of circular annuli, part of which are black and part gray. In response to this figure, we can see an illusory square filled with a gray color. FACADE theory has proposed an explanation of this percept in terms of interactions between the boundary and surface systems. In particular, the black boundaries cause small breaks, called *end gaps*, in the gray boundaries where they join (Grossberg, 1994). The gray color can spread through these breaks from the annuli into the illusory square. In this percept, filling-in spreads *outward* from the individual gray inducers in all directions. Its spread is thus *unoriented*.

How is this spread of activation contained? Signals from the boundary system to the surface system are predicted to define the regions within which filling-in is restricted via an interblob to blob stream interaction. These boundary signals act as barriers that block the spread of filling-in within the blob stream. Thus, filling-in is a type of anisotropic diffusion in which boundary signals nonlinearly gate, or inhibit, the diffusive flow of surface signal. Without these boundaries, filling-in would spread across space without restriction, and would thereby dissipate its activity, so that no visible surface percept could form. Invisible boundaries thereby indirectly ensure their own visibility through their interactions with the

surface stream, within which all visible percepts are predicted to form. In the neon color spreading example shown in Figure 110.2E, these boundary signals to the surface stream surround the annuli (except for their small breaks) and also form the square illusory contour. That is why the spread of gray is restricted to the square region.

We can now understand finer aspects of the other percepts derived from Figure 110.2. In Figure 110.2A, the square boundary is induced by four black pacmen that are all less luminant than the white background. In the surface stream, the process of discounting the illuminant has the side effect that the pacmen induce local brightness enhancements (the feature contours) adjacent to the pacmen and just within the square boundary. At a subsequent filling-in stage, these enhanced brightness signals spread within the square boundary, thereby causing the entire interior of the square to look uniformly brighter. The filled-in square is visible because the filled-in activity within the square is higher than the filled-in activity outside the square. Filling-in can thereby lead to visible percepts because it is *sensitive* to contrast polarity. These three properties of surface filling-in (outward, unoriented, sensitive to contrast polarity) are summarized in Figure 110.2. They are complementary to the corresponding properties (inward, oriented, insensitive to contrast polarity) of boundary completion. The surface system has been called the *Feature Contour System* (FCS) to denote that it builds up surface properties from *feature contours* that survive the process of discounting the illuminant and that are the basis for the features, such as brightness and color, that we can consciously see in surface percepts (Grossberg, 1994).

In Figure 110.2B, the opposite polarities of the pacmen with respect to the gray background can lead to approximately equal filled-in activities inside and outside the square. In particular, the black pacmen lead to enhanced brightness just within the square boundary, but the white pacmen lead to diminished brightness just within the boundary. When these opposite effects fill in, they can approximately cancel one another. As a result, the gray colors on the two sides of the boundary are approximately equal, so the boundary cannot be “seen.” On the other hand, the boundary can be consciously “recognized” as a salient perceptual event by brain processes that interact with the large boundary signals within the interblob stream. In Figure 110.2D, the vertical illusory contour is invisible because the white background can fill-in uniformly on both sides of the vertical boundary by spreading around the horizontal black lines.

Filling-in also clarifies how our brains can perceive brightnesses and colors across the retinal blind spot. Boundaries that form across the blind spot contain the filling-in of brightness and color there. Boundary completion and surface filling-in also help to explain how we see continuous blue surfaces (Grossberg, 1987a, Section 31), even though

blue cones have a sparse distribution on the retina (Boynton et al., 1985; Chapter 64, this volume). Interacting boundaries and surfaces will also be suggested below to play a fundamental role in three-dimensional (3D) vision and figure-ground perception.

Varied evidence for filling-in: constancy, contrast, and assimilation

Controversy persists about whether or not a physical filling-in interaction exists (Dennett, 1991; Pessoa et al., 1998). Such a question can be answered only by direct experimental test and by showing how neural models can explain more data by including a filling-in process. A number of early modeling articles explained perceptual data by using a neural filling-in process (e.g., Cohen and Grossberg, 1984; Grossberg, 1987a, 1987b; Grossberg and Mingolla, 1985a; Grossberg and Todorovic, 1988). Psychophysical data also supported a filling-in process by characterizing its temporal dynamics (Paradiso and Nakayama, 1991). Arrington (1994) simulated these data using the Grossberg–Todorovic model.

Since that time, neurophysiological evidence for filling-in has also been reported (e.g., Lamme et al., 1999; Lee et al., 1998). Interactions between boundary completion and surface filling-in have also played a key role in more recent explanations of data on 3D figure-ground perception (Grossberg, 1994, 1997; Grossberg and McLoughlin, 1997; Kelly and Grossberg, 2000), texture perception (Grossberg and Pessoa, 1998), brightness perception (Gove et al., 1995; Grossberg and Kelly, 1999; Neumann et al., 2001; Pessoa et al., 1995), visual persistence (Francis et al., 1994), negative aftereffects (Francis and Grossberg, 1996), and the McCollough effect (Grossberg et al., 2002). Most of these data have no other mechanistic explanation to date. Figure-ground perception will be discussed below.

Different combinations of mechanisms may be rate-limiting in explaining percepts which involve filling-in. Three simple mechanisms are sufficient to explain many data about brightness perception (Grossberg and Todorovic, 1988), but not all such data: (1) an on-center off-surround network of cells that obey shunting, or membrane, equations, (2) a boundary formation network, and (3) a surface filling-in network. The cells of the shunting on-center off-surround network preprocess visual inputs by discounting the illuminant and computing Weber-law modulated estimates of image reflectances that contrast-normalize input intensities. These contrast-normalized cell activities then input to the boundary formation and surface filling-in networks. The boundary signals to the surface filling-in network prevent filling-in from crossing boundaries.

Figure 110.3 gives four examples of how this simplest filling-in network works. The lowest row of each panel in the

figure shows a one-dimensional (1D) cross-section of image luminance. The next-lowest row shows how a shunting on-center off-surround network of cells can transform these image intensities. Comparing (A) and (B) shows that such a network can compensate for a gradient of illumination; see the patterns labeled FEATURE in the figure. In so doing, it can also distort the true pattern of image reflectances by generating cusps and dips in the profile of cell activities across space. One of these distortions is the attenuation of image reflectances away from object edges or other rapidly changing luminance gradients across space. This is the key mechanism whereby the illuminant is discounted. Boundary and surface interactions compensate for these distortions by exploiting the information that survives the discounting process. The boundaries create a frame within which the illuminant-discounted signals can fill-in within the surface processing stream; see the patterns labeled BOUNDARY in the figure. Thus, in Figures 110.3A and 110.3B, boundaries form at the luminance discontinuities of the image because the boundary system is sensitive to discontinuities in the activity profile of discounted signals. The pattern of these discounted signals is topographically mapped into filling-in domains (FIDOS) within the surface stream, or FCS. Here the discounted signals can begin to spread across space, contained within boundary signals that are topographically mapped from the BCS into the FIDOS. The result is given in the top row of each panel by the patterns labeled OUTPUT.

Figures 110.3A and 110.3B show how this network can discount the illuminant and recover the original pattern of image reflectances under some circumstances. This is an example of *brightness constancy*. However, due to the discounting process, image reflectances are not always veridically recovered. For example, the STIMULUS in Figure 110.3C contains two steps of equal luminance on a luminance that varies so gradually between them that no boundary is detected. In the OUTPUT profile, *brightness contrast* obtains; that is, the right step is more active than the left step in the OUTPUT activity profile. This is due to the sensitivity of the on-center off-surround network to image contrasts; see the FEATURE pattern. Remarkably, the luminance gradient that caused the brightness contrast is not visible in the final percept. The background has uniform brightness in the OUTPUT because no boundary exists to restrict the filling-in process between the two luminance steps, as also occurs in vivo under such conditions. Thus, this example also demonstrates a “visible effect of an invisible cause.”

Figure 110.3D shows that the same mechanisms can also cause the opposite of brightness contrast: *brightness assimilation* (Helson, 1963) from a display that was studied by Shapley and Reid (1986). Its luminance profile is derived from a standard brightness contrast profile by introducing

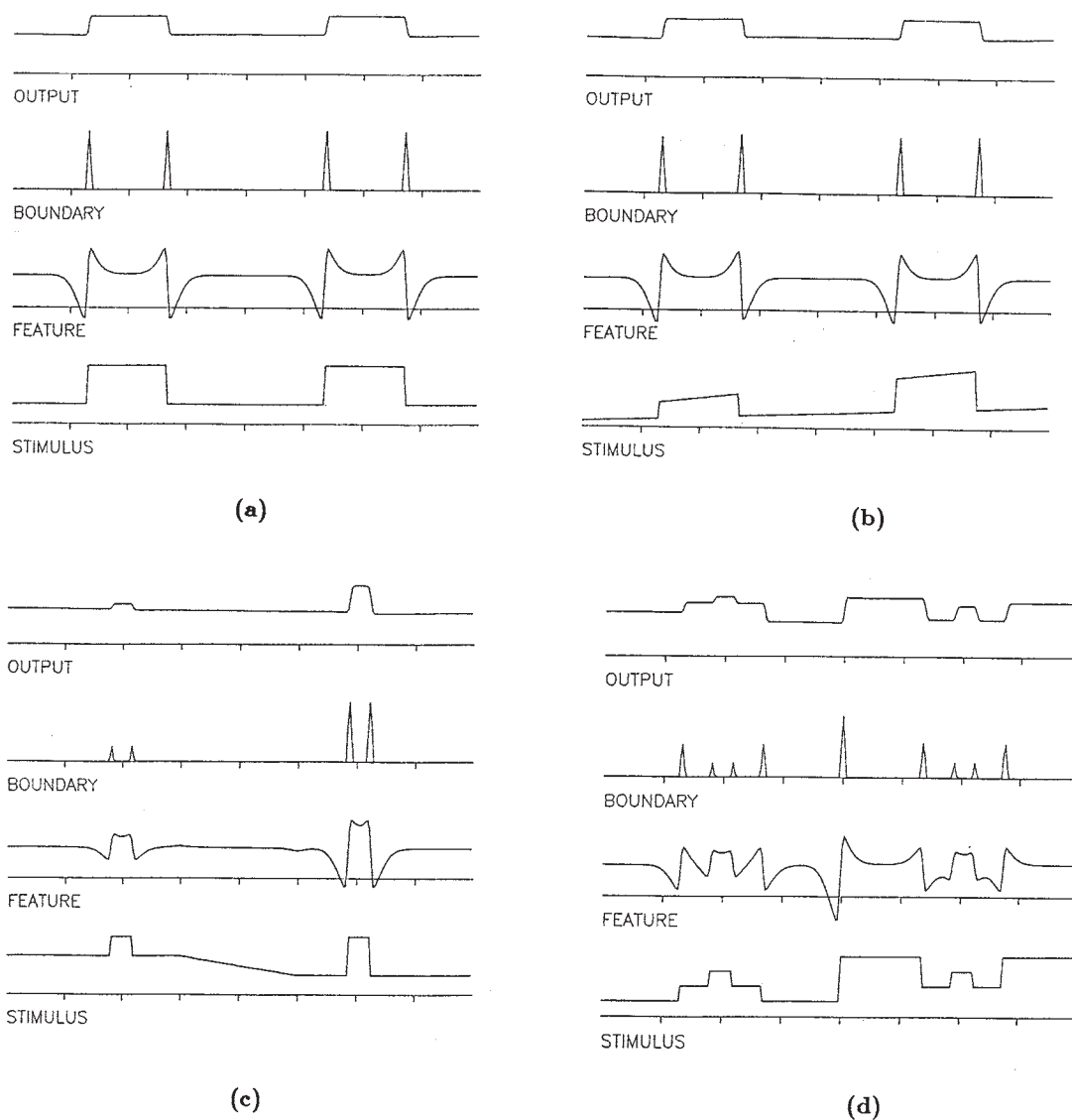


FIGURE 110.3. How filling-in can explain examples of brightness constancy (*a* and *b*), brightness contrast (*c*), and brightness assimilation (*d*). See text for details. (Adapted with permission from Grossberg and Todorovic, 1988.)

two additional test regions. These test luminance steps are the same and are placed on equally but less luminant backgrounds. A simple brightness contrast explanation would suggest that the two steps should have the same brightness. However, humans report that the left step looks brighter than the right one, as also occurs in the OUTPUT activity profile of the model. The perceived brightness of the background has been “assimilated” into the brightness of the steps. Figure 110.3D shows that a spatial pattern of activity cusps and dips is caused by the discounting process. These cusps and dips are broader than the boundaries that they induce. When this FEATURE profile fills-in within its narrower boundaries, assimilation obtains in the OUTPUT as an emergent property of network interactions.

The Grossberg-Todorovic model can explain many other brightness data, including the Craik-O’Brien-Cornsweet

effect, the Koffka-Benussi ring, Kanizsa-Minguzzi anomalous brightness differentiation, the Hermann grid, Land Mondrians, impossible staircases, bull’s-eyes, and nested combinations of luminance profiles. This explanatory success challenges other models of brightness perception. However, these mechanisms cannot, by themselves, explain data on brightness and lightness *scission* or *anchoring* during figure-ground perception. More comprehensive models can explain some scission and anchoring properties (Grossberg, 1999a; Grossberg et al., 1995).

Boundary completion and attention by the laminar circuits of visual cortex

How does visual cortex complete boundaries across gaps due to internal brain imperfections, such as the retinal blind spot,

or due to incomplete contours in external inputs, such as occluded surfaces, spatially discrete texture elements, illusory contour stimuli, or even missing pixels in impressionist paintings? The BCS model predicted how long-range horizontal cooperation interacts with shorter-range competition to do this. The cooperating cells were predicted to satisfy a *bipole* property. Such *bipole cells* achieve inward and oriented boundary completion by firing when they receive inputs from pairs of (almost) like-oriented and (almost) colinear scenic inducers. Von der Heydt et al. (1984) reported bipole cells in cortical area V2. Subsequent psychophysical studies also noted a bipole property during perceptual grouping. Field et al. (1993) called it an *association field*, and Shipley and Kellman (1992) called it a *reliability condition*.

More recently, the BCS was extended to clarify how laminar cortical circuits work (Grossberg, 1999b). This LAMINART model predicts how bottom-up, top-down, and horizontal interactions within the cortical layers achieve (1)

perceptual grouping, (2) attention, and (3) stable development and learning. The model proposes how mechanisms that achieve property (3) imply (1) and (2). That is, constraints on stable development of cortical circuits in the infant determine properties of learning, perception, and attention in the adult.

Figure 110.4 summarizes how known laminar cortical circuits may carry out perceptual grouping and attention. This summary omits binocular interactions for simplicity (but see below). The LGN directly activates V1 layers 4 and 6 (Fig. 110.4a). Layer 6, in turn, sends on-center off-surround inputs to layer 4. Layer 6 can strongly inhibit layer 4 through the off-surround, but the excitatory and inhibitory inputs in the on-center are approximately balanced. Layer 6 can thus modulate the excitability of layer 4 cells but cannot drive them to fire vigorously. This balance helps ensure stable cortical development (Grossberg and Williamson, 2001). The direct LGN-to-4 connections are proposed to drive layer 4 cells. The direct and indirect pathways from LGN-to-4 together form an on-center off-surround network. When layer 4 cells obey membrane, or shunting, equations, this network can contrast-normalize the responses of layer 4 cells (Grossberg, 1973; Heeger, 1992) and thus preserve their sensitivity to input differences over a wide dynamic range.

FIGURE 110.4. Boundary and attentional laminar circuits in interblob cortical areas V1 and V2. Inhibitory interneurons are shown filled-in black. *a*, The LGN provides bottom-up activation to layer 4 via two routes. It makes strong connections directly into layers 4 and 6. Layer 6 then activates layer 4 via a $6 \rightarrow 4$ on-center off-surround network. In all, LGN pathways to layer 4 form an on-center off-surround network, which contrast-normalizes layer 4 cell responses. *b*, *Folded feedback* carries attentional signals from higher cortex into layer 4 of V1 via the $6 \rightarrow 4$ path. Corticocortical feedback axons tend to originate in layer 6 of the higher area and to terminate in the lower cortex's layer 1, where they excite apical dendrites of layer 5 pyramidal cells, whose axons send collaterals into layer 6. Several other routes through which feedback can pass into V1 layer 6 exist. Having arrived in layer 6, the feedback is then "folded" back up into the feedforward stream by passing through the $6 \rightarrow 4$ on-center off-surround path. *c*, Connecting the $6 \rightarrow 4$ on-center off-surround to the layer 2/3 grouping circuit: like-oriented layer 4 simple cells with opposite contrast polarities compete (not shown) before generating half-wave rectified outputs that converge onto layer 2/3 complex cells in the column above them. Groupings that form in layer 2/3 enhance their own positions in layer 4 via the $6 \rightarrow 4$ on-center and suppress other groupings via the $6 \rightarrow 4$ off-surround. There exist direct layer 2/3 \rightarrow 6 connections in macaque V1, as well as indirect routes via layer 5. *d*, Top-down corticogeniculate feedback from V1 layer 6 to LGN also has an on-center off-surround anatomy similar to that of the $6 \rightarrow 4$ path. The on-center feedback selectively enhances LGN cells that are consistent with the activation that they cause, and the off-surround contributes to length-sensitive (endstopped) responses that facilitate grouping perpendicular to line ends. *e*, The model V1/V2 circuit: V2 repeats the laminar pattern of V1 circuitry on a larger spatial scale; notably, the horizontal layer 2/3 connections have a longer range in V2. V1 layer 2/3 projects to V2 layers 6 and 4, just as LGN projects to layers 6 and 4 of V1. Higher cortical areas send feedback into V2 which ultimately reaches layer 6, just as V2 feedback acts on layer 6 of V1. Feedback paths from higher cortical areas straight into V1 (not shown) can complement and enhance feedback from V2 into V1. (Reprinted with permission from Grossberg and Raizada, 2000.)

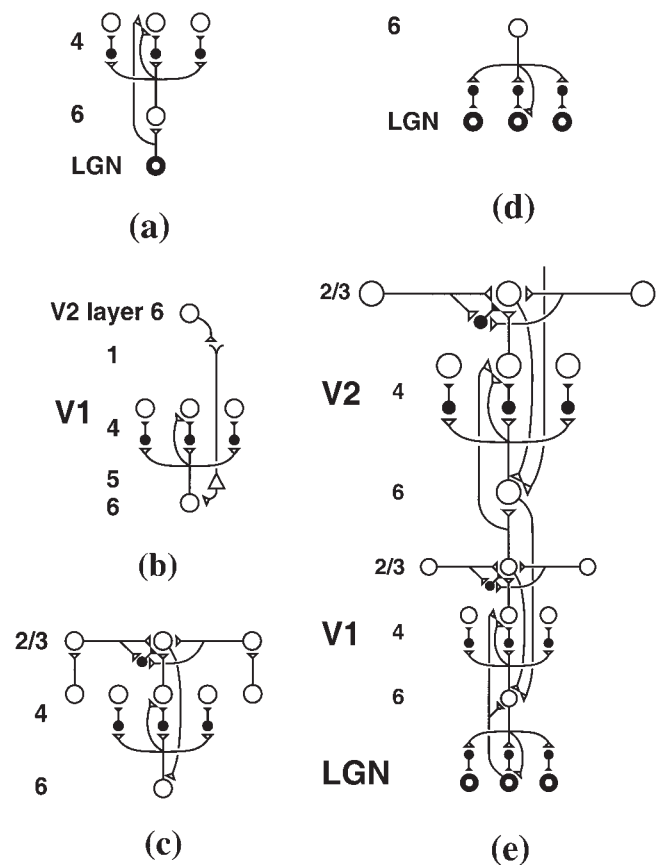


Figure 110.4*B* illustrates how the modulatory layer 6-to-4 circuit can also be used by top-down signals from V2 layer 6 to attentionally modulate the excitability of V1 layer 4 cells while inhibiting layer 4 cells that are not in the attentional focus.

Boundary completion that obeys a bipole property occurs as illustrated in Figure 110.4*C*. Layer 4 cells activate layer 2/3 cells, which communicate with their layer 2/3 neighbors via long-range horizontal excitatory connections and shorter-range inhibitory interneurons. The strengths of these excitatory and inhibitory interactions are approximately balanced. This balance also contributes to stable cortical development. Activation of a single layer 2/3 cell causes its horizontal excitatory and inhibitory connections to be approximately equally activated. The inhibition cancels the excitation, so a boundary cannot shoot out from individual scenic inducers. When two or more (approximately) like-oriented and (approximately) colinear layer 2/3 cells are activated, the excitation that converges on cells in between can summate, but the inhibitory interneurons form a recurrent inhibitory net that normalizes its total activity. As a result, total excitation exceeds total inhibition, and the cells can fire. A boundary can thereby be completed inwardly, but not outwardly.

If a scene has unambiguous groupings, then this horizontal interaction can rapidly complete boundaries (cf. Thorpe et al., 1996). In response to scenes with multiple possible groupings, competitive interactions in layers 2/3 and 4 can keep the layer 2/3 activities small, while positive feedback signals between layers $2/3 \rightarrow 6 \rightarrow 4 \rightarrow 2/3$ (Fig. 110.4*C*) have a chance to selectively amplify the strongest grouping, which can then generate outputs from layer 2/3, as its strong layer 6-to-4 off-surround signals inhibit weaker groupings. The layer 6-to-4 circuit thus has at least three functions: it contrast-normalizes bottom-up inputs, selects groupings via intracortical feedback from layer 2/3, and primes attention via intercortical feedback from higher cortical levels.

This intimate connection between grouping and attention enables attention to flow along a grouping and thereby selectively enhance an entire object, as Roelfsema et al. (1998) have shown in macaque V1. Because attention acts through an on-center off-surround circuit, it can “protect” feature detectors from inhibition by distractors by using its off-surround, as Reynolds et al. (1999) have shown in V2 and V4. Because both cooperation and competition influence groupings, the effects of colinear inducers can be either facilitatory or suppressive at different contrasts, as Polat et al. (1998) have shown in V1. Grossberg and Raizada (2000) and Raizada and Grossberg (2001) have quantitatively simulated these and related neurophysiological data.

A top-down on-center off-surround from V1 layer 6 to the LGN (Fig. 110.4*D*) can act in much the same way as the top-down signals from V2 layer 6 to V1, as Sillito et al.

(1994) have shown. Figure 110.4*E* synthesizes these circuits into a system architecture, which shows that the horizontal interactions within V2 layer 2/3 can have a broader spatial extent than those in V1 layer 2/3. The V2 interactions carry out perceptual groupings like illusory contours, texture grouping, completion of occluded objects, and bridging the blind spot. The V1 interactions improve the signal-to-noise ratio of feature detectors within the V1 cortical map.

The LAMINART model has been extended to clarify how depthful boundaries are formed (Grossberg and Howe, 2003) and how slanted surfaces are perceived in 3D (Swaminathan and Grossberg, 2001). This generalization is consistent with laminar anatomical and neurophysiological data. For example, suppose that a scenic feature activates monocular simple cells in layer 4 via the left and right eyes. These simple cells are sensitive to the same contrast polarity and orientation. Because they are activated by different eyes, they are positionally displaced with respect to one another on their respective retinas. These monocular simple cells activate disparity-selective binocular simple cells in layer 3B. Binocular simple cells that are sensitive to the same disparity but to opposite contrast polarities then activate complex cells in layer 2/3A. This two-stage process enables the cortex to match features binocularly with the same contrast polarity, yet also to form boundaries around objects in front of textured backgrounds, as in Figures 110.2*B* and 110.2*C*.

3D vision and figure-ground separation

How are depthful boundary and surface representations formed? How are percepts of occluding and occluded objects represented in depth? Multiple problems need to be solved to understand how boundaries and surfaces work together during 3D vision and figure-ground perception. The rest of this section summarizes some of these problems. Then model mechanisms that embody a proposed solution for all these problems will be summarized, as well as a simulation example of how the model works.

THREE-DIMENSIONAL SURFACE CAPTURE AND FILLING-IN

How are the luminance and color signals that are received by the two eyes transformed into 3D surface percepts? FACADE theory posits that multiple depth-selective boundary representations exist and interact with multiple depth-selective surface FIDOS to determine which surfaces in depth can be seen. The same filling-in processes which enable us to see perceptual qualities like brightness and color are predicted to also determine the relative depth of these surfaces. In particular, depth-selective boundaries selectively *capture* brightness and color signals at the subset of FIDOS that support depthful visual percepts. Such a viewpoint predicts that perceived depth and brightness

can interact. In fact, brighter surfaces can look closer (Egusa, 1983).

BINOCULAR FUSION, GROUPING, AND DA VINCI STEREOPSIS
 Granted that surface capture can achieve depth-selective filling-in, how are the depth-selective boundaries formed that control surface capture? Our two eyes view the world from slightly different perspectives. Their different views lead to relative displacements, or disparities, on their retinas of the images that they register. These disparate retinal images are binocularly matched at disparity-sensitive cells, as noted above. The disparity-sensitive cells are used to form depth-selective boundaries, which capture surface filling-in signals at the corresponding depth-selective FIDOs.

When two eyes view the world, part of a scene may be seen by only one eye. No disparity signals are available here to determine the depth of the monocularly viewed features, yet they are seen at the correct depth (Nakayama and Shimojo, 1990). FACADE theory proposes how depth-selective filling-in of a nearby binocularly viewed region spreads into the monocularly viewed region to impart the correct depth. This proposal also explains related phenomena like the *equidistance tendency*, whereby a monocularly viewed object in a binocular scene seems to lie at the same depth as the retinally most contiguous binocularly viewed object (Gogel, 1965). How this works leads to a number of new hypotheses, including how horizontal and monocularly viewed boundaries are added to all boundary representations and how an “asymmetry between near and far” distributes boundaries from nearer to farther surface representations. Without these mechanisms, all occluding objects would look transparent.

MULTIPLE SCALES INTO MULTIPLE BOUNDARY DEPTHS
 When a single eye views the image of an object in depth, the same size of the retinal image may be due to either a large object far away or a small object nearby. How is this ambiguity overcome to activate the correct disparity-sensitive cells? The brain uses multiple receptive field sizes, or scales, that achieve a *size-disparity correlation* between retinal size and binocular disparity. It has often been thought that larger scales code nearer objects and smaller scales more distant objects. For example, a nearer object can lead to a larger disparity that can be binocularly fused by a larger scale. In fact, each scale can fuse multiple disparities, although larger scales can fuse a wider range of disparities (Julesz and Schumier, 1981). This ambiguity helps to explain how higher spatial frequencies in an image can sometimes look closer, rather than more distant, than lower spatial frequencies in an image and how this percept can reverse during prolonged viewing (Brown and Weisstein, 1988). FACADE theory explains these reversals by analyzing how

multiple spatial scales interact to form depth-selective boundary groupings (Grossberg, 1994).

Multiple spatial scales also help to explain how shaded surfaces are seen. In fact, if boundaries were sensitive only to the bounding edge of a shaded surface, then shaded surfaces would look uniformly bright and flat after filling-in occurs, as in the background of Figure 110.3C. However, boundaries respond to shading gradients as well as to edges. Different scales react differently to different regions of the shading gradients, leading to a multiple-depth *boundary web* of small boundary compartments. Such a boundary web traps contrasts locally and leads to a shaded surface percept.

RECOGNIZING OBJECTS VERSUS SEEING THEIR UNOCCLUDED PARTS
 In many scenes, some objects lie partially in front of other objects and thereby occlude them. How do we know which features belong to the different objects, both in 3D scenes and in two-dimensional (2D) pictures? If we could not make this distinction, object recognition would be severely impaired. FACADE theory predicts how the mechanisms which solve this problem when we view 3D scenes also solve the problem when we view 2D pictures.

In the Bregman–Kanizsa image of Figure 110.5, the gray B shapes can be readily recognized even though they are partially occluded by the black snake-like occluder. In Figure 110.5B, the occluder is removed. Although the same amount of gray is shown in both images, the B shapes are harder to recognize in Figure 110.5B. This happens because the boundaries that are shared by the black occluder and the gray B shapes in Figure 110.5A are assigned by the brain to the black occluder. These boundaries form within a boundary representation that codes a nearer distance to the viewer than the boundary representation of the gray shapes. With the shared boundaries removed from the gray B shapes, the B boundaries can be completed behind the positions of the black occluder by using the bipole property. These completed boundaries help to recognize the Bs at the farther



FIGURE 110.5. *a*, Uppercase gray B letters that are partially occluded by a black snake-like occluder. *b*, Same B shapes as in *a* except that the occluder is white and therefore merges with the remainder of the white background. (Adapted with permission from Nakayama et al., 1989.)

depth. In Figure 110.5*B*, the shared boundaries are not removed from the gray shapes, and they prevent the completion of the gray boundaries.

To actually do this, the brain needs to solve several problems. First, it needs to figure out how geometrical and contrast factors work together. In Figure 110.5*A*, for example, the T-junctions where the gray shapes intersect the black occluders seem to be a cue signaling that the black occluder looks closer than the gray shapes. However, if you imagine the black occluder gradually getting lighter until it matches the white background in Figure 110.5*B*, it is clear that when the occluder is light enough, the gray shapes will no longer appear behind the occluder. Thus, geometrical factors like T-junctions are not sufficient to cause figure-ground separation. They interact with contrast relationships within the scene too.

The brain also needs to figure out how to complete the B boundaries “behind” the occluder in response to a 2D picture. In particular, how do different spatial scales get differentially activated by a 2D picture as well as a 3D scene so that the occluding and occluded objects can be seen in depth? Moreover, if the B boundaries can be completed and thereby recognized, then why do we not *see* completely filled-in B shapes too, including in the regions behind the black occluder? This state of affairs clarifies that there is a design tension between properties needed to recognize opaque objects, including where they are occluded, and our ability to see only their unoccluded surfaces. Here again, *the asymmetry between near and far* plays a key role, as noted below.

FROM BOUNDARY-SURFACE COMPLEMENTARITY TO CONSISTENCY Such subtle data make one wonder about how the brain evolved to behave this way. FACADE theory predicts how simple mechanisms that realize a few new perceptual principles can explain figure-ground data when they interact together. One such principle is that boundary and surface computations are complementary. How, then, do we see a single percept wherein boundaries and surfaces are consistently joined? How does *complementarity* become *consistency*? FACADE theory proposes how consistency is achieved by a simple kind of feedback that occurs between the boundary and surface streams. Remarkably, this feedback also explains many properties of figure-ground percepts, including the Bregman–Kanizsa percept. The remainder of the chapter sketches some of these principles and mechanisms, followed by a simulation of the Bregman–Kanizsa percept.

Three-dimensional boundary and surface formation

Figure 110.6 is a macrocircuit of FACADE theory in its present form. Monocular processing of left-eye and right-eye inputs by the retina and LGN discounts the illuminant and

generates parallel signals to the BCS and FCS. These signals go to model cortical simple cells via pathways 1 in Figure 110.6 and to monocular FIDOs via pathways 2. Model simple cells have oriented receptive fields and come in multiple sizes. Simple cell outputs are binocularly combined at disparity-sensitive complex and complex endstopped (or hypercomplex) cells via pathways 3. Complex cells with larger receptive fields can binocularly fuse a broader range of disparities than can cells with smaller receptive fields, thereby achieving a size-disparity correlation. Competition across disparity at each position and among cells of a given size scale sharpens complex cell disparity tuning (Fahle and Westheimer, 1995). Spatial competition (endstopping) and orientational competition convert complex cell responses into spatially and orientationally sharper responses at hypercomplex cells.

How are responses from multiple receptive field *sizes* combined to generate boundary representations of relative *depths* from the observer? Hypercomplex cells activate bipole cells via pathway 4. The bipole cells carry out long-range grouping and boundary completion via horizontal connections that occur in layer 2/3 of area V2 interstripes. Bipole grouping collects outputs from hypercomplex cells of all sizes that are sensitive to a given depth range. The bipole cells then send excitatory feedback signals via pathways 5 back to all hypercomplex cells within the same depth range that represent the same position and orientation, and inhibitory feedback signals to hypercomplex cells at nearby positions and orientations (cf. layer 2/3-6-4 inhibition in Fig. 110.4*E*). The feedback groups cells of multiple *sizes* into a BCS representation, or copy, that is sensitive to a prescribed range of *depths*. Multiple BCS copies are formed, each corresponding to different (but possibly overlapping) depth ranges.

Bipole cells play a key role in figure-ground separation. Each bipole cell has an oriented receptive field with two branches (Fig. 110.7). Long-range excitatory bipole signals combines with shorter-range inhibitory signals to make the system sensitive to T-junctions (Fig. 110.7). In particular, horizontally oriented bipole cells that are located where the top of the T joins its stem receive excitatory inputs to both of their receptive field branches. Vertically oriented bipole cells that process the stem of the T where it joins the top receive excitatory support only in the one branch that is activated by the stem. Because of this excitatory imbalance, inhibition of the stem by the top can cause a gap in the stem boundary (Fig. 110.7), termed an *end-gap*. During filling-in, boundaries contain the filling-in process. Where end-gaps occur, brightness or color can flow out of a figural region. FACADE theory predicts that this escape of color or brightness via filling-in is a key step that initiates figure-ground separation (Grossberg, 1994, 1997; Grossberg and McLoughlin, 1997; Kelly and Grossberg, 2000). Figure 110.8 shows a simulation from Kelly and Grossberg (2000) which illustrates

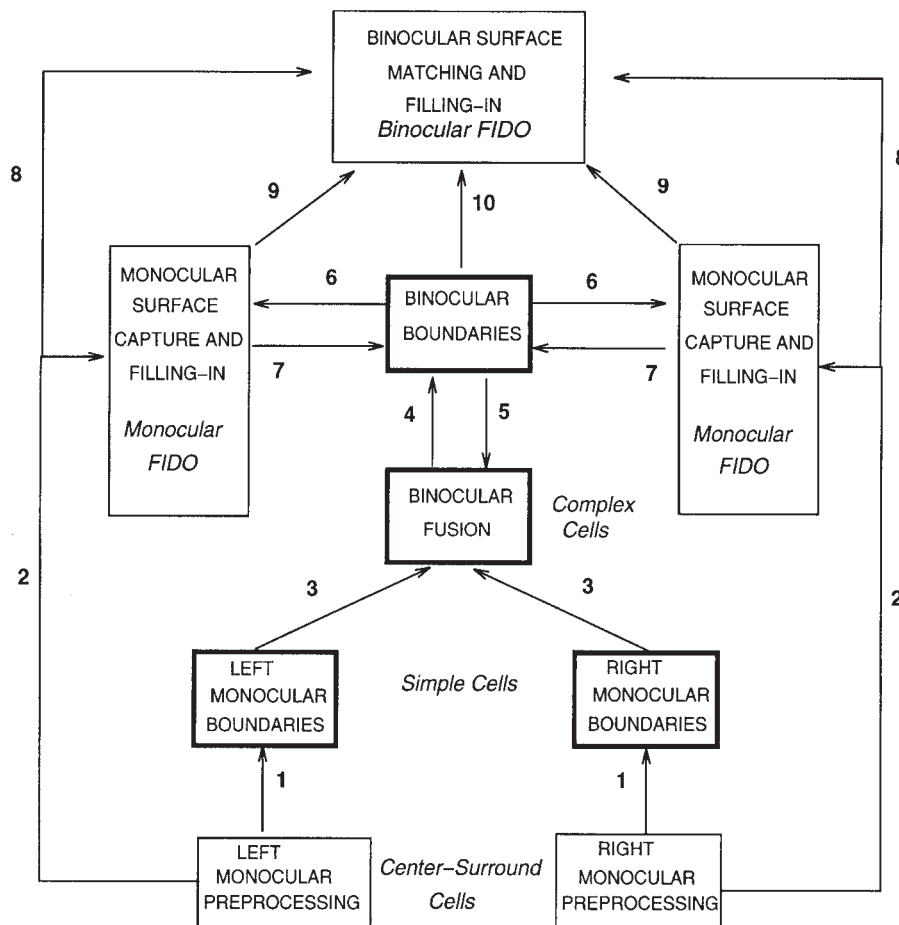


FIGURE 110.6. FACADE macrocircuit showing interactions of the BCS and FCS. See text for details. (Reprinted with permission from Kelly and Grossberg, 2000.)

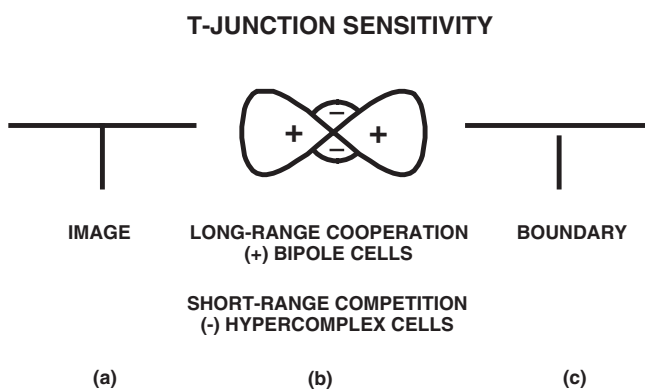


FIGURE 110.7. T-junction sensitivity in the BCS. *a*, T-junction in an image. *b*, Bipole cells provide long-range cooperation (+), whereas hypercomplex cells provide shorter-ranger competition (-). *c*, An end-gap in the vertical boundary arises due to this combination of cooperation and competition. (Reprinted with permission from Grossberg, 1997.)

end-gaps in response to the Bregman–Kanizsa image. End-gaps occur where the horizontal occluder touches the partially occluded B shape at both near (Fig. 110.8*A*) and far (Fig. 110.8*B*) depths.

How do multiple depth-selective BCS copies capture brightness and color signals within depth-selective FCS surface representations? This happens in at least two stages. The first stage of *monocular FIDO*s may exist in V2 thin stripes. Each monocular FIDO is broken into three pairs of opponent FIDOs (black/white, red/green, blue/yellow) that receive achromatic and chromatic signals from a single eye. A pair of monocular FIDOs, one for each eye, corresponds to each depth-selective BCS copy and receives its strongest boundary-gating signals from this BCS copy. Each monocular FIDO may also receive weaker boundary signals from BCS copies that represent depths close to that of its primary BCS copy. In this way, a finite set of FIDOs can represent a continuous change in perceived depth, much as three classes of retinal cones can be used to represent a continuum of perceived colors.

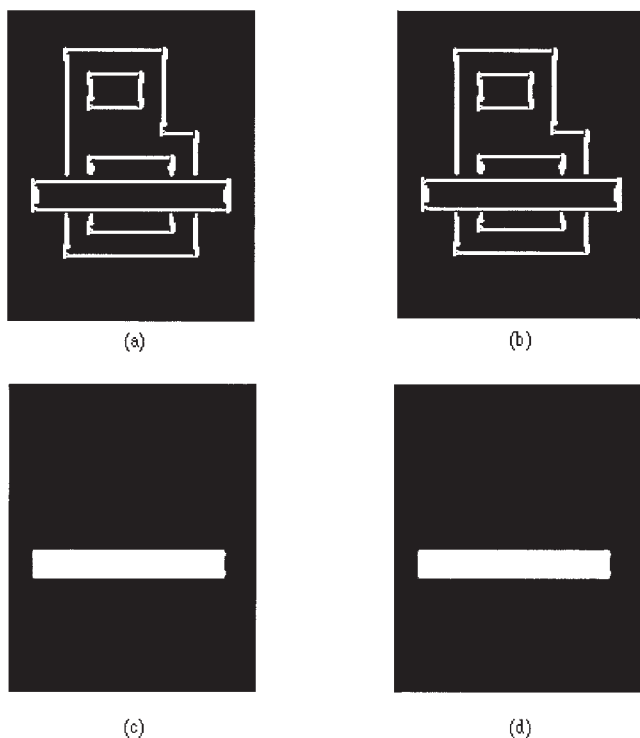


FIGURE 110.8. Binocular boundaries for monocular filling-in in response to a Bregman–Kanizsa image: (a) near depth and (b) far depth. Filled-in monocular FIDOs before boundary pruning occurs: (c) near depth and (d) far depth. (Reprinted with permission from Kelly and Grossberg, 2000.)

Surface capture is triggered when boundary-gating BCS signals interact with illuminant-discounted FCS signals. Pathways 2 in Figure 110.6 input discounted monocular FCS signals to *all* monocular FIDOs. Only some FIDOs will selectively fill-in these signals and thereby lift monocular FIDO signals into depth-selective surface representations for filling-in. The boundary signals along pathways 6 in Figure 110.6 determine which FIDOs will fill-in. These boundary signals selectively capture FCS inputs that are spatially coincident and orientationally aligned with them. Other FCS inputs are suppressed. These properties follow when double-opponent, boundary-gating, and filling-in processes interact. How this happens, and how it can explain data on binocular fusion and rivalry, among other percepts, are discussed in Grossberg (1987b).

Because these filled-in surfaces are activated by depth-selective BCS boundaries, they inherit the depths of their boundaries. Three-dimensional surfaces may thereby represent depth as well as brightness and color. This link between depth, brightness, and color helps to explain *proximity-luminance covariation*, or why brighter surfaces tend to look closer (e.g., Egusa, 1983).

Not every filling-in event can generate a visible surface. Because activity spreads until it hits a boundary, only sur-

faces that are surrounded by a *connected* BCS boundary are effectively filled-in. Otherwise, the spreading activity can dissipate across the FIDO. This property helps to explain data ranging from neon color spreading to how T-junctions influence 3D figure-ground perception (Grossberg, 1994). Figures 110.8C and 110.8D illustrate how filling-in occurs in response to the Bregman–Kanizsa boundaries of Figures 110.8A and 110.8B. The connected boundary surrounding the occluder can contain its filled-in activity, but activity spreads through the end-gaps of the B boundaries, thereby dissipating across space, at both near (Fig. 110.8C) and far (Fig. 110.8D) depths.

An analysis of how the BCS and FCS react to 3D images shows that too many boundary and surface fragments are formed as a result of the size-disparity correlation. This redundancy is clear in Figure 110.8. As noted above, larger scales can fuse a larger range of disparities than can smaller scales. How are the surface depths that we perceive selected from this range of possibilities across all scales? FACADE’s proposed answer to this question follows from its answer to the more fundamental question: how is perceptual *consistency* derived from boundary-surface *complementarity*? FACADE predicts how this may be achieved by feedback between the boundary and surface streams, which is predicted to occur no later than V2. This mutual feedback also helps to explain why blob and interblob cells share so many receptive field properties even though they carry out such different tasks. In particular, boundary cells, which summate inputs from both contrast polarities, can also be modulated by surface cells, which are sensitive to just one contrast polarity.

Boundary-surface consistency derives from a contrast-sensitive process that detects the contours of successfully filled-in regions within the monocular FIDOs. Only successfully filled-in regions *can* activate such a contour-sensitive process, because other regions either do not fill-in at all or their filling-in dissipates across space. These filled-in contours activate FCS-to-BCS feedback signals (pathways 7 in Fig. 110.5) that strengthen boundaries at their own positions and depths while inhibiting redundant boundaries at farther depths. This inhibition from near to far is called *boundary pruning*. It illustrates a perceptual principle called *asymmetry between near and far*. This principle is reflected in many phenomena, including 3D neon color spreading (Nakayama et al., 1990). Grossberg (1994, 1999a) discusses how to explain such data.

How does boundary pruning influence figure-ground separation? Boundary pruning spares the closest surface representation that successfully fills-in a region and inhibits redundant copies of occluding object boundaries that would otherwise form at farther depths. When these redundant occluding boundaries are removed, the boundaries of partially occluded objects can be completed behind them within

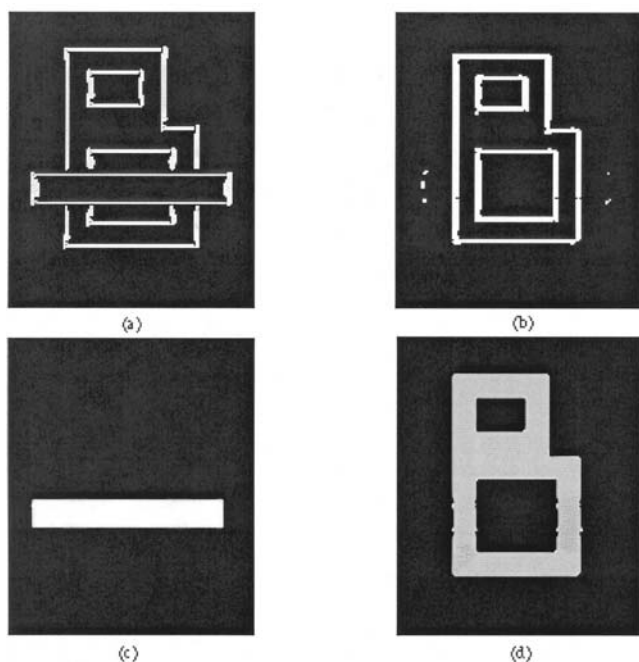


FIGURE 110.9. Amodal boundary and surface representations in response to a Bregman–Kanizsa image. Binocular boundaries after boundary pruning occurs: (a) near depth and (b) far depth. Filled-in amodal surface representations at the monocular FIDOs: (c) near depth and (d) far depth. (Reprinted with permission from Kelly and Grossberg, 2000.)

BCS copies that represent farther depths, as we perceive from Figure 110.5A but not 110.5B. Moreover, when the redundant occluding boundaries collapse, the redundant surfaces that they momentarily supported at the monocular FIDOs also collapse. Occluding surfaces thereby form in front of occluded surfaces.

Figures 110.9A and 110.9B illustrate boundary pruning and its asymmetric action from near to far. The near boundaries in Figure 110.8A are retained in Figure 110.9A, but the far boundary of the occluder in Figure 110.8B is inhibited by boundary pruning signals from the contour of the near filled-in surface representation in Figure 110.8C. When these occluder boundaries are eliminated, the B boundary can be colinearly completed, as in Figure 110.9B. Because the boundaries of both the horizontal occluder and the B are now connected, they can contain their filled-in activities within the monocular FIDOs, as shown in Figures 110.9C and 110.9D.

Boundary pruning also helps to explain data about depth/brightness interactions, such as: why do brighter Kanizsa squares look closer (Bradley and Dumais, 1984)? Why is boundary pruning relevant here? A Kanizsa square’s brightness is an emergent property that is determined after *all* brightness and darkness inducers fill-in within the square. This emergent brightness within the FIDOs then influences the square’s perceived depth. Within FACADE, this means

that the FIDO’s brightness influences the BCS copies that control relative depth. This occurs via the BCS-to-FCS feedback signals, including pruning, that ensure boundary-surface consistency (Grossberg, 1997, Section 22).

Visible brightness percepts are not represented within the monocular FIDOs. Model V2 representations of binocular boundaries and monocular filled-in surfaces are predicted to be *amodal*, or perceptually invisible. These representations are predicted to directly activate object recognition mechanisms in inferotemporal cortex and beyond, since they accurately represent occluding and occluded objects. In particular, boundary pruning enables boundaries of occluded objects to be completed within the BCS, which makes them easier to recognize, as is illustrated for the Bregman–Kanizsa display in Figure 110.9. The monocular FIDO surface representations fill-in an occluded object within these completed object boundaries, even behind an opaque occluding object. We can thereby *know* the color of occluded regions without *seeing* them. How, then, do we *see* opaque occluding surfaces? How does the visual cortex generate representations of occluding and occluded objects that can be easily recognized, yet also allow us to consciously see, and reach for, only the unoccluded parts of objects?

FACADE theory proposes that the latter goal is achieved at the binocular FIDOs using a different combination of boundary and surface representations than is found at the monocular FIDOs. The surface representations at the monocular FIDOs are depth-selective, but they do not combine brightness and color signals from both eyes. Binocular combination of brightness and color signals takes place at the binocular FIDOs, which are predicted to exist in cortical area V4. It is here that *modal*, or visible, surface representations occur, and we see only unoccluded parts of occluded objects, except when transparent percepts are generated by special circumstances.

To accomplish binocular surface matching, monocular FCS signals from both eyes (pathways 8 in Fig. 110.6) are binocularly matched at the binocular FIDOs. These matched signals are redundantly represented on multiple FIDOs. The redundant binocular signals are pruned by inhibitory contrast-sensitive signals from the monocular FIDOs (pathways 9 in Fig. 110.6). As in the case of boundary pruning, these *surface pruning* signals arise from surface regions that successfully fill-in within the monocular FIDOs. These signals inhibit the FCS signals at their own positions and farther depths. As a result, occluding objects cannot redundantly fill-in surface representations at multiple depths. Surface pruning is another example of the asymmetry between near and far. Figure 110.10 illustrates how surface pruning works for the Bregman–Kanizsa image. Figure 110.10A shows the signals that initiate filling-in at the near binocular FIDO, and Figure 110.10B shows them at the far

binocular FIDO. Surface pruning eliminates signals from the occluder in Figure 110.10B.

As in the monocular FIDOs, FCS signals to the binocular FIDOs can initiate filling-in only where they are spatially coincident and orientationally aligned with BCS boundaries. BCS-to-FCS pathways 10 in Figure 110.6 carry out depth-selective surface capture of the binocularly matched FCS signals that survive surface pruning. In all, binocular FIDOs fill in FCS signals that (1) survive within-depth binocular FCS matching and across-depth FCS inhibition; (2) are spatially coincident and orientationally aligned with BCS boundaries; and (3) are surrounded by a connected boundary (web).

One further property completes this summary: at the binocular FIDOs, nearer boundaries are added to FIDOs that represent their own and farther depths. This asymmetry

between near and far is called *boundary enrichment*. Enriched boundaries prevent occluding objects from looking transparent by blocking filling-in of occluded objects behind them. The total filled-in surface representation across all binocular FIDOs represents the visible percept. It is called a FACADE representation because it multiplexes the properties of Form-And-Color-And-DEpth that give this theory its name. Figures 110.10C and 110.10D show the enriched near and far binocular FIDO boundaries, respectively, for the Bregman–Kanizsa image. Note the superposition of occluder and occluding boundaries in Figure 110.10D. Figures 110.10E and 110.10F show the filled-in near and far modal surface representations that the surface signals in Figures 110.10A and 110.10B cause within the boundaries of Figures 110.10C and 110.10D. Note that only the unoccluded surface of the B is “visible” in the binocular FIDO representation, even though the entire B surface is completed within the amodal monocular FIDO representation in Figure 110.9D.

Conclusion

This chapter describes some of the complementary properties of boundary and surface computations in the interblob and blob cortical processing streams of visual cortex. These insights lead to a revision of classical views about how visual cortex works. In particular, visual cortex does not consist of independent processing modules. Rather, hierarchical and parallel interactions between the boundary and surface streams synthesize consistent visual percepts from their complementary strengths and weaknesses. Boundaries help to trigger depth-selective surface filling-in, and successfully filled-in surfaces reorganize the global patterning of boundary and surface signals via feedforward and feedback signals. Boundary-gated filling-in plays a key role in surface perception, ranging from lower-level uses, such as recovering surface brightness and color after discounting the illuminant and filling-in the blind spot, to higher-level uses, such as completing depthful modal and amodal surface representations during 3D vision and figure-ground separation. Nor is visual cortex a feedforward filter that passively detects visual features. Rather, it is an integrated system of bottom-up, top-down, and horizontal interactions which actively completes boundary groupings and fills-in surface representations as its emergent functional units. This interactive perspective has enabled recent neural models to simulate quantitatively the dynamics of individual cortical cells in laminar cortical circuits and visual percepts that emerge from their circuit interactions.

Acknowledgments

The author wishes to thank Robin Amos for his valuable assistance in the preparation of the manuscript. The research

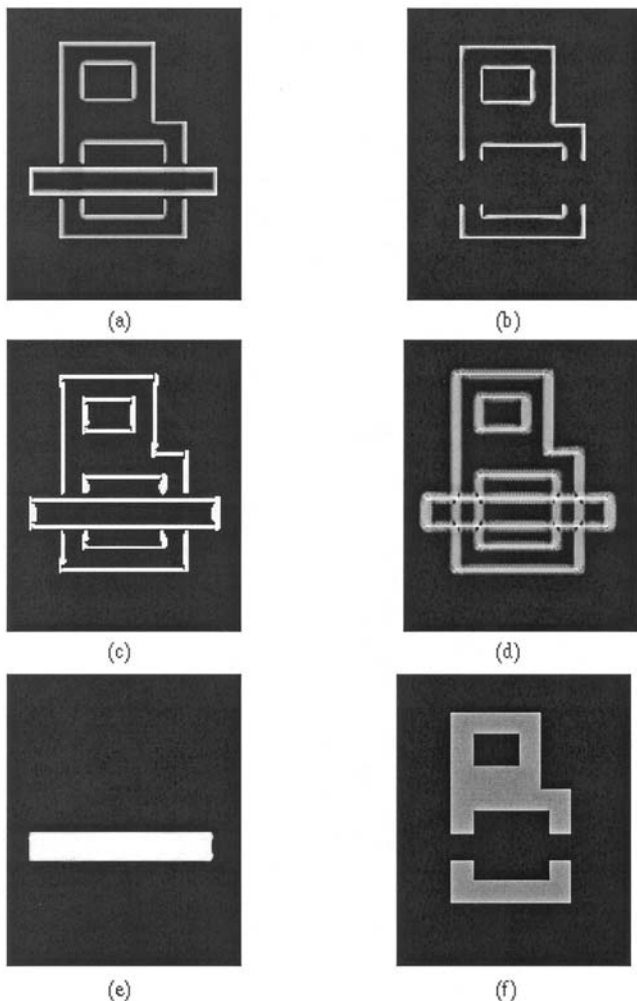


FIGURE 110.10. Enriched boundary and modal surface representations. Binocular FIDO filling-in signals at (a) near depth and (b) far depth. Enriched boundaries at (c) near depth and (d) far depth. Filled-in binocular FIDO activity consisting of two modal surfaces at two different depths: (e) near depth and (f) far depth. (Reprinted with permission from Kelly and Grossberg, 2000.)

was supported in part by the Air Force Office of Scientific Research (AFOSR F49620-01-1-0397) and the Office of Naval Research (ONR N00014-01-1-0624).

REFERENCES

- Arrington, K. F., 1994. The temporal dynamics of brightness filling-in, *Vis. Res.*, 34:3371–3387.
- Boynton, R. M., R. T. Eskew, Jr., and C. X. Olson, 1985. Research note: blue cones contribute to border distinctness, *Vis. Res.*, 25:1349–1352.
- Bradley, D. R., and S. T. Dumais, 1984. The effects of illumination level and retinal size on the depth stratification of subjective contour figures, *Perception*, 13:155–164.
- Brown, J. M., and N. Weisstein, 1988. A spatial frequency effect on perceived depth, *Percept. Psychophys.*, 43:53–56.
- Cohen, M. A., and S. Grossberg, 1984. Neural dynamics of brightness perception: features, boundaries, diffusion, and resonance, *Percept. Psychophys.*, 36:428–456.
- Dennett, D., 1991. *Consciousness Explained*, Boston: Little, Brown.
- De Yoe, E. A., and D. C. Van Essen, 1988. Concurrent processing streams in monkey visual cortex, *Trends Neurosci.*, 11:219–226.
- Egusa, H., 1983. Effects of brightness, hue, and saturation on perceived depth between adjacent regions in the visual fields, *Perception*, 12:167–175.
- Elder, J. H., and S. W. Zucker, 1998. Evidence for boundary-specific grouping, *Vis. Res.*, 38:143–152.
- Fahle, M., and G. Westheimer, 1995. On the time-course of inhibition in the stereoscopic perception of rows of dots, *Vis. Res.*, 35:1393–1399.
- Faubert, J., and M. von Grünau, 1995. The influence of two spatially distinct primers and attribute priming on motion induction, *Vis. Res.*, 36:149–173.
- Field, D. J., A. Hayes, and R. F. Hess, 1993. Contour integration by the human visual system; evidence for a local “association field,” *Vis. Res.*, 33:173–193.
- Francis, G., and S. Grossberg, 1996. Cortical dynamics of boundary segmentation and reset: persistence, afterimages, and residual traces, *Perception*, 25:543–567.
- Francis, G., S. Grossberg, and E. Mingolla, 1994. Cortical dynamics of feature binding and reset: control of visual persistence, *Vis. Res.*, 34:1089–1104.
- Gogel, W. C., 1965. Equidistance tendency and its consequences, *Psych. Bull.*, 64:153–163.
- Gove, A., S. Grossberg, and E. Mingolla, 1995. Brightness perception, illusory contours, and corticogeniculate feedback, *Vis. Neurosci.*, 12:1027–1052.
- Grossberg, S., 1973. Contour enhancement, short-term memory, and constancies in reverberating neural networks, *Studies Appl. Math.*, 52:217–257.
- Grossberg, S., 1984. Outline of a theory of brightness, color, and form perception, in (E. Degreaf and J. van Buggenhout eds.) *Trends in Mathematical Psychology*, Amsterdam: Elsevier/North-Holland, pp. 59–86.
- Grossberg, S., 1987a. Cortical dynamics of three-dimensional form, color, and brightness perception: I. Monocular theory, *Percept. Psychophys.*, 41:87–116.
- Grossberg, S., 1987b. Cortical dynamics of three-dimensional form, color, and brightness perception: II. Binocular theory, *Percept. Psychophys.*, 41:117–141.
- Grossberg, S., 1994. 3-D vision and figure-ground separation by visual cortex, *Percept. Psychophys.*, 55:48–120.
- Grossberg, S., 1997. Cortical dynamics of three-dimensional figure-ground perception of two-dimensional pictures, *Psychol. Rev.*, 104:618–658.
- Grossberg, S., 1999a. A comment on “Assimilation of achromatic color cannot explain the brightness effects of the achromatic neon effect” by Marc K Albert, *Perception*, 28:1291–1302.
- Grossberg, S., 1999b. How does the cerebral cortex work? Learning, attention, and grouping by the laminar circuits of visual cortex, *Spat. Vis.*, 12:163–186.
- Grossberg, S., 2000. The complementary brain: Unifying brain dynamics and modularity, *Trends Cogn. Sci.* 4:233–245.
- Grossberg, S., and F. Kelly, 1999. Neural dynamics of binocular brightness perception, *Vis. Res.*, 39:3796–3816.
- Grossberg, S., and P. D. L. Howe, 2003. A laminar cortical model of stereopsis and three-dimensional surface perception, *Vis. Res.*, 43:801–829.
- Grossberg, S., and E. Mingolla, 1985a. Neural dynamics of form perception: boundary completion, illusory figures, and neon color spreading, *Psychol. Rev.*, 92:173–211.
- Grossberg, S., and E. Mingolla, 1985b. Neural dynamics of perceptual grouping: Textures, boundaries, and emergent segmentations, *Percept. Psychophys.*, 38:141–171.
- Grossberg, S., S. Hwang, and E. Mingolla, 2002. Thalamocortical dynamics of the McCollough effect: boundary-surface alignment through perceptual learning, *Vis. Res.*, 42:1259–1286.
- Grossberg, S., E. Mingolla, and J. W. Williamson, 1995. Synthetic aperture radar processing by a multiple scale neural system for boundary and surface representation, *Neural Net.*, 8:1005–1028.
- Grossberg, S., and N. McLoughlin, 1997. Cortical dynamics of 3-D surface perception: binocular and half-occluded scenic images, *Neural Net.*, 10:1583–1605.
- Grossberg, S., and L. Pessoa, 1998. Texture segregation, surface representation, and figure-ground separation, *Vis. Res.*, 38:2657–2684.
- Grossberg, S., and R. D. S. Raizada, 2000. Contrast-sensitive perceptual grouping and object-based attention in the laminar circuits of primary visual cortex, *Vis. Res.*, 40:1413–1432.
- Grossberg, S., and D. Todorovic, 1988. Neural dynamics of 1-D and 2-D brightness perception: a unified model of classical and recent phenomena, *Percept. Psychophys.*, 43:241–277.
- Grossberg, S., and J. R. Williamson, 2001. A neural model of how horizontal and interlaminar connections of visual cortex develop into adult circuits that carry out perceptual grouping and learning, *Cereb. Cortex.*, 11:37–58.
- He, Z. J., and K. Nakayama, 1995. Visual attention to surface in three-dimensional space, *Proc. Natl. Acad. Sci. USA*, 21:11155–11159.
- Heeger, D. J., 1992. Normalization of cell responses in cat striate cortex, *Vis. Neurosci.*, 9:181–197.
- Helson, H., 1963. Studies of anomalous contrast and assimilation, *J. Opt. Soc. Am.*, 53:179–184.
- Hubel, D., and T. N. Wiesel, 1977. Functional architecture of macaque monkey visual cortex, *Proc. R. Soc. Lond. B*, 198:1–59.
- Julesz, B., and R. A. Schumer, 1981. Early visual perception, *Annu. Rev. Psychol.*, 32:572–627.
- Kanizsa, G., 1974. Contours without gradients or cognitive contours. *It. J. Psychol.*, 1:93–113.
- Kawabata, N., 1984. Perception at the blind spot and similarity grouping, *Percept. Psychophys.*, 36:151–158.
- Kelly, F., and S. Grossberg, 2000. Neural dynamics of 3-D surface perception: figure-ground separation and lightness perception, *Percept. Psychophys.*, 62:1596–1618.

- Lamme, V. A., V. Rodríguez-Rodríguez, and H. Spekreijse, 1999. Separate processing dynamics for texture elements, boundaries and surfaces in primary visual cortex of the macaque monkey, *Cereb. Cortex*, 9:406–413.
- Lee, T. S., D. Mumford, R. Romero, and V. A. Lamme, 1998. The role of the primary visual cortex in higher level vision, *Vis. Res.*, 38:2429–2454.
- Li, Z., 1998. A neural model of contour integration in the primary visual cortex, *Neural Comput.*, 10:903–940.
- Mumford, D., 1992. On the computational architecture of the neocortex. II. The role of corticocortical loops, *Biol. Cybern.*, 66:241–251.
- Nakayama, K., and S. Shimojo, 1990. DaVinci stereopsis: depth and subjective occluding contours from unpaired image points, *Vis. Res.*, 30:1811–1825.
- Nakayama, K., S. Shimojo, and V. S. Ramachandran, 1990. Transparency: relation to depth, subjective contours, luminance, and neon color spreading, *Perception*, 19:497–513.
- Nakayama, K., S. Shimojo, and G. H. Silverman, 1989. Stereoscopic depth: its relation to image segmentation, grouping, and the recognition of occluded objects, *Perception*, 18:55–68.
- Neumann, H., L. Pessoa, and T. Hansen, 2001. Visual filling-in for computing perceptual surface properties, *Biol. Cybern.*, 85:355–369.
- Paradiso, M. A., and K. Nakayama, 1991. Brightness perception and filling-in, *Vis. Res.*, 31:1221–1236.
- Pessoa, L., J. Beck, and E. Mingolla, 1996. Perceived texture segregation in chromatic element-arrangement patterns: high luminance interference, *Vis. Res.*, 36:1745–1761.
- Pessoa, L., E. Mingolla, and H. Neumann, 1995. A contrast- and luminance-driven multiscale network model of brightness perception, *Vis. Res.*, 35:2201–2223.
- Pessoa, L., E. Thompson, and A. Noë, 1998. Finding out about filling in: a guide to perceptual completion for visual science and the philosophy of perception, *Behav. Brain Sci.*, 21:723–802.
- Polat, U., K. Mizobe, M. W. Pettet, T. Kasamatsu, and A. M. Norcia, 1998. Collinear stimuli regulate visual responses depending on cell's contrast threshold, *Nature*, 391:580–584.
- Raizada, R. D. S., and S. Grossberg, 2001. Context-sensitive binding by the laminar circuits of V1 and V2: A unified model of perceptual grouping, attention, and orientation contrast, *Vis. Cogn.*, 8:431–466.
- Reynolds, J., L. Chelazzi, and R. Desimone, 1999. Competitive mechanisms subserve attention in macaque areas V2 and V4, *J. Neurosci.*, 19:1736–1753.
- Roelfsema, P. R., V. A. F. Lamme, and H. Spekreijse, 1998. Object-based attention in the primary visual cortex of the macaque monkey, *Nature*, 395:376–381.
- Rogers-Ramachandran, D. C., and V. S. Ramachandran, 1998. Psychophysical evidence for boundary and surface systems in human vision, *Vis. Res.*, 38:71–77.
- Shapley, R., and R. C. Reid, 1986. Contrast and assimilation in the perception of brightness, *Proc. Natl. Acad. Sci. USA*, 82:5983–5986.
- Shipley, T. F., and P. J. Kellman, 1992. Perception of partly occluded objects and illusory figures: evidence for an identity hypothesis, *J. Exp. Psych. Human Percept. Perform.*, 18:106–120.
- Sillito, A. M., H. E. Jones, G. L. Gerstein, and D. C. West, 1994. Feature-linked synchronization of thalamic relay cell firing induced by feedback from the visual cortex, *Nature*, 369:479–482.
- Smallman, H. S., and S. P. McKee, 1995. A contrast ratio constraint on stereo matching, *Proc. R. Soc. Lond. B*, 260:265–271.
- Swaminathan, G., and S. Grossberg, 2001. Laminar cortical circuits for the perception of slanted and curved 3-D surfaces, *Soc. Neurosci. (Abs.)*, 27:619.49.
- Thorpe, S., D. Fize, and C. Marlot, 1996. Speed of processing in the human visual system, *Nature*, 381:520–522.
- Von der Heydt, R., E. Peterhans, and G. Baumgartner, 1984. Illusory contours and cortical neuron responses, *Science*, 224:1260–1262.
- Waxman, A. M., M. C. Seibert, A. Gove, D. A. Fay, A. M. Bernardon, C. Lazott, W. R. Steele, and R. K. Cunningham, 1995. Neural processing of targets in visible, multispectral IR and SAR imagery, *Neural Net.*, 8:1029–1051.

How the Visual Cortex Recognizes Objects: The Tale of the Standard Model

MAXIMILIAN RIESENHUBER AND TOMASO POGGIO

OBJECT RECOGNITION is fundamental to the behavior of higher primates. It is also the most remarkable achievement of visual cortex and one that probably influences greatly its overall functional architecture.

Object recognition is a computationally hard problem. The visual system rapidly and effortlessly recognizes a large number of diverse objects in cluttered natural scenes. Computer vision systems are still far from passing the Turing test for vision, that is to “see” as well as human beings do. Very recent work in computer vision, however, has achieved impressive results on specific tasks such as object detection/categorization and face identification, suggesting that the problem is solvable with well-understood modern statistical learning algorithms.

The problem of object recognition is even more difficult from the point of view of neuroscience since it involves several levels of understanding, from the information processing or computational level to the level of circuits and of cellular and biophysical mechanisms. After decades of work in striate and extrastriate areas that have produced a significant and rapidly increasing amount of data, the emerging picture of how cortex performs object recognition may be becoming too complex for physiologists (as David Hilbert famously said about quantum mechanics: “Physics is too difficult for physicists”). Now, paralleling the very recent developments in bioinformatics, computational approaches may be riding to the rescue.

In this chapter, we attempt to take a first step. We review progress in the field. We do so by using a computational model as a tool to summarize, organize, and interpret existing data and discuss open questions. We first sketch the basic facts that have been established during the past three decades and that are now broadly accepted. We then describe a Standard Model that emerges from the data and represents in its basic architecture the average belief—often implicit—of many visual physiologists. In this sense, it is definitely not our model. The broad form of the model is suggested by the basic facts; we have made it quantitative and thereby predictive (through computer simulations). From the precise perspective it provides, we will discuss recent data, new experiments, and important open questions. We will also discuss specific alternative hypotheses

about modules and mechanisms of the model, as well as evidence that may possibly falsify the whole class of interpretations associated with the Standard Model.

Basic facts

Object recognition in cortex is thought to be mediated by the ventral visual pathway (Ungerleider and Haxby, 1994) running from primary visual cortex, V1, over extrastriate visual areas V2 and V4, to inferotemporal cortex IT. Based on physiological experiments in monkeys, IT has been postulated to play a central role in object recognition. IT, in turn, is a major source of input to prefrontal cortex (PFC), “the center of cognitive control” (Miller, 2000) involved in linking perception to memory.

Over the past decade, several physiological studies in non-human primates have established a core of basic facts about cortical mechanisms of recognition that seem to be widely accepted and that confirm and refine older data from neuropsychology. A brief summary of this consensus knowledge begins with the groundbreaking work of Hubel and Wiesel first in the cat (1962, 1965) and then in the macaque (1968). Starting from *simple cells* in primary visual cortex, V1, with small receptive fields that respond preferably to oriented bars, neurons along the ventral stream (Logothetis and Sheinberg, 1996; Perrett and Oram, 1993; Tanaka, 1996) show an increase in receptive field size as well as in the complexity of their preferred stimuli (Kobatake and Tanaka, 1994). At the top of the ventral stream, in anterior inferotemporal cortex (AIT), cells are tuned to complex stimuli such as faces (Desimone, 1991; Desimone et al., 1984; Gross et al., 1972; Perrett et al., 1992). The tuning of the view-tuned and object-tuned cells in AIT depends on visual experience as shown by Logothetis et al. (1995) and supported by Booth and Rolls (1998), DiCarlo and Maunsell (2000), and Kobatake et al. (1998). A hallmark of these IT cells is the robustness of their firing to stimulus transformations such as scale and position changes (Logothetis et al., 1995; Logothetis and Sheinberg, 1996; Perrett and Oram, 1993; Tanaka, 1996). In addition, as other studies have shown (Booth and Rolls, 1998; Hietanen et al., 1992; Logothetis et al., 1995; Perrett and Oram, 1993), most

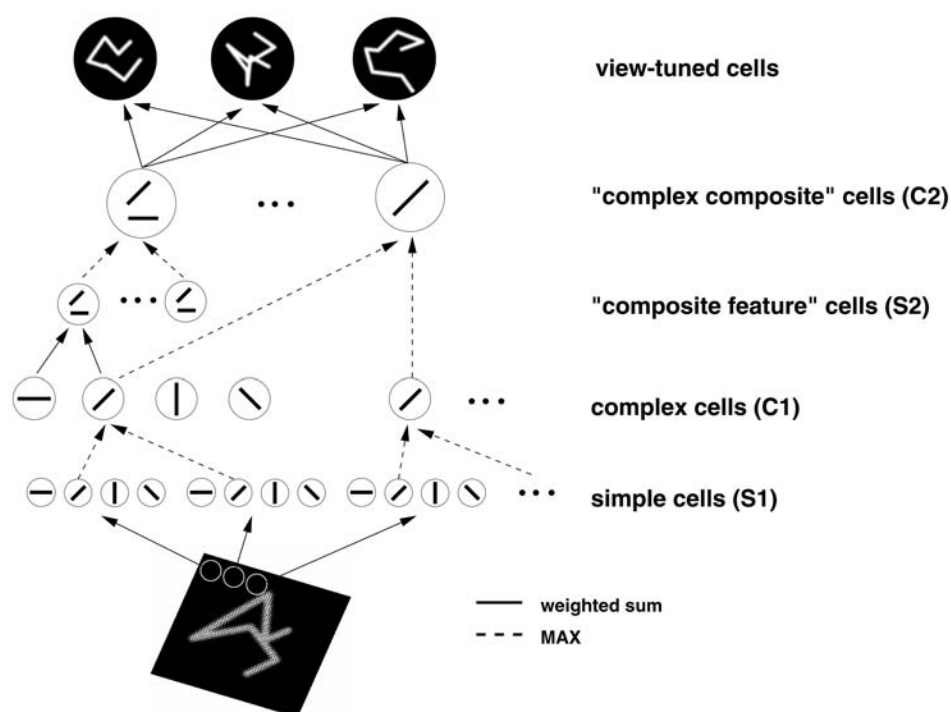


FIGURE 111.1. The figure shows the first part of the Standard Model. It extends several recent models (see especially Fukushima, 1980; see also Perrett and Oram, 1993; Poggio and Edelman, 1990; Riesenhuber and Poggio, 1999b; Wallis and Rolls, 1997). The view-based module, HMAX, shown here is an hierarchical extension of the classical paradigm (Hubel and Wiesel, 1962) of building complex cells from simple cells. The circuitry consists of a hierarchy of layers leading to greater specificity and greater invariance by using two different types of pooling mechanisms. The first layer in V1 represents linear oriented filters followed by input normalization, similar to simple cells (Carandini et al., 1997); each unit in the next layer (C1) pools the outputs of simple cells with the same orientation but at slightly different positions (scales) by using a maximum operation (see text and Riesenhuber and Poggio, 1999b). Each of these units is still orientation selective but more invariant to position (scale), similar to some complex cells. In the next stage, signals from complex cells with different orientations but similar positions are combined (in a weighted sum) to create neurons tuned to a dictionary of more complex features. The next layer (C2) is

similar to the C1 cells: by pooling together signals from S2 cells of the same type but at slightly different positions (and scales), the C2 units become more invariant to position (and scale) but preserve feature selectivity. They may correspond roughly to V4 cells. In the model, the C2 cells feed into view-tuned cells, with connection weights that are learned from exposure to a view of an object. There may be more levels in the hierarchy than are shown in the figure after the C2 layer. The output of the view-based module is represented by view-tuned model units that exhibit tight tuning to rotation in depth (as well as illumination and other object-dependent transformations such as facial expression) but are tolerant to scaling and translation of their preferred object view. Notice that the cells labeled here as view-tuned units encompass, between PIT and AIT, a spectrum of tuning from full views to components or complex features: depending on the synaptic weights determined during learning, each view-tuned cell becomes effectively connected to all or only a few of the units activated by the object view (Riesenhuber and Poggio, 1999a).

neurons show specificity for a certain object view or lighting condition. In particular, Logothetis et al. (1995) trained monkeys to perform an object recognition task with isolated views of novel three-dimensional objects ("paper clips"; see the objects at the top of Fig. 111.1). When recording from the animals' IT, they found that the great majority of neurons selectively tuned to the training objects were view-tuned (with a half-width of about 20 degrees for rotation in depth) to one of the training objects [about one-tenth of the tuned neurons were view-invariant, in agreement with earlier predictions (Poggio and Edelman, 1990)], but an average translation invariance of 4 degrees (for typical stimulus sizes of 2 degrees) and an average scale invariance of 2 octaves (Riesenhuber and Poggio, 1999b). Thus, whereas view-

invariant recognition requires visual experience of the specific novel object, position and scale invariance seems to be immediately present in the view-tuned neurons (Logothetis et al., 1995) without the need of visual experience for views of the specific object at different positions and scales. A very recent study (DiCarlo and Maunsell, 2003)—using different stimuli and training paradigm—reports translation invariance from one view of less than 3 degrees, pointing to a possible influence of training history and object shape on invariance ranges. Recent functional magnetic resonance imaging (fMRI) data have shown a similar pattern for the lateral occipital cortex (LOC), a brain region in human visual cortex central to object recognition and believed to be the homolog of monkey area IT (Grill-Spector et al., 2001;

Malach et al., 1995; Tanaka, 1997). Optical recordings in monkeys confirmed the view dependency of several face-tuned neurons (Wang et al., 1996).

A comment about the architecture is important: in its basic initial operation—akin to *immediate recognition*—the hierarchy is likely to be mainly feedforward (though local feedback loops almost certainly have key roles, e.g., possibly in performing a maximum-like pooling; see later) (Perrett and Oram, 1993). Event-related potential data (Thorpe et al., 1996) have shown that the process of object recognition appears to take remarkably little time, on the order of the latency of the ventral visual stream (Perrett et al., 1992), adding to earlier psychophysical studies using a rapid serial visual presentation (RSVP) paradigm (Intraub, 1981; Potter, 1975) that have found that subjects were still able to process images when they were presented as rapidly as eight per second.

In summary, the accumulated evidence points to six mostly accepted properties of the ventral stream architecture:

1. A hierarchical buildup of invariances first to position and scale and then to viewpoint and more complex transformations requiring the interpolation between several different object views
2. In parallel, an increasing size of the receptive fields
3. An increasing complexity of the optimal stimuli for the neurons
4. A basic feedforward processing of information (for “immediate” recognition tasks)
5. Plasticity and learning probably at all stages and certainly at the level of IT
6. Learning specific to an individual object is not required for scale and position invariance (over a restricted range)

The Standard Model

Invariance properties of IT neurons with respect to different transformations can be understood from a computational perspective (Riesenhuber and Poggio, 2000b): mathematically, the effects of two-dimensional (2D) affine transformations, such as scaling and translation in the image plane, can be estimated exactly from just one object view. There is no need then to, for example, collect examples of one object at all positions in the image to be able to generalize across positions from a single view. To determine the behavior of a specific object under transformations that depend on its three-dimensional (3D) shape, such as illumination changes or rotation in depth, however, one view generally is not sufficient. Unlike affine 2D transformations, 3D rotations, as well as illumination changes, usually require multiple example views during learning. Mathematically, the space of the orthographic views of one object is spanned by a single view for affine 2D transformations and by two or

more for affine 3D transformations (Poggio, 1990; Ullman and Basri, 1991).

The basic facts summarized earlier, together with the above computational considerations, lead to a Standard Model likely to represent the simplest class of models reflecting the known anatomical and biological constraints.

The model reflects the general organization of visual cortex in a series of layers from V1 to IT to PFC. From the point of view of invariance properties, it consists of a sequence of two main modules based on two key ideas. The first module, shown schematically in Figure 111.1, leads to model units showing the same scale and position invariance properties as the view-tuned IT neurons of Logothetis et al. (1995) using the same stimuli (Fig. 111.3). This is not an independent prediction since the model parameters were chosen to fit Logothetis’ data. It is, however, not obvious that an hierarchical architecture using plausible neural mechanisms could account for the measured invariance *and* selectivity. Computationally, this is accomplished by a scheme that can be best explained by taking striate complex cells as an example: invariance to changes in the position of an optimal stimulus (within a range) is obtained in the model by means of a *maximum operation (max)* performed on the simple cell inputs to the complex cells, where the strongest input determines the cell’s output. Simple cell afferents to a complex cell are assumed to have the same preferred orientation with their receptive fields located at different positions. Taking the maximum over the simple cell afferent inputs provides position invariance while preserving feature specificity. The key idea is that the step of filtering followed by a max operation is equivalent to a powerful signal processing technique: select the peak of the correlation between the signal and a given matched filter, where the correlation is either over position or over scale. The model alternates layers of units combining simple filters into more complex ones—to increase pattern selectivity—with layers based on the max operation—to build invariance to position and scale while preserving pattern selectivity.

In the second part of the architecture, shown in Figure 111.2, learning from multiple examples, that is, different view-tuned neurons, leads to view-invariant units as well as to neural circuits performing specific tasks. The key idea here is that interpolation and generalization can be obtained by simple networks, similar to Gaussian Radial Basis Function networks (GRBF) (Poggio and Girosi, 1990), that learn from a set of examples, that is, input-output pairs. In this case, the inputs are views and the outputs are the parameters of interest such as the label of the object or its pose or expression (for a face). The GRBF network has a hidden unit for each example view, broadly tuned to the features of an example image (see also opde Beeck et al., 2001). The weights from the hidden units to the output are learned from the set of examples, that is, input-output pairs. In principle,

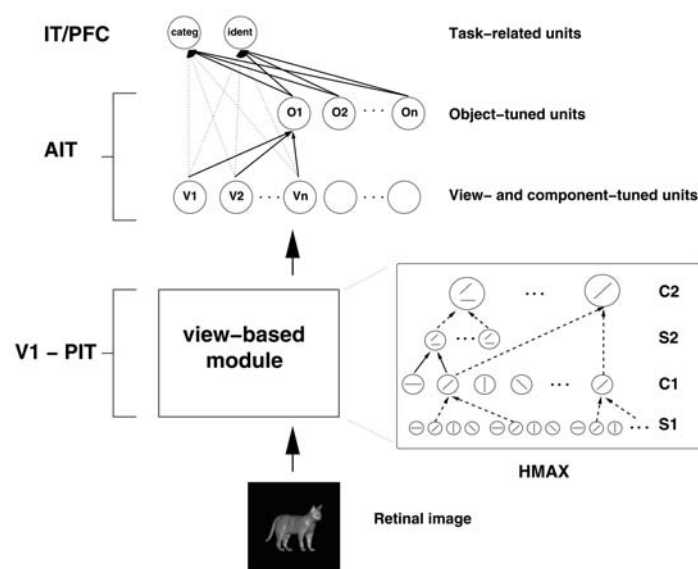


FIGURE 111.2. The figure shows the overall architecture of the Standard Model. The view-tuned module, described in Figure 111.1, is shown here in the inset (up to the C2 layer). The second part of the model starts with the view-tuned cells which represent the output of the view-based module. Invariance to rotation in depth is obtained by combining in a learning module several view-tuned units V_n tuned to different views of the same object (Poggio and Edelman, 1990), creating view-invariant (object-tuned) units O_n . These, as well as the view-tuned units, can then serve as input to task modules that learn to perform different visual tasks such as identification/discrimination or object categorization. They consist

of the same generic learning circuitry (similar to an RBF network; see text) but are trained with appropriate sets of examples to perform specific tasks. In addition to the feedforward processing, there are likely feedback pathways (not shown) for top-down modulation of neuronal responses throughout the processing hierarchy and to support the learning phase. The stages up to the object-centered units probably encompass V1 to anterior IT (AIT). The last stage of task-dependent modules may be localized in AIT or PFC. All the units in the model represent single cells modeled as simplified neurons with modifiable synapses. (Modified from Riesenhuber and Poggio, 2000b.)

two networks sharing the same hidden units but with different weights (from the hidden units to the output unit) could be trained to perform different tasks, such as pose estimation or view-invariant recognition. Depending just on the set of training examples, learning networks of this type can learn to categorize across exemplars of a class (Riesenhuber and Poggio, 1999c), as well as to identify an object across different illuminations and different viewpoints. The demonstration (Poggio and Edelman, 1990) that a view-based GRBF model could achieve view-invariant object recognition in fact-motivated psychophysical experiments (Bülthoff and Edelman, 1992; Gauthier and Tarr, 1997). In turn, the psychophysics provided strong support for the view-based hypothesis against alternative theories (for a review, see Tarr and Bülthoff, 1998) and, together with the model, triggered the physiological work of Logothetis et al. (1995).

Thus the two key ideas in the model are (1) the max operation to provide invariance at several steps of the hierarchy and (2) the RBF-like learning network to learn a specific task based on a set of cells tuned to example views.

Interpreting experimental data

The Standard Model summarizing the basic facts about the ventral pathways predicts additional experimental results

and provides interesting perspectives on still other data. For instance, the model accounts (see Riesenhuber and Poggio, 1999a, 1999c, 2000b) for the response of tuned IT cells to scrambled objects (Vogels, 1999) (see Fig. 5 in Riesenhuber and Poggio, 1999b), clutter (Missal et al., 1997) (Fig. 111.4), and mirror views (Logothetis and Sheinberg, 1996) (see Fig. 4 in Riesenhuber and Poggio, 1999b). It also shows a degree of performance roughly in agreement with physiological and psychophysical data in specific tasks (the same stimuli are used for simulations and experiments) such as the cat versus dog categorization task described by Freedman et al. (2001a) (Fig. 111.6), object identification (in separate experiments faces, cars, paper clips were used; see Figs. 111.5 and 111.7), gender classification, and possibly the face habituation effect of (Leopold et al., 2001).

A key function of models is to clarify key issues. Here we use the Standard Model to discuss several central topics concerning the neural mechanisms of object recognition.

SELECTIVITY Invariance is only one requirement for object recognition, the other one being selectivity. Several studies have established that IT neurons can become tuned to task-relevant objects and their full or partial (Vetter et al., 1995) views (DiCarlo and Maunsell, 2000; Kobatake et al., 1998; Logothetis et al., 1995) or to objects in the monkey's envi-

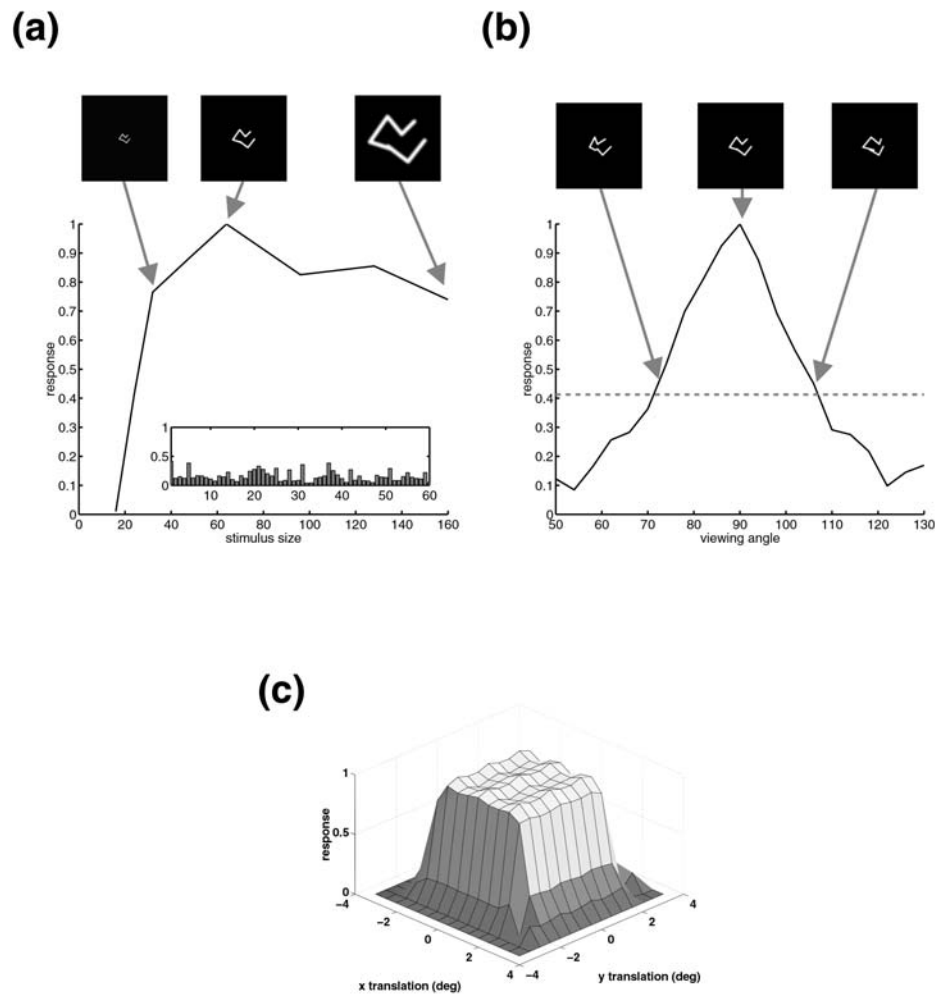


FIGURE 111.3. Responses of a sample model neuron to different transformations of its preferred stimulus. The different panels show the same neuron's response to (a) varying stimulus sizes [the inset shows the response to 60 distractor objects, selected randomly from the paper clips used in the physiology study (Logothetis et al.,

1995)], (b) experiments, rotation in depth, and (c) translation. The training size was 64×64 pixels corresponding to 2 degrees of visual angle. The simulation results shown here are in quantitative agreement with recordings in IT by Logothetis et al. (1995) (see Fig. 8 in that article), using the same stimuli.

ronment (Booth and Rolls, 1998), suggesting that these neurons provide a representation of objects occurring in an animal's environment. The preferred stimuli of neurons in intermediate stages of the ventral stream are less clear, partly owing to the difficulty of knowing which stimuli to use to probe the neural selectivity. Reports of preferred features of neurons in V4, the visual area preceding IT in the ventral pathway, vary, depending on the set of stimuli used to probe responses, including Cartesian gratings (Desimone and Schein, 1987) polar and hyperbolic sinusoidal gratings (Gallant et al., 1996), and contour features (Pasupathy and Connor, 1999). In V2, a recent study (Hegde and Van Essen, 2000) has reported preferences to complex stimuli such as arcs, intersecting lines, and non-Cartesian gratings. Instead of probing neuronal tuning with a fixed set of stimuli, a set of studies (Fujita et al., 1992; Kobatake and Tanaka, 1994; Tanaka, 1993, 1996) used a heuristic "simplification proce-

cedure" in an effort to arrive at the features crucial to activate a neuron. In this approach, a complex natural stimulus (such as a face) to which the neuron under study responds is progressively "simplified" (e.g., by removing color or texture or by reducing complex shapes to simpler geometric primitives) in a way that preserves or increases the neuronal firing. The stimulus that cannot be simplified further without significantly decreasing the firing rate is then labeled the *effective stimulus* for that cell. A study using this paradigm (Kobatake and Tanaka, 1994) has reported an increase in feature complexity from area V2 to anterior IT. However, a recent IT optical imaging study (Tsunoda et al., 2001), supported by single-cell recordings, demonstrates the fundamental difficulty of determining a neuron's preferred feature in higher visual areas. The authors report that simplifying a stimulus often causes additional IT neurons to respond relative to the more complex stimulus. Interestingly, the Standard Model

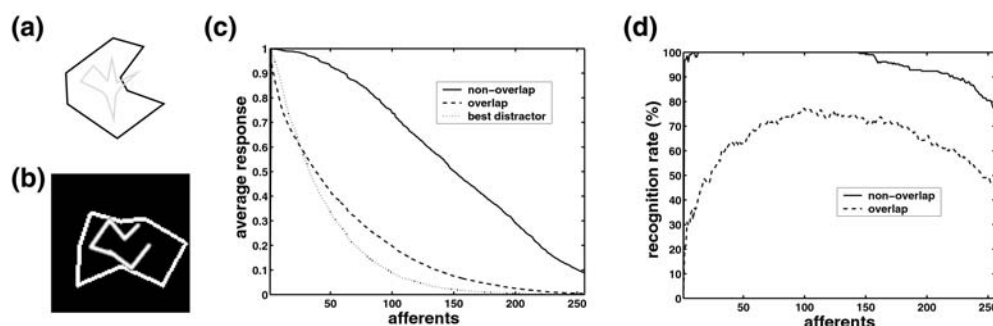


FIGURE 111.4. Recognition in clutter in the Standard Model. *a*, Example stimulus (light gray) and outline background (black) from the experiment by Missal et al. (1997) (redrawn from that source), in which a monkey was trained to recognize polygonal shapes in isolation and on a polygonal background. In the experiment, foreground and background stimuli were of different colors. The study found that while the monkeys' performance was only slightly impaired by the introduction of a background stimulus (from 98% to 89% correct), firing rates of IT neurons were affected much more strongly. *b*, Example stimulus for the corresponding experiment with the model, in which paper clip stimuli were superimposed on polygonal backgrounds (for details, see Riesenhuber and Poggio, 1999a). Unlike in the experiment (Missal et al., 1997), the stimuli and background were of the same color, increasing task difficulty. The foreground clip in *b* was correctly recognized by the corresponding model IT unit (which was the same as in Fig. 111.3).

does in fact predict qualitatively what is observed—neurons tuned to a dictionary of features at different levels of complexity. Moreover, preliminary simulations (Knoblich and Riesenhuber, 2002) suggest that for IT model units the effect of the simplification procedure may well lead to the observations of Tsunoda et al. (2001). In any case, it is important to emphasize that features are defined not only by the specific image but also by the system looking at it. A pattern that seems simple to us may activate more filters in a vision system looking at it than another stimulus that is apparently more complex, depending on the filters used by the system. Thus the Standard Model can provide specific hypotheses to guide experiments regarding how more complex features (and ultimately object-tuned cells) are built from simpler ones.

REPRESENTATION Related to the question of neuronal tuning is the question of the precise nature of object representation in cortex. It has recently been put forward, based on a set of human fMRI studies, that some object classes—faces (Kanwisher et al., 1997), places (Epstein and Kanwisher, 1998), body parts (Downing et al., 2001)—are processed by distinct modules in cortex. Interestingly, another fMRI study (Haxby et al., 2001) has shown that objects of a certain class (e.g., faces) evoke a distributed pattern of activity that is not confined to the aforementioned specialized modules [e.g., the fusiform face area (FFA), a brain area that is strongly activated by face stimuli

(Kanwisher et al., 1997)], and that the part of the activation pattern *outside* the specific module is sufficient for object categorization. Thus, some data appear to argue for a *modular* framework of object representation in cortex, where specific brain areas perform computations unique to the object class at hand, while others support a model in which the same computation is performed for different objects and represented in a distributed way. The latter claim is supported by the Standard Model, which also helps to reconcile the two sets of data. Model IT units have preferred C2 activation vectors that can be full or partial view of an object (Riesenhuber and Poggio, 1999a), depending on their connectivity. The distinction between *complex features* and *object* is largely semantic, since during training a cell can become tuned to a feature that is diagnostic for the object rather than to a full view (Pauls, 1997). What is relevant for object recognition is that the objects to be discriminated produce distinct activation patterns. From the point of view of the model, groups of neurons responding to representatives from the same object class do not have to be segregated but are expected to be interdigitated. Since the activity of one fMRI voxel is the average over typically hundreds of thousands of neurons,¹ strong activation of the FFA for faces would argue for a

(Kanwisher et al., 1997)], and that the part of the activation pattern *outside* the specific module is sufficient for object categorization. Thus, some data appear to argue for a *modular* framework of object representation in cortex, where specific brain areas perform computations unique to the object class at hand, while others support a model in which the same computation is performed for different objects and represented in a distributed way. The latter claim is supported by the Standard Model, which also helps to reconcile the two sets of data. Model IT units have preferred C2 activation vectors that can be full or partial view of an object (Riesenhuber and Poggio, 1999a), depending on their connectivity. The distinction between *complex features* and *object* is largely semantic, since during training a cell can become tuned to a feature that is diagnostic for the object rather than to a full view (Pauls, 1997). What is relevant for object recognition is that the objects to be discriminated produce distinct activation patterns. From the point of view of the model, groups of neurons responding to representatives from the same object class do not have to be segregated but are expected to be interdigitated. Since the activity of one fMRI voxel is the average over typically hundreds of thousands of neurons,¹ strong activation of the FFA for faces would argue for a

¹For cautionary notes about the interpretation of fMRI images see Logothetis et al. (2001).

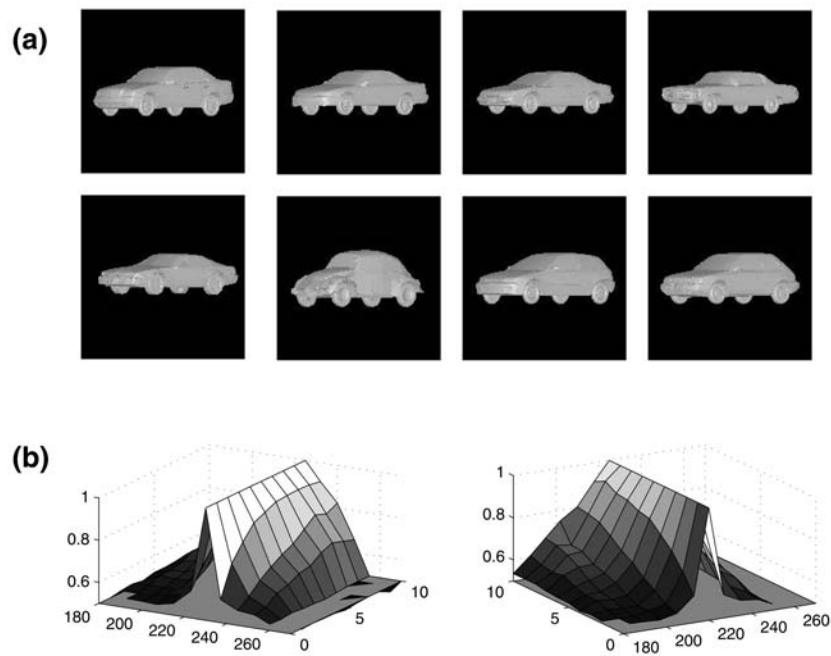


FIGURE 111.5. Recognition of non-paper clip objects (morphed cars) in HMAX. *a*, The eight prototype cars spanning the car morph space (Riesenhuber and Poggio, 2000a). *b*, Recognition performance of the model on the eight car morph space for a discrimination task in which first a target car was shown from a viewpoint $\phi_0 = 225$ degrees. This car, presented at viewpoint ϕ (varying between 180 and 270 degrees), then had to be discriminated from a distractor car presented at the same viewpoint ϕ . The similarity of the target and distractor cars was controlled by varying the separation of their corresponding parameter vectors in morph space. In particular, the parameter vectors were chosen to lie on lines connecting two prototypes from *a*. The *x*-axis shows viewpoint ϕ of the nonmatch object, *y*-axis target/distractor morph distance d (in steps along the morph line that the sample object lies on, a distance of 10 corresponds to the easiest case of the two cars being

different prototypes), and *z*-axis model discrimination performance for all (ϕ, d) stimulus pairs in the sample set. Stimulus identity was represented by a population code over 16 “car neurons.” The two subplots show the same graph from two different viewpoints to show positive rotations (i.e., toward the front, so that the front of the car is turning toward the viewer, as used in the psychophysical experiments), left plot, and negative rotations (i.e., toward the back, so that the side of the car faces the viewer), right plot. Note that the invariance range for the class of car stimuli is comparable to the results obtained with the paper clip stimuli in psychophysics and modeling (Bülthoff and Edelman, 1992; Logothetis et al., 1994; Poggio and Edelman, 1990) (see Fig. 111.3), demonstrating the generality of the model (over different object classes and representations).

higher density of face neurons in that part of cortex, possibly reflecting the great cognitive importance of face neurons. However, subjects with great expertise for other object classes might show significant activation of parts of cortex for objects from their field of expertise. Indeed, in bird and car experts, brain areas, overlapping with but not limited to the FFA, have been found to be specifically activated by birds and cars, respectively (Gauthier et al., 2000).

Thus the Standard Model suggests the following object representation in cortex [for the appropriate computational simulations, see Riesenhuber and Poggio (1999c, 2000a)], a related proposal can be found in Edelman (1999). A particular object, say a specific face, will elicit different activity in the view-specific V_n and object-specific O_n cells of Figure 111.2 (an example of which is shown in Fig. 111.7). Thus, the memory of the particular face is represented in the identification circuit in an implicit way by a sparse population code through the activation pattern over the coarsely tuned V_n and O_n cells, generally without cells dedicated to repre-

sent individual objects (*grandmother cells*).² Discrimination, or memorization of specific objects, can then proceed by comparing activation patterns over the strongly activated object- or view-tuned units (Riesenhuber and Poggio, 2000a) tuned to a small number of “prototypical” faces (Young and Yamane, 1992). For a certain level of specificity, only the activations of a small number of units have to be stored, forming a sparse code—in contrast to activation patterns on lower levels, where units are less specific and hence activation patterns tend to involve more neurons. In a similar fashion, categorization neurons, located putatively in the PFC, can be trained (Riesenhuber and Poggio, 1999c) to receive input from relevant object-tuned units.

²For special cases in which a small, fixed number of objects had to be discriminated [as, for example, it Logothetis et al. (1995)], the representations found in the model during learning turned out to be more grandmother-like.

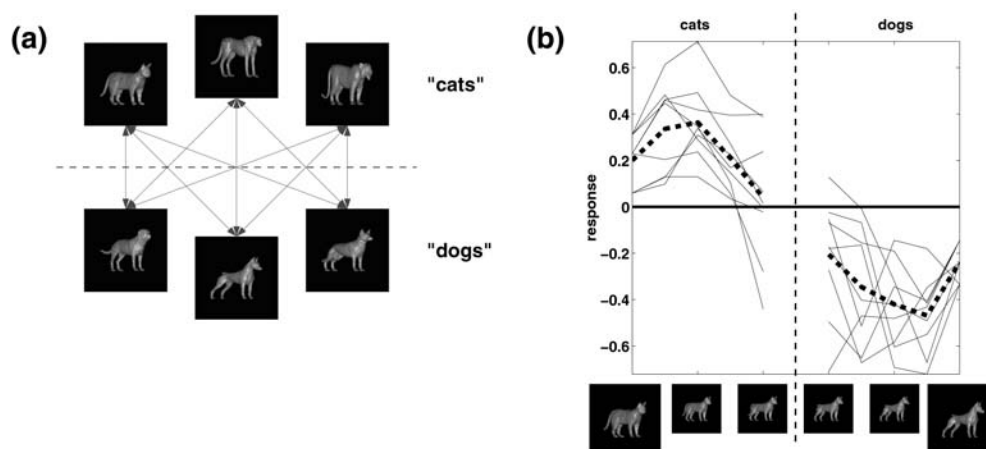


FIGURE 111.6. Example of categorization in the Standard Model. *a*, Illustration of the cat/dog stimulus space [used in the physiology experiments of Freedman et al. (2001a)]. The morph space is spanned by the pictures of three cats shown on top (“House Cat,” “Cheetah,” and “Tiger”) and the three dogs below (“House Dog,” “Doberman,” and “German Shepherd”). All prototypes have been normalized with respect to viewing angle, lighting parameters, size, and color. *b*, Response of a cat/dog categorization unit along the nine class boundary-crossing morph lines (*thin lines*). The unit receives input from 144 view-tuned units tuned to cat/dog training stimuli, as used in Freedman et al. (2001a), and was trained to respond differently to cats and dogs (cf. Fig. 111.7). The dashed line

shows the average over all morph lines. The solid horizontal line shows the class boundary in response space, and the dashed vertical line shows the category boundary in morph space the unit was trained on. The images on the bottom are taken from one morph line (from the House Cat to the Doberman) to illustrate the fine shape changes involved in categorization. All stimuli in the left half of the plot are “cats” and all stimuli in the right half are “dogs” (the class boundary is at the morph line center). The model unit correctly categorizes 94% of all stimuli [as good as the monkey trained on the same categorization task (Freedman et al., 2001a)], with errors occurring at the class boundary where categorization is most difficult (Riesenhuber and Poggio, 1999c).

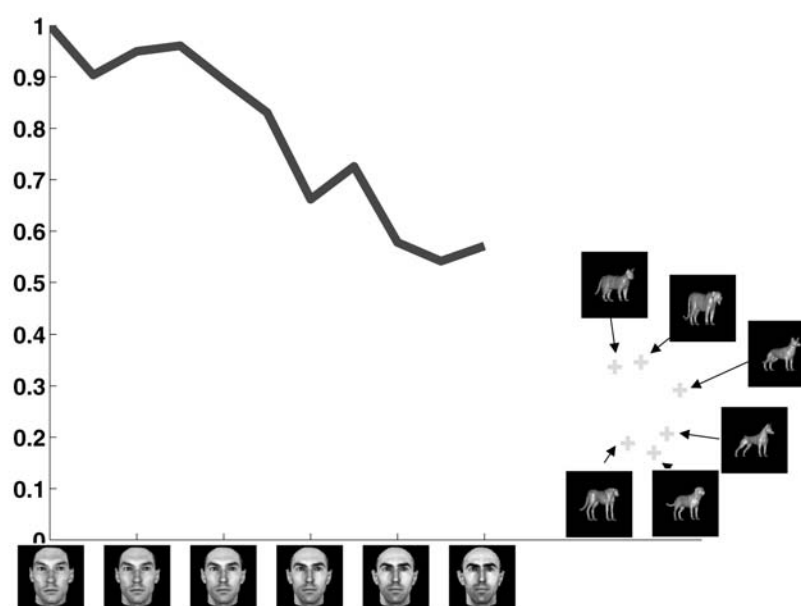


FIGURE 111.7. Tuning of a model face unit. The unit is a view-tuned unit, as shown in Figure 111.2, tuned to the face shown in the lower left. The solid line shows how the unit's response changes as the stimulus is gradually morphed away from the preferred stimulus to another face (faces shown at lower edge of plot). The unit's response changes gradually with changes in the stimulus, permitting subordinate-level discrimination [especially when using a population code consisting of several units tuned to different representatives of the class (Riesenhuber and Poggio, 2000a)]. The

same unit also responds to animal stimuli [cf. Freedman et al. (2001a); responses shown by crosses], but at a lower level than to the faces, permitting a coarse categorization of a stimulus as an animal stimulus based on the face unit's firing (cf. Haxby et al., 2001). As for subordinate-level recognition, combining several such units in a sparse population code (Young and Yamane, 1992), improves recognition performance (Riesenhuber and Poggio, 1999c). [Faces and morphing software courtesy of Thomas Vetter (Blanz and Vetter, 1999).]

CATEGORIZATION AND IDENTIFICATION An object can be recognized at different levels—a face can be recognized as a face, but also more specifically as a “male face,” “Tommy Poggio’s face,” or “Tommy Poggio’s smiling face.” It has been common in cognitive science to assume that recognition of an object at different levels is based on different computational mechanisms (Murphy and Brownell, 1985; Tversky and Hemenway, 1984). In particular, it has been proposed that *subordinate-level* recognition (identification) is based on *configurational* judgments (i.e., based on the spatial arrangement of features), whereas *basic-level* categorization (a face? a dog? a car?) is based on a qualitative representation based on the presence or absence of features. However, as Figure 111.2 makes clear and as we pointed out earlier (Riesenhuber and Poggio, 2000b), all supervised recognition tasks—in which the subject is trained with labeled examples—are identical from a computational point of view: they all involve a classification based on positive and negative exemplars. Indeed, it is not clear why different computations should be required in recognizing a face on the subordinate level and in, for example, determining its gender. Rather, in the simple framework of the Standard Model, the same learning algorithm and architecture can support a variety of object recognition tasks. In particular, identification and categorization circuits (possibly located in PFC) should receive signals from the same or equivalent cells tuned to specific objects or prototypes (in IT). This prediction is supported by recent results from physiology (Opde Beeck et al., 2001), where different monkeys were trained on a discrimination and a categorization task on the same stimuli. Subsequent recordings from neurons in the animals’ IT revealed no systematic differences in the representation of stimuli in the different animals. Further support comes from combined IT and PFC recordings (Freedman et al., in press) of monkeys trained on a cat/dog categorization task (Freedman et al., 2001a), where PFC neurons showed stronger category tuning than IT neurons. Simulation results (Knoblich et al., 2002) suggest that the tuning properties of these IT neurons could in fact arise without any explicit category information during training. Recent human fMRI data which indicate that the FFA is involved not just in subordinate-level face recognition but also in face detection (Grill-Spector et al., 2001) also argue against a specialization of brain areas for recognition tasks such as subordinate-level recognition independent of object class.

The problem with many experiments investigating the relationship between categorization and identification which claim that there is a time advantage of basic-level recognition versus subordinate-level recognition (Jolicoeur et al., 1984; Rosch et al., 1976) is that the tasks used for the different recognition levels are of different difficulty: discriminating a face from a chair (in categorization) is a much easier task than discriminating the faces of the two authors (in

identification), as the latter two are more similar to each other. Assuming that physically similar stimuli produce similar neuronal activation patterns, and that the ability to discriminate between two stimuli requires a certain level of evidence, finer discrimination would require the accumulation of evidence (in the form of firing rate differences) over a longer time period than when the activation patterns are very different.

POOLING AND MAX MECHANISM A key component of hierarchical models of cortical processing, such as Fukushima’s and Hubel and Wiesel’s, is pooling of afferents with similar tuning to increase the neuronal response invariance of certain stimulus transformations. Our version of the Standard Model—the HMAX model of Figure 111.1—assumes that this pooling is done—at some but not all levels in cortical processing—by a *maximum-like operation* rather than by a linear sum.

Invariance for translation and scaling is achieved by pooling the responses from noninvariant neural detectors over multiple spatial positions or scales using a maximum-like operation. Pooling by a maximum operation, as opposed to linear summation, ensures that the invariant response is robust against background clutter and does not lose the selectivity for the original feature. In neural terms, the firing rate of a maximum circuit corresponds to the firing rate of the strongest input pooled over some set of synaptic inputs. The maximum operation can be realized with biologically plausible neural circuits.

It will be critical to evaluate whether there are sets of neurons along the ventral pathway that implement such an operation. The model predicts (Riesenhuber and Poggio, 1999b) that the first stage showing a maximum-operation is a subset of complex cells in V1. Preliminary data (Lampl et al., 2001), obtained by intracellular recordings in simple and complex cells, are encouraging.

Extensions of the Standard Model and open issues

The Standard Model can serve as a conceptual tool to guide experiments and as the integrative “glue” between single-cell physiology and behavior. It also incorporates a large body of experimental data into one coherent framework. However, this framework needs to be extended in a number of directions. For instance, it has to take into account top-down and bottom-up attentional effects (Itti and Koch, 2000), learning at most stages of the hierarchy (Riesenhuber and Poggio, 2000b), and recognition of moving objects (Giese and Poggio, 2003).

ATTENTION Attention permeates most natural object recognition tasks. Thus, all the issues discussed earlier have also to be addressed in the context of task dependency,

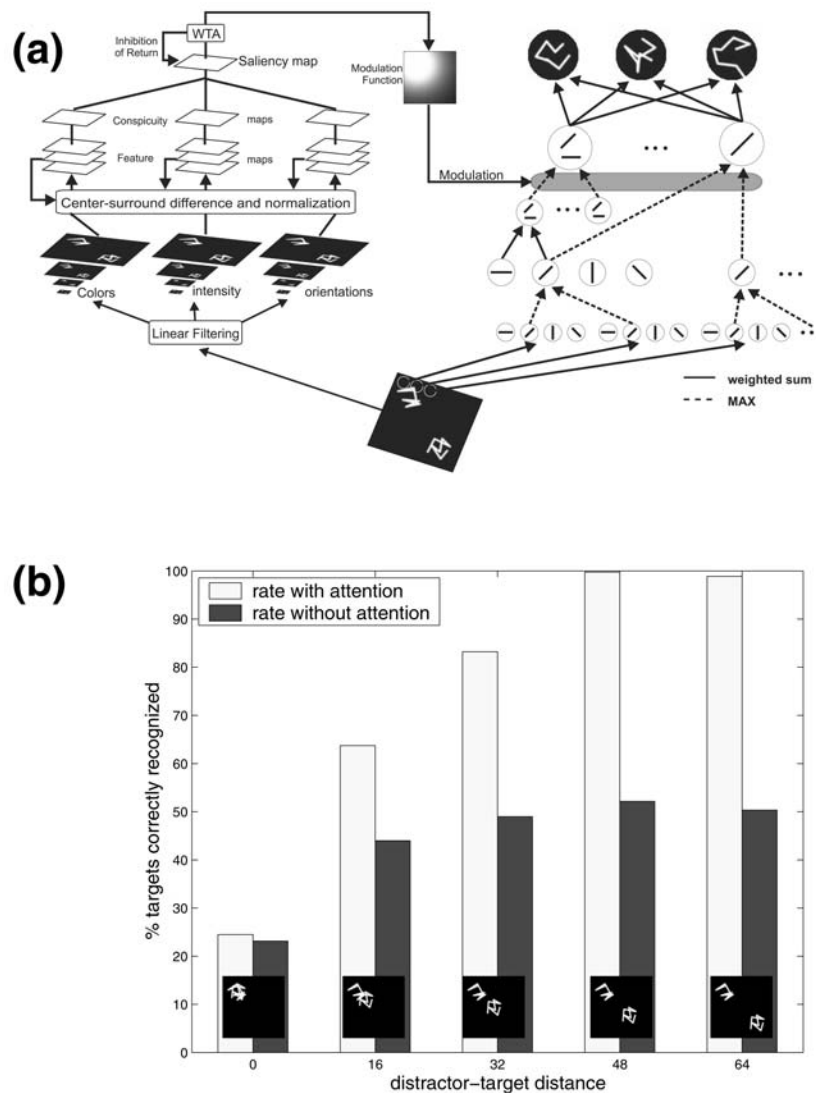


FIGURE 111.8. Coupling of the saliency map (Itti and Koch, 2000) and HMAX (Walther et al., 2002). *a*, Sketch of the integrated system. Targets in the saliency map (*left*) cause a modulation of receptive field size of C2 neurons in HMAX (*right*) by modulating their spatial pooling range (*center*). *b*, Recognition results in HMAX

with and without attentional modulation (cf. Fig. 111.4), depending on the separation of stimuli. Attentional modulation of the spatial extent of receptive fields dramatically improves recognition performance.

context, and attentional control. The experimental paradigms used so far in object recognition simplify these issues to a minimum. The Standard Model does not yet incorporate any attentional bias. This is justified by the fact that recognition is possible for scenes viewed in rapid visual presentation that do not allow sufficient time for shifts of attention (Potter, 1975). Furthermore, electroencephalographic studies (Thorpe et al., 1996) provide evidence that the human visual system is able to perform an object detection task—which includes categorization and search—within 150 msec, which is on the order of the latency of view- and object-tuned cells in IT (Perrett et al., 1992). Recent studies indeed suggest that such object detection tasks can be per-

formed in the near absence of attention (Li et al., 2002) and in parallel (Rousselet et al., 2002). None of this rules out, of course, the use of feedback processing, but it suggests a hierarchical feedforward architecture as the core circuitry underlying immediate recognition, with recursion and higher-level interactions playing a role only over longer time periods.

What should happen, however, in the model when the object to be detected is embedded in a large image? Saliency computation is likely to drive eye movement and to interact with the recognition machinery in this process (Fig. 111.8). Task-dependent priming may affect tuning of cells at different levels of the model.

This calls for investigating the relationship between object recognition and visual attention. The required quantitative theory will assume that object recognition derives its key properties of invariance and specificity from two cortical pathways working in parallel. An attentional system (which may be mapped in part onto the dorsal stream of primate cerebral cortex in addition to certain subcortical structures) selects salient or task-relevant candidate locations in the visual field. Attentional biases include both rapid, bottom-up, saliency-driven components as well as slower, top-down, task-dependent components. Attended locations are processed in a mainly feedforward (ventral) stream from primary visual cortex, to IT cortex, and PFC in order to recognize objects. We expect this cooperation between attentional and recognition systems to be especially relevant in object recognition situations too complex—due to, for instance, visual clutter or ambiguous displays—to be parsed by one feedforward pass through the object recognition pathway in isolation.

LEARNING In the Standard Model simulations described so far, *learning and adaptation* of synapses occur only at the last stages—from the dictionary of features produced by the view-based module in V4 and PIT to the view-tuned, object-tuned, and identification/categorization units. We believe, however, that experience-dependent learning occurs at all stages, possibly starting in V1. There is physiological evidence that the dictionary of complex features in PIT is affected by visual experience (Kobatake et al., 1998). Computationally, hard recognition tasks involving background and clutter require the selection of appropriate complex features, depending on the class of object [early simulations of feature selection used a HyperBF model (Bricolo et al., 1997; Vetter et al., 1995)]. It will be important to investigate with computer experiments how feature sets could be learned using plausible cortical mechanisms and how they may affect object recognition, in particular object detection performance. Simulation results have shown that the model's object detection performance in natural images can be significantly improved by learning target object class-specific intermediate features at the S2 level (Serre et al., 2002). Learning effects may also explain intriguing, recent data on limitations of position invariance (DiCarlo and Maunsell, 2003). It is likely that learning at different stages in cortex takes place over different time scales, the shortest in IT and PFC and the longer in V1.

RECOGNIZING OBJECTS IN MOTION Initial work on extending the Standard Model to the time domain for the recognition of biological movements and actions has begun (Giese and Poggio, 2003). The key idea in this extension of the model is that action recognition is based on learned proto-

typical complex motion patterns. Simulations consistently summarize many existing results and simultaneously provide a plausibility proof that the recognition of complex biological motion patterns might be based on relatively simple, well-established neural mechanisms. In addition, the model shows that biological motion recognition can be based on a relatively limited number of learned prototypical motion patterns. This representational principle is analogous to the encoding of complex stationary three-dimensional shapes in terms of learned *prototypical views*.

In this model, *view-tuned neurons* similar to the units that have been found in area IT of macaques can learn to respond selectively to configurations of the human body that are characteristic of biological movements or actions. The model further assumes that a sequence of such “snapshots” represents a limited number of prototypical example movement patterns. The highest level of the form pathway consists of neurons that respond selectively to whole motion patterns, like walking and running. These neurons integrate the activity of the view-tuned neurons at the previous level that code for the same motion pattern over time. Since recognition of complex movement patterns must be selective for temporal order, the model assumes a simple mechanism that is based on asymmetric lateral connections between the view-tuned, pattern-selective neurons. Lateral connections lead to a network dynamics that stabilizes a traveling activity pulse only if the stimulus frames are presented in the right temporal order. The effectiveness of this mechanism for sequence selectivity has been shown in simulations. Scrambling of the temporal order of the stimulus leads to competition between the stimulus input and the intrinsic dynamics of the network, resulting in a strong reduction of neural activity.

Falsifying the Standard Model

There is no doubt that existing and future data will force modifications of the Standard Model. But what kinds of experiments would falsify it completely and provide no-go results for the whole class of neural architectures associated with it? Data showing that the basic operation is *intrinsically* not feedforward are prime candidates. Dependency of recognition on different computations and computational modules for every object class would be difficult to reconcile with the Standard Model. Finding that supervised forms of categorization and identification do not use the same basic machinery to provide input signals would require a major revision of the Standard Model but not of its view-based HMAX module. The simplest interpretation of the model predicts that both categorization and identification rely on IT, but direct neural correlates of categorization are not in IT. Refutation of this prediction, however, would not falsify the Standard Model (cf. Fig. 111.2).

The road ahead

The architecture of the Standard Model allows us to quantitatively summarize and structure knowledge from experimental data and plan new experiments. It is an implicit map to future experimental work in terms of both its predictions and the questions that are left open. Clearly, the road ahead will require a very close interaction of experiments and computational work.

Acknowledgments

Supported by grants from ONR, Darpa, NSF, ATR, and Honda. M.R. is supported by a McDonnell-Pew Award in Cognitive Neuroscience. T.P. is supported by the Uncas and Helen Whitaker Chair at the Whitaker College, Massachusetts Institute of Technology. We are grateful to Nikos Logothetis for useful comments and suggestions, to Ulf Knoblich for creating Figure 111.6, and to Dirk Walther for creating Figure 111.8.

REFERENCES

- Blanz, V., and T. Vetter, 1999. A morphable model for the synthesis of 3D faces, in *SIGGRAPH '99 Proceedings*, ACM Computer Society Press, pp. 187–194.
- Booth, M. C., and E. T. Rolls, 1998. View-invariant representations of familiar objects by neurons in the inferior temporal visual cortex, *Cereb. Cortex*, 8:510–523.
- Bricolo, E., T. Poggio, and N. K. Logothetis, 1997. 3D object recognition: a model of view-tuned neurons, in *Advances in Neural Information Processing Systems*, vol. 9, Cambridge, MA: MIT Press, pp. 41–47.
- Bülthoff, H., and S. Edelman, 1992. Psychophysical support for a two-dimensional view interpolation theory of object recognition, *Proc. Natl. Acad. Sci. USA*, 89:60–64.
- Carandini, M., D. J. Heeger, and J. A. Movshon, 1997. Linearity and normalization in simple cells of the macaque primary visual cortex, *J. Neurosci.*, 17:8621–8644.
- Desimone, R., 1991. Face-selective cells in the temporal cortex of monkeys, *J. Cogn. Neurosci.*, 3:1–8.
- Desimone, R., T. D. Albright, C. G. Gross, and C. Bruce, 1984. Stimulus-selective properties of inferior temporal neurons in the macaque, *J. Neurosci.*, 4(8):2051–2062.
- Desimone R., and S. J. Schein, 1987. Visual properties of neurons in area V4 of the macaque: sensitivity to stimulus form, *J. Neurophysiol.*, 57:835–868.
- DiCarlo, J. J., and J. H. R. Maunsell, 2000. Form representation in monkey inferotemporal cortex is virtually unaltered by free viewing, *Nat. Neurosci.*, 3:814–821.
- DiCarlo, J. J., and J. H. R. Maunsell, 2003. Anterior intertemporal recognition can be highly sensitive to object retinal position, *J. Neurophysiol.*, 89:3264–3278.
- Downing, P. E., Y. Jiang, M. Shuman, and N. Kanwisher, 2001. A cortical area selective for visual processing of the human body, *Science*, 293:2470–2473.
- Edelman, S., 1999. *Representation and Recognition in Vision*, Cambridge, MA: MIT Press.
- Epstein, R., and N. Kanwisher, 1998. A cortical representation of the local visual environment, *Nature*, 392:598–601.
- Freedman, D., M. Riesenhuber, T. Poggio, and E. Miller, 2001a. Categorical representation of visual stimuli in the primate prefrontal cortex, *Science*, 291:312–316.
- Freedman, D. J., M. Riesenhuber, T. Poggio, and E. Miller, in press. Comparison of primate prefrontal and inferior temporal cortices during visual categorization, *J. Neurosci.*
- Fujita, I., K. Tanaka, M. Ito, and K. Cheng, 1992. Columns for visual features of objects in monkey inferotemporal cortex, *Nature*, 360:343–346.
- Fukushima, K., 1980. Neocognitron: a self-organizing neural network model for a mechanism of pattern recognition unaffected by shift in position, *Biol. Cybern.*, 36:193–202.
- Gallant, J. L., C. E. Connor, S. Rakshit, J. W. Lewis, and D. C. Van Essen, 1996. Neural responses to polar, hyperbolic, and cartesian gratings in area V4 of the macaque monkey, *J. Neurophysiol.*, 76:2718–2739.
- Gauthier, I., P. Skudlarski, J. C. Gore, and A. W. Anderson, 2000. Expertise for cars and birds recruits brain areas involved in face recognition, *Nat. Neurosci.*, 3:191–197.
- Gauthier, I., and M. J. Tarr, 1997. Becoming a “Greeble” expert: exploring mechanisms for face recognition, *Vis. Res.*, 37:1673–1682.
- Giese, M. A., and T. Poggio, 2003. Biological movement recognition, *Nature Reviews Neuroscience*, 4:179–192.
- Grill-Spector, K., and N. G. Kanwisher, 2001. The functional organization of human ventral temporal cortex is based on stimulus selectivity not recognition task, *Soc. Neurosci. Abstr.*, 27:122.10.
- Grill-Spector, K., Z. Kourtzi, and N. Kanwisher, 2001. The lateral occipital complex and its role in object recognition, *Vis. Res.*, 41:1409–1422.
- Gross, C. G., C. E. Rocha-Miranda, and D. B. Bender, 1972. Visual properties of neurons in inferotemporal cortex of the macaque, *J. Neurophysiol.*, 35:96–111.
- Haxby, J. V., M. I. Gobbini, M. L. Furey, A. Ishai, J. L. Schouten, and P. Pietrini, 2001. Distributed and overlapping representations of faces and objects in the ventral temporal cortex, *Science*, 293:2425–2430.
- Hegde, J., and D. C. Van Essen, 2000. Selectivity for complex shapes in primate visual area V2, *J. Neurosci.*, 20(R61):1–6.
- Hietanen, J. K., D. I. Perrett, P. J. Benson, and W. H. Dittrich, 1992. The effects of lighting conditions on responses of cells selective for face views in the macaque temporal cortex, *Exp. Brain Res.*, 89:157–171.
- Hubel, D. H., and T. N. Wiesel, 1962. Receptive fields, binocular interaction and functional architecture in the cat’s visual cortex, *J. Physiol.*, 160:106–154.
- Hubel, D. H., and T. N. Wiesel, 1965. Receptive fields and functional architecture in two nonstriate visual areas (18 and 19) of the cat, *J. Neurophysiol.*, 28:229–289.
- Hubel, D. H., and T. N. Wiesel, 1968. Receptive fields and functional architecture of monkey striate cortex, *J. Physiol.*, 195: 215–243.
- Intraub, H., 1981. Rapid conceptual identification of sequentially presented pictures, *J. Exp. Psych. Hum. Percept. Perform.*, 7:604–610.
- Itti, L., and C. Koch, 2000. A saliency-based search mechanism for overt and covert shifts of visual attention, *Vis. Res.*, 40:1489–1506.

- Jolicoeur, P., M. A. Gluck, and S. M. Kosslyn, 1984. Pictures and names: making the connection, *Cogn. Psychol.*, 16:243–275.
- Kanwisher, N., J. McDermott, and M. M. Chun, 1997. The fusiform face area: a module in human extrastriate cortex specialized for face perception, *J. Neurosci.*, 17:4302–4311.
- Knoblich, U., D. J. Freedman, and M. Riesenhuber, 2002. Categorization in IT and PFC: Model and experiments, CBCL paper #2110/AI Memo #2002-007. Cambridge, MA: Massachusetts Institute of Technology.
- Knoblich, U., and M. Riesenhuber, 2002. Stimulus simplification and object representation: a modeling study, CBCL Paper #215/AI Memo #2002-004, Massachusetts Institute of Technology, Cambridge, MA.
- Kobatake, E., and K. Tanaka, 1994. Neuronal selectivities to complex object features in the ventral visual pathway of the macaque cerebral cortex, *J. Neurophysiol.*, 71:856–867.
- Kobatake, E., G. Wang, and K. Tanaka, 1998. Effects of shape-discrimination training on the selectivity of inferotemporal cells in adult monkeys, *J. Neurophysiol.*, 80:324–330.
- Lampl, I., T. Poggio, D. Ferster, and M. Riesenhuber, 2001. Spatial integration of complex cells of the cat primary visual cortex.
- Leopold, D. A., A. J. O’Toole, T. Vetter, and V. Blanz, 2001. Prototype-references shape encoding revealed by high-level aftereffects, *Nat. Neurosci.*, 4:3–5.
- Li, F. F., R. van Rulien, C. Koch, and P. Perona, 2002. Rapid natural scene categorization in the near absence of attention. *Proc. Nat. Acad. Sci. USA*, 99:9596–9601.
- Logothetis, N. K., J. Pauls, M. Augath, T. Trinath, and A. Oeltermann, 2001. Neurophysiological investigation of the basis of the fMRI signal, *Nature*, 412:150–157.
- Logothetis, N. K., J. Pauls, H. H. Bülthoff, and T. Poggio, 1994. View-dependent object recognition by monkeys, *Curr. Biol.*, 4:401–414.
- Logothetis, N. K., J. Pauls, and T. Poggio, 1995. Shape representation in the inferior temporal cortex of monkeys, *Curr. Biol.*, 5:552–563.
- Logothetis, N. K., and D. L. Sheinberg, 1996. Visual object recognition, *Annu. Rev. Neurosci.*, 19:577–621.
- Malach, R., J. B. Reppas, R. R. Benson, K. K. Kwong, H. Jiang, W. A. Kennedy, P. J. Ledden, T. J. Brady, B. R. Rosen, and R. B. Tootell, 1995. Object-related activity revealed by functional magnetic resonance imaging in human occipital cortex, *Proc. Natl. Acad. Sci. USA*, 92:8135–8139.
- Miller, E., 2000. The prefrontal cortex and cognitive control, *Nat. Rev. Neurosci.*, 1:59–65.
- Missal, M., R. Vogels, and G. A. Orban, 1997. Responses of macaque inferior temporal neurons to overlapping shapes, *Cereb. Cortex*, 7:758–767.
- Murphy, G. L., and H. H. Brownell, 1985. Category differentiation in object recognition: typicality constraints on the basic category advantage, *J. Exp. Psychol. Learn. Mem. Cogn.*, 11:70–84.
- Opde Beeck, H., J. Wagemans, and R. Vogels, 2001. Inferotemporal neurons represent low-dimensional configurations of parametrized shapes, *Nat. Neurosci.*, 4:1244–1252.
- Pasupathy, A., and C. E. Connor, 1999. Responses to contour features in macaque area V4, *J. Neurophysiol.*, 82:2490–2502.
- Pauls, J., 1997. The Representation of 3-Dimensional Objects in the Primate Visual System. Ph.D. thesis, Baylor College of Medicine, Houston, TX.
- Perrett, D. I., J. K. Hietanen, M. W. Oram, and P. J. Benson, 1992. Organization and functions of cells responsive to faces in the temporal cortex, *Philos. Trans. R. Soc. B*, 335:23–30.
- Perrett, D. I., and M. Oram, 1993. Neurophysiology of shape processing, *Img. Vis. Comput.*, 11:317–333.
- Poggio, T., 1990. A theory of how the brain might work. *Cold Spring Harbor Symp. Quant. Biol.*, 55:899–910.
- Poggio, T., and S. Edelman, 1990. A network that learns to recognize 3D objects, *Nature*, 343:263–266.
- Poggio, T., and F. Girosi, 1990. Networks for approximation and learning, *Proc. IEEE*, 78(9):1481–1497.
- Potter, M. C., 1975. Meaning in visual search, *Science*, 187:565–566.
- Riesenhuber, M., and T. Poggio, 1999a. Are cortical models really bound by the “Binding Problem”? *Neuron*, 24:87–93.
- Riesenhuber, M., and T. Poggio, 1999b. Hierarchical models of object recognition in cortex, *Nat. Neurosci.*, 2:1019–1025.
- Riesenhuber, M., and T. Poggio, 1999c. A note on object class representation and categorical perception. Technical Report AI Memo 1679, CBCL Paper 183, Cambridge, MA: MIT AI Lab and CBCL.
- Riesenhuber, M., and T. Poggio, 2000a. The individual is nothing, the class everything: psychophysics and modeling of recognition in object classes, Technical Report AI Memo 1682, CBCL Paper 185, Cambridge, MA: MIT AI Lab and CBCL.
- Riesenhuber, M., and T. Poggio, 2000b. Models of object recognition, *Nat. Neurosci. Suppl.*, 3:1199–1204.
- Rosch, E., C. B. Mervis, W. Gray, D. Johnson, and P. Boyes-Braem, 1976. Basic objects in natural categories, *Cogn. Psychol.*, 8:382–439.
- Rousselet, G. A., M. Fabre-Thorpe, and S. J. Thorpe, 2002. Parallel processing in high-level categorization of natural images, *Nat. Neurosci.*, 5:629–630.
- Serre, T., M. Riesenhuber, J. Louie, and T. Poggio, 2002. On the role of object-specific features for real world object recognition in biological vision. In: Biologically Motivated Computer Vision, Second International workshop (BMCV 2002), H. H. Bülthoff, S.-W. Lee, T. Poggio, and C. Wallraven (eds.), Tübingen, Germany.
- Tanaka, K., 1993. Neuronal mechanisms of object recognition, *Science*, 262:685–688.
- Tanaka, K., 1996. Inferotemporal cortex and object vision, *Annu. Rev. Neurosci.*, 19:109–139.
- Tanaka, K., 1997. Mechanisms of visual object recognition: monkey and human studies, *Curr. Opin. Neurobiol.*, 7:523–529.
- Tarr, M. J., and H. H. Bülthoff, 1998. Image-based object recognition in man, monkey and machine, *Cognition*, 67:1–20.
- Thorpe, S. J., D. Fize, and C. Marlot, 1996. Speed of processing in the human visual system, *Nature*, 381:520–522.
- Tsunoda, K., Y. Yamane, M. Nishizaki, and M. Tanifuji, 2001. Complex objects are represented in macaque inferotemporal cortex by the combination of feature columns, *Nat. Neurosci.*, 4:832–838.
- Tversky, B., and K. Hemenway, 1984. Objects, parts, and categories, *J. Exp. Psych. Gen.*, 113:169–197.
- Ullman, S., and R. Basri, 1991. Recognition by linear combinations of models, *IEEE Trans. Patt. Anal. Mach. Intell.*, 13:992–1006.
- Ungerleider, L. G., and J. V. Haxby, 1994. “What” and “where” in the human brain, *Curr. Opin. Neurobiol.*, 4:157–165.
- Vetter, T., A. Hurlbert, and T. Poggio, 1995. View-based models of 3D object recognition: invariance to imaging transformations, *Cereb. Cortex*, 3:261–269.
- Vogels, R., 1999. Categorization of complex visual images by rhesus monkeys. Part 2: single-cell study, *Eur. J. Neurosci.*, 11:1239–1255.

- Wallis, G., and E. T. Rolls, 1997. A model of invariant object recognition in the visual system, *Prog. Neurobiol.*, 51:167–194.
- Walther, D., L. Itti, M. Riesenhuber, T. Poggio, and C. Koch, 2002. Attentional selection for object recognition—a gentle way. In: *Biologically Motivated Computer Vision, Second International Workshop (BMCV 2002)*, H. H. Bülthoff, S.-W. Lee, T. Poggio, and C. Wallraven (eds.). Tübingen, Germany, pp. 472–479.
- Wang, G., K. Tanaka, and M. Tanifuji, 1996. Optical imaging of functional organization in the monkey inferotemporal cortex, *Science*, 272:1665–1668.
- Young, M. P., and S. Yamane, 1992. Sparse population coding of faces in the inferotemporal cortex, *Science*, 256:1327–1331.

112 Plasticity of Orientation Processing in Adult Visual Cortex

VALENTIN DRAGOI AND MRIGANKA SUR

NEURONS IN THE PRIMARY visual cortex (V1) have been traditionally considered to be passive filters, extracting elementary features of visual stimuli such as local orientation or direction of motion and responding invariantly to the physical properties of stimuli present in their receptive fields. However, another view has emerged in the past 15 years. According to this view, V1 responses are strongly influenced by the spatial and temporal context in which local features are presented, and their responses are modulated as well by previous visual experience, including perceptual learning and adaptation.

Evidence that even the earliest areas of the adult cerebral cortex have the remarkable capacity to change as a result of experience, a phenomenon termed *plasticity*, has been accumulating steadily. The first reports of plasticity in primary sensory cortex of the adult brain came from studies in the somatosensory cortex, which contains a systematic sensory representation of the body surface. Partially removing inputs to the cortex by peripheral nerve transection or by amputation of a finger reorganized the cortical sensory representation such that the denervated cortex now responded to adjacent fingers or the hand (Merzenich et al., 1983, 1984). In V1, sensory map plasticity was first demonstrated using retinal lesions: cortical regions processing inputs from the lesioned parts of the retina were initially silenced, but then regained activity by shifting receptive fields toward regions of the retina surrounding the lesion (Gilbert and Wiesel, 1992; Kaas et al., 1990). Such lesion-induced plasticity implies either the unmasking of existing connections or the formation of new ones (Darian-Smith and Gilbert, 1994). New connections are typically associated with plasticity during development, when neurons are being wired together, but are unlikely to be a mechanism working on shorter time scales in adulthood during normal sensory processing. The latter kinds of plasticity include dynamic changes in neuronal responses mediating contextual effects and short-term plasticity associated with learning or adaptation.

Dynamics and plasticity of responses in V1

Dynamic effects induced by the spatial context of visual stimuli allow V1 neurons to integrate information from dif-

ferent parts of the visual scene. These effects are manifested when both the classical receptive field (i.e., the receptive field center), and the extraclassical receptive field (i.e., the surround), are stimulated together. The way in which surround stimulation modulates responses elicited by a center stimulus is highly nonlinear and often nonintuitive. Thus, stimuli in the surround can either facilitate or suppress cortical responses, depending on the relative orientation and contrast between the center and the surround. The presence of a surround stimulus with an orientation similar to that of the cell's preferred orientation suppresses the response to a high-contrast optimal stimulus within the receptive field center and facilitates the response to a low-contrast optimal stimulus within the receptive field center (Polat et al., 1998; Somers et al., 1998; Toth et al., 1996). On the other hand, stimulating the surround with a stimulus whose orientation differs significantly from the cell's preferred orientation facilitates responses to optimal stimulation within the center (Levitt and Lund, 1997; Sillito et al., 1995). In this case, the cell responds "supraoptimally," that is, beyond the level expected after stimulation with the optimal orientation.

In addition to integrating inputs from outside their classical receptive fields, V1 responses are sensitive to the history of visual stimulation or short-term experience. For instance, masking a portion of the visual field for several minutes (a situation akin to creating an artificial scotoma) while placing a patterned stimulus around the mask demonstrates the capacity of V1 neurons with receptive fields inside the artificial scotoma to alter their responses. Specifically, after a few minutes of conditioning with the artificial scotoma, the receptive fields of neurons close to the scotoma borders expand beyond their original limits and show an overall increase in responsiveness (Das and Gilbert, 1995; DeAngelis et al., 1995; Pettet and Gilbert, 1992). This type of receptive field plasticity has also been demonstrated at shorter time scales. De Weerd et al. (1995) have shown that after exposure to a static stimulus consisting of a similar artificial scotoma pattern, neurons with receptive fields inside the scotoma borders begin to respond despite the absence of retinal stimulation, a phenomenon associated with the perceptual filling-in effect (Ramachandran and Gregory, 1991).

The dependence of V1 neuron responses on short-term or recent experience is evident in the phenomenon of pattern adaptation: selective exposure for a period of time to patterned stimulation induces transient changes in the selectivity of V1 responses. Pattern adaptation has been characterized with respect to many stimulus dimensions, such as orientation (Blakemore and Campbell, 1969; Carandini et al., 1998; Dragoi et al., 2000; Hammond et al., 1986; Muller et al., 1999; Nelson, 1991), contrast (Carandini and Ferster, 1997; Carandini et al., 1998; Movshon and Lennie, 1979; Ohzawa et al., 1982), spatial frequency (Movshon and Lennie, 1979; Saul and Cynader, 1989), direction of motion (Hammond et al., 1985, 1986; Maffei et al., 1973), and velocity (Hammond et al., 1985).

Cortical neurons also have the adaptive capacity to change their responses with perceptual learning (Gilbert et al., 2001). Perceptual learning in vision is a particular form of plasticity that begins during postnatal life, continues throughout adulthood, and allows us to improve visual performance after active exposure to a structured visual environment. There are many examples of situations in which training has been shown to improve discrimination along a variety of visual stimulus dimensions. For instance, training can improve spatial resolution of the visual system (Fahle and Edelman, 1993; Poggio et al., 1992), the ability to discriminate orientations (Schoups et al., 2001; Vogels and Orban, 1985), the direction of motion (Ball and Sekuler, 1985, 1987), or the depth of visual targets (Fendick and Westheimer, 1983). However, importantly, unlike other forms of learning, in which enhanced performance in one task improves performance in related tasks, perceptual learning is highly specific for the stimulus dimension used in the training task, such as retinal position (e.g., Karni and Sagi, 1991b) or orientation (e.g., McKee and Westheimer, 1978; Ramachandran and Braddick, 1973). This high degree of specificity has important implications for the neuronal mechanisms underlying perceptual learning, for it argues that plasticity must be a phenomenon present in the early visual cortical areas. Indeed, recent work has demonstrated task-specific, learning-induced plasticity of V1 neurons in animals trained to perform either a three-line bisection task (Crist et al., 2001) or an orientation discrimination task (Schoups et al., 2001).

Orientation plasticity in V1

A prominent form of plasticity in the adult visual cortex is the plasticity of orientation tuning. Orientation plasticity can be simply demonstrated by an instant perceptual experiment. If we stare for a brief period of time at oblique lines, the perceived orientation of vertical lines appears tilted away from the obliques; this is the well-known *tilt aftereffect* (Gibson, 1933; Gibson and Radner, 1937; Magnussen and Kurten-

bach, 1980). At longer time scales, the ability of the visual system to discriminate differences in orientation can be improved through perceptual learning. This suggests that visual experience or learning could alter the functional properties of orientation-selective neurons and networks in the early visual cortex of the adult brain.

V1 neurons are selective for the orientation of lines which are presented in their receptive field center (Hubel and Wiesel, 1962). The development of orientation tuning does not require visual experience (Crair et al., 1998; Fregnac and Imbert, 1978; Godecke et al., 1997; Hubel and Wiesel, 1962), although selective experience in early life can modify the orientation preference of neurons (Blakemore, 1977; Blakemore and Cooper, 1970; Hirsch and Spinelli, 1970; Sengpiel et al., 1999; Stryker et al., 1978). The orientation preference of adult V1 neurons has long been considered a stable property that remains fundamentally unchanged after early life. However, recent evidence demonstrates that orientation selectivity of neurons and the way in which orientation is mapped onto the cortex can be altered by visual experience, and these changes have important consequences for visual perception.

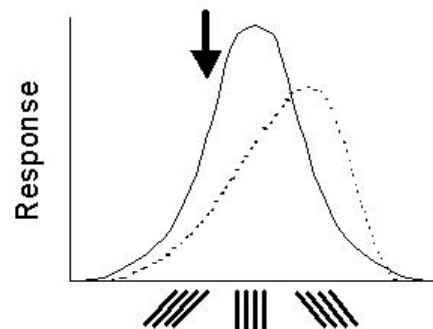
There are several ways in which orientation plasticity has been demonstrated in adult V1 neurons. While the details of the inducing procedures define the specifics of cortical plasticity, three major types of orientation plasticity stand out (Fig. 112.1).

ADAPTATION-INDUCED PLASTICITY Continuous visual stimulation for a period of seconds to minutes (a process defined as *adaptation*) at a fixed orientation induces a reversible shift in the preferred orientation of individual neurons away from the adapting stimulus (Fig. 112.1A) (Dragoi et al., 2000; Muller et al., 1999). Interestingly, this form of short-term plasticity induces not only a significant change in optimal orientation but also a reorganization of responses around the new preferred orientation. For instance, a long period of adaptation induces a reduction of responses on the flank of the tuning curve near the adapting stimulus and a facilitation of responses on the opposite flank. This suggests that adaptation-induced orientation plasticity involves an active process of network synaptic changes that lead to a new preferred orientation rather than simply a passive reduction of orientation-selective responses around the adapting orientation.

STIMULATION TIMING-DEPENDENT PLASTICITY Intracortical electrical stimulation paired with visual stimulation for several hours leads to a shift in the preferred orientation of individual neurons (Fig. 112.1B) (Schuett et al., 2001). The shift can occur toward or away from the orientation of the visual stimulus, depending on the temporal order of the visual stimulus and the delivery of the electrical pulses.

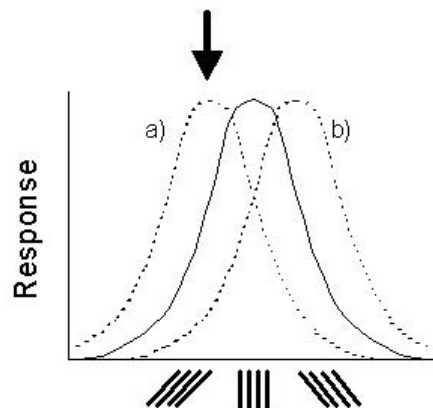
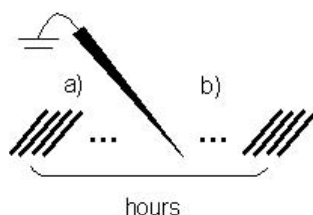
A

**ADAPTATION-INDUCED
PLASTICITY**



B

**STIMULATION TIMING-
DEPENDENT PLASTICITY**



C

**LEARNING-INDUCED
PLASTICITY**

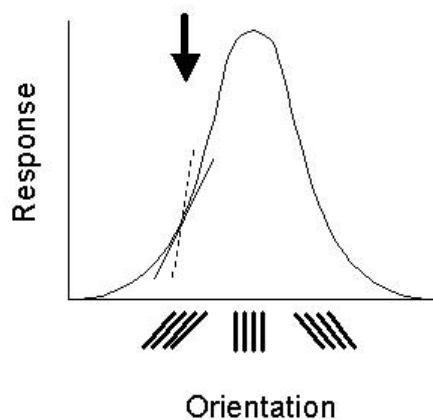


FIGURE 112.1. Different forms of orientation plasticity in V1. *A*, Adaptation-induced orientation plasticity. Short-term exposure for a period of seconds to minutes induces a repulsive shift in the preferred orientation of V1 neurons away from the adapting stimulus (*arrow*). The solid line represents the orientation tuning curve before adaptation, and the dotted line represents the tuning curve after adaptation. *B*, Stimulation timing-dependent orientation plasticity. The figure schematically shows orientation plasticity induced by a combination of cortical microstimulation and visual stimulation. When electrical microstimulation is delivered to a cortical site 65 msec after the visual stimulus (*arrow*), there is a shift in the preferred orientation of V1 neurons toward the visual stimulus orientation (*a*), whereas when electrical microstimulation is delivered after the

visual stimulus, there is a shift in preferred orientation away from the visual orientation (*b*). The solid line represents the tuning curve before microstimulation, and the dotted lines represent the tuning curves after forward (*a*) and backward (*b*) microstimulation. *C*, Learning-induced orientation plasticity. Improvement in orientation discrimination performance during learning is accompanied by an increase in the slope of the tuning curve near the trained orientation (*arrow*). The solid line represents the orientation tuning curve of a V1 neuron before training. The straight solid line represents the slope of the tuning curve at the trained orientation before training; the straight dashed line represents the slope of the tuning curve at the trained orientation after training.

Consistent with previously demonstrated rules of synaptic plasticity based on the precise timing of the presynaptic and postsynaptic activity (spike-timing-dependent plasticity) obtained in slice preparations (Markram et al., 1997; Zhang et al., 1998), electrical stimuli delivered after the visual stimulus-driven activity reaches cortex produces a shift in the preferred orientation of individual neurons toward the visually presented orientation, whereas reversing the temporal order between electrical and visual stimuli produces a shift in preferred orientation away from the visual orientation. Except for the timing between stimuli, this pairing protocol is similar to that introduced by Fregnac et al. (1988), in which the preferred orientation of individual neurons shifted toward the orientation of the visual stimulus. Similarly, the preferred orientation of individual neurons can be induced to shift toward the orientation at a cortical site that is stimulated pharmacologically (Toth et al., 1997) or electrically (Godde et al., 2002), even without a paired visual stimulus. However, the rules of synaptic plasticity underlying such shifts are still likely to involve the relative timing and correlations between input and output spikes of neurons. Yao and Dan (2001) specifically demonstrated that two gratings—one at a tilted orientation and the other at the cell's preferred orientation—flashed in quick succession (8 to 40 msec apart) causes a cell to shift its preferred orientation toward the first grating, whereas flashing the gratings in the opposite order causes the cell to shift its orientation away from the first grating.

LEARNING-INDUCED PLASTICITY Intensive practice in discriminating fine orientation differences increases neuronal orientation discrimination performance at the trained orientation (Shiu and Pashler, 1992; Vogels and Orban, 1985), but not at other orientations or visual field locations (Schoups et al., 2001). The proposed mechanism for this type of plasticity has been linked to the observed increase in the slope of the tuning curve of individual V1 neurons in the vicinity of the trained orientation (Fig. 112.1C) (Schoups et al., 2001).

These forms of orientation plasticity demonstrate the powerful effect of short- and long-term synaptic plasticity rules, such as those previously derived from work in reduced preparations, including cultured neurons and brain slices, on shaping fundamental properties of individual V1 neurons and networks in vivo (Sur et al., 2002). Two questions have recently emerged from our understanding of cortical plasticity: how is orientation plasticity represented across the cortex, and what is its significance for visual perception, including natural vision? Whereas orientation plasticity induced by electrical stimulation does not appear to have a direct impact on vision, adaptation and learning-induced changes in V1 responses offer powerful tools with which to address both questions. In the following sections, we will

focus on plasticity of orientation tuning induced by adaptation as a model system in which to understand the representation, mechanism, and significance of plasticity in V1 networks.

Adaptation-induced orientation plasticity

Our knowledge of adaptation in early visual cortex comes from studies demonstrating that exposure to a potent stimulus for several minutes (pattern adaptation) can cause a reduction in sensitivity to stimulus attributes such as contrast or spatial frequency (Blakemore and Campbell, 1969; Carandini et al., 1998; Movshon and Lennie, 1979; Nelson, 1991; Ohzawa et al., 1982). In light of these experiments, cortical adaptation has been viewed for many years as a local phenomenon mediated by depression of firing at the level of individual neurons, possibly involving tonic hyperpolarization of the membrane potential of V1 cells (Carandini and Ferster, 1997) due to synaptic depression (Abbott et al., 1997; Chance et al., 1998) or to a slow hyperpolarizing membrane potassium current (Sanchez-Vives et al., 2000).

In a recent study, Dragoi et al. (2000) studied adaptation-induced orientation plasticity in V1 and found, in contrast to previous results, that adaptation causes both depression and enhancement of responses to a range of stimulus orientations, along with reorganization of the entire profile of the orientation tuning curve. Figure 112.2A shows how the preferred orientation of a representative V1 cell changes after 2 minutes of exposure to one orientation located on one flank of the cell's tuning curve, followed by a period of recovery, subsequent adaptation to a different orientation located on the opposite flank with respect to the preferred orientation, and a final period of recovery. When the difference between the cell's preferred orientation and that of the adapting stimulus ($\Delta\theta$) is -22.5 degrees, that is, adapting orientation is on the left flank of the tuning curve, there is a shift in preferred orientation to the right, away from the adapting stimulus. In contrast, when the adapting stimulus is presented on the right flank of the tuning curve ($\Delta\theta = 45$ degrees), the preferred orientation shifts to the left and then returns to the original value after 10 minutes of recovery.

These effects of orientation adaptation are short term: the shift in preferred orientation increases with adaptation time until it asymptotes at about 10 minutes of adaptation and then reverses to the original level when the adapting stimulus is removed. Figure 112.2B shows the behavior of one cell that exhibits significant shifts in orientation following adaptation to a stimulus oriented 45 degrees away from the cell's peak orientation (Dragoi et al., 2000). Both the response reduction on the near flank and facilitation on the far flank build up gradually in time: increasing the adaptation time from 10 seconds to 10 minutes shows a progressive

depression of responses on the near flank and a progressive facilitation of responses on the far flank. Interestingly, adaptation and recovery develop at two different time scales, with the rate of recovery being at least an order of magnitude slower than the rate of adaptation (Fig. 112.2C).

Orientation plasticity and the cortical map of orientation preference

Adaptation-induced orientation plasticity is a cortical phenomenon that depends on changes in inputs from other neurons in a local network. Thus, it is conceivable that the

strength of adaptation effects would depend on the specific cortical location of a neuron within the map of orientation preference. V1 neurons are clustered according to their orientation preference in iso-orientation domains (Hubel and Wiesel, 1974), where the optimal orientation of individual neurons varies smoothly across the cortex, and singularities or pinwheel centers (Blasdel, 1992; Bonhoeffer and Grinvald, 1991), which are foci where the optimal orientation of neurons varies rapidly (Fig. 112.3A). The structure of the orientation map in V1 implies that the orientation distribution of local connections would vary with a neuron's position within the map: neurons in pinwheel centers are likely to be connected to neurons of a broader range of orientations than neurons in iso-orientation domains. This suggests that altering the efficacy of intracortical orientation-specific inputs to neurons in different locations of the orientation map in a manner that induces adaptive changes in tuning properties could show dependence on cortical location.

Dragoi et al. (2001) investigated the relationship between adaptation-induced orientation plasticity and a neuron's location in the orientation preference map in V1 of adult cats. Optical imaging of intrinsic signals was used to obtain the orientation map in a patch of V1, and then the vascular pattern of the cortical surface was used in relation to the orientation map to guide electrode penetrations aimed at iso-orientation domains or pinwheel centers (Fig. 112.3A). The specific question was whether the local orientation distribution at the recording site correlated with the degree of plasticity. Anatomical and physiological data in V1 (Das and Gilbert, 1999; Hata et al., 1991; Kisvarday et al., 1997;

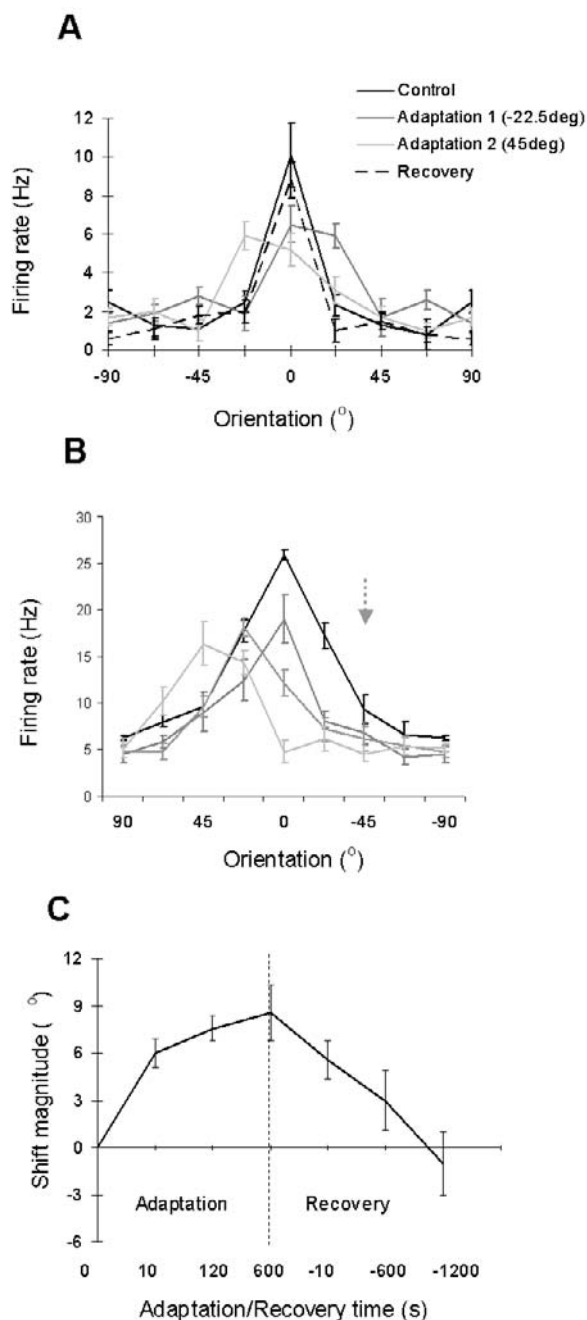


FIGURE 112.2. Adaptation-induced orientation plasticity. *A*, Orientation tuning curves of one representative V1 neuron that was successively adapted to two different orientations. Each graph represents orientation tuning during four conditions: control (black), adaptation to the first orientation (dark gray), adaptation to the second orientation (light gray), and recovery (black, dashed line). In this tuning curve display convention, the control optimal orientation is represented as 0 degrees, and all subsequent tuning curves (during adaptation and recovery) are represented relative to the control condition. *B*, Tuning curves of neurons that show adaptation-induced response suppression on the near flank and response facilitation on the far flank. Each cell was serially exposed to different adaptation periods: 10 seconds, 2 minutes, and 10 minutes. Tuning curves were calculated in each of the four conditions: control (black), 10 seconds adaptation (dark gray), 2 minutes adaptation (medium gray), and 10 minutes adaptation (light gray). The adapting orientation is marked by the gray arrow. *C*, Time course of adaptation and recovery. The graph shows the mean shift magnitude \pm S.E.M. as a function of adaptation and recovery time for a subpopulation of seven neurons. The orientation shift magnitude was calculated after adaptation to a stimulus presented for 10 seconds, 2 minutes, and 10 minutes, followed by recovery to a blank stimulus presented for 10 seconds, 10 minutes, and 20 minutes.

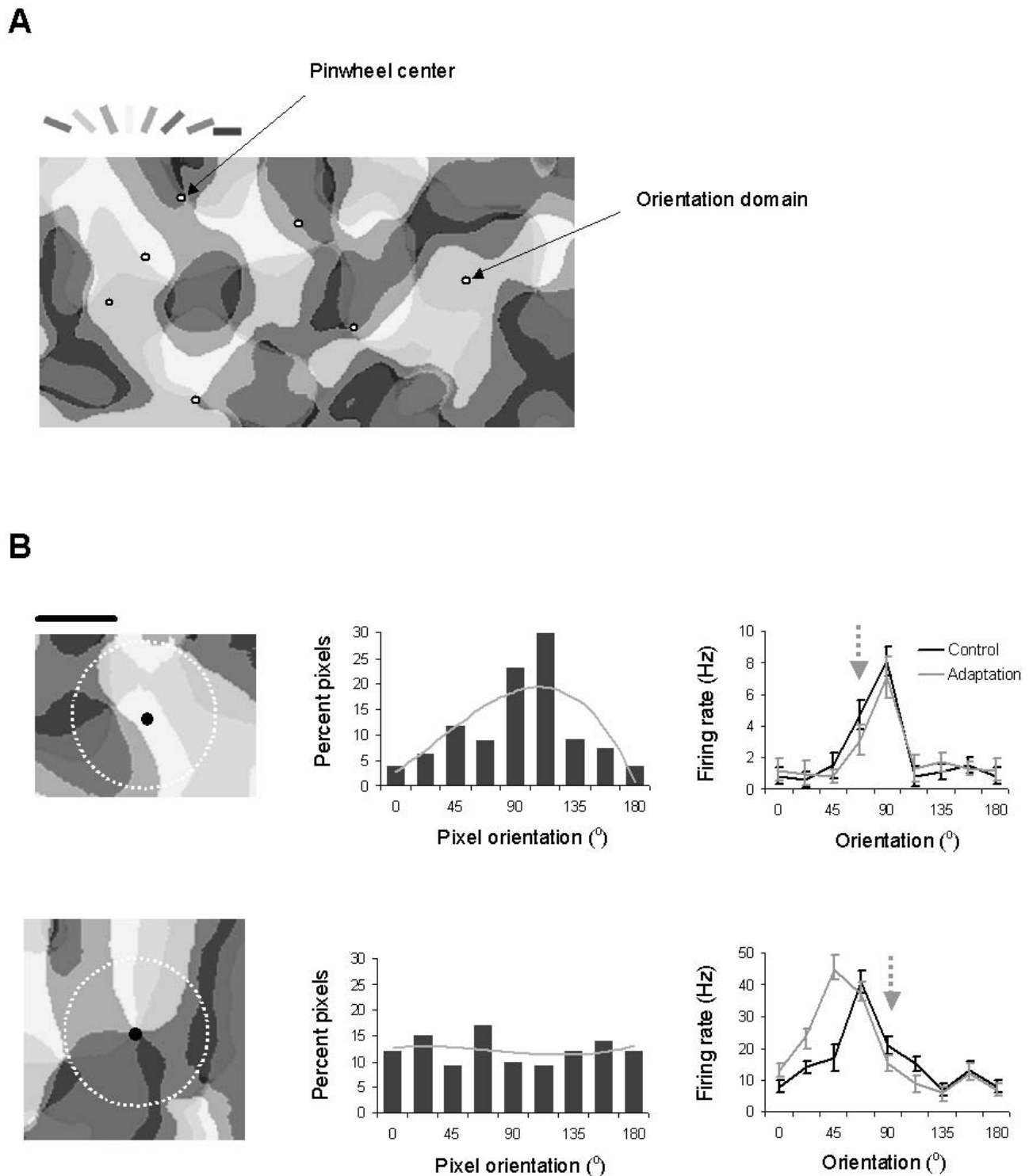


FIGURE 112.3. Adaptation-induced plasticity of orientation tuning and the orientation architecture of V1. *A*, Composite orientation map obtained by intrinsic signal optical imaging. The angle of preferred orientation of each pixel is shown in pseudo-color according to the key at the top. The circles show the location of seven representative neurons to illustrate the range of orientation distributions in recorded neurons. *B*, Relationship between the local orientation distribution at the recording site and the degree of orientation plasticity. *Left*: Two recording sites (filled circles) placed respectively within an iso-orientation domain and a pinwheel

center. The white dotted circle of radius $500\mu\text{m}$ represents the basin of local intracortical inputs. *Middle*: The percentage of pixels at each orientation within $500\mu\text{m}$ of the recording site after pooling the pixels into eight orientation bins between 0 and 180 degrees. The gray curve represents the best third-order polynomial fit to each histogram. *Right*: Orientation tuning curves in the control condition (black) and after adaptation (gray) for the cells recorded at the locations shown in the left panels. The adapting orientation is marked by the gray arrow. Error bars represent S.E.M. (See color plate 85)

Weliky et al., 1995) have demonstrated that local excitatory and inhibitory inputs to cortical cells originate from within an approximate 500 μm radius around the cell body. The critical feature for explaining orientation plasticity was found to be the distribution of local inputs to individual neurons. When the recording site is in the middle of an iso-orientation domain (Fig. 112.2*B*), neurons within a 500 μm radius have a preponderance of orientation preferences similar to that of the recorded neuron, whereas when the recording site is near a pinwheel center, local inputs arise from domains of all orientations. Qualitatively, the orientation distribution of inputs to a neuron is a predictor of the degree of change in its orientation preference. When it has a peaked profile, adaptation induces only minor changes in orientation selectivity (Fig. 112.3*B*), whereas the orientation tuning curve undergoes pronounced changes when the orientation distribution is flat.

What kind of mechanism could generate these effects? The changes in orientation selectivity following adaptation imply a network mechanism that reorganizes responses across a broad range of orientations. For instance, hyperpolarization of neurons at or close to the adapting orientation, due either to membrane mechanisms (such as slow hyperpolarizing Ca^{2+} - and Na^{+} -activated potassium channels; Sanchez-Vives et al., 2000), or to synaptic depression (Abbott et al., 1997), can cause suppression of responses on the near flank of the tuning curve, whereas facilitation of responses on the far flank requires disinhibition (Dragoi and Sur, 2000) and possibly amplification via local excitatory intracortical interactions (Somers et al., 2002). But what is important is that the strength of these effects, which determines the magnitude of the change in preferred orientation, depends on the location of neurons in the orientation map. Neurons in an iso-orientation domain would be only weakly activated by intracortical inputs with orientations that differ from the domain's preferred orientation, whereas neurons located at or near pinwheel centers would receive strong local inputs from neurons of all orientations. Therefore, altering the efficacy of these inputs through adaptation is likely to induce more profound changes in the orientation preference of neurons at or near pinwheel centers. This suggests that adaptation-induced orientation plasticity in V1 is an emergent property of a local cortical network overlaid on a nonuniform orientation map.

Rapid adaptation-induced plasticity

An important question about orientation plasticity is whether the different forms of response change have adaptive significance for vision. Whereas long-term cortical plasticity has been used to explain certain kinds of perceptual learning, the functional implications of the more rapid forms

of plasticity have been less clear. For instance, plasticity induced by short-term adaptation to oriented contours is considered to underlie the tilt aftereffect (see below), but the tilt aftereffect leads to an altered perception of contour orientation.

Two recent studies have demonstrated that the discrimination of orientations is actually improved by adaptation. Clifford et al. (2001) showed that orientation discrimination around vertical orientations improved in human observers after adaptation to either vertical or horizontal gratings but was impaired after adaptation to intermediate orientations. The improvement was greatest when the adapting and test gratings were orthogonal. The study, however, employed long adaptation times of several seconds to 1 minute, a duration unlikely to have a significant role in ongoing natural vision.

Dragoi et al. (2002) asked whether cortical plasticity is involved during the rapid processing of image patterns during natural viewing. During the viewing of a natural scene, we make saccadic eye movements several times a second (Andrews and Coppola, 1999; Yarbush, 1967). Between successive saccades, during visual fixation, the portions of a scene that fall within the receptive fields of V1 neurons are well correlated in local features. Brief adaptation during exposure to such spatially correlated image patches is known to induce short-term changes in the response of V1 neurons by reducing the response at the preferred orientation and hence possibly the correlation among neuronal responses (Attneave, 1954; Barlow, 1990). However, adaptation effects have been mainly described by examining how exposure to a certain image pattern affects the subsequent viewing and discrimination of similar patterns, thus ignoring the properties of natural viewing. Indeed, during natural vision we often make large saccades to explore new regions of visual space, with local attributes (e.g., orientation) that are typically uncorrelated to the previous fixation (Fig. 112.4). Therefore, fixation at one location is likely to be followed by a saccade to an image patch of dissimilar structure. How does brief adaptation affect the discrimination of local image patches of dissimilar structure and their encoding by visual cortical neurons?

Dragoi et al. (2002) showed that orientation discrimination by humans and monkeys is markedly improved when an adapting grating is presented briefly, for a few hundred milliseconds (i.e., for a time equivalent to one visual fixation), followed by a test grating that is orthogonal in orientation to the adapting grating. They also showed that rapid adaptation affects the signaling capabilities of V1 neurons. Specifically, while brief adaptation to an oriented grating broadens orientation selectivity and changes the preferred orientation of individual V1 neurons, it actually enhances the discrimination of orthogonal orientations by sharpening neuronal selectivity.



1°

FIGURE 112.4. Image statistics during natural vision. While viewing a scene, a short saccade is likely to land on an image patch of similar orientation structure, whereas a long saccade is likely to land on an image patch of dissimilar orientation structure.

While most work on adaptation effects on neuronal responses has employed long adaptation and stimulus-response times, stimuli which are presented briefly (Muller et al., 1999; Nelson, 1991) are necessary for examining both the effects of rapid adaptation on cortical responses and the temporal development of neuronal interactions underlying adaptation effects. These temporal interactions are critical for providing clues to the role of temporal interactions in natural vision, as the changing stimulus statistics between eye movements during free viewing introduces complex dynamics in cortical responses.

One efficient way to capture the dynamics of neuronal responses after adaptation would be to estimate the development of orientation tuning by implementing the reverse correlation procedure (de Boer and Kuyper, 1968; Dragoi et al., 1999; Mazer et al., 2002; Ringach et al., 1997). Dragoi et al. thus measured how the orientation tuning of V1 neurons evolves at the millisecond time scale before and after brief adaptation. They stimulated V1 neurons of awake monkeys with movie sequences in which each frame was a high-contrast sine-wave grating of pseudorandom orientation synchronized with the refresh of the monitor and flashed at 60 Hz. The orientation domain was sampled in steps of 11.25 degrees, and each orientation was presented seven times during each movie strip. Spikes were recorded during a control condition (in which movie strips were presented alone) or immediately after adaptation (in which movie strips were preceded by a 400 msec sine-wave drifting grating of fixed orientation). For each recorded action potential, the orientation that had been presented at various

preceding times in the movie sequence was determined. Spikes from completed trials were accumulated in a two-dimensional array based on stimulus orientation and time delay before spiking. A mean spike count was obtained for each stimulus orientation by dividing each spike counter by the number of rewarded trials and by the number of stimulus repetitions within each trial.

Figure 112.5 shows two examples of cells with distinct behaviors during brief adaptation. When the adapting stimulus orientation is near a cell's preferred orientation (small $\Delta\theta$), the development of orientation selectivity is delayed, whereas adaptation orthogonal to a cell's preferred orientation (large $\Delta\theta$) accelerates the development of orientation selectivity. More importantly, however, adaptation near the preferred orientation reduces responses on the near flank of the tuning curve, shifts the preferred orientation away from the adapting stimulus, and increases the width of the tuning curve, whereas adaptation far away from the optimal orientation maintains orientation preference and sharpens orientation tuning.

Significance of adaptation-induced orientation plasticity for vision

These effects of rapid adaptation (with the adapting grating presented for hundreds of milliseconds) on neuronal responses are fundamentally similar to the effects of short-term adaptation (with the adapting grating presented for seconds to minutes). In both cases (cf. Fig. 112.1A or the bottom part of Fig. 112.3B and Fig. 112.5), adaptation with a grating oriented near a cell's preferred orientation alters the tuning curve and broadens selectivity, whereas a grating oriented orthogonal to a cell's preferred orientation preserves the same orientation preference but sharpens selectivity (Dragoi et al., 2000, 2002). How do these neuronal changes explain the perceptual consequences of adaptation?

Population coding models that relate neuronal responses to perception assume that a cell is a "labeled line" for a stimulus, so that each neuron signals the presence of its preferred stimulus within its receptive field. The response of the population is inferred as the vector sum of the individual neuron responses. Two of the response changes induced by short-term adaptation—reduction in response at the adapting orientation and broadening of tuning width—are important for explaining at least the repulsive tilt aftereffect at intermediate orientation differences between adapting and test orientations (Clifford et al., 2001; Sur et al., 2002).

The consequences of rapid adaptation for natural vision can be understood qualitatively from the experimental data now available, and they suggest an interesting functional role for rapid as well as short-term adaptation. On the one hand,

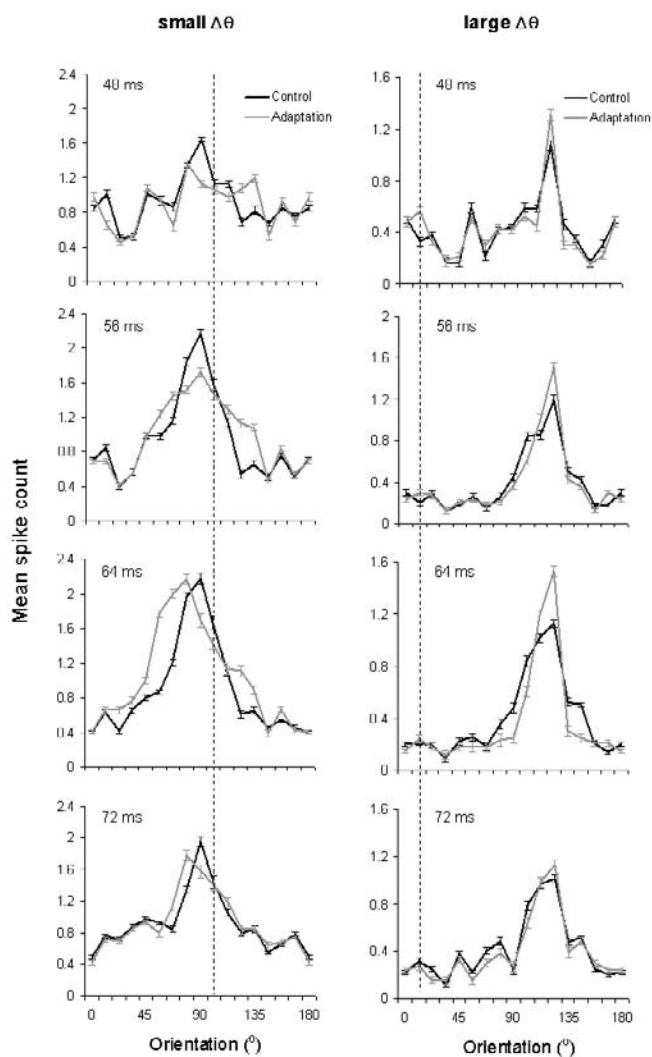


FIGURE 112.5. Temporal dynamics of brief adaptation in V1 neurons revealed by reverse correlation. *Left:* Adaptation near the cell's preferred orientation (small $\Delta\theta$) delays the development of orientation tuning, shifts the preferred orientation away from the adapting stimulus, and broadens orientation selectivity. *Right:* Adaptation at an orthogonal orientation relative to the cell's optimal orientation (large $\Delta\theta$) accelerates the development of orientation tuning, preserves orientation preference, and sharpens orientation selectivity. The graphs within each column show the development of orientation tuning for two neurons at different temporal delays during control (black) and adaptation (gray) conditions. The adapting orientation is marked by the dashed line. Error bars represent S.E.M.

rapid adaptation during fixation induces a suppression of responses on the flank of the tuning curve near the adapting stimulus and a facilitation of responses on the opposite flank, which together constitute a repulsive shift in the preferred orientation of V1 neurons. We suggest that brief adaptation improves the discrimination of orientations close to the neuron's optimal orientation by increasing the slope of the tuning curve in the vicinity of the preadaptation pre-

ferred orientation. This improvement in discrimination performance following iso-orientation adaptation has clear psychophysical support (Clifford et al., 2001; Regan and Beverley, 1985) and could be a mechanism that might be used by the visual system in order to resolve fine orientation details during visual fixation.

On the other hand, since the mean saccade length during free viewing is relatively large, successive fixations are likely to be made on image patches of dissimilar structure. In this case, adaptation to largely dissimilar image patterns improves neuronal performance in V1 by sharpening orientation tuning curves, and there is a corresponding improvement of psychophysical performance on orientation discrimination. Given the ubiquity of successive saccades to patches of dissimilar structure during natural vision, we suggest that the visual system has adapted to the correlational structure of images so as to encode local features more efficiently.

Conclusions

Examining how visual cortical neurons adapt their response properties to short-term exposure to patterned stimulation or to perceptual learning, and how the capacity for adaptive changes is mapped onto the cortex, is fundamental for understanding neuronal mechanisms of conscious visual perception. An astonishing property of adaptation-induced plasticity is the fact that its magnitude changes, depending on cortical location. This suggests that the visual cortex is not homogeneous in its capacity to undergo plastic changes and indicates the existence of a map of orientation plasticity, closely related to the map of orientation preference, in which pinwheel centers constitute foci of maximal plasticity and the rate of orientation change is a measure of the degree of plasticity across V1. Whether there are similar plasticity maps related to other functional maps, such as those for eye preference, spatial frequency, direction, or the effects of attention, remains an open and interesting question.

Plasticity is an integral part of information processing in the cortex. Visual cortex neurons change their responses as they are stimulated, and vision is continually shaped by these response changes. The findings on orientation plasticity induced by adaptation on the time scale of visual fixation demonstrate that these changes can be rapid indeed and can continuously influence vision.

REFERENCES

- Abbott, L. F., J. A. Varela, K. Sen, and S. B. Nelson, 1997. Synaptic depression and cortical gain control, *Science*, 275:220–224.
- Andrews T. J., and D. M. Coppola, 1999. Idiosyncratic characteristics of saccadic eye movements when viewing different visual environments, *Vis. Res.*, 39:2947–2953.

- Attneave, F., 1954. Informational aspects of visual processing, *Psychol. Rev.*, 61:183–193.
- Ball, K., and R. Sekuler, 1985. A specific and enduring improvement in visual motion discrimination, *Science*, 218:697–698.
- Ball, K., and R. Sekuler, 1987. Direction-specific improvement in motion discrimination, *Vis. Res.*, 27:953–965.
- Barlow, H. B., 1990. A theory about the functional role and synaptic mechanism of after-effects, in *Vision: Coding and Efficiency* (C. Blakemore ed.), Cambridge: Cambridge University Press, pp. 363–375.
- Blakemore, C., 1977. Genetic instructions and developmental plasticity in the kitten's visual cortex, *Philos. Trans. R. Soc. Lond. B Biol. Sci.*, 278:425–434.
- Blakemore, C., and F. W. J. Campbell, 1969. Adaptation to spatial stimuli, *J. Physiol. (Lond.)*, 200:11P–13P.
- Blakemore, C., and G. F. D. Cooper, 1970. Development of the brain depends on the visual environment, *Nature*, 228:477–478.
- Blasdel, G. G., 1992. Differential imaging of ocular dominance and orientation selectivity in monkey striate cortex, *J. Neurosci.*, 12:3115–3138.
- Bonhoeffer, T., and A. Grinvald, 1991. Iso-orientation domains in cat visual cortex are arranged in pinwheel-like patterns, *Nature*, 353:429–431.
- Carandini, M., and D. Ferster, 1997. A tonic hyperpolarization underlying contrast adaptation in cat visual cortex, *Science*, 276:949–952.
- Carandini, M., J. A. Movshon, and D. Ferster, 1998. Pattern adaptation and cross-orientation interactions in the primary visual cortex, *Neuropharmacology*, 37:501–511.
- Chance, F. S., S. B. Nelson, and L. F. Abbott, 1998. Synaptic depression and the temporal response characteristics of V1 cells, *J. Neurosci.*, 18:4785–4799.
- Clifford, C. W., A. M. Wyatt, D. H. Arnold, S. T. Smith, and P. Wenderoth, 2001. Orthogonal adaptation improves orientation discrimination, *Vis. Res.*, 41:151–159.
- Crair, M. C., D. C. Gillespie, and M. P. Stryker, 1998. The role of visual experience in the development of columns in cat visual cortex, *Science*, 279:566–570.
- Crist, R. E., W. Li, and C. D. Gilbert, 2001. Learning to see: experience and attention in primary visual cortex, *Nat. Neurosci.*, 4:519–525.
- Darian-Smith, C., and C. D. Gilbert, 1994. Axonal sprouting accompanies functional reorganization in adult cat striate cortex, *Nature*, 368:737–740.
- Das, A., and C. D. Gilbert, 1995. Long-range horizontal connections and their role in cortical reorganization revealed by optical recording of cat primary visual cortex, *Nature*, 375:780–784.
- Das, A., and C. D. Gilbert, 1999. Topography of contextual modulations mediated by short-range interactions in primary visual cortex, *Nature*, 399:655–661.
- DeAngelis, G. C., A. Anzai, I. Ohzawa, and R. D. Freeman, 1995. Receptive field structure in the visual cortex: does selective stimulation induce plasticity? *Proc. Natl. Acad. Sci. USA*, 92:9682–9686.
- de Boer, E., and P. Kuyper, 1968. *IEEE Trans. Biomed. Eng.*, 15:169–179.
- De Weerd, P., R. Gattass, R. Desimone, and L. G. Ungerleider, 1995. Responses of cells in monkey visual cortex during perceptual filling-in of an artificial scotoma, *Nature*, 377:731–734.
- Dragoi, V., J. Sharma, E. K. M. Miller, and M. Sur, 1999. Dynamics of orientation adaptation in awake monkey V1 revealed by reverse correlation, *Soc. Neurosci. Abstr.*, 25:1548.
- Dragoi, V., J. Sharma, E. K. M. Miller, and M. Sur, 2002. Dynamics of neuronal sensitivity in primate V1 underlying local feature discrimination, *Nat. Neurosci.*, 5:883–891.
- Dragoi, V., J. Sharma, and M. Sur, 2000. Adaptation-induced plasticity of orientation tuning in adult visual cortex, *Neuron*, 28:287–298.
- Dragoi, V., and M. Sur, 2000. Dynamic properties of recurrent inhibition in primary visual cortex: contrast and orientation dependence of contextual effects, *J. Neurophysiol.*, 83:1019–1030.
- Dragoi, V., C. Rivabulla, and M. Sur, 2001. Foci of orientation plasticity in visual cortex, *Nature*, 411:80–86.
- Fahle, M., and S. Edelman, 1993. Long-term learning in vernier acuity: effects of stimulus orientation, range and of feedback, *Vis. Res.*, 33:397–412.
- Fendick, M., and G. Westheimer, 1983. Effects of practice and the separation of test targets on foveal and peripheral stereoacuity, *Vis. Res.*, 23:145–150.
- Fregnac, Y., and M. Imbert, 1978. Early development of visual cortical cells in normal and dark-reared kittens: relationship between orientation selectivity and ocular dominance, *J. Physiol. (Lond.)*, 278:27–44.
- Fregnac, Y., D. Shulz, S. Thorpe, and E. Bienenstock, 1988. A cellular analogue of visual cortical plasticity, *Nature*, 333:367–370.
- Gibson, J. J., 1933. Adaptation, after-effect and contrast in the perception of curved lines, *J. Exp. Psychol.*, 16:1–33.
- Gibson, J. J., and M. Radner, 1937. Adaptation, after-effect and contrast in the perception of tilted lines. I. Quantitative studies, *J. Exp. Psychol.*, 20:453–467.
- Gilbert, C. D., and T. N. Wiesel, 1992. Receptive field dynamics in adult primary visual cortex, *Nature*, 356:150–152.
- Gilbert, C. D., H. Sigman, and R. E. Crist, 2001. The neural basis of perceptual learning, *Neuron*, 31:681–697.
- Godde, B., R. Leonhardt, S. M. Cords, and H. R. Dinse, 2002. Plasticity of orientation preference maps in the visual cortex of adult cats, *Proc. Natl. Acad. Sci. USA*, 99:6352–6357.
- Godecke, I., D. S. Kim, T. Bonhoeffer, and W. Singer, 1997. Development of orientation preference maps in area 18 of kitten visual cortex, *Eur. J. Neurosci.*, 9:1754–1762.
- Hammond, P., G. S. Mouat, and A. T. Smith, 1985. Motion after-effects in cat striate cortex elicited by moving gratings, *Exp. Brain Res.*, 60:411–416.
- Hammond, P., G. S. Mouat, and A. T. Smith, 1986. Motion after-effects in cat striate cortex elicited by moving texture, *Vis. Res.*, 26:1055–1060.
- Hata, Y., T. Tsumoto, H. Sato, and H. Tamura, 1991. Horizontal interactions between visual cortical neurones studied by cross-correlation analysis in the cat, *J. Physiol.*, 441:593–614.
- Hirsch, H. V., and D. N. Spinelli, 1970. Visual experience modifies distribution of horizontally and vertically oriented receptive fields in cats, *Science*, 168:869–871.
- Hubel, D. H., and T. N. Wiesel, 1962. Receptive fields, binocular interaction and functional architecture in the cat's visual cortex, *J. Physiol. (Lond.)*, 160:106–154.
- Hubel, D. H., and T. N. Wiesel, 1974. Sequence regularity and geometry of orientation columns in the monkey striate cortex, *J. Comp. Neurol.*, 158:267–293.
- Kaas, J. H., L. A. Krubitzer, Y. M. Chino, A. L. Langston, E. H. Polley, and N. Blair, 1990. Reorganization of retinotopic cortical maps in adult mammals after lesions of the retina, *Science*, 248:229–231.
- Karni, A., and D. Sagi, 1991a. Perceptual filling in of artificially induced scotomas in human vision, *Nature*, 350:699–702.

- Karni, A., and D. Sagi, 1991b. Where practice makes perfect in texture discrimination: evidence for primary visual cortex plasticity, *Proc. Natl. Acad. Sci. USA*, 88:4966–4970.
- Kisvarday, Z. F., E. Toth, M. Rausch, and U. T. Eysel, 1997. Orientation-specific relationship between populations of excitatory and inhibitory lateral connections in the visual cortex of the cat, *Cereb. Cortex*, 7:605–618.
- Levitt, J. B., and J. S. Lund, 1997. Contrast dependence of contextual effects in primate visual cortex, *Nature*, 387:73–76.
- Maffei, L., A. Fiorentini, and S. Bisti, 1973. Neural correlate of perceptual adaptation to gratings, *Science*, 182:1036–1038.
- Magnussen, S., and W. Kurtenbach, 1980. Adapting to two orientations: disinhibition in a visual aftereffect, *Science*, 207:908–909.
- Markram, H., J. Lubke, M. Frotscher, and B. Sakmann, 1997. Regulation of synaptic efficacy by coincidence of postsynaptic APs and EPSPs, *Science*, 275:213–215.
- Mazer, J. A., W. E. Vinje, J. McDermott, P. H. Schiller, and J. L. Gallant, 2002. Spatial frequency and orientation tuning dynamics in area V1, *Proc. Natl. Acad. Sci. USA*, 99:1645–1650.
- McKee, S. P., and G. Westheimer, 1978. Improvement in vernier acuity with practice, *Percept. Psychophys.*, 24:258–262.
- Merzenich, M. M., J. H. Kaas, J. T. Wall, M. Sur, R. J. Nelson, and D. J. Felleman, 1983. Progression of change following median nerve section in the cortical representation of the hand in areas 3b and 1 in adult owl and squirrel monkeys, *Neuroscience*, 10:639–665.
- Merzenich, M. M., R. J. Nelson, M. P. Stryker, M. S. Cynader, A. Schoppmann, and J. M. Zook, 1984. Somatosensory cortical map changes following digit amputation in adult monkeys, *J. Comp. Neurol.*, 224:591–605.
- Movshon, A., and P. Lennie, 1979. Pattern-selective adaptation in visual cortical neurones, *Nature*, 278:850–852.
- Muller, J. R., A. B. Metha, J. Krauskopf, and P. Lennie, 1999. Rapid adaptation in visual cortex to the structure of images, *Science*, 285:1405–1408.
- Nelson, S. B., 1991. Temporal interactions in the cat visual system. I. Orientation-selective suppression in the visual cortex, *J. Neurosci.*, 11:344–356.
- Ohzawa, I., G. Sclar, and R. D. S. Freeman, 1982. Contrast gain control in the cat visual cortex, *Nature*, 298:266–268.
- Pettet, M. W., and C. D. Gilbert, 1992. Dynamic changes in receptive-field size in cat primary visual cortex, *Proc. Natl. Acad. Sci. USA*, 89:8366–8370.
- Poggio, T., M. Fehle, and S. Edelman, 1992. Fast perceptual learning in visual hyperacuity, *Science*, 256:1018–1021.
- Polat, U., K. Mizobe, M. W. Pettet, T. Kasamatsu, and A. M. Norcia, 1998. Collinear stimuli regulate visual responses depending on cell's contrast threshold, *Nature*, 391:580–584.
- Ramachandran, V. S., and O. Braddick, 1973. Orientation-specific learning in stereopsis, *Perception*, 2:371–376.
- Ramachandran, V. S., and R. L. Gregory, 1991. Perceptual filling in of artificially induced scotomas in human vision, *Nature*, 350:699–702.
- Regan, D., and K. I. Beverley, 1985. Postadaptation orientation discrimination, *J. Opt. Soc. Am. A*, 2:147–155.
- Ringach, D. L., M. J. Hawken, and R. Shapley, 1997. Dynamics of orientation tuning in macaque primary visual cortex, *Nature*, 387:281–284.
- Sanchez-Vives, M. V., L. G. Nowak, D. A. McCormick, 2000. Membrane mechanisms underlying contrast adaptation in cat area 17 in vivo, *J. Neurosci.*, 20:4267–4285.
- Saul, A. B., and M. S. Cynader, 1989. Adaptation in single units in visual cortex: the tuning of aftereffects in the spatial domain, *Vis. Neurosci.*, 2:593–607.
- Schoups, A., R. Vogels, N. Qian, and G. Orban, 2001. Practising orientation identification improves orientation coding in V1 neurons, *Nature*, 412:549–553.
- Schuett, S., T. Bonhoeffer, and M. Hubener, 2001. Pairing-induced changes of orientation maps in cat visual cortex, *Neuron*, 32:325–337.
- Sengpiel, F., P. Stawinski, and T. Bonhoeffer, 1999. Influence of experience on orientation maps in cat visual cortex, *Nat. Neurosci.*, 2:727–732.
- Shiu, L. P., and H. Pashler, 1992. Improvement in line orientation discrimination is retinally local but dependent on cognitive set, *Percept. Psychophys.*, 52:582–588.
- Sillito, A. M., K. L. Grieve, H. E. Jones, J. Cudeiro, and J. Davis, 1995. Visual cortical mechanisms detecting focal orientation discontinuities, *Nature*, 378:492–496.
- Somers, D. C., V. Dragoi, and M. Sur, 2002. Orientation selectivity and its modulation by local and long-range connections in visual cortex, in *Cerebral Cortex: The Cat Primary Visual Cortex* (A. Peters and B. Payne, eds.), San Diego, CA: Academic Press.
- Somers, D. C., E. V. Todorov, A. G. Siapas, L. J. Toth, D. S. Kim, and M. Sur, 1998. A local circuit approach to understanding integration of long-range inputs in primary visual cortex, *Cereb. Cortex*, 8:204–217.
- Stryker, M. P., H. Sherk, A. G. Leventhal, and H. V. Hirsch, 1978. Physiological consequences for the cat's visual cortex of effectively restricting early visual experience with oriented contours, *J. Neurophysiol.*, 41:896–909.
- Sur, M., J. Schummers, and V. Dragoi, 2002. Cortical plasticity: time for a change, *Curr. Biol.*, 12:R168–R170.
- Toth, L. J., S. C. Rao, D. S. Kim, D. Somers, and M. Sur, 1996. Subthreshold facilitation and suppression in primary visual cortex revealed by intrinsic signal imaging, *Proc. Natl. Acad. Sci. USA*, 93:9869–9874.
- Toth, L. J., D. S. Kim, S. C. Rao, and M. Sur, 1997. Integration of local inputs in visual cortex. *Cereb. Cortex*, 7:703–710.
- Vogels, R., and G. A. Orban, 1985. The effect of practice on the oblique effect in line orientation judgments, *Vis. Res.*, 25:1679–1687.
- Weliky, M., K. Kandler, D. Fitzpatrick, and L. C. Katz, 1995. Patterns of excitation and inhibition evoked by horizontal connections in visual cortex share a common relationship to orientation columns, *Neuron*, 15:541–552.
- Yao, H., and Y. Dan, 2001. Stimulus timing-dependent plasticity in cortical processing of orientation, *Neuron*, 32:315–323.
- Yarbus, A. L., 1967. *Eye Movement and Vision*, New York: Plenum.
- Zhang, L. I., H. W. Tao, C. E. Holt, W. A. Harris, and M. Poo, 1998. A critical window for cooperation and competition among developing retinotectal synapses, *Nature*, 395:37–44.

113 Synchrony, Oscillations, and Relational Codes

WOLF SINGER

PSYCHOPHYSICAL AND neurophysiological evidence suggests that the visual system identifies objects by decomposing them into components, by extracting certain sets of features, and by analyzing the relations among the respective components and features. This is an efficient strategy for two reasons. First, it permits unambiguous descriptions of a virtually unlimited number of different objects with a limited set of descriptors for components, features, and relations. Second, it can be scaled and applied also for the description of entire visual scenes, that is, for the infinite variety of configurations in which visual objects can occur. Linguistic descriptions follow the same principle. By recombining in ever-changing configurations a rather limited set of descriptors for objects, components, properties, and relations, a virtually inexhaustible repertoire of descriptions can be composed, both of familiar and novel, concrete and abstract constellations.

This coding strategy is necessarily distributed in nature because it requires recombining and hence separate descriptors for components, features, and relations. Substituting a sentence by a single word that captures the full meaning of the sentence may be advantageous in exceptional cases—for example, if the description refers to a particularly important, frequently recurring event or scene. It would make no sense, however, to invent single-word descriptions for all possible sentences, as this would lead to a combinatorial explosion of the required vocabulary. This suggests an interesting trade-off between the size of the vocabulary, that is, the variety and complexity of the descriptors, on the one hand, and the complexity of the syntactic structures that define the relations between the descriptors, on the other hand. If descriptors address only very elementary components and features, relatively few types of descriptors are required because the diversity of elementary components of objects is limited: a few dozen different atoms suffice to generate a universe of molecules. However, if descriptors are available only for very-low-level components and features, full descriptions of complex objects require highly sophisticated syntactic structures to cope with the large number of nested relations that need to be specified. Conversely, if descriptors exist that not only define elementary components, features, and relations but already certain conjunctions of components and features, more descriptors

are required but the complexity of the syntactic structures necessary for the definition of relations can be reduced. Depending on the nature of the coding task, the cost of descriptors, and the versatility of the relation-defining mechanisms, cognitive systems can be expected to settle for optimally adapted compromises in this trade-off between the sophistication of descriptors and the sophistication of dynamic codes for relations.

Regarding the neuronal implementation of such coding strategies, one expects to find neurons whose responses signal the presence of very elementary components and features, as well as neurons whose responses encode conjunctions of variable complexity. In addition, one expects to find mechanisms that permit a flexible and context-dependent definition of relations among the responses of neurons that code for components, features, and some of their conjunctions.

The numerous investigations of single-cell responses performed over the past decades have provided robust support for the existence of neurons in sensory areas of the cerebral cortex that signal the presence of features and their conjunctions. Some of them encode elementary components and features of perceptual objects, while others are tuned to quite complex conjunctions of components and features. The former prevail at early and the latter at late stages of the processing streams. However, until recently, no systematic investigations were devoted to the analysis of mechanisms permitting flexible and context-dependent definitions of relations among the responses of these neurons. The reasons were mainly conceptual. First, the discovery of neurons responding to complex conjunctions of features indicated that relations are encoded by having feature-selective cells converge on specific conjunction cells, and it was assumed that this mechanism, if iterated sufficiently often, can cope with the definition of all conceivable relations. Second, neurons were considered insensitive to the precise temporal relations among afferent spike trains and to essentially evaluate average rate fluctuations. This predicted that all information about the relatedness of responses should be contained in the amplitude distribution of responses, a conjecture that was corroborated by the observation that in many instances such population rate vectors correlate very well with stimulus configurations or movement trajectories.

All relevant information appeared to be retrievable by recording the event-related responses of single cells, by computing averages of these responses in order to reduce noise, and by comparing the response amplitudes of the various successively recorded neurons. The tremendous explanatory power of single-cell responses made it appear unlikely that any additional information is encoded in the precise temporal relations between the discharges of simultaneously active neurons. These hypotheses provided little incentive to record from more than one unit at a time and to investigate relations among nonaveraged, simultaneously recorded responses. Research focused on the analysis of averaged responses from sequentially recorded neurons.

Systematic search for mechanisms permitting dynamic and flexible definition of relations among distributed responses began after the accidental finding that neurons in the cat visual cortex can engage in oscillatory firing patterns and coordinate the temporal fine structure of their responses by synchronizing their discharges with a precision in the millisecond range (Gray and Singer, 1987, 1989). This finding suggested the hypothesis that the cerebral cortex exploits its ability to coordinate the discharges of distributed neurons in order to define relations that are difficult to encode with conjunction neurons. In the following, some of the theoretical considerations which led to the hypothesis that synchronization could serve as a code for relations are reviewed. Then experiments that were designed to test predictions derived from the synchronization hypothesis are discussed.

Why synchrony?

Figure 113.1 illustrates how relations among features can be encoded by conjunction-specific neurons within hierarchically structured feedforward architectures. Representing relations among components by conjunction units has two undisputed advantages. First, it permits rapid processing because it can be realized in feedforward architectures. Second, it is unambiguous because the response of a particular cell always signals the same relation (labeled line coding). However, if not complemented by additional, more dynamic and context-sensitive mechanisms for the definition of relations, this strategy poses problems. First, excessively large numbers of conjunction units are required to cope with the manifold intramodal and cross-modal relations between the features of real-world objects. Second, it is hard to see how the entirely new relations among the features of novel objects can be represented, as there cannot be an exhaustive repertoire of a priori specified conjunction units for all possible feature constellations. Third, unresolved problems arise with the specification of the nested relations that need to be defined to represent composite objects or scenes containing numerous objects. (For a more detailed review

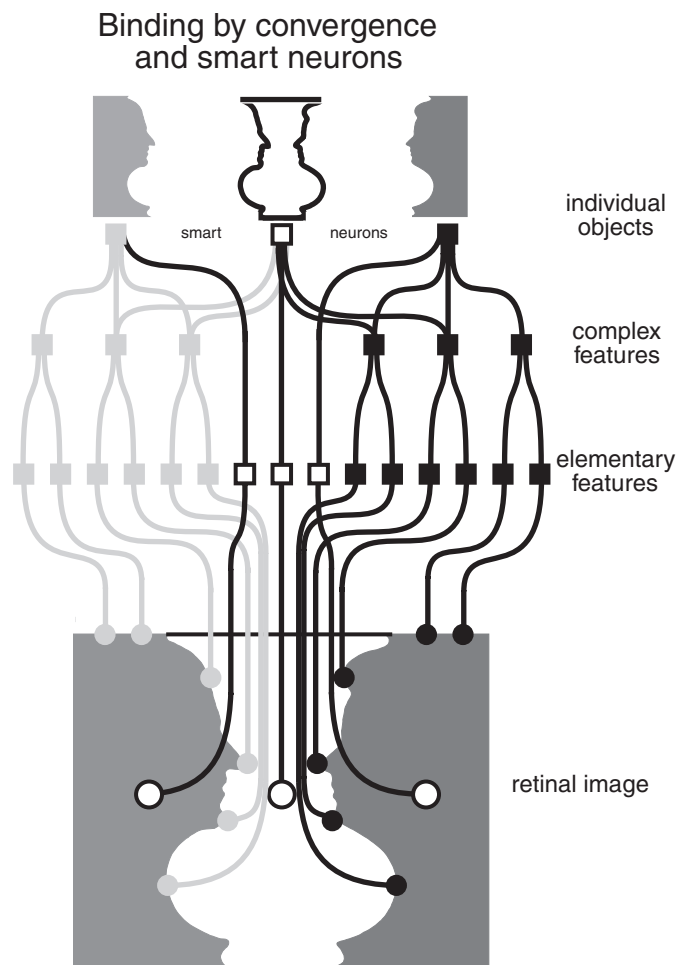


FIGURE 113.1. Schematic wiring diagram of a hierarchically organized feedforward network that generates conjunction-specific neurons which respond selectively to different perceptual objects. Note that the neurons representing the faces and the vase receive input partially from the same feature-specific neurons.

of the arguments, see Gray, 1999; Singer, 1999; von der Malsburg, 1999.)

These shortcomings can be overcome by assembly coding. Here individual cells signal only components of objects that may consist of rather complex conjunctions of elementary features—while the whole object is represented by the simultaneous responses of the respective component coding cells (Fig. 113.2). Individual neurons can then contribute at different times to the representation of different objects by forming ensembles with varying partners. This reduces dramatically the number of required conjunction units. It also solves the problem of representing novel relations, objects, and scenes because cells representing elementary features can be grouped dynamically in ever-changing constellations and then can represent as an assembly the particular combination of features characteristic of the novel object. However, this coding strategy requires a dynamic

Assembly coding

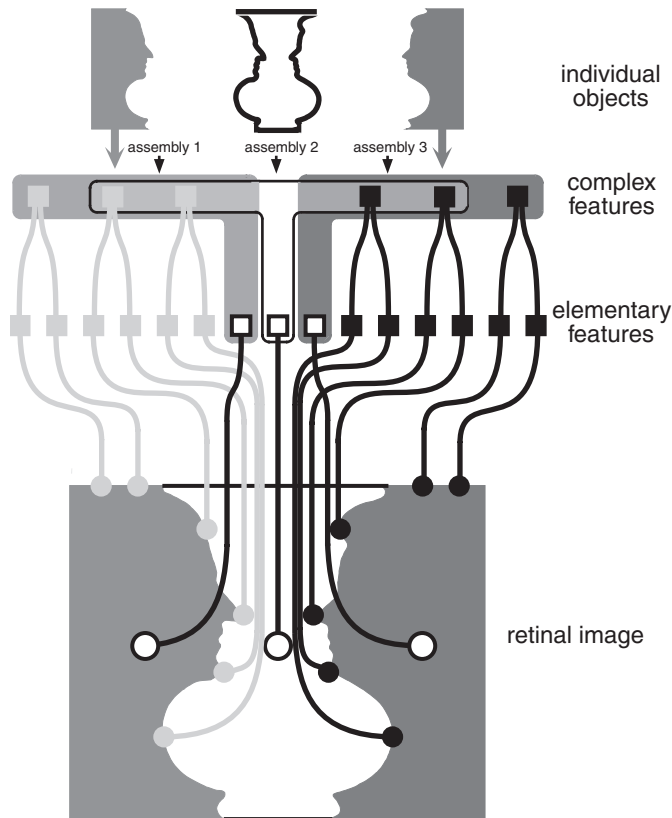


FIGURE 113.2. Schematic wiring diagram of neuronal architectures serving the representation of perceptual objects by assemblies. Note that the assembly representing the vase shares neurons with the assemblies representing the faces. To ensure stability of the respective assemblies, additional reciprocal connections among neurons constituting an assembly are required (*shaded regions*) that bind responses of neurons belonging to the same assembly.

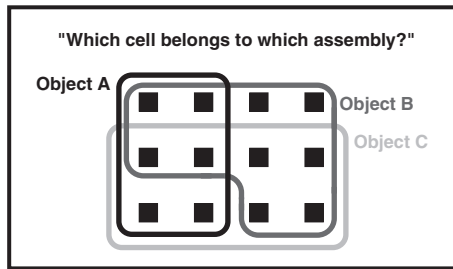
binding mechanism that can associate cells into assemblies and tag responses of distributed neurons as related once these have formed an assembly. Such dynamic binding mechanisms cannot be implemented in feedforward architectures, as they require additional reciprocal association connections and reentry loops.

An unambiguous signature of relatedness is absolutely crucial in assembly coding because, unlike in labeled line codes, the meaning of responses changes with the context in which they are embedded. It needs to be ensured that the responses of the neurons that constitute an assembly are processed and evaluated together at subsequent processing stages and are not confounded with other, unrelated responses. In principle, this can be achieved by raising jointly and selectively the saliency of the responses belonging to an assembly, and there are three options: first, unrelated responses can be inhibited and excluded from further processing. Second, the discharge frequency of the selected

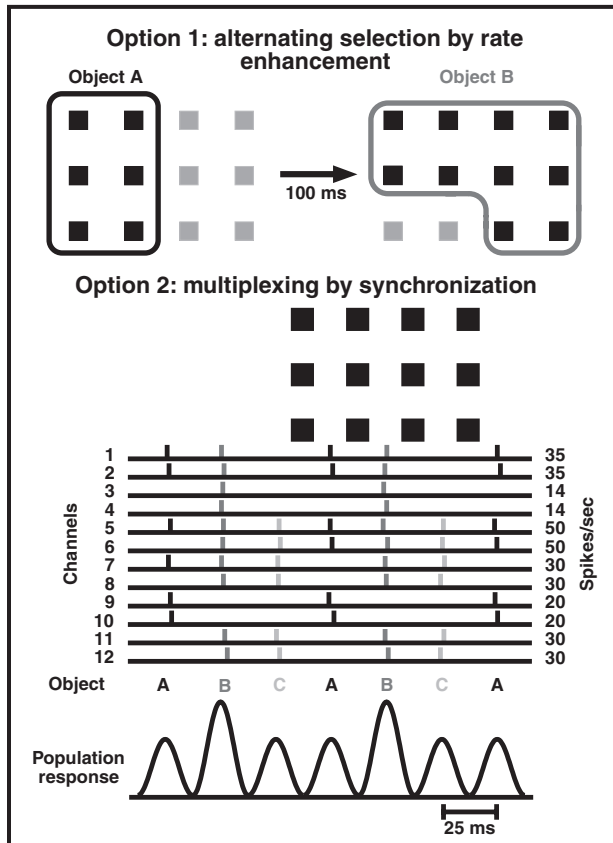
responses can be enhanced. Third, the selected cells can be made to discharge in precise temporal synchrony. All three mechanisms enhance the relative impact of the selected responses and can therefore be used to tag them as related. Problems arise, however, when several assemblies need to be formed at the same time and need to recruit partly the same neurons—a condition that is likely to occur when a scene contains several objects that have subsets of features in common. This problem has been addressed as the so-called superposition problem and can only be resolved by segregating assemblies in time (Fig. 113.3). One option is to raise jointly the discharge frequency of cells belonging to the first assembly for an interval sufficiently long to permit readout by subsequent stages and subsequently to increase the discharge rate of the cells belonging to the second assembly, and so on. Another option is to label responses of cells belonging to an assembly by synchronizing the respective discharges. As synchronization raises the saliency of individual discharges, it defines relations with much higher temporal resolution than rate modulation and, in principle, permits multiplexing of assemblies, as suggested in Figure 113.3. Single-cell studies have provided robust evidence that attentional mechanisms use inhibition and selective enhancement of the discharge rate for response selection and grouping. However, there is little evidence so far from multielectrode studies that joint increases in discharge rate are used for response selection and grouping in the context of assembly coding. This may be due to the paucity of multielectrode studies searching for such phenomena. However, it is also conceivable that synchronization and temporal multiplexing are better suited for the definition of relations in assembly coding than joint rate increases.

In assembly coding processing, speed is limited essentially by the rate at which relational codes can be generated and read out. If relations are defined by joint rate increases, readout requires temporal summation of successively arriving excitatory postsynaptic potentials (EPSPs) and hence integration over a sequence of EPSPs. If integration intervals are shorter than the average interspike intervals, EPSPs do not summate effectively and rate increases cannot be detected. Synchronization, by contrast, exploits exclusively spatial and no additional temporal summation to raise the saliency of responses. Therefore, relations can be defined—at least in principle—with a temporal resolution corresponding to the duration of individual EPSPs. Thus, assemblies can be reconfigured and multiplexed at much faster rate when synchronization is used as a tag of relatedness instead of joint rate enhancement. Another, potentially important advantage of using synchrony as a tag of relatedness is that relations can be specified independently of firing rate. Discharge rates depend on numerous variables, such as the physical energy of stimuli or the match between stimulus and receptive field properties. Response amplitudes

The superposition problem



The only solution: segregation in time



are thus rather ambiguous indicators of relatedness. As synchrony can be modulated by temporal regrouping of discharges and thus can be varied independently of firing rates, synchronicity and rate can be used as orthogonal codes. Signals indicating the presence and the properties of visual features can thus be kept separate from signals indicating how these features are related.

Another advantage of using synchronization as a tag of relatedness is that synchronized input is transmitted with minimal latency jitter (Abeles, 1982; Diesmann et al., 1999). Thus, signatures of relatedness can be relayed with great reliability across processing stages, which contributes to reducing the risk of false conjunctions. Finally, synchronization enhances processing speed by accelerating synaptic

FIGURE 113.3. Options for the solution of the superposition problem. Superposition problems arise if perceptual objects are present whose corresponding assemblies partly share the same neurons (*upper box*). In this case, different assemblies need to be segregated in time to avoid false conjunctions. One option is to raise successively the saliency of responses belonging to the respective assemblies by enhancing the discharge rate of the corresponding responses (*lower box*, option 1). An alternative solution is to enhance the saliency of responses belonging to a particular assembly by making the discharges of the respective neurons coincident in time (option 2). This permits rapid multiplexing of the different assemblies because coincidence can be evaluated within short time intervals, as it does not require temporal summation. Here it is assumed that the different assemblies alternate at intervals of approximately 25 msec. Note that this temporal structure can be, but does not have to be, obvious in the discharge sequences of individual neurons (channels 1 to 12) but that the spike density function of the population response shows an oscillatory modulation in the 40 Hz range. Note also that the constellation of neurons contributing spikes to the oscillatory population response changes from cycle to cycle.

transmission per se because synchronized EPSPs trigger action potentials with minimal delay.

Constraints of synchrony

In conclusion, these features make response synchronization an attractive strategy to encode relations. However, in order to be effective, several additional constraints need to be met. First, neuronal networks must be able to modify and to coordinate the temporal patterning of spike trains in a context-dependent manner. Second, it must be possible to structure episodes of coordinated firing and to change the constellations of synchronously discharging neurons within a few tens of milliseconds in order to be compatible with processing speed. Third, the temporal signatures of coordinated discharge sequences must be preserved with millisecond precision across processing stages. Fourth, neuronal networks must be able to distinguish synchronous from temporally dispersed activity with a precision in the millisecond range; that is, synchronous input must have a stronger impact on neurons than asynchronous input. Fifth, since Hebbian learning is based on the evaluation of relations, activity-dependent modifications of synaptic gain must be gated by the synchronicity of pre- and postsynaptic discharge patterns and not only by the mere covariation of rate changes if relations are encoded by synchrony.

However, even if all these constraints are met, this is still not proof that the cerebral cortex uses response synchronization to tag responses as related. It also needs to be shown that the occurrence and structure of synchronous discharge patterns are related in a meaningful way to perceptual or motor processes requiring dynamic grouping of responses. If synchronization matters, it should be possible to predict

behavior from measures of synchrony. Ideally, one would like to obtain not only correlative but also causal evidence for such relations by manipulating synchrony and studying the behavioral consequences.

Are the constraints met?

Evidence suggests that neuronal networks are capable of transmitting temporal patterns with the required precision and of distinguishing between coincident (synchronous) and noncoincident (temporally dispersed) input signals with the necessary temporal resolution. Specialized circuits of the auditory system can exploit latency differences in the sub-millisecond range for sound localization. Signal transduction in the retina is slower than in the ear, but the visual system is also capable of resolving temporal patterns with a precision in the millisecond range. Psychophysical experiments suggest that stimulus onset asynchronies of less than 10 msec can support perceptual grouping. The visual system binds simultaneously appearing pattern elements and segregates them from elements presented with temporal offset (Alais et al., 1998; Lee and Blake, 1999; Leonards et al., 1996; Usher and Donnelly, 1998).

This indicates that temporally modulated responses can be transmitted over several processing stages with a precision in the millisecond range. Supportive evidence comes from electrophysiological investigations. Cross-correlations between simultaneously recorded responses of retinal ganglion cells, relay neurons in the lateral geniculate nucleus, and cortical cells show that the oscillatory patterning of retinal responses is reliably transmitted to the cortex (Castelo-Branco et al., 1998). Given the high frequency of the retinal oscillations (up to 100 Hz), this implies that synchronized volleys of discharges are transmitted over several synaptic stages with a precision in the millisecond range. The well-synchronized cortical responses to flicker stimuli point in the same direction (Rager and Singer, 1998). As indicated by the precise temporal modulation of responses in area MT of the monkey visual cortex, temporal fidelity of synaptic transmission is not confined to primary sensory pathways but also holds for cortico-cortical connections (Buracas et al., 1998). Simulation studies indicate that such precision is readily obtained with neurons that operate with conventional time constants. The only prerequisite is that transmission occurs in parallel channels that interact through diverging and converging axon collaterals (Diesmann et al., 1999). Once neurons at the same processing level have synchronized their discharges, the highly coherent pulse packets are conveyed with minimal dispersion across several synaptic stages, as postulated for synfire chains (Abeles, 1991).

Evidence is also available that synchronization can be established and dissolved very rapidly (within maximally a

few tens of milliseconds). Simulations with spiking neurons revealed that networks of appropriately coupled units can indeed undergo very rapid transitions from uncorrelated to synchronized states and vice versa (Gerstner, 1996). In physiological recordings, it is not uncommon that neurons engage in synchronous activity, often with additional oscillatory patterning, at the same time that they increase their discharge rate in response to the light stimulus (Gray et al., 1992).

The postulate that synchronized activity must have a stronger impact in target structures than temporally dispersed firing is also supported by data. Simultaneous recordings from coupled neuron triplets along thalamocortical and intracortical pathways in the visual system have revealed that EPSPs synchronized within intervals below 2 or 3 msec are much more effective than EPSPs dispersed over longer intervals (Alonso and Martinez, 1998; Alonso et al., 1996; Usrey and Reid, 1999). Multielectrode recordings from several sites of the cat visual cortex and retinotopically corresponding loci in the superior colliculus indicated that the impact of a particular group of cortical cells on target cells in the colliculus increases substantially whenever the cortical cells synchronize their discharges with other cortical cell groups projecting to the same site in the tectum (Brecht et al., 1998). Enhanced saliency of synchronized responses can also be inferred from experiments in amblyopic cats which showed a close correlation between reduced synchrony in primary visual cortex and a loss of responses in higher visual areas (Roelfsema et al., 1994; Schröder et al., 2002). Similar conclusions are suggested by simulation studies (Bair and Koch, 1996; Niebur and Koch, 1994) and in vitro experiments (Stevens and Zador, 1998).

Several mechanisms, some of which have been identified only recently, can account for the enhanced efficacy of synchronously arriving EPSPs. First, because of their exponential decay, simultaneous EPSPs summate more effectively than temporally dispersed EPSPs, and there is some evidence for supralinear summation due to voltage-gated dendritic conductances (Schiller et al., 2000). Second, firing threshold is sensitive to the rising slope of the depolarization and lowers for fast-rising depolarizations such as those characteristic of synchronously arriving EPSPs (C. M. Gray, personal communication). Third, the effect of EPSPs is dramatically enhanced when they coincide with a back-propagating dendritic spike and hence with the input that generated this spike (Larkum et al., 1999). All three mechanisms are sensitive to temporal dispersions of EPSPs in the range of a few milliseconds.

Further evidence that precise temporal relations among neuronal discharges matter in cortical processing comes from investigations of synaptic plasticity. Varying the temporal relations between presynaptic EPSPs and postsynaptic spike responses in simultaneously recorded coupled cortical

cells revealed that long-term potentiation (LTP) results when the EPSP precedes the postsynaptic spike within intervals of 10 msec or less while the polarity of the modification reverses to long-term depression (LTD) as soon as the EPSP follows the spike (Markram et al., 1997). Thus, shifts of a few milliseconds in the timing relations between pre- and postsynaptic discharges suffice to invert the polarity of use-dependent synaptic modifications. The mechanism permitting such precise evaluation of the temporal contiguity of pre- and postsynaptic responses is the active dendritic response associated with the back-propagating spike. The following results obtained from visual cortex slices point in the same direction. They suggest that the temporal windows for Hebbian coincidence matching are sharpened further if neurons engage in oscillatory responses.

Pyramidal cells of rat visual cortex slices were made to discharge tonically at 20 or 40 Hz by injecting sinusoidally modulated current through a patch pipette. Simultaneously, EPSPs were evoked at 20 Hz by electrical stimulation of excitatory afferents. Changing the phase relations between pre- and postsynaptic activity revealed that the stimulated input tended to undergo LTP when the EPSPs were coincident with the spikes, while afferents consistently underwent LTD when the EPSPs fell in the troughs of the membrane potential oscillations. Thus, phase shifts of about 12 msec between individual EPSPs and spikes reversed the polarity of the synaptic modifications (Wespatat et al., 2001, 2003). This indicates that Hebbian modifications are sensitive to the precise phase relations of high-frequency discharges. If the modifications were gated solely by rate covariations, one would not expect such polarity reversals because pre- and postsynaptic discharge rates were the same in the two conditions. This implies further that precise synchrony serves as a signature of relatedness not only in the context of Hebbian learning but also in signal processing. The reason is that the temporal windows within which coincident synaptic events or spikes are treated as related must have the same duration in signal processing and learning, as any discrepancy would cause learning of false conjunctions.

In conclusion, there is converging evidence from different experimental approaches that cortical networks can handle temporal patterns with high precision and that precise timing relations among the discharges of distributed neurons are computationally relevant. Thus, the major constraints for the use of synchrony as a relation defining code are met. But does the brain exploit this option?

General properties of response synchronization

Synchronization of activity is defined operationally as a transient increase in coincident firing of two or more units that exceeds the level of coincidences predicted from estimations of actual discharge rates. Therefore, synchroniza-

tion must be assessed by correlation analysis and cannot be deduced from comparisons of rate fluctuations alone. Because the synchronization phenomena which are of interest here result from internal interactions, the time of occurrence of synchronized discharges is locked only loosely or not at all to external events. This intertrial variability precludes detection of synchronized response segments in histograms averaged over successive trials. Thus, episodes of enhanced response synchronization are detectable only if responses of different neurons are recorded simultaneously and subjected to a trial-by-trial correlation analysis.

The results of such analyses indicate that synchronization by internal neuronal interactions is a frequent phenomenon that occurs in many cerebral structures (for recent reviews, see Engel et al., 2001; Singer, 1999). It has also been noted that response synchronization is often associated with an oscillatory patterning which is best revealed by recording jointly the activity of several adjacent cells. The reasons for the better detectability of oscillations in population responses are two. First, individual cells tend to skip oscillation cycles in an irregular manner; second, oscillatory epochs are usually short and oscillation frequencies variable. Therefore, the periodicity of oscillatory population responses is often not apparent in the firing patterns of individual cells, even if their discharges are precisely phase locked to the oscillatory activity of the population. For this reason, synchronized oscillatory activity is detected best with methods that assess population responses such as recordings of multi-unit activity, local field potentials (LFPs), or the electroencephalogram (EEG). These global signals can then be correlated with the activity of individual cells to determine whether the discharges of the recorded cells are correlated with the synchronized activity of surrounding cell populations. Such measurements of spike-field coherence have proven highly efficient to detect changes in the synchronization of neurons and in the frequency of oscillatory patterning (see below).

Several properties make response synchronization, as it has been observed in the visual cortex, a good candidate mechanism for the definition of relations. First, synchronization is sufficiently precise, in particular when it occurs on the basis of beta and gamma oscillations, to raise the saliency of the synchronized responses and to be computationally effective. Second, joint firing is not simply the result of coherent, stimulus-locked variations in discharges rate, nor is it a trivial reflection of anatomical connectivity such as shared input. Rather, synchronization is generated by dynamic interactions within the cortical network, and its spatiotemporal patterning depends on a large number of variables; among these are the stimulus configuration (Engel et al., 1991b; Gray et al., 1989), the architecture of the intracortical synchronizing connections (Engel et al., 1991a; Löwel and Singer, 1992), the activation state of the cortical

network (Herculano-Houzel et al., 1999; Munk et al., 1996), and attention-dependent effects (Fries, et al., 2001b; Roelfsema et al., 1997; Steinmetz et al., 2000). These multiple influences endow synchronization with the required context sensitivity. Third, synchronization can be established across different cortical areas (Engel et al., 1991c; Roelfsema et al., 1997) and even hemispheres (Engel et al., 1991a) which is required for a relational code. Fourth, synchrony has been shown to vary independently of rate changes (Herculano-Houzel et al., 1999; Riehle et al., 1997), which is advantageous for the encoding of relations (see above). Fifth, synchronization is not an all-or-none phenomenon. When populations of cells engage in synchronous oscillatory activity, individual cells can skip cycles (Buzsaki, 1996; Buzsaki and Chrobak, 1995), and cells participating in population oscillations of different frequency can engage in partial correlations (Jensen and Lisman, 1998). This can be exploited to express graded and nested relations (Luck and Vogel, 1997). Sixth, when cells engage in synchronous oscillatory activity, the probability increases that the same cells synchronize in subsequent trials (Herculano-Houzel et al., 1997, 2003). In principle, this makes it possible to store information about relations by changing synchronization probability.

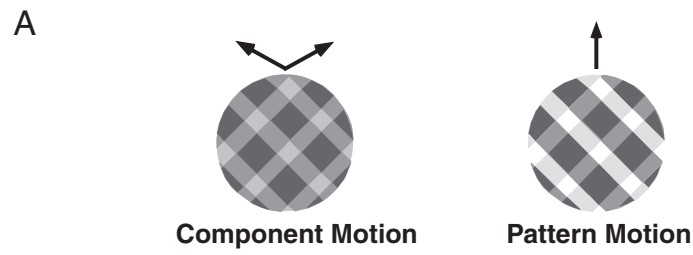
In the following some of these features of response synchronization will be discussed in more detail. Emphasis is placed on synchronization phenomena in the visual system and on relations between synchrony and cognitive processes.

Perceptual grouping

Scene segmentation and perceptual grouping are typical examples of low-level visual functions requiring flexible definition of relations. If internal synchronization of discharges serves to tag responses as related and to ensure their joint processing, synchronization probability among neurons in early visual areas should reflect some of the basic Gestalt criteria according to which the visual system groups related features during scene segmentation. Multielectrode studies designed to test this prediction revealed that neurons distributed across different columns within the same or different visual areas and even across hemispheres tend to synchronize their responses with close to zero phase lag when activated with a single contour but fire independently when stimulated simultaneously with two different contours (Engel et al., 1991a; Engel et al., 1991b; Engel et al., 1991c; Freiwald et al., 1995; Gray et al., 1989; Kreiter and Singer, 1996). Further analysis of the dependence of synchrony on receptive field and stimulus configurations confirmed that the probability and strength of response synchronization reflected elementary Gestalt criteria for perceptual grouping such as continuity, proximity, similarity in the orientation

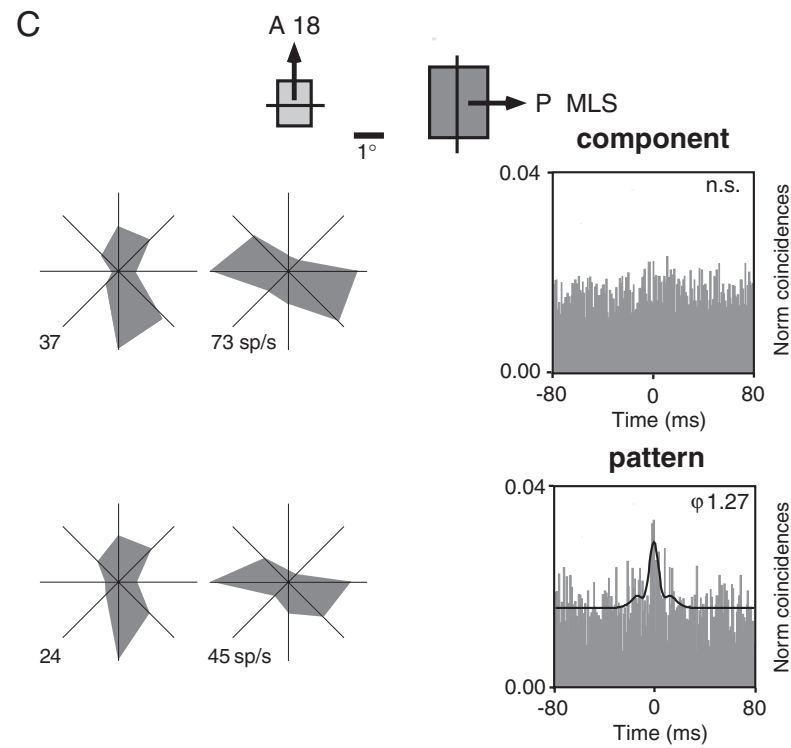
domain, colinearity, and common fate (for review, see Gray, 1999; Singer, 1993; Singer et al., 1997). These early experiments were performed in anesthetized animals, but more recent multielectrode recordings from awake cats and monkeys indicate that these synchronization phenomena are not artifacts of anesthesia but are even more pronounced when the animals are awake and attentive (Friedman-Hill et al., 2000; Fries et al., 1994; Fries et al., 1997; Gray and Viana Di Prisco, 1997; Kreiter and Singer, 1992, 1996; Maldonado et al., 2000). It is noteworthy that none of these systematic changes in synchronization probability have been associated with systematic stimulus-dependent changes of the neurons' discharge rate.

A particularly close correlation between neuronal synchrony and perceptual grouping has recently been observed in experiments with plaid stimuli. These stimuli are well suited for the study of dynamic binding mechanisms because minor changes of the stimulus cause a binary switch in perceptual grouping. Two superimposed gratings moving in different directions (plaid stimuli) may be perceived either as two surfaces, one being transparent and sliding on top of the other (component motion), or as a single surface, consisting of crossed bars, that moves in a direction intermediate between three of the component vectors (pattern motion) (Adelson and Movshon, 1982; Stoner et al., 1990). Which percept dominates depends on the luminance of grating intersections, because this variable defines the degree of transparency, or on the duty cycle of the gratings, because this variable determines changes in foreground-background assignments (Albright and Stoner, 1995). Component (pattern) motion is perceived when luminance conditions are compatible (incompatible) with transparency (Fig. 113.4*A*). Here is a case where the percept changes when the assignment of relations among stimulus components changes. If responses evoked by the two different gratings are treated as unrelated and only responses evoked by the contours of the same grating are bound together, one perceives two surfaces; conversely, if responses to all contours are treated as related, one perceives a single surface. If assignment of these different relations is achieved by selective synchronization, two predictions must hold (Fig. 113.4*B*): First, neurons whose responses represent the moving contours of the same grating should always synchronize. This is the case for cells that prefer the direction of motion of one of the two gratings and have colinearly aligned receptive fields. Second, groups of neurons that are tuned to respond to different gratings should synchronize their responses if they mediate the percept of pattern motion because in this case they must signal that all contours belong to the same surface and are related. By contrast, the same groups of cells should not synchronize if they mediate the percept of component motion because in this case their responses must be treated as unrelated. Such



B **Predictions on Synchronization**

Receptive field Configuration	Stimulus Configuration	Stimulus Configuration
	component: pattern:	sync sync
	component: pattern:	no sync sync
	component: pattern:	no sync sync



differential synchronization behavior should be particularly pronounced for cell pairs that have clear preferences for the two different gratings, that is, for cells with spatially offset receptive fields that are sharply tuned for the different directions of motion of the two gratings.

Cross-correlation analysis of responses from cell pairs distributed either within or across areas 18 and the postero-medial lateral suprasylvian complex (PMLS) of lightly anaesthetized cats confirmed these predictions. Cells synchronized their activity if they responded to contours that were perceived as belonging to the same surface (Castelo-Branco et al., 2000) (Fig. 113.4C). Analysis of the neurons' discharge rate confirmed that most of the cells in these visual areas respond preferentially to the component gratings of the plaids (component specific cells; Gizzi et al., 1990) and not to the pattern as a whole. However, in contrast to synchrony, variations in response amplitude failed to reflect the transition from component to pattern motion induced by transparency manipulation. Dynamic changes in synchronization could thus serve to encode in a context-dependent way the relations among the simultaneous responses to spatially superimposed contours and thereby bias their association with distinct surfaces.

In all experiments referred to in this review, trials with different stimulus configurations were interleaved randomly to counterbalance possible effects of slow drifts in central state that may have caused covariations of discharge rate at a slow time scale. Moreover, phasic response components were excluded from correlation analysis to avoid artifactual correlations due to instationarities in discharge rate (Brody, 1999a, 1999b). Accordingly, the shift predictors (correlograms between responses to the same stimulus configuration selected from different trials) were always flat, indicating that the changes in the correlations were caused by context-dependent changes of internal interactions and not by changes in stimulus-locked or state-dependent covariations of discharge rate.

Perceptual selection

If synchronization serves to raise the saliency of responses, one should expect that it is used as a mechanism for response selection that is complementary to response selection by rate

increases. The studies described in this paragraph deal with such aspects of response selection. A close relation between synchronization and response selection has been found in cats that suffered from strabismic amblyopia, a developmental impairment of vision associated with suppression of signals conveyed by the amblyopic eye, reduced visual acuity, and crowding. *Crowding* refers to the inability of amblyopic subjects to identify target stimuli if these are surrounded by nearby contours and is thought to result from false binding of responses evoked by the target and the embedding background. Quite unexpectedly, the response properties of individual neurons in the primary visual cortex appeared normal, and the neurons continued to respond vigorously to stimuli which the animals had been unable to resolve through the amblyopic eye during prior behavioral testing. The only significant correlate of amblyopia detected in this study was a reduction of response synchronization among neurons driven by the amblyopic eye. This reduction in synchrony became particularly pronounced when responses were evoked with gratings that had been identified in previous behavioral experiments as too fine to be resolvable by the animal through the amblyopic eye (Roelfsema et al., 1994). This impaired ability to synchronize responses is likely to account for at least some of the perceptual deficits: by reducing the saliency of responses, it could explain why signals from the amblyopic eye cannot compete successfully with the well-synchronized responses from the normal eye and are excluded from supporting perception when both eyes are open. Recent recordings from area 21, a higher visual area, have indeed shown that the poorly synchronized responses evoked from the amblyopic eye drive neurons in area 21 less efficiently than the well-synchronized responses from the normal eye (Schröder et al., 2002). Poor synchronization is also likely to be responsible for the reduction in visual acuity and for crowding. If grouping of responses related to the same contour and segregation of responses evoked by unrelated contours require intact synchronization mechanisms, then impaired synchronization is likely to impede the disambiguation of responses evoked by closely spaced stimuli.

A correlation between response synchronization and stimulus selection has also been documented in experiments on binocular rivalry that were again performed in strabismic

FIGURE 113.4. *A*, Two superimposed gratings that differ in orientation and drift in different directions are perceived either as two independently moving gratings (component motion) or as a single pattern drifting in the intermediate direction (pattern motion), depending on whether the luminance conditions at the intersections are compatible with transparency. *B*, Predictions on the synchronization behavior of neurons as a function of their receptive field configuration (*left*) and stimulation conditions (*right*). *C*, Changes in the synchronization behavior of two neurons recorded

simultaneously from areas 18 and the PMLS that were activated with a plaid stimulus under component (*upper graph*) and pattern motion conditions (*lower graph*). The two neurons preferred gratings with an orthogonal orientation (see the receptive field configuration at the top and the tuning curves obtained with the component and pattern, respectively) and synchronized their responses only when activated with the pattern stimulus (compare the cross-correlograms on the right). (Adapted from Castelo-Branco et al., 2000.)

animals (Fries et al., 1997, 2002). Perception in strabismic subjects always alternates between the two eyes. This can be exploited to investigate how neuronal responses to constant stimuli change if they pass from being selected and perceived to being suppressed and excluded from perception and vice versa (Fig. 113.5). The outcome of these experiments was surprising because the responses of neurons in areas 17 and 18 were not enhanced in amplitude when they supported perception and were not attenuated when they were excluded from supporting perception. A close and highly significant correlation existed, however, between changes in the strength of response synchronization and the outcome of rivalry. Cells mediating responses of the eye that won in interocular competition increased the synchronicity of their responses upon presentation of the rivalrous stimulus to the other, losing eye, while the reverse was true for cells driven by the eye that became suppressed. The synchronized responses exhibited an oscillatory modulation in the gamma frequency range, and rivalry-related changes in synchrony were particularly pronounced in measurements of spike-field coherence (see above). Thus, in primary visual cortex there are instances where internal selection of responses for further processing is associated with enhanced synchronization rather than increased firing. This agrees with rivalry experiments in awake, behaving monkeys which showed no systematic relation between the strength of visual responses and perception in early visual areas but a clear correlation between perceptual suppression and loss of neuronal responses in higher visual areas (Leopold and Logothetis, 1996; Logothetis and Schall, 1989; Sheinberg and Logothetis, 1997). This is what one expects if the saliency of the responses from the two eyes is adjusted at early processing stages by modulating synchronization rather than discharge rates.

Dependency on central states and attention

A characteristic feature of response synchronization is its marked state dependency. It is particularly prominent when the cortex is in an activated state, that is, when the EEG is desynchronized and exhibits high power in the beta and gamma frequency range (Fig. 113.6) (Herculano-Houzel et al., 1999; Munk et al., 1996). In particular, synchronization over long distances that requires oscillatory patterning of responses breaks down completely when the EEG gets “synchronized” and exhibits high power in the low-frequency range (<10 Hz). This close correlation between the occurrence of response synchronization, on the one hand, and EEG states characteristic of the aroused and performing brain, on the other hand, may be taken as support for a functional role of precise synchrony in cortical processing.

The magnitude and precision of synchronization in the beta and gamma frequency range also vary in the fully

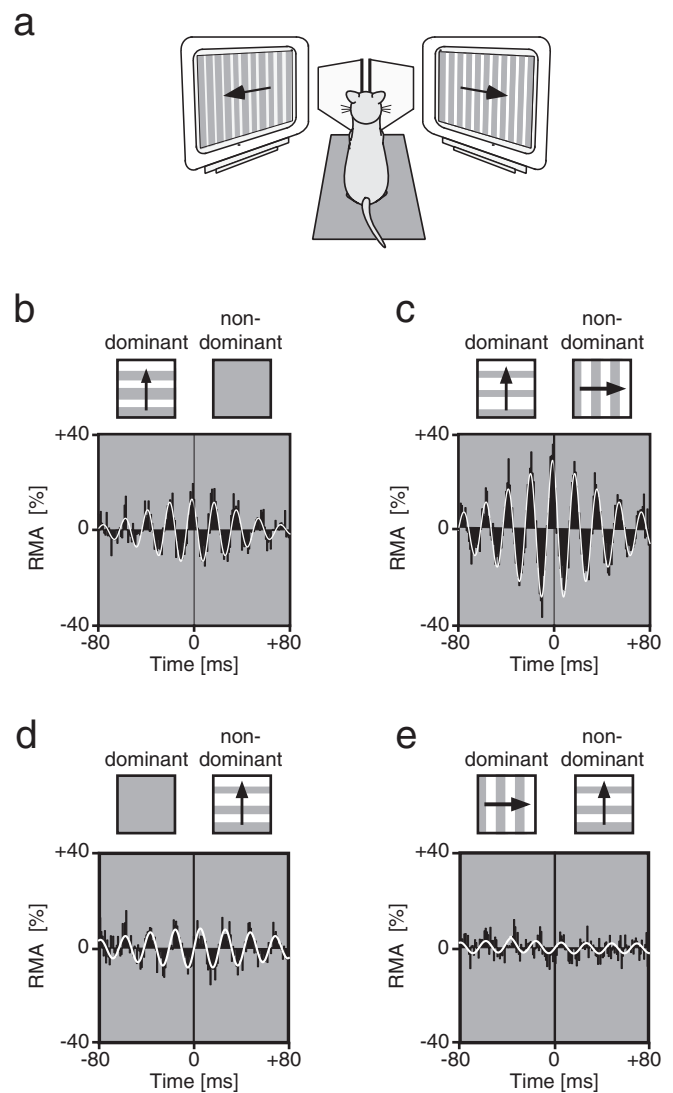


FIGURE 113.5. Neuronal synchronization under conditions of binocular rivalry. *A*, Using two mirrors, different patterns were presented to the two eyes of strabismic cats. Panels *B* to *E* show normalized cross-correlograms for two pairs of recording sites activated by the eye that won (*B*, *C*) and lost (*D*, *E*) in interocular competition, respectively. Insets above the correlograms indicate stimulation conditions. Under monocular stimulation (*B*), cells driven by the winning eye show a significant correlation, which is enhanced after introduction of the rivalrous stimulus to the other eye (*C*). The reverse is the case for cells driven by the losing eye (compare conditions *D* and *E*). The white continuous line superimposed on the correlograms represents a damped cosine function fitted to the data. RMA, relative modulation amplitude of the center peak in the correlogram, computed as the ratio of peak amplitude over offset of correlogram modulation. This measure reflects the strength of synchrony. (Modified from Fries et al., 1997.)

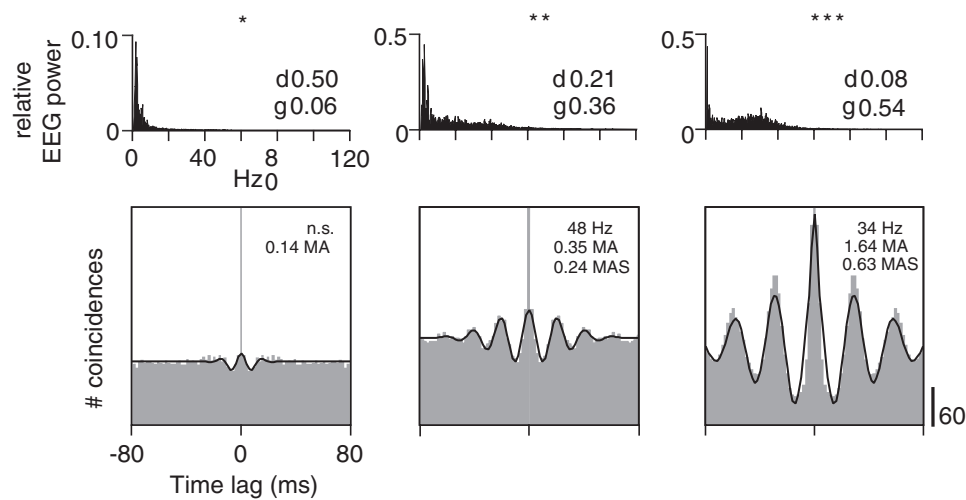


FIGURE 113.6. State dependence of response synchronization. *Upper row:* Power distribution in the EEG recorded during three episodes from an anesthetized cat. *Lower row:* Averaged cross-correlograms of multiunit responses evoked by a drifting grating and recorded from two different sites in A17 during corresponding episodes. Note that the synchronization of the responses and the oscillatory modulation in the gamma frequency range increase with

increasing gamma activity in the EEG. Inserts in the power spectra give the relative power in the delta and gamma frequency range. Inserts in the cross-correlograms give the oscillation frequency (Hz) and the relative modulation amplitude of the center peak (MA) and of the first side peak (MAS). (From Herculano-Houzel et al., 1999.)

aroused brain and are then correlated with fluctuations of attention. Such modulation of synchrony has been observed in cats trained to perform a visually triggered motor response. The visual, association, somatosensory, and motor areas involved in the execution of the task synchronized their oscillatory activity in the beta frequency range as soon as the animals focused their attention on the relevant stimulus; the strength of synchronization among areas reflected precisely the coupling of these areas by corticocortical connections. Immediately after the appearance of the visual stimulus, synchronization increased further, and these coordinated activation patterns were maintained until the task was completed. However, once the reward was available and the animals engaged in consummatory behavior, these coherent patterns collapsed and gave way to low-frequency oscillatory activity that did not exhibit any consistent relations with regard to phase and areal topology (Roelfsema et al., 1997). These results suggest that an attention-related process had imposed a coherent temporal patterning on the activity of cortical areas required for the execution of the task. Such anticipatory enhancement of coherence could facilitate rapid synchronization of responses both within and across areas once the stimulus appears, thereby accelerating selection and grouping of responses.

Anticipatory synchronization patterns would be particularly effective if they exhibited some topological specificity and reflected the architecture of tangential intracortical connections. In that case, they could serve as a readout mechanism that translates the grouping criteria defined by intercolumnar connections into dynamic patterns of coher-

ent activity against which incoming signals can be matched. Recent evidence supports such a scenario. Measurements of fluctuations in response latency revealed that self-generated gamma activity exhibits a specific patterning that reflects the grouping criteria of vicinity and colinearity. Response latencies of neurons in striate cortex fluctuate considerably for identical, repeatedly presented stimuli, but these fluctuations are not random. Rather, they are correlated across cortical columns sharing similar feature preferences (Fries et al., 2001a). Correlating response latencies of cells recorded from one site with the fluctuations of LFPs recorded from a site in the opposite hemisphere that had the same orientation preference revealed that response latencies could be predicted from the phase of the ongoing LFP oscillations if these were in the gamma frequency range. This suggests that the synchronization of the very first spikes of a response is due to ongoing oscillatory fluctuations of the cells' membrane potential and that these fluctuations can be coherent over large distances, in this case across hemispheres. These oscillations of membrane potential delay or advance responses to light stimuli, depending on the timing of the stimulus relative to the phase of the ongoing oscillation. The reason is that in oscillating cells the discharges evoked by a barrage of EPSPs are only loosely time-locked to the EPSPs and occur predominantly around the peak of the respective next depolarizing cycle because of an NMDA receptor-mediated delay mechanism (Volgushev et al., 1997). As a result, cells located in coherently oscillating columns become synchronized right from the beginning due to latency adjustment.

Analysis of the receptive field properties of cell pairs revealed that latency fluctuations are often coherent for cells that have overlapping receptive fields. For cells with nonoverlapping fields, these fluctuations are coherent only if the cells have a similar orientation preference. These results suggest that columns encoding spatially contiguous stimuli or contours with similar orientation tend to oscillate spontaneously in phase. This, in turn, enhances through latency adjustment the temporal coherence of responses to nearby contours or to contours with similar orientation preference. As contours appearing in such constellations tend to be grouped perceptually, this mechanism of response coordination could be exploited for perceptual grouping. Anatomical evidence indicates that the corticocortical association connections link preferentially columns coding for related features that tend to be grouped perceptually (Gilbert and Wiesel, 1989; Malach et al., 1993; Schmidt et al., 1997; Ts'o and Gilbert, 1988), and physiological data suggest that these corticocortical connections contribute to the synchronization of spatially segregated groups of neurons (Engel et al., 1991a; König et al., 1993; Löwel and Singer, 1992). Thus, spontaneous activity could serve to continuously translate the functional architecture of the association connections into coordinated fluctuations of neuronal excitability. The coherent oscillations of the LFP could then be regarded as the dynamic correlate of the grouping rules defined by the association connections. Inevitably, the pattern of these fluctuations is also modified by top-down influences from higher cortical areas and by immediately preceding changes of sensory input. Both effects would be equivalent to the functions commonly attributed to attentional mechanisms, the selection and binding of expected events as a consequence of either bottom-up priming or intentional top-down selection. The observed fluctuations could thus be equivalent to the system's updated expectancy that is determined by the fixed, locally installed grouping rules, by top-down influences, and by preceding sensory input. Seen in this context, ongoing activity assumes the function of a predictor against which incoming activity is matched (Grossberg, 1999). One of the effects of matching these predictions with incoming signals is a rapid temporal regrouping of output activity (see Fig. 113.7).

Direct evidence for an attention-dependent anticipatory modulation of synchronous gamma oscillations has recently been obtained in area V4 of the monkey visual cortex (Fries et al., 2001b). While the monkey expected a visual stimulus that needed to be discriminated, coherence between "spontaneous" unit discharges and LFP oscillations increased in the gamma frequency range. This increase was specific for the site where the relevant stimulus was expected to appear and was not associated with a modulation of discharge rate. When the stimulus appeared, responses exhibited better coherence when the stimulus was attended

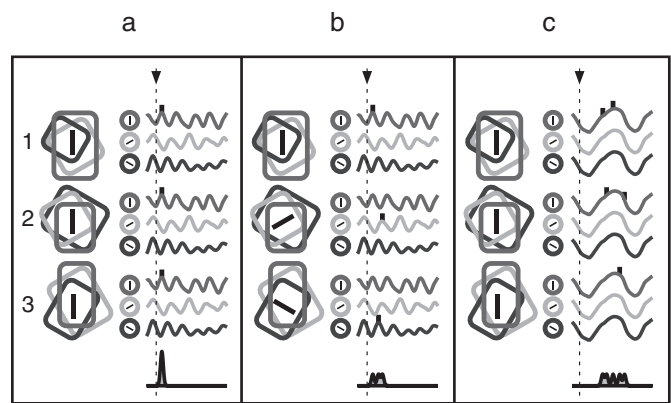


FIGURE 113.7. A model of rapid feature selective neuronal synchronization through correlated latency shifting. *A*, Three groups of neurons are shown schematically as circles (*middle column*). The three groups have relative frequencies at different locations in the visual field (*left column*), and each group contains neurons with three different orientation selectivities (*small black bars inside circles*). The graphs in the right column depict LFPs dominated by gamma frequency oscillations that reflect the neurons' membrane potential fluctuations. The model assumes that fluctuations are coherent for neurons of the same orientation preference but incoherent for neurons preferring dissimilar orientation. When a stimulus array of three vertical bars (*black bars over the relative frequencies*) is presented, only the neurons selective for vertical orientations respond. The arrow and the dotted vertical line over LFPs indicate the time when stimulus-driven synaptic input reaches the recorded neurons. As their response onsets are shifted coherently by the coherent membrane potential fluctuations, their first spikes are correlated and add up to a strong population response, shown as a spike density function in the lowest trace. Note that for the sake of clarity, we have focused on the effect of similarity of orientation selectivity and ignored relative frequency overlap as a factor influencing the strength of latency correlations. *B*, The same conventions as in *A*, but stimulation with bars of different orientations. Neurons of different orientation selectivities are activated by the three bars. As in this case, the neuronal membrane potentials fluctuate incoherently, the response onsets are not aligned, and the population response is spread out in time. *C*, The same conventions as in *A*, but the LFP is dominated by low-frequency oscillations. These low-frequency oscillations are globally synchronous (coherence is not dependent on orientation selectivity), but due to their low frequency, they have no latency-shifting effect. Upon stimulation with three aligned bars, the neurons fire more spikes than with gamma-dominated LFP (*A*), but the latency is long, the spikes are not synchronized, and the responses to nonaligned bars would exhibit the same temporal dispersion as the responses to aligned bars. (Courtesy of Pascal Fries.)

to than when attention was directed to another, distracting stimulus. Similar attention-dependent enhancement of synchrony has been observed among neurons in the somatosensory cortex of monkeys engaged in a tactile discrimination task (Steinmetz et al., 2000).

These results suggest that cognitive processes consist not simply of the extraction and recombination of features but also of an active matching operation in which afferent sensory activity is compared with self-generated dynamic

states. This anticipatory nature of cortical computations is probably one reason why processing of sensory signals is so fast (for a detailed review of relations between top-down processing and synchronous oscillations, see Engel et al., 2001).

Plasticity of synchronizing connections

If synchronization serves to establish relations between neuronal responses, synchronizing connections must be susceptible to use-dependent modifications. This is required to implement new grouping criteria by learning and to stabilize assemblies representing previously experienced conjunctions. Synchronization probability must increase durably for groups of cells that have been forced previously to engage repeatedly in highly synchronous firing, and the mechanism mediating these use-dependent changes in synchronization probability must be capable of distinguishing between synchronous and nonsynchronous firing with a temporal resolution that is in the same range as the temporal precision of observed synchrony. Both postulates have recently received experimental support. Herculano-Houzel et al. (1997, 2003) have shown that synchronization probability increases between groups of neurons if these engage repeatedly in synchronous oscillatory firing in the gamma frequency range. This enhanced tendency of neurons to synchronize their responses to coherent stimuli can be reduced again by having the same cells engage repeatedly in oscillatory firing patterns that are decorrelated. These increases and decreases of synchronization probability appeared to depend on the precise phase relations of the oscillatory discharges during conditioning because, on a coarser time scale (>50 msec), the neurons' activity overlapped completely in both conditioning paradigms.

To obtain these lasting modifications in synchronization probability in anesthetized cats, it was necessary to pair the light stimuli that induced synchronous (asynchronous) oscillatory firing of cortical cell pairs with electrical stimulation of the mesencephalic reticular formation (MRF). Activation of the MRF has several probably causally related effects. It desynchronizes the EEG, as is the case with arousal. This, in turn, enhances oscillatory modulation of visual responses in the gamma frequency range and increases the magnitude and precision of synchronization (see above). These effects are probably mediated by muscarinic receptors in the cortex that are activated by enhanced release of acetylcholine from projections originating in the basal forebrain. This is suggested by two observations: first, MRF stimulation enhances acetylcholine release in striate cortex, and in nonrodents the only source of cholinergic afferents to striate cortex is the basal forebrain (Mesulam et al., 1983). Second, iontophoretic application of scopolamine in the striate cortex abolishes both gamma oscillations and response synchrony

(Rodriguez et al., 2001, 2003). The facilitation of lasting modifications of synchronization probability by MRF stimulation could thus have two quite different causes. It could be due to enhanced synchrony and the resulting increase in cooperativity among synchronously active synaptic inputs, but it could also be due to the plasticity-enhancing effect of acetylcholine. Both scenarios are supported by experimental evidence. Experiments on use-dependent synaptic plasticity in slices of the hippocampus and the visual cortex have revealed that induction of modifications such as LTP and LTD is facilitated both by increasing cooperativity among synaptic inputs (Gustafsson and Wigstrom, 1986) and by application of carbachol, the latter effect being mediated by muscarinic receptors (Bröcher et al., 1992). Both increased cooperativity and muscarinic activation enhance depolarization, the latter via blockade of K^+ currents. This, in turn, augments entry of calcium via NMDA receptors and voltage-gated calcium channels, thus increasing the probability of the occurrence of LTP and LTD (Hansel et al., 1997). However, there are numerous other routes by which acetylcholine can facilitate plasticity because muscarinic receptors modulate a variety of intracellular signaling cascades that control NMDA receptor efficacy, Ca^{2+} release from internal stores, and gene expression.

The observation that synchronous and asynchronous firing had opposite effects on synchronization probability, although discharge rates were comparable in the two conditions, suggests that the mechanism mediating the long-term modifications is sensitive to the precise phase relations among the oscillatory discharges rather than to the covariation of discharge rates. The recent slice data on spike timing-dependent plasticity and the phase sensitivity of LTP and LTD are compatible with this interpretation (see above).

Synchronized gamma oscillations and visual perception in human subjects

In a series of pioneering EEG studies, evidence has been obtained that the engagement in cognitive tasks requiring figure-ground distinctions and feature binding (Tallon-Baudry et al., 1996, 1997) or perceptual switching during perception of bistable figures (Keil et al., 1999) or the retention of visual patterns in short-term memory (Tallon-Baudry et al., 1998, 1999) are associated with transient increases of gamma oscillations in cortical areas involved in the respective tasks. These findings have recently been extended by the demonstration that during a face recognition task, populations of neurons not only synchronize locally on the basis of gamma oscillations but also phase-lock across large distances with zero phase lag. A particularly interesting finding was that these large-scale synchronization patterns dissolved and settled into new configurations at exactly the time when

subjects recognized the pattern and prepared the execution of the motor response (Rodríguez et al., 1999).

A close correlation has also been found between the establishment of coherent gamma oscillations across cortical areas and the acquisition of a visuotactile association in classical conditioning. Once subjects have learned about the association between a visual and a tactile stimulus, the visual stimulus evokes gamma activity over the visual cortex that is coherent with gamma activity over the somatosensory cortex contralateral to the stimulated finger; this coherence breaks down again upon extinction (Miltner et al., 1999). Finally, evidence has been obtained in an MEG study on binocular rivalry that activity evoked from the eye that dominates perception during rivalry is better synchronized than activity evoked by the suppressed eye (Tononi and Edelman, 1998; Tononi et al., 1998). This agrees with the rivalry experiments in cats (Fries et al., 1997).

Consistent with a functional role of synchronized gamma oscillations is the observation that these oscillations are closely related to arousal and attention. In human subjects, gamma oscillations are enhanced in responses to attended as compared to nonattended stimuli (Gruber et al., 1999; Müller et al., 2001; Tiitinen et al., 1993). They disappear in deep anesthesia (Madler and Pöppel, 1987) but are present during paradoxical sleep, where dreaming, that is, reactivation of memories, is thought to occur (Llinas and Ribary, 1993; Steriade, 1999).

Conclusions

Taken together, the data and arguments presented in this chapter support the notion that neuronal networks are capable of evaluating with a precision in the millisecond range the temporal relations among the discharges of neuronal populations, and that precise timing relations are computationally relevant in the context of both signal processing and synaptic plasticity. Evidence suggests further that cortical networks exploit this ability not only to transmit with high temporal fidelity the temporal features of stimuli across processing stages but also to impose temporal signatures on neuronal activity that can be used in a variety of ways. Frequently observed signatures are an oscillatory patterning and precise synchronization of discharges. Evidence available so far suggests that the oscillatory patterning serves to synchronize responses at variable time scales and that synchronization enhances with high temporal resolution the saliency of the synchronized discharges. This, in turn, appears to be used for a variety of functions that require selection of responses for further joint processing. Changes in synchrony correlate with both preattentive switches in stimulus selection—as indicated by the rivalry experiments—and with attention-dependent stimulus selection. Furthermore, synchronization appears to be used to label responses as related

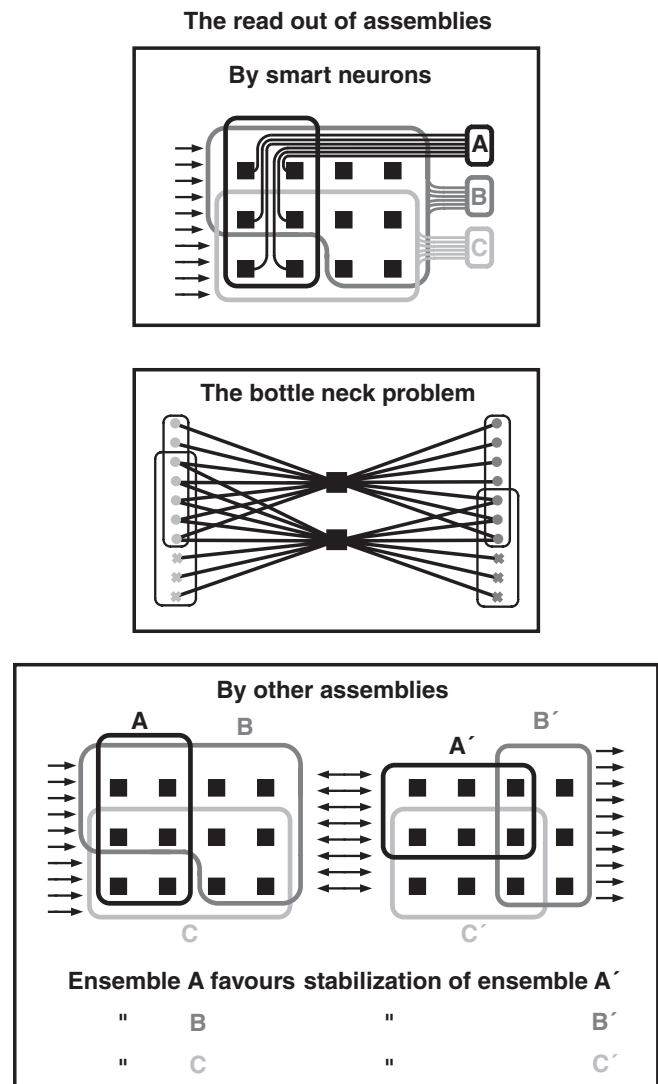


FIGURE 113.8. Representation of solutions for the readout of assemblies. The distributed responses of assemblies A to C could be read out (bound together) by conjunction-specific neurons that receive convergent input from the members of each of the three assemblies (*upper box*). This solution is not attractive because it leads to a combinatorial explosion of the number of required readout units. Moreover, it generates a bottleneck problem (*middle box*) because the activity of individual readout neurons needs to be redistributed onto large assemblies of neurons to orchestrate executive functions. The alternative option is the readout of assemblies by assemblies (*lower box*). This requires parallel reentry connections between the respective cortical areas in which “sending” and “receiving” assemblies are configured.

in the context of both signal processing and use-dependent synaptic modifications. This latter function has the characteristics of a binding mechanism that permits rapid context-dependent definition of relations in ever-changing constellations. It is therefore ideally suited to serve as a selection mechanism in assembly coding that associates distributed responses with one another and ensures their joint

processing. Assembly coding, in turn, appears necessary to cope with the representation of the astronomical number of possible relations that can exist among the features of real-world objects and among the objects constituting visual scenes. Thus, both theoretical considerations and experimental evidence converge in the conclusion that the cerebral cortex probably uses two complementary strategies to encode relations: first, an explicit representation of relations by the responses of conjunction specific neurons and, second, an implicit representation of relations by dynamically associated assemblies. The first strategy seems to be applied for the representation of a limited set of conjunctions and is probably reserved for items that occur very frequently and/or are of particular behavioral importance. The second strategy seems to be reserved for the representation of novel conjunctions and all those relations that do not warrant explicit representation, either because these would require too many neurons or because the contents to be represented are too infrequent to justify the implementation of specialized and henceforth committed neurons.

A frequently posed question is how the distributed activity of assemblies is read out in order to support decisions and instantiate actions. The intuitively most plausible solution would be to postulate readout neurons, as indicated in Figure 113.8, that receive convergent input from the respective assemblies and have their thresholds adjusted so that they discharge only if all members of the assembly discharge in synchrony. This, however, would jeopardize all the advantages of assembly coding and would reintroduce exactly those problems whose solution requires assembly coding: the combinatorial explosion of object specific units, the difficulty of representing novel contents, the lack of systematicity, and the bottleneck problem. Therefore, alternative readout strategies are required. The most straightforward scenario appears to consist of mapping assemblies onto assemblies without interposed convergence nodes (Fig. 113.8). If one assumes that executive commands are also implemented by assemblies of distributed neurons, sensory assemblies could be mapped directly onto motor assemblies. The only constraint is that distributed learning processes at the level of the reciprocal connections between sensory and motor assemblies ensure that the formation of a particular assembly at the input stage favors stabilization of the corresponding assembly at the output stage. In this case, processing could remain distributed all the way through the system. If so, this has consequences with respect to the formulation of working hypotheses and the design of experiments. If codes are distributed and if relations between responses are defined in the temporal domain, then the search for sensory or motor representations will require simultaneous recording from large numbers of neurons and evaluation of higher-order correlations among their responses.

REFERENCES

- Abeles, M., 1982. Role of the cortical neuron: integrator or coincidence detector? *Isr. J. Med. Sci.*, 18:83–92.
- Abeles, M., 1991. *Corticonics. Neural Circuits of Cerebral Cortex*, Cambridge: Cambridge University Press.
- Adelson, E. H., and J. A. Movshon, 1982. Phenomenal coherence of moving visual patterns, *Nature*, 300:523–525.
- Alais, D., R. Blake, and S.-H. Lee, 1998. Visual features that vary together over time group together over space, *Nat. Neurosci.*, 1:160–164.
- Albright, T. D., and G. R. Stoner, 1995. Visual motion perception, *Proc. Natl. Acad. Sci. USA*, 92:2433–2440.
- Alonso, J.-M., and L. M. Martinez, 1998. Functional connectivity between simple cells and complex cells in cat striate cortex, *Nat. Neurosci.*, 1:395–403.
- Alonso, J.-M., W. M. Usrey, and R. C. Reid, 1996. Precisely correlated firing in cells of the lateral geniculate nucleus, *Nature*, 383:815–819.
- Bair, W., and C. Koch, 1996. Temporal precision of spike trains in extrastriate cortex of the behaving macaque monkey, *Neural Comput.*, 8:1185–1202.
- Brecht, M., W. Singer, and A. K. Engel, 1998. Correlation analysis of corticotectal interactions in the cat visual system, *J. Neurophysiol.*, 79:2394–2407.
- Brody, C. D., 1999a. Disambiguating different covariation types, *Neural Comp.*, 11:1527–1535.
- Brody, C. D., 1999b. Correlation without synchrony, *Neural Comp.*, 11:1537–1551.
- Bröcher, S., A. Artola, and W. Singer, 1992. Agonists of cholinergic and noradrenergic receptors facilitate synergistically the induction of long-term potentiation in slices of rat visual cortex, *Brain Res.*, 573:27–36.
- Buracas, G., A. Zador, M. Deweese, and T. Albright, 1998. Efficient discrimination of temporal patterns by motion-sensitive neurons in primate visual cortex, *Neuron*, 20:959–969.
- Buzsaki, G., 1996. The hippocampo-neocortical dialogue, *Cereb. Cortex*, 6:81–92.
- Buzsaki, G., and J. J. Chrobak, 1995. Temporal structure in spatially organized neuronal ensembles: a role for interneuronal networks, *Curr. Opin. Neurobiol.*, 5:504–510.
- Castelo-Branco, M., R. Goebel, S. Neuenschwander, and W. Singer, 2000. Neural synchrony correlates with surface segregation rules, *Nature*, 405:685–689.
- Castelo-Branco, M., S. Neuenschwander, and W. Singer, 1998. Synchronization of visual responses between the cortex, lateral geniculate nucleus, and retina in the anesthetized cat, *J. Neurosci.*, 18:6395–6410.
- Diesmann, M., M.-O. Gewaltig, and A. Aertsen, 1999. Stable propagation of synchronous spiking in cortical neural networks, *Nature*, 402:529–533.
- Engel, A. K., P. Fries, and W. Singer, 2001. Dynamic predictions: oscillations and synchrony in top-down processing, *Nature Rev. Neurosci.*, 2:704–716.
- Engel, A. K., P. König, A. K. Kreiter, and W. Singer, 1991a. Inter-hemispheric synchronization of oscillatory neuronal responses in cat visual cortex, *Science*, 252:1177–1179.
- Engel, A. K., P. König, and W. Singer, 1991b. Direct physiological evidence for scene segmentation by temporal coding, *Proc. Natl. Acad. Sci. USA*, 88:9136–9140.
- Engel, A. K., A. K. Kreiter, P. König, and W. Singer, 1991c. Synchronization of oscillatory neuronal responses between striate

- and extrastriate visual cortical areas of the cat, *Proc. Natl. Acad. Sci. USA*, 88:6048–6052.
- Freiwald, W. A., A. K. Kreiter, and W. Singer, 1995. Stimulus dependent intercolumnar synchronization of single unit responses in cat area 17, *NeuroReport*, 6:2348–2352.
- Friedman-Hill, S., P. E. Maldonado, and C. M. Gray, 2000. Dynamics of striate cortical activity in the alert macaque: I. Incidence and stimulus-dependence of gamma-band neuronal oscillations, *Cereb. Cortex*, 10:1105–1116.
- Frien, A., R. Eckhorn, R. Bauer, T. Woelbern, and H. Kehr, 1994. Stimulus-specific fast oscillations at zero phase between visual areas V1 and V2 of awake monkey, *NeuroReport*, 5:2273–2277.
- Fries, P., S. Neuenschwander, A. K. Engel, R. Goebel, and W. Singer, 2001a. Rapid feature selective neuronal synchronization through correlated latency shifting, *Nat. Neurosci.*, 4(2):194–200.
- Fries, P., J. H. Reynolds, A. E. Rorie, and R. Desimone, 2001b. Modulation of oscillatory neuronal synchronization by selective visual attention, *Science*, 291:1560–1563.
- Fries, P., P. R. Roelfsema, A. K. Engel, P. König, and W. Singer, 1997. Synchronization of oscillatory responses in visual cortex correlates with perception in interocular rivalry, *Proc. Natl. Acad. Sci. USA*, 94:12699–12704.
- Fries, P., J.-H. Schröder, P. R. Roelfsema, W. Singer, and A. K. Engel, 2002. Oscillatory neuronal synchronization in primary visual cortex as a correlate of perceptual stimulus selection, *J. Neurosci.*, 22(9):3739–3754.
- Gerstner, W., 1996. Rapid phase locking in systems of pulse-coupled oscillators with delays, *Phys. Rev. Lett.*, 76:1755–1758.
- Gilbert, C. D., and T. N. Wiesel, 1989. Columnar specificity of intrinsic horizontal and cortico-cortical connections in cat visual cortex, *J. Neurosci.*, 9:2432–2442.
- Gizzi, M. S., E. Katz, R. A. Schumier, and J. A. Movshon, 1990. Selectivity for orientation and direction of motion of single neurons in cat striate and extrastriate visual cortex, *J. Neurophysiol.*, 63:1529–1543.
- Gray, C. M., 1999. The temporal correlation hypothesis of visual feature integration: still alive and well, *Neuron*, 24:31–47.
- Gray, C. M., A. K. Engel, P. König, and W. Singer, 1992. Synchronization of oscillatory neuronal responses in cat striate cortex—temporal properties, *Vis. Neurosci.*, 8:337–347.
- Gray, C. M., P. König, A. K. Engel, and W. Singer, 1989. Oscillatory responses in cat visual cortex exhibit inter-columnar synchronization which reflects global stimulus properties, *Nature*, 338:334–337.
- Gray, C. M., and W. Singer, 1987. Stimulus-dependent neuronal oscillations in the cat visual cortex: a cortical functional unit, *Soc. Neurosci. Abstr.*, 13:404.3.
- Gray, C. M., and W. Singer, 1989. Stimulus-specific neuronal oscillations in orientation columns of cat visual cortex, *Proc. Natl. Acad. Sci. USA*, 86:1698–1702.
- Gray, C. M., and G. Viana Di Prisco, 1997. Stimulus-dependent neuronal oscillations and local synchronization in striate cortex of the alert cat, *J. Neurosci.*, 17:3239–3253.
- Grossberg, S., 1999. The link between brain learning, attention, and consciousness, *Conscious. Cogn.*, 8:1–44.
- Gruber, T., M. M. Müller, A. Keil, and T. Elbert, 1999. Selective visual-spatial attention alters induced gamma band responses in the human EEG, *Clin. Neurophysiol.*, 110:2074–2085.
- Gustafsson, B., and H. Wigstroem, 1986. Hippocampal long-lasting potentiation produced by pairing single volleys and brief conditioning tetani evoked in separate afferents, *J. Neurosci.*, 6:1575–1582.
- Hansel, C., A. Artola, and W. Singer, 1997. Relation between dendritic Ca^{2+} levels and the polarity of synaptic long-term modifications in rat visual cortex neurons, *Eur. J. Neurosci.*, 9:2309–2322.
- Herculano-Houzel, S., M. H. J. Munk, S. Neuenschwander, and W. Singer, 1999. Precisely synchronized oscillatory firing patterns require electroencephalographic activation, *J. Neurosci.*, 19:3992–4010.
- Herculano-Houzel, S., M. H. J. Munk, and W. Singer, 1997. Use-dependent reversible modification in the composition of synchronously firing ensembles in cat visual cortex, *Soc. Neurosci. (Abs.)*, 23:13.5.
- Herculano-Houzel, S., W. Singer, and M. H. J. Munk, 2003. Use-dependent long-term modification of neuronal synchronization. In preparation.
- Jensen, O., and J. E. Lisman, 1998. An oscillatory short-term memory buffer model can account for data on the Sternberg task, *J. Neurosci.*, 18:10688–10699.
- Keil, K., M. M. Müller, W. J. Ray, T. Gruber, and T. Elbert, 1999. Human gamma band activity and perception of a Gestalt, *J. Neurosci.*, 19:7152–7161.
- König, P., A. K. Engel, S. Löwel, and W. Singer, 1993. Squint affects synchronization of oscillatory responses in cat visual cortex, *Eur. J. Neurosci.*, 5:501–508.
- Kreiter, A. K., and W. Singer, 1992. Oscillatory neuronal responses in the visual cortex of the awake macaque monkey, *Eur. J. Neurosci.*, 4:369–375.
- Kreiter, A. K., and W. Singer, 1996. Stimulus-dependent synchronization of neuronal responses in the visual cortex of the awake macaque monkey, *J. Neurosci.*, 16:2381–2396.
- Larkum, M. E., J. J. Zhu, and B. Sakmann, 1999. A new cellular mechanism for coupling inputs arriving at different cortical layers, *Nature*, 398:338–341.
- Lee, S.-H., and R. Blake, 1999. Visual form created solely from temporal structure, *Science*, 284:1165–1168.
- Leonards, U., W. Singer, and M. Fahle, 1996. The influence of temporal phase differences on texture segmentation, *Vis. Res.*, 36:2689–2697.
- Leopold, D. A., and N. K. Logothetis, 1996. Activity changes in early visual cortex reflect monkeys' percepts during binocular rivalry, *Nature*, 379:549–553.
- Llinas, R., and U. Ribary, 1993. Coherent 40 Hz oscillation characterizes dream state in humans, *Proc. Natl. Acad. Sci. USA*, 90:2078–2081.
- Logothetis, N. K., and J. D. Schall, 1989. Neuronal correlates of subjective visual perception, *Science*, 245:761–763.
- Löwel, S., and W. Singer, 1992. Selection of intrinsic horizontal connections in the visual cortex by correlated neuronal activity, *Science*, 255:209–212.
- Luck, S. J., and E. K. Vogel, 1997. The capacity of visual working memory for features and conjunctions, *Nature*, 390:279–281.
- Madler, C., and E. Pöppel, 1987. Auditory evoked potentials indicate the loss of neuronal oscillations during general anaesthesia, *Naturwissenschaften*, 74:42–43.
- Malach, R., Y. Amir, M. Harel, and A. Grinvald, 1993. Relationship between intrinsic connections and functional architecture revealed by optical imaging and in vivo targeted biocytin injections in primate striate cortex, *Proc. Natl. Acad. Sci. USA*, 90:10469–10473.
- Maldonado, P. E., S. R. Friedman-Hill, and C. M. Gray, 2000. Dynamics of striate cortical activity in the alert macaque: II. Fast time scale synchronization, *Cereb. Cortex*, 10:1117–1131.

- Markram, H., J. Lübke, M. Frotscher, and B. Sakmann, 1997. Regulation of synaptic efficacy by coincidence of postsynaptic APs and EPSPs, *Science*, 275:213–215.
- Mesulam, M. M., E. J. Mufson, A. I. LeVey, and B. H. Wainer, 1983. Cholinergic innervation of cortex by the basal forebrain: cytochemistry and cortical connections of the septal area, diagonal band nuclei, nucleus basalis (substantia innominata) and hypothalamus in the rhesus monkey, *J. Comp. Neurol.*, 214:170–197.
- Miltner, W. H. R., C. Braun, M. Arnold, H. Witte, and E. Taub, 1999. Coherence of gamma-band EEG activity as a basis for associative learning, *Nature*, 397:434–436.
- Müller, M. M., T. Gruber, and A. Keil, 2001. Modulation of induced gamma band activity in the human EEG by attention and visual information processing, *Int. J. Psychophysiol.*, 38:283–299.
- Munk, M. H. J., P. R. Roelfsema, P. König, A. K. Engel, and W. Singer, 1996. Role of reticular activation in the modulation of intracortical synchronization, *Science*, 272:271–274.
- Niebur, E., and C. Koch, 1994. A model for the neuronal implementation of selective visual attention based on temporal correlation among neurons, *J. Comput. Neurosci.*, 1:141–158.
- Rager, G., and W. Singer, 1998. The response of cat visual cortex to flicker stimuli of variable frequency, *Eur. J. Neurosci.*, 10:1856–1877.
- Riehle, A., S. Grün, M. Diesmann, and A. Aertsen, 1997. Spike synchronization and rate modulation differentially involved in motor cortical function, *Science*, 278:1950–1953.
- Rodriguez, E., N. George, J.-P. Lachaux, J. Martinerie, B. Renault, and F. J. Varela, 1999. Perception's shadow: long-distance gamma band synchronization of human brain activity, *Nature*, 397:430–433.
- Rodriguez, R., U. Kallenbach, W. Singer, and M. H. J. Munk, 2001. Reduction of gamma-oscillatory responses after scopolamine application in cat visual cortex, *Soc. Neurosci. Abstr.*, 27:123.3.
- Rodriguez, R., U. Kallenbach, W. Singer, and M. H. J. Munk, 2003. Short- and long-term effects of cholinergic modulation on gamma oscillations and response synchronization in the visual cortex, submitted. In preparation.
- Roelfsema, P. R., A. K. Engel, P. König, and W. Singer, 1997. Visuomotor integration is associated with zero time-lag synchronization among cortical areas, *Nature*, 385:157–161.
- Roelfsema, P. R., P. König, A. K. Engel, R. Sireteanu, and W. Singer, 1994. Reduced synchronization in the visual cortex of cats with strabismic amblyopia, *Eur. J. Neurosci.*, 6:1645–1655.
- Schiller, J., G. Major, H. J. Koester, and Y. Schiller, 2000. NMDA spikes in basal dendrites of cortical pyramidal neurons, *Nature*, 404:285–289.
- Schmidt, K. E., R. Goebel, S. Löwel, and W. Singer, 1997. The perceptual grouping criterion of colinearity is reflected by anisotropies of connections in the primary visual cortex, *Eur. J. Neurosci.*, 9:1083–1089.
- Schröder, J.-H., P. Fries, P. R. Roelfsema, W. Singer, and A. K. Engel, 2002. Ocular dominance in extrastriate cortex of strabismic amblyopic cats, *Vis. Res.*, 42:29–39.
- Sheinberg, D. L., and N. K. Logothetis, 1997. The role of temporal cortical areas in perceptual organization, *Proc. Natl. Acad. Sci. USA*, 94:3408–3413.
- Singer, W., 1993. Synchronization of cortical activity and its putative role in information processing and learning, *Annu. Rev. Physiol.*, 55:349–374.
- Singer, W., 1999. Neuronal synchrony: a versatile code for the definition of relations? *Neuron*, 24:49–65.
- Singer, W., A. K. Engel, A. K. Kreiter, M. H. J. Munk, S. Neuenschwander, and P. R. Roelfsema, 1997. Neuronal assemblies: necessity, signature and detectability, *Trends Cogn. Sci.*, 1:252–261.
- Steinmetz, P. N., A. Roy, P. J. Fitzgerald, S. S. Hsiao, K. O. Johnson, and E. Niebur, 2000. Attention modulates synchronized neuronal firing in primate somatosensory cortex, *Nature*, 404:187–190.
- Steriade, M., 1999. Coherent oscillations and short-term plasticity in corticothalamic networks, *Trends Neurosci.*, 22:337–345.
- Stevens, C. F., and A. M. Zador, 1998. Input synchrony and the irregular firing of cortical neurons, *Nat. Neurosci.*, 1:210–217.
- Stoner, G. R., T. D. Albright, and V. S. Ramachandran, 1990. Transparency and coherence in human motion perception, *Nature*, 344:153–155.
- Tallon-Baudry, C., O. Bertrand, C. Delpuech, and J. Pernier, 1996. Stimulus specificity of phase-locked and non-phase-locked 40 Hz visual responses in human, *J. Neurosci.*, 16:4240–4249.
- Tallon-Baudry, C., O. Bertrand, C. Delpuech, and J. Pernier, 1997. Oscillatory γ -band (30–70 Hz) activity induced by a visual search task in humans, *J. Neurosci.*, 17:722–734.
- Tallon-Baudry, C., O. Bertrand, F. Peronnet, and J. Pernier, 1998. Induced γ -band activity during the delay of a visual short-term memory task in humans, *J. Neurosci.*, 18:4244–4254.
- Tallon-Baudry, C., A. K. Kreiter, and O. Bertrand, 1999. Sustained and transient oscillatory responses in the gamma and beta bands in a visual short-term memory task in humans, *Vis. Neurosci.*, 16:449–459.
- Tiitinen, H., J. Sinkkonen, K. Reinikainen, K. Alho, J. Lavikainen, and R. Naatanen, 1993. Selective attention enhances the auditory 40-Hz transient response in humans, *Nature*, 364:59–60.
- Tononi, G., and G. M. Edelman, 1998. Consciousness and complexity, *Science*, 282:1846–1851.
- Tononi, G., R. Srinivasan, D. P. Russell, and G. M. Edelman, 1998. Investigating neural correlates of conscious perception by frequency-tagged neuromagnetic responses, *Proc. Natl. Acad. Sci. USA*, 95:3198–3203.
- Ts'o, D. Y., and C. D. Gilbert, 1988. The organization of chromatic and spatial interactions in the primate striate cortex, *J. Neurosci.*, 8:1712–1727.
- Usher, M., and N. Donnelly, 1998. Visual synchrony affects binding and segmentation in perception, *Nature*, 394:179–182.
- Usrey, W. M., and R. C. Reid, 1999. Synchronous activity in the visual system, *Annu. Rev. Physiol.*, 61:435–456.
- Volgushev, M., L. L. Voronin, M. Chistiakova, and W. Singer, 1997. Relations between long-term synaptic modifications and paired-pulse interactions in the rat neocortex, *Eur. J. Neurosci.*, 9:1656–1665.
- von der Malsburg, C., 1999. The what and why of binding: the modeler's perspective, *Neuron*, 24:95–104.
- Wespatat, V., F. Tennigkeit, J. Eilers, and W. Singer, 2001. State-dependence of phase-sensitive hebbian modifications during oscillations in rat visual cortex, *Soc. Neurosci. Abstr.*, 27:922.10.
- Wespatat, V., F. Tennigkeit, and W. Singer, 2003. Phase sensitivity of Hebbian modifications in oscillating cells of rat visual cortex, In preparation.

114 The Neuronal Basis of Visual Consciousness

CHRISTOF KOCH AND FRANCIS CRICK

WE OUTLINE IN THIS chapter some of our present ideas about consciousness in general and visual consciousness in particular. (For an up-to-date summary, see Crick and Koch, 2003.) For now, we believe that the most productive research strategy is to focus on the neuronal correlates of consciousness (NCC). The next step is to establish the exact nature of the causal relationship between neuronal events and subjective feelings and, finally, to understand the thorny philosophical problem of qualia or subjective feelings and how they can arise out of certain physical systems. We assume that higher mammals, such as rodents or primates, share certain forms of sensory consciousness with humans, even though these animals lack language skills.

To characterize the NCC, we have to contrast neural activity that directly gives rise to conscious sensations, thoughts, or action with neural activity that is associated with unconscious, stereotyped, and on-line visuomotor behavior. Where is the difference between these forms? How do these differences in activity relate to the ventral and dorsal streams (Ungerleider and Mishkin, 1982)? We emphasize the importance of explicit representations, the idea of essential nodes in a network, and whether such nodes correspond to the columnar properties of a patch of cortex. We also discuss whether the correlated firing of a set of neurons is needed for consciousness and the role of cortical area V1 and prefrontal areas in consciousness. We end by briefly describing some of the relevant experiments. For earlier versions of these ideas, see Crick and Koch (1998) and Koch and Crick (2000).

Prolegomenon to any study of consciousness

The most puzzling aspect of vision and visual perception is that it gives rise to conscious seeing: to the vivid sense of a hot pink shirt, the sight of the face of a loved one, or the profound sense of depth when gingerly stepping up to the edge of a bluff. After a hiatus of half a century or more (e.g., Westheimer, 1999), the physical origins of consciousness are once again being vigorously debated in numerous books and monographs published in the past decade. What is it that we can ascertain about the neurobiological basis of consciousness, in particular visual

consciousness, and what can we reasonably assume at this point in time? Neuroscientists have made a number of working assumptions that, in the fullness of time, need to be justified more fully.

Firstly, and most importantly, is the assumption there is something to be explained—that the subjective content associated with a conscious sensation exists and has its physical basis in the brain. Philosophers refer to this as *qualia*, *what-it-is-like*, the *aboutness of consciousness*, and other terms. At this point in time, no even remotely satisfactory accounts of why brains can produce subjective feelings have been presented. Our strategy is to focus for now on other aspects of qualia where progress can be made.

There is general agreement that much of consciousness is private. I cannot convey to you exactly how red looks to me, even if experiments show that you and I respond to colors in a very similar way. We have claimed (Crick and Koch, 1995a) that this is because, at each stage of processing in the cortex, the information symbolized is recoded, so that the more internal neural activity is expressed only very indirectly in any motor output, such as speech. On the other hand, a person can say whether two shades of red appear identical or not. It is not surprising that much of the content of consciousness is largely private. What is mysterious is the exact nature of these internal experiences.

Secondly, consciousness is one of the principal properties of the human brain, a highly evolved system. Therefore, it must have some useful function to perform. It is extremely unlikely that the well-structured nature of conscious representations are epiphenomena without any causal function, as is sometimes asserted by philosophers. We (Crick and Koch, 1995b) assume that the function of visual consciousness is to produce the best current interpretation of the visual scene—in the light of past experiences—and to make it available, for a sufficient time, to the parts of the brain which contemplate, plan, and execute voluntary motor outputs (including language). This needs to be contrasted with on-line or zombie behaviors that bypass consciousness but can generate stereotyped motor outputs (see below).

Thirdly, at least some animal species possess some aspects of consciousness. In particular, this is assumed to be true for nonhuman primates such as the macaque monkey. Visual

consciousness is likely to be similar in humans and monkeys for several reasons. (1) For most sensory tasks (e.g., for visual motion discrimination, as discussed in Chapters 81 to 83), trained monkeys behave as humans do under similar conditions. (2) The gross neuroanatomy of humans and nonhuman primates is the same once the difference in size has been accounted for. This is not to deny differences in the microcircuitry or the existence of cell types unique to humans and great apes (Nimchinsky et al., 1999). (3) As emphasized throughout this book, functional brain imaging in humans is confirming the existence of a functional organization similar to that characterized by single-cell electrophysiology in the monkey.

As a corollary, it follows that neither language nor a highly developed sense of the self or of others is necessary for consciousness to occur. Indeed, even severely autistic individuals can carry out very complex sensory discrimination tasks and show no evidence of deficits in sensory discrimination or detection tasks, conscious or not (Baron-Cohen, 2001). Of course, language does enrich consciousness considerably, but there is little hard evidence that it is necessary for conscious sensations to occur.

Conscious and nonconscious visual behaviors

We can state bluntly the question that neuroscience must ultimately answer: it is probable that at any moment some active neuronal processes in our heads correlate with consciousness, while others do not; what is the difference between them? We refer to the minimal neuronal mechanisms necessary and sufficient for any one specific conscious percept as the *neuronal correlates of consciousness* (NCC). We believe that at this point in time, it is empirically most profitable to seek to identify the NCC and to defer many of the other problems (such as qualia).

It is critical to distinguish levels of consciousness (as in drowsy versus awake) from the NCC associated with a specific phenomenal content. This distinction reflects everyday experience of the distinction between being conscious versus unconscious, on the one hand, and being conscious of a high C versus not being consciousness of this tone. *Enabling factors* are required for any conscious sensation to occur without reflecting any specific one.

Cognitive and clinical research demonstrates that much complex information processing can occur without involving consciousness. In normal subjects, such *unconscious* processing includes priming, many aspects of oculomotor behaviors, the implicit recognition of complex sequences, posture adjustment, and many highly trained behaviors, such as driving, climbing, dancing, playing tennis and so on (Koch and Crick, 2001; Velmans, 1991).

Milner and Goodale (1995) make a masterful case for the existence of *on-line* systems that bypass consciousness (see

also Rossetti, 1998). Their function is to mediate relatively stereotyped visuomotor behaviors, such as eye and arm movements, posture adjustments, and so on, in a very rapid manner. On-line agents—or *zombies*, as we call them—operating in the here and now and lacking direct access to working memory, are complemented by one or more networks for object classification, recognition, and identification. It is coalitions of neurons in these latter networks that give rise to conscious perception.

The exact relationship between zombie and conscious systems is unclear. In one reading, these might coexist as anatomically distinct streams in the brain. Milner and Goodale (1995) suggest that the on-line system mainly uses the dorsal visual stream (see Chapter 34), implying that all activity in this pathway is unconscious. They consider the ventral stream (see Chapters 77 and 79), on the other hand, to be largely conscious. Another interpretation holds that zombie and conscious systems share the same anatomical substrate but correspond to different modes. For instance, it is quite possible that feedforward activity that rapidly moves through the relevant networks to trigger motor action correspond to on-line behaviors, while sustained firing activity that is modulated by corticocortical feedback, in particular from prefrontal cortex, is a critical component of the NCC.

The broad properties of the two hypothetical entities—the on-line and the seeing systems—are shown in Table 114.1 following Milner and Goodale (1995; for critical evaluation and alternative views, see Boussaoud et al., 1996; Franz et al., 2000). The on-line system may have multiple subcomponents (e.g., for eye movements, arm movements, body posture adjustment). Under normal conditions, on-line behaviors coexist with conscious percepts, or actions. Indeed, there is evidence that in some circumstances the seeing system can interfere with the on-line system (Rossetti, 1998).

TABLE 114.1 <i>Comparison of the hypothetical on-line system and the seeing system</i>		
	On-Line System	Seeing System
Visual inputs handled	Must be simple	Can be complex
Motor outputs	Stereotyped responses	Many possible responses
Minimum time needed for response	Short	Longer
Effect of a few seconds' delay	May not work	Can still work
Coordinates used	Egocentric	Object-centered
Certain perceptual illusions	Not effective	Seen
Conscious	No	Yes

Source: Based on Milner and Goodale (1995).

One striking piece of evidence for on-line behaviors comes from studies on patient D. F. Her brain has diffuse damage produced by carbon monoxide poisoning. She is able to see color and texture very well but is very deficient in seeing orientation and form. In spite of this, she is very good at catching a ball. She can “post” her hand or a card into an elongated slot without difficulty, though she is unable to report the slot’s orientation. If the stimulus is removed and D.F. is asked to delay her response by a few seconds, she is unable to orient her hand properly. That is, her on-line visuomotor behaviors do not have access to working memory since they operate in the here and now. This observation might be used to distinguish all manner of zombie actions from conscious ones.

We suspect that while these suggestions about two systems are on the right lines, they are probably oversimplified. The little that is known of visual neuroanatomy would suggest that there are likely to be multiple cortical streams, with numerous anatomical connections between them (Distler et al., 1993). For example, recent data implicate the superior temporal cortex in humans as critical for spatial awareness, attention, and exploration (Karnath, 2001). It is difficult to assign this brain area unambiguously to either the ventral or the dorsal pathway, raising the possibility that it acts as an interface between the two. Furthermore, the neuroanatomy does not suggest that the sole pathway goes up to the highest levels of the visual system, and from there to the highest levels of the prefrontal system and then down to the motor output. There are numerous pathways from intermediate levels of the visual system to intermediate frontal regions.

Other examples of residual visual behaviors in the absence of conscious visual sensation in brain-damaged patients include *blindsight* (see Chapter 40) and the *visual neglect syndrome* (Driver and Mattingley, 1998). In extinction, the presence of a visual stimulus in the intact hemifield successfully competes with the stimulus in the lesioned hemifield: the latter one is simply not perceived. Typically, these symptoms are associated with lesions in the contralateral posterior parietal lobes (for an alternative view, see Karnath, 2001). This has been taken as *prima facie* evidence for the importance of these areas for visual consciousness.

Bilateral damage of both parietal lobes can give rise to *Balint syndrome*. Such patients see only one thing at a time, neglecting everything but the one object that currently captures their attention (Rafal, 1997). Yet the critical point is that they can still see something. This leads us to conclude that the areas involved in spatial neglect are not strictly necessary for conscious object vision per se. It is likely, though, that parietal areas provide attentional modulation of processing in the ventral pathway by biasing the competition among neuronal assemblies there.

Finally, two groups of people who appear to function, on occasion, in the absence of conscious sensations are a subset of patients with complex partial epileptic seizures (Penfield

and Jasper, 1954) and sleepwalkers (Revonuso et al., 2000). Both can execute routine behaviors, including mumbling, walking, moving furniture, driving, and other automatic behaviors without being able to interact in a meaningful manner (e.g., have a conversation) with their environment or recall anything that occurred during the seizure or the somnambulistic episode. It is possible that the NCC is shut down but that enough specific nervous activity remains to support zombie behaviors (Koch and Crick, 2001).

All of this evidence suggests that many behaviors occur in the absence of conscious sensation. This offers the possibility of a *contrastive program* in which the neural mechanisms underlying automatic or zombie behaviors are compared to those underlying any one conscious sensation, the NCC proper. However, the existence of unconscious behaviors also implies that one has to exercise great caution when working with animals, babies, or severely aphasic patients to infer conscious when some seeming “complex” task is carried out. It therefore becomes important to develop criteria to distinguish optomotor behaviors controlled by zombie agents from those that require consciousness. Interposing a delay of a few seconds between the visual stimulus and the required response seems currently the most promising litmus test.

The existence of a host of zombie behaviors also raises the question of why we need consciousness at all. Why aren’t we large bundles of on-line behaviors? We proposed (Crick and Koch, 1998) that while this might be appropriate for animals with a limited behavioral repertoire, such as a fruit fly, it would not do for mammals, with their enormous range of behaviors. Instead, evolution produced a general-purpose system which can deal with all sorts of contingencies and permits the animal to plan in parallel with a host of very rapid but special-purpose and stereotyped zombie behaviors. The price is speed: consciousness, reflection, and planning requires a fraction of a second or more.

The nature of the visual representation

We argued (Crick and Koch, 1995b) that to be aware of an object or event, the brain has to construct a multilevel, explicit, symbolic interpretation of part of the visual scene. By *multilevel* we mean, in psychological terms, different levels such as those that correspond, for example, to lines or eyes or faces. In neurological terms, we mean, loosely, the different levels in the visual hierarchy (Felleman and Van Essen, 1991).

The important idea is that the representation must be explicit. The word representation is used here in the sense that it should be easy to infer the presence or absence of the feature that is made explicit in the cellular response (one could formalize this using a perceptron).

Note that while the *information* needed to represent a face is contained in the firing of the ganglion cells in the retina, the retina lacks an *explicit* representation for faces.

The evidence from brain damage, especially in humans, suggests that certain parts of the cortex are essential for a person to be conscious of certain aspects of the visual sensation or percept, such as color, motion, and faces. Zeki and Bartels (1999) have, very reasonably, described such a piece of the cortex as an essential node for that aspect of the percept, though *key node* might be a better term. What should be considered *one aspect* must be decided by experiment. Thus, *motion* is not necessarily a single aspect. Indeed, there is evidence from brain damage (Vaina and Cowey, 1996) that F.D., a patient with rather limited brain damage, is impaired in the detection of second-order or texture-based motion but does perceive first-order or intensity-based motion.

The term *essential node* should not be taken to imply that a person who possessed only the relevant essential node would be conscious of that aspect of the percept. It is highly probable that to produce that aspect of consciousness, the node would have to interact with other parts of the brain. A node is a node, not a network. The point is that damage to that essential node would specifically remove that particular aspect of the sensation or percept while leaving other aspects relatively intact.

The concept of an essential node is important. It implies that if there is no essential node for some possible aspect of consciousness, the subject cannot be conscious of it. Zihl's patient (Zihl et al., 1983) can see a car, but if the car is moving, she does not see its movement because the essential nodes for movement have been damaged. So it is important not to assume that, for example, the brain can *necessarily* consciously detect some particular change in its firing activity. It will not be able to do so unless there is some essential node to *consciously* register that type of change.

It is plausible that an explicit representation (at an essential node) might be a smallish group of neurons employing coarse coding to represent some aspect of the visual scene. In the case of a particular face, all of these neurons can fire to somewhat face-like objects (see Chapter 78). We suggest that one set of such neurons will be all of one type, will probably be fairly close together, and will all project to roughly the same place. If all such groups of neurons (there may be several of them, stacked one above the other) were destroyed, then the person would not see a face, though he or she might be able to see the parts of a face, such as the eyes, the nose, and the mouth. There are other places in the brain that explicitly represent other aspects of a face, such as the emotion the face is expressing or its angle of gaze.

An attractive proposition is that the stimulus feature common to most neurons within a cortical column is what is made explicit there. Thus, orientation is one feature explicitly represented in V1, as are the direction and speed of motion in area V5. We call this the *columnar hypothesis*. Note that an explicit representation is a necessary but not sufficient condition for the NCC. As outlined in the section

"Bistable Percepts," it matters a great deal where these neurons project.

A representation of an object or event will usually consist of representations of many of the relevant aspects of it, and these are likely to be distributed, to some degree, over different parts of the visual system. How these properties are bound together is one aspect of the binding problem (see Chapter 113). It is possible that in many cases the firing of pyramidal neurons in all layers within a column that code for the object need to be synchronized for this to occur.

Much neural activity, a great deal of which is probably unconscious, is usually needed for the brain to construct a representation. It may prove useful to consider this unconscious activity as the computations needed to find the best interpretation, while the interpretation itself may be considered to be the results of the computations, only some of which the subject is then conscious of. To judge from perception, the results probably have something of a winner-take-all character.

In the past, we wondered whether only some types of specific neurons might express the NCC. Silence these, and a very specific loss of some specific content of consciousness might occur (such as the inability to perceive a certain type of motion). A weaker version of this hypothesis holds that the NCC depends on some crucial biophysical or anatomical property of some network in the brain. Again, blocking this feature could lead to a very specific loss of some aspect of subjective feelings.

An alternative possibility is that the NCC is necessarily global, usually identified with some emergent property of very large, diffuse assemblies of neurons. In one extreme form this would mean that, at one time or another, any neuron in cortex and associated structures could express the NCC, and it would be foolish to locate consciousness at the level of single neurons.

These possibilities are nonexclusive; it is possible that both local and global properties of the brain are necessary for consciousness to occur. While our thinking over the past decade has stressed particular neuronal mechanisms, that of Edelman and Tononi has focused on certain global aspects of networks (their *dynamic core* hypothesis; Edelman and Tononi, 2000). Both ideas might be valid.

Conscious visual representations are likely to be distributed over more than one area of the cerebral cortex and possibly over certain subcortical structures as well. We have argued that in primates—contrary to received opinion—they are not located in primary visual cortex (see below).

Whatever the NCC is, it must be present in the two hemispheres. Careful study of split brain patients demonstrates that one hemisphere usually supports language, while the linguistic competence of the other is severely reduced. Yet, even this nondominant hemisphere can clearly reason,

respond purposefully, and plan complex behaviors. From this, one can conclude that split-brain patients have, within the confines of a single skull, two brains with two conscious minds (Bogen, 1997; Sperry, 1974).

What is essential for visual consciousness?

The term *visual consciousness* almost certainly covers a variety of processes. When one is actually looking at a visual scene, the experience is very vivid. This should be contrasted with the much less vivid and less detailed visual images produced by trying to remember the same scene (a vivid recollection is usually called a *hallucination*). We are concerned here mainly with normal visual experiences. It is possible that our dimmer visual recollections, imagery, are mainly due to the back pathways in the visual hierarchy biasing the “noise” in earlier stages of the system.

Some form of very-short-term memory seems almost essential for consciousness, but this memory may be very transient, lasting for only a fraction of a second. The existence of *iconic memory*, as it is called, is well established experimentally (Coltheart, 1983; Gegenfurtner and Sperling, 1993).

Psychophysical evidence for short-term memory (Potter, 1976) suggests that if we do not pay attention to some part or aspect of the visual scene, our memory of it is very transient and can be overwritten (masked) by the following visual stimulus. This probably explains many of our fleeting memories when we drive a car over a familiar route. If we do pay attention (e.g., to a child crossing the road), our recollection of this can be longer-lasting.

Our impression that at any moment we see all of a visual scene very clearly and in great detail is illusory, partly due to ever-present eye movements and partly due to our ability to use the scene itself as a readily available form of memory, since in most circumstances the scene usually changes rather little over a short span of time (O'Regan, 1992; see Chapter 102). What we can grasp very rapidly and preattentively is the gist of a scene (Mack and Rock, 1998; Wolfe, 1998). It is this that provides us with the illusion of being able to apprehend the entire scene at once. It is likely that there are neurons at the higher visual levels whose firing directly encodes the *gist* of that scene. These neurons would then be key culprits for mediating the sensation of seeing everything at once.

Although working memory expands the time frame of consciousness, it is not obvious that it is essential for consciousness. It seems to us that working memory is a mechanism for maintaining one or a small sequence of items in consciousness. In a similar way, the episodic memory enabled by the hippocampal system (Zola-Morgan and Squire, 1993) is not essential for consciousness, though a person without it is severely handicapped.

Is attention necessary for consciousness? It seems that it is enriched by visual attention, though top-down attention is not essential for visual consciousness to occur (Braun and Julesz, 1998; Rock et al., 1992). Attention is broadly of two types: bottom-up, saliency-driven, and task-independent; and top-down, produced by the planning parts of the brain. Visual attention can be directed either to a location in the visual field, to a feature, or to one or more objects. The neural mechanisms that achieve this are still being debated. But they are likely to involve biasing the competition among groups of cells coding for neighbouring objects in favor of the attended one (Desimone and Duncan, 1995). See our earlier discussion of neglect and Balint syndromes.

How does the timing of events affect the percept?

The timing of the emergence of consciousness has been called *microgenesis* (Bachmann, 2000). We can easily see something of a visual input, such as a flash of lightening, even though it lasts for a very short time, provided that it is strong enough. Bloch's law states that for a stimulus duration less than about a tenth of a second (for a diffuse flash), the brightness of the stimulus appears the same, provided that the product of its intensity and its duration are constant. In some sense, the system is integrating the input over some short time interval.

How bright does a flash of light appear if its intensity is kept the same but its duration varies from trial to trial? This can be estimated by comparing its apparent brightness with the brightness of a similar but constant light. A typical result has been described by Efron (1967). As the duration increases, the light appears more intense until, for a duration of about 40 msec, it reaches a maximum, after which the subjective brightness declines to a steady value (Fig. 114.14). As Efron has pointed out, this description can be misleading. It expresses the results of *multiple* trials, each one for one particular duration of flash. It does not show what a person experiences at a *single* trial. That is, for a flash of length of, say, 125 msec, the subject does not see the brightness of the flash increasing rapidly and then decreasing somewhat. On the contrary, the subject reports that she saw a steady brightness. This distinction, which has been widely overlooked, is important.

The results suggest that the NCC comes into being abruptly rather than gradually. Once the relevant neural activity reaches some threshold, a constant percept of brightness results, at least for a short time.

Instead of a single flash of light, what do we see if a complex scene, such as people dining in a restaurant, is flashed for different short durations? The general result is that for very short exposures, one perceives the general nature of the scene—the gist, as mentioned earlier. As the flash is made longer, we can report more details. Once again,

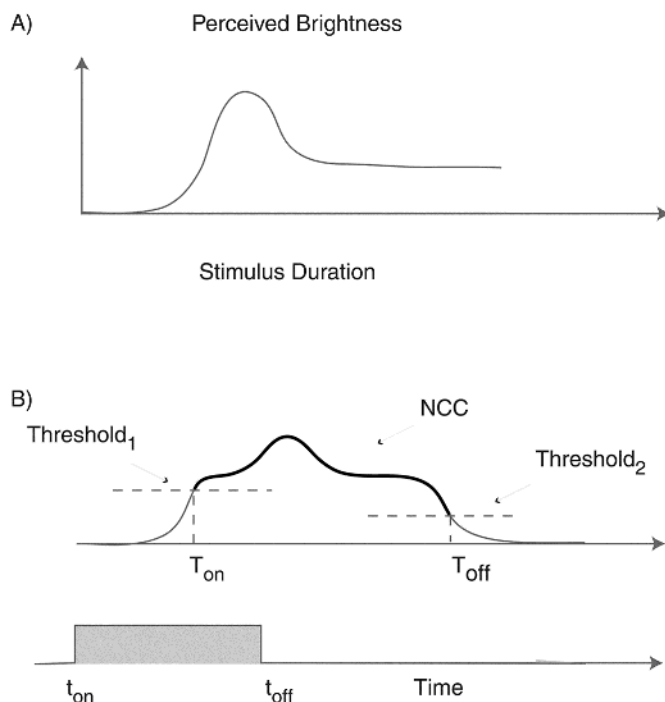


FIGURE 114.1. How does a conscious percept and the neural activity that encodes it evolve in time? *A*, Schematic drawing of the relationship between subjectively perceived brightness and stimulus duration. A flash of intermediate duration is perceived as brighter than a flash of much longer duration. Yet the percept associated with a single trial does not wax and wane, as suggested by this function; instead, it remains constant. *B*, Hypothetical time course of the critical activity at the essential node coding for the brightness percept. Once this exceeds some amplitude, this NCC activity is sustained enough to project widely throughout cortex, and the subject becomes consciousness of the stimulus and its brightness. Awareness is expressed until the NCC drops below some level (the two threshold values do not have to be identical: the phenomena of hysteresis).

in any one trial we do not see the scene change. We just see more for longer flashes.

This might suggest that some of the higher levels of the visual hierarchy reach the necessary threshold for consciousness before the lower levels do. Possibly the lower levels need some feedback from the higher levels to boost their activity above threshold.

In *masking*, two (or more) inputs are involved (Bachmann, 2000; Enns and DiLollo, 2000). When the two inputs blend, this is sometimes referred to as *integrative masking*, though the term *blending* might be preferable. Pattern masking occurs when two rather different spatially superimposed contours interfere. When two patterns are not superimposed but spatially adjacent, the interference is called *metaccontrast*. Masking can also occur when the masking pattern does not abut the target pattern but is nearby. This is now called *object-substitution masking* (Enns and DiLollo, 1997).

Suppose that a red circular disc and an otherwise identical green disc are flashed simultaneously onto the same place in the retina. Not surprisingly, the subject sees a yellow disc. If the red disc alone is flashed first, for only 10 msec, immediately followed by the green disc for 10 msec, the subject does not see a red disc turning green but just a yellow disc. The yellow has a greenish tinge compared to the yellow produced when the two colors are flashed simultaneously. If the green disc comes before the red disc, the yellow is a little redder (Yund, et al., 1983). The subject perceives a mixture of the inputs, with a bias toward the later one—this turns out to be a general rule. This suggests some form of integration, with the later signal having a somewhat greater weight. If one disc appears 100 msec before the other, little blending occurs. This suggests that, in this instance, the integration time is less than 100 msec.

When masking produces interference, this is because, in some sense, the mask is competing with the target. The subject can easily report the target if there is no mask, but if the mask is spatially superimposed on the target and occurs at about the same time, his responses are mostly at chance—he reports that he did not see the target. He does better if there is a delay of 100 msec or so between the onset of the target and the onset of the mask. The mask interferes with processing of the target in the integration period leading up to consciousness. It is plausible that once some kind of neural activity due to the target has reached a certain threshold, the following mask cannot interfere with it so easily. This suggests that the conscious activity may show hysteresis—as Libet (1973) has claimed—since the activity is probably held above a threshold to some extent by some mechanism, such as loops with positive feedback (Fig. 114.1*B*). This activity corresponds to the NCC for the attribute encoded by the essential node, say the target's brightness, location, or color. The attribute remains consciously accessible until the activity dips below a lower threshold (Fig. 114.1*B*), at which point it becomes perceptually invisible.

In *metaccontrast*, the subject can see the target if the onsets of the target and mask are simultaneous, but fails to see it if the onset of the mask is delayed by a short period, typically 50 to 100 msec or so. This is presumably because the target and the mask are initially activating different places in the brain, and it takes time for their activities to interfere with each other.

The most interesting case is *object-substitution masking*, that is, when the target and the mask are spatially separate. No masking occurs if the target and the mask come into view simultaneously and disappear simultaneously. Masking does occur if, instead, the mask continues beyond the disappearance of the target. No masking occurs if the target is especially salient or if attention is focused on the target location beforehand.

The phenomenon of *masked priming* implies that (unconscious) processing of the masked target proceeds to fairly high levels. That is, some level of priming occurs whether or not the prime was masked, suggesting that the physiological correlate of priming (short-term synaptic changes?) can occur in high-level cortical areas without giving rise to consciousness.

Enns and DiLollo (2000) suggest that one is not conscious of the details of the target until the activity it has produced first reaches a higher level (when there is integration) and then flows back to a lower level (possibly iteratively). They propose that it is at one of the lower levels that the activity of the sustained mask interferes with conscious seeing, presumably of the details of the pattern.

Until recently, visual psychologists did not relate their results to the complex organization of the primate visual system. The study of masking in the alert monkey by neurophysiologists has only just begun (Macknik and Livingstone, 1998; Thompson and Schall, 2000). A careful study of the neurophysiological effects of masking should throw light on the processes leading to consciousness, on the integration times for the signal to reach above the thresholds for consciousness, and on the ways interference works. In general, the times involved seem to range from 50 to 100 msec up to 200 msec or more. This upper limit approaches the typical time between eye movements.

The picture that emerges from these speculations is a rather curious one. It bears some resemblance to Dennett's multiple drafts model (Dennett, 1991), though Dennett's ideas, though suggestive, are not precise enough to be considered scientific. The content of consciousness, instead of being a continuous, ever-changing flux, may be more like a rapid series of "static snapshots." Movement, like other attributes, is signaled in a static way by special neurons. That is, movement is not symbolized by a change in time of the symbols for position, but by special neural symbols that represent movement of one sort or another. If the essential nodes for these symbols are lost, as in Zihl's patient, then though she can see the moving car, she cannot see it moving.

There is little evidence for a regular clock in the brain with a mechanism that integrates over intervals of constant duration and then starts afresh over the next interval. The duration of a snapshot is likely to depend on various factors, such as contrast, saliency, competition, and so on. Purves and his colleagues (1996) have described several psychological effects, such as a wagon-wheel effect under constant illumination, which hint that there are some clock-like effects in vision. This would be worth further study.

The brain has a problem with time, since time is needed to express a symbol (by neurons firing, a process spread out over time), so it is not surprising if it symbolized changes in time, such as movements, in a special way and differences in time in another way.

We are dealing with an intrinsically parallel system to which we have limited access introspectively. This is probably why we find it so hard to understand how it works. This does not mean that we cannot usefully analyze it into smaller parts that interact dynamically, just as the holistic properties of a complex organic molecule, such as a protein, can be understood by the interactions of its many amino acids and the atoms of which they are made. In the brain, an essential node may be a useful unit of analysis. It may turn out that the best way to describe the NCC for any one percept is in terms of the activities at the relevant essential nodes and their dynamic interactions. This suggestion resembles the dynamic core of Edelman and Tononi (2000).

Bistable percepts

Perhaps the most relevant experimental approach to tracking down the footsteps of the NCC for now is to study the behavior of single neurons while the subject is looking at something that produces a bistable percept. The visual input, apart from minor eye movements, is constant, but the subject's percept can take one of two alternative forms. This happens, for example, when one looks at a drawing of the Necker cube. Which neurons follow the constant retinal input and which ones the variable percept?

A more practical alternative is to study binocular rivalry (Myerson et al., 1981). If the visual input into each eye is different but perceptually overlapping, one usually sees the visual input as received by one eye alone, then by the other one, then by the first one, and so on. This approach has been explored by Logothetis and his colleagues, who trained macaque monkeys to report which of two rivalrous inputs they saw. The fairly similar distribution of switching times strongly suggests that monkeys and humans perceive these bistable visual inputs in the same way. In the first set of experiments, Logothetis and Schall (1989) investigated neurons in area MT (also referred to as V5). The stimuli were vertically drifting horizontal gratings. Of the relevant neurons, only about 35% were modulated according to the monkey's reported percept. Surprisingly, half of these responded in the opposite direction to the one expected. Leopold and Logothetis (1996) used stationary gratings. The orientation was chosen in each case to be optimal for the neuron studied and orthogonal to it in the other eye. The authors recorded how the neuron fired during several alterations of the reported percept. While only a small fraction of foveal V1/V2 neurons followed the percept, about 40% of neurons in V4 did. Interestingly, about half of V4 cells were anticorrelated with the stimulus.

The results of the Sheinberg and Logothetis (1997) experiments are striking. Instead of using binocular rivalry, they exploited a related paradigm: *flash suppression*. An image is presented to one eye for a second or longer. A different image

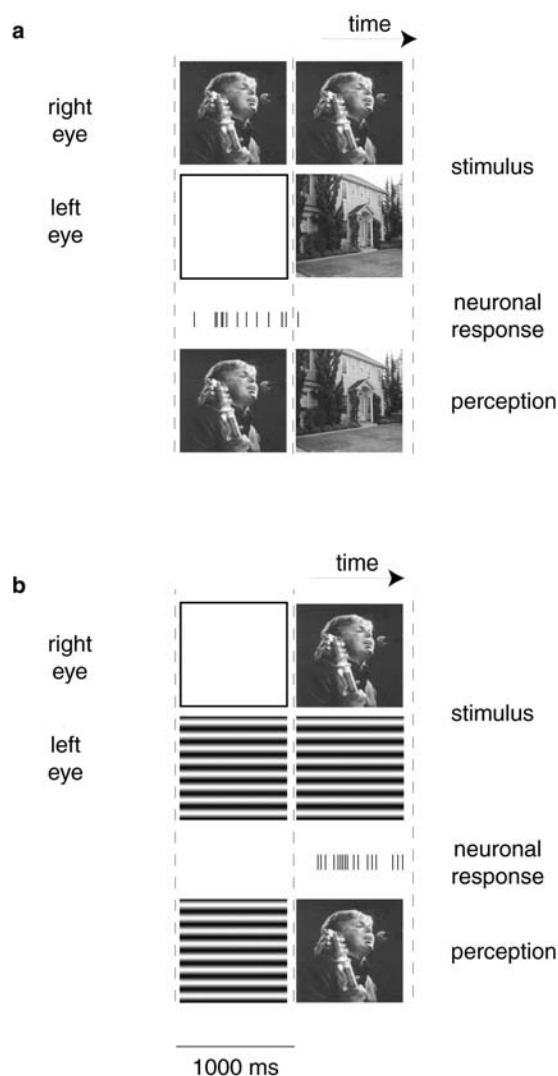


FIGURE 114.2. Example of a response of a single neuron in the left parahippocampal gyrus of a human patient during flash suppression. *A*, A photo of one of the Beatles, Paul McCartney, is projected into the right eye of the patient. After 1 second, a picture of a house is flashed into the left eye. This novel image completely suppresses the percept of McCartney and only the house is consciously seen. *B*, The converse situation: a horizontal grating is shown to the left eye. After 1 second, the image of McCartney is flashed into the right eye, completely suppressing the grating percept, although this image is still present on the left retina. The particular neuron recorded here follows the conscious percept of the patient rather than the retinal stimulus. It fires only to its preferred stimulus—McCartney—whenever the subject perceives this stimulus. (From Kreiman et al., 2002.)

is then flashed into the other eye. The former image is perceptually completely suppressed by the novel pattern, even though the first image is still present on the retina (Fig. 114.2). The mechanisms underlying flash suppression are unrelated to either forward masking, adaptation, or any other mechanism that reduces the visibility of the ipsilateral flash (Wolfe, 1984). Flash suppression is easy to obtain, is

very robust, and can be exactly timed, unlike the transitions occurring during binocular rivalry.

Sheinberg and Logothetis (1997) recorded from individual neurons in the monkey's superior temporal sulcus (STS) and inferior temporal cortex (IT). Overall, approximately 90% of the relevant neurons in STS and IT reliably predict the perceptual state of the animal. That is, these neurons follow the percept rather than the retinal stimulus. Moreover, many of these neurons respond in an almost all-or-none fashion, firing strongly for one percept, yet only at background levels for the alternative one.

Although the vast majority of electrophysiological single-cell experiments are carried out in animals, under exceptional circumstances such recordings are possible in humans. These occur in a subset of pharmacologically intractable epilepsy patients undergoing evaluation for surgical treatment. Kreiman et al. (2000) found many neurons to be tuned for specific categories of visually presented stimuli (e.g., famous people such as politicians or entertainers, faces of unknown actors expressing various emotions, animals or cars). Many of these cells fire selectively when their preferred stimulus is perceived but not when it is perceptually suppressed during flash suppression (Kreiman et al., 2002). About two-thirds of a total of 48 selective medial temporal lobe (MTL) neurons followed the percept (Figs. 114.2 and 114.3). No neuron responded in a significant manner to its preferred visual stimulus if this stimulus was physically present on the retina but perceptually suppressed. That is, there is no evidence for a neuronal representation of perceptually suppressed, that is unconscious, stimuli in the higher echelons of the visual hierarchy. Thus, both IT neurons in the macaque and MTL neurons in humans follow the subject's conscious percept.

Of course, without further experiments it is not possible to distinguish between correlation and causation. It does not automatically imply that just because a particular neuron follows the percept, its firing is part of the NCC. Do the MTL neurons carry a mere copy of the neuronal signal already expressed in IT for transfer into working memory or are neurons in the hippocampus, amygdala, and entorhinal cortex in normal also necessary for conscious perception? Where are these neurons projecting to? At the moment, it is technically difficult to interfere selectively, transiently, deliberately, and reversibly with these cellular populations in primates, but it is essential to have this knowledge or it will be almost impossible to understand the neural nature of consciousness.

What is the role of V1 in visual consciousness?

We have argued (Crick and Koch, 1995b) that primates are not directly conscious of the features represented by the neural activity in primary visual cortex. Activity in V1 may be necessary for vivid and veridical visual consciousness (as is activity in the retina), but we suggest that the firing of none

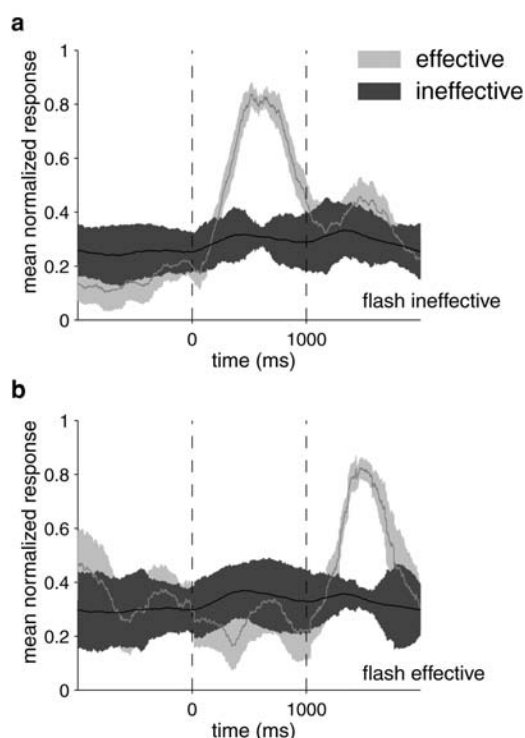


FIGURE 114.3. Averaged normalized spike density functions of 12 MTL neurons in human patients during flash suppression that followed the percept. These cells responded selectively to a specific face or image in the test set (as in Fig. 114.2). The light trace corresponds to the response for all trials when a stimulus from the cell's effective category was shown monocularly for 1 second (*A*) or during the 0.5 second long flash presentation period (*B*). The dark trace corresponds to the response to all other (ineffective) stimuli (shaded regions are the 95% confidence intervals). As all subjects perceive the effective stimuli during the monocular presentation (in *A*) or during flash suppression (in *B*), the cellular responses closely follow the subject's conscious visual experience. (From Kreiman et al., 2002.)

of the neurons in V1 directly correlates with what we consciously see.

Our reason is that at each stage in the visual hierarchy the explicit aspects of the representation we have postulated are recoded. We also assumed that any neurons expressing an aspect of the NCC must project directly, without recoding, to at least some of the parts of the brain that plan voluntary action—that is what we have argued seeing is for. We think that these plans are made in some parts of frontal cortex (see below).

The neuroanatomy of the macaque monkey shows that V1 cells do not project directly to any part of frontal cortex (see the references in Crick and Koch, 1995b).

The strategy used to verify or falsify this and similar hypotheses is to relate the receptive field properties of individual neurons in V1 or elsewhere to perception in a quantitative manner. Ultimately, this correlation has to be made on an individual trial-to-trial basis. If the structure of per-

ception does not map to the receptive field properties of V1 cells, it is unlikely that these neurons directly give rise to consciousness. In the presence of a correlation between perceptual experience and the receptive field properties of V1 cells, it is unclear whether these cells just correlate with consciousness or directly give rise to it. In that case, further experiments need to be carried out to untangle the exact relationship between neurons and perception.

Psychophysical evidence is broadly consistent with our proposal. The study by He et al. (1996) exploits a common visual aftereffect. If a subject stares for a fraction of a minute at a horizontal grating, and is then tested with a faint grating at the same location to decide whether it is oriented vertically or horizontally, the subject's sensitivity for detecting a horizontal grating will be reduced. This adaptation is orientation specific—the sensitivity for vertical gratings is almost unchanged—and disappears quickly. He and colleagues projected a single patch of grating onto a computer screen some 25 degrees from the fixation point. It was clearly visible, and their subjects showed the predictable orientation-selective adaptation effect. Adding one or more similar patches of gratings to either side of the original grating removes the lines of the grating from visibility; it is masked. Subjectively, one still sees something at the location of the original grating, but one is unable to make out its orientation, even when given unlimited viewing time. Yet despite this inability to see the adapting stimulus, the aftereffect was as strong and as specific to the orientation of the invisible grating as when the grating was visible. What this shows is that visual awareness must occur at a higher stage in the visual hierarchy than orientation-specific adaptation. This aftereffect is thought to be mediated by oriented neurons in V1 and beyond, implying that the NCC must be located past this stage.

Another case in point is the observation that very-high-frequency gratings that are perceptually indistinguishable from a uniform field nevertheless produce robust orientation-dependent aftereffects (He and MacLeod, 2001). The presence of aftereffects from stimuli that are not consciously perceived (Blake and Fox, 1974) indicates that stimulus properties must be represented outside of awareness. Thus, activity in V1 often does not correlate with awareness.

These inferences from behavior are complemented by direct electrophysiological measurements of neuronal activity in V1 in macaque monkeys. These measurements show that perceptual reports (presumably reflecting awareness) and the mean firing activity in V1 can change completely independently. For example, disparity-selective cells in V1 differentiate between local depth cues even when these do not give rise to an overall depth percept or may respond in an identical manner to two depth cues that yield very different global depth percepts (Cumming and Parker, 1997). This suggests that single V1 cells sensitive to binocular dis-

parity represent a first critical stage for generation of stereo cues but that conscious perception of depth is most likely generated further upstream. A similar lack of correlation between perceptual experience and the response properties of V1 cells can be seen during blinks. They produce profound and frequent interruptions in retinal stimulation, yet barely impinge on our visual experience (Volkman et al., 1980). Cells in the supragranular layers of V1 show responses to visual stimulation that decrease substantially during reflex blinks (Gawne and Martin, 2000), and this reduction is significantly more pronounced than when there is an equally long gap in visual stimulation. Similarly, microsaccades that occur continually do not alter our impression of the world but are reflected in the activity of neurons in V1 (Martinez-Conde et al., 2000). Or, when two isoluminant colors are alternated at frequencies beyond 10 Hz, humans perceive only a single fused color with a minimal sensation of brightness flicker. In spite of the perception of color fusion, color opponent cells in primary visual cortex of two alert macaque monkeys follow high-frequency flicker well above heterochromatic fusion frequencies (Gur and Snodderly, 1997). Lastly the brain automatically, and unconsciously, compensates for the incessant motion of the eyes. As a result, the external world looks stable. Yet V1 neurons can't tell the motion induced by smoothly pursuing a target with the eyes from pure image motion with the eyes stationary, contrary to visual experience (Ilg and Thier, 1996). In other words, neuronal activity in V1 can clearly represent certain retinal stimulation that is not perceived.

Changes in conscious perception can also occur in the absence of concomitant variations of neuronal activity in V1. As mentioned above, the majority of the V1/V2 cells recorded by Leopold and Logothetis (1996) do not covary with the animal's behavior during binocular rivalry. Instead, their firing reflects stimulus properties. Recently, two neuroimaging studies in humans have presented evidence arguing for a stronger role for V1 in binocular rivalry and hence, by implication, visual awareness. The most popular form of functional neuroimaging is blood oxygenation-level-dependent (BOLD) functional magnetic resonance imaging (fMRI). BOLD measures a component of the hemodynamic response associated with local neural activity (for the exact relationship between the two, see Logothetis et al., 2001). Averaged over the whole of human V1, reliable fluctuations in BOLD contrast activity are observed (Polonsky et al., 2000). The amplitude of these fluctuations is about half as large as those evoked by nonrivalrous stimuli, and is even larger in the part of V1 associated with the blind spot representation which contains cells receiving only monocular input from the non-blind spot eye (Tong and Engel, 2001). The reasons for this discrepancy are not yet clear but might well involve the complex nature of the relationship between

single-cell activity and BOLD measurements (Logothetis et al., 2001). In particular, it is possible that feedback activity from higher cortical areas to lower ones does give rise to a metabolic demand in the lower area due to the associated synaptic activity and so results in enhanced BOLD contrast. Yet the feedback is, by itself, not sufficiently powerful to affect spiking in the V1 cells. Other fMRI BOLD studies in humans show a poor correlation between V1 activity and visual awareness (for a review, see Rees et al., 2002).

Note that our hypothesis is not easy to prove, since it applies to all V1 cell populations. We hope that further neuroanatomical work will make our hypothesis plausible for humans. If correct, it would narrow the search to areas of the brain farther removed from the sensory periphery.

The frontal lobe hypothesis

As mentioned several times, we hypothesize that the NCC must have access to explicitly encoded visual information and project directly into the planning stages of the brain, associated with the frontal lobes in general and with prefrontal cortex in particular (Fuster, 1997). We would therefore predict that patients unfortunate enough to have lost their entire prefrontal cortex on both sides (including Broca's area due to the direct interhemispheric input from the right inferior temporal cortex to Broca's area [Di Virgilio and Clarke, 1997]) would not be visually conscious, although they might still have well-preserved, but unconscious, visual-motor abilities. No such patient is known to us (not even Brickner's famous patient; for an extensive discussion, see Damasio and Anderson, 1993). The visual abilities of any patient with frontal lobe damage needs to be carefully evaluated using a battery of appropriate psychophysical tests.

The fMRI study of the blindsight patient G.Y. (Sahraie et al., 1997) provides direct evidence for our view by revealing that prefrontal areas 46 and 47 are active when G.Y. is aware of a moving stimulus.

Findings of neurons in the inferior prefrontal cortex (IPC) of the macaque that respond selectively to faces—and that receive direct input from regions around STS and the inferior temporal gyrus that are well known to contain face-selective neurons—is very encouraging (Scalaidhe et al., 1997). This raises the question of why face cells would be represented in both IT and IPC. It is unlikely that exactly the same information is represented at two different locations, so it will be important to find out in what way they differ.

Large-scale lesion experiments carried out in the monkey suggest that the absence of frontal lobes leads to complete blindness (Gazzaniga, 1966; Nakamura and Mishkin, 1986). One would hope that future monkey experiments will reversibly (by cooling and/or injection of GABA agonists) inactivate specific prefrontal areas and demonstrate the

specific loss of abilities linked to visual perception while visual-motor behaviors—mediated by the on-line system—remain intact.

Some cognitive scientists (in particular, Jackendoff, 1987) have presented an *Intermediate-Level* theory of consciousness in which neither early sensory processing (the *outer world*) nor high-level three-dimensional information or thoughts (the *inner world*) is directly accessible to consciousness. The Intermediate-Level hypothesis raises the intriguing possibility that although much of the frontal lobes might be necessary for consciousness, the NCC might be preferentially located in more intermediate levels of cortex, such as the inferior temporal lobes (for a more detailed discussion of this and some experimental ramifications, see Crick and Koch, 2000).

Where are we and where should we be going?

We have reviewed the evidence in favor of the hypothesis that there might be anatomically localized neurons or neural pathways whose level of spiking activity mediates consciousness. The NCC is not likely to be found in V1, but among neurons in the ventral pathway (in particular in and around area IT) and in its recipient zones in the medial temporal and frontal lobes. Neurons from posterior parietal areas can modulate the competition in this stream without being strictly necessary for conscious perception of color, shape, objects, and form.

It is likely that a conscious percept requires that the relevant activity in the relevant neurons exceed some minimal amount. It is possible that such a threshold can only be exceeded by some type of feedback activity from a higher cortical area (Lamme and Roelfsema, 2000; Pollen, 1999). Furthermore, this minimal activity may have to persist for a minimum amount of time.

Yet the average firing activity need not be the only relevant variable. An alternative hypothesis is that consciousness may be associated with specific types of neural activity, such as oscillatory or synchronized discharges. These two hypotheses are not mutually exclusive, and a combination of synchronous activity and neural spike rates might be an important attribute of the NCC. Indeed, we suggested early on that synchronized oscillations in the broad 40 Hz range may underlie feature integration and form a substrate for visual consciousness, although the idea remains controversial (Crick and Koch, 1990; Engel and Singer, 2001; Chapter 113). In general, a synchronized neuronal population will be more efficient in evoking a strong postsynaptic response compared to a network of independently firing neurons; that is, it carries a more powerful postsynaptic “punch.” The brain may use correlated firing for more than one purpose. In particular, it might embody the effects of top-down attention. As consciousness frequently involves the suppression of competing percepts, such synchronized and oscillatory

firing might often accompany the NCC without being strictly necessary. Conversely, synchronized firing might also underlie other processes, such as figure-ground segregation, so that their mere presence might not reliably indicate a NCC.

At the moment, the most promising experiments used to discover the correlates of visual consciousness are those on bistable percepts, which need to be expanded to include other brain areas (in particular prefrontal cortex) in both the monkey and the human. It is important to discover which neurons express the NCC in each case (which neuronal subtype, in what layer, and so on), how they fire (do they fire in bursts? are discharge patterns across neurons synchronized?), does the time-course of the relevant activity correspond to the temporal dynamics of conscious perception? and, especially, where they project to. To assist this, more detailed neuroanatomy of the connectivity will be needed. It is also important to discover how the various on-line systems work so that one can contrast their (unconscious) neuronal activity with that of the NCC (Koch and Crick, 2001).

It will not be enough to show that certain neurons embody the NCC in certain—limited—visual situations. Rather, we need to identify the NCC for a sufficiently large and representative sample of visual inputs. One popular approach is to study the many visual illusions. For instance, humans clearly perceive, under appropriate circumstances, a transient motion aftereffect. On the basis of fMRI, it has been found that the human equivalent of cortical area MT is activated by the motion aftereffect (in the absence of any moving stimuli; Tootell et al., 1995). The time course of this illusion parallels the time course of activity as assayed using fMRI. In order to really pinpoint the NCC, one would need to identify individual cells expressing this and similar visual aftereffects.

This is not to argue that studying visual consciousness is the one and only means of cracking the mind-brain problem. Investigating other forms of consciousness might have practical advantages (e.g., the awareness of the exact unconditioned-conditioned stimulus contingency relationship during certain forms of associative conditioning; Clark and Squire, 1998). In order to understand consciousness, we need to understand cerebral cortex. We can only hope to achieve this goal by deliberately interfering with cortex and its components in a delicate, reversible, and transient manner. Molecular biology is beginning to provide the relevant tools (e.g., Lois et al., 2002). Whether these tools are best applied to the macaque’s visual system or to another modality in the more accessible mouse remains an open question.

Finding the NCC would only be the first, albeit critical, step in understanding consciousness. The next biggest challenge would be to bridge the gap between correlation and causation. For this to occur, we would need to understand

the postsynaptic action of neurons expressing the NCC, what happens to them in various diseases known to affect consciousness, such as schizophrenia or autism, and so on. And, of course, a final theory of consciousness would have to explain the central mystery: how a physical system with a particular architecture can have feelings and qualia (Chalmers, 1995). After several thousand years of speculation, it would be very gratifying to solve this puzzle.

Acknowledgments

We thank the J. W. Kieckhefer Foundation, the W. M. Keck Foundation Fund for Discovery in Basic Medical Research at Caltech, NIH, NIMH, and the NSF for support.

REFERENCES

- Bachmann, T., 2000. *Microgenetic Approach to the Conscious Mind*, Amsterdam: John Benjamins.
- Baron-Cohen, S., 2001. Consciousness of the physical and the mental, in *Finding Consciousness in the Brain* (P. G. Grossenbacher ed.), Amsterdam: John Benjamins, pp. 61–76.
- Blake, R., and R. Fox, 1974. Adaptation to invisible gratings and the site of binocular rivalry suppression, *Nature*, 249:488–490.
- Bogen, J. E., 1997. Some neurophysiologic aspects of consciousness, *Semin. Neurobiol.*, 17:95–103.
- Boussaoud, D., G. Di Pellegrino, and S. P. Wise, 1996. Frontal lobe mechanisms subserving vision-for-action versus vision-for-perception, *Behav. Brain Res.*, 72:1–15.
- Braun, J., and B. Julesz, 1998. Withdrawing attention at little cost: detection and discrimination tasks, *Percept. Psychophys.*, 60:1–23.
- Chalmers, D., 1995. *The Conscious Mind: In Search of a Fundamental Theory*, Oxford: Oxford University Press.
- Clark, R. E., and L. R. Squire, 1998. Classical conditioning and brain systems: the role of awareness, *Science*, 280:77–81.
- Coltheart, M., 1983. Iconic memory, *Philos. Trans. R. Soc. Lond. B*, 302:283–294.
- Crick, F., and C. Koch, 1990. Towards a neurobiological theory of consciousness, *Semin. Neurosci.*, 2:263–275.
- Crick, F., and C. Koch, 1995a. Why neuroscience may be able to explain consciousness, *Sci. Am.*, 273:84–85.
- Crick, F., and C. Koch, 1995b. Are we aware of neural activity in primary visual cortex? *Nature*, 375:121–123.
- Crick, F., and C. Koch, 1998. Consciousness and neuroscience, *Cereb. Cortex*, 8:97–107.
- Crick, F., and C. Koch, 2000. The unconscious homunculus. With commentaries by multiple authors, *Neuro-Psychoanalysis*, 2:3–59.
- Crick, F., and C. Koch, 2003. A framework for consciousness. *Nat. Neurosci.*, 6:119–126.
- Cumming, B. G., and A. J. Parker, 1997. Responses of primary visual cortical neurons to binocular disparity without depth perception, *Nature*, 389:280–283.
- Damasio, A. R., and S. W. Anderson, 1993. The frontal lobes, in *Clinical Neuropsychology*, 3rd ed. (K. M. Heilman and E. Valenstein, eds.), Oxford: Oxford University Press, pp. 409–460.
- Dennett, D. C. 1991. *Consciousness Explained*, Boston: Little, Brown.
- Desimone, R., and J. Duncan, 1995. Neural mechanisms of selective visual attention, *Annu. Rev. Neurosci.*, 18:193–222.
- Di Virgilio, G., and S. Clarke, 1997. Direct interhemispheric visual input to human speech areas, *Human Brain Map*, 5:347–354.
- Distler, C., D. Boussaoud, R. Desimone, and L. G. Ungerleider, 1993. Cortical connections of inferior temporal area TEO in macaque monkeys, *J. Comp. Neurol.*, 334:125–150.
- Driver, J., and J. B. Mattingley, 1998. Parietal neglect and visual awareness, *Nat. Neurosci.*, 1:17–22.
- Edelman, G. M., and G. Tononi, 2000. *A Universe of Consciousness*, New York: Basic Books.
- Efron, R., 1967. The duration of the present. *Annals New York Acad. Sci.*, 138:713–729.
- Engel, A. K., and W. Singer, 2001. Temporal binding and the neural correlates of sensory awareness, *Trends Cogn. Sci.*, 5:16–25.
- Enns, J. T. and V. DiLollo, 1997. Object substitution: a new form of masking in unattended visual locations, *Psych. Sci.*, 8:135–139.
- Enns, J. T., and V. DiLollo, 2000. What's new in visual masking? *Trends Cogn. Sci.*, 4:345–352.
- Felleman, D. J., and D. Van Essen, 1991. Distributed hierarchical processing in the primate cerebral cortex, *Cereb. Cortex*, 1:1–47.
- Franz, V. H., et al. 2000. Grasping visual illusions: no evidence for a dissociation between perception and action, *Psychol. Sci.*, 11:20–25.
- Fuster, J. M., 1997. *The Prefrontal Cortex: Anatomy, Physiology, and Neuropsychology of the Frontal Lobe*, 3rd ed., Philadelphia: Lippincott-Raven.
- Gawne, T. J., and J. M. Martin, 2000. Activity of primate V1 cortical neurons during blinks, *J. Neurophysiol.*, 84:2691–2694.
- Gazzaniga, M. S., 1966. Visuomotor integration in split-brain monkeys with other cerebral lesions, *Exp. Neurol.*, 16:289–298.
- Gegenfurtner, K. R., and G. Sperling, 1993. Information transfer in iconic memory experiments, *J. Exp. Psych. Hum. Percept. Perform.*, 19:845–866.
- Gur, M., and D. M. Snodderly, 1997. A dissociation between brain activity and perception: chromatically opponent cortical neurons signal chromatic flicker that is not perceived, *Vis. Res.*, 37:377–382.
- He, S., P. Cavanagh, and J. Intriligator, 1996. Attentional resolution and the locus of visual awareness, *Nature*, 383:334–337.
- He, S., and D. R. Macleod, 2001. Orientation-selective adaptation and tilt after-effect from invisible patterns, *Nature*, 411:473–476.
- Ilg, U. J., and P. Thier, 1996. Inability of rhesus monkey area V1 to discriminate between self-induced and externally induced refinal image slip. *European J. Neurosci.*, 8:1156–1166.
- Jackendoff, R., 1987. *Consciousness and the Computational Mind*, Cambridge, MA: MIT Press.
- Karnath, H. O., 2001. New insights into the functions of the superior temporal cortex, *Nat. Rev. Neurosci.*, 2:568–576.
- Koch, C., and F. C. Crick, 2000. Some thoughts on consciousness and neuroscience, in *The Cognitive Neurosciences*, 2nd ed. (M. S. Gazzaniga ed.), Cambridge, MA: MIT Press, pp. 1285–1294.
- Koch, C., and F. Crick, 2001. On the zombie within, *Nature*, 411:893.
- Kreiman, G., I. Fried, and C. Koch, 2002. Single neuron correlates of subjective vision in the human medial temporal lobe, *Proc. Natl. Acad. Sci. USA*, 99:8378–8383.
- Kreiman, G., C. Koch, and I. Fried, 2000. Category-specific visual responses of single neurons in the human medial temporal lobe, *Nat. Neurosci.*, 3:946–953.
- Lamme, V. A., and P. R. Roelfsema, 2000. Two distinct modes of vision offered by feedforward and recurrent processing, *Trends Neurosci.*, 23:571–579.

- Leopold, D. A., and N. K. Logothetis, 1996. Activity changes in early visual cortex reflect monkeys' percepts during binocular rivalry, *Nature*, 379:549–553.
- Libet, B. 1973. Electrical stimulation of cortex in human subjects and conscious sensory aspects, in *Handbook of Sensory Physiology*, vol. II: *Somatosensory Systems* (A. Iggo ed.), Berlin: Springer Verlag, pp. 743–790.
- Logothetis, N. K., J. Pauls, M. Augath, T. Trinath, and A. Oeltermann, 2001. Neurophysiological investigation of the basis of the fMRI signal, *Nature*, 412:150–157.
- Logothetis, N., and J. Schall, 1989. Neuronal correlates of subjective visual perception, *Science*, 245:761–763.
- Lois, C., E. J. Hong, S. Pease, E. J. Brown, and D. Baltimore, 2002. Germline transmission and tissue-specific expression of transgenes delivered by lentiviral vectors, *Science*, 295:868–872.
- Mack, A., and I. Rock, 1998. *Inattentional Blindness*, Cambridge, MA: MIT Press.
- Macknik, S. L., and M. S. Livingstone, 1998. Neuronal correlates of visibility and invisibility in the primate visual system, *Nat. Neurosci.*, 1:144–149.
- Martinez-Conde, S., S. L. Macknik, and D. H. Hubel, 2000. Microsaccadic eye movements and firing of single cells in the striate cortex of macaque monkeys, *Nat. Neurosci.*, 3:251–258.
- Milner, D., and M. Goodale, 1995. *The Visual Brain in Action*, Oxford: Oxford University Press.
- Myerson, J., F. Miezin, and J. Allman, 1981. Binocular rivalry in macaque monkeys and humans: a comparative study in perception, *Behav. Anal. Lett.*, 1:149–156.
- Nakamura, R. K., and M. Mishkin, 1986. Chronic blindness following lesions of nonvisual cortex in the monkey, *Exp. Brain Res.*, 62:173–184.
- Nimchinsky, E. A., E. Gilissen, J. M. Allman, D. P. Perl, J. M. Erwin, and P. R. Hof, 1999. A neuronal morphologic type unique to humans and great apes, *Proc. Natl. Acad. Sci. USA*, 96:5268–5273.
- O'Regan, J. K., 1992. Solving the “real” mysteries of visual perception: the world as an outside memory, *Can. J. Psychol.*, 46:461–488.
- Penfield, W., and H. Jasper, 1954. *Epilepsy and the Functional Anatomy of the Human Brain*, Boston: Little, Brown.
- Pollen, D. A., 1999. On the neural correlates of visual perception, *Cereb. Cortex*, 9:4–19.
- Polonsky, A., R. Blake, J. Braun J., and D. J. Heeger, 2000. Neuronal activity in human primary visual cortex correlates with perception during binocular rivalry, *Nat. Neurosci.*, 3:1153–1159.
- Potter, M. C., 1976. Short-term conceptual memory for pictures, *Exp. Psychol. Hum. Learn. Mem.*, 2:509–522.
- Purves, D., J. A. Paydartar, and T. J. Andrews, 1996. The wagon wheel illusion in movies and reality, *Proc. Natl. Acad. Sci. USA*, 93:3693–3697.
- Rafal, R. D., 1997. Balint syndrome, in *Behavioral Neurology and Neuropsychology* (T. E. Feinberg and M. J. Farah, eds.), New York: McGraw-Hill, pp. 337–356.
- Rees, G., G. Kreiman, and C. Koch, 2002. Neural correlates of consciousness in humans, *Nat. Rev. Neurosci.*, 3:261–270.
- Revonuso, A., M. Johanson, J.-E. Wedlund, and J. Chaplin, 2000. The zombie among us, in *Beyond Dissociation* (Y. Rossetti, and A. Revonuso, eds.), Amsterdam: John Benjamins, pp. 331–351.
- Rock, I., C. M. Linnett, P. Grant, and A. Mack, 1992. Perception without attention: results of a new method, *Cogn. Psychol.*, 24:502–534.
- Rossetti, Y., 1998. Implicit short-lived motor representations of space in brain damaged and healthy subjects, *Conscious. Cogn.*, 7:520–558.
- Sahraie, A., L. Weiskrantz, J. L. Barbur, A. Simmons, S. C. R. Williams, and M. J. Brammer, 1997. Pattern of neuronal activity associated with conscious and unconscious processing of visual signals, *Proc. Natl. Acad. Sci. USA*, 94:9406–9411.
- Scalaidhe, S. P. O., F. A. W. Wilson, and P. S. Goldman-Rakic, 1997. Areal segregation of face-processing neurons in prefrontal cortex, *Science*, 278:1135–1138.
- Sheinberg, D. L., and N. K. Logothetis, 1997. The role of temporal cortical areas in perceptual organization, *Proc. Natl. Acad. Sci. USA*, 94:3408–3413.
- Sperry, R. W., 1974. Lateral specialization in the surgically separated hemispheres, in *Neuroscience, 3rd Study Program* (F. O. Schmitt and F. G. Worden, eds.), Cambridge, MA: MIT Press.
- Thompson, K. G., and J. D. Schall, 2000. Antecedents and correlates of visual detection and awareness in macaque prefrontal cortex, *Vis. Res.*, 40:1523–1538.
- Tong, F., and S. A. Engel, 2001. Interocular rivalry revealed in the human cortical blind-spot representation, *Nature*, 411:195–199.
- Tootell, R. B. H., J. B. Reppas, A. M. Dale, R. B. Look, M. I. Sereno, R. Malach, T. J. Brady, and B. R. Rosen, 1995. Visual motion aftereffect in human cortical area MT revealed by functional magnetic resonance imaging, *Nature*, 375:139–141.
- Ungerleider, L. G., and M. Mishkin, 1982. Two cortical visual systems, in *Analysis of Visual Behavior* (D. J. Ingle, M. A. Goodale, and R. J. W. Mansfield, eds.), Cambridge, MA: MIT Press, pp. 549–586.
- Vaina, L., and A. Cowey, 1996. Impairment of the perception of second order motion but not first order motion in a patient with unilateral focal brain damage, *Proc. R. Soc. Lond. B*, 263:1225–1232.
- Velmans, M., 1991. Is human information processing conscious? *Behav. Brain Sci.*, 14:651–726.
- Volkman, F. C., L. A. Riggs, and R. K. Moore, 1980. Eye-blinks and visual suppression, *Science*, 207:900–902.
- Westheimer, G., 1999. Gestalt theory reconfigured: Max Wertheimer's anticipation of recent developments in visual neuroscience, *Perception*, 28:5–15.
- Wolfe, J., 1984. Reversing ocular dominance and suppression in a single flash, *Vis. Res.*, 24:471–478.
- Wolfe, J. M., 1998. Visual memory: what do you know about what you saw? *Curr. Biol.*, 8(9):R303–R304.
- Yund, E. W., H. Morgan, and R. Efron, 1983. The micropattern effect and visible persistence, *Percept. Psychophys.*, 34(3):209–213.
- Zeki, S., and A. Bartels, 1999. Toward a theory of visual consciousness, *Conscious. Cogn.*, 8:225–259.
- Zihl, J., D. Von Cramon, and N. Mai, 1983. Selective disturbance of movement after bilateral brain damage, *Brain*, 106:313–340.
- Zola-Morgan, S., and L. R. Squire, 1993. Neuroanatomy of memory, *Annu. Rev. Neurosci.*, 16:547–563.

LIST OF CONTRIBUTORS

- Albrecht, Duane G. Department of Psychology, University of Texas, Austin, Texas
- Albright, Thomas D. The Salk Institute for Biological Studies, San Diego, California
- Andersen, Richard A. Division of Biology, California Institute of Technology, Pasadena, California
- Anderson, Barton L. Department of Brain and Cognitive Sciences, Massachusetts Institute of Technology, Cambridge, Massachusetts
- Anzai, Akiyuki Washington University, St. Louis, Missouri
- Barbur, John L. Applied Vision Research Centre, City University, London, England
- Barlow, Horace Physiology Laboratory, Downing Site, Cambridge, England
- Barnstable, Colin J. Department of Ophthalmology and Visual Science, Yale University School of Medicine, New Haven, Connecticut
- Berardi, Nicoletta Istituto di Neuroscienze del CNR, Pisa, Italy; Dipartimento di Psicologia, Università di Firenze, Italy
- Blake, Randolph Vanderbilt Research Center, Department of Psychology, Vanderbilt University, Nashville, Tennessee
- Brainard, David H. Department of Psychology, University of Pennsylvania, Philadelphia, Pennsylvania
- Brecha, Nicholas C. Departments of Neurobiology and Medicine and the Jules Stein Eye Institute, UCLA School of Medicine, Los Angeles, California
- Britten, Kenneth H. Center for Neuroscience and Section of Neurobiology, Physiology, and Behavior, University of California, Davis, California
- Bruce, Charles J. Department of Neurobiology, Yale University, New Haven, Connecticut
- Buck, Steven L. Department of Psychology, University of Washington, Seattle, Washington
- Bullier, Jean Centre de Recherche Cerveau et Cognition, Toulouse, France
- Burkhalter, Andreas Department of Anatomy and Neurobiology, Washington School of Medicine, St. Louis, Missouri
- Burns, Marie E. Center for Neuroscience and Department of Psychiatry, University of California, Davis, California
- Burr, David C. Istituto di Neurofisiologia del CNR, Pisa, Italy; Dipartimento di Psicologia, Università di Firenze, Florence, Italy
- Calkins, David J. Departments of Ophthalmology; Neurobiology and Anatomy, and the Center for Visual Science, University of Rochester Medical Center, Rochester, New York
- Callaway, Edward M. The Salk Institute for Biological Studies, Systems Neurobiology Laboratories, La Jolla, California
- Casagrande, Vivien A. Departments of Cell and Developmental Biology, Psychology, and Ophthalmology and Visual Sciences, Vanderbilt University, Nashville, Tennessee
- Casanova, Christian Laboratory of Visual Neurosciences, School of Optometry, University of Montreal, Montreal, Canada

Chapman, Barbara Center for Neuroscience and Section of Neurobiology, Physiology, and Behavior, University of California, Davis, California

Chiu, Chiayu Interdepartmental Graduate Program in Neuroscience, University of Rochester, Rochester, New York

Cohn, Theodore E. School of Optometry, Department of Bioengineering, University of California, Berkeley, California

Conner, Charles E. Department of Neuroscience and Zanvyl Krieger Mind/Brain Institute, Johns Hopkins University, Baltimore, Maryland

Cook, Jeremy E. Department of Anatomy and Developmental Biology, University College London, London, England

Copenhagen, David R. Departments of Ophthalmology and Physiology, University of California, San Francisco, California

Crane, Alison M. Department of Psychology, University of Texas, Austin, Texas

Crick, Francis Kieckhefer Center for Theoretical Biology, The Salk Institute, La Jolla, California

Daw, Nigel W. Department of Ophthalmology and Visual Science, Yale University Medical School, New Haven, Connecticut

De Angelis, Gregory C. Department of Anatomy and Neurobiology, Washington University, St. Louis, Missouri

De Valois, Karen K. Psychology Department and Graduate Group in Vision Science, University of California, Berkeley, California

De Valois, Russell L. Psychology Department, University of California, Berkeley, California

Dobkins, Karen R. Department of Psychology, University of California, San Diego, California

Dragoi, Valentin Department of Brain and Cognitive Sciences, Center for Learning and Memory, Massachusetts Institute of Technology, Cambridge, Massachusetts

Duffy, Charles J. Department of Neurology, Rochester University, Rochester, New York

Ehrenstein, Walter H. Leibniz Research Center for Human Factors, University of Dortmund, Dortmund, Germany

Erskine, Lynda Departments of Visual Science and Molecular Genetics, Institute of Ophthalmology, University College London, London, England

Ferster, David Department of Neurobiology and Physiology, Northwestern University, Evanston, Illinois

Field, Daniel J. Department of Psychology, Cornell University, Ithaca, New York

Fiorentini, Adriana Istituto di Neurofisiologia del CNR, Pisa, Italy

Fitzpatrick, David Department of Neurobiology, Duke University Medical Center, Durham, North Carolina

Fleming, Roland Department of Brain and Cognitive Science, Massachusetts Institute of Technology, Cambridge, Massachusetts

Freeman, Ralph D. Group in Vision Science, School of Optometry, Helen Wills Neuroscience Institute, University of California, Berkeley, California

Friedman, Harriett R. Department of Neurobiology, Yale University, New Haven Connecticut

Gallant, Jack L. Department of Psychology, University of California, Berkeley, California

Gandhi, Neeraj J. Department of Otolaryngology, University of Pittsburgh, Pittsburgh, Pennsylvania

Gegenfurtner, Karl R. Department of Psychology, Gießen University, Gießen, Germany

Geisler, Wilson S. Department of Psychology, University of Texas, Austin, Texas

Glickstein, Mitchell Department of Anatomy, University College London, London, England

Godinho, Leanne Department of Anatomy and Neurobiology, Washington University School of Medicine, St. Louis, Missouri

Graham, Norma Department of Psychology, Columbia University, New York, New York

Grossberg, Stephen Department of Cognitive and Neural Systems, Boston University, Boston, Massachusetts

Grünert, Ulrike Department of Physiology, University of Sydney, Sydney, Australia

Guillery, R.W. Department of Anatomy, University of Wisconsin School of Medicine, Madison, Wisconsin

Hayes, Anthony Department of Psychology, University of Hong Kong, Hong Kong, China

Heinen, Stephen J. Smith-Kettlewell Institute, San Francisco, California

Hess, Robert F. Department of Ophthalmology, McGill University, Montreal, Canada

Hofer, Heidi Center for Visual Science, University of Rochester, Rochester, New York

Ishida, Andrew T. Section of Neurobiology, Physiology, and Behavior, University of California, Davis, California

Jacobs, Gerald H. Neuroscience Research Institute and Department of Psychology, University of California, Santa Barbara, California

Jones, Helen E. Department of Visual Science, Institute of Ophthalmology, University College London, London, England

Kaas, Jon H. Department of Psychology, Vanderbilt University, Nashville, Tennessee

Kamitani, Yukiyasu Department of Neurology, Harvard Medical School, Boston, Massachusetts

Kanwisher, Nancy Department of Brain and Cognitive Sciences, Massachusetts Institute of Technology, Cambridge, Massachusetts

Kaplan, Ehud Departments of Ophthalmology, Physiology, and Biophysics, Mount Sinai School of Medicine, New York, New York

Kastner, Sabine Department of Psychology, Princeton University, Princeton, New Jersey

Keller, Edward L. Smith-Kettlewell Institute, San Francisco, California

Kennedy, Henry INSERM, Bron, France

Kiorpes, Lynne Center for Neural Science, New York University, New York, New York

Kiper, Daniel C. Institute of Neuroinformatics, University of Zurich and Swiss Federal Institute of Technology, Zurich, Switzerland

Knoblauch, Kenneth INSERM, Cerveau et Vision, Bron, France

Koch, Christof Division of Biology, California Institute of Technology, Pasadena, California

Koenderink, Jan J. Utrecht University, Utrecht, The Netherlands

Kolb, Helga John Moran Eye Center, University of Utah, Salt Lake City, Utah

Kraus, Michael S. Department of Neurobiology, Yale University, New Haven, Connecticut

Lamb, Trevor D. Division of Neuroscience, John Curtin School of Medical Research, Australian National University, Canberra, Australia

Lamme, Victor A.F. Graduate School of Neuroscience, Department of Visual System Analysis, University of Amsterdam; The Netherlands Ophthalmic Research Institute, Amsterdam, The Netherlands

Land, Michael F. Sussex Centre for Neuroscience, School of Biological Sciences, University of Sussex, Brighton, England

Landy, Michael S. Department of Psychology and Center for Neural Science, New York University, New York, New York

Maffei, Lamberto Istituto di Neuroscienze del CNR, Laboratorio di Neurofisiologia, and Scuola Normale Superiore, Pisa, Italy

Makous, Walter Center for Visual Science, University of Rochester, Rochester, New York

Marc, Robert E. John Moran Eye Center, University of Utah School of Medicine, Salt Lake City, Utah

Martin, Paul R. National Vision Research Institute and Department of Optometry and Vision Sciences, University of Melbourne, Melbourne, Australia

Masland, Richard H. Howard Hughes Medical Institute, Massachusetts General Hospital, Harvard Medical School, Boston, Massachusetts

Mason, Carol Departments of Pathology, Anatomy, and Cell Biology, Center for Neurobiology and Behavior, Columbia University College of Physicians and Surgeons, New York, New York

Maunsell, John Division of Neuroscience, Baylor College of Medicine, Houston, Texas

Mays, Lawrence E. Department of Physiological Optics, University of Alabama, Birmingham, Alabama

Meijer, Johanna H. Department of Neurophysiology, Leiden University Medical Center, Leiden, The Netherlands

Miller, Earl K. Department of Brain and Cognitive Sciences, Massachusetts Institute of Technology, Cambridge, Massachusetts

Mitchell, Donald E. Psychology Department, Dalhousie University, Halifax, Canada

Moody, Sally Department of Anatomy and Cell Biology, Programs in Genetics and in Neuroscience, George Washington University Medical Center, Institute for Biomedical Sciences, Washington, D.C.

Morrone, M. Concetta Dipartimento di Psicologia, Università di Firenze, Florence, Italy; Università Vita-Salute San Raffaele, Milan, Italy

Movshon, J. Anthony Center for Neural Science, New York University, New York, New York

Neitz, Jay Department of Cell Biology, Neurobiology, and Anatomy, Medical College of Wisconsin, Milwaukee, Wisconsin

Neitz, Maureen Department of Ophthalmology, Medical College of Wisconsin, Milwaukee, Wisconsin

Nelson, Ralph Basic Neurosciences Program, National Institute of Neurological Disorders and Stroke, National Institutes of Health, Bethesda, Maryland

Norcia, Anthony M. The Smith-Kettlewell Eye Research Institute, San Francisco, California

Olshausen, Bruno A. Center for Neuroscience and Section of Neurobiology, Physiology, and Behavior, University of California, Davis, California

Orban, Guy A. Laboratorium voor Neuro- en Psychofysiologie, K.U. Leuven, Medical School, Campus Gasthuisberg, Leuven, Belgium

Parker, Andrew J. University Laboratory of Physiology, Oxford University, Oxford, England

Pasternak, Tatiana Department of Neurobiology and Anatomy, University of Rochester Medical Center, Rochester, New York

Perlman, Ido Department of Physiology, Technion University, Haifa, Israel

Poggio, Tomas Department of Brain and Cognitive Sciences, Massachusetts Institute of Technology, Cambridge, Massachusetts

Pokorny, Joel Visual Science Laboratories, University of Chicago, Chicago, Illinois

Reeves, Adam Department of Psychology, Northeastern University, Boston, Massachusetts

Reid, R. Clay Department of Neurobiology, Harvard University, Boston, Massachusetts

Riesenhuber, Maximilian Center for Biological and Computational Learning, Massachusetts Institute of Technology, Cambridge, Massachusetts

Ringach, Dario Department of Neurobiology, University of California, Los Angeles, California

Rolls, Edmund T. Department of Experimental Psychology, Oxford University, Oxford, England

Rubin, Nava Center for Neural Science, New York University, New York, New York

Schall, Jeffrey D. Vanderbilt Vision Research Center, Vanderbilt University, Nashville, Tennessee

Scherberger, Hansjörg Division of Biology, California Institute of Technology, Pasadena, California

Schor, Clifton M. School of Optometry, Visual Science Group, University of California, Berkeley, California

Shapley, Robert Center for Neural Science, New York University, New York, New York

Sherman, S. Murray Department of Neurobiology, State University of New York, Stony Brook, New York

Shevell, Steven K. Visual Science Laboratories, University of Chicago, Chicago, Illinois

Shimojo, Shinsuke Division of Biology, California Institute of Technology, Pasadena, California

Sillito, Adam M. Department of Visual Science, Institute of Ophthalmology, University College London, London, England

Silverman, Michael Department of Psychology, Harvard University, Boston, Massachusetts

Simoncelli, Eero P. Center for Neural Science, New York University, New York, New York

Simons, Daniel J. Department of Psychology, Harvard University, Boston, Massachusetts

Singer, Wolf Max Planck Institute for Brain Research, Frankfurt, Germany

Slaughter, Malcolm M. Department of Physiology and Biophysics, State University of New York at Buffalo School of Medicine, Buffalo, New York

Smith, Vivianne C. Visual Science Laboratories, University of Chicago, Chicago, Illinois

Sommer, Marc A. National Institutes of Health, Bethesda, Maryland

Sparks, David L. Division of Neuroscience, Baylor College of Medicine, Houston, Texas

Spillmann, Lothar Brain Research Unit, University of Freiburg, Freiburg, Germany

Srinivasan, Mandyam Research School for Biological Sciences, Centre for Visual Science, Australian National University, Canberra, Australia

Stanton, Gregory B. Department of Anatomy, College of Medicine, Howard University, Washington, D.C.

Steinman, Robert M. Department of Psychology, University of Maryland, College Park, Maryland

Sterling, Peter Department of Neuroscience, University of Pennsylvania School of Medicine, Philadelphia, Pennsylvania

Sur, Mriganka The Department of Brain and Cognitive Sciences, Massachusetts Institute of Technology, Cambridge, Massachusetts

Takahashi, Joseph S. Howard Hughes Medical Institute, Neurobiology and Physiology, Northwestern University, Evanston, Illinois

Tanaka, Keiji RIKEN Brain Research Institute, Saitama, Japan

Tucker, Thomas R. Department of Neurobiology, Duke University, Durham, North Carolina

Ungerleider, Leslie G. Laboratory of Brain and Cognition, National Institute of Mental Health, Bethesda, Maryland

Usrey, W. Martin Center for Neuroscience and Section of Neurobiology, Physiology, and Behavior, University of California, Davis, California

van Doorn, Andrea J. Department of Industrial Design, Delft Technical University, Delft, The Netherlands

Van Essen, David C. Department of Anatomy and Neurobiology, Washington University School of Medicine, St. Louis, Missouri

Vanduffel, Wim Laboratory of Neuro- and Psychophysiology, K.U. Leuven, Medical School, Leuven, Belgium

Vaney, David I. Vision, Touch, and Hearing Research Centre, School of Biomedical Sciences, University of Queensland, Queensland, Australia

von der Heydt, Rüdiger, the Zanvyl Krieger Mind/Brain Institute, Johns Hopkins University, Baltimore, Maryland

Walker, Mark F. Department of Neurology, Johns Hopkins University, Baltimore, Maryland

Wallis, Jonathan D. Department of Brain and Cognitive Sciences, Massachusetts Institute of Technology, Cambridge, Massachusetts

Warren, William H. Cognitive and Linguistic Sciences, Brown University, Providence, Rhode Island

Weale, Robert A. Age Concern Institute of Gerontology, King's College London; Eye Department, University College London Hospital, London, England

Webster, Michael A. Department of Psychology, University of Nevada, Reno, Nevada

Weliky, Michael Department of Brain and Cognitive Sciences, University of Rochester, Rochester, New York

Weiskrantz, Larry Department of Experimental Psychology, University of Oxford, Oxford, England

Wilkinson, Frances Department of Psychology, York University, Ontario, Canada

Williams, David R. Center for Visual Science, University of Rochester, Rochester, New York

Williams, Robert W. Center of Genomics and Bioinformatics, Center for Neuroscience, Department of Anatomy and Neurobiology, Department of Pediatrics, University of Tennessee Health Science Center, Memphis, Tennessee

Wilson, Hugh R. Department of Biology, York University, Ontario, Canada

Wilson, Martin Section of Neurobiology, Physiology, and Behavior, Division of Biological Sciences, University of California, Davis, California

Wong, Rachel O.L. Department of Anatomy and Neurobiology, Washington University School of Medicine, St. Louis, Missouri

Wurtz, Robert H. National Institutes of Health, Bethesda, Maryland

Xu, Xiangmin Department of Ophthalmology and Visual Science, Vanderbilt University, Nashville, Tennessee

Zee, David S. Department of Neurology, Johns Hopkins University, Baltimore, Maryland

Zeki, Semir Department of Anatomy, University College, London, England

Zhang, Shaowu Research School of Biological Sciences, Centre for Visual Science, Australian National University, Canberra, Australia

INDEX

Page numbers followed by *b*, *f*, or *t* denote boxes, figures, or tables, respectively.

A

- Abducens internuclear (AI) neurons, 1416–1417, 1416*f*, 1418*f*
- Abducens nucleus, neurons in, 1416–1417, 1416*f*, 1418*f*, 1424
- Aberration(s)
 - chromatic, 800–801, 805–807
 - adaptive optics and, 805, 807–808, 808*f*
 - axial, 800–801, 805–806
 - and image formation, 800–801
 - transverse, 800–801
 - correction of, effects of, 807–808, 808*f*
 - monochromatic, 796, 800–801, 805–806
 - correction of, effects of, 807–808, 808*f*
 - pupil size and, 799–800, 800*f*
 - and retinal image formation, 795–797
 - trade-off with diffraction, 799–800
 - wave, 795
 - in aberrated eye, 795, 796*f*
 - capture by pupil function, 796
 - in corrected eyes, 807–808
 - decomposition into component aberrations, 795–796, 797*f*
 - in perfect eye, 795, 796*f*
 - in real eyes, 795, 796*f*
 - Zernike modes of, 795–796, 797*f*
- Abney effect, 893
- Absolute disparity, 550, 780, 1303, 1303*f*, 1304
 - response of V1 neurons to, 783
- Absolute threshold. *See also* Detection threshold
 - of cone system, 841
 - dark light and, 816–817
 - in scotopic vision, 838–840
 - aging and, 846
 - in infants, 846
- Absolute threshold problem, 817
- Absorbance of lens, aging and, 208*t*, 208–209
- Abstract concepts
 - honeybees' formation of, 1502–1504
 - prefrontal cortex (PFC) and, 1555
- Accommodation, 1415, 1461–1462
 - ambient annual temperature and, 206, 206*t*
 - and convergence, 1415
 - cross-coupling between, 1301
 - and ganglion cell excitability, 436
 - loss of, 205–208. *See also* Presbyopia
 - neural pathway for, 1425
 - reading and, 207–208
 - vergence and
 - linkage of, 1419–1422, 1420*f*, 1421*f*, 1461–1462
 - synkinesis between, 1461–1462
- Accommodation gain
 - definition of, 1421*f*
 - and vergence gain, relationship between, 1419–1422, 1421*f*
- Acetylcholine, 311–313, 312*f*
 - amacrine cells expressing, 294–295, 295*f*, 312–313, 361, 403–404, 457–458
 - and calcium currents, 432
 - and cortical plasticity, 128, 134–135, 136*t*, 137*f*, 139
 - and direction selectivity, 457–458
 - future directions for study of, 313
 - ganglion cells expressing, 404, 457–458
 - horizontal cells expressing, 370
 - localization of, 311, 312*f*
 - and long-term depression, 134, 136*t*
 - and long-term potentiation, 134, 136*t*
 - metabolism of, 304, 311, 312*f*
 - modulatory actions of, 135
 - neurotrophins and, 55, 56*f*, 60
 - and orientation selectivity, 134, 136*t*
 - peptide action on, 337
 - retinal, 86*f*, 87
 - signals about nervous system state carried by, 134
 - species differences in systems of, 135
 - in synaptic transmission, 294–295, 295*f*, 304, 312–313
 - versus GABA, 312–313
 - transporters of, 311, 312*f*
 - mitochondrial, 312*f*
 - plasma membrane, 311, 312*f*
 - vesicular, 311, 312*f*
- Acetylcholine receptor(s), 311–312, 312*f*
 - heptahelical, 312, 312*f*
 - ionotropic, 311–312, 312*f*
- Acetylcholine receptor antagonists, and cortical plasticity, 134
- Acetylcholinesterase, 311, 312*f*
 - activity, thalamic, 592
 - and cortical connectivity, 151, 152*f*
- Achromatic appearance, 897–898, 897*f*
- Achromatic channel, 1008, 1217
- Achromatic contrast, 882
- Achromatic contrast sensitivity, 177, 186
- Achromatic observers
 - rod saturation in, 841–842
 - scotopic grating acuity in, 843, 844*f*
- Achromatic percepts, constancy of, 904
- Achromatic vision, bidimensional model of, 884–885
- Achromatopsia, 554, 975, 1014, 1015
 - central, 1029
 - cerebral, 1029, 1035
 - pupil responses in, 641–642, 651*f*, 652, 653
 - complete, 976
 - molecular genetics of, 983
 - incomplete, 976
 - autosomal recessive, 983
 - induced by fusiform gyrus lesions, 1034–1035
 - inheritance of, 976
 - transient, 1035
 - variations in, 1035
- Achromats, X-chromosome incomplete, 875
- ACPD (aminocyclopentane-trans-1, 3-dicarboxylic acid)
 - and cortical plasticity, 129, 132
 - and CREB, 132
- Actin filaments, in cones and rods, 216
- Action potential(s)
 - in area MT neurons, 1206

- Action potential(s) (cont.)
 with frequency adaptation, in basket cell, 688
 in ganglion cells
 bursts or events, 427–430, 428*f*, 429*f*
 calculations of, 434
 frequencies of, 415, 422–430
 accommodation and, 436
 calcium modulation of, 436–437
 current transformed into, 423, 424*f*, 425*f*
 currents facilitating, 424
 in dark-adapted retina, 426, 426*f*, 428, 436
 dopamine and, 438–443
 high versus low, 423–426
 Hodgkin-Huxley equations for, 425
 light intensity and, 423–425, 425*f*, 427, 428*f*, 429*f*
 in light-adapted retina, 426, 427*f*, 427–428
 prediction of, 443
 with presentations of flickering checkerboards, 426–427
 with presentations of spatially uniform random flicker, 427
 temporal contrast and, 437*f*, 437–438
 heterogeneity in, 434–435
 in LGN cells
 burst, 575–578, 612, 613*f*, 622
 in waking state, 612
 cortical feedback and, 611–612, 613*f*
 tonic, 575–578, 612, 613*f*
 in long-term depression, 127
 in long-term potentiation, 127
 synchrony of, horizontal cortical connections and, 742*f*, 742–743
 Action spectrum, of horizontal cells, 373, 375*f*
 Active zones, of photoreceptor axon terminals, 245, 247*f*
 Activin
 in retinal cell development, 65
 in retinal cell differentiation, 68
 Activity
 and cortical development, 165, 167, 170
 and cortical plasticity, importance of, 128
 deprivation of. *See* Binocular deprivation; Dark rearing; Monocular deprivation
 and eye-specific lamination in LGN, 109–110, 113–115
 instructive versus permissive role of, 113–115, 117, 122, 123–124, 165, 167, 170
 and ocular dominance column development, 110–115, 147
 and orientation selectivity, 117, 119–121, 121*f*, 147–148
 mechanisms in, 121–124
 spontaneous, of developing visual system, 88–89, 89*f*
 and LGN lamination, 109–110
 and ocular dominance development, 147
 and orientation selectivity, 117, 123–124
 Acuity. *See also* Grating acuity; Hyperacuity; Stereopsis; Vernier acuity; Visual acuity
 in blindsight, 658
 Adaptation, 851–861. *See also* Dark adaptation; Light adaptation; Sensitivity regulation
 to blur, 944–945, 944*f*
 chromatic, 900–902
 to color and luminance variations, 930
 and color vision, 939–942, 940*f*
 contingent, 939
 contrast, 940*f*, 941–942, 942
 and decorrelation, 943, 945
 definition of, 1655
 diagonal model for, 955–957
 evolutionary, of vision, 943
 in face perception, 944–945, 945*f*
 fMRI, 1184
 functions of, 942–943
 and gain control, 942
 to illuminant, 901
 and learning, 943
 to natural color distributions, 929, 943, 944*f*
 and natural visual environment, 943–945
 and normalization, 942–943
 and object recognition, 1650
 orientation plasticity induced by, 1657–1658, 1658*f*
 pattern. *See* Pattern adaptation
 perceptual, 936
 and phenomenology of perception, 945–946
 plasticity induced by, 1655, 1656*f*
 rapid, 1660–1661, 1661*f*
 as psychologist's electrode, 936
 in regulation of salience, 945
 in scotopic vision, 843
 short-term, to varying environments, 943–945, 944*f*
 spatial, rod-cone interactions and, 871
 spatial frequency, 1062
 von Kries, 940, 955–957
 Adaptation pool, 843
 Adaptive optics, and chromatic aberrations, 805, 807–808, 808*f*
 Adaptive staircases, 811–812
 Adenosine triphosphate (ATP)
 in photoreceptor metabolism, 216, 244
 in signal processing, 316
 Adenosine triphosphate (ATP) receptor(s), 316
 Adenylate cyclase
 activation of, 135, 137
 inhibition of, 135
 PACAP coupling to, 336
 peptide action on, 348
 somatostatin coupling to, 340
 stimulation by CRH, 348
 stimulation by VIP, 336, 345–346
 α -Adrenergic receptor antagonist(s), and ocular dominance plasticity, 134
 Adrian, E. D., 16, 23
 Barlow's recollections of, 26–28
 laboratory of, 27–28
 as research supervisor, 27
 Adult plateau of vigor, 210–211
 Affective significance, prefrontal cortex (PFC) and, 1557
 Affordance, 1114
 Aftereffects, 936–938, 943, 1690. *See also* Illusion
 contingent, 939
 face, 945
 interocular transfer of, discordant visual input and, 198
 motion, 1319–1320, 1692
 hMT/V5+ visual area activity during, 1237–1239
 negative, 1628
 of pattern adaptation, 939
 rod, 374–375, 376*f*
 surfaces and, 1131–1132
 tilt, 936–939, 937*f*, 938*f*
 Afterimages. *See also* Aftereffects
 of filled-in surfaces, 1130*f*, 1132–1135, 1133*f*, 1134*f*, 1135*f*
 rod saturation and, 841
 Agatoxin, calcium currents sensitive to, 433
 Age
 and long-term depression, 127–128
 and long-term potentiation, 127–128
 and NMDA receptor levels, 129
 and pupil size, 642, 846
 and scotopic vision, 846–847
 Age-related maculopathy (ARM), versus natural processes of aging, 846–847
 Aging, 205–211
 cellular dichotomy in (nervous versus non-nervous tissue), 209
 constancy of color vision in, 807
 dark adaptation in, 846
 decline of neural components in, 209, 210*t*
 and disease, mathematical analysis of, 210–211
 versus disease processes, 846–847
 environment and, 205–206
 epidemiology of, 205
 lens changes in, 206–207, 207*f*, 846

- errors and variations in, 208–209
- slopes of log magnitude versus log age for, 208, 208*t*
- and light scatter, 799
- linear decline of, 205
- mathematical analysis of, 210–211
- presbyopia in, 205–208
- pupil size in, 642, 846
- scotopic vision in, 846–847
- Agnosia, visual object, 554
- Airy disk, 796*f*, 798, 799
- AIT visual area, macaque
 - dorsal (AITd), 510*f*–511*f*, 512
 - ventral (AITv), 510*f*–511*f*, 512
- Akinetopsia, 554
- Albedo, 1092
- Albinism
 - and ganglion cells, 71, 100*f*, 102–103
 - optic chiasm defects in, 100*f*, 102–103
 - visual defects in, 102
- Algae, green, eyespots of, 967
- Al-Haithem, Ibn, 3
- Aliasing, 803
 - chromatic, 805–807
 - by cones, 803–805, 805–807
- Alignment. *See* Hyperacuity
- Alignment/misalignment response, 182, 182*f*
- Allelotropia, 1300
- Allocentric representations, 1183
- All-or-none nerve impulses, 15–16
- Alpha-amino-3-hydroxy-5-methylisoxazole-4-propionic acid receptor. *See* AMPA receptors
- Alzheimer's disease, pulvinar in, 602
- Amacrine cells, 5, 6*f*–7*f*, 235*f*, 395–405, 863, 864*f*, 997–998, 998*f*
- A13, 398
- A17, 396–398, 397*f*
- aberrant, 400
- acetylcholine expression in, 294–295, 295*f*, 312–313, 361, 403–404, 457–458
- acetylcholine receptors in, 312
- AI, 395, 396–398, 397*f*, 405
 - dendritic-field size of, 398
 - receptive field of, 398
- AII, 320–321, 395–396, 402, 405, 863, 864*f*
 - under dark-adapted conditions, 396
- dendritic-field size of, 396
- inhibition of, 364
- under light-adapted conditions, 396
- morphology of, 395
- number and density of, 396
- ON and OFF signals transferred by, 269–270, 398, 864
- output to cone bipolars, 864–865
- principal roles of, 269
- receptive fields of, 396
- changes under different lighting conditions, 396
- dopamine and, 396
- rod and cone signals in, 864–865
- stratification of, 269–270, 270*f*
- angiotensin II expression in, 347
- association, 395, 400–401, 401*f*
- axon-like processes of, 400–401, 401*f*
- Cajal's studies of, 395, 399, 400
- CCK expression in, 347
- classification of, 399–400
- clusters of, 68
- cone, 395–396, 398–399
- CRH expression in, 347–348
- DAPI-3, 402
- dendrites of, 396, 397*f*, 399–400, 400*f*
 - arborization of, 83
 - morphology of, 360
- dendritic-field size of, 396, 398, 399
- depolarizing spikes of, 400–401
- developing
 - spontaneous activity of, 88
 - tangential migration by, 469
- development of, 36–37, 37*f*, 395
- timing of, 77, 78*f*
- differentiation of, 38, 67–68, 78
 - in inner plexiform layer, 81–82
- diffuse, 399
- in direction selectivity, 361, 404–405, 456–460, 457*f*, 458*f*
- discovery of, 395
- displaced, 395
- dopaminergic, 67–68, 313, 383, 396, 400–401, 401*f*, 402, 405, 440
 - GABA interaction with, 365
- enigma of, 395
- excitation of, central, 360
- fire and reload model of, 294
- fireworks, 83, 84*f*
- function of, 395, 405
- GABA receptors in, 309, 358, 398
- GABA transporters in, 308–309
- GABAergic, 269, 291–295, 307, 309–310, 312–313, 359, 361, 395, 396–398, 402, 403*f*, 403–404, 405
 - and ganglion cell stratification, 85–86
- gap junctions between, 396–398
- glutamate receptors in, 291, 306–307
- glutamate transporters in, 306
- glycine receptors in, 311, 396
- glycinergic, 269, 291, 293–294, 304, 310–311, 359, 361, 364, 395–396, 402, 403*f*, 405
- Golgi-stained, 395, 399, 400
- indoleamine accumulation in, 398
- inhibition of, 355, 359, 364
 - peripheral, 360–361
- inhibitory roles of, 291, 355, 359, 364, 364*f*, 364–365
- lateral, 405
- vertical, 405
- lamination patterns of, 83–84, 269–270
- and low-light vision, 70
- medium-field, 399
- minimal spacing of, 469*f*, 470
- monoaminergic, 402
- morphological diversity of, 399–402
- mosaics of, 469, 469*f*, 470, 474
- neurochemical diversity of, 402–405
- neurochemical signature of, 402
- neurokinin receptors in, 343–344
- neuropeptide Y expression in, 337–338, 338*f*
- neurotransmitter expression and receptors in, 67–68, 279, 291, 402–405
- neurotransmitter release from, 294–295, 295*f*, 296*f*, 297*f*, 298
- nonlinearity of, 486–487
- numbers produced, regulation of, 38
- OFF, 400*f*, 403–404
 - stratification of, 269–270, 270*f*
- in ON and OFF pathways, 269–270, 398, 864
- ON, 400*f*, 403–405
 - stratification of, 269–270, 270*f*
- ON-OFF, 269
- opioid expression in, 348
- peptide expression in, 334–349
- peptide receptors in, 337
- photofilling of, 399–400, 400*f*
- polyaxonal, 335, 400–401, 401*f*, 402
- in primates, 399, 482–483
- process outgrowth from, 81–82, 83, 84, 84*f*
- progenitors biased to produce, 67
- prototypical, 395–399
- reciprocal cone, 398–399
- reciprocal rod, 395, 396–398, 397*f*, 400*f*
- rod, 395, 396–398, 397*f*, 400*f*
- serotonergic, 314, 316
- in signal transmission from
 - photoreceptors, 234, 235*f*, 236*f*
 - in starlight circuit, 248, 248*f*
- small-field, 395–396, 399
- somatostatin expression in, 339*f*, 339–340
- somatostatin receptors in, 340*f*, 340–341
- starburst, 293, 294, 400*f*, 403–405
 - dendrites of, directional and functional polarization of, 456–457, 457*f*
 - in direction selectivity, 361, 404–405, 456–460, 457*f*, 458*f*
 - excitation and inhibition of, 361, 403–405
 - ON and OFF, 403–405
 - signaling between, 293, 294, 312–313
 - stratification of, 269
 - synaptic asymmetries of, 456–457, 457*f*
 - stratification of, 86, 399

- Amacrine cells (cont.)
 structure-function relationship in, 405
 subtypes of, lineage bias of, 67–68
 synapses of, 290–295
 basic plan of, 280, 280*f*
 bipolar cell to, 291–292, 304, 306–307, 311, 316
 to bipolar cells, 280, 280*f*, 309–310, 311, 316, 361–362, 395–399
 cholinergic, 294–295, 295*f*, 312–313
 dopaminergic, 314
 formation of, 87–88
 GABAergic, 291–295, 292*f*, 295*f*, 309–310, 312–313, 402, 440
 to ganglion cells, 87, 280, 280*f*, 293, 309–310, 316, 359, 404–405, 412, 417, 440
 glutamatergic, 291, 293, 304, 306–307, 320–330
 glycinergic, 291, 304, 311, 364
 inhibitory, 359, 360*f*, 361–362, 364
 to other amacrine cells, 87, 293–295, 309–310, 312–313, 314, 402
 pharmacology of, 293
 serotonergic, 316
 tachykinin peptide expression in, 342*f*, 342–343
 terminology for, 395
 tracer-coupling studies of, 396, 401–402
 transcription factors expressed in, 68
 types of, 482
 VIP expression in, 344–345, 345*f*, 348
 wide-field, 395, 396–398, 399–400
 CCK expression in, 347
 characteristics of, 335
 coexpression of GABA and peptide in, 336
 functions of, 335
 neuropeptide Y expression in, 338
 peptide expression in, 334, 335–336, 338, 339, 344–345, 347, 348–349
 Ambient illumination, and pupil response, 641
 Ambient term, and shape from shading, 1093
 Ambient vision, 495
 Amblyopia
 anisometropic, 189. *See also* Anisometropia
 contrast differences in, 773
 definition of, 167
 deprivation, 189
 behavioral versus physiological changes in, 168–170, 169*f*
 and contour integration ability, 170–171
 cortical effects of, 46, 126
 and extrastriate development, 170–171
 human studies of, 197–198
 neuronal correlates of, 167–171
 prevention of, 51*f*–52*f*
 and spatial vision, 167–170, 168*f*, 169*f*
 meridional, 199–200, 200*f*
 neural deficits with, 804
 and neuronal synchrony, 1673
 patch therapy for, 196
 strabismic, 189. *See also* Strabismus
 in cats, 1673
 cis-Aminocrotonic acid (CACA), GABA receptor response to, 293, 356*t*, 357, 357*t*, 358, 363
 2-Amino-4-phosphonobutyric acid. *See* APB
 4-Aminopyridine, potassium currents blocked by, 433–434, 436
 Amodal completion. *See* Visual completion, amodal
 AMPA receptors, 306, 324
 in bipolar cells, 260
 in OFF pathway, 265*f*, 265–266, 268, 269*f*
 and cortical plasticity, 137, 138
 and direction selectivity, 361
 in ganglion cells, 288–289
 in horizontal cells, 378
 in A layers of cat LGN, 571
 in retina, 86
 in rod bipolar cells, 285
 in signal transmission from photoreceptors, 246, 250
 and spinule retraction, 297
 in synaptic transmission, 307
 amacrine cell-ganglion cell, 293
 bipolar cell-amacrine cell, 291
 bipolar cell-ganglion cell, 288–289
 photoreceptor-bipolar cell, 285
 photoreceptor-horizontal cell, 289, 307
 Amphibian(s)
 amacrine cells of, inhibition and excitation in, 360
 GABA receptors in, 293, 357
 optic chiasm in
 development of, 98
 organization of, 94
 retinal cell production in, regulation of, 38
 retinal synapses of, 289–290
 rod system of, versus primate, 843
 Amplifier(s), and gain control, 760–761
 Amygdala, 544
 activation by faces, 1167
 damage to, social/emotional problems caused by, 1167
 response to emotional content, 659–660
 and social/emotional responses to faces, 1167
 Anandamide, in signal processing, 316
 Anatomical correspondence, 779
 Anchoring problem, 957, 1629
 Anchoring theory, of lightness perception, 885
 Anesthesia, pupil constriction during, 642, 653
 Angiotensin converting enzyme (ACE), retinal expression of, 347
 Angiotensin converting enzyme (ACE) inhibitors, retinal effects of, 347
 Angiotensin II, retinal expression of, 347
 Angiotensinogen, retinal expression of, 347
 Angular gyrus, 11
 lesions of, behavioral effect of, 11, 11*f*
 Angular speed, and centering response in insects, 1196
 Animal models, of human visual system, 494
 Anisometropia, 189
 contrast differences in, 773
 in monkeys, 196–197
 neuronal correlates of, 167
 and ocular dominance columns, 126
 and spatial vision, 167, 169*f*
 Anomalous pigment, 981, 983
 Anomaly, color. *See* Color anomaly
 Anterior ectosylvian (AEV) cortex, inputs to pulvinar region, 595
 Anterior intraparietal area (AIP), sensorimotor transformation in, 1327–1328, 1328*f*
 Anticipation, and eye movement, in ball games, 1362–1363, 1363*f*
 Antidromic activation, 1468, 1469*f*
 Anti-neuron, 21
 Anti-plasticity genes (capgs), 134
 Antipreferred or null direction, 1204
 Antisaccades, 1382, 1433, 1439–1440
 Apamin, and spike frequency in ganglion cells, 437
 APB (2-amino-4-phosphonobutyric acid) and dendritic stratification in ganglion cells, 85
 and orientation selectivity, 122
 and ON pathway, 264–265, 265*f*, 269, 269*f*, 272–273
 and synaptic transmission, photoreceptor-bipolar cell, 283–284
 Ape(s). *See also* Primate(s)
 color vision in, 968
 evolution of, 1564
 lateral geniculate nucleus in, 6
 visual system of, 1567
 Aperture motion, 1584–1585
 Aperture problem, 1584, 1616–1617, 1617*f*
 Aphakic observers, spectral sensitivity of, 838
 APMPA, GABA receptor response to, 356*t*, 358
 Apoptosis, and mosaic formation, 470, 472
 Apparent motion, 1573, 1578–1579
 neuronal substrate for, 1579

- Apraxia
 constructional, 554
 gaze, 554
- Arborizations. *See also specific cell*
 axonal
 and corticocortical connections, 522, 523*f*, 524
 in corticocortical pathways, 523, 523*f*
 of inhibitory neurons in macaque V1, 689, 690*f*
 and ocular dominance development, 147
 of spiny stellate cells in macaque V1, 683
 cell-type specific, in retina cells, 82*f*, 82–83
- Arcuate sulcus, 1428, 1429*f*, 1430*f*, 1433
- Area(s)
 of complete summation (Ricco), 819
 smallest, of complete summation, 819
 and thresholds, 818–820, 819*f*
 visual. *See* Visual area(s); *specific area*
- Area centralis, 1564
 cell number and density in, 80
- Area contrast, 881
 border-induced, 885, 886*f*
 definition of, 885
 explanation of, 885
- Area MT. *See* Middle temporal (MT) visual area
- Area prostriata, 1565
- Argyle illusion, 887, 887*f*
- Arrestin
 cone, 222–223
 rhodopsin binding and inactivation by, 222–223
 effects of genetic mutations on, 222, 223–225, 224*f*, 225*f*
- Artificial scotoma, and receptive field size, 741–742
- aschaete-scute*, and neurogenesis in *Drosophila*, 38
- Ash1*, in retinal cell differentiation, 68
- Ash3*, in retinal cell differentiation, 68
- Aspartate, and horizontal cell function, 377*f*, 377–378, 378*f*
- Asperity scattering, 1096–1097, 1096*f*, 1097*f*
- Assembly coding, 1666–1667, 1667*f*, 1678–1679
- Assimilation, in perception of brightness, 888, 888*f*
- Association amacrine cells, 395, 400–401, 401*f*
- Association field, 1064, 1070, 1071*f*, 1072, 1630
 definition of, 722, 722*f*
 natural, 722
 perceptual, 722
- Association spongioblasts, 395
- Associative learning, 547
- Astigmatism, 796, 800–801
 and contour orientation, 199–200, 200*f*
- Astrocyte(s), retinal, 41, 66
- Asymmetric matching, 956–957
- Asymmetry between near and far, 1632–1633, 1635, 1636*f*
- Ath3*, in retinal cell differentiation, 68
- Ath5*, in retinal cell differentiation, 68
- Atlas(es), of visual areas
 computerized, surface-based, 507, 508*f*
 advantages of, 507, 508*f*
 probabilistic, 513
 software for, 513
 human, 513–515, 514*f*, 516*f*
 human and macaque comparison in, 515–518, 517*f*
 macaque, 507–513, 508*f*, 510*f*–511*f*
 technical impediments to, 508–509
- Atmospheric perspective, 1091
- atonal*, and neurogenesis in *Drosophila*, 38
- Atrial natriuretic peptide (ANP), retinal expression of, 347
- Attention
 behavioral effects of, 1514
 and binocular rivalry, 1316–1317
 in blind field, in blindsight, 660
 bottom-up (saliency-driven, task-independent), 1686
 in change detection, 1526
 to color, 1515–1516
 contextual modulation and, 728
 and control, comparison of, 1547
 cortical feedback to LGN and, 612
 definition of, 1514, 1538
 and dorsal stream processing, 547
 effects of, when no stimulus is present, 1540
 featural, 1538
 and MT/MST activation, 1276
 feedback connections in, 536
 as increased salience, 1541
 and intention, differentiation of, 1327
 K (konio cellular) pathway and, 503
 laminar cortical circuits and, 1630, 1630*f*
 modulation of neuronal responses by, 1538–1540
 within and between cortical areas, 1538–1539
 cortical hierarchy and, 1539, 1539*f*
 task difficulty and, 1539–1540
 to motion, 1239–1241
 direction of, 1240, 1240*f*
 global, 1239–1240
 speed of, 1241
 and MT visual area, 1208–1209, 1214
 neuronal correlates of, 1478, 1479*f*, 1538
 neuronal effects of
 and behavioral effects, relationship of, 1542–1543
 research on, advances in (future directions for), 1543
 and neuronal synchrony, 1541, 1675–1676, 1676*f*
 and object recognition, 1648–1650, 1649*f*
 and receptive fields, 1541
 role of, in visual cortex, 1538–1543
 selective, 1342–1343, 1538, 1585, 1596.
 See also Attention, visual
 sensory, 1538
 to shape, 1515–1516
 spatial, 1467, 1478, 1479*f*, 1514, 1538
 behavioral effects of, 1539
 deficit in, 1519
 distributed network for, 1519–1521, 1520*f*
 modulation of neuronal responses by, task difficulty and, 1539–1540
 and MT/MST activation, 1276
 neuronal effects of, 1539
 state of, and cortical plasticity, 128, 134
 tactile, and MT/MST activation, 1276
 top-down, 1517–1518, 1518*f*, 1596, 1686
 and ventral stream processing, 546–547
 visual, 1108
 biased competition model of, 1558–1559
 control of, 1596–1597
 mechanisms of, 1518–1521
 cortical processing in, 1514–1518
 endogenous stimuli for, 1514
 exogenous stimuli for, 1514, 1515*f*
 eye movements and, 1596–1599
 and facilitation of visual processing at attended locations, 1515
 of attended stimulus attributes or objects, 1515–1516
 in filtering out unwanted material, 1516–1517, 1517*f*
 human, neural basis of, 1514–1522
 impairments, ventral stream lesions and, 549
 model of, 1521–1522, 1522*f*
 and neural activity, 1517–1518
 neuronal substrate for, 565
 pulvinar in, 598–599, 601–602
 and sensory suppression, 1516–1517, 1517*f*
 and visual consciousness, 1686
 visual search and, 1369–1371, 1370*f*
- Attitude effect, 1092
- Auditory processing, in frontal eye field, 1439, 1439*f*
- Auditory target processing, 1327, 1329–1330, 1329*f*, 1397, 1397*f*
- Autocorrelation, of neuronal mosaics, 473
- Automatic processes, 1546
- Autonomic nervous system, neurotrophin action in, 46–48, 48*b*

- Axon(s)
 arborization of, and ocular dominance development, 147
 bifurcations, and corticocortical connections, 525–527
 of bipolar cells, 84
 stratification in inner plexiform layer, 267*f*, 268–269, 269*f*
 structure and information content of, 253
 of Cajal-Retzius neurons, 150
 of cones
 microtubules of, 245, 246*f*
 thickness of, 242*f*, 245, 246*f*
 in cortical connectivity, 149
 feedforward, 151
 corticofugal
 arborization of, 609, 610*f*
 feedback from, 609–611
 expansion of, and cortical plasticity, 137–138, 138*f*
 of ganglion cells
 arborization in LGN, 270–271, 271*f*
 chemosuppression of, 98
 contralateral, 94, 95*f*
 decussation at optic chiasm, 94–103
 cell and molecular mechanisms
 underlying, 97–101
 defects in, 97–98, 102–103
 maneuvers in, 98
 partial, 94
 regulation of, 95–103, 97*f*
 timing of, 95–96, 97*f*
 ectopic, 98
 growth cones of, 95, 100–101
 advancing and streamlined, 96, 97*f*
 behaviors at midline, 95–96
 pausing and complex, 96, 97*f*
 temporal and morphologic patterns of, 95–96, 97*f*
 guidance or regulation of, 95–103, 97*f*, 100*f*
 cellular specializations at midline and, 97–98
 cellular specializations at ventral midline and, 96, 97*f*
 Eph receptors/ephrin ligands and, 97*f*, 99
 GAP-43 and, 100*f*, 100–101
 genetic, 100*f*, 101–102
 molecular factors in, 98–101
 proteoglycans and, 97*f*, 100
 Roundabouts (Robos) and, 97*f*, 99–100, 100*f*
 Slits and, 97*f*, 99–100, 100*f*, 101
 interactions between fibers from each eye, 98
 ipsilateral, 94, 95*f*, 99, 101
 lack of pigment (albinism) and, 100*f*, 102–103
 in optic chiasm agenesis, 103
 organization of
 age-related, 94
 binocular plan of, 94, 95*f*
 changes in optic nerve, chiasm, and tract, 94–95
 quadrantic, 94
 retinorectal, 95
 retinotopic, 94
 outgrowth of, 81, 81*f*
 projections of, 413–415
 static and dynamic chronicles of
 behavior at chiasm, 95–96, 97*f*
 of horizontal cells, 369–370
 outgrowth of, in retinal neurons, 81, 81*f*
 retraction of
 and cortical connectivity, 148
 and cortical plasticity, 137–138, 138*f*
 of rods
 microtubules of, 245, 246*f*
 thickness of, 242*f*, 245, 246*f*
 Axon terminal, of photoreceptors, 245, 246*f*
 active zones of, 245, 247*f*
- B**
 b wave, of electroretinogram, 261, 261*f*
 in melanoma-associated retinopathy, 272, 273*f*
 Baboon(s), mapping of visual fields on cortex of, 10
 Back pocket model, of texture segregation, 1109, 1109*f*, 1110*f*, 1111
 Background, discrimination of objects
 from, by insects, motion cues for, 1200*f*, 1200–1201
 Background illumination, horizontal cell response to, 375, 386, 388–389
 Background inefficiency, high, and thresholds, 817–818
 Background invariance, 1171
 Background perturbation techniques, of studying pupil light reflex, 643, 644*f*
 Background sensitization, low, and thresholds, 816*f*, 818
 Background subtraction, 250
 Backscatter, 1096
 Backscatter lobe, 1096
 Backward masking, 868
 Baclofen, GABA receptor response to, 293, 356*t*, 357, 357*t*, 358, 359, 360, 360*f*, 361, 363
 Balance point, in color vision, 1219
 Balint syndrome, 1684
 Ball games, eye movements in, 1362–1363, 1363*f*
 Bandpass filtering, by cone synapses, 246, 249–251, 251*f*
- Bandwidth
 in area MT, 1204–1205
 spatial, of receptive fields, 165*f*
 Barber pole effect, 1131, 1131*f*, 1584
 Barlow, Horace, 10, 22
 Basal forebrain, signals about nervous system state from, 134
 Basal ganglia (BG)
 connections with ventral and dorsal streams, 544
 in dialogue between cerebral cortex and superior colliculus, 1467, 1468*f*, 1471–1472
 interconnections of, with prefrontal cortex (PFC), 1548
 and oculomotor system, 1371, 1372*f*
 Baseline shift, 1518
 Basic helix-loop-helix (bHLH)
 transcription factors
 expression of, in optic cup and optic vesicle, 34, 35*f*
 in retinal cell differentiation, 38, 39, 68
 Basis function tiling properties, 1608, 1610*f*
 Basket cells
 adapting (regular) spiking, 688
 burst spiking, 688
 fast-spiking, 688–689
 in primary visual cortex (V1) of macaque, 688–689
 in rat visual cortex, 689
 Bat(s)
 evolutionary history of, 1564
 megachiropteran
 evolutionary history of, 1564
 visual system of, 1566–1567
 BAT-1, and opsin expression, 40, 40*f*
 Bayesian ideal observer, 825–826
 constrained, 826–827
 Bayesian natural selection, 835–836
 Bayesian statistical decision theory, 825–826
 Bayliss et al. scheme, for partitioning macaque visual cortex, 510*f*–511*f*, 512
 BDNF. *See* Brain-derived neurotrophic factor
 Bee(s). *See also* Honeybee(s)
 centering response in, 1195*f*, 1195–1196
 motion cues in, 1193
 for controlling flight speed, 1196–1197, 1197*f*
 for discriminating objects at different distances, 1199–1200
 for discriminating objects from backgrounds, 1200*f*, 1200–1201
 for estimating distance flown, 1197–1198, 1198*f*
 for executing smooth landings, 1198–1199, 1199*f*

- for hovering, 1194–1195
- for negotiating narrow gaps, 1195*f*, 1195–1196
- waggle dance of, 119
- Beer's law, 838
- Behavior(s)
 - visual
 - conscious, 1683–1684
 - nonconscious, 1683–1684
- Belgian sheepdogs, optic chiasm agenesis in, 103
- Belongingness, 1581
- Benham illusion, 1505
- Benzodiazepine, GABA receptor response to, 358
- Bezold-Brücke effect, 893
- Bhl* transcription factor, in eye field development, 66
- Bias
 - in horizontal disparity, 1310
 - in perceived depth, 1310
 - in perceived visual direction, 1310
 - rod hue, 873–874, 875*f*
- Bicuculline
 - GABA receptor response to, 293, 356*t*, 358
 - and long-term potentiation, 127
 - and ocular dominance plasticity, 126, 131
- Bidirectional reflectance distribution
 - function (BRDF), 1091–1092, 1092*f*, 1094, 1097, 1098
 - specular lobe of, 1095
- Binding problem, 726
- Binocular advantage ratio, 773, 774*f*
- Binocular anticorrelation or decorrelation. *See* Binocular disparity
- Binocular competition, 49
 - during monocular deprivation, 49, 194
 - in normal development, 49
- Binocular correspondence, 779, 1301
- Binocular deprivation
 - animal studies of, 190–193
 - in cats, 191*f*, 191–192, 192*f*
 - and contrast sensitivity
 - in cats, 191, 193*f*
 - in humans, 193
 - in monkeys, 193
 - and cortical connectivity, 153
 - dark rearing versus eyelid suture, 190–191
 - effects of, 189, 190–193
 - human studies of, 190
 - congenital bilateral cataract, 190, 193
 - recovery from blindness, 190
 - in monkeys, 192–193
 - neuronal correlates of, 167–170
 - and ocular dominance columns, 108, 113, 147
 - and orientation selectivity, 117, 119–121, 121*f*, 123
 - recovery after, effect of experiment type on, 190–191
- Binocular disparity, 1145, 1145*f*, 1285, 1471
 - absolute, 550, 780, 1303, 1303*f*, 1304
 - response of V1 neurons to, 783
 - contrast differences, 773–774, 775*f*, 784–785
 - artificial changes in ocular dominance with, 775–776
 - definitions and diagrams of, 780*f*
 - and depth measurements, 1285
 - effects of, 198–199, 199*f*
 - energy model of, 785
 - far, 780
 - local, response of V1 neurons to, 784, 784*f*
 - in motion, effect of area MT, 1211
 - near, 780
 - neurons selective for, 550
 - complex cells, 715, 716
 - in extrastriate cortex, 781, 785–787
 - in MST visual area, 785, 786–787, 790, 1266–1267
 - in primary visual cortex, 550, 765–766, 766*f*, 767*f*, 779–785, 781*f*, 783*f*, 790
 - inconsistencies with stereoscopic vision properties, 782–785
 - range of disparities processed by, 781*f*, 781–782, 783*f*
 - in V5/MT visual areas, 788*f*, 788–790, 789*f*
 - perceptual signals in, indices of, 787–790
 - receptive field responses to, 765–768, 779, 782*f*, 783, 786–787
 - in nonlinear maps, 711, 712*f*, 713, 714, 715, 717
 - relative, 550, 780–781, 1303–1304
 - beginnings of, 786–787, 787*f*
 - and center-surround responses of receptive fields, 786–787
 - processing of, imaging of, 787
 - thresholds, for stereopsis, 1304, 1305*f*
 - and stereoscopic vision, 198–199, 199*f*, 765–766, 779–790, 784–785
- Binocular fusion, 1142*f*, 1316, 1320
- Binocular matching, 1301–1304
- Binocular rivalry, 1313–1321, 1688–1689, 1691
 - attention and, 1316–1317
 - bibliography on, 1313
 - characteristics of, 1313–1319
 - definition of, 1313
 - demonstrations of, 1313, 1314*f*
 - dissimilar images not producing, 1315, 1315*f*
 - dominance in, 1313, 1314*f*, 1317, 1318, 1318*f*
 - in everyday viewing, 1320–1321
 - interocular grouping during, 1317
 - literature on, reviews of, 1313
 - meaningful (familiar) versus less meaningful (unfamiliar) targets and, 1316
 - multistability in, 1321
 - neural operations in, 1319–1320
 - neuronal synchronization and, 1673–1674, 1674*f*
 - practical applications of, 1319
 - predominance in, 1316
 - spatial dynamics of, 1316–1319
 - suppression in, 1313, 1314*f*, 1318, 1320
 - versus Troxler's effect, 1313
 - temporal dynamics of, 1316–1319
 - triggers for, 1313–1316
 - and visual awareness, 1319–1320
- Binocular summation. *See* Summation, binocular
- Binocular vision
 - compensatory mechanism for unequal signal strength in, 774–775
 - complex cells in, 770*f*, 770–772, 771*f*, 772*f*
 - contrast differences between left and right eyes in, 773–774, 775*f*, 784–785
 - contrast gain control in, 773–775
 - contrast processing in, 772–773, 773*f*, 774*f*
 - contrast thresholds in, 772–773, 774*f*
 - cortical interactions for, 765–776, 779, 781–785
 - combination of left and right eye signals, 768, 770*f*
 - phase-shifted gratings for measurement of, 767–772, 768*f*–769*f*, 770*f*, 771*f*, 772*f*
 - depth of modulation in, 774, 775*f*
 - development of, 184–185, 776, 776*f*
 - correlogram of, 184–185
 - cyclopean VEP assessment of, 184–185
 - dichoptic tests for, need for, 767, 776, 777*f*
 - disparity-sensitive neurons in, 765–766, 766*f*, 767*f*
 - LGN cells in, 768, 770*f*
 - linear convergence for, 768, 770*f*
 - monocular tests of, inaccurate or misleading results from, 765, 767, 776, 777*f*
 - multiplicative convergence for, 768, 770*f*
 - ocular dominance for assessment of, 767, 775–776
 - physiological studies of, background of, 765–766
 - plasticity of, 776
 - in primates, 1567
 - retinal decussation and, 94, 95*f*
 - and scotopic vision, 840

- Binocular vision (cont.)
 simple cells in, 768–770, 770*f*, 774, 775*f*
 threshold mechanisms in, 768, 774–775
- Biological minipumps, for intravitreal
 administration of neurotrophins,
 50–51
- Biological motion, 1242, 1577
- Bipolar cells, 5, 6*f*–7*f*, 235*f*, 482, 909,
 1010, 1630
 axons of, 84
 stratification in inner plexiform layer,
 267*f*, 268–269, 269*f*
 structure and information content of,
 253
- blue-cone, 320
- CCK expression in, 347
- cell-specific markers of, 82
- chloride transporters in, 290, 291*f*
- color opponent, horizontal cells and,
 387–388, 388*f*
- cone
 AII amacrine cell output to, 864–865
 distribution of, 268
 cone OFF, 320–321, 321*f*
 cone ON, 320–321, 321*f*
 dendrites of, arborization of, 83
 developing, spontaneous activity of, 88
 development of, 36–37, 37*f*
 timing of, 77, 78*f*
 differentiation of, 39, 66, 67, 68, 78–79
 diffuse, 993, 1007
 DB2, 993
 DB3, 993
 types of, 1007
- dynamic range of, 423
- in figure-ground separation, 1633
- GABA receptors in, 309, 355, 356–357,
 358
 dopamine interaction with, 365
 GABAergic, 308, 355, 363
 ganglion cell connectivity of, 413, 418
 and ganglion cell stratification, 85–86
 glutamate expression in, 362
 glutamate receptors in, 260, 288,
 306–307
 excitatory versus inhibitory, 260
 in ON and OFF pathways, 264–266,
 265*f*, 266*f*, 268–269, 269*f*
 species diversity in, 266
 glutamate transporters in, 306
 glycine expression in, 310
 glycine receptors in, 311
 high-frequency (transient), 253
 inhibition of, 355, 360, 361–363
 GABA feedback and, 356, 359, 360,
 360*f*, 361–363, 362*f*
 inhibitory, 363
 innervation of X and Y cells by, 263
 kinetic properties of, 260
 lamination patterns of, 84–85, 268–269
- linkage to ganglion cells, 320
- low-frequency (sustained), 253
- Mb1
 neurotransmitter expression and
 synaptic transmission in, 286–288,
 287*f*, 292*f*, 292–293
 spinule formation in, 297–298
- midget, 997–998, 998*f*, 1007
- migration of, 80
- neurokinin receptors in, 344
- neuropeptide Y expression in, 338
- neurotransmitter expression and receptors
 in, 86–87, 279
- neurotransmitter release in, 286–288,
 287*f*
- number of, 69
- OFF (hyperpolarizing), 236*f*, 864
 chloride transporters of, 290, 291*f*
 classes of, 285
 direct pathway from rods to, 845
 discovery of, 263–264
 electroretinogram of response, 261*f*
 glutamate receptors in, 265–266, 266*f*
 sharp electrode recording of activity,
 263–264, 264*f*
 spinules of, 297
 stratification of, 84, 85, 267*f*, 268–269,
 269*f*
 synapses of, 279, 283, 284*f*
 postsynaptic mechanisms of, 285
- ON (depolarizing), 236*f*, 864
 chloride conductance in, 265, 266*f*, 290,
 291*f*
 discovery of, 263–264
 electroretinogram of response, 261*f*
 GABA receptor feedback to, 362
 glutamate receptors in, 264–265, 265*f*,
 266*f*
 sharp electrode recording of activity,
 263–264, 264*f*
 spinules of, 297
 stratification of, 84, 85, 267*f*, 268–269,
 269*f*
 synapses of, 283, 284*f*
 postsynaptic mechanisms of, 283–285,
 285*f*
- peptide expression in, 335–336, 338,
 340–341, 344, 347, 348
 effect on ion channels, 337, 341, 341*f*
- polarity of, 82
- progenitors biased to produce, 67
- receptive fields of, 264, 418
 organization of, horizontal cells and,
 386–388, 388*f*
- retinal position of, 41, 80
- rod
 distribution of, 268–269
 transmission of, 284
- rod ON, 320–321, 321*f*
- rod-cone signal interaction in, 864–865
- serotonin receptors in, 315
- in signal transmission from
 photoreceptors, 246
 in moonlight circuit, 248
 pathways for cone signals, 252*f*,
 252–253, 255
 in starlight circuit, 247–248, 248*f*, 249*f*
- somatostatin receptors in, 340*f*, 340–341
- stratification of, 86, 413
- sustained, 288
- synapses of, 283–289
 to amacrine cells, 280, 280*f*, 291–292,
 304, 306–307, 309–310, 311, 316,
 361–362, 395–399
 basic plan of, 280, 280*f*
 to cones, complexity of, 283, 284*f*
 formation of, 87
- GABAergic, 281*f*, 281–282, 283, 284*f*,
 286, 290, 292*f*, 292–293, 309–310,
 386
 to ganglion cells, 268, 279, 280, 280*f*,
 306–307, 412, 413, 418
 postsynaptic mechanisms of, 288–289
 presynaptic mechanisms of, 285–288,
 287*f*
 type-to-type connectivity of, 413
- glutamatergic, 264–266, 281*f*, 281–285,
 284*f*, 285*f*, 286, 288, 304, 306–307,
 320–330
- glycinergic, 311
- horizontal cell to, 290, 304, 309,
 386–388, 389
- inhibitory, 359, 360, 360*f*, 361–362
- invaginating, 283
- to photoreceptors, 264–266, 280, 280*f*,
 307
 image separation at, 260, 266
 postsynaptic mechanisms of, 283–285,
 285*f*
 presynaptic mechanisms of, 280–283,
 281*f*
- rectification of, 255
- to rods, 279, 280
- serotonergic, 316
- sign-inverting, 283
- sign-preserving, 283, 285
- spinule formation and retraction in,
 297–298
- superficial, 283
- synaptic vesicle cycling in, 286–288, 287*f*
- transient, 288
- transmission of light-evoked signals to,
 rod-cone gap junctions and, 322
- types of, 264, 1007
- VIP expression in, 348
- Birds
 color vision in, 964, 965, 968
 horizontal cells of, 370*f*, 370–371
 neuronal mosaics in, 467
- Bishop, George, 10–11, 495

- Bistable figures, 1321
- Bistable percepts, 1688–1689, 1692
- Blackness, 881–882
spectral efficiency of, 897
- Blank-wall problem, 1616–1617, 1617*f*
- Blastomere(s)
amacrine cell subtypes arising from, 67–68
retina competent and biased, in *Xenopus laevis*, 64–65, 65*f*
vegetal, 64–65, 65*f*
- Bleaching. *See* Dark adaptation
- Blending, 1687
- Blind spot, 1584, 1625, 1629
perception across, 1627–1628
- Blindness, 1691. *See also* Change blindness
cortical damage and, 747
face. *See* Prosopagnosia
inattentional, 728
motion-induced, 1321
night, congenital stationary, 272–273
recovery from, studies of, 190
- Blindsight, 643, 648–649, 1260, 1477, 1684
animal homologues of, 663
blind hemifield in
interactions with intact hemifield, 662
reflexes to visual stimuli in, 661–662, 661*f*, 662*f*
cortical lesion causing, 657
completeness of, and extensions to nonstriate cortex, 664–665
definition of, 657
incidence of, 664
neural substrate for, 599–600
neuroimaging in, 1691
and normal vision, qualitative versus quantitative differences between, 665–666
pulvinar in, 594
recovery from, 663
residual visual capacities in
assessment of, nonverbal indirect methods for, 661–662, 661*f*, 662*f*
categories of, 657–660
recovery of, 663
practice and, 663
type 1, 660
type 2, 660
visual assessment in
commentary key paradigm in, 660
eye movement and, 663–664
intraocular diffusion and, 663–664
optical artifacts and, 663–664
response assessment and, 665
response criteria and, 665
stray light and, 663–664
validation issues in, 663–666
verbal versus nonverbal approaches to, 657, 660–662
- Blinking, 1691
- Bloch's law, 820, 821, 1686
- Block copying task, 1363, 1364*f*
- Blood oxygenation level dependent (BOLD) imaging
of motion regions, 1232, 1233*f*
of relative disparity processing, 787
- Blue blindness, short-term. *See* Tritanopia, transient
- Blue cones, 372. *See also* S (short-wavelength sensitive or blue) cones
connections to horizontal cells, 370–371, 373–374, 376*f*
feedback from horizontal cells, 382, 383*f*
mosaics of, 468
visual pathway input from, 497–498
- Blue light, circadian sensitivity to, 627
- Blue-OFF ganglion cells, 419, 682
- Blue-ON ganglion cells, 411–412, 682, 865–866
- Blue/yellow chromatic channel, 1217, 1218*f*
and motion processing, 1217–1218
- Blue/yellow color, K cell response to, 1219–1220
- Blue/yellow color system, 1013
- Blue/yellow horizontal cells, 370, 370*f*, 373–374, 374*f*, 375*f*
- Blur
adaptation to, 944–945, 944*f*
perception of, scale and, 1055
- BMAL1* gene, 625
- Body shadow, 1092–1093, 1093*f*, 1094–1095, 1094*f*, 1095*f*, 1099
- Body-centric frame of reference, 1252
- Bone morphogenetic protein(s)
BMP-4
in eye field separation, 34
and retinal cell development, 65
BMP-5, in eye field separation, 34
BMP-7, and retinal cell development, 65
repression of, and retinal cell development, 65
in retinal cell differentiation, 68
- Border(s)
color, 930
shadow, 930
types of, 1106, 1107*f*
- Border contrast, 881, 885–886, 890
local energy model of, 887
models for, 886–888
multichannel model of, 887
theory of, 886–888
- Border ownership, 1135–1136, 1142–1145, 1142*f*, 1143*f*, 1144*f*, 1581
coding of, 1145, 1146, 1146*f*
low-level mechanisms and, 1146–1148, 1147*f*
neural mechanism for, 1126
- segmentation and, 1124–1126
signals for, time course of, 1146, 1147*f*
- Bottom-up processes, 1579
- Boundary(ies), 722–725, 1624–1638
amodal, 1625*f*, 1636, 1636*f*
and attentional laminar circuits, 1629–1630, 1630*f*
completion of, 1625*f*, 1626
sites of, 1626
depthful, formation of, 1631
formation of, 1626–1627. *See also* Grouping, perceptual
context-dependent, 1582
three-dimensional, 1633–1637
and illusions, 1625–1626, 1625*f*
luminance, 1108
modal representation of, 1636, 1637*f*
processing system for, 1582
and seeing versus recognizing, 1625–1626, 1625*f*
and surface, complementarity, and consistency, 1633, 1635
visual, and complementary cortical streams, 1624
- Boundary Contour System (BCS) model, 1626, 1630, 1634–1635, 1636
and Feature Contour System (FCS), interactions of, 1633, 1634*f*
T-junction sensitivity in, 1633, 1634*f*
- Boundary enrichment, 1637, 1637*f*
- Boundary pruning, 1635–1636, 1636*f*
- Boundary web, 1632
- Brain
Brodman's cytoarchitectonic map of, 1030, 1030*f*
color center in, 1026
evolution of, studying, methods for, 1563–1564
function of, theories of, 146
gene transcription in, and optic chiasm development, 101–102
honeybee, 1501
human, 1429*f*
and ape brain, comparison of, 1570
size of, 1570, 1570*f*
ventral and dorsal processing streams in, 554–555, 555*f*
monkey, 541, 542*f*, 1429*f*
Platonic understanding of, 146
processes of, perceptual and stimulus properties as correlational counterparts of, 1578
scaling issues related to, 1570
size of, 1563
in primates, 1570, 1570*f*
- Brain natriuretic peptide (BNP), retinal expression of, 347
- Brain-derived neurotrophic factor (BDNF), 46
activity and, 133

- Brain-derived neurotrophic factor (BDNF)
(cont.)
anterograde and retrograde actions of, 50*b*
cellular targets of, 55, 60
classical hypothesis of, 48*b*
in cortical development, 53–55, 60
in cortical plasticity, 53–55, 60, 128, 131, 133, 136*t*, 137, 139
and CREB, 132
deficiency of, 48*b*
and dendritic arborization in ganglion cells, 83
excitatory effects of, 54
exogenous administration of, during dark rearing, 50–52, 53*f*
in glaucoma, 42
inhibitory effects of, 55–58, 57*f*, 60, 60*f*
and long-term depression, 133, 136*t*
and long-term potentiation, 133, 136*t*
mechanisms of action, 133
and monocular deprivation, 54–55
overexpression of, 55–58
and acceleration of visual cortex development, 55–58, 57*f*, 58*f*, 136
and cortical connectivity, 154
during dark rearing, 51
and long-term potentiation, 131
and ocular dominance plasticity, 131, 133
and visual acuity, 55–58, 58*f*, 136
presynaptic action of, 133
proliferative action of, 133
receptors for, 46, 48*b*, 133
in retinal cell differentiation, 68
in synaptic plasticity, 59, 60
in synaptic transmission, 54, 55, 56*f*
and timing of critical period, 58
Brainstem. *See also* Neural integrator;
Saccade generator
area MT connections to, 1203, 1204*f*
and oculomotor system, 1371, 1372*f*
and pursuit behavior, 1402, 1408–1409
BrdU labeling, of retinal neurons, 36
Bregman-Kanizsa image, 1632–1633, 1632*f*, 1636, 1636*f*
response to, end gaps in, 1634, 1635*f*
Brewster's colors, 805
Bright-excitatory responses, in receptive field maps, 707
Brightness, 721, 872, 881–890, 893, 933–934
color, 1010
conscious percept of, 1686, 1687*f*
and darkness, 881–883
historical perspective on, 882–883
definition of, 881
depth and, interactions of, 1636
mesopic, rod-cone interactions and, 867
perception of, 883, 883*f*, 1628
mechanisms for, 1628
model of, 887
rod-cone interactions and, 867
Brightness assimilation, 1628–1629, 1629*f*
Brightness constancy, 1617–1618, 1622, 1628, 1629*f*
Brightness contrast, 1628–1629, 1629*f*
Brisk ganglion cells, 253–255, 254*f*
Brn-3 gene
Brn-3b
and optic chiasm development, 100*f*, 101–102
in process outgrowth of retinal cells, 81
Brn-3c, and optic chiasm development, 100*f*, 101–102
in retinal cell differentiation, 38, 78
Brodmann, K., cytoarchitectonic map of brain, 1030, 1030*f*
Buildup neurons, 1372, 1381
Bulla gouldiana snail, circadian cycle in, 633
Bumblebee(s), context-dependent learning in, 1507
Burst neurons, 1372, 1450
convergence, 1419, 1423
divergence, 1419
excitatory, 1408, 1423–1424, 1486, 1492
and pursuit- and saccade-related activity, 1410
inhibitory, 1408, 1492
long-lead, 1381
and pursuit- and saccade-related activity, 1410, 1433
Bushbabies, K (koniocellular) cells of, 489, 498, 499
C
CACNA1F gene, 273
Cajal, Santiago Ramon y, 5, 6*f*–7*f*, 15, 33, 95, 279, 395, 399, 400, 410
Cajal-Retzius neurons, and cortical connectivity, 150–151
Calbindin
as bipolar cell marker, 82
in dendrite-targeting interneurons, 689
as K cell marker, 497, 498, 502–503
Calcarine cortex. *See* Primary visual cortex
Calcineurin, and cortical plasticity, 130
Calcium
circadian role of, 633–634, 635*f*
and cortical plasticity, 128, 129, 130, 136*t*, 137, 137*f*, 139
in dark-adapted rods, purposes of, 227
in darkness
free cytoplasmic, resting concentration of, 226
influx and efflux of, 225–226
disc membrane cascade regulation by, 227, 228–229
biochemistry of, 227
electrophysiology of, 227
dynamic effect of, 228
in excitatory transmission, 326–327, 327*f*
feedback regulation of phototransduction by, 216, 217, 223, 225–228
GABA receptor response to, 359
and ganglion cell behavior, 288–289, 436–437
guanylate cyclase regulation by, 226–227
influx into cones, 282–283, 1006
horizontal cells and, 388–389
kinases and phosphatase stimulated by, 128, 130
and light adaptation, 228–229
light responsiveness of, 633
and long-term depression, 130, 136*t*
and long-term potentiation, 130, 136*t*
MAPK activation by, 634
and neurotransmitter release
by amacrine cells, 294–295, 295*f*, 296*f*, 297*f*
by photoreceptor, 377
potassium currents activated by
in ganglion cells, 425, 432, 433
in thalamocortical relays, 573
regulation of, 135
release of, glutamate receptors and, 25, 129, 633
and spinule formation/retraction, 297
steady-state effect of, 228–229
and synaptic plasticity, 130
uptake of, via NMDA receptors, 130
Calcium channels/currents
acetylcholine and, 432
angiotensin II and, 347
dopamine and, 432, 438–439, 441*f*
GABA and, 432
GABA receptor modulation of, 357*t*, 357–358, 358, 363, 363*f*, 363–364
in ganglion cells, 433, 436–437
conotoxin-sensitive, 432, 433
dihydropyridine-sensitive, 432, 433
high-threshold, 425, 433
low-threshold, 433
toxin-resistant, 432, 433
transient, 432, 433, 435–436
glutamate and, 432
horizontal cell feedback and, 383
in horizontal cells, 378–379
peptide action on, 334, 337, 341, 341*f*, 342, 344, 347, 348
somatostatin and, 341, 341*f*, 342, 348
substance P and, 344
in synaptic transmission
amacrine cell-amacrine cell, 294–295, 295*f*
amacrine cell-ganglion cell, 293
bipolar cell-ganglion cell, 289
horizontal cell-photoreceptor, 290

- photoreceptor-bipolar cell, 282–283, 284
- in thalamocortical relays, 573–574, 574*f*
- Calcium imaging, of retinal peptide action, 337
- Calcium ions, ganglion cell permeability to, 431
- Calcium/calmodulin kinase II
 - and cortical plasticity, 130, 132, 136*t*, 137, 137*f*, 138
 - and spinule retraction, 297
- Calcium-induced calcium release (CICR), 25
 - dendritic propagation of, speed of, 25
- Callosal connections, 522
- Calmodulin
 - and GABA receptor response, 293
 - in phototransduction, 227–228
 - and spinule retraction, 297
- Calretinin, in interneuron-targeting interneurons, 689
- Camera obscura, 3
- Camouflage, 1288–1292, 1297, 1300, 1302, 1504, 1504*f*, 1577
 - color and, 1290
 - environmental conditions and, 1290
- cAMP. *See* Cyclic adenosine monophosphate
- cAMP response element binding (CREB) protein
 - activation of, 59, 59*f*, 132, 634
 - and circadian rhythms, 629, 634, 635*f*
 - and cortical plasticity, 132–133, 136*t*, 137, 137*f*
 - light responses of, 634
 - monocular deprivation and, 132, 134
- Cancellation, in visual pathways, 845
- Candidate plasticity genes (cpgs), 133–134
- Cannabinoid receptor(s), in signal processing, 316
- Capacitance method, for studying neurotransmitter release in bipolar cells, 286–288, 287*f*
- Carbon monoxide, in signal processing, 316
- Cardinal axes, of color space, 1217, 1218*f*
- Cardinal channels, 1217, 1218*f*
- Caret software, for cortical mapping, 513
- Carnivore(s), lateral geniculate nucleus in, eye-specific lamination of, 108–109
- Cast shadows, 1092–1093, 1093*f*, 1094*f*, 1287–1288
- Cat(s)
 - amacrine cells of, 399
 - AI, 396–398, 397*f*
 - AII, 396
 - neurochemistry of, 402
 - ON and OFF stratification of, 269
 - tracer-coupling studies of, 402
 - axon terminals of, active zones of, 245
 - binocular deprivation in, 191–192
 - and contrast sensitivity, 191, 193*f*
 - dark rearing versus eyelid suture, 190–192, 191*f*, 192*f*
 - duration of and subsequent effects, 191*f*, 191–192, 192*f*
 - binocular disparity in, 198
 - binocular interaction in, 765, 776, 777*f*
 - bipolar cells of, ON and OFF
 - stratification of, 268
 - cortical connections in
 - feedback, 152–153
 - from area MT, 609
 - to lateral geniculate nucleus, 609, 611–612, 614
 - feedforward, 151
 - horizontal, 738
 - receptive field effects of, 734, 737
 - horizontal intrinsic, 148–149
 - neuronal synchrony in, 535–536
 - and synaptic organization, 154
 - synaptic transmission in, 527–528
 - visual deprivation and, 153
 - cortical optic flow responses in, 1268–1269
 - cortical plasticity in
 - BDNF and, 133
 - calcium and, 130
 - dark rearing and, 128, 131
 - GABA and, 131
 - nerve growth factor and, 135
 - NMDA receptors and, 129
 - corticocortical pathways in, 522
 - dark rearing in, 190–192, 191*f*, 192*f*
 - direction selectivity in, 532–533
 - selective visual exposure and, 201, 201*f*
 - disparity-sensitive cells in, 766, 766*f*
 - feedback connections in, synaptic transmission in, 528
 - feedforward connections in, functional roles of, 532–533
 - forced-choice preferential looking by, 190
 - functional connectivity in, 673–678
 - ganglion cells of, 495
 - dendrite development in, 82–83
 - dopamine and, 440, 442*f*
 - excitability of, 424–425, 426, 426*f*
 - inhibition of, 359
 - membrane time constant of, 430–431
 - mosaics of, 470
 - number of, 411
 - ON and OFF
 - stratification of, 266–267
 - sustained and transient, 262*f*, 262–263
 - projections of, 415, 496
 - receptive fields of, 415*f*, 419
 - spatial selectivity of, 418
 - within-type variation among, 464, 465
 - horizontal cells of, 370, 370*f*, 371*f*
 - and bipolar cell receptive field architecture, 386
 - ion channels in, 378–379
 - luminosity, 374
 - mixing of rod and cone signals in, 375, 376*f*
 - lateral cortical connections in, 1071, 1072
 - lateral geniculate nucleus in, 566–567, 567*f*, 695
 - C layers of, 585
 - cell types within, 568–573, 569*f*
 - functional connectivity versus anatomy of, 673
 - A layers of, 567, 567*f*, 585
 - afferents to, 568–571, 569*f*, 570*f*
 - interneurons in, 568, 569*f*, 573
 - intrinsic properties of cells in, 573–576
 - ionotropic receptors in, 571, 572
 - metabotropic receptors in, 571, 572
 - postsynaptic receptors in, 569*f*, 571
 - synaptic structures in, 571–572, 572*f*
 - lateral inhibition in, 17
 - lateral posterior pulvinar complex in, 592. *See also* Pulvinar region
 - M, P, and K cells of, X/Y/W homology of, 486–487
 - mapping of visual fields on striate cortex of, 10
 - as model of human visual system, 494
 - monocular deprivation in, 126, 194–196
 - alternating, 198
 - and contrast sensitivity, 196, 196*f*
 - and cortical connectivity, 153
 - duration and subsequent effects of, 194*f*, 194–196, 195*f*
 - effects of exogenous neurotrophins on, 50, 51*f*–52*f*
 - preventive effects of neurotrophins in, 53–54
 - recovery after, 113, 194*f*, 194–196, 195*f*, 196*f*
 - neurotrophin blockade in, 52, 54*f*
 - ocular dominance columns in
 - development of, 110, 110*f*, 113–114, 147
 - neurotrophins and, 53
 - optic chiasm in, organization of, 95, 95*f*
 - orientation selectivity in, 117–124, 179, 532–533
 - development of, 119–121
 - number of cells tuned for, 119
 - restricted range of exposures and, 199
 - visual experience and, 119–121
 - parabrachial region, inputs to A layers, 568, 569*f*, 570–571
 - parallel visual pathways in, 496, 496*f*
 - organization in primary visual cortex, 498

- Cat(s) (cont.)
- pulvinar region
 - afferents to, 579
 - cortical inputs to, 595
 - cortical projections from, 585
 - and eye movements, 601
 - retinal inputs to, 593
 - subdivisions of, 583, 592
 - visual functions of, 592–604, 599
 - receptive field dynamics in, 740
 - receptive field mapping in
 - linear, 707–710, 708*f*, 709*f*
 - nonlinear, 714*f*, 714–715
 - retina
 - inputs to A layers, 568–569, 569*f*, 570*f*
 - rod-cone interactions in, 864, 865
 - retina of, weight and area of, 234
 - retinal cell number and density in, 69
 - in domestic versus wild animals, 70–71
 - variations in, 70–71
 - retinal peptide expression in, 336
 - NPY, 338
 - somatostatin, 339–340
 - tachykinins, 342–343
 - retinal synapses of
 - amacrine cell-bipolar cell, 292
 - bipolar cell-ganglion cell, 288, 413
 - photoreceptor, 283
 - photoreceptor-horizontal cell, 289
 - retino-geniculo-cortical pathway in,
 - functional connectivity in, 673–678
 - rods of, outer segments of, 241
 - single-unit recording in, 17
 - Sprague effect in, 1472
 - strobe rearing in, 201, 201*f*
 - thalamic reticular nucleus, inputs to A
 - layers, 568, 569*f*, 570
 - visual area 17, 1605
 - visual area 18, receptive field size in, 1045
 - visual areas outside primary visual cortex in, 10–11
 - visual cortex of, 1581, 1582
 - receptive fields in, 695
 - visual deprivation studies in, 189. *See also specific study types*
 - visual processing in, anatomical and
 - functional organization of early stages of, 117–119
 - visual system of, 1569
 - X, Y, and W cells of, 495, 566–567, 568–573, 569*f*, 673, 681
- Cataract(s)
- age-related
 - development of, 209
 - glutathione decrease and, 205, 206*f*
 - prevalence of, 205, 206*f*
 - bilateral congenital, 190, 193
 - correction of, visual deficits after, 804
 - unilateral congenital, 46, 126
- Catarrhines, vision of, 968
- Caudate nucleus, in dialogue between
 - cerebral cortex and superior colliculus, 1468*f*
- CD44 neurons, and regulation of
 - ganglion cell axons, 96, 97*f*, 98, 99, 100
- Cell(s). *See also* Cortex; Lateral geniculate nucleus; Neuron(s)
- amacrine. *See* Amacrine cells
 - bipolar. *See* Bipolar cells
 - chattering, and neuronal synchrony, 742, 742*f*
 - complex. *See* Complex cells
 - dividing versus non-dividing, age-related decline of, 209
 - double-bouquet, in primary visual cortex (V1) of macaque, 689
 - far, in stereoscopic vision, 766, 767*f*
 - ganglion. *See* Ganglion cell(s)
 - glial. *See* Glial cells; Müller glia cell(s)
 - grandmother. *See* Grandmother cell
 - horizontal. *See* Horizontal cells
 - hypercomplex
 - orientation-selective, 118
 - receptive fields of, 118
 - interplexiform. *See* Interplexiform cells (IPCs)
 - K. *See* Koniocellular pathway, cells of
 - M. *See* Magnocellular pathway, cells of
 - Martinotti, in primary visual cortex (V1) of macaque, 689
 - midget. *See* Midget cells
 - near, in stereoscopic vision, 766, 767*f*
 - neurogliaform, in primary visual cortex (V1) of macaque, 689
 - P. *See* Parvocellular pathway, cells of
 - parasol. *See* Parasol cells
 - polymer-encapsulated, neurotrophin administration via, 51
 - pyramidal. *See* Pyramidal cell(s)
 - retinal, 5, 6*f*–7*f*, 234, 235*f*. *See also* Retinal cells
 - mosaics of, 463–475
 - patterns and tiles of, 463
 - spatial regularity among, 463–475
 - simple. *See* Simple cells
 - S-opponent, 1008
 - types of
 - functional correlates of, 481
 - taxonomical notion of, 481
 - W. *See* W cells
 - X. *See* X cells
 - Y. *See* Y cells
- Cell assemblies, 25
- Cell cycle, of retinal cells, 77
 - exit from, 77
 - spatiotemporal pattern of, 66
- Center of best vision, 1343
- Center of interest effect, 1526
- Centering response
 - angular speed and, 1196
 - in insects, 1195*f*, 1195–1196
 - versus optomotor response, 1196
 - nondirectional nature of, 1196
- Center-surround organization
 - feedback connections and, 535
 - of receptive fields, 89, 415–417, 416*f*, 483
 - of area MT neurons, 1205–1206
 - dynamics of, intracortical circuits and, 739*f*, 739–742, 740*f*
 - of ganglion cells, 23, 89, 415–417, 416*f*, 422, 708
 - horizontal cells and, 386–388, 388*f*
 - horizontal connections and, 733, 734, 736*f*, 737, 739*f*, 739–741, 740*f*
 - of LGN neurons, 708–709
 - cortical feedback and, 612–614
 - relative disparity and, 786–787
 - stimulus contrast and, 739*f*, 739–741, 740*f*
 - summation and, 739*f*, 739–741, 740*f*
- Central nervous system
 - neurotrophin action in, 48–49, 50*b*, 61
 - retinal models of, 33
 - single-unit recording in, 17
- Central performance drop, 1112
- Central visual field
 - cortical representation of, 9
 - relative immaturity of cones in, 176
 - visual acuity in, 176
- Central visual pathway, linear receptive
 - field maps for neurons of, 707–708, 708*f*
- Cephalopods, vision of, 964
- Cerebellum
 - and binocular ocular motor control, 1494–1495
 - and eye movement control, 1405, 1425, 1485–1496
 - anatomical approach to, 1486–1487
 - in pursuit behavior, 1408–1409, 1485
 - lesions of, disorders of static alignment caused by, 1494–1495
 - ocular motor learning and, 1495–1496, 1495*f*
 - in oculomotor system, 1405, 1425, 1485–1496
 - research on, advances in (future directions for), 1496
 - and pursuit behavior, 1408–1409, 1485
 - structural-functional correlations for, 1486–1487
- Cerebral achromatopsia, pupil responses in, 641–642, 651*f*, 652, 653
- Cerebral blood flow, regional, in cortical optic flow responses, 1269
- Cerebral cortex. *See also* Primary visual cortex; Visual cortex

- concentration of synapses in, 148
connections of, ontogenesis of, 146–154
development of, 146
 extrinsic control of, 146
 intrinsic control of, 146
 protocortex theory of, 146
 protomap theory of, 146
fiber layer of (striping), 7–8, 8*f*
functional localization in, 8
human, visual areas of, 513–515
 comparison with macaque, 507, 515–518, 517*f*
macaque, visual areas of, 507–513
 comparison to humans, 507, 515–518, 517*f*
 organization of, 507–513, 508*f*, 510*f*–511*f*, 513*f*
mapping techniques for, 507
 technical impediments in, 508–509
representation of visual fields in, 6–9
structure of, 7–8
 regional variability in, 7–8
c-FOS, and CREB, 132
cGMP. *See* Cyclic guanosine monophosphate
cGMP-gated cation channel, and rod maturation, 41
CGP35348, GABA receptor response to, 356*t*, 358
CGP55845, GABA receptor response to, 356*t*, 358
Chandelier cells, axo-axonic, in primary visual cortex (V1) of macaque, 689
Change blindness, 546, 728, 1148, 1525, 1526–1527
 and change detection, dissociation of, 1534
 from comparison failure, 1528
 and driving, 1527
 evidence for, historical perspective on, 1525–1527
 preserved representations in, behavioral measures of, 1527–1528
 saccade-contingent, 1525
Change detection, 1524–1535
 attention in, 1526
 comparisons in, 1524–1525
 event-related potentials (ERP) in, 1528, 1531–1533, 1534
 explicit processing for, 1528–1529, 1534–1535
 eye movements in, 1528, 1529–1531
 failure of, preserved representations in, 1527–1531
 fixation duration in, 1528, 1530
 fixation patterns in, 1530–1531
 functional magnetic resonance imaging (MRI) studies of, 1528, 1533–1534
 implicit, 1534–1535
 behavioral evidence for and against, 1528–1529
 explicit mechanism for, 1528–1529
 eye movements and, 1529–1531
 neuroimaging and, 1528, 1531–1534
 orientation of changed item and, 1529
 during reading, 1525
 representations in, 1524–1525, 1526
 verbal reports in, cautions about, 1531
 without awareness, 1528
Channels, 1302
 color-sensitive, 939
 L-M, 939–940, 940*f*
 S-LM, 939–940, 940*f*
 spatial. *See* Spatial channels
 visual. *See* Visual channels
Charybdotoxin, and spike frequency in ganglion cells, 437
Chattering cells, and neuronal synchrony, 742, 742*f*
Chemosuppression, of ganglion cell axons, 98
Chevreul illusion, 886, 889
Chicken(s)
 color vision in, 965
 optic chiasm in
 development of, 99
 organization of, 94, 95, 95*f*
 process outgrowth from amacrine cells in, 84*f*
 retina neurotransmitters in, 87
 retinal cells of, 6*f*–7*f*
 differentiation of, 67
 tangential migration by, 469
Chimpanzee(s), binocular deprivation in, 191, 192
Chloride, intracellular concentration of, in immature ganglion cells, 87
Chloride channels/currents
 in ON bipolar cells, 265, 266*f*, 290, 291*f*
 and direction selectivity, 455
 GABA receptors and, 356, 356*t*
 glycine receptors and, 356, 356*t*
 peptide action on, 337, 346, 346*f*
 in signal transmission from cones, 250
Chloride ions, ganglion cell permeability to, 431
Chloride transporters, in bipolar cells, 290, 291*f*
Choice probabilities
 in binocular disparity/stereopsis experiments, 789
 in perception decision experiments, 1211
 in single-unit recording, 21–22
Cholecystokinin (CCK)
 expression of, in basket cell, 688
 retinal, 334, 347
Choline acetyltransferase (ChAT), 311, 312*f*
 in retina, 87
Choline transporters, 311, 312*f*
Chondroitin sulfate proteoglycans (CSPGs)
 degradation of, and restoration of plasticity, 137
 and optic chiasm development, 100
Chondroitinase-ABC, and restoration of plasticity, 137
Chow, K. L., 12
Chroma, 899, 900*f*
 definition of, 899
Chromatic aberrations. *See* Aberration(s), chromatic
Chromatic adaptation. *See* Adaptation, chromatic
Chromatic aliasing, 805–807
 and image acquisition, 805–807
Chromatic assimilation, 900, 901*f*
Chromatic channels, 1217
 and motion processing, 1217–1218
Chromatic contrast. *See* Color contrast
Chromatic discrimination, 908–921
 chromaticity variation and, 914–915, 915*f*
 colorimetric purity variation and, 913–914, 914*f*
 L and S axes' combination and, 916–917
 luminance level and, 914–915
 models of, 917–921
 modern theory of, based on retinal physiology, 918–920, 918*f*, 919*f*
 rods and, 874–875
 studies of, 908, 913–917
 modern approaches to, 915–917, 916*f*
 wavelength variation and, 913, 913*f*
Chromatic extent, and thresholds, 820
Chromatic induction, 900. *See also* Color contrast
Chromatic information, transmission via K (konio cellular) pathway, 497–498
Chromatic opponent valences, 917–918
Chromatic sensitivity, during saccades, 1393–1394, 1393*f*
Chromatic threshold, dark adaptation and, 873
Chromaticity, average, in natural scenes, 807
Chromaticity coordinates, 951
Chromaticity diagrams, 910, 910*f*
 CIE XYZ, 910–911
 modified, 910–911, 910*f*
 MacLeod-Boynton, 910*f*, 911
 physiological, 910*f*, 911
Chromaticity horizontal cells, 370*f*, 370–371, 372–374
 biphasic, 373
 monophasic, 373
 polarity reversal in, 373–374, 374*f*
 spatial properties of, 381
 triphasic, 373
 wavelength dependency of, 373–374, 374*f*

- Chromophore, 976
- CIE chromaticity diagram, 951
- Ciliary ganglion, and pupil responses, 642
- Ciliary margin, 35*f*, 36
- Ciliary muscle
- age-related changes in
 - angular shape of, 207
 - human versus monkey, 207
 - and presbyopia, 207–208
 - reading and, 207–208
- Ciliary nerves, short, and pupil responses, 642
- Ciliary neurotrophic factor (CNTF)
- production of, by Müller glia cells, 41
 - in retinal cell differentiation, 39, 43, 68, 78–79
 - in retinitis pigmentosa, 43
 - rod production inhibited by, 39, 43
- Ciliary stalk, 216, 216*f*
- Circadian clock
- anatomical location of, 625
 - light input pathways to, 625, 628–629, 629*f*, 635*f*
 - light-induced phase shifts in, 625–628
 - mammalian, light responsiveness and
 - photoc entrainment of, 625–636
- Circadian oscillators, 625
- genetic components of, 635
 - light responses of, 627
 - negative elements of, 625
 - positive elements of, 625
- Circadian pacemaker. *See* Suprachiasmatic nuclei (SCN)
- Circadian rhythms
- behavioral, light responses of, 625–628, 626*f*
 - cellular generation of, 625
 - darkness/light pulse experiments on, 626–628
 - evolution of, 625
 - future directions for study of, 635–636
 - genetic control of, 625, 634*f*, 634–636
 - light responses in, 625–636
 - complexity of, 627
 - light-responsive intracellular signaling and, 633–636
 - melatonin and, 628
 - neuronal knowledge of, 24
 - neurotransmitters and, 628–629
 - period changes in, 627
 - phase advance of, 626*f*, 626–628, 632
 - phase delay of, 626*f*, 626–628, 632
 - phase response curve of, 626, 626*f*, 636
 - phase shifts in, 625–628
 - behavior and, 628, 631, 632*f*
 - duration of light pulse and, 627
 - light intensity and, 627
 - light-induced, 625–628, 626*f*
 - magnitude of, factors affecting, 627
 - saturation of, 627
 - threshold intensity for, 627
 - transient cycles in, 626*f*, 627
 - two-pulse paradigm of, 627
- photoc entrainment of, 625–636
- as photon counter, 627
- and SCN neuron responses, 631–632, 632*f*, 633*f*
- wavelength sensitivity of, 627, 628
- CIT visual area, macaque
- dorsal (CITd), 510*f*–511*f*, 512
 - ventral (CITv), 510*f*–511*f*, 512
- Clare, Margaret, 10–11
- Classification image, 833–834
- Clathrin-induced endocytosis, in bipolar cells, 286
- Clastrum, connections with ventral and dorsal streams, 544
- Climate, and presbyopia, 206, 206*t*
- Clipped cells, 1451
- Clock* gene, 625
- Clock genes, 625, 634–636
- Closed-loop behavior, 1485
- Closure, 1581
- Gestalt factor of, 1148, 1575, 1576*f*
- Cognition/cognitive processes
- architecture of, 1547, 1547*f*
 - color vision and, 933
 - as corollary discharge function, 1466
 - definition of, 1466
 - and dialogue between cerebral cortex and superior colliculus, 1473
 - feedforward and feedback pathways in, 150
 - as forward function, 1466
 - and gaze control, 1343, 1370
 - in honeybee, 1501–1512
 - levels of, 1547, 1547*f*
 - neural pathway for, and neural pathway for visuomotor processing, 1406–1407, 1407*f*
 - neuronal synchrony and, 1671, 1675–1676, 1677–1678
 - as reverse function, 1466
 - and smooth pursuit eye movements, 1402, 1405, 1410
 - types of, 1466
- Cognitive control
- capacity limitation and, 1547
 - definition of, 1546
 - need for, detection of, 1559
 - neural system for, 1546–1547
 - prefrontal cortex (PFC) in, 1546, 1554
 - and selection, 1546–1547
 - system for, plasticity of, 1547
- Colinear facilitation, 1063–1064, 1064*f*, 1066–1067
- Collimated beam, 1092
- and shape from shading, 1093, 1094*f*
- Collimation, 1092
- Collision test, 1468
- Color
- achromatic, invariance of, with
 - illumination changes, 883–884
 - animals' experience of, 971–972
 - binary, 894
 - and camouflage, 1290
 - dark, context and, 899
 - dimensions of, 893
 - illuminant variation and, 948, 949*f*
 - and intensity, separation of, 1003
 - K cell responses to, 1219–1220
 - large-scale effects of, 1583–1584
 - and luminance, 930–933
 - separation of, 1012–1014, 1013*f*
 - M cell responses to, 1219–1220
 - in natural scenes, 807
 - and occlusion, 1290
 - P cell responses to, 1219–1220
 - and pattern segregation, 929–930
 - preferred, of color cells, 1019–1020
 - pupil response to, 641–642, 650*f*, 650–652, 651*f*
 - clinical applications of research on, 654
 - damage to dorsal midbrain and, 653–654
 - representation of, 905
 - rivalry of forms and, 1316, 1317, 1318*f*
 - rod response to, 838
 - in spatial vision, 924–934. *See also* Color spatial vision
 - spreading of, 1583–1584
 - in temporal vision, 924
 - unitary, 894
 - antagonistic relation of, 894
 - and binary, distinguishing, 893–894
- Color anomaly, 1005
- Color appearance, 892–905, 1113
- achromatic, 897–898, 897*f*
 - versus color matching, 892–893
 - colorimetric coordinates and, 895–896
 - dimensions of, 893. *See also* Brightness; Hue(s); Saturation
 - perceptual organization of, 893
 - physiologic relation of, 898–899
 - study of, achromatic judgments in, 950
 - von Kries Coefficient Law for, 900–901
- Color blindness. *See also* Color anomaly; Dichromacy; Monochromacy
- cerebral, 1029
 - molecular genetics of, 977, 979*f*
- Color center, 1026
- central, 1014
 - in humans, 1034–1036, 1035*f*
 - location of, 1029–1031
 - as salience center, 1035
 - visual field representation within, 1029–1031
- Color channels
- definition of, 1217, 1218*f*
 - and motion processing, 1217–1218

- Color coding, 892, 905, 1003–1015, 1017
in bee, 971
in extrastriate cortex, 1018–1026
- Color constancy, 902–905, 948–959, 966, 969, 1024–1026, 1578. *See also* Color memory
across illumination changes, 948, 949*f*
definition of, 902, 948
early adaptive gain control and, 956
image ensemble studied and, 953–955
measurement of, 949–953
data from, 951–952
sample experiment for, 950–953, 950*f*
mechanisms of, 902
paradox in, 952–953, 953*f*, 954*f*
simultaneous, 949, 958–959
studies of
computational approach in, 954, 956, 957–958
mechanistic approach in, 954, 955–957
successive, 949, 958
theory of, 903
V1 cells and, 1018
- Color constancy index, 952
- Color contrast, 900, 900*f*
photopic, 872–873
scotopic, 872–874, 872*f*
simultaneous, 1011
successive, 658, 1011
- Color contrast sensitivity (chromatic contrast sensitivity), 177, 186, 186*f*, 800–801
cone ratio variations and, 806*f*, 807
in ganglion cells, 418–419, 488–489
ideal observer analysis of, 831
in M (magnocellular) cells, 488–489
in P (parvocellular) cells, 488–489, 497, 501
in W cells, 498
- Color cues
for motion integration and segregation, 1223–1226
plaid stimulus in, 1223–1226, 1224*f*
stochastic motion stimulus in, 1225, 1225*f*
for motion processing, 1023–1024, 1023*f*, 1210, 1217–1226, 1237
chromatic input to MT visual area and, 1218–1220
koniocellular pathway and, 1219–1220, 1223, 1223*f*
magnocellular pathway and, 1219–1223, 1221*f*, 1222*f*
neural correlates of, 1218–1219
parvocellular pathway and, 1219–1220, 1223–1226
plaid stimulus in, 1223–1226, 1224*f*
psychophysical evidence for, 1217–1218
stochastic motion stimulus in, 1225, 1225*f*
- Color discrimination. *See also* Chromatic discrimination
in dogs, 962, 963*f*
- Color fusion, 1691
- Color identification, ideal observer analysis of, 834
- Color matching, 909–911, 962, 1113
versus color appearance, 892–893
experiment, in dogs, 962
isomeric, 892
linearity of, 910
metameric, 892
prefrontal cortex (PFC) damage and, 1552
- Color matching task, in diagnosis of color vision defect, 982
- Color memory, 905
- Color opponency, 17, 296, 894, 894*f*, 909, 917, 943, 1691
blue-yellow, 681, 989, 990
and red-green opponency, comparison of, 996–997, 996*f*
retinal circuit for, 992–996
cascade model of, 387
cone antagonism and, 989–990, 990*f*
critical locus of, 990, 990*f*
in ganglion cells, 418–419, 483, 488–489
horizontal cells in, 370*f*, 370–371, 372–374, 387–388, 388*f*
in M (magnocellular) cells, 488
in P (parvocellular) cells, 488
red-green, 681, 989, 990*f*
and blue-yellow opponency, comparison of, 996–997, 996*f*
new views of, 996–999
P-cell hypothesis for, 997–998, 998*f*
role of cortex in, 999–1000
variability in, 999
retinal circuits and, 989–1000
- Color perception, 892, 905
achromatic, 890
areas beyond striate cortex and, 1014–1015
with change of illumination, 904–905
cone responses in, 896, 897*f*
context and, 899–902
cortical areas in, 1685
cortical region essential for, 1014
in humans, 971
motion and, 1034
physiologic basis of, 989–992
in pigeons, 971
in primates, 971
during saccades, 1393–1394, 1393*f*
- Color problem, in single-unit recording, 16–17
- Color processing
in extrastriate cortex, 1017–1026
interactions with other visual attributes, 1023–1024, 1023*f*
in striate cortex, 1011–1014, 1013*f*, 1014*f*, 1017
- Color responsivity (CR) index, 1018
- Color signal, 948
spectral power distribution $[C(\lambda)]$ of, 948
- Color space, encoding of, 1010–1011, 1010*f*
- Color spatial vision, 924–934
constraints on, 924–925
- Color [term], 892
- Color vision, 720, 1339
aberrations in (chromatic aberrations). *See* Aberration(s), chromatic
adaptation and, 939–942, 940*f*
advantages of, 924, 933, 969
aliasing in, 805–807
and image acquisition, 805–807
in animals
distribution of, 964–967
oil droplets and, 968–969, 969*f*
study of, 962–964
variations of, 964–967, 968
dimensional, 964–966
and wavelength-specific behaviors, 966–967
in blindsight, 658, 662
blue-yellow, 974
defects of, 983
and cognitive functions, 933
comparative, 962–972
cones and, 215, 801–802, 1217, 1218*f*, 1237
sampling in, 805–807
variation in cone ratio and, 806*f*, 807
in conspecific communication, 933
constancy in aging, 807
and contour integration, 929
contrast adaptation in, 940*f*, 941–942
contrast sensitivity in (chromatic contrast sensitivity). *See* Color contrast sensitivity
cortical specialization for, 942, 1035
defects. *See also* Color blindness
deutan, 974–975, 980–982, 980*f*
inheritance of, 975–976
molecular genetics of, 980–983
protan, 974–975, 980*f*, 982–983
rare, molecular genetics of, 983
tritan, 975
inheritance of, 976
types of, 974–976
X-chromosome visual pigment genes in, 980–983, 980*f*
definition of, 908
and depth perception, 928
dimensions of, 965–966, 1217
limitations on, 970
variations of, in animals, 964–966
early studies of, 3, 12
evolution of, 967–970

- Color vision (cont.)
in food foraging, 933
functions of, 933–934
geniculate processing in, 1006–1011
horizontal cells in, 370*f*, 370–371, 372–374
biphasic, 373
monophasic, 373
polarity reversal in, 373–374, 374*f*
spatial properties of, 381
triphasic, 373
wavelength dependency of, 373–374, 374*f*
human, molecular genetics of, 974–986
ideal observer analysis of, 831
improbable areas in, 1029–1037
cross-species analysis of, 1034
definition of, 1031
at isoluminance, 930
K (konioecellular) pathway for, 497–498, 1217, 1219–1220
light adaptation and, 859–860
versus luminance vision, 933
M (magnocellular) cells in, 488, 1217, 1219–1220
mechanics of, 989
in memory enhancement, 933–934
molecular biology of, 964, 974
in motion perception, 933
and motion processing, 1023–1024, 1023*f*, 1210, 1217–1226, 1237
multiple tasks and bottlenecks in, 1003–1004
neural organization underlying, 1003–1015
normal, 974
in object segregation, 933
one-stage model of, 1007
opponent-color model of, 1007
P (parvocellular) cells in, 488–489, 497, 501, 1217, 1219–1220
pathways for
characteristics of, 990–991
chromatic signature of, 991
L/M, 989, 990, 991
S/(M+L), 989, 990, 991
in pattern recognition, 933
primary cortical processing in, 1011–1012
receptors in, 969, 1005–1006
linear transduction cascade of, 1006
nonlinear adaptational processes of, 1006
red-green, 974
defects, 981
deficiency of, 974
human, evolution of, 977
reflectance in, and illuminant, separation of, 1003
requirements for, 908
retinal processing in, 1006–1011
rods and, 866, 872–875, 872*f*, 874*f*, 875*f*
scale and, 1051, 1053*f*
spatial factors in, 924. *See also* Color spatial vision
spatial selectivity and, 942
temporal factors in, 924
three-stage LGN-cortical cell responses in, 1013–1014
thresholds for, 820
two-color threshold test of Stiles in, 940, 940*f*
two-stage model of, 939, 940*f*, 1007
utility of, 970–972
ventral stream lesions and, 547–548
visual pathways and, 488, 490, 497–498, 1217, 1219–1220
visual stimulus in, confounds in, 1003
Colorimetric purity, 892, 918
definition of, 913
Colorimetric purity discrimination, 913–914, 914*f*
Colorimetry, 893
Color-selective cells, 1017–1018
linear, 1020
luminance, 1020
narrowly tuned, 1020
properties of, 1018–1019
Columnar hypothesis, 1685
Columnar organization
of cortex, 733
of MT visual area, 1204–1205, 1205*f*
Common fate, 1577
Gestalt factor of, 1148, 1575–1576, 1576*f*, 1580
Communication, human, overcomplete coding in, 1606
Comparison-and-decision stage, in texture segregation, 1109, 1111
Compartmental model of neurons, 24–25
Completion
Gestalt, across scotomata, 1584
visual. *See* Visual completion
Complex cells, 750, 1584–1585
binocular disparity selectivity in, 715, 716
binocular interaction in, 770*f*, 770–772, 771*f*, 772*f*
contrast processing, 772–773, 773*f*, 774*f*
contrast adaptation in, 754, 754*f*
contrast response function in, 752*f*, 752–753, 753, 753*f*
contrast-set gain control in, 753, 753*f*
in cortical feedback system, 617, 621, 622
direction selectivity in, 617, 715, 716, 1621
linear and nonlinear properties of, 753
energy model of, 706, 715–716, 716*f*, 717
invariance properties of, 1611, 1613
latency shift in, 753–754, 754*f*
maximum operation in, 1648
neurometric function for, 822, 822*f*
nonlinear interactions of, 714–715, 715*f*, 717
second-order, 714–715
nonlinear properties of, 751–754
temporal dynamics of, 754–759
ON/OFF, 270, 715–716
pharmacologic blockade of, 273, 274*f*
orientation selectivity in, 1621
orientation selectivity of, 714, 715, 770, 770*f*, 771*f*
linear and nonlinear properties of, 753
receptive fields of
construction of, 716
feature selectivity of, 1611
linear map of, 708, 708*f*, 709*f*, 710
nonlinear map of, 706, 708, 714–716, 715*f*, 717
singular value decomposition (SVD) analysis of, 716
spatiotemporal map of, 709*f*, 710
subunits of, 714–716
response expansion in, 752*f*, 752–753
response properties of
nonlinear, 1611
relation to image representation model, 1611
response rectification in, 751*f*, 751–752
response refractory period of, 751
response saturation in, 753, 753*f*
selectivity of and generalization by, 18
and signal pooling, 1626
versus simple cells, 750
spatial frequency selectivity in, 714, 715, 770, 770*f*, 771*f*, 1621
linear and nonlinear properties of, 753
speed preference of, 715
system structure of, 715–716, 716*f*
temporal frequency selectivity in, 1621
tuning of, 1302
Complex trait analysis, of retina cells, 63, 71
Compression, perceptual, during saccades, 1396–1397, 1398–1399, 1399*f*
Computational model(s), 1044, 1074–1076, 1640
of contour integration, 1074–1076
of natural vision, 1596
of stereopsis, 1303
of visual search, 1597
Concealment, 1577
Concepts, abstract, prefrontal cortex (PFC) and, 1555
Conditional learning, prefrontal cortex (PFC) damage and, in monkeys, 1552
Cone(s), 908, 911
absorption spectra, in dogs, 963, 963*f*
age-related failure of, 210*t*
aliasing by, 803–805

- chromatic, 805–807
- amacrine cells of, 395–396
 - reciprocal, 398–399
- anomalous, 982, 983
- antagonism
 - and color opponency, 989, 990*f*
 - retinal circuitry and, 991–992
- aperture
 - size of, 801
 - spatial filtering by, 801
- axon terminal of, 245, 246*f*
- active zones of, 245, 247*f*
- axons of
 - microtubules of, 245, 246*f*
 - thickness of, 242*f*, 245
- bipolar cells of
 - neurokinin receptors in, 344
 - stratification of, 268
- blue, 372. *See also* Cone(s), S (short-wavelength sensitive)
 - connections to horizontal cells, 370–371, 373–374, 376*f*
 - feedback from horizontal cells, 382, 383*f*
 - mosaics of, 468
 - visual pathway input from, 497–498
- calcium influx in, 282–283
 - horizontal cells and, 388–389
- ciliary stalk of, 216, 216*f*
- circuitry relaying signals of, 234–255, 235*f*, 236*f*
 - bipolar pathways in, 252*f*, 252–253
 - daylight circuits in, 249–251
 - ganglion cell pathways for, 253–255, 254*f*
- in color vision, 215, 801–802, 1217, 1219–1220, 1237
 - sampling and, 805–807
 - variation in cone ratio and, 806*f*, 807
- as contrast encoders, 851
- conversion tables for analysis of, 838, 839*f*
- in dark adaptation, 845, 847
- in daylight vision, 70, 239*f*–240*f*, 240, 249–251
- death or loss of
 - in macular degeneration, 42–43
 - secondary, in retinitis pigmentosa, 42–43
- development of, 36–37, 37*f*, 159–163, 162*f*, 176, 467–468
- functional, 176
- ideal observer model of, 160–163, 162*f*, 163*t*
- in primates, 159–163
- tangential migration in, 469
- timing of, 77, 78*f*
- visual evoked potentials in, 176, 186, 186*f*
- in dichromats, 372
- distribution and morphology of, 3–5, 4*f*
- dynamic range of, 423
- foveal, 244–245, 801–802, 802*f*
 - concentration of, 69, 159–160, 162*f*, 166–167
 - and image acquisition, 801–808
 - mean center-to-center spacing of, 802
 - mosaic of, 159–160, 162*f*, 239*f*–240*f*, 240
 - and receptive fields of cortical neurons, 166*f*, 166–167
 - Nyquist limit of, 803–805, 804*f*
 - relative immaturity of, 176
- function of, 237–240
- functional constraints of, 236–237
- functional domains of, 215
- functions of, 215, 974
- GABA receptors in, 309
- glutamate receptors in, 306–307
- glutamate transporters in, 306
- green, 372. *See also* Cone(s), M (mid-wavelength sensitive)
 - connections to horizontal cells, 370–371, 373–374, 376
 - feedback from horizontal cells, 382, 383*f*
 - and horizontal cells
 - connections between, 370–372, 372–374, 373–374, 375–376, 376*f*
 - contributions to, 374–376
 - effect of dopamine on, 384
 - feedback from horizontal cells, 381–383, 382*f*, 388–389
 - modulatory effects on cones, 388–389
 - signal mixing with rods, 374–375, 376*f*
 - and image acquisition, 801–808
 - image properties reported by, 260
 - information capacity of, 244
 - inner segments of, 176, 216, 216*f*, 235*f*, 239*f*–240*f*, 242*f*
 - variation in, 244–245
- intensity ranges of, 215, 228, 229, 240
- L (long-wavelength sensitive), 176, 186, 186*f*, 372, 805, 806*f*, 908, 924–925, 939, 955, 974, 1003, 1004
- chromatic aberration and, 800–801
- chromatic discrimination, model for, 918–920, 918*f*, 919*f*
- in chromatic motion processing, 1219–1220, 1237
- in color vision, 800–801, 1217, 1218*f*, 1219–1220, 1237
- connections to horizontal cells, 373–374, 376
- feedback from horizontal cells, 382, 383*f*
- identity of, determinants of, 985
- input to P cells, 1219–1220
- photopigment genes, 1005
- photopigment peak, 1005
- retinal distribution of, 1006
- sampling by, 805, 806–807
- sensitivity regulation in, 912–913
- spectral sensitivity of, 908
- spectral variants of, in protanomaly, 983
- maintenance of, 216
- migration of, 80, 159–160, 162*f*, 166–167
- mosaic of, 159–160, 162*f*, 239*f*–240*f*, 240–241
 - comparison across species, 472
 - development of, 467–469, 468*f*
 - minimal-spacing rules and, 469–470
 - and receptive fields of cortical neurons, 166*f*, 166–167
 - sampling by, 802–807
 - by different cone classes/submosaics, 805–807
 - trichromatic, 805–807
- in motion processing, 845, 1219–1220, 1223, 1237
- neurotransmitter release from, 245, 246–247
- noise and, 240–241
- number of, 69–71, 215, 801–802
- sampling by, 805, 806–807
- sensitivity regulation in, 912–913
- spectral sensitivity of, 908
- spectral variants of, in deuteranomaly, 981, 983
- lateral integration of, 237*f*
- light adaptation in, 228–230
 - calcium-dependent mechanisms in, 228–229
 - composite effect of mechanisms in, 230
 - elevated steady-state activity of
 - phosphodiesterase and, 229, 230
 - gain reduction in, 229
 - mechanisms of, 228–230
 - pigment bleaching and, 215, 229–230
 - response compression and, 228
- L:M ratio of, 71, 985–986
 - and chromatic discrimination, 915
 - and color vision, 806*f*, 807
- M (mid-wavelength sensitive), 176, 186, 186*f*, 372, 805, 806*f*, 908, 924–925, 939, 955, 974, 1003, 1004
- chromatic aberration and, 800–801
- chromatic discrimination, model for, 918–920, 918*f*, 919*f*
- in chromatic motion processing, 1219–1220, 1237
- in color vision, 800–801, 1217, 1218*f*, 1219–1220, 1237
- connections to horizontal cells, 370–371, 373–374, 376
- feedback from horizontal cells, 382, 383*f*
- identity of, determinants of, 985
- input to P cells, 1219–1220
- photopigment genes, 1005
- photopigment peak, 1005
- retinal distribution of, 1006
- sampling by, 805, 806–807
- sensitivity regulation in, 912–913
- spectral sensitivity of, 908
- spectral variants of, in protanomaly, 983
- maintenance of, 216
- migration of, 80, 159–160, 162*f*, 166–167
- mosaic of, 159–160, 162*f*, 239*f*–240*f*, 240–241
 - comparison across species, 472
 - development of, 467–469, 468*f*
 - minimal-spacing rules and, 469–470
 - and receptive fields of cortical neurons, 166*f*, 166–167
 - sampling by, 802–807
 - by different cone classes/submosaics, 805–807
 - trichromatic, 805–807
- in motion processing, 845, 1219–1220, 1223, 1237
- neurotransmitter release from, 245, 246–247
- noise and, 240–241
- number of, 69–71, 215, 801–802

- Cone(s) (cont.)
- functional correlate of, 69
 - large, need for, 69
 - ratio of L and M cones, 71
 - ratio to rods, 215, 240–241
 - variation in, 71
 - and spatial resolution, 80
 - variations in, 71
 - outer segments of, 176, 215–216, 216*f*, 235*f*, 239*f*–240*f*
 - calcium-induced changes in, 225–228
 - design of, effect on speed, 241–244
 - elongation and maturation of, 160, 167
 - length of, 241
 - mammalian, 241, 242*f*
 - nonmammalian, 241
 - shedding and renewal of, 216
 - size of, 241, 242*f*
 - surface-to-volume ratio of, 226
 - volume of, 241
 - performance of, versus rods, 215
 - peripheral, 245
 - in photopic (daylight) vision, 851, 852
 - photopigments of, 976–980
 - alleles for, 1005
 - evolution of, 967
 - genes for, 976–980
 - spacing of, 1005
 - spectral sensitivities of, 1004, 1005*f*
 - spectral tuning of, 976–977
 - phototransduction (light response) by, 215–230
 - activation of, 217–221
 - calcium feedback regulation of, 216, 217, 223, 225–228
 - inactivation of, 221–225
 - mutations of proteins involved in, comparison of effects of, 222, 223–225, 224*f*, 225*f*
 - overview of, 216–217
 - physical limits to, 215
 - plateau, in dark adaptation, 841
 - postnatal changes in, 159–163
 - process outgrowth from, 82
 - quantum fluctuations in, 820
 - red, 372. *See also* Cone(s), L (long-wavelength sensitive)
 - connections to horizontal cells, 373–374, 376
 - feedback from horizontal cells, 382, 383*f*
 - retinal distribution of, 1006
 - and rod saturation, 842
 - S (short-wavelength sensitive), 176, 186, 805, 806*f*, 856*f*, 857, 860, 908, 924, 939, 955, 974, 1004–1005
 - chromatic aberration and, 800–801
 - chromatic discrimination, model for, 918–920, 918*f*, 919*f*, 920–921
 - in chromatic motion processing, 1219–1220, 1223, 1237
 - and color channels, 999
 - in color vision, 800–801, 1217, 1218*f*, 1219–1220, 1223, 1237
 - input to K cells, 1219, 1223
 - input to M cells, 1219–1220
 - photopigment genes, 1005
 - mutations of, 983
 - photopigment peak, 1005
 - sampling by, 805–806
 - sensitivity regulation in, 913
 - spectral sensitivity of, 908
 - visual pathway input from, 497–498, 502, 503
 - sampling by, 802–807
 - by different cone classes, 805–807
 - and image acquisition, 802–807
 - trichromatic, 805–807
 - saturation of, 229
 - sensitivity of, 237, 244
 - monocular deprivation and, 196
 - signal-to-noise ratio of, 244
 - in spatial vision, 80, 239*f*–240*f*, 240–241, 801–802
 - specialized mechanisms of, 230
 - spectral sensitivity of, 908, 909*f*, 989–990, 990*f*
 - at equal luminance, 908, 909*f*
 - spectral types of, 370, 372
 - speed of, 215
 - Stiles-Crawford effect in, 216, 841, 846–847
 - structure of, 215–216, 216*f*
 - postnatal changes in, 160, 167
 - subdivision of mammalian mosaic for, 239*f*–240*f*, 240–241
 - summation of signals from, 848
 - survival advantages from, 215
 - synapses of, 280, 280*f*
 - bandpass filtering by, 246, 249–251, 251*f*
 - to bipolar cells, 280–285, 281*f*, 285
 - complexity of, 283, 284*f*
 - engineered spillover of, 247, 247*f*
 - formation of, 87–88
 - to ganglion cells, interaction with cones, 418–419
 - glycinergic, 311
 - horizontal cell to, 290, 381–383, 382*f*, 383*f*, 386, 388–389
 - to horizontal cells, 370–372, 371*f*, 372–374, 373–374, 375–376
 - invaginating, 246, 247*f*, 281*f*, 281–282
 - to rods, 279
 - superficial, 281, 281*f*
 - three-dimensional structure and function of, 246–247, 247*f*
 - synaptic terminal of, 216, 216*f*, 242*f*
 - in tetrachromats, 372
 - thresholds of, 820, 841
 - topography of, 801–802
 - topology of, versus rods, 216
 - in trichromats, 372
 - types of, 908, 939
 - ultraviolet light-sensitive, 372
 - in vertical pathway, 320
 - visual pathways from, 844
 - cancellation in, 845
 - shared with rods, 841, 845
 - Cone excitation coordinates, 955
 - Cone trolands, 911. *See also* Troland value(s)
 - Configural pooling, 1066, 1067
 - Conformity ratio, in mosaic measurement, 473
 - Congenital stationary night blindness, 272–273
 - Conjugate eye position, 1300
 - Connexin, 251, 290, 307–308, 309, 372
 - Connexon channels, 322, 372
 - Conotoxin, calcium currents sensitive to, in ganglion cells, 432, 433
 - Consciousness
 - in animals, 1682–1683
 - content of
 - multiple drafts model of, 1688
 - private quality of, 1682
 - enabling factors and, 1683
 - function of, 1682
 - intermediate-level theory of, 1692
 - language and, 1683
 - levels of, 1683
 - neurobiological basis of, 1682
 - physical origins of, 1682
 - qualia of, 1682
 - visual. *See also* Visual awareness
 - area V1 in, 1689–1691
 - definition of, 1686
 - function of, 1682
 - neural activity in, 1692
 - neuronal basis of, 1682–1693
 - percepts for, timing and, 1686–1688, 1687*f*
 - requirements for, 1686
 - research on, advances in (future directions for), 1692–1693
 - visual representation in, nature of, 1684–1686
 - what-it-is-like of, 1682
 - Constrained Bayesian ideal observer, 826–827
 - Constraint function, in ideal observer analysis, 827
 - Context(s)
 - and color perception, 899–902
 - and shape from shading, 1094, 1094*f*
 - Contextual field, 1070
 - Contextual modulation
 - in anesthetized versus awake animals, 726
 - and attention, 728
 - and awareness, 728

- excitation-inhibition balance and, 725
- feedback connections and, 725–726
- and figure-ground segregation, 722–725, 728, 729*f*
- functions of, 726–728
- horizontal connections and, 725–726
- mechanisms of, 725–726
- and perceptual grouping, 726–728
- and V1 responses, 720–729
- Contingent adaptation, 939
- Continuation, good (smooth). *See* Law of good continuation
- Continuity, 1069
 - representation of, 1069
- Continuity constraint, 1304
- Contour(s)
 - amodal, 1574
 - cognitive, 1119
 - detection of, ideal observer analysis of, 834
 - disparity, neurons sensitive to, 787, 787*f*
 - identification of, 1011
 - illusory (ICs), 544, 1076, 1076*f*, 1119–1120, 1129, 1130*f*, 1136, 1139–1142, 1140*f*, 1505, 1579–1580, 1581, 1584, 1585
 - dynamics of, 1120–1121
 - meridional asymmetry in, 1121–1122, 1123*f*
 - neurophysiology of, 1123–1124, 1125*f*
 - perception of
 - in bees, 1504–1505, 1506*f*
 - in nonhuman species, 1142
 - physiologic correlations with, 1141–1142, 1142*f*
 - upper/lower field asymmetry in, 1121, 1122*f*
 - perceptual learning of, 1123
 - processing stages of, 1141
 - psychophysics of, 1120–1123, 1120*f*
 - thin-fat task for, 1120, 1120*f*
 - spatial scale and, 1120, 1121*f*
 - support ratio for, 1120
 - universality of, 1142
 - vertical meridian and, 1121–1122, 1123*f*
- kinetic, 1036
- processing of, 1047, 1581
- representation of, 1069
- and shape from shading, 1099
- and surface attributes, 1146, 1146*f*
- Contour fragments, shape representation
 - by, 1081–1082, 1081*f*
 - in area V4, 1081*f*, 1084–1086, 1084*f*, 1085*f*, 1086*f*
- Contour integration, 929, 1070
 - ability for, development of, 170–171
 - computational models of, 1074–1076
 - definition of, 1070–1071
 - mechanism of, 1072
 - psychophysics of, 1073–1074, 1073*f*
 - research on, advances in (future directions for), 1076–1077
- Contour orientation
 - and binocular rivalry, 1313–1316
 - selective exposure to, effects of, 121, 199–200, 200*f*
- Contour units, 1613
- Contrast
 - achromatic, 882
 - apparent, 888
 - binocular processing of, 772–773, 773*f*, 774*f*
 - encoding of, in light-adapted eye, 851
 - induction of
 - neural mechanisms for, 889–890, 889*f*
 - spatial texture interactions and, 888–889, 889*f*
 - low, creating optical image at, 237
 - minimum detectable, 237
 - modulation, detection of, 1046–1047
 - objective, 888
 - and pattern adaptation, 1655
 - in pictures, 1097–1098
 - and receptive field dynamics, 739*f*, 739–741, 740*f*
 - simultaneous, 881–882, 882*f*
 - structure defined by, 1046–1047
 - successive, 882
- Contrast adaptation, 940*f*, 941–942, 942
 - in cortical neurons, 754, 754*f*
 - temporal dynamics of, 755
- Contrast depth asymmetry principle, 1286*f*, 1287, 1296–1297
 - application of, 1288
- Contrast differences, interocular
 - artificial changes in ocular dominance with, 775–776
 - binocular responses to, 773–774, 775*f*, 784–785
- Contrast discrimination, ideal observer analysis of, 832
- Contrast enhancement, 250
- Contrast envelope, 1304
- Contrast flash, 868
- Contrast gain
 - of M (magnocellular) cells, 485–487, 486*f*, 488*f*
 - of P (parvocellular) cells, 485–487, 486*f*, 488*f*
 - in pupil, 642, 653
 - saccades and, 1393*f*, 1394
- Contrast gain control, 178, 181, 888–890, 1063–1064, 1066
 - in binocular vision, 773–775
 - definition of, 888
 - electrophysiological evidence for, 889–890
 - in ganglion cells, 416, 487
 - in humans, 889–890
- interocular transfer of, 774–775
- neuronal activity level and, 741
- short-range horizontal cortical connections and, 736–737
- Contrast induction, 1046
- Contrast perception, 1046
- Contrast response function
 - binocular processing of, 772–773, 773*f*, 774*f*
 - of cortical neurons, 752*f*, 752–753, 753, 753*f*
 - descriptive model of, 759
 - during first 16 msec., 756, 756*f*
 - as function of contrast, 755*f*, 755–756
 - as function of contrast through time, 756, 756*f*
 - functional model of, 759–760
 - poststimulus time histograms of, 755*f*, 755–757, 756*f*
 - temporal dynamics of, 755*f*, 755–757, 756*f*
- Contrast sensitivity
 - achromatic, 177, 186
 - binocular deprivation and
 - in cats, 191, 193*f*
 - in humans, 193
 - in monkeys, 193
 - chromatic, 177, 186, 186*f*, 800–801
 - cone ratio variations and, 806*f*, 807
 - in ganglion cells, 418–419, 488–489
 - ideal observer analysis of, 831
 - in M (magnocellular) cells, 488–489
 - in P (parvocellular) cells, 488–489, 497, 501
 - in W cells, 498
- cone distribution and, 239*f*–240*f*
- contour orientation restrictions and, 200
- development of, 176–178, 177*f*, 186
 - behavioral versus physiological changes in, 164*f*, 164–165
- ideal observer model of, 160–163, 162*f*, 163*t*
- in macaque monkeys, 159, 160–163, 161*f*, 162*f*, 163*t*
- neural factors in, 159–163
- noise as limiting factor in, 177–178, 178*f*
- forced-choice, in laser interferometry, 804, 805*f*
- function, 1043, 1044*f*
- in ganglion cells, 416*f*, 416–419, 484–486, 486*f*
- grating (resolution) acuity and, 178–179
- in hMT/V5+ visual area, 1239
- ideal observer analysis of, 831, 831*f*, 832
 - photon noise-limited, 828–829, 829*f*
- in M (magnocellular) cells, 484, 485–486, 486*f*
- mean light level and, 1046, 1046*f*

- Contrast sensitivity (cont.)
 measurement of, 176–177, 177*f*
 spatial scale and, 1044, 1045*f*
 monocular deprivation and
 in cats, 196, 196*f*
 in humans, 197–198
 in monkeys, 196–197, 197*f*
 for natural images, 237, 238*f*
 newborn versus adult levels, in primates,
 159, 160*f*
 orientation selectivity and, 181
 in P (parvocellular) cells, 484, 485–486,
 486*f*
 receptive field responses and, 163–165,
 164*f*
 regional variation of, 1044–1045, 1045*f*
 and response timing, 185–186
 saccades and, 1391–1392, 1392*f*
 in scotopic vision, 843–844, 844, 844*f*
 in infants, 846
 spatiotemporal, development of, 176–178,
 177*f*
 visual deprivation and, 167–170, 168*f*
 Contrast sensitivity function(s), 177
 for achromatic and chromatic stimuli,
 1051, 1053*f*
 in scotopic vision, 844, 844*f*
 spatial, 925–927, 926*f*, 1060–1061,
 1062*f*
 Contrast signals, 1285
 Contrast threshold(s), 1073–1074, 1073*f*
 binocular, 772–773, 774*f*
 monocular, 773
 monocular-to-binocular ratio of, 773,
 774*f*
 in swept-parameter VER, 175–176, 176*f*
 Contrastive program, 1684
 Contrast-set gain control, 760–761
 in cortical neurons, 753, 753*f*, 760–761
 temporal dynamics of, 756–757
 Control
 and attention, comparison of, 1547
 cognitive. *See* Cognitive control
 Controlled processes, 1546–1547
 Convergence, 1300, 1415
 and accommodation, 1415
 cross-coupling between, 1301
 accommodative, 1415
 in corticocortical connections, 524
 excyclotorsion with, 1417
 of feedback connections, 535
 motoneurons in, 1415
 in retino-geniculo-cortical pathway, upper
 limit of, 675
 Convergence accommodation, 1415
 Convergence cells, 1418
 Conversion tables, for rods and cones, 838,
 839*f*
 Cornea, light scatter from, 798–799
 Corner frequency, 858
 Corollary discharge
 definition of, 1466
 and saccades, 1391, 1466–1481
 and visual processing in monkey,
 1466–1481
 Corpus callosum, 1564
 in cortical connectivity, 148
 Correlation-based models
 for mapping receptive fields, 706–707,
 707*f*
 of MT role in motion perception,
 1209–1211
 of orientation selectivity, 123*f*, 123–124
 quantitative, 1209
 trial-by-trial, 1209
 Correlogram, 184–185
 of stimulus-linked synchronization of
 LGN cell-pairs, 614, 616*f*–617*f*
 Correspondence
 anatomical, 779
 binocular, 779
 and binocular matching, 1301–1304
 Correspondence noise, 22
 Cortex. *See also* Cerebral cortex; Primary
 visual (striate) cortex; Visual cortex
 optic flow responses in
 in cat, 1268–1269
 in human, 1269
 organization of, 541, 554
 prefrontal, volition and, 1546–1559
 Cortical plate, 148
 neurons of, interareal connections of, 150
 Corticocortical connections. *See*
 Corticocortical pathways
 Corticocortical pathways, 1579
 convergence in, 524
 development of, 148–154
 divergence in, 524
 excitatory and inhibitory effects of,
 522–523
 function of, 522–528
 interarea, 522–523
 interarea, laminar specificity of, 150–151
 interhemispheric, 522
 laminar organization of, 529–530, 529*f*
 local, 523
 long-distance, 523
 patchy organization and axonal
 bifurcations in, 525–527, 526*f*
 retinotopic organization of, 524–525,
 525*f*
 structure of, 522–528
 synaptic transmission in, 527–528
 temporal aspects of, 530–532, 531*f*
 transthalamic, 580–582, 580*f*, 582*f*, 586
 types of, 523–524
 Corticofugal axons
 arborization of, 609, 610*f*
 asymmetry of, 611, 611*f*
 feedback from, 609–611
 and firing patterns in LGN cells,
 611–612, 613*f*, 622
 Corticofugal feedback, 609–614, 610*f*,
 611*f*
 Cortico-thalamo-cortical loop, 565, 593*f*,
 595, 599
 extrageniculate, pulvinar complex and,
 602–603
 functional specificity of, 603
 in neurodegenerative disease, 602
 Corticotropin-releasing hormone (CRH),
 retinal, 347–348
 Coverage factor
 anatomical, 674, 675
 definition of, 674
 geniculate, 674
 physiological, 674
 of thalamic afferents, 675
 Cow(s), rods of, outer segments of, 241
cpg-15 gene, 134
 Craik-O'Brien-Cornsweet illusion, 885,
 886*f*, 888, 889
 Cranioscopists, 8
 CREB. *See* cAMP response element
 binding protein
 Cricket (game), eye movements in, 1363,
 1363*f*
 Critical flicker frequency
 in scotopic vision, 844–845, 845*f*
 for visual evoked potentials, 177
 Critical period, 46, 47*f*
 for direction selectivity, 127
 for monocular deprivation, 46, 47*f*, 49,
 126, 193
 prolonged, neurotrophin blockade and,
 52, 54*f*
 for ocular dominance columns, 108, 112,
 126, 129, 133
 for orientation selectivity, 122, 127
 precocious closure of, overexpression of
 BDNF and, 55–58, 58*f*
 time course of
 inhibition and, 58
 neurotrophins and, 58
 Cross-correlation
 of horizontal connections and orientation
 selectivity, 735
 for mapping receptive fields, 706–707,
 707*f*
 of neuronal mosaics, 473
 of stimulus-linked synchronization
 between LGN cell-pairs, 614,
 616*f*–617*f*
 Cross-orientation inhibition, 701–702, 754
 Crossovers, genetic, and color vision
 defects, 979, 979*f*, 980*f*, 981–982
 Crowding, 1673
 Crustaceans
 color vision in, 964, 965–966
 vision of, 965

- CRX*
in macular degeneration, 43
and opsin expression, 40
in retinitis pigmentosa, 43
Cryptochrome genes, 625, 635
C-type natriuretic peptide, retinal
expression of, 347
Cue invariance, 1036
Cuneus, motion-sensitive regions of,
functional mapping of, 1234
Curl, in optic flow, 1250
Curvature, 1081
mathematical definition of, 1081
negative, 1081, 1081*f*
neuronal processing of, 1087
positive, 1081, 1081*f*
Cyclic adenosine monophosphate (cAMP)
and cortical plasticity, 129, 131–132, 137,
137*f*
and dopaminergic inhibition of ganglion
cells, 438, 439*f*
peptides and, 334, 336, 338, 340, 346,
348
Cyclic guanosine monophosphate (cGMP)
calcium regulation of, 227–228, 1006
circadian role of, 633, 635*f*
cytoplasmic concentration of, 219
dark concentration of, 244
and ganglion cell permeability, 431
hydrolysis of
maximal catalytic rate of, 219
by phosphodiesterase, 217*f*, 219, 1006
effect of genetic mutations on, 223,
224*f*, 225
predicted time course of, 219–220, 220*f*
rate constant of, 219
speed of, size of outer segment and,
241–244, 243*f*
ion channel opening/closing by, 217*f*, 219
in light adaptation, 229
nitric oxide and, 633–634
in phototransduction, 217*f*, 217–220,
223, 227–228
in synaptic transmission
amacrine cell-ganglion cell, 293
cone-bipolar cell, 283
photoreceptor-bipolar cell, 284, 285*f*
Cycloheximide, and cortical plasticity, 138
Cyclopean eye, 1300, 1415, 1424
Cyclopean gaze, 1350
Cyclopean percepts, 728, 729*f*
Cyclopean VEP, in binocular vision and
sensory fusion, 184–185
Cytochalasin, 296
Cytochrome oxidase-rich blobs, 681–683,
683*f*, 1568, 1568*f*, 1569
functions of, 502
versus interblobs, 502, 682–683
K (koniocellular) cells projecting to, 483,
485, 496, 496*f*, 497–498, 499, 503
reasons for, 502
in nocturnal versus diurnal animals, 502
and ocular dominance column
development, 147
Cytokine(s)
inhibition of rod production by, 39
and retinal cell differentiation, 67
- D**
d wave, of electroretinogram, 261, 261*f*
da Vinci, Leonardo, on image formation, 3
Dalmation dog, 1504, 1504*f*, 1576
Dark adaptation, 838, 851–858. *See also*
Scotopic (night) vision
adaptive independence and, 852–853
aging and, 846
amacrine cells in, 396
anomalies of, 855–856, 856*f*
bleaching in, 853
photoproducts of, 853–854
protective function of, 853
recovery from, 853, 854*f*
and chromatic discrimination, 874–875
chromatic thresholds in, 873
cone plateau in, 841
definition of, 851
ganglion cell excitability in, 426, 426*f*,
428, 436, 855
horizontal cell response in, 290
hue-pathway anomalies and, 856–857,
856*f*
inhibitory surrounds in, 364, 364*f*
luminance anomalies and, 858
peptides and, 334, 349
photopic threshold and, 852–858
red/green anomaly and, 857, 858*f*
of red/green pathway, 856–857, 858*f*
rod-cone break in, 845, 847, 852, 854,
855*f*
rod-cone interactions in, 854–855
retinal or cortical origins of, 855, 855*f*
rods in, 873
scotopic threshold and, 852–858
spinule retraction in, 296–298, 297*f*
summary of, 858
synaptic plasticity and, 295–298
veiling effect in, 853
of yellow/blue pathway, 856–857, 856*f*
Dark current, 244
calcium concentration and, 226
in photoreceptors, 216
restoration of, calcium and, 227
Dark light, 215, 859, 912
and absolute threshold, 816–817
concept of, application of, 817
in cones, 215
in rods, 215
Dark rearing
administration of neurotrophins during,
60
as replacement for visual experience,
50–52, 53*f*
technical difficulties in, 50–51
and BDNF levels, 133, 136*t*
versus binocular eyelid suture, 190–192,
191*f*, 192*f*
in cats, 190–192, 191*f*, 192*f*
classical signs of, 50, 53*f*
and cortical connectivity, 149
and cortical plasticity, 128, 129, 130, 131,
132, 133–134
and cyclic AMP levels, 132
effects of, 189
and GABA, 131
and glutamate receptors, 129, 136*t*
and light response, 89–90
and long-term depression, 128
and long-term potentiation, 128
in monkeys, 192–193
and NMDA receptors, 129, 136*t*
and ocular dominance columns, 132
developmental effects of, 112
plasticity effects of, 128
and orientation selectivity, 117, 119–121,
121*f*, 122, 123
and receptive field development, 89–90
Dark-excitatory responses, in receptive
field maps, 707
Darkness
calcium influx and efflux during, 225–
226
perception of, 883, 883*f*
Darwin, Charles, 63
Daughter cells, retinal, 77
Day
circadian responses to, 625–626
SCN neuron responses during, 631–632,
632*f*
subjective, 631
Daylight, natural, linear model for, 956,
956*f*
Daylight vision, *See* Photopic vision
De Vries-Rose law, 1046, 1046*f*
Decorrelated binocular input. *See*
Binocular disparity
Decrement thresholds, in DeVries-Rose
regime, 816, 817*f*
Decussation, in optic chiasm
defects of, 97–98, 102–103
development of, 94–103
lack of pigment (albinism) and, 100*f*,
102–103
partial, 94
pattern of, 5, 94–95
Deferred-saccade tasks, 1436
presaccadic burst activity for, 1437–1439
Defocus, 796, 800–801
Deformation, in optic flow, 1250
Degus, light responses of SCN neurons in,
630–631

- Delay activity, in visuosaccadic behavior, 1468–1470, 1469*f*
- Delay tasks, 1436
- Delayed match-to-sample (DMTS) task
in honeybees, 1507, 1510
symbolic, in honeybees, 1508
across sensory modalities, learning of, 1509–1510
in visual modality, learning of, 1508–1509, 1509*f*, 1510*f*
- Delayed nonmatch-to-sample (DNMTS) task, in honeybees, 1510
- Delayed reach task, 1326, 1326*f*
- Delayed-response task
matching-to-sample, prefrontal cortex (PFC) damage and, in monkeys, 1551, 1552*f*
prefrontal cortex (PFC) damage and in humans, 1551
in monkeys, 1551–1552
spatial, prefrontal cortex (PFC) damage and, in monkeys, 1551, 1552*f*
- Delayed-saccade tasks, 1436
- Delta ligand in Notch system, and retinal cell differentiation, 38, 79
- Dendrite(s)
of amacrine cells, 360, 399–400, 400*f*
AI, 396, 397*f*
AII, 396
arborization of, 83
starburst, directional and functional polarization of, 456–457, 457*f*
of bipolar cells, arborization of, 83
competitive, territorial nature of, 463
expansion and retraction of, and cortical plasticity, 137–138, 138*f*
filopodia of, and synapses formation, 88
of ganglion cells, 360, 410, 411*f*
arborization of, 82*f*, 82–83, 410, 411*f*
cell density and, 83
cell-cell interactions and, 83
in ON and OFF pathways, 266–268, 267*f*
functional maturation of, 84
growth patterns of, 470–471
lateral extent of territory, 85
midget, 410–411, 411*f*
outgrowth of, 81*f*, 81–82
parasol, 410–411, 411*f*
shunting inhibition of, and direction selectivity, 455
stratification and organization of, 84–86, 85*f*, 412–413
in synapse formation, 87
of horizontal cells, 370, 376
in visual cortex, neurotrophins and, 53
- Dendritic field(s)
of amacrine cells, size of, 396, 398, 399
competition among, and mosaic formation, 470–471
of ganglion cells
correspondence with receptive field, 417, 417*f*
diameter of, 413
stratification of, 412–413
- Dense noise, as stimuli for mapping receptive fields, 706, 714
- Density recovery profile (DRP), of neuronal mosaics, 473
- 2-Deoxyglucose autoradiography, of extrastriate cortex, 170
- 2-Deoxyglucose labeling, in ocular dominance columns, 111
- Deprivation, visual. *See* Binocular deprivation; Dark rearing; Monocular deprivation
- Depth
asymmetries in, 1286–1287, 1286*f*
binocular cues for, 928
and brightness, interactions of, 1636
constancy of, 1307
cues for, at isoluminance, 928
distortions of, analogous to Mach bands, 1305
inversion of
geometrical asymmetry in, 1296
photometric asymmetry in, 1296
monocular cues for, 928
of object surfaces, 1153–1154
perceptual organization of. *See* Depth perception
relative, judgments of, frame of reference for, 1306
reversal of, 1296–1297
stereoscopic, 1145–1146, 1145*f*, 1307
- Depth discontinuity, 1287–1288
- Depth measurement(s), local
contrast depth asymmetry principle and, 1284–1288
occlusion and, 1284–1288
- Depth of modulation, in binocular vision, 774, 775*f*
- Depth pedestal, 1304, 1305*f*
- Depth perception, 550, 928, 1284–1298, 1300, 1471, 1485, 1690–1691. *See also* Stereopsis
color vision and, 928
and form perception, 1302
multiple depth planes and, 1292–1297
visual completion and, 1288–1289, 1289*f*, 1291–1292, 1292*f*
- Depth stratification, 1292–1295
- Depth-detecting neurons, 765–766
- Descartes, René, 3
- Descriptive models
of cortical neurons, 759
goal of, 759
- Detection, in blindsight, 658
- Detection sensitivity, rod-cone interactions in, 867–869, 868*f*, 869*f*
- Detection tasks, ideal observer analysis of, 825, 827–834
quantum fluctuation-limited, 813–814
- Detection threshold, rod and cone signals and, 866
- Detective quantum efficiency, 816
- Deutan, 974
- Deuteranomaly, 975, 981, 983
- Deuteranopia, 875, 975. *See also* Dichromacy
- Development
of optic chiasm, 94–103
of retinal cells, 36–37, 37*f*, 63–68, 77–78
spatial overlap in, 36–37
temporal overlap in, 36–37, 77
of spatial selectivity, in humans, 174–186
of vision, 46–61
critical period for, 46, 47*f*
electrical activity and, 46
in humans
quantitative and qualitative characteristics of, 174
research methods for studying, 174–176
ideal observer model of, 160–163, 162*f*, 163*t*
neurotrophins and, 46–61, 47*f*
postnatal changes and, 159–163
in primates, neural limitations on, 159–171
of visual cortex
accelerated, overexpression of BDNF and, 55–58, 57*f*, 58*f*, 136
neural factors in, 165–170
visual deprivation and, 167–170
- DeVries-Rose law/regime, 815–816, 816*f*
decrement thresholds in, 816, 817*f*
explanation of thresholds in, 816
- Diazepam, and ocular dominance plasticity, 131, 133
- Dichlorokynurenic acid (DCKA), glycine receptor response to, 356*t*, 357, 358
- Dichoptic tests, of binocular vision, need for, 767, 776, 777*f*
- Dichromacy, 965, 968, 971
in animals, 964
in dogs, 962–963
in humans, 963
- Dichromats, 372
pupil responses in, 650–652, 651*f*
pupil responses of, 641–642
- Diencephalic neurons, early-born, and regulation of ganglion cell axons, 96, 97*f*
- Difference-of-Gaussians model, of ganglion cell receptive fields, 415, 416*f*
limitations of, 418
- Differential motion, 1253

- Differentiation, of retinal cells, 37–39, 63, 66–68, 78–79, 467–471. *See also specific retinal cells*
- environment and, 66–67, 79
- extrinsic control of, 67
- in inner and outer plexiform layers, 81–86
- inner cells, 37–38
- lineage regulation of, 66–67
- outer cells, 39
- at quantitative level, 72. *See also* Retinal cells, number and density of
- transcription factors and, 38–39, 68, 78
- Diffraction, 798
- and image formation, 798, 798f, 799–800
- trade-off with aberrations, 799–800
- Dihydropyridine, calcium currents sensitive to, in ganglion cells, 432, 433
- Dihydroxyphenylacetaldehyde (DOPAL), 313f, 314
- Dihydroxyphenylamine (DOPA), 313, 313f
- Dilator muscle of iris, and pupil responses, 642, 652–653
- Dim flash response
- mutations of inactivation proteins and, 222, 223–225, 224f, 225f
- recovery from, calcium and, 227
- Dim light responses, 838
- ON pathways and, 273
- Diplopia, 1300
- Dipper phenomena, 815, 818
- DIPSA visual area, motion sensitivity of, functional mapping of, 1234–1235, 1235f
- DIPSM/L visual area, motion sensitivity of, functional mapping of, 1234–1235, 1235f, 1239
- Direction, discrimination of. *See also* Motion perception
- in blindsight, 658, 660, 660f, 662
- saccades and, 1397, 1397f
- spatial scale and, 1049, 1049f
- Direction selectivity
- amacrine cells and, 361, 404–405, 456–460, 457f, 458f, 459f
- in area MT, 20–21, 619, 621f, 621–623, 1204–1205, 1205f, 1211–1212
- chromatic input and, 1218–1219
- calcium and, 25
- color cues and, 1220–1221, 1221f
- and color processing, 1023–1024, 1023f
- in complex cells, 617, 715, 716
- linear and nonlinear properties of, 753
- critical period for, 127
- development of, 182–184, 184f
- developmental motion asymmetry and, 183–184, 184f, 185f
- evolutionary variation and, 71
- feedforward connections and, 532–533
- fundamental features of, 451
- in ganglion cells, 404–405, 451–461
- acetylcholine and, 457–458
- amacrine cells and, 404–405, 456–460, 457f, 458f, 459f
- Barlow-Levick model of, 453, 455f
- challenges in studying, 455–456
- excitatory model of, 453–455, 455f
- feedforward inhibition and, 451–452, 454f
- fundamental features of, 451
- GABA and, 355, 361, 452, 457
- general requirements for, 453–455
- independence of sign contrast, 451, 454f
- inhibitory model of, 453, 454f, 455f
- injected after recording, 451, 453f
- lateral inhibition and, 453–455, 454f
- mosaic organization and, 466–467
- mosaics of, 466–467
- motion detection and, 453–455, 456–459, 458f
- nonlinearity and, 454f, 454–455, 455f
- nonlinearity in, 454f, 454–455, 455f
- ON-OFF cells in, 451, 452f, 453f
- crosstalk between, 457
- physical asymmetry for, 453–455, 454f, 455f
- alternative anatomical locations for, 459–460
- postsynaptic mechanisms in, 454f, 454–456
- postsynaptic model of, 454f, 454–456
- presynaptic mechanisms in, 454f, 454–456
- presynaptic model of, 454f, 454–456
- presynaptic versus postsynaptic computation of, 455–456
- Reichart's model of, 453–455, 455f
- responses to light and dark edges, 451, 454f
- synaptic connections and, 460f, 460–461
- time delay for, 453–455
- tracer-coupling studies of, 466
- general requirements for, 453–455
- in hMT/V5+ visual area, 1239, 1240, 1240f
- inhibition and, 361
- in lateral geniculate nucleus, cortical feedback and, 612–613, 615f, 617
- lateral inhibition and, 127, 453–454, 454f
- linear and nonlinear properties of, 753
- motion processing and, 183–184, 184f, 185f, 453–459, 458f, 549–550, 1240f, 1250
- during natural fixation, 758f, 758–759
- of optomotor response in insects, 1196
- plasticity of, 126–127
- in primary visual cortex, 549
- linear and nonlinear properties of, 753
- MT feedback and, 621f, 621–622
- spatiotemporal mechanisms underlying, 710–711, 711f
- temporal dynamics of, 758f, 758–759
- in receptive fields, 89, 165f, 165–166, 451, 452f
- spatiotemporal mechanisms of, 710–711, 711f
- selective visual exposure and, 201, 201f
- in simple cells, 617
- linear and nonlinear properties of, 753
- spatiotemporal mechanisms of, 710–711, 711f
- of single neurons, 17, 18
- spatiotemporal mechanism underlying, 710–711, 711f
- Stiles-Crawford effect in, 216, 797
- temporal and spatial inseparability in, 26
- temporal dynamics of, 758f, 758–759
- testing of, 126
- visual deprivation and, 189
- visual evoked potentials in, 182–184, 184f
- Direction selectivity index (DSI)
- comparison with linear receptive field maps, 710–711, 711f
- in MT neurons, 1204
- of receptive fields, 165f, 165–166
- Directional tuning, of reach-related activity in posterior parietal cortex, 1325–1326, 1325f
- Disc membrane, of rods, 216, 216f
- rhodopsin density in, 241–244, 243f
- Discrimination
- chromatic. *See* Chromatic discrimination
- color. *See* Color discrimination
- colorimetric purity, 913–914, 914f
- contrast, ideal observer analysis of, 832
- of direction. *See* Direction, discrimination of; Motion perception
- object. *See* Object discrimination
- optimal, given statistically independent sources of information, 827–828
- of orientation, by honeybees, 1502, 1503f
- of shape, in blindsight, 659
- tritan, rods and, 874–875
- wavelength. *See* Wavelength discrimination
- Discrimination tasks, ideal observer analysis of, 825, 827–834
- Disparity, retinal image, 1485, 1632. *See also* Binocular disparity; Binocular vision; Stereopsis
- absolute, 550, 780, 783, 1303, 1303f, 1304
- coded from edges and contrast information, 1304
- coding, 1306–1307, 1306f
- phase, 1306–1307, 1306f
- position, 1306–1307, 1306f
- horizontal, 1308, 1308f, 1310

- Disparity, retinal image (cont.)
 local contrasts and, 1296–1297
 phase, 1306–1307, 1306*f*
 position, 1306–1307, 1306*f*
 processing of, by early spatial filters, 1306
 relative, 550, 1303–1304
 thresholds, for stereopsis, 1304, 1305*f*
 in stereopsis, 1300
 upper limit of, 1304
 vertical, 1308, 1308*f*
- Disparity-selective neurons, 550, 715, 716, 765–766, 766*f*, 767*f*, 779–781, 781*f*
- Displaced amacrine cells, 395
- Distance flown, estimation by insects,
 motion cues for, 1197–1198, 1198*f*
- Diurnal animals, K (koniocellular) cells of, 498, 499, 502
- Diurnal rhythm, neuronal knowledge of, 24
- Divergence, 1415
 in corticocortical connections, 524
 of feedback connections, 535
 motoneurons in, 1415
 in optic flow, 1250
 versus radial flow, 1250
 in retino-geniculo-cortical pathway, upper limit of, 675
- Divergence cells, 1418
- DNA replication, in retina, 77
- Dog(s)
 color vision in, 965
 parameters for, 962, 963*f*
 study of, 962–964
 diurnal knowledge in neurons of, 24
 optic chiasm agenesis in, 103
 effect on LGN lamination, 114–115
 retinal cells of, 6*f*–7*f*
 number in domestic animals versus wolves, 70
 visual areas outside primary visual cortex in, 10
- Dominance, definition of, 976
- Dominance waves, 1314*f*, 1318–1319
- Dominator spectral sensitivity curve, 16–17
- Donders' law, 1493–1494
- Dopamine (DA), 313*f*, 313–314
 amacrine cells expressing, 313–314, 365, 383, 400–401, 401*f*, 402, 405, 440
 lineage bias of, 67–68
 receptive field size of, 396
 and calcium currents, 432, 438–439, 441*f*
 future directions for study of, 314
 GABA interaction with, 365
 ganglion cell inhibition by, 438–443
 feedforward, 439–440
 mechanisms of, 438–439, 439*f*, 440*f*, 441*f*
 and ganglion cell light responses, 440–443, 442*f*
 as global modulator, 313–314
 and horizontal cell function, 372, 380, 383–384, 384*f*
 interaction with glutamate, 384
 light and, 440
 localization of, 313*f*, 313–314
 metabolism of, 304, 313*f*, 313–314
 peptide action on, 337, 344
 signals about nervous system state carried by, 134
 and sodium currents, 438–439, 441*f*
 and spinule formation, 296
 transporters of, 313*f*, 314
 plasma membrane, 313*f*, 314
 vesicular, 313*f*, 314
 volume diffusion of, 383
- Dopamine receptor(s), 313*f*, 314
 heptahelical, 313*f*, 314
 in synaptic transmission, 314
- Dorsal raphe nucleus, inputs to A layers, 568, 571
- Dorsal stream, 489, 530, 541, 542*f*, 1371, 1372*f*, 1585
 anatomical organization of, 541, 542–544, 543*f*
 anterior, motion processing in, 1261–1262
 color processing in, 548
 connections beyond modality-specific visual system, 553–554
 feedforward inputs to, 150
 integration of information about motion, color, and form in, 553, 554*f*
 lesions of, behavioral effects of, 541–542, 541*f*, 551–553
 motion processing in, 549–550, 551–552, 1261–1262
 neurons in, 541
 attention and, 547
 latency of, 530–532, 531*f*
 properties of, 549–551
 on-line system and, 1683
 posterior, motion processing in, 1261
 processing in, visuomotor aspects of, 530, 532
 subcortical connections with, 544
 visual areas corresponding to, in macaque, 510*f*–511*f*, 511–512
- Dorsal terminal nucleus, connections with area MT, 1203, 1204*f*
- Dorsoventral axis, maturation of, 34
- Dot product decoding, 1169, 1170, 1171*f*
- Double vision, 1485
- Double-bouquet cells, in primary visual cortex (V1) of macaque, 689
- Double-flash procedures, rod-cone interactions reported for, 868
- Double-step saccade task, 1440–1442
- DP (dorsal prelunate) visual area, macaque, 510*f*–511*f*, 512
 homology with human visual area, 518
- d*-prime measure
 in ideal observer analysis, 828
 in signal detection theory, 19
- Drifting gratings, simple cell responses to, 750
- Drifting steady-state measurements, of cortical neurons, 749–750, 757
- Drivers
 feedforward connections as, 533
 properties of, 533
 of pulvinar cells, 580, 582–583
 pulvinar region, 596
 retinogeniculate, 572–573, 578–580, 582–583, 586
 in thalamocortical relays, 572–573, 578, 579
- Driving
 change blindness and, 1527
 eye movements in, 1360–1362, 1361*f*
- Drosophila*
 ectopic eye formation in, 33–34
 imaginal disc of
 neurogenesis in, 37–38
Pax-6 expression in, 33–34
- DSR (direction, size, rotation) region, 1262
- Duplicity theory, 851–852
- Duration, and threshold, 819*f*, 820
- Dynamic core hypothesis, 1685, 1688
- Dynamic noise experiments
 in functional mapping of motion regions, 1236–1237
 for studying pupil responses, 643, 644*f*, 645, 647, 650–652, 651*f*
- Dynamic pupil light reflex, 641, 642, 643*f*
- Dyschromatopsia, 1035
- Dysexecutive syndrome, 1548
- Dyslexia, magnocellular pathway in, 490
- ## E
- EAAT glutamate transporters, 305*f*, 306, 307
- Ebenbreite*, in Gestalt psychology, 1575
- Eccentricity. *See* Retina, eccentricity of
- Ecological approach, to perception and action, 1247
- Ectopic eyes
Pax-6 gene and, 33–34, 66
 retina competent/biased blastomeres and, 64
- Edge(s)
 boundary, 1070
 coding of, 1056
 definition of, 1070
 luminance, 1108, 1581
 in scenes, 1070
 stereo, 1581
 neuronal selectivity for, 1145, 1145*f*
 texture-defined, 1107*f*, 1108
- Edge detection
 scale and, 1053

- scale combination in, 1056
- Edge detector, 747–748
- Edinger-Westphal (EW) nucleus, and pupil responses, 642, 653, 654*f*
- Effective stimulus, 1644
- Effector protein, in phototransduction, 217
optimization for speed, sensitivity, gain, and noise, 241–244
- Efference copy, saccades and, 1391, 1442
- Efference copy error signals, 1496
- Egocentric representations, 1183
- Ehrenstein figure, 1574, 1575*f*
- Einstellung*, 1576, 1576*f*
- Electrical activity
in binocular competition, 49
and cortical plasticity, 54
interactions with neurotrophins, 46, 47*f*, 49, 54, 59
MAPK activation by, 59*f*, 59–60
during monocular deprivation, 49
and visual development, 46
- Electrical stimulation studies
of binocular disparity and stereoscopic vision, 789–790
of horizontal cortical connections, 733–734
of long-term potentiation and depression, 127–128
of MT role in motion perception, 1212*f*, 1212–1213
of neural activity in primary visual cortex, 9–10
of orientation selectivity, 122–123
of SCN neurons, 629
of visual areas outside primary visual cortex, 10–11
of visual field representation on cortex, 9–10, 10*f*
- Electroencephalogram (EEG), versus steady-state visual evoked potentials, 174–175, 175*f*
- Electron microscopy, of synapses, 87, 268, 279, 292, 293–294, 396, 413
- Electrophysiological studies. *See also* Visual evoked potential(s)
of calcium-regulated disc membrane reactions, 227
of human visual development, 174
of ocular dominance columns, 108, 111
of primary visual cortex, 108
of SCN neurons, 629–632, 630*f*–631*f*
of spatial vision development, 159
- Electroretinogram
ACE inhibitor effects on, 347
in congenital stationary night blindness, 272–273
in melanoma-associated retinopathy, 272, 273*f*
ON and OFF signals in, 260–261, 261*f*
in ON pathway knockout mice, 272
of peptide action in retina, 337
scotopic, in infants, 846
suppressive rod-cone interaction (SRCI) in, 389
- Ellipsoid, 216, 216*f*
- Embryonic cells, retina competent and specific, 64*f*, 64–65
- End gaps, 1627, 1633–1634
in response to Bregman-Kanizsa image, 1634, 1635*f*
- Endocytosis, of synaptic vesicles
in bipolar cells, 286–288, 287*f*
in photoreceptors, 282
- Endoplasmic reticulum, of cones and rods, 216, 216*f*
- Endstopping
horizontal cortical connections and, 739*f*, 739–741, 740*f*
vertical cortical connections and, 740
- Energy model
binocular, 785
of complex cells, 706, 715–716, 716*f*, 717
- Engineered spillover, of photoreceptor synapses, 247, 247*f*
- Enkephalin(s)
cellular physiology studies/calcium imaging of, 337
and circadian rhythms, 628
retinal, 334, 348
- Entorhinal cortex, 529*f*
- Eph A receptor, and optic chiasm development, 97*f*, 99
- Eph B2, and positioning of retinal cells, 42
- Eph B3, and positioning of retinal cells, 42
- Eph B receptor, and optic chiasm development, 97*f*, 99
- Eph receptor tyrosine kinases
and optic chiasm development, 97*f*, 99
retinal positioning information conveyed by, 42
- EphA3 receptor, and positioning of retinal cells, 42
- Ephrin A2
overexpression of, 99
and positioning of retinal cells, 42
- Ephrin A5
overexpression of, 99
and positioning of retinal cells, 42
- Ephrin ligands
and optic chiasm development, 97*f*, 99
and positioning of retinal cells, 42
- Epilepsy, photosensitive, 890
- Equal-luminance gratings, pupil responses to, 649*f*, 649–650, 650*f*
- Equidistance tendency, 1632
- Equiluminant stimuli, 1217
- Equivalent background hypothesis, 957
- Equivalent background light, in photoreceptors, 215
- Equivalent light, photoproducts of bleaching as, 853–854
- Equivalent luminance contrast (EqLC), 1218
for blue/yellow gratings, 1218
in paradigm to measure chromatic input to MT visual area, 1221–1222, 1222*f*
for red/green gratings, 1218
univariant, in humans, 1223
- Equivalent noise paradigm, in contrast sensitivity, 177–178, 178*f*
- Equivalent surface, 951
- Equivalent surface reflectance, 951–952
- ERK 1, 2 cascade, and plasticity, 58–60
- Error signals
efference copy, 1496
and ocular motor learning, 1496
proprioceptive, 1496
visual, 1496
- Escherichia coli*, biophysical mechanisms in, 25
- Esotropia, 1494
- ET* gene, expression of, in eye fields, 34
- Evanescent wave microscopy, of synaptic vesicle cycling in bipolar cells, 287–288
- Event-related potentials (ERP), in change detection, 1528, 1531–1533, 1534
- Evoked potential(s). *See also* Visual evoked potential(s)
from areas outside primary visual cortex, 10–11
in map of visual field representation, 9–10, 10*f*
monocular deprivation and, 51*f*–52*f*
effects of exogenous neurotrophins on, 51*f*–52*f*
in spatial vision development, 159
- Evolution
adaptations of vision in, 943
of brain, studying, methods for, 1563–1564
of color vision, 967–970
of visual systems, 825
in primates, 1563–1570
- Excitatory neurotransmitters, in retina, 86*f*, 86–87
- Excitatory postsynaptic potential(s) (EPSP)
GABA_B receptor and, 363*f*, 363–364
horizontal connections and, 733–734
in long-term depression, 127
in long-term potentiation, 127
and neuronal synchrony, 742*f*, 742–743
retinal, 571, 573
age and, 321–322
size of, BDNF and, 133
synchronization and, 1667–1669

- Exclusion ratio, in spatial correlograms,
resistance to undersampling in mosaic
measurement, 473, 474*f*
- Executive function. *See also* Volition
models of, 1556–1558, 1558*f*
- Exocytosis, of synaptic vesicles
in bipolar cells, 286–288, 287*f*
in photoreceptors, 282
- Expansion of response, in cortical neurons,
752*f*, 752–753, 759
temporal dynamics of, 756–757
- Experience. *See also* Activity
deprivation of. *See* Binocular deprivation;
Dark rearing; Monocular deprivation
and orientation selectivity, 119–121, 121*f*
and ventral stream processing, 547
- Express saccades, 1440
- External fiber layer, of retina, 4*f*
- Extinction, 1131
visual, 1519
- Extracellular recording
of peptide action in retina, 337
of SCN neurons, 629–632
- Extraretinal theory, of rotation problem,
1252
- Extrastriate body area (EBA), 1180*f*, 1183,
1184
- Extrastriate cortex, 1371, 1372*f*
attention and, 546–547
binocular disparity selectivity in, 781,
785–787
color processing in, 1017–1026
interactions with other visual attributes,
1023–1024, 1023*f*
isoluminant stimuli and, 1021–1023,
1022*f*, 1023*f*
connections of, exuberant, 170
development of
neural, 170–171
visual deprivation and, 170–171
- dorsal
input to, 1260–1261
in spatial perception, 1260
- image parsing in, 1139–1149
- macaque, 680–681
- neuronal responses in, modulation by
attention, 1538–1539
- neurons, 1139
and oculomotor system, 1372*f*
receptive field size in, 1045
shape coding in, 1594
and stereoscopic vision, 781, 785–787
visual areas of, 11, 515
behavioral evidence for functions of, 11
- Extrinsic noise, importance of, 19
- Exuberant cortical connections, 146, 148,
170
- Eye field(s)
development of, 33–34, 64–66, 68
frontal. *See* Frontal eye field (FEF)
- initial demarcation of, 33–34
occipital, 1429*f*
parietal. *See* Parietal eye field (PEF)
posterior, 1429*f*
separation into two eye primordia, 34
stem cells of, heterogeneity of, 67
supplementary. *See* Supplementary eye
field (SEF)
- Eye movement(s). *See also* Gaze; Saccades
abnormal
cerebellar dysfunction and, 1493–1494
in nondeussating retinofugal fiber
syndrome, 103
and actions
in domestic tasks, 1359–1360, 1359*f*,
1360*f*
spatial accuracy of, 1364–1365, 1364*f*
in activity, 1357–1363
buffers in, timing and role of, 1360*f*,
1361*f*, 1365
intrinsic salience and, 1359*f*, 1365
with (involving) movement, 1359–1363
and top-down control, 1359*f*, 1365
without movement (sedentary
conditions), 1357–1359
anticipation and, in ball games,
1362–1363, 1363*f*
and attention, 1596–1597, 1596–1599
in change detection, 1528, 1529–1531
conjugate, 1415
conjugate versus monocular commands
for, 1423–1424
control of
brainstem substrate for, 1486
cerebellar, 1408–1409, 1485–1496
cortical
in humans, 1429*f*
in primates, 1428, 1429*f*
motion-sensitive visual regions in, 1241
premotor control signals for, 1486
in copy typing, 1358–1359, 1358*f*
and cortical plasticity, 128
in daily life, 1357–1367. *See also* Gaze
control, under ecologically relevant
conditions
directionally appropriate, development of,
182
disconjugate, cerebellar lesions and,
1494–1495
in driving, 1360–1362, 1361*f*
dysjunctive, 1415
FEF and, 1445
electrically elicited from frontal eye field
characteristics of, 1428–1432
presaccadic burst activity and,
1433–1435, 1434*f*
evoked by optic flow, 1271
fast, 1342
and functional mapping of motion
regions, 1229
- information flow for, 1367, 1367*f*
in manipulative tasks, 1363–1364, 1364*f*
measurement of
in humans
corneal reflex method for, 1340
optical lever technique for, 1340–1341,
1344
methods for, 1339
requirement for, 1339
multisensory integration and, 1327,
1329–1330, 1329*f*, 1370
in musical sight reading, 1358, 1358*f*
neural substrate for, 1371, 1372*f*
planning of, posterior parietal cortex in,
1326–1328
pulvinar and, 601
pursuit, 1369, 1370*f*. *See also* Eye
movement(s), smooth pursuit
and cortical motion processing,
1270–1271
optic flow responses during, 1272–1274,
1274*f*, 1275*f*
rapid shifts in, 1347. *See also*
Microsaccades
in reading, 1343, 1344*f*, 1357–1358, 1525
rotational, 1489–1490
saccadic. *See* Saccades
in sedentary activity, 1357–1359
slow, 1342, 1485
involuntary, 1344
and noisy drifts, 1344
optokinetic, 1485
vestibular, 1485
slow control, 1342
smooth, 1342, 1343–1344
anticipatory, 1344
smooth pursuit, 1342–1343, 1402–1410,
1485
alternative cortical pathway for,
1407–1408
anticipatory, 1402, 1405–1406, 1406*f*
in ball games, 1363
cognitive aspects of, 1402, 1405, 1410
neural pathways supporting,
1406–1407, 1407*f*
control of, 1422, 1487
cortical, 1402
cortical regions for, 1428, 1429*f*, 1430*f*
extraretinal and retinal image motion
substrates for, 1406–1409
frontal eye field and, 1443–1445,
1443*f*–1444*f*
gain control for, 1408
initiation of
smooth and saccadic components of,
1403
vector averaging during, 1402–1403
to larger and more complex stimuli,
1403–1405, 1404*f*
MT lesions and, 551

- in natural scene, 1402–1406
 - neural pathway for, 1425, 1431, 1432*f*, 1492–1493, 1493*f*
 - and neural pathway for saccades, 1409–1410, 1422, 1432*f*
 - and optokinetic reflex, distinction between, 1403–1405
 - postsaccadic enhancement of, 1403
 - to step-ramp target motion, 1403
 - superior colliculus and, 1458–1460
 - target selection for, 1402–1403
 - study of
 - device for, 1359
 - ecologically relevant conditions for, 1339–1340, 1349–1350
 - top-down influence on, 1365, 1366*f*
 - torsional, 1415, 1417, 1486
 - abnormalities of, during fixation, 1493–1494
 - tracking, 544
 - type V, 1348–1349, 1348*f*, 1349*f*
 - types of, 1342, 1348, 1485
 - vergence. *See* Vergence
 - wave, 1344
 - Eye position
 - and optic flow responses, 1269–1270
 - primary, 1493
 - Eye velocity, premotor commands for, 1486
 - Eye-hand movement, neural control of, 1462
 - Eye-head movement(s), coordinated,
 - superior colliculus in, 1454–1458
 - Eyelid suture
 - binocular, versus dark rearing, 190–192, 191*f*, 192*f*
 - monocular, versus chronic monocular cycloplegia, in monkeys, 196–197, 197*f*
 - Eye-specific segregation
 - historic studies of, 108
 - in lateral geniculate nucleus lamination, 108–110
 - instructive versus permissive role of activity in, 113–115
 - in retino-geniculo-striate pathway, development of, 108–115
- F**
- F actin, and spinule formation, 297
 - FACADE (Form-And-Color-And-Depth)
 - theory, 1626, 1627, 1631–1632, 1633, 1636, 1637
 - Face(s)
 - emotional salience of, perception of, 1580
 - expression on, neuronal response to, 1166–1167
 - identity of, distributed coding of, 1167–1170
 - advantages of, 1170
 - social/emotional responses to, neural substrate for, 1167
 - Face aftereffects, 945
 - Face blindness. *See* Prosopagnosia
 - Face cells, 545, 546, 1087, 1153, 1553, 1580, 1640
 - view dependency of, 545, 1171–1172, 1642
 - Face detectors, 18
 - Face perception, 1580
 - adaptation in, 944–945, 945*f*
 - cortical areas in, 1685
 - neurons in, 1691
 - Face processing, afferent systems for, 1167
 - Face recognition, 1066, 1153, 1165–1175, 1179–1182, 1180*f*
 - in blindsight, 659–660
 - levels of, 1648
 - neuronal activation in, 1156–1157, 1157*f*
 - synchronized gamma oscillations in, 1677–1678
 - tuning in, 1646, 1647*f*
 - ventral pathway in, 1534
 - visual areas for, 515, 516*f*
 - Face representation, distributed nature of, 1167–1169, 1168*f*, 1169*f*
 - advantages of, 1170
 - Facial movement, and motion processing, 1242
 - False alarms, 812, 818, 854
 - Far cells, 1425
 - in stereoscopic vision, 766, 767*f*
 - Far disparity, 780, 788
 - Far response cells, 1425
 - Farnsworth-Munsell 100 hue test, 915
 - Fast Fourier transform, for mosaic measurement, 474
 - Fastigial nucleus
 - posterior, in eye movement control, 1491–1493
 - and pursuit- and saccade-related activity, 1409
 - Fastigial oculomotor region (FOR)
 - in eye movement control, 1486, 1491–1494
 - in ocular motor learning, 1495–1496, 1495*f*
 - and pursuit behavior, 1408–1409, 1492–1493, 1493*f*
 - Feature(s)
 - processing system for, 603, 1158, 1582
 - selectivity of cortical neurons for, 747–748, 1158
 - Feature binding
 - pulvinar region in, 603
 - TE area in, 1158
 - Feature Contour System (FCS), 1627, 1635
 - Feature contours, 1627
 - Feature detection. *See* Segmentation
 - Feature detectors, ON and OFF pathways
 - as, 260, 273–274
 - Feature map, visual information encoded as, 1139
 - Fechnerian threshold, 811, 812*f*
 - Feedback. *See also* Feedback connections
 - in cortical function, 695–697
 - static, 1453–1454
 - subtractive, 913
 - in visual processing, 609–623
 - Feedback connections, 720
 - and contextual modulation, 725–726, 727*f*
 - cortical, 146–147, 522, 523–524, 523*f*, 543–544, 609–623, 695–697, 1071, 1579
 - activity and, 153, 154
 - anatomical considerations in, 523–524
 - anterograde tracing of, 152–153
 - from area MT, 609, 614–622
 - effects of, 619–622, 620*f*, 621*f*
 - in associating objects, 547
 - in attention, 536
 - to bipolar cells, 356, 359, 360, 360*f*, 361–363, 362*f*
 - between boundary and surface streams, 1633
 - and center-surround interactions, 535
 - convergence of, 535
 - development of, 152*f*, 152–153
 - divergence of, 535
 - elimination of, 152*f*, 153
 - experimental evidence for, 697–702
 - versus feedforward connections, 153, 154
 - in figure-ground segregation, 536
 - folded, 1630*f*
 - functional roles of, 533–536
 - future directions for study of, 622–623
 - hierarchical models of, 1613
 - from horizontal cells, 290, 381–383, 382*f*, 383*f*, 386, 388–389
 - in image representation, 1613
 - inhibitory and excitatory responses in, 154
 - interareal, 149–150
 - laminar specificity of, 150–151
 - to lateral geniculate nucleus, 609–614, 622
 - anatomical considerations in, 609–611, 610*f*, 611*f*
 - and LGN cell firing patterns, 611–612, 613*f*, 622
 - and LGN spatial interactions, 612–614, 614*f*
 - and orientation selectivity, 612–614, 615*f*, 616*f*–617*f*, 695–702
 - maturation of, 152*f*, 153, 154
 - and neuronal synchrony in lower-order areas, 535–536

- Feedback connections (cont.)
 number of, 150
 organization of, 524–525, 525*f*
 patchy organization and axonal bifurcations in, 526–527, 526*f*
 to perigeniculate nucleus, 609, 610
 and phototransduction, 216, 217, 223, 225–228
 remodeling of, 152*f*, 153
 and responses to receptive field center stimulation, 533–535
 retrograde tracing of, 152–153
 role of, 150
 in superior colliculus, 1451–1454
 and synaptic organization, 153–154
 synaptic transmission in, 527–528
 termination of, 150
 to thalamic reticular nucleus, 609
 in top-down processes, 536
 and eye movements in driving, 1360–1362
- Feedforward connections, 720
 cortical, 146–147, 522, 523–524, 523*f*, 543–544, 695–697, 1069, 1071, 1579
 anatomy of, 523–524, 674
 clusters of, 151, 153
 conjunction-specific neurons in, 1666, 1666*f*
 in cortical function, 695–697
 cortico-cortical, 147
 development of, 151, 152*f*
 directed growth and target selection by, 151, 154
 experimental evidence for, 697–702
 versus feedback connections, 153, 154
 functional roles of, 532–533
 and ganglion cell inhibition, 439–440, 451–452, 454*f*
 inhibitory and excitatory responses in, 154
 interareal, 149–150
 laminar specificity of, 150–151
 number of, 150
 in object recognition, 1642
 organization of, 524–525, 525*f*
 patchy organization and axonal bifurcations in, 525–527, 526*f*
 retrograde tracing of, 151, 152*f*
 role of, 150
 in superior colliculus, 1451, 1453–1454
 and synaptic organization, 153–154
 synaptic transmission in, 527–528
 termination of, 150, 154
 thalamocortical, 146–147
 visual deprivation and, 153
 and eye movements in driving, 1360–1362
- FEF (frontal eye field) visual area. *See* Frontal eye field (FEF)
- Felderfüllung*, 1573
- Felleman and Van Essen scheme, for partitioning macaque visual cortex, 508, 510*f*–511*f*, 512
- Ferret(s)
 binocular deprivation in, dark rearing versus eyelid suture, 190–191
 dendritic development in, neurotrophins and, 53
 ganglion cells of
 dendrite development in, 83
 developing, spontaneous activity in, 88–89
 lateral cortical connections in, 1071
 lateral geniculate nucleus in, lamination of, 114
 monocular deprivation in, 126
 preventive effects of neurotrophins in, 53
 ocular dominance columns in, development of, 110, 147
 ON and OFF leaflets in LGN of, 271
 optic chiasm in
 development of, 98
 organization of, 95, 95*f*
 orientation selectivity in, 117–124
 activity-dependent, mechanisms in, 121–124
 development of, 119–121, 121*f*
 first detection of, 119
 map of, 119, 120*f*
 visual experience and, 119–121
 process outgrowth from retinal neurons of, 82
 visual processing in, anatomical and functional organization of early stages of, 117–119, 118*f*
- Ferrier, David, 11, 11*f*
- FFA. *See* Fusiform face (FF) visual area
- Fiber layer, of cerebral cortex, 7–8, 8*f*
- Fibroblast growth factor(s)
 and opsin expression, 39
 production of, by Müller glia cells, 41
 and retinal cell development, 65
 and retinal cell differentiation, 68
- Field potentials, retinal, ON and OFF signals in, 260–261, 261*f*
- Figure-ground correlates, 1581
- Figure-ground segregation, 545, 722–725, 1106, 1115
 contextual modulation and, 722–725, 725–726, 727*f*, 728, 729*f*
 feedback connections in, 536
 neural correlate of, 722, 724*f*
- Figure-ground separation (assignment), 1519, 1580, 1582, 1631–1633
 bipole cells in, 1633
 boundary pruning and, 1635
 in Gestalt psychology, 1574–1576
 neural mechanism for, 1126, 1576
 reversals, human cortical analysis of, 1126
 segmentation and, 1124–1126
 three-dimensional, 1628, 1635
 T-junctions and, 1635
- Filling-in domains (FIDOS), in surface perception, 1628, 1631–1637
 binocular, 1636–1637
 monocular, 1634–1635, 1635*f*, 1636
 opponent, 1634
- Filling-in effect, 1129–1130, 1130*f*, 1139, 1140*f*, 1573, 1627–1628, 1631–1632, 1654–1655
 evidence for, 1628–1629
 surface, 1129–1130, 1582
- Filopodia, dendritic, and synapses formation, 88
- Filter(s)
 bandpass, cone synapses as, 246, 249–251, 251*f*
 cortical neurons as, 747–748, 747–749
 highpass, 250
 linear
 for ganglion cell excitability, 428
 simple cells as, 712*f*, 713–714, 717, 750
 for rod signals, 845
 spatial, cone aperture as, 801
 spatiotemporal
 cortical neurons as, 748–749
 receptive fields as, 717
 simple cells as, 750
- Filtering task, pulvinar activity in, 601
- Fireworks amacrine cell, 83, 84*f*
- First-order linear spatial filter, 1109–1110, 1109*f*
- First-order [term], 1110
- Fish. *See also specific fish*
 GABA receptors in, 357
 ganglion cells of
 excitability of, 426, 434–435
 sodium currents in, 432
 horizontal cells of, 370*f*, 370–371, 371*f*
 chromaticity, 373
 and color opponency, 387
 dopamine and, 384, 384*f*
 gap junctions between, 372
 ion channels in, 378–379, 379*f*
 morphology of, 369, 370*f*
 nitric oxide and, 385
 retinoic acid and, 386, 387*f*
 S-potentials of, 369, 370*f*
 neuronal mosaics in, development of, 467–468, 468*f*
 optic chiasm in
 development of, 99, 100
 organization of, 94, 95*f*
 retina of
 cell production in, regulation of, 38
 color opponency in, 17
 retinal peptide expression in, 344
 retinal synapses of, 289–290

- Six3* gene overexpression in, 66
- vision of, 964, 965, 1577
- Fitness utility function, in ideal observer analysis, 834–836, 835*f*
- Fixation(s)
 - and actions in domestic tasks, 1359–1360, 1360*f*
 - checking, 1366
 - directing, 1366
 - duration, in change detection, 1528, 1530
 - functions of, 1365–1367
 - guiding, 1366
 - in humans, recording of, historical perspective on, 1340–1342
 - locating, 1366
 - measurement of, in humans
 - corneal reflex method for, 1340
 - historical perspective on, 1340–1342
 - optical lever technique for, 1340–1341, 1344
 - patterns, in change detection, 1530–1531
 - status signals for, in frontal eye field, 1440, 1441*f*
 - torsional abnormalities during, 1493–1494
- Fixation duration, 1380
- Fixation zone, in superior colliculus, 1452–1453
- Fixation-disengagement discharge (FDD), 1440, 1441*f*
- FK506 calcineurin inhibitor, and cortical plasticity, 130
- Fkh4*, in eye field development, 66
- Flash suppression, 1688–1689, 1689*f*
- Flicker
 - cone-mediated thresholds for, dark-adapted rods and, 870, 870*f*
 - detection of, dark adaptation and, 857–858, 858*f*
 - perception of, rod-cone contributions to, 854–855
 - rate of, and light adaptation, 860–861, 860*f*
 - and rod-cone interactions, 866–869, 869–871
- Flicker hypothesis, of honeybee pattern recognition, 1501
- Flicker responses
 - of hMT/V5+ visual area, 1236–1237, 1238*f*, 1239
 - of MT visual area, 1237, 1238*f*
- Flicker sensitivity, cone-mediated, rods and, 866
- Flight speed control, in insects, motion cues for, 1196–1197, 1197*f*
- Flight stabilization, in insects, motion cues for, 1194
- Flocculus
 - in eye movement control, 1408–1409, 1486, 1487–1489, 1490
 - in ocular motor learning, 1495
 - and pursuit behavior, 1408–1409
- Flourens, P., 8
- Flower(s)
 - color of, bee color vision and, 970–971, 971*f*
 - spectral reflectance patterns of, 970–971, 971*f*
- Fluorescence of lens
 - aging and, 208*t*, 208–209
 - geographical location and, 208–209
- Fly(ies)
 - motion cues in, 1193
 - for flight speed control, 1196
 - for flight stabilization, 1194
 - patterning of compound eyes in, comparison with cone mosaic, 467
- Flying insects, 1194–1201
 - centering response in, 1195*f*, 1195–1196
 - angular speed and, 1196
 - nondirectional nature of, 1196
 - versus optomotor response, 1196
 - motion cues in, 1193–1201, 1194–1201
 - for discriminating objects from backgrounds, 1200*f*, 1200–1201
 - for distinguishing objects at different distances, 1199–1200
 - for estimating distance flown, 1197–1198, 1198*f*
 - for executing smooth landings, 1198–1199, 1199*f*
 - for flight speed control, 1196–1197, 1197*f*
 - for flight stabilization, 1194
 - for hovering, 1194–1195
 - for negotiating narrow gaps, 1195*f*, 1195–1196
- FM 1-43, for studying neurotransmitter release in bipolar cells, 286–288, 287*f*
- fMRI, *See* functional magnetic resonance imaging
- Focal vision, 495
- Focus of expansion (FOE), 1247, 1251
- Food object detectors, 18
- Food source identification, ideal observer analysis of, 834
- Forced-choice preferential looking (FPL), 190
 - direction selectivity in, 182–183
- Forebrain, basal, signals about nervous system state from, 134
- Form analysis, 530
 - in blindsight, 659
 - MT/MST lesions and, 551–552, 552*f*
 - P (parvocellular) cells in, 489
 - ventral stream lesions and, 547–548
- Form perception
 - depth perception and, 1302
 - pattern-selective adaptation in, 936–946
- Form recognition, temporal lobe lesions and, 11–12
- Fos* gene, and cortical plasticity, 134
- Fourier channels, 1111
- Fourier optics, 795
- Fourier [term], 1111
- Fovea, 1339
 - cell number and density in, 69, 71, 80–81
 - functional correlate of, 69
 - central, absence of rods in, 841
 - cone concentration in, 4*f*, 69, 159–160, 162*f*, 166–167, 239*f*–240*f*, 240, 801–802, 802*f*
 - cone immaturity in, 176
 - cone mosaic in, 159–160, 162*f*, 239*f*–240*f*, 240
 - and receptive fields of cortical neurons, 166–167
 - cone Nyquist limit in, 803–805, 804*f*
 - distance from, and ganglion cell morphology, 413, 414*f*
 - image acquisition in, 800–808, 801–808
 - image formation in, 795–800
 - receptive field size in, 1045
 - rods in, 4*f*
 - synapse formation in, 87
- Foveal pit, 80
- Fractal edge(s), 1047
- Fractures, in orientation maps, 119
- Frequency domain, retinal image computation in, 799
- Frequency domain analysis
 - of cortical neurons, 748–749
 - of MT speed tuning, 1206–1207, 1207*f*
- Frequency response, 751
- Frequency seen curve (psychometric function), 811, 813*f*, 820–822, 840, 847
- FRF (filter, rectify, filter) model, of texture segregation, 1109
- Frog(s)
 - amacrine cell subtypes in, lineage bias of, 67–68
 - lateral inhibition in, 17
 - neuronal mosaics in, 467
 - ON and OFF ganglion cells of, 261*f*, 261–262
 - optic chiasm in
 - development of, 99
 - organization of, 95
 - retinal cell development in, 63
 - retinal synapses of, 293
 - rods of, regulation by calcium in, 227
 - single-unit recording in, 17, 23
 - three-eyed, ocular dominance columns in tectum of, 111–112, 112*f*

- Frontal cortex. *See also* Frontal eye field (FEF)
- connections with area MT, 1203, 1204*f*
 - in dialogue between cerebral cortex and superior colliculus, 1470–1471
 - human versus macaque, 517
 - visual areas of, in macaque, 510*f*–511*f*, 512
- Frontal eye field (FEF), 529, 529*f*, 1429*f*, 1568*f*
- auditory responses in, 1439, 1439*f*
 - connections with area MT, 1203, 1204*f*
 - in dialogue between cerebral cortex and superior colliculus, 1468*f*, 1470–1471, 1477
 - discovery of, 1428
 - and dysjunctive eye movements, 1445
 - eye movements electrically elicited from, characteristics of, 1428–1432
 - fixation responses in, 1440, 1441*f*
 - lesions, and saccades, 1433
 - low-threshold, and presaccadic burst activity, 1433
 - macaque, 510*f*–511*f*, 512
 - motion sensitivity of, functional mapping of, 1235*f*, 1236, 1239
 - motor function of, 1241, 1378
 - in natural scene perception, 1599
 - neural network models of, 1443
 - neurons
 - latencies of, 530–532, 531*f*
 - perisaccadic receptive field shifts in, 1398
 - in oculomotor system, 1379, 1425, 1428
 - postsaccadic activity in, 1442
 - presaccadic burst activity in, 1433, 1469*f*, 1470
 - and electrically elicited saccades, 1433–1435, 1434*f*
 - incidence of, 1433, 1434*f*
 - memory-saccade, versus for visually guided saccades, 1436–1437, 1438*f*
 - and purposive saccades, 1435–1437
 - as signature neuronal activity, 1435
 - significance of, 1433, 1434*f*
 - suppression of, by saccade execution, 1442
 - primate, 1428–1445
 - and pursuit- and saccade-related activity, 1410, 1443–1445, 1443*f*–1444*f*
 - and pursuit behavior, 1407–1408, 1410, 1428
 - in pursuit gain control, 1403
 - remapped visual activity in, 1441
 - saccade-related activities and phenomena in, summary of, 1442–1443
 - and saccades, 1371, 1372*f*, 1378–1383, 1410, 1428–1443, 1432*f*
 - neurophysiology of, 1433–1435
 - sensorimotor transformation in, for smooth pursuit, 1443–1445, 1443*f*–1444*f*
 - in spatially directed attention, 1379, 1379*f*, 1519–1521, 1520*f*
 - and vergence, 1445
 - vergence and accommodation zone of, 1445
 - in vergence control, 1415
 - in visual function, 1378–1379
 - in visual target selection, 1379, 1379*f*, 1381, 1381*f*
 - visuomovement cells in, 1439
 - in visuosaccadic system, 1467, 1467*f*
- Frontal lobe
- damage to, social/emotional problems caused by, 1167
 - and pursuit behavior, 1408
 - and visual consciousness, 1691–1692
 - and visual processing, 1371, 1372*f*
- frq* gene, 636
- Fruitflies, flight speed control in, 1196
- FST (floor of superior temporal area) visual area, 1569
- connections with area MT, 1203, 1204*f*
 - macaque, 510*f*–511*f*, 511
- Full-wave rectification, 751*f*, 751–752
- uses of, 752
- Functional architecture, definition of, 673
- Functional connectivity
- and anatomy, differentiation of, 673
 - in cat, 673–678
 - definition of, 673, 677
 - in retina-striate cortex pathway, 673–678
- Functional magnetic resonance imaging. *See also* magnetic resonance imaging.
- and functional mapping, 1229–1236
- Functional mapping. *See also specific imaging modality*
- of motion regions, 1229–1243
- Functional models
- of cortical neurons, 759–760
 - goal of, 759
- Fundal superior temporal area (FST), interconnections/projections of, 1260
- Fundus, light scatter from, 798–799
- Fusiform cortex, motion processing in, functional mapping of, 1235
- Fusiform face (FF) visual area, 515, 516*f*, 1153, 1179–1182, 1180*f*, 1184, 1534, 1645–1646
- attentional response modulation in, 1516
 - development of, 1186
 - and nonpreferred stimuli, 1181*f*, 1184–1185
- Fusiform gyrus
- activation by faces, 1167
 - attentional response modulation in, 1515–1516
 - color center in, 1032, 1034–1036, 1035*f*
 - in color vision, 1029
 - color-selective region in, 1034–1035, 1035*f*
 - lesions of, achromatopsia induced by, 1034–1035
- Fusion
- assessment of
 - correlogram of, 184–185
 - cyclopean VEP for, 184–185
 - development of, 184–185
- G**
- G protein(s)
- activation of, in phototransduction, 216–218, 217*f*. *See also* Transducin
 - signaling of, regulators of, 223
 - in synaptic transmission, photoreceptor-bipolar cell, 284
- GABA. *See* Gamma aminobutyric acid
- Gabor patches, 929, 1063–1064, 1064*f*, 1581, 1581*f*
- Gain(s)
- accommodation
 - definition of, 1421*f*
 - and vergence gain, relationship between, 1419–1422, 1421*f*
 - contrast
 - of M (magnocellular) cells, 485–487, 486*f*, 488*f*
 - of P (parvocellular) cells, 485–487, 486*f*, 488*f*
 - in pupil, 642, 653
 - definition and description of, 760–761
 - optimization of transduction proteins and ion channels for, 241–244
 - vergence, 1416, 1417*f*, 1418*f*
 - and accommodation gain, relationship between, 1419–1422, 1421*f*
 - definition of, 1421*f*
 - version, 1416, 1417*f*, 1418*f*
- Gain control, 760–761, 1064, 1115
- adaptation and, 942
 - and color constancy, 956
 - contrast, 178, 181
 - in binocular vision, 773–775
 - in ganglion cells, 416, 487
 - interocular transfer of, 774–775
 - neuronal activity level and, 741
 - short-range horizontal cortical connections and, 736–737
 - contrast-set, 760–761
 - in cortical neurons, 753, 753*f*, 760–761
 - temporal dynamics of, 756–757
 - in ganglion cells, 416, 422, 427, 487
 - in light adaptation, 229, 760–761
 - in multidimensional feature space, 761
 - in receptors, 1006

- and target selection for pursuit, 1402–1403
- and thresholds, 817–818, 819–820
- Gain field, 1252
- Galagos, visual system of, 1568*f*, 1569
- Gambling task, prefrontal cortex (PFC)
 - damage and, 1550*f*, 1551, 1557
- Gamma aminobutyric acid (GABA), 307–310, 308*f*
 - amacrine cell release and use of, 269, 291–295, 307, 309–310, 312–313, 359, 361, 395, 396–398, 402, 403*f*, 403–404, 405
 - BDNF and, 133
 - bipolar cell release and use of, 308
 - and calcium currents, 432
 - and circadian rhythms, 628
 - coexpression with other neurotransmitters, 402
 - coexpression with peptides, 336, 402
 - and cortical plasticity, 127, 130–131, 133, 136–137, 137*f*, 139
 - gate hypothesis of, 131, 137
 - restorative effects of inhibition, 136–137
 - and direction selectivity, 355, 361, 452, 457
 - future directions for study of, 310
 - and ganglion cell light responses, 443
 - horizontal cell release and use of, 250, 289–290, 307–308, 361, 382–383
 - in horizontal cortical connections, 736, 740
 - inhibitory role of, 86*f*, 87, 307–310, 355–365
 - in direction selectivity, 355, 361, 452, 457
 - effect on amacrine cells, 359
 - effect on ganglion cells, 355–356, 359, 412, 412*f*, 443, 452, 457
 - feedback from horizontal cells, 382–383
 - feedback to bipolar cells, 356, 359, 360, 360*f*, 361–363, 362*f*
 - versus glycine, 355
 - ON pathway preference of, 355, 362
 - pathways for, 361–364
 - in sustained inhibition, 355–356
 - interaction with dopamine, 365
 - interplexiform neurons expressing, 307, 355, 361, 365
 - ion channel modulation by, 357*t*, 357–358, 358, 363*f*, 363–364
 - localization of, 307–308, 308*f*
 - and long-term potentiation, 127, 131
 - metabolism of, 304, 307, 308*f*
 - neuronal expression of, 361
 - neurotrophins and, 55, 56*f*, 60*f*
 - in ON and OFF pathways, 355–356
 - peptide action on, 334, 336, 337, 344, 346, 346*f*, 348
 - retinal, 86*f*, 87, 279
 - in signal transmission from cones, 250–251, 253
 - in synaptic transmission, 279, 304, 309–310, 355, 412
 - versus acetylcholine, 312–313
 - amacrine cell-amacrine cell, 294, 312–313, 402
 - amacrine cell-bipolar cell, 292*f*, 292–293, 396–398
 - amacrine cell-ganglion cell, 293, 440
 - bipolar cell-ganglion cell, 286
 - cone-bipolar cell, 283, 284*f*
 - horizontal cell-bipolar cells, 290, 386
 - horizontal cell-horizontal cell, 289–290
 - horizontal cell-photoreceptor, 290, 382–383
 - photoreceptor-bipolar cell, 281*f*, 281–282
 - synergy with glycine, 358
 - synthesis of, 131, 307, 308*f*
 - transporters of, 308*f*, 308–309, 382–383
 - mitochondrial, 308*f*
 - plasma membrane, 308*f*, 308–309
 - vesicular, 250, 289, 308*f*, 308–309, 311
- Gamma aminobutyric acid receptor(s), 308*f*, 309, 356*t*, 356–358
 - in amacrine cells, 309, 358, 398
- baclofen-sensitive, 293, 356*t*, 357, 357*t*, 358, 359, 360, 360*f*, 361, 363
- CACA-sensitive, 293, 356*t*, 357, 357*t*, 358, 363
- colocalization with glycine receptors, 358
- GABA_A, 356, 356*t*, 357*t*, 357–358
- GABA_B, 356*t*, 356–357, 357, 357*t*
 - feedback to bipolar cells, 362*f*, 363
- neural discriminator created by, 363*f*, 363–364
- GABA_C, 356*t*, 356–357, 357*t*, 357–358
 - feedback to bipolar cells, 362, 362*f*
- in ganglion cells, 309, 357, 358, 359, 412, 412*f*
- heptahelical, 308*f*, 309
- inhibitory roles of, 356–359
 - effect on amacrine cells, 359
 - effect on bipolar cells, 360, 360*f*, 360–363, 362*f*
 - effect on ganglion cells, 359, 412, 412*f*, 452, 457
- ionotropic, 308*f*, 309, 356, 356*t*, 357*t*
 - pharmacology of, 358
- in A layers of cat LGN, 571
- metabotropic, 356*t*, 356–357, 357*t*
 - pharmacology of, 358
- modulators of, 356*t*, 358, 359
- peptide action on, 334, 336, 337, 346, 346*f*, 348
- pharmacology of, 293, 358
- relative properties of, 357*t*
- rho subunit of, 357, 358, 362
- spatial distribution of, 357–358
- subtypes of, 357, 358
- varieties of, 357–358
- Gamma aminobutyric acid receptor
 - agonists, 356*t*
- Gamma aminobutyric acid receptor
 - antagonists, 356*t*, 358
 - and cortical feedback to LGN, 612, 613*f*
 - and MT feedback to V1, 620*f*, 621
 - and orientation selectivity, 702
- Ganglion cell(s), 5, 6*f*–7*f*, 235*f*, 410–419, 482–485, 909, 918, 1010
 - acetylcholine receptors in, 312
 - age-related failure of, 210*t*, 846–847
 - albinism and, 71, 100*f*, 102–103
 - alpha, 430–431
 - versus beta, 464
 - evolution of, 472, 472*f*
 - opposite-sign pairs among, 470
- axons of
 - arborization in LGN, 270–271, 271*f*
 - chemosuppression of, 98
 - contralateral, 94, 95*f*
 - decussation at optic chiasm, 94–103
 - cell and molecular mechanisms underlying, 97–101
 - defects in, 97–98, 102–103
 - maneuvers in, 98
 - partial, 94
 - regulation of, 95–103, 97*f*
 - timing of, 95–96, 97*f*
- ectopic, 98
- growth cones of, 95, 100–101
 - advancing and streamlined, 96, 97*f*
 - behaviors at midline, 95–96
 - pausing and complex, 96, 97*f*
 - temporal and morphologic patterns of, 95–96, 97*f*
- guidance or regulation of, 95–103, 97*f*
 - cellular specializations at midline and, 97–98
 - cellular specializations at ventral midline and, 96
- Eph receptors/ephrin ligands and, 97*f*, 99
- GAP-43 and, 100*f*, 100–101
- genetic, 100*f*, 101–102
- molecular factors in, 98–101
- netrin/deleted in colorectal cancer and, 98–99
- proteoglycans and, 97*f*, 100
- Roundabouts (Robos) and, 97*f*, 99–100, 100*f*
- Slits and, 97*f*, 99–100, 100*f*, 101
- interactions between fibers from each eye, 98
- ipsilateral, 94, 95*f*, 99, 101
- lack of pigment (albinism) and, 100*f*, 102–103

- Ganglion cell(s) (cont.)
 in optic chiasm agenesis, 103
 organization of
 age-related, 94
 binocular plan of, 94, 95*f*
 changes in optic nerve, chiasm, and tract, 94–95
 quadrantic, 94
 retinorectal, 95
 retinotopic, 94
 outgrowth of, 81, 81*f*
 projections of, 413–415
 static and dynamic chronicles of
 behavior at chiasm, 95–96, 97*f*
 beta, 430
 versus alpha, 464
 bipolar cell connectivity of, 413, 418
 and bipolar cells, linkage of, 320
 birth dates of, 95
 bistratified, 1008
 blue-OFF, 419
 blue-ON, 411–412, 865–866
 brisk, 253–255, 254*f*
 broad-band, 483, 488
 Cajal's studies of, 410
 calcium currents in, 433, 436–437
 conotoxin-sensitive, 432, 433
 dihydropyridine-sensitive, 432, 433
 high-threshold, 425, 433
 low-threshold, 433
 toxin-resistant, 432, 433
 transient, 432, 433, 435–436
 CCK expression in, 347
 central projections of, 117–118, 270–271, 412, 413–415, 483, 484*f*, 496, 497–498
 definition of classes by, 414–415
 cholinergic, 312, 404, 457–458
 chromatic contrast sensitivity in, 418–419, 488–489
 circadian role of, 628, 629, 635*f*, 636
 classes of, 260, 262–263, 402, 566
 color opponent, 483, 488–489, 992
 horizontal cells and, 387–388
 computational role of, 70
 cone-driven, 240–241
 connections of, 485, 486*f*
 connections with photoreceptors, 3–5
 constant properties of, 410
 contrast gain control in, 416, 487
 contrast gain of, 485–488, 486*f*, 488*f*
 contrast sensitivity in, 416*f*, 416–419, 484, 486*f*
 coverage factor of, 674
 CRH expression in, 347–348
 dark rearing and, 192
 and daylight vision, 70
 death or loss of, 80
 excitotoxic injury from glutamate and, 42
 in glaucoma, 42
 and mosaic formation, 470
 delta, 430
 dendrites of, 360, 410, 411*f*
 arborization of, 82*f*, 82–83, 410–411, 411*f*
 in ON and OFF pathways, 266–268, 267*f*
 functional maturation of, 84
 growth patterns of, 470–471
 lateral extent of territory, 85
 outgrowth of, 81*f*, 81–82
 shunting inhibition of, and direction selectivity, 455
 stratification and organization of, 84–86, 85*f*, 412–413
 in synapse formation, 87
 development of, 36–37, 37*f*, 77
 tangential migration in, 469
 timing of, 77, 78*f*
 differentiation of, 37–38, 66, 68, 72, 77–78, 467
 in inner and outer plexiform layers, 81*f*, 81–86
 diffuse, 411
 direction-selective (DSGCs), 404–405, 451–461
 acetylcholine and, 457–458
 amacrine cells and, 404–405, 456–460, 457*f*, 458*f*, 459*f*
 Barlow and Levick's classic studies of, 451, 452*f*
 Barlow-Levick model of, 453, 455*f*
 challenges in studying, 455–456
 excitatory model of, 453–455, 455*f*
 feedforward inhibition and, 451–452, 454*f*
 fundamental features of, 451
 GABA and, 355, 361, 452, 457
 general requirements for, 453–455
 independence of sign contrast, 451, 454*f*
 inhibitory model of, 453, 454*f*, 455*f*
 lateral inhibition and, 453–455, 454*f*
 mosaic organization and, 466–467
 mosaics of, 466–467
 motion detection and, 453–455, 456–459, 458*f*
 nonlinearity and, 454*f*, 454–455, 455*f*
 nonlinearity in, 454*f*, 454–455, 455*f*
 ON-OFF, 451, 452*f*, 453*f*
 crosstalk between, 457
 physical asymmetry for, 453–455, 454*f*, 455*f*
 alternative anatomical locations for, 459–460
 postsynaptic mechanisms in, 454*f*, 454–456
 postsynaptic model of, 454*f*, 454–456
 presynaptic mechanisms in, 454*f*, 454–456
 presynaptic model of, 454*f*, 454–456
 presynaptic versus postsynaptic computation of, 455–456
 Reichart's model of, 453–455, 455*f*
 responses to light and dark edges, 451, 454*f*
 synaptic connections and, 460*f*, 460–461
 time delay for, 453–455
 tracer-coupling studies of, 466
 discovery of, 410
 dynamic range of, 422, 423, 424*f*, 425*f*
 emergent property of, 255
 excitability of, 260, 422–444
 burst firing in, 427–430, 428*f*, 429*f*
 calcium modulation of, 436–437
 central, 360
 in dark-adapted retina, 426, 426*f*, 428, 436
 depolarization and, 428, 436–438
 dopamine and, 438–443
 fixed versus variable mechanism of, 422
 heterogeneity of, 422, 434–435
 hyperpolarization and, 426, 426*f*, 428, 435–436
 input-dependent, 435, 438–443, 444
 integrate-and-fire model of, 423, 428
 ion conductances and, 422, 424–426, 432–434, 443–444
 in light-adapted retina, 426, 427*f*, 427–428
 linear filter for, 428
 peptides and, 337, 341–342, 342*f*, 344, 346, 349
 response-dependent, 435–438, 444
 somatostatin and, 341–342, 342*f*, 349
 substance P and, 344
 synaptic input and, 428, 434–435
 temporal contrast and, 437*f*, 437–438
 transient responses in, 426–430
 two signal-processing stages of, 428
 VIP and, 346, 349
 functions of, 422
 morphology as guide to, 410
 GABA receptors in, 309, 357, 358, 359, 412, 412*f*
 gain control in, 416, 422, 427, 487
 generalization by, 17–18
 glutamate receptors in, 306, 412, 412*f*, 431–432
 glutamate transporters in, 306
 in glutamatergic pathways, 320–330
 glycine receptors in, 311, 357, 359, 412, 412*f*
 highlight and shadow detection by, 260
 historical perspective on study of, 410
 hue-encoding, 855
 ideal observer analysis at level of, 832
 immature
 chloride concentration in, 87

- spontaneous activity of, 88–89, 89*f*, 109–110
- inhibition of, 355–356, 359
 - by dopamine, 438–443
 - mechanisms of, 438–439, 439*f*, 440*f*, 441*f*
- feedforward, 439–440, 451–452, 454*f*
- GABA and, 355–356, 359, 412, 412*f*, 443, 452
- glycine and, 355–356, 359, 412, 412*f*, 443
- lateral, and direction selectivity, 453–455, 454*f*
- peripheral, 360
- intensity discriminator in, GABA_B receptor and, 363*f*, 363–364
- inwardly rectifying cation current in, 432, 434, 435–436
- ion channels/currents in, 422, 424–426, 430, 432–434
 - dopamine and, 438–439, 441*f*
- identification and characterization of, 434
- progress in study of, 434, 443–444
- voltage-gated, 432–434
- kinetic properties of, 288
- koniocellular-projecting, 416, 416*f*, 483, 484*f*, 1219. *See also* Koniocellular pathway, cells of (K cells)
- lamination patterns of, 84–86, 85*f*, 266–268
 - in lateral geniculate nucleus, 108–110, 109–110, 114
- of lateral geniculate nucleus, 117–118, 270–271, 413–415, 483–484, 484*f*, 485, 496, 497–498
- light adaptation in, 422, 427–428, 487
- light responses of, 117, 423–430
 - cellular mechanisms of, 428–430
 - and circadian rhythms, 628, 629, 636
- development of, 89–90
- dopamine and, 440–443, 442*f*
- GABA and, 443
- glycine and, 443
- luminance-encoding, 855
- magnocellular-projecting, 413–414, 416, 416*f*, 418, 483, 484*f*, 1219. *See also* Magnocellular pathway, cells of (M cells)
- medium, 430
- melanopsin-containing, 628, 629, 635*f*, 636
- membrane resistance of, 431
- membrane time constant of, 430–431
 - range between species, 431
 - range within species, 431
- synaptic input and, 431–432
- midget, 262, 268, 410–411, 411*f*, 483–485, 997–998, 998*f*, 1007
 - in peripheral retina, 998–999
 - rods and, 865–866
- migration of, 79
- morphology of
 - distance from fovea and, 413, 414*f*
 - eccentricity-dependent, 413, 414*f*
 - properties of, 410–415, 411*f*
- mosaics of, 465–467, 466*f*, 470
 - and cellular evolution, 472, 472*f*
- multiplexing of chromatic and luminance information in, 488–489
- narrow-field, 237, 238*f*, 253–255, 254*f*
- in natural scene visualization, 237, 238*f*
- neurokinin receptors in, 343–344
- neurometric function for, 821–822, 822*f*
- neuromodulators of, 438
- neuropeptide Y expression in, 337–338
- neurotransmitter expression and receptors in, 86–87, 279, 288, 412, 412*f*
- and neurotrophin action, 52
- non-midget, non-parasol, 411
- number of, 69–72, 80
 - diffusible factor limiting, 79, 98
 - in domestic versus wild animals, 70–71
 - evolutionary flexibility of, 70
 - genetic analysis of, 71–72
 - high and low, crossing of strains with, for genetic mapping, 72
 - in isogenic lines, 72
 - large, need for, 69
 - ratio to horizontal cells, 70
 - ratio to projection neurons, 69
- regulation of, 38
 - and spatial resolution, 80
- tyrosinase gene mutation and, 71
- variation within species and genotype, 70–71
- OFF, 17, 83, 260, 419
 - central projections of, 270–271
 - developing, spontaneous spiking patterns of, 88–89
 - discovery of, 261–262
 - Golgi, flat-mount image of, 263, 263*f*
 - inhibition of, 355–356
 - membrane time constant of, 432
 - projections to LGN, 117–118, 118*f*, 270–271, 271*f*
 - retinal circuits and, 235*f*, 236*f*
 - segregation of, 86, 122
 - specification of, versus ON-OFF combination, 253
 - stratification of, 266–268, 267*f*
 - sustained and transient, 262*f*, 262–263
 - synapses of, 285–286
 - to LGN neurons, 270
- OFF-center, 881, 882–883, 883*f*, 909
- olivary pretectal nucleus-projecting, 412
- ON, 17, 83, 260, 411–412
 - central projections of, 270–271
 - developing, spontaneous spiking patterns of, 88–89
 - discovery of, 261–262
 - Golgi, flat-mount image of, 263, 263*f*
 - inhibition of, 355–356
 - membrane time constant of, 432
 - projections to LGN, 117–118, 118*f*, 270–271, 271*f*
 - retinal circuits and, 235*f*, 236*f*
 - segregation of, 86, 122
 - specification of, versus ON-OFF combination, 253
 - stratification of, 266–268, 267*f*
 - sustained and transient, 262*f*, 262–263
 - synapses of, 285–286
 - to LGN neurons, 270
- ON-center, 881, 882–883, 883*f*, 909
- ON-OFF, 261*f*, 261–262, 320, 321*f*
 - bi-stratification of, 267
 - membrane time constant of, 432
 - versus ON or OFF specification, 253
- (M+L)-ON/S-OFF, 996
- opioid expression in, 348
- orientation of, radial or tangential, 418
- orientation selectivity in, 117–118, 118*f*, 122, 418
 - as output neurons, 410
- PACAP in, 345
- parallel pathways of, 495, 496, 496*f*
- parasol, 262, 268, 410–411, 411*f*, 483–485
- parvocellular-projecting, 411–412, 416, 416*f*, 418, 483, 484*f*, 1219. *See also* Parvocellular pathway, cells of (P cells)
- passive properties of, 430–432
- peptide expression in, 334–349
- perikaryal translocation of, 79
- phasic, 483, 485
 - and photoreceptors, linkage of, 320
- physiological properties of, 485–489
- polarity of, 81–82
- potassium channels in, 433–434, 435, 436
 - calcium-activated, 425, 432, 433, 437
 - high-threshold, 425, 433
 - low-threshold, 425, 433
 - slowly activating, 432
 - transient, 432, 433, 436
- in primates, 482–485, 1567
- process outgrowth from, 81*f*, 81–82
- quantum fluctuation fingerprint of, 822
- range fractionation by, 422–423
- receptive fields of, 17, 261, 261*f*, 288, 415–419
 - asymmetric or elliptical, 417*f*, 418
 - center-surround organization of, 23, 89, 415–417, 416*f*, 422, 708
 - cone antagonism and, 991–992
 - cone input to, 488
 - correspondence with dendritic field, 417, 417*f*
 - dark rearing and, 89–90

- Ganglion cell(s) (cont.)
 difference-of-Gaussians model of, 415, 416*f*
 limitations of, 418
 and direction selectivity, 451, 452*f*
 excitatory versus inhibitory, 360–361, 415, 415*f*
 extraclassical properties of, 419
 light response in, development of, 89–90
 linear maps of, 708, 708*f*
 ON/OFF, 117–118, 118*f*
 organization of, horizontal cells and, 386
 parameters of, 20
 properties of, 415–419
 development of, 163–165
 relation to synaptic input, 417
 responses of, development of, neural factors in, 163–165
 size of, 18, 1044
 newborn versus adult, 163
 somatostatin and, 342, 349
 spectral variations in, 991
 subregions of, 415
 trigger features for, 18
 response dynamics of, 485
 resting ion permeabilities of, 431
 retinal, 529*f*
 NMDA receptors on, 330
 non-NMDA receptors on, 330
 transmission of light-evoked signals to
 delay in, 323–324, 323*f*
 filtering in, 323–324, 323*f*
 slow nonspiking responses and, 322
 small-amplitude signals in, 322–323
 voltage gain with, 323, 323*f*
 in retinal circuits, 234, 235*f*, 236*f*
 retinal circuits and, 234, 235*f*
 retinal position of, 33, 41–42, 79–80
 retrograde labeling of, 411
 rods and, 865–866
 sampling density of, 483–484
 SCN-projecting, 628
 in scotopic (low light) vision, 487–488, 488*f*
 selectivity of, 17–18
 in signal transmission from cones, 253–255, 254*f*
 signal-to-noise ratio of, 240–241
 somatostatin and, 341–342
 single-unit recording of, 16–17
 slow, 430
 sluggish (W), 255
 small bistratified, 898–899, 993, 995
 across retinal eccentricity, 994–995
 presynaptic circuitry of, 993–994, 993*f*
 rods and, 865–866
 spatial sampling of, 995
 spectral sensitivity of, 992, 993*f*
 small-field bistratified, 411–412, 483, 484*f*
 central projections of, 414, 497–498
 ON and OFF responses of, 483
 S cone inputs to, 497–498
 sodium channels in, 417, 425–426, 432–433, 435–436
 high-threshold, 432
 low-threshold, 432
 persistent, 432–433
 temporal contrast and, 437*f*, 437–438
 transient, 432–433
 S-OFF, 996
 somatostatin expression in, 340
 somatostatin receptors in, 340–341
 S-ON, 993–994, 993*f*
 S-ON/(M+L)-OFF, 992–993, 992*f*
 across retinal eccentricity, 994–995, 994*f*
 and blue-yellow opponency, 992–993
 mosaic of, 995
 receptive fields of, cone antagonism and, 993–994
 and spatial acuity, 240–241
 spatial frequency selectivity in, 708
 spatial resolution of, 483–484, 484*f*
 spatial selectivity of, 418
 spatial summation in, 418, 486–487, 495, 751
 spectral sensitivity of, 628
 spike bursts or events in, 427–430, 428*f*, 429*f*
 spike calculations in, 434
 spike frequencies of, 415, 422–430
 accommodation and, 436
 calcium modulation of, 436–437
 current transformed into, 423, 424*f*, 425*f*
 currents facilitating, 424
 in dark-adapted retina, 426, 426*f*, 428, 436
 dopamine and, 438–443
 high versus low, 423–426
 Hodgkin-Huxley equations for, 425
 light intensity and, 423–425, 425*f*, 427, 428*f*, 429*f*
 in light-adapted retina, 426, 427*f*, 427–428
 prediction of, 443
 with presentations of flickering checkerboards, 426–427
 with presentations of spatially uniform random flicker, 427
 temporal contrast and, 437*f*, 437–438
 spike heterogeneity in, 434–435
 stratification of, 84–86, 266–268, 411–412, 412–413
 substance P-containing, 629
 surround responses from, 675
 sustained, 288, 483
 inhibition of, 355–356
 synapses of, 412–413
 amacrine cell to, 293, 309–310, 316, 359, 412, 417, 440
 to amacrine cells, 87, 280, 280*f*
 basic plan of, 280, 280*f*
 to bipolar cells, 268, 279, 280, 280*f*, 304, 306–307, 412, 413, 417, 418
 postsynaptic mechanisms of, 288–289
 presynaptic mechanisms of, 285–288, 287*f*
 type-to-type connectivity of, 413
 and direction selectivity, 460*f*, 460–461
 dopaminergic, 439–440
 electron microscopy of, 413
 excitatory, 412, 412*f*, 440
 formation of, 87–88
 GABAergic, 286, 293, 309–310, 359, 412, 412*f*, 440
 glutamatergic, 286, 288, 293, 304, 306–307, 320–330, 412, 412*f*
 glycinergic, 311, 359, 412, 412*f*
 inhibitory, 359, 360*f*, 412, 412*f*, 417, 439–440
 to lateral geniculate nucleus, 88
 receptive field correspondence with, 417
 rod-cones interaction in, 418–419
 serotonergic, 316
 terminology for, 483
 tiling of, 483–484
 tonic, 483, 485
 topographic connectivity of, 33
 transcription factors expressed in, 68
 transient, 288, 483
 inhibition of, 355–356
 types of, 410–411, 483, 484*f*, 496, 1566
 methods for identifying, 411
 variable properties of, 410
 VIP expression in, 348
 in vitro recording of, 411
 wide-field, 237, 238*f*, 253–255, 254*f*, 411, 412
 central projections of, 414
 stratification of, 412–413
 within-type variation among, 464–465
 mosaics as guide to, 465–466, 466*f*
 X. *See* X cells
 Y. *See* Y cells
 zeta, 430
 Ganzfeld, 1093
 GAP-43, and optic chiasm development, 100*f*, 100–101
 Gap effect, 1440
 Gap junctions
 between amacrine cells, 396–398
 between cones and rods, 375
 and transmission of light-evoked signals to bipolar cells, 322
 between horizontal cells, 371*f*, 379–380, 380*f*
 dopamine and, 384

- nitric oxide and, 385
- physiological consequences of, 380
- rod-cone, 863–864, 864*f*
- GATs (GABA transporters), 250, 289, 308*f*, 308–309, 311
- GAT-1, 289
- Gauss map, 1099–1100
- Gaussian blobs, 929
- Gaussian noise, as stimuli for mapping receptive fields, 706
- Gaussian Radial Basis Function (GRBF) networks, 1642–1643
- Gaze
 - cyclopean, 1350
 - definition of, 1339, 1454
 - direction of
 - and perceived auditory direction, 1585
 - and version, 1301
 - in reading, 1357–1358
 - targets for
 - salience of, 1365
 - selection of, neural mechanisms of, 1369–1384
 - in visual search, 1369, 1370*f*
- Gaze angle, modulation of optic flow responses, 1269–1270
- Gaze control, 1369, 1370*f*
 - accurate, mechanisms of, 1350
 - cognitive factors in, 1343, 1370
 - under ecologically relevant conditions, 1339–1340, 1349–1350. *See also* Eye movement(s), in daily life
 - in humans, 1350, 1351*f*–1354*f*
- human
 - first accurate but unnatural studies of, 1340–1342
 - first accurate natural studies of, 1342
- study of
 - ecologically relevant conditions for, 1339–1340, 1349–1350
 - natural, 1339–1340, 1349–1350
 - rationale for, 1339
 - unnatural, 1340–1342
 - relevance of, 1344–1350
 - superior colliculus in, 1449–1462
- Gaze shift, 1428, 1485
 - amplitude of, 1454
 - and attention allocation, 1369–1371, 1370*f*
 - control of, 1425
 - eye-head contributions to, 1454
 - in natural vision, 1378
 - neural pathway for, 1425
 - neural substrate for, 1371, 1372*f*
 - parameters for, collicular encoding of, 1454
 - timing of, 1380
- Gaze-displacement hypothesis, collicular neurons and, 1456–1458, 1457*f*
- Gaze-holding, 1487–1488
- GCAP1, 226
- GCAP2, 226
- GCAP3, 226
- GDNF, in retinal cell differentiation, 68
- Gelb effect, 1578
- Gene(s). *See also specific genes*
 - anti-plasticity (capgs), 134
 - candidate plasticity (cpgs), 133–134
 - changes in, pleiotropic effects of, 68–72
 - expression of, and cortical plasticity, 133–134
 - housekeeping, 64
 - master, in eye development, 33–34
 - neurogenic, mapping of, 72
 - retina-specific, 36
 - rod-specific, 41
- Generalization
 - by neurons in ventral stream, 546
 - by single neurons, 17–18
- Genetic(s)
 - and individual differences in retina structure, 71–72
 - Mendelian, 71
 - quantitative, 71
- Genetic polymorphism, within species, and retina structure, 71
- Geniculate relay(s), 565. *See also* Lateral geniculate nucleus (LGN)
- Geniculocortical loop/pathway, 609–614
 - anatomical considerations in, 609–611, 610*f*, 611*f*, 675–676
 - linear receptive field maps for neurons of, 707–708, 708*f*
 - physiological studies of, 676–677, 677*f*
- Geniculostriate pathway, spatiotemporal receptive field maps along, 708–709, 709*f*
- Geniculostriate projection, and pupil responses, 641, 643, 647
- Gennari, Francesco, 7–8, 8*f*
- Geographical location, and lens fluorescence, 208–209
- Geometric module, for shape, 1182
- Geons, 1083
- Gestalt (term), 1573
- Gestalt factors, 1069, 1108, 1119, 1148
 - in animals, 1577
 - autochthonous, 1574
 - as bottom-up mechanism, 1585
 - definition of, 1573
 - in dynamic displays, 1576–1577
 - equilibrium of, 1574
 - in visual neuroscience, 1573–1585
- Gestalt formation, mechanism for, 1580
- Gestalt laws, 1139
- Gestalt psychology, 1139, 1142
 - basic concepts of, 1573–1578
 - and neuroscience, 1578–1580
 - current research in, 1581–1582
 - perceptual constraints in, 1574
- subjective factors in, 1576
- Glass patterns, structure recognition in, spatial tuning for, 1054*f*, 1055
- Glaucoma
 - causes of, 42
 - magnocellular pathway in, 490
 - versus natural processes of aging, 846–847
- Glial cells. *See also* Müller glia cell(s)
 - avoidance of photoreceptor synaptic terminals by, 247, 247*f*
 - glutamate export by, 304
 - as guides for retina cell migration, 79
 - and outgrowth of axons and dendrites, 81
 - radial, and regulation of ganglion cell axons, 96, 97*f*, 99
 - role in retinal development and function, 41
- Glial knot, and regulation of ganglion cell axons, 96
- Glissade, 1488–1489
- Global attention, to motion, 1239–1240
- Glomeruli, 572
- Glucagon, retinal, 334–335
- Glutamate, 304–307, 305*f*
 - bipolar cell release and use of, 362
 - and calcium currents, 432
 - and circadian rhythms, 628–629, 635*f*
 - coexpression with PACAP, 336
 - excess, in glaucoma, 42
 - future directions for study of, 307
 - and horizontal cell function, 377*f*, 377–378, 378*f*
 - interaction with dopamine, 384
 - localization of, 304, 305*f*
 - metabolism of, 304, 305*f*
 - as neurotransmitter, 993
 - nitric oxide and, 385–386
 - peptide action on, 334
 - recycling, at glutamatergic synapses, 327–328, 327*f*
 - and relay cells in cat LGN, 568
 - release of, neurotrophins and, 55, 56*f*, 133
 - retinal, 86, 86*f*, 279, 304–307
 - in signal transmission from photoreceptors, 246, 252–253, 320–330
 - signals about nervous system state carried by, 134
 - in synaptic transmission, 279, 291, 304, 306–307, 320–330, 412
 - amacrine cell-ganglion cell, 293
 - bipolar cell-amacrine cell, 304, 306–307
 - bipolar cell-ganglion cell, 286, 288, 304, 306–307
 - cone-bipolar cell, 283, 284*f*
 - photoreceptor-bipolar cell, 264–266, 281*f*, 281–285, 285*f*, 304, 307

- Glutamate (cont.)
 photoreceptor-ganglion cell, 320–330
 photoreceptor-horizontal cell, 289, 304, 307, 377*f*, 377–378, 378*f*
 synaptically released, in feedback control of light-evoked signal transmission, 327*f*, 328
 transporters of, 304–306, 305*f*, 307
 in excitatory transmission, 328–330, 329*f*
 expressed in retina, 306
 mitochondrial, 305*f*
 plasma membrane, 304–306, 305*f*
 vesicular, 304, 305*f*, 307
 as vertical channel neurotransmitter, 304–311
- Glutamate decarboxylase (GAD)
 GAD1, 307
 GAD2, 307
 GAD65, 57*f*, 58, 307
 and cortical plasticity, 131, 136*t*
 GAD67, 307
 and cortical plasticity, 131
- Glutamate receptor(s), 305*f*, 306–307
 in amacrine cells, 291, 306–307
 antagonists, effects of, 129–130
 in bipolar cells, 260, 288, 306–307
 excitatory versus inhibitory, 260
 in ON and OFF pathways, 264–266, 265*f*, 266*f*, 268–269, 269*f*, 320–330
 species diversity in, 266
 and calcium release, 25, 129, 633
 and circadian rhythms, 628–629, 633
 dark rearing and, 129, 136*t*
 in ganglion cells, 306, 412, 412*f*, 431–432
 heptahelical, 305*f*, 306–307
 in horizontal cells, 289, 307, 377*f*, 378
 ionotropic, 305*f*, 306–307
 in ON bipolar cells, 265, 266, 266*f*
 diversity of, 306
 in excitatory transmission, 328–330, 329*f*
 mixed expression of, 306
 in OFF bipolar cells, 265–266, 266*f*
 metabotropic, 993
 in ON bipolar cells, 264–265, 265*f*
 and cortical plasticity, 126, 128, 129–130, 132, 136*t*, 137, 137*f*
 in excitatory transmission, 328–330, 329*f*
 Group I, 129
 Group II, 129
 Group III, 129
 and long-term depression, 130, 132, 136*t*
 and long-term potentiation, 130, 132, 136*t*
 sustained and transient, 265
 mGluR6, 306, 307
 deficiency of, 265, 265*f*, 272–273
 in ON pathway, 264–265
 phosphorylation sites of, 132
 in retina, 86, 288–289
- Glutamic acid decarboxylase, 131
 amacrine cell expression of, 402
 inhibition of, and restoration of plasticity, 136–137
- Glutamine, recycling, at glutamatergic synapses, 327–328, 327*f*
- Glutamine synthetase, in glaucoma, 42
- Glutamine transporters, in glaucoma, 42
- Glutathione, lenticular concentration of, age-related decrease in, 205, 206*f*
- Glycine, 310*f*, 310–311
 amacrine cell release and use of, 269, 291, 293–294, 304, 310–311, 359, 361, 364, 395–396, 402, 403*f*, 405
 avoidance of inhibitory occlusion by, 311
 coexpression with other neurotransmitters, 402
 currents produced by, 357
 and ganglion cell light responses, 443
 inhibitory role of, 86*f*, 87, 310–311, 355–365
 effect on amacrine cells, 359, 364
 effect on ganglion cells, 355–356, 359, 412, 412*f*, 443
 versus GABA, 355
 in ON pathway, 364
 pathways for, 361, 364
 in transient inhibition, 355–356, 358
 interplexiform neurons expressing, 311, 365
 localization of, 310*f*, 310–311
 metabolism of, 304, 310*f*, 310–311
 neuronal expression of, 361
 in ON and OFF pathways, 355–356
 peptide action on, 337
 in synaptic transmission, 291, 304, 311, 355, 395–396, 412
 synergy with GABA, 358
 transporters of, 310*f*, 311, 396, 402
 mitochondrial, 310*f*
 plasma membrane, 310*f*, 311
 vesicular, 310*f*, 311
- Glycine receptor(s), 310*f*, 311, 356*t*, 356–358, 396
 colocalization with GABA receptors, 358
 in ganglion cells, 311, 357, 359, 412, 412*f*
 inhibitory roles of, 356–359
 effect on amacrine cells, 359
 effect on ganglion cells, 359, 412, 412*f*
 ionotropic, 310*f*, 311, 356*t*
 metabotropic, lack of, 357
 modulators of, 356*t*, 358–359
 pharmacology of, 358
 spatial distribution of, 357–358
 varieties of, 357–358
- Glycine receptor agonists, 356*t*
- Glycine receptor antagonists, 356*t*, 358
- GlyT1 glycine transporter, 310*f*, 311, 396, 402
- Gnostic cell, 1167
- Goal neglect, prefrontal cortex (PFC)
 damage and, 1548–1550
- Goal-directed behavior, prefrontal cortex (PFC) and, 1554
- Goldfish
 amacrine cells of, 291
 neurochemistry of, 402
 color vision in, 965, 966*f*
 GABA receptors in, 357
 ganglion cells of
 excitability of, 426, 434–435
 sodium currents in, 432
 horizontal cells of, ion channels in, 378–379
 Mb1 bipolar cell of
 neurotransmitter expression and synaptic transmission in, 286–288, 287*f*, 292*f*, 292–293
 spinule formation in, 297–298
 retinal cell differentiation in, 467
- Golgi apparatus, of cones and rods, 216
- Golgi staining, 5
- Gompertz constants, 210, 211*f*
- G-protein coupled receptors, 976
- Grandmother cell, 18, 726, 1167, 1593, 1646
- Granit, Ragnar, 16–17, 27, 260–261
- Grasshoppers, peering by, 1194
- Grating acuity, 178–179, 179*f*
 binocular deprivation and
 in cats, 191–192, 192*f*
 in humans, 193
 in monkeys, 192–193
 contour orientation restrictions and, 199–200, 200*f*
 as function of retinal eccentricity, 832, 832*f*
 in scotopic vision, 843–844, 844*f*
- Grating stimuli
 phase-shifted, for measurement of binocular interaction, 767–772, 768*f*–769*f*, 770*f*, 771*f*, 772*f*
 pupil responses to, 649*f*, 649–650, 650*f*
 damage to dorsal midbrain and, 653–654
- Grazing landings, by flying insects, motion cues for execution of, 1198–1199, 1199*f*
- Green cones, 372. *See also* M (mid-wavelength sensitive or green) cones
 connections to horizontal cells, 370–371, 373–374, 376
 feedback from horizontal cells, 382, 383*f*
- Green light, circadian sensitivity to, 627

- Ground squirrel
 cone function in, 240
 cone-specific opsin kinase in, 222
 light responses of SCN neurons in, 630–631
 OFF bipolar cells of, glutamate receptors in, 265–266, 266*f*
 synaptic transmission in, 285
- Grouping, 1519
 contextual modulation and, 726–728
 of line segments, 722, 722*f*
 axial offset in, 722
 perceptual, 1626–1627, 1630, 1630*f*. *See also* Boundary(ies), formation of in Gestalt psychology, 1574–1576
 neural basis of, 1626
 neuronal synchrony and, 1671–1673, 1672*f*
- Growth cone(s), of ganglion cell axons, 95, 100–101
 advancing and streamlined, 96, 97*f*
 and optic chiasm development, 95–96, 97*f*
 pausing and complex, 96, 97*f*
 temporal and morphologic patterns of, 95–96, 97*f*
- Growth factor(s), and visual acuity, 136
- Guanylate cyclase
 calcium regulation of, 226–227
 coupling to natriuretic peptides, 347
 isoforms of, 226
- Guanylate cyclase-activating proteins (GCAPs), 223, 224*f*, 226–227
- Guinea pig, retinal peptide expression in, 336
 NPY, 338
 opioids, 348
 somatostatin, 339
- GYKI 52466, and OFF bipolar cell responses, 265–266
- H**
- Habituation, in dark rearing, 50, 53*f*
- Half-wave rectification, 751*f*, 752
 beneficial consequences of, 752
- Hallucination, 1686
- Hamster(s)
 circadian rhythms in
 light responses of SCN neurons in, 629–630, 630, 631
 phase shifts in, 626*f*
 monocular deprivation in, 198
 retinal peptide expression in, 342–343
- Hand detectors, 18
- Hand movements, control of, motion-sensitive visual areas in, 1241
- Hartline, Keffer, 16–17, 23, 27, 261*f*, 261–262, 273
- Head movements, and visual processing, 1345–1346, 1345*f*, 1346*f*
- Head thrust, 1489
- Head-centric frame of reference, 1252, 1308
- Heading, 1247, 1300
 absolute, 1252, 1256, 1256*f*
 determination of, 1247–1248
 judgments of, 1263–1264, 1264*f*
 dorsal medial superior temporal area (MSTd) and, 1251–1252
 flow structure and, 1251
 in presence of moving objects, 1251
 during pursuit, 1272–1273
 rotation problem in, 1249*f*, 1252–1254
 spatial integration and, 1250–1251
 speed gradients and, 1251
 object-relative, 1252, 1254–1255, 1255*f*, 1256, 1256*f*
 and obstacle avoidance in locomotion, 1257
 and steering in locomotion, 1257
 oculo-centric, 1256, 1256*f*
 and path, differentiation of, 1254
 perception of
 extraretinal signals in, 1255–1256, 1256*f*
 during rotation, 1253–1254, 1254*f*
 translational, perception of, 1250–1252
- Heading task, 1240
- Hearing loss, low versus high frequency in, 209
- Hebb, Donald, 25, 52, 1119
- Hebbian synapses, 25
 and cortical plasticity, 113–114, 137–138
 NMDA receptors and, 129
 in orientation selectivity, 117, 123
- Helmholtz, H. von, 882
- Helmholtz-Kohlsrausch effect, 893
- Hemichromatopsia, cerebral, lesion producing, 1029
- Hemianopia, 8–9, 663. *See also* Blindsight
 pupil responses in, 654
 to color, 641–642, 651*f*, 652
 to grating stimuli, 650, 650*f*
 to light, 643, 644*f*, 647, 648*f*
 to motion, 648–649, 649*f*
 residual visual function in, 664
 Wollaston's experience with, 5
- Hemidecussation, 5
- Hemispherical diffuse beam, 1093, 1093*f*
- Heptahelical receptors, 304. *See also specific receptors*
- Hering, E., 882, 884
- Hering's law, 1415, 1416*f*, 1419, 1422, 1424
- Hering's rules for visual direction, 1300
 exceptions to, 1300–1301
- Hermann grid illusion, 886
- Hes-1* gene, in retinal cell differentiation, 39
- High background inefficiency, and thresholds, 817–818, 819–820
- Highlights, detection of, 260
 electroretinogram recording of, 260–261, 261*f*
- Highpass filtering, 250, 845
- Hippocampal formation, 529*f*
- Hippocampus
 Cajal-Retzius neurons of, 150–151
 electrical activity in, increase in, and neurotrophins, 49
 long-term potentiation in, 132
 synaptic plasticity in, calcium and, 130
- Histogram contrast analysis, 1111
- Hitzig, Eduard, 8
- hMT/V5+ visual area
 behavioral functions of, 1239
 cone input to, 1237
 direction selectivity in, 1239, 1240, 1240*f*
 flicker responses in, 1229, 1236–1237, 1238*f*
 identification of, 1229–1233, 1233*f*
 ipsilateral overlap in, 1231
 during motion aftereffect, 1237–1239
 motion processing in
 attention to direction of motion and, 1240, 1240*f*
 attention to motion and, 1239–1241
 attention to speed of motion and, 1241
 dynamic noise and, 1236–1237
 functional mapping of, 1229–1243, 1230*f*
 stimulus parameters for, 1236
 stimulus patterns for, 1236
 incoherent motion and, 1236–1237
 motion perception and, 1237–1239
 nonluminance-defined stimuli and, 1237
 versus primary visual cortex, 1230–1231, 1231*f*
 and movement control, 1241
 response during pursuit, 1231
 responsiveness to optic flow, 1231
 subdivision of, 1231
 three-dimensional structure
 determination in, 1242
- Hodgkin-Huxley equations, for ganglion cell excitability, 425
- Holmes, Gordon, 9, 11
- Hominids, evolution of, 1564
- Honeybee(s). *See also* Bee(s)
 abstraction of pattern properties by, 1502–1504, 1511–1512
 brain of, 1501, 1511
 visual and olfactory pathways of, 1511
 cognition in, 1501–1512
 color vision in, 963, 965, 966*f*
 and floral colors, 970–971, 971*f*
 context-dependent learning in, 1507, 1508*f*
 cross-modal associative recall in, 1510
 detection of camouflaged objects, 1504, 1511

- Honeybee(s) (cont.)
 learning of *sameness* and *difference*, 1510–1511, 1510f
 maze negotiation by, 1505–1507, 1507f, 1511
 using color mark, 1506, 1507f
 using symbolic cue, 1506–1507
 motion-sensitive vision in, 1511
 navigational skills of, 1508
 pattern recognition in, 1501–1502
 perception of illusory contours, 1504–1505, 1506f
 photoreceptors of, properties of, 970–971
 shape perception in, 1512
 spatial vision in, 1511
 symbolic matching tasks done by, 1507–1510
 top-down processes in, 1504, 1505f
 trichromatic color vision in, 1511–1512
 visual perception in, 1501–1512
- Horizontal cells, 5, 6f–7f, 235f, 369–389, 997–998, 998f
 acetylcholine expression in, 370
 action spectrum of, 373, 375f
 adaptation to background light, 375
 aspartate and, 377f, 377–378, 378f
 A-type (axonless), 370f, 370–371, 371f, 373, 375
 and bipolar cell receptive field
 architecture, 386–388, 388f
 blue-yellow types, 370, 370f, 373–374, 374f, 375f
 broad-field, 250
 B-type (with axons), 369–370, 370f, 373, 375–376
 CCK expression in, 347
 chromaticity (C-type), 370f, 370–371, 372–374
 biphasic, 373
 monophasic, 373
 polarity reversal in, 373–374, 374f
 spatial properties of, 381
 triphasic, 373
 wavelength dependency of, 373–374, 374f
 circuitry of, 369–372
 classification of, 381
 and color opponency, 370f, 370–371, 372–374, 387–388, 388f
 computational role of, 70
 cone connections of, 370–372, 372–374, 373–374, 375–376, 376f
 dendrites of, 370, 376
 development of, 36–37, 37f
 tangential migration in, 469, 469f
 timing of, 77, 78f
 differentiation of, 67
 dopamine and, 372, 380, 383–384, 384f
 feedback from, 290, 381–383, 382f, 383f, 386, 388–389
 functional roles of, 386–389
 GABA receptors in, 309, 358
 dopamine interaction with, 365
 GABA release from, 250, 289–290, 307–308
 GABA transporters in, 308–309, 382–383
 GABAergic, 250, 289–290, 307–308, 361, 382–383
 gap junctions between, 371f, 379–380, 380f
 dopamine and, 384
 nitric oxide and, 385
 physiological consequences of, 380
 retinoic acid and, 386
 glutamate and, 377f, 377–378, 378f
 glutamate receptors in, 289, 307, 377f, 378
 glutamate transporters in, 306
 H1, 370, 370f, 373, 374, 376f
 H2, 370f, 370–371, 374
 networks of, 380, 380f
 H3, 370f, 370–371
 H4, 370f
 ionic conductances in, 376–379
 ligand-gated, 376–378
 voltage- and time-dependent, 378–379, 379f
 L1, 372–373
 L2, 372–373
 large receptive field, 381
 in lateral inhibition, 289
 as lateral pathway for retina, 289
 light responses of, 290
 dopamine and, 383–384, 384f
 electrical recording of, 369, 370f
 in L-type cells, 372f, 372–373
 in luminosity-type cells, 372f, 372–373
 nitric oxide and, 384–386, 385f
 retinoic acid and, 386, 387f
 rod and cone signals in, 374–375
 slowness of, 290
 wavelength dependency of, 373–374, 374f
 luminosity (L-type), 370, 370f, 372–374
 photoreponses of, 372f, 372–373
 receptive fields of, 380f, 380–381
 spatial properties of, 381
 membrane potential of, 377f, 377–378, 378f
 migration of, 80
 minimal spacing of, 470
 modulation of, 383–386
 morphology of, 369–372, 370f
 narrow-field, 250
 neurochemical properties of, debate over, 307–308
 neurotransmitter expression and receptors in, 279, 289, 376–378
 neurotransmitter-free signaling by, 307–309
 nitric oxide and, 371, 384–386, 385f
 number of, 70
 ratio of ganglion cells to, 71
 variations in, 71
 passive electrical models of, 375–376
 peptide expression in, 335–336, 338, 340, 347
 in photoreceptor modulation, under
 different lighting conditions, 388–389
 physiological types of, 372–374
 in primates, 482–483
 synapses of, spinule formation and retraction in, 296–298, 297f
 transmission from, 289
 within-type variation among, 465f
 Y receptors in, 338
 yellow-blue types of, 373–374, 374f, 375f
- process outgrowth from, 82
 progenitors biased to produce, 67
 receptive fields of, 380f, 380–381
 dopamine and, 383–384, 384f
 equations for calculating, 381
 nitric oxide and, 385, 385f
 retinoic acid and, 386
 red-green types of, 373–374, 374f, 375f
 retinoic acid and, 372, 380, 386, 387f
 rod after effect in, 374–375, 376f
 rod and cone contributions to, 374–376
 rod-cone mixing in, 374–375, 376f
 in signal transmission from
 photoreceptors, 246
 daylight circuit for cones, 250–251, 251f
 small receptive field, 381
 somatostatin receptors in, 340
 spatial characteristics of, 379–381
 spatial surround organization created by, 386–388, 388f
 spectral properties of, 372–374, 374f, 375f
 spinules of, 371f, 371–372, 382
 dopamine and, 384
 nitric oxide and, 386
 retinoic acid and, 386
 S-potentials of, 369, 370f, 374–375
 wavelength dependency of, 373–374, 374f
 S-space of, 372
 synapses of, 289–290, 370
 basic plan of, 280, 280f
 to bipolar cells, 290, 304, 309, 386–388, 389
 dopaminergic, 314
 formation of, 87–88
 GABAergic, 289–290, 309, 382–383, 386
 glutamatergic, 289, 304, 377f, 377–378, 378f
 glycinergic, 311
 at lateral elements, 371f, 371–372

- to other horizontal cells, 289–290, 314
- to photoreceptor, 290, 381–383, 382*f*, 383*f*, 386, 388–389
- photoreceptor to, 314, 369–372, 372–374, 373–374, 375–376, 376–378
- postsynaptic mechanisms of, 289
- Horizontal cortical connections, 522, 523*f*, 535, 720, 733–743
 - anisotropy of, 738
 - and contextual modulation, 725–726, 727*f*
 - and endstopping, 739*f*, 739–741, 740*f*
 - functional contributions of, 733
 - functional relationship with vertical connections, 734, 743
 - functional specificity of, 734
 - identification of, 733–734
 - intrinsic, 148–149
 - in TE visual area, 1158–1159
 - and length summation, 739*f*, 739–741, 740*f*
 - local or short-range, 734–737, 737*f*
 - functional significance of, hypotheses of, 736–737
 - as modulators, 733
 - and neuronal synchrony, 742*f*, 742–743
 - organization of, 525, 525*f*
 - orientation selectivity and, 734, 734*f*, 735, 737, 737*f*, 738, 742
 - patchy organization and axonal bifurcations in, 525–527, 526*f*
 - receptive field effects of
 - on minimum discharge field, 733–739, 736*f*, 738*f*
 - size effects, 734, 736*f*, 741–742
 - surround effects of, 733, 734, 736*f*, 737, 739*f*, 739–741, 740*f*
 - and response properties of cortical neurons, 733–743
 - spatial overlap with vertical connections, 734, 738–739
- Horoptyer, 1302*f*
 - curvature of, spatial variation in, 1301
 - definition of, 1301
 - shape of, 1301
- Housekeeping genes, 64
- Hovering, by insects, motion cues for, 1194–1195
- Howler monkeys
 - color vision in, 977
 - vision of, 968
- Hubel, David, 11, 17, 18, 23, 49, 108, 126, 127, 147
- Hue(s), 872, 893, 917–918, 933–934, 974, 989, 990, 1010, 1011
 - definition of, 881, 893, 894*f*
 - detection of, 855
 - dark adaptation and, 854–855, 855*f*, 856–858, 856*f*, 858*f*
 - equilibrium, 894–895
 - of isolated lights, 894–895
 - perception of, 895
 - spectral sensitivity and, 990
 - red-green equilibrium, 894
 - rods and, 872–874, 872*f*, 874*f*
 - specific threshold for, 855, 855*f*
 - stimulus, threshold for, 856
 - unique, 895
 - scalar invariance of, 895, 896*f*
 - Hue cancellation, 893–897, 917–918
 - Hue threshold, specific, in dark adaptation, 873
 - Human(s). *See also specific anatomy and functions*
 - blindsight in. *See* Blindsight
 - brain of. *See* Brain
 - color vision in, 968
 - lifespan of, 205
 - newborn versus adult visual capacities in, 159, 160*f*
 - photopigment genes of, 979–980
 - primary visual cortex of
 - architectonic boundary of, 513
 - individual variability in, 513
 - surface area of, 513
 - visual areas of, 513–515
 - comparison with macaque, 515–518, 517*f*
 - criteria for, 1231
 - functional modalities of, 513, 515, 516*f*
 - organization of, 513–515, 514*f*, 516*f*
 - total cortical area occupied by, 513
 - visual deprivation studies in, 46, 126, 189, 190, 193, 197–198
 - visual system of, evolution of, 1569–1570
 - Huxley, Andrew, 27
 - 6-Hydroxydopamine (6-OHDA), lesions
 - induced by, and cortical plasticity, 134
 - Hyperacuity, 69
 - Hypercomplex cells, 1633
 - orientation-selective, 118
 - receptive fields of, 118
 - Hypothalamus, lateral, food object detectors in, 18
 - Hysteresis, of conscious activity, 1687

I

 - I4AA, GABA receptor response to, 356*t*, 358
 - Iceberg effect, 698, 699
 - modification of, 700–701
 - Ideal observer, 825
 - Bayesian, 825–826
 - constrained, 826–827
 - Ideal observer analysis, 160, 835–836
 - basic concepts and formulas for, 825
 - Bayesian natural selection in, 835–836
 - biological constraints in, 826–827
 - central concept of, 825
 - central efficiency in, 832–834
 - of color identification, 834
 - of color vision, 831
 - of detection, discrimination, and identification, 825, 827–834
 - key parameters for, 160, 163*t*
 - maximum fitness in, 834–836, 835*f*
 - of natural scene statistics and natural selection, 834
 - neural factors of retina and primary visual cortex in, 832, 832*f*, 833*f*
 - neural noise in, 832–834
 - optics in, 829–831, 830*f*, 831*f*
 - photon noise-limited, 828–829, 829*f*
 - at photoreceptor level, 829–831, 830*f*, 831*f*
 - pixel noise in, 832–834
 - purpose of, 825
 - quantum fluctuation-limited, 813–814
 - relationship with real observer, 831, 833, 834–835
 - retinal eccentricity in, 832, 832*f*
 - of spatial vision, 160–163, 162*f*, 830–831
 - statistically independent sources of information in, 827–828
 - of thresholds, 813–814, 816
 - value of, 825
 - Identification tasks, ideal observer analysis of, 825, 827–834
 - Illuminant
 - adaptation to, 901
 - discounting, 1627
 - Illumination, modeling of, 903–904
 - Illusion(s)
 - Argyle, 887, 887*f*
 - Benham, 1505
 - Chevreul, 886, 889
 - Craik-O'Brien-Cornsweet, 885, 886*f*, 888, 889
 - geometric-optical, 928–929, 1574, 1575*f*, 1577
 - luminance versus color contrast in, 929
 - Hermann grid, 886
 - lightness, 887
 - Mueller-Lyer, 1505
 - perceptual, 1574
 - visual, 1692. *See also* Aftereffects
 - boundary formation and, 1625–1626, 1625*f*
 - definition of, 1625
 - serrated-edge, 1291–1292, 1292*f*
 - surface formation and, 1625–1626, 1625*f*
 - wallpaper, 1302, 1302*f*
 - watercolor, 1583, 1583*f*
 - waterfall, 936
 - hMT/V5+ visual area activity during, 1237–1239
 - waterfall, 1505
 - Illusory conjunctions, 1108

- Illusory contours. *See* Illusion(s)
- Image, 948
- probabilistic inference on, 1604
 - retinal, natural and unnatural motion of, and visual processing, 1344–1347, 1345*f*, 1346*f*
 - separation into components by retina, 260
 - transformation to neuronal response, in receptive field, 704–706, 705*f*
- Image acquisition, retinal, 800–808
- chromatic aliasing and, 805–807
 - cone ratio variations and, 806*f*, 807
 - laser interferometry studies of, 802–805, 803*f*, 804*f*, 805*f*
 - limits in, 807–808
 - sampling and, 802–805
 - sampling by cones and, 802–807
 - trichromatic sampling and, 805–807
- Image computation, retinal, 799
- Image formation, 3
- retinal, 795–800
 - chromatic aberration and, 800–801
 - in corrected eyes, 807–808, 808*f*
 - diffraction and, 798, 798*f*, 799–800
 - light scatter and, 798–799
 - limits in, 807–808
 - point spread function and, 796*f*, 797–798
 - estimates of, 799–800, 800*f*
 - pupil function and, 796–797
 - wave aberrations and, 795–797
- Image parsing. *See also* Border ownership; Figure-ground segregation
- definition of, 1139
 - low-level mechanisms and, 1146–1148, 1147*f*
 - mechanisms of, 1139–1149
- Image representation. *See also* Pattern analysis
- feedback pathways in, 1613
 - linear superposition model of, 1606–1607, 1606*f*
 - coefficients for, neural circuit for sparsifying, 1607, 1608*f*
 - overcomplete, 1604–1606
 - probabilistic model for
 - adaptation of, for statistics of natural images, 1607–1608
 - and contextual effects, 1611–1612
 - extension beyond V1, 1613
 - and horizontal connections, 1611–1612
 - relation to V1 response properties, 1609–1612
 - sparseness in, 1605, 1606*f*, 1607, 1610–1611, 1612
 - alternatives to, 1612–1613
 - spatiotemporal, 1608–1609, 1609*f*
 - with time-varying images, 1608–1609, 1609*f*
 - redundancy reduction and, 1604
 - simple probabilistic model of, 1606–1609
 - sparse, 1604–1606
 - in visual cortex, principles of, 1603–1613
- Imidazole-4-acetic acid (IAAA), GABA receptor response to, 293
- Immediate early genes, and cortical plasticity, 128, 134
- Impulse response, 751
- Inattention blindness, 728
- Incoherent motion, in functional mapping of motion regions, 1236–1237
- Incomplete penetrance, definition of, 976
- Increment threshold, 911, 912*f*
- Increment threshold curves, 815–816, 816*f*
- photopic, 858–859, 859–860, 859*f*
 - scotopic, 858–859, 859*f*
 - theory of, 859–861, 860*f*
- Increment-sensitivity regulation, 868–869
- Independence, in independent components analysis, 1592
- Independent components (ICs)
- analysis, applied to natural images, 1612–1613
 - for image coding, 1592
- Independent components analysis (ICA), 1592
- Indoleamine accumulation, in amacrine cells, 398
- Inducers, of visual completion, 1289
- Infant(s), scotopic vision of, 846
- Inferior olive, 1487, 1491
- Inferior parietal lobule (IPL)
- interconnections/projections of, 1261
 - in spatially directed attention, 1520
- Inferior temporal area, and visual consciousness, 1689
- Inferior temporal cortex (IT), object coding in, 1599
- Inferior temporal sulcus (ITS), motion regions of, functional mapping of, 1230–1233
- Inferotemporal cortex, 529*f*, 1568*f*, 1569. *See also* TE visual area
- anterior (AIT), 1640
 - in object recognition, 1641*f*, 1643*f*, 1644
 - binocular disparity selectivity in, 787, 790
 - binocular disparity sensitivity in, 550
 - central, structural representation in, 1084
 - color cells in, 1019
 - preferred colors of, 1020
 - and color processing, 1014
 - corticocortical connections of, 523
 - face cells of, 1580
 - face detectors in, 18
 - feedback projections from, 524–525
 - hand detectors in, 18
 - lesions of
 - behavioral effects of, 548
 - and memory impairments, 548–549
 - in monkeys, 541, 542*f*
 - neurons
 - attention and, 1540
 - invariance properties of, 1170–1172, 1641–1642
 - latencies of, 530–532, 531*f*
 - properties of, 1165
 - receptive fields of, 522, 1171
 - selectivity of
 - changes in, in adults, 1159–1161, 1159*f*, 1160*f*
 - task requirements and, 1161–1162
 - specificity of, 1640–1641
 - in object recognition, 1158, 1640, 1641*f*, 1642, 1643*f*, 1644–1645, 1648–1650
 - and oculomotor system, 1372*f*
 - and perceptual constancy, 548
 - posterior (PIT)
 - in object recognition, 1641*f*, 1642, 1650
 - structural representation in, 1084, 1086–1087
 - response properties of, 1151–1162
 - and saccades, 1375–1376
 - structural representation in, 1084–1088
 - visual areas of
 - human, 515, 516*f*
 - human versus macaque, 518
 - in macaque, 510*f*–511*f*, 512
 - visual function of, 12
- Inflow theory, 1391
- Information bottleneck, 1004
- Information processing, 544
- unconscious, 1683
- Information storage, 544
- Infragranular neurons, connectivity of, 148, 149, 153
- Inhibition. *See also specific agents, cells, and functions*
- amacrine cells in, 405
 - development of, accelerated, overexpression of BDNF and, 55–58, 57*f*
 - lateral, 17
 - between amacrine cells, 355
 - amacrine cells in, 359, 405
 - contact-mediated, 79
 - and direction selectivity, 127, 453–455, 454*f*
 - horizontal cells in, 289
 - and orientation selectivity, 127
 - retinal, 355–365
 - anatomy of, 359–360
 - background history of, 355–356
 - direct functions in, 355–356
 - GABA versus glycine in, 355
 - morphology of, 360–361
 - peripheral, 360–361
 - sustained, 355–356
 - transient, 355–356, 358
 - vertical, amacrine cells in, 405

- Inhibitory control, orbital prefrontal cortex (PFC) and, 1554
- Inhibitory pathways, 361–364
- Inhibitory postsynaptic currents (IPSCs), 57*f*
- Inhibitory postsynaptic potentials (IPSPs)
GABA transporters and, 309
GABAergic, 355
glycinergic, 355, 365
horizontal connections and, 733–734
long-term depression of, 127
and neuronal synchrony, 742*f*, 742–743
retinal, 571
- Inhibitory surrounds, 364–365
of amacrine cells, 364
GABA and, 364*f*, 364–365
of ganglion cells, 23, 89, 355, 364*f*, 364–365, 422
glycine and, 364*f*, 364–365
horizontal cells and, 386–388, 388*f*
of LGN cells, cortical feedback and, 612–614
of receptive fields, 165*f*, 165–166. *See also* Center-surround organization, of receptive fields
- Inhibitory synapses, 359–360
development of, precocious, BDNF overexpression and, 55–58, 57*f*
- Inner plexiform layer of retina
absolute width of, 412
formation of, 81–86
ganglion cell stratification in, 412–413
glutamate receptors in, 86, 288
inhibitory surrounds in, 364*f*, 364–365
ON and OFF stratification in, 266–270, 267*f*
organization of, 83–86
synapse formation in, 87
synaptic transmission in, 288, 290–292
- Input-dependent excitability, of ganglion cells, 435, 438–443, 444
- Insect(s). *See also* Honeybee(s)
brain of, mushroom bodies in, 1512
centering response in, 1195*f*, 1195–1196
angular speed and, 1196
nondirectional nature of, 1196
versus optomotor response, 1196
color vision in, 963, 964, 965
flying, 1194–1201
learning and perception in, 1511
motion cues in, 1193–1201
for discriminating objects from backgrounds, 1200*f*, 1200–1201
for distinguishing objects at different distances, 1199–1200
for estimating distance flown, 1197–1198, 1198*f*
for flight speed control, 1196–1197, 1197*f*
for flight stabilization, 1194
- future directions for study of, 1201
for hovering, 1194–1195
for negotiating narrow gaps, 1195*f*, 1195–1196
for smooth landings, 1198–1199, 1199*f*
optomotor response in, 1193, 1194, 1201
direction selectivity of, 1196
temporal frequency and, 1196
patterning of compound eyes in, comparison with cone mosaic, 467
peering, 1193–1194, 1194*f*
screening pigments in, 965
visual anatomy of, 1193
- Instructive role of activity, 113
in cortical development, 165, 167
in LGN lamination, 113–115
in ocular dominance column development, 113–115
in orientation selectivity, 117, 122, 123–124
- Insulin-like growth factor (IGF), in retinal cell differentiation, 78
- Integrate-and-fire model, of ganglion cell excitability, 423, 428
- Integrate-and-fire neurons, 24, 26
- Integration, cortical feedback systems and, 614, 616*f*–617*f*, 621, 621*f*, 622
- Integration field, 1070
- Integration interval, in cortical neurons, 758
- Intensity, threshold versus, 815–816, 816*f*, 842
- Intensity coding
definition of, 932
hue-selective, in spatial vision, 932–933
- Intention
and attention, differentiation of, 1327
coding of, in posterior parietal cortex, 1324–1328
definition of, 1324
reach, reading out, 1333–1334, 1333*f*
- Intentional maps, in posterior parietal cortex, 1327–1328, 1328*f*
- Interareal cortical connections, 149–151
of preplate neurons, 150–151
and synaptic organization, 153–154
topographic organization of, 150
- Interblobs, 1626
versus CO blobs, 502, 682–683
- Intercalated layers. *See* Koniocellular layers; Koniocellular pathway
- Interference fringe, in laser interferometry studies, 802–805, 803*f*, 804*f*, 805*f*
- Intergeniculate leaflet (IGL), ganglion cells innervating, 628
- Interhemispheric connections, 522
morphology of, 524
organization of, 525
- Interkinetic migration, of retinal progenitor cells, 77
- Interlaminar layers. *See* Koniocellular layers; Koniocellular pathway(s)
- Interleukin(s), IL-6, inhibition of rod production by, 39
- Intermediate-level vision, 1139
- Intermediate-type projections, 544
- Intermedullary nuclei of thalamus, signals about nervous system state from, 134
- Interneurons
in cat LGN, I_f current in, 575–576
dendrite-targeting, in primary visual cortex (V1) of macaque, 689
inhibitory, 696
inhibitory GABAergic, 522
interneuron-targeting, in primary visual cortex (V1) of macaque, 689
of lateral geniculate nucleus, in cat, 568, 569*f*, 573
cable modeling for, 573
multiplexing by, 573
- Internuclear ophthalmoplegia, 1418
- Interocular light adaptation effect, 855, 855*f*
- Interocular transfer. *See* Aftereffects
- Interplexiform cells (IPCs), 395
dopaminergic, 313–314, 383, 401, 440
GABAergic, 307, 355, 361, 365
glycinergic, 311, 365
peptide expression in, 335
- Interstitial nucleus of Cajal, 1432*f*, 1486
- Intraareal cortical connections, 148–149
- Intracellular recording
of horizontal cortical connections, 733–734
of peptide action in retina, 337
of SCN neurons, 629
- Intraocular pressure, elevated, in glaucoma, 42
- Intraparietal sulcus
motion sensitivity in
functional mapping of, 1234–1235, 1235*f*, 1240
and structure determination, 1242
optic flow responses in, 1267–1268
- Intrinsic cortical connections. *See* Horizontal cortical connections
- Intrinsic noise, 19, 177
- Invariance
background, 1171
complex cells and, 1611, 1613
cue, 1036
in neuronal representation of stimuli, 1170–1172, 1641–1642
perceptual, 1154, 1574
mechanisms of, 1577–1578
position, 1250, 1262–1263, 1578
simple cells and, 1610, 1613
translation (shift), 1171
viewpoint, 1591
- Inverse mapping problem, 1307

Inversion of image, 3
 Invertebrates
 color vision in, and wavelength-specific behaviors, 966–967
 photopigments of, phylogeny of, 967
 Inverted-response polarity, in
 phototransduction, 217
 Inwardly rectifying cation current, in
 ganglion cells, 432, 434, 435–436
 Iodopsin, 215
 Ion channels/currents
 cGMP-gated, calcium regulation of, 227–228
 during darkness, 225–226
 GABA receptor modulation of, 357*t*, 357–358, 358, 363*f*, 363–364
 in ganglion cells, 422, 424–425, 430, 432–434
 identification and characterization of, 434
 progress in study of, 434, 443–444
 high-threshold, 432
 in horizontal cells, 376–379
 low-threshold, 432
 mixed cation, 431
 and neuronal activity, 24–25
 peptides and, 334, 337, 341, 341*f*, 342, 344, 346, 346*f*, 347, 348
 in phototransduction, 217
 opening and closing of, 217*f*, 219, 226
 optimization for speed, sensitivity, gain, and noise, 241–244
 somatostatin and, 341, 341*f*, 342
 substance P and, 344
 in synaptic transmission, photoreceptor-bipolar cell, 282–283, 284
 VIP and, 346, 346*f*
 Ion permeability, resting, in ganglion cells, 431
 Ionotropic receptors, 304. *See also specific receptors*
 IPa visual area, 1165, 1166*f*
 macaque, 510*f*–511*f*, 512
 Iris
 function of, 641
 movement of, 642
 muscles of, and pupil responses, 642, 652–653, 654*f*
 size of, and light capture, 642
 Isogenic lines, for mapping retina cell populations, 71–72
 Isomorphism
 Gestalt factor of, 1578
 second-order, 1080, 1082

J
 Jaybird, vision of, 1577
 Jitter, 1307, 1395
 Jumping stand tests, in visually deprived cats, 190–192, 191*f*, 194

K
 K cells. *See* Koniocellular pathway, cells of
 K layers. *See* Koniocellular layers
 Kainate receptors, 306
 in bipolar cells, 260
 in OFF pathway, 265*f*, 265–266, 268, 269*f*
 and direction selectivity, 361
 in horizontal cells, 378
 in synaptic transmission, 307
 bipolar cell-amacrine cell, 291
 bipolar cell-ganglion cell, 288
 photoreceptor-bipolar cell, 285, 307
 photoreceptor-horizontal cell, 289
 Kainic acid
 and horizontal cell function, 377, 378, 384, 384*f*
 and production of retinal cells, 38
 Kanizsa figures, 1142, 1579
 Kanizsa square, 1120, 1129, 1130*f*, 1625, 1625*f*
 Kanizsa triangle, 929, 1076, 1076*f*, 1119, 1120*f*, 1139, 1140*f*, 1142, 1286–1287, 1286*f*, 1288, 1290, 1574, 1575*f*
 KCC2 transporter, 87, 290, 291*f*
 Kinase(s), calcium-stimulated, and cortical plasticity, 128, 130, 137
 Kinesin, in ribbon synapses, 282
 Kinesthetic sense, in flying insects, 1194
 Kinetic boundaries, motion-sensitive visual regions and, 1241–1242, 1242*f*
 Kinetic contours, 1036
 Kinetic depth effect, 1211, 1577
 Kinetic occipital region
 and kinetic boundaries, 1241–1242, 1242*f*
 motion sensitivity of, functional mapping of, 1236
 Knockout mice, for neurotransmitter study, 87
 Köhler, Wolfgang, 1573–1574, 1579, 1580
 Koniocellular layers, 483, 485, 1219
 Koniocellular pathway(s), 481–491, 898, 909, 1007–1008
 cells of (K cells), 416, 416*f*, 481, 483–489, 484*f*, 566, 1219, 1566, 1567–1568
 chromatic information transmitted by, 497–498
 classes of, 499
 color responses of, 497–498, 1217, 1219–1220
 cone input to, 497–498
 functional properties of, 681
 heterogeneity of, 498, 499, 500*f*
 homogeneity versus heterogeneity of, 489
 homology to W cells, 487
 neurochemical signature of, 496–497

in nocturnal versus diurnal animals, 498, 499, 502
 parallel projections of, 496, 496*f*
 physiological properties of, 489
 projections to cytochrome oxidase-rich blobs, 483, 485, 496, 496*f*, 497–498, 499, 503
 reasons for, 502
 response properties of, 1008–1009
 spectrally opponent organization of, 1008
 visual latencies of, 503
 and chromatic discrimination, 920–921
 and chromatic motion processing, 1219–1220, 1223, 1223*f*
 color responses of, 1217
 connectivity of, 485, 486*f*
 to cortical layer 1, 502–503
 with MT visual area, 1220, 1223, 1223*f*
 to primary visual cortex, 498–501, 500*f*, 501*f*
 in cortical feedback systems, 610–611
 functions of, 489–491
 difficulties in lesion studies of, 490
 future directions for study of, 491
 independence versus interdependence of, 490–491
 macaque, 680–682
 parallel, 496–498
 functional implications of, 502
 organization in primary visual cortex, 498–501, 500*f*, 501*f*
 properties of, 482, 482*t*
 underlying anatomical certainty for, 482–485
 Kuffler, S. W., 17, 20, 23
 Kynurenic acid, and horizontal cell function, 377

L
 L (long-wavelength sensitive or red) cones, 176, 186, 186*f*, 372, 805, 806*f*
 chromatic aberration and, 800–801
 in chromatic motion processing, 1219–1220, 1237
 in color vision, 800–801, 1217, 1218*f*, 1219–1220, 1237
 connections to horizontal cells, 373–374, 376
 feedback from horizontal cells, 382, 383*f*
 input to P cells, 1219–1220
 ratio to M cones, 71
 effect on color vision, 806*f*, 807
 sampling by, 805, 806–807
lacZ gene, as marker of lateral movement by developing neurons, 468–469, 469*f*
 Lagged neurons, of lateral geniculate nucleus, 709
 receptive field maps for, 709, 709*f*

- Lambertian sphere, 1091–1092, 1092*f*
 Lambertian surface, 1098
 Lamellar motion, 1248
 definition of, 1247
 in optic flow field, 1250
 sensitivity to, in dorsal medial superior temporal area (MSTd), 1250
 LAMINART model, 1630, 1631
 Lamination
 of lateral geniculate nucleus, 270–271, 485
 in achiasmatic animals, 114–115
 activity and, 109–110
 instructive versus permissive role of, 113–115
 adult pattern of, 108
 eye-specific, development of, 108–110
 molecular cues for, 114–115
 patches versus layers in, 114–115
 of retina, 36, 37*f*, 83–86
 ON and OFF pathways in, 83–86, 266–270, 267*f*
 specificity of cortical connections for, 150–151
 Language, and consciousness, 1683
 Laser interferometry
 forced-choice contrast sensitivity in, 804, 805*f*
 for image acquisition studies, 802–805, 803*f*, 804*f*, 805*f*
 Latency
 of contextual effects, 725–726
 in different visual pathways, 503, 530–532, 531*f*
 in MT visual area, 530–532, 531*f*, 1206
 onset, in pupil responses, 642, 643*f*, 648, 650
 in SCN neurons, 630
 of visual response, development of, 163–165, 185*f*, 185–186
 Latency shift, in cortical neurons, 753–754, 754*f*, 759
 temporal dynamics of, 755
 Lateral channel neurotransmitters, 304
 dominant fast inhibitory, 307–310
 fast excitatory, 311–313
 minor fast inhibitor, 310–311
 Lateral cortical connections, 148–149, 1069
 anatomy of, 1071–1072
 orientation specificity of, 1071–1072, 1071*f*
 physiology of, 1071–1072
 specificity of, 1071–1072, 1071*f*
 of V1 neurons, and contour integration, 1069–1077
 Lateral elements, horizontal cell synapses at, 371*f*, 371–372
 Lateral geniculate nucleus (LGN), 529*f*, 565, 592, 695, 883, 1564–1565, 1566
 afferents to, 568–571, 569*f*, 570*f*, 578
 eye-specific segregation of, 108
 nonretinal, 566
 anatomy of, 485
 binocular interaction in, 768, 770*f*
 cells, 1010
 input to simple cells
 cortical inactivation experiments and, 697–698
 spatial organization of, 697
 strength of, 697
 untuned component of, 699–700
 L/M-opponent, 1013
 number and density of, 69
 OFF-center, 695
 ON-center, 695, 696*f*
 peak chromaticities of, 1011
 responses
 to chromatic flicker, 1010
 and color perception, 1013–1014
 spectral-response characteristics of, and color perception, 1013, 1013*f*
 circadian role of, 628
 circuitry of, 609–611, 610*f*, 611*f*
 color and space representation in, 488
 color cells in, preferred colors of, 1019, 1020*f*
 color opponency in, 17, 488
 cortical connections of, 154, 496
 feedback from cortex, 609–614, 622
 anatomical considerations in, 609–611, 610*f*, 611*f*
 effect on LGN cell firing patterns, 611–612, 613*f*, 622
 effect on LGN spatial interactions, 612–614, 614*f*
 interactions with layer 6, 568, 569*f*, 570, 578, 610*f*, 610–611, 612, 614–617, 622
 multiple, functional implications of, 501–503
 to primary visual cortex, 485, 486*f*, 494–503, 498–501, 499*f*, 500*f*, 501*f*
 signaling to cortical layer 1, 502–503
 corticofugal axons innervating, 609–611, 610*f*, 611*f*
 direction selectivity in, cortical feedback and, 612–613, 615*f*, 617
 dorsal, 565
 and oculomotor system, 1372*f*
 firing patterns of cells in
 burst, 575–578, 586, 612, 613*f*, 622
 in waking state, 612
 cortical feedback and, 611–612, 613*f*, 622
 tonic, 575–578, 586, 612, 613*f*, 622
 functional organization of, 566–578, 566*f*
 ganglion cell projections to, 413–414, 483–484, 485
 ON and OFF, 117–118, 118*f*, 270–271, 271*f*
 ganglion cell ratio to projection neurons in, 69
 human, 567
 innervation of, by nonretinal afferent axons, 566
 input from contralateral eye, 485
 input from ipsilateral eye, 485
 integration in, cortical feedback and, 614, 616*f*–617*f*, 622
 koniocellular layers of. *See* Koniocellular layers; Koniocellular pathway(s)
 labeling studies of, in ocular dominance column development, 110–111
 lagged neurons in, 709
 receptive field maps for, 709, 709*f*
 layering/lamination in, 117–118, 118*f*, 270–271, 485, 566–567, 567*f*, 1008, 1567–1568, 1567*f*. *See also* Koniocellular layers; Magnocellular layers; Parvocellular layers
 in achiasmatic animals, 114–115
 activity and, 109–110
 instructive versus permissive role of, 113–115
 adult pattern of, 108
 eye-specific, development of, 108–110
 molecular cues for, 114–115
 patches versus layers in, 114–115
 spontaneous activity of retinal cells and, 109–110
 length tuning in, cortical feedback and, 612, 614*f*
 M, P, and K cells of, 485, 566
 magnocellular layers of. *See* Magnocellular layers; Magnocellular pathway(s)
 maps of, 566, 566*f*
 monocular deprivation and, preventive effects of neurotrophins in, 53
 MT effects on, 619, 622
 nonlagged neurons in, 709
 receptive field maps for, 709, 709*f*
 ON and OFF leaflets in, 271
 opponent cells
 chromo-temporal receptive fields of, 1010–1011, 1012*f*
 response types of, 1010, 1011*f*
 optimization in, for natural scene perception, 1593
 organization of, 6
 in apes, 6
 in squirrel monkeys, 6
 orientation selectivity in, 117–118, 118*f*, 123–124, 127, 768, 770*f*
 cortical feedback and, 612–614, 615*f*, 616*f*–617*f*
 orthograde and retrograde degeneration in, 6–7

- Lateral geniculate nucleus (LGN) (cont.)
parvocellular layers of. *See* Parvocellular layers; Parvocellular pathway(s)
phase-specific responses in, 768, 770*f*
plasticity of, 114–115
projections to V1, 1568
receptive fields of cells in, 117–118, 118*f*, 123, 123*f*, 127
center-surround organization of, 612–614, 708–709
inhibitory surround of, cortical feedback and, 612–614
linear maps of, 707–709, 708*f*, 709*f*
responses of
behavioral versus physiological changes in, 164*f*, 164–165
development of, 163–165
spatial properties of, 166*f*, 166–167
spatiotemporal maps of, 708–709, 709*f*
representation of visual fields in, 6–7
and retina, functional connectivity
between, 674–675, 676*f*
retinal input to, in cat, 572
rod input to, 865–866
S cone signals to, 497–498, 502, 503
segmentation in, cortical feedback and, 612–614, 615*f*, 622
separation of eye inputs in, 270–271
spatial frequency selectivity in, 708, 768, 770*f*
spectrally opponent units in, 17, 1007
striped appearance of, 6
synaptic connections of
with ganglion cells, long-term potentiation between, 88
with layer 4 simple cells, 118, 118*f*
synchronization of cells in, cortical feedback and, 614, 616*f*–617*f*, 618*f*, 622
temporal dynamics in, 708–709
termination of optic tract fibers in, 6
thin layers of, 1008
transneuronal atrophy in, 6
ventral, 565
and visual cortex, functional connectivity
between, 675–677, 677*f*
visual pathways of
animal models of, 494
differing visual latencies of, 503, 530–532, 531*f*
M, P, and K, 481–491
parallel, 494–503
functional implications of, 501–503
number of, 496–498
organization in primary visual cortex, 498–501, 499*f*, 501*f*
unanswered questions about, 503
in visuosaccadic system, 1467
Lateral inhibition, 17
between amacrine cells, 355
amacrine cells in, 359, 405
contact-mediated, 79
and direction selectivity, 127, 453–455, 454*f*
horizontal cells in, 289
and orientation selectivity, 127
Lateral integration, of cones, 237*f*
Lateral intraparietal visual area. *See* LIP
(lateral intraparietal) visual area
Lateral masking, 1065
Lateral occipital area
human, 515, 516*f*, 517–518
and illusory contour perception, 1124
Lateral occipital complex (LOC), neuronal response properties of, 1183–1184
Lateral posterior nucleus, 565
Lateral posterior pulvinar complex, in cats, 592. *See also* Pulvinar region
Lateral processes, 1579
Lateral suprasylvian visual area, 10–11
Law of good continuation, Gestalt factor of, 1069, 1140, 1575, 1576*f*, 1581–1582, 1581*f*
and motion, 1576
Learning
associative, synchronized gamma oscillations in, 1678
context-dependent, in bees, 1507, 1508*f*
and object recognition, 1650
ocular motor
acquisition versus maintenance of, 1496
and cerebellum, 1495–1496, 1495*f*
context-specific, 1496
error signals as triggers for, 1496
short- versus long-term, 1496
in posterior parietal cortex, 1332–1333, 1332*f*
and visual target selection, 1382–1383, 1382*f*
Least displacement, in Gestalt psychology, 1576
Lemur, flying
evolutionary history of, 1564
visual system of, 1567
Length summation
horizontal cortical connections and, 739*f*, 739–741, 740*f*
vertical cortical connections and, 740
Length tuning, of LGN cells, cortical feedback and, 612, 614*f*
Lens
absorbance of, aging and, 208*t*, 208–209
accommodation of
ambient annual temperature and, 206, 206*t*
loss of, 205–208. *See also* Presbyopia
reading and, 207–208
age-related changes in, 206–207, 207*f*, 846
errors and variations in, 208–209
slopes of log magnitude versus log age for, 208, 208*t*
crystallins of, spatial arrangement of, age-related unraveling of, 209
curvature of, aging and, 207
distance from retina, reading and, 207–208
elasticity of, aging and, 206–207, 208, 208*t*
fluorescence of
aging and, 208*t*, 208–209
geographical location and, 208–209
geometric properties of, age-related changes in, 206–207
glutathione concentration in, age-related decline of, 205, 206*f*
light scatter from, 798–799
light transmission by, aging and, 208–209
mechanical properties of, age-related changes in, 206–207
metabolic decay of, 208
optical density of
aging and, 846
and spectral sensitivity, 838
size of, aging and, 206–207
yellowing and darkening of, aging and, 208–209
Leukemia inhibitory factor (LIF), inhibition of rod production by, 39
Levick, W. R., 17–18
Lewis and Van Essen scheme, for partitioning macaque visual cortex, 508, 510*f*–511*f*, 512
L-glutamate. *See* Glutamate
LGN. *See* Lateral geniculate nucleus
Ligand-gated ion channels, in horizontal cells, 376–378
Light, 1090
dark, 215
in cones, 215
in rods, 215
equivalent background, in photoreceptors, 215
isolated, perceptual attributes of, 893–899
mesopic. *See* Mesopic range
for natural images, 237, 238*f*
perceptual attributes of, in context, 899–902
Light adaptation, 858–861, 940–941, 940*f*
in amacrine cells, 396
chromatic, 859–860
definition of, 851
gain control in, 760–761
in ganglion cells, 422, 426, 427*f*, 427–428, 487
increment threshold curves in, 858–859, 859*f*
inhibitory surrounds in, 364, 364*f*

- in M (magnocellular) cells, 487
- opponent site and, 856*f*, 857, 860
- in P (parvocellular) cells, 487
- peptides and, 334, 349
- in photoreceptors, 228–230
 - calcium-dependent mechanisms in, 228–229
 - cellular events contributing to, 228
 - composite effect of mechanisms in, 230
 - elevated steady-state activity of
 - phosphodiesterase and, 229, 230
 - gain reduction in, 229
 - mechanisms of, 228–230
 - pigment bleaching and, 215, 229–230
 - response compression and, 228
- to polarizing field, 857
- rapid adaptational changes in, 860–861, 860*f*
- scale and, 1045–1046
- second-sight adjustments in, 940–941
- spinule formation in, 296–298, 297*f*
- synaptic plasticity and, 295–298
- and temporal sensitivity, 861
- Light field, 1090–1091
 - objects in, 1091–1094, 1092*f*, 1093*f*, 1094*f*
- Light offset, detection of,
 - electroretinogram of, 260–261, 261*f*
- Light onset, detection of, electroretinogram of, 260–261, 261*f*
- Light responses
 - of circadian clock, 625–636
 - behavioral, 625–628, 626*f*
 - phase shifts in, 625–628, 626*f*
 - dark rearing and, 89–90
 - development of, 89–90, 117, 176
 - of ganglion cells, 117, 423–430
 - cellular mechanisms of, 428–430
 - and circadian rhythms, 628, 629, 636
 - development of, 89–90
 - dopamine and, 440–443, 442*f*
 - GABA and, 443
 - glycine and, 443
 - of horizontal cells, 290
 - dopamine and, 383–384, 384*f*
 - electrical recording of, 369, 370*f*
 - in L-type cells, 372*f*, 372–373
 - in luminosity-type cells, 372*f*, 372–373
 - nitric oxide and, 384–386, 385*f*
 - retinoic acid and, 386, 387*f*
 - rod and cone signals in, 374–375
 - slowness of, 290
 - wavelength dependency of, 373–374, 374*f*
 - in intracellular signaling, 632–636
 - in melatonin production, 628
 - of photoreceptors, 215–230
 - activation of, 217–221
 - molecular mechanisms of, 217, 217*f*, 217–221
 - calcium feedback regulation of, 216, 217, 223, 225–228
 - versus chemoreceptive systems, 217
 - defects in, 217
 - inactivation of, 221–225
 - mutations of proteins involved in,
 - comparison of effects of, 222, 223–225, 224*f*, 225*f*
 - inverted-response polarity in, 217
 - noise during, calcium and, 227
 - onset phase of, predicted form of, 219–220, 220*f*
 - theory versus experiment, 220, 221*f*
 - overview of, 216–217
 - physical limits to, 215
 - proteins in, optimization for sensitivity, speed, gain, and noise, 241–244
 - speed of, size of outer segment and, 241–244, 243*f*
- of pupil, 641, 642–648
 - clinical applications of research on, 654–655
 - cortical damage and, 647, 648*f*, 654*f*
 - damage to dorsal midbrain and, 652*f*, 652–654, 654*f*
 - dilator muscle of iris and, 652–653
 - dynamic, 641, 642, 643*f*
 - dynamic noise experiments on, 643, 644*f*, 647
 - as example of servomechanism, 641, 653
 - function of, 641
 - optic nerve damage and, 645, 645*f*
 - pathways for, 641, 642, 653–654, 654*f*
 - single, hypothesis of, 641
 - two-component hypothesis of, 642–643, 647, 654
 - perimetry studies of, 645–647, 646*f*, 647*f*, 648*f*
 - steady-state component of, 642, 643*f*, 654*f*
 - transient component of, 642–643, 643*f*, 647, 654*f*
- of suprachiasmatic nucleus/SCN neurons, 625–636, 629–632, 630*f*–631*f*, 635*f*
- Light scatter
 - in aging eye, 799
 - and image formation, 798–799
 - sources of, 798–799
 - in young eye, 799
- Light transmission, by lens, aging and, 208–209
- Lightness, 881–890, 933
 - and chroma, 899
 - definition of, 881, 899
- Lightness constancy, 883–885, 884*f*
 - definition of, 884
 - limits of, 884–885
 - verification of, 884–885
- Lightness perception
 - stages of, 959
 - theories of, 959
- Light-scattering signal, 221
- Limb effect, 1092, 1096–1097, 1096*f*
- Limbic system, interconnections of, with prefrontal cortex (PFC), 1548
- Line detector, 747–748
- Line Element Model, 1044
- Line element theory
 - of chromatic discrimination, 917
 - definition of, 917
- Line of projection, 566
- Lineage
 - bias, of amacrine cell subtypes, 67–68
 - of retinal cells, 37, 63, 64–65, 66–67
- Linear chemical synapse, 248
- Linear convergence, of left and right eye signals, 768, 770*f*
- Linear decline, in human biological systems, 205
- Linear model, 956
 - for natural daylight, 956, 956*f*
- Linear neurons, response properties of, 704–706, 705*f*
- Linear properties
 - of cortical neurons, 750–751
 - of simple cells, 750–751
- Linear receptive field map(s), 705*f*, 705–706, 707–711, 716–717
 - comparison with direction selectivity index, 710–711, 711*f*
 - for complex cells, 708, 708*f*
 - for geniculocortical neurons, 707–708, 708*f*
 - for geniculostriate neurons, 708–709, 709*f*
 - methods for obtaining, 706–707, 707*f*
 - negative values of, 707
 - OFF or dark-excitatory responses in, 707
 - ON or bright-excitatory responses in, 707
 - positive values of, 707
 - for simple cells, 708, 708*f*, 709*f*, 709–710, 750
- Linear system identification, 1594–1595
- Linear systems analysis, 176–177, 495
 - of cortical neurons, 749
 - linear and nonlinear properties revealed by, 749
 - and receptive field mapping, 706
- Lingual cortex, motion sensitivity of, functional mapping of, 1235
- Lingual gyrus, in color vision, 1029
- LIP (lateral intraparietal) visual area, 543, 1429*f*
 - in attention and eye movements, 1326–1327, 1597
 - attentional response modulation in, 1515, 1540

- LIP (lateral intraparietal) visual area (cont.)
in dialogue between cerebral cortex and superior colliculus, 1468*f*, 1469*f*, 1471
in eye movement planning, 1327, 1328
eye-centered response fields in, gain modulation of, 1330–1331
lesions of, behavioral effects of, 552–553
macaque, 510*f*–511*f*, 511–512
dorsal (LIPv), 510*f*–511*f*, 511–512
homology with human visual area, 518
ventral (LIPv), 510*f*–511*f*, 511–512
neurons
attention and, 1515, 1540
delay period activity of, 1325–1326
and oculomotor system, 1376–1378
in oculomotor system, 1425
in saccades, 1398
sensorimotor transformation in, 1327–1328, 1328*f*
in spatial processing in active observers, 550–551
in spatially directed attention, 1325–1327, 1521
in visuosaccadic system, 1467, 1467*f*
Listing's law, 1418, 1493–1494
Listing's plane, 1493
Lizard(s), color vision in, 968
L-N model, of simple cells, 712*f*, 713–714, 714*f*, 717
LNL (linear, nonlinear, linear) model, of texture segregation, 1109
LO visual area, human, 515, 516*f*, 517–518
Local cortical connections. *See* Horizontal cortical connections
Local disparity, response of V1 neurons to, 784, 784*f*
Local edge detectors, 17
Localization, in blindsight, 658
LOC/LOP complex. *See also* Lateral occipital complex (LOC)
human, 515, 516*f*
Locomotion
control of, with optic flow, 1256–1257
obstacle avoidance in, object-relative heading and, 1257
steering in, object-relative heading and, 1257
Locomotor flow line, 1254
Locus coeruleus, signals about nervous system state from, 134
Locus control region, 978*f*, 985
deletion of, 983
as stochastic selector of L and M cone identity, 985–986
Locusts, peering by, 1193–1194, 1194*f*
Logical space, 813
Logistic growth curve, 846
Long-lead burst neurons, 1381
and pursuit- and saccade-related activity, 1410, 1433
Long-term depression, 127–128, 1670
acetylcholine and, 134, 136*t*
age and, 127–128
BDNF and, 133, 136*t*
calcium and, 130, 136*t*
dark rearing and, 128
electrical stimulation studies of, 127–128
glutamate receptors and, 130, 132, 136*t*
nerve growth factor and, 135, 136*t*
physiologic efficacy in, 137–138, 138*f*
presynaptic and postsynaptic changes in, 138–139, 139*f*
protein kinase A and, 131, 136*t*
relationship with ocular dominance
plasticity and long-term potentiation, 136, 136*t*, 137–138
serotonin and, 134, 136*t*
Long-term potentiation, 127–128, 1670
acetylcholine and, 134, 136*t*
age and, 127–128
BDNF and, 131, 133, 136*t*
calcium and, 130, 136*t*
dark rearing and, 128
electrical stimulation studies of, 127–128
GABA and, 131
glutamate receptors and, 130, 132, 136*t*
MAPK and, 59*f*, 59–60, 132, 136*t*
nerve growth factor and, 135, 136*t*
neurotrophins and, 49
nitric oxide and, 132
NMDA receptors and, 129, 136*t*
physiologic efficacy in, 137–138, 138*f*
presynaptic and postsynaptic changes in, 138–139, 139*f*
protein kinase A and, 131, 136*t*
protein kinase G and, 132, 136*t*
protein synthesis and, 133
relationship with ocular dominance
plasticity and long-term depression, 136, 136*t*, 137–138
serotonin and, 134, 136*t*
of synapses between ganglion cells and lateral geniculate nucleus, 88
Long-wavelength sensitive cones. *See* L (long-wavelength sensitive or red) cones
Looking
selective, 1524
without seeing, 1524
Looking-time habituation methods, direction selectivity in, 182–183
LOP (lateral occipital parietal) visual area, macaque, 510*f*–511*f*, 512
homology with human visual area, 518
Low area thresholds, 818–819
Low background sensitization, and thresholds, 816*f*, 818
Lower-luminance gratings, pupil responses to, 649*f*, 649–650, 650*f*
Low-light vision. *See* Scotopic vision
L-threo-3-dihydroxyphenylserine, and restoration of plasticity, 137
Lumanopia, transient, 858
Luminance, 721, 908
and binocular rivalry, 1316
and chromatic discrimination, 914–915
and color, 927–928
separation of, 1012–1014, 1013*f*
definition of, 881
detection of, 855
estimation of, 925
modulation, detection of, 1046
physiological substrate for, 909
spatial patterns of, 1080
of surfaces, 884
and visual completion, 1290, 1291*f*
Luminance channel, 1217, 1218*f*
and motion processing, 1217
Luminance contrast (LC)
and cortical neuron responses, 752*f*, 752–753
equivalent (EqLC), 1218
for blue/yellow gratings, 1218
invariant, in humans, 1223
in paradigm to measure chromatic input to MT visual area, 1221–1222, 1222*f*
for red/green gratings, 1218
M cell response to, 1219–1220
and motion processing, 1217–1218
and pupil light reflex, 642–643, 643*f*
Luminance contrast noise, and pupil responses, 643, 644*f*, 645, 647, 650–652, 651*f*
Luminance edge(s), 1285, 1286*f*, 1581
Luminance sensitivity, during saccades, 1393–1394, 1393*f*
Luminosity, mesopic, rod-cone interactions and, 867
Luminosity horizontal cells, 370, 370*f*, 372–374
receptive fields of, 380*f*, 380–381
spatial properties of, 381
Luminous atmosphere, 1094
Lunar effects, 1092
- M**
M cells. *See* Magnocellular pathway, cells of
M (mid-wavelength sensitive or green) cones, 176, 186, 186*f*, 372, 805, 806*f*
chromatic aberration and, 800–801
in chromatic motion processing, 1219–1220, 1237
in color vision, 800–801, 1217, 1218*f*, 1219–1220, 1237
connections to horizontal cells, 370–371, 373–374, 376

- feedback from horizontal cells, 382, 383*f*
- input to P cells, 1219–1220
- ratio to L cones, 71
 - effect on color vision, 806*f*, 807
- sampling by, 805, 806–807
- Macaques
 - amacrine cells of
 - AII, 396
 - GABAergic, 361
 - glycinergic, 361
 - area MT in, 510*f*–511*f*, 511
 - anatomy of, 1203–1204, 1204*f*
 - attentional effects in, 1208–1209, 1214
 - binocular disparity selectivity in, 550, 788*f*, 788–790, 789*f*
 - columnar organization of, 1204–1205, 1205*f*
 - correlation of response properties with motion perception, 1209–1210
 - direction selectivity in, 20–21, 619, 621*f*, 621–623, 1204–1205, 1205*f*, 1211–1212
 - motion integration and segregation in, 1207–1208
 - in motion perception, 1203, 1209–1213
 - color cues and, 1217
 - lesion studies of, 1211–1212
 - microstimulation studies of, 1212*f*, 1212–1213
 - real-time correlation with perception decisions, 1210–1211
 - sufficiency of, 1213
 - in motion processing, 1203–1214
 - neuronal bandwidth in, 1204–1205
 - physiological response properties of, 1204–1209
 - receptive fields of neurons in, 1205–1206
 - single neuronal responses in, 20–23
 - spatial properties of, 1205–1206
 - spatiotemporal profiles of neurons in, 1206–1207, 1207*f*
 - specialization of, 1213
 - speed tuning in, 1206–1207, 1207*f*, 1213
 - and stereoscopic vision, 788–790, 1205*f*, 1208, 1210
 - temporal properties of, 1206
 - binocular disparity selectivity in, 550, 779, 781*f*, 784, 787–788, 788*f*, 789*f*
 - brain of, 1429*f*
 - ciliary muscle of, age-related changes in, 207
 - color processing in, in extrastriate cortex, 1017–1026
 - color vision in, 908, 966*f*
 - cones of
 - development and migration in, 159–163, 162*f*
 - mosaics of, 468
 - size of, 241
 - consciousness in, 1682–1683
 - cortical plasticity in, 131
 - cortical processing streams in, 1624, 1625*f*
 - evolution of, 1564
 - extrastriate cortex of, color processing in, 1017–1026
 - ganglion cells of, 496
 - contrast sensitivity in, 418
 - small bistratified, 411–412
 - wide-field, 412
 - horizontal cortical connections in, 740
 - ideal observer analysis in, 829–830, 832
 - K (konio cellular) cells of, 496, 499
 - lateral cortical connections in, 1072
 - lateral geniculate nucleus in, 566, 567*f*
 - neurons of, 485
 - M (magnocellular) cells of, contrast gain of, 486, 486*f*
 - as model of human visual system, 494
 - neuronal correlates of visual deprivation in, 167–170
 - newborn versus adult visual capacities in, 159, 160*f*
 - orientation selectivity in, 179
 - P (parvocellular) cells of, contrast gain of, 486, 486*f*
 - parallel visual pathways of, 496–498
 - functional implications of, 501–503
 - organization in primary visual cortex, 498–499, 501*f*
 - parasol cell-to-midget cell ratio in, 484
 - photopigments in, genes for, 977
 - prefrontal cortex (PFC) of, 1547–1548, 1549*f*
 - primary visual cortex (V1) of
 - axo-axonic chandelier cells in, 689
 - basket cells in, 688–689
 - cell types in, 680
 - columnar (blob, interblob) division of, 681, 682–691
 - dendrite-targeting interneurons in, 689
 - excitatory cell types in, 683–686, 683*f*, 685*f*, 687*f*
 - and connections from layer 4C to superficial layers, 683–684, 683*f*, 685*f*
 - in deep layers, and their connections, 684–686, 687*f*
 - local connectivity of, 683–686
 - relationships to extrastriate cortical areas, 683–686
 - functional compartments of, 681
 - inhibitory cell types in, 686–688
 - morphology of, 689–690, 690*f*
 - interneuron-targeting interneurons in, 689
 - laminar (4B, 4C α , 4C β) division of, 681–691
 - local circuits in, 680–691
 - organization of, 680–681
 - pathways from LGN to, 680–683
 - projections to extrastriate cortical areas, 682–683
 - pulvinar region
 - retinal inputs to, 593–594
 - visual functions of, 599
 - receptive field properties in, development of, 163–165
 - retina of, weight and area of, 234
 - retinal cell number and density in, 69
 - variations in, 70–71
 - retinal peptide expression in, 336
 - CRH, 347–348
 - NPY, 338
 - somatostatin, 339
 - VIP, 345
 - rods of
 - noise and, 840
 - outer segments of, 241
 - spatial frequency and orientation
 - bandwidths in, 1062–1063
 - spatial vision in
 - development of, 159–171, 161*f*
 - visual deprivation and, 167–170, 168*f*, 169*f*
 - superior temporal sulcus in, 1165, 1166*f*
 - vertical cortical connections in, 733
 - visual areas in cerebral cortex of
 - comparison to humans, 507, 515–518, 517*f*
 - composite map of, 512, 513*f*
 - frontal, 510*f*–511*f*, 512
 - individual variability in, 509, 512–513
 - inferotemporal, 510*f*–511*f*, 512
 - number of subdivisions in, 512
 - occipital, 508, 509–511, 510*f*–511*f*
 - organization of, 507–513
 - parietal, 508, 510*f*–511*f*, 512
 - posterior, 510*f*–511*f*, 511–512
 - partitioning schemes for, 507–513, 510*f*–511*f*, 513*f*
 - differences among, reasons for, 509
 - multiple, coping with, 512–513
 - relationship to other sensory modalities, 507, 508*f*
 - temporal, 508, 510*f*–511*f*, 511–512
 - dorsal, 510*f*–511*f*, 511–512
 - ventral, 510*f*–511*f*, 512
 - total cortical area occupied by, 507, 747
 - visual cortex of
 - hierarchical organization of, 528–530, 529*f*
 - role of attention in, 1538–1543
 - visual development in
 - ideal observer model of, 160–163, 162*f*, 163*t*

- Macaques (cont.)
 neural limitations on, 159–171
 postnatal changes and, 159–163
 visual system of, 1569
 visuosaccadic system of, 1467–1468, 1467*f*
 afferent limb of, 1467, 1467*f*, 1480*f*
 efferent limb of, 1467, 1467*f*, 1480*f*
 intermediary limb of, 1467, 1467*f*, 1480*f*
- Macbeth ColorChecker, 902, 904*f*
- Mach bands, 885–886, 886*f*, 887, 888, 889
 depth distortions analogous to, 1305
- MacLeod-Boynton chromaticity diagram, 910*f*, 911
- Macula lutea, cones and rods of, 4*f*
- Macular degeneration
 age-related, mathematical analysis of, 210–211, 211*f*
 causes of, 42–43
- Magnetic resonance imaging
 functional
 of attention, 1516, 1520, 1520*f*
 in blindsight, 662–663, 1691
 blood oxygen level dependent (BOLD), 1691
 of cortical optic flow responses, 1269
 of V1 activity and visual awareness, 1691
 of human ventral visual pathway, 1179–1187
 interpretation of, 1645
 for mapping motion regions, 1229–1243
 attention to direction of motion and, 1240, 1240*f*
 attention to motion and, 1239–1240, 1239–1241
 attention to speed of motion and, 1241
 biological motion and, 1242
 BOLD versus MION methods of, 1232, 1233*f*
 dynamic noise and, 1236–1237
 in human homologue of area MT, 1229–1233, 1230*f*
 incoherent motion and, 1236–1237
 in monkeys, 1231–1235, 1233*f*, 1235, 1242–1243
 motion perception and, 1237–1239
 nonluminance-defined stimulus and, 1237
 in parietal cortex, 1234–1235, 1235*f*
 in primary visual cortex, 1233–1234, 1234*f*
 stimulus parameters for, 1236
 stimulus patterns for, 1236
 in V3A visual area, 1234
 in ventral cortex, 1234*f*, 1235–1236
 for mapping visual areas, 513, 514*f*, 518
 of object recognition, 1645
 in pattern adaptation, 939
 of posterior parietal cortex, 1324
 of relative disparity processing, 787
 of texture segregation, 1115
 of ventral visual object pathway in humans, 1179–1187
 of pupil responses
 to light, 643, 644*f*
 to motion, 649
 structural, for mapping visual areas, 507, 508*f*, 513, 514*f*
- Magnetic resonance imaging (MRI), functional
 in change detection, 1528, 1533–1534
 of color analysis, 1034
- Magnitude constraint, 1293–1294
- Magnocellular layers, 483, 485, 529*f*, 1219, 1567, 1567*f*
- Magnocellular pathway(s), 481–491, 529*f*, 898, 909, 1007
 activation of, 1315
 cells of (M cells), 413–414, 416, 416*f*, 418, 483–489, 484*f*, 566, 1219, 1566, 1570
 chromatic selectivity of, 488
 classes of, 499
 color responses of, 488, 1217, 1219–1220
 unsigned, 1220
 contrast gain control of, 487
 contrast gain of, 485–488, 486*f*, 488*f*
 contrast sensitivity of, 484, 485–486, 486*f*
 electrical coupling of, 484
 functional properties of, 681
 homogeneity versus heterogeneity of, 489
 light adaptation in, 487
 linearity/nonlinearity of, 486–487
 neurochemical signature of, 496–497
 parallel projections of, 496, 496*f*
 physiological properties of, 485–489
 ratio to P (parvocellular) cells, 484
 receptive fields of, 164, 164*f*
 size of, 484–485, 486
 response dynamics of, 485
 response properties of, 1008
 sampling density of, 483–484
 in scotopic (low light) vision, 487–488, 488*f*
 spatial resolution of, 483–484, 484*f*, 501
 spatially opponent organization of, 1008
 temporal profile of, 709
 temporal resolution of, 496, 501
 terminology for, 483
 tiling of, 483–484
 visual latencies of, 503
 X/Y cell homology of, 486–487
 color and space representation in, 488
 connection to “where” pathway, 489
 connectivity of, 485, 486*f*
 to primary visual cortex, 498–501, 501*f*
 in cortical feedback systems, 610–611
 dysfunctions attributed to, 490
 functional segregation of, 496, 497*f*
 functions of, 489–491
 based on clustering or functional properties, 489
 independence versus interdependence of, 490–491
 lesion studies of, 489–490, 490*f*
 future directions for study of, 491
 macaque, 680–681
 in motion processing, 489–490, 496, 501, 1206
 chromatic, 1219–1223, 1221*f*, 1222*f*
 MT connections with, 619, 1219–1223
 parallel, 496–497, 498–501, 501*f*
 functional implications of, 501
 organization in primary visual cortex, 498–501, 501*f*
 and photopic luminance, 867
 properties of, 482, 482*t*
 retinal eccentricity and, 484–485
 saccadic suppression and, 1394–1395, 1394*f*, 1399
 segregation from parvocellular pathway, 483, 496, 497*f*
 underlying anatomical certainty for, 482–485
- Magritte, René
The Blank Signature, 1576, 1577*f*
Paysage de Baucis, 1140*f*
- Maltese cross figure, 1124–1125, 1125*f*
- Mammal(s)
 color vision in, 964
 evolutionary history of, 1564, 1565*f*
 marine, vision of, 964
 visual system of, characteristics of, 1564–1566
- Mantids, peering by, 1194
- Marmoset
 ganglion cells of, peripheral inhibition of, 361
 parallel visual pathways in, 498
- Marshall, Wade, 9–10, 27
- Marsupial, optic chiasm in
 development of, 98
 organization of, 95, 95*f*
- Marsupials, evolutionary history of, 1564, 1565*f*
- Martinotti cells, in primary visual cortex (V1) of macaque, 689
- Masked priming, 1688
- Masking, 927–928, 1687
 backward, in stereopsis, 1310
 integrative, 1687
 lateral, 1065
 mask contrast and, 1063, 1063*f*
 object-substitution, 1687
 spatial, 930

- simultaneous, for color and luminance, 931–932, 931*f*
- suprathreshold, 930–931
- spatial frequency and orientation
 - bandwidth measurements using, 1062–1063
- spatiotemporal, 1310
- temporal, 1310
- Master gene, in eye development, 33–34
- Matching problem, 1302
- Math5*, in retinal cell differentiation, 38
- Maximum A Posterior (MAP) estimate, 1607
- Maximum fitness ideal observers, 834–836, 835*f*
- Maximum operation, 1642–1643, 1648
- Mb1 bipolar cell
 - neurotransmitter expression and synaptic transmission in, 286–288, 287*f*, 292*f*, 292–293
 - spinule formation in, 297–298
- MBDKL space, 1010, 1010*f*, 1011*f*
- McCollough effect, 1132, 1628. *See also* Aftereffects
- mCry1* and *mCry2* genes, 635
- MD cells, type-specific tiling behavior of, 471
- MDP (medial dorsal parietal) visual area, macaque, 510*f*–511*f*, 512
- Medial interlaminar nucleus, 569
- Medial intraparietal area (MIP)
 - movement planning in, 1327–1328, 1328*f*
 - sensorimotor transformation in, 1327–1328, 1328*f*
- Medial longitudinal fasciculus, 1416, 1416*f*, 1486
- Medial superior temporal area (MST), 543, 1568*f*, 1569, 1584–1585
 - attentional response modulation in, 1515–1516
 - binocular disparity selectivity in, 785, 786–787, 790
 - color cells in, 1019
 - connections with area MT, 1203, 1204*f*, 1260
 - human homologue of, 1231
 - in heading detection, 1252
 - optic flow responses in, 1269
 - lesions of, behavioral effects of, 551
 - macaque, 510*f*–511*f*, 511, 512, 513*f*
 - dorsal (MSTd)
 - columnar organization of, 1264
 - flow-selective units in, 1249–1250
 - functional organization of, 1264, 1265*f*
 - heading selectivity in, 1263–1264, 1264*f*
 - motion processing in, 549–550, 1274–1276, 1276*f*
 - motion processing in, pursuit eye movements and, 1270–1271
 - neuronal response mechanisms of, 1264–1267, 1266*f*
 - neuronal sensitivity to binocular disparity, 1266–1267
 - neurons, 1262–1263, 1263*f*
 - optic flow responses in, 1262–1263, 1263*f*, 1277, 1277*f*
 - and self-motion determination, 1251–1252
 - in spatial processing in active observers, 550–551
 - vestibular input and, 1271–1272
 - motion processing in, pursuit eye movements and, 1270
 - subdivisions of, 510*f*–511*f*, 511
 - ventrolateral (MSTv, MSTl)
 - motion processing in, 550, 1261
 - motion processing in, pursuit eye movements and, 1270
 - vestibular input and, 1272
- motion processing in, 549–550, 1212, 1261, 1270, 1274–1276
- neurons
 - latencies of, 530–532, 531*f*
 - responses of, modulation by surrounding stimuli, 1375
- neurons in
 - optic flow responses in, 1262–1263
 - receptive fields of, attention and, 1541
 - in oculomotor system, 1405
 - perisaccadic compression of space in, 1398–1399, 1399*f*
 - and pursuit behavior, 1407, 1408
 - and stereoscopic vision, 786–787, 790
 - in vergence control, 1425
- Medial temporal lobe (MTL), and visual consciousness, 1689, 1690*f*
- MEK, 59
- Melanin, and optic chiasm development, 102–103
- Melanoma-associated retinopathy, 272, 273*f*
- Melanopsin
 - and circadian rhythms, 628, 629, 635*f*
 - coexpression with PACAP, 345, 629
 - ganglion cells containing, 628, 629, 635*f*
- Melatonin
 - and circadian rhythm, 628, 630–631
 - light responsiveness of, 628, 630
 - in signal processing, 316
 - suppression of, light intensity and, 630–631
- Melatonin receptors, 316
- Membrane time constant, of ganglion cells, 430–431
 - range between species, 431
 - range within species, 431
 - synaptic input and, 431–432
- Memory. *See also* Cognition; Color memory; Working memory
 - and anticipatory pursuit, 1405
 - in conjunction search, 1383
 - enhancement of, color and, 933–934
 - iconic, 1686
 - impairments, ventral stream lesions and, 548–549
 - implicit, and visual target selection, 1370
 - long-term, 544
 - short-term, 1525, 1540
 - neural substrate for, 1406
 - psychophysical evidence for, 1686
 - synapses and, 25
 - in visual consciousness, 1686
 - working. *See* Working memory
- Memory reach task, posterior parietal cortex in, 1327
- Memory saccades, 1441*f*
 - FEF activity and, 1435–1436, 1436*f*, 1437–1439, 1437*f*
- Mendelian genetics, 71
- Mercaptopropionic acid, and restoration of plasticity, 136–137
- Meridional amblyopia, 199–200, 200*f*
- Mesopic light. *See* Mesopic range
- Mesopic range, 841, 845, 851, 863, 865
- Mesopic sensitivity, rod-cone interactions and, 867
- Mesopic spectral efficiency function, 867, 867*f*
- Metacontrast, 868, 1687. *See also* Masking
- Metamers, 910
- Metarhodopsin I (M_I), 218
- Metarhodopsin II (M_{II}), 218
- α -Methyl-4-carboxyphenylglycine (MCPG), and cortical plasticity, 129–130
- N*-Methyl-D-aspartate receptor(s). *See* NMDA (*N*-methyl-D-aspartate) receptor(s)
- 2-Methyl-6-(phenylethynyl)-pyridine hydrochloride (MPEP), and cortical plasticity, 130
- Meynert cells, 527
- Mice
 - BDNF overexpression in, 55–58, 57*f*
 - during dark rearing, 51
 - bipolar cell transmission in, 284
 - circadian rhythms in, genetic expression and, 634*f*, 634–635
 - cortical connections in
 - feedback, 152
 - feedforward, 151
 - patchy organization and axonal bifurcations in, 525
 - of preplate neurons, 150
 - and synaptic organization, 154
 - cortical plasticity in
 - calcium and, 130
 - GABA and, 131

- Mice (cont.)
 immediate early genes and, 134
 protein synthesis and, 138
dark rearing of, and light response of
 receptive fields, 89–90
direction selectivity of, starburst amacrine
 cells and, 457–459
eye field demarcation in, 33
GABA transport in, 289
ganglion cells of
 calcium currents in, 433
 light responses of, 443
horizontal cells of, retinoic acid and, 386,
 387*f*
knockout, for neurotransmitter study, 87
mi/mi mutant, rod maturation in, 41
monocular deprivation in, 126, 198
 effects of exogenous neurotrophins on,
 50, 51*f*–52*f*
neurotrophin deficiencies in, 48, 48*b*
optic chiasm in
 development of, 99, 100, 101
 ganglion cell axon behavior in, 95–96
 organization of, 94, 95
ON pathway knockout in, 272
phototransduction in, mutations of
 inactivation proteins and, 222,
 223–225, 224*f*, 225*f*
positioning information across retina in,
 41
retina of, developing, spontaneous activity
 of, 89*f*
retinal cell development in, bone
 morphogenetic proteins and, 65
retinal cell differentiation in, 38, 67
retinal cell number and density in, 69–70
 genetic polymorphism and, 71
 in isogenic lines, 72
 tyrosinase gene mutation and, 71
 variations in, 70–71
retinal peptide expression in, 336
 NPY, 338
 somatostatin, 340
 tachykinins, 342–343
retinitis pigmentosa in, 43
rhodopsin in, phosphorylation of, 222
rod-cone interactions in, retinal pathways
 of, 865
Six3 gene overexpression in, 66
visual areas of, 518
visual deprivation studies in, 189
Michelson contrasts, 1294–1295
Microgenesis, 1686
Microglia, retinal, 41
Microsaccades, 1343, 1347, 1350, 1395
Microtubule(s)
 in cones and rods, 216, 245, 246*f*
 and mosaic formation, 470
Midbrain
 connections with area MT, 1203, 1204*f*
 dorsal, damage to, and pupil responses,
 641–642, 652*f*, 652–654, 653*f*
 signals about nervous system state from,
 134
 as target of ganglion cell axons, 94
Middle temporal (MT) visual area,
 510*f*–511*f*, 511, 528, 529*f*, 543, 1371,
 1372*f*, 1568, 1568*f*, 1569
 anatomy of, 1203–1204, 1204*f*
 attentional effects in, 1208–1209, 1214
 attentional response modulation in,
 1515–1516
 behavioral functions of, 1239
 binocular disparity selectivity in, 550,
 788*f*, 788–790, 789*f*
 binocular disparity sensitivity in, 550
 chromatic input to
 effect on motion perception, 1218–
 1226
 equivalent luminance contrast (EqLC)
 paradigm for measuring, 1221–1222,
 1222*f*
 sources of, 1219–1220
 color cells in, 1019
 preferred colors of, 1020
 tuning of, 1020–1021
 columnar organization of, 1204–1205,
 1205*f*
 component cells in, 1584–1585
 connections of
 cortical and subcortical, 1203, 1204*f*
 with koniocellular pathway, 1220, 1223,
 1223*f*
 with magnocellular pathway, 619,
 1219–1223
 with parvocellular pathway, 619, 1220,
 1223–1226
 with primary visual cortex, 619, 1203,
 1204*f*
 cooling experiments on, 619–620
 development of, 170
 direction selectivity in, 20–21, 619, 621*f*,
 621–622, 1204–1205, 1205*f*,
 1211–1212
 chromatic input and, 1218–1219
 feedback to V1, 609, 614–622
 effects of, 619–622, 620*f*, 621*f*
 future directions for study of, 622–623
 flicker responses of, 1237, 1238*f*
 functional specializations of, receptive
 field tuning properties and, 720
 future directions for study of, 1213–1214
 human homologue of (hMT/V5+)
 behavioral functions of, 1239, 1241
 cone input to, 1237
 direction selectivity in, 1239, 1240,
 1240*f*
 flicker responses in, 1236–1237, 1238*f*,
 1239
 identification of, 1229–1233, 1233*f*
 motion processing in
 attention to direction of motion and,
 1240, 1240*f*
 attention to motion and, 1239–1241
 functional mapping of, 1229–1243,
 1230*f*
 motion perception and, 1237–1239,
 1252
 nonluminance-defined stimuli and,
 1237
 versus primary visual cortex,
 1230–1231, 1231*f*
 stimulus parameters for mapping,
 1236
 stimulus patterns for mapping, 1236
 subdivision of, 1231
 and movement control, 1241
 optic flow responses in, 1269
 three-dimensional structure
 determination in, 1242
 interconnections/projections of,
 1260–1261
 latencies in, 1206
 lesions of, behavioral effects of, 551
 and LGN responses, 619, 622
 motion integration and segregation in,
 1207–1208
 color cues for, 1223–1226
 in motion perception, 1203, 1209–1213
 correlation of response properties with
 perception, 1209–1210
 lesion studies of, 1211–1212
 microstimulation studies of, 1212*f*,
 1212–1213
 necessity of, 1213
 real-time correlation with perception
 decisions, 1210–1211
 sufficiency of, 1213
 in motion processing, 619–622, 620*f*,
 621*f*, 1203–1214, 1261–1262, 1274,
 1619–1620
 color cues and, 1210, 1217, 1218–1226
 functional mapping of, 1231–1233,
 1233*f*, 1242–1243
 epoch duration and, 1236, 1236*f*
 stimulus parameters for, 1236
 pursuit eye movements and, 1270–1271
 motion processing in, 549
 myelination of, 1203
 neuronal bandwidth in, 1204–1205
neurons
 attentional modulation of, 1541, 1542,
 1542*f*
 directional selectivity of, attention and,
 1540–1541
 integration of information about
 motion, color, and form in, 1024
 luminance response of, 1020
 optic flow responses in, 1262–1263
 pattern-selective, 1619

- responses of, modulation by surrounding stimuli, 1375
- neurons in, receptive fields of, attention and, 1541
- pattern cells of, 1209–1210, 1584–1585
- perisaccadic compression of space in, 1398–1399, 1399*f*
- physiological response properties of, 1204–1209
- and pursuit behavior, 1407
- receptive fields of neurons in, 1205–1206
- retinotopy of, 1203–1204
- single neuronal responses in, 20–23
- spatial properties of, 1205–1206
- spatiotemporal profiles of neurons in, 1206–1207, 1207*f*
- specialization of, 1213
- speed tuning in, 1206–1207, 1207*f*, 1213
- spikes or spike trains in, 1206
- and stereoscopic vision, 788–790, 1205*f*, 1208, 1210
- study of
 - experimental approaches to, 1203
 - importance of, 1203
- temporal properties of, 1206
- variance in location and extent, 511
- in vergence control, 1425
- visual deprivation and, 170–171
- Midget cells
 - bipolar, 997–998, 998*f*, 1007
 - ganglion cells, 262, 268, 410–411, 411*f*, 483–485, 997–998, 998*f*, 1007
 - central projections of, 413–414, 483, 484*f*, 497
 - color responses of, 1219–1220
 - connections of, 485, 486*f*
 - connectivity to midget bipolar cells, 413, 418
 - contrast sensitivity of, 416*f*, 416–417, 484, 486*f*
 - morphology of
 - distance from fovea and, 413, 414*f*
 - eccentricity-dependent, 413, 414*f*
 - neurotransmitter receptors in, 412, 412*f*
 - ratio to parasol cells, 484
 - receptive fields of, center-surround organization of, 415
 - response dynamics of, 485
 - sampling density of, 483–484
 - spatial resolution of, 483–484, 484*f*
 - stratification of, 412–413
 - synaptic input to, 412–413, 418–419, 483
 - terminology for, 483
 - tiling of, 483–484
 - tonic nature of, 485
 - types of, 489
- in peripheral retina, 998–999, 998*f*
- rods and, 865–866
- Midget system, 483
- Mid-wavelength sensitive cones. *See* M (mid-wavelength sensitive or green) cones
- Minimal-spacing rules, and formation of neuronal mosaics, 469*f*, 469–470, 474
- Minimum discharge field
 - of cortical neurons
 - horizontal connections and, 733–739, 736*f*, 738*f*
 - stimulation of, and activation of horizontally linked neurons, 737–739, 738*f*
 - size of, regulation of, 741
- Mink(s), ON and OFF leaflets in LGN of, 271
- Miosis, 1415
- MIP (medial intraparietal) visual area, macaque, 510*f*–511*f*, 512
- MIRAGE model, 1044, 1055
- Mirror stereoscope, 779
- Misalignment/misalignment response, 182, 182*f*
- Mislocalization(s), perisaccadic, 1397–1399
- Mismatching loss, 819
- Misreaching, 554
- MITF* gene
 - expression of, in optic cup and optic vesicle, 34, 35*f*, 36
 - mutations of, 36
- Mitochondria, in cones and rods, 216, 216*f*
- Mitochondrial genes, and cortical plasticity, 134
- Mitogen-activated protein kinase (MAPK)
 - activation of, 59*f*, 59–60
 - calcium and, 634
 - circadian role of, 634, 635*f*
 - CREB activation by, 132
 - and long-term potentiation, 132, 136*t*
 - and ocular dominance, 132, 136*t*
 - and plasticity, 58–60, 59*f*, 132, 136*t*, 137, 137*f*
 - in retinal cell differentiation, 39
- Mitosis, in retina, 77
- MK-801, and circadian rhythms, 629
- Mnemonic enhancement, 547
- Modal completion. *See* Visual completion, modal
- Models. *See* specific models
- Modulation
 - first-order, 1046
 - push-pull, of pulvinar cells, 598–599
 - second-order, 1046
- Modulation transfer function, 1097
 - of retinal images, 799
 - estimates of, 799–800, 801*f*
 - in monochromatic and broadband light, 801, 801*f*
- pupil size and, 799–800, 801*f*
- relationship with foveal cone Nyquist limit, 803–804, 804*f*
- Modulator spectral sensitivity curve, 16–17
- Modulators
 - horizontal cortical connections as, 733
 - properties of, 533
 - pulvinar region, 596
 - retinogeniculate, 572–573, 578–580, 582–583, 586
 - in thalamocortical relays, 572–573, 578, 579
- Molecular gradients, and retinal cell development, 41–42, 63
- Mondrian world, 948, 956
- Monkey(s). *See also* Macaques; Primate(s)
 - amacrine cells of, 400–401
 - GABAergic, 361
 - glycinergic, 361
 - neurochemistry of, 402
 - tracer-coupling studies of, 402
- angular gyrus lesions in, 11, 11*f*
- anticipatory pursuit in, 1405–1406, 1406*f*
- asymmetric response to motion in, 184
- awake, behaving, experimental arrangement for, 766, 766*f*
- binocular deprivation in, 192–193
- dark rearing versus eyelid suture, 190–191
- binocular disparity selectivity in, 550, 766, 766*f*, 779, 781*f*, 1266–1267
- blindsight in. *See* Blindsight
- brain of, 541, 542*f*, 1429*f*. *See also* Brain
- ciliary muscle of, age-related changes in, 207
- cones of
 - development and migration in, 159–163, 162*f*
 - mosaic of, 468
 - size of, 241
- cortical connections in
 - feedback, 150, 152*f*, 152–153
 - feedforward, 151, 152*f*
 - horizontal, 737–738, 738*f*
 - patchy organization and axonal bifurcations in, 526*f*
 - of preplate neurons, 150
 - and synaptic organization, 154
- cortical development in, 165–167
- receptive field properties in, 165*f*, 165–167, 166*f*
- cortical neurons of, contrast response function in, 755*f*, 755–756
- cortical plasticity in, 131
- corticocortical pathways in, 523
- conduction speed in, 532
- decorrelated binocular input in, 198–199, 199*f*
- feedforward connections in, functional roles of, 532–533

- Monkey(s) (cont.)
 ganglion cells of
 excitability of, 426
 peripheral inhibition of, 361
 horizontal cells of, luminosity, 372, 372*f*
 horizontal cortical connections in, 737–738, 738*f*
 inferotemporal cortex of, hand and face detectors in, 18
 K (koniocellular) cells of, 489, 498, 499
 lateral geniculate nucleus in, 6
 color opponency in, 17
 receptive field properties of, development of, 163–165
 spectrally opponent units in, 17, 1007
 microsaccades in, 1347
 as model of human visual system, 494
 monocular deprivation in, 196–197
 eyelid suture versus chronic monocular cycloplegia, 196–197, 197*f*
 motion regions in, functional mapping of, 1229–1235, 1233*f*, 1234*f*, 1242–1243
 MT visual area of. *See* Middle temporal (MT) visual area
 neuronal correlates of visual deprivation in, 167–170
 New World
 color vision in, 977, 979
 polymorphism of, 968, 968*f*
 evolution of, 1564
 lateral geniculate nucleus in, 566, 567
 visual system of, 1567, 1569, 1570
 newborn versus adult visual capacities in, 159, 160*f*
 occipital lobe lesions in, 8, 9*f*
 ocular dominance in, development of, 147
 OFF and ON pathways in, stratification of, 268
 ON and OFF leaflets in LGN of, 271
 Old World. *See also* Macaques
 color and food source identification in, ideal observer analysis of, 834
 color vision in, 908, 968, 977, 979
 evolution of, 1564
 lateral geniculate nucleus in, 6, 566
 receptive fields in, responses and properties of, development of, 163–165
 retinal cell types in, 483
 visual system of, 1567, 1569, 1570
 orientation selectivity in, 179
 measurement in awake, behaving animal, 758
 parallel visual pathways of, 496–498
 functional implications of, 501–503
 organization in primary visual cortex, 498–499, 499*f*, 501*f*
 parasol cell-to-midget cell ratio in, 484
 perception of illusory contours, 1505
 photopigment genes of, 979–980
 posterior parietal cortex in, 1324
 prefrontal cortex (PFC) damage in, behavioral effects of, 1551–1554
 pulvinar region
 cortical projections from, 585
 retinal inputs to, 593–594
 subdivisions of, 583, 592
 visual functions of, 592–604
 receptive field dynamics in, 739*f*, 740
 receptive field mapping in, linear, 710
 retina of, weight and area of, 234
 retinal cell number and density in, 69
 variations in, 70–71
 retinal peptide expression in, 336
 CRH, 347–348
 NPY, 338
 somatostatin, 339–340
 tachykinins, 342–343
 VIP, 345
 rods of, outer segments of, 241
 single-unit recording in, 17, 18
 spatial frequency selectivity in, measurement in awake, behaving animal, 758
 spatial vision in
 development of, 159–171, 161*f*
 visual deprivation and, 167–170, 168*f*, 169*f*
 striate cortex of
 lesions of, 657
 mapping of visual fields on, 10, 10*f*
 superior colliculus in, 1455
 temporal lobe lesions in, 11–12
 visual areas of, 518, 541, 542*f*, 544*t*
 comparison to humans, 507, 515–518, 517*f*
 organization of, 507–513, 508*f*, 510*f*–511*f*, 513*f*
 outside primary visual cortex, 11
 parietal, 11
 V1, 1581–1582
 removal of, 657
 visual cortex of, 1582
 contextual modulation in, 720–729
 visual deprivation studies in, 189. *See also specific study types*
 visual development in
 ideal observer model of, 160–163, 162*f*, 163*t*
 neural limitations on, 159–171
 Monochromacy, 796, 800–801, 805–806
 blue cone, 975
 inheritance of, 976
 molecular genetics of, 983
 correction of, effects of, 807–808, 808*f*
 rod, 975, 983
 Monocrystalline iron oxide nanoparticle (MION), in MRI of motion regions, 1232, 1233*f*, 1236
 Monocular cycloplegia, chronic, in monkeys, 196–197, 197*f*
 Monocular deprivation, 189, 193–198
 alternating, 189, 198–199
 binocular competition during, 49, 194
 and binocular vision, 776
 in cats, 194–196
 and contrast sensitivity
 in cats, 196, 196*f*
 in monkeys, 196–197, 197*f*
 and cortical connectivity, 147, 153, 154
 and CREB, 132, 134
 critical period for, 46, 47*f*, 49, 126, 193
 prolonged, neurotrophin blockade and, 52, 54*f*
 effects of, 46, 50, 51*f*–52*f*, 126, 167, 189, 193–198
 and Hebbian synapses, 113–114
 in humans, 46, 126, 197–198
 MAPK activation and, 59*f*, 59–60
 in monkeys, 196–197
 neuronal correlates of, 167–170
 neurotrophins and
 effects of BDNF overexpression, 55–58, 58*f*
 effects of endogenous NGF blockade, 52, 54*f*
 effects of exogenous administration, 50, 51*f*–52*f*, 135, 136, 137
 ocular dominance column shift prevented by, 53–55
 shrinkage of lateral geniculate nucleus neurons prevented by, 53
 and ocular dominance, 49, 51*f*–52*f*
 developmental effects of, 108, 112–114, 115, 147
 effects of exogenous neurotrophins on, 50, 51*f*–52*f*, 135, 136
 effects of MAPK activation in, 59*f*, 59–60
 plasticity effects of, 126, 128, 130–131, 132, 133, 135, 137, 138
 preventive effects of neurotrophins in, 53–55
 and orientation selectivity, 121, 132, 133
 and plasticity, of visual cortex, 126
 recovery after, 113, 121, 132, 137
 in cats, 194*f*, 194–196, 195*f*, 196*f*
 cooperative mechanisms in, 195
 in monkeys, 196–197, 197*f*
 reverse occlusion in
 in cats, 194–196, 195*f*
 and orientation selectivity, 121
 in rodents, 198
 Wiesel and Hubel's pioneering studies on, 147
 Monocular response, asymmetric, to oscillating motion, 183–184, 184*f*, 185*f*

- Monocular rivalry, 1321
- Monocular tests, of binocular vision,
inaccurate or misleading results from,
765, 767, 776, 777*f*
- Monotremes, evolutionary history of, 1564,
1565*f*
- Morphogenetic furrow, 467
- Morphology. *See* Neuroanatomy
- Mosaic(s), 463–475
- cone, 159–160, 162*f*, 239*f*–240*f*, 240–
241
- comparison across species, 472
- formation of, 467–468, 468*f*
- minimal-spacing rules and, 469–470
- and receptive fields of cortical neurons,
166*f*, 166–167
- sampling by, 802–807
- by different cone classes/submosaics,
805–807
- trichromatic, 805–807
- development of, 467–471
- computer-modeling studies of, 467–
468
- dendritic field competition and,
470–471
- inductive interactions and molecular
markers in, 467–468, 468*f*
- lateral movements of developing
neurons and, 468–469, 469*f*
- mechanical, cytoskeleton-mediated basis
for, 470
- neuronal death and, 470, 472
- evolutionary information from, 471–472,
472*f*, 475
- future directions for study of, 474–475
- as guide to within-type variation,
465–466, 466*f*
- hidden, exposure of, 466–467
- identification and characterization of
neuronal types via, 464–467
- measurement of, 472–474
- methods for, 472–474
- nearest-neighbor distance in, 472–473
- spatial autocorrelograms for, 469–470,
473
- spatial correlograms for, 467, 473
- undersampling resistance of exclusion
ratio in, 473, 474*f*
- Voronoi domain analysis in, 473
- minimal-spacing rules and, 469*f*,
469–470, 474
- paired, in mammals, 472, 472*f*
- photoreceptor, mammalian, 237–245
- subdivision of, 239*f*–240*f*, 240–241
- regularity of, nucleus position and, 470
- spacing and scale of, variation across
species, 463, 464*f*
- and visual function, 463
- Motion. *See also* Phi motion
- apparent, 1573, 1578–1579
- attention to
- and functional mapping of motion
regions, 1239–1241
- global, 1239–1240
- biological, 1577
- coherent, detection of, 1580
- complex, deficits in, MT/MST lesions
and, 551–552, 552*f*
- component, neuronal synchrony and,
1671–1673, 1672*f*
- depth structure from, 1576–1577
- detection of, 1566
- attention and, 1542, 1542*f*
- in blindsight, 662
- models of, 1047
- scale and, 1053, 1054
- spatial scale and, 1048–1049
- direction of
- attention to, 1240, 1240*f*
- discrimination of, spatial scale and,
1049, 1049*f*
- and pattern adaptation, 1655
- exaggerated, and visual processing, 1344
- feature model of, 1048
- incoherent, in functional mapping of
motion regions, 1236–1237
- independent scale model of, 1048
- local, 1616–1617
- local analysis of, 1616–1622
- Bayesian model for, 1618–1619, 1622
- computational framework for,
1617–1619
- local combination of constraints in,
1618
- measurement noise in, 1618
- physiological interpretation of,
1619–1621
- prior probability distribution on velocity
in, 1618–1619
- spatial combination and, 1618
- object, and anticipatory pursuit,
1405–1406
- and object recognition, 1650
- pattern, neuronal synchrony and,
1671–1673, 1672*f*
- pupil responses to, 641, 648–649, 649*f*
- scale and, 1047–1049
- speed of, attention to, 1241
- velocity of
- and pattern adaptation, 1655
- perception of, scale and, 1055
- visual, processing
- and anticipatory pursuit, 1405–1406
- and smooth pursuit control, 1406–
1409
- Motion aftereffect, 1319–1320
- hMT/V5+ visual area activity during,
1237–1239
- Motion asymmetry, developmental,
183–184, 184*f*, 185*f*
- Motion contrast, 1582, 1582*f*
- Motion correspondence, 1217
- color and, 1223
- Motion cues, in insect vision, 1193–1201
- centering response, 1195*f*, 1195–1196
- for discriminating objects from
backgrounds, 1200*f*, 1200–1201
- for distinguishing objects at different
distances, 1199–1200
- in flying insects, 1194–1201
- future directions for study of, 1201
- in peering insects, 1193–1194, 1194*f*
- Motion energy, 1047
- computation of, full-wave rectification for,
752
- Motion estimator
- brightness-based, 1617–1618
- second-order (non-Fourier), 1618
- Motion field
- definition of, 1616
- estimation of, 1616
- Motion integration, in area MT,
1207–1208
- color cues for, 1223–1226
- Motion opponency, 1204
- Motion parallax cues, 1200*f*, 1200–1201,
1247, 1248, 1248*f*, 1253, 1253*f*, 1256,
1256*f*, 1257
- in camouflage, 1504, 1504*f*
- Motion pathway, 1619
- Motion perception, 720, 1584, 1584–1585.
See also Optic flow
- aperture problem in, 1207–1208
- in blindsight, 658–659
- color and, 1023–1024, 1023*f*, 1217–1226
- neural correlates in, 1218–1219
- cortical areas in, 1685
- and hMT/V5+ visual area activity,
1237–1239, 1252
- MT visual area in, 1203, 1209–1213
- correlation of MT response properties
and perception, 1209–1210
- lesion studies of, 1211–1212
- microstimulation studies of, 1212*f*,
1212–1213
- necessity of, 1213
- real-time correlation with perception
decisions, 1210–1211
- sufficiency of, 1213
- during saccades, 1392–1393
- Motion processing, 1344–1347
- aperture problem in, 1207–1208
- area MT in, 619–622, 620*f*, 621*f*,
1203–1214
- chromatic input and, 1218–1226
- functional mapping in human
homologue of (hMT/V5),
1229–1243, 1230*f*
- functional mapping of, 1231–1233,
1233*f*, 1242–1243

- Motion processing (cont.)
 stimulus parameters for, 1236, 1236*f*
 basic task in, 1217
 biological motion in, 1242
 blue/yellow input to, 1217–1218
 color cues for, 1023–1024, 1023*f*, 1210, 1217–1226, 1237
 chromatic input to MT visual area and, 1218–1220
 koniocellular pathway and, 1219–1220, 1223, 1223*f*
 magnocellular pathway and, 1219–1223, 1221*f*, 1222*f*
 neural correlates of, 1218–1219
 parvocellular pathway and, 1219–1220, 1223–1226
 plaid stimulus in, 1223–1226, 1224*f*
 psychophysical evidence for, 1217–1218
 stochastic motion stimulus in, 1225, 1225*f*
 cortical, pursuit eye movements and, 1270–1271
 and direction selectivity, 183–184, 184*f*, 185*f*, 453–459, 458*f*, 1240*f*, 1250
 functional mapping of regions involved in, 1229–1243
 attention to direction of motion and, 1240, 1240*f*
 attention to motion and, 1239–1241
 attention to speed of motion and, 1241
 dynamic noise and, 1236–1237
 incoherent motion and, 1236–1237
 motion perception and, 1237–1239
 nonluminance-defined stimuli and, 1237
 stimulus parameters for, 1236
 stimulus patterns for, 1236
 higher-order, thalamic involvement in, 597–598, 598*f*
 in insect vision, 1193–1201
 and kinetic boundaries, 1241–1242, 1242*f*
 luminance input to, 1217
 magnocellular pathway in, 489–490, 496, 501, 1206, 1219–1223
 and movement control, 1241
 MST visual area in, 1212
 in parietal cortex, functional mapping of, 1234–1235, 1235*f*, 1239, 1240
 in primary visual cortex
 functional mapping of, 1233–1234, 1234*f*
 MT feedback and, 619–622, 620*f*, 621*f*
 pulvinar region in, 596–598, 598*f*
 red/green input to, 1217–1218
 rods and cones in, 845
 selective visual exposure and, 201, 201*f*
 single-cell studies of, 1229
 spatiotemporal receptive fields and, 751
 structure determination in (structure-from-motion), 1211, 1239, 1242
 in V3A visual area, functional mapping of, 1234
 in ventral cortex, functional mapping of, 1234*f*, 1235–1236
- Motion regions
 behavioral functions of, 1239, 1241
 functional mapping of, 1229–1243
 advances in monkey, 1229, 1243
 attention to direction of motion and, 1240, 1240*f*
 attention to motion and, 1239–1241
 attention to speed of motion and, 1241
 in awake subjects, 1229
 biological motion and, 1242
 dynamic noise and, 1236–1237
 eye movements and, 1229
 in human occipito-temporal cortex, 1229–1233
 incoherent motion and, 1236–1237
 motion perception and, 1237–1239
 in MT visual area, 1229–1233, 1230*f*, 1235–1236
 nonluminance-defined stimuli in, 1237
 in parietal cortex, 1234–1235, 1235*f*, 1239, 1240
 in passive subject, 1229
 in primary visual cortex, 1233–1234, 1234*f*
 region of interest approach to, 1230
 single-cell recording of, 1229
 stimulus parameters for, 1236
 stimulus patterns for, 1236
 technical difficulties in, 1229
 in V3A visual area, 1234
 in ventral cortex, 1234*f*, 1235–1236
 and kinetic boundaries, 1241–1242, 1242*f*
 and movement control, 1241
 three-dimensional structure
 determination in, 1242
- Motion segregation, in area MT, 1207–1208
 color cues for, 1223–1226
- Motion sensitivity, reduction of, during saccades, 1392–1393
- Motion velocity, and binocular rivalry, 1313–1316
- Motoneuron(s)
 lateral rectus (LR), 1416*f*, 1417, 1418*f*, 1419
 medial rectus (MR, MR*), 1416–1417, 1416*f*, 1418*f*, 1419
 in vergence, extraocular, 1415–1418, 1416*f*
- Mouse. *See* Mice
- Movement(s)
 control of, motion-sensitive visual regions in, 1241
 visual guidance of, angular gyrus lesions and, 11, 11*f*
- Movement fields, 1449
mPer1 and *mPer2* genes, 24, 634*f*, 634–635, 635*f*
 Msh-like family of transcription factors, in optic cup regionalization, 35*f*, 36
- MST visual area. *See* Medial superior temporal area (MST)
- Msx-1 transcription factor, in optic cup regionalization, 35*f*, 36
- Msx-2 transcription factor, in optic cup regionalization, 35*f*, 36
- MT visual area. *See* Middle temporal (MT) visual area
- MT+ visual area, human, 515, 516*f*
- MTc visual area, macaque, 510*f*–511*f*, 511
- Mu opioid receptor, retinal expression of, 348
- Mudpuppy retina
 ganglion cells of, membrane time
 constant of, 430–431
 ON and OFF bipolar cells of, 263–264, 264, 264*f*, 265*f*
 substance P in, 344
- Mueller-Lyer illusion, 1505
- Müller glia cell(s), 235*f*
 avoidance of photoreceptor synaptic terminals by, 247, 247*f*
 barrier function of, 41
 development of, 36, 39
 timing of, 77, 78*f*
 differentiation of, 37, 39, 66, 68
 GABA transporters in, 308–309
 in glaucoma, 42
 glutamate and glutamate transporters in, 304, 306
 and glutamate expression, 86
 metabolic role of, 41, 42
 migration of, 80
 and outgrowth of axons and dendrites, 81
 renin expression in, 347
 role in retinal development and function, 41
 structural role of, 41
- Müller's doctrine of specific nerve energies, 15
- Multidimensional feature space, 1081
 gain control in, 761
- Multiple Errands Test, 1550
- Multiple-motion problem, 1617
- Multiplicative convergence, of left and right eye signals, 768, 770*f*
- Multistability
 in binocular rivalry, 1321
 definition of, 1321
- Munc13-3* gene, 134
- Munk, Hermann, 8, 9*f*, 10
- Muscarinic receptor(s), 312, 312*f*
- Muscarinic receptor antagonists, and ocular dominance plasticity, 134

- Muscimol
 GABA receptor response to, 356*t*
 and ocular dominance plasticity, 126, 130–131
- Mushroom bodies, in insect brain, 1512
- Musical sight reading, eye movements in, 1358, 1358*f*
- Myelin, 532
- Myopia, reading and, 207
- Myosin, in ribbon synapses, 282
- N**
- NADPH-diaphorase activity
 in horizontal cells, 385
 in retinal neurons, 384–385
- Naka-Rushton equation
 applications of, 759
 for contrast response function, 752–753, 753*f*, 756, 757, 759
- Narrow gaps, negotiation by insects,
 motion cues for, 1195*f*, 1195–1196
- Natural images, 1591*f*
 average chromaticity in, 807
 basis functions learned from, 1607–1608, 1609*f*
 independent component analysis applied to, 1612–1613
 light and contrast requirements for, 237, 238*f*
 properties of, 1047
 spatial frequency of, 804
 time-varying, basis functions learned from, 1608, 1609*f*
- Natural scene
 adaptation to, 929
 characterization of, independent components analysis in, 1592
 definition of, 1590
 interpretation of, contextual modulation of, 721
 investigation of shape representation using, 1594–1595
 pursuit in, 1402–1406
 and receptive field size in inferotemporal cortex, 1171
 spatial power spectrum of, 1604
- Natural scene perception, 1590–1599
 higher-order structure for, 1591
 neurophysiological studies of, 1597–1599, 1597*f*–1598*f*
 optimization for, 1592–1594
 representation in, 1594–1595
 research on, advances in (future directions for), 1599
- Natural scene statistics, 1590–1592, 1599
 ideal observer analysis of, 834
 and probabilistic model of image representation, 1607–1608
- Natural selection
 Bayesian, 835–836
- ideal observer analysis of, 834
 and retinal circuits, 234–237
- Navigation, in insect vision, motion cues and, 1193–1201
- Near cells, in stereoscopic vision, 766, 767*f*
- Near disparity, 780, 788
- Near response, 1415, 1418
- Near response cells, 1418–1419, 1419*f*
 accommodation, 1419–1422, 1420*f*, 1421*f*
 vergence, 1419–1422, 1420*f*, 1421*f*
- Near triad, 1415
- Nearest-neighbor distance (NND), mosaic measurement based on, 472–473
- Nearest-neighbor match, 1303
- Negative feedback mechanisms, 226
 in phototransduction, 225–228
- Neglect
 hemispatial, 554
 spatial, visual areas involved in, 1684
 visual, 1684
 visuospatial, 1519
- Neocortex, 1565
 electrical activity in, increase in, and neurotrophins, 49
- Neon color spreading, 1129, 1130*f*, 1583, 1625*f*, 1627, 1635
- Nerve conduction, age-related decline in, 209
- Nerve growth factor (NGF), 46
 and acuity, 136
 anterograde and retrograde actions of, 50*b*
 blockade of, effects on visual development, 52, 54*f*
 cellular targets of, 55
 classical hypothesis of, 48*b*
 in cortical development and plasticity, 54–55, 60
 and cortical plasticity, 135, 136*t*, 137
 deficiency of, 48, 48*b*
 exogenous administration of
 during dark rearing, 50–52, 53*f*
 and monocular deprivation, 50, 51*f*–52*f*, 135, 136, 137
 and long-term depression, 135, 136*t*
 and long-term potentiation, 135, 136*t*
 receptors for, 46, 48*b*, 55
 and retinal cell differentiation, 78
 retrograde transport of, 55
 in synaptic plasticity, 60
 and synaptic transmission, 55, 56*f*
 and timing of critical period, 58
- Net flux vector, 1090, 1091*f*
- Netrin(s), and optic chiasm development, 98–99
- Neural activity, single-unit recording of, 10–11, 15–28
- Neural integrator, 1431, 1432*f*, 1486, 1487–1488
- Neural limitations, on visual development
 in primates, 159–171
- Neural networks, 1585
 as FEF models, 1443
- Neural plate
 anterior-posterior axis of, 33
 development of, 33–34, 64–66
- Neural processing, retinal, 234, 235*f*
 reasons for, 234–237, 237*f*
- Neural prosthesis
 posterior parietal cortical control of, 1333–1334
 for reading out reach intention, 1333–1334, 1333*f*
- Neural representation scheme(s)
 distributed, 1080
 local (labeled line), 1080
 viewpoint dependence of, 1083
- Neural streams, reasons for studying, 481
- Neural tube, development of, 64–65, 77
- Neurite(s)
 patterning of, 82–83
 process outgrowth of, 81–82
- Neuro D
 in retinal cell differentiation, 38, 39, 68
 in rod formation, 39, 40
- Neurobiotin injections
 for amacrine cell visualization, 396–398, 397*f*, 399–400, 401*f*
 for horizontal cell visualization, 380, 380*f*
- Neuroblast(s), postmitotic, 77
 migration of, 79
- Neurogenic genes, mapping of, 72
- Neurogliaform cells, in primary visual cortex (V1) of macaque, 689
- Neuroimaging
 in binocular rivalry, 1319
 in blindsight, 662–663, 1691
 in change detection, 1528, 1531–1534
 functional, for mapping motion regions, 1229–1243
 of ventral and dorsal processing streams, 554–555
 of ventral processing stream, in humans, 1179–1187
 of visual cortex/visual areas, 507, 513–515, 514*f*, 518
 attention-related activity in, 1514
- Neurokinin A, retinal, 342–343
 binding sites of, 343
 localization of, 343
- Neurokinin B, retinal, 342–343
 binding sites of, 343
 localization of, 343
- Neurokinin receptors
 mRNA of, 336
 retinal, 336, 337, 343–344
 retinal localization of, 337
- Neuromedin K. *See* Neurokinin B

- Neurometric functions, 821–822, 822*f*
 Neuromodulators, 383
 Neuron(s). *See also* Burst neurons;
 Interneurons; Motoneuron(s);
 Omnipause neurons; specific neuron
 types
 arm movement-related, 1462
 binocular disparity sensitivity of, 550,
 765–766, 766*f*, 767*f*
 biophysical knowledge in, 24–25
 circadian or diurnal, 24
 build-up, in superior colliculus,
 1452–1453
 collicular, 1449–1451
 with saccade-related bursts, 1451
 collinearity-coding, 1581
 compartmental model of, 24–25
 competition among, for neurotrophic
 factors, 46–48
 computational capacity of, 24–26
 conjunction-specific, 1666, 1666*f*
 direction-selective, 526, 532–533,
 549–550, 1261–1262
 disparity-sensitive, 550, 765–766, 766*f*,
 767*f*, 1632
 in *Drosophila* imaginal disc, development
 of, 37
 excitatory, and synaptic transmission in
 cortical connections, 527–528
 face-selective, 1165, 1166–1167, 1691
 learning new representations in,
 1172–1173
 figure-ground direction-selective, 1581
 firing rate of, as binding tag, 728
 fixation, in superior colliculus, 1452–1453
 glutamate import by, 304
 identification and characterization of,
 mosaics and, 464–467
 inhibitory
 in primary visual cortex (V1) of
 macaque, 686–688
 classification of, 688–690
 morphology of, 689–690, 690*f*
 properties of, 689–690, 690*f*
 and synaptic transmission in cortical
 connections, 527–528
 integrate-and-fire, 24, 26
 interactions of, types of, 1579
 linear, response properties of, 704–706,
 705*f*
 motion-sensitive, in insects, 1194
 multimodal, 1450–1451
 multipurpose, 1579
 nonlinear, response properties of,
 704–706, 705*f*
 object-based responses in, 1170–1172
 object-selective, 1167
 opponent vector, 1261–1262
 orientation preference of, 1655
 orientation selectivity of, 532–533
 orientation tuning of, attention and,
 1540–1541
 orientation-selective, 1568
 context-sensitive, 1582
 pattern-selective, 1619
 perceptive, 1579–1580
 readout, 1678*f*, 1679
 response properties of, attention and,
 1540–1541
 responses of
 and limitations on visual development,
 159–171
 modulation by attention, 1538–1540
 within and between cortical areas,
 1538–1539
 cortical hierarchy and, 1539, 1539*f*
 task difficulty and, 1539–1540
 variability of, attention and, 1541
 retinal, 234, 235*f*
 comparisons across species, 471–472
 development of, 36–37, 37*f*
 mosaics of, 463–475
 identification and characterization of
 neuronal types via, 464–467
 multiple dimensions of, 481, 482*f*
 natural type of, 465, 471, 474
 anomalies among, 466
 patterns and tiles of, 463
 spatial regularity among, 463–475
 selectivity of, 544–545, 546
 attention and, 1540–1541, 1541
 extraretinal input and, 1541
 sensitive to collinearity, 1575
 Sherringtonian model of, 24
 spatiotemporal processing by, 704–717
 specialization of, 1579
 spike rate of, membrane potential and,
 701, 701*f*
 survival of, neurotrophins and, 46–48,
 48*b*, 61
 sustained activity of, in biased
 competition model of attention,
 1558–1559
 temporal and spatial inseparability in, 26
 types of
 functional correlates of, 481
 taxonomical notion of, 481
 view-tuned, 1641, 1641*f*, 1642, 1647*f*,
 1650
 Neuronal correlates of consciousness
 (NCC), 1682–1693
 definition of, 1683
 neural substrate of, 1692
 research on, advances in (future
 directions for), 1692–1693
 time course of, 1686–1688, 1687*f*
 and visual representation, 1685–1696
 Neuronal streams
 anatomical versus physiological
 classification of, 482
 reasons for studying, 482
 Neuronal synchrony. *See* Synchrony
 Neuronal theory, 410
 Neuropeptide Y (NPY)
 amacrine cells expressing, 337–338, 338*f*
 lineage bias of, 67–68
 coexpression with GABA, 336
 ganglion cells expressing, 337–338
 modulation of transmitter release by, 337
 retinal, 67–68, 334, 336, 337–338
 Neuropeptide Y (NPY) receptors, retinal,
 338
 functional, 336
 Neurotransmitter(s), 304–316. *See also*
 specific neurotransmitter
 bipolar cell release of, 286–288, 287*f*
 cone release of, 245, 246–247
 and cortical plasticity, 128, 134–135,
 136*t*, 137*f*, 139
 excitatory, in retina, 86*f*, 86–87
 global, dopamine as, 313–314
 inhibitory, 86*f*, 86–87, 307–311, 355–365
 lateral channel, 304
 fast excitatory, 311–313
 fast inhibitory, 307–310
 minor fast inhibitor, 310–311
 modulation of
 neurotrophins and, 55, 56*f*, 60, 60*f*
 peptides and, 337, 348–349
 modulatory actions of, 135
 in ocular motor learning, 1496
 retinal, 279, 304–316
 expression of, 86*f*, 86–88, 234
 before visual processing, 87
 rod release of, 245, 246–247, 282
 serotonin, 314–316
 vertical channel, 304–307
 Neurotrophin(s)
 action in central nervous system, 48–49,
 50*b*
 action in peripheral and autonomic
 nervous systems, 46–48, 48*b*, 61
 anterograde action of, 47*f*, 49, 50*b*, 52
 blockade of, effects on visual
 development, 52, 54*f*
 cellular targets of, 55, 60
 classical hypothesis of, 46–48, 48*b*, 61
 competition for, 46–48, 49
 and cortical connectivity, 154
 and cortical plasticity, 47*f*, 48–49, 52–55,
 58–60, 59*f*, 61, 128
 possible sites of action for, 60, 60*f*
 deficiency of, neuronal losses in, 46–48,
 48*b*
 and dendritic arborization in ganglion
 cells, 83
 differing roles for different types of,
 52–55
 exogenous administration of
 during dark rearing, 60

- as replacement for visual experience, 50–52, 53*f*
- technical difficulties in, 50–51
- and monocular deprivation, 50, 51*f*–52*f*, 135, 136, 137
- experience and, 52, 58–60
- in glaucoma, 42
- interactions with electrical activity, 46, 47*f*, 49, 54, 59, 60
- intraventricular administration of, 50–51
- MAPK activation by, 59*f*, 59–60
- new hypothesis of, 48–49, 61
- NT3, 46
 - classical hypothesis of, 48*b*
 - in cortical development and plasticity, 54
 - deficiency of, 48, 48*b*
 - receptors for, 46, 48*b*
- NT4, 46
 - cellular targets of, 55, 60
 - classical hypothesis of, 48*b*
 - in cortical development and plasticity, 53–55, 60
 - and cortical plasticity, 128, 133
 - deficiency of, 48*b*
 - and dendritic arborization in ganglion cells, 83
 - receptors for, 46, 48*b*
 - in synaptic plasticity, 60
 - and synaptic transmission, 55, 56*f*
- NT5, 46
 - and cortical plasticity, 128, 133
 - receptor binding of, 46, 48*b*
 - release of, 47*f*
 - and retinal cell differentiation, 78–79
 - retrograde action of, 46, 47*f*, 48*b*, 50*b*, 52, 55
 - and synaptic plasticity, 47*f*, 49, 58–60, 61
 - and synaptic transmission, 54, 55, 56*f*
 - uptake of, 47*f*
 - and visual development, 46–61, 47*f*
- Newt(s), ganglion cells of, excitability of, 425
- Newton, Isaac, on course of optic nerve fibers, 5
- Ngn2*, in retinal cell differentiation, 68
- Nicotinic receptor(s), 87, 311–312, 312*f*
 - and direction selectivity, 361
 - in A layers of cat LGN, 571
- Night
 - circadian responses to, 625–626
 - SCN neuron responses during, 631–632, 632*f*
 - subjective, 626, 631
- Night blindness, congenital stationary, 272–273
- Night vision, 838–848. *See also* Scotopic (night) vision
- Nitric oxide
 - and calcium entry in photoreceptors, 283
 - and cGMP activation, 633–634
 - circadian role of, 633–634, 635*f*
 - and ganglion cell behavior, 289
 - and horizontal cell function, 384–386, 385*f*
 - and horizontal cell functioning, 371, 380
 - and long-term potentiation, 132, 138–139
 - in signal processing, 316
- Nitric oxide synthase
 - in horizontal cells, 385
 - in retinal neurons, 384–385
- NKCC transporters, in ON bipolar cells, 290, 291*f*
- NMDA (*N*-methyl-D-aspartate) receptor(s), 306
 - activation of, 129
 - age and overall levels of, 129
 - antagonists, effects of, 129
 - in bipolar cells, in OFF pathway, 265–266
 - and calcium levels, 633
 - calcium uptake through, 130
 - and circadian rhythms, 628–629, 631, 633, 634
 - as correlation between pre- and postsynaptic activity, 123
 - and CREB phosphorylation, 634
 - dark rearing and, 129, 136*t*
 - and direction selectivity, 361
 - downregulation of, 129
 - in ganglion cells, 432
 - in horizontal cells, 378
 - and long-term potentiation, 129, 136*t*
 - nonlinear response of, 129
 - NR1 subunit of, 129
 - NR2 subunit of, 129
 - developmental switch from NR2B to NR2A, 129
 - NR3 subunit of, 129
 - and orientation selectivity, 123, 129, 136*t*
 - and plasticity
 - of ocular dominance columns, 129, 136*t*, 137, 137*f*, 139
 - of visual cortex, 129, 136*t*, 137, 137*f*, 139
 - in retina, 86
 - on retinal ganglion cells, 330
 - serotonin and, 135
 - in synaptic transmission, 307
 - amacrine cell-ganglion cell, 293
 - bipolar cell-amacrine cell, 307
 - bipolar cell-ganglion cell, 288–289, 307
 - photoreceptor, 282, 283
 - photoreceptor-horizontal cell, 289
- Nociceptin, retinal expression of, 348
- Nocturnal animals
 - K (koniocellular) cells of, 498, 499, 502
 - rod system in, 241
- Nodulus, in eye movement control, 1486, 1489–1490
- Noise, 18
 - added, as analytical tool, 822–823
 - in cone system, 240–241
 - and contrast sensitivity, 177–178, 178*f*
 - in contrast sensitivity, as limiting factor, 177–178, 178*f*
 - correspondence, 22
 - dynamic
 - and functional mapping of motion regions, 1236–1237
 - and pupil responses, 643, 644*f*, 645, 647, 650–652, 651*f*
 - equivalent, 177–178, 178*f*
 - external versus internal, 822–823
 - extrinsic, importance of, 19
 - 1/*f*, 1591, 1591*f*
 - in human vision, importance of, 20
 - intrinsic, 19, 177
 - measurement, in local analysis of motion, 1618
 - neural, retinal cell numbers and, 69–70
 - photon, 237
 - in ideal observer analysis, 828–829, 829*f*
 - pixel, in ideal observer analysis, 832–834
 - in rod system, 240–241, 840
 - and scotopic vision, 840
 - signal ratio to. *See* Signal-to-noise ratio
 - smoothing by, of membrane potential and spike rate, 701, 701*f*
 - and thresholds, 811–823, 840
 - and visual evoked potentials, 174–175
 - white, 1591, 1591*f*
 - domain analysis with, 748
 - in ideal observer analysis, 833, 833*f*
 - in MT speed tuning analysis, 1206–1207, 1207*f*
 - as stimuli for mapping receptive fields, 706–707, 714
- Noise maskers, in orientation selectivity, 179–181, 180*f*, 181*f*
- Noncorresponding points, and binocular disparity, 779, 780*f*
- Nondecussating retinofugal fiber syndrome, 103
- Non-Fourier envelope responses, 754
- Non-Fourier stimuli, 1111
- Nonlagged neurons, of lateral geniculate nucleus, 709
 - receptive field maps for, 709, 709*f*
- Nonlinear amplification, in starlight circuit, 247–248, 248*f*, 249*f*
- Nonlinear neurons, response properties of, 704–706, 705*f*
- Nonlinear receptive field map(s), 705*f*, 705–706, 711–717
 - for complex cells, 706, 708, 714–716, 715*f*, 717
 - for interaction order of *p*, 707

- Nonlinear receptive field map(s) (cont.)
 methods for obtaining, 706–707
 negative values of, 707
 polarity-matched responses in, 707, 712, 713
 polarity-mismatched responses in, 707, 712, 713
 positive values of, 707
 second-order, 705–706, 707, 711–717
 for simple cells, 712*f*, 712–714, 714*f*, 717
- Nonlinear systems analysis, and receptive field mapping, 706
- Nonlinear transducer explanation, of psychometric function, 821
- Nonluminance-defined stimuli, in functional mapping of motion regions, 1237
- Noradrenaline/norepinephrine
 and cortical plasticity, 128, 134–135, 136*t*, 137*f*, 139
 restorative effects of, 137
 modulatory actions of, 135
 and pupil responses, 642
 signals about nervous system state carried by, 134
 and signal-to-noise ratio, 135
- Notch system, in retinal cell differentiation, 38, 39, 79
- NRE, and opsin expression, 40*f*
- Nrl, and opsin expression, 40
- Nucleus of the optic tract (NOT)
 connections with area MT, 1203, 1204*f*
 receptive fields of neurons in, responses of, development of, 163
- Nucleus prepositus hypoglossi, 1424, 1486
 in eye movement control, 1491
 and pursuit- and saccade-related activity, 1408, 1432*f*
- Nucleus reticularis tegmenti pontis (NRTP), 1425
 in eye movement control, 1491
 and pursuit- and saccade-related activity, 1408, 1432*f*
- Null direction, 1204
- Null phase position, of simple cells, 751
- Nyctalopen deficiency, 273
- Nyquist frequency, 159–160, 162*f*, 240
- Nyquist limit, 803–805
- Nystagmus
 divergence-beating, 1494
 downbeat, 1488, 1488*f*
 periodic alternating, 1490
 physiological, 1341
- O**
- Obersteiner, H., 8
- Object(s), 1094
 and complex features, differentiation of, 1645
- identity of, distributed coding of, 1167–1170
 advantages of, 1170
 invariant, recognition of, 1165–1175
 invariant aspects of, extraction by ventral stream, 546, 1154
 representations of
 distributed versus local, 1184–1185
 in lateral occipital complex, 1183–1184
- Object discrimination
 CO blobs and, 502
 development of, 179
 feedback processing of, 150
 in insects, motion cues for, 1199–1201, 1200*f*
 stimulus selectivity and, 748
 visual areas for, 515, 516*f*
- Object primitives, 1080–1088
 definition of, 1080
- Object recognition, 541, 542*f*, 1080, 1585, 1640–1651
 adaptation and, 1650
 attention and, 1648–1650, 1649*f*
 basic facts about, 1640–1642
 basic-level, 1648
 categorization and, 1648
 with clutter, 1643, 1645*f*
 coding strategy for, 1665
 configurational judgments in, 1648
 cortical analysis in, 542, 1173–1174, 1173*f*
 cortical computational mechanisms for, 1173–1174, 1173*f*
 cortical modularity and, 1185–1186
 development of, 179
 hierarchical processing in, 1173–1174, 1173*f*
 in humans, functional MRI studies of, 1179–1187
 identification in, 1648
 learning and, 1642, 1650
 levels of, 1648
 maximum-like operation in, 1648
 with mirror views, 1643
 with morphed objects, 1643, 1646*f*, 1647*f*
 motion and, 1650
 neural mechanisms of, 1643
 object-centered (view independent), 546
 optic flow in, 1260
 pooling in, 1648
 prefrontal cortex (PFC) damage and, in monkeys, 1553
 relational codes in, 1665
 representation in, 1645–1647
 modular framework for, 1645
 research on, advances in (future directions for), 1651
 with scrambled objects, 1643, 1644*f*
 versus seeing unoccluded parts of objects, 1632–1633, 1632*f*
- selectivity in, 1643–1645, 1644*f*
 Standard Model for, 1640, 1641*f*, 1642–1643
 architecture of, 1642, 1643*f*
 categorization in, 1643, 1646, 1647*f*
 extensions of, 1648–1650
 falsifying, 1650
 and interpretation of experimental data, 1643–1648, 1645*f*, 1646*f*, 1647*f*
 subordinate-level, 1647*f*, 1648
 ventral stream in, 544–545
 viewer-centered (view dependent), 546
- Object representation
 distributed nature of, 1167–1169, 1168*f*, 1169*f*
 advantages of, 1170
 feedforward processing of, 150
 partially view-independent, 1171–1172
 view-dependent, 1171–1172
 view-independent, 1171–1172
 view-invariant, distributed encoding of, 1169
- Object self-ordered search task, prefrontal cortex (PFC) damage and, in monkeys, 1552*f*, 1553
- Object volume, 1300
- Objective contrast, definition of, 881
- Object-substitution masking, 1687
- Occipital cortex
 in binocular rivalry, 1319
 corticocortical connections of, 523
 lateral (LOC), in object recognition, 1641
 lesions of, 8–9
 visual areas of
 human, 515, 516*f*
 in macaque, 512, 513*f*
 visual function of, 8–9, 9*f*, 530
- Occipital eye field, 1429*f*
- Occipital lobe, in color vision, 1029
- Occipitoparietal cortex, lesions of, syndromes caused by, 554
- Occipitoparietal stream. *See* Dorsal stream
- Occipito-temporal cortex
 human motion complex of, functional mapping of, 1229–1233
 lesions of, syndromes caused by, 554
- Occipitotemporal stream. *See* Ventral stream
- Occlusion, 1096, 1284, 1631, 1632–1633, 1632*f*
 and camouflage, 1288–1292
 color and, 1290
 environmental conditions and, 1290
 geometry of, 1286
 interpretation of, 1147, 1147*f*
 and interpretation of local depth measurements, 1284–1288

- Octaves, in measurement of spatial resolution, 190
- Ocular albinism 1 gene, 102
- Ocular dominance
- artificial changes in, interocular contrast differences and, 775–776
 - in binocular vision assessment, inadequacy of approach, 767, 775–776
 - decorrelated binocular input and, 198
 - monocular deprivation and, 49, 51*f*–52*f*, 108, 112–115
 - effects of exogenous neurotrophins on, 50, 51*f*–52*f*, 135, 136
 - effects of MAPK activation in, 59*f*, 59–60
 - effects on plasticity, 126
 - preventive effects of neurotrophins in, 53–55
 - reverse shift in, 130–131, 133
- Ocular dominance columns
- and cortical connectivity, 148
 - desegregation of, 111
 - development of, 110–113, 118*f*, 147
 - activity and, 110–113, 147
 - artificial manipulations of, 113–114
 - instructive versus permissive role of, 113–115
 - in animals without eyes, 111
 - in animals without functioning retinas, 111, 147
 - binocular deprivation and, 108, 113, 147
 - competitive process in, 108, 147
 - computational models of, 112
 - controversy over timing and mechanism of, 110–112
 - critical period for, 108, 112, 126, 129, 133
 - defined precritical period of, 112–113
 - LGN injection studies of, 110–111
 - methods for assessing, 111
 - monocular deprivation and, 108, 112–114, 115, 147
 - neurotrophins and, 52, 53, 54*f*
 - normal, 110*f*, 110–113
 - spontaneous activity of visual system and, 147
 - in tectum of three-eyed frog, 111–112, 112*f*
 - transneuronal labeling studies of, 108, 110*f*, 110–111
 - maintenance of, 111, 148
 - number of, variation in, 71
 - plasticity of, 108, 112–113, 115, 126
 - activity and, importance of, 128
 - BDNF and, 131, 133, 136*t*
 - calcium and, 130, 136*t*, 137, 137*f*, 139
 - CREB and, 132–133, 136*t*, 137, 137*f*
 - cyclic AMP and, 131–132
 - dark rearing and, 128, 132
 - factors in, 137*f*, 137–139
 - versus activity-related factors, 128
 - evaluation of, 128–139
 - instructive, 128–134
 - modulatory, 128, 134–139
 - summary of, 136, 136*t*
 - feedback pathways in, 137
 - GABA and, 130–131, 133, 137, 137*f*, 139
 - gene expression and, 133–134
 - glutamate receptors and, 126, 129–130, 136*t*, 137, 137*f*
 - Hebbian synapses and, 113–114
 - instructive versus permissive role of activity in, 113–115
 - MAPK and, 132, 136*t*, 137, 137*f*
 - monocular deprivation and, 126, 128, 130–131, 132, 133, 135, 137, 138
 - neurotransmitters and, 134–135, 136*t*, 137*f*, 139
 - NMDA receptors and, 129, 136*t*, 137, 137*f*, 139
 - physiologic efficacy in, 137–138, 138*f*
 - presynaptic and postsynaptic changes in, 138–139, 139*f*
 - protein kinase A and, 131–132, 136*t*, 137*f*, 137–139
 - protein kinase C and, 132, 136*t*
 - protein synthesis and, 133–134, 138–139, 139*f*
 - relationship with long-term depression and potentiation, 136, 136*t*, 137–138
 - restoration of, 131
 - in older animals, 137
 - transsynaptic labeling of, 147
- Ocular following, 1403–1405
- Ocular motor learning. *See* Learning, ocular motor
- Oculo-centric frame of reference, 1252
- Oculomotor control, and optic flow analysis, 1278
- Oculomotor internuclear (OI) neurons, 1416, 1416*f*, 1417*f*
- Oculomotor nucleus, neurons in, 1416, 1416*f*, 1417*f*
- Oculomotor subsystems, 1342
 - vergence, 1348–1349, 1348*f*
- Oculomotor system, input to, 1342–1343
- OFF amacrine cells, 400*f*, 403–405
 - stratification of, 269–270, 270*f*
- OFF bipolar cells, 236*f*
 - chloride transporters of, 290, 291*f*
 - classes of, 285
 - direct pathway from rods to, 845
 - discovery of, 263–264
 - electroretinogram response, 261*f*
 - glutamate receptors of, 265–266, 266*f*
 - sharp electrode recording of activity, 263–264, 264*f*
 - spinules of, 297
 - stratification of, 84, 85, 267*f*, 268–269, 269*f*
 - synapses of, 279, 283, 284*f*
 - postsynaptic mechanisms of, 285
- OFF ganglion cells, 17, 83, 260, 419
 - central projections of, 270–271
 - developing, spontaneous spiking patterns of, 88–89
 - discovery of, 261–262
 - Golgi, flat-mount image of, 263, 263*f*
 - inhibition of, 355–356
 - membrane time constant of, 432
 - projections to dorsal LGN, 270–271, 271*f*
 - projections to LGN, 117–118, 118*f*, 270–271, 271*f*
 - retinal circuits and, 235*f*, 236*f*
 - segregation of, 86, 122
 - specification of, versus ON-OFF combination, 253
 - stratification of, 266–268, 267*f*
 - sustained and transient, 262*f*, 262–263
 - synapses of, 285–286
 - to LGN neurons, 270
- OFF pathways. *See* ON and OFF pathways
- Old World monkeys
 - cone mosaics of, 468
 - mapping of visual fields on cortex of, 10
 - visual areas outside primary visual cortex in, 11
- Olivary pretectal nucleus (OPN)
 - ganglion cells projecting to, 412
 - and pupil responses, 642, 652–653, 654*f*
- Ommatidia, development of, 63
- Omnipause neurons, 1408, 1423, 1451–1452, 1492
 - and pursuit- and saccade-related activity, 1409–1410
- ON amacrine cells, 400*f*, 403–405
 - stratification of, 269–270, 270*f*
- ON and OFF complex cells, 270, 715–716
 - pharmacologic blockade of, 273, 274*f*
- ON and OFF leaflets, in LGN, 271
- ON and OFF pathways, 260–274
 - amacrine cell function in, 269–270, 320, 321*f*, 398
 - behavioral and clinical implications of, 272–273
 - and cortical feedback systems, 622
 - crosstalk between, amacrine cells for, 269–270
 - as feature detectors, 260, 273–274
 - GABA and, 355–356
 - in glutamatergic pathways from photoreceptors to ganglion cells, 320–330
 - glycine and, 321*f*, 355–356
 - Hartline's experiments on, 17, 261*f*, 261–262, 272
 - inhibition in, 355–356, 362, 364

- ON and OFF pathways (cont.)
 and orientation selectivity, 117–118, 118*f*, 122–123, 123*f*
 perspectives on, 273–274
 projections of, 270–271
 retinal lamination and, 83–86, 266–270
 segregation of, 122–123, 123*f*
 serotonin and, 316
 stratification in inner plexiform layer, 266–270, 267*f*
 sustained and transient, 262–263
 in vertebrate retinal and visual system, 260–274
- ON and OFF receptive fields, 117–118, 118*f*, 673, 674*f*, 704
 mapping of, 707
- ON and OFF signals, in retinal field potentials, 260–261, 261*f*
- ON and OFF simple cells, 118, 118*f*, 123, 123*f*, 270, 673–674, 674*f*
 pharmacologic blockade of, 273
- ON bipolar cells, 236*f*, 320–324
 chloride conductance in, 265, 266*f*, 290, 291*f*
 discovery of, 263–264
 electroretinogram response, 261*f*
 GABA receptor feedback to, 362
 glutamate receptors of, 264–265, 265*f*, 266*f*
 sharp electrode recording of activity, 263–264, 264*f*
 spinules of, 297
 stratification of, 84, 85, 267*f*, 268–269, 269*f*
 synapses of, 283, 284*f*
 postsynaptic mechanisms of, 283–285, 285*f*
- ON ganglion cells, 17, 83, 260, 323–324, 411–412
 central projections of, 270–271
 developing, spontaneous spiking patterns of, 88–89
 discovery of, 261–262
 Golgi, flat-mount image of, 263, 263*f*
 inhibition of, 355–356
 membrane time constant of, 432
 projections to dorsal LGN, 270–271, 271*f*
 projections to LGN, 117–118, 118*f*, 270–271, 271*f*
 retinal circuits and, 235*f*, 236*f*
 segregation of, 86, 122
 specification of, versus ON-OFF combination, 253
 stratification of, 266–268, 267*f*
 sustained and transient, 262*f*, 262–263
 synapses of, 285–286
 to LGN neurons, 270
- ON pathways. *See also* ON and OFF pathways
 dim light responses conveyed by, 273
 diseases of, 272–273
 pharmacologic blockade of, 272–273, 274*f*
- On-line system
 evidence for, 1684
 properties of, 1683, 1683*t*
- ON-OFF amacrine cells, 269
- ON-OFF direction-selective neurons, 451, 452*f*, 453*f*
 crosstalk between, 457
- ON-OFF ganglion cells, 261*f*, 261–262
 bistratification of, 267
 membrane time constant of, 432
 versus ON or OFF specification, 253
- Open-loop behavior, 1430, 1485
- Open-loop period, pursuit in, 1405–1406
- Opioid(s), retinal, 337, 348
- Opioid receptor(s)
 delta, 348
 kappa, 348
 mu, 348
 retinal, 337, 348
- Opponent colors theory
 of chromatic discrimination, 917–918
 definition of, 917
- Opponent motion computation, 1620
- Opsin, 976
 and circadian rhythms, 628
 expression of, molecular regulation of, 39
 genes for, 964, 965, 967, 967*f*, 969
 sequences upstream of, 40, 40*f*
 and photoreceptor differentiation, 39–40, 467–468
 in retinitis pigmentosa, 42–43
- Opsin kinase, cone-specific (GRK7), 222
- Optic ataxia, 554
- Optic chiasm
 agenesis of, 97–98
 in absence of other brain abnormalities, 100*f*, 103
 and LGN lamination, 114–115
 decussation in, 5, 94–103, 97*f*
 defects of, 97–98, 102–103, 114–115
 lack of pigment (albinism) and, 100*f*, 102–103
 development of, 94–103
 cell and molecular mechanisms underlying, 97–101
 cellular environment and, 95–96
 cellular specializations at midline and, 97–98
 cellular specializations at ventral midline and, 96
 Eph receptors/ephrin ligands and, 97*f*, 99
 GAP-43 and, 100*f*, 100–101
 gene transcription and, 101–102
 growth cone behaviors at midline and, 95–96
 molecular factors critical for, 98–101, 103
 netrin/deleted in colorectal cancer and, 98–99
 proteoglycans and, 97*f*, 100
 Roundabouts (Robos) and, 97*f*, 99–100, 100*f*
 Slits and, 97*f*, 99–100, 100*f*, 101
 ectopic, 100
 ganglion cell axons in
 organization of, 94–95
 projections (decussation) of, 94–103
 static and dynamic chronicles of
 behavior of, 95–96, 97*f*
 growth cone morphology in, 96, 97*f*
 organization of
 binocular plan of, 94, 95*f*
 principles of, 94–95
 position of, establishment of, 96
- Optic cup
 cell differentiation in, 66, 67
 lineage regulation of, 66
 formation of, 34–36, 35*f*
 regionalization of, 34–36
 transcription factors in, 34–36, 35*f*, 68
 interactions among, 34–36, 36*f*
- Optic flow, 1247–1257, 1616
 analysis of, 1260
 cortical analysis of, 1260–1278
 behavioral influences on, 1276–1277
 behavioral response to, 1274–1276, 1276*f*
 cortical responses to
 in cat, 1268–1269
 in human, 1269
 decomposition of, 1250
 definition of, 1247
 detection of, 1249–1250
 estimation of, 1616
 illusory perception of, MSTd and, 1275
 locomotion control with, 1256–1257
 in object recognition, 1260
 observer rotation and, 1247–1248
 ocular following evoked by, 1271
 parietal cortical responses to, 1267–1268
 perception of, and behavior, 1274–1276
 perception of self-motion from, 1247
 responses to
 in dorsal medial superior temporal area (MSTd), 1262–1263, 1263*f*
 eye position and, 1269–1270
 during pursuit, 1272–1274, 1274*f*, 1275*f*
 visual-vestibular interactions and, 1271–1272
 rotational component of, 1247, 1248*f*, 1249*f*
 templates (filters) for, 1250
 temporal cortical responses to, 1267
 translational component of, 1247, 1248*f*, 1249*f*

- Optic flow field, 1247–1249, 1248*f*
- Optic nerve
 bottleneck at, 1004
 carrying capacity of, 320
 damage to, and pupil light reflex, 645, 645*f*
 electrical stimulation of
 and long-term potentiation, 127
 and orientation selectivity, 122–123
 SCN neuron responses to, 629
 fibers
 age-related failure of, 210*t*
 central course of, 5
 single-unit recording of, Hartline's technique for, 17
 formation of, 81, 260, 270, 482
 ganglion cell axon organization in, 94, 95
 growth cone morphology in, 96, 97*f*
 hypoplasia of, netrin/deleted in colorectal cancer and, 98–99
 neurotrophin transport in, 50*b*
 parallel processing by, 495
- Optic stalk, 64, 64*f*
 formation of, 34, 35*f*, 36
- Optic tectum, ganglion cells projecting to, 270
- Optic tract
 fibers, termination in lateral geniculate nucleus, 6
 ganglion cell axon organization in, 94–95
 growth cone morphology in, 96, 97*f*
 nucleus of, inputs to A layers, 568, 571
- Optic vesicle
 cell differentiation in, 67
 expression patterns of transcription factors in, 34–36, 35*f*, 66
 formation of, 34, 35*f*, 77
 invagination of, 34, 35*f*, 77
 transcription factor expression in, 68
- Optical density of lens
 aging and, 846
 and spectral sensitivity, 838
- Optical transfer function (OTF), 799
- Optics, in ideal observer analysis, 829–831, 830*f*, 831*f*
- Optimization, for natural scene perception, 1592–1594
 in area V1, 1593–1594
 in retina and lateral geniculate nucleus, 1593
- Optokinetic eye movements. *See* Optokinetic reflexes (OKN)
- Optokinetic nystagmus (OKN), 183–184
 and activation of motion-sensitive visual regions, 1241
- Optokinetic reflexes (OKN), 1342–1343, 1403, 1485
 and smooth pursuit, distinction between, 1403–1405
- Optomotor response, in insects, 1193, 1194, 1201
 versus centering response, 1196
 direction selectivity of, 1196
 temporal frequency and, 1196
- Optx* gene
 expression of
 in eye fields, 34, 66
 in optic vesicle, 66
 in optic cup development and regionalization, 35*f*, 36, 68
 overexpression of, 68
- Orbitofrontal cortex
 activation by faces, 1167
 and social/emotional responses to faces, 1167
- Orientation, 1081, 1081*f*
 in blindsight, 658
 and change detection, 1529
 and contrast induction, 1046
 definition of, 1081
 discrimination of, by honeybees, 1502, 1503*f*
 and pattern adaptation, 1655
 plasticity
 adaptation-induced, 1657–1658, 1658*f*
 and cortical map of orientation preference, 1658–1660, 1659*f*
 significance for vision, 1660–1662, 1661*f*
 in V1, 1655–1657, 1656*f*
 and salience, 721
 scale and, 1053
 tuning, 1087, 1655
- Orientation contrast, 1582, 1582*f*
- Orientation maps, 118–119, 122–124
 development of, 119–121, 120*f*, 147–148
- Orientation pinwheel centers, 119, 737
- Orientation selectivity, 695
 activity and, 119–121, 147–148
 instructive versus permissive role of, 117, 122, 123–124
 mechanisms in, 121–124
 animal models of, 117
 astigmatism and, 199–200, 200*f*
 in awake, behaving monkey, measurement of, 758
 binocular deprivation and, 117, 119–121, 121*f*, 123
 cellular and molecular mechanisms in, 123
 in complex cells, 714, 715, 770, 770*f*, 771*f*
 linear and nonlinear properties of, 753
 correlation-based models of, 123*f*, 123–124
 and cortical connections, 148
 horizontal, 734, 734*f*, 735, 737, 737*f*, 738, 742
 cortical inactivation experiments and, 697–698
- critical period for, 122, 127
 cross-modal rewiring experiments on, 148
 dark rearing and, 117, 119–121, 121*f*, 122, 123
 development of, 147–148, 179–181
 neural activity and, 117–124
 dynamic property of, 127
 establishment of, 117, 124
 feedback model of, 696–697, 696*f*
 feedforward connections and, 532–533
 in ganglion cells, 117–118, 118*f*, 122, 418
 of input to simple cells, 695–697
 spatial organization of, 697
 strength of, 697
 laminar analysis of, 122
 in lateral geniculate nucleus, 117–118, 118*f*, 123–124, 127, 768, 770*f*
 cortical feedback and, 612–614, 615*f*, 616*f*–617*f*
 lateral inhibition and, 127
 linear and nonlinear properties of, 753
 maintenance of, 117, 148
 maturation of, 117
 monocular deprivation and, 121, 132, 133
 ON/OFF visual pathways and, 117–118, 118*f*, 122–123, 123*f*
 optical imaging of, 118–119, 122–123, 148
 plasticity of, 126–127
 BDNF and, 133, 136*t*
 neurotransmitters and, 134, 136*t*
 NMDA receptors and, 129, 136*t*
 protein kinase A and, 132, 136*t*
 of receptive fields, 165*f*, 165–166
 restricted range of exposures and, 121, 199–200, 200*f*
 reverse correlation measurement of, 757–758
 in simple cells, 118, 118*f*, 768, 770*f*
 linear and nonlinear properties of, 753
 in single neurons, 17, 18
 single-unit recording of, 118
 stages of, 117
 stripe-rearing studies of, 121, 199–200, 200*f*
 temporal dynamics of, 757–758
 testing of, 126
 visual evoked potentials in, 179–181, 180*f*, 181*f*
 visual experience and, 119–121, 121*f*
- Orientation tuning
 measured from spikes, 698
 measured from synaptic input, 698
 of simple cells
 contrast invariance of, 699, 699*f*
 dynamics of, 698–699
 prediction of, from spatial organization of receptive field map, 698

- Orientation-selective cells, 117–119, 118*f*, 1655
 mapping of, 118–121
 organization of, 118*f*, 118–119
 Orientation-specific pattern masking,
 development of, 179–181, 180*f*, 181*f*
 Orphan receptor-like 1, retinal expression
 of, 348
orphan receptors, 306
 Orphanin FQ, retinal expression of, 348
 Orthodromic activation, 1468, 1469*f*
 Orthograde degeneration, in lateral
 geniculate nucleus, 6–7
 Oscillating motions
 asymmetric response to, developmental,
 183–184, 184*f*, 185*f*
 detection of, 26
 direction sensitivity to, 183–184
 position sensitivity to, 182, 182*f*, 183*f*
 thresholds, in visual evoked potential,
 183, 183*f*
 Oscillations, synchronous. *See also*
 Synchrony, neuronal
 detectability of, 1670
 gamma, and visual perception in humans,
 1677–1678
 Oscillopsia, 1485
Otx-2 gene
 expression of, in optic vesicle, 34
 in eye field development, 34, 65–66
 in retinal cell differentiation, 38, 39, 43,
 68
 and selection of retinal stem cells, 66
 Outer plexiform layer of retina, 235*f*
 formation of, 81–86
 neurotransmitter expression in, 87
 organization of, 83–86
 synapse formation in, 87–88
 Overcompleteness
 in human communication, 1606
 in image representation, 1605
 and sparseness, combination of, 1605
 Overlay, interpretation of, 1147, 1147*f*
 Owl monkey
 horizontal cortical connections in, 738
 K (konio) cells of, 489, 498,
 499
 lateral cortical connections in, 1072
 parallel visual pathways in, organization
 in primary visual cortex, 498–499,
 499*f*
 visual areas of, 518
 outside primary visual cortex, 11
 visual system of, 1568
 Oxen, retinal cells of, 6*f*–7*f*
- P**
 P cells. *See* Parvocellular pathway, cells of
 P100 component, of pattern reversal
 response, development of, 185, 185*f*
 p75 receptor
 for neurotrophins, 46, 48*b*, 55
 in visual cortex, 50
 Panum's fusional area, 1300
 Parabrachial region
 cat, inputs to A layers, 568, 569*f*,
 570–571
 inputs to A layers, 568
 Paraflocculus
 in eye movement control, 1408–1409,
 1486, 1487–1489, 1490
 in ocular motor learning, 1495
 and pursuit behavior, 1408–1409
 Parafoveal sensitivity, in infants, 846
 Parahippocampal area(s), 544
 Parahippocampal gyrus, cortical
 connections of, 544
 Parahippocampal place area (PPA), 1180*f*,
 1182–1183, 1184–1185, 1534
 attentional response modulation in, 1516
 Parahippocampal place (PP) visual area,
 515, 516*f*
 Parallel visual pathways, 481–482, 485,
 494–503
 ambient versus focal, 495
 anatomical classification of, 496, 496*f*
 comparative perspective on, 494–503
 functional basis of, 496, 497*f*
 functional implications of, 501–503
 historical perspective on, 494–496
 linear systems approach to, 495
 number projecting to and through
 primate LGN, 496–498
 organization in primary visual cortex,
 498–501, 499*f*, 501*f*
 unanswered questions about, 503
 Parallelism, Gestalt factor of, 1575, 1576*f*
 Parasol cells, 262, 268, 410–411, 411*f*,
 483–485, 898, 1007
 central projections of, 413–414, 483,
 484*f*, 497
 color responses of, 1219–1220
 connections of, 485, 486*f*
 contrast sensitivity in, 416*f*, 416–417,
 484, 486*f*
 eccentricity-dependent morphology of,
 413, 414*f*
 electrical coupling of, 484
 neurotransmitter receptors in, 412, 412*f*
 phasic nature of, 485
 and photopic luminance, 867
 physiological properties of, 485–489
 ratio to midget cells, 484
 receptive fields of, center-surround
 organization of, 415
 response dynamics of, 485
 rods and, 865–866
 sampling density of, 483–484
 spatial resolution of, 483–484, 484*f*
 stratification of, 412–413
 synaptic input to, 412–413, 418–419, 483
 terminology for, 483
 tiling of, 483–484
 Parietal area 7a, 529*f*, 543
 in attention and eye movements, 1597
 neurons, latencies of, 530–532, 531*f*
 and oculomotor system, 1376–1378
 posterior, in motion processing,
 1261–1262
 in spatial processing, 551, 552–553
 Parietal area 7b, in spatial processing, 553
 Parietal cortex
 connections with area MT, 1203, 1204*f*
 corticocortical connections of, 523
 in dialogue between cerebral cortex and
 superior colliculus, 1469*f*, 1471, 1477
 inferior, in visuospatial neglect, 1519
 lesions of, 11, 11*f*
 in macaque, posterior, 510*f*–511*f*,
 511–512
 motion processing in, 550
 motion-sensitive regions of, functional
 mapping of, 1234–1235, 1235*f*, 1239,
 1240
 neurons, receptive fields of, 522
 in oculomotor system, 1425
 optic flow responses in, 1267–1268
 posterior
 lesions of, behavioral effects of, 552–553
 optic flow responses in, 1267
 in vergence control, 1415
 visual areas of, 11
 human, 515, 516*f*
 human versus macaque, 517–518
 in macaque, 508, 510*f*–511*f*, 512, 513*f*
 visual functions of, 530
 in “where” visual pathway, 495
 Parietal eye field (PEF), 1429*f*
 discovery of, 1428
 and pursuit- and saccade-related activity,
 1432*f*
 Parietal lobe, 1371, 1372*f*
 in binocular rivalry, 1319
 and oculomotor system, 1376–1378,
 1377*f*
 and pursuit behavior, 1402
 Parietal reach region (PRR)
 arm movement planning in, 1326, 1326*f*,
 1327
 eye-centered response fields in
 and coordinate transformation,
 1331–1332
 gain modulation of, 1330–1331
 sensory stimuli encoding in, 1329–1330,
 1329*f*
 Parietal-occipital (PO) visual area,
 macaque, 510*f*–511*f*, 511
 Parieto-occipital sulcus, motion sensitivity
 of, functional mapping of, 1234–1235,
 1235*f*

- Parinaud's syndrome, 652*f*, 652–654, 654*f*
- Parvalbumin
expression of, in basket cell, 688
as marker of M and P cells, 497, 498
- Parvo-blob stream, 529*f*
- Parvocellular layers, 483, 485, 529*f*, 1219, 1567, 1567*f*
- Parvocellular pathway(s), 481–491, 898, 909, 991, 1007
and binocular rivalry, 1315
cells of (P cells), 411–412, 413–414, 418, 483–489, 484*f*, 566, 1219, 1566, 1567, 1570
chromatic selectivity of, 488, 496, 497, 501
classes of, 499
color responses of, 488–489, 497, 501, 1217, 1219–1220
cone-input map of, 1009
contrast gain of, 485–488, 486*f*, 488*f*
contrast sensitivity of, 484, 485–486, 486*f*
functional properties of, 681
homogeneity versus heterogeneity of, 489
light adaptation in, 487
linearity/nonlinearity of, 486–487
multiplexing of chromatic and luminance information by, 488–489
neurochemical signature of, 496–497
parallel projections of, 496, 496*f*
physiological properties of, 485–489
ratio to M (magnocellular) cells, 484
receptive field map of, 1009
receptive fields of, 164, 164*f*, 1009–1010, 1009*f*
size of, 484–485, 486
surrounds of, cone input to, 488
response characteristics of, 1009–1010
response dynamics of, 485
sampling density of, 483–484
in scotopic (low light) vision, 487–488, 488*f*
spatial frequency tuning of, for chromatic versus achromatic stimuli, 1009
spatial resolution of, 483–484, 484*f*, 496, 497, 501
spatially and spectrally opponent organization of, 1009
temporal profile of, 709
terminology for, 483
tiling of, 483–484
visual latencies of, 503
wavelength selectivity of, 488
X cell homology of, 486–487
and chromatic discrimination, 919, 920
and chromatic motion processing, 1219–1220, 1223–1226
color and space representation in, 488
connectivity of, 485, 486*f*
to MT visual area, 619, 1220, 1223–1226
to primary visual cortex, 498–501, 501*f*
to “what” pathway, 489
in cortical feedback systems, 610–611
functional segregation of, 496, 497*f*
functions of, 489–491
based on clustering or functional properties, 489
independence versus interdependence of, 490–491
lesion studies of, 489–490, 490*f*
future directions for study of, 491
macaque, 680–682
parallel, 496–497
functional implications of, 501–502
organization in primary visual cortex, 498–501, 501*f*
properties of, 482, 482*t*
retinal eccentricity and, 484–485
segregation from magnocellular pathway, 483, 496, 497*f*
underlying anatomical certainty for, 482–485
- Parvo-interblob stream, 529*f*
- Patch therapy, for amblyopia, 196
- Path
absolute, 1256, 1256*f*
and heading, differentiation of, 1254
object-relative, 1256, 1256*f*
perception of, 1254–1255
extraretinal signals in, 1255–1256, 1256*f*
of self-motion, 1254
- Path problem, 1248, 1254–1255
- Pathway(s). *See* Visual pathways
- Pattern adaptation, 927, 936, 1655
aftereffects of, 939
in form perception, 936–946
functions of, 942–943
with refractive errors, 944
sites of, 938–939
and visual channels, 936–938
- Pattern analysis, 1603
probabilistic approach to, 1603–1606, 1612
theory of, 1603
- Pattern cells, of area MT, 1209–1210, 1619
- Pattern electroretinogram, with contrast increase, 890
- Pattern masking, 927–928
orientation-specific, development of, 179–181, 180*f*, 181*f*
- Pattern matching, sparseness and, 1606
- Pattern recognition, ganglion cells in, 865
- Pattern reversal response, development of, 185*f*, 185–186
- Pattern segregation, color and, 929–930
- Pax-2* gene
expression of, in optic cup and optic vesicle, 34, 35*f*
and optic chiasm development, 101
- Pax-6* gene, 63
and eye field development, 33–34, 66
and formation of ectopic eyes, 33–34, 66
and optic vesicle formation, 43
and retinal cell differentiation, 68
and selection of retinal stem cells, 66
- PCE, and opsin expression, 40
- PDZ-like domains, of glutamate receptors, 306
- Pedunculopontine tegmental nucleus, 568
- Peering insects, 1193–1194, 1194*f*
- Peptide(s)
actions of, characteristics of, 334, 337, 348
GABA coexpression with, 336, 402
glycine coexpression with, 402
paracrine mode of action, 334, 336, 338
retinal, 334–349, 335*t*
binding sites of, 336
calcium imaging of, 337
cellular physiology studies of, 337
coexpression with GABA, 336
content of, 334–335
developmental effects of, 33
expression of, 334–348
functional studies of, 337
functions of, 334–337, 348–349
and ganglion cell excitability, 337, 341–342, 342*f*, 344, 346, 349
ion channel modulation by, 334, 337, 341, 341*f*, 342, 344, 346, 346*f*, 347, 348
localization of, 334, 335–336
modulation of transmitter release by, 337, 348–349
molecular structure of, 335
mRNAs of, 335
- Peptide histidine isoleucine (PHI),
coexpression with VIP, 344–345
- Peptide receptor(s)
functional, 336
mRNAs, 336
retinal, 334, 335*t*, 336
retinal functions of, 334–337
retinal localization of, 337
- Perception. *See also specific perception modalities*
area 17 neurons and, 202
dynamic self-organization in, 1574
early visual deprivation and, 189–202
motives for studies of, 189
feedforward and feedback circuits in, 150
as organization, 1585
visual
brain theory of, 1573
in honeybee, 1501–1512
without awareness, 1528

- Perceptive field, 1579, 1579*f*
 properties of, 886
- Perceptual constancy, 1585
 impairments of, ventral stream lesions and, 548
 inferotemporal cortex and, 548
- Perceptual invariance, 1154, 1574
 mechanisms of, 1577–1578
- Perceptual learning, 1065, 1655
 of illusory contours, 1123
- Perforated-patch recording, of ion conductances in ganglion cells, 434, 443
- Perigeniculate nucleus, cortical feedback to, 609, 610
- Perikaryal translocation, of retina cells, 79
- Perimetry studies, of pupil light reflex, 645–647, 646*f*, 647*f*, 648*f*
- Period changes, in circadian rhythms, 627
- Period* gene, 625, 634–635
- Peripheral inhibition, 360–361
- Peripheral nervous system, neurotrophin action in, 46–48, 48*b*, 61
- Peripheral sensory nerve fibers, single-unit recording of, 16
- Peripheral visual field, cortical representation of, 9
- Peripherin
 in retinitis pigmentosa, 42
 and rod maturation, 41
- Peristriate visual cortex, prominent expansion of, 69
- Permissive role of activity, 113
 in cortical development, 165, 167, 170
 in LGN lamination, 113–115
 in ocular dominance column development, 113–115
 in orientation selectivity, 117, 122, 124
- Perseveration, prefrontal cortex (PFC)
 damage and, 1550
 in monkeys, 1552*f*, 1553
- Petter's law, 1289*f*, 1290
- PGa visual area, 1165, 1166*f*
 macaque, 510*f*–511*f*, 512
- Phase advance, of circadian rhythms, 626*f*, 626–628, 632
 intracellular signaling and, 632–636
- Phase delay, of circadian rhythms, 626*f*, 626–628, 632
 intracellular signaling and, 632–636
- Phase response curve, of circadian rhythms, 626, 626*f*
- Phase shift(s), in circadian rhythms, 625–628
 behavior and, 628, 631, 632*f*
 duration of light pulse and, 627
 intracellular signaling and, 632–636
 light intensity and, 627
 light-induced, 625–628, 626*f*
 magnitude of, factors affecting, 627
 neurotransmitters affecting, 628–629
 saturation of, 627
 threshold intensity for, 627
 transient cycles in, 626*f*, 627
 two-pulse paradigm of, 627
- Phase transfer function (PTF), of retinal images, 799
- Phase volume element, 1090
- Phase-shifted gratings, for measurement of binocular interaction, 767–772, 768*f*–769*f*, 770*f*, 771*f*, 772*f*
- Phi motion, 1573–1574
- Phoria adaptation, 1495
- Phoria cover test, 1350
- Phosphenes, 9
- Phosphatase(s), calcium-stimulated, and cortical plasticity, 128, 130, 137
- Phosphodiesterase
 activation of, 217, 217*f*, 218–219
 calcium and, 227
 predicted time course of, 219–220, 220*f*
 rate of, 220–221
 mean, 219
 ratio to transducin activation rate, 219
 bathtub analogy of relationship with cGMP, 229
 coupling of G protein transducin to, 217, 217*f*, 218–219, 220–221
 elevated steady-state activity of, and light adaptation, 229, 230
 hydrolysis of cGMP by, 217*f*, 219
 inactivation of, 223, 224*f*, 225
 in phototransduction, 217*f*, 217–220, 223, 225, 227, 229
 in retinitis pigmentosa, 42
 and rod maturation, 41
 speed of action, size of outer segment and, 241, 243*f*
- Phosphoinositide(s)
 and cortical plasticity, 129
 modulation of, 135
- Phospholipase C
 modulation of, 135
 peptide action on, 343, 348
- Photic entrainment, of circadian clock, 625–636
 as photon counter, 627
- Photochromatic interval, 873
- Photofilling, of amacrine cells, 399–400, 400*f*
- Photometric effects, 1094–1097
- Photon(s), 1090
 capture
 cone inner segment variation and, 244–245
 outer segment size and, 241, 243*f*
 in daylight vision, 237, 238*f*
 detection of, 851
 threshold for, 813–814. *See also* Threshold(s)
- photoreceptor absorption of
 calculation of mean number absorbed, 830
 in ideal observer analysis, 829–831, 830*f*, 831*f*
 response to. *See* Phototransduction
- rhodopsin activation by, 217*f*, 217–218
 single
 absorption and transduction by cones, 240
 detection by rods, 215
 inactivation of rhodopsin and, 223
- Photon counter, circadian photic entrainment system as, 627
- Photon noise, 237
 in cone system, 240–241
 in ideal observer analysis, 828–829, 829*f*
 in rod system, 240–241
- Photon-counting mode, of visual system, 215
- Photopic threshold, and dark adaptation, 852–858
- Photopic (daylight) vision, 851, 863. *See also* Light adaptation
 adaptive independence and, 852–853
 cones in, 70, 239*f*–240*f*, 240, 249–251
 ganglion cells in, 70
 photon integration/noise and, 237, 238*f*
 retinal circuits for signal transmission in, 249–251
 temporal integration for, 237, 238*f*
 transition from scotopic vision, in infants and adults, 846
- Photopigment(s), 215–216, 965, 974, 1004–1005. *See also* Melanopsin; Opsin; Rhodopsin
 absorption spectra of, 965, 966*f*, 969
 alleles for, multiple, 1005
 in animals, 964
 anomalous, 981, 983
 and circadian rhythms, 628
 cone, 976–980
 genes for, 976–980
 development of, 176
 in dogs, 962
 evolution of, 967–968, 976
 L (long-wavelength sensitive), 974
 absorption spectra of, 977
 genes for, 976
 expression of, 983–986, 984*f*
 in normal color vision, 977–980
 normal variations of, 974
 spectral tuning of, 977, 975*f*
- M (middle-wavelength sensitive), 974
 absorption spectra of, 977
 genes for, 976
 expression of, 983–986, 984*f*
 in normal color vision, 977–980

- normal variations of, 974
- spectral tuning of, 977, 975*f*
- measurement of, and predictions about
 - color vision, 964
- molecular biology of, 964
- phylogeny of, 967, 967*f*
- regeneration of, 853
- S (short-wavelength sensitive), 974
 - genes for, 976
 - spectral tuning of, 976–977
- spectrally distinct, number of, 965
- UV, 965
- Photoreceptor(s), 12, 234, 908, 924–925, 1139. *See also* Cone(s); Rod(s)
 - axons of, 245, 246*f*
 - circadian role of, 628
 - circuitry relaying signals of, 234–255, 235*f*, 236*f*
 - cone. *See* Cone(s)
 - connections of, 3–5
 - conversion tables for analysis of, 838, 839*f*
 - development of, 63, 176, 467–468
 - functional, 176
 - visual evoked potentials in, 176, 186, 186*f*
 - distribution of, 3, 4*f*
 - equivalent background light in, 215
 - functional domains of, 215
 - functions of, 422
 - gap junctions between, 375
 - ideal observer analysis at level of, 829–831, 830*f*, 831*f*, 832
 - and image acquisition, 801–808
 - inner segments of, 242*f*
 - light adaptation in, 228–230
 - calcium-dependent mechanisms in, 228–229
 - cellular events contributing to, 228
 - composite effect of mechanisms in, 230
 - elevated steady-state activity of
 - phosphodiesterase and, 229, 230
 - mechanisms of, 228–230
 - pigment bleaching and, 215, 229–230
 - response compression and, 228
 - linkage to ganglion cells, 320
 - maintenance of, 216
 - mammalian mosaic of, 237–245
 - subdivision of, 239*f*–240*f*, 240–241
 - migration of, 80
 - modulation of, by horizontal cells, under
 - different lighting conditions, 388–389
 - need for two types of, 237–240
 - neurometric function for, 821–822, 822*f*
 - neurotransmitter expression and receptors in, 86–87
 - neurotransmitter release from, calcium and, 377
 - outer segments of
 - design of, effect on speed, 241–244, 243*f*
 - mammalian, uniformity and size of, 241, 242*f*
 - nonmammalian, 241
 - peptide expression in, 336
 - effect on ion channels, 337
 - photon absorption by
 - calculation of mean number absorbed, 830
 - in ideal observer analysis, 829–831, 830*f*, 831*f*
 - phototransduction (light response) by, 215–230
 - activation of, 217–221
 - calcium feedback regulation of, 216, 217, 223, 225–228
 - inactivation of, 221–225
 - mutations of proteins involved in,
 - comparison of effects of, 222, 223–225, 224*f*, 225*f*
 - overview of, 216–217
 - physical limits to, 215
 - speed of, size of outer segment and, 241–244, 243*f*
 - in primates, 482
 - rod. *See* Rod(s)
 - saturation of, 229, 816, 841–843
 - serotonin receptors in, 315
 - spatial organization of, horizontal cells and, 386–388, 388*f*
 - specialized mechanisms of, 230
 - structure of, 215–216, 216*f*
 - synapses of, 280–283
 - bandpass filtering by, 246, 249–251, 251*f*
 - basic plan of, 280, 280*f*
 - to bipolar cells, 264–266, 279, 280, 280*f*, 307
 - image separation at, 260, 266
 - postsynaptic mechanisms of, 283–285, 285*f*
 - presynaptic mechanisms of, 280–283, 281*f*
 - sign-inverting, 283
 - sign-preserving, 283, 285
 - dopaminergic, 314
 - formation of, 87–88
 - GABAergic, 281*f*, 281–283, 284*f*, 290
 - to ganglion cells, interaction of rods and cones in, 418–419
 - glutamatergic, 264–266, 281*f*, 281–285, 285*f*, 289, 304, 307, 320–330, 377*f*, 377–378, 378*f*
 - glycinergic, 311
 - horizontal cell to, 290, 309, 381–383, 382*f*, 383*f*, 386, 388–389
 - to horizontal cells, 280, 280*f*, 307, 314, 370–371, 372–374, 373–374, 375–376, 376–378
 - postsynaptic mechanisms of, 289
 - invaginating, 281*f*, 281–282
 - negative feedback on, 283
 - postsynaptic partners in, patterns of
 - connection, 282
 - superficial, 281, 281*f*
 - three-dimensional structure and function of, 246–247, 247*f*
 - thresholds of, 820, 821–822, 822*f*
 - topography of, 801–802
 - in vertical pathway, 320–330
 - Photoreceptor degenerative diseases, 39, 42–43
 - Phototransduction, 215–230
 - activation of, 217–221
 - molecular mechanisms of, 217*f*, 217–221
 - calcium feedback regulation of, 216, 217, 223, 225–228
 - versus chemoreceptive systems, 217
 - dark rearing and, 89–90
 - defects in, 217
 - development of, 89–90, 117, 176
 - in horizontal cells, 290
 - inactivation of, 221–225
 - mutations of proteins involved in,
 - comparison of effects of, 222, 223–225, 224*f*, 225*f*
 - inverted-response polarity in, 217
 - noise during, calcium and, 227
 - onset phase of, predicted form of, 219–220, 220*f*
 - theory versus experiment, 220, 221*f*
 - overview of, 216–217
 - in photoreceptors, 215–230
 - physical limits to, 215
 - proteins in, optimization for sensitivity,
 - speed, gain, and noise, 241–244
 - speed of, size of outer segment and, 241–244, 243*f*
 - Phrenology, 8
 - pi* mechanisms, 940
 - Picrotoxin
 - and cortical plasticity, 131
 - restorative effects of, 136–137
 - GABA receptor response to, 293, 356*t*, 358, 362, 452, 457
 - Picture priming, 1320
 - Piéron's law, 820
 - Pigeon(s)
 - color vision in, 965, 971
 - retinal synapses of, 293
 - Pigment, 215–216. *See also* Rhodopsin
 - absence of, and optic chiasm defects, 100*f*, 102–103
 - bleaching of, and light adaptation, 215, 229–230
 - Pigmented retina, 64, 64*f*, 68, 235*f*
 - Pineal gland
 - melatonin production in, 628, 630

- Pineal gland (cont.)
Rax/Rx gene expression in, 66
 tumor of, and pupil responses, 652
- Pinwheel centers, in orientation, 119, 737
- PIT visual area, macaque
 dorsal (PITd), 510*f*–511*f*, 512
 ventral (PITv), 510*f*–511*f*, 512
- Pituitary adenylate cyclase activating polypeptide (PACAP)
 and circadian rhythms, 628–629, 634, 635, 635*f*
 coexpression with glutamate, 336
 coexpression with melanopsin, 345, 629
 coupling to adenylate cyclase, 336
 CREB stimulation by, 634
 ganglion cells expressing, 345
 molecular forms of, 345
 retinal, 334, 336, 345–346, 348
 binding sites of, 345–346
 coupling to adenylate cyclase, 345–346
 localization of, 345–346
- Pituitary adenylate cyclase activating polypeptide (PACAP) receptor
 mRNA of, 336
 retinal, 336, 346
- Pixel noise, in ideal observer analysis, 832–834
- Place cells, 1183
- Plaid stimuli, for chromatic motion processing, 1223–1226, 1224*f*
- Planning, prefrontal cortex (PFC) damage and, 1550–1551
- Plasticity
 adaptation-induced, 1655, 1656*f*
 rapid, 1660–1661, 1661*f*
 anti-plasticity genes (capgs) and, 134
 of binocular vision, 776
 candidate genes (cpgs) in, 133–134
 of cognitive control system, 1547
 cortical
 activity and, importance of, 128
 BDNF and, 53–55, 60, 128, 131, 133, 136*t*
 calcium and, 128, 129, 130, 136*t*, 137, 137*f*, 139
 CREB and, 132–133, 136*t*, 137, 137*f*
 cyclic AMP and, 129, 131–132
 dark rearing and, 128, 129, 130, 131, 132, 133–134
 electrical activity and, 54
 factors in, 137*f*, 137–139
 versus activity-related factors, 128
 evaluation of, 128–139
 instructive, 128–134
 modulatory, 128, 134–139
 summary of, 136, 136*t*
 feedback pathways in, 137
 forms of, 126
 GABA and, 127, 130–131, 133, 136–137, 137, 137*f*, 139
 gate hypothesis of, 131, 137
 gene expression and, 133–134
 glutamate receptors and, 126, 128, 129–130, 132, 136*t*, 137, 137*f*
 inhibition and, 58
 MAPK cascade and, 59*f*, 59–60, 132, 136*t*, 137, 137*f*
 mechanisms of, 126–139
 as model for nervous system, 126
 monocular deprivation and, 126, 132, 135
 nerve growth factor and, 135, 136*t*
 nervous system states and, 128, 134
 neurotransmitters and, 128, 134–135, 136*t*, 137*f*, 139
 neurotrophins and, 47*f*, 48–49, 52–55, 58–60, 59*f*, 61
 possible sites of action for, 60, 60*f*
 NMDA receptors and, 129, 136*t*, 137, 137*f*, 139
 physiologic efficacy in, 137–138, 138*f*
 presynaptic and postsynaptic changes in, 138–139, 139*f*
 protein kinase A and, 131–132, 136*t*, 137, 137*f*, 137–139
 protein synthesis and, 133–134, 138–139, 139*f*
 restoration of, in older animals, 136–137
 definition of, 1332, 1654
 direction selectivity, 126–127
 lateral geniculate nucleus, 114–115
 learning-induced, 1656*f*, 1657
 lesion-induced, 1654
 ocular dominance, 108, 112–113, 115, 126
 activity and, importance of, 128
 BDNF and, 131, 133, 136*t*
 calcium and, 130, 136*t*, 137, 137*f*, 139
 CREB and, 132–133, 136*t*, 137, 137*f*
 cyclic AMP and, 131–132
 dark rearing and, 128, 132
 factors in, 137*f*, 137–139
 versus activity-related factors, 128
 evaluation of, 128–139
 instructive, 128–134
 modulatory, 128, 134–139
 summary of, 136, 136*t*
 feedback pathways in, 137
 GABA and, 130–131, 133, 137, 137*f*, 139
 gene expression and, 133–134
 glutamate receptors and, 126, 129–130, 136*t*, 137, 137*f*
 Hebbian synapses and, 113–114
 instructive versus permissive role of
 activity in, 113–115
 MAPK and, 132, 136*t*, 137, 137*f*
 monocular deprivation and, 126, 128, 130–131, 132, 133, 137, 138
 neurotransmitters and, 134–135, 136*t*, 137*f*, 139
 NMDA receptors and, 129, 136*t*, 137, 137*f*, 139
 physiologic efficacy in, 137–138, 138*f*
 presynaptic and postsynaptic changes in, 138–139, 139*f*
 protein kinase A and, 131–132, 136*t*, 137*f*, 137–139
 protein kinase C and, 132, 136*t*
 protein synthesis and, 133–134, 138–139, 139*f*
 relationship with long-term depression and potentiation, 136, 136*t*, 137–138
 restoration of, 131
 in older animals, 137
 orientation
 adaptation-induced, 1657–1658, 1658*f*
 and cortical map of orientation preference, 1658–1660, 1659*f*
 significance for vision, 1660–1662, 1661*f*
 in V1, 1655–1657, 1656*f*
 of orientation processing in adult visual cortex, 1654–1662
 orientation selectivity, 126–127
 BDNF and, 133, 136*t*
 neurotransmitters and, 134, 136*t*
 NMDA receptors and, 129, 136*t*
 protein kinase A and, 132, 136*t*
 in posterior parietal cortex, 1332–1333, 1332*f*
 in primary sensory cortex, 1654
 of sensory map, in V1, 1654
 spike-timing-dependent, 1657
 stimulation timing-dependent, 1655–1657, 1656*f*
 synaptic, 25, 127–128, 295–298, 1669–1670
 calcium and, 130
 excitatory, age and, 321–322
 MAPK cascade and, 59*f*, 59–60
 neurotrophins and, 47*f*, 49, 58–60, 61
 in ocular dominance columns, 113–114
 presynaptic and postsynaptic changes in, 138–139, 139*f*
 spinules in, 296–298, 297*f*
 in teleost fish retinas, 295–298
 in visual cortex, 126
 of synchronizing connections, 1676
 in V1, 1654–1655
- Platyrrhines, vision of, 968, 969
- Plenoptic function, 1091
- Plexiform layers of retina
 formation of, 81–86
 neurotransmitter expression in, 86–87
 organization of, 83–86
 synapse formation in, 87–88
- PLR. *See* Pupil light reflex

- POa visual area, macaque
 external (POa-e), 510*f*–511*f*, 511–512
 internal (POa-i), 510*f*–511*f*, 511–512
- Point image, 525
- Point spread function, 797–798
 calculation of, 798
 in corrected eyes, 807–808, 808*f*
 diffraction-limited, 798, 798*f*
 estimates of, 799–800, 800*f*
 and image formation, 796*f*, 797–798
 light scatter and, 798–799
 pupil size and, 798, 798*f*, 799–800, 800*f*
- Point-to-point connectivity, of visual system, 146
- Poisson distribution, 814
- Polarity constraint, 1293–1294, 1294*f*
- Polarity-matched responses, in nonlinear receptive field maps, 707, 712, 713
- Polarity-mismatched responses, in nonlinear receptive field maps, 707, 712, 713
- Polyak, Stephan, 12, 279
- Polyaxonal amacrine cells, 335, 400–401, 401*f*, 402
- Polychromatic light, retinal images in, 800–801, 801*f*
- Polymerase chain reaction (PCR), for quantitative trait loci mapping, 71
- Polymer-encapsulated cells, neurotrophin administration via, 51
- Polymorphisms, genetic, within species, and retina structure, 71
- Pontine areas, in oculomotor system, 1425
- Pontine nucleus, dorsolateral, in oculomotor system, 1405
- Pontine reticular formation, and pursuit- and saccade-related activity, 1410, 1432*f*
- Popout effect, 721, 1581
- Population coding, 726, 1450–1451
- Population statistics, 1107–1108
- Porphyropsin, 215. *See also* Rhodopsin
- Position, perceived, saccades and, 1395–1397, 1396*f*
- Position invariance, 1250, 1262–1263, 1578
- Position selectivity, development of, 181–182, 182*f*, 183*f*
- Positron emission tomography
 in blindsight, 662–663
 of cortical optic flow responses, 1269
 for mapping motion regions, 1229, 1230, 1235
- Positron emission tomography (PET), of pulvinar region, 601
- Posterior eye field, 1429*f*
- Posterior intraparietal (PIP) visual area, macaque, 510*f*–511*f*, 511
- Posterior parietal complex (PPcx), macaque, 512, 513*f*
- Posterior parietal cortex, 1568*f*, 1569
 activity planning in, 1324–1326
 decision processes for, 1327
 temporal evolution of, 1326–1327
 cognitive functions of, 1324
 in delayed reach task, 1326, 1326*f*
 eye-centered response fields in, gain modulation of, 1330–1331
 intention coding in, 1324–1328, 1330
 intentional maps in, 1327–1328, 1328*f*
 in intervening reach task, 1326, 1326*f*
 learning in, 1332–1333, 1332*f*
 lesions of, 1324
 in monkeys, 541, 542*f*
 multisensory integration in, 1327, 1329–1330, 1329*f*
 neural prosthesis controlled by, 1333–1334
 neurons, directional tuning of, 1325–1326, 1325*f*
 and oculomotor system, 1372*f*
 plasticity in, 1332–1333, 1332*f*
 reach-related activity in, spatial tuning of, 1325–1326, 1325*f*
 and saccades, 1376–1378
 sensorimotor transformation in, 1324–1334
 combinatorial model of, 1331
 coordinate frames and, 1328–1330
 coordinate transformation in, 1330*f*, 1331–1332, 1331*f*
 direct model of, 1331, 1331*f*
 gain fields in, 1330–1331
 sequential model of, 1331
 space representation in, 1328–1332, 1330*f*
 subregions of, 1324, 1328
- Posterior probability, in ideal observer analysis, 826
- Posterolateral lateral suprasylvian sulcus (PLLS), inputs to pulvinar region, 579, 595
- Posteromedial lateral suprasylvian sulcus (PMLS)
 inputs to pulvinar region, 579, 595, 600
 synaptic transmission in, 527
- Postsaccadic drift, 1487–1488
- Poststimulus time histogram, of contrast response function, in cortical neurons, 756, 756*f*
 as function of contrast, 755*f*, 755–756
 as function of contrast through time, 756, 756*f*
 to optimal and non-optimal stimuli, during first 20 msec., 756*f*, 756–757
- Postsynaptic density (PSD), reactions in, and cortical plasticity, 138–139, 139*f*
- Potassium channels/currents
 dopamine and, 438–439, 441*f*
- GABA receptor modulation of, 357*t*, 357–358, 363*f*, 363–364
- in ganglion cells, 433–434, 435, 436
 calcium-activated, 425, 432, 433, 437
 high threshold, 425, 433
 low threshold, 425, 433
 slowly activating, 432
 transient, 432, 433, 436
- in horizontal cells, 378–379
- peptide action on, 334, 337, 341, 341*f*, 342, 348
- in photoreceptors, 216
- Shab-type, 435
- Shaker-type, 435, 436
- Shaw-type, 435
- somatostatin and, 341, 341*f*, 342, 348
- in thalamocortical relays, 571, 573–575, 574*f*
- POU-domain transcription factors, in retinal cell differentiation, 38, 78
- p42/p44 MAPK cascade, 58–60, 59*f*
- Prägnanztendenz*, 1148, 1574
- Prechordal mesoderm, in eye field separation, 34
- Precritical period, of ocular dominance column development, 112–113
- Predictive index, in single-unit recording, 21–22
- Predictive saccades, 1440
- Predominance, in binocular rivalry, 1316
- Prefrontal cortex (PFC), 544
 anatomy of, 1547–1548, 1549*f*
 in cognitive control, 1546
 and cognitive functions, theories of, 1556–1559
 cytoarchitecture of, 1549*f*
 damage to
 behavioral effects of
 in humans, 1548–1551
 in monkeys, 1551–1554
 cognitive architecture and, 1547*f*, 1554
 tasks sensitive to
 in humans, 1550, 1550*f*, 1551
 in monkeys, 1551–1552, 1552*f*
- dorsal, interconnections of, 1548
- dorsolateral, and visual target selection, 1383–1384
- function of, models of, 1556–1559, 1558*f*
- functional topography of, 1553–1554
- lateral, interconnections of, 1548
- of macaque, 1547–1548, 1549*f*
- medial, interconnections of, 1548
- multiple processing levels in, 1557
- neurophysiology of, 1554–1556
- in object recognition, 1640, 1641*f*, 1642, 1648
- orbital, and inhibitory control, 1554
- orbitofrontal, interconnections of, 1548
- rapid learning in, 1555–1556
- subdivisions of, 1549*f*

- Prefrontal cortex (PFC) (cont.)
 and visual consciousness, 1691
 volition and, 1546–1559
- Prelude neurons, 1372, 1381
- Premotor commands, in eye movement control, 1418–1422, 1486
- Preplate neurons, interareal connections of, 150–151
- Preprotachykinin I and II (PPT1 and PPT2), retinal, 335, 342
- Presbyopia, 205–208
 aging and, 205–208
 ambient annual temperature and, 206, 206*t*
 biophysical properties in, 206–207, 207*f*
 ciliary muscle and, 207–208
 rapid development of, 209
 reading and, 207–208
- Prestriate cortex, 1031, 1031*f*
 relation to striate cortex, 1031, 1031*f*
- Presynaptic terminals, reactions in, and cortical plasticity, 138–139, 139*f*
- Pretectal area/pretectum
 circadian role of, 628, 630
 pulvinar connections of, 599
 and pupil responses, 641–642, 652*f*, 652–654, 654*f*
 sustained neuronal responses in, 630
- Primary visual (striate) cortex, 7–9, 509, 510*f*–511*f*, 541, 747, 1371, 1372*f*. *See also* Visual area(s), V1
- binocular interaction in, 765–776, 779, 781–785, 790
 combination of left and right eye signals, 768, 770*f*
 phase-shifted gratings for measurement of, 767–772, 768*f*–769*f*, 770*f*, 771*f*, 772*f*
 in binocular rivalry, 1319
 cell number and density in, 69
 functional correlate of, 69
 variation within species and genotype, 71
- chromatically responsive cells in, multiplicity of, 1011–1012
- circuitry of, 614–619
- color processing in, 1011–1014, 1013*f*, 1014*f*, 1017
- color-selective cells in, 1017
- connections of
 with area MT, 619, 1203, 1204*f*
 horizontal, 733–743
 identification of, 733–734
 local or short-range, 734–737, 737*f*
 and neuronal synchrony, 742*f*, 742–743
 receptive field effects of, 733–743
 with inferotemporal cortex, 12
 with lateral geniculate nucleus, 485, 486*f*, 494–503, 498–501, 499*f*, 500*f*, 501*f*
 multiple, functional implications of, 501–503
 receptive field effects of, 146, 148–151, 733–743
 vertical, 733–743
 identification of, 733–734
- damage to, and blindness, 747
- development of
 activity/experience and, 165, 167
 neural factors in, 165–170
 visual deprivation and, 167–170
- in dialogue between cerebral cortex and superior colliculus, 1468*f*, 1472
- direction selectivity in
 linear and nonlinear properties of, 753
 MT feedback and, 621*f*, 621–622
 spatiotemporal mechanisms underlying, 710–711, 711*f*
 temporal dynamics of, 758*f*, 758–759
- electrophysiological recordings in, 108
- functions of, 146, 747–748
- human
 architectonic boundary of, 513
 individual variability in, 513
 surface area of, 513
- layer 1, LGN signaling to, 502–503
- layer 2/3
 horizontal connections to, 733, 737–739
 vertical connections to, 733
- layer 4, collaterals of corticogeniculate cells in, 614–619
- layer 5, interactions with pulvinar region, 579, 583–584, 585*f*
- layer 6
 cell function in, 614–619
 effects on layer 4 cell responses, 617–622
 interactions with lateral geniculate nucleus, 568, 569*f*, 570, 578, 610*f*, 610–611, 612, 614–617, 622
 interactions with pulvinar region, 579, 583–584, 585*f*
 organization of, 610–611
- lesions of, 5, 657
- LGN afferents in, eye-specific segregation of, 108
- motion processing in
 functional mapping of, 1233–1234, 1234*f*
 versus hMT/V5+ visual area, 1230–1231, 1231*f*
 MT feedback and, 619–622, 620*f*, 621*f*
 and movement control, 1241
- MT feedback to, 609, 614–622
 effects of, 619–622, 620*f*, 621*f*
 future directions for study of, 622–623
- neural activity in, electrical recording of, 9–10
- neural factors in, and ideal observer analysis, 832, 833*f*
- neurons of. *See* Primary visual cortex neurons
- as pattern adaptation site, 939
- and pupil responses, 643
- receptive fields in, assembly of, 695–702
- representation of visual fields on, 8–10, 9–10, 10*f*
- and saccades, 1374–1376
- in stereoscopic vision, 765–766, 766*f*, 767*f*, 781–785, 790
- subthreshold responses in, 734, 736*f*
- surface area of, variations in, 71
- synaptic organization of, 614–619
- transfer of visual information through, 614–622
- visual pathways to, 494–503
 parallel, 680
 functional implications of, 501–503
 organization of, 498–501, 499*f*, 500*f*, 501*f*
 unanswered questions about, 503
 “what” and “where,” 489, 495–496
- Primary visual cortex neurons
 analysis of, 747
 models at different levels of, 759–760
- binocular disparity sensitivity of, 550, 765–766, 766*f*, 767*f*, 779–785, 781*f*, 783*f*, 790
- inconsistencies with stereoscopic vision properties, 782–785
- range of, 781*f*, 781–782, 783*f*
- response to absolute disparity, 783
- response to local disparity, 784, 784*f*
 and stereoscopic vision, 765–766, 779, 781–785, 790
- binocular interaction in, 768–772, 770*f*, 771*f*, 772*f*, 781–785, 790
- contrast adaptation in, 754, 754*f*
 temporal dynamics of, 755
- contrast response function in, 752*f*, 752–753, 753, 753*f*
 as function of contrast, 755*f*, 755–756
 as function of contrast through time, 756, 756*f*
- models of, 759–760
- to optimal and non-optimal stimuli during first 20 msec., 756*f*, 756–757
- poststimulus time histograms of, 755*f*, 755–757, 756*f*
- temporal dynamics of, 755*f*, 755–757, 756*f*
- contrast-set gain control in, 753, 753*f*, 760–761
- temporal dynamics of, 756–757
- as depth detectors, 765–766
- descriptive models of, 759
- drifting steady-state measurements of, 749–750, 757
- as filters, 747–748, 747–749
- spatiotemporal, 748–749

- frequency domain analysis of, 748–749
functional models of, 759–760
ideal observer analysis at level of, 832
integration interval in, 758
latency shift in, 753–754, 754*f*, 759
temporal dynamics of, 755
linear properties of, 750–751
nonlinear properties of, 747–761
linear systems analysis of, 749
rapid and slow, 754–755
temporal dynamics of, 749–750, 754–759
orientation selectivity in, 117–119, 124, 179
temporal dynamics of, 757–758
performance of, assessment of, 748
receptive fields of
behavioral development versus
physiological changes in, 165–167
complexity of, 747
dynamics of, intracortical circuits and, 739*f*, 739–742, 740*f*
horizontal connections and, 733–743
effect on minimum discharge field, 733–739, 736*f*, 738*f*
size effects, 734, 736*f*, 741–742
surround effects, 733, 734, 736*f*, 737, 739*f*, 739–741, 740*f*
properties of, development of, 165*f*, 165–167, 166*f*
spatial properties of, 166*f*, 166–167
visual deprivation and, 167–170
response expansion in, 752*f*, 752–753, 759
temporal dynamics of, 756–757
response rectification in, 751*f*, 751–752
temporal dynamics of, 755
response refractory period of, 751
temporal dynamics of, 755
response saturation in, 753, 753*f*, 759
spatial frequency selectivity in, linear and nonlinear properties of, 753
spatial frequency selectivity of, temporal dynamics of, 757–759
spatiotemporal processing by, 704–717
stimulus selectivity of, 747–748, 761
temporal dynamics of, 754–759
structural models of, 760, 760*t*
synchrony of
horizontal connections and, 742*f*, 742–743
vertical connections and, 743
systems analysis of, 747, 748–749
temporal dynamics of, 749–750, 754–759
transient stationary measurements of, 749–750, 757
types of, 750
Primate(s). *See also* Monkey(s)
amacrine cells of, 399, 482–483
anthropoid, 1564
color and food source identification in,
ideal observer analysis of, 834
color vision in, 965, 971
and retinal circuitry, reviews of, 991*t*
cone development and migration in,
159–163, 162*f*
cortical connections in, 148
feedback
from area MT, 609
to lateral geniculate nucleus, 609, 610
feedforward, 151
early
brains of, 1566
visual cortex in, 1568–1569, 1568*f*
visual system of, 1566–1568
forced-choice preferential looking by, 190
frontal eye field (FEF) in, 1428–1445. *See also* Frontal eye field (FEF)
ganglion cells of, 410–412
central projections of, 413–415
contrast sensitivity in, 416*f*, 416–417, 418
eccentricity-dependent morphology of, 413, 414*f*
receptive fields of, 418
small bistratified, 411–412
spatial selectivity of, 418
spatial summation in, 418
types of, 410–412
wide-field, 411, 412
horizontal cells of, 370, 370*f*
luminosity, 374
rod and cone mixing in, 375
S-potentials of, 369
lateral cortical connections in, 1071
lateral geniculate nucleus in
eye-specific lamination of, 108–109
parallel visual pathways of, 496–498
M, P, and K visual pathways of, 481–491
midget cells in, 262, 268, 410–411, 411*f*
neuronal correlates of visual deprivation in, 167–170
newborn, visual capacities of, 159
versus adult capacities, 159, 160*f*
nocturnal, vision of, 964
optic chiasm in, organization of, 94, 95, 95*f*
origin of, 1564
parasol cells in, 262, 268, 410–411, 411*f*
photopigments of, 968
phylogeny of, 1564
primary visual cortex of, layer 6 of, 617. *See also* Primary visual (striate) cortex
prosimian, 1564
pulvinar region, 1568
cortical inputs to, 594*f*, 595–596
evolution of, 592
and eye movements, 601
response properties of, 597
retinal inputs to, 593–594
visual functions of, 599
radiation of, 1564
receptive fields in
dynamics of, 740
responses and properties of,
development of, 163–165
retina of, 908–909
cell distribution in, 80
cell number and density in, 69–70
cell types in, 483
general scheme of, 482–483
retinal peptide expression in, 336
tachykinins, 342–343
rod system of, versus cold-blooded vertebrates, 843
scotopic vision of, adaptation in, 843
spatial vision in
development of, 159–171, 161*f*
visual deprivation and, 167–170, 168*f*, 169*f*
synapse formation in, 87
tarsier, 1564
visual system of, 1566, 1567–1568
visual development in
ideal observer model of, 160–163, 162*f*
neural limitations on, 159–171
postnatal changes and, 159–163
visual input and, 159–163
visual system of
comparison to other mammals, 1564–1566
evolution of, 1563–1570
Primitives
object, 1080–1088
definition of, 1080
shape, 1082
Principles, general, prefrontal cortex (PFC) and, 1555
Prior probability
definition of, 1618
distribution on velocity, in local analysis of motion, 1618–1619
in ideal observer analysis, 826
Prism(s), decorrelated binocular input with, effects of, 198–199, 199*f*
Probabilistic inference
definition of, 1604
perception as, 1604
Probabilistic methods
in ideal observer analysis, 826
for mapping visual areas, 513
Probabilistic models
as experimental tools, 1612
of image representation, 1603–1606, 1612
simple, 1606–1609
Probability density function (PDF), 1592
Process outgrowth
from amacrine cells, 84

- Process outgrowth (cont.)
 from retinal neurons, 81*f*, 81–82, 83, 84*f*
 in inner retina, 81–82
 in outer retina, 82
- Processing efficiency, 813
- Processing streams, 1579
- Progenitors of retinal cells, 37, 63
 competence of, 64*f*, 64–65
 limited, 78
 timing of, 67
 determinative states of, 67
 differentiation of, 78–79
 embryonic versus neonatal, 67
 fate of, 66–68, 77–78. *See also* Retinal cells, differentiation of
 heterogeneity of, 67, 78
 interkinetic migration of, 77
 lineage tracing of, 37, 66–68
 producing layer-restricted clones, 67
 producing radial clones, 67
 regionalization of, 64*f*, 65
 regulation of, 79
 selection of, 64*f*, 64–65
- Projection neurons, number of
 ratio of ganglion cells to, 69
 variation within species and genotype, 71
- Prosimians, visual system of, 1568*f*, 1569, 1570
- Prosopagnosia, 548, 554, 1153, 1165, 1580
 developmental, 1186
- Protan, 974
- Protanomaly, 975, 983
- Protanopia, 875, 975. *See also* Dichromacy
- Protein kinase A
 and circadian rhythms, 634
 and cortical plasticity, 131–132, 136*t*, 137*f*, 137–139
 restorative effects of, 137
 and dopaminergic inhibition of ganglion cells, 438–439
 GABA receptor modulation by, 356*t*, 359
 glycine receptor modulation by, 358
 and long-term depression, 131, 136*t*
 and long-term potentiation, 131, 136*t*
 and orientation selectivity, 132, 136*t*
- Protein kinase C
 as bipolar cell marker, 82
 GABA receptor modulation by, 356*t*, 359
 and ganglion cell permeability, 431
 glycine receptor modulation by, 356*t*, 358–359
 and ocular dominance plasticity, 132, 136*t*
 rhodopsin phosphorylation by, 222
 and spinule formation, 296, 298
- Protein kinase G, and long-term potentiation, 132, 136*t*
- Protein phosphatase 1, and cortical plasticity, 132, 137, 137*f*
- Protein phosphatase 2A, and cortical plasticity, 132, 137, 137*f*
- Protein synthesis, and cortical plasticity, 133–134, 138–139, 139*f*
- Proteoglycan(s)
 composition of, 100
 and optic chiasm development, 97*f*, 100
 and restoration of plasticity, 137
 structure of, 100
- Protocortex theory, of cortical development, 146
- Protomap theory, of cortical development, 146
- Proximity
 equivalent in motion, 1576
 Gestalt factor of, 1575, 1576*f*, 1578
- Proximity-luminance covariation, 1635
- Psychometric function, 811, 813*f*, 820–822, 840, 847
 definition of, 820–821
 nonlinear transducer explanation of, 821
 physiological, 821–822, 822*f*
 uncertainty explanation of, 821
- Psychophysics, 1573
 in blindsight, and pupillometry, comparison of, 661–662, 661*f*
- Ptois, 197–198
- Pulvinar. *See* Pulvinar region
- Pulvinar region, 565, 1565
 as active partner of cortical areas, 600, 602–603, 602*f*
 afferents to, 579, 593–596, 594*f*
 cortical, 583–584, 585*f*, 595–596, 603–604
 in Alzheimer's disease, 602
 anterior, 592–593
 in attention, 503, 598–599, 600, 600*f*, 1478, 1479*f*
 connectional and cellular properties in, 582–583
 connections with area MT, 1203, 1204*f*
 connections with ventral and dorsal streams, 544
 cortical projections from, 585
 in corticocortical communication, 580–582, 580*f*, 582*f*
 definition of, 565
 in dialogue between cerebral cortex and superior colliculus, 1468, 1468*f*, 1476–1480, 1479*f*
 efferent connectivity of, 585, 593–596, 594*f*, 603–604
 and eye movements, 601
 in feature binding, 603
 filtering of irrelevant information in, 600*f*, 601
 functional organization of, 578–585, 603
 in higher-order motion processing, 597–598, 598*f*
 as higher-order nucleus, 593, 597–598, 598*f*
 as higher-order visual relay, 579
 inferior, 592–593
 chemoarchitectonic subdivisions of, 1568
 lateral, 592–593
 dorsomedial part of, 593
 layers of, 583
 location of, 592, 593*f*
 maps of, 583
 medial, 592–593
 interconnections/projections of, 1261
 midbrain inputs to, 594–595
 as monitor of motor outputs, 582
 in motion processing, 596–598, 598*f*, 603
 neurons in
 push-pull modulation of, 598–599
 receptive field properties of, 592, 596–599, 597*f*, 598*f*
 and oculomotor system, 1372*f*
 organization of
 structural, 592–593
 visuotopic, 592–593
 parallel pathways through, 584–585, 585*f*
 in pattern recognition, 603
 in primates, 1568
 cortical inputs to, 594*f*, 595–596
 evolution of, 592
 and eye movements, 601
 organization of, 592–593
 response properties of, 597
 retinal inputs to, 593–594
 visual functions of, 599
 research on, advances in (future directions for), 603–604
 retinal inputs to, 593–594
 in schizophrenia, 602
 subdivisions of, 583, 592, 1568
 tectal inputs to, 579–580
 in texture analysis, 596
 visual functions of, 592–604
 human studies of, 601–602
 “not so strong” relay hypothesis for, 599–600
 visual noise and, 596
 as visual relay, 578–579
 zones of, 583
- Pupil(s), 641–655
 basic mechanisms of, 641–655
 constriction of (miosis), 642. *See also* Pupil light reflex
 during anesthesia, 642, 653
 during sleep, 642, 653
 contrast gain in, 642, 653
 dilation of (mydriasis), 642
 in light regulation, 851
 movement of, control of, 642
 pathways, 641, 642, 653–654, 654, 654*f*
 inhibitory, 642

parasympathetic, 642
 responses of
 in cerebral achromatopsia, 641–642, 651*f*, 652, 653
 to color, 641–642, 650*f*, 650–652, 651*f*
 clinical applications of research on, 654
 damage to dorsal midbrain and, 653–654
 cortical damage and, 647, 648*f*, 654*f*
 damage to dorsal midbrain and, 652*f*, 652–654, 654*f*
 dynamic noise studies of, 643, 644*f*, 645, 647, 650–652, 651*f*
 as example of servomechanism, 641, 653
 geniculostriate projection and, 641, 643, 647
 to grating stimuli, 649*f*, 649–650, 650*f*
 damage to dorsal midbrain and, 653–654
 in hemianopia, 641–643, 644*f*, 647–650, 648*f*, 649*f*, 650*f*, 651*f*, 652, 654
 to light. *See* Pupil light reflex
 to luminance flicker, 641
 to motion, 641, 648–649, 649*f*
 onset latency of, 642, 643*f*, 648, 650
 in Parinaud's syndrome, 652*f*, 652–654, 654*f*
 spatial summation of, 642, 647, 647*f*, 653, 654*f*
 to spatially structured patterns, 641, 645–647
 to specific stimuli other than light, 641–642, 648–652
 size of
 and aberrations, 799–800, 800*f*
 age and, 642, 846
 and image formation, 798, 798*f*, 799–800, 800*f*
 and modulation transfer function, 799–800, 801*f*
 optimum, task-specificity of, 800
 and point spread function, 798, 798*f*, 799–800, 800*f*
 slow oscillations, during sleepiness, 642, 653, 654*f*
 studies of, 641–655
 clinical applications of, 641, 654–655
 difficulties in, 641
 dynamic morphing of images in, 654
 Pupil function, 796–797
 and image formation, 796–797
 Pupil light reflex (PLR), 641, 642–648
 clinical applications of research on, 654–655
 cortical damage and, 647, 648*f*, 654*f*
 damage to dorsal midbrain and, 652*f*, 652–654, 654*f*

dilator muscle of iris and, 652–653
 dynamic, 641, 642, 643*f*
 dynamic noise experiments on, 643, 644*f*, 647
 as example of servomechanism, 641, 653
 function of, 641
 optic nerve damage and, 645, 645*f*
 pathways for, 641, 642, 653–654, 654*f*
 single, hypothesis of, 641
 two-component hypothesis of, 642–643, 647, 654
 perimetry studies of, 645–647, 646*f*, 647*f*, 648*f*
 steady-state component of, 642, 643*f*, 654*f*
 transient component of, 642–643, 643*f*, 647, 654*f*
 Pupillometry
 in blindsight, 661–662, 661*f*
 and psychophysics, comparison of, 661–662, 661*f*
 P-scan, in blindsight, 661–662, 661*f*
 Pupillomotor system, central inhibition of, 641
 Purkinje cells, 1486, 1488
 spike discharges from, 1486–1487
 Purkinje shift, 658, 852, 867
 Pursuit. *See* Eye movement(s), smooth pursuit
 Pursuit field, 1405
 Push-pull modulation, of pulvinar cells, 598–599
 Pyramidal cell(s), 24–26, 522
 BDNF expression in, 133
 as BDNF target, 55
 biophysical knowledge in
 circadian or diurnal, 24
 evolution of, 24–25
 Cajal-Retzius neurons and, 150–151
 chattering, and neuronal synchrony, 742, 742*f*
 computational capacity of, 24–26
 cortical connections originating from, 148–149
 in corticocortical pathways, 522
 in cortico-pulvinar connection, 595
 discharges, temporal relations among, 1670
 horizontal connections originating from, 733, 734–735
 lateral projections of, 1071–1072
 long-range projections of, 1072
 of macaque V1, 683*f*, 684–686, 685*f*, 687*f*
 phase sequences and, 25
 short-range projections of, 1072
 super-Hebbian, 26
 synapses of, to interareal cortical connections, 154
 synaptic transmission in, 528

Q

Quadrat analysis, in mosaic measurement, 474
 Quantitative genetics, 71
 Quantitative trait loci (QTLs), 71–72
 Quantum efficiency, 814
 detective, 816
 of retina, 797
 of rods, 816
 Quantum fluctuation fingerprint, 814–815, 815*f*, 820, 822
 Quantum fluctuation limit
 predicted square-root laws for, 814–815
 for thresholds, 813–815, 820, 822

R

Rabbit(s)
 amacrine cells of, 399–400, 400*f*, 482
 AII, 396
 association, 400, 401*f*
 effects on direction selectivity, 404–405
 reciprocal rod (S1 and S2), 398
 tracer-coupling studies of, 402
 direction selectivity in, 127, 451
 starburst amacrine cells and, 456–459
 ganglion cells of, 89
 direction-selective, 361, 455
 mosaics of, 466
 dopamine and, 440–441, 442*f*
 excitability of, 424–425
 inhibitory surrounds in, 364–365
 light responses of, 443
 ON and OFF, stratification of, 267
 spatial selectivity of, 418
 synapses of, 417
 horizontal cells of
 gap junctions between, 380, 380*f*
 ion conductances in, 377*f*, 378–379, 379*f*
 luminosity, 372*f*, 372–373
 nitric oxide and, 385, 385*f*
 receptive fields of, 380*f*
 retinoic acid and, 386, 387*f*
 rod and cone mixing in, 375
 optic nerve of, parallel processing by, 495
 process outgrowth from amacrine cells in, 84*f*
 receptive fields in, 89–90
 retinal peptide expression in, 336
 effect on ion channels, 337
 effect on neurotransmitter release, 337
 renin and angiotensin, 347
 somatostatin, 339–341
 tachykinins, 342–344
 VIP/PACAP, 344–346
 retinal synapses of, horizontal cell-
 horizontal cell, 289–290
 rods of, outer segments of, 241
 single-unit recording in, 17, 18
 visual system of, 1569

- Radial clones, retinal stem cells producing, 67
- Radial flow
and divergence, differentiation of, 1250
sensitivity to, in dorsal medial superior temporal area (MSTd), 1250
- Radial frequency, 1087–1088
- Radial glia, and regulation of ganglion cell axons, 96, 97*f*, 99
- Radial order, of Zernike modes, 795–796
- Radial pathway. *See* Vertical pathway
- Radiance, 1090–1091
- Radiation
definition of, 1090
scattered, 1092, 1093, 1093*f*
volume (photon) density of, 1090
volume (ray) density of, 1090
- Radiator(s)
primary, 1090, 1091
secondary, 1090
- Radiosity, 1098–1099
- Random dot cinematogram (RDC), 597, 603, 1403, 1404*f*
- Random dot kinematograms (RDKs), 597, 603, 1403, 1404*f*
- Range fractionation, by ganglion cells, 422–423
- Raphe nuclei
circadian role of, 628, 630
signals about nervous system state from, 134
sustained neuronal responses in, 630
- Rapid serial visual presentation (RSVP), 1642
- Rat(s)
circadian rhythms in
genetic expression and, 634–635
light responses of SCN neurons and, 629–630, 630, 631
cortical connections in, 148
feedback, 152
feedforward, 151
of preplate neurons, 150
and synaptic organization, 154
synaptic transmission in, 527
cortical plasticity in, 127
BDNF and, 133
nerve growth factor and, 135
NMDA receptors and, 129
corticocortical pathways in, 522
conduction speed in, 532
GABA receptors in, 293
GABA transport in, 289
ganglion cells of
calcium currents in, 433
dopaminergic inhibition of, 438
excitability of, 435
inwardly rectifying cation current in, 434
sodium currents in, 432
long-term potentiation in, 127, 129
monocular deprivation in, 126, 198
effects of exogenous neurotrophins on, 50, 51*f*–52*f*
preventive effects of neurotrophins in, 54–55
neurotrophin blockade in, 54*f*
OFF and ON pathways in, stratification of, 268
optic nerve of, neurotrophin transport in, 50*b*
retina in, developing, spontaneous activity of, 88
retinal cell development in, bone
morphogenetic proteins and, 65
retinal cell differentiation in, 78, 79
retinal peptide expression in, 334, 336
angiotensin II, 347
CRH, 347–348
NPY, 338
somatostatin, 339–341
tachykinins, 342–343
VIP/PACAP, 344–346
retinal synapses of, photoreceptor, 283
retinitis pigmentosa in, 43
visual areas of, 518
visual cortex, basket cells in, 689
visual deprivation studies in, 189
- Rax/Rx* gene
expression of
in eye fields, 33–34, 66
in pineal gland, 66
in retina, 66
and opsin expression, 40
in retinal cell differentiation, 68
and selection of retinal stem cells, 66
- Ray(s), 1090, 1091
- Ray tracing, 1098–1099
- Rayleigh color match, 982
- Reach task
delayed, posterior parietal cortex in, 1326, 1326*f*
intervening, posterior parietal cortex in, 1326, 1326*f*
- Reaching cells, 1462
in pulvinar, 599
- Reading. *See also* Musical sight reading
and accommodation, 207–208
change detection during, 1525
eye movements in, 1343, 1344*f*, 1357–1358, 1525
- Readout neurons, 1678*f*, 1679
- Receiver operating characteristic (ROC)
analysis, 577
of binocular processing of contrast, 772–773
of MT response properties and motion perception, 1210
photon noise and, 829
of thresholds, 814–815, 815*f*, 818, 820
- Receptive field(s), 565, 704–717, 1579, 1579*f*. *See also specific cell type*
of AI amacrine cells, 398
of AII amacrine cells, 396
changes under different lighting conditions, 396
dopamine and, 396
assembly of, in primary visual cortex, 695–702
attention and, 1541
binocular responsive, 765–768, 779, 782*f*, 783
in nonlinear maps, 711, 712*f*, 713, 714, 715, 717
of bipolar cells, 264, 418
organization of, horizontal cells and, 386–388, 388*f*
and border contrast, 886–887
center stimulation, responses to, feedback connections and, 533–535
center-surround organization of, 89, 415–417, 416*f*, 483
for area MT neurons, 1205–1206
dynamics of, intracortical circuits and, 739*f*, 739–742, 740*f*
for ganglion cells, 23, 89, 415–417, 416*f*, 422, 708
horizontal cells and, 386–388, 388*f*
horizontal connections and, 733, 734, 736*f*, 737
for LGN neurons, 708–709
cortical feedback and, 612–614
relative disparity and, 786–787
stimulus contrast and, 739*f*, 739–741, 740*f*
summation and, 739*f*, 739–741, 740*f*
in central visual pathway, spatial organization of, 707–708, 708*f*
classical, 545, 1069, 1654
limitations in characterization of, 704
modern view of, 704–717
color, 926, 926*f*
of complex cells
construction of, 716
linear map of, 708, 708*f*, 709*f*, 710
nonlinear map of, 706, 708, 714–716, 715*f*, 717
singular value decomposition (SVD) analysis of, 716
spatiotemporal map of, 709*f*, 710
subunits of, 714–716
conceptual framework for, 704–706
of cortical neurons
behavioral development versus physiological changes in, 165–167
complexity of, 747
cortical connectivity and, 146, 148–151, 733–743
dynamics of, intracortical circuits and, 739*f*, 739–742, 740*f*

horizontal connections and
 effect on minimum discharge field,
 733–739, 736*f*, 738*f*
 reconciling properties of, 734
 size effects, 734, 736*f*, 741–742
 surround effects, 739*f*, 739–741, 740*f*
 surround effects of, 733, 734, 736*f*, 737
 properties of, development of, 165*f*,
 165–167, 166*f*
 spatial properties of, 166*f*, 166–167
 visual deprivation and, 167–170
 definition of, 704, 705*f*, 1579
 direction index of, 165*f*, 165–166
 direction selectivity in, 89, 165*f*, 165–166,
 451, 452*f*
 spatiotemporal mechanisms of, 710–711,
 711*f*
 dynamic changes in, 1654
 dynamics of, intracortical circuits and,
 739*f*, 739–742, 740*f*
 extraclassical, 1654
 as functional micro-Gestalt, 1579
 of ganglion cells, 17, 261, 261*f*, 288,
 415–419
 asymmetric or elliptical, 417*f*, 418
 center-surround organization of, 23, 89,
 415–417, 416*f*, 422, 708
 cone input to, 488
 correspondence with dendritic field,
 417, 417*f*
 dark rearing and, 89–90
 difference-of-Gaussians model of, 415,
 416*f*
 limitations of, 418
 and direction selectivity, 451, 452*f*
 establishment of, 89–90
 excitatory versus inhibitory, 360–361,
 415, 415*f*
 extraclassical properties of, 419
 light response in, development of, 89–90
 linear maps of, 708, 708*f*
 ON/OFF, 117–118, 118*f*
 organization of, horizontal cells and,
 386
 parameters of, 20
 properties of, 415–419
 development of, 163–165
 relation to synaptic input, 417
 responses of, development of, neural
 factors in, 163–165
 size of, 18
 newborn versus adult, 163
 somatostatin and, 342, 349
 subregions of, 415
 trigger features for, 18
 hierarchy of, 1069
 of horizontal cells, 380*f*, 380–381
 dopamine and, 383–384, 384*f*
 equations for calculating, 381
 nitric oxide and, 385, 385*f*
 of hypercomplex cells, 118
 in ideal observer analysis, 827, 832
 of LGN cells, 117–118, 118*f*, 123, 123*f*,
 127
 center-surround organization of,
 612–614, 708–709
 inhibitory surround of, cortical feedback
 and, 612–614
 linear maps of, 707–708, 708*f*, 708–709,
 709*f*
 responses of
 behavioral versus physiological changes
 in, 164*f*, 164–165
 development of, 163–165
 spatial properties of, 166*f*, 166–167
 spatiotemporal maps of, 708–709, 709*f*
 linear maps of, 705*f*, 705–706, 707–711,
 716–717, 750
 comparison with direction selectivity
 index, 710–711, 711*f*
 for geniculostriate neurons, 708–709,
 708*f*, 709*f*
 methods for obtaining, 706–707, 707*f*
 negative values of, 707
 OFF or dark-excitatory responses in,
 707
 ON or bright-excitatory responses in,
 707
 positive values of, 707
 linear response properties of, 704–706,
 705*f*
 luminance, 926, 926*f*
 of M (magnocellular) cells, 164, 164*f*,
 484–485, 486
 mapping/maps of, 705–717
 in alert, fixating animals, 707
 in anesthetized, paralyzed animals, 707
 goal of, 706
 in space and time, 706–707
 spatiotemporal, along geniculostriate
 pathway, 708–709, 709*f*
 white noise approach to, 706–707, 714
 minimum discharge field
 horizontal cortical connections and,
 733–739, 736*f*, 738*f*
 size of, regulation of, 741
 of MT neurons, 1205–1206
 nonclassical (nCRF), in natural scene
 perception, 1594
 nonlinear maps of, 705*f*, 705–706,
 711–717
 for interaction order of p , 707
 methods for obtaining, 706–707
 negative values of, 707
 polarity-matched responses in, 707,
 712
 polarity-mismatched responses in, 707,
 712
 positive values of, 707
 second-order, 705–706, 707, 711–717
 nonlinear response properties of,
 704–706, 705*f*
 of NOT neurons, responses of,
 development of, 163
 ON and OFF, 117–118, 118*f*, 673, 704
 mapping of, 707
 orientation tuning of, 165*f*, 165–166
 of P (parvocellular) cells, 164, 164*f*,
 484–485, 486
 cone input to, 488
 perisaccadic shifts of, 1398
 properties of, 1069
 variation of, with eccentricity in retina,
 524, 524*f*, 1043–1045
 for pursuit, 1405
 of relay cells in cat LGN, 568
 response properties of, 704
 of SCN neurons, 630
 selectivity of, indices of, 165*f*, 165–166
 of simple cells, 118, 118*f*, 123, 123*f*
 linear map of, 708, 708*f*, 709*f*, 709–710,
 716–717, 750
 nonlinear maps of, 712*f*, 712–714, 714*f*,
 717
 ON and OFF regions of, 673, 674*f*, 768
 space-time inseparable, 709*f*, 710, 713
 space-time separable, 709*f*, 709–710
 spatiotemporal map of, 709*f*, 709–710
 spatiotemporal properties of, 751
 subregions of, 750
 temporal profile of, 709–710
 single-unit recording of, 118
 size of, 18, 524, 524*f*, 541, 720
 artificial scotoma and, 741–742
 definition of, 165*f*
 developmental changes in, 165*f*,
 165–167
 horizontal cortical connections and, 734,
 736*f*, 741–742
 newborn versus adult, 163
 object-related, 1171
 retinal position and, 546, 1043–1044
 and spatial extent in visual cortex, 522,
 1578
 space-time inseparable, 705*f*, 706, 709*f*,
 710
 construction of, 710
 space-time separable, 705*f*, 706, 709*f*,
 709–710
 spatial bandwidth of, 165*f*, 1062–1063
 spatial organization of, 704
 spatial resolution of, 165*f*, 165–166
 spatial structure of, 943
 and spatial vision, 163–167, 165*f*, 166*f*
 as spatiotemporal filters, 717
 spatiotemporal transfer function of,
 750–751
 specialized properties of, 89
 structure of, in retino-geniculo-cortical
 pathway, 673

- Receptive field(s) (cont.)
of superior colliculus neurons, responses
of, development of, 163
surround suppression of, 165*f*, 165–166
temporal dynamics of, 704, 706, 707,
708–709
reverse correlation method for, 707,
707*f*
traditional descriptions of, 704
limitations of, 704
transformation of visual image to
neural response in, 704–706, 705*f*
trigger features for, 18
tuning properties of
and combining distributed information,
720–721
and functions of visual areas, 720
and visual acuity, 166, 166*f*
- Receptor(s). *See also* Photoreceptor(s)
in color vision, 1005–1006
- Receptor potential. *See* Cone(s);
Electroretinogram; Photoreceptor(s);
Rod(s)
- Receptor protein, in phototransduction,
217
- Reciprocating synapses, 292
- Recoverin, 229
as bipolar cell marker, 82
and phototransduction, 227
- Recovery from blindness studies, 190
- Rectification
of bipolar cell synapses, 255
in cortical neurons, 751*f*, 751–752
temporal dynamics of, 755
full-wave, 751*f*, 751–752
uses of, 752
half-wave, 751*f*, 752
beneficial consequences of, 752
- Red cones, 372. *See also* L (long-wavelength
sensitive or red) cones
connections to horizontal cells, 373–374,
376
feedback from horizontal cells, 382, 383*f*
- Red light, circadian sensitivity to, 627
- Red/green anomaly, and dark adaptation,
857, 858*f*
- Red/green chromatic channel, 1217, 1218*f*
and motion processing, 1217–1218
- Red/green color dimension
M cell response to, 1219–1223
P cell response to, 1219–1220
- Red/green color system, 1013
- Red/green horizontal cells, 373–374, 374*f*,
375*f*
- Red/green luminance balance point, 1219
- Reelin, and dendritic arborization in
amacrine cells, 83
- Reflectance
definition of, 881
equivalent surface, 951–952
modeling of, 903–904
of surfaces, 884
- Reflectance edges, 1287–1288
- Region of interest approach, to functional
mapping of motion regions, 1230
- Relational code(s), 1665–1666
cortical formation of, complementary
strategies for, 1679
neuronal synchrony as, 1666–1668
advantages of, 1667–1668
- Relative disparity, 550, 780–781,
1303–1304
beginnings of, 786–787, 787*f*
and center-surround responses of
receptive fields, 786–787
processing of, imaging of, 787
thresholds, for stereopsis, 1304, 1305*f*
- Relative motion, 1253
- Relative position, determination of, 929
- Relay cells
in cat LGN, 568, 569*f*
cable modeling for, 573
dendritic arbors of, 572
distal region, 572
proximal region, 572
firing modes of, 575
burst, 575, 576–578, 576*f*, 577*f*, 586,
612, 613*f*, 622
and control of response mode, 578
and initial stimulus detectability,
577–578
and linearity of relay mode, 576*f*, 577
and stimulus detectability, 577, 577*f*
tonic, 575, 576–578, 576*f*, 577*f*, 586,
612, 613*f*, 622
inputs to, distribution of, 572
ion channels in, 573–575
I_T current in, 573–575, 576*f*
of lateral geniculate nucleus, feedback to,
609–611, 610*f*, 611*f*
effect on firing patterns, 611–612, 613*f*,
622
- Relay nucleus, simple, 599
- Relevant information, and signal-to-noise
ratio, 19–20
- Remapping, 550–551
- Renin, retinal expression of, 347
- Representation(s). *See also* Image
representation; Neural representation
scheme(s)
in change detection, 1524–1526
in color appearance, 892
holistic, 1083
in natural scene perception, 1594–1595
in object recognition, 1645–1647
of place
allocentric (world-centered), 1183
egocentric (body-centered), 1183
preserved, in change blindness,
1527–1531
behavioral measures of, 1527–1528
structural
by components, 1080
evidence for, 1084–1088
by parts, 1080
spatial arrangement information for,
1083
theory of, 1080–1084
in ventral pathway, 1086–1088
- Reptiles, vision of, 965
- Research methods, for studying human
visual development, 174–176
- Resolution. *See also* Spatial resolution
development of, 159–163
newborn versus adult, 159, 160*f*
in pictures, 1097–1098
- Response compression, and light
adaptation in photoreceptors, 228
- Response expansion, in cortical neurons,
752*f*, 752–753, 759
temporal dynamics of, 756–757
- Response invariance, of neurons in ventral
stream, 546, 1154, 1170–1172
- Response rectification
in cortical neurons, 751*f*, 751–752
temporal dynamics of, 755
full-wave, 751*f*, 751–752
uses of, 752
half-wave, 751*f*, 752
beneficial consequences of, 752
- Response refractory period, of cortical
neurons, 751
temporal dynamics of, 755
- Response saturation, in cortical neurons,
753, 753*f*, 759
- Response timing, development of, 174,
185*f*, 185–186, 186*f*
- Response-dependent excitability, of
ganglion cells, 435–438, 444
- Restricted Mondrian world, 956
- RET-4, and opsin expression, 40, 40*f*
- Reticular theory, 410
of nervous system organization, 3–5
- Retina. *See also* Retinal cells; Retinal
circuits; Retinal synapses
area of, 234
barriers for, 41
cat, inputs to A layers, 568–569, 569*f*,
570*f*
central
cell number and density in, 69, 80–81
functional correlate of, 69
development of, 37
positional information for, 41–42
relative immaturity of, 176
underdevelopment of, in albinism, 102
circadian role of, 628
color opponency in, 991
connections of, 234, 279–280. *See also*
Retinal synapses

- decussations of, development of, 94–103
- developing
 - physiology of, 88–90
 - spontaneous activity of, 88–89, 89*f*, 109–110, 147
- development of, 63, 77–90
 - flexibility of, 64
 - genetics of, 64
 - local intercellular signals and, 63, 65, 68
 - molecular regulation of, 33–43
 - postnatal changes and, 159
 - reliability of, 64
 - role of glia in, 41
- distance from lens, reading and, 207–208
- duplex nature of, 851, 863–866
 - and shared neural pathways, 863–866
- early studies of, 3–5, 4*f*
- eccentricity of, 413, 414*f*, 484–485
 - in ideal observer analysis, 832, 832*f*
 - S-ON/(M+L)-OFF ganglion cell across, 994–995, 994*f*
- external fiber layer of, 4*f*
- feedforward input from, 154
- function of, 3–5
 - heterogeneity of, 1339
 - role of glia in, 41
- functional constraints in, 236–237
- gene transcription in, and optic chiasm development, 101–102
- illuminance of, pupil response and, 641, 642, 653
- inhibition in, 355–365
 - anatomy of, 359–360
 - background history of, 355–356
 - direct functions in, 355–356
 - GABA versus glycine in, 355
 - morphology of, 360–361
 - pathways of, 361–364
 - peripheral, 360–361
 - sustained, 355–356
 - transient, 355–356, 358
- lamination of, 36, 37*f*, 83–86
- light response (phototransduction) in, 215–230, 1339
 - activation of, 217–221
 - molecular mechanisms of, 217, 217*f*, 217–221
 - calcium feedback regulation of, 216, 217, 223, 225–228
 - development of, 89–90, 117, 176
 - inactivation of, 221–225
 - mutations of proteins involved in, comparison of effects of, 222, 223–225, 224*f*, 225*f*
 - onset phase of, predicted form of, 219–220, 220*f*
 - overview of, 216–217
- light scatter from, 798–799
- metabolism of, 41
- mitosis in, 77
 - as model for central nervous system, 33
 - molecular complexity of, 64
 - morphological specialization of, 34–36
 - neural, 64, 64*f*, 68, 77
 - function of, 77
 - neural integration time in, 185
 - neural processing in, 234, 235*f*
 - reasons for, 234–237, 237*f*
 - neurochemical architecture of, 234, 235*f*
 - neurogenesis in, 36–37, 37*f*
 - neurotransmitters in, 279, 304–316
 - expression of and receptors for, 86*f*, 86–88, 234
 - before visual processing, 87
 - ON and OFF pathways of, 83–86, 260–274
 - optimization in, for natural scene perception, 1593
 - peptides and peptide receptors in, 334–349
 - expression of, 334–348
 - functions of, 334, 348–349
 - peripheral
 - development of, 37
 - positional information for, 41–42
 - pigmented, 64, 64*f*, 68, 235*f*
 - plexiform layers of, formation of, 81–86
 - positional information across, 41–42
 - molecular gradients determining, 41–42
 - proliferative ventricular layer of, 36
 - quantum efficiency of, 797
 - redundancy in, 64, 71
 - regionalization of, 34–36
 - spatial resolution of, 80
 - spectral performance of, aging and, 208
 - structure of, 3–5, 4*f*, 77, 234, 235*f*
 - diversity of, 63, 69
 - genetic polymorphism and, 71
 - individual difference in, genetic basis of, 71–72
 - topographical organization of, 41–42
 - understanding of, 279
 - meaning and purpose of, 234–237
 - vertebrate, 33–43, 77–90
 - vitreal surface of, 36
 - weight of, 234
- Retina-derived POU-domain factor-1, in retinal cell differentiation, 78
- Retinal cells, 234, 235*f*. *See also* Amacrine cells; Bipolar cells; Ganglion cell(s); Horizontal cells
 - between-type variation among, 464–465
 - birth date of, 77
 - cell cycle of, 77
 - exit from, 66, 77
 - cell-type specific arborizations in, 82–83
 - classification of, 464–467
 - complex trait analysis of, 63, 71
 - components of, genesis of, 77–78
 - computational roles of, 70
 - death of, 41, 42–43, 63
 - and mosaic formation, 470, 472
 - development of, 36–37, 37*f*, 63–68, 77–78
 - centro-peripheral sequence of, 77
 - inherited maternal determinants of, 63, 64
 - local intercellular signals and, 63, 65
 - spatial overlap in, 36–37
 - specifying stem cells for, 64*f*, 65–66
 - temporal overlap in, 36–37, 77
 - differences among, functional and genetic analysis of, 68–72
 - differentiation of, 37–39, 63, 66–68, 77, 467–471
 - environment and, 66–67, 79
 - extrinsic control of, 67
 - in inner and outer plexiform layers, 81–86
 - lineage regulation of, 66–67
 - local intercellular signals and, 68
 - at quantitative level, 72. *See also* Retinal cells, number and density of
 - transcription factors and, 38–39, 68, 78
 - distribution of, 80–81
 - division of, 63
 - glial, 41
 - inner, 395
 - differentiation of, 37–38
 - laminated structure of, 36, 37*f*, 83–86
 - lineage of, 37, 63, 64–65, 66–67, 72
 - differential bias of, 67
 - maturation of, 40–41
 - Mendelian and quantitative genetics of, 71
 - migration of, 66, 79–80
 - glial guides for, 79
 - radial, 80
 - tangentially, 79, 80*f*
 - molecular gradients and, 41–42, 63
 - mosaics of, 463–475
 - and cellular evolution, 471–472, 472*f*, 475
 - classification of cells via, 464–467
 - development of, 467–471
 - dendritic field competition and, 470–471
 - inductive interactions and molecular markers in, 467–468, 468*f*
 - lateral movements of developing neurons and, 468–469, 469*f*
 - neuronal death and, 470, 472
 - future directions for study of, 474–475
 - hidden, exposure of, 466–467
 - measurement of, 472–474
 - minimal-spacing rules and, 469*f*, 469–470
 - paired, in mammals, 472, 472*f*
 - and visual function, 463

- Retinal cells (cont.)
- multiple dimensions of, 481, 482*f*
 - natural type of, 465, 471, 474
 - anomalies among, 466
 - negative feedback for, 38
 - number and density of, 63–72, 80–81
 - in area centralis, 80
 - centroperipheral gradients in, 80
 - in domestic versus wild animals, 70–71
 - evolutionary flexibility of, 70
 - in fovea, 69, 71, 80
 - functional perspective on, 69–71
 - genetic analysis of, 71–72
 - heritability estimates for traits, 71
 - isogenic lines for mapping, 71–72
 - large, need for, 69
 - in lateral geniculate nucleus, 69
 - for low-light vision, 69–70
 - metabolic costs of, 71
 - and neural noise, 69
 - regulation of, 38
 - developmental and genetic, 63–72
 - selection of retinal stem cells and, 66
 - variation in, 68–72
 - high, paradox of, 71
 - within species and genotype, 70–71
 - and visual performance, 68–72
 - outer, differentiation of, 39
 - patterns and tiles of, 463
 - perikaryal translocation of, 79
 - polarity of, 81–82
 - positional specification of, 33, 41–42, 77, 79–80
 - primate
 - distribution of, 80
 - number and density of, 69–70
 - types of, 483
 - process outgrowth of, 81*f*, 81–82
 - progenitors of, 37, 63
 - competence of, 64*f*, 64–65
 - limited, 78
 - timing of, 67
 - determinative states of, 67
 - differentiation of, 78–79
 - embryonic versus neonatal, 67
 - fate of, 66–68, 77–78. *See also* Retinal cells, differentiation of
 - heterogeneity of, 67, 78
 - interkinetic migration of, 77
 - lineage tracing of, 37, 66–68
 - producing layer-restricted clones, 67
 - producing radial clones, 67
 - regionalization of, 64*f*, 65
 - regulation of, 79
 - selection of, 64*f*, 64–65
 - somata of, stratification of, and cell
 - identification, 465, 465*f*, 466*f*
 - spatial regularity among, 463–475
 - survival of, 42–43
 - synapse formation between, 87–88
 - temporal order of appearance, 77, 78*f*
 - topographical connectivity of, 33
 - transplantation of, 42, 43
 - types of, 5, 6*f*–7*f*, 33, 63, 77
 - comparisons across species, 471–472
 - functional correlates of, 481
 - identification and characterization of,
 - mosaics and, 464–467
 - in Old World primates, 483
 - taxonomical notion of, 481
 - within-type variation among, 464–465, 465*f*
 - mosaics as guide to, 465–466, 466*f*
- Retinal circuits, 234, 235*f*, 236*f*
- bipolar cell pathways in, 252*f*, 252–253
 - daylight, 249–251
 - dividing rod system's intensity range, 247–249
 - evolution of, 234–237
 - ganglion cell pathways in, 253–255, 254*f*
 - moonlight, 247, 248
 - optimization of information transfer in, 234–255
 - peptides and, 348–349
 - specialization of, 234
 - starlight, 247–248, 248*f*, 249*f*
 - symmorphosis of, 234–237
 - synapses in
 - bandpass filtering by, 246, 249–251, 251*f*
 - three-dimensional structure and function of, 246–247, 247*f*
 - twilight or dawn, 247–249, 248*f*
 - wire volume of, correlation with
 - information capacity, 245, 255
- Retinal cultures, cell regulation in, 38
- Retinal field potentials, ON and OFF
 - signals in, 260–261, 261*f*
- Retinal flow. *See* Optic flow
- Retinal flow theories, of heading
 - determination, 1252–1253
- Retinal image(s)
- acquisition of, 800–808
 - chromatic aliasing and, 805–807
 - cone ratio variations and, 806*f*, 807
 - laser interferometry studies of, 802–805, 803*f*, 804*f*, 805*f*
 - limits in, 807–808
 - sampling by cones and, 802–807
 - trichromatic sampling and, 805–807
 - computation of, 799
 - formation of, 795–800
 - chromatic aberration and, 800–801
 - in corrected eyes, 807–808, 808*f*
 - diffraction and, 798, 798*f*, 799–800
 - light scatter and, 798–799
 - limits in, 807–808
 - point spread function in, 796*f*, 797–798
 - estimates of, 799–800, 800*f*
 - pupil function and, 796–797
 - magnification of, postnatal growth and, 159
 - modulation transfer function of, 799
 - estimates of, 799–800
 - in monochromatic and broadband light, 801, 801*f*
 - pupil size and, 799–800, 801*f*
 - relationship with foveal cone Nyquist limit, 803–804, 804*f*
 - phase transfer function of, 799
 - in polychromatic light, 800–801, 801*f*
 - resolution and contrast of, postnatal optic changes and, 159
- Retinal pigment epithelium (RPE)
- age-related failure of, 210*t*
 - formation of, 34, 35*f*, 36, 77
 - glutamate in, 304
 - lack of pigment in, and optic chiasm
 - development, 102–103
 - in macular degeneration, 43
 - and rod maturation, 41
 - transcription factor expression in, 34–36
- Retinal synapses, 279–298. *See also specific synaptic connections*
- amacrine cell, 290–295
 - amacrine cell-amacrine cell, 87, 293–295
 - amacrine cell-bipolar cell, 292*f*, 292–293
 - amacrine cell-ganglion cell, 280, 280*f*, 293
 - basic plan of, 280, 280*f*
 - bipolar cell, 283–289
 - bipolar cell-amacrine cell, 280, 280*f*, 291–292
 - bipolar cell-ganglion cell, 268, 279, 280, 280*f*
 - postsynaptic mechanisms of, 288–289
 - presynaptic mechanisms of, 285–288, 287*f*
 - bipolar cell-horizontal cell, 280, 280*f*
 - cholinergic, 294–295, 295*f*, 312–313
 - direct pathway of, 279–289
 - and direction selectivity, 460*f*, 460–461
 - dopaminergic, 314
 - electron microscopy of, 87, 268, 279, 292, 293–294, 413
 - formation of, 87–88
 - function of, 279
 - future directions for study of, 298
 - GABAergic, 279, 281*f*, 281–283, 284*f*, 286, 289–290, 292*f*, 292–294, 309–310, 355, 396–398
 - glutamatergic, 264–266, 279, 281*f*, 281–285, 284*f*, 285*f*, 286, 288, 293, 304, 306–307, 320–330
 - glycinergic, 291, 304, 311, 355, 395–396
 - horizontal cell-bipolar cell, 290, 304, 309
 - horizontal cell-horizontal cell, 289–290
 - horizontal cell-photoreceptor, 290, 309
 - inhibitory, 359–360

- inner, 280, 280*f*
- invaginating, 246, 247*f*, 281*f*, 281–282, 281–283, 289, 296
- lateral pathways of, 289–295
- layers of, 234, 235*f*
- number of, 69
- order of appearance, 88
- outer, 280, 280*f*
- outer versus inner, 279
- photoreceptor, 280–283
 - bandpass filtering by, 246, 249–251, 251*f*
 - in signal transmission, 246–251
 - three-dimensional structure and function of, 246–247, 247*f*
- photoreceptor-bipolar cell, 279, 280, 280*f*
- image separation at, 260, 266
- postsynaptic mechanisms of, 283–285, 285*f*
- presynaptic mechanisms of, 280–283, 281*f*
- photoreceptor-horizontal cell, 280, 280*f*
- postsynaptic mechanisms of, 289
- plasticity of, 295–298
- reciprocating, 292
- ribbon, 246, 247*f*, 281*f*, 281–282, 296
- serial, 293–294
- serotonergic, 304, 315–316
- sign-inverting, 283, 304, 312–313, 395
- sign-preserving, 283, 285, 304, 309, 395
- spinule formation and retraction in, 296–298, 297*f*
- superficial, 281, 281*f*, 283
- Retina-specific genes, 36
- Retinex, 956
- Retinitis pigmentosa, causes of, 42–43
- Retinogeniculate cells
 - receptive fields of, 673, 674*f*
 - response properties of, 1008–1010
- Retinogeniculate pathway, 566
 - conduction velocity through, 185
 - functional connectivity in
 - anatomy of, 674–675
 - physiological studies of, 675, 676*f*
- Retinogeniculate synapse, 565
- Retino-geniculo-cortical pathway
 - functional connectivity in, 673–678, 1007–1008
- macaque, 680–683
- neuronal connections in, upper limits of, 675, 677
- Retino-geniculo-striate pathway, eye-specific segregation in, development of, 108–115
- Retinohypothalamic tract (RHT)
 - circadian role of, 628–629, 629, 635*f*
 - light-responsive SCN neurons of, 629
 - neurotransmitters of, 628–629
 - SCN projections of, 628
- Retinoic acid
 - and horizontal cell function, 372, 380, 386, 387*f*
 - in retinal cell differentiation, 68, 78–79
 - retinal positioning information conveyed by, 41
 - and spinule formation, 296, 386
 - and synaptic plasticity, 296, 386
- Retinoic acid alpha receptor, and retinal development, 64, 72
- Retinoid(s)
 - in macular degeneration, 43
 - and opsin expression, 39
- Retinopathy, melanoma-associated, 272, 273*f*
- Retino-tectal connectivity, Eph receptor-ephrin ligand system and, 42
- Retinotopic mapping, 1034, 1083, 1565
- Retinotopic organization, 542, 1578
 - of corticocortical connections, 524–525, 525*f*
 - in superior colliculus, 1566*f*, 1567
- Retrograde degeneration, in lateral geniculate nucleus, 6–7
- Reversal tasks, prefrontal cortex (PFC)
 - damage and, in monkeys, 1552*f*, 1553
- Reverse correlation method
 - for mapping receptive fields, 707, 707*f*
 - for measuring orientation selectivity, 757–758
 - for measuring spatial frequency selectivity, 757–758
- Reverse occlusion
 - application of studies to amblyopia, 196
 - in cats, 194–196, 195*f*
 - in monkeys, 196
 - and orientation selectivity, 121
- Reverse ocular dominance shift, 130–131, 133
- Reward prediction error, 1558
- Reward-related activity, prefrontal cortex (PFC) and, 1554
- RGCs. *See* Ganglion cell(s)
- RGS (regulators of G protein signaling) proteins, 223
- RGS9/Gβ5L, and inactivation of light response, 223, 224*f*
- Rhesus monkey. *See* Macaques
- Rhodopsin, 215–216
 - absorption spectrum of, and spectral sensitivity, 838
 - activated (R*)
 - encounter rate with transducin, 218
 - rate of transducin activation by, 218
 - speed of action, size of outer segment and, 241–244, 243*f*
 - activation of, 217*f*, 217–218, 854
 - by photon, 217*f*, 217–218
 - predicted time course of, 219–220, 220*f*
- arrestin binding of, 222–223
- density of, in rod membrane disc, 241–244, 243*f*
- ground state of, crystal structure of, 218
- inactivation of, 221–223
 - effects of genetic mutations on, 222, 223–225, 224*f*, 225*f*
 - molecular mechanisms of, 221–222
 - and reproducibility of single photon response, 223
- lateral diffusion of, 218
- in light adaptation
 - effects of bleaching on, 229–230
 - gain reduction and, 229
- optimization for sensitivity, speed, gain, and noise, 241–244
- overexpression of, 224
- peak sensitivity of, 852
- phosphorylation of, 222
 - calcium concentration and, 227
 - experimental prevention of, effects of, 224*f*, 224–225, 225*f*
 - potential sites for, 222
- in phototransduction, 215–228
- retinal component of, photoisomerization of, 1006
- in rod outer segment, 215
- term, use of, 215–216
- thermal isomerization of, 854
- underexpression of, 224
- Rhodopsin kinase (RK), rhodopsin
 - phosphorylation by, 222
 - experimental prevention of, effects of, 224*f*, 224–225, 225*f*
 - recoverin and, 227
- Ribbon synapses, 246, 247*f*, 281*f*, 281–282, 283, 286, 296, 395, 398
 - composition of, 282
 - lateral elements at, 371*f*, 371–372
- RIBEYE, in ribbon synapses, 282
- Ricco area, 819, 846
- Ricco's law, 818–819, 819*f*, 820, 821
- Richardson effect, 1096
- robo2*, and optic chiasm development, 97*f*, 99
- Robos, and optic chiasm development, 97*f*, 99–100, 100*f*
- Rod(s), 908, 911, 925
 - absence in central fovea, 841
 - adaptation of, 843
 - and signal-to-noise ratio, 843, 845
 - age-related failure of, 210*t*, 846–847
 - amacrine cells of, 395, 396–398, 397*f*, 400*f*
 - reciprocal, 395, 396–398, 397*f*, 400*f*
 - asymptotic limit of, 841
 - axon terminal of, 245, 246*f*
 - active zones of, 245, 247*f*
 - axons of
 - microtubules of, 245, 246*f*

- Rod(s) (cont.)
- thickness of, 242*f*, 245, 246*f*
 - binary response of, 237–240, 247*f*, 248*f*
 - bipolar cells of
 - peptide expression in, 337, 340–341
 - somatostatin receptors in, 340*f*, 340–341
 - stratification of, 268–269
 - transmission of, 284, 292–293
 - calcium influx in, 282–283
 - and chromatic discrimination, 874–875
 - ciliary stalk of, 216, 216*f*
 - circuitry relaying signals of, 234–255, 235*f*, 236*f*
 - pathways of, 247–249
 - color responses of, 838
 - and color vision, 866, 872–875, 872*f*, 874*f*, 875*f*
 - conversion tables for analysis of, 838, 839*f*
 - cytokine-induced inhibition of, 39
 - in dark adaptation, 845, 847
 - dark-adapted
 - and acuity, 871
 - calcium functions in, 227
 - and cone-mediated flicker threshold, 870, 870*f*
 - and cone-mediated spatial threshold, 871
 - at dawn or twilight, 240, 247–249, 248*f*
 - death or loss of, in retinitis pigmentosa, 42–43
 - development of, 36–37, 37*f*, 176
 - functional, 176
 - timing of, 77, 78*f*
 - visual evoked potentials in, 176
 - differentiation of, 38, 39, 67, 78–79
 - opsin expression and, 39–40
 - disc membrane of, 216, 216*f*
 - calcium regulation of reactions in, 227, 228–229
 - rhodopsin density in, 241–244, 243*f*
 - distribution and morphology of, 3–5, 4*f*
 - dynamic range of, 423
 - excitation of, 838
 - filtering of signals from, 845
 - functional constraints of, 236–237
 - functional domains of, 215
 - functions of, 215, 237–240, 974
 - glutamate receptors in, 307
 - glutamate transporters in, 306
 - and horizontal cells, 864
 - aftereffect, 374–375, 376*f*
 - connections between, 375–376
 - contributions to, 374–376
 - effect of dopamine on, 384
 - signal mixing with cones, 374–375, 376*f*
 - and hue, 872–874, 872*f*, 874*f*
 - image properties reported by, 260
 - inner segments of, 176, 216, 216*f*, 235*f*, 242*f*
 - intensity ranges of, 215, 228, 240
 - pathways dividing, 247–249
 - light adaptation in, 228–230
 - calcium-dependent mechanisms in, 228–229
 - composite effect of mechanisms in, 230
 - elevated steady-state activity of
 - phosphodiesterase and, 229, 230
 - gain reduction in, 229
 - mechanisms of, 228–230
 - pigment bleaching and, 215, 229–230
 - response compression and, 228
 - lower limits of, 838–840
 - and low-light vision, 69–70
 - maintenance of, 216
 - maturation of, 40–41
 - in moonlight, 247, 248
 - in motion processing, 845
 - neurotransmitter release from, 245, 246–247, 282, 843
 - in night vision, 237–240, 239*f*–240*f*, 272–273, 838–848
 - in nocturnal species, 241
 - noise and, 240–241, 840
 - number and density of, 69–70, 215
 - albinism and, 102
 - evolutionary flexibility of, 70
 - ratio to cones, 215, 240–241
 - variation in, 71
 - onset phase of response, predicted time course of, 220, 221*f*
 - outer segments of, 176, 215–216, 216*f*, 235*f*
 - calcium-induced changes in, 225–228
 - cGMP-gated ion channels of, 244
 - design of, effect on speed, 241–244, 243*f*
 - diameter of, 241
 - length of, 241
 - mammalian, 241, 242*f*, 243*f*
 - morphological specialization of, 40–41
 - nonmammalian, 241
 - rhodopsin in, 215
 - shedding and renewal of, 216
 - size of, 241, 242*f*, 243*f*
 - uniformity of, 241
 - ON pathway disease and, 272–273
 - performance of, versus cones, 215
 - as photon counters, 851
 - photon detection by, 215
 - inactivation of rhodopsin and, 223
 - photopigments of, evolution of, 967
 - phototransduction (light response) by, 215–230
 - activation of, 217–221
 - calcium feedback regulation of, 216, 217, 223, 225–228
 - inactivation of, 221–225
 - mutations of proteins involved in,
 - comparison of effects of, 222, 223–225, 224*f*, 225*f*
 - noise during, 227
 - overview of, 216–217
 - physical limits to, 215
 - primate versus cold-blooded vertebrates, 843
 - process outgrowth from, 82
 - progenitor cells biased to produce, 67
 - quantum efficiency of, 816
 - retinal distribution of, 1006
 - and retinal output pathways, 865–866
 - saturation of, 816, 841–843
 - data from studies of, 842*f*, 842–843
 - technical difficulties in measuring, 841–842
 - in scotopic vision, 69–70, 237–240, 247–249, 272–273, 838–848, 851, 852
 - sensitivity of, 237
 - monocular deprivation and, 196
 - sensitivity regulation in, 911–912
 - signals from, alternative pathways for, 320–321
 - signal-to-noise ratio of, 240–241, 243–244
 - size of, 69–70
 - specialized mechanisms of, 230
 - spectral sensitivity of, 838
 - in steady light, 240
 - Stiles-Crawford effect in, 846–847
 - structure of, 215–216, 216*f*
 - subdivision of mammalian mosaic for, 239*f*–240*f*, 240–241
 - summation of signals from, 848
 - synapses of, 280, 280*f*, 843
 - to bipolar cells, 280–283, 281*f*
 - sign-preserving, 285
 - electrical, 248
 - engineered spillover of, 247, 247*f*
 - formation of, 87–88
 - to ganglion cells, interaction with cones, 418–419
 - horizontal cell to, 290
 - to horizontal cells, 370, 375–376
 - invaginating, 246, 247*f*, 280–281
 - linear chemical, 248
 - to OFF cone bipolar cells, 279
 - postsynaptic partners in, patterns of connection, 282
 - superficial, 281
 - three-dimensional structure and function of, 246–247, 247*f*
 - synaptic terminal of, 216, 216*f*, 242*f*
 - thresholds of, 820, 838–840
 - topology of, versus cones, 216
 - and tritan discrimination, 874–875
 - in vertical pathway, 320
 - visual pathways from, 844–845
 - cancellation in, 845
 - direct to off-bipolar cells, 845
 - dual, 848

- maximal frequency for, 844–845
- shared with cones, 841, 845
- Rod aftereffect, 374–375, 376*f*
- Rod-cone break, 845, 847, 852, 854, 855*f*
- Rod-cone color mixture studies, 873–874, 875*f*
- Rod-cone dystrophies, 42
- Rod-cone gap junctions, 863–864, 864*f*
 - and transmission of light-evoked signals to bipolar cells, 322
- Rod-cone interactions, 863–875. *See also* Cone(s); Rod(s)
 - adaptation-state-dependent, 870–871
 - and brightness, 867
 - in dark adaptation, 854–855
 - retinal or cortical origins of, 855, 855*f*
 - in detection sensitivity, 867–869, 868*f*, 869*f*
 - for flickering stimuli, 866–869, 869–871
 - functional network properties of retina and, 863
 - in human vision, 863–875
 - isolated lateral, 869
 - pathways for, 863, 864*f*
 - psychophysics of, 866–875
 - reported for double-flash procedures, 868
 - retinal substrate of, 863–866
 - and shared neural pathways, 863–866
 - sites of, 863–865
 - in spatial sensitivity, 871–872
 - summation of rod and cone signals in, 866–867
 - suppressive, 870–871
 - photopic analog of, 871
 - in temporal sensitivity, 869–871, 870*f*, 871*f*
- Rodents. *See also* Mice; Rabbit(s); Rat(s); Squirrel(s)
 - vision of, 964
 - visual system of, 1569
- Rom-1, and rod maturation, 41
- Rotary motion
 - definition of, 1247
 - sensitivity to, in dorsal medial superior temporal area (MSTd), 1250
- Rotation
 - definition of, 1247
 - observer, 1247–1248, 1248*f*, 1249*f*
 - heading perception during, 1253–1254, 1254*f*
 - actual rotation condition for, 1253
 - simulated rotation condition for, 1253
- Rotation problem, 1248
 - in heading determination, 1249*f*, 1252–1254
 - extraretinal theories of, 1252
 - retinal flow theories of, 1252–1253
- Roundabouts (Robos), and optic chiasm development, 97*f*, 99–100, 100*f*
- Rubin's vase, 1142*f*
- Rule acquisition, prefrontal cortex (PFC) and, 1557–1558
- Rule representation, prefrontal cortex (PFC) and, 1555, 1557–1558
- Ryanodine receptors, circadian role of, 633, 635*f*
- S**
- S (short-wavelength sensitive or blue)
 - cones, 176, 186, 372, 805, 806*f*
 - chromatic aberration and, 800–801
 - in chromatic motion processing, 1219–1220, 1223, 1237
 - in color vision, 800–801, 1217, 1218*f*, 1219–1220, 1223, 1237
 - connections to horizontal cells, 370–371, 373–374, 376*f*
 - feedback from horizontal cells, 382, 383*f*
 - input to K cells, 1219, 1223
 - input to M cells, 1219–1220
 - mosaics of, 468
 - sampling by, 805–806
 - visual pathway input from, 497–498, 502, 503
- S layers. *See* Koniocellular layers; Koniocellular pathway
- Saccade generator, 1431, 1432*f*
- Saccades. *See also* Microsaccades; Suppression, saccadic
 - and actions in domestic tasks, 1359–1360
 - aurally guided, 1439, 1439*f*
 - chromatic sensitivity during, 1393–1394, 1393*f*
 - compression during, 1396–1399, 1399*f*
 - and contrast sensitivity, 1391–1392, 1392*f*
 - control of, 1425, 1458–1459, 1486
 - cortical regions for, 1429*f*, 1430*f*
 - by superior colliculus, 1449
 - and corollary discharge, 1391, 1466–1481
 - deferred, 1436
 - presaccadic burst activity for, 1437–1439
 - definition of, 1342, 1369, 1391, 1449, 1466, 1485
 - disjunctive, FEF and, 1445
 - displacement detection across, 1525
 - duration of, 1430
 - early visual activity during, extraretinal suppression of, 1391, 1393–1395
 - and efferent copy, 1391, 1442
 - electrically elicited from frontal eye field, presaccadic burst activity and, 1433–1435, 1434*f*
 - express, 1440
 - frontal eye field lesions and, 1433
 - gaze, control of, 1425
 - horizontal, neural substrate for, 1491–1492, 1491*f*
 - initiation of, 1430
 - timing of, and time of target selection, 1380–1382, 1380*f*, 1381*f*
- ipsipulsion of, 1492
- latency of, 1430
- lateropulsion of, 1492
- luminance sensitivity during, 1393–1394, 1393*f*
- main sequence of, 1343, 1350
- memory, 1441*f*
 - FEF activity and, 1435–1436, 1436*f*, 1437–1439, 1437*f*
- memory-guided, posterior parietal cortex and, 552–553
- mislocalizations during, 1397–1399
- motion desensitization during, 1392–1393
- motion perception during, 1392–1393
- motor responses during, 1397–1398
- to moving targets, 1442
- neural substrate for, 1371, 1372*f*, 1431, 1432*f*, 1491–1492, 1491*f*, 1493
 - and neural pathway for pursuit, 1409–1410, 1422, 1432*f*
- to new targets, 1365
- as open-loop movements, 1430
- and perceived position, 1395–1397, 1396*f*
- planning of, 1327–1328, 1328*f*
- posterior parietal cortex and, 1376–1378
- predictive, 1440
- presaccadic neuronal activity for, 1433–1439, 1469*f*, 1470
- primary visual (striate) cortex and, 1374–1376
- production of, superior colliculus in, 1371–1373, 1373*f*
- properties of, 1428–1431
- pulvinar and, 601
- purposive
 - FEF presaccadic burst activity and, 1435–1437
 - neural substrate for, 1433
- refractory period for, 1431
- remapped, 1440–1442
- and stereopsis, 1309
- superior colliculus and, 1449–1450
- targets for, 1369–1384
 - compression of perceptual space toward, 1396–1399, 1399*f*
 - selection of, 1466
 - dialogue between cerebral cortex and superior colliculus in, 1466–1481
 - frontal eye field and, 1378–1383
 - learning and, 1382–1383, 1382*f*
 - from multiple targets, 1442
 - posterior parietal cortex and, 1376–1378
 - primary visual cortex and, 1374–1376
 - progression of, from cortex to superior colliculus, 1469*f*, 1472–1474
 - superior colliculus and, 1373–1374, 1374*f*
 - timing of, and time of saccade initiation, 1380–1382, 1380*f*, 1381*f*

- Saccades (cont.)
 three-dimensional, 1460–1461
 torsional, 1486
 unequal horizontal, 1422–1423, 1423*f*
 uses of, 1343
 ventral processing stream and, 1374–1376
 and vergence, interaction of, 1422–1423, 1423*f*, 1460–1461
 facilitation hypothesis for, 1422, 1423–1424
 monocular control hypothesis for, 1422, 1423–1424
 veridical information available during, 1398
 vertical, 1486
 visual perception during, 1391–1400
 physiological mechanisms of, 1398–1399
 research on, advances in (future directions for), 1399–1400
- Salamander(s)
 axon terminals of, active zones of, 245
 ganglion cells of
 excitability of, 424, 425*f*, 425–426, 434–435
 light responses of, 443
 membrane time constant of, 430–431
 horizontal cell feedback pathways in, 381–382, 382*f*, 383*f*
 OFF and ON pathways in, stratification of, 268
 photoreceptor outer segments in, 241
 retinal peptide expression in, 341
 effect on ion channels, 337
 retinal synapses of, 288, 290, 293
 rods of
 predicted time course of onset phase in, 220, 221*f*
 rhodopsin activity in, calcium and, 227
- Salience
 attention and, 1541
 definition of, 1365, 1370
 of gaze targets, 1365
 in object recognition, 1648–1650, 1649*f*
 regulation of, adaptation in, 945
 of stimulus, 1515*f*
 factors affecting, 1514
 visual, pulvinar and, 598–599, 601–602
- Salience map, 1365, 1370–1371, 1374, 1377–1378, 1384, 1649, 1649*f*
- Sampling
 by cones, 802–807
 by different cone classes, 805–807
 trichromatic, 805–807
 Nyquist limit for, 803–805
 and retinal image acquisition, 802–805
 trichromatic, 805–807
- Sampling theorem, 803
- Saturating background, 842
- Saturation, 893, 933–934
 of circadian phase shifts, 627
 color, 872, 1010
 of cones, 229
 definition of, 893, 894*f*, 899
 of neuron, 911
 in neuronal response, cortical, 753, 753*f*, 759
 of rods, 816, 841–843
 data from studies of, 842*f*, 842–843
 technical difficulties in measuring, 841–842
- Scale(s). *See also* Receptive field(s), size of;
 Spatial scale
 analysis of, in vision, 1043–1056
 and blur perception, 1055
 and color vision, 1051, 1053*f*
 and functional specialization of central vision, 1044–1045
 levels of, 1094
 and light adaptation, 1045–1046
 and motion, 1047–1049, 1055
 multiple, and multiple boundary depths, 1632
 processing of, 1046–1051
 across-scale, 1056
 within-scale, 1056
 selection of, 1051–1053
 and space, 1046–1047, 1053*f*, 1054–1055
 and stereo processing, 1049–1051, 1050*f*
 and texture perception, 1054*f*, 1055
- Scale combination, in vision, 1043
 for edge features, 1056
 evidence for, 1053–1055, 1053*f*, 1054*f*
 rules for, 1044, 1055–1056
- Scene(s), 1094
 definition of, 948
 edges in, 1070
 geometry of, and color perception, 958
 gist of, 1686
 natural. *See* Natural scene
 outdoor, ventral pathway activity with, 1534
- SCH-23390, and ganglion cell cAMP levels, 438
- Schultze, Max, 3–5, 4*f*
- Schwann cells, genetically engineered, neurotrophin administration via, 51
- Scission, 1284, 1629
 and depth perception, 1293, 1295–1296, 1296*f*
 figural conditions for, 1295
 local cue to, 1294
 photometric conditions for, 1293–1295, 1294*f*
- SCN. *See* Suprachiasmatic nuclei
- Scotoma(s), 9
 artificial, and receptive field size, 741–742
 central, and scotopic vision, 841
 Gestalt completion across, 1584
 TMS-induced, 1136, 1137*f*
- Scotomata. *See* Scotoma(s)
- Scotopic light levels, 912
- Scotopic spectral efficiency function, 867
- Scotopic (night) vision, 237–240, 247–249, 838–848, 851, 863
 adaptation in, 843
 age and, 846–847
 aging and, 846–847
 versus effects of disease processes, 846–847
 binocular effects in, 840
 central processing in, 845
 cone thresholds and, 841, 852–858
 contrast sensitivity functions in, 844, 844*f*
 contrast sensitivity in, 843–844, 844, 844*f*
 in infants, 846
 conversion tables for analysis of, 838, 839*f*
 critical flicker frequency in, 844–845, 845*f*
 dimmest surface seen in, 840
 of infants, 846
 large number of retinal cells required for, 69–70
 lower limits of, 838–840
 maximal frequency in, 844–845
 noise and, 840
 versus other vision properties, 838
 ON pathway and, 272–274
 rod saturation and, 841–843
 rods in, 69–70, 237–240, 239*f*–240*f*, 247–249, 272–273, 838–848, 851, 852–858
 SCN neurons in, 631
 sensitivity of, boundaries of, 838–843
 single-channel system of, 838
 spatial sensitivity of, 843–844, 844*f*
 in infants, 846
 spectral sensitivity of, 838–843
 Stiles-Crawford effect in, 841, 845, 847*f*, 847–848
 temporal sensitivity of, 844–845
 thresholds in, 820, 838–840, 846–847, 852–858
 aging and, 846
 in infants, 846
 transition to photopic vision, in infants and adults, 846
 univariant system of, 838
 unresolved issues in study of, 847–848
 upper limits of, 841–843
 visual pathways in, 487–488, 488*f*, 841, 844–845
 cancellation in, 845
 dual, 848
- Screening pigments, in insects, 965
- Search. *See* Visual search
- Second messenger(s), 25
 and cortical plasticity, 128, 129

- modulation of, 135
- in phototransduction, 217
- Second-order linear spatial filter, 1109–1110, 1109*f*
- Second-order nonlinear receptive field maps, 705–706, 707, 711–717
- Second-order [term], 1109*f*, 1110
- Second-sight adjustments, in light adaptation, 940–941
- SEF (supplementary eye field) visual area. *See* Supplementary eye field (SEF)
- Segmentation, 1119–1127, 1519
- and border ownership, 1124–1126
- cortical feedback systems and, 612–614, 615*f*, 621, 621*f*, 622
- in depth perception, 1284
- and figure-ground assignment, 1124–1126
- textural, 1106–1113, 1107*f*
- Selectivity. *See also* Direction selectivity; Orientation selectivity; Spatial frequency selectivity; Spatial selectivity; Stimulus selectivity; Velocity selectivity
- of single neurons, 17–18
- Self-motion
- determination of, dorsal medial superior temporal area (MSTd) and, 1251–1252
- path of, 1248–1249, 1249*f*
- perception of, 1250
- Self-splitting object, 1289*f*
- Seltzer and Pandya scheme, for partitioning macaque visual cortex, 510*f*–511*f*, 512
- Semisaturation coefficient, 842, 843, 846
- Sender operating characteristics, in single-unit recording, 21–22
- Sensitivity regulation, 911–913
- in L cones, 912–913
- in M cones, 912–913
- multiplicative, 912–913
- in rods, 911–912
- in S cones, 913
- second-site, 913
- subtractive, 913
- Sensitization
- concept of, 818
- low background, and thresholds, 818
- Sensory deficiency, threshold behavior as indicator of, 823
- Sensory deprivation, developmental effects of, 46, 47*f*
- Sensory fusion, development of, 184–185
- Sensory integration, cross-modal, 1585
- Sensory nerve fibers, peripheral, single-unit recording of, 16
- Separate-channel hypothesis, for eye-head movements, collicular neurons and, 1456–1458, 1457*f*
- Serial synapses, 293–294
- Serotonin, 314–316, 315*f*
- amacrine cells expressing, lineage bias of, 67–68
- and circadian rhythms, 628
- and cortical plasticity, 128, 134–135, 136*t*, 137*f*, 139
- future directions for study of, 316
- localization of, 314, 315*f*
- and long-term depression, 134, 136*t*
- and long-term potentiation, 134, 136*t*
- metabolism of, 304, 314, 315*f*
- modulatory actions of, 135
- as mystery neurotransmitter, 314–316
- and NMDA receptors, 135
- in ON and OFF pathway modulation, 316
- peptide action on, 337
- release of, neurotrophins and, 55, 60*f*
- signals about nervous system state carried by, 134
- in synaptic transmission, 304, 315–316
- transporters of, 314, 315*f*
- plasma membrane, 314, 315*f*
- vesicular, 314, 315*f*
- Serotonin receptor(s), 314–315, 315*f*
- heptahelical, 315, 315*f*
- ionotropic, 314–315, 315*f*
- Serotonin receptor antagonists, and ocular dominance plasticity, 134
- SERT, 314, 315*f*
- Shab-type potassium channels, 435
- Shack-Hartmann wave front sensor, 799
- Shading. *See also* Shape, from shading
- in artistic renderings, 1104
- definition of, 1092
- Shadow
- colored, 1583
- detection of, 260
- electroretinogram recording of, 260–261, 261*f*
- Shaker-type potassium channels, 435, 436
- Shape. *See also* Representation, structural
- analysis of, for form vision, 1067
- aspect ratio of, 1154
- and TE neuronal invariance, 1154
- characterization of, 1011
- coding of, in extrastriate cortex, 1594
- definition of, 1098
- discrimination of, in blindsight, 659
- local definition of, 1099–1100
- local linear orientation and, 1082
- from motion, 550
- perceived, 1104
- persistence in, Gestalt tendency of, 1577
- representation of, investigation of, using natural scenes, 1594–1595
- from shading, 1091
- collimated beam and, 1093, 1094*f*
- multiple sources and, 1093
- open problems related to, 1101–1104
- point source and, 1093, 1094*f*
- psychophysical findings on, 1100–1101, 1101*f*
- theories of, computer vision and, 1103–1104
- from texture, 1114–1115
- Shape coding, based on contour fragments, 1081–1082, 1081*f*
- Shape descriptors, 1082
- axial, 1082–1083
- boundary-based, 1082–1083
- higher-level, 1082–1083
- surface-based, 1082–1083
- volumetric, 1082–1083
- Shape dimensions, 1080–1088, 1082
- Shape impressions, 1101, 1104
- Shape perception, 1090–1104. *See also* Form perception
- Shape primitives, 1082
- Shape processing, hierarchical, 1087
- Shape recognition, models for, 1082–1084
- Shaw-type potassium channels, 435
- Sherringtonian model of neuron, 24
- Short-wavelength sensitive cones. *See* S (short-wavelength sensitive or blue) cones
- Side-of-figure selectivity, 1143–1144, 1143*f*, 1144*f*, 1146
- Signal detection theory, 15, 18–19
- and blindsight, 665
- in visual neurophysiology, 20
- Signal-to-noise ratio (SNR), 15, 18–20
- choice probabilities and, 21–22
- expressing single neuron's performance as, 21
- improvement of, 19–20
- integration interval and, 758
- noradrenaline and, 135
- optimal, 20
- in photoreceptors, 240–241, 243–244
- retinal cell numbers and, 69
- rod adaptation and, 843, 845
- somatostatin and, 341–342
- in swept-parameter visual evoked potential, 175
- three rules about, 19–20
- Similarity, Gestalt factor of, 1575, 1576*f*
- Simple cells, 532, 750, 1584–1585, 1626, 1640
- binocular, 1631
- binocular interaction in, 768–770, 770*f*, 774, 775*f*
- contrast processing, 772–773, 773*f*, 774*f*
- versus complex cells, 750
- contrast adaptation in, 754, 754*f*
- contrast response function in, 752*f*, 752–753, 753, 753*f*

- Simple cells (cont.)
 contrast-set gain control in, 753, 753*f*
 in cortical feedback system, 614, 617, 621, 622
 direction selectivity in, 617, 1621
 linear and nonlinear properties of, 753
 spatiotemporal mechanisms of, 710–711, 711*f*, 713
 excitatory input to, 696, 697
 input to, orientation selectivity of, 695–697
 invariance properties of, 1610, 1613
 latency shift in, 753–754, 754*f*
 LGN input to, 695–697
 cortical inactivation experiments and, 697–698
 spatial organization of, 697
 strength of, 697
 untuned component of, 699–700
 as linear filter, 750
 with static nonlinearity, 712*f*, 713–714, 717
 linear properties of, 750–751
L-N model of, 712*f*, 713–714, 714*f*, 717
 monocular, 1631
 nonlinear interactions of, 712*f*, 712–713
 nonlinear properties of, 751–754
 temporal dynamics of, 754–759
 null phase position of, 751
 ON/OFF, 118, 118*f*, 123, 123*f*, 270
 pharmacologic blockade of, 273
 orientation selectivity in, 118, 118*f*, 768, 770*f*, 1621
 linear and nonlinear properties of, 753
 orientation tuning of
 contrast invariance of, 699, 699*f*
 dynamics of, 698–699
 prediction of, from spatial organization of receptive field map, 698
 position selectivity in, 1621
 receptive field map, spatial organization of, prediction of orientation tuning from, 698
 receptive fields of, 118, 118*f*, 673–674, 695, 696*f*
 development of, 123, 123*f*
 linear maps of, 708, 708*f*, 709*f*, 709–710, 716–717, 750
 nonlinear maps of, 712*f*, 712–714, 714*f*, 717
 ON and OFF regions of, 673, 674*f*, 768
 space-time inseparable, 709*f*, 710, 713
 space-time separable, 709*f*, 709–710, 713
 spatiotemporal maps of, 709*f*, 709–710
 spatiotemporal properties of, 751
 subregions of, 750
 temporal profile of, 709–710
 ON regions, 695, 696*f*
 response expansion in, 752*f*, 752–753
 response properties of, relation to image representation model, 1609–1611, 1610*f*, 1611*f*
 response rectification in, 751*f*, 751–752
 response refractory period of, 751
 response saturation in, 753, 753*f*
 responses of
 to drifting gratings, 750
 as function of spatial phase, 750
 selectivity of, 18
 spatial frequency selectivity in, 751, 768, 770*f*
 linear and nonlinear properties of, 753
 spatial summation in, 750
 synaptic connections of, with LGN cells, 118, 118*f*
 system structure of, 712*f*, 713–714
 tuning of, 1302
 Simultanagnosia, 1684
 Simultaneous contrast effects, 881–882, 882*f*
 Single-channel system, in scotopic vision, 838
 Singular value decomposition (SVD)
 analysis, of complex cell receptive fields, 716
 Sinusoidal spatial gratings
 for contrast sensitivity measurement, 176–177, 177*f*
 pupil responses to, 645–647, 646*f*, 647*f*, 648*f*
 X and Y cell responses to, 17
Six3 gene
 expression of
 in eye fields, 34, 66
 in optic vesicle, 66
 in optic cup development and regionalization, 35*f*, 36
 overexpression of, 66
 in retinal cell differentiation, 68
 Size-disparity correlation, 1632
 SKF-38393, and ganglion cell excitability, 438
 Sleep
 and cortical plasticity, 128, 134
 pupil constriction during, 642, 653
 Sleepiness, slow oscillations of pupils during, 642, 653, 654*f*
 Slits, and optic chiasm development, 97*f*, 99–100, 100*f*, 101
 Sloan's notch, 1394, 1394*f*
 Sluggish ganglion cells, 255
 Smooth landings, by insects, motion cues for execution of, 1198–1199, 1199*f*
 Smooth pursuit eye movements. *See* Eye movement(s), smooth pursuit
 Smoothness constraint, 1304
 Sodium channels/currents
 in bipolar cells, 263
 cGMP-activated, 431
 dopamine and, 438–439, 441*f*
 epithelial-type, 431
 in ganglion cells, 417, 425–426, 432–433, 435–436
 high-threshold, 432
 low-threshold, 432
 persistent, 432–433
 temporal contrast and, 437*f*, 437–438
 transient, 432–433
 in horizontal cells, 378–379
 voltage-gated, 435
 Sodium ions
 in current flow to photoreceptors, in darkness, 225
 ganglion cell permeability to, 431
 non-synaptic routes for influx of, 431
 Sodium-calcium exchanger, and amacrine cell release of neurotransmitter, 295, 297*f*
 Sodium/potassium transporters, in cone inner segments, 244
 Somatostatin (SRIF)
 amacrine cells expressing, 339*f*, 339–340
 in dendrite-targeting interneurons, 689
 ganglion cells expressing, 340
 in light/dark adaptation, 349
 retinal, 334–335, 336, 339–342, 348–349
 binding sites of, 336, 340
 cellular physiology studies/calcium imaging of, 337, 341, 341*f*
 coupling to adenylate cyclase, 340
 functional studies of, 337, 341–342
 ganglion cell effects of, 341–342, 342*f*, 349
 ion channel modulation by, 341, 341*f*, 342, 348
 localization of, 340
 Somatostatin (SRIF) receptors
 functional, 336
 mRNA of, 336
 retinal, 336, 337, 340*f*, 340–341
 retinal localization of, 337
 sst subtype of, 336, 337, 340*f*, 340–341
 Sonic hedgehog (Shh)
 in eye field separation, 34
 in optic chiasm development, 101
 in optic cup development, 34–36
 in retinal cell differentiation, 37–38, 68, 467
 Space
 encoding of, posterior parietal cortex lesions and, 552–553
 scale and, 1046–1047, 1053*f*, 1054–1055
 Space representation
 in posterior parietal cortex, 1328–1332, 1330*f*
 in visual pathways, 488
 Space-time inseparable receptive fields, 705*f*, 706

- construction of, 710
- in simple cells, 709*f*, 710, 713
- Space-time separable receptive fields, 705*f*, 706
 - of simple cells, 709*f*, 709–710, 713
- Sparse code, 1592, 1593, 1605, 1606*f*
 - in image representation, 1605, 1606*f*, 1612
- Sparse noise, as stimuli for mapping receptive fields, 706
- Spatial adaptation. *See* Adaptation, spatial
- Spatial autocorrelograms, for measuring neuronal mosaics, 469–470, 473
- Spatial bandwidth, of receptive fields, 165*f*
- Spatial channels, 1043, 1060–1067
 - bandwidths, measurement of, 1062
 - evidence for, 1060–1062
- Spatial contrast, 881, 885–888
- Spatial contrast sensitivity, 925–927
- Spatial correlograms, for measuring neuronal mosaics, 467, 473
 - undersampling resistance of exclusion ratio in, 473, 474*f*
- Spatial filtering
 - by cone aperture, 801
 - in texture segregation, 1109–1112, 1109*f*
- Spatial frequency, 1043, 1044*f*, 1062–1063
 - and binocular rivalry, 1313–1316
 - and contrast induction, 1046
 - in contrast sensitivity, 176–177, 177*f*, 186, 186*f*
 - in developmental motion asymmetry, 183–184, 184*f*, 185*f*
 - in laser interferometry studies of image acquisition, 802–805, 803*f*, 804*f*, 805*f*
 - of natural images, 804
 - and orientation channels, 927–928
 - in orientation selectivity, 179–181, 180*f*, 181*f*
 - and pattern adaptation, 1655
 - in resolution acuity, 178–179, 179*f*
 - sensitivity to, development of, 164*f*, 164–165
 - in swept-parameter VEP, 175–176, 176*f*
- Spatial frequency adaptation, 1062
- Spatial frequency detector, 747–748
- Spatial frequency masking, ideal observer analysis of, 832
- Spatial frequency selectivity
 - in complex cells, 714, 715, 753, 770, 770*f*, 771*f*
 - in ganglion cells, 708
 - in LGN neurons, 708, 768, 770*f*
 - linear and nonlinear properties of, 753
 - measurement of
 - in awake, behaving monkey, 758
 - reverse correlation method for, 757–758
 - transient spatial stimuli for, 758
 - of MT neurons, 1205–1206
 - during natural fixation, 758–759
 - in simple cells, 751, 753, 768, 770*f*
 - temporal dynamics of, 757–759
- Spatial integration
 - and heading judgments, 1250–1251
 - neuronal, 26
- Spatial perception, 541, 542*f*
 - cortical analysis in, 543
 - dorsal association cortex and, 1260
- Spatial phase
 - during natural fixation, 758–759
 - simple cell responses as function of, 750
 - temporal dynamics of, 758–759, 759*f*
- Spatial pooling, 1065–1066
 - higher-level, 1066
 - in stereopsis, 1304–1305
- Spatial processing, in active observers, 550–551
- Spatial regularity, among retinal neurons, 463–475
- Spatial resolution
 - cone inner segments and, 244
 - deficits in, measurement of, 190
 - development of, 178–179, 179*f*
 - of ganglion cells, 483–484, 484*f*
 - of M (magnocellular) cells, 483–484, 484*f*, 501
 - in macaque monkeys, development of, 159, 161*f*
 - neuronal mosaics and, 463
 - newborn versus adult levels, in primates, 159, 160*f*
 - of P (parvocellular) cells, 483–484, 484*f*, 496, 497, 501
 - of receptive fields, 165*f*, 165–167, 166*f*
 - visual deprivation and, 167–170, 168*f*, 169*f*
- Spatial scale, 1043–1056. *See also* Scale
 - concept of, historical perspective on, 1043–1044
 - and eccentricity, 1044–1045
- Spatial selectivity
 - in ganglion cells, 418
 - in humans, development of, 174–186
- Spatial sensitivity
 - rod-cone interactions in, 871–872
 - in scotopic vision, 843–844, 844*f*
 - in infants, 846
- Spatial summation
 - in ganglion cells, 418, 486–487, 495, 751
 - low-contrast, 931–932
 - nonlinear, 754
 - of pupil responses, 642, 647, 647*f*, 653, 654*f*
 - in simple cells, 750
- Spatial view cells, 1183
- Spatial vision, 530
 - with both color and luminance variations, 930–933
 - color in, 924–934. *See also* Color spatial vision
 - advantages of, 933–934
 - cones and, 80, 801–802
 - distribution effects, 239*f*–240*f*, 240–241
 - development of, 159–171
 - behavioral versus physiological changes in, 164*f*, 164–165
 - in humans, 159
 - ideal observer model of, 160–163, 162*f*
 - in macaque monkeys, 159, 161*f*
 - neural factors in, 159–171
 - feedforward processing of, 150
 - hue-selective intensity coding mechanisms in, 932–933
 - ideal observer analysis of, 160–163, 162*f*, 830–831
 - at isoluminance, 925–930
 - monocular deprivation and
 - in humans, 197–198
 - in monkeys, 196–197
 - newborn versus adult levels, in primates, 159, 160*f*
 - receptive field responses and, 163–167, 165*f*, 166*f*
 - visual deprivation and, 167–170, 168*f*, 169*f*
- Spatial-frequency analyzers, in parallel visual pathways, 495
- Spatiotemporal contrast, development of, 176–178, 177*f*
- Spatiotemporal filters
 - cortical neurons as, 748–749
 - receptive fields as, 717
 - simple cells as, 750
- Spatiotemporal mechanism, underlying direction selectivity, 710–711, 711*f*
- Spatiotemporal processing, by neurons of primary visual cortex, 704–717
- Spatiotemporal receptive field (STRF)
 - definition of, 1595
 - estimation of, 1595
 - in area V1, 1595, 1596*f*
- Spatiotemporal receptive field maps, 708–710
- Spatiotemporal transfer function, of simple cells, 750–751
- Specific nerve energies, Müller's doctrine of, 15
- Spectral analysis, of visual evoked potentials, 174
- Spectral opponency, 969
- Spectral power distribution $[E(\lambda)]$, 948
- Spectral reflectance function $[S(\lambda)]$, 948
- Spectral sensitivity, 908, 989
 - in blindsight, 658
 - of cones, 989–990, 990*f*
 - in dogs, 962, 963*f*
 - ideal observer analysis of, 835–836
 - of scotopic vision, 838–843
 - in single-unit recording, 16–17

- Specularity(ies), 1095, 1096*f*, 1099
- Speed of motion
attention to, 1241
discrimination of, MT/MST lesions and, 551
- Speed (velocity) selectivity
in area MT neurons, 1206–1207, 1207*f*, 1213
of complex cells, 715
of single neurons, 17
temporal and spatial inseparability in, 26
- Spherical aberration. *See* Aberration(s)
- Spherical coordinates, for visual area maps, 507
- Spherical image, 1099–1100
- Sphincter muscle of iris, and pupil responses, 642, 654*f*
- Spikes
in area MT neurons, 1206
in cortical neurons, synchrony of, horizontal connections and, 742*f*, 742–743
in ganglion cells
bursts or events, 427–430, 428*f*, 429*f*
calculations of, 434
frequencies of, 415, 422–430
accommodation and, 436
calcium modulation of, 436–437
current transformed into, 423, 424*f*, 425*f*
currents facilitating, 424
in dark-adapted retina, 426, 426*f*, 428, 436
dopamine and, 438–443
high versus low, 423–426
Hodgkin-Huxley equations for, 425
light intensity and, 423–425, 425*f*, 427, 428*f*, 429*f*
in light-adapted retina, 426, 427*f*, 427–428
prediction of, 443
with presentations of flickering checkerboards, 426–427
with presentations of spatially uniform random flicker, 427
temporal contrast and, 437*f*, 437–438
heterogeneity in, 434–435
- in LGN cells
burst, 575, 576*f*, 612, 613*f*, 622
in waking state, 612
cortical feedback and, 611–612, 613*f*
tonic, 575, 612, 613*f*
orientation tuning measured from, 698
Purkinje cell, 1486–1487
- Spinocerebellar ataxia type 6, 1487, 1487*f*
- Spinules
formation and retraction of, 296–298, 297*f*
of horizontal cells, 371*f*, 371–372, 382
dopamine and, 384
nitric oxide and, 386
retinoic acid and, 386
- Spiny stellate neurons, cortical connections originating from, 148–149
- Split-brain patients, 1685–1686
- Spongioblasts
amacrine cell development from, 395
association, 395
- Spontaneous activity, of developing visual system, 88–89, 89*f*
and LGN lamination, 109–110
and ocular dominance development, 147
and orientation selectivity, 117, 123–124
- Spontaneously splitting objects (SSOs), 1289*f*, 1290
- S-potentials, 369, 370*f*
mixing of rod and cone signals in, 374–375, 376*f*
wavelength dependency of, 373–374, 374*f*
- Sprague effect, 1472
- Square-root laws
measurement of, 815–820
of quantum fluctuation-limited detection performance, 814–815
for thresholds, 814–820
- Square-wave gratings, pupil responses to, 645–647, 647*f*, 648*f*
- Squirrel(s)
cone function in, 240
cone-specific opsin kinase in, 222
horizontal cortical connections in, 738
light responses of SCN neurons in, 630–631
OFF bipolar cells of, glutamate receptors in, 265–266, 266*f*
synaptic transmission in, 285
- Squirrel monkeys
horizontal cortical connections in, 737–738, 738*f*
lateral cortical connections in, 1072
lateral geniculate nucleus in, 6
- SR95531, GABA receptor response to, 356*t*, 358
- SRIF. *See* Somatostatin
- S-space, of horizontal cells, 372
- sst receptor
retinal, 336, 340*f*, 340–341
retinal localization of, 337
- Stable target saccade task, 1436
- Stage-specific embryonic antigen-1 (SSEA-1), and regulation of ganglion cell axons, 96, 97*f*, 98, 99, 100
- Standard-observer functions, 867
for photopic conditions mediated only by cones, 867
for scotopic conditions mediated only by rods, 867
- Starburst amacrine cells, 400*f*, 403–405
acetylcholine receptors in, 312
in direction selectivity, 361, 404–405, 456–460, 457*f*, 458*f*
excitation and inhibition of, 361, 403–405
motion discrimination by, 456–459, 458*f*
ON and OFF, 403–405
stratification of, 269
signaling between, 293, 294, 312–313
synaptic asymmetries of, 456–457, 457*f*
- Starlight
retinal circuits for signal transmission in, 247–248, 248*f*, 249*f*
rod function under, 237–240, 247–248, 248*f*, 249*f*
- STAT pathway, in rod formation, 39
- Static feedback, 1453–1454
- Statistical analysis, of single unit responses
experimental studies using, 20–23
power and pitfalls of, 15, 18–23
using neural and behavioral responses, 20–23
- Statistical decision theory, 18
- Statistics
population, 1107–1108
simple, 1107
third-order, 1107–1108
- Steady-state visual evoked potentials, 174–175, 175*f*
amplitude of, 174–175
versus EEG, 174–175, 175*f*
phase value of, 174–175
- Stellate cells
in corticocortical pathways, 522
dendrites of, 675
of macaque V1, 683–684
- Stem cell(s), retinal
differentiation of, 66–67
multiple types of, 67
producing layer-restricted clones, 67
producing radial clones, 67
specified, 63, 64*f*
selection of, 65–66
transcription factors expressed by, 68
transplantation of, 42, 43
- Step-flash effect, 228–229
- Step-ramp stimulus, 1485, 1492, 1493*f*
- Step-saccade task, presaccadic burst
activity for, 1437–1439
- Stereo acuity, 1304
measurement of, 1306
spatial scale and, 1306
- Stereo edge(s), 1581
- Stereo-depth scaling, 1307
- Stereograms, 1142*f*
- Stereopsis, 928, 1300–1310, 1424
calibration errors in, 1310
computational models of, 1303
and correspondence problem, 1054, 1285–1286, 1285*f*
neural mechanism of, 1307

- second-order, 1304
- sensorimotor interactions and, 1309–1310
- sequential, 1309–1310
- simultaneous
- definition of, 1308
 - versus sequential, 1308–1309
- spatial pooling and, 1304–1305
- spatial scale and, 1049–1051, 1050*f*, 1052*f*
- sustained, 1304
- temporal masking in, 1310
- transient, 1304
- uncertainty in, 1304–1305
- Weber fraction for, 1304
- Stereoscopic vision (stereopsis)
- area MT and, 788–790, 1205*f*, 1208, 1210
 - binocular deprivation and
 - in cats, 191
 - in monkeys, 193
 - binocular disparity and, 198–199, 199*f*, 550, 765–766, 779–790, 784–785
 - V1 neuron properties versus properties of, 782–785
 - development of, 184–185
 - discordant visual input and, 198
 - disparity-selective neurons and, 765–766, 766*f*, 767*f*, 780–781
 - extrastriate cortex and, 781, 785–787
 - MST visual area and, 786–787, 790
 - primary visual cortex and, 765–766, 779, 781–785, 790
 - selectivity of single neurons for, 18
 - V5/MT visual areas and, 788–790
 - Wheatstone's studies of, 779
- Stereo-slant scaling, 1307–1308, 1307*f*
- Stiles curves, 815–816, 816*f*
- Stiles-Crawford effect
- in direction selectivity, 216, 797
 - in scotopic vision, 841, 845, 847*f*, 847–848
- Stimulus contrast, and receptive field dynamics, 739*f*, 739–741, 740*f*
- Stimulus onset asynchrony (SOA), 1309–1310
- Stimulus selectivity
- contrast-set gain control and, 753
 - of cortical neurons, 747–750, 753, 761
 - functional significance of, 748
 - half-wave rectification and, 752
 - in multidimensional feature space, 761
 - stimulus dimensions in, 748
 - temporal dynamics of, 749–750, 754–759
- Stingray, retinal synapses of, 289
- Stochastic model, of L and M cone identity, 985–986
- Stochastic motion stimulus, for chromatic motion processing, 1225, 1225*f*
- Strabismus, 189, 1300, 1320. *See also* Amblyopia
- alternating, 1300
 - artificial, decorrelated binocular input with, effects of, 198–199, 199*f*
 - and binocularity, 184–185
 - contrast differences in, 773
 - and extrastriate development, 171
 - and motion asymmetry, 184
 - neuronal correlates of, 167–170
 - neurotrophins and, 50
 - and ocular dominance columns, 112–114, 126
 - and spatial vision, 167–170, 168*f*, 169*f*
 - and stereoscopic vision, 191, 198–199
 - unilateral, 1300
- Stream(s), visual, 541. *See also* Dorsal stream; Ventral stream; Visual pathways
- in macaque, 1624, 1625*f*
- Strehl ratio, 807–808, 808*f*
- Strepsirrhines, vision of, 968
- Striate cortex. *See* Primary visual (striate) cortex
- Striatorecipient zone, of pulvinar, 595
- Stripe of Gennari, 8
- Stripe-rearing studies, 199–200, 200*f*
- of orientation selectivity, 121, 199–200, 200*f*
- Strobe rearing, and direction selectivity, 201, 201*f*
- Stroboscopic rearing, 189
- Stroop test, 1550, 1550*f*
- Structural models
- of cortical neurons, 760, 760*t*
 - goal of, 760
- Structure-from-motion, 1211, 1239, 1242
- Strychnine, glycine receptor response to, 356*t*, 357, 358, 364
- Subcortical visual structures, development of, neural factors in, 163–165
- Sublamina *a*, OFF pathways in, 267, 267*f*, 269
- Sublamina *b*
- OFF pathways in, 267, 267*f*
 - ON pathways in, 269
- Subplate neurons
- connections of, 151
 - pioneering role in cortical development, 151
- Substance K. *See* Neurokinin A
- Substance P
- binding sites of, 336
 - cellular physiology studies/calcium imaging of, 337
 - and circadian rhythms, 628–629, 635*f*
 - coexpression with GABA, 336
 - ion channel modulation of, 337
 - retinal, 334, 342–343, 348
- binding sites of, 343
 - cellular physiology studies of, 344
 - functional studies of, 344
 - and ganglion cell excitability, 344
 - ion channel modulation by, 344
 - localization of, 343
 - in tecto-pulvinar pathway, 595
- Substantia nigra pars reticulata, in dialogue between cerebral cortex and superior colliculus, 1467, 1468*f*, 1471–1472
- Subthreshold summation, 928, 1062
- Summation
- binocular, 772–773, 779
 - and center-surround organization of receptive fields, 739*f*, 739–741, 740*f*
- complete
- area of, 819
 - smallest area of, 819
- length
- horizontal cortical connections and, 739*f*, 739–741, 740*f*
 - vertical cortical connections and, 740
- low-contrast, 931–932
- perfect, 819
- and receptive field dynamics, 739*f*, 739–741, 740*f*
- of rod and cone signals, 848
- in rod-cone interactions, 866–867
- spatial
- in ganglion cells, 418, 486–487, 495, 751
 - nonlinear, 754
 - of pupil responses, 642, 647, 647*f*, 653, 654*f*
 - in simple cells, 750
 - subthreshold, 928, 1062
 - subthreshold, 928, 1062
- Superadditivity, 1573–1574
- Superficial synapses, 281, 281*f*, 283
- Superior colliculus, 592, 1466, 1565, 1566
- anatomical organization in, 1449–1450
 - and cerebral cortex
 - ascending pathways connecting, 1468*f*, 1474–1480, 1475*f*, 1479*f*, 1480, 1480*f*
 - descending projections connecting, 1468–1474, 1468*f*, 1480, 1480*f*
 - dialogue between, 1466–1481, 1480*f*
 - interconnections between, 1467–1468, 1467*f*
 - connections with area MT, 1203, 1204*f*
 - in coordinated eye-head movements, 1454–1458
 - cortical connections of, 1466–1467
 - feedback signal incorporation in, 1451–1454
 - ganglion cell axon guidance in, 99, 101
 - ganglion cells projecting to, 415
 - ON and OFF, 270
 - in gaze control, 1449–1462

- Superior colliculus (cont.)
hamster, 1450
interconnections of, 1449
layers in, 1449–1450
 deep, 1449–1450
 intermediate, 1449–1450
 superficial, 1449–1450
lesions in, 1428
in monkeys, 1455
motor map in, 1451
neurons in
 buildup, 1452–1453
 classification of, 1452–1453
 fixation, 1452–1453
 perisaccadic receptive field shifts in, 1398
 response characteristics of, 1371, 1373*f*
 spatial control scheme for, 1452–1453
 temporal control scheme for, 1451–1452
and oculomotor system, 1371, 1372*f*, 1491
in oculomotor system, 1425
in orienting responses, 1454–1462
pulvinar connections of, 594–595, 599
and pursuit- and saccade-related activity, 1409, 1432*f*
receptive field properties of neurons in, development of, 163
retinal projections to, 1566
retinotopic organization in, 1566*f*, 1567
and saccades, 1371–1374, 1449–1450
single-unit recording in, 17
in spatial vision, 530
superficial layer of, signals from striate cortex to, 1472
topographical map of, 99, 101
in vergence control, 1415
and visual grasp response, 1431
in “where” visual pathway, 495–496
Superior parietal lobule (SPL), in spatially directed attention, 1519–1521, 1520*f*, 1521
Superior temporal cortex
 fundus of, 543
 in spatial perception, 1684
Superior temporal gyrus (STG), in visuospatial neglect, 1519
Superior temporal polysensory area (STP), 543, 1267
 connections with area MT, 1203, 1204*f*
 integration of information about motion, color, and form in, 553, 554*f*
 vestibular input and, 1272
Superior temporal sulcus, 541
 connections with area MT, 1203, 1204*f*
 face cells in, 1087
 fundal area of, 1568*f*
 interconnections/projections of, 1260–1261
 macaque, 1165, 1166*f*
 in motion perception, 1274
 motion sensitivity of, 543
 functional mapping of, 1236
neurons
 direction selectivity of, 1262
 optic flow responses in, 1262–1263
 response characteristics of, 1165, 1166
 and pursuit behavior, 1402, 1407, 1408
 visual areas of, in macaque, 510*f*–511*f*, 512
 and visual consciousness, 1689
Superposition, 1590, 1667, 1668*f*
Supplementary eye field (SEF), 1429*f*
 in dialogue between cerebral cortex and superior colliculus, 1470–1471
 discovery of, 1428
 and pursuit- and saccade-related activity, 1410, 1432*f*
 and pursuit behavior, 1408
 in pursuit gain control, 1403
 in spatially directed attention, 1519–1521, 1520*f*
Supplementary motor area (SMA), interconnections of, with prefrontal cortex (PFC), 1548
Suppression. *See also* Binocular rivalry
 flash, 1688–1689, 1689*f*
 saccadic, 1391–1395, 1399, 1430
 and magnocellular pathway, 1394–1395, 1394*f*
 and visual masking, time course of, 1393*f*, 1394
 sensory, and attentional modulation in cortex, 1516–1517, 1517*f*
 weak signal, 822
Suppression theory, 1320
Suppressive rod-cone interaction (SRCI), 389
Suprachiasmatic nuclei (SCN)
 circadian role of, 625–636
 ganglion cells projecting to, 628
 genetic expression in, 634*f*, 634–635
 inhibition of, 628
 intracellular signaling in, light-responsive, 633–636
 light input pathways to, 625, 628–629, 629*f*, 635*f*
 light responses of, 625–636, 635*f*
 light-induced phase shifts in, 625–628
 and melatonin production, 628, 630–631
 neuronal input pathways of, 628–629, 629*f*
 neurons of
 absence of center-surround organization in, 630
 behavior/activity and, 631, 632*f*
 circadian cycle and responsiveness of, 631–632, 632*f*, 633*f*
 conductance in, circadian variation in, 629
 in day versus night, 631–632, 632*f*
 discharge rates of, 629–632, 630*f*–631*f*
 electrophysiological response properties of, 629–632, 630*f*–631*f*
 extracellular recording of, 629–632
 intensity response curve of, 630–631
 intracellular recordings of, 629
 light intensity and, 630–631, 632, 633*f*, 636
 light responses of, 629–632, 630*f*–631*f*
 light-activated, 630, 630*f*–631*f*
 light-suppressed, 630, 630*f*–631*f*
 under photopic conditions, 631
 preferred firing rates of, 629–630
 receptive fields of, 630
 response latencies of, 630
 retinorecipient
 input resistance of, 629
 membrane potential of, 629
 under scotopic conditions, 631
 sustained responses of, 630, 636
 retinal innervation of, 628, 629*f*
Supragranular neurons, connectivity of, 148, 149, 151, 153
Surface(s), 722–725. *See also* Equivalent surface
 aftereffects induced by, 1131–1132
 attributes of, contour and, 1146, 1146*f*
 and complementary cortical streams, 1624
 creases in, 1287–1288
 features and, 1287–1288
 filled-in, afterimages of, 1130*f*, 1132–1135, 1133*f*, 1134*f*, 1135*f*
 filling-in, 1129–1130, 1582
 formation of
 in early visual processing, 1131, 1131*f*
 three-dimensional, 1633–1637
 and illusions, 1625–1626, 1625*f*
 local inputs to global percepts of, 1129–1131, 1130*f*
 luminance of, 884
 perceptual, neural substrates for, 1135–1136
 reflectance of, 884
 representing zero disparity, 1301
 shaded, perception of, 1632
 slanted, perception of, 1631
 three-dimensional capture of, 1631–1632
 visual, 1624–1638
Surface capture, 1634*f*, 1635
Surface representation, 1129–1137, 1582
 modal, 1636, 1637*f*
Surface slant (orientation), 1300, 1307–1308, 1307*f*
Surface-based atlases
 computer software for, 513
 of cortical organization, 507, 508*f*
 advantages of, 507, 508*f*

- comparison of macaque and human, 515–518, 517*f*
- probabilistic, 513
- Surround inhibition/suppression, 364–365
 - of amacrine cells, 364
 - GABA and, 364*f*, 364–365
 - of ganglion cells, 23, 89, 355, 364*f*, 364–365, 422
 - glycine and, 364*f*, 364–365
 - horizontal cells and, 386–388, 388*f*
 - of LGN cells, cortical feedback and, 612–614
 - of receptive fields, 165*f*, 165–166. *See also* Center-surround organization, of receptive fields
- Surround stimulation, and responses in V1, 1654
- Surroundedness, 1143
- Swept-parameter (sweep) visual evoked potential, 175–176, 176*f*
 - in grating acuity (resolution acuity), 178–179, 179*f*
 - in position sensitivity, 182, 183*f*
- SYM 2081, and OFF bipolar cell responses, 265–266
- Symmetry
 - bilateral, detection of, by honeybees, 1502
 - circular, detection of, by honeybees, 1502
 - Gestalt factor of, 1575, 1576*f*
 - radial, detection of, by honeybees, 1502
- Symmorphosis, of retinal circuits, 234–237
- Synapse(s), 279–298. *See also specific synaptic connections*
 - amacrine cell, 290–295
 - amacrine cell-amacrine cell, 87, 293–295
 - amacrine cell-bipolar cell, 292*f*, 292–293
 - amacrine cell-ganglion cell, 87, 280, 280*f*, 293
 - asymmetric, 571
 - bipolar cell, 283–289
 - rectification of, 255
 - bipolar cell-amacrine cell, 280, 280*f*, 291–292
 - bipolar cell-cone, 87
 - bipolar cell-ganglion cell, 268, 279, 280, 280*f*
 - postsynaptic mechanisms of, 288–289
 - presynaptic mechanisms of, 285–288, 287*f*
 - bipolar cell-horizontal cell, 280, 280*f*
 - canonical circuit of, 154
 - cholinergic, 294–295, 295*f*, 312–313
 - cone-bipolar cell, complexity of, 283, 284*f*
 - conventional, 87
 - cortical
 - concentration of, 148
 - organization in primary visual cortex, 614–619
 - dopaminergic, 314
 - efficacy of, neurotrophins and, 49, 55
 - extrastriate development of, 170
 - formation of, neurotrophins and, 49
 - GABAergic, 279, 281*f*, 281–283, 284*f*, 286, 289–290, 292*f*, 292–294, 309–310, 355, 396–398, 402
 - ganglion cell-LGN neuron, 270
 - glutamatergic, 264–266, 266, 279, 281*f*, 281–285, 284*f*, 285*f*, 288, 289, 293, 304, 306–307, 320–330
 - glycinergic, 291, 304, 311, 355, 395–396
 - Hebbian, 25
 - and cortical plasticity, 113–114, 137–138
 - NMDA receptors and, 129
 - in orientation selectivity, 117, 123
 - horizontal cell-bipolar cell, 290, 304, 309
 - horizontal cell-horizontal cell, 289–290
 - horizontal cell-photoreceptor, 290, 309
 - inhibitory, 359–360
 - development of, precocious, BDNF overexpression and, 55–58, 57*f*
 - invaginating, 246, 247*f*, 281*f*, 281–282, 281–283, 289, 296
 - in lateral geniculate nucleus, connections of, 88, 118, 118*f*
 - in A layers of cat LGN, 571–572, 572*f*
 - F1 terminals, 571–572
 - F2 terminals, 572, 572*f*
 - RL terminals, 571–572
 - RS terminals, 571–572
 - triadic arrangements of, 572, 572*f*
 - linear chemical, 248
 - neurotrophins and, 54, 55, 56*f*
 - organization of, cortical connectivity and, 150, 153–154
 - photoreceptor, 280–283
 - bandpass filtering by, 246, 249–251, 251*f*
 - delay and, 323–324
 - engineered spillover of, 247, 247*f*
 - formation of, 87–88
 - in moonlight circuit, 247, 248
 - negative feedback on, 283
 - in signal transmission, 246–251
 - in starlight circuit, 247–248
 - temporal properties of, 323–324
 - three-dimensional structure and function of, 246–247, 247*f*
 - in twilight or dawn circuit, 247–249
 - photoreceptor-bipolar cell, 264–266, 279, 280, 280*f*
 - image separation at, 260, 266
 - postsynaptic mechanisms of, 283–285, 285*f*
 - presynaptic mechanisms of, 280–283, 281*f*
 - photoreceptor-horizontal cell, 87, 280, 280*f*
 - postsynaptic mechanisms of, 289
 - reciprocating, 292
 - retinal, 279–298
 - basic plan of, 280, 280*f*
 - direct pathway of, 279–289
 - and direction selectivity, 460*f*, 460–461
 - electron microscopy of, 87, 268, 279, 292, 293–294, 413
 - formation of, 87–88, 88
 - function of, 279
 - future directions for study of, 298
 - inner, 280, 280*f*, 298
 - lateral pathways of, 289–295
 - layers of, 234, 235*f*
 - number of, 69
 - order of appearance, 88
 - outer, 280, 280*f*, 298
 - outer versus inner, 279
 - in signal transmission from photoreceptors, 246–251
 - understanding of, 279
 - ribbon, 246, 247*f*, 281*f*, 281–282, 283, 286, 296, 395, 398
 - composition of, 282
 - lateral elements at, 371*f*, 371–372
 - rod electrical, 248–249
 - serial, 293–294
 - serotonergic, 304, 315–316
 - sign-inverting, 283, 304, 312–313, 395
 - sign-preserving, 283, 285, 304, 309, 395
 - spinule formation and retraction in, 296–298, 297*f*
 - superficial, 281, 281*f*, 283
 - super-Hebbian, 26
 - symmetric, 571
- Synaptic cleft, photoreceptor-bipolar cell, 282–283
- Synaptic depression, 700
- Synaptic plasticity, 25, 127–128, 295–298. *See also* Long-term depression; Long-term potentiation
 - calcium and, 130
 - excitatory, age and, 321–322
 - MAPK cascade and, 59*f*, 59–60
 - neurotrophins and, 47*f*, 49, 58–60, 61
 - in ocular dominance columns, 113–114
 - presynaptic and postsynaptic changes in, 138–139, 139*f*
 - retinoic acid and, 296, 386
 - spinules in, 296–298, 297*f*
 - in teleost fish retinas, 295–298
 - in visual cortex, 126
- Synaptic terminal
 - of cones, 216, 216*f*, 242*f*
 - of rods, 216, 216*f*, 242*f*
- Synaptic vesicles
 - acetylcholine transporter in, 311, 312*f*
 - amine transporters in, 313*f*, 314, 315*f*
 - docking of, in bipolar cells, 286–288, 288*f*

- Synaptic vesicles (cont.)
 endocytosis of
 in bipolar cells, 286–288, 287*f*
 in photoreceptors, 282
 in excitatory transmission, 326
 exocytosis of
 in bipolar cells, 286–288, 287*f*
 in photoreceptors, 282
 formation of, 87
 fusion of, in bipolar cells, 286–288, 288*f*
 GABA transporter in, 250, 289, 308*f*,
 308–309, 311
 glutamate transporter in, 304, 305*f*, 307
 glycine transporter in, 310*f*, 311
 inhibitory amino acid transporters in, 311
 Synaptosomes, neurotrophin action in, 55,
 56*f*
 Synchronization. *See* Synchrony, neuronal
 Synchrony, neuronal, 727, 1158
 across cortical areas, 1671
 amblyopia and, 1673
 assessment of, by correlation analysis,
 1670
 attention and, 1541, 1675–1676, 1676*f*
 binding by, 1580
 and binocular rivalry, 1673–1674, 1674*f*
 cell participation in, 1671
 chattering cells and, 742, 742*f*
 and cognitive processes, 1671,
 1675–1676, 1677–1678
 connections for, plasticity of, 1676
 constraints of, 1668–1670
 dynamic properties of, 1670
 excitatory mechanisms for, 742*f*, 742–743
 horizontal cortical connections and, 742*f*,
 742–743
 inhibitory mechanisms for, 742*f*, 743
 in lower-order areas, feedback
 connections and, 535–536
 operational definition of, 1670
 and oscillatory patterning, 1670
 and perceptual grouping, 1671–1673,
 1672*f*
 and perceptual selection, 1673–1674
 precision of, 1670
 properties of, 1670–1671
 as relational code, 1666–1668
 advantages of, 1667–1668
 and salience, 1670, 1673
 as selective mechanism in assembly
 coding, 1678–1679
 state dependency of, 1674–1675, 1675*f*
 and stimulus selection, correlation of,
 1673–1674
 variation of, independent of rate changes,
 1671
 Syntaxin-1, in retinal cell differentiation,
 78
 Systems analysis
 basic principles of, 748
 of cortical neurons, 747, 748–749
 linear, 176–177, 495
 of cortical neurons, 749
 linear and nonlinear properties revealed
 by, 749
 and receptive field mapping, 706
 nonlinear, and receptive field mapping,
 706
T
 TAa visual area, 1165, 1166*f*
 Table tennis, eye movements in,
 1362–1363, 1363*f*
 Tachykinin peptide(s)
 amacrine cells expressing, 342*f*, 342–343
 ganglion cells expressing, 342–343
 retinal, 335, 336, 337, 342–343
 binding sites of, 343
 cellular physiology studies of, 344
 coupling to phospholipase C, 343
 functional studies of, 344
 ion channel modulation by, 344
 localization of, 343
 Tachykinin peptide receptors
 functional, 336
 mRNA of, 336
 retinal, 336, 337
 retinal localization of, 337
 Talbot, William, 10–11, 27
 Tangential cortical connections, 148–149
 Taurine
 as neurotransmitter, 358
 and opsin expression, 39
 and retinal cell differentiation, 78–79
 TE visual area, 529*f*, 542, 1151, 1152*f*
 columnar organization in, 1155, 1155*f*
 columns of, 545
 functions of, 1159
 spatial arrangement of, 1155–1158,
 1156*f*, 1157*f*, 1158*f*
 in depth perception, 1153–1154
 in face recognition, 1153
 intrinsic horizontal connections in,
 1158–1159
 learning new representations in,
 1172–1173
 loss of retinotopy in, 542
 neurons of
 activation of, luminosity gradient and,
 1152*f*, 1153
 experience and, 547
 form-cue invariance in, 546
 invariance of, 1154, 1170–1172
 object features for, 1158
 object-based responses in, 1170–1172
 optimal object features for, reductive
 determination of, 1151, 1152*f*
 pair coding by, 547
 stimulus selectivity of, determination of,
 1151–1153, 1152*f*
 TE1 visual area, 1165
 macaque, 510*f*–511*f*, 512
 TE2 visual area, 1165
 macaque, 510*f*–511*f*, 512
 TE3 visual area, 1165
 macaque, 510*f*–511*f*, 512
 TEa visual area, 1154, 1165, 1166, 1166*f*
 macaque, 510*f*–511*f*, 512
 dorsal (TEad), 510*f*–511*f*, 512
 ventral (TEav), 510*f*–511*f*, 512
 Tectopulvinar connections, 579–580,
 594–595
 Tectorecipient zone, of pulvinar region,
 594
 Tectum
 of three-eyed frog, ocular dominance
 columns in, 111–112, 112*f*
 topographical map of, Eph
 receptors/ephrin ligands and, 99
 TE1-3d visual area, macaque, 510*f*–511*f*,
 512
 Teleost fish
 ON and OFF bipolar cells of, 265
 synaptic plasticity in, 295–298
 synaptic transmission in
 cone-ON bipolar cell, 284
 dopaminergic, 314
 TEm visual area, 1154, 1165, 1166,
 1166*f*
 macaque, 510*f*–511*f*, 512
 Temperature, ambient annual, and
 presbyopia, 206, 206*t*
 Template hypothesis, of honeybee pattern
 recognition, 1502
 Temporal contrast
 definition of, 437
 and ganglion cell excitability, 437*f*,
 437–438
 Temporal cortex, 1565. *See also* TE visual
 area
 neurons
 face-selective, 1166–1167
 object-selective, 1167
 responses to optic flow, 1267
 visual areas of, 1165, 1166*f*
 human, 515, 516*f*
 versus macaque, 517–518
 in macaque, 508, 510*f*–511*f*, 511–512,
 512, 513*f*
 dorsal, 510*f*–511*f*, 511–512
 ventral, 510*f*–511*f*, 512
 medial superior (MST). *See* Medial
 superior temporal area (MST)
 middle (MT). *See* Middle temporal (MT)
 visual area
 neuronal responses in, 1165–1166
 specialization of function in, 1165–1166
 visual deficits following lesioning of,
 11–12
 in “what” visual pathway, 495

- Temporal dynamics
 of contrast adaptation, 755
 of contrast-set gain control, 756–757
 of cortical neurons, 749–750, 754–759
 of direction selectivity, 758*f*, 758–759
 of latency shift, 755
 of neural performance, 749–750
 of nonlinear properties, 754–759
 of orientation selectivity, 757–758
 of response expansion, 756–757
 of response rectification, 755
 of response refractory period, 755
 of spatial frequency selectivity, 757–759
 of spatial phase, 758–759, 759*f*
 of stimulus selectivity, 749–750, 754–759
- Temporal frequency
 in developmental motion asymmetry, 183–184, 184*f*, 185*f*
 and optomotor response in insects, 1196
- Temporal frequency tuning
 in complex cells, 715
 in MT neurons, 1206
- Temporal impulse response, 820
- Temporal integration
 in daylight vision, 237, 238*f*
 neuronal, 26
- Temporal lobe, 1371, 1372*f*
 in binocular rivalry, 1319
 and color processing, 1014–1015
 and oculomotor system, 1375–1376, 1376*f*
- Temporal resolution, of M (magnocellular) cells, 496, 501
- Temporal sensitivity
 rod-cone interactions in, 869–871, 870*f*, 871*f*
 in scotopic vision, 844–845
- Tenrecs
 brain of, 1565*f*
 evolutionary history of, 1564
- TEO visual area, 542, 545
 attentional response modulation in, 1515, 1516–1517
 lesions of, and visual attention impairments, 549
 macaque, 510*f*–511*f*, 512
 homology with human visual area, 517–518
 in texture segregation, 1115
- TEr visual area, macaque, 510*f*–511*f*, 512
- Ternary noise, as stimuli for mapping receptive fields, 706
- Tetrachromats, 372, 965, 966*f*
 rods in, 872
- Tetraethylammonium (TEA), potassium currents blocked by, 433–434
- Tetrodotoxin (TTX)
 and cortical connectivity, 149
 ion currents blocked by, 432–433, 437–438
- and mosaic formation, 470, 471
 and neurotrophins, 49
 and ocular dominance, 128
 and orientation selectivity, 121–122
- TE1-3v visual area, macaque, 510*f*–511*f*, 512
- Textons, 1107
- Texture, 1094. *See also* Camouflage
 appearance of, 1113–1114, 1113*f*
 characterization of, 1106
 contrasts of, and disparity, 1296
 co-occurrence in stimulus with other cues, 1108
 elemental descriptors of, 1106
 features of, 1106–1108, 1107*f*
 illusory, 1583–1584, 1584*f*
 light matter of, and disparity, 1297
 perception of, 1066, 1106–1115, 1628
 scale and, 1052, 1053, 1054*f*, 1055
 shape from, 1114–1115
 and shape from shading, 1093–1094, 1093*f*, 1095, 1095*f*, 1099
 spreading of, 1583–1584, 1584*f*
 statistical characterization of, 1106, 1113–1114
- Texture contrast sensitivity function, second-order, 1111–1112, 1112*f*
- Texture gradients
 compression, 1114
 density, 1114
 size, 1114
- Texture segregation, 1106–1113, 1107*f*
 asymmetries of, 1108
 back pocket model of, 1109, 1109*f*, 1110*f*, 1111
 comparison-and-decision stage in, 1109, 1111
 current models of, 1108–1111
 models of, specification, 1111–1113
 neurophysiology of, 1115
 second-order models of, 1109–1110
 third-order models of, 1110*f*, 1111
 and visual search, 1108
- TF (temporal area F) visual area, macaque, 510*f*–511*f*, 511, 512, 513*f*
- TH (temporal area H) visual area, macaque, 510*f*–511*f*, 511, 512, 513*f*
- Thalamic reticular nucleus
 cat
 cells of, cable modeling for, 573
 inputs to A layers, 568, 569*f*, 570
 cortical feedback to, 609
 inputs to A layers, 568, 569*f*, 570
 I_r current in, 576
- Thalamocortical pathway, 146–147, 146–148, 154
 development of, 147–148
 organization of, 524
 visual relays in, 565–586
- Thalamus. *See also* Pulvinar region
 cortical connections to and from, 146–147, 146–148, 154
 lateral geniculate nucleus of. *See* Lateral geniculate nucleus
 mediodorsal
 in dialogue between cerebral cortex and superior colliculus, 1468*f*, 1474–1476, 1475*f*
 and oculomotor system, 1371, 1372*f*
 signals from, and cortical plasticity, 128
 synaptic circuitry of, 567
 as target of ganglion cell axons, 94
 visual relays in, 565–586. *See also* Lateral geniculate nucleus (LGN)
 attentional modulation of, 580
 circuit properties of, 565
 complex cells of, 565
 first-order, 565, 579–580, 580*f*, 582, 586
 higher-order, 565, 579–580, 580*f*, 582, 586
 and motor function, 582
 research on, advances in (future directions for), 586
- Threshold(s), 811–823. *See also* Detection threshold
 absolute
 of cone system, 841
 dark light and, 816–817
 in scotopic vision, 838–840
 aging and, 846
 in infants, 846
 added noise as analytical tool of, 822–823
 area and, 818–820, 819*f*
 behavior of, as indicator of sensory deficiency, 823
 in binocular vision, 768, 772–773, 774*f*, 774–775
 chromatic extent and, 820
 classical (Fechnerian), 811, 812*f*
 concept of, 811
 of cone system, 820, 841
 contrast
 binocular, 772–773, 774*f*
 monocular, 773
 monocular-to-binocular ratio of, 773, 774*f*
 in swept-parameter VEP, 175–176, 176*f*
 definition of, 811
 DeVries-Rose law of, 815–816, 816*f*
 in DeVries-Rose regime
 decrement, 816, 817*f*
 explanation of, 816
 duration and, 819*f*, 820
 gain control and, 817–818, 819–820
 high background inefficiency and, 817–818, 819–820
 ideal observer analysis of, 813–814, 816
 implied by irreducible noise implicit in light, 813–815

- Threshold(s) (cont.)
 versus intensity, 815–816, 816*f*, 842
 at large areas, 819–820
 low area, 818–819
 low background sensitization and, 816*f*, 818
 modern, 812–813
 noise and, 811–823, 840
 oscillating motion, in visual evoked potentials, 183, 183*f*
 for phase shifts in circadian rhythms, 627
 psychometric function of, 811, 813*f*, 820–822, 840, 847
 definition of, 820–821
 nonlinear transducer explanation of, 821
 physiological, 821–822, 822*f*
 uncertainty explanation of, 821
 quantum fluctuation limit for, 813–814, 820, 822
 fingerprint of, 814–815, 815*f*, 820
 of rod system, 820, 838–840, 842
 in scotopic vision, 820, 838–841, 846–847
 aging and, 846
 in infants, 846
 sensory, and extrapolation of VEP response functions, 175
 square-root laws for, 814–820
 measurement of, 815–820
 theory of, 813–815
 traditional, 811–812
 vernier offset, in visual evoked potentials, 182–183, 183*f*
- Threshold versus duration curves, 819*f*, 820
- Threshold versus intensity (TVI) curves, 815–816, 816*f*, 817, 842
- Threshold versus radiance (TVR) function, 911–912
 linear region of, 912
- Thymidine labeling
 of retinal neurons, 36, 77
 of rods, 39
- Thyroid hormone, in retinal cell differentiation, 68, 78
- Thyroid hormone alpha receptor, and retinal development, 72
- Tilt aftereffect, 936–939, 937*f*, 938*f*
- Time-dependent ion channels, in horizontal cells, 378–379, 379*f*
- timeless* gene, 636
- T-junction sensitivity
 in Boundary Contour System (BCS) model, 1633, 1634*f*
 in figure-ground perception, 1635
- Toad(s)
 dark adaptation in, 854
 ganglion cells of, excitability of, 424
 horizontal cells of, luminosity, 372, 372*f*
 rods in, single photon response of, 223
- Top-down processes, 1579
 in eye movement, 1365, 1366*f*
 feedback connections in, 536
 in honeybees, 1504, 1505*f*
- Torsional eye movements. *See* Eye movement(s), torsional
- TPMPA, GABA receptor response to, 356*t*, 358
- TPO (temporal parietal occipital) visual area, 1165–1166, 1166*f*
 macaque, 510*f*–511*f*, 512
 caudal (TPOc), 510*f*–511*f*, 512
 intermediate (TPOi), 510*f*–511*f*, 512
 rostral (TPOr), 510*f*–511*f*, 512
- TRAAK, and ganglion cell permeability, 431
- Tracer-coupling studies
 of amacrine cells, 396, 401–402
 of direction-selective ganglion cells, 466
- Tract of postoptic commissure (TOPC), 96
- Transcranial magnetic stimulation (TMS), scotomas induced by, 1136, 1137*f*
- Transcription factors. *See also specific transcription factors*
 expression of
 in eye fields, 33–34, 65–66, 68
 in optic vesicle and optic cup, 34–36, 35*f*, 68
 in retina development, 33
 interactions of, 34–36, 36*f*
 and opsin expression, 39–40, 40*f*
 and optic chiasm development, 101–102
 in process outgrowth of retinal cells, 81
 reciprocal inhibition of, 34, 36*f*, 38
 in retinal cell differentiation, 38–39, 68, 78
- Transducin, 1006
 activation of, 217*f*, 217–218
 rate of, 218
 mean, 219
 ratio to PDE activation rate, 219
 coupling to phosphodiesterase, 217, 217*f*, 218–219, 220–221
 encounter rate with activated rhodopsin, 218
 inactivation of, 223, 224*f*, 225
 lateral diffusion of, 218
 in light adaptation, gain reduction and, 229
 in phototransduction, 217*f*, 217–219, 223, 225
 and rod maturation, 41
 speed of action, size of outer segment and, 241–244, 243*f*
- Transduction, by photoreceptors, 215–230. *See also* Phototransduction
- Transforming growth factor- α , in retinal cell differentiation, 68, 78
- Transient stationary measurements
 of cortical neurons, 749–750, 755, 757
- of spatial frequency selectivity, 758
- Transient stimuli, perception of, in blindsight, 658–659
- Translation
 definition of, 1247
 observer, 1247–1248, 1248*f*, 1249*f*
 oculo-centric, 1256, 1256*f*
- Transneuronal labeling, in ocular dominance columns, 108, 110*f*, 110–111
- Transparency, 1284
 and depth perception, 1292–1297, 1293*f*, 1303
 cues to, 1295
 for global stereopsis, 1051, 1052*f*
 perceptual
 magnitude constraint and, 1293–1294
 polarity constraint and, 1293–1294, 1294*f*
- Tree shrew
 evolutionary history of, 1564
 horizontal cortical connections in, 733, 737
 lateral cortical connections in, 1071, 1071*f*, 1072
 ON and OFF leaflets in LGN of, 271
 visual system of, 1566, 1567, 1568, 1569
- Triad(s), 572, 572*f*
- Trichromacy, 892, 910, 917, 951, 964, 965, 966*f*, 968, 969, 971, 974, 1010, 1011
 anomalous, 942, 975, 983, 1005
 evolution of, 977, 978*f*
 female, 969–970, 977
 processing for, 1005
- Trichromatic sampling, and image acquisition, 805–807
- Trichromats, 372
 normal, 910
 pupil responses in, 650–652, 651*f*
 rod saturation in, 842–843
 scotopic grating acuity in, 843, 844*f*
- Tristimulus coordinates, 951
- Tritan, 975
- Tritan discrimination, rods and, 874–875
- Tritanopia. *See also* Dichromacy
 molecular genetics of, 983
 transient, 856–857, 856*f*, 940
- trkA ligand, and cortical plasticity, 128
- trkA receptor, 46, 48*b*, 55
 deficiency of, 48, 48*b*
 in visual cortex, 50
- trkA-IgG receptor, 135
- trkB ligands, and cortical plasticity, 128, 131, 133
- trkB receptor, 46, 48*b*, 133
 deficiency of, 48*b*
- trkB-IgG infusion, and ocular dominance, 52, 54*f*, 133
- trkC receptor, 46, 48*b*
 deficiency of, 48*b*

- Trochlear nucleus, neurons in, 1417
- Troland value(s)
for color discrimination, 841
of cone input in Stiles-Crawford effect, 841
for critical flicker frequency, 844–845, 845*f*
of rod saturation, 841–842, 841–843
of Stiles-Crawford effect, 846*f*, 846–847
- Troxler's effect, 1313
- Tryptophan hydroxylase, 314, 315*f*
- TS visual area, 1165, 1166*f*
- Tuberomammillary nucleus, inputs to A layers, 568, 571
- Tuned excitatory neurons, in stereoscopic vision, 766, 767*f*
- Tuned inhibitory neurons, in stereoscopic vision, 766, 767*f*
- Tupaia belangeri*, retinal somatostatin expression in, 339–340
- Turtle(s)
color vision in, 965, 968
dark rearing of, and light response of receptive fields, 89–90
direction-selective ganglion cells of, 404–405
ganglion cells of
direction-selective, 455
dopaminergic inhibition of, 439
excitability of, 424, 425*f*, 434–435
membrane time constant of, 430–431
horizontal cells of
acetylcholine expression in, 370
action spectrum of, 373, 375*f*
chromaticity (C-type), 371, 373, 374*f*
feedback from, 382–383, 383*f*
gap junctions between, 372
ion channels in, 378*f*, 378–379
luminosity, 373, 374*f*
morphology of, 370*f*, 370–371
nitric oxide and, 385
receptive fields of, 380*f*, 380–381
rod and cone mixing in, 375
ON and OFF stratification in, 267
- Twilight
retinal circuits for signal transmission at, 247–249, 248*f*
rod function at, 240, 247–249, 248*f*
- Two-back task, prefrontal cortex (PFC)
damage and, 1551
- Tyrosinase gene, mutation of, and ganglion cells, 71, 100*f*, 102–103
- Tyrosine hydroxylase, 313, 313*f*
- Tyrosine kinase receptor(s), neurotrophin binding to, 46, 48*b*
- U**
- Ultraviolet light
circadian sensitivity to, 627
cones sensitive to, 372
Ultraviolet photopigment, 965
Unawareness, in blindsight, 659, 660–661
Uncertainty
definition of, 1624
hierarchical resolution of, 1624, 1627
in stereopsis, 1304–1305
Uncertainty explanation, of psychometric function, 821
Uncertainty principles, 1624
Unclipped cells, 1451
Univariance, 909, 1003, 1004
Univariant system, in scotopic vision, 838
Uvula, ventral, in eye movement control, 1486, 1489–1490
- V**
- Varin figure, 1129–1130, 1130*f*, 1132, 1136
- Vascular endothelial growth factor (VEGF), production of, by Müller glia cells, 41
- Vasoactive intestinal polypeptide (VIP)
adenylate cyclase stimulation by, 336, 345–346
amacrine cells expressing, 344–345, 345*f*
binding sites of, 336
cellular physiology studies/calcium imaging of, 337
coexpression with GABA, 336
retinal, 334–335, 344–346, 348–349
binding sites of, 345–346
cellular physiology studies of, 346, 346*f*
functional studies of, 346
ion channel modulation by, 346, 346*f*
localization of, 345–346
- Vasoactive intestinal polypeptide (VIP)
receptors
mRNA of, 336
retinal, 336, 346
- Vax-1* gene
expression of, in optic cup and optic vesicle, 34, 35*f*
and optic chiasm development, 100*f*, 101
- Vax-2* gene
and opsin expression, 40
and optic chiasm development, 101
and positioning of retinal cells, 42
- VC1.1, in retinal cell differentiation, 78
- Veiling effect, in dark adaptation, 853
- Velocity (speed) selectivity
in area MT neurons, 1206–1207, 1207*f*, 1213
of complex cells, 715
of single neurons, 17
temporal and spatial inseparability in, 26
- Ventral cortex, motion sensitivity of, functional mapping of, 1234*f*, 1235–1236
- Ventral diencephalon
albinism and, 102
cellular specializations in, 96–98
diffusible signal from, and regulation of retinal cell axons, 98
gene transcription in, 101–102
optic chiasm development in, 94–103
- Ventral intraparietal area. *See* VIP (ventral intraparietal) visual area
- Ventral intraparietal sulcus, motion sensitivity of, functional mapping of, 1234–1235
- Ventral midline, cellular specializations at, 96
- Ventral pathway. *See* Ventral stream
- Ventral stream, 489, 502, 541, 542*f*, 1080, 1151, 1152*f*, 1165, 1371, 1372*f*, 1585. *See also* TE visual area
anatomical organization of, 541, 542–544, 543*f*
architecture of, properties of, 1642
areas in, reciprocity among, 541, 543
category-general regions of, 1183–1184
category-selective regions of, 1179–1183, 1180*f*
development of
experiential factors in, 1186–1187
genetic factors in, 1186–1187
origins of, 1186–1187
connections beyond modality-specific visual system, 553–554
and consciousness, 1683
and dorsal stream, interactions of, anatomic substrate for, 544
in face recognition, 545, 1534. *See also* Face cells
feedforward inputs to, 150
functional organization of, 1179–1184
functions of, 1151
human, functional MRI of, 1179–1187
integration of information about motion, color, and form in, 553, 554*f*
lesions of, behavioral effects of, 541–542, 541*f*, 547–549
neurons in, 541
attention and, 546–547
experience and, 547
latency of, 530–532, 531*f*
properties of, 544–547
in object recognition, 544–546, 1086–1087, 1151, 1640
in outdoor scenes, 1534
processing in, 541
and saccades, 1374–1376
structural representation in, 1086–1088
subcortical connections with, 544
visual areas corresponding to, in macaque, 510*f*–511*f*, 512
- VEP. *See* Visual evoked potential(s)

- Vergence, 1301–1302, 1309, 1350, 1485 and accommodation
linkage of, 1419–1422, 1420*f*, 1421*f*, 1461–1462
synkinesis between, 1461–1462
control of
brain mechanisms for, 1415, 1445
conjugate versus monocular commands for, 1423–1424
higher-order, 1425
definition of, 1415, 1459
disparity-driven, 1419
fast smooth, 1349, 1349*f*
horizontal, 1415
motoneurons in, extraocular, 1415–1418, 1416*f*
muscle pulleys in, 1416*f*, 1418
under natural conditions, 1348–1349, 1349*f*
neural control of, 1415–1426, 1494
premotor commands in, 1418–1422
and saccades, interaction of, 1422–1423, 1423*f*, 1460–1461
saccadic, 1348–1349, 1349*f*
slow, 1348
smooth, 1348–1349, 1349*f*
torsional, 1415
vertical, 1415
Vergence gain, 1416, 1417*f*, 1418*f*
and accommodation gain, relationship between, 1419–1422, 1421*f*
definition of, 1421*f*
Vergence velocity, 1422, 1423*f*
Vermis
dorsal, in eye movement control, 1491–1493
in eye movement control, 1489–1490
oculomotor
in eye movement control, 1486, 1491–1494
in ocular motor learning, 1495–1496, 1495*f*
posterior cerebellar, and pursuit behavior, 1408, 1409
Vernier acuity, 69. *See also* Hyperacuity
development of, 181–182, 182*f*, 183*f*
as function of retinal eccentricity, 832, 832*f*
linear and nonlinear properties of, 753
luminance and, 1291
in scotopic vision, 844
Vernier acuity task, 929
Vernier offset thresholds, in visual evoked potentials, 182–183, 183*f*
Verrey, Louis, 1029–1030, 1030*f*
Version, 1301–1302
definition of, 1415, 1460
Version gain, 1416, 1417*f*, 1418*f*
Vertebrate(s)
extinct, color vision in, 964
lower, color vision in, 964
photopigments of, phylogeny of, 967, 967*f*
Vertebrate retina, development of, 77–90
molecular regulation of, 33–43
Vertical channel neurotransmitters, 304–307
Vertical cortical connections
functional contributions of, 733
functional relationship with horizontal connections, 734, 743
identification of, 733–734
intrinsic, 149
in length summation and endstopping, 740
and neuronal synchrony, 743
and response properties of cortical neurons, 733–743
spatial overlap with horizontal connections, 734, 738–739
Vertical pathway
linkage of photoreceptors and bipolar cells to ganglion cells in, 320
visual signaling in, 320–330
Vesicular acetylcholine transporter (VACHT), 311, 312*f*
Vesicular amine transporters (VMATs), 313*f*, 314, 315*f*
Vesicular GABA transporter (VGAT), 250, 289, 308*f*, 308–309, 311
Vesicular glutamate transporters (VGluT1 and VGluT2), 304, 305*f*, 307
Vesicular glycine transporters, 310*f*, 311
Vesicular inhibitory amino acid transporter (VIAAT), 311
Vestibular cortex, and optic flow neurons, 1271–1272
Vestibular nuclei, and pursuit behavior, 1408
Vestibulocerebellum, in eye movement control, 1487–1489
Vestibulo-ocular reflex, 1343, 1403, 1485, 1489, 1490
cross-coupled, 1489
latency of, 1430
rotational (r-VOR), 1485, 1489
translational (t-VOR), 1485, 1489, 1490*f*
View(s)
canonical, 1083
neuronal tuning for, 1171–1172, 1641
prototypical, 1650
Viewpoint problem, 1083
Vignetting, 1093, 1093*f*, 1094–1095, 1099
Vimentin, 79
VIP (ventral intraparietal) visual area, 529*f*, 543
in dialogue between cerebral cortex and superior colliculus, 1471
macaque, 510*f*–511*f*, 511–512, 529*f*
connections with area MT, 1203, 1204*f*
lateral (VIPl), 510*f*–511*f*, 511
medial (VIPm), 510*f*–511*f*, 511
motion sensitivity of, functional mapping of, 1234–1235
neurons
attentional modulation of, 1542, 1542*f*
response characteristics of, 1425
in vergence control, 1425
optic flow responses in, 1267–1268
in spatial processing, 551
VIP* visual area, macaque, 510*f*–511*f*, 512
VIP/PACAP receptors, retinal, 336, 346
Visual acuity, 1339
binocular deprivation and
in cats, 191*f*, 191–192, 192*f*
in humans, 193
in monkeys, 192–193
blockade of endogenous neurotrophins and, 52, 54*f*
in central visual field, 176
contour orientation restrictions and, 199–200, 200*f*
dark rearing and, 50, 53*f*
effects of exogenous neurotrophins on, 50–52, 53*f*
development of, 46, 47*f*
and eccentricity, 1044
growth factors and, 136
in low-light conditions, 70
monocular deprivation and, 51*f*–52*f*
in cats, 194*f*, 194–196, 195*f*
effects of exogenous neurotrophins on, 50, 51*f*–52*f*, 135, 136
overexpression of BDNF and, 55–58, 58*f*, 136
receptive field properties and, 166, 166*f*
retinal cell numbers and, 69
spatial, development of, 178–179, 179*f*
Visual area(s), 541
AIT, macaque
dorsal (AITd), 510*f*–511*f*, 512
ventral (AITv), 510*f*–511*f*, 512
anatomical connections of, 541, 543*f*
asymmetries in, 509
boundaries of
subtlety in, 509
uncertainty in, 509, 512–513
CIT, macaque
dorsal (CITd), 510*f*–511*f*, 512
ventral (CITv), 510*f*–511*f*, 512
connections between, 149–150
distinctiveness of, 149
dorsolateral (DL), 1568*f*, 1569
dorsomedial (DM), 1568, 1568*f*, 1569
dorsomedial occipital complex (DMOcx), macaque, 512, 513*f*
DP (dorsal prelunate), macaque, 510*f*–511*f*, 512
homology with human visual area, 518
extrastriate, 11, 515

- behavioral evidence for functions of, 11
- FEF (frontal eye field). *See* Frontal eye field (FEF)
- frontal, in macaque, 510*f*–511*f*, 512
- FST (floor of superior temporal area)
 - connections with area MT, 1203, 1204*f*
 - macaque, 510*f*–511*f*, 511
- functional specializations of, 149
 - receptive field tuning properties and, 720
- fusiform face (FF), 515, 516*f*
- genuine incompatibility of, 509
- gradients in, 509
- hierarchy of, 528–530, 529*f*
- human, 513–515
 - comparison with macaque, 515–518, 517*f*
 - criteria for, 1231
 - functional modalities of, 513, 515, 516*f*
 - organization of, 513–515, 514*f*, 516*f*
 - total cortical area occupied by, 513
- identification of
 - criteria for, 507
 - robustness, consistency, and replication in, 509
 - technical impediments to, 508–509
- individual variability in, 509, 512–513
- inferotemporal
 - human, 515, 516*f*
 - human versus macaque, 518
 - in macaque, 510*f*–511*f*, 512, 513*f*
- internal heterogeneity in, 509
- IPa, macaque, 510*f*–511*f*, 512
- KO (kinetic occipital), 1029, 1036–1037
- LIP (lateral intraparietal), macaque, 510*f*–511*f*, 511–512
 - dorsal (LIPv), 510*f*–511*f*, 511–512
 - homology with human visual area, 518
 - ventral (LIPv), 510*f*–511*f*, 511–512
- LO (lateral occipital)
 - human, 515, 516*f*, 517–518
 - and illusory contour perception, 1124
- LOC/LOP complex, human, 515, 516*f*
- LOP (lateral occipital parietal), macaque, 510*f*–511*f*, 512
 - homology with human visual area, 518
- lumping versus splitting of, 509
- macaque
 - comparison to human, 507, 515–518, 517*f*
 - composite map of, 512, 513*f*
 - frontal, 510*f*–511*f*, 512
 - inferotemporal, 510*f*–511*f*, 512
 - number of subdivisions in, 512
 - occipital, 508, 509–511, 510*f*–511*f*
 - organization of, 507–513
 - parietal, 508, 510*f*–511*f*
 - posterior, 510*f*–511*f*, 511–512
 - partitioning schemes for, 507–513, 510*f*–511*f*, 513*f*
 - differences among, reasons for, 509
 - multiple, coping with, 512–513
 - temporal, 508, 510*f*–511*f*, 511–512
 - dorsal, 510*f*–511*f*, 511–512
 - ventral, 510*f*–511*f*, 512
 - total cortical area occupied by, 507
 - mapping techniques for, 507
 - impediments in, 508–509
 - magnetic resonance imaging, 507, 508*f*, 513, 514*f*, 518
 - probabilistic, 513
- MDP (medial dorsal parietal), macaque, 510*f*–511*f*, 512
- MIP (medial intraparietal), macaque, 510*f*–511*f*, 512
- modularity of, 509
- monkey, 541, 542*f*, 544*t*
- motion-sensitive
 - behavioral functions of, 1239, 1241
 - functional mapping of, 1229–1243
 - and movement control, 1241
- mouse, 518
- MST. *See* Medial superior temporal area (MST)
- MT+, human, 515, 516*f*
- MT (middle temporal). *See* Middle temporal (MT) visual area
- MTc, macaque, 510*f*–511*f*, 511
- occipital
 - human, 515, 516*f*
 - in macaques, 508, 509–511, 510*f*–511*f*, 512, 513*f*
- outside primary visual cortex, 10–11
- owl monkey, 11, 518
- parahippocampal place (PP), 515, 516*f*
- parietal, 11
 - human, 515, 516*f*
 - human versus macaque, 517–518
 - in macaque, 508, 510*f*–511*f*, 512, 513*f*
 - posterior, 510*f*–511*f*, 511–512
- PGa, macaque, 510*f*–511*f*, 512
- PIP (posterior intraparietal), macaque, 510*f*–511*f*, 511
- PIT, macaque
 - dorsal (PITd), 510*f*–511*f*, 512
 - ventral (PITv), 510*f*–511*f*, 512
- PO (parietal-occipital), macaque, 510*f*–511*f*, 511
- POa, macaque
 - external (POa-e), 510*f*–511*f*, 511–512
 - internal (POa-i), 510*f*–511*f*, 511–512
- posterior parietal complex (PPcx), macaque, 512, 513*f*
- prenatal specification of, 153
- rat, 518
- STP (superior temporal polysensory),
 - connections with area MT, 1203, 1204*f*
- subdivisions of, 509
 - number in macaques, 512
- TE1, macaque, 510*f*–511*f*, 512
- TE2, macaque, 510*f*–511*f*, 512
- TE3, macaque, 510*f*–511*f*, 512
- TEa, macaque, 510*f*–511*f*, 512
 - dorsal (TEad), 510*f*–511*f*, 512
 - ventral (TEav), 510*f*–511*f*, 512
- TE1-3d, macaque, 510*f*–511*f*, 512
- TEm, macaque, 510*f*–511*f*, 512
- temporal
 - human, 515, 516*f*
 - human versus macaque, 517–518
 - in macaque, 508, 510*f*–511*f*, 511–512, 512, 513*f*
 - dorsal, 510*f*–511*f*, 511–512
 - ventral, 510*f*–511*f*, 512
- TEO, macaque, 510*f*–511*f*, 512
 - homology with human visual area, 517–518
- TEr, macaque, 510*f*–511*f*, 512
- TE1-3v, macaque, 510*f*–511*f*, 512
- TF (temporal area F), macaque, 510*f*–511*f*, 511, 512, 513*f*
- TH (temporal area H), macaque, 510*f*–511*f*, 511, 512, 513*f*
- TPO (temporal parietal occipital), macaque, 510*f*–511*f*, 512
 - caudal (TPOc), 510*f*–511*f*, 512
 - intermediate (TPOi), 510*f*–511*f*, 512
 - rostral (TPOr), 510*f*–511*f*, 512
- V1, 513, 516*f*, 528, 529*f*, 541, 1031, 1031*f*, 1565, 1568–1569, 1568*f*. *See also* Primary visual (striate) cortex
- attentional response modulation in, 1515, 1517*f*
- in binocular rivalry, 1691
- color cells in, 1018
 - preferred colors of, 1019, 1020*f*
 - tuning of, 1020, 1021*f*
- contextual modulation in, 720–729
 - grouping of line segments and, 722, 722*f*
- phenomenology of, 721–725
 - simple versus multiple image elements and, 721, 721*f*
- dynamics of responses in, 1654–1655
- functional specializations of, receptive field tuning properties and, 720
- human, 1570
 - architectonic boundary of, 513
 - individual variability in, 513
 - surface area of, 513
- integration of information about motion, color, and form in, 553, 1023–1024
- lateral connections in. *See also* Lateral cortical connections
 - and contour integration, 1069–1077
- layer 4 of, 522

Visual area(s) (cont.)

- lesions of. *See also* Blindsight
 - retrograde transneuronal degeneration after, 666
- local feature representation of, 1139
- M scales for, 1578
- macaque, 509, 510*f*–511*f*
 - and figure-ground assignment, 1126
 - neuronal responses in, modulation by attention, 1538–1539
- in motion analysis, 1621–1622
- motion processing in, 549
- MT feedback to, 609, 614–622
- neuronal response properties in
 - contextual modulation of, 720–729
 - image representation model and, 1609–1613
- neurons, latencies of, 531–532, 531*f*
- neurons in
 - orientation tuning of, attention and, 1540–1541
 - response characteristics of, 1580
 - as spatial filters, 544
- optimization in, for natural scene perception, 1593–1594
- orientation architecture of, adaptation-induced orientation plasticity and, 1658–1660, 1659*f*
- orientation plasticity in, 1655–1657, 1656*f*
 - adaptation-induced, 1658–1660, 1659*f*
- plasticity in, 1654–1655
- receptive field size in, 720–721, 1045
- receptive field tuning properties in, 720–721
- sensory map plasticity in, 1654–1655
- shape tuning dimensions in, 1087
- spatial interactions in, 1115
- spatiotemporal receptive field (STRF)
 - estimation in, 1595, 1596*f*
- in texture segregation, 1115
- in vergence control, 1425
- in visual consciousness, 1689–1691
- in visuosaccadic system, 1467, 1467*f*
- V2, 10, 528, 529*f*, 544–545, 1031, 1031*f*, 1565, 1568–1569, 1568*f*
 - binocular disparity sensitivity in, 550
 - color cells in
 - preferred colors of, 1019, 1020*f*
 - tuning of, 1020, 1021*f*
 - connections with area MT, 1203, 1204*f*
 - human, 515, 516*f*
 - illusory contour responses in, 1140–1141, 1140*f*, 1141*f*
 - integration of information about motion, color, and form in, 1023–1024, 1023*f*
 - macaque, 509, 510*f*–511*f*
 - attentional response modulation in, 1515, 1516–1517
 - dorsal (V2d), 509, 510*f*–511*f*
 - dorsoventral asymmetry of, 509
 - and figure-ground assignment, 1126
 - and illusory contour perception, 1124
 - ventral (V2v), 509, 510*f*–511*f*
 - modules in, 542
 - motion processing in, 549
 - functional mapping of, 1235
 - neurons, 1139
 - latencies of, 531*f*
 - orientation-selective, 1144
 - side-of-figure selectivity of, 1143–1144, 1143*f*, 1144*f*, 1146
 - neurons in
 - perisaccadic receptive field shifts in, 1398
 - preferred features of, 1644
 - response characteristics of, 1579–1580
 - receptive field size in, 1045
 - shape tuning dimensions in, 1087
 - stripe and interstripe neurons in,
 - integration of information about motion, color, and form in, 553
 - in texture segregation, 1115
- V3, 11, 529*f*, 1031, 1031*f*, 1568, 1568*f*, 1569
 - binocular disparity sensitivity in, 550
 - color cells in, 1018
 - preferred colors of, 1020, 1020*f*
 - tuning of, 1020, 1021*f*
 - connections with area MT, 1203, 1204*f*
 - dorsal (V3d), 1031, 1569
 - human, 515, 516*f*
 - macaque, 509, 510*f*–511*f*
 - human, 515, 516*f*
 - and illusory contour perception, 1124
 - integration of information about motion, color, and form in, 1023–1024, 1023*f*
 - macaque, 509, 510*f*–511*f*
 - dorsoventral asymmetry of, 509
 - motion processing in, 549
 - neurons, latencies of, 531–532, 531*f*
 - in texture segregation, 1115
 - ventral (V3v), 1031, 1569
 - human, 515, 516*f*
 - macaque, 509, 510*f*–511*f*
- V4, 542, 545, 1032, 1033*f*, 1371, 1372*f*
 - in attention and eye movements, 1597
 - attentional response modulation in, 1516–1517, 1517*f*
 - binocular disparity sensitivity in, 550
 - color cells in, 1018–1019
 - preferred colors of, 1020
 - in color constancy, 1024–1026
 - contour fragment representation in, 1081*f*, 1084–1086, 1084*f*, 1085*f*, 1086*f*
 - dorsal (V4d), macaque, 509–511, 510*f*–511*f*, 517–518
 - functional specializations of, receptive field tuning properties and, 720
 - higher-level pooling in, 1066
 - lesions of, behavioral effects of, 548, 551–552, 552*f*
 - macaque, 509–511, 510*f*–511*f*, 1036
 - attentional response modulation in, 1515–1516
 - and color vision, 1034
 - dorsal (V4d), 1036–1037
 - dorsoventral asymmetry in, 509–511
 - homology with human visual area, 517–518
 - individual variability in, 509–511
 - neurons, 1139
 - color selectivity of, 1021
 - latencies of, 531–532, 531*f*
 - responses of, modulation by surrounding stimuli, 1375
 - neurons in
 - attention and, 1540
 - attentional modulation of, 1541, 1542, 1542*f*
 - color tuning of, attention and, 1540–1541
 - orientation tuning of, attention and, 1540–1541
 - perisaccadic receptive field shifts in, 1398
 - preferred features of, 1644
 - receptive fields of, attention and, 1541
 - and saccades, 1375, 1376*f*
 - shape tuning in, 1087
 - subdivisions of, 1034
 - in texture segregation, 1115
 - topographic organization of, 1034–1035
 - ventral (V4v)
 - human, 515, 516*f*, 517–518
 - macaque, 509–511, 510*f*–511*f*
 - in visual search, 1597
- V5. *See* Middle temporal (MT) visual area
- V5+. *See* Middle temporal (MT) visual area, human homologue of
- V6, macaque, 510*f*–511*f*, 511
- V7, human, 515, 516*f*
 - homology with macaque visual area, 518
- V8, 1033–1034, 1033*f*
 - human, 515, 516*f*
 - homology with macaque visual area, 517–518
 - macaque, 510*f*–511*f*, 512
- V17, 513. *See also* Primary visual cortex
 - binocular deprivation and, in monkeys, 193
 - cortical connections in, 148, 149
 - discordant visual input and, 199
 - monocular deprivation and, 193–194
 - and perception, 202
 - visual deprivation and, 189, 202
- V46, macaque, 510*f*–511*f*, 512
- V3A

- human, 515, 516*f*
 - macaque, 510*f*–511*f*, 511
 - motion sensitivity of, functional mapping of, 1234, 1240, 1241
 - V3a, neurons in, perisaccadic receptive field shifts in, 1398
 - V6A, macaque, 510*f*–511*f*, 512
 - V3B, 1036
 - human, 515, 516*f*
 - ventral superior temporal complex (VSTcx), macaque, 512, 513*f*
 - VIP* (heavily myelinated division of VIP), macaque, 510*f*–511*f*, 512
 - VIP (ventral intraparietal), macaque, 510*f*–511*f*, 511–512
 - connections with area MT, 1203, 1204*f*
 - lateral (VIPl), 510*f*–511*f*, 511
 - medial (VIPm), 510*f*–511*f*, 511
 - VOT (ventral occipitotemporal), macaque, 510*f*–511*f*, 512
 - homology with human visual area, 517–518
 - VP (ventral posterior), 1029, 1031–1032
 - human, 515, 516*f*
 - macaque, 509, 510*f*–511*f*
 - motion processing in, functional mapping of, 1235
 - V4t, macaque, 510*f*–511*f*, 511
 - VTE, macaque, 510*f*–511*f*, 511
 - V4v, 1029, 1032–1034, 1033*f*, 1034
 - zones of, 509
 - Visual attention. *See* Attention, visual
 - Visual awareness. *See also* Change detection; Consciousness, visual
 - binocular rivalry and, 1319–1320
 - in blindsight, 659, 660–661
 - contextual modulation and, 728
 - failures of, 1524
 - Visual channels. *See also specific channel*
 - bandwidths (profiles) of, 938
 - colinear facilitation and, 1063–1064, 1064*f*, 1067
 - functional interaction of, 1063
 - pattern adaptation and, 936–938
 - subject to gain control, coupling of, 1063
 - Visual completion
 - amodal, 1126–1127, 1126*f*, 1129, 1131, 1131*f*, 1289, 1289*f*, 1297–1298
 - and depth perception, 1291–1292, 1292*f*
 - definition of, 1288
 - and depth perception, 1288–1289, 1289*f*, 1291–1292, 1292*f*
 - dual mechanism hypothesis of, 1289, 1292
 - identity hypothesis of, 1289–1291
 - inducers of, 1289
 - luminance and, 1290, 1291*f*
 - mechanisms of, 1298
 - modal, 1129, 1289, 1289*f*, 1297–1298
 - and depth perception, 1291–1292, 1292*f*
 - Visual consciousness, neuronal basis of, 1682–1693
 - Visual cortex, 541. *See also* Primary visual cortex
 - areas of. *See* Visual area(s)
 - attentional response modulation in, 1514–1518
 - binocular interaction in, 765–776
 - combination of left and right eye signals, 768, 770*f*
 - phase-shifted gratings for measurement of, 767–772, 768*f*–769*f*, 770*f*, 771*f*, 772*f*
 - ON cells of, pharmacologic blockade of, 272–273, 274*f*
 - columnar organization of, 733
 - connections of, 146–154
 - Cajal-Retzius neurons and, 150–151
 - callosal pathway of, 148
 - clusters of, 148–149, 151, 153
 - corticocortical, 147, 148–154
 - excitation and inhibition in, 154
 - extrinsic, 148
 - exuberant, 146, 148
 - feedback, 146–147
 - activity and, 153, 154
 - anterograde tracing of, 152–153
 - between cortical layers, 149–150
 - development of, 152*f*, 152–153
 - elimination of, 152*f*, 153
 - inhibitory and excitatory responses in, 154
 - laminar specificity of, 150–151
 - to lateral geniculate nucleus, 609–614, 610*f*, 611*f*, 622
 - maturation of, 152*f*, 153, 154
 - to perigeniculate nucleus, 609, 610
 - remodeling of, 152*f*, 153
 - retrograde tracing of, 152–153
 - to thalamic reticular nucleus, 609
 - feedback versus feedforward, 153, 154
 - feedforward, 146–147
 - between cortical layers, 149–150
 - development of, 151, 152*f*
 - directed growth and target selection by, 151, 154
 - inhibitory and excitatory responses in, 154
 - laminar specificity of, 150–151
 - to and from LGN, 154
 - retrograde tracing of, 151, 152*f*
 - termination of, 154
 - horizontal, 733–743
 - identification of, 733–734
 - local or short-range, 734–737, 737*f*
 - horizontal intrinsic, 148–149
 - interareal, 149–151
 - laminar specificity of, 150–151
 - of preplate neurons, 150–151
 - and synaptic organization, 153–154
 - topographic organization of, 150
 - intraareal, 148–149
 - intrinsic, 148–149
 - maximum extent of, 148–149
 - molecular cues for, 146
 - ontogenesis of, 146–154
 - precision of early, 146
 - pruning or elimination of, 146, 148, 153
 - receptive field effects of, 146, 148–151, 733–743
 - of subplate neurons, 151
 - thalamocortical, 146–148, 154
 - tracer injection size in experiments on, effect of, 149
 - vertical, 733–743
 - identification of, 733–734
 - and neuronal synchrony, 743
 - vertical intrinsic, 149
 - visual deprivation and, 153
- damage to
 - and blindness, 747
 - and pupil responses, 647, 648*f*, 654*f*
- development of, 146
 - accelerated, overexpression of BDNF and, 55–58, 57*f*, 58*f*, 136
- activity/experience and, 165, 167, 170
- extrinsic control of, 146
- intrinsic control of, 146
- neural factors in, 165–170
- pioneering role of subplate neurons in, 151
- protocortex theory of, 146
- protomap theory of, 146
- visual deprivation and, 167–170
- in early primates, 1568–1569, 1568*f*
- in form vision, 530
- functional areas of, 522
 - communications between, 522–536
- functional segregation in, 496, 497*f*
- geniculostriate projection of, and pupil responses, 641, 643
- hierarchical organization of, 528–530, 529*f*
- human
 - comparison with macaque, 515–518, 517*f*, 555
 - organization of, 513–515, 514*f*, 516*f*, 554, 555*f*
 - total cortical area occupied by, 513
- image parsing mechanisms of, 1139–1149
- integration time in, 185
- macaque
 - comparison with human, 515–518, 517*f*, 555
 - organization of, 507–513
 - partitioning schemes for, 507–513, 510*f*–511*f*, 513*f*

- Visual cortex (cont.)
 relationship to other sensory modalities, 507, 508*f*
 total cortical area occupied by, 507
 mapping techniques for, 507
 neurons of. *See* Visual cortex neurons
 ON and OFF cells of, 270
 organization of, hierarchical, 146, 149–150, 153, 541, 609
 passive versus dynamic role of, 146
 physiology of, interpretation of, 146–147
 plasticity of
 activity and, importance of, 128
 BDNF and, 53–55, 60, 128, 131, 133, 136*t*
 calcium and, 128, 129, 130, 136*t*, 137, 137*f*, 139
 CREB and, 132–133, 136*t*, 137, 137*f*
 cyclic AMP and, 129, 131–132
 dark rearing and, 128, 129, 130, 131, 132, 133–134
 electrical activity and, 54
 factors in, 137*f*, 137–139
 versus activity-related factors, 128
 evaluation of, 128–139
 instructive, 128–134
 modulatory, 128, 134–139
 summary of, 136, 136*t*
 feedback pathways in, 137
 forms of, 126
 GABA and, 127, 130–131, 133, 136–137, 137*f*, 139
 gate hypothesis of, 131, 137
 gene expression and, 133–134
 glutamate receptors and, 126, 128, 129–130, 132, 136*t*, 137, 137*f*
 inhibition and, 58
 MAPK cascade and, 59*f*, 59–60, 132, 136*t*, 137, 137*f*
 mechanisms of, 126–139
 as model for nervous system, 126
 monocular deprivation and, 126, 132, 135
 nerve growth factor and, 135, 136*t*
 nervous system states and, 128, 134
 neurotransmitters and, 128, 134–135, 136*t*, 137*f*, 139
 neurotrophins and, 47*f*, 48–49, 52–55, 58–60, 59*f*, 61
 possible sites of action for, 60, 60*f*
 NMDA receptors and, 129, 136*t*, 137, 137*f*, 139
 physiologic efficacy in, 137–138, 138*f*
 presynaptic and postsynaptic changes in, 138–139, 139*f*
 protein kinase A and, 131–132, 136*t*, 137, 137*f*, 137–139
 protein synthesis and, 133–134, 138–139, 139*f*
 restoration of, in older animals, 136–137
 primate, 1568–1570, 1568*f*, 1570*f*
 sparse coding in, quantitative evidence for, 1605
 subdivisions of, 1568–1569, 1568*f*
 synaptic organization in, 153–154
 synaptic transmission in, modulation by neurotrophins, 55, 56*f*
 Visual cortex neurons
 analysis of, 747
 models at different levels of, 759–760
 binocular interaction in, 768–772, 770*f*, 771*f*, 772*f*
 contrast adaptation in, 754, 754*f*
 temporal dynamics of, 755
 contrast response function in, 752*f*, 752–753, 753, 753*f*
 as function of contrast, 755*f*, 755–756
 as function of contrast through time, 756, 756*f*
 models of, 759–760
 to optimal and non-optimal stimuli during first 20 msec., 756*f*, 756–757
 poststimulus time histograms of, 755*f*, 755–757, 756*f*
 temporal dynamics of, 755*f*, 755–757, 756*f*
 contrast-set gain control in, 753, 753*f*, 760–761
 temporal dynamics of, 756–757
 as depth detectors, 765–766
 descriptive models of, 759
 drifting steady-state measurements of, 749–750, 757
 as filters, 747–748, 747–749
 spatiotemporal, 748–749
 frequency domain analysis of, 748–749
 functional models of, 759–760
 functions of, 747–748
 ideal observer analysis at level of, 832
 integration interval in, 758
 latency shift in, 753–754, 754*f*, 759
 temporal dynamics of, 755
 linear properties of, 750–751
 neurometric function for, 821–822, 822*f*
 nonlinear properties of, 747–761
 linear systems analysis of, 749–750
 rapid and slow, 754–755
 temporal dynamics of, 749–750, 754–759
 orientation selectivity in, 117–119, 124, 179
 temporal dynamics of, 757–758
 performance of, assessment of, 748
 receptive fields of
 behavioral development versus physiological changes in, 165–167
 complexity of, 747
 development of properties of, 165*f*, 165–167, 166*f*
 horizontal connections and, 733–743
 spatial properties of, 166*f*, 166–167
 visual deprivation and, 167–170
 response expansion in, 752*f*, 752–753, 759
 temporal dynamics of, 756–757
 response properties of, cortical
 connections and, 733–743
 response rectification in, 751*f*, 751–752
 temporal dynamics of, 755
 response refractory period of, 751
 temporal dynamics of, 755
 response saturation in, 753, 753*f*, 759
 spatial frequency selectivity in, linear and nonlinear properties of, 753
 spatial frequency selectivity of, temporal
 dynamics of, 757–759
 stimulus selectivity of, 747–748, 761
 temporal dynamics of, 754–759
 structural models of, 760, 760*t*
 synchrony of
 horizontal connections and, 742*f*, 742–743
 vertical connections and, 743
 systems analysis of, 747, 748–749
 temporal dynamics of, 749–750, 754–759
 transient stationary measurements of, 749–750, 757
 types of, 750
 Visual deprivation. *See also* Binocular deprivation; Dark rearing; Monocular deprivation
 animal studies of, 189
 behavioral testing methods in, benefits and shortcomings of, 189–190
 behavioral versus physiological changes in, 168–170, 169*f*
 and extrastriate cortex development, 170–171
 human studies of, 46, 126, 189, 190, 193, 197–198
 magnitude of deficits induced by, in different species, 190
 motives for studies of, 189
 neuronal correlates of, 167–171
 perceptual effects of, 189–202
 and spatial vision, 167–170, 168*f*, 169*f*
 and visual cortex
 connectivity effects of, 153
 developmental effects of, 165, 167–170
 Wiesel and Hubel's pioneering studies on, 147
 Visual dimensions, represented in visual system, 481–482
 Visual direction, 1300–1301
 Hering's rules of, 1300

- Visual discrimination learning, 12
- Visual evoked potential(s), 174–176
 chromatic waveforms in, 186, 186*f*
 in contrast sensitivity, 176–178, 186, 186*f*
 cortical, and contrast gain control, 889–890
 critical flicker frequency for, 177
 cyclopean, in binocular response, 184–185
 in direction selectivity, 182–184, 184*f*
 in early elements of visual pathways, 174
 latencies in, development of, 185*f*, 185–186
 monocular deprivation and, 51*f*–52*f*
 effects of exogenous neurotrophins on, 51*f*–52*f*
 motion asymmetry and, 183–184, 184*f*, 185*f*
 noise and, 174–175
 in orientation selectivity, 179–181, 180*f*, 181*f*
 oscillating motion thresholds in, 183, 183*f*
 in photoreceptor development, 176, 186, 186*f*
 in position selectivity, 181–182, 182*f*, 183*f*
 response functions of, sensory thresholds-
 base extrapolation of, 175
 in spatial vision development, 159
 steady-state, 174–175, 175*f*
 amplitude of, 174–175
 versus EEG, 174–175, 175*f*
 phase value of, 174–175
 swept-parameter (sweep), 175–176, 176*f*
 in grating acuity (resolution acuity), 178–179, 179*f*
 in position sensitivity, 182, 183*f*
 synchronization of response to stimulus
 in, 174
 time- or phase-locked, 174
 vernier offset thresholds in, 182–183, 183*f*
- Visual features. *See* Feature(s)
- Visual fields
 mapping/representation of
 on areas outside primary visual cortex, 10–11
 on cerebral cortex, 6–10
 electrical stimulation studies of, 9
 on lateral geniculate nucleus, 6–7
 on primary visual cortex, 8–10
 on striate cortex, 9–10, 10*f*
 spatial localization in, 11
 visual acuity in, 176
- Visual grasp reflex, 1431
- Visual latency. *See* Latency
- Visual memory. *See also* Memory
 storage of, 10
- Visual neglect syndrome, 1684. *See also*
 Neglect
- Visual pathways. *See also specific pathway*
 anatomical versus physiological
 classification of, 482
 animal models of, 494
 cancellation in, 845
 central, linear receptive field maps for
 neurons of, 707–708, 708*f*
 color and space representation in, 488
 in color vision, 488, 490, 497–498, 1217,
 1219–1220
 connectivity of, 485, 486*f*
 dorsal. *See* Dorsal stream
 dysfunctions attributed to, 490
 functions of, 489–491
 based on clustering or functional
 properties, 489
 lesion studies of, 489–490, 490*f*
 future directions for study of, 491
 independence versus interdependence of,
 490–491
 koniocellular. *See* Koniocellular pathway(s)
 of lateral geniculate nucleus, 481–491
 magnocellular. *See* Magnocellular
 pathway(s)
 in motion processing, 1206
 chromatic, 1217–1226
 ON and OFF, 260–274. *See also* ON and
 OFF pathways
 parallel, 481–482, 485, 494–503
 ambient versus focal, 495
 anatomical classification of, 496, 496*f*
 comparative perspective on, 494–503
 functional basis of, 496, 497*f*
 functional implications of, 501–503
 historical perspective on, 494–496
 linear systems approach to, 495
 number projecting to and through
 primate LGN, 496–498
 organization in primary visual cortex,
 498–501, 499*f*, 501*f*
 unanswered questions about, 503
 parvocellular. *See* Parvocellular pathway(s)
 retinal eccentricity and, 484–485
 for rod system, 844–845
 direct, to OFF bipolar cells, 845
 dual, 848
 in scotopic vision, 487–488, 488*f*, 841,
 844–845
 dual, 848
 underlying anatomical certainty for,
 482–485
 ventral. *See* Ventral stream
 “what” and “where,” 489, 495–496
- Visual persistence, 1628
- Visual processing. *See also specific visual processes*
 attentional influences on, 546–547
 color and motion streams of, merging of,
 1217–1226
 early stages of, anatomical and functional
 organization of, 117–119, 118*f*
 early studies of, 3–12
 experience and, 547
 feedback systems in, 609–623
 hierarchical nature of, 146, 149–150,
 153, 541, 609
 stimulus selectivity and, 747–748
 transduction by photoreceptors in,
 215–230
- Visual radiations, lesions of, 5
- Visual recognition, prefrontal cortex (PFC)
 damage and, in monkeys, 1553
- Visual response, in visuosaccadic behavior,
 1468–1470, 1469*f*
- Visual search, 728, 1108
 and attention, 1369–1371, 1370*f*
 computational models of, 1597
 definition of, 1369
 gaze in, 1369, 1370*f*
 V4 activity in, 1597
 and visual target selection, 1369–1371,
 1370*f*
- Visual search flicker task, 1526
- Visual streams. *See also* Dorsal stream;
 Ventral stream
 blob, 1625*f*, 1627
 and complementary properties, 1624
 as independent modules, 1624
 interactions of, 1624
 processing stages in, 1624
 surface, seeing by, 1627–1628
- Visual target(s)
 localization of, auditory, 1327,
 1329–1330, 1329*f*, 1397, 1397*f*
 for pursuit, selection of, 1402–1403
 selection of, 1369–1384, 1402. *See also*
 Saccades, targets for
- Visuosaccadic behavior, in monkey,
 neuronal activity in, stages of,
 1468–1470, 1469*f*
- Vitreous space, increase in, reading and,
 207–208
- Volition. *See also* Executive function
 and prefrontal cortex, 1546–1559
- Voltage-clamp amplifiers, for recording ion
 conductances in ganglion cells, 434
- Voltage-gated ion channels
 and ganglion cell excitability, 424–425,
 432–434
 in ganglion cells, 435
 in horizontal cells, 378–379, 379*f*
 von Kries adaptation, 900–901, 940,
 955–957
- Voronoi domain analysis, neuronal mosaic
 measurement based on, 473
- VOT (ventral occipitotemporal) visual
 area, macaque, 510*f*–511*f*, 512
 homology with human visual area,
 517–518
- VP (ventral posterior) visual area
 human, 515, 516*f*

VP (ventral posterior) visual area (cont.)
macaque, 509, 510*f*–511*f*
motion processing in, functional mapping
of, 1235
VTF visual area, macaque, 510*f*–511*f*, 511

W

W cells, 495, 566–567
chromatic sensitivity in, 498
circadian role of, 628
cortical connections of, 499
homology to K cells, 487
parallel projections of, 496, 496*f*
S-cone driven, 502
subgroups of, 499
Waggle dance, of bees, 1197
Waking state, burst firing patterns of LGN
cells in, 612
Wallenberg's syndrome, 1492
Wallpaper illusion, 1302, 1302*f*
Wasp(s), color vision in, 963
Watercolor effect, 1583, 1583*f*
Waterfall illusion, 936, 1505
hMT/V5+ visual area activity during,
1237–1239
Wave aberration(s), 795
in aberrated eye, 795, 796*f*
capture by pupil function, 796
in corrected eyes, 807–808
decomposition into component
aberrations, 795–796, 797*f*
and image formation, 795–797
in perfect eye, 795, 796*f*
in real eyes, 795, 796*f*
Zernike modes of, 795–796, 797*f*
Wavelength
cone sensitivity to, 176, 186, 186*f*
dominant, 892
horizontal cell dependency on, 373–374,
374*f*
and thresholds, 820
Wavelength discrimination, 658, 913, 913*f*.
See also Color discrimination
in dogs, 963, 963*f*
Weber law region, 912
Weber's law, 815–816, 817, 817*f*, 859, 912,
917, 1046, 1046*f*
Weber fraction, 1304
Wertheimer, Max, 1573–1574, 1578, 1585
“What” visual pathway, 489, 495–496

“Where” visual pathway, 489, 495–496
White noise, 1591, 1591*f*
domain analysis with, 748
in ideal observer analysis, 833, 833*f*
in MT speed selectivity analysis,
1206–1207, 1207*f*
as stimuli for mapping receptive fields,
706–707, 714
White-black dimension, 894, 894*f*,
897–898, 897*f*
Whiteness, 1092
Wiesel, Torgsten, 11, 17, 18, 23, 49, 108,
126, 127, 147
Wire volume, retinal, correlation with
information capacity, 245, 255
Wisconsin Card Sorting Test, 1550, 1550*f*
Working memory, 544
in cognitive control, 1547
definition of, 1547, 1551
prefrontal cortex (PFC) and, 1556–1557
prefrontal cortex (PFC) damage and,
1551, 1552
spatial, and MSTd neuronal responses to
optic flow, 1277, 1277*f*
and visual consciousness, 1686

X

X cells, 17, 495, 566–567, 568, 569*f*
cortical connections of, 498–499, 681
firing patterns of, cortical feedback and,
611–612
Golgi, flat-mount image of, 263, 263*f*
homology to M and P cells, 486–487
inhibitory surrounds of, 355
morphology of, 568
ON and OFF, 262*f*, 262–263, 673
axonal arborization in LGN, 271, 271*f*
distribution of, 267–268
parallel projections of, 496, 496*f*
subgroups of, 499
X chromosome
and color vision defects, 975–976
photopigment genes on, 979–980, 980*f*,
1005
expression of, 983–986
X inactivation, 976, 977
X-chromosome incomplete achromats, 875
Xenopus
eye field demarcation in, 33
optic chiasm development in, 99

optic chiasm in, organization of, 94
retinal cell development in, 63, 64–65,
65*f*
retinal cell differentiation in, 79
retinal progenitor cells in, 37

Y

Y cells, 17, 495, 566–567, 568, 569*f*
axonal bifurcations, 527
central projections of, 270
cortical connections of, 498–499, 681
firing patterns of, cortical feedback and,
611–612
Golgi, flat-mount image of, 263, 263*f*
homology to M cells, 486–487
inhibitory surrounds of, 355
morphology of, 568
ON and OFF, 262*f*, 262–263, 673
axonal arborization in LGN, 271, 271*f*
distribution of, 267–268
parallel projections of, 496, 496*f*
subgroups of, 499
Young, Thomas, 3, 12

Z

Zebrafish
astray mutants of, optic chiasm
development in, 100, 100*f*
bipolar axons in, stratification of, 268,
269*f*
cyclops mutant in, 34
lakritz mutants, retina lamination in, 83
ON and OFF pathways in, 266
electroretinogram of, 261, 261*f*
Pax2 (noi) mutants of, optic chiasm
development in, 101
positioning information across retina in,
41
retinal cell differentiation in, 467
young mutants, retina lamination in, 83
Zernike modes
average magnitude in normal population,
796, 797*f*
radial order of, 795–796
of wave aberrations, 795–796, 797*f*
Zinc
GABA receptor response to, 356*t*, 359
glycine receptor response to, 356*t*,
358–359
Zone models, 895–896, 917